

**JANUARY/FEBRUARY 2003**  
**Volume 14, Number 1**

© Copyright 2003 by the American Chemical Society

# ***Bioconjugate Chemistry***

## **EDITORIAL**

We welcome Professor Teruo Okano as Associate Editor of *Bioconjugate Chemistry*. Dr. Okano is Professor and Director of the Institute of Advanced Biomedical Engineering and Science at Tokyo Women's Medical University. He has an outstanding record in biomaterials and drug delivery, and we look forward to his service to the journal.

At the same time, Professor Mitsuru Hashida has finished his term as Associate Editor and will be stepping down. We thank Professor Hashida for his help, advice, and contributions to *Bioconjugate Chemistry*, and we wish him all the best in his future endeavors.

## **Thanks to Our Reviewers**

It is a pleasure to acknowledge the contributions of the reviewers of manuscripts submitted in 2002 for publication in *Bioconjugate Chemistry*. Their unselfish service has been essential in the shaping of the 13th volume of the journal. The scientific community is fortunate that its members are willing to share their time and specialized knowledge in this way. The reviewers are listed on the following page.

*Claude F. Meares*  
*Editor-in-Chief*

## List of Reviewers

Maciej Adamczyk  
Greg Adams  
Steven Ansell  
Ulysse Asseline  
Mariusz Banaszczyk  
Joel Barrish  
Serge Beaucage  
Craig Beeson  
Jean-Paul Behr  
Carolyn Bertozzi  
Erik Biessen  
Gary Bignami  
Alexei Bogdanov, Jr.  
Elijah Bolotin  
Martin Brechbiel  
Merlin Bruening  
Art Broom  
David Corey  
Masad Damha  
Gary David  
Mark Davis  
Vincent de Groot  
Mahendra Deonarain  
Mrinal Dewanjee  
Mark Distefano  
Gene Dubowchik  
Peter Fischer  
Warren Ford  
Keith Fox  
Ari Gafni  
Elisa Garcia-Garayoa  
Jerome Gaucheron  
Julia Gee  
Kyle Gee  
Catherine Gebhart

Lars Gedda  
Kieran Geoghegan  
David Goodwin  
David Grainger  
Mark Green  
Richard Greenwald  
Gary Griffiths  
Anne Gruaz-Guyon  
Hermann Gruber  
Elisha Haas  
Robert Hammer  
Fred Hawthorne  
Claude Hélène  
Donald Hnatowich  
Leaf Huang  
Yuji Inada  
Gérard Jaouen  
Knud Jørgen Jensen  
Lee Josephson  
Kazunori Kataoka  
John Keana  
David Kerr  
Thomas Kissel  
Hiromi Kitano  
Toni Kline  
Hisataka Kobayashi  
Kenji Kono  
Jindrich Kopecek  
Ulo Langel  
Christopher Leamon  
Robert Lee  
Jean-Christophe Leroux  
Susan Lever  
Stephen Lippard  
Shuang Liu

Harri Lönnberg  
Timo Lovgren  
Helmut Mäcke  
Hiroshi Maeda  
Ram Mahato  
Atsushi Maruyama  
Akira Matsuda  
Damon Meyer  
Lyle Middendorf  
Patrick Midoux  
Mark Mrksich  
Michel Monsigny  
Barbara Mueller  
Tom Muir  
Akira Murakami  
Dario Neri  
Peter Nielsen  
Makoto Oketani  
Ichiro Okura  
Leslie Orgel  
David Oupicky  
Roger Pak  
William Pardridge  
Marguerite Pitié  
David Piwnica-Worms  
Richard Pon  
Marco Ponzi  
Alain Rabie  
Tariq Rana  
Michael Reed  
Jean-Serge Remy  
Mark Reynolds  
Kevin Rice  
Blanka Rihová  
Keith Rose

Vincent Rotello  
Hideo Saji  
Russell Sanderson  
Etienne Schacht  
Roger Schibli  
August Schubiger  
Peter Seeburger  
Jolanta Sereikaite  
Lonnie Shea  
Terry Sheppard  
John Shively  
Kevin Smith  
Stanley Stein  
Russell Stewart  
Francis Szoka, Jr.  
Jonathan Tait  
Thomas Thompson  
Donald Tomalia  
Vladimir Torchilin  
Ching-Hsuan Tung  
Ganesan Vaidyanathan  
Pierre Vierling  
Wynn Volkert  
Ernst Wagner  
Alan Wahl  
Michael Welch  
George Whitesides  
Eric Wickstrom  
Scott Wilbur  
David Wilson  
Wolfgang Wrasidlo  
John Yates  
Samuel Zalipsky  
Michael Zalutsky



# REVIEWS

## Synthesis of Target-Specific Radiolabeled Peptides for Diagnostic Imaging

Jakub Fichna and Anna Janecka\*

Department of Medicinal Chemistry, Medical University of Lodz, Lindleya 6, 90-131 Lodz, Poland.  
Received April 23, 2002

### INTRODUCTION

Radiopharmaceuticals are drugs containing atoms of some radioactive elements. They are designed for diagnostic or therapeutic purposes, to deliver small doses of ionizing radiation to the disease sites in the body. Radiopharmaceuticals, unlike classical chemotherapeutics, act against malignant cells with high specificity. Radiopharmaceuticals are mostly small organic molecules, such as peptides or peptidomimetics, but they can also be macromolecules, for example antibodies.

Biodistribution of radiopharmaceuticals can be determined either by their chemical and physical properties or by their biological interactions. Radiopharmaceuticals, which act through receptor binding, are called target-specific. Ideally, these radiopharmaceuticals are designed to locate with high specificity at cancerous tumors, even if their location in the body is unknown, while producing minimal radiation damage to normal tissues (1–6). In the past decade significant progress has been made in the development of peptide-based target-specific radiopharmaceuticals, which have become an important class of imaging agents for the detection of various diseases, such as tumors, thrombosis, and inflammation.

Many excellent reviews have been published discussing different aspects of radionuclide chemistry and therapy (7–9) and the use of radiopharmaceuticals for diagnosis and treatment of different pathological conditions (10–19). Most popular technetium radiopharmaceuticals (20–28), as well as those incorporating other radionuclides (29, 30), have been reviewed. Antibodies (24, 25), peptides (23, 30–35), and steroids (36) as targeting molecules have been described.

In this review, which is limited to the use of small peptides as targeting molecules, we attempt to summarize, from the chemical point of view, the development of labeling methods, in particular the application of different bifunctional chelating agents. We also give a short description of radionuclides used with these agents. Radiopharmaceuticals based on small peptides, which are in clinical use or under investigation in preclinical and clinical trials, are also mentioned.

### LABELING METHODS

**Direct Labeling.** Direct labeling methods (Table 1) are mostly based on the binding of a radionuclide to thiol groups in the targeting molecule, that seems relatively

easy to perform (37, 38). However, such a labeling process is difficult to control, for its detailed chemistry is unknown and may lead to unplanned changes in the structure, stability, and pharmacokinetic properties of the labeled molecule. Furthermore, very little is known about the number of donor atoms in the labeled molecule and the geometry of radionuclide coordination. The stability in vivo of a synthesized complex also remains uncertain.

The direct labeling approach is rather unsuitable for small peptides, which either do not possess disulfide linkage or are unable to maintain their activity after reduction. For example Thakur (39) has reported the alteration of the receptor binding properties of the radiolabeled somatostatin analogues, when the disulfide bridge was reduced to free thiol groups and subsequently radiolabeled with  $^{99m}\text{Tc}$ . However, direct labeling has been successfully applied for labeling of the platelet receptor-binding peptide with  $^{99m}\text{Tc}$  (40, 41) and for high molecular weight proteins such as antibodies and their fragments (42, 43).

**Chelate Methods.** In chelate methods (Table 1) a radionuclide is bound to the targeting molecule indirectly, through a bifunctional chelating agent (BFCA) (Figure 1).

In general, a radiopharmaceutical containing a BFCA consists of the following parts: a targeting molecule, BFCA, radionuclide, and a linker (22). The targeting molecule is a carrier of a radionuclide to the receptor site in vivo. A radionuclide serves as a radiation source. A BFCA, covalently attached to the targeting molecule, functions as the coordinator of the radionuclide. A linker, not always necessary, is a spacer residue, which separates a targeting molecule from a chelating agent.

Functional groups, naturally present in the peptide or introduced synthetically, are responsible for covalent attachment of BFCA. Naturally occurring functional groups include terminal, as well as side-chain amino and carboxy groups, thiol groups from cysteine, and *p*-hydroxyphenyl from tyrosine. BFCA must contain a conjugation group, which is used for attachment of the peptide.

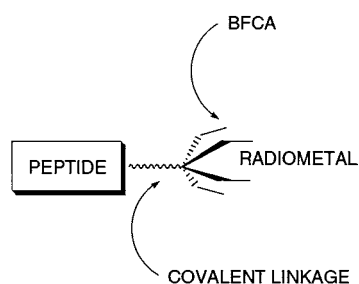
Several types of conjugation groups, active esters, isothiocyanates, maleimides, hydrazides, and  $\alpha$ -haloamides are used to form BFCA–peptide linkages (Figure 2).

Active esters can be used to form an amide bond between a carboxy group of a BFCA and an amino group in a peptide ligand. Since they are at a low level of activation, side-reactions during coupling are generally less of a problem than with most amide bond forming procedures. Commonly used are *p*-nitrophenyl, pen-

\* Address for correspondence: Dr. Anna Janecka, Department of Medicinal Chemistry, Medical University of Lodz, Lindleya 6, 90-131 Lodz, Poland. Tel/fax: (4842) 6784277. E-mail: ajanecka@csk.am.lodz.pl.

**Table 1. General Overview of Applied Labeling Methods**

labeling method	main principle	targeting molecule	advantages	disadvantages	ref
direct labeling	radionuclide binds directly to active groups present in the targeting molecule	high molecular weight molecules	easy to perform	unknown chemistry	(32, 35, 37, 38)
chelate methods				unknown geometry of a radionuclide-targeting molecule complex possible damage to targeting molecule during labeling process	
prelabeling	labeling of BFCA followed by conjugation with the targeting molecule	small peptides	relatively easy to control, well-defined chemistry	time-consuming	(26, 32)
postlabeling	conjugation of BFCA to targeting molecule, followed by labeling of conjugate	small peptides	most popular method	complicated purification of obtained radiopharmaceutical possible damage to targeting molecule during labeling process	(35, 44)
			targeting molecule functional groups remain unlabeled		
			well-defined chemistry possible use of classical solid-phase or solution methods of the peptide synthesis		

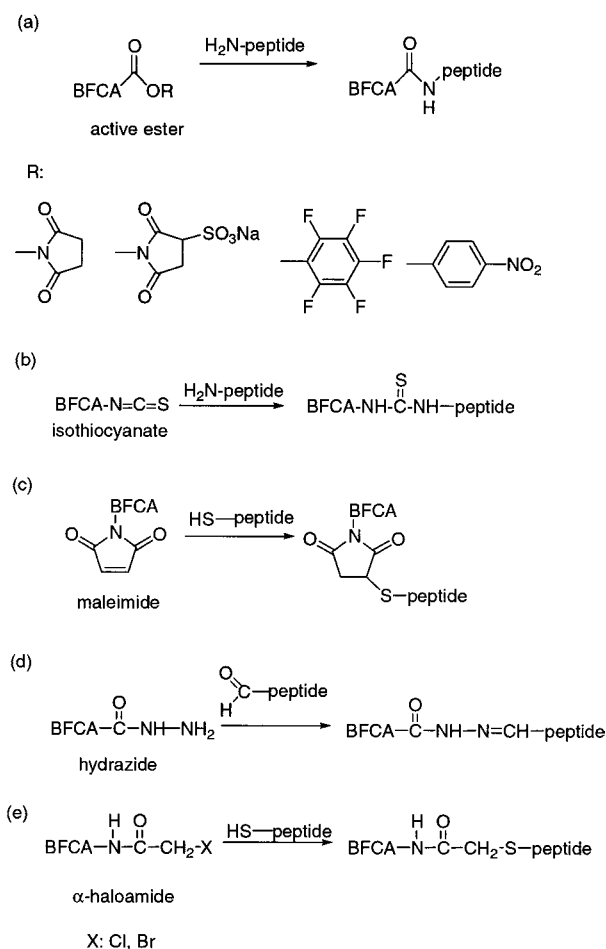
**Figure 1.** Schematic structure of a radiopharmaceutical. BFCA can complex a metal and also contains a functional group which forms a covalent linkage to a biological molecule, such as peptide.

tafluorophenyl, *N*-hydroxysuccinimide, and sulfo-*N*-hydroxysuccinimide active esters. The *N*-hydroxysuccinimide esters are very reactive with high selectivity toward aliphatic amines (22, 45). The choice of an active ester to be used for BFCA-peptide bond formation is partly dictated by sheer reactivity, but the ease of coproduct removal is also an important consideration. Thus, for water-insoluble BFCA-peptide conjugates, a succinimide ester coupling is especially convenient because both *N*-hydroxysuccinimide and sulfo-*N*-hydroxysuccinimide are very water-soluble (46, 47) and easy to remove. But for water-soluble BFCA-peptide conjugates *p*-nitrophenyl or pentafluorophenyl esters, which are ether-soluble, may be a better choice (48).

Isothiocyanates, like active esters, react with amino groups of a peptide forming thiourea bonds. Since they react best in the higher pH, they cannot be used with peptides susceptible to alkaline conditions.

The third class are maleimides, which react with thiols and form thioether bonds. The optimum pH for the reaction is near 7. At higher pH maleimides may hydrolyze to form nonreactive maleic acids (49, 50).

Hydrazides are conjugation groups which react with the aldehyde group of a peptide to form a hydrazone-

**Figure 2.** Reaction schemes for BFCA-peptide conjugation.

peptide conjugate. They are suitable for peptides containing 2-amino alcohol structure like in serine, threonine, and hydroxylysine, which can be very rapidly oxidized

by periodate at pH = 7 to generate an aldehyde. The use of a low molar ratio of periodate to peptide minimizes the potential for side-reactions during the oxidation. The formed hydrazones are stable at pH 6–8 for at least 12 h at 22 °C (51).

$\alpha$ -Haloamides are suitable for conjugation with peptides containing a free SH group. Chloroacetyl- or bromoacetyl amides are used (52, 53).

The bifunctional approach is often associated with the term 'pharmacokinetic modifier' (PKM). Liu and Edwards (22) define PKM as a linker between a targeting molecule and a BFCA. PKM is a spacer residue, separating the radionuclide from the binding site of the molecule to minimize the risk of its undesired modification. The use of a linker helps to choose a BFCA and a radionuclide more independently. The most popular linkers are long poly(ethylene glycol) (PEG) or hydrocarbon chains to increase the lipophilicity and polyamino acid sequences, such as polyglycine, to increase the hydrophilicity, as well as esters and disulfides capable of rapid metabolism.

The distinction between chelate methods can be made depending on the sequence of the steps used for the synthesis of a radiolabeled peptide.

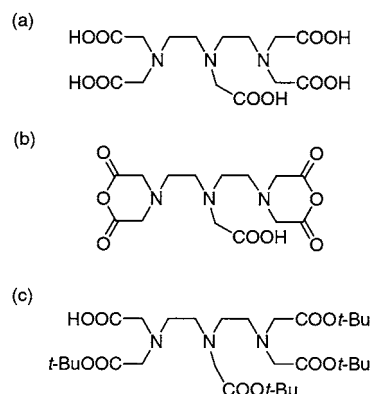
**Prelabeling Method.** The pre-labeling method (pre-formed chelate approach) is based on the labeling of a BFCA with its subsequent activation and conjugation, through covalent bonds, to a peptide. In this approach the chemistry of a process is well defined and easily controlled. As the labeling and conjugation steps are separated, it can be ensured that the radionuclide is attached directly to a chelate moiety and the peptide amino groups remain unlabeled (22). However, the pre-labeling of a BFCA may impair the conjugation process and complicate purification of a radiopharmaceutical. The method is time-consuming, so not appropriate for use with short-lived isotopes, generally associated with imaging. As such the prelabeling method is rarely used for synthesis of radiolabeled peptides.

**Postlabeling Method.** The postlabeling method (indirect labeling approach), the most popular approach in the synthesis of radiopharmaceuticals, requires the synthesis of a BFCA–peptide conjugate and is followed by its labeling. In this method BFCA may be attached to N- or C-terminus, as well as to a side chain of a peptide or it can be even incorporated into a peptide backbone. The postlabeling method is characterized by a well-defined chemistry and relative simplicity. For convenient, high yield synthesis of radiopharmaceuticals, applied BFCA should be compatible with the solid-phase or solution methods of peptide synthesis. However, harsh conditions required for effective labeling of conjugates may sometimes cause changes in the amino acid sequence or peptide backbone conformation and even begin the decomposition of the whole radiopharmaceutical (35).

## BIFUNCTIONAL CHELATING AGENTS

BFCAs are used to connect a radionuclide and a targeting molecule to form a radiopharmaceutical. An ideal BFCA should coordinate the radionuclide with a high yield, to form a relatively stable complex. The agent must comply with the nature and oxidation state of a radionuclide and should prevent any accidental changes in its redox potential.

It is important to carefully choose a proper BFCA, as the conjugation with targeting molecule requires specific conditions: pH, temperature, reaction time. The stereochemistry of a BFCA is important when synthesizing radiopharmaceuticals targeting specific receptors.



**Figure 3.** Structure of DTPA and its analogues: (a) DTPA; (b) cDTPA; (c) mDTPA.

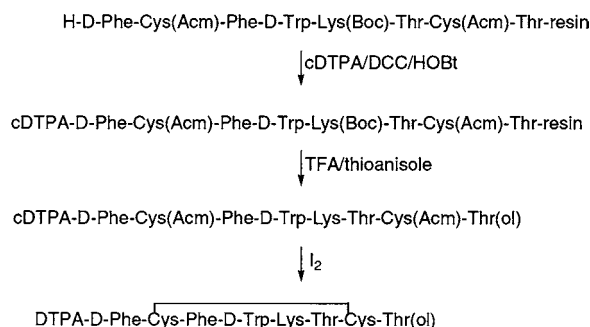
**DTPA.** DTPA (*N*<sup>5</sup>-diethylenetriaminopentaacetic acid) belongs to the group of polyaminocarboxy chelates (Figure 3a). It is a strong chelating group, mostly linked with <sup>111</sup>In, a trivalent radionuclide. It can be attached to larger proteins, e.g., albumins and antibodies (49, 50, 54), as well as to small peptides, like somatostatin analogues (55, 56). The conjugation of DTPA with macromolecules has been successfully performed by the use of isobutyl chloroformate as a coupling reagent (57). For small peptides, however, DTPA derivatives such as DTPA bicyclic anhydride (cDTPA) and monoreactive DTPA derivative, 3,6-bis(carboxymethyl)-9-(((2-maleimidoethyl)-carbamoyl)methyl)-3,6,9-triazaundecanedioic acid (mDTPA), have been applied (Figure 3b and 3c).

Hnatowich et al. (54) have developed a simple method of covalent coupling of cDTPA to peptides at their amino groups. The efficiency of this method is relatively high and it has several advantages. The coupling reaction runs in an aqueous solution and is a simple, one-step process. The side product of the reaction, a double substituted DTPA derivative, and unreacted material can be both easily separated from the main product by gel chromatography. The conjugated peptide maintains its affinity toward specific receptors. The sample, purified before the addition of a radionuclide, can be stored and labeled only when required. For peptides containing lysine the conjugation occurs especially at its  $\epsilon$ -amino group, as more basic than N-terminal amino group. The method is therefore inappropriate for somatostatin analogues, as the lysine residue is situated within the active site of the molecule and the conjugation may result in the loss of receptor binding activity. For that reason a modified method, proposed by Bakker et al. (55) for DTPA-octreotide, is used to conjugate the somatostatin analogue with cDTPA. In this approach lysine residue within the active site of the peptide is protected with *tert*-butoxy-carbonyl group (Boc), before the reaction with cDTPA and deprotected after the conjugation (Figure 4). This method enables a selective reaction of the N-terminal amino group with BFCA, whereas the lysine residue within the bioactive site remains unsubstituted.

A monoreactive DTPA derivative, mDTPA, with four carboxy groups protected as *tert*-butyl esters, was introduced by Arano et al. (57) (Figure 5). Since mDTPA possesses only one free carboxy group, the formation of undesired intermolecular linkages with peptides is prevented. High solubility of mDTPA in various solvents makes this BFCA appropriate for both liquid- and solid-phase peptide synthesis.

A great obstacle in the efficient radiolabeling of DTPA conjugates is the presence of trace metals in the prepara-





**Figure 4.** Synthesis of DTPA–octreotide, starting with cDTPA.

tion, as they compete with radionuclides in the process of labeling. For that reason a significant, 40- to 70-fold molar excess of peptide conjugate and ultrapure radionuclide derivative of the highest possible specific activity are required (55).

DTPA conjugates have been shown to form  $^{111}\text{In}$ -chelate structures (Figure 6), which are eight coordinate, using all three amino and four carboxy groups, while the eighth position around the radionuclide is occupied by the amide carbonyl oxygen (58).  $^{111}\text{In}$ –DTPA conjugates possess excellent *in vivo* stability (59–61).

Many research groups put much effort in the synthesis of kinetically stable DTPA–peptide conjugates that form complexes with  $^{90}\text{Y}$  (62). Substitutions, particularly in the carbon atoms of the DTPA backbone, sterically hinder the opening of the chelate ring that must occur during radionuclide complex dissociation and increase the *in vivo* stability of the radiopharmaceutical. The first class of modified DTPA conjugates was constructed by attaching *p*-isothiocyanatobenzyl moiety to one DTPA backbone ethylene group and appending methyl to another ethylene group in the same backbone (Figure 7a,b). The second class of modified DTPA conjugates was developed by replacing one of the ethylene groups by a cyclohexyl moiety (Figure 7c). Such modifications increase the rigidity in the DTPA backbone and the *in vivo* stability of obtained radiopharmaceuticals (62–64). Synthesis of new derivatives constructed on DTPA core has been recently reported (65, 66).

$^{99\text{m}}\text{Tc}$  is less suitable for the labeling of DTPA–peptide conjugates, as this radionuclide, even at high concentrations, has low affinity and poor selectivity to the binding sites of this BFCA (67).

**DOTA.** DOTA (1,4,7,10-tetraazacyclododecane-*N,N,N',N''*-tetraacetic acid) (Figure 8a) and its derivatives proved to be a good alternative for DTPA. They play an important role in clinical applications, as they form

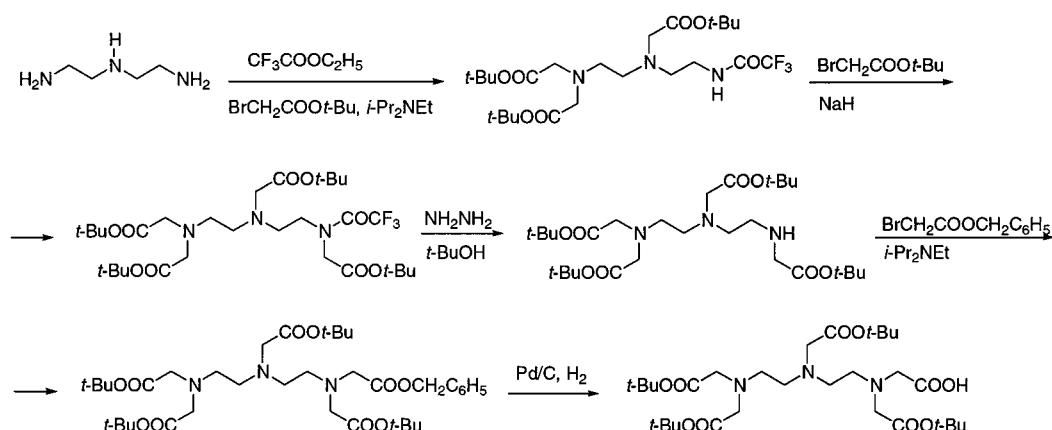
very stable complexes with a variety of trivalent radionuclides, such as  $^{66,67,68}\text{Ga}$ ,  $^{86,90}\text{Y}$ ,  $^{111}\text{In}$ ,  $^{149}\text{Pm}$ ,  $^{177}\text{Lu}$  (68–73) and divalent radionuclides,  $^{27}\text{Mg}$ ,  $^{47}\text{Ca}$ ,  $^{64}\text{Cu}$  (74).

Two different approaches for DOTA conjugation with peptides have been developed. In the first approach one of the four carboxy groups in DOTA is activated to facilitate the reaction with primary amines in the peptide and form a stable amide bond linkage. In the second approach DOTA derivatives with additional side chains are used. A peptide ligand is attached to the side chain of DOTA derivative. Several DOTA derivatives have been synthesized so far, like PA–DOTA ( $\alpha$ -[2-(4-aminophenyl)-ethyl]-1,4,7,10-tetraazacyclododecane-1,4,7,10-tetraacetic acid) and *p*-NCS-Bz–DOTA ((2-(4-isothiocyanatobenzyl)-1,4,7,10-tetraazacyclododecane-*N,N',N'',N'''*-tetraacetic acid) (Figure 8b and 8c) (69). Recently Eisenwiener et al. (44) have introduced two new DOTA derivatives, DOTASA(*t*-Bu)<sub>4</sub>, (1-(1-carboxy-2-carbo-*tert*-butoxyethyl)-4,7,10-(carbo-*tert*-butoxymethyl)-1,4,7,10-tetraazacyclododecane) and DOTAGA(*t*-Bu)<sub>4</sub>, (1-(1-carboxy-3-carbo-*tert*-butoxypropyl)-4,7,10-(carbo-*tert*-butoxymethyl)-1,4,7,10-tetraazacyclododecane) (Figure 8d), which convenient synthesis is outlined in Figure 9. The conjugation of all DOTA derivatives to a peptide is performed through an amino group of a peptide.

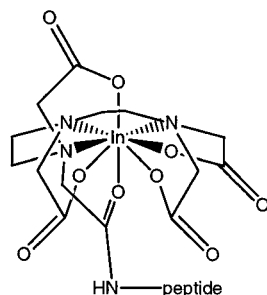
Fully eight coordinate structure has been reported for all DOTA complexes (60) using four amino and four carboxy groups. In the case when one carboxy group is used for conjugation, the amide carbonyl oxygen occupies the eighth position around the radionuclide.

DOTA and derivatives were successfully conjugated to a number of somatostatin analogues, and obtained radiopharmaceuticals had good pharmacological parameters (72–78). DOTA conjugates are especially suitable for radionuclide therapy, as they can be radiolabeled with  $^{67}\text{Ga}$  (75),  $^{90}\text{Y}$  (71, 76), and  $^{111}\text{In}$  (73). De Jong et al. (68) have demonstrated that  $^{90}\text{Y}$ –DOTA conjugates have very good pharmacokinetic properties *in vivo*. However, in these conjugates the chelate is situated closer to the peptide, the labeled conjugate is more rigid and less flexible, which makes binding with the receptor more difficult. Reubi et al. (79) reported the best pharmacological properties for  $^{67}\text{Ga}$ –DOTA complexes. The radionuclide coordination geometry, including the number of uncomplexed carboxy and amino groups, increases the flexibility of a ligand and allows its better adjustment to the receptor binding site.

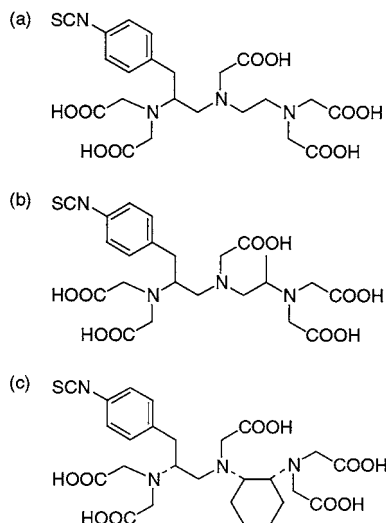
**TETA.** TETA (1,4,8,11-tetraazacyclotetradecane-1,4,8,11-tetraacetic acid) (Figure 10) is one of the most studied chelating agents for copper in peptide targeted radio-



**Figure 5.** Reaction scheme for synthesis of mDTPA.



**Figure 6.** Possible structure of  $\text{In}^{3+}$ -DTPA-peptide.



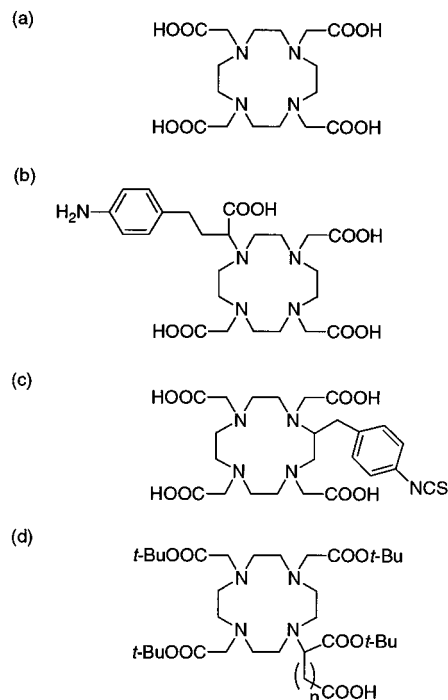
**Figure 7.** Structures of DTPA derivatives: (a) 2-(*p*-isothiocyanatobenzyl) diethylenetriaminopentaacetic acid; (b) 2-(*p*-isothiocyanatobenzyl)-6-methyldiethylene-triaminopentaacetic acid (1B4H-DTPA); (c) 2-(*p*-isothiocyanatobenzyl) cyclohexyldiethylene-triaminopentaacetic acid (CHX-DTPA).

therapy. TETA has been successfully used as a BFCA with somatostatin analogues (30).

**NOTA.** NOTA (1,4,7-triazacyclononane-1,4,7-triacetic acid) (Figure 11a), its phosphonate analogue NOTP (1,4,7-triazacyclononane-*N,N,N'*-tris(methylenephosphonic) acid) (Figure 11b) and the monoethyl ester of NOTP, NOTPME (1,4,7-triazacyclononane-*N,N,N'*-tris(methylenephosphonate-monoethyl ester)) (Figure 11c) were studied for possible use in radiopharmaceuticals. Complexes with  $^{67}\text{Ga}$  (80) and  $^{111}\text{In}$  (81) were reported.

A monoreactive NOTA derivative, NODAGA(*t*Bu)<sub>3</sub> (1-(1-carboxy-3-carbo-*tert*-butoxypropyl)-4,7-(carbo-*tert*-butoxymethyl)-1,4,7-triazacyclononane) (Figure 11d) was synthesized by Eisenwiener et al. (82). The synthesis is outlined in Figure 12. This BFCA is useful for the coupling to the N-terminus of peptides on solid-phase and in solution. The NODAGA-peptide conjugates were labeled with  $^{67}\text{Ga}$  and  $^{111}\text{In}$  in high yields and good specific activities. NODAGA-based derivatives carry a spacer function between the BFCA and the peptide which improves the receptor binding affinity.

**HYNIC.** HYNIC (2-hydrazinonicotinic acid) (Figure 13), first described by Abrams et al. (83) has been used as a BFCA for radiolabeling of different groups of molecules, such as  $\gamma$ -globulins (83, 84), chemotactic peptides (85, 86), and somatostatin analogues (87–90). Structural organization of HYNIC determines its application, as it can only occupy one or two coordination sites of the radionuclide. That is why a coligand such as tricine or EDDA (ethylenediaminediacetic acid) should be also coordinated to complete the coordination sphere

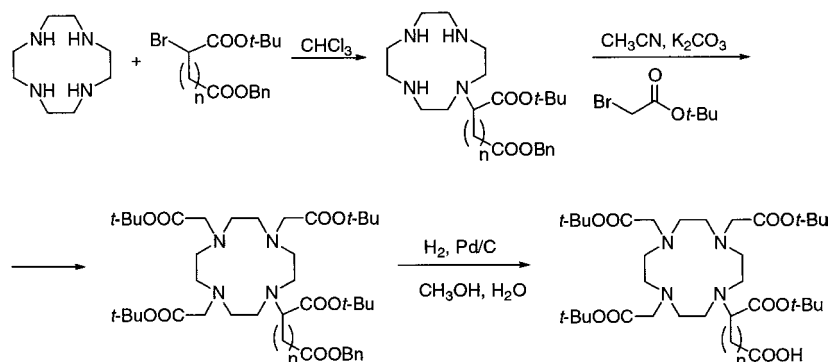


**Figure 8.** Structures of DOTA and its derivatives: (a) DOTA; (b) PA-DOTA; (c) *p*-NCS-Bz-DOTA; (d) DOTASA(*t*-Bu)<sub>4</sub>, *n* = 1 and DOTAGA(*t*-Bu)<sub>4</sub>, *n* = 2.

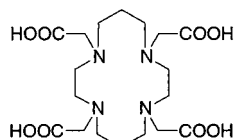
of a radionuclide (91, 92) (Figure 14). The conjugation of coligands helps in modifying the properties of obtained radiopharmaceutical, such as hydrophilicity or pharmacokinetics. However, the requirement for the use of coligands makes the chemistry of the synthesis more complicated, and multiple possible products and side-products can be obtained.

HYNIC-coligand conjugates were reported to have low stability (22). The search for stable HYNIC-coligand complexes is now carried on and phosphines seem to be the most promising coligands so far (92, 93). HYNIC derivatives, together with phosphines and tricine, form ternary complexes [ $^{99\text{m}}\text{Tc}(\text{HYNIC-TM})(\text{tricine})(\text{phosphine})$ ] (TM-targeting molecule). Such complexes are stable in solution, and their hydrophilicity can be modified by changing functional groups attached to phosphine backbone or by substitution of tricine by other glycine derivatives.

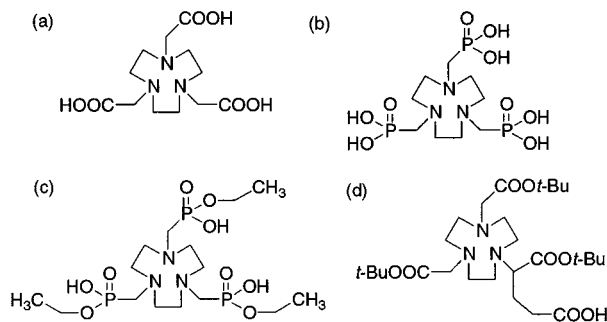
HYNIC is often used as a BFCA for somatostatin analogues. The desired amide bond formation should occur between the carboxy group of HYNIC and the N-terminal amino group of a peptide. However, in somatostatin analogues the presence of lysine makes it difficult to obtain a monosubstituted product. Krois et al. (87) have compared available methods of HYNIC-octreotide conjugation, and none of them seemed efficient enough. The method of protecting the lysine amino group with (Boc)<sub>2</sub>O reported by Bakker et al. (55) proved to be unsatisfactory, as the final product was contaminated with Boc-disubstituted derivative, difficult to separate. The activation of HYNIC to *N*-hydroxysuccinimide ester to facilitate the conjugation step, a method suggested by Abrams et al. (83), also produced poor results. An improved method of HYNIC-octreotide conjugation, reported by Krois et al. (87), is based on the incorporation of the chelator at an early stage of *ab ovo* peptide synthesis performed by solution method. That approach produced high yield of conjugate, practically free of any contamination.



**Figure 9.** Synthesis of DOTASA(*t*-Bu)<sub>4</sub> and DOTAGA(*t*-Bu)<sub>4</sub>.



**Figure 10.** Structure of TETA.



**Figure 11.** Structures of NOTA and its derivatives: (a) NOTA, (b) NOTP, (c) NOTPME, (d) NODAGA(*t*-Bu)<sub>3</sub>.

**Multidentate Chelators.** The class of tetradentate chelators includes N<sub>3</sub>S triamidothiol, N<sub>2</sub>S<sub>2</sub> diamidodithiols (94), and N<sub>2</sub>S<sub>4</sub> diaminotetrathiols (26) (Figure 15) and a number of their derivatives, containing sulfur and nitrogen atoms, incorporated into chelating backbones.

N<sub>2</sub>S<sub>4</sub> chelators contain two amino and four thiol donors and they have been used for <sup>99m</sup>Tc- and <sup>186</sup>Re-labeling of antibodies (95, 96). N<sub>2</sub>S<sub>2</sub> containing two amido and two thiol donors have been used for <sup>99m</sup>Tc- and <sup>186</sup>Re-labeling of proteins, peptides, and oligonucleotides. Since most of the N<sub>2</sub>S<sub>2</sub> derivatives form highly lipophilic rhenium and technetium complexes, they are used whenever hydrophobic targeting systems are applied (97). Both N<sub>3</sub>S- and

N<sub>2</sub>S<sub>2</sub>-derived BFCAs form high specific activity complexes, and for that reason they can be used in the preformed chelate labeling method. In case of small molecules (steroids, low molecular weight peptides) these BFCAs complex <sup>186/188</sup>Re in the postconjugation labeling process (28). BFCAs based on N<sub>3</sub>S backbone are used for the synthesis of <sup>168/188</sup>Re radiopharmaceuticals (98).

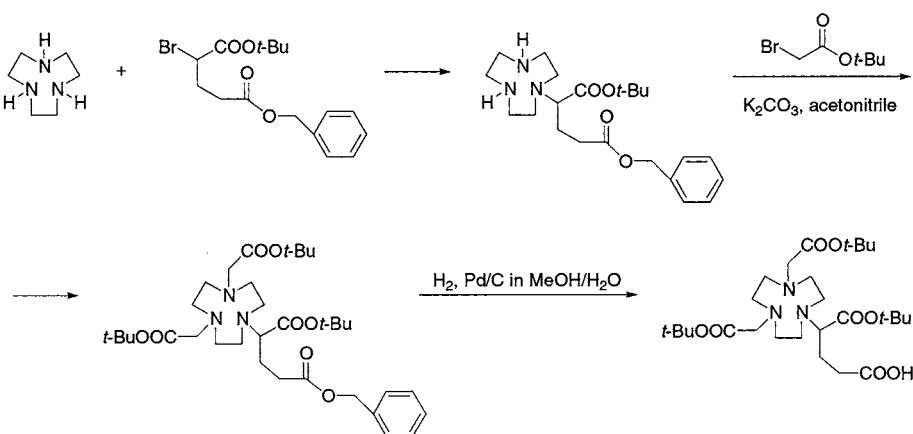
The most frequently applied BFCAs from that group are MAG<sub>3</sub> (mercaptoacetyl-glycylglycylglycine) and MAG<sub>2</sub>-GABA (mercaptoacetyl-glycylglycyl-γ-butyric acid), containing the spacer groups glycine and GABA, respectively (Figure 16). GABA spacer group is two carbon units longer than glycine; therefore, it may exhibit more useful properties, such as higher yield in radionuclide labeling or better receptor binding due to the changes in intramolecular organization (99–101).

BFCAs listed above have been widely used as metal chelating agents in both diagnostic and therapeutic procedures. Attempts to design new derivatives with improved properties are still under way (66, 102).

## RADIONUCLIDES

Each radionuclide is characterized by a specific coordination chemistry and therefore must be conjugated with a specific BFCA with specific donor atoms and ligand frameworks to retain its own radioactivity.

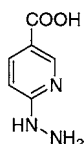
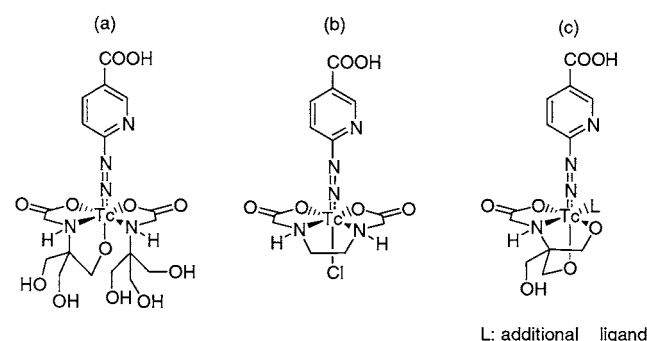
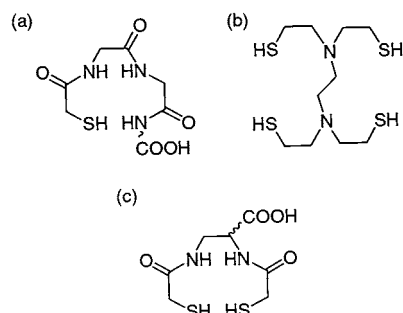
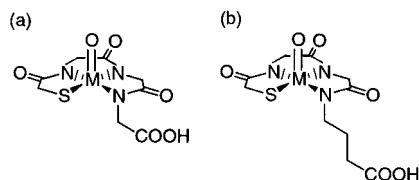
The selection of an appropriate radionuclide is an inherent determinant in developing any therapeutic radiopharmaceutical. Important factors to consider include half-life of the radioactive nuclide, its mode of decay, and its cost and availability (Table 2). The half-life is a critical factor. For diagnostic imaging the half-life of a radionuclide must be long enough to enable the synthesis of the labeled compound and to facilitate the accumulation in the target tissue, while allowing clear-



**Figure 12.** Synthesis of NODAGA(*t*-Bu)<sub>3</sub>.

**Table 2.**  $\gamma$ -,  $\beta^-$ -, and  $\beta^+$ -Emitting Radionuclides<sup>a</sup> Used for Radiolabeling of Radiopharmaceuticals (103)

radionuclide	$t_{1/2}$ (h)	$\gamma$ -energy (keV)	$\beta^-$ -energy (keV)	$\beta^+$ -energy (keV)	decay mode
<sup>64</sup> Cu	12.7	-	579	653	$\beta^+$ (17.4%) $\beta^-$ (39%) EC
<sup>66</sup> Ga	9.5	-	-	4150, 935	$\beta^+$ (56%) EC (44%)
<sup>67</sup> Ga	78.3	91, 93, 185, 296, 388	-	-	EC (100%)
<sup>68</sup> Ga	1.1	-	-	1880, 770	$\beta^+$ (90%) EC (10%)
<sup>86</sup> Y	14.7	-	-	2335, 2019, 1603, 1248, 1043	$\beta^+$ (33%) EC (66%)
<sup>90</sup> Y	64.1	-	2288	-	$\beta^-$ (72%)
<sup>99m</sup> Tc	6.0	141	-	-	IT (100%)
<sup>111</sup> In	67.9	245, 172	-	-	EC (100%)
<sup>149</sup> Pm	53.0	286	1070	-	$\beta^-$ (95.9%)
<sup>177</sup> Lu	160.8	-	236	-	$\beta^-$ (100%)

**Figure 13.** Structure of HYNIC.**Figure 14.** Structures of HYNIC–technetium complexes: (a) [Tc(HYNIC)(tricine)<sub>2</sub>]; (b) [Tc(HYNIC)(EDDA)Cl]; (c) [Tc(HYNIC)(tricine)(L)].**Figure 15.** Structures of multidentate chelators: (a) N<sub>3</sub>S triamidethiol; (b) N<sub>2</sub>S<sub>4</sub> diaminotetrathiol; (c) N<sub>2</sub>S<sub>2</sub> diamidodithiol.**Figure 16.** Structures of: (a) MAG<sub>3</sub>; (b) MAG<sub>2</sub>-GABA.

ance through the nontarget organs. Ideally, the half-life should be as short as possible to reach these two goals. Radionuclides most commonly used in radiopharmaceuticals range in half-lives from minutes (<sup>62</sup>Cu) to days (<sup>177</sup>Lu).

**Copper (<sup>64</sup>Cu).** There are two radionuclides of copper used in the radiopharmaceutical labeling. <sup>64</sup>Cu ( $t_{0.5}$  = 12.7 h) is a  $\beta^+$ -, 0.653 MeV (17.4% abundance), and  $\beta^-$ -emitter, 0.579 MeV (39% abundance), and it decays by electron capture. A good review on the biological chemistry of copper is a book by Linder (104).

**Gallium (<sup>66</sup>Ga, <sup>67</sup>Ga, <sup>68</sup>Ga).** Gallium radionuclides can be either used for  $\gamma$ -scintigraphy or positron emission tomography (PET) imaging. <sup>66</sup>Ga ( $t_{0.5}$  = 9.5 h) is a medium half-life  $\beta^+$ -emitting radionuclide obtained from <sup>66</sup>Zn(p,n)<sup>66</sup>Ga cyclotron, applied in the limited number of cases. <sup>67</sup>Ga ( $t_{0.5}$  = 78.3 h) is produced in <sup>68</sup>Zn(p,2n)<sup>67</sup>Ga cyclotron. <sup>68</sup>Ga ( $t_{0.5}$  = 1.1 h) is obtained from the <sup>68</sup>Ge/<sup>68</sup>Ga generator and it has been used in a limited number of clinical studies (105, 106).

**Yttrium (<sup>86</sup>Y, <sup>90</sup>Y).** There are two radionuclides of yttrium used in the radiopharmaceutical labeling. <sup>86</sup>Y ( $t_{0.5}$  = 14.7 h) is a  $\beta^+$ -emitting radionuclide, often used as an equivalent for <sup>90</sup>Y in the PET imaging. <sup>90</sup>Y ( $t_{0.5}$  = 64 h) is a  $\beta^-$ -emitter, which is probably the most frequently used radionuclide for targeted radiotherapy in human studies. It has a relatively high energy transfer and therefore can be used for imaging of bulky disease sites of solid tumors. <sup>90</sup>Y can be relatively easily obtained in a high-specific activity from <sup>90</sup>Sr (107–109). <sup>90</sup>Y is also available as a GMP commercial product.

**Technetium (<sup>99m</sup>Tc).** <sup>99m</sup>Tc is used in about 85% of all diagnostic applications. It has ideal properties for diagnostic imaging. The half-life of 6 h is long enough to synthesize the <sup>99m</sup>Tc-labeled radiopharmaceuticals and perform imaging studies, yet short enough to minimize the radiation dose to a patient. <sup>99m</sup>Tc emits a 140 keV  $\gamma$ -ray with 89% abundance which is close to optimum for imaging with the present  $\gamma$  cameras. This energy is sufficient for emerging from inside the body and for imaging internal organs. <sup>99m</sup>Tc is readily available at low costs from its parent nuclide <sup>99</sup>Mo ( $t_{0.5}$  = 66 h) from a <sup>99</sup>Mo/<sup>99m</sup>Tc generator. At the concentration levels used for imaging ( $<10^{-6}$  M) neither its  $\gamma$ -radiation nor the soft  $\beta$ -decay is hazardous (110).

**Indium (<sup>111</sup>In).** <sup>111</sup>In has the half-life of 67 h which makes this isotope ideal for labeling immunoglobulins, where imaging is performed over intervals of several days. This nuclide decays by electron capture with emission of  $\gamma$ -photons of 173 and 247 keV (89% and 95% abundance, respectively), which allows its use in  $\gamma$ -scintigraphy.

The first peptide radiopharmaceutical approved for clinical use was the <sup>111</sup>In labeled somatostatin analogue OctreoScan. Nevertheless, because of its less favorable half-life, <sup>111</sup>In is inferior to <sup>99m</sup>Tc for diagnosis. <sup>111</sup>In is often used as an equivalent for <sup>90</sup>Y in scintigraphic



**Table 3. Regulatory Peptides**

regulatory peptide	no. of amino acid residues	receptor type (subtypes)	in vivo activity
SST (somatostatin)	14	SST receptors (sst1/sst2/sst3/sst4/sst5)	inhibition of hormone and exocrine secretion
BN/GRP (bombesin/gastrin releasing peptide)	14	BN/GRP receptors (GRP, NMB, BRS-3)	gut hormone release, regulation of exocrine secretion
VIP (vasoactive intestinal peptide)	28	VIP receptors (–)	vasodilation, water, and electrolyte secretion in the gut
RGD-containing peptides/RGD-peptidomimetics	–	GPIIb/IIIa/platelet and vitronectin/integrin receptors	inhibition of adhesive and aggregatory functions of platelets
$\alpha$ -MSH ( $\alpha$ -melanocyte stimulating hormone)	13	$\alpha$ -MSH receptors (–)	melanogenesis
NT (neurotensin)	13	NT receptors (NT1, NT2, NT3)	vasoconstriction, regulation of cardiac activity raise in vascular permeability
SP (substance P)	11	SP receptors (NK1)	hypotension, salivary gland secretion, transmission of pain

**Table 4. Radiopharmaceuticals Based on Small Peptides<sup>a</sup>**

group	peptide	BFCA	targeted disease	ref
SST analogues	octreotide	DTPA	tumor (neuroendocrine)	(3, 113)
		TETA		(152, 153)
		HYNIC		(61, 118)
	Tyr <sup>3</sup> -octreotide (Y3-TETA)	TETA	tumor (neuroendocrine)	(152, 153)
		HYNIC		(114, 115)
	vapreotide (RC-160)	S–S (direct)	tumor (neuroendocrine)	(116)
		HYNIC		(117)
BN/GRP analogues	BN	N <sub>2</sub> S <sub>2</sub>	tumor	(94)
		HYNIC	tumor	(119)
VIP analogues	VIP	MAG <sub>3</sub>	tumor	(120–122)
RGD-containing peptides/RGD-peptidomimetics		HYNIC	thrombosis	(40, 41, 123, 124)
$\alpha$ -MSH analogues	CCMSH	S–S (direct)	tumor (breast, prostate)	(125, 126)
SP analogues	SP	DTPA	tumor	(127, 128)
chemotactic peptides	fMLF	HYNIC	infection/inflammation	(129, 130)

<sup>a</sup> ST, somatostatin; BN, bombesin; GRP, gastrin releasing peptide; VIP, vasoactive intestinal peptide; RGD sequence, Arg-Gly-Asp sequence;  $\alpha$ -MSH,  $\alpha$ -melanocyte stimulating hormone; SP, substance P.

imaging in humans by using dosimetry cameras, since <sup>90</sup>Y radionuclide does not emit  $\gamma$ -rays (32).

**Promethium (<sup>149</sup>Pm).** <sup>149</sup>Pm is a moderate energy  $\beta^-$ -emitter (1.07 MeV, 95.9% abundance) with a half-life of 53 h. <sup>149</sup>Pm also emits a low abundance of an imageable  $\gamma$ -ray (286 keV, 3%) that may allow in vivo tracking of the therapeutic dose (111).

**Lutetium (<sup>177</sup>Lu).** The most frequently used radionuclide of lutetium is <sup>177</sup>Lu ( $t_{0.5}$  = 160.8 h) which is a  $\beta^-$ - and also a  $\gamma$ -emitter (103).

#### RADIOPHARMACEUTICALS BASED ON SMALL PEPTIDES

Small peptides play a very important role in vivo, where they regulate many physiological processes (Table 3). Low molecular weight peptides have attracted much attention recently as radiopharmaceuticals due to their relatively low immunogenicity, good pharmacokinetic properties, and binding affinities. They are relatively easier to synthesize and modify than larger molecules (112). Many radiopharmaceuticals based on small peptides have been used as diagnostics for clinical purposes (Table 4). They have been radiolabeled with various radionuclides (Table 5).

Because of the lack of tertiary structure, small peptides are less susceptible to a loss of integrity through labeling conditions. However, when minor modifications occur in their structure, they can result in important changes in the lipophilicity and charge with consequences for biodistribution and kinetics.

The physicochemical properties of the radiopharmaceuticals based on small peptides, including binding affinity in vivo, are determined not only by the nature of

**Table 5. Radionuclides Used with Different Peptide Ligands<sup>a</sup>**

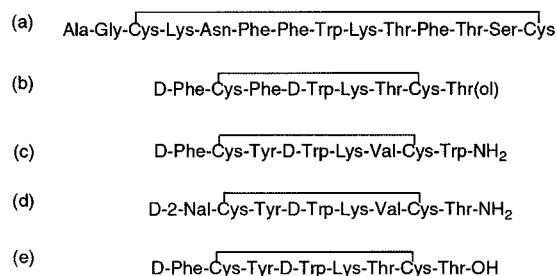
radionuclide	labeled peptide	ref
<sup>64</sup> Cu	SST analogues	(152, 153)
	chemotactic peptides	(18, 30)
<sup>66/67/68</sup> Ga	SST analogues	(131)
<sup>86/90</sup> Y	SST analogues	(18, 30, 132–136)
	SST analogues	(114, 115, 117, 118, 137)
<sup>99m</sup> Tc	BN/GRP analogues	(119)
	VIP analogues	(120–122)
	RGD-containing peptides/RGD-peptidomimetics	(40, 41, 123, 124)
	$\alpha$ -MSH analogues	(125, 126)
	chemotactic peptides	(129, 130, 138)
<sup>111</sup> In	SST analogues	(113)
	$\alpha$ -MSH analogues	(139, 140)
	NT analogues	(141, 142)
	SP analogues	(127, 128, 143)
	chemotactic peptides	(144)

<sup>a</sup> ST, somatostatin; BN, bombesin; GRP, gastrin releasing peptide; VIP, vasoactive intestinal peptide; RGD sequence, Arg-Gly-Asp sequence;  $\alpha$ -MSH,  $\alpha$ -melanocyte stimulating hormone; NT, neurotensin; SP, substance P.

the targeting molecule. They are also influenced by the radionuclide–BFCA complex properties, as a BFCA contributes greatly to the overall size and molecular weight of a conjugate. Furthermore, the incorporation of a spacer-linker between the radionuclide–BFCA complex and a peptide can also modify the binding interactions (22, 142, 143).

**Somatostatin Analogues.** The peptide that has attracted the greatest interest as an imaging agent is somatostatin (SST). Somatostatin is a tetradecapeptide that regulates the secretion of numerous hormones. In addition, receptors for somatostatin are expressed on a variety of human tumors and that fact has become a basic





**Figure 17.** Structure of somatostatin and its analogues: (a) somatostatin; (b) octreotide; (c) vapreotide (RC-160); (d) lanreotide; (e) Tyr<sup>3</sup>-octreotide (Y3-TATE).

**Table 6.** Radiopharmaceuticals Based on ST Analogs

ST analog	BFCA	radionuclide
octreotide (OC)	DTPA	<sup>111</sup> In
	TETA	<sup>64</sup> Cu
	HYNIC	<sup>99m</sup> Tc
Tyr <sup>3</sup> -octreotide (Y3-TATE)	DTPA	<sup>111</sup> In
	DOTA	<sup>66,67,68</sup> Ga, <sup>86/90</sup> Y, <sup>111</sup> In
	TETA	<sup>64</sup> Cu
vapreotide (RC-160)	DTPA	<sup>111</sup> In
	DOTA	<sup>66,67,68</sup> Ga, <sup>86/90</sup> Y, <sup>111</sup> In
	HYNIC	<sup>99m</sup> Tc
lanreotide (LAN)	DOTA	<sup>111</sup> In

principle for the use of somatostatin analogues in radiochemistry and tumor imaging (147–150).

Although the first report of *in vivo* imaging with a somatostatin analogue appeared in 1976 (151), further development was delayed because the native peptide is rapidly degraded by plasma and tissue proteases. In years that followed somatostatin analogues that are more resistant to biological degradation have been developed.

The cyclic octapeptide, octreotide (152), is a good replacement for somatostatin in the clinical application, since it shows similar bioactivity, it has a relatively high metabolic stability and its pharmacokinetic properties are better. Octreotide is less susceptible to enzymatic degradation *in vivo* due to the incorporation of the N-terminal D-Phe and the C-terminal amino alcohol, Thr(ol), into its molecule (153, 154).

The pharmacophoric group in octreotide is a sequence of four amino acids: -Phe<sup>3</sup>-D-Trp<sup>4</sup>-Lys<sup>5</sup>-Thr<sup>6</sup>-, organized into a  $\beta$ -turn conformation by a disulfide bond, formed between cysteine residues at the N- and C-terminus of the peptide backbone (112).

Many octreotide analogues have been synthesized and some of them proved to be useful as targeting molecules (113). Their structures are shown in Figure 17.

Somatostatin radiopharmaceuticals which have received the most attention were octreotide conjugates with DTPA, DOTA (132–136), and HYNIC (115–118, 137) (Table 6). Since the *in vivo* stability of DOTA octreotide conjugates is higher than DTPA derivatives, the former draw more attention of research groups.

<sup>64</sup>Cu-TETA-octreotide and <sup>64</sup>Cu-TETA-Tyr<sup>3</sup>-octreotide can be used to detect somatostatin receptor-positive tumors in humans. Their favorable dosimetry and pharmacokinetics indicate that they are promising radiopharmaceuticals for PET imaging of patients with endocrine tumors. The radiotherapy results, along with absorbed dose estimates to target and clearance organs, confirm that <sup>64</sup>Cu-labeled somatostatin analogues warrant continued consideration as agents for targeted radiotherapy (152, 153).

**Bombesin Analogues.** Bombesin (BN), a 14-amino acid peptide originally isolated from frog skin and its mammalian equivalent, a 27-amino acid gastrin-releas-

ing peptide (GRP) (157, 158) belong to the bombesin family of peptides. Receptors for bombesin/GRP are expressed in the central nervous system and peripheral tissues such as intestines or pancreas. They are also present on tumors, which include lung, prostate, breast, gastric, colon, and pancreatic cancer. Since bombesin/GRP peptides function in most cases as autocrine growth factors, the disruption of bombesin/GRP triggered biochemical pathways would result in the inhibition of cancer growth. This is the main principle of bombesin/GRP analogues application in tumor diagnosis (159–161).

Several attempts have been made to synthesize and evaluate the properties of bombesin/GRP analogues as future radiopharmaceuticals. Baidoo et al. (119) have synthesized N<sub>2</sub>S<sub>2</sub>-bombesin derivative, subsequently labeled with <sup>99m</sup>Tc, which proved to be a promising diagnostic agent. Bombesin-DTPA conjugates labeled with <sup>99m</sup>Tc have also been reported (162, 163).

**Vasoactive Intestinal Peptide Analogues.** Vasoactive intestinal peptide (VIP) is a 28-amino acid neuroendocrine mediator, one of the inhibitory neurotransmitters in the gut (62). VIP receptors are expressed on central nervous system and pancreatic tissues, as well as on adenocarcinomas.

The synthesis of VIP analogue conjugates seems complicated, since both N- and C-terminus play an important role and their substitution effects intrinsic activity and receptor binding, respectively. However, the <sup>99m</sup>Tc-radio-labeled derivatives of VIP have been reported (124, 164).

**RGD-Containing Peptides and RGD Peptidomimetics.** Peptides containing RGD (Arg-Gly-Asp) sequence interact *in vivo* with integrins, adhesion molecules present on cell membranes of most tissues, responsible for platelet adhesion and activation and leukocyte mobility, as well as cancer cell dissemination. As a result, RGD-containing peptides and RGD peptidomimetics bind to cancer cells and may be used as tumor diagnostic agents (123). Peptides with RGD sequence bind also to glycoprotein IIb/IIIa receptors expressed on activated platelets and are used as thrombus imaging agents or antithrombotics (165–169).

A group of potent RGD-containing analogues, candidates for thrombus imaging agents, was reported (170–172). To minimize the effect of <sup>99m</sup>Tc-labeling on RGD sequence integrity, Jackson et al. (170) have incorporated spacers between a BFCA and a targeting molecule. New thrombus imaging agents contain modified RGD sequences (52, 165, 173), so that the amino acid residue in the peptidomimetic triplet forms a N<sub>2</sub>S<sub>2</sub> group and functions also as a BFCA.

**$\alpha$ -Melanocyte Stimulating Hormone.** Labeled analogues of a tridecapeptide  $\alpha$ -melanocyte stimulating hormone ( $\alpha$ -MSH) are used for melanoma tumor imaging, as its receptors are overexpressed on the membranes of malignant cells (174–176). The most promising derivatives so far are <sup>111</sup>In-labeled conjugates with DTPA, as well as analogues containing N<sub>3</sub>S chelating moiety, labeled with <sup>99m</sup>Tc at the N-terminus (139, 140, 177).

**Neurotensin Analogues.** Neurotensin (NT) is a 13-amino acid neurotransmitter in the central nervous system and a local hormone stimulating growth functions. Neurotensin analogues are used for detection of tumors, such as meningiomas or pancreas, prostate, lung, and colon carcinomas. So far, DTPA conjugates with NT and analogues were synthesized (141, 142).

**Substance P Analogues.** The receptors for substance P (SP), an 11-amino acid neuromodulator and neurotransmitter, are overexpressed on breast, thyroid, and

glial tumors (143). DTPA conjugates of SP analogues, complexed with  $^{111}\text{In}$ , were reported (127, 128).

**Chemotactic Peptides.** *N*-Formylmethionyleucylphenylalanine (fMLF) is a microbial product, which binds to receptors present on inflammatory cells, granulocytes, and leukocytes.  $^{99\text{m}}\text{Tc}$ -HYNIC and  $^{111}\text{In}$ -DTPA conjugates were synthesized by means of SPPS method and evaluated as potential infection and inflammation imaging agents (144).

## CONCLUSIONS

Nature has designed peptides to regulate many body functions. The concept of designing radiopharmaceuticals based on small peptides is very promising. In the past decade radiolabeled peptide-based radiopharmaceuticals have become an important class of imaging agents for the detection of a wide variety of tumors, as well as thrombosis, infection, and inflammation. The major advantage of developing peptide-based radiopharmaceuticals is that, once the receptor-binding sequence of the peptide molecule is identified, it may be readily synthesized and modified according to pharmacokinetic requirements.

The application of radiolabeled peptides for diagnostic imaging and therapy is rapidly gaining importance in nuclear medicine. Biologically active molecules that selectively interact with specific cell types are attractive vehicles for the delivery of radioactivity to target tissues. The typical approach for imaging a cellular receptor is to synthesize appropriate radiolabeled peptide analogues that possess high binding affinity for the receptor of interest. Various receptors are overexpressed on particular tumor types, and peptides binding to these receptors can be used to visualize tumor lesions scintigraphically.

Small radiolabeled synthetic peptides are preferred over macromolecules such as proteins and antibodies for imaging applications, since they present several advantages. Small peptides can be easily synthesized. They can withstand harsher chemical conditions for radiolabeling. They penetrate tumors more easily than bigger molecules, and they are less likely to induce an immunogenic response.

However, the negative aspects of use of radiolabeled peptides should also be pointed out. Among them one should take into consideration a low tumor uptake relative to a total dose and a normal tissue uptake, very rapid targeting and clearance which creates the necessity to use shorter-lived isotopes. Other pharmacokinetic and toxicity issues still need to be addressed.

The synthesis of radiolabeled peptides is not an easy process. Binding of a radionuclide to a peptide can be achieved either directly or through a bifunctional chelating agent (BFCA). In the latter approach two methods can be distinguished: prelabeling method, based on the labeling of BFCA with its subsequent conjugation to a peptide and postlabeling method which requires the synthesis of BFCA-peptide conjugate, followed by its labeling. The postlabeling chelate method is the most popular approach in the synthesis of radiopharmaceuticals. Several BFCAs have been designed so far. The most popular are DTPA, DOTA, NOTA, and HYNIC. Conjugation of a BFCA to a peptide is not easy to perform considering multiple functional groups in a BFCA, as well as in a peptide molecule. Not many radiopharmaceuticals based on bioactive peptides have been in clinical use so far. The majority of them are somatostatin analogues. Further studies must be undertaken to explain the chemistry of radiolabeling and to develop better methods

of BFCA-peptide conjugate synthesis. The development of new radiopharmaceuticals is a multidisciplinary effort and requires the collaboration from scientists in organic, inorganic, and analytical chemistry, as well as biochemistry and nuclear medicine.

## ACKNOWLEDGMENT

This research was supported by grant of the Medical University of Lodz No. 502-11-812.

## LITERATURE CITED

- (1) Hoefnagel, C. A. (1991) Anticancer radiopharmaceuticals. *Anticancer Drugs* 2, 107–132.
- (2) Schubiger, P. A., Alberto, R., and Smith, A. (1996) Vehicles, chelators, and radionuclides: choosing the "building blocks" of an effective therapeutic radioimmunoconjugate. *Bioconjugate Chem.* 7, 165–179.
- (3) Reubi, J. C. (1995) Neuropeptide receptors in health and disease: the molecular basis for in vivo imaging. *J. Nucl. Med.* 36, 1825–1835.
- (4) Verbruggen, A. M. (1990) Radiopharmaceuticals: state of the art. *Eur. J. Nucl. Med.* 17, 346–364.
- (5) Antar, M. A. (1990) Radiopharmaceuticals: state of the art. *Nucl. Med. Biol.* 17, 103–128.
- (6) Pauwels, E. K., McCready, V. R., Stoot, J. H. M. B., and van Deurzen, D. F. P. (1998) The mechanism of accumulation of tumour-localising radiopharmaceuticals. *Eur. J. Nucl. Med.* 25, 277–305.
- (7) Wessels, B. W., and Meares, C. F. (2000) Physical and chemical properties of radionuclide therapy. *Semin. Radiat. Oncol.* 10, 115–122.
- (8) Liu, S., and Edwards, D. S. (1995) *Technetium and Rhenium in Chemistry and Nuclear Medicine* (Nicolini, M., Banoli, G., Mazzi, U., Eds.) pp 383–393, SG Editoriali, Padova.
- (9) Park, C. H. (1997) The role of radioisotopes in radiation oncology. *Semin. Oncol.* 24, 639–654.
- (10) Saha, G. B., Go, R. T., and Macintyre W. J. (1992) Radiopharmaceuticals for cardiovascular imaging. *Nucl. Med. Biol.* 19, 1–20.
- (11) Walovitch, R. C., Williams, S. J., and Lafrance, N. D. (1990) Radiolabeled agents for SPECT imaging of brain perfusion. *Nucl. Med. Biol.* 17, 77–83.
- (12) Nunn, A. D. (1990) Radiopharmaceuticals for imaging myocardial perfusion. *Semin. Nucl. Med.* 20, 111–118.
- (13) Britton, K. E. (1990) The development of new radiopharmaceuticals. *Eur. J. Nucl. Med.* 16, 373–385.
- (14) Eckelman, W. C. (1994) The application of receptor theory to receptor-binding and enzyme-binding oncologic radiopharmaceuticals. *Nucl. Med. Biol.* 21, 759–769.
- (15) Seregni, E., Chiti, A., and Bombardieri, E. (1998) Radionuclide imaging of neuroendocrine tumours: biological basis and diagnostic results. *Eur. J. Nucl. Med.* 25, 639–658.
- (16) Schmidt, M., Scheidhauer, K., Luyken, C., Voth, E., Hildebrandt, G., Klug, N., and Schicha, H. (1998) Somatostatin receptor imaging in intracranial tumours. *Eur. J. Nucl. Med.* 25, 675–686.
- (17) Spencer, R. P. (1991) Receptor-mediated radiopharmaceutical imaging of the liver. *Targeted Diagn. Ther.* 4, 321–338.
- (18) Volkert, W. A., and Hoffmann, T. J. (1999) Therapeutic radiopharmaceuticals. *Chem. Rev.* 99, 2269–2292.
- (19) Weiner, R. E., and Thakur, M. L. (2001) Radiolabeled peptides in diagnosis and therapy. *Semin. Nucl. Med.* 31, 296–311.
- (20) Lister-Jones, J., Moyer, B. R., and Dean, R. T. (1990) Small peptides radiolabeled with  $^{99\text{m}}\text{Tc}$ . *Q. J. Nucl. Med.* 40, 221–233.
- (21) Eckelman, W. C. (1995) Radiolabeling with technetium- $^{99\text{m}}$  to study high-capacity and low-capacity biochemical systems. *Eur. J. Nucl. Med.* 22, 249–263.
- (22) Liu, S., and Edwards, D. S. (1999)  $^{99\text{m}}\text{Tc}$ -labeled small peptides as diagnostic radiopharmaceuticals. *Chem. Rev.* 99, 2235–2268.



- (23) Jurisson, S. S., and Lydon, J. D. (1999) Potential technetium small molecule radiopharmaceuticals. *Chem. Rev.* **99**, 2205–2218.
- (24) Hnatovich, D. J. (1990) Recent developments in the radiolabeling of antibodies with iodine, indium, and technetium. *Semin. Nucl. Med.* **20**, 80–91.
- (25) Schwachau, K. (1994) Technetium radiopharmaceuticals – fundamentals, synthesis, structure and development. *Angew. Chem., Int. Ed. Engl.* **33**, 2258–2267.
- (26) Liu, S., Edwards, D. S., and Barrett, J. A. (1997)  $^{99m}\text{Tc}$  labeling of highly potent small peptides. *Bioconjugate Chem.* **8**, 621–636.
- (27) Okarvi, S. M. (1999) Recent developments in  $^{99m}\text{Tc}$ -labeled peptide-based radiopharmaceuticals: An overview. *Nucl. Med. Commun.* **20**, 1092–1112.
- (28) Hom, R. K., and Katzenellenbogen, J. A. (1997) Technetium-99m-labeled receptor-specific small-molecule radiopharmaceuticals: recent developments and encouraging results. *Nucl. Med. Biol.* **24**, 485–498.
- (29) Okarvi, S. M. (2001) Recent progress in fluorine-18 labeled peptide radiopharmaceuticals. *Eur. J. Nucl. Med.* **28**, 929–938.
- (30) Anderson, C. J., and Welch, M. J. (1999) Radiometal-labeled agents (non-technetium) for diagnostic imaging. *Chem. Rev.* **99**, 2219–2234.
- (31) Srivastava, S. C., and Mease, R. C. (1991) Progress in research on ligands, nuclides and techniques for labeling monoclonal antibodies. *Int. J. Rad. Appl. Instrum. B.* **18**, 589–603.
- (32) Fischman, A. J., Babich, J. W., and Strauss, W. (1993) A ticket to ride: Peptide radiopharmaceuticals. *J. Nucl. Med.* **34**, 2253–2263.
- (33) Ehrhardt, G. J., Ketrang, A. R., and Ayers, L. M. (1998) Reactor-produced radionuclides at the University of Missouri Research Reactor. *Appl. Radiat. Isot.* **49**, 295–297.
- (34) Langer, M., and Beck-Sickinger, A. G. (2001) Peptides as carrier for tumor diagnosis and treatment. *Curr. Med. Chem.-Anti-Cancer Agents* **1**, 71–93.
- (35) Thakur, M. L. (1995) Radiolabeled peptides: Now and the future. *Nucl. Med. Commun.* **16**, 724–732.
- (36) Katzenellenbogen, J. A. (1995) Designing steroid receptor-based radiotracers to image breast and prostate tumors. *J. Nucl. Med.* **36**(Suppl), 8S-13S.
- (37) Baidoo, K. E., Scheffel, U., and Stathis, M. (1998) High-affinity no-carrier-added  $^{99m}\text{Tc}$ -labeled chemotactic peptides for studies of inflammation in vivo. *Bioconjugate Chem.* **9**, 208–217.
- (38) Zamora, P. O., Gohlke, S., Bender, H., Diekmann, D., Rhodes, B. A., Biersack, H., and Knapp, F. F., Jr. (1996) Experimental radiotherapy of receptor-positive human prostate adenocarcinoma with  $^{188}\text{Re}$ -RC-160, a directly radiolabeled somatostatin analogue. *Int. J. Cancer* **65**, 214–220.
- (39) Thakur, M. L. (1993) Tc-99m labeled sandostatin: preparation and preliminary evaluation. *J. Labeled Compd. Radiopharm.* **32**, 365–367.
- (40) Lister-James, J., Vallabhajosula, S., Moyer, B. R., Pearson, D. A., McBride, B. J., De Rosch, M. A., Bush, L. R., Machac, J., and Dean, R. T. (1997) Pre-clinical evaluation of technetium-99m platelet receptor binding peptide. *J. Nucl. Med.* **38**, 105–111.
- (41) Lister-James, J., Knight, L. C., Maurer, A. H., Bush, L. R., Moyer, B. R., and Dean, R. T. (1996) Thrombus imaging with a technetium-99m-labeled, activated platelet receptor-binding peptide. *J. Nucl. Med.* **37**, 775–781.
- (42) Eckelman, W. C. (1990) Development of radiochemically pure antibodies. *Cancer Res.* **50**, 686–692.
- (43) Delmon-Moingeon, L. I., Mahmood, A., Davison, A., and Jones, A. G. (1991) Strategies for labeling monoclonal antibodies and antibody-like molecules with technetium-99m. *J. Nucl. Biol. Med.* **35**, 47–59.
- (44) Eisenwiener, K. P., Powell, P., and Maecke, H. R. (2000) A convenient synthesis of novel bifunctional prochelators for coupling to bioactive peptides for radionuclide labeling. *Bioorg. Med. Chem. Lett.* **10**, 2133–2135.
- (45) Anderson, G. W., Zimmerman, J. E., and Callahan, F. M. (1967) A reinvestigation of the mixed carbonic anhydride method of peptide synthesis. *J. Am. Chem. Soc.* **89**, 5012–5017.
- (46) Anderson, G. W., Zimmerman, J. E., and Callahan, F. M. (1964) The use of esters of *N*-hydroxysuccinimide in peptide synthesis. *J. Am. Chem. Soc.* **86**, 1839–1842.
- (47) Grumbach, I. M., and Veh, R. W. (1991) Sulpho-*N*-hydroxysuccinimide activated long chain biotin. A new microtitre plate assay for the determination of its stability at different pH values and its reaction rate with protein bound amino groups. *J. Immunol. Methods* **140**, 205–210.
- (48) Gohlke, S., Diekmann, D., Zamora, P. O., Knapp, F. F., and Biersack, H. J. (1995) MAG3 *p*-nitrophenyl ester for  $^{99m}\text{Tc}$  and  $^{188}\text{Re}$  labeling of amines and peptides. *Technetium and Rhenium in Chemistry and Nuclear Medicine 4* (M. Nicolini, G. Bandoli, U. Mazzi, Eds.) pp 363–366, SGEEditoriali, Padua.
- (49) Meares, C. F. (1986) Chelating agents for the binding of metals to antibodies. *Nucl. Med. Biol.* **13**, 311–318.
- (50) McMurphy, T. J., Pippin, C. G., Wu, C., Deal, K. A., Brechbiel, M. W., Mirzadeh, S., and Gansow, O. A. (1998) Physical parameters and biological stability of yttrium(III) diethylene-triaminepentaacetic acid derivative conjugates. *J. Med. Chem.* **41**, 3546–3549.
- (51) Geoghegan, K. F., Stroh, J. G. (1992) Site-directed conjugation of nonpeptide groups to peptides and proteins via periodate oxidation of a 2-amino alcohol. Application to modofocation at N-terminal serine. *Bioconjugate Chem.* **3**, 138–146.
- (52) Pearson, D. A., Lister-James, J., McBride, W. J., Wilson, D. M., Martel, L. J., Civitello, E. R., and Dean, R. T. (1996) Thrombus imaging using technetium-99m-labeled high-potency GPIIb/IIIa receptor antagonists. Chemistry and initial biological studies. *J. Med. Chem.* **39**, 1372–1382.
- (53) Pearson, D. A., Lister-James, J., McBride, W. J., Wilson, D. M., Martel, L. J., Civitello, E. R., Taylor, J. E., Moyer, B. R., and Dean, R. T. (1996) Somatostatin receptor-binding peptides labeled with technetium-99m: chemistry and initial biological studies. *J. Med. Chem.* **39**, 1361–1371.
- (54) Hnatowich, D. J., Layne, W. W., Childs, R. L., Lantaigne, D., Davis, M. A., Griffin, T. V., and Doherty, P. W. (1983) Radioactive labeling of antibody: A simple and efficient method. *Science* **220**, 613–615.
- (55) Bakker, W. H., Albert, R., Bruns, C., Breeman, W. A. P., Hofland, L. J., Marbach, P., Pless, J., Pralet, D., Stolz, B., Koper, J. W., Lamberts, S. W. J., Visser, T. J., and Krenning, E. P. (1991) [ $^{111}\text{In}$ -DTPA-D-Phe]-octreotide, a potential radiopharmaceutical for imaging of somatostatin receptor-positive tumors: synthesis, radiolabeling and in vitro validation. *Life Sci.* **49**, 1583–1591.
- (56) Krejcarek, G. E., and Tucker, K. L. (1977) Covalent attachment of chelating groups to macromolecules. *Biochem. Biophys. Res. Commun.* **2**, 581–585.
- (57) Arano, Y., Akizawa, H., Uezono, T., Akaji, K., Ono, M., Funakoshi, S., Koizumi, M., Yokoyama, A., Kiso, Y., and Saji, H. (1997) Conventional and high-yield synthesis of DTPA-conjugated peptides: application of a monoreactive DTPA to DTPA-D-Phe<sup>1</sup>-octreotide synthesis. *Bioconjugate Chem.* **8**, 442–446.
- (58) Maecke, H. R., Riesen, A., and Ritter, W. (1989) The molecular structure of Indium-DTPA. *J. Nucl. Med.* **30**, 1235–1239.
- (59) Wang, S., Luo, J., Lantrip, D. A., Waters, D. J., Mathias, C. J., Green, M. A., Fuchs, P. L., and Low, P. S. (1997) Design and synthesis of [ $^{111}\text{In}$ ]DTPA-folate for use as a tumor-targeted radiopharmaceutical. *Bioconjugate Chem.* **8**, 673.
- (60) Breeman, W. A. P., van Hagen, P. M., Kwekkeboom, D. J., Visser, T. J., and Krenning, E. P. (1998) Somatostatin receptor scintigraphy using [ $^{111}\text{In}$ -DTPA<sup>0</sup>]RC-160 in humans: a comparison with [ $^{111}\text{In}$ -DTPA<sup>0</sup>]octreotide. *Eur. J. Nucl. Med.* **25**, 182–186.
- (61) Kolan, H., Li, J., and Thakur, M. L. (1996) Sandostatin labeled with  $^{99m}\text{Tc}$ : In vitro stability, in vivo validity and comparison with  $^{111}\text{In}$ -DTPA-Octreotide. *Pept. Res.* **9**, 144–150.

- (62) Brechbiel, M. W., and Gansow, O. A. (1991) Backbone-substituted DTPA ligands for 90Y radioimmunotherapy. *Bioconjugate Chem.* 2, 187–194.
- (63) Kobayashi, H., Wu, C., Yoo, T. M., Sun, B. F., Drumm, D., Pastan, I., Paik, C. H., Gansow, C. A., Carrasquillo, J. A., and Brechbiel, M. N. (1998) Evaluation of the in vivo biodistribution of yttrium-labeled isomers of CHX-DTPA-conjugated monoclonal antibodies. *J. Nucl. Med.* 39, 829–836.
- (64) Wu, C., Kobayashi, H., Sun, B., Yoo, T. M., Paik, C. H., Gansow, O. A., Carrasquillo, J. A., Pastan, I., and Brechbiel, M. W. (1997) Stereochemical influence on the stability of radio-metal complexes in vivo. Synthesis and evaluation of the four stereoisomers of 2-(p-nitrobenzyl)-trans-CyDTPA. *Bioorg. Med. Chem.* 5, 1925–1934.
- (65) Safavy, A., Smith, D. C., Bazooband, A., and Buchsbaum, D. J. (2002) De novo synthesis of a new diethylenetriamine-pentaacetic acid (DTPA) bifunctional chelating agent. *Bioconjugate Chem.* 13, 317–326.
- (66) Safavy, A., Smith, D. C., Jr., Bazooband, A., and Buchsbaum, D. J. (2002) Synthesis of the first diethylenetriamine-pentahydroxamic acid (DTPH) bifunctional chelating agent. *Bioconjugate Chem.* 13, 327–332.
- (67) Blok, D., Feitsma, R. I. J., Vermeij, P., and Pauwels, E. J. K. (1999) Peptide radiopharmaceuticals in nuclear medicine. *Eur. J. Nucl. Med.* 26, 1511–1519.
- (68) de Jong, M., Bakker, W. H., Krenning, E. P., Breeman, W. A. P., van der Pluijm, M. E., Bernard, B. F., Visser, T. J., Jermann, E., Behe, M., Powell, P., and Maecke, H. R. (1997) Yttrium-90 and indium-111 labeling, receptor binding and biodistribution of [DOTA<sup>0</sup>, D-Phe<sup>1</sup>, Tyr<sup>3</sup>]octreotide, a promising somatostatin analogue for radionuclide therapy. *Eur. J. Nucl. Med.* 24, 368–371.
- (69) McMurry, T. J., Brechbiel, M., Kumar, K., and Gansow, O. A. (1992) Convenient synthesis of bifunctional tetraaza macrocycles. *Bioconjugate Chem.* 3, 108–117.
- (70) DeNardo, S. J., Kukis, D. L., Miers, L., Winthrop, M. D., Kroger, L. A., Salako, Q., Shen, S., Lamborn, K. R., Gumerlock, P. H., Meares, C. F., and DeNardo, G. L. (1998) Yttrium-90-DOTA-peptide-chimeric L6 radioimmunoconjugate: efficacy and toxicity in mice bearing p53 mutant human breast cancer xenografts. *J. Nucl. Med.* 39, 842–849.
- (71) DeNardo, S. J., Zhong, G. R., Salako, Q., Li, M., DeNardom G. L., and Meares, C. F. Pharmacokinetics of chimeric L6 conjugated to indium-111- and yttrium-90-DOTA-peptide in tumor-bearing mice. *J. Nucl. Med.* 36, 829–836.
- (72) Otte, A., Jermann, E., Behe, M., Goetze, M., Bucher, H. C., Roser, H. W., Heppeler, A., Mueller-Brand, J., and Maecke, H. R. (1997) DOTATOC: a powerful new tool for receptor mediated radionuclide therapy. *Eur. J. Nucl. Med.* 24, 792–795.
- (73) Virgolini, I., Szilvasi, I., Kurtaran, A., Angelberger, P., Raderer, M., Havlik, E., Vorbeck, F., Bischof, C., Leimer, M., Dorner, G., Kletter, K., Niederle, B., Scheithauer, W., and Smith-Jones, P. (1998) Indium-111-Dota-lanreotide: biodistribution, safety and radiation absorbed dose in tumour patients. *J. Nucl. Med.* 39, 1928–1936.
- (74) Keire, D. A., Jang, Y. H., Li, L., Dasgupta, S., Goddard, W. A., III, and Shively, J. E. (2001) Chelators for radioimmunotherapy: I. NMR and ab initio calculation studies on 1,4,7,10-tetra(carboxyethyl)-1,4,7,10-tetraazacyclododecane (DO4Pr) and 1,4,7-tris(carboxymethyl)-10-(carboxyethyl)-1,4,7,10-tetraazacyclododecane (DO3A1Pr). *Inorg. Chem.* 40, 4310–4318.
- (75) Otte, A., Mueller-Brand, J., Dellas, S., Nitzsche, E. U., Herrmann, R., and Maecke, H. R. (1998) Yttrium-90-labeled somatostatin-analogue for cancer treatment. *Lancet* 351, 417–418.
- (76) Smith-Jones, P., Bischof, C., Leimer, D., Gludovacz, D., Angelberger, P., Pangerl, T., Peck-Radosavljevic, M., Hamilton, G., Kaserer, K., Steiner, G., Schlagbauer-Wadl, H., Maecke, H., and Virgolini, I. (1998) "Mauritius", a novel somatostatin analogue for tumour diagnosis and therapy. *J. Nucl. Med.* 39 Suppl: 223P.
- (77) Heppeler, A., Behe, M., Froidevaux, S., Hennig, M., Jermann, E., and Maecke, H. R. (1998) Metal coordination chemical aspects and tumour targeting of a promising somatostatin analogue. *J. Nucl. Med.* 39 Suppl, 63P.
- (78) Stolz, B., Weckbecker, G., Smith-Jones, P., Albert, R., Raulf, F., and Bruns, C. (1998) The somatostatin receptor targeted radiotherapeutic [<sup>90</sup>Y-DOTA-D-Phe<sup>1</sup>, Tyr<sup>3</sup>]octreotide (<sup>90</sup>Y-SMT 487) eradicates experimental rat pancreatic CA20948 tumours. *Eur. J. Nucl. Med.* 7, 668–674.
- (79) Reubi, J. C., Waser, B., Schaer, J. C., Laederach, U., Erion, J., Srinivasan, A., Schmidt, M. A., and Bugaj, J. E. (1998) Unsulfated DTPA- and DOTA-CCK analogues as specific high affinity ligands for CCK-B receptor- expressing human and rat tissues in vitro and in vivo. *Eur. J. Nucl. Med.* 25, 481–490.
- (80) Broan, C. J., Cox, J. P. L., Craig, A. S., Katoky, R., Parker, D., Harrison, A., Randall, A. M., and Ferguson, G. (1991) Structure and solution stability of indium and gallium complexes of 1,4,7-triazacyclononanetriacetate and of Yttrium complexes of 1,4,7,10-tetraazacyclododecanetetracetate and related ligands: Kinetically stable complexes for use in imaging and radioimmunotherapy. X-ray molecular structure of the indium and gallium complexes of 1,4,7-triazacyclononan-1,4,7-triacetic acid. *J. Chem. Soc., Perkin Trans.* 2, 87–98.
- (81) Clarke, E. T., and Martell, A. (1991) Stabilities of the Fe(III), Ga(III) and In(III) chelates of N,N',N''-triazacyclononanetriacetic acid. *Inorg. Chem. Acta* 181, 273–280.
- (82) Eisenwiener, K. P., Prata, M. I., Buschmann, I., Zhang, H. W., Santos, A. C., Wenger, S., Reubi, J. C., and Macke, H. R. (2002) NODAGATOC, a new chelator-coupled somatostatin analogue labeled with [67/68Ga] and [111In] for SPECT, PET and targeted therapeutic applications of somatostatin receptor (hsst2) expressing tumors. *Bioconjugate Chem.* 13, 530–541.
- (83) Abrams, M. J., Juweid, M., tenKate, C. I., Schwartz, D. A., Hauser, M. M., Gaul, F. E., Fuccello, A. J., Rubin, R. H., Strauss, H. W., and Fischman, A. J. (1990) Technetium-99m-human polyclonal IgG radiolabeled via the hydrazino nicotinamide derivative for imaging focal sites of infection in rats. *J. Nucl. Med.* 31, 2022–2028.
- (84) Schwartz, D. A., Abrams, M. J., Hauser, M. M., Gaul, F. E., Larsen, S. K., Rauh, D., and Zubieta, J. A. (1991) Preparation of hydrazino-modified proteins and their use for the synthesis of 99mTc-protein conjugates. *Bioconjugate Chem.* 2, 333–336.
- (85) Babich, J. W., Solomon, H., Pike, M. C., Kroon, D., Graham, W., Abrams, M. J., Tompkins, R. G., Rubin, R. H., and Fischman, A. J. (1993) Technetium-99m-labeled hydrazino nicotinamide derivatized chemotactic peptide analogues for imaging focal sites of bacterial infection. *J. Nucl. Med.* 34, 1964–1974.
- (86) Babich, J. W., and Fischman, A. J. (1995) Effect of "co-ligand" on the biodistribution of 99mTc-labeled hydrazino nicotinamide acid derivatized chemotactic peptides. *Nucl. Med. Biol.* 22, 25–30.
- (87) Krois, D., Riedel, C., Angelberger, P., Kalchauer, H., Virgolini, I., and Lehner, H. (1996) Synthesis of N-α-(6-hydrazinonicotinoyl)-octreotide: a precursor of a [<sup>99m</sup>Tc] complex. *Liebig's Ann.* 1463–1469.
- (88) Bangard, M., Behe, M., Guhlke, S., Otte, R., Bender, H., Maecke, H., and Biersack, H.-J. (1998) Detection of somatostatin receptor -positive tumours using the new 99mTc-tricine-HYNIC-d-Phe1-Tyr3-octreotide: first results in patients and comparison with 111In-DTPA-d-Phe1-octreotide. *Eur. J. Nucl. Med.* 27, 628–637.
- (89) Decristoforo, C., and Mather, S. J. (1999) Technetium-99m somatostatin analogues: effect of labeling methods and peptide sequence. *Eur. J. Nucl. Med.* 26, 869–876.
- (90) Decristoforo, C., Melendez-Alafort, L., Sosabowski, J. K., and Mather, S. J. (2000) 99mTc-HYNIC-[Tyr3]-octreotide for imaging somatostatin-receptor-positive tumors: preclinical evaluation and comparison with 111In-octreotide. *J. Nucl. Med.* 41, 1114–1119.
- (91) Edwards, D. S., Liu, S., Barrett, J. A., Harris, A. R., Looby, R. J., Ziegler, M. C., Heminway, S. J., and Carroll, T. R. (1997) New and versatile ternary ligand system for technetium radiopharmaceuticals: water soluble phosphines and tricine as coligands in labeling a hydrazinonicotinamide-modified



- cyclic glycoprotein IIb/IIIa receptor antagonist with  $^{99m}\text{Tc}$ . *Bioconjugate Chem.* 8, 146–154.
- (92) Liu, S., Edwards, D. S., and Harris, A. R. (1998) A novel ternary ligand system for  $^{99m}\text{Tc}$ -labeling of hydrazino nicotinamide-modified biologically active molecules using imine-N-containing heterocycles as coligands. *Bioconjugate Chem.* 9, 583–595.
- (93) Barrett, J. A., Crocker, A. C., Damphousse, D. J., Hem-inway, S. J., Liu, S., Edwards, D. S., Lazewatsky, J. L., Kagan, M., Mazaika, T. J., and Carroll, T. L. (1997) Biological evaluation of thrombus imaging agents utilizing water soluble phosphines and tricine as coligands when used to label a hydrazinonicotinamide-modified cyclic glycoprotein IIb/IIIa receptor antagonist with  $^{99m}\text{Tc}$ . *Bioconjugate Chem.* 8, 155–160.
- (94) Liu, S., and Edwards, D. S. (1995) New  $\text{N}_2\text{S}_2$  diamidedithiol and  $\text{N}_3\text{S}$  triamidethiols as bifunctional chelating agents for labeling small peptides with technetium-99m. In *Technetium and Rhenium in Chemistry and Nuclear Medicine 4* (Nicolini M., Banoli G., Mazzi U., Eds.) pp 383–393, SG Editoriali, Padova.
- (95) Najafi, A., Alauddin, M. M., Siegel, M. E., and Epstein, A. L. (1991) Synthesis and preliminary evaluation of a new chelate  $\text{N}_2\text{S}_4$  for use in labeling proteins with metallic radionuclides. *Int. J. Rad. Appl. Instrum. B.* 18, 179–185.
- (96) Najafi, A., Alauddin, M. M., Sosa, A., Ma, G. Q., Chen, D. C., Epstein, A. L., and Siegel, M. E. (1992) The evaluation of  $^{186}\text{Re}$ -labeled antibodies using  $\text{N}_2\text{S}_4$  chelate in vitro and in vivo using tumor-bearing nude mice. *Int. J. Rad. Appl. Instrum. B.* 19, 205–212.
- (97) Kasina, S., Rao, T. N., Srinivasan, A., Sanderson, J. A., Fitzner, J. N., Reno, J. M., Beaumier, P. L., and Fritzberg, A. R. (1991) Development and biologic evaluation of a kit for preformed chelate technetium-99m radiolabeling of an antibody Fab fragment using a diamide dimercaptide chelating agent. *J. Nucl. Med.* 32, 1445–1451.
- (98) Wong, E., Fauconnier, T., Bennett, S., Valliant, J., Nguyen, T., Lau, F., Lu, L. F. L., Pollak, A., Bell, R. A., and Thornback, J. R. (1997) Rhenium(V) and Technetium(V) Oxo Complexes of an  $\text{N}(2)\text{N}'\text{S}$  Peptidic Chelator: Evidence of Interconversion between the Syn and Anti Conformations. *Inorg. Chem.* 36, 5799–5808.
- (99) Mathias, C. J., Sun, Y., Welch, M. J., Green, M. A., Thomas, J. A., Wade, K. R., and Martell, A. E. (1988) Targeting radiopharmaceuticals: comparative biodistribution studies of gallium and indium complexes of multidentate ligands. *Int. J. Rad. Appl. Instrum. B.* 15, 69–81.
- (100) Gohlke, S., Schaffland, A., Zamora, P. O., Sartor, J., Diekmann, D., Bender, H., Knapp, F. F., and Biesack, H. J. (1998)  $^{188}\text{Re}$ - and  $^{99m}\text{Tc}$ -MAG3 as prosthetic groups for labeling amines and peptides: approaches with pre- and postconjugate labeling. *Nucl. Med. Biol.* 25, 621–631.
- (101) Gano, L., Patricio, L., Marques, E., Cantino, G., Pena, H., Martins, T., and Hnatowich, D. J. (1998) Human polyclonal immunoglobulin labeled with technetium-99m via NHS-MAG3: a comparison of radiochemical behavior and biological efficacy with other labeling methods. *Nucl. Med. Biol.* 25, 395–403.
- (102) Benshafrut, R., Haran, A., Shvarts, D., and Schneider, B. (2002) Synthesis and characterization of a new tetradentate ligand for  $\text{Cu(II)}$  metal ions. *J. Org. Chem.* 67, 4040–4044.
- (103) Firestone, R. B. (1996) *Table of isotopes* (Shirley, W. S., Ed.), Horizon Pubs & Distributors Inc.,
- (104) Linder, M. C. (1991) *Biochemistry of copper*, Plenum Press, New York.
- (105) Goethals, P., Coene, M., Slegers, G., Agon, P., Deman, J., and Schelstraete, K. (1988) Cyclotron production of carrier-free  $^{66}\text{Ga}$  as a positron emitting label of albumin colloids for clinical use. *Eur. J. Nucl. Med.* 14, 152–154.
- (106) Loc'h, C., Maziere, B., and Comar, D. (1980) A new generator for ionic gallium-68. *J. Nucl. Med.* 21, 171–173.
- (107) Herzog, H., Rosch, F., Stocklin, G., Lueders, C., Quaim, S. M., and Feinendegen, L. E. (1993) Measurement of pharmacokinetics of yttrium-86 radiopharmaceuticals with PET and radiation dose calculation of analogous yttrium-90 radiotherapeutics. *J. Nucl. Med.* 34, 2222–2226.
- (108) Wester, H. J., Brockmann, J., Rosch, F., Wutz, W., Herzog, H., Smith Jones, P., Stolz, B., Bruns, C., and Stocklin, G. (1997) PET-pharmacokinetics of  $^{18}\text{F}$ -octreotide: a comparison with  $^{67}\text{Ga}$ -DFO- and  $^{86}\text{Y}$ -DTPA-octreotide. *Nucl. Med. Biol.* 24, 275–286.
- (109) Rosch, F., Herzog, H., Stolz, B., Brockmann, J., Kohle, M., Muhlensiepen, H., Marbach, P., and Muller-Gartner, H. W. (1999) Uptake kinetics of the somatostatin receptor ligand  $^{86}\text{Y}$ [DOTA-DPhe1-Tyr3-octreotide] ( $^{86}\text{Y}$ [SMT487]) using positron emission tomography in nonhuman primates and calculation of radiation doses of the  $^{90}\text{Y}$ -labeled analogue. *Eur. J. Nucl. Med.* 26, 358–366.
- (110) Sattlerberger, A. P., and Atcher, R. W. (1999) Nuclear medicine finds the right chemistry. *Nat. Biotechnol.* 17, 849–850.
- (111) Hu, F., Cutler, C. S., Hoffman, T., Sieckman, G., Volkert, W. A., and Jurisson, S. S. (2002) Pm-149 DOTA bombesin analogues for potential radiotherapy, in vivo comparison with Sm-153 and Lu-177 labeled  $\text{DO}_3\text{A}$ -amide-betaAla-BBN(7–14)NH(2). *Nucl. Med. Biol.* 29, 423–430.
- (112) Signore, A. (1995) Receptor ligands. *Q. J. Nucl. Med.* 39, 83–85.
- (113) Bakker, W. H., Krenning, E. P., and Breeman, W. A. (1990) Receptor scintigraphy with a radiolabeled somatostatin analog: radiolabeling, purification, biological activity and in vivo application in animals. *J. Nucl. Med.* 31, 1501–1509.
- (114) Bangard, M., Behe, M., and Bender, H. (1998) Technetium-99m-octreotide for the detection of somatostatin receptor positive (SSTR+) tumors: preliminary results. *Eur. J. Nucl. Med.* 25, 837.
- (115) Maecke, H. R., Heppeler, A., and Nock, B. (1999) Somatostatin Analogues Labeled with Different Radionuclides. *Technetium, Rhenium and Other Metals in Chemistry and Nuclear Medicine 5* (M. Nicolini, U. Mazzi, Eds.) pp 77–91, SGEditoriali, Padova.
- (116) Thakur, M. L., Kolan, H. R., and Rifat, S. (1996) Vapreotide labeled with  $^{99m}\text{Tc}$  for imaging tumors: preparation and preliminary evaluation. *Int. J. Oncol.* 9, 445–451.
- (117) Decristoforo, C., and Mather, S. J. (1999) In vitro and in vivo Comparison of HYNIC Versus  $\text{N}_3\text{S}$  Derivatized Somatostatin Analogues Labeled with  $^{99m}\text{Tc}$ . *Technetium, Rhenium and Other Metals in Chemistry and Nuclear Medicine 5* (M. Nicolini, U. Mazzi, Eds.) pp 77–91, SGEditoriali, Padova.
- (118) Thakur, M. L., Eshbach, J., Wilder, S., John, E., and McDevitt, M. R. (1993)  $\text{Tc-99m}$  labeled Sandostatin: Preparation and preliminary evaluation. *J. Label. Compds. Radiopharm.* 32, 365–367.
- (119) Baidoo, K. E., Lin, K. S., Zhan, Y. G., Finley, P., Scheffel, U., and Wagner, H. N., Jr. (1998) Design, synthesis and initial evaluation of high-affinity technetium bombesin analogues. *Bioconjugate Chem.* 9, 218–225.
- (120) Rao, P. S., Thakur, M. L., Pallela, V. R., Patti, R., Reddy, K., Li, H., Sharma, S., Pham, H. L., Diggles, L., Minami, C., and Marcus, C. S. (2001)  $^{99m}\text{Tc}$  labeled VIP analog: evaluation for imaging colorectal cancer. *Nucl. Med. Biol.* 28, 445–450.
- (121) Pallela, V. R., Thakur, M. L., Chakder, S., and Rattan, S. (1999)  $^{99m}\text{Tc}$ -labeled vasoactive intestinal peptide receptor agonist: functional studies. *J. Nucl. Med.* 40, 352–360.
- (122) Virgolini, I., Kurtaran, A., and Raderer, M. (1995) Vasoactive intestinal peptide receptor scintigraphy. *J. Nucl. Med.* 36, 1732–1739.
- (123) Sivolapenko, G. B., Skarlos, D., and Pectasides, D. (1998) Imaging of metastatic melanoma utilizing a technetium-99m labeled RGD-containing synthetic peptide. *Eur. J. Nucl. Med.* 25, 1383–1389.
- (124) Varner, J. A., and Cheresh, D. A. (1996) Integrins and cancer. *Curr. Opin. Cell Biol.* 8, 724–730.
- (125) Chen, J., Cheng, Z., Hoffman, T. J., Jurisson, S. S., and Quinn, T. P. (2000) Melanoma-targeting properties of ( $^{99m}\text{Tc}$ )-technetium-labeled cyclic alpha-melanocyte-stimulating hormone peptide analogues. *Cancer Res.* 60, 5649–5658.

- (126) Chen, J., Giblin, M. F., Wang, N., Jurisson, S. S., and Quinn, T. P. (1999) In vivo evaluation of  $^{99m}\text{Tc}/^{188}\text{Re}$ -labeled linear alpha-melanocyte stimulating hormone analogues for specific melanoma targeting. *Nucl. Med. Biol.* **26**, 687–693.
- (127) van Hagen, P. M., Breeman, W. A., Reubi, J. C., Postema, P. T., van der Anker-Lugtenburg, P. J., Kwekkeboom, D. J., Laissue, J., Waser, B., Lamberts, S. W., Visser, T. J., and Krenning, E. P. Visualization of the thymus by substance P receptor scintigraphy in man. *Eur. J. Nucl. Med.* **23**, 1508–1513.
- (128) Breeman, W. A., van Hagen, P. M., Visser-Wisselaar, H. A., van der Pluijm, M. E., Koper, J. W., Setyono-Han, B., Bakker, W. H., Kwekkeboom, D. J., Hazenberg, M. P., Lamberts, S. W., Visser, T. J., and Krenning, E. P. (1996) In vitro and in vivo studies of substance P receptor expression in rats with the new analogue [Indium-111-DTPA-Arg1]-substance P. *Eur. J. Nucl. Med.* **37**, 108–117.
- (129) Babich, J., Graham, W., Barrow, S. A., Fischman, A. J. (1995) Comparison of the infection imaging properties of a  $^{99m}\text{Tc}$  labeled chemotactic peptide with  $^{111}\text{In}$  IgG. *Nucl. Med. Biol.* **22**, 643–648.
- (130) Babich, J. W., Graham, W., Barrow, S. A., Dragotakes, S. C., Tompkins, R. G., Rubin, R. H., and Fischman, A. J. (1993) Technetium-99m-labeled chemotactic peptides: comparison with indium-111-labeled white blood cells for localizing acute bacterial infection in the rabbit. *J. Nucl. Med.* **34**, 2176–2181.
- (131) Moerlein, S. M., Welch, M. J., and Hotchkiss, R. M. (1993) A gallium-68-labeled chemotactic peptide analogue for imaging focal sites of bacterial infection. *J. Labeled. Compds. Radiopharm.* **32**, 426–427.
- (132) Otte, A., Jermann, E., Behe, M., Bucher, H. C., Roser, H. W., Heppeler, A., Mueller-Brand, J., and Maecke, H. R. (1997) DOTATOC: a powerful new tool for receptor-mediated radionuclide therapy. *Eur. J. Nucl. Med.* **24**, 792–795.
- (133) de Jong, M., Bakker, W. H., Breeman, W. A. P., Hofland, L. J., Visser, T. J., Srinivasan, A., Schmidt, M., Behe, M., Maecke, H., and Krenning, E. P. (1998) Pre-clinical comparison of [DTPA0] octreotide, [DTPA0, Tyr3] octreotide and [DOTA0, Tyr3] octreotide as carriers for somatostatin receptor-targeted scintigraphy and radionuclide therapy. *Int. J. Cancer* **5**, 406–411.
- (134) Krenning, E. P., Kwekkeboom, D. J., Bakker, W. H., Breeman, W. A., Kooij, P. P., Oei, H. Y., van Hagen, M., Postema, P. T., de Jong, M., and Reubi, J. C. (1993) Somatostatin receptor scintigraphy with [ $^{111}\text{In}$ -DTPA-D-Phe1]- and [ $^{123}\text{I}$ -Tyr3]-octreotide: the Rotterdam experience with more than 1000 patients. *Eur. J. Nucl. Med.* **20**, 716–731.
- (135) Heppeler, A., Froidevaux, S., Eberle, A. N., and Maecke, H. R. (2000) Receptor targeting for tumor localisation and therapy with radiopeptides. *Curr. Med. Chem.* **7**, 971–994.
- (136) de Jong, M., Bernard, B. F., de Bruin, E., van Gasteren, A., Bakker, W. H., Visser, T. J., Maecke, H. R., and Krenning, E. P. (1988) Internalization of radiolabeled [DTPA0]octreotide and [DOTA0, Tyr3]octreotide: peptides for somatostatin receptor-targeted scintigraphy and radionuclide therapy. *Nucl. Med. Commun.* **19**, 283–288.
- (137) Maina, T., Stolz, B., Albert, R., Bruns, C., Koch, P., and Maecke, H. (1994) Synthesis, radiochemistry and biological evaluation of a new somatostatin analogue (SDZ 219–387) labeled with technetium-99m. *Eur. J. Nucl. Med.* **21**, 437–444.
- (138) Fischman, A. J., Babich, J. W., and Rubin, R. H. (1994) Infection imaging with technetium-99m-labeled chemotactic peptide analogues. *Semin. Nucl. Med.* **24**, 154–168.
- (139) Bagutti, C., Stolz, B., Albert, R., Bruns, C., Pless, J., and Eberle, A. N. (1993) [ $^{111}\text{In}$ ]DTPA-labeled analogues of alpha-MSH for the detection of MSH receptors in vitro and in vivo. *Ann. N.Y. Acad. Sci.* **680**, 445–447.
- (140) Bard, D. R. (1995) An improved imaging agent for malignant melanoma, based on [Nle4, D-Phe7]alpha-melanocyte stimulating hormone. *Nucl. Med. Commun.* **16**, 860–866.
- (141) Reubi, J. C., Waser, B., Friess, H., Buchler, M., and Laissue, J. (1998) Neurotensin receptors: a new marker for human ductal pancreatic adenocarcinoma. *Gut* **42**, 546–550.
- (142) Reubi, J. C., Waser, B., Schaer, J. C., and Laissue, J. (1999) Neurotensin receptors in human neoplasms: high incidence in Ewing's sarcomas. *Int. J. Cancer* **82**, 213–218.
- (143) Hennig, I. M., Laissue, J. A., Horisberger, U., and Reubi, J. C. (1995) Substance-P receptors in human primary neoplasms: tumoral and vascular localization. *Int. J. Cancer* **61**, 786–792.
- (144) Fischman, A. J., Pike, M. C., and Kroon, D. (1991) Imaging focal sites of bacterial infection in rats with indium-111-labeled chemotactic peptide analogues. *J. Nucl. Med.* **32**, 483–491.
- (145) Liu, S., Edwards, D. S., Looby, R. J., Poirier, M. J., Rajopadhye, M., Bourque, J. P., and Carroll, T. R. (1996) Labeling cyclic glycoprotein IIb/IIIa receptor antagonists with  $^{99m}\text{Tc}$  by the preformed chelate approach: effects of chelators on properties of [ $^{99m}\text{Tc}$ ]chelator-peptide conjugates. *Bioconjugate Chem.* **7**, 196–202.
- (146) Barrett, J. A., Damphousse, D. J., Heminway, S. J., Liu, S., Edwards, D. S., Looby, R. J., and Carroll, T. R. (1996) Biological evaluation of  $^{99m}\text{Tc}$ -labeled cyclic glycoprotein IIb/IIIa receptor antagonists in the canine arteriovenous shunt and deep vein thrombosis models: effects of chelators on biological properties of [ $^{99m}\text{Tc}$ ]chelator-peptide conjugates. *Bioconjugate Chem.* **7**, 203–208.
- (147) Lamberts, S. W. J. (1988) The role of somatostatin in the regulation of anterior pituitary hormone secretion and the use of its analogues in the treatment of human pituitary tumors. *Endocr. Rev.* **9**, 417–436.
- (148) Lamberts, S. W. J., Krenning, E. P., and Reubi, J. C. (1991) The role of somatostatin and its analogues in the diagnosis and treatment of tumours. *Endocrine Rev.* **19**, 450–482.
- (149) Thakur, M. L., Kolan, H., Li, J., Wiaderkiewicz, R., Pallela, V. R., Duggaraju, R., and Schally, A. V. (1997) Radiolabeled somatostatin analogues in prostate cancer. *Nucl. Med. Biol.* **24**, 105–113.
- (150) de Jong, M., Breeman, W. A. P., and Bernard, H. F. (1999) Therapy of neuroendocrine tumours with radiolabeled somatostatin analogues. *Q. J. Nucl. Med.* **43**, 356–366.
- (151) Bardfeld, P. A., Chervu, L. R., and Myrty, D. R. K. (1976) The organ distribution of [ $^{131}\text{I}$ -tryosyl somatostatin. *Br. J. Radiol.* **49**, 381–382.
- (152) Anderson, C. J., Dehdashti, F., Cutler, P. D., Schwarz, S. W., Laforest, R., Bass, L. A., Lewis, J. S., and McCarthy, D. W. (2001)  $^{64}\text{Cu}$ -TETA-octreotide as a PET imaging agent for patients with neuroendocrine tumors. *J. Nucl. Med.* **42**, 213–221.
- (153) Lewis, J. S., Lewis, M. R., Cutler, P. D., Srinivasan, A., Schmidt, M. A., Schwarz, S. W., Morris, M. M., Miller, J. P., and Anderson, C. J. (1999) Radiotherapy and dosimetry of  $^{64}\text{Cu}$ -TETA-Tyr3-octreotate in a somatostatin receptor-positive, tumor-bearing rat model. *Clin. Cancer Res.* **5**, 3608–3616.
- (154) Bauer, W., Briner, U., Doepfner, W., Haller, R., Huguenin, R., Marbach, P., Petcher, T. J., and Pless, J. (1982) SMS 201–995: a very potent and selective octapeptide analogue of somatostatin with prolonged action. *Life Sci.* **31**, 1133–1140.
- (155) Pless, J., Bauer, W., Briner, U., Doepfner, W., Marbach, P., Maurer, R., Pletcher, T. J., Reubi, J. C., and Vonderscher, J. (1986) Chemistry and pharmacology of SMS 201–995, a long acting octapeptide analogue of somatostatin. *Scand. J. Gastroenterol. Suppl.* **119**, 54–64.
- (156) Edwards, W. B., Fields, C. G., Anderson, C. J., Pajean, T. S., Welch, M. J., and Fields, G. B. (1994) Generally applicable, convenient solid-phase synthesis and receptor affinities of octreotide analogues. *J. Med. Chem.* **37**, 3749–3757.
- (157) McDonald, T. J., Jornvall, J., Nilsson, G., Vagne, M., Ghatei, M., Bloom, S. R., and Mutt, V. (1979) Characterization of a gastrin releasing peptide from porcine nontral gastric tissue. *Biochem. Biophys. Res. Commun.* **90**, 227–233.
- (158) Moody, T. W., Carney, D. N., Cuttita, F., Quattrocchi, K., and Minna, J. D. (1985) High affinity receptors for bombesin/GRP-like peptides on human small cell lung cancer. *Life Sci.* **37**, 105–113.

- (159) Moody, T. W., Mahmoud, S., Staley, J. S., Naldini, L., Cirillo, D., South, V., Felder, S., and Kris, R. (1989) Human glioblastoma cell lines have neuropeptide receptors for bombesin/GRP. *J. Mol. Neurosci.* **1**, 235–242.
- (160) Yano, T., Pinski, J., Szepeshazi, K., Groot, K., and Schally, A. V. (1992) Stimulation by bombesin/gastrin releasing peptide antagonist RC-3095 of growth of human breast cancer lines. *Cancer Res.* **52**, 4545–4547.
- (161) Breeman, W. A., Hofland, L. J., de Jong, M., Bernard, B. F., Srinivasan, A., Kwekkeboom, D. J., Visser, T., and Krenning, E. P. (1999) Evaluation of radiolabeled bombesin analogues for receptor-targeted scintigraphy and radiotherapy. *Int. J. Cancer* **81**, 658–665.
- (162) Breeman, W. A., de Jong, M., Bernard, B. F., Kwekkeboom, D. J., Srinivasan, A., van der Pluijm, M. E., Hofland, L. J., Visser, T. J., and Krenning, E. P. (1999) Pre-clinical evaluation of [(111)In-DTPA-Pro(1), Tyr(4)]bombesin, a new radioligand for bombesin-receptor scintigraphy. *Int. J. Cancer* **83**, 657–663.
- (163) Moody, T. W., and Perry, D. C. (1989) Peptide Receptors. *Receptor Pharmacology and Function* (M. Williams, R. A. Glennon, P. B. M. W. M. Timmermans, Eds.) pp 527–570, Dekker, New York.
- (164) Pallela, V. R., Reddy, M. V. R., Senadhi, V. K., and Thakur, M. L. (1998) Synthesis and evaluation of Tc-99m-labeled VIP analogues as potential tumour imaging agents. *J. Nucl. Med.* **39**, 226P.
- (165) Ali, F. E., Bennett, D. B., Calvo, R. R., and Elliott, J. D. (1994) Conformationally constrained peptides and semipeptides derived from RGD as potent inhibitors of the platelet fibrinogen receptor and platelet aggregation. *J. Med. Chem.* **37**, 769–780.
- (166) Cheng, S., Craig, W. S., Mullen, D., Tschopp, J. F., Dixon, D., and Pierschbacher, M. D. (1994) Design and synthesis of novel cyclic RGD-containing peptides as highly potent and selective integrin  $\alpha_{IIb}\beta_3$  antagonists. *J. Med. Chem.* **37**, 1–8.
- (167) Teng, W., Rose, J. W., Philips, D. R., Nannizzi, L., Arsen, A., Campbell, A. M., and Charo, I. F. (1993) Design of potent and specific integrin antagonists. *J. Biol. Chem.* **268**, 1066–1073.
- (168) Zablocki, J. A., Miyano, M., and Garland, R. B. (1993) Potent in vitro and in vivo inhibitors of platelet aggregation based upon the Arg-Gly-Asp-Phe sequence of fibrinogen. A proposal on the nature of the binding interaction between the Arg-guanidine of RGD mimetics and the platelet GP IIb/IIIa receptor. *J. Med. Chem.* **36**, 1811–1919.
- (169) Bach, A. C., Eyermann, C. J., and Gross, J. D. (1994) Structural studies of a family of a high affinity ligands for GPIIb/IIIa. *J. Am. Chem. Soc.* **116**, 3220–3230.
- (170) Jackson, S., DeGrado, W. F., and Dwivedi, A. (1994) Template-constrained cyclic peptides: design of high affinity ligands for GPIIb/IIIa. *J. Am. Chem. Soc.* **116**, 3207–3219.
- (171) Xue, C. B., and DeGrado, W. F. (1995) An Efficient synthesis of GPIIb/IIIa inhibitor DMP 728. A novel synthesis of N $^{\alpha}$ -methylarginine-containing peptide. *J. Org. Chem.* **60**, 946–952.
- (172) Muto, P., Lastoria, S., and Varrella, P. (1995) Detecting deep venous thrombosis with technetium-99m-labeled synthetic peptide P280. *J. Nucl. Med.* **36**, 1384–1391.
- (173) Lister-Jones, J., Knight, L. C., Mauer, A. H., Bush, L. R., Moyer, B. R., and Dean, R. T. (1996) Thrombus imaging with technetium-99m-labeled, activated platelet receptor binding peptide. *J. Nucl. Med.* **37**, 775–781.
- (174) Siegrist, W., Oestreicher, M., Stutz, S., Girard, J., and Eberle, A. N. (1988) Radioreceptor assay for alpha-MSH using mouse B16 melanoma cells+. *J. Recept. Res.* **8**, 323–343.
- (175) Siegrist, W., Solca, F., Stutz, S., Giuffre, L., Carrel, S., Girard, J., and Eberle, A. N. (1989) Characterization of receptors for alpha-melanocyte-stimulating hormone on human melanoma cells. *Cancer Res.* **49**, 6352–6358.
- (176) Tatro, J. B., Atkins, M., Mier, J. W., Hardarson, S., Wolfe, H., Smith, T., Entwistle, M. L., and Reichlin, S. (1990) Melanotropin receptors demonstrated in situ in human melanoma. *J. Clin. Invest.* **85**, 1825–1832.
- (177) Chen, J., Giblin, M. F., Wang, N., Jurisson, S. S., and Quinn, T. P. (1999) In vivo evaluation of 99mTc/188Re-labeled linear alpha-melanocyte stimulating hormone analogues for specific melanoma targeting. *Nucl. Med. Biol.* **26**, 687–693.

BC025542F



# ARTICLES

## Synthesis of Antisense Oligonucleotides Conjugated to a Multivalent Carbohydrate Cluster for Cellular Targeting

Martin A. Maier,<sup>†</sup> Constantin G. Yannopoulos,<sup>‡</sup> Nazim Mohamed,<sup>‡</sup> Arlene Roland,<sup>‡</sup> Hans Fritz,<sup>§</sup> V. Mohan,<sup>†</sup> George Just,<sup>‡</sup> and Muthiah Manoharan<sup>\*,†</sup>

Department of Medicinal Chemistry, Isis Pharmaceuticals, Inc., 2292 Faraday Avenue, Carlsbad, California 92008, Department of Chemistry, McGill University, 801 Sherbrooke Street West, Montreal, PQ H3A2K6, Canada, and Beckman Coulter GmbH, Europark Fichtenhain B13, D-47807 Krefeld, Germany. Received April 10, 2002; Revised Manuscript Received July 18, 2002

Carrier-mediated delivery holds great promise for significantly improving the cellular uptake and therefore the therapeutic efficacy of antisense oligonucleotides in vivo. A multivalent carbohydrate recognition motif for the asialoglycoprotein receptor has been designed for tissue- and cell-specific delivery of antisense drugs to parenchymal liver cells. To combine low molecular weight with high receptor affinity, the synthetic ligand contains three galactosyl residues attached to a cholane scaffold via  $\epsilon$ -aminocapramide linkers. Three-dimensional structural calculations indicate that this unique design provides proper spacing and orientation of the three galactosyl residues to accomplish high affinity binding to the receptor. Covalent conjugation of the bulky carbohydrate cluster to oligonucleotides has been achieved by solid-phase synthesis using low-loaded macroporous resins and optimized synthesis protocols.

### INTRODUCTION

Specific inhibition of a gene through hybridization of a short single-stranded oligonucleotide (ON)<sup>1</sup> to complementary mRNA to prevent translation is known as the antisense strategy (1–3). This therapeutic technology originates from the specific molecular recognition event between the mRNA of the gene to be inhibited and the synthetic oligonucleotide drug. In addition to this key pharmacodynamic process, many pharmacokinetic processes must occur for gene inhibition to result. Between delivery into the patient's body and degradation or inhibition of translation of the target mRNA, the success of this drug development technology relies on many receptor–ligand recognition processes.

Unmodified ONs<sup>1</sup> lack stability against enzymatic degradation and, due to their size and polyanionic character, suffer from poor cellular uptake. Under in vivo conditions they are cleared rapidly from the body through renal excretion. To address these problems, numerous modifications have been introduced (4–7). Most, however, simply alter the chemical and physicochemical properties of the nucleic acids and enhance the biological efficacy of the derivatives by increasing their nuclease stability, binding affinity, and overall uptake. On the other hand, tissue- and cell-specific drug targeting can only be achieved by employing carrier-drug complexes or conju-

gates that contain a ligand recognized by a receptor on the target cell. Carbohydrate-based conjugates allow targeting of a certain class of cell membrane receptors that are referred to as lectins (8, 9). These receptors recognize a specific carbohydrate motif and internalize their ligands by endocytosis.

The ASGP-R<sup>1</sup> first identified by Pricer and Ashwell (10) is specifically located on parenchymal liver cells, i.e., hepatocytes, and recognizes terminal galactose or lactose residues (9). In the case of lactose, the glucose moiety functions as a tether and the galactose serves as the ligand. The ligands are internalized via receptor-mediated endocytosis (11) and transferred to lysosomes (12). On the basis of previous binding studies with isolated glycoproteins and glycopeptides, various synthetic cluster galactosides have been prepared and used to elucidate the structural requirements for high affinity binding to the receptor. The studies have demonstrated that the binding affinity of a carbohydrate ligand to the ASGP-R is highly influenced by the number and orientation of the

\* To whom correspondence should be addressed. Phone: +1 760 603 2381, Fax: +1 760 929 0036, E-mail: mmanoharan@isisph.com.

<sup>†</sup> Isis Pharmaceuticals, Inc.

<sup>‡</sup> McGill University.

<sup>§</sup> Beckman Coulter GmbH.

<sup>1</sup> Abbreviations: ONs, oligonucleotides; ASGP-R, asialoglycoprotein receptor; YEE(ahGalNAc)<sub>3</sub>, Tyr-Glu-Glu-(aminohexyl-*N*-acetylgalactosamine)<sub>3</sub>; CI, chemical ionization; ES-MS, electrospray mass spectrometry; TEA, triethylamine; DMT-Cl, 4,4'-dimethoxytrityl chloride; BOP, benzotriazol-1-yloxytris(dimethylamino)phosphonium hexafluorophosphate; HOBT, 1-hydroxybenzotriazole; HOSu, *N*-hydroxysuccinimide; tBDPSiCl, *tert*-butyldiphenylchlorosilane; DIEA, *N,N*-diisopropylethylamine; HATU, *O*-(7-azabenzotriazol-1-yl)-1,1,3,3-tetramethyluronium hexafluorophosphate; DMT/Fmoc, 9-fluorenylmethoxycarbonyl; CPG, controlled pore glass; ETT, 5-ethylthio-1*H*-tetrazole; PS-PEG, polystyrene poly(ethylene glycol); PTOs, phosphorothioate oligonucleotides; CGE, capillary gel electrophoresis; 2'-*O*-MOE, 2'-*O*-(2-methoxyethyl).

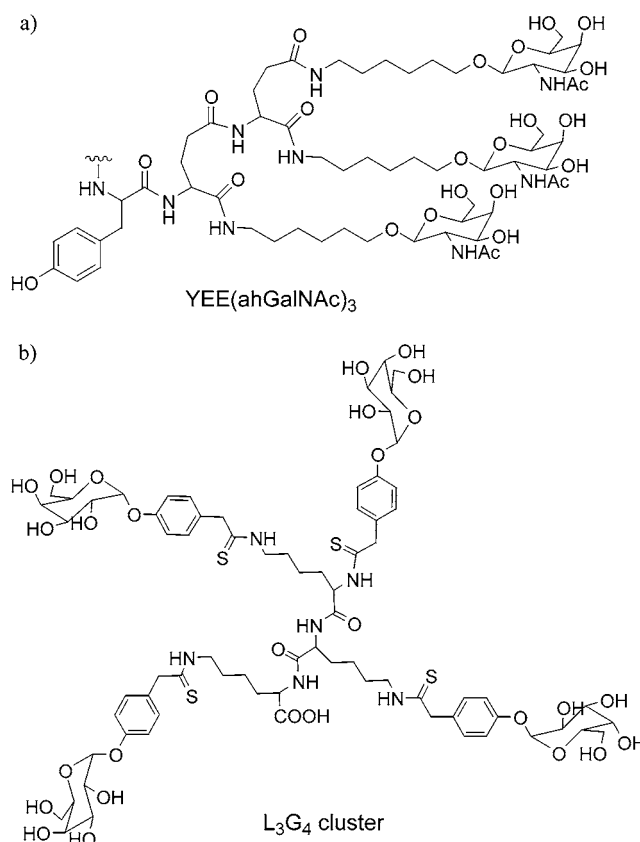


sugar residues, while the aglycon part plays a minor role in ligand recognition (13, 14). A dramatic increase in binding affinity was observed when mono- and triantennary galactosides were compared; this led to the term 'cluster effect' (15, 16). Furthermore, the distance between the vicinal sugar residues seems to have great influence on the binding. Elongation of the spacer from 4 to 20 Å led to a 2000-fold increase in the binding affinity of a synthetic galactoside cluster (17).

Several different approaches have been used to enable the glyco-targeted delivery of nucleic acids to hepatocytes. Wu and Wu developed a DNA carrier system based on a soluble noncovalent complex between nucleic acids and an ASGP-poly-L-lysine conjugate (18, 19). Polylysine covalently linked to asialoorosomucoid complexed with ON facilitated uptake of the ON into human hepatocellular carcinoma (HepG2) cells. In another noncovalent approach, DNA electrostatically bound to galactosylated polyethylenimine was used for *in vitro* gene delivery (20). Transfection with these complexes was found to be highly efficient and selective for hepatocytes. Similarly, additional coating of neutral lipopolyamine-condensed nucleic acids with lipids bearing a triantennary galactosyl residue drives the nucleolipidic particles to the asialoglycoprotein receptor of human hepatoma HepG2 cells (21, for a review of ligand-mediated gene delivery see ref 22). Transfection increases approximately 1000-fold with 25% galactolipid. Covalent conjugates of antisense ONs and ASGP were prepared via disulfide linkages and were found to exhibit an increased biological activity compared to the noncovalent complexes (23).

Chemically and structurally homogeneous conjugates have been prepared by covalent attachment of ONs to multivalent synthetic galactoside clusters (24, 25). Hangel et al. reported a 20- to 40-fold enhancement in cellular uptake in HepG2 cells when methylphosphonate ONs were conjugated to the triantennary *N*-acetylgalactosamine neoglycopeptide YEE(ahGalNAc)<sub>3</sub> (Figure 1a). This glycotriptide was reported to bind to Gal/GalNAc receptor sites on hepatocytes with a *K<sub>d</sub>* of 7 nM. Duff et al. showed that oligonucleotide phosphorothioates conjugated to this glycotriptide sequence specifically suppressed (greater than 90% inhibition) the integrated HBV viral expression in hepatoma cells at 1 μM concentration (26). Compared to the unconjugated compound, this was an increase in efficacy of at least 20-fold. Moreover, no toxicity was observed in the entire concentration range studied (1 to 20 μM). The studies indicated that the cellular delivery was not affected by the backbone charge of the ONs, as conjugates of both anionic oligodeoxyphosphorothioates and neutral oligodeoxymethylphosphonates showed a 20- to 40-fold increase in cellular uptake. *In vivo* experiments in mice showed rapid and high uptake of the conjugate in the liver after tail-vein injection (26).

More recently, improved targeted delivery of oligonucleotides to parenchymal liver cells has been demonstrated by Biessen et al. (25, 27). The ONs were conjugated to the ligand L<sub>3</sub>G<sub>4</sub> (Figure 1b) for the ASGP receptor. *In vitro* uptake studies and confocal laser scan microscopy studies demonstrated that L<sub>3</sub>G<sub>4</sub>-conjugated ONs were far more efficiently bound to and taken up by parenchymal liver cells than nonderivatized ONs. *In vivo* studies in rats showed that hepatic uptake was greatly enhanced from 19% for the unconjugated oligonucleotide to 77% of the injected dose after glycoconjugation. Importantly, accumulation into parenchymal liver cells was improved almost 60-fold after derivatization with



**Figure 1.** Carbohydrate clusters reported for liver cell specific targeting.

L<sub>3</sub>G<sub>4</sub>, and uptake has been attributed to the asialoglycoprotein receptor.

In the present work, the synthesis of a low molecular weight galactoside cluster (Gal<sub>3</sub>Chol) and its covalent conjugation to antisense ONs is described (28, 29). The chemically and structurally defined conjugates were made for targeted delivery to hepatocytes. The unique design of the carrier is based on structural features of known high affinity ligands for the ASGP-R and involves three β-aminogalactosyl residues attached to a rigid cholane scaffold via ε-aminocapramide linkers. In contrast to the reported glycopeptide approaches (Figure 1a/b), the rigid steroid scaffold was chosen to achieve a proper preorganization of the galactose residues and to minimize the loss in receptor binding due to entropic effects (30, 31). To circumvent solution phase conjugation, which generally requires high excess of valuable glycosylated carrier and laborious postsynthetic purification steps, we developed a solid-phase strategy for the conjugation of the carbohydrate cluster to the antisense ONs. The conjugation is compatible to the chemistry of oligonucleotide synthesis.

## EXPERIMENTAL PROCEDURES

**Materials.** Low resolution CI,<sup>1</sup> EI, and FAB mass spectra were obtained on a KRATOS MS 25RFA spectrometer in the direct-inlet mode. High-resolution FAB mass spectra were obtained on a ZAB 2F HS spectrometer from the McGill Biomedical Spectrometry Unit in the direct inlet mode. Positive mode ES-MS<sup>1</sup> of the carbohydrate cluster was performed on a Fisons VG Quattro II spectrometer from the McGill Biomedical Spectrometry Unit. Negative mode ES-MS of the carbohydrate cluster-oligonucleotide conjugates was performed on a Hewlett-Packard 1100 MSD Electrospray Mass

Spectrometer. Melting points were determined on a Gallenkamp block and are uncorrected. Thin-layer chromatography was performed using Kieselgel 60 F<sub>254</sub> aluminum-backed plates (0.2 mm thickness). Spots were visualized by UV and then by dipping in solution A followed by heating. (Solution A: Ammonium molybdate (2.5 g), ceric sulfate (1.0 g), and 10 mL of concentrated sulfuric acid in 100 mL of distilled water). <sup>1</sup>H NMR spectra were recorded on JEOL CPF 270 and Varian UNITY 500 spectrometers at 270 and 500 MHz, respectively. Peak assignments were made with homonuclear spin (H–H) decoupling experiments and COSY. <sup>13</sup>C NMR spectra were recorded on JEOL CFP 270 and Varian UNITY 500 spectrometers at 67.9 and 125.7 MHz, respectively. Peak assignments were made with 2D-heteronuclear correlation and 2D-heteronuclear Multiple Quantum Coherence spectroscopy. <sup>31</sup>P NMR spectra were recorded at 200 MHz on a Varian Gemini 200 Spectrometer. Spin multiplicities are given with the following abbreviations: s, singlet; d, doublet; t, triplet; q, quartet; m, multiplet. All air sensitive reactions were carried out under argon flow with freshly distilled solvents (BDH grade). Pyridine was refluxed for 4 h with fine BaO and distilled over granular BaO under N<sub>2</sub>. TEA<sup>1</sup> and acetonitrile were distilled from CaH<sub>2</sub>. Methanol was distilled from magnesium. Anhydrous DMF was purchased from Aldrich. THF was distilled from sodium benzophenone ketyl. Dimethoxyethane was distilled from sodium benzophenone ketyl. Dry acetone was distilled from anhydrous calcium sulfate. The following chemicals were purchased from Aldrich: D-galactose, sodium azide, tetrabutylammonium hydrogen sulfate, hydrogen bromide (30%) in acetic acid, acetic anhydride, DMT-Cl,<sup>1</sup> DMAP, BOP,<sup>1</sup> citric acid, succinic anhydride, triphosgene, borane–THF complex (1 M in anhydrous THF), HOBT,<sup>1</sup> HOSu,<sup>1</sup> palladium on carbon (10%). tBDPSiCl,<sup>1</sup> DIEA<sup>1</sup> and cholic acid were purchased from Fluka (Milwaukee, WI) and HATU<sup>1</sup> was obtained from Applied Biosystems (Foster City, CA). The DMT/Fmoc<sup>1</sup> precursor 1-O-DMT-6-N–Fmoc-2-hydroxymethylhexane was provided by Clontech Labs (Palo Alto, CA). CPG<sup>1</sup> supports with pore sizes of 2000 Å and 3000 Å and ETT<sup>1</sup> were purchased from Glen Research (Sterling, VA). Macroporous aminofunctionalized polystyrene was obtained from Amersham-Pharmacia (Piscataway, NJ) and the PS-PEG<sup>1</sup> copolymer (TentaGel) from Rapp Polymere (Tübingen, Germany). The other reagents used for solid-phase synthesis were purchased from Applied Biosystems.

**Pentaacetyl-D-galactose 1.** To a solution of D-galactose (3 g, 16.65 mmol) in dry pyridine (33 mL) at 0 °C under Ar was slowly added acetic anhydride (31.5 mL, 333 mmol). The reaction mixture was stirred at 0 °C for 1 h before a catalytic amount of DMAP (200 mg, 1.67 mmol) was added. As the reaction mixture was allowed to reach rt, the reaction became slightly exothermic. After 6 h, the clear yellow mixture was slowly poured into 500 mL of fast stirring ice–water, giving a sticky solid. After ethyl acetate extraction (75 mL), evaporation of the solvent, and coevaporations with dry toluene, acetylated galactose **1** was obtained as an oil (5.77 g, 89%). <sup>1</sup>H NMR (270 MHz, CDCl<sub>3</sub>) δ 6.34 (br s, <sup>3</sup>J<sub>1'–2'</sub> = 1.2 Hz, 1H) H1'; 5.46–5.47 (m, 1H) H2'; 5.29–5.31 (m, 2H) H3' and H4'; 4.29–4.33 (m, 1H) H5'; 4.02–4.10 (m, 2H) H6a' and H6b'; 1.96–2.12 (4 × br s, 15H) acetyl H's. <sup>13</sup>C NMR (67.9 MHz, CD<sub>3</sub>OD) δ [170.3, 170.1, 170.1, 169.8] (4 s) all C=O C's, 89.7 C-1', 68.7, 67.4, 67.3, 66.4, 61.2, [20.9, 20.6, 20.6, 20.6, 20.5] all acetyl C's. LRMS (CI/NH<sub>3</sub>) *m/e*: 408 ([M + NH<sub>3</sub>]<sup>+</sup>, 12.2), 331 (100). *R<sub>f</sub>* = 0.71 in 10% methanol/ethyl acetate.

**1-α-Bromo-2,3,4,6-tetraacetyl-D-galactose 2.** Acetylated galactose **1** (5.77 g, 14.7 mmol) was dissolved in 20 mL of a solution of HBr in acetic acid (30% w/w, 14.7 mmol). After 1 h, all the acetic acid was evaporated and coevaporated with dry toluene. Bromogalactoside **2** was obtained as a brown oil (5.69 g, 94%). Due to instability of bromogalactoside, no further purification was done. <sup>1</sup>H NMR (270 MHz, CDCl<sub>3</sub>) δ 6.66 (d, <sup>3</sup>J<sub>1'–2'</sub> = 3.9 Hz, 1H) H1'; 5.45–5.48 (m, 1H) H4'; 5.36 (dd, <sup>3</sup>J<sub>3'–2'</sub> = 10.6 Hz, <sup>3</sup>J<sub>3'–4'</sub> = 3.2 Hz, 1H) H3'; 5.00 (dd, <sup>3</sup>J<sub>2'–1'</sub> = 3.9 Hz, <sup>3</sup>J<sub>2'–3'</sub> = 10.6 Hz, 1H) H2'; 4.41–4.46 (m, 1H) H5'; 4.05–4.10 (dddd, <sup>2</sup>J<sub>6b'–6a'</sub> = 11.3 Hz, <sup>3</sup>J<sub>6b'–5'</sub> = 6.2 Hz, <sup>3</sup>J<sub>6a'–5'</sub> = 6.8 Hz, 2H) H6a' and H6b'; [2.09 (s); 2.05 (s); 1.99 (s); 1.95 (s)] 12 H, all acetyl H's. <sup>13</sup>C NMR (67.9 MHz, CDCl<sub>3</sub>) δ [170.2, 169.9, 169.8, 169.7] all C=O C's, 88.3 C-1', 71.1, 68.0, 67.8, 67.0, 60.9, [20.7, 20.6, 20.6, 20.6, 20.5] all acetyl C's. LRMS (CI/NH<sub>3</sub>) *m/e*: 412 ([M + H]<sup>+</sup>, 1.4), 169 (100).

**1-β-Azido-2,3,4,6-tetraacetyl-D-galactose 3.** To a solution of bromogalactoside **2** (5.69 g, 13.8 mmol) in CH<sub>2</sub>Cl<sub>2</sub> (57 mL) at room temperature was added NaN<sub>3</sub> (4.5 g, 69.1 mmol), tetrabutylammonium hydrogen sulfate (4.7 g, 13.8 mmol) and 57 mL of a saturated solution of NaHCO<sub>3</sub>. The reaction mixture was stirred vigorously at room temperature for 3 h and diluted with ethyl acetate (500 mL). The organic layer was washed with 200 mL of a saturated solution of NaHCO<sub>3</sub> and evaporated under reduced pressure. Azidogalactoside **3** was obtained as a pale yellow solid (5.02 g, 97%). Recrystallization from methanol yielded **3** as white crystals. mp 94–96 °C (reported: 103–104°). <sup>1</sup>H NMR (270 MHz, CDCl<sub>3</sub>) δ 5.37 (dd, <sup>3</sup>J<sub>4'–3'</sub> = 3.3 Hz, <sup>3</sup>J<sub>4'–5'</sub> = 1.1 Hz, 1H) H4'; 5.12 (dd, <sup>3</sup>J<sub>2'–1'</sub> = 8.6 Hz, <sup>3</sup>J<sub>2'–3'</sub> = 10.4 Hz, 1H) H2'; 5.00 (dd, <sup>3</sup>J<sub>3'–2'</sub> = 10.4 Hz, <sup>3</sup>J<sub>3'–4'</sub> = 3.3 Hz, 1H) H3'; 4.56 (d, <sup>3</sup>J<sub>1'–2'</sub> = 8.6 Hz, 1H) H1'; 4.11–4.13 (m, 2H) H5' and H-6b'; 3.95–4.00 (m, 1H) H-6a'; [2.12 (s); 2.04 (s); 2.01 (s); 1.94 (s)] 12 H, all acetyl H's. <sup>13</sup>C NMR (67.9 MHz, CDCl<sub>3</sub>) δ [170.3, 170.1, 169.9, 169.3] all C=O C's, 88.2, 72.8, 70.6, 68.1, 66.9, 61.2, [20.6, 20.6, 20.6, 20.6] all acetyl C's. LRMS (CI/NH<sub>3</sub>) *m/e*: 391 ([M + NH<sub>3</sub>]<sup>+</sup>, 34.5), 331 (100). *R<sub>f</sub>* = 0.48 in ethyl acetate/hexanes (1:1).

**1-β-Amino-2,3,4,6-tetraacetyl-D-galactose 4.** Azidogalactoside **3** (2.61 g, 6.98 mmol) was dissolved with 25 mL of methanol in a 100 mL hydrogenation flask. After 10–15 min of Ar purging, Pd on charcoal (10% w, 500 mg) was added. Under 40 p.s.i of H<sub>2</sub>, the reaction was allowed to proceed for 1 h. After filtration and evaporation, aminogalactoside **4** was obtained as a pale yellow oil (2.40 g, quantitative). <sup>1</sup>H NMR (270 MHz, CDCl<sub>3</sub>) δ 5.37–5.39 (m, 1H) H1'; 4.98–5.03 (m, 2H) H2' and H3'; 4.06–4.16 (m, 3H) H4', H5', and H6b'; 3.82–3.90 (m, 1H) H6a'; [2.13; 2.06; 2.03; 1.97] 4 (s), 12 H, all acetyl H's. <sup>13</sup>C NMR (67.9 MHz, CDCl<sub>3</sub>) δ [170.5, 170.4, 170.3, 170.1] all C=O C's, 85.3, 85.3, 71.5, 71.3, 69.8, 67.6, 61.8, [20.9, 20.79, 20.74, 20.67] all acetyl C's. LRMS (EI) *m/e*: 347 ([M]<sup>+</sup>, 51.4), 331 (100). *R<sub>f</sub>* = 0.08 in ethyl acetate/hexanes (1:1).

**1-(N-Carboxybenzyl-ε-aminocaproamidyl)-2,3,4,6-tetraacetyl-D-galactose 5.** To a solution of dry N-Cbz-ε-aminocaproic acid (1.93 g, 7.28 mmol) in dry DMF (3 mL) at room temperature under Ar were added BOP reagent (3.22 g, 7.28 mmol), 1-HOBT (0.98 g, 7.28 mmol), and TEA (1.47 mL, 10.59 mmol). The reaction mixture was stirred vigorously at room temperature for 30 min before addition of aminogalactoside **4** (2.3 g, 7.28 mmol). After 36 h, the reaction mixture was diluted with ethyl acetate (150 mL). The organic layer was washed with a saturated solution of NaHCO<sub>3</sub> (50 mL) and a 10% aq citric acid solution (50 mL) and dried under reduced



pressure. After flash column chromatography using (1)  $\text{CH}_2\text{Cl}_2$  and (2) 1.5% methanol/ $\text{CH}_2\text{Cl}_2$  as eluent mixture, galacto-amide **5** was obtained as a pale yellow oil (2.32 g, 60%).  $^1\text{H}$  NMR (500 MHz,  $\text{CDCl}_3$ )  $\delta$  7.25–7.29 (m, 5H) benzyl H's; 6.43 (d,  $^3J_{\text{NH-H}'} = 9.3$  Hz, 1H) amide NH; 5.37 (m, 1H) H4'; 5.20 (dd,  $^3J_{\text{H}1'-\text{H}2'} = 9.3$  Hz,  $^3J_{\text{H}1'-\text{H}2'} = 8.7$  Hz, 1H) H1'; 5.03–5.10 (m, 5H) H2', H3',  $\text{C}_6\text{H}_6\text{CH}_2\text{O}$ - and carbamate NH; 3.96–4.09 (m, 3H) H-5', H6a' and H6b'; 3.11 (br s, 2H)  $\text{CH}_2\text{NHC(O)}$ ; 2.09–2.14 (m, 2H) sugar-NHC(O) $\text{CH}_2$ -; [2.07; 1.98; 1.97; 1.93] 4 s 12H, all acetyl  $\text{CH}_3$  H's; 1.51–1.57 (m, 2H) C(O) $\text{CH}_2\text{CH}_2\text{CH}_2\text{CH}_2\text{CH}_2\text{NH}$ ; 1.41–1.47 (m, 2H) C(O) $\text{CH}_2\text{CH}_2\text{CH}_2\text{CH}_2\text{CH}_2\text{NH}$ ; 1.21–1.30 (m, 2H) C(O) $\text{CH}_2\text{CH}_2\text{CH}_2\text{CH}_2\text{CH}_2\text{NH}$ .  $^{13}\text{C}$  NMR (125.7 MHz,  $\text{CDCl}_3$ )  $\delta$  [173.1, 171.1, 170.4, 170.0, 169.7] all acetyl and amide C=O, 156.5 C=O carbamate, [128.5 and 128.1] benzyl C's, 78.4 C1', 72.3 C2', 70.9 C5', 68.4, 67.2, 66.5, 61.1 C6', 40.8 C(O) $\text{CH}_2\text{CH}_2\text{CH}_2\text{CH}_2\text{CH}_2\text{NH}$ , 36.6 C(O) $\text{CH}_2\text{CH}_2\text{CH}_2\text{CH}_2\text{CH}_2\text{NH}$ , 29.6 C(O) $\text{CH}_2\text{CH}_2\text{CH}_2\text{CH}_2\text{CH}_2\text{NH}$ , 26.1 C(O) $\text{CH}_2\text{CH}_2\text{CH}_2\text{CH}_2\text{CH}_2\text{NH}$ , 24.7 C(O) $\text{CH}_2\text{CH}_2\text{CH}_2\text{CH}_2\text{CH}_2\text{NH}$ , [20.76, 20.70, 20.60, 20.57] all acetyl  $\text{CH}_3$ . LRMS (FAB-NBA)  $m/e$ : 595 ([M + H]<sup>+</sup>, 24.4); 487 ([M + H –  $\text{C}_6\text{H}_6\text{CH}_2\text{O}$ ]<sup>+</sup>, 9.0). ES-MS  $m/z$ : 617.4 ([M + Na]<sup>+</sup>, 100), 595.4 ([M + H]<sup>+</sup>, 26.6). HRMS (FAB-NBA)  $m/e$ : 595 [M + H]<sup>+</sup>, calcd for  $\text{C}_{28}\text{H}_{38}\text{N}_2\text{O}_{12}$ , 595.2424; found 595.2503.  $R_f = 0.17$  in ethyl acetate/hexanes (1:1).

**$\epsilon$ -Aminocaproamidyl-2,3,4,6-tetraacetyl-D-galactose 6.** Galacto-amide **5** (50 mg, 0.084 mmol) was dissolved with 5 mL of ethyl acetate containing 1 mL of distilled  $\text{H}_2\text{O}$  and 0.5 mL of a 1 M acetic acid solution, in a 100 mL hydrogenation flask. After 10–15 min of Ar purging, Pd on charcoal (10% w, 10 mg) was added. Under 40 psi of  $\text{H}_2$ , the reaction was allowed to proceed for 1 h. After filtration and evaporation, aminogalactoside **6** was obtained as a thick, pale yellow oil (155 mg, 90%). Note: ethyl acetate was used for all subsequent hydrogenolytic reactions.  $^1\text{H}$  NMR (500 MHz,  $\text{CDCl}_3$ )  $\delta$  6.99 (d,  $^3J_{\text{NH-H}'} = 9.0$  Hz, 1H) amide NH; 5.40 (d,  $J = 1.9$  Hz, 1H) H4'; 5.22 (dd,  $^3J_{\text{H}1'-\text{H}2'} = 8.5$  Hz,  $^3J_{\text{H}1'-\text{H}2'} = 9.0$  Hz, 1H) H1'; 5.05–5.12 (m, 2H) H2' and H3'; 4.00–4.09 (m, 3H) H5', H6a' and H6b'; 2.88–2.91 (m, 2H)  $\text{CH}_2\text{NH}_2$ ; 2.12–2.20 (m, 2H) Gal-NHC(O) $\text{CH}_2$ ; 2.11 (s, 2H)  $\text{CH}_2\text{NH}_2$ ; [2.02; 2.01; 1.99, 1.96] 4 s 12H, all acetyl  $\text{CH}_3$  H's; 1.66–1.69 (m, 2H) C(O) $\text{CH}_2\text{CH}_2\text{CH}_2\text{CH}_2\text{CH}_2\text{NH}$ ; 1.58–1.62 (m, 2H) C(O) $\text{CH}_2\text{CH}_2\text{CH}_2\text{CH}_2\text{CH}_2\text{NH}$ ; 1.33–1.36 (m, 2H) C(O) $\text{CH}_2\text{CH}_2\text{CH}_2\text{CH}_2\text{CH}_2\text{NH}$ . LRMS (FAB-NBA)  $m/e$ : 461 ([M + H]<sup>+</sup>, 100); 331(7.08), 289(4.08), 129(1.8).  $R_f = 0.0$  in  $\text{CH}_2\text{Cl}_2$ .

**3 $\alpha$ ,7 $\alpha$ ,12 $\alpha$ ,24-Tetrahydroxycholeane 7.** To a solution of cholic acid (3.0 g, 7.34 mmol) in dry THF (30 mL) at 0 °C under Ar was slowly added  $\text{BH}_3\cdot\text{THF}$  (30 mL, 29.4 mmol) over a 20 min period. The reaction mixture solidified and was allowed to reach rt. After 2 h, slow addition of methanol (20 mL) resulted in a clear reaction mixture, which upon evaporation gave tetraol **7**. Purification by two recrystallizations from 2-propanol gave **7** as a white powder (2.15 g, 75%). mp 224–225 °C.  $^1\text{H}$  NMR (270 MHz,  $\text{CDCl}_3$ )  $\delta$  3.95 (br s, 1H) 12- $\text{HCOH}$  (equatorial); 3.78 (br s, 1H) 7- $\text{HCOH}$  (equatorial); 3.50 (m,  $J = 6.4$  Hz, 2H) 23- $\text{CH}_2\text{OH}$  H's; 3.34–3.42 (m, 1H) 3- $\text{HCOH}$  (axial); 3.29–3.31 (m, 3H) 3,7,12  $\text{OH}$  H's; 0.71–2.35 All steroid ring H's and  $\text{CH}_3$  groups.  $^{13}\text{C}$  NMR (67.9 MHz,  $\text{CDCl}_3$ )  $\delta$  74.2, 73.0, 69.2, 63.8, 48.5, 47.6, 43.3, 43.1, 41.2, 40.6, 37.2, 36.6, 36.0, 33.4, 31.3, 30.8, 30.5, 29.7, 28.9, 28.0, 25.4, 24.4, 23.3, 18.2, 13.1. LRMS (FAB-glycerol/NaCl)  $m/e$ : 789 ([2M + H]<sup>+</sup>, 11.5), 395 ([M + H]<sup>+</sup>, 5.7).  $R_f = 0.25$  in 10% methanol/ $\text{CH}_2\text{Cl}_2$ .

**3 $\alpha$ ,7 $\alpha$ ,12 $\alpha$ -Trihydroxy-24-(dimethoxytrityloxy)-choleane 8.** To a solution of cholanetetraol **7** (2 g, 5.06 mmol) in dry pyridine (15 mL) at 0 °C under Ar were

added DMT-Cl (1.88 g, 5.58 mmol) and DMAP (62 mg, 0.506 mmol). The reaction was allowed to proceed at room temperature for 6 h before pouring it into 200 mL of a saturated  $\text{NaHCO}_3$  solution. The crude product was extracted with ethyl acetate (3  $\times$  75 mL), washed with brine (1  $\times$  100 mL), dried with  $\text{MgSO}_4$ , and evaporated to dryness under reduced pressure. After flash column chromatography using (1) 100%  $\text{CH}_2\text{Cl}_2$  and (2) 2% methanol/ $\text{CH}_2\text{Cl}_2$  as eluent, triol **8** was obtained as a yellow solid (2.2 g, 64%).  $^1\text{H}$  NMR (500 MHz,  $\text{DMSO}-d_6$ )  $\delta$  6.85–7.36 (9H) phenyl H's of DMT group; 4.31 (d,  $^3J_{\text{OH-C}3\text{H}} = 4.4$  Hz, 1H) 3- $\text{HCOH}$  of choleane; 4.08 (d,  $^3J_{\text{OH-C}12\text{H}} = 3.4$  Hz, 1H) 12- $\text{HCOH}$  of choleane; 4.00 (d,  $^3J_{\text{OH-C}7\text{H}} = 3.4$  Hz, 1H) 7- $\text{HCOH}$  of choleane; 3.75–3.76 (m, 1H) 12- $\text{HCOH}$  (equatorial H); 3.71 (br s, 6H) two  $\text{OCH}_3$  groups; 3.59 (br s, 1H) 7- $\text{HCOH}$  (equatorial) of choleane; 3.14–3.19 (m, 1H) 3- $\text{HCOH}$  (axial) of choleane; 2.86–2.94 (m, 2H) 24- $\text{CH}_2\text{ODMT}$  H's; 0.79–1.97 All steran ring H's and  $\text{CH}_3$ -groups; 0.54 (s, 3H) 18- $\text{CH}_3$ .  $^{13}\text{C}$  NMR ( $\text{DMSO}-d_6$ )  $\delta$  157.94, 145.30, 136.07, 129.55, 127.73, 127.62, 126.52, 113.07, 85.07, 71.01, 70.43, 66.24, 63.20, 59.74, 54.98, 46.13, 45.68, 41.51, 41.34, 35.30, 35.05, 34.87, 34.37, 32.09, 30.40, 28.55, 27.34, 26.19, 26.05, 22.80, 22.61, 20.74, 17.27, 14.07, 12.30. LRMS (FAB-NBA)  $m/e$ : 697 ([M + H]<sup>+</sup>, 1.4), 303.05 ([M + H –  $\text{C}_{24}\text{H}_{41}\text{O}_4$ ]<sup>+</sup>, 100).

**3 $\alpha$ ,7 $\alpha$ ,12 $\alpha$ -Tri(*N*-hydroxysuccinimidyl carbonate)-24-(dimethoxytrityloxy)choleane 9.** To a solution of triol **8** (500 mg, 0.717 mmol) in dry pyridine (10 mL) was added triphosgene (425 mg, 1.43 mmol) at room temperature. The reaction mixture was stirred for 15 min before HOSu (825 mg, 7.17 mmol) was added. After 10 min, the reaction mixture was slowly poured into ice water (200 mL), giving rise to a fine beige precipitate. After filtration and drying under reduced pressure, 713 mg of active ester **9** were obtained (89%).  $^1\text{H}$  NMR (500 MHz,  $\text{DMSO}-d_6$ )  $\delta$  6.81–7.37 (9H) phenyl H's of DMT group; 5.03 (br s, 1H) 12- $\text{HCOH}$  (equatorial H); 4.87 (br s, 1H) 7- $\text{HCOH}$  (equatorial) of choleane; 4.55–4.61 (m, 1H) 3- $\text{HCOH}$  (axial) of choleane; 3.71 (br s, 6H) two  $\text{OCH}_3$  groups; 2.86–2.93 (m, 2H) 24- $\text{CH}_2\text{-ODMT}$  H's; 2.78–2.83 (m, 12H) all succinimidyl  $\text{CH}_2\text{CH}_2$ - H's; 0.77–1.97 All steran ring H's and  $\text{CH}_3$ -groups; 0.68 (s, 3H) 18- $\text{CH}_3$ .  $^{13}\text{C}$  NMR ( $\text{DMSO}-d_6$ )  $\delta$  169.88, 169.71, 157.95, 150.63, 145.28, 136.09, 136.07, 129.58, 127.76, 127.66, 126.54, 113.10, 85.10, 83.30, 81.58, 80.08, 63.02, 54.98, 47.98, 47.09, 44.85, 42.97, 36.54, 33.93, 33.70, 33.60, 33.59, 33.49, 31.68, 31.66, 30.32, 30.31, 28.01, 26.48, 26.46, 25.68, 25.33, 25.22, 24.54, 21.79, 21.63, 21.09, 17.26, 11.46. LRMS (FAB-NBA)  $m/e$ : 1143.38 ([M + Na]<sup>+</sup>, 0.4), 1120.47 ([M + H]<sup>+</sup>, 1.1), 303.21 ([M + H –  $\text{C}_{39}\text{H}_{50}\text{N}_3\text{O}_4$ ]<sup>+</sup>, 100).

**24-[[ $\alpha$ , $\alpha$ -Bis(*p*-methoxyphenyl)benzyl]oxy]-5 $\beta$ -choleane-3 $\alpha$ ,7 $\alpha$ ,12 $\alpha$ -tris[[5-[2,3,4,6-tetra-*O*-acetyl- $\beta$ -D-galactopyranosyl]carbamoyl]pentyl]carbamate] 10.** To a solution of activated ester **9** (188 mg, 0.17 mmol) in dry DMF (1 mL) at room temperature under argon was added amine **6** (258 mg, 56 mmol). The reaction mixture was stirred at room temperature for 15 h before pouring it into 50 mL of cold water. The crude yellowish precipitate was subjected to flash chromatography using 2.5% methanol/ $\text{CH}_2\text{Cl}_2$ , giving mainly trisubstituted adduct **10** (>90% by electrospray mass spectroscopy) as one streaky spot. Some deacetylated product(s) were observed by ES-MS. Therefore, repeated acetylation with 20 equiv of acetic anhydride in pyridine (5 mL) was performed prior to the detritylation step (286 mg, 79%). TLC (5% methanol/ $\text{CH}_2\text{Cl}_2$ ):  $R_f$  0.48–0.56.  $^1\text{H}$  NMR (500 MHz,  $\text{DMSO}-d_6$ )  $\delta$  8.63–8.66 (3  $\times$  m, 3H) three amide NH; 6.82–7.33 (13H) phenyl H's of DMT group; 6.60–6.84 (3  $\times$  m, 3H)

three carbamate NH; 5.35 (multiplet with a doublet of doublets-like character,  $^3J_{\text{H1}'-\text{NH}} = 8.8$  Hz,  $^3J_{\text{H1}'-\text{H2}'} = 8.8$  Hz, 3H) three  $\alpha$ -H1' of galactose; 5.22–5.27 (m, 6H) three H3' and H4'; 4.95 ( $J = 9$  Hz, 3H) three H2'; 4.62–4.77 (2  $\times$  br s) 7,12-equatorial H's of cholane; 4.30 (m,  $J = 6.3$  Hz, 4H) three H5' and 3-axial H of cholane; 4.03 (multiplet, 3H) three H6b'; 3.94 (multiplet, 3H) three H6a'; 3.33–3.41 (m, 2H) 24-CH<sub>2</sub>-ODMT; 2.84–3.02 (3  $\times$  m, 6H) three CH<sub>2</sub>NHC(O)); {0.62–2.10 (complex set of multiplets) all steran ring H's, CH<sub>3</sub>-groups and all caproic CH<sub>2</sub> groups; only assignments possible: 1.99–2.10 (m, 6H) Gal-NHC(O)CH<sub>2</sub> 1.89–2.07 (36H) all acetyl CH<sub>3</sub> H's; 0.62 (s, 3H) 18-CH<sub>3</sub>. <sup>13</sup>C NMR (125.7 MHz, DMSO-*d*<sub>6</sub>)  $\delta$  Only assignments possible 170.31, 170.23, 169.44, 169.40, 169.38, 169.23, 169.10, 167.45, 166.74, 165.88, 164.33, all C=O, 157.92, 145.33, 136.08, 129.50, 128.00, 127.66, 126.57, 113.04, all phenyl C's, 85.37, 78.20 C1', 74.67 C12-steran, 70.92 C2', 68.33, 67.16 C4', 63.40 C24-steran, 61.05 C6', 29.23, 25.76, 24.73 all caproic CH<sub>2</sub>C's, 20.63, 20.45, 20.41, 20.22, 20.11, 20.03, 18.99 all acetyl CH<sub>3</sub> and cholane CH<sub>3</sub>. Electrospray MS (DMF)  $m/z$ : 2179.9 ([M + Na]<sup>+</sup>, 100), 2195.9 ([M + K]<sup>+</sup>, 12.6).

**24-Hydroxy-5 $\beta$ -cholane-3 $\alpha$ ,7 $\alpha$ ,12 $\alpha$ -tris[[5-[2,3,4,6-tetra-*O*-acetyl- $\beta$ -D-galactopyranosyl]carbamoyl]pentyl]carbamate] 11.** The DMT-protected trigalactosyl glycoconjugate derivative **10** (0.41 g, 0.19 mmol) was dissolved in a solution of 3% trichloroacetic acid in 25 mL of CH<sub>2</sub>Cl<sub>2</sub>/MeOH and stirred at room temperature for 5 min. The reaction was monitored by TLC (CH<sub>2</sub>Cl<sub>2</sub>/methanol 6:4). After the DMT group was completely removed, the reaction mixture was evaporated. The residual solid was purified by flash chromatography on a silica gel column using a stepwise gradient of 0–10% methanol in ethyl acetate/hexanes (6:4) as eluents to give 0.32 g (90%) of the deprotected glycoconjugate **11** as a white foam: TLC (CH<sub>2</sub>Cl<sub>2</sub>/methanol 6:4):  $R_f$  0.35. <sup>1</sup>H NMR (500 MHz, DMSO-*d*<sub>6</sub>)  $\delta$  8.64–8.66 (2  $\times$  m, 3H) three amide NH; 6.60–6.84 (3  $\times$  m, 3H) three carbamate NH; 5.32 (multiplet with a doublet of doublets-like character,  $^3J_{\text{H1}'-\text{NH}} = \sim 9$  Hz,  $^3J_{\text{H1}'-\text{H2}'} = \sim 9$  Hz, 3H) three  $\alpha$ -H1' of galactose; 5.19–5.26 (m, 6H) three H3' and H4'; 4.97–5.02 (multiplet with triplet-like character,  $J = \sim 9$  Hz, 3H) three H2'; 4.60–4.75 (2  $\times$  br s) 7,12-equatorial H's of cholane; 4.28 (m,  $J = 6.3$  Hz, 4H) three H5' and 3-axial H of cholane; 4.00 (multiplet with a doublet of doublets-like character,  $^3J_{\text{H6b}'-\text{H6a}'} = \sim 11$  Hz,  $^3J_{\text{H6b}'-\text{H5}'} = \sim 5$  Hz, 3H) three H6b'; 3.94 (multiplet with a doublet of doublets-like character,  $^3J_{\text{H6a}'-\text{H6b}'} = \sim 11$  Hz,  $^3J_{\text{H6a}'-\text{H5}'} = \sim 6$  Hz, 3H) three H6a'; 3.30–3.40 (m,  $\sim 6$ H) 24-CH<sub>2</sub>OH and residual H<sub>2</sub>O; 2.86–2.99 (br m, 7H) three CH<sub>2</sub>NHC(O)) and 24-CH<sub>2</sub>-OH; {0.65–2.08 (complex set of multiplets) all steran ring H's, CH<sub>3</sub> groups and all caproic CH<sub>2</sub> groups; 2.00–2.09 (m, 6H) Gal-NHC(O)CH<sub>2</sub> 1.89–2.08 (36H) all acetyl CH<sub>3</sub> H's; 0.66 (s, 3H) 18-CH<sub>3</sub>. <sup>13</sup>C NMR (125.7 MHz, DMSO-*d*<sub>6</sub>)  $\delta$  Only assignments possible 170.31, 170.23, 169.44, 169.40, 169.38, 169.23, 169.10, 167.45, 166.74, 165.88, 164.33, all C=O, 85.32, 78.20 C1', 74.67 C12-steran, 70.92 C2', 68.33, 67.16 C4', 63.40 C24-steran, 61.05 C6', 29.23, 25.76, 24.73 all caproic CH<sub>2</sub>C's, 20.63, 20.45, 20.41, 20.22, 20.11, 20.03, 18.99 all acetyl CH<sub>3</sub> and cholane CH<sub>3</sub>. Electrospray MS (DMF/AcOH)  $m/z$ : 1877.2 ([M + Na]<sup>+</sup>, 100), 1855.1 ([M + H]<sup>+</sup>, 5.15).

**24-[*O*-(*N,N*-Diisopropylamino)(2-cyanoethyl)phosphite]-5 $\beta$ -cholane-3 $\alpha$ ,7 $\alpha$ ,12 $\alpha$ -tris[[5-[2,3,4,6-tetra-*O*-acetyl- $\beta$ -D-galactopyranosyl]carbamoyl]pentyl]carbamate] 12.** A 0.274 mL amount of 0.5 M tetrazole in CH<sub>3</sub>CN was added dropwise to a stirred solution of **11** (0.32 g, 0.17 mmol) and *O*-cyanoethyl-bis(diisopropylamino)phosphine (0.065 mL, 0.206 mmol) in 10 mL of

anhydrous CH<sub>3</sub>CN under argon atmosphere and the mixture was stirred at room temperature for 30 min. The reaction was monitored by TLC (5% TEA in ethyl acetate/hexanes/methanol 6:3:1). After completion, tetrazole was neutralized with a few drops of TEA, and the mixture was diluted with ethyl acetate to a volume of 50 mL. The organic solution was washed twice with NaHCO<sub>3</sub> solution (10% in H<sub>2</sub>O) followed by brine, dried over Na<sub>2</sub>SO<sub>4</sub>, and concentrated to an oil. The product was precipitated twice in hexanes at 0 °C and dried in vacuo to give 0.3 g (85%) of pure phosphoramidite **12**: TLC (5% TEA in ethyl acetate/hexanes/methanol 6:3:1):  $R_f$  0.63; <sup>31</sup>P NMR (CDCl<sub>3</sub>)  $\delta$  147.1.

**Preparation of Solid Supports for the Synthesis of 5'-Conjugates.** Prior to coupling of the nucleoside succinates, the aminofunctionalized resins were washed twice with 5% DIEA in CH<sub>2</sub>Cl<sub>2</sub> followed by three washing steps with DMF. For 1 g of resin, a solution of 0.019 mmol of nucleoside succinate, 0.06 mmol of DIEA, and 0.019 mmol of HATU in DMF was prepared, allowed to pre-activate for 1–2 min, and added to the resin. After shaking the suspension overnight, the resin was washed three times with DMF and three times with CH<sub>3</sub>CN and dried in vacuo. The resin substitution was determined by a spectrometric DMT-assay and the remaining NH<sub>2</sub> groups were capped using a 1:1 mixture of the capping reagents from oligonucleotide synthesis (CapA/CapB). Finally, the resin was washed with CH<sub>3</sub>CN and dried in vacuo.

**3 $\alpha$ ,7 $\alpha$ ,12 $\alpha$ -Trihydroxyallyl Cholate 13.** To a solution of cholic acid (2 g, 4.895 mmol) in anhydrous DMF (12 mL) was added cesium carbonate (1.73 g, 4.895 mmol) at room temperature and under inert atmosphere. The mixture was stirred for 1 h before adding 7 equiv of allyl bromide (2.96 mL, 34.26 mmol). The reaction was monitored by TLC and, after being stirred for 2 h 40 min, 80 mL of water was added, and the solution was acidified with 2 N KHSO<sub>4</sub>. Extraction of crude **13** was carried out with CH<sub>2</sub>Cl<sub>2</sub> and ethyl acetate. The organic layers were washed with brine, dried with MgSO<sub>4</sub>, filtered, and evaporated to dryness under reduced pressure. After flash chromatography on silica gel with 70–100% ethyl acetate in hexanes as the eluent, the allyl ester **13** was isolated as a white solid (2.05 g, 93%).  $R_f = 0.43$  in ethyl acetate/hexane 7/3. °F = 152–154 °C. <sup>1</sup>H NMR (200 MHz, CD<sub>3</sub>OD, ppm)  $\delta$  6.05–5.63 (ddt,  $J_{\text{ab}} = 22.5$  Hz,  $J_{\text{ac}} = 10.4$  Hz,  $J_{\text{ad}} = 5.6$  Hz, 1H) –CH= (allyl); 5.37–5.15 (2dq,  $J_{\text{ba}} = 17.3$  Hz,  $J_{\text{bc}} = J_{\text{cb}} = 1.6$  Hz,  $J_{\text{ca}} = 10.4$  Hz, 2H) CH<sub>2</sub>= (allyl); 4.90 (s, 3 OH); 4.56 (dt,  $J_{\text{ddr}} = 1.4$  Hz,  $J_{\text{da}} = 5.6$  Hz, 2H) CH<sub>2</sub>O (allyl); 4.00–3.90 (broad, 1 H) 17-H; 3.80 (broad, 1H) 7-H; 3.45–3.27 (m, 1 H) 3-H; 2.50–1.10 (m, 23 H) CH and CH<sub>2</sub> (steran rings); 1.05 (d,  $J = 6$  Hz, 3H) 18-CH-CH<sub>3</sub>; 0.90 (s, 3H) 13-C-CH<sub>3</sub>; 0.70 (s, 3H) 10-C-CH<sub>3</sub>. <sup>13</sup>C NMR (25 MHz, CD<sub>3</sub>OD)  $\delta$  175.0, 133.8, 118.5, 74.7, 73.6, 69.8, 66.8, 49.0, 48.5, 44.3, 44.1, 42.1, 41.6, 37.9, 37.7 (2 peaks), 37.1, 33.5, 33.3, 32.4, 30.8, 30.0, 29.1, 25.6, 24.6, 19.1, 14.5. LRMS (FAB–NBA)  $m/e$ : 897 (dimer), 449 [M + H]<sup>+</sup>, 431 [M + H–H<sub>2</sub>O]<sup>+</sup>, 413 [M + H–2H<sub>2</sub>O]<sup>+</sup>, 395 [M + H–3H<sub>2</sub>O]<sup>+</sup>.

**3 $\alpha$ ,7 $\alpha$ ,12 $\alpha$ -Tris(*N*-hydroxysuccinimidyl carbonate)-allyl Cholate 14.** A solution of allyl cholate **13** (200 mg, 0.446 mmol) in freshly distilled pyridine (4 mL) was cooled to 0 °C before adding 2 equiv of triphosgene (265 mg, 0.892 mmol). The reaction mixture was stirred for 30 min at 0 °C before adding another 1 equiv of triphosgene (132 mg, 0.446 mmol). Stirring was continued for 10 min at room temperature, and another 2 mL of anhydrous pyridine was added. Again the reaction mixture was cooled to 0 °C before 513 mg (4.460 mmol) of



*N*-hydroxysuccinamide (HOSu) was added. After 15 min, the light orange solution was slowly poured into ice-water (100 mL), to give a pale yellow precipitate. After purification by flash chromatography on silica gel (70–100% ethyl acetate in hexanes), **14** was obtained as a white solid (209 mg, 53%).  $R_f = 0.18$  (ethyl acetate/hexanes 7:3).  $F = 140\text{--}145^\circ\text{C}$ .  $^1\text{H}$  NMR (200 MHz,  $\text{CDCl}_3$ )  $\delta$  6.10–5.80 (ddt,  $J_{ab} = 16.5$  Hz,  $J_{ac} = 10.4$  Hz,  $J_{ad} = 5.6$  Hz, 1H) CH= (allyl); 5.39–5.19 (2dq,  $J_{ba} = 17.8$  Hz,  $J_{bc} = J_{cb} = 1.6$  Hz,  $J_{ca} = 10.3$  Hz, 2H) CH<sub>2</sub>= (allyl); 5.10 and 4.92 (2 broad peaks, 2 OH) 7-H, 12-H; 4.64–4.50 (2 broad peaks, 3H) CH<sub>2</sub>O (allyl); 3-H; 3.00–2.75 (2 s (12 H) CH<sub>2</sub> (N-Suc); 2.50–1.10 (m, ~26 H) CH and CH<sub>2</sub> (steran rings); 0.95 (m, 6H) 18-CH-CH<sub>3</sub> and 13-C-CH<sub>3</sub>; 0.75 (s, 3H) 10-C-CH<sub>3</sub>. LRMS (FAB–NBA)  $m/e$ : 872 [ $M + H$ ]<sup>+</sup>, 713 [ $M - \text{OSu} - \text{CO}_2$ ]<sup>+</sup>, 554 [ $M - 2(\text{OSu} - \text{CO}_2)$ ]<sup>+</sup>, 395 [ $M - 3(\text{OSu} - \text{CO}_2)$ ]<sup>+</sup>.

**3 $\alpha$ ,7 $\alpha$ ,12 $\alpha$ -Tris[[5-[2,3,4,6-tetra-*O*-acetyl- $\beta$ -D-galactopyranosyl]carbamoyl]pentyl]carbamate]allyl Cholate **15**.** To a solution of activated ester **14** (200 mg, 0.229 mmol) in dry DMF (1.3 mL) at room temperature and under nitrogen, 4.3 equiv of the aminogalactoside **6** (600 mg, 0.998 mmol) were added. The reaction mixture was stirred for 15 h before pouring it into 50 mL of ice-water. The crude yellowish precipitate was filtered and purified by flash chromatography on silica gel (gradient of 70% to 100% of ethyl acetate in hexane) to give a white solid (325 mg). MALDI-TOF demonstrated the loss of one or two acetyl group(s), which were reinstalled by standard acetylation using 4 equiv acetic anhydride in dry pyridine (2.5 mL) in the presence of 0.1 equiv of DMAP. The reaction mixture was stirred overnight and after evaporation of the solvent, the residual oil was added to cold water, yielding a white precipitate **15** (308 mg, 95%). Analysis before reacetylation:  $^{13}\text{C}$  NMR (25 MHz,  $\text{CDCl}_3$ )  $\delta$  173.0, 173.4, 173.3, 173.2, 173.2, 173.2, 171.2, 171.1, 170.4, 170.3, 170.0, 169.7, 156.2, 156.0 all C=O (esters and carbamates), 132.3, 118.3 (allyl group), 78.3 C1', 72.2 C12-steran, 70.8 C2', 68.4 C4', 67.5, 67.4, 67.3, 67.1, 65.0 C3, 61.0 C6', 47.2, 45.2, 43.6, 40.6, 37.7, 36.4, 36.3, 34.8, 34.3, 31.1, 30.8, 29.7, 28.9, 27.3, 26.1, 25.5, 24.8, 22.9, 22.8, 22.4, 20.7, 20.6, 20.5, 17.4, 12.2. MALDI-TOF: 1891 [ $M - \text{acetyl} + \text{Li} + \text{Na}$ ]; Analysis after re-acetylation: MALDI-TOF: 1911 [ $M - \text{H} + \text{Li}$ ].

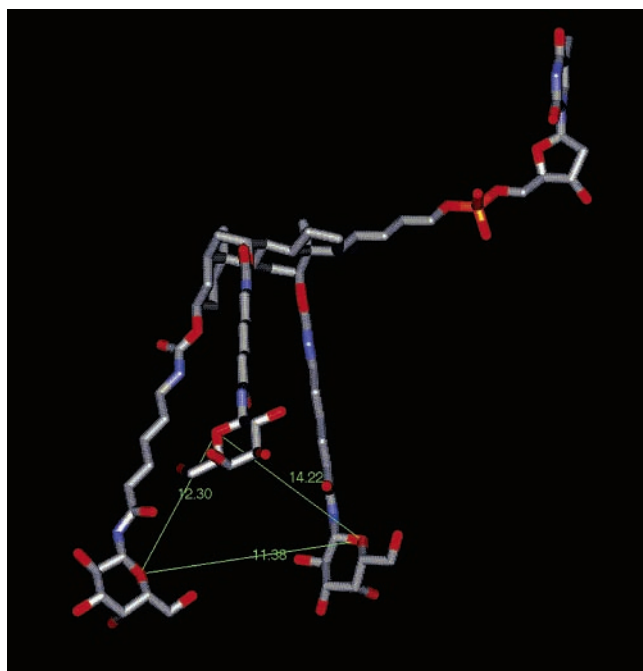
**3 $\alpha$ ,7 $\alpha$ ,12 $\alpha$ -tris[[5-[2,3,4,6-tetra-*O*-acetyl- $\beta$ -D-galactopyranosyl]carbamoyl]pentyl]carbamate]cholic Acid **16**.** To a solution of **15** (644 mg, 0.337 mmol) in anhydrous THF (7.7 mL) were added successively at room temperature and under inert atmosphere tetrakis(triphenylphosphine)palladium (160 mg, 0.135 mmol) and morpholine (305  $\mu\text{L}$ , 3.370 mmol). The reaction mixture was stirred for 20 min. Subsequently, the solvent was evaporated, and the crude compound was purified by chromatography on silica gel (0–20% methanol in ethyl acetate). The fractions containing **16** were collected, the solvent was evaporated, and the residual oil was poured in cold ether and stirred for 30 min to yield the cholic acid derivative **16** as a white precipitate. ( $R_f = 0.6$  in ethyl acetate/methanol 9:1); MALDI-TOF: 1874 [ $M - \text{H} + \text{Li}$ ].

**Functionalization of a Solid Support with Gal<sub>3</sub>Chol for the Synthesis of 3'-Conjugates (**17**).** The DMT/Fmoc linker succinate was prepared from 1.5 g (2.23 mmol) of 1-*O*-DMT-6-*N*-Fmoc-2-hydroxymethylhexane, 0.335 g (3.35 mmol) of succinic anhydride, and 0.14 g of DMAP, which were dissolved in 12 mL of  $\text{CH}_2\text{Cl}_2$ /pyridine (5:1) and stirred for 24 h. The reaction was monitored by TLC (1% TEA in  $\text{CH}_2\text{Cl}_2$ /methanol 9:1). After completion, the mixture was diluted with 50 mL of  $\text{CH}_2\text{Cl}_2$  and washed twice with 10% aq citric acid and once with brine.

The organic phase was dried over  $\text{Na}_2\text{SO}_4$  and evaporated in vacuo to give 1.46 g (85%) of the succinate. Loading of the succinate onto macroporous aminofunctionalized PS was performed as described above for the preparation of the solid supports for 5'-conjugation, whereas 0.03 mmol (23.2 mg) of succinate, 0.03 mmol (11.4 mg) of HATU, and 0.09 mmol (15  $\mu\text{L}$ ) of DIEA were used for 1 g of support. The loading of the support, as determined by DMT-assay, was 24  $\mu\text{mol/g}$ . Subsequently, the Fmoc group was removed from the amino terminus of the branched linker by treating the resin twice with a solution of 20% piperidine in DMF for 20 min. Finally, the carboxylic acid derivative of Gal<sub>3</sub>Chol **16** was attached to the amino group on the resin utilizing the HATU/DIEA activation described above. Briefly, 2 equiv (0.048 mmol/g resin) of **16** (87.7 mg), 2 equiv. (0.048 mmol) of HATU (18.3 mg), and 6 equiv (0.144 mmol) of DIEA (25  $\mu\text{L}$ ) were dissolved in DMF. After 3 min of preactivation, the mixture was added to the resin, and the suspension was shaken overnight. Subsequently, the Gal<sub>3</sub>Chol-substituted solid support **17** was washed thoroughly with DMF and  $\text{CH}_2\text{Cl}_2$ . The applied Kaisertest indicated a quantitative coupling reaction. However, a mixture of CapA/CapB (1:1) was applied to acetylate any residual unreacted amino groups.

**BET Surface Analysis of the Solid Supports.** The specific surface areas of the resins preloaded with the starting nucleoside were determined by BET analysis of the nitrogen adsorption isotherms using a SA 3100 Surface Area and Pore Size Analyzer from Beckman-Coulter (Krefeld, Germany). Therefore, samples of approximately 1 g of each material were degassed under reduced pressure for 10 h at 45  $^\circ\text{C}$  and 16 h at 40  $^\circ\text{C}$  for the CPG and PS supports, respectively. Nitrogen was added incrementally, and the data points derived from the adsorption isotherm were used to determine the monolayer volume and the specific surface area of the materials by BET calculation (32).

**Synthesis and Purification of Oligonucleotide–Gal<sub>3</sub>Chol Conjugates.** Solid-phase synthesis of PTOs<sup>1</sup> was carried out on an Applied Biosystems DNA/RNA synthesizer 380B using standard phosphoramidite chemistry and Beaucage reagent (0.05 M in  $\text{CH}_3\text{CN}$ ) as the sulfurizing agent. For synthesis of 5'-conjugates, the carbohydrate cluster was introduced as a phosphoramidite **12**. Prior to conjugation, the support-bound oligonucleotide (DMT-off) was placed in a Merrifield flask and washed thoroughly with anhydrous  $\text{CH}_3\text{CN}$ . The coupling was performed under argon atmosphere as a manual batch step using 3–30 equiv of phosphoramidite (0.05 M in  $\text{CH}_3\text{CN}$ ) and 15–150 equiv of the activation reagent tetrazole (0.5 M in  $\text{CH}_3\text{CN}$ ) or ETT (0.25 M in  $\text{CH}_3\text{CN}$ ). The suspension was shaken for 1 h. Subsequently, the solid support was washed three times with acetonitrile and the terminal P(III)-linkage was oxidized with Beaucage reagent (0.05 M in  $\text{CH}_3\text{CN}$ ) for 20 min. Finally, the resin was washed with  $\text{CH}_3\text{CN}$  before the conjugate was cleaved from the support and deprotected with concentrated aqueous ammonia (55  $^\circ\text{C}$ , 6 h). Using the Gal<sub>3</sub>Chol-modified PS **17** as the solid support, automated syntheses of 3'-conjugates were performed using standard protocols. The conjugates were purified by RP-HPLC using a 306 Piston Pump System, a 811C Dynamic Mixer, a 170 Diode Array Detector and a 215 Liquid Handler together with the Unipoint Software from Gilson (Middleton, WI). The HPLC conditions were as follows. Column: Waters Deltapak C<sub>18</sub> reversed phase (300  $\times$  3.9 mm, 15  $\mu$ , 300  $\text{\AA}$ ); Solvent A: 0.1 M  $\text{NH}_4\text{OAc}$  in  $\text{H}_2\text{O}$ ; Solvent B: 0.1 M  $\text{NH}_4\text{OAc}$  in  $\text{CH}_3\text{CN}/\text{H}_2\text{O}$  (80:20);



**Figure 2.** Geometry and conformation of the carbohydrate cluster conjugated to the 5'-position of a nucleoside via a thiophosphate linkage.

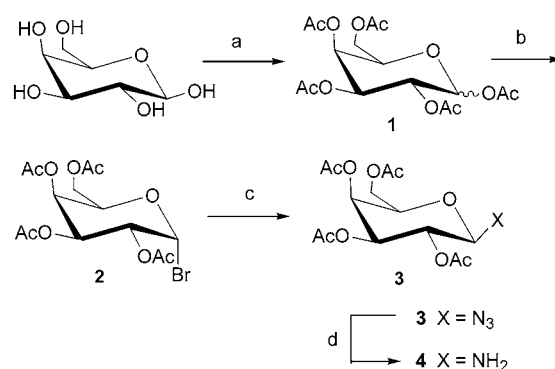
Gradient: 0–32 min 0–50% B. After chromatographic purification the oligonucleotides were desalted by RP-HPLC, analyzed by CGE<sup>1</sup> and ES-MS, lyophilized, and stored at  $-20^{\circ}\text{C}$ .

## RESULTS AND DISCUSSION

**Design and Synthesis of the Galactoside Cluster (Gal<sub>3</sub>Chol).** The application of glycosylated ligands for targeted delivery of antisense oligonucleotides has been shown to enhance their cell-specific uptake and efficacy in vitro and in vivo and may have significant implications for the antisense therapy (19, 23–25, 33–36). We report here on the development of a synthetic vector for targeting antisense ONs to parenchymal liver cells and the synthesis of various carrier–oligonucleotide conjugates.

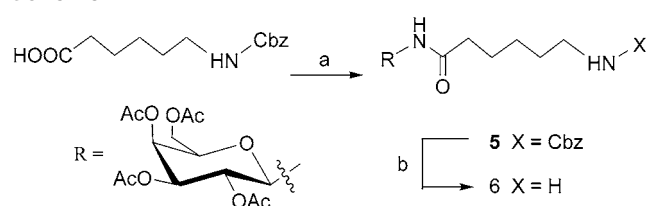
According to the known structural features required for high affinity binding to the ASGP-R, a triantennary conjugate was chosen as the synthetic carbohydrate carrier. Synthesis of the carrier was achieved by connecting three  $\beta$ -aminogalactosyl residues to a rigid cholane scaffold via  $\epsilon$ -aminocapramide linkers. With this design, we created a ligand with favorable spacing and orientation of the galactose moieties for high affinity recognition by the membrane lectins. Three-dimensional molecular modeling involving structural calculations with energy minimization indicate that Gal<sub>3</sub>Chol has an umbrella-like conformation with the three galactosyl residues protruding from one side of the steroid backbone. The cluster forms a triangle with distances of about 11, 12, and 14 Å measured from tetrahydropyran ring oxygen to tetrahydropyran ring oxygen (Figure 2). Given the flexibility of the  $\epsilon$ -aminocapramide spacers, however, the cluster system will be able to adopt a wide range of conformations with varying intergalactosyl distances. Molecular dynamics simulations of a known high affinity oligosaccharide ligand indicate a relatively constant distance of 15 Å between two of the Gal residues (37). The spacing is crucial for the recognition by the receptor, while the distances to the other residue show a considerable degree of flexibility. Thus, the required flexibility

### Scheme 1<sup>a</sup>



<sup>a</sup> Reagents and conditions: (a) acetic anhydride, pyridine, DMAP,  $0^{\circ}\text{C}$ , 1 h, rt, 6 h, 89%; (b) HBr, acetic acid, rt, 1 h, 94%; (c)  $\text{NaN}_3$ ,  $\text{Bu}_4\text{NHOSO}_4$ ,  $\text{CH}_2\text{Cl}_2$ ,  $\text{NaHCO}_3$ , rt, 3 h, 97%; (d) 10% Pd/C, 40 psi  $\text{H}_2$ , methanol, rt, 1 h, 98%.

### Scheme 2<sup>a</sup>



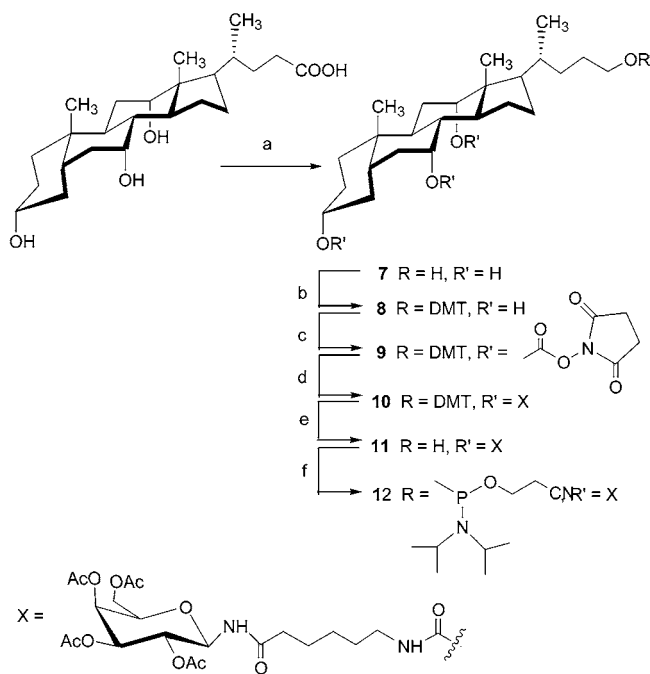
<sup>a</sup> Reagents and conditions: (a) BOP, HOBT, TEA, DMF; 4, rt, 36 h, 60%; (b) 10% Pd/C, 40 psi  $\text{H}_2$ , acetic acid, ethyl acetate,  $\text{H}_2\text{O}$ , rt, 1 h, 90%.

and proper spacing between the galactose residues can be achieved with the present design. The actual binding affinity of the conjugates for the ASGP-R, however, has not yet been determined.

Our goal was to combine high affinity binding with low molecular weight in order to enable the synthesis of structurally and chemically homogeneous conjugates through a straightforward solid-phase approach. Therefore, the carrier was designed to be chemically stable under the conditions of oligonucleotide synthesis and deprotection. Acyl groups, removable under the conditions of oligonucleotide deprotection, were chosen to protect the hydroxy functions of the sugar residues.

The acyl-protected  $\beta$ -aminogalactoside **4** was prepared in a four-step procedure (overall yield: 80%) from D-galactose (Scheme 1). After peracetylation of the sugar with acetic anhydride in pyridine, the anomeric position of **1** was converted to the bromide **2** with HBr/AcOH and subsequently treated with  $\text{NaN}_3$  under phase-transfer catalysis. The resulting azide **3** was reduced to the 1- $\beta$ -amino-2,3,4,6-tetraacetyl-D-galactose **4**. Subsequently, the acylated  $\beta$ -aminogalactoside was coupled to N-Cbz-protected  $\epsilon$ -aminocaproic acid (Scheme 2). With a coupling yield of about 60%, the combination of BOP/HOBT/TEA in DMF proved to be most suitable among the activation reagents tested. CBz provided stable protection of the  $\epsilon$ -amino group without any loss of acyl groups during the subsequent deprotection step. After removal of the CBz protection group from **5** ( $\text{H}_2$ , 10% Pd/C), the spacer 1-( $\epsilon$ -aminocaproamide)-2,3,4,6-tetraacetyl-D-galactose **6** was obtained in an isolated yield of 90%.

The scaffold was derived from cholic acid, with three hydroxyl groups as the anchors for triantennary linkers. Cholic acid was converted to the activated tricarboxylate **9** in three consecutive steps with an overall yield of 43%, to which the galactosylated spacers **6** were attached (Scheme 3). To achieve this, cholic acid was first converted to tetrahydroxycholane **7** using a  $\text{BH}_3\cdot\text{THF}$  com-

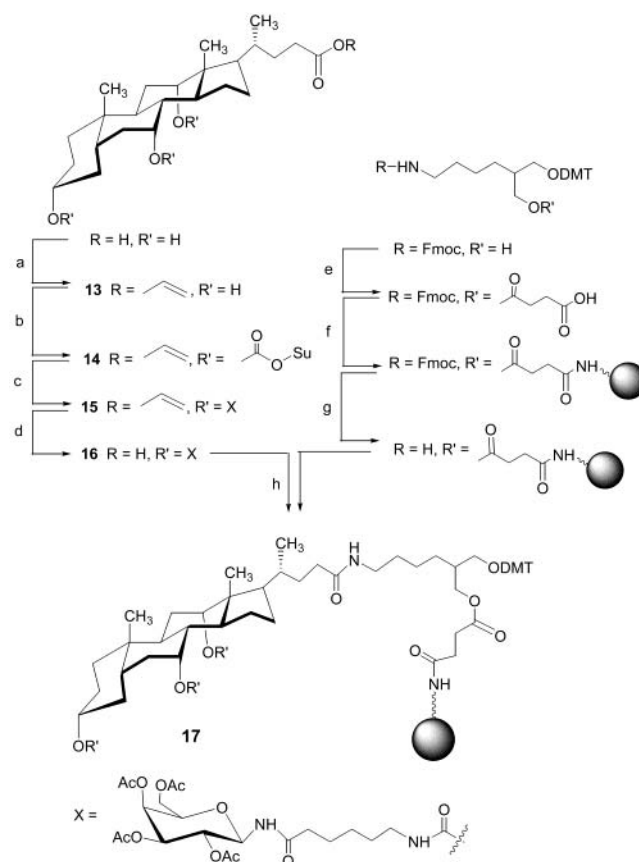
Scheme 3<sup>a</sup>

<sup>a</sup> Reagents and conditions: (a)  $\text{BH}_3\cdot\text{THF}$ , THF, 0 °C to room temperature, 2 h, 75%; (b) DMT-Cl, pyridine, 0 °C to room temperature, 6 h, 64%; (c) 1. triphosgene, pyridine, rt, 15 min, 2. HOSu, 10 min, 89%; (d) 1. **6**, DMF, rt, 15 h, 2. acetic anhydride, pyridine, rt, 12 h, 79%; (e) TCA,  $\text{CH}_2\text{Cl}_2$ , methanol, rt, 5 min, 90%; (f)  $\text{NC}(\text{CH}_2)_2\text{-OP[N}(\text{iPr})_2\text{]}_2$ , tetrazole,  $\text{CH}_2\text{Cl}_2$ , rt, 2 h, 85%.

plex in THF for reduction of the carboxyl group. In the second step, the primary hydroxy function was protected with DMT. The DMT group was chosen since it is orthogonal to the acyl protection on the Gal residues and can be easily removed under mild acidic conditions. Finally, the remaining hydroxy functions of **8** were converted to HOSu-activated carbonates using triphosgene followed by *N*-hydroxysuccinimide.

The final assembly of the carbohydrate cluster was achieved by coupling the galactosylated spacers **6** to the activated cholane backbone **9** (Scheme 3, step d). This turned out to be the most difficult step of the entire synthesis, since attachment of all three bulky spacer molecules to the cholane backbone was apparently hampered by steric effects. The choice of the solvent turned out to be crucial for this process, and best results were obtained when the reaction was carried out in dry DMF at room temperature for about 15 h (79%). Subsequently, the crude product **10** was treated with acetic anhydride in pyridine to reinstall any acyl groups lost during the coupling reaction. Finally, the DMT group was removed with 3% TCA in  $\text{CH}_2\text{Cl}_2$ /methanol (90% isolated yield). The triantennary galactoside **11** was reacted with *O*-cyanoethyl-bis(diisopropylamino)phosphine and tetrazole in  $\text{CH}_2\text{Cl}_2$  to give the phosphoramidite **12** in 85% isolated yield.

As a second building block, a functionalized solid support was prepared for solid-phase synthesis of oligonucleotides 3'-conjugated to the Gal<sub>3</sub>Chol cluster. The cholic acid analogue **16** of the carbohydrate cluster was synthesized and attached to macroporous polystyrene, which was functionalized with a branched amino-C7-linker by using HATU/DIEA activation (Scheme 4). The solid support with a loading of 24  $\mu\text{mol NH}_2/\text{g}$  could be completely substituted with the Gal<sub>3</sub>Chol cluster using 2 equiv of the carboxylic acid. The triantennary galac-

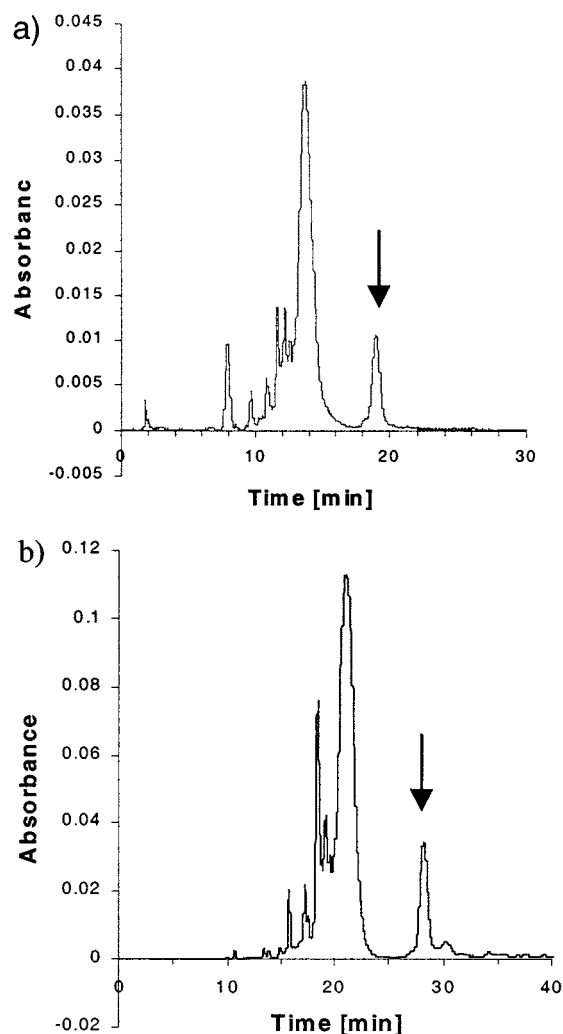
Scheme 4<sup>a</sup>

<sup>a</sup> Reagents and conditions: (a)  $\text{Cs}_2\text{CO}_3$ , allyl bromide, DMF, rt, 3.6 h; (b) 1. triphosgene, pyridine, 0 °C to room temperature, 40 min, 2. HOSu, 0 °C to room temperature, 15 min, 53%; (c) 1. **6**, DMF, rt, 15 h, 2. acetic anhydride, pyridine, rt, 12 h, 71%; (d)  $\text{Pd[P(Ph)}_3\text{]}_4$ , morpholine, pyridine, rt, 20 min; (e) FmocNH-( $\text{CH}_2$ )<sub>4</sub>CH( $\text{CH}_2\text{-OH}$ ) $\text{CH}_2\text{-O-DMT}$ , succinic anhydride, DMAP,  $\text{CH}_2\text{Cl}_2$ , pyridine, rt, 24 h; (f) succinate, HATU, DIEA, DMF, amino polystyrene resin, rt, 16 h; (g) piperidine, DMF, rt, 2  $\times$  20 min; (h) **16**, HATU, DIEA, DMF,  $\text{H}_2\text{N}(\text{CH}_2)_4\text{CH}(\text{CH}_2\text{O-amino polystyrene})\text{CH}_2\text{O-DMT}$ , rt, 16 h.

toside **16** was synthesized analogously to the procedure described above for the cluster galactoside **11**, except that the activated cholane precursor **14** was prepared from allyl-protected cholic acid **13**.

**Solid-Phase Synthesis of Oligonucleotide-Gal<sub>3</sub>Chol Conjugates.** In previous reports of synthesis of covalent conjugates between ONs and synthetic glycosylated ligands, solution-phase strategies have been applied for conjugate formation. Hangeland and co-workers (24) reported a 14% yield for the covalent coupling of a synthetic triantennary glycopeptide to ON in solution by using 10 equiv of the glycopeptide. A 100-fold molar excess of a synthetic galactoside cluster was used for its solution-phase conjugation to antisense ON and a coupling yield of 31% was obtained (25). In contrast, we favored a solid-phase strategy for conjugate formation. We rationalized that this technique would minimize consumption of the precious galactoside cluster and would enable a facile isolation and purification of the products. Two different approaches were investigated, both being compatible with the conditions of oligonucleotide synthesis and deprotection. For a straightforward and chemically stable conjugation to the 5'-terminus, Gal<sub>3</sub>Chol was introduced as a phosphoramidite generating a phosphodiester or thiophosphate linkage to the resin-bound oligonucleotide. The lipophilic cholane backbone was expected to facilitate the purification of the





**Figure 3.** HPLC analysis of crude 5'-Gal<sub>3</sub>Chol conjugates of PTO 20mers (ON-1) synthesized on CPG (2000 Å) using (a) a 30-fold and (b) a 3-fold excess of Gal<sub>3</sub>Chol amidite. The signal of the conjugate is marked with an arrow.

conjugates by reversed phase HPLC. On the other hand, a solid support, prefunctionalized with Gal<sub>3</sub>Chol, was prepared for the synthesis of the 3'-conjugates.

**5'-Conjugation.** The coupling of Gal<sub>3</sub>Chol amidite to the 5'-end of resin-bound ON was performed in a manual batch step in order to allow extended reaction times and maximum coupling efficiency without the need for a large excess of amidite. Initial attempts were made on CPG support, a rigid, nonswellable silica matrix functionalized with long chain alkylamine spacers. CPG is the most commonly used solid support for ON synthesis. Rather low overall yields of about 10% were obtained despite the fact that the support had a large pore size of 2000 Å and the Gal<sub>3</sub>Chol amidite was applied in a 30-fold molar excess. Interestingly, however, reducing the molar excess of amidite to 3 equiv did not affect the overall synthesis yields (Figure 3). The HPLC profiles of crude 20mer PTOs 5'-conjugated to Gal<sub>3</sub>Chol (ON-1) are almost identical for 3 equiv and 30 equiv of amidite with overall yields of 10.0% and 9.8%, respectively. Differences in the intensity scale of the chromatograms are due to variations in the concentration of the samples injected and do not reflect any differences in the total yield of crude product. These results indicated that the moderate synthesis yields were not a consequence of an inherent low reactivity of the Gal<sub>3</sub>Chol amidite. Presumably, the 5'-termini of the resin-bound oligonucleotides (molecular weight: 6–7 kDa)

exhibited limited accessibility for the bulky Gal<sub>3</sub>Chol cluster (molecular weight: > 2 kDa).

We rationalized that the low coupling yields observed could either be a consequence of hindered diffusion of the cluster amidite through the macroporous interior of the resin beads or steric hindrance of the coupling reaction caused by a too dense loading of the ONs on the particle surface. Both effects are closely related to the microscopic structure of the solid support. To determine the main factor influencing the coupling reaction and to improve the yields of the conjugation reaction, several different amino-functionalized solid supports were prepared and evaluated. Supports were loaded with starting nucleoside to obtain a low substitution in the range of 10–20 μmol/g. Then, the materials were physicochemically characterized to determine their specific surface area by using the BET method to analyze the isotherm data derived from N<sub>2</sub> adsorption. Finally, their performance was compared in the synthesis of 20-mer PTOs 5'-conjugated to Gal<sub>3</sub>Chol. The results of this study are summarized in Table 1.

Apparently, the nature of the solid support has a major influence on the conjugation reaction. The lowest synthesis yields of about 2% were observed for the PS-PEG copolymer resin. Moderate synthesis yields could be obtained with all the CPG supports investigated. Surprisingly, an increase in the average pore size from 2000 to 3000 Å did not improve but rather led to a reduction of the synthesis yields from 10% to 6%. Best results were achieved by using a highly cross-linked PS as the solid support. An overall yield of about 25% was obtained with an initial resin substitution of 10–15 μmol nucleoside/g and by using tetrazole as the activation reagent. Assuming an average stepwise coupling yield of 98.5% for ON synthesis, this translates to a coupling yield for the Gal<sub>3</sub>Chol amidite of more than 34%. Most importantly, under these conditions the consumption of the valuable Gal<sub>3</sub>Chol amidite could be kept at a minimum of a 3-fold molar excess. Increasing the amount of amidite did not lead to further improvement in yield (data not shown).

The significant differences in the performance of the resins can be explained by looking at the physicochemical characteristics of the polymers, namely their microscopic structure and morphology. The applied PS-PEG copolymer, consists of a minimally cross-linked PS matrix, to which PEG chains with an average length of 3000 Da are grafted. The reaction sites are on the free end of the PEG tentacles and are almost quantitatively located in the lumen of the large swellable beads. The nature of this beaded gel resin makes a determination of porosity or specific surface area impossible. However, the poor synthesis yields indicate that the structure of the beads did not allow the unhindered diffusion of the bulky carrier molecules through the matrix and that only the easily accessible sites on the outer surface of the particles reacted with the Gal<sub>3</sub>Chol amidite.

CPG consists of a rigid, nonswelling silica matrix, functionalized with alkylamine spacers and available in a range of pore sizes. The particles exhibit an irregular shape with average sizes between 75 and 125 μm. CPG supports with average pore diameters of 2000 and 3000 Å, which were investigated in the present study, are commonly used for the synthesis of long oligonucleotides (>50 nucleotides). The inferior performance of the latter, even though it has the larger pore sizes, could be a consequence of the amount of water adsorbed on the silica surface in combination with the small excess of

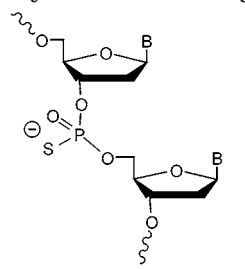
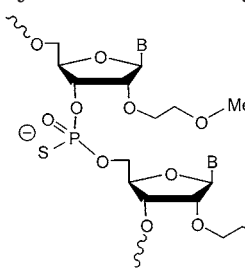


**Table 1. Physicochemical Characterization of the Solid Supports and Their Effects on the Overall Yields Determined for the Synthesis of PTO 20Mers 5'-Conjugated to Gal<sub>3</sub>Chol**

solid support	substitution [μmol/g]	particle size [μm]	surface area [m <sup>2</sup> /g]	surface area [nm <sup>2</sup> /molecule]	excess of gal <sub>3</sub> chol amidite	overall yield <sup>a</sup> [%]
PS-PEG <sup>b</sup>	18	90 <sup>c</sup>	n.a.	n.a.	5-fold	2.0
CPG (2000 Å) <sup>b</sup>	18	75–125	11.5	1.1	30-fold	10.0
CPG (2000 Å) <sup>b</sup>	18	75–125	11.5	1.1	3-fold	9.8
CPG (3000 Å) <sup>b</sup>	10	75–125	8.9	1.5	3-fold	5.9
PS (1000 Å) <sup>d</sup>	14	50–70	42.5	5.0	3-fold	20.8
PS (1000 Å) <sup>d</sup>	14	50–70	42.5	5.0	3-fold	25.2

<sup>a</sup> As determined by HPLC. <sup>b</sup> Activation reagent: ETT. <sup>c</sup> Dry state. <sup>d</sup> Activation reagent: tetrazole.

**Table 2. Oligonucleotide–Carbohydrate Cluster Conjugates Synthesized for Biological Studies**

			
2'-deoxy phosphorothioate DNA		2'-O-MOE: 2'-O-(2-Methoxyethyl) RNA	
oligo	sequence 5' → 3'	backbone	
ON-1	<b>Gal<sub>3</sub>Chol</b> -ATG CAT TCT GCC CCC AAG GA	all PS, 2'-deoxy	
ON-2	ATG C'AT TCT GCC CCC AAG GA- <b>Gal<sub>3</sub>Chol</b>	all PS, _ = 2'-O-MOE, C' = C <sup>5me</sup>	
ON-3	<b>Gal<sub>3</sub>Chol</b> -TCC AGC ACT <u>TTC TTT</u> TCC GG	all PS, _ = 2'-O-MOE, C' = C <sup>5me</sup>	
ON-4	<b>Gal<sub>3</sub>Chol</b> -CTG CTA GCC TCT GGA <u>TTT</u> GA	all PS, _ = 2'-O-MOE, C' = C <sup>5me</sup>	

amidite used. The surface area of the CPG (3000 Å) used in the synthesis was about 1.5-fold higher than of CPG (2000 Å).

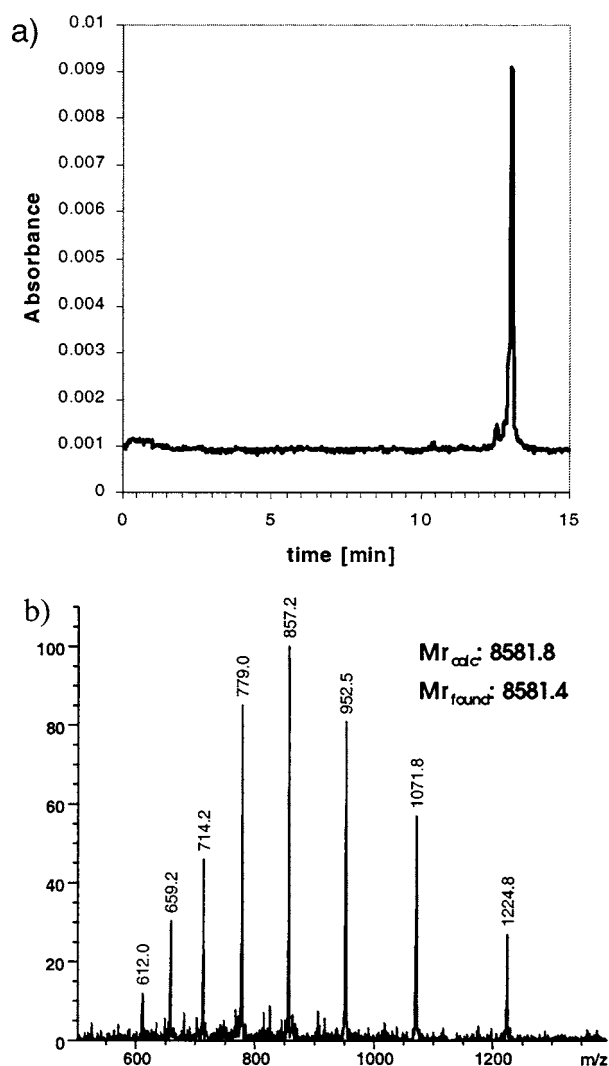
The PS support has an average pore size of 1000 Å, lower than of the CPG supports, indicating that another structural feature must be responsible for the differences in the synthesis yields observed for these macroporous CPG and polystyrene resins. In other words, hindered diffusion of the amidite due to narrow pores can be excluded as the main factor determining the yield of the coupling reaction. The physicochemical characterization of the materials by BET analysis revealed significant differences in the specific surface areas, from which the average surface area/molecule was calculated (Table 1). PS shows the highest value of surface area per g and also per molecule, 4- to 5-fold higher than the corresponding values for the two CPG supports. Therefore, it can be concluded that the density of the oligonucleotides on the particle surface had the most influence on the yield of conjugation reaction. Furthermore, the reduced average particle size of the PS support not only increases the available surface area/g but also provides an advantageous ratio of outer to inner surface functional groups. The application of the more reactive activator ETT instead of tetrazole did not lead to an improvement but rather a reduction of the synthesis yields. This result underscores the conclusion that steric factors rather than the reactivity of the amidite were crucial for the coupling efficiency.

**3'-Conjugation.** Given the results described above, macroporous PS was also considered to be the most suitable support for the synthesis of 3'-conjugates. Prior to the oligonucleotide synthesis, the galactoside cluster was attached to a branched amino-C7 linker on the support via an amide linkage. Interestingly, the amino groups present in an initial substitution of 24 μmol/g could be quantitatively functionalized with the activated ester of Gal<sub>3</sub>Chol, and the modified resin was suitable

for the automated synthesis of homogeneous oligonucleotide-3'-Gal<sub>3</sub>Chol conjugates (ON-2) using standard synthesis protocols. The 3'-conjugation, due to the absence of oligonucleotides on the support, proved to be a more facile and efficient method for introduction of the bulky galactoside cluster. These findings also confirm the conclusion that the density of the ONs on the surface of the resin particles plays the key role in determining the synthesis yields for 5'-conjugation.

In Table 2, the various ON-carbohydrate cluster conjugates that have been synthesized for biological studies are summarized. As an example, the analysis of purified ON-3 is shown in Figure 4. The 5'-Gal<sub>3</sub>Chol conjugate of a gapmer oligonucleotide containing 2'-O-MOE<sup>1</sup> sugars (38) in the wings and a 2'-deoxy center appears as a homogeneous product in the CGE profile and the ES-MS analysis confirms the correct molecular weight.

Since glycoconjugates are internalized via receptor-mediated endocytosis, the escape of the antisense ONs from the endosomal pathway is a prerequisite for hybridization to target mRNA in the cytosol or nucleus and to inhibit protein expression. For a specific release of ON from the carrier inside the target cell, the drug-carrier linkage has to be degradable under the conditions present in late endosomal or lysosomal compartments. This is not the case for the conjugates presented in this work. These conjugates were designed to be biologically stable in order to facilitate studies of the cellular uptake of these derivatives. However, the applied methods of solid-phase conjugation provide a variety of possibilities to further modify the ON-Gal<sub>3</sub>Chol linkage for a specific cleavage under biological conditions. For instance, commercially available disulfide-containing building blocks, introduced as the linkage between the ON and the carrier, can be cleaved under mild reducing conditions. Natural phosphodiester linkages at the 5' or 3' end of the ON are subject of hydrolysis by the nucleases present in the



**Figure 4.** (a) CGE and (b) ESI-MS analysis of a 2'-MOE gapmer oligonucleotide 5'-conjugated to the carbohydrate cluster Gal<sub>3</sub>Chol (ON-2); MW<sub>calc</sub>: 8581.8, MW<sub>found</sub>: 8581.4.

lysosomes and could also be utilized for a gradual release from the carrier.

#### CONCLUDING REMARKS

A synthetic ligand for the asialoglycoprotein receptor has been developed for tissue- and cell-specific targeting of antisense oligonucleotides to parenchymal liver cells. To combine low molecular weight with high receptor affinity, three galactosyl residues were attached to a rigid cholane scaffold via  $\epsilon$ -aminocapramide linkers. Computational calculations reveal an umbrella-like geometry with the galactosylated spacers protruding from one side of the steroid backbone and forming an almost equilateral triangle. Compared to the published results of known high affinity ligands, it can be assumed that the present tri-antennary setup provides proper spacing and orientation of the galactosyl residues required for high affinity binding. The galactoside cluster has been prepared in a convergent multistep synthesis starting from inexpensive natural products. It has been designed to be chemically stable under the conditions of oligonucleotide synthesis and deprotection, allowing its covalent conjugation to antisense oligonucleotides through solid-phase methods. On macroporous PS supports, efficient 5'-conjugation has been achieved while reducing the consumption of Gal<sub>3</sub>-Chol amidite to a level of 3 equiv, drastically lower than

the molar excess generally used for solution-phase conjugation. The results of the 3'-conjugation demonstrate that utilizing prefunctionalized supports provides an even more efficient way to introduce bulky synthetic ligands. A number of antisense ON-Gal<sub>3</sub>Chol conjugates have been prepared and characterized for initial biological studies. Future work will include the solid-phase synthesis of conjugates specifically cleavable under the conditions present in endosomes or lysosomes and studies of the in vivo fate, subcellular distribution, and pharmacological effects of these conjugates. To this end, medium-scale syntheses of these conjugates for three different target genes have been achieved.

#### ACKNOWLEDGMENT

The authors would like to thank Hans Norbert Grzeski for his technical assistance in BET surface analysis of the solid supports.

#### LITERATURE CITED

- (1) Crooke, S. T. (1998) Antisense therapeutics. *Biotechnol. Genet. Eng. Rev.* 15, 121–157.
- (2) Stein, C. A., and Cheng, Y. C. (1993) Antisense oligonucleotides as therapeutic agents – is the bullet really magical? *Science* 261, 1004–1012.
- (3) Cook, P. D. (1998) Antisense medicinal chemistry. *Handb. Exp. Pharmacol.* 131, 51–101.
- (4) Manoharan, M. (2001) Oligonucleotide conjugates in antisense technology. *Antisense Drug Technology*, 391–469; Manoharan, M. (2002) Oligonucleotide conjugates as potential antisense drugs with improved uptake, biodistribution, targeted delivery, and mechanism of action. *Antisense Nucleic Acid Drug Dev.* 12, 103–128.
- (5) Uhlmann, E., and Peyman, A. (1990) Antisense oligonucleotides: a new therapeutic principle. *Chem. Rev.* 90, 543–584.
- (6) Matteucci, M. (1997) Oligonucleotide analogues: an overview. *Ciba Found. Symp.* 5–18.
- (7) Manoharan, M., Tivel, K. L., Andrade, L. K., Mohan, V., Condon, T. P., Bennett, C. F., and Cook, P. D. (1995) Oligonucleotide conjugates: alteration of the pharmacokinetic properties of antisense agents. *Nucleosides Nucleotides* 14, 969–973.
- (8) Wadhwa, M. S., and Rice, K. G. (1995) Receptor mediated glycotargeting. *J. Drug Target.* 3, 111–127.
- (9) Ashwell, G., and Harford, J. (1982) Carbohydrate-specific receptors of the liver. *Annu. Rev. Biochem.* 51, 531–554.
- (10) Pricer, W. E., Jr., and Ashwell, G. (1971) Binding of desialylated glycoproteins by plasma membranes of rat liver. *J. Biol. Chem.* 246, 4825–4833.
- (11) Ashwell, G., and Morell, A. G. (1974) Role of surface carbohydrates in the hepatic recognition and transport of circulating glycoproteins. *Adv. Enzymol. Relat. Areas Mol. Biol.* 41, 99–128.
- (12) Schwartz, A. L., Fridovich, S. E., and Lodish, H. F. (1982) Kinetics of internalization and recycling of the asialoglycoprotein receptor in a hepatoma cell line. *J. Biol. Chem.* 257, 4230–4237.
- (13) Lee, Y. C., Townsend, R. R., Hardy, M. R., Lonngren, J., Arnarp, J., Haraldsson, M., and Lonn, H. (1983) Binding of synthetic oligosaccharides to the hepatic Gal/GalNAc lectin. Dependence on fine structural features. *J. Biol. Chem.* 258, 199–202.
- (14) Kawaguchi, K., Kuhlenschmidt, M., Roseman, S., and Lee, Y. C. (1981) Differential uptake of D-galactosyl- and D-glucosyl-neoglycoproteins by isolated rat hepatocytes. *J. Biol. Chem.* 256, 2230–2234.
- (15) Connolly, D. T., Townsend, R. R., Kawaguchi, K., Bell, W. R., and Lee, Y. C. (1982) Binding and endocytosis of cluster glycosides by rabbit hepatocytes. Evidence for a short-circuit pathway that does not lead to degradation. *J. Biol. Chem.* 257, 939–945.

- (16) Lee, Y. C., and Lee, R. T. (1995) Carbohydrate-Protein Interactions: Basis of Glycobiology. *Acc. Chem. Res.* **28**, 321–327.
- (17) Biessen, E. A. L., Beuting, D. M., Roelen, H. C. P. F., van de Marel, G. A., Van Boom, J. H., and Van Berkel, T. J. C. (1995) Synthesis of Cluster Galactosides with High Affinity for the Hepatic Asialoglycoprotein Receptor. *J. Med. Chem.* **38**, 1538–1546.
- (18) Wu, G. Y., and Wu, C. H. (1987) Receptor-mediated in vitro gene transformation by a soluble DNA carrier system. *J. Biol. Chem.* **262**, 4429–4432.
- (19) Wu, G. Y., and Wu, C. H. (1992) Specific inhibition of hepatitis B viral gene expression in vitro by targeted antisense oligonucleotides. *J. Biol. Chem.* **267**, 12436–12439.
- (20) Zanta, M.-A., Boussif, O., Adib, A., and Behr, J.-P. (1997) In Vitro Gene Delivery to Hepatocytes with Galactosylated Polyethylenimine. *Bioconjugate Chem.* **8**, 839–844.
- (21) Remy, J.-S., Kichler, A., Mordvinov, V., Schuber, F., and Behr, J.-P. (1995) Targeted gene transfer into hepatoma cells with lipopolyamine-condensed DNA particles presenting galactose ligands: a stage toward artificial viruses. *Proc. Natl. Acad. Sci. U.S.A.* **92**, 1744–1748.
- (22) Schuber, F., Kichler, A., De Souza, D. L., and Frisch, B. (2000) Ligand-mediated gene delivery. *NATO Science Series, Series A: Life Sciences* **323**, 210–225.
- (23) Rajur, S. B., Roth, C. M., Morgan, J. R., and Yarmush, M. L. (1997) Covalent Protein-Oligonucleotide Conjugates for Efficient Delivery of Antisense Molecules. *Bioconjugate Chem.* **8**, 935–940.
- (24) Hangeland, J. J., Flesher, J. E., Deamond, S. F., Lee, Y. C., Ps'O, P. O. P., and Frost, J. J. (1997) Tissue distribution and metabolism of the [<sup>32</sup>P]-labeled oligodeoxynucleoside methylphosphonate-neo-glycopeptide conjugate, [YEE(ah-GalNAc)3]-SMCC-AET-pUmpT7, in the mouse. *Antisense Nucleic Acid Drug Dev.* **7**, 141–149.
- (25) Biessen, E. A. L., Vietsch, H., Rump, E. T., Fluiter, K., Kuiper, J., Bijsterbosch, M. K., and Van Berkel, T. J. C. (1999) Targeted delivery of oligodeoxynucleotides to parenchymal liver cells in vivo. *Biochem. J.* **340**, 783–792.
- (26) Duff, R. J., Deamond, S. F., Roby, C., Zhou, Y., and Ts'o, P. O. P. (2000) Intrabody tissue-specific delivery of antisense conjugates in animals: ligand-linker-antisense oligomer conjugates. *Methods Enzymol.* **313**, 297–321.
- (27) Biessen, E. A. L., Vietsch, H., Rump, E. T., Flutter, K., Bijsterbosch, M. K., and Van Berkel, T. J. C. (2000) Targeted delivery of antisense oligonucleotides to parenchymal liver cells in vivo. *Methods Enzymol.* **313**, 324–342.
- (28) Maier, M. A., Yannopoulos, C., Mohamed, N., Just, G., and Manoharan, M. (2000) Synthesis of oligonucleotides conjugated to multivalent carbohydrate clusters for cellular targeting of antisense drugs. *Book of Abstracts*, 219th ACS National Meeting, San Francisco, CA, March 26–30, 2000, CARB-077.
- (29) Manoharan, M. (2001) Targeted Oligonucleotide Conjugates. US 6,300,319, Isis Pharmaceuticals, Inc., Carlsbad, CA.
- (30) Li, C., Peters, A. S., Meredith, E. L., Allman, G. W., and Savage, P. B. (1998) Design and Synthesis of Potent Sensitizers of Gram-Negative Bacteria Based on a Cholic Acid Scaffolding. *J. Am. Chem. Soc.* **120**, 2961–2962.
- (31) Janout, V., Lanier, M., and Regen, S. L. (1997) Design and Synthesis of Molecular Umbrellas. *J. Am. Chem. Soc.* **119**, 640–647.
- (32) Brunauer, S., Emmett, P. H., and Teller, E. (1938) Adsorption of gases in multimolecular layers. *J. Am. Chem. Soc.* **60**, 309–319.
- (33) Bonfils, E., Depierreux, C., Midoux, P., Thuong, N. T., Monsigny, M., and Roche, A. C. (1992) Drug targeting: synthesis and endocytosis of oligonucleotide-neoglycoprotein conjugates. *Nucleic Acids Res.* **20**, 4621–4629.
- (34) Reinis, M., Damkova, M., and Korec, E. (1993) Receptor-mediated transport of oligodeoxynucleotides into hepatic cells. *J. Virol. Methods* **42**, 99–106.
- (35) Sugano, M., and Makino, N. (1996) Changes in plasma lipoprotein cholesterol levels by antisense oligodeoxynucleotides against cholesteryl ester transfer protein in cholesterol-fed rabbits. *J. Biol. Chem.* **271**, 19080–19083.
- (36) Sugano, M., Makino, N., Sawada, S., Otsuka, S., Watanabe, M., Okamoto, H., Kamada, M., and Mizushima, A. (1998) Effect of antisense oligonucleotides against cholesteryl ester transfer protein on the development of atherosclerosis in cholesterol-fed rabbits. *J. Biol. Chem.* **273**, 5033–5036.
- (37) Balaji, P. V., Qasba, P. K., and Rao, V. S. R. (1993) Molecular dynamics simulations of asialoglycoprotein receptor ligands. *Biochemistry* **32**, 12599–12611.
- (38) Altmann, K.-H., Dean, N. M., Fabbro, D., Freier, S. M., Geiger, T., Häner, R., Hüsken, D., Martin, P., Monia, B. P., Müller, M., Natt, F., Nicklin, P., Phillips, J., Pieves, U., Sasmor, H., and Moser, H. E. (1996) Second generation of antisense oligonucleotides: from nuclease resistance to biological efficacy in animals. *Chimia* **50**, 168–176.



## Chemical Defense in Ascidians of the *Didemnidae* Family†

Madeleine M. Joullié,<sup>\*,‡</sup> Michael S. Leonard,<sup>‡</sup> Padma Portonovo,<sup>‡</sup> Bo Liang,<sup>‡</sup> Xiaobin Ding,<sup>‡</sup> and James J. La Clair<sup>§</sup>

Department of Chemistry, University of Pennsylvania, Philadelphia, Pennsylvania 19104-6323, and Bionic Brothers, Postfach 51 11 07, D-13371 Berlin, Germany. Received July 16, 2002;

Revised Manuscript Received October 17, 2002

Fluorescent analogues (DB1 and TA1) of the secondary metabolites didemnin B (DB) and tamandarin A (TA) were synthesized to investigate the potential chemical defense mechanisms of tunicates in the family *Didemnidae*. These compounds were found to alter predator–prey relations. Five species of freshwater fish and one marine fish, the damselfish *Amphiprion ocellaris*, were acclimated to a diet of mosquito larvae. Fish showed an immediate, negative reaction to mosquito larvae treated with  $\geq 5$  ng of DB1 or TA1, with consumption of larvae resulting in regurgitation. Both freshwater and marine fish learned to avoid tainted prey by associating species of larvae with “distaste”. Distaste for a given organism also arose when depsipeptides DB1 or TA1 were transferred to the fish from the surrounding medium. Fluorescence microscopy in fish indicated that a similar processing and localization followed ingestion and absorption of DB1 or TA1. Fluorescent labeling of DB or TA provided an ideal tool to conduct short-term studies of predator–prey relationships between fish and marine invertebrate larvae.

### INTRODUCTION

Tunicates of the family *Didemnidae* produce a class of depsipeptides called the didemnins (Rinehart et al., 1981; Sakai et al., 1996; Li and Joullié, 1992; Rinehart, 2000; Vera and Joullié, 2002). Didemnin B (DB,<sup>1</sup> Figure 1) was one of the first members of this class to show biological activity. Recently, Vervoort et al. (2000) reported the isolation and characterization of tamandarin A (TA, Figure 1) from an unclassified didemnid from a shallow-water reef in Brazil. While the chemical structure and cellular activity of TA is comparable to that of DB, the two metabolites have not yet been shown to exhibit a common biochemical and ecological function. Here we provide further insight into the mechanisms underlying these activities.

Modification of a marine natural product (i.e., addition of a fluorescent tag) requires knowledge of its biological and ecological function (Faulkner, 2000a; Faulkner, 2000b; Moore, 1999). Both naturally occurring and synthetic didemnins are known to inhibit protein synthesis, initiate apoptosis, and reduce cell proliferation (Fimiani, 1987; LeGrue et al., 1988; Maldonado et al.,

1982; Montgomery et al., 1987; Rinehart et al., 1982). While the biochemical action of DB has not been fully determined (Beidler et al., 1999; Crews et al., 1994; Crews et al., 1996), a compilation of cellular, affinity and structure–activity relationship studies suggest that protein synthesis inhibition and cell proliferative activities arise through different pathways (Meng et al., 1998). Therefore, it was critical to demonstrate that incorporation of a fluorescent marker preserved the biological activity of the depsipeptides.

Using known structure–activity relationships (Rinehart, 2000; Sakai et al., 1996; Vera and Joullié, 2002), we appended a fluorescently labeled side-chain onto the didemnin and tamandarin macrocycles (Figure 1). A 7-*N,N*-dimethylaminocoumarin-4-acetic acid (DACA) label was used for this study (Portonovo et al., 2000), as its fluorescence (photophysical properties of probes DB1 and TA1 provided in Table 1) allowed visualization in vivo at concentrations comparable to those naturally expressed by the tunicates (Rinehart et al., 1981; Vervoort et al., 2000). As shown through established assays (Table 1), the didemnin analogue DB1 was better at reducing cell proliferation (GI<sub>50</sub> and TGI) than DB, offering activity at less than 1 nM. The activity of TA1 was comparable to that of TA. With these labels in hand, we examined their role in altering predator–prey relations.

Lindquist and Hay (1995) found that extracts of *Trididemnum solidum* (containing DA, DB, as well as other derivatives) deterred predators. In these and preceding studies (Lindquist et al., 1992), DB was shown to be critical in protecting the tunicate larvae (Young and Bingham, 1987; Van Duyl et al., 1981; Ford, 1996). Upon consuming bait containing  $\sim 23$   $\mu\text{g}$  of extract  $\text{mg}^{-1}$ , the pinfish *Lagodon rhomboides* regurgitated. These fish quickly learned to avoid this bait. Other organisms such as the anemone *Aiptasia pallida* consumed the depsipeptide-containing food and rapidly lost fitness, as expressed by a profound decrease in growth as well as sexual and asexual reproduction.

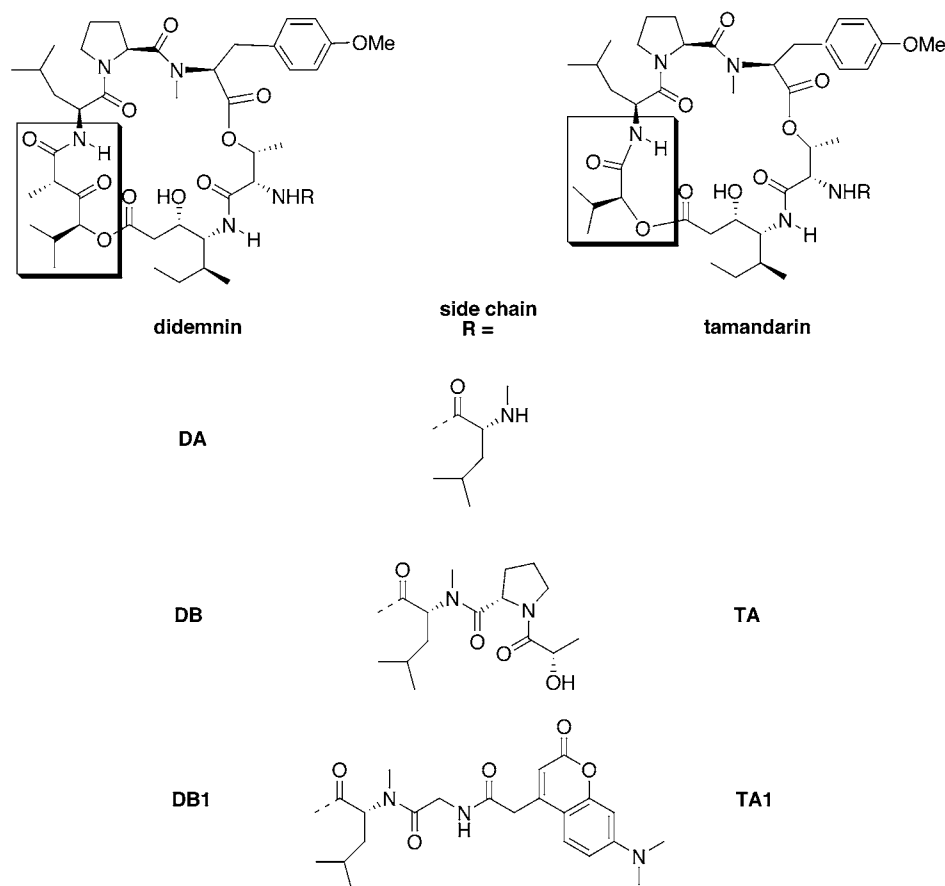
\* To whom correspondence should be addressed: Madeleine M. Joullié, Ph.D., University of Pennsylvania, Department of Chemistry, 231 S. 34th St., Philadelphia, PA 19104-6323. Telephone: (215) 898–3158. E-mail: mjoullie@sas.upenn.edu.

† Dedicated to Professor Koji Nakanishi.

‡ University of Pennsylvania.

§ Bionic Brothers.

<sup>1</sup> Abbreviations: DA = didemnin A; DACA = 7-dimethylaminocoumarin-4-acetic acid; DB = didemnin B; DB1 = coumarin-tagged didemnin analogue;  $\epsilon$  = extinction coefficient;  $F$  = number of feedings; GI<sub>50</sub> = growth inhibition of 50%; IC<sub>50</sub> = protein synthesis inhibition of 50%;  $\lambda_a$  = absorption maximum;  $\lambda_f$  = fluorescence maximum; LC<sub>50</sub> = lethal concentration 50%;  $M$  = number of schools;  $N$  = a given population of fish;  $\Phi_f$  = fluorescence quantum yield; PBS = phosphate buffer solution;  $S$  = school size; SAR = structure/activity relationships; TA = tamandarin A; TA1 = coumarin-tagged tamandarin analogue; TGI = total growth inhibition.



**Figure 1.** Structures of DA, DB, TA, and their fluorescent analogues DB1 and TA1. Structural differences in the macrocycles are accentuated.

**Table 1. Biological and Photophysical Activity of Selected Depsipeptides<sup>a</sup>**

	DB range <sup>b</sup>	DB <sup>c</sup>	TA	DB1 <sup>c</sup>	TA1 <sup>c</sup>
GI <sub>50</sub>	5–46 nM	13 nM	1.5 nM <sup>d</sup>	11 nM	49 nM
TGI	5–270 nM	66 nM		295 nM	589 nM
LC <sub>50</sub>	0.036–50 μM	3.8 μM		7.2 μM	22.4 μM
IC <sub>50</sub>		0.89 μM	1.3 μM	16 ± 1.2 μM	19 ± 0.9 μM
λ <sub>a</sub>				369 nm	370 nm
ε				23 200 cm <sup>-1</sup> M <sup>-1</sup>	21 000 cm <sup>-1</sup> M <sup>-1</sup>
λ <sub>f</sub>				459 nm	460 nm
Φ <sub>f</sub>				0.21	0.19

<sup>a</sup> GI<sub>50</sub>, TGI, and LC<sub>50</sub> were determined by screening through NCI's Developmental Therapeutics Program. Determination of protein synthesis inhibition (IC<sub>50</sub>) and photophysical properties are described in the methods. <sup>b</sup> The range provided illustrates the minimum and maximum activity found when screening DB against a series of tumor cell lines. <sup>c</sup> NCI-60 mean data from NCI-60 tumor cell screen. <sup>d</sup> Activity is measured in pancreatic carcinoma BX-PC3.

These studies showed that the didemnin-containing extracts protect both adult and larval tunicates from fish and invertebrate predators. What remained to be explained was how the tunicates could produce powerful inhibitors of cell proliferation and growth (Table 1) and yet not inhibit their own development. We hypothesized that fish might learn to avoid prey containing didemnins so that, over time, very low tissue concentrations would suffice to deter predation. We synthesized fluorescent analogues of the didemnins and tamandarins so that their uptake by predators of didemnin-containing organisms could be examined using analytically pure samples. To this end, five species of common freshwater fish and

one marine species, the damsselfish *Amphiprion ocellaris*, were chosen for the study of response to the uptake of DB1 and TA1. The reason for using multiple species was to ensure that the findings were generally applicable to fish from a variety of taxa and habitats. We used two species of mosquito larvae as prey and, in a series of experiments, examined the response of predators to both species, when containing the depsipeptides as well as when unprotected by these chemical defense agents.

#### MATERIALS AND METHODS

**Fish.** Studies were conducted in a laboratory setting from August 1999 to March 2000. A marine system was developed using the damsselfish *Amphiprion ocellaris*. This species was complemented with five freshwater species, all of which lack natural exposure to marine tunicates. Both fresh and marine systems were housed in 100 × 40 × 50 cm tanks (200 L), unless otherwise noted. The systems were recirculated and aerated. Five freshwater species were used: firehead tetra *Hemigrammus bleheri* (Gery and Mahnert, 1986); peppered corydoras *Corydoras paleatus* (Jenyns, 1840); common zebrafish *Danio rerio* (Hamilton, 1822); celebes medaka *Oryzias celebensis* (Weber, 1894); and glass catfish *Kryptopterus bicirrhus* (Cuvier and Valenciennes, 1840). *H. bleheri* and *K. bicirrhus* were kept at 13 dGH (hardness), pH 6.5 ± 0.3 and 23 ± 3 °C, *C. paleatus* and *D. rerio* at 13 dGH, pH 7.0 ± 0.8 and 20 ± 2 °C, *O. celebensis* at pH 8.5 ± 0.2 and 25 ± 2 °C, and *A. ocellaris* at 26 ± 2 °C with a salinity of 1.018, pH 8.1 ± 0.1. The media were changed weekly. Freshwater media were maintained at less than 0.05 ppm ammonia, 0.5 ppm of nitrite, and 50.0 ppm of nitrate. The adjustment of the pH was necessary to provide the ideal medium for the given fish. Using the

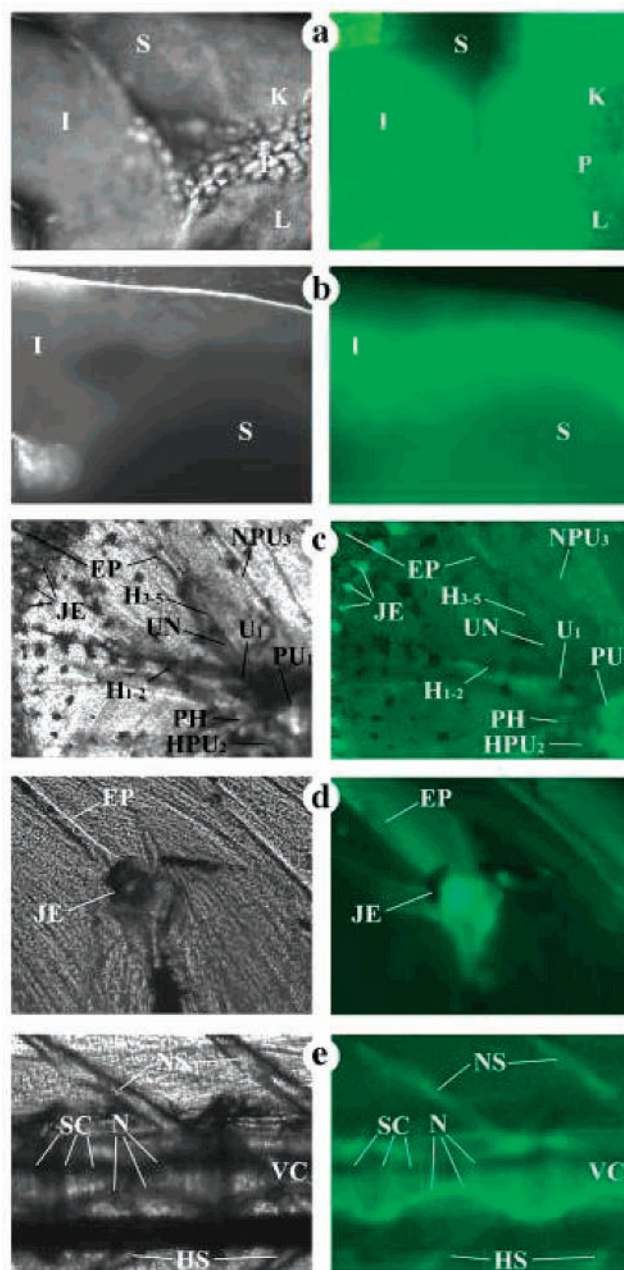
intensity of DACA fluorescence (Table 1), the rate of absorption of DB1 and TA1 either through larvae or the medium randomly deviated within 1.2% over the pH range of 5.5–7.5. Under the conditions used in the preceding experimentation, the variance of pH was irrelevant to the transfer of the analogues DB1 and TA1.

Studies were conducted on a given population of fish ( $N$ ) distributed into small schools ( $M$ ). Each school was held in an individual tank. The school size ( $S$ ), as given by  $S = NM^{-1}$ , was set to  $S = 2$  for *A. ocellaris*,  $S = 5$  for *C. paleatus*,  $S = 10$  for *H. bleheri*,  $S = 10$  for *K. bicirrhys*,  $S = 13$  for *O. celebensis*, and  $S = 30$  for *D. rerio*, unless otherwise noted. The number of feedings ( $F$ ) served to calibrate contact between fish (predator) and mosquito larvae (prey). Each fish species was acclimated over 3 weeks ( $F = 20$ ) to a diet of mosquito larvae by a daily feeding with *Anopheles stephensi* and *Culex pipiens* (referred to herein as acclimation). Each feeding consisted of a 20% excess of larvae in 1:1 ratio of *A. stephensi* to *C. pipiens* (i.e., the number of larvae added was 20% more than the number of fish). Feedings lasted for 30 min, at which point the remaining larvae were removed by net.

During acclimation, none of the six species of fish favored a given species of mosquito larvae, as determined by calculating the percentage of *A. stephensi* selected. Over the acclimation period, the percentage of *A. stephensi* selected was  $49.4 \pm 6.8$  for *H. bleheri* ( $N = 100$ ,  $M = 10$ ),  $52.7 \pm 4.3$  for *C. paleatus* ( $N = 50$ ,  $M = 10$ ),  $50.1 \pm 1.2$  for *D. rerio* ( $N = 300$ ,  $M = 10$ ),  $53.2 \pm 2.9$  for *O. celebensis* ( $N = 26$ ,  $M = 2$ ),  $49.0 \pm 5.6$  for *K. bicirrhys* ( $N = 100$ ,  $M = 10$ ), and  $49.4 \pm 6.8$  for *A. ocellaris* ( $N = 20$ ,  $M = 10$ ). The percentage of the fish that did not consume at each feeding was determined by counting the number of mosquito larvae that remained after feeding. Over repetitive feedings ( $F = 50$ ), 96.5% of *H. bleheri* ( $N = 100$ ,  $M = 10$ ), 97.5% of *C. paleatus* ( $N = 50$ ,  $M = 10$ ), 98.6% of *D. rerio* ( $N = 300$ ,  $M = 10$ ), 96.1% of *O. celebensis* ( $N = 26$ ,  $M = 2$ ), and 97.8% of *K. bicirrhys* ( $N = 100$ ,  $M = 10$ ), and 95.9% of *A. ocellaris* ( $N = 20$ ,  $M = 10$ ) consumed at least a single larva per feeding.

**Mosquito Larvae.** *A. stephensi* and *C. pipiens* larvae were selected with a length of 10–12 mm and weight of 8–12 mg. This size is  $\sim 6$ –12 times that of the larval tunicate *Trididemnum solidum* (Lindquist and Hay, 1995; Lindquist et al., 1992). While DB is not uniformly distributed throughout the adult tunicate (Rinehart, 2000), one can estimate the average tissue concentration based on the amount of metabolite isolated per mass of tunicate. For DB and TA, this concentration lies between 50 and 100 ppm. Since the larval mimics employed in this study were larger than tunicate larva, we charged each mosquito larva with  $50 \pm 4$  ng of DB1 or TA1, providing an average tissue concentration of  $\sim 4$ –6 ppm. This was accomplished by gently shaking each larva for 5 min in sterile Eppendorf tubes containing 50  $\mu$ L of 42 nM DB1 (or 45 nM TA1) diluted in 1 mL of sterilized mineral water. This transfer was verified by measuring the amount of analogue absorbed from the medium (using fluorescence spectroscopy) and/or by tissue analysis (method described below). By linearly adjusting the solution concentration of DB1 or TA1, this procedure could be used to load larvae with  $10 \pm 2$  to  $250 \pm 12$  ng larva $^{-1}$ .

**Molecular Tracking System.** The transmission between prey and predator was monitored using fluorescence from DB1 and TA1. Physiological processing of these ligands was examined on an Axiovert 100 with a conventional Zeiss DAPI filter set with excitation, G365; beam splitter, FT 395; emission, LP 420. Images were



**Figure 2.** *K. bicirrhys*. Physiological processing after ingestion of a *C. pipiens* larva containing  $50 \pm 4$  ng of DB1. Images provided in two views: white light (left) and fluorescence (right). Abbreviations: liver (L), kidney (K), pancreas (P), stomach (S), intestine (I), epurals (EP), hypurals ( $H_{1-5}$ ), hermal spines of the preural centra ( $HPU_2$ ), epural joint (JE), neural spines of the preural centra ( $NPU_3$ ), preural centra ( $PU_1$ ), parhypural (PH), ural centrum ( $U_1$ ), and uroneural (UN), neural spine (NS), hemal spine (HS), spinal chord (SC), vertebral centrum (VC), notochord (N). (a) Dorsal view of the digestive system. (b) Lateral view of stomach and intestine. In addition to the digestive system, DB1 also localizes within the skeleton. (c) Lateral view of the caudal fin. (d) Close-up of an epural joint. (e) Lateral view of posterior vertebrate. Comparable images were also produced by ingestion of a larva containing  $50 \pm 4$  ng of TA1 or exposure for 5 min to 100 mL of media containing  $10 \pm 2$  ng of either DB1 or TA1.

collected on a Zappa digital camera. Physiological examinations were performed after dissection of a random subsample of 3–5 fish per school. Advantageously, the lack of pigment in *Kryptopterus bicirrhys* allowed direct investigation in vivo. Images from this fish are provided in Figure 2. The localization studies were controlled by



comparing transfer with that of *N*-methyl-7-*N,N*-dimethylaminocoumarin-4-acetamide (i.e., a nondepsipeptide containing derivative of DACA). This derivative, unlike DB1 and TA1, provided weak nonspecific localization in fish tissue, therein further verifying that localization of fluorescence shown in Figure 2 arose from the depsipeptide-function of DB1 and TA1. Furthermore, a "no treatment" negative control revealed that any intrinsic fluorescence was below the limit of detection.

**Tissue Concentration Analysis.** Tissue concentrations of DB1 or TA1 were determined by ultramicrosonicating ~10 mg of tissue (either mosquito larvae or fish) in 30  $\mu$ L of phosphate buffer solution (PBS). The concentration of depsipeptide in the resulting sample was determined fluorometrically using the DACA label (excitation at  $\lambda_{\text{max}} = 370$  nm and emission at  $\lambda_{\text{max}} = 460$  nm, see Table 1).

**Rejection Studies.** After acclimation, colonies of fish were given mosquito larvae containing DB1 or TA1 (exposed larvae). The fish were allowed to feed on the larvae for 30 min, at which point excess larvae were collected using a net, and counted. After removal, the fish were again fed with an excess of a 1:1 mixture of nontreated *C. pipiens* and *A. stephensi* larvae. This method was used to collect data presented in Figures 3–8.

**Larval Success Study.** Modified 10 L tanks were constructed with a 2 mm mesh barrier that divided the vessel in two equal volumes. This barrier restricted fish to one side of the tank, while allowing larvae to freely access the entire tank. Larvae were added in a single transfer to the side of the tank containing the fish. Twenty larvae (either *C. pipiens* or *A. stephensi* larvae) were challenged to avoid consumption by fish ( $S = 20$ ). Larvae that crossed to the right side of the tank were removed and tallied (referred to as escaped). Without prior exposure to DB1 or TA1, naive *D. rerio* ( $N = 400$ ,  $M = 20$ ,  $S = 20$ ) hunted  $98 \pm 0.5\%$  of the larvae before they crossed the barrier (control). These fish were then removed and individually exposed for 30 min to 100 mL of media containing  $50 \pm 4$  ng of DB1 followed by a 5 min wash in 100 mL of depsipeptide-free media. The ability of these fish to learn was determined by counting the number of larvae that escaped and comparing with control. The data from this study is depicted in Figure 9.

**Fish Diversity Study.** Thirty tanks (200 L) were loaded with *Danio rerio* ( $N = 600$ ,  $M = 30$ ) and *Kryptopterus bicirrhys* ( $N = 600$ ,  $M = 30$ ). Each tank contained 20 *D. rerio* and 20 *K. bicirrhys*. The *D. rerio* were acclimated and pretrained over 10 feedings to avoid *C. pipiens* larvae, while the *K. bicirrhys* were only acclimated. Each of the tanks was fed over a period of 30 d ( $F = 30$ ) with a diet consisting of 30 *C. pipiens* containing  $50 \pm 4$  ng of DB1 and 20 depsipeptide-free *A. stephensi*. Five minutes after feeding, excess mosquito larvae were removed and the stomachs of the fish examined. Fish that failed to hunt a depsipeptide-free *A. stephensi* (i.e., consume no larvae or a fluorescent *C. pipiens*) were marked with a drop of paint. Fish that failed three times were removed from the tank. The results of this study are presented in Figure 11.

## RESULTS

**Biochemical Analyses.** Cell proliferation and protein synthesis assays were conducted on DB1 and TA1 to ensure proper biological activity. The effects of DB1 and TA1 on cell growth and proliferation were determined

via the NCI-60 tumor cell screen (Boyd and Paul, 1995). Protein synthesis inhibition was measured in MCF-7 cells using a protocol described by Toogood (Ahuja et al., 2000; Beidler, 1999). The results of these assays are summarized in Table 1.

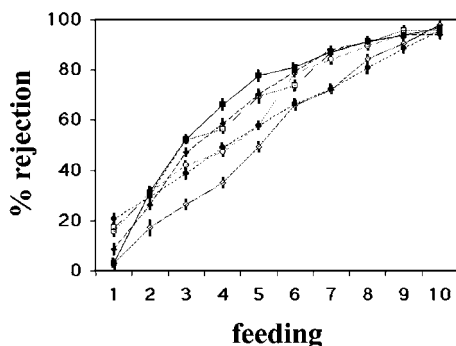
**Transfer by Consumption.** Given its favorable lack of pigmentation, physiological studies began with *Kryptopterus bicirrhys*. Individual *K. bicirrhys* were fed with a larva containing  $50 \pm 4$  ng of DB1 or TA1 (exposed larva) and monitored over the course of 10 d. Immediately after swallowing the exposed larva, fluorescence from DB1 or TA1 crossed the stomach wall of the fish. Soon thereafter, fluorescence spread throughout the stomach and entered the intestine. This path was followed by regurgitation. Within 15 min of this regurgitation, fluorescence from DB1 was no longer apparent in the stomach, but remained within the intestine (Figure 2a,b). At a dose of  $50 \pm 4$  ng larva<sup>-1</sup>, fluorescence from DB1 remained in the intestine for up to 3 d. The rate of transfer, physiological processing, and intensity of localization could not be differentiated between DB1 and TA1 on *Kryptopterus bicirrhys*.

The amount of DB1 or TA1 required to cause regurgitation was then determined by measuring the residual concentration of depsipeptide in regurgitated mosquito larvae (using tissue concentration analysis, see methods). After 65 regurgitations in *D. rerio*,  $42 \pm 3$  ng of DB1 remained within the mosquito larva, indicating that each *D. rerio* regurgitated after absorbing a dose less than  $8 \pm 2$  ng of DB1. Under identical conditions,  $12 \pm 4$  ng of TA1 was transferred. The increased dose of TA1 may be explained by its reduced biological activity (Table 1). Comparable analysis in the other fish indicated that *H. bleheri* absorbed  $8 \pm 2$  ng DB1 and  $11 \pm 3$  ng TA1; *C. paleatus*,  $8 \pm 2$  ng DB1 and  $12 \pm 2$  ng TA1; *O. celebensis*,  $7 \pm 3$  ng DB1 and  $9 \pm 3$  ng TA1; *K. bicirrhys*,  $5 \pm 3$  ng DB1 and  $8 \pm 2$  ng TA1; and *A. ocellaris*,  $10 \pm 2$  ng DB1 and  $19 \pm 4$  ng TA1.

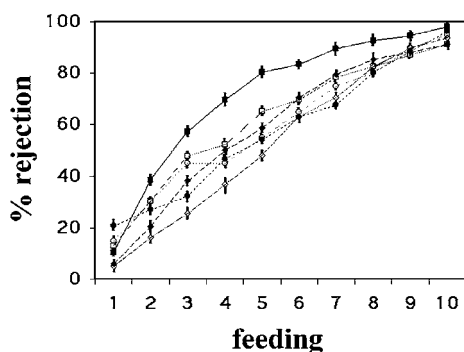
In addition to localization in the digestive system, fluorescence from DB1 and TA1 was also observed in the skeleton of all six fish species. This staining became visible 2 min after consumption and lasted for over a week. As illustrated Figure 2c–e, DB1 showed particular affinity for the endoskeleton at the joints of the eplurals and hypurals. In the spine (Figure 2e), there was a clear affinity for the notochord. The depsipeptides did not bind neural tissue, as even faint DACA fluorescence was not seen in the spinal chord, nerves, or motor neurons. Staining was seen not only in the caudal fin and spine but also in the jaw, chest, pelvic girdle, and dorsal fin.

We then compared this delivery with transfer of the depsipeptide from the medium. The rate and physiological accumulation of depsipeptides DB1 or TA1 in *K. bicirrhys* upon exposure for 5 min to 100 mL of media containing  $10 \pm 2$  ng of DB1 or TA1 was indistinguishable from that observed after ingestion of an exposed larva containing  $50 \pm 4$  ng of DB1 or TA1 (Figure 2). When transmitted from the medium, fluorescence from DB1 was initially observed in the skin, gills, and mouth of *K. bicirrhys*. Within minutes, this fluorescence disappeared and again localized in the intestine and joints. This observation suggests that the physiological target of DB1 and TA1 is independent of the digestive system. It also further indicates that the staining in Figure 2 arises from intact DB1 or TA1, and not from products of digestion or metabolism.

**Calibrating Rejection.** A series of experiments were conducted to examine the response of fish to the analogues. As shown in Figure 3, rejection was readily



**Figure 3.** Rejection of DB1. Fish given a *C. pipiens* larvae containing  $50 \pm 4$  ng of DB1 quickly learn to avoid the bait. The data are presented as the percentage of the school that did not consume a larva at each feeding. Six species are shown: *H. bleheri* (■,  $N = 100$ ,  $M = 10$ ), *C. paleatus* (◆,  $N = 50$ ,  $M = 5$ ), *D. rerio* (●,  $N = 300$ ,  $M = 10$ ), *O. celebensis* (□,  $N = 26$ ,  $M = 2$ ), *K. bicirrhys* (◇,  $N = 100$ ,  $M = 10$ ), and *A. ocellaris* (○,  $N = 20$ ,  $M = 10$ ).

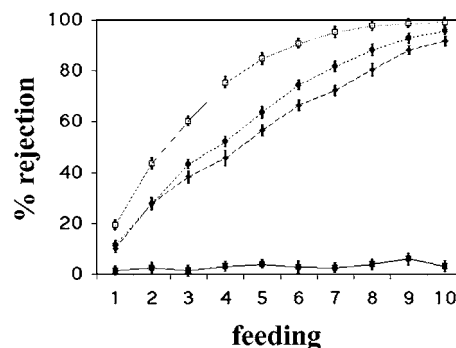


**Figure 4.** Rejection of TA1. Fish given *C. pipiens* larvae containing  $50 \pm 4$  ng of TA1 learn to avoid the bait. The data are presented as the percentage of the school that did not consume a larva at each feeding. Six species are shown: *H. bleheri* (■,  $N = 100$ ,  $M = 10$ ), *C. paleatus* (◆,  $N = 50$ ,  $M = 5$ ), *D. rerio* (●,  $N = 300$ ,  $M = 10$ ), *O. celebensis* (□,  $N = 26$ ,  $M = 2$ ), *K. bicirrhys* (◇,  $N = 100$ ,  $M = 10$ ), and *A. ocellaris* (○,  $N = 20$ ,  $M = 10$ ).

reproduced when mosquito larvae were dosed with  $50 \pm 4$  ng of DB1 or TA1. Over 50% of all six species of fish avoided *C. pipiens* larvae containing  $50 \pm 4$  ng of DB1 after 5 feedings (Figure 3). After 10 feedings, only ~5% of these fish continued to consume the exposed larvae. A comparable outcome was observed with TA1 (Figure 4).

The intensity of this rejection increased with dose of depsipeptide (Figure 5). When loaded at  $10 \pm 2$  ng larva<sup>-1</sup>,  $20 \pm 1\%$  of the *Danio rerio* ( $N = 300$ ,  $M = 10$ ) avoided the exposed larvae after two feedings. When enhanced to  $50 \pm 4$  ng larva<sup>-1</sup>, the rejection after two feedings improved only slightly to  $25 \pm 2\%$ . A comparable response was seen in the other species of fish. Over the same regime ( $10 \pm 2$  ng larva<sup>-1</sup> vs  $50 \pm 4$  ng larva<sup>-1</sup>), the number of *H. bleheri* ( $N = 100$ ,  $M = 10$ ) deterred after 2 feedings improved from  $17 \pm 2\%$  to  $23 \pm 3\%$ , in *C. paleatus* ( $N = 40$ ,  $M = 4$ ) from  $18 \pm 3\%$  to  $26 \pm 2\%$ , in *O. celebensis* ( $N = 26$ ,  $M = 2$ ) from  $19 \pm 5\%$  to  $21 \pm 4\%$ , in *K. bicirrhys* ( $N = 100$ ,  $M = 10$ ,  $N = 10$ ) from  $16 \pm 3\%$  to  $28 \pm 3\%$ , and in *A. ocellaris* ( $N = 20$ ,  $M = 13$ ) from  $17 \pm 6\%$  to  $24 \pm 4\%$ .

While dosages above  $10 \pm 2$  ng larva<sup>-1</sup> modestly improved the induction of rejection, fluorescent examinations (Figure 2) indicated that the bulk of this effect arose from increasing the rate of analogue transfer. Fluorescent studies indicated that increasing the dose of DB1 above  $50 \pm 4$  ng larva<sup>-1</sup> did not alter the intensity of fluores-



**Figure 5.** *Danio rerio*. Concentration profile. Increasing concentration of DB1 in the larvae increases the rejection of *C. pipiens*. These data were collected by repeating Figure 3 with 0 ng (■),  $10 \pm 2$  ng (▲),  $50 \pm 4$  ng (●), and  $250 \pm 12$  ng (XXXXXX) of DB1 per larva.

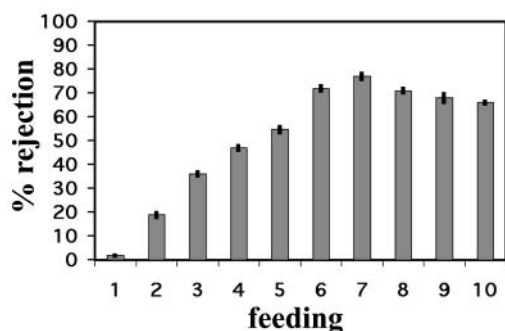
cence observed in the joints of fish, rather, it enhanced the rate at which DB1 was absorbed in (or transferred to) the stomach of the fish. Given a larva that is 10 mg,  $50 \pm 4$  ng larva<sup>-1</sup> corresponds to 50 ppm, a concentration that lies at the lower end of that known to be expressed in tunicate tissue (i.e. 50–100 ppm). While this transfer could operate for the protection of adults, a single didemnid larvae is 0.8–1 mg (Lindquist and Hay, 1995). At this size a single 3 g fish would have to swallow at least 10 larvae to feel the effects of these agents.

A curious facet of these tunicate metabolites lies in their expression in the larval stage (Lindquist et al., 1992; Lindquist and Hay, 1995). In the preceding study, we found that the optimal tissue expression of DB1 and TA1 was around  $10 \pm 2$  ng larvae<sup>-1</sup>. At this expression, critical cell proliferation in the tunicate's larvae would also be at risk (i.e., anti-proliferative activity occurs at the pM range, Table 1), raising the question of how the tunicate and its larvae express the required amounts of depsipeptide without inhibiting their own growth. Consequently, we examined how predators (fish) assimilated the biochemical information provided by the chemical defense agents.

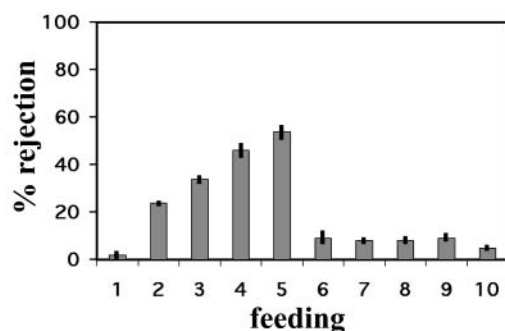
**Learned Avoidance.** Lindquist and Hay (1995) verified that fish learned to avoid the "distaste" of DB (Hay, 1996). While learning is well documented in fish, we were interested in understanding how this response was processed. We found that the toxicity of DB1 and TA1 was associated with the identity of the prey and not by a chemosensing (Rittschof, 1993). *Danio rerio* trained to avoid *C. pipiens* larvae avoided the larvae even when they did not contain DB1 (Figure 6). Not surprisingly, *D. rerio* trained to avoid *C. pipiens* readily consumed larvae from a second species, *A. stephensi* (Figure 7). *Danio rerio* trained to avoid *C. pipiens* however had to relearn to avoid *A. stephensi* containing either DB1 or TA1 (Figure 8). These observations indicate that *D. rerio* learned to avoid the depsipeptide by processing the structural or behavioral trait(s) of the larvae. This advantageously allowed fish to minimize their contact with the analogues.

**Indirect Transmission.** While not yet examined in the field, logistic analysis suggests that release mechanisms are also feasible. When a 3.8 g *Amphiprion ocellaris* was exposed to 200 ng of DB1 in 10 L of media for 5 min, the level of fluorescence from DB1 in its joints was indistinguishable from that shown in Figure 2. At this level of transfer, tunicates would have to deliver 20 ng L<sup>-1</sup> to their local medium. In a sea with a depth of 10 m and a density of 50 adult tunicates m<sup>-2</sup>, a single tunicate would need to release 4 μg of depsipeptide

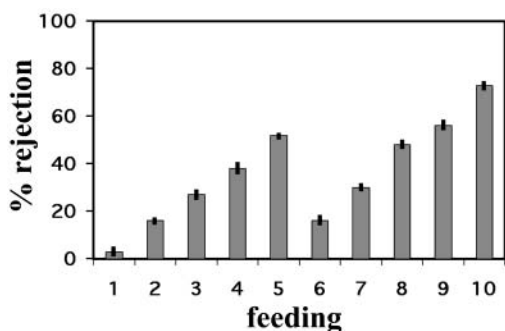




**Figure 6.** *Danio rerio*. Rejection and learning. Schools of zebrafish ( $N = 300$ ,  $M = 10$ ) learned to reject *C. pipiens* containing  $50 \pm 4$  ng of DB1 over 5 daily feedings and continued to reject *C. pipiens* not containing DB1 thereafter. Data presented by plotting the percentage of zebrafish that did not consume a larva over a total of 10 feedings.



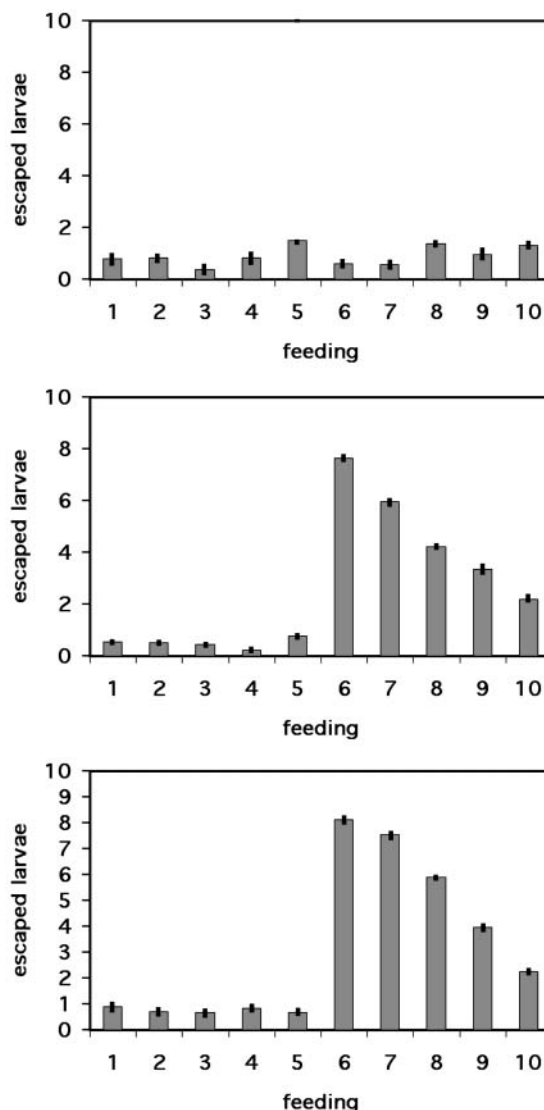
**Figure 7.** *Danio rerio*. Rejection and acceptance. Schools of zebrafish ( $N = 300$ ,  $M = 10$ ) that learned to reject *C. pipiens* containing  $50 \pm 4$  ng of DB1 over 5 daily feedings accepted DB1-free *A. stephensi* (feedings 6–10). Data presented depicts the percentage of zebrafish that did not consume a larva over a total of 10 feedings.



**Figure 8.** *Danio rerio*. Rejection and relearning. Schools of zebrafish ( $N = 300$ ,  $M = 10$ ) that learned to reject *C. pipiens* containing  $50 \pm 4$  ng of DB1 over 5 daily feedings had to relearn to avoid *A. stephensi* containing  $50 \pm 4$  ng of DB1 (feedings 6–10). Data presented depicts the percentage of zebrafish that did not consume a larva over a total of 10 feedings.

(typically  $50\text{--}250$   $\mu\text{g}$  of depsipeptide are isolated per tunicate). Here the colonial nature of these tunicates could be used to further concentrate the release and targeting of the metabolites.

We also examined the possibility of media transfer by examining the appetite of the fish after exposures to media-born DB1. As shown in Figure 9, fish quickly lost their appetite after exposure to  $0.5$  ng mL<sup>-1</sup> of DB1. Dose relation studies indicated that this effect required an exposure of 5 min in media containing  $80$  pM, or  $0.1$  ng mL<sup>-1</sup> of DB1. While temporary, this loss of appetite allowed the mosquito larvae to escape consumption (i.e., crossing the barrier). Interestingly, fish exposed to media

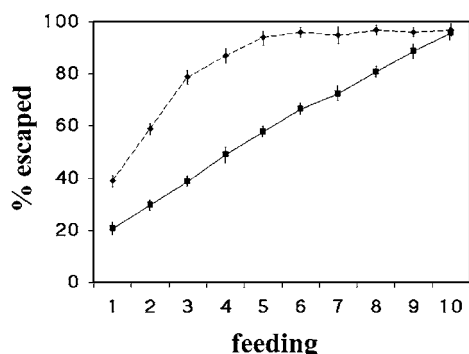


**Figure 9.** *Danio rerio*. Larval success study. (top) Zebrafish ( $N = 300$ ,  $M = 10$ ) in media without DB1 feed normally. (middle) Zebrafish ( $N = 300$ ,  $M = 10$ ) that were individually exposed to  $100$  mL media containing  $50 \pm 4$  ng of DB1 after the fifth feeding lost their ability to hunt depsipeptide-free *C. pipiens*. This loss was not permanent, as shown by the reduction in escaped larvae. (bottom) A comparable outcome was also observed by exposure to  $50 \pm 4$  ng of TA1 after the fifth feeding.

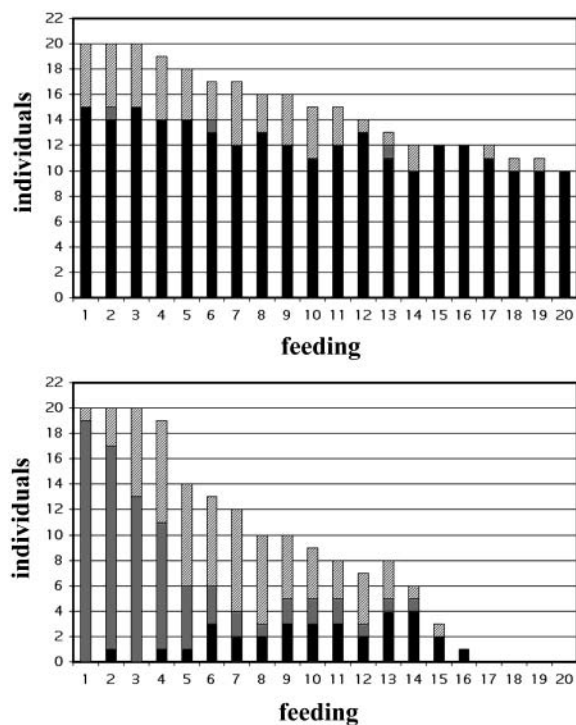
containing DB1 apparently improved their recognition of DB1-exposed *C. pipiens* (Figure 10). *Danio rerio* that only had brief contact to media containing DB1 learned to avoid the exposed *C. pipiens* much faster than fish that had no prior contact to DB1.

We then examined how media transfer could alter the competition between two species of fish. A total of five tanks were prepared with an equivalent number of *D. rerio* ( $N = 100$ ,  $M = 5$ ) and *K. bicirrhys* ( $N = 100$ ,  $M = 5$ ). Each tank was fed daily with  $30$  *C. pipiens* containing  $50 \pm 4$  ng of DB1 and  $20$  unexposed *A. stephensi* larvae. When examined without training, *D. rerio* and *K. bicirrhys* competed for bait at the same rate and success (not shown). The schools of *D. rerio* were then removed and trained over 10 feedings to avoid *C. pipiens*. As indicated in Figure 11, *D. rerio* excelled at catching the depsipeptide-free *A. stephensi*, while *K. bicirrhys* continued to consume the exposed *C. pipiens*.

We then modeled the effects that this competition would have on short-term decline, by tagging each fish



**Figure 10.** *Danio rerio*. Fish learn from media exposure. Exposure to media containing DB1 improved *D. rerio*'s ability to avoid exposed *C. pipiens*. Schools of *D. rerio* trained by exposure to media containing  $50 \pm 4$  ng of DB1 (◆,  $N = 300$ ,  $M = 10$ ) were more apt to avoid treated *C. pipiens* than naïve *D. rerio* (■,  $N = 300$ ,  $M = 10$ ). This experiment was conducted using the conditions described in the larval success study (see methods). The percent of *C. pipiens* larvae that escaped is shown.



**Figure 11.** *D. rerio* and *K. bicirrhys*. Fish diversity study. The influence of DB1 on an artificial ecosystem containing schools of *D. rerio* ( $N = 200$ ,  $M = 10$ ) and *K. bicirrhys* ( $N = 200$ ,  $M = 10$ ) was calibrated by examining the ability to hunt. Feedings were conducted with *C. pipiens* containing  $50 \pm 4$  ng of DB1 and depsipeptide-free *A. stephensi*. Fish that failed to hunt *A. stephensi* were marked with paint. Once they failed three times (three dots of paint), they were removed from the tank. (top) *D. rerio*, trained to avoid DB1, outlasted (bottom) naïve *K. bicirrhys*. The members of each species remaining are displayed as those who did not consume a larva (black), caught a *C. pipiens* (gray), and caught an *A. stephensi* (stripes).

after it failed to hunt properly. Tanks were prepared with 20 *D. rerio* trained to avoid *C. pipiens* and 20 untrained *K. bicirrhys*. Each of the tanks was provided over a period of 30 d ( $F = 30$ ) with a diet consisting of 30 *C. pipiens* containing  $50 \pm 4$  ng of DB1 and 20 depsipeptide-free *A. stephensi*. After 20 feedings, an average of  $11 \pm 3$  trained *D. rerio* ( $N = 100$ ,  $M = 20$ ) remained in each school. The naïve *K. bicirrhys* ( $N = 100$ ,  $M = 20$ ) were not as successful (Figure 11). Even after five feedings, the

number of successful or remaining *K. bicirrhys* was four less than that of the trained *D. rerio*. After 16 feedings (average presented graphically), no *K. bicirrhys* remained.

## DISCUSSION

There was a rapid, definitive response by six species of fish to larval mosquitoes containing analogues DB1 or TA1. Transfer of the chemical-defense agent from prey (mosquito larvae) to predator (fish) was rapid. Once localized in the intestine and skeleton, DB1 and TA1 were not cleared for several days. In all six species of fish, the processing of DB1 and TA1 was indistinguishable with respect to the kinetics of transfer and thermodynamic localization, as all species of fish displayed a comparable rate of absorption as well as physiological processing. The intensity of this response was sufficient to cause 50% of the fish that consumed larvae containing  $50 \pm 4$  ng of depsipeptide to avoid the treated larvae after only five daily feedings. Subsequent analyses indicated that this response arose after transfer of only 5–10 ng of depsipeptide. The effect was dose dependent and led to association of the larval species with distaste. Thus, once conditioned, the fish did not consume untreated larvae of the same species but fed upon another species of mosquito larvae.

The analog-mediated effect did not require ingestion. Transfer of the analogue from the medium to the fish also resulted in a decreased efficiency of hunting. Furthermore, the physiological localization of the analogues in fish was not altered by this mode of delivery.

Predator fitness potentially increases with their ability to recognize treated larvae. Fish that had been preconditioned to avoid the depsipeptide-treated larvae were able to hunt other species of larvae selectively and benefit; whereas, unconditioned fish had to learn to avoid the tainted larvae before they could effectively compete for food.

This study is among the first to show that TA has similar activity to DB (Liang et al., 2001). Analogues DB1 and TA1 shared a common potency and localization in the predators. The two species of family *Didemnidae* that produce DB and TA, while from remote geographic locations, use a common method to defend themselves and their otherwise vulnerable larvae by producing two structurally similar but not identical depsipeptides. The results of this study might be used to investigate predator–prey interactions in marine species other than tunicates.

## ACKNOWLEDGMENT

We thank W. Müller, W. Rettig, and B. Mallioux for their assistance. This work has been supported in part by grants from the National Institutes of Health (CA-40081) and the National Science Foundation (CHE 99-01449). This work was conducted under protocols that met standards of the National Institutes of Health, and the countries where experimentation was conducted.

## LITERATURE CITED

- (1) Ahuja, D., Vera, M. D., SirDeshpande, B. V., Morimoto, H., Williams, P. G., Joullié, M. M., and Toogood, P. L. (2000) Inhibition of protein synthesis by Didemnin B: How EF-1 $\alpha$  mediates inhibition of translocation. *Biochemistry* 39, 4339–4346.
- (2) Beidler, D. R., Ahuja, D., Wicha, M. S., and Toogood, P. L. (1999) Inhibition of protein synthesis by Didemnin B is not sufficient to induce apoptosis in human mammary carcinoma (MCF7) cells. *Biochem. Pharmacol.* 58, 1067–1074.

- (3) Boyd, M. R., and Paull, K. D. (1995) Some practical considerations and applications of the National Cancer Institute in vitro anticancer drug discovery screen. *Drug Dev. Res.* 34, 91–109.
- (4) Crews, C. M., Collins, J. L., Lane, W. S., Snapper, M. L., and Schreiber, S. L. (1994) GTP-dependent binding of the antiproliferative agent didemnin to elongation factor 1 $\alpha$ . *J. Biol. Chem.* 269, 15411–15414.
- (5) Crews, C. M., Lane, W. S., and Schreiber, S. L. (1996) Didemnin binds to the protein palmitoyl thioesterase responsible for infantile neuronal ceroid lipofuscinosis. *Proc. Natl. Acad. Sci. U.S.A.* 93, 4316–4319.
- (6) Cuvier, G., and Valenciennes, A. (1840) Histoire naturelle des poissons. Tome quatorzième. Suite du livre seizième. Labroides. Livre dix-septième. Des Malacopterygiens. *Hist. Nat. Poiss.* i–xxii, 1–464.
- (7) Faulkner, D. J. (2000a) Highlights of marine natural products (1972–1999). *Nat. Prod. Rep.* 17, 1–6.
- (8) Faulkner, D. J. (2000b) Marine natural products. *Nat. Prod. Rep.* 17, 7–55.
- (9) Fimiani, V. (1987) In vivo effect of Didemnin B on two tumors of the rat. *Oncology* 44, 42–46.
- (10) Ford, P. W. (1996) Studies of marine macro- and microorganisms. Part I. The chemistry of ascidians from the family Didemnidae. Part II. Metabolites from marine sediment-derived actinomycetes. Ph. D. dissertation, University of Hawaii.
- (11) Gery, J., and Mahnert, V. (1986) A new rummy-nose tetra from the Rio Negro, Brazil: *Hemigrammus bletheri*. *Trop. Fish Hobby* 37, 40–41.
- (12) Hamilton, F. (1822) An account of the fishes found in the river Ganges and its branches. Edinburgh, London.
- (13) Hay, M. E. (1996) Marine chemical ecology: What is known and what is next? *J. Exp. Marine Biol.* 200, 103–134.
- (14) Jenyns, L. (1840–2) Fish, in *The zoology of the voyage of H. M. S. Beagle, under the command of Captain Fitzroy, R. N. during the years of 1832 to 1836*. Smith, Elder and Co., London.
- (15) Kats, L. B. (1998) The scent of death: Chemosensory assessment of predation risk by prey animals. *Ecoscience* 5, 361–394.
- (16) Kerfoot, W. C. (1982) A question of taste: crypsis and waring coloration in freshwater zooplankton communities. *Ecology* 63, 538–554.
- (17) LeGrue, S. J., Sheu, T.-L., Carson, D. D., Laidlaw, J. L., and Sanduja, S. K. (1988) Inhibition of T-lymphocyte proliferation by the cyclic polypeptide Didemnin B: No inhibition of lymphokine stimulation. *Lymphokine Res.* 7, 21–29.
- (18) Li, W.-R., and Joullie, M. M. (1992) The Didemnins: biological properties, chemistry, and total synthesis. *Studies in Natural Products Chemistry* (Atta-ur-Rahman, Ed.) pp 241–302, Vol. 10, Stereoselective Synthesis (Part F), Elsevier, Amsterdam.
- (19) Liang, B., Richard, D. J., Portonovo, P., and Joullie, M. M. (2001) Total syntheses and biological investigations of Tamandarins A and B and Tamandarin A analogues. *J. Am. Chem. Soc.* 123, 4469–4474.
- (20) Lindquist, N., and Hay, M. E. (1995) Can small rare prey be chemically defended? The case for marine larvae. *Ecology* 76, 1347–1358.
- (21) Lindquist, N., Hay, M. E., and Fenical, W. (1992) Defense of ascidians and their conspicuous larvae: adult vs larval chemical defenses. *Ecol. Monogr.* 62, 547–568.
- (22) Maldonado, E., Lavergne, J. A., and Kraiselburd, E. (1982) Didemnin A inhibits the in vitro replication of dengue virus types 1, 2 and 3. *P. R. Health Sci. J.* 1, 22–25.
- (23) Meng, L., Sin, N., and Crews, C. M. (1998) The antiproliferative agent didemnin B uncompetitively inhibits palmitoyl protein thioesterase. *Biochemistry* 37, 10488–10492.
- (24) Montgomery, D. W., Celniker, A., and Zukoski, C. F. (1987) Didemnin B-An immunosuppressive cyclic peptide that stimulates murine hemagglutinating antibody responses and induces leukocytosis in Vivo. *Transplantation* 43, 133.
- (25) Moore, B. S. (1999) Biosynthesis of marine natural products: microorganisms and macroalgae. *Nat. Prod. Rep.* 16, 653–674.
- (26) Portonovo, P., Ding, X., Leonard, M. S., and Joullie, M. M. (2000) First total synthesis of a fluorescent Didemnin. *Tetrahedron* 56, 3687–3690.
- (27) Rinehart, K. L. (2000) Antitumor compounds from tunicates. *Med. Res. Rev.* 20, 1–27.
- (28) Rinehart, K. L., Cook, J. C., Jr., Pandey, R. C., Gaudioso, L. A., Meng, H., Moore, M. L., Gloer, J. B., Wilson, G. R., Gutowsky, R. E., Zierath, P. D., Shield, L. S., Li, L. H., Renis, H. E., McGovern, J. P., and Canonico, P. G. (1982) Biologically active peptides and their mass spectra. *Pure Appl. Chem.* 54, 2409–2424.
- (29) Rinehart, K. L., Gloer, J. B., Hughes, R. G., Jr., Renis, H. E., McGovern, J. P., Swynenberg, E. B., Stringfellow, D. A., Kuentzel, S. L., and Li, L. H. (1981) Didemnins: antiviral and antitumor depsipeptides from a Caribbean tunicate. *Science* 212, 933.
- (30) Rittschof, D. (1993) Body odors and neutral-basic peptide mimics: A review of responses by marine organisms. *Am. Zool.* 33, 487–493.
- (31) Sakai, R., Rinehart, K. L., Kishore, V., Kundu, B., Faircloth, G., Gloer, J. B., Carney, J. R., Namikoshi, M., Sun, F., Hughes, R. G., Jr., Gravalos, G., De Quesada, T. G., Wilson, G. R., and Heid, R. M. (1996) Structure–activity of the Didemnins. *J. Med. Chem.* 39, 2819–2834.
- (32) Van Duyl, F. C., Bak, R. P. M., and Sybesma, J. (1981) The ecology of the tropical compound ascidian *Trididemnum solidum*. I. Reproductive strategy and larval behavior. *Ecol. Prog. Ser.* 6, 35–42.
- (33) Vera, M. D., and Joullie, M. M. (2002) Natural Products as Probes of Cell Biology: 20 Years of Didemnin Research. *Med. Res. Rev.* 22, 102–145.
- (34) Vervoort, H., Fenical, W., and De A. Epifanio, R. (2000) Tamandarins A and B: New cytotoxic depsipeptides from a Brazilian ascidian of the family Didemnidae. *J. Org. Chem.* 65, 782–792.
- (35) Weber, M. (1894) The freshwater fish of the Indian Archipelago, the finding of a new fauna from Celebes. *Zool. Ergebn. Reise Nederl. Ost-Ind.* 405–476.
- (36) Wolfe, G. V. (2000) The chemical defense ecology of marine unicellular plankton: Constraints, mechanisms, and impacts. *Biol. Bull. Woods Hole* 198, 225–244.
- (37) Young, C. M., and Bingham, B. L. (1987) Chemical defense and aposematic coloration in larvae of the ascidian *Ecteinascidia turbinata*. *Marine Biol.* 96, 539–554.

BC025576N



## Blue Fluorescent Antibodies as Reporters of Steric Accessibility in Virus Conjugates

Qian Wang,<sup>†</sup> Krishnaswami S. Raja,<sup>†</sup> Kim D. Janda,<sup>†</sup> Tianwei Lin,<sup>\*,‡</sup> and M. G. Finn<sup>\*,†</sup>

Departments of Chemistry and Molecular Biology, The Skaggs Institute for Chemical Biology, and the Center for Integrative Molecular Biosciences, The Scripps Research Institute, 10550 N. Torrey Pines Road, La Jolla, California 92037 Received July 29, 2002; Revised Manuscript Received November 13, 2002

Nonenveloped viruses provide the chemist with large, preassembled polyvalent protein scaffolds for modification. These structures are typically porous to small molecules but not to large ones. The solution-phase structures and reactivities of such assemblies may be substantially different than indicated by X-ray crystal structures. Here, the attachment of organic compounds to either the inside or outside surface of the cowpea mosaic virus (CPMV) coat protein was verified with an indicating antibody–antigen interaction. Antibody binding was subsequently blocked by the installation of poly(ethylene glycol) chains. These results typify the type of site-specific control that is available with CPMV and related virus building blocks.

### INTRODUCTION

Cowpea mosaic virus (CPMV) is a prototypical icosahedral plant virus having qualities that render it useful as a supramolecular chemical compound as well as a biological entity. It can be made and purified in large quantities (1, 2), is structurally characterized to near-atomic resolution (3), is stable to a variety of conditions compatible with both hydrophobic and hydrophilic molecules (4), and can be manipulated at the genetic level to introduce mutations at desired positions (5–9). Sixty identical asymmetric protein units, each composed of “large” and “small” polypeptide chains, comprise the CPMV coat protein (capsid). The virion is approximately 300 Å in diameter, with an average capsid thickness of 30 Å and RNA packaged in the interior. The structure therefore possesses inside and outside protein surfaces, which are chemically different. The most obvious distinction is the disposition of multiple positively charged residues on the interior surface, which presumably serve as points of association with the encapsidated polynucleotide. Thus, X-ray crystallography shows more than 10 lysines per asymmetric unit to be arrayed on the capsid interior, whereas only five lysine residues per asymmetric unit are found on the exterior surface. We have taken advantage of some of these properties to demonstrate the attachment of lysine- and cysteine-reactive small molecules to specific positions on the CPMV capsid (4, 10, 11).

While the positions of attachment to the coat protein sequence may be engineered and/or elucidated, such experiments do not provide independent information about the location of the reactive site relative to other structural elements of the virion in solution. In other words, the crystal structure of a virus provides a useful initial guide to its chemistry, but such a structure offers little information about capsid dynamics, which may bring apparently blocked residues to the surface. In fact,

dynamic structural transitions occur in many virions (12). For example, cleavage of an *N*-terminal sequence of flock house virus by added trypsin occurs readily, although the crystal structure shows this sequence to be attached to the interior surface of the capsid (13). Another example of dynamic behavior is afforded by cowpea chlorotic mottle virus, which undergoes reversible pH-dependent swelling, changing the virus diameter by approximately 10% (14). To evaluate the solution-phase chemical behavior of the lysine and cysteine residues, we require solution-phase methods to determine if the chemical linkages have been made on the inside vs the outside capsid surface. Here we describe the use of a Lerner-Janda blue fluorescent antibody to report on the position of its stilbene hapten (15, 16) and the modulation of this antibody–antigen interaction by covalent modification of the virus surface. The result of an initial version of this experiment was included in a previous report (4).

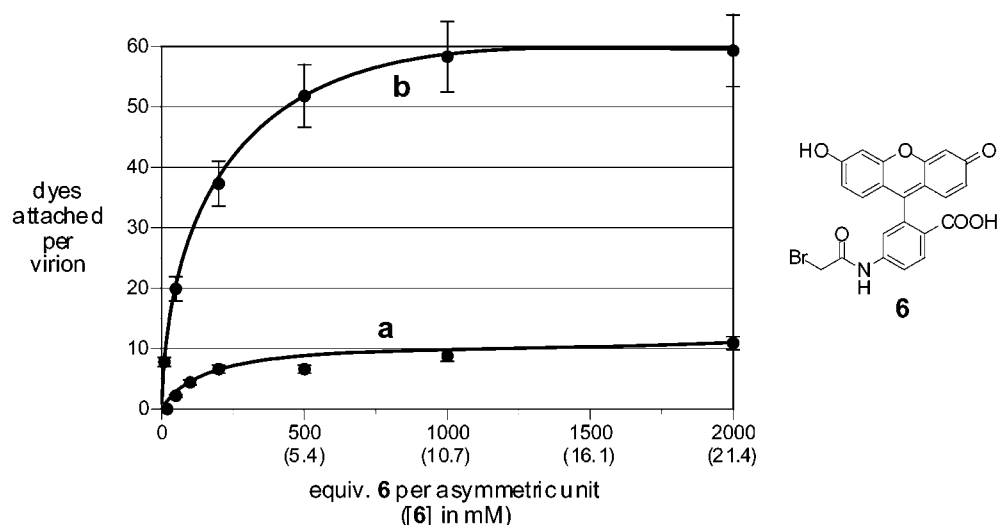
### EXPERIMENTAL PROCEDURES

*trans*-4-Aminostilbene, 5-aminofluorescein, and bromoacetyl bromide were purchased from Aldrich. Poly(ethylene oxide) reagents “mPEG-succinimidyl propionate-5000” (MW 5000) and “mPEG-succinimidyl propionate-2000” (MW 2000) were purchased from Shearwater Polymer Inc. Wild-type and mutant (VEFCysα) viruses were prepared as previously described (10, 11). Unless otherwise noted, “buffer” refers to 0.1 M potassium phosphate, pH 7.0. The virus was stored in buffer at a concentration of about 10 mg/mL. Size exclusion columns for purification of virus from reaction mixtures were prepared by preswelling Bio-Gel P-100 Gel (BioRad, 23 g) in buffer (400 mL, degassed overnight for use with mutants displaying exterior cysteine residues) and loading the gel into Bio-Spin disposable chromatography columns (BioRad). For 80 µL of virus solution (1 mg/mL), approximately 1 mL of the prepared gel is required. Sucrose gradient ultracentrifugation separation of virus samples was performed on 30 mL gradients [made of 20% (w/w) sucrose solution in buffer, frozen at –20 °C, and defrosted just before use] with centrifugation at 38000 rpm for 3 h (Beckman SW41 Ti rotor), giving rise to well-separated bands.

\* To whom correspondence should be addressed. Fax: (858) 784-8850. e-mail: mgfinn@scripps.edu, twlin@scripps.edu.

<sup>†</sup> Department of Chemistry.

<sup>‡</sup> Department of Molecular Biology.



**Figure 1.** Plots showing the amount of the covalently attached fluorescein to (a) wild-type CPMV, and (b) the mutant virus VEFcys $\alpha$ , as a function of the ratio of reagent **6** to virus. Note that there are 60 asymmetric units per virus particle. Each data point shown is the average of three independent experiments with maximum error of  $\pm 9\%$  of the reported attachment value.

TEM analyses were performed by depositing 20  $\mu$ L aliquots of each sample onto 100-mesh carbon-coated copper grids for 2 min. The grids were then stained with 20  $\mu$ L of 2% uranyl acetate and viewed with Philips CM100 electron microscope. FPLC analyses were performed with AKTA Explorer (Amersham Pharmacia Biotech) equipment, using Superose-6 size-exclusion or Hitrap-Q ion-exchange columns. In the former case, 0.05 M potassium phosphate buffer (pH 7.0) was used as eluent; intact virions show retention times of approximately 25 min at an elution rate of 0.4 mL/min, whereas broken particles and individual subunit proteins elute only after 50–60 min. Ion-exchange FPLC was performed with 0.05 M potassium phosphate as the low-salt buffer and 1.0 M NaCl in 0.05 M potassium phosphate as high-salt eluent.

**4-(4-*E*-Styryl-phenylcarbamoyl)butyric Acid (1).** *trans*-4-Aminostilbene (426 mg, 2.18 mmol) and glutaric anhydride (250 mg, 2.19 mmol) were stirred in  $\text{CH}_2\text{Cl}_2$  (10 mL) at room temperature, the solution depositing a white precipitate within a few minutes. After 5 h, the solvent was removed to give carboxylic acid **1** as a pale yellow solid (671 mg, 99% yield).  $^1\text{H}$  NMR ( $\text{DMSO}-d_6$ )  $\delta$  12.02 (br s, 1H), 9.97 (s, 1H), 7.6 (m, 6H), 7.35 (t,  $J = 7.9$  Hz, 2H), 7.23 (d,  $J = 7.9$  Hz, 1H), 7.15 (s, 2H), 2.32 (m, 4H), 1.80 (m, 2H).  $^{13}\text{C}$  NMR ( $\text{DMSO}-d_6$ )  $\delta$  174.8, 171.3, 139.5, 137.9, 132.5, 129.3, 128.7, 127.9, 127.6, 126.9, 119.8, 36.2, 33.7, 21.2.

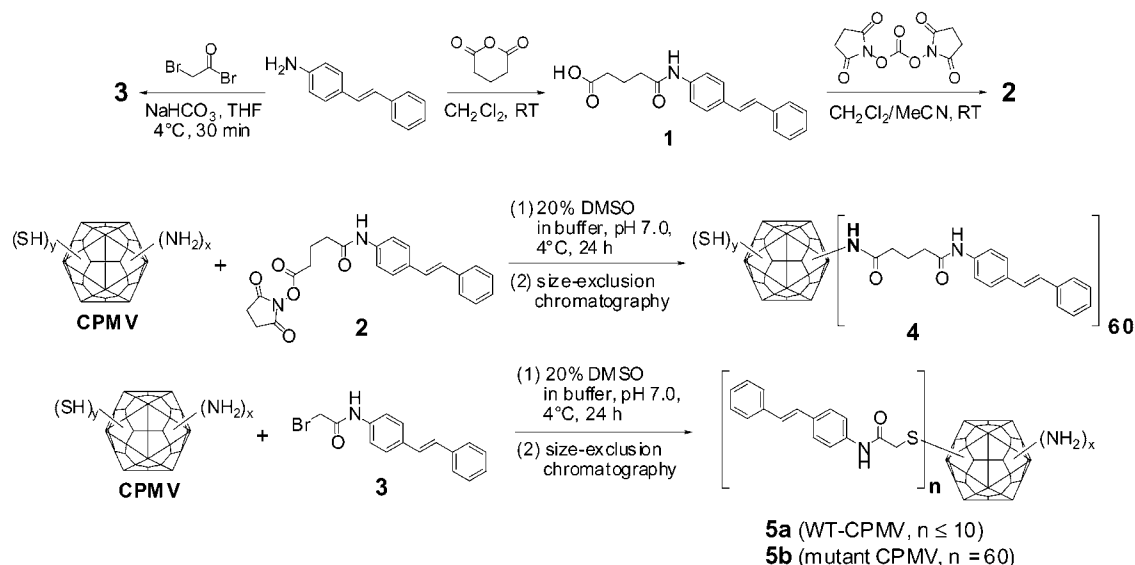
**4-(4-*E*-Styryl-phenylcarbamoyl)butyric Acid 2,5-Dioxo-pyrrolidin-1-yl Ester (2).** A solution of **1** (200 mg, 0.65 mmol) in 1:1:0.1  $\text{CH}_2\text{Cl}_2$ :MeCN:pyridine was treated with disuccinimidyl carbonate (182 mg, 0.71 mmol), and the reaction was stirred at room temperature under a drying tube. The small amount of solid that was undissolved at the beginning of the reaction was solubilized after several hours. After 12 h, the solvent was removed to give a wet, off-white solid;  $\text{CH}_2\text{Cl}_2$  was added and then removed to give a dry white solid. This material was purified by column chromatography on silica gel, using 2:1  $\text{CH}_2\text{Cl}_2$ :MeCN as eluent. The desired product, **2**, eluted near the solvent front and was isolated as a white solid (186 mg, 70% yield).  $^1\text{H}$  NMR ( $\text{CDCl}_3$ )  $\delta$  7.96 (br s, 1H), 7.5 (m, 6H), 7.35 (m, 2H), 7.28 (m, 1H), 7.05 (s, 2H), 2.89 (s, 4H), 2.74 (t,  $J = 7.0$  Hz, 2H), 2.49 (t,  $J = 6.8$  Hz, 2H), 2.22 (m, 2H).

**(*E*)-4-Bromoacetamidostilbene (3).** A suspension of *trans*-4-aminostilbene (0.98 g, 5 mmol) and  $\text{NaHCO}_3$  (1.3 g, 15 mmol) in dry tetrahydrofuran (15 mL) was stirred at 0  $^\circ\text{C}$  for 15 min, followed by dropwise addition of a solution of bromoacetyl bromide (2.0 g, 10 mmol) in dry tetrahydrofuran (5 mL). After the mixture was stirred for 30 min, diethyl ether (50 mL) and saturated aqueous  $\text{NaHCO}_3$  (50 mL) were added. The organic layer was separated and concentrated to afford 1.4 g (91%) of the desired product as a brown powder. Further purification was performed by recrystallization from acetone.  $^1\text{H}$  NMR ( $\text{CDCl}_3$ ):  $\delta$  8.16 (br, 1 H), 7.53–7.26 (m, 9 H), 7.08 (s, 2 H), 4.04 (s, 2 H).

**6- $\alpha$ -Bromoacetamidofluorescein (6)** (17). This compound was prepared analogously to **3**, using 6-aminofluorescein (1.74 g, 5 mmol). The crude product was purified by column chromatography over silica gel, eluting with ethyl acetate, giving **6** as a yellow powder (1.85 g, 79%).  $^1\text{H}$  NMR ( $\text{CDCl}_3$ , 500 Hz):  $\delta$  9.95 (s, 1 H), 7.98–7.70 (m, 4 H), 6.75–6.61 (m, 6 H), 4.00 (s, 2 H).

**General Procedure for Modification of CPMV with Chemical Reagents.** Organic reagents in DMSO solution were introduced into a solution of virus, such that the final solvent mixture was composed 80% buffer and 20% DMSO. Following incubation at 4  $^\circ\text{C}$  for 24–48 h, the mixture was purified by passage through a P-100 size exclusion column (centrifugation at 800  $g$  for 3–5 min). This filtration was repeated (typically two or three times) with fresh columns until all the excess reagents were removed. Purification of larger quantities of derivatized virus ( $>1$  mg) was performed by ultracentrifugation at 42000 rpm (Beckman 50.2 Ti rotor) through a 2 cm sucrose cushion, followed by solvation of the resulting material in buffer. Mass recoveries of derivatized viruses were typically 60–90%; all such samples were composed of  $>95\%$  intact particles as determined by analytical size-exclusion FPLC. Virus concentrations were measured by absorbance at 260 nm; virus at 0.1 mg/mL gives a standard absorbance of 0.8. The average molecular weight of the CPMV virion is  $5.6 \times 10^6$ .

**Stoichiometry of Virus Derivatization (Figure 1).** The reactions were performed at constant virus concentration (1 mg/mL) under the above conditions. After purification, the concentration of viruses and dyes were determined by absorbance spectroscopy. Fluorescein

**Scheme 1. Preparation of Virus–Stilbene Conjugates**

concentrations were obtained by measurement of absorbance at 495 nm, using a calibrated value of molar absorptivity ( $77\,000\text{ cm}^{-1}\text{ M}^{-1}$ ) determined by mixing known quantities of dye with CPMV (1 mg/mL). Each data point is the average of values obtained from three independent parallel reactions. The average deviation was 5%, and the maximum deviation was 9%. Most samples were also analyzed by anion-exchange FPLC to verify the integrity of the particles and the quantitation of their dye attachments.

**Wild-Type CPMV Lysine–Stilbene Conjugate (4) and Cysteine–Stilbene Conjugates (5a, 5b).** Wild-type CPMV (10 mg) and **2** (20  $\mu\text{mol}$ , ca. 200-fold excess relative to viral protein) in a solution of DMSO (1 mL) and buffer (4 mL) were shaken gently at 4  $^\circ\text{C}$  for 24 h. Initial separation of virus from reagent was accomplished by adding another 4 mL of buffer to induce precipitation of the organic reagent and spinning at 16000*g* for 2 min. The supernatant was further purified by ultracentrifugation at 42000 rpm over a 2 cm 40% (w/w) sucrose cushion, and the resulting transparent pellets were dissolved in 1 mL buffer. Measurement of  $\text{OD}_{260}$  provided a concentration of virus **4** of 9.1 mg/mL (91% yield). The syntheses of **5a** and **5b** were performed analogously, using wild-type or mutant CPMV (5 mg) and **3** (100  $\mu\text{mol}$ , ca. 2000-fold excess relative to viral protein), with the only difference being the reaction time (48 h for **5a** and 12 h for **5b**), reflecting the difference in reactivity between the two viruses.

**PEGylation of 5b.** Conjugate **5b** (2 mg) and **7a** or **8a** (20-fold excess with respect to viral protein) were incubated in 0.1 M  $\text{NaHCO}_3$  buffer (pH 8.4) at 4  $^\circ\text{C}$  for 48 h. The resulting viruses were purified by sucrose gradient sedimentation. The bands corresponding to virus were collected, concentrated by ultracentrifugation through a 2 cm sucrose cushion, and dissolved in PBS buffer.

**Formation of Antibody 19G2 Complexes.** All samples were dialyzed into PBS buffer at 4  $^\circ\text{C}$  before mixing with antibody 19G2. The concentration of 19G2 was 1.5 mg/mL and virus concentrations were made constant at 1.0 mg/mL. For denaturation, the viruses were heated for 1 h at 60  $^\circ\text{C}$  in 50 mM ammonium carbonate buffer containing 20% acetonitrile.

**RESULTS AND DISCUSSION**

**Preparation of CPMV–Stilbene Conjugates.** Stilbene derivatives **2** and **3**, prepared from *trans*-4-amino-

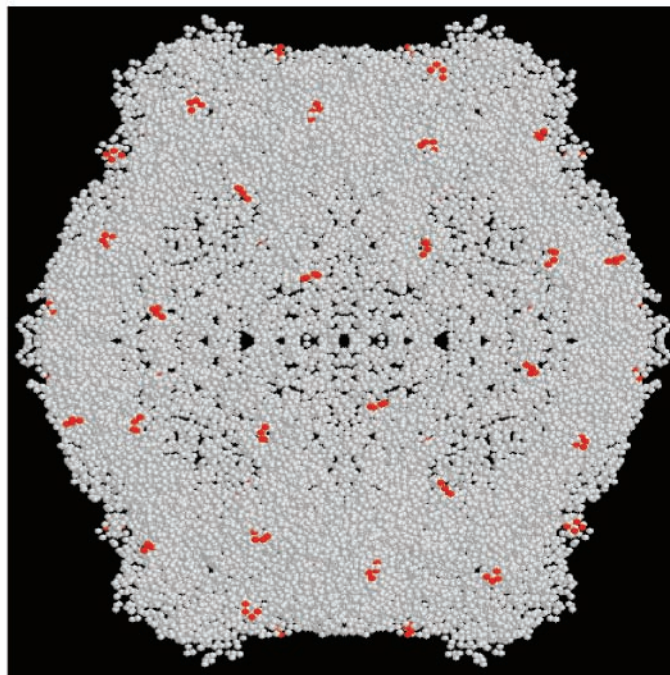
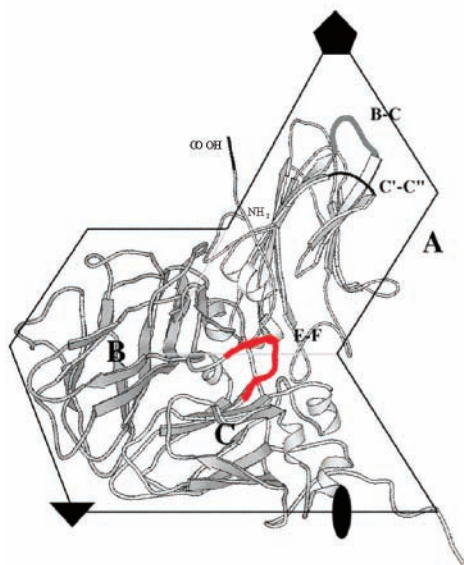
stilbene, were used to modify wild-type and mutant CPMV, as shown in Scheme 1. Reactions with **2** were performed under the conditions previously shown with dye-NHS esters to provide attachment of the small molecule predominantly at a single lysine residue of the coat protein (K38 in the small subunit), giving 60 stilbenes per virus particle (virus **4**) (10).

Stilbene bromoacetamide **3**, a readily available reagent for specific modification of sulfhydryl groups, was chosen for the derivatization of the cysteine mutant viruses and the modification of the cysteines of wild-type CPMV (Scheme 1). The use of **3** required a preliminary assessment of the reactivity of a model bromoacetamide with the virus. Thus, fluorescein derivative **6** was employed to establish the proper conditions for stilbene attachment to thiol residues of CPMV. Wild-type CPMV proved to be poorly reactive toward **6**, showing no dye attachment in a 6-h reaction and modest levels of covalent modification of the virus after 2 days. The dose–response for attachment under the latter conditions is shown in Figure 1; under the most forcing conditions (2000:1 molar ratio of **6** to viral protein), a maximum of 10 dye molecules per capsid were attached.

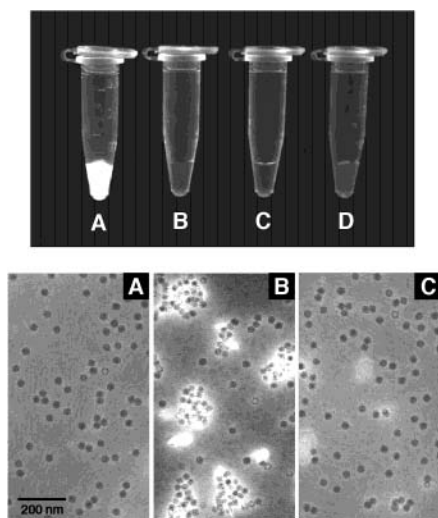
The CPMV mutant designated VEFcys $\alpha$  was chosen for comparison to the wild-type particle for reasons of stability and spacing of the inserted cysteine moieties. Figure 2 shows the site of the five-residue (GGCGG) insert made in the  $\beta\text{E}$ – $\beta\text{F}$  loop of the large subunit, between residues G98 and K99, and the roughly equidistant disposition of these sites about the external surface of the particle. The preparation and chemistry of this virus has been described elsewhere (11). As observed previously with maleimides, this mutant virus displayed much greater reactivity, in this case loading fluorescein bromoacetamide to the maximum value of 60 per particle within 12 h (Figure 1). On the basis of these results, stilbene bromoacetamide **3** was used to derivatize both wild-type and mutant CPMV at a reagent:protein ratio of 2000:1, to give viruses **5a** and **5b** (Scheme 1) in excellent chemical yield.

**Recognition of *trans*-Stilbene on CPMV with Blue-Fluorescent Antibody.** The addition of the monoclonal antibody 19G2 to a solution of virus **5b**, which bears stilbene groups at the designed cysteine residues on the exterior  $\beta\text{E}$ – $\beta\text{F}$  loop, gave an intense blue fluorescence under ultraviolet irradiation (Figure 3). No fluo-



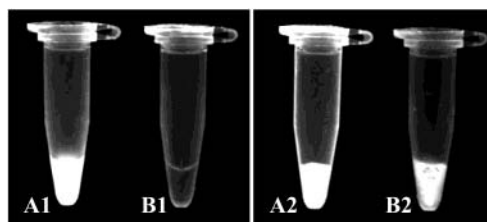


**Figure 2.** (Left) Ribbon diagram of the asymmetric unit of the CPMV coat protein, showing the two component proteins (small subunit = domain A; large subunit = domains B + C), and the  $\beta$ E- $\beta$ F loop in red. (Right) View down the 2-fold axis of the wild-type CPMV structure ( $\alpha$  carbons only), depicting the pattern created on the surface of the particle by mutational insertion between R97-G98 and K99-Y100 of the  $\beta$ E- $\beta$ F loop, shown in red.



**Figure 3.** (Top) Black-and-white photographs taken under ultraviolet illumination of the following 50  $\mu$ L samples in PBS buffer, pH 7.4: (A) virus **5b** + 19G2; (B) **5b** alone; (C) 19G2 alone; (D) VEF-Cys $\alpha$  + 19G2 (concentrations: 19G2, 1.5 mg/mL; viruses, 1.0 mg/mL). (Bottom) representative TEM pictures (negative staining with uranyl acetate) showing the binding of **5b** with 19G2. (A) **5b**. (B) **5b** + 19G2; approximately 90% of all virus particles visualized in an exhaustive examination of these samples were found in the type of small clusters shown here. (C) **5b** + 19G2, subsequently treated with **1** (10 mg/mL, approximately 3500 molar equivalents relative to viral protein, at 4  $^{\circ}$ C for 12 h). All samples were diluted to a virus concentration of 0.2 mg/mL before TEM analysis.

rescence was observed for the underivatized virus in the presence of 19G2. The relatively low binding affinity of 19G2 for the stilbene hapten (in the  $\mu$ M range) (15) precludes the chromatographic purification of such adducts. However, the interaction could be independently visualized by transmission electron microscopy (TEM) as shown in Figure 3. The polyvalent display of hapten on the virus and the presence of two binding sites per

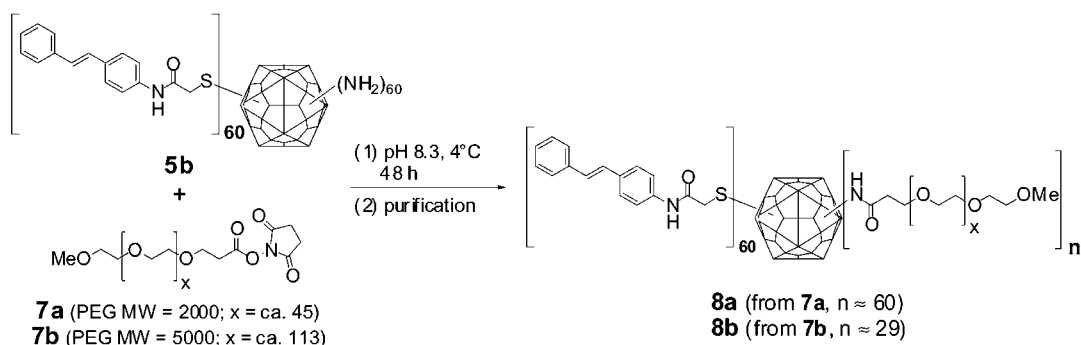


**Figure 4.** Black-and-white photographs taken under ultraviolet illumination of antibody 19G2 complexed with stilbene-decorated wild-type CPMV (A1) **4** + 19G2; (B1) **5a** + 19G2; (A2) denatured **4** + 19G2; (B2) denatured **5a** + 19G2. Sample volumes and conditions were as described in Figure 3.

immunoglobulin gave rise to clusters of virus particles formed only in the presence of both components; the addition of soluble, monomeric stilbene **1** breaks up these clusters. The blue fluorescent response was similarly observed for four other cysteine-containing mutants (11) of CPMV derivatized with reagent **2** (data not shown).

The basic function of the outer protein shell is to protect the fragile nucleic acid genome from physical, chemical, or enzymatic damage (18). While small molecules can pass through the capsid of CPMV easily, it should be difficult for proteins or other big molecules to reach the virus interior. The ability of blue-fluorescent antibodies to recognize *trans*-stilbene on the exterior CPMV surface thereby offers a convenient way to distinguish between attachments made to the inside vs the outside surface of CPMV, when the site of attachment is less certain than it is for **5b**.

Incubation of virus **4** with antibody 19G2 resulted in strong blue fluorescence under UV irradiation (Figure 4), confirming that NHS ester **1** reacts to a significant extent at exterior residues, consistent with the expected site of attachment (K38). Furthermore, the antibody should not give a strong positive response when presented with a hapten structure that is accessible only in a transient sense by virtue of an energetically unfavorable dynamic

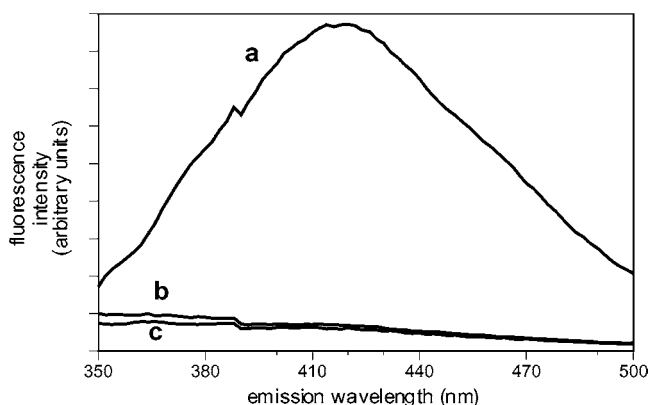
**Scheme 2. Preparation of Virus–Stilbene-PEG Conjugates**

conformational change, unless the antibody-hapten binding energy (relatively weak in these systems) (15) is sufficient to overcome the conformational cost. In other words, residues recognized by this method as being on the virus exterior are likely to reside there in the most stable solution-phase structures of the capsid. In contrast, assays that involve a rapid and irreversible chemical reaction can more easily intercept an energetically disfavored subpopulation of conformers (12).

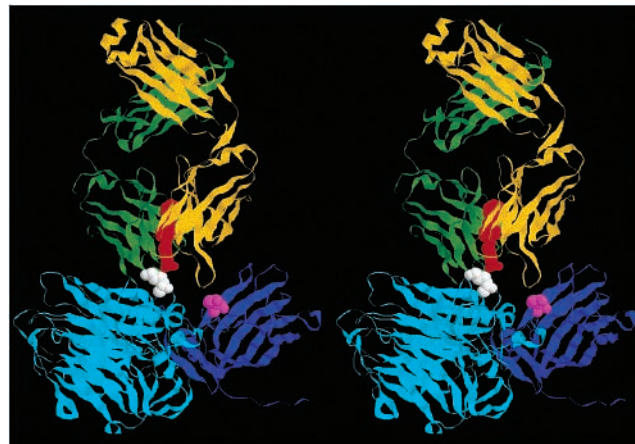
As shown in Figure 4, the S-alkylated product from wild-type CPMV, **5a**, was not recognized by the antibody, and thus the reactive residues are assigned to a position *inside* the particle. This is consistent with the X-ray crystal structure of CPMV, in which no cysteines are visibly exposed on the exterior surface. In the case of both **4** and **5a**, denaturing the derivatized virus allows for antibody binding and strong fluorescence with 19G2 (Figure 4). The capsid is thereby found to be sufficiently permeable to allow small molecules such as **2** and **3** to diffuse through, but the antibody is too large to do likewise.

**Position-Dependent Blocking of Antibody–Antigen Interaction.** Many therapeutic proteins have been coupled to poly(ethylene oxide) [commonly referred to as poly(ethylene glycol), or PEG] in order to prolong their circulating lifetimes and increase their potencies *in vivo* (19, 20). PEG attachment is also commonly used to passivate the immune response toward proteins (21, 22) and viruses (23). Here we show that PEGylation can be used to block the binding of a blue fluorescent antibody to its antigen. The decoration of CPMV with PEG produces substantial changes in the physical and chemical properties of the virus, which will be discussed elsewhere (24).

The cysteine-added mutants we have described thus far all retain the natural chemical reactivity of exposed lysines, and especially K38 (11). Derivatization of **5b** at lysine with commercially available *N*-hydroxysuccinimide PEG reagents **7a** and **7b** afforded virus conjugates **8a** and **8b**, as shown in Scheme 2. In this case, the virus products were purified by filtration through size-exclusion resin to remove the excess PEG reagent, followed by sucrose gradient sedimentation, ultracentrifugation pelleting, and resuspension in 0.1 M potassium phosphate buffer (pH 7.0). From previous studies under identical conditions with wild-type CPMV, we have established that approximately 60 copies of PEG-2000 are attached per virion with **7a**, and approximately 29 copies of PEG-5000 are attached per virion in the presence of **7b** (24). The products here were shown to be composed of intact virus particles by their sedimentation properties in sucrose gradients as well as by electron microscopy (data not shown). Upon incubation with 19G2, neither PEG-decorated virus showed fluorescence under



**Figure 5.** Steady-state fluorescence emission spectra with excitation at 327 nm: (a) **5b** + 19G2; (b) **8a** + 19G2; (c) **8b** + 19G2. For all samples, concentrations were 1.5 mg/mL in antibody and 1.0 mg/mL in virus.



**Figure 6.** Stereoimage of the 19G2  $F_{ab}$  fragment (green and orange) containing hapten **1** (red) docked with the CPMV coat protein asymmetric unit (small subunit in dark blue; large subunit in light blue), as described in the text. The orientation is chosen to minimize the distance between the carboxylate group of **1** and the site of VEFCys $\alpha$  mutation (residue 99 of the large subunit, shown in white). Lysine 38 of the small subunit is shown in purple.

UV irradiation (Figure 5), presumably because the PEG chains block the binding of antibody with the attached *trans*-stilbene on the virus.

An appreciation for the qualitative aspects of the interactions between antibody and a virus–hapten conjugate can be obtained by considering the crystal structure of the 19G2–**1** complex (involving only the antibody  $F_{ab}$  fragment (Protein Data Bank structure 1FL3, [www.rcsb.org/pdb/](http://www.rcsb.org/pdb/)). The hapten is bound in the expected planar, *trans*-configuration with the long axis directed toward the center of the mAb and the carboxy-terminated



linker at its periphery. Most of the side chains adjacent to the stilbene moiety are nonpolar, forming an uncharged, hydrophobic pocket (15). While not intended to be a detailed model, docking of this structure with that of the wild-type CPMV asymmetric unit, as seen in Figure 6, shows that the stilbene unit of **5b** should be easily accessible to the binding pocket of 19G2. The structures are positioned such that the carboxylic acid group of the hapten **1** (in red) is as close as possible to the location of the GGCGG insert (residue 99 of the large subunit, shown in white). Note the close approach of these two fragments, suggesting that the stilbene-decorated virus should suffer few steric barriers to forming a complex with the antibody. Furthermore, the attachment of a PEG chain to lysine 38 (purple) is likely to result in an unfavorable interaction with a loop of the antibody structure (marked with an arrow) that overhangs this position, preventing antigen–antibody binding, as observed.

## CONCLUSIONS

We have shown here that decoration of CPMV by bromoacetamide reagents is specific and selective for displayed cysteine residues, with the degree of loading controlled by reaction conditions in a predictable manner. It is noteworthy that these electrophilic reagents are quite hydrophobic, demonstrating that the virus survives the attachment of such species and the use of aqueous–organic cosolvent mixtures. Cysteine residues on the wild-type capsid are at least 6-fold less reactive than those displayed on the inserted loop of the VEF<sub>Cys</sub> mutant. Most importantly, the blue fluorescent antibody can be employed as a convenient probe of the location of its stilbene hapten on a nanoparticle scaffold, and that this interaction can be inhibited by the site-directed attachment of a PEG chain. These tools and insights will be employed in the design of virus-displayed antigens and other species.

## ACKNOWLEDGMENT

We thank The Skaggs Institute of Chemical Biology and the David and Lucille Packard Foundation (Interdisciplinary Science Program) for support of this work. Q.W. and K.S.R. are Skaggs Postdoctoral Fellows. We are grateful to Dr. L. Tang for assistance with representations of the CPMV–antibody interactions shown in Figure 6.

## LITERATURE CITED

- (1) Goldbach, R., and van Kammen, A. (1985). Structure replication and expression of the bipartite genome of cowpea mosaic virus. In *Molecular Plant Virology* (J. Davies, Ed.) pp 83–120, CRC Press, Boca Raton.
- (2) Spall, V. E., Porta, C., Taylor, K. M., Lin, T., Johnson, J. E., and Lomonosoff, G. P. (1998). Antigen Expression on the Surface of a Plant Virus for Vaccine Production. In *Engineering Crops for Industrial End Uses* (P. R. Shewry, J. A. Napier, and P. Davis, Eds.) pp 35–46, Portland Press, London.
- (3) Lin, T., Chen, Z., Usha, R., Stauffacher, C. V., Dai, J.-B., Schmidt, T., and Johnson, J. E. (1999). The Refined Crystal Structure of Cowpea Mosaic Virus at 2.8 Å Resolution. *Virology* 265, 20–34.
- (4) Wang, Q., Lin, T., Tang, L., Johnson, J. E., and Finn, M. G. (2002). Icosahedral Virus Particles as Addressable Nanoscale Building Blocks. *Angew. Chem., Int. Ed.* 41, 459–462.
- (5) Lin, T., Porta, C., Lomonosoff, G., and Johnson, J. E. (1996). Structure-Based Design of Peptide Presentation on a Viral Surface: the Crystal Structure of a Plant/Animal Virus Chimera at 2.8 Å Resolution. *Fold. Des.* 1, 179–187.
- (6) Porta, C., Spall, V. E., Lin, T., Johnson, J. E., and Lomonosoff, G. P. (1996). The Development of Cowpea Mosaic Virus as a Potential Source of Novel Vaccines. *Intervirology* 39, 79–84.
- (7) Johnson, J., Lin, T., and Lomonosoff, G. (1997). Presentation of Heterologous Peptides on Plant Viruses. *Annu. Rev. Phytopathol.* 35, 67–86.
- (8) Taylor, K. M., Lin, T., Porta, C., Mosser, A., Giesing, H., Lomonosoff, G. P., and Johnson, J. E. (2000). Influence of 3-Dimensional Structure on the Immunogenicity of a Peptide Expressed on the Surface of a Plant Virus. *J. Mol. Recogn.* 13, 71–82.
- (9) Lomonosoff, G. P., and Hamilton, W. D. O. (1999). Cowpea Mosaic Virus-Based Vaccines. *Curr. Top. Microbiol. Immun.* 240, 177–189.
- (10) Wang, Q., Kaltgrad, E., Lin, T., Johnson, J. E., and Finn, M. G. (2002). Natural Supramolecular Building Blocks: Wild-Type Cowpea Mosaic Virus. *Chem. Biol.* 9, 805–811.
- (11) Wang, Q., Lin, T., Johnson, J. E., and Finn, M. G. (2002). Natural Supramolecular Building Blocks: Cysteine-Added Mutants of Cowpea Mosaic Virus. *Chem. Biol.* 9, 813–819.
- (12) Johnson, J. E., and Speir, J. A. (1997) Quasi-equivalent viruses: A paradigm for protein assemblies. *J. Mol. Biol.* 269, 665–675.
- (13) Bothner, B., Dong, X. F., Bibbs, L., Johnson, J. E., and Siuzdak, G. (1998). Evidence of Viral Capsid Dynamics Using Limited Proteolysis and Mass Spectrometry. *J. Biol. Chem.* 273, 673–676.
- (14) Speir, J. A., Munshi, S., Wang, G., Baker, T. S. and Johnson, J. E. (1995) Structures of the native and swollen forms of cowpea chlorotic mottle virus determined by X-ray crystallography and cryo-electron microscopy. *Structure* 3, 63–68.
- (15) Simeonov, A., Matsushita, M., Juban, E. A., Thompson, E. H. Z., Hoffman, T. Z., Beuscher, A. E. I., Taylor, M. J., Wirsching, P., Rettig, W., McCusker, J. K., Stevens, R. C., Millar, D. P., Schultz, P. G., Lerner, R. A., and Janda, K. D. (2000). Blue-Fluorescent Antibodies. *Science* 290, 307–313.
- (16) Chen, D. W., Beuscher, A. E., Stevens, R. C., Wirsching, P., Lerner, R. A., and Janda, K. D. (2001). Preparation of stilbene-tethered nonnatural nucleosides for use with blue-fluorescent antibodies. *J. Org. Chem.* 66, 1725–1732.
- (17) The designation of this compound as the 6-substituted isomer corresponds to common usage by vendors and in other publications; the structure is more properly described as the 4-substituted isomer. The use of this reagent in bioconjugation is described in Heiman, D. F., Yang, H. H. Y., and Flentge, C. A. (1986) Eur. Pat. Appl., EP199042.
- (18) Cann, A. J. (1997) *Principles of molecular virology*, pp 22–49, 2nd ed., Academic Press, New York
- (19) Zalipsky, S. (1995). Chemistry of poly(ethylene glycol) conjugates with biologically active molecules. *Adv. Drug Delivery Rev.* 16, 157–182.
- (20) Abuchowski, A., Van Es, T., Palcank, N. C., and Davis, F. F. (1977). Alteration of immunological properties of bovine serum albumin by covalent attachment of poly(ethylene glycol). *J. Biol. Chem.* 252, 3578–3581.
- (21) Zalipsky, S., and Lee, C.-H. (1992). Poly(Ethylene Glycol) Chemistry: Biotechnical and Biomedical Applications (J. M. Harris, Ed.) pp 347–367, Plenum Press, New York.
- (22) Delgado, C., Francis, G. E., and Fisher, D. (1992). The uses and properties of PEG-linked proteins. *Crit. Rev. Ther. Drug Carrier Syst.* 9, 249–304.
- (23) O’Riordan, C. R., Lachapelle, A., Delgado, C., Parkes, V., Wadsworth, S. C., Smith, A. E., and Francis, G. E. (1999). PEGylation of Adenovirus with Retention of Infectivity and Protection from Neutralizing Antibody in Vitro and in Vivo. *Hum. Gene Ther.* 10, 1349–1358.
- (24) Raja, K. S., Wang, Q., Gonzalez, M., Manchester, M., Johnson, J. E., Finn, M. G., unpublished results.



# Tat-Conjugated Synthetic Macromolecules Facilitate Cytoplasmic Drug Delivery To Human Ovarian Carcinoma Cells

Aparna Nori,<sup>†</sup> Keith D. Jensen,<sup>†</sup> Monica Tijerina,<sup>†</sup> Pavla Kopečková,<sup>†,‡</sup> and Jindřich Kopeček<sup>\*,‡</sup>

Department of Pharmaceutics and Pharmaceutical Chemistry/CCCD, and Department of Bioengineering, University of Utah, Salt Lake City, Utah 84112. Received August 1, 2002;  
Revised Manuscript Received October 3, 2002

We have synthesized N-(2-hydroxypropyl)methacrylamide (HPMA) copolymer–cell penetrating peptide Tat conjugates and evaluated their subcellular distribution in A2780 human ovarian carcinoma cells by confocal fluorescence microscopy and subcellular fractionation. Our data indicate the transport of these conjugates by a single Tat molecule to both the cytoplasm and nucleus via a nonendocytotic and concentration independent process. The uptake was observed to occur within 3 min, as confirmed by live cell microscopy. In contrast, HPMA copolymers lacking the Tat peptide were internalized solely by endocytosis. For the first time, Tat-mediated cytoplasmic delivery of a polymer bound anticancer drug, doxorubicin, was also demonstrated. These findings establish the feasibility of overcoming major cellular and subcellular obstacles to intracellular macromolecular delivery and hold great promise for the development of polymer-based systems for the cytoplasmic delivery of therapeutic molecules.

## INTRODUCTION

Water-soluble polymers such as N-(2-hydroxypropyl)methacrylamide (HPMA)<sup>1</sup> copolymers are frequently employed as drug carriers because of their ability to improve the solubility of hydrophobic compounds, reduce nonspecific toxicity, and increase the therapeutic index of low molecular weight anticancer drugs (1, 2). Anticancer drugs bound to water-soluble polymeric carriers such as HPMA copolymers have exhibited decreased systemic toxicity, a result of the altered biodistribution of polymer-bound drugs as compared to free drugs. Further, cationic polymers poly(L-lysine) and polyethyleneimine are being increasingly investigated as nonviral vectors for nucleic acids and oligonucleotides due to the immunogenicity and toxicity problems associated with conventional viral vectors.

Binding a drug or nucleic acid to a polymer directs the conjugate to the lysosomes by endocytosis. Due to the impermeable nature of the lysosomal membrane, such vesicular entrapment poses a hindrance to molecules expressing biological activity in the cytoplasm or nucleus, thus necessitating the endosomal escape of the polymer conjugate. Drug release from the lysosomes can be facilitated by introducing drug–polymer linkages such as the tetrapeptide spacer glycylphenylalanylleucylglycine (GFLG), which are stable in the bloodstream but susceptible to enzymatic cleavage in the lysosomes (3). However, this approach cannot be implemented for the delivery of therapeutic molecules such as oligonucleotides

or proteins, as these molecules not only lack inherent membrane penetrating capabilities but are susceptible to both the acidic environment of the lysosomes and enzymatic degradation (4).

Recently, the ability of several peptides, called cell penetrating peptides or protein transduction domains (PTDs), to translocate across the cell membrane into the cytoplasm in an energy-independent (5), receptor-less manner has been discovered (6). These peptides which have been successfully employed as vectors for cytoplasmic and nuclear macromolecular transport include synthetic/chimeric peptides and protein derived peptides such as the *Drosophila* homeotic transcription factor ANTP, the herpes simplex virus type-1 transcription factor VP22 and the Tat peptide from the HIV-1 transactivating factor Tat. While the Tat protein itself has been proven to be taken up rapidly by cells in culture (7, 8), shorter sequences such as the Tat peptide (Y<sub>47</sub>GRKKRRQRRR<sub>57</sub>) have also been shown to transport full-length proteins such as a  $\beta$ -galactosidase–Tat fusion protein across not only the plasma membrane in different tissues but also the blood brain barrier, in mice (9). Additionally, the Tat PTD has successfully ferried derivatized nanoparticles (45 nm) into progenitor cells, thus allowing their facile detection by magnetic resonance imaging (10). Tat peptide containing peptide-based chelates of technetium-99m and rhenium have also been efficiently delivered to the cytoplasm and nucleus of living human cells (11). Both the Tat and ANTP peptides have shown prowess in delivering 2'-O-methyl phosphorothioate antisense oligonucleotides to the cytoplasm and nucleus, resulting in an increase in pharmacological activity without an accompanying loss in specificity of the antisense oligonucleotides (12).  $\lambda$  bacteriophages expressing the Tat peptide on their surface have also been shown to deliver DNA intracellularly (13). Recently, 200 nm liposomes bearing a Tat peptide-modified surface (500 Tat peptide molecules per liposome) were transported intracellularly in an energy independent fashion (14). Additionally, the Tat peptide has facilitated the

\* Corresponding author. Phone: (801) 581-4532. Fax: (801)-581-7848. E-mail: Jindrich.Kopecek@m.cc.utah.edu.

<sup>†</sup> Department of Pharmaceutics and Pharmaceutical Chemistry/CCCD.

<sup>‡</sup> Department of Bioengineering.

<sup>1</sup> Abbreviations: AIBN, 2,2'-azobis-isobutyronitrile; DMF, dimethylformamide; DMSO, dimethyl sulfoxide; Dox, Doxorubicin; HPMA, N-(2-hydroxypropyl)methacrylamide; MWCO, molecular weight cut off; SAMSA, 5-((2-S-acetylmercapto)succinoyl)-amino fluorescein; SMCC, succinimidyl 4-(N-maleimidomethyl)cyclohexane-1-carboxylate; TR, Texas Red.

uptake of cysteine-tagged antibody fragments in a compartmentalized manner; however, this suggests that the transport capabilities of the Tat peptide may be limited by size or the biological activity of the cargo (15).

We hypothesized that attachment of the Tat peptide to a water-soluble synthetic macromolecule will result in cytoplasmic delivery of the conjugate. To test this hypothesis, we synthesized several HPMA copolymer-Tat peptide conjugates and evaluated their internalization and subcellular trafficking in A2780 human ovarian carcinoma cells by confocal fluorescence microscopy and subcellular fractionation. We showed that these conjugates were localized to the cytoplasm and nucleus by a Tat-facilitated pathway as opposed to conjugates without the Tat peptide, which accumulated only in endocytotic vesicles.

#### EXPERIMENTAL PROCEDURE

**Synthesis of Polymer Precursors.** The HPMA copolymer containing amino groups in the side chains (**P-NH<sub>2</sub>**, where P represents the polymeric backbone), was prepared by copolymerization of HPMA and 3-(aminopropyl)methacrylamide hydrochloride (MA-AP), using 2,2'-azo-bis-isobutyronitrile (AIBN, Fluka) as the initiator and 3-mercaptopropionic acid (MPA) as the chain transfer agent (molar ratio 93:7.5:0.5, respectively) in methanol (10 wt % monomers in the mixture) at 50 °C for 24 h. The polymer was precipitated into ether, extensively dialyzed (MWCO 6–8 kDa), and freeze-dried.

The maleimide containing HPMA copolymer (**P-MAL**) was obtained by reaction of 160 mg P-NH<sub>2</sub> (0.070 mmol NH<sub>2</sub> groups) with 46.8 mg (0.140 mmol) of succinimidyl 4-(N-maleimidomethyl) cyclohexane-1-carboxylate (SMCC, Molecular Probes) and 22 mg (0.18 mmol) of diisopropylethylamine in DMF at room temperature for 12 h with stirring. The solvent was removed in vacuo, and the polymer was precipitated into acetone.

**Synthesis of Polymer Conjugates.** *P-Tat-FITC.* Tat-containing HPMA copolymer (P-Tat-FITC) was obtained by reaction of 40 mg (0.015 mmol maleimide groups) of P-MAL in 0.8 mL PBS buffer (pH 7.2), with 11.4 mg (0.0052 mmol) of Tat-FITC (Emory University Microchemical Facility, Atlanta) dissolved in 0.2 mL PBS (under nitrogen). The reaction mixture was stirred overnight in dark at room temperature. Five microliters of mercaptoethanol was added to inactivate the residual maleimide groups, and the polymer was then separated on a PD-10 column in PBS. P-Tat-FITC was isolated by dialysis (MWCO 6–8 kDa) against DI water and freeze-dried.

*P(TR)-Tat(FITC).* Double-label HPMA copolymer-Tat conjugate P(TR)-Tat(FITC) containing TR-labeled polymer backbone and Tat-FITC was prepared in several steps. HPMA copolymer containing TR and NH<sub>2</sub> (**P-TR-NH<sub>2</sub>**) was obtained by reaction of 100 mg P-NH<sub>2</sub> (0.044 mmol NH<sub>2</sub>) with 5 mg Texas Red succinimidyl ester (Molecular Probes) (0.0061 mmol) and 6 mg diisopropylethylamine (8  $\mu$ L) in 0.8 mL DMSO with stirring for 3 h. The mixture was then diluted with ethanol/H<sub>2</sub>O (1:1, 5 mL) and dialyzed against water acidified with dilute HCl (pH 3) followed by extensive dialysis against water. The content of TR in the freeze-dried polymer determined spectrophotometrically ( $\epsilon = 1.16 \times 10^5 \text{ M}^{-1} \text{ cm}^{-1}$ ,  $\lambda_{\text{max}}$  586 nm) in MeOH was 0.055 mmol/g. The residual amino groups present in P-TR-NH<sub>2</sub> were reacted with SMCC to yield a polymer containing both maleimide groups as well as TR. This polymer was treated with Tat-FITC to form a thioether linkage between the Tat and the polymer using similar procedures as described above.

*P-GFLG-Dox-Tat.* Dox containing HPMA copolymer-Tat conjugate (P-GFLG-Dox-Tat) was synthesized in several steps. First, the Dox containing monomer N-methacryloylglycylphenylalanylleucylglycylidoxorubicin (**MA-GFLG-DOX**) was synthesized (16) and copolymerized with HPMA and MA-AP (molar ratio 90.5:2.5:7) using AIBN as the initiator in methanol (12.5 wt % monomers in the mixture) at 50 °C for 24 h. The volume of the polymerization mixture was reduced by half, and the product precipitated in acetone/ether (3:1). The polymer was first dialyzed against 50% ethanol/H<sub>2</sub>O (containing 0.1% HCl) and then against DI water. The polymer isolated by freeze-drying contained 0.38 mmol/g (6.1 mol %) of the amino group containing side chains as determined by the Ninhydrin assay. The content of Dox determined spectrophotometrically ( $\epsilon = 11\,000 \text{ M}^{-1} \text{ cm}^{-1}$ ) in water was 0.11 mmol Dox/g (1.8 mol %; 6.4 wt %). The HPMA copolymer containing both Dox and maleimide groups (**P-Mal-Dox**) was then obtained by modification of amine groups with SMCC as described above. To purify the conjugate from free Dox, the polymer was purified twice on a Sephadex LH-20 column using MeOH/DMSO/CH<sub>3</sub>COOH (89:10:1) solvent mixture. The polymer was isolated after MeOH evaporation and precipitation in acetone/ether mixture. In the last step, the Tat peptide was conjugated to P-Mal-Dox via a thioether linkage as described above. The product was purified by dialysis and isolated by freeze-drying.

*Control Polymers.* The control polymers P-FITC and P-GFLG-Dox lacking the Tat peptide were synthesized as described (16, 17).

**Characterization of Polymer Precursors and Polymer Conjugates.** The polymer precursor P-NH<sub>2</sub> contained 6.6 mol % (0.44 mmol/g) of the amino group containing side chains as determined by the Ninhydrin assay. The molecular weight determined by size exclusion chromatography (SEC) on a Superose 6 (HR 10/30) column, AKTA system, PBS buffer was 26 000 Da;  $M_w$ :  $M_n$  = 1.5 and  $dn/dc = 0.156$ , using MiniDawn laser light scattering detector (Wyatt Technology, Santa Barbara).

The maleimide content of the polymer precursor **P-MAL** as determined by the SAMSA assay (Molecular Probes) was 0.37 mmol/g. The polymer did not contain any residual amine groups as determined by the Ninhydrin assay.

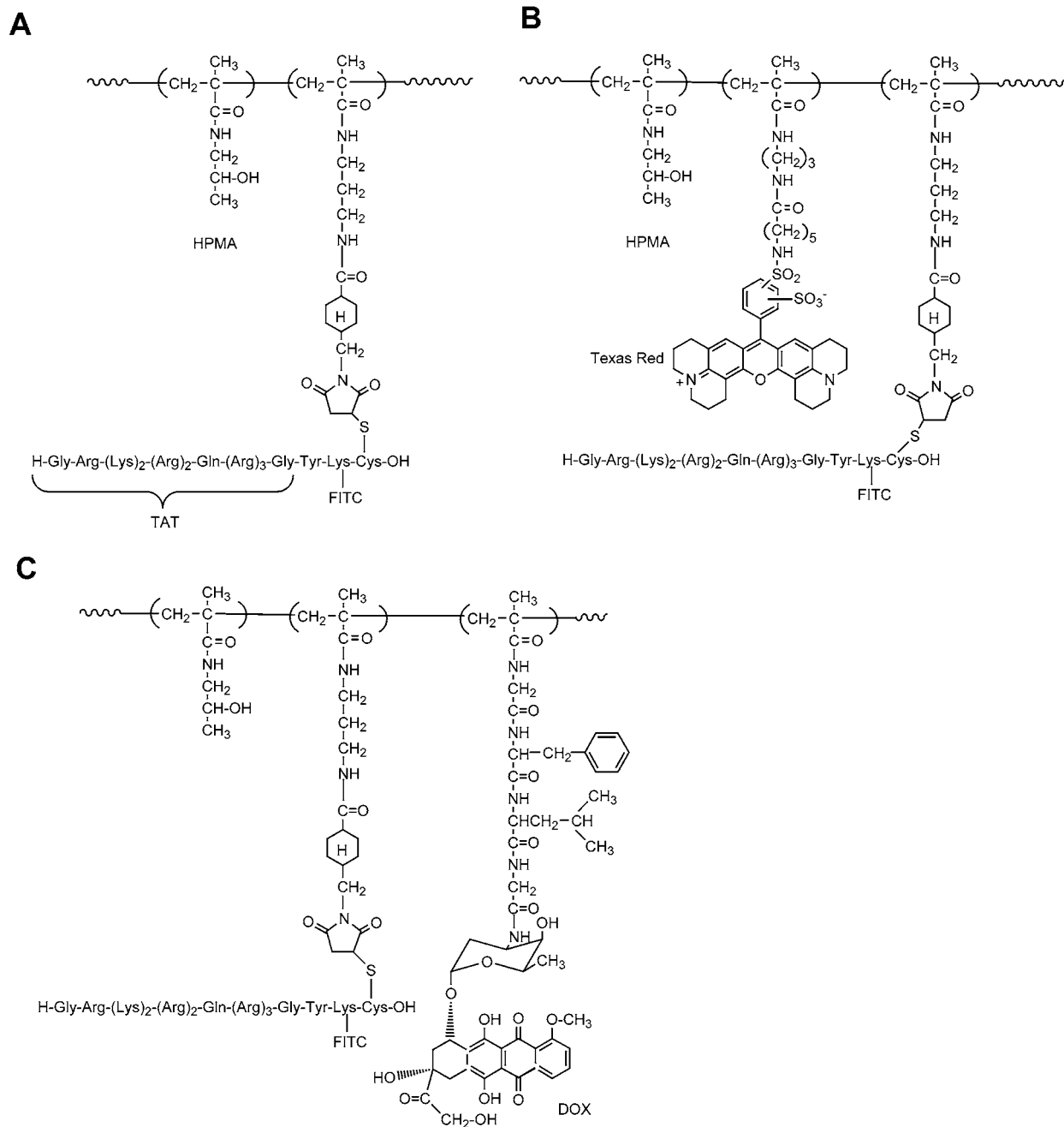
*P-Tat-FITC.* The Tat-FITC content in the polymer was determined by spectrophotometric determination of FITC ( $\epsilon = 80\,000 \text{ M}^{-1} \text{ cm}^{-1}$ ,  $\lambda_{\text{max}}$  500 nm) in 0.1 M borate buffer (pH 9.2).

*P(TR)-Tat(FITC).* The TR and Tat-FITC contents in the final polymer were determined spectrophotometrically at  $\lambda_{\text{max}} = 588 \text{ nm}$ ,  $\epsilon = 1.16 \times 10^5 \text{ M}^{-1} \text{ cm}^{-1}$  and  $\lambda_{\text{max}} = 504 \text{ nm}$ ,  $\epsilon = 80\,000 \text{ M}^{-1} \text{ cm}^{-1}$ , respectively.

*P-GFLG-Dox-Tat.* The content of Dox and Tat-FITC in this polymer was measured by two methods: (a) UV spectra in alkaline conditions (0.01 M NaOH), where the  $\lambda_{\text{max}}$  of Dox shifts to 590 nm and can be separated from FITC ( $\lambda_{\text{max}} = 500 \text{ nm}$ ); (b) amino acid analysis after acidic hydrolysis (Glu, Tyr).

**Cell Lines.** The A2780 human ovarian carcinoma cell line obtained from Dr. T. C. Hamilton (Fox Chase Cancer Center) was cultured in RPMI 1640 media (Sigma) supplemented with 10% fetal bovine serum (FBS, Hyclone) and 10  $\mu$ g/mL insulin and kept at 37 °C in a humidified atmosphere of 5% CO<sub>2</sub>.

**Confocal Fluorescence Microscopy.** For all studies, 500 000 A2780 cells were seeded on previously sterilized glass coverslips in 35 mm dishes (Becton Dickinson) 24 h before incubation to reach 90% confluence.



**Figure 1.** Structures of HPMA copolymer Tat conjugates (A) P-Tat-FITC, (B) P(TR)-Tat(FITC), and (C) P-GFLG-Dox-Tat.

For live microscopy (17), the cells were cultured in MEM Eagle media (Sigma) without phenol red, buffered with 0.25 mM HEPES (Sigma), containing 10% FBS and 0.292 mg/mL L-glutamine (Hyclone) in open air. A BioRad MRC 1024 confocal system with a krypton-argon laser, and a Nikon Diaphot microscope (100 X plan-apo objective, NA = 1.3, oil; for FITC, excitation = 488 nm, emission = 515 nm long pass filter) was used. For all fixed cell microscopy studies, cells were washed with DPBS after incubation with the polymer conjugates, fixed with 3% paraformaldehyde for 20 min at room temperature, mounted with SlowFade Light antifade medium, and sealed. In case of the nuclear localization study, cells were first incubated with 7.3  $\mu$ M P-Tat-FITC and then permeated with 0.1% Triton-X (Sigma). They were then treated with RNase in 2X SSC buffer (Sigma) at 37 °C for 20 min, followed by incubation with 1  $\mu$ M nuclear marker propidium iodide (Molecular Probes). Time de-

pendence studies were conducted by incubating cells with 7.3  $\mu$ M P-Tat-FITC for different time periods from 5 min to 1 h. For the concentration dependence studies, cells were incubated with concentrations ranging from 1.8 to 18  $\mu$ M P-Tat-FITC for 1 h at 37°C.

For all studies, the cells were imaged on a Zeiss (Thornwood, NY) LSM 510 confocal imaging system with an Axioplan 2 microscope (100 $\times$  plan-apo objective, NA = 1.4, oil) and an argon laser. (FITC, excitation = 488 nm, emission = 505 nm long-pass filter; propidium iodide, excitation = 543 nm, emission = 650 nm long-pass filter; Texas Red and Rhodamine, excitation = 543 nm, emission = 560 nm long-pass filter). The settings for all the confocal systems were adjusted so that control cells always yielded dark images.

**Subcellular Fractionation.** Percoll was used as the separation medium for subcellular fractionation. Ten million A2780 cells were cultured in 75 cm<sup>2</sup> flasks for 24



h prior to exposure to polymer–Tat conjugates. Cells were exposed to the conjugate P(TR)-Tat(FITC) for 4 h at 37 °C and then treated to the procedure as previously described(21) to obtain the lysosomal, plasma membrane, cytoplasmic and nuclear fractions. Fluorescence of FITC in each of these subcellular fractions was analyzed with an LS 55 luminescence spectrometer (Perkin-Elmer) (excitation-495 nm, emission-518 nm) and normalized to the protein content of each fraction (Coomassie Plus Protein Assay, Pierce). The fluorescence per microgram of protein associated with each fraction was expressed as a percentage of the total fluorescence per microgram of all fractions.

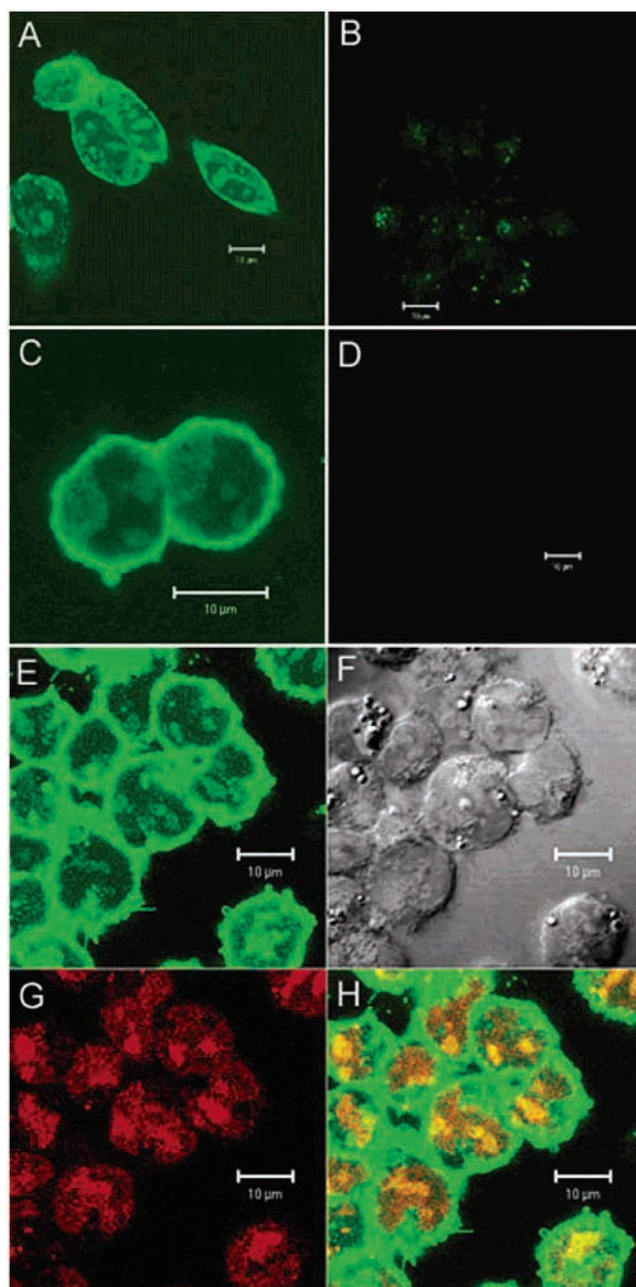
## RESULTS AND DISCUSSION

Several fluorescently labeled HPMa copolymer–Tat conjugates were synthesized by reacting the Tat peptide [H-Gly-Arg-(Lys)<sub>2</sub>-(Arg)<sub>2</sub>-Gln-(Arg)<sub>3</sub>-Gly-Tyr-Lys(FITC)-Cys-OH] with maleimide containing HPMa copolymer to form a thioether linkage (Figure 1). The Tat-FITC content in the P-Tat-FITC polymer as determined by UV spectroscopy was 0.038 mmol/g (one Tat peptide molecule per chain), indicating 40% binding efficiency of the Tat peptide to the polymer backbone. The double-label conjugate P(TR)-Tat(FITC) contained 0.034 mmol/g of TR and 0.056 mmol/g Tat-FITC. The content of Dox and Tat-FITC in the Dox containing HPMa copolymer–Tat conjugate P-GFLG-Dox-Tat determined by UV spectroscopy and amino acid analysis was 0.099 mmol/g (1.7 mol %) Dox and 0.064 mmol/g (1.2 mol %) Tat-FITC, respectively. The control polymer P-FITC and P-GFLG-Dox contained 0.038 mmol/g of FITC and 0.121 mmol/g of Dox, respectively, as determined by UV spectroscopy.

Confocal fluorescence microscopy of polymer–Tat conjugate P-Tat-FITC after 1 h incubation with the cells at 37 °C, exhibited powerful fluorescence associated with the plasma membrane. Diffuse fluorescence observed throughout the cell implied that the conjugate localized to the cytoplasm. Faint fluorescence in the nuclear region accompanied by areas of intense staining indicative of putative nucleolar accumulation were also seen (Figure 2A). Earlier reports demonstrate Tat-mediated transport of liposomes only into the cytoplasm (14); however, our data indicate both cytoplasmic as well as nuclear delivery of the polymer. The presence of punctate staining suggested that the conjugate was also internalized via endocytosis, which is typical of macromolecular uptake (18). In contrast, a control FITC-labeled polymer lacking the Tat peptide, P-FITC, was internalized solely by endocytosis even when high concentrations of the polymer were tested (Figure 2B).

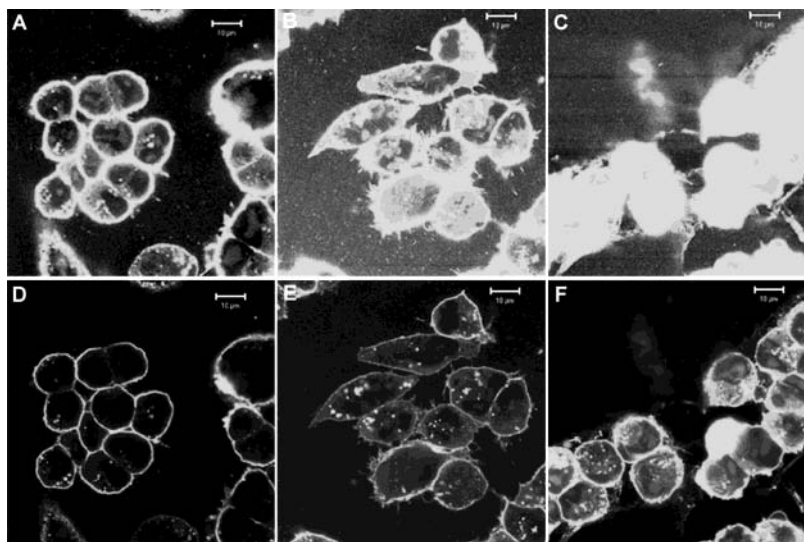
To determine whether the Tat peptide mediated transport was by endocytosis, cells were incubated with either P-Tat-FITC or P-FITC at 4 °C for 1 h. Endocytosis, an energy dependent process is blocked at 4 °C (19). The internalization of P-Tat-FITC by the Tat mediated pathway was not inhibited, suggesting an energy independent, nonendocytotic uptake process (Figure 2C). However, cells incubated with P-FITC did not exhibit any fluorescence, as the endocytotic uptake of P-FITC was suppressed (Figure 2D).

Nuclear localization was corroborated by co-incubating the cells with P-Tat-FITC and the nuclear marker propidium iodide for 1 h at 37 °C. Confocal microscopy performed by separately tracking the FITC label on the conjugate (green) and propidium iodide (red) demonstrated areas of orange-yellow staining representing co-



**Figure 2.** Subcellular trafficking of various polymer conjugates incubated with A2780 cells by confocal fluorescence microscopy. (A) HPMa copolymer–Tat conjugate (P-Tat-FITC) for 1 h at 37 °C showed intense plasma membrane, cytoplasmic, and nuclear uptake. (B) FITC-labeled polymer lacking Tat peptide (P-FITC) for 1 h at 37 °C exhibited only endocytotic vesicles. (C) P-Tat-FITC for 1 h at 4 °C demonstrated Tat-mediated nonendocytotic transport of the conjugate. (D) P-FITC for 1 h at 4 °C showed no uptake. (E) P-Tat-FITC (green), (F) DIC image, and (G) nuclear marker propidium iodide (red) for 1 h at 37 °C. (H) Colocalization of the two dyes (orange-yellow staining) implied nuclear localization. Scale bar represents 10 μm.

localization of the two dyes in the nucleus (Figure 2E–H). One possible explanation for nuclear entry of the conjugate could be the presence of a nuclear localization signal RKKRR embedded in the Tat peptide sequence (6). Similarly, cytoplasmic import was verified by treating the cells with the membrane permeant cytoplasmic marker chloromethylbenzoylamino tetramethyl rhodamine (CMTMR) and P-Tat-FITC. The FITC label on the polymer–Tat conjugate (green) and CMTMR (red) were separately tracked and were found to co-localize,



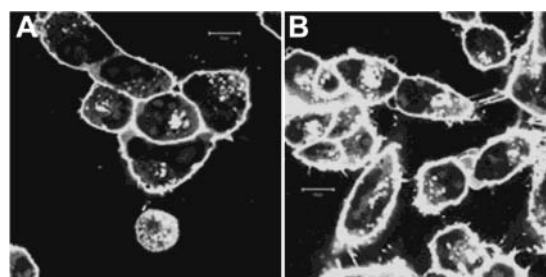
**Figure 3.** Fluorescence images of cells incubated with P-Tat-FITC after 20 min, 2 h, and 4 h. Panels A–C represent images taken at high microscope settings in order to visualize the cytoplasm and nucleus. Panels D–F are images of the same cells taken at lower settings in order to observe the plasma membrane. Scale bar represents 10  $\mu\text{m}$ .

thus confirming the cytoplasmic delivery of P-Tat-FITC (data not shown).

Recent studies have exhibited that fixing agents such as methanol, commonly employed for fixing cells in microscopy studies, lead to artificial cytoplasmic and nuclear accumulation as a consequence of membrane permeabilization (20). Microscopy of live cells, which precludes the use of fixing agents, was utilized to examine the subcellular distribution of the polymer–Tat conjugate. In agreement with data from fixed cell microscopy, cytoplasmic as well as nuclear uptake of the conjugate was observed, thus excluding the likelihood of artificial subcellular localization. Live microscopy studies also revealed internalization within 3 min, thus verifying the rapidity of the process (see movie in Supporting Information).

The time and concentration dependence of the internalization process was also investigated. Increasing incubation periods of P-Tat-FITC with the cells resulted in persistent membrane staining as well as a proportional increase in the fluorescence intensity within the cytoplasm and the nucleus, signifying augmented distribution of the conjugates with time. Images of the cells were taken at both low as well as high microscope settings in order to better visualize the changes in the plasma membrane and cytoplasm at different time points. Accumulation of the conjugate in the cytoplasm and nucleus was observed as quickly as 5 min. Endocytotic vesicles were more prominent at time points greater than 1 h as expected (Figure 3A–F). In the concentration dependent study, cells incubated with higher concentrations of P-Tat-FITC showed stronger fluorescence as compared to cells incubated with lower concentrations. Cytoplasmic and nuclear localization was observed for the entire concentration range (1.8–18  $\mu\text{M}$ ) tested, indicating concentration-independent subcellular fate (Figure 4A,B).

In the above experiments, the FITC label on the Tat peptide was traced, as the polymeric backbone was unlabeled. One concern was that subcellular proteolytic enzymes could potentially cleave the labeled Tat peptide from the polymeric backbone, resulting in the release of free, labeled Tat peptide within the cells. Thus, fluorescence in the cytoplasm and nucleus could represent the subcellular distribution of the cleaved fluorescent Tat peptide and not the polymer–Tat conjugate itself. To

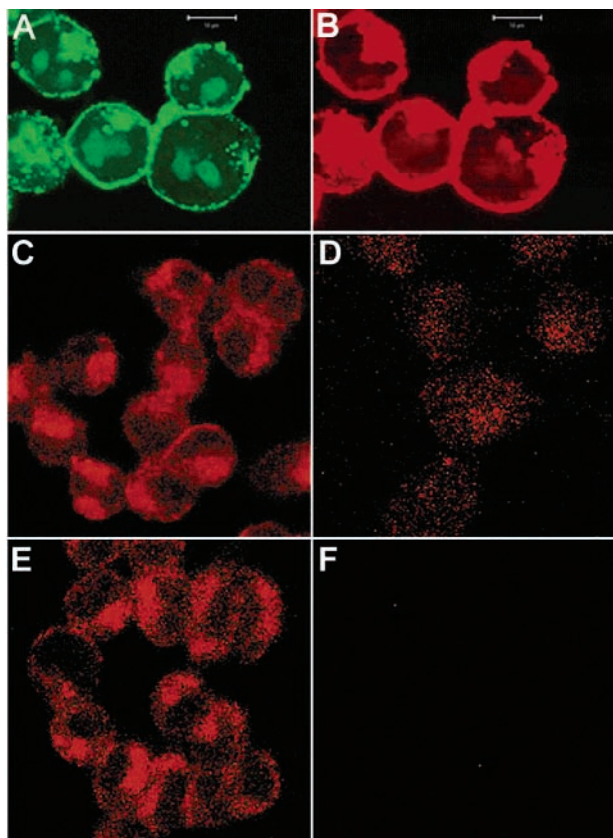


**Figure 4.** Fluorescence images of cells incubated with (A) 1.8 and (B) 18  $\mu\text{M}$  P-Tat-FITC show both cytoplasmic as well as nuclear uptake. Scale bar represents 10  $\mu\text{m}$ .

address this problem, a double-label polymer–Tat conjugate [P(TR)-Tat(FITC)] was synthesized (Figure 1B). This conjugate bore a Texas Red (TR) label attached to the polymeric backbone in addition to the FITC label on the Tat peptide. Its subcellular distribution was evaluated by fluorescence microscopy. Similar uptake patterns in the cytoplasm and nucleus were observed with both dyes, establishing the Tat mediated cytoplasmic and nuclear delivery of the polymer–Tat conjugate (Figure 5A,B).

The ability of the Tat peptide to efficiently transport a drug across the plasma membrane into the cytoplasm was also assessed. To this end, Dox containing HPMA copolymer–Tat conjugate [P-GFLG-Dox-Tat] was synthesized (Figure 1C). This system was chosen as a model for demonstrating the significant nuclear and cytoplasmic transport achieved by the Tat peptide in comparison with that of the GFLG spacer. The subcellular distribution pattern in A2780 cells was studied by tracking the inherent fluorescence of Dox by confocal microscopy. At 37  $^{\circ}\text{C}$ , cytoplasmic as well as nuclear uptake of P-GFLG-Dox-Tat was observed (Figure 5C). The intensity of the Dox fluorescence signal was significantly stronger than that of the control P-GFLG-Dox copolymer lacking the Tat peptide (Figure 5D). This enhancement in the Dox uptake has two independent components—the enzymatic hydrolysis of the lysosomally degradable spacer GFLG (3) and Tat-mediated cytoplasmic delivery of Dox; a large contribution was attributed to the Tat mediated transport, as evidenced by studies at 4  $^{\circ}\text{C}$ . The intense fluorescent signal of P-GFLG-Dox-Tat observed at 4  $^{\circ}\text{C}$



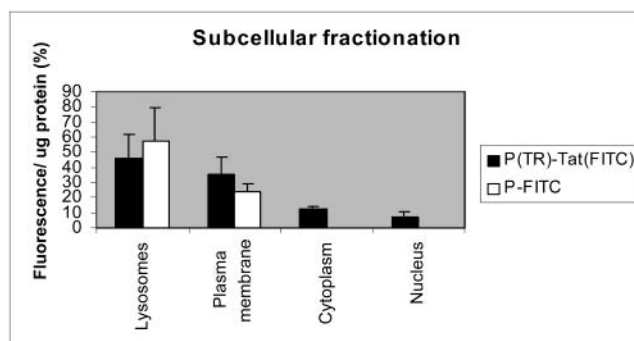


**Figure 5.** Confocal fluorescence images of A2780 cells incubated with double label HPMA copolymer–Tat conjugate (P(TR)-Tat(FITC)) for 1 h at 37 °C. The two dyes (A) FITC and (B) TR show similar distribution, confirming the intracellular delivery of the polymer–Tat conjugate. Fluorescence images of cells incubated with different polymer conjugates containing anticancer drug doxorubicin with or without Tat. (C) P-GFLG-Dox-Tat for 4 h at 37 °C showed both cytoplasmic as well as nuclear localization. (D) P-GFLG-Dox for 4 h at 37 °C showed weaker signal. (E) P-GFLG-Dox-Tat at 4 °C continued to show cytoplasmic uptake in contrast with (F) P-GFLG-Dox at 4 °C, where uptake was completely abolished. Scale bar represents 10  $\mu$ m.

proved that the Tat peptide could successfully transport polymer bound doxorubicin into the cytoplasm independent of the GFLG spacer (Figure 5E). In contrast, no signal was visible with P-GFLG-Dox, as endocytosis was inhibited, as expected (Figure 5F). The use of the P-GFLG-Dox-Tat model system clearly demonstrates the superior transducing capabilities of the Tat peptide.

The cytoplasmic and nuclear uptake of the polymer–Tat conjugate was independently verified by subcellular fractionation. The polymer–Tat conjugate mainly amassed in the lysosomal and plasma membrane fraction after 4 h incubation. Further, the conjugate localized in smaller fractions in the cytoplasm and nucleus. This subcellular distribution pattern was a significant improvement over that of the P-FITC conjugate, which localized to the lysosomes (Figure 6). Our approach utilizing subcellular fractionation in conjunction with live and fixed cell confocal microscopy shows advantages over conventional methods such as flow cytometry (which represents surface binding and not internalization) and functional assays, which may be typical only of a sub-population of cells (20).

In conclusion, these results validate our hypothesis that the Tat peptide can transport a synthetic macromolecule across the plasma membrane and deliver it into the cytosol as shown by confocal fluorescence microscopy and subcellular fractionation. Our data indicated that



**Figure 6.** Subcellular fractionation showing the subcellular distribution of the polymer–Tat conjugate and control polymer P-FITC in the different organelle fractions.

incubation of HPMA copolymer–Tat conjugate with human ovarian carcinoma cells resulted in internalization of the conjugate by two processes, namely, endocytosis and a Tat-mediated nonendocytotic process. The Tat-mediated process, characterized by intense membrane staining and cytoplasmic and nuclear uptake, was not inhibited at 4 °C, indicating an energy independent pathway. Studies performed so far have demonstrated the delivery of proteins, nanoparticles, and liposomes; however, this is the first time the Tat peptide has been shown to efficiently transport a polymer bound drug to the cytosol by a nonendocytotic pathway. These systems hold great potential, due to the immense utility of water soluble polymers as drug carriers, mainly attributed to their ability to alter the biodistribution and reduce nonspecific toxicity of low molecular weight anticancer drugs. Though the lack of cell specificity of the Tat peptide makes its applicability universal, it is this very property of the Tat peptide that also causes it to be disadvantageous. The use of water-soluble polymers which allow the facile attachment of targeting moieties such as carbohydrates and antibodies may well render a Tat containing conjugate selectively biorecognizable to a specific cell population resulting in a change in both its uptake and distribution. Further, the binding of nonimmunogenic polymers to antibodies results in the decreased immunogenicity of the antibody due to steric hindrance of the polymer conjugate (1).

Although further investigations are warranted, these results suggest that the development of polymer–Tat based cytoplasmic delivery systems, especially for gene and antisense therapy, which combine the advantages of macromolecules and exploit the unique transport capabilities of the Tat peptide, will be beneficial.

#### ACKNOWLEDGMENT

We thank Drs. E. J. King and C. Anderson for their assistance with the confocal microscopy studies. This work was supported in part by NIH Grant CA51578 from the National Cancer Institute.

**Supporting Information Available:** Movie demonstrating the intracellular uptake of the HPMA copolymer–Tat conjugate in A2780 cells by live microscopy. This material is available free of charge via the Internet at <http://pubs.acs.org>.

#### LITERATURE CITED

- (1) Putnam, D.; Kopeček, J. (1995) Polymer conjugates with anticancer activity. *Adv. Polym. Sci.* 122, 55–123.



- (2) Kopeček, J., Kopečková, P., Minko, T., and Lu, Z.-R. (2000) HPMA copolymer-anticancer drug conjugates: design, activity, and mechanism of action. *Eur. J. Pharm. Biopharm.* **50**, 61–81.
- (3) Kopeček, J., Rejmanová, P., Strohalm, J., Ulbrich, K., Říhová, B., Chytrý, V., Lloyd, J. B., and Duncan, R. (1991) Synthetic polymeric drugs. US Patent 5,037,883.
- (4) Lindgren, M., Hallbrink, H., Prochiantz, A., and Langel, U. (2000) Cell penetrating peptides. *Trends Pharmacol. Sci.* **21**, 99–103.
- (5) Vivès, E., Brodin, P., and Lebleu, B. (1997) A truncated HIV-1 Tat protein basic domain rapidly translocates through the plasma membrane and accumulates in the cell nucleus. *J. Biol. Chem.* **272**, 16010–16017.
- (6) Schwarze, S. R., Hruska, K., and Dowdy, S. F. (2000) Protein transduction: unrestricted delivery into all cells? *Trends Cell Biol.* **10**, 290–295.
- (7) Frankel, A. D., and Pabo, C. O. (1988) Cellular uptake of the Tat protein from human immunodeficiency virus. *Cell* **55**, 1189–1193.
- (8) Green, M., and Loewenstein, P. M. (1988) Autonomous functional domains of chemically synthesized human immunodeficiency virus Tat *trans*-activator protein. *Cell* **55**, 1179–1188.
- (9) Schwarze, S. R., Ho, A., Vocero-Akbani, A., and Dowdy, S. F. (1999) In vivo protein transduction: delivery of a biologically active protein into the mouse. *Science* **3**, 1569–1572.
- (10) Lewin, M., Carlesso, N., Tung, C. H., Tang, X. W., Cory, D., Scadden, D. T., et al. (2000) Tat peptide-derivatized magnetic nanoparticles allow in vivo tracking and recovery of progenitor cells. *Nat. Biotechnol.* **18**, 410–414.
- (11) Polyakov, V., Sharma, V., Dahlheimer, J. L., Pica, C. M., Luker, G. D., and Piwnica-Worms, D. (2000) Novel Tat-peptide chelates for direct transduction of technetium-99m and rhenium into human cells for imaging and radiotherapy. *Bioconjugate Chem.* **11**, 762–771.
- (12) Astriab-Fisher, A., Sergueev, D., Fisher, M., Ramsay Shaw, B., and Juliano, R. L. (2002) Conjugates of antisense oligonucleotides with the Tat and Antennapedia cell-penetrating peptides: Effects on cellular uptake, binding to target sequences, and biologic actions. *Pharm. Res.* **19**, 744–754.
- (13) Eguchi, A., Akuta, T., Okuyama, H., Senda, T., Yokoi, H., Inokuchi, H. et al. (2001) Protein transduction domain of HIV-1 Tat protein promotes efficient delivery of DNA into mammalian cells. *J. Biol. Chem.* **276**, 26204–26210.
- (14) Torchilin, V. P., Rammohan, R., Weissig, V., and Levchenko, T. S. (2001) Tat peptide on the surface of liposomes affords their efficient intracellular delivery even at low temperature and in the presence of metabolic inhibitors. *Proc. Natl. Acad. Sci. U.S.A.* **98**, 8786–8791.
- (15) Niesner, U., Halin, C., Lozzi, L., Günthert, M., Neri, P., Wunderli-Allenspach, H. et al. (2002) Quantitation of the tumor-targeting properties of antibody fragments conjugated to cell-permeating HIV-1 TAT peptides. *Bioconjugate Chem.* **13**, 729–736.
- (16) Ulbrich, K., Šubr, V., Strohalm, J., Plocová, D., Jelínková, M., and Říhová, B. (2000) Polymeric drugs based on conjugates of synthetic and natural macromolecules I. Synthesis and physico-chemical characterization. *J. Controlled Release* **64**, 63–79.
- (17) Jensen, K. D., Kopečková, P., Bridge, J. H. B.; Kopeček, J. (2001) The cytoplasmic escape and nuclear accumulation of endocytosed and microinjected HPMA copolymers and a basic kinetic study in Hep G2 cells. *AAPS Pharm. Sci* [serial online] **3**, Article 32.
- (18) Omelyanenko, V., Kopečková, P., Gentry, C.; Kopeček, J. (1998) Targetable HPMA copolymer-adriamycin conjugates. Recognition, internalization, and subcellular fate. *J. Controlled Release* **53**, 25–37.
- (19) Duncan, R., and Lloyd, J. B. (1978) Pinocytosis in the rat visceral yolk sac. Effects of temperature, metabolic inhibitors and some other modifiers. *Biochim. Biophys. Acta* **544**, 647–655.
- (20) Lundberg, M., and Johansson, M. (2002) Positively charged DNA-binding proteins cause apparent cell membrane translocation. *Biochem. Biophys. Res. Commun.* **22**, 367–371.
- (21) Tijerina, M., Kopečková, P., and Kopeček, J. (2002) unpublished results.

BC0255900

# Endosomolysis by Masking of a Membrane-Active Agent (EMMA) for Cytoplasmic Release of Macromolecules

David B. Rozema,<sup>\*,†</sup> Kirk Ekena,<sup>†</sup> David L. Lewis,<sup>†</sup> Aaron G. Loomis,<sup>†</sup> and Jon A. Wolff<sup>‡</sup>

Mirus Corporation, 505 S. Rosa Road, Madison, Wisconsin 53711, and Waisman Center, Department of Pediatrics and Medical Genetics, Medical School, University of Wisconsin—Madison, Madison, Wisconsin 53705. Received August 15, 2002; Revised Manuscript Received November 6, 2002

Endosomolysis, a critical barrier to efficient delivery of macromolecules such as nucleic acids, has been breached using a novel approach: endosomolysis by masking of a membrane-active agent (EMMA). To demonstrate the concept of EMMA, a cationic membrane-active peptide, melittin, was reversibly inhibited using a maleic anhydride derivative. At neutral pH, the lysines of melittin are covalently acylated with the anhydride, thereby inhibiting melittin's membrane disruption activity. Under acidic conditions such as those present within endosomes, the amide bond of the maleamate is cleaved, thus unmasking melittin. The active melittin can then disrupt the endosomal membrane resulting in release of biologically active molecules into the cytoplasm. This approach avoids cellular toxicity by restricting melittin's activity until it reaches the endosomal compartment. The utility of this approach was demonstrated by delivery phosphorodiamidate morpholino oligonucleotides (PMOs).

## INTRODUCTION

In the rational design of synthetic delivery vehicles for biologically active compounds and macromolecules such as nucleic acids, endosomal escape can be a critical barrier for their efficient delivery to cytoplasmic and nuclear sites of action (1–3). Endosomal escape can be enabled by the use of liposomes that hypothetically fuse with the endosomal membrane in a process akin to that used by enveloped viruses such as influenza (4, 5). Alternatively, nonliposomal vehicles (e.g., polymer-based systems) and nonenveloped viruses (e.g., adenoviruses) must escape from endosomes by disrupting their membranes (termed endosomolysis) (6). Despite some advances, our understanding of endosomal release and ability to synthetically enhance it remain at a rudimentary level.

Both viral and synthetic processes for accomplishing endosomal release often rely upon the changing environment of the endosome and/or lysosome to trigger either membrane fusion or disruption (7, 8). Endosomal acidification is frequently exploited to facilitate escape, given that as the endosome matures into a lysosome, the pH progressively drops to less than 5 (9–11). The pH gradient between cytoplasm and endosome causes endosomolytic monoamines such as chloroquine to concentrate within endosomes and destroy the pH gradient (12). The pH-sensitive amines within polyamines such as polyethyleneimine also play a role in endosomal release (13–15). For some liposome-based systems, pH-sensitive groups, typically carboxylic or amino groups, have been incorporated into lipids that undergo phase transitions upon protonation (4, 16). Peptides and synthetic polymers containing protonable groups have been modeled after viral sequences to become more amphipathic and membrane active in acidic environments (17–19). By limiting membrane activity to acidic vesicles, effects on the

plasma membrane and thereby cellular toxicity are attenuated.

The use of protonation to effect membrane disruption is beset with a potential conundrum. Endosome disruption by a pH-sensitive agent will destroy the pH gradient, which may reverse the membrane activity of the endosomolytic agent. As a consequence, the endosome membrane could reseal before the macromolecule diffuses out of the endosome, thereby limiting delivery. To avoid the swift reversibility of the protonation-based membrane active agents, we have developed an irreversible process that relies upon chemical bond cleavage to unmask a peptide's endosomolytic activity. The use of linkages that are labile within the endosomal or lysosomal milieu has previously been used in liposomes or for coupling drugs with carriers (4, 7, 20, 21). We chose to work with the cationic peptide melittin that contains several lysines required for its membrane activity and to use maleic anhydrides to reversibly modify the  $\epsilon$  amino groups of the lysine residues. Maleic anhydrides react with amines to form pH-labile amides, called maleamic acids, that are cleaved when the carboxylic group becomes protonated (22). A series of cyclic, maleic anhydride derivatives were evaluated for their ability to reversibly inhibit melittin (Figure 1A). Citraconic anhydride had previously been used to reversibly modify the primary amine of dioleoylphosphatidylethanolamine, but this reagent was not effective for our purposes (21). A previously unstudied maleic anhydride derivative, 2-propionic-3-methylmaleic anhydride (termed CDM for carboxylated dimethyl maleic acid), was synthesized to incorporate two design features that were found to be required: disubstitution of the maleic anhydride to increase pH-lability and an additional carboxylic acid to inhibit membrane activity of the peptide.

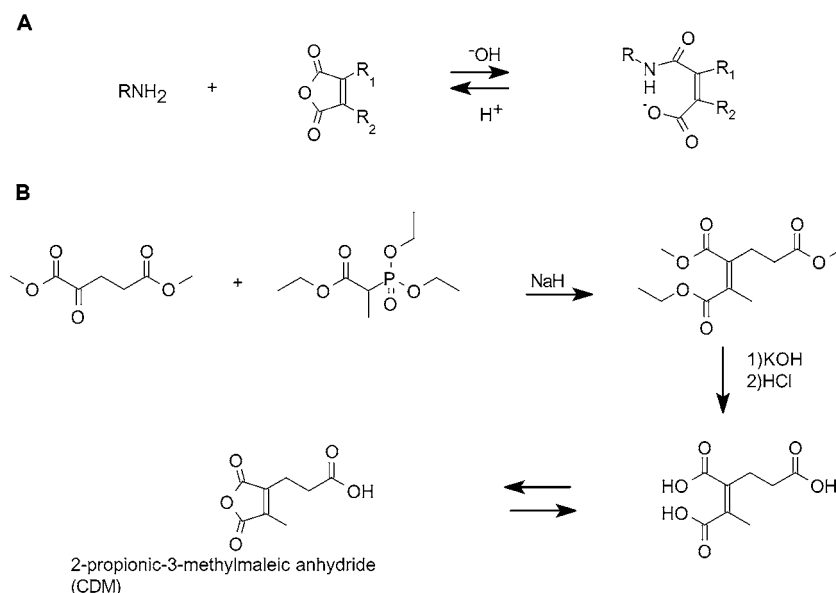
## MATERIALS AND METHODS

### Maleic Anhydride Derivatives and Synthesis of 2-Propionic-3-methylmaleic Anhydride (Carboxydimethylmaleic Anhydride or CDM). 2-Propionic-3-

\* Corresponding author. E-mail: daver@genetransfer.com.

<sup>†</sup> Mirus Corporation.

<sup>‡</sup> University of Wisconsin—Madison.



**Figure 1.** (A) Maleic anhydride and maleamate derivatives: maleic R<sub>1</sub> and R<sub>2</sub> = H, dimethyl maleic R<sub>1</sub> and R<sub>2</sub> = CH<sub>3</sub>, citraconic R<sub>1</sub> or R<sub>2</sub> = H and R<sub>2</sub> or R<sub>1</sub> = CH<sub>3</sub>, *cis*-aconitic R<sub>1</sub> or R<sub>2</sub> = H and R<sub>2</sub> or R<sub>1</sub> = CH<sub>2</sub>CO<sub>2</sub>H, and 2-propionic-3-methylmaleic (CDM) R<sub>1</sub> or R<sub>2</sub> = CH<sub>3</sub> and R<sub>2</sub> or R<sub>1</sub> = C<sub>2</sub>H<sub>4</sub>CO<sub>2</sub>H. (B) Synthesis of 2-propionic-3-methylmaleic anhydride (CDM): a Horner–Emmons reaction between dimethyl-2-oxoglutarate and triethyl-2-phosphonopropionate, followed by saponification of the ester groups.

methylmaleic anhydride was synthesized according to a published procedure (23). To a suspension of sodium hydride (0.58 g, 25 mmol) in 50 mL anhydrous tetrahydrofuran was added triethyl-2-phosphonopropionate (7.1 g, 30 mmol). After evolution of hydrogen gas had stopped, dimethyl-2-oxoglutarate (3.5 g, 20 mmol) in 10 mL anhydrous tetrahydrofuran was added and stirred for 30 min. Water, 10 mL, was then added, and the tetrahydrofuran was removed by rotary evaporation. The resulting solid and water mixture was extracted with 3 × 50 mL ethyl ether. The ether extractions were combined, dried with magnesium sulfate, and concentrated to a light yellow oil. The oil was purified by silica gel chromatography elution with 2:1 ether:hexane to yield 4 g (82% yield) of pure triester. The 2-propionic-3-methylmaleic anhydride was then formed by dissolving of this triester into 50 mL of a 50/50 mixture of water and ethanol containing 4.5 g (5 equiv) of potassium hydroxide. This solution was heated to reflux for 1 h. The ethanol was then removed by rotary evaporation, and the solution was acidified to pH 2 with hydrochloric acid. This aqueous solution was then extracted with 200 mL ethyl acetate, which was isolated, dried with magnesium sulfate, and concentrated to a white solid. This solid was then recrystallized from dichloromethane and hexane to yield 2 g (80% yield) of 2-propionic-3-methylmaleic anhydride (CDM).

Citraconic, *cis*-aconitic, dimethylmaleic, and succinic anhydrides were purchased from Aldrich.

**Quantification of Amines by TNBS.** To determine the amine content of a sample, 50–200 nmol of amine is added to a 0.5 mL solution of 100 mM Borax solution containing 0.4 mM 2,4,6-trinitrobenzenesulfonic acid (TNBS) (Sigma). Fifteen minutes later the absorbance of the solution was measured at 420 nm. The amount of amine may be calculated by the absorbance of a solution of known amine concentration.

**Acylation of Poly-L-lysine (PLL) with CDM, Dimethylmaleic, Succinic, Citraconic, and *cis*-Aconitic Anhydrides and Assessment of Charge Density.** To a solution containing 200 μg PLL (MW 34 000 from Aldrich), 2 mg HEPES, and 0.4 mg NaOH in 100 μL water was added 0.4 mg of CDM, dimethylmaleic, suc-

cinic, or citraconic anhydride in 20 μL ethanol with rapid vortexing. For *cis*-aconitic anhydride, there was a substantial amount of hydrolyzed anhydride present in the sample; therefore, 2 mg of anhydride, 12 mg of HEPES, and 2.4 mg of NaOH were used. By TNBS assay there was no detectable amount of amine upon acylation under these conditions.

The charge density of these polyanions was determined by adapting a technique used for assessing DNA condensation (24, 25). A compacted, interpolyelectrolyte complex is formed when the polyanions (PLL completely reacted with the anhydrides) are mixed with fluorescein-labeled PLL. The compaction causes the fluorescein residues on PLL to be in closer proximity and self-quench, which enables the condensation state and by inference the effective charge density of the polyanions to be conveniently determined. To measure the condensation of PLL by acylated PLL, 10 μg of fluorescein-labeled PLL was placed in 0.5 mL of 5 mM HEPES buffer at pH 7.8. The fluorescence intensity of this solution was measured (excitation at 495 nm, emission at 530 nm). A 1 μg sample of acylated PLL (weight based on the starting weight of PLL, not on the weight of acylated PLL) was added to the fluorescein-labeled PLL, and the fluorescence intensity was again measured. This was repeated until the decrease in fluorescence intensity ceased. The amount of acylated PLL needed to quench fluorescein–PLL to the maximum degree was assumed to be point at which an equal amount of polyanion was added to the polycation.

**Acylation of Melittin with CDM, dimethylmaleic, Citraconic, and *cis*-Aconitic Anhydrides.** To a solution containing 200 μg melittin, 500 μg HEPES, and 100 μg NaOH in 20 μL water was added 100 μg of CDM, dimethylmaleic, or citraconic anhydride in 50 μL ethanol with rapid vortexing. For *cis*-aconitic anhydride 250 μg of anhydride, 1.25 mg of HEPES, and 250 mg of NaOH were used. By TNBS assay there was no detectable amount of amine upon acylation under these conditions.

**Fluorescein Labeling of PLL.** To a solution of PLL (10 mg) in 1 mL 10 mM K<sub>2</sub>CO<sub>3</sub> was added 0.4 mg of fluorescein isothiocyanate (0.02 functional eq). After 2 h, the polymer was placed into dialysis tubing (12 000 MW cutoff) and dialyzed for 72 h against 3 × 2 L deionized



water. The polymer was then removed from the tubing, and the water was removed by lyophilization. The yield of the reaction was estimated to be 50% by measurement of the absorbance of fluorescein-labeled PLL at 494 nm in a solution of 10 mM  $\text{NaHCO}_3$  using the extinction coefficient  $77\,000\text{ M}^{-1}\text{cm}^{-1}$  (Molecular Probes).

**Synthesis of Fluorescein-PEG.** A 100 mg sample of monoamine PEG (MW 5000, Shearwater) was dissolved in 1 mL of dimethylformamide. To this solution was added  $3.5\text{ }\mu\text{L}$  of diisopropylethylamine and 8 mg of fluorescein isothiocyanate. After 1 h, the PEG was precipitated by addition of 10 mL of diethyl ether. The PEG was then dissolved in 5 mL of water and purified by size exclusion chromatography using a  $30 \times 150\text{ mm}$  column of sephadex G10 (Sigma) eluting with water.

**Kinetics of Acid-Catalyzed Cleavage of Maleamylated Glycylalanine.** CDM, dimethyl maleic, and citraconic modified glycylalanine (GA, from Sigma) were synthesized by addition of  $400\text{ }\mu\text{g}$  of CDM, citraconic, or dimethylmaleic anhydride in  $20\text{ }\mu\text{L}$  of ethanol to a solution of  $200\text{ }\mu\text{g}$  of GA and 2.4 mg of HEPES base in  $44\text{ }\mu\text{L}$  of water. The solutions were mixed by rapid vortexing. The acylated peptide was acidified by addition of  $0.8\text{ }\mu\text{L}$  glacial acetic acid and  $10\text{ }\mu\text{L}$  of 1 M sodium acetate to bring the pH to 5.0. At various times,  $10\text{ }\mu\text{g}$  aliquots were removed and added to 0.5 mL of 100 mM  $\text{NaHCO}_3$  solution containing 0.4 mM TNBS. Fifteen minutes later the absorbance of the solution was measured at 420 nm. A plot of  $\ln[1 - (A_t/A_0)]$  as a function of time was a straight line whose slope is  $-k$ , the rate constant for the cleavage reaction, where  $A_t$  is the absorbance at time  $t$  and  $A_0$  is the absorbance of unmodified GA.

For *cis*-aconitic modification of GA, 3-fold more anhydride, base, and acid were used to synthesize and cleave the acylated peptide.

**Hemolysis Assay.** The membrane activity of polymers and peptides was measured using a red blood cell (RBC) hemolysis assay (26). Porcine whole blood was isolated in heparin-containing vacutainers. The RBC's were isolated by centrifugation at 500 RCF for 5 min. They were washed three times with 100 mM dibasic sodium phosphate at the desired pH and resuspended to the initial volume. The desired pH phosphate buffer was obtained by acidification of a dibasic sodium phosphate stock with HCl. (Buffers made from mixing of mono- and dibasic phosphate lysed red blood cells at acidic pH.) A  $20\text{ }\mu\text{L}$  sample of the washed RBC suspension, which is approximately  $10^8$  cells (26), was added to 500  $\mu\text{L}$  of phosphate buffer. To this solution was added various amounts of peptide or polymer. The samples were incubated for 1.5 h in a  $37^\circ\text{C}$  incubator. They were then spun for 1 min at 15 000 RCF. Lysis was determined by measuring the absorbance of the supernatant at 541 nm. Percent hemolysis was calculated assuming 100% lysis to be the absorbance of hemoglobin released upon addition of deionized water; all sample absorbances had the absorbance of buffer alone subtracted.

**Fluorescein-PEG Delivery Assay.** HeLa (human epitheloid) cells were grown in Dulbecco's Modified Eagle's Medium (DMEM, Cellgro, Herndon, VA) containing 10% fetal bovine serum (Hyclone Laboratories, Logan, Utah) in a humidified incubator at  $37^\circ\text{C}$  with 5%  $\text{CO}_2$  atmosphere. Cells were plated in 6-well culture dishes containing untreated glass coverslips at a density of  $1.0\text{--}1.5 \times 10^5$  cells/well and incubated for 24–48 h. Media were replaced with 1.0 mL DMEM containing 1.0 mg fluorescein-PEG3000 either with or without  $400\text{ }\mu\text{g}$  CDM-melittin. Cells were then incubated for 10 min at

$37^\circ\text{C}$ , washed once with warm  $37^\circ\text{C}$  DMEM, and incubated for an additional 35 min in DMEM containing 10% bovine serum. Cells were then washed three times with PBS (Sigma), fixed for 30 min at  $4^\circ\text{C}$  in PBS + 4% formaldehyde (Sigma), and washed three times in PBS. Coverslips were mounted onto glass slides for fluorescent microscopy. Images of the samples were collected by confocal microscopy on a Zeiss LSM510 confocal microscope (Zeiss, Germany) using a  $63\times$  oil plan apo objective with NA 1.4. Similar methods were used with 1 mg/mL of fluorescein-dextran (10 kDa, purchased from Molecular Probes).

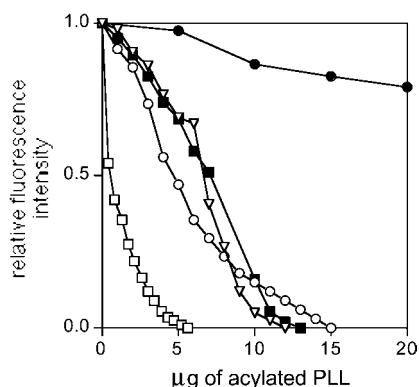
To assay or cellular toxicity,  $2\text{ }\mu\text{L}$  of saturated solution propidium iodide in water was added to cells in 3 mL PBS after 35 min incubation in DMEM. After 3 min, the PBS solution was removed and cells were washed and fixed as described above. To study the effect of a proton pump inhibitor on the release of fluorescein-PEG, the cells were incubated with 200 nM bafilomycin A, while the cells were loaded with fluorescein-PEG and during their incubation in the presence of DMEM. The cells were then washed and fixed as described above. No diffuse cytoplasmic staining was observed for cells incubated with bafilomycin A.

**Oligonucleotide Delivery Assay.** HeLa Luc/705 cells (Gene Tools, Philomath OR) were grown under conditions used for HeLa cells. The cells were plated in 24-well culture dishes at a density of  $3 \times 10^6$  cells/well and incubated for 24 h. Media were then replaced with 1.0 mL DMEM or 1.0 mL DMEM containing 10% FBS. To these samples was added 2.5 nmol PMO (CCT CTT ACC TCA GTT ACA ATT TAT A, Gene Tools, Philomath, OR) with or without 2.5 or 5.0 nmol CDM-melittin, citraconylated melittin, or *cis*-aconitylated melittin. The cells were incubated for 4 h in a humidified, 5%  $\text{CO}_2$  incubator at  $37^\circ\text{C}$ . The medium was then replaced with DMEM containing 10% fetal bovine serum. The cells were then incubated for an additional 48 h. The cells were then harvested and the lysates were then assayed for luciferase expression as previously reported using a Lumat LB 9507 (EG&G Berthold, Bad-Wildbad, Germany) luminometer (27).

## RESULTS AND DISCUSSION

Synthesis of a carboxylic acid-containing derivative of dimethylmaleic anhydride(CDM). Two features of maleic anhydride derivatives were systematically evaluated. The first was the degree of substitution at the unsaturated carbon-carbon bond since it has been shown that the greater amount of substitution increases pH-lability (28, 29). The parent anhydride, maleic anhydride, has no substitution and forms the most stable maleamic acid (Figure 1). Citraconic and *cis*-aconitic-derived maleamic acids have one substitution and are more pH-labile. Maleamic acids derived from disubstituted dimethyl maleic anhydride are the most pH-labile (30). The second parameter evaluated was the effect of the addition of a carboxylate-containing group, which increases charge and water solubility. The *cis*-aconitic anhydride has such a carboxylic acid group. To complete the series and have a disubstituted anhydride with an additional carboxylic acid group, CDM was synthesized via a Horner-Emmons reaction between dimethyloxoglutarate and triethyl-2-phosphonopropionate, followed by saponification of the ester groups (Figure 1B) (23).

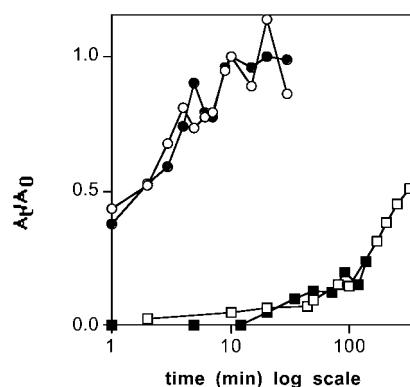
**Acylation of a Polyamine with Cyclic Anhydrides and the Effect on Charge Density.** To confirm the ability of the anhydrides to modify a polyamine and to



**Figure 2.** The quenching of fluorescein-labeled PLL upon addition of PLL modified with succinic anhydride ( $\nabla$ ), dimethylmaleic anhydride ( $\bullet$ ), CDM anhydride ( $\circ$ ), citraconic ( $\blacksquare$ ), or *cis*-aconitic anhydride ( $\square$ ).

evaluate the effect of acylation on the charge of the amines, the cyclic anhydrides were reacted with the polyamine PLL. The effect of acylation on the charge of the modified polyamine is important, given that the membrane activity of melittin is presumably dependent on its positive charge (*vide infra*). After reaction of PLL with succinic, citraconic, *cis*-aconitic, dimethylmaleic, and CDM anhydrides, the TNBS assay indicated that there was complete conversion of the  $\gamma$ -amines of PLL to carboxylates. The charge density of these polyanions was determined by assessing their ability to condense cationic, fluorescein-labeled PLL (24). At slightly basic pH, 1–1.2 functional equiv of succinylated PLL is required to condense PLL, which is estimated from our observation that 10–12  $\mu\text{g}$  of succinylated PLL is required to fully quench 10  $\mu\text{g}$  of fluorescein-labeled PLL (Figure 2). Similarly, 1–1.3 equiv of citraconylated PLL and 1.5 equiv of *cis*-aconitylated PLL, which has two carboxylate groups per repeating unit, are required to condense PLL. In contrast, PLL that is modified with dimethylmaleic anhydride requires ca. 20 equiv to condense PLL. Similarly, the charge density of CDM-modified PLL is roughly one charge per two carboxylates. It appears that the distal carboxylate of CDM anhydride adds charge to the modified polymer while the carboxylate of the anhydride contributes very little charge to the polyanion. This deficiency of effective charge density for dimethylmaleamates may be due to a hydrogen bond interaction between the amide proton and the carboxylate of the dimethylmaleamylate group. Another hypothesis is that the steric bulk of the two methyl groups prevents any interaction. The reported  $\text{pK}_a$  of the carboxylate of dimethylmaleamylate is 4.2 (28), and the  $\text{pK}_a$  of citraconylates is 3.2. These values suggest that the carboxylate is not hydrogen bonded to the amide proton because one would expect that a hydrogen bond between the carboxylate and amide proton would *decrease*, not increase the  $\text{pK}_a$  of dimethylmaleamylate. Whatever the reason for dimethylmaleamate's apparent lack of charge density, these results indicate that CDM can modify the amines of lysine, thereby converting a positive charge into a negative one.

**The Acylation of the Dipeptide Glycylalalanine and the Kinetics of Cleavage.** The rates of acid-catalyzed cleavage of the maleamates were evaluated using the dipeptide glycylalalanine (GA) (Figure 3). GA was chosen because it (1) contains one amine group, which simplifies kinetics, and (2) contains a carboxylate distant from the amine, which keeps the peptide soluble in the assay conditions without greatly affecting the  $\text{pK}_a$  of the amine. The rate of maleamate cleavage was studied

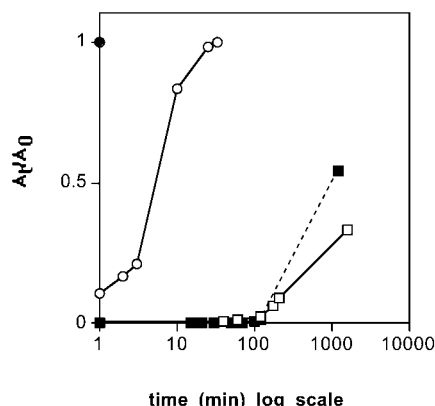


**Figure 3.** The cleavage of maleamic acid modifications of the glycylalalanine dipeptide modified with dimethylmaleic ( $\bullet$ ), CDM ( $\circ$ ), citraconic ( $\blacksquare$ ), or *cis*-aconitic anhydride ( $\square$ ).

by addition of the modified peptides to a pH 5 solution, and at various times the cleavage reaction was quenched by addition to a pH 9 solution containing TNBS. As expected, the disubstituted maleamic acids cleave much more rapidly than monosubstituted maleamic acids (Figure 3) (29). At early time points, the reverse reaction is negligible, and the reaction can be treated as unimolecular; but at later time points, the reverse reaction between amine and anhydride affects the concentration of amine, and the reaction is no longer strictly unimolecular. Data points where the reaction is less than 50% complete can be fitted to the equation  $\ln[1 - (A_t/A_0)] = -kt$ , where  $A_t$  is the absorbance at time  $t$  and  $A_0$  is the absorbance of PLL that was not modified by anhydride. We calculated rate constants of  $0.4 \text{ min}^{-1}$  for dimethylmaleamic acid cleavage and  $0.3 \text{ min}^{-1}$  for the cleavage of CDM modified GA, which correspond to half-lives of 1.5 and 2 min, respectively. Similar measurements of the reversal of citraconic and *cis*-aconitic modification revealed much slower cleavage kinetics with an approximate half-life of 300 min.

**Acylation of the Membrane Disruptive Peptide Melittin.** To investigate the effect of acylation on the activity of membrane-active, cationic peptides, we chose melittin. Melittin is a 26-residue peptide from bee venom (GIGAILKVLATGLPTLISWIKNKRKQ from the little honey bee), which is highly cytotoxic and hemolytic (31). Many synthetic analogues of melittin have been studied to determine which residues are important for membrane disruptive ability (17). The lysine at position 7 has been shown to be important for hemolytic activity (32). This importance of lysine 7 and the presence of four other amine groups, from three lysines and the amino terminus, suggest that regulating these amino groups could control the activity of melittin.

To test this hypothesis, we acylated melittin at pH 7.5 with two molar equiv, relative to the four lysine residues with succinic, *cis*-aconitic, dimethylmaleic, citraconic, and CDM anhydrides. Modification by all of the anhydrides except dimethylmaleic anhydride resulted in a complete loss of membrane activity as measured by red blood cells lysis. Measurement of amine content by TNBS revealed that the inactivation of melittin by dimethylmaleic anhydride modification was not the result of incomplete amine acylation. A possible explanation for the activity of dimethylmaleamylated melittin is the lack of effective charge for dimethylmaleamates. As we observed that dimethylmaleamylated PLL possessed very little charge density, we would expect that dimethylmaleamylated melittin would not be entirely inhibited from interacting with the anionic cellular membrane.



**Figure 4.** The return of melittin hemolytic activity at various times after incubation of maleamic-modified melittin at pH 5.0, for dimethylmaleic- (●), CDM- (○), citraconic- (■), or *cis*-aconitic-anhydride- (□) modified melittin.

**Restoration of Membrane Activity of Melittin upon Acidification.** To test whether the reversibility of the acylation reaction restores membrane activity, melittin modified with CDM, citraconic, or *cis*-aconitic anhydride was incubated at pH 5. At various times, the acidification was stopped by addition to pH 7.5 phosphate buffer and the membrane disruptive ability of each sample was measured by the addition of red blood cells. The membrane activity for CDM-melittin returned to 100% within 25 min (Figure 4). Analysis of the kinetics of the return of activity using an analysis method similar to that used for the TNBS assay (plotting of  $\ln[1 - (A_t/A_0)]$  as a function of time to determine the slope,  $-k$ ) revealed a rate constant of  $0.07 \text{ min}^{-1}$ , or a half-life of 10 min for CDM-melittin. The half-life for the restoration of melittin's activity is roughly 4 times longer than the half-life of cleavage. This increase suggests that most, if not all, of the CDM groups must be cleaved from melittin for it to be active. Despite this delay for the return of activity, these results suggest that the new reagent CDM is able to reversibly inhibit melittin's membrane activity in a time frame consistent with endocytosed materials' transit to late endosomes (11).

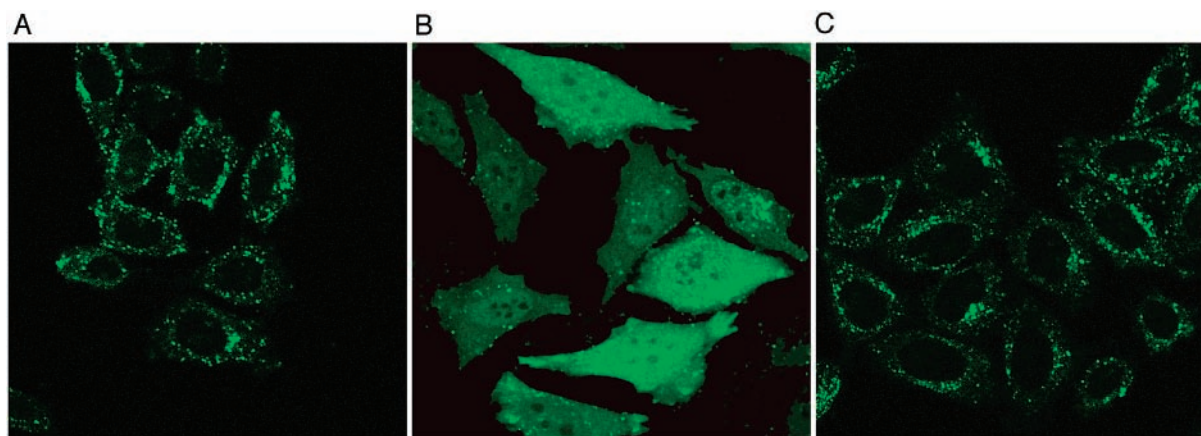
As one would expect from the kinetics for the cleavage of monosubstituted maleamic acids, the cleavage of citraconic and *cis*-aconitic anhydride modifications of melittin were much slower (Figure 4). Incubation of *cis*-aconitylated melittin at pH 5 for 27 h resulted in only a 30% return in activity, and citraconylated melittin had only a 50% return of activity. Analysis of the kinetics of

the cleavage of *cis*-aconityl modified melittin reveals a rate constant of  $0.015 \text{ h}^{-1}$  or a half-life of 47 h, while citraconylated melittin has a half-life of 24 h. The difference between modification by *cis*-aconitic and citraconic anhydrides may be due to the charge upon modification. As mentioned previously, *cis*-aconitic modification results in two carboxylate groups, while citraconic modification results in only one carboxylate group.

**Release of Fluorescein-Labeled Polyethylene Glycol from the Endocytic Compartment by CDM-Melittin.** To assess the ability of CDM-melittin to function as an endosomolytic agent, its ability to facilitate release of fluorescein-labeled poly(ethylene glycol) (PEG) from endosomes was examined (Figure 5). Similar assays have been used to examine the endosomolytic properties of viruses (33). Cells were incubated with  $1 \text{ mg/mL}$  fluorescein-PEG  $\pm 400 \text{ } \mu\text{g/mL}$  modified melittin for 10 min at  $37^\circ\text{C}$ . After this pulse, cells were washed and chased for an additional 35 min at  $37^\circ\text{C}$  in DMEM + 10% bovine serum. In the absence of CDM-melittin, the fluorescein-PEG had a punctuate appearance, indicative of localization in endosomes and/or lysosomes (Figure 5A). In contrast, when CDM-melittin was included, there was diffuse fluorescence throughout the cell, indicating release of fluorescein-PEG from internal endosomes/lysosomes (Figure 5B). Addition of *cis*-aconitic modified melittin resulted in the punctate fluorescence from the endocytosis of the fluorophore (Figure 5C), just as in the absence of melittin. The persistence of a punctate endosomal signal in the CDM-modified melittin indicates that organelle rupture was not 100% efficient. Similar results were observed when fluorescein-labeled 10kDa dextran was used as the marker molecule (data not shown). In addition, bafilomycin A, an inhibitor of endosomal acidification, inhibited release of the fluorescein-PEG (data not shown).

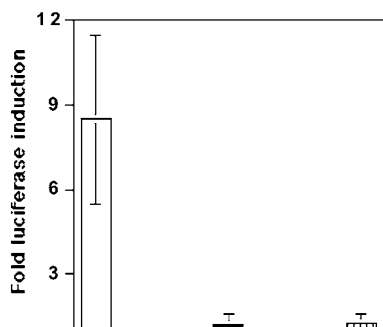
Visual inspection indicated that  $400 \text{ } \mu\text{g/mL}$  of CDM-melittin had no apparent cytopathic effect, whereas  $10 \text{ } \mu\text{g/mL}$  unmodified melittin completely destroyed the cells in less than 10 min. Additionally, propidium iodide staining was used to provide a more sensitive indication of cellular toxicity (34). In the cells exposed to CDM-melittin and after the 10 min wash,  $\sim 1\%$  of the cells showed nuclear staining with propidium iodide, which is similar to control samples (data not shown). Thus, CDM modification of melittin enabled endosomal release while substantially reducing melittin's cellular toxicity.

**Delivery of Oligonucleotide.** To assay the ability of CDM-modified melittin to aid in the delivery of a biologi-



**Figure 5.** Confocal fluorescent photomicrographs showing the sub-cellular distribution of endocytosed PEG-fluorescein in HeLa cells without any melittin(A), with CDM-modified melittin(B), or with *cis*-aconitic modified melittin(C). Settings were identical for all three pictures.





**Figure 6.** The effect of 2.5 nmol of maleamate modified melittin on PMO delivery as measured by their induction of luciferase expression in a HeLa cell line stably transformed with the luciferase gene containing an intron with a mutant splice site. The values are normalized to cells treated with PMO alone and represent the means of four separate experiments. The error bars encompass entire range of induction. Data presented for PMO with CDM-melittin (white bar), *cis*-aconitylated melittin (black bar), and citraconylated melittin (striped bar).

cally active molecule, we chose to study the delivery of phosphorodiamidate morpholino oligonucleotides (PMOs) (35, 36). These agents exert their effects by steric hindrance mechanisms and can be used to block translation or splicing of a target RNA (37–39). PMOs are uncharged nucleotide analogues in which a six-membered morpholine ring is substituted for ribose and an uncharged phosphorodiamidate linkage replaces the phosphodiester linkage (40). Like PEG and dextran, oligonucleotides are internalized by endocytosis (8) and are unable to diffuse across cell membranes (41, 42).

The most common method for delivery of anionic oligonucleotides is the use of cationic lipids (43, 44) and polymers (45). However, to use these strategies for the delivery of uncharged oligonucleotides, such as PMO's, they must first be complexed with a complimentary strand of anionic oligonucleotide to form a charged complex. Two other methods for delivering PMOs, scrape-loading and syringe-loading, both involve physically damaging cells to create transient lesions in the plasma membrane (37) and do not give consistent results.

To assay the delivery of PMO by CDM-melittin, we used a commercially available HeLa cell line that carries an integrated luciferase gene with a mutant splice site (39). This mutant splice site results in production of a mRNA coding for a truncated inactive luciferase protein. Blocking this splice site with an oligonucleotide enables expression of the full-length active enzyme. Thus, the luciferase activity in this cell line is directly proportional to the amount of PMO released from the endosomal compartment.

Co-incubation of 2.5  $\mu$ M blocking PMO with 2.5  $\mu$ M CDM-melittin resulted in 5–12-fold increase in luciferase expression above incubation with PMO alone (Figure 6, white bar). The CDM-melittin facilitated induction was comparable to the induction we obtained using scrape-loading. Neither *cis*-aconitylated nor citraconylated melittin resulted in any increase in PMO delivery (Figure 6, black and striped bars respectively), supporting our hypothesis that these modifications are too stable to aid in endosome disruption.

The presence of 10% serum decreased the amount of delivery observed for CDM-modified melittin and increased the amount of peptide required for optimal delivery. For example, incubation of 2.5 nmol PMO with 5.0 nmol CDM-modified melittin resulted in a 4–5-fold increase in luciferase production. As observed in the absence of serum, citraconylated and *cis*-aconitylated

melittin did not increase the delivery of PMO in the presence of serum.

## CONCLUSIONS

The research presented in this report is a demonstration of the concept of endosomolysis by masking of a membrane-active agent (EMMA). This study demonstrates the ability of a new chemical reagent, CDM, to reversibly inhibit the membrane active peptide melittin and enable endosomal release. Melittin is only representative of the many membrane active compounds whose activity can be potentially controlled in order to deliver impermeable compounds. CDM modification could also be used to reversibly inhibit other amine-containing molecules, including membrane-active peptides or polymers. Further studies are in progress to incorporate the CDM modification and CDM-melittin into a variety of synthetic delivery systems for the delivery of oligonucleotides, plasmid DNA and other membrane impermeable drugs.

Delivery of the morpholino-based oligonucleotide by CDM-modified melittin relies on the co-endocytosis of oligonucleotide and melittin. This event is possible in the relatively high concentration of the culture dish, but is impossible in vivo. In order for CDM-based EMMA to facilitate delivery in vivo, the masked membrane-active agent must be associated, with the compound to be delivered. This association may occur by covalent attachment of the membrane-active agent to the compound to be delivered or noncovalent attachment via electrostatic interaction, for example in DNA-polycation complexes. Studies are in progress to attach compounds to be delivered to the masked endosomolytic agent.

## ACKNOWLEDGMENT

The authors would like to thank Lori Higgs for the synthesis of melittin. We would also like to thank the National Institute of Standards and Technology for financial support through Advanced Technology Program (ATP).

## LITERATURE CITED

- (1) Brown, M. D., Schatslein, A. G., and Uchegbu, I. F. (2001) Gene delivery with synthetic (non viral) carriers. *Int. J. Pharm.* 229, 1–21.
- (2) Lloyd, J. B. (2000) Lysosome membrane permeability: implications for drug Del.ery. *Adv. Drug Del. Rev.* 41, 189–200.
- (3) Nishikawa, M., and Huang, L. (2001) Nonviral vectors in the new millenium: delivery Barrier in Gene Transfer. *Human Gene Ther.* 12, 861–870.
- (4) Drummond, D. C., Zignani, M., and Leroux, J.-C. (2000) Current status of pH-sensitive liposomes in drug delivery. *Prog. Lipid Res.* 39, 409–460.
- (5) Eckert, D. M., and Kim, P. S. (2001) Mechanisms of viral membrane fusion and its inhibition. *Annu. Rev. Biochem.* 70, 777–810.
- (6) Nemerow, G. R., and Stewart, P. L. (1999) Role of alpha v integrins in adenovirus cell entry and gene delivery. *Microbiol. Mol. Biol. Rev.* 63, 725–734.
- (7) Asokan, A., and Cho, M. J. (2002) Exploitation of intracellular pH gradients in the cellular delivery of macromolecules. *J. Pharm. Sci.* 91, 903–913.
- (8) Carrasco, L. (1994) Entry of animal viruses and macromolecules into cells. *FEBS Lett.* 350, 151–4.
- (9) Clague, M. J. (1998) Molecular aspects of the endocytic pathway. *Biochem. J.* 336, 271–282.
- (10) Gruenberg, J. (2001) The endocytic pathway: A mosaic of domains. *Nat. Rev.: Mol. Cell. Biol.* 2, 721–730.

- (11) Mukherjee, S., Ghosh, R. N., and Maxfield, F. R. (1997) Endocytosis. *Physiol. Rev.* 77, 759–803.
- (12) Ciftci, K., and Levy, R. J. (2001) Enhanced plasmid DNA transfection with lysosomotropic agents in cultured fibroblasts. *Int. J. Pharm.* 218, 81–92.
- (13) Kichler, A., Leborgne, C., Coeytaux, E., and Danos, O. (2001) Polyethylenimine-mediated gene Delivery: a mechanistic study. *J. Gene Med.* 3, 135–144.
- (14) Klemm, A. R., Young, D., and Lloyd, J. B. (1998) Effects of polyethylenimine on endocytosis and lysosome stability. *Biochem. Pharm.* 56, 41–46.
- (15) Zuber, G., et al. (2001) Towards synthetic viruses. *Adv. Drug Del. Rev.* 52, 245–53.
- (16) Budker, V., et al. (1996) pH-sensitive, cationic liposomes: a new synthetic virus-like vector. *Nat. Biotech.* 14, 760–764.
- (17) Sitaram, N., and Nagaraj, R. (1999) Interaction of antimicrobial peptides with biological and model membranes: structural and charge requirements for activity. *Biochim. Biophys. Acta* 1462, 29–54.
- (18) Cheung, C. Y., Murthy, N., Stayton, P. S., and Hoffman, A. S. (2001) A pH-sensitive polymer that enhances cationic lipid-mediated gene transfer. *Bioconjugate Chem.* 12, 906–910.
- (19) Plank, C., Zauner, W., and Wagner, E. (1998) Application of membrane-active peptides for drug and gene delivery across cellular membranes. *Adv. Drug Del. Rev.* 34, 21–35.
- (20) Guo, X., and Szoka, F. C. (2001) Steric Stabilization of Fusogenic Liposomes by a Low-pH Sensitive PEG-Diortho Ester-Lipid Conjugate. *Bioconjugate Chem.* 12, 291–300.
- (21) Reddy, J. A., and Low, P. S. (2000) Enhanced folate receptor mediated gene therapy using a novel pH-sensitive lipid formulation. *J. Controlled Release* 64, 27–37.
- (22) Blattler, W. A., Kuenzi, B. S., Lambert, J. M., and Senter, P. D. (1985) New Heterobifunctional Protein Cross-Linking Reagent That Forms an Acid-Labile Link. *Biochemistry* 24, 1517–1524.
- (23) Naganawa, A., Ichikawa, Y., and Isobe, M. T. (1994) Synthetic Studies on Tautomycin Synthesis of 2,3-Disubstituted Maleic Anhydride Segment. *Tetrahedron* 50, 8969.
- (24) Trubetskoy, V. S., et al. (1999) Quantitative assessment of DNA condensation. *Anal. Biochem.* 267, 309–13.
- (25) Tang, M. X., and Szoka, F. C. (1997) The influence of polymer structure on the interactions of cationic polymers with DNA and morphology of the resulting complexes. *Gene Ther.* 4, 823–32.
- (26) Lackey, C. A., et al. (1999) Hemolytic Activity of pH-Responsive Polymer-Streptavidin Bioconjugates. *Bioconjugate Chem.* 10, 401.
- (27) Wolff, J. A., et al. (1990) Direct gene transfer into mouse muscle in vivo. *Science* 247, 1465–8.
- (28) Kirby, A. J., and Lancaster, P. W. (1972) Structure and Efficiency in Intramolecular and Enzymic Catalysis. Catalysis of Amide Hydrolysis by the Carboxy-group of Substituted Maleamic Acids. *J. Chem. Soc., Perkin Trans. 2* 1206–1214.
- (29) Nieto, M. A., and Palacian, E. (1983) Effects of temperature and pH on the regeneration of the amino groups of ovalbumin after modification with citraconic and dimethylmaleic anhydrides. *Biochim. Biophys. Acta* 749, 204–210.
- (30) Kirby, A. J. (1980) Effective Molarities for Intramolecular Reactions. *Adv. Phys. Org. Chem.* 17, 183–278.
- (31) Dempsey, C. E. (1990) The actions of melittin on membranes. *Biochim. Biophys. Acta* 1031, 143–161.
- (32) Blondelle, S. E., and Houghten, R. A. (1991) Hemolytic and antimicrobial activities of the twenty-four individual omission analogues of melittin. *Biochemistry* 30, 4671–8.
- (33) Yoshimura, A. (1985) Adenovirus-induced leakage of co-endocytosed macromolecules into the cytosol. *Cell Struct. Funct.* 10, 391–404.
- (34) Budker, V., et al. (1997) Protein/amphipathic polyamine complexes enable highly efficient transfection with minimal toxicity. *Biotechniques* 23, 139, 142–147.
- (35) Heasman, J., Kofron, M., and Wylie, C. (2000) Beta-catenin signaling activity dissected in the early *Xenopus* embryo: a novel antisense approach. *Dev. Biol.* 222, 124–34.
- (36) Nasevicius, A., and Ekker, S. C. (2000) Effective targeted gene 'knockdown' in zebrafish. *Nat. Genetics* 26, 216–20.
- (37) Ghosh, C., and Iversen, P. L. (2000) Intracellular delivery strategies for antisense phosphorodiamidate morpholino oligomers. *Antisense Nucleic Acid Drug Dev.* 10, 263–74.
- (38) Giles, R. V., Spiller, D. G., Clark, R. E., and Tidd, D. M. (1999) Antisense morpholino oligonucleotide analogue induces missplicing of C-myc mRNA. *Antisense Nucleic Acid Drug Dev.* 9, 213–20.
- (39) Kang, S. H., Cho, M. J., and Kole, R. (1998) Up-regulation of luciferase gene expression with antisense oligonucleotides: implications and applications in functional assay development. *Biochemistry* 37, 6235–9.
- (40) Summerton, J., and Weller, D. (1997) Morpholino antisense oligomers: design, preparation, and properties. *Antisense Nucleic Acid Drug Dev.* 7, 187–95.
- (41) Akhtar, S., Basu, S., Wickstrom, E., and Juliano, R. L. (1991) Interactions of antisense DNA oligonucleotide analogues with phospholipid membranes (liposomes). *Nucleic Acids Res.* 19, 5551–9.
- (42) Akhtar, S., et al. (2000) The delivery of antisense therapeutics. *Adv. Drug Del. Rev.* 44, 3–21.
- (43) Audouy, S., and Hoekstra, D. (2001) Cationic lipid-mediated transfection in vitro and in vivo. *Mol. Membr. Biol.* 18, 129–43.
- (44) Hope, M. J., Mui, B., Ansell, S., and Ahkong, Q. F. (1998) Cationic lipids, phosphatidylethanolamine and the intracellular delivery of polymeric, nucleic acid-based drugs (Review). *Mol. Mem. Biol.* 15, 1–14.
- (45) Robaczewska, M., et al. (2001) Inhibition of hepadnaviral replication by polyethylenimine-based intravenous delivery of antisense phosphodiester oligodeoxynucleotides to the liver. *Gene Ther.* 8, 874–881.

BC0255945

# Light-Harvesting Ionic Dendrimer Porphyrins as New Photosensitizers for Photodynamic Therapy

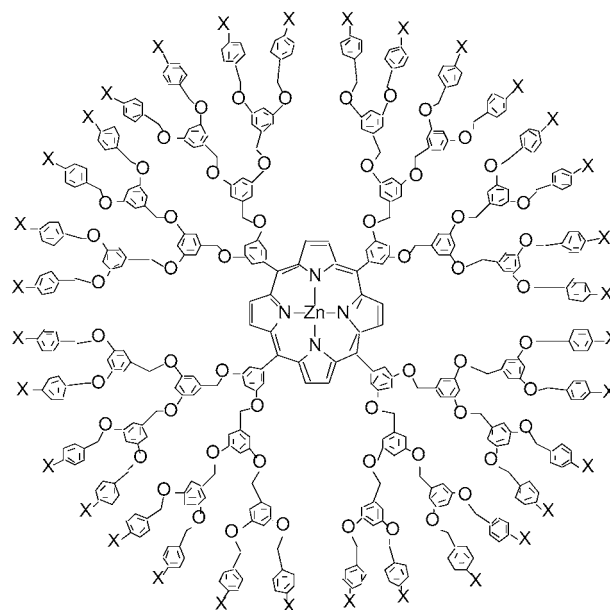
Nobuhiro Nishiyama,<sup>†</sup> Hendrik R. Stapert,<sup>†,‡</sup> Guo-Dong Zhang,<sup>†</sup> Daisuke Takasu,<sup>§</sup> Dong-Lin Jiang,<sup>§</sup> Tetsuo Nagano,<sup>||</sup> Takuzo Aida,<sup>§</sup> and Kazunori Kataoka<sup>\*,†</sup>

Department of Materials Science and Engineering, Graduate School of Engineering, The University of Tokyo, Hongo 7-3-1, Bunkyo-ku, Tokyo 113-8656, Japan, Department of Chemistry and Biotechnology, Graduate School of Engineering, The University of Tokyo, Japan, and Department of Bioorganic Chemistry, Graduate School of Pharmaceutical Sciences, The University of Tokyo. Received August 23, 2002

Photodynamic therapy (PDT) is a promising therapeutic modality for treatment of solid tumors. In this study, third-generation aryl ether dendrimer porphyrins (DPs) with either 32 quaternary ammonium groups (32(+)-DPZn) or 32 carboxylic groups (32(-)-DPZn) were evaluated as a novel, supramolecular class of photosensitizers for PDT. DPs showed a different cell-association profile depending on the positive or negative charge on the periphery, and both DPs eventually localized in membrane-limited organelles. In contrast, protoporphyrin IX (PIX), which is a hydrophobic and relatively low molecular weight photosensitizer used as a control in this study, diffused through the cytoplasm except the nucleus. Confocal fluorescent imaging using organelle-specific dyes indicated that PIX induced severe photodamage to disrupt membranes and intracellular organelles, including the plasma membrane, mitochondrion, and lysosome. On the other hand, cells treated with DPs kept the characteristic fluorescent pattern of such organelles even after photoirradiation. However, notably 32(+)-DPZn achieved remarkably higher  $^1\text{O}_2$ -induced cytotoxicity against LLC cells than PIX. Furthermore, both dendrimer porphyrins had far lower dark toxicity as compared with PIX, demonstrating their highly selective photosensitizing effect in combination with a reduced systemic toxicity.

## INTRODUCTION

Molecular nanomeric-scaled devices prepared through chemical process have recently been recognized to be useful for high-throughput screening, molecular diagnosis, and targeting therapy (*1*). In particular, dendrimers, the three-dimensional tree-like branched macromolecules, have received intense attention especially in the field of drug and gene delivery (*1–5*). On the basis of the delivery of modern organic synthetic chemistry, dendrimers having intriguing structures can be tailored in size, functional peripheral groups, and inner cavity for incorporation of a variety of molecules. Such custom-made dendrimers offer the design of novel types of delivery systems used for nanomedicines, with controlled interaction with cells and biological compounds. We have recently reported extensively on dendrimer porphyrins in which a porphyrin chromophore is spatially isolated by the aryl ether dendrimer framework (Figure 1) (*6–9*). The dendrimer porphyrins can transport absorbed energy to the porphyrin center over relatively large distance via the dendritic architecture, thereby mimicking the antenna complex and bacteriochlorophyll photo-



**Figure 1.** Chemical structure of third-generation ionic dendrimer porphyrins. 32(+)-DPZn, X =  $\text{CONH}(\text{CH}_2)_2\text{N}^+\text{Me}_3\text{Cl}^-$ ; 32(-)-DPZn, X =  $\text{COO}^-\text{H}^+$

\* Corresponding author. Phone: +81-3-5841-7138. Fax: +81-3-5841-7139. E-mail: kataoka@bmw.t.u-tokyo.ac.jp.

<sup>†</sup> Department of Materials Science and Engineering, Graduate School of Engineering, The University of Tokyo.

<sup>‡</sup> Present address: Philips Research, prof. Holstlaan 4, 5656 AA, Eindhoven, The Netherlands. E-mail: henk.stapert@philips.com.

<sup>§</sup> Department of Chemistry and Biotechnology, Graduate School of Engineering, The University of Tokyo.

<sup>||</sup> Department of Bioorganic Chemistry, Graduate School of Pharmaceutical Sciences, The University of Tokyo.

system (*8, 9*). On the other hand, a series of porphyrin compounds is known to effectively produce highly toxic singlet oxygen ( $^1\text{O}_2$ ) through excitation by light of a characteristic wavelength, and some are being used as photosensitizers for photodynamic therapy (PDT). Consequently, dendrimer porphyrins may have a potential as a novel type of photosensitizer used for PDT.



PDT is a topical and promising method for the localized treatment of solid tumors, and an increasing number of the photosensitizers are presently being explored in the preclinical and clinical study (10–15). However, most of them cause toxic side effects such as prolonged skin photosensitivity due to lack of the specificity to tumors (16). The efficiency of photosensitizers in situ is most likely to be dependent on their local accumulation and specific cellular uptake in the tumor site, stimulating research toward the development of water-soluble and efficient in vivo sensitizer–delivery system with a high potential to target specific organs (17–20). Notably, the higher molecular weight of the dendrimer porphyrins are promising in this regard, since macromolecular compounds can preferentially accumulate in solid tumor due to the enhanced permeability of tumor vascular endothelium and the lack of functional lymphatic drainage in the tumor tissue, known as the so-called enhanced permeability and retention (EPR) effect (21, 22). In addition, being different from low molecular weight photosensitizers currently in clinical use which exhibit nonspecific intracellular distribution, the dendrimer porphyrins with the relatively large size and three-dimensional structure are expected to be internalized in membrane-limited organelles, thereby achieving controlled localization in the intracellular compartment. Further, modification of the periphery of dendrimers with various ligands, including charged groups, sugars, and peptides, may open the way to design molecular-targeted PDT to accomplish highly selective death of tumorous cells with minimal side effects to the normal tissue. Here, we report for the first time the feasibility of dendrimer porphyrins with positive or negative charged groups on their periphery as an effective photosensitizer with little nonspecific, dark toxicity for PDT.

## MATERIALS AND METHODS

**Photosensitizers.** The synthesis and characterization of the ionic dendrimer porphyrins as given in Figure 1 have been reported previously (6–8). The third-generation aryl ether dendrimer with a Zn–porphyrin center and 32 positively charged  $(\text{C}(\text{O})\text{N}(\text{H})(\text{CH}_2)_2\text{N}^+\text{Me}_3)$  groups on its periphery and third-generation aryl ether dendrimer with a Zn–porphyrin center and 32 negatively charged  $(\text{COO}^-)$  groups on its periphery are abbreviated to 32(+)DPZn and 32(–)DPZn, respectively (Figure 1). The protoporphyrin IX (PIX, 8,13-divinyl-3,7,12,17-tetramethyl-21H,23H-porphine-2,18-dipropionic acid) (Aldrich Chemical Co., Inc., U.S.A.) was used as a control photosensitizer in this study.

**Evaluation of Singlet Oxygen Quantum Yield.** The singlet oxygen quantum yield was measured via direct observation of the near-infrared emission at 1268 nm, corresponding to the  $\text{O}_2(^1\Delta_g) \rightarrow \text{O}_2(^3\Sigma_g^-)$  transition (23). The experimental setup consists of Ar laser equipment (Innova 70–4; Coherent Inc., U.S.A.) and a near-infrared Ge detector (model 403HS; Applied Detector Co., U.S.A.) cooled by liquid nitrogen, connected to the exit slit of the monochromator (model CT10; JASCO, Japan) with a blaze wavelength at 1250 nm to minimize the grating loss. An IR-80 cutoff filter with 0% transmittance at less than 750 nm and 35% transmittance at 800 nm was placed at the entrance slit of the monochromator. A collecting lens focused the monochromator output onto the detector crystal. The Ar laser output at 514.5 nm was chopped with 800 Hz by an acousto-optic modulator (A-160; HOYA, Japan) operated by a driver (110-DS; HOYA, Japan). The signal output from the Ge detector was fed into a model 124A lock-in amplifier via a model 116

preamplifier (both from E.G. & G. Princeton Applied Research, U.S.A.) and synchronized with the internal reference signal of the lock-in amplifier. The signal output from the lock-in amplifier was fed to an XY recorder, and the emission spectrum was recorded by scanning the grating with a monitor. To minimize photobleaching, the solution was circulated at 4 mL/min using a peristaltic pump through a quartz flow cell ( $3 \times 3$  mm). MeOD was used as the solvent. Solutions were bubbled with pure  $\text{O}_2$  for 1 min before measurement.

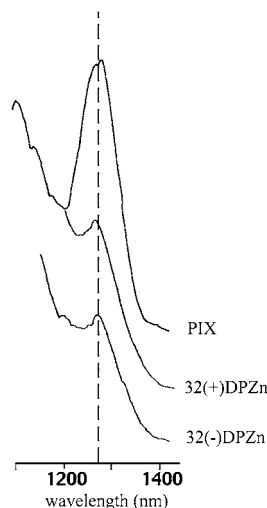
Molar absorption coefficients at 514.5 nm were determined in MeOD using a JASCO UV/VIS apparatus (model: Ubest-series V-550).

**Quantitative Analysis of Photosensitizers Associated with the Cells.** Quantification of the amount of dendrimers or PIX associated with Lewis Lung Carcinoma (LLC) cells at 4 or 37 °C was performed by utilizing the fluorescence of PIX at 630 nm (excitation at 400 nm) and of 32(+)DPZn and 32(–)DPZn at 600 nm (excitation at 430 nm). Following exposure to dendrimers or PIX for 30 min, 3 h, and 8 h, the cells were washed three times with sterile PBS, harvested after treated with trypsin–EDTA solution, and then dissolved in 20% SDS solution prior to fluorescence measurement ( $n = 3$ ). Fluorescent measurement was performed by JASCO spectrofluorometer FP-777 (Tokyo, Japan).

**Confocal Microscopy.** For confocal microscopy, LLC cells were cultured onto fibronectin (from bovine plasma, Itoham Foods, Inc., Japan)-coated sterile 35 mm glass-base dishes (Iwaki Glass, Japan). The cells were then incubated with each photosensitizer. In the case of dendrimer porphyrins, the cells were coinocubated with Tex-Red dextran (Molecular Probes, U.S.A.) as a neutral endocytosis marker (24). At definite time intervals, the cells were washed two times with sterile PBS, followed by confocal microscopy observation. Confocal microscopy was conducted using LSM 510 (Carl Zeiss Co., Ltd., Germany) at excitation wavelengths of 458 nm (Ar laser) for dendrimers and 543 nm (He–Ne laser) for Tex-Red dextran.

**Photoirradiation and Cell Viability Assay.** The cytotoxicity of each photosensitizer in vitro was assessed against LLC cells. In the darkened room, photosensitizers with different concentration in medium (Dulbecco's modified eagle's medium (DMEM) + 10% Fetal Bovine Serum (FBS)) were added to cell solutions in 96-well culture plates ( $n = 4$ ). After a defined incubation time (30 min, 3 h, and 8 h) at either 4 or 37 °C, the photosensitizers were removed, and then the plates were photoirradiated for 10 min with broad-band visible light using a Xenon lamp (150 W) equipped with a filter passing light of 377–700 nm (Estimated incident light irradiance: 150 mW/cm<sup>2</sup>). The viability of photoirradiated and nonphotoirradiated cells was evaluated by using the mitochondrial respiration via the 3-(4,5-dimethyl thiazol-2-yl)-2,5-diphenyltetrazolium bromide cleavage assay (MTT) following incubation for 24 h after photoirradiation.

**Detection of Photodamage by Fluorescent Probes.** Photodamaged sites in the cell were detected by three different fluorescent probes, Rhodamine 123 (Rh123; excitation 450–490 nm, emission 520–600 nm), 1-(4-trimethylammoniumphenyl)-6-phenyl-1,3,5-hexatriene iodide (tma-DPH; excitation 330–380 nm, emission 420–550 nm) (Dojindo Laboratories, Inc., Japan), and LysoTracker Red DND-99 (LysoTracker; excitation 577 nm, emission 590 nm) (Molecular Probes, U.S.A.), which is used for the staining of the mitochondrion, plasma membrane, and lysosome, respectively, in the living cell (25). Twenty minutes after irradiation, control or photo-



**Figure 2.** Near-infrared singlet oxygen luminescence emission spectrum of PIX, 32(+)-DPZn and 32(-)-DPZn excited by Ar laser light of 514.5 nm with 300 mW output power.

**Table 1.** The Efficiency of the  $^1\text{O}_2$  Emission at 1268 nm and the Absorption Coefficient at 514.5 nm of Each Photosensitizer

	$\epsilon$ (L/mol)	$^1\text{O}_2$ emission (V L mol $^{-1}$ )	$I/\epsilon$ (V)	$I/\epsilon$ (rel.)
Rose Bengal	31480	257 $\pm$ 34	8.2 $\pm$ 1.1	1.00
PIX	8705	32.5 $\pm$ 7.7	3.7 $\pm$ 0.9	0.45
P32(+)-DPZn	6239	25.1 $\pm$ 3.4	4.0 $\pm$ 0.5	0.49
P32(-)-DPZn	4849	16.6 $\pm$ 2.3	3.4 $\pm$ 0.5	0.41

damaged cells on fibronectin-coated sterile 35 mm glass-base dishes were incubated with 10  $\mu\text{g}/\text{mL}$  Rh123 for 10 min or 25  $\mu\text{M}$  LysoTracker for 40 min at 37  $^\circ\text{C}$  before the observation. To detect the plasma membrane photo-damage, a drop of tma-DPH in dimethylformamide (DMF) (0.5 mg/mL) was added to control or photodamaged cells detached from the culture dish by cell scraper 20 min after irradiation. Fluorescent images were acquired using confocal microscopy (LSM 510, Carl Zeiss Co, Germany).

## RESULTS

### Quantum Yield for Singlet Oxygen Production.

To compare the singlet oxygen quantum yield, direct observation of the  $\text{O}_2(^1\Delta_g) \rightarrow \text{O}_2(^3\Sigma_g^-)$  transition at 1270 nm ((0,0) vibronic band) was performed for PIX, 32(+)-DPZn, and 32(-)-DPZn in MeOD excited by Ar laser light bundle of 514.5 nm with 300 mW output power. The emission intensity was linear with output power over the range of at least 0–300 mW. Figure 2 presents the near-

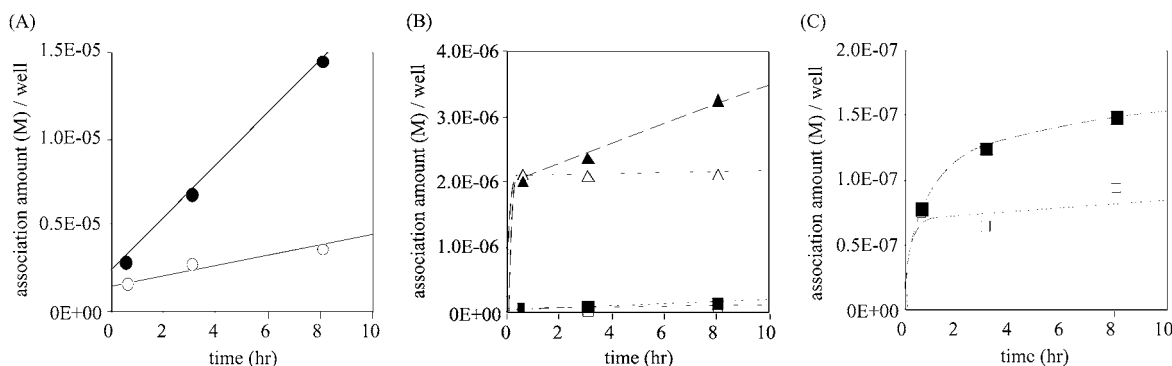
infrared singlet oxygen luminescence emission spectrum of the photosensitizers in MeOD. The linear relation between the emission intensity and the concentration of photosensitizers in the range of this measurement was confirmed for Rose Bengal, which was used as a reference. The emission efficiency defined as the molar ratio of the  $^1\text{O}_2$  emission intensity to the absorption coefficient at 514.5 nm of each photosensitizer is listed in Table 1. Small differences in the ratio of the  $^1\text{O}_2$  emission intensity to the absorption coefficient ( $I/\epsilon$ ) were observed between PIX and the dendrimer porphyrins. The observation that PIX and both dendrimers have similar singlet oxygen quantum efficiencies gave basis to directly compare the effects of 3D architecture and surface groups on the photodynamic activity of these sensitizers.

### Amount of Cellular Associated Photosensitizers.

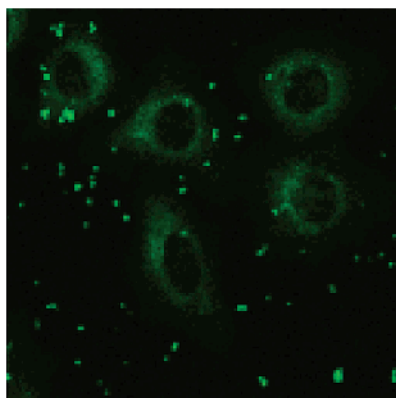
The time-dependent association of PIX and dendrimers with Lewis Lung Carcinoma (LLC) cells at different temperature (4 or 37  $^\circ\text{C}$ ) was evaluated from their fluorescence and shown in panels A and B, respectively, of Figure 3. The amount of PIX associated with the cells increased linearly with the exposure time for both 4 and 37  $^\circ\text{C}$ ; yet the slope is remarkably steeper for the latter condition (Figure 3A). The association profile of 32(+)-DPZn comprised two-phases: the first temperature-independent rapid association accomplished within 30 min, and the subsequent slow association particularly observed at 37  $^\circ\text{C}$  (Figure 3B). 32(-)-DPZn showed a similar trend to 32(+)-DPZn, although the associated amount was about one-order of magnitude lower (Figure 3B,C).

**Intracellular Localization.** The intracellular localization of dendrimers in LLC cells was observed by confocal microscopy. Figure 4 shows the fluorescent image of PIX after incubation with LLC cells for 3 h at 37  $^\circ\text{C}$ . Diffuse PIX fluorescence was present throughout the cell except for the nuclei, which is consistent with the intracellular distribution of in situ biosynthesized PIX in  $\Delta^5$ -aminolevulinic acid (ALA)-based PDT, as previously reported by Madsen et al. (13).

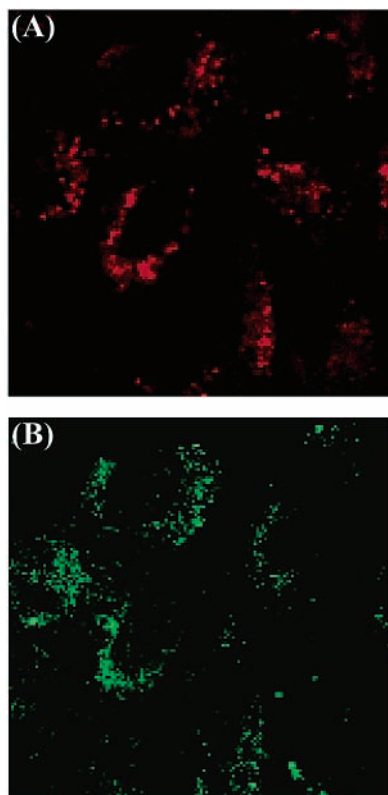
Confocal fluorescent images of Texas-Red dextran (red fluorescence) and 32(+)-DPZn (green fluorescence) after incubation with LLC cells for 3 h at 37 $^\circ\text{C}$  are shown in panels A and B, respectively, of Figure 5. Texas-Red dextran, which is known to be internalized by endocytosis leading to long time location in a lysosomal vesicle, was used as a marker molecule (24). The cellular nuclei appeared not fluorescent for both Texas-Red dextran and 32(+)-DPZn, indicating their localization in the extra-nuclear region of the intracellular compartment. Texas-Red dextran revealed the tiny dotted fluorescence around the perinuclear region, resulting from localization in



**Figure 3.** Amount of photosensitizers associated with LLC cells as a function of incubation time (○: PIX(4  $^\circ\text{C}$ ); ●: PIX(37  $^\circ\text{C}$ ); △: 32(+)-DPZn(4  $^\circ\text{C}$ ); ▲: 32(+)-DPZn(37  $^\circ\text{C}$ ); □: 32(-)-DPZn(4  $^\circ\text{C}$ ); ■: 32(-)-DPZn(37  $^\circ\text{C}$ )).



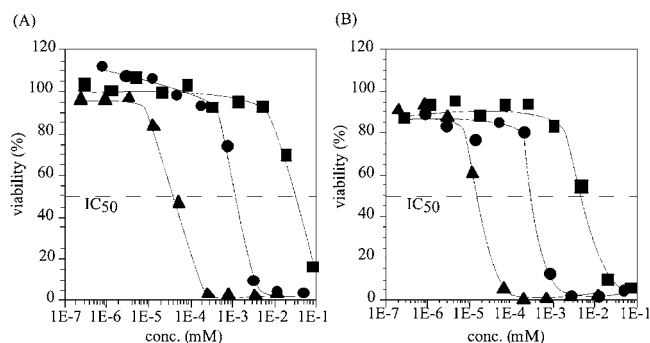
**Figure 4.** Confocal images of PIX in LLC cells after incubation of 3 h at 37 °C.



**Figure 5.** Confocal images of Texas-Red dextran (A) and 32(+)DPZn (B) in LLC cells after incubation of 3 h at 37 °C.

lysosomes (Figure 5A), and 32(+)DPZn showed a similar fluorescent image. The superposition of both fluorescent images revealed that 32(+)DPZn partially colocalized with Texas-Red dextran, suggesting that 32(+)DPZn is likely to be internalized via endocytosis, followed by localization in membrane-limited organelles such as lysosomes. 32(−)DPZn showed subcellular localization similar to that of 32(+)DPZn (data not shown).

**In Vitro PDT Effect.** The viability of LLC cells upon photoirradiation was evaluated by MTT assay and determined as a function of the concentration and the exposure time of photosensitizers, PIX, 32(+)DPZn, and 32(−)DPZn. In this assay, photosensitizers were incubated with LLC cells for a definite time period (30 min, 3 h, and 8 h), and nonassociated photosensitizers were removed prior to photoirradiation. The cellular viability upon photoirradiation indicates the in vitro photodynamic (PD) effect ( $^1\text{O}_2$ -induced toxicity). Panels A and B of Figure 6 illustrate the PD effect for LLC cells



**Figure 6.** The viability of LLC cells treated with PIX (●), 32(+)DPZn (▲), and 32(−)DPZn (■) after photoirradiation and at incubation times of 30 min (A) or 8 h (B).

**Table 2.** The in Vitro PDT Effect ( $^1\text{O}_2$ -Induced Toxicity) of PIX, 32(+)DPZn, and 32(−)DPZn in LLC Cell Line<sup>a</sup>

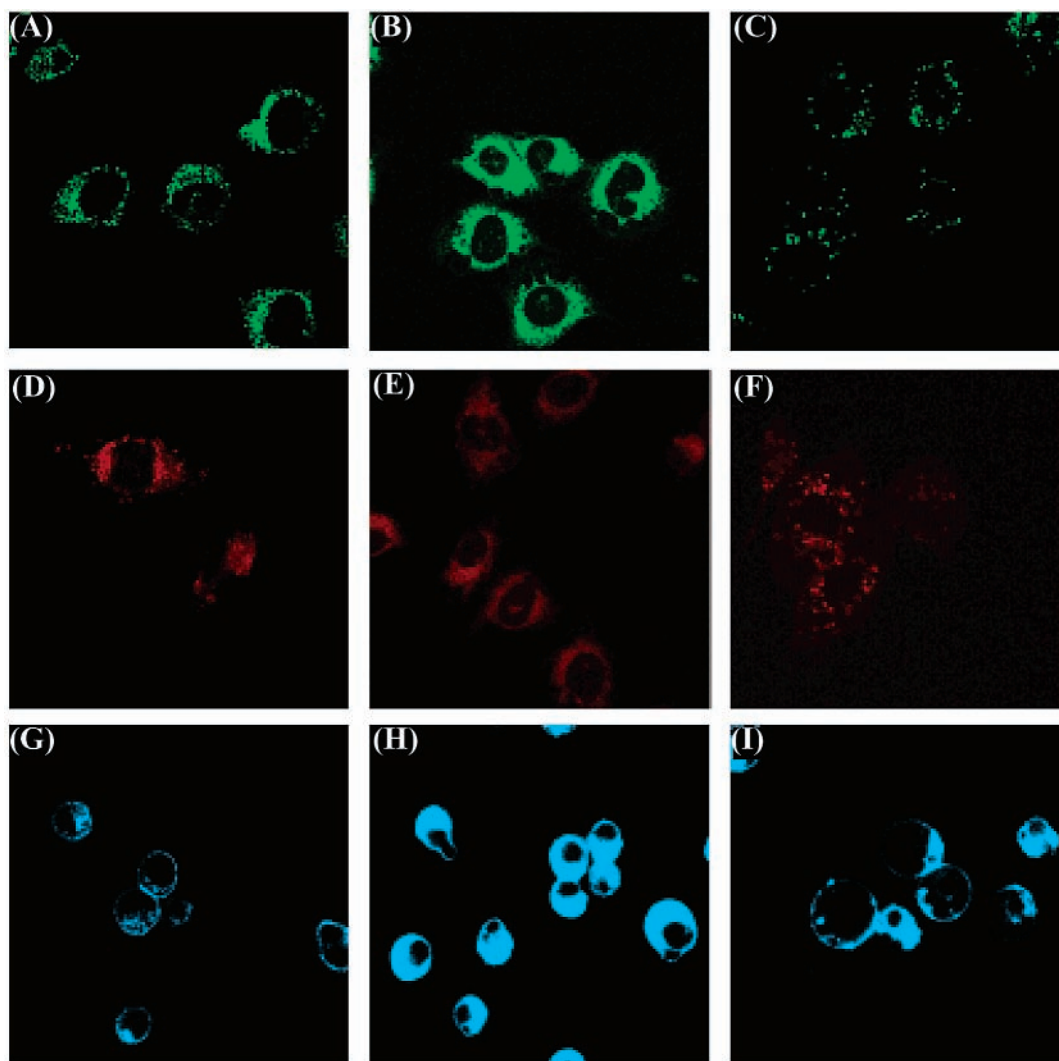
		IC <sub>50</sub> (μM)		IC <sub>50</sub> (4 °C)/ IC <sub>50</sub> (37 °C)
		4 °C	37 °C	
PIX	30 min	2.48	1.84	1.34
	3 h	1.02	0.980	1.04
	8 h	1.33	0.503	2.64
P32(+)	30 min	0.0986	0.0469	2.10
	3 h	0.0330	0.0280	1.18
	8 h	0.0237	0.0250	0.95
P32(−)	30 min	>80.0	35.8	—
	3 h	30.1	4.31	6.96
	8 h	38.7	5.76	6.72

<sup>a</sup> All data were presented by 50% inhibitory concentration (IC<sub>50</sub>) (unit: μM).

incubated with an increasing concentration of PIX (circle), 32(+)DPZn (trigon), and 32(−)DPZn (square) for 30 min (A) and 8 h (B), respectively. Obviously, the PD effect observed decreased in the order of 32(+)DPZn, PIX, and 32(−)DPZn. Table 2 summarizes 50% inhibitory concentration (IC<sub>50</sub>) of each photosensitizer at which fifty percent of tumor cells survive after photoirradiation, calculated from the cell viability–concentration curve (Figure 6). At 37 °C with 30 min and 8 h incubation, respectively, 32(+)DPZn has 39 and 20 times lower IC<sub>50</sub> values than PIX and 763 and 230 times lower IC<sub>50</sub> values than 32(−)DPZn, indicating a remarkably high PD efficiency of 32(+)DPZn. Notably, 32(+)DPZn achieved an extremely high PD effect even after a short exposure period (30 min), whereas the PD effect of 32(−)DPZn was low and appeared in a time-dependent manner particularly at 37 °C, where appreciable decrease in IC<sub>50</sub> value by increasing temperature was observed. On the other hand, significant differences in IC<sub>50</sub> between 4 and 37 °C were not observed for 32(+)DPZn, especially for the sample with prolonged incubation time, but were observed for 32(−)DPZn, as can be concluded from Table 2. It should be noted that the level of endocytotic activity of cells is greatly diminished at 4 °C.

**Dark Toxicity.** It is of primary importance to evaluate the dark toxicity (inherent toxicity) of photosensitizers in long time exposure from the standpoint of their application in vivo. Therefore, each photosensitizer, PIX, 32(+)DPZn, and 32(−)DPZn, was examined in terms of IC<sub>50</sub> values without photoirradiation after 72 h exposure in a dark room, and the results are shown in Table 3. 32(+)DPZn and 32(−)DPZn, respectively, exhibited 113- and 157-fold lower dark toxicity than PIX, indicating the remarkably high light-induced toxicity of dendrimer porphyrins, especially for 32(+)DPZn.





**Figure 7.** Photodamage from PIX and 32(+)DPZn in LLC cells as detected by three fluorescent probes: Rh123(A–C), LysoTracker (D–F), and tma-DPH (G–I). Control cells with photoirradiation alone are shown in panels A, D, and G, cells photodamaged with PIX in panels B, E, and H, and cells photodamaged with 32(+)DPZn in panel C, F, and I.

**Table 3.** Dark Toxicity of PIX, 32(+)DPZn, and 32(–)DPZn in LLC Cell Line after Incubation of 72 h at 37 °C

	PIX	P32(+)	P32(–)
IC <sub>50</sub> (μM)	0.200	22.6	31.3

**Photodamaged Sites in the Cell.** Control and photodamaged cells were stained with Rh123, LysoTracker, and tma-DPH to detect the mitochondrial, lysosomal, and plasma membrane photodamage, respectively. In this experiment, LLC cells were incubated with each photosensitizer at the concentration of 10-fold IC<sub>50</sub> for a definite time period (30 min and 3 h) at 4 or 37 °C prior to photoirradiation. Note that the fluorescent patterns of every probe in control cells were not altered by photoirradiation alone.

Fluorescent images of Rh123, LysoTracker, and tma-DPH-stained LLC cells are shown in panels A–C, D–F, and G–I, respectively, of Figure 7. Irradiated control cells without incubated photosensitizers showed spotted fluorescence of Rh123 and LysoTracker corresponding to the mitochondrion and lysosome, respectively (Figure 7A,D). The fluorescence of tma-DPH was mainly present at the cell surface (Figure 7G). After photodamage by PIX, diffuse fluorescence of Rh123 and LysoTracker (Figure 7B,E) and penetration of tma-DPH into submembrane

loci (Figure 7H) were detected, suggesting a disruption of mitochondrion, lysosome, and plasma membrane, respectively. On the other hand, photodamage by 32(+)DPZn seemed to induce no substantial change in the characteristic fluorescent pattern of each probe, except that a small portion of LysoTracker fluorescence became diffuse and the number of spotted fluorescence of Rh123 evidently decreased (Figure 7C,F,I). Photodamage by 32(–)DPZn rendered the fluorescent pattern of LysoTracker diffusive in small part similar to 32(+)DPZn but kept the characteristic fluorescent pattern of each probe, as observed in control cells (data not shown).

## DISCUSSION

32(+)DPZn and 32(–)DPZn aryl ether dendrimer zinc porphyrins both absorb light at 415, 434 (Soret bands), and 559 nm (Q-band) and emit fluorescent light at 610 and 660 nm. Due to their well-defined three-dimensional shape, which is morphologically trying to mimic biological light-harvesting antennae, they are of interest as artificial antennae for large distance energy transfer. Recently it has been shown that the efficiency of photoinduced energy transfer to the porphyrin core is enhanced via the rigid dendritic architecture (8, 9). The encapsulation of the reactive porphyrin center into a dendritic architecture

was also expected to have additional interesting properties, like the possibility to influence the interactions of the ionic groups on the periphery with biocomponents. The above considerations initiate our interest to investigate the potential of porphyrin dendrimers as photosensitizers for PDT. We have chosen third-generation water soluble ionic dendrimers which have an interesting combination of their size ( $\sim 5$  nm), surface charge, and water solubility (7).

The time-dependent profile of 32(+)DPZn association with LLC cells comprised two distinct phases: first, temperature-independent rapid association accomplished within 30 min, followed by temperature-dependent slow association (Figure 3B). The first rapid association appears to correspond to 32(+)DPZn adsorption to the negatively charged plasma membrane through electrostatic interaction, and the second phase, which is apparent at 37 °C, is likely to be internalization of dendrimers by adsorptive endocytosis. Note that the size of dendrimer ( $\sim 5$  nm) is obviously too large to diffuse through the plasma membrane. On the other hand, 32(-)DPZn showed a very low initial adsorption, which is less than 1/10 of the 32(+)DPZn adsorption. The slow and small increase in the associated amount after the initial adsorption was only observed at 37 °C (Figure 3C), suggesting that 32(-)DPZn is taken up by fluid-phase endocytosis. Both dendrimers internalized into the cells finally appear to localize in endosomal compartments because they colocalized with Tex-Red dextran, a fluid-phase endocytic marker (Figure 5). The PD effect ( $^1\text{O}_2$ -induced cytotoxicity) at 37 °C of 32(+)DPZn was 230 times higher than that of 32(-)DPZn (Table 2), while the associated amount of 32(+)DPZn was estimated to be only 22–25 times higher than that of 32(-)DPZn (Figure 3B), illustrating the higher PD efficiency of 32(+)DPZn compared to 32(-)DPZn. Because both compounds have similar efficiencies of singlet oxygen production, difference in the photoinduced cytotoxicity cannot solely be attributed to the different internalized amounts. The difference in the efficiency of PD effect between 32(+)DPZn and 32(-)DPZn should be due to the different interactions of both compounds with cellular components. 32(+)DPZn is likely to adsorb strongly with negatively charged membrane components, for example, glycoproteins, through electrostatic interactions, whereas negatively charged 32(-)DPZn seems not to be in a close contact with membrane components due to electrostatic repulsion. Consequently, the photodamage to the plasma membranes may be more vigorous for 32(+)DPZn as compared to 32(-)DPZn and may cause lipid peroxidation, protein cross-linking, and loss of ionic homeostasis (26–29). Further, the photodamage to the lysosomal membranes may cause release of hydrolases into the cytoplasm (30). The direct possible interaction of dye radicals with biocomponents can be excluded in the present case because the dendrimers have a relatively dense 3D structure in which the dye molecule (porphyrin) is protected by aryl ether dendrons. Thus, it is likely that only singlet oxygen or other reactive oxygenic species are responsible for the PD effect of dendrimer porphyrins. Singlet oxygen has a quite short lifetime, and the diffusion distance of  $^1\text{O}_2$  is estimated to be less than 10 nm (10). Nevertheless, the 3D structure of dendrimers with the size of 5 nm appears not to be a barrier for the  $^1\text{O}_2$ -induced PD effect, as 32(+)DPZn showed a remarkably high cytotoxicity upon photoirradiation.

The protoporphyrin (PIX) used as a control in this study is one of primitive but effective photosensitizers well-studied by many research groups and is a component

of protoheme (28, 29, 31–33). Excessive levels of PIX in circulating red blood cells cause erythropoietic protoporphyria, leading to cutaneous photosensitivity (33). The PIX, which is rather unpolar and only slightly soluble in water, may penetrate into cells through the plasma membrane by simple diffusion (Figure 3A) and partitions into the plasma as well as subcellular membrane components, including the mitochondrial, lysosomal, endoplasmic reticulum, and nuclear membranes (31, 32). Indeed, PIX showed a diffuse pattern of fluorescence throughout the cell except the nuclei. It seems that the mitochondrion is most likely susceptible to the PIX-induced photodamage (32), since PIX can be ligands for the mitochondrial peripheral benzodiazepine receptor (PBR) (10). The reason many PD efficient photosensitizers are hydrophobic appears to be because the plasma as well as subcellular membranes are critical sites for the  $^1\text{O}_2$ -induced photodamage to the cells (25, 27, 33, 34). Worth noting is that 32(+)DPZn showed a 20 times higher PD effect than PIX (Table 2) even though the former cell association after 8 h incubation was 4.5 times lower (Figure 3A,B). These results suggest that 32(+)-DPZn has a markedly enhanced efficiency of PD effect even compared with PIX, which should be explained by the their different localization in the plasma and subcellular membranes such as plasma membrane proteins, including transporters, ion channels, enzymes or cytoskeleton, lipids, etc. (26, 27, 35), as well as the differences in photodamaged sites in the organelles in the cells (25, 30, 31, 33, 34, 36, 37). Kochevar et al. demonstrated that the photodamaged sites and functions vary with the localization or distribution of the dye molecules in the cell membranes (27). PIX is known to accumulate primarily in the lipophilic compartments of the cell membranes (31, 32), while 32(+)DPZn appears to interact electrostatically with cell membranes, leading to different localization and/or distribution on the membranes as compared to PIX. Dendrimer porphyrins with a size of 5 nm are likely too large to penetrate into the cytoplasm, so that their internalization does occur in membrane-limited organelles (Figure 5). Therefore, the PD effect of 32(+)DPZn may also be different from that of low molecular weight photosensitizers with a cationic charge, which have been shown to localize selectively within mitochondria leading to efficient cell death (10). Furthermore, 32(+)DPZn may overcome the drawback of low molecular weight, cationic photosensitizers, as they clear very rapidly from tumor tissues (38, 39). Macromolecules retain in tumor tissue at higher levels due to the EPR effect (21, 22). Recently, several studies have demonstrated that nucleic acid compounds can be an alternative potential target of  $^1\text{O}_2$ -induced photodamage (40, 41). However, this mechanism seems to be unlikely for the PD effect of 32(+)DPZn because, as seen in Figure 5, fluorescence of 32(+)DPZn was hardly detectable in cellular nuclei. Although the exact molecular targets of 32(+)DPZn are an issue to be clarified in future, it is apparently important to control the intracellular disposition of the dye molecules based on the nature of the interaction forces to achieve an efficient PD effect.

Photodamage by 32(+)DPZn maintained the characteristic structure of membrane and intracellular organelles (the plasma membrane, mitochondria, and lysosomes), whereas such organelles were severely photodamaged by PIX (Figure 7). Thus, the question is raised how photodamage by 32(+)DPZn nevertheless leads to the most efficient cell death. In this regard, the number of spotted fluorescence of the mitochondrion marker Rh123 decreased due to photodamage by 32(+)DPZn even

after incubation of 30 min (Figure 7C). The fluorescent intensity of Rh123 is known to be correlated with the amount of adenosine triphosphate (ATP) in the cell (42). Therefore, photodamage by 32(+)-DPZn may have clipped the ATP production in the cell, resulting in the efficient cell death. In general, the eliminated ATP production is characteristic for necrosis or caspase-independent programmed cell death (43, 44) (oncosis (45)). Similar necrosis-like cell death was previously observed when the plasma membrane was targeted as the photodamaged site (25, 34, 46). It was suggested that such necrotic process could be induced by photodynamically stimulating some critical targets on the plasma membrane, which results in a delayed or arrested apoptotic signaling pathway. The target sites are thought to be transporters, ion channels, or lipids rather than direct disruption of the outer cell membrane (25, 34, 46). This hypothesis appears to be consistent with our observation that the efficient PD-induced cell death combined with extremely low dark toxicity and the maintained characteristic organella structure after photoirradiation of 32(+)-DPZn-treated LLC cells. However, the mechanism of necrosis-like cell death following photodamage to the plasma membrane remains to be studied. Elucidation of the PD mechanism of dendrimer-based photosensitizers is ongoing in our laboratory.

PIX exhibited remarkably high dark toxicity after prolonged incubation of 72 h (Table 3). On the other hand, both dendrimers, 32(+)-DPZn and 32(-)-DPZn showed extremely low dark toxicity even after 72 h incubation. Upon prolonged incubation, PIX tends to localize largely in the mitochondrial membrane (32), causing mitochondrial dysfunction. Further, it can diffuse to every other organelle in the cytoplasm as shown in Figure 4 (13, 33). The high dark toxicity of PIX may result from such complexity in the intracellular localization. In contrast, the extremely low dark toxicity of dendrimer porphyrins may result from the distinctive intracellular disposition characteristics due to their relative large size and anionic or cationic periphery. Note that a low dark toxicity is one of the important criteria for assessing the usefulness of photosensitizers because unwanted toxicity to normal tissues is one of the major side effects in clinical PDT (33). The low dark toxicity of 32(+)-DPZn is consistent with previous results obtained for cationic dendrimers used for gene transfection, which are known to have lower inherent cytotoxicity than other cationic linear polymers (5). The inherent low toxicity of dendrimers may originate from their monodispersed spherical nature as compared with conventional synthetic polymers having a three-dimensional configuration as well as chemical heterogeneity. Thus, the dendrimers are of great interest as the materials for drug delivery system (DDS).

The porphyrin dendrimers used in this study have a maximum optical absorption at approximately 559 nm (Q-band), which has only limited tissue penetration efficiency. Therefore, the development of dendrimers having increased absorbance of light in the higher wavelength region may be desirable for clinical use. In this regard, synthesis of dendrimers encapsulating a metallo-phthalocyanine, which has an optical absorption at 675 nm where the light can penetrate the tissues approximately 2 times deeper than Photofrin (630 nm) (18), is in principle feasible in our laboratory (47). Alternatively, two-photon excitation by using near-infrared lasers may have great potential for dendrimer porphyrin-based PDT of diseases in the deeper tissue (e.g., brain tumors) (48). The possibility of two photon absorption is known to depend linearly on the intrinsic

two-photon cross section of the compounds,  $\delta$ , and quadratically on the incident light intensity (48). Although the two-photon cross section of molecules is typically small compared with one-photon absorption, neodymium: YAG (Nd:YAG) laser emitting at 1,064 nm or tunable solid state lasers generating far-red/near-infrared light could significantly increase the possibility of two photon absorption of the compounds due to high laser output (49).

On the other hand, substituting peripheral ionic groups of dendrimers with alternative ligands to target particular types of tumor cells is likely a key to performing the most efficient PDT (36, 50). This has wide-reaching implications for achieving efficient cell type-specific PDT because it will enable the active dose of dyes administered to the patients to be reduced. The development of appropriate in vivo carrier system of 32(+)-DPZn is of primary importance for systemic PDT of solid tumor with suppression of side effects (17–20). The desirable properties of such in vivo carrier system are (i) improved water-solubility, (ii) specific accumulation in tumor, (iii) safety to the body, and (iv) prompt excretion from the body following PDT. To achieve these requirements, we have developed poly-ion complex (PIC) micelles entrapping dendrimer porphyrins in their core through the self-association of ionic dendrimer porphyrins with oppositely charged poly(ethylene glycol) PEG–poly(amino acid) block copolymers (51). In this way, PIC micelle carriers of dendrimer porphyrins, surrounded by a hydrophilic palisade of PEG strands, were prepared. As previously reported, several types of polymeric micelles with PEG shell were demonstrated to accumulate effectively and specifically in solid tumor (52–54). Thus, we expect PIC micelles with dendrimer porphyrins in the core may hold a promise for tumor-directed targeting of photosensitizers, and research in this direction is now ongoing in our laboratory.

#### ACKNOWLEDGMENT

The authors like to thank Ms A. Ryu, Kose Co. for assisting with the singlet oxygen quantum efficiency measurements. This work was supported in part by Core Research for Evolutional Science and Technology (CREST), Japan Science and Technology Corporation (JST).

#### LITERATURE CITED

- Alivisatos, A. P. (2001) Less is more in medicine. *Sci. Am.* September, 67–74.
- Wang, D., Kopeckova, P., Minko, T., Nanayakkara, V., and Kopecek, J. (2000) Synthesis of starlike N-(2-hydroxypropyl)-methacrylamide copolymers: potential drug carriers. *Bio-macromolecules* 1, 313–319.
- Malik, N., Wiwattanapatapee, R., Klopsch, R., Lorenz, K., Frey, H., Weener, J. W., Meijer, E. W., Paulus, W., and Duncan, R. (2000) Dendrimers: relationship between structure and biocompatibility in vitro, and preliminary studies on the biodistribution of  $^{125}\text{I}$ -labeled polyamidoamine dendrimers in vivo. *J. Contrlled Release* 65, 133–148.
- Kukowska-Latallo, J. F., Bielinska, A. U., Johnson, J., Spindler, R., Tomalia, D. A., and Baker, J. R., Jr. (1996) Efficient transfer of genetic material into mammalian cells using Starburst polyamidoamine dendrimers. *Proc. Natl. Acad. Sci. U.S.A.* 93, 4987–4992.
- Bielinska, A., Kukowska-Lattalo, J.-F., Johnson, J., Tomalia, D. A., and Baker, J. R., Jr. (1996) Regulation of in vitro gene expression using antisense oligonucleotides or antisense expression plasmids transfected using starburst PAMAM dendrimers. *Nucleic Acids Res.* 24, 2176–2182.



- (6) Tomoyose, Y., Jiang, D.-L., Jin, R.-H., Aida, T., Yamashita, T., Horie K., Yashima, E., and Okamoto, Y. (1996) Aryl ether dendrimers with an interior metalloporphyrin functionality as a spectroscopic probe: interpenetrating interaction with dendritic imidazoles. *Macromolecules* 29, 5236–5238.
- (7) Tomioka, N., Takasu, D., Takahashi, T., and Aida, T. (1998) Electrostatic assembly of dendrimer electrolytes: negatively and positively charged dendrimer porphyrins. *Angew. Chem., Int. Ed. Engl.* 37, 1531–1534.
- (8) Sadamoto, R., Tomioka, N., and Aida, T. (1996) Photo-induced electron-transfer reactions through dendrimer architecture. *J. Am. Chem. Soc.* 118, 3978–3979.
- (9) Jiang, D.-L., and Aida, T. (1998) Morphology-dependent photochemical events in aryl ether dendrimer porphyrins: cooperation of dendron subunits for singlet energy transduction. *J. Am. Chem. Soc.* 120, 10895–10901.
- (10) Macdonald, I. J., and Dougherty, T. J. (2001) Basic principles of photodynamic therapy. *J. Porphyrins Phthalocyanines* 5, 105–129.
- (11) McCaughan, J. M., Jr. (1999) Photodynamic therapy: a review. *Drug Aging* 15, 49–68.
- (12) Veenhuizen, R. B., Ruevekamp, M. C., Oppelaar, H., Helmerhorst, T. J. M., Kenemans, P., and Stewart, F. A. (1997) Foscan-mediated photodynamic therapy for a peritoneal-cancer model: drug distribution and efficacy studies. *Int. J. Cancer* 73, 230–235.
- (13) Madsen, S. J., Sun, C.-H., Tromberg, B. J., Wallance, V. P., and Hirschberg, H. (2000) Photodynamic therapy of human glioma spheroids using 5-aminolevulinic acid. *Photochem. Photobiol.* 72, 128–134.
- (14) Songca, S. P., and Mbatha, B. (2000) Solubilization of meso-tetraphenylporphyrin photosensitizers by substitution with fluorine and with 2,3-dihydroxy-1-propyloxy groups. *J. Pharm. Pharmacol.* 52, 1361–1367.
- (15) Bousset, N., Vonarx, V., Eleouet, S., Carre, J., Bourre, L., Lajat, Y., and Patrice, T. (2000) Cellular distribution and phototoxicity of benzoporphyrin derivative and Photofrin. *Res. Exp. Med.* 199, 341–357.
- (16) Hamblin, M. R., and Newman, E. L. (1994) On the mechanism of the tumour-localising effect in photodynamic therapy. *J. Photochem. Photobiol. B: Biol.* 23, 3–8.
- (17) Allemann, E., Rousseau, J., Brasseur, N., Kudrevich, S. V., Lewis, K., and van Lier, J. E. (1996) Photodynamic therapy of tumours with hexadecafluoro zinc phthalocyanine formulated in PEG-coated poly(lactic acid) nanoparticles. *Int. J. Cancer* 66, 821–824.
- (18) Brasseur, N., Ouellet, R., Madeleine, C. L., and van Lier, J. E. (1991) Water-soluble aluminium phthalocyanine-polymer conjugates for PDT: photodynamic activities and pharmacokinetics in tumour-bearing mice. *Br. J. Cancer* 80, 1533–1541.
- (19) Ris, H.-B., Krueger, T., Giger, A., Lim, C. K., Stewart, J. C. M., Althaus, U., and Altermatt, H. J. (1999) Photodynamic therapy with mTHPC and polyethylene glycol-derived mTHPC: a comparative study on human tumour xenografts. *Br. J. Cancer* 79, 1061–1066.
- (20) Tabata, Y., Murakami, Y., and Ikada, Y. (1997) Photodynamic effect of polyethylene glycol-modified fullerene on tumor. *Jpn. J. Cancer Res.* 88, 1108–1116.
- (21) Matsumura, Y., and Maeda, H. (1986) A new concept for macromolecular therapeutics in cancer chemotherapy: mechanism of tumorotropic accumulation of proteins and the antitumor agent Smancs. *Cancer Res.* 46, 6387–6392.
- (22) Maeda, H. (2001) SMANCS and polymer-conjugated macromolecular drugs: advantages in cancer chemotherapy. *Adv. Drug Deliv. Rev.* 46, 169–185.
- (23) Arakane, K., Ryu, A., Takarada, K., Masunaga, T., Shimoto, K., Kobayashi, R., Mashiko, S., Nagano, T., and Hirobe, M. (1996) Measurement of 1268 nm emission for comparison of singlet oxygen ( $^1D_2$ ) production efficiency of various dyes. *Chem. Pharm. Bull.* 44, 1–4.
- (24) Ferris, A. L., Brown, J. C., Park, R. D., and Storrle, B. (1987) Chinese hamster ovary cell lysosomes rapidly exchange contents. *J. Cell Biol.* 105, 2703–2712.
- (25) Kessel, D., Luo, Y., Deng, Y., and Chang, C. K. (1997) The role of subcellular localization in initiation of apoptosis by photodynamic therapy. *Photochem. Photobiol.* 65, 422–426.
- (26) Kessel, D. (1977) Effects of photoactivated porphyrins at the cell surface of leukemia. *Biochemistry* 16, 3443–3449.
- (27) Kochevar, I. E., Bouvier, J., Lynch, M., and Lin, C.-W. (1994) Influence of dye and protein location on photosensitization of the plasma membrane. *Biochim. Biophys. Acta* 1196, 172–180.
- (28) Wakulchik, S. D., Schiltz, J. R., and Bickers, D. R. (1980) Photolysis of protoporphyrin-treated human fibroblasts in vitro: studies on the mechanism. *J. Lab. Clin. Med.* 96, 158–167.
- (29) Girotti, A. W. (1976) Photodynamic action of protoporphyrin IX on human erythrocytes: cross-linking of membrane proteins. *Biochem. Biophys. Res. Com.* 72, 1367–1374.
- (30) Santus, R., Kohen, E., Reyftmann, J. P., Morliere, P., Dubertret, L., and Tocci, P. M. (1983) Permeation of lysosomal membranes in the course of photosensitization with methylene blue and hematoporphyrin: study of cellular microspectrofluorometry. *Photochem. Photobiol.* 38, 71–77.
- (31) Moan, J., Pettersen, E. O., and Christensen, T. (1979) The mechanism of photodynamic inactivation of human cells in vitro in the presence of haematoporphyrin. *Br. J. Cancer* 39, 398–407.
- (32) Stanberg, S., and Romslo, I. (1981) Porphyrin-induced photodamage at the cellular and the subcellular level as related to the solubility of the porphyrin. *Clin. Chim. Acta* 109, 193–201.
- (33) Sandberg, S., and Romslo, I. (1981) Phototoxicity of protoporphyrin as related to its subcellular localization in mice livers after short-term feeding with griseofulvin. *Biochem. J.* 198, 67–74.
- (34) Dellinger, M. (1996) Apoptosis or Necrosis following Photofrin photosensitization: influence of the incubation protocol. *Photochem. Photobiol.* 64, 182–187.
- (35) Boegheim, J. P. J., Scholte, H., and Dubbelman, T. M. A. R. (1987) Photodynamic effects of hematoporphyrin-derivative on enzyme activities of murine L929 fibroblasts. *J. Photochem. Photobiol. B: Biol.* 1, 61–73.
- (36) Akhlynina, T. V., Rosenkranz, A. A., Jans, D. A., and Sobolev, A. S. (1995) Insulin-mediated intracellular targeting enhances the photodynamic activity of chlorin  $e_6$ . *Cancer Res.* 55, 1014–1019.
- (37) Brenner, C., and Kroemer, G. (2000) Mitochondria-the death signal integrators. *Science* 289, 1150–1151.
- (38) Bellnier, D. A., Young, D. N., Detty, M. R., Camacho, S. H., and Oseroff, A. R. (1999) pH-dependent chalcogenopyrylium dyes as potential sensitizers for photodynamic therapy: selective retention in tumors by exploiting pH differences between tumor and normal tissue. *Photochem. Photobiol.* 70, 630–636.
- (39) Villanueva, A., and Jori, G. (1993) Pharmacokinetic and tumour-photosensitizing properties of the cationic porphyrin meso-tetra(4-N-methylpyridyl)porphine. *Cancer Lett.* 73, 59–64.
- (40) Akhlynina, T. V., Jans, D. A., Rosenkranz, A. A., Statsyuk, N. V., Balashova, I. Y., Toth, G., Pavo, I., Rubin, A. B., and Sobolev, A. S. (1997) Nuclear targeting of chlorin  $e_6$  enhances its photosensitizing activity. *J. Biol. Chem.* 272, 20328–20331.
- (41) Bisland, S. K., Singh, D., and Gariepy, J. (1999) Potentiation of chlorin  $e_6$  photodynamic activity in vitro with peptide-based intracellular vehicles. *Bioconjug. Chem.* 10, 982–992.
- (42) Downes, C. S., Ord, M. J., Mullinger, A. M., Collins, A. R., and Johnson, R. T. (1985) Novobiocin inhibition of DNA excision repair may occur through effects on mitochondrial structure and ATP metabolism, not on repair topoisomerases. *Carcinogenesis* 6, 1343–1352.
- (43) Chi, S., Kitanaka, C., Noguchi, K., Mochizuki, T., Nagashima, Y., Shirouzu, M., Fujita, H., Yoshida, M., Chen, W., Asai, A., Himeno, M., Yokoyama, S., and Kuchino, Y. (1999) Oncogenic Ras triggers cell suicide through the activation of

- a caspase-independent cell death program in human cancer cells. *Oncogene* 18, 2281–2290.
- (44) Xiang, J., Chao, D. T., and Korsmeyer, S. J. (1996) Bax-induced cell death may not require interleukin 1 $\beta$ -converting enzyme-like proteases. *Proc. Natl. Acad. Sci. U.S.A.* 93, 14559–14563.
- (45) Majno, G., and Joris, I. (1995) Apoptosis, oncosis, and necrosis: an overview of cell death. *Am. J. Pathol.* 146, 3–15.
- (46) Luo, Y., and Kessel, D. (1997) Initiation of apoptosis versus necrosis by photodynamic therapy with chloroaluminum phthalocyanine. *Photochem. Photobiol.* 66, 479–483.
- (47) Aida, T., and Jiang, D.-L. (2000) Dendrimer porphyrins and metalloporphyrins: syntheses, structures and functions. In *The Porphyrin Handbook, Inorganic, Organometallic and Coordination Chemistry* (Kadish, K. M., Smith, K. M., and Guillard, R., Eds.) Volume 3, pp 369–384, Academic Press, New York.
- (48) Oh, D. H., Stanley, R. J., Lin, M., Hoeffler, W. K., Boxer, S. G., Berns, M. W., and Bauer, E. (1997) Two-photon excitation of 4'-hydroxymethyl-4,5',8-trimethylpsoralen. *Photochem. Photobiol.* 65, 91–95.
- (49) Fisher, A. M. R., Murphree, A. L., and Gomer, C. J. (1995) Clinical and preclinical photodynamic therapy. *Lasers Surgery Med.* 17, 2–31.
- (50) Lu, Z.-R., Kopeckova, P., and Kopecek, J. (1999) Polymerizable Fab' antibody fragments for targeting of anticancer drugs. *Nat. Biotechnol.* 17, 1101–1104.
- (51) Stapert, H. R., Nishiyama, N., Kataoka, K., Jiang, D.-L., and Aida, T. (2000) Poly-ion complex micelles encapsulating light-harvesting dendrimer porphyrins. *Langmuir* 16, 8182–8188.
- (52) Kwon, G. S., and Kataoka, K. (1995) Block copolymer micelles as long-circulating drug vehicles. *Adv. Drug Deliv. Rev.* 16, 295–309.
- (53) Yokoyama, M., Okano, T., Sakurai, Y., Fukushima, S., Okamoto, K., and Kataoka, K. (1999) Selective delivery of adriamycin to a solid tumor using a polymeric micelle carrier system. *J. Drug Target.* 7, 171–186.
- (54) Nishiyama, N., Kato, Y., Sugiyama, Y., and Kataoka, K. (2001) Cisplatin-loaded polymer-metal complex micelle with time-modulated decaying property as a novel drug delivery system. *Pharm. Res.* 18, 1035–1041.

BC025597H

# Non-Natural Cell Surface Receptors: Synthetic Peptides Capped with N-Cholesterylglycine Efficiently Deliver Proteins into Mammalian Cells

Scott E. Martin and Blake R. Peterson\*

Department of Chemistry, The Pennsylvania State University, 152 Davey Lab, University Park, Pennsylvania 16802. Received September 5, 2002; Revised Manuscript Received October 9, 2002

Protein toxins such as shiga toxin and cholera toxin penetrate into cells by binding small molecule-based cell surface receptors localized to cholesterol and sphingolipid-rich lipid raft subdomains of cellular plasma membranes. Molecular recognition between these toxins and their receptors triggers endocytic protein uptake through endogenous membrane trafficking pathways. We report herein the synthesis of functionally related non-natural cell surface receptors comprising peptides capped with N-cholesterylglycine as the plasma membrane anchor. The peptide moieties of these receptors were based on high-affinity epitopes of anti-hemagglutinin antibodies (anti-HA), anti-Flag antibodies, and a moderate-affinity *Strep* Tag II peptide ligand of the streptavidin protein from *Streptomyces avidini*. These non-natural receptors were directly loaded into plasma membranes of Jurkat lymphocytes to display peptides from lipid rafts on the cell surface. Molecular recognition between these receptors and added cognate anti-HA, anti-Flag, or streptavidin proteins resulted in rapid clathrin-mediated endocytosis; fluorescent target proteins were completely internalized within 4–12 h of protein addition. Analysis of protein uptake by epifluorescence microscopy and flow cytometry revealed intracellular fluorescence enhancements of 100-fold to 200-fold (10  $\mu$ M non-natural receptor) with typically >99% efficiency. This method enabled intracellular delivery of a functional *Escherichia coli*  $\beta$ -galactosidase enzyme conjugated to Protein A from *Staphylococcus aureus*. We termed this novel delivery strategy “synthetic receptor targeting”, which is an efficient method to enhance macromolecular uptake by decorating mammalian cells with chemically defined synthetic receptors that access the molecular machinery controlling the organization of cellular plasma membranes.

## INTRODUCTION

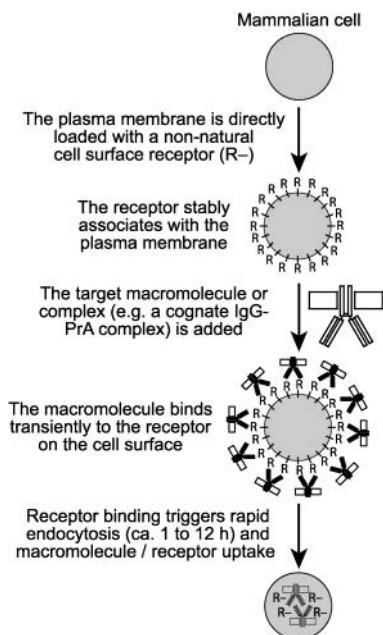
The hydrophobic character of cellular plasma membranes effectively seals the inner machinery of cells away from many molecules in the extracellular environment. Typically only moderately hydrophobic compounds of low molecular weight undergo rapid passive diffusion across low-polarity cellular membranes; macromolecules such as proteins and DNA generally require specific active transport mechanisms to access the cell interior (1). To circumvent this obstacle, many methods have been developed to enhance the cellular uptake of poorly permeable molecules (2–9). Many such methods involve covalent or noncovalent modification of macromolecules with polymers, lipids, or other agents that favorably alter the chemical properties of macromolecular cargo. In particular, peptides that mediate membrane translocation comprise an important class of oligomeric delivery vectors (2). However, the molecular mechanisms underlying many cellular delivery systems are not yet well enough understood to consistently and efficiently deliver macromolecules to desired targets in diverse cell lines. Hence, improved delivery systems with well-defined molecular mechanisms of action are needed in basic cell biology, tumor therapy, and genetic therapy.

Mammalian cells internalize nutrients and other macromolecular entities through the active transport mechanism of endocytosis (10, 11). This mechanism typically

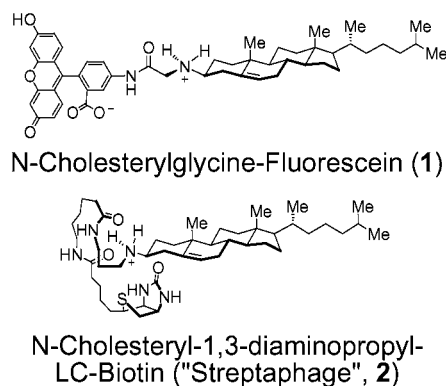
involves recognition of molecules by plasma-membrane-associated receptors, clustering of receptor–ligand complexes, and invagination of these regions of the plasma membrane to form intracellular vesicles. These vesicles fuse to form organelles termed endosomes that are directed to compartments for degradation or recycling of internalized contents. Under certain conditions, endosomal contents can also be released into the cytosol (10, 11). Endocytosis is a mechanism of cellular penetration employed by many viruses and toxins such as shiga toxin from *Shigella dysenteriae* and cholera toxin from *Vibrio cholerae* (12). These toxins are members of the AB<sub>5</sub> family of protein toxins (13) that penetrate into mammalian cells by binding of the toxin to small molecule cell surface receptors such as the glycosphingolipid Gb3 (shiga toxin receptor) and ganglioside GM1 (cholera toxin receptor). These low molecular weight receptors are sphingolipids that comprise tri- or pentasaccharide headgroups linked to the lipid ceramide (N-acyl sphingosine). These receptors reside in sphingolipid-rich lipid raft subdomains of cellular plasma membranes. Lipid rafts are composed of cholesterol packed with sphingolipids in a liquid ordered phase (14–17), and these subdomains are key elements involved in the control of numerous signal transduction pathways (18). Although both shiga toxin and cholera toxin penetrate into cells (12) primarily through the mechanism of clathrin-mediated endocytosis (19), the precise interactions that link these toxins to clathrin through their receptors and the role played by lipid rafts in this process are not yet well understood (20, 21).

\* Corresponding author. Email: brpeters@chem.psu.edu. Tel: (814) 865-2969. Fax: (814) 863-8403.



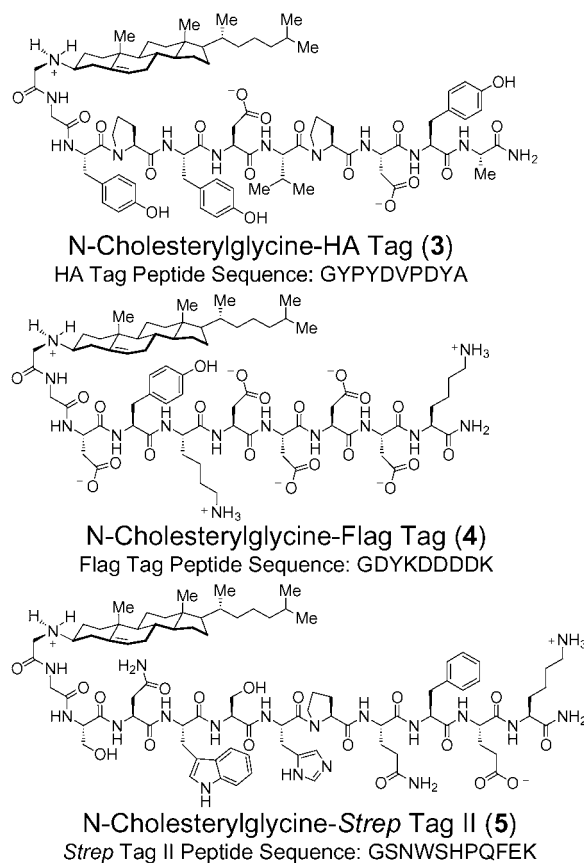


**Figure 1.** Delivery of macromolecules to cells by synthetic receptor targeting. Non-natural cell surface receptors directly loaded into cellular plasma membranes enable delivery of cognate macromolecules through endogenous membrane trafficking pathways.



**Figure 2.** Structures of previously reported non-natural cell surface receptors.

Our laboratory is investigating a novel macromolecular delivery system termed here as "synthetic receptor targeting" (Figure 1). This method employs non-natural cell surface receptors such as compounds **1** and **2** (Figure 2) based on lipids that insert into cellular plasma membranes. These receptors comprise derivatives of  $\beta$ -cholesterylamine linked to protein-binding motifs including fluorescein (22) and biotin (23). These compounds functionally mimic natural small-molecule receptors such as glycosphingolipid Gb3 or ganglioside GM1 by persistently associating with lipid raft subdomains of cellular plasma membranes. For example, the cholesterylamine-derived fluorescent probe **1** is primarily plasma-membrane-associated even 16 h after addition to living cells (22). However, as shown in Figure 1, binding of cognate proteins such as immunoglobulins (IgGs) or streptavidin to these plasma membrane-anchored small molecules rapidly triggers clathrin-mediated endocytosis of the receptor-protein complex (22, 23). This approach is conceptually related to elegant studies of metabolic cell surface engineering that display non-natural functional groups such as ketones and azides on cell surfaces (24–27). These ketones and other functional groups can



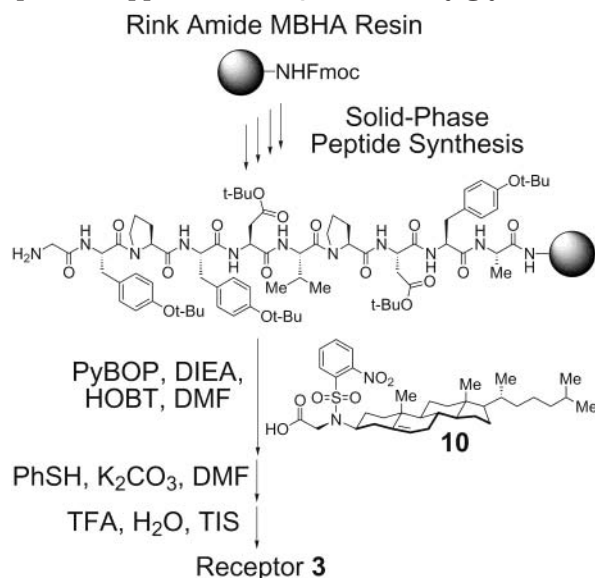
**Figure 3.** Structures of non-natural receptors based on N-( $\beta$ )-cholesteryl-glycine-capped peptides.

be incorporated into diverse glycolipids and glycoproteins on cells by accessing endogenous pathways of oligosaccharide biosynthesis with engineered monosaccharide precursors (28–30).

We describe here three novel non-natural small-molecule receptors (Figure 3, **3–5**) that deliver proteins into Jurkat lymphocytes. These receptors comprise protein-binding peptides capped with N-cholesteryl-glycine. As shown in Figure 3, peptide derivatives **3** and **4** are membrane-anchored antigens designed to bind commercially available anti-hemagglutinin (anti-HA) and anti-Flag IgGs. Peptide **5** is a derivative of the previously reported *Strep* Tag II peptide, which is a ligand of the streptavidin protein from *Staphylococcus aureus* (31). We report that receptors **3–5** dramatically enhance endocytic uptake of cognate proteins by mammalian cells, and this approach can deliver functional enzymes such as  $\beta$ -galactosidase conjugated to Protein A from *Staphylococcus aureus*.

## EXPERIMENTAL PROCEDURES

**General.** Chemical reagents and solvents were obtained from Aldrich, Alfa Aesar, Fluka, or VWR Scientific. Media and antibiotics were obtained from Gibco BRL. Streptavidin Alexa Fluor 488 (SA488), Cholera toxin Alexa Fluor 594, Protein A Alexa Fluor 488 (PrA488), and Lysotracker Red were purchased from Molecular Probes. Protein A- $\beta$ -galactosidase (PrA- $\beta$ -Gal), chlorpromazine, sucrose, methyl- $\beta$ -cyclodextrin, rabbit anti-Flag IgG, and rabbit anti-HA IgG were obtained from Sigma. Fmoc-protected amino acids, coupling reagents, and Rink Amide MBHA resin (75–150  $\mu$ m, 0.7 mmol/g) were purchased from Novabiochem. Analytical and semipreparative HPLC analysis/purifica-

**Scheme 1. General Strategy for Synthesis of Peptides Capped with N-( $\beta$ )-Cholesterylglycine**

tion employed a Hewlett-Packard HP 1100 instrument with StableBond C18 columns (analytical column: 300 SB-C18, 4.6 mm  $\times$  25 cm, 1 mL/min flow rate; semi-preparative column: 300 SB-C18, 9.4 mm  $\times$  25 cm, 3 mL/min flow rate) using a gradient from 9:1:0.001 ddw/CH<sub>3</sub>CN/TFA to 0.9:9.1:0.001 ddw/CH<sub>3</sub>CN/TFA over 40 min. Peptide mass spectrometry was obtained on a Perseptive Voyager DE-STR MALDI-TOF instrument. Epifluorescence micrographs were captured through a Zeiss Fluor (100 $\times$ ) objective by a Zeiss Axiocam digital camera interfaced to a Zeiss Axiovert S100TV microscope. Images were processed with Adobe Photoshop 5.0.

**Control and Fluorescent Peptides.** Two peptides were synthesized as C-terminal carboxamides to provide nonmembrane binding competitors. Peptide **6** sequence, YPYDVPDYA; peptide **7**, GDYKDDDDK. Biotin provided the soluble streptavidin competitor. Two peptides were synthesized as C-terminal carboxamides for fluorescence polarization assays. Peptide **8**, Fluor-GYPYDVPDYA; peptide **9**, Fluor-GDYKDDDDK. Fluor = fluorescein-5(6)-carboxamidohexanoamide. Peptide sequences are listed in single letter amino acid codes.

**Peptide Synthesis.** Peptides were synthesized with an Advanced Chemtech FBS-357 automated batch-mode synthesizer. Peptide synthesis employed standard N $\alpha$ -Fmoc methodology with *tert*-butyl ester, *tert*-butyl ether, *tert*-butyl carbamate, and methyltrityl side chain protection. Deprotection of Fmoc carbamates on Rink Amide MBHA resin (50 mg, 35  $\mu$ mol) was effected by the addition of 30% piperidine in DMF (2  $\times$  1 mL for 5 min followed by 1 mL for 20 min). N $\alpha$ -Fmoc amino acids were coupled as previously described (32). Peptide precursors to **3–5** were capped with the cholesteryl moiety by coupling with the nosyl-protected N-( $\beta$ )-cholesterylglycine (**10**, Scheme 1) prepared as previously reported (22). Peptides were capped with **10** by sequential addition of the following reagents in DMF: **10**/HOBT (250  $\mu$ L, 0.5 M of each component), followed by PyBOP (250  $\mu$ L, 0.5 M) and DIEA (500  $\mu$ L, 0.5 M). The resin was subsequently agitated for 1 h at 23  $^{\circ}$ C. This coupling step was repeated, and all amines were acylated as evidenced by Kaiser test. Deprotection of the nosyl sulfonamide was effected by treatment with K<sub>2</sub>CO<sub>3</sub> (70 mg) and thiophenol (25 mg) in DMF (2 mL) for 16 h. Fluorescent peptides **8** and **9** were synthesized with 23 mg of Rink Amide MBHA

**Table 1. Analytical Data for Peptides 3–9**

peptide, formula	yield	M + H <sub>calcd</sub>	M + H <sub>obs</sub>
<b>3</b> , C <sub>84</sub> H <sub>118</sub> N <sub>12</sub> O <sub>18</sub>	15%	1583.9	1583.9
<b>4</b> , C <sub>72</sub> H <sub>111</sub> N <sub>13</sub> O <sub>21</sub>	19%	1494.8	1494.8
<b>5</b> , C <sub>88</sub> H <sub>129</sub> N <sub>19</sub> O <sub>18</sub>	23%	1741.0	1741.0
<b>6</b> , C <sub>53</sub> H <sub>68</sub> N <sub>10</sub> O <sub>16</sub>	58%	1101.5	1101.5
<b>7</b> , C <sub>43</sub> H <sub>64</sub> N <sub>12</sub> O <sub>20</sub>	59%	1069.4	1069.4
<b>8</b> , C <sub>82</sub> H <sub>92</sub> N <sub>12</sub> O <sub>24</sub>	42%	1629.7	1629.6
<b>9</b> , C <sub>70</sub> H <sub>85</sub> N <sub>13</sub> O <sub>27</sub>	20%	1540.6	1540.6

resin (16  $\mu$ mol). After N $\alpha$ -Fmoc deprotection of the N-terminal amino acid of resin-bound precursors to peptides **8** and **9**, fluorescein-5(6)-carboxamidohexanoic acid succinimidyl ester (12 mg, 24  $\mu$ mol in 500  $\mu$ L of DMF) and DIEA (500  $\mu$ L, 0.5 M in DMF) were added with shaking for 16 h at 23  $^{\circ}$ C. Cleavage of peptides from the resin and side chain deprotection employed TFA/H<sub>2</sub>O/TIS (1 mL, 95:2.5:2.5) for 1 h. Peptides were purified by reverse-phase HPLC to >90% homogeneity, and peptides were analyzed by MALDI-TOF mass spectrometry as shown in Table 1.

**Flow Cytometry.** Analyses were performed with a Beckman-Coulter XL-MCL benchtop flow cytometer equipped with a 15 mW air-cooled argon-ion laser. Fluorescence detection was derived from excitation at 488 nm, splitting the emission with a 550 nm dichroic and long pass filter, and optical filtering through 530/30-nm band-pass filter. Forward-scatter (FS) and side-scatter (SSC) dot plots afforded cellular physical properties of size and granularity that allowed gating of living cells. After gating, 10 000 cells were counted.

**Confocal Microscopy.** Sequential scans were performed on an Olympus FV300 laser scanning confocal microscope fitted with a UplanFl objective (100 $\times$ ). Alexa Fluor 488 was excited with a 488 nm Argon ion laser, and emitted photons were collected through 510 nm LP and 530 nm SP filters. Excitation of Alexa Fluor 594 employed a 543 nm HeNe laser and a 605 nm BP filter.

**Antibody Uptake Assays.** Human Jurkat T lymphocytes were maintained in Roswell Park Memorial Institute (RPMI) 1640 media supplemented with Fetal Bovine Serum (FBS, 10%), penicillin (100 units/mL), and streptomycin (100  $\mu$ g/mL). Receptors **3–5** were dissolved in dimethyl sulfoxide (DMSO), which was diluted with media to yield a final DMSO concentration of 1%. For antibody/PrA488 uptake assays, Jurkat cells ( $5 \times 10^6$ ) were incubated with receptors **3–5** at 37  $^{\circ}$ C for 1 h, washed with media (2  $\times$  0.5 mL), and resuspended in media (490  $\mu$ L). To these cells was added a mixture of antibody (2.7  $\mu$ g) and PrA488 (0.5  $\mu$ g) in phosphate buffered saline (PBS, 10  $\mu$ L, pH 7.4). This protein mixture was preincubated at 23  $^{\circ}$ C for 1 h prior to addition to cells. Cells were maintained at 37  $^{\circ}$ C for 12 h. Cells were then washed with media (1  $\times$  0.5 mL), incubated with the appropriate free peptide (100  $\mu$ M, **6** or **7**) in media (2  $\times$  0.5 mL  $\times$  30 min) to compete away any noninternalized protein, washed with media (1  $\times$  0.5 mL), resuspended in media (0.75 mL), and analyzed by flow cytometry.

**Cellular Uptake of Protein A- $\beta$ -Galactosidase (PrA- $\beta$ -Gal).** The antibody/PrA- $\beta$ -Gal uptake assays employed Jurkat cells ( $5 \times 10^6$ ) incubated with receptor **3** (10  $\mu$ M) at 37  $^{\circ}$ C for 1 h. The cells were washed with media (2  $\times$  0.5 mL) and resuspended in media (490  $\mu$ L). A mixture of rabbit anti HA antibody (2.7  $\mu$ g) and PrA- $\beta$ -Gal (4  $\mu$ L, 0.3 units) in PBS (10  $\mu$ L, pH 7.4) was incubated at 23  $^{\circ}$ C for 1 h and then added to the cells treated with **3**. Cells were maintained at 37  $^{\circ}$ C for 12 h, washed with media (1  $\times$  0.5 mL), and incubated with free



HA peptide in media ( $100\ \mu\text{M}$ ,  $3 \times 0.5\ \text{mL} \times 30\ \text{min}$ ) to competitively displace any plasma membrane-bound protein. Uptake of PrA- $\beta$ -Gal was detected by incubation with fluorescein di-( $\beta$ -D-galactopyranoside) in media ( $1\ \text{mM}$ ,  $2\%$  DMSO) for  $30\ \text{min}$  at  $37\ ^\circ\text{C}$ . After this incubation, cells were washed with media ( $1 \times 1\ \text{mL}$ ), resuspended in media ( $0.75\ \text{mL}$ ), and analyzed by flow cytometry.

**Streptavidin Uptake Assay.** Receptors **3–5** were dissolved in DMSO and diluted with media to yield a final DMSO concentration of  $1\%$ . Jurkat cells ( $5 \times 10^6$ ) were incubated with receptors **3–5** at  $37\ ^\circ\text{C}$  for  $1\ \text{h}$ , washed with media ( $2 \times 0.5\ \text{mL}$ ), and resuspended in media ( $198\ \mu\text{L}$ ). To these cells was added streptavidin Alexa Fluor 488 (SA 488,  $2\ \mu\text{g}$ ), and cells were maintained at  $37\ ^\circ\text{C}$  for  $4\ \text{h}$ . Cells were washed with media ( $1 \times 0.5\ \text{mL}$ ), followed by media containing biotin ( $50\ \mu\text{M}$ ,  $1\%$  DMSO,  $2 \times 0.5\ \text{mL}$ ) as a nonmembrane binding competitor to displace any noninternalized protein. The cells were washed again with media ( $1 \times 0.5\ \text{mL}$ ) and resuspended in media ( $0.75\ \text{mL}$ ) for analysis by flow cytometry.

**Inhibition of Uptake Experiments.** Receptor **3** ( $1\ \mu\text{M}$ ) was subjected to the uptake assay with an antibody/PrA 488 incubation time of  $4\ \text{h}$ .

**Depletion of Cellular Cholesterol with Methyl- $\beta$ -Cyclodextrin (CD).** Cells were suspended in PBS (pH 7.4) containing BSA ( $1\ \text{mg/mL}$ ) and CD ( $10\ \text{mM}$ ) for  $30\ \text{min}$  prior to the protein uptake assay, and BSA ( $1\ \text{mg/mL}$ ) was included in subsequent assay media.

**Treatment with Hypertonic Sucrose.** Cells were suspended in media containing sucrose ( $400\ \text{mM}$ ) for  $1\ \text{h}$  prior to the protein uptake assay, and sucrose ( $400\ \text{mM}$ ) was included in subsequent assay media.

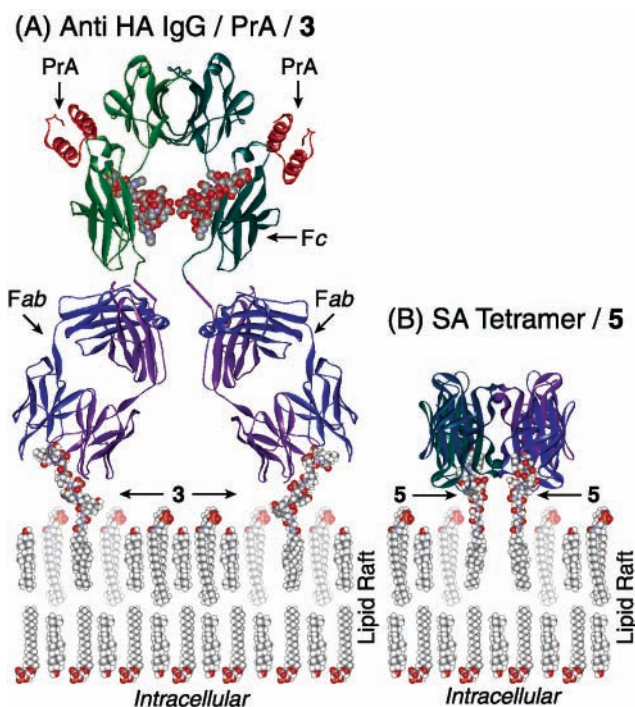
**Treatment with Chlorpromazine.** Cells were suspended in media containing chlorpromazine ( $100\ \mu\text{M}$ ) for  $1\ \text{h}$  prior to the protein uptake assay, and chlorpromazine ( $100\ \mu\text{M}$ ) was included in subsequent assay media.

**Fluorescence Polarization Assays.** Apparent binding constants for rabbit anti-HA and anti-Flag IgGs were determined by fluorescence polarization measurements with a Packard Fusion microtiterplate reader utilizing a  $485\ \text{nm}$  excitation filter and a  $535\ \text{nm}$  fluorescence polarization emission filter. All fluorescence polarization experiments employed black 384 well plates (Costar) with a fixed concentration of **8** or **9** ( $10\ \text{nM}$ ) in PBS (pH 7.4,  $40\ \mu\text{L}$ ). Fluorescent peptides **8** and **9** were equilibrated with cognate antibodies for  $10\ \text{min}$  prior to fluorescence polarization measurements. Dissociation constants were calculated by nonlinear regression with a one-site binding model (GraphPad Prism 3 software). Errors reflect calculated standard errors of the mean.

## RESULTS AND DISCUSSION

**Design and Synthesis of Non-Natural Cell Surface Receptors.** Receptors **3** and **4** were designed on the basis of known short peptide epitopes of anti-HA (epitope sequence: YPYDVPDYA) (**33**) and anti-Flag (epitope sequence: DYKDDDDK) IgGs (**34**). Receptor **5** was designed from the previously reported *Strep* Tag II peptide (sequence: SNWSHPQFEK), which is a moderate affinity ( $K_d = 72\ \mu\text{M}$ ) peptide ligand of the protein streptavidin (SA) (**31**).

To examine hypothetical geometries of receptors **3** and **5** bound to cognate proteins, models of molecular complexes interacting with a model membrane were constructed (Figure 4). These models employed X-ray crystal structures of a peptide-bound anti-HA Fab fragment

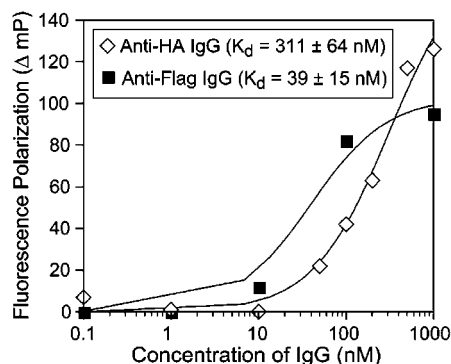


**Figure 4.** Molecular models of proteins (ribbon diagrams) bound to Macromodel-minimized peptidic receptors (CPK models) inserted into a model lipid raft (CPK models). (A) Model of anti-HA/PrA bound to **3**. (B) Model of SA bound to **5**.

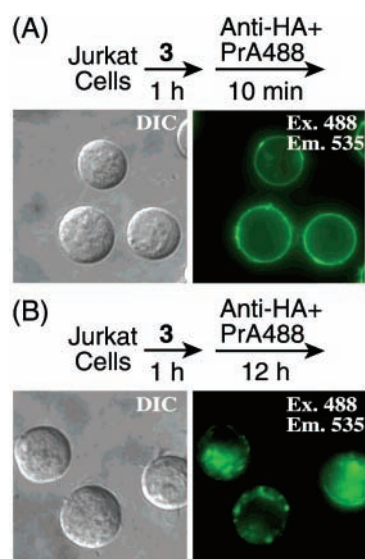
(PDB# 1FRG) (**33**) and *Strep* Tag II-bound SA (PDB# 1KL5) (**35**). The anti-HA model was embellished by inclusion of the invariant Fc fragment from an X-ray structure of IgG2a (PDB# 1IGT) (**36**) and the structure of a Fc-bound fragment of PrA (PDB# 1FC2) (**37**). Model construction involved modification of the X-ray structure of the anti-HA epitope peptide and the SA-bound *Strep* Tag II peptide by addition of a flexible glycine residue appended to the peptide N-terminus, which was further capped with N-( $3\beta$ )-cholesteryl glycine (**22**). The model cholesteryl glycine-Gly moiety was minimized with the Macromodel (v. 6.5) (**38**) Amber\* force field prior to attachment to the bound peptide ligands of cognate proteins (Figure 4). WebLab ViewerLite (Molecular Simulations Inc., v. 3.2) was employed to display the complexes. The model membrane bilayer was constructed to mimic the composition of a lipid raft subdomain composed of cholesterol packed with sphingomyelin in the outer leaflet and cholesterol packed with saturated phosphatidylserine in the inner leaflet (Figure 4) (**17**). These modeling studies suggested that a glycine linker between the protein-bound peptides and N-( $3\beta$ )-cholesteryl glycine would be sufficient to enable complete insertion of the bound steroid into the model membrane. The length of linker between the steroid and protein ligand has been shown to be critical in structurally related systems (**23**).

Receptors **3–5** were synthesized as shown in Scheme 1. The peptide precursors were synthesized and capped with a previously reported nosyl-protected N-( $3\beta$ )-cholesteryl glycine (**10**) (**22**). The nosyl protecting group was removed on solid phase with deprotonated thiophenol prior to cleavage of peptides from the solid support. Analogous control peptides **6** and **7** were synthesized lacking the N-cholesteryl glycine moiety to serve as non-membrane binding competitors. Because the affinities of rabbit anti-HA and rabbit anti-Flag IgGs have not been previously reported, fluorescent peptides **8** and **9** were





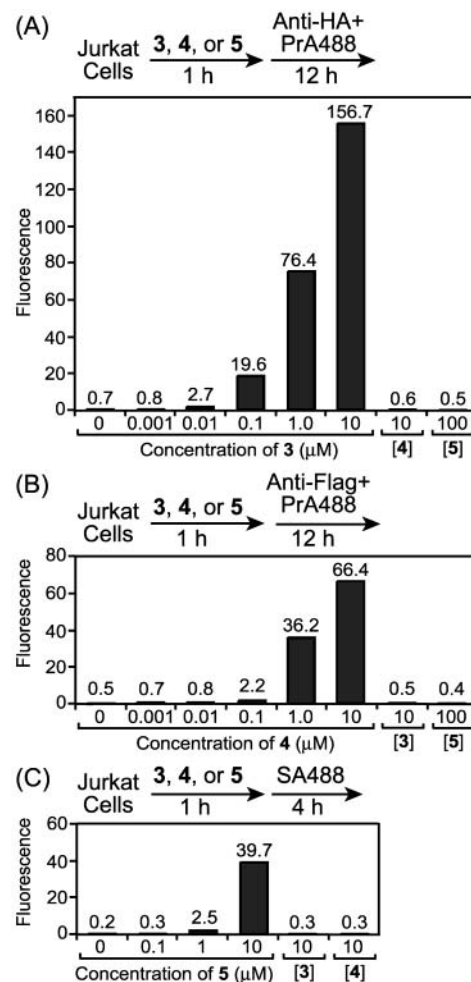
**Figure 5.** Determination of apparent dissociation constants ( $K_d$ ) of anti-HA and anti-Flag IgGs by quantification of the fluorescence polarization of peptides **8** and **9**.



**Figure 6.** Differential interference contrast (DIC) and epifluorescence micrographs of Jurkat lymphocytes treated with receptor **3** ( $10\ \mu\text{M}$ ), anti-HA, and green fluorescent PrA488. Fluorescence excitation (Ex.) and emission (Em.) wavelengths (nm) are explicitly shown.

synthesized as analogues of **3** and **4** that substitute the N-cholesteryl-glycine moiety with a fluorescein derivative to enable determination of peptide affinities by fluorescence polarization (FP) measurements (39). As shown in Figure 5, quantification of FP values as a function of IgG concentration yielded apparent  $K_d$  values of  $311 \pm 64\ \text{nM}$  for the anti-HA-binding peptide **8** and  $39 \pm 15\ \text{nM}$  for the anti-Flag-binding peptide **9**. In these experiments, the concentration of the fluorescent tracer peptide was fixed at  $10\ \text{nM}$ .

**Uptake of Proteins by Mammalian Cells Bearing Non-Natural Cell Surface Receptors.** Initial qualitative analysis of protein uptake mediated by receptors **3**–**5** employed epifluorescence microscopy. As shown in Figure 6, Jurkat lymphocytes treated with receptor **3** for 1 h followed by addition of anti-HA and green fluorescent PrA (PrA488) as a probe exhibited bright fluorescence at the cellular periphery within 10 min of protein addition. This peripheral fluorescence was localized to the plasma membrane of practically 100% of viable cells as compared with fluorescent plasma membrane probes such as the fluorescent analogue **1** (22, 40). After 12 h of protein treatment, the fluorescence was observed in defined compartments in the cell interior, indicating that the protein complex was internalized (Figure 6). Cells treated with receptor **4** followed by anti-Flag IgG/PrA488 or

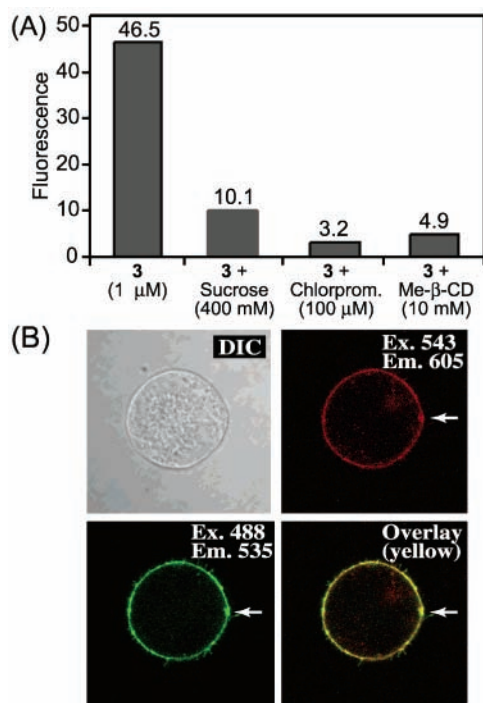


**Figure 7.** Analysis of dose-dependent cellular uptake of proteins by flow cytometry. Each bar represents the median fluorescence of 10 000 living cells.

treated with receptor **5** followed by SA488 showed highly similar patterns of cellular fluorescence (data not shown).

To quantitatively examine this uptake process, dose-dependent effects on intracellular fluorescence were measured by flow cytometry. Because flow cytometry cannot distinguish membrane-associated from intracellular fluorescence, cells were extensively washed with soluble competitor peptides ( $100\ \mu\text{M}$ ) or biotin ( $50\ \mu\text{M}$ ) prior to analysis to displace any noninternalized protein. As shown in Figure 7A, pretreatment of cells with **3** for 1 h followed by addition of anti-HA and PrA488 for 12 h dramatically enhanced intracellular fluorescence with significant effects observed at concentrations of **3** as low as  $100\ \text{nM}$ . The intracellular fluorescence of cells pretreated with  $10\ \mu\text{M}$  **3** was enhanced by over 200-fold compared with cells treated with the anti-HA/PrA488 complex alone. This effect on anti-HA/PrA488 specifically required receptor **3**; no uptake of this complex was mediated by receptors **4** or **5** (Figure 7A). However, receptor **4** efficiently and specifically mediated the dose-dependent uptake of anti-Flag/PrA488 with over a 100-fold enhancement of intracellular fluorescence at  $10\ \mu\text{M}$  (Figure 7B). Furthermore, green fluorescent streptavidin (SA488) was specifically internalized by receptor **5**, which enhanced uptake by over 100-fold at  $10\ \mu\text{M}$  (Figure 7C).

**Non-Natural Cell Surface Receptors Direct Cognate Proteins to Lipid Rafts and Effect Protein Uptake via Clathrin-Mediated Endocytosis.** The biotin-derived “streptaphage” receptor (**2**) was previously

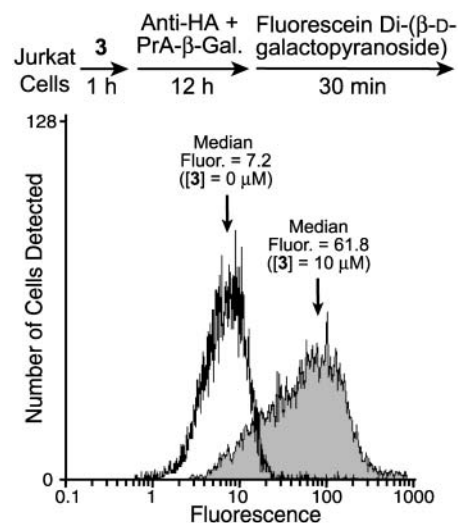


**Figure 8.** Analysis of inhibition of protein uptake and protein subcellular localization. (A) Uptake of anti-HA/PrA488/3 measured by flow cytometry in the presence of inhibitors of clathrin-mediated endocytosis. (B) Confocal laser scanning microscopy of cells treated with **3** for 1 h followed by anti-HA/PrA488 and red fluorescent Alexa fluor-594 Cholera toxin B subunit for 5 min. White arrows illustrate colocalization of green and red fluorescence.

shown to mediate uptake of streptavidin by targeting this protein to lipid rafts and promoting clathrin-mediated endocytosis (23). To examine the mechanism of uptake of structurally related receptors **3–5**, protein uptake under conditions that block clathrin-mediated endocytosis was examined (Figure 8A). Cells treated with hypertonic sucrose exhibit defects in clathrin-coated lattices (41), and these conditions were found to diminish receptor **3**-mediated uptake of anti-HA/PrA488 measured by flow cytometry. In addition, the cationic amphiphatic drug chlorpromazine disrupts the assembly/disassembly of clathrin associated with coated pits and endosomes (42), and this drug inhibited protein uptake. Furthermore, depletion of cellular cholesterol by treatment with methyl- $\beta$ -cyclodextrin to disrupt lipid rafts (43) blocked protein uptake. These results indicate that lipid rafts may be important for this process, and protein uptake mediated by receptors **3–5** is most likely controlled by a clathrin-mediated endocytosis mechanism.

To examine the localization of proteins binding to non-natural receptors in cellular plasma membranes, cells were treated with **3** followed by addition of anti-HA/PrA488 and red fluorescent cholera toxin B subunit. Cholera toxin binds ganglioside GM1 in lipid rafts and provides a probe of these membrane subdomains. As shown in Figure 8B, confocal laser scanning microscopy revealed a heterogeneous distribution of anti-HA/PrA488/3 in plasma membranes of Jurkat lymphocytes. Moreover, this complex extensively colocalized with cholera toxin, indicating that receptor **3** mediates protein association with lipid rafts.

**Non-Natural Receptor-Mediated Delivery of Functional  $\beta$ -Galactosidase into Cells.** Functional enzymes such as caspases (9), ribonuclease (44), and horseradish peroxidase (45) have been delivered into cells by a variety



**Figure 9.** Flow cytometry of Jurkat lymphocytes treated with receptor **3**, anti-HA IgG, and PrA- $\beta$ -galactosidase.

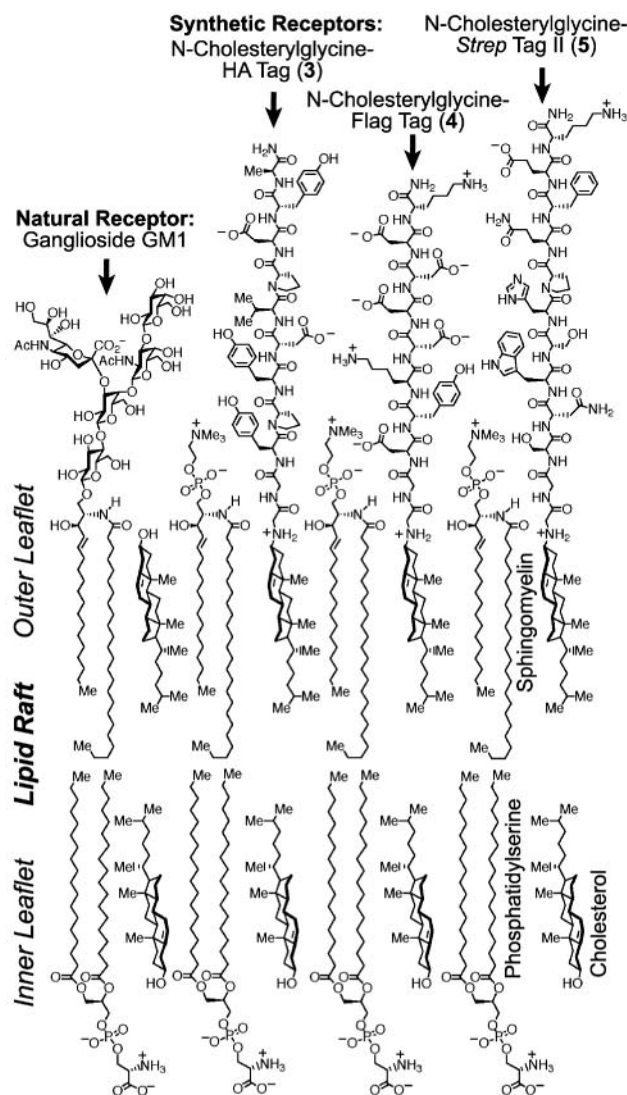
of carrier mechanisms and are under investigation as components of antitumor agents. To investigate whether a synthetic cell surface receptor might enable delivery of a functional enzyme into mammalian cells, uptake of a commercially available Protein A- $\beta$ -galactosidase conjugate (PrA- $\beta$ -Gal) was examined. As shown in Figure 9, Jurkat lymphocytes were treated with receptor **3** and the anti-HA/PrA- $\beta$ -Gal conjugate. Cells were treated with a fluorescent substrate of  $\beta$ -galactosidase, and fluorescence was analyzed by flow cytometry. These experiments revealed that receptor **3** engendered a ca. 9-fold enhancement of median cellular fluorescence compared with identically treated cells in the absence of receptor **3**. Under these conditions, this fluorescence enhancement was detected in 75% of the treated cells (Figure 9). This result established that non-natural cell surface receptors such as **3** can deliver at least transiently functional enzymes into cells.

## CONCLUSION

We describe three novel non-natural cell surface receptors (**3–5**) that enable dose-dependent uptake of specific macromolecules by mammalian cells. These compounds comprise peptides capped with N-(3 $\beta$ )-cholesteryl glycine, which is a mimic of cholesterol that can stably integrate into cellular plasma membranes of mammalian cells (22, 23). Addition of cognate IgGs or streptavidin proteins to cells displaying these non-natural cell surface receptors triggers endocytic protein uptake through endogenous membrane trafficking pathways.

Proteins delivered through this "synthetic receptor targeting" approach can span a wide range of affinities for non-natural cell surface receptors. For example streptavidin can be delivered to cells by surface display of either very high affinity biotin (100 fM) (23) or the modest affinity Strep Tag II peptide (receptor **5**, ca. 72  $\mu$ M). However, the magnitude of delivery of streptavidin is ca. 6.5-fold greater with the high-affinity biotin-derived receptor **2** compared with the modest-affinity receptor **5**. Despite these vast affinity differences, similarities in the magnitude of delivery may relate to the high effective concentration of non-natural receptors on cell surfaces and the multivalent nature of cell surface recognition by bivalent IgGs and tetrameric streptavidin. Interestingly, the higher affinity anti-Flag receptor **4** ( $K_d \sim 39$  nM) delivered 2.4-fold less IgG/PrA complex than the lower





**Figure 10.** Model of a plasma membrane raft segment containing the non-natural receptors **3–5** and the natural receptor ganglioside GM1.

affinity anti-HA receptor **3** ( $K_d \sim 311$  nM). This result may relate to the highly acidic nature of the Flag epitope peptide, which has been shown to diminish the affinity of fusion proteins for cellular plasma membranes (34).

The non-natural receptors described herein appear to associate with lipid raft subdomains of cellular plasma membranes as evidenced by colocalization with cholera toxin on cell surfaces, and these receptors cause proteins to penetrate into cells by clathrin-mediated endocytosis. In this regard, as shown in a model of a lipid raft in Figure 10, these compounds functionally mimic natural cell surface receptors such as ganglioside GM1, which resides in lipid rafts and enables the cellular penetration of cholera toxin through endocytic uptake mechanisms. Given that non-natural cell surface receptors can be used for the delivery of functional enzymes of high molecular weight such as *E. Coli*  $\beta$ -galactosidase (tetramer  $\sim 540$  000 Da) (46) conjugated to Protein A ( $\sim 42$  000 Da) and bound to IgGs ( $\sim 150$  000 Da), this “synthetic receptor targeting” approach may have potential applications in tumor therapy by enabling the delivery of lethal enzymes into tumor cells. This approach may also facilitate studies in other areas requiring the delivery of macromolecules into mammalian cells including basic cell biology, genetic therapy, and immunology.

## ACKNOWLEDGMENT

We thank the National Institutes of Health (RO1-CA83831) for financial support.

## LITERATURE CITED

- (1) Smith, D. A.; van de Waterbeemd, H. *Curr. Opin. Chem. Biol.* **1999**, *3*, 373–378.
- (2) Fischer, P. M.; Krausz, E.; Lane, D. P. *Bioconjugate Chem.* **2001**, *12*, 825–841.
- (3) Garnett, M. C. *Crit. Rev. Ther. Drug Carrier Syst.* **1999**, *16*, 147–207.
- (4) Hawiger, J. *Curr. Opin. Chem. Biol.* **1999**, *3*, 89–94.
- (5) Lindgren, M.; Hallbrink, M.; Prochiantz, A.; Langel, U. *Trends Pharmacol. Sci.* **2000**, *21*, 99–103.
- (6) Schwarze, S. R.; Hruska, K. A.; Dowdy, S. F. *Trends Cell Biol.* **2000**, *10*, 290–295.
- (7) Wender, P. A.; Mitchell, D. J.; Pattabiraman, K.; Pelkey, E. T.; Steinman, L.; Rothbard, J. B. *Proc. Natl. Acad. Sci. U.S.A.* **2000**, *97*, 13003–13008.
- (8) Umezawa, N.; Gelman, M. A.; Haigis, M. C.; Raines, R. T.; Gellman, S. H. *J. Am. Chem. Soc.* **2002**, *124*, 368–369.
- (9) Zelfathi, O.; Wang, Y.; Kitada, S.; Reed, J. C.; Felgner, P. L.; Corbeil, J. J. *J. Biol. Chem.* **2001**, *276*, 35103–35110.
- (10) Mukherjee, S.; Ghosh, R. N.; Maxfield, F. R. *Physiol. Rev.* **1997**, *77*, 759–803.
- (11) Mellman, I. *Annu. Rev. Cell Dev. Biol.* **1996**, *12*, 575–625.
- (12) Sandvig, K.; Van Deurs, B. *Annu. Rev. Cell Dev. Biol.* **2002**.
- (13) Merritt, E. A.; Hol, W. G. J. *Cur. Opin. Struct. Biol.* **1995**, *5*, 165–171.
- (14) Hooper, N. M. *Mol. Mem. Biol.* **1999**, *16*, 145–156.
- (15) Brown, D. A.; London, E. *Annu. Rev. Cell Dev. Biol.* **1998**, *14*, 111–136.
- (16) Simons, K.; Ikonen, E. *Nature* **1997**, *387*, 569–572.
- (17) Simons, K.; Ikonen, E. *Science* **2000**, *290*, 1721–1726.
- (18) Simons, K.; Toomre, D. *Nat. Rev. Mol. Cell. Biol.* **2000**, *1*, 31–39.
- (19) Kirchhausen, T. *Annu. Rev. Biochem.* **2000**, *69*, 699–727.
- (20) Shogomori, H.; Futerman, A. H. *J. Biol. Chem.* **2001**, *276*, 9182–9188.
- (21) Torgersen, M. L.; Skretting, G.; van Deurs, B.; Sandvig, K. *J. Cell Sci.* **2001**, *114*, 3737–3747.
- (22) Hussey, S. L.; He, E.; Peterson, B. R. *J. Am. Chem. Soc.* **2001**, *123*, 12712–12713.
- (23) Hussey, S. L.; Peterson, B. R. *J. Am. Chem. Soc.* **2002**, *124*, 6265–6273.
- (24) Sampson, N. S.; Mrksich, M.; Bertozzi, C. R. *Proc. Natl. Acad. Sci. U.S.A.* **2001**, *98*, 12870–12871.
- (25) Saxon, E.; Bertozzi, C. R. *Annu. Rev. Cell Dev. Biol.* **2001**, *17*, 1–23.
- (26) Jacobs, C. L.; Yarema, K. J.; Mahal, L. K.; Nauman, D. A.; Charters, N. W.; Bertozzi, C. R. *Methods Enzymol.* **2000**, *327*, 260–275.
- (27) Mahal, L. K.; Yarema, K. J.; Bertozzi, C. R. *Science* **1997**, *276*, 1125–1128.
- (28) Jacobs, C. L.; Goon, S.; Yarema, K. J.; Hinderlich, S.; Hang, H. C.; Chai, D. H.; Bertozzi, C. R. *Biochemistry* **2001**, *40*, 12864–12874.
- (29) Saxon, E.; Bertozzi, C. R. *Science* **2000**, *287*, 2007–2010.
- (30) Hang, H. C.; Bertozzi, C. R. *J. Am. Chem. Soc.* **2001**, *123*, 1242–1243.
- (31) Schmidt, T. G.; Koepke, J.; Frank, R.; Skerra, A. *J. Mol. Biol.* **1996**, *255*, 753–766.
- (32) Martin, S. E.; Peterson, B. R. *J. Pept. Sci.* **2002**, *8*, 227–233.
- (33) Churchill, M. E.; Stura, E. A.; Pinilla, C.; Appel, J. R.; Houghten, R. A.; Kono, D. H.; Balderas, R. S.; Fieser, G. G.; Schulze-Gahmen, U.; Wilson, I. A. *J. Mol. Biol.* **1994**, *241*, 534–556.
- (34) Chen, J.; Skehel, J. J.; Wiley, D. C. *Biochemistry* **1998**, *37*, 13643–13649.
- (35) Korndorfer, I. P.; Skerra, A. *Protein Sci.* **2002**, *11*, 883–893.
- (36) Harris, L. J.; Larson, S. B.; Hasel, K. W.; McPherson, A. *Biochemistry* **1997**, *36*, 1581–1597.



- (37) Deisenhofer, J. *Biochemistry* **1981**, *20*, 2361–2370.
- (38) Mohamadi, F.; Richards, N. G. J.; Guida, W. C.; Liskamp, R.; Lipton, M.; Caufield, C.; Chang, G.; Hendrickson, T.; Still, W. C. *J. Comput. Chem.* **1990**, *11*, 440–467.
- (39) Dubowchik, G. M.; Ditta, J. L.; Herbst, J. J.; Bollini, S.; Vinitsky, A. *Bioorg. Med. Chem. Lett.* **2000**, *10*, 559–562.
- (40) Creaser, S. P.; Peterson, B. R. *J. Am. Chem. Soc.* **2002**, *124*, 2444–2445.
- (41) Heuser, J. E.; Anderson, R. G. W. *J. Cell Biol.* **1989**, *108*, 389–400.
- (42) Wang, L. H.; Rothberg, K. G.; Anderson, R. G. *J. Cell Biol.* **1993**, *123*, 1107–1117.
- (43) Ikonen, E. *Curr. Opin. Cell Biol.* **2001**, *13*, 470–477.
- (44) Leland, P. A.; Staniszewski, K. E.; Kim, B. M.; Raines, R. T. *J. Biol. Chem.* **2001**, *276*, 43095–43102.
- (45) Wardman, P. *Curr. Pharm. Des.* **2002**, *8*, 1363–1374.
- (46) Jacobson, R. H.; Zhang, X. J.; DuBose, R. F.; Matthews, B. W. *Nature* **1994**, *369*, 761–766.

BC025601P

# Preparation of Bioconjugates by Solid-Phase Conjugation to Ion Exchange Matrix-Adsorbed Carrier Proteins

G. Houen,<sup>\*,†</sup> D. T. Olsen,<sup>†</sup> P. R. Hansen,<sup>‡</sup> K. B. Petersen,<sup>†</sup> and V. Barkholt<sup>§</sup>

Department of Research and Development, Statens Serum Institut, Artillerivej 5, DK-2300 Copenhagen, Denmark, Department of Chemistry, Royal Veterinary and Agricultural University, Thorvaldsensvej 40, DK-1871 Frederiksberg, Denmark, and BioCentrum-DTU, Biochemistry and Nutrition, Technical University of Denmark, DK-2800 Lyngby, Denmark. Received October 8, 2002; Revised Manuscript Received October 23, 2002

A solid-phase conjugation method utilizing carrier protein bound to an ion exchange matrix was developed. Ovalbumin was adsorbed to an anion exchange matrix using a batch procedure, and the immobilized protein was then derivatized with iodoacetic acid *N*-hydroxysuccinimid ester. The activated protein was conjugated with glutathione, the conjugation ratio determined by acid hydrolysis, and amino acid analysis performed with quantification of carboxymethyl cysteine. Elution of conjugates from the resin by a salt gradient revealed considerable heterogeneity in the degree of derivatization, and immunization experiments with the eluted conjugates showed that the more substituted conjugates gave rise to the highest titers of glutathione antibodies. Direct immunization with the conjugates adsorbed to the ion exchange matrix was possible and gave rise to high titers of glutathione antibodies. Conjugates of ovalbumin and various peptides were prepared in a similar manner and used for production of peptide antisera by direct immunization with the conjugates bound to the ion exchanger. Advantages of the method are its solid-phase nature, allowing fast and efficient reactions and intermediate washings, and the ability to release conjugates from the solid phase under mild conditions.

## 1. INTRODUCTION

Sequence-specific peptide antibodies are important tools for protein chemistry, histochemistry, cytochemistry, and immunology. Such antibodies are fairly easily prepared, but most peptides require conjugation to a carrier protein in order to elicit high titers of antibodies. The same applies to hapten antibodies, which are also valuable reagents in immunoassays, histochemistry, and cytochemistry.

Peptides and haptens may be conjugated in solution to the carrier protein using various condensing agents (e.g., carbodiimides) or homo- and heterobifunctional cross-linking reagents such as glutaraldehyde, SPDP,<sup>1</sup> iminothiolane, and others (Briand et al., 1985; Regemortel et al., 1988; Carter, 1994). In relation to this, it has been shown that preactivation of the carrier proteins followed by conjugation may have some advantages, including increased stereochemical control of the reaction (Houen and Jensen, 1995).

Solid-phase synthesis of peptides directly on carrier proteins has also been described, but the properties of the resulting conjugates were found to be unsuitable for routine use (Hansen et al., 1993). Solid-phase conjugation to carrier proteins preadsorbed to aluminum hydroxide was developed by Houen et al. (1997) as a method for producing well defined conjugates, which simultaneously incorporated an adjuvant as the solid phase. The adjuvant-carrier-peptide particles thus produced were found to

elicit high titers of specific peptide antibodies. However, the physical strength of the interaction between carrier protein and aluminum hydroxide is very sensitive to pH and to the ionic strength and composition of the buffers used for washing and conjugation, making it essential to carefully control these parameters during all steps. For this reason we have further explored the principle of solid-phase conjugation, and here we describe a procedure for solid-phase conjugation to ion exchange matrix-adsorbed carrier proteins and immunization with the conjugates. This method has the added advantage of allowing elution of the conjugates for analysis of the conjugation ratios and for separation of conjugates with different conjugation ratios. We believe this method will be useful for preparation and analysis of a wide range of bioconjugates.

## 2. MATERIALS AND METHODS

**2.1. Reagents.** Glycine, urea, trishydroxymethylaminomethane (Tris), dithiothreitol (DTT), iodoacetic acid, ovalbumin, phenol, dithiodipropionic acid, *ortho*-phthalaldehyde (OPA), diethanolamine, *p*-nitrophenyl phosphate tablets, 5-bromo-4-chloro-3-indolyl phosphate/nitro blue tetrazolium tablets, bromophenol blue, and bovine serum albumin (BSA) were from Sigma (St. Louis, MO). Methanol, NaCl, CH<sub>3</sub>COOH, CH<sub>3</sub>COONa, HCl, NaHCO<sub>3</sub>, Na<sub>2</sub>CO<sub>3</sub>, Na<sub>2</sub>HPO<sub>4</sub>, NaH<sub>2</sub>PO<sub>4</sub>, (NH<sub>4</sub>)<sub>2</sub>SO<sub>4</sub>, Pyronin G, Tween 20, and acetonitrile were from Merck (Darmstadt, Germany). Glutathione (reduced and oxidized) was from Boehringer (Mannheim, Germany). Tris-glycine gels (12% and 4–20%) were from NOVEX (San Diego, CA). GELCODE Blue Stain Reagent was from Pierce (Rockford, IL). Sodium dodecyl sulfate (SDS) was from BDH (Poole, Dorset, England). Prestained low molecular weight standard proteins, acrylamide, bisacrylamide, ammonium persulfate, *N,N,N,N*-tetramethylethylenediamine,

\* Corresponding author. E-mail: gh@ssi.dk. Tel.: +45 32683276. Fax.: +45 32683149.

<sup>†</sup> Statens Serum Institut.

<sup>‡</sup> Royal Veterinary and Agricultural University.

<sup>§</sup> Technical University of Denmark.

<sup>1</sup> Abbreviations: Fmoc, 9-fluorenylmethyloxycarbonyl; SPDP, *N*-hydroxysuccinimidyl-3-(2-pyridyldithio)-propionate

and DEAE cellulose were from Bio-Rad (Hercules, CA). Q Sepharose High Performance (HP), DEAE Sephadex, CNBr Sepharose were from Pharmacia (Uppsala, Sweden). Nitrocellulose (NC) membranes (0.2  $\mu$ m) were from Schleicher & Schuell (Dassel, Germany). Milli Q water equipment was from Millipore (Bedford, MA).

Iodoacetic acid *N*-hydroxysuccinimid ester was synthesized according to Hampton et al. (1976).

Peptides were made by solid-phase synthesis using Fmoc protection and diisopropylcarbodiimide/1-hydroxybenzotriazol activation (Chang and White, 2000).

Rabbit immunoglobulins against glutathione conjugated to BSA using divinylsulfone were produced as described (Houen and Jensen, 1995).

**2.2. Amino Acid Analysis.** Amino acid analysis was carried out as described by Barkholt and Jensen (1989). In short, samples were hydrolyzed in 6 M HCl, 0.05% phenol, 0.05% dithiodipropionic acid for 24 h at 110 °C, dried in vacuo, redissolved, and analyzed by ion exchange chromatography with postcolumn OPA derivatization.

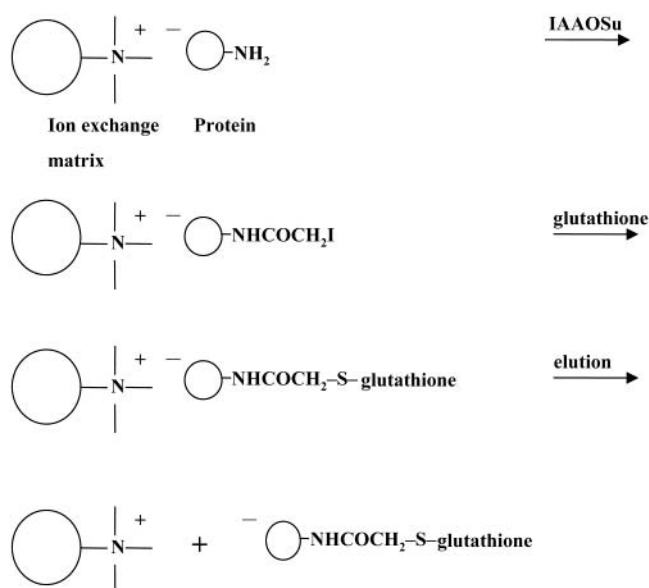
**2.2. SDS-PAGE.** SDS-PAGE was performed according to Laemmli (1970) and Studier (1973) using precast 12% or 4–20% Tris-glycine gels following the prescriptions of the manufacturer. Electrophoresis was performed for about 90 min at 150 V using Tris-glycine running buffer (25 mM Tris, 192 mM glycine, 0.1% sodium dodecyl sulfate, pH 8.3).

Coomassie Brilliant Blue staining was performed using GELCODE stain reagent. The gel was washed three times for 5 min in milli Q water, followed by staining for 1 h or overnight with GELCODE Blue Stain Reagent, and finally washed with milli Q water.

**2.3. Immunoblotting.** SDS-PAGE gels were electroblotted overnight (0.1 mA/cm<sup>2</sup>) to nitrocellulose membranes using a semi-dry apparatus (Bio-Rad) and 2.5 mM Tris, 19.2 mM glycine, pH 8.3, 20% EtOH as transfer buffer. Membranes were pre-blocked in 50 mM Tris, pH 7.5, 1% Tween 20, 0.3 M NaCl (TTN), and incubated with primary antibodies (mouse or rabbit sera) diluted in TTN. After 1 h incubation the membrane was washed three times for 5 min in TTN and incubated 1 h with alkaline phosphatase-conjugated rabbit immunoglobulins against mouse immunoglobulins or goat immunoglobulins against rabbit immunoglobulins. After washing in TTN three times for 5 min, the membranes were developed with BCIP/NBT (one tablet per 10 mL water).

**2.4. Conjugation to Activated Ion Exchange Matrix-Adsorbed Ovalbumin.** Ten milliliters of ion exchange matrix was washed in 0.1 M sodium phosphate, pH 8.8, and then in 10 mM sodium phosphate, pH 9.0. The matrix was then incubated with 10 mL ovalbumin (25 mg/mL) overnight at 4 °C on a rotator. The matrix was washed three times in 10 mM sodium phosphate, pH 9.0, with intermittent centrifugations. The washed matrix was resuspended with 10 mL sodium phosphate, pH 9.0, and 1 mL of iodoacetic acid *N*-hydroxysuccinimide (10 mg/mL DMF) was added. After incubation 1 h at 4 °C on a rotator, the matrix was washed three times in 10 mM sodium phosphate, pH 8, with intermittent centrifugations. The washed matrix was resuspended with 10 mL sodium phosphate, pH 8.0, and then incubated with glutathione (1 mg/mL) for 1 h or peptides (0.1 mg/mL) overnight at 4 °C. Finally, the matrix was washed three times in 10 mM sodium phosphate, pH 8, with intermittent centrifugations.

**2.5. Elution of Conjugates from Ion-Exchange Resins.** The ion exchange matrix with glutathione-conjugated ovalbumin (10 mL) was packed in a column (16 mm diameter) washed with 10 mM sodium phos-



**Figure 1.** Schematic presentation of the principle of solid-phase conjugation to ion exchange matrix-adsorbed carrier proteins. IAAOSu: iodoacetic acid *N*-hydroxysuccinimid ester.

phate, pH 8, and eluted with a linear gradient of NaCl in the same buffer (0–1 M over 200 min; flow, 1 mL/min).

**2.6. ELISA.** Antigens were diluted 1:1000 and coated in wells of microtiter plates using 50 mM sodium carbonate, pH 9.6, as coating buffer. The wells were washed three times for 5 min with TTN and incubated for 1 h with primary antibodies diluted 1:1000 in TTN. After washing in TTN three times for 5 min, the wells were incubated 1 h with alkaline phosphatase-conjugated secondary antibodies (rabbit immunoglobulins against mouse immunoglobulins or goat immunoglobulins against rabbit immunoglobulins) diluted 1:2000 in TTN. The wells were washed three times for 5 min in TTN and developed with pNPP (1 tablet (15 mg) per 15 mL 1 M diethanolamine, 0.5 mM MgCl<sub>2</sub> pH 9.8). Absorbances were read at 405 nm with background subtraction at 690 nm.

**2.7. Immunizations.** Ion exchange matrix-adsorbed conjugates were washed three times in water, and eluted conjugates were dialyzed three times against water. They were then mixed with an equal volume Al(OH)<sub>3</sub> before immunization. Mice were immunized intraperitoneally or subcutaneously with 100  $\mu$ L. Rabbits were immunized subcutaneously with 1 mL. In some experiments aluminum hydroxide was substituted with Freund's complete adjuvant for the first immunization and Freund's incomplete adjuvant for the following immunizations. The titer of a serum was defined as the dilution giving half-maximal response when analyzed by ELISA.

### 3. RESULTS

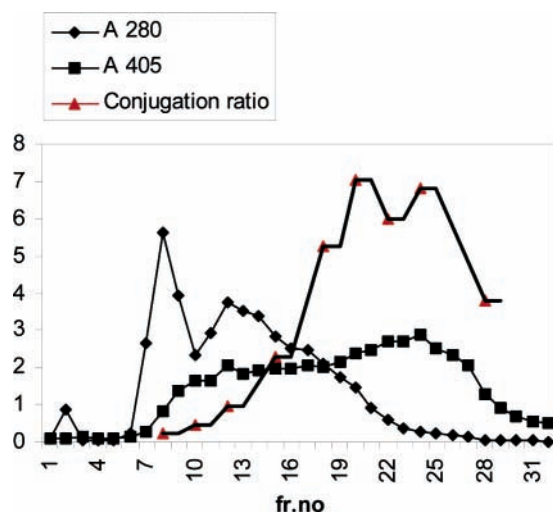
To determine the feasibility of solid-phase carrier protein activation and peptide conjugation, we initially compared immobilization of ovalbumin on three ion exchange matrixes in combination with iodoacetic acid *N*-hydroxysuccinimide ester activation and subsequent conjugation of glutathione using batch procedures for all steps (Figure 1, Table 1). As illustrated in Figure 1, this procedure takes advantage of the immobilization of proteins on ion exchange matrixes at low ionic strength. This allows the protein to be manipulated by solid-phase methods, and it allows the resulting conjugate to be



**Table 1. Binding of Ovalbumin to Different Ion Exchange Matrices Combined with Solid-Phase Activation with Iodoacetic Acid *N*-Hydroxysuccinimid Ester (1 mg/mL) and Conjugation of Glutathione (1 mg/mL) and Antibody Titers against Ovalbumin (OVA) and Glutathione (GS) Induced by the Conjugates in Mice (groups of four animals) after Four Immunizations**

matrix	ovalbumin conc. (mg/mL) <sup>a</sup>	conjugation ratio (GS/OVA)	titers	
			OVA	GS
Q Sepharose HP	19.0	9.2	41250	2075
DEAE Sephadex	14.4	6.4	33500	303
DEAE cellulose	3.0	7.1	37333	537

<sup>a</sup> Settled matrix



**Figure 2.** Elution of glutathione-IAA-ovalbumin conjugates from Q Sepharose HP after solid-phase activation of ovalbumin with iodoacetic acid *N*-hydroxysuccinimid ester (1 mg/mL) and conjugation of glutathione (1 mg/mL). The protein profile (A280), the reactivity with an antiserum against glutathione (A405), and the conjugation ratio between glutathione and ovalbumin as determined by amino acid analysis are shown.

eluted from the ion exchange matrix by increasing the ionic strength. As shown in Table 1, and in agreement with the capacities of the matrixes, the highest amounts were immobilized on Q Sepharose High Performance (HP) (about 20 mg/mL settled matrix) and the lowest amounts on DEAE cellulose. The average conjugation ratios (the number of glutathione molecules covalently bound to each ovalbumin molecule) as determined by amino acid analysis were almost equal for the ion exchange matrix-bound ovalbumin conjugates and reached a value of about 9 on Q Sepharose HP.

Immunization of mice with the ion exchange matrix-bound conjugates showed that essentially equal titers of ovalbumin antibodies were elicited, whereas the average titers for glutathione antibodies ranged from 300 for DEAE Sephadex to about 2000 for Q Sepharose HP (Table 1).

To analyze the extent of conjugation further, we immobilized ovalbumin on 30 mL Q Sepharose HP anion exchange matrix, activated the immobilized protein with iodoacetic acid *N*-hydroxysuccinimid ester and derivatized 10 mL immediately with glutathione. The rest was frozen at 20 °C for later derivatization. The glutathione-derivatized resin was then packed in a column and subjected to elution with a salt gradient (Figure 2). As expected, this revealed a broad elution pattern reflecting a heterogeneous distribution of conjugated molecules. Analysis with an antiserum against glutathione (Houen and Jensen, 1995) showed the lowest reactivity in the

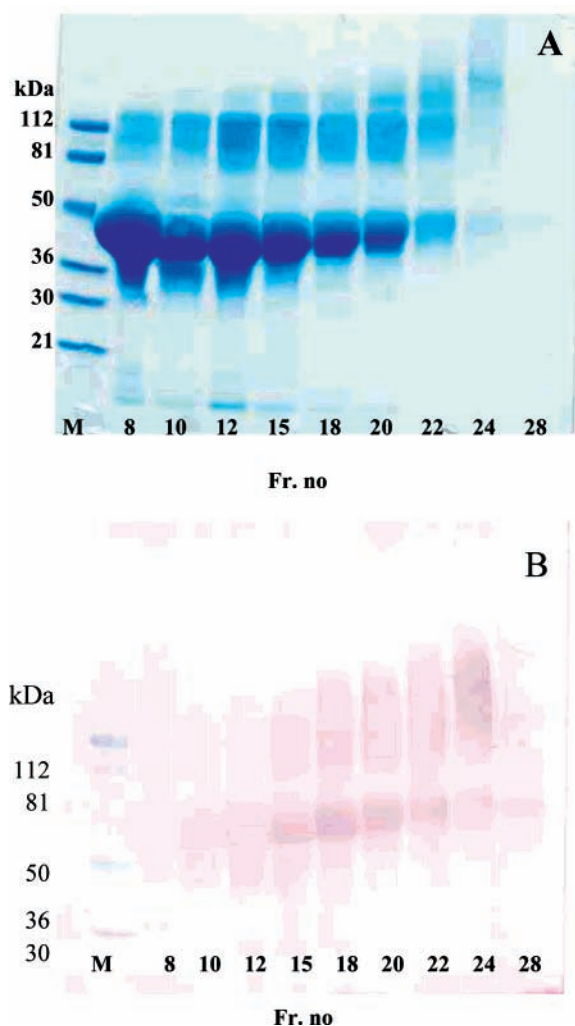
**Table 2. Conjugation Ratios of Selected Fractions from Figure 2 and Titers for Ovalbumin (OVA) and Glutathione (GS) Antibodies in Sera from Mice (groups of four animals) Immunized Four Times with Selected Fractions**

fraction	protein conc. (mg/mL)	conjugation ratio (GS/OVA)	titers	
			OVA	GS
8	8.3	0.22		
10	3.2	0.45	41250	—
12	5.0	0.94		
15	3.6	2.29		
18	2.6	5.25	15000	252
20	1.9	7.02		
22	0.7	6.01		
24	0.3	6.83	11250	2540
28	0.1	3.80		

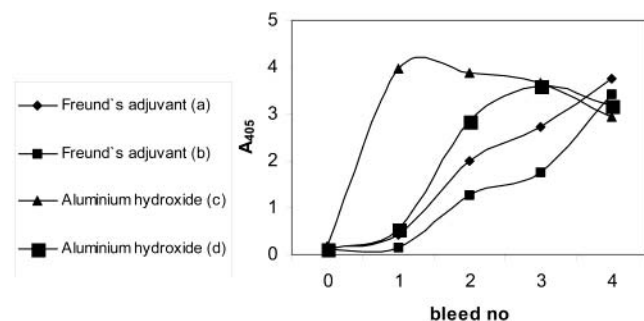
early eluting fractions and increasing reactivity at the end of the elution profile. This reflects that ovalbumin molecules with more glutathione conjugated are more negatively charged (for each lysine activated one positive charge is lost, and for each glutathione molecule conjugated one negative charge is gained). Amino acid analysis of selected fractions confirmed this and revealed the actual conjugation ratios (Table 2), which ranged from 0.22 to 7.02. Compared to the average conjugation ratio in Table 1, these values are somewhat lower, which is due to the use of less iodoacetic acid *N*-hydroxysuccinimid ester in the activation step (1 mg/30 mg ovalbumin vs 1 mg/10 mg ovalbumin). SDS-PAGE analysis and immunoblotting of selected fractions from the elution are shown in Figure 3. These analyses correspond to the elution pattern, showing a relatively large amount of protein early in the chromatogram with an electrophoretic mobility corresponding to nonconjugated ovalbumin and with a low reactivity with the glutathione antiserum. Fractions eluting later in the chromatogram showed a more heterogeneous electrophoretic mobility pattern and reacted stronger with the antiserum. Immunization of mice with selected fractions representing low (fraction 10), intermediate (fraction 18), and high (fraction 24) conjugation ratios induced antibodies against glutathione for the two latter fractions (Table 2), while no antibodies against glutathione were induced by the essentially nonconjugated fraction. The highest titers of glutathione antibodies were achieved with the fraction containing the more substituted conjugate, whereas the titers for ovalbumin antibodies were highest for the fractions with the lowest conjugation ratios. For one particular mouse, immunized with the highly conjugated fraction, the level of ovalbumin antibodies was remarkably low, while the glutathione antibody titer reached a level of almost 6000.

Immunization of rabbits with a pool of fractions (15–25) representing the more substituted conjugates showed that high titers of glutathione antibodies were rapidly induced. Aluminum hydroxide adjuvant was more effective than Freund's adjuvant since the antibody levels increased faster (Figure 4).

Thawing of the frozen iodoacetic acid *N*-hydroxysuccinimid ester-activated matrix and derivatization with glutathione revealed a lower average conjugation ratio, showing that freezing leads to inactivation of some of the reactive iodine groups. Similarly, in situ activation of ion exchange matrix-immobilized carrier protein packed in a column and conjugation by recirculation of reagents was attempted but was found to be inferior to batch activation and conjugation, presumably due to the absence of stirring, which is important for heterogeneous reactions (results not shown).

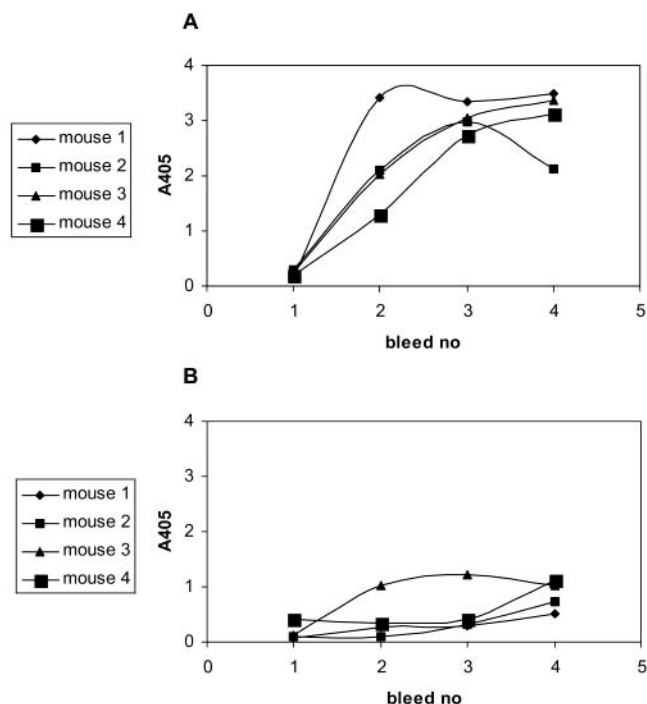


**Figure 3.** Analysis of eluted conjugates from Figure 2 by SDS-PAGE (A) and by immunoblotting (B) with an antiserum against glutathione. M: molecular weight marker proteins.



**Figure 4.** Time course for induction of antibodies against glutathione in rabbits immunized with eluted glutathione-ovalbumin conjugates using aluminum hydroxide (a, b) or Freund's adjuvant (c, d).

Conjugation of various peptides (1 mg/mL), with N- or C-terminally added cysteines, to ion exchange matrix-adsorbed ovalbumin was carried out using the batch procedure. Conjugation ratios of 1–2 were found by amino acid analysis. The conjugation ratios were lower for the synthetic peptides than for glutathione because lower concentrations were used. However, immunization of mice with the peptide-ovalbumin conjugates bound to Q Sepharose HP showed induction of antibodies, although different peptides were not equally immunogenic (Figure 5). As seen in Figure 5A, the conjugate of ovalbumin and peptide CGHEKEGFMEAEQC bound to



**Figure 5.** Antibody levels in mice immunized with Q Sepharose HP-immobilized ovalbumin conjugates of the following peptides (one letter amino acid code): (A) CGHEKEGFMEAEQC, (B) CADQLDPIYVAYNM.

Q Sepharose HP induced antibodies in all four mice reaching titers of 1:1600, whereas the conjugate of ovalbumin and peptide CADQLDPIYVAYNM bound to Q Sepharose HP was less immunogenic and only induced low titers of antibodies ( $\leq 1:200$ ).

#### 4. DISCUSSION

In this study we have shown that a carrier protein can be immobilized on an ion exchange matrix, activated with iodoacetic acid *N*-hydroxysuccinimid ester and then conjugated with glutathione or peptides containing a cysteine residue. The resulting conjugates could be eluted from the matrix for use in immunization experiments but the matrix-immobilized conjugates could also be used directly for immunization. Immunization of mice with eluted glutathione-ovalbumin conjugates showed that the more substituted conjugates elicited the highest titers of glutathione antibodies, and immunization experiments with matrix-bound peptide-ovalbumin conjugates revealed varying degrees of peptide antibody induction depending on the peptide.

Compared to previously described methods such as peptide synthesis directly on carrier proteins (Hansen et al., 1993), preactivation of carrier proteins in solution (Houen and Jensen, 1995), or preactivation of carrier proteins adsorbed to aluminum hydroxide (Houen et al., 1997), the present method is more versatile and easier to carry out. Peptide synthesis on proteins results in highly substituted conjugates with low solubility and requires simultaneous synthesis of the peptide itself for binding studies and absorption experiments. Preactivation of carrier proteins in solution with heterobifunctional reagents (eg., iodoacetic acid *N*-hydroxysuccinimid ester) is an efficient way of achieving conjugation to specific groups in haptens and peptides (eg., cysteine SH group), but this method requires extensive dialyses in order to remove activation reagents. Preactivation of carrier proteins adsorbed to aluminum hydroxide substitutes

dialysis for reagent removal with washing-centrifugation steps and therefore incorporates the advantages of solid-phase chemistry. This procedure, however, has the disadvantage that aluminum hydroxide is sensitive to variations in pH, and that the aluminum hydroxide-carrier interactions are rather weak and therefore sensitive to low concentrations of salt even at physiological pH. Adsorption of the carrier protein on ion exchange matrixes is much more robust compared to aluminum hydroxide, since the matrix itself is very stable and since the ionic interactions involved are strong. Furthermore, elution of the conjugates may be easily achieved by a salt gradient.

Compared to conjugation methods using homobifunctional reagents for cross-linking of carrier and peptide/hapten, the use of preactivation and heterobifunctional cross-linking reagents provides for better conjugation ratios and lower degrees of multimeric aggregate formation. When this is combined with solid-phase technology, which has proven its efficacy in peptide and oligonucleotide synthesis, the conjugation procedures can be carried out with optimal convenience, speed, and control of the conjugations. For this purpose, we have explored the use of ion exchange matrixes as the solid support in bioconjugate preparations, and we find that this is currently the optimal choice with respect to convenience, speed, stability, robustness, and versatility. Compared to the use of aluminum hydroxide as the solid support, ion exchange matrixes have the drawback of being less effective as adjuvants, and it may therefore be desirable to add aluminum hydroxide or another adjuvant prior to immunization. However, for several conjugates we observed efficient induction of antibodies without addition of adjuvant (results not shown), indicating that the matrix-bound conjugates are capable of activating a sufficient immune response.

In conclusion, we have developed a convenient and robust solid-phase conjugation method, which will be useful in preparation of many types of bioconjugates. Future investigations could therefore be aimed at incorporating the adjuvant into the solid-phase matrix or linking it through ionic interactions. Also, the combination of an affinity matrix and an immobilized ligand will offer protection of the ligand binding site during subse-

quent conjugations. Elution of the conjugate afterwards should provide a functional conjugate.

#### ACKNOWLEDGMENT

We thank Birgitte Gudmand and Anne Blicher for excellent technical assistance.

#### LITERATURE CITED

- (1) Barkholt, V., and Jensen, A. L. (1989). Amino acid analysis: determination of cysteine plus half-cystine in proteins after hydrochloric acid hydrolysis with a disulfide compound as additive. *Anal. Biochem.* 177, 318–22.
- (2) Briand, J. P., Muller, S., and Regenmortel, M. H. (1985). Synthetic peptides as antigens: Pitfalls of conjugation methods. *J. Immunol. Methods* 78, 59–69.
- (3) Carter, J. M. (1994). Techniques for conjugation of synthetic peptides to carrier molecules. *Methods Mol. Biol.* 36, 155–91.
- (4) Chan, W. C., and White, P. D. (2000). *Fmoc Solid-Phase Synthesis*, Oxford University Press, Oxford.
- (5) Hampton, A., Slotin, L. A., and Chawla, R. R. (1976). Evidence for species-specific substrate-site-directed inactivation of rabbit adenylate kinase by N6-(6-iodoacetamido-*n*-hexyl)adenosine 5'-triphosphate. *J. Med. Chem.* 19, 1279–83.
- (6) Hansen, P. R., Holm, A., and Houen, G. (1993). Solid-phase peptide synthesis on proteins. *Int. J. Pept. Protein Res.* 41, 237–45.
- (7) Houen, G., and Jensen, O. M. (1995). Conjugation to preactivated proteins using divinyl sulfone and iodoacetic acid. *J. Immunol. Methods* 181, 187–200.
- (8) Houen, G., Jakobsen, M. H., Svaerke, C., Koch, C., and Barkholt, V. (1997). Conjugation to preadsorbed preactivated proteins and efficient generation of anti peptide antibodies. *J. Immunol. Methods* 206, 125–34.
- (9) Laemmli, U. K. (1970) Cleavage of structural proteins during the assembly of the head of bacteriophage T4. *Nature* 227, 680–685.
- (10) Regenmortel, M. H. V., Briand, J. P., Muller, S., and Plaue, S. (1988). Synthetic polypeptides as antigens. In *Laboratory Techniques in Biochemistry and Molecular Biology* (R. H. Burdon and P.H. Knippenberg, Eds.), pp 1–227, Elsevier, Amsterdam.
- (11) Studier, F. W. (1973). Analysis of bacteriophage T7 early RNAs and proteins on slab gels. *J. Mol. Biol.* 79, 237–248.

BC025622J



# Reversible Biotinylation Phosphoramidite for 5'-End-Labeling, Phosphorylation, and Affinity Purification of Synthetic Oligonucleotides

Shiyue Fang<sup>†,§</sup> and Donald E. Bergstrom<sup>\*,†,§</sup>

Department of Medicinal Chemistry and Molecular Pharmacology, Purdue University, West Lafayette, Indiana 47907 and Walther Cancer Institute, Indianapolis, Indiana 46208. Received October 14, 2002

A fluoride/amine-cleavable phosphoramidite designed for biotinylation, phosphorylation, and affinity purification of synthetic oligonucleotides was synthesized and coupled efficiently to the 5'-end of DNA on a solid-phase automatic synthesizer. The two hydroxyl groups of diethyl bis(hydroxymethyl)malonate were used to link biotin and the 5'-end of DNA together through a diisopropylsilyl acetal functionality and a phosphate ester group, respectively. The DNA was cleaved from solid support and fully deprotected by treating with a mixture of MeNH<sub>2</sub> (~40%) and NH<sub>4</sub>OH (~29%) (1:1, v/v, 65 °C, 30 min), and the linkage between biotin and DNA was found completely stable under these conditions. The biotinylated full-length DNA was efficiently attached to NeutrAvidin coated microspheres and failure sequences and other impurities were simply removed by washing with buffer and water. The microspheres were then treated with HF/pyridine/THF (rt, 1 h) and MeNH<sub>2</sub> (~40%, rt, 15 min) sequentially to yield high quality full-length 5'-end phosphorylated unmodified DNA as revealed by HPLC analysis. It is anticipated that this method will find applications in areas that require efficient isolation of 5'-end phosphorylated DNA from a complex mixture.

## INTRODUCTION

The high affinity between biotin and streptavidin or avidin (association constant 10<sup>15</sup>/M) has been widely used as a means to label DNA and RNA (1), and as a result, chemical biotinylation of these biopolymers has received considerable attention (2–9). For some applications, reversible biotinylation may be required in order to regenerate unmodified DNA/RNA that can be biochemically or biologically processed. For 5'-end reversibly biotinylated DNA/RNA, after cleavage, both 5'-end non-phosphorylated and 5'-end phosphorylated DNA/RNA are required to meet different applications. For the former purpose, Gildea and co-workers reported an acid-labile biotinylation phosphoramidite (8). For the latter purpose, Rothschild and co-workers reported a photocleavable biotinylation phosphoramidite (9). Although they successfully applied their methods for affinity purification of synthetic oligonucleotides, Gildea's method requires a challenging and inconvenient reagent synthesis, and in Rothschild's method, formation of thymine–thymine photodimer under UV irradiation is a concern (10–12). We recently reported a fluoride-cleavable biotinylation phosphoramidite for 5'-end-labeling, affinity purification of synthetic oligonucleotides (13). In this method, non-phosphorylated unmodified DNA was obtained after removal of the biotin tag. Complementary to this method, we describe here a reversible biotinylation phosphoramidite that on removal of the biotin tag affords 5'-end phosphorylated unmodified DNA.

## MATERIALS AND METHODS

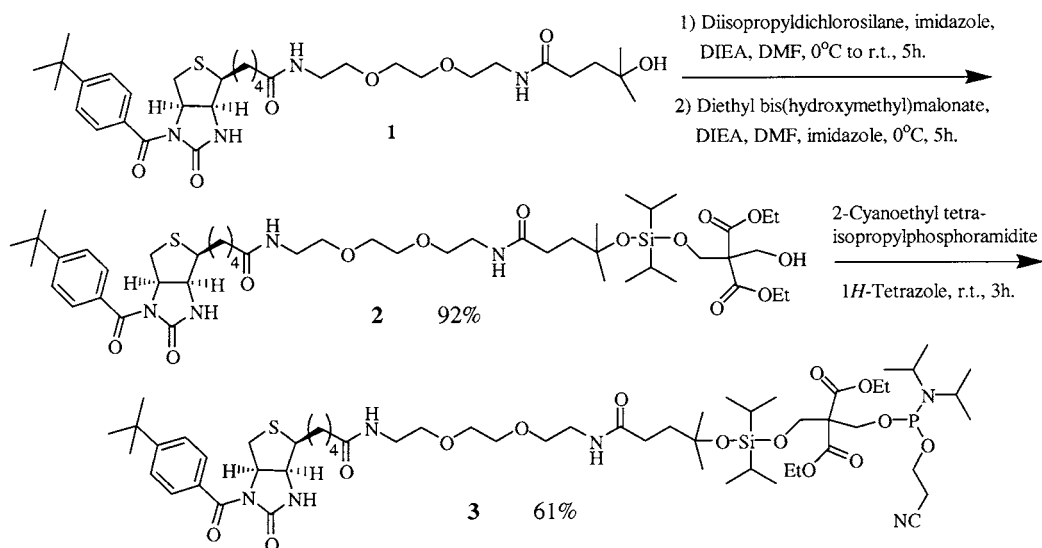
**General.** All reactions were performed under a blanket of dry argon. Reagents and solvents available from commercial sources were used as received unless otherwise noted. Tetrahydrofuran was distilled from a Na/benzophenone ketyl. Acetonitrile was distilled over CaH<sub>2</sub>. Acetone was dried over anhydrous Na<sub>2</sub>SO<sub>4</sub>, and the supernatant was used directly. Thin-layer chromatography (TLC) was performed using Sigma-Aldrich TLC plates, silica gel on aluminum 60F-254, 200 μm thickness. Flash column chromatography was performed using 'Baker' silica gel (40 μm). NMR spectra were obtained using a 250 or 500 MHz Bruker spectrometer. Chemical shifts (δ) are reported relative to CHCl<sub>3</sub> (δ = 7.27 ppm for <sup>1</sup>H and 77.23 ppm for <sup>13</sup>C) or triphenyl phosphate (δ = 0.00 ppm for <sup>31</sup>P). Infrared spectra were recorded on a Nicolet FTIR spectrophotometer. High-resolution mass spectra were obtained on a Finnigan Mat 95XL spectrometer. UltraLink Immobilized NeutrAvidin (slurry in water, approximately 50% v/v, containing 0.02% sodium azide; pore size, 1000 Å; particle size, 50–80 μm; biotin-binding capacity, ~0.08 μmol biotin/mL gel) was purchased from Pierce. Aqueous MeNH<sub>2</sub> (~40%) and NH<sub>4</sub>OH (~29%), HF/pyridine (HF, ~70%; pyridine, ~30%), diethyl bis(hydroxymethyl)malonate and Me<sub>3</sub>SiOMe were purchased from Aldrich Inc. Diisopropylchlorosilane was purchased from Gelest Inc. Succinic ester linked DMTr-dT-lcaa-CPG (pore size 1000 Å), (2-cyanoethyl)-[2,2-bis(ethoxycarbonyl)-3-(4,4'-dimethoxytrityloxy)propyl-1]-N,N-diisopropylphosphoramidite and 5'-DMTr, 2-cyanoethyl phosphoramidites: benzoyl-dA, isobutryl-dG, acetyl-dC, and dT were purchased from Glen Research Inc. PBS buffer: 136.9 mM NaCl, 2.7 mM KCl, 10.1 mM Na<sub>2</sub>HPO<sub>4</sub>, 1.8 mM KH<sub>2</sub>PO<sub>4</sub>, adjusted to pH 7.0 with HCl. HPLC: C-18 reverse phase column (100 Å, 250 × 4.6 mm for analysis, 250 × 10.0 mm for preparation, Varian

\* To whom correspondence should be addressed. . Telephone: 765-494-6275 Fax: 765-494-9193 email: bergstrom@purdue.edu.

<sup>†</sup> Purdue University.

<sup>§</sup> Walther Cancer Institute.

Scheme 1

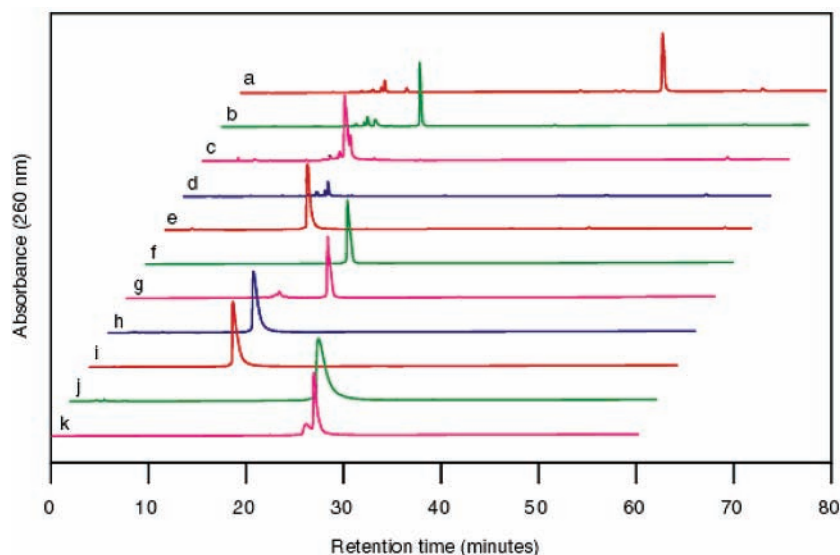


Analytical Instruments); solvent A: 0.1 M triethylammonium acetate, 5% acetonitrile; solvent B: 90% acetonitrile; profiles were generated by detection of the absorbance of DNA at 260 nm using two linear gradient solvent systems: Gradient A: solvent B (0–45%) in solvent A over 60 min at flow rates of 1 mL/min (analysis) and 3 mL/min (preparation); Gradient B: solvent B (0–20%) in solvent A over 60 min at a flow rate of 1 mL/min (analysis). In all cases, gradient A was used unless otherwise noted.

**Biotin Diethyl Bis(hydroxymethyl)malonate Conjugate 2.** A one-necked round-bottomed flask was charged with biotinyl alcohol **1** (605 mg, 0.93 mmol), synthesized following procedures described previously (13), and imidazole (63 mg, 0.93 mmol) and flushed with Ar. DMF (2 mL) and diisopropylethylamine (498  $\mu$ L, 2.79 mmol) were added via syringe. After the mixture was cooled to 0 °C, diisopropyldichlorosilane (252  $\mu$ L, 1.40 mmol) was added via syringe in one portion. The light yellow solution was stirred at 0 °C for 1 h and at rt for 4 h and then added to a solution of diethyl bis(hydroxymethyl)malonate (500 mg, 2.20 mmol) and imidazole (126 mg, 1.86 mmol) in DMF (2 mL) via syringe very slowly (over 45 min). After being stirred at 0 °C for 5 h, the reaction mixture was partitioned between CH<sub>2</sub>Cl<sub>2</sub> (30 mL  $\times$  5) and 5% citric acid (50 mL). The organic phase was washed with brine (30 mL) and dried over anhydrous Na<sub>2</sub>SO<sub>4</sub>. Removal of volatile components gave a light yellow residue, which was purified by flash column chromatography (3.0  $\times$  12 cm, SiO<sub>2</sub>, 19:1, CH<sub>3</sub>Cl/CH<sub>3</sub>OH). The highest UV active spot (the major one) on TLC ( $R_f$  = 0.5; 9:1, CH<sub>3</sub>Cl/CH<sub>3</sub>OH) was easily isolated, giving **2** (Scheme 1) as a white foam (839 mg, 92%): IR (thin film, cm<sup>-1</sup>)  $\nu$  3318, 2954, 2864, 1739, 1652, 1555, 1040; <sup>1</sup>H NMR (CDCl<sub>3</sub>, 500 MHz)  $\delta$  0.88–1.01 (m, 14H), 1.24–1.27 (m, 12H), 1.32 (s, 9H), 1.47–1.53 (m, 2H), 1.65–1.85 (m, 6H), 2.18–2.31 (m, 4H), 3.03–3.10 (m, 2H), 3.25 (dt, 1H,  $J$  = 7.4, 4.7 Hz), 3.38–3.50 (m, 4H), 3.54–3.56 (m, 4H), 3.60 (s, 4H), 4.14–4.27 (m, 9H), 5.22–5.24 (m, 1H), 6.37 (t, 1H,  $J$  = 5.5 Hz), 6.58 (t, 1H,  $J$  = 5.3 Hz), 7.39 (d, 2H,  $J$  = 8.5 Hz), 7.57 (d, 2H,  $J$  = 8.5 Hz); <sup>13</sup>C NMR (CDCl<sub>3</sub>, 500 MHz)  $\delta$  13.4, 14.2, 17.7, 27.8, 29.8, 30.5, 31.3, 32.0, 35.1, 35.6, 38.4, 39.2, 39.5, 40.0, 55.2, 57.5, 61.6, 61.7, 61.8, 62.7, 70.0, 70.1 (X 2), 70.3, 73.8, 124.7, 129.1, 131.9, 155.1, 156.3, 169.2, 170.2, 173.3, 174.2. HRMS (ESI, M + H<sup>+</sup>) Calcd for C<sub>48</sub>H<sub>81</sub>N<sub>4</sub>O<sub>13</sub>SSi 981.5290, found 981.5295.

**Biotin Diethyl Bis(hydroxymethyl)malonate Conjugate Phosphoramidite 3.** To a solution of **2** (715 mg, 0.72 mmol) in dry acetonitrile (2 mL) were added 2-cyanoethyl-*N,N,N,N*-tetraisopropylphosphoramidite (264  $\mu$ L, 0.80 mmol) and 1*H*-tetrazole (0.45 M in acetonitrile, 1.68 mL, 0.76 mmol) sequentially. After stirring at rt for 3 h, some white precipitate formed. The reaction was quenched with NaHCO<sub>3</sub> (5%, 50 mL), and the mixture was extracted by CH<sub>2</sub>Cl<sub>2</sub> (30 mL  $\times$  5). The organic phase was dried over anhydrous Na<sub>2</sub>SO<sub>4</sub>, solvents were removed under reduced pressure, and the residue was purified by flash column chromatography (3.0  $\times$  10 cm, SiO<sub>2</sub>, 7:3:0.5, CHCl<sub>3</sub>/THF/Et<sub>3</sub>N), giving **3** as a white foam (520 mg, 61%):  $R_f$  = 0.5 (7:3:0.5, CHCl<sub>3</sub>/THF/Et<sub>3</sub>N); <sup>1</sup>H NMR (CDCl<sub>3</sub>, 250 MHz)  $\delta$  0.91–1.07 (m, 14H), 1.14–1.18 (m, 12H), 1.22–1.29 (m, 12H), 1.32 (s, 9H), 1.41–1.51 (m, 2H), 1.65–1.82 (m, 4H), 2.16–2.34 (m, 4H), 2.60 (t, 2H,  $J$  = 6.8 Hz), 3.04–3.06 (m, 2H), 3.21–3.26 (m, 1H), 3.40–3.48 (m, 4H), 3.52–3.61 (m, 8H), 3.76–3.82 (m, 2H), 4.05–4.25 (m, 11H), 5.19–5.22 (m, 1H), 6.28 (t, 1H,  $J$  = 5.5 Hz), 6.39 (t, 1H,  $J$  = 5.3 Hz), 7.39 (d, 2H,  $J$  = 8.0 Hz), 7.57 (d, 2H,  $J$  = 8.3 Hz); <sup>31</sup>P NMR (CDCl<sub>3</sub>, 250 MHz)  $\delta$  166.36.

**Biotinyl Oligonucleotide 4, Synthesis, Cleavage, Deprotection, and HPLC Analysis.** The oligonucleotide was synthesized on an ABI DNA/RNA synthesizer at 1  $\mu$ mol scale, using the following 5'-DMTr, 2-cyanoethyl phosphoramidites: benzoyl-dA, isobutyryl-dG, acetyl-dC and dT. The manufacturer recommended synthetic cycles were used except that **3** (0.1 M in acetonitrile) was coupled for 15 min. The CPG was dried under nitrogen flow and then divided into two portions (0.52  $\mu$ mol, 0.48  $\mu$ mol). To the 0.52  $\mu$ mol portion in a screw-capped 5-mL vial was added NH<sub>4</sub>OH (~29%, 200  $\mu$ L) and methylamine (~40%, 200  $\mu$ L), and the resulting suspension was heated to 65 °C for 30 min. After being cooled to -20 °C, the supernatant was taken out, and the CPG was washed with water (200  $\mu$ L  $\times$  5). The supernatant and water washes were combined and dried on a SpeedVac. The residue was redissolved in 1.0 mL water, of which 10  $\mu$ L was diluted to 100  $\mu$ L, and 50  $\mu$ L was analyzed by HPLC to generate trace a (Figure 1). From the 1.0 mL solution was taken out a 100  $\mu$ L portion and dried on a SpeedVac. The residue was suspended in dry THF (200  $\mu$ L) in an Eppendorf tube, 30  $\mu$ L of HF/pyridine was added via pipet. The mixture was vortexed for 1 min and then



**Figure 1.** HPLC traces of (a) crude oligonucleotide **4**, containing failure sequences. (b) HF/pyridine-treated crude **4**. (c) HF/pyridine- and aqueous methylamine-treated crude **4**. (d) Unbiotinylated failure sequences left after treating crude **4** with NeutrAvidin gel. (e) Affinity-purified oligonucleotide **7**. (f) Authentic **6**. (g) Authentic **6** and HF/pyridine-treated crude **4**. (h) Authentic **7** and affinity-purified **7**. (i) Authentic **7**. (j) Authentic **7** and affinity-purified **7** eluted with solvent gradient B. (k) Authentic **8** and affinity-purified **7** eluted with solvent gradient B.

allowed to stand at rt for 1 h with occasional shaking. The excess fluoride ion was quenched with Me<sub>3</sub>SiOMe (500  $\mu$ L) by gentle shaking at rt for 30 min. Volatile components were removed on a SpeedVac, the residue was dissolved in 500  $\mu$ L water, and 50  $\mu$ L was analyzed by HPLC to generate trace **b** (Figure 1). From the 1.0 mL solution was taken out another 100  $\mu$ L portion, which was treated with HF/pyridine and Me<sub>3</sub>SiOMe exactly as described above. To the resulting residue was added MeNH<sub>2</sub> (~40%, 200  $\mu$ L), the mixture was gently shaken at rt for 15 min and then dried on a SpeedVac. The residue was dissolved in 500  $\mu$ L water, and 50  $\mu$ L was analyzed by HPLC to generate trace **c** (Figure 1). The coupling efficiency of **3** was estimated to be more than 81% by comparing the area of the peak with retention time near 43 min to that of the major peak near 15 min in trace **a** (Figure 1).

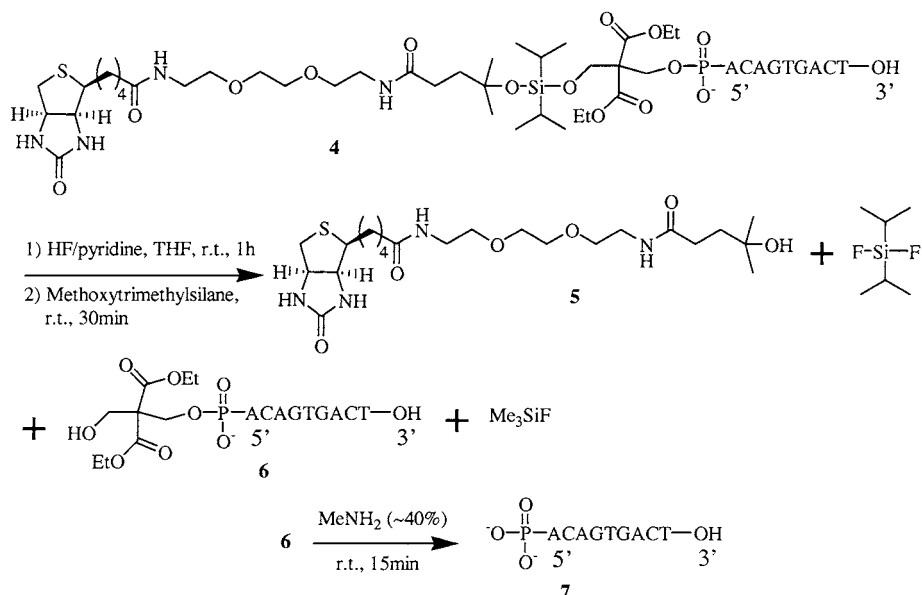
**Affinity Purification and HPLC Analysis.** Another 100  $\mu$ L was taken out from the above-described 1.0 mL solution of crude oligonucleotide **4**, dried on a SpeedVac, redissolved in 300  $\mu$ L of PBS buffer, and incubated with UltraLink Immobilized NeutrAvidin gel (0.5 mL gel, 1.0 mL gel slurry), which was washed with PBS buffer (300  $\mu$ L  $\times$  3), for 1 h at rt with gentle shaking (it is important to handle the gel gently, otherwise, gel material may leak, and recovery yield of full-length DNA may be low). The mixture was centrifuged, the supernatant removed, and the gel washed with PBS buffer (300  $\mu$ L  $\times$  2). The supernatant and PBS buffer washes were combined, dried on a SpeedVac, redissolved in 500  $\mu$ L water, and 100  $\mu$ L was analyzed by HPLC to generate trace **d** (Figure 1). The gel was further washed with PBS buffer (500  $\mu$ L  $\times$  3) and water (500  $\mu$ L  $\times$  3), dried by washing with dry acetone (500  $\mu$ L  $\times$  3) and THF (500  $\mu$ L  $\times$  3), and then suspended in THF (300  $\mu$ L). To the suspension was added HF/pyridine (30  $\mu$ L), and the mixture was incubated at rt for 1 h with gentle shaking. The excess fluoride ion was quenched with Me<sub>3</sub>SiOMe (500  $\mu$ L, rt, 30 min), the mixture was centrifuged, and the supernatant was removed. The gel was washed with THF (300  $\mu$ L  $\times$  2) and then incubated in MeNH<sub>2</sub> (~40%, 500  $\mu$ L) at rt for 15 min. The mixture was centrifuged, the supernatant obtained, and the gel washed with water (300  $\mu$ L  $\times$  8).

The supernatant and water washes were combined and dried on a SpeedVac. The residue was redissolved in water (1.5 mL), and 100  $\mu$ L was analyzed by HPLC to give trace **e** (Figure 1). The recovery yield of full-length 5'-end phosphorylated DNA **7** (see Scheme 2 for structure) was estimated to be 72% by comparing the area of the peak in trace **e** to that in trace **a** with a retention time of near 43 min. The presence of the 5'-phosphate group on **7** was supported by HPLC analysis through coinjection of authentic **6** (authentic samples were synthesized as described below) with the sample used to generate trace **b** (trace **g**, Figure 1). Coinjection of the affinity purified **7** with authentic **7** gave trace **h** (Figure 1). Coinjection of affinity purified **7** with the nonphosphorylated authentic sample HOACAGTGACTOH (**8**) eluting with solvent gradient A, however, gave a single peak (HPLC trace not shown). To resolve affinity purified **7** and authentic **8**, solvent gradient B was used, and HPLC trace **k** was generated. Coinjection of affinity purified **7** with authentic **7** under these conditions gave trace **j**. The identity of affinity purified **7** was also confirmed by MALDI mass spectrum analysis of the failure sequences and full-length **7** (**14**). The samples, which were used to generate HPLC traces **d** and **e**, were desalted by Sep-Pac cartridge independently according to the reported procedure and analyzed separately (**14**). The failure sequences gave the following peaks: 2718.4 for (HO-TCAGTGACA-OH - H)<sup>-</sup> calcd 2721.9, 2405.7 for (HO-TCAGTGAC-OH - H)<sup>-</sup> calcd 2408.7, 2117.7 for (HO-TCAGTGA-OH - H)<sup>-</sup> calcd 2119.5, 1804.3 for (HO-TCAGTG-OH - H)<sup>-</sup> calcd 1806.3, 1476.5 for (HO-TCAGT-OH - H)<sup>-</sup> calcd 1477.1, 1173.2 for (HO-TCAG-OH - H)<sup>-</sup> calcd 1172.8, 844.9 for (HO-TCA-OH - H)<sup>-</sup> calcd 843.6, 531.0 for (HO-TC-OH - H)<sup>-</sup> calcd 530.4. The affinity purified **7** gave a peak of 2804.8 for (HO-TCAGTGACA-OPO<sub>3</sub>H<sub>2</sub> - H)<sup>-</sup> calcd 2801.9.

**Synthesis and Purification of Authentic Oligonucleotides **6**, **7**, and **8**.** Oligonucleotide **6** and **7** were synthesized independently on an ABI DNA/RNA synthesizer at 1  $\mu$ mol scale, using the following 5'-DMTr, 2-cyanoethyl phosphoramidites: benzoyl-dA, isobutyryl-dG, acetyl-dC and dT; and (2-cyanoethyl)[2,2-bis(ethoxycarbonyl)-3-(4,4'-dimethoxytrityloxy)propyl-1]-*N,N*-diiso-



## Scheme 2



propylphosphoramidite. Manufacture recommended synthetic cycles were used. Cleavage/deprotection was performed by  $\text{NH}_4\text{OH}$  (~29%) and  $\text{MeNH}_2$  (~40%) (1:1, v/v) at 65 °C for 15 min. Following the procedure described by Guzaev (15), trityl-on reverse phase preparative HPLC purification, detritylation gave **6** (HPLC trace f, Figure 1); removal of the 5'-end diethyl bis(hydroxymethyl)malonate moiety gave **7** (HPLC trace i, Figure 1). Authentic **8** was synthesized following a procedure described previously (13).

## RESULTS AND DISCUSSION

We recently reported the design and synthesis of a fluoride-cleavable phosphoramidite for 5'-end biotinylation and affinity purification of synthetic oligonucleotides (13). The biotinylated structure obtained by such a method after cleavage of the oligonucleotide from solid support and ammonia deprotection is illustrated in Figure 2 (**9**). The diisopropylsilyl acetal linkage, which connects the biotin moiety and the 5'-OH of the synthetic oligonucleotide through a tertiary hydroxide group, was found completely stable under certain postsynthetic DNA cleavage/deprotection conditions. However, this linkage can be readily broken by treating with HF/pyridine under mild conditions to yield unmodified DNA carrying a free 5'-OH. In 1995, Guzaev and co-workers described an approach that used the dimethoxytrityl protected diethyl bis(hydroxymethyl)malonate phosphoramidite for chemical phosphorylation of oligonucleotides at the 5'-terminus (15). The structure of DNA obtained by their method is also shown in Figure 2 (**10**). The DMTr-protected diethyl bis(hydroxymethyl)malonate moiety that is linked to the 5'-OH of DNA through a phosphodiester group is stable under common amino cleavage/deprotection conditions.

This property is useful for purification of synthetic DNA by reverse phase HPLC. After purification and removal of the DMTr group, the 5'-end phosphate group is released by briefly treating with aqueous amine under mild conditions. On the basis of these two reports, we reasoned that substitution of the DMTr group in **10** by the diisopropylsilyl acetal functionality linked to biotin as in **9** would provide a simple method for reversible biotinylation and phosphorylation of DNA. This led to design of the reversible biotinylation phosphoramidite **3** (Scheme 1). The new linkage between DNA and biotin, like **9** and **10**, should be stable under certain postsynthetic DNA cleavage/deprotection conditions. Removal of the silyl acetal group by treating with fluoride ion should generate the same species as treating **10** with acid, and 5'-end phosphorylated DNA should be produced in the presence of aqueous amine under mild conditions.

Synthesis of the phosphoramidite **3** is shown in Scheme 1. The biotinyl tertiary alcohol **1** was prepared according to procedures described previously (13). The tertiary hydroxyl group of **1** was first silylated by diisopropylchlorosilane in DMF in the presence of diisopropylethylamine (2 equiv) and imidazole. This solution was added to a solution of diethyl bis(hydroxymethyl)malonate and imidazole in DMF via syringe very slowly to avoid possible deformylation of the hydroxymethylmalonate under basic conditions, and **2** was obtained as a white foam in excellent yield. The biotinyl alcohol **2** was then phosphorylated under a slightly acidic conditions following Guzaev's procedure to give **3** (61%) (15).

The biotinyl oligonucleotide **4** (Scheme 2) was synthesized on an automatic DNA/RNA synthesizer according to standard synthetic cycles. The following 5'-DMTr, 2-cyanoethyl phosphoramidites were used: benzoyl-dA,

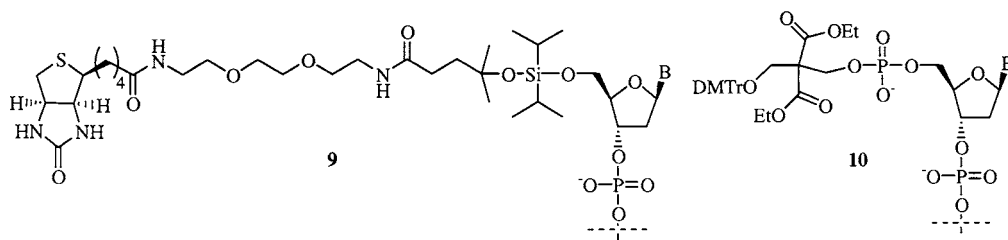


Figure 2.

isobutyryl-dG, acetyl-dC and dT, and in the last cycle, **3** (0.1 M in acetonitrile) was coupled for 15 min. Protection of C with an acetyl group allowed fast cleavage/deprotection of the DNA by treating with MeNH<sub>2</sub> (~40%)/NH<sub>4</sub>-OH (~29%) (1:1, v/v, 65 °C, 30 min) (16, 17). The 4-tertiary butyl benzoyl protecting group on biotin was also removed under these conditions, giving the diisopropylsilyl acetal linked biotinyl oligonucleotide **4** as the product (13). Analysis by HPLC generated *trace a* (Figure 1); the major peak with a retention time near 43 min should be the biotinylated oligonucleotide **4** (Scheme 2). A portion was treated with HF/pyridine, followed by quenching the excess fluoride ion by methoxytrimethylsilane (18), dried, redissolved in water, and analyzed by HPLC to give *trace b* (Figure 1); the major peak with a retention time near 20 min should be **6** (Scheme 2). The peaks with retention time around 15 min in *traces a* and *b* should be failure sequences and other impurities. Another portion was treated similarly with HF/pyridine, followed by methoxytrimethylsilane, but was then further incubated in aqueous MeNH<sub>2</sub> (~40%) at room temperature to give the 5'-end phosphorylated unmodified oligonucleotide **7** (Scheme 2) (15). As expected, HPLC analysis (*trace c*, Figure 1) indicated that the major peaks in *traces a* (retention time ~43 min) and *b* (retention time ~20 min) was replaced by a peak near 15 min. Comparison of *traces a* with *b* and *c* indicates that the linkage between biotin and the 5'-end of DNA is completely stable under these postsynthetic DNA cleavage/deprotection conditions. The coupling efficiency of phosphoramidite **3** was estimated to be 81% by comparing the area of the peak in *trace a* with a retention time of near 43 min to that of the largest peak with retention time near 15 min.

To demonstrate application of this biotinylation strategy, the crude oligonucleotide **4**, contaminated by failure sequences and other impurities (see *trace a*, Figure 1), was then purified by NeutrAvidin-coated microsphere-mediated affinity purification. Because the failure sequences and other impurities do not contain biotin, incubation of the crude product with the microsphere followed by washing with buffer should leave only the biotinylated full-length **4** on the solid phase. In practice, crude **4** was incubated with the microspheres in PBS buffer at room temperature for 1 h. After being centrifuged, the supernatant was removed and analyzed by HPLC (*trace d*, Figure 1). The major peak in *trace a* (retention time ~43 min) disappeared in *trace d*, showing the high efficiency of binding **4** to the NeutrAvidin-coated microspheres. The microspheres were then further washed with buffer and water, dried by washing with anhydrous acetone and THF, and then suspended in dry THF. The cleavage reagent HF/pyridine was added, incubated at room temperature, followed by quenching excess fluoride ion by methoxytrimethylsilane to give **6** (Scheme 2). The mixture was centrifuged and the supernatant removed. The gel was washed with THF and incubated at room temperature in aqueous MeNH<sub>2</sub> (~40%) to remove the diethyl bis(hydroxymethyl)malonate moiety and generate 5'-end phosphorylated **7** (15). After centrifugation, the supernatant was obtained, and the gel was washed with water. The supernatant and water washes were combined, dried on a SpeedVac, redissolved in water, and analyzed by HPLC to give *trace e* (Figure 1). As can be seen, the full-length, 5'-end phosphorylated DNA **7** is very pure. The recovery yield of **7** by this purification method was estimated by comparing the area of the peak in *trace e* (Figure 1) with that in *trace a* with a retention time of near 43 min, and it was 72%. To confirm the identity of **7**, authentic samples of **6** and **7** were prepared

following the published procedure (15). We first confirmed the structure of **6** by coinjection of the sample used to generate HPLC *trace b* with authentic **6** to give *trace g*. The identity of **7** was confirmed by coinjection of affinity purified sample with authentic **7**, whereupon only one peak was observed (*trace h*, Figure 1). However, when we coinjected affinity purified **7** with nonphosphorylated authentic sample HOACAGTGACTOH (**8**), prepared according to procedures described previously (13), a single peak was also observed (HPLC trace not shown). To resolve affinity purified **7** and authentic **8**, the solvent gradient B was used, and HPLC *trace k* was generated, which had two peaks. To make certain the affinity purified **7** and authentic **7** were also identical under these conditions, they were also coinjected for HPLC analysis, eluting with solvent gradient B; as expected, a single peak was observed (*trace j*). The identity of **7** was also conveniently confirmed by MALDI mass spectrum analysis of the failure sequences and full-length **7** (samples used to generate HPLC *traces d* and *e*, respectively), because the failure sequences were easily enriched after efficient separation from the full-length biotinylated **4** (14).

In conclusion, we designed and synthesized a novel reversible biotinylation, phosphorylation phosphoramidite, and successfully used it to biotinylate and phosphorylate the 5'-end of DNA on an automatic synthesizer. We demonstrated the use of this method by application in affinity purification of a synthetic oligonucleotide. The full-length biotinylated DNA was efficiently attached to NeutrAvidin-coated microspheres by brief incubation, and failure sequences and other impurities were removed by simple washing with buffer and water. High quality full-length 5'-end phosphorylated DNA was recovered by brief treatments with fluoride ion and aqueous amine, sequentially. The procedure is simple, and the recovery yield is high. We anticipate that this method will find applications in areas that require efficient isolation of 5'-end phosphorylated DNA from complex mixtures.

#### ACKNOWLEDGMENT

Grant support from the National Institutes of Health (GM53155) and the Showalter Trust Fund is gratefully acknowledged. Assistance from the National Cancer Institute Grant (P30 CA23168) awarded to Purdue University is also gratefully acknowledged.

#### LITERATURE CITED

- (1) McInnes, J. L., and Symons, R. H. (1989) Preparation and detection of nonradioactive nucleic acid and oligonucleotide probes. *Nucleic Acid Probes* (R. H. Symons, Ed.) pp 33–80, CRC Press, Boca Raton, FL.
- (2) Zhao, Z., and Ackroyd, J. (1999) A biotin phosphoramidite reagent for the automated synthesis of 5'-biotinylated oligonucleotides. *Nucleosides Nucleotides* 18, 1231–1234.
- (3) Kumar, P., Bhatia, D., Garg, B. S., and Gupta, K. C. (1994) An improved method for synthesis of biotin phosphoramidites for solid-phase biotinylation of oligonucleotides. *Bioorg. Med. Chem. Lett.* 4, 1761–1766.
- (4) Neuner, P. (1996) New non nucleosidic phosphoramidite reagent for solid-phase synthesis of biotinylated oligonucleotides. *Bioorg. Med. Chem. Lett.* 6, 147–152.
- (5) Piele, U., Sproat, B. S., and Lamm, G. M. (1990) A protected biotin containing deoxycytidine building block for solid-phase synthesis of biotinylated oligonucleotides. *Nucleic Acids Res.* 18, 4355–4360.
- (6) Shimkus, M., Levy, J., and Herman, T. (1985) A chemically cleavable biotinylated nucleotide: usefulness in the recovery of protein-DNA complexes from avidin affinity columns. *Proc. Natl. Acad. Sci. U.S.A.* 82, 2593–2597.

- (7) Herman, T. M., and Fenn, B. J. (1990) Chemically cleavable biotin-labeled nucleotide analogs. *Methods Enzymol.* **184**, 584–588.
- (8) Gildea, B. D., Coull, J. M., and Koster, H. (1990) A versatile acid-labile linker for modification of synthetic biomolecules. *Tetrahedron Lett.* **31**, 7095–7098.
- (9) Olejnik, J., Krzymanska-Olejnik, E., and Rothschild, K. J. (1996) Photocleavable biotin phosphoramidite for 5'-end-labelling, affinity purification and phosphorylation of synthetic oligonucleotides. *Nucleic Acids Res.* **24**, 361–366.
- (10) Greenberg, M. M. (1995) Photochemical release of protected oligodeoxyribonucleotides containing 3'-glycolate termini. *Tetrahedron* **51**, 29–38.
- (11) Greenberg, M. M., and Gilmore, J. L. (1994) Cleavage of oligonucleotides from solid-phase supports using *o*-nitrobenzyl photochemistry. *J. Org. Chem.* **59**, 746–753.
- (12) Cadet, J., and Vigny, P. (1990) The photochemistry of nucleic acids. *Bioorganic Photochemistry* (H. Morrison, Ed.) Vol. 1, pp 170–184, John Wiley & Sons, New York.
- (13) Fang, S., and Bergstrom, D. E. (2003) Fluoride-cleavable biotinylation phosphoramidite for 5'-end-labeling, affinity purification of synthetic oligonucleotides. *Nucleic Acids Res.*, in press.
- (14) Alazard, D., Filipowsky, M., Raeside, J., Clarke, M., Majlessi, M., Russell, J., and Weisburg, W. (2002) Sequencing of production-scale synthetic oligonucleotides by enriching for coupling failures using matrix-assisted laser desorption/ionization time-of-flight mass spectrometry. *Anal. Biochem.* **301**, 57–64.
- (15) Guzaev, A., Salo, H., Azhayev, A., and Lönnberg, H. (1995) A new approach for chemical phosphorylation of oligonucleotides at the 5'-terminus. *Tetrahedron* **51**, 9375–9384.
- (16) Reddy, M. P., Hanna, N. B., and Farooqui, F. (1994) Fast cleavage and deprotection of oligonucleotides. *Tetrahedron Lett.* **35**, 4311–4314.
- (17) Wincott, F., DiRenzo, A., Shaffer, C., Grimm, S., Tracz, D., Workman, C., Sweedler, D., Gonzalez, C., Scaringe, S., and Usman, Z. (1995) Synthesis, deprotection, analysis and purification of RNA and ribozymes. *Nucleic Acids Res.* **23**, 2677–2684.
- (18) Tallarico, J. A., Depew, K. M., Pelish, H. E., Westwood, N. J., Lindsley, C. W., Shair, M. D., Schreiber, S. L., and Foley, M. A. (2001) An alkylsilyl-tethered, high-capacity solid support amenable to diversity-oriented synthesis for one-bead, one-stock solution chemical genetics. *J. Comb. Chem.* **3**, 312–318.

BC0256260



# Multiple-Peptide Conjugates for Binding $\beta$ -Amyloid Plaques of Alzheimer's Disease

Guobao Zhang,<sup>†,‡</sup> Michael J. Leibowitz,<sup>§,⊥</sup> Patrick J. Sinko,<sup>||,⊥</sup> and Stanley Stein<sup>\*,†,‡,§,||,⊥</sup>

Center for Advanced Biotechnology and Medicine, Piscataway, New Jersey 08854, Department of Chemistry, Rutgers University, Piscataway, New Jersey 08854, Department of Molecular Genetics and Microbiology, Robert Wood Johnson Medical School-UMDNJ, Piscataway, New Jersey 08854, Department of Pharmaceutics, Ernest Mario School of Pharmacy, Rutgers University, Piscataway, New Jersey 08854, and Cancer Institute of New Jersey, New Brunswick, New Jersey 08903. Received March 8, 2002;

Revised Manuscript Received July 18, 2002

Formation of  $\beta$ -amyloid plaques in Alzheimer's disease is initiated by intermolecular contact of the 5-amino acid sequence, KLVFF, in  $\beta$ -amyloid peptides ranging in size from 40 to 43 residues. Through optimization of binding avidity using structure/function studies, we have found that the retro-inverso peptide, ffvlk, binds artificial fibrils made from  $A\beta^{1-40}$  with moderate affinity ( $K_d = 5 \times 10^{-7}$  M). Conjugates having two copies of this peptide, whether connected by a long poly(ethylene glycol) (PEG) spacer or just two amino acids, display about 100-fold greater affinity for fibrils. Placing six copies of ffvlk on a branched PEG resulted in a 10 000-fold greater affinity ( $K_d = 1 \times 10^{-10}$  M) than the monomer peptide. This increased affinity was accompanied by more effective inhibition of the thioflavin T fluorescence signal, which correlates with neurotoxicity of plaques and fibrils. We propose that conjugates bearing several copies of ffvlk may be useful as diagnostic and therapeutic agents for Alzheimer's disease.

## INTRODUCTION

In Alzheimer's disease (AD), the brain is characterized by diffuse atrophy, especially of the cortex and hippocampus, and by the presence of senile plaques, the hallmark of AD. The plaques are complex extracellular lesions composed of a central deposition of  $\beta$ -amyloid peptide. Genetic, neuropathological, and biochemical evidence has shown that these deposits of  $\beta$ -amyloid peptide play an important role in the pathogenesis of AD (Glenner et al., 1984; Master et al., 1985; Selkoe, 1994).  $\beta$ -Amyloid ( $A\beta$ ) peptide refers to a 39–43 amino acid peptide derived from the amyloid precursor protein (APP) by proteolytic processing (Figure 1). Both the  $A\beta^{1-40}$  and  $A\beta^{1-42}$  amyloid peptides are components of the deposits of amyloid fibrils found in brain tissue of AD patients.  $A\beta^{1-42}$  is believed to play a more important role in the early stage of fibril formation and to have a seeding effect, thus being more "amyloidogenic" than  $A\beta^{1-40}$ . The fibril formation process is proposed to have two phases, nucleation followed by extension. The nucleation phase requires unfavorable, rate-limiting association steps from monomers. Once the nucleus of aggregated monomers has been formed, further addition of monomers becomes thermodynamically favorable, resulting in rapid extension of amyloid peptides into fibrils and then plaques (Harper and Lansbury, 1997).

```

651      660      670      680      690      700
TTRPGSGLT N IKTEEISEVK MDAEFRHDSG YEVHHQKLVE FAEDVGSNKG
701      710      720      730      740      750
AIIGLMVGGV VIATVIVITL VMLKKKQYTS IHHGVVEVDA AVTPEERHLS
751      760      770
KMQQNGYENP TYKFFEQQMN

```

**Figure 1.** Partial sequence of APP770. The  $\beta$ -amyloid peptide,  $A\beta^{1-43}$ , is shown in bold;  $A\beta^{1-40}$  would have the three amino acids, IAT, truncated from the C-terminus. The motif of  $A\beta$  that is the initial contact site in fibril formation is underlined.

Finding an inhibitor of the proteolytic process that is believed to excise the  $\beta$ -amyloid peptide from APP has been suggested as an approach to plaque elimination (Esler and Wolfe, 2001). Alternatively, plaque elimination could involve blocking or reversing the process of  $A\beta$  monomer aggregation into amyloid fibrils and plaques. This latter approach does not necessarily require a complete blockade, but is based on the hypothesis that aggregated  $A\beta$  in its disordered form is not neurotoxic. The fact that  $A\beta$  is also produced in normal people indicates that there may be certain functions associated with it (Haass et al., 1992; Seubert et al., 1992). Therefore, preventing  $A\beta$  from forming highly ordered amyloid fibrils and then plaques, rather than interfering with its synthesis and proteolytic processing, may be preferable as a therapeutic strategy.

The earliest studies on the aggregation process were done by Hilbich et al. (1992). They identified the critical region of  $A\beta$  involved in amyloid fibril formation by substituting the hydrophobic amino acids in  $A\beta$  by more hydrophilic amino acids and testing the effects of these changes. Their results showed that the hydrophobic core at residues 17–20 of  $A\beta$ , LVFF, is crucial for the formation of the  $\beta$ -sheet structure and the amyloid properties of  $A\beta$ . The  $A\beta^{1-40}$  analogues, where the amino acids in 17–20 are substituted by more hydrophilic amino acids, are still able to bind to full length  $A\beta^{1-40}$ . Further-

\* Corresponding author: Stanley Stein, Department of Pharmaceutics, Ernest Mario School of Pharmacy, Rutgers University, Piscataway, NJ 08854. Tel.: 732-445-3831 ext. 224. Fax: 732-445-3134. E-mail: stein@cabm.rutgers.edu.

<sup>†</sup> Center for Advanced Biotechnology and Medicine.

<sup>‡</sup> Department of Chemistry, Rutgers University.

<sup>§</sup> Robert Wood Johnson Medical School-UMDNJ.

<sup>||</sup> Department of Pharmaceutics, Rutgers University.

<sup>⊥</sup> Cancer Institute of New Jersey.

more, they were reported (Hilbich et al. 1992) to inhibit fibril formation in vitro, and therefore these analogues were suggested as therapeutic reagents for AD.

Similarly, Tjernberg et al. (1996) first synthesized the 31 possible decamers (corresponding to amino acid residues 1–10 through 31–40) of the  $A\beta^{1-40}$  molecule on a cellulose membrane matrix. The  $A\beta$  fragments capable of binding full length  $A\beta$  were identified by radioligand binding. A series of overlapping peptides, representing a region located in the central part of  $A\beta$  ( $A\beta^{9-18}$  to  $A\beta^{13-22}$ ), displayed prominent binding to  $A\beta^{1-40}$ .  $A\beta^{11-20}$ , which comprises the center of the binding region, was selected for further studies of the structural requirements for binding. This peptide, as well as N- and C-terminally truncated fragments, were synthesized and tested. It was found that the shortest peptide still displaying consistently high  $A\beta$  binding capacity had the sequence KLVFF (corresponding to  $A\beta^{16-20}$ ). This result agreed with Hilbich et al. (1992). This peptide was studied by microscopy and was found to be able to interfere with fibril formation in vitro. Having shown that the short peptide KLVFF can bind to  $A\beta$  and disrupt ordered fibril formation, Tjernberg et al. (1997) showed that peptide KLVFF binds stereospecifically to the homologous sequence in  $A\beta$ , i.e.,  $A\beta^{16-20}$ . Also, molecular modeling suggested that association of the two homologous sequences leads to the formation of an atypical antiparallel  $\beta$ -sheet structure stabilized primarily by interaction between the Lys, Leu, and Phe residues. The self-recognition property of the peptide, KLVFF, without any additional amino acids, has recently been confirmed (Watanabe et al., 2001).

On the basis of these results, Ghanta et al. (1996) presented an approach to the design of inhibitors of  $A\beta$  toxicity. In their strategy, a recognition element, which interacts specifically with  $A\beta$ , is combined with a disrupting element, which alters  $A\beta$  aggregation pathways. They synthesized a peptide composed of residues 15–25 of  $A\beta$ , designed as the recognition element, linked to an oligolysine disrupting element. This inhibitor does not alter the apparent secondary structure of  $A\beta$  nor prevent its aggregation; rather, it causes changes in aggregation kinetics and higher order structural characteristics of the aggregate. In addition to its influence on the physical properties of  $A\beta$  aggregates, the inhibitor completely blocks  $A\beta$  toxicity to PC-12 cells. These results suggest that formation of disordered aggregates rather than complete blockade of amyloid fibril formation might be sufficient for abrogation of toxicity.

Many peptide fragments, homologous to the  $\beta$ -amyloid peptide, have been synthesized and tested, and they can block the orderly aggregation of the  $\beta$ -amyloid peptide. For example, Soto et al. (1998) designed small peptides to interfere with the development of  $\beta$ -sheet structures. Their so-called ' $\beta$ -sheet breaker', a pentapeptide with partial homology to the  $\beta$ -amyloid peptide, was shown to be capable of preventing  $\beta$ -amyloid fibril formation and disassembling preformed fibrils in vitro when a 20-fold excess of inhibitor peptide was used. However, specific binding to plaques was not shown. More recently, a peptidase-resistant congener based on the KLVFF motif, having *N*-methyl amino acids at alternate positions, was shown to prevent ordered fibril formation (Gordon et al., 2001). Although interesting, the ability of these  $\beta$ -sheet breakers to oppose the accumulation of toxic plaques has been demonstrated only in model in vitro systems. To be useful therapeutically, these inhibitory compounds must be able to cross the blood–brain barrier (BBB). Furthermore, there must be specificity in the ability of the proposed inhibitory compounds to recognize aggregates

of  $\beta$ -amyloid peptide, rather than bonding and disrupting  $\beta$ -sheet structures in unrelated proteins.

We now present results that address the issues of target specificity, in addition to  $\beta$ -sheet disruption. Our research focuses on the design of multifunctional conjugates. We are using branched PEG as a scaffold and the peptide motif, KLVFF, as the plaque recognition element for preparing diagnostic and therapeutic agents for AD. Studies are presented on a PEG–peptide conjugate that cannot only bind to  $\beta$ -amyloid plaques much more avidly than those described above, but also can efficiently disrupt ordered  $\beta$ -sheet formation.

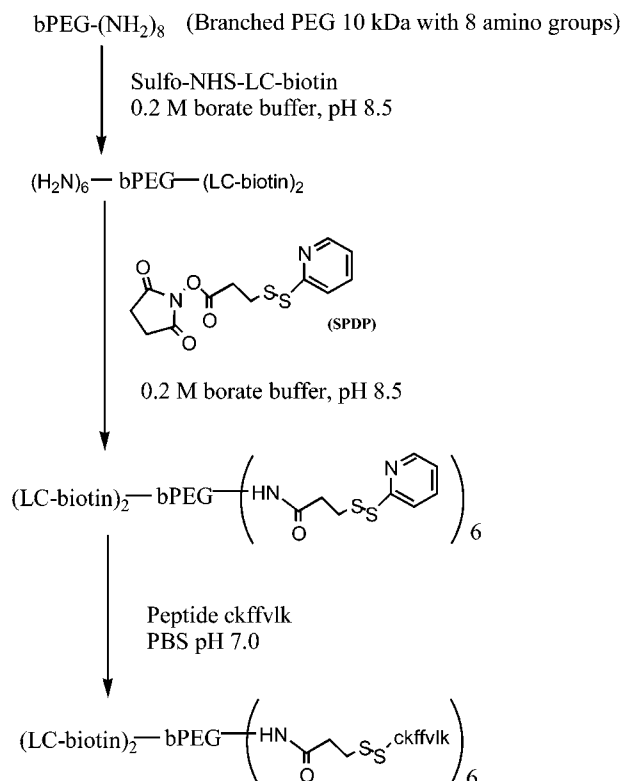
## MATERIALS AND METHODS

**Synthesis of Conjugates.** Peptides were synthesized manually by solid phase, Fmoc chemistry using reagents from Bachem and other commercial sources. Note that capital letters refer to the L-isomer, whereas lower case letters refer to the D-isomer. To prepare the tandem dimer peptide,  $\alpha$ -Fmoc (fluorenylmethoxycarbonyl),  $\epsilon$ -Mtt (methoxytrityl)-Lys was placed at the C-terminus. The Fmoc group was removed by treating the resin with 20% piperidine, and Fmoc- $\beta$ -alanine was coupled. After piperidine followed by 1% trifluoroacetic acid deprotection, the dimer peptide was produced by continuing the synthesis in the normal manner. Thus, the tandem dimer comprised two identical sequences, fvlk, joined at their C-termini by a Lys- $\beta$ -Ala spacer. A different dimer was produced by coupling KLVFF to  $\alpha,\omega$ -di-*N*-hydroxysuccinimide-PEG (Shearwater Polymers, Huntsville, AL). Peptides were cleaved from the resin and deprotected using 90% trifluoroacetic acid, 5% thioanisole, 3% ethanedithiol, and 2% anisole. After purification by reverse-phase HPLC, molecular weights were determined by MALDI-TOF mass spectrometry (Perkin-Elmer) and found to be within 1 Da of the predicted value. Unless otherwise indicated, all peptides have a free N-terminus and an amidated C-terminus. Peptide concentration was determined by absorbance at 260 nm using a standard solution of phenylalanine for calibration.

The PEG conjugate of the retro-inverso peptide, ckffvlk (Scheme 1), was prepared from eight-arm-branched amino-PEG, 10 kDa total molecular weight (Shearwater Polymers). In this process, two biotin residues were appended to PEG via amide bond formation, as quantitated by the fluorescamine reaction (Udenfriend et al., 1972). This assay measures primary amines, and coupling two out of eight amino groups gives a decrease of 25% in the fluorescence signal of an aliquot compared with an aliquot of the original reaction mixture.

**Binding to Fibrils.** The dissociation constant ( $K_d$ ) for each peptide and for the PEG conjugate with preformed fibrils was determined by Scatchard plot analysis (Scatchard, 1949). This method is necessary when one of the binding components (fibrils) is a solid and cannot be expressed in units of concentration. The  $A\beta^{1-40}$  (Quality Control Biochemicals) was dissolved in phosphate-buffered saline (PBS) with 0.05% sodium azide to form a clear solution (0.5 mg/mL, 0.1 mM). The solution was shaken for 3 days to allow fibrils to form. The preformed fibrils were checked visually, and an aliquot of each fibril suspension was checked for  $\beta$ -amyloid quality by the ThT assay (see below). Fibrils are considered to be highly representative of  $\beta$ -amyloid plaques in the brain.

The peptides and conjugates to be tested were labeled with either fluorescein isothiocyanate or [ $^3$ H]acetic anhydride for quantitation. Labeled peptide that bound fibrils was separated from unbound labeled peptide by

**Scheme 1. Multipetide Conjugate Synthesis**

ultrafiltration. Furthermore, the molecular weight cutoff of the ultrafilter was sufficiently high to permit even the largest nonfibrillar conjugates to pass through. In a typical binding assay, the total volume was 400  $\mu\text{L}$ . In each Centricon filter unit (100 kDa cutoff), 50  $\mu\text{L}$  of a preformed fibril suspension (0.5 mg/mL) and 50  $\mu\text{L}$  of peptide or conjugate solutions of various concentrations, typically diluted down from 0.1 mM, were added. PBS solution was used to adjust the total volume to 400  $\mu\text{L}$ . After incubation at room temperature with gentle shaking, some of the original mixture was taken, and the fluorescence or the radioactivity was measured to determine total peptide concentration. Then the mixture was centrifuged for 5 min at 5000 rpm at room temperature. The fluorescence or the radioactivity of the ultrafiltered permeate was measured to determine the free (unbound) peptide concentration. Then the ratio of bound concentration/free concentration was plotted against the bound concentration. The  $K_d$  was calculated from the slope of the linear plot. For Scatchard analysis of binding of conjugates to monomer peptide, the biotinylated conjugate was immobilized on streptavidin-coated plates.

**Thioflavin T Assay.** The benzothiazole dye, thioflavin T (ThT), is a classical amyloid stain for senile plaques containing  $\text{A}\beta$  in AD brain.  $\text{A}\beta^{1-40}$  was dissolved in HPLC grade DMSO to yield a clear stock solution (10 mg/mL). Before use, the solution was centrifuged for 10 min at 12 000 rpm to remove potential fibril formed during storage. In a typical ThT assay, the test sample (peptide or peptide conjugate) was diluted serially into PBSA (PBS with 0.05% sodium azide). Then 95  $\mu\text{L}$  of such diluted test sample solution was mixed with 5  $\mu\text{L}$  of  $\text{A}\beta^{1-40}$  stock solution in a 1.5 mL polypropylene tube. The mixtures were shaken vigorously at room temperature for 2 days. Then, 500  $\mu\text{L}$  of 12  $\mu\text{M}$  ThT solution in sodium phosphate buffer pH 6.0 was added. The tubes were vortexed briefly. The mixture was left standing at room temperature for 30 min. Then fluorescence was measured at excitation

and emission wavelengths of 450 and 482 nm, respectively. The fluorescence was plotted against the molar ratio of test sample to  $\text{A}\beta^{1-40}$ .

**RESULTS**

**Binding Properties.** The goal of these experiments was to maximize the avidity of interaction with amyloid plaques while preserving the natural KLVFF motif. Fibrils made similarly to our procedure are commonly used to represent amyloid plaques in the brain. According to the Scatchard equation, the data form a straight line in which the slope is the negative reciprocal of the dissociation constant. The various peptides and peptide-PEG conjugates and their binding avidity to preformed fibrils are summarized in Table 1. Note the relative standard deviation of about 30% for the prototype peptide, KLVFF (Table 1), when evaluating the data.

Peptide KLVFF is the natural sequence of residues 16–20 from  $\text{A}\beta$ , the nucleation site for peptide aggregation. Peptide ffvfk is a retro-inverso peptide, made of all D-amino acids and having the reverse of the natural sequence. Peptide ffvkk is the retro-inverso peptide with one extra lysine at the C-terminus. That extra lysine provides an additional positive charge that might increase the avidity of the peptide for binding to fibrils. Peptide FLKVF is a control peptide having a scrambled sequence. We confirmed that the binding to preformed fibrils is sequence specific since the control peptide has much lower affinity than does KLVFF. We also found that the retro-inverso peptides ffvk and ffvkk both have slightly higher affinity (2–3-fold lower dissociation constants) with  $\beta$ -amyloid fibrils than does the natural KLVFF (Table 1; Figure 2A) peptide. More importantly, these retro-inverso peptides are made of all D-amino acids and are resistant to protease digestion in vivo.

A PEG conjugate containing two copies of the prototype fibril-binding peptide had a dissociation constant ( $K_d$ ) that was 100-fold lower than the free peptide, KLVFF. The tandem dimer peptide (Table 1), having two closely spaced copies of the retro-inverso peptide, gave a  $K_d$  of the same magnitude as the peptide-PEG-peptide conjugate having one peptide appended at either end of the polymer chain. The markedly increased avidity of both dimer peptides for preformed fibrils suggested that increasing the number of  $\text{A}\beta$ -derived peptides on a single polyvalent carrier molecule might even further increase the binding strength. Therefore, we tested the fibril-binding ability of a hexameric conjugate of the retro-inverso peptide, ckffvfk, on a branched PEG carrier. The conjugate  $\text{PEG}_{10\text{kDa}}(\text{biotin})_2(\text{ckffvfk})_6$  was made for this purpose. The PEG used in this conjugate was branched PEG of molecular weight 10 kDa with eight primary amines used for attaching other components. The  $K_d$  for binding of this hexameric peptide conjugate to fibrils was determined to be  $1.1 \times 10^{-10}$  M (Figure 2B), which is 4 orders of magnitude higher avidity than the single peptide. Thus, we have found the means to increase binding avidity by using multiple interactions between the "ligand" and the "receptor" molecules (i.e., the peptide conjugate and the fibril, respectively).

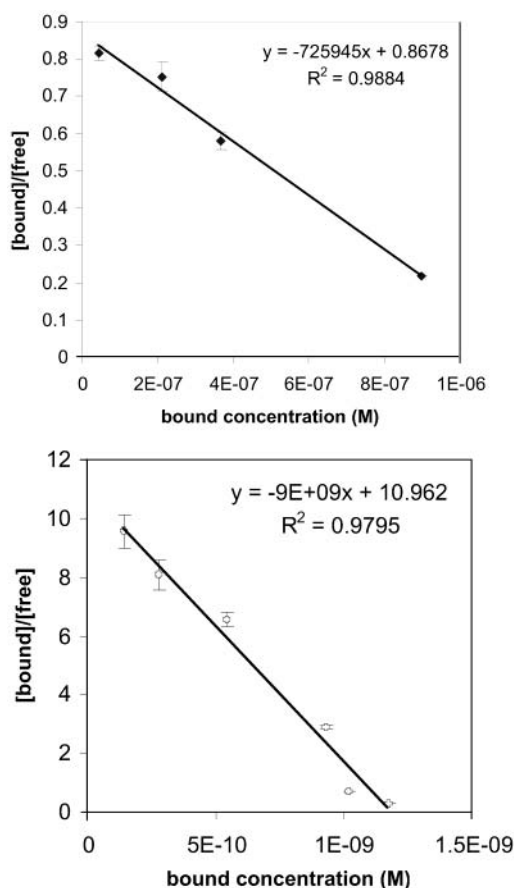
Besides binding to plaques, inhibitor peptides could hypothetically interfere with plaque formation by binding to monomer or oligomeric  $\text{A}\beta$  peptides before they have a chance to form  $\beta$ -sheets. To test this possibility, the target was monomeric  $\text{A}\beta^{1-40}$  instead of fibrils. The tandem dimer peptide was found to bind  $\text{A}\beta^{1-40}$  moderately ( $K_d = 1.7 \mu\text{M}$ ), while the hexameric peptide conjugate had about 10-times greater avidity ( $K_d = 0.16 \mu\text{M}$ )



**Table 1. Summary of  $K_d$  Values Determined by Scatchard Plot**

binding compound	binding target	$K_d$ ( $\mu$ M)	$R^2$ <sup>b</sup>
KLVFF (prototype)	preformed fibrils	$1.1 \pm 0.3^a$	0.998
ffvlk (retro-inverso)	preformed fibrils	0.50	0.973
ffvlkk	preformed fibrils	0.33	0.985
FLKVF (scrambled)	preformed fibrils	52	0.997
PEG-(KLVFF) <sub>2</sub> (dimer)	preformed fibrils	$1.0 \times 10^{-2}$	0.917
(ffvlk) <sub>2</sub> ( $\beta$ A)k (tandem dimer)	preformed fibrils	$1.3 \times 10^{-2}$	0.910
PEG <sub>10k8a</sub> (biotin) <sub>2</sub> (ckffvlk) <sub>6</sub>	preformed fibrils	$1.1 \times 10^{-4}$	0.980
tandem dimer	fluorescein-A $\beta^{1-40}$ monomer	1.7	0.980
PEG <sub>10k8a</sub> (biotin) <sub>2</sub> (ckffvlk) <sub>6</sub>	fluorescein-A $\beta^{1-40}$ monomer	0.16	0.862
ffvlk	biotinylated tandem dimer	1.8	0.973

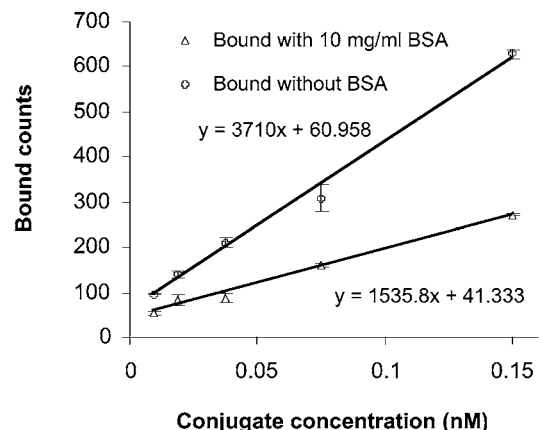
<sup>a</sup> Standard deviation for three analyses done on different days. Scatchard plot was done on triplicate samples at each concentration in one experiment for each of the other binding compounds. <sup>b</sup> Correlation coefficient.



**Figure 2.** Scatchard plot analysis of binding to preformed fibrils. Panels A and B are for the peptide, KLVFF, and the conjugate PEG(ckffvlk)<sub>6</sub>(biotin)<sub>2</sub>, respectively. Both peptides have a free N-terminus and an amidated C-terminus. The peptides were labeled using tritiated acetic anhydride. Triplicate samples were analyzed at each concentration within the same experiment.

for the A $\beta^{1-40}$  peptide (Table 1). By having six copies of the binding peptide present in each conjugate, there is a 10-fold greater binding (relative to the dimeric peptide) when the target is monomer peptide. In contrast, when the target is fibrils, there is a 100-fold difference between the dimeric and hexameric binding peptides. However, binding constants alone are not predictors of in vivo antiplaque activity.

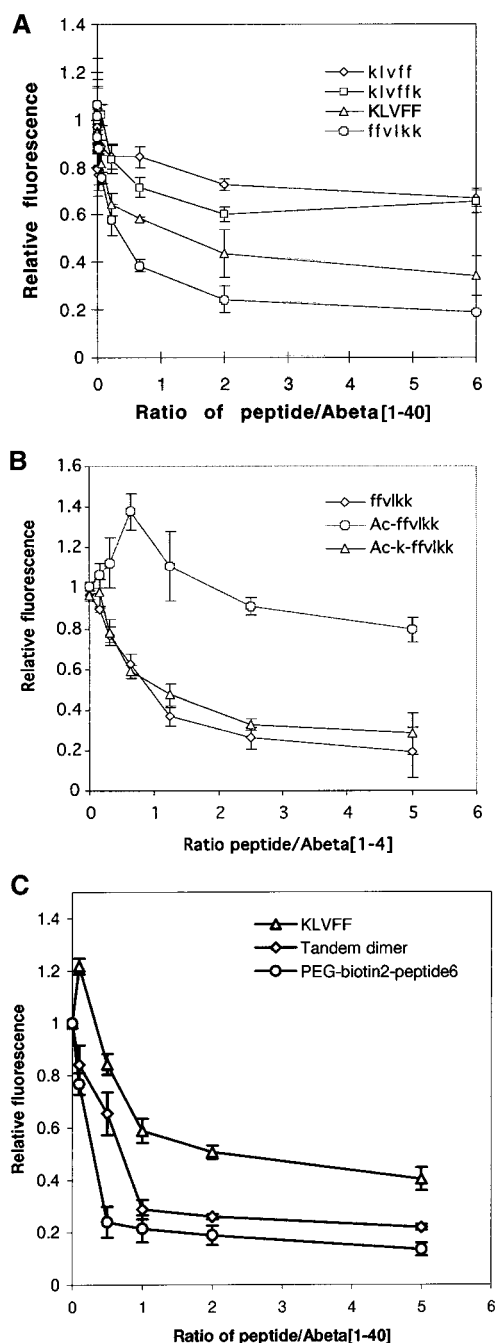
Specificity of binding was tested by measuring the binding to preformed fibrils in the presence of a large excess of serum albumin. That is, if some form of the KLVFF peptide were to be used clinically, would albumin interfere with binding to fibrils? Not only is albumin the most abundant protein in blood, but it is known to bind hydrophobic substances, such as the anticancer drug,



**Figure 3.** Specificity of binding. Binding of [<sup>3</sup>H]-PEG(ckffvlk)<sub>6</sub>(biotin)<sub>2</sub> to preformed fibrils was done in the presence and absence of bovine serum albumin. The percent nonspecific binding to albumin was essentially independent of concentration of conjugate. Triplicate samples were analyzed at each concentration within the same experiment.

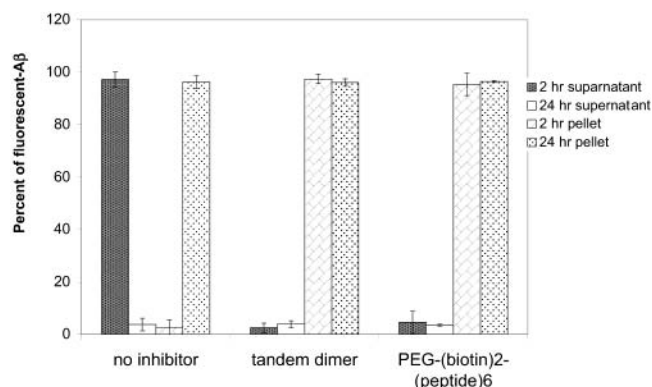
camptothecin (Mi et al., 1995). As seen in Figure 3, there was about a 60% decrease in binding of the six-peptide conjugate across the entire dosage range in the presence of bovine serum albumin at 10 mg/mL. In this assay, the amount of A $\beta^{1-40}$  peptide was only 0.017 mg/mL, about 600-fold lower than albumin. Indeed, the amount of six-peptide conjugate tested was as low as 0.01 nM ( $10^{-14}$  mol/mL), which is on the order of 0.01 ng/mL or 1 part per trillion of albumin. Thus, the pharmacokinetic result of this interaction might be to extend the in vivo half-life of the KLVFF-related peptides and conjugates. Albumin does not appear to sequester the binding peptide conjugate in an inactive form.

**Inhibition of Ordered Fibril Formation.** While the Scatchard plot is a good way to evaluate a peptide or conjugate by determining the  $K_d$  for binding to preformed fibrils, it does not provide information on inhibition of ordered fibril formation, as opposed to disordered aggregation. ThT binds rapidly and specifically to the antiparallel  $\beta$ -sheet fibrils formed from synthetic A $\beta^{1-40}$ , but it does not bind to monomer or oligomeric intermediates (LeVine, 1993). A $\beta$  in the  $\beta$ -amyloid fibrils in senile plaque is arranged in a highly ordered, condensed antiparallel  $\beta$ -sheet structure, and neuronal toxicity is attributed to this structural characteristic. That is, an amorphous aggregate of amyloid peptide is not neurotoxic, while a highly ordered, condensed antiparallel  $\beta$ -sheet structure is neurotoxic. For this reason, completely preventing the aggregation of A $\beta$  may not be necessary for achieving a therapeutic effect. It has been shown that the fluorescence in the ThT assay is correlated with both neurotoxicity and with the aggregation morphology being highly ordered (Ghanta et al., 1996).



**Figure 4.** Thioflavin T assays for inhibition of ordered fibril formation. The monomer peptide,  $A\beta^{1-40}$ , was incubated with each test sample for 2 days to determine inhibition of ordered fibril formation. Amorphous aggregates are observed as low fluorescence intensity, while well-ordered fibrils are observed as high fluorescence signal. Each of panels A, B, and C depict the concentration curves for several variations in the KLVFF motif done at the same time. Triplicate samples were analyzed at each concentration within the same experiment.

The inhibitory effect of the various peptides and conjugates in preventing ordered fibril formation, as monitored by the ThT assay, is presented in Figure 4. While peptide KLVFF and retro-inverso ffvlkk show an inhibitory effect in reducing the fluorescence signal, corresponding to preventing ordered fibril formation, inverso peptides klvff and klvfk were found to be relatively ineffective at all concentrations (Figure 4A). This result confirmed that the effect on ordered aggregation of  $A\beta^{1-40}$  by KLVFF analogues is specific with respect to both sequence and three-dimensional structure. The



**Figure 5.** Kinetics of fibril formation. A fresh solution of  $A\beta^{1-40}$  (0.1 mM), spiked with fluorescein-labeled  $A\beta^{1-40}$ , was incubated with or without an inhibitor peptide (0.5 mM). Samples were centrifuged at either 2 or 24 h, and peptide content in the pellet (if present) and supernatant were measured by fluorescence. Results are the average data from two separate experiments.

effect on ordered aggregation of  $A\beta^{1-40}$  by the positive charge at the N-terminus of the retro-inverso peptide, ffvlk, was examined using the *N*-acetylated peptide, *N*-acetyl-ffvlkk; there was no suppression of ThT fluorescence even at a 6-fold excess of the hexapeptide. However, an extra lysine residue in the peptide, *N*-acetyl-kffvlkk, which restored a positive charge at the N-terminus, was able to inhibit the ThT fluorescence identically to the retro-inverso hexapeptide, ffvlkk (Figure 4B). Indeed, there was actually an increase in ThT fluorescence with *N*-acetyl-ffvlkk. In a repeat experiment with *N*-acetyl-ffvlkk, this increase was qualitatively reproducible, including the large variability in the fluorescence signal (Figure 4B).

The tandem dimer retro-inverso peptide was found to be much more effective in preventing ordered fibril formation than the prototype peptide, KLVFF, or any of the monomer peptides, as indicated by both the amount of fluorescence reduction in the ThT assay and the relative amount needed for inhibition (Figure 4C). The conjugate  $PEG_{10k8a}(biotin)_2(peptide)_6$  was even more effective in preventing the ThT signal (Figure 4C). Indeed, the six-copy conjugate is about 3 times more potent than the dimer when expressed per mole of peptide subunit, as in Figure 4C, but 9 times more potent when expressed per mole of conjugate molecule. That is, maximal inhibition is attained at a ratio of one inhibitor peptide per three  $A\beta^{1-40}$  peptides in the context of the conjugate, but at a 1:1 ratio in the tandem dimer form of the same retro-inverso peptide.

**Other Studies.** Experiments were done to determine if the peptides or conjugates can disaggregate preformed fibrils. Preformed fibrils were incubated with peptides or conjugates at different ratios for 3 days at room temperature. Then the ThT assay was done to quantify the amount of ordered fibrils remaining after treatment. None of the peptides or peptide conjugates were able to break preformed fibrils under these conditions, according to the ThT assay (data not shown).

The kinetics of aggregation of  $A\beta^{1-40}$  was also monitored in the absence and presence of inhibitory peptides.  $A\beta^{1-40}$  was incubated under conditions typically used to prepare fibrils, normally taking 2–3 days to complete. Since the transition from a soluble to an insoluble form of  $A\beta^{1-40}$  was at about 15 h (data not shown), the experimental samples were spun down at either 2 or 24 h to observe any change in the kinetics of aggregation. As shown in Figure 5, all of the  $A\beta^{1-40}$  peptide was in

the supernatant at 2 h, while all was in the pellet at 24 h, in agreement with the transition occurring at 15 h. However, in the presence of either the dimer or the six-copy conjugate inhibitor, all of the  $A\beta^{1-40}$  appeared in the pellet after only 2 h. On the basis of the ThT assay (Figure 4C), this increased kinetics results in nonordered aggregates rather than highly ordered beta-sheet structures, in agreement with Ghanta et al. (1996). Essentially the same conclusion, that a decrease in the rate of aggregation (i.e., transition time going from 30 to 43 h) of  $A\beta$  increased the tendency to form  $\beta$ -amyloid plaques, was drawn in studies on the Flemish variant, Ala<sup>692</sup>Gly, which results in early onset AD (Walsh et al., 2001).

## DISCUSSION

This work confirms and extends the structure/function studies on  $A\beta$  fibrils of the peptide motif, KLVFF. We show that the retro-inverso analogue, fflvk, is preferable for use as a target recognition element. Not only does it have a 2-fold greater affinity for fibrils, but it is composed of peptidase-resistant D-amino acids. According to the ThT assay, a positively charged group at the N-terminus is essential in order to inhibit ordered fibril formation. Furthermore, this work demonstrates the cooperative effect that multiple copies of the KLVFF motif can have on the binding to fibrils and the aggregation of  $A\beta^{1-40}$  into fibrils. Two different dimers displayed 100-fold stronger avidity than their respective monomers for fibrils. In one dimeric form, (KLVFF)-PEG-(KLVFF), the two copies of the L-amino acid binding peptide were linked by a long, flexible PEG chain. In the other dimeric form, the two copies of the retro-inverso peptide, fflvk, were linked by just a pair of amino acids. The synergistic effect is so substantial that a six-copy conjugate of the retro-inverso peptide, kfflvk, can bind preformed fibrils 10 000-times more avidly than does the monomer peptide. Furthermore, the multicopy conjugates block the formation of well ordered fibrils from monomer  $A\beta$  peptide. Thus, the KLVFF motif might be useful not only as a target recognition element, but also as a  $\beta$ -sheet breaker.

The concept of increased avidity due to multivalent interactions is certainly not new. For example, combining multiple weak but specific receptor-ligand interactions was recently illustrated by Mourez et al. (2001). Using phage display libraries directed to the heptameric cell-binding subunit of anthrax toxin, they selected a peptide sequence, synthesized that peptide, and appended multiple copies to a flexible polymer. This polyvalent inhibitor was able to block toxin action in an animal model. Similarly, we showed the relationship between the number of copies of the macrophage chemoattractant peptide, *N*-formyl-Met-Leu-Phe-OH, and macrophage receptor avidity, being 1000-fold stronger with the eight-copy versus the single-copy PEG adducts (Pooyan et al., 2002).

In this study, the biotin groups were included in the hexameric conjugate for future use as a reporter for a quantitative ELISA or for a qualitative tissue stain. Recently, we have described the ability of an appended biotin group to impart oral bioavailability to a fragment of the HIV-1-encoded Tat protein (Ramanathan et al. 2001a). The permeability across the intestinal barrier was even greater for PEG conjugates comprising as many as eight copies of the Tat peptide (Ramanathan et al. 2001b). Indeed, the membrane-penetrating properties of Tat peptide and other small cationic peptides has been documented by several laboratories, as reviewed by

Fischer et al. (2001). Since delivery of plaque-binding compounds across the blood-brain barrier (BBB) might be a requirement for a diagnostic or therapeutic agent for AD, the presence of biotin or another transport ligand might be important for clinical applications. However, recent results (DeMattos et al., 2002) suggest that a therapeutic or diagnostic agent, comprising a monoclonal antibody against  $A\beta$  peptide in their studies, can be useful when administered peripherally. Apparently, the pools of soluble plaque-forming  $A\beta$  peptide in the central nervous system and in the periphery are in equilibrium, implying that  $A\beta$  is able to cross the BBB. Injection of their antibody was shown to produce a "sink" effect, drawing soluble  $A\beta$  from the brain into the bloodstream (DeMattos et al., 2002). This could remove  $A\beta$  from the brain, potentially halting or even reversing plaque formation. The antibody results suggest that even if the multivalent conjugates described above do not cross the BBB, they may be useful for diagnosis and treatment of AD.

## LITERATURE CITED

- (1) DeMattos, R. B., Bales, K. R., Cummins, D. J., Paul, S. M., and Holtzman, D. M. (2002) Brain to plasma  $\beta$ -amyloid efflux: a measure of brain amyloid burden in a mouse model of Alzheimer's disease. *Science* 295, 2264-2267.
- (2) Esler, W. P., and Wolfe, M. S. (2001) A portrait of Alzheimer secretases—New features and familiar faces. *Science* 293, 1449-1454.
- (3) Fischer, P. M., Krausz, E., and Lane, D. P. (2001) Cellular delivery of impermeable effector molecules in the form of conjugates with peptides capable of mediating membrane translocation. *Bioconjugate Chem.* 12, 825-841.
- (4) Ghanta, J., Shen, C. L., Kiessling, L. L., and Murphy, R. M. (1996) A strategy for designing inhibitor of  $\beta$ -Amyloid toxicity. *J. Biol. Chem.* 271, 29525-29528.
- (5) Glenner, G., and Wong, C. W. (1984) Alzheimer's Disease: Initial report of the purification and characterization of a novel cerebrovascular amyloid protein. *Biochem. Biophys. Res. Commun.* 120, 885-890.
- (6) Gordon, D. J., Sciarretta, K. L., and Meredith, S. C. (2001) Inhibition of  $\beta$ -amyloid(40) fibrillogenesis and disassembly of  $\beta$ -amyloid(40) fibrils by short  $\beta$ -amyloid congeners containing *N*-methyl amino acids at alternate residues. *Biochemistry* 40, 8237-8245.
- (7) Haass, C., Schlossmacher, M. G., Hung, A. Y., Vigo-Pelfrey, C., Mellon, A., Ostaszewski, B. L., Lieberburg, I., Koo, E. H., Schenk, D., and Teplow, D. B. (1992) Amyloid beta-peptide is produced by cultured cells during normal metabolism. *Nature* 359, 322-325.
- (8) Harper, J. D., and Lansbury, P. T. (1997) Models of amyloid seeding in Alzheimer's disease and scrapie: Mechanistic truths and physiological consequences of the time-dependent solubility of amyloid proteins. *Annu. Rev. Biochem.* 66, 385-407.
- (9) Hilbich, C., Kisters-Woike, B., Reed, J., Masters, C. L., and Beyreuther, K. (1992) Substitutions of hydrophobic amino acids reduce the amyloidogenicity of Alzheimer's disease  $\beta$ A4 peptides. *J. Mol. Biol.* 228, 460-473.
- (10) LeVine, H. (1993) Thioflavin T interaction with synthetic Alzheimer's disease  $\beta$ -amyloid peptides: Detection of amyloid aggregation in solution. *Protein Sci.* 2, 404-410.
- (11) Master, C. L., Simms, G., Weinman, N. A., Multhap, G., McDonald, B. L., and Beyreuther, K. (1985) Amyloid plaque core protein in Alzheimer Disease and Down Syndrome. *Proc. Natl. Acad. Sci. U.S.A.* 82, 4245-4249.
- (12) Mi, Z., Malak, H., and Burke, T. G. (1995) Reduced albumin binding promotes the stability and activity of topotecan in human blood. *Biochemistry* 34, 13722-13728.
- (13) Mourez, M., Kane, R. S., Mogridge, J., Metallo, S., Deschatelets, O., Sellman, B. R., Whitesides, G. M., and Collier, R. J. (2001) Designing a polyvalent inhibitor of anthrax toxin. *Nature Biotechnol.* 19, 958-961.



- (14) Pooyan, S., Qiu, B., Chen, M., Fong, D., Sinko, P., Leibowitz, M. J., and Stein, S. Conjugates bearing multiple formyl-methionyl peptides display enhanced binding to but not activation of phagocytic cells. *Bioconjugate Chem.* **13**, 216–223.
- (15) Ramanathan, S., Pooyan, S., Stein, S., Prasad, P. D., Wang, J., Leibowitz, M. J., Ganapathy, V., and Sinko, P. (2001a) Targeting the sodium dependent multivitamin transporter (SMVT) for improving the oral absorption properties of a retro-inverso Tat nonapeptide. *Pharm. Res.* **18**, 950–956.
- (16) Ramanathan, S., Pooyan, S., Qiu, B., Zhang, G., Stein, S., Leibowitz, J., and Sinko, P. (2001b) Targeted PEG-based bioconjugates enhance the cellular uptake and transport of an HIV-1 Tat nonapeptide. *J. Controlled Release* **77**, 199–212.
- (17) Scatchard, G. (1949) The attraction of proteins for small molecules and ions. *Ann. New York Acad. Sci.* **51**, 660–672.
- (18) Selkoe, D. J. (1994) Cell biology of the amyloid-protein precursor and the mechanism of Alzheimer's disease. *Annu. Rev. Cell Biol.* **10**, 373–403.
- (19) Seubert, P., Vigo-Pelfrey, C., Esch, F., Lee, M., Dovey, H., Davis, D., Sinha, S., Schlossmacher, M., Whaley, J., and Swindlehurst, C. (1992) Isolation and quantification of soluble Alzheimer's  $\beta$ -peptide from biological fluids. *Nature* **359**, 325–327.
- (20) Soto, C., Sigurdsson, E. M., Morelli, L., Kumar, R. A., Castaño, E. M., and Frangione, B. (1998)  $\beta$ -sheet breaker peptides inhibit fibrillogenesis in a rat brain model of amyloidosis: Implications for Alzheimer's therapy. *Nat. Med.* **4**, 822–826.
- (21) Tjernberg, L. O., Lilliehook, C., Callaway, D. J., Näslund, J., Hahne, S., Thyberg, J., Terenius, L., and Nordstedt, C. (1997) Controlling amyloid  $\beta$ -peptide fibril formation with protease-stable ligands. *J. Biol. Chem.* **272**, 12601–12605.
- (22) Tjernberg, L. O., Naslund, J., Lindqvist, F., Johansson, J., Karlström, A. R., Thyberg, J., Terenius, L., and Nordstedt, C. (1996) Arrest of  $\beta$ -amyloid fibril formation by a pentapeptide ligand. *J. Biol. Chem.* **271**, 8545–8548.
- (23) Udenfriend, S., Stein S., Bohlen P., and Dairman, W. (1972) Applications of fluorescamine, a new reagent for assay of amino acids, peptides, proteins and other primary amines in the picomole range. *Science* **178**, 871–872.
- (24) Walsh, D. M., Hartley, D. M., Condron, M. M., Selkoe, D. J., and Teplow, D. B. (2001) In vitro studies of amyloid protein fibril assembly and toxicity provide clues to the aetiology of Flemish variant (Gly<sup>692</sup>Ala) Alzheimer's disease. *Biochem. J.* **355**, 869–877.
- (25) Watanabe, K., Segawa, T., Nakamura, K., Kodaka, M., Konakara, T., and Okuno, H. (2001) Identification of the molecular interaction site of amyloid  $\beta$  peptide by using a fluorescence assay. *J. Pept. Res.* **58**, 342–346.

BC025526I

# Radiochemical Investigations of $^{99m}\text{Tc}-\text{N}_3\text{S}-\text{X}-\text{BBN}[7-14]\text{NH}_2$ : An in Vitro/in Vivo Structure–Activity Relationship Study Where X = 0-, 3-, 5-, 8-, and 11-Carbon Tethering Moieties

C. Jeffrey Smith,<sup>†</sup> Hariprasad Gali,<sup>†</sup> Gary L. Sieckman,<sup>‡</sup> Chris Higginbotham,<sup>‡</sup> Wynn A. Volkert,<sup>†,‡</sup> and Timothy J. Hoffman<sup>\*,‡,§</sup>

Research Services, Harry S. Truman Memorial Veterans' Hospital, Columbia, Missouri 65201, and Departments of Internal Medicine and Radiology, University of Missouri—Columbia School of Medicine, Columbia, Missouri 65211. Received April 24, 2002; Revised Manuscript Received July 15, 2002

Bombesin (BBN), a 14 amino acid peptide, is an analogue of human gastrin releasing peptide (GRP) that binds to GRP receptors (GRPr) with high affinity and specificity. The GRPr is overexpressed on a variety of human cancer cells, including prostate, breast, lung, and pancreatic cancers. The specific aim of this study was to develop  $^{99m}\text{Tc}$ -radiolabeled BBN analogues that maintain high specificity for the GRPr in vivo. A preselected synthetic sequence via solid-phase peptide synthesis (SPPS) was designed to produce  $\text{N}_3\text{S}-\text{BBN}$  ( $\text{N}_3\text{S}$  = dimethylglycyl-L-seryl-L-cysteinylglycinamide) conjugates with the following general structure:  $\text{DMG-S-C-G-X-Q-W-A-V-G-H-L-M}(\text{NH}_2)$ , where the spacer group,  $\text{X}$  = 0 (no spacer),  $\omega\text{-NH}_2(\text{CH}_2)_2\text{COOH}$ ,  $\omega\text{-NH}_2(\text{CH}_2)_4\text{COOH}$ ,  $\omega\text{-NH}_2(\text{CH}_2)_7\text{COOH}$ , or  $\omega\text{-NH}_2(\text{CH}_2)_{10}\text{COOH}$ . The new BBN constructs were purified by reversed phase-HPLC (RP-HPLC). Electrospray mass spectrometry (ES-MS) was used to characterize the nonmetalated BBN conjugates.  $\text{Re(V)}-\text{BBN}$  conjugates were prepared by the reaction of  $\text{Re(V)}\text{gluconate}$  with  $\text{N}_3\text{S-X-BBN}[7-14]\text{NH}_2$  ( $\text{X}$  = 0 carbons,  $\beta\text{-Ala}$  ( $\beta$ -alanine), 5-Ava (5-aminovaleric acid), 8-Aoc (8-aminooctanoic acid), and 11-Aun (11-aminoundecanoic acid)) with gentle heating.  $\text{Re}-\text{N}_3\text{S-5-Ava-BBN}[7-14]\text{NH}_2$  was also prepared by the reaction of  $[\text{Re(V)}\text{dimethylglycyl-L-seryl-L-cysteinylglycinamide}]$  with 5-Ava-BBN[7–14] $\text{NH}_2$ . ES-MS was used to determine the molecular constitution of the new  $\text{Re(V)}$  conjugates. The  $^{99m}\text{Tc}$  conjugates were prepared at the tracer level by each the prelabeling, post-conjugation and pre-conjugation, postlabeling approaches from the reaction of  $\text{Na}^{99m}\text{TcO}_4$  with excess  $\text{SnCl}_2$ , sodium gluconate, and corresponding ligand. The  $^{99m}\text{Tc}$  and  $\text{Re(V)}$  conjugates behaved similarly under identical RP-HPLC conditions. In vitro and in vivo models demonstrated biological integrity of the new conjugates.

## INTRODUCTION

Detection and treatment of cancers using radiopharmaceuticals that selectively target cancers in human patients has been employed for several decades (1–10). There is accelerated interest in developing new radiolabeled drugs due to the emergence of more sophisticated biomolecular vectors that exhibit high affinity and specificity for in vivo targeting of tumors. Several types of targeting agents are being developed and have been investigated, including monoclonal antibodies and other immuno-derived fragments and assemblies and receptor-avid peptides (11–15). The potential utility of using radiolabeled receptor-avid peptides to formulate site-directed radiopharmaceuticals is readily exemplified by the radiolabeled conjugates of octreotide and analogues that bind to cancer cells that overexpress somatostatin receptors (16–21).  $^{111}\text{In}$ -DTPA-octreotide (Octreoscan, Mallinckrodt Medical Inc.) is available for routine use in patients,<sup>16</sup> and other derivatized forms are currently

being developed as anti-cancer radiolabeled diagnostics and therapeutics (16–21).

Bombesin (BBN), a 14 amino acid peptide, is an analogue of human gastrin releasing peptide (GRP) that binds to GRP receptors with high affinity and specificity (22–24). GRP receptors have been shown to be overexpressed on several types of cancer cells including prostate, breast, lung, and pancreatic cancers (22–24). Since BBN agonistically binds to GRP receptors on cancer cells and may function as an autocrine or paracrine growth stimulator, a great deal of work has been devoted to development of BBN or GRP analogues that are antagonists as potential agents for inhibition and control of GRP-expressing tumors (23, 24). These antagonists are designed to competitively inhibit endogenous GRP binding to GRP receptors and reduce the rate of cancer cell proliferation (23, 24). Treatment of cancers using these nonradioactive antagonists requires chronic injection regimens using large quantities of the drug.<sup>25</sup> In designing receptor-avid radiopharmaceuticals for use as diagnostic or therapeutic agents, it is important that the drug not only exhibit cancer-specific in vivo targeting and acceptable pharmacokinetic properties, but it must be available as high specific activity products and exhibit long-term residualization in the tumor (26–28).

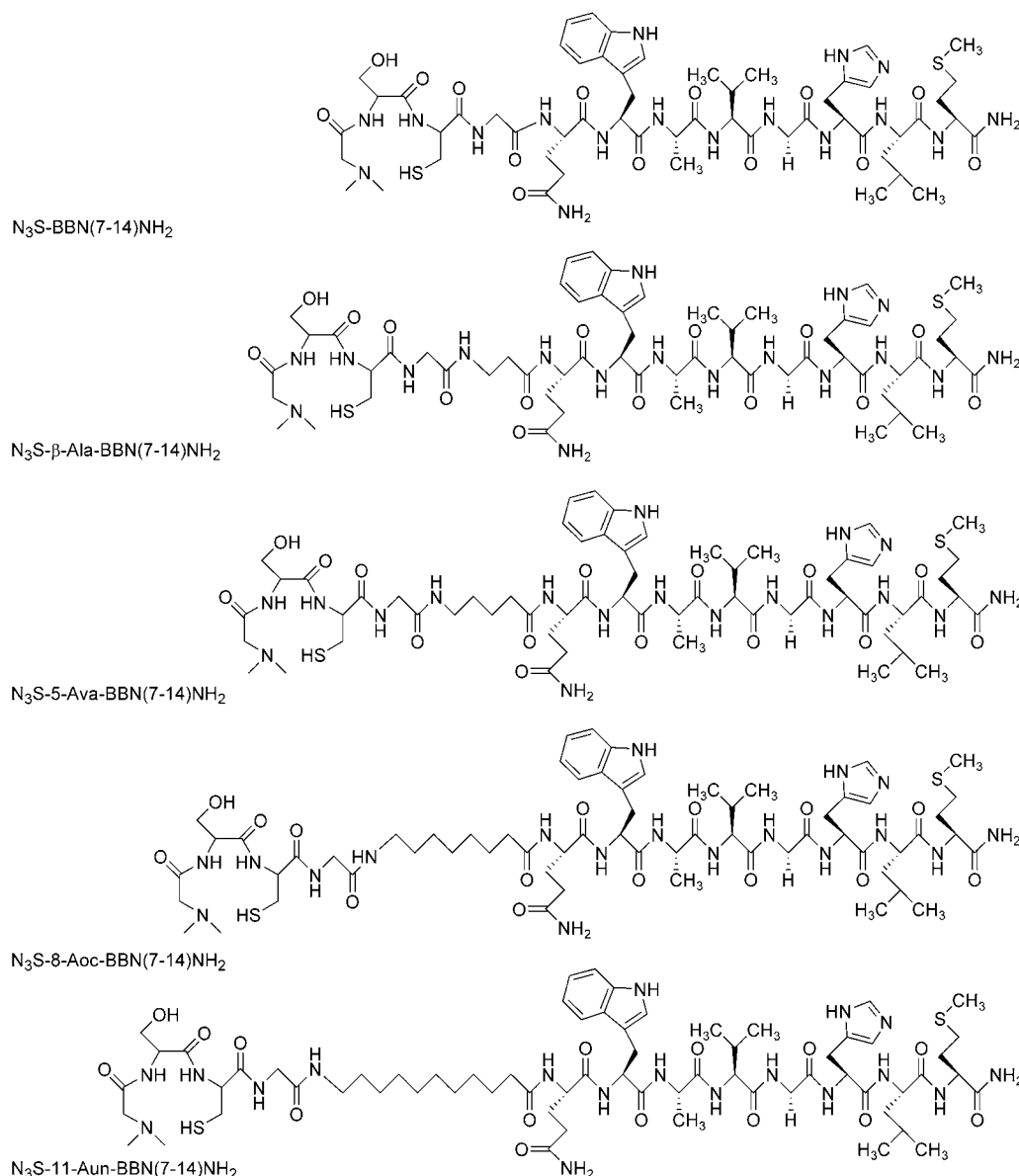
The synthesis and characterization of radiolabeled BBN or GRP analogues has been reported by several groups (26–35). Several of these analogues, labeled with radioiodine and radiometals, have been shown to bind

\* Corresponding author. Address: Harry S. Truman VA Hospital, 800 Hospital Drive, Research F-003, Columbia, MO 65211. E-mail: HoffmanT@health.missouri.edu. Phone: (573)-814-6000 ext. 2593. Fax: (573)882-1663.

<sup>†</sup> Department of Radiology, University of Missouri—Columbia.

<sup>‡</sup> Harry S. Truman Memorial Veterans Hospital.

<sup>§</sup> Department of Internal Medicine, University of Missouri—Columbia.



**Figure 1.** Structures of DMG-S-C-G-X-Q-W-A-V-G-H-L-M-NH<sub>2</sub>, where the spacer group, X = 0 (no spacer),  $\omega\text{-NH}_2(\text{CH}_2)_2\text{COOH}$ ,  $\omega\text{-NH}_2(\text{CH}_2)_4\text{COOH}$ ,  $\omega\text{-NH}_2(\text{CH}_2)_7\text{COOH}$ , or  $\omega\text{-NH}_2(\text{CH}_2)_{10}\text{COOH}$ .

selectively and avidly to GRP receptors on cancer cells, both in vitro and in vivo (26–35). The various BBN analogues studied range from structures in which the radiolabeled moiety is conjugated to the nearly full-length BBN (1–14) sequence, to where it is attached to a smaller truncated amino acid sequence comprising the GRP-receptor binding moiety (e.g., BBN[8–14]NH<sub>2</sub>). Results of studies to evaluate these conjugates demonstrate that radiolabeled BBN/GRP analogues hold important promise as cancer specific radiopharmaceuticals (26–35).

Our laboratory has focused on the design of BBN-agonist analogues in which the radiolabeled moiety (e.g., radiometal chelate) is linked either directly to the N-terminal amine group of BBN[7–14]NH<sub>2</sub> or via hydrocarbon spacer groups (Figure 1) (33–38). The length and composition of the spacer group, or tether, as well as the physio-chemical properties of the radiolabeled moiety will influence the GRP receptor binding affinity, residualization of radioactivity in cancer cells, and pharmacokinetics of the BBN conjugate (33–38). In this study, we have complexed <sup>99m</sup>Tc to a triamido-thiol (N<sub>3</sub>S) bifunctional chelating agent (BFCA). The <sup>99m</sup>Tc chelate has been conjugated to the N-terminal amine of BBN[7–14]NH<sub>2</sub>

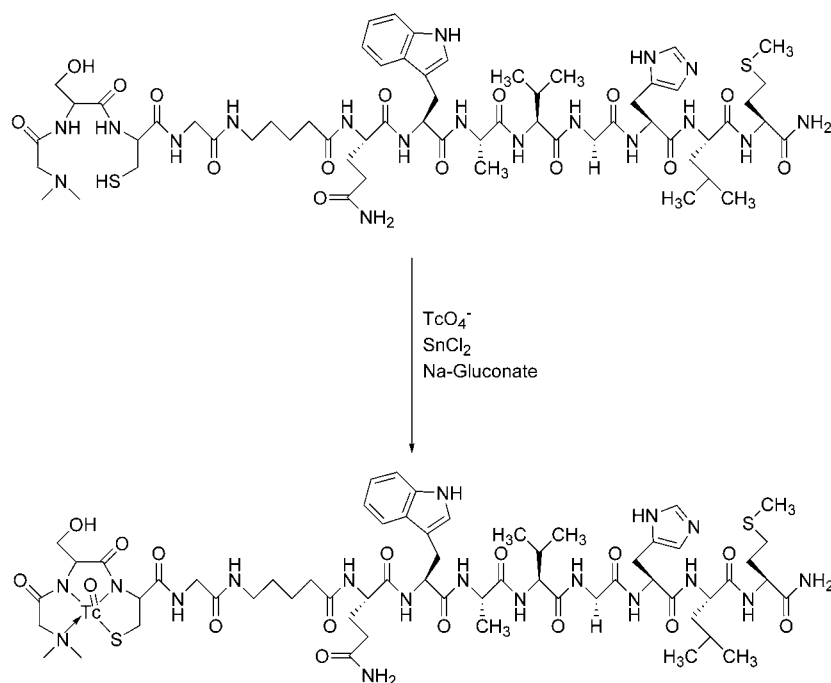
via a limited series of hydrocarbon spacers of increasing length (i.e., 3, 5, 8, and 11 carbon atoms in length). The purpose of this study is to determine the effects of varying the length of hydrocarbon spacer groups on the in vitro binding affinity with GRP receptors expressed on human prostate PC-3 cells and their in vivo pharmacokinetics in normal CF-1 mice. It would be beneficial to formulate new <sup>99m</sup>Tc-labeled site-specific tracers since <sup>99m</sup>Tc is currently the most widely used radionuclide used for diagnostic SPECT imaging studies (39). The N<sub>3</sub>S-BFCA used to complex <sup>99m</sup>Tc is N-dimethylglycyl-L-seryl-L-cysteinyglycyl[(CH<sub>3</sub>)<sub>2</sub>-G-S-C-G], which has been shown to form a well-defined and stable complex with TcO<sup>3+</sup> (40).

#### EXPERIMENTAL SECTION

All solvents were either ACS certified or HPLC grade. All solvents were obtained from Fisher Scientific and used as received. Fmoc-amino acids, coupling agents and resins were purchased from Calbiochem-Novabiochem Corp., San Diego, CA. All other reagents were purchased from either Aldrich Chemical Co., Fisher Scientific or ACROS Chemicals. <sup>99m</sup>TcO<sub>4</sub><sup>−</sup> was obtained as the sterile



## Scheme 1



0.9% aqueous NaCl eluant solution from a  $^{99}\text{Mo}/^{99m}\text{Tc}$  generator (Mallinckrodt Medical, Inc.). Electrospray mass spectral (ESMS) Analyses were performed by SynPep Corporation, Dublin, CA.  $^{125}\text{I}$ -Tyr<sup>4</sup>-BBN was obtained from NEN Life Sciences Products, Inc., Boston, MA.

**Solid-Phase Peptide Synthesis (SPPS).** Peptide synthesis was performed on a Perkin-Elmer-Applied Biosystem Model 432 automated peptide synthesizer employing traditional Fmoc Chemistry. The reaction of HBTU activated carboxyl groups on the reactant with the N-terminal amino group on the growing peptide, anchored via the C-terminus to the resin, provided for stepwise amino acid addition. Rink Amide MBHA resin (25  $\mu\text{mole}$ ) and Fmoc-protected amino acids, with appropriate side-chain protections, and the Fmoc-protected  $\omega$ - $\text{NH}_2(\text{CH}_2)_n\text{COOH}$  compounds used as spacer groups (75  $\mu\text{mol}$ ), were used for SPPS of the nonmetalated BBN conjugates. The preselected synthetic sequence was designed to produce the  $\text{N}_3\text{S}$ -BBN conjugates with the following general structure DMG-S-C-G-X-Q-W-A-V-G-H-L-M-NH<sub>2</sub>, where the spacer group, X = 0 (no spacer),  $\omega$ - $\text{NH}_2(\text{CH}_2)_2\text{COOH}$ ,  $\omega$ - $\text{NH}_2(\text{CH}_2)_4\text{COOH}$ ,  $\omega$ - $\text{NH}_2(\text{CH}_2)_7\text{COOH}$ , or  $\omega$ - $\text{NH}_2(\text{CH}_2)_{10}\text{COOH}$  (See Figure 1 for structures of these  $\text{N}_3\text{S-X-BBN}[7-14]\text{NH}_2$  conjugates). The final products were cleaved by a standard procedure using a cocktail containing thioanisole, water, ethanedithiol and trifluoroacetic acid in a ratio of 2:1:1:36 and precipitated into methyl-*tert*-butyl ether. The crude peptides were purified by HPLC and the solvents removed on a SpeedVac concentrator. Typical yields of the crude peptides were 80–85%. ES-MS was used in order to determine the molecular constitution of the  $\text{N}_3\text{S-X-BBN}[7-14]\text{NH}_2$  conjugates.

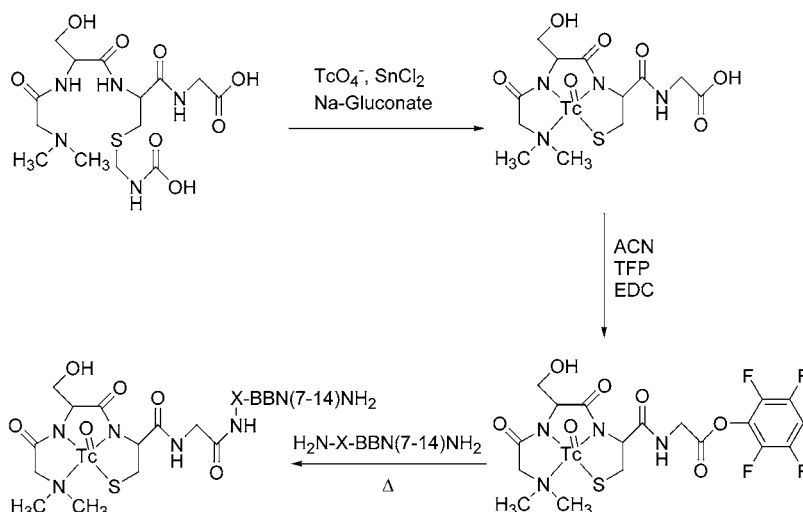
**HPLC Purification and Analysis.** HPLC analyses and purification of all peptide conjugates and their metal complexes were performed on a Waters 600E instrument equipped with a Varian 2550 variable absorption detector, a Packard Radiometric 150 TR flow scintillation analyzer or a sodium iodide crystal radiometric detector, and an Eppendorf TC-50 column temperature controller and Hewlett-Packard HP3395 integrator. HPLC solvents consisted of H<sub>2</sub>O containing 0.1% trifluoroacetic acid

**Table 1. Mass-Spectral Analyses and IC<sub>50</sub> (IC<sub>50</sub>*nM*(SD), *n* = 3) Determination of the Peptide Series and Re Conjugates**

peptide/ conjugate	calculated mass	actual mass	IC <sub>50</sub> (PC-3)
Re-0	1471.7	1472.4	3.97(1.07)
Re-3	1542.8	1543.6	0.67(0.21)
Re-5	1570.8	1571.4	1.00(0.20)
Re-8	1612.9	1612.9	0.53(0.25)
Re-11	1655.0	1655.6	1.50(0.26)

(Solvent A) and acetonitrile containing 0.1% trifluoroacetic acid (Solvent B). A Phenomenex Jupiter C-18 (5  $\mu\text{m}$ , 4.6  $\times$  250 mm) column was used with a flow rate of 1.5 mL/min. The HPLC gradient system begins with a solvent composition of 95% A and 5% B and follows a linear gradient of 30% A:70% B from 0 to 25 min, and 30% A:70% B to 5% A:95% B from 25 to 30 min.

**$^{99m}\text{Tc}$ - and Re- $\text{N}_3\text{S-X-BBN}[7-14]\text{NH}_2$  Conjugate Synthesis.** The  $\text{N}_3\text{S-X-BBN}[7-14]\text{NH}_2$  analogues were labeled with  $^{99m}\text{Tc}$  and Re using pre-conjugation, post-transmetalation from  $^{99m}\text{Tc(V)}$ <sup>41</sup> or Re(V)-gluconate<sup>42</sup> synthons, respectively (Scheme 1). Preparation of Re(V)-gluconate was performed as previously described.<sup>42</sup> In brief, the preparation of the Re(V) conjugates was performed by addition of excess Re(V)-gluconate solution to a solution of  $\text{N}_3\text{S-X-BBN}[7-14]\text{NH}_2$ . Each mixture was heated for 2h at 60 °C. After incubation of the resulting solutions at room temperature, the Re- $\text{N}_3\text{S-X-BBN}[7-14]\text{NH}_2$  complexes were purified by RP-HPLC. Each of the new complexes were peak-collected and evaporated to dryness. ES-MS analysis was used to determine the molecular constitution of the new Re conjugates (Table 1). For  $^{99m}\text{Tc}$ , this method involved preparation of a stannous gluconate stock solution by mixing 20 mg  $\text{SnCl}_2$  in 1 mL ultrapure deoxygenated water. Twenty microliters of this stock solution was mixed with 1.0 mL of a 13 mg/mL sodium gluconate solution. To 100  $\mu\text{L}$  of this solution was added 500  $\mu\text{L}$  of an isotonic saline solution containing approximately 370 MBq of  $^{99m}\text{TcO}_4^-$  and 50  $\mu\text{g}$  of the  $\text{N}_3\text{S-X-BBN}[7-14]\text{NH}_2$  conjugate.<sup>10,30,40</sup> After incubation of the resulting solution at room temperature, the  $^{99m}\text{Tc}-\text{N}_3\text{S-X-BBN}[7-14]\text{NH}_2$  complexes were puri-

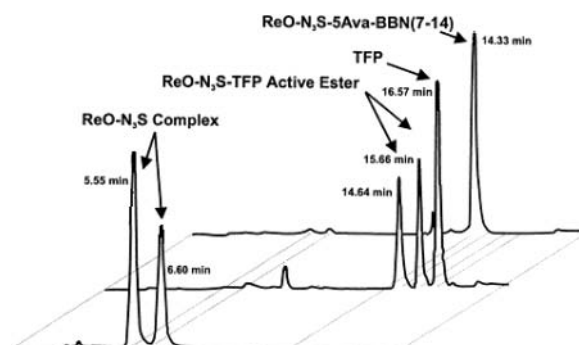
**Scheme 2**

fied by RP-HPLC and the peaks collected into a 1 mL solution of 0.02 M sodium phosphate buffered saline at pH 7.4, containing 0.1 mg of bovine serum albumin (BSA). Prior to use of the purified conjugates for in vitro GRP receptor binding and in vivo biodistribution studies, the residual acetonitrile was evaporated from the solution under a stream of nitrogen. These  $^{99m}\text{Tc}$ - $\text{N}_3\text{S}$ - $\text{X}$ -BBN[7-14] $\text{NH}_2$  conjugates were of high specific activity as the  $\text{N}_3\text{S}$ - $\text{X}$ -BBN[7-14] $\text{NH}_2$  analogues eluted approximately 1 min prior to the corresponding metalated  $^{99m}\text{Tc}$ - $\text{N}_3\text{S}$ - $\text{X}$ -BBN[7-14] $\text{NH}_2$  conjugates.

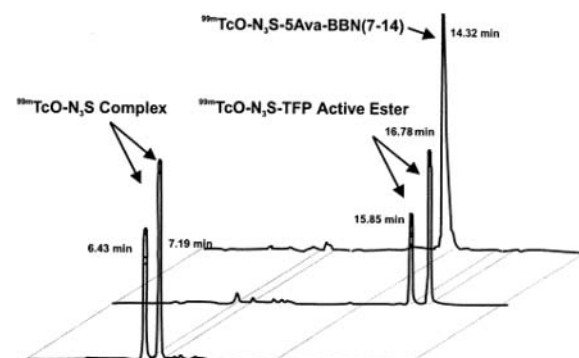
$^{99m}\text{Tc}$ - $\text{N}_3\text{S}$ -5-Ava-BBN[7-14] $\text{NH}_2$  was also synthesized by the prechelat post-conjugation approach, as was  $\text{Re}$ - $\text{N}_3\text{S}$ -5-Ava-BBN[7-14] $\text{NH}_2$  (Scheme 2). The  $^{99m}\text{Tc}$ - $\text{N}_3\text{S}$  bifunctional chelate (BFC) was prepared by transchelation from  $^{99m}\text{Tc(V)}$ -gluconate similar to the method described earlier. The  $\text{Re}$ - $\text{N}_3\text{S}$  BFC was prepared by trans-metalation of  $\text{Re(V)}$  to the  $\text{N}_3\text{S}$ -BFCA from the  $[\text{ReO}_2(\text{en}_2)]\text{Cl}$  ( $\text{en}$  = ethylenediamine) synthon using a method previously reported (40).  $\text{ReO}$ - $\text{N}$ -dimethylglycyl-L-seryl-L-cysteinyl-glycine ( $\text{ReO}$ - $\text{N}_3\text{S}$ -BFCA) was provided by Resolution Pharmaceuticals (Toronto, Canada).

The C-terminal carboxy group on both the  $^{99m}\text{Tc}$ - and  $\text{Re}$ - $\text{N}_3\text{S}$ -BFCA were converted to the corresponding tetrafluoro-phenyl (TFP) ester precursors. To produce the  $\text{Re}$ - $\text{N}_3\text{S}$ -TFP precursor, 0.011 g (0.02 mmol) of  $\text{Re}$ - $\text{N}_3\text{S}$ -BFCA was dissolved in 500  $\mu\text{L}$  of deionized water with gentle stirring. To this solution was added 7 mg of TFP (0.042 mmol) in 500  $\mu\text{L}$  of acetonitrile, followed by addition of 7 mg (0.044 mmol) of  $N,N$ -dicyclohexylcarbodiimide. The reaction mixture was heated gently for 2 h. Synthesis of  $\text{Re}$ - $\text{N}_3\text{S}$ -5-Ava-BBN[7-14] $\text{NH}_2$  was performed by dissolving 0.011 g ( $0.11 \times 10^{-5}$  moles) of  $\text{N}_3\text{S}$ -5-Ava-BBN[7-14] $\text{NH}_2$  in a water/acetonitrile mixture (50:50) with gentle stirring, followed by addition of 1.8 mL of 0.2N  $\text{NaHCO}_3$ . The crude  $\text{Re}$ - $\text{N}_3\text{S}$ -TFP solution was added to this solution and the reaction mixture was heated at 60  $^\circ\text{C}$  for 2 h. The progress of the reaction was incrementally followed by RP-HPLC (Figure 2). The HPLC purified  $\text{Re}$ - $\text{N}_3\text{S}$ -5-Ava-BBN[7-14] $\text{NH}_2$  product was analyzed by ES-MS ( $m/z$  for  $(\text{M}+\text{H})^+$  was found to be 1570.0; calculated 1569.9).

The  $^{99m}\text{Tc}$ - $\text{N}_3\text{S}$ -5-Ava-BBN[7-14] $\text{NH}_2$  product was prepared by the same procedure (Scheme 1), however, the HPLC purified  $^{99m}\text{Tc}$ - $\text{N}_3\text{S}$ -BFCA reagent was present at tracer levels when reacted with excess TFP to produce the  $^{99m}\text{Tc}$ - $\text{N}_3\text{S}$ -TFP precursor. The progress of the reactions leading to production of the  $^{99m}\text{Tc}$ - $\text{N}_3\text{S}$ -5-Ava-BBN-



**Figure 2.** HPLC elution profile of  $\text{ReO}$ - $\text{N}_3\text{S}$ -5-Ava-BBN[7-14] $\text{NH}_2$  and reaction intermediates (prechelate, post-conjugation labeling method).



**Figure 3.** HPLC elution profile of  $^{99m}\text{TcO}$ - $\text{N}_3\text{S}$ -5-Ava-BBN[7-14] $\text{NH}_2$  and reaction intermediates (prechelate, post-conjugation labeling method).

[7-14] $\text{NH}_2$  product was also incrementally monitored by HPLC (Figure 3).

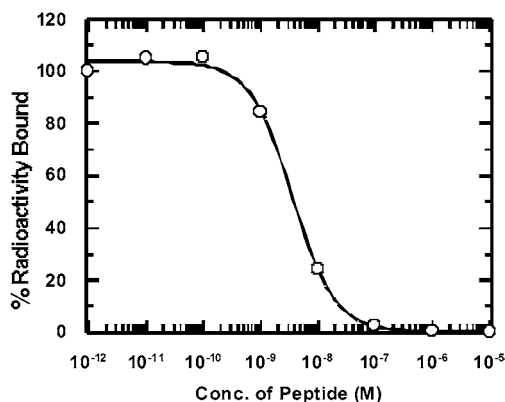
$^{99m}\text{Tc}$ - and  $\text{Re}$ - $\text{N}_3\text{S}$  BFCs and their respective TFP-activated esters reveal the presence of two readily identifiable peaks for each chelate reflecting the presence of *syn*- and *anti*-isomers<sup>40</sup> (Figures 2 and 3). The final  $^{99m}\text{Tc}$ - and  $\text{Re}$ - $\text{N}_3\text{S}$ -5-Ava-BBN[7-14] $\text{NH}_2$  conjugates, which eluted at retention times of 14.32 and 14.33 min, respectively, are single Gaussian peaks (Figures 2 and 3) which are expected to include both the *syn*- and *anti*- $\text{N}_3\text{S}$ -BFCA conjugates which are not resolvable by this HPLC elution method.  $^{99m}\text{Tc}$ - $\text{N}_3\text{S}$ -5-Ava-BBN[7-14] $\text{NH}_2$  and  $\text{Re}$ - $\text{N}_3\text{S}$ -5-Ava-BBN[7-14] $\text{NH}_2$ , synthesized by each the preformed chelate method and the post-conjugation transmetalation approach, produce  $^{99m}\text{Tc}/\text{Re}$  species that

have identical HPLC retention times (i.e., approximately 14.3 min).  $^{99m}\text{Tc}-\text{N}_3\text{S}-5\text{-Ava}-\text{BBN}[7-12]$  was also synthesized. This analogue has both the C-terminal Leu<sup>13</sup> and Met<sup>14</sup> deleted and is expected to exhibit neither agonist nor antagonist binding to GRP receptors (43–44).

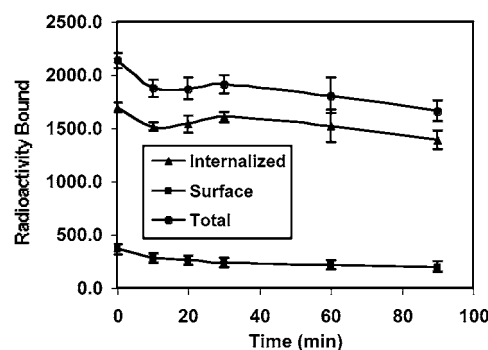
**In Vitro Cell Binding Studies.** In vitro GRP receptor binding affinities and specificities of the BBN conjugates were assessed utilizing displacement cell-binding assays using  $^{125}\text{I}-\text{Tyr}^4\text{-BBN}$  as the GRP receptor specific radioligand with PC-3 human prostate cancer cells (ATCC, Manassas, VA) by a method previously described.<sup>22</sup> Briefly, the PC-3 cells were grown in HAM's F-12K media supplemented with 7% fetal calf serum. The  $3 \times 10^4$  PC-3 cells were suspended in 300  $\mu\text{L}$  RPMI 1640 media at pH 7.4 containing 2.4 mg/mL HEPES, 0.1  $\mu\text{g}/\text{mL}$  Bacitracin, and 2 mg/mL BSA. They were incubated at 37 °C (5%  $\text{CO}_2$ ) for 40 min in the presence of approximately 20,000 cpm of  $^{125}\text{I}-\text{Tyr}^4\text{-BBN}$  and increasing concentrations of the  $\text{N}_3\text{S}-\text{X}-\text{BBN}[7-14]\text{NH}_2$  conjugates or the  $\text{Re}-\text{N}_3\text{S}-\text{X}-\text{BBN}[7-14]\text{NH}_2$  conjugate ranging from  $10^{-11}\text{M}$  to  $10^{-5}\text{M}$ . After incubation, the reaction medium was centrifuged (1 min, 8000 rpm) and aspirated and the cells washed three times with media. The radioactivity bound to the cells was counted in a Packard Riastar gamma counting system. The percent  $^{125}\text{I}-\text{Tyr}^4\text{-BBN}$  bound to the cells was plotted versus increasing concentration of the BBN-[7-14] $\text{NH}_2$  conjugates to determine the specific  $\text{IC}_{50}$  values (Table 1,  $n = 3$ ). The degree of specific  $^{99m}\text{Tc}-\text{N}_3\text{S}-\text{X}-\text{BBN}$  analogue binding to the GRP receptors expressed on PC-3 cells was determined by incubating approximately 0.01–0.02  $\mu\text{Ci}$  of each  $^{99m}\text{Tc}$  analogue with  $3 \times 10^4$  PC-3 cells in the absence of displacing BBN[7-14] $\text{NH}_2$  ligands and in the presence of  $10^{-5}\text{M}$  of the corresponding  $\text{N}_3\text{S}-\text{X}-\text{BBN}[7-14]\text{NH}_2$  analogue.

**Internalization Studies.** In vitro studies were performed to determine the efficiency of internalization of  $^{99m}\text{Tc}-\text{N}_3\text{S}-5\text{-Ava}-\text{BBN}[7-14]\text{NH}_2$  (Scheme 2) and the degree of residualization of  $^{99m}\text{Tc}$  in the cells as a function of time. These studies were performed by a method similar to that described by Rogers et al. (28). In short,  $3 \times 10^4$  PC-3 cells were suspended in RPMI 1640 media at pH 7.4 containing 2.4 mg/mL HEPES, 0.1  $\mu\text{g}/\text{mL}$  Bacitracin and 2 mg/mL BSA in the presence of approximately 20 000 cpm  $^{99m}\text{Tc}-\text{N}_3\text{S}-5\text{-Ava}-\text{BBN}[7-14]\text{NH}_2$  (3) for a period of 40 min at 37 °C (5%  $\text{CO}_2$ ). After incubation, the reaction medium was centrifuged (1 min, 8000rpm) and aspirated, and cells were washed with the incubation media. The percent of  $^{99m}\text{Tc}$  cell-associated activity were determined as a function of time (in the incubating medium at 37 °C). The percentage of  $^{99m}\text{Tc}$  activity trapped in the cells was determined after removing  $^{99m}\text{Tc}$  activity bound to the surface of the cells by washing with a pH 2.5 (0.2 M acetic acid and 0.5 M NaCl) buffer at 10, 20, 30, 60, and 90 min ( $n = 3$ ) following the washing with incubation media (Figure 5). A control study with  $^{125}\text{I}-\text{Tyr}^4\text{-BBN}$  was performed using the same method (Figure 6).

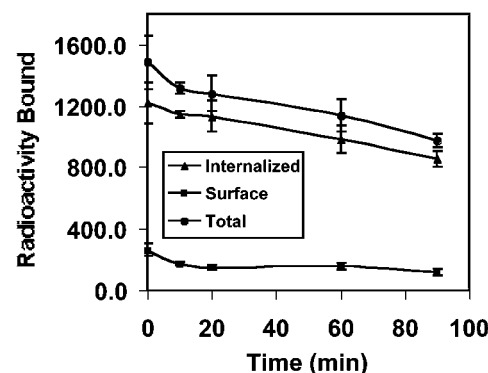
**Biodistribution of  $^{99m}\text{Tc}-\text{N}_3\text{S}-\text{X}-\text{BBN}[7-14]\text{NH}_2$  Analogues in Normal Mice.** Normal CF-1 mice (average weight 20–25 g) were used for the biodistribution studies (Tables 2–5). The pH of the HPLC-purified  $^{99m}\text{Tc}-\text{N}_3\text{S}-\text{X}-\text{BBN}[7-14]\text{NH}_2$  solutions was adjusted to physiological conditions using a 0.01 M phosphate buffer (pH 7.4). Aliquots (80–100  $\mu\text{L}$ ) of the labeled peptide solution (55–75 kBq) were injected into each animal via the tail vein. Tissues and organs were excised from the sacrificed animals 30 min, 1 h, and 4 h post-injection (p.i.). The organs and tissue were weighed and the



**Figure 4.** Typical  $\text{IC}_{50}$  cell-binding studies of  $\text{ReO}-\text{N}_3\text{S}-5\text{-Ava}-\text{BBN}[7-14]\text{NH}_2$  in human prostate (PC-3) cancerous cells ( $\text{IC}_{50} = 1.0 \pm 0.2\text{nM}$ ). Each point is an average of three separate values.  $\text{IC}_{50}$  values from the best-fit line from four separate studies with each conjugate were used to calculate the means and respective standard deviations reported in Table 1.



**Figure 5.** Efflux determination of  $^{99m}\text{TcO}-\text{N}_3\text{S}-5\text{-Ava}-\text{BBN}[7-14]\text{NH}_2$  in human prostate (PC-3) cancerous cells.



**Figure 6.** Efflux determination of  $^{125}\text{I}-\text{Tyr}^4\text{-BBN}$  in human prostate (PC-3) cancerous cells.

activity was counted in a NaI counter. The percent-injected dose per organ and the percent-injected dose per gram were calculated. The % ID in whole blood was estimated assuming a blood volume of 6.5% of the total body weight. Receptor blocking studies were also carried out where excess BBN was administered to animals prior to injection of  $^{99m}\text{Tc}-\text{N}_3\text{S}-5\text{-Ava}-\text{BBN}[7-14]\text{NH}_2$ . In these studies, each animal received a subcutaneous injection of 1 mg of BBN dissolved in 100  $\mu\text{L}$  of the solvent mixture of saline/acetonitrile/DMF (90:5:5) 35 min prior to the injection of  $^{99m}\text{Tc}-\text{N}_3\text{S}-5\text{-Ava}-\text{BBN}[7-14]\text{NH}_2$ . Control (unblocked) animals received an injection of 100  $\mu\text{L}$  of the solvent mixture without BBN 35 min prior to the injection of  $^{99m}\text{Tc}-\text{N}_3\text{S}-5\text{-Ava}-\text{BBN}[7-14]\text{NH}_2$ . The animals were sacrificed 30 min post-injection and the tissues removed, weighed, and counted as previously described.



**Table 2. In Vivo Biodistribution Analyses (%ID/organ (SD), 1 h p.i.,  $n = 5$ ) of  $^{99m}\text{Tc}$ -N<sub>3</sub>S-X-BBN[7-14]NH<sub>2</sub> in Non-Tumor-Bearing Mice Models (CF-1)**

tissue/ organ	0 carbon	3 carbon	5 carbon	8 carbon	11 carbon
blood <sup>a</sup>	1.85(0.36)	0.24(0.08)	0.34(0.12)	0.31(0.06)	2.97(2.01)
heart	0.03(0.01)	0.01(0.00)	0.00(0.00)	0.01(0.01)	0.07(0.03)
lung	0.07(0.01)	0.02(0.01)	0.03(0.01)	0.05(0.01)	0.30(0.27)
liver	5.09(0.62)	1.94(0.36)	1.79(0.70)	4.62(1.06)	6.00(2.80)
spleen	0.04(0.02)	0.10(0.03)	0.03(0.01)	0.06(0.02)	0.13(0.11)
stomach	0.28(0.03)	0.36(0.07)	0.43(0.10)	0.38(0.05)	2.37(0.79)
l. intestine	11.4(17.1)	14.2(8.60)	16.1(9.26)	21.2(18.3)	4.71(6.45)
s. intestine	36.9(18.4)	24.1(10.0)	33.7(8.64)	46.0(17.3)	58.0(18.5)
kidney	1.87(0.18)	1.26(0.14)	0.90(0.19)	1.30(0.15)	1.99(2.13)
pancreas	1.48(0.13)	5.54(0.67)	3.19(0.35)	2.87(0.35)	0.99(0.16)
muscle	0.01(0.01)	0.01(0.00)	0.00(0.00)	0.00(0.00)	0.02(0.01)
urine	38.0(2.45)	47.5(2.08)	38.8(1.71)	19.7(0.31)	14.3(10.5)
(%ID)					

<sup>a</sup> %ID in blood was estimated assuming the whole blood volume to be 6.5% of the total body weight.

The biodistribution of  $^{99m}\text{Tc}$ -N<sub>3</sub>S-5-Ava-BBN[7-12] analogue, which does not bind with high affinity to GRP receptors, was also determined at 1 h p.i.

## RESULTS

The N<sub>3</sub>S-X-BBN[7-14]NH<sub>2</sub> (Figure 1) conjugates were conveniently synthesized by SPPS. The yields of the HPLC purified conjugates were approximately 50%. ES-MS analyses were consistent with the molecular weights calculated for each conjugate.

Figure 4 shows an example of the displacement binding of  $^{125}\text{I}$ -Tyr<sup>4</sup>-BBN from GRP receptors expressed on PC-3 cells as a function of increasing concentrations of the metalated N<sub>3</sub>S-X-BBN[7-14]NH<sub>2</sub> conjugate, Re-N<sub>3</sub>S-5-Ava-BBN[7-14]NH<sub>2</sub>. In the absence of competitors, approximately 5% of the  $^{125}\text{I}$ -Tyr<sup>4</sup>-BBN was bound to the cells after 40 min incubation. In the presence of 10<sup>-5</sup> M cold Tyr<sup>4</sup>-BBN, <10% of the  $^{125}\text{I}$ -Tyr<sup>4</sup>-BBN activity was bound to the cells relative to the absence of cold ligand. This demonstrates that >90% of the  $^{125}\text{I}$ -Tyr<sup>4</sup>-BBN associated with the cells corresponds to specific GRP receptor binding.

The IC<sub>50</sub> values obtained for the series of ReO-N<sub>3</sub>S-X-BBN[7-14]NH<sub>2</sub> conjugates are summarized in Table 1. These results show that the metalated N<sub>3</sub>S-X-BBN[7-14]NH<sub>2</sub> derivatives with 3-, 5-, and 8-carbon spacers (i.e., X = ω-NH<sub>2</sub>(CH<sub>2</sub>)<sub>2</sub>COOH, ω-NH<sub>2</sub>(CH<sub>2</sub>)<sub>4</sub>COOH and ω-NH<sub>2</sub>(CH<sub>2</sub>)<sub>7</sub>COOH) exhibit IC<sub>50</sub> values in the single direct nanomolar range which are lower than derivatives containing the 0- and 11-carbon spacers. The IC<sub>50</sub> for N<sub>3</sub>S-5-Ava-BBN[7-12], the analogue with deletion of Leu<sup>13</sup> and Met<sup>14</sup>, is >10<sup>-6</sup> M. The IC<sub>50</sub> for ReO-N<sub>3</sub>S-5-Ava-BBN[7-14]NH<sub>2</sub> is 1.0 nM.

Radiolabeling of the N<sub>3</sub>S-X-BBN[7-14]NH<sub>2</sub> series of chelates with  $^{99m}\text{Tc}$  was performed by the pre-conjugation post-labeling approach using  $^{99m}\text{Tc}$ (V) gluconate as the synthon (40). The yields of the  $^{99m}\text{Tc}$ -N<sub>3</sub>S-X-BBN[7-14]NH<sub>2</sub> conjugates ranged from 90% to 95%.  $^{99m}\text{Tc}$ -N<sub>3</sub>S-X-BBN[7-14]NH<sub>2</sub> products were purified by RP-HPLC to produce the respective  $^{99m}\text{Tc}$  conjugates in high radiochemical purity (RCP). The  $^{99m}\text{Tc}$ (metalated) conjugates eluted 1 min later than the corresponding nonmetalated N<sub>3</sub>S-X-BBN[7-14]NH<sub>2</sub> reactants, making it possible to collect the  $^{99m}\text{Tc}$  N<sub>3</sub>S-X-BBN[7-14]NH<sub>2</sub> conjugates as high specific activity products. The HPLC chromatograms in Figures 2 and 3 show the elution profiles of the prechelated  $^{99m}\text{Tc}$  and Re reactants and the final  $^{99m}\text{Tc}$ - and Re-N<sub>3</sub>S-5-Ava-BBN[7-14]NH<sub>2</sub> products. These figures also show that both the Re- and  $^{99m}\text{Tc}$ -N<sub>3</sub>S-5-Ava-BBN[7-14]NH<sub>2</sub> species coelute at 14.3 min retention times.

Specific binding of all of the  $^{99m}\text{Tc}$ -N<sub>3</sub>S-X-BBN[7-14]NH<sub>2</sub> conjugates to GRP receptors expressed on PC-3 cells was demonstrated following incubation (40min) of 3 × 10<sup>4</sup> PC-3 cells with high specific activity  $^{99m}\text{Tc}$  analogues. In the absence of the corresponding nonmetalated analogue, approximately 3–6% of the  $^{99m}\text{Tc}$  activity was associated with the PC-3 cells. In contrast, if 10<sup>-5</sup> M of the corresponding unlabeled N<sub>3</sub>S-X-BBN[7-14]NH<sub>2</sub> conjugate or BBN(1-14) is present during the 30 min incubation, less than 0.5% of the  $^{99m}\text{Tc}$  activity is cell associated.

Figure 5 summarizes the results of studies to assess the degree of trapping (or internalization) of the  $^{99m}\text{Tc}$ -N<sub>3</sub>S-5-Ava-BBN[7-14]NH<sub>2</sub> in PC-3 cells. The total  $^{99m}\text{Tc}$  activity associated with the cells after the 40 min incubation was measured following washing the cells with the pH 7.4 incubation media. After washing these cells with the pH 2.5 buffer to remove surface bound  $^{99m}\text{Tc}$  activity, approximately 84% remained trapped by the cells (Figure 5). Results of measurements at 10, 20, 30, 60, and 90 min show that the majority of activity remains trapped by the PC-3 cells, with approximately 70% of the  $^{99m}\text{Tc}$  activity associated with the cells at  $t = 0$  remaining residualized at 90 min. Thus, at 90 min, approximately 83% of the activity remains residualized when normalized to the 84% trapped in the cells at  $t = 0$ . The same studies, when performed with  $^{125}\text{I}$ -Tyr<sup>4</sup>-BBN, show that after a 40 min incubation of PC-3 cells with  $^{125}\text{I}$ -Tyr<sup>4</sup>-BBN, nearly 100% of the cell-associated  $^{125}\text{I}$  activity is internalized (Figure 6). Furthermore, efflux of radioactivity is comparable to that of the  $^{99m}\text{Tc}$  conjugate. Therefore, incorporation of the  $^{99m}\text{Tc}$ -N<sub>3</sub>S chelate onto BBN[7-14]NH<sub>2</sub> has little or no effect on the internalization properties of the  $^{99m}\text{Tc}$  conjugate in GRP receptor-specific PC-3 cells. The binding of these radioligands to PC-3 cells is receptor-specific since the addition of 10<sup>-5</sup> M of the corresponding unlabeled BBN analogues essentially eliminated the uptake of radioactivity by these cells. Furthermore, incubation of  $^{99m}\text{Tc}$ -N<sub>3</sub>S-5-Ava-BBN[7-14]NH<sub>2</sub> and  $^{125}\text{I}$ -Tyr<sup>4</sup>-BBN with MDA-MB-438 human breast cancer cells, a cell line that exhibits no measurable GRPr expression, showed no significant uptake or internalization of the radioligand.

**Biodistribution of  $^{99m}\text{Tc}$ -N<sub>3</sub>S-BBN[7-14]NH<sub>2</sub> Conjugates.** Tables 2 and 3 summarize the results of the biodistribution studies in normal CF-1 mice at 1 h post-intravenous injection for the series of  $^{99m}\text{Tc}$ -N<sub>3</sub>S-X-BBN[7-14]NH<sub>2</sub> conjugates. As the hydrocarbon chain length of the spacer group, X, increases from 0 to 11, the % ID cleared by the renal-urinary pathway decreases. There is no significant uptake or retention in the stomach

**Table 3. In Vivo Biodistribution Analyses (%ID/g (SD), 1h p.i.,  $n = 5$ ) of  $^{99m}\text{Tc}-\text{N}_3\text{S}-\text{X}-\text{BBN}[7-14]\text{NH}_2$  in Non-Tumor-Bearing Mice Models (CF-1)**

tissue/ organ	0 carbon	3 carbon	5 carbon	8 carbon	11 carbon
blood <sup>a</sup>	0.48(0.10)	0.14(0.04)	0.23(0.09)	0.20(0.04)	1.66(1.21)
heart	0.15(0.02)	0.10(0.07)	0.02(0.04)	0.09(0.08)	0.64(0.29)
lung	0.24(0.03)	0.14(0.10)	0.25(0.10)	0.31(0.06)	1.48(1.39)
liver	2.30(0.42)	1.18(0.18)	1.22(0.58)	2.85(0.61)	3.74(1.68)
spleen	0.21(0.02)	1.04(0.45)	0.59(0.25)	0.70(0.26)	0.97(0.67)
stomach	0.44(0.05)	1.13(0.29)	1.05(0.31)	1.05(0.36)	5.51(1.83)
l. intestine	8.65(13.0)	16.5(10.7)	22.9(11.8)	28.2(25.7)	4.54(5.76)
s. intestine	19.2(10.4)	17.4(7.59)	25.0(7.90)	31.3(11.5)	35.3(11.2)
kidney	3.29(0.45)	3.15(0.30)	2.89(0.67)	3.47(0.60)	5.04(5.40)
pancreas	2.79(0.33)	19.5(2.24)	13.8(1.62)	10.5(1.07)	3.43(0.31)
muscle	0.04(0.03)	0.10(0.05)	0.10(0.06)	0.06(0.05)	0.12(0.09)
urine	38.0(2.45)	47.5(2.08)	38.8(1.71)	19.7(0.31)	14.3(10.5)
(%ID)					

**Table 4. In Vivo Biodistribution Analyses (%ID/organ (SD),  $n = 5$ ) of  $^{99m}\text{Tc}-\text{N}_3\text{S}-5-\text{Ava}-\text{BBN}[7-14]\text{NH}_2$  in Normal Mice Models (CF-1)**

tissue/ organ	0.5 h	1 h	4 h
blood <sup>b</sup>	0.55(0.07)	0.34(0.12)	0.17(0.16)
heart	0.01(0.01)	0.00(0.00)	0.00(0.00)
lung	0.04(0.02)	0.03(0.01)	0.01(0.01)
liver	3.96(1.40)	1.79(0.70)	1.20(0.53)
spleen	0.08(0.03)	0.03(0.01)	0.02(0.01)
stomach	0.46(0.08)	0.43(0.10)	0.29(0.04)
l. intestine <sup>a</sup>	2.89(0.73)	16.1(9.26)	36.6(11.9)
s. intestine <sup>a</sup>	45.8(3.52)	33.7(8.64)	5.64(3.32)
kidney <sup>a</sup>	1.45(0.24)	0.90(0.19)	0.49(0.09)
pancreas	4.34(1.60)	3.19(0.35)	1.36(0.27)
muscle	0.01(0.00)	0.00(0.00)	0.00(0.00)
urine <sup>a</sup>	34.2(6.05)	38.8(1.71)	52.0(9.35)

<sup>a</sup> At 4 h, feces containing  $^{99m}\text{Tc}$  had been excreted from each animal, and the % in the urine was estimated to be approximately 35% of the ID. <sup>b</sup>%ID in blood was estimated assuming the whole blood volume to be 6.5% of the total body weight.

**Table 5. In Vivo Biodistribution Analyses (%ID/g (SD),  $n = 5$ ) of  $^{99m}\text{Tc}-\text{N}_3\text{S}-5-\text{Ava}-\text{BBN}[7-14]\text{NH}_2$  in Normal Mice Models (CF-1)**

tissue/organ	0.5 h	1 h	4 h
blood	0.38(0.05)	0.23(0.09)	0.12(0.12)
heart	0.16(0.13)	0.02(0.04)	0.06(0.06)
lung	0.30(0.13)	0.25(0.10)	0.10(0.07)
liver	2.53(0.91)	1.22(0.58)	0.82(0.28)
spleen	1.10(0.47)	0.59(0.25)	0.29(0.22)
stomach	1.04(0.28)	1.05(0.31)	0.82(0.11)
l. intestine	3.88(1.03)	22.9(11.8)	50.6(13.8)
s. intestine	29.8(3.43)	25.0(7.90)	4.04(2.38)
kidney	4.22(0.81)	2.89(0.67)	1.53(0.31)
pancreas	20.3(6.15)	13.8(1.62)	6.28(1.29)
muscle	0.18(0.13)	0.10(0.06)	0.01(0.01)
pancreas/blood	53.4(23.0)	60.0(24.5)	52.3(53.4)
pancreas/muscle	113(88.3)	138(84.4)	628(641)

indicating that there is minimal, if any, in vivo dissociation of  $^{99m}\text{Tc}$  from these ligands to produce  $^{99m}\text{TcO}_4^-$ . Pancreatic uptake of this series of conjugates at 1 h p.i. shows considerable variability, with the highest value associated with the three-carbon conjugate (Tables 2 and 3). As the tethering moiety is lengthened beyond three carbons, the uptake in normal pancreas decreases. There is retention of the  $^{99m}\text{Tc}$  activity localized in the pancreas; however, there is some efflux. For example, for the  $^{99m}\text{Tc}-\text{BBN}$  analogue where  $\text{X} = \text{NH}_2(\text{CH}_2)_4\text{COOH}$  (5-Ava), the percent  $^{99m}\text{Tc}$  activity retained in the pancreas at 1 and 4 h, relative to  $^{99m}\text{Tc}$  activity localized in that organ at 30 min is approximately 75% and 35%, respectively. Tables 4 and 5 summarize the results of the biodistribution studies in normal CF-1 mice at 30 min, 1 h, and

4 h post-intravenous injection for the  $^{99m}\text{Tc}-\text{N}_3\text{S}-5-\text{Ava}-\text{BBN}[7-14]\text{NH}_2$  conjugate. There is  $4.22 \pm 0.81\%$  ID/gm retained in the kidneys at 30 min p.i., but in all cases, the  $^{99m}\text{Tc}$  activity in the kidneys decreases to a level at 4 h p.i., which is approximately 35% of that observed at 30 min p.i. The  $^{99m}\text{Tc}-\text{N}_3\text{S}-5-\text{Ava}-\text{BBN}[7-12]$  analogue with the Leu<sup>13</sup> and Met<sup>14</sup> deletion does not bind to GRP receptors and shows no significant accumulation in pancreatic tissue. Blocking studies in which high levels of cold BBN[1–14] was administered 35 min prior to the  $^{99m}\text{Tc}$  ligands, reduced the % ID/gm uptake/retention in the pancreas at 30 min p.i. by a factor of 8–10, demonstrating the in vivo specificity of these analogues for GRP-receptor expressing cells.

## DISCUSSION

Considerable efforts have been made by several research groups to identify structural features of BBN-analogues that produce binding and stability properties necessary for in vivo targeting of GRP receptor expressing cancers (43–48). Insights gained from these research efforts can provide the basis for designing radiolabeled conjugates of BBN derivatives that maintain high GRP receptor-binding affinities. The W-A-V-G-H-L sequence BBN[8–13] has been shown to be a sequence that is directly involved in a specific high-affinity binding interaction with GRP receptors (44, 49). Modifications or a deletion at position 14 (i.e., the position normally occupied by methionine Met<sup>14</sup>) is an important factor in determining whether or not the derivative will possess antagonistic or agonistic properties (23, 45, 47, 48). Minor structural variations (e.g., reduction of the Leu<sup>13</sup>–Met<sup>14</sup> peptide bond or cyclization of Met<sup>14</sup> on the BBN analogue structure) can confer agonist or antagonist properties (44, 47, 50). While the vast majority of research with BBN analogues has been devoted to the development of antagonists, BBN[8–14]NH<sub>2</sub> is an example of a truncated BBN[1–14] sequence that will form conjugates that frequently bind GRP receptors as agonists (34, 43, 44).

The strategy used in designing the limited series of  $^{99m}\text{Tc}-\text{N}_3\text{S}-\text{X}-\text{BBN}[7-14]\text{NH}_2$  derivatives was to covalently link the  $^{99m}\text{Tc}-\text{N}_3\text{S}$  chelate via a spacer group to the BBN[8–14]NH<sub>2</sub> binding sequence (32). Previous studies demonstrated that the inclusion of Gln<sup>7</sup> in linking radiometal chelates to BBN[8–14]NH<sub>2</sub> was beneficial in reducing renal retention of  $^{105}\text{Rh}-\text{S}_4-\text{BBN}$  analogues and is compatible with maintaining high GRP receptor binding affinity (15, 35). For these reasons, the various hydrocarbon spacer groups used in this study were linked to the BBN[8–14]NH<sub>2</sub> receptor binding sequence via the Gln<sup>7</sup> residue (Figure 1).

Since the Re–N<sub>3</sub>S-5-Ava-BBN[7–14]NH<sub>2</sub> and  $^{99m}\text{Tc}-\text{N}_3\text{S}-5-\text{Ava}-\text{BBN}[7-14]\text{NH}_2$  conjugates each have a 14.3

min retention time by RP-HPLC (Figures 2 and 3), it can be deduced that both the Re and  $^{99m}\text{Tc}$  conjugates have the same structure. These results provide evidence that  $^{99m}\text{Tc}$  is present as the  $^{99m}\text{TcO}-\text{N}_3\text{S}$  chelate, attached via the spacer groups to the BBN[7–14] $\text{NH}_2$  GRP receptor binding sequence. These results are consistent with previous studies which show that  $^{99m}\text{Tc}(\text{V})$  precursors react with  $\text{N}_3\text{S}$  ligand systems to form stable chelates that contain the mono-oxo- $\text{Tc}(\text{V})$  (i.e.,  $\text{TcO}^{3+}$ ) core, as do the corresponding Re(V) chelates (40). Complexation of  $\text{ReO}^{3+}$  and  $\text{TcO}^{3+}$  with these types of  $\text{N}_3\text{S}$  ligands results in deprotonation of two amide groups to produce metal chelate structures that have an overall neutral charge (40). The observation that  $^{99m}\text{TcO}-\text{N}_3\text{S}-5\text{-Ava-BBN}[7-14]\text{NH}_2$  is formed in high yields by transchelation from  $^{99m}\text{Tc}$ -gluconate (Scheme 1), and, coelutes with  $^{99m}\text{TcO}-$  and  $\text{ReO}-\text{N}_3\text{S}-5\text{-Ava-BBN}[7-14]\text{NH}_2$  conjugates synthesized by the preformed chelate route demonstrates the feasibility of producing well defined  $^{99m}\text{Tc}-\text{N}_3\text{S}-\text{BBN}[7-14]\text{NH}_2$  chemical entities via the post conjugation labeling method. These results are consistent with previous studies that utilized other  $\text{N}_3\text{S}$  bioconjugates to formulate  $^{99m}\text{Tc}(\text{V})\text{O}$ -labeled radiopharmaceuticals in high specific activities using similar labeling approaches (40, 41).

In vitro binding studies with the  $\text{N}_3\text{S}-\text{X}-\text{BBN}[7-14]\text{NH}_2$  analogues demonstrate that derivatives where the spacer group, **X**, comprises a 3-, 5-, and 8-carbon tether (i.e.,  $\beta$ -Ala, 5-Ava and 8-Aoc), produce derivatives that have high GRP-receptor binding affinities (i.e.,  $\text{IC}_{50} < 10 \text{ nM}$ ) (Table 1). In the absence of a spacer group and with an 11-carbon (11-Aun) tether, the  $\text{IC}_{50}$  values increase (Table 1). This is similar to the results obtained with analysis of  $^{105}\text{Rh}-\text{S}_4-\text{X}-\text{BBN}[7-14]\text{NH}_2$  constructs (35). These data, therefore, indicate that the most promising analogues of this design, for in vivo targeting of cells expressing GRP receptors, are those with **X** = 3–8 carbon atoms.

Maximizing residualization of radioactivity in tumors after binding of the activity is an important factor in optimizing the diagnostic and/or therapeutic efficacy of radiotracers (1, 36, 51). Results of studies with  $^{99m}\text{Tc}-\text{N}_3\text{S}-5\text{-Ava-BBN}[7-14]\text{NH}_2$  show that most of the  $^{99m}\text{Tc}$  activity associated with the PC-3 cells is not surface bound and is not lost from the cells by incubation in pH 2.5 buffer (Figure 5). Furthermore, there is only minimal efflux of  $^{99m}\text{Tc}$  activity from the cells for at least 90 min. These results indicate that residualization of  $^{99m}\text{Tc}$  activity results from GRP receptor-mediated endocytosis of  $^{99m}\text{Tc}-\text{N}_3\text{S}-5\text{-Ava-BBN}[7-14]\text{NH}_2$  with subsequent trapping of activity. Similar studies with  $^{125}\text{I}-\text{Tyr}^4\text{-BBN}$  demonstrate that GRP receptor mediated trapping and efflux of  $^{125}\text{I}$  radioactivity is comparable to that of the  $^{99m}\text{Tc}$  conjugate (Figure 6).

Internalization of both the  $^{125}\text{I}$  and  $^{99m}\text{Tc}-\text{BBN}$  analogues can be attributed to their agonistic binding to GRP receptors (26, 28, 36, 44). GRP receptors are 7-TMS-G-protein coupled receptors which are capable of internalizing the agonist-receptor complex (48, 49, 52, 53). Since the BBN[7–14] $\text{NH}_2$  receptor binding sequence is consistent with agonistic binding, GRP receptor mediated endocytosis of the  $^{99m}\text{Tc}-\text{N}_3\text{S}-\text{X}-\text{BBN}[7-14]\text{NH}_2$  constructs used in this study is not unexpected. The specific intracellular trapping mechanism of the  $^{99m}\text{Tc}$  activity in these PC-3 cells is not understood. It is likely that following internalization of  $^{99m}\text{Tc}-\text{N}_3\text{S}-\text{X}-\text{BBN}[7-14]\text{NH}_2$ , that lysosomal proteases degrade the  $^{99m}\text{Tc}-\text{BBN}$  conjugate to peptide fragments.<sup>54,55</sup> The fragments to which  $^{99m}\text{Tc}$  remain attached would be the chemical species that are residualized in the cell for extended

periods. Further work is needed to identify the structure of the  $^{99m}\text{Tc}$  fragments to help elucidate the trapping mechanisms. Efflux of  $^{125}\text{I}$  activity (Figure 6), on the other hand, is expected, as lysosomal breakdown of the  $^{125}\text{I}-\text{Tyr}^4$ -containing peptides results in the production of free  $^{125}\text{I}$  tyrosine, which is exported from the lysosome and the cell by specific transport pathways (55–57). The degree of efflux for the  $^{125}\text{I}-\text{Tyr}^4\text{-BBN}$  species does occur at a slightly more rapid rate than that of the corresponding  $^{99m}\text{Tc}$  conjugate (Figures 5 and 6).

Results from the biodistribution studies, where **X** = 0–11 carbons, are summarized in Tables 2 and 3. These data, along with the data acquired from in vitro cell binding assays, suggest that those  $^{99m}\text{Tc}-\text{N}_3\text{S}-\text{X}-\text{BBN}[7-14]\text{NH}_2$  conjugates, where **X** = 3–8, are the most promising candidates for further in vivo evaluation. It is interesting to note that with this limited series of  $^{99m}\text{Tc}-\text{BBN}$  conjugates, the 3-carbon spacer ( $\beta$ -Alanine) analogue exhibits the highest localization in the pancreas at 1 h p.i. As the length of the spacer increases, there is a decline in pancreatic uptake (Tables 2 and 3). The reasons for this observation are not clear. However, this relationship may result from the higher degree of plasma protein binding of the  $^{99m}\text{Tc}-\text{BBN}$  analogues as their hydrophobicity increases. As plasma protein binding increases, the availability of the respective  $^{99m}\text{Tc}$  analogue for binding to the GRP expressing cells in the pancreas possibly decreases.

Results from biodistribution studies with  $^{99m}\text{Tc}-\text{N}_3\text{S}-5\text{-Ava-BBN}[7-14]\text{NH}_2$  in normal CF-1 mice at 30 min, 1 h, and 4 h p.i. are summarized in Tables 4 and 5. This  $^{99m}\text{Tc}$  conjugate clears efficiently from the blood with only  $0.34 \pm 0.12 \text{ ID}$  remaining in the blood at 1 h p.i. (Table 3).  $^{99m}\text{Tc}-\text{N}_3\text{S}-5\text{-Ava-BBN}[7-14]\text{NH}_2$  clears by each the hepatobiliary and renal/urinary pathways. Retention in the kidneys is significant (i.e.,  $2.89\% \pm 0.67\%$  and  $1.53\% \pm 0.31\% \text{ ID/g}$  at 1 and 4 h, respectively, Table 4) but is less than the level of retention in that organ reported for several other radiolabeled peptides and proteins.<sup>12</sup> Uptake and retention of  $^{99m}\text{Tc}-\text{N}_3\text{S}-5\text{-Ava-BBN}[7-14]\text{NH}_2$  in the pancreas is high (i.e.,  $13.8\% \pm 1.62\%$  and  $6.05\% \pm 0.28\% \text{ ID/g}$  at 1 and 4 h p.i., respectively, Table 4). The observation that the uptake of this  $^{99m}\text{Tc}$  conjugate in the pancreas is reduced to  $2.10\% \pm 0.80\% \text{ ID/g}$  at 0.5 h p.i., when the animals were administered 1 mg of BBN 35 min prior to injection of the radiotracer, demonstrates the high specificity of  $^{99m}\text{Tc}-\text{N}_3\text{S}-5\text{-Ava-BBN}[7-14]\text{NH}_2$  for in vivo targeting of the GRP receptor expressing cells in this organ. The high pancreas-to-blood and pancreas-to-muscle ratios that are maintained at  $\geq 4 \text{ h p.i.}$  (Table 4) is a reflection of the high GRP binding affinity of this  $^{99m}\text{Tc}-\text{BBN}$  analogue and its receptor-mediated transport to promote intracellular trapping. While retention of  $^{99m}\text{Tc}-\text{N}_3\text{S}-5\text{-Ava-BBN}[7-14]\text{NH}_2$  is extended, washout of  $^{99m}\text{Tc}$  activity from the organ occurs over time with  $1.36\% \pm 0.27\% \text{ ID}$  remaining at 4 h p.i. in comparison to  $3.19\% \pm 0.35\% \text{ ID}$  at 1 h p.i. (Table 2). For this reason, the pancreas to blood and pancreas-to-muscle ratios at 4 h are not significantly different than those at 1 h p.i.

## CONCLUSION

The results of this study demonstrate that the  $^{99m}\text{Tc}-\text{N}_3\text{S}-\text{X}-\text{BBN}[7-14]\text{NH}_2$  construct provides flexibility for designing  $^{99m}\text{Tc}$ -labeled conjugates that retain high in vitro and in vivo specificity targeting of GRP receptor expressing cells. In this particular instance, it was shown that the length of the hydrocarbon spacer group can be



varied from at least 3–8 carbon atoms in length without comprising agonistic binding affinity to GRP receptors. These findings, coupled with previous reports, show that there is a significant degree of bulk tolerance when attaching radiometals via the N-terminal end of the BBN[8–14] $\text{NH}_2$  sequence (31–35). The potential clinical utility of the  $^{99m}\text{Tc}-\text{N}_3\text{S}-\text{X}-\text{BBN}[7-14]\text{NH}_2$  constructs as cancer specific imaging agents was recently demonstrated by Van de Weile et al. (10, 30) in human patients with either prostate or breast cancer. Their studies showed that  $^{99m}\text{Tc}-\text{N}_3\text{S}-5\text{-Ava}-\text{BBN}[7-14]\text{NH}_2$  localizes in tumors with high specificity producing good tumor-to-normal tissue uptake ratios and high-quality SPECT images (10, 30). To design improved radiolabeled synthetic BBN analogues for diagnostic or therapeutic applications, it is essential to devote more effort to better understand the structurally sensitive mechanisms involved in the binding of these derivatives to GRP receptors and subsequent residualization of the radiotracer in cancer cells.

#### ACKNOWLEDGMENT

This material is the result of work supported with resources and the use of facilities at the Harry S. Truman Memorial Veterans' Hospital, Columbia, MO 65201, and the University of Missouri-Columbia School of Medicine Departments of Radiology and Internal Medicine, Columbia, MO 65211. This work was also funded in part by grants from the American Cancer Society (RPG-99-331-01-CDD), the National Cancer Institute (DHHS-RO1-CA72942), the National Institute of Health (DHHS-1P20-CA86290), and Resolution Pharmaceuticals Inc., Mississauga, Ontario, Canada. The University of Missouri holds a patent on the bombesin agonists cited in this paper.

#### LITERATURE CITED

- (1) Anderson, C. J., and Welch, M. J. (1999) Radiometal-labeled agents (non-technetium) for diagnostic imaging. *Chem. Rev.* 99, 2219–2234.
- (2) Behr, T. M., and Goldenberg, D. M. (1996) Improved prospects for cancer therapy with radiolabeled antibody fragments and peptides? *J. Nucl. Med.* 37, 834–836.
- (3) Bakker, W. H., Albert, R., Bruns, C., Breeman, W. A., Hoffland, L. J., Marbach, P., Pless, J., Pralet, D., Stolz, B., and Koper, J. W. (1991) [Indium-111-DTPA-D-Phe<sup>1</sup>]octreotide, a potential radiopharmaceutical for imaging somatostatin receptor positive tumors: Synthesis, radiolabeling, and in vivo validation. *Life Sci.* 49, 1583–1591.
- (4) deJong, M., Bakker, W. H., Krenning, E. P., Breeman, W. A. P., van der Pluijm, M. E., Bernard, B. F., Visser, T. J., Jermann, E., Behe, M., Powell, P., and Macke, H. (1997) Yttrium-90 and Indium-111 labeling, receptor binding, and biodistribution of [DOTA-o-D-Phe<sup>1</sup>, Tyr<sup>3</sup>]octreotide, a promising somatostatin analogue for radionuclide therapy. *Eur. J. Nucl. Med.* 24, 368–371.
- (5) Eckelman, W. C., and Gibson, R. E. (1993) The design of site-directed radiopharmaceuticals for use in drug discovery. In *Nuclear Imaging in Drug Discovery, Development, and Approval* (H. D. Burns, R. E. Gibson, R. Dannals, and P. Siegl, Eds.) Birkhauser, Boston.
- (6) Hom, R. K., and Katzenellenbogen, J. A. (1997) Technetium-99m-labeled receptor-specific small-molecule radiopharmaceuticals: Recent developments and encouraging results. *Nucl. Med. Biol.* 24, 485–498.
- (7) Kvols, L. K. (1999) Somatostatin receptor imaging of neuroendocrine carcinomas: Implications for patient management and radiotherapy. In *Technetium, Rhenium and Other Metals in Chemistry and Nuclear Medicine* (M. Nicolini and U. Mazzi, Eds.) pp 153–756, SGEditionali, Padova, Italy.
- (8) Press, O. W., Appelbaum, F. R., Early, J. F., and Bernstein, I. D. (1994) Radiolabeled antibody therapy of lymphomas. *Biol. Ther. Cancer Update* 4, 1–13.
- (9) Seregini, E., Chiti, A., and Bombardieri, E. (1998) Radionuclide imaging of neuroendocrine tumors: Biological basis and diagnostic results. *Eur. J. Nucl. Med.* 25, 639–658.
- (10) Van de Wiele, C., Broecke, R. V., Cocquyt, V., Dumont, F., Oosterlinck, W., Thornback, J., and Peers, S. H. (2000)  $^{99m}\text{Tc}$ -RP-527, a gastrin releasing peptide (GRP) analogue for visualization of GRP receptor expressing malignancies: A feasibility study. *Nucl. Med. Commun.* 21, 21.
- (11) Boerman, O. C., Oyen, W. J. G., and Corstens, F. H. M. (2000) Radio-labeled receptor-binding peptides: A new class of radiopharmaceuticals. *Sem. Nucl. Med.* 30, 195–208.
- (12) Giblin, M. F., Wang, N., Hoffman, T. J., Jurisson, S. S., and Quinn, T. P. (1998) Design and characterization of alpha-melanotropin peptide analogues cyclized through rhenium and technetium metal coordination. *Proc. Natl. Acad. Sci. U.S.A.* 95, 12814–12818.
- (13) Ugur, O., Kostakoglu, L., Hui, E. T., Fisher, D. R., Garmestani, K., Gansow, O. A., Cheung, N. V., and Larson, S. M. (1996) Comparison of the targeting characteristics of various radioimmunoconjugates for radioimmunotherapy of neuroblastoma: Dosimetry calculations incorporating cross-organ beta doses. *Nucl. Med. Biol.* 23, 1–8.
- (14) Brechbiel, M. W., Gansow, O. A., Atcher, R. W., Schlom, J., Esteban, J., Simpson, D. E., and Colcher, D. (1986) Synthesis of 1-(p-Isothiocyanatobenzyl) derivatives of DTPA and EDTA. Antibody labeling and tumor-imaging studies. *Inorg. Chem.* 25, 2772–2781.
- (15) Ning, L., Ochymowycz, L. A., Higginbotham, C., Struttman, M., Abrams, M. J., Vollano, J. F., Skerlj, R. T., Ketrang, A. R., and Volkert, W. A. (1995) Pharmacokinetic studies of  $^{105}\text{Rh}(\text{III})$  Complexes with macrocycles. *J. Labeled Compd. Radiopharm.* 37, 426–428.
- (16) Krenning, E. P., Kwekkeboom, D. J., Bakker, W. H., Breeman, W. A., Kooij, P. P., Oei, H. Y., van Hagen, M., Postema, P. T., de Jong, M., and Reubi, J. C. (1993) Somatostatin receptor scintigraphy with [ $^{111}\text{In}$ -DTPA-D-Phe<sup>1</sup>] and [ $^{123}\text{I}$ -Tyr<sup>3</sup>]Octreotide: The Rotterdam experience with more than 1000 patients. *Eur. J. Nucl. Med.* 20, 716–731.
- (17) Lewis, J. S., Lewis, M. R., Srinivasan, A., Schmidt, M. A., Wang, J., and Anderson, C. J. (1999) Comparison of four  $^{64}\text{Cu}$ -labeled somatostatin analogues in vitro and in a tumor-bearing rat model: Evaluation of new derivatives for positron emission tomography imaging and targeted radiotherapy. *J. Med. Chem.* 42, 1341–1347.
- (18) Smith-Jones, P. M., Stolz, B., Albert, R., Ruser, G., Maecke, H., Briner, U., Tolcfai, L., Weckbecker, G., and Bruns, C. (1995) Synthesis, radiolabeling, and evaluation of DTPA/Octreotide conjugates for radiotherapy. *J. Labeled Compd. Radiopharm.* 37, 499–501.
- (19) Stolz, B., Smith-Jones, P. M., Weckbecker, G., Albert, R., Knecht, H., Haller, R., Tolcsvai, L., Hofman, G., Pollehn, K., and Bruns, C. (1997) Radiotherapy with Yttrium-90 labeled DOTA-Tyr<sup>3</sup>-Octreotide in tumor bearing rodents. *J. Nucl. Med.* 38, 18p.
- (20) Otte, A., Mueller-Brand, J., Goetze, M., Hermann, R., Knecht, H. R., and Maecke, H. R. (1998) Yttrium-90-DOTA-Octreotide treatment of somatostatin receptor positive tumors. *J. Nucl. Med.* 39, 70P.
- (21) Anderson, C. J., Jones, L. A., Bass, L. A., Sherman, E. L. C., McCarthy, D. W., Cutler, P. D., Lanahan, M. V., Cristel, M. E., Lewis, J. S., and Schwarz, S. W. (1998) Radiotherapy, toxicity, and dosimetry of Copper-64-TETA-Octreotide in tumor-bearing Rats. *J. Nucl. Med.* 39, 1944–1951.
- (22) Mahmoud, S., Staley, J., Taylor, J., Bogden, A., Moreau, J.-P., Coy, D., Avis, I., Cuttitta, F., Mulshine, J. L., and Moody, T. W. (1985) [ $^{125}\text{I}$ ] Bombesin analogues inhibit growth of small cell lung cancer in vitro and in vivo. *Life Sci.* 37, 105–113.
- (23) Qin, Y., Ertl, T., Cai, R.-Z., Halmos, G., and Schally, A. V. (1994) Inhibitory effect of bombesin receptor antagonist RC-3095 on the growth of human pancreatic cancer cells in vivo and in vitro. *Cancer Res.* 54, 1035–1041.
- (24) Qin, Y., Ertl, T., Cai, R.-Z., Horvath, J. E., Groot, K., and Schally, A. V. (1995) Antagonists of bombesin/gastrin-releasing peptide inhibit growth of SW-1990 human pancreatic

- adenocarcinoma and production of cyclic AMP. *Int. J. Cancer* 63, 257–262.
- (25) Plonowski, A., Nagy, A., Schally, A. V., Sun, B., Groot, K., and Halmos, G. (2000) In vivo inhibition of PC-3 human androgen-independent prostate cancer by a targeted cytotoxic bombesin analogue, AN-215. *Int. J. Cancer* 88, 652–657.
- (26) Breeman, W. A. P., Hofland, L. J., De Jong, M., Bernard, B. F., Srinivasan, A., Kwekkeboom, D. J., Visser, T. J., and Krenning, E. P. (1999) Evaluation of radio-labeled bombesin analogues for receptor-targeted scintigraphy and radiotherapy. *Int. J. Cancer* 81, 658–665.
- (27) Breeman, W. A. P., De Jong, M., Bernard, B. F., Kwekkeboom, D. J., Srinivasan, A., van der Pluijm, M. E., Hofland, L. J., Visser, T. J., and Krenning, E. P. (1999) Pre-clinical evaluation of [ $^{111}\text{In}$ -DTPA-Pro<sup>1</sup>, Tyr<sup>4</sup>]Bombesin, a new radioligand for bombesin-receptor scintigraphy. *Int. J. Cancer* 83, 657–663.
- (28) Rogers, B. E., Brechbiel, M. W., Kirkman, R. L., Clarkson, M., and Buchsbaum, D. J. (1999) In Vitro binding and internalization of an Indium-111 labeled bombesin derivative to cells expressing the gastrin releasing peptide receptor. In *Technetium, Rhenium and Other Metals in Chemistry and Nuclear Medicine* (M. Nicolini and U. Mazzi, Eds.) pp 519–525, SGE Editoriale, Padova, Italy.
- (29) Rogers, B. E., Curiel, D. T., Mayo, M. S., Laffoon, K. K., Bright, S. J., and Buchsbaum, D. J. (1997) Tumor localization of a radiolabeled bombesin analogue in mice bearing human ovarian tumors induced to express the gastrin-releasing peptide receptor by an adenoviral vector. *Cancer Suppl.* 80, 2419–2424.
- (30) Van de Wiele, C., Dumont, F., Broecke, R. V., Oosterlinck, W., Cocquyt, V., Serreyn, R., Peers, S., Thornback, J., Slegers, G., and Dierckx, R. A. (2000) Technetium-99m RP525, a GRP analogue for visualization of GRP receptor-expressing malignancies: A feasible study. *Eur. J. Nucl. Med.* 27, 1694–1699.
- (31) Breeman, W. A. P., Hofland, L. J., DeJong, M., Bernard, B. F., Srinivasan, A., Kwekkeboom, D. J., Visser, T. J., and Krenning, E. P. (1999) Evaluation of radio-labeled bombesin analogues for receptor-targeted scintigraphy and radiotherapy. *Int. J. Cancer* 81, 658–665.
- (32) Baidoo, K. E., Lin, K.-S., Zhan, Y., Finley, P., Scheffel, U., and Wagner, Jr. H. N. (1998) Design, synthesis, and initial evaluation of high-affinity technetium bombesin analogues. *Bioconjugate Chem.* 9, 218–225.
- (33) Karra, S. R., Schibli, R., Gali, H., Katti, K. V., Hoffman, T. J., Higginbotham, C., Sieckman, G. L., and Volkert, W. A. (1999)  $^{99\text{m}}\text{Tc}$ -labeling and in vivo studies of a bombesin analogue with a novel water-soluble dithiadiphosphine-based bifunctional chelating agent. *Bioconjugate Chem.* 10, 254–260.
- (34) Hoffman, T. J., Quinn, T. P., and Volkert, W. A. (2001) Radio-metalated receptor-avid peptide conjugates for specific in vivo targeting of cancer cells. *Nucl. Med. Biol.* 28, 527–539.
- (35) Hoffman, T. J., Li, N., Volkert, W. A., Sieckman, G. L., Higginbotham, C., and Ochrymowycz, L. A. (1997) Synthesis and characterization of  $^{105}\text{Rh}$  labeled bombesin analogues: Enhancement of GRP receptor binding affinity utilizing aliphatic carbon chain linkers. *J. Labeled Compd. Radiopharm.* 40, 490–493.
- (36) Volkert, W. A., and Hoffman, T. J. (1999) Therapeutic radiopharmaceuticals. *Chem. Rev.* 99, 2269–2292.
- (37) Gali, H., Hoffman, T. J., Owen, N. K., Sieckman, G. L., and Volkert, W. A. (2000) In vitro and in vivo evaluation of  $^{111}\text{In}$ -labeled DOTA-8-Aoc-BBN[7–14] $\text{NH}_2$  conjugate for specific targeting of tumors expressing gastrin releasing peptide receptors (GRP-R). *J. Nucl. Med. (Supplement)*, 41(5), 119P.
- (38) Smith, C. J., Hoffman, T. J., Hayes, D. L., Owen, N. K., Sieckman, G. L., and Volkert, W. A. (2001) Radiochemical investigations of  $^{177}\text{Lu}$ -DOTA-8-Aoc-BBN[7–14] $\text{NH}_2$ : A new gastrin releasing peptide receptor (GRPr) targeting radiopharmaceutical. *J. Labeled Compd. Radiopharm.* 44, 706–708.
- (39) Jurisson, S., Berning, D., Jia, W., and Ma, D. (1993) Coordination compounds in nuclear medicine. *Chem. Rev.* 93, 1137–1156.
- (40) Wong, E., Fauconnier, T., Bennett, S., Valliant, J., Nguyen, T., Lau, F., Lu, L. F. L., Pollak, A., Bell, R. A., and Thornback, J. R. (1997) Rhenium(V) and technetium(V) oxo complexes of an  $\text{N}_2\text{N}'\text{S}$  peptidic chelator: Evidence of interconversion between the syn and anti conformations. *Inorg. Chem.* 36, 5799–5808.
- (41) Guhlke, S., Schaffland, A., Zamora, A., P. O., Sartor, J., Diekmann, D., Bender, H., Knapp, F. F., and Biersack, H.-J. (1998)  $^{188}\text{Re}$ - and  $^{99\text{m}}\text{Tc}$ -MAG<sub>3</sub> as prosthetic groups for labeling amines and peptides: Approaches with pre- and postconjugation labeling. *Nucl. Med. Biol.* 25, 621–631.
- (42) Noll, B., Kniess, T., Friebe, M., Spies, H., and Johannsen, B. (1996) Rhenium (V) gluconate, a suitable precursor for the preparation of rhenium (V) complexes. *Isotopes Environ. Health Stud.* 32, 21–29.
- (43) Jensen, R. T., Mrozinski, J. E. Jr., and Coy, D. H. (1993) Bombesin receptor antagonists: different classes and cellular basis of action. *Recent Results Cancer Res.* 129, 87–113.
- (44) Moody, T. W. (1996) Peptides and growth factors in non-small cell lung cancer. *Peptides* 17, 545–555.
- (45) Leban, J. J., Landavazo, A., McDermed, J. D., Diliberto, E. J. Jr., Jansen, M., Stockstill, B., and Kull, F. C. Jr. (1994) Potent gastrin-releasing peptide (GRP) antagonists derived from GRP (19–27) with a C-terminal DPro psi [ $\text{CH}_2\text{NH}$ ]Phe-NH<sub>2</sub> and N-terminal aromatic residues. *J. Med. Chem.* 37, 439–445.
- (46) Kahan, Z., Sun, B., Schally, A. V., Arencibia, J. M., Cai, R. Z., Groot, K., and Halmos G. (2000) Inhibition of growth of MDA-MB-468 estrogen-independent human breast carcinoma by bombesin/gastrin-releasing peptide antagonists RC-3095 and RC-3940-II. *Cancer* 88, 1384–1392.
- (47) Cai, R. Z., Reile, H., Armatis, P., and Schally, A. V. (1994) Potent bombesin antagonists with C-terminal Leu-psi( $\text{CH}_2$ -N)-Tac-NH<sub>2</sub> or its derivatives. *Proc. Natl. Acad. Sci. U.S.A.* 91, 12664–12668.
- (48) Coy, D. H., Heinz-Erian, P., Jiang, N. Y., Taylor, J., Moreau, J. P., Gardner, J. D., and Jensen, R. T. (1988) Progress in the development of competitive bombesin antagonists. *Ann. N.Y. Acad. Sci.* 547, 150–157.
- (49) Coy, D. H., Jensen, R. T., Jiang, N. Y., Lin, J. T., Bogden, A. E., and Moreau, J. P. (1992) Systematic development of bombesin/gastrin-releasing peptide antagonists. *J. Natl. Cancer Inst. Monogr.* 13, 133–139.
- (50) Davis, T. P., Crowell, S., Taylor, J., Clark, D. L., Coy, D., Staley, J., and Moody, T. W. (1992) Metabolic stability and tumor inhibition of bombesin/GRP receptor antagonists. *Peptides* 13, 401–407.
- (51) Schubiger, P. A., Alberto, R., and Smith, A. (1996) Vehicles, chelators, and radionuclides: choosing the “building blocks” of an effective therapeutic radioimmunoconjugate. *Bioconjugate Chem.* 7, 165–179.
- (52) Bijsterbosch, M. K. (1995) Selective drug delivery by means of receptor-mediated endocytosis. *Q. J. Nucl. Med.* 39, 4–9.
- (53) Beck-Sickinger, A. G. (1996) Structural characterization and binding sites of G-protein-coupled receptors. *Drug Discovery Today* 1, 502–513.
- (54) Duncan, J. R., Stephenson, M. T., Wu, H. P., and Anderson, C. J. (1997) Indium-111-diethylenetriaminepentaacetic acid-octreotide is delivered in vivo to pancreatic, tumor cell, renal, and hepatocyte lysosomes. *Cancer Res.* 57, 659–671.
- (55) Press, O. W., Shan, D., Howell-Clark, J., Eary, J., Appelbaum, F. R., Matthews, D., King, D. J., Haines, A. M., Hamann, P., Hinman, L., Shochat, D., and Bernstein, I. D. (1996) Comparative metabolism and retention of iodine-125, yttrium-90, and indium-111 radioimmunoconjugates by cancer cells. *Cancer Res.* 56, 2123–2129.
- (56) Naruki, Y., Carrasquillo, J. A., Reynolds, J. C., Maloney, P. J., Frincke, J. M., Neumann, R. D., and Larson, S. M. (1990) Differential cellular catabolism of  $^{111}\text{In}$ ,  $^{90\text{Y}}$  and  $^{125\text{I}}$  radiolabeled T101 anti-CD5 monoclonal antibody. *Int. J. Radiat. Appl. Instrum. – Part B, Nucl. Med. Biol.* 17, 201–207.
- (57) Mattes, M. J., Griffiths, G. L., Diril, H., Goldenberg, D. M., Ong, G. L., and Shih, L. B. (1994) Processing of antibody-radioisotope conjugates after binding to the surface of tumor cells. *Cancer* 73 (Suppl. 3), 787–793.



# A High-Capacity Streptavidin-Coated Microtitration Plate

Lasse Välimaa,\* Kim Pettersson, Markus Vehniäinen, Matti Karp, and Timo Lövgren

University of Turku, Department of Biotechnology, Tykistökatu 6 A, FIN-20520, Turku, Finland. Received June 14, 2002; Revised Manuscript Received October 30, 2002

A majority of current immunoassays rely on capturing a specific analyte on a solid phase to allow the separation of the bound analyte from nonbound components. Streptavidin-coated microtitration plates are widely used for immobilization of capturing antibodies, since they provide a generic surface for immobilization of any biotinylated molecule and preserve biomolecule activity much better than direct passive adsorption. Our trials to further improve the properties of the plates resulted in a development of a modified plate, which has higher binding capacity than currently used control plate. The modified coat was prepared by cross-linking streptavidin chemically prior to adsorption onto the microtitration well surfaces. The binding capacities of the plates were measured with biotinylated, europium-labeled molecules and labeled antigen. The immunoassay performance of the plates was studied with noncompetitive, sandwich-type assays of prostate specific antigen (PSA) and human chorionic gonadotropin (hCG). The maximum immobilization capacity of the modified plate was up to 2.5 times higher than that of the control plate. The higher binding capacity was especially emphasized with small-size molecules. The modified high capacity plate increased the linear ranges of the immunoassays and thus delayed the high-dose hook effect. At high antigen concentrations the signal increased up to 59%, and at the conventional linear ranges of the assays, the increase was up to 29%. We conclude that the modified coating method will be valuable for the future miniaturized systems, where high immobilization capacity is needed at limited areas.

## INTRODUCTION

Most of the presently used immunoassays utilize binding of a specific antigen or antibody on a solid phase followed by the removal of nonbound analyte and the sample matrix by extensive washing procedure (1). Commonly used solid phases are 96-well microtitration plates or single wells prepared of polystyrene. For the immunoassay purposes, the microtitration well surfaces are precoated with capturing protein like antibody to allow analyte immobilization. However, direct adsorption of antibodies on the plastic surface may destroy the functional sites to even less than one-tenth of the original activity (2–4). These studies have shown also that the protein activity could be preserved when the capturing antibody was immobilized as a secondary layer over a primary coated layer such as via streptavidin–biotin linkage. Therefore, streptavidin-coated wells are preferred to antibody or antigen coated wells. In addition, streptavidin-coated wells provide a universal immobilization surface for any biotinylated molecule and therefore tedious optimization of adsorption conditions for a number of different antibodies or antigens could be avoided. Generally, the streptavidin–biotin technology provides a valuable tool in clinical diagnostics (5) like immobilization of the molecules on the solid phases or signal amplification (6, 7). Therapeutic applications of biotin–streptavidin use are, e.g., delivery of drug molecules to pretargeted cancer cells (8, 9).

Streptavidin, like its counterpart hen egg-white avidin, is a tetrameric protein consisting of four identical subunits each about 14 kDa in size. These proteins are known for their ability to bind biotin very tightly (10, 11). Unlike avidin, streptavidin is from microbial source;

it is produced by the bacteria *Streptomyces avidinii*. In diagnostic applications streptavidin is preferred to avidin due to reduced nonspecific binding which is because of lower isoelectric point and lack of carbohydrate moieties. Biotin, also known as vitamin H, is a small molecule (MW = 244) with a double-ring structure and a carboxyl acid side chain. The side chain can be extended with different linker molecules and active groups enabling chemical coupling of biotin to other molecules. The coupling can be done under gentle conditions (12), and the biological activity of protein is thus well preserved. The biotin–streptavidin interaction is nearly irreversible since the binding affinity ( $K_a$ ) in liquid phase is about  $2.5 \times 10^{13} \text{ M}^{-1}$  (13). However, decreased affinity (around  $10^8$ – $10^{10} \text{ M}^{-1}$ ) was shown between biotinylated macromolecule and solid-phase adsorbed streptavidin (14). This may be due to partial rupture of the critical binding sites and adoption of stiff conformation upon adsorption and attachment on the solid phase. Nevertheless, the binding tightness is still strong enough to separate the biotinylated molecules from nonbiotinylated ones in the immunoassays.

The influence of the solid phase is significant in noncompetitive, two-site immunoassays (1). The binding capacity of the surface must be high enough to provide a real reagent excess, wide dynamic range without high-dose hook effect, and rapid kinetics. Nonspecific binding must be negligible in order to acquire the highest possible assay sensitivity. It is also evident that correct orientation of the immobilized antibody has a significant role (15, 16). Besides immunoassays, streptavidin surfaces are used for nucleic acid assays to immobilize biotinylated oligonucleotide probes or biotinylated amplification products (17). The immobilization of oligonucleotides directly on the plastic surface is often complicated, since they are too small in size for proper passive adsorption to take

\* Corresponding author. Phone: +358-2-333 8089. Fax: +358-2-333 8050. E-mail: lasse.valimaa@utu.fi.



place. Nucleic acid amplifications usually utilize a large excess of biotinylated primers, and therefore detection of the products at streptavidin wells requires a large number of binding sites.

Dissolving streptavidin in appropriate buffer and subsequent plain passive adsorption into the microtitration wells usually results in quite poor coating densities and low binding capacities. Therefore, the advantageous effect of streptavidin–biotin immobilization to the features of immunoassays may be abolished by the poor quality of the primary streptavidin coat. Some trials have been made to improve the coats. High-capacity plates have been prepared by coupling streptavidin to hydrophobic proteins prior to adsorption or by immobilizing streptavidin on biotinylated macromolecule coats (18, 19). We introduce here a simple method to prepare streptavidin-coated plates having improved binding capacities. The method relies on the chemical cross-linking of streptavidin prior to the routine coating procedure. The properties of the high-capacity plate were compared to the control plate coated without pretreatment of streptavidin. These types of the wells are widely used, and this is the way a number of commercial plates are still prepared. The properties of the plates were studied in different capacity tests and in noncompetitive, sandwich-type immunoassays.

#### MATERIALS AND METHODS

**Coating Procedure.** Streptavidin was obtained from BioSpa, Società Prodotti Antibiotici (Milan, Italy). Lyophilized protein was dissolved in pure water (Milli-Q) 10 mg/mL and stored frozen in aliquots. Maxisorp™ microtitration plates in C12-strips or single well formats were from Nunc A/S (Roskilde, Denmark). The normal coating procedure for streptavidin, the preparation of the control plate, is briefly described below. Streptavidin was diluted in the coating buffer (100 mM Na<sub>2</sub>HPO<sub>4</sub>/50 mM citric acid, pH 5.0) to the final concentration 5.0 µg/mL. Then 200 µL of the coating solution was dispensed into each well, giving 1 µg streptavidin per well. The plates were closed in a humidified box and incubated overnight at +35 °C. Then the plates were washed in a DELFIA Platewash (Perkin-Elmer Life Sciences, Turku, Finland) with DELFIA Wash Solution supplemented with Tween 20 (Merck, Hohenbrunn, Germany) to the final concentration 0.05%. After washing, 250 µL of saturation solution (50 mM Tris-HCl, pH 7.0; 150 mM NaCl; 0.05% NaN<sub>3</sub>; 0.2% bovine serum albumin and 6% D-sorbitol) was added per well. The plates were saturated overnight at +25 °C. The saturation solution was aspirated and the plates were dried (+35 °C, relative humidity < 5%) for 2 h. Finally the plates were packed with moisture adsorbent and stored dry at +4 °C.

The procedure leading to the high-capacity, modified plate included a pretreatment step prior to addition of streptavidin into the coating buffer. A reaction mixture was prepared, containing 2 mg/mL streptavidin, 10 mM NaH<sub>2</sub>PO<sub>4</sub>/Na<sub>2</sub>HPO<sub>4</sub> (pH 7.0), 150 mM NaCl, and 1.0% glutaraldehyde (J. T. Baker, Deventer, The Netherlands). The mixture was incubated 2 h at +4 °C. The excess glutaraldehyde was removed by purifying the reaction in gel filtration through NAP-5 and NAP-10 columns or PD-10 column (Amersham Biosciences AB, Uppsala, Sweden). The cross-linked glutaraldehyde–streptavidin (GA–SAv)<sup>1</sup> was eluted in TSA buffer (50 mM Tris-HCl, pH 7.75; 150 mM NaCl; 0.05% NaN<sub>3</sub>). The streptavidin concentration of the eluate was determined in a Bradford dye-binding assay following the instructions of the kit

supplier (Bio-Rad Laboratories, Hercules, CA). Originally dissolved streptavidin was used as a reference standard. GA–SAv was then diluted in the coating buffer (5.0 µg/mL), and the coating was proceeded according to the procedure described above.

**Size-Exclusion Chromatography of Cross-Linked Streptavidin.** GA–SAv was analyzed and fractionated in a preparative size-exclusion chromatography through Superose 12 HR 10/30 column driven by ÄKTA explorer system (both from Amersham Biosciences AB). An aliquot of completed cross-linking reaction mixture (before purification through NAP-columns) was injected into the column through a 2.0 mL sample loop, followed by isocratic elution in buffer consisting of 50 mM Tris-HCl (pH 8.40) and 0.05% NaN<sub>3</sub> with flow rate 0.5 mL/min. The purification was monitored at 280 nm, and 0.5 mL fractions were collected in an automatic fraction collector. Molecular weight calibration standards of Gel filtration calibration kits (Amersham Biosciences AB) were run separately in identical conditions. The protein concentrations of the fractions were determined with the Bradford method as above.

On the basis of absorbance and protein concentration profiles, adjacent fractions from the appropriate sites were combined to give three pools representing different molecular sizes. An aliquot from each pool was coated on the microtitration plates as described above.

**MALDI-TOF Mass Spectrometric Analyses.** Bound proteins were eluted from ZipTip C<sub>4</sub> reverse-phase matrix (Millipore, Bedford, U.S.A.) in 2.5% formic acid (Rathburn Chemicals, Walkerburn, Scotland), 50% acetonitrile (Rathburn Chemicals), and 10 mg/mL sinapinic acid (Sigma-Aldrich, Steinheim, Germany) to the sample plate. Perseptive Biosystems (Framingham, MA) Voyager DE-PRO mass spectrometer with a pulsed nitrogen laser at 337 nm was operated in a linear mode. The instrument operated at a 25 kV accelerating potential. At least 120 scans were collected for data acquisition. For calibration we used lysozyme (Sigma-Aldrich) and bovine serum albumin (Sigma-Aldrich).

**Biotinylation and Labeling.** The immobilization capacities of the streptavidin-coated plates were measured with molecules bearing both biotin moieties and europium (Eu) chelates as measurable labels. A monoclonal intact antibody H117 (20) was biotinylated with an isothiocyanate derived active biotin, BITC (21). The biotinylation was performed with an 80-fold molar excess (500 µM) of BITC in 50 mM carbonate buffer (pH 9.8). After 4 h incubation at room temperature the biotinylated antibody was separated from noncoupled BITC through NAP-5 and NAP-10 columns. The biotinylated antibody was labeled with an isothiocyanate-activated fluorescent Eu chelate, 2,2',2'',2'''-[[4-[(4-isothiocyanatophenyl)ethynyl]pyridine-2,6-diyl]bis(methylenenitrilo)]tetrakis(acetic acid) (22). The labeling was performed with a 20–40-fold molar excess (125–250 µM) of activated Eu chelate in 50 mM carbonate buffer (pH 9.8). After overnight incubation at +25 °C the biotinylated and labeled antibody (Bio-H117–Eu) was separated from noncoupled chelate in a Superdex 200 HR 10/30 column (Amersham Biosciences AB). The antibody was eluted in TSA buffer, and the fractions containing the purified labeled antibody were pooled. The protein concentration

<sup>1</sup> Abbreviations: BITC, biotin isothiocyanate; DELFIA, dissociation-enhanced lanthanide fluoroimmunoassay; GA–SAv, glutaraldehyde pretreated streptavidin; hCG, human chorionic gonadotropin; MS, mass spectrometry; PSA, prostate specific antigen; SAv, streptavidin.

of the pool was determined by measuring absorbance at 280 nm. Eu contents of the pool was measured by preparing a dilution series of the solution in DELFIA Enhancement Solution and measuring time-resolved fluorescence in a Victor 1420 multilabel counter (Perkin-Elmer Life Sciences) after 30 min shaking. A dilution series of europium standard calibrator was run together with the sample. The labeling degree (Eu chelates/antibody molecule) was calculated on the basis of measured Eu and protein concentrations.

We used also horse skeletal muscle myoglobin (Sigma-Aldrich) and biotinylated peptide for the capacity measurements. Those represented smaller molecular weights (myoglobin  $\approx$  17 000 Da and peptide = 1672 Da) than the intact antibody ( $\approx$ 160 000 Da). Myoglobin (Mb) was biotinylated, labeled, and purified as described above. The protein concentration of the purified, pooled Bio-Mb-Eu solution was determined in the Bradford assay using originally dissolved myoglobin as a reference standard. The labeling degree was calculated based on the measured Eu and protein concentrations. The biotinylated and Eu-labeled peptide (Bio-Eu-peptide) was purchased from Perkin-Elmer Life Sciences. The peptide consisted of 11 amino acids and its molecular weight was 1672. The peptide bore two Eu chelates ([2-(4-isothiocyano-benzyl)]diethylenetriaminetetraacetic acid), described by Mukkala et al. (23).

**Production and Purification of Recombinant Fab Fragment.** Hybridoma cell line H117 was previously (24) cloned as a recombinant Fab fragment. It contains an engineered five amino acid long Thr-Ser-Cys-Ala-Ala peptide at C-terminus of the Fd chain. Fab fragments were expressed to periplasmic space of *Escherichia coli* in a 5-L BioFlo3000 fermentor (New Brunswick Scientific, New Jersey) and purified with osmotic shock, Streamline SP (75 mL in Streamline25 column) expanded bed adsorption chromatography and finally 5 mL HiTrap Protein G affinity column (all from Amersham Biosciences AB). Unpaired cysteine in C-terminal peptide was used for site-specific biotinylation with 3-(N-maleimido-propionyl) biocytin (Sigma-Aldrich), and the biotinylated fraction was collected using 5 mL monomeric avidin column (SoftLink avidin resin, Promega, Madison, USA).

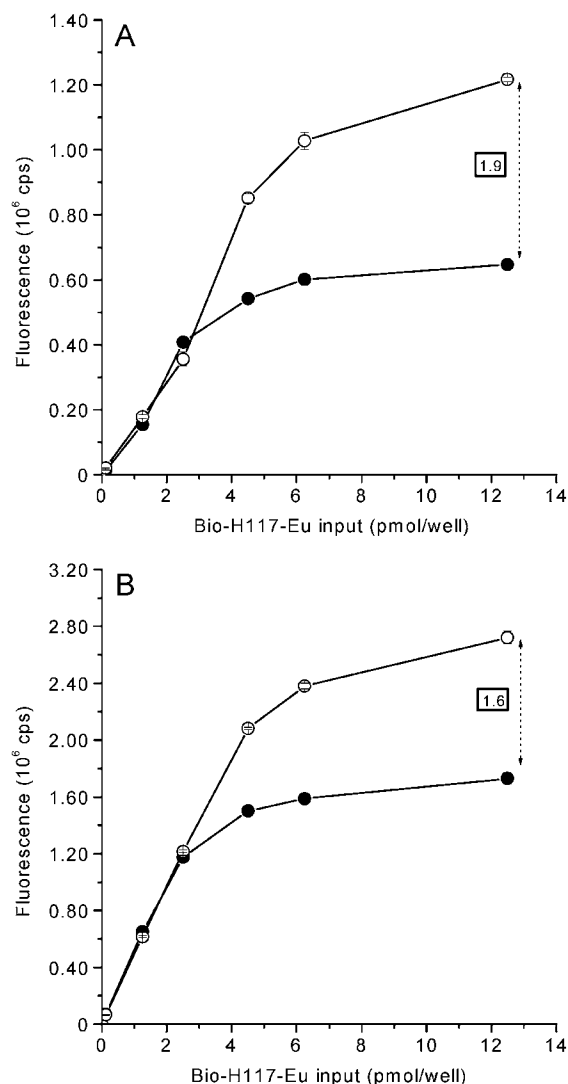
**The Determination of the Binding Capacities of the Coated Wells.** Dilution series of Bio-H117-Eu or Bio-Mb-Eu were prepared in Assay Buffer (Perkin-Elmer Life Sciences) shortly before use. One hundred microliters of each dilution was added into four replicate wells of streptavidin-coated microtitration plates, giving 0.125–12.5 pmol protein inputs per well. The plates were sealed with tape and shaken for 1 h in the DELFIA Plateshake and washed six times with DELFIA Wash solution (5 mM Tris-HCl, pH 7.75; 154 mM NaCl; 0.1% Germall II<sup>+</sup>; 0.005% Tween20) in the Platewash. The plates were dried at +65 °C air blow for 3 min and were cooled to the room temperature for 10 min. The time-resolved fluorescence signal was measured from the bottom of the dried wells in the Victor counter. For this surface readout measurement the measurement focus was custom-adjusted close to the bottom of the well. An area of a few square millimeters in the bottom of the well becomes excited and measured. After the surface readout measurement, the plates were passed to the conventional dissociation enhancement (DELFA) measurement. Two hundred microliters of Enhancement Solution was added into each well, and the time-resolved fluorescence was measured in the Victor counter after 30 min shaking. Known amounts of europium calibrators were measured

parallel. A standard curve was derived and the Eu concentrations of the wells containing immobilized Bio-Eu-molecules were calculated. Since the label degrees of the molecules were known, the actual immobilized quantities of Bio-Eu-molecules (pmol/well) could be calculated.

The capacity test utilizing successive incubations with free biotin and Bio-Eu-peptide was performed as follows. D-Biotin (Sigma-Aldrich) was first dissolved in 1 M NaOH and diluted in the Assay Buffer to give a 11.9 mM stock solution from which the work dilutions containing up to  $2.5 \times 10^{13}$  molecules (41.5 pmol) D-biotin per 200  $\mu$ L were prepared. Two hundred microliters of each dilution was added into four replicate wells of the streptavidin-coated plates. The plates were shaken at room temperature for 1 h and washed twice in the Platewash. Bio-Eu-peptide was diluted in Assay Buffer and 200  $\mu$ L of the dilution was added into each well giving 0.17 pmol peptide input per well. After 1 h shaking the wells were washed six times, and Enhancement Solution was added. Time-resolved fluorescence was measured in Victor counter after 5 min shaking.

For the antigen-binding capacity test, biotinylated intact antibody H117 or site-specifically biotinylated recombinant Fab fragments of that were diluted in Assay Buffer and immobilized in streptavidin-coated wells during a 30 min shaking. Four hundred nanograms of Bio-H117 and two hundred nanograms of Bio-Fab per well were used. Prostate-specific antigen (PSA) standard was a kind gift from Professor Hans Lilja (Lund University, Malmö, Sweden). PSA was labeled with Eu chelate (22) as described above. A dilution series of Eu-PSA was prepared in Assay Buffer, and 30  $\mu$ L of each dilution (5–500 ng Eu-PSA) was added into the wells harboring the immobilized Bio-H117 or Bio-Fab fragments. The reaction was incubated 40 min at +30 °C in iEMS incubator shaker (LabSystems, Helsinki, Finland). The plates were then washed six times, Enhancement Solution was added, and time-resolved fluorescence was measured in Victor after five minutes shaking.

**Immunoassays. Prostate Specific Antigen.** Four hundred nanograms of Bio-H117 (in 50  $\mu$ L Assay Buffer) were added into streptavidin coated wells. The plates were shaken for 1 h at the room temperature in the Plateshake and washed twice in the Platewash. A series of PSA antigen standard dilutions (0.19–5000  $\mu$ g/L) were prepared in 7.5% TSA-BSA (50 mM Tris-HCl, pH 7.75; 150 mM NaCl; 0.05% NaN<sub>3</sub>; 7.5% bovine serum albumin). Ten microliters of each standard dilution was added into the wells containing immobilized Bio-H117. The tracer antibody 5F7 was produced at our department as characterized by Nurmikko et al. (25). The antibody 5F7 was labeled with the fluorescein Eu chelate (22) as described above. Eu-5F7 was diluted in Assay Buffer and 20  $\mu$ L of the dilution containing 200 ng antibody was added to each well shortly after the addition of the standard dilutions. The plates were shaken 30 min at room temperature, followed by washing six times. Enhancement Solution was added (200  $\mu$ L), and the signal was measured in Victor after 30 min shaking. In the other PSA assay, recombinant Fab fragment of H117 antibody (produced as described above) was used as capturing antibody instead of intact Bio-H117. The assay was run as above, except that the amount of Bio-Fab used for the immobilization in the first step was 600 ng/well, and the tracer antibody Eu-5F7 was used 800 ng/well to provide sufficient reagent excess to satisfy increased binding capacity.

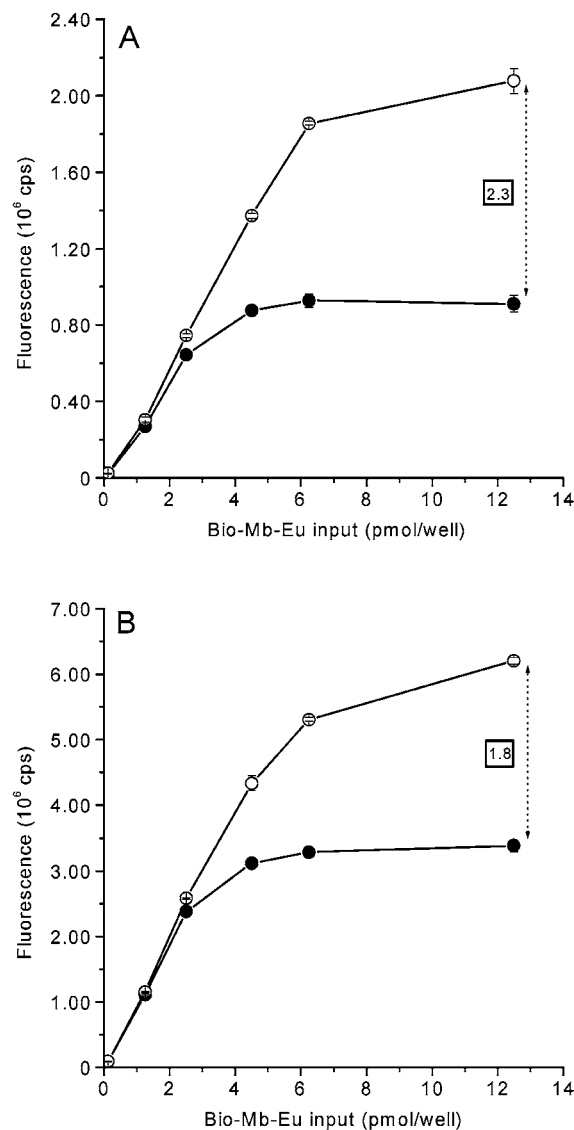


**Figure 1.** The capacities of the streptavidin-coated plates measured with a biotinylated, Eu-labeled antibody Bio-H117-Eu. The signal was measured either with a surface readout method from the dried bottom of the well (A) or with dissociation enhancement (DELFA) method (B). The filled symbols (●) denote the control plate and the open symbols (○) the GA-SAv plate. The error bars indicate the within-assay standard deviations of four replicate wells.

*Human Chorionic Gonadotropin (hCG).* Biotinylated monoclonal antibody Bio-E27, hCG standards, and tracer antibody Eu-8D10 were from Perkin-Elmer Life Sciences. Four hundred nanograms of Bio-E27 was used for immobilization into streptavidin-coated microtitration wells in 50  $\mu$ L Assay Buffer. The hCG standard dilutions including 2–80 000 units per liter hCG (1 U/L corresponds to about 0.1  $\mu$ g/L) were prepared in 7.5% BSA-TSA. Shortly after the addition of the standard dilution, 300 ng/well of Eu-8D10 was added in 20  $\mu$ L Assay Buffer. The plates were shaken 30 min at +36 °C in iEMS incubator shaker and washed six times. The signal measurement was run as described above for the surface readout method.

## RESULTS

**The Immobilization Capacities of the Streptavidin-Coated Plates.** The binding capacities of the plates measured with Bio-H117-Eu are shown in Figure 1. The GA-SAv plate shows up to 1.9 times higher signal than the control plate when the surface readout mea-

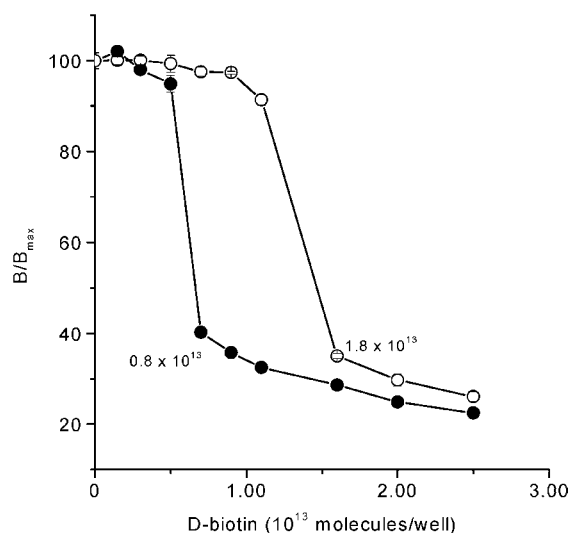


**Figure 2.** The capacities of the streptavidin-coated control plate (●) and GA-SAv plate (○) measured with a biotinylated Eu-labeled myoglobin, Bio-Mb-Eu. The signal was measured either with a surface readout method from the dried bottom of the well (A) or with dissociation enhancement (DELFA) method (B). The error bars indicate the within-assay standard deviations of four replicate wells.

surement was used and up to 1.6 times higher signal with dissociation enhanced (DELFA) method. The surface readout method measures only a certain area in the bottom of the well, while the latter method rather represents an integrated signal of the total coated area. The capacity curves of Bio-Mb-Eu measurement are shown in Figure 2. Compared to the control plate, the GA-SAv plate presented 2.3-fold increase in signal with surface readout and 1.8-fold increase in DELFA method. It was noted that as the size of the immobilized detection molecule decreased the differences between the control and GA-SAv plates increased, which most probably indicates less steric hindrance in the case of Bio-Mb-Eu. The actual immobilized quantities were calculated from the DELFA signals and were found to be 2.2 and 3.6 pmol for Bio-H117-Eu and 2.8 and 5.2 pmol for Bio-Mb-Eu at the control well and GA-SAv well, respectively.

The results of the capacity test based on the successive incubations with D-biotin and Bio-Eu-peptide are shown in Figure 3. The measured fluorescence signals





**Figure 3.** The capacities of the plates as measured in the D-biotin test. D-Biotin was first immobilized in the wells, and the unoccupied sites were detected with biotinylated, Eu-labeled peptide (Bio-Eu-peptide). The capacities of the control plate (●) and GA-SAv plate (○) can be read at the lower turn-points of the curves. The error bars indicate the within-assay standard deviations of the replicate wells.

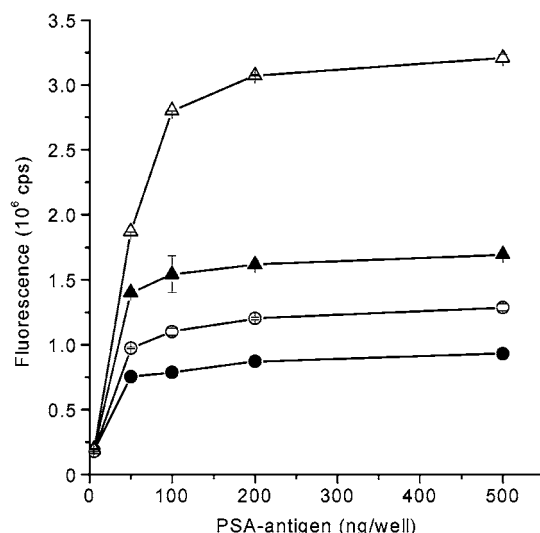
**Table 1. The Capacities of the Control Plate and the GA-SAv Plate to Immobilize Different Biotinylated Molecules**

biotinylated molecule	MW	capacity (pmol/well)	
		control plate	GA-SAv plate
intact antibody (IgG)	160 000	2.2	3.6
myoglobin	17 000	2.8	5.2
peptide (direct immob.)	1672	3.8	8.3
D-biotin/peptide	1672	13	30

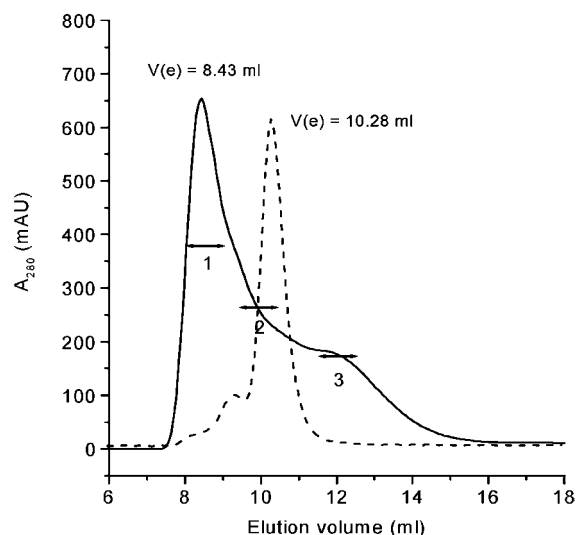
were compared to the maximum signal measured from the zero wells (no D-biotin input), and the percentage values were calculated. The capacities of the plates were estimated at the lower turn-points of the curves. The capacity of the control plate was  $0.8 \times 10^{13}$  molecules (13 pmol), that of the modified plate  $1.8 \times 10^{13}$  molecules (30 pmol), and the difference between the plates thus 2.3. It was noted that the signal level did not reach close to zero but stayed around 20% of the maximum signal despite large excess of D-biotin used. We assume that some of the bound D-biotin dissociated out of the surface and thus the method overestimates the binding capacities. The binding capacities of the wells in the case when Bio-Eu-peptide was immobilized direct (like Bio-H117-Eu and Bio-Mb-Eu above) were 3.8 pmol for the control well and 8.3 pmol for the GA-SAv well. Table 1 summarizes the binding capacities of the control and GA-SAv plates as measured with different biotinylated molecules.

Figure 4 compares the capacities of immobilized biotinylated intact antibody (Bio-H117) or biotinylated Fab fragment (Bio-Fab) to bind cognate Eu-labeled PSA antigen. Changing from Bio-H117 to Bio-Fab resulted in around 1.8-fold increase in the binding capacity. Immobilizing Bio-Fab in the GA-SAv well resulted in 1.9-fold more increase in the binding capacity. Thus, combining Bio-Fab with high capacity GA-SAv plate altogether resulted in 3.5-fold increase compared to the case of intact antibody immobilized in the control well.

**Size-Exclusion Analysis and Fractionation of Cross-Linked Streptavidin.** The elution profile of cross-linked streptavidin is shown in Figure 5. Under the

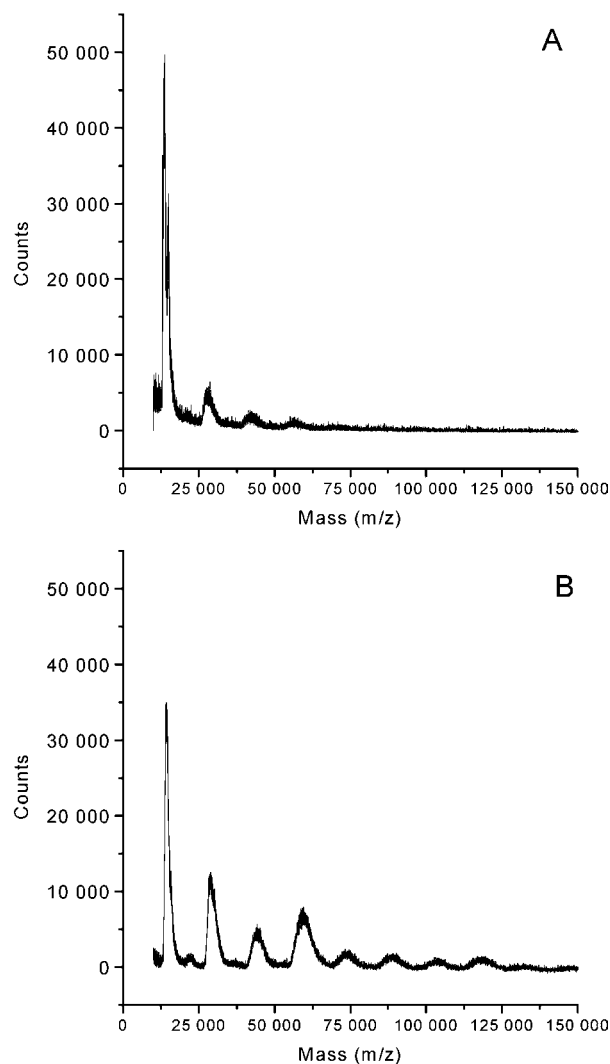


**Figure 4.** Antigen-binding capacities of the intact antibody (● and ○) and Fab fragments (▲ and △) at the control plate (filled symbols) or GA-SAv-plate (open symbols). The error bars indicate the within-assay standard deviations of the replicate wells.



**Figure 5.** Elution profiles of cross-linked streptavidin (straight line) and BSA as a molecular weight marker (dashed line). The fractionation of GA-SAv was performed in a Superose 12-gel filtration column. The profile represents molecular weights extending from around 200 to 25 kDa. The locations of the adjacent fractions combined to three pools are shown with bars.

described conjugation conditions (+4 °C, 2 h, 2 mg/mL SAv), the reaction resulted in a mixture of products ranging in molecular weights from around 25 to around 200 kDa. The exact determination of the highest molecular weights turned out to be inaccurate, since those eluted quite close to the column void volume determined with Blue Dextran 2000 from the calibration kit. The peak representing free glutaraldehyde appeared at an elution volume of 21 mL. The first one of the pooled fractions represented molecular weights from 95 to 200 kDa, the second 65 to 85 kDa, and the third 45 to 55 kDa. Prolonged incubation of the conjugation reaction at the room temperature increased the proportion of larger molecular weight products slightly. A considerable change was noted when protein concentration in the conjugation reaction was increased from 2 to 4 mg/mL. This resulted in an almost complete cross-linking; i.e., only one peak

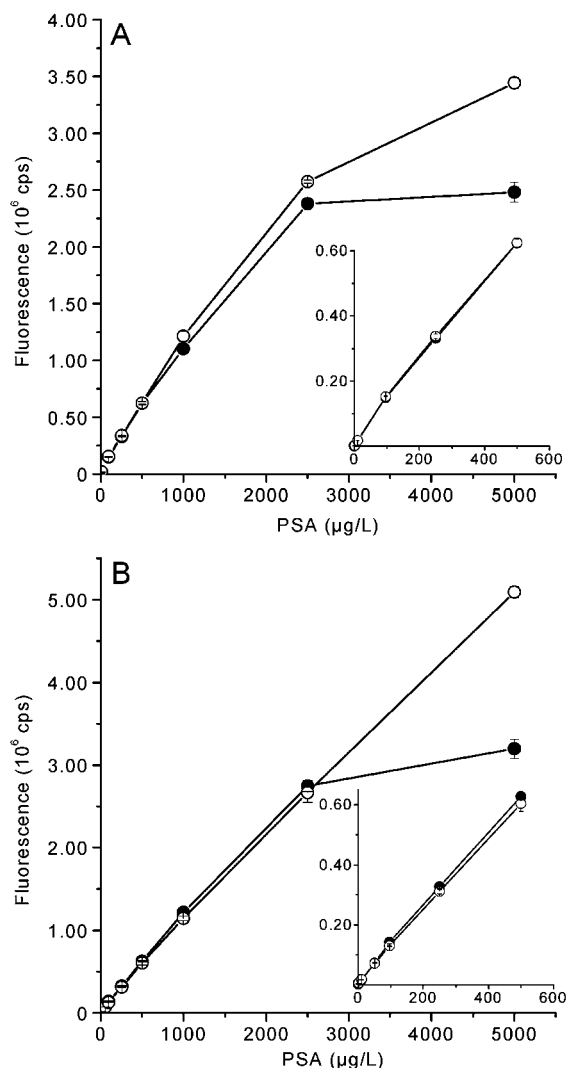


**Figure 6.** Mass spectra of streptavidin. Native streptavidin (A) is mainly found as monomeric form ( $m/z$  13 140) while di-, tri-, and tetrameric forms are hardly present. Glutaraldehyde-treated streptavidin (B) is stabilized over native streptavidin and up to octameric subunit compositions are found.

appeared representing the largest conjugate sizes (data not shown).

The binding capacities of the wells coated from the three pools of cross-linked, fractionated streptavidin (see Figure 5) did not exceed that coated from nonfractionated mixture. The immobilization capacities of the pools 1 and 2 were 80% and pool 3 around 50% of a nonfractionated, total mixture. The capacity of the pool 3 was close to the control plate. Neither the coated wells prepared from the cross-linking reaction with 4 mg/mL protein concentration introduced improved capacity compared to the 2 mg/mL reaction but the capacities were equal or slightly decreased (data not shown).

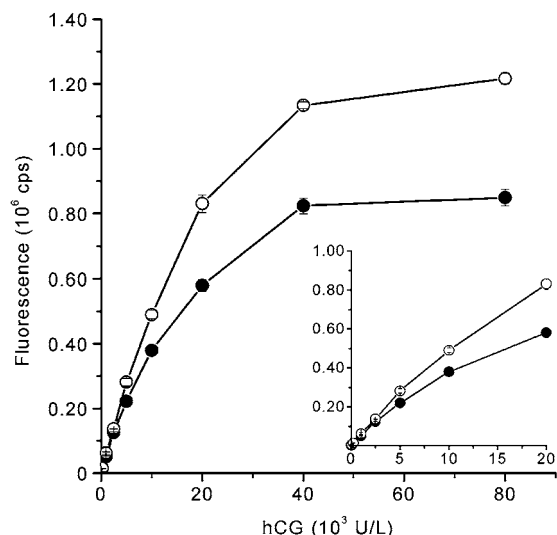
**Analysis of Mass Spectrometry Results.** Streptavidin from *Streptomyces avidinii* is synthesized as a 183 amino acids long precursor. After cleavage of a 24 aa long signal sequence, mature 159 aa long streptavidin (calculated mass 16 490 Da) is released. It undergoes proteolytic digestions, and finally a core streptavidin of 127 aa is formed. Monomeric core streptavidin has an expected molecular mass of 13 270 daltons (10), and thus calculated mass for tetrameric core streptavidin (native existence) is 53 080 daltons. For non-glutaraldehyde-treated streptavidin (Figure 6 A), we found four peaks



**Figure 7.** The standard curves of the PSA-assays. Either biotinylated intact antibody (A) or a recombinant Fab fragment of the antibody (B) was used as the immobilized capturing agent. The filled symbols (●) denote the assays run at the control plate and open symbols (○) at the GA-SAv plate. The inset graphs show the standard curve ranges up to 500 µg/L. The error bars show the within-assay standard deviations of four replicate wells.

corresponding to mono- (13 140 Da) to tetrameric streptavidin masses (56 782 Da). Monomeric peak dominated in the results. Glutaraldehyde treatment increased di- to tetrameric streptavidin peak intensities 2- to 10-fold. Also, new peaks differing in size at average intervals of 14 880 Da appeared clearly up to size 118 152 Da, which presumably corresponds to a dimer of streptavidin (Figure 6 B).

**PSA Immunoassay.** Figure 7 A shows the standard curves of PSA immunoassays with the intact Bio-H117 antibody immobilized as the capturing antibody. The figure shows that the assay performed at the high-capacity GA-SAv plate has improved high-dose hook efficiency; i.e., the hook is avoided, or it tends to appear at higher antigen concentrations. The background signals were 637 cps at the control plate and 937 at the GA-SAv plate. The detection limits of the assays (background + 3 × SD) were 0.191 µg/L at the control plate and 0.239 µg/L at the GA-SAv plate. Figure 7 B shows the standard curves of the assays utilizing recombinant Bio-Fab immobilized as the capturing agent. This assay clearly shows the potential of the high capacity GA-SAv



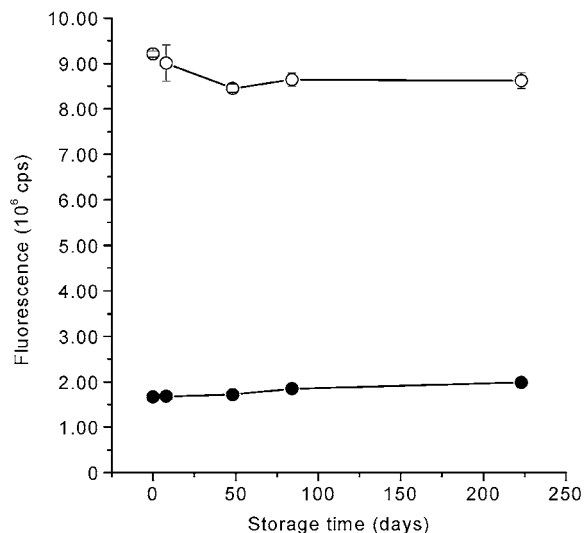
**Figure 8.** The standard curves of the hCG-assays at the control plate (●) and GA-SAv plate (○). The inset graph shows the range of the assay up to 20 000 U/L. The error bars show the within-assay standard deviations of four replicate wells.

plate since excellent linearity of the assay extends at least up to 5000  $\mu\text{g/L}$ , while the standard curve at the control plate declines earlier. Because nonoptimal excess amounts of the labeled tracer antibody had to be used to satisfy increased capacities, the background signals tended to increase and thus lower detection limits of these assays were 0.795  $\mu\text{g/L}$  at the control plate and 0.717  $\mu\text{g/L}$  at the GA-SAv plate.

**hCG Immunoassays.** The standard curves of the hCG immunoassays, measured by surface readout method, are shown in Figure 8. The assay shows improved linearity and higher binding capacities of the GA-SAv plate. Since hCG concentration in pregnancy can be as high as 200 000 IU/L or above, it is essential to have high binding capacity and improved linearity to avoid the high-dose hook effect. The background signals were 1782 at the control plate and 1876 at the GA-SAv plate. The detection limits of the assays were 4.5 U/L at the control plate and 4.2 U/L at the GA-SAv plate. The hCG assay was also run at the GA-SAv plates coated from the pools of fractionated cross-linking reactions. No improvement in linearity or binding capacity was obtained compared to the nonfractionated mixture (data not shown), as would have been expected also on the basis of the Bio-Mb-Eu capacity test.

**Reproducibility and Storage Stability.** Thirteen separate batches of GA-SAv plates were coated independently of each other. The coated plates were collected together, and the capacities of the plates were measured with Bio-Mb-Eu. The CV% values within one coated batch varied from 0.6% to 4.3%. The batch to batch CV% values varied from 10.0% to 14.3%.

The stability of one batch of GA-SAv-coated plates was followed several months. The plates were stored in separate sealed boxes with moisture adsorbent at +4 °C after coating. One plate at a time was taken out and the capacity was measured with Bio-Mb-Eu using low input (1.25 pmol/well) and high input (12.5 pmol/well). Figure 9 shows the results of the assays measured during those 225 days of storage. A slight increase (19%) in the signal level was noted when measured with low amount of Bio-Mb-Eu but a slight drop (6%) when measured with 12.5 pmol Bio-Mb-Eu.



**Figure 9.** The storage stability of the GA-SAv plate. Bio-Mb-Eu was used to measure the capacities of GA-SAv plates after different storage periods. The measurements were performed either with 1.25 (●) or 12.5 pmol/well (○) inputs. The storage stability was followed up to 225 days. The error bars indicate the standard deviations of the replicate wells.

## DISCUSSION

The streptavidin-coated plates allow an immobilization of any biotinylated molecule and thus provide flexibility for the solid phase assays compared to the antibody- or antigen-coated plates. Streptavidin-coated plates are widely used in clinical diagnostics and there are numbers of manufacturers. Though the plates are widely used, the optimal coating conditions are based more or less on experimental optimization and the adsorption mechanisms are not well understood, as is the case for proteins in general. Also, the influence of the solid phase on the immunoassay performance is often underestimated.

We presented a preparation of high-capacity streptavidin-coated microtitration plate with a convenient and cost-effective method. The properties of the plates were characterized in terms of binding capacities and immunoassay performance. The capacity increased considerably compared to the control plate but the size of the immobilized biotinylated molecule affected the difference, a result that is quite obvious from steric point of view. Furthermore, surface readout measurement gave larger differences between the plates than dissociation enhancement method. Probably adsorption to the bottom of the well was thus favored in GA-SAv coating, which is promising for the future surface measurement applications. Taking into account the different molecular sizes and measurement methods, we can deduce that the maximum binding capacity of the GA-SAv plate is at least 2–2.5-fold higher than that of the control plate.

Fractionation of GA-SAv by gel filtration and coating from pooled peaks showed that the largest molecular weight products are mainly responsible for the increased capacities, but none of the fractions alone exceeded the capacities of a nonfractionated mixture. It shows that a range of molecular sizes is needed in order to achieve the highest performance. The fractionation also showed products that were smaller in size than a native streptavidin consisting of four identical subunits. A reason may be that some element in conjugation process had partially dissociated tetrameric structure to smaller units from which the cross-linking and building of the larger species was started. On the other hand, our gel filtration runs with native, nontreated streptavidin showed that some



of the original protein had dissociated to subunit dimers and thus peaked at around 25–30 kDa.

The MALDI-TOF mass spectrometry results of non-treated streptavidin showed a dominance of the peak corresponding to one subunit of streptavidin. Most probably the tetrameric structure, held together by non-covalent interactions, was disrupted to subunits by intensive laser radiation. The MALDI-TOF results of GA-SAv showed peaks representing larger sizes, which were multiples of one subunit size. The existence of the peak corresponding to one subunit confirmed that the conjugation did not go to completion in the conditions we used for cross-linking.

Noncompetitive reagent excess immunoassays are widely used to assay clinical analytes demanding high sensitivity, wide dynamic range, speed, and robustness. Minimal nonspecific binding, even background signal and high slope of the standard curve result in sensitive assays having low detection limits. The high-dose hook effect, caused by blocking of all antibody binding sites before sandwich formation, can be avoided or shifted to higher concentrations by increasing the number of binding sites for antigen. Our immunoassay results showed that the hook performance could be improved with high capacity solid phases. The influence of the high capacity plates to the assay sensitivities was insignificant, since the standard curves worked quite equally in the "conventional" linear ranges of the assays at both types of plates. In that area, the capacity of the control plate was high enough to immobilize the required quantity of the biotinylated antibody to give optimal binding of the antigen. It must be considered that the actual quantities of the antigens we used were quite low since small sample volumes (10  $\mu$ L per well) were used. The GA-SAv coating protocol is likely to be important when the solid phases are reduced in area as in spots or in chip technologies. In these cases a considerable high density of the coat at the unit area is required to give enough binding capacity.

A large increase in antigen binding capacity was obtained when Fab fragments were immobilized in GA-SAv plates (Figure 4). This shows clearly how dramatic the influence is of steric hindrance caused by the large size of the intact antibody. Large antibody molecules mask the streptavidin binding sites on the surface and therefore full potential of the GA-SAv plates is not available. In the Bio-Fab-based PSA-assay (Figure 7 B), we did not reach such improvement in assay performance as would have been expected on the basis of labeled antigen-binding assay. There are at least two reasons for that. First, the actual antigen amounts were quite small as discussed above. Second, we had to use intact whole size antibody as the tracer and this rises again the influence of steric factors. There was not a proper recombinant Fab fragment of any appropriate tracer antibody available.

Nonspecific binding of the labeled antibody causes increase in the assay background signal (wells with zero standard), and especially background variation impairs the lower detection limit. The immunoassays run at the GA-SAv plate showed none or up to some 1.5–2-fold increase in background signals, but as the variation kept quite constant, the detection limits were only slightly affected. A higher degree of nonspecific binding is usually obvious when there are larger amounts of coated proteins or immobilized antibodies present. It must be anyhow considered that the background values and the effects of the solid phase may vary between the assays of different analytes, and even within one analyte if different batches of antibodies are used.

In principle, the assay equilibrium should be reached faster (kinetics improved) as more antigen binding sites are introduced and therefore high-capacity plates provide potential for faster kinetics. Our hCG and PSA assays had quite fast kinetics (equilibration at  $\leq 30$  min) in the optimized assay conditions, but no substantial improvement in kinetics beyond that point was noted when control plates were replaced to GA-SAv plates. The assays utilized well-selected antibody–antigen pairs that allowed fast kinetics as such. The effect of the solid-phase capacity may have become more remarkable in the case of slower-reacting antibodies.

## CONCLUSIONS

We have developed a modified streptavidin coating method, which leads to surfaces having high binding capacity for immobilization of biotinylated molecules. The method relies on a chemical cross-linking of streptavidin prior to the routine coating procedure. The treatment was also upscaled and tested in pilot production facilities. The maximum binding capacity of the modified plate increased up to 2.5 times compared to the control plate.

The high-capacity surface increased the linear ranges of the sandwich-type immunoassays and improved the high-dose hook performance. Especially biotinylated Fab fragments immobilized in GA-SAv plate resulted in considerable increase in antigen binding capacities. Some of the potential of the high-capacity plates was masked by steric factors caused by the large size of the immobilized antibody. Furthermore, the coated area of a microtitration well is quite large, and the total binding capacity of low capacity plates is considered adequate for many purposes. We anticipate that the benefits of the GA-SAv coatings will be more evident when reduced surface areas are combined with small biotinylated antibody fragments.

## ACKNOWLEDGMENT

The study was financially supported by the National Technology Agency of Finland (TEKES) and InnoTrac Diagnostics Oy. We thank Mrs Pirjo Laaksonen for technical assistance.

## LITERATURE CITED

- (1) Gosling, J. P. (2000) Analysis by specific binding. In *Immunoassays. A Practical Approach* (J. P. Gosling, Ed.) pp 1–15, Oxford University Press, Oxford.
- (2) Butler, J. E., Ni, L., Nessler, R., Joshi, K. S., Suter, M., Rosenberg, B., Chang, J., Brown, W. R., and Cantarero, L. A. (1992) The physical and functional behavior of capture antibodies adsorbed on polystyrene. *J. Immunol. Methods* 150, 77–90.
- (3) Davies, J., Dawkes, A. C., Haymes, A. G., Roberts, C. J., Sunderland, R. F., Wilkins, M. J., Davies, M. C., Tendler, S. J., Jackson, D. E., and Edwards, J. C. (1994) A scanning tunnelling microscopy comparison of passive antibody adsorption and biotinylated antibody linkage to streptavidin on microtiter wells. *J. Immunol. Methods* 167, 263–269.
- (4) Butler, J. E. (2000) Solid supports in enzyme-linked immunosorbent assay and other solid-phase immunoassays. *Methods* 22, 4–23.
- (5) Schettters, H. (1999) Avidin and streptavidin in clinical diagnostics. *Biomol. Eng.* 16, 73–78.
- (6) Scorilas, A., Bjartell, A., Lilja, H., Moller, C., and Diamandis, E. P. (2000) Streptavidin-polyvinylamine conjugates labeled with a europium chelate: applications in immunoassay, immunohistochemistry, and microarrays. *Clin. Chem.* 46, 1450–1455.

- (7) Qin, Q. P., Lovgren, T., and Pettersson, K. (2001) Development of highly fluorescent detection reagents for the construction of ultrasensitive immunoassays. *Anal. Chem.* **73**, 1521–1529.
- (8) Ohno, K., Levin, B., and Meruelo, D. (1996) Cell-specific, multidrug delivery system using streptavidin-protein A fusion protein. *Biochem. Mol. Med.* **58**, 227–233.
- (9) Wilbur, D. S., Pathare, P. M., Hamlin, D. K., Stayton, P. S., To, R., Klumb, L. A., Buhler, K. R., and Vessella, R. L. (1999) Development of new biotin/streptavidin reagents for pretargeting. *Biomol. Eng.* **16**, 113–118.
- (10) Bayer, E. A., Ben-Hur, H., and Wilchek, M. (1990) Isolation and properties of streptavidin. *Methods Enzymol.* **184**, 80–89.
- (11) Green, N. M. (1990) Avidin and streptavidin. *Methods Enzymol.* **184**, 51–67.
- (12) Bayer, E. A., and Wilchek, M. (1990) Protein biotinylation. *Methods Enzymol.* **184**, 138–160.
- (13) Wilchek, M., and Bayer, E. A. (1999) Foreword and introduction to the book (strept)avidin–biotin system. *Biomol. Eng.* **16**, 1–4.
- (14) Huang, S. C., Stump, M. D., Weiss, R., and Caldwell, K. D. (1996) Binding of biotinylated DNA to streptavidin-coated polystyrene latex: effects of chain length and particle size. *Anal. Biochem.* **237**, 115–122.
- (15) Lu, B., Smyth, M. R., and O'Kennedy, R. (1996) Oriented immobilization of antibodies and its applications in immunoassays and immunosensors. *Analyst* **121**, 29R–32R.
- (16) Vijayendran, R. A., and Leckband, D. E. (2001) A quantitative assessment of heterogeneity for surface-immobilized proteins. *Anal. Chem.* **73**, 471–480.
- (17) Ylikoski, A., Karp, M., Lilja, H., and Lovgren, T. (2001) Dual-label detection of amplified products in quantitative RT-PCR assay using lanthanide-labeled probes. *Biotechniques* **30**, 832–836.
- (18) Tischer, W., Maier, J., and Deeg, R. (1991) Process for preparing a carrier useful in immunoassays by deposition of a complex of a specifically binding substance with hydrophobic protein, and the resulting carrier. U.S. Patent Number 5,061,640.
- (19) Immer, U., and Strohner, P. (2001) Surfaces coated with streptavidin/avidin. U.S. Patent Number 6,270,983.
- (20) Piironen, T., Villoutreix, B. O., Becker, C., Hollingsworth, K., Vihinen, M., Bridon, D., Qiu, X., Rapp, J., Dowell, B., Lovgren, T., Pettersson, K., and Lilja, H. (1998) Determination and analysis of antigenic epitopes of prostate specific antigen (PSA) and human glandular kallikrein 2 (hK2) using synthetic peptides and computer modeling. *Protein Sci.* **7**, 259–269.
- (21) Mikkala, V.-M., Hänninen, E., and Hemmälä, I. (1993) Synthesis of two biotin isothiocyanate derivatives. In *Proceedings of 8th European Symposium on Organic Chemistry*, p 86, Universitat Autònoma de Barcelona, Sitges, Barcelona, Spain.
- (22) Takalo, H., Mikkala, V. M., Mikola, H., Liitti, P., and Hemmälä, I. (1994) Synthesis of europium(III) chelates suitable for labeling of bioactive molecules. *Bioconjugate Chem.* **5**, 278–282.
- (23) Mikkala, V. M., Mikola, H., and Hemmälä, I. (1989) The synthesis and use of activated N-benzyl derivatives of diethylenetriaminetetraacetic acids: alternative reagents for labeling of antibodies with metal ions. *Anal. Biochem.* **176**, 319–325.
- (24) Eriksson, S., Vehniainen, M., Jansen, T., Meretoja, V., Saviranta, P., Pettersson, K., and Lovgren, T. (2000) Dual-label time-resolved immunofluorometric assay of free and total prostate-specific antigen based on recombinant Fab fragments. *Clin. Chem.* **46**, 658–666.
- (25) Nurmikko, P., Vaisanen, V., Piironen, T., Lindgren, S., Lilja, H., and Pettersson, K. (2000) Production and characterization of novel anti-prostate-specific antigen (PSA) monoclonal antibodies that do not detect internally cleaved Lys145-Lys146 inactive PSA. *Clin. Chem.* **46**, 1610–1618.

BC020058Y

# Design, Synthesis, and Evaluation of Gadolinium Cationic Lipids As Tools for Biodistribution Studies of Gene Delivery Complexes

Francoise Leclercq,<sup>†</sup> Mirit Cohen-Ohana,<sup>‡</sup> Nathalie Mignet,<sup>†</sup> Andrea Sbarbati,<sup>§</sup> Jean Herscovici,<sup>\*,†</sup> Daniel Scherman,<sup>†</sup> and Gerardo Byk<sup>\*,‡</sup>

Bar Ilan University, Department of Chemistry, Laboratory of Peptidomimetics and Genetic Chemistry, 52900-Ramat Gan, Israel, Department of Morphological and Biomedical Sciences, Section of Anatomy and Histology, University of Verona, Verona, Italy, and UMR 7001 (CNRS/ENSCP/Aventis), E.N.S.C.P., 11 rue P. & M. Curie, 75231-Paris Cedex, France. Received July 3, 2002; Revised Manuscript Received October 28, 2002

Gadolinium-chelating cationic lipids have been synthesized to obtain lipoplexes with MRI contrast properties. These compounds were designed to follow the biodistribution of synthetic DNA for gene delivery by nuclear magnetic resonance imaging. The lipid MCO-I-68 was synthesized, and chelate complexes with gadolinium were formed and characterized in terms of physicochemical and DNA binding properties. The transfection activity of MCO-I-68-Gd/DNA complexes was assayed in vitro on NIH 3T3. Different formulations of the product were tested. When up to 5% of the gadolinium lipid complexes were co-formulated with the cationic lipid RPR120535 used as a reference, the transfection levels were maintained as compared to RPR120535 alone. To date, only a liposomal formulation of a gadolinium–cationic lipid chelate without DNA had been observed using magnetic resonance imaging. In vivo intratumoral administration of MCO-I-68-Gd/DNA lipoplexes to tumor model led to an important increase of the NMR signal. It was demonstrated that the new complexes also acted as transfection carriers when they were formulated from liposomes.

## INTRODUCTION

The different self-assembling systems presented since the pioneering works of Felgner (1) on nonviral approaches for gene delivery have explored the nature and geometry of the cationic moiety, the type of lipid, the biodegradability properties, the controlled release of DNA from complexes, and the introduction of some targeting elements (2–3). During the last five years, a great effort has been devoted to the elucidation of the physicochemical properties of the different cationic lipid/DNA complexes (named lipoplexes). Moreover, it seems increasingly crucial to develop efficiently tissue-targeted lipoplexes, taking advantage of the growing number of tissue targeting molecules emerging from phage libraries (4) and other selection technologies.

Histological processing commonly monitors visualization of gene expression in opaque tissues. Noninvasive techniques such as PET (positron emission tomography),  $\gamma$  cameras, and SPECT (single-photon emission tomography) operate in the range of cubic millimeters or larger. Magnetic resonance imaging (MRI) provides an alternative to these technologies and its use for noninvasive visualization of gene delivery complexes is an exciting emerging technique (5–9). In particular, it was studied with contrast agents whose activity depends of an enzymatic process (7–8). With the aim to follow the biodistribution of lipoplexes and correlate their transfecting ability with in vivo biodistribution, we present

here a new strategy based on magnetic resonance imaging using gadolinium-chelating cationic lipid associated to DNA.

Our approach included the design and synthesis of a new building block precursor of DTPA in which the carboxylic acids in DTPA are protected as *tert*-butyl esters and only one of them remains free for coupling to the cationic lipid. This synthesis could be accomplished using a solid-phase methodology. This precursor was coupled to a free amino group placed in the side chain of the protected cationic lipid backbone to result in the desired cationic lipid bearing a gadolinium-complexing moiety as side chain.

## EXPERIMENTAL PROCEDURES

**General.** <sup>1</sup>H NMR spectra were recorded on Bruker 300 and 600 MHz spectrometers. Samples were dissolved in CDCl<sub>3</sub> or CD<sub>3</sub>OD. Chemical shifts are in parts per million relative to TMS internal standard.

We have performed a complete NMR analysis of the final product MCO-I-68, including <sup>1</sup>H NMR recorded with an Avance DMX 600 Bruker (2D, COSY, and HOHAHA methods, *t* = 40ms) and <sup>13</sup>C NMR (heteronuclear 2D techniques HMQC and HMBC with a delay of 3.45 and 60 ms, respectively, in the reverse mode).

Analytical and preparative HPLC were performed on Waters HPLC system equipped with a 717-plus autosampler, a 600-controller pump, a 996-photodiode array detector with tunable wavelength set at 220 nm, and a fraction collector Gilson 202. Mobile phases were (A) H<sub>2</sub>O (0.1%TFA) and (B) MeCN (0.08% TFA). Separation conditions are as follows. *Analytical.* Method A: column C18 Vydac-218TP-54, gradient H<sub>2</sub>O/MeCN, 3 min [80/20], 3–25 min [0/100], 25–50 min [0/100], 51min [80/20]; flow, 1 mL/min. Method B: Column BU-300 aquapore Butyl 7 m, 30 × 4.6 mm from Perkin-Elmer,

\* Corresponding authors. G.B.: e-mail, bykger@mail.biu.ac.il; phone, (972)-3-5318325; fax, (972)-3-5351250. J.H.: e-mail, herscovi@ext.jussieu.fr; phone: (33)-001-53-10-12-95; fax, (33)-001-53-10-12-92.

<sup>†</sup> UMR 7001.

<sup>‡</sup> Bar Ilan University.

<sup>§</sup> University of Verona.



gradient H<sub>2</sub>O/MeCN, 3 min [80/20], 3–25 min [0/100], 25–35 min [0/100], 36 min [80/20]; flow, 1 mL/min. Method C: Column BU-300 aquapore Butyl 7 m, 30 × 4.6 mm, 3 min [100/0], 3–20 min [50/50], 20–30 min [0/100], 30–40 min [0/100], 41 min [100/0]; flow, 1 mL/min. Preparative. Method D: column C<sub>4</sub> Vydac-214TP1022, 250 × 26 mm gradient H<sub>2</sub>O/MeCN, 3 min [60/40], 3–10 min [38/62], 10–15 min [34/66], 15–20 min [30/70], 20–30 min [60/40]; flow, 10 mL/min.

Fluorescence measurements were carried out on a Jobin-Yvon Spex fluoromax-2 spectrofluorimeter (Longjumeau, France). The size distribution of the liposomes and the lipoplexes was determined by dynamic light scattering using a coulter N4 Plus particle sizer (Coulter, Margency, France). Solid supports were purchased from Nova-Biochem (Switzerland), polyamine, and other reagents and solvents from Aldrich. Solvents for HPLC were purchased from Merck (Germany), and DOPE was purchased from Avanti Polar Lipids, Inc. (Alabaster, AL).

**Solid-Phase Synthesis of Protected DTPA Harboring a Single Free Carboxylate (1).** 2-Chloro trityl chloride resin (2 g, 1.5 mmol) was placed in a solid phase synthesis flask, and DCM was added, followed by bromoacetic acid (1.43 g, 10.3 mmol) and DIEA (4 mL). The flask was placed into a motor flask shaker and was shaken overnight at room temperature. MeOH was added as capping reagent, and the reaction was left for 10 additional minutes; the solution was filtered, and the resin was washed alternatively using DCM and <sup>3</sup>PrOH (×3) and finally MeOH (×2) and then dried.

Diethylenetriamine (29.4 mmol, 10 equiv) was dissolved in DCM, added to the flask containing the bromoacetyl resin, and agitated for 4 h. The solvent was filtered, and the resin was washed by alternating between DCM and <sup>3</sup>PrOH (×3), distilled water (×2), and again DCM and <sup>3</sup>PrOH (×2). The Kaiser test (90 °C) was positive. The resin was then washed with DMF (×2). *tert*-Butyl bromoacetate (5.2 mL, 35.3 mmol) and TEA (6.9 mL, to pH 7–8 on wet pH paper) were dissolved in DMF and added to the flask shaker containing the resin. The reaction was left overnight at room temperature under shaking. The solvent was filtered, and the resin was washed with <sup>3</sup>PrOH and distilled water. Additional washings were performed alternating between DCM and <sup>3</sup>PrOH (×3), then MeOH (×2), and finally ether (×1) and dried under vacuo. The Kaiser test was negative. The resin was washed with 20 %TEA in DCM (×2) and alternatively with DCM and <sup>3</sup>PrOH (×3) and then MeOH (×1) and removed to a round-bottomed flask equipped with a magnetic stirrer. A solution composed of DCM and trifluoroethanol in ratio of 2:1 was added and stirred for 2 h at room temperature. The solution was filtered and the resin washed with DCM. The organic fractions were collected and evaporated to give the expected product 0.81 g (89%). <sup>1</sup>H NMR (300 MHz, CDCl<sub>3</sub> δ in ppm): 1.45–1.48 (36H, s, *t*-Bu), 2.95–3.05 (8H, m, NCH<sub>2</sub>CH<sub>2</sub>NCH<sub>2</sub>CH<sub>2</sub>N), 3.45 (4H, s, NCH<sub>2</sub>COO-*t*-Bu), 3.53 (2H, s, NCH<sub>2</sub>COO-*t*-Bu), 3.54 (2H, s, NCH<sub>2</sub>COO-*t*-Bu), 3.56 (2H, s, NCH<sub>2</sub>COOH). HPLC analysis *t*<sub>R</sub> = 17.14 min (analytical method A). HRMS: calcd for C<sub>30</sub>H<sub>55</sub>N<sub>3</sub>O<sub>10</sub>, 618.3965; found [M + H<sup>+</sup>], 618.3982.

**Synthesis of [(Boc)NH(CH<sub>2</sub>)<sub>2</sub>]<sub>2</sub>N(CH<sub>2</sub>)<sub>2</sub>N(Boc)-CH<sub>2</sub>CO-Lys(Z)-ditetradecylamide (2).** Ditetradecylamine (1 g, 2.4 mmol) was dissolved in DCM. TEA (1 mL, 7.3 mmol) was added until the solution reached pH 8. BOC-Lys (Z)-OH (0.93 g, 2.4 mmol) was dissolved in DCM and added to the flask. Then PyBOP coupling reagent (1.3 g, 2.4 mmol) was added. The reaction mixture was stirred at room temperature for 3 h. The reaction was

followed to completion by TLC (EtOAc:Hex 1:1, ninhydrin). The DCM was then removed under reduced pressure. EtOAc was added and the organic layer was washed with aq. KHSO<sub>4</sub> (×3), aq. NaHCO<sub>3</sub> (×3), brine (×3), dried over MgSO<sub>4</sub>, filtered, and evaporated to give 1.76 g (93.3%). TFA (6 mL) was added to the flask-containing product (2). The solution was stirred for 1.5 h at room temperature. The TFA was removed under reduced pressure using ether in order to removed excess of TFA to give 1.48 g (96.9%). This product was used without further purification. H-Lys(Z)-ditetradecylamide (1 g, 1.5 mmol) was dissolved in DCM. The BOC-protected mono functionalized polyamine obtained as previously reported (12) (0.76 g, 1.5 mmol) was then added. TEA was added until the mixture showed pH 8 and then the PyBOP (0.78 g, 1.5 mmol). The reaction mixture was stirred at room temperature for 4 h. The coupling was followed using TLC (EtOAc:chloroform 3:1, ninhydrin) to completion. The DCM was removed under reduced pressure, and EtOAc was added. The organic layer was washed with aq. KHSO<sub>4</sub> (×3), aq. NaHCO<sub>3</sub> (×3), brine (×2), and dried over MgSO<sub>4</sub>, filtered, and evaporated, and the product was chromatographed on silica gel (EtOAc:chloroform 3:1) to give 0.63 g (36.4%). This intermediate was used without further purification.

**Synthesis of [NH<sub>3</sub><sup>+</sup>(CH<sub>2</sub>)<sub>2</sub>]<sub>2</sub>N(CH<sub>2</sub>)<sub>2</sub>NH<sub>2</sub><sup>+</sup> CH<sub>2</sub>CO-Lys(DTPA)-ditetradecylamide (MCO-I-68).** Product 2 (0.6 g, 0.5 mmol) was dissolved in EtOH. Pd/C 10% (0.6 g) was added, and H<sub>2</sub> gas was bubbled continuously into the reaction solution. The reaction was followed by TLC (EtOAc:chloroform 3:1, ninhydrin, and fluorescamine) to completion after 1 h. MeOH was added and the reaction solution was filtered and evaporated to give 0.43 g (82%) of the desired product.

The crude [BocNH(CH<sub>2</sub>)<sub>2</sub>]<sub>2</sub>N(CH<sub>2</sub>)<sub>2</sub>N(Boc)CH<sub>2</sub>CO-Lys-ditetradecylamide (0.4 g, 0.4 mmol) was dissolved in DCM, and TEA was added until the mixture showed pH 8. A solution of product 1 (0.4 g, 0.64 mmol) in DCM was added; then BOP (0.25 g, 0.56 mmol) was used as coupling reagent. The reaction was followed by TLC (EtOAc:chloroform 3:1, ninhydrin, and fluram) to completion (overnight). The DCM was evaporated, and EtOAc was added. The organic layer was washed with aq. NaHCO<sub>3</sub> (×3), brine (×2), dried over MgSO<sub>4</sub>, filtered, and evaporated to give 0.67 g (99.2% of crude product). TFA was added, and the solution was stirred at room temperature for 1.5 h. The TFA was evaporated, and the crude was purified by preparative HPLC according to method D. The appropriate fractions were pooled and lyophilized to afford pure product, 0.22 g (48.5%). <sup>1</sup>H NMR (600 MHz, CD<sub>3</sub>OD δ in ppm): 0.9 (6H, CH<sub>3</sub>), 1.3–1.35 (44H lipid CH<sub>2</sub>'s), 1.36 (2H, COCHCHCH<sub>2</sub>), 1.4–1.6 (2H, NCH<sub>2</sub>CH<sub>2</sub>(CH<sub>2</sub>)<sub>11</sub>CH<sub>3</sub>), 1.54 (2H, NCH<sub>2</sub>CH<sub>2</sub>(CH<sub>2</sub>)<sub>11</sub>CH<sub>3</sub>), 1.6–1.8 (4H, COCHCH<sub>2</sub>CH<sub>2</sub>CH<sub>2</sub>CH<sub>2</sub>NH), 2.8 (4H, N(CH<sub>2</sub>CH<sub>2</sub>NH<sub>2</sub>)<sub>2</sub>), 2.8–2.9 (4H, HNCH<sub>2</sub>CH<sub>2</sub>N), 3.14 (2H, CONHCH<sub>2</sub>(CH<sub>2</sub>)<sub>3</sub>CH), 3.16–3.48 (2H, CONCH<sub>2</sub> lipid), 3.2–3.3 (4H, N(CH<sub>2</sub>CH<sub>2</sub>NH<sub>2</sub>)<sub>2</sub>), 3.21 (2H, CONCH<sub>2</sub>lipid), 3.3 (8H, HO<sub>2</sub>CCH<sub>2</sub>N-(CH<sub>2</sub>CH<sub>2</sub>N)<sub>2</sub>), 3.37 (1H, CHCON), 3.64 (2H, (CH<sub>2</sub>CH<sub>2</sub>)<sub>2</sub>NCH<sub>2</sub>CO<sub>2</sub>H), 3.72 (2H, Lys-NHCO-CH<sub>2</sub>NCH<sub>2</sub>CO<sub>2</sub>H), 3.74 (4H, N(CH<sub>2</sub>CO<sub>2</sub>H)<sub>2</sub>), 3.84–3.9 (2H, Lys-NHCOCH<sub>2</sub>N), 3.92–4.09 (2H, HNCH<sub>2</sub>CO NH).

<sup>13</sup>C NMR (600 MHz, CD<sub>3</sub>OD δ in ppm): 14.49 (Me), 23.78 (CH<sub>2</sub>Me), 27.92–28.0/28.61 (N(CH<sub>2</sub>CH<sub>2</sub>CH<sub>2</sub>(CH<sub>2</sub>)<sub>10</sub>-Me), 30–31 (central lipid CH<sub>2</sub>'s), 33.12 (CH<sub>2</sub>CH<sub>2</sub>Me), 38.14 (CONHCH<sub>2</sub>(CH<sub>2</sub>)<sub>3</sub>CH), 46.4 (N(CH<sub>2</sub>CH<sub>2</sub>NH<sub>2</sub>)<sub>2</sub>), 47.75 (NCH<sub>2</sub>(CH<sub>2</sub>)<sub>12</sub>Me), 49.3 (COCH<sub>2</sub>NH), 49.3 (NCH<sub>2</sub>(CH<sub>2</sub>)<sub>12</sub>Me), 51.23 (CHCO), 51.55/52.14 (HNCH<sub>2</sub>CH<sub>2</sub>N), 52.31 (N(CH<sub>2</sub>CH<sub>2</sub>NH<sub>2</sub>)<sub>2</sub>), 52.85/53.02/53.21 ((CH<sub>2</sub>CH<sub>2</sub>)<sub>2</sub>-NCH<sub>2</sub>CO<sub>2</sub>H), 55.82 (NCH<sub>2</sub>CONH), 57.25 (N(CH<sub>2</sub>CO<sub>2</sub>H)<sub>2</sub>).

57.85 ( $\text{HO}_2\text{CCH}_2\text{NCH}_2\text{CONH}$ ), 57.88 ( $(\text{CH}_2\text{CH}_2)_2\text{NCH}_2\text{CO}_2\text{H}$ ), 166.6–173.4 (CO's). HPLC analysis  $t_R = 17.14$  min (analytical method B) and  $t_R = 25.38$  min (analytical method C). MS analysis: calcd for  $\text{C}_{56}\text{H}_{110}\text{N}_{10}\text{O}_{11}$ , 1098; found  $[\text{MH}^+]$ , 1099.

**Preparation of the Chelate Complex (MCO-I-68-Gd).** MCO-I-68 (33 mg, 30  $\mu\text{mol}$ ) was dissolved in  $\text{H}_2\text{O}$ , the pH was adjusted to 5–6.5, and  $\text{GdCl}_3 \cdot 6\text{H}_2\text{O}$  (52 mg, 150  $\mu\text{mol}$ ) was added. The mixture was stirred overnight and then dialyzed over  $\text{H}_2\text{O}$ . After filtration on sephadex G25, the compound was lyophilized. Electrospray mass spectrometry confirmed the mass of the expected product: calcd for  $\text{C}_{56}\text{H}_{107}\text{N}_{10}\text{O}_{11}$  ( $\text{MH}^+$ ), 1254.78; found, 1254.8.

**Preparation of MCO-I-68-Gd/DOPE Liposomes.** MCO-I-68-Gd (3.7 mg, 3  $\mu\text{mol}$ ) was dissolved in sterile water (150  $\mu\text{L}$ ) by heating at 30 °C. Dioleoylphosphatidylethanolamine (DOPE, 2.2 mg, 3  $\mu\text{mol}$ ) was added to the solution and the mixture was sonicated for an hour (Laboratory Supplies Co., Inc., model G112sp1t). When all the co-lipid had been incorporated, 150  $\mu\text{L}$  of  $\text{H}_2\text{O}$  was added to get a 10 mM solution. Integrity of the lipid MCO-I-68-Gd after sonication was checked by mass spectrometry. Peaks compatible with calculated DOPE (744) and MCO-I-68-Gd (1254) were found. Mean size of the particles was measured at 160 nm by dynamic light scattering.

**Preparation of MCO-I-68-Gd as Micelles.** MCO-I-68-Gd (3.7 mg, 3  $\mu\text{mol}$ ) was dissolved in sterile water (300  $\mu\text{L}$ ) by heating at 30 °C. Mean size of the particles was measured at 110 nm by dynamic light scattering.

**Preparation of Liposomes of RPR120535/DOPE/MCO-I-68-Gd.** The cationic lipid RPR120535 (5.3 mg, 5  $\mu\text{mol}$ ) was dissolved in a DOPE chloroform solution (373  $\mu\text{L}$ , 10 g/L, 5  $\mu\text{mol}$ ). A solution of MCO-I-68-Gd was added to get 1% and 5% of the gadolinium lipid incorporated as compared to the cationic lipid (0.05 and 0.25  $\mu\text{mol}$ , respectively). The solvent was removed via rotary vacuum evaporation resulting in the formation of a thin film, which was hydrated at 4 °C in  $\text{H}_2\text{O}$ . Slow vortex and sonication of the film lead to particles sizing 100–300 nm.

**Preparation of the Lipoplexes.** For size measurements, complexation, and in vitro experiments, lipoplexes were formed by mixing volume to volume 8  $\mu\text{g}$  DNA (200  $\mu\text{g}/\text{mL}$  plasmid pCMV-luc+, pCOR plasmid) with different charge ratio of MCO-I-68-Gd, formulated as micelles or liposomes, in 5% glucose/20 mM NaCl.

For in vivo experiments, 25  $\mu\text{L}$  (7.5 mM) liposome or micelle of MCO-I-68-Gd were mixed with 25  $\mu\text{L}$  DNA (400  $\mu\text{g}/\text{L}$  in 5% glucose, 20 mM NaCl).

**Fluorescence Studies.** Complexes were prepared as described above. Ethidium bromide (3  $\mu\text{L}$ , 1 mM) was added to the lipoplexes, and fluorescence was read at 590 nm upon a 260 nm excitation wavelength with 5 nm slit width.

**In Vitro Transfections.**  $5 \times 10^4$  NIH 3T3 cells were seeded in 24-well plates in Dubelcco Modified Eagle Medium (DMEM) at 37 °C, in 5%  $\text{CO}_2$ . After 24 h, cells were washed twice with 0.5 mL of serum free medium and then supplemented with 0.5 mL of medium ( $\pm$  serum). Plasmid DNA (1  $\mu\text{g}/\text{well}$ ) containing the luciferase gene under the dependency of the cytomegalovirus (CMV) immediate early promoter purified according to standard procedure was mixed with 0.5, 1.5, and 6 nmol of cationic lipid per  $\mu\text{g}$  DNA in 75 mM NaCl. For each condition a triplicate determination was performed. Extemporaneous prepared complexes were added dropwise to the cells in the medium  $\pm$  serum. After 2 h of transfection, fetal calf

serum was added to a 10% final concentration in the wells free of serum. The cells were then incubated at 37 °C for an additional period of 24 h, then the medium removed, the cells washed with PBS and lysed with 100  $\mu\text{L}/\text{well}$  of passive lysis buffer (Promega, Madison, WI) for 30 min at RT. Protein concentration of cell extracts was determined using the Bradford protein assay kit (Bio-Rad). Luminescence was measured using a luminometer (Multilabel counter 1420 Victor, EG&G Wallac) equipped with a co-injector that delivered 80  $\mu\text{L}$  of luciferase substrate into 20  $\mu\text{L}$  of cells extracts. The indicated luciferase activity corresponds to the ratio between the detected light unit and the protein amount.

**Animals.** Nude mice were bilaterally implanted in the subcutaneous tissue of the flanks with fragments of human lung tumor NCIH-1299. Human tumors have been used because they develop slowly and with less necrosis than murine tumors. As the cationic lipid has no targeting group, injection in the blood flow leads to a wide dispersion in the body, so that the low gadolinium concentration is not sufficient to expect an increasing of the MRI signal. As our purpose was the validation of the DNA/lipid cationic/gadolinium complex as a lipoplex imaging agent, we have tested the distribution of the lipoplex after direct injection into the tumoral mass. After 4–6 weeks from implant, tumors were large enough (about 1 cm in diameter) to be injected with lipoplex. The mice were anaesthetized with aqueous chloral hydrate (8 mg in 100  $\mu\text{L}$  of  $\text{H}_2\text{O}$ ) administrated intraperitoneally. Then, 50  $\mu\text{L}$  of the lipoplex (formulated as MCO-I-68-Gd/DNA or MCO-I-68-Gd/DOPE/DNA) was injected locally in one of the two tumors, the other contralateral tumor being a control. Experiments were performed with 25 mice (12 injected with micelles and 13 with liposomes).

In each mouse, imaging was performed after 4 h, 24 h, 48 h, 72 h, 8 days, and 10 days from the lipoplex injection. Before each imaging sequence, the animals were anesthetized with an intraperitoneal injection of pentobarbital (2.4 mg in 400  $\mu\text{L}$  of water).

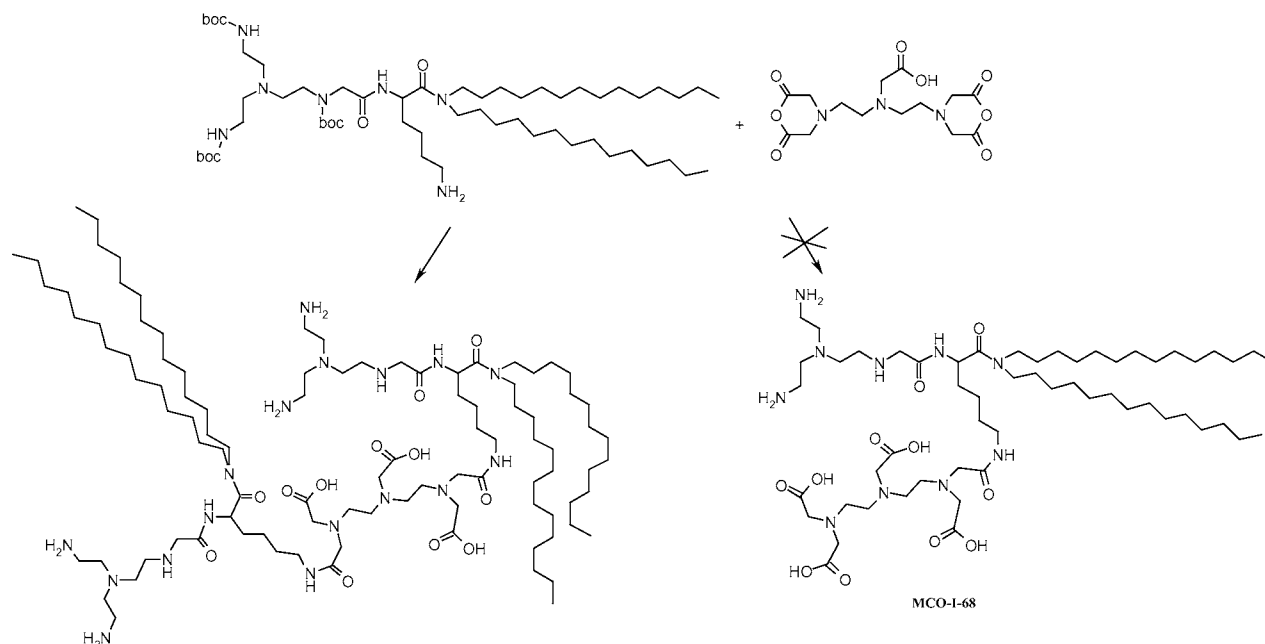
For transfection measurements, the animals were euthanased 1, 2, 3, or 10 days after injection, and the tumors were removed and homogenized in 1 mL of PLB (Promega, Madison, WI). After centrifugation at 3000 g for 20 min at 4 °C, luciferase was assessed on 10  $\mu\text{L}$  supernatant, using a luminometer (Multilabel counter 1420 Victor, EG&G Wallac).

**MRI Experiments.** Magnetic Resonance images were acquired using a Bruker AMX300 spectrometer equipped with a mini-imaging accessory (RF probe 38 mm, gradient strength 0.5 G/cm/A). A spin-echo sequence was used to obtain T1 weighted MR images ( $\text{TE}/\text{TR} = 10/500$  ms;  $\text{NEX} = 6$ ). Typically, a FOV of  $3 \times 3$  cm with a slice thickness of 1 mm was used with a  $256 \times 256$  matrix data. Sixteen consecutive transverse slices, and then eight sagittal slices through the tumor were acquired.

## RESULTS AND DISCUSSION

**Synthesis of Gadolinium Cationic Lipids.** According to previously reported results (9) using DTPA dianhydride as precursor, our attempts to synthesize MCO-I-68 failed to give good yields of the desired product, since the second anhydride function reacted with another equivalent of the amino-free lipopolyamine to result in a dimeric molecule containing two lipid units linked through a DTPA diamide spacer (Figure 1).

To develop our integrated imaging approach, it was necessary to use large quantities of the Gd-cationic lipid. Therefore, we decided to use a protected DTPA harboring

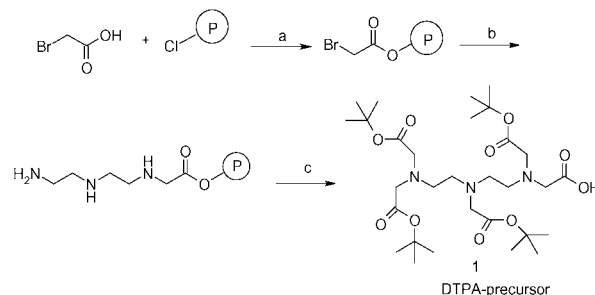


**Figure 1.** Attempts to use DTPA anhydride to obtain MCO-I-68.

a single free carboxylic acid precursor. To our surprise, there are only two methods to obtain the desired DTPA harboring a single free carboxylic acid. In one of them, the building block is obtained by biodegradation of a single methyl ester using an esterase to form a DTPA protected with methyl esters in small quantities (10). This approach is complicated and necessitates the final deprotection by basic ester hydrolysis.

The second approach is a seven-step process for obtaining DTPA *tert*-butyl esters with a free carboxylic acid at one extremity (11). This tedious multistep process prompted us to propose the simplified and versatile method presented here. The approach is based on our previous works for the synthesis of protected monofunctionalized polyamines using solid support techniques (12–13). In those works, we have taken advantage of the dilution effect induced by the coupling of an alkylating agent to a solid support, which prevents polyalkylation when treating a polyamine with the solid supported alkylating agent. Thus, we have attached bromoacetic acid to chlorotriethyl resin and reacted the solid supported bromide with an excess of free diethylenetriamine. In a second step, the supported polyamine was reacted with excess *tert*-butyl-bromoacetate under basic conditions to afford the protected DTPA. Finally, the product was cleaved from the solid support using mild acidic conditions (trifluoroethanol) to prevent *tert*-butyl ester deprotection, thus resulting in the desired DTPA building block **1** with a single free carboxylic acid (see Figure 2).

Unlike our previous works using spermine as polyamine, we did not observe any of the symmetric free carboxymethylene DTPA product which could have been obtained, in theory, by the reaction between the central secondary amine of the diethylenetriamine and the solid supported bromoacetyl group. This is probably mainly due to the statistical ratio of 1/2 secondary/primary amines in diethylenetriamine, contrary to the 1/1 ratio in the case of spermine. This, together with small steric and inductive effects favoring the reaction of the primary amine, results in the absence of the symmetric product. The advantage of this new method is that no isolation of intermediates is necessary. Thus, product **1** is obtained rapidly without needing any purification step. (Figure 2).



**Figure 2.** Synthesis of asymmetrically protected DTPA building block **1**. (a) Diethylisopropylamine  $\text{CH}_2\text{Cl}_2$  overnight, (b) diethylenetriamine  $\text{CH}_2\text{Cl}_2$ , 4 h, and (c) *tert*-butyl-bromoacetate triethylamine overnight then trifluoroethanol/ $\text{CH}_2\text{Cl}_2$ , 1 h.

The lipopolyamine precursor was obtained by coupling of previously reported protected building block tris-aminoethylcarboxymethylene to a preformed H-Lys(Z)-ditetradecylamide (13). After deprotection of the Lys side chain of product **2** by hydrogenolysis, product **1** was coupled with the free amino group of the obtained product **3** using regular peptide coupling techniques to give **4**.

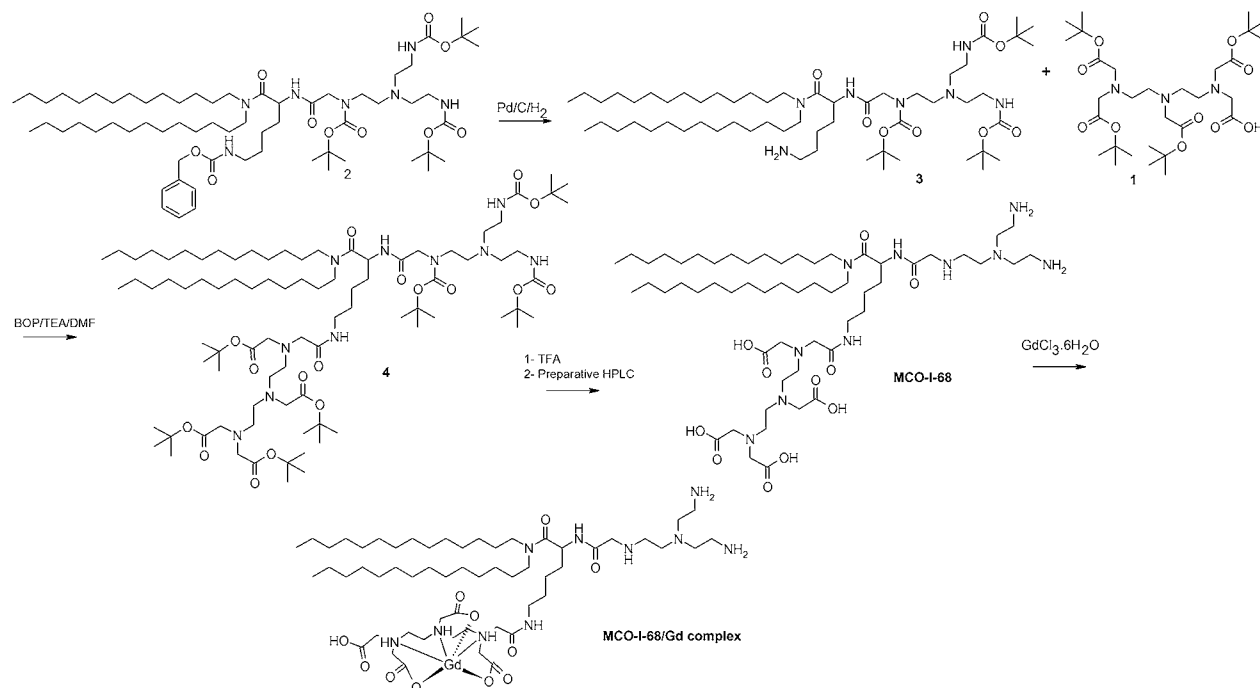
The final product was obtained after exhaustive deprotection of **4** using trifluoroacetic acid (see Figure 3). The cationic lipid MCO-I-68 was fully characterized using two different HPLC gradients, multidimensional NMR, and high-resolution mass spectroscopy. The gadolinium ion was complexed to the DTPA moiety of the lipid as previously described (9).

The excess of  $\text{GdCl}_3 \cdot 6\text{H}_2\text{O}$  was removed via subsequent dialysis and gel filtration to remove all traces of toxic  $\text{GdCl}_3 \cdot 6\text{H}_2\text{O}$ . The full conversion of MCO-I-68 to MCO-I-68-Gd was checked by electrospray mass spectroscopy. (See Figure 3).

**Physicochemical Characterization of DNA/MCO-I-68-Gd Complexes.** Dilution of MCO-I-68-Gd in water gave a micellar suspension. The cationic polyamine moiety of this lipid allowed to form MCO-I-68-Gd/DNA lipoplexes by direct mixing of the micelles with DNA. Liposomes were prepared by direct mixing of the gadolinium lipid with a co-lipid.

The lipid chains of the widely used dioleoylphosphatidylethanolamine (DOPE), and the gadolinium lipid or-



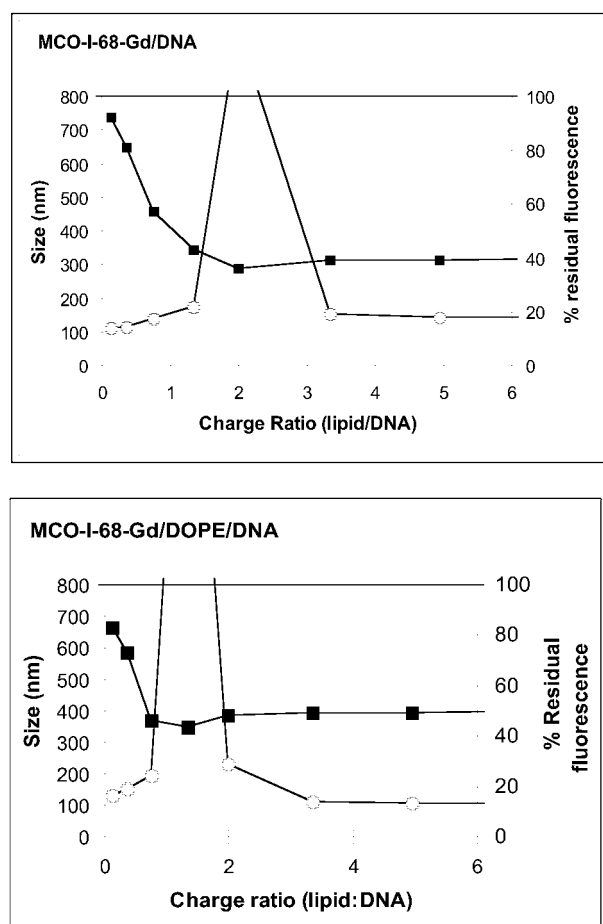


**Figure 3.** Synthesis of MCO-I-68 and its complex with gadolinium.

ganized together under liposome type of structures when both lipids were sonicated together, as described in materials and methods and in (9). On the other hand, the usual way of preparing liposomes via formation of a film under vacuum elimination of CHCl<sub>3</sub> did not allow us to form homogeneous liposomal structures. Lipoplexes (MCO-I-68-Gd/DOPE/ DNA) were then formed by diluting different amounts of the preformed liposomes with a constant amount of DNA.

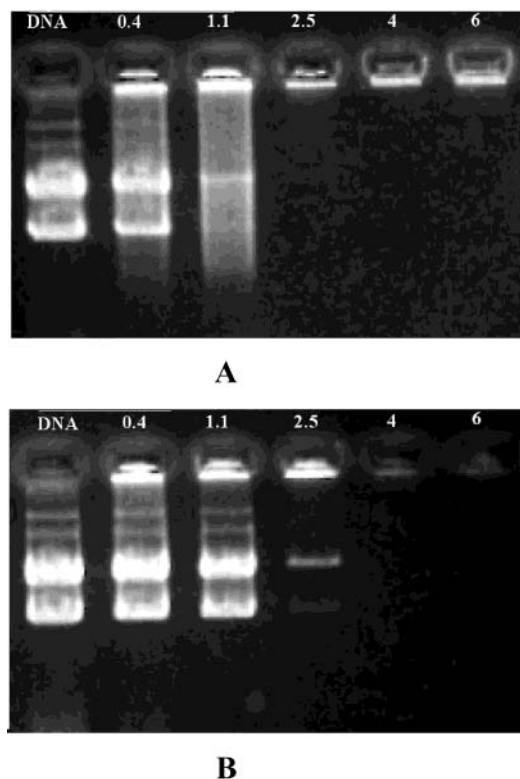
The ability of MCO-I-68-Gd as micelles or liposomes to complex DNA and to form small particles was studied. The size of lipoplexes obtained either by association of micelles to DNA or by association of liposomes to DNA was evaluated by dynamic light scattering experiments (Figure 4). Results are represented as a function of the ratio of positive charges (MCO-I-68-Gd) to negative charges (DNA Phosphate) equivalents, considering that the MCO-I-68-Gd compound carried three positive charges.

Complexes, formulated either from micelles or liposomes, exhibit comparable size for the different studied charge ratio (MCO-I-68-Gd/DNA) studied. Moreover, the characteristics of lipoplexes are similar to those previously observed with lipopolyamine RPR120535 (14). We found that, when lipoplex self-assembly is formed with negative charges in excess (charge ratio MCO-I-68-Gd/DNA < 1), lipoplexes are colloidally stable and exhibit a small size around 110 nm when starting from micelles and 150 nm when starting from liposomes. Aggregation (size > 1  $\mu$ m) occurs at lipid/DNA ratio between 1 and 2, corresponding to charge neutrality of the complexes. As the amount of cationic lipid was increasing relative to the DNA, colloidally stable 100 nm size particles are obtained. We also carried out fluorescence experiments in order to estimate DNA entrapment into the lipoplexes. Intercalation of ethidium bromide between the free DNA base pairs gives a fluorescent signal taken as 100%. When DNA is complexed with the cationic lipids, the ethidium bromide signal decreases due to its exclusion from DNA. This allows monitoring the percentage of compacted DNA. Figure 4 shows the diminution of fluorescence depending on the degree of DNA complexation. Fluorescence level decreases to 50% or 60% for



**Figure 4.** Size of the lipoplexes and ethidium bromide residual fluorescence in function of the charge ratio lipid/DNA ( $\pm$ ). Open circles represent the size of the lipoplexes, measured by dynamic light scattering. Full squares represent complexation of DNA, measured by emission fluorescence (100% = complete intercalation in absence of cationic lipid).

micelle or liposome-based lipoplexes, respectively. This is less than what had been previously observed with



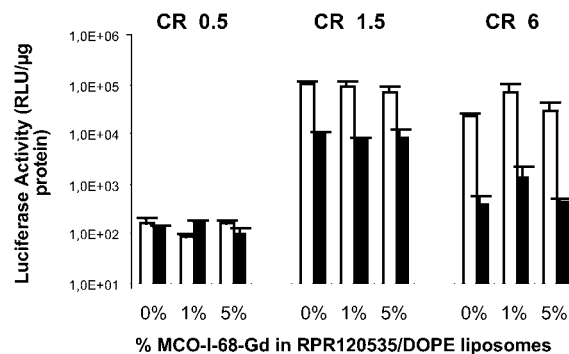
**Figure 5.** Lipoplexes were loaded on a 0.8% agarose gel at the different DNA complexation zone identified in Figure 2. Free DNA was loaded on the first well as a control. Then mixtures of MCO-I-68-Gd/DNA at the lipid/DNA charge ratio 0.4, 1.1, 2.5, 4, and 6 were loaded either when starting from liposomes (A) or micelles (B).

RPR120535 (13), thus suggesting incomplete DNA compaction or association to lipoplexes. However, MCO-I-68-Gd/DNA lipoplexes did not migrate on agarose gel electrophoresis (Figure 5). Thus, it appeared in both liposome and micelle-based lipoplexes that a charge ratio of 2.5 was enough to get a full DNA complexion. Nevertheless, the ethidium bromide test indicates a lower affinity of the MCO-I-68-Gd lipid for DNA as compared to the RPR120535 lipopolyamine control.

**In Vitro Transfection.** The gadolinium lipid had been designed as a tracer co-lipid for MRI studies in order to follow the biodistribution of our new homemade DNA lipidic vectors. As this lipid presents the same type of structure as other cationic lipids, it should not alter in vivo lipoplex biodistribution.

Moreover, the physico-chemistry shown above indicates that this lipid behaves very closely to previously studied cationic lipids). In vitro transfection activity of MCO-I-68-Gd lipid was studied on NIH3T3 cells and compared to reference lipid RPR120535. MCO-I-68-Gd was used either alone or by co-formulation with cationic RPR120535, which represents the way this method will be used in future MRI studies. The gadolinium lipid, to be used as a co-lipid, should not modify the activity, nor reduce the efficiency of the lipid tested. The cationic lipid RPR120535 formulated with DOPE (1/1) was chosen as a reference, since it was shown that this lipid did transfect efficiently NIH 3T3 cells in absence of serum (15). We incorporated 1–5% gadolinium lipid into the cationic formulation (materials and methods) and evaluated the transfection activity of these new gadolinium-based formulations (see Figure 6).

With the MCO-I-68-Gd/DNA complex was used, transfection efficiency was reduced as compared to the



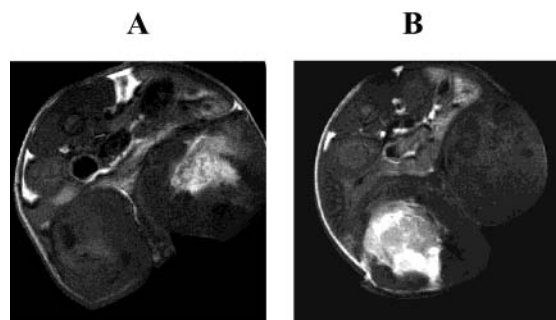
**Figure 6.** Lipid-mediated DNA transfection of NIH 3T3 cells using cationic liposomes RPR120535/DOPE, RPR120535/DOPE + 1% MCO-I-68-Gd, RPR120535/DOPE, /DOPE+5% MCO-I-68-Gd in three different charge ratio (RPR120535/DNA) 0.5, 1.5, and 6, in the presence (gray) or absence (white) of calf serum. Data are the mean of triplicate determination (error bars: SD).

RPR120535/DNA complex (not shown). This may be explained by the reduced affinity of the MCO-I-68-Gd for DNA as compared to RPR120535, as measured by ethidium bromide. Complexes formed out of MCO-I-68-Gd are likely less stable and release DNA faster than the RPR120535. On the other hand, addition of 1 and 5% of the MCO-I-68-Gd into the RPR120535/DOPE formulation did not significantly affect the DNA transfection efficiency, as compared to DNA complexed with RPR120535/DOPE, indicating that MCO-I-68-Gd does not interfere with in vitro transfection efficiency of RPR120535 (Figure 6).

**MRI Experiments.** The efficiency of a DNA delivery vehicle depends of the pharmacokinetics that determines distribution and concentration in targeted tissue. With the aim to explore the possibility of imaging a DNA transfection event, Nantz et al. (9) brought to the fore a contrast enhancement in lymph nodes after subcutaneous injection of a polymerizable lipid chelated with gadolinium. They formulated afterward this gadolinium lipid with DOTAP and DNA and showed that the lipoplex formed was able to transfect NIH 3T3 cells in vitro. However, visualization DNA complexes were not shown in those works so far.

The most important objective of this work was to design and assess a new tool visualizable in MRI for the biodistribution monitoring of cationic lipid/DNA complexes. For this purpose we have tested the ability of MCO-I-68-Gd/DNA complex to act as a MRI contrast agent and to follow lipoplex biodistribution in vivo. Imaging studies were performed after intratumoral injection of the complexes. Tumors were bilaterally implanted in the flanks of the animals, and only one tumor was injected, the contralateral one serving as a control.

Noninjected tumors appeared as multinodular masses with a thin layer of oedematous tissue at their boundary (Figure 7). The neoplastic tissue appeared as rather homogeneous nodules emitting a signal of medium intensity. Hypointense areas were visible within the mass, probably corresponding to necrotic tumoral tissue. In lipoplex injected tumor, areas of hyperintensity were visible. In some cases (2 out of 13), these areas appeared only 24 h after injection, probably because little or no exchange water with the gadolinium could occur in the injection site (Figure 8). The contrast agent diffused slowly (up to 10 days) out of the neoplastic mass, in the healthy tissue. The injection of the contrast agent labeled lipoplexes did not cause any increase of the necrosis, but both with liposomes and micelles small hemorrhages were associated to the injection site. After 24 h, the



**Figure 7.** (A) 48h after injection of the left side tumor with MCO-I-68-Gd/DOPE/ DNA complexes. Right side tumor is thenon injected tumor control. (B) 48 h after injection of the right side tumor with MCO-I-68-Gd/DNA lipoplex. Left side tumor is the noninjected tumor control.

contrast agent diffused in the surrounding neoplastic tissue, creating areas of medium intensity signal with irregular margins. However, injection site was still visible by its hyperintensity. In the cases in which a necrotic core was involved in the injection site, the diffusion of the hyperintensity signal was poor and mainly limited around the injection site. The different behavior of the complex from a mouse to another was correlated to the intern structure of the tumor. No difference could be obviously detected between micelles and liposomes. Diffusion of the hyperintensity signal reached a maximum after 52 h from injection and decreased slowly thereafter. Nevertheless, hyperintensity was still visible after 10 days (Figure 8).

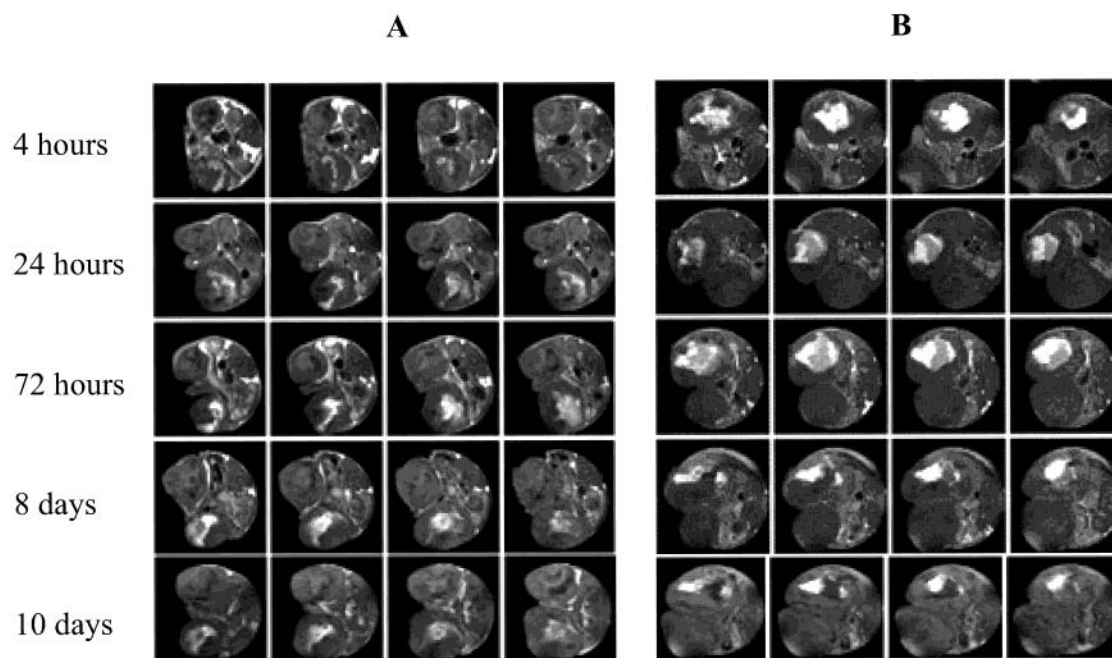
The presence of hyperintensity demonstrates that gadolinium complex interacts with water molecules and is not sequestered in small intracellular compartments (i.e., secondary lysosomes). The clearance of the gadolinium from the tumor is probably hampered by the hypovascularity of the tumoral core. The displacement of the contrast agent in the tumor could be due to both diffusive and convective movements of the interstitial fluid.

In these MR imaging experiments, the injected plasmid coded for the reporter gene luciferase, thus allowing

assaying transfection efficiency. After 1, 2, 3, and 10 days, mice were euthanased, tumors were removed, and the luciferase activity was quantified. No significant luciferase activity was detected in the tumors injected with micelle-based complexes. On the other hand, in most of the tumors injected with liposome-based lipoplexes, the luciferase activity was noteworthy although with low levels during the first 3 days. Nevertheless, as shown from the corresponding imaging, the transfection level seems to depend essentially on the possible diffusion of the complex in nonnecrotic zones. Because of the variability between the tumors observed, we could not evaluate the decrease of transfection from day 1 to day 3. No luciferase activity could be detected at day 10. This was expected, as it had been shown that cationic lipid mediated gene transfer results in a temporary transgene expression with a maximal expression after 24 h which decreases rapidly afterward (data not shown).

It should be noted that all the MRI experiments were performed using MCO-I-68-Gd to form the DNA complexes, without adding cationic lipid RPR120535. On the other hand the transfection level was lower when using MCO-I-68-Gd/DNA complexes than when diluting 1–5% MCO-I-68-Gd in a RPR120535/DOPE/DNA. Thus, we are currently working on the MRI of the co-formulated cationic lipid, which has been shown to be more efficient *in vitro*. In this way we will aim at adjusting the *in vivo* formulation so that gadolinium contrast can be observed with a lower concentration of MCO-I-68-Gd in a co-formulation, hence, increasing *in vivo* transfection and thus correlating the imaging observation to transfection.

According to the *in vivo* results, the transfection occurs only during the first 3 days after injection and is paralleled by hyperintensity at MRI examination. In the following days, there is a mismatch between hyperintensity and transfection. This mismatch seems to suggest that lipoplexes although remain in the tumor, their ability to transfect is lost. We speculate that the loss of transfection ability could arise from DNA damage; however, we cannot demonstrate this assumption to date.



**Figure 8.** Visualization of lipoplex-Gd in tumor NCIH-1299 at 4 h, 24 h, 72 h, 8 days, and 10 days after injection. (A) Lipoplexes formed from liposomes injected on left side tumor. (B) Lipoplexes formed from micelles injected on right side tumor.



## CONCLUSIONS

We have designed and applied a new tool based on in vivo magnetic resonance imaging of cationic lipid/DNA complexes. A new versatile solid phase synthesis of asymmetrically protected DTPA building block for covalent conjugation to cationic lipids has been demonstrated.

The DTPA-cationic lipid obtained was chelated with gadolinium and complexed with plasmid DNA. We have shown that these complexes display significant levels of transgene expression after in vitro transfection. Our present studies show, for the first time, that cationic lipid/DNA complexes can be observed in vivo using magnetic resonance imaging after intratumoral administration. We could visualize cationic lipid/DNA complexes and observe their distribution in the tumor area as a function of time. We have shown that lipoplexes formulated from both micelles and liposomes can be observed during long periods of time. However, transgene expression could be detected on tissue extract only when complexes were formulated as liposomes.

Overall, this technique opens the field of gene delivery to the design and the in vivo observation DNA/cationic targeted to various tissues or tumors. Works exploiting these possibilities are currently ongoing.

## ACKNOWLEDGMENT

This project was funded by Arc-en-Ciel and AFIRST Israel/France (programs of the French Ministry of Foreign Affairs and the Israeli Ministry of Sciences). Dr. Gerardo Byk is also indebted to the Marcus Center of Medicinal Chemistry and to TEVA Pharmaceuticals Inc. The imaging system was purchased with a grant of the Association pour la Recherche sur le Cancer (ARC).

## LITERATURE CITED

- (1) Felgner, J. H., Kumar, R., Sridhar, C. N., Wheeler, C. J., Tsai, Y. J., Border, R., Ramsey, P., Martin, M., and Felgner, P. L. (1994) Enhanced gene delivery and mechanism studies with a novel series of cationic lipid formulations. *J. Biol. Chem.* 269, 2550–2661.
- (2) Schatzlein, A. G. (2001) Nonviral vectors in cancer gene therapy: principles and progress. *Anti-Cancer Drugs* 12, 275–304.
- (3) Miller, A. D. (1998) Cationic Liposomes for Gene Therapy. *Angew. Chem.* 37, 1768–1785.
- (4) Pasqualini, R., and Ruoslahti, E. (1996) Tissue targeting with phage peptide libraries. *Mol. Psychiatr.* 6, 421–423.
- (5) Bell, J. D., and Taylor-Robinson, S. D. (2000) Assessing gene expression in vivo: magnetic resonance imaging and spectroscopy. *Gene Ther.* 7, 1259–1264.
- (6) Goffeney, N., Bulte, J. W. M., Duyn, J., Bryant Jr, L. H., and van Zijl, P. C. M. (2001) Sensitive NMR detection of cationic-polymer-based gene delivery systems using saturation transfer via proton exchange. *J. Am. Chem. Soc.* 123, 8628–8629.
- (7) Louie, A. Y., Hüber, M. M., Ahrens, A. T., Rothbächer, U., Moats, R., Jacobs, R. E., Fraser, S. E., and Meade, T. J. (2000). In vivo visualization of gene expression using magnetic resonance imaging. *Nat. Biotechnol.* 18, 321–325.
- (8) Bhorade, R., Weissleder, R., Nakakoshi, T., Moore, A., and Tung, C.-H. (2000) Macrocyclic chelators with paramagnetic cations are internalized into mammalian cells via a HIV-tat derived membrane translocation peptide. *Bioconjugate Chem.* 11, 301–305.
- (9) Wisner, E. R., Aho-Sharon, K. L., Bennett, M. J., Penn, S. G., Lebrilla, C. B., and Nantz, M. H. (1997) A modular lymphographic magnetic resonance imaging contrast agent: contrast enhancement with DNA transfection potential. *J. Med. Chem.* 40, 3992–3996.
- (10) Burks, E., Koshti, N., Jacobs, H., and Gopalan, A. (1998) Selective Monohydrolysis of Esters of Polyaminocarboxylic acids using Pig Liver Esterase. *Synlett* 11, 1285–1287.
- (11) Arano, Y., Uezono, T., Akizawa, H., Ono, M., Wakisaka, K., Nakayama, M., Sakahara, H., Konishi, J., and Yokoyama, A. (1996) Reassessment of diethylenetriaminepentaacetic acid (DTPA) as a chelating agent for indium-111 labeling of polypeptides using a newly synthesized monoreactive DTPA derivative. *J. Med. Chem.* 39, 3451–3460.
- (12) Byk, G., Frederic, M., and Scherman, D. (1997) One Pot Synthesis of Unsymmetrically Functionalized polyamines by a solid-phase strategy starting from their symmetrical polyamine counterparts. *Tetrahedron Lett.* 38, 3219–3222.
- (13) Byk, G., Dubertret, C., Escriou, V., Frederic, M., Jaslin, G., Rangara, R., Pitard, B., Crouzet, J., Wils, P., Schwartz, B., Scherman, and D. (1998) Synthesis, activity, and structure–activity Relationship studies of novel cationic lipids for DNA Transfer. *J. Med. Chem.* 41, 224–235.
- (14) Pitard, B., Oudrihiri, N., Vigneron, J. P., Hauchecorne, M., Aguerre, O., Toury, R., Airiau, M., Ramasawny, R., Scherman, D., Crouzet, J., Lehn, J. M., and Lehn, P. (1999) Structural characteristics of supramolecular assemblies formed by guanidinium-cholesterol reagents for gene transfection. *Proc. Natl. Acad. Sci.* 96, 2621–2626.
- (15) Escriou, V., Ciolina, C., Lacroix, F., Byk, G., Scherman, D., and Wils, P. (1998) Cationic lipid-mediated gene transfer: effect of serum on cellular uptake and intracellular fate of lipopolyamine/DNA complexes. *Biochim. Biophys. Acta* 1368, 276–288.

BC025567E

# Synthesis and Binding Properties of Oligo-2'-deoxyribonucleotides Conjugated with Triple-Helix-Specific Intercalators: Benzo[e] and Benzo[g] Pyridoindoles

Serguei Vinogradov,<sup>†,‡</sup> Victoria Roig,<sup>†</sup> Zinaida Sergueeva,<sup>§,||</sup> Chi Hung Nguyen,<sup>§</sup> Paola Arimondo,<sup>⊥</sup> Nguyen T. Thuong,<sup>†</sup> Emile Bisagni,<sup>§</sup> Jian-Sheng Sun,<sup>⊥</sup> Claude Hélène,<sup>⊥</sup> and Ulysse Asseline\*,<sup>†</sup>

Centre de Biophysique Moléculaire, CNRS UPR 4301, Rue Charles Sadron, 45071 Orléans Cedex 02, France, UMR 176 CNRS–Institut Curie, Section de Recherche, Bâtiments 110-112, 15 Rue Georges Clemenceau, 91405 Orsay, France, and Laboratoire de Biophysique, Muséum National d'Histoire Naturelle, INSERM U 201-UMR 8643 CNRS, 43 rue Cuvier, 75231 Paris Cedex 05, France. Received July 10, 2002; Revised Manuscript Received October 12, 2002

DNA binding compounds, such as benzo[e] (BePI) and benzo[g] pyridoindole (BgPI) derivatives, exhibit preferential stabilization of triple helices. We report here the synthesis of a series of pyrimidine triple-helix-forming oligo-2'-deoxyribonucleotides conjugated with these molecules. BePI was coupled to the 5-position of 2'-deoxyuridine via two linkers of different sizes attached to its 11-position and placed at either the 5'-end, inside the sequence, or at both the 5'-end and the internal positions using periodate oxidation of a diol-containing oligonucleotide followed by reductive coupling with amino-linked BePI. The same BePI derivatives were also linked to the oligonucleotide chain via internucleotidic phosphorothiolate or phosphoramidate linkages. A mixture of diastereoisomers was prepared as well as separate pure Rp and Sp isomers. A BePI derivative, with two different linkers attached to its 3-position, and BgPI derivatives were also linked to the 5-position of a 2'-deoxyuridine located at either the 5'-end or inside the sequence, as well as to the  $\beta$ -anomeric position of an additional 2'-deoxyribose placed inside the sequence. The binding properties of these oligonucleotide–benzopyridoindoles conjugates with their double-stranded DNA target was studied by absorption spectroscopy.

## INTRODUCTION

Since their first description with polynucleotides by Felsenfeld et al. (1) in 1957, followed 30 years later by the discovery that they can also be formed upon binding of synthetic oligonucleotides to double-helical DNA (2, 3), nucleic acid triple helices have been the focus of considerable attention because of their possible applications in biotechnology, diagnostics, and therapeutics (for reviews, see ref 4). Short triple-stranded complexes can compete with the cellular machinery to inhibit either transcription initiation (5) or transcription elongation (6, 7). In addition, reactive triple-helix-forming oligonucleotides (TFOs) have been shown to induce targeted mutations (8, 9) and have been used to demonstrate the accessibility of the DNA target sequence in the cell nuclei (10–12). TFOs covalently linked to camptothecin, an inhibitor of topoisomerase I, have been proven to induce in vitro sequence-specific cleavage of one strand of the double-stranded DNA target by recruiting topoisomerase I (13, 14). More recently a TFO was shown to induce mutations in mice

(15). However, in many cases the stability of triple-helical complexes is not strong enough to compete efficiently with transcription activating factors or to arrest the transcription machinery. The mechanism of sequence-specific DNA triplex formation involves the formation of hydrogen bonds between the bases of the third strand and the purine bases of the double stranded DNA target. The stability of triple helices involving a natural oligo-2'-deoxyribonucleotide third strand is in most cases inferior to that of double helices. Only a few (G,A)-containing third strands form very stable complexes (16). The requirement for cytosine protonation destabilizes triplexes involving (C,T)-containing third strands under physiological conditions, especially when they contain adjacent cytosines. To increase the stability of the complexes, the third-strand oligonucleotides have to be modified. This can be achieved by modification of the oligonucleotide either at the backbone or at the base level. Another strategy consists of the covalent attachment of stabilizing agents such as groove binding ligands (17–18), peptides (19), or intercalators (20–28). The covalent attachment of intercalators at the end of the oligonucleotides has been shown to strongly stabilize triple helical complexes due to intercalation at the junction between the duplex and triplex regions along the DNA template. One example of strong stabilization of a triple helix by covalent coupling of two intercalators derivatives at both the 5' and the 3'-ends of a pyrimidine triple-helix-forming oligonucleotide has also been reported (27). The design of triple-helix-specific intercalating agents (29) has opened the possibility of stabilizing triplexes by attaching this kind of triplex-specific ligand at any site along the third strand oligonucleotide. Benzopyridoindole and Benzopy-

\* Corresponding author. Fax: + 33-2-38-63-15-17. E-mail: asseline@cnrs-orleans.fr.

<sup>†</sup> Centre de Biophysique Moléculaire, CNRS UPR 4301 (affiliated with the University of Orléans and with INSERM).

<sup>‡</sup> Present address: Department of Pharmaceutical Sciences, College of Pharmacy, 986025 Nebraska Medical Center Omaha, NE 68198-6025.

<sup>§</sup> UMR 176 CNRS–Institut Curie.

<sup>||</sup> Present address: Department of Chemistry, Duke University, Box 90349, Durham, NC, 27708.

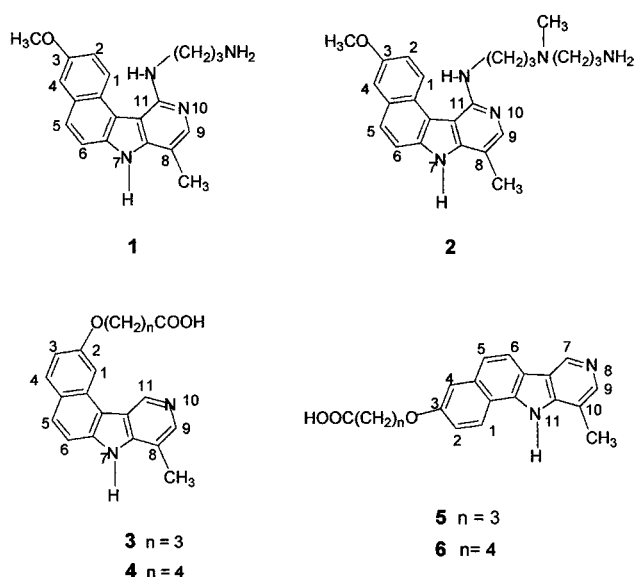
<sup>⊥</sup> Laboratoire de Biophysique, Muséum National d'Histoire Naturelle.

ridoquinoxaline derivatives have been covalently attached to either the 5'-end, via a phosphoramidate linkage, or an internal position, via an abasic site generated after *in situ* depurination followed by reductive amination of the generated aldehyde group by the amino-containing intercalator-linker derivative (24, 25). Two derivatives, a benzopyridoquinoxaline attached to the 5'-end and a benzopyridoindole attached to the internal position, notably stabilized the triple helix.

On the basis of these results and in order to further explore the possibility of increasing the stability of triplexes, we chose to covalently attach a few benzo[e] pyridoindole and benzo[g] pyridoindole derivatives to different positions of a pyrimidine third strand: the 5-position of 2'-deoxyuridine incorporated in place of thymidine at various locations inside the sequence, the  $\beta$ -anomeric position of a 2'-deoxyribose residue inserted between the second and third nucleotides of the third strand and at internucleotidic positions via a phosphorothiolate or a phosphoramidate linkage. We also chose to study the influence of the position of the linker attachment site to the intercalator as well as that of the linker size to connect the intercalator to the oligonucleotide. We report here the preparation of these oligonucleotide-BePI and oligonucleotide-BgPI conjugates and their binding properties with a complementary double-stranded DNA target sequence.

#### EXPERIMENTAL PROCEDURES

**General Methods.** All solvents used were dried, distilled, and stored as described in ref 30. All chemicals were used as obtained unless otherwise stated. Triethylamine and sodium sulfate were from Merck. Pyridine and dichloromethane were from SDS. Analytical thin-layer chromatography (TLC) was performed on precoated alumina plates (Merck silica gel 60F 254 ref. 5554). For flash chromatography, Merck silica gel 60 (70–230 mesh) (ref. 7734) or Aldrich neutral alumina oxide (150 mesh) (ref. 19,997-4) and anhydrous solvents were used. Melting points (mp, uncorrected) were measured using an Electrothermal IA 9200 melting point apparatus. NMR spectroscopy was performed on a Bruker AC 200 or AM 300WB Spectrometer.  $^1\text{H}$  chemical shifts were referenced to either residual solvent peak DMSO (2.54 ppm) or  $\text{Me}_4\text{Si}$ . Elemental analysis was performed by Service Central de microanalyses du CNRS, 91190 Gif sur Yvette, France. The results are within  $\pm 0.4\%$  of the theoretical values corresponding to the mentioned formulas. Mass analysis was performed on a Quattro II (Micromas) instrument. Oligonucleotides, including those with an internucleotidic thiophosphate group, were synthesized using cyanoethyl phosphoramidite chemistry using either a Pharmacia Gene Assembler or an Expedite Nucleic Acid Synthesis system 8909 from Perseptive Biosystems. Analysis and purification by ion-exchange chromatography were carried out on a Pharmacia FPLC with a DEAE column (8  $\mu\text{m}$ , 100 mm  $\times$  10 mm, Waters) with a linear gradient of NaCl in Tris/HCl, 25 mM buffer, pH 7, containing 10%  $\text{CH}_3\text{CN}$ . Reversed-phase chromatography analysis was performed on a 600 E System Controller equipped with a photodiode array detector Waters 990 using a Lichrospher 100 RP18 (5  $\mu\text{m}$ ) column (125 mm  $\times$  4 mm) from Merck with a linear gradient of  $\text{CH}_3\text{CN}$  in 0.1 M aqueous triethylammonium acetate, pH 7, with a flow rate of 1 mL/min. The concentration of unmodified oligonucleotides was calculated using molar extinction coefficients at 260 nm using a nearest-neighbor model (31). The extinction coefficients for oligo-2'-deoxyribonucleotide-BePI and oligo-2'-deoxyribonucleotide-BgPI conjugates



**Figure 1.** Structures of the BePI and BgPI derivatives 1–6.

were approximated by adding the experimentally determined extinction coefficient at 260 nm of the unconjugated BePI or BgPI in  $\text{H}_2\text{O}$  to the extinction coefficient for oligonucleotide  $5'\text{TTTTCTTTTC}'$  ( $\epsilon_{260} = 80\ 100\ \text{M}^{-1}\ \text{cm}^{-1}$ ). All concentrations are given on a per strand basis.

#### A. Synthesis of BePI and BgPI Derivatives 1–20.

**I. Synthesis of the BePI Derivatives 1 and 2 Involving an Amino-Containing Linker Attached to Their 11-Position.** The 11-amino-substituted benzo[e]pyridoindole derivatives 1 and 2 (Figure 1) were obtained as described in the literature (32, 33).

**II. Synthesis of the BePI and BgPI Derivatives 3–6 Involving a Carboxylated Linker (Schemes 1 and 2).** **1. 11-Chloro-3-hydroxy-8-methyl-7H-benzo[e]pyrido[4,3-b]indole 8.** To a suspension of the methoxybenzo[e]pyrido[4,3-b]indole 7 (1 g, 3.4 mmol) in 12 N hydrochloric acid (100 mL) was added benzyltriethylammonium chloride (3 g, 13 mmol). The mixture was heated at reflux under nitrogen atmosphere for 72 h. Evaporation to dryness under reduced pressure provided a solid residue, which was taken up in water (100 mL), and the pH was adjusted to 14 by 14%  $\text{NH}_4\text{OH}$ . The precipitate was collected by filtration and washed with water, dried and chromatographed on neutral alumina column with gradient of ethanol (0 to 10%) in  $\text{CH}_2\text{Cl}_2$  as eluent, giving 820 mg (86%) of **8**: mp 236  $^\circ\text{C}$  (dioxane);  $^1\text{H}$  NMR,  $\delta$  12.5 (s, 1H, NH), 9.57 (d, 1H, H-1), 8.07 (s, 1H, H-9), 7.90 (d, 1H, H-5), 7.76 (d, 1H, H-6), 7.36 (d, 1H, H-4), 7.27 (dd, 1H, H-2), 2.58 (s, 3H,  $\text{CH}_3$ -8). Anal. Calcd for  $\text{C}_{16}\text{H}_{11}\text{N}_2\text{ClO} \cdot \text{H}_2\text{O}$ : C, 63.89; H, 4.32; N, 9.31. Found: C, 63.72; H, 4.1; N, 9.22.

**2. 7-Chloro-3-hydroxy-10-methyl-11H-benzo[g]pyrido[4,3-b]indole 12.** This compound was prepared according to the procedure described above for **8** (starting from the methoxybenzo[g]pyrido[4,3-b]indole 11) in 85% yield mp 298  $^\circ\text{C}$  (acetonitrile);  $^1\text{H}$  NMR,  $\delta$  12.50 (s, 1H, NH), 9.96 (s, 1H, OH), 8.66 (d, 1H, H-1), 8.35 (d, 1H, H-6), 8.07 (s, 1H, H-9), 7.63 (d, 1H, H-5), 7.36 (d, 1H, H-4), 7.29 (dd, 1H, H-2), 2.66 (s, 3H,  $\text{CH}_3$ -10). Anal. Calcd for  $\text{C}_{16}\text{H}_{11}\text{N}_2\text{ClO} \cdot \text{H}_2\text{O}$ : C, 63.89; H, 4.32; N, 9.32. Found: C, 63.72; H, 4.63; N, 9.78.

**3. Alkylation and Hydro-Dechlorination Reactions for the Production of the O-Substituted Derivatives 9, 10, 13, and 14.** **Preparation of Ethyl 4-(7H-Benzo[e]pyrido[4,3-b]indol-3-yloxy)butanoate 9: An Example of the General Method.** A solution of ethyl 4-bromobutyrate (1.9 g; 9.7



mmol) in DMF (20 mL) was added over a 4 h period at 0 °C to the mixture of 3-hydroxybenzo[*e*]pyrido[4,3-*b*] indole **8** (2.3 g; 8.1 mmol) in DMF (60 mL) and K<sub>2</sub>CO<sub>3</sub> (5.6 g; 40 mmol). After 8 h at 0 °C, the mixture was kept under stirring at room temperature for 72 h. Water (250 mL) was added, and the mixture was extracted with ethyl acetate. Evaporation of the solvent gave a gum which was chromatographed on a silica column with a gradient of ethanol (0–1.5%) in CH<sub>2</sub>Cl<sub>2</sub> as eluent. A residue (1.77 g) was obtained, and it was submitted to hydrogenation in absolute ethanol (150 mL) in the presence of 10% palladium on activated charcoal (900 mg) and triethylamine (1.5 mL). After 48 h at room temperature, the catalyst was removed by filtration and washed with hot ethanol, and the filtrate was evaporated to dryness. To the residue was added 50 mL of water, and the pH was adjusted to 14 by 14% NH<sub>4</sub>OH. The precipitate was collected by filtration and washed with water, dried, and chromatographed on a neutral alumina column with a gradient of ethanol (0–2%) in CH<sub>2</sub>Cl<sub>2</sub> as eluent to give the titled compound **9** (1.3 g; 45%); <sup>1</sup>H NMR, δ 12.31 (s, 1H, NH), 9.87 (s, 1H, H-11), 8.94 (d, 1H, H-1), 8.54 (s, 1H, H-9), 8.18 (d, 1H, H-5), 8.04 (d, 1H, H-6), 7.82 (d, 1H, H-4), 7.63 (dd, 1H, H-2), 4.5–4.3 (m, 4H, OCH<sub>2</sub>CH<sub>2</sub> + CH<sub>2</sub>CH<sub>3</sub>), 2.86 (s, 3H, CH<sub>3</sub>-8), 2.9–2.8 (m, 2H, CH<sub>2</sub>CO), 2.4–2.3 (m, 2H, CH<sub>2</sub>CH<sub>2</sub>CH<sub>2</sub>), 1.46 (t, 3H, CH<sub>3</sub>CH<sub>2</sub>). Anal. Calcd for C<sub>22</sub>H<sub>22</sub>N<sub>2</sub>O<sub>3</sub>: C, 72.92; H, 6.07; N, 7.73. Found: C, 72.84; H, 5.96; N, 8.01. Similar preparation from 3-hydroxybenzopyridoindoles **8** or **12** and ethyl 4-bromobutyrate or ethyl 5-bromovalerate gave ester derivatives **10**, **13**, and **14**, respectively.

*Ethyl 5-(7H-benzo[*e*]pyrido[4,3-*b*]indol-3-yloxy)pentanoate* **10** was obtained in 47% yield; <sup>1</sup>H NMR, δ 12.07 (s, 1H, NH); 9.64 (s, 1H, H-11), 8.70 (d, 1H, H-1), 8.31 (s, 1H, H-9), 7.94 (d, 1H, H-5), 7.80 (d, 1H, H-6), 7.58 (d, 1H, H-4), 7.40 (dd, 1H, H-2), 4.2–4.0 (m, 4H, OCH<sub>2</sub>CH<sub>2</sub> + CH<sub>2</sub>CH<sub>3</sub>), 2.62 (s, 3H, CH<sub>3</sub>-8), 2.45 (t, 2H, CH<sub>2</sub>CO), 2.0–1.8 (m, 4H, OCH<sub>2</sub>CH<sub>2</sub>CH<sub>2</sub>), 1.22 (t, 3H, CH<sub>3</sub>CH<sub>2</sub>). Anal. Calcd for C<sub>23</sub>H<sub>24</sub>N<sub>2</sub>O<sub>3</sub>·2 H<sub>2</sub>O: C, 70.05; H, 6.59; N, 7.10. Found: C, 70.16; H, 6.44; N, 6.92.

*Ethyl 4-(11H-benzo[*g*]pyrido[4,3-*b*]indol-3-yloxy)butanoate* **13** was obtained in 46% yield; <sup>1</sup>H NMR, δ 12.18 (s, 1H, NH), 9.24 (s, 1H, H-7), 8.67 (d, 1H, H-1), 8.3–8.2 (m, 2H, H-6+H-9), 7.68 (d, 1H, H-5), 7.54 (d, 1H, H-4), 7.38 (dd, 1H, H-2), 4.25–4.05 (m, 4H, OCH<sub>2</sub>CH<sub>2</sub> + CH<sub>2</sub>CH<sub>3</sub>), 2.67 (s, 3H, CH<sub>3</sub>-10), 2.5–2.4 (m, 2H, CH<sub>2</sub>CO), 2.2–2.0 (m, 2H, CH<sub>2</sub>CH<sub>2</sub>CH<sub>2</sub>), 1.23 (t, 3H, CH<sub>3</sub>CH<sub>2</sub>). Anal. Calcd for C<sub>22</sub>H<sub>22</sub>N<sub>2</sub>O<sub>3</sub>: C, 72.92; H, 6.07; N, 7.73. Found: C, 73.02; H, 6.14; N, 7.80.

*Ethyl 5-(11H-benzo[*g*]pyrido[4,3-*b*]indol-3-yloxy)pentanoate* **14** was obtained in 45% yield; <sup>1</sup>H NMR, δ 12.17 (s, 1H, NH), 9.24 (s, 1H, H-7), 8.67 (d, 1H, H-1), 8.3–8.2 (m, 2H, H-6+H-9), 7.67 (d, 1H, H-5), 7.54 (d, 1H, H-4), 7.38 (dd, 1H, H-2), 4.3–4.0 (m, 4H, OCH<sub>2</sub>CH<sub>2</sub> + CH<sub>2</sub>CH<sub>3</sub>), 2.66 (s, 3H, CH<sub>3</sub>-10), 2.45 (t, 2H, CH<sub>2</sub>CO), 1.9–1.7 (m, 4H, OCH<sub>2</sub>CH<sub>2</sub>CH<sub>2</sub>), 1.22 (t, 3H, CH<sub>3</sub>CH<sub>2</sub>). Anal. Calcd for C<sub>23</sub>H<sub>24</sub>N<sub>2</sub>O<sub>3</sub>: C, 73.40; H, 6.38; N, 7.44. Found: C, 73.04; H, 6.53; N, 7.59.

**4. Saponification Reaction for the Production of the Acid Derivatives 3–6.** Preparation of 4-(7H-Benzo[*e*]pyrido[4,3-*b*]indol-3-yloxy)butanoic acid **3**: Example of the General Method. To a solution of NaOH (600 mg; 15 mmol) in water (30 mL) and ethanol (83 mL) was added the ester derivative **9** (1.0 g; 2.7 mmol), and the mixture was heated at reflux for 1 h. Evaporation to dryness under reduced pressure provided a solid residue, which was taken up in water (80 mL), and 1N HCl (15 mL) was added. The precipitate was collected by filtration and washed with water and dried, giving 900 mg (87%) of **3**;

<sup>1</sup>H NMR, δ 13.35 (s, 1H, NH), 12.20 (br.s, 1H, OH), 9.99 (s, 1H, H-11), 8.79 (d, 1H, H-1), 8.56 (s, 1H, H-9), 8.14 (d, 1H, H-5), 7.93 (d, 1H, H-6), 7.69 (d, 1H, H-4), 7.47 (dd, 1H, H-2), 4.21 (t, 2H, OCH<sub>2</sub>CH<sub>2</sub>), 2.76 (s, 3H, CH<sub>3</sub>), 2.55–2.45 (m, 2H, CH<sub>2</sub>CO), 2.2–2.0 (m, 2H, CH<sub>2</sub>CH<sub>2</sub>CH<sub>2</sub>). Anal. Calcd for C<sub>20</sub>H<sub>18</sub>N<sub>2</sub>O<sub>3</sub>·2.75 H<sub>2</sub>O: C, 62.58; H, 6.12; N, 7.30. Found: C, 62.41; H, 5.84; N, 7.24.

Similar preparation from ester derivatives **10**, **13**, and **14** gave acid derivatives **4**, **5**, and **6**, respectively.

*5-(7H-Benzo[*e*]pyrido[4,3-*b*]indol-3-yloxy)pentanoic acid* **4** was obtained in 98% yield; <sup>1</sup>H NMR, δ 12.89 (s, 1H, NH), 12.10 (br.s, 1H, OH), 9.84 (s, 1H, H-11), 8.75 (d, 1H, H-1), 8.45 (s, 1H, H-9), 8.06 (d, 1H, H-5), 7.88 (d, 1H, H-6), 7.64 (d, 1H, H-4), 7.44 (dd, 1H, H-2), 4.19 (t, 2H, OCH<sub>2</sub>CH<sub>2</sub>), 2.69 (s, 3H, CH<sub>3</sub>), 2.38 (t, 2H, CH<sub>2</sub>CO), 1.95–1.65 (m, 4H, OCH<sub>2</sub>CH<sub>2</sub>CH<sub>2</sub>). Anal. Calcd for C<sub>21</sub>H<sub>20</sub>N<sub>2</sub>O<sub>3</sub>·2.25 H<sub>2</sub>O: C, 64.86; H, 6.43; N, 7.21. Found: C, 64.79; H, 6.03; N, 7.05.

*4-(11H-Benzo[*g*]pyrido[4,3-*b*]indol-3-yloxy)butanoic acid* **5** was obtained in 94% yield; <sup>1</sup>H NMR, δ 12.87 (s, 1H, NH), 9.48 (s, 1H, H-7), 8.77 (d, 1H, H-1), 8.45–8.30 (m, 2H, H-6+H-9), 7.78 (d, 1H, H-5), 7.60 (d, 1H, H-4), 7.45 (dd, 1H, H-2), 4.22 (t, 2H, OCH<sub>2</sub>CH<sub>2</sub>), 2.76 (s, 3H, CH<sub>3</sub>), 2.6–2.5 (m, 2H, CH<sub>2</sub>CO), 2.2–2.0 (m, 2H, CH<sub>2</sub>CH<sub>2</sub>CH<sub>2</sub>). Anal. Calcd for C<sub>20</sub>H<sub>18</sub>N<sub>2</sub>O<sub>3</sub>·2.7 H<sub>2</sub>O: C, 62.73; H, 6.12; N, 7.32. Found: C, 62.46; H, 5.79; N, 7.13.

*5-(11H-Benzo[*g*]pyrido[4,3-*b*]indol-3-yloxy)pentanoic acid* **6** was obtained in 95% yield; <sup>1</sup>H NMR, δ 12.30 (s, 1H, NH), 9.28 (s, 1H, H-7), 8.69 (d, 1H, H-1), 8.3–8.2 (m, 2H, H-6+H-9), 7.68 (d, 1H, H-5), 7.55 (d, 1H, H-4), 7.39 (dd, 1H, H-2), 4.19 (t, 2H, OCH<sub>2</sub>CH<sub>2</sub>), 2.68 (s, 3H, CH<sub>3</sub>), 2.37 (t, 2H, CH<sub>2</sub>CO), 1.9–1.7 (m, 4H, OCH<sub>2</sub>CH<sub>2</sub>CH<sub>2</sub>). Anal. Calcd for C<sub>21</sub>H<sub>20</sub>N<sub>2</sub>O<sub>3</sub>·2 H<sub>2</sub>O: C, 65.62; H, 6.25; N, 7.29. Found: C, 65.83; H, 6.08; N, 7.37.

**III. Preparation of the Activated Esters 15–18 of the BePI and BgPI Derivatives 3–6.** Compounds **3–6** individually (0.13 mmol) were placed in a round-bottomed flask, and anhydrous CH<sub>3</sub>CN (5 mL) was added. Triethylamine (0.1 mL) was added, and the reaction mixture was stirred at room temperature for 5 min and then concentrated to dryness. The process was repeated three times, and the obtained salt was dried overnight in a desiccator which was filled with argon before being opened. Dichloromethane (5 mL) triethylamine (1.1 equiv) and then pentafluorophenyltrifluoroacetate (1 equiv) were successively added. The reaction mixture became homogeneous under vigorous stirring. After 15 min stirring, silica gel TLC analysis using ethyl acetate/hexane and then CH<sub>3</sub>CN as eluent showed the formation of a new compound *R*<sub>f</sub> = 0.7–0.8 (blue-colored spot after spraying with a 2,6-dibromo-4-benzoquinone-*N*-chloroimine solution in ethanol). (Starting material *R*<sub>f</sub> = 0.) The reaction mixture was concentrated and the residue purified on a small silica gel column using an ethyl acetate/hexane (1:1, v/v) mixture and then CH<sub>3</sub>CN as eluent.

**Mass Analysis.** ESI, polarity-positive. Calcd for compound **15** C<sub>26</sub>H<sub>17</sub>N<sub>5</sub>O<sub>3</sub>F<sub>5</sub>: 500.16. Found: M + H = 501.2. Calcd for compound **16** C<sub>27</sub>H<sub>19</sub>N<sub>5</sub>O<sub>3</sub>F<sub>5</sub>: 514.13. Found M + H = 515.2. Calcd for compound **17** C<sub>26</sub>H<sub>17</sub>N<sub>5</sub>O<sub>3</sub>F<sub>5</sub>: 500.16. Found: M + H = 501.1. Calcd for compound **18** C<sub>27</sub>H<sub>19</sub>N<sub>5</sub>O<sub>3</sub>F<sub>5</sub>: 514.13. Found M + H = 515.2.

**IV. Preparation of Iodoacetamido BePI Derivatives 19 and 20 from BePI Derivatives 1 and 2.** To modify the thiophosphate-containing oligonucleotides, two BePI derivatives with amino-containing linkers were transformed into activated acetamide derivatives following a previously published procedure (34). Compounds **19** and **20** were obtained as a pale yellow powder, after stirring

in hexane, with 75% yield. Silica gel TLC analysis using dichloromethane/methanol (90:10, v/v) mixture as eluent  $R_{f19} = 0.36$  (starting material  $R_f = 0$ ) and  $R_{f20} = 0.40$  (starting material  $R_f = 0$ ). Mass analysis. ESI, polarity-positive. Calcd for compound **19**  $C_{22}H_{23}N_4O_2I$ : 503.09. Found: M + H = 504.0.

**B. Synthesis of the Modified Oligo-2'-deoxyribonucleotides.** *I. Synthesis of Oligonucleotides 28–30 Containing Modified 2'-Deoxyuridine Involving a Linker Ending with cis Diol at the 5-Position.* *1. Synthesis of the Modified 2'-Deoxyuridine-Linker Derivative 27 (Scheme 3).* *3',5'-O-(Tetraisopropylidisiloxane-1,3-diyl)-5-N-(2,3-dihydroxypropyl)amino-2'-deoxyuridine 23.* To a solution of 5-bromo-2'-deoxyuridine **21** (1.58 g, 5 mmol) in anhydrous pyridine (20 mL) was added a solution of 1,3-dichloro-1,1,3,3-tetraisopropylidisiloxane (1.88 g, 6 mmol) in dry dichloromethane (10 mL) over 30 min under stirring. After 2 h of stirring at room temperature, the reaction was completed as shown by silica TLC analysis using dichloromethane/methanol (9:1, v/v) mixture as eluent ( $R_{f22} = 0.75$ ). The reaction mixture was quenched with 2 mL of methanol and the solvents removed under reduced pressure. The residue was dissolved with dichloromethane (70 mL) and washed with 5% aqueous sodium bicarbonate (3 × 70 mL). The organic phase was dried over  $Na_2SO_4$  and concentrated, and the residue was dried by coevaporation with toluene to leave a white foam. Yield 93% (2.21 g, 4.65 mmol). This product, **22**, was used in the next step without purification.

A solution of **22** (2.14 g, 4.5 mmol) and 3-amino-1,2-propanediol (4.2 g, 45 mmol) in ethanol (15 mL) was heated at 80 °C for 17 h. TLC analysis using the elution system reported above showed the formation of a new more polar product ( $R_{f23} = 0.2$ ). The solvent was evaporated under reduced pressure and the residue dissolved in ethyl acetate (50 mL) and washed with water (5 × 50 mL) to eliminate excess aminodiol. The organic solution was dried over  $Na_2SO_4$  and evaporated to dryness. Compound **23** was purified by silica gel column chromatography using dichloromethane/methanol (9:1, v/v) mixture as eluent. Yield: 76% (1.66 g, 3.42 mmol).  $^1H$  NMR ( $CDCl_3$ ),  $\delta$  ppm: 6.57 (s, 1H, H-6), 6.14 (m, 1H, H-1'), 4.55 (m, 1H, H-3'), 4.04 (m, 2H, H-4' + OH), 3.94 (t, 1H, NH), 3.78–3.60 (m, 3H, CH +  $CH_2$ ), 3.04 (d, 1H, OH), 3.00 (m, 2H, H-5', H-5''), 2.43 (m, 2H, H-2', H-2''), 2.30 (m, 2H,  $CH_2$ ), 1.09–1.06 (s, 28 H, 'Pr).

*5-N-(2,3-O-Dibenzoyloxypropyl)amino-2'-deoxyuridine 25.* To a stirred solution of **23** (1.56 g, 3.2 mmol) in anhydrous pyridine (20 mL) at 0 °C was added benzoyl chloride (1.12 mL, 1.35 g, 9.6 mmol) for 15 min, and the mixture was left under stirring for 2 h at room temperature. Methanol (2 mL) was added under cooling in an ice bath, and the resulting solution was poured into a 5% aqueous sodium bicarbonate solution (200 mL). The reaction mixture was extracted with dichloromethane (3 × 100 mL), the organic phases pooled, dried over  $Na_2SO_4$ , and concentrated to dryness, and the residue dried by coevaporation with toluene. Compound **24**, obtained as a yellow oil ( $R_{f24} = 0.85$  in the above-described TLC analysis system), was used in the next step without purification.

A solution of **24** in dry tetrahydrofuran (15 mL) was added to a 1.1 M solution of tetrabutylammonium fluoride in tetrahydrofuran (14 mL) with stirring. Silica gel TLC analysis using a dichloromethane/methanol (9:1, v/v) mixture as eluent showed complete reaction after 10 min with the apparition of a new spot ( $R_{f25} = 0.35$ ). The reaction was quenched by addition of a pyridine/methanol/water (3:1:1, v/v/v) mixture (15 mL), and a

suspension of Dowex 50W × 4-200 resin (pyridinium form) (15 g) was added in the above solvent mixture with gentle stirring. The final suspension was stirred for 0.5 h. The resin was filtered off and washed with the above-described solvent mixture (3 × 50 mL). The combined filtrates were evaporated to dryness under reduced pressure. Compound **25** was purified by silica gel column chromatography using 10% methanol in dichloromethane as eluent. Compound **25** was obtained as a white foam. Yield 72% (1.21 g, 2.30 mmol).  $^1H$  NMR ( $CDCl_3$ ),  $\delta$  ppm: 8.05–6.70 (m, 10 H, Ar-H), 5.70 (d, 1H, OH-3'), 5.30 (m, 1H, OH-5'), 3.44–3.30 (m, 3H, CH +  $CH_2$ ), 2.64 (m, 2H,  $CH_2$ ).

*5'-O-(4,4'-Dimethoxytrityl)-5-N-(2,3-O-dibenzoyloxypropyl)amino-2'-deoxyuridine-3'-O-(2-cyanoethyl)-N,N-diisopropylphosphoramidite 27.* Compound **25** (1.16 g, 2.2 mmol) was dried by coevaporation with anhydrous pyridine (3 × 10 mL), and a solution of 4,4'-dimethoxytrityl chloride (0.85 g, 2.5 mmol) in 10 mL of pyridine was added with exclusion of moisture. The reaction was quenched after 2 h by addition of methanol (1 mL), and the mixture was poured into a 5% aqueous sodium bicarbonate solution (70 mL). The crude product was extracted with dichloromethane (3 × 70 mL) and the organic phase pooled, dried over  $Na_2SO_4$ , and concentrated under reduced pressure. The residue was purified by silica gel column chromatography using a dichloromethane/methanol (98:2, v/v) mixture to give compound **26** ( $R_{f26} = 0.75$ , using the TLC analysis system described above). Yield: 90% (1.62 g, 1.98 mmol). Compound **26** (0.83 g, 1 mmol) was dried by coevaporation with anhydrous pyridine (5 mL) then with anhydrous  $CH_3CN$  (5 mL, three times) and left in a desiccator under vacuum overnight. The next day, the desiccator was filled with argon before its opening. The residue was solubilized with 1,2-dichloroethane (10 mL), and diisopropylethylamine (0.52 mL, 0.387 g, 3 mmol) was added, and then 2-cyanoethyldiisopropylchlorophosphoramidite (0.301 mL, 0.319 g, 1.35 mmol) was added dropwise under stirring at room temperature. After 15 min, silica gel TLC analysis using ethyl acetate/triethylamine mixture (95:5, v/v) mixture as eluent showed complete reaction, with the formation of two new spots corresponding to both isomers of the phosphoramidite derivative. The reaction mixture was diluted with methanol (1 mL) and after 10 min stirring concentrated to dryness. The residue was dissolved with ethyl acetate (50 mL) previously washed with a cold aqueous 10% sodium carbonate solution. The organic phase was washed with a cold 10% aqueous sodium carbonate solution (10 mL) and with cold saturated aqueous sodium chloride solution (10 mL), dried over  $Na_2SO_4$ , and concentrated to dryness. The residue was purified on a silica gel column using a ethyl acetate/triethylamine (99:1, v/v) mixture. After precipitation from hexane, compound **27** was obtained as a white powder. Yield 78% (0.8 g, 0.78 mmol).  $^1H$  NMR ( $CDCl_3$ ),  $\delta$  ppm: 7.94–6.76 (m, 23H, Ar), 6.2 (m, 1H, H1'), 5.25 (s, 1H, H-6), 4.75–3.25 (m, 5H, H-3', H-4', H-5', H-5'' + CH), 3.80 (s, 6H,  $OCH_3$ ), 3.60–3.23 (m, 8H,  $CH_2OH$  +  $CH_2OP$  +  $2CH$  +  $OCH_2$ ), 2.60–2.34 (m, 6H,  $CH_2CN$  + H-2', H-2'' + HN- $CH_2$ ), 1.17–1.12 (m, 12H, 4  $CH_3$ ).

*2. Synthesis of the Modified Oligo-2'-deoxyribonucleotides 28–30 Involving Modified 2'-Deoxyuridine Containing a Linker Ending with cis Diol (Scheme 3).* The oligo-2'-deoxyribonucleotides were assembled using classical phosphoramidite chemistry on a CPG support at a  $\mu$ mol scale. To introduce the modified 2'-deoxyuridine residue into the oligonucleotides, an automated prolonged coupling step (5 min) was used for compound **27**.



**Table 1.**  $\lambda$  Max Values for Oligo-2'-deoxyribonucleotide–BePI and Oligo-2'-deoxyribonucleotide–BgPI Conjugates, Retention Times<sup>a</sup> for the Modified Oligonucleotides 28–32 and for the Oligo-2'-deoxyribonucleotide–BePI and Oligo-2'-deoxyribonucleotide–BgPI Conjugates II–X, and  $T_m$  Values for Triplexes Formed between Various Conjugates and the Double-Stranded Target<sup>b,c</sup>

oligonucleotides	$\lambda_{\text{uv}}^{\text{uv}}$ (nm)	$\lambda_{\text{max}}^{\text{vis}}$ (nm)	$t_R$ (min) C18 column	$T_m$ (°C) ( $\pm 1$ °C)
<b>I</b> 5'-d-(TTTTCTTTTC) <sup>3'</sup>	267.7	—	5 min	~12
<b>28</b> 5'-d-(dU*TTTCTTTTC) <sup>3'</sup>	268.8	—	6 min 10 s	n.m.
<b>29</b> 5'-d-(TTTTCTTdU*TC) <sup>3'</sup>	268.8	—	5 min 56 s	n.m.
<b>30</b> 5'-d-(dU*TTTCTTdU*TC) <sup>3'</sup>	268.8	—	6 min 58 s	n.m.
<b>31</b> 5'-d-(dU+TTTCTTTTC) <sup>3'</sup>	267.6	—	12 min 32 s	n.m.
<b>32</b> 5'-d-(TTTTCTTdU+TC) <sup>3'</sup>	267.6	—	12 min	~12
<b>II</b> 5'-d-(TTTTCTTTTC) <sup>3'</sup>	268.8	365.1	12 min 44 s	42
<b>III</b> 5'-d-(X'TTTCTTTTC) <sup>3'</sup>	268	365.1	13 min 04 s	34
<b>IV</b> 5'-d-(TTTTCTTXXTC) <sup>3'</sup>	268.8	362.9	12 min 15 s	≤12
<b>V</b> 5'-d-(TTTTCTTXXTC) <sup>3'</sup>	268.8	363.9	12 min 52 s	≤12
<b>VI</b> 5'-d-(XTTCTTXXTC) <sup>3'</sup>	268.8	367.5	16 min 56 s	≤12
<b>VII</b> 5'-d-(WTTTCTTTTC) <sup>3'</sup>	268.8	362.9	20 min 36 s	<12
<b>VIII</b> 5'-d-(TTTTCTTWTC) <sup>3'</sup>	268.8	362.9	20 min 13 s	<12
<b>IX</b> 5'-d-(WTTTCTTTTC) <sup>3'</sup>	270.0	<i>d</i>	21 min 39 s	<12
<b>X</b> 5'-d-(TTTTCTTWTC) <sup>3'</sup>	270.0	<i>d</i>	19 min 53 s	<12

<sup>a</sup> Obtained by reversed-phase HPLC analyses, performed on a Lichrospher 100 RP18 (5  $\mu$ M) column (125 mm  $\times$  4 mm) from Merck using a linear gradient of CH<sub>3</sub>CN (12.5–31.25% over 15 min for compounds **28–32** and **I–VI**) and (8–32% over 30 min for compounds **11–12** and **VII–X**) in 0.1 M aqueous triethylammonium acetate, pH 7, with a flow rate of 1 mL/min. <sup>b</sup> In a 10 mM sodium cacodylate, pH 6, containing 100 mM NaCl and 10 mM MgCl<sub>2</sub>. <sup>c</sup> Oligonucleotide concentrations were 1  $\mu$ M of the duplex target D (with a 1/1.2 ratio of purine/pyrimidine-containing strands), and 1.5  $\mu$ M of the third strand. n.m. = not measured.

<sup>d</sup> For these conjugates a weak absorption is observed between 320 and 420 nm, and the  $\lambda_{\text{max}}$  of the UV band is slightly red-shifted as compared to the UV  $\lambda_{\text{max}}$  of other conjugates.

The average coupling efficacy was 85–95%. The deprotection step was performed by 28% aqueous ammonia treatment for 3 h at 55°C or for 18 h at 20°C. Purifications were performed either on 20% PAGE in denaturing conditions or by reversed-phase HPLC (see legend for Table 1). Oligonucleotides **28** and **29** with one modified 2'-deoxyuridine or oligonucleotide **30** with two modified 2'-deoxyuridines gave the following retention times: 6 min 10 s, 5 min 56 s, and 6 min 58 s.

**II. Synthesis of Oligonucleotides 31 and 32 Containing Modified 2'-Deoxyuridine Involving a Linker at the 5-Position Ending with an Amino Function.** Oligonucleotides **31** and **32** were obtained via phosphoramidite chemistry using the Amino-Modifier C2 dT from Glen Research. Deprotection and purification steps were performed using classical procedures. Retention times obtained by reversed-phase analysis are given in Table 1

**III. Synthesis of the Modified Oligonucleotide 43 Involving the Sugar-Linker Derivative between the Second and the Third Nucleotides.** 1. **Synthesis of the 2'-Deoxyribose-Linker Derivatives 42** (Scheme 4). *N*-Fmoc-3-aminopropan-1-ol **33**. To a 9-fluorenylmethyl chloroformate (2.058 g, 10 mmol) solution in dry ether (120 mL) was added dropwise, under stirring at 0°C, a solution of 3-amino-1-propanol (0.75 g, 20 mM) in 1,2-dichloroethane (30 mL) over 10 min. The mixture was maintained at 0°C for 20 min and then left to warm to room temperature for 20 min. Silica gel TLC analysis using a hexane/ethyl acetate (1:1, v/v) mixture as eluent showed complete reaction with a new spot ( $R_{33}$  = 0.2). The mixture was concentrated to dryness, and then dichloromethane (60 mL) was added. The organic phase was washed with H<sub>2</sub>O (15 mL, twice). The organic phase was dried over Na<sub>2</sub>SO<sub>4</sub> and then concentrated to dryness. The residue was

purified on a silica gel column using dichloromethane/methanol (99:1, v/v, then 98:2, v/v) as eluent. Yield 90% (1.62 g, 9 mmol). <sup>1</sup>H NMR (CDCl<sub>3</sub>),  $\delta$  ppm: 7.77–7.26 (m, 8H, Ar), 5.03 (s, 1H, NH), 4.43 (d, 2H,  $J$  = 6.64 Hz, O–CH<sub>2</sub>), 4.20 (t, 1H fmoc,  $J$  = 6.6 Hz), 3.64 (d, 2H,  $J$  = 5.48, CH<sub>2</sub>), 3.34 (d, 2H,  $J$  = 5.92 CH<sub>2</sub>), 1.69 (t, 2H,  $J$  = 5.64, CH<sub>2</sub>).

*1'*-Deoxy-1'-(*N*-fmoc-3-aminopropyl)-2,3,5-tri-*O*-acetyl- $\beta$ -D-ribofuranose **35**. Compound **33** (3.12 g, 10.5 mmol) and  $\beta$ -D-ribofuranose 1,2,3,5-tetraacetate **34** (3.18 g, 10 mmol) were dried overnight in a desiccator containing P<sub>2</sub>O<sub>5</sub>. The mixture was partially dissolved by addition of 1,2-dichloroethane (85 mL) and cooled to –10°C with an NaCl-ice bath, and trimethylsilyltrifluoromethanesulfonate (2.17 mL, 2.67 g, 12 mmol) was added slowly with a syringe over 10 min. The reaction mixture was stirred for 15 min at –10°C and then for 1 h at room temperature. Silica gel TLC in hexane/ethyl acetate (1:1, v/v) showed complete reaction with a new spot  $R_{35}$  = 0.46 and a side product with  $R_f$  = 0.63. The reaction mixture was cooled, pyridine (8 mL) was added, and the mixture was left to react for 15 min. The reaction mixture was then concentrated to dryness, the residue solubilized with dichloromethane (100 mL), and the organic phase washed with a 5% aqueous sodium hydrogenocarbonate solution (20 mL) and then with saturated sodium chloride aqueous solution (20 mL). The organic phase was dried over Na<sub>2</sub>SO<sub>4</sub> and concentrated to dryness. The residue was purified on a silica gel column using a hexane/ethyl acetate mixture (60:40, v/v) then (55:45, v/v) as eluent. Yield 30% (1.7 g, 3.15 mmol).

<sup>1</sup>H NMR (CDCl<sub>3</sub>),  $\delta$  ppm: 7.76–7.25 (m, 8H, Ar), 5.22 (d, 1H,  $J$  = 3.73, H-1'), 5.13 (br s, 1H, NH), 4.38 (d, 2H,  $J$  = 6.58 O–CH<sub>2</sub>), 4.31–4.10 (m, 5H, H-3', H-4', H-5', H-5'' + C–H fmoc), 3.85–3.72 (m, 2H, CH<sub>2</sub>), 3.50–3.15 (m, 3H, CH<sub>2</sub>O, H-2'), 2.1–2.00 (m, 9H, CH<sub>3</sub>–C(O)), 1.83–1.70 (m, 2H, CH<sub>2</sub>).

*1'*-Deoxy-1'-(*N*-fmoc-3-aminopropyl)- $\beta$ -D-ribofuranose **36**. Compound **35** (2 g, 3.6 mmol) was dissolved at room temperature in a 0.1 M solution of KCN in methanol (105 mL, 3.6 mmol). After 1 h stirring, silica gel TLC analysis using hexane/ethyl acetate (1:1, v/v) mixture as eluent, showed complete reaction with a new spot  $R_{36}$  = 0.21. The solution was evaporated to dryness. The residue was solubilized with dichloromethane (80 mL) and the organic phase was washed with a 5% aqueous sodium hydrogenocarbonate solution (15 mL) and water (15 mL), dried over Na<sub>2</sub>SO<sub>4</sub>, and concentrated to dryness. The residue was purified on a silica gel column using a dichloromethane/methanol (97:3, v/v) mixture as eluent. Yield 70% (1 g, 2.52 mmol). <sup>1</sup>H NMR (CDCl<sub>3</sub>),  $\delta$  ppm: 7.77–7.24 (m, 8H, Ar), 5.8 (br s, 1H, NH), 5.3 (m, 1H, H1'), 4.36 (d, 2H,  $J$  = 3.22 Hz, O–CH<sub>2</sub>), 4.14 (m, C–H fmoc), 4.17–3.60 (m, 7H, H-3', H-4', H-5', H-5'' + 3 OH), 3.44–3.10 (m, 5H, CH<sub>2</sub>, H-2' + CH<sub>2</sub>O), 1.70–1.60 (m, 2H, CH<sub>2</sub>).

*1'*-Deoxy-1'-(*N*-fmoc-3-aminopropyl)-3,5-*O*-(tetraisopropylidisiloxane-1,3-diyl)- $\beta$ -D-ribofuranose **37**. Compound **36** (0.9 g, 2 mmol) and imidazole (0.57 g, 8 mmol) were dried by coevaporation with anhydrous pyridine (10 mL, three times) and left overnight in a desiccator containing P<sub>2</sub>O<sub>5</sub>. The residue was solubilized with anhydrous pyridine (20 mL), and 1,3-dichloro-1,1,3,3-tetraisopropylidisiloxane (0.73 mL, 0.72 g, 2.2 mmol) in 1,2-dichloromethane solution (1 mL) was added dropwise at 0°C under stirring. The reaction mixture was left to react at room temperature, under stirring, for 1 h. Silica gel TLC analysis using a hexane/ethyl acetate (1:1, v/v) mixture as eluent showed complete reaction with a new spot  $R_{37}$  = 0.75. Methanol (5 mL) was added and the stirring maintained for 15 min.



The reaction mixture was concentrated to dryness, and the residue was dissolved with dichloromethane (60 mL). The organic phase was washed with a 5% aqueous sodium hydrogenocarbonate solution (15 mL) and with water (15 mL), dried over  $\text{Na}_2\text{SO}_4$ , and concentrated to dryness. The residue was purified on a silica gel column using a dichloromethane and then a dichloromethane/methanol (98:2, v/v) mixture as eluent. Yield 85% (1.2 g, 1.7 mmol).

$^1\text{H}$  NMR ( $\text{CDCl}_3$ ),  $\delta$  ppm: 7.77–7.26 (m, 8H, Ar), 5.09 (m, 1H, H-1'), 4.92 (br s, 1H, NH), 4.52–4.49 (m, 2H, H-5', H-5''), 4.39 (d, 2H,  $J = 6.9$  Hz, O-CH<sub>2</sub>), 4.24–4.18 (m, 1H, CH-fmoc), 4.07–3.7 (m, 5H, OH, H-3', H-4' + CH<sub>2</sub>O), 3.50–3.15 (m, 3H, CH<sub>2</sub>N, H-2'), 1.76 (m, 2H, CH<sub>2</sub>), 1.15–1.03 (m, 28H,  $^i\text{Pr}$ ).

*1'-Deoxy-1'-(N-fmoc-3-aminopropyl)-2'-O-phenoxythiocarbonyl-3,5'-O-(tetraisopropylidisiloxane-1,3-diyl)- $\beta$ -D-ribofuranose 38.* Compound **37** (1.2 g, 1.8 mmol) was dried by coevaporation with anhydrous pyridine (10 mL, three times). The residue was solubilized with anhydrous pyridine (20 mL), and phenylchlorothionoformate (0.37 mL, 0.46 g, 27 mmol) was added under stirring. The reaction mixture was stirred for two additional hours. Silica gel TLC analysis using a hexane/ethyl acetate (5:2, v/v) mixture as eluent showed complete reaction with a new spot  $R_{38} = 0.55$  (starting material  $R_{37} = 0.33$ ). The reaction mixture was concentrated to dryness under vacuum and the residue dissolved with dichloromethane (60 mL). The organic phase was washed with a 5% aqueous sodium hydrogenocarbonate solution (15 mL) and with water (15 mL), dried over  $\text{Na}_2\text{SO}_4$ , and concentrated to dryness. The residue was purified on a silica gel column using a hexane:ethyl acetate (5:0.5 to 5:2, v/v) mixture as eluent. Yield 71% (1 g, 1.27 mmol).  $^1\text{H}$  NMR ( $\text{CDCl}_3$ ),  $\delta$  ppm: 7.77–7.10 (m, 8H, Ar), 5.71 (m, 1H, H-1'), 5.08 (br s, 1H, NH), 4.68–4.72 (m, 1H, H-5'), 4.40 (d, 2H,  $J = 5.61$  Hz, O-CH<sub>2</sub>), 4.26–4.19 (m, 1H, CH fmoc), 4.04–3.70 (m, 3H, H-3', H-4', H-5''), 3.56–3.14 (m, 5H, CH<sub>2</sub>O + CH<sub>2</sub>N + H-2'), 1.80–1.70 (m, 2H, CH<sub>2</sub>), 1.15–1.00 (m, 28H,  $^i\text{Pr}$ ).

*1'-Deoxy-1'-(N-fmoc-3-aminopropyl)-3,5'-O-(tetraisopropylidisiloxane-1,3-diyl)- $\beta$ -D-2'-deoxyribofuranose 39.* Compound **38** (0.8 g, 1 mmol) was coevaporated three times with dry toluene (10 mL). The residue was left in a desiccator for 3 h, which was then filled with argon before its opening. The residue was solubilized with freshly distilled toluene (over  $\text{P}_2\text{O}_5$ ). Tributyltin hydride (0.4 mL, 0.43 g, 1.5 mmol) was added at room temperature and then  $\alpha$ ,  $\alpha'$ -azaisobutyronitrile (0.05 g, 0.3 mmol). The mixture was stirred for a few min at room temperature and then refluxed for 1 h. Another amount of  $\alpha$ ,  $\alpha'$ -azaisobutyronitrile (0.03 g, 0.2 mmol) was added, and the mixture was refluxed for an additional 1 h. Silica gel TLC analysis using a dichloromethane/methanol (98:2, v/v) mixture as eluent showed complete reaction with a new spot  $R_{39} = 0.83$  (starting material  $R_f = 0.90$ ). The reaction mixture was concentrated to dryness under vacuum and the residue dissolved with dichloromethane (50 mL). The organic phase was washed with a 5% aqueous sodium hydrogenocarbonate solution (10 mL) and with water (10 mL), dried over  $\text{Na}_2\text{SO}_4$  and concentrated to dryness. The residue was purified on a silica gel column using a dichloromethane/ethyl acetate (98:2 to 96:4, v/v) mixture as eluent. Yield: 66% (0.43 g, 0.66 mmol).  $^1\text{H}$  NMR ( $\text{CDCl}_3$ ),  $\delta$  ppm: 7.77–7.28 (m, 8H, Ar), 5.23 (br s, 1H, NH), 5.03 (m, 1H, H-1'), 4.70–4.60 (m, 1H, H-5'), 4.36 (d, 2H,  $J = 6.10$  Hz, O-CH<sub>2</sub>), 4.22–4.19 (m, 1H, CH fmoc), 4.05–3.66 (m, 3H, H-3', H-4', H-5''),

3.35–3.21 (m, 4 H, CH<sub>2</sub>O + CH<sub>2</sub>N), 2.30–2.05 (m, 2H, H-2', H-2''), 1.80–1.71 (m, 2H, CH<sub>2</sub>), 1.14–0.98 (m, 28 H,  $^i\text{Pr}$ ).

*1'-Deoxy-1'-(N-fmoc-3-aminopropyl)- $\beta$ -D-2'-deoxyribofuranose 40.* Compound **39** (0.43 g, 0.66 mmol) was dried by coevaporation with  $\text{CH}_3\text{CN}$  (10 mL, three times). The residue was solubilized with anhydrous THF (6 mL), and the reaction mixture was cooled to 0 °C with an ice–water bath. Tetrabutylammonium fluoride (1.3 mL of 1.1 M solution in THF, 1.3 mmol) was added. The reaction mixture was stirred for 15 min at 0 °C. Silica gel TLC in dichloromethane/methanol (90:10, v/v) showed complete reaction with a new spot  $R_{40} = 0.44$  (starting material  $R_f = 0.88$ ). The reaction mixture was diluted with water (1 mL) and concentrated to dryness. The residue was purified on a silica gel column using a dichloromethane/ethyl acetate (98:2 to 96:4, v/v) mixture as eluent. Yield 70% (0.19 g, 0.46 mmol).  $^1\text{H}$  NMR ( $\text{CDCl}_3$ ),  $\delta$  ppm: 7.77–7.28 (m, 8H, Ar), 5.21–5.16 (m, 2H, H1', NH), 4.48–4.41 (m, 3H, H-5' + O-CH<sub>2</sub>), 4.20 (m, 1H, CH fmoc), 4.01–3.99 (m, 1H, OH), 3.84–3.54 (m, 4H, H-3', H-4', H-5'', OH), 3.47–3.24 (m, 4 H, 2 CH<sub>2</sub>), 2.23–2.07 (m, 2H, 2', 2''), 1.77–1.73 (m, 2H, CH<sub>2</sub>).

*1'-Deoxy-1'-(N-fmoc-3-aminopropyl)- $\beta$ -D-2'-deoxyribofuranose-5'-O-(4,4'-dimethoxytrityl) 41.* Compound **40** (0.070 g, 0.17 mmol) was coevaporated with anhydrous pyridine (5 mL, three times). The residue was solubilized with pyridine (5 mL), and dimethoxytritylchloride (170 mg, 0.5 mmol) was added under stirring. Silica gel TLC analysis using a dichloromethane/methanol (90:10, v/v) mixture as eluent showed complete reaction with a new spot  $R_{41} = 0.75$  (starting material  $R_f = 0.44$ ). The reaction mixture was diluted with methanol (1 mL) and after 15 min stirring concentrated to dryness. The residue was dissolved with dichloromethane (20 mL). The organic phase was washed with a 5% aqueous sodium hydrogenocarbonate solution (5 mL) and with water (5 mL), dried over  $\text{Na}_2\text{SO}_4$ , and concentrated to dryness. The residue was purified on a silica gel column using dichloromethane and then a dichloromethane/methanol (99:1, v/v) mixture as eluent. Yield 72% (0.086 g, 0.124 mmol).  $^1\text{H}$  NMR ( $\text{CDCl}_3$ ),  $\delta$  ppm: 7.76–6.78 (m, 21 H Ar), 5.11 (m, 1H, H-1'), 4.93 (br s, 1H, NH), 4.36 (d, 2H,  $J = 6.77$  Hz, O-CH<sub>2</sub>), 4.19–4.17 (m, 1H, CH fmoc), 4.0–3.98 (m, 1H, OH), 3.77–3.66 (m, 6H, H-3', H-4', H-5', H-5'' + CH<sub>2</sub>O), 3.75 (s, 6H, OCH<sub>3</sub>), 3.12–3.07 (m, 2H, CH<sub>2</sub>N), 2.17–2.02 (m, 2H, H-2', H-2''), 1.61–1.56 (m, 2H, CH<sub>2</sub>).

*1'-Deoxy-1'-(N-fmoc-3-aminopropyl)- $\beta$ -D-2'-deoxyribofuranose-5'-O-(4,4'-dimethoxytrityl)-3'-O-(2-cyanoethyl N,N-diisopropylphosphoramidite 42.* Compound **41** (0.08 g, 0.11 mmol) was dried by coevaporation with anhydrous pyridine (5 mL, twice) and then with anhydrous  $\text{CH}_3\text{CN}$  (5 mL, twice) and left in a desiccator under vacuum overnight. The next day the desiccator was filled with argon before its opening. The residue was solubilized with 1,2-dichloroethane (2 mL); then diisopropylethylamine (0.1 mL, 0.072 g, 0.55 mmol) was added, and finally 2-cyanoethyl diisopropylchlorophosphoramidite (0.040 g, 0.165 mmol) was added dropwise under stirring at room temperature. After 20 min, silica gel TLC analysis using a ethyl acetate/triethylamine (95:5, v/v) mixture as eluent showed complete reaction with the formation of a new spot  $R_{42} = 0.82$  (starting material  $R_{41} = 0.61$ ). The residue was dissolved with ethyl acetate (5 mL) previously washed with a cold aqueous 10% sodium carbonate solution. The organic phase was washed with a cold 10% aqueous sodium carbonate solution (5 mL) and with a cold saturated aqueous sodium chloride solution (5 mL), dried over  $\text{Na}_2\text{SO}_4$ , and concentrated to dryness. The

residue was purified on a silica gel column using a dichloromethane/triethylamine (99:1, v/v) mixture as eluent. The collected product was dried in a desiccator overnight, solubilized with ethyl acetate (3 mL), and precipitated in anhydrous hexane (50 mL) at  $-70^{\circ}\text{C}$ . Yield 85% (0.085 g, 0.093 mmol).  $^1\text{H}$  NMR ( $\text{CDCl}_3$ ),  $\delta$  ppm: 7.76–6.78 (m, 21H, Ar), 5.20 (m, 1H, H1'), 5–4.90 (br s, 1H, NH), 4.34 (d, 2H,  $J = 7.04$  Hz, O–CH<sub>2</sub>), 4.27–4.16 (m, 1H, fmoc), 3.75–3.13 (m, 12H, H-3', H-4', H-5', H-5'' + 3CH<sub>2</sub> + 2CH), 3.74 (s, 6H, OCH<sub>3</sub>), 2.56 (t, 2H,  $J = 6.45$  Hz, CH<sub>2</sub>CN), 2.20–2.17 (m, 2H, H-2', H-2''), 1.65–1.63 (m, 2H, CH<sub>2</sub>), 1.17–1.12 (m, 12H, 4 CH<sub>3</sub>).

$^{31}\text{P}$  NMR ( $\text{CDCl}_3$ ),  $\delta$  ppm: 149.3–150 ppm.

**2. Preparation of the Modified Oligo-2'-deoxyribonucleotide 43 Involving the Sugar-Linker Derivative between the Second and the Third Nucleotides.** The oligo-2'-deoxyribonucleotide was assembled using classical phosphoramidite chemistry on a CPG support at a  $\mu\text{mol}$  scale. To introduce the modified 2'-deoxyribose-linker residue into the oligonucleotide, a manual coupling step (10 min) was used for compound **42**. The coupling efficacy was 85–95%. The deprotection step was performed by 28% aqueous ammonia treatment for 18 h at  $20^{\circ}\text{C}$ . Purification was performed by ion exchange chromatography on a DEAE column (8  $\mu\text{m}$ , 100 mm  $\times$  10 mm, Waters) using a linear gradient of NaCl (0 to 0.725 M over 30 min) in Tris/HCl pH 7, 25 mM buffer containing 10% MeOH. After the desalting and detritylation steps (using an 80% acid acetic treatment for 20 min), reversed-phase chromatography analyses were performed on a Lichrospher 100 RP18 (5  $\mu\text{m}$ ) column (125 mm  $\times$  4 mm) from Merck with a linear gradient of CH<sub>3</sub>CN (12.5–35% over 30 min) in 0.1 M aqueous triethylammonium acetate, pH 7, with a flow rate of 1 mL/min. One peak was obtained with  $t_{\text{R}43} = 5$  min.

**IV. Synthesis of Modified Oligonucleotides Involving One or Two Internucleotidic Thiophosphate Groups 44 and 45, Respectively.** The oligonucleotides involving one or two phosphorothioate groups were assembled using classical phosphoramidite chemistry at the  $\mu\text{mol}$  scale, except that at the site preselected for the introduction of a phosphorothioate group, the oxidation step by iodine was replaced by a sulfuration step using a 15 min treatment with a 0.5 M tetraethylthiuram disulfide solution in anhydrous CH<sub>3</sub>CN (35). The deprotection step was carried out using aqueous concentrated (28%) ammonia treatment overnight at room temperature. Purification was performed by reversed-phase chromatography or 20% PAGE in denaturing conditions. In the case of monothiophosphate, oligonucleotides were eluted as two peaks with very close retention times ( $t_{\text{R}} = 5$  min 36 s and  $t_{\text{R}} = 6$  min) corresponding to the two diastereoisomers. In the case of oligonucleotides with two phosphorothioate groups, three main peaks were observed by reversed-phase analysis (see Table 2) corresponding to the mixture of isomers. 20% PAGE analysis in denaturing conditions (Figure 7) exhibited only one band for the mixture of isomers of either the monophosphorothioate oligonucleotide **44** (lane 1) or the diphosphorothioate-containing oligonucleotide **45** (lane 4) with very close mobilities for oligonucleotides **44** and **45**.

**C. Preparation of the Oligo-2'-deoxyribonucleotide-intercalator Conjugates II–XXI. I. Base-Linked BePI Derivatized Oligo-2'-deoxyribonucleotides II–VI (Figure 2).** Diol-containing oligonucleotide **28**, **29**, or **30** (25–50 nmol) were oxidized with a 20 mM sodium periodate solution (25  $\mu\text{L}$ ) for 1 h at room temperature. The resulting aldehyde-containing oligonucleotide was

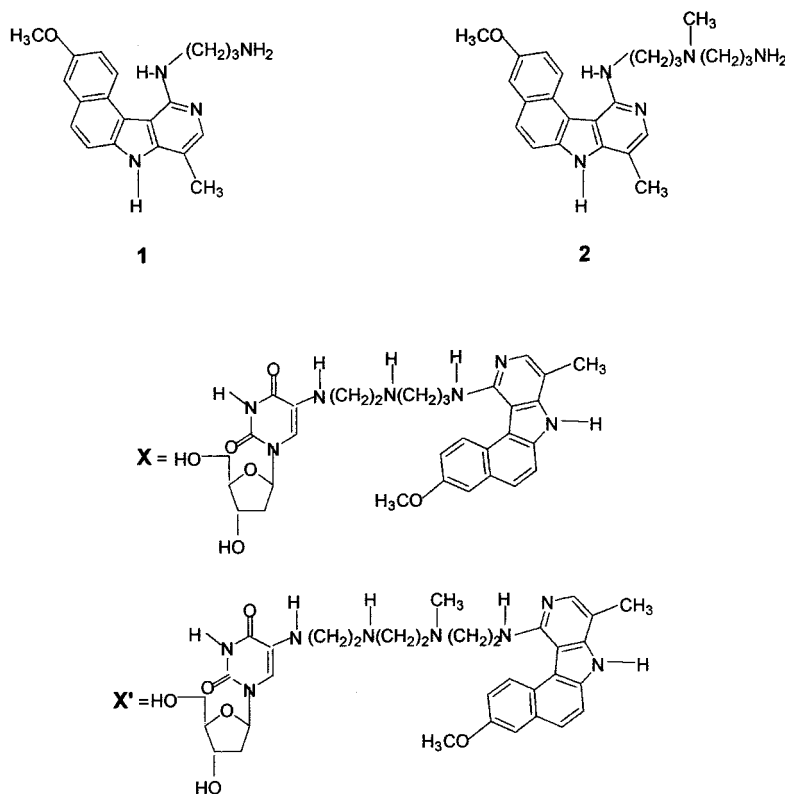
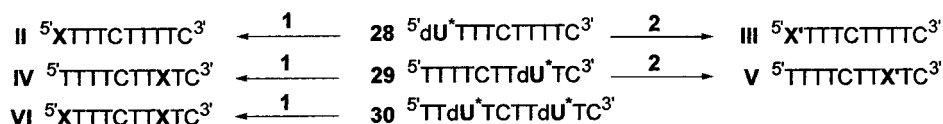
**Table 2.**  $\lambda$  Max Values for the Modified Oligo-2'-deoxyribonucleotides **43**, **44**, and **45** and Oligo-2'-deoxyribonucleotide–BePI and Oligo-2'-deoxyribonucleotide–BgPI Conjugates **XI–XXI**, Retention Times<sup>a</sup> for the Modified Oligonucleotides **41**, **44**, and **45** and for the Oligo-2'-deoxyribonucleotide–BePI and Oligo-2'-deoxyribonucleotide–BgPI Conjugates **XI–XXI**, and  $T_{\text{m}}$  Values for Triplexes Formed between Various Conjugates and the Double-Stranded Target<sup>b,c</sup>

oligonucleotides	$\lambda_{\text{max}}^{\text{uv}}$ (nm)	$\lambda_{\text{max}}^{\text{vis}}$ (nm)	$t_{\text{R}}$ (min)	$T_{\text{m}}$ ( $^{\circ}\text{C}$ )
<b>I</b> 5'-d-(TTTTCTTTTC) <sup>3'</sup>	267.7	—	5 min 10 s	$\approx 12$
<b>43</b> 5'-d-(TTS*TTCTTTTC) <sup>3'</sup>	267.6	—	5 min	n.m.
<b>44</b> 5'-d-(TTTTCTTp(S)TTC) <sup>3'</sup>	267.6	—	5 min 36 s	n.m.
	267.6	—	6 min	
<b>45</b> 5'-d-(TTP(S)TTCTTp(S)TTC) <sup>3'</sup>	267.6	—	6 min 8 s	n.m.
	267.6	—	6 min 30 s	
	267.6	—	6 min 52 s	
<b>XI</b> 5'-d-(TTY <sub>1</sub> TTCTTTTC) <sup>3'</sup>	268.8	362.9	11 min 28 s	$\leq 12$
<b>XII</b> 5'-d-(TTY <sub>2</sub> TTCTTTTC) <sup>3'</sup>	268.8	362.9	13 min 56 s	$\leq 12$
<b>XIII</b> 5'-d-(TTZ <sub>1</sub> TTCTTTTC) <sup>3'</sup>	270.0	<i>d</i>	17 min 09 s	$\leq 12$
<b>XIV</b> 5'-d-(TTZ <sub>2</sub> TTCTTTTC) <sup>3'</sup>	271.2	<i>d</i>	14 s 20 s	$\leq 12$
<b>XV</b> 5'-d-(TTTTCTTpTTC) <sup>3'</sup> fast	267.6	363.9	12 min 52 s	$\leq 13$
<b>R</b>				
<b>XVI</b> 5'-d-(TTTTCTTpTTC) <sup>3'</sup> slow	267.6	366.3	13 min 15 s	$\leq 15$
<b>R</b>				
<b>XVII</b> 5'-d-(TTTTCTTpTTC) <sup>3'</sup> fast	268.8	366.3	11 min 35 s	$\leq 12$
<b>R'</b>				
<b>XVIII</b> 5'-d-(TTTTCTTpTTC) <sup>3'</sup> slow	267.6	362.9	12 min 19 s	$\leq 12$
<b>R'</b>				
<b>XIX</b> 5'-d-(TTP <sub>1</sub> TTCTTpTTC) <sup>3'</sup>	267.6	366.3	15 min 22 s	$\leq 18$
<b>R</b> <b>R</b>	267.6	367.5	16 min.	
	267.6	366.3	16 min 26 s	
<b>XX</b> 5'-d-(TTP <sub>2</sub> TTCTTpTTC) <sup>3'</sup>	267.6	367.5	15 min 14 s	$< 12$
<b>R'</b> <b>R'</b>	267.6	367.5	15 min 51 s	
	268.8	363.9	16 min 15 s	
<b>XXI</b> 5'-d-(TTTTCTTpTTC) <sup>3'</sup>	268.8	362.9	12 min 17 s	$< 12$
<b>V</b>				

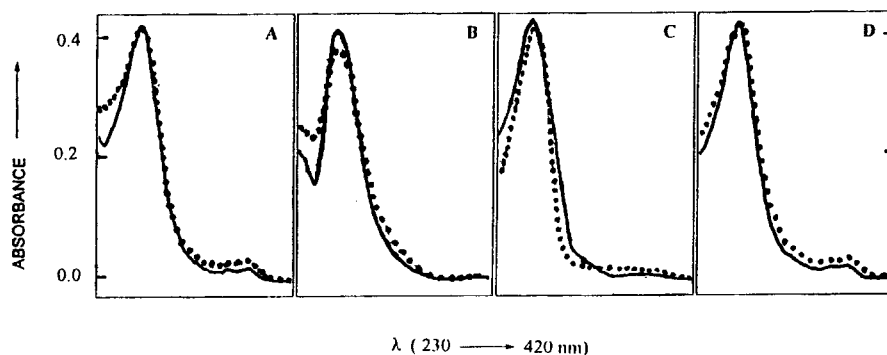
<sup>a</sup> Obtained by reversed-phase HPLC analyses, performed on a Lichrospher 100 RP18 (5 mM) Column (125 mm  $\times$  4 mm) from Merck using a linear gradient of CH<sub>3</sub>CN (12.5–31.25% over 15 min) in 0.1 M aqueous triethylammonium acetate, pH 7, with a flow rate of 1 mL/min. <sup>b</sup> Conditions used are the same as described in Table 1. <sup>c</sup> n.m. = not measured. <sup>d</sup> For these conjugates a weak absorption is observed between 320 and 420 nm and the  $\lambda_{\text{max}}$  of the UV band is slightly red-shifted as compared to the UV  $\lambda_{\text{max}}$  of other conjugates.

precipitated as cetyl trimethylammonium salt, washed with water (50  $\mu\text{L}$ ) and redissolved in methanol (50  $\mu\text{L}$ ). A solution of a BePI reagent (0.1 M in methanol) (25–50  $\mu\text{L}$ ) was then added and then sodium cyanoborohydride in a 0.5 M aqueous sodium acetate solution (1 mg in 10  $\mu\text{L}$ ), pH 5. The mixture was allowed to rest for 24 h at  $40^{\circ}\text{C}$ . Next, a 0.1 M SDS solution in methanol (10  $\mu\text{L}$ ) was added, followed by addition of water (500  $\mu\text{L}$ ). Excess BePI was extracted with *n*-butanol (3  $\times$  300  $\mu\text{L}$ ), and the oligonucleotide–BePI conjugate was precipitated with a 4% lithium perchlorate solution in acetone. PAGE analysis showed the formation of a slower migrating band with a visible fluorescence at  $\lambda = 350$  nm. The reaction yields of the reaction usually reached 60–85% as determined for the HPLC-purified oligonucleotide–BePI conjugates. Retention times are given in Table 1. The oligonucleotide–BePI conjugates **II** to **VI** were characterized by UV–visible spectroscopy.  $\lambda_{\text{max}}$  values are given in Table 1. Absorption spectra recorded between 230 and 420 nm of the oligonucleotide–BePI conjugates **II** and **VI** are shown in Figure 3A.

**II. Base-Linked BePI and Base-Linked BgPI Derivatized Oligo-2'-deoxyribonucleotides VII–X (Figure 4) and Sugar-Linked BePI and BgPI Derivatized Oligo-2'-deoxyribonucleotides XI–XIV (Figure 5).** Oligonucleotide **31**, **32**, or **43** (7 OD units) was dissolved in anhydrous DMSO



**Figure 2.** Oligo-2'-deoxyribonucleotide-BePI conjugates **II**–**VI** with linkage of the intercalators at the 5-position of a 2'-deoxyuridine residue.

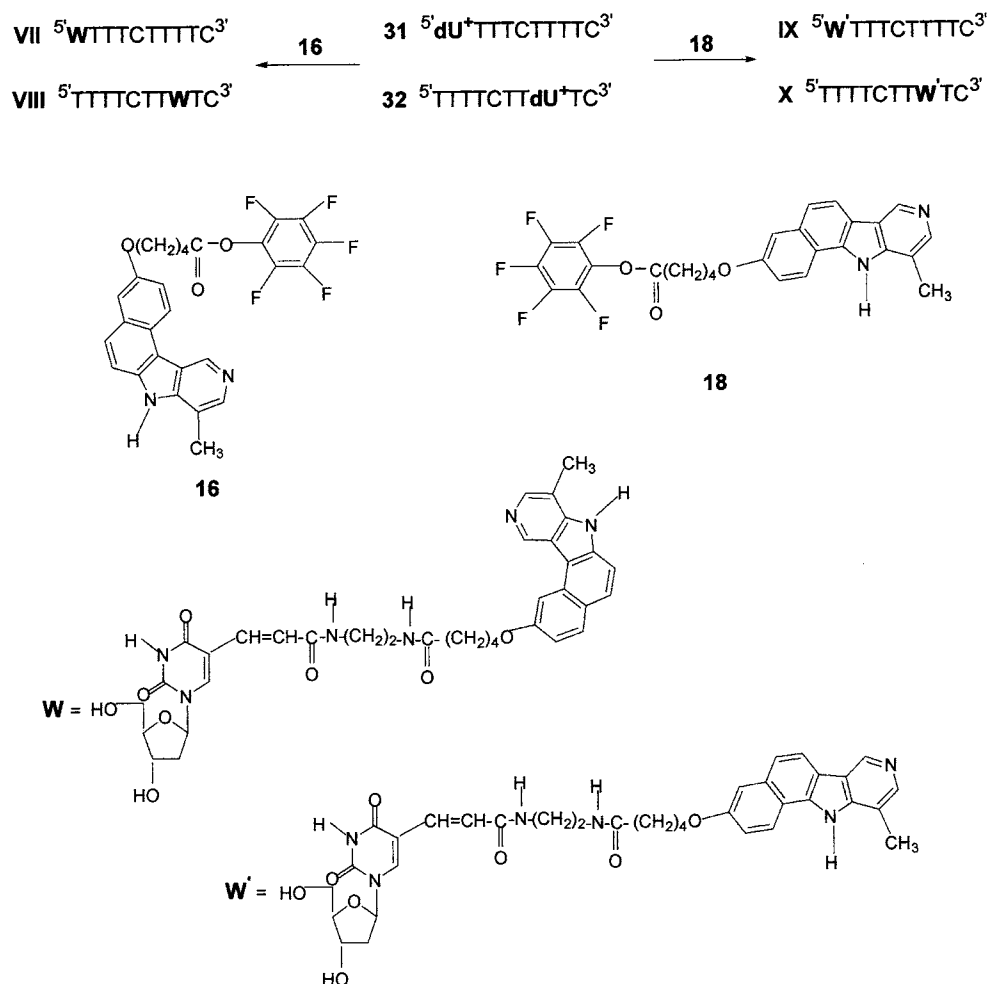


**Figure 3.** Absorption spectra recorded between 230 and 420 nm of the oligo-2'-deoxyribonucleotide-BePI conjugates **II** (full line) and **VI** (dotted line) (A), oligo-2'-deoxyribonucleotide-BePI conjugate **VIII** (dotted line) and oligo-2'-deoxyribonucleotide-BgPI conjugate **IX** (full line) (B), oligo-2'-deoxyribonucleotide-BePI conjugate **XII** (full line) and oligo-2'-deoxyribonucleotide-BgPI conjugate **XIII** (dotted line) (C), and oligo-2'-deoxyribonucleotide-BePI conjugates **XV** (full line) and **XIX** (dotted line) (D).

(50  $\mu\text{L}$ ) containing diisopropylethylamine (5  $\mu\text{L}$ ). The activated ester (10 equiv) solubilized with DMSO (50  $\mu\text{L}$ ) was added. The mixture was left at room-temperature overnight. The reaction mixture was precipitated by addition of a 3% solution of lithium perchlorate in acetone. The precipitate was washed twice with acetone and solubilized with water. The residue was purified by reversed-phase chromatography on a Lichrospher 100 RP18 (5  $\mu\text{M}$ ) column (125 mm  $\times$  4 mm) from Merck with a linear gradient of  $\text{CH}_3\text{CN}$  in 0.1 M aqueous triethylammonium acetate, pH 7, with a flow rate of 1 mL/min. Retention times obtained for the purified conjugates by

reversed-phase analysis performed on the same column but using different linear gradients of  $\text{CH}_3\text{CN}$  are given in Tables 1 and 2. The oligonucleotide-BePI and oligonucleotide-BgPI conjugates **VII**–**XIV** were characterized by UV-visible spectroscopy.  $\lambda_{\text{max}}$  values are given in Tables 1 and 2. Absorption spectra recorded between 230 and 420 nm of the oligonucleotide-BePI conjugates **XIII** and oligonucleotide-BgPI conjugate **IX** are shown in Figure 3B. Absorption spectra recorded between 230 and 420 nm of the oligonucleotide-BePI conjugates **XII** and oligonucleotide-BgPI conjugate **XIII** are shown in Figure 3C.



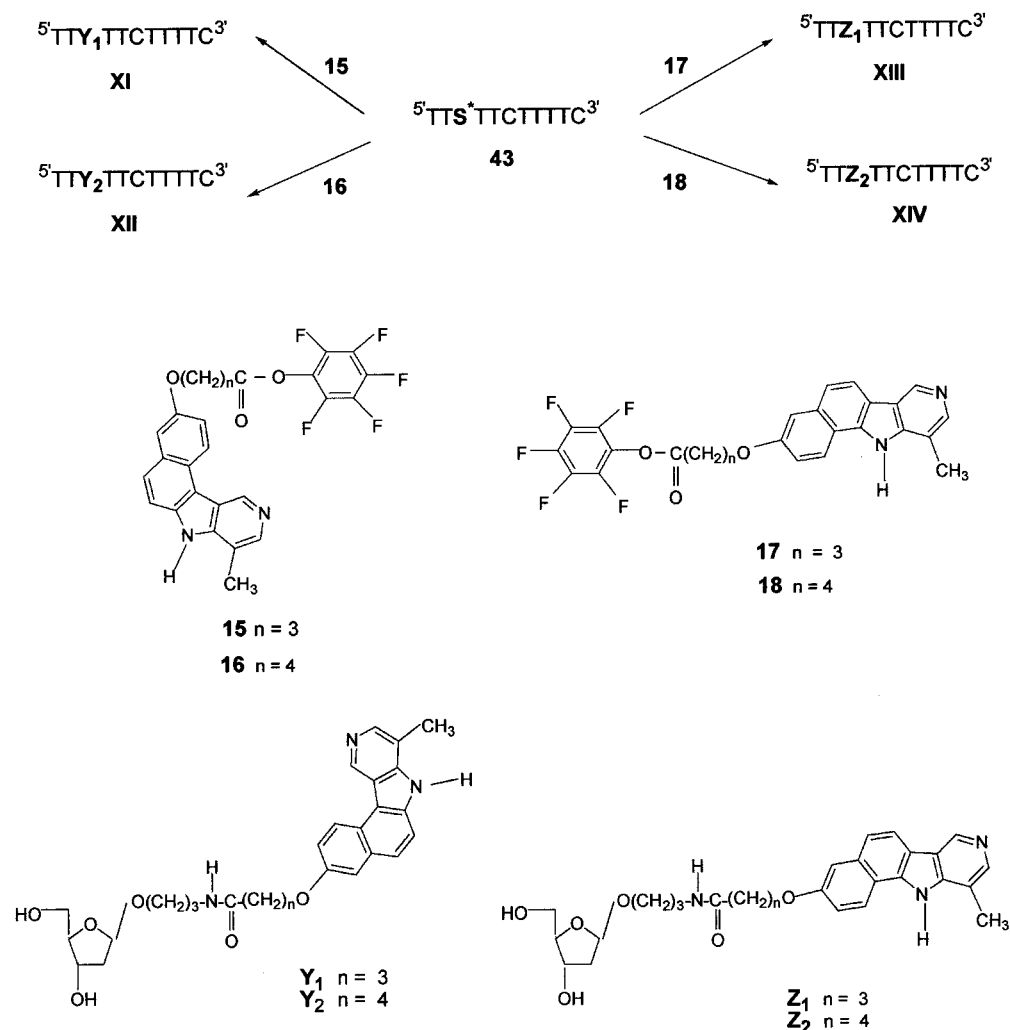


**Figure 4.** Oligo-2'-deoxyribonucleotide-BePI and oligo-2'-deoxyribonucleotide-BgPI conjugates **VII–X** with linkage of the intercalators at the 5-position of a 2'-deoxyuridine residue.

**III. Internucleotidic Thiophosphate-Linked BePI-Derivatized Oligo-2'-deoxyribonucleotides **XV–XX**** (Figure 6). To a water solution of oligonucleotides **44** or **45** (sodium salt) (25–50 nmol) (10  $\mu\text{L}$ ) were added 15-crown 5 (2  $\mu\text{L}$ ) and methanol (50  $\mu\text{L}$ ) to obtain a homogeneous solution. A BePI reagent solution (0.1 M in methanol) (25–50  $\mu\text{L}$ ) was then added, and the mixture was allowed to rest for 48 h at 40  $^{\circ}\text{C}$ . Oligonucleotide-BePI conjugates were precipitated with a 4% lithium perchlorate solution in acetone and purified by reversed-phase chromatography. Yields of purified conjugates usually reached 50–60%. In addition 20% PAGE analysis in denaturing conditions (see Figure 7) indicated that the coupling of oligonucleotide **44** (lane 1) with the BePI derivative **1** gave a new band with lower mobility as compared to that of oligonucleotide **44**. The mobilities for oligonucleotide-BePI conjugates **XV** (lane 2) and **XVI** (lane 3) (corresponding to each stereoisomer at the phosphorus level) were similar. The coupling of oligonucleotide **45** involving two phosphorothioate groups (mixture of stereoisomers) (lane 4) with two BePI derivatives **1** (compound **XIX**) gave a new band (lane 5) with a retarded mobility as compared to those of the conjugates **XV** and **XVI**. The oligonucleotide-BePI conjugates were characterized by UV-visible spectroscopy.  $\lambda_{\text{max}}$  values are given in the Table 1. Oligonucleotide-BePI conjugates **XVII**, **XVIII**, and **XX** involving BePI derivative **2** with a longer linker were obtained and characterized as described above for the preparation of conjugates **XV**, **XVI**, and **XIX** (see Table 2). Absorption spectra recorded between 230 and

420 nm of the oligonucleotide-BePI conjugates **XV** and **XIX** are shown in Figure 3D.

**IV. Internucleotidic Phosphoramidite linked-BePI Derivatized Oligo-2'-deoxyribonucleotide **XXI**** (Figure 6). The oligo-2'-deoxyribonucleotide was assembled using classical phosphoramidite chemistry on a CPG support at a  $\mu\text{mol}$  scale except that at the site selected for the introduction of the intercalator linker residue, a coupling step using H-phosphonate chemistry was manually performed. The syntheses were performed as follows. After the assembly of the first three nucleotides, an additional detritylation step was performed. 5'-O-(4,4'-dimethoxytrityl)- $\beta$ -thymidine-3'-H-phosphonate (0.05 g, 0.056 mmol) in a pyridine/ $\text{CH}_3\text{CN}$  (50:50, v/v) mixture (0.4 mL) and pivaloyl chloride (0.02 g, 0.166 mmol) in a pyridine/ $\text{CH}_3\text{CN}$  (50:50, v/v) mixture (0.5 mL) were then added simultaneously to the trinucleotide bound to the support. After a 2.5 min reaction, the solution was removed and the support washed with an anhydrous pyridine/ $\text{CH}_3\text{CN}$  (50:50, v/v) mixture (1 mL, three times). Then BePI derivative **1** (0.135 g, 0.87 mmol) solubilized by a pyridine/ $\text{CCl}_4$  (50:50, v/v) mixture (1 mL) was added. After 1 h, the solution was removed and the support washed with an anhydrous pyridine/ $\text{CH}_3\text{CN}$  (50:50, v/v) mixture (1 mL) three times and then with anhydrous  $\text{CH}_3\text{CN}$  (1 mL) three times. The support was treated with a mixture of capping solutions used on the synthesizer (0.5 mL each) for 10 min, washed with  $\text{CH}_3\text{CN}$  (1 mL, four times), and dried. The oligonucleotide chain assembly was completed via phosphoramidite chemistry to give the fully protected



**Figure 5.** Oligo-2'-deoxyribonucleotide-BePI and oligo-2'-deoxyribonucleotide-BgPI conjugates **XI–XIV** with linkage of the intercalators at the  $\beta$ -anomeric position of a 2'-deoxyribose residue.

oligo-2'-deoxyribonucleotide bound to the support bearing the BePI derivative at the seventh internucleotidic phosphate. At the end of the chain assembly, an additional detritylation step was performed to deblock the 5'-terminal hydroxyl function. The deprotection step was completed by overnight concentrated ammonia treatment at room temperature. Purification was performed by 20% PAGE in denaturing conditions. After the desalting steps, reversed-phase chromatography analyses were performed on a Lichrospher 100 RP18 (5  $\mu$ M) column (125 mm  $\times$  4 mm) from Merck with a linear gradient of CH<sub>3</sub>CN (12.5–35% over 30 min) in 0.1 M aqueous triethylammonium acetate, pH 7, with a flow rate of 1 mL/min.

**V.  $T_m$  Measurements by UV Absorption Experiments.** UV melting curves were obtained using a UVikon 940 spectrophotometer interfaced to an IBM computer. The temperature of the cell holders was regulated by an 80% water/20% ethylene glycol circulating liquid. Sample temperature was decreased from 70 to 0  $^{\circ}$ C and increased back to 80  $^{\circ}$ C at 0.2  $^{\circ}$ C/min with absorption readings at 260 and 440 nm taken every 1–1.2  $^{\circ}$ C. Samples were kept for an additional 30 min at the lowest and highest temperature. Experiments were carried out using a double-stranded DNA target (5'-CCACTTTTAAAGAA-AAGGGGGACTGG-3' / 3'-GGTGAAAAATTTTCTTTTC-CCCCCTGACC-5') (D) in a 10 mM sodium cacodylate buffer (pH 6) containing 10 mM MgCl<sub>2</sub> and 100 mM NaCl. A cacodylate buffer was chosen because of its limited dependence of pH versus temperature. Oligonucleotide

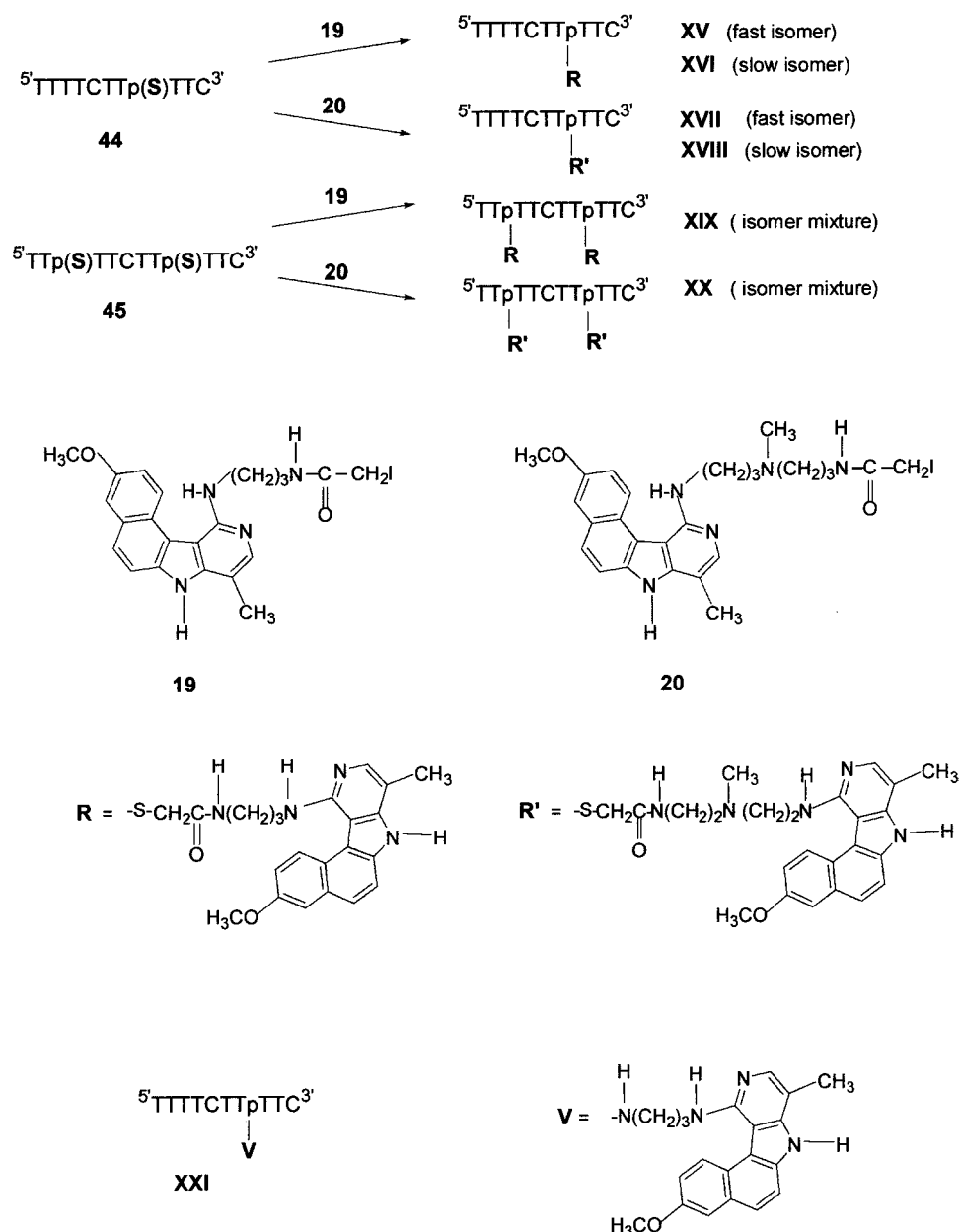
concentrations were 1  $\mu$ M of the duplex target D (with a 1/1.2 ratio of purine/pyrimidine-containing strands) and 1.5  $\mu$ M of the third strand (see sequences in Table 1). For the melting temperature ( $T_m$ ) analysis, the drift of baseline was corrected by subtracting absorptions at 440 nm from those at 260 nm and plotted against temperature ( $^{\circ}$ C). The maximum of the first derivative  $dA/dT$  was taken as a first estimation of the  $T_m$  value. The uncertainty in the  $T_m$  values reported is estimated at  $\pm 1$   $^{\circ}$ C.

## RESULTS AND DISCUSSION

Triple-helix-specific intercalators benzo[e] and benzo[g] pyridoindole [BePI and BgPI] were covalently linked to various positions of a triple-helix-forming 10-mer oligopyrimidine sequence [TFO] 5'-TTTTCTTTTC-3'. Parameters such as the size of the linker chosen to connect the intercalators and the third pyrimidine strand as well as the position of attachment of the linker to the intercalator in the case of BePI derivatives were investigated. We report here the synthesis of the various families of oligonucleotide intercalator conjugates and the results of their binding properties evaluated by absorption spectroscopy.

### A. Synthesis of BePI and BgPI Derivatives 1–20.

**1. Synthesis of the BePI Derivatives 1 and 2 Involving an Amino-Containing Linker Attached to Their Position 11.** The 11-amino-substituted benzo[e]pyridoindole deriva-



**Figure 6.** Oligo-2'-deoxyribonucleotide–BePI conjugates with linkage of the intercalators at an internucleotidic phosphate position via phosphothiotriester **XV–XX** or phosphoramidate **XXI** bonds.

tives **1** and **2** (Figure 1) were obtained as described in the literature (32, 33).

**II. Syntheses of the BePI and BgPI Derivatives Involving a Carboxylated Linker 3–6 and of Activated Esters 15–18.** New benzo[*e*]pyridoindoles substituted at the 3-position (**3** and **4**) (Figure 1, Scheme 1) were synthesized starting from the known 11-chloro-3-methoxy-8-methyl-7H-benzo[*e*]pyrido[4,3-*b*]indole **7** (36). Demethylation of this methoxy derivative in standard conditions under reflux of concentrated HBr or using cetyltrimethylammonium bromide by phase transfer catalysis under reflux of concentrated HCl described in ref 37 was unsuccessful, and the unaltered starting material was recovered, even after a prolonged heating time. To overcome this disappointing result, we examined new conditions for this transformation. It was found that under reflux of concentrated HCl and in the presence of benzyltriethylammonium chloride, compound **7** led to the 3-hydroxybenzo[*e*]pyridoindole **8** in good yield. Treatment of this phenolic derivative **8** with ethyl 4-bromobutyrate

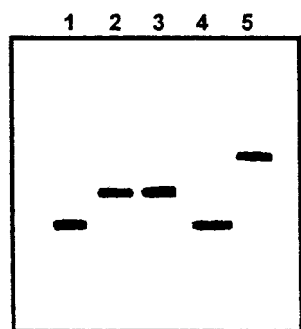
or ethyl 5-bromovalerate, followed by catalytic (Pd/C) hydrogenation, gave the corresponding O-substituted ester derivatives **9** and **10**, and their saponification led to the expected compounds **3** and **4** (Scheme 1).

For compounds **5** and **6** belonging to the benzo[*g*]pyridoindole series, the same transformations were performed under similar conditions starting from the known 7-chloro-3-methoxy-10-methyl-11H-benzo[*g*]pyrido[4,3-*b*]indole **11** (36) via **12**, **13**, and **14** (Scheme 2).

The corresponding activated esters **15–18** of BePI and BgPI derivatives **3–6** were obtained by reaction of pentafluorophenyltrifluoroacetate with the amino-containing linker derivatives **3–6** and directly used after purification on a silica gel column. The iodoacetamide derivatives **19** and **20** were obtained from the BePI derivatives **1** and **2** using a previously reported procedure (34).

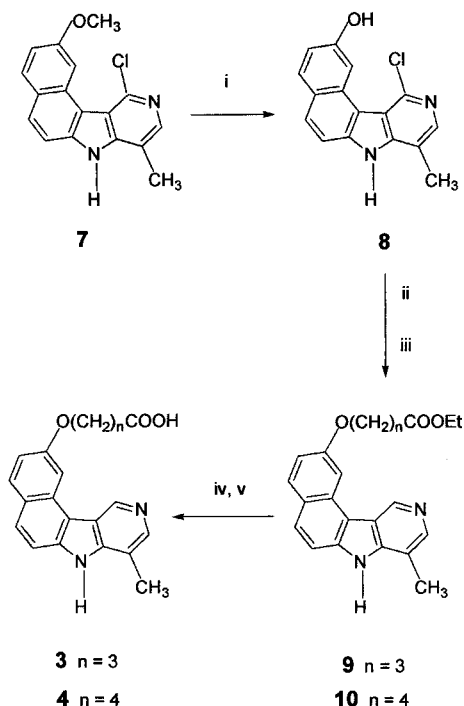
**B. Synthesis of the Oligo-2'-deoxyribonucleotide-BePI and Oligo-2'-deoxyribonucleotide–BgPI Conjugates.** BePI derivatives **1** and **2** with different linker sizes attached





**Figure 7.** Denaturing polyacrylamide (20%) gel electrophoresis of phosphorothioate-containing oligo-2'-deoxyribonucleotides and oligo-2'-deoxyribonucleotide-BePI conjugates stained with methylene blue: lane 1, oligo-2'-deoxyribonucleotide **44** with one phosphorothioate group; lane 2, oligo-2'-deoxyribonucleotide-BePI conjugate **XV** (fast isomer); lane 3, oligo-2'-deoxyribonucleotide-BePI conjugate **XVI** (slow isomer); lane 4, oligo-2'-deoxyribonucleotide **45** with two phosphorothioate groups; lane 5, oligo-2'-deoxyribonucleotide-BePI conjugate **XIX** with two BePI derivatives.

**Scheme 1. Synthesis of the BePI Derivatives 3 and 4<sup>a</sup>**

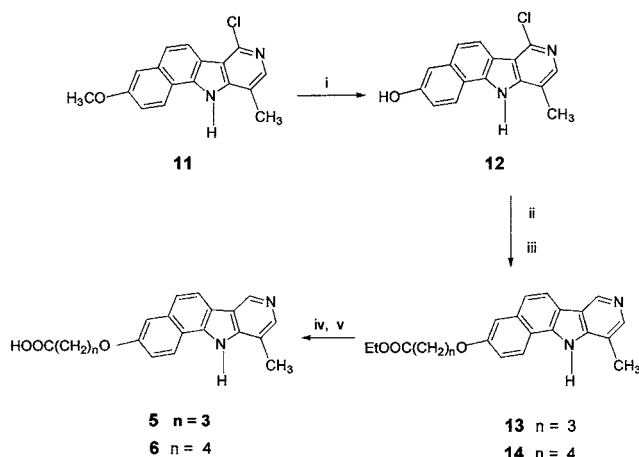


<sup>a</sup> (i) Conc HCl/BnEt<sub>3</sub>NCl. (ii) Br(CH<sub>2</sub>)<sub>n</sub>COOEt. (iii) H<sub>2</sub>, Pd/C. (iv) NaOH. v: HCl.

to their 11-position were covalently linked to the 5-position of a 2'-deoxyuridine located in place of either the first or the eighth nucleotide of the sequence. These positions were chosen to allow intercalation of the BePI derivatives between the TxA.T base triplets since studies carried out with free BePI derivatives and various triple helices have shown a preferential binding for sequences involving runs of TxA.T triplets (29). The preparation of these conjugates **II–VI** was performed by postsynthetic coupling of the BePI derivatives with modified oligonucleotides involving a modified 2'-deoxyuridine at the site preselected for the linkage of intercalators.

The modified 2'-deoxyuridine-linker derivative was obtained as reported in Scheme 3. First, the 5-bromo-2'-deoxyuridine **21** was reacted with 1,3-dichloro-1,1,3,3-tetraisopropylidisiloxane (**38**) in order to protect the 5'- and 3'-functions (compound **22**). The latter was then reacted with 10-fold excess of 3-amino-1,2-propanediol to

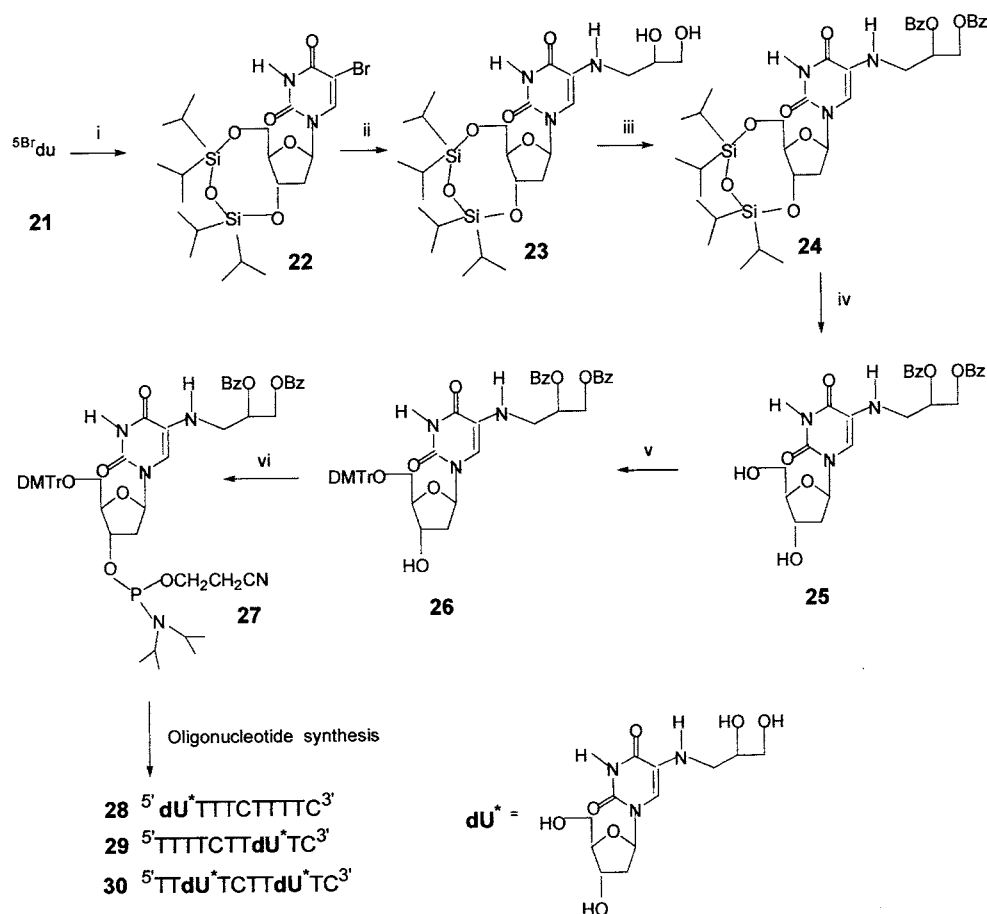
**Scheme 2. Synthesis of the BgPI Derivatives 5 and 6<sup>a</sup>**



<sup>a</sup> (i) Conc HCl/BnEt<sub>3</sub>NCl. (ii) Br(CH<sub>2</sub>)<sub>n</sub>COOEt. (iii) H<sub>2</sub>, Pd/C. (iv) NaOH. v: HCl.

give the 2'-deoxyuridine-linker derivative **23** in 76% yield. The hydroxyl function of the amino-1,2-propanediol linker was protected with benzoyl groups to give compound **24**. The protective group of the 5'- and 3'-hydroxyl functions was then removed by tetrabutylammonium fluoride treatment to give compound **25**, which was dimethoxytritylated at the 5'-position (compound **26**) and transformed into its phosphoramidite derivative **27** following a standard procedure. The modified 2'-deoxyuridine-linker derivative was then incorporated during the oligonucleotide chain elongation, via phosphoramidite chemistry, in replacement of the thymidines at the positions chosen for the linkage of the BePI derivatives. After a standard deprotection step, purification was carried out by reversed-phase HPLC or PAGE to give oligonucleotides **28–30**. The linkage between the BePI-linker derivatives **1** and **2**, ending with an amino group, and the oligonucleotides **28–30** containing the modified 2'-deoxyuridine bearing a diol-containing linker at their 5-position was performed via an amino reductive coupling step (Figure 2). This included periodate treatment to generate the aldehydic derivative, reaction of the latter with amino containing BePI derivatives **1** or **2** and finally a reduction step by sodium cyanoborohydride. Purification of the conjugates was performed by reversed-phase chromatography. The retention times for the conjugates involving one BePI derivative **II** to **V** were higher than those of oligonucleotides **28** and **29** ( $\Delta t_R \approx 6$  min); in the case of compound **30** with two BePI derivatives (compound **VI**), the retention time was even more increased ( $\Delta t_R \approx 10$  min) (Figure 2, Table 1). These results indicate the formation of more lipophilic compounds. UV spectra recorded between 230 and 420 nm indicate the presence of a band corresponding to the BePI derivatives (Table 1 and Figure 3A).

BePI derivative **4** involving a linker attached to its 3-position instead of the 11-position for the above-described conjugates and BgPI derivative **6** with a linker attached to its 3-position (Figure 1) were also covalently linked to the 5-position of another modified 2'-deoxyuridine inserted at the same positions as those reported above. In this case the modified 2'-deoxyuridine involved a more rigid linker ending with an amino function. Oligonucleotides involving these modified 2'-deoxyuridines **31** and **32** were reacted with the carboxyl function (as pentafluorophenyl esters **16** and **18**) of the BePI and BgPI-linker derivatives (including four methylenes) **4** and **6** to give the oligonucleotide-BePI and BgPI conjugates

**Scheme 3. Synthesis of the Modified 2'-Deoxyuridine 26 and Its Incorporation into Oligo-2'-Deoxyribonucleotides<sup>a</sup>**

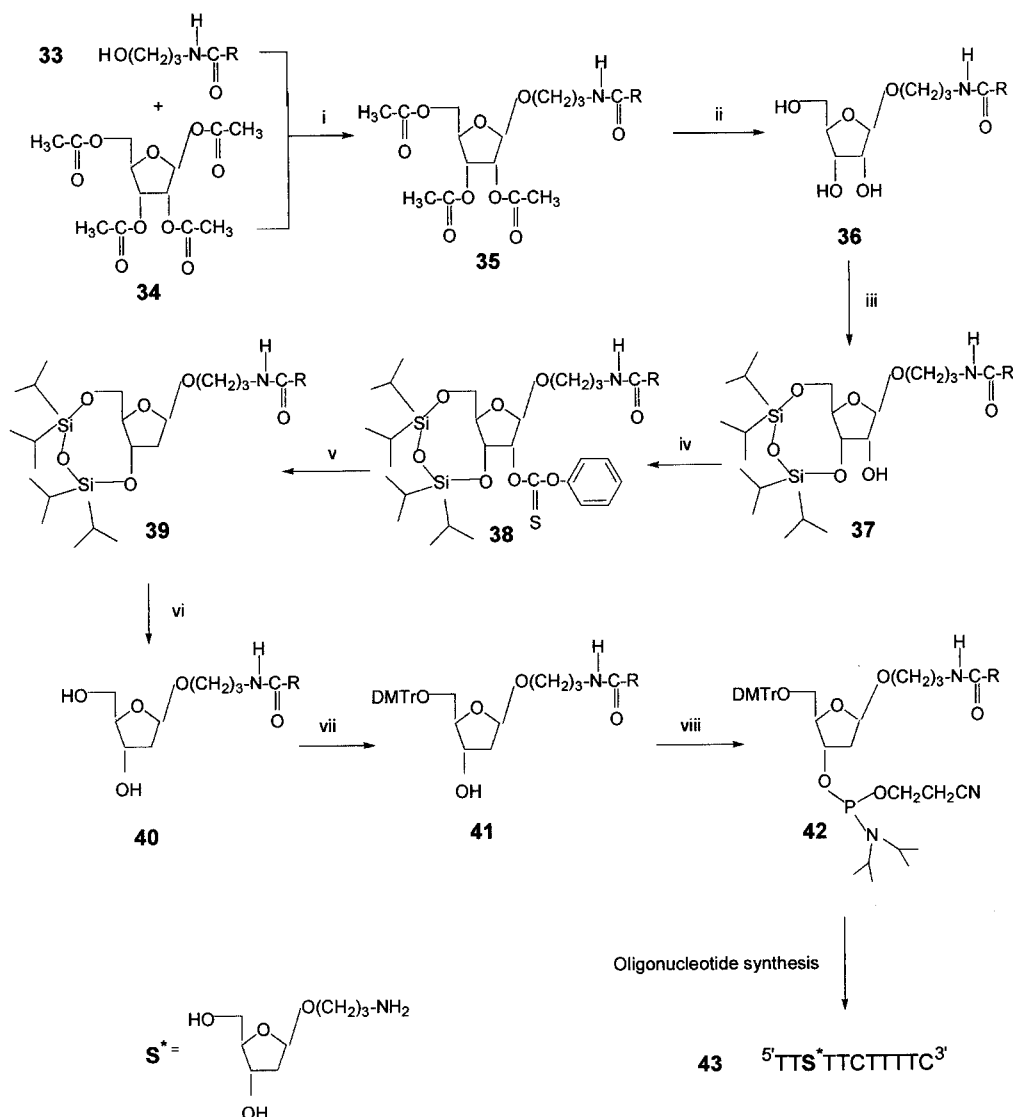
<sup>a</sup> 5BrdU = 5-bromo-2'-deoxyuridine, DMTr = dimethoxytrityl, Bz = benzoyl. (i) 1, 3-dichloro-1, 2, 3, 3-tetraisopropylidisiloxane, pyridine. (ii) 3-Amino-1, 2-propanediol, EtOH, 80 °C, 17 h. (iii) Benzoylchloride, pyridine. (iv) Tetrabutylammonium fluoride, THF. (v) DMTrCl, pyridine. (vi) 2-Cyanoethoxy-*N,N*-diisopropylaminophosphine, DIEA, CH<sub>2</sub>Cl<sub>2</sub>.

**VII** to **X** (Figure 4). Purification was performed by reversed-phase chromatography. In all cases the retention time for conjugates **VII–X** was a few minutes ( $\Delta t_R \approx 7$  min) higher than that of the starting oligonucleotides **31** or **32** (Table 1). The oligonucleotide–BePI conjugates were characterized by UV–visible spectroscopy.  $\lambda_{max}$  values are given in Table 1. Absorption spectra recorded between 230 and 420 nm of the oligonucleotide–BePI conjugate **VIII** and the oligonucleotide–BgPI conjugate **IX** are shown in Figure 3B.

The BePI with a linker attached to its 3-position and BgPI derivatives described above were then covalently linked to an internal position of the TFO pyrimidine sequence via an additional 2'-deoxyribose moiety bearing a propylamino linker at its 1'-position in the  $\beta$ -anomeric configuration. The 2'-deoxyribose residue was added between the second and third thymidines of the sequence. This strategy was chosen in order to favor intercalation between the two neighboring T.AxT base triplets.

The 2'-deoxyribose-linker derivative was obtained following Scheme 4. The amino function of aminopropanol was protected with the fmoc group to give compound **33**. The latter was reacted with  $\beta$ -D-ribofuranose 1,2,3,5 tetraacetate **34** to give the 2'-deoxyribose-linker derivative **35**. The 5', 3', and 2'-hydroxyl functions were released by KCN treatment (**39**) to give compound **36** protected on the amino function with a fluorenylmethyl group in 30% yield. The 5'- and 3'-functions were then protected using Markiewicz reagent to give compound **37**. The 2'-hydroxyl function was then removed following a

two-step procedure involving its activation with the phenoxythiocarbonyl group (compound **38**) followed by radical deoxygenation in the presence of tributyltin hydride and AIBN (compound **39**). After release of its 5'- and 3'-hydroxyl functions by treatment with tetrabutylammonium fluoride, the modified 2'-deoxyribose **40** was tritylated at its 5'-position (compound **41**) and transformed into its phosphoramidite derivative **42**. The 2'-deoxyribose-linker derivative was incorporated into the sequence by manual coupling and increased time reaction between the second and third thymidines. The modified trityl-on oligonucleotide was then deprotected by concentrated ammonia treatment overnight at room temperature. Purification was performed by ion-exchange chromatography and, after detritylation, analyzed and purified by reversed-phase chromatography. Oligonucleotide **43** was then reacted with the carboxyl function (as pentafluorophenyl ester **15–18**) of the BePI and BgPI-linker derivatives **3–6** (including three or four methylenes) to give the oligonucleotide–BePI and BgPI conjugates **XI** to **XIV** (Figure 5). Purifications were performed by reversed-phase chromatography. In all cases the retention times for the conjugates were a few minutes longer than that for the starting oligonucleotide **43** ( $\Delta t_R \approx 8–11$  min) (Table 2). The oligonucleotide–BePI conjugates were characterized by UV–visible spectroscopy.  $\lambda_{max}$  values are given in Table 2. Absorption spectra recorded between 230 and 420 nm of the oligonucleotide–BePI conjugate **XII** and oligonucleotide–BgPI conjugate **XIII** are shown in Figure 3C.

**Scheme 4. Synthesis of the Modified 2'-Deoxyribose Linker Derivative 41 and Its Incorporation into an Oligo-2'-deoxyribonucleotide<sup>a</sup>**

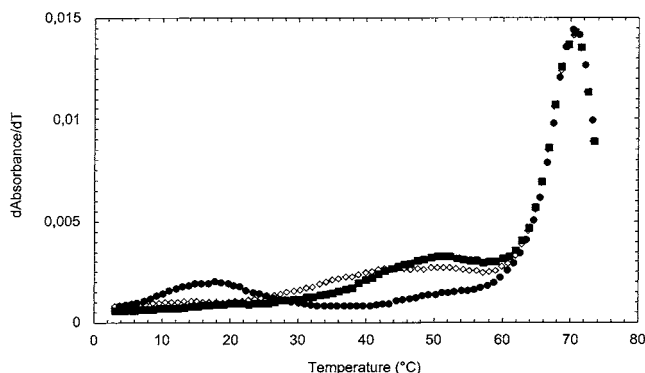
<sup>a</sup> R = fluorenylmethyl; DMTr = dimethoxytrityl. (i) Trimethylsilyltrifluoromethane sulfonate, 1,2-dichloroethane. (ii) KCN, MeOH. (iii) 1,3-Dichloro-1,1,3,3-tetraisopropylidisiloxane, imidazole, 1,1-dichloromethane. (iv) Phenylchlorothionochloroformate, pyridine. (v) AIBN, toluene. (vi) Tetrabutylammonium fluoride, THF. (vii) DMTrCl, pyridine. (viii) 2-Cyanoethoxy-*N,N*-diisopropylaminochlorophosphine, DIEA, CH<sub>2</sub>Cl<sub>2</sub>.

BePI derivatives **1** and **2**, involving a linker attached to their 11-position were then covalently linked at an internal position of the TFO pyrimidine sequence via internucleotidic thiophosphate and amidophosphate bonds. Purification was performed by reversed-phase chromatography. Iodoacetamide derivatives of BePI derivatives **1** (compound **19**) and **2** (compound **20**) were reacted with oligonucleotides containing either one thiophosphate group **44** or two thiophosphate groups **45** (Figure 6) at preselected positions chosen for the attachment of the BePI derivatives. Compounds **XV–XX** were obtained (Figure 6, Table 2). Purification and analysis steps were performed both by reversed-phase chromatography and 20% PAGE in denaturing conditions. Retention times for the conjugates were higher than for the starting oligo-2'-deoxyribonucleotides:  $\Delta t_R \approx 6$  min in the case of the coupling of one BePI derivative and  $\Delta t_R \approx 10$  min in the case of the coupling of two BePI derivatives (Table 2). Compounds **XV** and **XVI** correspond to each pure diastereoisomer of the oligonucleotide–BePI conjugate. They were separated by reversed-phase chromatography using a weak gradient. PAGE analysis revealed that the con-

jugates **XI** and **XII** possess the same mobilities in denaturing gels (Figure 7). However, their mobilities are lower than that of the starting oligonucleotide involving a thiophosphate group **24**. In the case of conjugate **XIX** involving two BePI residues, the mixture of stereoisomers (four isomers) was not separated. PAGE analysis showed only one band for compound **XIX** with a retarded mobility as compared to the conjugates involving only one BePI derivative **XV** and **XVI**. On the contrary, reversed-phase analysis revealed three peaks (with a higher intensity for the central one) with increased retention times as compared to those of the conjugates involving one BePI residue **1**. UV analysis indicated the presence of BePI in the products corresponding to all three peaks (Table 2). Similar results were obtained with the conjugates **XVII**, **XVIII**, and **XX** involving either one or two BePI derivatives **2**. Absorption spectra recorded between 230 and 420 nm of the oligonucleotide–BePI conjugates **XV** and **XIX** are shown in Figure 3D.

Oligonucleotide–BePI **1** conjugate **XXI** (Table 2) (Figure 6) involving a phosphoramidate linkage was obtained by performing an H-phosphonate coupling step (**40**) at





**Figure 8.** First derivative  $d\text{Absorbance}/dT$  of the UV melting profiles recorded at 260 nm of the duplex in the presence of oligonucleotide **I** (●), oligonucleotide **II** (■), and oligonucleotide **III** (◇).

the selected site for the attachment of the intercalator followed by an oxidation step in the presence of the BePI derivative **1**. Coupling of the BePI derivative resulted in an increase in retention time for conjugate **XXI**.

**C. Stabilities of the Triplexes Formed between Conjugates II–XVII and the Double-Stranded DNA Target (Tables 1 and 2).** The results obtained for the described conjugates, listed in Tables 1 and 2, indicate that the binding of the third strand to the target duplex was stabilized only with BePI-oligo-2'-deoxyribonucleotide conjugates **II** and **III** (Figure 8). In these conjugates, the BePI derivative is attached by its 11-position, via a flexible linker, to the 5-position of a modified 2'-deoxyuridine located at the 5'-end of the sequence. In these cases, BePI probably intercalates at the duplex–triplex junction as previously reported for acridine–oligonucleotide conjugates. Stabilization was more efficient with a shorter linker (conjugate **II**) between the BePI and the third strand compared to that with a longer linker (conjugate **III**). In the case of the shorter linker (conjugate **II**), the  $T_m$  increase is 6 °C superior to that observed with an acridine–oligonucleotide conjugate used as a reference [ $\text{Acr}(\text{CH}_2)_6\text{-P}^5' \text{TTTTCTTTT}^3$ ] (**41**). In this oligonucleotide–acridine conjugate, the cytosine was replaced with 5-methylcytosine. When BePI derivatives, with any position of the linker attachment on the intercalator residue and any linker size, were attached to other positions of the oligonucleotide chain: 5-position of a modified 2'-deoxyuridine (conjugates **IV–VIII**),  $\beta$ -anomeric position of an internal 2'-deoxyribose residue (conjugates **XI** and **XII**), or internucleotidic position (conjugates **XV–XXI**)—only very weak or no stabilization of the triplex was observed. This was also true with BgPI derivatives fixed at internal positions of the sequence either on a modified 2'-deoxyuridine (conjugates **IX** and **X**) or on the  $\beta$ -anomeric position of a 2'-deoxyribose residue (conjugates **XIII** and **XIV**).

We have reported the synthesis and binding properties of a series of oligopyrimidine sequences covalently linked to triple-helix-specific intercalators (BePI and BgPI) derivatives. The influence of the linker attachment position on both the intercalating agent and the oligonucleotide chain as well as the linker size were studied. The syntheses of new BePI and BgPI derivatives (**3–6**) were reported. The preparation of the oligonucleotide–BePI and oligonucleotide–BgPI conjugates (compounds **II–XXI**) was performed by specific coupling reactions between suitable functional groups present on both the intercalating agents and the deprotected oligonucleotides (**28–32**, **43–45**). The incorporation of the functional groups into the modified oligonucleotide at the site preselected

for the coupling of the intercalating agents was performed by using either well-known procedures including phosphorothioate or H-phosphonate chemistry or new modifications such as a modified 2'-deoxyuridine containing a linker ending with a cis-diol or a 2'-deoxyribose residue involving an amino-containing linker at its  $\beta$ -anomeric position. The binding properties of the conjugates synthesized with the double-stranded DNA target were studied by absorption spectroscopy (Tables 1 and 2). The results indicated that a significant stabilization was observed only when BePI derivatives with the linker attached to their 11-position are covalently linked, via a flexible linker, to the 5-position of a modified 2'-deoxyuridine located at the 5'-end of the oligopyrimidine sequence (conjugates **II** and **III**). The strongest stabilization ( $\Delta T_m = 30$  °C) was observed with the shorter linker (conjugate **II**).

#### ACKNOWLEDGMENT

This work is supported by funds from the Agence Nationale de Recherches sur le SIDA (ANRS). We thank M. Novello for the preparation of oligonucleotides **31** and **32**, H. Labbé for recording NMR spectra, and C. Buré for running the electrospray mass spectrometer.

#### LITERATURE CITED

- (1) Felsenfeld, G., Davies, D., and Rich, A. (1957) Formation of a three-stranded polynucleotide molecule. *J. Am. Chem. Soc.* **79**, 2023–2024.
- (2) Moser, H. E., and Dervan, P. B. (1987) Sequence-specific cleavage of double helical DNA by triplex helix formation. *Science* **238**, 645–650.
- (3) Le Doan, T., Perrouault, L., Praseuth, D., Habhouh, N., Decout, J. L., Thuong, N. T., Lhomme, J., and Hélène, C. (1987) Sequence-specific recognition, photo-cross-linking, and cleavage of the DNA double-helix by an oligo-[ $\alpha$ ]-thymidylate covalently linked to an azidoproflavine derivative. *Nucleic Acids Res.* **15**, 7749–7760.
- (4) Hélène, C. (1999) In *Triple Helix Forming Oligonucleotides* (C. Malvy, A. Harel-Bellan, and L. L. Pritchard, Eds.) pp 3–16, Kluwer Academic Publishers, Dordrecht, The Netherlands.
- (5) Grigoriev, M., Praseuth, D., Guieysse, A.-L., Robin, P., Thuong, N. T., Hélène, C., and Harel-Bellan, A. (1993) Inhibition of gene expression by triple helix-directed DNA cross-linking at specific genes. *Proc. Natl. Acad. Sci. U.S.A.* **90**, 3501–3505.
- (6) Giovannangeli, C., Perrouault, L., Escudé, C., Gryaznov, S. N., and Hélène, C. (1996) Efficient inhibition of transcription elongation in vitro by oligonucleotide phosphoramidates targeted to proviral HIV DNA. *J. Mol. Biol.* **261**, 386–398.
- (7) Faria, M., Wood, C. D., Perrouault, L., Nelson, J. S., White, M. R. H., Hélène, C., and Giovannangeli, C. (2000) Targeted inhibition of transcription elongation in cells mediated by triplex-forming oligonucleotides. *Proc. Natl. Acad. Sci. U.S.A.* **97**, 3862–3867.
- (8) Faruqi, A. F., Krawczyk, S. H., Matteucci, M. D., and Glazer, P. M. (1997) Potassium-resistant triple helix formation and improved intracellular gene targeting by oligo-2'-deoxyribonucleotides containing 7-deazaxanthine. *Nucl. Acids Res.* **25**, 633–640.
- (9) Majumdar, A., Khorlin, A., Dyatkina, N., Lin, F.-L. M., Powell, J., Liu, J., Fei, Z., Khripine, Y., Watanabe, K. A., George, J., Glazer, P. M., and Seidman, M. M. (1998) Targeted gene knockout mediated by triple helix forming oligonucleotide. *Nat. Genet.* **20**, 212–214.
- (10) Giovannangeli, C., Diviacco, S., Labrousse, V., Gryaznov, S., Charneau, P., and Hélène, C. (1997). Accessibility of nuclear DNA to triplex-forming oligonucleotides: the integrated HIV-1 provirus as a target. *Proc. Natl. Acad. Sci. U.S.A.* **94**, 79–84.

- (11) Belousov, E. S., Afonina, I. A., Kutyavin, I. V., Gall, A. A., Reed, M. W., Gamper, H. B., Wydro, R. M., and Meyer, R. B. (1998) Triplex targeting of a native gene in permeabilized intact cells: covalent modification of the gene for the chemokine receptor CCR5. *Nucleic Acids Res.* **26**, 1324–1328.
- (12) Barre, F.-X., Ait-Si-Ali, S., Giovannangeli, C., Luis, R., Robin, P., Pritchard, L. L., Hélène, C., and Harel-Bellan, A. (2000) Unambiguous demonstration of triple-helix-directed gene modification. *Proc. Natl. Acad. Sci. U.S.A.* **94**, 3084–3088.
- (13) Matteucci, M., Lin, K.-Y., Huang, T., Wagner, R., Sternbach, D. D., Mehrotra, M.; and Bestermann, J. M. (1997) Sequence-specific targeting of duplex DNA using a camptothecin-triple helix forming oligonucleotide conjugate and topoisomerase I. *J. Am. Chem. Soc.* **119**, 6939–6940.
- (14) Arimondo, P., Bailly, C., Boutorine, A., Sun, J. S., Garestier, T., and Hélène, C. (1999) Targeting topoisomerase I cleavage to specific sequences of DNA by triple helix-forming oligonucleotide conjugates. A comparison between a rebeccamycin derivative and camptothecin. *C. R. Acad. Sci. III/Life Sci.* **322**, 785–790.
- (15) Vasquez, K. M., Narayanan, L., and Glazer, P. M. (2000) Specific mutations induced by triplex-forming oligonucleotides in mice. *Science* **290**, 530–533.
- (16) Debin, A., Malvy, C., and Svinarchuk, F. (1997) Investigation of the formation and intracellular stability of purine-(purine/pyrimidine) triplexes. *Nucleic Acids Res.* **25**, 1965–1974.
- (17) Robles, J., Rajur, S. B. and McLaughlin, L. W. (1996) A parallel-stranded DNA triplex tethering a Hoechst 33258 analogue results in complex stabilization by simultaneous major groove and minor groove binding. *J. Am. Chem. Soc.* **118**, 5820–5821.
- (18) Szewczyk, J. W., Baird, E. E. and Dervan, P. B. (1996) Sequence-specific recognition of DNA by a major and minor groove binding ligand. *Angew. Chem., Int. Ed. Engl.* **35**, 1487–1489.
- (19) Tung, C.-H., Breslauer, K., J., and Stein S. (1996) Stabilization of DNA triple-helix formation by appended cationic peptides. *Bioconjugate Chem.* **7**, 529–531.
- (20) Sun, J. S., Giovannangeli, C., François, J. C., Kurfürst, R., Montenay-Garestier, T., Asseline, U., Thuong, N. T., and Hélène, C. (1991) Triple-helix formation by  $\alpha$ -oligodeoxynucleotide intercalator conjugates. *Proc. Natl. Acad. Sci. U.S.A.* **88**, 6023–6027.
- (21) Koshkin, A. A., Kropachev, K. Y., Mamaev, S. V., Bulychev, N. V., Lokhov, S. G., Vlassov, V. V., and Lebedev, A. V. (1994) Ethidium and azidoethidium oligonucleotide derivatives: Synthesis, complementary complex formation and sequence-specific photomodification of the single-stranded and double-stranded target oligo- and polynucleotides. *J. Mol. Recognit.* **7**, 177–198.
- (22) Mouscadet, J. F., Ketterlé, C., Goulaouic, H., Carteau, S., Subra F., Le Bret, M., and Auclair C. (1994) Triple helix formation with short oligonucleotide intercalator conjugates matching the HIV-1 U3 LTR end sequence. *Biochemistry* **33**, 4187–4196.
- (23) Garbesi, A., Bonazzi, S., Zanella, S., Capobianco, M. L., Giannini, G., and Arcamone, F. (1997) Synthesis and binding properties of conjugates between oligodeoxynucleotides and daunorubicin derivatives. *Nucleic Acids Res.* **25**, 2121–2128.
- (24) Silver, G. C., Nguyen, C. H., Boutorine, C. H., Bisagni, E., Garestier, T. and Hélène, C. (1997) Conjugates of oligonucleotides with triplex-specific intercalating agents. Stabilization of triple-helical DNA in the promoter region of the gene for the  $\alpha$ -subunit of interleukin 2 (IL-2R $\alpha$ ). *Bioconjugate Chem.* **8**, 15–22.
- (25) Silver, G. C., Sun, J. S., Nguyen, C. H., Boutorine, C. H., Bisagni, E. and Hélène, C. (1997) Stable triple-helical DNA complexes formed by benzopyridoindole and benzopyridoquinoline-oligonucleotide conjugates. *J. Am. Chem. Soc.* **119**, 263–268.
- (26) Keppler, M. D., McKeen C. M., Zegrocka, O., Strekowski, L., Brown, T., and Fox, K. R. (1999) DNA triple helix stabilisation by covalent attachment of a triplex-specific ligand. *Biochim. Biophys. Acta* **137**–145.
- (27) Gianolio, D. A., Segismundo, J. M., and McLaughlin, L. W. (2000) Tethered naphthalene diimide-based intercalators for DNA triplex stabilisation. *Nucleic Acids Res.* **28**, 2128–2134.
- (28) Asseline, U., and Cheng, E. Synthesis and binding properties of perylene-oligo-2'-deoxyribonucleotides conjugates. (2001) *Tetrahedron Lett.* **42**, 9005–9010.
- (29) Mergny, J.-L., Duval-Valentin, G., Nguyen, C. H., Perrouault, L., Faucon, B., Rougée, M., Montenay-Garestier, T., Bisagni, E. and Hélène, C. (1992) Triple helix-specific ligands. *Science* **256**, 1681–1684.
- (30) Atkinson, T., and Smith, M. (1984) Solid-phase synthesis of oligo-2'-deoxyribonucleotides by the phosphite triester approach. In *Oligonucleotides Synthesis: A Practical Approach* (F. Eckstein, Ed.) pp 283–308, IRL Press, Oxford.
- (31) Cantor, C., R., Warshaw, M. M., and Shapiro, H. (1970) Oligonucleotide interactions. III. Circular dichroism studies of the conformation of deoxyoligonucleotides. *Biopolymers* **9**, 1059–1077.
- (32) Nguyen, C. H., Lavelle, F., Riou, J.-F., Bisserey, M.-C., Huel, C., and Bisagni, E. (1992) Further SAR in the new antitumor 1-amino-substituted  $\gamma$ -carboline and 5H-benzo[e]pyrido[4,3-b]indoles series. *Anti-Cancer Drug Des.* **7**, 235–251.
- (33) Escudé, C., Nguyen, C. H., Mergny, J.-L., Sun, J. S., Bisagni, E., Garestier, T., and Hélène, C. (1995) Selective stabilization of DNA triple helices by benzopyridoindole derivatives. *J. Am. Chem. Soc.* **117**, 10212–10219.
- (34) Asseline, U., Bonfils, E., Dupret, D., and Thuong, N. T. (1996) Synthesis and binding properties of oligonucleotides covalently linked to an acridine derivative: New study of the influence of the dye attachment site. *Bioconjugate Chem.* **7**, 369–379.
- (35) Vu, H., and Hirschbein, B. L. (1991) Internucleotide phosphite sulfurization with tetraethylthiuram disulfide: Phosphorothioate oligonucleotide synthesis via phosphoramidite chemistry. *Tetrahedron Lett.* **32**, 3005–3008.
- (36) Nguyen, C.-H., Lhoste, J.-M., Lavelle, F., Bissery, M. C., and Bisagni, E. (1990) Synthesis and antitumor activity of 1-(dialkylamino) alkylamino-4-methyl-5H-pyrido [4,3-b] benzo[e] (and benzo[g]) indoles. A new class of antineoplastic agents. *J. Med. Chem.* **33**, 1519–1528.
- (37) Jursic, B. (1989) Cleavage of ethers with aqueous hydrochloric acid in the presence of surfactants. *J. Chem. Res.*, **284**.
- (38) Markiewicz, W. T., and Wiewiorowski, M. (1978) A new type of silyl protecting groups in nucleoside chemistry. *Nucl. Acids Res. Spec. Pub.* **4**, 185–188.
- (39) Herzig, J., Nudelman, A., Gottlieb, H. E., and Fischer, B. (1986) Studies in sugar chemistry. A simple method for O-deacylation of polyacylated sugars. *J. Org. Chem.* **51**, 727–730.
- (40) Froehler, B. C., and Matteucci, M. D. (1986) Nucleoside H-phosphonates: valuable intermediates in the synthesis of deoxyoligonucleotides. *Tetrahedron Lett.* **27**, 469–472.
- (41) Giovannangeli, C., Perrouault, L., Escudé, C., Thuong, N. T., and Hélène C. (1996) Specific inhibition of in vitro transcription elongation by triplex-forming oligonucleotide intercalator conjugates targeted to HIV proviral DNA. *Biochemistry* **35**, 10539–10548.

# Synthesis, Characterization, and Biological Evaluation of Technetium(III) Complexes with Tridentate/Bidentate S,E,S/P,S Coordination (E = O, N(CH<sub>3</sub>), S): A Novel Approach to Robust Technetium Chelates Suitable for Linking the Metal to Biomolecules

Hans-Juergen Pietzsch,<sup>\*,†</sup> Sepp Seifert,<sup>†</sup> Rosemarie Syhre,<sup>†</sup> Francesco Tisato,<sup>‡</sup> Fiorenzo Refosco,<sup>‡</sup> Peter Leibnitz,<sup>§</sup> and Hartmut Spies<sup>†</sup>

Forschungszentrum Rossendorf, Institut für Bioanorganische und Radiopharmazeutische Chemie, PF 510119, D-01314 Dresden, Germany, Istituto di Chimica Inorganica e delle Superfici, Consiglio Nazionale delle Ricerche, Corso Stati Uniti 4, 35127 Padova, Italy, and Bundesanstalt für Materialforschung, Richard-Willstätter-Str. 11, D-12489 Berlin, Germany. Received July 16, 2002; Revised Manuscript Received November 13, 2002

A novel type of mixed-ligand Tc(III) complexes, [Tc(SCH<sub>2</sub>CH<sub>2</sub>-E-CH<sub>2</sub>CH<sub>2</sub>S)(PR<sub>2</sub>S)] (E = S, N(CH<sub>3</sub>); PR<sub>2</sub>S = phosphinothiolate with R = aryl, alkyl) is described. These “3+2”-coordinated complexes can be prepared in a two-step reduction/substitution procedure via the appropriate chloro-containing oxotechnetium(V) complex [TcO(SES)Cl] {E = S, N(CH<sub>3</sub>)}. Tc(III) compounds have been fully characterized both in solid and solution states and found to adopt the trigonal-bipyramidal coordination geometry. The equatorial trigonal plane is formed by three thiolate sulfur atoms, whereas the phosphorus of the bidentate P,S ligand and the neutral donor of the tridentate chelator occupy the apical positions. The <sup>99m</sup>Tc(III) complexes have been proven to be identical with the <sup>99m</sup>Tc agents prepared at the no-carrier-added level by comparison of the corresponding UV/vis and radiometric HPLC profiles. Challenge experiments with glutathione clearly indicate that this tripeptide has no effect on the stability of the <sup>99m</sup>Tc complexes in solutions. Biodistribution studies have been carried out in rats at 5 and 120 min postinjection. The substituents at the bidentate P,S ligand significantly influence the biodistribution pattern. Remarkable differences are observed especially in brain, blood, lungs, and liver. All the complexes are able to penetrate the blood–brain barrier of rats and showed a relatively fast washout from the brain.

## INTRODUCTION

This paper reports on the synthesis and biological characterization of a novel class of technetium(III) mixed-ligand complexes with tridentate S,E,S and bidentate P,S coordination (E = S, N(R), O). The syntheses of these mixed-ligand species represent an alternative approach for the development of radiotracers because they offer manifold possibilities to combine the metal with a biologically active fragment and to vary bio-relevant molecular properties.

Mixed-ligand complexes of technetium and rhenium contain the metal ion stabilized in an appropriate oxidation state by a suitable ligand framework, which only partially fills the coordination sphere. Examples for such arrangements are described, beside the technetium(I) and rhenium(I) tricarbonyl moiety [M(CO)<sub>3</sub>]<sup>+</sup> (1), mainly for Tc(V). These include the “super-nitrido” fragment [Tc(N)(PNP)]<sup>2+</sup> (PNP = tridentate aminediphosphine ligand) (2), the substitution-inert [Re(O)(L)]<sup>2+</sup> moiety (L = bidentate functionalized phosphine) (3), and the [M(O)-(SES)]<sup>+</sup> group (SES = tridentate dithiol ligand; E = S, NR, O) forming the well-known “3+1” Tc and Re complexes (4, 5). In all cases the coordination sphere of the metal ion is completed by additional mono-, bi-, or

tridentate co-ligands. Among these species, the so-called “3+1” complexes suffer in vitro and in vivo substitution reaction with thiol-containing molecules such as cysteine or glutathione (6–9). To overcome this problem, labile oxo-Tc(V) compounds have been replaced by electron-rich Tc(III) ones in the search for neutral and stable mixed-ligand complexes. So, “4+1” Re and Tc complexes containing 2,2',2''-nitritoltris-(ethanethiol) as a tripodal ligand and tertiary phosphines or isocyanides as co-ligands have shown superior properties compared to the “3+1” complexes in terms of stability (10–12).

Another type of neutral Tc(III) complexes derived from the reaction of oxo-Tc(V) “3+1” precursors with tertiary phosphines, namely, the “3+1+1” complexes of general formula [M(PR<sub>3</sub>)(SES)(SR)] (SES = tridentate dithiol ligand; E = S, NR, O), are still unstable against cysteine and GSH and, sometimes, re-oxidize to the original starting material (13, 14). Stability of this class of compounds can be enhanced by combining the monodentate ligands, i.e., tertiary phosphine and thiol, into a bidentate P,S phosphinothiol to produce “3+2” Tc(III) mixed-ligand complexes of the type [Tc(SES)(R<sub>2</sub>PS)]. Previous investigations have demonstrated that P,S functionalized phosphines allow the synthesis of Tc(III) species of different geometry by varying either the nature of the carbon chain between the phosphorus and the sulfur atoms and/or the substituents at the phosphorus atom (15, 16). Furthermore bis- and monosubstituted nitrido-Tc(V) complexes with phosphinothiolate ligands have been described (17).

\* Corresponding author. Fax: (0351) 260 3232. E-mail: h.j.pietzsch@fz-rossendorf.de.

<sup>†</sup> Institut für Bioanorganische und Radiopharmazeutische Chemie.

<sup>‡</sup> Istituto di Chimica Inorganica e delle Superfici.

<sup>§</sup> Bundesanstalt für Materialforschung.



The aim of the work presented here was to prepare neutral and stable "3+2" Tc(III) complexes both at macroscopic and at nca level, to confirm their identity by using chromatographic techniques coupled with UV/vis and radiometric detection, to study their reactivity in various media and to check the biodistribution properties in rats of a number of model complexes.

## EXPERIMENTAL PROCEDURES

**General.** All solvents and commercially available substances were of reagent grade and used without further purification. The P,S ligands were prepared by ARGUS Chemicals according to the method reported by Chatt et al. (18). The tridentate ligands 3-thiapentane-1,5-dithiol and 3-oxapentane-1,5-dithiol were obtained from Aldrich. 3-(*N*-Methyl)azapentane-1,5-dithiol was prepared according to standard procedures starting from *N*-methyl-2,2'-iminodiethanol (MERCK-Schuchart) (19).

$^{99}\text{Tc}$  as  $\text{NH}_4\text{TcO}_4$  was obtained from Amersham as 0.3 M aqueous solution.  $^{99\text{m}}\text{TcO}_4^-$  was eluted from a commercial  $^{99}\text{Mo}/^{99\text{m}}\text{Tc}$  generator (Mallinckrodt).

**Instrumentation.** Elemental analyses were performed on a LECO Elemental Analyzer CHNS-932. Melting points were obtained on a Boëtius-Mikroheitzisch and are uncorrected. IR spectra were measured as KBr pellets on a Perkin-Elmer FTIR-spectrometer SPECTRUM 2000. UV/vis spectra were recorded on a SPECORD S10 spectrometer from Carl Zeiss Jena. Proton,  $^{13}\text{C}$ , and  $^{31}\text{P}$  NMR spectra were collected on a Bruker 300 instrument, using  $\text{SiMe}_4$  as internal reference ( $^1\text{H}$  and  $^{13}\text{C}$ ) and 85% aqueous  $\text{H}_3\text{PO}_4$  as external reference ( $^{31}\text{P}$ ). Samples were dissolved in deuterated chloroform at a concentration of ca. 2%. Chemical shifts are reported as  $\delta$  in ppm. Cyclic voltammetry of complexes 1–5 was carried out in dichloromethane solutions ( $3.5 \times 10^{-3} \text{ mol dm}^{-3}$ ), with  $[n\text{-Bu}_4\text{N}][\text{ClO}_4]$  ( $0.1 \text{ mol dm}^{-3}$ ) as supporting electrolyte, at a stationary platinum-disk electrode (area ca.  $1.28 \text{ mm}^2$ ), which was cleaned after each run, with scan rate  $0.2 \text{ V s}^{-1}$  at  $T = 293 \text{ K}$ . Potentials were measured relative to an Ag-wire pseudo-electrode using the  $\text{Fc}/\text{Fc}^+$  couple as internal reference. Controlled potential coulometries of dichloromethane solutions of 1 were performed using an Amel model 721 integrator, in a H-shaped cell containing, in arm 1, a platinum-gauze working electrode and an  $\text{Ag}/\text{Ag}^+$  reference isolated inside a salt bridge by a medium glass frit and, in arm 2, an auxiliary platinum-foil electrode. Thin-layer chromatography (TLC) and high-performance liquid chromatography (HPLC) analyses were performed for controlling the identity, the radiochemical purity, and the stability of the preparations. For TLC studies silica gel plates (Merck 60F $_{254}$ ) and mobile phases of  $\text{MeOH}/0.1 \text{ N HCl}$  (95/5), acetone, or  $\text{BuOH}/\text{water}/\text{MeOH}/25\%$  ammonia (60/20/20/1) were used. The plates were scanned with a Raytest Rita radioanalyzer. HPLC analyses were performed on a Perkin-Elmer device consisting of a Turbo LC System with a quaternary pump (Series 200 LC Pump), a Programmable Absorbance Detector Model 785A, and a homemade  $\gamma$ -ray detector (Bohrloch, NaI-(Ti) crystal). HPLC analyses were carried out with a Hypersil ODS column ( $250 \times 4 \text{ mm}$ ) using a gradient eluent of acetonitrile/ $0.05 \text{ M NH}_4\text{Ac}$  pH 4, and a flow rate of  $1.0 \text{ mL/min}$ . The effluent from the column was monitored by UV absorbance at  $254 \text{ nm}$  for  $^{99}\text{Tc}$  reference complexes or  $\gamma$ -ray detection for the  $^{99\text{m}}\text{Tc}$  complexes.

**X-Ray Data Collection and Processing.** The X-ray data were collected at room temperature ( $293 \text{ K}$ ) on a SMART-CCD diffractometer (SIEMENS), using graphite

**Table 1. Crystal Data and Structure Refinement for Complexes  $^{99}\text{Tc}$ 1 and  $^{99}\text{Tc}$ 4**

complex	$^{99}\text{Tc}$ 1	$^{99}\text{Tc}$ 4
formula	$\text{C}_{18}\text{H}_{22}\text{PS}_4\text{Tc}$	$\text{C}_{19}\text{H}_{25}\text{NPS}_3\text{Tc}$
f.w.	495.57	492.55
crystal system	triclinic	monoclinic
space group	$P\bar{1}$	$P2(1)/n$
$a$ [Å]	7.11(2)	14.8299(7)
$b$ [Å]	17.00(4)	8.0082(4)
$c$ [Å]	19.18(5)	17.7414(9)
$\alpha$ [deg]	64.06(8)	90
$\beta$ [deg]	88.60(9)	97.0470(10)
$\gamma$ [deg]	87.95(9)	90
$V$ [Å $^3$ ]	2084(9)	2091.1(2)
$Z$	4	4
temp [K]	293(2)	293(2)
$d$ [g/cm $^3$ ]	1.579	1.565
abs. coeff. [mm $^{-1}$ ]	1.167	1.067
$F(000)$	1008	1008
$\mu$ [Å] radiation	0.71073	0.71073
crystal size [mm $^3$ ]	$0.540 \times 0.072 \times 0.036$	$0.9 \times 0.54 \times 0.18$
$2\theta$ range	2.13–28.84	1.69–28.91
$hkl$	$-9 \leq h \leq 9$ $-22 \leq k \leq 17$ $-18 \leq l \leq 24$	$-20 \leq h \leq 11$ $-10 \leq k \leq 10$ $-23 \leq l \leq 23$
no. of coll. reflns	6175	12200
no. of indep. reflns.	6154	5029
GOF	1.195	1.093
$R$ [ $I > 2s$ ( $I$ )]	$R1 = 0.0814$ $wR2 = 0.1779$	$R1 = 0.0372$ $wR2 = 0.1025$
$R$ (all data)	$R1 = 0.1015$ $wR2 = 0.2017$	$R1 = 0.0399$ $wR2 = 0.1048$
largest diff. peak	1.875	0.779
largest diff. hole	−1.019	−0.736

monochromatized Mo- $\text{K}_\alpha$  radiation ( $\lambda = 0.71073 \text{ Å}$ ). A summary of the crystallographic data is given in Table 1. The positions of the non-hydrogen atoms were determined by the heavy atom technique. After anisotropic refinement of these positions, the hydrogen positions were calculated according to ideal geometries. Empirical absorption corrections were made using psi scans. Most of the calculations were carried out in the SHELXTL system with some local modifications.

Relevant bond lengths and angles are contained in Table 3. Atomic positional and thermal parameters, full lists of bond lengths and angles, and  $F_o/F_c$  values have been deposited (20).

**Synthesis of  $[\text{TcO}(\text{SCH}_2\text{CH}_2\text{SCH}_2\text{CH}_2\text{S})\text{Cl}]$  (I) and  $[\text{TcO}(\text{SCH}_2\text{CH}_2\text{N}(\text{CH}_3)\text{CH}_2\text{CH}_2\text{S})\text{Cl}]$  (II).** These precursor complexes were prepared by ligand-exchange reaction of  $[\text{N}(\text{C}_4\text{H}_9)]_3[\text{TcOCl}_4]$  with the appropriate tridentate ligand as described elsewhere (21, 22).

**Synthesis Procedure for the Tc(III) Complexes  $[\text{Tc}(\text{SCH}_2\text{CH}_2\text{SCH}_2\text{CH}_2\text{S})(\text{PR}_2\text{S})]$ – $^{99}\text{Tc}$ 1– $^{99}\text{Tc}$ 3.** A  $100 \mu\text{mol}$  sample of the oxotechnetium(V) complex I and  $400 \mu\text{mol}$  of the appropriate phosphinethiol were dissolved in 3 mL of acetonitrile. After addition of  $0.5 \text{ mL}$  of acetic acid, the mixture was stirred at room temperature under argon for 60 min. The color of the solution turned from yellowish-brown to violet. The reaction mixture was reduced in volume to  $1 \text{ mL}$ , and methanol was added until the solution became turbid. The mixture was then allowed to stand overnight in the refrigerator. Recrystallization of the raw precipitates from chloroform/methanol at  $-20 \text{ °C}$  gave  $^{99}\text{Tc}$ 1,  $^{99}\text{Tc}$ 2, and  $^{99}\text{Tc}$ 3 as dark-violet crystals.

$[\text{Tc}(\text{SCH}_2\text{CH}_2\text{SCH}_2\text{CH}_2\text{S})(\text{PPh}_2\text{S})]$ – $^{99}\text{Tc}$ 1. Yield (rel. to I): 66%. mp =  $175 \text{ °C}$ . Anal. ( $\text{C}_{18}\text{H}_{22}\text{PS}_4\text{Tc}$ ) Calcd: C 43.5%, H 4.5%, S 25.8%. Found: C 43.3%, H 4.8%, S 25.3%. UV/vis ( $\text{CHCl}_3$ ):  $\lambda_{\text{max}}(\text{lg}\epsilon) = 286 \text{ nm}$  (4.0),  $358$  (3.6),  $538$  (2.7). IR (KBr):  $\nu_{\text{C-H}} = 2912\text{--}3070 \text{ cm}^{-1}$ ,  $\nu_{\text{C=C(arat)}}$  =  $1582, 1619 \text{ cm}^{-1}$ ,  $\nu_{\text{P-C}} = 1433 \text{ cm}^{-1}$ .  $^1\text{H}$  NMR: 2.49 (m,

**Table 2. Selected Data for  $^{99}\text{Tc(III)}$  Complexes**

complex	ligand set		$\text{Tc}-\text{P}^a$	$\text{Tc}-\text{E}^{a,b}$	$^{31}\text{P}\{^1\text{H}\}^{c,d}$	$E^e$ $\text{Tc}^{\text{III}}/\text{Tc}^{\text{II}}$	$E_p^{a,e}$ $\text{Tc}^{\text{III}}/\text{Tc}^{\text{IV}}$
	SES	R in $\text{PR}_2\text{S}$					
$^{99}\text{Tc}$ 1	SSS	Ph	2.320	2.402	81.5 (+99.0)	-0.468	0.294
$^{99}\text{Tc}$ 2	SSS	Cy			87.8 (+92.0)	-0.550	0.200
$^{99}\text{Tc}$ 3	SSS	Me			56.6 (+107.8)	-0.565	0.215
$^{99}\text{Tc}$ 4	SNS	Ph	2.298	2.248	88.5 (+106.0)	-0.556	0.144
$^{99}\text{Tc}$ 5	SNS	Me			62.8 (+114.0)	-0.568	0.247
$^{99}\text{Tc}$ "3+1+1" (13)	SSS	$\text{Me}_2\text{Ph/S}$	2.358	2.398	20.4 (+65.2)	-0.335	0.262
$^{99}\text{Tc}$ "3+1+1" (13)	SNS	$\text{Me}_2\text{Ph/S}$	2.318	2.273	31.4 (+76.2)	-0.520	0.063

<sup>a</sup> In Å. <sup>b</sup> E is the central atom of the tridentate ligand. <sup>c</sup> In ppm. <sup>d</sup> The chemical shift between uncoordinated and coordinated phosphinothiol or phosphine is reported in parentheses. <sup>e</sup> In mV, potentials are vs the ferricinium/ferrocene couple.

**Table 3. Selected Bond Lengths and Angles of Complexes  $^{99}\text{Tc}$ 1 and  $^{99}\text{Tc}$ 4**

$^{99}\text{Tc}$ 1		$^{99}\text{Tc}$ 4	
Tc-S(1)	2.251(6)	Tc(1)-S(3)	2.2202(9)
Tc-S(2)	2.216(6)	Tc(1)-S(1)	2.2396(8)
Tc-S(3)	2.239(7)	Tc(1)-S(2)	2.2427(8)
Tc-S(4)	2.402(7)	Tc(1)-N(1)	2.248(2)
Tc-P(1)	2.320(7)	Tc(1)-P(1)	2.2979(7)
S(2)-Tc-S(3)	114.9(2)	S(3)-Tc(1)-S(1)	121.27(3)
S(2)-Tc-S(1)	118.5(2)	S(3)-Tc(1)-S(2)	116.57(3)
S(3)-Tc-S(1)	126.4(2)	S(1)-Tc(1)-S(2)	121.73(3)
S(2)-Tc-P(1)	93.8(2)	S(3)-Tc(1)-N(1)	85.30(8)
S(3)-Tc-P(1)	94.4(2)	S(1)-Tc(1)-N(1)	92.64(8)
S(1)-Tc-P(1)	85.2(2)	S(2)-Tc(1)-N(1)	85.30(8)
S(2)-Tc-S(4)	87.9(2)	S(3)-Tc(1)-P(1)	92.29(3)
S(3)-Tc-S(4)	87.0(2)	S(1)-Tc(1)-P(1)	85.28(3)
S(1)-Tc-S(4)	91.9(2)	S(2)-Tc(1)-P(1)	99.27(3)
P(1)-Tc-S(4)	177.04(10)	N(1)-Tc(1)-P(1)	175.42(8)

4H), 2.96 (m, 8H), 7.35–7.60 (10H,  $\text{PPh}_2$ ).  $^{13}\text{C}$  NMR: 34.99 (s), 35.72 (d), 36.53 (d), 38.75 (d), 128.14 (d), 129.74 (s), 132.73 (d), 135.48 (d).  $^{31}\text{P}$  NMR: 81.48 (bs).

$[\text{Tc}(\text{SCH}_2\text{CH}_2\text{SCH}_2\text{CH}_2\text{S})(\text{P}(\text{C}_6\text{H}_{11})_2\text{S})]-^{99}\text{Tc}$ 2. Yield (rel. to **I**): 63% rel. to **I**. mp = 158 °C. Anal. ( $\text{C}_{18}\text{H}_{34}\text{PS}_4\text{Tc}$ ) Calcd: C 42.5%, H 6.7%, S 25.2%. Found: C 42.4%, H 6.8%, S 24.7%. UV/vis ( $\text{CHCl}_3$ ):  $\lambda_{\text{max}}(\text{lg}\epsilon) = 285$  nm (4.0), 356 (3.6), 552 (2.8). IR (KBr):  $\nu_{\text{C-H}} = 2910$ –3075  $\text{cm}^{-1}$ ,  $\nu_{\text{C=C(arat)}} = 1582$ , 1615  $\text{cm}^{-1}$ ,  $\nu_{\text{P-C}} = 1436$   $\text{cm}^{-1}$ .  $^1\text{H}$  NMR: 1.59 (d, 6H;  $\text{P-CH}_3$ ), 1.84 (dt, 2H;  $\text{P-CH}_2$ ), 2.89 (m, 8H), 3.03 (s, 3H;  $\text{N-CH}_3$ ), 3.25 (m, 2H).  $^{13}\text{C}$  NMR: 17.82 (d), 36.10 (d), 37.83 (d), 39.44 (d), 49.99 (s), 61.57 (s).  $^{31}\text{P}$  NMR: 62.80 (bs).

$[\text{Tc}(\text{SCH}_2\text{CH}_2\text{SCH}_2\text{CH}_2\text{S})(\text{PMe}_2\text{S})]-^{99}\text{Tc}$ 3. Yield (rel. to **I**): 71%. mp = 162 °C. Anal. ( $\text{C}_8\text{H}_{18}\text{PS}_4\text{Tc}$ ) Calcd: C 25.8%, H 4.9%, S 34.4%. Found: C 25.7%, H 4.9%, S 34.0%. UV/vis ( $\text{CHCl}_3$ ):  $\lambda_{\text{max}}(\text{lg}\epsilon) = 283$  nm (4.0), 355 (3.6), 548 (2.7). IR (KBr):  $\nu_{\text{C-H}} = 2850$ –3065  $\text{cm}^{-1}$ ,  $\nu_{\text{P-C}} = 1435$   $\text{cm}^{-1}$ .  $^1\text{H}$  NMR: 1.25–2.35 (20H + 2H), 2.43 (m, 2H), 2.93 (m, 8H).  $^{13}\text{C}$  NMR: 26.0–29.3 (Cyclohexyl), 34.53 (d), 37.48 (d), 39.02 (d), 40.10 (d).  $^{31}\text{P}$  NMR: 87.80 (bs).

**Synthesis Procedure for the Tc(III) Complexes  $[\text{Tc}(\text{SCH}_2\text{CH}_2\text{N}(\text{CH}_3)\text{CH}_2\text{CH}_2\text{S})(\text{PR}_2\text{S})]-^{99}\text{Tc}$ 4,  $^{99}\text{Tc}$ 5.** A 100  $\mu\text{mol}$  sample of the oxotechnetium(V) complex **II** and 400  $\mu\text{mol}$  of the appropriate phosphinothiol were dissolved in 3 mL of acetonitrile. After addition of 0.5 mL of acetic acid, the mixture was stirred at room temperature under argon for 90 min. The color of the solution turned from yellowish-brown to violet. After reduction of the reaction mixture in volume to 0.5 mL, the complexes were isolated by column chromatography (column 10  $\times$  250 mm, stationary phase silica gel 0.04–0.063 mm, eluent  $\text{CHCl}_3$ /acetone 12:1 v/v). Recrystallization from chloroform/methanol (1:3 v/v) gave violet crystals of  $^{99}\text{Tc}$ 4 and  $^{99}\text{Tc}$ 5.

$[\text{Tc}(\text{SCH}_2\text{CH}_2\text{N}(\text{CH}_3)\text{CH}_2\text{CH}_2\text{S})(\text{PPh}_2\text{S})]-^{99}\text{Tc}$ 4. Yield (rel. to **II**): 68%. mp = 185 °C. Anal. ( $\text{C}_{19}\text{H}_{25}\text{NPS}_3\text{Tc}$ )

Calcd: C 46.2%, H 5.1%, N 2.8%, S 19.5%. Found: C 46.6%, H 5.5%, N 2.8%, S 18.9%. UV/vis ( $\text{CHCl}_3$ ):  $\lambda_{\text{max}}(\text{lg}\epsilon) = 280$  nm (4.2), 349 (3.7), 545 (2.9). IR (KBr):  $\nu_{\text{C-H}} = 2915$ –3070  $\text{cm}^{-1}$ ,  $\nu_{\text{C=C(arat)}} = 1580$ , 1623  $\text{cm}^{-1}$ ,  $\nu_{\text{P-C}} = 1433$   $\text{cm}^{-1}$ .  $^1\text{H}$  NMR: 2.39 (q, 2H), 2.85 (m, 4H), 2.99 (m, 4H), 3.11 (s, 3H;  $\text{N-CH}_3$ ), 3.23 (m, 2H), 7.35–7.55 (10H,  $\text{PPh}_2$ ).  $^{13}\text{C}$  NMR: 35.01 (d), 37.29 (d), 39.55 (d), 49.95 (s), 61.78 (s), 127.90 (d), 129.27 (s), 132.48 (d), 137.21 (d).  $^{31}\text{P}$  NMR: 88.50 (bs).

$[\text{Tc}(\text{SCH}_2\text{CH}_2\text{N}(\text{CH}_3)\text{CH}_2\text{CH}_2\text{S})(\text{PMe}_2\text{S})]-^{99}\text{Tc}$ 5. Yield (rel. to **II**): 64%. mp = 167 °C. Anal. ( $\text{C}_9\text{H}_{21}\text{NPS}_3\text{Tc}$ ) Calcd: C 29.3%, H 5.7%, N 3.8%, S 26.1%. Found: C 29.6%, H 5.8%, N 3.5%, S 25.8%. UV/vis ( $\text{CHCl}_3$ ):  $\lambda_{\text{max}}(\text{lg}\epsilon) = 276$  nm (4.3), 345 (3.8), 509 (2.8). IR (KBr):  $\nu_{\text{C-H}} = 2860$ –3069  $\text{cm}^{-1}$ ,  $\nu_{\text{P-C}} = 1434$   $\text{cm}^{-1}$ .  $^1\text{H}$  NMR: 1.59 (d, 6H;  $\text{P-CH}_3$ ), 1.84 (dt, 2H;  $\text{P-CH}_2$ ), 2.89 (m, 8H), 3.03 (s, 3H;  $\text{N-CH}_3$ ), 3.25 (m, 2H).  $^{13}\text{C}$  NMR: 17.82 (d), 36.10 (d), 37.83 (d), 39.44 (d), 49.99 (s), 61.57 (s).  $^{31}\text{P}$  NMR: 62.80 (bs).

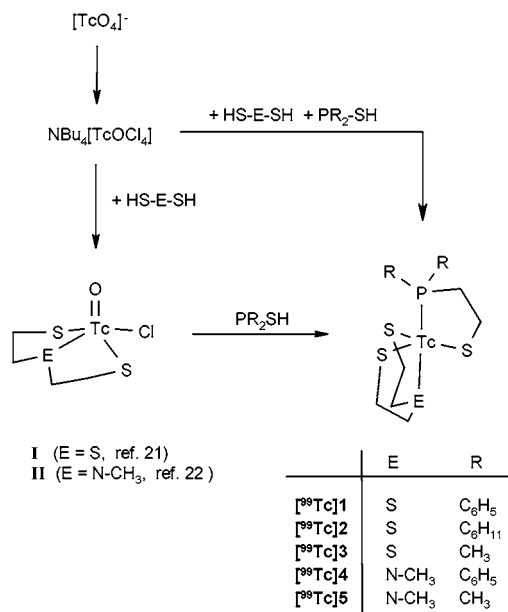
**General Synthesis Procedure for the No-Carrier-Added Preparation of the Compounds  $^{99}\text{mTc}(\text{SES})-(\text{PR}_2\text{S})]-^{99}\text{mTc}$ 1,  $^{99}\text{mTc}$ 2,  $^{99}\text{mTc}$ 4,  $^{99}\text{mTc}$ 6– $^{99}\text{mTc}$ 11.** No-carrier-added preparations of "3+2"  $\text{Tc(III)}$  compounds were studied with the tridentate SES ligands 3-thiapentane-1,5-dithiol, 3-(*N*-methyl)azapentane-1,5-dithiol and 3-oxapentane-1,5-dithiol and bidentate P,S ligands illustrated in Figure 4.

A 0.10 mg (for preparing  $[\text{Tc}(\text{SSS}/\text{PR}_2\text{S})]$ ) or 0.05 mg (for preparing  $[\text{Tc}(\text{SNMeS}/\text{PR}_2\text{S})]$  and  $[\text{Tc}(\text{SOS}/\text{PR}_2\text{S})]$ ) sample of the bidentate P,S ligand, dissolved in 0.10 mL of ethanol, and 0.05 mg of the appropriate tridentate SES ligand, dissolved in 0.10 mL of ethanol, were added to a mixture of 0.50–1.0 mL pertechnetate, 0.25 mL propylene glycol, and 0.75 mL of acetonitrile. After addition of 40  $\mu\text{L}$  0.1 N NaOH, the complexes were formed by reduction of pertechnetate with 40  $\mu\text{L}$   $\text{SnCl}_2$  solution (2.0 mg  $\text{SnCl}_2$  dissolved in 5.0 mL 0.1 N HCl). The reaction was completed by heating at 50 °C within 15 min (yields between 60 and 90%).

The preparations were purified for stability and bio-distribution studies by HPLC using a semipreparative Hypersil column (250  $\times$  8 mm, 10  $\mu\text{m}$ ).

**Determination of Partition Coefficients.** Partition coefficients of the  $^{99}\text{mTc}$  complexes were determined by shake-flask method by mixing 0.5 mL of the complex solution (0.9% NaCl solution and 20% propylene glycol) and 0.5 mL *n*-octanol and shaking for 5 min. After centrifugation aliquots of both phases were counted and the partition coefficient calculated.

**Ligand Exchange (Challenge) Experiments with Glutathione (GSH).**  $^{99}\text{mTc}$  complexes, dissolved in a mixture of propylene glycol/MeOH (2:1 v/v), were diluted with an equivalent volume of an aqueous solution of 20 mM GSH containing 25% of propylene glycol immediately

**Scheme 1. Reaction Routes to Tc(III) Complexes with "3+2" Coordination (E = N(CH<sub>3</sub>), S)**


after HPLC separation, resulting in a final glutathione concentration of 10 mM. The analyses were performed by HPLC as described above.

**Stability Studies in Plasma.** A 50  $\mu$ L sample of the appropriate <sup>99m</sup>Tc complex solution (0.9% NaCl, 12% propylene glycol) was incubated in 200  $\mu$ L of rat plasma at 37 °C. After an incubation time of 30 min, the samples were analyzed by HPLC with a Supelguard column (20  $\times$  4.6 mm, 10  $\mu$ m, flow rate 1.0 mL/min) using a linear gradient 95% to 40% A in 15 min [A, 2-propanol/0.1% trifluoroacetic acid (TFA) (10/90); B, 2-propanol/0.1% TFA (90/10)].

**Biodistribution Studies.** The animal studies in male Wistar rats (5–6 weeks old) were carried out according to the relevant national regulations. A 500  $\mu$ L sample of <sup>99m</sup>Tc complex solution (saline, propylene glycol 25%) was injected into the tail vein of rats. After the injection the rats were sacrificed by heart puncture under ether anaesthesia at 5 and 120 min p.i.. Selected organs were isolated for weighing and counting. The accumulated radioactivity in the organs tissue were calculated in terms of percentage of injected dose per organ as well as percent injected dose per gram of blood.

## RESULTS AND DISCUSSION

**Technetium-99 Chemistry. Synthesis.** As shown in Scheme 1, the Tc(III) mixed-ligand complexes can be prepared in a two-step substitution-reduction procedure starting from the prereduced precursor [TcOCl<sub>4</sub>]<sup>−</sup> via the appropriate chloro-containing oxotechnetium(V) complex **I** or **II**. In this case, sequential addition of the relevant dithiol followed by the bidentate phosphinothiol is required. An alternative one-pot reaction with the simultaneous addition of the ligands to the labile [TcOCl<sub>4</sub>]<sup>−</sup> precursor is possible, but the yield of the Tc(III) species is lower. In these reactions the phosphinethiols work as reducing agent as well as coordinating ligand. Both procedures are characterized by a typical change in color from orange to deep-violet indicating the transfer from Tc(V) to Tc(III). There is no evidence for the formation of other oxo-Tc(V) species.

**Characterization.** The Tc(III) complexes have been characterized by (i) elemental analyses, which are in

agreement with the proposed formulations, (ii) cyclic voltammetry, (iii) spectroscopic measurements, including IR, UV/vis, NMR, and (iv) X-ray structure analyses of two prototypic representatives.

The IR spectra of all compounds show characteristic absorptions of the Tc–P stretching vibrations. No bands assignable to the Tc=O core are observed in the range 900–1000 cm<sup>−1</sup> indicating the absence of oxotechnetium species.

The UV/vis spectra of the Tc(III) complexes exhibit very similar and characteristic intense bands at 345–353 nm and less intense absorptions in the visible region (509–552 nm).

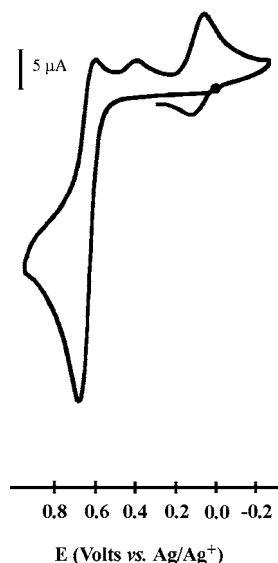
The diamagnetism exhibited by this class of Tc(III) complexes is in agreement with low-spin d<sup>4</sup> trigonal bipyramidal configuration (vide infra). Consequently, NMR spectra show sharp proton and carbon signals and allow to distinguish both coordinated dithiolate and phosphinothiolate fragments. On the contrary, room-temperature <sup>31</sup>P{<sup>1</sup>H} spectra exhibit rather broad signals due to the quadrupolar relaxation induced by the <sup>99</sup>Tc nucleus (*I* = 9/2) at the neighbor P atom (23). The <sup>31</sup>P signal moves significantly downfield by ca. 100 ppm upon phosphine coordination (see Table 2) compared to the values exhibited by uncoordinated PMe<sub>2</sub>S = −51.2, PPh<sub>2</sub>S = −17.5, and PCy<sub>2</sub>S = −4.2 ppm. Despite the more shielded values exhibited by those complexes containing the more basic phosphine of the series (i.e., PMe<sub>2</sub>S), this ligand induces the highest chemical shift variation (+114 and +107.8 ppm for [<sup>99</sup>Tc]5 and [<sup>99</sup>Tc]3, respectively), indicating a strong contribution of the phosphine lone pair to the metal-phosphorus bond. Less pronounced is the chemical shift variation induced by the less basic PCy<sub>2</sub>S and PPh<sub>2</sub>S ligands (see Table 2). The nature of the *trans*-axial heteroatom of the tridentate ligand (S or N) affects the <sup>31</sup>P signal and the Tc–P bond as well. In fact, by increasing the  $\pi$ -accepting combination in the series (thioether/phosphine in [<sup>99</sup>Tc]1 vs amine/phosphine in [<sup>99</sup>Tc]4), the Tc–P bond distance elongates from 2.298 to 2.320 Å, whereas the <sup>31</sup>P signal is less downfield shifted. These "3+2" species do not rearrange back to the original oxo-Tc(V) precursors, as it was observed in the case of some isostructural Tc(III) "3+1+1" complexes containing a monodentate phosphine and a monodentate thiolate (13).

Cyclic voltammetric (CV) data support the observations pointed out above. CV oxidation (*E*<sub>p</sub><sup>a</sup>) and reduction (*E*<sup>o</sup>) potentials are reported in Table 2 and a representative voltammogram is depicted in Figure 1. The redox stability window for this class of Tc(III) "3+2" complexes is about 700–800 mV. This range is ca. 100–200 mV larger when compared to the redox windows found in similar T(III) "3+1+1" complexes, indicating an increased stability of the more chelated "3+2" compounds.

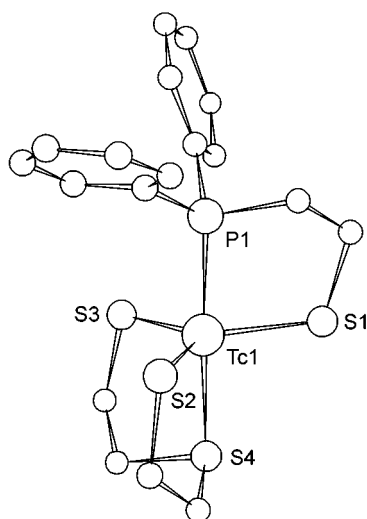
Complexes [<sup>99</sup>Tc]1 and [<sup>99</sup>Tc]4, as prototypic representatives of this novel class of neutral Tc(III) compounds, were studied by X-ray structure analysis. A summary of the crystallographic data is given in Table 1. Selected bond lengths and angles are cumulated in Table 3.

As illustrated in Figures 2 and 3, the complexes adopt the trigonal-bipyramidal geometry comprised by three sulfur atoms, the neutral heteroatom of the tridentate ligand, and the tertiary phosphorus atom. The trigonal plane is formed by the three thiolate sulfurs of the tridentate ligand and the bidentate P,S chelator. The phosphorus and the neutral heteroatom of the tridentate chelate ligand occupy the apical positions. This arrange-





**Figure 1.** Cyclic voltammogram of complex  $[^{99m}\text{Tc}]\mathbf{5}$  in 1 mM  $\text{CH}_2\text{Cl}_2$  solution. Potentials are vs  $\text{Ag}/\text{Ag}^+$ . The scan rate is  $200 \text{ mV s}^{-1}$ .

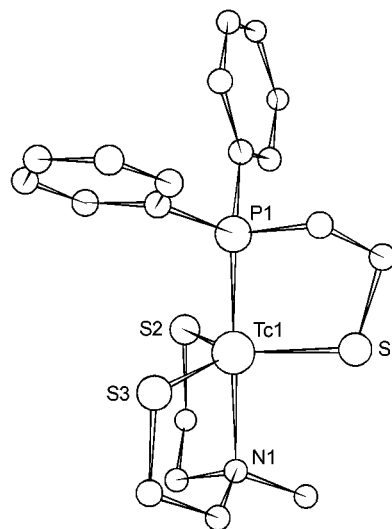


**Figure 2.** Molecular structure of complex  $[^{99m}\text{Tc}]\mathbf{1}$ .

ment is quite common for transition-metal complexes containing two  $\pi$ -acceptor groups (12, 13, 15, 24–26).

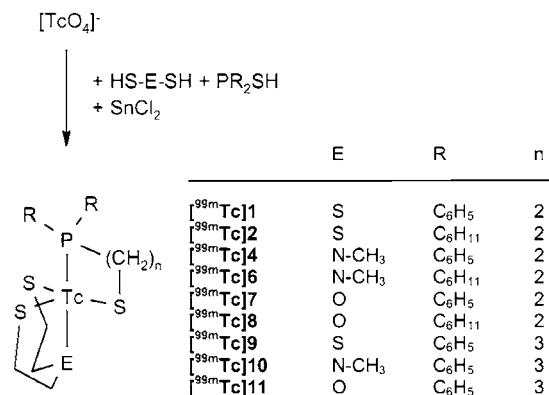
The  $\text{Tc}-\text{S}_{\text{thiolato}}$  distances are restricted in a narrow range (2.21–2.24 Å) and compares well with those previously reported for similar trigonal-bipyramidal complexes (12, 13, 26). The unique axial metal thioether-sulfur bond in  $[^{99m}\text{Tc}]\mathbf{1}$  elongates to 2.427 Å. The  $\text{P}-\text{Tc}-\text{E}$  axis shows only slight deviation from linearity. Other angles of the inner coordination sphere are consistent with the *tbp* arrangement. A special order/disorder phenomenon was detected in the crystal packing of  $[^{99m}\text{Tc}]\mathbf{4}$ . As frequently observed in this type of complexes, the “SNS” chelator can change its conformation by a flip-flop mechanism giving rise to a statistical distribution of two equal isomers within the crystal (27).

**Technetium-99m Chemistry and Biodistribution Studies.** *No-Carrier-Added Preparation of the  $^{99m}\text{Tc}$  Complexes.* The “3+2” coordinated  $^{99m}\text{Tc}$  complexes  $[^{99m}\text{Tc}]\mathbf{1}$ ,  $[^{99m}\text{Tc}]\mathbf{2}$ ,  $[^{99m}\text{Tc}]\mathbf{4}$ , and  $[^{99m}\text{Tc}]\mathbf{6}$ – $[^{99m}\text{Tc}]\mathbf{11}$  were prepared by a one-step procedure starting from  $^{99m}\text{TcO}_4^-$  with stannous chloride as reducing agent in nearly neutral solutions using optimized amounts of the bidentate P,S ligands as well as of the tridentate S,E,S



**Figure 3.** Molecular structure of complex  $[^{99m}\text{Tc}]\mathbf{4}$ .

**Scheme 2. No-Carrier-Added Preparation of “3+2” Coordinated  $^{99m}\text{Tc}$  Complexes**



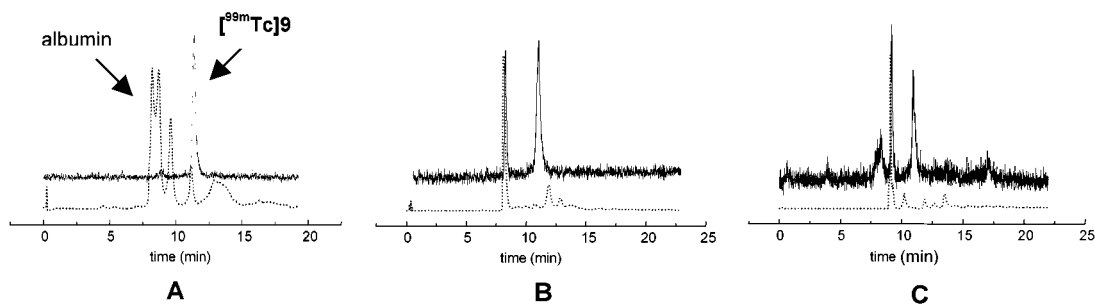
**Table 4.  $\log P_{o/w}$  Values and Reaction against Rat Plasma of “3+2”  $^{99m}\text{Tc}$  Model Complexes**

complex	$\log P_{o/w}$	plasma binding
$[^{99m}\text{Tc}]\mathbf{1}$	3.1	—
$[^{99m}\text{Tc}]\mathbf{2}$	1.5	—
$[^{99m}\text{Tc}]\mathbf{4}$	1.5	—
$[^{99m}\text{Tc}]\mathbf{6}$	1.2	—
$[^{99m}\text{Tc}]\mathbf{7}$	1.5	+
$[^{99m}\text{Tc}]\mathbf{8}$	1.6	+
$[^{99m}\text{Tc}]\mathbf{9}$	2.2	—
$[^{99m}\text{Tc}]\mathbf{10}$	1.8	—
$[^{99m}\text{Tc}]\mathbf{11}$	1.2	+

ligands (Scheme 2). While 0.05 mg of the P,S chelators are sufficient for the preparation of the complexes with S,N,S/P,S and S,O,S/P,S coordination, the formation of the S,S,S/P,S complexes needs 1.0 mg of the P,S ligand. For all products the amount of the tridentate ligand was determined to be 0.05 mg.

To establish the structure of the  $^{99m}\text{Tc}$  complexes, comparison by HPLC with the well-characterized  $^{99m}\text{Tc}$  analogues was pursued applying parallel radiometric and photometric detection. Thus, after co-injection of appropriate  $^{99m}\text{Tc}/^{99}\text{Tc}$  complex couples, practically identical retention times were observed, while the recovery through the column was quantitative.

Examination of the octanol/water partition coefficients suggests high lipophilicity for the resulting “3+2”  $^{99m}\text{Tc}$  species (Table 4).



**Figure 4.** Plasma binding of [ $^{99m}\text{Tc}$ ]9 and [ $^{99m}\text{Tc}$ ]7 determined by HPLC. (A) [ $^{99m}\text{Tc}$ ]9 after 5 min incubation at 37 °C; (B) after 150 min; (C) [ $^{99m}\text{Tc}$ ]7 after 5 min. Dotted line, UV detection (220 nm); solid line,  $\gamma$  detection [ $^{99m}\text{Tc}$ ]9

**Table 5.** Biodistribution of “3+2” Coordinated  $^{99m}\text{Tc}$  Complexes in the Blood and in Selected Organs of Wistar Rats (%ID/g, 5 and 120 min p.i., mean  $\pm$  SD,  $N = 5$ )

complex	[min p.i.]	%ID/g					
		blood	brain	heart	lung	kidney	liver
[ $^{99m}\text{Tc}$ ]1	5	0.3 $\pm$ 0.1	0.40 $\pm$ 0.03	1.3 $\pm$ 0.2	1.2 $\pm$ 0.2	1.2 $\pm$ 0.2	5.8 $\pm$ 0.4
	120	$\leq 0.1$	$< 0.05$	0.2 $\pm$ 0.05	0.4 $\pm$ 0.1	0.6 $\pm$ 0.1	2.8 $\pm$ 0.2
[ $^{99m}\text{Tc}$ ]2	5	0.6 $\pm$ 0.1	$\leq 0.1$	1.6 $\pm$ 0.2	1.5 $\pm$ 0.2	2.3 $\pm$ 0.5	10.8 $\pm$ 1.4
	120	0.2 $\pm$ 0.05	$< 0.05$	0.3 $\pm$ 0.1	0.2 $\pm$ 0.1	0.7 $\pm$ 0.1	4.8 $\pm$ 0.6
[ $^{99m}\text{Tc}$ ]4	5	0.6 $\pm$ 0.1	0.62 $\pm$ 0.06	1.3 $\pm$ 0.2	2.3 $\pm$ 0.4	2.2 $\pm$ 0.1	5.2 $\pm$ 0.4
	120	$\leq 0.1$	$< 0.05$	0.1 $\pm$ 0.05	0.6 $\pm$ 0.1	0.8 $\pm$ 0.1	4.0 $\pm$ 0.6
[ $^{99m}\text{Tc}$ ]6	5	1.8 $\pm$ 0.2	$\leq 0.1$	1.1 $\pm$ 0.1	2.0 $\pm$ 0.2	1.7 $\pm$ 0.1	10.0 $\pm$ 0.8
	120	0.3 $\pm$ 0.1	$< 0.05$	0.2 $\pm$ 0.5	0.5 $\pm$ 0.1	1.7 $\pm$ 0.1	4.8 $\pm$ 0.2
[ $^{99m}\text{Tc}$ ]7	5	1.5 $\pm$ 0.1	0.37 $\pm$ 0.04	0.8 $\pm$ 0.0	2.3 $\pm$ 0.1	1.3 $\pm$ 0.2	5.6 $\pm$ 0.5
	120	0.8 $\pm$ 0.2	$< 0.05$	0.3 $\pm$ 0.1	2.5 $\pm$ 0.6	1.5 $\pm$ 0.2	5.7 $\pm$ 0.8
[ $^{99m}\text{Tc}$ ]8	5	3.8 $\pm$ 0.6	0.16 $\pm$ 0.02	1.3 $\pm$ 0.2	3.1 $\pm$ 0.3	3.9 $\pm$ 0.3	5.3 $\pm$ 0.3
	120	2.3 $\pm$ 0.3	0.15 $\pm$ 0.03	0.7 $\pm$ 0.1	2.0 $\pm$ 0.3	6.2 $\pm$ 0.6	3.4 $\pm$ 0.4
[ $^{99m}\text{Tc}$ ]9	5	0.4 $\pm$ 0.1	0.66 $\pm$ 0.11	1.4 $\pm$ 0.3	2.3 $\pm$ 0.6	2.5 $\pm$ 0.7	13.2 $\pm$ 2.4
	120	0.1 $\pm$ 0.05	$< 0.05$	0.1 $\pm$ 0.05	0.9 $\pm$ 0.1	1.1 $\pm$ 0.1	9.0 $\pm$ 1.9
[ $^{99m}\text{Tc}$ ]10	5	0.4 $\pm$ 0.1	0.32 $\pm$ 0.04	1.3 $\pm$ 0.1	1.3 $\pm$ 0.2	1.6 $\pm$ 0.2	4.7 $\pm$ 0.5
	120	0.2 $\pm$ 0.05	$< 0.05$	0.1 $\pm$ 0.05	1.0 $\pm$ 0.1	1.6 $\pm$ 0.1	6.4 $\pm$ 0.6
[ $^{99m}\text{Tc}$ ]11	5	0.9 $\pm$ 0.1	0.37 $\pm$ 0.03	0.8 $\pm$ 0.1	4.2 $\pm$ 0.8	1.5 $\pm$ 0.1	9.5 $\pm$ 1.2
	120	0.5 $\pm$ 0.1	$< 0.05$	0.2 $\pm$ 0.05	4.9 $\pm$ 0.4	1.3 $\pm$ 0.1	8.1 $\pm$ 0.3

**Glutathione Challenge Experiments.** Glutathione (GSH), the most abundant thiol-containing compound in tissues, is present in almost all animal cells in relatively high concentrations (0.5–12 mM) (28, 29). Therefore, it has to be considered as a potential agent for transchelation reactions in vivo. In fact, GSH is responsible for the in vivo reactivity of “3+1” mixed-ligand  $^{99m}\text{Tc(V)}$  complexes which consist of a monodentate thiol ligand and a tridentate dithiol (9–11). Here a ligand exchange in terms of the replacement of the monodentate ligand by GSH occurs both in vitro and in vivo (6–9). For this reason, we investigated the behavior of  $^{99m}\text{Tc(III)}$  “3+2” complexes against GSH.

Saline-containing preparations of the  $^{99m}\text{Tc}$  compounds were diluted 1:1 (v/v) with a 20 mM GSH solution immediately after HPLC purification. For the complexes formed by the S,S,S and S,N,S tridentate ligand, no additional peaks of hydrophilic Tc-GSH mixed ligand species are observed in HPLC studies. These results clearly indicate that glutathione has no negative effect on the stability of  $^{99m}\text{Tc}$  complexes in solutions. This property exhibited by  $^{99m}\text{Tc(III)}$  “3+2” complexes constitutes an important improvement over oxo- $^{99m}\text{Tc(V)}$  “3+1” and similar Tc(III) “3+1+1” complexes (14).

On the contrary, incubation of  $^{99m}\text{Tc(III)}$  “3+2” compounds containing the S,O,S ligand with GSH leads to the formation of hydrophilic species which are not glutathione related. The reason of such instability is not clear yet. However, this behavior parallels the difficulty encountered in the isolation of the corresponding [ $^{99}\text{Tc}(\text{SOS})(\text{PR}_2\text{S})$ ] compounds. Reoxidation processes may play a role in the reduced stability of these solutions.

**Stability in Aqueous Solution.**  $^{99m}\text{Tc}$  preparations containing the S,S,S/P,S and S,N(CH<sub>3</sub>),S/P,S combinations are stable for hours after HPLC purification. However, species with S,O,S/P,S coordination are slowly transformed into more hydrophilic compounds after dilution with saline or phosphate buffer solution. When the appropriate complex solution is diluted about 1:200 (v/v), as it is normally done for the determination of the partition coefficient in octanol/water, the radiochemical purity of the diluted sample decreases to about 80% after 1 h. Due to the formation of hydrophilic impurities the calculated partition coefficients are too low. For this reason we diluted the original complex solution only 1:1 (v/v) with phosphate buffer solution, added octanol immediately, shaken the solution for 5 min, separated the phases, and measured the partition the following day in a Bohrloch scintillation counter (Table 4).

**Stability in Rat Plasma.** Slight differences in stability between the complexes are confirmed by their incubation in rat plasma. While the S,S,S/P,S and S,N,S/P,S coordinated complexes are stable, the analogous S,O,S/P,S species are bound to plasma proteins, especially to albumin (Figure 4). It remains unclear whether the complex itself or decomposition products are bound to albumin.

**Biodistribution Studies in Rats.** The uptake and clearance behavior of the  $^{99m}\text{Tc}$  complexes was determined by distribution studies in Wistar rats at 5 and 120 min postinjection (Table 5). The results indicate that the substituents at the bidentate P,S chelator significantly influence the distribution pattern. Remarkable differences were observed, especially in brain, blood, lungs, and

liver of rats. All of the complexes are able to penetrate the blood-brain-barrier and show a relatively fast wash-out from the brain. However, no correlation was found between brain uptake and lipophilicity of the complexes. The phenyl derivatives ( $[^{99m}\text{Tc}]\mathbf{1}$ ,  $[^{99m}\text{Tc}]\mathbf{4}$ ,  $[^{99m}\text{Tc}]\mathbf{7}$ ,  $[^{99m}\text{Tc}]\mathbf{9}$ – $[^{99m}\text{Tc}]\mathbf{11}$ ) exhibit the highest initial uptake (0.4–1.0% ID/g at 5 min p.i.), whereas the cyclohexyl-bearing species ( $[^{99m}\text{Tc}]\mathbf{2}$ ,  $[^{99m}\text{Tc}]\mathbf{6}$ ,  $[^{99m}\text{Tc}]\mathbf{8}$ ) show only a moderate uptake up to 0.2% ID/g at 5 min postinjection.

The elimination behavior of the complexes differs significantly. In contrast to the S,S,S and S,N,S donor atom sequence ligands, the S,O,S moiety leads to a high blood activity and to a persistent high activity in lungs and liver. The cyclohexyl derivative  $[^{99m}\text{Tc}]\mathbf{8}$  shows increased activity in the kidneys up to 6.2% ID/g (120 min p.i.).

The liver uptake of the phenyl-bearing complexes  $[^{99m}\text{Tc}]\mathbf{9}$  and  $[^{99m}\text{Tc}]\mathbf{11}$  was found to be extremely high (13.2% ID/g, 5 min p.i. for the S,S,S ligand and 9.5% ID/g, 5 min p.i. for the S,O,S moiety) and is connected with a slow elimination of 9.0% and 8.1% ID/g, respectively, up to 120 min postinjection. The S,N,S derivative  $[^{99m}\text{Tc}]\mathbf{10}$  shows an increasing liver uptake up to 6.4% ID/g, 120 min p.i. (47.5% ID). This uptake and elimination pattern does not correlate with the lipophilicity of the complexes. Corresponding to the observed unstability and plasma protein binding of complexes with S,O,S/P,S coordination (see Table 4), the different in vivo behavior, dependent on the tridentate ligand, can be explained as an unspecific binding on proteins of plasma and tissue in vivo.

## CONCLUSION

The association of a tridentate HS–E–SH ligand ( $E = \text{N}(\text{CH}_3)_3$ , S) with a bidentate  $\text{PR}_2$ –SH chelator leads to the formation of nonpolar, lipophilic technetium complexes,  $[\text{Tc}(\text{SCH}_2\text{CH}_2\text{–E–CH}_2\text{CH}_2\text{S})(\text{PR}_2\text{S})]$ , which contain sterically shielded oxo-free Tc(III) ions. This combination enables easy functionalization in order to fine-tune physicochemical properties of the complexes as well as linking of the chelate unit to biomolecules.

$^{99m}\text{Tc}$  analogues can be prepared at no-carrier-added level in high radiochemical yields. With the exception of complexes containing the S,O,S moiety all other complexes are stable toward ligand exchange in challenge experiments with glutathione. This behavior is considered to be an important advantage over oxo- $^{99m}\text{Tc}(\text{V})$  “3+1” complexes. Furthermore, there are no indications for reoxidation of Tc(III) to Tc(V) species or pertechnetate. There is no tendency of these complexes to bind on plasma components. The substituents at the bidentate P,S chelator significantly influence the biodistribution pattern in rats.

Therefore, we propose this new type of Tc(III) complexes as a useful tool in designing of lipophilic, tunable  $^{99m}\text{Tc}$  radiopharmaceuticals.

## LITERATURE CITED

- Alberto, R., Schibli, R., Angst, D., Schubiger, P. A., Abram, U., Abram, S., and Kaden, T. A. (1997) Application of technetium and rhenium carbonyl chemistry to nuclear medicine. *Trans. Met. Chem.* 22, 597–601.
- Bolzati, C., Boschi, A., Duatti, A., Prakash, S., Uccelli L., Refosco, F., Tisato, F., and Bandoli, G. (2000) Geometrically controlled selective formation of nitrido technetium(V) asymmetrical heterocomplexes with bidentate ligands. *J. Am. Chem. Soc.* 122, 4510–4511.
- Bolzati, C., Porchia, M., Bandoli, G., Boschi, A., Malagò, E., and Uccelli, L. (2001) Oxorhenium(V) mixed-ligand complexes with bidentate functionalized phosphines and tridentate Schiff base ligands. *Inorg. Chim. Acta* 315, 205–212.
- Pietzsch, H.-J., Spies, H., and Hoffmann, S. (1989) Lipophilic technetium complexes. VI. Neutral Tc(V) complexes with tridentate dithiol/monothiol ligand coordination. *Inorg. Chim. Acta* 165, 163–166.
- Spyriounis, D. M., Pelecanou, M., Stassinopoulou, C. I., Raptopoulou, C. P., Terzis, A., and Chiotellis, E. (1995) Synthesis and characterization of oxotechnetium(V) complexes with aza-substituted 2,6-dimethyl-4-azaheptane-2,6-dithiol ligands and benzyl mercaptan as coligand. *Inorg. Chem.* 34, 1077–1082.
- Sybre, R., Seifert, S., Spies, H., Gupta, A., and Johannsen, B. (1998) Stability versus reactivity of “3+1” mixed-ligand technetium-99m complexes *in vitro* and *in vivo*. *Eur. J. Nucl. Med.* 793–796.
- Pelecanou, M., Pirmettis, I. C., Nock, B. A., Papadopoulos, M., Chiotellis, E., and Stassinopoulou, C. I. (1998) Interaction of  $[\text{ReO}(\text{SNS})(\text{S})]$  and  $[\text{Tc}(\text{SNS})(\text{S})]$  mixed ligand complexes with glutathione: isolation and characterization of the product. *Inorg. Chim. Acta* 281, 148–152.
- Nock, B. A., Maina, T., Yannoukakos, D., Ioannis, C., Papadopoulos, M., and Chiotellis, E. (1999) Glutathione-mediated metabolism of technetium-99m SNS/S mixed ligand complexes: a proposed mechanism of brain retention. *J. Med. Chem.* 42, 1066–1075.
- Gupta, A., Seifert, S., Sybre, R., Scheunemann, M., Brust, P., and Johannsen, B. (2001) Reactivity of  $^{99m}\text{Tc}(\text{V})$  “3+1” mixed-ligand complexes towards glutathione. *Radiochim. Acta* 89, 43–49.
- Spies, H., Glaser, M., Pietzsch, H.-J., Hahn, F. E., Kintzel, O., and Lügger, T. (1994) Trigonal-bipyramidal Technetium- und Rhenium-Komplexe mit vierzähligen tripodalen  $\text{NS}_3$  Liganden. *Angew. Chem.* 106, 1416–1419.
- Spies, H., Glaser, M., Pietzsch, H.-J., Hahn, F. E., Kintzel, O., and Lügger, T. (1995) Synthesis and reactions of trigonal bipyramidal rhenium and technetium complexes with a tripodal  $\text{NS}_3$  ligand. *Inorg. Chim. Acta* 240, 465–478.
- Pietzsch, H.-J., Gupta, A., Sybre, R., Leibnitz, P., and Spies, H. (2001) Mixed-ligand technetium(III) complexes with tetradentate/monodentate  $\text{NS}_3$ /isocyanide coordination: A new non-polar Technetium chelate system for the design of neutral and lipophilic complexes stable in vivo *Bioconjugate Chem.* 12, 538–544.
- Pietzsch, H.-J., Tisato, F., Refosco, F., Leibnitz, P., Drews, A., Seifert, S., and Spies, H. (2001) Synthesis and characterization of novel trigonal bipyramidal technetium(III) mixed-ligand complexes with SES/S/P coordination ( $E = \text{O}$ ,  $\text{N}(\text{CH}_3)_3$ , S). *Inorg. Chem.* 40, 59–64.
- Seifert, S., Drews, A., Gupta, A., Pietzsch, H.-J., Spies, H., and Johannsen, B. (2000) Stability studies on  $^{99m}\text{Tc}$  technetium(III) complexes with tridentate/monodentate thiol ligands and phosphine “3+1+1” complexes. *Appl. Radiat. Isot.* 53, 431–438.
- Tisato, F., Refosco, F., Bandoli, G., Bolzati, C., and Moresco, A. (1994) Synthesis and Characterization of neutral Tc(III) complexes with mixed S,P-bidentate phosphine-thiolate ligands. Crystal structure of  $[\text{Tc}(\text{SCH}_2\text{CH}_2\text{PPh}_2)_2(\text{SCH}_2\text{CH}_2\text{PPh}_2\text{O})]$ . *J. Chem. Soc., Dalton Trans.* 1453–1461.
- Bolzati, C., Uccelli, L., Boschi, A., Malagò, E., Duatti, A., Tisato, F., Refosco, F., Pasqualini, R., and Piffanelli, A. (2000) Synthesis of a novel class of nitrido Tc-99m radiopharmaceuticals with phosphino-thiol ligands showing transient heart uptake. *Nucl. Med. Biol.* 27, 369–374.
- Bolzati, C., Malagò, E., Boschi, A., Cagnolini, A., Porchia, M., and Bandoli, G. (1999) Symmetric bis-substituted and asymmetric mono-substituted nitridotechnetium complexes with heterofunctionalized phosphinothiolate ligands. *New J. Chem.* 23, 807–809.
- Chatt, J., Dilworth, J. R., Schmutz, J. A., and Zubieta, J. A. (1979) Preparation and crystal and molecular structure of  $[\text{MoO}(\text{SCH}_2\text{CH}_2\text{–PPh}_2)_2]$ . *J. Chem. Soc., Dalton Trans.* 1595–1599.
- Gloe, K., Stephan, H., Jacobi, R., and Beger, J. (1995) Liquid–liquid extraction of mercury chloride with thiaoxaaza alkanes. *Solvent Extraction Res. Dev., Jpn. Vol. 2*, 18–35.



- (20) Crystallographic data (excluding structure factors) for the structures reported in this paper have been deposited with the Cambridge Crystallographic Data Centre as supplementary publication no. CCDC-156313 (complex  $^{99}\text{Tc}1$ ), 159498 ( $^{99}\text{Tc}4$ ). Copies of the data can be obtained free of charge on application to CCDC, 12 Union Road, Cambridge CB2 1EZ, U.K. (fax, +44-1223/336-033; e-mail, deposit@ccdc.cam.ac.uk).
- (21) Noll, B., Leibnitz, P., and Spies, H. (1999) *Synthesis and Molecular Structure of Chloro(3-thiapentane-1,5-dithiolato)-oxotechnetium(V)*, pp 151–152, Annual Report FZR-270, Forschungszentrum Rossendorf, Dresden.
- (22) Mastrostamatis, S. G., Papadopoulos, M. S., Pirmettis, I. C., Paschali, E., Varvarigou, A. D., Stassinopoulou, C. I., Raptopoulou, C. R., Terzis, A., and Chiotellis E. (1994) Tridentate ligands containing the SNS donor atom set as a novel backbone for the development of Technetium brain-imaging agents. *J. Med. Chem.* 37 S.3212–3218.
- (23) Abram, U., Lorenz, B., Kaden, L., and Scheller, D. (1988) Nitrido Complexes of Technetium with Tertiary Phosphines and Arsines. *Polyhedron* 7, 285–289.
- (24) de Vries, N., Dewan, J., Jones, A., and Davison, A. (1988) Complexes of technetium(III) with sterically hindered arenethiolates and their interactions with small  $\pi$ -accepting molecules. *Inorg. Chem.* 27, 1574–1580.
- (25) de Vries, N., Davison, A., and Jones, A. (1989) Trigonal-bipyramidal compounds of technetium with tetradentate umbrella ligand. *Inorg. Chim. Acta* 165, 9–10.
- (26) de Vries, N., Cook, J., Jones, A., and Davison, A. (1991) Technetium(III) complexes with the tetradentate “umbrella” ligand tris(o-mercaptophenyl)phoshinate: X-ray structural characterization of  $\text{Tc}(\text{P}(\text{o}-\text{C}_6\text{H}_4\text{S})_3(\text{CNC}_3\text{H}_7))$ . *Inorg. Chem.* 30, 2662–2665.
- (27) Leibnitz, P., Reck, G., Pietzsch, H.-J., and Spies, H. (2001) *Structures of Technetium and Rhenium Complexes*, p 21, Scientific-Technical Report FZR-311, Forschungszentrum Rossendorf, Dresden.
- (28) Kosower, E. M. (1976) Chemical properties of glutathione. In *Glutathione – Metabolism and Function* (J. M. Arias and W. B. Jakoby, Eds.) Raven Press, New York.
- (29) Sies, H., (1989) Zur Biochemie der Thiolgruppe: Bedeutung des Glutathions. *Naturwissenschaften* 76, 57–64.

BC025575V

# Synthetic Approaches to Multivalent Lipopeptide Dendrimers Containing Cyclic Disulfide Epitopes of Foot-and-Mouth Disease Virus

Eliandre de Oliveira,<sup>†</sup> Judit Villén,<sup>†</sup> Ernest Giralt, and David Andreu<sup>\*,†</sup>

Department of Organic Chemistry, University of Barcelona, Barcelona, Spain Received July 17, 2002;  
Revised Manuscript Received November 5, 2002

The synthesis of a multiantigenic peptide dendrimer incorporating four copies of a cyclic disulfide epitope has been undertaken. Since standard chemoselective ligation procedures involving thioether formation are inadvisable in the presence of a preformed disulfide, conjugation through a peptide bond between the lipidated branched lysine scaffold and a suitably protected version of the cyclic disulfide has been used instead. Several synthetic approaches to the partially protected cyclic disulfide peptide have been explored. The most effective involves building a minimally protected version of the peptide by Boc solid phase synthesis, using fluorenyl-based anchorings and cysteine protecting groups. Peptide–resin cleavage and cysteine deprotection/oxidation are performed simultaneously by base-promoted elimination. The cyclic disulfide epitope is readily obtained in sufficient amounts by this procedure and subsequently incorporated to the lipidated lysine core by peptide bond formation in solution. A final acid deprotection step in anhydrous HF yields a peptide construction containing a maximum of three copies of the cyclic disulfide epitope, the lower substitution being attributable to steric constraints. This immunogen has been successfully used in an experimental vaccination trial against foot-and-mouth disease virus.

## INTRODUCTION

Interest in peptide-based vaccines remains high despite the limited number of practical applications reported to date (1–4). A particular concern in the design and production of peptide vaccines is defining an appropriate carrier/adjuvant system that enhances the generally reduced immunogenicity of free peptides (5). Conjugation of the peptide to a carrier protein (6) is an effective solution but suffers from drawbacks such as poor chemical definition, unwanted peptide or carrier modification during the coupling steps, or undesired response to the carrier (7). Other alternatives, such as encapsulation of the peptide antigen into liposomes (8) or conjugation to poly-lysine-based synthetic carriers (9), have been proposed. A particularly fruitful strategy has been the multiple antigenic peptide (MAP)<sup>1</sup> system (10), a dendrimeric construction that displays four or eight copies of peptide on a branched lysine scaffold. The MAP concept has been further expanded by combining in a single molecular entity the antigen multiplicity provided by the MAP with the adjuvant effect of lipid moieties (11–13). This type of constructs are regarded as promising candidates for a new generation of fully synthetic, peptide-based vaccines.

MAP immunogens have been prepared by either stepwise or convergent synthetic approaches. In the original procedure (10), the construct was synthesized entirely in the solid phase: the four (or eight) amino groups of a tri- (or hepta-) lysine core were used as starting points

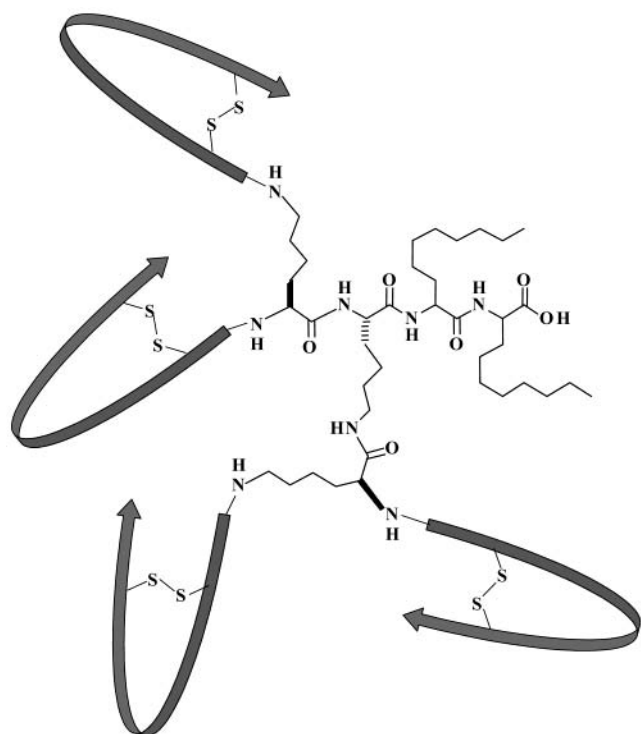
for assembly of the immunogenic peptide sequence. The potential advantages of this approach, namely, simplicity and expediency, are usually offset by the difficulties of achieving quantitative couplings within a sterically crowded dendrimer network (14), which result in heterogeneous products. More recently, chemoselective ligation (15) strategies have been shown as convenient alternatives to this procedure. A typical approach involves suitable functionalization (e.g., haloacetylation) of the lysine core followed by conjugation in solution, e.g., S<sub>N</sub>2 reaction with the Cys thiol group of an independently synthesized, well characterized peptide (16–18), to give four (eight) copies of immunogen conjugated to the lysine core through thioether bonds.

The serious economical impact of foot-and-mouth disease (19) has been acutely highlighted by the 2001 outbreak in the U.K. (20). Disadvantages of the use of conventional vaccines against foot-and-mouth disease virus (FMDV), as well as considerable hurdles for new vaccine design, have been described (21). As a result, new

\* Corresponding author. Address: Department of Experimental and Health Sciences, Pompeu Fabra University, Doctor Aiguader 80, E-08003 Barcelona, Spain. Phone/Fax: (34) 935 422 934. E-mail: david.andreu@cexs.upf.es.

<sup>†</sup> Present address: Department of Experimental and Health Sciences, Pompeu Fabra University, Doctor Aiguader 80, 08003 Barcelona, Spain.

<sup>1</sup> Abbreviations: AAA, amino acid analysis; AcM, acetamidomethyl; Ada, 2-aminodecanoic acid; DCM, dichloromethane; DIC, diisopropylcarbodiimide; DIEA, *N,N*-diisopropylethylamine; DMAP, 4-(dimethylamino)pyridine; DMF, *N,N*-dimethylformamide; DMSO, dimethyl sulfoxide; EDT, 1,2-ethanedithiol; ES, electrospray; Fm, fluorenylmethyl; FMDV, foot-and-mouth disease virus; HMFS, *N*-[(9-oxymethyl)-2-fluorenyl]-succinamic acid; HMPB, 4-(4-hydroxymethyl-3-methoxyphenoxy)butyric acid; HOBt, 1-hydroxybenzotriazole; HOObt, 3,4-dihydro-3-hydroxy-4-oxo-1,2,3-benzotriazine; MALDI-TOF, matrix-assisted laser desorption with time-of-flight detection; MAP, multiple antigenic peptide; MBHA, 4-methylbenzhydrylamine; MeCN, acetonitrile; MeOH, methanol; MS, mass spectrometry; NMP, *N*-methylpyrrolidone; PEG-PS, poly(ethylene glycol)-polystyrene; TBTU, 2-(1*H*-benzotriazol-1-yl)-1,1,3,3-tetramethyluronium tetrafluoroborate; TEA, triethylamine; TFA, trifluoroacetic acid; TFE, trifluoroethanol; TIS, triisopropylsilane; Trt, trityl; WSC, 1-ethyl-3-(3'-dimethylaminopropyl)carbodiimide.



**Figure 1.** Schematic view of multiantigenic peptide system consisting of four cyclic disulfide peptide epitopes (depicted as ribbons) conjugated to a lipidated core of (Lys)<sub>2</sub>-Lys-Ada<sub>2</sub>-NH<sub>2</sub>.

efforts to develop FMDV vaccines requiring no handling or administration of virus particles are under way. Use of synthetic peptides reproducing relevant antigenic sites (22) is particularly attractive in the case of FMDV, given the relevance of the humoral response in the control of the disease (23). We have recently shown (24) that cyclic disulfide versions of the main antigenic site of FMDV (site A) provide excellent mimicry of the bioactive conformation, with a substantial (10–100-fold) improvement in antigenic recognition over the consensus sequence (YTASARGDLAHLTTT, residues 136–150 of viral protein 1 (VP1), isolate C-S8c1). We are seeking to develop these cyclic peptide antigens into practical vaccine candidates by combining them with the known immunogenic properties of lipo-MAP systems. Our target, a lipidated lysine core displaying four copies of the cyclic disulfide peptide (Figure 1), is substantially more complex from the synthetic point of view than any of the MAP constructs reported so far. In this case, the thioether-based ligation strategy described above is not advisable due to the incompatibility of a free thiol and an internal disulfide within the same molecule. In view of these difficulties, we have opted for a more elaborate approach, involving the conjugation, through a peptide bond, of the lipo-MAP core to a protected version of the cyclic disulfide peptide epitope. In this paper we analyze several approaches to this challenging synthetic goal and propose a feasible solution to the problem.

## EXPERIMENTAL SECTION

**General.** 2'-Chlorotrityl chloride resin and *p*-methylbenzhydrylamine resin were from Novabiochem. Poly(ethylene glycol)-polystyrene resin (0.31 mmol/g) was from Perseptive Biosystems (Framingham, MA). Protected (Boc and Fmoc) amino acids were from Bachem (Bubendorf, Switzerland), Neosystem (Strasbourg, France), or Novabiochem (Läufelfingen, Switzerland). In the

Fmoc-based synthesis, the side chain protections were Arg(Pmc), Asn(Trt), Asp(OtBu), Cys(Trt), Cys(Acm), Gln(Trt), Lys(Boc), and Ser(tBu). The Boc-based synthetic runs used Asp(OcHex), Cys(Fm), Lys(ClZ), and Ser(Bn). Peptide-synthesis grade DCM and DMF, and HPLC-grade acetonitrile were from Scharlau (Barcelona, Spain). 2-Aminodecanoic acid (Ada) was a gift from Prof. William Gibbons (School of Pharmacy, University of London). All other chemicals for peptide synthesis were of the highest quality available from Sigma-Aldrich (Madrid, Spain).

Analytical HPLC was performed on Nucleosil C<sub>18</sub> or C<sub>4</sub> reverse-phase columns (4.6 × 250 mm, 5 μm particle size) on a Shimadzu system. Preparative HPLC runs were done on Vydac C<sub>8</sub> column (20 × 250 mm, 10 μm particle size) columns in a Waters Delta Prep 4000 system. Semipreparative HPLC runs were performed on Vydac C<sub>4</sub> (25 × 300 mm, 15–20 μm particle size). Amino acid analyses (AAA) of peptide hydrolysates (6 N HCl, 150 °C, 3 h) were run in a Beckmann 6300 autoanalyzer. MALDI-TOF and ES mass spectra were recorded in Voyager DE-RP (Applied Biosystems, Foster City, CA) and VG-Quattro (Micromass, U.K.) instruments, respectively.

**Lipitated Lysine Core.** The branched Lys<sub>2</sub>-(Lys)-Ada<sub>2</sub>-NH<sub>2</sub> scaffold was synthesized manually by standard Boc chemistry protocols (25) on 0.2 mmol (286 mg) of MBHA resin. The two residues of Boc-Ada (0.4 mmol, 115 mg for each coupling, 2× molar excess) were followed by one, then (after deprotection of both α and ε amino groups) two residues of Boc-Lys(Boc) [0.6 mmol (208 mg) per residue, 3× molar excess], to give the tetravalent dendrimer core. Couplings were mediated by TBTU (equimolar to amino acid) and DIEA (2× molar excess relative to TBTU) in DMF for 1.5 h. The peptide-resin was deprotected at the N-termini with 40% TFA in DCM and then treated with HF/anisole (9:1 v/v, 0 °C, 1 h) to release the lipidated Lys core, which was eluted in 10% HOAc and lyophilized. Purification by preparative HPLC using a linear gradient of 10–50% MeCN in water (+0.05% TFA) over 180 min at a flow rate of 3 mL/min afforded 32.3 mg (22% yield) of the branched lipopeptide. Since two residues of racemic Ada had been used, four clustered peaks were observed by analytical HPLC, corresponding to the possible diastereomers of the product, each of them with the correct mass by MALDI-TOF MS (theoretical: 740.27 Da, found: 740.67 Da).

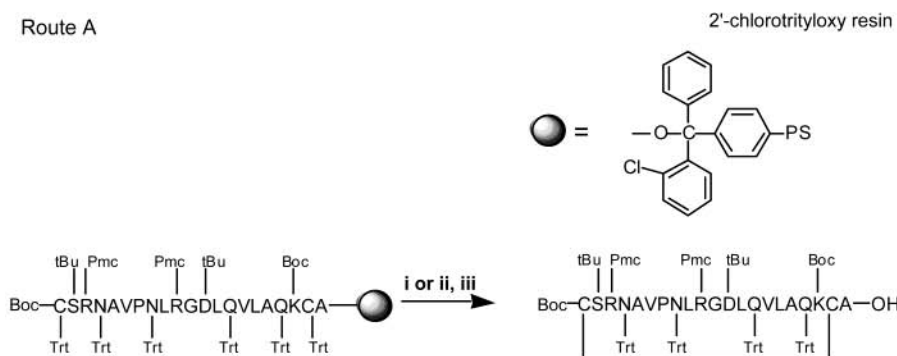
**Partially Protected Cyclic Disulfide Version of Site A Epitope Peptide.** Four different synthetic approaches (Scheme 1) were attempted, as follows:

**Route A.** The initial substitution (1–1.5 mmol/g) of 300 mg of commercial 2'-chlorotrityl chloride resin was lowered by coupling of a substoichiometrical amount of Fmoc-Ala (0.18 mmol, 56 mg, 0.5 equiv) in the presence of DIEA (1.8 mmol, 308.3 μL) in DCM for 1 h, followed by capping with MeOH (400 μL, 10 min). A new substitution of 0.38 mmol/g was determined by AAA. The remaining amino acids in the target sequence were incorporated by standard Fmoc protocols (26) in a Milligen 9050 synthesizer. Deprotections were done with 20% (v/v) piperidine in DMF (6 min, continuous flow), and couplings with 5 equiv (1.9 mmol) of Fmoc-amino acid and TBTU and 10 equiv of DIEA (3.8 mmol) in DMF for 60 min. After the target sequence was assembled, formation of the internal disulfide was attempted by two different procedures: (i) peptide-resin cleavage and selective deprotection of the two Cys(Trt) residues with simultaneous oxidation and (ii) cleavage and Cys(Trt) deprotection followed by oxidative treatment. In procedure i, 20 mg peptide-resin (ca. 2.5 μmol) were treated

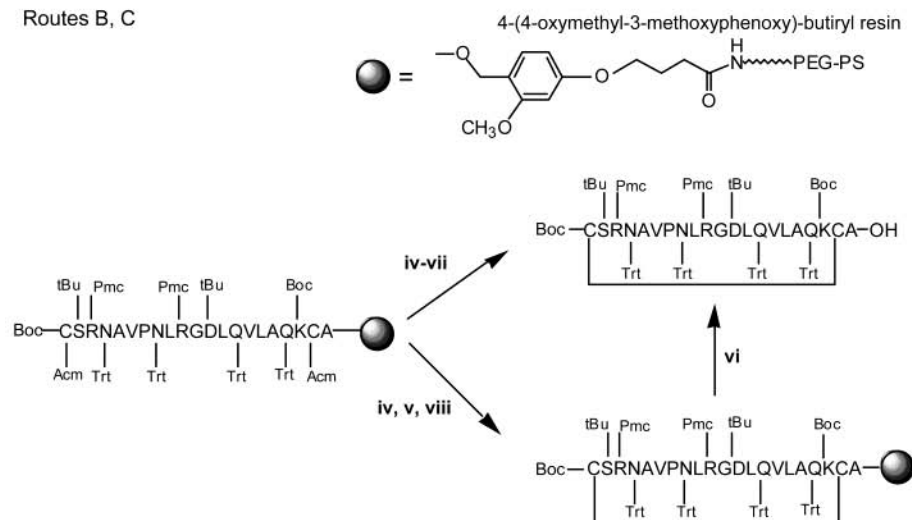


**Scheme 1. Synthetic Approaches to Protected Cyclic Disulfide Epitope Peptides<sup>a</sup>**

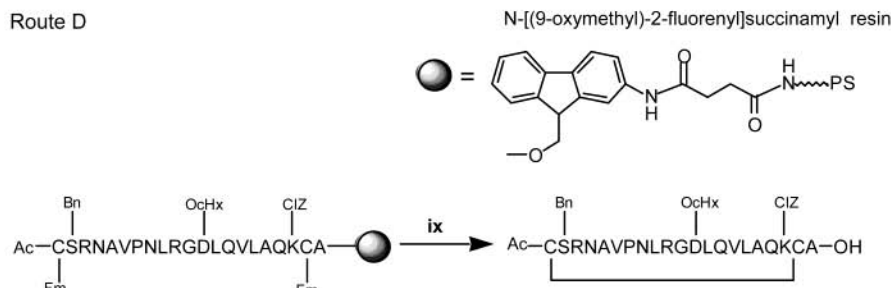
Route A



Routes B, C



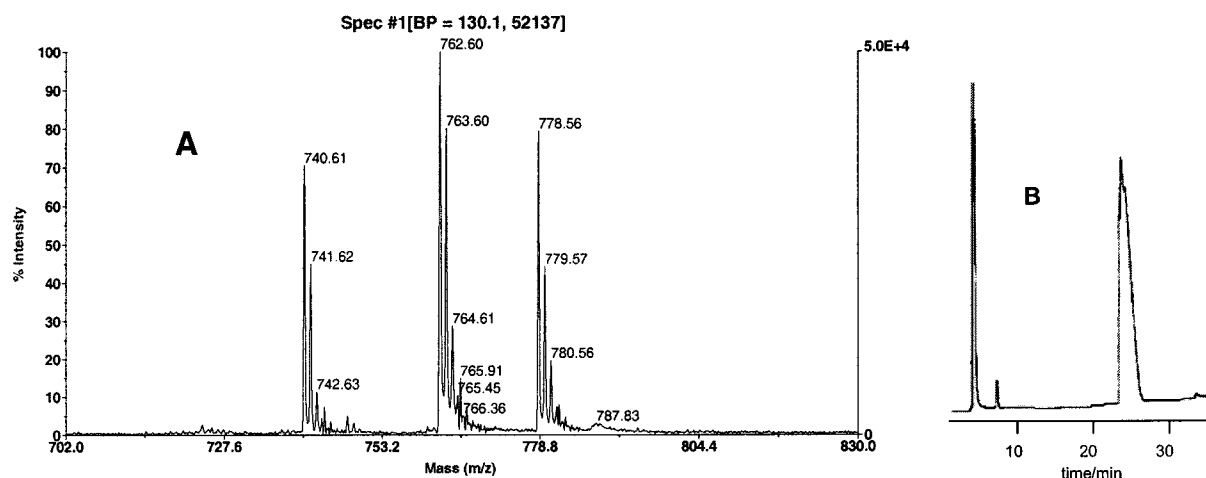
Route D



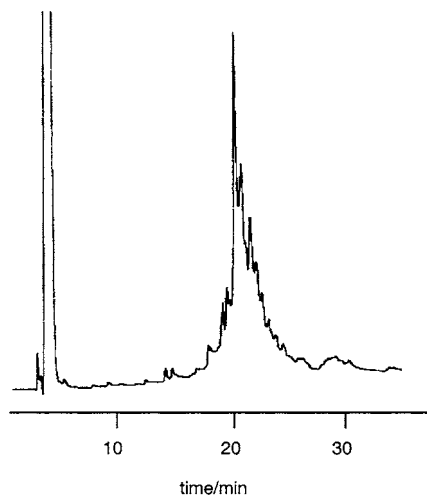
<sup>a</sup> (i) I<sub>2</sub> (10 eq) in DCM/TFE/HOAc (7:2:1); (ii) DCM/TFE/HOAc (7:2:1); (iii) I<sub>2</sub> (10 eq); (iv) 0.1 M Hg(OAc)<sub>2</sub> in DMF; (v) β-mercaptoethanol/DMF (1:9); (vi) DCM/TFA (98:2); (vii) 0.1 M NH<sub>4</sub>HCO<sub>3</sub>, pH 8/DMSO (1:1); (viii) DMSO/NMP (2:8) or 20 mM TEA/20 mM CCl<sub>4</sub> in NMP; (ix) piperidine/DMF (1:1).

with 500 μL of a DCM/TFE/HOAc (7:2:1) solution containing 25 μmol iodine (27) for 10 min at 25 °C. The resin was filtered and washed twice with 500 μL DCM/TFE/HOAc (7:2:1), and the combined filtrates were stirred into 1.5 mL of a 0.1% solution of Na<sub>2</sub>S<sub>2</sub>O<sub>3</sub>·5H<sub>2</sub>O in water until complete disappearance of the brownish color. The aqueous phase was washed with DCM, and the combined organic phases were briefly dried with anhydrous MgSO<sub>4</sub> and evaporated to dryness under vacuum. In procedure ii, the same amount of peptide-resin was stirred with 500 μL of DCM/TFE/HOAc (7:2:1) for 15 min at 25 °C, filtered, and washed with 500 μL of the same reagent. The combined filtrates were then added dropwise to a solution of 25 μmol I<sub>2</sub> in 1 mL DCM/TFE/HOAc (7:2:1), stirred for 10 min, and worked up as in procedure i.

**Route B.** Fmoc-Ala (0.75 mmol, 5 equivalent) was manually coupled (3 × 30 min) in the presence of DMAP (0.075 mmol, 0.5 equiv) and TBTU (0.75 mmol, 5 equiv) to a PEG-PS resin (0.22 mmol/g) functionalized with the HMPB (28) handle. A substitution of 0.13 mmol/g was determined by AAA. The remaining residues in the target sequence were incorporated by standard Fmoc protocols in a Milligen 9050 synthesizer as in approach A, except that Cys(Acm) (29) instead of Cys(Trt) was used. Recouplings of Arg<sup>138,145</sup>, Asn<sup>139,143</sup>, and Leu<sup>144</sup> were performed. After chain assembly was completed, the Cys(Acm) residues were selectively deprotected by treatment with a 0.1 M solution of Hg(OAc)<sub>2</sub> in DMF for 3 h in the dark (30). The resin was then washed with DMF (6 × 1 min) and treated with β-mercaptoethanol/DMF (1:9 v/v, 6 × 1



**Figure 2.** MALDI-TOF mass spectrum (A) and analytical HPLC (B) of the lipidated lysine core. The peak at 740.61 Da, which fits with the theoretical mass of Lys<sub>2</sub>-Lys-Ada<sub>2</sub>-NH<sub>2</sub> (740.27 Da), is accompanied by its sodium (762.6 Da) and potassium (778.56 Da) adducts. The unusually broad HPLC peak is due to the diastereomeric mixture resulting from use of racemic Ada (see text). HPLC was performed on a C<sub>4</sub> column eluted with a linear gradient of 10–60% B in 30 min, flow rate 1.0 mL/min.



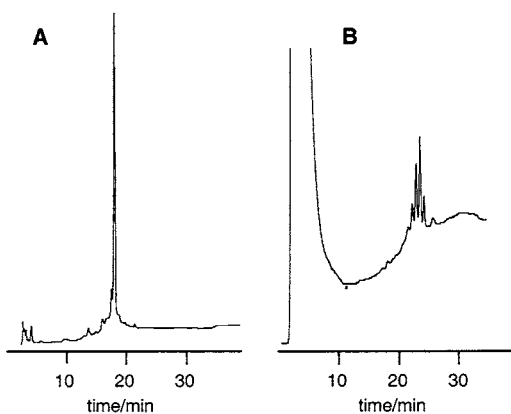
**Figure 3.** Analytical HPLC of a fully deprotected version of the 21-residue peptide epitope prepared by route A. HPLC was performed on a C<sub>18</sub> column eluted with a linear gradient of 10 to 60% B in 30 min, flow rate 1.0 mL/min.

min and overnight) to remove the mercuric salts from the peptide-resin and release the free thiols, which gave a positive (orange) Ellman (31) test. The protected peptide (in free dithiol form) was then cleaved from the resin by treatment with TFA/DCM (1:99 v/v, 4 × 10 mL, 30 s). The filtrates from each treatment were poured over 40 mL H<sub>2</sub>O, combined, concentrated on a rotary evaporator and lyophilized. The residue was dissolved in a 1:1 (v/v) solution of DMSO in 0.1 M NH<sub>4</sub>HCO<sub>3</sub> (1:1), pH 8, to 49 μM peptide concentration, and the progress of the oxidation reaction was monitored by both HPLC and a qualitative Ellman test. For HPLC analysis, 100 μL aliquots of the oxidation solution were neutralized with HOAc, injected into a C<sub>4</sub> column, and eluted with a linear 60–100% gradient of MeCN (+0.036% TFA) into water (+0.045% TFA) over 30 min at 1 mL/min flow rate. Oxidation was judged to be complete after 128 h.

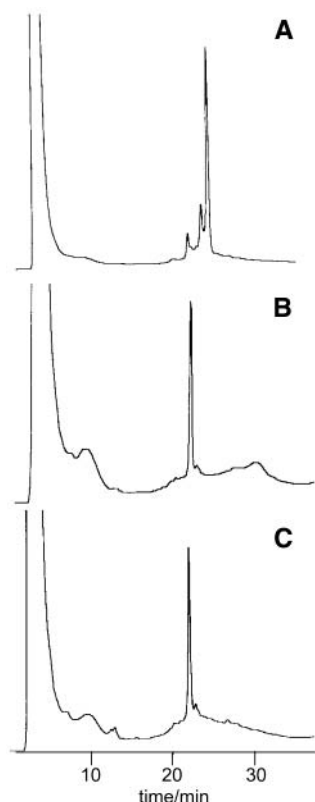
**Route C.** Peptide synthesis and Cys deprotection were performed as in approach B. After the removal of the mercuric salts, the oxidation step was carried out in the solid phase by treating the peptide-resin with either DMSO/NMP (2:8 v/v) or 20 mM carbon tetrachloride-triethylamine (CCl<sub>4</sub>/TEA) in NMP. In both cases, the peptide-resin gave a negative (faint yellow) qualitative

Ellman test after 24 h. The protected peptide was cleaved from the resin by treatment with TFA/DCM (2:98 v/v, 4 × 1 min) and analyzed by HPLC. The identity of the cyclic peptide was further confirmed by AAA and by ES-MS after complete deprotection in TFA/H<sub>2</sub>O/TIS (95:2.5:2.5; v/v/v) (theoretical, 2255.16 Da; found, 2253.35 Da).

**Route D.** The substitution of 1 g of commercial MBHA resin (0.7 mmol/g) was reduced to 0.25 mmol/g by coupling of Boc-Gly (0.3 mmol, 52 mg) with DIC for 2 h in DCM. Next, the HMFS handle (32) (0.375 mmol, 79 mg) was coupled with DIC/HOBt (1:1:1 molar ratio) in DMF (overnight + 2 h recoupling). The first amino acid in the target sequence (Ala) was esterified to the polymer using two 60 min couplings with 5 eq each of Boc-Ala (1.25 mmol, 237 mg) in the presence of DIC (1.25 mmol) and DMAP (0.125 mmol) in DCM. The remaining residues in the target sequence were incorporated by a manual protocol that included (i) Boc deprotection (neat TFA, 1 + 10 min), (ii) washes (DCM, 6 × 1 min), (iii) neutralization (5% DIEA/DCM, 3 × 1 min), washes (DCM, 6 × 1 min), and (iv) single couplings with 5 equiv of both Boc-amino acid and DIC in DCM; for Asn, Arg, and Gln residues that were incorporated without side chain protection, HOBt (5 equiv) was added to the coupling mixture and DCM/DMF (1:1 v/v) was used as solvent. Coupling reactions were run for 30–40 min, until a negative Kaiser ninhydrin test was obtained. Upon completion of chain assembly, the peptide resin was treated with 500 mL piperidine/DMF (1:1) to selectively deprotect/oxidize (33) the Cys(Fm) residues at positions 136 and 155 and simultaneously cleave the peptide from the resin. The oxidation/cyclization reaction was monitored by analytical HPLC of the filtrates and judged to be complete after 3 h. The filtrate was then cooled in an ice bath, acidified to pH 4 by dropwise glacial HOAc addition, and concentrated in a rotary evaporator to induce precipitation of salts, which were removed by filtration. The resulting solution was loaded onto a Vydac preparative C<sub>8</sub> HPLC column (20 × 250 mm) equilibrated with 0.1% TFA in water (solvent A) in a Waters Delta Prep 4000 system. Purification was done by a linear gradient of 0–20% solvent B (0.1% TFA in MeCN) into A over 5 min followed by another linear gradient of 20–70% B into A over 100 min, at a 25 mL/min flow rate.



**Figure 4.** HPLC analysis of epitope peptide prepared according to route B, (A) with protected side chains but Cys in free dithiol form and (B) after oxidative treatment with DMSO in pH 8 buffer. HPLC was performed on a  $C_4$  column eluted with a linear gradient of 60–100% B in 30 min, flow rate 1.0 mL/min.



**Figure 5.** HPLC analysis of epitope peptide prepared according to route C, with protected side chains and free Cys (dithiol form) (A), and after solid-phase oxidation with either DMSO/NMP (2:8) (B) or 20 mM  $CCl_4$ /TEA in NMP (C). HPLC was performed on a  $C_4$  column eluted with a linear gradient of 60–100% B in 30 min, flow rate 1.0 mL/min.

Fractions judged to be homogeneous by analytical HPLC were pooled and lyophilized. The purified partially protected peptide was satisfactorily characterized by MALDI-TOF (theoretical, 2650.19 Da; found, 2644.42 Da) and AAA.

**Synthesis of the Branched Multiple Antigenic Peptide.** The lipidated lysine core (0.05  $\mu$ mol), the partially protected cyclic disulfide site A peptide (prepared by route D, 0.6  $\mu$ mol, 12 equ), WSC, and HOOBt (0.6  $\mu$ mol each) were dissolved in 100  $\mu$ L of DMF and allowed to react for 48 h at 25  $^{\circ}$ C. The reaction mixture was diluted with water (10 mL) and lyophilized and the lipopeptide fully deprotected with HF/anisole (90:10,

0  $^{\circ}$ C, 1 h). After evaporation, the residue was dissolved in 1 M HOAc and lyophilized, and then filtered through a Sephadex G 25 column (300  $\times$  10 mm) eluted with 0.1 M HOAc at 20 mL/h. Fractions shown by MALDI-TOF MS to contain the conjugation product were pooled and lyophilized. The resulting product was characterized by HPLC, AAA, and MALDI-TOF.

## RESULTS AND DISCUSSION

The goal of this work was to develop an efficient synthetic approach to a multivalent format of the previously described, antigenically optimized cyclic disulfide version of site A peptide from FMDV (24). For serotype O<sub>1</sub>BFS, the specific epitope was a 21-residue cyclic

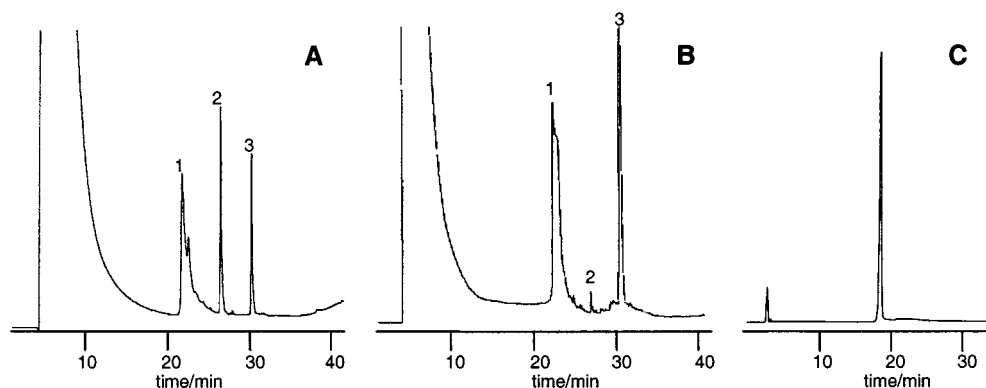
disulfide (CSRNAVPNLRGDLQVLAQKCA) displayed 4-fold on a lipidated branched lysine core (Figure 1). Although this type of structure is conceptually identical to other MAP constructions, the need to incorporate several copies of a large cyclic disulfide (predictably bulkier and less flexible than a linear peptide chain of similar length) substantially increases its synthetic difficulty.

To synthesize MAP type structures, the most reliable approaches involve ligation strategies, i.e., the lysine core and the epitope peptide, are synthesized independently and, after adequate purification and characterization, conjugated in solution. Such an approach has been shown to provide much better products fully stepwise solid phase schemes, where sterical crowding in the dendrimeric structure increases the risk of incomplete couplings and consequently heterogeneous products (34, 35). Thioether-based ligation, a widely used approach for this type of constructs, is clearly unadvisable in the present case, since the integrity of any disulfide (four in our target structure) cannot be guaranteed in the presence of the free thiol required for thioether formation. This drawback forced us to consider as an alternative approach the ligation of the cyclic disulfide epitope to the lipidated MAP core by means of a peptide bond, i.e., linking a suitably protected version of the cyclic disulfide peptide through its C-terminus to the lipo-MAP scaffold. This relatively elaborated approach to disulfide-containing MAP constructions has, to our knowledge, not been previously attempted. In the present work, we have explored several potentially useful synthetic routes and settled for one which in our hands has turned out to be most efficient.

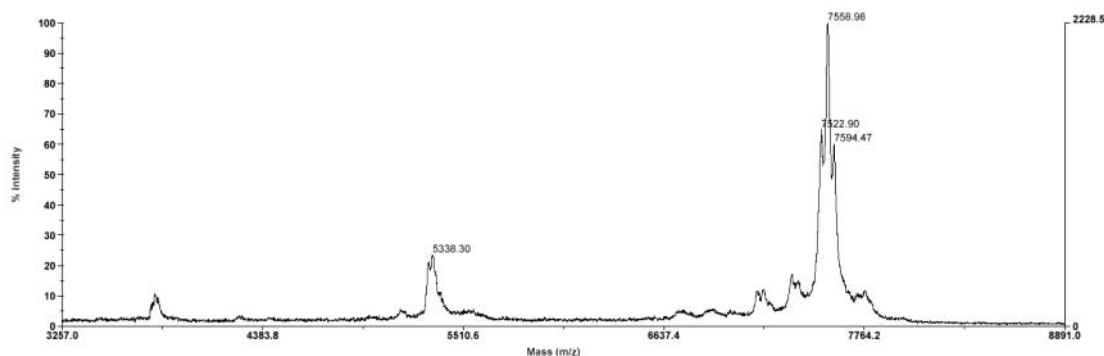
**A. Lipidated Lysine Core.** The carrier structure chosen for our conjugate was a branched lysine scaffold bearing two residues of 2-aminodecanoic acid (Ada) (36) at its C-terminus. The synthesis of this lipo-MAP core was straightforward by standard Boc solid-phase methods. Since the lipoamino acid was used in racemic form, the final product obtained after HF cleavage was an almost equimolar mixture of the four possible diastereomers. We found it expedient to work with this mixture, after ensuring that each of the four peaks observed by HPLC (Figure 2) had a MALDI-TOF spectrum consistent with the desired structure. The amphipathic character of the MAP facilitated its purification by reverse phase HPLC using a simple  $H_2O$ /MeCN gradient.

**B. Partially Protected Cyclic Disulfide Version of Site A Epitope Peptide.** Several synthetic approaches (routes A–D, see Experimental Section) were explored to access the cyclic disulfide version of 21-residue FMDV site A peptide (O<sub>1</sub>BFS serotype) ( $C^{136}$ SRNAVPNLRGDLQVLAQKCA $^{156}$ ) in protected form;





**Figure 6.** HPLC analysis of epitope peptide prepared according to route D, after (A) 20 min and (B) 180 min cleavage and oxidation with piperidine/DMF (1:1). Peaks 1–3 are, respectively, a non-peptide byproduct, the dithiol form of the peptide, and the expected cyclic disulfide, which after preparative HPLC was obtained in highly homogeneous form (C). HPLC was performed on a  $C_4$  column eluted with a linear gradient of 5–95% B in 35 min (A and B) or 35–65% B in 30 min (C), flow rate 1.0 mL/min.



**Figure 7.** MALDI-TOF mass spectrum of the lipidated lysine core conjugated with the cyclic disulfide epitope peptide. The peak at 7558 Da is consistent with a conjugate consisting of three copies of the epitope bound to the  $\text{Lys}_2\text{--Lys--Ada}_2\text{--NH}_2$  core (theoretical mass 7570 Da).

three approaches were based on Fmoc chemistry (Scheme 1, routes A–C) and one on Boc chemistry (route D).

**Route A.** In our first attempt to synthesize the site A cyclic disulfide in protected form, we opted for a maximal protection scheme relying on the 2'-chlorotrytyl chloride resin and trityl-type protection groups, which allowed (i) selective (iodine-mediated) Cys(Trt) deprotection, (ii) disulfide formation, and (iii) peptide–resin cleavage in a single operation (27). An initial synthesis was planned for a 20- (not 21-) residue target, namely, the above sequence lacking the  $\text{Ala}^{156}$  residue. In this case, the first amino acid coupled to the 2'-chlorotrytyl chloride resin was Fmoc–Cys(Trt). A very low incorporation of this amino acid occurred (detectable by the weak absorbance of the Fm–piperidine adduct solution obtained upon deprotection), probably due to steric conflict between the Trt groups of both solid support and Cys side chain. Once chain assembly was complete, treatment with DCM/TFE/HOAc (7:2:1) containing iodine (10 equivalent) was expected to achieve peptide–resin cleavage, Cys deprotection, and disulfide formation in a single step. However, MALDI-TOF or ES MS analysis of the resulting product showed no peaks assignable to the target sequence or related species. Since low solubility might be expected for the protected peptide and eventually complicate its detection, a small amount of peptide resin was cleaved and fully deprotected by means of reagent R (TFA/thioanisole/EDT/anisole; 90:5:3:2) (37). Again, no peaks consistent with the expected structure could be detected in the cleavage mixture.

A new synthetic attempt was done with a one-residue longer peptide as target, i.e., the sterically nonconflicting, native  $\text{Ala}^{156}$  anchored (0.38 mmol/g) to 2'-chlorotrytyl

chloride resin instead of Cys<sup>155</sup>. Again, analysis of the fully deprotected (reagent R) crude by HPLC and MALDI-TOF (Figure 3) showed unsatisfactory results: only traces of the expected peptide, plus a number of peaks attributable to single deletions (Arg, Leu, or Asn) were detected. Thus, despite its well-documented usefulness for the preparation of protected peptides, 2'-chlorotrytyl chloride resin was in our hands inadequate to synthesize this particular peptide.

**Route B.** Our next attempt to synthesize the 21-mer used PEG-PS as solid support, functionalized with the HMPB (28) handle. Since this handle is less acid-labile than 2'-chlorotrytyl chloride resin, we opted for the Acn group as Cys side chain protection. In view of past difficulties, double couplings were done for Arg<sup>138,145</sup>, Asn<sup>139,143</sup>, and Leu<sup>144</sup>. To evaluate the quality of the synthetic product, a small aliquot was fully deprotected and cleaved, showing a rather homogeneous HPLC profile with the expected molecular weight by MALDI-TOF MS (expected 2255.2; found 2256.2). Once the presence of the correct sequence on the resin was assured, we performed selective solid-phase deprotection of the thiol group with 0.1 M  $\text{Hg}(\text{OAc})_2$  in DMF. Mercury salts were removed from the polymer by extensive treatment with  $\beta$ -mercaptoethanol/DMF (1:9), and then the peptide–resin bond was cleaved with TFA/DCM (1:99) to give the partially protected peptide in reasonably pure dithiol form (Figure 4A), ready for oxidation in solution. Unfortunately, this protected precursor was totally insoluble in aqueous solution, even at the high dilution (49  $\mu\text{M}$ ) required to avoid aggregation and intermolecular disulfide bond formation. To improve its solubility we resorted to DMSO, a denaturing cosolvent known for its

added advantage of promoting thiol-disulfide oxidation (38, 39). In our case, the protected peptide could be dissolved in an oxidation buffer containing ca. 40% DMSO, but HPLC monitoring of the reaction showed a complex oxidation mixture (Figure 4B). In addition, and as described by other authors (40), we experienced severe difficulties in removing DMSO, either by reverse-phase HPLC or by selective adsorption of the peptide (carrying several aromatic side chain protections) on an aromatic-binding Diaion column (41). Since our efforts to devise efficient, preparative scale purification conditions were unsuccessful, this synthetic approach was finally abandoned.

**Route C.** Oxidation of free bis-thiol precursors in the solid phase, i.e., while the partially protected peptide remains anchored to the polymeric support, is a well-known strategy for disulfide formation (42–47). Use of a low-substitution resin creates pseudo-dilution conditions that favor intramolecular cyclization (48). Other obvious additional advantages are the facile removal of oxidizing agents by washing and filtration, and the fact that the solubility behavior of the peptide is not an issue. On the down side, the efficiency of solid phase cyclizations tends to depend strongly on the distance between the thiol groups. Though no systematic studies have been performed, not many cycles larger than 18 amino acids have been described (49). A number of Cys protecting groups, oxidizing agents, and conditions have been described for this type of strategy, both for Fmoc [e.g., Trt/iodine (50), AcM/iodine (51), AcM/thallium trifluoroacetate (52), etc.] and for Boc-based [Fm/piperidine (33)] synthetic chemistries.

Our attempt of on-resin oxidation/cyclization used the same anchoring and protection scheme as those in route B. The Cys(AcM) residues were also deprotected with Hg(OAc)<sub>2</sub>, and after removal of Hg(II) salts, the resin-bound bis-thiol was treated with a mild oxidation mixture [NMP/DMSO (8:2)] (to our knowledge not previously reported) or, for comparison, with a well-known solid-phase oxidation reagent, 20 mM CCl<sub>4</sub>/TEA in NMP (53). The reactions were monitored by qualitative Ellman test (31), which after 24 h gave only a very faint yellow coloration (vs strong orange color for the non-oxidized peptide resin). As shown in Figure 5, analytical HPLC profiles of small aliquots of both peptide–resins after full deprotection and cleavage (reagent R) show much cleaner materials than those obtained in solution (approach B). Difficulties, however, appeared when cleavage of the peptide in protected form from the solid support was attempted. Standard cleavage conditions (TFA/DCM (2:98, v/v) were ineffectual. Higher percentages of TFA (5:95 and 10:90, v/v) improved only slightly the cleavage yield but were associated to complex HPLC profiles indicative of undesired partial deprotection of side chains. Due to these difficulties, this initially promising scheme had also to be abandoned.

**Route D.** In view of the shortcomings of the previous Fmoc-based synthetic schemes, a rather different approach was explored, on the basis of (i) Boc chemistry for chain elongation, (ii) minimalist protection scheme (Asn, Arg, and Gln side chains unblocked) to favor solubility of the partially protected cyclic disulfide epitope during coupling to the lipo-MAP core, and (iii) base-labile, fluorenyl-based chemistries for both Cys protection (Fm) and peptide anchoring to the solid support (HMFS handle, 54), which allow deprotection/oxidation and peptide–resin cleavage in a simultaneous step, under conditions orthogonal with other (acid-labile) protecting groups. A potential further advantage of Boc chemistry, vis-à-

vis the difficulties experienced in building up the epitope sequence using Fmoc chemistry in routes A–C, would be a reduced risk of aggregation (and thus of ensuing incomplete couplings) by the use of TFA, an excellent disaggregating agent, at the repetitive N<sup>α</sup>-deprotection steps.

In practice, this last approach turned out to be quite satisfactory. Thus, a single treatment of the peptide–resin with piperidine readily produced the peptide epitope in (partially protected) cyclic disulfide form. An unusually large solvent-to-resin ratio was used at this step, to achieve high dilution conditions favoring the formation of the internal disulfide over other undesirable Cys pairings. Neutralization of the large amount of piperidine in the cleavage/oxidation mixture slightly complicated the work up: after filtering off the initially formed piperidine acetate, recurrent precipitation of this salt upon concentrating the solution in the rotary evaporator made several additional filtration steps necessary. This inconvenience aside, the procedure furnished in adequate purity and yield a correctly oxidized, minimally protected cyclic disulfide peptide epitope, which was further purified to satisfactory specifications by preparative HPLC (Figure 6).

**C. Conjugation of the Cyclic Disulfide Epitope to the Lipidated MAP Core.** The purified, partially protected cyclic disulfide version of antigenic site A of FMDV prepared by route D above was incorporated to the tetravalent lipo-MAP by peptide bond formation between the C-terminal carboxyl of the epitope peptide and the amino groups of the lipidated lysine core. A 3-fold excess of peptide over each amino group (12 equiv in total) was used, with activation by carbodiimide (water-soluble) and HOObt in DMF over 48 h. When HPLC monitoring of this conjugation reaction showed no significant progress (48 h at 25 °C), the reaction mixture was evaporated and submitted to acidolysis with anhydrous HF to remove the protecting groups remaining on the Ser, Asp, and Lys side chains of the disulfide epitope (see Figure 6). The resulting lipopeptide was shown by MALDI-TOF MS (Figure 7) to be predominantly the trivalent version of the conjugate (theoretical, 7565.1 Da; found, 7570.4 Da). The fact that no peak corresponding to the tetravalent conjugate could be detected in the mass spectra, together with the aforementioned lack of progress of the conjugation reaction after 48 h, led us to the temporary conclusion that the tetravalent version of the conjugate was not readily accessible, perhaps due to the predictably substantial steric crowding caused by the cyclic disulfide. This point is currently under investigation. Despite the less-than-optimal result in this particular case, the synthetic approach based on route D is in our opinion the most straightforward and reliable procedure for preparing dendrimeric conjugates of cyclic disulfide epitopes.

The dendrimeric, lipidated, cyclic disulfide version of antigenic site A of FMDV which has been the object of the present study has been preliminarily evaluated as a vaccine candidate with very promising results (De Oliveira et al., manuscript in preparation). Thus, guinea pigs immunized with 500 µg of the trivalent conjugate and boosted with another 500 µg after 27 days elicited antibodies with neutralization titers comparable to control animals immunized with conventional (guinea pig-adapted) FMDV vaccine. When challenged (experimentally infected) with live virus, two out of three animals turned out to be protected (vs three out of three for the conventional vaccine). We look forward to using this type

of conjugate, in combination with other replicas of FMDV antigenic sites, in future synthetic vaccine trials.

## ACKNOWLEDGMENT

Support from Generalitat de Catalunya (CERBA) and the Ministry of Education and Science (DGICYT Grants PB97-0873 and BIO99-0484), Spain, and from the European Union (Grant FAIR5-CT97-3577) is gratefully acknowledged. J.V. is a predoctoral fellow from DURSI (Generalitat de Catalunya, Spain).

## LITERATURE CITED

- (1) Arnon, R., and Horwitz, R. J. (1992) Synthetic peptides as vaccines. *Curr. Opin. Immunol.* 4, 449–453.
- (2) Ben Yedidia, T., and Arnon, R. (1997) Design of peptide and polypeptide vaccines. *Curr. Opin. Biotechnol.* 8, 442–448.
- (3) Patarroyo, M. E., Amador, R., Clavijo, P., Moreno, A., Guzmán, F., Romero, P., Tascón, R., Franco, A., Murillo, L. A., Pontón, G., and Trujillo, G. (1988) A synthetic vaccine protects humans against challenge with asexual blood stages of *Plasmodium falciparum* malaria. *Nature* 332, 158–161.
- (4) Meloen, R. H., Casal, J. I., Dalsgaard, K., and Langeveld, J. P. M. (1995) Synthetic peptide vaccines: success at last. *Vaccine* 13, 885–886, and references therein.
- (5) Van Regenmortel, M. H. V., and Muller, S. (1999) Immunization with peptides. In *Synthetic Peptides as Antigens* (Pillai, S., and Van der Vliet, Eds.) pp 136–167, Elsevier, Amsterdam.
- (6) Müller, G. M., Shapiro, M., and Arnon, R. (1982) Anti-influenza response achieved by immunization with a synthetic conjugate. *Proc. Natl. Acad. Sci. U.S.A.* 79, 569–573.
- (7) Schutze, M. P., Deriaud, E., Przewlocki, G., and Leclerc, C. (1989) Carrier-induced epitopic suppression is initiated through clonal dominance. *J. Immunol.* 142, 2635–2640.
- (8) Pintó, R. M., González-Dankaart, J. F., Sánchez, G., Guix, S., Gómara, M. J., García, M., Haro, I., and Bosch, A. (1998) Enhancement of the immunogenicity of a synthetic peptide bearing a VP3 epitope of hepatitis A virus. *FEBS Lett.* 438, 106–110.
- (9) Mezö, G., Mezö, I., Pimm, M. V., Kajtár, J., Seprödi, A., Teplán, I., Kovács, M., Vincze, B., Pályi, I., Idei, M., Szekerke, M., and Hudecz, F. (1996) Synthesis, conformation, biodistribution, and hormone-related *in-vitro* antitumor activity of a gonadotropin-releasing hormone antagonist-branched polypeptide conjugate. *Bioconjugate Chem.* 7, 642–650.
- (10) Tam, J. P. (1988) Synthetic peptide vaccine design. Synthesis and properties of a high-density multiple antigenic peptide system. *Proc. Natl. Acad. Sci. U.S.A.* 85, 5409–5413.
- (11) Defoort, J.-P., Nardelli, B., Huang, W., Ho, D. D., and Tam, J. P. (1992) Macromolecular assemblage in the design of a synthetic AIDS vaccine. *Proc. Natl. Acad. Sci. U.S.A.* 89, 3879–3883.
- (12) Beekman, N. C. J. M., Schaaper, W. M. M., Turkstra, J. A., and Meloen, R. H. (1999) Highly immunogenic and fully synthetic peptide-carrier constructs targeting GNRH. *Vaccine* 17, 2043–2050.
- (13) Gómara, M. J., Riedemann, S., Vega, I., Ibarra, H., Ercilla, G., and Haro, I. (2000) Use of linear and multiple antigenic peptides in the immunodiagnosis of acute hepatitis A virus infection. *J. Immunol. Methods* 234, 23–34.
- (14) See, however, Keah, H. H., Kecorius, E., and Hearn, M. T. W. (1988) *J. Pept. Res.* 51, 2–8, for a possible partial solution.
- (15) Schnolzer, M., and Kent, S. B. H. (1992) Constructing proteins by dovetailing unprotected synthetic peptides. Backbone-engineered HIV protease. *Science* 256, 221–225.
- (16) Lu, Y.-A., Clavijo, P., Galantino, M., Shen, Z.-Y., Liu, W., and Tam, J. P. (1991). Chemically unambiguous peptide immunogen preparation. Orientation and antigenicity of purified peptide conjugated to the multiple antigen peptide system. *Mol. Immunol.* 28, 623–630.
- (17) Zeng, W., Ghosh, S., Macris, M., Pagnon, J., and Jackson, D. C. (2001) Assembly of synthetic peptide vaccines by chemoselective ligation of epitopes: influence of different chemical linkages and epitope orientations on biological activity. *Vaccine* 19, 3843–3852.
- (18) Cavallaro, V., Thompson, P., and Hearn, M. T. W. (2001) Solid-phase synthesis of a dendritic peptide related to a retinoblastoma protein fragment utilizing a combined Boc- and Fmoc-chemistry approach. *J. Pept. Sci.* 7, 262–269.
- (19) Pereira, H. G. (1981) Foot-and-mouth disease. In *Virus Diseases of Food Animals*, Vol. 2, (Gibbs, E. P. J., Ed.) pp 333–336, Academic Press, New York.
- (20) Sobrino, F., and Domingo, E. (2001) Foot-and-mouth disease in Europe. *EMBO Rep.* 2, 459–461.
- (21) Brown, F. (1992) New approach to vaccination against foot-and-mouth disease. *Vaccine* 10, 1022–1026.
- (22) Bittle, J. L., Houghten, R. A., Alexander, H., Sutcliffe, J. G., Lerner, R. A., Rowlands, D. J., and Brown, F. (1982) Protection against foot-and-mouth disease by immunization with a chemically synthesized peptide predicted from the viral nucleotide sequence. *Nature* 298, 30–33.
- (23) McCulloch, K. C., De Simone, F., Brocchi, E., Capucci, L., Crowther, J. R., and Kihm, O. (1992) Protective immune response against foot-and-mouth disease. *J. Virol.* 66, 1835–1840.
- (24) Valero, M. L., Camarero, J. A., Haack, T., Mateu, M. G., Domingo, E., Giral, E., and Andreu, D. (2000) Nativelike cyclic peptide models of viral antigenic site: finding a balance between rigidity and flexibility. *J. Mol. Recognit.* 13, 5–13.
- (25) Stewart, J. M., and Young, J. D. (1984) *Solid-Phase Peptide Synthesis*, pp 18–47, Pierce Chemical Co., Rockford, Illinois.
- (26) Fields, G. B., Tian, Z., and Barany, G. (1982) In *Synthetic Peptides: A User's Guide* (Grant, G. A., Ed.) pp 77–183, Freeman, New York.
- (27) Barlos, K., Gatos, D., Kutsogianni, S., Papaphotiu, G., Poulos, C., and Tseganidis, T. (1991) Solid phase synthesis of partially protected and free peptides containing disulfide bonds by simultaneous cysteine oxidation-release from 2-chlorotrityl resin. *Int. J. Pept. Protein Res.* 38, 562–568.
- (28) Flörsheimer, A., and Riniker, B. (1991) Solid-phase synthesis of peptides with the highly acid-sensitive HMPB linker. *Peptides 1990*. In *Proceedings of the 21st European Peptide Symposium*, Platja d'Aro, Spain, 1990 (Giral, E., and Andreu, D., Eds.), pp 131–133, Escom, Leiden.
- (29) Veber, D. F., Milkowski, J. D., Varga, S. L., Denkwalter, R. G., and Hirschman, R. (1972) Acetamidomethyl, a novel thiol protecting group for cysteine. *J. Am. Chem. Soc.* 94, 5456–5461.
- (30) Liu, W.; Shiue, G. H., and Tam, J. P. (1989) A novel strategy for the desprotection of S-acetamidomethyl containing peptides: an approach to the efficient synthesis of endothelin. *Peptides: Chemistry, structure and biology. Proceedings of the 11th American Peptide Symposium*, San Diego, 1989 (Rivier, J. E., and Marshall, G. R., Eds) pp 271–271, Escom, Leiden.
- (31) Ellman, G. L. (1958) A colorimetric method for determining low concentrations of mercaptans. *Arc. Biochem. Biophys.* 74, 443–450.
- (32) Rabanal, F., Giral, E., and Albericio, F. (1995) Synthesis and applications of a new base-labile fluorene derived linker for solid-phase peptide synthesis. *Tetrahedron* 51, 1449–1458.
- (33) Albericio, F., Hammer, R. P., García-Echeverría, C., Molins, M. A., Chang, J. L., Munson, M. L., Pons, M., Giral, E., and Barany, G. (1991) Cyclization of disulfide-containing peptides in solid-phase synthesis. *Int. J. Pept. Protein Res.* 37, 402–413.
- (34) Dubois, P., and Baleux, F. (1992) Novel version of multiple antigenic peptide allowing incorporation on a cysteine functionalized lysine tree. *Int. J. Pept. Protein Res.* 40, 7–12.
- (35) Liu, C. F., and Tam, J. P. (1994) Chemical ligation approach to form a peptide bond between unprotected peptide segments. Concept and model study. *J. Am. Chem. Soc.* 116, 4149–4153.
- (36) Gibbons, W. A. (1990) Synthesis, resolution and structural elucidation of lipidic amino acids and their homo- and hetero-oligomers. *Liebigs Ann. Chem.* 1175–1183.



- (37) Albericio, F., Kneib-Cordonier, N., Biancalana, S., Gera, L., Masada, R. I., Hudson, D., and Barany, G. (1990) Preparation and application of the 5-(4-(9-fluorenylmethoxycarbonyl)aminomethyl-3,5-dimethoxyphenoxy)-valeric acid (PAL) handle for the solid-phase synthesis of C-terminal peptide amides under mild conditions. *J. Org. Chem.* **55**, 3730–3743.
- (38) Wallace, T. J., and Mahon, J. J. (1965) Reactions of thiols with sulfoxides. III. Catalysis by acids and bases. *J. Org. Chem.* **30**, 1502–1506.
- (39) Tam, J. P., Wu, C. R., Liu, W., and Zhang, J. W. (1991) Disulfide bond formation in peptides by dimethyl sulfoxide. Scope and applications. *J. Am. Chem. Soc.* **113**, 6657–6662.
- (40) Munson, M. C., and Barany, G. (1993) Synthesis of  $\alpha$ -conotoxin SI, a bicyclic tridecapeptide amide with two disulfide bridges: Illustration of novel protection schemes and oxidation strategies. *J. Am. Chem. Soc.* **115**, 10203–10210.
- (41) Vijayakumar, E. K. S., Roy, K., Chatterjee, S., Deshmukh, S. K., and Ganguli, B. N. (1996). Arthrithitin. A new cell wall active metabolite from *Arthrinium phaeospermum*. *J. Org. Chem.* **61**, 19, 6591–93.
- (42) Eritja, R., Ziehler-Martin, J. P., Walker, P. A., Lee, T. D., Legesse, K., Albericio, F., and Kaplan, B. E. (1987) On the use of S-*tert*-butylsulphenyl group for protection of cysteine in solid-phase peptide synthesis using Fmoc-amino acids. *Tetrahedron* **43**, 2675–2680. Ponsati, B., Giralt, E., and Andreu, D. (1990) Solid-phase approaches to regiospecific double disulfide formation. Application to a fragment of bovine pituitary peptide. *Tetrahedron* **46**, 8255–8266 (f). See also refs 32, 38, and 42.
- (43) García-Echeverría, C., Albericio, F., and Pons, M. (1989) Convenient synthesis of a cyclic peptide disulfide: A type II  $\beta$ -turn structural model. *Tetrahedron Lett.* **30**, 2441–2444.
- (44) Ponsati, B., Giralt, E., and Andreu, D. (1990) Solid-phase approaches to regiospecific double disulfide formation. Application to a fragment of bovine pituitary peptide. *Tetrahedron* **46**, 8255–8266.
- (45) Shih, H. (1993) New approaches to the synthesis of cystine peptides using N-iodosuccinimide in the construction of disulfide bridges. *J. Org. Chem.* **58**, 3003–3008.
- (46) Nishino, N., Mihara, H., Izumi, N., Fujimoto, T., Ando, S., and Ohba, M. (1993) Disulfide cyclization of protected peptide assembled on oxime resin. *Tetrahedron Lett.* **34**, 1295–1298.
- (47) See also refs 33, 40, and 49.
- (48) Andreu, D., Albericio, F., Solé, N. A., Munson, M. C., Ferrer, M., and Barany, G. (1994). Formation of disulfide bonds in synthetic peptides and proteins. In *Methods in Molecular Biology 35: Peptide Synthesis Protocols*. (Pennington, M. W., and Dunn, B. M., Eds.) pp 105–109. Humana Press, Totowa, NJ.
- (49) Camarero, J. A., Giralt, E., and Andreu, D. (1995) Cyclization of a large disulfide peptide in the solid phase. *Tetrahedron Lett.* **36**, 1137–1140.
- (50) Kamber, B., Hartmann, A.; Eiler, K., Riniker, B.; Rink, H., Sieber, P., and Rittel, W. (1980) The synthesis of cystine peptides by iodine oxidation of S-trityl-cysteine and S-acetamidomethyl cysteine peptides. *Helv. Chim. Acta* **63**, 899–915.
- (51) Ruiz-Gayo, M., Albericio, F., Royo, M., García-Echevarría, C., Pedrosa, E., Pons, M., and Giralt, E. (1989) A convenient procedure for synthesis of cystine peptides via iodine oxidation of S-acetamidomethyl-cysteine peptides. *An. Quim.* **85C**, 116–118.
- (52) Fujii, N., Otaka, A., Funakoshi, S., Bessho, K., Watanabe, T., Akaji, K., and Yajima, H. (1987) Studies on peptides. CLI. Syntheses of cystine-peptides by oxidation of S-protected cysteine-peptides with thallium (III) trifluoroacetate. *Chem. Pharm. Bull.* **35**, 2339–2347.
- (53) Wenschuh, E., Heydenreich, M., Runge, R., and Fisher, S. (1989) CCl<sub>4</sub> as mildes Oxidans in der Schwefelchemie: Oxidation von Thiolen zu Disulfiden. *Sulfur Lett.* **8**, 251–260.
- (54) Nishiuchi, Y., Nishio, H., Inui, T., Bodi, J., and Kimura, T. (2000) Combined solid-phase and solution approach for the synthesis of large peptides or proteins. *J. Pept. Sci.* **6**, 84–93.

BC025577F

# Signal Peptide Mimics Conjugated to Peptide Nucleic Acid: A Promising Solution for Improving Cell Membrane Permeability

Xiaoxu Li,<sup>†</sup> Liangren Zhang,<sup>†</sup> Jingfen Lu,<sup>†</sup> Yaozu Chen,<sup>‡</sup> Jimei Min,<sup>†</sup> and Lihe Zhang<sup>\*,†</sup>

National Laboratory of Natural and Biomimetic Drugs, Peking University, Beijing 100083, P. R. China and Department of Chemistry, Lanzhou University, Lanzhou 730000, P. R. China. Received July 24, 2002; Revised Manuscript Received October 8, 2002

The specific binding ability and biostability of PNA (peptide nucleic acid) with DNA or RNA make PNA not only a good tool for the studies of molecular biology but also the candidate for gene-targeting drugs. However, the main obstacle for its potential usage as a therapeutic is the low cell uptake caused by the poor cell membrane permeability. In this paper the hydrophobic pentadecapeptide and two signal peptide mimics, hexa- and decapeptides ending with a positively charged amino acid, were proposed as the linked carrier for the transportation of PNA T10 through the cell membrane; stable spin label was coupled to the peptide–PNA conjugate so that the ESR measurements can be used for the assessment of their transmembrane movements. The syntheses of spin-labeled peptide–PNA conjugates were carried out on MBHA resin with Boc strategy. The cell membrane permeability of the spin-labeled conjugates of peptides and PNA can be determined with ESR, during the incubation of erythrocyte with the samples. According to ESR measurements, the three conjugates exhibit enhanced uptake into erythrocytes. The hexa- and decapeptide-modified PNA showed suitable water solubility. The peptide–PNA conjugates retained their binding ability to complementary DNA. The results suggest that peptide modification of PNA might be a promising solution for improving cell membrane permeability toward PNA.

## INTRODUCTION

Peptide nucleic acid (PNA) is a structural DNA mimic in which the entire backbone has been replaced by a polyamide backbone composed of *N*-(2-aminoethyl)glycine units (1, 2). PNA can hybridize to the complementary DNA and RNA or dsDNA strand with higher affinity than their oligonucleotide counterparts, obeying either Watson–Crick or Hoogsteen base pairing rules (2–5). Upon binding to DNA or mRNA, PNA exerts biological effects including in vitro transcription and translation modulation (6, 7), and PNA is stable toward both nuclease and protease (8). This character of PNA not only makes it a new tool for the studies of molecular biology but also the potential candidate for gene-targeting drugs (9, 10). However, the main obstacle for its potential usage as a therapeutic is the low cell uptake caused by the poor cell membrane permeability (11). Many physical delivery methods such as microinjection and cell treatment by detergent were reported for the studies of antisense or antigene PNA (6, 12). The efforts via chemical modification have also been made to improve cell uptake of PNA. Receptor-mediated cell or tissue internalization mechanism has been proposed for the specific delivery of PNA; for example, lactose (13), dihydrotestosterone (14), and D-peptide analogue of insulin-like growth factor 1 (IGF1) (15) modified PNAs were designed and exhibited rapid and specific entry into the corresponding cells. The transferrin receptor-mediated endocytosis system (16, 17) was also used to transport PNA through the blood–brain barrier in vivo, and gelatin or protein nanoparticles were

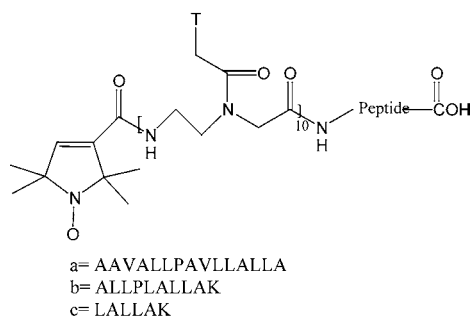
also explored as carriers for PNA (18, 19). On the other hand, PNAs attached with lipophilic groups such as adamantyl (20, 21), phosphonium cation (22), and hydrophobic peptides (23) showed significantly improved membrane penetration in either liposome models or biomembrane systems. Different types of peptides with membrane permeability could be used as a carrier for the membrane transportation of PNA by chemical conjugation. PNA coupled to a retro-inverso delivery peptide was rapidly taken up by cultured cerebral cortex neurons (24); PNA coupled with the cellular transporter peptide, Antennapedia, was efficiently taken up into Bowes cells (25); the cationic peptide (26) linked at the N-end of a PNA pentamer directed at the RNA template of telomerase resulted in enhanced inhibition of telomerase activity; Antennapedia peptide also showed both cell uptake and inhibition of telomerase activity in human melanoma cells (27, 28); SV40 nuclear localization signal (NLS) demonstrated its efficiency for the transportation of PNA as well as the hybridized DNA (29, 30). The accumulated results suggest that peptide conjugation is an attractive strategy for the intracellular delivery of PNA.

Signal peptide is an N-terminal extension of premature secretory protein and directs the translocation of protein through the membrane of endoplasmic reticulum of eukaryotes or the inner membrane of prokaryotes. The sequences of most signal peptides have a hydrophobic core consisting of a stretch of hydrophobic amino acids, basic residues near the N-terminal, and small neutral residues (31, 32). The studies strongly support that the hydrophobic interaction between the hydrophobic region (h-region) of the signal peptide and the lipid bilayer of cell membrane is the main cause of transmembrane movement (33–37). Some signal peptides have been used

\* To whom correspondence should be addressed. E-mail: dzszlh@mail.bjmu.edu.cn.

<sup>†</sup> Peking University.

<sup>‡</sup> Lanzhou University.



**Figure 1.** Structure of spin-labeled peptide–PNA conjugates.

as a carrier of certain protein domains to bring the whole polypeptide through the cell membrane (38–41).

In this paper, the peptide corresponding to the h-region of signal sequences from Kaposi FGF (38, 39) (Figure 1a) and two signal peptide mimics hexa- and decapeptides (Figure 1b,c) were designed as the carriers to conjugate with the model PNA T10 at the N-end. To evaluate the transmembrane behavior of the conceived adducts of peptide and PNA, the stable nitroxyl free radical 3-carboxyl-2,2,5,5-tetramethyl-pyrroline-1-oxyl as reporter group (42) was coupled at the N-end of the PNA moiety (Figure 1). Cell membrane penetration can be exhibited by the changes of the ESR signal during the incubation of erythrocyte with the samples (43, 44).

#### EXPERIMENTAL PROCEDURES

**General.** The PNA monomer *N*-(2-Boc-aminoethyl)-*N*-(thymine-1-ylacetyl)glycine<sup>1</sup> (45) and the stable free radical 3-carboxyl-2,2,5,5-tetramethyl-3-pyrroline-1-oxyl (42) are synthesized as described. Boc-protected amino acids MBHA resin are from Pennisular, and DCC is from Aldrich. DCC and DMF are dried with K<sub>2</sub>CO<sub>3</sub> and molecular sieves, respectively, before use; other chemicals are reagent grade from local commercial sources. Solid-phase synthesis is conducted with manual apparatus. Standard Ninhydrin test (46) is used for monitoring the coupling reaction. HPLC purification is performed with a Waters system on C-18 reverse phase column (0.8 × 20 mm); mobile phase gradient is B: 20–80% or 0–50% in A within 50 min (A: H<sub>2</sub>O containing 0.1% TFA; B: acetonitrile containing 0.1% TFA/H<sub>2</sub>O). UV spectra and *T<sub>m</sub>* are recorded with a Pharmacia LKB Biochrom 4060 spectrophotometer. MALDI-TOF mass spectra are recorded with ZAB-HS, and ESR measurements are conducted with a Bruker ESP 300 ESR spectrometer.

**Synthesis.** *Spin-Labeled Pentadecapeptide PNAT10 Conjugate (R15T10).* Oligomerization of spin-labeled peptide conjugated PNAT10 was conducted by manual solid-phase peptide synthesis on MBHA resin (213 mg, substitution 0.35 mmol/g) with Boc strategy in the order of peptide synthesis, PNA monomer condensation (45, 47), and in situ spin labeling. The cycle procedure for the solid-phase peptide synthesis was as follows: Boc-deprotection was completed with TFA/DCM (1:2, v/v), 3 mL, 1 × 2 min and 1 × 30 min, and then neutralization by using TEA/DCM (1:10, v/v), 3 mL, 2 × 2 min. Condensation was carried out with DCC (2 equiv) as coupling

**Table 1.** Properties and Characterization of Spin-Labeled Conjugates of Peptide and PNA, R15T10, R10T10, R6T10, RT10, and Decamer PNA T10

	R15T10	R10T10	R6T10	RT10	T10 <sup>a</sup>
calcd MS	4244	3848	3453	2972	2806
found MS	4245	3848	3454	2973	2808
<i>T<sub>m</sub></i> (°C)	---	77	76	78	78
solubility	water/DMSO	water	water	water	water
(mg/mL)	<5	5	>5	>5	>5
ESR signal (standard)	+	+	+	+	<sup>b</sup>

<sup>a</sup> Composed of thymine monomer. <sup>b</sup> No ESR signal.

agent. Two equivalents of Boc-protected amino acid or PNA monomer was dissolved in DCC/DMF (1:1, v/v), giving the final concentration of 0.1 M of Boc amino acid or PNA monomer; after the coupling reaction, the unreacted amino groups were blocked by acetylation with a mixture of 2.5 mL of Ac<sub>2</sub>O/DCM (1:1, v/v) and 2.5 mL of TEA/DCM (1:1, v/v) for 20 min. The coupling reaction was allowed to proceed for 2 h with stirring at rt. The Kaiser test (46) was used to monitor the completion of Boc-deprotection and coupling reaction, respectively. For the peptide synthesis, the first Boc-Ala (0.1 mmol) was loaded on MBHA resin, and the coupling was done sequentially with Boc-protected Leu, Leu, Ala, Leu, Leu, Val, Ala, Pro, Leu, Leu, Ala, Val, Ala, and Ala. The PNA monomer condensation was conducted continuously after the completion of amino acid coupling cycles. Following the 10th PNA monomer coupling cycle, 2.5 equiv of 3-carboxy-2,2,5,5-tetramethyl-3-pyrroline-1-oxyl (final concentration was 0.1 M in DCM) was added to the reaction vessel and stirred with PNAT10-peptide-resin in the presence of DCC (2.5 equiv, 0.1 M). The coupling reaction was completed within 2 h according to the Kaiser test. After capping and wash procedures, the product-resin was dried and treated with anhydrous HF (at 0 °C, 1 h) for cleavage of the oligomer from the resin, and the crude product was purified on C-18 RP-HPLC (20–80% B containing 0.1% TFA in A within 50 min, detected at 260 nm). The final product revealed the standard nitroxyl free radical signals under ESR spectrum measurement (three peaks, *g* = 2.0029, *a<sub>N</sub>* = 15.8 G,  $\Delta H_0$  = 2.5 G). MALDI-TOF MS result: 4245, calculated: 4244.

*Spin-Labeled Decapeptide PNAT10 Conjugate (R10T10).* The procedure of oligomerization, cleavage, and purification is the same as spin-labeled pentadecapeptide PNAT10 conjugate, except the coupling order of amino acids is K, A, L, L, A, L, P, L, L, A; MALDI-TOF MS found: 3848, calculated: 3848; ESR measurement gives the standard three-peak signal as above.

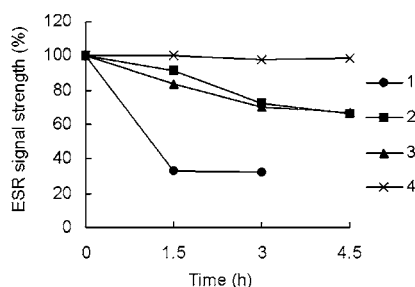
*Spin-Labeled Hexapeptide PNAT10 Conjugate (R6T10).* The procedure of oligomerization, cleavage, and purification is the same as spin-labeled pentadecapeptide-conjugated PNA, except the coupling order of amino acids is K, A, L, L, A, L; MALDI-TOF MS found: 3454, calculated: 3453; ESR measurement gives the standard three-peak signal as above.

*Spin-Labeled PNAT10 (RT10).* The procedure of oligomerization and cleavage is the same as the described in spin-labeled pentadecapeptide-conjugated PNAT10, but only K is coupled on the resin before condensation of the PNA monomers. HPLC purification is carried out with B: 0–50% in A within 50 min. MALDI-TOF MS found: 2972, calculated: 2973; ESR measurement gives the standard three-peak signal as above.

*PNA T10 (T10).* The procedure for synthesis of PNA T10 is the same as described above without the spin labeling. MALDI-TOF MS found: 2808, calculated: 2806.

<sup>1</sup> Abbreviations: Boc, *tert*-butoxycarbonyl; DCC, *N,N*-dicyclohexylcarbodiimide; DMF, *N,N*-dimethylformamide; DCM, dichloromethane; ESR, electron spin resonance; HOBT, 1-hydroxybenzotriazole; MBHA, methylbenzhydrylamine; RP-HPLC, reverse phase high-pressure liquid chromatography; T, thymine; TEA, triethylamine; TFA, trifluoroacetic acid; Z, benzyloxycarbonyl.





**Figure 2.** ESR signal strength of spin-labeled conjugates of peptide and PNA R15T10 (1), R10T10 (2), R6T10 (3), and spin-labeled PNA RT10 (4) incubated with erythrocyte. The strength is presented as the percentage of the initial peak height at low field.

**Table 2. Molecular Total Energy Calculated by the Computer Simulating Method for the  $\alpha$  Helix of Pentapeptides**

sequence	total energy (kcal/mol)	sequence	total energy (kcal/mol)
LVALL	49.49	AVLLA	61.44
VLLAL	49.49	LALLA	40.20
AVALL	59.92	AAVAL	71.60

**Computer Simulation.** The molecular total energy was calculated on an SGI indy workstation using the Biopolymer module in INSIGHT II 95.0 (Biosym).

**Observation of Membrane Permeability by ESR Measurement.** Healthy adult's erythrocytes were washed three times with isoosmotic phosphate buffer solution (PBS, pH 7.0) by centrifugation (10 min  $\times$  2000 rpm) (43, 44). The erythrocytes were suspended with PBS, and the density of cell in the suspension was adjusted to 50 million/mL and was incubated at 37 °C for 15 min prior to use. The spin-labeled peptide-conjugated PNA or spin-labeled PNA (2 mM) in 200  $\mu$ L PBS (containing 2% DMSO) was mixed with 200  $\mu$ L erythrocyte suspension. The mixture was incubated at 37 °C. The same volume of sample was picked out from the mixture at beginning of incubation, and thereafter periodically, and submitted to ESR measurement on a Bruker ESP 300 ESR spectrometer, respectively, and the spectra as well as signal strength at the same field was recorded. The percentage of ESR signal strength was calculated from the changes of ESR measurements before and after the incubation of erythrocyte with samples (Figure 2).

## RESULTS AND DISCUSSION

The mechanism of signal peptide in transmembrane movement is complex, but in most cases, the hydrophobic region composed of 5–15 amino acid residues is critical to the hydrophobic interaction with the phospholipids on the membrane. Studies also showed that the polarity and the conformation adopted by the signal sequence played an important role to facilitate the crossing membrane behavior: with the basic residue near the N-end, and most of the h-region in the signal sequence, it more readily formed an  $\alpha$ -helix (31, 32). To design the peptide sequences used for PNA modification, computer-aided modeling was used to search the ideal sequence with the lowest systemic energy in simulation of the  $\alpha$ -helix. According to the data of the simulation, two new sequences LALLAK and ALLPLALLAK with the system energy of 40.20 kcal/mol and 90.65 kcal/mol respectively (Table 2, 3) were proposed as the signal peptide mimics for the modification of PNA. A positively charged lysine was selected as a polarity enhancer which can be appended at the end of peptide, and the lysine would also

**Table 3. Molecular Total Energy Calculated by the Computer Simulating Method for the  $\alpha$  Helix of Nanopeptides**

sequence	total energy (kcal/mol)	sequence	total energy (kcal/mol)
ALLPAVLLA	112.9	AAVALPAVL	146.20
ALLPLALLA	90.65	AAVALPLLA	124.08
VALLPAVLL	124.67	AAVAPAVLL	144.02
VALLPALLA	112.80	AAVAPALLA	132.35
AVALLPAVL	134.56	AAVPAVLLA	142.47
AVALLPLLA	112.39	AAVPLALLA	120.12

contribute to its solubility, as well as the possible role of directing the adduct to access the partial polar cell membrane surface (49, 50). To assess the membrane permeability of the conceived peptide-linked PNA, we designed nitroxyl free radical as a report group so that the permeability of the spin-labeled adduct of peptide and PNA could be detected by the measurement of the ESR signal changes. Therefore, three spin-labeled peptide PNA conjugates (R15T10, R10T10, and R6T10) and the control sample, spin-labeled PNA (RT10), were designed and synthesized by standard solid-phase peptide chemistry. After cleavage with HF treatment, the products show the correct molecular weights by MALDI-TOF MS and the ESR signal with standard nitroxyl free radical parameters: three peaks,  $g = 2.0029$ ,  $a_N = 15.8$  G,  $\Delta H_0 = 2.5$  G. The results also demonstrate that the selected spin label molecule cannot be chemically influenced through a series of peptide synthesis conditions including HF treatment (Table 1).  $T_m$  values of R15T10, R10T10, R6T10, and RT10 measured with the complementary sequence dA<sub>10</sub>, respectively, show that such modification has only little influence on its hybridizing behavior (Table 1).

Stable nitroxyl free radical can be readily reduced to hydroxylamine by reductive agent. In erythrocyte the concentration of the reductive agent is 2–3 mM which can reduce the free radical and dramatically quench the ESR signals inside the cell (43, 44). In our experiments, the erythrocyte suspension in isoosmic buffer was free of plasma via a washing procedure so that the changes of ESR signal were only due to the intracellular chemical conditions. The results (Figure 2, curve 1) showed that the ESR signal strength decreased significantly after 3 h incubation of the pentadecapeptide-conjugated PNA (R15T10) with erythrocyte suspension, and no change was observed in the case of control sample (RT10) at the same condition (Figure 2, curve 4). It indicated that the free radical of R15T10 was reduced by the reductive agents inside the cells. The signal changes after 1.5 h incubation was also observed and showed the same as that determined after 3 h. It may infer that peptide-PNA conjugate R15T10 can penetrate the cell membrane rapidly and reach an equilibrium within 1.5 h. The same ESR measurements were used to assess the cell membrane permeability of hexapeptide- and decapeptide-conjugated PNAs, respectively. R10T10 and R6T10 showed almost the same decrease of the ESR signal strength after the incubation with erythrocyte for over 4 h (Figure 2, curve 2 and 3). After 4 h of incubation, no more decrease of ESR signal was exhibited. It means that the two peptide-PNA conjugates bear a similar extent of cell uptake.

Although pentadecapeptide-PNA conjugate R15T10 appears to have a faster penetrating rate than that of the hexa- and decapeptide modifiers, the pentadecapeptide modification makes the whole PNA T10 adduct difficult to dissolve in water. Lower water solubility may constitute another disadvantage for the feasibility of

therapeutics. However, the hexa- and decapeptide modification both improve the cell membrane permeability and in the meantime bear acceptable water solubility (Table 1). To support the ESR results, an antisense oligonucleotide-peptide conjugate containing LALLAK was synthesized, and the antisense activities targeting GLUT-1 in HepG-2 and MCF-7 cells were investigated (51). It was found that the synthetic antisense oligonucleotide-peptide conjugate showed up to 50% inhibition of cell proliferation in HepG-2 and MCF-7 cells. Compared to the previous paper, the same antisense oligonucleotide without peptide conjugated only showed a transient inhibition of HL-60 proliferation of about 25% and the expressed antisense RNA produced over 50% inhibition (52). Therefore, it seems that the efficiency of the synthetic antisense oligonucleotide peptide conjugate is the same as the expressed antisense RNA in the intact cells.

In conclusion, the hydrophobic pentadecapeptide and two signal peptide mimics, hexa and decapeptides ended with a positively charged amino acid, were proposed as the linked carrier for the transportation of PNA T10 through the cell membrane. Stable spin label was coupled to the peptide-PNA conjugate so that the ESR measurements can be used for the assessment of their transmembrane movements. The syntheses of spin-labeled peptide-PNA conjugates were carried out on MBHA resin with Boc strategy. According to the measurement of ESR, the three conjugates, R15T10, R10T10, R6T10, exhibit an enhanced rate of uptake across the erythrocyte membrane. The hexa- and decapeptide modified PNAs, R10T10 and R6T10, show suitable water solubility. The peptide-PNA conjugates retain their binding ability to the complementary DNA. The results suggest that peptide modification of PNA might be a promising solution for improving cell membrane permeability toward PNA.

#### ACKNOWLEDGMENT

This work is financially supported by the National Natural Science Foundation of China and the research grant G 1998051103 awarded by The ministry of Science and Technology, People's Republic of China.

#### LITERATURE CITED

- Nielsen, P. E., Egholm, M., Berg, R. H., and Buchardt, O. (1991) Sequence-selective recognition of DNA by strand displacement with a thymine-substituted polyamide. *Science* 254, 1497–1500.
- Egholm, M., Buchardt, O., Christensen, L., Behrens, C., Freier, S. M., Driver, D. A., Berg, R. H., Kim, S. K., Norden, B., and Nielsen, P. E. (1993) PNA hybridizes to complementary oligonucleotides obeying the Watson-Crick hydrogen-bonding rules. *Nature* 365, 566–568.
- Leijon, M., Gräslund, A., Nielsen, P. E., Buchardt, O., Nordén, B., Kristensen, S. M., and Eriksson, M. (1994) Structural characterization of PNA-DNA duplexes by NMR. Evidence for DNA in a B-like conformation. *Biochemistry* 33, 9820–9825.
- Brown, S. C., Thomson, S. A., Veal, J. M., and Davis, D. G. (1994) NMR Solution structure of a peptide nucleic acid complexed with RNA. *Science* 265, 777–780.
- Cherny, D. Y., Belotserkovskii, B. P., Frank-Kamenetskii, M. D., Egholm, M., Buchardt, O., Berg, R. H., and Nielsen, P. E. (1993) DNA unwinding upon strand-displacement binding of a thymine-substituted polyamide to double-stranded DNA. *Proc. Natl. Acad. Sci. U.S.A.* 90, 1667–1670.
- Hanvey, J. C., Pepper, N. J., Bisi, J. E., Thomson, S. A., Cadilla, R., Josey, J. A., Ricca, D. J., Hassman, C. F., Bonham, M. A., Au, K. G., Carter, S. G., Bruckenstein, D. A., Boyd, A. L., Noble, S. A., and Babiss, L. E. (1992) Antisense and antigene properties of peptide nucleic acids. *Science* 258, 1481–1485.
- Nielsen, P. E., Egholm, M., and Buchardt, O. (1994) Sequence-specific transcription arrest by peptide nucleic acid bound to the DNA template strand. *Gene* 149, 139–145.
- Demidov, V. V., Potaman, V. N., Frank-Kamenetskii, M. D., Egholm, M., Buchardt, O., Sönnichsen, S. H., and Nielsen, P. E. (1994) Stability of peptide nucleic acids in human serum and cellular extracts. *Biochem. Pharmacol.* 48, 1310–1313.
- Good, L., and Nielsen, P. E. (1997) Progress in developing PNA as a gene-targeted drug. *Antisense Nucleic Acid Drug Dev.* 7, 431–437.
- Ray, A., and Nordén, B. (2000) Peptide nucleic acid (PNA): its medical and biotechnical applications and promise for the future. *FASEB J.* 14, 1041–1060.
- Wittung, P.; Kajan, J., Edwards, K., Nielsen, P. E., Norden, B., and Malmström, B. G.; Phospholipid membrane permeability of peptide nucleic acid. (1995) *FEBS Lett.* 365, 27–29.
- Norton, J. C., Piatyszek, M. A., Wright, W. E., Shay, J. W., Corey, D. R. (1996) Inhibition of human telomerase activity by peptide nucleic acids. *Nat. Biotechnol.* 14, 615–619.
- Zhang, X., Simmons, C. G., and Corey, D. R. (2001) Liver cell specific targeting of peptide nucleic acid oligomers. *Bioorg. Med. Chem. Lett.* 11, 1269–1272.
- Boffa, L. C., Scarfi, S., Mariani, M. R., Damonte, G., Allfrey, V. G., Benatti, U., and Morris, P. L. (2000) Dihydrotestosterone as a selective cellular/nuclear localization vector for anti-gene peptide nucleic acid in prostatic carcinoma cells. *Cancer Res.* 60, 2258–2262.
- Basu, S., and Wickstrom, E. (1997) Synthesis and characterization of a peptide nucleic acid conjugated to a D-peptide analogue of insulin-like growth factor 1 for increased cellular uptake. *Bioconjugate Chem.* 8, 481–488.
- Pardridge W. M., Boado R. J., and Kang Y. S. (1995) Vector-mediated delivery of a polyamide ("peptide") nucleic acid analogue through the blood-brain barrier in vivo. *Proc. Natl. Acad. Sci. U.S.A.* 92, 5592–5596.
- Shi, N., Boado, R. J., and Pardridge, W. M. (2000) Antisense imaging of gene expression in the brain in vivo. *Proc. Natl. Acad. Sci. U.S.A.* 97, 14709–14714.
- Langer, K., Coester, C., Weber, C., von Briesen, H., and Kreuter, J. (2000) Preparation of avidin-labeled protein nanoparticles as carriers for biotinylated peptide nucleic acid. *Eur. J. Pharmacol. Biopharmacol.* 49, 303–307.
- Coester, C., Kreuter, J., von Briesen, H., and Langer, K., (2000) Preparation of avidin-labeled gelatin nanoparticles as carriers for biotinylated peptide nucleic acid (PNA). *Int. J. Pharm.* 196, 147–149.
- Mologni, L., Marchesi, E., Nielsen, P. E., and Gambacorti-Passerini, C., (2001) Inhibition of promyelocytic leukemia (PML)/retinoic acid receptor- $\alpha$  and PML expression in acute promyelocytic leukemia cells by anti-PML peptide nucleic acid. *Cancer Res.* 61, 5468–5473.
- Ardhammar, M., Norden, B., Nielsen, P. E., Malmström, B. G., and Wittung-Stafshede, P. (1999) In vitro membrane penetration of modified peptide nucleic acid (PNA). *J. Biomol. Struct. Dyn.* 17, 33–40.
- Muratovska, A., Lightowlers, R. N., Taylor, R. W., Turnbull, D. M., Smith, R. A. J., Wilce, J. A., Martin, S. W., and Murphy, M. P. (2001) Targeting peptide nucleic acid (PNA) oligomers to mitochondria within cells by conjugation to lipophilic cations: implications for mitochondrial DNA replication, expression and disease. *Nucleic Acids Res.* 29, 1852–1863.
- Scarfi, S., Gasparini, A., Damonte, G., and Benatti, U. (1997) Synthesis, uptake, and intracellular metabolism of a hydrophobic tetrapeptide-peptide nucleic acid (PNA)-biotin molecule. *Biochem. Biophys. Res. Commun.* 236, 323–326.
- Aldrian-Herrada, G., Desarménien, M. G., and Orsel, H., Boissin-Agasse L., Méry, J., Brugidou, J. and Rabié, A. (1998) A peptide nucleic acid (PNA) is more rapidly internalized in cultured neurons when coupled to a *retro-inverso* delivery peptide. The antisense activity depresses the target mRNA

- and protein in magnocellular oxytocin neurons. *Nucleic Acids Res.* 26, 4910–4916.
- (25) Pooga, M., Soomets, U., Hallbrink, M., Valkna, A., Saar, K., Rezaei, K., Kahl, U., Hao, J. X., Xu, X. J., Wissenfeld-Hallin, Z., Hökfelt, T., Bartfai, T., and Langel, U. (1998) Cell penetrating PNA constructs regulate galanin receptor levels and modify pain transmission in vivo. *Nat. Biotechnol.* 16, 857–861.
- (26) Harrison, J. G., Frier, C., Laurant, R., Dennis, R., Raney, K. D., and Balasubramanian, S. (1999) Inhibition of human telomerase by PNA-cationic peptide conjugates. *Bioorg. Med. Chem. Lett.* 9, 1273–1278.
- (27) Villa, R., Folini, M., Lualdi, S., Veronese, S., Daidone, M. G., and Zaffaroni, N. (2000) Inhibition of telomerase activity by a cell-penetrating peptide nucleic acid construct in human melanoma cells. *FEBS Lett.* 473, 241–248.
- (28) Simmons, C. G., Pitts, A. E., Mayfield, L. D., Shay, J. W., and Corey, D. R. (1997) Synthesis and membrane permeability of pna-peptide conjugates. *Bioorg. Med. Chem. Lett.* 7, 3001–3006.
- (29) Cutrona, G., Carpaneto, E. M., Ulivi, M., Roncella, S., Landt, O., Ferrarini, M., and Boffa, L. C. (2000) Effects in live cells of a c-myc anti-gene PNA linked to a nuclear localization signal. *Nat. Biotechnol.* 18, 300–303.
- (30) Branden, L. J., Mohamed, A. J., and Smith C. I. (1999) A peptide nucleic acid-nuclear localization signal fusion that mediates nuclear transport of DNA. *Nat. Biotechnol.* 17, 784–787.
- (31) von Heijne, G. (1985) Signal sequence: the limits of variation. *J. Mol. Biol.* 184, 99–105.
- (32) von Heijne, G. (1990) The signal peptide. *J. Membr. Biol.* 115, 195–201.
- (33) McKnight, C. J., Stradley, S. J., Jones, J. D., and Gierasch, L. M. (1991) Conformational and Membrane-Binding Properties of a Signal Sequence are Largely Unaltered by Its Adjacent Mature Region. *Proc. Natl. Acad. Sci. U.S.A.* 88, 5799–5803.
- (34) Hoyt, D. W., and Gierasch, L. M. (1991) A peptide corresponding to an export-defective mutant OmpA signal sequence with asparagine in the hydrophobic core is unable to insert into model membranes. *J. Biol. Chem.* 266, 14406–14412.
- (35) Rusch, S. L., Chen, H., Izard, J. W., and Kendall, D. A. (1994) Signal peptide hydrophobicity is finely tailored for function. *J. Cell Biochem.* 55, 209–217.
- (36) Jacobs, R. E., and White, S. H. (1989) The nature of the hydrophobic binding of small peptides at the bilayer interface: implications for the insertion of transbilayer helices. *Biochemistry* 28, 3421–3437.
- (37) Killian, J. A., de Jong, A. M. Ph., Bijvelt, J., Verkleij, A. J., and de Kruijff, B. (1990) Induction of nonbilayer lipid structures by functional signal peptides. *EMBO J.* 9, 815–819.
- (38) Lin, Y.-Z., Yao, S. Y., Veach, R. A., Torgerson, T. R., and Hawiger, J. (1995) Inhibition of nuclear translocation of transcription factor NF- $\kappa$ B by a synthetic peptide containing a cell membrane-permeable motif and nuclear localization sequence. *J. Biol. Chem.* 270, 14255–14258.
- (39) Bovi, P. D., Curatola, A. M., Kern, F. G. Greco, A., Ittmann, M., and Basilico, C. M. (1987) An Oncogene Isolated by Transfection of Kaposi's Sarcoma DNA Encodes a Growth Factor That Is a Member of the FGF Family. *Cell* 50, 729–737.
- (40) Fischer, P. M., Krausz, E., and Lane, D. P. (2001) Cellular Delivery of Impermeable Effector Molecules in the Form of Conjugates with Peptides Capable of Mediating Membrane Translocation. *Bioconjugate Chem.* 12, 825–841.
- (41) Rojas, M., Donahue, J. P., Tan, Z., and Lin, Y.-Z. (1998) Genetic engineering of proteins with cell membrane permeability. *Nat. Biotechnol.* 16, 370–375.
- (42) Couet, W. R., Brasch, R. C., Sosnovsky, G., Lukszo, J., Prakash, I., Gnewuch, C. T., and Tozer, T. N. (1985) Influence of chemical structure of nitroxyl spin labels on their reduction by ascorbic acid. *Tetrahedron* 41, 1165–1172.
- (43) Ross, A. H., and McConnell, H. M. (1975) Permeation of a spin-label phosphate into the human erythrocyte. *Biochemistry* 14, 2793–2798.
- (44) Eriksson, U. G., Tozer, T. N., Sosnovsky, G., Lukszo, J., and Brasch, R. C. (1986) Human erythrocyte membrane permeability and nitroxyl spin-label reduction. *J. Pharm. Sci.* 75, 334–337.
- (45) Dueholm, K. L., Egholm, M., Behrens, C., Christensen, L., Hansen, H. F., Vulpius, T., Petersen, K. H., Berg, R. H., Nielsen, P. E., and Buchardt, O. (1994) Synthesis of peptide nucleic-acid monomers containing the four natural nucleobases: thymine, cytosine, adenine, and guanine and their oligomerization. *J. Org. Chem.* 59, 5767–5773.
- (46) Sarin, V. K., Kent, S. B. H., Tam, J. P., and Merrifield, R. B. (1981) Quantitative monitoring of solid-phase peptide synthesis by the ninhydrin reaction. *Anal. Biochem.* 117, 147–157.
- (47) Christensen, L., Fitzpatrick, R., Gildea, B., Petersen, K. H., Hansen, H. F., Koch, T., Egholm, M., Buchardt, O., Nielsen, P. E., Coull, J., and Berg, R. H. (1995) Solid-phase synthesis of peptide nucleic acids. *J. Pept. Sci.* 3, 175–183.
- (48) Chou, P. Y., and Fasman, G. D. (1974) Conformational parameters for amino acids in helical,  $\beta$ -sheet, and random coil regions calculated from proteins. *Biochemistry* 13, 211–222.
- (49) Scheller, A., Oehlke, J., Wiesner, B., Dathe, M., Krause, E., Beyermann, M., Melzig, M., and Bienert, M. (1999) Structural requirements for cellular uptake of  $\alpha$ -helical amphipathic peptides. *J. Pept. Sci.* 5, 185–194.
- (50) Oehlke, J., Scheller, A., Wiesner, B., Krause, E., Beyermann, M., Klauschen, E., Melzig, M., and Bienert, M. (1998) Cellular uptake of an  $\alpha$ -helical amphipathic model peptide with the potential to deliver polar compounds into the cell interior nonendocytically. *Biochim. Biophys. Acta* 1414, 127–139.
- (51) Chen, C. P., Li, X. X., Zhang, L. R., Min, J. M., Chan, J. Y.-W., Fung, K. P., and Zhang, L. H. (2002) Synthesis of Antisense Oligonucleotide-Peptide Conjugate Targeting to GLUT-1 in HepG-2 and MCF-7 Cells. *Bioconjugate Chem.* 13, 525–529.
- (52) Chan, J. Y.-W., Kong, S. K., Choy, Y. M., Lee, C. Y., and Fung, K. P. (1999) Inhibition of Glucose Transporter Gene Expression by Antisense Nucleic Acid in HL-60 Leukemia Cells. *Life Sci.* 65, 63–70.



# Synthesis and Biological Evaluation of Folate Receptor-Targeted Boronated PAMAM Dendrimers as Potential Agents for Neutron Capture Therapy

Supriya Shukla,<sup>†</sup> Gong Wu,<sup>‡</sup> Madhumita Chatterjee,<sup>†</sup> Weilian Yang,<sup>‡</sup> Masaru Sekido,<sup>†</sup> Lamine A. Diop,<sup>§</sup> Rainer Müller,<sup>†</sup> Jennifer J. Sudimack,<sup>†</sup> Robert J. Lee,<sup>†</sup> Rolf F. Barth,<sup>‡</sup> and Werner Tjarks<sup>\*,†</sup>

College of Pharmacy and Department of Pathology, The Ohio State University, Columbus, Ohio 43210, and Collège Universitaire de Saint-Boniface, Winnipeg, Manitoba R2H 0H7, Canada. Received July 27, 2002; Revised Manuscript Received October 8, 2002

Successful treatment of cancer by boron neutron capture therapy (BNCT) requires the selective delivery of  $^{10}\text{B}$  to constituent cells within a tumor. The expression of the folate receptor is amplified in a variety of human tumors and potentially might serve as a molecular target for BNCT. In the present study we have investigated the possibility of targeting the folate receptor on cancer cells using folic acid conjugates of boronated poly(ethylene glycol) (PEG) containing 3rd generation polyamidoamine dendrimers to obtain  $^{10}\text{B}$  concentrations necessary for BNCT by reducing the uptake of these conjugates by the reticuloendothelial system. First we covalently attached 12–15 decaborate clusters to 3rd generation polyamidoamine dendrimers. Varying quantities of PEG units with varying chain lengths were then linked to these boronated dendrimers to reduce hepatic uptake. Among all prepared combinations, boronated dendrimers with 1–1.5 PEG<sub>2000</sub> units exhibited the lowest hepatic uptake in C57BL/6 mice (7.2–7.7% injected dose (ID)/g liver). Thus, two folate receptor-targeted boronated 3rd generation polyamidoamine dendrimers were prepared, one containing ~15 decaborate clusters and ~1 PEG<sub>2000</sub> unit with folic acid attached to the distal end, the other containing ~13 decaborate clusters, ~1 PEG<sub>2000</sub> unit, and ~1 PEG<sub>800</sub> unit with folic acid attached to the distal end. In vitro studies using folate receptor (+) KB cells demonstrated receptor-dependent uptake of the latter conjugate. Biodistribution studies with this conjugate in C57BL/6 mice bearing folate receptor (+) murine 24JK-FBP sarcomas resulted in selective tumor uptake (6.0% ID/g tumor), but also high hepatic (38.8% ID/g) and renal (62.8% ID/g) uptake, indicating that attachment of a second PEG unit and/or folic acid may adversely affect the pharmacodynamics of this conjugate.

## INTRODUCTION

BNCT,<sup>1</sup> which has been the subject of recent reviews (1, 2), is a binary approach to cancer therapy based on the nuclear reaction that occurs when  $^{10}\text{B}$  is irradiated with low energy neutrons to yield high LET  $\alpha$ -particles and lithium nuclei. These particles have a short range (<10  $\mu\text{m}$ ) and essentially deposit their energy within single cells. The efficacy of BNCT depends on the selective delivery of a relatively high amount of  $^{10}\text{B}$  to tumor cells while sparing adjacent normal cells. It has been estimated that ~15  $\mu\text{g}$  of  $^{10}\text{B}$  must be delivered to each gram of tumor in order to sustain lethal tumor cell damage (3). Numerous tumor selective low and high MW  $^{10}\text{B}$  carrier systems for BNCT are under investigation (1). High MW  $^{10}\text{B}$  carrier systems include, e.g., monoclonal and bispecific antibodies (4–6); EGF (7–9) as well as receptor-, antigen-, and nontargeted liposomes (10–16).

FR expression is amplified in a variety of human cancers and concomitantly is restricted in most normal

tissues (17, 18). FR-overexpressing tumors that may be suitable for treatment by NCT include those of the brain, lung, and some sarcomas (18). The vitamin FA (MW: 441 Da) [Figure 1 (3)] is transported into cells via FR mediated endocytosis (17, 18) and it has been established that the attachment of FA via its  $\gamma$ -carboxylic function to almost any type of molecule produces conjugates that

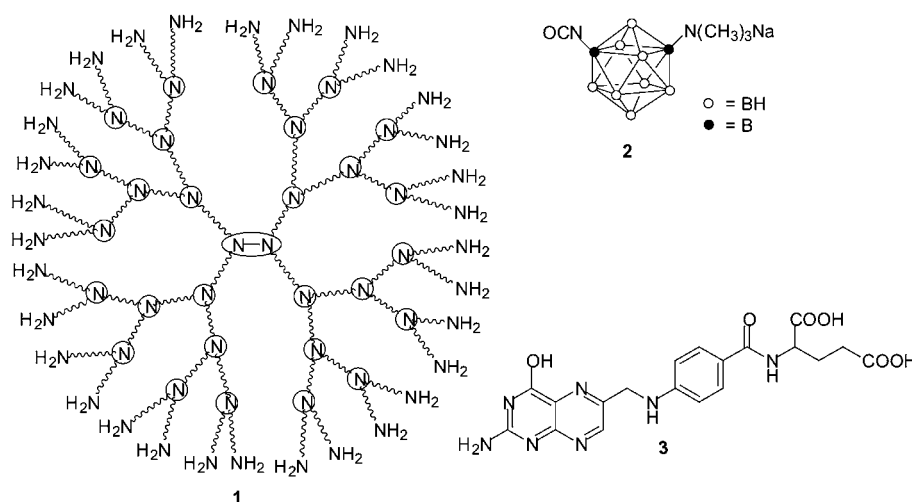
<sup>1</sup> Abbreviations: BNCT, boron neutron capture therapy; BSA, bovine serum albumin; Da, Dalton; DCC, dicyclohexylcarbodiimide; DCP-AES, direct current plasma-atomic emission spectroscopy; *D*, polydispersity; DE, dendrimer; DEAE, diethylaminoethyl; DMAP, (dimethylamino)pyridine; DMSO, dimethyl sulfoxide; DTT, dithiothreitol; EDA, ethylenediamine; EGF, epidermal growth factor; EGFR, epidermal growth factor receptor; FA, folic acid; FR, folate receptor; G3-BDE, EDA core boronated 3rd generation PAMAM dendrimer; GdNCT, gadolinium neutron capture therapy; % ID, % injected dose; ip, intraperitoneal; iv, intravenous; MALDI-TOFMS, matrix-assisted laser desorption/ionization time-of-flight mass spectroscopy; MePEG, poly(ethylene glycol) monomethyl ether; MM, molecular mechanics; MRI, magnetic resonance imaging; MW, molecular weight;  $M_n$ , number-average MW;  $M_w$ , weight-average MW; NCT, neutron capture therapy; NHS, *N*-hydroxysuccinimide; PAMAM, polyamidoamine; PBS, phosphate buffered saline; PEG, poly(ethylene glycol); RES, reticuloendothelial system; RT, room temperature; SPDP, *N*-succinimidyl 3-(2-pyridyldithio) propionate; SD, standard deviation; sulfo-MBS, *m*-maleimidobenzoyl-*N*-hydroxysulfosuccinimide ester; G, generation; UV/vis, ultraviolet/visible.

\* To whom correspondence should be addressed at the College of Pharmacy, The Ohio State University, 500 W. 12th Ave., Columbus, OH 43210-1291. Phone: (614)-292-7624, FAX: (614)-292-2435, E-mail: tjarks.1@osu.edu.

<sup>†</sup> College of Pharmacy, The Ohio State University.

<sup>‡</sup> Department of Pathology, The Ohio State University.

<sup>§</sup> Collège Universitaire de Saint-Boniface, Winnipeg, Manitoba, Canada.



**Figure 1.** Schematic presentation of an EDA core 3rd generation PAMAM dendrimer [G3-DE] (1), Na(CH<sub>3</sub>)<sub>3</sub>NB<sub>10</sub>H<sub>8</sub>NCO (2), and folic acid [FA](3).

can be endocytosed by FR-expressing cells in a fashion similar to that which occurs with FA (17, 18). FA-containing conjugates of a variety of diagnostic and therapeutic agents can selectively target FR-expressing cancer cells both in vitro and in vivo (17, 18). In BNCT-related studies, significant quantities of boron were delivered to FR(+) KB cells in vitro by receptor-mediated endocytosis using FA conjugated liposomes (13, 14).

PAMAM DEs [Figure 1 (1)] are spherical precision macromolecules with defined MWs and, depending upon the generation of the DE, an exponentially increasing number of terminal amino groups (19). Biomedical applications of PAMAM and other types of DEs have been reviewed recently (20, 21). These include the delivery of low MW drugs (22), oligonucleotides (23), transgenes (24), MRI contrast agents (25–29), radionuclides (30), as well as boron (4, 8, 9, 31, 32) and gadolinium (33) for NCT. FA-conjugated DEs, in particular, have been prepared as model drug carriers (34) and for MRI (27, 28).

Barth et al. have reported biodistribution studies with an ammonia core G4-BDE-monoconal antibody conjugate using B16 melanoma bearing C57BL/6 mice (4). G4-DE boronation was carried out using a negatively charged decaborate cluster, Na(CH<sub>3</sub>)<sub>3</sub>NB<sub>10</sub>H<sub>8</sub>NCO (35) [Figure 1 (2)]. Following ip injection, 0.4% ID/g of the G4-BDE-monoconal antibody conjugate localized in the tumor and concomitantly there was a high hepatic uptake (20% ID/g). Interestingly, the G4-BDE per se, which contained ~25 decaborate clusters (250 boron atoms), as well as non-boronated ammonia core G2-, G3-, and G4-DEs used in this study had similar hepatic uptake as the G4-BDE-antibody conjugate (4). Another biodistribution study with an ammonia core G4-BDE-EGF conjugate carried out in rats bearing intracerebral implants of the C6 glioma that had been transfected with the gene encoding EGFR resulted in 0.01% ID/g tumor and 12% ID/g liver for the bioconjugate following iv injection (8). The high hepatic uptake observed in this study may in part have been due to the expression of EGFR in the liver (36).

Numerous reports have described PEG modification of a wide variety of molecules, including low MW drugs, proteins, liposomes, and viruses (37–40). Benefits of the PEGylation of these molecules include, for example, improved aqueous solubility, prolonged blood circulation due to reduced renal, and RES clearance as well as reduced enzymatic degradation and toxicity (37). Indeed, during the past decade the FDA has approved several PEGylated agents including the antiviral drug PEGinter-

feron Alfa-2B (PEG-Intron) and the anticancer drug PEGasparaginase (Oncaspar). PEG units, ranging in MW from 5000 Da to 40000 Da, frequently have been used to improve the biological properties of proteins such as enzymes, interferons, and antibodies (37, 38, 40). In the case of liposomes maximum prolongation of blood circulation times has been attained with formulations containing 5–10 mol % PEG<sub>2000</sub> (41–43) although other liposomal formulations, containing both longer and shorter PEG units, also have proven to be effective in prolonging blood circulation times (40, 44). PEGylation also has been applied with some success to improve the biodistribution profiles of therapeutic and diagnostic DEs (22, 24, 26, 29, 32).

On the basis of the studies described above, we report here the synthesis of FA conjugated and nonconjugated PEGylated G3-BDEs as well as their in vitro evaluation using FR(+) cells and in vivo evaluation using a murine tumor model. PEG units were attached to the G3-BDEs in an attempt to reduce hepatic uptake previously observed with non-PEGylated BDEs (4). The in vivo biodistribution profiles of nonconjugated/PEGylated G3-BDEs were determined in nontumor bearing mice. In this pilot study, we have focused on G3-BDEs because of the experience previously obtained in our laboratories with medium sized BDEs (4, 8, 9). If necessary, G5- or even G6-BDEs, suitable for containing up to 250 decaborate clusters (2500 boron atoms), could be used for the preparation of FA conjugated PEGylated BDEs in order to obtain sufficient boron concentrations in FR-overexpressing tumors.

## EXPERIMENTAL PROCEDURES

**General Synthetic/Analytical Methods and Materials.** <sup>1</sup>H NMR and <sup>13</sup>C NMR spectra were obtained on Bruker FT-NMRs (250 or 400 MHz) at The Ohio State University College of Pharmacy. Chemical shifts (δ) are reported in ppm from an internal tetramethylsilane standard and coupling constants are reported in hertz. High-resolution MALDI-TOFMS were obtained by The Ohio State University Campus Chemical Instrumentation Center—Mass Spectrometry Facility (CCIC-MS) group members including Dr. Kari Green-Church, Dr. Johnnie Brown, Nan Kleinholz, Ben Jones, and Rhonda Pitsch on a Bruker Reflex III (Bruker, Bremen, Germany) mass spectrometer. Bond lengths were calculated by MM2 energy minimization calculations using CS Chem

3D Pro Version 4.0 (Cambridge Soft). Precoated glass-backed TLC plates with silica gel 60 F<sub>254</sub> (0.25 mm layer thickness) and silica gel 60 (70–230 mesh) from Merck were used for TLC and column chromatography, respectively. For compound visualization on TLC plates, UV light as well as KMnO<sub>4</sub> and molybdenum phosphate reagent sprays were used. DEAE-Trisacryl Sepharose (Sigma-Aldrich, St. Louis, MO) was used for ion exchange chromatography; Sephadex G-25, Sephadex G-50, and Superdex G-75 (Pharmacia, Piscataway, NJ) were used for size exclusion chromatography.

G3-DE was purchased from Dendritech Inc, Midland MI. Na(CH<sub>3</sub>)<sub>3</sub>NB<sub>10</sub>H<sub>8</sub>NCO was prepared as previously described (35) from (CH<sub>3</sub>)<sub>3</sub>NB<sub>10</sub>H<sub>8</sub>CO, which was purchased from Katchem Ltd., Prague, Czech Republic. Other reagents were purchased from commercial sources as indicated: MBS and SPDP from Pierce, Rockford, IL; MePEG<sub>3000</sub> and MePEG<sub>5000</sub> from Shearwater Polymers Inc., Huntsville, AL; FA, DCC, DMAP, 4-fluoro-3-nitrobenzoic acid, MePEG<sub>550</sub> and MePEG<sub>750</sub> from Sigma-Aldrich Corp., St. Louis, MO; *O,O*-bis(2-aminopropyl)-poly(ethylene glycol)<sub>800</sub> and MePEG<sub>2000</sub> from Fluka, Milwaukee, WI; *O,O*-bis(2-aminoethyl)poly(ethylene glycol)<sub>2000</sub> was gift from Shearwater Polymers Inc., Huntsville, AL; anhydrous DMSO and CH<sub>2</sub>Cl<sub>2</sub> were purchased from EM Science, Gibbstown, NJ. Other chemicals were of reagent grades and obtained from major suppliers.

**Synthesis of Compounds 5a–e.** Compounds **5a–e** were prepared from 4-fluoro-3-nitrobenzoic acid and **4a–e** as described previously (45). Briefing at the example of **5c**: Compound **4c** (4 g, 2 mmol) and 4-fluoro-3-nitrobenzoic acid (0.37 g, 2 mmol) in dichloromethane were treated with DCC (0.453 g, 2.2 mmol) and DMAP (25 mg, 0.2 mmol). The reaction mixture was stirred under an atmosphere of argon at RT overnight and subsequently filtered. The filtrate was washed with water, dried over MgSO<sub>4</sub>, and concentrated in a vacuum. The crude product (**5c**) was purified by silica gel column chromatography using 10% MeOH in CH<sub>2</sub>Cl<sub>2</sub>. The same solvent system was used for compounds **5d** and **5e** while 7.5% MeOH in CH<sub>2</sub>Cl<sub>2</sub> was used for **5a** and **5b**.

**5c.** Yield: 79%; NMR: <sup>1</sup>H NMR (CDCl<sub>3</sub>) δ: 8.8–8.6 (m, 1H, ArH), 8.4–8.1 (m, 1H, ArH), 7.5 (t, 1H, ArH), 4.6 (s, 2H, OCOCH<sub>2</sub>), 3.9–3.4 (m, ~176H, CH<sub>2</sub>CH<sub>2</sub>O), 3.35 (s, 3H, OMe). <sup>13</sup>C NMR (CDCl<sub>3</sub>) δ: 58.8 (OMe), 61.5 (MeO–CH<sub>2</sub>), 69.8, 70.4 (CH<sub>2</sub>O), 159.0 (NO<sub>2</sub>C), 165.0 (C=O). MALDI-TOFMS produced a characteristic bell shaped distribution of spectral lines spaced equally at 44 ± 1 Da apart, corresponding to the MW of one ethylene oxide repeat unit and centered at ~2200 Da (theoretical value: 2167 Da, based on the approximate MW of the PEG<sub>2000</sub> unit indicated by the supplier to be 2000 Da). The *M<sub>n</sub>* (number-average MW) is 2186.3283 and the *M<sub>w</sub>* (weight-average MW) is 2202.8476 with a polydispersity, *D* (*D* = *M<sub>w</sub>*/*M<sub>n</sub>*), of 1.0076. This method of analyzing mass spectroscopic data of PEG containing molecules has been previously described (46–49).

The yields for **5a**, **5b**, **5d**, and **5e** were in the same range as for **5c**. <sup>1</sup>H NMR and <sup>13</sup>C NMR spectra of **5a**, **5b**, **5d**, and **5e** were identical to those of **5c** except for differing signal intensities of the PEG protons around δ 3.9–3.4 [**5a** (~44 H), **5b** (~64H), **5d** (~264H), and **5e** (~448H)] as well as the PEG carbons around δ 71–70 ppm. MALDI-TOFMS produced similar characteristic bell shaped distribution of spectral lines spaced equally at 44 ± 1 Da apart, and centered around ~675 Da, ~1000 Da, ~3100 Da, ~5100 Da with *D*s of 1.0044, 1.0130, 1.0118, and 1.0079 for **5a**, **5b**, **5d** and **5e**, respectively.

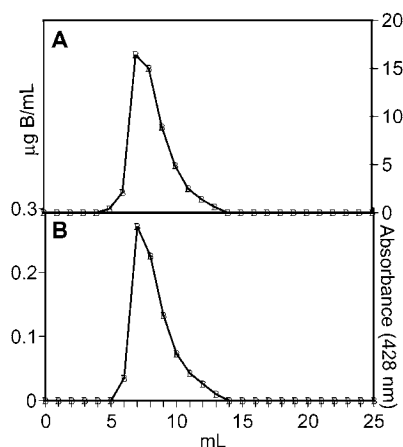
**Synthesis of Compounds 6 and 7.** A solution of FA (441 mg, 1 mmol) in anhydrous DMSO (10 mL) and triethylamine (2.5 mL) was reacted with NHS (230 mg, 2 mmol) in the presence of DCC (248 mg, 1.2 mmol) at RT. The reaction was stirred for 4 h followed by the addition of *O,O*-bis(2-aminopropyl)poly(ethylene glycol)<sub>800</sub> (800 mg, 1 mmol) or *O,O*-bis(2-aminoethyl)poly(ethylene glycol)<sub>2000</sub> (2 g, 1 mmol). The resulting mixture was stirred overnight at RT. Dicyclohexylurea was removed by filtration, and the crude product was precipitated with excess acetone, filtered, washed three times with acetone, and dried in a vacuum. The crude product was applied to a DEAE-Trisacryl Sepharose column. Compounds **6** and **7** were eluted with 10 mM NH<sub>4</sub>HCO<sub>3</sub> (pH 8.0). Fractions containing either **6** or **7** were pooled and lyophilized.

**6:** Yield: 52%; <sup>1</sup>H NMR (DMSO-*d*<sub>6</sub>) δ: 8.58 (s, 1H, C<sub>7</sub>-H); 7.75 (d, *J* = 8.4 Hz, 2H, Ar-H); 6.95 (br s, 1H, NH); 6.60 (d, *J* = 8.4 Hz, 2H, Ar-H); 5.09 (br s, 1H, NH); 4.55 (d, *J* = 5.1 Hz, 2H, C<sub>9</sub>-H); 3.60–3.30 (br m, PEG protons, ~56H); 1.11 (m, 6H, 2-CH<sub>3</sub>). MALDI-TOFMS produced a slightly deformed bell shaped distribution of spectral lines spaced equally at 44 ± 1 Da apart, corresponding to the MW of one ethylene oxide repeat unit and centered around ~1175 Da (calculated 1223 Da, taking the approximate MW of the PEG<sub>800</sub> unit indicated by the supplier to be 800 Da). *M<sub>n</sub>*: 1093.7049; *M<sub>w</sub>*: 1107.7550; *D*: 1.0128.

**7:** Yield 58%; <sup>1</sup>H NMR (DMSO-*d*<sub>6</sub>) δ: 8.63 (s, 1H, C<sub>7</sub>-H); 7.87 (d, *J* = 8.4 Hz, 2H, Ar-H); 6.92 (br s, 1H, NH); 6.62 (d, *J* = 8.4 Hz, 2H, Ar-H); 4.46 (d, *J* = 5.1 Hz, 2H, C<sub>9</sub>-H); 3.60–3.30 (br m, PEG protons, ~176H). MALDI-TOFMS produced a characteristic bell shaped distribution of spectral lines spaced equally at 44 ± 1 Da apart, corresponding to the MW of one ethylene oxide repeat unit and centered at ~2425 Da (calculated 2423 Da, taking the approximate MW of the PEG<sub>2000</sub> unit indicated by the supplier to be 2000 Da). *M<sub>n</sub>*: 1938.3420; *M<sub>w</sub>*: 1938.3420; *D*: 1.0000.

**Synthesis of Compounds 10 and 11a–e.** The introduction of Na(CH<sub>3</sub>)<sub>3</sub>NB<sub>10</sub>H<sub>8</sub>NCO (**2**, Figure 1) to G3-DE (**1**, Figure 1) was carried out as described previously (4). Briefly, compound **1** (53.3 mg, 25.9% w/w in 10% aqueous MeOH, 2 mmol) and **2** (10.29 mg, 44 mmol) were reacted in 1.0 mL of 0.1 M carbonate/bicarbonate buffer, pH 9.0, at RT for 24 h to yield **10** and **5a–e** (4.0 or 24 mmol) were added, and the reaction mixture was incubated in the dark at RT for 4 h. The reaction mixture was then applied to a Sephadex G-50 column in case of **11a** and **11b** and to a Superdex G-75 column in case of **11c–e** and eluted with carbonate/bicarbonate buffer, pH 9.0. The fractions containing both boron and MePEG were pooled and concentrated by ultrafiltration (Amicon, Bedford, MA). The number of PEG units attached to G3-BDE was determined spectrophotometrically by measuring the absorbance at 428 nm (nitroaniline chromophore, ε = 5.45 × 10<sup>3</sup> M<sup>−1</sup>cm<sup>−1</sup>) using a Beckman DU-6 spectrophotometer (Beckman Instruments, Inc., Irvine CA) [Figure 2]. Boron was quantified by means of DCP-AES as previously described (50) [Figure 2] using a Spectraspan VB spectrometer (Applied Research Laboratories, La Brea, CA). Briefly, 10 μL of boron compound solution was diluted to 1 mL with 0.1 M phosphate buffer, pH 8.5, and determined by DCP-AES at 249 nm. The instrument was calibrated by standard boron solution (VHG labs, Manchester, NH). The number of the PEG units and boron clusters in **10**, **11a–e** obtained by using varying molar ratios of **5a–e** are given in Table 1.





**Figure 2.** Sephadex G-50 column chromatographic profile of **11c**. Fractions of 1 mL were collected and analyzed by DCP-AES (A) and spectrophotometrically at 428 nm (B).

**Table 1. Composition and Hepatic Uptake of G3-BDE and PEGylated G3-BDEs<sup>a</sup>**

compd	number of MePEG units	number of boron clusters	% ID/g liver
<b>10</b>	0	15	17.0 ± 1.4
<b>10</b>	0	13	14.0 ± 2.1
<b>11a*</b>	2.5	15	17.1 ± 2.2
<b>11a**</b>	11.0	15	29.0 ± 9.0
<b>11b*</b>	2.0	15	20.0 ± 4.9
<b>11b**</b>	7.0	15	34.0 ± 12.3
<b>11c*</b>	1.0	13	7.7 ± 2.2
<b>11c*</b>	1.5	15	7.2 ± 1.1
<b>11c**</b>	6.5	15	20.6 ± 3.8
<b>11d*</b>	1.0	12	17.8 ± 2.8
<b>11d**</b>	4.0	12	17.8 ± 0.9
<b>11e*</b>	1.0	12	18.1 ± 2.0
<b>11e**</b>	4.0	12	17.2 ± 3.0

<sup>a</sup> C57BL/6 mice were injected ip with **10**, **11a–e**. The % ID/g were determined 6 h postinjection by DCP-AES. Mean ± SDs are based on four animals per group. Compounds **11a–e** were prepared using 2-fold (\*) and 12-fold (\*\*) molar excesses of MePEGs **5a–e** to compound **1**.

**Synthesis of Compounds 15 and 16.** Compound **1** (53.3 mg, 25.9% w/w in 10% aqueous MeOH, 2 mmol) and SPDP (3.12 mg, 10 mmol) were incubated in 1.0 mL of 0.1 M phosphate buffer (pH 7.5) at RT for 30 min and then applied to a Sephadex G-25 column and intermediate **12** was eluted with 0.1 M carbonate buffer (pH 9.0). Subsequently, **5c** (8.8 mg, 4 mmol) and then **2** (10.29 mg, 44 mmol) were reacted with **12** as described for the synthesis of compounds **11a–e** from compound **1**. The disulfide bond was subsequently cleaved using DTT (7.7 mg, 50 mmol) in 0.1 M phosphate buffer (10% DMSO, pH 7.5) for 30 min at RT. The reaction mixture was applied to a Sephadex G-25 column and the intermediate **14** was eluted with 0.1 M phosphate buffer (10% DMSO, pH 7.5). For the synthesis of **13**, compounds **12** and **2** (10.29 mg, 44 mmol) were reacted as described for the synthesis of compound **10** from compound **1**. The disulfide bond subsequently was cleaved using DTT (7.7 mg, 50 mmol) in 0.1 M phosphate buffer (10% DMSO, pH 7.5) for 30 min at RT. The reaction mixture was then applied to a Sephadex G-25 column and intermediate **13** was eluted with 0.1 M phosphate buffer (10% DMSO, pH 7.5). As determined spectrophotometrically by measuring the absorption of released pyridine-2-thione at 343 nm, ~2 free SH-groups were introduced to **13** and **14**. Compound **6** (4.9 mg, 4 mmol) and **7** (9.8 mg, 4 mmol) were reacted with sulfo-MBS (8.32 mg, 20 mmol) in 1.0 mL of 0.1 M

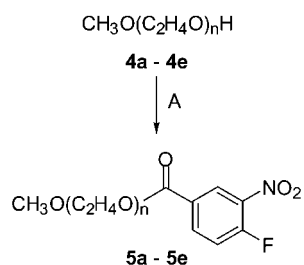
phosphate buffer (pH 7.5) at RT for 30 min to yield compounds **8** and **9**, respectively. After elution from a Sephadex G-25 column, fractions containing **8** and **9** were added directly to solution of **14** and **13**, respectively, resulting in a total reaction volume of 5 mL (0.1 M phosphate buffer and 10% DMSO, pH 7.5). The reaction was terminated after 30 min at RT to yield **15** and **16**, respectively. Both compounds were purified by column chromatography using a Superdex G-75 column and were eluted with 0.1 M phosphate buffer (pH 8.5). The number of MePEG<sub>2000</sub> and FA-PEG<sub>800/2000</sub> units were determined spectrophotometrically by measuring absorbance at 428 nm (nitroaniline chromophore,  $\epsilon = 5.45 \times 10^3 \text{ M}^{-1}\text{cm}^{-1}$ ) and 363 nm (folate,  $\epsilon = 7.5 \times 10^3 \text{ M}^{-1}\text{cm}^{-1}$ ). Boron was quantified by means of DCP-AES. According to these measurements, compound **15** was composed of ~15 boron clusters and ~1 FA-PEG<sub>2000</sub> while compound **16** was composed of ~13 boron clusters, ~1 MePEG<sub>2000</sub> unit, and ~1 FA-PEG<sub>800</sub> unit.

**Cell Culture.** Human FR(+) KB cancer cells (American Type Culture Collection # CCL 17), derived from an epidermal carcinoma of the oral cavity, were obtained as a gift from Dr. Philip S. Low at Purdue University (West Lafayette, IN). The cells were maintained in FA-free RPMI 1640 (Invitrogen, Grand Island, NY) medium supplemented with 100 units/mL penicillin, 100  $\mu\text{M}$ /mL streptomycin, and 5% fetal bovine serum, which provided the only source of FA. The cells were cultured as a monolayer at 37 °C in a humidified atmosphere containing 5% CO<sub>2</sub>. 24JK-FBP, a mouse sarcoma cell line transfected with the gene for human FR (5I), was maintained under the same culture conditions as those used to propagate KB cells.

**In Vitro Uptake of Compounds 15 and 16 in KB Cells.** KB cells were seeded into T-150 flasks and cultured (RPMI 1640, FA free) for 3 days to establish a complete monolayer. Cells were washed with 2 × PBS and harvested with 5 mM EDTA and then briefly exposed to 0.1 M acetate buffer, pH 3.5. Following removal of the acetate buffer, the cells were incubated with RPMI 1640 media (FA free) containing 2% BSA for 20 min at room temperature. Three tubes each containing  $13.3 \times 10^6$  cells were used for each uptake study, which was carried out by adding amounts of **15** and **16** corresponding to 40  $\mu\text{g}$  boron to each tube. The cells then were incubated for 20 min at RT, sedimented, and washed 3 × with PBS. The number of cells was determined by counting in a hemocytometer, and the boron concentration was determined by DCP-AES. For FR blocking studies, the cells were incubated with **15** or **16** in the presence of 1.0 mM FA.

**Hepatic Uptake of Compounds 10, 11a–e in C57BL/6 Mice.** C57BL/6 male mice were purchased from the Animal Production Unit of the National Cancer Institute, Frederick, MD. For hepatic uptake studies, groups of four animals were injected ip with 500  $\mu\text{g}$  of conjugates **10**, **11a–e** in 0.2 mL of 0.1 M phosphate buffer, pH 8.5. The animals were euthanized by cervical dislocation 6 h postinjection and liver samples were obtained. The boron contents in the liver samples were determined by DCP-AES.

**Biodistribution of Compounds 10, 11c, and 16 in C57BL/6 Mice Bearing 24JK-FBP.** For biodistribution studies of **10**, **11c**, and **16**, C57BL/6 male mice were injected subcutaneously with  $2 \times 10^6$  24JK-FBP cell in the back after 10 days on a FA free diet (Dyets, Inc, Bethlehem, PA). Within 10–14 d after implantation, by which time the tumors had attained a size of 100–500 mg, groups of four animals were injected ip with amounts of **10**, **11c**, and **16** corresponding to 120  $\mu\text{g}$  boron in 0.2

**Scheme 1<sup>a</sup>**

<sup>a</sup> Key: (A) DCC, 3-fluoro-2-nitrobenzoic acid, DMAP/ $\text{CH}_2\text{Cl}_2$ , 12 h, RT. **4a, 5a**:  $n = \sim 12$  (MePEG<sub>550</sub>), **4b, 5b**:  $n = \sim 17$  (MePEG<sub>750</sub>), **4c, 5c**:  $n = \sim 45$  (MePEG<sub>2000</sub>), **4d, 5d**:  $n = \sim 67$  (MePEG<sub>3000</sub>), **4e, 5e**:  $n = \sim 113$  (MePEG<sub>5000</sub>). Chromatography: silica gel 60.

mL of 0.1 phosphate buffer, pH 8.5. Blood, liver, spleen, kidneys, tumor, and skeletal muscle samples were obtained after euthanizing the animals 6 h postinjections, and the boron contents in the tissue samples were determined by DCP-AES.

**RESULTS**

**Synthesis of PEG Units, PEGylated G3-BDEs, and FA Conjugated/PEGylated G3-BDEs.** Compounds **5a–e** were prepared and purified as previously reported (45) by reacting 4-fluoro-3-nitrobenzoic acid with MePEGs **4a** [MW: 550], **4b** [MW: 750], **4c** [MW: 2000] (45), **4d** [MW: 3000], and **4e** [MW: 5000] (45) (Scheme 1). Aromatic nucleophilic substitution of the fluorine atom in 4 position of the aryl function in **5a–e** with aliphatic amines generates chromophoric *o*-nitroaniline moieties. This chromophore has been used to quantify the MePEG content of Bovine superoxide dismutase, to which **5c** and **5e** were attached via protein amino groups, by measuring its absorbance at 428 nm (45). We decided to use the same procedure to attach PEG units to the terminal amino functions of G3-BDEs, as shown in Schemes 3 and 4, since this permitted the convenient spectrophotometric quantification of the attached PEG units in the presence or absence of FA, which absorbs UV/vis at 363 nm. The maximum absorbance of FA did not interfere with that of the *o*-nitroaniline group, which permitted the spectrophotometric quantification of FA attached to G3-BDEs in the presence or absence of the *o*-nitroaniline group. MePEGs with MWs ranging from 550 to 5000 were chosen for the attachment to G3-BDE (Scheme 3) in order to evaluate the impact on MePEG chain length on hepatic uptake of MePEG-G3-BDE conjugates (Table 1).

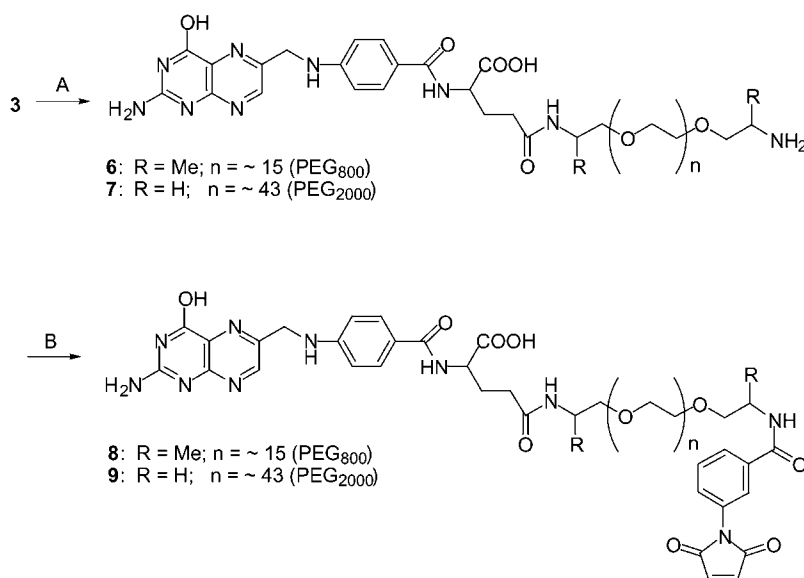
Compounds **6** and **7** were synthesized and purified using a combination of two methods described by Lee et al. for the preparation and purification of FA-PEG<sub>3400</sub>-NH<sub>2</sub> (52, 53) (Scheme 2). Isomeric mixtures of both **6** and **7** were generated with  $\sim 20\%$  substitution at the  $\alpha$ - and  $\sim 80\%$  substitution at the  $\gamma$ -carboxylic function of FA. These were purified, but not separated, by DEAE-trisacryl sepharose ion exchange chromatography as reported previously (54). Compounds **6** and **7** were treated with sulfo-MBS to afford the respective succinimidyl derivatives **8** and **9**, which were used directly for the preparation of G3-BDEs **15** and **16** (Scheme 4).

Boronation of a G3-DE [Figure 1 (1)] was carried out, as previously described (4, 8, 9, 55), using the polyhedral decaborate,  $\text{Na}(\text{CH}_3)_3\text{NB}_{10}\text{H}_8\text{NCO}$  (35) [Figure 1 (2)], carrying a single negative charge (Scheme 3). A 22-fold molar excess of **1** relative to **2** was used ensuring a substitution level of 12–15 boron clusters or 120–150 boron atoms per G3-DE. G3-DE (**1**) has 32 terminal

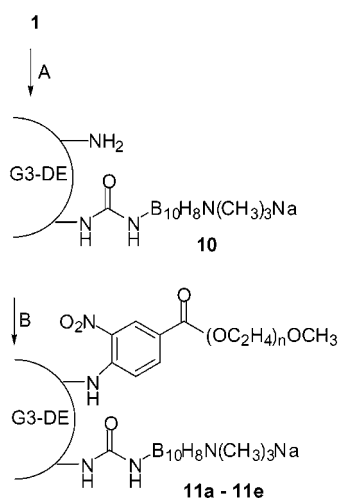
amino groups, a MW of 6909 Da, and a measured diameter of 36 Å (56). As determined by MM calculations, the total length of all bonds, including EDA core, between two terminal nitrogen atoms in G3-DE was 64.5 Å. The terminal amino groups of G3-DE should be partially protonated under physiological conditions in contrast to the interior tertiary amino groups, which are not sufficiently basic (19). This would leave the G3-DE with a maximum of about 32 positively charged ammonium groups under physiological conditions.

Based on MM calculations, the total length of all bonds between two nitrogen atoms of two terminal boron clusters in **10** (Scheme 3), including the EDA core, is  $\sim 78$  Å. The MW of G3-BDE (**10**) substituted with 15 boron clusters is 10164 Da (excluding sodium). We therefore estimate the actual diameter of **10** to be in the range of  $\sim 40$  Å since the effective diameter of G4-DE (MW: 14,215 Da) is 45 Å (56). Both nitrogens of the urea linker between boron clusters and G3-DE should not be sufficiently basic to be protonated under physiological conditions. Thus, G3-BDE (**10**) should be close to neutral or slightly positively charged under these conditions because the negative charges of the 15 boron clusters would almost completely neutralize the positive charges of the unsubstituted protonated terminal amino groups. MePEGs with MWs ranging from 550 to 5000 were chosen for the attachment to G3-BDE (Scheme 3) in order to evaluate the impact on MePEG chain length on the hepatic uptake of MePEG-G3-BDE conjugates (Table 1).

Introduction of the **5a–e** to G3-BDE (**10**) was carried out as previously described for the attachment of **5c** and **5e** to bovine superoxide dismutase (45). The reaction was carried out using 2-fold and 12-fold molar excess of **5a–e** relative to G3-DE (**1**) in an attempt to obtain substitution levels of about 1–2 and  $\sim 10$  PEG chains, respectively, at **10**. Different substitution levels were chosen in order to evaluate their impact on the hepatic uptake of MePEG-G3-BDE conjugates. The results are summarized in Table 1. The actual substitution levels indicated that it became increasingly more difficult to attach the desired number of MePEGs to G3-BDE (**10**) as the length of the MePEG chain increased. This was most striking when **10** was treated with a 12 molar excess of **5d** (MePEG<sub>3000</sub>) and **5e** (MePEG<sub>5000</sub>), which resulted in only four attached MePEGs in case of **11d** and **11e**, respectively. However, the shielding effect of the MePEGs was noticeably evident when a 2 molar excess of shorter MePEGs chain was used. This, in part, may explain the hepatic uptake levels observed for **11a,b**. It should be noted that the amino function in *N*-alkyl-*o*-nitroanilines, which constitute the chromophoric linker between MePEGs and G3-BDE in **11a–e**, is not sufficiently basic to be protonated under physiological conditions (57). Therefore, compounds **11a–e** should be close to neutral or even negatively charged, depending on the degree of MePEG substitution under these conditions. For reasons outlined in detail later, two FA conjugated PEGylated G3-BSDs were prepared adopting procedures previously described by us (4, 8, 9, 55), one containing  $\sim 15$  boron clusters and  $\sim 1$  PEG<sub>2000</sub> unit with FA attached to the distal end (**15**, Scheme 4), the other containing  $\sim 13$  boron clusters,  $\sim 1$  MePEG<sub>2000</sub>, and  $\sim 1$  PEG<sub>800</sub> unit with FA attached to the distal end (**16**, Scheme 4). Approximately two 3-(2-pyridyldithio) propionate groups were introduced to G3-DE (**1**) using a 5-fold excess of SPDP to yield intermediate **12**. The chromophoric MePEG unit (**5c**) and/or the boron clusters (**2**) were then attached to **12** in accordance with the procedure described above for the synthesis of compounds **11a–e** and **10**. The disulfide bonds in the 3-(2-py-

Scheme 2<sup>a</sup>

<sup>a</sup> Key: (A) i. **3**, triethylamine, DCC, DMSO, NHS, RT, 4 h; ii. *O,O*-bis(2-aminopropyl)poly(ethylene glycol)-800 and *O,O*-bis(2-aminoethyl)poly(ethylene glycol)-2000, RT, 12 h. (B) Sulfo-MBS, 0.1 M phosphate buffer, pH 7.5, RT, 30 min; Chromatography: DEAE-Trisacryl Sepharose for **6** and **7** and Sephadex G-25 for **8** and **9**.

Scheme 3<sup>a</sup>

<sup>a</sup> Key: (A) Na(CH<sub>3</sub>)<sub>3</sub>NB<sub>10</sub>H<sub>8</sub>NCO, carbonate-bicarbonate buffer, pH 9.0, RT, 24 h; (B) **5a-e**, carbonate-bicarbonate buffer, pH 9.0, RT, 4 h; Chromatography: Sephadex G-50 for **10**, **11a**, and **11b** and Superdex G-75 for **11c-e**; **a**: n = ~12 (MePEG<sub>550</sub>), **b**: n = ~17 (MePEG<sub>750</sub>), **c**: n = ~45 (MePEG<sub>2000</sub>), **d**: n = ~67 (MePEG<sub>3000</sub>); **e**: n = ~113 (MePEG<sub>5000</sub>).

ridyldithio) propionate groups subsequently were reduced to yield compounds **14** and **13**, respectively, each containing about two free sulfhydryl functions. Compounds **13** and **14** then were treated with compounds **9** and **8**, respectively, to afford target compounds **15** and **16**, respectively. In accordance with preceding considerations, both compound **15** and **16** should be neutral or slightly positively charged under physiological conditions.

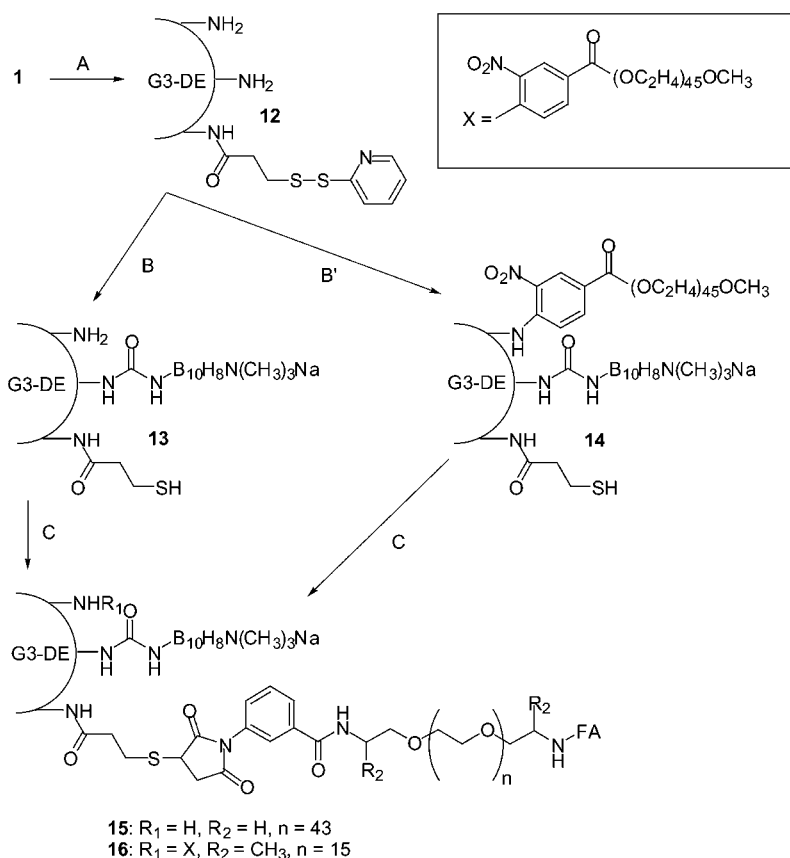
**Hepatic Uptake of Compounds G3-BDE and PEGylated G3-BDEs.** The hepatic uptake of G3-BDE (**10**) and PEGylated G3-BDEs (**11a-e**) was studied in C57BL/6 mice and the results are summarized in Table 1. The % IDs/g liver of G3-BDEs (**10**) with 13 and 15 attached boron clusters were  $17.0 \pm 1.4$  and  $14.0 \pm 2.1$ , respectively. These values are comparable with those obtained by Barth et al. using an ammonia core G4-BDE with ~25 attached boron clusters (**4**). Among all prepared

combinations, PEGylated G3-BDEs (**11c**) with 1 MePEG<sub>2000</sub> chain and 13 boron clusters and 1.5 MePEG<sub>2000</sub> chains and 15 boron clusters showed the lowest hepatic uptake with  $7.7 \pm 2.2$  and  $7.2 \pm 1.1\%$  ID/g liver, respectively. The highest hepatic uptake was observed for **11a** (11 MePEG<sub>550</sub> chains, 15 boron cluster) with  $29.0 \pm 9.0\%$  ID/g liver and **11b** (7 MePEG<sub>750</sub> chains, 15 boron cluster) with  $34.0 \pm 12.3$ . Both compounds show similarities in as far as that they possess high numbers of short MePEG chains and are probably negatively charged under physiological conditions. All other PEGylated G3-BDEs had hepatic uptake values, which were in the range of G3-BSD (**10**).

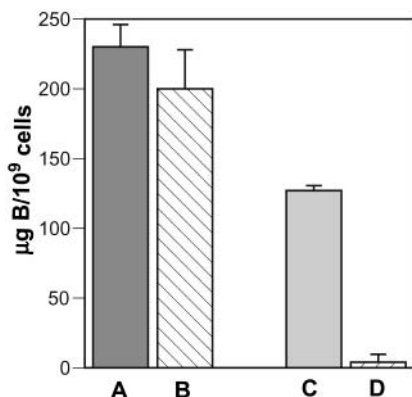
On the basis of these results, it appears that PEGylated G3-BSDs must be carefully designed to reduce opsonization and that there may be a very narrow window for optimal reduction demanding a small number (1–1.5) of PEG<sub>2000</sub> chains for a sufficiently large and flexible shielding layer. Thus, we have applied two different design strategies for the synthesis of FA conjugated/PEGylated G3-BDEs. First, attachment of a single PEG<sub>2000</sub> unit with FA linked to the distal end to a G3-BDE for shielding and FR targeting (compound **15**, Scheme 4). Second, attachment of a MePEG<sub>2000</sub> unit for shielding as well as attachment of an additional second PEG<sub>800</sub> unit with FA linked to the distal end for targeting (compound **16**, Scheme 4).

**In Vitro Evaluation of FA Conjugated PEGylated G3-BDEs.** As shown in Figure 3, both **15** and **16** were taken up in large amounts by FR(+) KB cells. Cellular uptake of **15** was 1.84 times higher than that of **16**. Cellular uptake in the presence of free FA, however, was effectively blocked only with **16**, indicating that it was taken up by FR-mediated endocytosis. In the case of conjugate **15**, the FA moiety may have been shielded from FRs by the coating layer generated by the PEG<sub>2000</sub> chain thereby preventing FR dependent cellular uptake. However, we cannot provide any explanation for the high, and obviously nonspecific, uptake of **15** by KB cells. Gabizon et al. have reported a high degree of nonspecific binding of FA conjugated liposomes to extracellular components in vitro, which may have resulted in inaccurate values for the cellular uptake of FA conjugated liposomes (**58**)



Scheme 4<sup>a</sup>

<sup>a</sup> Key: (A) SPDP, 0.1 M phosphate buffer, pH 7.5, RT, 30 min; (B) i. Na(CH<sub>3</sub>)<sub>3</sub>NB<sub>10</sub>H<sub>8</sub>NCO, carbonate-bicarbonate buffer, pH 9.0, RT, 24 h; ii. DTT, phosphate buffer (10% DMSO, pH 7.5), RT, 30 min; (B') i. 5 c, carbonate-bicarbonate buffer, pH 9.0/RT, 4 h; ii. Na(CH<sub>3</sub>)<sub>3</sub>NB<sub>10</sub>H<sub>8</sub>NCO, carbonate-bicarbonate buffer, pH 9.0, RT, 24 h; iii. DTT, phosphate buffer (10% DMSO, pH 7.5), RT, 30 min; (C) 8 or 9, 0.1 M phosphate buffer (10% DMSO, pH 7.5), RT, 30 min; Chromatography: Sephadex G-25 for 12, 13, and 14 and Superdex G-75 for 15 and 16.



**Figure 3.** Uptake of compounds 15 and 16 by KB cells. Cells were incubated with 15 or 16 in the presence and absence of FA at RT for 20 min. Boron uptake was determined by DCP-AES. A: Compound 15; B: Compound 15 + 1 mM FA; C: Compound 16; D: Compound 16 + 1 mM FA. Mean  $\pm$  SDs are based on three experiments.

and similar problems may have affected the cellular uptake of compound 15 in our studies. On the basis of the in vitro uptake data, conjugate 16 was chosen for biodistribution studies in C57BL/6 mice bearing FR(+) 24JK-FBP tumors.

**Biodistribution of G3-BDE (10), PEGylated G3-BDE (11c), and FA Targeted/PEGylated G3-BDE (16).** The biodistribution of conjugates 10 (~15 boron clusters), 11c (~1 MePEG<sub>2000</sub>, 13 boron cluster), and 16 6 h after ip injection into C57BL/6 mice bearing FR(+) 24JK-FBP tumors are summarized in Table 2. High tumor uptake only was observed for the FA conjugated/PEGylated G3-BDE 16 (6.0%  $\pm$  1.6 ID/g). The hepatic uptake values of 10 and 11c were comparable to those observed in nontumor bearing mice (Table 1). However, conjugate 16 showed a markedly increased hepatic uptake (38.8  $\pm$  5.9%ID/g) compared to 11c, indicating that the low RES clearance of 11c was completely abolished by the attachment of an additional FA-PEG<sub>800</sub> unit, either by the presence of the PEG<sub>800</sub> moiety, FA, or both. The very high renal uptake of 10 (104.2  $\pm$  20.7%ID/g) was consistent with renal uptake values previously reported for low and mid generation DEs (25, 26, 28, 59, 60). Modification of 10 with a MePEG<sub>2000</sub> chain increased the MW and, subsequently, decreased renal retention, as observed for 11c (45.0  $\pm$  13.4 ID/g). This also was consistent with previously reported data of Kobayashi et

**Table 2. Biodistribution of Compounds 10, 11c, and 16<sup>a</sup>**

tissue	% ID of 10/ g tissue	% ID of 11c/ g tissue	% ID of 16/ g tissue
blood	1.1 $\pm$ 1.3	n.m.	n.m.
liver	20.6 $\pm$ 5.0	7.1 $\pm$ 4.0	38.8 $\pm$ 5.9
spleen	14.7 $\pm$ 3.9	20.2 $\pm$ 8.8	25.0 $\pm$ 7.4
kidney	104.2 $\pm$ 20.7	45.0 $\pm$ 13.4	62.8 $\pm$ 14.5
muscle	n.m.	n.m.	n.m.
tumor	n.m.	n.m.	6.0 $\pm$ 1.6

<sup>a</sup> 24JK-FBP tumor bearing C57BL/6 mice were injected ip with 10, 11c, and 16. The % ID/g were determined 6 h post injection by DCP-AES. Mean  $\pm$  SDs are based on four animals per group. n.m.: not measurable.

al. (25, 26). Additional attachment of FA-PEG<sub>800</sub> again increased the renal uptake ( $62.8 \pm 14.5\%$  ID/g), which was expected because of the high expression of FR in the kidneys (61). In case of **10**, **11c**, and **16** high boron accumulation was also detected in the spleen while blood and muscle values were low. Preliminary studies with **10**, **11c**, and the FA-PEG<sub>350</sub>-G3-BDE derivative of **16** in a small number of FR(+) 24JK-FBP tumor bearing mice at 3 and 24 h after ip injection, indicating that uptake values shown in Table 2 were almost constant over a 21 h period for the indicated tissues (data not shown).

## DISCUSSION

Despite growing interest in the use of PAMAM DEs as macromolecular carriers (20, 21), little is known about their biological behavior following in vivo administration, which ultimately is critical for their use in biomedical applications. In an early study using ammonia core DE-monoclonal antibody conjugates, we observed that <sup>125</sup>I-labeled DE-monoclonal antibodies showed an increasing propensity to localize in the liver and spleen of B16 melanoma bearing mice as the size of the DE increased from 0 to 4th generation (4). Both an ammonia core G3-DE (59) and an EDA core <sup>125</sup>I-labeled iodo-benzoyl-biotinylated G2-DE (60) had high renal uptake in Swiss-Webster rats and athymic nude mice, respectively. In another study carried out with Wistar rats both cationic and anionic DEs showed high hepatic uptake (62). Kobayashi et al. evaluated the biodistribution pattern of EDA core G3-, G4-, G5-, and G6-DEs, that had been heavily substituted with Gd-DTPA chelates, in BALB/c mice and found that hepatic and renal uptake of the DEs was generation dependent. G6-DE had the highest hepatic uptake and lowest renal uptake while G3-DE had the lowest hepatic and highest renal uptake (25). Kobayashi et al. also explored the biodistribution of Gd-DTPA-G4-DEs either mono- or disubstituted with PEG<sub>2000</sub> with that of a non-PEGylated Gd-DTPA-G4-DE in mice (26). Renal uptake was extremely high for the non-PEGylated conjugates and decreased significantly with increasing MW in case of monoPEGylation and even more pronounced in case of diPEGylation. The hepatic uptake of the non-PEGylated conjugate was high and decreased significantly with diPEGylation but not with monoPEGylation. Margerum et al. prepared a G3-DEs substituted with Gd-chelates and noticed moderate hepatic uptake for this conjugate in Sprague-Dawley rats, which appeared to increase when this conjugate was modified with varying quantities of PEG<sub>2000</sub> or PEG<sub>5000</sub> units (29).

Overall, it appears that hepatic uptake depends to a significant degree on the MW and, consequently, the size of a DE. The attachment of PEG units to a DE increases its MW/size. The affinity of PEGylated DEs for the RES system may therefore depend strongly on a finely tuned balance between overall MW/size and shielding effect of the PEG layer. Studies have shown that the level of substitution with PEG units drastically affects the actual size of a PEGylated liposome and that the size, as well as a dense and rigid surface coating, may negatively affect its biodistribution pattern (63–65). In contrast, a relatively small number of hydrophilic and highly flexible liposomal surface polymers may effectively protect a liposome from being opsonized and filtered out of the vascular compartment by the RES (65).

In case of G3-BDEs **11a** and **11b**, a small number of short PEG<sub>550</sub> and PEG<sub>750</sub> chains may not effectively shield the G3-BDE surface while a large number of short PEG<sub>550</sub>

and PEG<sub>750</sub> chains may generate a dense and fairly rigid surface layer, which simply increases the MW/size of the G3-BDE but does not effectively shield the conjugate from opsonization. The latter also may apply to some extent to large numbers of PEG<sub>2000</sub> chains (**11c**) as well as small and large numbers of PEG<sub>3000</sub> (**11d**) and PEG<sub>5000</sub> (**11e**) chains attached to G3-BDE.

Wiener et al. have evaluated the biodistribution of a FA conjugated gadolinium containing G4-DE in athymic nude mice carrying FR(+) SKOV3 tumors and found tumor selective uptake of the conjugate (3.62% ID/g tumor), high hepatic uptake (6.35%/g), and very high renal uptake (70.77% ID/g) (28). The results reported by Wiener et al. are similar to those obtained with **16** in our biodistribution study. In another study, Kobayashi et al. compared the biodistribution of avidine targeted Gd-DTPA-G6-DE with nontargeted Gd-DTPA-G6-DE in SHIN3 tumor bearing BALB/c mice and found highly tumor selective uptake for the former conjugate (103% ID/g) compared with the latter conjugate (~30% ID/g) while the hepatic uptake of both bioconjugates were similarly (~17.5% ID/g) (33). The results obtained by us, Wiener et al. (28), and Kobayashi et al. (33) clearly demonstrate that receptor/antigen targeted DEs may have significant potential in MRI and NCT applications.

In summary, we have developed synthetic methods for the preparation of chromophorically labeled PEGylated BDEs and FA conjugated/PEGylated BDEs. The number of MePEGs and FA units attached to BDE can be easily determined spectrophotometrically by taking advantage of the differences in the absorbance maxima of FA and an attached *o*-nitroaniline moiety. PEGylated G3-BDEs with 1 MePEG chain and 13 boron clusters and 1.5 MePEG chains and 15 boron clusters showed the lowest hepatic uptake of all evaluated conjugates with  $7.7 \pm 2.2$  and  $7.2 \pm 1.1\%$  ID/g liver, respectively. The optimal modification of BDEs, as well as DEs in general, with PEG chains to reduce RES affinity appears to be highly complex endeavor that depends on a variety of factors, which will require extensive evaluation. A FA conjugated/PEGylated G3-BDE was prepared, which was taken up in vitro by FR(+) KB cells apparently by FR mediated endocytosis. The same conjugate showed significantly increased tumor selectivity compared with non-PEGylated BDE-antibody and BDE-EGF conjugates previously evaluated for potential application in BNCT (4, 8). However, the hepatic and renal uptake of this conjugate was very high. The results obtained in this study warrant further effort in the optimization of biodistribution profiles of receptor/antigen targeted PEGylated BDEs.

## ACKNOWLEDGMENT

This work was supported by the National Institutes of Health grant R01CA79758. The authors thank Ms. Dianne M. Adams for technical assistance.

## LITERATURE CITED

- (1) Soloway, A. H., Tjarks, W., Barnum, B. A., Rong, F. G., Barth, R. F., Codogni, I. M., and Wilson, J. G. (1998) The chemistry of neutron capture therapy. *Chem. Rev.* 98, 1515–1562.
- (2) Barth, R. F., Soloway, A. H., Goodman, J. H., Gahbauer, R. A., Gupta, N., Blue, T. E., Yang, W., and Tjarks, W. (1999) Boron neutron capture therapy of brain tumors: an emerging therapeutic modality. *Neurosurgery* 44, 433–450.
- (3) Fairchild, R. G., and Bond, V. P. (1985) Current status of <sup>10</sup>B-neutron capture therapy: Enhancement of tumor dose via beam filtration and dose rate, and the effects of these

- parameters on minimum boron content: A theoretical evaluation. *Int. J. Radiat. Oncol., Biol., Phys.* **11**, 831–840.
- (4) Barth, R. F., Adams, D. M., Soloway, A. H., Alam, F., and Darby, M. V. (1994) Boronated starburst dendrimer-mono-clonal antibody immunoconjugates: evaluation as a potential delivery system for neutron capture therapy. *Bioconjugate Chem.* **5**, 58–66.
  - (5) Liu, L., Barth, R. F., Adams, D. M., Soloway, A. H., and Reisfeld, R. F. (1996) Critical evaluation of bispecific antibodies as targeting agents for boron neutron capture therapy of brain tumors. *Anticancer Res.* **16**, 2581–2588.
  - (6) Guan, L. F., Wims, L. A., Kane, R. R., Smuckler, M. B., Morrison, S. L., and Hawthorne, M. F. (1998) Homogeneous immunoconjugates for boron neutron-capture therapy: Design, synthesis, and preliminary characterization. *Proc. Natl. Acad. Sci. U.S.A.* **95**, 13206–13210.
  - (7) Gedda, L., Olsson, P., Ponten, J., and Carlsson, J. (1996) Development and *in vitro* studies of epidermal growth factor-dextran conjugates for boron neutron capture therapy. *Bioconjugate Chem.* **7**, 584–591.
  - (8) Yang, W., Barth, R. F., Adams, D. M., and Soloway, A. H. (1997) Intratumoral delivery of boronated epidermal growth factor for neutron capture therapy of brain tumors. *Cancer Res.* **57**, 4333–4339.
  - (9) Barth, R. F., Yang, W., Adams, D. M., Rotaru, J. H., Shukla, S., Sekido, M., Tjarks, W., Fenstermaker, R. A., Ciesielski, M., Nawrocky, M. M., and Coderre, J. A. (2002) Molecular targeting of the epidermal growth factor receptor for the neutron capture therapy of gliomas. *Cancer Res.* **62**, 3159–3166.
  - (10) Feakes, D. A., Waller, R. C., Hathaway, D. K., and Morton, V. S. (1999) Synthesis and *in vivo* murine evaluation of Na<sub>4</sub>[1-(1'-B<sub>10</sub>H<sub>9</sub>)-6-SHB<sub>10</sub>H<sub>8</sub>] as a potential agent for boron neutron capture therapy. *Proc. Natl. Acad. Sci. U.S.A.* **96**, 6406–6410.
  - (11) Hawthorne, M. F., and Kelly, S. (1997) Liposomes as drug delivery vehicles for boron agents. *J. Neuro-Oncol.* **33**, 53–58.
  - (12) Yanagie, H., Tomita, T., Kobayashi, H., Fujii, Y., Nonaka, Y., Saegusa, Y., Hasumi, K., Eriguchi, M., Kobayashi, T., and Ono, K. (1997) Inhibition of human pancreatic cancer growth in nude mice by boron neutron capture therapy. *Br. J. Cancer* **75**, 660–665.
  - (13) Pan, X. Q., Wang, H., Shukla, S., Sekido, M., Adams, D. M., Tjarks, W., Barth, R. F., and Lee, R. J. (2002) Boron-containing folate receptor-targeted liposomes as potential delivery agents for neutron capture therapy. *Bioconjugate Chem.* **13**, 435–442.
  - (14) Sudimack, J. J., Adams, D., Rotaru, J., Shukla, S., Yan, J., Sekido, M., Barth, R. F., Tjarks, W., and Lee, R. J. (2002) Folate receptor-mediated liposomal delivery of a lipophilic boron agent to tumor cells *in vitro* for neutron capture therapy. *Pharm. Res.* **19**, 1502–1508.
  - (15) Kullberg, E. B., Bergstrand, N., Carlsson, J., Edwards, K., Johnsson, M., Sjöberg, S., and Gedda, L. (2002) Development of EGF-conjugated liposomes for targeted delivery of boronated DNA-binding agents. *Bioconjugate Chem.* **13**, 737–743.
  - (16) Ishida, O., Maruyama, K., Tanahashi, H., Iwatsuru, M., Sasaki, K., Eriguchi, M., and Yanagie, H. (2001) Liposomes bearing poly(ethylene glycol)-coupled transferrin with intracellular targeting property to the solid tumors *in vivo*. *Pharm. Res.* **18**, 1042–1048.
  - (17) Leamon, C. P., and Low, P. S. (2001) Folate-mediated targeting: From diagnostics to drug and gene delivery. *Drug Discov. Today* **6**, 44–51.
  - (18) Sudimack, J., and Lee, R. J. (2000) Targeted drug delivery via the folate receptor. *Adv. Drug Delivery Rev.* **41**, 147–162.
  - (19) a) Tomalia, D. A., Naylor, A. M., and Goddard, W. A., III. (1990) Starburst dendrimers: Control of size, shape, surface chemistry, topology and flexibility in the conversion of atoms to macroscopic materials. *Angew. Chem., Int. Ed. Engl.* **102**, 119–157. (b) <http://www.dendritech.com/pamam.html>.
  - (20) Esfand, R., and Tomalia, D. A. (2001) Poly(amidoamine) (PAMAM) dendrimers: From biomimicry to drug delivery and biomedical application. *Drug Discov. Today* **6**, 427–436.
  - (21) Stiribara, S. E., Frey, H., and Haag, R. (2002) Dendritic polymers in biomedical applications: From potential to clinical use in diagnostic and therapy. *Angew. Chem., Int. Ed. Engl.* **41**, 1329–1334.
  - (22) Kojima, C., Kono, K., Maruyama, K., and Takagishi, T. (2000) Synthesis of polyamidoamine dendrimers having poly(ethylene glycol) grafts and their ability to encapsulate anticancer drugs. *Bioconjugate Chem.* **11**, 910–917.
  - (23) Yoo, H., and Juliano, R. L. (2000) Enhanced delivery of antisense oligonucleotides with fluorophore-conjugated PAMAM dendrimers. *Nucleic Acids Res.* **28**, 4225–4231.
  - (24) Luo, D., Haverstick, K., Belcheva, N., Han, E., and Saltzman, W. M. (2002) Poly(ethylene glycol)-conjugated PAMAM dendrimer for biocompatible, high-efficiency DNA delivery. *Macromolecules* **35**, 3456–3462.
  - (25) Kobayashi, H., Sato, N., Hiraga, A., Saga, T., Nakamoto, Y., Ueda, H., Konishi, J., Togashi, K., and Brechbiel, M. W. (2001) 3D-micro-MR angiography of mice using macromolecular MR contrast agents with polyamidoamine dendrimer core with reference to their pharmacokinetic properties. *Magn. Reson. Med.* **45**, 454–460.
  - (26) Kobayashi, H., Kawamoto, S., Saga, T., Sato, N., Hiraga, A., Ishimori, T., Konishi, J., Togashi, K., and Brechbiel, M. W. (2001) Positive effects of poly(ethylene glycol) conjugation to generation-4 polyamidoamine dendrimers as macromolecular MR contrast agents. *Magn. Reson. Med.* **46**, 781–788.
  - (27) Konda, S. D., Aref, M., Wang, S., Brechbiel, M., and Wiener, E. C. (2001) Specific targeting of folate-dendrimer MRI contrast agents to the high affinity folate receptor expressed in ovarian tumor xenografts. *Magn. Reson.* **12**, 104–113.
  - (28) Konda, S. D., Wang, S., Brechbiel, M., and Wiener, E. C. (2002) Biodistribution of a <sup>153</sup>Gd-folate dendrimer, generation = 4, in mice with folate-receptor positive and negative ovarian tumor xenografts. *Invest. Radiol.* **37**, 199–204.
  - (29) Margerum, L. D., Campion, B. K., Koo, M., Shargill, N., Lai, J.-J., Marumoto, A., and Sontum, P. C. (1997) Gadolinium(III) DO3A macrocycles and poly(ethylene glycol) coupled to dendrimers. Effect of molecular weight on physical and biological properties of macromolecular magnetic resonance imaging contrast agents. *J. Alloys Compd.* **249**, 185–190.
  - (30) Kobayashi, H., Wu, C., Kim, M.-K., Paik, C. H., Carrasquillo, J. A., and Brechbiel, M. W. (1999) Evaluation of the *in vivo* biodistribution of indium-111 and yttrium-88 labeled dendrimer-1B4M-DTPA and its conjugation with anti-tac monoclonal antibody. *Bioconjugate Chem.* **10**, 103–111.
  - (31) Newkome, G. R., Moorefield, C. N., Keith, J. M., Baker, G. R., and Escamilla, G. H. (1994) Chemistry of micelles. 37. Internal chemical transformations in a precursor of a unimolecular micelle: boron supercluster via site-specific addition of B<sub>10</sub>H<sub>14</sub> to cascade molecules. *Angew. Chem., Int. Ed. Engl.* **33**, 666–668.
  - (32) Qualmann, B., Kessels, M. M., Musiol, H. J., Sierralta, W. D., Jungblut, P. W., and Moroder, L. (1996) Synthesis of boron-rich lysine dendrimers as protein labels in electron microscopy. *Angew. Chem., Int. Ed. Engl.* **35**, 909–911.
  - (33) Kobayashi, H., Kawamoto, S., Saga, T., Sato, N., Ishimori, T., Konishi, J., Ono, K., Togashi, K., and Brechbiel, M. W. (2001) Avidin-dendrimer-(1B4M-Gd)(254): A tumor-targeting therapeutic agent for gadolinium neutron capture therapy of intraperitoneal disseminated tumor which can be monitored by MRI. *Bioconjugate Chem.* **12**, 587–593.
  - (34) Kono, K., Liu, M., and Fréchet, J. M. J. (1999) Design of dendritic macromolecules containing folate or methotrexate residues. *Bioconjugate Chem.* **10**, 1115–1121.
  - (35) Alam, F., Soloway, A. H., Barth, R. F., Mafune, N., Adams, D. M., and Knuth, W. H. (1989) Boron neutron capture therapy: Linkage of a boronated macromolecule to monoclonal antibodies directed against tumor-associated antigens. *J. Med. Chem.* **32**, 2326–2330.
  - (36) Vinter-Jensen, L., Froekiaer, J., Joergensen, P. E., Marquers, J., Rehling, M., Dajani, E. Z., and Nexoe, E. (1995) Tissue distribution of <sup>131</sup>I-labeled epidermal growth factor in the pig visualized by dynamic scintigraphy. *J. Endocrinol.* **144**, 5–12.



- (37) Chapman, A. P. (2002) PEGylated antibodies and antibody fragments for improved therapy: A review. *Adv. Drug Delivery Rev.* 54, 531–545.
- (38) Greenwald, R. B. (2001) PEG drugs: An overview. *J. Controlled Release* 74, 159–171.
- (39) Mastrobattista, E., Koning, G. A., and Storm, G. (1999) Immunoliposomes for the targeted delivery of antitumor drugs. *Adv. Drug Delivery Rev.* 40, 103–127.
- (40) Monfardini, C., and Veronese, F. M. (1998) Stabilization of substances in circulation. *Bioconjugate Chem.* 9, 418–450.
- (41) Allen, T. M., Austin, G. A., Chonn, A., Lin, L., and Lee, K. C. (1991) Uptake of liposomes by cultured mouse bone marrow macrophages: Influence of liposome composition and size. *Biochim. Biophys. Acta* 1061, 56–64.
- (42) Hansen, C. B., Kao, G. Y., Moase, E. H., Zalipsky, S., and Allen, T. M. (1995) Attachment of antibodies to sterically stabilized liposomes: Evaluation, comparison and optimization of coupling procedures. *Biochim. Biophys. Acta* 1239, 133–144.
- (43) Suzuki, S., Watanabe, S., Masuko, T., and Hashimoto, Y. (1995) Preparation of long-circulating immunoliposomes containing adriamycin by a novel method to coat immunoliposomes with poly(ethylene glycol). *Biochim. Biophys. Acta* 1245, 9–16.
- (44) Woodle, M. C., Matthey, K. K., Newman, M. S., Hidayat, J. E., Collins, L. R., Redemann, C., Martin, F. J., and Papahadjopoulos, D. (1992) Versatility in lipid compositions showing prolonged circulation with sterically stabilized liposomes. *Biochim. Biophys. Acta* 1105, 193–200.
- (45) Ladd, D. L., and Snow, R. A. (1993) Reagents for the preparation of chromophorically labeled poly(ethylene glycol)-protein conjugates. *Anal. Biochem.* 210, 258–261.
- (46) Lee, S., Winnik, M. A., Whittall, R. M., and Li, L. (1996) Synthesis of symmetric fluorescently labeled poly(ethylene glycols) using phosphoramidites of pyrenebutanol and their characterization by MALDI mass spectrometry. *Macromolecules* 29, 3060–3072.
- (47) Montaudo, G., Montaudo, M. S., Puglisi, C., and Samperi, F. (1995) Characterization of polymers by matrix-assisted laser desorption/ionization time-of-flight mass spectrometry: molecular weight estimates in samples of varying polydispersity. *Rapid Commun. Mass Spectrom.* 9, 453–460.
- (48) Zalipsky, S., Mullah, N., Harding, J. A., Gittelman, J., Guo, L., and DeFrees, S. A. (1997) Poly(ethylene glycol)-grafted liposomes with oligopeptide or oligosaccharide ligands appended to the termini of the polymer chains. *Bioconjugate Chem.* 8, 111–118.
- (49) Wu, K. J., and Odom, R. W. (1998) Characterizing synthetic polymers by MALDI MS. *Anal. Chem. News Features*, 456A–461A.
- (50) Barth, R. F., Adams, D. M., Soloway, A. H., Mechetner, E. B., Alam, F., and Anisuzzaman, A. K. (1991) Determination of boron in tissues and cells using direct-current plasma atomic emission spectroscopy. *Anal. Chem.* 63, 890–893.
- (51) Hwu, P., Yang, J. C., Cowherd, R., Treisman, J., Shafer, G. E., Eshhar, Z., and Rosenberg, S. A. (1995) In vivo antitumor activity of T cells redirected with chimeric antibody/T-cell receptor genes. *Cancer Res.* 55, 3369–3373.
- (52) Lee, R. J., and Low, P. S. (1994) Delivery of liposomes into cultured KB cells via folate receptor-mediated endocytosis. *J. Biol. Chem.* 269, 3198–3204.
- (53) Lee, R. J., and Low, P. S. (1995) Folate-mediated tumor cell targeting of liposome-entrapped doxorubicin in vitro. *Biochim. Biophys. Acta* 1233, 134–144.
- (54) Guo, W., Hinkle, G. H., and Lee, R. J. (1999)  $^{99m}\text{Tc}$ -HYNIC-folate: A novel receptor-based targeted radiopharmaceutical for tumor imaging. *J. Nucl. Med.* 40, 1563–1569.
- (55) Capala, J., Barth, R. F., Bendayan, M., Lauzon, M., Adams, D. M., Soloway, A. H., Fenstermaker, R. A., and Carlsson, J. (1996) Boronated epidermal growth factor as a potential targeting agent for boron neutron capture therapy of brain tumors. *Bioconjugate Chem.* 7, 7–15.
- (56) Tomalia, D. A., Naylor, A. M., and Goddard, W. A., III (1990) Starburst dendrimers: Control of size, shape, surface chemistry, topology and flexibility in the conversion of atoms to macroscopic materials. *Angew. Chem., Int. Ed. Engl.* 102, 119–157.
- (57) Eastes, J. W., Aldridge, M. H., and Kamlet, M. J. (1969) Effects of *N*-alkylation and *N,N*-dialkylation on  $\text{pK}_a$  of anilinium and nitroanilinium ions. *J. Chem. Soc. B* 922–928.
- (58) Gabizon, A., Horowitz, A. T., Goren, D., Tzemach, D., Mandelbaum-Shavit, F., Qazen, M. M., and Zalipsky, S. (1999) Targeting folate receptor with folate linked to extremities of poly(ethylene glycol)-grafted liposomes: In vitro studies. *Bioconjugate Chem.* 10, 289–298.
- (59) Roberts, J. C., Bhalgat, M. K., and Zera, R. T. (1996) Preliminary biological evaluation of polyamidoamine (PAM-AM) starburst(TM) dendrimers. *J. Biomed. Mater. Res.* 30, 53–65.
- (60) Wilbur, D. S., Pathare, P. M., Hamlin, D. K., Buhler, K. R., and Vessella, R. L. (1998) Biotin reagents for antibody pretargeting. 3. Synthesis, radioiodination, and evaluation of biotinylated starburst dendrimers. *Bioconjugate Chem.* 9, 813–825.
- (61) Weitman, S. D., Lark, R. H., Coney, L. R., Fort, D. W., Frasca, V., Zurawski, V. R., Jr., and Kamen, B. A. (1992) Distribution of the folate receptor GP38 in normal and malignant cell lines and tissues. *Cancer Res.* 52, 3396–3401.
- (62) Malik, N., Wiwattanapatapee, R., Klopsch, R., Lorenz, K., Frey, H., Weener, J. W., Meijer, E. W., Paulus, W., and Duncan, R. (2000) Dendrimers: Relationship between structure and biocompatibility in vitro, and preliminary studies on the biodistribution of  $^{125}\text{I}$ -labeled polyamidoamine dendrimers in vivo. *J. Controlled Release* 65, 133–148.
- (63) Hristova, K., and Needham, D. (1995) Physical properties of polymer-grafted bilayers. *Stealth Liposomes* (D. Lasic, and M. Martin, Eds.) pp 35–49, CRC Press, Inc., Boca Raton.
- (64) MacIntosh, T. J., Kenworthy, A. K., and Needham, D. (1995) Measurement of the range and magnitude of the repulsive pressure between PEG-coated liposome. *Stealth Liposomes* (D. Lasic, and F. Martin, Eds.) pp 63–71, CRC Press, Inc., Boca Raton.
- (65) Torchilin, V. P., Papisov, M. I., Bogdanov, A. A., Trubetskoy, V. S., and Omelyanenev, V. G. (1995) Molecular mechanism of liposome and immunoliposome steric protection with poly (ethylene glycol): Theoretical and experimental proof of the role of polymer chain flexibility. *Stealth Liposomes* (D. Lasic, and F. Martin, Eds.) pp 51–62, CRC Press, Inc., Boca Raton.

BC0255860

## Modulation of the T Cell Response to $\beta$ -Lactoglobulin by Conjugation with Carboxymethyl Dextran

Kazuo Kobayashi, Tadashi Yoshida, Koji Takahashi, and Makoto Hattori\*

Department of Applied Biological Science, Faculty of Agriculture, Tokyo University of Agriculture and Technology, Tokyo, Japan. Received July 31, 2002; Revised Manuscript Received October 22, 2002

We have previously prepared  $\beta$ -lactoglobulin ( $\beta$ -LG)–carboxymethyl dextran (CMD) conjugates with water-soluble carbodiimide and achieved reduced immunogenicity of  $\beta$ -LG. In the present study, to elucidate the mechanism for the reduced immunogenicity of  $\beta$ -LG, we investigated changes in the T cell response to  $\beta$ -LG after conjugation with CMDs differing in molecular weight (about 40 and 162 kDa). Lymph node cells from BALB/c, C3H/He, and C57BL/6 mice that had been immunized with  $\beta$ -LG or the conjugates were stimulated with  $\beta$ -LG, and the *in vivo* T cell response was then evaluated by BrdU (5-bromo-2'-deoxyuridine) ELISA as the *ex vivo* proliferative response. T cells from the conjugate-immunized mice showed a lower proliferative response than those from the  $\beta$ -LG-immunized mice. T cell epitope scanning, using synthesized peptides, showed that the T cell epitope profiles of the conjugates were similar to those of  $\beta$ -LG, whereas the proliferative response to each epitope was reduced. These results indicate that the lower *in vivo* T cell response with the conjugates was not due to induction of conjugate-specific T cells, but due to a decrease in the number of  $\beta$ -LG-specific T cells. After the lymph node cells from  $\beta$ -LG-immunized mice had been stimulated with  $\beta$ -LG or the conjugates, the efficiency of the antigen presentation of the conjugate to  $\beta$ -LG-specific T cells was evaluated by BrdU ELISA as the *in vitro* proliferative response. The antigen presentation of  $\beta$ -LG to the T cells was reduced by conjugation with CMD. In addition, conjugation with CMD enhanced the resistance of  $\beta$ -LG to cathepsin B and cathepsin D, which suggest that conjugation with CMD inhibited the degradation of  $\beta$ -LG by proteases in APC and led to suppression of the generation of antigenic peptides including T cell epitopes from  $\beta$ -LG. It is therefore considered that the suppressive effect on the generation of T cell epitopes reduced the antigen presentation of the conjugates and that this reduction led to a decrease in the number of  $\beta$ -LG-specific T cells *in vivo*. As a result, the decreased help to B cells by T cells would have reduced the antibody response to  $\beta$ -LG. We conclude that suppression of the generation of T cell epitopes by conjugation with CMD is important to the mechanism for the reduced immunogenicity of  $\beta$ -LG.

### INTRODUCTION

Allergic reactions to food and dietary components have shown a tendency to increase in advanced countries, and food allergies have become an important human health problem. It has been reported that 12.6% of children in Japan had experienced an allergic reaction within 1 h after ingesting food and that the most common sources of food allergens involved were eggs (52.3% of food allergy cases), milk (31.8%), and seafoods (10.6%) (1). Although the fundamental therapy for food allergy is a food elimination diet, a prolonged period of food elimination affects a child's growth (1). In particular, milk is a basic food component that plays a predominant role in the first

years of life. The major allergen in cow's milk is  $\beta$ -lactoglobulin ( $\beta$ -LG), and about 82% of milk allergy patients are sensitive to this protein (2).  $\beta$ -LG, a major whey protein, is a globular protein of MW 18 400 consisting of 162 amino acids and possesses two disulfide bonds and one free cysteine (3). Although the physiological function of  $\beta$ -LG still remains unclear, it is tentatively considered to be the binding and transportation of small hydrophobic ligands such as retinol and fatty acids, and the protein is categorized as a member of the lipocalin superfamily (4).  $\beta$ -LG has a  $\beta$ -barrel structure (5, 6) which is a common feature among the lipocalins. This kind of molecule has high allergenic potential, and several allergens of animal origin belong to the lipocalin superfamily (7, 8).

In terms of food science,  $\beta$ -LG is considered to be a valuable protein because it has useful functional properties such as emulsifying, foaming and gelling properties (9–11), as well as a high content of essential amino acids (3). It is therefore desirable to develop new methods that would reduce the allergenicity of  $\beta$ -LG. Although attempts to reduce the allergenicity of proteins have been made by enzymatic digestion and denaturation (12–15), these methods destroy the physiological functions of the proteins and bring about problems with their taste. In contrast, protein conjugation is superior to other hypoallergenic methods in that it can simultaneously

\* Corresponding author. Address: Department of Applied Biological Science, Tokyo University of Agriculture and Technology, 3-5-8 Saiwai-cho, Fuchu-City, Tokyo 183-8509, Japan. Telephone: +81-42-367-5879. Fax: +81-42-360-8830. E-mail: makoto@cc.tuat.ac.jp.

<sup>1</sup> Abbreviations: APC, antigen-presenting cells;  $\beta$ -LG,  $\beta$ -lactoglobulin; BrdU, 5-bromo-2'-deoxyuridine; CD, circular dichroism; CMD, carboxymethyl dextran; EDC, 1-ethyl-3-(3-dimethylaminopropyl)carbodiimide; ELISA, enzyme-linked immunosorbent assay; mAb, monoclonal antibody; 2-ME, 2-mercaptoethanol; MHC, major histocompatibility complex; PAGE, polyacrylamide gel electrophoresis; PBS, phosphate-buffered saline; PEG, poly(ethylene glycol); SDS–PAGE, sodium dodecyl sulfate-polyacrylamide gel electrophoresis.

achieve improved functions (thermal stability, solubility, emulsifying ability, etc.) and low allergenicity and immunogenicity, while maintaining the physiological functions of proteins (16–20).

Many attempts to reduce the antigenicity and immunogenicity of proteins by conjugation methods have been made. Poly(ethylene glycol) (PEG) conjugates of recombinant IL-2 have been reported to elicit a 100–1000-fold lower level of antigen-specific IgG antibody production than recombinant IL-2 (21). High lipophilization of  $\beta$ -LG has been shown to be effective in reducing the production of anti- $\beta$ -LG IgG and IgE (22). Conjugates of monoclonal and polyclonal antibodies with oxidized dextrans of low molecular weight have been reported to have optimal immunoreactivity, in vivo pharmacokinetics, and tumor localization properties, as well as low immunogenicity in vivo (23). The conjugation of allergens with oligodeoxynucleotides having CpG sequences has been shown to suppress allergic responses (24, 25). However, the mechanism for the reduced antigenicity and immunogenicity of the proteins is still unclear despite such work.

Our objective in this study was to create hypoallergenic neoglycoconjugates of  $\beta$ -LG with high thermal stability and improved functional properties, while maintaining retinol-binding activity, and to elucidate the mechanism involved. We have achieved, in our previous studies (16–18, 26, 27), reduced immunogenicity, high thermal stability, improved emulsifying ability, and retained the retinol-binding activity, while maintaining an almost nativelike conformation, by conjugating  $\beta$ -LG with carboxymethyl dextran (CMD). We have shown that the molecular weight of the polysaccharides used as modifiers and the saccharide content in the conjugates affected the immunogenicity of  $\beta$ -LG and that one mechanism involved in the reduced immunogenicity of  $\beta$ -LG by conjugation with CMD was responsible for masking B cell epitopes by the saccharide chain from the results of B cell epitope scanning of  $\beta$ -LG and the conjugates (26, 27).

We investigated, in the present study, changes in the T cell response to  $\beta$ -LG after conjugation with CMD to further elucidate the mechanism. Antigens delivered from an extracellular source are processed by proteases within APC to create antigenic peptides including T cell epitopes and then presented on the APC surface by major histocompatibility complex (MHC) class II molecules for recognition by T cells (28). The T cells provide help to B cells through direct cell–cell interaction and secretion of cytokines that promote their proliferation and differentiation into antibody-producing cells (29). Thus, modulation of the T cell response by conjugation is considered to affect the immunogenicity of proteins. In particular, we focus on changes in the epitope profiles of  $\beta$ -LG after conjugation in elucidating the mechanism. Although the T cell epitope profiles of proteins, including  $\beta$ -LG (30–32), have been reported, there have been hardly any reports on the changes in epitope profiles of proteins after conjugation with saccharides. Epitope scanning of proteins after conjugation provides useful information such as the elimination of epitopes and generation of neo-epitopes. After preparing covalently bonded  $\beta$ -LG-CMD conjugates with CMDs of different molecular weight ( $M_r$  = about 40 and 162 kDa), we investigate the in vivo T cell response, T cell epitope profiles, antigen presentation to  $\beta$ -LG-specific T cells, and the susceptibility to cathepsin B and cathepsin D. Our data show that suppression of the generation of T cell epitopes by conjugation with CMD was involved in the mechanism for the reduced immunogenicity of  $\beta$ -LG.

## MATERIALS AND METHODS

**Materials.** Dextran T40 ( $M_r$  = about 40 kDa) and Dextran 162 ( $M_r$  = about 162 kDa) were purchased from Amersham Pharmacia Biotech (Buckinghamshire, U.K.) and Sigma Chemical Co. (St. Louis, MO), respectively. 1-Ethyl-3-(3-dimethylaminopropyl)carbodiimide (EDC) hydrochloride was purchased from Dojindo (Kumamoto, Japan).

**Carboxymethylation of Dextran.** Each dextran sample was carboxymethylated with monochloroacetic acid under alkaline conditions as previously described (16–18, 26). The carboxymethyl dextrans prepared from Dextran T40 and Dextran 162 are termed CMD 40 and CMD 162, respectively. The numbers of carboxyl groups attached to one molecule of dextran were determined by  $^1\text{H}$  NMR (400 MHz JEOL AL-400, Japan) to be 39 and 162, respectively, for CMD 40 and CMD 162.

**Preparation and Purification of  $\beta$ -LG.** Crude  $\beta$ -LG (genotype AA) was prepared from fresh milk of a Holstein cow according to the method of Armstrong et al. (33). Crude  $\beta$ -LG was purified with a DEAE-Sepharose Fast Flow column (3.0 ID  $\times$  40 cm; Amersham Pharmacia Biotech, Buckinghamshire, U.K.) by referring to the method described previously (16). The purity of  $\beta$ -LG was confirmed by polyacrylamide gel electrophoresis (PAGE), performed by the method of Davis (34).

**Preparation and Purification of the  $\beta$ -LG-CMD Conjugates.** The  $\beta$ -LG-CMD conjugates were prepared by using EDC as previously described (27). In brief,  $\beta$ -LG (1 g) and each CMD (CMD 40, 8.48 g; CMD 162, 9.375 g) in the molar ratio of amino groups of  $\beta$ -LG:carboxyl groups of CMD = 1:10 were dissolved in distilled water (125 mL), and the pH value of the solution was adjusted to 4.75 with 1 M HCl. An EDC solution (1.67 g/10 mL) in a molar ratio of amino groups of  $\beta$ -LG:EDC = 1:10 was added over a 30 min period, the pH value being maintained at 4.75 by adding 1 M HCl. The reaction mixture was incubated at 25 °C for 3 h before a 2 M acetate buffer at pH 5.5 (10 mL) was gradually added over a period of 10 min to stop the reaction. After dialyzing against distilled water at 4 °C and lyophilizing, the crude  $\beta$ -LG-CMD conjugates were obtained. These crude conjugates were purified by hydrophobic chromatography and anion-exchange chromatography as described previously (27). The conjugates prepared from CMD 40 and CMD 162 are termed Conj. 40 and Conj. 162, respectively. The amount of protein in each conjugate was determined by measuring the absorbance at 280 nm. The amount of CMD bound to  $\beta$ -LG was determined by measuring the absorbance at 490 nm after coloring by the phenol-sulfuric acid method (35).

**Immunization.** Female BALB/c, C3H/He, and C57BL/6 mice (Clea Japan, Tokyo, Japan) at 6 weeks of age (7–8 animals/group) were subcutaneously immunized in the hind footpads and base of the tail with  $\beta$ -LG or the conjugates (100  $\mu\text{g}$  as protein) emulsified in Freund's complete H37 Ra adjuvant (Difco Laboratories, Detroit, MI). After 7 days, the inguinal and popliteal lymph nodes were removed.

**T Cell Proliferation Assay and T Cell Epitope Scanning.** The T cell proliferation assay and T cell epitope scanning were performed in 96-well culture plates (Beckton Dickinson, Franklin Lakes, NJ) in 200  $\mu\text{L}$ /well of an RPMI1640 medium (Nissui Pharmaceutical, Tokyo, Japan) supplemented with 0.03% glutamine, 0.2%  $\text{NaHCO}_3$ , 2-mercaptoethanol (2-ME; 50  $\mu\text{M}$ ), penicillin (100 U/mL), streptomycin (100  $\mu\text{g}/\text{mL}$ ), and 1% autologous normal mouse serum. For T cell epitope scanning,



**Table 1. Immunological Properties of the  $\beta$ -LG-CMD Conjugates<sup>a</sup>**

mice	immunogenicity (%) <sup>b</sup> (anti- $\beta$ -LG antibody response)		novel immunogenicity (anti-conjugate antibody response)		B cell epitope distribution		antibody response to epitopes	
	Conj. 40	Conj. 162	Conj. 40	Conj. 162	Conj. 40	Conj. 162	Conj. 40	Conj. 162
BALB/c	54.2	39.5	not emerged		not changed		reduced (Conj. 40 < Conj. 162)	
C3H/He	54.0	44.0	not emerged		not changed		reduced (Conj. 40 < Conj. 162)	
C57BL/6	59.7	34.5	not emerged		not changed		reduced (Conj. 40 < Conj. 162)	

<sup>a</sup> This table summarized the data reported previously (27). <sup>b</sup>BALB/c, C3H/He, and C57BL/6 mice were immunized i.p. with  $\beta$ -LG, Conj. 40, or Conj. 162 emulsified in Freund's complete adjuvant and boosted 14 days later with the proteins emulsified in Freund's incomplete adjuvant. Seven days after secondary immunization, each antiserum was prepared. Immunogenicity was evaluated by ELISA using the antisera. Anti- $\beta$ -LG antibody response in the antisera prepared from the  $\beta$ -LG-immunized mice was as 100%, and that from conjugate-immunized mice was relatively calculated.

a series of overlapping 15-mer peptides moving one amino acid residue at a time in accordance with the amino acid sequence of  $\beta$ -LG were synthesized with a five-in-one B cell and T cell epitope scanning kit (Chiron Mimotopes, Clayton, Victoria, Australia) as described previously (26). The concentration of the synthesized peptides was approximately 1 nmol/ $\mu$ L from the results of an amino acid analysis. The lymph node cells were suspended at  $5 \times 10^5$  cells/well in the culture plates and then stimulated with protein ( $\beta$ -LG or the conjugates) at various concentrations, a synthesized peptide solution (10  $\mu$ L) or PBS (blank). Cultures were set up in triplicate for stimulation with the proteins, while one well for each peptide was tested for the peptide series. After culturing in a humidified atmosphere of 5% CO<sub>2</sub> in air for 3 days at 37 °C, the T cell proliferative response was measured with a BrdU proliferation kit (Roche Molecular Biochemicals, Basel, Switzerland). In short, the cells in the culture plates were pulsed with a 100  $\mu$ M BrdU solution (20  $\mu$ L/well) for 2 h under the same culture conditions. The culture plates were centrifuged at 1250 rpm for 10 min at 4 °C and the supernatant was removed, before the plates were dried for 1 h at 60 °C. A FixDenat solution (200  $\mu$ L) was added to each well, and the plates were incubated for 1 h at 25 °C. The FixDenat solution was removed, and peroxidase-labeled anti-BrdU mAb (100  $\mu$ L/well) that had been diluted 100-fold with the Antibody dilution solution was added, before the plates were incubated for 2 h at 25 °C. The peroxidase-labeled anti-BrdU mAb solution was removed, and each well was washed three times with PBS (200  $\mu$ L each). A tetramethylbenzidine solution (100  $\mu$ L/well) was added, and the plates were incubated for 5–10 min. After adding 1 M H<sub>2</sub>SO<sub>4</sub> (25  $\mu$ L/well) to stop the enzymatic reaction, the absorbance at 450 nm was measured with an MPR-A4i microplate reader (Tosoh, Tokyo, Japan).

The following criteria were used for the peptides adopted as positive in determining the T cell epitopes: (1) those which showed response greater than the mean value plus three times the standard deviation of the absorbance to the peptide (PLAQGGGGGGGGGG) in the absence of the  $\beta$ -LG sequence (31), (2) those which showed positive response to at least two consecutive overlapping peptides, and (3) those which showed reproducibility in two individual experiments (31). The common amino acid sequences among the peptides that fulfilled these criteria were identified as the epitopes according to the method of Gammon et al. (36).

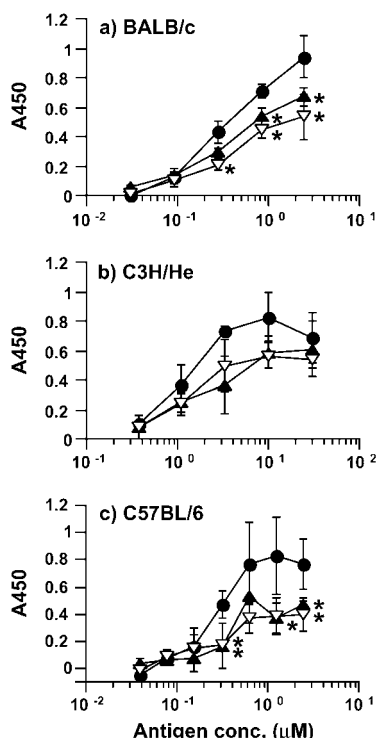
**Digestion of the  $\beta$ -LG-CMD Conjugates with Cathepsin B and Cathepsin D.**  $\beta$ -LG or each conjugate (0.1% (w/v) as the protein concentration) was dissolved in a 0.2 M citric acid/Na<sub>2</sub>HPO<sub>4</sub> buffer (pH 5.0) containing EDTA (1 mM) and 2% (v/v) 2-ME, and the solution was incubated at 37 °C for 12 h. Cathepsin B (EC 3.4.22.1) or cathepsin D (EC 3.4.23.5) from bovine spleen (Sigma

Chemical Co., St. Louis, MO) was added to the solution (enzyme:substrate = 1:10), and the mixture was incubated at 37 °C for various times. Digestion was stopped by adding the loading buffer for sodium dodecyl sulfate-polyacrylamide gel electrophoresis (SDS-PAGE) and by heating at 100 °C for 5 min. The digested sample was applied to SDS-PAGE (37), and the gel was stained with Coomassie Brilliant Blue R-250. After destaining, the digestibility of each sample was evaluated by densitometry.

## RESULTS AND DISCUSSION

To reduce the immunogenicity of  $\beta$ -LG by conjugation with polysaccharides and to elucidate the mechanism involved, we have previously prepared two  $\beta$ -LG-CMD conjugates (Conj. 40 and Conj. 162) by using EDC and investigated the immunological properties of each conjugate in BALB/c, C3H/He and C57BL/6 mice (27). We prepared conjugates having a similar saccharide content with CMDs of different molecular weight to evaluate the influence of the molecular weight of the polysaccharides on the immunological properties of the conjugates. The respective molar ratios of  $\beta$ -LG to CMD in the conjugates were 8:1 and 7:1 for Conj. 40 and Conj. 162. The immunological properties of the conjugates are shown in Table 1. In all the three strains of mice, the immunogenicity of  $\beta$ -LG (production of the  $\beta$ -LG-specific antibody) was reduced without inducing any novel immunogenicity (production of a conjugate-specific antibody) by conjugation with CMD. The reduced immunogenicity was more evident in the case of Conj. 162 than Conj. 40. To elucidate the mechanism for the reduced immunogenicity of  $\beta$ -LG, we investigated changes in the B cell epitope profiles of the conjugates by ELISA, using the overlapping 15-mer peptides synthesized on the basis of the amino acid sequence of  $\beta$ -LG (27). The linear B cell epitope profile of each conjugate was similar to that of  $\beta$ -LG in terms of the epitope distribution, whereas the antibody response to each epitope was reduced. The reducing effect was Conj. 40 < Conj. 162, so we concluded that masking of the B cell epitopes by the saccharide chain was responsible for reducing the immunogenicity of  $\beta$ -LG.

**In Vivo T Cell Response of the  $\beta$ -LG-CMD Conjugates.** Since T cells provide help to B cells through direct cell-cell interaction and secretion of cytokines that promote their proliferation and differentiation into antibody-producing cells (29), T cells are considered to play an important role in antibody response. To elucidate the mechanism for the reduced immunogenicity of  $\beta$ -LG by conjugation with CMD, we investigated the in vivo T cell response of each conjugate. After BALB/c, C3H/He, and C57BL/6 mice had been immunized with  $\beta$ -LG or the conjugates, the lymph node cells from the mice were



**Figure 1.** Proliferative response to  $\beta$ -LG of lymph node cells from mice immunized with  $\beta$ -LG or the  $\beta$ -LG-CMD conjugates. After immunizing BALB/c (a), C3H/He (b), and C57BL/6 (c) mice with  $\beta$ -LG (●), Conj. 40 (▲), or Conj. 162 (▽), the lymph node cells from the mice were removed and stimulated with  $\beta$ -LG at various concentrations. The magnitude of the in vivo T cell response was evaluated as the ex vivo proliferative response by BrdU ELISA. Each value is expressed as the mean absorbance at 450 nm and standard deviation of triplicate cultures after subtracting the background values (stimulated with PBS). Significant differences ( $p < 0.05$ ) between  $\beta$ -LG and each conjugate were determined by Student's  $t$ -test and are indicated by asterisks.

removed and then stimulated with  $\beta$ -LG at various concentrations. The magnitude of the in vivo T cell response was evaluated as the ex vivo proliferative response by BrdU ELISA (Figure 1). In BALB/c mice (Figure 1a), T cells from the groups immunized with the conjugates showed lower response than those from  $\beta$ -LG-immunized mice, this being particularly evident with Conj. 162. In C3H/He (Figure 1b) and C57BL/6 mice (Figure 1c), although the T cell proliferative responses of the Conj. 40- and Conj. 162-immunized groups were similar, the proliferative response of T cells from the conjugate-immunized groups was lower than that from the  $\beta$ -LG-immunized group. This result indicates that the response of the T cells to  $\beta$ -LG in the conjugate-immunized mice was reduced by conjugation with CMD. Two possibilities are considered as the reason for this result. (1) A decrease in the number of  $\beta$ -LG-specific T cells: since the induction of  $\beta$ -LG-specific T cells was suppressed by conjugation with CMD, the number of  $\beta$ -LG-specific T cells might have been reduced. (2) Changed T cell epitopes by conjugation: McCool et al. (38) have found that lymph node cells from mice immunized with a protein-polysaccharide conjugate recognized additional peptides that were not recognized by lymph node cells from mice immunized with the original protein. In our study, T cells in the conjugate-immunized mice might have shown the reduced response to  $\beta$ -LG owing to the induction of conjugate-specific T cells which could not recognize native  $\beta$ -LG by the generation of the

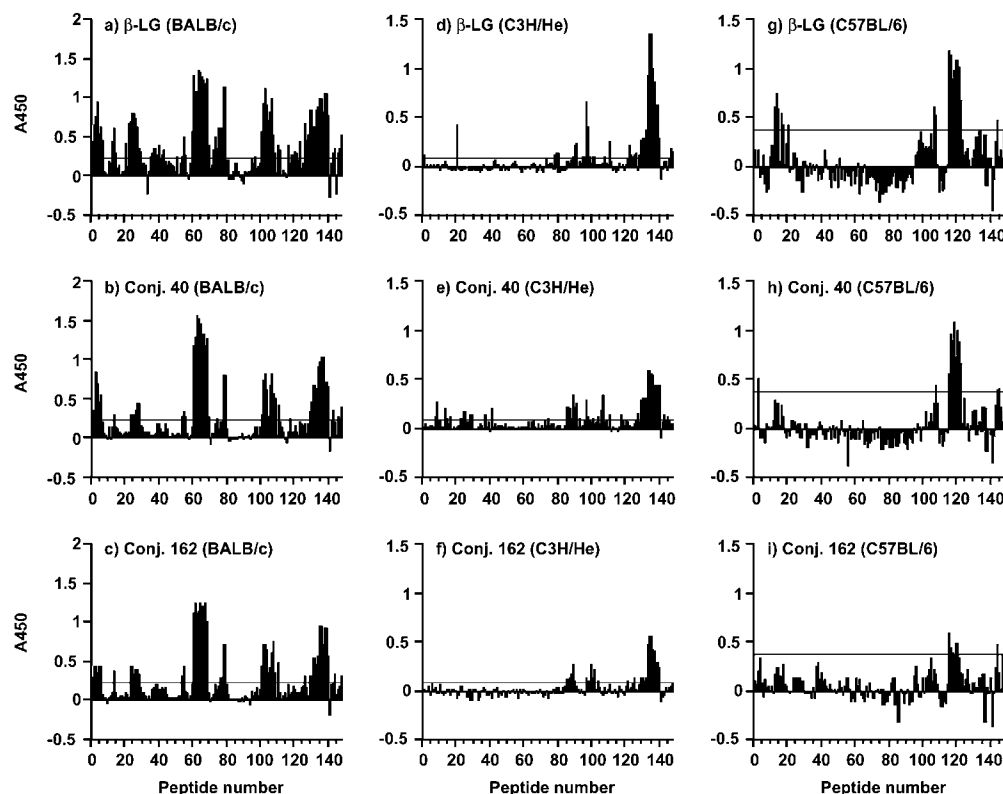
neo-epitopes that are not recognized by  $\beta$ -LG-specific T cells after conjugation with CMD.

**T Cell Epitope Profiles of the  $\beta$ -LG-CMD Conjugates.** Since the proliferative response of T cells to whole proteins is polyclonal, we next investigated in detail the T cell epitope profiles of the conjugates. After the lymph node cells from BALB/c, C3H/He, and C57BL/6 mice immunized with  $\beta$ -LG or the conjugates had been stimulated with the overlapping peptides synthesized on the basis of the sequence of  $\beta$ -LG, the T cell proliferative response to the peptides was measured by BrdU ELISA. Figure 2 shows the T cell epitope profiles of  $\beta$ -LG and the  $\beta$ -LG-CMD conjugates. The horizontal axis indicates the N-terminal amino acid residue number of each 15-mer peptide corresponding to the position in the  $\beta$ -LG sequence, and the vertical axis indicates the T cell proliferative response to each peptide. The T cell epitopes identified according to the method of Gammon et al. (36) are summarized in Figure 3, in which the horizontal axis indicates the sequence number in  $\beta$ -LG and the line thickness indicates the intensity of the response to each epitope.

The T cells from BALB/c mice immunized with  $\beta$ -LG showed proliferative response to peptides 1–7, 14–15, 23–29, 35–40, 42–43, 54–55, 60–70, 73–79, 101–109, 111–112, 119–122, 127–133, 133–140, 143–144, and 147–148 (Figure 2a). The T cell epitopes of  $\beta$ -LG that had been recognized in BALB/c mice were determined to be  $^{15}\text{Met}$ – $^{28}\text{Val}$ ,  $^{15}\text{Val}$ – $^{28}\text{Asp}$ ,  $^{29}\text{Ile}$ – $^{37}\text{Ala}$ ,  $^{40}\text{Arg}$ – $^{49}\text{Thr}$ ,  $^{43}\text{Val}$ – $^{56}\text{Ile}$ ,  $^{55}\text{Glu}$ – $^{68}\text{Gln}$ ,  $^{70}\text{Lys}$ – $^{74}\text{Glu}$ ,  $^{79}\text{Pro}$ – $^{87}\text{Leu}$ ,  $^{109}\text{Asn}$ – $^{115}\text{Gln}$ ,  $^{112}\text{Glu}$ – $^{125}\text{Thr}$ ,  $^{122}\text{Leu}$ – $^{133}\text{Leu}$ ,  $^{133}\text{Leu}$ – $^{141}\text{Lys}$ ,  $^{140}\text{Leu}$ – $^{147}\text{Ile}$ ,  $^{144}\text{Pro}$ – $^{157}\text{Glu}$  and  $^{148}\text{Arg}$ – $^{161}\text{His}$ , the dominant epitopes being  $^{70}\text{Lys}$ – $^{74}\text{Glu}$ ,  $^{109}\text{Asn}$ – $^{115}\text{Gln}$ , and  $^{140}\text{Leu}$ – $^{147}\text{Ile}$  (Figure 3). No changes in the epitope distribution was apparent for T cells from the conjugate-immunized BALB/c mice, but the proliferative response to the epitopes was lower throughout the entire amino acid sequence than that of the  $\beta$ -LG-immunized group (Figure 2a–c). The magnitude of the response to Conj. 162 was lower than that to Conj. 40. The T cell epitopes of the conjugates recognized in BALB/c mice were determined to be  $^{6}\text{Thr}$ – $^{15}\text{Val}$ ,  $^{25}\text{Ala}$ – $^{38}\text{Pro}$ ,  $^{28}\text{Asp}$ – $^{41}\text{Val}$ ,  $^{70}\text{Lys}$ – $^{75}\text{Lys}$ ,  $^{109}\text{Asn}$ – $^{115}\text{Gln}$ ,  $^{140}\text{Leu}$ – $^{144}\text{Pro}$  and  $^{148}\text{Arg}$ – $^{161}\text{His}$  for Conj. 40, and  $^{6}\text{Thr}$ – $^{15}\text{Val}$ ,  $^{28}\text{Asp}$ – $^{38}\text{Pro}$ ,  $^{69}\text{Lys}$ – $^{75}\text{Lys}$ ,  $^{109}\text{Asn}$ – $^{115}\text{Gln}$ , and  $^{140}\text{Leu}$ – $^{146}\text{His}$  for Conj. 162 (Figure 3).

The results obtained with the C3H/He and C57BL/6 mice are shown in Figure 2d–f, and the T cell epitope profiles of  $\beta$ -LG and the conjugates were determined as shown in Figure 3. The T cell epitopes of  $\beta$ -LG recognized in the C3H/He mice were determined to be  $^{91}\text{Lys}$ – $^{103}\text{Leu}$ ,  $^{99}\text{Tyr}$ – $^{111}\text{Ala}$ ,  $^{102}\text{Tyr}$ – $^{115}\text{Gln}$ ,  $^{125}\text{Thr}$ – $^{137}\text{Asp}$ ,  $^{137}\text{Asp}$ – $^{143}\text{Leu}$ , and  $^{148}\text{Arg}$ – $^{161}\text{His}$ , the dominant epitope being  $^{137}\text{Asp}$ – $^{143}\text{Leu}$  (Figure 3). In the C3H/He mice immunized with the conjugates, the epitope distribution of both conjugates was similar to that of  $\beta$ -LG, whereas the proliferative response to the epitopes was lower throughout the entire amino acid sequence than that of the  $\beta$ -LG-immunized group (Figure 2d–f). The signal intensity to the epitopes in the Conj. 162-immunized group was weaker than that in the Conj. 40-immunized group. The T cell epitopes of each conjugate recognized in C3H/He mice were determined to be  $^{91}\text{Lys}$ – $^{101}\text{Lys}$ ,  $^{98}\text{Asp}$ – $^{111}\text{Ala}$ ,  $^{119}\text{Cys}$ – $^{132}\text{Ala}$ ,  $^{137}\text{Asp}$ – $^{144}\text{Pro}$  and  $^{140}\text{Leu}$ – $^{151}\text{Phe}$  for Conj. 40, and  $^{90}\text{Asn}$ – $^{101}\text{Lys}$ ,  $^{101}\text{Lys}$ – $^{114}\text{Glu}$ ,  $^{131}\text{Glu}$ – $^{144}\text{Pro}$ , and  $^{139}\text{Ala}$ – $^{147}\text{Ile}$  for Conj. 162 (Figure 3).

The T cell epitopes of  $\beta$ -LG recognized in C57BL/6 mice were determined to be  $^{15}\text{Val}$ – $^{27}\text{Ser}$ ,  $^{108}\text{Glu}$ – $^{121}\text{Cys}$ , and  $^{123}\text{Val}$ – $^{130}\text{Asp}$ , the dominant epitope being  $^{123}\text{Val}$ –



**Figure 2.** Proliferation of the lymph node cells from mice immunized with  $\beta$ -LG or the  $\beta$ -LG-CMD conjugates to the overlapping 15-mer peptides covering the amino acid sequence of  $\beta$ -LG. After immunizing BALB/c (a–c), C3H/He (d–f), and C57BL/6 mice (g–i) with  $\beta$ -LG (a, d, g), Conj. 40 (b, e, h), or Conj. 162 (c, f, i), the lymph node cells from the mice were removed and stimulated with the overlapping synthesized peptides. The proliferative response of T cells to the peptides was measured by BrdU ELISA. The horizontal lines in the figures indicate cutoff values to judge whether the observed response was positive. Representative epitope profiles from two individual experiments are shown.

<sup>130</sup>Asp (Figure 3). No changes in the epitope distribution were apparent for the T cells from the conjugate-immunized C57BL/6 mice, but the proliferative response to the epitopes was lower throughout the entire amino acid sequence than that of the  $\beta$ -LG-immunized group (Figure 2g–i). The signal intensity to the epitopes in the Conj. 162-immunized group was weaker than that in the Conj. 40-immunized group. The T cell epitopes of the conjugates recognized in C57BL/6 mice were determined to be <sup>123</sup>Val–<sup>130</sup>Asp for Conj. 40 and <sup>118</sup>Val–<sup>30</sup>Asp and <sup>121</sup>Cys–<sup>134</sup>Glu for Conj. 162 (Figure 3).

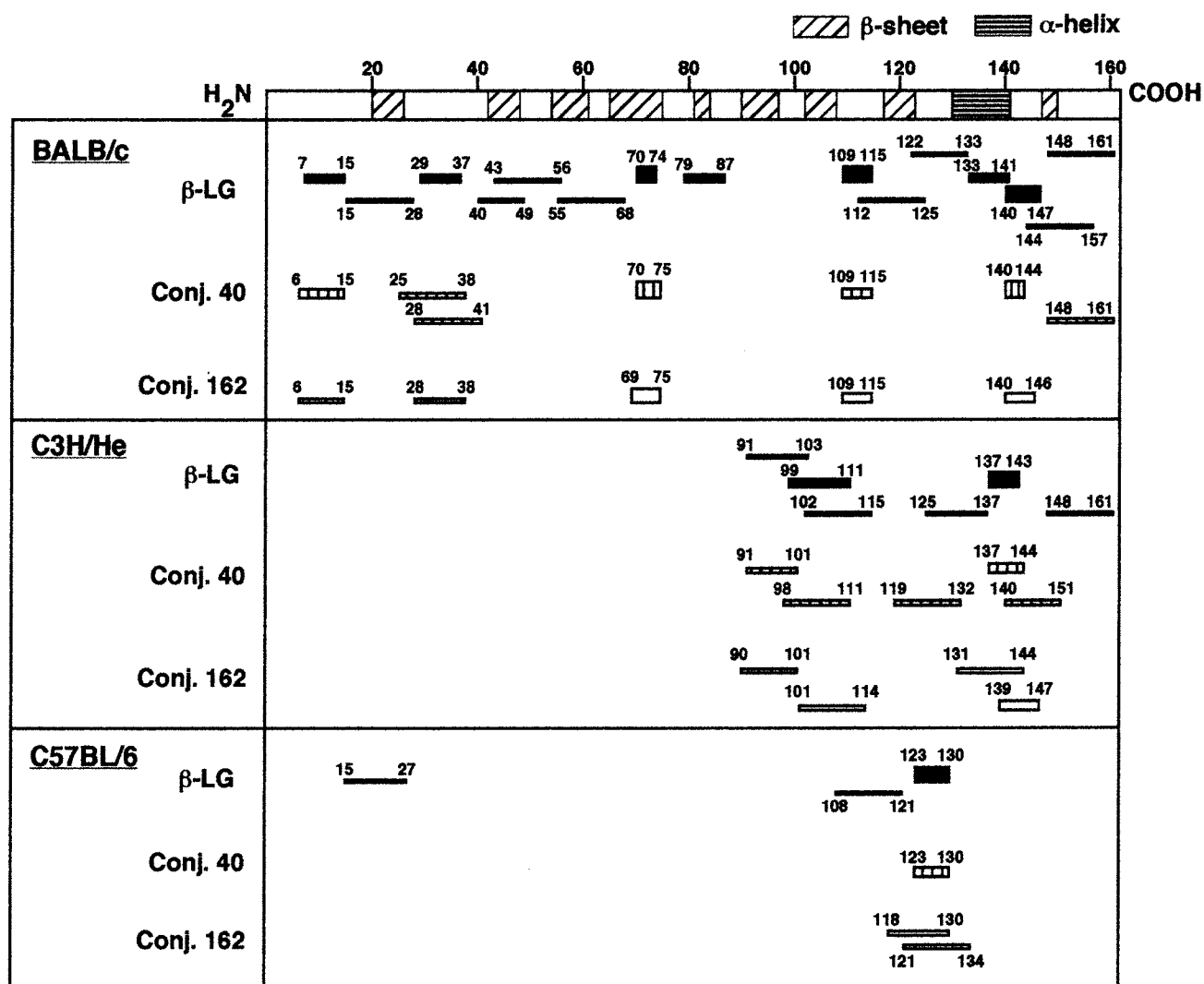
Totsuka et al. (31) have clarified the T cell epitope profiles of  $\beta$ -LG in BALB/c, C3H/He and C57BL/6 mice by a conventional <sup>3</sup>H-thymidine incorporation assay. Although some differences are apparent between our results and those of Totsuka et al. with respect to the signal intensity, the epitope distribution is similar. We have previously shown that the glycosylation sites in  $\beta$ -LG after conjugation with CMD of 10 kDa were <sup>47</sup>Lys, <sup>60</sup>Lys, <sup>101</sup>Lys, and <sup>138</sup>Lys (26). Other investigators (39–41) have reported that the preferential lactosylation sites of  $\beta$ -LG by the Maillard reaction were <sup>47</sup>Lys and/or <sup>100</sup>Lys. The conjugates prepared in this study tended to reduce the response to the epitope regions around these Lys residues. The human T cell epitopes of  $\beta$ -LG have recently been identified as <sup>1</sup>Leu–<sup>21</sup>Ser, <sup>14</sup>Lys–<sup>29</sup>Ile, <sup>30</sup>Ser–<sup>47</sup>Lys, <sup>47</sup>Lys–<sup>67</sup>Ala, <sup>77</sup>Lys–<sup>97</sup>Thr, <sup>97</sup>Thr–<sup>117</sup>Leu, and <sup>142</sup>Ala–<sup>162</sup>Ile by using synthesized peptides (32). Since most of these T cell epitopes are located in the vicinity of the plausible glycosylation sites just mentioned, the conjugates prepared in this study would modulate the T cell response in humans.

It has been reported that a protein–polysaccharide conjugate showed a different pattern of T cell reactivity

to epitopes derived from original protein (38); however, our results from the epitope scanning of Conj. 40 and Conj. 162 show that the T cell epitope profiles of the conjugates were similar to those of  $\beta$ -LG in all the strains of mice tested, which indicates that the location of epitopes recognized by T cells induced in vivo in the conjugate-immunized mice did not change by conjugation with CMD. In fact, when lymph node cells from the conjugate-immunized mice were stimulated with  $\beta$ -LG or the conjugates, the proliferative response to the conjugate was no higher than that to  $\beta$ -LG (data not shown). The signal intensity to the epitopes in the conjugate-immunized groups was lower than that in the  $\beta$ -LG-immunized group in the three strains of mice, indicating a decrease in the number of  $\beta$ -LG-specific T cells owing to the low induction of  $\beta$ -LG-specific T cells in vivo after conjugation with CMD. Therefore, the low in vivo T cell response in the conjugate-immunized groups, as shown in Figure 1, is considered to have been due to the lower number of  $\beta$ -LG-specific T cells induced in vivo by conjugation with CMD.

**Antigen Presentation of the  $\beta$ -LG-CMD Conjugates to  $\beta$ -LG-Specific T Cells.** To elucidate the mechanism for the decrease in number of  $\beta$ -LG-specific T cells in vivo by conjugation with CMD, we investigated antigen presentation of the conjugates to  $\beta$ -LG-specific T cells. After the three strains of mice had been immunized with  $\beta$ -LG, the lymph node cells were removed and stimulated with  $\beta$ -LG or the conjugates at various concentrations. The efficiency of the antigen presentation was evaluated as the in vitro T cell proliferative response by BrdU ELISA (Figure 4). In the BALB/c (Figure 4a) and C3H/He mice (Figure 4b), the proliferative response of the  $\beta$ -LG-specific T cells to Conj. 40 was similar to that



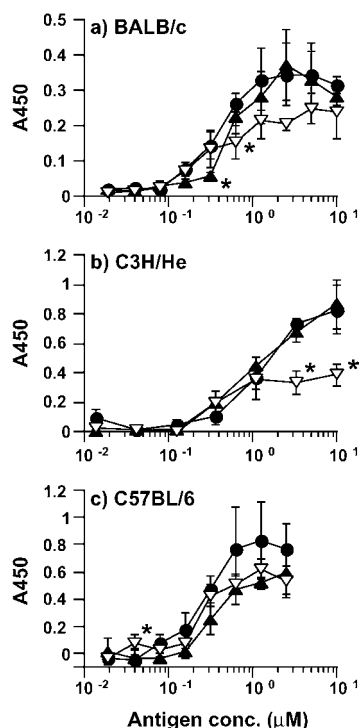


**Figure 3.** T cell epitope profiles of  $\beta$ -LG and the  $\beta$ -LG-CMD conjugates. The common regions of at least two overlapping peptides, which showed a response greater than the mean value plus three times the standard deviation of the absorbance when the lymph node cells were stimulated with the peptide (PLAQGGGGGGGGGG) in the absence of the  $\beta$ -LG sequence and which showed reproducibility in two individual experiments, were identified as epitopes according to the method of Gammon et al. (36).

to  $\beta$ -LG, whereas the response to Conj. 162 was lower than that to  $\beta$ -LG. In C57BL/6 mice (Figure 4c), Conj. 40 and Conj. 162 both showed lower T cell proliferative response than that to  $\beta$ -LG. CMD 40 and CMD 162 had no effect on the T cell proliferative response, even at a concentration of 10  $\mu$ M/well (data not shown). This lower T cell proliferative response indicates that the antigen presentation of  $\beta$ -LG to the  $\beta$ -LG-specific T cells was suppressed by the conjugation with CMD. In particular, the proliferative response of  $\beta$ -LG-specific T cells to Conj. 162 from CMD of the higher molecular weight was lower than that to  $\beta$ -LG in the three strains of mice. Hence, conjugation with CMD of high molecular weight is considered to be effective for suppression of the antigen presentation of  $\beta$ -LG which would lead to a decrease in the number of  $\beta$ -LG specific T cells in vivo.

**Susceptibility of the  $\beta$ -LG-CMD Conjugates to Cathepsin B and Cathepsin D.** Three possible mechanisms are considered plausible for suppressing the antigen presentation of  $\beta$ -LG to T cells by conjugation with CMD: (1) suppression of the generation of T cell epitopes, (2) inhibition of binding between MHC and the antigenic peptide, and (3) inhibition of MHC-peptide complex recognition by the T cell receptor. To examine the first possibility, we investigated the susceptibility of

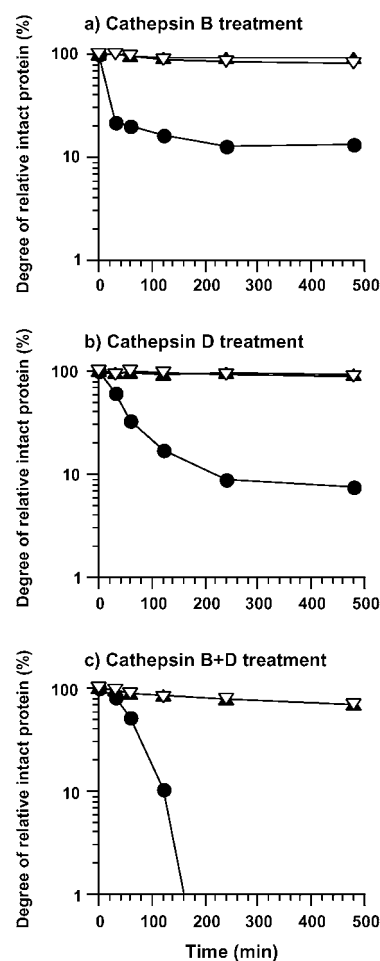
the conjugates to cathepsin B and cathepsin D, which are regarded as representative enzymes involved in the generation of antigenic epitopes (28). The processing of many antigens requires reduction of the disulfide bonds (28, 42) as well as proteolysis in APC, so the conjugates were digested with the cathepsins in the presence of 2-ME (Figure 5). About 90% of  $\beta$ -LG was digested with cathepsin B (Figure 5a) and cathepsin D (Figure 5b) after 8 h, whereas no more than 10% of the conjugates was digested. In respect of the endosomal protease involved in antigen processing, it has been suggested that the processing of most antigens occurs through the sequential action of more than one enzyme, that endoproteases including cathepsin D may be important in revealing and releasing antigens, and that exopeptidases including cathepsin B may trim epitopes to their final size (28, 43). Hence, the conjugates were digested with a mixture (1:1) of cathepsin B and cathepsin D (Figure 5c).  $\beta$ -LG was completely digested after about 2 h, whereas about 70% of each conjugate remained intact even after 8 h of digestion.  $\beta$ -LG was not digested when incubated for 8 h in the absence of the cathepsins (data not shown). In all experiments, both conjugates showed much higher resistance to the cathepsins than  $\beta$ -LG. These results indicate that conjugation with CMD inhibited the deg-



**Figure 4.** Proliferative response to  $\beta$ -LG and the  $\beta$ -LG-CMD conjugates of the lymph node cells from the mice immunized with  $\beta$ -LG. After immunizing BALB/c (a), C3H/He (b), and C57BL/6 (c) mice with  $\beta$ -LG, the lymph node cells from the mice were removed and stimulated with  $\beta$ -LG (●), Conj. 40 (▲), or Conj. 162 (▽) at various concentrations. The T cell proliferative response to the proteins was measured by BrdU ELISA. Each value is expressed as the mean absorbance at 450 nm and standard deviation of triplicate cultures after subtracting the background values (stimulated with PBS). Significant differences ( $p < 0.05$ ) between  $\beta$ -LG and each conjugate were determined by Student's  $t$ -test and are indicated by asterisks.

radiation of  $\beta$ -LG by proteases in APC and would have led to suppression of the generation of T cell epitopes from  $\beta$ -LG. It is considered that this suppressive effect on the generation of T cell epitopes by conjugation with CMD reduced the antigen presentation of the conjugates. This proposal is supported by the findings that the lysozyme stabilized by intramolecular cross-linking depressed T cell epitope generation by increasing the resistance to proteolysis (44) and that proteophosphoglycan, a major product secreted from *Leishmania mexicana* amastigotes, did not elicit a specific CD4<sup>+</sup> T cell response due to no degradation occurring in macrophages (45). The reduced antigen presentation of the conjugates would bring about a decrease in the number of  $\beta$ -LG-specific T cells in vivo and, as a result, the decreased help to B cells by T cells would reduce the antibody response to  $\beta$ -LG. Consequently, we conclude that suppression of the generation of T cell epitopes by conjugation with CMD played an important role in the mechanism for reducing the immunogenicity of  $\beta$ -LG. As for the other possibilities, the inhibition of binding between MHC and the antigenic peptide must be taken into consideration, because the plausible glycosylation sites already mentioned are located within some of the T cell epitopes identified in this study. In fact, T cell epitopes with internal but not external glycosylation did not bind MHC class II molecules and had less T cell proliferative response (46).

**Concluding Remarks.** We have shown in this study that the suppressive effect on the generation of T cell epitopes by conjugation with CMD played an important role in the mechanism for the reduced immunogenicity



**Figure 5.** Susceptibility of  $\beta$ -LG and the  $\beta$ -LG-CMD conjugates to cathepsin B and cathepsin D.  $\beta$ -LG (●), Conj. 40 (▲), and Conj. 162 (▽) were digested with cathepsin B (a), cathepsin D (b), and a mixture (1:1) of cathepsin B and cathepsin D (c) for various times in the presence of 2-ME. The digested samples were applied to SDS-PAGE, and the digestibility of the samples was evaluated by densitometry. The intensity of the bands of each sample at 0 min is taken as 100%, and that of the samples at subsequent times is relative to the value at 0 min. All results are expressed relative to the intact protein (%).

of  $\beta$ -LG. Our work is valuable in that we could clarify the change in the T cell epitope profile of a protein after conjugation with polysaccharides differing in molecular weight to elucidate the mechanism for the reduced immunogenicity. Taken together with our previous results (26, 27), both masking of the B cell epitopes by the saccharide chain and suppression of the generation of T cell epitopes in APC are considered to be important for the reduced immunogenicity of protein by conjugation with a polysaccharide. Both factors would be involved in the induction of a low IgE response by conjugation methods, and further studies focusing on these aspects should be carried out. We have particular interest in the change in qualitative T cell response to proteins after conjugation or modification (47–51). With regard to the difference in the molecular weight of CMD used as a modifier, although not all experiments showed a distinct difference between Conj. 40 and Conj. 162, the effect of Conj. 40 did not exceed that of Conj. 162. Conjugation with a polysaccharide of high molecular weight is therefore considered to be effective for modulating the T cell response to proteins. The results of the present study are essential to develop the design of novel hypoallergenic foods.

## ACKNOWLEDGMENT

This work was supported in part by grant from Asahi Breweries Foundation and Kyowa Hakko Kogyo Co. Ltd.

## LITERATURE CITED

- (1) Iikura, Y., Imai, Y., Imai, T., Akasawa, A., Fujita, K., Hoshiyama, K., Nakura, H., Kohno, Y., Koike, K., Okudaira, H., and Iwasaki, E. (1999) Frequency of immediate-type food allergy in children in Japan. *Int. Arch. Allergy Immunol.* **118**, 251–252.
- (2) Spies, J. (1973) Milk allergy. *J. Milk Food Technol.* **36**, 225–231.
- (3) McKenzie, H. A. (1971)  $\beta$ -Lactoglobulins. In *Milk Proteins: Chemistry and Molecular Biology* (H. A. McKenzie, Ed.) pp 257–330, Academic Press, New York.
- (4) Sawyer, L., and Kontopidis, G. (2000) The core lipocalin, bovine  $\beta$ -lactoglobulin. *Biochim. Biophys. Acta* **1482**, 136–148.
- (5) Papiz, M. Z., Sawyer, L., Eliopoulos, E. E., North, A. C. T., Findlay, J. B. C., Sivaprasadarao, R., Jones, T. A., Newcomer, M. E., and Kraulis, P. J. (1986) The structure of  $\beta$ -lactoglobulin and its similarity to plasma retinol-binding protein. *Nature* **324**, 383–385.
- (6) Brownlow, S., Cabral, J. H. M., Cooper, R., Flower, D. R., Yewdall, S. J., Polikarpov, I., North, A. C. T., and Sawyer, L. (1997) Bovine  $\beta$ -lactoglobulin at 1.8 Å resolution – still an enigmatic lipocalin. *Structure* **5**, 481–495.
- (7) Virtanen, T., Zeiler, T., Rautiainen, J., and Mäntyjärvi, R. (1999) Allergy to lipocalins: a consequence of misguided T-cell recognition of self- and nonself? *Immunol. Today* **20**, 398–400.
- (8) Wal, J. M. (1998) Cow's milk allergens. *Allergy* **53**, 1013–1022.
- (9) Shimizu, M., Saito, M., and Yamauchi, K. (1985) Emulsifying and structural properties of  $\beta$ -lactoglobulin at different pHs. *Agric. Biol. Chem.* **49**, 189–194.
- (10) Waniska, R. D., and Kinsella, J. E. (1988) Foaming and emulsifying properties of glycosylated  $\beta$ -lactoglobulin. *Food Hydrocolloids* **2**, 439–449.
- (11) Foegeding, E. A., Kuhn, P. R., and Hardin, C. C. (1992) Specific divalent cation-induced changes during gelation of  $\beta$ -lactoglobulin. *J. Agric. Food Chem.* **40**, 2092–2097.
- (12) Ishizaka, K., Okudaira, H., and King, T. (1975) Immunogenic properties of modified antigen E. II. Ability of urea-denatured antigen and a polypeptide chain to prime T cells specific for antigen C. *J. Immunol.* **114**, 110–115.
- (13) Kurisaki, J., Nakamura, S., Kaminogawa, S., and Yamauchi, K. (1982) The antigenic properties of  $\beta$ -lactoglobulin examined with mouse IgE antibody. *Agric. Biol. Chem.* **46**, 2069–2075.
- (14) Watanabe, M., Suzuki, T., Ikezawa, Z., and Arai, S. (1994) Controlled enzymatic treatment of wheat proteins for production of hypoallergenic flour. *Biosci. Biotechnol. Biochem.* **58**, 388–390.
- (15) del Val, G., Yee, B. C., Lozano, R. M., Buchanan, B. B., Ermel, R. W., Lee, Y. M., and Frick, O. L. (1999) Thioredoxin treatment increases digestibility and lowers allergenicity of milk. *J. Allergy Clin. Immunol.* **103**, 690–697.
- (16) Hattori, M., Nagasawa, K., Ametani, A., Kaminogawa, S., and Takahashi, K. (1994) Functional changes in  $\beta$ -lactoglobulin by conjugation with carboxymethyl dextran. *J. Agric. Food Chem.* **42**, 2120–2125.
- (17) Nagasawa, K., Takahashi, K., and Hattori, M. (1996) Improved emulsifying properties of  $\beta$ -lactoglobulin by conjugating with carboxymethyl dextran. *Food Hydrocolloids* **10**, 63–67.
- (18) Nagasawa, K., Ohgata, K., Takahashi, K., and Hattori, M. (1996) Role of the polysaccharide content and net charge on the emulsifying properties of  $\beta$ -lactoglobulin-carboxymethyl dextran conjugates. *J. Agric. Food Chem.* **44**, 2538–2543.
- (19) Hattori, M., Numamoto, K., Kobayashi, K., and Takahashi, K. (2000) Functional changes in  $\beta$ -lactoglobulin by conjugation with cationic saccharides. *J. Agric. Food Chem.* **48**, 2050–2056.
- (20) Babiker, E. E., Azakami, H., Matsudomi, N., Iwata, H., Ogawa, T., Bando, N., and Kato, A. (1998) Effect of polysaccharide conjugation or transglutaminase treatment on the allergenicity and functional properties of soy protein. *J. Agric. Food Chem.* **46**, 866–871.
- (21) Katre, N. (1990) Immunogenicity of recombinant IL-2 modified by covalent attachment of polyethylene glycol. *J. Immunol.* **144**, 209–213.
- (22) Akita, E. M., and Nakai, S. (1990) Lipophilization of  $\beta$ -lactoglobulin: Effect on allergenicity and digestibility. *J. Food Sci.* **55**, 718–723.
- (23) Fagnani, R., Hagan, M. S., and Bartholomew, R. (1990) Reduction of immunogenicity by covalent modification of murine and rabbit immunoglobulins with oxidized dextrans of low molecular weight. *Cancer Res.* **50**, 3638–3645.
- (24) Shirota, H., Sano, K., Kikuchi, T., Tamura, G., and Shirato, K. (2000) Regulation of murine airway eosinophilia and Th2 cells by antigen-conjugated CpG oligodeoxynucleotides as a novel antigen-specific immunomodulator. *J. Immunol.* **164**, 5575–5582.
- (25) Tighe, H., Takabayashi, K., Schwartz, D., Nest, G. V., Tuck, S., Eiden, J. J., Kagey-Sobotka, A., Creticos, P. S., Lichtenstein, L. M., Spiegelberg, H. L., and Raz, E. (2000) Conjugation of immunostimulatory DNA to the short ragweed allergen Amb a 1 enhances its immunogenicity and reduces its allergenicity. *J. Allergy Clin. Immunol.* **106**, 124–134.
- (26) Hattori, M., Nagasawa, K., Ohgata, K., Sone, N., Fukuda, A., Matsuda, H., and Takahashi, K. (2000) Reduced immunogenicity of  $\beta$ -lactoglobulin by conjugation with carboxymethyl dextran. *Bioconjugate Chem.* **11**, 84–93.
- (27) Kobayashi, K., Hirano, A., Ohta, A., Yoshida, T., Takahashi, K., and Hattori, M. (2001) Reduced immunogenicity of  $\beta$ -lactoglobulin by conjugation with carboxymethyl dextran differing in molecular weight. *J. Agric. Food Chem.* **49**, 823–831.
- (28) Fineschi, B., and Miller, J. (1997) Endosomal proteases and antigen processing. *Trends Biochem. Sci.* **22**, 377–382.
- (29) Kaminogawa, S. (1996) Food Allergy, oral tolerance and immunomodulation – Their molecular and cellular mechanisms. *Biosci. Biotechnol. Biochem.* **60**, 1749–1756.
- (30) Tsuji, N. M., Kurisaki, J., Mizumachi, K., and Kaminogawa, S. (1993) Localization of T-cell determinants on bovine  $\beta$ -lactoglobulin. *Immunol. Lett.* **37**, 215–221.
- (31) Totsuka, M., Ametani, A., and Kaminogawa, S. (1997) Fine mapping of T-cell determinants of bovine  $\beta$ -lactoglobulin. *Cytotechnology* **25**, 101–113.
- (32) Inoue, R., Matsushita, S., Kaneko, H., Shinoda, S., Sakaguchi, H., Nishimura, Y., and Kondo, N. (2001) Identification of  $\beta$ -lactoglobulin-derived peptides and class II HLA molecules recognized by T cells from patients with milk allergy. *Clin. Exp. Allergy* **31**, 1126–1134.
- (33) Armstrong, J. M., McKenzie, H. A., and Sawyer, W. H. (1967) On the fractionation of  $\beta$ -lactoglobulin and  $\alpha$ -lactalbumin. *Biochim. Biophys. Acta* **147**, 60–72.
- (34) Davis, B. J. (1964) DISC ELECTROPHORESIS – II: Method and application to human serum proteins. *Ann. N.Y. Acad. Sci.* **121**, 404–427.
- (35) Dubois, M., Gilles, K. A., Hamilton, J. L., Rebers, P. A., and Smith, F. (1956) Colorimetric method for determination of sugars and related substances. *Anal. Chem.* **28**, 350–356.
- (36) Gammon, G., Geysen, H. M., Apple, R. J., Pickett, E., Palmer, M., Ametani, A., and Sercarz, E. E. (1991) T cell determinant structure: cores and determinant envelopes in three mouse major histocompatibility complex haplotypes. *J. Exp. Med.* **173**, 609–617.
- (37) Laemmli, U. K. (1970) Cleavage of structural proteins during the assembly of the head of bacteriophage T4. *Nature* **227**, 680–685.
- (38) McCool, T. L., Harding, C. V., Greenspan, N. S., and Schreiber, J. R. (1999) B- and T-cell immune response to pneumococcal conjugate vaccines: Divergence between carrier- and polysaccharide-specific immunogenicity. *Infect. Immun.* **67**, 4862–4869.
- (39) Leonil, J., Molle, D., Fauquant, J., Maubois, J. L., Pearce, R. J., and Bouhallab, S. (1997) Characterization by ionization mass spectrometry of lactosyl  $\beta$ -lactoglobulin conjugates



- formed during heat treatment of milk and whey and identification of one lactose-binding site. *J. Dairy Sci.* 80, 2270–2281.
- (40) Fogliano, V., Monti, S. M., Visconti, A., Randazzo, G., Facchiano, A. M., Colonna, G., and Ritieni, A. (1998) Identification of a  $\beta$ -lactoglobulin lactosylation site. *Biochim. Biophys. Acta* 1388, 295–304.
- (41) Siciliano, R., Rega, B., Amoresano, A., and Pucci, P. (2000) Modern mass spectrometric methodologies in monitoring milk quality. *Anal. Chem.* 72, 408–415.
- (42) Collins, D. S., Unanue, E. R., and Harding, C. V. (1991) Reduction of disulfide bonds within lysosomes is a key step in antigen processing. *J. Immunol.* 147, 4054–4059.
- (43) Riese, R. J., and Chapman, H. A. (2000) Cathepsins and compartmentalization in antigen presentation. *Curr. Opin. Immunol.* 12, 107–113.
- (44) So, T., Ito, H.-O., Koga, T., Watanabe, S., Ueda, T., and Imoto, T. (1997) Depression of T-cell epitope generation by stabilizing hen lysozyme. *J. Biol. Chem.* 272, 32136–32140.
- (45) Aebischer, T., Harbecke, D., and Ilg, T. (1999) Proteophosphoglycan, a major secreted product of intracellular *Leishmania mexicana* amastigotes, is a poor B-cell antigen and does not elicit a specific conventional CD4<sup>+</sup> T-cell response. *Infect. Immun.* 67, 5379–5385.
- (46) Mouritsen, S., Meldal, M., Christiansen-Brams, I., Elsner, H., and Werdelin, O. (1994) Attachment of oligosaccharides to peptide antigen profoundly affects binding to major histocompatibility complex class II molecules and peptide immunogenicity. *Eur. J. Immunol.* 24, 1066–1072.
- (47) Yang, X., Gieni, R. S., Mosmann, T. R., and HayGlass, K. T. (1993) Chemically modified antigen preferentially elicits induction of Th1-like cytokine synthesis patterns in vivo. *J. Exp. Med.* 178, 349–353.
- (48) Kohno, K., Ohtsuki, T., Suemoto, Y., Inoue, T., Taniguchi, Y., Usui, M., Ikeda, M., and Kurimoto, M. (1996) Regulation of cytokine production by sugi allergen-pullulan conjugate. *Cell. Immunol.* 168, 211–219.
- (49) Singh, N., Bhatia, S., Abraham, R., Basu, S. K., George, A., Bal, V., and Rath, S. (1998) Modulation of T cell cytokine profiles and peptide-MHC complex availability in vivo by delivery to scavenger receptors via antigen maleylation. *J. Immunol.* 160, 4869–4880.
- (50) Korematsu, S., Tanaka, Y., Hosoi, S., Koyanagi, S., Yokota, T., Mikami, B., and Minato, N. (2000) C8/119S mutation of major mite allergen Derf-2 leads to degenerate secondary structure and molecular polymerization and induces potent and exclusive Th1 cell differentiation. *J. Immunol.* 165, 2895–2902.
- (51) So, T., Ito, H.-O., Hirata, M., Ueda, T., and Imoto, T. (2001) Contribution of conformational stability of hen lysozyme to induction of type 2 T-helper immune responses. *Immunology* 104, 259–268.

BC0200500

# Lactose-Installed Poly(ethylene glycol)–Poly(D,L-lactide) Block Copolymer Micelles Exhibit Fast-Rate Binding and High Affinity toward a Protein Bed Simulating a Cell Surface. A Surface Plasmon Resonance Study

Eduardo Jule,<sup>†,§</sup> Yukio Nagasaki,<sup>‡</sup> and Kazunori Kataoka<sup>\*,†</sup>

Department of Materials Science and Engineering, Graduate School of Engineering, The University of Tokyo, 7–3–1 Hongo, Bunkyo-ku, Tokyo 113-8656, Japan, and Department of Materials Science, Science University of Tokyo, 2641 Yamazaki, Noda, Chiba 278-8510, Japan. Received August 26, 2002; Revised Manuscript Received October 15, 2002

Lactose molecules were installed on the surface of poly(ethylene glycol)–poly(D,L-lactide) (PEG–PLA) block copolymer micelles in the scope of seeking specific recognition by cell surface receptors at hepatic sites. This, in turn, is expected to result in the formation of a complex displaying prolonged retention times and thus enhanced cellular internalization by receptor-mediated endocytosis. The so-obtained particles based on a block copolymer of molecular weight 9400 g/mol (4900/4500 g/mol for the PEG and PLA blocks, respectively) were found to have an average hydrodynamic diameter of 31.8 nm, as measured by dynamic light scattering. Further, the particle size distribution ( $\mu_2/\bar{\Gamma}^2$ ) was found to be lower than 0.08. Lactose–PEG–PLA micelles (Lac-micelles) were then injected over a gold surface containing *Ricinus communis* agglutinin lectins simulating the aforementioned glycoreceptors, and their interaction was studied by surface plasmon resonance. Then, a kinetic evaluation was carried out, by fitting the observed data mathematically. It appears that Lac-micelles bind in a multivalent manner to the lectin protein bed, which logically results in low dissociation constants. Micelles bearing a ligand density of 80% (Lac-micelles 80%: 80 lactose molecules per 100 copolymer chains) exhibit fast association phases ( $k_{a1} = 3.2 \times 10^4 \text{ M}^{-1} \text{ s}^{-1}$ ), but also extremely slow dissociation phases ( $k_{d1} = 1.3 \times 10^{-4} \text{ s}^{-1}$ ). Recorded sensorgrams were fitted with a trivalent model, conveying a calculated equilibrium dissociation constant ( $K_{D1} = k_{d1}/k_{a1}$ ) of about 4 nM. The importance of cooperative binding was also assessed, by preparing Lac-micelles bearing different ligand densities, and by discussing the influence of the latter on kinetic constants. Interestingly enough, whereas Lac-micelles 80% bind in a trivalent manner to the protein bed, Lac-micelles 20% are still capable of forming bivalent complexes with the same protein bed ( $K_{D1} = 1360 \text{ nM}$ ). Therefore, despite enhanced kinetic values brought about by a supplementary bond, lower ligand densities appear to be more effective on a molecular basis.

## 1. INTRODUCTION

Combining the properties of colloidal particles such as liposomes or polymeric micelles with those of certain biomolecules such as antibodies, peptides, or carbohydrates can bring about a new array of properties to the bioconjugates. This, in turn, can be exploited in fields not applicable to each of the separate species. For quite some time now, it has been acknowledged that carbohydrates and proteins play a fundamental role in cellular processes such as growth, recognition, and inflammation (1), so that extensive research has focused on the design of carbohydrate analogues, for example to target receptors such as the asialoglycoprotein receptor at hepatic sites (2). Yet, these efforts are undermined by the intrinsic low affinity of carbohydrates toward proteins such as lectins, which of course presents only limited interest for the design of drug delivery systems. Multivalency is known to greatly

enhance kinetic values, and starlike particles greatly enhance binding constants (3). Much in the same manner, colloidal particles bearing an important ligand density on their surface could be expected to enhance such parameters and demonstrate interesting properties from the standpoint of cellular uptake by receptor-mediated endocytosis (RME).

Macromolecular assemblies such as polymeric micelles are promising systems, as they can ensure the actual transport and delivery of a wide variety of compounds (4–6). Indeed, block copolymers bearing blocks of dissimilar natures, i.e., a hydrophilic and a hydrophobic block, are known to spontaneously associate into colloidal particles. Micelles have thus a hydrophobic inner core surrounded by an external hydrophilic corona, a unique feature that permits the entrapment of compounds otherwise poorly soluble in body fluids such as the bloodstream. Micelles based on acetal-poly(ethylene glycol)–poly(D,L-lactide) (Ac-PEG–PLA) block copolymers meet these stipulations, forming particles in the tens-of-nanometers scale, a good compromise for avoiding urinary excretion while escaping recognition by reticuloendothelial systems (6). Aside from this, cellular surface receptors could be targeted by bioconjugates such as Ac-

\* To whom correspondence should be addressed. Telephone: +81.3.5841.7145. Fax: +81.3.5841.7139. E-mail: kataoka@bmw.t.u-tokyo.ac.jp.

<sup>†</sup> The University of Tokyo.

<sup>‡</sup> Science University of Tokyo.

<sup>§</sup> Coauthor e-mail address: eduardo@bmw.mm.t.u-tokyo.ac.jp.

PEG-PLA micelles bearing a specific ligand on their surface. Indeed, the acetal end of the PEG block can be deprotected into an aldehyde reactive group through which surface formulation of micelles can be achieved, as previously reported (7, 8). Whereas charged peptides have been shown to regulate the uptake of particles in the liver and spleen (9), carbohydrates are expected to form a complex with the receptor protein in a highly specific manner, displaying selective accumulation at target cells. The affinity of complex formation shall be well characterized, then, if one is to optimize the uptake by RME (10). Another factor that appears to be critical in the design of multivalent devices is the ligand density, or the amount of ligands to be displayed to targeted receptors. As shall be explained herein, lactose-bearing PEG-PLA micelles (Lac-micelles) appear to be an interesting model for a detailed study on this matter, since what will be referred to as the lactose functionality or density can be controlled in a facile way.

*Ricinus communis* agglutinin (RCA) lectins were thus immobilized on a gold surface plasmon resonance (SPR) surface, to simulate asialoglycoprotein receptors on the surface of hepatocytes whereas Lac-micelles were injected in order to evaluate their interaction. A kinetic evaluation was carried out, to further characterize in a more qualitative manner what has previously been reported (11). The interaction was found to be highly specific and of many orders superior to that of micelles bearing no such ligand, rendering the former of obvious therapeutic interest. As shall be exposed herein, Lac-micelles exhibit fast-rate binding kinetics to the protein bed, whereas the ligand density on their surface results in multivalent binding to the protein bed, which in turn yields diminished kinetic dissociation and thus lowered equilibrium dissociation constants. Furthermore, micelles bearing different ligand densities were analyzed so that the influence of multivalency on kinetic values is also discussed. An innovative technique, SPR, demonstrates the perspective of recording responses in real time, so that kinetic assays can readily be conducted, if one is to set aside the inherent difficulty of controlling mass transport phenomena which heavily compromise such evaluations.

## 2. EXPERIMENTAL SECTION

**2.1. Materials and Methods.** Commercial tetrahydrofuran (THF), 3,3'-diethoxypropanol (DEP), and ethylene oxide (EO) were purified by conventional distillations under argon atmosphere. Commercial D,L-lactide (LA) was recrystallized from ethyl acetate twice, under argon atmosphere, and sublimated under vacuum at 110 °C. Potassium naphthalene was used in a THF solution, the concentration of which was determined by an appropriate titration. *Ricinus communis* agglutinin (RCA-I) lectins (Funakoshi Corporation, Japan) were used as received. Water was purified with a Milli-Q instrument (Millipore, Bedford, MA).

Gel permeation chromatography (GPC) measurements of the prepared polymers were conducted using a JASCO liquid chromatograph equipped with TSK gel columns (G4000H<sub>HR</sub> and G3000H<sub>HR</sub>) and an internal refractive index (RI) detector (930-R1, JASCO, Japan). Dimethyl formamide (DMF) containing 10 mM LiBr was used as eluent at a flow rate of 0.8 mL/min. Molecular weight calibrations were done using a series of standard PEGs (Polymer Laboratories, UK). Samples dissolved in the eluent at a concentration of 2 mg/mL were injected into the GPC circuit through a 100  $\mu$ L loop. The <sup>1</sup>H NMR spectra of polymer samples were established at 80 °C in

DMSO-*d*<sub>6</sub> or at 25 °C in CDCl<sub>3</sub>-*d* with a JEOL GSX-270 spectrometer at 270 MHz.

**2.2. Preparation and Characterization of Block Copolymers.** The Ac-PEG-PLA block copolymer was synthesized via an anionic ring-opening polymerization at room temperature under argon atmosphere. The typical procedure is described hereafter: 0.16 mL (1 mmol) of DEP and 3.2 mL (1 mmol) of a 0.31 M naphthalene potassium solution in THF were introduced in a flask containing 20 mL of dry THF and stirred for 10 min. A 5.7 mL (114 mmol) volume of EO was then added and polymerized for 2.5 days. After sampling a small volume of the solution for GPC analysis, 46 mL (40 mmol) of a LA solution in THF (0.88 mol/L) was introduced in the medium, and the polymerization was allowed to proceed for 4 h. The polymer was then precipitated into a 50-fold excess of ice-cooled isopropyl alcohol (IPA) and then centrifuged at 8000g for 30 min. The polymer was then freeze-dried from benzene, affording white flakes in a yield of 90%. The sample was stored at -20 °C until use.

The molecular weight of the PEG segment was determined by GPC using the fraction sampled at the end of the first stage of the copolymerization. Given that interference of the block copolymers with the GPC separating columns, often yielding apparent lower molecular weights, has been observed, the size of the PLA block was calculated based on the molecular weight of the PEG block as obtained by GPC and the NMR spectrum of the block copolymer. Therefore, it is possible to correlate the number average molecular weight (*M<sub>n</sub>*) of the PEG block and the intensity ratio of methine protons on the PLA block (COCH(CH<sub>3</sub>)O:  $\delta$  = 5.2 ppm) and methylene protons on the PEG block (OCH<sub>2</sub>CH<sub>2</sub>:  $\delta$  = 3.6 ppm).

**2.3. Preparation and Characterization of Micelles.** The Ac-PEG-PLA copolymer was dissolved in *N,N*-dimethylacetamide (DMAc), a good solvent of both the hydrophilic and hydrophobic blocks, in a 5 mg/mL solution. The solution was then filtered through a 0.2  $\mu$ m PTFE filter (Ekicrodisk, Japan) into a preswollen semi-permeable membrane (Spectra/Por, Spectrum, Rancho Dominguez, CA, molecular weight cutoff 3500) and dialyzed for 24 h against a 100-fold excess of distilled water. The dialysate was exchanged at times 2, 5, and 8 h. The micelles were eventually filtered through a 0.45  $\mu$ m PTFE filter (Millipore).

The hydrodynamic radius and the size distribution of micelles were determined by dynamic light scattering (DLS). The gyration radius and the apparent molecular weight of micelles were established by static light scattering (SLS). All measurements were carried out at 25 °C on a light scattering spectrophotometer (DLS-7000, Photol, Otsuka Electronics, Japan), and the scattering was carried out with a vertically polarized incident beam at 488 nm supplied by an argon ion laser. A scattering angle of 90° was used for the DLS evaluations, and the particle size distribution was estimated from the correlation function profile using the cumulant method (12).

SLS measurements of a colloidal dispersion yield values for *K<sub>c</sub>/R<sub>90</sub>* that can be used to determine the apparent molecular weight of the particles (13). A plot of this value against the particle concentration is known as a Debye plot and can be analyzed with the equation:

$$Kc/R_{90} = 1/M_w + A_2c + \dots$$

where *K* is a constant, given for vertically polarized light by the expression  $7\pi n_0^2(N_A^2\lambda^4)^{-1}(dn/dc)^2$ , for which *n*<sub>0</sub> is



the solvent refractive index;  $N_a$ , Avogadro's number,  $\lambda$  the wavelength of the scattered light, and  $dn/dc$  the gradient in the refractive index against the sample concentration  $c$ .  $R_\theta$  is the experimentally measured excess Rayleigh ratio,  $\theta$  is the scattering angle,  $M_w$  is the apparent molecular weight of the particle, and  $A_2$  is the second virial coefficient. A series of polymer solutions, ranging from 0.5 mg/mL to 4 mg/mL (0.5, 1, 2, 3, and 4) were thus scattered at angles spanning from 30° to 135° (30, 45, 60, 75, 90, 105, 120, and 135). Deionized water and benzene were used as references for the scattering and refractive index gradient evaluations, respectively.

The increment of the refractive index ( $dn/dc$ ) of the polymer solutions was evaluated using a DRM-120 double-beam differential refractometer (Otsuka Electronics Co., Ltd., Osaka, Japan).

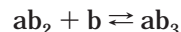
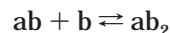
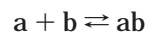
**2.4. Sugar Installation on the Surface of the Micelles.** Deprotection of the acetal functions at the PEG block end was conducted by mild acidification of the corresponding Ac-PEG-PLA micellar solution to pH 2, using a 0.1 M HCl solution. The solution was stirred for 2 h before being brought back to the initial pH of micelles (pH 5) with a 0.1 M NaOH solution. At this stage, a small volume was sampled in order to evaluate the aldehyde functionality. The system was then concentrated to 4 mg/mL and placed in a phosphate buffer saline (PBS, pH 7.4;  $I = 0.1$  M) before introducing a 10-fold molar excess of *p*-aminophenyl- $\beta$ -D-lactopyranoside, the amine terminal group of which forms a Schiff base with the aldehyde groups previously obtained by deprotection of the acetal groups. After another hour of stirring, the Schiff base was reduced to a secondary amine using a 10-fold molar excess of  $\text{NaH}_3\text{BCN}$ , and the system was stirred for another 96 h. Unreacted species were removed by dialysis on a preswollen membrane (Spectra/Por, Spectrum, molecular weight cutoff 1000). Micelles were eventually filtered through a 0.45  $\mu\text{m}$  PTFE filter (Millipore). The polymer was once more freeze-dried and stored at  $-20^\circ\text{C}$  until use.

The sugar functionality, defined as the number of sugar ends bound at the end of the PEG block per 100 polymer chains, was determined by NMR measurements of the freeze-dried polymer in  $\text{DMSO}-d_6$  at  $80^\circ\text{C}$ . The intensity of the methine peaks on the phenyl groups of the lactopyranoside at 6.4 and 6.8 ppm was then related to the intensity of the methine peak on the PLA block ( $\delta = 5.2$  ppm).

**2.5. Surface Plasmon Resonance Measurements.** Surface plasmon resonance (SPR) evaluations were carried out on a BIACORE 3000 device (Biacore AB, Uppsala, Sweden). Proteins were bound to the carboxymethyl dextran gel on the surface of a CM5 chip by amine coupling. Both the ends of the gel matrix and the protein to be bound on the gel were electrostatically activated by flowing a buffer at a pH lower than the pI of the protein (acetate buffer pH 5,  $I = 0.01$  M) as a preparation for the chemical binding of the proteins. Then, 70  $\mu\text{L}$  of a freshly prepared 1:1 mixture of 0.2 M *N*-ethyl-*N*-(3-dimethylaminopropyl)carbodiimide hydrochloride (EDC) and 0.05 M *N*-hydroxysuccinimide (NHS) was injected, chemically activating the surface of the gel. This was followed by the injection of a 50  $\mu\text{g/mL}$  RCA-I solution, the volume of which depended on the amount of bound proteins desired. Finally, the injection of 70  $\mu\text{L}$  of 1 M ethanolamine/HCl pH 8.5 ensured the deactivation of nonreacted carboxyl ends on the surface of the gel. A similar procedure was carried out over a reference channel, for which the ligand injection was a blank injection of buffer. Internal reference subtraction was

then used to establish all data in the report. The buffer was subsequently changed to a PBS (pH 7.4, 0.1 M) and flowed until reaching a stable baseline. All buffers were degassed and filtered through a 0.45  $\mu\text{m}$  PTFE filter (Millipore).

**2.6. Fitting Models.** Aside from the Langmuir and bivalent models included within the BIAevaluation Software provided with the SPR apparatus, a trivalent model was introduced to fit the obtained data. In the trivalent model, the binding process is described as follows:



where  $a$  would be a lactose molecule on the surface of a micelle,  $b$  a lectin on the protein bed,  $ab$  the complex subsequently formed, and  $ab_2$  the complex formed between two lactose molecules on the same micelle and two lectins on the protein bed, etc. These equations can be transcribed into the following equations:

$$\begin{aligned} d[ab]/dt = & (k_{a1}[a][b] - k_{d1}[ab]) - \\ & (k_{a2}[ab][b] - k_{d2}[ab_2]) - (k_{a3}[ab_2][b] - k_{d3}[ab_3]) \end{aligned}$$

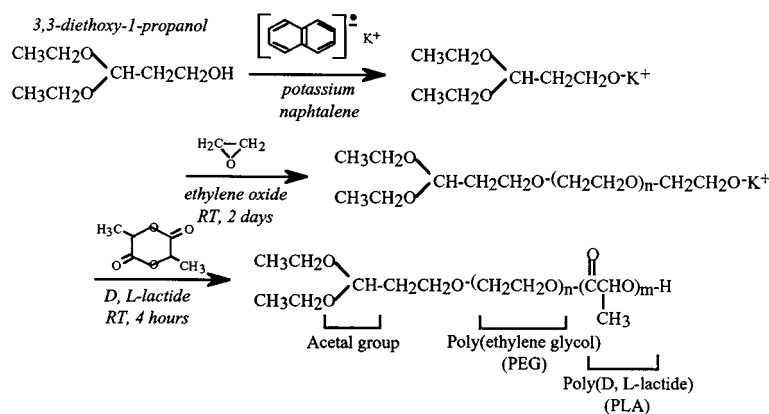
$$\begin{aligned} d[ab_2]/dt = & (k_{a2}[ab][b] - k_{d2}[ab_2]) - \\ & (k_{a3}[ab_2][b] - k_{d3}[ab_3]) \end{aligned}$$

$$d[ab_3]/dt = (k_{a3}[ab_2][b] - k_{d3}[ab_3])$$

where  $[a]$  is the concentration of Lac-micelles and  $[b]$  the concentration of lectins.  $[a]$  is equal to 0 at time  $t = 0$  or to the Lac-micelles concentration at time  $t$ .  $[b]$  can then be expressed as  $[b] = \text{lectin concentration at time } t - ([ab] + [ab_2] + [ab_3])$ , if steric hindrance or the binding of more than one lactose molecule to the same protein is neglected. These issues are to be discussed in a later section.

### 3. RESULTS AND DISCUSSION

**3.1. Preparation of the Block Copolymer.** As thoroughly described in our previous reports, ring-opening anionic polymerizations result in block copolymers, the final block molecular weights being dependent on initial monomer/initiator ratios. Furthermore, these polymers display low size distributions, a feature particularly desirable for drug delivery, as micelles prepared from these polymers also to display low size distributions (14). After polymerization of the poly(ethylene glycol) (PEG) block, a small amount of mixture was sampled and analyzed by GPC, exhibiting an average  $M_n$  and  $M_w$  of 4876 g/mol and 5099 g/mol, respectively, as compared to the 5016 g/mol theoretically calculated from initial ratios. The polydispersity index,  $I_p = M_w/M_n$  was found to be 1.046. After subsequent copolymerization of the lactide and purification of the resulting Ac-PEG-PLA block copolymer (Figure 1 presents the synthetic route to the block copolymer), the molecular weight of the latter was analyzed by GPC and by combined GPC/NMR measurements. GPC conveys an average  $M_n$  and  $M_w$  of 8125 g/mol and 8872 g/mol, respectively, with an  $I_p = 1.092$ . Combined GPC and NMR evaluations convey an average molecular weight of 4500 g/mol for the lactide block, and of 9400 g/mol for the copolymer, for a theoretical value of 10000 g/mol. Noteworthy is the fact that the size



**Figure 1.** Synthetic route to an acetal-poly(ethylene glycol)-poly(D,L-lactide). The one-pot, ring-opening polymerization was carried out at room temperature under argon atmosphere in tetrahydrofuran (THF).

distribution of the polymer remains low even after copolymerization of the second block.

**3.2. Preparation and Characterization of Sugar-Installed Micelles.** Micelles were found to have a particle size of  $30 \pm 0.2$  nm. The cumulant method also provides the value  $\mu_2/\bar{\Gamma}^2$ , a measure of the particle size distribution, found to be in average lower than 0.09.

Deprotection of acetal ends is carried out more efficiently in micellar solution, because, first of all, aldehyde groups located at the distal end of the PEG block are presented at the surface of micelles. Thus, they are more accessible than those in random-coiled PEG strands are. Second, aldol groups are prone to undergo an aldol condensation in solution, thus reducing the yield of the subsequent coupling reaction. This phenomenon is remarkably quenched in micellar solution, most probably due to the restricted motion of polymer chains that prevents the condensation of aldehyde groups, which would be moreover entropically unfavorable (15).

What will be defined hereupon as the aldehyde functionality, that is, the number of aldehyde groups per 100 copolymer chains, was calculated using NMR measurements. Certainly, by relating the intensity of the aldehyde proton peak ( $\delta = 9.8$  ppm) to that of the methine peak of the PLA block ( $\delta = 5.2$  ppm), it is possible to assess to what extent acetal groups can be converted to aldehyde groups. As the former peak is not always readily detectable by such spectroscopy, a second calculation based on the ratio of the intensity of the  $\alpha$ -methine proton peak ( $\delta = 1.6$  ppm) to that of the aforementioned methine peak is carried out. For both evaluations, the aldehyde functionality was found to be of 80%. A similar evaluation, carried out with the final lactose-poly(ethylene glycol)-poly(D,L-lactide) (Lac-PEG-PLA) block copolymer and based on the correlation of intensities of the aromatic protons on the phenyl group of the *p*-aminophenyl- $\beta$ -D-lactopyranoside ( $\delta = 6.4$  and 6.8 ppm) and the methine peak on the PLA block demonstrated similar results. The coupling reaction would then proceed in a quantitative way. Of deeper relevance is the fact that the size of the particle was not greatly modified, despite the chemical nature of the process, as, indeed, lactose-micelles (Lac-micelles) were found to have a hydrodynamic diameter of  $31.8 \pm 0.2$  nm and a size distribution of 0.12. The slight increase in the former value might be explained by the creation of a thin lactose layer around micelles.

**3.3. Kinetic Evaluations.** As thoroughly described elsewhere, not only has surface plasmon resonance (SPR) analysis provided evidence of the specific recognition and retention of Lac-micelles by a lectin bed, it has also provided a quite original tool for dealing with fundamen-

tal parameters that would severely affect the efficiency of any ligand-installed micelles. Such parameters, the ligand density or, more fundamentally, the critical association concentration (cac), are most crucial in that they would have direct consequences on the biodistribution of Lac-micelles after intravenous administration. Therefore, multivalency in the binding has been shown to greatly enhance complex formation in a clear example of cooperativity. Moreover, recorded sensorgrams have allowed the observation of complex formation between micelles and lectins due to the specific interaction between lactose molecules on the surface of micelles and binding sites on the protein bed. Beyond this specificity, the intensity of complex formation has indicated a link between binding ability and self-assembling structure of the polymer in aqueous solution and thus to calculating the cac of Lac-micelles. More interestingly, the SPR evaluation has resulted in values in good accordance with those obtained using the environment-dependent fluorescence of pyrene (11).

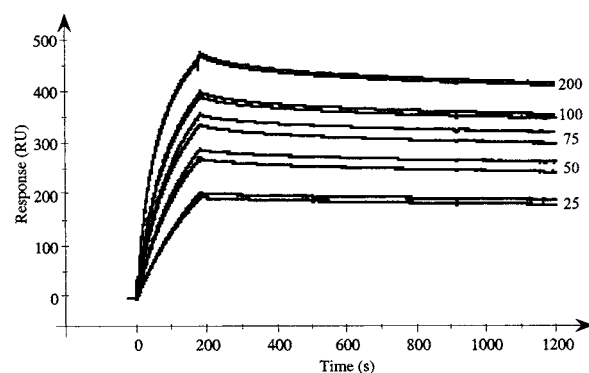
Yet, all of the data discussed in our previous report was recorded at equilibrium, which is somehow the completion of the binding between Lac-micelles and a protein bed. It shall, however, be recalled that of a nonetheless fundamental relevance is the rate of complex formation since it is to have a direct repercussion on the binding of Lac-micelles to target sites. In this regard, further information can be obtained by a closer and more careful analysis of the recorded sensorgrams. Indeed, recording the change of the angle at which the total reflection effect takes place, the fundamental principle of SPR, is carried out in real time under a constant buffer flow over the ligand-installed surface. Therefore, as the response of the adsorption and desorption processes can be recorded and plotted on a sensorgram, a function of time, information about the speed at which these processes take place can be obtained. The subsequent use of simulation software demonstrates the possibility of fitting the observed data with kinetic models, allowing the calculation of kinetic binding rates as the apparent association and dissociation rate constants ( $k_a$  and  $k_d$ , respectively), or the equilibrium constants  $K_A$  or  $K_D$ . In such regard, the evaluation itself is not especially difficult, if one takes precautions such as to diminish mass transport phenomena, nonspecific adsorption, and avidity, which heavily compromise SPR analysis (16). What certainly poses a far more delicate problem is to fit the experimental data with a model that fully accounts of all the involved parameters. In this evaluation, the multivalency of micelles (17) and the bivalency of the protein and its density on the surface of the gel are all

to be taken into account to reach a proper understanding of the system. It is quite apparent that several assumptions have to be accepted if a valid and accurate evaluation is to be undertaken.

**3.4. Preliminary Considerations.** For the sake of simplicity, the amount of bound lectins on the surface of the chip is to be kept as low as accuracy in the measurements will allow (18). Previous evaluations showed that no coherence in the binding of micelles was observed for lectin densities lower than 2000 resonance units (RU), as recorded values varied randomly and were not reproducible. Thus, this value was set as a standard for all kinetic evaluations. Because the equivalence  $1 \text{ RU} = 1 \text{ pg/mm}^2$  (provided by BIAcore), it is possible to convert resonance units into molecular concentrations and further into intermolecular distances; 2000 RU are thus equivalent to  $2000 \text{ pg/mm}^2$ . Given that the molecular weight of RCA-I lectins is  $\sim 120\,000 \text{ g/mol}$ , it follows that  $2000 \text{ pg/mm}^2 = 1.67 \times 10^{-14} \text{ mol/mm}^2 = 1.00 \times 10^{10} \text{ proteins/mm}^2 = 1.00 \times 10^{-2} \text{ proteins/nm}^2$ . Thus, 2000 RU are equivalent to 1 protein/99.6  $\text{nm}^2$ . The distance between two protein molecules at the very surface of the protein bed can then be approximated to  $D_{\text{prot-prot}} \sim 10 \text{ nm}$  (8.9–9.0 nm for a protein density of 2500 RU, the maximum protein density used for these experiments), that is, if all the proteins are considered to be at the surface of the gel as a first approximation.

Another consideration, the distance between two lactose molecules on the surface of a single micelle, was assessed. In this view, the association numbers of Ac-micelles and that of Lac-micelles were evaluated by static light scattering (SLS) measurements. The so-obtained Debye plots (data not shown) convey increments of the refractive index ( $dn/dc$ ) of 0.1070 and 0.1148, as well as micelle apparent molecular weights of 1100000 g/mol and 1050000 g/mol for acetal-poly(ethylene glycol)-poly(D,L-lactide) micelles (Ac-micelles) and Lac-micelles, respectively. Considering that the molecular weight of one copolymer chain is 9400 g/mol, it can be readily established that the association number accounts for  $\sim 112$  chains of copolymer per Lac-micelle. Taking into account the lactose functionality calculated by NMR, it can be presumed there are about 89 lactose molecules on the surface of a single Lac-micelle 80%, and that a single lactose molecule centers in an area of  $(4\pi r^2)/89 = 31 \text{ nm}^2$  ( $r$  was calculated by either DLS measurement). In the simplest case of molecules distributed in a grid, this is equivalent to an interlactose distance of 5.6 nm. Given the distance between two lactose molecules on the surface of a micelle, it is then possible to simplify lectin bivalency to monovalency, as it is not likely that two sugar molecules bind to the same protein unless the micelle structure is heavily distorted.

**3.5. Specificity of the Binding.** Injection of Lac-micelles led to a considerable increase in the signal of the lectin-installed flow cell due to the specific interaction between lectins and lactose molecules on the surface of micelles. Conversely, only feeble responses (less than 8 RU) were recorded for injections of Lac-micelles on the reference flow cell bearing no such receptors. Ac-micelles, used as a control of the specificity in the recognition by lectins, exhibited low responses on both flow cells (data not shown). Therefore, a double specificity can be claimed, as both types of micelles bind to the dextran gel in negligible levels (i.e., nonspecific binding) and as Lac-micelles bind to the protein bed due to the molecular recognition between lactose molecules on the surface of micelles and lectins (i.e., specific binding).



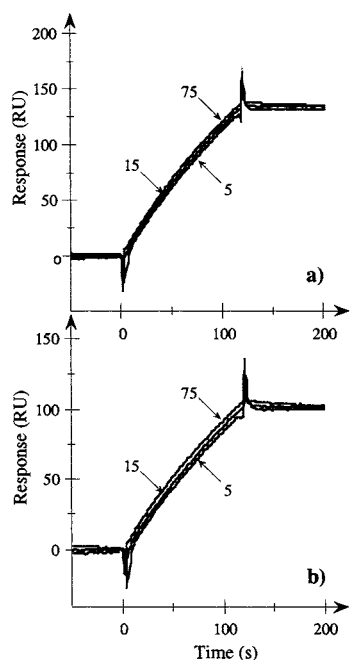
**Figure 2.** Recorded sensorgrams for Lac-micelles 80% at different micelle concentrations. Values next to sensorgrams express the micelle concentration, in  $\mu\text{g/mL}$ .

**3.6. Kinetic Evaluations.** Prior to fitting the data comes the evaluation itself. A series of concentrations: 0 (blank injection), 25, 50, 75, 100, and 200  $\mu\text{g/mL}$  (23.8, 47.6, 71.4, 95.2, and 190.5 nM, as established from the apparent molecular weight obtained by SLS measurements) was randomly injected over both a protein bed and a blank cell. The latter cell serves as reference for subsequent internal signal subtraction in order to discard nonspecific binding. Special care was taken in choosing the lowest, readily detectable polymer concentration, as this concentration should be above the  $\text{cac}$  of 7.5  $\mu\text{g/mL}$ . Every sample was then injected for 3 min at a flow rate of 30  $\mu\text{L/min}$ , followed by a 10-min dissociation time. Since only low dissociation from the protein bed has been observed even after several hours of buffer flow (data not shown), regeneration of the surface was ensured by a 15  $\mu\text{L}$  injection of free galactose. Each measurement was carried out twice.

As seen in Figure 2, after subtraction of the reference cell signal, the slopes of all association phases are quite steep, reaching complex formation rates close to 30 RU/s. But far more remarkable is the fact that dissociation phases are characterized by poor slopes. Lac-micelles 80% exhibit fast association and slow dissociation rates at any given concentration. This behavior has been previously observed and proven to be due to the multivalent interaction between micelles and the protein bed (11). Yet another point that is worth mentioning is the reproducible character of the measurements, as responses varied from 0.54% to 3.25% from the average value.

The obtained data was subsequently fitted with BIAcore software models. Yet, most of the equations used in the software illustrate, of course, the behavior of an ideal system. Several factors complicate the kinetic evaluation, the most important being the presence of several binding sites available to the several molecules of lactose on the surface of micelles which makes it difficult to attain a 1:1 interaction with lectins on the protein bed. Second, one might cite cooperative effects between neighboring lactose molecules that are to enhance association rates, especially at the beginning of the adsorption phase, again probably conveying a deviation from the simplest Langmuir model. Third, if the association rate is considerably high, diffusion or mass transport can occur, compromising the validity of the equations discussed beforehand, complicating the proper fitting of the experimental data or the creation of a new kinetic model, should this be required. Of the three considerations, it is mass transport control experiments which are to be assessed first, as these are independent of the fitting model used and therefore of a far more critical importance.



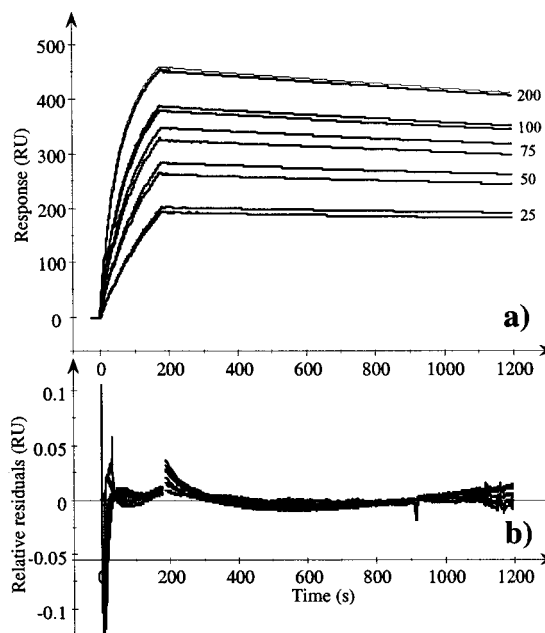


**Figure 3.** (a) Response generated by the injection of Lac-micelle 80% solution at 25  $\mu\text{g/mL}$ , as a function of time. The values above the arrows correspond to the flow rate expressed in  $\mu\text{L/min}$ . (b) Injection of Lac-micelle 60% solution under the same conditions.

**3.7. Mass Transport Control Experiments.** Mass transport occurs when the binding rate of the analyte to the ligand is faster than the diffusion of the analyte to the ligand. This phenomenon results in the existence of concentration gradients of the analyte over the ligand bed and heavily complicates the use of kinetic models. Furthermore, and due to the same reasons, the analyte concentration does not instantly drops to zero at the end of the sample injection, favoring rebinding phenomena. In which case, as the dissociation phase proceeds, binding sites become available so that the analyte can rebind to the surface (19). This generally results in apparently lower dissociation constants.

Kinetic processes are independent of the flow rate. Should association rates considerably vary with it, mass transport phenomena have a non-negligible repercussion on the reaction, and far more complicated models have to be used in order to fit the data. Bearing this in mind, micelles at the lowest, yet readily detectable, concentration (25  $\mu\text{g/mL}$ ) were injected over a fixed period of time at different flow rates (5, 15, and 75  $\mu\text{L/min}$ ). The sensorgrams are plotted in Figure 3. It is obvious that the slopes of the association phases do not greatly differ from one curve to the other. Combined with the above-described evaluation, safe ground can be laid as to state that this evaluation is mainly kinetically driven, most probably due to the colloidal nature of polymeric micelles, which ensures fast diffusion over the SPR surface and thus prevents the generation of a concentration gradient.

**3.8. Fitting of the Data.** *3.8.1. The Langmuir and Bivalent Models.* As one has to start from the beginning, the basic Langmuir model was assessed and shown to demonstrate a poor fitting of the data (fitting not shown). Whether the variables are fitted globally or locally,  $\chi^2$ , a measure of the accuracy of the fitting, was found to be disparate and superior to 100. Since fitting with a Langmuir-based model conveyed results lacking any coherence, a bivalent model was used. Within this model, binding would be ensured by the sequential complex



**Figure 4.** (a) Fitting of the sensorgrams recorded for Lac-micelles 80%, using the trivalent model. (b) Relative deviation to the trivalent model, or relative residuals, expressed in RU. Values next to sensorgrams express the micelle concentration, in  $\mu\text{g/mL}$ .

formation between two lactose molecules on the surface of a micelle and two receptor sites on the lectin bed. This model correlates well the sensorgrams obtained for micelles bearing lower lactose densities, as will be explained in the following section, but not sensorgrams obtained for Lac-micelles 80%. A more complex model has to be used in order to fit these data, as association with lectins seems to be ensured by more than two lactose molecules. Indeed, applying the bivalent model conveys both a visual appearance and thus a  $\chi^2$  that are far from being ascertained (data not shown). Be that as it may, it seems appropriate at this point to reflect upon what is the most likely situation to evolve for the studied system. Clearly, Lac-micelles 80% bind in a multivalent manner, with a valency  $\geq 3$ . This can be approached by using a simple theoretical calculation, that a 30 nm particle approaching the protein bed will "shadow" an area of  $A = \pi R^2 = \pi(15^2) \sim 707 \text{ nm}^2$ . If this value is to be related to the interprotein distance calculated in section 3.4 (10 nm), one single micelle will cover an area occupied by about seven binding sites, of which not all are attainable for lactose molecules on the surface of a micelle, given the spherical shape of the latter. Roughly, it can be thus stated that the valency of the binding is likely to be somewhere between 3 and 7 and most probably less than 7, as far as the beginning of the adsorption phase is concerned. Subsequent relaxation of the micelle structure, or further interaction with lectins not at the very surface of the protein bed, might result in an increased multivalent effect. These two cases will not be taken into account in this first approximation, since none of them can be experimentally assessed.

*3.8.2. The Trivalent Model.* The recorded sensorgrams were then fitted using the trivalent model described in section 2.5. In Figure 4, not only is a relatively satisfactory visual appearance observed, but also a narrow scatter of relative residuals (that is, residuals divided by recorded responses) around 0, except for the very beginning of the desorption phase, for which a small trend can be discerned. Still, this deviation is feeble, representing

**Table 1. Kinetic Binding Constants Obtained for the Kinetic Assay of Lac-micelles 80%, Using the Trivalent Model<sup>a</sup>**

sample name	$k_{a1}$ ( $M^{-1} s^{-1}$ )	$k_{d1}$ ( $s^{-1}$ )	$k_{a2}$ ( $RU^{-1} s^{-1}$ )	$k_{d2}$ ( $s^{-1}$ )	$k_{a3}$ ( $RU^{-1} s^{-1}$ )	$k_{d3}$ ( $s^{-1}$ )	$K_{D1}$ (nM)	$\chi^2$
Lac-micelles 80%	$3.18 \times 10^4 \pm 0.37$	$1.28 \times 10^{-4}$	$4.68 \times 10^{-5}$	0.019	$6.46 \times 10^{-6}$	$4.65 \times 10^{-5}$	3.4	6.34

<sup>a</sup>  $k_{a1}$  was fitted locally, while the rest of the parameters were done so globally. The statistical value  $\chi^2$  assesses the goodness of the fitting.

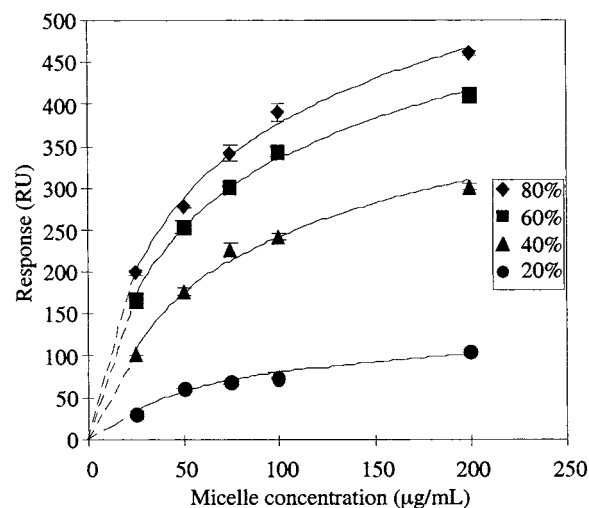
at most a 3.5% deviation from recorded values. Yet, this trend might be due to a detail of the dissociation process, a feature that shall be studied in detail in the future.  $\chi^2$ , a statistical measure of the goodness of the numerical fitting, was found to be 6.3. Kinetic constants are presented in Table 1, and  $K_{D1}$ , calculated as  $k_{d1}/k_{a1}$ , was thus found to be 3.4 nM. Equilibrium constants are expressed as  $K_{D1}$ , as the first binding appears to be the critical step in the binding to the protein bed. As estimated in the previous section, the valency of the binding is restrained here by the amount of protein sites available to one micelle and somewhere between 3 and 7. To discard a higher cooperative effect, a tetravalent model was also devised, and the data recorded for Lac-micelles 80% fitted accordingly. Yet, no enhancement in the fitting was observed; quite the contrary, a stronger deviation was found (data not shown). These observations point in the direction that the binding between Lac-micelles 80% and the protein bed would occur through the driving force of the binding of one lactose molecule. A similar study conducted by Lortat-Jacob et al. dealt with an adenovirus fiber binding in a trivalent manner to its receptor immobilized on a SPR chip (20). Their analysis indicated that the leading event in the fiber attachment to the receptor bed was the binding of the first fiber head molecule to one receptor, with a  $K_{D1}$  of 23 nM.

**3.9. Kinetic Constants and Multivalency.** Another point that is worth discussing is the influence of multivalency on kinetic constants. It is known that the transition between monovalency and multivalency induces a nonlinear increase of kinetic rates. Certainly, the ligand density influences parameters such as the stoichiometry of the binding, the rate of complex formation, and the inter-receptor distance (21).

Lac-micelles bearing different ligand functionalities were prepared by mixing the Lac-PEG-PLA with its Ac-PEG-PLA counterpart in different ratios, in DMAc solution. After that, the mixtures were dialyzed against water following the conventional procedure to prepare micelles. Predictably enough, the size of the particles was not altered but rather in a negligible manner (data not shown). Thus, Lac-micelles 60%, Lac-micelles 40%, Lac-micelles 20%, and Lac-micelles 10% were chosen to be analyzed to assess the influence of multivalency on kinetic values, following a similar procedure as that described in section 3.6.

No coherent data was recorded for micelles bearing a lactose functionality of 10% (data not shown). Indeed, response values varied randomly and in a nonreproducible manner, so any kinetic values obtained would have been anyway of a quite dubious nature. Although we cannot explain this behavior, it might be suggested that low ligand densities generate important areas where no single lactose molecule is present. That is, 11 lactose molecules would be present in an area of more than 2800 nm<sup>2</sup>, conveying an average interligand distance of about 16 nm, generating highly heterogeneous ligand surfaces and thus nonreproducible responses.

The recorded sensorgrams for all other batches, on the other hand, appeared to be more reliable. The first



**Figure 5.** Recorded response at equilibrium for micelles bearing different ligand densities, at different concentrations. The numbers next to the symbols correspond to the ligand density. Dotted fragments indicate the transition phase between unimers and micelles.

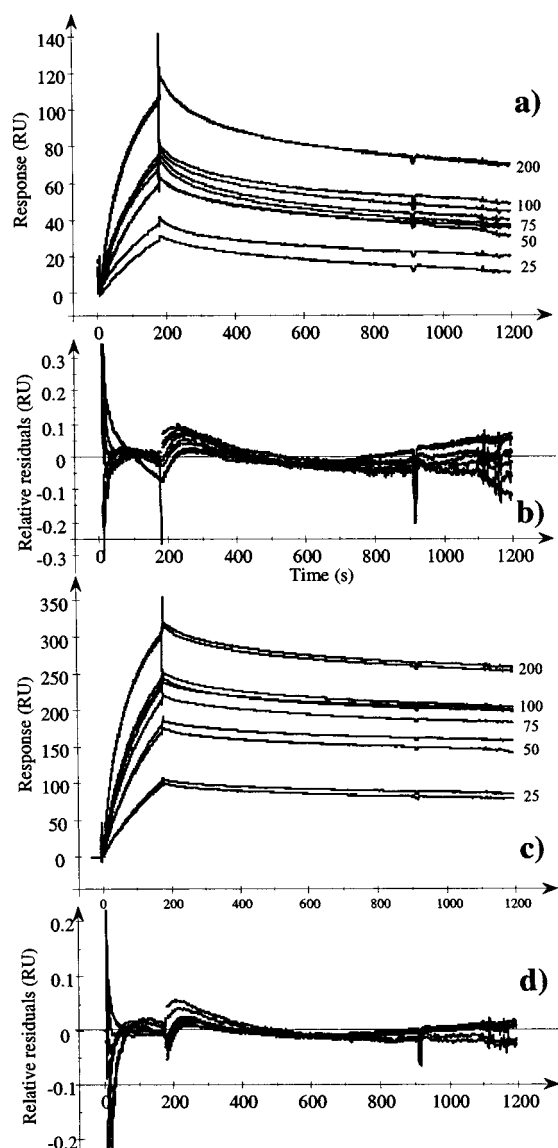
observation originating from the recorded sensorgrams is that the intensity of the binding to the protein bed increases with, quite logically, an increasing concentration. Second, at any given concentration, the amount of complex formation increases with an increasing ligand density, conferring a equilibrium binding of about 110 RU for Lac-micelles 20% and of 460 RU for Lac-micelles 80% (Figure 5).

Sensorgrams recorded for Lac-micelles 20% and 40% were successfully fitted using the bivalent model provided within the original BIAevaluation Software.  $\chi^2$  was found to be 3.4 in the case of the former and 4.0 in the case of the latter. Small tendencies also appear on the relative residues, but remain small scatters, representing less than 3% of the recorded values. The trivalent model described in section 3.8.3 was also used to fit the data, but no enhancement in the fitting was observed, even though certain comments should be made regarding Lac-micelles 40%. Certainly, using the trivalent model did not improve the accuracy of the fitting of the sensorgrams, but still a low enough  $\chi^2$  was recorded (6.0), making this fit also acceptable by BIAcore standards ( $\chi^2 < 10$ ). This led to the difficult choice of which model is most adequate for the ongoing discussion. This is not an isolated remark, but is based on the following consideration. As can be seen in Figure 5, and as it was reported in detail in a previous paper (11), there is a nonlinear increase in complex formation between micelles and the lectin bed when the lactose functionality exceeds what seems to be a critical value of 40%. Similar experiments carried out by measuring the turbidity of the system had conveyed comparable results but a lower value (20%), an observation that can be understood through the differing conditions and spatial geometry of the measurement systems, as discussed by the Kiessling group (22). In any way, a ligand density of 40% seems to set a transition in the valence of the binding and is most probably to be set somewhere between 2 and 3.

**Table 2. Kinetic Binding Constants Obtained for the Kinetic Assay of Lac-micelles 20% and 40%, Using the Bivalent Model<sup>a</sup>**

sample name	$k_{a1}$ ( $M^{-1} s^{-1}$ )	$k_{d1}$ ( $s^{-1}$ )	$k_{a2}$ ( $RU^{-1} s^{-1}$ )	$k_{d2}$ ( $s^{-1}$ )	$K_{D1}$ (nM)	$\chi^2$
Lac-micelles 20%	$1.36 \times 10^4 \pm 0.33$	0.0185	$2.43 \times 10^{-5}$	$3.05 \times 10^{-4}$	1360	3.44
Lac-micelles 40%	$2.48 \times 10^4 \pm 0.27$	0.0225	$3.84 \times 10^{-5}$	$1.23 \times 10^{-4}$	907	3.96

<sup>a</sup>  $k_{a1}$  was fitted locally, while the rest of the parameters were done so globally.



**Figure 6.** (a, c) Recorded sensorgrams for Lac-micelles 20% and Lac-micelles 40%, using the bivalent model. (b, d) Relative deviation to the bivalent model, or relative residuals, expressed in RU. Values next to sensorgrams express the micelle concentration, in  $\mu g/mL$ .

Be that as it may, it appears that the main driving force of the kinetic process is the initial binding, characterized by  $k_{a1}$  and  $k_{d1}$ , as their values are of far more consequence than those of the other two steps.  $K_{D1}$ , calculated as  $k_{d1}/k_{a1}$ , was thus found to be 1360 nM for Lac-micelles 20% and 907 nM (28 nM when fitted with the trivalent model) for Lac-micelles 40% (Table 2). Figure 6 presents both recorded sensorgrams and the relative residuals from the fitted data (fittings are not shown) for both micelle batches.

Sensorgrams recorded for Lac-micelles 60% were accurately fitted using the trivalent model, even if the fitting was of lower quality ( $\chi^2 = 8.69$ , data not shown) (Table 3).  $K_{D1}$ , in this case, was calculated to be 8.4 nM.

Another interesting observation to be made is that the  $K_{D1}$  of Lac-micelles 60% is more than double that of Lac-micelles 80%. Even still, the stoichiometry of the binding was not altered.

As mentioned earlier in this section, equilibrium complex formation is of about 110 RU for Lac-micelles 20%, whereas it reaches 460 RU for Lac-micelles 80%. The former exhibited a  $k_{d1}$ , the main driving constant in the dissociation process, of  $1.85 \times 10^{-2} s^{-1}$ . When fitted with the trivalent model, Lac-micelles 80% yielded a  $k_{d1}$  of  $1.28 \times 10^{-4} s^{-1}$ , which represents a 145-fold decrease in the main dissociation constant. Much in the opposite way, the  $k_{a1}$  of both micelles are in the same range of values ( $1.36 \times 10^4 M^{-1} s^{-1}$  for Lac-micelles 20%;  $3.18 \times 10^4 M^{-1} s^{-1}$  for Lac-micelles 80%, or a 2.3-fold difference), an observation in good accordance to what was discussed earlier. An increase in the ligand density seems to bring about a tremendous decrease in kinetic dissociation constants, not an increase in kinetic association constants (Figure 7). If one is to next analyze the behavior of the second binding step,  $k_{a2}$  varies from  $8.36 \times 10^{-6} RU^{-1} s^{-1}$  for Lac-micelles 60% to  $4.68 \times 10^{-5} RU^{-1} s^{-1}$  for Lac-micelles 80%, which represents a 5.6-fold difference between these two maximums. Albeit an inverse tendency is observed for Lac-micelles 60%, it can be said that the second kinetic association constant tends to increase as the lactose functionality increases. The second binding between lactose molecules and lectins occurs at a faster rate with increasing lactose functionality. This observation is not unreasonable, as at higher ligand functionalities, a higher number of lactose molecules are available to bind locally to the protein bed, thus favoring the second binding to the protein bed. Conversely,  $k_{d2}$  shifts from a minimum of  $1.23 \times 10^{-4} s^{-1}$  for Lac-micelles 40% to  $0.019 s^{-1}$  for Lac-micelles 80%, accounting for a 154-fold difference between the two values. Quite surprisingly, the second kinetic dissociation constant increases with an increase in the ligand functionality (Figure 8), yielding an overall increase of the second equilibrium constant  $K_{D2}$ . To this tendency, it can be hypothesized that the second binding is ensured by the equilibrium of more than one complex formed between one or more lactose molecule(s) and several binding sites on the protein bed. This observation should become more pronounced at higher ligand densities as, logically enough, more lactose molecules are available. As for the third step, no firm conclusions can be drawn, as only two sets of values are available. Briefly, it can be said that the system as a whole appears to be further stabilized at higher ligand densities, as the third equilibrium constant  $K_{D3}$  decreases.

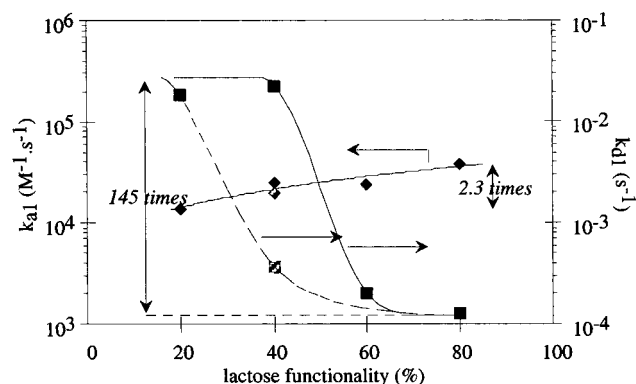
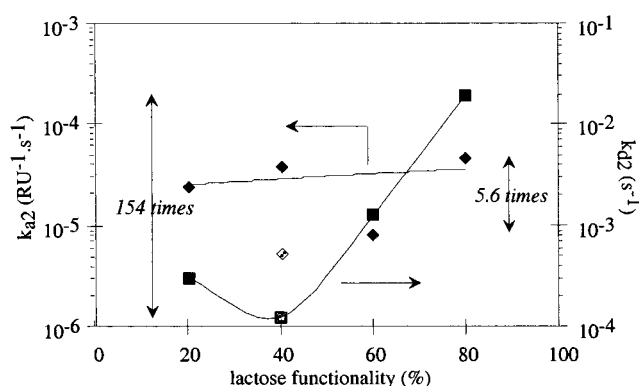
Yet another curious observation about the ligand density is its influence on the binding ability of the system. Lac-micelles 80% would have an interligand distance half that of Lac-micelles 20% (5.6 and 11.2 nm, respectively), if one is to trust the calculations presented earlier in this paper (see section 3.4). And remarkably enough, the former would bind to the protein bed in a trivalent way whereas the latter in a bivalent way. In other words, despite a higher ligand density, Lac-micelles 80% are only able to bind in a trivalent manner to the



**Table 3. Kinetic Binding Constants Obtained for the Kinetic Assay of Lac-micelles 60% and 80%, Using the Trivalent Model<sup>a</sup>**

sample name	$k_{a1}$ ( $M^{-1} s^{-1}$ )	$k_{d1}$ ( $s^{-1}$ )	$k_{a2}$ ( $RU^{-1} s^{-1}$ )	$k_{d2}$ ( $s^{-1}$ )	$k_{a3}$ ( $RU^{-1} s^{-1}$ )	$k_{d3}$ ( $s^{-1}$ )	$K_{D1}$ (nM)	$\chi^2$
Lac-micelles 40%	$1.94 \times 10^4 \pm 0.34$	$3.68 \times 10^{-4}$	$5.41 \times 10^{-6}$	0.000128	$3.01 \times 10^{-4}$	$2.07 \times 10^{-3}$	18.9	6.07
Lac-micelles 60%	$2.38 \times 10^4 \pm 0.34$	$1.99 \times 10^{-4}$	$8.36 \times 10^{-6}$	0.00128	$5.19 \times 10^{-5}$	$3.28 \times 10^{-3}$	8.4	8.69
Lac-micelles 80%	$3.18 \times 10^4 \pm 0.37$	$1.28 \times 10^{-4}$	$4.68 \times 10^{-5}$	0.019	$6.46 \times 10^{-6}$	$4.65 \times 10^{-5}$	3.4	6.34

<sup>a</sup>  $k_{a1}$  was fitted locally, while the rest of the parameters were done so globally.

**Figure 7.** Driving kinetic constants  $k_{a1}$  ( $\square$ ) and  $k_{d1}$  ( $\blacksquare$ ) as a function of lactose functionality. Slanting squares represent kinetic constants for Lac-micelles 40% fitted with the trivalent model.**Figure 8.** Kinetic constants  $k_{a2}$  ( $\square$ ) and  $k_{d2}$  ( $\blacksquare$ ) as a function of lactose functionality. Slanting squares represent kinetic constants for Lac-micelles 40% fitted with the trivalent model.

lectin bed. To put it in yet another way, a 2-fold decrease in the interligand distance only brings about one extra ligand binding to the protein bed. Therefore, whereas Lac-micelles 80% present an enhanced binding in terms of kinetic and equilibrium constants, Lac-micelles 20% seem to be more effective if understood through the amount of available lactose molecules, as reported by Cairo et al. (23). Their data clearly shows how, on a molecular basis, the most efficient compounds are those bearing the lowest ligand densities whereas higher ligand densities convey the largest ligand–receptor clusters.

Perhaps the flexible structure of PEG and micelles in general is to be accounted for this trend. Certainly, the mobility of micelles is to be restricted as the first binding takes place. This will of course draw the micelle into closer contact with the protein bed, and yet, lactose molecules at the distal end of the hydrophilic block are to remain mobile due to the extreme high mobility and elongation of PEG chains (24) so that further bindings are rather facilitated. Therefore, independently of the ligand density, Lac-micelles will tend to form multivalent bindings to the protein bed, a property of certain interest in the design of drug delivery systems devised to achieve specific accumulation at defined sites.

#### 4. CONCLUSION

Lac-micelles form highly specific complexes when interacting with a lectin bed. These complexes are furthermore stable, since little dissociation is observed even after hours of buffer flow. Lac-micelles also exhibit colloidal properties such as fast diffusion over a surface, remarkably quenching mass transport limitations, a quite common handicap in kinetic studies carried out by SPR. They exhibit fast-rate binding as well as decreased dissociation rates. Such properties are expected to facilitate binding and subsequent complex formation with specific asialoglycoprotein receptors present in high levels at hepatic sites. Due to the strength of the association, prolonged retention at these sites is expected, which should certainly favor uptake by receptor-mediated endocytosis. Data otherwise obtained in cellular assays point in this direction and are to be published soon.

Multivalency once more has been shown to considerably alter kinetic values toward slower dissociation processes and thus enhanced equilibrium constants. An increase in the ligand functionality on the surface of micelles will lead to higher levels of complex formation, as well as to stronger affinities essentially brought about by decreased kinetic dissociation constants. Although the stoichiometry of the systems does not dramatically increase, there is a remarkable decrease in equilibrium dissociation constants.

#### ACKNOWLEDGMENT

The authors wish to express their gratitude to Biacore Japan, for invaluable discussions on the use of Biaevaluation software. Much in the same manner, they wish to express their thankfulness to Professor Yukihiro Shimogaki, Faculty of Engineering at the University of Tokyo, for enriching discussions. This work was supported by the Core Research Program for Evolutional Science and Technology (CREST), the Japan Science and Technology Corporation (JST), and by the Special Coordination Fund for Promoting Science and Technology of the Ministry of Education, Science, Sports and Culture of Japan (MEXT).

#### LITERATURE CITED

- (1) Lis, H., and Sharon, N. (1998) *Chem. Rev.* 98, 637–674.
- (2) Ashwell, G., and Harford, J. (1982) *Annu. Rev. Biochem.* 21, 531–554.
- (3) Dam, T., Roy, R., Das, S., Oscarson, S., and Brewer, F. (2000) *J. Biol. Chem.* 275, 14223–14230.
- (4) Kataoka, K., Kwon, G., Yokoyama, M., Okano, T., and Sakurai, Y. (1993) *J. Controlled Release* 24, 119–132.
- (5) Cammas, S., and Kataoka, K. (1996) Site Specific Drug Carriers: Polymeric Micelles as High Potential Vehicles for Biologically Active Molecules. *Solvents Self-Organ. Polym.* 1996, 83–113.
- (6) Kataoka, K., Harada, A., and Nagasaki, Y. (2001) *Adv. Drug Delivery Rev.* 47, 113–131.
- (7) Yamamoto, Y., Nagasaki, Y., Kato, M., and Kataoka, K. (1999) *Colloids Surf., B* 16, 135–146.
- (8) Yasugi, K., Nakamura, T., Nagasaki, Y., Kato, M., and Kataoka, K. (1999) *Macromolecules* 32, 8024–8032.

- (9) Yamamoto, Y., Nagasaki, Y., Kato, Y., Sugiyama, Y., Kataoka, K. (2001) *J. Controlled Release* 77, 27–38.
- (10) Kato, Y., Seita, T., Kuwabara, T., Sugiyama, Y. (1996) *J. Controlled Release* 39, 191–200.
- (11) Jule, E., Nagasaki, Y., and Kataoka, K. A Surface Plasmon Resonance Study on the Interaction between Lactose-Installed Poly(Ethylene Glycol)-poly(D,L-Lactide) Block Copolymer Micelles and Lectins Immobilized on a Gold Surface. *Langmuir*, in press.
- (12) Gulari, E., Gulari, E., Tsunashima, Y., and Chu, B. (1979) *J. Chem. Phys.* 70, 3965–3972.
- (13) Nolan, S., Philips, R., Cotts, P., Dungan, S. (1997) *J. Colloidal Interface Sci.* 191, 291–302.
- (14) Yasugi, K., Nagasaki, Y., Kato, M., and Kataoka, K. (1999) *J. Controlled Release* 62, 89–100.
- (15) Nagasaki, Y., Okada, T., Scholz, C., Iijima, M., Kato, M., and Kataoka, K. (1998) *Macromolecules* 31, 1473–1479.
- (16) Myszk, D. (1999) *J. Mol. Recog.* 12, 279–284.
- (17) Nagasaki, Y., Yasugi, K., Yamamoto, Y., Harada, A., and Kataoka, K. (2001) *Biomacromolecules* 2, 1067–1070.
- (18) Biacore 3000 Instrument Handbook, March 1999, Biacore AB, Uppsala, Sweden.
- (19) Rich, R.; Myszk, D. (2000) *Curr. Opin. Biotechnol.* 11, 54–61.
- (20) Lortat-Jacob, H., Chouin, E., Cusack, S., and van Raaij, M. (2000) *J. Biol. Chem.* 276, 9009–9015.
- (21) MacKenzie, C., Hiram, T., Deng, S., Bundle, D., Narang, S., and Young, N. (1996) *J. Biol. Chem.* 271, 1527–1533.
- (22) Mann, D., Kanai, M., Maly, D., and Kiessling, L. (1998) *J. Am. Chem. Soc.* 120, 10575–10582.
- (23) Cairo, C., Gestwicki, J., Kanai, M., and Kiessling, L. (2002) *J. Am. Chem. Soc.* 124, 1615–1619.
- (24) Otsuka, H., Nagasaki, Y., and Kataoka, K. (2000) *Biomacromolecules* 1, 39–48.

BC025598+

# A Stable Bis-Allyloxycarbonyl Biotin Aldehyde Derivative for Biotinylation via Reductive Alkylation: Application to the Synthesis of a Biotinylated Doxorubicin Derivative

Brigitte Allart,<sup>†</sup> Pauliina Lehtolainen,<sup>‡</sup> Seppo Ylä-Herttuala,<sup>‡</sup> John F. Martin,<sup>§</sup> and David L. Selwood<sup>\*,†</sup>

The Wolfson Institute for Biomedical Research, University College London, The Cruciform Building, Gower Street, London, WC1E 6BT, United Kingdom, BHF Laboratories, Department of Medicine, University College London, 5 University Street, London, WC1E 6JJ, United Kingdom, and University of Kuopio, A.I. Virtanen-Institute, P.O. Box 1627, FIN-70211 Kuopio, Finland. Received August 29, 2002; Revised Manuscript Received October 10, 2002

A novel, stable, biotin aldehyde derivative is reported in which the biotin moiety is *N*1,*N*3-protected by the allyloxycarbonyl group. The derivative is stable to sodium cyanoborohydride mediated reductive alkylation and is cleaved under mild Pd [0] catalysis. This novel biotin aldehyde should have wide application in avidin- and streptavidin-based detection systems and bioassays. The derivative is utilized in the synthesis of a biotinylated doxorubicin analogue that retains topoisomerase activity.

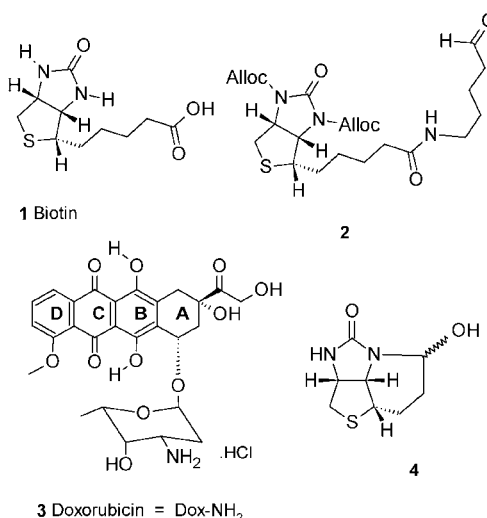
## INTRODUCTION

The avidin–biotin interaction is one of the strongest between a small molecule and a protein, with a  $K_d$  measured at  $10^{-15}$ . This pseudo-irreversible interaction has found many applications in biology, mostly in visualization or detection systems. In most cases biotin **1** (Chart 1) is attached to proteins, peptides, and small molecules via an amide bond or by conjugate addition of a protein or peptide thiol to a biotin–enone. We report here a novel stable biotin-aldehyde derivative **2** suitable for attachment of biotin by reductive alkylation. The method is compatible with highly functionalized molecules and is illustrated here, by the preparation of a biotinylated doxorubicin derivative. This molecule can be used as a probe for cancer therapy systems, employing avidin (*1*) or streptavidin targeting.

Such systems include three step radioimmunotherapy and the Scavidin gene therapy system (*2*). Three step immunotherapy (*3*) relies on predelivery of a tumor targeting antibody, followed by the streptavidin protein and finally delivery of a biotinylated radionuclide. The Scavidin gene therapy system induces expression of a synthetic hybrid receptor at the cell surface. This receptor comprises the avidin protein linked to the macrophage scavenger class A receptor (*4*), the avidin portion of the receptor binds biotin tightly and enables cellular internalization of biotinylated molecules.

One could imagine that molecular probes for such systems could come in many forms; however, a doxorubicin **3** probe was attractive in that extracellular and intracellular localization could be monitored by confocal fluorescence microscopy (*5*). It was desirable to maintain the topoisomerase activity of doxorubicin in order to have an additional functional readout of activity. A metaboli-

## Chart 1. Structures



cally stable linker had the advantage of allowing us to observe the fate of the molecule without the complication of ongoing cleavage. In the design of our linker, we needed to retain the basic nitrogen on the glycoside of doxorubicin **3**, as this is a prerequisite for topoisomerase II activity of anthracycline cytotoxics. This is also an attractive position for attachment via reductive alkylation, as the basicity of the nitrogen is maintained and several potent analogues of doxorubicin, substituted at this position, are known (*6*). Furthermore, the reductive alkylation reaction conditions do not affect the sensitive functionality of doxorubicin (*7*).

These initial experiments directed us toward employing a reductive alkylation approach. There are few reports, however, on the successful preparation of biotin aldehyde derivatives. These are limited to the low-temperature generation of biotin-4-aldehyde by DIBALH (*8*). *N*1,*N*3-Dibenzylated aldehydes were prepared during a total synthesis of biotin (*9*). Intramolecular formation of hemiaminal derivatives such as **4** is indicated (*10*) for

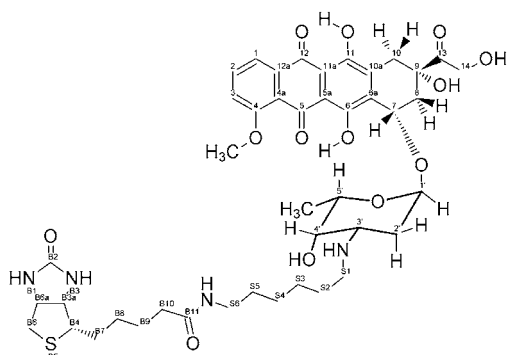
\* To whom correspondence should be addressed. E-mail: d.selwood@ucl.ac.uk.

<sup>†</sup> Wolfson Institute, University College London.

<sup>‡</sup> BHF laboratories, University College London.

<sup>§</sup> University of Kuopio.



**Chart 2. Numbering Convention**

biotin aldehydes. The literature evidence and our preliminary work demonstrated the need for a stable *N*-3-blocked biotin aldehyde derivative, which would avoid formation of intra and intermolecular hemiaminal derivatives and would allow single step reaction with highly functionalized cytotoxic agents followed by mild deprotection.

A survey of protecting groups identified allyloxycarbonyl (alloc) as a likely candidate. This group would be stable to reductive amination ( $\text{NaCNBH}_3$ ) and be removed utilizing palladium [0] catalysis. We envisaged that these conditions would be compatible with attachment to doxorubicin or other antineoplastic agents such as mitomycin C, bleomycin, or methotrexate. The direct introduction of ureido protecting groups on urea is rare. Some photolabile urethanes (*11*) represent the only example reported for biotin derivatives. We also included a long linker chain to maintain tight binding interaction with the avidin protein (*12*).

**EXPERIMENTAL DETAILS**

**General. Chemicals.** Biotin and tetrakis(palladium) (0) triphenylphosphine were purchased from Avocado. Doxorubicin was purchased from LKT laboratories (USA). *N,N*-Dimethylformamide di-*tert*-butyl acetal was obtained from Lancaster and was used without further purification. Avidin was purchased from Pierce. Other common reagents were purchased from Sigma or Lancaster. Anhydrous organic solvents were used as the highest quality grade packaged under nitrogen and were not distilled prior to use, unless otherwise indicated.

**Equipment.** NMR spectra were recorded on a Bruker AMX-300 (or an Avance-500) spectrometer, operating at 300 (or 500) MHz for  $^1\text{H}$  NMR and 75.41 (or 125.65) MHz for  $^{13}\text{C}$  NMR. NMR spectra of compounds **2** and **5–10** were recorded in  $\text{CDCl}_3$ , using TMS as external reference ( $\delta$  0.0 ppm) for  $^1\text{H}$  NMR and using  $\text{CDCl}_3$  ( $\delta$  77.0 ppm) for  $^{13}\text{C}$  NMR. For  $^1\text{H}$  and  $^{13}\text{C}$  NMR spectra of compounds **3**, **12**, and **11**, chemical shifts were reported in the scale relative to the solvent used as an internal reference. FAB and HRMS mass spectra were recorded on a VG ZO-SE spectrometer. Electrospray mass and LC/MS data were recorded either on a Micromass Quattro LC-mass spectrometer or a Finnigan AQA LC-mass spectrometer. IR spectra were recorded from KBr pellets or  $\text{CHCl}_3$  solutions using NaCl plates, on a Perkin-Elmer Spectrum One FT-IR spectrophotometer. UV spectra were recorded on a Unicam Helios  $\alpha$  spectrometer. Melting points were determined on a Gallenkamp melting point apparatus and are uncorrected. Microanalyses were performed by the Analytical Services Section, Department of Chemistry, University College London.

**Chromatography.** Column chromatography was performed either with bulk silica gel Merck (40–63  $\mu\text{m}$ ) or

on Isolute Flash-Si prepacked columns (FlashMaster automated chromatographic system, Jones chromatography). Reverse-phase Isolute Flash-C18 support (40–70  $\mu\text{m}$ , Jones chromatography) was used for the purification of compound **11** (see procedure below). HPLC and LC/MS analyses of compounds **5–12** were conducted on a Gilson gradient pumping system with a variable wavelength UV/visible detector. Reverse phase HPLC chromatography was carried out using a Hypersil BDS C18 column (5  $\mu\text{m}$ , 100  $\times$  4.6 mm) with a gradient solvent system at a flow rate of 1 mL/min, the solvents A (water) and B (acetonitrile) composing the gradient mixture contained 0.1%  $\text{CF}_3\text{COOH}$  as additive. Size exclusion HPLC analyses used in the avidin binding assay were conducted on a Shimadzu HPLC equipped with a gradient solvent pumping system and a diode array detector (Shimadzu, SPD-M10A), using a Spherogel TSK G5000PW column (10  $\mu\text{m}$ , 7.5 mm  $\times$  300 mm, stainless steel, Tosoh Biosep). HPLC analyses were run at a flow rate of 1.0 mL/min using a 50 mM potassium phosphate buffer (300 mM NaCl, 1 mM EDTA, 1 mM  $\text{NaN}_3$ , pH 6.8) as the mobile phase.

**Numbering Conventions and NMR Data.** *Numbering Conventions.* The numbering system adopted below uses the trivial systems commonly adopted for numbering biotin and anthracyclines (Chart 2).

For simplicity, numbers for atoms of the biotin moiety are preceded by B (to avoid confusion with the atoms of the anthracyclic moiety), whereas the numbers referring to atoms from the spacer moiety are preceded by an S.

*NMR data.* All the NMR spectra summarized below were assigned on the basis of 2D  $^1\text{H}$ – $^1\text{H}$  (COSY) and  $^1\text{H}$ – $^{13}\text{C}$  (HMQC) correlation experiments performed at 500 MHz. As an illustration, the 2D  $^1\text{H}$ – $^1\text{H}$  and  $^1\text{H}$ – $^{13}\text{C}$  spectra for compound **10** are represented in Figures S1 and S2 see Supporting Information. The assignment of compounds **5–9** and compound **12** is unambiguous. The assignment proposed for the conjugates **10** and **11** is in agreement with NMR data published in the literature for biotin (*13*) and Doxorubicin (*14*). The methylenic protons on the carbon 6 of the biotin pattern ( $\text{C}^{\text{B}6}$ ) are labeled  $\text{H}^{\text{B}6}_{\text{syn}}$  and  $\text{H}^{\text{B}6}_{\text{anti}}$  (where “syn” and “anti” refer to the relative configuration vs the proton  $\text{H}^{\text{B}6a}$ ), when the difference in their respective vicinal coupling constant with  $\text{H}^{\text{B}6a}$  is sufficient to allow an unambiguous assignment (see compounds **5** and **11**). In intermediates **7**, **9**, **2**, and **10**, the presence of the sterically demanding alloc protecting groups on the urea moiety of the biotin pattern induces a conformational change (strain), which results in vicinal coupling constants  $^3J(\text{H}^{\text{B}6a}, \text{H}^{\text{B}6}_{\text{syn}})$  and  $^3J(\text{H}^{\text{B}6a}, \text{H}^{\text{B}6}_{\text{anti}})$  being within the same range. In addition, the respective signals for protons  $\text{H}^{\text{B}3a}$  and  $\text{H}^{\text{B}6a}$  (at the junction of the bicyclic biotin pattern) overlap with the resonance of the allylic protons from the two alloc groups. As a consequence, NOE experiments could not be envisaged to resolve the assignment of the two protons  $\text{H}^{\text{B}6}$ . Therefore, NMR data reported for intermediates **7**, **2**, and **10** refer to protons  $\text{H}^{\text{B}6}$  as  $\text{H}^{\text{B}6}_{\text{I}}$  and  $\text{H}^{\text{B}6}_{\text{II}}$ , when a particular chemical shift could not be assigned to a particular configuration (syn/anti). For the same reason as mentioned above, in the case of intermediates **7**, **2**, and **10**, the three vicinal coupling constants ( $^3J$ ) observed for the resonance of the proton  $\text{H}^{\text{B}4}$  cannot be assigned unambiguously to the respective couplings of  $\text{H}^{\text{B}3a}$ ,  $\text{H}^{\text{B}7}_{\text{I}}$ , and  $\text{H}^{\text{B}7}_{\text{II}}$  with  $\text{H}^{\text{B}4}$ .

**Synthesis and Characterization of Conjugate 11 (B-Dox).** Biotin *tert*-Butyl Ester **5**. Biotin (10.03 g, 41.07 mmol) was suspended in 38 mL (158.48 mmol, 3.85 equiv) of *N,N*-dimethylformamide di-*tert*-butyl acetal.

The suspension was stirred vigorously under a nitrogen pressure and heated progressively to 80 °C in order to get a homogeneous brown solution after 20 min. The mixture was then gently stirred at 80 °C for 48 h. The reaction mixture was then cooled to ambient temperature, affording massive precipitation of the remaining starting material. The precipitate was washed several times with cold CH<sub>2</sub>Cl<sub>2</sub> and discarded in order to be recycled. The CH<sub>2</sub>Cl<sub>2</sub> washings were combined to the filtrate, and after evaporation, the residue was suspended in CH<sub>2</sub>Cl<sub>2</sub> (1 L) and water (300 mL). The organic layer was washed successively with saturated NaHCO<sub>3</sub> (3 × 300 mL) and brine (3 × 300 mL). After drying (MgSO<sub>4</sub>), the crude product was purified by silica gel chromatography, using CHCl<sub>3</sub>–MeOH (100:0 to 24:1) as eluent, to afford 5.075 g of Biotin *tert*-butyl acetal (16.89 mmol, 41% yield) as a white powder. <sup>1</sup>H NMR (300 MHz, CDCl<sub>3</sub>, 27 °C, TMS) δ 5.73 (br s, 1H; NH), 5.46 (br s, 1H; NH), 4.48 (dd, <sup>3</sup>J(H-<sup>B</sup>3a, H-<sup>B</sup>6a) = 7.36 Hz, <sup>3</sup>J(H-<sup>B</sup>6<sub>anti</sub>, H-<sup>B</sup>6a) = 4.96 Hz, 1H; H-<sup>B</sup>6a), 4.29 (dd, <sup>3</sup>J(H-<sup>B</sup>3a, H-<sup>B</sup>6a) = 7.36 Hz, <sup>3</sup>J(H-<sup>B</sup>3a, H-<sup>B</sup>4) = 4.95 Hz, 1H; H-<sup>B</sup>3a), 3.15 (1H, m, H-<sup>B</sup>4), 2.90 (dd, <sup>2</sup>J = 12.75 Hz, <sup>3</sup>J(H-<sup>B</sup>6<sub>anti</sub>, H-<sup>B</sup>6a) = 4.96 Hz, 1H; H-<sup>B</sup>6<sub>anti</sub>), 2.73 (d, <sup>2</sup>J = 12.75 Hz, 1H; H-<sup>B</sup>6<sub>syn</sub>), 2.23 (t, <sup>3</sup>J(H-<sup>B</sup>9, H-<sup>B</sup>10) = 7.43 Hz, 2H; CH<sub>2</sub>-<sup>B</sup>10), 1.52–1.70 (m, 4H; CH<sub>2</sub>-<sup>B</sup>7, CH<sub>2</sub>-<sup>B</sup>8 or CH<sub>2</sub>-<sup>B</sup>9), 1.43 (s, 9H; 3 CH<sub>3</sub>), 1.43 (m, 2H; CH<sub>2</sub>-<sup>B</sup>9 or CH<sub>2</sub>-<sup>B</sup>8). <sup>13</sup>C NMR (75 MHz, CDCl<sub>3</sub>, 27 °C) δ = 173.01 (COO-), 163.54 (C-<sup>B</sup>2), 80.13 (C(CH<sub>3</sub>)<sub>3</sub>), 61.97 and 60.15 (C-<sup>B</sup>6a, C-<sup>B</sup>3a), 55.39 (C-<sup>B</sup>4), 40.51 (C-<sup>B</sup>6), 35.19 (C-<sup>B</sup>10), 28.12 (3 CH<sub>3</sub>), 28.39, 28.27 and 24.92 (C-<sup>B</sup>7, C-<sup>B</sup>8 and C-<sup>B</sup>9). mp 124 °C. MS (ES<sup>+</sup>) 300.8 [M + H]<sup>+</sup>. HRMS (FAB<sup>+</sup>) Calcd for C<sub>14</sub>H<sub>25</sub>N<sub>2</sub>O<sub>3</sub>S, [M + H]<sup>+</sup>: 301.1586. Found: 301.1582 (error: 1.3 ppm). Anal. Calcd for C<sub>14</sub>H<sub>24</sub>N<sub>2</sub>O<sub>3</sub>S: C, 55.97; H, 8.05; N, 9.32. Found: C, 55.74; H, 7.66; N, 9.02. FT-IR(KBr): ν = 3241, 2981, 2936, 2872, 1727, 1705, 1470, 1368, 1234, 1162 cm<sup>-1</sup>.

**Allyl *para*-Nitrophenyl Carbonate 6.** Allyl alcohol (9.40 mL, 135.60 mmol) was added to a vigorously stirred solution of bis(*para*-nitrophenyl) carbonate (50 g, 162.72 mmol, 1.2 equiv) in 420 mL of CH<sub>2</sub>Cl<sub>2</sub>. After 10 min, *N,N*-diisopropylethylamine (72 mL, 406.80 mmol, 3 equiv) was added dropwise, affording a bright yellow coloration of the reaction mixture. The experiment was run overnight at ambient temperature. The reaction mixture was then diluted with 1 L of CH<sub>2</sub>Cl<sub>2</sub> and extracted successively with 15% citric acid (3 × 300 mL), water (2 × 250 mL), and brine (2 × 250 mL). After drying (MgSO<sub>4</sub>) and evaporation of the solvent, the crude product was adsorbed on silica and purified by silica gel chromatography using EtOAc–cyclohexane (1:9 to 1:1) as the eluent. Concentration of the corresponding fractions afforded precipitation of the allyl *para*-nitrophenyl carbonate (28.41 g, 127.29 mmol, 94% yield) as pale yellow needles, the purity of which was sufficient for the following step. <sup>1</sup>H NMR (400 MHz, CDCl<sub>3</sub>, 27 °C, TMS) δ = 8.29 (dt, <sup>3</sup>J(Ar H-o, Ar H-m) = 9.21 Hz, <sup>4</sup>J(Ar H-m, Ar H-m') ~ <sup>5</sup>J(Ar H-m, Ar H-o') ~ 2.70 Hz, 2H; 2 Ar H-m/m'), 7.39 (d, <sup>3</sup>J(Ar H-o, Ar H-m) = 9.21 Hz, <sup>4</sup>J(Ar H-o, Ar H-o') ~ <sup>5</sup>J(Ar H-o, Ar H-m') ~ 2.70 Hz, 2H; 2 Ar H-o/o'), 6.01 (ddt, <sup>3</sup>J(vinyl H, cis vinyl H) ~ 17.0 Hz, <sup>3</sup>J(vinyl H, trans vinyl H) ~ 11.8 Hz, <sup>3</sup>J(vinyl H, allyl H) = 5.56 Hz, 1H; vinyl CH), 5.46 (ddd, <sup>3</sup>J = 17.18 Hz, <sup>2</sup>J = 2.45 Hz, <sup>4</sup>J = 1.38 Hz, 1H; terminal cis vinyl CH), 5.38 (dd, <sup>3</sup>J = 9.34 Hz, <sup>2</sup>J = 2.45 Hz, <sup>4</sup>J = 1.07 Hz, 1H; terminal trans vinyl CH), 4.78 (dt, <sup>4</sup>J(allyl H, cis vinyl H) ~ 1.27 Hz, <sup>3</sup>J(allyl H, vinyl H) = 5.56 Hz, 2H; allyl CH<sub>2</sub>O). <sup>13</sup>C NMR (75 MHz, CDCl<sub>3</sub>, 27 °C) δ = 155.56 and 152.30 (Ar CNO<sub>2</sub> and Ar CO(CO)), 145.48 (O(CO)O), 130.63 (CH=CH<sub>2</sub>), 125.28 and 121.75 (4 Ar CH), 120.11 (CH=CH<sub>2</sub>), 69.72 (CH<sub>2</sub>–allyl). mp 45 °C. HRMS (FAB<sup>+</sup>) Calcd for C<sub>10</sub>H<sub>10</sub>NO<sub>5</sub>, [M + H]<sup>+</sup>:

224.0559. Found: 224.05567 (error: 1.0 ppm). Anal. Calcd for C<sub>10</sub>H<sub>9</sub>NO<sub>5</sub>: C, 53.82; H, 4.06; N, 6.28. Found: C, 53.82; H, 4.04; N, 6.00.

**[N1,N3-bis(alloc)]Biotin *tert*-Butyl Ester 7.** Sodium hydride, 90% in mineral oil (755 mg, 28.23 mmol, 1.0 equiv), was added progressively at ambient temperature to a solution of Biotin *tert*-butyl ester (8.48 g, 28.23 mmol) in DMF (110 mL) stirred under a nitrogen atmosphere. After 1 h, allyl *p*-nitrophenyl carbonate (6.3 g, 28.23 mmol, 1.0 equiv) was added to the solution, which instantly became bright yellow. The reaction mixture was stirred further for 1 h before the introduction of an additional equivalent of sodium hydride (755 mg). After another hour, a second sample of allyl *p*-nitrophenyl carbonate (7.56 g, 33.88 mmol, 1.2 equiv) was added to the mixture in order to get the bis(carbamate) protection of the urea function. The reaction mixture became progressively orange. Since the free position of the mono(alloc) protected intermediate is less reactive than the starting material, the mixture was heated progressively to 80 °C, but due to the instability of the bis(alloc) protected urea compound at high temperature, the experiment was stopped after 15 h, even if TLC analysis (using CHCl<sub>3</sub>–MeOH 49:1 as eluent) indicated incomplete bis-protection. After evaporation of the solvent at 40 °C under a high vacuum, the resulting oil was suspended into CH<sub>2</sub>Cl<sub>2</sub> (2 L) and extracted with 5% NaHCO<sub>3</sub> (at least 15 × 650 mL, until the aqueous layer was not bright yellow anymore) and then with brine (5 × 500 mL). The organic phase was dried (MgSO<sub>4</sub>) and evaporated. The brown oily residue was purified by flash chromatography on silica gel using CHCl<sub>3</sub>–MeOH 100:0 to 49:1 as eluent. The [N1,N3-bis(alloc)]biotin *tert*-butyl ester **7** (6.085 g, 12.99 mmol, 46% yield) was eluted first, followed by the residual *p*-nitrophenol and the mono(alloc)biotin *tert*-butyl ester (**8a/8b** in mixture, 3.256 g, 8.47 mmol, 30% yield). The mixture of **8a** and **8b** was then recycled in a similar experiment using 1.0 equiv of sodium hydride and 1.2 equiv of allyl *p*-nitrophenyl carbonate, to afford after workup and chromatography 2.73 g of additional [N1,N3-bis(alloc)]biotin *tert*-butyl ester **7** (7.11 mmol). The colorless oil was stored at 4 °C in the absence of light. <sup>1</sup>H NMR (300 MHz, CDCl<sub>3</sub>, 27 °C, TMS) δ = 5.94 (m, 2H; 2 vinyl CH), 5.44 (dt, <sup>3</sup>J = 18.50 Hz, <sup>2</sup>J = <sup>4</sup>J = 1.31 Hz, 2H; 2 terminal cis vinyl CH), 5.30 (dt, <sup>3</sup>J ~ 8.36 Hz, <sup>2</sup>J = <sup>4</sup>J = 1.20 Hz, 2H; 2 terminal trans vinyl CH), 4.67–4.79 (m, 6H; 2 allyl CH<sub>2</sub>–O, H-<sup>B</sup>3a, H-<sup>B</sup>6a), 3.50 (m, 1H; H-<sup>B</sup>4), 3.29 (dd, 1H; <sup>2</sup>J = 13.10 Hz, <sup>3</sup>J(H-<sup>B</sup>6a, H-<sup>B</sup>6<sub>I</sub>) = 6.07 Hz, H-<sup>B</sup>6<sub>I</sub>), 2.92 (dd, <sup>2</sup>J = 13.10 Hz, <sup>3</sup>J(H-<sup>B</sup>6a, H-<sup>B</sup>6<sub>II</sub>) = 5.11 Hz, 1H; H-<sup>B</sup>6<sub>II</sub>), 2.04 (t, <sup>3</sup>J(H-<sup>B</sup>9, H-<sup>B</sup>10) ~ 6.78 Hz, 2H; CH<sub>2</sub>-<sup>B</sup>10), 1.45–1.85 (m, 4H; CH<sub>2</sub>-<sup>B</sup>7, CH<sub>2</sub>-<sup>B</sup>8 or CH<sub>2</sub>-<sup>B</sup>9), 1.44 (s, 4H; 3 CH<sub>3</sub>), 1.18–1.45 (m, 2H; CH<sub>2</sub>-<sup>B</sup>9 or CH<sub>2</sub>-<sup>B</sup>8). <sup>13</sup>C NMR (75 MHz, CDCl<sub>3</sub>, 27 °C) δ = 172.76 (COO-), 151.53 and 151.33 (2 NC(O)O–allyl), 148.18 (C-<sup>B</sup>2), 130.98 and 130.94 (2 CH=CH<sub>2</sub>), 119.58 and 119.40 (2 CH=CH<sub>2</sub>), 80.12 (C(CH<sub>3</sub>)<sub>3</sub>), 67.72 and 67.66 (2 CH<sub>2</sub>–allyl), 60.41 and 58.60 (C-<sup>B</sup>6a, C-<sup>B</sup>3a), 52.43 (C-<sup>B</sup>4), 36.20 (C-<sup>B</sup>6), 35.34 (C-<sup>B</sup>10), 28.11 (3 CH<sub>3</sub>), 27.71, 27.30, and 24.57 (C-<sup>B</sup>7, C-<sup>B</sup>8, and C-<sup>B</sup>9). MS (ES<sup>+</sup>) 491.2 [M + Na]<sup>+</sup>. FT-IR(CHCl<sub>3</sub>): ν = 3027, 3014, 2980, 2944, 1810, 1783, 1721, 1367, 1330, 1298, 1278, 1251, 1158, 989 cm<sup>-1</sup>.

**[N1,N3-bis(alloc)]Biotin 9.** [N1,N3-bis(alloc)]Biotin *tert*-butyl ester (3.30 g, 7.05 mmol) was treated for 1 h at 0 °C with 35 mL of CF<sub>3</sub>COOH:CH<sub>2</sub>Cl<sub>2</sub> (1:1) mixture. The oily residue obtained after evaporation of the solvents was chromatographed on silica gel using CHCl<sub>3</sub>–MeOH (100:0 to 25:1) as eluent, to yield 2.72 g of crude [N1,N3-bis(alloc)]biotin as a pale yellow oil. <sup>1</sup>H NMR



(CDCl<sub>3</sub>, 300 MHz, 27 °C, TMS)  $\delta$  = 5.94 (m, 2H; 2 vinyl CH), 5.46 (dt,  $^3J$  = 17.17 Hz,  $^2J$  =  $^4J$  = 1.36 Hz, 2H; 2 terminal cis vinyl CH), 5.30 (dt,  $^3J$  = 9.11 Hz,  $^2J$  =  $^4J$  ~ 1.42 Hz, 2H; 2 terminal trans vinyl CH), 4.57–4.83 (m, 6H; 2 allyl CH<sub>2</sub>-O, H-<sup>B</sup>3a, H-<sup>B</sup>6a), 3.50 (m, 1H; H-<sup>B</sup>4), 3.30 (dd, 1H;  $^2J$  = 12.97 Hz,  $^3J$ (H-<sup>B</sup>6a, H-<sup>B</sup>6<sub>l</sub>) = 6.02 Hz, H-<sup>B</sup>6<sub>l</sub>), 2.94 (dd,  $^2J$  = 13.12 Hz,  $^3J$ (H-<sup>B</sup>6a, H-<sup>B</sup>6<sub>l</sub>) = 4.74 Hz, 1H; H-<sup>B</sup>6<sub>l</sub>), 2.34 (t,  $^3J$ (H-<sup>B</sup>9, H-<sup>B</sup>10) ~ 6.66 Hz, 2H; CH<sub>2</sub>-<sup>B</sup>10), 1.45–1.76 (m, 4H; CH<sub>2</sub>-<sup>B</sup>8, CH<sub>2</sub>-<sup>B</sup>9), 1.12–1.45 (m, 2H; CH<sub>2</sub>-<sup>B</sup>7). <sup>13</sup>C NMR (CDCl<sub>3</sub>, 75 MHz, 27 °C)  $\delta$  = 178.12 (COOH), 151.56 and 151.30 (2 NC(O)O-allyl), 148.23 (C-<sup>B</sup>2), 130.93 and 130.91 (2 CH=CH<sub>2</sub>), 119.62 and 119.44 (2 CH=CH<sub>2</sub>), 67.78 and 67.70 (2 CH<sub>2</sub>-allyl), 60.41 and 58.60 (C-<sup>B</sup>6a, C-<sup>B</sup>3a), 52.35 (C-<sup>B</sup>4), 36.23 (C-<sup>B</sup>6), 33.59 (C-<sup>B</sup>10), 27.71 (C-<sup>B</sup>7), 27.29 and 24.09 (C-<sup>B</sup>8 and C-<sup>B</sup>9). MS (ES<sup>+</sup>) 434.9 [M + Na]<sup>+</sup>. FT-IR(CHCl<sub>3</sub>):  $\nu$  = 2948, 1810, 1721, 1365, 1330, 1297, 1252, 906 cm<sup>-1</sup>.

**[N1,N3-bis(alloc)]Biotinyl-6-aminoalcohol.** HATU (1.87 g, 4.91 mmol, 1 equiv) was added to a solution of [N1,N3-bis(alloc)]biotin (2.013 g, 4.88 mmol), 6-aminoalcohol (711 mg, 5.885 mmol, 1.2 equiv) and *N,N*-diisopropylethylamine (2.56 mL, 14.64 mmol, 3.0 equiv) in CH<sub>2</sub>Cl<sub>2</sub> (20 mL). The solution was stirred at ambient temperature under a nitrogen atmosphere overnight. The reaction mixture was then diluted with 750 mL of CH<sub>2</sub>Cl<sub>2</sub> and worked up successively with a 15% citric acid solution (4 × 200 mL), brine, and water. The organic phase was dried (MgSO<sub>4</sub>) and evaporated. Chromatography of the oily residue using CHCl<sub>3</sub>-MeOH (50:1 to 20:1) afforded 1.90 g (3.71 mmol, 71% yield for two steps) of [N1,N3-bis(alloc)]biotinyl-6-aminoalcohol as a colorless oil. The compound was stored under nitrogen, in the absence of light at -20 °C. <sup>1</sup>H NMR (500 MHz, CDCl<sub>3</sub>, 27 °C, TMS)  $\delta$  = 5.96 (m, 2H; 2 vinyl CH), 5.60 (br t, 1H; C(O)-NH), 5.45 (ddt,  $^3J$  = 17.16 Hz,  $^2J$  =  $^4J$  = 1.38 Hz, 2H; 2 terminal cis vinyl CH), 5.31 (m, 2H; 2 terminal trans vinyl CH), 4.63–4.81 (m, 6H; 2 allyl CH<sub>2</sub>-O, H-<sup>B</sup>3a, H-<sup>B</sup>6a), 3.64 (t,  $^3J$ (H-<sup>S</sup>1, H-<sup>S</sup>2) = 6.51 Hz, 2H; CH<sub>2</sub>-<sup>S</sup>1), 3.51 (ddd,  $^3J$ (H-<sup>B</sup>4, H-<sup>B</sup>7<sub>l</sub>) = 12.09 Hz,  $^3J$ (H-<sup>B</sup>4, H-<sup>B</sup>7<sub>l</sub>) = 5.85 Hz,  $^3J$ (H-<sup>B</sup>3a, H-<sup>B</sup>4) = 3.25 Hz, 1H; H-<sup>B</sup>4), 3.29 (dd,  $^2J$  = 13.07 Hz,  $^3J$ (H-<sup>B</sup>6a, H-<sup>B</sup>6<sub>l</sub>) = 6.32 Hz, 1H; H-<sup>B</sup>6<sub>l</sub>), 3.25 (t,  $^3J$ (H-<sup>S</sup>5, H-<sup>S</sup>6) ~ 6.98 Hz, 1H; H-<sup>S</sup>6<sub>l</sub>), 3.24 (t,  $^3J$ (H-<sup>S</sup>5, H-<sup>S</sup>6) ~ 6.98 Hz; H-<sup>S</sup>6<sub>l</sub>), 2.94 (dd,  $^2J$  = 13.07 Hz,  $^3J$ (H-<sup>B</sup>6a, H-<sup>B</sup>6<sub>l</sub>) = 5.27 Hz, 1H; H-<sup>B</sup>6<sub>l</sub>), 2.14 (m, 2H; CH<sub>2</sub>-<sup>S</sup>10), 1.85 (br s, 1H; OH), 1.18–1.72 (m, 14H; CH<sub>2</sub>-<sup>B</sup>7, CH<sub>2</sub>-<sup>B</sup>8, CH<sub>2</sub>-<sup>B</sup>9, CH<sub>2</sub>-<sup>S</sup>2, CH<sub>2</sub>-<sup>S</sup>3, CH<sub>2</sub>-<sup>S</sup>4, CH<sub>2</sub>-<sup>S</sup>5). <sup>13</sup>C NMR (125 MHz, CDCl<sub>3</sub>, 27 °C)  $\delta$  = 173.64 (CH<sub>2</sub>C(O)NH), 152.28 and 152.01 (2 NC(O)O-allyl), 149.13 (C-<sup>B</sup>2), 131.79 and 131.70 (2 CH=CH<sub>2</sub>), 120.39 and 120.23 (2 CH=CH<sub>2</sub>), 68.53 and 68.46 (2 CH<sub>2</sub>-allyl), 63.26 (C-<sup>S</sup>1), 61.20 (C-<sup>B</sup>3a), 59.46 (C-<sup>B</sup>6a), 54.33 (2 CH=CH<sub>2</sub>), 53.31 (C-<sup>B</sup>4), 40.11 (C-<sup>S</sup>6), 37.21 and 37.06 (C-<sup>B</sup>6, C-<sup>B</sup>10), 33.35 (C-<sup>B</sup>7), 30.39 (C-<sup>B</sup>9), 28.74, 28.18, 27.36, 26.16 and 26.04 (C-<sup>B</sup>8, C-<sup>S</sup>2, C-<sup>S</sup>3, C-<sup>S</sup>4, C-<sup>S</sup>5). MS (ES<sup>+</sup>) 534.6 [M + Na]<sup>+</sup>. HRMS (FAB<sup>+</sup>) Calcd for C<sub>24</sub>H<sub>38</sub>N<sub>3</sub>O<sub>7</sub>S, [M + H]<sup>+</sup>: 512.2430. Found: 512.24341 (error: 0.8 ppm).

**[N1,N3-bis(alloc)]Biotinyl-6-aminoalcohol 2.** A 70  $\mu$ L sample of water (3.85 mmol) was solvated in 70 mL of CH<sub>2</sub>Cl<sub>2</sub> by drawing the solvent mixture into and expelling it from a disposable pipet several times. The wet CH<sub>2</sub>Cl<sub>2</sub> was added slowly via a dropping funnel to a vigorously stirring solution of [N1,N3-bis(alloc)]biotinyl-6-aminoalcohol (1.77 g, 3.46 mmol) and Dess–Martin periodinane (2.231 g, 5.19 mmol, 1.5 equiv) in 21 mL of dry CH<sub>2</sub>Cl<sub>2</sub> at ambient temperature under a nitrogen atmosphere. The clear solution grew cloudy toward the end of wet CH<sub>2</sub>Cl<sub>2</sub> addition, which required 1 h. After 3 h, the reaction mixture was diluted with EtOAc and then concentrated into a few mL of solvent by rotary evapora-

tor. The residue was taken up in 500 mL of EtOAc and then washed (2 × 150 mL) with a (1:1) mixture of 10% Na<sub>2</sub>S<sub>2</sub>O<sub>3</sub> and 5% NaHCO<sub>3</sub>, followed by water (2 × 200 mL) and brine (2 × 150 mL). The aqueous washings were back-extracted with EtOAc (5 × 75 mL), and this organic layer was washed with water and brine. The combined organic layers were dried with MgSO<sub>4</sub> and concentrated. Flash chromatography (50:1 to 20:1 of CHCl<sub>3</sub>-MeOH) afforded [N1,N3-bis(alloc)]biotinyl-6-aminoalcohol (1.57 g, 3.08 mmol, 89% yield) as a colorless oil. The compound was stored under nitrogen, in the absence of light at -20 °C. <sup>1</sup>H NMR (500 MHz, CDCl<sub>3</sub>, 27 °C, TMS)  $\delta$  = 9.76 (t,  $^3J$ (H-<sup>S</sup>1, H-<sup>S</sup>2) = 1.60 Hz, 1H; CHO), 5.95 (m, 2H; 2 vinyl CH), 5.62 (br t, 1H; C(O)-NH), 5.45 (ddt,  $^3J$  = 17.16 Hz,  $^2J$  =  $^4J$  ~ 1.49 Hz, 2H; 2 terminal cis vinyl CH), 5.31 (ddd,  $^3J$  = 10.46 Hz,  $^4J$  = 4.03 Hz,  $^2J$  ~ 1.20 Hz, 2H; 2 terminal trans vinyl CH), 4.64–4.82 (m, 6H; 2 allyl CH<sub>2</sub>-O, H-<sup>B</sup>3a, H-<sup>B</sup>6a), 3.51 (ddd,  $^3J$  = 11.96 Hz,  $^3J$  = 5.70 Hz,  $^3J$  = 3.20 Hz, 1H; H-<sup>B</sup>4), 3.29 (dd,  $^2J$  = 13.06 Hz,  $^3J$ (H-<sup>B</sup>6a, H-<sup>B</sup>6<sub>l</sub>) = 6.32 Hz, 1H; H-<sup>B</sup>6<sub>l</sub>), 3.26 (t,  $^3J$ (H-<sup>S</sup>5, H-<sup>S</sup>6) ~ 6.09 Hz, 1H; H-<sup>S</sup>6<sub>l</sub>), 3.24 (t,  $^3J$ (H-<sup>S</sup>5, H-<sup>S</sup>6) ~ 6.09 Hz, 1H; H-<sup>S</sup>6<sub>l</sub>), 2.95 (dd,  $^2J$  = 13.06 Hz,  $^3J$ (H-<sup>B</sup>6a, H-<sup>B</sup>6<sub>l</sub>) = 5.26 Hz, 1H; H-<sup>B</sup>6<sub>l</sub>), 2.45 (td,  $^3J$ (H-<sup>S</sup>2, H-<sup>S</sup>3) = 7.22 Hz,  $^3J$ (H-<sup>S</sup>1, H-<sup>S</sup>2) = 1.57 Hz, 2H; CH<sub>2</sub>-<sup>S</sup>2), 2.15 (m, 2H; CH<sub>2</sub>-<sup>B</sup>10), 1.47–1.73 (m, 8H; CH<sub>2</sub>-<sup>B</sup>8, CH<sub>2</sub>-<sup>B</sup>9, CH<sub>2</sub>-<sup>S</sup>3, CH<sub>2</sub>-<sup>S</sup>5), 1.31–1.42 (m, 2H; CH<sub>2</sub>-<sup>S</sup>4), 1.20–1.30 (m, 2H; CH<sub>2</sub>-<sup>B</sup>7). <sup>13</sup>C NMR (125 MHz, CDCl<sub>3</sub>)  $\delta$  = 202.36 (C-<sup>S</sup>1), 172.46 (CH<sub>2</sub>C(O)NH), 151.34 and 151.08 (2 NC(O)O-allyl), 148.06 (C-<sup>B</sup>2), 130.77 and 130.73 (2 CH=CH<sub>2</sub>), 119.42 and 119.29 (2 CH=CH<sub>2</sub>), 67.58 and 67.51 (2 CH<sub>2</sub>-allyl), 60.19 (C-<sup>B</sup>3a), 58.41 (C-<sup>B</sup>6a), 52.25 (C-<sup>B</sup>4), 43.53 (C-<sup>S</sup>2), 38.94 (C-<sup>S</sup>6), 36.29 and 36.06 (C-<sup>B</sup>6, C-<sup>B</sup>10), 29.23, 27.73, 27.15, 26.16 and 21.39 (C-<sup>B</sup>7, C-<sup>B</sup>8, C-<sup>B</sup>9, C-<sup>S</sup>3, C-<sup>S</sup>4, C-<sup>S</sup>5), 25.00 (C-<sup>S</sup>4). MS (ES<sup>+</sup>) 532.15 [M + Na]<sup>+</sup>. HRMS (FAB<sup>+</sup>) Calcd for C<sub>24</sub>H<sub>36</sub>N<sub>3</sub>O<sub>7</sub>S, [M + H]<sup>+</sup>: 510.2274. Found: 510.22716 (error: 0.5 ppm).

### Comparative Analytical Data for Doxorubicin

**HCl 3.** <sup>1</sup>H NMR (500 MHz, D<sub>2</sub>O, 27 °C)  $\delta$  = 7.46 (t,  $^3J$ (H-1, H-2) ~  $^3J$ (H-2, H-3) ~ 7.51 Hz, 1H; H-2), 7.20 (d,  $^3J$ (H-1, H-2) = 8.18 Hz, 1H; H-1), 7.12 (app s,  $J$  = 8.20 Hz, 1H; H-3), 5.40 (s, 1H; H-1'), 4.79 (d,  $^2J$  = 4.40 Hz, 2H; CH<sub>2</sub>-14), 4.67 (app s, 1H; H-7), 4.21 (q,  $^3J$ (H-5', CH<sub>3</sub>) = 6.56 Hz, 1H; H-5'), 3.85 (app s, 1H; H-4'), 3.77 (s, 3H; OCH<sub>3</sub>), 3.73 (m, 1H; H-3'), 2.81 (d,  $^2J$  = 17.56 Hz, 1H; H-10<sub>eq</sub>), 2.50 (d,  $^2J$  = 17.56 Hz, 1H; H-10<sub>ax</sub>), 2.23 (d,  $^2J$  = 10.11 Hz, 1H; H-8<sub>eq</sub>), 2.02 (m, 2H; CH<sub>2</sub>-2'), 1.93 (app d,  $^2J$  = 10.11 Hz, 1H; H-8<sub>ax</sub>), 1.29 (d,  $^3J$ (H-5', CH<sub>3</sub>) = 6.56 Hz, 3H; CH<sub>3</sub>). <sup>13</sup>C NMR (125 MHz, D<sub>2</sub>O, 27 °C)  $\delta$  = 213.75 (C-13), 185.84 and 185.64 (C-5, C-12), 160.61 (C-4), 155.89 (C-6), 154.28 (C-11), 136.99 (C-2), 134.11 (C-6a, C-12a), 133.66 (C-10a), 119.88 and 119.66 (C-1, C-3), 118.76 (C-4a), 110.67 and 111.60 (C-5a, C-11a), 99.10 (C-1'), 76.11 (C-9), 68.67 (C-7), 67.46 (C-5'), 66.59 (C-4'), 64.79 (C-14), 56.76 (OCH<sub>3</sub>), 47.17 (C-3'), 35.62 (C-8), 32.45 (C-10), 27.95 (C-2'), 16.16 (CH<sub>3</sub>). FT-IR (KBr) 3420, 1724, 1617, 1583, 1445, 1412, 1284, 1211, 11118, 1076, 1014, 987 cm<sup>-1</sup>. MS (ES<sup>+</sup>) 544.8 [M + H]<sup>+</sup>. HRMS (FAB<sup>+</sup>) Calcd for C<sub>27</sub>H<sub>29</sub>NO<sub>11</sub>, [M + H]<sup>+</sup>: 544.18187. Found: 544.18174 (error: 0.01 ppm). UV (H<sub>2</sub>O)  $\lambda_{\max}$  = 482 nm ( $\epsilon$  = 8277).

**N-[3-Phenyl-propyl]-doxorubicin 12.** The reductive alkylation of Doxorubicin hydrochloride was attempted first on a 50 mg scale using phenyl propionaldehyde as the substrate. (refer to compound **10** for details of the procedure). Chromatography on silica gel using chloroform-methanol (from 90:10 to 80:20) as eluent provided 21 mg of **12** as a red amorphous film (35% yield).

**Selected Analytical Data for Compound 12:** <sup>1</sup>H NMR (500 MHz, CD<sub>3</sub>OD, 27 °C)  $\delta$  = 7.88 (m, 1H; H-1), 7.81 (t,  $^3J$ (H-1, H-2) ~  $^3J$ (H-2, H-3) = 7.59 Hz, 1H; H-2),



7.55 (d,  $^3J(\text{H-2,H-3}) = 8.20$  Hz, 1H; H-3), 7.06–7.17 (m, 5H; Ar), 5.44 (s, 1H; H-1'), 5.05 (s, 1H; H-7), 4.70 (d,  $^2J = 3.30$  Hz, 2H; CH<sub>2</sub>-14), 4.24 (q,  $^3J(\text{H-5'},\text{CH}_3) = 6.54$  Hz, 1H; H-5'), 4.01 (s, 3H; OCH<sub>3</sub>), 3.75 (s, 1H; H-4'), 3.54 (m, 1H; H-3'), 3.05 (d,  $^2J = 18.36$  Hz, 1H; H-10<sub>eq</sub>), 2.97 (m, 2H; CH<sub>2</sub>-1'), 2.88 (d,  $^2J = 18.36$  Hz, 1H; H-10<sub>ax</sub>), 2.63 (app t,  $J = 8.50$  Hz, 2H; CH<sub>2</sub>-3'), 2.33 (d,  $^2J = 14.57$  Hz, 1H; H-8<sub>eq</sub>), 2.14 (app d,  $^2J = 14.57$  Hz, 1H; H-8<sub>ax</sub>), 1.91–2.06 (m, 4H; CH<sub>2</sub>-2', CH<sub>2</sub>-2''), 1.28 (d,  $^3J(\text{H-5'},\text{CH}_3) = 6.54$ , 3H; CH<sub>3</sub>). <sup>13</sup>C NMR (125 MHz, CD<sub>3</sub>OD, 27 °C)  $\delta = 215.90$  (C-13), 189.45 (C-5, C-12), 163.82 (C-4), 158.66 (C-6), 157.44 (C-11), 142.76 (Ar C-i), 138.61 (C-2), 137.68 (C-6a), 136.87 and 136.50 (C-10a, C-12a), 130.88 and 130.57 (Ar C-o, C-m), 128.65 (Ar C-p), 122.82 (C-4a), 121.85 and 121.70 (C-1, C-3), 113.52 (C-5a, C-11a), 102.44 (C-1'), 78.27 (C-9), 72.91 (C-7), 69.14 (C-5'), 67.59 (C-4'), 66.87 (C-14), 58.43 (OCH<sub>3</sub>), 56.35 (C-3'), 46.26 (C-1'), 38.62 (C-8), 34.86 (C-10, C-3''), 29.99 and 29.73 (C-2', C-2''), 18.24 (CH<sub>3</sub>). MS (ES<sup>+</sup>) 662.3 [M + H]<sup>+</sup>. HRMS (FAB<sup>+</sup>) Calcd for C<sub>36</sub>H<sub>39</sub>NO<sub>11</sub>, [M + H]<sup>+</sup>: 662.26011. Found: 662.25892 (error: 1.8 ppm).

**N3'-[N1,N3-bis(alloc)]Biotinyl-6-aminohexanyl]-doxorubicin 10.** A 1 M solution of NaCNBH<sub>3</sub> in tetrahydrofuran (200  $\mu$ L, 0.200 mmol, 0.255 equiv) was added to a stirred solution of doxorubicin hydrochloride (457.5 mg, 0.7888 mmol), [N1,N3-bis(alloc)]biotinyl-6-aminohexanal (982 mg, 1.9269 mmol, 2.44 equiv) and glacial AcOH (100  $\mu$ L, 2.13 equiv) in degassed CH<sub>3</sub>CN–H<sub>2</sub>O (2:1) (50 mL). The mixture was maintained under a nitrogen atmosphere at ambient temperature in the absence of light. The progress of the reaction was monitored by TLC in CHCl<sub>3</sub>/MeOH (4:1). When reaction was complete (after 5h30), the solution was concentrated under vacuum, then diluted with CH<sub>2</sub>Cl<sub>2</sub> (250 mL), and extracted repeatedly (5  $\times$  80 mL) with CH<sub>2</sub>Cl<sub>2</sub>–MeOH (9:1). The product was purified by column chromatography on silica gel using CHCl<sub>3</sub>–MeOH (from 95:5 to 50:50) as the eluent to yield 268 mg (0.2584 mmol, 33% yield) of N3'-[N1,N3-bis(alloc)]biotinyl-6-aminohexanyl]-doxorubicin ( $R_f = 0.5$  in CHCl<sub>3</sub>–MeOH 4:1) as a red amorphous film. A 76 mg (0.07314 mmol, 9%) sample of the reduced form of the conjugate (both rings B and C in hydroquinone form) ( $R_f = 0.27$  in CHCl<sub>3</sub>–MeOH 4:1) was additionally isolated from the chromatography.

<sup>1</sup>H NMR (500 MHz, CDCl<sub>3</sub>, 27 °C)  $\delta = 7.98$  (d,  $^3J(\text{H-1,H-2}) = 7.62$  Hz, 1H; H-1), 7.58 (t,  $^3J(\text{H-1,H-2}) \sim ^3J(\text{H-2,H-3}) \sim 8.08$  Hz, 1H; H-2), 7.37 (d,  $^3J(\text{H-2,H-3}) = 8.44$  Hz, 1H; H-3), 5.92 (ddd,  $J = 22.76$  Hz, 10.68 Hz, 5.48 Hz, 2H; 2 vinyl CH), 5.51 (d,  $^3J(\text{H-1'},\text{H-2'}) = 2.79$  Hz, 1H; H-1'), 5.41 (dd,  $^3J = 17.16$  Hz,  $^2J \sim 1.23$  Hz, 2H; 2 terminal cis vinyl CH), 5.27 (dt,  $^3J = 10.44$  Hz,  $^2J \sim 1.23$  Hz, 2H; 2 terminal trans vinyl CH), 5.24 (br s, 1H; H-7), 4.58–4.80 (m, 8H; 2 allyl CH<sub>2</sub>–O, CH<sub>2</sub>-14, H-B<sub>3a</sub>, H-B<sub>6a</sub>), 3.98–4.07 (m, 1H; H-5'), 4.05 (s, 3H; OCH<sub>3</sub>), 3.89 (br s, 1H; H-4'), 3.46 (m, 1H; H-B<sub>4</sub>), 3.26 (m, 2H; H-S<sub>6i</sub>, H-10<sub>i</sub>), 3.15 (m, 3H; H-3', H-S<sub>6ii</sub>, H-B<sub>6i</sub>), 2.99 (d,  $^2J = 18.72$  Hz, 1H; H-10<sub>ii</sub>), 2.92 (dd,  $^2J = 13.10$  Hz,  $^3J(\text{H-B}_{6a},\text{H-B}_{6ii}) = 5.24$  Hz, 1H; H-B<sub>6ii</sub>), 2.75 (m, 2H; CH<sub>2</sub>-S<sub>1</sub>), 2.35 (d,  $^2J = 14.59$  Hz, 1H; H-8<sub>i</sub>), 1.80–2.20 (m, 5H; CH<sub>2</sub>-2', CH<sub>2</sub>-B<sub>10</sub>, H-8<sub>ii</sub>), 1.40–1.70 (m, 6H; CH<sub>2</sub>-B<sub>9</sub>, CH<sub>2</sub>-S<sub>2</sub>, CH<sub>2</sub>-S<sub>5</sub>), 1.31 (d,  $^3J(\text{H-5'},\text{CH}_3) = 6.41$  Hz, 3H; CH<sub>3</sub>), 1.13–1.38 (m, 8H; CH<sub>2</sub>-B<sub>7</sub>, CH<sub>2</sub>-B<sub>8</sub>, CH<sub>2</sub>-S<sub>3</sub>, CH<sub>2</sub>-S<sub>4</sub>). <sup>13</sup>C NMR (125 MHz, CDCl<sub>3</sub>, 27 °C)  $\delta = 213.74$  (C-13), 186.65 and 186.35 (C-5, C-12), 172.84 (CH<sub>2</sub>C(O)NH), 160.91 (C-4), 156.20 (C-6), 155.38 (C-11), 151.32 and 151.06 (2 NC(O)O–allyl), 148.32 (C-B<sub>2</sub>), 135.69 (C-2), 135.15 (C-6a), 133.76 and 133.67 (C-10a, C-12a), 130.89 and 130.87 (2 CH=CH<sub>2</sub>), 120.53 (C-4a), 119.64 (C-1), 119.54 and 119.37 (2 CH=CH<sub>2</sub>), 118.47 (C-3), 111.25 and 111.10 (C-5a, C-11a),

100.14 (C-1'), 76.37 (C-9), 69.30 (C-7), 67.66 and 67.57 (2 CH<sub>2</sub>-allyl), 66.90 (C-5'), 65.95 (C-4'), 65.35 (C-14), 60.29 (C-B<sub>3a</sub>), 58.56 (C-B<sub>6a</sub>), 56.58 (OCH<sub>3</sub>), 53.84 (C-3'), 52.42 (C-B<sub>4</sub>), 45.31 (CH<sub>2</sub>-S<sub>1</sub>), 39.09 (CH<sub>2</sub>-S<sub>6</sub>), 36.21 and 36.16 (C-2', C-B<sub>10</sub>, C-10 or C-B<sub>6</sub>), 35.48 (C-8), 33.53 (C-B<sub>6</sub> or C-10), 29.60, 29.12, 27.84, 27.26, 27.02, 26.27, 26.17 and 25.10 (C-B<sub>7</sub>, C-B<sub>8</sub>, C-B<sub>9</sub>, C-S<sub>2</sub>, C-S<sub>3</sub>, C-S<sub>4</sub>, C-S<sub>5</sub>), 16.87 (CH<sub>3</sub>). MS (ES<sup>+</sup>) 1037.4 [M]<sup>+</sup>.

**N3'-[Biotinyl-6-aminohexan]-yl]-doxorubicin Hydrochloride 11.** A solution of N3'-[N1,N3-bis(alloc)]-biotinyl-6-aminohexanyl]-doxorubicin (206 mg, 0.1986 mmol) in degassed CH<sub>2</sub>Cl<sub>2</sub>–MeOH (2:1) (6 mL) was treated with *N,N*-dimethylbarbituric acid (24 mg, 0.1537 mmol, 0.77 equiv) and tetrakis(palladium) (0) triphenylphosphine (46 mg, 0.03972 mmol, 0.2 equiv). The reaction mixture was stirred in the absence of light under a nitrogen atmosphere at ambient temperature for 3 h. The solvents were evaporated (30 °C), and the dark red film was suspended in 2 mL of MeOH. The suspension was filtered, and the material soluble in MeOH was treated at 0 °C with diethyl ether (10 mL) and a 1 M solution of HCl in diethyl ether (1.55 mL). After 10 min, the mixture was cooled to –40 °C to afford more efficient precipitation of the N3'-[biotinyl-6-aminohexan]-yl]-doxorubicin hydrochloride. The filtrate was decanted, and the precipitate was repeatedly suspended in cold diethyl ether (10 mL), triturated, and sonicated until the pH of the filtrate was approximately 3–4. Then the precipitate was suspended in degassed water (10 mL) and worked up with diethyl ether (5  $\times$  3 mL). The crude material insoluble in MeOH was suspended in water (20 mL) and the insoluble residue discarded. The aqueous solution was treated at 0 °C with a few drops of a 0.1M HCl in order to adjust the pH to  $\sim$ 3. The solution was then diluted with water (50 mL) and worked up with diethyl ether. Aqueous layers were combined and filtered through a small layer of reverse-phase C18 support in order to discard the palladium salts. The support was washed with degassed water (2  $\times$  10 mL) and the product eluted selectively with degassed water–acetonitrile mixture (1:1) (6  $\times$  10 mL). The fractions were analyzed by TLC and by (ES<sup>+</sup>)MS. The fractions containing the conjugate **11** ( $R_f = 0.15$  in CHCl<sub>3</sub>–MeOH 4:1) were evaporated, and the combined residue was lyophilised to afford N3'-[Biotinyl-6-aminohexan]-yl]-doxorubicin hydrochloride (136 mg, 0.1504 mmol, 76% yield) as an orange solid. <sup>1</sup>H NMR (500 MHz, CD<sub>3</sub>OD, 27 °C)  $\delta = 7.79$  (m, 2H; H-1, H-3), 7.52 (app t,  $^3J(\text{H-1,H-2}) \sim ^3J(\text{H-2,H-3}) \sim 4.81$  Hz, 1H; H-2), 5.47 (app s, 1H; H-1'), 4.99 (app d,  $^3J(\text{H-7,H-8}) = 2.33$  Hz, 1H; H-7), 4.77 (d,  $^2J = 4.55$  Hz, 2H; CH<sub>2</sub>-14), 4.51 (m, 1H; H-B<sub>6a</sub>), 4.30 (m, 2H; H-B<sub>3a</sub>, H-5'), 4.02 (s, 3H; OCH<sub>3</sub>), 3.88 (app s, 1H; H-4'), 3.59 (app t,  $^3J(\text{H-2'},\text{H-3'}) \sim 8.68$  Hz, 1H; H-3'), 3.19 (m, 2H; H-B<sub>4</sub>, H-S<sub>6i</sub>), 3.10 (app t,  $J = 6.87$  Hz, 1H; H-S<sub>6ii</sub>), 2.92–3.06 (m, 3H; H-10<sub>eq</sub>, CH<sub>2</sub>-S<sub>1</sub>), 2.92 (dd,  $^2J = 12.84$  Hz,  $^3J(\text{H-B}_{6a},\text{H-B}_{6anti}) = 8.15$  Hz, 1H; H-B<sub>6anti</sub>), 2.81 (d,  $^2J = 18.34$  Hz, 1H; H-10<sub>ax</sub>), 2.71 (d,  $^2J = 12.84$  Hz, 1H; H-B<sub>6syn</sub>), 2.36 (app dd,  $^2J \sim 15.56$  Hz,  $^3J(\text{H-7,H-8}_{eq}) \sim 1.72$  Hz, 1H; H-8<sub>eq</sub>), 2.12–2.31 (m, 3H; H-8<sub>ax</sub>, CH<sub>2</sub>-B<sub>10</sub>), 2.09 (app d,  $^3J(\text{H-2'},\text{H-3'}) = 8.21$  Hz, 2H; CH<sub>2</sub>-2'), 1.24–1.81 (m, 14H; CH<sub>2</sub>-B<sub>7</sub>, CH<sub>2</sub>-B<sub>8</sub>, CH<sub>2</sub>-B<sub>9</sub>, CH<sub>2</sub>-S<sub>2</sub>, CH<sub>2</sub>-S<sub>3</sub>, CH<sub>2</sub>-S<sub>4</sub>, CH<sub>2</sub>-S<sub>5</sub>), 1.33 (d,  $^3J(\text{H-5'},\text{CH}_3) = 6.87$  Hz, 3H; CH<sub>3</sub>). <sup>13</sup>C NMR (125 MHz, CD<sub>3</sub>OD, 27 °C)  $\delta = 215.59$  (C-13), 188.58 and 188.35 (C-5, C-12), 176.79 (CH<sub>2</sub>C(O)NH), 166.76 (C-B<sub>2</sub>), 163.20 (C-4), 158.09 (C-6), 156.81 (C-11), 138.09 (C-2), 136.91 (C-6a), 136.35 and 135.98 (C-10a, C-12a), 122.09 (C-4a), 121.29 and 121.22 (C-1, C-3), 113.12 and 112.87 (C-5a, C-11a), 101.88 (C-1'), 77.79 (C-9), 72.20 (C-7), 68.69 (C-5'), 67.04 (C-4'), 66.49 (C-14), 64.29 (C-B<sub>3a</sub>), 62.56 (C-B<sub>6a</sub>),

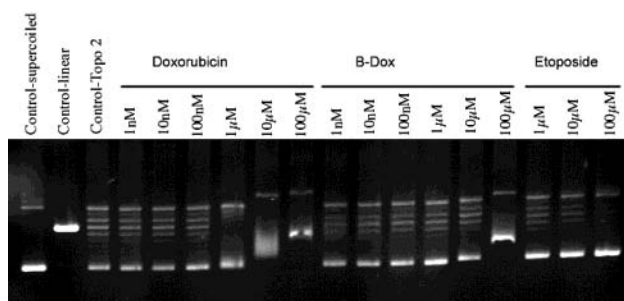
57.98 and 57.78 (OCH<sub>3</sub>, C-<sup>B</sup>4), 55.95 (C-3'), 46.29 (C-<sup>S</sup>1), 41.81 (C-<sup>B</sup>6), 40.78 (C-<sup>S</sup>6), 38.05 (C-8), 34.43 (C-10), 29.23 (C-2'), 37.55, 37.49, 30.89, 30.26, 28.02, 27.95, 27.77, and 27.67 (C-<sup>B</sup>10, C-<sup>B</sup>7, C-<sup>B</sup>8, C-<sup>B</sup>9, C-<sup>S</sup>2, C-<sup>S</sup>3, C-<sup>S</sup>4, C-<sup>S</sup>5), 17.82 (CH<sub>3</sub>). MS (ES<sup>+</sup>) 869.4 [M]<sup>+</sup>. HRMS (FAB<sup>+</sup>) Calcd for C<sub>43</sub>H<sub>56</sub>N<sub>4</sub>O<sub>13</sub>S, [M + H]<sup>+</sup>: 869.36426. Found: 869.36293 (error: 1.5 ppm). FT-IR(KBr):  $\nu$  = 3378, 2936, 2860, 1683, 1618, 1579, 1445, 1414, 1286, 1211, 1117, 1082, 1018, 992 cm<sup>-1</sup>. UV/Vis (H<sub>2</sub>O):  $\lambda_{\text{max}}$  = 487 nm ( $\epsilon$  = 9240).

**Avidin Binding Assay.** The conjugate **11** (B-Dox) was assayed for avidin binding using the size exclusion HPLC methodology developed by Wilbur et al. (15, 16), where the Doxorubicin moiety of the conjugate is the dye, and with a few modifications described below: (1) Duplicate samples containing avidin (4.4 nmol) in phosphate buffer and compound **11** (18 nmol) in 10% aq. DMSO were incubated at 25 °C for 1 h before an aliquot of 100  $\mu$ L was removed for HPLC analysis. Then, 233 nmol (76 equiv.) of biotin was added to the samples, and the very low displacement of avidin-bound **11** by biotin was monitored by size exclusion HPLC for at least 48 h (using triplicate samples). (2) Since the free conjugate **11** (MW 869) was not eluted from the TSK G5000 PW column after 2 h, the HPLC analysis was performed in a slightly different way to that reported in refs 15 and 16: only the avidin-bound **11** was detected at the maximum wavelength corresponding to the biotinylated dye ( $\lambda_{\text{max}}$  = 487 nm). Integration of this peak compared to the integration of the peak corresponding to the "total" quantity of avidin in the sample (HPLC trace at 280 nm) allows monitoring the percentage of displacement by biotin of the avidin-bound **11** over the time, using the "total avidin" as an internal standard. Due to the very small relative increase in molecular weight generated by binding of **11** to avidin (MW ~ 68 kDa) free avidin and avidin-bound **11** coelute in the conditions of the HPLC assay (retention time  $t_R$  = 8.95 min). Diode array detection (Shimadzu, SPD-M10A) affords a straightforward dual-wavelength readout. B-Dox (**11**) binds tightly to avidin, since the incubation of **11** with 76 mol equiv of biotin affords only 27% of displacement after 24 h. HPLC analysis of a blank (avidin incubated in absence of conjugate **11**) affords a complete flat chromatogram at 487 nm, whereas the analysis of a sample containing avidin (4.4 nmol) and Doxorubicin (18 nmol) in place of **11** after a 12 h incubation as described above allowed to ensure that if some nonspecific avidin binding occurs (due to possible hydrophobic interactions with the drug), it is not detectable in the conditions of the assay.

**Topoisomerase II Relaxation Assay.** Each reaction contained 250ng supercoiled plasmid pBR322 (New England Biolabs). Reactions in a final volume of 20  $\mu$ L were carried out in 10mM Tris-HCl, pH 7.9, containing 50 mM NaCl, 50 mM KCl, 5 mM MgCl<sub>2</sub>, 100  $\mu$ M EDTA, 15  $\mu$ g/mL BSA, 1mM ATP. Test compound and 5 units Topoisomerase II (Amersham Pharmacia Biotech) were added on ice, and the mixture was incubated at 30 °C for 15 min. Reactions were stopped by the addition of 2  $\mu$ L 7mM EDTA/0.77% SDS. A 2  $\mu$ L gel loading buffer was added, and samples electrophoresed on a 1% agarose gel for approximately 2.5 h at 100V. DNA was stained with ethidium bromide (0.5  $\mu$ g/mL) and visualized under UV. Data are shown in Figure 1.

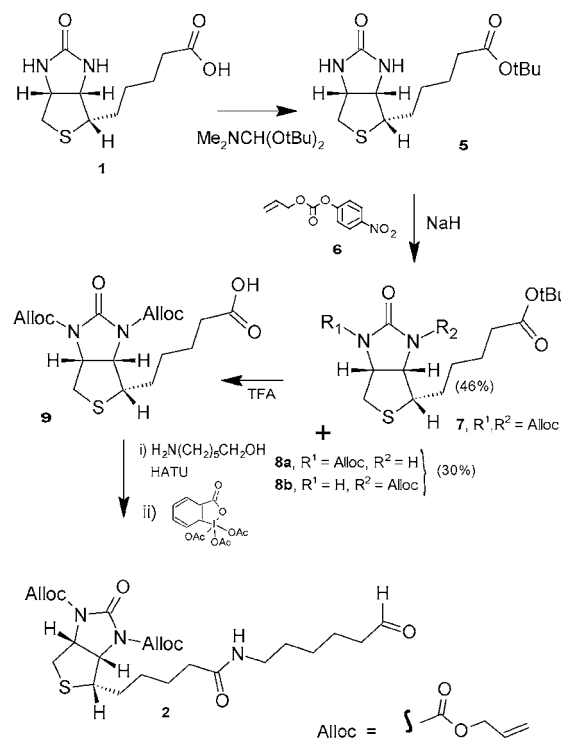
## RESULTS AND DISCUSSION

The bis-alloc-protected biotin aldehyde derivative was synthesized as shown in Scheme 1. Biotin *tert*-butyl ester **5** was treated with allyl *para*-nitrophenyl carbonate, in

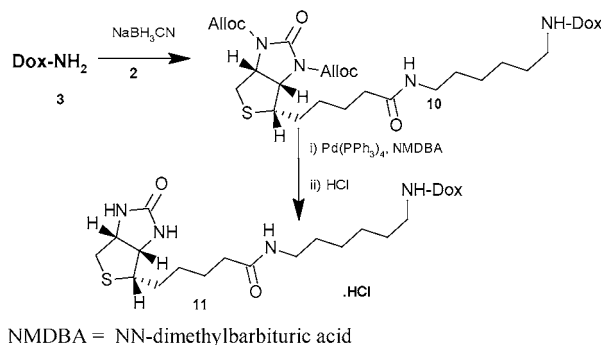


**Figure 1.** Topoisomerase II activity of biotinylated doxorubicin (B-dox) **11** compared to free doxorubicin and etoposide.

## Scheme 1. Synthesis of the Biotin Aldehyde

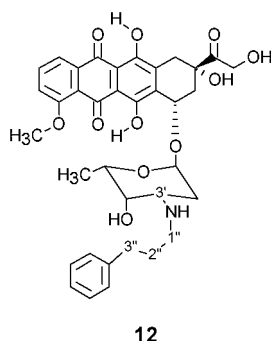


## Scheme 2. Reductive Alkylation of Doxorubicin



a two step procedure to give the *N1,N3*-bis-alloc compound **7** together with the mono alloc regioisomers **8a**/**8b** in 46% and 30% yield. Difficulty in realizing clean bis-protection of *N1* and *N3* positions of biotin has been noted by others (17, 18). Cleavage to the acid **9** was followed by coupling with 6-aminohexanol using HATU. Dess–Martin periodinane oxidation gave bis-(*N1,N3*)-alloc protected biotinyl-6-aminohexanal **2**.

The reductive alkylation of doxorubicin HCl **3** by **2** using NaCNBH<sub>3</sub> is shown in Scheme 2. This procedure gave the alloc protected conjugate **10** in 33% yield. The

**Chart 3. Doxorubicin Derivative Utilized as a Model Compound**

structure of **10** was confirmed with the aid of 2D COSY and HMQC spectra. Deprotection of **10** using Pd[0] in the presence of *N,N*-dimethylbarbituric acid (NMDBA) as scavenger gave biotin-doxorubicin conjugate **11** (B-Dox) in 76% yield.

B-Dox **11** showed strong binding to avidin protein and was not displaced by a large excess of free biotin (data not shown). Electrophoretic analysis of DNA topoisomerase activity is shown in Figure 1. Each lane contains 250 ng of supercoiled plasmid DNA (pBR322). Addition of topoisomerase II cuts the DNA and the fragments appear as separate bands. This activity is inhibited by doxorubicin (1–10  $\mu$ M) and etoposide (100  $\mu$ M). The B-Dox **11** has activity in the range of 10–30-fold less than doxorubicin (10–100  $\mu$ M). Some loss in activity for attachment of a reporter molecule is observed in other systems (3).

The reductive alkylation of Doxorubicin hydrochloride was conducted first on a 50 mg scale using phenyl propionaldehyde as the substrate. The "test" conjugate **12** (Chart 3) obtained in this way proved very useful for the complete assignment of NMR data of the bis(alloc)-biotin-doxorubicin conjugate **10** and its deprotected derivative **11**.

**CONCLUSIONS**

Reductive alkylation is a process carried out under weakly acidic (NaCNBH<sub>3</sub>) or neutral (pyridine–BH<sub>3</sub>) conditions and is compatible with sensitive and complex functionality. It is also compatible with attachment to proteins (19), via their lysine side chains, without altering the charge state on the amine functionality. Alloc removal using Pd[0] may be effected under aqueous conditions (20, 21), in addition biocompatible Pd[0] Sonogashira couplings are reported (22). Our novel derivative may find therefore find use as an alternative biotinylation reagent for proteins. Experiments to validate the use of **2** and similar reagents for biotinylation of proteins are in progress.

**ACKNOWLEDGMENT**

The authors thank Prof John Hartley Cancer Research-UK, for the topoisomerase assays. This work was supported by Ark Therapeutics Ltd.

**Supporting Information Available:** 2D NMR spectra for **10**. This material is available free of charge via the Internet at <http://pubs.acs.org>.

**LITERATURE CITED**

- (1) Green, N. M. (1975). *Adv. Protein Chem.* 29, 85–133.
- (2) Lehtolainen, P., Taskinen, A., Laukkanen, J., Airenne, K. J., Heino, S., Lappalainen, M., Ojala, K., Marjomaki, V., Martin, J. F., Kulomaa, M. S., and Yla-Herttuala, S. (2002) Cloning and characterisation of scavadin, a fusion protein for the targeted delivery of biotinylated molecules. *J. Biol. Chem.* 277, 8545–50.
- (3) Wang, Y., Yuan, H., Wright, S. C., Wang, H., and Larrick, J. W. (2002) Synthesis and cytotoxicity of a biotinylated CC-1065 analogue. *BMC. Chem. Biol.* 2, 1. For optimization of the design of the biotin linkers see Wilbur, D. S., Chyan, M. K., Pathare, P. M., Hamlin, D. K., Frownfelter, M. B., Kegley, B. B. (2000) Biotin reagents for antibody pretargeting 4. Selection of biotin conjugates for in vivo application based on their dissociation rate from avidin and streptavidin. *Bioconjugate Chem.* 11, 569–583.
- (4) Kodama, T., Doi, T., Suzuki, H., Takahashi, K., Wada, Y., and Gordon, S. (1996) Collagenous macrophage scavenger receptors. *Curr. Opin. Lipidol.* 7, 287–291.
- (5) Rodrigues, P. C., Beyer, U., Schumacher, P., Roth, T., Fiebig, H. H., Unger, C., Messori, L., Orioli, P., Paper, D. H., Mulhaupt, R., and Kratz, F. (1999) Acid-sensitive polyethylene glycol conjugates of doxorubicin: preparation, in vitro efficacy and intracellular distribution. *Bioorg. Med. Chem.* 7, 2517–2524.
- (6) Farquhar, D., Cherif, A., Bakina, E., and Nelson, J. A. Intensely potent doxorubicin analogues: structure–activity relationship (1998) *J. Med. Chem.* 41, 965–972.
- (7) Cherif, A., and Farquhar, D. (1992) N–(5,5-diacetoxypent-1-yl)doxorubicin: a new intensely potent doxorubicin analogue. *J. Med. Chem.* 35, 3208–3214.
- (8) Liu, F. T., and Leonard, N. J. (1979) Avidin–biotin interaction. Synthesis, oxidation, and spectroscopic properties of linked models. *J. Am. Chem. Soc.* 101, 996–1005.
- (9) Lavielle, S., Bory, S., Moreau, B., Luche, M. J., and Marquet, A. (1978) A total synthesis of biotin based on the stereoselective alkylation of sulfoxides. *J. Am. Chem. Soc.* 100, 1558–1563.
- (10) Field, G. F., Zally, W. J., Sternbach, L. H., and Blount, J. F. (1976) *J. Org. Chem.* 41, 3853–3857.
- (11) Sundberg, S. A., Barrett, R. W., Pirrung, M., Lu, A. L., Kiangsoontra, B., and Holmes, C. P. (1995) Spatially-Addressable Immobilization of Macromolecules on Solid Supports *J. Am. Chem. Soc.* 117, 12050–12057.
- (12) Finn, F. M., Titus, G., and Hofmann, K. (1984) Ligands for insulin receptor isolation. *Biochemistry.* 23, 2554–2558.
- (13) Ikura, M., and Hikichi, K. (1982) Application of two-dimensional NMR spectroscopy to the complete analysis of the proton and carbon-13 NMR spectra of d-biotin in aqueous solution. *Organic Magnetic Resonance.* 20(4), 266–273.
- (14) Barthwal, R., Srivastava, N., Sharma, U., and Govil, G. (1994) A 500 MHz proton NMR study of the conformation of adriamycin. *J. Mol. Struct.* 327, 201–220. See also: Mondelli, R., Ragg, E., Fronza, G., and Arnone, A. (1987) *J. Chem. Soc., Perkin Trans. 2*, 15–32.
- (15) Wilbur, D. S., Chyan, M.-K., Pathare, P. M., Hamlin, D. K., Frownfelter, M. B., and Kegley, B. B. (2000) Biotin reagents for antibody pretargeting. 4. Selection of biotin conjugates for in vivo application based on their dissociation rate from avidin and streptavidin. *Bioconjugate Chem.* 11 (4), 569–583.
- (16) Wilbur, D. S., Pathare, P. M., Hamlin, D. K., Frownfelter, M. B., Kegley, B. B., Leung, W.-Y., Gee, K. R. (2000) Evaluation of biotin-dye conjugates for use in an HPLC assay to assess relative binding of biotin derivatives with avidin and streptavidin. *Bioconjugate Chem.* 11 (4), 584–598.
- (17) Alves, A. M., Holland, D., and Edge, M. D. (1989) A chemical method of labeling oligodeoxyribonucleotides with biotin: A single step procedure using a solid-phase methodology. *Tetrahedron Lett.* 30, 3089–3092.
- (18) Amspacher, D. R., Blanchard, C. Z., Fronczek, F. R., Saraiva, M. C., Waldrop, G. L., and Strongin, R. M. (1999) Synthesis of a reaction intermediate analogue of biotin-dependent carboxylases via a selective derivatization of biotin. *Organic Lett.* 1, 99–102.



- (19) Carlsson, J., Blomquist, E., Gedda, L., Liljegren, A., Malmstrom, P. U., Sjostrom, A., Sundin, A., Westlin, J. E., Zhao, Q., Tolmachev, V. et al. (1999) Conjugate chemistry and cellular processing of EGF-dextran. *Acta Oncol.* 38, 313–321.
- (20) Genet, J. P., Blart, E., Savignac, M., Lemeune, S., and Paris, J. M. (1993) Palladium-catalyzed reactions in aqueous media. An efficient removal of allyloxycarbonyl protecting group from oxygen and nitrogen. *Tetrahedron Lett.* 34, 4189–4192.
- (21) Lemaire-Audoire, S., Savignac, M., Blart, E., Bernard, J. M., and Genet, J. P. (1997) Synthesis of Peptides Using Palladium Promoted Selective Removal of Allyloxycarbonyl Protecting Groups in Aqueous Medium. *Tetrahedron Lett.* 38, 2955–2958.
- (22) Dibowski, H., Schmidtchen, F. P. (1998) Sonogashira Cross-Couplings Using Biocompatible Conditions in Water. *Tetrahedron Lett.* 39, 525–528.

BC0255992

# Spectroscopic Study and Evaluation of Red-Absorbing Fluorescent Dyes

Volker Buschmann,<sup>†</sup> Kenneth D. Weston,<sup>‡</sup> and Markus Sauer<sup>\*,†</sup>

Physikalisch-Chemisches Institut, Universität Heidelberg, Im Neuenheimer Feld 253, 69120 Heidelberg, Germany and Department of Chemistry and Biochemistry, Florida State University, Tallahassee, Florida 32306. Received September 4, 2002; Revised Manuscript Received October 21, 2002

The spectroscopic characteristics (absorption, emission, and fluorescence lifetime) of 13 commercially available red-absorbing fluorescent dyes were studied under a variety of conditions. The dyes included in this study are Alexa647, ATTO655, ATTO680, Bodipy630/650, Cy5, Cy5.5, DiD, DY-630, DY-635, DY-640, DY-650, DY-655, and EVOblue30. The thorough characterization of this class of dyes will facilitate selection of the appropriate red-absorbing fluorescent labels for applications in fluorescence assays. The influences of polarity, viscosity, and the addition of detergent (Tween20) on the spectroscopic properties were investigated, and fluorescence correlation spectroscopy (FCS) was utilized to assess the photophysical properties of the dyes under high excitation conditions. The dyes can be classified into groups based on the results presented. For example, while the fluorescence quantum yield of ATTO655, ATTO680, and EVOblue30 is primarily controlled by the polarity of the surrounding medium, more hydrophobic and structurally flexible dyes of the DY-family are strongly influenced by the viscosity of the medium and the addition of detergents. Covalent binding of the dyes to biotin and subsequent addition of streptavidin results in reversible fluorescence quenching or changes in the relaxation time of other photophysical processes of some dyes, most likely due to interactions with tryptophan residues in the streptavidin binding site.

## INTRODUCTION

The interest in fluorescent dyes for qualitative and quantitative assays has increased considerably during the last 20 years (1–4). The sensitivity, simplicity, and selectivity of fluorescence-based techniques make them particularly attractive for *in vitro* and *in vivo* cellular and molecular biology studies (5). There are several major advantages of using fluorescent dyes that absorb in the red over those that absorb at shorter blue and green wavelengths. The most important of these advantages is the reduction in background that ultimately improves the sensitivity achievable. There are three major sources of background: (i) elastic scattering, i.e., Rayleigh scattering, (ii) inelastic scattering, i.e., Raman scattering, and (iii) fluorescence from impurities. The efficiencies of both Rayleigh and Raman scattering are dramatically reduced by shifting to longer wavelength excitation. (scales with the  $1/\lambda^4$ ). Likewise, the number of fluorescent impurities is significantly reduced with longer excitation and detection wavelengths (6–8). Besides reduced background, a further advantage is that low-cost, energy efficient, rugged diode lasers can be used in place of the more expensive and shorter lived gas lasers. A variety of highly sensitive detectors in the visible-near-IR region are now available. A recent report demonstrated that the use of red-absorbing fluorescent labels and diode laser excitation at 635 nm provides sufficiently low autofluorescence of biological samples so that individual antigen and antibody molecules can be detected in human serum samples (21, 22).

The advantages of red-absorbing fluorophores has prompted current efforts to develop new fluorescent dyes which absorb and emit above 620 nm but still exhibit a sufficient fluorescence quantum yield, especially in an aqueous surrounding (9–11). Among these new red-absorbing dyes are rhodamine (10, 12), bora-diaza-indacene (4, 13), oxazine (10, 14), squaraine (15, 16), and indocarbocyanine dyes (17–20). Excitation in the red spectral region is also advantageous when working with live cells because of reduced cell damage (23).

Several applications benefit from efficient red-absorbing fluorescent dyes when used in combination with shorter wavelength dyes to increase the spectral range over which detection is possible. In multicolor imaging, the number of simultaneously imaged species can be increased by including red and near-IR absorbing dyes (24). Red-absorbing fluorescent dyes are also needed as acceptors in fluorescence resonance energy transfer (FRET) measurements (25–27). Red-absorbing dyes are also useful in dual-laser fluorescence cross-correlation experiments (28, 29).

The absorption and emission spectra, fluorescence quantum yield, and fluorescence lifetime of dyes often vary with environmental conditions. Thus, many fluorescent dyes can be used as sensors to probe their local environments in biological and analytical applications. For example, coumarin (30), rhodamine (10, 31, 32), oxazine (33), and bora-diaza-indacene (34) dyes are known to be efficiently quenched by the nucleobase guanosine (dG) and the amino acid tryptophan (Trp). It has been proposed that the mechanism of fluorescence quenching is a photoinduced electron transfer reaction from the guanosine or tryptophan ground-state to the excited singlet state of the dye. The difference between dG or Trp and the other DNA bases and amino acids can

\* To whom correspondence should be addressed. Phone: +49-6221-548460, Fax: +49-6221-544255, E-mail: sauer@urz.uni-heidelberg.de.

<sup>†</sup> Universität Heidelberg.

<sup>‡</sup> Florida State University.

be attributed to their low oxidation potential (30, 35). Although this quenching effect is not always desirable, it can be used to develop new, highly sensitive probes for the detection of specific DNA sequences (36) or proteins (22). Others examples of the sensitivity of fluorescent dyes to their local surroundings is the increase in fluorescence intensity and lifetime of some dyes, such as DY-630 and DY-635, upon binding to bovine serum albumin (BSA) (37) and the dependence of the cis/trans isomerization rate in some indocarbocyanine dyes on the viscosity of the surrounding medium (38, 39).

An understanding of the dependence of the spectroscopic properties of fluorescent dyes on environmental conditions is crucial for the development of new fluorescence-based assays. Fluorescence quenching effects such as those mentioned above are especially important in fluorescence resonance energy transfer (FRET)-applications, where spectral shifts, fluorescence lifetime, quantum yield changes, and changes in the isomerization rates of the donor or acceptor dye influence the measured FRET efficiencies.

Motivated by these considerations, we studied the spectroscopic characteristics of most of the commercially available fluorescent dyes that absorb and emit in the wavelength range of 640–700 nm and can be conjugated to biological molecules. The fluorescence quantum yield and excited state lifetime of dyes are influenced by the rate of internal conversion, which is controlled by the rigidity of the dye structure (40). Since highly viscous solvents impair structural mobility, an increase in fluorescence lifetime and quantum yield is expected with increasing solvent viscosity. The influence of viscosity on the spectroscopic parameters was examined by measuring the spectral properties of the dyes in solvent mixtures of water and glycerin. The influence of solvent polarity on the spectral properties was investigated by comparing measurements in water and ethanol.

To reveal the photophysical properties of the dyes under high excitation conditions, fluorescence correlation spectroscopy (FCS) measurements were performed. FCS permits measurements of a number of photophysical properties of fluorescent dyes such as the triplet lifetime, intersystem crossing yield, photoinduced isomerization, and photobleaching rates (41) and is commonly used in fluorescence assays. An often-neglected effect that dramatically influences the achievable detection sensitivity is the hydrophobicity of the dye structure. Very hydrophobic dyes often aggregate or form dimers in aqueous solvents. Therefore, often in fluorescence assays utilizing hydrophobic fluorophores, a detergent such as Tween20 (a nonionic detergent) is included in the buffer to facilitate solvation and prevent dimerization. Consequently, the photophysical characteristics of all red-absorbing fluorescent dyes were also investigated in aqueous medium containing Tween20.

The strong binding of biotin to the 60 kDa protein streptavidin ( $K_D = 10^{-15}$  M) has become a standard tool in molecular biology (42, 43). Each hydrophobic binding pocket of streptavidin contains four tryptophan residues that are involved in strong biotin binding (46). Because of the importance of the biotin–streptavidin techniques, dyes were covalently attached to biotin and the effect of binding the conjugates to streptavidin was investigated. Quenching or dequenching of the dye's fluorescence upon binding have been observed and were attributed to dye/dye interactions, such as the formation of nonfluorescent dimers or quenching interactions between the dye and the tryptophan-containing binding pocket of streptavidin (44, 45).

## EXPERIMENTAL PROCEDURES

**Fluorescent Dyes and Conjugates.** The dyes used in this study were obtained as *N*-hydroxysuccinimidyl esters. ATTO 655 and ATTO 680 were purchased from ATTO-TEC (Siegen, Germany), Alexa 647, DiD (DiIC<sub>18</sub> (5)), and Bodipy630/650 from Molecular Probes (Göttingen, Germany), Cy5 and Cy5.5 from Amersham Pharmacia Biotech (Freiburg, Germany), and DY-630, DY-635, DY-640, DY-650, DY-655, and EvoBlue30 from Dyomics (Jena, Germany). When dissolved in water, *N*-hydroxysuccinimidyl esters are believed to be deactivated within minutes to hours.

For the biotin–streptavidin studies, the activated dye was coupled with biotin cadaverine (Molecular Probes, Göttingen, Germany) in dimethylformamide with 1% *N*-ethyl-diisopropylamine. The reaction solution was incubated for 90 min at room temperature, and the product was purified by HPLC (Hewlett-Packard, Böblingen, Germany) using a reversed-phase column (Knauer, Berlin, Germany) with octadecylsilan-hypersil C18. Separation was performed in 0.1 M triethylammonium acetate, using a linear gradient from 0% to 75% acetonitril in 20 min. Yields >80% were obtained. For coupling to biotin, the dyes Alexa 647 (elution time: 6.5 min), Bodipy 630/650 (15.0 min), Cy5 (8.9 min), DY-630 (14.5 min), and DY-640 (14.5 min) were used. Biotin conjugates of ATTO 655 (9.3 min) and ATTO 680 (9.5 min) were obtained from ATTO-TEC (Siegen, Germany). All of the dyes, with the exception of DiD, could be linked to biotin–cadaverine in DMF; the HPLC elution time was between the free dye and the activated ester.

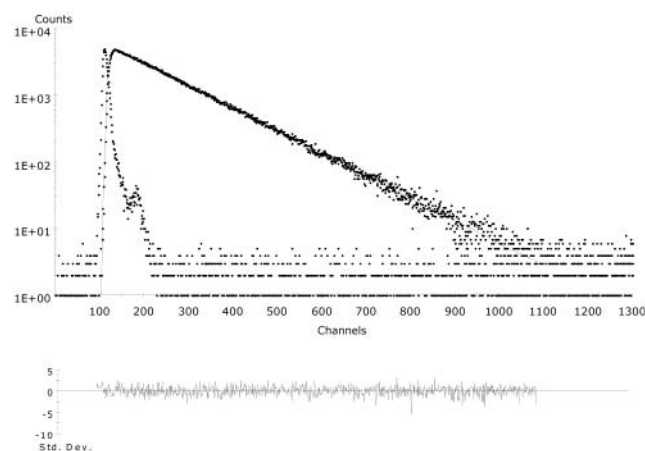
**Ensemble Spectroscopy.** Absorption spectra were taken on a Cary 500 UV–vis–NIR spectrometer (Varian, Darmstadt, Germany). Steady-state fluorescence spectra were measured in standard quartz cuvettes with a LS100 spectrometer (Photon Technology International, Wedel, Germany). Corrected fluorescence spectra were obtained using a high-pressure xenon flash lamp as excitation source. To avoid re-absorption and re-emission effects, concentrations were kept strictly below 1  $\mu$ M (typically 0.1  $\mu$ M) in all measurements. Ensemble fluorescence lifetime measurements were performed on a 5000MC spectrometer (IBH, Glasgow, U.K.) using the time-correlated single-photon counting (TCSPC) technique. The excitation source was a pulsed laser diode emitting at 635 nm with a repetition rate of 1 MHz and pulse lengths of  $\sim$ 200 ps (fwhm). With this setup an instrument response function (IRF) of 220 ps (fwhm) was measured. To exclude polarization effects, fluorescence was observed under magic angle (54.7°) conditions. Typically, 5000 photon counts were collected in the maximum channel using 2056 channels (Figure 1). The decay parameters were determined by least-squares deconvolution, and their quality was judged by the reduced  $\chi^2$  values and the randomness of the weighted residuals. In the case that a monoexponential model was not adequate to describe the measured decay, a multiexponential model was used to fit the decay (eq 1),

$$I(t) = I(0) \sum a_i \tau_i \quad (1)$$

where  $a_i$  are the preexponential factors that describe the ratio of the excited species and  $\tau_i$  denote their lifetimes.

**Fluorescence Correlation Spectroscopy (FCS).** The setup for fluorescence correlation spectroscopy (FCS) measurements has been described recently (13). A pulsed diode laser served as excitation source operating at a repetition rate of 64 MHz (PicoQuant, Berlin, Germany).





**Figure 1.** Fluorescence decay of ATTO 680 in EtOH. The instrument response function (IRF), and corresponding fit revealed a monoexponential fluorescence lifetime of 3.04 ns with a reduced  $\chi^2$  of 1.160. The weighted residuals of the fit are also shown.

The laser beam passed an excitation filter (639DF9; Omega Optics, Brattleboro, MA) and entered an inverted microscope (Axiovert 100TV, Zeiss, Jena, Germany) through the back port. It was coupled into an oil immersion objective (100 $\times$ , NA = 1.4, Nikon, Japan) by a dichroic beam splitter (645DLRP, Omega Optics, Brattleboro, MA). The fluorescence signal was collected through the same objective, filtered by two band-pass filters (680HQ60, 675DF50), and imaged onto a 100  $\mu$ m pinhole diameter directly in front of the avalanche diode (SPAD, AQ 141, EG&G Optoelectronics, Canada). The APD output was connected to a correlator card (model 5000/E, ALV, Langen, Germany). For a correlation curve, 6 runs of 30 s were averaged. All fluorescence measurements were done at room temperature (25  $^{\circ}$ C).

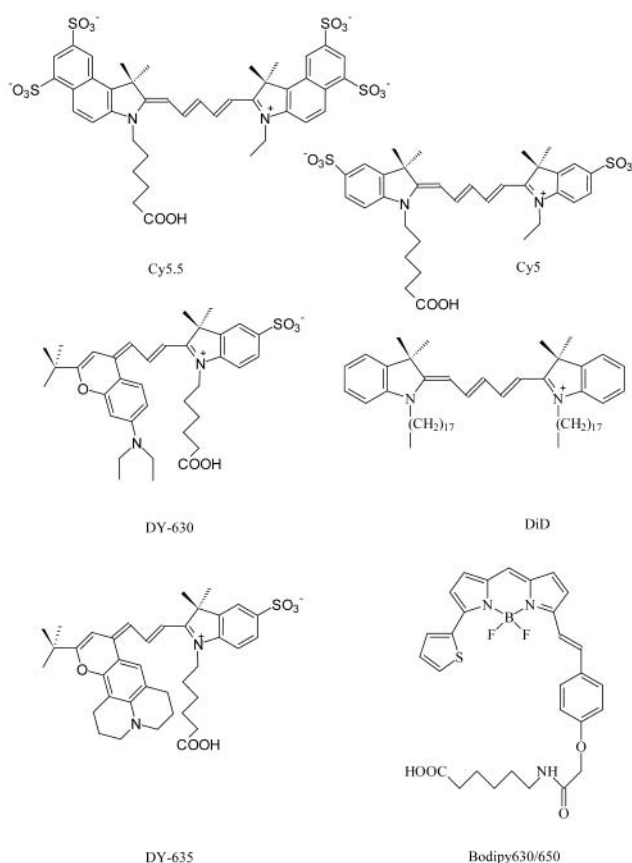
**Data Analysis.** Fluorescence intensity autocorrelation functions were calculated by the correlator board and saved as ASCII files. The autocorrelation functions were analyzed with Origin (Microcal Software, Northampton, MA). Fluorescence correlation spectroscopy (FCS) measures the fluorescence fluctuations arising from fluorescent molecules as they pass the detection volume to obtain information about dynamic processes at the molecular level (47). Using FCS, the time dependent fluorescence signal  $F = \delta F + \langle F \rangle$  is described by the fluorescence fluctuations  $\delta F(t)$  about an average value  $\langle F \rangle$ . These fluctuations are analyzed in the form of a normalized autocorrelation function  $G(\tau)$ , where  $\tau$  denotes the correlation time (eq 2).

$$G(\tau) = \frac{\langle F(t)F(t+\tau) \rangle}{\langle F(t) \rangle^2} = 1 + \frac{\langle \delta F(t)\delta F(t+\tau) \rangle}{\langle F(t) \rangle^2} \quad (2)$$

FCS can be used to gain information about all processes influencing the fluorescence intensity in the detection volume, e.g., translational diffusion, triplet states, or equilibrium constants (38, 39, 41, 47).

## RESULTS AND DISCUSSION

**Absorption and Emission Characteristics of Red-Absorbing Fluorescent Dyes.** The molecular structures of some of the investigated dyes are available (Bodipy 630/650, Cy5, Cy5.5, DiD, DY-630, DY-635; see Figure 2), while for other red-absorbing dyes the structures are proprietary (Alexa 647, ATTO 655, ATTO 680, DY-640, DY-650, DY-655, EvoBlue30). Absorption and



**Figure 2.** Molecular structures (the free carboxyl group structure without succinimidyl ester) of some of the red-absorbing fluorescent dyes used in this study.

emission maxima of all red-absorbing dyes in different solvents are listed in Table 1. Starting from water, all dyes except DiD show a red-shift in the absorption and emission maximum with increasing glycerol concentration. For most dyes, the absorption and emission maximum is also shifted to the red in ethanol. In contrast, some chromophores, such as ATTO 655, ATTO 680, and DY-640 show distinct shifts to shorter wavelengths in ethanol, especially for the absorption maxima.

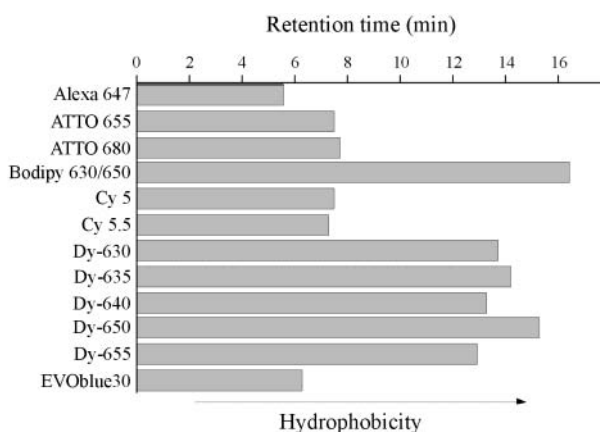
Due to long alkyl side chains ( $C_{18}$ ) and the lack of sulfonate groups, the carbocyanine dye DiD shows a strong aggregation tendency in aqueous solvents which promotes the formation of nonfluorescent dimers and aggregates. DiD and related dyes exhibit a strong fluorescence increase when incorporated into membranes (48), organic solvents, or immobilized on dry glass surfaces (49). The addition of 0.05% (v/v) Tween20 reduces the aggregation tendency and increases the fluorescence lifetime and intensity significantly (Table 1). The absorption and emission characteristics of dyes of the DY-family are also strongly influenced by the addition of Tween20. For example, the absorption maximum of DY-635 is 16 nm red-shifted from 635 to 651 nm upon addition of the detergent.

Figure 3 shows the retention times of the red-absorbing dyes measured by HPLC on a reversed-phase column using a water/acetonitrile gradient. The measured retention times suggest the classification of the dyes into two groups: hydrophilic dyes (Alexa 647, ATTO 655, ATTO 680, Cy5, Cy5.5, and EvoBlue30) and hydrophobic dyes (DiD, Bodipy 630/650, and the dyes of the DY-family). In general, the more hydrophobic chromophores are influenced by the addition of Tween20 while more hydrophilic dyes are not. The spectroscopic data of the

**Table 1. Spectroscopic Characteristics (absorption maxima,  $\lambda_{\text{abs}}$  (nm), Emission Maxima,  $\lambda_{\text{em}}$  (nm), and Fluorescence Lifetimes,  $\tau$  (ns)) of Red-Absorbing Fluorescent Dyes in Different Solvents<sup>a,b</sup>**

	$\lambda_{\text{abs}} \text{ (nm)}/\lambda_{\text{em}} \text{ (nm)}/\tau \text{ (ns)}$													
	Alexa 647	ATTO 655	ATTO 680	Bodipy630/650	Cy5	Cy5.5	DiD <sup>c</sup>	DY-630	DY-635	DY-640	DY-650	DY-655	EVOblue30	
water	649	661	680	629	647	675	652	627	635	627	646	637	650	
	666	678	695	646	663	692	—	651	669	667	670	676	667	
	1.04	1.87	1.69	3.89	0.91	0.83	—	0.21	0.48	0.59	0.64	0.54	0.64	
20% glycerol	652	664	682	631	649	677	649	629	640	628	649	641	653	
	667	680	699	648	666	695	—	653	668	662	668	683	670	
	1.22	2.02	1.83	4.01	1.13	1.03	—	0.36	0.72	0.84	0.97	0.79	0.79	
40% glycerol	654	666	685	633	652	680	648	632	644	631	650	646	655	
	670	683	701	648	669	698	—	655	669	667	674	683	673	
	1.44	2.17	1.96	4.06	1.39	1.27	—	0.62	0.99	1.19	1.28	1.09	1.01	
ethanol	655	655	675	628	652	685	647	636	647	624	654	645	649	
	674	677	695	643	672	706	668	657	671	651	675	672	666	
	1.51	3.31	3.04	4.42	1.32	1.23	1.12	0.30	0.98	3.33	0.95	0.97	1.16	
0.05% Tween20	649	661	680	633	647	675	648	637	651	628	656	648	650	
	665	677	694	648	663	692	667	660	675	659	676	680	667	
	1.03	1.87	1.68	4.96	0.92	0.86	1.62	0.94	1.66	3.64	1.82	2.07	0.66	

<sup>a</sup> The extinction coefficients reported by the manufacturers,  $\epsilon$  (L mol<sup>-1</sup> cm<sup>-1</sup>) are  $2.5 \times 10^5$  for Cy5, Cy5.5, and Alexa 647,  $0.97 \times 10^5$  for Bodipy630/650,  $>1.2 \times 10^5$  for DY-630 and DY-635,  $2.6 \times 10^5$  for DiD, and  $1.0 \times 10^5$  for ATTO 655 and ATTO 680. <sup>b</sup> The quality of the fit was judged by the reduced  $\chi^2$  values and the randomness of the weighted residuals (Figure 1). For all fits,  $\chi^2$  values between 0.900 and 1.200 were obtained. Viscosities of the solvents at 20 °C are 1.00 mPa s (water), 2.025 mPa s (20% glycerol, v/v), 4.95 mPa s (40% glycerol, v/v), and 1.2 mPa s (ethanol). Fluorescent dyes of the DY-family show only weak fluorescence intensity and nonexponential fluorescence kinetics. Therefore average fluorescence lifetimes,  $\tau_{\text{av}} = a_1\tau_1 + a_2\tau_2$ , are given. <sup>c</sup> The carbocyanine dye DiD shows a strong aggregation tendency in aqueous solvents which promotes the formation of nonfluorescent dimers or aggregates.



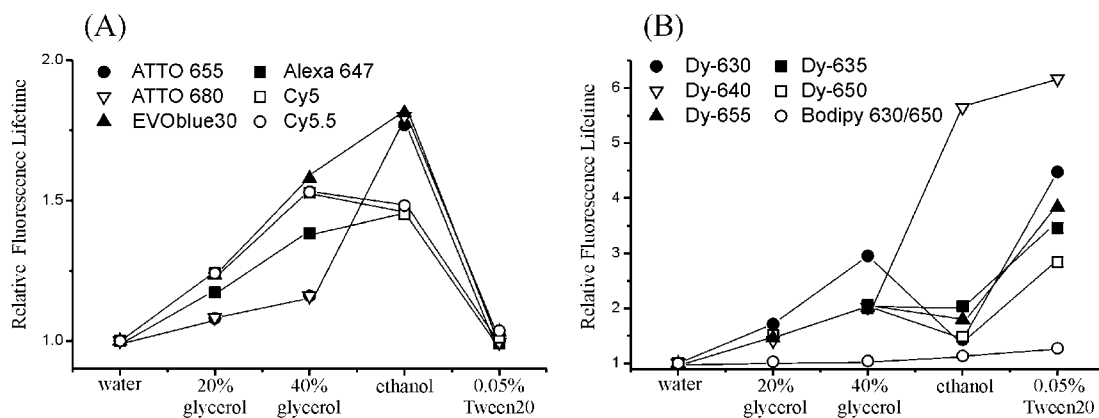
**Figure 3.** Retention times of red-absorbing fluorescent dyes measured by HPLC. The dye DiD did not elute under the applied experimental conditions. Separation was performed in 0.1 M triethylammonium acetate, using a linear gradient from 0% to 75% acetonitril in 20 min.

hydrophobic bora-diaza-indacene dye Bodipy 630/650 are nearly unaffected by the surrounding medium (Table 1).

Neglecting the dielectric constant,  $\epsilon$ , dye-solvent interactions are, in general, described by the refractive index of the solvent,  $n$ , if the interactions are predominated by dispersion forces (50). Generally, an increase of the refractive index is expected to result in a red-shift of the absorption maximum. The refractive indices of the solvents used in our experiment are 1.33 (water), 1.36 (ethanol), 1.36 (20% glycerol in water), and 1.40 (40% glycerol in water). As can be seen from Table 1, the absorption and emission maxima of all dyes investigated show a red-shift with increasing glycerol concentration. Using ethanol as the solvent also increases the refractive index, but the effect on the absorption and emission spectra is less pronounced. This, and the fact that some dyes (ATTO 655, ATTO 680, EVOblue30, and Bodipy 630/650) show a blue-shift in ethanol mixtures means that other effects, such as the polarity and the solvation of the different chromophore structures must also influence the absorption and emission maxima.

**Fluorescence Lifetimes of Red-Absorbing Fluorescent Dyes.** Due to problems associated with adsorption of hydrophobic dyes to the walls of the quartz cuvettes, we have not attempted to report the measured values of the fluorescence quantum yields. However, since the fluorescence quantum yield,  $\Phi_f$ , is defined as  $\Phi_f = \tau/\tau_n$  in the absence of static fluorescence quenching ( $\tau_n$ : native radiative lifetime without any nonradiative processes), an increase or decrease in the measured fluorescence lifetime is always related to an increase or decrease in fluorescence quantum yield.

Figure 4 shows the relative fluorescence lifetimes (relative to pure water value) measured for each dye in each of the various solvent conditions tested. On the basis of the dependence of the fluorescence lifetime on the different solvents, the red-absorbing dyes investigated in this study can be divided into the following groups: (i) fluorescent dyes for which the lifetime is independent of the surrounding medium (Bodipy 630/650), (ii) fluorescent dyes for which the lifetime is much longer in ethanol than water, but does not change significantly in the presence of Tween20 (ATTO 655, ATTO 680, Alexa 647, EVOblue30, Cy5, and Cy5.5; see Figure 4A), and (iii) fluorescent dyes from the DY-family for which the lifetime is much longer with Tween20 than in pure water. Within these groups there are still some differences: For example, the fluorescence lifetimes of ATTO 655, ATTO 680, and EVOblue30 dyes are less sensitive to solvent viscosity, e.g., in 40% glycerol, than they are to solvent polarity (ethanol). These observations, especially the strong increase in fluorescence lifetime of ATTO 655, ATTO 680, and EvoBlue30 in ethanol, indicate a more rigid chromophore structure. It was recently shown that several red-absorbing rhodamine and oxazine dyes (both xanthene dyes with rigid structures) exhibit shorter fluorescence lifetimes in water than in ethanol (3, 10). On the other hand, the viscosity (and temperature) dependence of the fluorescence characteristics is only weak. From these findings, we assume that the three red-absorbing fluorescent dyes ATTO 655, ATTO 680, and EVOblue30 have a rigid planar chromophore structure which do not show cis/trans isomerization processes



**Figure 4.** Relative fluorescence lifetimes measured for the red-absorbing fluorescent dyes in different solvents. Relative fluorescence lifetimes were calculated by dividing the measured values by the value obtained in water.

commonly observed for chromophores with flexible polymethine groups.

The other three dyes of this group (Figure 4A), Alexa 647, Cy5, and Cy5.5 show shorter fluorescence lifetimes but otherwise absolutely identical dependencies. Due to the flexibility of the polymethine backbone of carbocyanine dyes and consequential cis/trans isomerization possibilities, the fluorescence lifetimes and quantum yields are strongly influenced by the viscosity (Figure 4A). This is in good agreement with earlier findings for most cyanine dyes at room temperature in alcoholic or aqueous solutions which demonstrated that viscosity is the dominating solvent property influencing the fluorescence intensity and that the polarity of the solvent plays only a minor role (51). As expected for more hydrophilic dyes (Figure 3), the fluorescence properties of all red-absorbing fluorescent dyes of this group (Figure 4A) are very weakly influenced by the addition of 0.05% Tween20 (v/v) to an aqueous solution.

The fluorescent dyes from the DY-family (Figure 4B) all show a similar increase in fluorescence lifetime upon changing the solvent from water to water/glycerol mixtures or pure ethanol. Only for the dye DY-640, both the viscosity and the polarity strongly influence the fluorescence intensity and lifetime to the same degree (see lifetimes in ethanol and upon addition of Tween20). Nevertheless, the strong increase in fluorescence lifetime and intensity upon addition of 0.05% Tween20 (v/v) to an aqueous solution (up to 6-fold) is unexpected. Certainly, the addition of Tween20 reduces the aggregation tendency and promotes the solubility of these rather hydrophobic dye structures in aqueous solutions (Figure 3), but the degree of this increase in fluorescence intensity indicates that other effects have to be taken into account. For example, as can be seen in Figure 2, at least two dyes of the DY-family are asymmetric carbocyanine dyes (DY-630, DY-635). It may be that those dyes associate with Tween20 molecules or micelles thereby increasing the solubility and decreasing the internal conversion rate by reducing the flexibility of the polymethine backbone.

**Fluorescence Correlation Spectroscopy (FCS) Measurements.** The dyes used in this study, particularly the more hydrophobic dyes, show dynamic adsorption on the cover slides used for FCS measurements. Furthermore, some dyes show strong adsorption to nonfluorescent impurities, e.g., dust particles, in aqueous solutions. These problems render the analysis of the normalized autocorrelation functions more difficult. There-

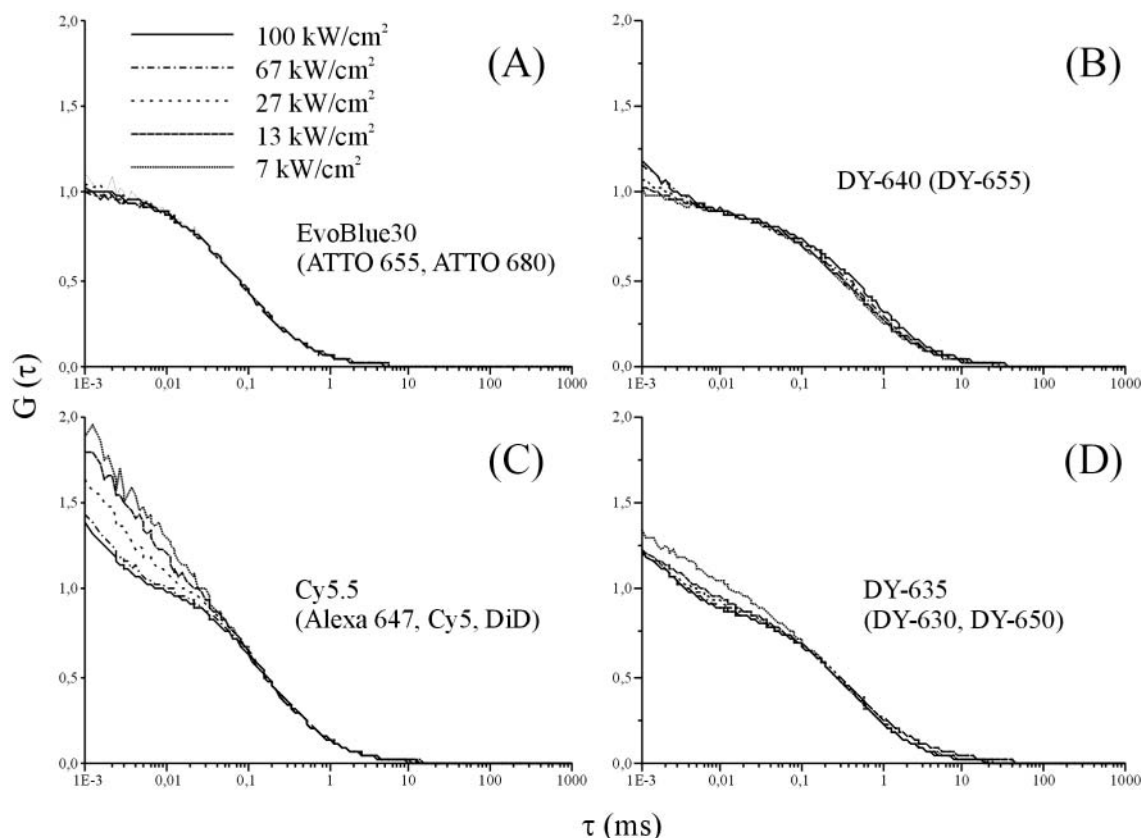
fore, experiments were performed in water containing 0.05% Tween20 (v/v), which effectively eliminates these problems.

In FCS measurements, transient nonfluorescent states such as triplet states or cis-conformations (as in the case of the carbocyanine dye Cy5) (38) give rise to fluorescence fluctuations that are superimposed on those caused by 3D-translational motion (Brownian motion) of the fluorescent molecule in and out of the sample volume element. Since the lifetime of these transient states are usually shorter, i.e., in the range of several microseconds, than the typical diffusion time of a fluorescent dye molecule through the sample volume element, they can be analyzed separately (41). While translational diffusion is, as a first approximation, independent of the laser excitation energy (neglecting photobleaching effects), intersystem crossing and photoinduced cis/trans isomerization is not. Widengren and Schille recently showed that the correlation times for cis/trans isomerization for the carbocyanine dye Cy5 are drastically reduced with higher excitation intensities but that the amplitude of this process (about 50%) is not excitation power dependent (38).

Figure 5 shows representative FCS curves of the red-absorbing fluorescent dyes for a range of excitation intensities in water containing 0.05% Tween20 (v/v). In these experiments, four different types of FCS curves and excitation intensity dependencies were observed. The FCS curves obtained for EVOblue30 under various excitation intensities (Figure 5A) are representative for FCS curves measured for ATTO 655, ATTO 680. They are also representative for Bodipy 630/650, except that Bodipy 630/650 has a slightly longer diffusion time. FCS curves of these fluorescent dyes can be described exclusively by translational diffusion up to an excitation energy of 100 kW/cm<sup>2</sup>. This indicates that the intersystem crossing yield is very low under moderate excitation conditions. Figure 5B shows the FCS curves measured for DY-640 under various excitation intensities. Similar curves were obtained for DY-655. For these dyes, a second exponential process could be observed at excitation intensities of > 27 kW/cm<sup>2</sup> with an amplitude of 30–35% (at 100 kW/cm<sup>2</sup>). This second process can be ascribed to intersystem crossing into the triplet state. In addition, at excitation intensities above 27 kW/cm<sup>2</sup> a distinctly faster decay of the autocorrelation curves due to photobleaching is evident.

The normalized intensity autocorrelation curves presented in Figure 5C are representative for carbocyanine dyes showing photoinduced cis/trans isomerization. These





**Figure 5.** FCS curves of some red-absorbing fluorescent dyes in water containing 0.05% Tween20 (v/v) at excitation intensities of 7, 13, 27, 67, and 100 kW/cm<sup>2</sup>. (A) EVOblue30; similar curves were obtained for ATTO 655, ATTO 680 and, with a longer diffusion time, for Bodipy 630/650. (B) DY-640; similar traces were obtained for DY-655. (C) Cy5.5; similar curves were obtained for Alexa 647, Cy5 and DiD. (D) DY-635; similar curves were obtained for DY-630 and DY-650.

dyes, Cy5, Cy5.5, DiD, and Alexa 647, all show identical excitation intensity dependence in FCS curves. The relaxation times for cis/trans isomerization are drastically reduced with higher excitation intensities. At the highest excitation intensity (100 kW/cm<sup>2</sup>) weak triplet state population is observed. Although the molecular structure of Alexa 647 has not been published, the FCS curves and fluorescence lifetimes strongly indicate that it has a carbocyanine structure. For DiD, significant photobleaching, manifested by faster decays of the FCS curves for excitation intensities above 20 kW/cm<sup>2</sup>, is evident.

The FCS curves recorded for DY-630, DY-635, and DY-650 under various excitation intensities (Figure 5D) exhibit behavior similar to those shown in Figure 5C. The major difference is that a second component (other than translational diffusion) is required to describe the curves even under weak excitation conditions. Besides the apparent photobleaching at higher excitation intensities, the more hydrophobic red-absorbing dyes, especially the dyes of the DY-family shown in Figs. 5B and 5D and Bodipy630/650, show slower translational diffusion. This implies that those dyes tend to adsorb to Tween20 micelles, which increases the observed diffusion time.

To summarize, the best signal-to-noise ratios in the FCS measurements were obtained for all dyes applying an excitation intensity of 67 kW/cm<sup>2</sup>. For our excitation wavelength and filter combination, Alexa 647, Cy5, ATTO 655, DY-640, and Bodipy 630/650 proved to be the brightest red-absorbing fluorescent dyes in aqueous solutions containing 0.05% Tween 20. Since the cis and triplet states of dyes such as Cy5, Cy5.5, or Alexa 647 are also potential nonfluorescent energy transfer acceptors, the use of these dyes as acceptors in FRET mea-

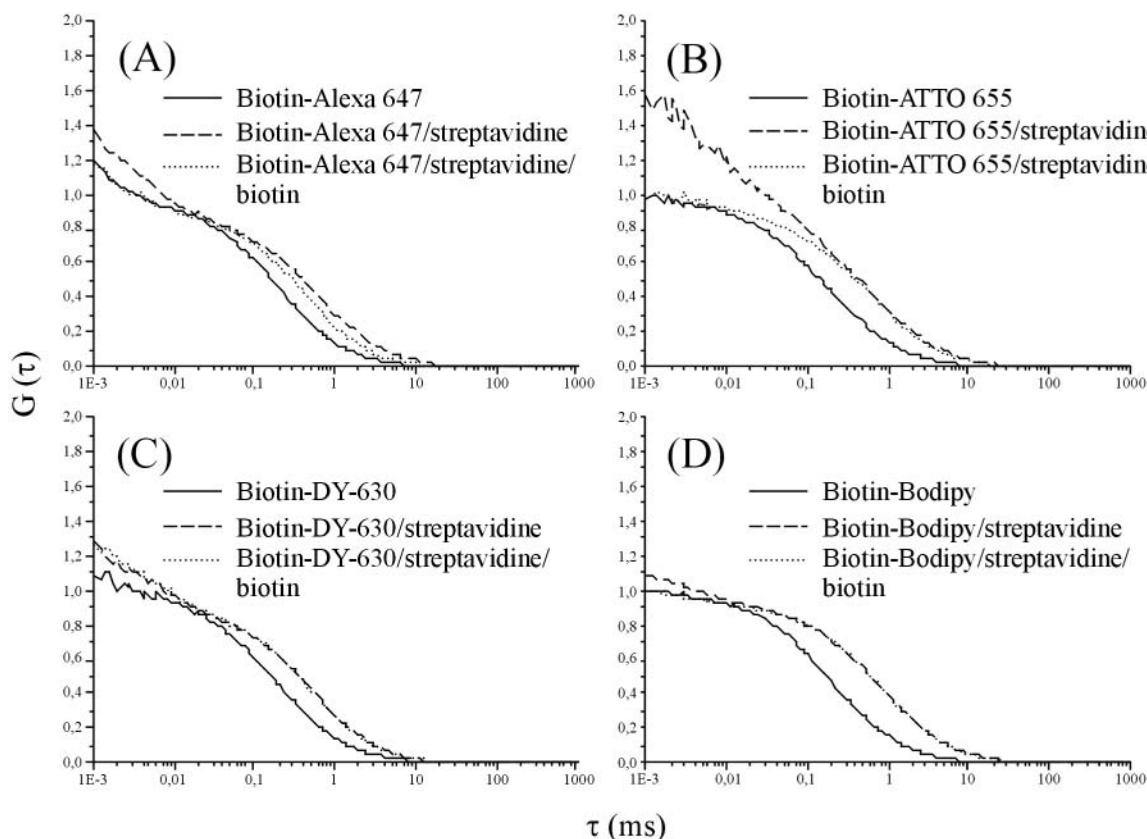
surements is more problematic (39, 52). Due to their low intersystem crossing yields, ATTO 655, ATTO 680, DY-640, and Bodipy 630/650 offer efficient alternatives. Fluorescent dyes of the DY-family require the addition of detergents to compete.

**Biotin Conjugates and Streptavidin Binding.** The steady-state absorption and fluorescence spectra of the biotin conjugates of Alexa 647, ATTO 655, ATTO 680, Cy5, DY-630, and DY-640 are all shifted slightly to the red compared to the free dyes (Table 2). In addition, most biotin conjugated dyes exhibit a slight increase in fluorescence lifetime. However, the absorption and fluorescence excitation spectra of the Bodipy 630/650 biotin conjugate indicate the formation of nonfluorescent dimers. From the data shown in Table 2, it is clear that the addition of streptavidin significantly alters the spectroscopic properties of all conjugates investigated. To prevent dye/dye interactions between biotin conjugated dyes bound to neighboring binding sites of the same streptavidin, an excess of streptavidin was used (44). Carbocyanine dyes such as Cy5 show bathochromic shifts in absorption and emission and a considerable increase in fluorescence lifetime. The fact that Cy5 and Alexa 647 both show this behavior is another indicator that they are similar in structure. The two conjugates from the DY-family (DY-630, DY-640) show a strong increase in fluorescence lifetime and intensity upon addition of streptavidin. The fluorescence decays of the DY-630 and DY-640 biotin conjugates show a second dominant component with a long fluorescence lifetime, similar to the fluorescence lifetimes obtained upon addition of Tween20 to an aqueous solution of the free dyes. Surprisingly, the emission maximum of the DY-640 biotin conjugate showed a 10 nm blue-shift upon addition of streptavidin.

**Table 2. Spectroscopic Characteristics (Absorption Maxima,  $\lambda_{\text{abs}}$  (nm), Emission Maxima,  $\lambda_{\text{em}}$  (nm), Fluorescence Lifetimes,  $\tau$  (ns)) of Dye–Biotin Conjugates in the Absence/Presence of an Excess of Streptavidin in Water<sup>a</sup>**

	$\lambda_{\text{abs}}$ (nm)	$\lambda_{\text{em}}$ (nm)	$\tau_1$ (ns)	$a_1$	$\tau_2$ (ns)	$a_2$
Alexa 647	649/655	667/669	1.24/0.98	1.00/0.67	–/1.96	–/0.33
ATTO 655	662/667	677/677	2.06/2.01	1.00/0.86	–/0.34	–/0.14
ATTO 680	681/687	701/700	1.84/1.79	1.00/0.74	–/0.35	–/0.26
Bodipy 630/650	645*/635	650/662	3.82/3.11	1.00/0.85	–/0.54	–/0.15
Cy5	647/653	664/668	1.07/1.84	1.00/1.00	–/–	–/–
Dy-630	629/634	652/654	0.30/0.77	0.44/0.30	0.59/1.74	0.56/0.70
Dy-640	630/631	667/657	0.74/0.57	0.96/0.05	2.06/3.87	0.05/0.95

<sup>a</sup> The quality of the fit was judged by the reduced  $\chi^2$  values and the randomness of the weighted residuals. Most biotin conjugates show a biexponential fluorescence decay upon binding to streptavidin.



**Figure 6.** FCS curves of some biotin conjugates in water measured at an excitation intensity of 67 kW/cm<sup>2</sup>. The solid lines give the FCS curves of the biotin conjugates, the dashed line upon addition of an excess of streptavidin, and the dotted line upon a subsequent addition of an excess of unlabeled biotin. (A) Biotin–Alexa 647, similar curves were obtained for Cy5. (B) Biotin–ATTO 655, similar curves were obtained for ATTO 680. (C) Biotin–DY-630, similar curves were obtained for DY-640. (D) Biotin–Bodipy 630/650.

In contrast, the biotin conjugates of ATTO 655, ATTO 680, and Bodipy 650/680 show fluorescence quenching upon addition of an excess of streptavidin, indicated by the appearance of a shorter component in the fluorescence decay (Table 2). In the case of the Bodipy 630/650 biotin conjugate, the dimers disappear completely upon binding to streptavidin.

Figure 6 shows FCS curves recorded for some biotin conjugates in water with and without the addition of an excess of streptavidin (solid line and dashed line, respectively). The binding of the biotin conjugates to streptavidin can be confirmed and monitored by the shift of the diffusional correlation times. Because we want to observe this shift, these measurements were performed in pure water, i.e., without Tween20.

Upon addition of streptavidin, all the FCS curves showed an increased translational diffusion time, confirming that streptavidin binds each dye conjugate. The FCS curves also showed additional fast correlation times in the presence of an excess of streptavidin for all biotin-conjugated dyes. For example, biotin conjugates of Alexa

647 (Figure 6A) and DY-630 (Figure 6C) that show the expected short correlation times due to cis/trans isomerization and intersystem crossing in the absence of streptavidin show an increase of the short correlation terms after streptavidin binding in the short-time range. In almost the same manner, the FCS curves of the Bodipy 630/650 conjugates show an additional term in the short time range in the presence of streptavidin (Figure 6D). However, the biotin conjugates of ATTO 655 and ATTO 680 show the most pronounced changes upon addition of streptavidin (Figure 6B, FCS curves for ATTO 655). The data shown in Table 2 indicate fluorescence quenching of the dye due to binding of the biotin conjugate to streptavidin. This quenching correlates with the appearance of the additional short-time FCS decay components.

It is likely that the additional short correlation times observed in the FCS curves upon streptavidin binding is caused by reversible quenching of the dye with tryptophan residues of streptavidin. The quenching could be from tryptophan residues at the streptavidin binding site, or from one (or more) of the three neighboring, unoc-

cupied binding sites. To distinguish these two possibilities, an excess of unlabeled biotin was added. The addition of excess free biotin blocks neighboring binding sites and suppresses possible interactions between the dye and those tryptophan residues. Another possible process to consider is that unlabeled and labeled biotins compete for the same streptavidin binding sites, i.e., dye-labeled biotin may be displaced (42–45). The FCS curves of the biotin conjugates of hydrophobic dyes (DY-630, DY-640, Bodipy 630/650; see Figures 6C and 6D) do not change upon addition of excess free biotin, but the conjugates of more hydrophilic dyes such as Alexa 647, Cy5, ATTO 655, and ATTO 680 do show a decrease in the translational diffusion times (Figures 6A and 6B).

Hydrophilic dyes bind in the binding pocket, hence they can be displaced by competing free biotin; hydrophobic dyes bind nonspecifically, i.e., not at the binding sites, therefore they are not displaced by free biotin.

With the exception of DY-630 and DY-640 (Figure 6C), the additional short-time FCS decay component disappears when an excess of biotin is added to the streptavidin–biotin–dye complexes. The disappearance of the additional fast process for Alexa 647, Cy5, ATTO 655, ATTO 680, and Bodipy 630/650 indicates that these dyes interact with neighboring binding sites, likely with the tryptophan residues, that are inhibited upon addition and binding of unlabeled biotin molecules. In the case of ATTO 655, ATTO 680, and Bodipy 630/650, the quenching probably occurs via an electron transfer reaction from the ground state tryptophan residue to the first excited singlet state of the dye (22, 33, 34, 36). Since carbocyanine dyes such as Cy5 exhibit a lower electron accepting tendency, they are not quenched (14). The loss of the additional short-time component for the Alexa 647 and Cy5 streptavidin complexes in excess free biotin are not easily explained. It is likely that the observed changes are related to a change in the cis/trans isomerization rate brought on by a conformational change that occurs when the neighboring binding sites are filled. The reason that the additional short-time FCS decay components do not disappear on addition of free biotin for DY-630 and DY-640 conjugates is that these biotin–dye complexes are in fact bound to streptavidin nonspecifically through hydrophobic interactions of the dye and the protein interior. As a result, the binding to streptavidin is independent of whether free biotin is present at the streptavidin binding sites.

## CONCLUSIONS

The spectroscopic data of 13 commercially fluorescent dyes absorbing in the red-wavelength range (620–700 nm)—a very promising wavelength range for diagnostic applications—are measured and compared using ensemble steady-state and time-resolved fluorescence spectroscopy as well as fluorescence correlation spectroscopy (FCS). The best signal-to-noise ratios in aqueous solutions are obtained for the relatively hydrophilic dyes Cy5, Cy5.5, Alexa 647, ATTO 655, and ATTO 680. The data obtained strongly suggest that besides Cy5 and Cy5.5, Alexa 647 also belongs to the class of symmetric carbocyanine dyes which show excitation intensity dependent cis/trans isomerization and short fluorescence lifetimes of ~1 ns in aqueous solutions. Due to their similar spectroscopic behavior, the red-absorbing dyes EVOblue30 and the two ATTO-dyes probably belong to the same class of structurally rigid chromophores such as rhodamines or oxazines. ATTO 655 and ATTO 680 exhibit longer fluorescence lifetimes in aqueous solutions than the

carbocyanine dyes, thus allowing an improved discrimination against autofluorescent impurities which normally have very fast fluorescence decays. On the other hand, both chromophore classes might be used to probe the local environment due to specific quenching processes or changes in the cis/trans isomerization rates. Although the fluorescence intensity and lifetime of Bodipy 630/650 is superior and nearly independent of the surrounding medium, the strong dimerization and nonspecific adsorption tendency renders its application more difficult in aqueous solutions. The relatively hydrophobic fluorescent dyes of the DY-family proved to be only weakly fluorescent in aqueous solutions. However, upon addition of Tween20 or binding of biotin conjugates to streptavidin, the fluorescence drastically increases.

The results presented demonstrate that knowledge of the spectroscopic behavior of the dyes used under various conditions is crucial for the design of any application. As an example, the binding of labeled biotin conjugates to streptavidin was monitored. Selective fluorescence quenching of dyes by tryptophan residues in proteins has great potential for the development of diagnostic applications (22). Furthermore, the data show that changes in the fluorescence lifetime of the dye or any other photophysical properties such as cis/trans isomerization might be used advantageously in developing fluorescence-based assays. Finally, the data suggest that the fluorescent dye that exhibits the highest signal-to-noise ratio is not necessarily the best dye for any desired application. It is also important to consider experimental details such as the excitation intensity, the optimum solvent conditions, and the protein/peptide or DNA/RNA sequence of the probe or target molecule.

## ACKNOWLEDGMENT

This work was supported by the Bundesministerium für Bildung, Wissenschaft, Forschung und Technologie (Grant 311864).

## LITERATURE CITED

- (1) Smith, L. M., Fung, S., Hunkapillar, M. W., and Hood, L. E. (1985) The synthesis of oligonucleotides containing an aliphatic amine group at the 5'-terminus: synthesis of fluorescent DNA primers for use in DNA sequence analysis. *Nucleic Acids Res.* 13, 2328–2410.
- (2) Waggoner, A. (1995) Covalent labeling of proteins and nucleic acids with fluorophores. In *Methods in Enzymology* (Abelson, J. N., and Simon, M. I., Eds.) Vol. 246, pp 362–373, Academic Press, San Diego, CA.
- (3) Daehne, S. (1998) Near-infrared dyes for high technology applications. Kluwer, Dordrecht.
- (4) Haugland, R. P. (1996) Handbook of fluorescent probes and research chemicals, Sixth Edition, Molecular Probes, Eugene.
- (5) Hovius, R., Vallotton, P., Wohland, T., and Vogel, H. (2000) Fluorescence techniques: shedding light on ligand acceptor interactions. *Trends Pharmacol. Sci.* 21, 266–273.
- (6) Aubin, J. E. (1979) Autofluorescence of viable cultured mammalian cells. *J. Histochem. Cytochem.* 27, 35–43.
- (7) Cheng, P. C., and Kriete, A. (1995) Image contrast in confocal light microscopy. In *Handbook of biological confocal microscopy* (Pawley, J. B., Ed.) 2nd ed., pp 327–346, Plenum Press, New York.
- (8) Affleck, R. L., Ambrose, W. P., Demas, J. N., Goodwin, P. M., Schecker, J. A., Wu, M., and Keller, R. A. (1996) Reduction of luminescent background in ultrasensitive fluorescence detection by photobleaching. *Anal. Chem.* 68, 2270–2276.
- (9) Patonay, G., and Antoine, M. D. (1991) Near-infrared fluorogenic labels: New approach to an old problem. *Anal. Chem.* 63, 321A–327A.
- (10) Sauer, M., Han, K. T., Ebert, V., Müller, R., Schulz, A., Seeger, S., Wolfrum, J., Arden-Jacob, J., Deltau, G., Marx,



- N. J., Zander, C., and Drexhage, K. H. (1995) New fluorescent dyes in the red region for biodiagnostics. *J. Fluoresc.* **5**, 247–261.
- (11) William, D. C., and Soper, S. A. (1995) Ultrasensitive near-IR fluorescence detection for capillary gel electrophoresis and DNA sequencing applications. *Anal. Chem.* **67**, 3427–3432.
- (12) Arden-Jacob, J., Marx, N. J., and Drexhage, K. H. (1997) New fluorescent probes for the red spectral region. *J. Fluoresc.* **7**, 91S–93S.
- (13) Sauer, M., Arden-Jacob, J., Drexhage, K. H., Göbel, F., Lieberwirth, U., Mühlegger, K., Müller, R., Wolfrum, J., and Zander, C. (1998) Time-resolved identification of individual mononucleotide molecules in aqueous solution with pulsed semiconductor lasers. *Bioimaging* **6**, 14–24.
- (14) Lieberwirth, U., Arden-Jacob, J., Drexhage, K. H., Hertel, D. P., Müller, R., Neumann, M., Schulz, A., Siebert, S., Sagner, G., Klingel, S., Sauer, M., and Wolfrum, J. (1998) Multiplex dye DNA sequencing in capillary gel electrophoresis by diode laser-based time-resolved fluorescence detection. *Anal. Chem.* **70**, 4771–4779.
- (15) Terpetschnig, E., Szmazinski, H., Ozinskas, A., and Lakowicz, J. R. (1994) Synthesis of squaraine-N-hydroxysuccinimide esters and their biological application as long-wavelength fluorescent labels. *Anal. Biochem.* **217**, 197–204.
- (16) Oswald, B., Patsenker, L., Duschl, J., Szmazinski, H., Wolfbeis, O. S., and Terpetschnig, E. (1999) Synthesis, spectral properties, and detection limits of reactive squaraine dyes, a new class of diode laser compatible fluorescent protein labels. *Bioconjugate Chem.* **10**, 925–931.
- (17) Mujumdar, R. B., Ernst, L. A., Mujumdar, S. R., and Waggoner, A. S. (1989) Cyanine dye labeling reagents containing isothiocyanate groups. *Cytometry* **10**, 11–19.
- (18) Southwick, P. L., Ernst, L. A., Tauriello, E. V., Parker, S. R., Mujumdar, R. B., Mujumdar, S. R., Clever, H. A., and Waggoner, A. S. (1990) Cyanine dye labeling reagents: carboxymethylindocyanine esters. *Cytometry* **11**, 418–430.
- (19) Mujumdar, R. B., Ernst, L. A., Mujumdar, S. R., Lewis, C. J., and Waggoner, A. S. (1993) Cyanine dye labeling reagents: Sulfoindocyanine succinimidyl esters. *Bioconjugate Chem.* **4**, 105–111.
- (20) Flanagan, J. H., Jr., Khan, S. H., Menchen, S., Soper, S. A., and Hammer, R. P. (1997) Functionalized tricarboquinone dyes as near-infrared fluorescent probes for biomolecules. *Bioconjugate Chem.* **8**, 751–756.
- (21) Sauer, M., Zander, C., Müller, R., Ullrich, B., Drexhage, K. H., Kaul, S., and Wolfrum, J. (1997) Detection and identification of individual antigen molecules in human serum with pulsed semiconductor lasers. *Appl. Phys. B* **65**, 427–431.
- (22) Neuweiler, H., Schulz, A., Vaiana, A., Smith, J., Kaul, S., Wolfrum, J., and Sauer, M. (2002) Peptide-based molecular beacons for the detection of p53-autoantibodies in human sera. *Angew. Chemie*, in press.
- (23) Terasaki, M., and Dailey, M. E. (1995) Confocal microscopy on living cells. In *Handbook of biological confocal microscopy* (Pawley, J. B., Ed.) 2nd ed., pp 327–346, Plenum Press, New York.
- (24) Sawano, A., Hama, H., Saito, N., and Miyawaki, A. (2002) Multicolor imaging of  $\text{Ca}^{2+}$  and protein kinase C signals using novel epifluorescence microscopy. *Biophys. J.* **82**, 1076–1085.
- (25) Förster, T. (1949) Experimentelle und theoretische Untersuchung des zwischenmolekularen Übergangs von Elektronenanregungsenergie. *Z. Naturforsch.* **4a**, 321–327.
- (26) Weiss, S. (1998) Fluorescence spectroscopy of single biomolecules. *Science* **283**, 1676–1683.
- (27) Gordon, G. W., Berry, G., Liang, X. H., Levine, B., and Herman, B. (1998) Quantitative fluorescence resonance energy transfer measurements using fluorescence microscopy. *Biophys. J.* **74**, 2702–2713.
- (28) Schwille, P., Meyer-Almes, F. J., and Rigler, R. (1997) Dual-color fluorescence cross-correlation spectroscopy for multi-component diffusional analysis in solution. *Biophys. J.* **72**, 1878–1886.
- (29) Hom, E. F. Y., and Verkman, A. S. (2002) Analysis of coupled bimolecular reaction kinetics and diffusion by two-color fluorescence correlation spectroscopy: Enhanced resolution of kinetics by resonance energy transfer. *Biophys. J.* **83**, 533–546.
- (30) Seidel, C. A. M., Schulz, A., and Sauer, M. (1996) Nucleobase-specific quenching of fluorescent dyes. 1. Nucleobase one-electron redox potentials and their correlation with static and dynamic quenching efficiencies. *J. Phys. Chem.* **100**, 5541–5553.
- (31) Edman, L., Mets, Ü., and Rigler, R. (1996) Conformational transitions monitored for single molecules in solution. *Proc. Natl. Acad. Sci. U.S.A.* **93**, 6710–6715.
- (32) Eggeling, C., Fries, J. R., Brand, L., Günther, R., and Seidel, C. A. M. (1998) Monitoring conformational dynamics of a single molecule by selective fluorescence spectroscopy. *Proc. Natl. Acad. Sci. U.S.A.* **95**, 1556–1561.
- (33) Sauer, M., Drexhage, K. H., Lieberwirth, U., Müller, R., Nord, S., and Zander, C. (1998) Dynamics of the electron-transfer reaction between an oxazine dye and DNA oligonucleotides monitored at the single molecule level. *Chem. Phys. Lett.* **284**, 153–163.
- (34) Kurata, S., Kanagawa, T., Yamada, K., Torimura, M., Yokomaku, T., Kamagata, Y., and Kurane, R. (2001) Fluorescent quenching-based quantitative detection of specific DNA/RNA using BODIPY FL-labeled probe or primer. *Nucleic Acids Res.* **29**, e34.
- (35) Wagenknecht, H. A., Stemp, E. D. A., and Barton, J. K. (2000) Evidence of electron transfer from peptides to DNA: Oxidation of DNA-bound tryptophan using the flash-quench technique. *J. Am. Chem. Soc.* **122**, 1–7.
- (36) Knemeyer, J. P., Marmé, N., and Sauer, M. (2000) Probes for the detection of specific DNA sequences at the single-molecule level. *Anal. Chem.* **72**, 3717–3724.
- (37) Czerney, P., Lehmann, F., Wenzel, M., Buschmann, V., Dietrich, A., and Mohr, G. J. (2001) Tailor-made dyes for fluorescence correlation spectroscopy (FCS). *Biol. Chem.* **382**, 495–498.
- (38) Widengren, J., and Schwille, P. (2000) Characterization of photoinduced isomerization and back-isomerization of the cyanine dye Cy5 by fluorescence correlation spectroscopy. *J. Phys. Chem. A* **104**, 6416–6428.
- (39) Widengren, J., Schweinberger, E., Berger, S., and Seidel, C. A. M. (2001) Two new concepts to measure fluorescence resonance energy transfer via fluorescence correlation spectroscopy: Theory and experimental realizations. *J. Phys. Chem. A* **105**, 6851–6866.
- (40) Drexhage, K. H. (1973) Structure and properties of laser dyes. In *Dye Lasers* (Schäfer, F. P., Ed.), pp 144–193, Springer-Verlag, Berlin.
- (41) Widengren, J. (2001) Photophysical aspects of FCS. In *Fluorescence Correlation Spectroscopy* (Rigler, R., and Elson, E. S., Eds.), pp 276–301, Springer-Verlag, Berlin.
- (42) Weber, P. C., Ohlendorf, D. H., Wendolowski, J. J., and Salemme, F. R. (1989) Structural origins of high-affinity biotin binding to streptavidin. *Science* **243**, 85–88.
- (43) Chevalier, J., Yi, J., Michel, O., and Ming, T. X. (1997) Biotin and digoxigenin as labels for light and electron microscopy in situ hybridization probes: Where do we stand? *J. Histochem. Cytochem.* **45**, 481–491.
- (44) Gruber, J. H., Kahn, C. D., Kada, G., Riener, C. K., Harms, G. S., Ahrer, W., Dax, T. G., and Knaus, H. (2000) Anomalous fluorescence enhancement of Cy3 and Cy3.5 versus anomalous fluorescence loss of Cy5 and Cy7 upon covalent linking to IgG and noncovalent binding to avidin. *Bioconjugate Chem.* **11**, 696–704.
- (45) Emans, N., Biwerski, J., and Verkman, A. S. (1995) Imaging of endosome fusion in BHK fibroblasts based on a novel fluorometric avidin-biotin binding assay. *Biophys. J.* **69**, 716–728.
- (46) Watt, R. M., and Voss, E. W., Jr. (1977) Mechanism of quenching of fluorescein by anti-fluorescein IgG antibodies. *Immunochemistry* **14**, 533–541.
- (47) Magde, D., Elson, E. L., and Webb, W. W. (1972) Thermodynamic fluctuations in a reacting system – Measurement by fluorescence correlation spectroscopy. *Phys. Rev. Lett.* **29**, 705–708.

- (48) Honig, M. G., and Hume, R. I. (1986) Fluorescent carbocyanine dyes allow living neurons of identified origin to be studied in long-term cultures. *J. Cell Biol.* 103, 171–187.
- (49) Weston, K. D., and Goldner, L. (2001) Measuring the orientation and reorientation dynamics of single molecules. *J. Phys. Chem. B* 105, 3453–3460.
- (50) Bayliss, N. S. (1950) The effect of electrostatic polarization of the solvent on electronic absorption spectra. *J. Chem. Phys.* 18, 292–298.
- (51) Rodriguez, J., Scherlis, D., Estrin, D., Aramendia, P. F., and Negri, R. M. (1997) AM1 study of the ground and excited-state potential energy surfaces of symmetric carbocyanines. *J. Phys. Chem.* 101, 6998–7006.
- (52) Tinnefeld, P., Buschmann, V., Weston, K. D., and Sauer, M. (2002) Direct Observation of Collective Blinking and Energy Transfer in a Bichromophoric System. *J. Phys. Chem. A*, in press.

BC025600X

# Capture of Peptides with N-Terminal Serine and Threonine: A Sequence-Specific Chemical Method for Peptide Mixture Simplification

Dirk Chelius\* and Thomas A. Shaler

Thermo Finnigan, 355 River Oaks Parkway, San Jose, California. Received September 13, 2002;  
Revised Manuscript Received October 24, 2002

The objective of this study was to evaluate a sequence-specific chemistry for the ability to specifically capture peptides that contain N-terminal serine or threonine residues from mixtures. The first step is the oxidation of the 1,2-amino alcohol structure  $-\text{CH}(\text{NH}_2)\text{CH}(\text{OH})-$  of peptides containing N-terminal serine or threonine with periodate. The newly formed aldehyde reacts with a labeling reagent containing a hydrazide,  $\text{RCONHNH}_2$ , to form a hydrazone-peptide conjugate,  $\text{RCONHN}=\text{CH}-$  peptide. Biotin-labeled conjugates can then be isolated by affinity purification with streptavidin. The method described in this report can be useful in simplifying the complex mixtures of peptides that are generated in typical proteomic analysis, where proteins are digested with trypsin and analyzed using liquid chromatography mass spectrometry data. The sequence-specific peptide selection not only reduces the complexity of digest mixtures, but also provides additional information for peptide identification. The targeted peptides are those that have either serine or threonine adjacent to a protease cleavage site. The sequence information should greatly aid in both database matching for protein identification and for de novo sequence determination.

## INTRODUCTION

Large-scale analysis of a proteome typically includes separation of complex biological mixtures into individual proteins followed by the identification of the fractionated proteins. Typically, two-dimensional gel electrophoresis followed by mass spectrometry analysis is used (1–3). Alternative methods are based on two-dimensional chromatography coupled with mass spectrometry (4). The identification of proteins in both approaches includes tryptic digestion of the protein and identification of the tryptic peptides either directly by mass or by fingerprinting of these peptides during tandem mass spectrometry. Large numbers of peptides are typically generated during such experiments and the separation and identification remains a challenge.

The objective of this study was to develop a method to reduce the large number of peptides that are generated during large-scale protein identification techniques. To evaluate if peptides containing N-terminal serine or threonine are distributed in sufficient amounts in all proteins, a computer program was written to generate and identify all peptides that fit the criteria from the *C. elegans* database.

The sequence-specific chemistry to isolate peptides containing N-terminal serine or threonine residues was optimized for our purpose, including oxidation with periodate, linkage to biocytin hydrazide, and binding and release from streptavidin-coated beads. The oxidation by periodate of N-terminal 1,2-amino alcohols serine ( $\text{R} = \text{CH}_2\text{OH}$ ) or threonine [ $\text{R} = \text{CH}(\text{OH})\text{CH}_3$ ] residues  $\text{NH}_2-\text{CHR}-\text{CO}-$  of a polypeptide to an aldehyde func-

tion  $\text{O}=\text{CH}-\text{CO}-$  has been known for many years (5). This mild oxidation has been exploited for the synthesis of bioconjugates through formation of hydrazone, thiazolidine, or oxime ( $-\text{ON}=\text{CH}-\text{CO}-$ ) bonds (6–11). Reaction of the aldehyde with a hydrazide was reported to be very effective and could be achieved quantitatively (6). The conjugation reaction was used to generate biocytinylated peptides that could be isolated on streptavidin-coated beads. The biocytin is similar to biotin and has a very strong affinity to streptavidin. Elution of the captured peptides could be achieved by incubation in acid conditions.

The results presented in this study described a method to specifically capture peptides containing N-terminal serine or threonine residues. The method can potentially lead to improvements in large-scale protein identification strategies. Additionally the potential for an alternative method for protein quantitation similar to the isotope-coded affinity tags (ICAT) method is demonstrated (12).

## EXPERIMENTAL PROCEDURES

**Theoretical Modeling.** Bioinformatic modeling of theoretical digests and the simplifications resulting for different types of peptide selection for the *C. Elegans* database was performed with software written in-house. The *C. Elegans* protein database was obtained from the National Center for Biotechnology Information (NCBI).

**Chemistry.** Ten microgram pure peptides (Sigma, St. Louis, MO) or peptide mixtures (Table 1) were incubated with 10  $\mu\text{L}$  sodium periodate (40  $\mu\text{mol}$ ) in 20  $\mu\text{L}$  PBS (pH 7.2) at room temperature for 10 min in the dark. Peptides were exchanged into 100 mM sodium acetate (pH 4.5), and 100  $\mu\text{g}$  biocytin hydrazide (EZ-Link, Pierce, Rockford, IL) was added. The mixture was incubated for 1 h at room temperature and then incubated with streptavidin-coated magnetic beads (CPG Inc., Palo Alto, CA). After 1 h at room temperature, the beads were washed five times

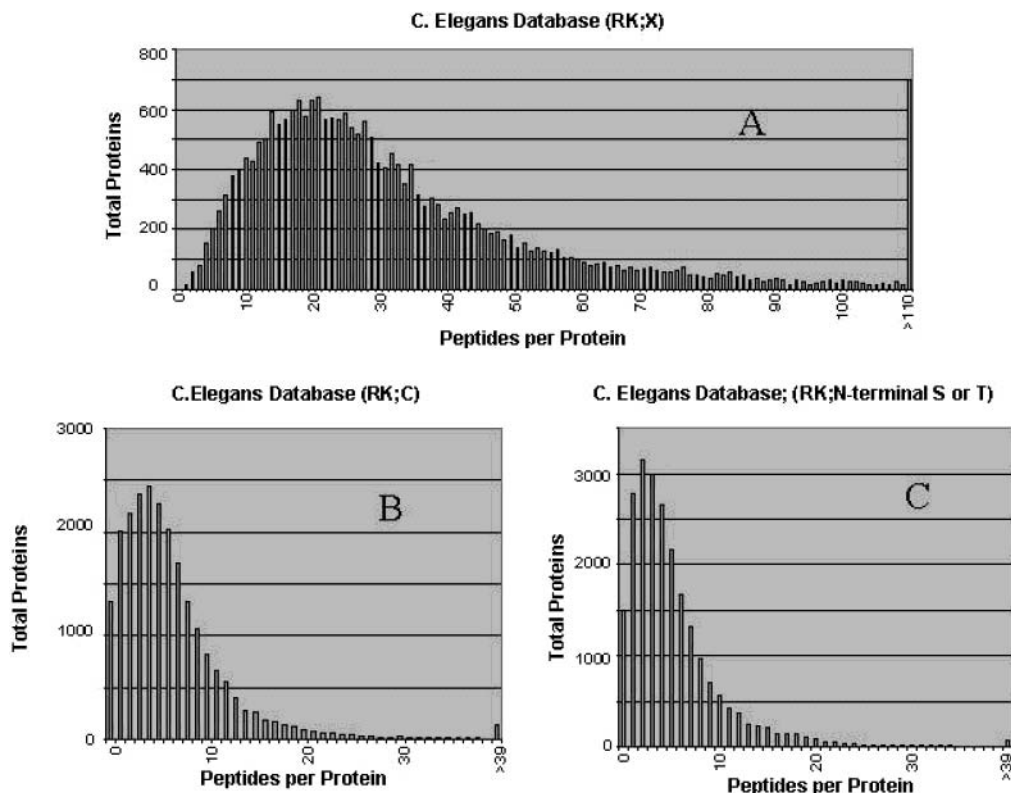
\* Corresponding author. Address: ThermoFinnigan, Proteomics Division, 355 River Oaks Parkway, San Jose, CA 95134. Phone: (408) 965-6326. Fax: (408) 965-6138. E-mail: dchelius@thermofinnigan.com.



**Table 1. Amino Acid Sequence and Molecular Weight (MW) of Peptides Used in This Study<sup>a</sup>**

#	peptide	<i>m/z</i>	observed MW	calculated MW
1	TFQAYPLREA	598.9 (2 <sup>+</sup> ); 1195.6 (1 <sup>+</sup> )	1195.2 ± 0.6	1195.3
2	SGQSWRPQGRF	436.5 (3 <sup>+</sup> ); 653.3 (2 <sup>+</sup> ) 1304.7 (1 <sup>+</sup> )	1304.9 ± 0.8	1304.4
3	SIPSKDALLK	536.7 (2 <sup>+</sup> )	1072.4	1071.3
4	MNYLAFPRM	572.0 (2 <sup>+</sup> ); 1141.6 (1 <sup>+</sup> )	1141.3 ± 0.7	1141.4

<sup>a</sup> Peptides were analyzed by LC/MS as described in the Experimental Procedure section. Although ions were observed in a variety of multiple charge states, observed masses are calculated as molecular masses of neutrals. The masses are identified as average.



**Figure 1.** Bioinformatic modeling of theoretical digests and the simplifications resulting for different types of peptide selection for the *C. Elegans* database (NCBI) was performed with software written in-house. A: Distribution of the numbers of peptides per protein generated by tryptic digestion from *C. Elegans* database. B: Peptides per protein containing cysteine residues from tryptic digestion of the *C. Elegans* database. C: Peptides per protein containing N-terminal serine or threonine residues from tryptic digestion of the *C. Elegans* database.

with the sodium acetate buffer to remove nonbiotinylated peptides. The aldehyde form of the peptides could be eluted from the beads by incubation of the beads at 60 °C for 1 h in 10% formic acid. Each step in the reaction scheme (Figure 2) was monitored by LC/MS/MS on an LCQ DECA ion trap mass spectrometer (Thermo Finnigan, San Jose, CA).

**Sample Analysis.** The peptide samples were analyzed using a fully automated nanoflow LC/MS/MS system (13). Aliquots of the sample digest (250 fmol each peptide) were placed in wells of a 96-well plate (Nalge Nunc International, Rochester, NY). The plate was sealed with plastic film to minimize evaporation and inserted into the auto-sampler of a Surveyor HPLC system (Thermo-Finnigan, San Jose, CA), where it was kept at 4 °C while waiting for analysis. The auto-sampler was equipped with no-waste injection capability, which enables injection volumes as low as 1  $\mu$ L. The injected peptides were first loaded onto a reversed-phase poly(styrene-divinylbenzene) peptide trap (Michrom Bioresources, Auburn, CA) with a flow rate of 10  $\mu$ L/min for 3 min. The peptides were eluted from the trap and separated on a reversed-phase capillary column (PicoFrit; 5  $\mu$ m BioBasic C18, 300 Å pore size; 75  $\mu$ m  $\times$  10 cm; tip 15  $\mu$ m, New Objective, Woburn, MA) with a 30 min linear gradient of 0–60% acetonitrile in 0.1% formic acid/water at a flow rate of

approximately 0.1  $\mu$ L/min after split. The HPLC was directly coupled to a ThermoFinnigan LCQ Deca ion trap mass spectrometer equipped with a nano-spray ionization source. The spray voltage was 2.0 kV, and the capillary temperature was 200 °C. The ion-trap collisional fragmentation spectra were obtained using collision energies of 35%. Each full-scan mass spectrum was followed by one MS/MS spectra of the most intense peak. Full mass spectra and tandem mass spectra were analyzed manually by comparing the data with the predicted data based on the amino acid sequence of the peptides.

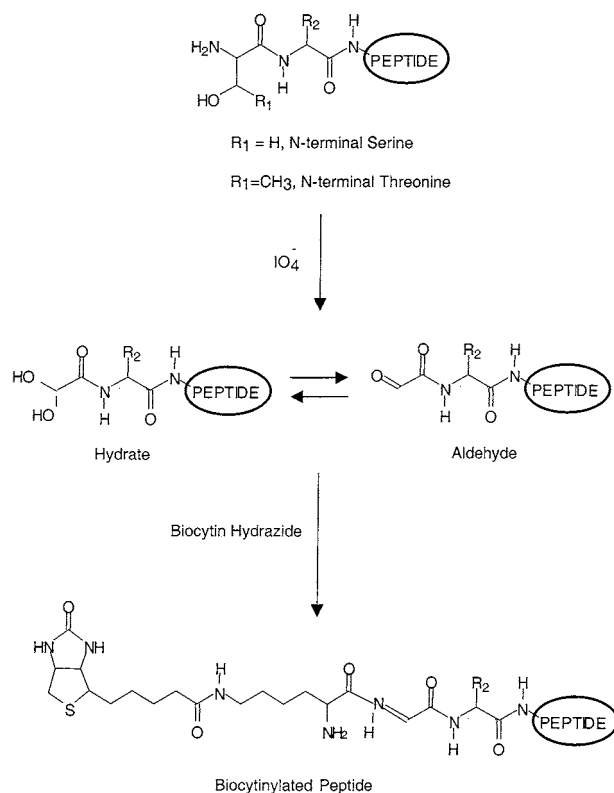
## RESULTS

**Computer Modeling.** A computer program was written to generate and identify all peptides from a tryptic digest that contain N-terminal serine or threonine residues from the *C. elegans* database. The results are summarized in Figure 1. Only 1500 proteins from the *C. elegans* database do not contain such peptides (Figure 1C). Therefore, our proposed method of peptide reduction would not be able to identify these proteins. However, the *C. elegans* database contains 63 394 proteins, so that only 2.3% of all proteins would be missed. This result was compared to peptides containing cysteine residues (Figure 1b). Capture of cysteine residue is commonly used for reduction of peptide complexity and for quantitation

**Table 2. Calculated and Observed Molecular Weights (MW) of Peptides after Oxidation with Periodate<sup>a</sup>**

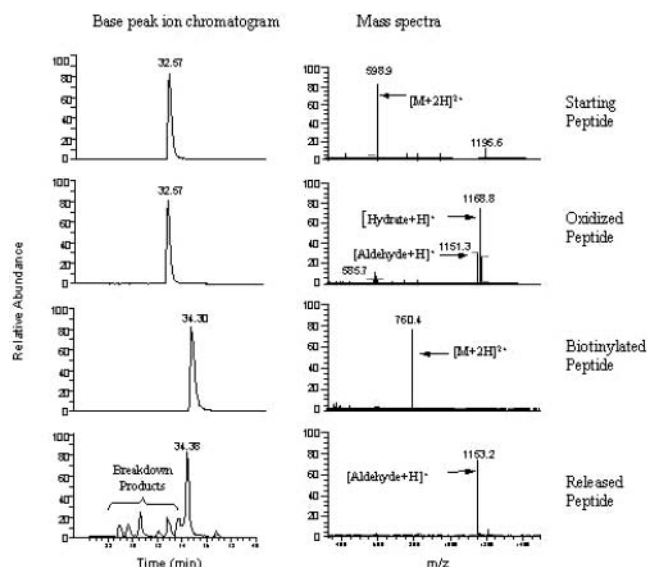
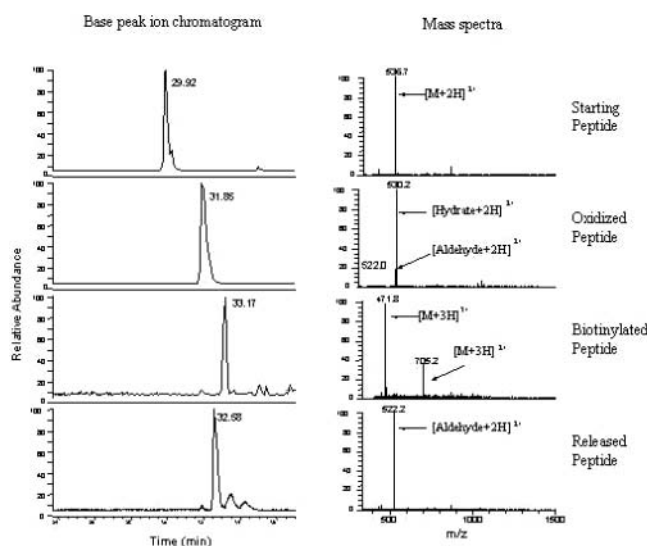
#	<i>m/z</i>	observed MW	calculated MW (hydrate)	calculated MW (aldehyde)
1	1151.3 (1 <sup>+</sup> ); 1168.8 (1 <sup>+</sup> )	1150.3; 1167.8	1168.3	1150.3
2	646.9 (2 <sup>+</sup> );	1291.8	1291.4	1273.4
3	530.2 (2 <sup>+</sup> ); 522.0 (2 <sup>+</sup> )	1058.4; 1042.0	1058.3	1040.3
4	588.0 (2 <sup>+</sup> ); 1173.6 (1 <sup>+</sup> )	1174.0	1173.4 <sup>b</sup>	—

<sup>a</sup> Peptides were oxidized with periodate and the products were analyzed by LC/MS as described in the Experimental Procedures section. Although ions were observed in a variety of multiple charge states, observed masses are calculated as molecular masses of neutrals. The masses are identified as average. <sup>b</sup> The molecular weight of peptide 4 MNLYAFPRM was calculated under the assumption that both methionines were oxidized which correlates to the addition of 32 Da to the molecular weight.

**Figure 2.** Schematically representation of the peptide derivatization chemistry performed in this study.

applications such as the ICAT method. The distribution of cysteine containing tryptic peptides is similar to the distribution of tryptic peptides containing N-terminal serine or threonine residues. The result demonstrates that our proposed method would generate sufficient amounts of peptides to identify more than 97% of all proteins of the *C. elegans* database.

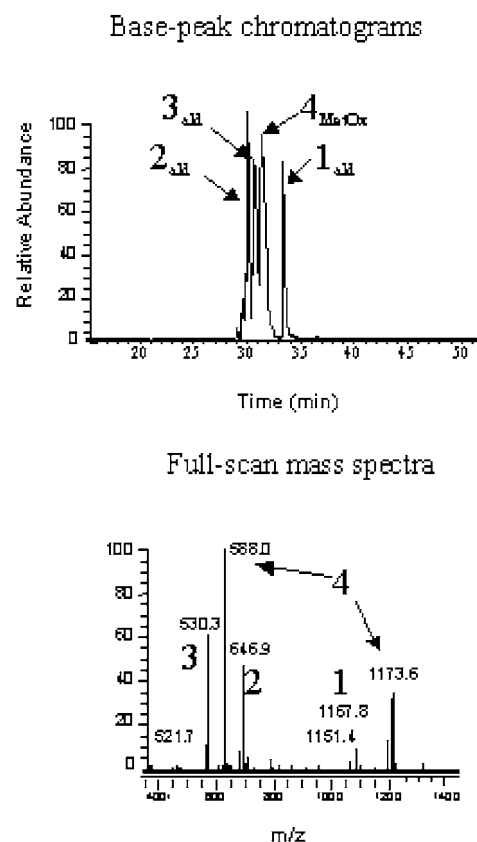
**Chemistry.** The four peptides used in this study, including two peptides with N-terminal serine residue and one peptide with N-terminal threonine residue, were analyzed by LC/MS/MS analysis to ensure the purity and to confirm the molecular weight. The results are summarized in Table 1. The oxidation of N-terminal 1,2 amino alcohols with periodate was optimized using one synthetic peptide containing a N-terminal threonine residue and one peptide containing an N-terminal serine residue. Oxidation of peptide 1 (TFQAYPLREA) resulted in the formation of the aldehyde form and the aldehyde-hydrate form (to be referred to as hydrate). The calculated molecular weight and the measured molecular weight are shown in Table 2. The singly charged ion with an *m/z* value of 1151.3 correlates well with the calculated molecular weight of the aldehyde (1150.3). Additionally the hydrate form could be detected with an *m/z* value of 1168.8 (calculated 1168.3). The corresponding chromato-

**Figure 3.** LC/MS/MS analysis of reaction products after each step during capture of peptide 1 (TFQAYPLREA). See the Experimental Procedures for details.**Figure 4.** LC/MS/MS analysis of reaction products after each step during capture of peptide 3 (SIPSKDALLK). See the Experimental Procedures for details.

grams and mass spectra are shown in Figure 3. The reaction was found to be quantitative. Similar results could be obtained with the oxidation of peptide 3 (SIPSKDALLK). The doubly charged ions with *m/z* values of 522.0 and 530.2 correspond to peptides with apparent molecular weight of 1042.0 and 1058.4 Da, which agrees well with the calculated molecular weight for the aldehyde (1040.4 Da) and the hydrate-form (1058.3). The results are shown in Table 2 and Figure 4. The alde-

hyde-hydrate was the major product in both reactions. Incubation of the oxidation products with biocytin hydrazide yields the biocytinylated peptides. For peptide **1** the bioconjugate was calculated to have a molecular weight of 1518.8 (the molecular weight of the linker 386.5 Da plus the molecular weight of the aldehyde 1150.3 Da minus 18 ( $\text{H}_2\text{O}$ ) = 1518.8). This correlates very well with the major peak found in the chromatogram, where the doubly charge ion of 760.4 corresponds to a molecular weight of 1518.8 Da (Figure 3). The conjugation reaction of peptide **3** shows two major peaks with  $m/z$  values of 471.8 ( $3^+$ ) and 705.2 ( $2^+$ ), corresponding to a molecule with a molecular weight of  $1410.4 \pm 2.0$  Da (Figure 4). This corresponds well with the calculated molecular weight of peptide **3** linked to biocytin hydrazide of 1408.8 Da (same calculation as above). The reaction appears to be quantitative on the basis of the chromatogram. In the final step the biocytinylated peptides were bound to streptavidin-coated beads, washed and eluted with 10% formic acid. LC/MS analysis of the eluted samples showed the aldehyde form of either peptide **1** or peptide **3** as major peaks. Elution of peptide **1** shows one major peak with an  $m/z$  value of 1153.2 corresponding to the aldehyde form of peptide **1** (Figure 3). Several smaller peaks could be detected but not identified. Most likely, these peaks correspond to breakdown products of peptide **1**. Elution of peptide **3** shows one major peak with an  $m/z$  value of 522.2, corresponding to the aldehyde form of peptide **3** (Figure 4). Additionally, several smaller peaks could be also detected but not identified. LC/MS analysis of the products after every step of chemical synthesis confirms that the peptide modifications were performed as planned and complete.

The method was further evaluated to test if this approach could be used to specifically capture peptides, which contain N-terminal serine or threonine residues from a mixture of four synthetic peptides, two containing N-terminal serine (peptide **2** SGQSWRPQGRF and peptide **3** SIPSKDALLK), one containing N-terminal threonine (peptide **1** TFQAYPLREA), and one containing neither N-terminal serine nor threonine but N-terminal methionine (peptide **4** MNYLAFPRM). The peptide mixture was first oxidized with periodate as described in the Experimental Procedure section. The sample mixture was analyzed by LC/MS, and the results are shown in Figure 5. The four major peaks in the chromatogram could be identified as the oxidized isoforms of peptides **1**, **2**, **3**, and **4**. The aldehyde form and the hydrate form of peptide **1** (calculated MW of 1150.3 and 1168.3 Da) can be identified as a singly charged ions with an  $m/z$  value of 1151.4 and 1167.8, respectively. The doubly charge ion with an  $m/z$  value of 646.9 corresponds to the hydrate form of peptide **2**, and the doubly charge ions with an  $m/z$  value of 521.7 and 530.3 corresponds to the aldehyde form and the hydrate form of peptide **3**. Additionally peptide **4** was identified in the oxidized form as a doubly charged ion with an  $m/z$  value of 588.0 and a singly charge ion with an  $m/z$  value of 1173.6. The observed molecular weight of peptide **4** differs by 32 from the calculated molecular weight of peptide **4** (1141.4). The difference can be explained with the oxidation of the two methionines in peptide **4**. The oxidized peptide mixture was incubated with biocytin hydrazide as described in the Experimental Procedures section, and the bioconjugates were bound to the streptavidine-coated beads. After several washing steps to remove all unspecific bound material, the peptides were eluted with 10% formic acid as described in the Experimental Procedures section. The eluate was analyzed by LC/MS/MS, and the ion chromatograms and



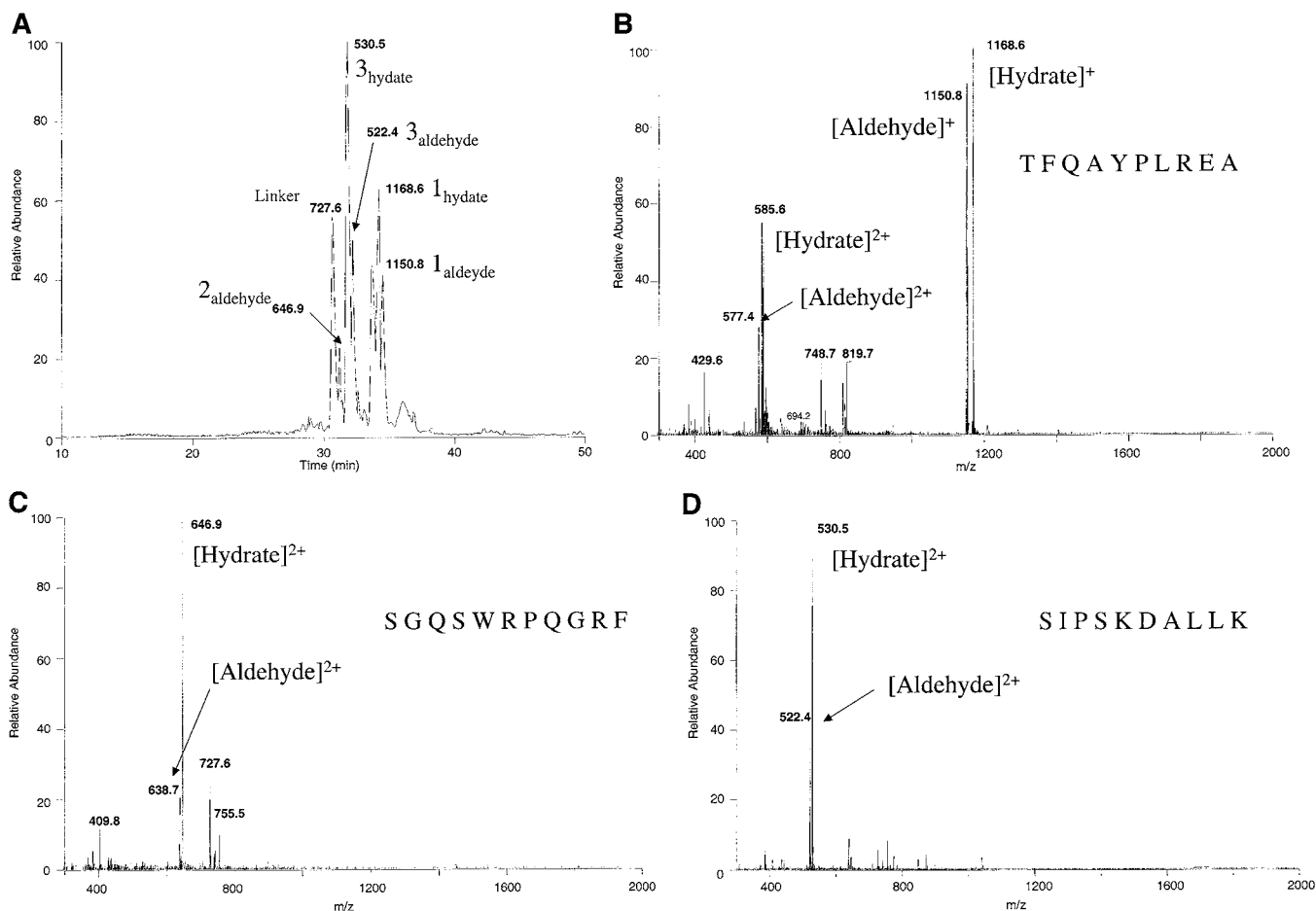
**Figure 5.** LC/MS/MS analysis of the four peptides after oxidation with periodate. See the Experimental Procedures for details. The amino acid sequence of the four peptides is shown in Table 1. The full-scan mass spectrum is the sum of all mass spectra recorded during the elution of the peptides (elution time: 28–35 min).

mass spectra are shown in Figure 6. As predicted peptide **4** could not be identified. However, peptides **1**, **2**, and **3** could be identified as both, the aldehyde form and the hydrate form. Peptide **1** showed ions with  $m/z$  values of 1150.8 ( $1^+$ ) and 577.4 ( $2^+$ ) that correlate well with the predicted molecular weight of the aldehyde form of peptide **1** (see Table 2). Additionally the hydrate form of peptide **1** could be identified as singly charge ion with a  $m/z$  value of 1168.6 (calculated molecular weight of hydrate 1168.3 Da) and as a doubly charged ion with a  $m/z$  value of 585.6. Peptide **2** could be identified as doubly charge ions at  $m/z$  values of 646.9 (hydrate) and 638.7 (aldehyde), and peptide **3** could be identified as doubly charged ions with  $m/z$  values of 530.5 (hydrate) and 522.4 (aldehyde) (see Table 2). Additionally a species with an  $m/z$  value of 727.6 (singly charged ion) could be detected. Fragmentation of the 727.6 ion resulted in a major peak with an  $m/z$  value of 387.4 (data not shown), which correlates with the molecular weight of the linker (386.5) indicating that the unidentified peak at 727.6 might be a linker related adduct. The results demonstrated that the peptide modifications were performed as planned and the specific capture of peptides, containing N-terminal serine or threonine residues was successful.

## DISCUSSION

Analysis of the theoretical tryptic digest of the *C. elegans* database showed that 1500 proteins do not generate tryptic peptides that contain N-terminal serine or threonine residues. These proteins could not be identified if the proposed method for protein identifications would be used. However, the NCBI database contains a





**Figure 6.** A mixture of peptides 1–4 (the amino acid sequences of the peptides are shown in Table 1) was oxidized and biotinylated as described in the Experimental Procedures section. The biotinylated peptides were captured on magnetic beads and released by acid hydrolysis. The eluate was analyzed by LC/MS/MS as described in the Experimental Procedures section. A: Base peak ion chromatogram. B: Full mass spectra at a retention time of 34.2 min (peptide 1 TFQAYPLREA). C: Full mass spectra at a retention time of 31.3 min (peptide 2 SGQSWRPQGRF). D: Full mass spectra at a retention time of 32.0 min (peptide 3 SIPSKDALLK).

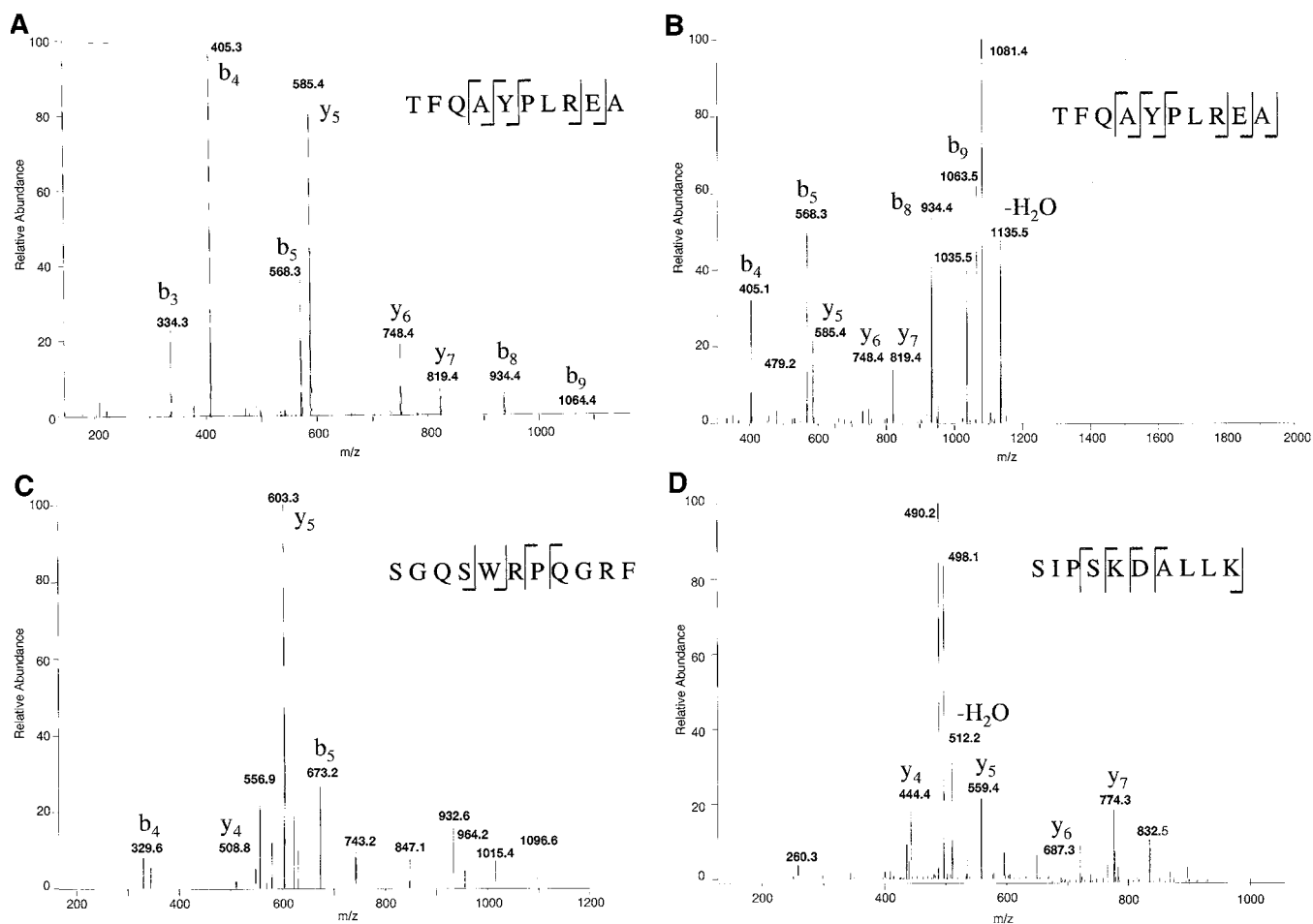
total of 63394 protein entries for *C. elegans* so that only 2.3% of all proteins would be missed. The reduction of total numbers of peptides in a complex mixture should greatly enhance the peptide ionization efficiency during electrospray process and should therefore facilitate the identification of low abundant proteins. The percentage of proteins missed using this technology depends on the database and it is possible that more proteins would be missed for other organisms. The ICAT (isotope-coded affinity tags) method for protein quantitation uses cysteine residues to specifically label and isolate certain peptides (12). The distribution of tryptic peptides containing cysteine residues is very similar to tryptic peptides containing N-terminal serine or threonine residues in the *C. elegans* database. The distribution of tryptic peptides containing cysteine or N-terminal serine or threonine residues might also be different for other databases.

After theoretical proof of the concept, that indeed the capture of peptides containing N-terminal serine or threonine residues could reduce the complexity of a complex mixture of tryptic peptides without losing a significant amount of protein information, a chemistry was developed to capture those peptides. The oxidation of N-terminal 1,2 amino alcohols serine or threonine with periodate was optimized. Alcohols were converted to aldehydes within 10 min reaction time, and the reaction was found to be quantitative. The aldehyde is in equilibrium with the diol form (in the text revert to as aldehyde–hydrate or hydrate), and under the conditions

used in this experiment, the hydrate form is the predominant species. This fact does not affect the next reaction step with hydrazide as shown in results. The reaction was performed under mild conditions however oxidation of methionine was also observed. This unwanted side reaction should not present any problems for our proposed method, since oxidation of methionine to the thiol form seems to be quantitative, too.

The next step was the linkage of the generated aldehydes to the biocytin hydrazide reagent. The reaction was also found to be quantitative demonstrating that our method of specifically labeling peptides containing N-terminal serine or threonine was successful. As expected, peptides that do not contain N-terminal serine or threonine do not react with the biocytin hydrazide.

Finally the labeled peptides could be bound to streptavidin-coated beads, allowing the isolation of the labeled peptides. Elution of the peptides was found to be somewhat tricky. The biocytin–streptavidine interaction is very strong. In fact, initial attempts to remove the peptides with guanidine hydrochloride and incubation at high temperature resulted in very bad yields (data not shown). Fortunately the peptides could be released by incubation in 10% formic acid at 60° for 30 min. The chemistry was not studied in detail, however hydrolysis of hydrazone bonds is well reported in the literature (6). The main product for the three peptides tested was the aldehyde form of those peptides. Several other fragments could be eluted from the beads. These fragments could not be identified but are most likely breakdown product



**Figure 7.** Tandem mass spectra analysis of peptides eluted from the streptavidin-coated magnetic beads (see Experimental Procedures for details). The full scan mass spectra are shown in Figure 6B–D. A: Tandem mass spectrum derived by collision induced dissociation of the  $(M + 2H)^{2+}$  precursor ion,  $m/z = 577.4$  of peptide **1** (retention time 34.2). B: Tandem mass spectrum derived by collision induced dissociation of the  $(M + H)^+$  precursor ion,  $m/z = 1150.8$  of peptide **1** (retention time 34.2). C: Tandem mass spectrum derived by collision induced dissociation of the  $(M + 2H)^{2+}$  precursor ion,  $m/z = 646.9$  of peptide **2** (retention time 31.3). And D: Tandem mass spectrum derived by collision induced dissociation of the  $(M + 2H)^{2+}$  precursor ion,  $m/z = 522.4$  of peptide **3** (retention time 32.0). Fragment ions in all four spectra represent mainly singly event preferential cleavage of the peptide bonds resulting in the sequence information recorded from both N (b-ions) and C (y-ions) termini of the peptides simultaneously.

of the bioconjugates. Either peptide bonds are hydrolyzed under the acid conditions or other parts of the linker are labile to acid hydrolyzation.

Clearly the acid hydrolysis for peptide release is not the optimal solution. Although all three peptides could be identified, the appearance of additional peptide fragments is not desirable and could complicate the peptide identification. However, several linkers are commercially available that contain a cleavable linker attached to a biotin or biocytin label and a hydrazine reactive group. The use of such linkers should greatly enhance the yield of our proposed method and reduce the formation of breakdown products. Additionally one could imagine the construction of linkers, which are different only in certain isotopes that could be used similar to the ICAT method in protein quantitation (12). The idea behind such quantitation method is the labeling of control and experimental sample with tags that are different in mass but chemically identical ( $H/D$  or  $C^{12}/C^{13}$ ). After labeling, the control and experimental samples are combined and differences in the protein profile can be analyzed by comparing the signal intensity of the labeled peptides. The labeling of peptides containing N-terminal serine or threonine residues could complement the ICAT method, which labels peptides containing cysteine residues.

The huge advantage of our proposed method becomes obvious when looking at the tandem mass spectra in

Figure 7. Although all peptides could be identified in the full mass spectra, the tandem mass spectra frequently do not contain sufficient fragmentation information for automatic peptide identification. Our method is sequence-specific, and the targeted peptides are those that have either serine or threonine adjacent to a protease cleavage site. This additional sequence information should greatly aid in both database matching for protein identification and for de novo sequence determination.

## CONCLUSIONS

Peptides that contain serine or threonine at the N-terminus can be specifically modified and captured from mixtures. The initial oxidation step with periodate occurs under mild conditions and is rapid and quantitative, although methionine sulfoxide formation occurs. Treatment of the N-terminal aldehydes with biocytin hydrazide allows the modified peptides to be tagged with affinity selection groups. These bioconjugates can be captured on streptavidin-coated magnetic beads. The release of the peptide aldehydes from the solid support was achieved by acidic hydrolysis of the hydrazone. This release reaction can lead to peptide degradation. However, all peptides containing N-terminal serine or threonine could be isolated from a mixture of peptides with this method. The described approach to simplify complex

peptide mixture could have an impact on large-scale protein identification and quantification.

#### ACKNOWLEDGMENT

The authors would like to thank Chris Becker for the encouragement and fruitful discussions.

#### LITERATURE CITED

- (1) Hanash, S. M. (2000) Biomedical applications of two-dimensional electrophoresis using immobilized pH gradients: current status. *Electrophoresis* 21, 1202–1209.
- (2) Pandey, A., and Mann, M. (2000) Proteomics to study genes and genomes. *Nature* 405, 837–846.
- (3) Washburn, M. P., and Yates, J. R., III. (2000) Analysis of the microbial proteome. *Curr. Opin. Microbiol.* 3, 292–297.
- (4) Washburn, M. P., Wolters, D., and Yates, J. R., III. (2001) Large-scale analysis of the yeast proteome by multidimensional protein identification technology. *Nat. Biotechnol.* 19, 242–247.
- (5) Fields, R., and Dixon, H. B. (1968) A spectrophotometric method for the microdetermination of periodate. *Biochem. J.* 108, 883–887.
- (6) Geoghegan, K. F., and Stroh, J. G. (1992) Site-directed conjugation of nonpeptide groups to peptides and proteins via periodate oxidation of a 2-amino alcohol. Application to modification at N-terminal serine. *Bioconjugate Chem.* 3, 138–146.
- (7) Gaertner, H. F., Rose, K., Cotton, R., Timms, D., Camble, R., and Offord, R. E. (1992) Construction of protein analogues by site-specific condensation of unprotected fragments. *Bioconjugate Chem.* 3, 262–268.
- (8) Mikołajczyk, S. D., Meyer, D. L., Starling, J. J., Law, K. L., Rose, K., Dufour, B., and Offord, R. E. (1994) High yield, site-specific coupling of N-terminally modified beta-lactamase to a proteolytically derived single-sulfhydryl murine Fab'. *Bioconjugate Chem.* 5, 636–646.
- (9) Zhang, L., and Tam, J. P. (1996) Thiazolidine formation as a general and site-specific conjugation method for synthetic peptides and proteins. *Anal. Biochem.* 233, 87–93.
- (10) Rose, K., Zeng, W., Regamey, P. O., Chernushevich, I. V., Standing, K. G., and Gaertner, H. F. (1996) Natural peptides as building blocks for the synthesis of large protein-like molecules with hydrazone and oxime linkages. *Bioconjugate Chem.* 7, 552–556.
- (11) Nardin, E. H., Calvo-Calle, J. M., Oliveira, G. A., Clavijo, P., Nussenzweig, R., Simon, R., Zeng, W., and Rose, K. (1998) Plasmodium falciparum polyoximes: highly immunogenic synthetic vaccines constructed by chemoselective ligation of repeat B-cell epitopes and a universal T-cell epitope of CS protein. *Vaccine* 16, 590–600.
- (12) Gygi, S. P., Rist, B., Gerber, S. A., Turecek, F., Gelb, M. H., and Aebersold, R. (1999) Quantitative analysis of complex protein mixtures using isotope-coded affinity tags. *Nat. Biotechnol.* 17, 994–999.
- (13) Chelius, D., Hühmer, A. F. R., Shieh, C. H., Lehmberg, E., Traina, J. A., Slattey, T. K., and Pungor, E., Jr. (2002) Analysis of the adenovirus type 5 proteome by liquid chromatography and tandem mass spectrometry methods. *J. Proteome Res.* 501–513.

BC025605U



# Vanadyl–Thiazolidinedione Combination Agents for Diabetes Therapy

Tim Storr,<sup>†</sup> Devin Mitchell,<sup>†,‡</sup> Péter Buglyó,<sup>†,§</sup> Katherine H. Thompson,<sup>†</sup> Violet G. Yuen,<sup>||</sup> John H. McNeill,<sup>\*,||</sup> and Chris Orvig<sup>\*,†</sup>

Medicinal Inorganic Chemistry Group, Department of Chemistry, University of British Columbia, Vancouver, BC, V6T 1Z1, Canada, and Faculty of Pharmaceutical Sciences, University of British Columbia, Vancouver, BC, V6T 1Z3, Canada. Received September 16, 2002; Revised Manuscript Received October 9, 2002

A series of vanadium compounds, chelated by ligands containing a thiazolidinedione moiety as an additional insulin-enhancing component, were produced in this study to create potentially synergistic compounds. A set of four bifunctional ligand precursors were synthesized: ( $\pm$ )-5-[4-[(5-hydroxy-4-oxo-4H-pyran-2-ylmethyl)amino]benzyl]thiazolidine-2,4-dione (HL<sup>1</sup>), ( $\pm$ )-5-[4-[(5-hydroxy-1-methyl-4-oxo-1,4-dihydro-pyridin-2-ylmethyl)amino]benzyl]thiazolidine-2,4-dione (HL<sup>2</sup>), 5-[4-(5-hydroxy-4-oxo-4H-pyran-2-ylmethoxy)benzylidene]thiazolidine-2,4-dione (HL<sup>3</sup>), and ( $\pm$ )-5-[4-(5-hydroxy-4-oxo-4H-pyran-2-ylmethoxy)benzyl]thiazolidine-2,4-dione (HL<sup>4</sup>), each containing a metal chelating portion as well as a thiazolidinedione moiety. From this set of ligand precursors, air-stable VO(L<sup>1</sup>)<sub>2</sub>, VO(L<sup>3</sup>)<sub>2</sub>, and VO(L<sup>4</sup>)<sub>2</sub> were prepared. The four ligand precursors and three complexes were tested for insulin-enhancing potential in STZ-diabetic rats and compared to rosiglitazone and BMOV, respectively. Both the ligand precursors HL<sup>1</sup> and HL<sup>3</sup> showed enhanced activity compared with that of rosiglitazone. The complex VO(L<sup>3</sup>)<sub>2</sub> showed the most efficacious hypoglycemic effects in this study; however, neither additive nor synergistic effects were observed using this acute animal model.

## INTRODUCTION

Diabetes mellitus includes a heterogeneous group of diseases which have become an important health concern in our society, affecting 1 in 20 persons in industrialized nations. The disease is characterized by hyperglycemia, alterations in carbohydrate and lipid metabolism, and vascular and neurological complications. It can be roughly divided into two classes: type 1, insulin-dependent diabetes mellitus (IDDM), and type 2, non-insulin-dependent diabetes mellitus (NIDDM). Treatment may involve daily subcutaneous injections of insulin (most common for type 1), diet and exercise, administration of one or more of the currently available hypoglycemic agents (type 2), or combination therapy. Numerous therapies designed to supplement or enhance insulin action have been developed to aid in the treatment of NIDDM. Combined with diet and exercise, these regimens have proven to be fairly effective, but none are ideal. Thus, there is a need to find effective, orally active drugs that mimic or enhance the properties of insulin.

Vanadium was first demonstrated to have insulin-like properties in vitro in 1979 (1), in skeletal muscle and adipose tissue, and in vivo in 1985 (2). Since this time there has been a great deal of interest in determining the biological role of vanadium, including its mechanism of action, and in the development of new vanadium

compounds as alternatives to conventional diabetes therapy. The mechanism of vanadium's in vivo effects has been the subject of much debate (3–8), most probably due to the multiplicity of its effects (5, 9). Current evidence points to a site (or sites) of action downstream from the insulin receptor (10) in the insulin signaling cascade. The therapeutic value of inorganic vanadium, in the form of vanadate ([VO<sub>4</sub>]<sup>3-</sup>) or vanadyl ([VO]<sup>2+</sup>), as an orally active agent against diabetes has been well documented (5, 11). Poor absorption from the gastrointestinal tract (GI) into the bloodstream, as well as a narrowness of the window of optimal effectiveness in vivo, limits the utility of administering vanadium to diabetic patients in this form. However, vanadium complexes such as bis(maltolato)oxovanadium(IV), commonly known by its acronym BMOV (12, 13) (Chart 1), have shown increased efficacy over inorganic vanadium in STZ-diabetic rat studies (14). BEOV (the ethyl analog) has recently completed phase 1 human clinical trials. Complexation of vanadyl ([VO]<sup>2+</sup>) with the approved food additive maltol improved GI (gastrointestinal) absorption, thereby decreasing the vanadium dose required for effective glucose lowering (14, 15). Numerous small ligands have been subsequently used in this manner to increase the potency of the vanadium center (15, 16). In an effort to further increase the efficacy of the drug candidates, the coupling of vanadium with a ligand that contains an insulin-action-enhancing drug has been explored (17). The coupling of vanadyl with a series of biguanides failed to produce additive or synergistic effects; however, this was most likely due to the large dosage differences required for these two classes of drugs (17–19). In an advance on this approach herein, we have chelated the vanadium center to a series of thiazolidinedione-containing ligands; dosage differences be-

\* Corresponding authors. E-mails: orvig@chem.ubc.ca and jmcneill@unixg.ubc.ca.

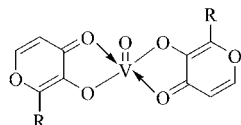
<sup>†</sup> Department of Chemistry, University of British Columbia.

<sup>‡</sup> Present address: Department of Chemistry, University of Victoria, Victoria, BC, V8W 3V6, Canada.

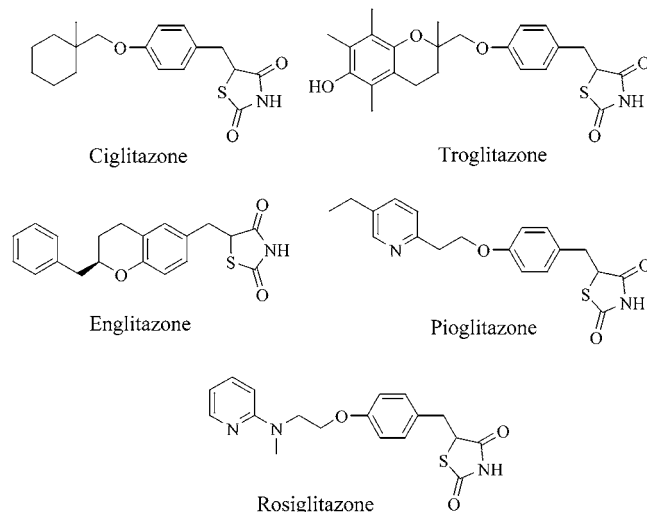
<sup>§</sup> Present address: Department of Inorganic and Analytical Chemistry, University of Debrecen, H-4010 Debrecen, P.O. Box 21, Hungary.

<sup>||</sup> Faculty of Pharmaceutical Sciences, University of British Columbia.

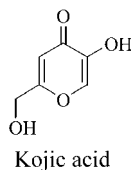
**Chart 1.** Bis(maltolato)oxovanadium(IV) (BMOV,  $R = CH_3$ ), bis(ethylmaltolato)oxovanadium(IV) (BEOV,  $R = C_2H_5$ )



**Chart 2**



**Chart 3**



tween oxovanadium(IV) compounds and representative thiazolidinediones are small (18, 20).

The thiazolidinediones are named for the five-membered heteronuclear ring common to all compounds of this class (Chart 2). Of the thiazolidinedione compounds, ciglitazone, troglitazone, englitazone, pioglitazone, and rosiglitazone have been clinically examined as potential antidiabetic compounds (21). Both pioglitazone and rosiglitazone are available on the market for the treatment of type 2 diabetes. Thiazolidinediones act by indirectly enhancing peripheral insulin sensitivity, thereby lowering the levels of both glucose and insulin (22). Thiazolidinediones are known to activate the peroxisome proliferator-activated receptor gamma ( $PPAR\gamma$ ).  $PPAR\gamma$  regulates numerous metabolic pathways involving lipoprotein lipase, glucose transporters and insulin signaling pathways (23). Nonetheless, binding affinity of the thiazolidinediones for  $PPAR\gamma$  does not always correlate with euglycemic activity (24). A major benefit of the thiazolidinediones is that unlike sulfonylurea derivatives,  $\alpha$ -glucosidase inhibitors, or insulin, they influence insulin resistance. Compounds which improve insulin resistance enable the continued treatment of NIDDM patients without inducing hypoglycemia (21).

To form stable neutral complexes with the vanadyl ion, bifunctional ligands were developed, tethering the active portion of the thiazolidinedione molecule to a suitable chelator. Kojic acid **1** (Chart 3) was chosen for this purpose because, like maltol, it forms water soluble, neutrally charged complexes with appropriate metal ions (25). Simple kojic acid complexes with  $VO^{2+}$  have shown

significant antidiabetic activity (16). The planar ring system of kojic acid was also well suited for interacting with the binding domain of the  $PPAR\gamma$  receptor (26). It was hypothesized that kojic acid would be the most versatile binding moiety, as the planar ring system is also capable of chelating vanadium.

The concept of combining vanadium and a thiazolidinedione-containing ligand to form a compound that exhibits additive or synergistic effects is quite appealing. The preparation and characterization of a series of such bifunctional ligand precursors and their associated oxovanadium(IV) complexes are presented herein. Results from preliminary acute STZ-diabetic rat studies of four ligand precursors and three of the corresponding complexes are also reported and compared to rosiglitazone and BMOV, respectively.

## RESULTS AND DISCUSSION

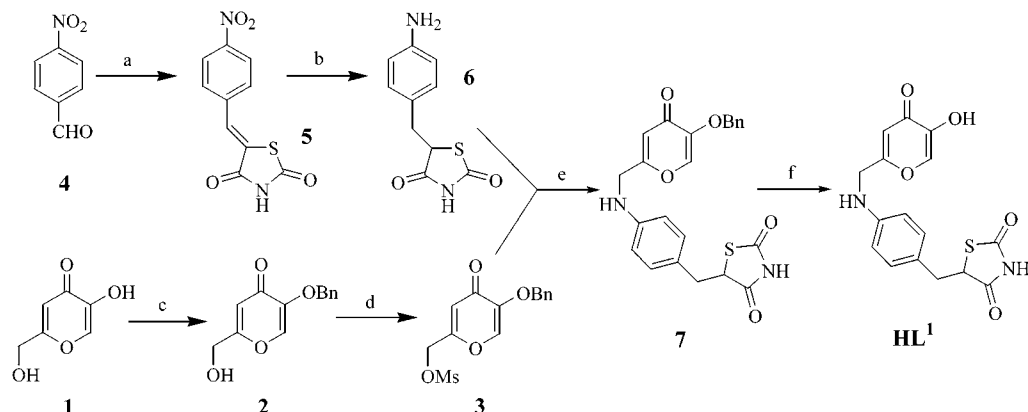
**Ligand Preparation.** All four ligand precursors **HL**<sup>1</sup>, **HL**<sup>2</sup>, **HL**<sup>3</sup>, and **HL**<sup>4</sup> were prepared by various routes from kojic acid **1**. Kojic acid **1** was first protected at the ring hydroxyl using the method of Thomas and Marxer (27) to afford the benzyl protected compound **2**. This compound was further elaborated to synthesize the four distinct ligand precursors. An effort was made to preserve the active portion of the thiazolidinediones (the 5-(4-substituted-benzyl)thiazolidine-2,4-dione moiety) in these bifunctional ligands (Chart 2).

For the amino-tethered ligand (Scheme 1), 5-benzyloxy-2-hydroxymethyl-pyran-4-one **2** was reacted with methanesulfonyl chloride to afford the mesylate **3**. Compound **3** was then coupled with ( $\pm$ )-5-(4-amino-benzyl)thiazolidine-2,4-dione **6**, which was synthesized by a more direct route than that available in the literature (28), to afford **7**. To synthesize **6**, 4-nitrobenzaldehyde **4** was coupled with thiazolidine-2,4-dione using reported conditions (29) to afford **5**, which was then reduced using  $NaBH_4$  in the presence of a cobalt/dimethylglyoxime catalyst formed in situ (30). Using this method, both the nitro group and the double bond were reduced simultaneously. Benzyl group removal from the coupled product **7** in strong acid afforded the amino-tethered thiazolidinedione ligand **HL**<sup>1</sup>.

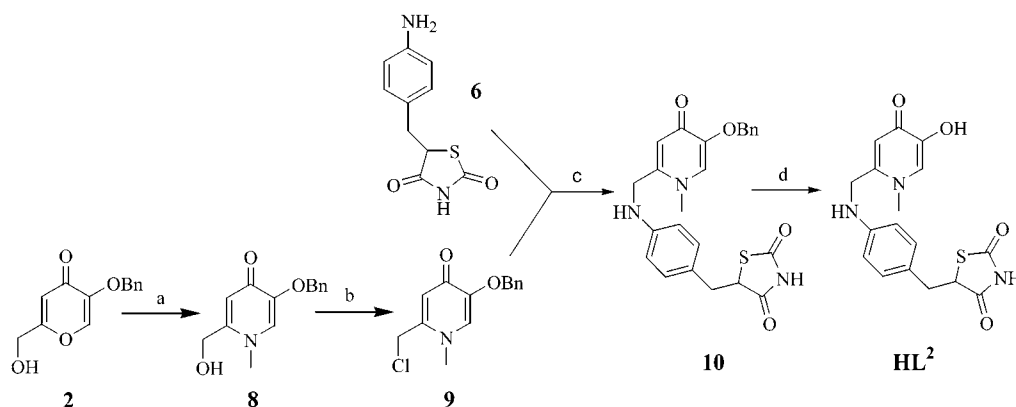
Synthesis of the pyridinone-type ligand (Scheme 2) proceeded in much the same manner as with **HL**<sup>1</sup>. A pyridinone-type chelator was examined because N-substitution into a pyrone ring has been shown to increase metal binding affinity (31, 32). Benzyl-protected kojic acid **2** was reacted with methylamine to form the pyridinone **8** in an improved yield over that reported (33). Compound **8** was then converted to the chloride **9** with thionyl chloride in good yield. The coupling step proceeded to give the protected compound **10** from which the benzyl group was removed to afford the pyridinone-type ligand precursor **HL**<sup>2</sup>.

The unsaturated ether-tethered ligand (Scheme 3) **HL**<sup>3</sup> was synthesized using the mesylate **3** as the starting material. Compound **3** was coupled with 4-hydroxybenzaldehyde to afford the aldehyde **11**, which then underwent a Knoevenagel condensation with thiazolidine-2,4-dione to yield compound **12**. The original intent at this point was to reduce the C–C double bond connecting the thiazolidinedione ring. Unfortunately we were not able to effect this transition selectively, despite employing a variety of conditions, because of the many other unsaturation points in the molecule. Because previous work (34, 35) had shown that the activity of certain thiazolidinediones with an unsaturation point in an identical

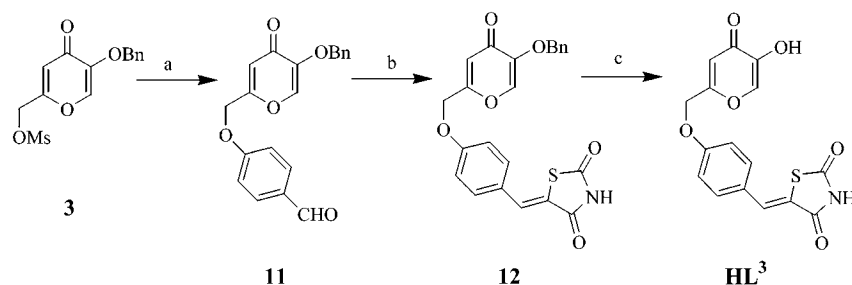
**Scheme 1. The Synthesis of HL<sup>1</sup>:** (A) Thiazolidine-2,4-dione, Piperidine, Benzoic Acid, Toluene, 55%; (B) CoCl<sub>2</sub>, Dimethylglyoxime, NaBH<sub>4</sub>, H<sub>2</sub>O, 71%; (C) Na, Benzyl Chloride, CH<sub>3</sub>OH, 55%; (D) Triethylamine, Methanesulfonyl Chloride, CH<sub>2</sub>Cl<sub>2</sub>; (E) K<sub>2</sub>CO<sub>3</sub>, CH<sub>3</sub>CN, 69%; (F) HCl, CH<sub>3</sub>COOH, 70%



**Scheme 2. The Synthesis of HL<sup>2</sup>:** (A) Methylamine, EtOH/H<sub>2</sub>O, 77%; (B) SOCl<sub>2</sub>, CH<sub>2</sub>Cl<sub>2</sub>, 96%; (C) Triethylamine, DMF, 88%; (D) HCl, CH<sub>3</sub>COOH, 73%



**Scheme 3. The Synthesis of HL<sup>3</sup>:** (A) 4-Hydroxybenzaldehyde, K<sub>2</sub>CO<sub>3</sub>, DMF, 64%; (B) Thiazolidine-2,4-dione, Piperidine, Benzoic Acid, Toluene, 57%; (C) HCl, CH<sub>3</sub>COOH, 67%



location exhibited equal or more impressive activity than their saturated analogues, we decided to continue by deprotecting **12** to form the unsaturated ether-tethered ligand **HL<sup>3</sup>**.

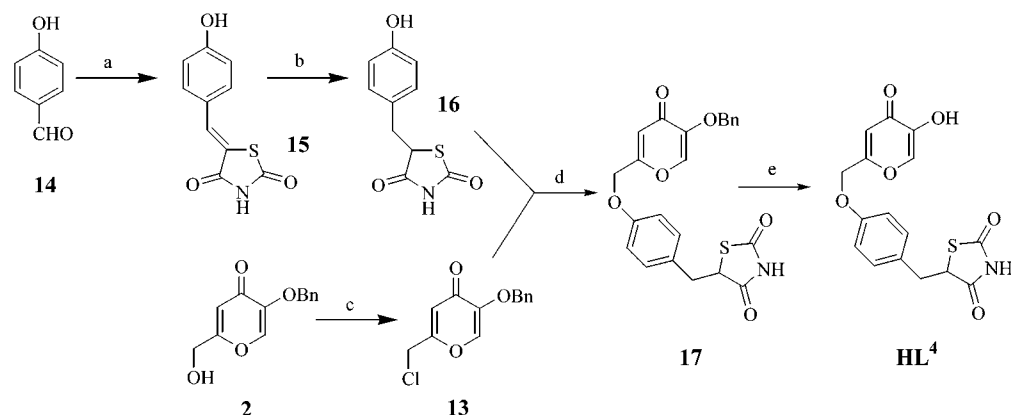
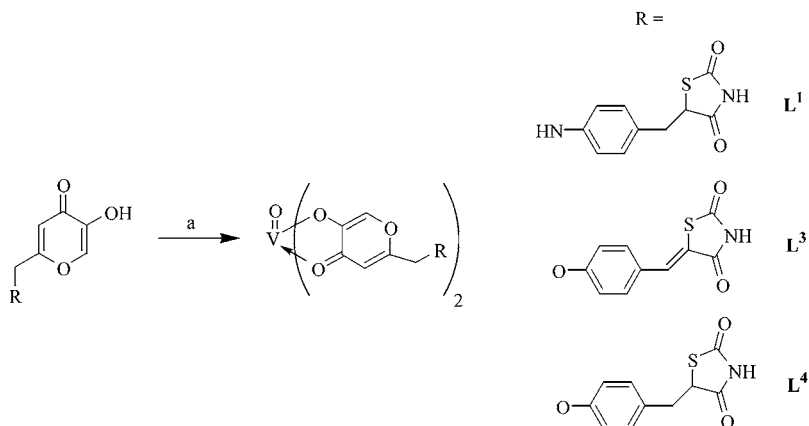
The ether-tethered ligand (Scheme 4) **HL<sup>4</sup>** was synthesized in a manner similar to that employed for **HL<sup>1</sup>**. In this case 5-benzyloxy-2-chloromethyl-pyran-4-one **13** was used in the coupling step because the mesylate **3** did not afford any coupled product. The slower reactivity of the chloride derivative presumably minimized side-reactions allowing the coupling reaction to take place. Compound **13** was coupled with 5-(4-hydroxy-benzyl)-thiazolidine-2,4-dione (**28**) **16**, which was synthesized by a Knoevenagel condensation of 4-hydroxybenzaldehyde **14** with thiazolidine-2,4-dione to form **15**, and then subsequent reduction. The coupled product **17** was then deprotected to afford the ether-tethered ligand **HL<sup>4</sup>**. The low yield of the coupling step here is most likely because of the similar nucleophilicities of the thiazolidinedione

nitrogen and the ring hydroxyl oxygen of compound **16**. Indeed, both coupling products were isolated, with the O-alkylation product occurring in a higher proportion.

The saturated ligand precursors **HL<sup>1</sup>**, **HL<sup>2</sup>**, and **HL<sup>4</sup>** are presumed to exist as a mixture of enantiomers with the stereogenic center located at C-5 of the thiazolidinedione ring. No attempt was made to synthesize or isolate selectively one enantiomer because this center is prone to rapid racemization at physiological pH (36). Interestingly, it has been reported that the (S)-(−)-enantiomer of rosiglitazone **5** was responsible for the binding affinity to PPAR $\gamma$  with a  $t_{1/2}$  for racemization of 3 h at pH 7.2(36).

**Vanadyl–Thiazolidinedione Complexes.** The neutral oxovanadium(IV)–thiazolidinedione complexes were prepared (Scheme 5) by refluxing vanadyl sulfate and two equivalents of the appropriate ligand precursor in mildly acidic aqueous medium (pH ~5). The precipitated products were isolated and washed with water and



**Scheme 4. The Synthesis of HL<sup>4</sup>:** (A) Thiazolidine-2,4-dione, Piperidine, Benzoic Acid, Toluene, 98%; (B) CoCl<sub>2</sub>, Dimethylglyoxime, NaBH<sub>4</sub>, H<sub>2</sub>O, 64%; (C) SOCl<sub>2</sub>, CH<sub>2</sub>Cl<sub>2</sub>, 60%; (D) NaH, DMF, 35%; (E) HCl, CH<sub>3</sub>COOH, 93%**Scheme 5. The Synthesis of VO(L<sup>1</sup>)<sub>2</sub> (83%), VO(L<sup>3</sup>)<sub>2</sub> (93%), and VO(L<sup>4</sup>)<sub>2</sub> (88%)<sup>a</sup>**<sup>a</sup> VOSO<sub>4</sub>, H<sub>2</sub>O.

diethyl ether to afford, after drying in vacuo light brown, gray, and brown solids, characterized as VO(L<sup>1</sup>)<sub>2</sub>, VO(L<sup>3</sup>)<sub>2</sub>, and VO(L<sup>4</sup>)<sub>2</sub>, respectively. Unfortunately, the extremely low solubility of the pyridinone-type ligand HL<sup>2</sup> precluded complexation to vanadium under a variety of conditions.

Characteristic stretching frequencies of the V=O bond in oxovanadium(IV) complexes generally occur in the region 930–1030 cm<sup>-1</sup> (37). The complexes VO(L<sup>1</sup>)<sub>2</sub>, VO(L<sup>3</sup>)<sub>2</sub>, and VO(L<sup>4</sup>)<sub>2</sub> exhibit V=O stretching frequencies of 982, 985, and 975 cm<sup>-1</sup>, respectively. The corresponding bis(kojato)oxovanadium(IV) (VO(ka)<sub>2</sub>) complex exhibits a similar V=O stretch at 980 cm<sup>-1</sup> (16).

Elemental analyses of the three complexes were consistent with the calculated values. All exhibited one molecule of residual water which could not be eliminated with prolonged drying. The mass spectra (+ ESIMS) support the VO(L)<sub>2</sub> formulation showing parent ion M + 1 peaks ([HVOL<sub>2</sub>]<sup>+</sup>), as well as expected fragmentation patterns.

All complexes prepared were paramagnetic in the solid state. Room-temperature paramagnetic susceptibilities were obtained. By correcting for the diamagnetic susceptibilities of the ligands using Pascal's constants, the effective magnetic moments of the complexes were calculated. With an electronic configuration of [Ar]3d<sup>1</sup>, vanadium(IV) has one unpaired electron for which the spin-only formula predicts a magnetic moment of 1.73 μ<sub>B</sub>. The experimental values are in the range 1.69–1.75 μ<sub>B</sub> for the three vanadyl complexes.

Electron paramagnetic resonance spectroscopic data for the three complexes showed the characteristic eight-line

**Table 1. Spin Hamiltonian Parameters for VO(L)<sub>2</sub>; L = L<sup>1</sup>, L<sup>3</sup>, L<sup>4</sup>, Ma, Ka**

complex	<i>g</i> <sub>iso</sub> <sup>a</sup>	<i>A</i> <sub>iso</sub> <sup>b</sup>
VO(L <sup>1</sup> ) <sub>2</sub> (MeOH:CH <sub>2</sub> Cl <sub>2</sub> 1:1)	1.967	104.0
VO(L <sup>3</sup> ) <sub>2</sub> (MeOH:CH <sub>2</sub> Cl <sub>2</sub> 1:1)	1.967	108.0
VO(L <sup>4</sup> ) <sub>2</sub> (MeOH:CH <sub>2</sub> Cl <sub>2</sub> 1:1)	1.967	105.0
VO(ma) <sub>2</sub> (BMOV) (CHCl <sub>3</sub> ) <sup>c</sup>	1.963	103.7
VO(ka) <sub>2</sub> (CHCl <sub>3</sub> ) <sup>d</sup>	1.963	104.5

<sup>a</sup> Error, ±0.001. <sup>b</sup> Units for the vanadium hyperfine coupling are ± 0.1 × 10<sup>-4</sup> cm<sup>-1</sup>. <sup>c</sup> Ref 12. <sup>d</sup> Ref 16.

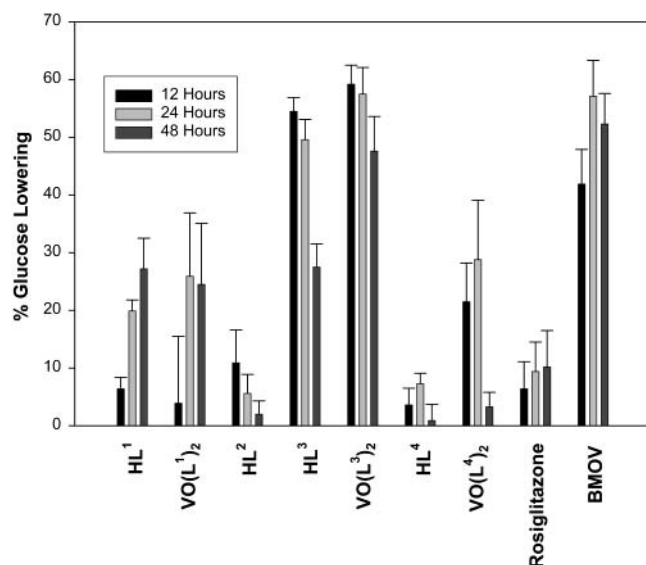
pattern expected for V (IV). The three vanadium–thiazolidinedione complexes exhibited identical *g*-values and very similar isotropic vanadium nuclear hyperfine couplings (Table 1). In addition, the experimental values compare very well with those reported for BMOV (12) and VO(ka)<sub>2</sub> (16) (Table 1). Dissolution of each vanadium–thiazolidinedione complex in MeOH:CH<sub>2</sub>Cl<sub>2</sub> (1:1) most probably results in solvated MeOH species. Possible sites for solvent coordination are trans (T) or cis (C) to the oxo-O, yielding six possible species in solution (38). X-ray crystal-structure analysis would give a much more detailed understanding of the coordination environment; however, many crystallization attempts did not produce the required single crystals.

**In Vivo Results.** Animal studies were completed in four sets of trials the first three of which used, in each trial, a diabetic control, a ligand precursor, the associated vanadyl complex of the ligand precursor, and BMOV as a representative standard. The fourth trial used a diabetic control, a ligand precursor, rosiglitazone, and BMOV. The percent decrease in blood glucose was

**Table 2.** Glucose Lowering of Four Thiazolidinedione Ligand Precursors and Three of Their Corresponding Complexes Compared with BMOV, and Rosiglitazone

compound	% decrease in blood glucose <sup>a,b</sup>		
	12 h	24 h	48 h
HL <sup>1</sup>	6.4 ± 2.0	19.9 ± 1.9	27.2 ± 5.3
VO(L <sup>1</sup> ) <sub>2</sub>	3.9 ± 11.6	25.9 ± 11.0	24.5 ± 10.6
HL <sup>2</sup>	10.9 ± 5.7	5.6 ± 3.3	2.0 ± 2.3
HL <sup>3</sup>	54.5 ± 2.4	49.6 ± 3.5	27.5 ± 4.0
VO(L <sup>3</sup> ) <sub>2</sub>	59.2 ± 3.3	57.5 ± 4.6	47.6 ± 6.0
HL <sup>4</sup>	3.6 ± 2.9	7.3 ± 1.8	0.9 ± 2.8
VO(L <sup>4</sup> ) <sub>2</sub>	21.5 ± 6.7	28.8 ± 10.3	3.3 ± 2.5
Rosiglitazone	6.4 ± 4.7	9.4 ± 5.1	10.2 ± 6.3
BMOV (average) <sup>c</sup>	41.9 ± 6.0	57.1 ± 6.2	52.3 ± 5.3

<sup>a</sup> Glucose lowering of test compounds in STZ-diabetic rats was calculated as in eq 1 (21). Each value represents the mean ± SEM (*n* = 10). <sup>b</sup> Dose: 0.1 mmol/kg. <sup>c</sup> Combination of four trials (*n* = 26).

**Figure 1.** Hypoglycemic activity (% plasma glucose lowering) of four thiazolidinedione ligand precursors and three of their corresponding complexes compared with BMOV and rosiglitazone.

calculated for each compound utilizing a common method (21, 39), and the results are displayed in Table 2. A visual representation of the data is presented in Figure 1. The BMOV results are a combination of the four trials.

The results for the amine tethered ligand precursor **HL<sup>1</sup>** and the associated complex **VO(L<sup>1</sup>)<sub>2</sub>** suggest that these compounds may be taken up more slowly because there was no observed glucose lowering at 12 h. Positive effects were evident, however, at the 24 and 48 h time points, with both compounds exhibiting half of the *in vivo* activity of BMOV in acute testing. The pyridinone-type ligand precursor **HL<sup>2</sup>** showed minimal glucose lowering at 12 h, but the effect was not sustained. The very low solubility of this compound leading to a lack of absorption *in vivo* was most probably responsible for the observed response. This low solubility precluded complexation with vanadium as well.

The unsaturated ether-tethered ligand precursor **HL<sup>3</sup>** and complex **VO(L<sup>3</sup>)<sub>2</sub>** showed the most efficacious hypoglycemic effects in this study. Both compounds exhibited enhanced glucose lowering compared to BMOV at the 12 h time point. Whereas the glucose lowering effect of the ligand was lessened from 12 to 48 h, the effect of **VO(L<sup>3</sup>)<sub>2</sub>** on blood glucose levels was sustained, similar to BMOV. On the basis of these promising results, we

tested the saturated analogues **HL<sup>4</sup>** and **VO(L<sup>4</sup>)<sub>2</sub>**. The ligand precursor did not show any glucose lowering, while the complex exhibited glucose-lowering at 12 and 24 h but the effect was not sustained to 48 h. The results for **VO(L<sup>4</sup>)<sub>2</sub>** contrast that for **VO(L<sup>1</sup>)<sub>2</sub>** in that the former complex was faster acting but the positive effects were not sustained. These results could be explained by quicker uptake of **VO(L<sup>4</sup>)<sub>2</sub>** followed by faster metabolism and/or excretion.

Both the ligand precursors **HL<sup>1</sup>** and **HL<sup>3</sup>** were more proficient in lowering plasma glucose levels in this testing protocol when compared with rosiglitazone (Avandia), a marketed PPAR $\gamma$  agonist. While these results are preliminary, the increased activity of **HL<sup>1</sup>** and **HL<sup>3</sup>** compared to that of rosiglitazone is very encouraging. **HL<sup>2</sup>** showed minimal hypoglycemic activity at 12 h, but the effect was not sustained. The very low solubility of this compound most probably hampered its activity. **HL<sup>3</sup>** lowered plasma glucose much more effectively than rosiglitazone, a significant finding that warrants further attention. It has been reported that unsaturated thiazolidinediones show lesser fold transactivation of PPAR $\alpha$  and PPAR $\gamma$  than their saturated analogues (29, 40). This suggests that **HL<sup>3</sup>** and other unsaturated thiazolidinediones exhibit their antidiabetic effects through other, yet to be determined, mechanisms. Interestingly the saturated analogue **HL<sup>4</sup>** did not show any activity in this testing protocol. This lack of activity could have been due to poor pharmacokinetics as the solubility of this ligand precursor was satisfactory. Further testing in a more specific animal model of type 2 diabetes, such as db/db mice, is planned to elucidate more clearly the potential of these structurally novel thiazolidinediones, especially **HL<sup>3</sup>** (34, 35).

Studies of the combined effects of treatment with rosiglitazone and BMOV on glucose-lowering in STZ-diabetic rats have shown possible additivity (41). Neither additive nor synergistic effects were observed in this study; however, this could be due to the limited amount of information available from this short-term testing protocol. With these preliminary results in hand, it is clear that **VO(L<sup>3</sup>)<sub>2</sub>** is comparable to BMOV in lowering plasma glucose levels in STZ diabetic rats. Again, further testing would be prudent in a specific model of type 2 diabetes whereby effects on other important parameters such as plasma triglycerides and insulin could be determined (39).

## CONCLUDING REMARKS

To design vanadyl-thiazolidinedione complexes was appealing because of the potential for associative or synergistic effects via complexation of vanadium to thiazolidinedione-containing compounds. There is considerable evidence for the orally effective glucose-lowering properties of V(V) and V(IV), and a number of thiazolidinediones are either in late-stage clinical trials or are available for the treatment of type 2 diabetes. In preliminary animal investigations with this class of compounds the ligand precursors **HL<sup>1</sup>** and **HL<sup>3</sup>** showed enhanced activity in lowering blood glucose compared with that of rosiglitazone. The complex **VO(L<sup>3</sup>)<sub>2</sub>** exhibited comparable activity to BMOV and had a more prolonged treatment effect than the ligand alone.

## EXPERIMENTAL PROCEDURES

**Chemicals and Instrumentation.** All solvents and chemicals (Fisher, Aldrich) were reagent-grade and used without further purification unless otherwise specified.

Rosiglitazone was a gift from Kinetek Pharmaceuticals Inc. Water was deionized (Barnstead D9802 and D9804 cartridges) and distilled (Corning MP-1 Megapure Still) before use. Melting points were measured on a Mel-Temp apparatus and are uncorrected.

The ligands and complexes synthesized were characterized by infrared (IR) spectroscopy, mass spectrometry, elemental analysis, magnetic susceptibility, and  $^1\text{H}$  NMR, where appropriate. Infrared spectra were recorded as KBr disks in the range  $4000\text{--}400\text{ cm}^{-1}$  on a Galaxy Series FTIR spectrometer. Mass spectra (+ ion) were obtained with a Kratos MS 50 (electron-impact ionization, EI), a Kratos MS 80 (desorption chemical ionization, DCI), or a Macromass LCT (electrospray ionization, ESI) instrument. Room-temperature (293 K) magnetic susceptibilities were measured on a Johnson Matthey balance, using  $\text{Hg}[\text{Co}(\text{NCS})_4]$  as the susceptibility standard; diamagnetic corrections were estimated using Pascal's constants (42). C, H, and N analyses were performed either in this department by Mr. Peter Borda (Carlo Erba analytical instrumentation) or by Delta Microanalytical Services.  $^1\text{H}$  NMR spectra of samples were recorded on either a Bruker AM-300 or an AX-400 instrument at 300.13 or 400.13 MHz, respectively. Room-temperature X-band EPR spectra were recorded on a Bruker ECS-106 EPR spectrometer in  $20\text{ }\mu\text{L}$  quartz capillaries. Computer simulations of the isotropic EPR spectra were performed using Bruker's WINEPR/SIMFONIA package.

**Synthesis of Bifunctional Ligands.** *5-Benzyloxy-2-hydroxymethyl-pyran-4-one (2)*. This compound was prepared in a manner similar to that in the literature (27). To a solution of sodium (2.3 g, 100 mmol) in dry MeOH (200 mL) was added kojic acid **1** (14.2 g, 100 mmol) in portions. To this solution was added benzyl chloride (14 mL, 100 mmol) dropwise, and the mixture was heated to reflux for 5 h, cooled to room temperature, and then poured into  $\text{H}_2\text{O}$  (1 L). The precipitate was collected and recrystallized from a minimum of hot EtOH (80 mL) to afford 12.7 g (55%) of the title compound **2** as colorless crystals; mp  $120\text{--}122\text{ }^\circ\text{C}$ .  $^1\text{H}$  NMR ( $\text{CD}_3\text{OD}$ , 300 MHz):  $\delta$  8.00 (s, 1H), 7.38 (m, 5H), 6.50 (s, 1H), 5.01 (s, 2H), 4.39 (s, 2H). EIMS  $m/z$  (relative intensity) = 232 ( $\text{M}^+$ , 60), 91 (100). Anal. Calcd. (found) for  $\text{C}_{13}\text{H}_{12}\text{O}_4$ : C, 67.23 (67.42); H, 5.21 (5.26).

*Methanesulfonic Acid 5-Benzyloxy-4-oxo-4H-pyran-2-ylmethyl Ester (3)*. To a suspension of 5-benzyloxy-2-hydroxymethyl-pyran-4-one **2** (0.303 g, 1.3 mmol) in dry  $\text{CH}_2\text{Cl}_2$  (10 mL) was added triethylamine (0.36 mL, 2.6 mmol). The suspension was then cooled in an ice bath and methanesulfonyl chloride (0.12 mL, 1.6 mmol) was added dropwise. The mixture was stirred for 0.5 h, quenched with saturated  $\text{NaHCO}_3$  (15 mL), and then extracted with  $\text{CH}_2\text{Cl}_2$  ( $2 \times 15\text{ mL}$ ); the combined organic extracts were dried over anhydrous  $\text{Na}_2\text{SO}_4$ , and then concentrated. The slightly colored oil **3** was used without further purification.  $^1\text{H}$  NMR ( $\text{CDCl}_3$ , 300 MHz):  $\delta$  7.57 (s, 1H), 7.38 (m, 5H), 6.55 (s, 1H), 5.08 (s, 2H), 4.95 (s, 2H), 3.08 (s, 3H).

*5-(4-Nitro-benzylidene)thiazolidine-2,4-dione (5)*. To a solution of 4-nitrobenzaldehyde **4** (5.00 g, 33.0 mmol) and thiazolidine-2,4-dione (3.87 g, 33.0 mmol) in toluene (200 mL) was added benzoic acid (0.68 g, 5.5 mmol) and piperidine (0.55 mL, 5.5 mmol). The resulting mixture was refluxed for 2 h with the continuous removal of water using a Dean–Stark water separator. The reaction was then cooled to room temperature and the resulting precipitate was collected and washed with  $\text{CH}_2\text{Cl}_2$  and  $\text{Et}_2\text{O}$  to yield 4.50 g (55%) of compound **5** as a pale yellow solid; mp  $250\text{ }^\circ\text{C}$ .  $^1\text{H}$  NMR ( $\text{DMSO}-d_6$ , 300 MHz):  $\delta$  8.35

(d,  $J = 8.6\text{ Hz}$ , 2H), 7.91 (s, 1H), 7.87 (d,  $J = 8.6\text{ Hz}$ , 2H). EIMS  $m/z$  (relative intensity) = 250 ( $\text{M}^+$ , 35), 179 (100), 89 (70). Anal. Calcd. (found) for  $\text{C}_{10}\text{H}_6\text{N}_2\text{O}_4\text{S}$ : C, 48.00 (48.00); H, 2.42 (2.46); N, 11.20 (10.99).

( $\pm$ )-5-(4-Amino-benzyl)thiazolidine-2,4-dione (**6**). This compound was prepared by a more direct method than that reported in the literature (28).  $\text{CoCl}_2 \cdot 6\text{H}_2\text{O}$  (0.30 g, 1.3 mmol) and dimethylglyoxime (0.56 g, 4.9 mmol) were added to  $\text{H}_2\text{O}$  (300 mL). After addition of NaOH (3 mL, 1 M), the brown solution was cooled to  $0\text{ }^\circ\text{C}$  in an ice bath and  $\text{NaBH}_4$  (7.90 g, 209 mmol) was added in portions. 5-(4-Nitro-benzylidene)thiazolidine-2,4-dione **5** (5.22 g, 20.9 mmol) was then added slowly as a slurry in THF (50 mL). The reaction mixture was stirred at room-temperature overnight. The pH was then adjusted to 9 with  $\text{CH}_3\text{COOH}$ , and the mixture was extracted with THF ( $3 \times 200\text{ mL}$ ). The combined organic extracts were dried over  $\text{Na}_2\text{SO}_4$  and concentrated. The residue was chromatographed over silica gel using a mixture of MeOH and  $\text{CH}_2\text{Cl}_2$  (5:95) as the eluent to afford 3.31 g (71%) of the title compound **6** as a pale yellow solid; mp  $152\text{--}153\text{ }^\circ\text{C}$ .  $^1\text{H}$  NMR ( $\text{DMSO}-d_6$ , 300 MHz):  $\delta$  6.89 (d,  $J = 8.3\text{ Hz}$ , 2H), 6.49 (d,  $J = 8.3\text{ Hz}$ , 2H), 4.65 (dd,  $J = 9.3, 4.4\text{ Hz}$ , 1H), 3.20 (dd,  $J = 14.4, 4.4\text{ Hz}$ ), 2.91 (dd,  $J = 14.4, 9.3\text{ Hz}$ ). EIMS  $m/z$  (relative intensity) = 222 ( $\text{M}^+$ , 60), 106 (100). Anal. Calcd. (found) for  $\text{C}_{10}\text{H}_{10}\text{N}_2\text{O}_2\text{S}$ : C, 54.04 (54.26); H, 4.53 (4.53); N, 12.60 (12.45); S, 14.42 (14.26).

( $\pm$ )-5-[4-[(5-Benzyloxy-4-oxo-4H-pyran-2-ylmethyl)amino]benzyl]thiazolidine-2,4-dione (**7**). Methanesulfonic acid 5-benzyloxy-4-oxo-4H-pyran-2-ylmethyl ester **3** (2.67 g, 9.05 mmol) and ( $\pm$ )-5-(4-amino-benzyl)thiazolidine-2,4-dione **6** (2.00 g, 9.0 mmol) were dissolved in dry  $\text{CH}_3\text{CN}$  (50 mL).  $\text{K}_2\text{CO}_3$  (2.50 g, 18 mmol) was then added as a solid, and the resulting mixture was heated at  $50\text{ }^\circ\text{C}$  for 24 h with stirring. The solvent was then removed and the residue partitioned between  $\text{CH}_2\text{Cl}_2$  (50 mL) and saturated  $\text{NaHCO}_3$  (30 mL). The mixture was extracted with  $\text{CH}_2\text{Cl}_2$  ( $2 \times 50\text{ mL}$ ); the organic extracts were dried over  $\text{Na}_2\text{SO}_4$  and concentrated. The crude product was chromatographed on silica gel using a mixture of MeOH and  $\text{CH}_2\text{Cl}_2$  (3:97) as the eluent to afford 2.73 g (69%) of the title compound **7** as a pale yellow solid; mp  $57\text{--}59\text{ }^\circ\text{C}$ .  $^1\text{H}$  NMR (acetone- $d_6$ , 300 MHz):  $\delta$  7.86 (s, 1H), 7.37 (m, 5H), 6.95 (d,  $J = 8.3\text{ Hz}$ , 2H), 6.59 (d,  $J = 8.3\text{ Hz}$ , 2H), 6.21 (s, 1H), 5.02 (s, 2H), 4.82 (dd,  $J = 8.4, 4.1\text{ Hz}$ , 1H), 4.57 (s, 1H), 3.33 (dd,  $J = 14.1, 4.1\text{ Hz}$ , 1H), 3.09 (dd,  $J = 14.1, 8.4\text{ Hz}$ , 1H). EIMS  $m/z$  (relative intensity) = 436 ( $\text{M}^+$ , 10), 196 (20), 106 (100), 91 (55). Anal. Calcd. (found) for  $\text{C}_{23}\text{H}_{20}\text{N}_2\text{O}_5\text{S}$ : C, 63.29 (63.39); H, 4.62 (4.59); N, 6.42 (6.43).

( $\pm$ )-5-[4-[(5-Hydroxy-4-oxo-4H-pyran-2-ylmethyl)amino]benzyl]thiazolidine-2,4-dione (**HL<sup>1</sup>**). 5-[4-[(5-Benzyloxy-4-oxo-4H-pyran-2-ylmethyl)amino]benzyl]thiazolidine-2,4-dione **7** (3.75 g, 8.6 mmol) was dissolved in a mixture of concentrated HCl (20 mL) and  $\text{CH}_3\text{COOH}$  (40 mL) and heated at  $70\text{ }^\circ\text{C}$  with stirring for 48 h. The yellow solution was rotary evaporated to dryness and then  $\text{H}_2\text{O}$  (3 mL) was added and the pH adjusted to 5. The precipitate was isolated and washed with a minimum of cold  $\text{H}_2\text{O}$  to afford, after drying, 2.71 g (70%) of the title compound as a pale yellow solid; mp  $146\text{ }^\circ\text{C}$ .  $^1\text{H}$  NMR ( $\text{D}_2\text{O}$ , 300 MHz):  $\delta$  7.85 (s, 1H), 7.29 (d,  $J = 8.5\text{ Hz}$ , 2H), 7.22 (d,  $J = 8.5\text{ Hz}$ , 2H), 5.76 (s, 1H), 4.58 (dd,  $J = 6.4, 4.8\text{ Hz}$ , 1H), 4.5 (s, 2H), 3.76 (dd,  $J = 15.5, 6.4\text{ Hz}$ , 1H), 3.63 (dd,  $J = 15.5, 4.8\text{ Hz}$ , 1H). EIMS  $m/z$  (relative intensity) = 346 ( $\text{M}^+$ , 4), 106 (100). Anal. Calcd. (found) for  $\text{C}_{16}\text{H}_{14}\text{N}_2\text{O}_5\text{S} \cdot 0.5\text{H}_2\text{O}$ : C, 54.08 (54.21); H, 4.25 (4.06); N, 7.88 (7.74).



5-Benzyloxy-2-hydroxymethyl-1-methyl-1H-pyridin-4-one (**33**) (**8**). This compound was synthesized in a higher yield than that reported in the literature (**33**). 5-Benzyloxy-2-hydroxymethyl-pyran-4-one **2** (0.99 g, 4.27 mmol) was suspended in a mixture of EtOH and H<sub>2</sub>O (10 mL/10 mL), and methylamine (0.56 mL, 40% w/w, 6.42 mmol) was added. The mixture was heated to reflux for 6 h and then cooled to r.t., at which time the product crystallized from the solution. The solid was washed with Et<sub>2</sub>O and dried in vacuo to afford 0.81 g (77%) of the title compound **8** as an off-white solid; mp 218–220 °C. <sup>1</sup>H NMR (CD<sub>3</sub>OD, 300 MHz): δ 7.60 (s, 1H), 7.48 (d, *J* = 7.2 Hz, 2H), 7.37 (m, 3H), 6.61 (s, 1H), 5.10 (s, 2H), 4.55 (s, 2H), 3.77 (s, 3H). DCIMS *m/z* = 245 (M<sup>+</sup>, 100), 168 (15), 139 (85), 91 (74). Anal. Calcd. (found) for C<sub>14</sub>H<sub>15</sub>N O<sub>3</sub>: C, 68.56 (68.42); H, 6.16 (6.22); N, 5.71 (5.81).

5-Benzyloxy-2-chloromethyl-1-methyl-1H-pyridin-4-one Hydrochloride Salt (**9**). 5-Benzyloxy-2-hydroxymethyl-1-methyl-1H-pyridin-4-one **8** (2.10 g, 8.57 mmol) was added with stirring to form a suspension in dry CH<sub>2</sub>Cl<sub>2</sub> (20 mL). Thionyl chloride (5.0 mL, 68.9 mmol) was then added dropwise. The resulting light yellow solution was stirred overnight under Ar, and then the solvent was removed under reduced pressure. Ethyl acetate (15 mL) was added, and the triturated solid was collected and washed with hexanes to afford 2.45 g (96%) of the title compound **9** as a white solid; mp 170–172 °C. <sup>1</sup>H NMR (DMSO-*d*<sub>6</sub>, 300 MHz): δ 8.62 (s, 1H), 7.40 (m, 6H), 5.17 (s, 2H), 5.04 (s, 2H). DCIMS *m/z* = 263 (M<sup>+</sup>, 16), 228 (20), 157 (30), 91 (100). Anal. Calcd. (found) for C<sub>14</sub>H<sub>14</sub>ClNO<sub>2</sub>: C, 56.00 (56.00); H, 5.00 (5.04); N, 4.67 (4.72).

(±)-5-{4-[(5-Benzyloxy-1-methyl-4-oxo-1,4-dihydro-pyridin-2-ylmethyl)amino]benzyl}thiazolidine-2,4-dione (**10**). (±)-5-(4-Amino-benzyl)thiazolidine-2,4-dione **6** (1.55 g, 6.98 mmol) and 5-benzyloxy-2-chloromethyl-1-methyl-1H-pyridin-4-one hydrochloride salt **9** (2.08 g, 6.98 mmol) were dissolved in DMF (50 mL). Triethylamine (3 mL, 21 mmol) was added dropwise, and the resulting mixture was stirred for 22 h. Water (60 mL) was added and the resulting mixture extracted with CH<sub>2</sub>Cl<sub>2</sub> (2 × 70 mL). The combined organic extracts were dried over Na<sub>2</sub>SO<sub>4</sub>, filtered, and then evacuated. The crude product was chromatographed on silica gel eluting with MeOH:CH<sub>2</sub>Cl<sub>2</sub> (5:95) to afford 2.65 g (88%) of the title compound **10** as a pale yellow solid; mp 85–87 °C. <sup>1</sup>H NMR (CDCl<sub>3</sub>, 300 MHz): δ 7.32 (m, 5H), 6.85 (s, 1H), 6.84 (d, *J* = 8.3 Hz, 2H), 6.43 (d, *J* = 8.3 Hz, 2H), 6.12 (s, 1H), 5.08 (s, 2H), 4.44 (dd, *J* = 8.0, 3.9 Hz, 1H), 4.42 (s, 2H), 3.35 (s, 3H), 3.20 (dd, *J* = 14.2, 3.9 Hz, 1H), 3.06 (dd, *J* = 14.2, 8.0 Hz, 1H); EIMS *m/z* = 449 (M<sup>+</sup>, 45), 344(10), 238(35), 106(80), 91(100). Anal. Calcd. (found) for C<sub>24</sub>H<sub>23</sub>N<sub>3</sub>O<sub>4</sub>S·HCl: C, 59.32 (59.52); H, 4.98 (4.90); N, 8.65 (8.49).

(±)-5-{4-[(5-Hydroxy-1-methyl-4-oxo-1,4-dihydro-pyridin-2-ylmethyl)amino]benzyl}thiazolidine-2,4-dione (**HL**<sup>2</sup>). The title compound **HL**<sup>2</sup> (1.50 g, 73%) was prepared as a light yellow solid from (±)-5-{4-[(5-benzyloxy-1-methyl-4-oxo-1,4-dihydro-pyridin-2-ylmethyl)amino]benzyl}thiazolidine-2,4-dione **10** (2.60 g, 5.80 mmol) by a procedure analogous to that described for **HL**<sup>1</sup>; mp 108–110 °C. <sup>1</sup>H NMR (DMSO-*d*<sub>6</sub>, 300 MHz): δ 7.58 (s, 1H), 6.94 (d, *J* = 8.1 Hz, 2H), 6.58 (d, *J* = 8.1 Hz, 2H), 5.99 (s, 1H), 5.06 (dd, *J* = 8.9, 4.2 Hz, 1H), 4.69 (s, 2H), 3.69 (s, 3H), 3.34 (dd, *J* = 14.1, 4.2 Hz, 1H), 3.04 (dd, *J* = 14.1, 8.9 Hz, 1H). EIMS *m/z* = 359 (M<sup>+</sup>, 30), 254 (60), 181 (30), 106 (100). Anal. Calcd. (found) for C<sub>17</sub>H<sub>17</sub>N<sub>3</sub>O<sub>4</sub>S·0.5H<sub>2</sub>O: C, 55.42 (55.19); H, 4.92 (4.75); N, 11.41 (11.28).

4-(5-Benzyloxy-4-oxo-4H-pyran-2-ylmethoxy)benzaldehyde (**11**). Methanesulfonic acid 5-benzyloxy-4-oxo-4H-pyran-2-ylmethyl ester **3** (5.37 g, 17.3 mmol) was dis-

solved in DMF (150 mL) and 4-hydroxybenzaldehyde **14** (2.11 g, 17.3 mmol) was added. To this stirred solution K<sub>2</sub>CO<sub>3</sub> (7.18 g, 52 mmol) was added and the mixture was heated at 60 °C overnight. Water (250 mL) was then added and the mixture extracted with CH<sub>2</sub>Cl<sub>2</sub> (3 × 200 mL). The combined organic extracts were washed with brine (50 mL), dried over Na<sub>2</sub>SO<sub>4</sub>, and concentrated. The crude material was washed with acetone to afford 3.72 g (64%) of **11** as a white solid; mp 155 °C. <sup>1</sup>H NMR (acetone-*d*<sub>6</sub>, 300 MHz): δ 9.93 (s, 1H), 8.04 (s, 1H), 7.92 (d, *J* = 8.5 Hz, 2H), 7.40 (m, 5H), 7.25 (d, *J* = 8.5 Hz, 2H), 6.54 (s, 1H), 5.15 (s, 2H), 5.07 (s, 2H). EIMS *m/z* (relative intensity) = 336 (M<sup>+</sup>, 4), 214 (10), 91 (100). Anal. Calcd. (found) for C<sub>20</sub>H<sub>16</sub>O<sub>5</sub>: C, 71.42 (71.59); H, 4.79 (4.72).

5-[4-(5-Benzyloxy-4-oxo-4H-pyran-2-ylmethoxy)benzylidene]thiazolidine-2,4-dione (**12**). The title compound **12** (1.50 g, 57%) was prepared as a light orange solid from 4-(5-benzyloxy-4-oxo-4H-pyran-2-ylmethoxy)benzaldehyde (2.11 g, 6.28 mmol), thiazolidine-2,4-dione (0.74 g, 6.28 mmol), benzoic acid (0.15 g, 1.25 mmol), and piperidine (0.12 mL, 1.25 mmol) by a procedure analogous to that described for **5**; mp 253–254 °C. <sup>1</sup>H NMR (DMSO-*d*<sub>6</sub>, 300 MHz): δ 12.52 (s, 1H), 8.27 (s, 1H), 7.75 (s, 1H), 7.58 (d, *J* = 8.6 Hz, 2H), 7.39 (m, 5H), 7.20 (d, *J* = 8.6 Hz, 2H), 6.56 (s, 1H), 5.10 (s, 2H), 4.94 (s, 2H). EIMS *m/z* (relative intensity) = 435 (M<sup>+</sup>, 7), 91 (100). Anal. Calcd. (found) for C<sub>23</sub>H<sub>17</sub>NO<sub>6</sub>S: C, 63.44 (63.16); H, 3.93 (4.06); N, 3.22 (3.21).

5-[4-(5-Hydroxy-4-oxo-4H-pyran-2-ylmethoxy)benzylidene]thiazolidine-2,4-dione (**HL**<sup>3</sup>). The title compound **HL**<sup>3</sup> (1.60 g, 67%) was prepared as a light beige solid from 5-[4-(5-benzyloxy-4-oxo-4H-pyran-2-ylmethoxy)benzylidene]thiazolidine-2,4-dione **12** (3.00 g, 6.90 mmol) by a procedure analogous to that described for **HL**<sup>1</sup>; mp 275–276 °C. <sup>1</sup>H NMR (DMSO-*d*<sub>6</sub>, 300 MHz): δ 12.54 (s, 1H), 9.26 (s, 1H), 8.12 (s, 1H), 7.76 (s, 1H), 7.59 (d, *J* = 8.8 Hz, 2H), 7.20 (d, *J* = 8.8 Hz, 2H), 6.57 (s, 1H), 5.10 (s, 2H). DCIMS *m/z* (relative intensity) = 346 (M<sup>+</sup>, 100), 221 (40), 203 (35), 150 (60), 125 (100). Anal. Calcd. (found) for C<sub>16</sub>H<sub>11</sub>NO<sub>6</sub>S: C, 55.65 (55.23); H, 3.21 (3.19); N, 4.06 (4.03).

5-Benzyloxy-2-chloromethyl-pyran-4-one (**13**). The title compound **13** (2.01 g, 62%) was prepared as a white solid from 5-benzyloxy-2-hydroxymethyl-pyran-4-one (3.00 g, 12.9 mmol) by a procedure analogous to that described for **9**; mp 109–110 °C. <sup>1</sup>H NMR (CDCl<sub>3</sub>, 300 MHz): δ 7.58 (s, 1H), 7.38 (m, 5H), 6.56 (s, 1H), 5.09 (s, 2H), 4.29 (s, 2H). EIMS *m/z* (relative intensity) = 250 (M<sup>+</sup>, 7), 126 (10), 108 (28), 91 (100). Anal. Calcd. (found) for C<sub>13</sub>H<sub>11</sub>ClO<sub>3</sub>: C, 62.29 (62.41); H, 4.42 (4.41).

5-(4-Hydroxy-benzylidene)thiazolidine-2,4-dione (**15**). The title compound (17.69 g, 98%) was prepared as a bright yellow solid from 4-hydroxybenzaldehyde **14** (10.00 g, 81.9 mmol), thiazolidine-2,4-dione (9.58 g, 81.9 mmol), benzoic acid (1.51 g, 12.3 mmol), and piperidine (1.2 mL, 12.1 mmol) by a procedure analogous to that described for **5**; mp 291–292 °C. <sup>1</sup>H NMR (CD<sub>3</sub>OD, 300 MHz): δ 7.72 (s, 1H), 7.43 (d, *J* = 8.6 Hz, 2H), 6.90 (d, *J* = 8.6 Hz, 2H). EIMS *m/z* (relative intensity) = 221 (M<sup>+</sup>, 40), 151 (10), 150 (100), 121 (17), 75 (11). Anal. Calcd. (found) for C<sub>10</sub>H<sub>7</sub>NO<sub>3</sub>S: C, 54.29 (54.69); H, 3.19 (3.30); N, 6.33 (6.44).

(±)-5-(4-Hydroxy-benzyl)thiazolidine-2,4-dione(**28**) (**16**). CoCl<sub>2</sub>·6H<sub>2</sub>O (0.02 g, 0.08 mmol) and dimethylglyoxime (0.04 g, 0.3 mmol) were added to H<sub>2</sub>O (80 mL). After the addition of NaOH (1 M, 1 mL), the brown solution was cooled to 0 °C in an ice bath and NaBH<sub>4</sub> (1.20 g, 31.7 mmol) was added in portions. 5-(4-Hydroxy-benzylidene)-

thiazolidine-2,4-dione **15** (1.00 g, 4.5 mmol) was then added slowly as a solid over 15 min, and then the reaction mixture was stirred at room-temperature overnight. The pH was adjusted to 6 with  $\text{CH}_3\text{COOH}$ , and then the mixture was extracted with  $\text{CHCl}_3$  ( $3 \times 60$  mL). The combined organic extracts were dried over  $\text{Na}_2\text{SO}_4$ , filtered, and decolorized with charcoal (refluxed for 5 min and filtered). Evaporation of the solvents afforded 0.64 g (64%) of the title compound **16** as a white solid; mp 156–157 °C.  $^1\text{H}$  NMR ( $\text{CD}_3\text{OD}$ , 300 MHz):  $\delta$  7.06 (d,  $J = 8.6$  Hz, 2H), 6.71 (d,  $J = 8.6$  Hz, 2H), 4.65 (dd,  $J = 9.2$ , 3.9 Hz, 1H), 3.34 (dd,  $J = 14.2$ , 3.9 Hz, 1H), 3.03 (dd,  $J = 14.2$ , 9.2 Hz, 1H). EIMS  $m/z$  (relative intensity) = 223 ( $\text{M}^+$ , 35), 107 (100), 91 (4), 77, (13). Anal. Calcd. (found) for  $\text{C}_{10}\text{H}_9\text{O}_3\text{S}$ : C, 53.80 (53.76); H, 4.06 (3.95); N, 6.27 (6.15).

( $\pm$ )-5-[4-(5-Benzyloxy-4-oxo-4H-pyran-2-ylmethoxy)benzyl]thiazolidine-2,4-dione (**17**). Sodium hydride (0.40 g, 16.7 mmol) was added to DMF (45 mL) cooled in an ice bath. To this stirring mixture ( $\pm$ )-5-(4-hydroxy-benzyl)-thiazolidine-2,4-dione **16** (1.70 g, 7.6 mmol) was added as a solid in portions causing considerable gas evolution. After 0.5 h 5-benzyloxy-2-chloromethyl-pyran-4-one **13** (2.00 g, 8.0 mmol) was added dropwise as a solution in DMF (30 mL). The resulting mixture was warmed to room temperature and stirred for 18 h. Saturated  $\text{NaHCO}_3$  (125 mL) was then added and the mixture was extracted with  $\text{CH}_2\text{Cl}_2$  ( $3 \times 125$  mL). The combined organic portions were washed with brine (100 mL), dried over  $\text{Na}_2\text{SO}_4$ , and then the solvent was evaporated. The crude product was chromatographed on silica gel eluting with  $\text{MeOH}:\text{CH}_2\text{Cl}_2$  (1:99) to afford 1.20 g (35%) of **17** as a pale yellow solid; mp 165–166 °C.  $^1\text{H}$  NMR ( $\text{CDCl}_3$ , 400 MHz):  $\delta$  8.71 (s, 1H), 7.57 (s, 1H), 7.40 (m, 5H), 7.16 (d,  $J = 8.6$  Hz, 2H), 6.86 (d,  $J = 8.6$  Hz, 2H), 5.07 (s, 2H), 4.80 (s, 2H), 4.47 (dd,  $J = 9.2$ , 3.9 Hz, 1H), 3.42 (dd,  $J = 14.2$ , 3.9 Hz, 1H), 3.11 (dd,  $J = 14.2$ , 9.2 Hz, 1H). EIMS  $m/z$  (relative intensity) = 437 ( $\text{M}^+$ , 3), 214 (10), 107 (53), 91 (100). Anal. Calcd. (found) for  $\text{C}_{23}\text{H}_{19}\text{NO}_6\text{S}$ : C, 63.15 (63.09); H, 4.38 (4.40); N, 3.20 (3.32).

( $\pm$ )-5-[4-(5-Hydroxy-4-oxo-4H-pyran-2-ylmethoxy)benzyl]thiazolidine-2,4-dione (**HL<sup>4</sup>**). The title compound **HL<sup>4</sup>** (0.50 g, 93%) was prepared as a white solid from ( $\pm$ )-5-[4-(5-benzyloxy-4-oxo-4H-pyran-2-ylmethoxy)benzyl]thiazolidine-2,4-dione **17** (0.68 g, 1.6 mmol) by a procedure analogous to that described for **HL<sup>1</sup>**; mp 174 °C.  $^1\text{H}$  NMR ( $\text{CD}_3\text{OD}$ , 300 MHz):  $\delta$  8.04 (s, 1H), 7.24 (d,  $J = 8.6$  Hz, 2H), 6.98 (d,  $J = 8.6$  Hz, 2H), 6.60 (s, 1H), 4.99 (s, 2H), 4.73 (dd,  $J = 8.9$ , 4.2 Hz, 1H), 3.42 (dd,  $J = 14.2$ , 4.2 Hz, 1H), 3.11 (dd,  $J = 14.2$ , 8.9 Hz, 1H); EIMS  $m/z$  (relative intensity) = 347 ( $\text{M}^+$ , 10), 231 (70), 125 (100), 107 (63). Anal. Calcd. (found) for  $\text{C}_{16}\text{H}_{13}\text{NO}_6\text{S}$ : C, 55.33 (54.87); H, 3.77 (3.75); N, 4.03 (4.03).

**Synthesis of Vanadyl–Thiazolidinedione Complexes.** *Bis*( $\pm$ )-5-[4-(5-alkoxy-4-oxo-4H-pyran-2-ylmethyl)-amino]benzylthiazolidine-2,4-dionato)oxovanadium(IV) Hydrate (**VO(L<sup>1</sup>)<sub>2</sub>·H<sub>2</sub>O**). **HL<sup>1</sup>** (0.91 g, 2.64 mmol) was dissolved in  $\text{H}_2\text{O}$  (15 mL) and  $\text{VOSO}_4 \cdot 5\text{H}_2\text{O}$  (0.28 g, 1.12 mmol) was added. The pH was adjusted to 5 with 1 M  $\text{NaOH}$  and the mixture was refluxed under Ar for 22 h. The reaction mixture was filtered hot and the precipitate was washed with  $\text{H}_2\text{O}$  to afford, after drying in vacuo, 0.71 g (83% based on V) of the title compound as a brown solid; mp 175–176 °C. IR ( $\text{cm}^{-1}$ , KBr disk): 3500–3000 ( $\nu_{\text{N-H}}$ ,  $\nu_{\text{C-H}}$ ); 1752, 1681 ( $\nu_{\text{C=O}}$  thiazolidinedione); 1610, 1563, 1516, 1475 (pyrone  $\nu_{\text{C=O}}$ , ring  $\nu_{\text{C=C}}$ ); 982 ( $\nu_{\text{V=O}}$ ). ESIMS  $m/z$  (relative intensity) = 758 ( $[\text{HVO}(\text{L}^1)_2]^+$ , ( $\text{M}+1$ )<sup>+</sup>, 6), 740 (16), 444 (15), 412 (60), 347 (100). The room-temperature solid-state magnetic moment was 1.75

$\mu_{\text{B}}$ . Anal. Calcd. (found) for  $\text{C}_{32}\text{H}_{26}\text{N}_4\text{O}_{11}\text{S}_2\text{V} \cdot \text{H}_2\text{O}$ : C, 49.55 (49.25); H, 3.64 (3.54); N, 7.22 (6.94).

*Bis*( $\pm$ )-5-[4-(5-alkoxy-4-oxo-4H-pyran-2-ylmethoxy)benzyl]thiazolidine-2,4-dionato)oxovanadium(IV) Hydrate (**VO(L<sup>3</sup>)<sub>2</sub>·H<sub>2</sub>O**). The title compound **VO(L<sup>3</sup>)<sub>2</sub>·H<sub>2</sub>O** (1.00 g, 88%) was prepared as a gray solid from **HL<sup>3</sup>** (1.03 g, 2.98 mmol) and  $\text{VOSO}_4 \cdot 5\text{H}_2\text{O}$  (0.38 g, 1.60 mmol) by a procedure analogous to that described for **VO(L<sup>1</sup>)<sub>2</sub>**; mp 189–192 °C. IR ( $\text{cm}^{-1}$ , KBr disk): 3500–3000 ( $\nu_{\text{N-H}}$ ,  $\nu_{\text{C-H}}$ ); 1745, 1679 ( $\nu_{\text{C=O}}$  thiazolidinedione); 1596, 1562, 1510, 1472 (pyrone  $\nu_{\text{C=O}}$ , ring  $\nu_{\text{C=C}}$ ); 985 ( $\nu_{\text{V=O}}$ ). ESIMS  $m/z$  = 756 ( $[\text{HVO}(\text{L}^3)_2]^+$ , ( $\text{M}+1$ )<sup>+</sup>, 9), 685 (4), 593 (25), 458 (100), 443 (56), 368 (20). The room-temperature solid-state magnetic moment was 1.72  $\mu_{\text{B}}$ . Anal. Calcd. (found) for  $\text{C}_{32}\text{H}_{20}\text{N}_2\text{O}_{13}\text{S}_2\text{V} \cdot \text{H}_2\text{O}$ : C, 49.68 (50.01); H, 2.87 (2.67); N, 3.62 (3.71).

*Bis*( $\pm$ )-5-[4-(5-alkoxy-4-oxo-4H-pyran-2-ylmethoxy)benzyl]thiazolidine-2,4-dionato)oxovanadium(IV) Hydrate (**VO(L<sup>4</sup>)<sub>2</sub>·H<sub>2</sub>O**). The title compound **VO(L<sup>4</sup>)<sub>2</sub>·H<sub>2</sub>O** (0.51 g, 93%) was prepared as a brown solid from **HL<sup>4</sup>** (0.71 g, 2.05 mmol) and  $\text{VOSO}_4 \cdot 5\text{H}_2\text{O}$  (0.29 g, 1.21 mmol) by a procedure analogous to that described for **VO(L<sup>1</sup>)<sub>2</sub>**; mp 174 °C. IR ( $\text{cm}^{-1}$ , KBr disk): 3500–3000 ( $\nu_{\text{N-H}}$ ,  $\nu_{\text{C-H}}$ ); 1750, 1692 ( $\nu_{\text{C=O}}$  thiazolidinedione); 1610, 1563, 1510, 1476 (pyrone  $\nu_{\text{C=O}}$ , ring  $\nu_{\text{C=C}}$ ); 975 ( $\nu_{\text{V=O}}$ ). ESIMS  $m/z$  = 760 ( $[\text{HVO}(\text{L}^4)_2]^+$ , ( $\text{M}+1$ )<sup>+</sup>, 50), 445 (100), 413 (49), 370 (10). The room-temperature solid-state magnetic moment was 1.69  $\mu_{\text{B}}$ . Anal. Calcd. (found) for  $\text{C}_{32}\text{H}_{24}\text{N}_2\text{O}_{13}\text{S}_2\text{V} \cdot \text{H}_2\text{O}$ : C, 49.43 (48.98); H, 3.37 (3.25); N, 3.60 (3.52).

**Glucose-Lowering Studies.** Male Wistar rats weighing 190–210 g (Animal Care Unit, UBC) were housed two per cage (polycarbonate) on a 12 h light:dark cycle. Animals were allowed ad libitum access to food (Purina Rat Chow #5001) and water, and were cared for in accordance with the principles and guidelines of the Canadian Council for Animal Care. Animals were allowed to acclimatize for a period of 7 days, and then diabetes was induced by a single tail vein injection of streptozotocin (STZ) (60 mg  $\text{kg}^{-1}$  in 0.9%  $\text{NaCl}$ ) under light halothane anesthesia. Diabetes was confirmed 3 days after STZ-injection by tail-vein blood glucose determination (Ames Glucometer II and Glucostix), with blood levels over 13 mM being accepted as diabetic. One week after STZ-injection, animals were divided into treatment groups: carboxymethylcellulose (CMC) alone, thiazolidinedione compound, congeneric vanadium complex, or BMOV. All drugs were administered as suspensions in 1% CMC. Animals were not fasted prior to drug administration. Blood, 50  $\mu\text{L}$ , was collected for glucose analysis immediately prior to drug administration and at selected times up to 72 h after drug administration. Blood was collected from the tail vein into heparinized capillary tubes and centrifuged (10 000g  $\times$  15 min), and plasma was collected for immediate determination of glucose using Boehringer Mannheim kits (glucose oxidase method). The hypoglycemic activity of the test compounds was calculated as shown in eq 1 (21, 39):

$$\text{Hypoglycemic activity (\%)} = \left( \frac{\text{PG}_c - \text{PGT}}{\text{PG}_c} \right) \times 100\% \quad (1)$$

$\text{PG}_c$  is plasma glucose in control mice, and  $\text{PG}_T$  is plasma glucose in the mice treated with test compounds. Values are presented as means  $\pm$  SEM at 12, 24, and 48 h. At all time points, the animals were observed for signs of toxicity (e.g. diarrhea).

**Intraperitoneal (i.p.) Administration in STZ-Diabetic Rats.** Studies were done on 4 separate occa-



sions, in each study four groups were examined CMC, BMOV, ligand, and vanadyl complex. For  $\text{VO}(\text{L}^1)_2$ , the animals were divided into CMC ( $n = 5$ ), BMOV ( $n = 5$ ),  $\text{HL}^1$  ( $n = 10$ ),  $\text{VO}(\text{L}^1)_2$  ( $n = 10$ ); for  $\text{HL}^2$ , CMC ( $n = 5$ ), BMOV ( $n = 6$ ),  $\text{HL}^2$  ( $n = 10$ ), rosiglitazone ( $n = 10$ ); for  $\text{VO}(\text{L}^3)_2$ , CMC ( $n = 6$ ), BMOV ( $n = 10$ ),  $\text{HL}^3$  ( $n = 10$ ),  $\text{VO}(\text{L}^3)_2$  ( $n = 10$ ); and for  $\text{VO}(\text{L}^4)_2$ , ( $n = 5$ ), BMOV ( $n = 5$ ),  $\text{HL}^4$  ( $n = 10$ ),  $\text{VO}(\text{L}^4)_2$  ( $n = 10$ ). All drug candidates were administered by i.p. injection in a volume of  $2.5 \text{ mL kg}^{-1}$  at a dose of  $0.1 \text{ mmol kg}^{-1}$ . The control groups (CMC) received an equivalent volume of 1% CMC alone. There was no significant effect of drug administration on body weight over the treatment period in any of the trials.

#### ACKNOWLEDGMENT

The authors gratefully acknowledge the Canadian Institutes of Health Research (CHIR) for an operating grant and Kinetek Pharmaceuticals Inc. for personnel support. We also thank Dr. B.D. Liboiron for his assistance with the EPR spectra. T.S. acknowledges NSERC (Natural Sciences and Engineering Research Council) of Canada for a postgraduate fellowship, and P.B. acknowledges a NATO Science Fellowship.

#### LITERATURE CITED

- (1) Tolman, E. L., Barris, E., Burns, M., Pansini, A., and Partridge, R. (1979) Effects of vanadium on glucose metabolism in vitro. *Life Sci.* 25, 1159–1164.
- (2) Heyliger, C. E., Tahilliani, A. G., and McNeill, J. H. (1985) Effect of vanadate on elevated blood glucose and depressed cardiac performance of diabetic rats. *Science* 227, 1474–1477.
- (3) Li, J., Elberg, G., Crans, D. C., and Shechter, Y. (1996) Evidence for the distinct vanadyl(+4)-dependent activating system for manifesting insulin-like effects. *Biochemistry* 35, 8314–8318.
- (4) Fantus, I. G., Ahmad, F., and Deragon, G. (1994) Vanadate augments insulin-stimulated insulin receptor kinase activity and prolongs insulin action in rat adipocytes. Evidence for transduction of amplitude of signaling into duration of response. *Diabetes* 43, 375–383.
- (5) Shechter, Y., Meyerovitch, J., Farfel, Z., Sack, J., Bruck, R., BarMeir, S., Amir, S., Degani, H., and Karlsh, S. J. D. (1990) In *Vanadium in Biological Systems* (N. D. Chasteen, Ed.), pp 129, Kluwer, Dordrecht, The Netherlands.
- (6) Shechter, Y., Li, J., Meyerovitch, J., Gefel, D., Bruck, R., Elberg, G., Miller, D. S., and Shisheva, A. (1995) Insulin-like actions of vanadate are mediated in an insulin-receptor-independent manner via nonreceptor protein tyrosine kinases and protein phosphotyrosine phosphatases. *Mol. Cell. Biochem.* 153, 39–47.
- (7) Shisheva, A., and Shechter, Y. (1993) Mechanism of per-vanadate stimulation and potentiation of insulin-activated glucose transport in rat adipocytes: dissociation from vanadate effect. *Endocrinology* 133, 1562–1568.
- (8) Meyerovitch, J., Farfel, Z., Sack, J., and Shechter, Y. (1987) Oral administration of vanadate normalizes blood glucose levels in streptozotocin-treated rats. Characterization and mode of action. *J. Biol. Chem.* 262, 6658–6662.
- (9) Nechay, B. R. (1984) Mechanisms of action of vanadium. *Annu. Rev. Pharmacol. Toxicol.* 24, 501–524.
- (10) Tsiani, E., and Fantus, I. G. (1997) Vanadium compounds. Biological actions and potential as pharmacological agents. *Trends Endocrinol. Metab.* 8, 51–58.
- (11) Thompson, K. H., Yuen, V. G., McNeill, J. H., and Orvig, C. (1998) Chemical and pharmacological studies of a new class of antidiabetic vanadium complexes. In *Chemistry, Biochemistry and Therapeutic Applications*, ACS Symposium Series 711, pp 329, American Chemical Society, New York.
- (12) Caravan, P., Gelmini, L., Glover, N., Herring, F. G., Li, H., McNeill, J. H., Rettig, S. J., Setyawati, I. A., Shuter, E., Sun, Y., Tracey, A. S., Yuen, V. G., and Orvig, C. (1995) Reaction chemistry of BMOV, bis(maltolato)oxovanadium(IV)-A potent insulin mimetic agent. *J. Am. Chem. Soc.* 117, 12759–12770.
- (13) McNeill, J. H., Yuen, V. G., Hoveyda, H. R., and Orvig, C. (1992) Bis(maltolato)oxovanadium(IV) is a potent insulin mimic. *J. Med. Chem.* 35, 1489–1491.
- (14) Yuen, V. G., Orvig, C., and McNeill, J. H. (1995) Comparison of the glucose-lowering properties of vanadyl sulfate and bis(maltolato)oxovanadium(IV) following acute and chronic administration. *Can. J. Physiol. Pharmacol.* 73, 55–64.
- (15) McNeill, J. H., Yuen, V. G., Dai, S., and Orvig, C. (1995) Increased potency of vanadium using organic ligands. *Mol. Cell. Biochem.* 153, 175–180.
- (16) Yuen, V. G., Caravan, P., Gelmini, L., Glover, N., McNeill, J. H., Setyawati, I. A., Zhou, Y., and Orvig, C. (1997) Glucose-lowering properties of vanadium compounds: comparison of coordination complexes with maltol or kojic acid as ligands. *J. Inorg. Biochem.* 68, 109–116.
- (17) Woo, L. C. Y., Yuen, V. G., Thompson, K. H., McNeill, J. H., and Orvig, C. (1999) Vanadyl-biguanide complexes as potential synergistic insulin mimics. *J. Inorg. Biochem.* 76, 251–257.
- (18) Cohen, N., Halberstam, M., Shlimovich, P., Chang, C. J., Shamoon, H., and Rossetti, L. (1995) Oral vanadyl sulfate improves hepatic and peripheral insulin sensitivity in patients with noninsulin-dependent diabetes mellitus. *J. Clin. Invest.* 95, 2501–2509.
- (19) Asagami, T., Abbasi, F., Stuelinger, M., Lamendola, C., McLaughlin, T., Cooke, J. P., Reaven, G. M., and Tsao, P. S. (2002) Metformin treatment lowers asymmetric dimethylarginine concentrations in patients with type 2 diabetes. *Metabolism* 51, 843–846.
- (20) Chen, C. (1998) Troglitazone: an antidiabetic agent. *Am. J. Health-Syst. Pharm.* 55, 905–925.
- (21) Oguchi, M., Wada, K., Honma, H., Tanaka, A., Kaneko, T., Sakakibara, S., Ohsumi, J., Serizawa, N., Fujiwara, T., Horikoshi, H., and Fujita, T. (2000) Molecular design, synthesis, and hypoglycemic activity of a series of thiazolidine-2,4-diones. *J. Med. Chem.* 43, 3052–3066.
- (22) Wagenaar, L. G., Kuck, E. M., and Hoekstra, J. B. L. (1999) Troglitazone. Is it all over? *Neth. J. Med.* 55, 4–12.
- (23) Santiago, J. V. (1997) Troglitazone. *Compr. Ther.* 23, 560–562.
- (24) Raginato, M. J., Bailey, S. T., Krakow, S. L., Minami, C., Ishii, S., Tanaka, H., and Lazar, M. A. (1998) A potent antidiabetic thiazolidinedione with unique peroxisome proliferator-activated receptor  $\gamma$ -activating properties. *J. Biol. Chem.* 273, 32679–32684.
- (25) Finnegan, M. M., Lutz, T. G., Nelson, W. O., Smith, A., and Orvig, C. (1987) Neutral water-soluble post-transition-metal chelate complexes of medical interest: aluminum and gallium tris(3-hydroxy-4-pyronates). *Inorg. Chem.* 26, 2171–2176.
- (26) Nolte, R. T., Wisely, G. B., Westin, S., Cobb, J. E., Lambert, M. H., Kurokawa, R., Rosenfeld, M. G., Wilson, T. M., Glass, C. K., and Milburn, M. K. (1998) Ligand binding and co-activator assembly of the peroxisome proliferator-activated receptor- $\gamma$ . *Nature* 395, 137–143.
- (27) Thomas, A. F., and Marxer, A. (1960) Heilmittelchemische studien in der heterocyclischen reihe. Die reaktion von kojisaure mit hydrazin. Umsetzung von kojisaureathern mit hydrazin. *Helv. Chim. Acta* 61, 469–477.
- (28) Sohda, T., Mizuno, K., Imamiya, E., Sugiyama, Y., Fujita, T., and Kawamatsu, Y. (1982) Studies on antidiabetic agents. II. Synthesis of 5-[4-(1-methylcyclohexylmethoxy)-benzyl]-thiazolidine-2,4-dione (ADD-3878) and its derivatives. *Chem. Pharm. Bull.* 30, 3580–3600.
- (29) Cantello, B. C. C., Cawthorne, M. A., Cottam, G. P., Duff, P. T., Haigh, D., Hindley, R. M., Lister, C. A., Smith, S. A., and Thurlby, P. L. (1994) [ $\omega$ -(Heterocyclamino)alkoxy]-benzyl]-2,4-thiazolidinediones as potent antihyperglycemic agents. *J. Med. Chem.* 37, 3977–3985.
- (30) Tanis, S. P., Parker, T. T., Colca, J. R., Fisher, R. M., and Kletzein, R. F. (1996) Synthesis and biological activity of metabolites of the antidiabetic, antihyperglycemic agent pioglitazone. *J. Med. Chem.* 39, 5053–5063.



- (31) Finnegan, M. M., Rettig, S. J., and Orvig, C. (1986) A neutral water-soluble aluminum complex of neurological interest. *J. Am. Chem. Soc.* **108**, 5034–5035.
- (32) Nelson, W. O., Rettig, S. J., and Orvig, C. (1987) The Exoclathrate  $\text{Al}(\text{C}_7\text{H}_8\text{NO}_2)_3 \cdot 12\text{H}_2\text{O}$ . A facial geometry imposed by extensive hydrogen bonding with the ice I structure. *J. Am. Chem. Soc.* **109**, 4121–4123.
- (33) Teitei, T. (1983) Chemistry of kojic acid: one-step syntheses of benzothiazoles and other fused heterocycles from kojic acid derivatives. *Aust. J. Chem.* **36**, 2307.
- (34) Reddy, K. A., Lohray, B. B., Bhushan, V., Reddy, A. S., Mamidi, N. V. S. R., Reddy, P. P., Saibaba, V., Reddy, N. J., Suryaprakash, A., Misra, P., Vikramadithyan, R. K., and Rajagopalan, R. (1999) Novel antidiabetic and hypolipidemic agents 5. Hydroxyl versus benzyloxy containing chroman derivatives. *J. Med. Chem.* **42**, 3265–3278.
- (35) Prabhakar, C., Madhusudhan, G., Sahadev, K., Maheedara, C., Reddy, R., Sarma, M. R., Reddy, G. O., Chakrabarti, R., Rao, C. S., Kumar, T. D., and Rajagopalan, R. (1998) Synthesis and biological activity of novel thiazolidinediones. *Bioorg. Med. Chem. Lett.* **8**, 2725–2730.
- (36) Parks, D. J., Tomkinson, N. C. O., Villeneuve, M. S., Blanchard, S. G., and Willson, T. M. (1998) Differential activity of rosiglitazone enantiomers at PPAR- $\gamma$ . *Bioorg. Med. Chem. Lett.* **8**, 3657–3658.
- (37) Boas, L. V., and Pessoa, J. C. (1987) *Comprehensive Coordination Chemistry*, p 455, Pergamon, New York.
- (38) Hanson, G. R., Sun, Y., and Orvig, C. (1996) Characterization of the potent insulin mimetic agent bis(maltolato)-oxovanadium(IV) (BMOV) in solution by EPR spectroscopy. *Inorg. Chem.* **35**, 6507–6512.
- (39) Sauerberg, P., Pettersson, I., Jeppesen, L., Bury, P. S., Mogenson, J. P., Wassermann, K., Brand, C. L., Sturis, J., Woldike, H. F., Fleckner, J., Anderson, A. T., Mortensen, S. B., Svensson, L. A., Rasmussen, H. B., Lehmann, S. V., Polivka, Z., Sindelar, K., Panajoto (2002) Novel tricyclic- $\alpha$ -alkyloxyphenylpropionic acids: dual PPAR  $\alpha/\gamma$  agonists with hypolipidemic and antidiabetic activity. *J. Med. Chem.* **45**, 789–804.
- (40) Cantello, B. C. C., Cawthorne, M. A., Haigh, D., Hindley, R. M., Smith, S. A., and Thurlby, P. L. (1994) The synthesis of BRL-49653 – a novel and potent antihyperglycemic agent. *Bioorg. Med. Chem. Lett.* **4**, 1181–1184.
- (41) Yuen, V. G., and McNeill, J. H. (2002) Manuscript in preparation.
- (42) Mabbs, F. E., and Machin, D. J. (1961) *Magnetism and Transition Metal Complexes*, p 5, Chapman and Hall, London.

BC025606M

# Novel Shielded Transferrin–Polyethylene Glycol–Polyethylenimine/DNA Complexes for Systemic Tumor-Targeted Gene Transfer

Malgorzata Kursa,<sup>†</sup> Greg F. Walker,<sup>‡</sup> Vanessa Roessler,<sup>†</sup> Manfred Ogris,<sup>‡</sup> Wolfgang Roedel,<sup>‡</sup> Ralf Kircheis,<sup>†,§</sup> and Ernst Wagner<sup>\*,‡</sup>

Pharmaceutical Biology-Biotechnology, Department for Pharmacy, Ludwig-Maximilians-Universitaet, Butenandtstrasse 5-13, D-81377 Muenchen, Germany, and Boehringer Ingelheim Austria, Dr Boehringer Gasse 5-11, A-1121 Vienna, Austria. Received September 20, 2002; Revised Manuscript Received November 7, 2002

Tumor-targeting DNA complexes which can readily be generated by the mixing of stable components and freeze–thawed would be very advantageous for their subsequent application as medical products. Complexes were generated by the mixing of plasmid DNA, linear polyethylenimine (PEI22, 22 kDa) as the main DNA condensing agent, PEG–PEI (poly(ethylene glycol)-conjugated PEI) for surface shielding, and Tf–PEG–PEI (transferrin–PEG–PEI) to provide a ligand for receptor-mediated cell uptake. Within the shielding conjugates, PEG chains of varying size (5, 20, or 40 kDa) were conjugated with either linear PEI22 (22 kDa) or branched PEI25 (25 kDa). The three polymer components were mixed together at various ratios with DNA; particle size, surface charge, in vitro transfection activity, and systemic gene delivery to tumors was investigated. In general, increasing the proportion of shielding conjugate in the complex reduced surface charge, particle size, and in vitro transfection efficiency in transferrin receptor-rich K562 cells. The particle size or surface charge of the complexes containing the PEG–PEI conjugate did not significantly change after freeze–thawing, while complexes without the shielding conjugate aggregated. Complexes containing PEG–PEI conjugate efficiently transfected K562 cells after freeze–thawing. Furthermore the systemic application of freeze–thawed complexes exhibited in vivo tumor targeted expression. For complexes containing the luciferase reporter gene the highest expression was found in tumor tissue of mice. An optimum formulation for in vivo application, PEI22/Tf–PEG–PEI/PEI22–PEG5, containing plasmid DNA encoding for the tumor necrosis factor (TNF- $\alpha$ ), inhibited tumor growth in three different murine tumor models. These new DNA complexes offer simplicity and convenience, with tumor targeting activity in vivo after freeze–thawing.

## INTRODUCTION

The ability of nonviral DNA complexes to deliver genes specifically to cells and tissues in vivo offers a potential therapy for many diseases that are currently considered incurable, including some disseminated tumors (1). To date, the main developmental focus for nonviral DNA complexes for systemic tumor targeting has been improving their gene transfer in vivo. Beside the need to improve delivery efficiency, the formulation of well-defined, easily prepared complexes that can be stored over long periods is also necessary for their practical administration and development as a pharmaceutical product. For tumor-specific uptake, polyplexes (2) are usually made in relatively small batches and are required to be freshly prepared before use as they form large aggregates when stored by freezing or freeze-drying (3, 4). Furthermore, nonviral-based gene delivery systems have to be administered many times, and the formation of many types of DNA complexes requires sequential reaction steps which are both laborious and inconvenient.

Polyplexes are formed by the mixing of a solution of plasmid DNA with a solution of a cationic polymer which

collapses the DNA via electrostatic interactions. Of the cationic polymers, PEI is the most popular for gene delivery as DNA/PEI complexes display high transfection efficiency in cell culture and have potential for gene delivery in vivo (5, 6). For tumor specific uptake a ligand such as epidermal growth factor (7), folate (8), or transferrin (9) is conjugated to the cationic polymer. However, in vivo PEI/DNA complexes have been shown to interact with blood components and nontarget cells, strongly reducing their tumor targeting efficiency (10). To overcome this problem a shielding molecule such as the hydrophilic PEG molecule is conjugated to the surface of the DNA complex (11). It is believed that the highly mobile and hydrated PEG strands sterically prevent nonspecific interactions with the biological environment, prolonging the circulation time of the complex in vivo (10).

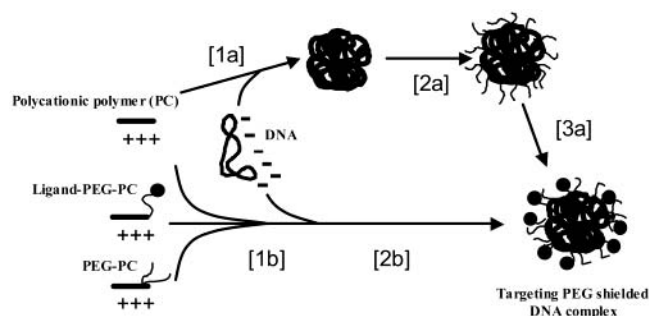
Improved systemic circulation of DNA/PEI complexes by their PEGylation was first described by Ogris et al. (10) with TF–PEI 800 kDa/DNA complexes. PEG was covalently attached to the cationic polymer after DNA polymer condensation (post-PEGylation). PEGylation not only improves systemic tumor targeting but improves solubility of the DNA complexes allowing for formulations to be prepared at the higher therapeutic concentrations without aggregation (10, 12). Furthermore, PEGylation reduces the in vivo toxicity of DNA complexes containing PEI (10, 13).

\* Corresponding author. Telephone: ++49-89-2180-77841. Fax: ++49-89-2180-77798. E-mail: ernst.wagner@cup.uni-muenchen.de.

<sup>†</sup> Boehringer Ingelheim Austria.

<sup>‡</sup> Ludwig-Maximilians-University, Muenchen.

<sup>§</sup> Present address: Igeneon AG, Vienna, Austria.



**Figure 1.** A schematic presentation of alternative strategies for the formation of a PEG shielded, ligand-containing DNA-polymer complex. Strategy A: DNA is condensed with a polycation (step 1), heterobifunctional PEG is covalently attached to the amino groups of the polycation at the surface (step 2), ligands are covalently attached to the distal end of the PEG chain (step 3). Strategy B: DNA-condensing agent PEI, targeting conjugate ligand-PEG-PEI and shielding conjugate PEG-PEI are mixed together (step 1), DNA in buffer is then added and mixed (step 2).

Recently, it was observed that DNA complexes with lower molecular weight PEIs (25 kDa branched, 22 kDa linear) display less systemic toxicity than the PEI 800 kDa complexes (9). Subsequently it was shown that DNA complexes of low molecular weight PEI could also be successfully post-PEGylated.

The major drawback of post-PEGylation of DNA complexes is that they require an additional sequential synthesis step which is time-consuming; furthermore, the degree of surface PEGylation is not well defined. Another strategy for the PEGylation of DNA complexes is to synthesize a copolymer of the condensing and the shielding agent prior to the mixing of DNA, for instance, polylysine-PEG (8, 14–16) and PEI-PEG (17–19) copolymers. However, the major limitation of these copolymers is that the hydrophilic part appears to hinder proper DNA condensation and particle formation (14, 17).

Work with an alternative shielding agent, transferrin, showed that although Tf-PEI (22 and 25 kDa) conjugates were not able to condense DNA either, the inclusion of extra unmodified PEI25 in the complex enabled efficient DNA condensation and particle formation (9, 20). Since post-PEGylation was not required for these complexes, they could be quickly and easily generated by the flash mixing of three components, Tf-PEI, unmodified linear PEI22, and DNA.

In this work we present novel tumor-targeting PEG shielded DNA complexes which can be formed more quickly and easily generated than post-PEGylation strategies (7) (Figure 1). Furthermore these new DNA complexes containing the PEI-PEG shielding conjugate were shown to have tumor-targeting activity after freeze-thawing.

## MATERIALS AND METHODS

**Reagents and Assays.** Branched PEI with an average molecular weight of 25 kDa (PEI25) was obtained from Sigma-Aldrich (Vienna, Austria). Linear PEI with an average molecular weight of 22 kDa (PEI22) is available from Euromedex (Exgen 500, Euromedex, Souffelweyersheim, France). For complex preparation, PEI was used as a 1 mg/mL working solution, neutralized with HCl. Liquid chromatography of conjugates was performed with a Merck-Hitachi L-6220 pump, with a L-4500A UV-vis diode array detector. PEI content of conjugate fractions was determined spectrophotometrically by ninhydrin assay at 570 nm (21) and DNA mobility shift assay by

**Table 1.** Conjugation Ratio of Shielding Conjugates Generated

conjugate	ratio (PEI:PEG)
PEI22-PEG20	1/0.9
PEI25-PEG20	1/0.9
PEI22-PEG5	1/4.4
PEI25-PEG5	1/23
PEI22-PEG40	1/0.1 <sup>a</sup> , 1/0.3 <sup>b</sup>
PEI25-PEG40	1/0.4
PEI22-ss-PEG5	1/0.7

<sup>a</sup> PEI was incubated with PEG succinimide for 1 h. <sup>b</sup> PEI was incubated with PEG succinimide for 24 h.

agarose gel electrophoresis. PEG derivatives were obtained from Shearwater Polymers (Birmingham, AL). The modification of PEI with PEG (molar ratio of PEI/PEG) in conjugates was determined by proton NMR spectrometry (400 MHz, Bruker, Germany). Succinimidyl 3-(2-pyridyldithio)propionate (SPDP) was purchased from Fluka (Buchs, Switzerland) and 2-iminothiolane from Sigma (Vienna, Austria). The amount of dithiopyridine linkers in modified PEI was determined after reduction of an aliquot with dithiothreitol (DTT) followed by absorption measurement of released pyridine-2-thione at 340 nm. The amount of free mercapto groups was determined by Ellman assay at 412 nm (22) using 5,5'-dithiobis(2-nitrobenzoic acid) (Sigma, Vienna, Austria). Transferrin (iron-free) was obtained from Biotest (Dreieich, Germany), cell culture media, antibiotics, fetal calf serum (FCS) from Life Technologies (Gaithersburg, MD). Plasmid pCMVLuc (*Photinus pyralis* luciferase under control of the CMV enhancer/promoter) described in Plank et al. (23) was purified with the EndoFree Plasmid Kit from Qiagen (Hilden, Germany). Plasmid pGSmtNF $\alpha$  coding for murine TNF $\alpha$  was purified by ELIM Biopharmaceuticals (San Francisco, CA). Endotoxin (LPS) levels were <0.1 endotoxin units/50  $\mu$ g DNA as determined by Limulus Amebocyte Lysate assay (BioWhittaker, Walkersville, MD).

**Synthesis of PEG-PEI Conjugates.** *PEI22-PEG20 and PEI25-PEG20 Conjugate.* A gel-filtered (Sephadex G-25 superfine, Pharmacia, Sweden) solution of PEI22 HCl (0.7  $\mu$ mol), at pH of 6 in 1 mL of 0.25 M NaCl, was mixed with a 2  $\mu$ mol of PEG succinimidyl propionate (methoxy-PEG-SPA; MW 20 kDa) dissolved in 0.8 mL of water. The pH of the solution was adjusted to 7.1 by the addition of 25  $\mu$ L of 2 M HEPES, pH 7.9. After 24 h, 0.6 mL of 3 M NaCl and 1.6 mL of water were added to the incubate to give a final NaCl concentration of 0.5 M. The reaction mixture was loaded on a cation-exchange column (Macro-prep High S; HR 10/10, BioRad, München, Germany) and fractionated with a salt gradient from 0.5 to 3.0 M NaCl in 20 mM HEPES pH 7.1. The product (6 mL) was eluted between 2.3 and 2.8 M NaCl. All PEI-PEG conjugates were dialyzed against 2 L of HBS (20 mM HEPES pH 7.3, containing 150 mM NaCl), and the conjugation ratio of PEI modified with PEG was determined by 400 MHz proton NMR (Table 1). The yield of the PEI22-PEG20 and PEI25-PEG20 synthesized in a similar manner based on PEI was 63% and 95%, respectively. The conjugate was diluted to 1 mg/mL PEI equivalent concentration by addition of HBS buffer, pH 7.3, and then divided into convenient small aliquots and stored at -20 °C.

*PEI22-PEG5 and PEI25-PEG5 conjugates* were prepared in analogous manner to PEI-PEG20 conjugates by mixing 0.7  $\mu$ mol of PEI HCl salt in 1 mL of 20 mM HEPES pH 7.1 with 42 equiv (in case of PEI22) or 50 equiv (in case of PEI25) of PEG succinimidyl propionate



(Methoxy-PEG-SPA; MW 5000) dissolved in 0.7 mL of DMSO. After 1 h incubation, the PEI conjugates were isolated by a cation-exchange column and dialyzed.

**PEI22-PEG40 Conjugate.** A gel-filtered solution of PEI22 (0.7  $\mu$ mol) in 1 mL of 0.25 M NaCl was mixed with a 0.8 mL aqueous solution of 2  $\mu$ mol branched PEG succinimide (branched-PEG2-NHS ester; MW 40 kDa). The solution was incubated at pH 7.1 for 1 h (a) or 24 h (b), respectively; 0.6 mL of 3 M NaCl and 1.5 mL of water were added to bring the solution to 0.5 M NaCl. The reaction mixture was loaded on a cation-exchange column (BioRad Macro-prep High S; HR 10/10) and fractionated with a salt gradient from 0.5 to 3.0 M NaCl in 20 mM HEPES, pH 7.1, buffer. The conjugate product (4 mL) was eluted between 2.6 and 2.9 M NaCl.

**PEI25-PEG40 conjugate** was similarly prepared as for PEI22-PEG40. Gel-filtered PEI25 (0.6  $\mu$ mol, HCl form) in 1 mL of 0.15 M NaCl was mixed with a 0.8 mL aqueous solution of 1.8  $\mu$ mol of branched PEG succinimide (branched-PEG2-NHS ester; MW 40 kDa). After 24 h, PEI conjugate was isolated on the cation-exchange column and dialyzed.

**PEI22ssPEG5 conjugate** was prepared as follows: to a solution of 1.4  $\mu$ mol of PEI22 as HCl salt in 1 mL of 0.25 M NaCl, 20 mM HEPES, pH 7.1, 0.27 mL of 10 mM ethanol containing of 2.9  $\mu$ mol of SPDP was added, and after purification by gel filtration (Sephadex G-25 superfine; HR 10/30 column; 0.25 M NaCl, 20 mM HEPES, pH 7.1), 5 mL of product containing 30 mg of PEI22 and 1.5  $\mu$ mol of dithiopyridine linker was obtained and quantified spectrophotometrically at 343 nm by release of thiopyridone after reduction of an aliquot with excess DTT (24). To 2 mL of this solution (0.6  $\mu$ mol of PEI), 30  $\mu$ mol of DTT in 0.1 mL of 20 mM HEPES buffer, pH 7.1, containing 0.25 M NaCl was added to yield (after gel filtration) 0.5  $\mu$ mol of PEI22 modified with 0.5  $\mu$ mol of mercaptopropionate linker. A solution of 0.6  $\mu$ mol of PEG-orthopyridyl-disulfide (methoxy-PEG-OPSS; MW 5000) in 0.1 mL of 20 mM HEPES, pH 7.1, was added under argon and incubated for 48 h and then purified by cation-exchange chromatography.

**Synthesis of Tf-PEG-PEI25 Conjugate.** To a solution of 4.1  $\mu$ mol of PEI25 (HCl form, after gel filtration with Sephadex G-25 superfine) in 1.3 mL of 0.7 M NaCl, 810  $\mu$ L of a 10 mM ethanolic solution of SPDP (8.1  $\mu$ mol) was added while mixing vigorously. After 1 h at room temperature, purification was performed by gel filtration (Sephadex G-25 superfine, HR 10/30 column; 20 mM HEPES, pH 7.1, containing 0.25 M NaCl) to give 5 mL of a solution of 3.9  $\mu$ mol of PEI25 modified with 6  $\mu$ mol of dithiopyridine linker (molar ratio of 1/1.5). Half of the solution (containing 49 mg of PEI25) was treated with 150  $\mu$ mol of DTT in 0.1 mL of 20 mM HEPES, pH 7.1, containing 0.25 M NaCl, and the reaction mixture was kept under argon for 1 h. After gel filtration (Sephadex G-25 superfine, HR 10/10 column; 0.25 M NaCl, 20 mM HEPES, pH 7.1; under argon), a solution of 1.6  $\mu$ mol of PEI25 modified with 2.7  $\mu$ mol of mercaptopropionate linker (1.7 linker for each PEI chain) was obtained.

A solution of 2.5  $\mu$ mol of transferrin (human, iron-free) in 4 mL of a 0.15 M NaCl was subjected to gel filtration with 30 mM sodium acetate pH 5.0 on a Sephadex G-25 superfine column (Pharmacia; HR 10/30). The resulting 6.6 mL of product was concentrated (speed-vac) to a volume of 2.7 mL, containing 2  $\mu$ mol of transferrin. The pH was adjusted to 7.3 by addition of sodium bicarbonate and 25  $\mu$ L of 2 M HEPES, pH 7.3. Part of the solution (0.9  $\mu$ mol) of transferrin in 1.25 mL was mixed with a

solution of 1.05  $\mu$ mol of *N*-hydroxysuccinimide-PEG-maleimide (NHS-PEG-MAL; MW 3400) in 0.1 mL of water. After 3 h at room temperature, the reaction mixture was added under argon to the mercaptopropionate-modified PEI25 solution (0.8  $\mu$ mol of PEI; 1.3  $\mu$ mol of mercaptopropionate linker) in 1.5 mL of 20 mM HEPES, pH 7.1, containing 0.25 M NaCl, at a molar ratio of 1/1.2 (maleimide linker/SH group) and kept under argon for 24 h at room temperature. The mixture was diluted with 0.9 mL of 3 M NaCl and 2.5 mL of water, and conjugate was isolated by cation-exchange chromatography (BioRad Macro-prep High S; HR 10/10 column) with a salt gradient from 0.5 to 3.0 M NaCl with a constant content of 20 mM HEPES, pH 7.1. The 8 mL of product was eluted between 2.2 and 3.0 M NaCl. After dialysis against 2 L of HBS (20 mM HEPES pH 7.3, 150 mM NaCl), 11.4 mL of conjugate consisting of 170 nmol of transferrin modified through PEG bridges with 0.4  $\mu$ mol PEI25 at a molar ratio of 1/2.4 was obtained. The yield (based on PEI25) was 52%.

Iron incorporation into transferrin was performed by addition of 1.25  $\mu$ L of 10 mM iron(III) citrate buffer (containing 200 mM citrate and adjusted to pH 7.8 by sodium bicarbonate addition) per milligram of transferrin content. The conjugate was left at 0.9 mg PEI/mL concentration, divided into convenient small aliquots, and stored at  $-20^{\circ}\text{C}$ .

**Synthesis of Tf-PEG-PEI22 Conjugate.** PEI22 (1.3  $\mu$ mol, hydrochloride salt, after gel filtration with Sephadex G-25 superfine) in 2.45 mL of 0.18 M NaCl was mixed under argon with a solution of 0.4  $\mu$ mol of 2-iminothiolane in 50  $\mu$ L of 15 mM HEPES, pH 8.5, and kept under argon for 2 h. The mixture was diluted with 1.3 mL of 3 M NaCl and 5.2 mL of water and separated by cation-exchange chromatography under argon (BioRad Macro-prep High S, HR 10/10 column; gradient elution 22–100% buffer A; buffer A, 20 mM HEPES, pH 7.1, containing 3 M NaCl; buffer B, 20 mM HEPES pH 7.1). The 4.5 mL of PEI product was eluted at a NaCl concentration of approximately 2.5–2.9 M. After gel filtration under argon with 20 mM HEPES, pH 7.1, containing 0.25 M NaCl (Sephadex G-25 superfine, HR 10/30 column), 4.3 mL solution containing 0.8  $\mu$ mol of PEI22 modified with 0.6  $\mu$ mol of thiolane linker (molar ratio of 1.5/1) was obtained.

A solution of 0.4  $\mu$ mol of transferrin in 1.6 mL of 30 mM HEPES, pH 8.5, was mixed under argon with a solution of 1.3  $\mu$ mol of 2-iminothiolane in 100  $\mu$ L of 15 mM HEPES, pH 8.5. After 3 h at room temperature, purification was performed by gel filtration under argon with HBS, pH 7.3, on a Sephadex G-50 superfine column (HR 10/10) to give 2.8 mL of a solution of 0.3  $\mu$ mol of transferrin modified with 0.55  $\mu$ mol of thiolane linker (molar ratio of 1/1.8). This solution was mixed under argon with a solution of 0.55  $\mu$ mol of PEG-bis-orthopyridyl-disulfide (PEG-[OPSS]<sub>2</sub>; MW 3400) in 0.2 mL of HBS, pH 7.3, and kept at room temperature for approximately 70 h. After gel filtration (Sephadex G-50, HR 10/30; HBS pH 7.3), 3.3 mL of product containing 0.3  $\mu$ mol of transferrin modified with PEG with 0.15  $\mu$ mol of dithiopyridine linker (molar ratio of 2/1) was obtained. The modified transferrin solution was added under argon to the thiolane-modified PEI22 solution (0.2  $\mu$ mol of PEI; 0.15  $\mu$ mol of thiolane linker) in 1.15 mL of 20 mM HEPES, pH 7.1, containing 0.25 M NaCl, at a molar ratio 1/1 (SS-pyridine linker/SH group). After 24 h at room temperature, 1.1 mL of 3 M NaCl and 2.5 mL of water were added to bring the solution to a salt concentration of about 0.5 M. The reaction mixture was loaded on a

cation-exchange column (BioRad Macro-prep High S; HR 10/10) and fractionated with a salt gradient from 0.5 to 3.0 M NaCl with a constant content of 20 mM HEPES pH 7.1. The 7.6 mL of product was eluted between 1.9 and 2.8 M salt and concentrated (speed-vac) to a volume of 4.5 mL. The resulting 4.5 mL of solution was subjected to gel filtration with HBS, pH 7.3, on a Superdex-75 column (HR 10/30) to give 6 mL of conjugate consisting of 63 nmol of transferrin modified through PEG linker with 68 nmol of PEI22 (molar ratio of 1/1.1). The yield based on PEI was 32%. The iron incorporation into conjugates was performed as described above.

**Formation of Transfection Complexes.** DNA complexes were prepared by first diluting and mixing free PEI22 with various amounts of PEG-PEI and Tf-PEG-PEI conjugates in the indicated ratios and buffer. Plasmid DNA diluted in buffer was mixed with the PEI-conjugate buffer solution. Complexes were formed at a molar ratio of PEI nitrogen atoms to DNA phosphate (N/P) of 6. Complexes were prepared in either 0.5× HBS for in vitro application or 20 mM HEPES, pH 7.1, for in vivo application. Complexes were allowed to stand for at least 20 min at room temperature before use. Final concentration of DNA in complexes for in vitro application was 10  $\mu\text{g/mL}$ , while for in vivo it was 200  $\mu\text{g/mL}$ . DNA complexes prepared at the higher DNA concentration for in vivo application (200  $\mu\text{g/mL}$ ) were shock-frozen in liquid nitrogen and stored at  $-20^\circ\text{C}$ . To obtain isosmolarity glucose stock (50% w/v) was added to give a final glucose concentration of 5% (w/v). For determining the biophysical parameters, glucose was added to the DNA complex solution either before freezing or after thawing. For all DNA complexes that are applied systemically to mice, glucose was added after thawing. DNA complexes were thawed rapidly with mixing in a water bath at  $37^\circ\text{C}$  and then placed on ice and stood at room temperature for at least 1 h before use.

For example, for in vitro transfection complexes were generated containing 20  $\mu\text{g}$  of DNA in 1 mL total volume. For this purpose, 20  $\mu\text{g}$  (60.6 nmol phosphate) of pCMV-Luc plasmid was diluted to a volume of 0.5 mL with 0.5× HBS buffer and added to 363 nmol nitrogen of PEI (including PEI conjugates) in 0.5 mL of the same buffer with rapid mixing by pipetting.

Measurement of particle size and zeta-potential. Particle size of transfection complexes was measured by laser-light scattering using a Malvern Zetasizer 3000HS (Malvern Instruments, Worcestershire, UK). For particle sizing, complexes were diluted in the appropriate buffer to give a final DNA concentration of 10  $\mu\text{g/mL}$ . For estimation of the surface charge, transfection complexes were diluted in 10 mM NaCl to give a DNA final concentration of 2  $\mu\text{g/mL}$ , and the zeta-potential was measured as previously described (25).

**Cells Culture and Transfection.** K562 suspension cells (ATCC CCL-243) were grown in RPMI 1640 medium supplemented with 10% FCS and 6 mM L-glutamine, at  $37^\circ\text{C}$  in a 5%  $\text{CO}_2$  humidified atmosphere. Cells were placed in fresh medium containing 50  $\mu\text{M}$  desferrioxamine 16 h before transfection. Before transfection, the cells were collected, resuspended in fresh medium (10% FCS, 68 mM L-glutamine), and plated in a 24-well plate at a density of  $5 \times 10^5$  cells in 1.5 mL per well. Transfection complexes (0.5 mL, 5  $\mu\text{g}$  DNA) were added to the cells, and after 4 h incubation at  $37^\circ\text{C}$ , transfection medium was replaced by 2 mL of fresh culture medium. The cells were harvested 20–22 h after transfection and lysed with 1 mL of lysis buffer (25 mM Tris-phosphate, pH 7.8, 2 mM DTT, 2 mM CDTA pH 7.8, 10% glycerol, 1% Triton

X-100) per well. Luciferase activity was determined from aliquots of the lysate using a luminometer (Lumat LB9507, Berthold, Bad Wildbad, Germany). Values are given as light units and represent the total luciferase activity per  $5 \times 10^5$  cells as mean  $\pm$  standard deviations of at least triplicates.

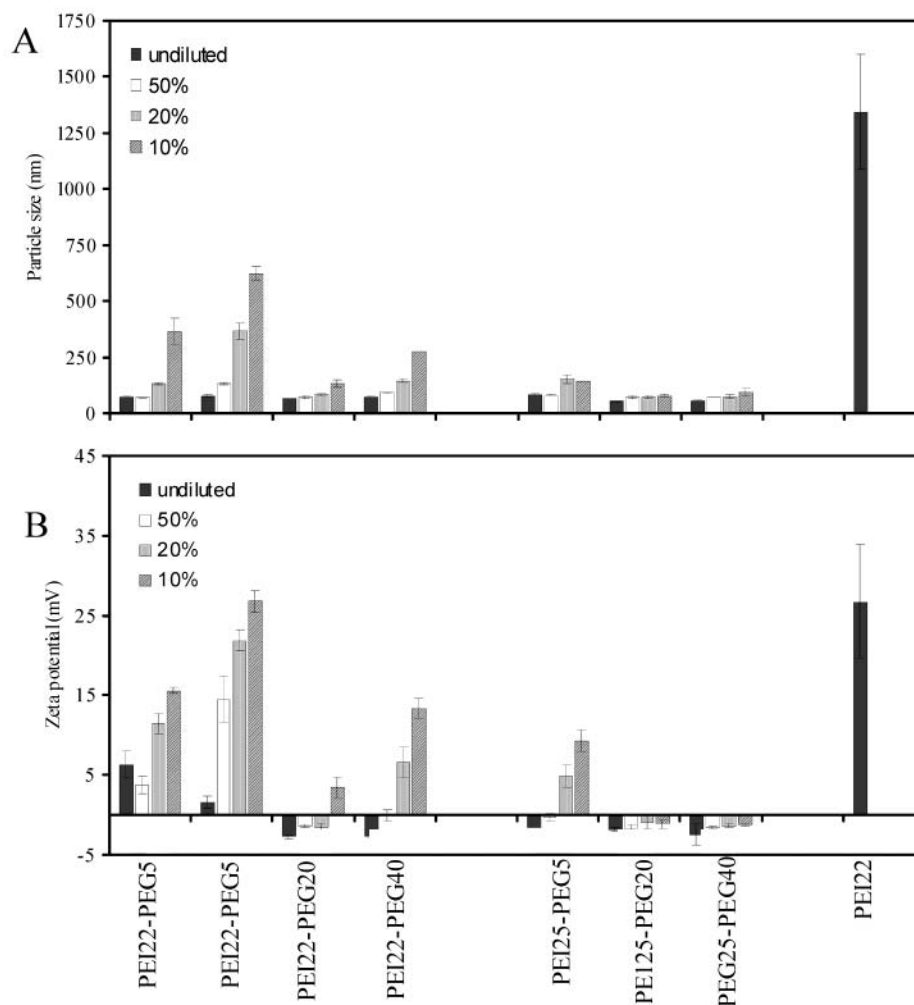
**Systemic Application of Transfection Complexes in Tumor-Bearing Mice.** A/J mice (7–8 weeks, female) were purchased from Harlan, Bicester, UK. Mice were injected subcutaneously with  $1 \times 10^6$  Neuro2a neuroblastoma cells (ATCC CCL 131). After 2 weeks, when tumors had reached approximately 10–13 mm in diameter, transfection complexes were applied. The thawed transfection complexes with the pCMVL plasmid (50  $\mu\text{g}$  DNA, at 200  $\mu\text{g/mL}$ ) coding the luciferase prepared in 20 mM HEPES, pH 7.1, were injected into the tail vein. At 24 h after injection, animals were sacrificed and the indicated tissues were resected, frozen in liquid nitrogen, and stored at  $-80^\circ\text{C}$ . Tissues were homogenized in 250 mM Tris-buffer, pH 7.5, using an IKA-Homogenizer, and frozen in liquid nitrogen, and the tissue lysates were stored at  $-80^\circ\text{C}$  until assay of luciferase activity (as described above). Luciferase background (100–200 RLU) was subtracted from each value and transfection efficacy is expressed as RLU per tumor. One million RLU correspond approximately to 2 ng of luciferase.

**Systemic Application of TNF $\alpha$  DNA Complexes in Therapeutic Models.** A/J mice were injected subcutaneously with  $1 \times 10^6$  syngeneic Neuro2a tumor cells, DBA/2 mice were injected with  $1 \times 10^6$  M-3 (ATCC CCL131) cells, and C57Bl6 mice were injected with  $1 \times 10^6$  B16F10 cells (kindly provided by Dr. Fidler, M. D. Anderson Hospital, Houston, TX). Starting at indicated time points after tumor setting, when tumors reached sizes of 5–8 mm in diameter, thawed DNA complex containing 50  $\mu\text{g}$  of plasmid pGSmuTNF $\alpha$  coding for murine TNF $\alpha$  in 20 mM HEPES, pH 7.1, and 5% (w/w) glucose was injected into the tail vein. For control animals, 0.25 mL 0.9% (w/v) NaCl was injected into the tail vein. Injections were repeated 5–7 times as indicated, and tumor sizes of the animals were monitored. Differences in tumor growth were statistically analyzed using one-way ANOVA, using GraphPad Prism software.

## RESULTS AND DISCUSSION

**Synthesis of PEG-PEI and Tf-PEG-PEI Conjugates.** Several different PEG-PEI shielding conjugates were generated by modifying amino groups of 22 kDa linear PEI or the 25 kDa branched PEI with *N*-hydroxysuccinimide ester derivatives of PEG of 5, 20, or 40 kDa. In addition, a disulfide-bridged conjugate, PEI22ssPEG5, was synthesized by reacting mercaptopropionate-modified 22 kDa PEI with 5 kDa PEG-orthopyridyl disulfide. Conjugates were purified by cation exchange chromatography, and PEG:PEI ratios were analyzed by proton NMR. These coupling efficiencies are shown in Table 1. The highest coupling ratio of 23 was generated for the PEI25-PEG5 conjugate. This is most likely due to the highly branched PEI25 core having a large number of primary amines available to react with PEG. Likewise a much lower coupling ratio of 4.4 was observed for the PEI22-PEG5 conjugate, which has a linear PEI core. The size of the PEG molecule conjugated also influences the efficiency of the coupling reaction. For copolymers with either branched or linear PEI core the coupling efficiency decreases with increasing PEG size.

For receptor-specific targeting of the complexes, transferrin was linked to either 22 kDa linear or 25 kDa



**Figure 2.** Particle size (A) and zeta-potential (B) of DNA complexes generated in  $0.5\times$  HBS at a final DNA concentration of  $20\text{ }\mu\text{g/mL}$  at a PEI/DNA charge ratio of  $N/P = 6$ . PEG–PEI conjugates were mixed with unmodified PEI22; the percentage of PEG–PEI conjugate was 50, 20, and 10 by weight relative to PEI. Measurements were made approximately 30 min after mixing of the components. Each data value represents mean  $\pm$  SD of three experiments.

branched PEI via a PEG bridging molecule to form the Tf–PEG–PEI, the targeting conjugate. The Tf–PEG–PEI25 conjugate was generated by first modifying PEI25 with SPDP and conversion into the mercaptopropionate form, reaction of transferrin amino groups with heterobifunctional ( $\alpha$ -maleimide- $\omega$ -*N*-hydroxysuccinimide ester) 3.4 kDa PEG derivative, and reacting the maleimide group at the distal end of the PEG-chain in the Tf conjugate with the thiol-functionalized PEI25. The resulting Tf–PEG–PEI25 polymer after purification contained approximately one Tf ligand on average per two PEI molecules.

In the Tf–PEG–PEI22 targeting conjugate, both PEI and transferrin were modified separately with iminothiolane. The modified transferrin was reacted with bifunctional PEG derivative PEG-bis-orthopyridyl-disulfide. The reaction mixture was subsequently reacted with the sulfhydryl groups of the iminothiolane-modified PEI22. The purified conjugate contained approximately one Tf ligand to one PEI molecule.

**Formation of DNA Complexes.** The concept of how post-PEGylated and the new PEGylated DNA particles described here are formed is presented in Figure 1. The previous post-PEGylation method involves three sequential steps (path a). First, DNA is condensed to the cationic PEI, and then PEG is covalently attached to the surface.

For receptor-mediated cell uptake, the targeting ligand is covalently attached to some of the surface-exposed PEG chains.

For the new method of PEGylation described here, complex formation requires only two quick sequential steps (path b). Unlike the postPEGylation method, conjugation of shielding and targeting agents is performed prior to DNA complex formation. The two copolymers, PEG–PEI for surface shielding and Tf–PEG–PEI for receptor-mediated cell uptake, are synthesized as described above and stored at  $-20\text{ }^{\circ}\text{C}$  until required. The two copolymers and unmodified PEI22, the main DNA condensing agent, are mixed together, followed by the addition of plasmid DNA.

To explore the effect of PEG conjugates, in the first physical characterization studies, the targeting conjugate was omitted. The shielding conjugate was mixed with PEI22 at various ratios with plasmid DNA at  $10\text{ }\mu\text{g/mL}$ . These complexes were analyzed fresh by laser-light scattering (Figure 2). The size and surface charge of these particles varied depending upon the amount and type of shielding conjugate in the complex. The particle size and zeta potential of DNA complexes generated from the various shielding conjugates is shown in Figures 2, parts A and B, respectively. Figure 2A shows that for the linear PEI shielding PEG conjugate there is an increase in particle size when its fraction is reduced in the complex.



This effect was greatest for the low molecular weight 5 kDa PEG shielding conjugates, followed by the branched 40 kDa PEG and the linear 20 kDa PEG. In contrast, it appears that decreasing amount of branched PEI shielding PEG conjugate in the complex has less effect on the particle size (Figure 2A).

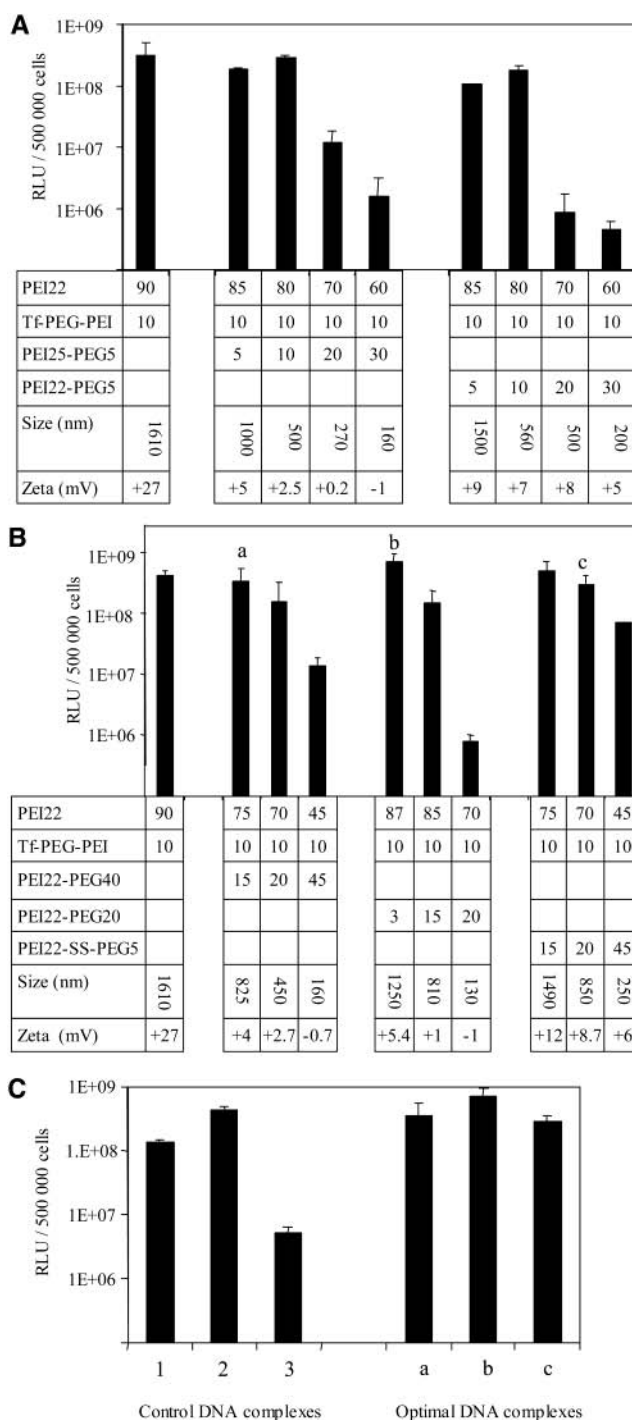
The zeta potential data (Figure 2B) is also shown to be influenced by the ratio of the linear shielding PEG conjugate in the complex, while the branched PEI shielding conjugate has lesser effect on the zeta potential. Decreasing the amount of linear PEI shielding conjugate in the complex results in an increase in the surface charge. For the branched shielding conjugate, the complexes have a surface charge near neutral with the exception of the 5 kDa PEG at the two lowest concentrations in the complexes.

**In Vitro Transfection Efficiency of DNA Complexes.** To determine the effect of the shielding conjugate on receptor-mediated cell uptake in vitro, the complexes were prepared with the targeting conjugate, Tf-PEG-PEI, which was maintained at 10% of total PEI (w/w) in the complex. Luciferase transfection efficiency was determined with freshly prepared complexes in the transferrin receptor-rich erythromyeloid cell line K562 (26, 27). Gene expression was determined by luciferase activity using a luminometer (Figure 3). Figure 3A compares the transfection efficiency of branched and linear PEI shielding conjugates, with the low molecular weight shielding PEG (5 kDa). There appears to be little difference in transfection efficiencies for both branched and linear PEI conjugates, with maximum transfection efficiency when the shielding conjugate represents 5 and 10% of the complex.

Figure 3B compares the transfection efficiencies of the linear PEI22 conjugated with 40, 20, or 5 kDa PEG. Transfection efficiency of these complexes was highest when the fraction of the shielding conjugate was at the two lowest fractions tested in the complex. The maximum transfection efficiencies for all complexes tested were similar to the control complex, which consists of PEI22 and the targeting conjugate Tf-PEG-PEI only. Although the control has a high transfection efficiency, it has a high positive surface charge of +27 mV, while the shielded conjugates have a surface charge in the range of -1 to +12 mV. The high positive surface charge on the control complex is expected to result in the complex interacting with serum proteins when applied systemically, resulting in particle aggregation and loss of systemic targeting activity (10).

On the basis of the biophysical properties of the complexes and their in vitro transfection efficiency, complexes a, b, and c (Figure 3B) were chosen as optimal. Optimum ratios for the 40 and 20 kDa PEG shielding conjugates was based on their high transfection efficiency. For the low molecular weight 5 kDa PEGylated conjugates, the complex with the highest transfection efficiency had a high surface positive charge of +12 mV and was not expected to be effective in vivo, therefore a formulation of medium PEG conjugate content was chosen.

Figure 3C gives a direct comparison of the transfection efficiency of the three optimal complexes from Figure 3B with two additional control complexes. The three optimal formulations tested all showed similar transfection efficiencies, comparable to the control complex "2" consisting of Tf-PEG-PEI/PEI22. The DNA/PEI22 control complex "1", without the targeting conjugate, has slightly lower transfection efficiency. The high transfection efficiency of the DNA/PEI complex is believed to be due to



**Figure 3.** In vitro transfection efficiency of DNA complexes. Complexes were prepared in  $0.5 \times$  HBS at a DNA concentration of  $10 \mu\text{g/mL}$ , N/P ratio of 6.0. First, the Tf-PEG-PEI conjugate was mixed with various amounts of PEI-PEG conjugate and PEI22 in 0.25 mL buffer (containing  $3.9 \mu\text{g}$  of PEI in total), and then  $5 \mu\text{g}$  of pCMVL in 0.25 mL of buffer was added. The percentages of components in the complex are based on PEI: (A) 5 kDa PEG conjugated with branched or linear core PEI; (B) linear core PEI conjugated with 40, 20, or 5 kDa PEG. (C) Transferrin is required for gene transfer to K562 cells. Control DNA complexes, 1; PEI22, without shielding and targeting conjugate, 2; PEI22 (90%) and Tf-PEG-PEI targeting conjugate (10%), without shielding conjugate, 3; PEI22 (85%) and PEI-PEG40 shielding conjugate (15%), without targeting conjugate. Optimal DNA complexes a, b, and c as described in Figure 3B. All DNA complexes were applied fresh to the K562 cells; luciferase activity of transfected K562 cells ( $5 \mu\text{g}$  DNA per 500,000 cells) is shown as mean  $\pm$  SD, of four to six experiments.

**Table 2.** Effect of Freeze–Thawing on Particle Size and Zeta Potential of DNA Complexes Formed with and without PEG–PEI Shielding Conjugate

complex	components (%)	fresh		frozen	
		size (nm)	zeta (mV)	size (nm)	zeta (mV)
non PEG–PEI shielded	Tf–PEI (25) PEI22 (75)	270 ± 34	+4.9 ± 0.7	> 1000 (aggregates)	aggregates
PEG–PEI shielded	Tf–PEG–PEI (10)	214 ± 22	+5.6 ± 1.5	271 ± 34 <sup>a</sup>	+2.8 ± 0.2 <sup>a</sup>
	PEG20–PEI22 (20)			1250 ± 118 <sup>b</sup>	+2.3 ± 0.1 <sup>b</sup>
	PEI22 (70)				

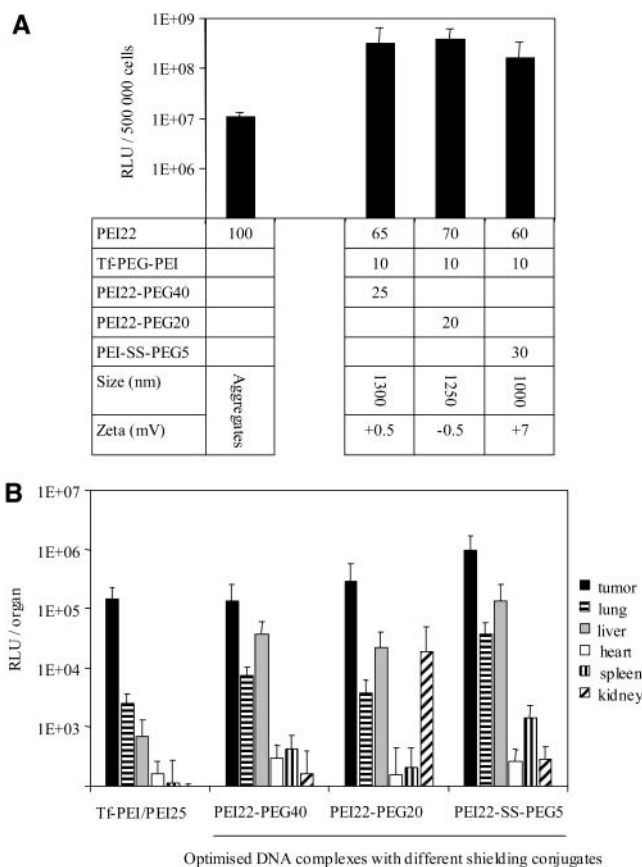
<sup>a</sup> Glucose was added after complex formation and before freezing. <sup>b</sup> Glucose was added after thawing.

its high surface charge of +31 mV (data not shown) which will facilitate its binding to the cell surface by electrostatic attraction (28). The third control “3” consists of DNA, PEI, and the shielding conjugate PEI22–PEG40, analogous to formulation “a” but lacking the targeting conjugate. The inclusion of the shielding conjugate in the complex reduced the surface charge of the complex to +10 mV (data not shown). The transfection efficiency of this complex was about 100-fold lower than the analogous complexes containing Tf ligand (Figure 3C, compare with formulation “a”). The lower transfection efficiency in comparison to the other control complexes can be attributed to the lower surface charge of the complex, resulting in reduced electrostatic interactions with the cell surface. The higher transfection rate of the transferrin targeting DNA complexes “a” indicates transferrin receptor-mediated internalization of the complexes in K562 cells, which is consistent with our previous work (26, 27, 29).

**Freeze–Thawing of DNA Complexes for in Vivo Application.** It would be of great convenience to store DNA complexes frozen and thaw them prior to their in vivo application. Since previous work demonstrated a strong correlation between the maintenance of particle size/zeta potential and retention of transfection rates (30), the biophysical parameters (particle size and zeta potential) of complexes before and after freeze–thawing was first determined. To determine whether the inclusion of PEG conjugates in the complex affords greater freeze–thawing stability, we compared Tf-targeting DNA complexes with and without PEG conjugates. The ratio of the components in the complexes is shown in Table 2.

To deliver therapeutic amounts of DNA to tumor-bearing mice, a higher concentration of DNA (200 µg/mL) is required. The physical parameters of the complexes were determined with DNA at the higher in vivo concentration of 200 µg/mL, with an N/P of 6. However complexes containing such high concentrations of DNA have been shown to have a higher tendency to aggregate (30). To prevent aggregation of DNA particles, a greater amount (20–30%) of the shielding conjugate in the complexes is required to maintain particles sizes similar to those in the earlier in vitro transfection studies (Figure 4A). In these biophysical studies, PEGylated complexes contained 20% shielding conjugate (Table 2). Complexes were prepared in 20 mM HEPES, pH 7.1, in the absence of NaCl, as previously it was shown that NaCl is a driving force for particle aggregation (30, 31). Furthermore, previous work showed that sugars (sucrose, trehalose, or maltose) were required to maintain size and transfection efficiency of DNA/polymer complexes after freeze–thawing (32). Therefore to minimize aggregation, glucose was added to the complexes after complex formation and before freezing at 5% (w/v) to obtain iso-osmolarity. The effect of adding glucose only after thawing was also investigated as indicated in Table 2.

Both PEGylated and non-PEGylated complexes freshly prepared had similar particle size and a surface charge



**Figure 4.** Transfection efficiency of optimized DNA complexes prepared with DNA at a higher concentration for in vivo application. Complexes were prepared with DNA at 200 µg/mL, N/P ratio of 6.0, in 20 mM HEPES pH 7.1, snap frozen in liquid nitrogen and stored at –20 °C. DNA complexes were thawed in glucose (5% w/v, final concentration). (A) In vitro transfection: the complexes were diluted after thawing with 20 mM HEPES, pH 7.1, to a DNA concentration of 10 µg/mL. Luciferase activity of K562 cells transfected with 5 µg pCMVL DNA per 5 × 10<sup>5</sup> cells represents the mean ± SD of four to five experiments. (B) Biodistribution of reporter gene expression after systemic gene delivery. The DNA complexes (pCMVL, 50 µg per mouse) after thawing in glucose were injected into the tail vein of Neuro2a tumor-bearing A/J mice. The control complexes (Tf-PEI/PEI25, N/P of 4.8) were freshly prepared as previously described. The biodistribution of gene expression was determined after 24 h by luciferase activity (mean ± SD, *n* = 6 animals per group).

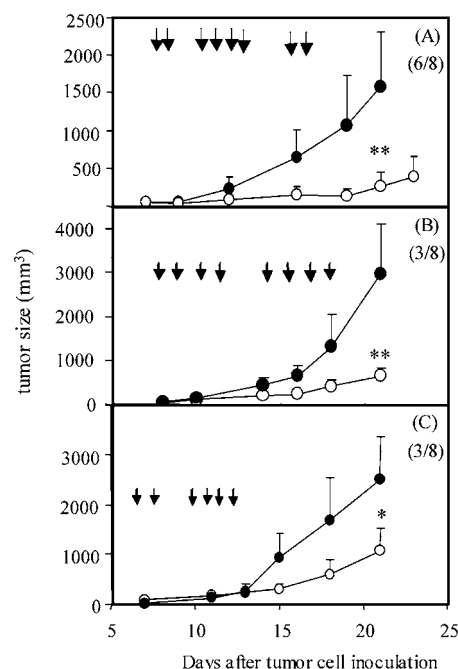
near neutral (Table 2). After freeze–thawing of these complexes, the particle size and zeta potential of the PEGylated complex was comparable to the fresh complex, while the non PEGylated complexes grew in size (Table 2). These results suggest that PEGylation can not only stabilize DNA/polymer particles in solution but also prevent aggregation upon the freeze–thawing process. Similarly, it was shown that a DNA–peptide condensing agent when PEGylated was an efficient lyoprotectant, with respect to maintaining particle size (33).

Interestingly, larger but stable PEGylated particles could be generated when glucose was only added after thawing (Table 2). Larger Tf-PEI/DNA complexes ( $\sim 1 \mu\text{m}$ ) have previously been shown to have higher transfection efficiencies (30). Therefore these large, stable DNA complexes were used to deliver plasmid DNA systemically to mice.

**Formulation of DNA Complexes for in Vivo Application.** DNA complexes were formed with the higher concentration of DNA ( $200 \mu\text{g/mL}$ ) and shielding conjugate (20–30%). Complexes were snap frozen and stored, and glucose was added to the complexes after they were thawed, as described in Table 2. Figure 4A shows the physical characteristics and in vitro transfection efficiencies of the three optimized formulations generated at the higher DNA concentration of  $200 \mu\text{g/mL}$ . The particles which we have chosen for further evaluation have a diameter of around  $1 \mu\text{m}$ , slightly larger in size than those prepared with lower amounts of DNA (compare with Figure 3). Importantly for in vivo application, the increased amount of the shielding conjugate in the complex maintains the zeta potential at near neutral. The in vitro transfection efficiencies of the optimized formulations are all much higher than the control DNA/PEI22 complex which aggregated upon the freeze/thaw process. Furthermore, there was no significant difference in the transfection efficiency of all three optimized formulations.

To test these optimized formulations in vivo (Figure 4B), each formulation was thawed, glucose added, and the formulation injected into the tail vein of A/J Neuro2a neuroblastoma tumor-bearing mice. The major internal tissues were recovered after 1 day. The control DNA/Tf-PEI/PEI25 complexes had to be prepared fresh before application as previously described (9). Figure 4B shows the luciferase protein expressed in the respective tissues. For all formulations, the highest expression was observed in the tumor cells. The highest expression in the tumor tissue was observed for PEI22-SS-PEG5 shielded formulation, with an expression level almost 1 log unit higher than the other formulations tested. The luciferase was found to be also expressed at low but significant levels in the liver, followed by the lung. The gene expression in the kidney for the PEI22-PEG20 formulation was due to expression in only 1 mouse out of 6 and in no other treatment group. It is therefore believed that this single observation is animal-specific (possibly due to a dysfunctional kidney) and not formulation-specific.

**Systemic Administration of a Therapeutic Gene (TNF $\alpha$ ).** Previously we demonstrated that freshly prepared transferrin-shielded DNA complexes mediate the expression of the highly potent and toxic protein tumor necrosis factor (TNF $\alpha$ ) in distant tumors, resulting in therapeutic effects in several murine tumor models (3, 34). On the basis of the previous luciferase experiments, we now selected the cryoconserved formulation shielded by PEI22-SS-PEG5 and tested for its ability to target the TNF $\alpha$  gene expression in distant tumors after systemic application. This was assessed by the reduction in growth and necrosis of tumors in three different murine tumor models, Neuro2a, M-3, and B16F10 (Figure 5). Complexes containing the plasmid pGSmuTNF $\alpha$  coding for murine TNF $\alpha$  were formed in 20 mM HEPES pH 7.1 and stored at  $-20^\circ\text{C}$ . Prior to injection, DNA formulations were thawed, glucose was added, and the formulation was injected into the tail vein of mice, between 5 and 7 times at the intervals indicated in Figure 5, and tumor sizes of the animals were recorded. Administration of the formulation was well tolerated by the mice; out of the 174 applications no sign of toxicity was



**Figure 5.** Tumor growth after the systemic application of Tf-PEG-PEI22/PEI22/PEI22ssPEG5/DNA (pGSmuTNF $\alpha$ ) to (A) Neuro2a tumor-bearing A/J mice, (B) M-3 tumor-bearing DBA/2 mice, or (C) B16F10 tumor-bearing C57Bl6 mice. Complexes were prepared in 20 mM HEPES, pH 7.1, using a molar PEI ratio of 1:6:3. DNA complexes were snap frozen in liquid nitrogen and stored at  $-20^\circ\text{C}$ . At indicated time points (see arrows), the DNA complex was thawed in glucose (5% w/v final concentration), and the complex ( $50 \mu\text{g}$  DNA per mouse) was injected into the tail vein of the mouse (open circles). Control mice were injected with 0.9% (w/v) NaCl (closed circles). Tumor sizes were monitored, mean  $\pm$  SD are presented;  $n = 10$  animals in Neuro2a control group,  $n = 8$  animals per group in all other control and treatment groups. Number of treatment animals with tumor necrosis is indicated in brackets. (\*)  $p < 0.1$ , (\*\*)  $p < 0.05$ , compared to control.

observed. Retardation in tumor development was observed in all three tumor models (Figure 5) accompanied with pronounced tumor necrosis. This is in agreement with transferrin-shielded DNA complexes which localized TNF $\alpha$  activity to the tumor without systemic toxicity (3). Of the models tested, the Neuro2a model showed the strongest response with regard to tumor necrosis with strong necrosis in six of the eight mice treated with the plasmid coding for TNF $\alpha$ , while for the control, two out of the 10 mice only showed weak central necrosis. For both M-3 and B16F10 tumor models, three of the eight mice showed tumor necrosis, while for the controls, no change in tumor growth was observed.

Current literature suggests that biodistribution of therapeutic particles following intravenous administration is modulated by the size of the particle and surface charge. A hydrophilic and uncharged surface on the particle reduces their uptake by the phagocytic cells of the RES and aggregation, significantly prolonging circulation time. For targeting DNA complexes to cancer cells, particles should be small enough to pass through the fenestrations in the tumor vasculature (35). These two parameters, particle size and surface hydrophilicity, can easily be modulated by this new streamlined system for generating PEGylated DNA particles. For instance, particle size and surface charge was reduced by increasing the amount of the shielding conjugate in the complex (Figure 2). The in vivo studies (Figure 4B) show that the PEGylated DNA complexes encoding TNF $\alpha$  were effective



in tumor necrosis in three different murine tumor models (Figure 5). Despite these promising *in vivo* results, the tumors were only rarely regressed and there was a variable response in the different tumor models tested. The variable response of the different tumor models to the formulation may be a reflection of the different tumor types having varying leakiness (35). Future studies will use this system to optimize size and surface charge of the transferrin-targeted formulations for targeting different tumors *in vivo*.

## CONCLUSION

This work describes a simple and quick method for the formation of PEG shielded transferrin-targeting PEI/DNA complexes. We demonstrate that the PEG shielded DNA/polymer vector can maintain its size/charge and transfection efficiency after freeze–thawing. For the first time we show that freeze–thawed polyplex vectors have systemic targeting activity toward disseminated tumors. Furthermore, the ratios of the shielding and targeting components in the complex can easily be varied, producing well defined particles with varying size and surface charge. This will enable such biophysical parameters to be easily investigated for their ability to target tumors, leading to DNA vectors which are tailor-made for their application. The simplicity of their preparation and storage in frozen form is a major step forward in the development of nonviral vectors as pharmaceutical products.

## ACKNOWLEDGMENT

We are grateful to Alexandra Schreiber and Sandra Fandl for help in the animal experiments.

## LITERATURE CITED

- Ogris, M., and Wagner, E. (2002) Targeting tumors with nonviral gene delivery systems. *Drug Discovery Today* 15, 479–485.
- Felgner, P. L., Barenholz, Y., Behr, J. P., Cheng, S. H., Cullis, P., Huang, L., Jessee, J. A., Seymour, L., Szoka, F., Thierry, A. R., Wagner, E., and Wu, G. (1997) Nomenclature for synthetic gene delivery systems [editorial]. *Hum. Gene Ther.* 8, 511–512.
- Kirchheis, R., Wightman, L., Kursa, M., Ostermann, E., and Wagner, E. (2002) Tumor-targeted gene delivery: an attractive strategy to use highly active effector molecules in cancer treatment. *Gene Ther.* 9, 731–735.
- Anchordoquy, T. J., Dean Allison, S., Molina, M., Girouard, L. G., and Carson, T. K. (2001) Physical stabilization of DNA-based therapeutics. *Drug Discovery Today* 6, 463–470.
- Boussif, O., Lezoualc'h, F., Zanta, M. A., Mergny, M. D., Scherman, D., Demeneix, B., and Behr, J. P. (1995) A versatile vector for gene and oligonucleotide transfer into cells in culture and *in vivo*: polyethylenimine. *Proc. Natl. Acad. Sci. U.S.A.* 92, 7297–7301.
- Ferrari, S., Moro, E., Pettenazzo, A., Behr, J. P., Zacchello, F., and Scarpa, M. (1997) ExGen 500 is an efficient vector for gene delivery to lung epithelial cells *in vitro* and *in vivo*. *Gene Ther.* 4, 1100–1106.
- Blessing, T., Kursa, M., Holzhauser, R., Kirchheis, R., and Wagner, E. (2001) Different strategies for formulation of PEGylated EGF-conjugated PEI/DNA complexes for targeted gene delivery. *Bioconjugate Chem.* 12, 529–537.
- Leamon, C. P., Weigl, D., and Hendren, R. W. (1999) Folate copolymer-mediated transfection of cultured cells. *Bioconjugate Chem.* 10, 947–957.
- Kirchheis, R., Wightman, L., Schreiber, A., Robitza, B., Rossler, V., Kursa, M., and Wagner, E. (2001) Polyethylenimine/DNA complexes shielded by transferrin target gene expression to tumors after systemic application. *Gene Ther.* 8, 28–40.
- Ogris, M., Brunner, S., Schuller, S., Kirchheis, R., and Wagner, E. (1999) PEGylated DNA/transferrin-PEI complexes: reduced interaction with blood components, extended circulation in blood and potential for systemic gene delivery. *Gene Ther.* 6, 595–605.
- Oupicky, D., Ogris, M., and Seymour, L. (2002) Development of long-circulating polyelectrolyte complexes for systemic delivery of genes. *J. Drug Targeting* 10, 93–98.
- Kichler, A., Chillón, M., Leborgne, C., Danos, O., and Frisch, B. (2002) Intranasal gene delivery with a polyethylenimine-PEG conjugate. *J. Controlled Release* 379–388.
- Kirchheis, R., Schuller, S., Brunner, S., Ogris, M., Heider, K. H., Zauner, W., and Wagner, E. (1999) Polycation-based DNA complexes for tumour targeted gene delivery *in vivo*. *J. Gene Med.* 1, 111–120.
- Wolfert, M. A., Schacht, E. H., Toncheva, V., Ulbrich, K., Nazarova, O., Seymour, L. W., Dash, P. R., and Oupicky, D. (1996) Characterization of vectors for gene therapy formed by self-assembly of DNA with synthetic block copolymers. *Hum. Gene Ther.* 7, 2123–2133.
- Katayose, S., and Kataoka, K. (1997) Water Soluble Polyion Complex Associates of DNA and Poly(ethylene glycol) Poly(L-lysine) Block Copolymer. *Bioconjugate Chem.* 8 (5), 702–707.
- Toncheva, V., Wolfert, M. A., Dash, P. R., Oupicky, D., Ulbrich, K., Seymour, L. W., and Schacht, E. H. (1998) Novel vectors for gene delivery formed by self-assembly of DNA with poly(L-lysine) grafted with hydrophilic polymers. *Biochim. Biophys. Acta* 1380, 354–368.
- Erbacher, P., Bettinger, T., Belguise, Valladier P., Zou, S., Coll, J. L., Behr, J. B., and Remy, J. S. (1999) Transfection and physical properties of various saccharide, poly(ethylene glycol), and antibody-derivatized polyethylenimines (PEI). *J. Gene Med.* 1, 210–222.
- Nguyen, H. K., Lemieux, P., Vinogradov, S. V., Gebhart, C. L., Guérin, N., Paradis, G., Bronich, T. K., Alakhov, V. Y., and Kabanov, A. V. (2000) Evaluation of polyether-polyethylenimine graft copolymers as gene transfer agents. *Gene Ther.* 7, 126–138.
- Woodle, M. C., Scaria, P., Ganesh, S., Subramanian, K., Titmas, R., Cheng, C., Yang, J., Pan, Y., Weng, K., Gu, C., and Torkelson, S. (2001) Sterically stabilized polyplex: ligand-mediated activity. *J. Controlled Release* 74, 309–311.
- Ogris, M., Steinlein, P., Carotta, S., Brunner, S., and Wagner, E. (2001) DNA/polyethylenimine transfection particles: influence of ligands, polymer size, and PEGylation on internalization and gene expression. *AAPS PharmSci.* 3, E21.
- Sarin, V. K., Kent, S. B., Tam, J. P., and Merrifield, R. B. (1981) Quantitative monitoring of solid-phase peptide synthesis by the ninhydrin reaction. *Anal. Biochem.* 117, 147–157.
- Riddles, P. W., Blakeley, R. L., and Zerner, B. (1979) Ellman's reagent: 5,5'-dithiobis(2-nitrobenzoic acid)-a re-examination. *Anal. Biochem.* 94, 75–81.
- Plank, C., Zatloukal, K., Cotten, M., Mechtler, K., and Wagner, E. (1992) Gene transfer into hepatocytes using asialoglycoprotein receptor mediated endocytosis of DNA complexed with an artificial tetra-antennary galactose ligand. *Bioconjugate Chem.* 3, 533–539.
- Carlsson, J., Drevin, H., and Axen, R. (1978) Protein thiolation and reversible protein–protein conjugation. N-Succinimidyl 3-(2-pyridyldithio)propionate, a new heterobifunctional reagent. *Biochem. J.* 173, 723–737.
- Kirchheis, R., Wightman, L., and Wagner, E. (2001) Design and gene delivery activity of modified polyethylenimines. *Adv. Drug Delivery Rev.* 53, 341–358.
- Kirchheis, R., Kichler, A., Wallner, G., Kursa, M., Ogris, M., Felzmann, T., Buchberger, M., and Wagner, E. (1997) Coupling of cell-binding ligands to polyethylenimine for targeted gene transfer. *Gene Ther.* 4, 409–418.
- Cotten, M., Langle, Rouault, Kirlappos, H., Wagner, E., Mechtler, K., Zenke, M., Beug, H., and Birnstiel, M. L. (1990) Transferrin-polycation-mediated introduction of DNA into human leukemic cells: stimulation by agents that affect the survival of transfected DNA or modulate transferrin receptor levels. *Proc. Natl. Acad. Sci. U.S.A.* 87, 4033–4037.

- (28) Mislick, K. A. and Baldeschwieler, J. D. (1996) Evidence for the role of proteoglycans in cation-mediated gene transfer. *Proc. Natl. Acad. Sci. U.S.A.* **93**, 12349–12354.
- (29) Wagner, E., Curiel, D., and Cotten, M. (1994) Delivery of drugs, proteins and genes into cells using transferrin as a ligand for receptor-mediated endocytosis. *Adv. Drug Delivery Rev.* **14**, 113–136.
- (30) Ogris, M., Steinlein, P., Kursa, M., Mechtler, K., Kircheis, R., and Wagner, E. (1998) The size of DNA/Transferrin-PEI complexes is an important factor for gene expression in cultured cells. *Gene Ther.* **5**, 1425–1433.
- (31) Wightman, L., Kircheis, R., Rössler, V., Carotta, S., Ruzicka, R., Kursa, M., and Wagner, E. (2001) Different behavior of branched and linear polyethylenimine for gene delivery in vitro and in vivo. *J. Gene Med.* **3**, 362–372.
- (32) Cherng, J. Y., Wetering P., Talsma, H., Crommelin, D. J., and Hennink, W. E. (1999) Stabilization of polymer-based gene delivery systems. *Int. J. Pharm.* **183**, 25–28.
- (33) Kwok, K. Y., Adami, R. C., Hester, K. C., Park, Y., Thomas, S., and Rice, K. G. (2000) Strategies for maintaining the particle size of peptide DNA condensates following freeze-drying. *Int. J. Pharm.* **203**, 81–88.
- (34) Kircheis, R., Ostermann, E., Wolschek, M. F., Lichtenberger, C., Magin-Lachmann, C., Wightman, L., Kursa, M., and Wagner, E. (2002) Tumor-targeted gene delivery of tumor necrosis factor- $\alpha$  induces tumor necrosis and tumor regression without systemic toxicity. *Cancer Gene Ther.* **9**, 673–680.
- (35) Hashizume, H., Baluk, P., Morikawa, S., McLean, J. W., Thurston, G., Roberge, S., Jain, R. K., and McDonald, D. M. (2000) Openings between defective endothelial cells explain tumor vessel leakiness. *Am. J. Pathol.* **156**, 1363–1380.

BC0256087

# Synthesis of Maleimide-Activated Carbohydrates as Chemoselective Tags for Site-Specific Glycosylation of Peptides and Proteins

Jiahong Ni, Suddham Singh, and Lai-Xi Wang\*

Institute of Human Virology, University of Maryland Biotechnology Institute, University of Maryland, 725 W. Lombard Street, Baltimore, Maryland 21201. Received September 30, 2002; Revised Manuscript Received November 14, 2002

An array of maleimide-activated mono- and oligosaccharides were synthesized to permit site-specific glycosylation of cysteine-containing peptides and proteins. Maleimide-activated monosaccharides, in which the native  $\alpha$ - or  $\beta$ -O-glycosidic linkages found for nonreducing terminal sugars of native glycoproteins are preserved, were prepared using 2'-aminoethyl glycosides as the key intermediates. In addition, a native high-mannose type oligosaccharide, Man<sub>9</sub>GlcNAc<sub>2</sub>Asn, was converted into its maleimide-activated form by taking advantage of the existing amino group in the Asn portion. The application of these maleimide-activated carbohydrates was exemplified by the site-specific glycosylation of a 36-mer HIV-1 gp41 peptide, T20, which is a potent inhibitor against HIV infection. The chemoselective ligation was found to be rapid, highly efficient, and essentially quantitative. Tagging the biologically active peptide with a mannose and/or oligomannose moiety will be useful for targeting the drug to macrophage and dendritic cells, which are primary targets for HIV-1 infection and are expressing mannose- and oligomannose-specific receptors on their surface. In combination with site-specific mutagenesis, the maleimide-activated carbohydrates can serve as generally applicable tags for site-specific glycosylation of proteins via the highly efficient maleimide–thiol ligation reaction.

## INTRODUCTION

Protein glycosylation, the covalent attachment of carbohydrates to the side chains of proteins, is one of the most common co- and posttranslational modifications of proteins. The carbohydrate portions of glycoproteins have been implicated to play a role in many important biological recognition processes such as cell adhesion, host–pathogen interaction, and host immune responses (1–3). In addition, it is known that correct glycosylation is critical for protein expression and folding and increases protein's thermal and proteolytic stability (4). However, a thorough understanding of the functions and properties of glycoproteins has been hindered by the complexity of glycoprotein biosynthesis. Generally, natural and recombinant glycoproteins occur as a heterogeneous mixture of glycoforms that share the same peptide backbone but differ in the carbohydrate portions and/or in the sites of linkage. This micro-heterogeneity makes it extremely difficult to obtain a pure, homogeneous glycoprotein from natural and recombinant sources (5). To better understand the molecular basis of the oligosaccharides in biological processes and to exploit these molecular properties for pharmaceutical applications, e.g., drug targeting, there is an urgent need for chemical methods that will allow site-specific attachment of homogeneous and natural as well as unnatural carbohydrates to proteins. For the purpose, several nonnative chemoselective ligation methods have been developed to introduce carbohydrate moieties at specific sites of peptides and proteins (6, 7). For example, iodoacetamide-containing mono- and oligosaccharides were first employed for site-specific glycosylation of cysteine-containing peptides/proteins (8, 9). Glyco-methanethiosulfonates that are reactive to

cysteines via disulfide formation have been developed for controlled site-selective glycosylation of proteins (10). In combination with sited-directed mutagenesis to introduce cysteine residue(s) at predetermined sites, the above-mentioned methods allow regio- and glycan-specific glycosylation of some biologically important proteins (10–12). In addition, aminooxy-, hydrazide-, and thiosemicarbazide-functionalized saccharides have been prepared as versatile reagents for glycoconjugate synthesis via chemoselective formation of oxime or hydrazone linkages (13). The development of these chemoselective ligation methods significantly extends our abilities to design and synthesize novel glycoproteins and analogues for biological and biomedical applications. Nevertheless, some drawbacks exist for some current methods that limit their potentials. For example, glycosylation via nucleophilic substitution of a thiol group with iodoacetyl moieties requires an alkaline condition (pH 8–9). Under the alkaline conditions, side reactions from other nucleophiles (e.g., histidine and lysine residues) may occur (12). The effective formation of an oxime or hydrazone needs an acidic condition (pH 4–5) that may cause stability and solubility problems for certain peptides and proteins.

In an attempt to develop milder alternative approaches toward chemoselective site-specific glycosylation of peptides and proteins, we turned our attention to the highly efficient and selective ligation between maleimide and thiol functionalities. Maleimide-functionalized moieties have been widely used for selective modification and conjugation of cysteine-containing biomolecules in bioconjugate chemistry (14–16). The maleimide–thiol ligation is rapid, highly selective, and essentially quantitative under physiological conditions. Recently we have successfully exploited the potential of this highly chemoselective ligation for the synthesis of very large and complex multivalent HIV-1 peptides (17). In the design of carbo-

\* Corresponding author. Tel. 410-706-4982. Fax 410-706-5068. E-mail: wangx@umbi.umd.edu.



hydrate-based vaccine, a maleimide group was introduced into the carbohydrate antigen for final coupling to a carrier protein (18). More recently, 1-maleimido sugars were prepared and used for the synthesis of neoglycopeptides and neoglycoproteins via maleimide–thiol ligation (19). The major drawback of the reported synthesis is that the  $\beta$ -*N*-glycosidic linkage in the 1-maleimido sugars does not represent most native glycosidic forms of nonreducing terminal sugars found in native glycoproteins. In this paper, we describe a general synthesis of an array of maleimide-activated carbohydrates using 2'-aminoethyl glycosides as the key intermediates, in which the native  $\alpha$ - or  $\beta$ -*O*-glycosidic linkages found for the nonreducing terminal sugars of native glycoproteins are preserved. The preservation of native  $\alpha$ - or  $\beta$ -*O*-glycosidic linkages is important for the interactions between the terminal sugars and carbohydrate-specific lectins or cell surface receptors (20). On the other hand, a native high-mannose type oligosaccharide, Man<sub>9</sub>GlcNAc<sub>2</sub>-Asn, was converted into its maleimide-activated form by taking advantage of the existing amino group in the Asn portion. The application of these maleimide-activated carbohydrates was exemplified by the site-specific glycosylation of a 36-mer HIV-1 gp41 peptide, T20, which is a potent inhibitor against HIV infection.

## EXPERIMENTAL PROCEDURES

**General.** *N,N*-Dimethylformamide, dichloromethane, and methanol were purchased from Aldrich and stored over 4A molecular sieves. All other chemicals were purchased from Aldrich/Sigma and used as received. <sup>1</sup>H NMR spectra were recorded at 300 MHz on a QE 300 with Me<sub>4</sub>Si ( $\delta$  0) as the internal standard. <sup>13</sup>C NMR spectra were recorded at 125 MHz with a Varian 500. The ESI-MS spectra were measured on a Waters ZMD mass spectrometer. Analytical TLC was performed on glass plates coated with silica gel 60 F<sub>254</sub> (E. Merck). Carbohydrates were detected by charring with 10% ethanolic sulfuric acid. Amines were detected by ninhydrin spraying (0.3% in ethanol and acetic acid (97:3)). Flash chromatography was performed on silica gel 60 (200–400 mesh, EM Science). Analytical HPLC was carried out with a Waters 626 HPLC instruments on Waters Nova-Pak C18 column (3.9  $\times$  150 mm) at 40 °C, with a linear gradient of 0–30% (Method A) or 10–90% (Method B) acetonitrile containing 0.1% TFA in 25 min at a flow rate of 1 mL/min with UV detection (at 214 and/or 280 nm).

**2'-Chloroethyl 2,3,4-Tri-*O*-acetyl- $\alpha$ -L-fucopyranoside (9).** A mixture of L-fucose (1.64 g, 10.00 mmol), 2-chloroethanol (10 mL), and Dowex 50W-100 (H<sup>+</sup>) (1.00 g) was stirred at 80 °C for 2 h. The mixture was cooled to room temperature and filtered. The resin was washed with ethanol (2  $\times$  3 mL). The combined filtrates were evaporated at a reduced pressure. The residue was purified by flash column chromatography on silica gel using dichloromethane and MeOH (9:1) as the eluent to give a crude product, which was recrystallized with ethanol to afford a crystalline 2-chloroethyl  $\alpha$ -L-fucopyranoside (1.01 g, 45%); <sup>1</sup>H NMR (300 MHz, D<sub>2</sub>O):  $\delta$  4.92 (d, *J* = 3.9 Hz, 1 H, H-1), 4.14 (q, *J* = 6.6 Hz, 1 H, H-5), 3.96–3.73 (m, 7 H, H-2, H-3, H-4, OCH<sub>2</sub>CH<sub>2</sub>Cl), 1.20 (d, *J* = 6.6 Hz, 3 H, H-6); ESI-MS: 251.30 (M(<sup>37</sup>Cl) + Na)<sup>+</sup>, 249.30 (M(<sup>35</sup>Cl) + Na)<sup>+</sup>.

A solution of 2'-chloroethyl  $\alpha$ -L-fucopyranoside (320.0 mg, 1.41 mmol) in pyridine–acetic anhydride (1:1, v/v, 4 mL) was stirred at room temperature for 2 h, then ice (5 g) was added. The resulting mixture was stirred for 1 h

and extracted with dichloromethane (50 mL). The organic layer was separated, washed with solution of hydrogen chloride (1 M, 3  $\times$  30 mL) and brine (3  $\times$  30 mL), dried over sodium sulfate, filtered, and evaporated. The residue was purified by flash column chromatography on silica gel using dichloromethane–EtOAc (9:1, v/v) as the eluent to give the per-*O*-acetylated glycoside **9** (478.6 mg, 97%); *R*<sub>f</sub> = 0.58 (CH<sub>2</sub>Cl<sub>2</sub>–EtOAc 9:1); <sup>1</sup>H NMR (300 MHz, CDCl<sub>3</sub>/TMS):  $\delta$  5.40 (dd, *J* = 10.1, 3.4 Hz, 1 H, H-3), 5.33 (d, *J* = 3.9 Hz, 1 H, H-1), 5.16 (d, *J* = 3.4 Hz, 1 H, H-4), 5.13 (dd, *J* = 10.1, 3.9 Hz, 1 H, H-2), 4.27 (q, *J* = 6.6 Hz, 1 H, H-5), 3.95 (ddd = dt, *J* = 11.2, 5.6, Hz, 1 H, OCHHCH<sub>2</sub>Cl), 3.77 (ddd = dt, *J* = 11.2, 5.3, 3.4 Hz, 1 H, OCHHCH<sub>2</sub>Cl), 3.47 (dd, *J* = 5.6, 5.3, 2 H, OCH<sub>2</sub>CH<sub>2</sub>Cl), 2.19 (s, 3 H, (O)CCH<sub>3</sub>); 2.11 (s, 3 H, (O)CCH<sub>3</sub>); 2.02 (s, 3 H, HN(O)CCH<sub>3</sub>), 1.17 (d, *J* = 6.6 Hz, 3 H, H-6); ESI-MS: 377.14 (M(<sup>37</sup>Cl) + Na)<sup>+</sup>, 375.16 (M(<sup>35</sup>Cl) + Na)<sup>+</sup>, 273.17 (M – OCH<sub>2</sub>CH<sub>2</sub>Cl)<sup>+</sup>.

**2'-Azidoethyl 2,3,4-Tri-*O*-acetyl- $\alpha$ -L-fucopyranoside (10).** A suspension of the 2-chloroethyl glycoside **9** (459.0 mg, 1.30 mmol), NaI (193.6 mg, 13.00 mmol), and sodium azide (845.1 mg, 13.00 mmol) in *N,N*-dimethylformamide (6 mL) was stirred at 80 °C for 18 h. The *N,N*-dimethylformamide was evaporated at a reduced pressure, and the residue was partitioned between dichloromethane (150 mL) and water (30 mL). The organic layer was separated, washed with brine (3  $\times$  30 mL), dried over sodium sulfate, filtered, and evaporated. The residue was purified by flash column chromatography on silica gel using dichloromethane–EtOAc (9:1, v/v) as the eluent to give the per-*O*-acetylated 2-azidoethyl glycoside **10** (454.5 mg, 98%); *R*<sub>f</sub> = 0.64 (CH<sub>2</sub>Cl<sub>2</sub>–EtOAc 9:1); <sup>1</sup>H NMR (300 MHz, CDCl<sub>3</sub>/TMS):  $\delta$  5.38 (dd, *J* = 10.0, 3.3 Hz, 1 H, H-3), 5.33 (d, *J* = 3.3 Hz, 1 H, H-4), 5.13 (dd, *J* = 10.0, 3.7 Hz, 1 H, H-2), 5.12 (d, *J* = 3.7 Hz, 1 H, H-1), 4.19 (q, *J* = 6.6 Hz, 1 H, H-5), 3.87 (ddd, *J* = 10.5, 6.1, 3.2 Hz, 1 H, OCHHCH<sub>2</sub>N<sub>3</sub>), 3.62 (ddd, *J* = 10.5, 6.8, 3.4 Hz, 1 H, OCHHCH<sub>2</sub>N<sub>3</sub>), 3.47 (ddd, *J* = 13.2, 6.8, 3.2, 1 H, OCH<sub>2</sub>CHHN<sub>3</sub>), 3.38 (ddd, *J* = 13.2, 6.1, 3.4, 1 H, OCH<sub>2</sub>CHHN<sub>3</sub>), 2.18 (s, 3 H, (O)CCH<sub>3</sub>); 2.09 (s, 3 H, (O)CCH<sub>3</sub>); 2.00 (s, 3 H, HN(O)CCH<sub>3</sub>), 1.16 (d, *J* = 6.6 Hz, 3 H, H-6); ESI-MS: 382.18 (M + Na)<sup>+</sup>, 273.17 (M – OCH<sub>2</sub>CH<sub>2</sub>Cl)<sup>+</sup>.

**2'-Azidoethyl  $\alpha$ -L-Fucopyranoside (11).** The per-*O*-acetylated glycoside **10** (408.0 mg, 1.14 mmol) was treated with catalytic amount of MeONa in MeOH (10 mL) for 30 min, and then the reaction was neutralized with Dowex 50W(H<sup>+</sup>). The resin was removed by filtration and the filtrate was evaporated to give the 2-azidoethyl fucoside **11** (251.7 mg, 95%); *R*<sub>f</sub> = 0.34 (CH<sub>2</sub>Cl<sub>2</sub>–MeOH 90:10); <sup>1</sup>H NMR (300 MHz, D<sub>2</sub>O):  $\delta$  4.89 (d, *J* = 3.7 Hz, 1 H, H-1), 4.09 (m, 1 H, H-5), 3.92–3.38 (m, 7 H, H-2, H-3, H-4, OCH<sub>2</sub>CH<sub>2</sub>NH<sub>2</sub>), 1.20 (d, *J* = 6.4 Hz, 3 H, H-6); <sup>13</sup>C NMR (125 MHz, D<sub>2</sub>O):  $\delta$  98.7 (C-1), 72.0 (C-3), 69.6 (C-5), 68.1 (C-2), 67.0 (C-4), 66.9 (OCH<sub>2</sub>CH<sub>2</sub>N<sub>3</sub>), 50.6 (OCH<sub>2</sub>CH<sub>2</sub>N<sub>3</sub>), 15.5 (C-6); ESI-MS: 256.24 (M + Na)<sup>+</sup>.

**2'-Aminoethyl Glycosides. General Procedures for Hydrogenation of 2'-Azidoethyl Glycosides.** A solution of the respective 2'-azidoethyl  $\beta$ -D-galactoside (**1**) (2f),  $\alpha$ -D-mannoside (**3**) (2f),  $\beta$ -D-glucoside (**5**) (2f), 2-acetamido-2-deoxy- $\alpha$ -D-galactoside (**7**) (2f), or  $\alpha$ -L-fucoside (**11**) (1 mmol), in methanol (10 mL) containing Pd–C (30.0 mg), was stirred at room temperature under hydrogen atmosphere for 12–18 h until the disappearance of the starting material (TLC). The mixture was filtered through a pad of Celite. The solid was washed with methanol (2  $\times$  2 mL), and the combined filtrates were evaporated at a reduced pressure to give the

corresponding 2-aminoethyl glycosides **2**, **4**, **6**, **8**, and **12**, respectively.

**2'-Aminoethyl  $\beta$ -D-Galactopyranoside (2).** Yield: 100%;  $^1\text{H}$  NMR (300 MHz,  $\text{D}_2\text{O}$ ):  $\delta$  4.38 (d,  $J = 7.8$  Hz, 1 H, H-1), 3.97–3.90 (m, 1 H,  $\text{OCHHCH}_2\text{NH}_2$ ), 3.89 (d,  $J = 3.2$  Hz, 1 H, H-4), 3.80–3.64 (m, 4 H, H-5, H-6, H-6',  $\text{OCHHCH}_2\text{NH}_2$ ), 3.63 (dd,  $J = 9.8$ , 3.2 Hz, 1 H, H-3), 3.50 (dd,  $J = 9.8$ , 7.8 Hz, 1 H, H-2), 2.94–2.76 (m, 2 H,  $\text{OCH}_2\text{CH}_2\text{NH}_2$ );  $^{13}\text{C}$  NMR (125 MHz,  $\text{D}_2\text{O}$ ):  $\delta$  103.3 (C-1), 75.5 (C-3), 73.0 (C-5), 71.1 (C-2), 71.2 ( $\text{OCH}_2\text{CH}_2\text{NH}_2$ ), 68.9 (C-4), 61.3 (C-6), 40.4 ( $\text{OCH}_2\text{CH}_2\text{NH}_2$ ); ESI-MS: 246.24 ( $\text{M} + \text{Na}$ ) $^+$ , 224.24 ( $\text{M} + \text{H}$ ) $^+$ .

**2'-Amidoethyl  $\alpha$ -D-Manopyranoside (4).** Yield: 100%;  $^1\text{H}$  NMR (300 MHz,  $\text{D}_2\text{O}$ ):  $\delta$  4.88 (d,  $J = 1.6$  Hz, 1 H, H-1), 4.00–3.50 (m, 8 H, H-2, H-3, H-4, H-5, H-6, H-6',  $\text{OCH}_2\text{CH}_2\text{NH}_2$ ), 2.94–2.76 (m, 2 H,  $\text{OCH}_2\text{CH}_2\text{NH}_2$ );  $^{13}\text{C}$  NMR (125 MHz,  $\text{D}_2\text{O}$ ):  $\delta$  100.1 (C-1), 72.9 (C-4), 70.7 (C-3), 70.2 (C-2), 68.7 ( $\text{OCH}_2\text{CH}_2\text{NH}_2$ ), 67.0 (C-5), 61.1 (C-6), 40.1 ( $\text{OCH}_2\text{CH}_2\text{NH}_2$ ); ESI-MS: 246.17 ( $\text{M} + \text{Na}$ ) $^+$ , 224.12 ( $\text{M} + \text{H}$ ) $^+$ .

**2'-Aminoethyl  $\beta$ -D-Glucopyranoside (6).** Yield: 100%;  $^1\text{H}$  NMR (300 MHz,  $\text{D}_2\text{O}$ ):  $\delta$  4.43 (d,  $J = 7.8$  Hz, 1 H, H-1), 3.95–3.85 (m, 2 H, H-6,  $\text{OCHHCH}_2\text{NH}_2$ ), 3.74–3.64 (m, 2 H, H-6',  $\text{OCHHCH}_2\text{NH}_2$ ), 3.50–3.30 (m, 3 H, H-3, H-4, H-5), 3.24 (dd,  $J = 9.1$ , 7.8 Hz, 1 H, H-2), 2.94–2.76 (m, 2 H,  $\text{OCH}_2\text{CH}_2\text{NH}_2$ );  $^{13}\text{C}$  NMR (125 MHz,  $\text{D}_2\text{O}$ ):  $\delta$  102.5 (C-1), 76.1 (C-3), 75.8 (C-5), 73.3 (C-2), 70.6 ( $\text{OCH}_2\text{CH}_2\text{NH}_2$ ), 69.8 (C-4), 60.9 (C-6), 40.2 ( $\text{OCH}_2\text{CH}_2\text{NH}_2$ ); ESI-MS: 246.14 ( $\text{M} + \text{Na}$ ) $^+$ , 224.15 ( $\text{M} + \text{H}$ ) $^+$ .

**2'-Aminoethyl 2-Acetylamino-2-deoxy- $\alpha$ -D-galactopyranoside (8).** Yield: 100%;  $^1\text{H}$  NMR (300 MHz,  $\text{D}_2\text{O}$ ):  $\delta$  4.87 (d,  $J = 3.7$  Hz, 1 H, H-1), 4.15 (dd,  $J = 11.0$ , 3.7 Hz, 1 H, H-2), 3.96 (d,  $J = 3.2$  Hz, 1 H, H-4), 3.93 (t,  $J = 6.1$  Hz, 1 H, H-5), 3.91 (dd,  $J = 11.0$ , 3.2 Hz, 1 H, H-3), 3.80–3.69 (m, 3 H, H-6, H-6',  $\text{OCHHCH}_2\text{NH}_2$ ), 3.46 (ddd,  $J = 10.5$ , 5.9, 4.6 Hz, 1 H,  $\text{OCHHCH}_2\text{NH}_2$ ), 2.92–2.76 (m, 2 H,  $\text{OCH}_2\text{CH}_2\text{NH}_2$ ), 2.02 (s, 3 H,  $\text{HN}(\text{O})\text{CCH}_3$ );  $^{13}\text{C}$  NMR (125 MHz,  $\text{D}_2\text{O}$ ):  $\delta$  174.9 ( $\text{COCH}_3$ ), 97.5 (C-1), 71.2 (C-3), 68.7 (C-5), 68.1 ( $\text{OCH}_2\text{CH}_2\text{NH}_2$ ), 67.9 (C-4), 61.5 (C-6), 50.0 (C-2), 40.0 ( $\text{OCH}_2\text{CH}_2\text{NH}_2$ ), 22.1 ( $\text{COCH}_3$ ); ESI-MS: 287.30 ( $\text{M} + \text{Na}$ ) $^+$ , 265.31 ( $\text{M} + \text{H}$ ) $^+$ , 247.23 ( $\text{M} - \text{NH}_3$ ) $^+$ , 204.14 ( $\text{M} - \text{OCH}_2\text{CH}_2\text{NH}_2$ ) $^+$ .

**2'-Aminoethyl  $\alpha$ -L-Fucopyranoside (12).** Yield: 100%;  $^1\text{H}$  NMR (300 MHz,  $\text{D}_2\text{O}$ ):  $\delta$  4.86 (d,  $J = 4.1$  Hz, 1 H, H-1), 4.06 (m, 1 H, H-5), 3.86 (dd,  $J = 10.3$ , 3.3 Hz, 1 H, H-3), 3.83–3.67 (m, 3 H, H-2, H-4,  $\text{OCHHCH}_2\text{NH}_2$ ), 3.5–3.43 (m, 1 H,  $\text{OCHHCH}_2\text{NH}_2$ ), 2.92–2.75 (m, 2 H,  $\text{OCH}_2\text{CH}_2\text{NH}_2$ ), 1.19 (d,  $J = 6.6$  Hz, 3 H, H-6);  $^{13}\text{C}$  NMR (125 MHz,  $\text{D}_2\text{O}$ ):  $\delta$  98.6 (C-1), 72.0 (C-3), 69.7 (C-5), 69.0 ( $\text{OCH}_2\text{CH}_2\text{NH}_2$ ), 68.2 (C-2), 66.8 (C-4), 40.2 ( $\text{OCH}_2\text{CH}_2\text{NH}_2$ ), 15.5 (C-6); ESI-MS: 230.09 ( $\text{M} + \text{Na}$ ) $^+$ , 208.11 ( $\text{M} + \text{H}$ ) $^+$ .

**6'-Maleimidohexanamidoethyl Glycosides. General Procedures for the Introduction of Maleimide Functionality into the 2-Aminoethyl Glycosides.** To a stirred solution of the 2-aminoethyl glycoside (1 mmol) in MeOH (10 mL) was added a solution of 6-maleimidoheptanoic acid *N*-hydroxysuccinimide ester (1.5 mmol) in MeOH (5 mL). The reaction mixture was stirred at room temperature for 1–2 h, when TLC showed the disappearance of the starting 2-aminoethyl glycosides. The reaction mixture was concentrated to dryness. The residue was subject to flash column chromatography on silica gel using  $\text{CH}_2\text{Cl}_2$ –MeOH (4:1 to 1:1) as the eluent to give the corresponding 6-maleimidohexanamidoethyl glycosides.

**6'-Maleimidohexanamidoethyl  $\beta$ -D-Galactopyranoside (13).** Yield: 67%;  $R_f = 0.37$  ( $\text{CH}_2\text{Cl}_2$ –MeOH 80:20);  $^1\text{H}$  NMR (300 MHz,  $\text{D}_2\text{O}$ ):  $\delta$  6.82 (s, 2 H,  $\text{CH}=\text{CH}$ ),

4.38 (d,  $J = 7.8$  Hz, 1 H, H-1), 3.99–3.91 (m, 1H,  $\text{OCHHCH}_2\text{NH}$ ), 3.90 (d,  $J = 3.2$  Hz, 1 H, H-4), 3.81–3.61 (m, 4 H, H-5, H-6, H-6',  $\text{OCHHCH}_2\text{NH}$ ), 3.64 (dd,  $J = 10.1$ , 3.2 Hz, 1 H, H-3), 3.51 (dd,  $J = 10.1$ , 7.8 Hz, 1 H, H-2), 3.49 (t,  $J = 6.8$  Hz, 2 H,  $\text{CH}_2\text{CH}_2\text{CH}_2\text{CH}_2\text{CH}_2\text{N}$ ), 3.47–3.32 (m, 2 H,  $\text{OCH}_2\text{CH}_2\text{NH}$ ), 2.23 (t,  $J = 7.3$  Hz, 2 H,  $\text{CH}_2\text{CH}_2\text{CH}_2\text{CH}_2\text{CH}_2\text{N}$ ), 1.64–1.51 (m, 4 H,  $\text{CH}_2\text{CH}_2\text{CH}_2\text{CH}_2\text{CH}_2\text{N}$ ), 1.31–1.19 (m, 2 H,  $\text{CH}_2\text{CH}_2\text{CH}_2\text{CH}_2\text{CH}_2\text{N}$ ); ESI-MS: 439.49 ( $\text{M} + \text{Na}$ ) $^+$ , 417.49 ( $\text{M} + \text{H}$ ) $^+$ .

**6'-Maleimidohexanamidoethyl  $\alpha$ -D-Manopyranoside (14).** Yield 65%;  $R_f = 0.32$  ( $\text{CH}_2\text{Cl}_2$ –MeOH 80:20);  $^1\text{H}$  NMR (300 MHz,  $\text{D}_2\text{O}$ ):  $\delta$  6.90 (s, 2 H,  $-\text{CH}=\text{CH}-$ ), 4.84 (d,  $J = 1.6$  Hz, 1 H, H-1), 3.90 (dd,  $J = 3.2$ , 1.7 Hz, 1 H, H-2), 3.84 (dd,  $J = 12.5$ , 1.7 Hz, 1 H, H-6), 3.80–3.351 (m, 6 H, H-3, H-4, H-5, H-6',  $\text{OCH}_2\text{CH}_2\text{NH}$ ), 3.47 (t,  $J = 6.9$  Hz, 2 H,  $\text{CH}_2\text{CH}_2\text{CH}_2\text{CH}_2\text{CH}_2\text{N}$ ), 3.44–3.31 (m, 2 H,  $\text{OCH}_2\text{CH}_2\text{NH}$ ), 2.21 (t,  $J = 7.3$  Hz, 2 H,  $\text{CH}_2\text{CH}_2\text{CH}_2\text{CH}_2\text{CH}_2\text{N}$ ), 1.64–1.49 (m, 4 H,  $\text{CH}_2\text{CH}_2\text{CH}_2\text{CH}_2\text{CH}_2\text{N}$ ), 1.30–1.18 (m, 2 H,  $\text{CH}_2\text{CH}_2\text{CH}_2\text{CH}_2\text{CH}_2\text{N}$ ); ESI-MS: 439.36 ( $\text{M} + \text{Na}$ ) $^+$ , 417.37 ( $\text{M} + \text{H}$ ) $^+$ .

**6'-Maleimidohexanamidoethyl  $\beta$ -D-Glucopyranoside (15).** Yield 70%;  $R_f = 0.40$  ( $\text{CH}_2\text{Cl}_2$ –MeOH 80:20);  $^1\text{H}$  NMR (300 MHz,  $\text{D}_2\text{O}$ ):  $\delta$  6.87 (s, 2 H,  $\text{CH}=\text{CH}$ ), 4.44 (d,  $J = 8.2$  Hz, 1 H, H-1), 3.97–3.89 (m, 1H,  $\text{OCHHCH}_2\text{NH}$ ), 3.89 (dd,  $J = 12.2$ , 5.7 Hz, 1 H, H-6'), 3.77–3.69 (m, 1 H,  $\text{OCHHCH}_2\text{NH}$ ), 3.68 (dd,  $J = 12.2$ , 2.4 Hz, 1 H, H-6), 3.52–3.31 (m, 7 H, H-3, H-4, H-5,  $\text{CH}_2\text{CH}_2\text{CH}_2\text{CH}_2\text{CH}_2\text{N}$ ,  $\text{OCH}_2\text{CH}_2\text{NH}$ ), 3.54 (dd,  $J = 8.8$ , 8.2 Hz, 1 H, H-2), 2.22 (t,  $J = 7.3$  Hz, 2 H,  $\text{CH}_2\text{CH}_2\text{CH}_2\text{CH}_2\text{CH}_2\text{N}$ ), 1.63–1.49 (m, 4 H,  $\text{CH}_2\text{CH}_2\text{CH}_2\text{CH}_2\text{CH}_2\text{N}$ ), 1.30–1.19 (m, 2 H,  $\text{CH}_2\text{CH}_2\text{CH}_2\text{CH}_2\text{CH}_2\text{N}$ ); ESI-MS: 439.28 ( $\text{M} + \text{Na}$ ) $^+$ , 417.29 ( $\text{M} + \text{H}$ ) $^+$ .

**6'-Maleimidohexanamidoethyl 2-Acetylamino-2-deoxy- $\alpha$ -D-galactopyranoside (16).** Yield: 61%;  $R_f = 0.26$  ( $\text{CH}_2\text{Cl}_2$ –MeOH 85:15);  $^1\text{H}$  NMR (300 MHz,  $\text{D}_2\text{O}$ ):  $\delta$  6.81 (s, 2 H,  $\text{CH}=\text{CH}$ ), 4.85 (d,  $J = 3.4$  Hz, 1 H, H-1), 4.15 (dd,  $J = 11.0$ , 3.4 Hz, 1 H, H-2), 3.95 (d,  $J = 3.2$  Hz, 1 H, H-4), 3.88 (t,  $J = 5.7$  Hz, 1 H, H-5), 3.84 (dd,  $J = 11.0$ , 3.2 Hz, 1 H, H-3), 3.78–3.69 (m, 3 H, H-6, H-6',  $\text{OCHHCH}_2\text{NH}$ ), 3.55–3.45 (m, 2 H,  $\text{OCHHCH}_2\text{NH}$ ), 3.47 (t,  $J = 6.8$  Hz, 2 H,  $\text{CH}_2\text{CH}_2\text{CH}_2\text{CH}_2\text{CH}_2\text{N}$ ), 3.35–3.24 (m, 1 H,  $\text{OCH}_2\text{CH}_2\text{NH}$ ), 2.22 (t,  $J = 7.3$  Hz, 2 H,  $\text{CH}_2\text{CH}_2\text{CH}_2\text{CH}_2\text{CH}_2\text{N}$ ), 2.02 (s, 3 H,  $\text{NH}(\text{O})\text{CCH}_3$ ), 1.63–1.49 (m, 4 H,  $\text{CH}_2\text{CH}_2\text{CH}_2\text{CH}_2\text{CH}_2\text{N}$ ), 1.30–1.18 (m, 2 H,  $\text{CH}_2\text{CH}_2\text{CH}_2\text{CH}_2\text{CH}_2\text{N}$ ); ESI-MS: 480.42 ( $\text{M} + \text{Na}$ ) $^+$ , 458.49 ( $\text{M} + \text{H}$ ) $^+$ .

**6'-Maleimidohexanamidoethyl  $\alpha$ -L-Fucopyranoside (17).** Yield: 55%;  $R_f = 0.72$  ( $\text{CH}_2\text{Cl}_2$ –MeOH 80:20);  $^1\text{H}$  NMR (300 MHz,  $\text{D}_2\text{O}$ ):  $\delta$  6.82 (s, 2 H,  $-\text{CH}=\text{CH}-$ ), 4.84 (d,  $J = 3.7$  Hz, 1 H, H-1), 3.99 (m, 1 H, H-5), 3.81 (dd,  $J = 10.1$ , 3.1 Hz, 1 H, H-3), 3.78–3.67 (m, 3 H, H-2, H-4,  $\text{OCHHCH}_2\text{NH}$ ), 3.55–3.47 (m, 1 H,  $\text{OCHHCH}_2\text{NH}$ ), 3.47 (t,  $J = 7.1$  Hz, 2 H,  $\text{CH}_2\text{CH}_2\text{CH}_2\text{CH}_2\text{CH}_2\text{N}$ ), 3.47–3.38 (m, 1 H,  $\text{OCH}_2\text{CH}_2\text{NH}$ ), 3.38–3.30 (m, 1 H,  $\text{OCH}_2\text{CH}_2\text{NH}$ ), 2.21 (t,  $J = 7.3$  Hz, 2 H,  $\text{CH}_2\text{CH}_2\text{CH}_2\text{CH}_2\text{CH}_2\text{N}$ ), 1.63–1.49 (m, 4 H,  $\text{CH}_2\text{CH}_2\text{CH}_2\text{CH}_2\text{CH}_2\text{N}$ ), 1.30–1.19 (m, 2 H,  $\text{CH}_2\text{CH}_2\text{CH}_2\text{CH}_2\text{CH}_2\text{N}$ ), 1.18 (d,  $J = 6.6$  Hz, 3 H, H-6); ESI-MS: 423.43 ( $\text{M} + \text{Na}$ ) $^+$ , 401.38 ( $\text{M} + \text{H}$ ) $^+$ .

***N*-(6'-Maleimidohexacarbonyl) Man<sub>9</sub>GlcNAc<sub>2</sub>Asn (19).** To a solution of Man<sub>9</sub>GlcNAc<sub>2</sub>Asn **18** (**23**) (2.25 mg, 1.13  $\mu\text{mol}$ ) in phosphate buffer (pH 7.4, 50 mM) and acetonitrile (2:1, v/v, 1.5 mL) was added a solution of 6-maleimidoheptanoic acid *N*-hydroxysuccinimide ester (3.47 mg, 11.26  $\mu\text{mol}$ ) in acetonitrile (0.5 mL). The reaction mixture was stirred at room temperature for 2 h and then lyophilized to dryness. The residue was purified on reverse-phase preparative HPLC to yield the maleimide-activated product **19** (1.68 mg, 68%). The



purified **19** appeared at 10.48 min as a single peak under the HPLC condition with a linear gradient (method A) as described in General Methods. ESI-MS: 2192.17 ( $M + H$ )<sup>+</sup>, 1118.60 ( $M + 2Na$ )<sup>2+</sup>, 1096.72 ( $M + 2H$ )<sup>2+</sup>, 1015.60 ( $M - Man + 2H$ )<sup>2+</sup>, 934.41 ( $M - 2Man + 2H$ )<sup>2+</sup>, 853.35 ( $M - 3Man + 2H$ )<sup>2+</sup>, 772.28 ( $M - 4Man + 2H$ )<sup>2+</sup>, 691.21 ( $M - 5Man + 2H$ )<sup>2+</sup>, 610.06 ( $M - 6Man + 2H$ )<sup>2+</sup>.

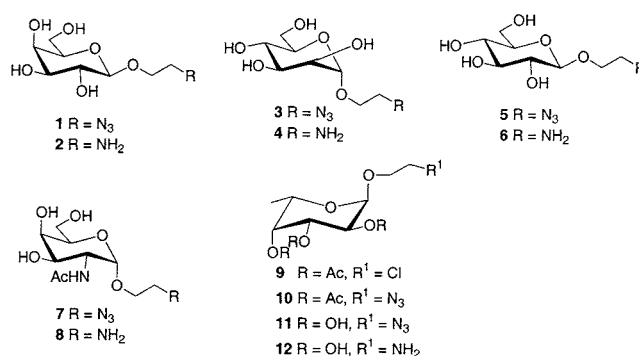
**The Cysteine-Containing Peptide 20.** Peptide **20** was synthesized on a Pioneer Peptide Synthesizer (Applied Biosystems, Foster City, CA) using standard Fmoc-chemistry on Fmoc-PAL-PEG-PS resin, according to the reported method (17). Briefly, 4-fold excess of *N*<sup>t</sup>-Fmoc-protected amino acids were used for each coupling and HATU/DIPEA were used as the coupling reagents. The N-terminus of the peptide was capped with an acetyl group, and the C-terminus is in the amide form after release from the resin and simultaneous deprotection. The peptide was purified with HPLC and characterized by ESI-MS. The purified peptide **20** appeared at 15.84 min as a single peak under the HPLC condition with a linear gradient (method B) as described in General Methods. ESI-MS of **20**: 1532.84 ( $M + 3H$ )<sup>3+</sup>, 1149.83 ( $M + 4H$ )<sup>4+</sup>, and 920.12 ( $M + 5H$ )<sup>5+</sup>.

**Glycopeptide 21.** To a solution of peptide **20** (20 mg, 4.35  $\mu$ mol) in phosphate buffer (pH 6.6, 50 mM, 3 mL) and acetonitrile (3.0 mL) was added dropwise a solution of the maleimide-activated mannose **14** (1.21 mg, 2.90  $\mu$ mol) in DMF (242  $\mu$ L). The mixture was kept at room temperature for 1 h and lyophilized. The residue was subject to reverse-phase preparative HPLC to give the glycopeptide **21** (11.6 mg, 80%). The purified glycopeptide **21** appeared at 15.18 min as a single peak under the HPLC condition with a linear gradient (method B) as described in General Methods. ESI-MS of **21**: 1671.50 ( $M + 3H$ )<sup>3+</sup>, 1253.97 ( $M + 4H$ )<sup>4+</sup>, 1213.34 ( $M - Man + 4H$ )<sup>4+</sup>, 1003.64 ( $M + 5H$ )<sup>5+</sup>, 971.08 ( $M - Man + 5H$ )<sup>5+</sup>.

**Glycopeptide 22.** A mixture of peptide **20** (4.33 mg, 0.94  $\mu$ mol) and the maleimide-activated high-mannose oligosaccharide **19** (1.03 mg, 0.47  $\mu$ mol) in a phosphate buffer (pH 6.6, 50 mM, 1.0 mL) and acetonitrile (1.0 mL) was kept at room temperature for 1 h. After the reaction mixture was lyophilized to dryness, the residue was subject to preparative RP-HPLC to give the glycopeptide **22** (2.56 mg, 82%). The purified glycopeptide **22** appeared at 14.43 min as a single peak under the HPLC condition with a linear gradient (Method B) as described in General Methods. ESI-MS of **22**: 2262.96 ( $M + 3H$ )<sup>3+</sup>, 1698.34 ( $M + 4H$ )<sup>4+</sup>, 1657.26 ( $M - Man + 4H$ )<sup>4+</sup>, 1358.62 ( $M + 5H$ )<sup>5+</sup>, 1326.18 ( $M - Man + 5H$ )<sup>5+</sup>, 1293.80 ( $M - 2Man + 5H$ )<sup>5+</sup>, 1261.29 ( $M - 3Man + 5H$ )<sup>5+</sup>, 1229.04 ( $M - 4Man + 5H$ )<sup>5+</sup>, 1196.39 ( $M - 5Man + 5H$ )<sup>5+</sup>, 1164.08 ( $M - 6Man + 5H$ )<sup>5+</sup>, 1131.63 ( $M + 6H$ )<sup>6+</sup>.

## RESULTS AND DISCUSSION

Glycosides and oligosaccharides with a terminal amino group in the aglycon moiety are frequently used in the synthesis of neoglycoconjugates (24). One way to introduce an amino group at later stage of oligosaccharide synthesis is to use an azido group as a latent functionality, which can be easily converted into amino group through reduction (21). Therefore, to introduce maleimide functionality into carbohydrates while preserving the native  $\alpha$ - or  $\beta$ -*O*-glycosidic linkages, we chose 2'-aminoethyl  $\alpha$ - and  $\beta$ -glycosides as the key intermediates. Accordingly, the 2'-azidoethyl  $\beta$ -D-galactopyranoside (**1**),  $\alpha$ -D-mannopyranoside (**3**),  $\beta$ -D-glucopyranoside (**5**), and 2-acetamido-2-deoxy- $\alpha$ -D-galactopyranoside (**7**) were synthesized following the reported procedures (21, 22). To



**Figure 1.** Structures of 2'-azidoethyl and 2'-aminoethyl glycosides.

prepare the corresponding 2'-azidoethyl fucopyranoside (**11**) with an  $\alpha$ -L-glycosidic linkage found in native glycoproteins, L-fucose was refluxed with 2-chloroethanol under acid catalysis to give the 2'-chloroethyl  $\alpha$ -L-fucopyranoside, which was isolated as its per-acetate (**9**) after *O*-acetylation. Treatment of 2'-chloroethyl glycoside (**9**) with NaN<sub>3</sub>/NaI in DMF gave the corresponding 2'-azidoethyl per-*O*-acetylated glycoside (**10**), which was de-*O*-acetylated with MeONa/MeOH to afford the 2'-azidoethyl  $\alpha$ -L-fucopyranoside (**11**) in excellent yield. Catalytic hydrogenation of the 2'-azidoethyl glycosides **1**, **3**, **5**, **7**, and **11** was performed using palladium/charcoal as the catalyst to afford the corresponding 2'-aminoethyl glycosides **2**, **4**, **6**, **8**, and **12** in essentially quantitative yield (Figure 1). With a terminal amino group in the aglycon moiety, a maleimide moiety was readily introduced into the carbohydrates through reaction with an activated ester of maleimide. Thus, treatment of the 2'-aminoethyl glycosides **2**, **4**, **6**, **8**, and **12** with 6-maleimido-hexanoic acid *N*-hydroxysuccinimide ester in MeOH gave the 6-maleimido-hexanamidoethyl glycosides **13–17**, respectively (Table 1).

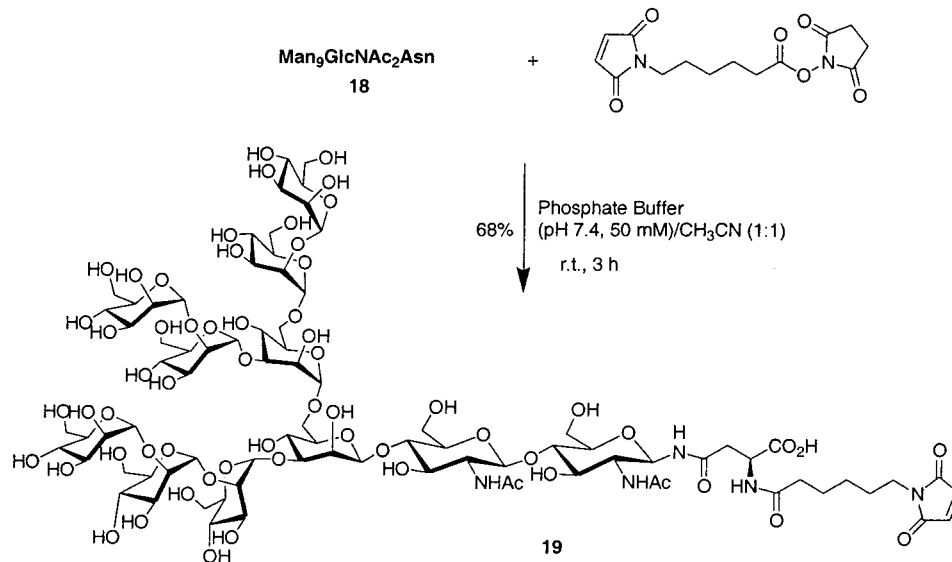
For some native glycopeptides that can be isolated from native glycoproteins to homogeneity via thorough protease digestion, the free amino group in the resulting glycopeptide or glyco-asparagine moiety can be used directly for introducing a maleimide moiety. As an example, a high-mannose type oligosaccharide, Man<sub>9</sub>GlcNAc<sub>2</sub>Asn (**18**), was prepared via thorough Pronase digestion of soybean agglutinin that was isolated from soybean flour according to the literature (23). The released Man<sub>9</sub>GlcNAc<sub>2</sub>Asn (**18**) was purified by HPLC, which is identical to an authentic sample in HPLC. Its identity was further characterized by ESI-MS [1998.73 ( $M + H$ )<sup>+</sup>, 999.69 ( $M + 2H$ )<sup>2+</sup>, and 918.65 ( $M - Man + 2H$ )<sup>2+</sup>, 837.68 ( $M - 2Man + 2H$ )<sup>2+</sup>, 756.70 ( $M - 3Man + 2H$ )<sup>2+</sup>, 675.52 ( $M - 4Man + 2H$ )<sup>2+</sup>, 594.61 ( $M - 5Man + 2H$ )<sup>2+</sup>]. Introduction of a maleimide moiety was achieved by treatment of Man<sub>9</sub>GlcNAc<sub>2</sub>Asn (**18**) with excess of the activated ester of 6-maleimido-hexanoic acid in an aqueous organic solvent (Scheme 1). After reverse-phase HPLC purification, the resulting maleimide-activated oligosaccharide (**19**) was isolated in 68% yield. The ESI-MS of **19**, showing typical ionic species at 2192.17 ( $M + H$ )<sup>+</sup>, 1118.60 ( $M + 2Na$ )<sup>2+</sup>, 1096.72 ( $M + 2H$ )<sup>2+</sup>, 1015.60 ( $M - Man + 2H$ )<sup>2+</sup>, 934.41 ( $M - 2Man + 2H$ )<sup>2+</sup>, 853.35 ( $M - 3Man + 2H$ )<sup>2+</sup>, 772.28 ( $M - 4Man + 2H$ )<sup>2+</sup>, 691.21 ( $M - 5Man + 2H$ )<sup>2+</sup>, 610.06 ( $M - 6Man + 2H$ )<sup>2+</sup>, is in good agreement with its structure. The procedure should be readily extendable to other native high-mannose type as well as complex type glyco-asparagine/glycopeptides, when their isolation from native glycoproteins is achievable (25, 26).



**Table 1.** Synthesis of Maleimide-Activated Carbohydrates<sup>a</sup>

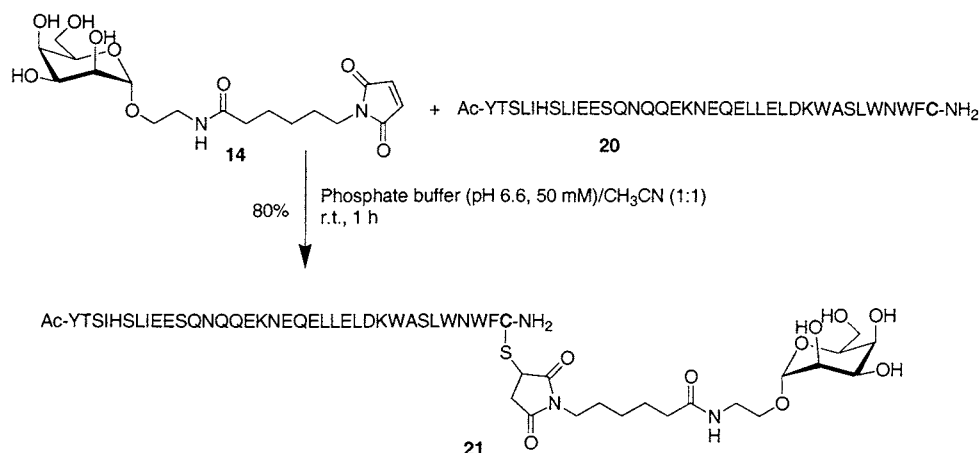
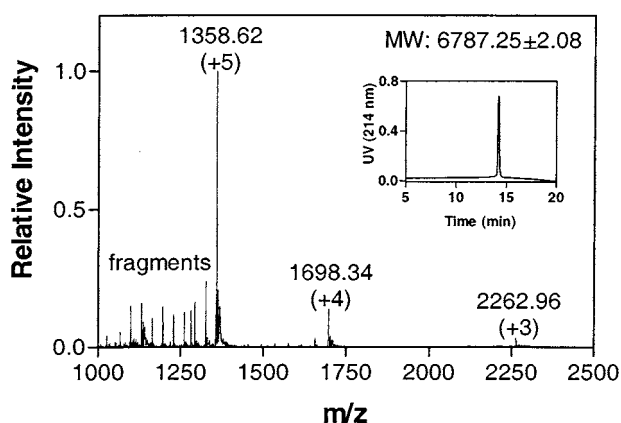
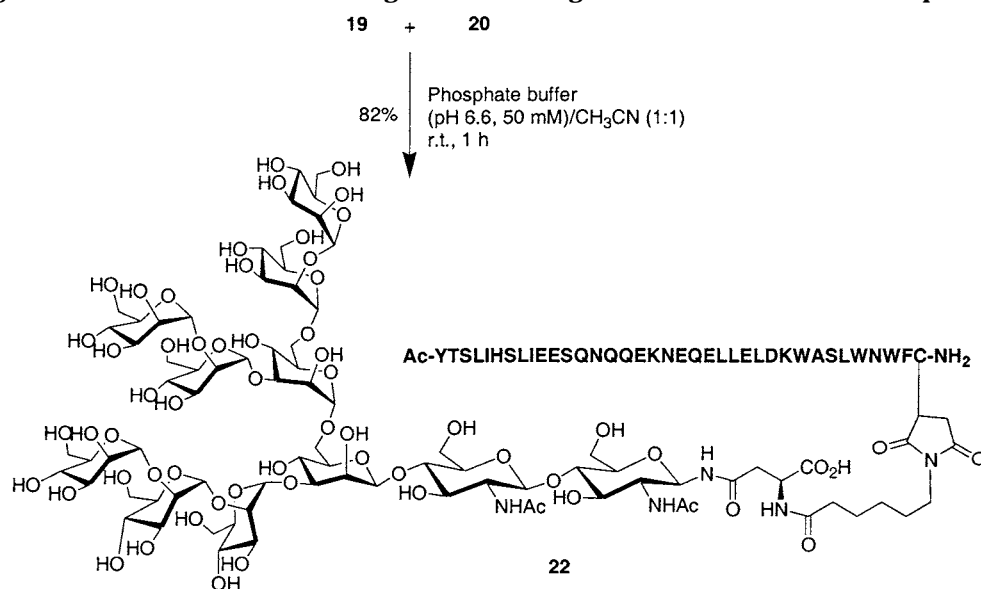
	2'-Aminoethyl glycosides	Products	Yields
2			67%
4			65%
6			70%
8			61%
12			55%

<sup>a</sup> Reaction conditions: 2'-Aminoethyl glycosides and 6-maleimido-hexanoic acid *N*-hydroxysuccinimide ester (1:1.5 mol equiv), MeOH, rt, 2 h.

**Scheme 1.** Synthesis of Maleimide-Activated High Mannose Oligosaccharide

The application of the maleimide-activated mono- and oligosaccharides were exemplified by the synthesis of two neoglycopeptides. A biologically active HIV-1 gp41 peptide, T20, was chosen as the model peptide. T20 is a 36-mer peptide from the C-terminal ectodomain of HIV-1 glycoprotein gp41. It exhibits strong inhibitory activity against HIV-1 infection, and is currently in clinical trials for the treatment of HIV/AIDS (27, 28). For chemoselective ligation to maleimide-activated carbohydrates, a cysteine residue was introduced at the C-terminus of the peptide T20 during solid-phase synthesis to give the cysteine-containing peptide **20**. The ligation of the maleimide-activated mannose (**14**) and peptide **20** was readily achieved in a phosphate buffer (pH 6.6)

containing acetonitrile (Scheme 2). The neoglycopeptide **21** thus formed was purified by reverse phase HPLC. The ESI-MS of **21** revealed typical ionic species at 1671.50 ( $M + 3H$ )<sup>3+</sup>, 1253.97 ( $M + 4H$ )<sup>4+</sup>, 1213.34 ( $M - \text{Man} + 4H$ )<sup>4+</sup>, 1003.64 ( $M + 5H$ )<sup>5+</sup>, 971.08 ( $M - \text{Man} + 5H$ )<sup>5+</sup>, which confirms the identity of **21**. It should be pointed out that the peptide **20** was found to aggregate in aqueous solution even at a relatively low concentration (50  $\mu\text{M}$  and above), which prevents the ligation and gives unidentified byproducts (data not shown). We found that addition of acetonitrile in the reaction mixture efficiently prevented the aggregation of the peptide and allowed the ligation reaction to proceed smoothly (Scheme 2).

**Scheme 2. Ligation of Maleimide-Activated Mannose **14** and HIV-1 Peptide **20******Scheme 3. Ligation of Maleimide-Activated High-Mannose Oligosaccharide **19** and HIV-1 Peptide **20******Figure 2.** The ESI-MS and HPLC profile of glycopeptide **21**.

Similarly, a high-mannose oligosaccharide was conjugated to the HIV-1 peptide through chemoselective ligation of the maleimide-activated oligosaccharide **19** and peptide **20** to give the neoglycopeptide **22** (Scheme 3). The ligation proceeded rapidly and specifically to give a single product, as monitored by HPLC, even if a large oligosaccharide was involved. The HPLC and ESI-MS profile of **22** was shown in Figure 2. Typical ionic species in the ESI-MS of **22** include 2262.96 ( $M + 3H$ )<sup>3+</sup>, 1698.34 ( $M + 4H$ )<sup>4+</sup>, 1657.26 ( $M - \text{Man} + 4H$ )<sup>4+</sup>, 1358.62 ( $M +$

5H)<sup>5+</sup>, 1326.18 ( $M - \text{Man} + 5H$ )<sup>5+</sup>, 1293.80 ( $M - 2\text{Man} + 5H$ )<sup>5+</sup>, 1261.29 ( $M - 3\text{Man} + 5H$ )<sup>5+</sup>, 1229.04 ( $M - 4\text{Man} + 5H$ )<sup>5+</sup>, 1196.39 ( $M - 5\text{Man} + 5H$ )<sup>5+</sup>, 1164.08 ( $M - 6\text{Man} + 5H$ )<sup>5+</sup>, and 1131.63 ( $M + 6H$ )<sup>6+</sup>. These data are in good agreement with the structure of the neoglycopeptide **22**. The introduction of mannose and/or high-mannose oligosaccharide moiety at the C-terminus of the biologically active HIV-1 peptide should have the potential to target the drug to macrophage and dendritic cells through specific carbohydrate ligand–receptor recognition. Macrophage and dendritic cells are major target cells for HIV-1 infection and express rich mannose- and oligomannose-specific receptors on their surface (29, 30).

In summary, an array of maleimide-activated monosaccharides and a maleimide-tagged, native high-mannose oligosaccharide were synthesized. The application of these maleimide-activated carbohydrates as chemoselective tags for site-specific glycosylation of peptides via the highly efficient maleimide–thiol ligation was exemplified by the site-specific introduction of mannose and oligomannose ligands at the C-terminus of a 36-mer HIV-1 gp41 peptide, which is a potent inhibitor against HIV infection. Tagging the biologically active peptide with a mannose and/or oligomannose moiety will be useful for targeting the drug to macrophage and dendritic cells, which are primary targets for HIV-1 infection and are expressing

mannose- and oligomannose-specific receptors on their surface. In combination with site-specific mutagenesis, the maleimide-activated carbohydrates described can serve as generally applicable tags for site-specific glycosylation of proteins via the highly efficient maleimide-thiol ligation reaction.

#### ACKNOWLEDGMENT

The work was financially supported by the Institute of Human Virology, University of Maryland Biotechnology Institute.

#### LITERATURE CITED

- Varki, A. (1993) Biological roles of oligosaccharides: all of the theories are correct. *Glycobiology* 3, 97–130.
- Dwek, R. A. (1996) Glycobiology: Toward understanding the function of sugars. *Chem. Rev.* 96, 683–720.
- Rudd, P. M., Elliott, T., Cresswell, P., Wilson, I. A., and Dwek, R. A. (2001) Glycosylation and the immune system. *Science* 291, 2370–2376.
- Aplin, J. D., and Wriston, J. C., Jr. (1981) Preparation, properties, and applications of carbohydrate conjugates of proteins and lipids. *CRC Crit. Rev. Biochem.* 10, 259–306.
- Rudd, P. M., Joao, H. C., Coghill, E., Fiten, P., Saunders, M. R., Opdenakker, G., and Dwek, R. A. (1994) Glycoforms modify the dynamic stability and functional activity of an enzyme. *Biochemistry* 33, 17–22.
- Davis, B. G. (2002) Synthesis of glycoproteins. *Chem. Rev.* 102, 579–601.
- Grogan, M. J., Pratt, M. R., Marcaurelle, L. A., and Bertozzi, C. R. (2002) Homogeneous glycopeptides and glycoproteins for biological investigation. *Annu. Rev. Biochem.* 71, 593–634.
- Davis, N. J., and Flitsch, S. L. (1991) A novel method for the specific glycosylation of proteins. *Tetrahedron Lett.* 32, 6793–6796.
- Wong, S. Y., Guile, G. R., Dwek, R. A., and Arsequell, G. (1994) Synthetic glycosylation of proteins using N-(beta-saccharide) iodoacetamides: applications in site-specific glycosylation and solid-phase enzymic oligosaccharide synthesis. *Biochem. J.* 300, 843–850.
- Davis, B. G., Lloyd, R. C., and Jones, J. B. (1998) Controlled site-selective glycosylation of proteins by a combined site-directed mutagenesis and chemical modification approach. *J. Org. Chem.* 63, 9614–9615.
- Davis, B. G., Lloyd, R. C., and Jones, J. B. (2000) Controlled site-selective protein glycosylation for precise glycan structure-catalytic activity relationships. *Bioorg. Med. Chem.* 8, 1527–1535.
- Macmillan, D., Bill, R. M., Sage, K. A., Fern, D., and Flitsch, S. L. (2001) Selective in vitro glycosylation of recombinant proteins: semi-synthesis of novel homogeneous glycoforms of human erythropoietin. *Chem. Biol.* 8, 133–145.
- Rodriguez, E. C., Marcaurelle, L. A., and Bertozzi, C. R. (1998) Aminoxy-, Hydrazide-, and Thiosemicarbazide-Functionalized Saccharides: Versatile Reagents for Glycoconjugate Synthesis. *J. Org. Chem.* 63, 7134–7135.
- Hermanson, G. T. (1996) *Bioconjugate Techniques*, Academic Press, San Diego, CA.
- Elliott, J. T., and Prestwich, G. D. (2000) Maleimide-functionalized lipids that anchor polypeptides to lipid bilayers and membranes. *Bioconjugate Chem.* 11, 832–841.
- Schelte, P., Boeckler, C., Frisch, B., and Schuber, F. (2000) Differential reactivity of maleimide and bromoacetyl functions with thiols: application to the preparation of liposomal diepitope constructs. *Bioconjugate Chem.* 11, 118–123.
- Wang, L. X., Ni, J., and Singh, S. (2003) Carbohydrate-centered maleimide cluster as a new type of templates for multivalent peptide assembling: Synthesis of multivalent HIV-1 gp41 peptides. *Bioorg. Med. Chem.* 11, 129–136.
- Ragupathi, G., Koganty, R. R., Qiu, D., Lloyd, K. O., and Livingston, P. O. (1998) A novel and efficient method for synthetic carbohydrate conjugate vaccine preparation: synthesis of sialyl Tn-KLH conjugate using a 4-(4-N-maleimido-methyl) cyclohexane-1-carboxyl hydrazide (MMCCH) linker arm. *Glycoconjugate J.* 15, 217–221.
- Shin, I., Jung, H. J., and Lee, M. R. (2001) Chemoselective ligation of maleimidosugars to peptides/protein for the preparation of neoglycopeptides/neoglycoprotein. *Tetrahedron Lett.* 42, 1325–1328.
- Lee, Y. C., and Lee, R. T. (1995) Carbohydrate-protein interactions: Basis of glycobiology. *Acc. Chem. Res.* 28, 321–327.
- Ya. Chernyak, A., Sharma, G. V. M., Kononov, L. O., Krishna, P. R., Levinsky, A. B., and Kochetkov, N. K. (1992) 2-azidoethyl glycosides: Glycosides potentially useful for the preparation of neoglycoconjugates. *Carbohydr. Res.* 223, 303–309.
- Roy, R., and Kim, J. M. (1999) Amphiphilic p-tert-butylcalix-(4)arene scaffolds containing exposed carbohydrate dendrons. *Angew. Chem., Int. Ed.* 38, 369–372.
- Lis, H., and Sharon, N. (1978) Soybean agglutinin—a plant glycoprotein. Structure of the carbohydrate unit. *J. Biol. Chem.* 253, 3468–3476.
- Lee, Y. C., and Lee, R. T. (1994) *Neoglycoconjugates: Preparation and Applications*, Academic Press, San Diego, CA.
- Oda, Y., Nakayama, K., Abdul-Rahman, B., Kinoshita, M., Hashimoto, O., Kawasaki, N., Hayakawa, T., Kakehi, K., Tomiya, N., and Lee, Y. C. (2000) Crocus sativus lectin recognizes Man3GlcNAc in the N-glycan core structure. *J. Biol. Chem.* 275, 26772–26779.
- Rice, K. G., and Da Silva, M. L. C. (1996) Preparative purification of tyrosinamide N-linked oligosaccharides. *J. Chromatogr. A* 720, 235–249.
- Wild, C. T., Shugars, D. C., Greenwell, T. K., McDaniel, C. B., and Matthews, T. J. (1994) Peptides corresponding to a predictive alpha-helical domain of human immunodeficiency virus type 1 gp41 are potent inhibitors of virus infection. *Proc. Natl. Acad. Sci. U.S.A.* 91, 9770–9774.
- Kilby, J. M., Hopkins, S., Venetta, T. M., DiMassimo, B., Cloud, G. A., Lee, J. Y., Alldredge, L., Hunter, E., Lambert, D., Bolognesi, D., Matthews, T., Johnson, M. R., Nowak, M. A., Shaw, G. M., and Saag, M. S. (1998) Potent suppression of HIV-1 replication in humans by T-20, a peptide inhibitor of gp41-mediated virus entry. *Nat. Med.* 4, 1302–1307.
- Feinberg, H., Park-Snyder, S., Kolatkar, A. R., Heise, C. T., Taylor, M. E., and Weis, W. I. (2000) Structure of a C-type carbohydrate recognition domain from the macrophage mannose receptor. *J. Biol. Chem.* 275, 21539–21548.
- Feinberg, H., Mitchell, D. A., Drickamer, K., and Weis, W. I. (2001) Structural basis for selective recognition of oligosaccharides by DC-SIGN and DC-SIGNR. *Science* 294, 2163–2166.

BC025617F



# Solid-Phase Synthesis of Multivalent Glycoconjugates on a DNA Synthesizer

Michael Dubber and Jean M. J. Fréchet\*

Department of Chemistry, University of California, Berkeley, California 94720-1460. Received October 9, 2002

Carbohydrate–oligonucleotide conjugates and glycodendrimers were synthesized utilizing a DNA synthesizer. The synthesis of multivalent glycoconjugates on solid-phase allows custom tailoring of their structure to the requirements of biological assays within hours, as opposed to traditional approaches that require weeks or months of work in the laboratory. Therefore it will become much easier to investigate carbohydrate–protein interactions and optimize for objectives such as the receptor-mediated targeting of antisense oligonucleotides.

## INTRODUCTION

Many recognition events in biology are based on multivalent carbohydrate protein interactions (1). Numerous examples from recent years demonstrate that molecules capable of presenting multiple carbohydrates in an appropriate way to viruses, bacteria, and toxins can efficiently target or inhibit them (2). Tremendous inhibition properties have been achieved, when structurally well defined, monodisperse glycoconjugates matched the carbohydrate receptors of bacterial AB5 toxins. These toxins recognize their host cells through the simultaneous interaction of their five carbohydrate-binding proteins with gangliosides on human cell surfaces. Critical information from the X-ray crystallographic structure of AB5 toxins led to the syntheses of pentameric glycoconjugates with optimized spacer lengths that exhibited binding at a level  $10^7$ -fold higher than that for single ligands (3, 4). However, in most cases the exact structure of receptors for biologically active carbohydrates are unknown, making the screening of glycoconjugates with different structures of special interest. Recently, the chemotactic response of *Escherichia coli* to galactose-functionalized oligomers was optimized by tuning the valency of these galactose arrays (5); in another study, the inhibition of influenza viruses by sialic acid-conjugated dendritic polymers with various backbone structures was investigated (6).

Numerous attempts have been made to utilize carbohydrate–protein interactions to enhance the cellular uptake and the targeting of drug delivery vehicles by coating them with carbohydrates ligands (7). Currently, only a few examples are known in which carbohydrate ligands have been used to increase the uptake of antisense oligonucleotides (8). Carbohydrate-coated structures have been used to achieve the receptor-mediated endocytosis of antisense oligonucleotides by either complexation with mannosylated polylysine (9) or chemical ligation to galactosylated polylysine (10). However, a drawback in the synthesis of multivalent glycoconjugates is the complexity of their synthesis and the difficulty of their purification (11). This becomes even more problematic if only biocompatible connections are allowed (12). Recently, the synthesis of oligosaccharides and simple

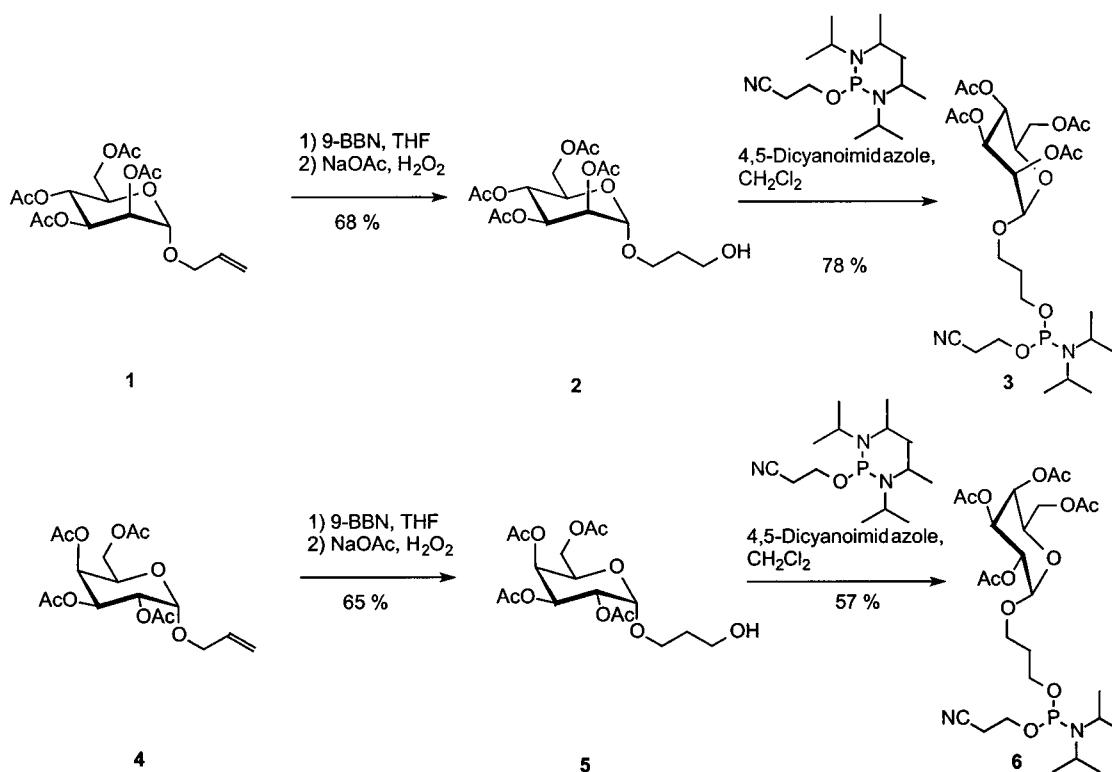
glycoconjugates was facilitated by their automated assembly on solid phase (13). The automated synthesis of multivalent glycoconjugates on solid phase would allow their custom tailoring to the requirements of biological assays within hours, whereas solution phase strategies require weeks or months of work in the laboratory.

In the course of an ongoing antisense project with macrophages in our laboratory, it became of interest to synthesize oligonucleotides with mannosylated dendrons for receptor-mediated endocytosis. Therefore a flexible methodology to attach multivalent carbohydrate structures to oligonucleotides that allows for easy modification of the bouquet of presented carbohydrates was necessary. The most appealing way to synthesize such hybrid molecules involved the use of a consistent type of chemistry enabling the preparation of the hybrid as a whole instead of synthesizing two separate moieties using distinct carbohydrate and nucleic acid methodologies. In previous work a DNA synthesizer has been used to assemble dendritic structures that present multiple DNA strands (14, 15) or dyes (16). Branched phosphoramidites as well as mannose-containing phosphoramidites have been described in the literature for different purposes (17–21). Therefore, it was reasonable to try and complete the whole synthesis of our oligonucleotides with mannosylated glycodendrons on the DNA synthesizer. Herein we demonstrate that a standard DNA synthesizer may be used for the small-scale assembly of a variety of multivalent glycoconjugates with biological relevance, which may or may not contain DNA fragments.

## RESULTS AND DISCUSSION

The DNA synthesizer is an ideal tool for the assembly of complex, multivalent glycoconjugates from versatile components, such as spacer units, branching points, or terminal carbohydrates. Therefore it should be possible to select the combination, number, and arrangement of building blocks to create a variety of structures. Originally, DNA synthesizers were designed to assemble oligonucleotides from cyanoethyl phosphoramidites on solid supports (22). Numerous functional groups have since been introduced in the middle or at the end of the oligonucleotide by adapting the desired functionality into an appropriate phosphoramidite (23). Utilizing this approach, the synthesis of mannose, galactose, and branched functional phosphoramidites is described, followed by the

\* To whom correspondence should be addressed. E-mail: frechet@cchem.berkeley.edu.

**Scheme 1. Synthesis of Carbohydrate Phosphoramidites**

assembly of an oligonucleotide with mannosylated glycodendron and other glycoconjugates.

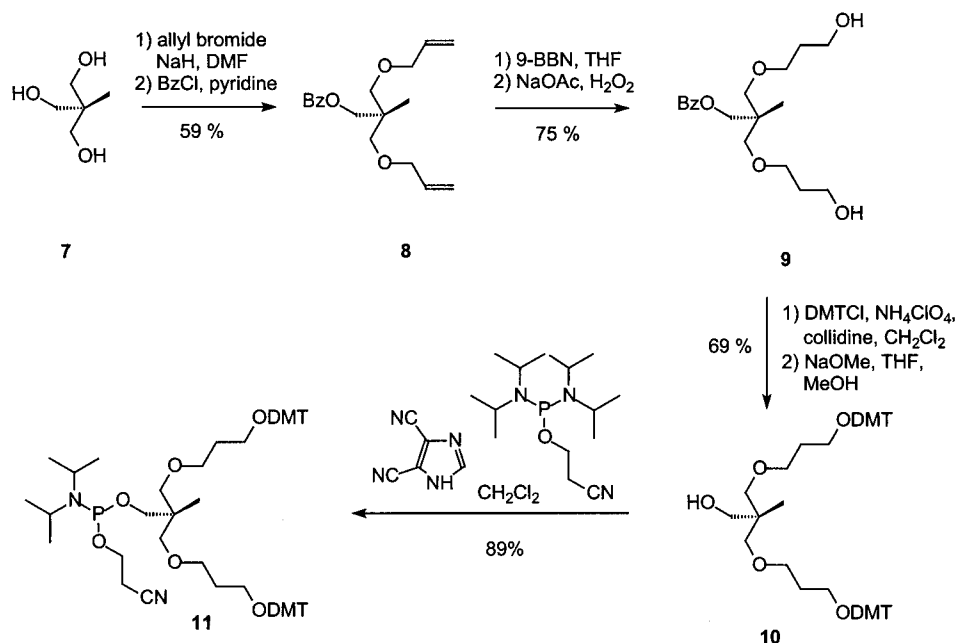
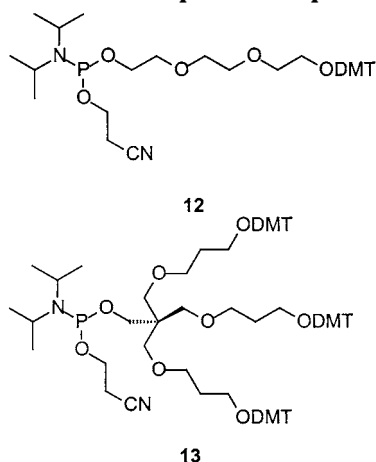
**Phosphoramidite Syntheses.** The mannose- and galactose-derivatized phosphoramidites, **3** and **6**, respectively, were synthesized by hydroboration of the acetylated allyl glycosides, **1** and **4**, and subsequent reaction with 2-cyanoethyl tetraisopropylphosphordiamidite (Scheme 1). The hydroboration was performed with 9-BBN to achieve a stereoselective anti-Markovnikoff addition of the borane (24). Nonbasic conditions were required to retain the four ester protecting groups on the carbohydrate. Therefore, the normal hydroboration workup procedure was replaced with aqueous 3 M NaOAc and 30% H<sub>2</sub>O<sub>2</sub>; less than 1 equiv of 9-BBN was used to avoid base formation by hydrolysis of excess 9-BBN. Best results for the synthesis of phosphoramidites such as **3** and **6** were achieved by a modification of a recently published procedure with 2-cyanoethyl tetraisopropylphosphordiamidite and 4,5-dicyanoimidazole (25). Only 0.1 equiv of 4,5-dicyanoimidazole were used to avoid the formation of side products, in which both diisopropylamino groups reacted with the alcohol donor. Furthermore, the suggested aqueous workup was eliminated, and the reaction products were directly purified with dichloromethane over basic alumina, which was made less polar by increasing the Brokmann factor (26), so that the use of reactive solvents such as methanol could be avoided.

Branched functional phosphoramidite **11** was synthesized by selective extension and protection of two hydroxyl groups of 1,1,1-trihydroxymethylethane and its transformation into a phosphoramidite (Scheme 2). After allylation of two hydroxyl groups of 1,1,1-trihydroxymethylethane, the remaining third hydroxyl group was protected with the UV-active benzoyl group to facilitate reaction monitoring. The bis allyl ether **8** was hydroborated as described earlier with less than 1 equiv of 9-BBN followed by workup with 3 M NaOAc/30% H<sub>2</sub>O<sub>2</sub> to afford the diol **9**. The sterically hindered diol **9** was protected

with 4,4'-dimethoxytrityl chloride (DMTCl) using a procedure with DMTCl, NH<sub>4</sub>ClO<sub>4</sub>, and 2,4,6-trimethylpyridine, thereby generating in situ the active protection reagent 4,4'-dimethoxytrityl perchlorate (27). After debenzoylation with sodium methoxide in a THF/methanol mixture, the resulting alcohol **10** was reacted with 2-cyanoethyl tetraisopropylphosphordiamidite and 4,5-dicyanoimidazole to yield the branched phosphoramidite **11**, which was purified with basic alumina.

Spacer functionalized phosphoramidites and triple branched functional phosphoramidites are required in addition to the phosphoramidites described above to vary the spacer length and multiplicity of the targeted multivalent glycoconjugates. The previously known spacer phosphoramidite **12** and the triply branched phosphoramidite **13** meet these requirements perfectly (Chart 1) (17, 28). Following a synthetic approach different from that previously reported, we synthesized **12** by mono DMT-protection of triethylene glycol and subsequent reaction with 2-cyanoethyl tetraisopropylphosphordiamidite and 4,5-dicyanoimidazole. The triply branched phosphoramidite **13** was synthesized following the procedure for the branched phosphoramidite **11** starting with pentaerythritol triallyl ether instead of 1,1,1-trihydroxymethylethane.

**Assembly of Phosphoramidites.** With the mannose, galactose, spacer, and branched phosphoramidites in hand, all the building blocks for the synthesis of multivalent glycoconjugates on a DNA synthesizer are complete and model compounds can be assembled. Initially, the coupling parameters for each novel phosphoramidite needed to be optimized. Several simple structures were synthesized with different reaction times and flow parameters to optimize the coupling conditions for both the new carbohydrate presenting phosphoramidites and the branched phosphoramidites **3**, **6**, and **11**. The purity of the desired products was monitored by MALDI-TOF MS. It revealed that, when used in the synthesizer, all the functional phosphoramidites we prepared were much

**Scheme 2. Synthesis of Branched Phosphoramidites****Chart 1. Branched and Spacer Phosphoramidites.**

less reactive than the phosphoramidites of the four nucleotides adenosine, guanosine, cytosine, and thymidine, and that a simple increase in the normal reaction time was not sufficient to achieve complete coupling. Instead it was found that best results were obtained when the phosphoramidite-activator mixture was regularly renewed over the solid support every 1 or 2 min over a period of 6 or 18 min, respectively. Details about the use of this procedure on an Expedite 8909 synthesizer can be found in the Supporting Information.

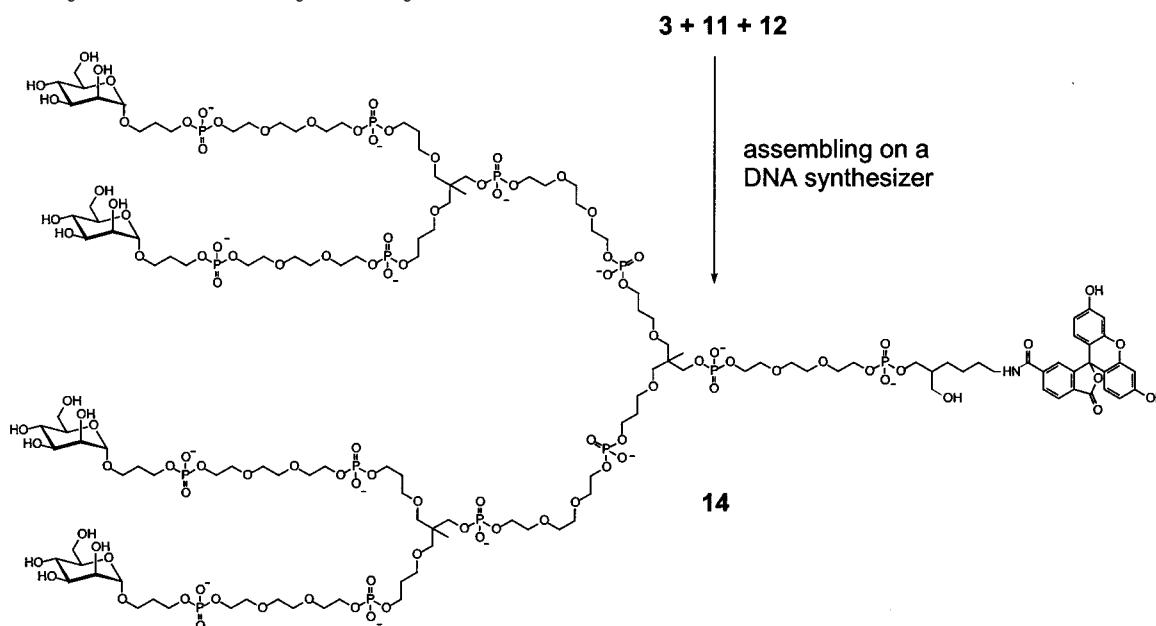
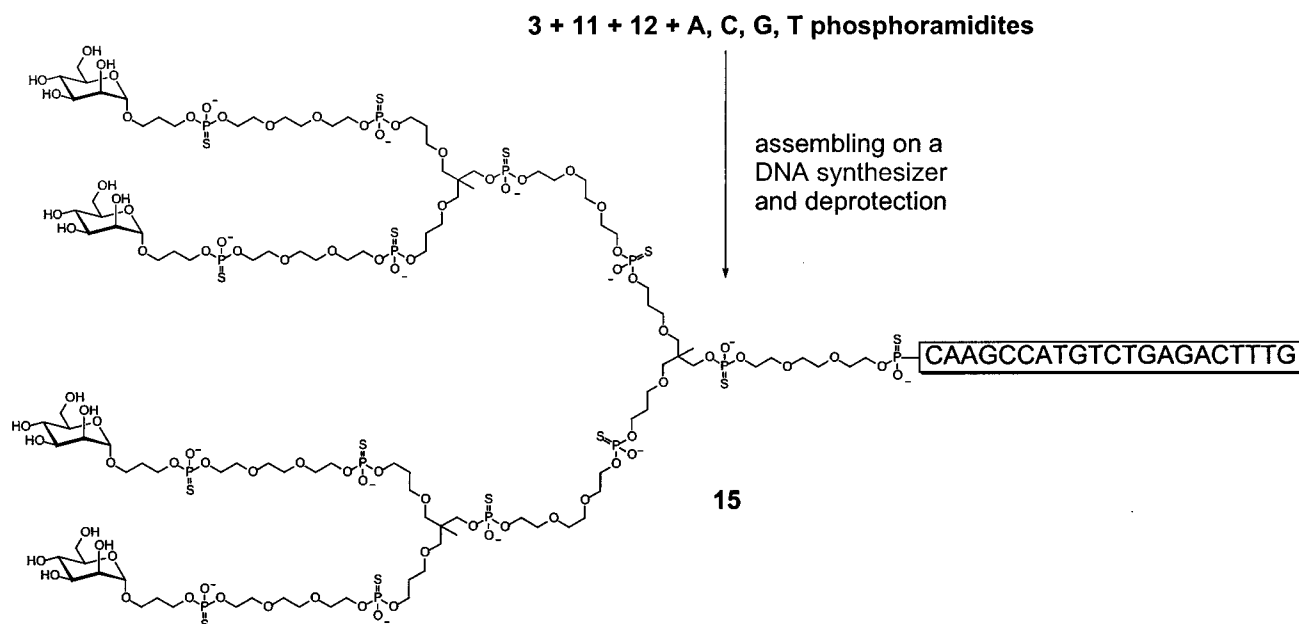
**Assembly of Glycodendrimer 14.** The first glycoconjugates targeted was glycodendrimer **14** (Scheme 3). A solid support tagged with 6-fluorescein was used, to obtain fluorescently tagged glycoconjugates that will facilitate monitoring within biological assays. Since the Applied Biosystems Expedite 8909 synthesizer allows the assignment of letters to certain reagents together with corresponding reaction protocols, the automated synthesis became as simple as entering a "XVWVWV" code into the synthesizer computer. Typically the codes X, W, and V were assigned to reagent bottles with phosphoramidites **3**, **11**, and **12**, respectively, together with their appropriate reaction times and flow parameters. It is possible to cleave glycodendrimer **14** from the solid support and deprotect it under normal oligonucleotide

deprotection conditions, for example with aqueous ammonia, but it is more convenient to use standard carbohydrate deprotection conditions. The only protecting group used, acetate ester, becomes volatile methyl acetate, if sodium methoxide in methanol is used for the deprotection. The glycodendrimer **14** was characterized by  $^1\text{H}$  NMR spectroscopy and MALDI-TOF mass spectroscopy.

**Assembly of Oligonucleotide-Glycodendrion Conjugate 15.** The thioated oligonucleotide (5-CAAGCCATGTCTGAGACTTTG) coded for the antisense inhibition of inducible nitric oxide synthase (**29**) with mannosylated glycodendrion **15** was grown divergently in the same manner as **14** on a standard guanosine-support (Scheme 4). The standard oxidizing reagent iodine, which yields oligonucleotides with phosphate backbone, was replaced by the sulfurization reagent 3*H*-1,2-benzodithiole-3-one 1,1-dioxide to obtain a phosphorothioate backbone that increases the stability against nucleases. The deprotection was done with aqueous ammonia/methylamine 1:1 at 40 °C (**30**). The oligonucleotide-glycodendrion conjugate **15** was purified by an ethanol precipitation and subsequently characterized by MALDI-TOF mass spectroscopy and gel electrophoresis. The sterically bulky glycodendrion causes delayed elution in gel electrophoresis, and **15** behaves like a 38mer though it only has 34 negative charges. The formation of duplexes of **15** with complementary oligonucleotide strands was not hindered, due to the good solubility properties of the glycodendrion. A melting point of 44.2 °C (50 mM NaCl) was measured for the hybridization product of **15** with a complementary DNA strand with two short PEG chains at its 5' end, compared to 44.1 °C (50 mM NaCl) for the unmodified DNA strands.

**Assembly of Cluster Glycoside 16.** Galactosylated cluster glycosides were used in the first example of the exponential affinity enhancement of carbohydrate-protein interactions through multiple contacts by multivalent glycoconjugates, also known as cluster effect (**31**, **32**). Using the galactose phosphoramidite **6**, the triple branched phosphoramidite **13**, and the spacer phosphoramidite **12**, it is easy to use the DNA synthesizer to assemble such cluster glycosides with variable spacer



**Scheme 3. Synthesis of Mannosylated Glycodendrimer 14****Scheme 4. Synthesis of Thioated Antisense Oligonucleotide with Mannosylated Glycodendron 15**

lengths. The negatively charged backbone may increase inhibition potency of antisense-oligonucleotide-glycodendrimer conjugates in some cases (33) and may obstruct structural investigations with the presented cluster glycosides. In such cases it is possible to avoid the negative charges, by using methyl phosphoramidites instead of cyanoethyl phosphoramidites, though in this case the resulting structures will be mixtures of diastereomers with neutral methylphosphonate backbone. The cluster glycoside **16** with phosphate backbone was synthesized as a model compound and characterized by MALDI-TOF and  $^1\text{H}$  NMR (Scheme 5). As was the case for the syntheses of **14** and **15**, this synthesis was carried out on a 1  $\mu\text{mol}$  scale. This scale is normally sufficient to meet the amount of glycoconjugate needed for in vitro biological investigations.

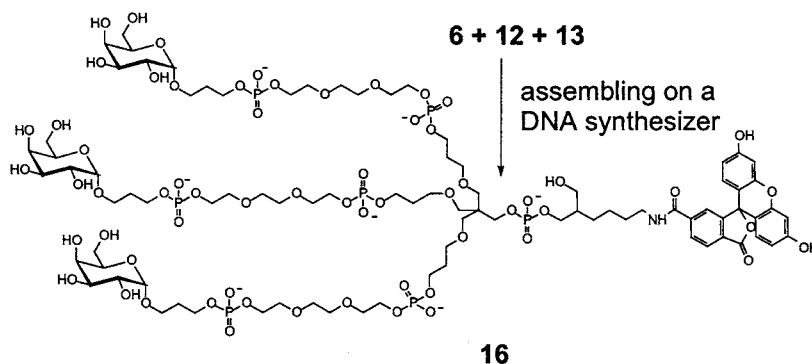
**CONCLUSION**

In conclusion, a methodology for the facile, fast, and efficient synthesis of oligonucleotides with glycodendrons

for receptor-mediated endocytosis was presented. This approach also allowed the synthesis of high molecular-weight, multivalent glycoconjugates, such as glycodendrimers and cluster glycosides. The large glycoconjugates prepared are highly soluble in water and present potential high affinity ligands for carbohydrate binding proteins. The syntheses of multivalent glycoconjugates on a DNA synthesizer allows the custom-tailoring of their structure to meet the requirements of biological assays and affords the desired samples within hours, while normal approaches to the synthesis of multivalent glycoconjugates take weeks or months of work in the laboratory. Therefore, it should be possible to generate biological results much faster and optimize for instance the affinity of antisense oligonucleotides fitted with glycodendrons to their target cells.

**EXPERIMENTAL SECTION**

**General Procedures.** For the preparation of Brockmann type II or III alumina, 3% or 6% water was added

**Scheme 5. Synthesis of Galactosylated Cluster Glycoside 16**

to basic alumina type I, respectively, and the resulting material was agitated for 10 min and equilibrated overnight. Vanillin (2.5 g) in 5%  $\text{H}_2\text{SO}_4$  in ethanol (100 mL) was used as the staining reagent for phosphoramidites. Simple alcohols and unsaturated compounds were stained with basic  $\text{KMnO}_4$ -staining reagent [ $\text{KMnO}_4$ , (3 g),  $\text{K}_2\text{CO}_3$  (20 g) in 300 mL water plus 5% (w/v) aqueous  $\text{NaOH}$  (5 mL)]. Carbohydrate-containing compounds were stained with 5%  $\text{H}_2\text{SO}_4$  in ethanol. Dimethoxytrityl-containing compounds were monitored by UV light 254 nm. MALDI-TOF spectra were measured on a Voyager DE MALDI-TOF mass spectrometer from Perseptive Biosystems using 3-hydroxy picolinic acid (HPA) as a matrix [0.7 M HPA, 0.07 M ammonium citrate dibasic, acetonitrile/water 1:1].  $^1\text{H}$  NMR,  $^{13}\text{C}$  NMR, and  $^{31}\text{P}$  NMR spectra were recorded on Bruker VBAMX-400 or DRX-500 spectrometers. Melting points were measured on a Lambda 35 UV spectrometer from Perkin-Elmer with PTP 6 Peltier unit.

**Oligonucleotide Synthesis.** Assembly of the phosphoramidites was done on an Expedite 8909 synthesizer from Applied Biosystems with 1*H*-tetrazole as activator. All synthesizer reagents and controlled glass pore (CPG) supports were obtained from Glen Research. A 1  $\mu\text{mol}$  500 Å 3-(6-fluorescein)-LCAA-CPG (LCAA: Long Chain Alkylamine) was used for fluorescein-labeling of **14** and **16**, and 1  $\mu\text{mol}$  G-1000 Å-LCAA-CPG support was used for the synthesis of **15**. Optimized long coupling procedures were used for the phosphoramidites **3**, **6**, **11**, **12**, and **13**. A short coupling procedure with 16  $\mu\text{mol}$  0.06 M reagent/1  $\mu\text{mol}$  support in five equal injections over 6 min and a longer coupling procedure with 26  $\mu\text{mol}$  0.06 M reagent/1  $\mu\text{mol}$  support in eight equal injections over 18 min was used for the introduction of the more sterical hindered branched phosphoramidites **11** and **13**, as well as for the extension of branched structures. Both procedures use a larger phosphoramidite excess than normal 6  $\mu\text{mol}$  0.06 M reagent/1  $\mu\text{mol}$  support to achieve a better than 98% coupling yield.

**3-Hydroxypropyl 2,3,4,6-Tetra-*O*-acetyl  $\alpha$ -D-mannopyranoside (**2**).** Allyl 2,3,4,6 tetra-*O*-acetyl  $\alpha$ -D-mannopyranoside (**1**) (1.43 g, 3.68 mmol) was dissolved in dry THF (40 mL). 9-BBN (7 mL, 3.5 mmol) was added, and the solution was stirred for 1 day at room temperature. Ice (5 g) and 3 M  $\text{NaOAc}$  (3.5 mL) were added followed by 30% hydrogen peroxide (3.5 mL) added slowly while stirring at 0 °C in an ice bath. The solution was stirred for 8 h and then quickly saturated with  $\text{K}_2\text{CO}_3$  at 0 °C. The phases were carefully separated and the aqueous phase washed twice with THF. The combined organic layers were filtered, dried over  $\text{MgSO}_4$ , filtered, concentrated, and purified over silica gel with ethyl acetate/cyclohexane 2:1 to yield **2** as white amorphous solid (1.01 g, 68%).  $^1\text{H}$  NMR ( $\text{CDCl}_3$ , 400 MHz):  $\delta$  5.23

(dd,  $J$  3.2 Hz and  $J$  9.9 Hz, 1H), 5.18 (dd $\approx$ t,  $J$  9.5 Hz, 1H), 5.15 (dd,  $J$  1.8 Hz,  $J$  3.1 Hz, 1H), 4.74 (d,  $J$  1.6 Hz, 1H), 4.19 (dd,  $J$  12.3 Hz,  $J$  5.4 Hz, 1H), 4.03 (dd,  $J$  12.1 Hz,  $J$  2.5 Hz, 1H), 3.93 (m, 1H), 3.77 (m, 1H), 3.66 (t,  $J$  6.1 Hz, 2H), 3.50 (m, 1H), 2.07, 2.02, 1.97, 1.91 (each s, each 3H), 1.77 (m, 2H) ppm.  $^{13}\text{C}$  NMR ( $\text{CDCl}_3$ , 400 MHz):  $\delta$  170.8, 170.1, 169.9, 169.8, 97.6, 69.5, 69.1, 68.3, 66.1, 65.1, 62.5, 59.3, 32.0, 20.9, 20.8, 20.7, 20.6 ppm. Anal. Calcd for  $\text{C}_{17}\text{H}_{26}\text{O}_{11}$ : C, 50.24; H, 6.45. Found: C, 49.99; H, 6.49.

**3-(2,3,4,6-Tetra-*O*-acetyl  $\alpha$ -D-mannopyranosyloxy)-propyl (2-Cyanoethyl) (*N,N*-Diisopropyl)phosphoramidite (**3**).** To a solution of **2** (410 mg, 1.01 mmol) in dry dichloromethane were added 2-cyanoethyl tetraisopropylphosphordiamidite (0.45 mL, 1.4 mmol) and 4,5-dicyanoimidazole (12 mg, 0.1 mmol). The reaction mixture was stirred for 2 h and then directly purified by column chromatography on Brockmann Type III alumina with dichloromethane as the eluent to yield **3** as colorless viscous liquid (480 mg, 78%).  $^1\text{H}$  NMR ( $\text{CDCl}_3$ , 400 MHz):  $\delta$  5.34–5.24 (m, 2H), 5.22 (m, 1H), 4.80 (m, 1H), 4.28 (m, 1H), 4.08 (dd,  $J$  12.3 Hz,  $J$  2.4 Hz, 1H), 3.99 (m, 1H), 3.89–3.52 (m, 8H), 2.63 (t,  $J$  11.4 Hz, 2H), 2.14, 2.09, 2.02, 1.98 (each s, each 3H), 1.90 (m, 2H), 1.18, 1.16 (each d,  $J$  2.0 Hz, each 6H) ppm.  $^{13}\text{C}$  NMR ( $\text{CDCl}_3$ , 400 MHz):  $\delta$  170.6, 169.9, 169.8, 169.6, 117.5, 97.6, 69.5, 69.0, 68.3, 66.0, 64.9 (d,  $J$  6.0 Hz), 62.3, 59.9 (d,  $J$  17.5 Hz), 58.2 (d,  $J$  9.8 Hz), 42.9 (d,  $J$  12.3 Hz), 30.8 (d,  $J$  6.8 Hz), 24.6, 24.5, 24.5, 24.4, 20.8, 20.7, 20.6, 20.6, 20.3 (d,  $J$  7.2 Hz) ppm.  $^{31}\text{P}$  NMR ( $\text{CDCl}_3$ , 400 MHz):  $\delta$  146.6 ppm. Anal. Calcd for  $\text{C}_{26}\text{H}_{43}\text{N}_2\text{O}_{12}\text{P}$ : C, 51.48; H, 7.14; N, 4.62. Found: C, 51.52; H, 7.18; N, 4.65.

**3-(2,3,4,6-Tetra-*O*-acetyl  $\alpha$ -D-galactopyranosyloxy)-propyl (2-Cyanoethyl) (*N,N*-Diisopropyl)phosphoramidite (**6**).** To a solution of **5** (386 mg, 0.950 mmol) in dry dichloromethane (20 mL) were added 2-cyanoethyl tetraisopropyl phosphordiamidite (0.44 mL, 1.39 mmol) and 4,5-dicyanoimidazole (14 mg, 0.2 mmol). The reaction mixture was stirred for 2 h and directly purified by column chromatography on Brockmann type III alumina using dichloromethane as eluent, to yield **6** as colorless syrup (330 mg, 54%).  $^1\text{H}$  NMR ( $\text{CDCl}_3$ , 400 MHz):  $\delta$  5.41 (m, 1H), 5.31 (dd,  $J$  10.6 Hz,  $J$  3.4 Hz, 1H), 5.11–5.05 (m, 2H), 4.20 (m, 1H), 4.11–4.01 (m, 2H), 3.88–3.45 (m, 8H), 2.61 (dt,  $J$  6.3 Hz,  $J$  1.8 Hz, 2H), 2.10, 2.05, 2.01, 1.95 (each s, each 3H), 1.87 (m, 2H), 1.16–1.13 (m, 12H) ppm.  $^{13}\text{C}$  NMR ( $\text{CDCl}_3$ , 400 MHz):  $\delta$  170.4, 170.3, 170.2, 170.0, 117.6, 96.3, 68.2, 68.1, 68.0, 67.6, 65.1 (d,  $J$  3.6 Hz), 61.6, 60.2 (t,  $J$  18.0 Hz), 58.3 (dd,  $J$  19.5 Hz,  $J$  7.9 Hz), 43.1 (dd,  $J$  2.3 Hz,  $J$  12.5 Hz), 31.1 (t,  $J$  7.5 Hz), 24.6, 24.5, 20.8, 20.8, 20.7, 20.7, 20.4 (d,  $J$  7.0 Hz) ppm.  $^{31}\text{P}$  NMR ( $\text{CDCl}_3$ , 400 MHz):  $\delta$  146.6 ppm. Anal. Calcd for  $\text{C}_{26}\text{H}_{43}\text{N}_2\text{O}_{12}\text{P}$ : C, 51.48; H, 7.14; N, 4.62. Found: C, 51.17; H, 6.97; N, 4.27.

**4,8-Dioxa-6-[(benzoyloxy)methyl]-6-methylnona-1,10-diene (8).** 1,1,1-Trihydroxymethylethane (12.4 g, 103.5 mmol) and allyl bromide (17.9 mL, 206.8 mmol) were dissolved in DMF (60 mL), and NaH (12.0 g, 327 mmol) was added at 0 °C over 1 h. The solution was stirred for 12 h. Ice and brine (400 mL) were added at 0 °C, and the solution was extracted five times with cyclohexane (50 mL each). The combined cyclohexane fractions were dried over MgSO<sub>4</sub> and purified over silica gel using a toluene → toluene/ethyl acetate 10:1 gradient, to obtain the bis-allyl ether as a colorless viscous liquid. The syrup was dissolved in pyridine (100 mL), and benzoyl chloride (10 mL) was added at 0 °C over 10 min. The solution was stirred overnight. Methanol (5 mL) was added at 0 °C to quench the reaction, and the solution was poured into ice–water (300 mL). Dichloromethane was added, the phases were separated, and the aqueous phase was extracted twice with dichloromethane. The combined organic phases were dried (MgSO<sub>4</sub>), concentrated, and purified over silica gel with cyclohexane/ethyl acetate 9:1 to yield **8** as colorless viscous liquid (18.6 g, 59%). <sup>1</sup>H NMR (CDCl<sub>3</sub>, 400 MHz): δ 8.02 (d, *J* 8.2 Hz, 2H), 7.53 (t, *J* 7.4 Hz, 1H), 7.43 (t, *J* 7.4 Hz, 2H), 5.85 (m, 2H), 5.26 (m, 2H), 5.12 (m, 2H), 4.27 (s, 2H), 3.96 (t, *J* 1.5 Hz, 2H), 3.95 (t, *J* 1.5 Hz, 2H), 3.41 (s, 4H), 1.08 (s, 3H) ppm. <sup>13</sup>C NMR (CDCl<sub>3</sub>, 400 MHz): δ 166.4, 135.0, 132.9, 130.5, 129.6, 128.4, 116.5, 72.7, 72.3, 67.5, 40.3, 17.5 ppm. Anal. Calcd for C<sub>18</sub>H<sub>24</sub>O<sub>4</sub>: C, 71.03; H, 7.95. Found: C, 70.70; H, 7.96.

**4,8-Dioxa-6-[(benzoyloxy)methyl]-6-methylnonane-1,11-diol (9).** To a solution of **8** (5.85 g, 19.2 mmol) in dry THF (40 mL) was added 9-BBN (75.7 mL, 37.8 mmol), and the solution was stirred for 3 d at room temperature. Ice (10 g) and 3 M NaOAc (38 mL) were added followed by 30% hydrogen peroxide (37.5 mL) added slowly while stirring at 0 °C in an ice bath. The solution was stirred for 6 h and then quickly saturated with K<sub>2</sub>CO<sub>3</sub> at 0 °C. The phases were carefully separated, and the aqueous phase was washed twice with THF. The combined organic layers were filtered, dried over MgSO<sub>4</sub>, filtered, concentrated, and purified over silica gel with dichloromethane/methanol 50:3 to yield **9** as colorless viscous liquid (4.89 g, 75%). <sup>1</sup>H NMR (CDCl<sub>3</sub>, 400 MHz): δ 8.02 (d, *J* 8.3 Hz, 2H), 7.56 (t, *J* 7.4 Hz, 1H), 7.46 (t, *J* 7.4 Hz, 2H), 4.24 (s, 2H), 3.73 (t, *J* 5.5 Hz, 4H), 3.58 (t, *J* 5.5 Hz, 4H), 3.39 (s, 2H), 3.38 (s, 2H), 2.77 (s, 2H), 1.78 (m, 4H), 1.02 (s, 3H) ppm. <sup>13</sup>C NMR (CDCl<sub>3</sub>, 400 MHz): δ 166.1, 133.0, 129.6, 128.5, 73.7, 70.2, 67.5, 61.3, 40.1, 31.8, 17.8 ppm. Anal. Calcd for C<sub>18</sub>H<sub>28</sub>O<sub>6</sub>: C, 63.51; H, 8.29. Found: C, 63.15; H, 8.31.

**1,11-Bis(4,4'-dimethoxytrityloxy)-4,8-dioxa-6-(hydroxymethyl)-6-methylnonane (10).** The diol **9** (2.0 g, 5.9 mmol) was dissolved in dry CH<sub>2</sub>Cl<sub>2</sub> (100 mL). 2,4,6-Trimethylpyridine (3.16 mL, 23.8 mmol), NH<sub>4</sub>ClO<sub>4</sub> (5.43 g, 15.9 mmol), and 4,4'-dimethoxytrityl chloride (5.38 g, 15.9 mmol) were added, and the solution was stirred for 5 d. For workup, the solution was washed with saturated aqueous NaHCO<sub>3</sub> and water, dried (Na<sub>2</sub>SO<sub>4</sub>), filtered through a alumina Brockmann III pad, concentrated, and dried in high vacuum. For debenzoylation, the residue was dissolved in THF (50 mL), and NaOMe in methanol (0.1 M, 20 mL) was added. The solution was stirred overnight, concentrated, redissolved in CH<sub>2</sub>Cl<sub>2</sub> and washed with brine (2×), dried (Na<sub>2</sub>SO<sub>4</sub>), concentrated, and purified over silica gel with toluene/ethyl acetate 9:1 to yield **10** as colorless viscous liquid (3.42 mg, 69%). <sup>1</sup>H NMR (CDCl<sub>3</sub>, 400 MHz): δ 7.47–7.43 (m, 4H), 7.36–7.16 (m, 14H), 6.86–6.83 (m, 8H), 3.81 (s, 12H), 3.54 (t, *J* 6.5 Hz, 4H), 3.48 (d, *J* 5.8 Hz, 2H), 3.36 (d, *J* 8.9 Hz, 2H), 3.29

(d, *J* 8.9 Hz, 2H), 3.15 (t, *J* 6.2 Hz, 4H), 2.84 (t, *J* 5.7 Hz, 1H), 1.86 (m, 4H), 0.78 (s, 3H) ppm. <sup>13</sup>C NMR (CDCl<sub>3</sub>, 400 MHz): δ 158.7, 145.6, 136.9, 130.3, 128.5, 128.1, 127.0, 113.3, 86.1, 75.8, 69.7, 69.1, 60.6, 55.5, 40.7, 30.6, 17.8 ppm. Anal. Calcd for C<sub>60</sub>H<sub>64</sub>O<sub>10</sub>: C, 76.25; H, 6.83. Found: C, 75.85; H, 7.18.

**2,2-Bis[5-(4,4'-dimethoxytrityloxy)-2-oxapentyl]-propyl (2-Cyanoethyl) (N,N-Diisopropyl)phosphoramidite (11).** **10** (940 mg, 1.12 mmol) was dissolved in dry dichloromethane (10 mL). 2-Cyanoethyl tetraisopropyl phosphordiamidite (1.2 mL, 3.78 mmol) and 4,5-dicyanoimidazole (11.2 mg, 0.095 mmol) were added to the solution. The reaction mixture was stirred for 15 h and directly purified by column chromatography on Brockmann type II alumina using dichloromethane as eluent, to yield **11** as colorless viscous liquid (1.04 mg, 89%). <sup>1</sup>H NMR (CDCl<sub>3</sub>, 400 MHz): δ 7.41–7.15 (m, 18H), 6.81–6.76 (m, 8H), 3.76 (s, 12H), 3.57–3.45 (m, 9H), 3.18 (s, 4H), 3.11 (t, *J* 6.3 Hz, 4H), 2.54 (t, *J* 6.7 Hz, 2H), 1.82 (m, 4H), 1.16–1.13 (m, 12H), 0.83 (s, 3H) ppm. <sup>13</sup>C NMR (CDCl<sub>3</sub>, 400 MHz): δ 158.3, 145.4, 136.7, 130.1, 128.2, 127.7, 126.6, 117.7, 113.0, 85.7, 73.2, 68.6, 66.4 (d, *J* 16.3 Hz), 60.5, 58.2 (d, *J* 18.5 Hz), 55.2, 43.0 (d, *J* 13.3 Hz), 41.1 (d, *J* 8.2 Hz), 30.3, 24.7, 24.6, 20.3 (d, *J* 6.4 Hz), 17.3 ppm. <sup>31</sup>P NMR (CDCl<sub>3</sub>, 400 MHz): δ 146.9 ppm. Anal. Calcd for C<sub>62</sub>H<sub>77</sub>N<sub>2</sub>O<sub>10</sub>P: C, 71.52; H, 7.45; N, 2.69. Found: C, 71.37; H, 7.61; N, 2.71.

#### Synthesis of Mannosylated Glycodendrimer 14.

At the DNA synthesizer, 6 coupling cycles using the functional phosphoramidites in the sequence **12**, **11**, **12**, **11**, **12**, and **3** were applied to a 1 μmol 3'-(6-fluorescein) support. The first coupling step was done with 16 μmol 0.06 M reagent in five equal injections over 6 min, the second to fifth coupling steps were done with 26 μmol 0.06 M reagent in 8 equal injections over 18 min. The product was deprotected with 0.1 M NaOMe in MeOH at 40 °C over 3 h and neutralized with Dowex 50WX2 to obtain **14** as an amorphous orange solid (2.9 mg). <sup>1</sup>H NMR (d<sub>4</sub>-MeOH, 500 MHz): δ 8.04 (m, 2H), 7.67 (s, 1H), 7.03 (d, *J* 9.2 Hz, 2H), 6.51 (m, 4H), 4.90 (s, 4H), 3.98–3.30 (m, 172H + MeOH), 1.90 (m, 20H), 1.65–1.30 (m, 7H), 0.97 (s, 9H) ppm. MALDI-TOF MS: *m/z* 4087.8 (Calcd for C<sub>139</sub>H<sub>255</sub>N<sub>107</sub>P<sub>14</sub>: 4086.1).

**Synthesis of Thioated Oligonucleotide with Mannosylated Glycodendron 15.** The iNOS-sequence (5'-CAAGCCATGTCTGAGACTTTG-3') was synthesized on a 1 μmol G-support at the DNA synthesizer using standard phosphoramidites. After the last coupling cycle, a sequence of six further coupling cycles using the functional phosphoramidites in the sequence **12**, **11**, **12**, **11**, **12**, and **3** was added. The first additional coupling step was done with 16 μmol 0.06 M reagent in five equal injections over 6 min, the second to sixth coupling steps were done with 26 μmol 0.06 M reagent in eight equal injections over 18 min. For each step the sulfurization reagent 3*H*-1,2-benzodithiole-3-one 1,1-dioxide was used to oxidize the intermediate phosphotriester. The product was deprotected with aqueous ammonia/aqueous methyllamine (1:1; 1 mL) at 40 °C over 1 h and concentrated at the SpeedVac. The crude product was subjected to a standard ethanol precipitation to yield 151 OD of **15**. A MALDI-TOF MS spectrum was obtained after precipitation of a sample with 3 volume equivalents of 3 M NH<sub>4</sub>-OAc with 0.01 M EDTA overnight at –20 °C. MALDI-TOF MS: *m/z* 10575.7 (calcd for C<sub>316</sub>H<sub>487</sub>N<sub>77</sub>O<sub>190</sub>P<sub>34</sub>S<sub>34</sub>: 10547.9).

The melting behavior of **15** with complementary DNA strand (5'-CAAAGTCTCAGACATGGCTTG-3') was analyzed by UV spectrometry in 0.05 M aqueous NaCl from



20 °C to 70 °C. A melting point of 44.2 °C (50 mM NaCl,  $2 \times 0.2$  OD) was observed for the hybridization of **15** with a complementary DNA strand with two short PEG chains at its 5' end, compared to 44.1 °C (50 mM NaCl,  $2 \times 0.2$  OD) for the unmodified DNA strands.

The mobility shift caused by the glycodendron, was monitored by gel electrophoresis using a 13% denaturing polyacrylamide gel (200 V, 45 min). The oligonucleotide was compared with thioated iNOS DNA (21 bases) and a 10 bp ladder. The iNOS oligonucleotide with mannosylated glycodendron behaved like a 38mer though it has only 34 negative charges.

**Synthesis of Galactosylated Cluster Glycoside 16.** At the DNA synthesizer, three coupling cycles using the synthesized phosphoramidites in the sequence **12**, **13** and **6** were applied to a 1  $\mu$ mol 3'-(6-fluorescein) support. All coupling steps were done with 26  $\mu$ mol 0.06 M reagent in eight equal injections over 18 min. The product was deprotected overnight with 0.06 M NaOMe in MeOH (1 mL) at 37 °C over 6 h and neutralized with Amberlite IR120 to obtain **16** as an amorphous orange solid (2.0 mg). <sup>1</sup>H NMR (*d*<sub>4</sub>-MeOH, 500 MHz):  $\delta$  8.05 (m, 2H), 7.51 (s, 1H), 7.03 (d, *J* 9.3 Hz, 2H), 6.52 (m, 4H), 4.95 (s, 3H), 3.99–3.30 (m, 92H + MeOH), 1.92 (m, 12H), 1.65–1.30 (m, 7H) ppm. MALDI-TOF MS: *m/z* 2416.2 (calcd for C<sub>87</sub>H<sub>146</sub>NO<sub>62</sub>P<sub>7</sub> 2414.90).

#### ACKNOWLEDGMENT

Financial support of this research by the Department of Energy (Basic Energy Sciences; DE-AC03-76SF00098) and the DOE's Biomolecular Program at Lawrence Berkeley National Laboratory is acknowledged with thanks.

**Supporting Information Available:** The synthesizer program for the Expedite 8909 DNA synthesizer. <sup>1</sup>H NMR for **14** and **16**. MALDI-TOF spectra **14**, **15**, and **16**. Gel electrophoresis and melting point diagram for **15**. This material is available free of charge via the Internet at <http://pubs.acs.org>.

#### LITERATURE CITED

- (1) Lee, R. T., Lee, Y. C. (2000) Affinity enhancement by multivalent lectin-carbohydrate interaction. *Glycoconjugate J.* 17, 543–551.
- (2) Choi, I. S., Bowden, N., and Whitesides, G. M. (1998) Polyvalent Interactions in Biological Systems: Implications for Design and Use of Multivalent Ligands and Inhibitors. *Angew. Chem.* 110, 2908–2953; *Angew. Chem., Int. Ed.* 37, 2754–2794.
- (3) Fan, E., Zhang, Z., Minke, W. E., Hou, Z., Verlinde, C. L. M. J., and Hol, W. G. J. (2000) High-Affinity Pentavalent Ligands of *Escherichia coli* Heat-Labile Enterotoxin by Modular Structure-Based Design. *J. Am. Chem. Soc.* 122, 2663–2664.
- (4) Kitov, P. I., Sadowska, J. M., Mulvey, G., Armstrong, G. D., Ling, H., Pannu, N. S., Read, R. J., and Bundle, D. R. (2000) Shiga-like toxins are neutralized by tailored multivalent carbohydrate ligands. *Nature* 403, 669–672.
- (5) Gestwicki, J. E., Strong, L. E., and Kiessling, L. L. (2000) Tuning chemotactic responses with synthetic multivalent ligands. *Chem. Biol.* 7, 583–591.
- (6) Reuter, J. D., Myc, A., Hayes, M. M., Gan, Z., Roy, R., Qin, D., Yin, R., Piehler, L. T., Esfand, R., Tomalia, D. A., and Baker, J. R., Jr. (1999) Inhibition of Viral Adhesion and Infection by Sialic-Acid-Conjugated Dendritic Polymers. *Bioconjugate Chem.* 10, 271–278.
- (7) Sihorkar, V., Vyas, S. P. (2001) Potential of polysaccharide anchored liposomes in drug delivery, targeting and immunization. *J. Pharm. Pharmacol. Sci.* 4, 138–158.
- (8) Akhtar, S., Hughes, M. D., Khan, A., Bibby, M., Hussain, M., Nawaz, O., Double, J., Sayyed, P. (2000) The delivery of antisense therapeutics. *Adv. Drug Deliv. Rev.* 44, 3–21.
- (9) Liang, W., Shi, X., Desphande, D., Malanga, C. J., and Rojanasakul, Y. (1996) Oligonucleotide targeting to alveolar macrophages by mannose receptor-mediated endocytosis. *Biochim. Biophys. Acta* 1279, 227–234.
- (10) Biessen, E. A. L., Vietsch, H., Rump, W. T., Fluiter, K., Kuiper, J., Bijsterbosch, M. K., and Van Berkel, T. J. C. (2000) Targeted delivery of oligodeoxynucleotides to parenchymal liver cells in vivo. *Biochem. J.* 314, 324–342.
- (11) Turnbull, W. B., Stoddart, J. F. (2002) Design and synthesis of glycodendrimers. *Rev. Mol. Biotechnol.* 90, 231–255.
- (12) Dubber, M., Lindhorst, Th. K. (2001) Synthesis of Carbohydrate-Centered Oligosaccharide Mimetics Equipped with a Functionalized Tether. *J. Org. Chem.* 65, 5275–5281.
- (13) Plante, O. J., Palmacci, E. R., and Seeberger, P. H. (2001) Automated solid-phase synthesis of oligosaccharides. *Science* 291 (5508), 1523–1527.
- (14) Shchepinov, M. S., Mir, K. U., Elder, J. K., Frank-Kamenetskii, M. D., and Southern, E. M. (1999) Oligonucleotide dendrimers: stable nano-structures. *Nucleic Acids Res.* 27, 3035–3041.
- (15) Goh, S. L., Francis, M. B., and Fréchet, J. M. J. (2002) Self-assembled oligonucleotide-polyester dendrimers. *Chem. Commun.*, submitted.
- (16) Shchepinov, M. S., Korshun, V. A. (2001) Design of multi-dye systems for fret-based applications. *Nucleosides, Nucleotides Nucleic Acids* 20, 369–374.
- (17) Shchepinov, M. S., Udalo, I. A., Bridgman, A. J., and Southern, E. M. (1997) Oligonucleotide dendrimers: synthesis and use as polylabeled DNA probes. *Nucleic Acids Res.* 25, 4447–4454.
- (18) Polushin, N. N. (2000) The precursor strategy: terminus methoxyoxaamido modifiers for single and multiple functionalisation of oligodeoxyribonucleotides. *Nucleic Acids Res.* 28, 3125–3133.
- (19) Hovinen, J., Hakala, H. (2001) Versatile Strategy for Oligonucleotide Derivatization. Introduction of Lanthanide(III) Chelates to Oligonucleotides. *Org. Lett.* 3, 2473–2476.
- (20) Akhtar, S., Routledge, A., Patel, R., and Gardiner, J. M. (1995) Synthesis of Mono- and Dimannoside Phosphoramidite Derivatives for Solid-Phase Conjugation to Oligonucleotides. *Tetrahedron Lett.* 36, 7333–7336.
- (21) Sheppard, T. L., Wong, C.-H., and Joyce, G. F. (2000) Nucleoglycoconjugates: Design and Synthesis of a new Class of DNA-Carbohydrate Conjugates. *Angew. Chem., Int. Ed.* 39, 3660–3663.
- (22) Ellington, A., Pollard, J. D., Jr. (1998) Synthesis and purification of oligonucleotides. *Current Protocols Molecular Biology* (John Wiley & Sons, Inc., New York) Chapt. 2.11.1–2.11.25.
- (23) Beaucage, S. L., and Iyer, R. P. (1993) The Functionalization of Oligonucleotides Via Phosphoramidite Derivatives. *Tetrahedron* 49, 1925–1963.
- (24) Brown, H. C., and Chen, J. C. (1981) Hydroboration. 57. Hydroboration with 9-borabicyclo[3.3.1]nonane of alkenes containing representative functional groups. *J. Org. Chem.* 46, 3978–3988.
- (25) Vargeese, C., Carter, J., Yegge, J., Krivjansky, S., Settle, A., Kropp, E., Peterson, K., and Pieken, W. (1998) Efficient activation of nucleoside phosphoramidites with 4,5-dicyanoimidazole during oligonucleotide synthesis. *Nucleic Acids Res.* 26, 1046–1050.
- (26) (1984) Camag Aluminas for Chromatography. *Aldrichimica Acta* 17, 42.
- (27) Reddy, M. P., Rampal, J. B., and Beaucage, S. L. (1987) An Efficient Procedure for the Solid-Phase Tritylation of Nucleosides and Nucleotides. *Tetrahedron Lett.* 28, 23–26.
- (28) Ma, M. Y. X., Reid, L. S., Climie, S. C., Lin, W. C., Kuperman, R., Sumner-Smith, M., Barnett, R. W. (1993) Design and synthesis of RNA miniduplexes via a synthetic linker approach. *Biochemistry* 32, 1751–1758.
- (29) Ding, M., Zhang, M., Wong, J. L., Rogers, N. E., Ignarro, L. J., and Voskuhl, R. R. (1998) Cutting Edge: Antisense Knockdown of Inducible Nitric Oxide Synthase Inhibits

- Induction of Experimental Autoimmune Encephalomyelitis in SJL/J Mice. *J. Immunol.* **160**, 2560–2564.
- (30) Reddy, M. P., Hanna, and N. B., Farooqui, F. (1997) Ultrafast cleavage and deprotection of oligonucleotides: synthesis and use of CAc derivatives. *Nucleosides Nucleotides* **16**, 1589–1598.
- (31) Lee, Y. C., Lee, R. T. (1995) Carbohydrate-Protein Interactions: Basis of Glycobiology. *Acc. Chem. Res.* **28**, 321–327.
- (32) Lundquist, J. J., Toone, E. J. (2002) The Cluster Glycoside Effect. *Chem. Rev.* **102**, 555–578.
- (33) Benimetskaya, L., Loike, J. D., Khaled, Z., Loike, G., Silverstein, S. C., Cao, L., El Khoury, J., Cai, T.-Q., and Stein, C. A. (1997) Mac-1 (CD11b/CD18) is an oligodeoxynucleotide-binding protein. *Nature Medicine* **3**(4), 414–420.

BC0256244

# Structural Effects of Carbohydrate-Containing Polycations on Gene Delivery. 1. Carbohydrate Size and Its Distance from Charge Centers

Theresa M. Reineke<sup>†</sup> and Mark E. Davis\*

Division of Chemistry and Chemical Engineering, California Institute of Technology, Pasadena, California 91125. Received August 9, 2002; Revised Manuscript Received October 10, 2002

Cationic polymers have the ability to bind plasmid DNA (pDNA) through electrostatic interactions and condense it into particles that can be readily endocytosed by cultured cells. The effects that polycation structure has on toxicity and gene delivery efficiency are investigated here by synthesizing a series of amidine-based polycations that contain the carbohydrates D-trehalose and  $\beta$ -cyclodextrin (CD) within the polycation backbone. The carbohydrate size (trehalose vs CD) and its distance from the charge centers affect the gene delivery behavior in BHK-21 cells. It is found that as the charge center is further removed from the carbohydrate unit, the toxicity is increased. Also, as the size of the carbohydrate moiety is enlarged from trehalose to  $\beta$ -cyclodextrin, the toxicity is reduced. The absence of a carbohydrate in the polycation produces high toxicity. All carbohydrate polycations transfect BHK-21 cells to approximately the same level of gene expression.

## INTRODUCTION

One of the hurdles to successful application of gene therapy is the development of a viable nucleic acid delivery vehicle. Although viruses are the foremost-investigated gene transfer agents, several problems with this technology have surfaced and nonviral alternatives, such as cationic polymers, are currently being explored (1, 2). While synthetic vectors have been found to be more toxic and have lower transgene expression than viral vectors, several benefits remain. Advantages of utilizing nonviral carriers include the lack of immune and/or inflammatory responses, the lower cost and ease of manufacture on a larger scale, and the ability to carry an unlimited amount of genetic information (viruses can only contain a finite gene size within their capsid) (2–4).

Polylysine (PLL), polyethylenimine (PEI), polyamidoamine (PAA), chitosan, and other polycations have the ability to bind pDNA through electrostatic interactions and condense it into colloidal particles that have been termed polyplexes (5–9). Numerous studies have shown that these systems can carry pDNA into cultured cells. However, substantial differences in transfection efficiency and degree of toxicity have been observed. Several reviews on this topic have recently been published, and they discuss the many vectors that are currently under investigation (4, 10–14).

As various structure–property studies are completed, the influence of polycation composition on gene delivery is beginning to be identified. Numerous reports have suggested that physical and chemical differences play a significant role in the delivery efficiency and toxicity of these systems (3, 15–22). For example, Godbey and co-workers have shown that the transfection efficiency of

PEI increases as the molecular weight increases (6). Also, Murphy et al. have synthesized and studied a diverse set of peptoids and revealed that although several variations were able to bind and condense DNA, only a small subset containing a repeated cationic–hydrophobic–hydrophobic motif were able to transfect cultured cells (21). Moreover, Jones and colleagues have found that very minor structural changes in PAAs have profound effects on the DNA binding ability and colloidal stability, which in turn affected transfection efficiency of the polyplexes (16).

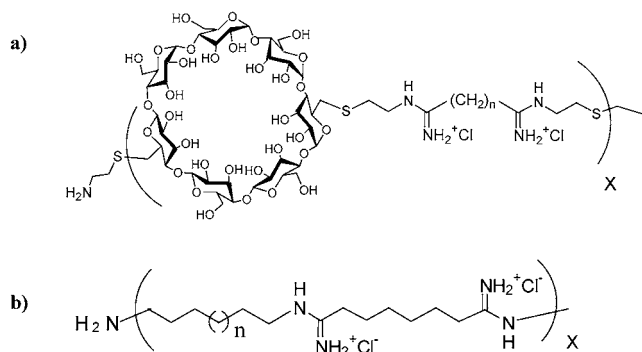
Hwang et al. have shown that the inclusion of  $\beta$ -cyclodextrin into a polyamidine backbone significantly lowers the toxicity associated with polymeric vectors (15). This study suggested that the presence of a large carbohydrate in the polycation backbone was responsible for a remarkable decrease in the toxicity of these systems since polyamidines lacking a carbohydrate were very toxic. Also, the spacing between the charge centers was modified (Figure 1a) and found to affect the toxicity and gene expression. The most efficient vector in the series by Hwang et al. was the  $\beta$ -cyclodextrin polycation with six methylene units between the cationic amidine groups. It was observed that a reduction in the charge separation by only 2 Å (from six to five methylenes), decreased the transfection efficiency of the  $\beta$ -cyclodextrin polycation by an order of magnitude. Furthermore, the  $\beta$ -cyclodextrin polycation with charge centers separated by eight methylenes was found to be the least toxic.

In the previous study by Hwang et al., amidine polymers lacking the repeated sugar moieties (Figure 1b) were initially examined as controls with approximately the same charge distribution along the polycation backbone as the  $\beta$ -cyclodextrin-containing polymers (15). Unfortunately, the long hydrophobic regions in these polyamidine structures are not ideal models for examining the effects of the polymer hydration and determining the parameters responsible for the cytotoxic effects of polycation vectors. Here, several polycations that contain hexamethylenediamine, D-trehalose, and  $\beta$ -cyclo-

\* To whom correspondence should be addressed. E-mail: mdavis@cheme.caltech.edu.

<sup>†</sup> Current address: Department of Chemistry, University of Cincinnati, Cincinnati, OH 45221.





**Figure 1.** (a) Schematic structure of the  $\beta$ -cyclodextrin polycations that were studied previously to elucidate structure–property relationships (15). The charge separation was varied by  $n = 4, 5, 6, 7, 8$ , and 10 methylene units between the amidine charge centers. (b) Schematic structure of the amidine polycations lacking a sugar moiety (15). The value of  $n$  was varied by  $n = 1$  or 4 methylene units.

dextrin were created to give further insight into the physiochemical and structural contributions of synthetic gene carriers on toxicity and gene expression in vitro. Trehalose was selected to provide a smaller carbohydrate than the CD since it contains two glucose units (as compared to the seven of the CD). Because the highest gene expression levels were obtained previously with a charge spacing of six methylene units, we chose to keep the charge separation constant at six and vary other parameters in an attempt to (i) understand and elucidate the effects of additional structural differences on the toxicity and delivery efficiency, and (ii) compare the results to our previous investigations. Here, a series of amidine polymers (AP1–AP7) were synthesized with variations in the size of the carbohydrate as well as the distance of the carbohydrate from the charge center. In this examination, each polycation was synthesized and characterized by molecular weight, binding to pDNA, size and zeta potential of the formed polyplexes, and delivery efficiency and toxicity to BHK-21 cells.

## MATERIALS AND METHODS

**Monomer and Polycation Synthesis.** All reagents were purchased from Aldrich Chemical Co. (Milwaukee, WI) with the exception of the dimethyl suberimidate·2HCl (DMS), dimethyl adipimidate·2HCl (DMA), and cysteamine, which were purchased from Pierce Chemical Co. (Rockford, IL) and  $\beta$ -cyclodextrin, which was purchased from Wacker Biochem. Corp. (Adrian, MI). Electrospray mass spectra were obtained from the Beckman Institute Mass Spectrometry Center on a Perkin-Elmer SCIEX API 365 in either positive or negative ion mode as indicated. NMR spectra were collected on a Varian 300 MHz spectrometer (75.5 MHz for  $^{13}\text{C}$ ) with trimethylsilylpropionic acid sodium salt as an internal standard. All amine products were purified using a Toyopearl SP-650M ion-exchange column using a gradient of ammonium bicarbonate (0–0.3 M) as the eluant. TLC on amine products were performed as previously described (15) and spots were detected by using 0.2% ninhydrin in ethanol. Monomers **8** and **9** (Schemes 3 and 4) as well as polymers AP1, AP4, and AP5 were synthesized as previously described (3, 15).

**6,6'-Diiodo-6,6'-dideoxy-D-trehalose 2** (Scheme 1) (23). Anhydrous D-trehalose **1** (4.00 g, 11.7 mmol) was dissolved in anhydrous dimethylformamide (100 mL) under  $\text{N}_2(\text{g})$ . Triphenylphosphine ( $\text{PPh}_3$ ) (15.325 g, 58.5 mmol) and iodine solid (11.875 g, 46.8 mmol) were added to this

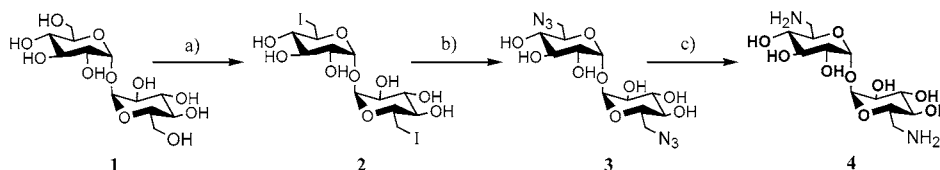
reaction and heated to 80 °C for 1.5 h. This mixture was then concentrated to about 1/3 the starting volume, and methanol (150 mL) was added. Sodium methoxide was added to this solution to pH = 8 and then stirred for another 1.5 h. This mixture was then desalted with the addition of ion-exchange resin (IWT TMD-8). The resin was filtered off, and the solution was concentrated to a residue. This product was then triturated with water, and the residual  $\text{PPh}_3$  was filtered off. This solution was then extracted with  $4 \times 100$  mL of chloroform, and the aqueous layer was concentrated to yield a white solid, **2** (5.472 g, 83%). ES/MS:  $m/z$  561  $[\text{M} - \text{H}]^-$ , 689  $[\text{M} + \text{I}]^-$ .  $^{13}\text{C}$  NMR ( $\text{D}_2\text{O}$ ):  $\delta$  95.81, 76.11, 74.49, 73.51, 73.30, 9.53.

**6,6'-Diazido-6,6'-dideoxy-D-trehalose 3** (Scheme 1) (23). To a solution of **2** (2.089 g, 3.72 mmol) in dimethylformamide (40 mL) was added sodium azide (1.446 g, 22.2 mmol), and the mixture was stirred at 80 °C for 16 h. The mixture was then cooled, the residual salts were filtered, and the remaining solution was concentrated. This mixture was then dissolved in water, and ion-exchange resin (IWT TMD-8) was added to the mixture to desalt the solution. The mixture was filtered, and the aqueous solution was concentrated yielding **3** (0.534 g, 37%) ES/MS:  $m/z$  391  $[\text{M} - \text{H}]^-$ .  $^{13}\text{C}$  NMR ( $\text{D}_2\text{O}$ ):  $\delta$  96.37, 74.96, 73.66, 73.49, 73.10, 53.53.

**6,6'-Diamino-6,6'-dideoxy-D-trehalose 4** (Scheme 1) (23). **3** (0.437 g, 1.11 mmol) was dissolved in anhydrous pyridine (19 mL) under  $\text{N}_2(\text{g})$ .  $\text{PPh}_3$  (2.04 g, 7.77 mmol) was added to the mixture, and the mixture was stirred for 1 h at room temperature. Next, concentrated ammonium hydroxide (4.8 mL) was added via syringe to the mixture, and the solution was stirred at room temperature for 16 h. The pyridine was then removed, and the dry material was triturated with water. The solids were filtered off, the aqueous mixture was brought to a pH < 4, and the liquid was added to the Toyopearl column to purify. The appropriate fractions were combined and lyophilized to dryness, yielding a white solid, **4** (0.355 g, 94%). ES/MS:  $m/z$  341  $[\text{M} + \text{H}]^+$ .  $^{13}\text{C}$  NMR ( $\text{D}_2\text{O}$ ):  $\delta$  96.18, 74.44, 73.79, 73.16, 70.61, 43.07.

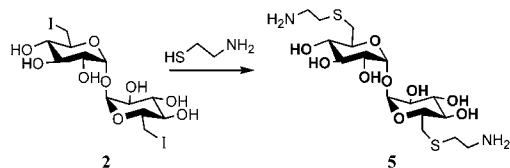
**6,6'-Dicysteamino-6,6'-dideoxy-D-trehalose 5** (Scheme 2). To a solution containing freshly sublimed cysteamine (0.312 g, 4.0 mmol) in degassed water (50 mL) was added **2** (0.573 g, 1.0 mmol) in four aliquots to the mixture over 30 min. The mixture was heated to 80 °C and stirred for 3 h. The heat was shut off, and the solution was stirred overnight at room temperature. This mixture was concentrated, redissolved in water, and acidified to a pH = 1.8. The mixture was then purified on the Toyopearl column and lyophilized to dryness, yielding a white solid, **5** (0.306 g, 67%). ES/MS:  $m/z$  461  $[\text{M} + \text{H}]^+$ .  $^{13}\text{C}$  NMR ( $\text{D}_2\text{O}$ ):  $\delta$  95.85, 75.25, 73.88, 43.42, 41.45, 35.13.

***N,N*-(Dithiodibutane-4,1-diyl)bis[phthalimide] 11** (Scheme 5) (26). A solution of *N*-(4-bromobutyl)phthalimide **10** (4.250 g, 15.1 mmol) was refluxed in a 1:1 mixture of methanol:water (60 mL) with  $\text{Na}_2\text{S}_2\text{O}_3$  (3.78 g, 15.2 mmol) for 4 h. Next, the Bunte salt was formed by treating the hot solution with small aliquots of iodine solid (2.22 g, 8.74 mmol) over 30 min until the brown color remained. The residual iodine was reduced by adding a small amount of  $\text{Na}_2\text{S}_2\text{O}_5$ . The solution was then cooled to room temperature and stored overnight in the refrigerator. The methanol/water layer was decanted, the solid pellet was dissolved in chloroform, and the remaining salts were removed with ion-exchange resin (IWT TMD-8). A white-yellow solid, **11** (3.78 g, 66%), remained after evaporation of the chloroform. ES/MS:  $m/z$  486  $[\text{M} + \text{H}]^+$ ,  $^{13}\text{C}$  NMR ( $\text{D}_2\text{O}$ ):  $\delta$  168.03, 133.68, 131.83, 122.98, 38.03, 37.33, 27.33, 26.28.

Scheme 1<sup>a</sup>

<sup>a</sup> Reagents and conditions: (a) PPh<sub>3</sub>, I<sub>2</sub>, DMF, 80 °C; (b) NaN<sub>3</sub>, DMF; (c) PPh<sub>3</sub>, pyridine, NH<sub>4</sub>OH.

## Scheme 2



**4,4'-Dithiobisbutane-1-amine Dihydrochloride 12** (Scheme 5) (26). **11** (3.784 g, 7.8 mmol) was refluxed in anhydrous ethanol (90 mL) and hydrazine hydrate (1.1 mL) under N<sub>2</sub>(g). The reaction was stirred for 1 h in which a white precipitate formed after about 30 min. The ethanol was then removed, and the solid was refluxed in 1 M HCl for 1.5 h to form the dihydrochloride salt. The solid hydrazide residue was filtered off, and the aqueous layer was concentrated. The crude product was purified on the Toyopearl column using a gradient of 0–1.0 M of aqueous ammonium bicarbonate. The appropriate fractions were combined and lyophilized to dryness, yielding a white product, **12** (1.38 g, 85%). ES/MS: *m/z* 209 [M + H]<sup>+</sup>, <sup>13</sup>C NMR (D<sub>2</sub>O):  $\delta$  39.63, 37.55, 26.05, 25.76.

**6<sup>A</sup>,6<sup>D</sup>-Dithiobutaneamino-6<sup>A</sup>,6<sup>D</sup>-dideoxy- $\beta$ -cyclodextrin 14** (Schemes 5 and 6). **12** (0.434 g, 2.09 mmol) was dissolved in 70 mL of degassed dH<sub>2</sub>O, and Ar(g) was bubbled through this solution for 30 min. Triscarboxyethylphosphine dihydrochloride (TCEP) (Molecular Probes, Eugene, OR) (0.719 g, 2.51 mmol) was then added to this solution, and the mixture was stirred for 1 h under Ar(g) to reduce the disulfide. The TCEP oxide was removed by quickly passing the solution through a column of Amberlite IRA-400 (OH) resin that was prepared by rinsing with several portions of He(g) sparged water. The freshly cleaved sulfhydryl form, **13**, was then immediately heated to 80 °C, and **6** (0.583 g, 0.43 mmol) was added to the solution in three aliquots over 20 min and left to stir for 4 h. The mixture was then concentrated, dissolved in water, acidified to a pH = 2.0, filtered to remove undissolved solids, and purified. The proper fractions were recovered and lyophilized to dryness to give a white solid, **14** (0.250 g, 44%). ES/MS: *m/z* 1309 [M + H]<sup>+</sup>, 1332 [M + Na]<sup>+</sup>, <sup>13</sup>C NMR (DMSO-*d*<sub>6</sub>):  $\delta$  104.39, 86.95, 83.57, 75.57, 74.53, 62.57, 43.32, 35.46, 34.91, 31.65, 29.09.

**Polymerization.** Each polycation was synthesized as previously described through condensation polymerization (Scheme 7) of an amine monomer with DMS (AP1–AP6) or DMA (AP7) (3, 15). For example, 0.102 g (0.3 mmol) of **2** was combined with DMS (0.067 g, 0.25 mmol) in a small scintillation vial. Na<sub>2</sub>CO<sub>3</sub> (0.5 M, 0.500 mL) was added, and the mixture was stirred for 16 h. This solution was then diluted with about 5 mL of water, brought to a pH < 4.0 with 0.1 M HCl, and added to a dialysis membrane (3500 MWCO for the  $\beta$ -cyclodextrin polycations and 1000 MWCO for the hexamethylenediamine and trehalose polycations). The solution was then dialyzed for 36 h with several water changes and lyophilized to dryness.

**Polycation Characterization.** Polycation molecular weights were determined by static light scattering. The

polycations were analyzed on a Waters 515 HPLC system equipped with a Wyatt Technologies Corp. DAWN EOS in conjunction with an Optilab DSP interferometric refractometer or on a Hitachi D6000 HPLC system equipped with a ERC-7512 refractive index detector and a Precision Detectors PD2020/DLS. Each sample was prepared at a concentration between 50 and 70 mg/mL and injected onto a Polymer Labs Aquagel-OH 30 column with an eluant flow rate of 0.7 mL/min. The eluant was 0.8 M ammonium acetate, brought down to a pH = 2.8 with phosphoric acid. The refractive index increment values were determined in the same eluant at 25 °C (633 nm).

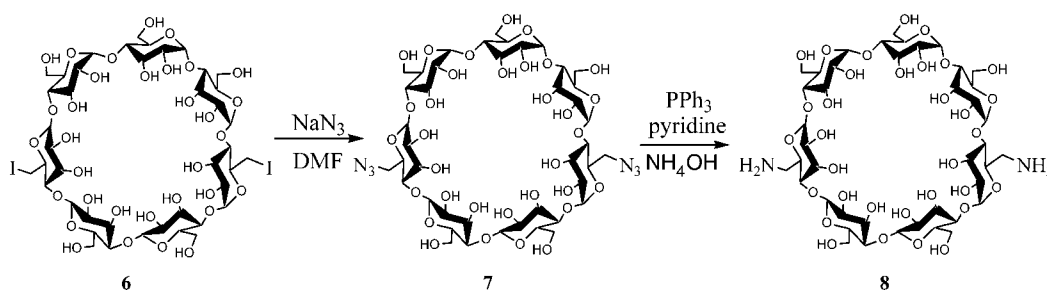
**Gel Retardation Experiments.** Each polycation was examined for its ability to bind pDNA through gel electrophoresis experiments as previously described (3). pGL3-CV (1  $\mu$ g; 10  $\mu$ L of a 0.1  $\mu$ g/ $\mu$ L in DNase free water) was mixed with an equal volume of polymer at charge ratios between 0 and 5.0  $\pm$ . Each solution was incubated for approximately 30 min. Loading buffer (2  $\mu$ L) was added to each sample, and then 10  $\mu$ L of each sample was pipetted into the wells of a 0.6% agarose gel containing 6  $\mu$ g of ethidium bromide/100 mL TAE buffer (40 mM Tris-acetate, 1 mM EDTA) and electrophoresed.

**Dynamic Light Scattering and Zeta-Potential.** The polyplex size and zeta-potential were measured using a ZetaPals dynamic light scattering instrument (Brookhaven Instruments Corporation, Holtsville, NY) as previously described (15). pGL3-CV (2  $\mu$ g) was complexed with each polymer at a charge ratio of 10  $\pm$  in dH<sub>2</sub>O and allowed to stand for 30 min before diluting to 1.2 mL of dH<sub>2</sub>O. The results for each sample are reported as an average of five measurements for the polyplex size and an average of 10 data points for the zeta-potential.

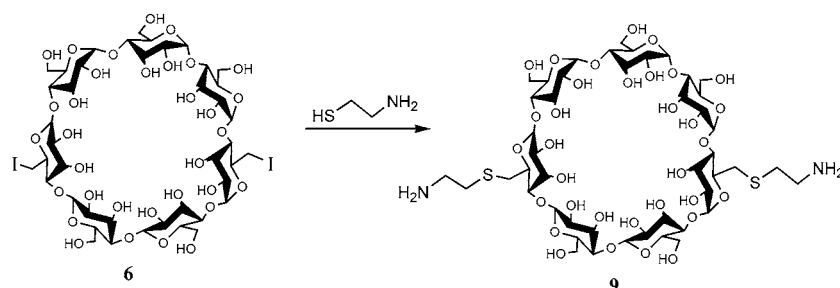
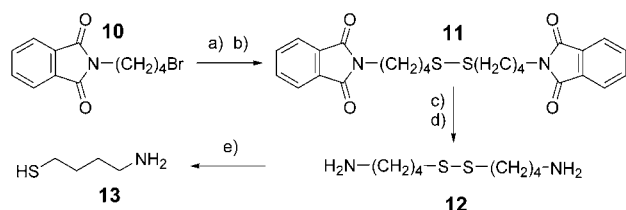
**Cell Culture Experiments.** Plasmid pGL3-CV (Promega, Madison WI) containing the luciferase gene under the control of the SV40 promoter was amplified by *Escherichia coli* strain DH5 $\alpha$  and was then purified using a Novagen Ultramobius 1000 plasmid kit. BHK-21 cells were purchased from ATCC (Rockville, MD) and maintained in Dulbecco's Modified Eagle Medium (DMEM) supplemented with 10% FBS, 100 units/mg penicillin, 100  $\mu$ g/mL streptomycin, and 0.25  $\mu$ g/mL amphotericin at 37 °C and 5% CO<sub>2</sub>. Media and supplements were purchased from Gibco BRL (Gaithersburg, MD). BHK-21 cells were plated at 50000 cells per well in 24 well plates and incubated for 24 h.

Sixty microliters of cationic polymer dissolved in DNase free water (Gibco BRL) was added to 60  $\mu$ L of pDNA (0.05  $\mu$ g/ $\mu$ L in DNase free water) at charge ratios of 3, 5, 10, 15, 20 (polymer +/DNA –). The mixtures were incubated for 30 min and then diluted to 600  $\mu$ L with serum free media. Twenty four hours after cell plating, the cells were transfected with 1  $\mu$ g of pGL3-CV complexed with each of the polymers (AP1–AP7) at the various charge ratios (200  $\mu$ L of each solution above) and with naked pDNA in triplicate in serum free media. After 4 h, 800  $\mu$ L of DMEM was added to each well. Twenty four hours after transfection, the media was replaced

Scheme 3



Scheme 4

Scheme 5<sup>a</sup>

<sup>a</sup> (a) MeOH/H<sub>2</sub>O 1:1, Na<sub>2</sub>S<sub>2</sub>O<sub>3</sub>; (b) I<sub>2</sub>; (c) EtOH, H<sub>2</sub>N-NH<sub>2</sub>; (d) 1 M HCl; (e) TCEP.

with 1 mL of DMEM. Forty eight hours after transfection, cell lysates were analyzed for luciferase protein activity with results reported in relative light units (RLUs) as previously described (3). Toxicities were determined by a modified version of the Lowry protein assay with a Bio-Rad (Hercules, CA) DC Protein Assay Kit also as previously described (3).

## RESULTS

**Monomer and Polycation Synthesis and Characterization.** Each monomer was synthesized in accordance to the procedures described above (depicted in Schemes 1–6). All yields and spectra were in agreement with literature values where applicable. The polycations were synthesized in the same manner as previously described via AABB condensation polymerization by combining amine-functionalized comonomers with DMS or DMA in aqueous sodium carbonate as shown in Scheme 7 (3, 15). The polycation yield, molecular weight, degree of polymerization, and polydispersity index were determined by static light scattering and the results given in Table 1 for each polycation (see Figure 2 for schematics of structures).

**pDNA Binding Studies and Polyplex Characterization.** The polycations were complexed with pDNA at several charge ratios, and the point of charge neutralization was determined by agarose gel electrophoresis. All polycations bound pDNA at and above a charge ratio of 1.0 ±.

To determine both the particle size and the surface charge of the polyplexes, each polycation was complexed with pDNA at a charge ratio of 10 ± and analyzed for

particle size using dynamic light scattering and surface charge using zeta-potential. As shown in Figure 3a, the polyplexes formed by each of the polycations were all between 80 and 100 nm in diameter. In addition, the polyplex surface charge was very positive (Figure 3b), indicating an excess of polycation charge relative to the charge of the pDNA. Positive zeta-potentials provide appropriate characteristics for endocytosis of the polyplexes (24).

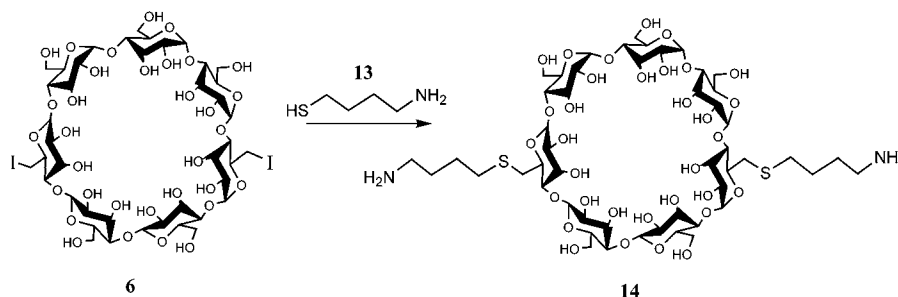
**In Vitro Toxicity and Transfection of the Polyplexes.** BHK-21 cells were plated in 24-well plates and transfected under serum-free conditions using 1 µg of pGL3-CV complexed with each polycation at various charge ratios. Toxicities associated with the polyplexes at various charge ratios were determined by measuring the total protein concentration in the cell lysates after 48 h following initial transfection and normalizing the data to protein levels from untransfected cells. As shown in Figure 4, at a charge ratio of 3 ± and above, the toxicity associated with AP1 becomes evident and only 20% cell survival is found. At charge ratios of both 15 and 20 ±, only 40% of the cells survived with polyplexes from AP3. AP6 displays slight toxicity to BHK-21 cells at a charge ratio of 15 and 20 ± where 70% cell survival was noticed, and AP4, AP5, and AP7 show essentially no toxicity to BHK-21 cells at all charge ratios shown in Figure 4.

IC<sub>50</sub> values for AP1, AP3, AP6, and AP7 (6.6 µM, 23 µM, 58 µM, and 71 µM, respectively) were calculated from transfection experiments (AP1 and AP3 from charge ratios of 3, 5, 10, 15, and 20 ± and AP6 and AP7 from charge ratios of 10, 20, and 50 ±). Results for AP5 (formerly denoted CDP6), CDP8, and CDP4 were obtained from the previous study (1100 µM, 2200 µM, and 380 µM, respectively) and were determined via the MTT assay (15). A comparison of all the IC<sub>50</sub> data is shown in Figure 5.

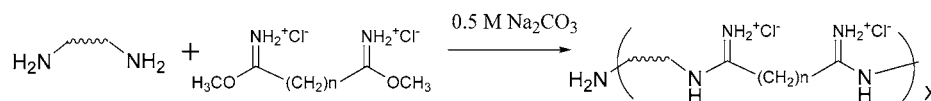
Transfection efficiencies of the polyplexes were determined by assaying for luciferase protein activity, and the results are reported in relative light units (RLUs) per mg of protein. Several polycation (+) to DNA (−) charge ratios were tested and the results are shown in Figure 6. AP3 was found to have the highest transfection efficiency at lower charge ratios. At a charge ratio of 20



### Scheme 6



### Scheme 7



Where  $n = 4$  or  $6$

**Table 1. the Polycation Percent Yield, Refractive Index Increment, Molecular Weight, Polydispersity, and Degree of Polymerization Data for the Amidine Polymers AP1–AP7 (Figure 2) As Determined by Static Light Scattering**

polycation	yield, %	$dn/dc$	$M_w$ (kDa)	$M_w/M_n$	degree of polymerization
AP1	31	0.154	3.2	1.15	10
AP2	23	0.154	4.5	1.25	8
AP3	45	0.172	5.4	1.91	8
AP4	29	0.135	6.2	1.07	5
AP5	35	0.155	4.9	1.13	4
AP6	27	0.125	9.0	1.20	6
AP7	32	0.159	6.5	1.06	4

±, AP2–AP7 all revealed expression levels within an order of magnitude from one another. The lowest gene expression values were obtained with AP1 where maximum transfection was reached at a charge ratio of 3 ± and significantly decreased at higher charge ratios.

## DISCUSSION

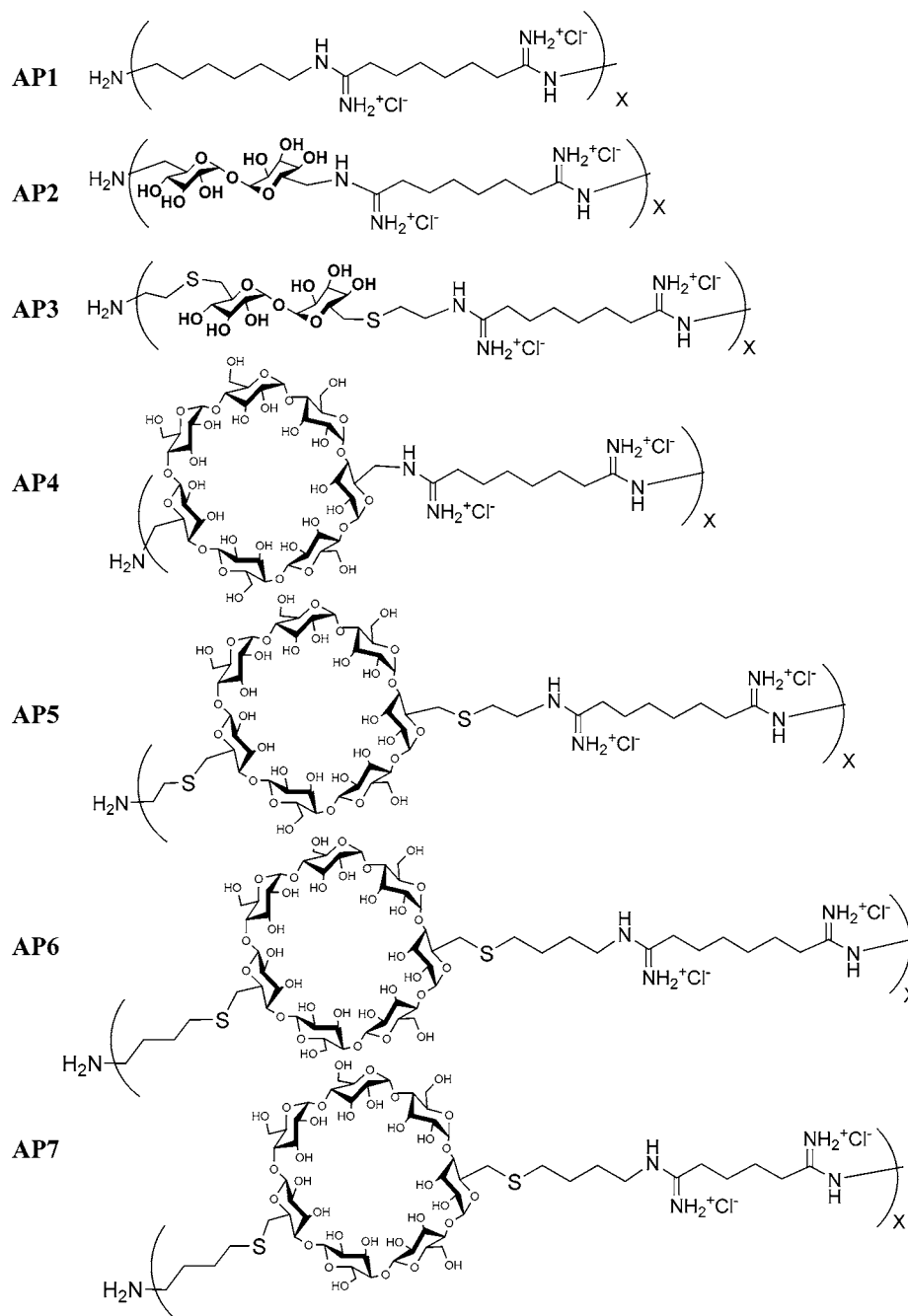
Previously, Hwang and co-workers demonstrated with  $\beta$ -cyclodextrin-containing polyamidines that interchange spacing was an important parameter, and significant differences in the toxicity and gene expression were noted for this family of delivery vehicles (15). Here, further investigation of the charge spacing is studied by systematically changing the distance from the charge center to the carbohydrate unit within the backbone to determine whether there is a relationship between this distance and toxicity and gene expression. Likewise, the carbohydrate size was varied to determine if increasing the size and therefore the degree of backbone hydration affects these parameters. Such parameter changes were accomplished through preparing a new set of carbohydrate monomers. The trehalose amine monomer **4** was synthesized in a manner similar to Garcia Fernandez et al. using slight modifications to the various steps by exploiting the greater reactivity of the primary hydroxyl groups to halogenation (23). As shown in Scheme 1, the final amine product **4** was created through a Staudinger reduction of the azide **3**. A literature preparation of the trehalose dicysteamine analogue **5** was found where the product was synthesized via a tosyl intermediate step (25). However, here a nucleophilic substitution of the iodo group with cysteamine was used and proceeded in an efficient manner as pictured in Scheme 2. The  $\beta$ -cyclodextrin monomers (**8** and **9**) were synthesized as previously described (depicted in Schemes 3 and 4) with the

exception of the dithiobutaneamino  $\beta$ -cyclodextrin derivative, **14**, that was produced by a new method (vide infra). **12** (Scheme 5) was prepared through a similar route published by Pfammatter and co-workers to create C6–C12 alkanethiols (26). The synthesis of **14**, as shown in Scheme 6, was found to be slightly complicated by the fact that the TCEP interfered with the nucleophilic substitution step with **13**, and that the reducing agent must be removed from the solution via anion-exchange chromatography in order for the desired reaction to proceed. Also, after TCEP removal, the disulfide, **12**, can reform quickly after cleavage, and therefore the substitution step must take place immediately upon disulfide reduction.

The  $\beta$ -cyclodextrin and trehalose polycations were prepared in an effort to modify the charge distribution along the polyamidinium backbone, and to compare how the size of the carbohydrate moiety affects both the toxicity and gene delivery efficiency. The structures of the polycations used in this study are illustrated in Figure 2. Molecular weights were determined by static light scattering, and results are listed Table 1. Note that as the monomer is changed, the degree of polymerization is affected; the hexamethylenediamine derivative (AP1) showed the highest degree of polymerization (DP = 10, 3.2 kDa), the trehalose polycations (AP2 and AP3) had intermediate degrees of polymerization (DP = 8, 4.5, and 5.4 kDa, respectively), and the  $\beta$ -cyclodextrin polycations (AP4–AP7) showed the lowest degrees of polymerization (DP = 5, 6.2 kDa; DP = 4, 4.9 kDa; DP = 6, 9.0 kDa; and DP = 4, 6.5 kDa). This influence is more pronounced in the  $\beta$ -cyclodextrin derivatives than in the trehalose polycations, and could be due to the steric affects of the bulk cyclodextrin cup hindering further monomer coupling during the polymerization steps.

Polyplexes formed from all the polycations were between 80 and 100 nm in diameter. Therefore, it is unlikely that differences noted in the transfection efficiency are due to changes in polyplex size. The zeta-potential measurements reveal that all polyplexes contain a large positive charge on the surface of the polyplexes. It is somewhat surprising that AP6 and AP7 have quite high values (above 50 mV).

Figure 4 shows the toxicity observed for each polycation. AP1 is clearly the most toxic, where only 20% cell survival is found at a charge ratio of  $3 \pm$  and above. This effect is likely due to the lack of a carbohydrate within the polycation structure, but some of the increase in toxicity could also be from the slightly higher degree of



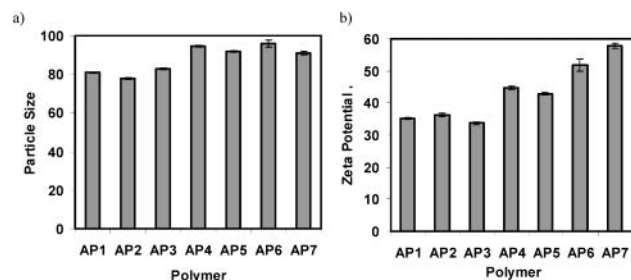
**Figure 2.** Schematic structures of the amidine polycations AP1–AP7.

polymerization. Several groups have observed the effect of higher polymer toxicity with increasing polymer molecular weight (19, 27). AP3 is more toxic to BHK-21 cells than the remaining carbohydrate polyamidine systems; cell survival decreases systematically as the charge ratio increases for AP3, and only 40% cell survival is obtained at  $20 \pm$ . In addition, AP6 also exhibits some degree of toxicity at charge ratios of 15 and  $20 \pm$ . Polycations AP2, AP4, AP5, and AP7 revealed almost no toxic effects to BHK-21 cells at charge ratios up to  $20 \pm$ , with AP2 showing only a small amount of toxicity at a charge ratio of  $20 \pm$ .

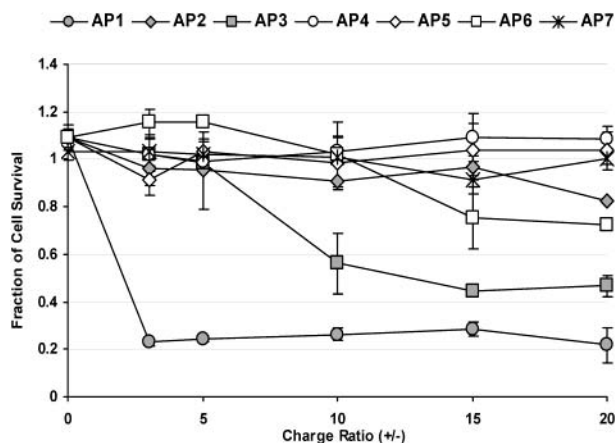
$\text{IC}_{50}$  values were calculated from a series of transfection experiments that were conducted to charge ratios as high as  $50 \pm$ . As shown in Figure 5, AP1, which lacks a carbohydrate, is clearly the most toxic of the series to BHK-21 cells ( $\text{IC}_{50} = 6.6 \mu\text{M}$ ). AP3 also displays a low  $\text{IC}_{50}$  value ( $23 \mu\text{M}$ ) and was shown to be more toxic than

AP2 in the transfection experiments. AP2 did display a small amount of toxicity at a charge ratio of  $20 \pm$  (83% cell survival), but the CD analogue, AP4, as well as AP5 did not display any toxicity. These data reinforce the idea that larger carbohydrates contribute to lowering the toxicity of polycations in BHK-21 cells.

The  $\text{IC}_{50}$  values for the  $\beta$ -cyclodextrin polycations (Figure 5), AP6 and AP7, are considerably lower ( $58 \mu\text{M}$  and  $71 \mu\text{M}$ , respectively) than those obtained in a previous study for CDP4 (Figure 1a,  $n = 4$ ), AP5 (formerly CDP6), and CDP8 (Figure 1a,  $n = 8$ ) where  $\text{IC}_{50}$  results were found to be  $380 \mu\text{M}$ ,  $1100 \mu\text{M}$ , and  $2200 \mu\text{M}$ , respectively (15). As mentioned earlier, transfection experiments revealed that AP4 and AP5 were nontoxic to BHK-21 cells up to a charge ratio of  $20 \pm$ . However, as the charge was moved further from the CD (AP6), the toxicity did increase. It is interesting to note that this effect was not as dramatic with AP7 at a charge ratio of



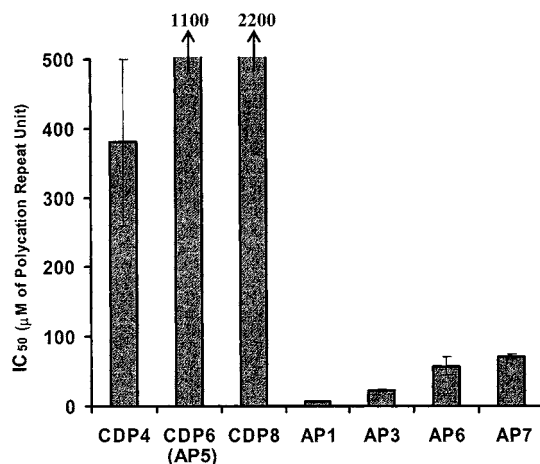
**Figure 3.** (a) Comparison of the hydrodynamic diameter of the polyplexes formed by complexing AP1–AP7 with pDNA as measured by dynamic light scattering. The results shown are reported as an average of five measurements. (b) The particle charge as determined by zeta-potential measurements. The results are reported as an average of 10 measurements. Polyplexes were prepared by combining 2  $\mu$ g of DNA with polycations AP1–AP7 at a charge ratio of  $10 \pm$  and diluting to 1.2 mL.



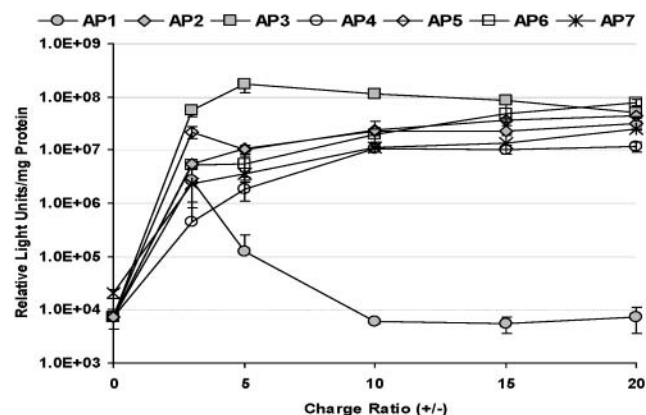
**Figure 4.** Comparison of the relative toxicities of the polycations AP1–AP7 at charge ratios of 3, 5, 10, 15, and 20  $\pm$  with BHK-21 cells. Cell survival was determined by assaying for total protein content and normalizing each sample with the protein concentration for untransfected cells. The data are reported as a mean  $\pm$  SD of three samples.

20  $\pm$  and may be because AP7 has a lower degree of polymerization than AP6 (19, 27). When transfection experiments were performed at a charge ratio of 50  $\pm$  for AP6 and AP7, the calculated  $IC_{50}$  values were similar. These data support the idea that toxicity increases as the DNA-binding charge center is further removed from carbohydrate moiety within the polycation backbone (see particularly CDP8 versus AP7 where both polycations have exactly the same composition but different arrangements of the charge centers).

All polyplexes were able to transfect BHK-21 cells with differing degrees of efficiency (Figure 6). AP1 revealed the lowest transfection efficiency, which is most likely attributable to the high degree of cell death obtained from this polycation. While all the carbohydrate-containing polymers demonstrate relatively high transfection efficiency, the best gene expression is obtained with AP3 at a charge ratio of 5  $\pm$ . Similar gene expression values resulted from polyplexes using AP2–AP7 (within the same order of magnitude at 20  $\pm$ ). Additionally, it is observed that the trehalose polyplexes reach maximum gene expression levels at lower charge ratios than the  $\beta$ -cyclodextrin polyplexes. The CD-containing polyplexes exhibited escalating gene expression levels with increasing charge ratio, which may be due to the lower degrees of polymerization for the  $\beta$ -cyclodextrin polymers. This trend has also been observed by Plank et al. with branched cationic peptides, where optimum transfection



**Figure 5.** Comparison of the  $IC_{50}$  values calculated for CDP4, CDP6 (AP5), CDP8, AP1, AP3, AP6, and AP7.  $IC_{50}$  values for CDP4, CDP6, and CDP8 were obtained from the previous study (15) and values for AP1, AP3, AP6, and AP7 were calculated from transfection experiments.



**Figure 6.** Comparison of transfection efficiencies of the AP1–AP7 polyplexes at charge ratios of 3, 5, 10, 15, and 20  $\pm$  with BHK-21 cells as determined by luciferase protein activity. Data are presented as a mean  $\pm$  SD of three replicates.

shifted to higher charge ratios with decreasing peptide length (28).

In conclusion, a series of polycations containing hexamethylenediamine, D-trehalose, and  $\beta$ -cyclodextrin were synthesized and studied for their toxicity and gene delivery efficiency in BHK-21 cells. It is found that the distance of the charge center from the carbohydrate unit in the polycation backbone affects the toxicity to BHK-21 cells. Also, it appears that the size of the carbohydrate moiety affects toxicity since the  $\beta$ -cyclodextrin polycations all display lower toxicity than the trehalose polycations. Further structure–property studies are ongoing in order to fully understand these effects. In Part 2 of this study, we investigate a series of polyquaternary ammonium vectors that are analogous to the amidine systems studied herein, and compare the effects of charge type on toxicity and delivery efficiency in cell culture.

#### ACKNOWLEDGMENT

We thank Insert Therapeutics, Inc. for partial support of this project. T.M.R. would like to thank the NIH for a National Research Service Award (1-F32 GM64919-01). Also, we are grateful to Swaroop Mishra for amplifying the pDNA and Jeremy Heidel for helpful discussions regarding the cell culture experiments and performing some of the toxicity studies on polymers AP6 and AP7.



## LITERATURE CITED

- (1) Rolland, A. P. (1998) From genes to gene medicines: Recent advances in nonviral gene delivery. *Crit. Rev. Ther. Drug Carrier Syst.* **15**, 143–198.
- (2) Mahato, R. I., Smith, L. C., and Rolland, A. P. (1999) Pharmaceutical perspectives of nonviral gene therapy. *Adv. Genet.* **41**, 95–156.
- (3) Gonzalez, H., Hwang, S. J., and Davis, M. E. (1999) New class of polymers for the delivery of macromolecular therapeutics. *Bioconjugate Chem.* **10**, 1068–1074.
- (4) Han, S., Mahato, R. I., Sung, Y. K., and Kim, S. W. (2000) Development of biomaterials for gene therapy. *Mol. Ther.* **2**, 302–317.
- (5) Zauner, W., Ogris, M., and Wagner, E. (1998) Polylysine-based transfection systems utilizing receptor-mediated delivery. *Adv. Drug Deliv. Rev.* **30**, 97–113.
- (6) Godbey, W. T., Wu, K. K., and Mikos, A. G. (1999) Size matters: Molecular weight affects the efficiency of poly(ethylenimine) as a gene delivery vehicle. *J. Biomed. Mater. Res.* **45**, 268–275.
- (7) Ferruti, P., Manzoni, S., Richardson, S. C. W., Duncan, R., Patrick, N. G., Mendichi, R., and Casolaro, M. (2000) Amphoteric linear poly(amido-amines)s as endosomolytic polymers: Correlation between physicochemical and biological properties. *Macromolecules* **33**, 7793–7800.
- (8) Leong, K. W., Mao, H.-Q., Truong-Le, V. L., Roy, K., Walsh, S. M., and August, J. T. (1998) DNA-polycation nanospheres as nonviral gene delivery vehicles. *J. Controlled Release* **53**, 183–193.
- (9) Felgner, P. L., Barenholz, Y., Behr, J.-P., Cheng, S. H., Cullis, P., Huang, L., Jessee, J. A., Seymour, L., Szoka, F., Thierry, A. R., Wagner, E., and Wu, C. (1997) Nomenclature for synthetic gene delivery systems. *Hum. Gene Ther.* **8**, 511–512.
- (10) Davis, M. E. (2002) Nonviral gene delivery systems. *Curr. Opin. Biotech.* **13**, 128–131.
- (11) Li, S., and Ma, Z. (2001) Nonviral gene therapy. *Curr. Gene Ther.* **1**, 201–226.
- (12) Ma, H., and Diamond, S. L. (2001) Nonviral gene therapy and its delivery systems. *Curr. Pharm. Biotech.* **2**, 1–17.
- (13) Hwang, S. J., and Davis, M. E. (2001) Cationic polymers for gene delivery: Designs for overcoming barriers to systematic administration. *Curr. Opin. Mol. Ther.* **3**, 183–191.
- (14) De Smedt, S. C., Demeester, J., and Hennink, W. E. (2000) Cationic polymer based gene delivery systems. *Pharm. Res.* **17**, 113–126.
- (15) Hwang, S. J., Bellocq, N. C., and Davis, M. E. (2001) Effects of structure of  $\beta$ -cyclodextrin-containing polymers on gene delivery. *Bioconjugate Chem.* **12**, 280–290.
- (16) Jones, N. A., Hill, I. R. C., Stolnik, S., Bignotti, F., Davis, S. S., and Garnett, M. C. (2000) Polymer chemical structure is a key determinant of physicochemical and colloidal properties of polymer-DNA complexes for gene delivery. *Biochim. Biophys. Acta* **1517**, 1–18.
- (17) Neiman, Z., and Quinn, F. R. (1981) Quantitative structure–activity relationships of purines I: Choice of parameters and prediction of  $pK_a$  values. *J. Pharm. Sci.* **70**, 425–430.
- (18) Tang, M., and Szoka, F. (1997) The influence of polymer structure on the interactions of cationic polymers with DNA and the morphology of the resulting complexes. *Gene Ther.* **4**, 823–832.
- (19) Wadhwa, M. S., Collard, W. T., Adami, R. C., McKenzie, D. L., and Rice, K. G. (1997) Peptide-mediated gene delivery: Influence of peptide structure on gene expression. *Bioconjugate Chem.* **8**, 81–88.
- (20) van de Wetering, P., Moret, E. E., Schuurmans-Nieuwenbroek, N. M. E., van Steenbergen, M. J., and Hennink, W. E. (1999) Structure–activity relationships of water-soluble cationic methacrylate/methacrylamide polymers for nonviral gene delivery. *Bioconjugate Chem.* **10**, 589–597.
- (21) Murphy, J. E., Uno, T., Hamer, J. D., Cohen, F. E., Dwarki, V., and Zuckerman, R. N. (1998) A combinatorial approach to the discovery of efficient cationic peptoid reagents for gene delivery. *Proc. Natl. Acad. Sci. U.S.A.* **95**, 1517–1522.
- (22) Azzam, T., Eliyahu, H., Shapira, L., Linial, M., Barenholz, Y., and Domb, A. J. (2002) Polysaccharide-oligoamine based conjugates for gene delivery. *J. Med. Chem.* **45**, 1817–1824.
- (23) Garcia Fernandez, J. M., Mellet, C. O., Blanco, J. L. J., Mota, J. F., Gadelle, A., Coste-Sarguet, A., and Defaye, J. (1995) Isothiocyanates and cyclic thiocarbamates of  $\alpha,\alpha'$ -trehalose, sucrose, and cyclomaltooligosaccharides. *Carbohydr. Res.* **268**, 57–71.
- (24) Mislick, K. A., and Baldeschwieler, J. D. (1996) Evidence for the role of proteoglycans in cation-mediated gene transfer. *Proc. Natl. Acad. Sci. U.S.A.* **93**, 12349–12354.
- (25) Cucinotta, V., Grasso, G., and Vecchio, G. (1998) From capped to three-dimensional cyclodextrins: The first example of a new class of receptors by trehalose capping of a  $\beta$ -cyclodextrin. *J. Incl. Phenom. Mol. Recogn. Chem.* **31**, 43–55.
- (26) Pfammatter, M. J., Siljegovic, V., Darbre, T., and Keese, R. (2001) Synthesis of  $\omega$ -substituted alkanethiols and (bromomethyl)methylthiomalonates. *Helv. Chim. Acta* **84**, 678–689.
- (27) Fischer, D., Bieber, T., Li, Y., Elsasser, H.-P., and Kissel, K. (1999) A novel nonviral vector for DNA delivery based on low molecular weight, branched polyethylenimine: Effect of molecular weight on transfection efficiency and cytotoxicity. *Pharm. Res.* **16**, 1273–1279.
- (28) Plank, C., Tang, M. X., Wolf, A. R., and Szoka, F. C. (1999) Branched cationic peptides for gene delivery: Role of type and number of cationic residues in formation and in vitro activity of DNA polyplexes. *Hum. Gene Ther.* **10**, 319–332.

BC025592K

# TECHNICAL NOTES

## Structural Effects of Carbohydrate-Containing Polycations on Gene Delivery. 2. Charge Center Type

Theresa M. Reineke<sup>†</sup> and Mark E. Davis\*

Division of Chemistry and Chemical Engineering, California Institute of Technology, Pasadena, California 91125. Received August 9, 2002

Recent polycation structure–gene delivery studies reveal that subtle changes in the molecular structure of polycations have substantial influences on DNA-binding and condensation and on in vitro toxicity and gene delivery efficiency. In Part 1 of this structure–property study using carbohydrate-containing polycations (1), it is demonstrated that as the amidine charge center is removed further from the carbohydrate unit within the polycation structure, the toxicity increases. Inclusion of larger carbohydrate species within the polycation backbone also reduces the toxicity. Here, the effect that polycation charge center type has on toxicity and gene delivery efficiency is investigated. A series of quaternary ammonium polycations containing *N,N,N,N*-tetramethyl-1,6-hexanediamine, D-trehalose, and  $\beta$ -cyclodextrin are synthesized in order to elucidate the effects of charge center type (by comparison to the data given in Part 1) on gene delivery. In all cases, it is found that the quaternary ammonium analogues exhibit lower gene expression values and similar toxicities to their amidine analogues. Additionally, transfection experiments conducted in the presence of chloroquine reveal increased gene expression from quaternary ammonium containing polycations and not from their amidine analogues.

### INTRODUCTION

Cationic polymers are under investigation as alternatives to viral systems for the delivery of therapeutic genes (1–6). Several recent reports have indicated that structural differences in polycations have a considerable effect on nucleic acid condensation, polyplex stability, toxicity, and cellular uptake (1, 7–21). In Part 1 of our study (1), efforts aimed at elucidating structure–property relationships between carbohydrate-containing polyamides and their ability to deliver plasmid DNA (pDNA) are described. It was found that the structure indeed played a role in the toxicity of the polycation in cultured cells, and as the charge center was moved away from the carbohydrate unit within the polycation backbone, the toxicity increased (1). In addition, by increasing the size of the carbohydrate moiety, a reduction in the toxicity was observed.

The identification of subtle structure–property relationships prompted us to further investigate other changes within this family of polycations in hopes of enhancing the understanding of how charge variations affect the properties of carbohydrate-containing, polycationic, gene delivery vectors. A number of studies have recently indicated that there is a relationship between charge center type, toxicity, and delivery efficiency. For instance, van de Wetering et al. investigated a series of cationic methacrylate and methacrylamide polymers and determined that small changes in the structure and charge type did not have a large effect on the pDNA condensing

properties, although substantial changes in the cytotoxicity and transfection capabilities were observed (14). Molecular modeling studies were used to help clarify their findings, and it was discovered that polycations having a low number of interactions with DNA possessed higher gene expression. Wolfert and co-workers also investigated a family of polymethacrylates for the influence of charge spacing, charge type, and molecular weight and found that as the pendant charge was further removed from the polymer backbone, pDNA condensation was less efficient (21). In addition, gene expression levels were influenced by charge type where polymethacrylates containing quaternary ammonium charges exhibited low transfection efficiency.

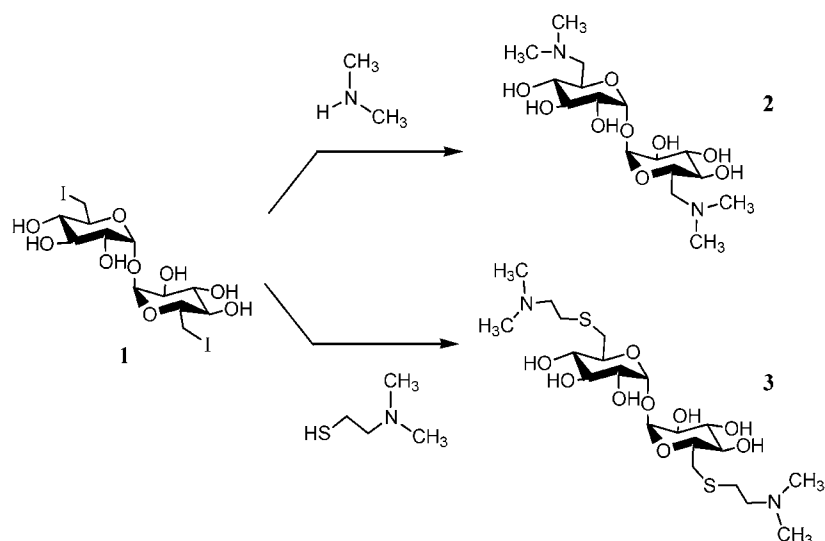
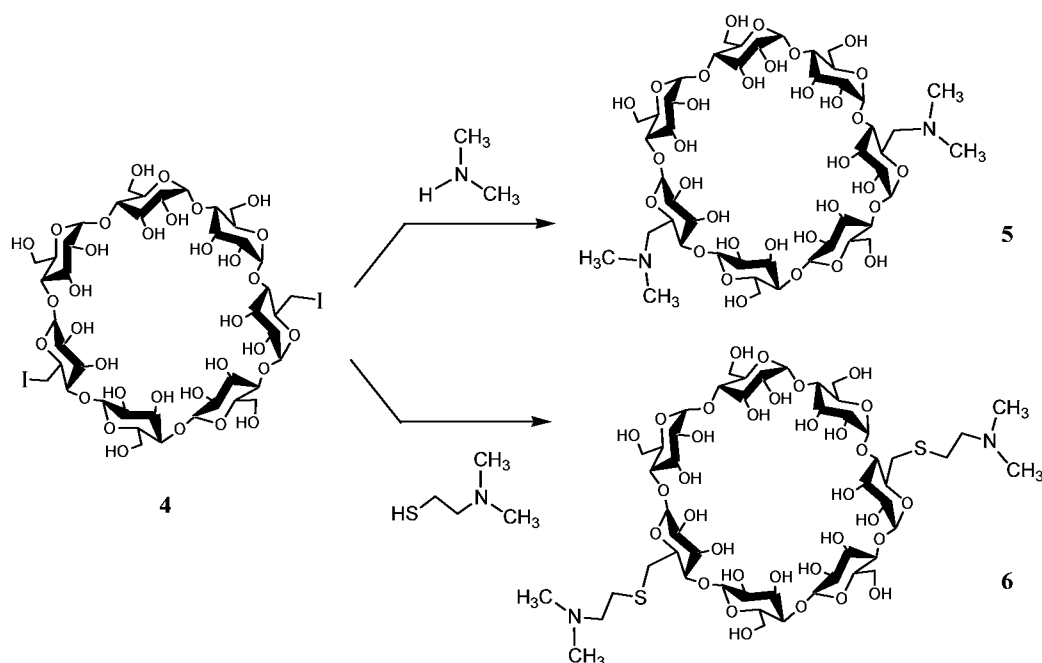
Here, we describe the synthesis and characterization of a new family of carbohydrate-containing polyquaternary ammonium vectors. The polycations were synthesized from *N,N,N,N*-tetramethyl-1,6-hexanediamine, D-trehalose, and  $\beta$ -cyclodextrin in an effort to create a group of polycations related to the amidine carbohydrate polycations (1) and to compare the results of transfection experiments between the two polycation families.

### MATERIALS AND METHODS

**Monomer and Polycation Synthesis.** All reagents were purchased from Aldrich Chemical Co. (Milwaukee, WI) with the exception of the dimethylaminoethanethiol that was obtained from Research Organics, Inc. (Cleveland, OH) and the  $\beta$ -cyclodextrin, which was purchased from Wacker Biochem Corp (Adrian, MI). Electrospray mass spectra were obtained from the Beckman Institute Mass Spectrometry Center on a Perkin-Elmer SCIEX API 365 in positive ion mode. NMR spectra were collected on a Varian 300 MHz spectrometer (75.5 MHz for <sup>13</sup>C)

\* To whom correspondence should be addressed. mdavis@cheme.caltech.edu.

<sup>†</sup> Current address: Department of Chemistry, University of Cincinnati, Cincinnati, OH 45221.

**Scheme 1****Scheme 2**

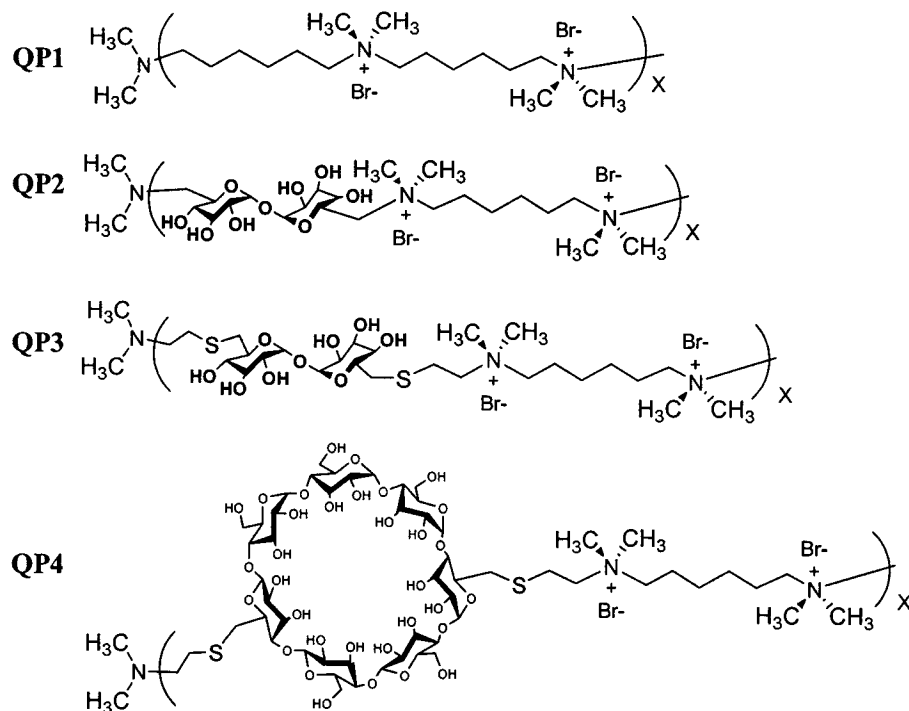
with trimethylsilylpropionic acid sodium salt as an internal standard. All amine products were purified over a Toyopearl SP-650M ion-exchange column using a gradient of ammonium bicarbonate (0–0.3 M) as the eluant. TLC on amine products were performed as previously described and spots were detected by using  $\text{I}_2$  (**8**). 6,6'-diiodo-6,6'-dideoxy-D-trehalose **1** and 6A,6B-diiodo-6A,6B-dideoxy- $\beta$ -cyclodextrin **4** were synthesized as previously described in Part 1 of this study (**1**, **7**, **8**).

*N,N,N,N*-Tetramethyl-6,6'-diamino-6,6'-dideoxy-D-trehalose **2** (Scheme 1). **1** (0.364 g, 0.648 mmol) was dissolved in 25 mL of 2.0 M dimethylamine in methanol. The reaction was stirred at 70 °C for 6 h, stirred at room-temperature overnight, and then concentrated. The residue was redissolved in 25 mL of water, brought to a pH = 1.8, and then purified on the cation exchange column. The appropriate fractions were combined and lyophilized to dryness yielding a white solid, **2** (0.134 g, 52%). ES/MS:  $m/z$  397  $[\text{M} + \text{H}]^+$ , 419  $[\text{M} + \text{Na}]^+$ .  $^{13}\text{C}$  NMR ( $\text{D}_2\text{O}$ ):  $\delta$  95.93, 74.77, 74.69, 73.21, 71.16, 62.13, 46.80.

*N,N,N,N*-Tetramethyl-6,6'-diaminoethanethio-6,6'-dideoxy-D-trehalose **3** (Scheme 1). To a flask containing 60 mL of degassed  $\text{dH}_2\text{O}$  was added dimethylaminoethanethiol (0.693 g, 6.6 mmol). Under constant stirring, **1** (0.606 g, 1.10 mmol) was then added in 4 equal installments over 30 min and then stirred at 75 °C for 5 h. This mixture was then concentrated to a residue, resuspended in 20 mL of  $\text{dH}_2\text{O}$ , and acidified to a pH = 1.8. After purification with the Toyopearl column, the appropriate fractions were combined and lyophilized to dryness yielding a white product, **3** (0.347 g, 61%) ES/MS:  $m/z$  517  $[\text{M} + \text{H}]^+$ .  $^{13}\text{C}$  NMR ( $\text{D}_2\text{O}$ ):  $\delta$  95.27, 74.97, 74.84, 73.58, 73.43, 59.96, 46.07, 35.23, 31.33.

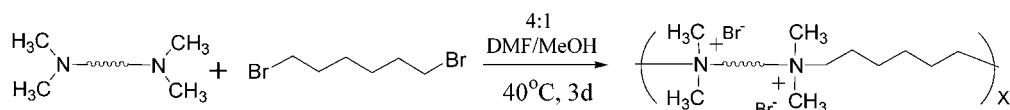
*N,N,N,N*-Tetramethyl-6A,6B-diamino-6A,6B-dideoxy- $\beta$ -cyclodextrin **5** (Scheme 2). **4** (2.169 g, 1.6 mmol) was dissolved in 2 M dimethylamine in methanol (77 mL) and was stirred at 70 °C. After 7 h the reaction was cooled to room temperature and stirred overnight. The methanol was evaporated, the crude product redissolved in methanol, evaporated again, and pumped on overnight to remove residual dimethylamine. The crude product was





**Figure 1.** Schematic structures of the quaternary ammonium polycations QP1–QP4.

### Scheme 3



then dissolved in water, acidified to pH = 2.0, and purified yielding a white solid, **5** (0.528 g, 28%). ES/MS:  $m/z$  1190  $[M + H]^+$ ,  $^{13}\text{C}$  NMR ( $\text{D}_2\text{O}$ ):  $\delta$  104.16, 103.47, 86.39, 83.64, 82.84, 82.70, 75.45, 74.43, 74.30, 71.82, 62.72, 61.56, 47.26.

*N,N,N,N*-Tetramethyl-6<sup>A</sup>,6<sup>D</sup>-diaminoethanethio-6<sup>A</sup>,6<sup>D</sup>-dideoxy- $\beta$ -cyclodextrin **6** (Scheme 2). To a flask containing  $\text{dH}_2\text{O}$  was added dimethylaminoethanethiol (0.630 g, 6.0 mmol), and the mixture was stirred at 80 °C. Next, **4** (1.350 g, 1.0 mmol) was added to this mixture in 4 aliquots over 30 min and then stirred for an additional 4.5 h at temperature. The mixture was then dried in vacuo, resuspended in water, acidified to a pH = 1.5, and purified on the ion exchange column. Fractions containing the product were combined and lyophilized yielding a white solid, **6** (0.53 g, 53%). ES/MS:  $m/z$  1310  $[M + H]^+$ ,  $^{13}\text{C}$  NMR ( $\text{D}_2\text{O}$ ): 104.79, 104.55, 87.53, 84.34, 75.88, 74.65, 63.11, 60.95, 46.98, 35.95, 32.23

**Polymerization.** The polycations QP1–QP4 (see Figure 1) were synthesized via Menschutkin polymerization (Scheme 3) by combining a ditertiary amine comonomers with dibromohexane and mixing the reaction in a solvent for 3 days at temperature (22). For example, **3** (0.103 g, 0.20 mmol) was combined in a small scintillation vial with 0.6 mL of a 4:1 dimethylformamide:methanol solution. Next, 1,6-dibromohexane (0.055 g, 0.23 mmol) was added, and the mixture was stirred for 3 days at 40 °C. The solution was then suspended in a 50% solution of methanol in  $\text{dH}_2\text{O}$ , added to a 1000 MWCO dialysis membrane (Spectrum Laboratories) (1000 MWCO was used for the tetramethyl-1,6-hexanediamine and trehalose polycations, 2000 MWCO membranes were used for the  $\beta$ -cyclodextrin analogues), dialyzed in 30% methanol

in water for 3 h to remove residual dibromohexane, and then dialyzed exhaustively with several water changes for 72 h.

**Polycation Characterization.** Polycation molecular weights were determined by static light scattering. The polycations were analyzed on a Waters 515 HPLC system equipped with a Wyatt Technologies Corp. DAWN EOS in conjunction with an Optilab DSP interferometric refractometer or on a Hitachi D6000 HPLC system equipped with a ERC-7512 refractive index detector and a Precision Detectors PD2020/DLS. Each sample was prepared at a concentration between 50 and 70 mg/mL and injected onto a Polymer Labs Aquagel-OH 30 column with an eluant flow rate of 0.7 mL/min. The eluant was 0.8 M ammonium acetate, brought down to pH = 2.8 with formic acid. The refractive index increment values were determined in the same eluant at 25 °C (633 nm).

**Gel Retardation Experiments.** Each polycation was examined for its ability to bind pDNA through gel electrophoresis experiments as previously described (7). A 1  $\mu\text{g}$  amount of pGL3-CV (10  $\mu\text{L}$  of a 0.1  $\mu\text{g}/\mu\text{L}$  in DNase free water) was mixed with an equal volume of polymer at charge ratios between 0 and 5.0  $\pm$ . Each solution was incubated for approximately 30 min. A 2  $\mu\text{L}$  volume of loading buffer was added to each sample, and then 10  $\mu\text{L}$  of each sample was pipetted into the wells of a 0.6% agarose gel containing 6  $\mu\text{g}$  of ethidium bromide/100 mL TAE buffer (40 mM Tris-acetate, 1 mM EDTA) and electrophoresed.

**Dynamic Light Scattering and Zeta-Potential.** The polyplex size and zeta-potential were measured using a ZetaPals dynamic light scattering instrument (Brookhaven Instruments Corporation, Holtsville, NY) as

**Table 1. The Polycation Percent Yield, Refractive Index Increment, Molecular Weight, Polydispersity, and Degree of Polymerization Data for the Carbohydrate-Containing Quaternary Ammonium Polycations QP1–QP4 (Figure 1) As Determined by Static Light Scattering**

polycation	yield, %	dn/dc	$M_w$ (kDa)	$M_w/M_n$	degree of polymerization
QP1	53	0.149	12.5	1.68	30
QP2	38	0.154	6.0	1.53	14
QP3	32	0.162	3.4	2.60	12
QP4	37	0.140	9.8	1.30	6

previously described (7, 8). A 2  $\mu$ g amount of pGL3-CV was complexed with each polymer at a charge ratio of  $10 \pm$  and allowed to stand for 30 min before diluting to 1.2 mL of dH<sub>2</sub>O. The results for each sample are reported as an average of five measurements for the polyplex size and an average of 10 data points for the zeta-potential.

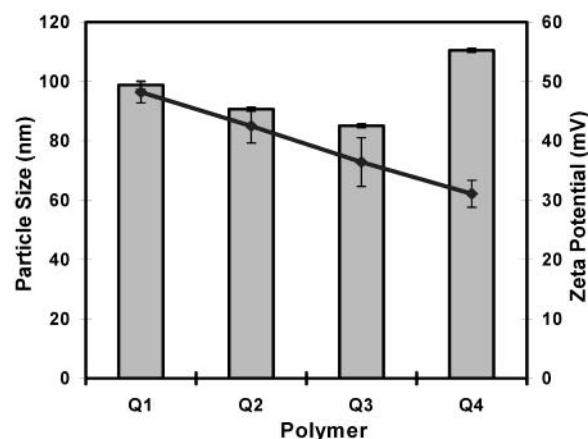
**Cell Culture Experiments.** Plasmid pGL3-CV (Promega, Madison WI) containing the luciferase gene under the control of the SV40 promoter was amplified by *Escherichia coli* strain DH5 $\alpha$  and was then purified using a Novagen Ultramobius 1000 plasmid kit. BHK-21 cells were purchased from ATCC (Rockville, MD) and maintained in Dulbecco's Modified Eagle Medium (DMEM) supplemented with 10% FBS, 100 units/mg penicillin, 100  $\mu$ g/mL streptomycin, and 0.25  $\mu$ g/mL amphotericin at 37 °C and 5% CO<sub>2</sub>. Media and supplements were purchased from Gibco BRL (Gaithersburg, MD). BHK-21 cells were plated at 50000 cells per well in 24 well plates and incubated for 24 h.

A 60  $\mu$ L volume of polycation dissolved in DNase free water (Gibco BRL) was added to 60  $\mu$ L of plasmid DNA (0.05  $\mu$ g/ $\mu$ L in DNase free water) at charge ratios of 3, 5, 10, 15, 20 (polymer +/DNA –). The mixtures were incubated for 30 min and then diluted to 600  $\mu$ L with serum free media. Twenty four hours after cell plating, the cells were transfected with 1  $\mu$ g of pGL3-CV complexed with each of the polymers above (QP1–QP4) at the various charge ratios (200  $\mu$ L of each solution above) and with naked pDNA in triplicate in serum free media. After 4 h, 800  $\mu$ L of DMEM was added to each well. Twenty four hours after transfection, the media was replaced with 1 mL of DMEM. Forty eight hours after transfection, cell lysates were analyzed for luciferase protein activity with results reported in relative light units (RLUs) as previously described (7). Toxicities were determined by a modified version of the Lowry protein assay with a Bio-Rad (Hercules, CA) DC Protein Assay Kit also as previously described (7).

Transfections were also completed with polyplexes prepared from pDNA and polycations AP3 and QP3 at charge ratios of 3, 5, and  $10 \pm$  in the presence of chloroquine. These experiments were carried out using the same procedure above with the exception that chloroquine was added at concentrations of 0, 50, 100, and 200  $\mu$ M to the serum free media in which the polyplexes were diluted in.

## RESULTS

**Monomer and Polycation Synthesis and Characterization.** Each monomer was synthesized in accordance to the procedures described above (depicted in Schemes 1 and 2). Monomers were prepared via nucleophilic substitution of the halogenated analogue with the corresponding amine derivative. All of the polycations were prepared via the Menshutkin reaction by combining the tertiary amine-functionalized comonomers with dibromohexane in a solution of dimethylformamide and



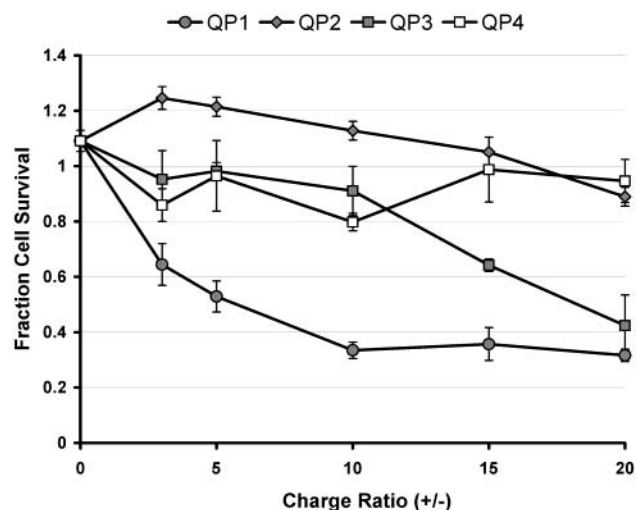
**Figure 2.** Comparison of the hydrodynamic diameter of the polyplexes formed by complexing QP1–QP4 with pDNA as measured by dynamic light scattering (illustrated by the bars on the graph). The results shown are reported as an average of five measurements. The particle charge is denoted by (◆) as determined by zeta-potential measurements. The results are reported as an average of 10 measurements. Polyplexes were prepared by combining 2  $\mu$ g of DNA at a charge ratio of  $10 \pm$  and diluting to a total volume 1.2 mL.

methanol as shown in Scheme 3. Polymerizations proceeded accordingly with the exception of monomer 5, which would not undergo polymerization. The reaction of 5 with 1,6-dibromohexane was attempted in several solvent combinations without success. The polymer yield, molecular weight, degree of polymerization, and polydispersity index were determined by static light scattering, and the results are given in Table 1 for each polycation.

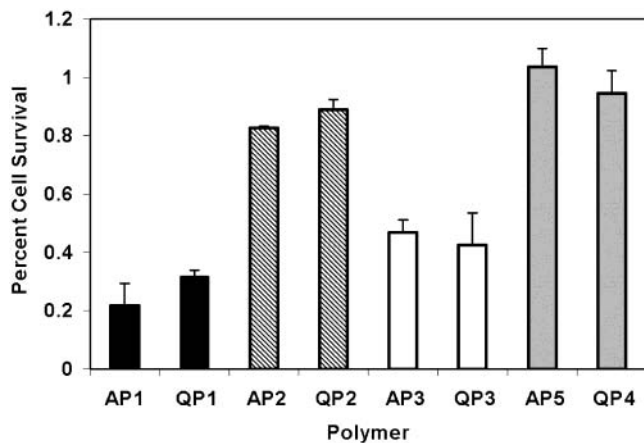
**pDNA Binding Studies and Polyplex Characterization.** The polycations were complexed with pDNA at several charge ratios between 0 and  $5.0 \pm$  and the point of charge neutralization determined by agarose gel electrophoresis. All polycations bound and neutralized pDNA at and above a charge ratio of  $1.0 \pm$ .

To determine both the particle size and the surface charge of the polyplexes, each polycation was complexed with pDNA at a charge ratio of  $10 \pm$  and analyzed for particle size using dynamic light scattering and surface charge using zeta-potential. As shown in Figure 2, the polyplexes formed by each of the polycations were all between 90 and 110 nm. In addition, the surface charge of these the polyplexes was positive indicating an excess of polycation charge relative to the charge of the pDNA. Positive zeta-potentials provide for endocytosis with cultured cells (23).

**In Vitro Toxicity and Transfection of the Polyplexes.** BHK-21 cells were plated in 24-well plates and transfected under serum-free conditions using 1  $\mu$ g of pGL3-CV complexed with each polycation at charge ratios of 3, 5, 10, 15, and  $20 \pm$ . Toxicities associated with the polyplexes at various charge ratios were determined by measuring the total protein concentration in the cell lysates after 48 h following initial transfection and normalizing the data with protein levels from untransfected cells. As shown in Figure 3, at a charge ratio of  $3 \pm$ , the toxicity associated with polymer QP1 becomes evident where about 70% cell survival is obtained. At a charge ratio of  $20 \pm$ , only about 30% of the cells survived. Polycation QP3 also shows elevated toxicity levels, and at a charge ratio of  $20 \pm$ , approximately 40% of the cells survived. Polycations QP2 and QP4 were essentially nontoxic to BHK-21 cells. Toxicity comparisons between AP and QP type polycations are shown in Figure 4.



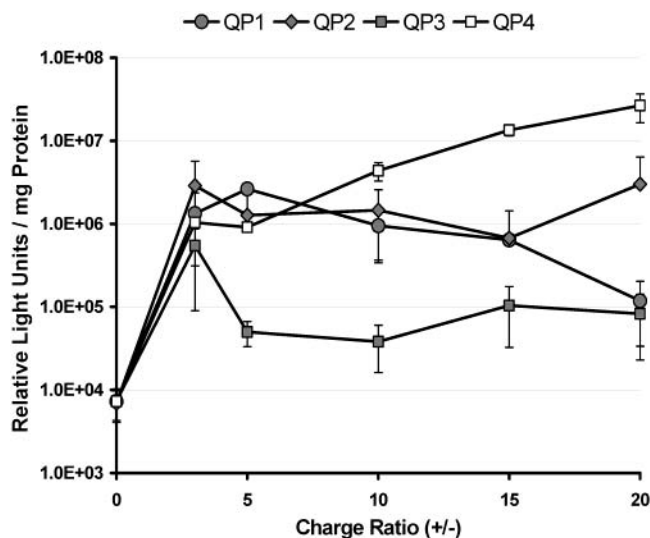
**Figure 3.** Comparison of the relative toxicities of the carbohydrate quaternary ammonium polymers QP1–QP4 at charge ratios of 0, 3, 5, 10, 15, and 20 with BHK-21 cells. Cell survival was determined by assaying for total protein content and normalizing each sample with the protein concentration for untransfected cells. The data are reported as a mean  $\pm$  SD of three samples.



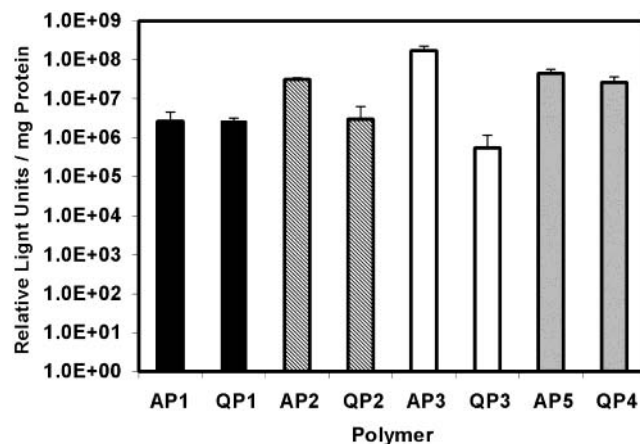
**Figure 4.** Toxicity comparison of analogous AP and QP polyplexes at a charge ratio of  $20 \pm$  in BHK-21 cells. Data were normalized to untransfected cells for each study.

Transfection efficiencies of the polyplexes were determined by assaying for luciferase protein activity, and the results are reported in relative light units (RLUs) per mg of protein. Several polycation (+) to DNA (–) charge ratios were tested, and the results are shown in Figure 5. QP4 is found to have the highest transfection efficiency, but only at higher charge ratios. Both QP1 and QP2 give similar gene expression values at lower charge ratios; however, at  $20 \pm$ , QP2 exhibits higher expression (likely due to the high toxicity of QP1). The lowest gene expression was obtained from QP3. Transfection efficiency comparisons between AP and QP type polycations are illustrated in Figure 6.

Transfections were also conducted in the presence of 0, 50, 100, and  $200 \mu\text{M}$  chloroquine in serum free media with naked pDNA and with polyplexes formed with polymers AP3 and QP3 at charge ratios of 3, 5, and  $10 \pm$ . Polycations AP3 and QP3 were compared in this experiment because of the large difference in gene expression values obtained for these polycations (Figure 6). As depicted in Figure 7, for almost all cases, the addition of chloroquine to transfection experiments using polyplexes formed from AP3 actually resulted in a



**Figure 5.** Comparison of transfection efficiencies of the QP1–QP4 polyplexes with BHK-21 cells at charge ratios of 0, 3, 5, 10, 15, and  $20 \pm$  as determined by luciferase protein activity. Data are presented as a mean  $\pm$  SD of three replicates.



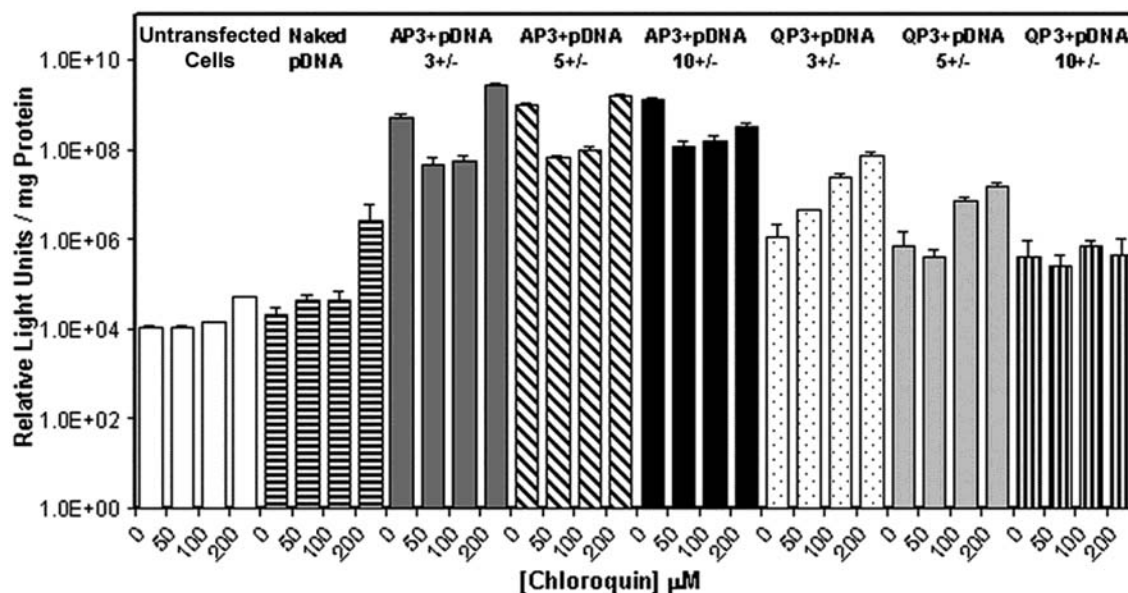
**Figure 6.** Comparison of transfection efficiencies for the analogous AP and QP polyplexes with BHK-21 cells as determined by luciferase protein activity. Data points represent the maximum transfection for each vector.

decrease in gene expression (most likely due to an increase in cell death from the associated toxicity of chloroquine). It is shown that at charge ratios of both 3 and  $5 \pm$ , the addition of  $200 \mu\text{M}$  of chloroquine did cause a small increase in gene expression. However, for polymer QP3, a substantial increase in gene expression is observed at both charge ratios of 3 and  $5 \pm$ . At a charge ratio of  $3 \pm$ , gene expression increases systematically with increasing concentration of chloroquine, and at a concentration of  $200 \mu\text{M}$ , a 63-fold increase in gene expression is observed. At a charge ratio of  $5 \pm$ , an overall 20-fold increase in gene expression is noted. At a charge ratio of  $10 \pm$ , gene expression levels do not increase with QP3 and this is likely due to the high degree of cell death (between 20 and 40% cell survival) that is observed at this charge ratio.

## DISCUSSION

A series of carbohydrate-containing polycations with quaternary ammonium DNA-binding centers were synthesized to study the effect of charge center type on toxicity and gene delivery efficiency. The effect of charge center type was assessed by comparing the results obtained to those from polycations possessing amidine





**Figure 7.** The effects of chloroquine on the transfection efficiency of polyplexes formed with polycations AP3 and QP3. Chloroquine concentrations of 0, 50, 100, and 200  $\mu\text{M}$ , and polycation charge ratios of 3, 5, and 10  $\pm$  were tested with BHK-21 cells.

charges (investigated in Part 1). Synthesis of the tertiary amine monomers is accomplished through the substitution of the diiodo-carbohydrate molecule with the corresponding nucleophile as depicted in Schemes 1 and 2. Polymerizations of the tertiary amine comonomers with dibromohexane proceed efficiently through Menshutkin quaternization, as shown in Scheme 3, with the exception of monomer **5**, which did not react. Previous synthetic studies with this type of polymerization reaction by Rembaum and co-workers indicate that solvent is an important variable in the kinetics of formation (22). Polymerization of **5** was attempted with several batches of monomer as well as in several solvent systems including dimethylformamide, methanol, water, and dimethyl sulfoxide without success. The polymerization of **5** may not be possible due to the steric hindrance around the amine from the bulky cyclodextrin unit. All other monomers were successfully polymerized (Figure 1). Polycation data such as molecular weights, degrees of polymerization, and polydispersity indices are displayed in Table 1. Clearly, the degree of polymerization is dependent on the structure of the diamine.

As expected, all polycations neutralize pDNA above a charge ratio of 1.0 according to agarose gel electrophoresis experiments. Polyplexes prepared from the quaternary ammonium polymers QP1–QP4 were analyzed using dynamic light scattering and found to be less than 110 nm (QP4 forms the largest polyplexes at 110 nm). zeta-potential measurements show that all polyplexes have high positive surface charge (Figure 2).

Toxicity studies (Figure 3) reveal that QP1 (lacks a carbohydrate unit) is the most toxic polycation to BHK-21 cells where only 30% cell viability is observed at a charge ratio of 20  $\pm$ . In addition, the trehalose polymer, QP3 is found to be relative toxic (40% cell survival at 20  $\pm$ ). These observations are consistent to those found with polyamides (Part 1) where the amidine analogue of QP3 (AP3) was found to be the most toxic of the carbohydrate-containing polycations. QP2 exhibits only slight toxicity with 90% cell viability at 20  $\pm$ , and QP4 is essentially nontoxic. Figure 4 shows the toxicity comparison between the amidine and the quaternary ammonium polycations. Both polycations that lack a carbohydrate, AP1 and QP1, are the most toxic to cells. Note that these polycations

have higher degrees of polymerization and this may influence the toxicity. However, since QP1 is approximately 3 times longer than AP1, and their toxicities to BHK-21 cells are similar, the toxicity of these non-carbohydrate polycations may not be influenced by chain length in the range investigated here. A similar trend exists between the both polycation families where toxicity increases as the charge center is moved further away from the carbohydrate moiety (AP2, AP3, QP2, QP3). However, the effect is not as severe with the  $\beta$ -cyclodextrin polycations. In general, the toxicity does not appear to significantly vary between each analogous quaternary ammonium and amidine polycation (Figure 4).

Transfection efficiencies as determined by luciferase protein activity show that QP3 generally gives lower transfection efficiency than QP1, QP2, and QP4 (Figure 5). QP4 reveals increasing gene expression with increasing polycation amount. This effect is also noted with  $\beta$ -cyclodextrin polyamides and may be attributed to the slight membrane disruption ability of cyclodextrins (24). Figure 6 shows a comparison of the transfection efficiencies for both families of polycations (polyamides and the polyquaternary ammonium). The data displayed in Figure 6 are for the maximum transfection. In every case with carbohydrate-containing polycations, it is observed that the quaternary ammonium polycations give lower gene expression values than the amidine analogues, and the largest difference is noted between AP3 and QP3.

Transfections with AP3 and QP3 polyplexes were performed with the lysosomotropic agent, chloroquine (Figure 7). Chloroquine is known to promote endosomal release of some types of polyplexes. In Part 1 (1), it was noticed that AP3 exhibited the highest transfection efficiency in the series of amidine polymers. However, here it is shown that the quaternary ammonium analogue of AP3 (QP3) displays the lowest transfection efficiency. If this discrepancy is due to the inability of the quaternary ammonium polycations to be released from the endosomes, then the addition of chloroquine may affect the gene expression. There is not a significant increase in gene expression in the presence of chloroquine for AP3, while for QP3 at charge ratios of 3 and 5  $\pm$ , gene expression increases with chloroquine concentration (Figure 7). These results could indicate that the amidine

analogues have improved endosomal escape properties relative to the quaternary ammonium analogues. An exception to this finding is QP4, where at a charge ratio of  $20 \pm$ , relatively high transfection efficiency is noted. As previously mentioned, this may be due to the slight membrane disruption ability of the  $\beta$ -cyclodextrin moiety that may contribute to increase the endosomal escape (24).

Reports by Wolfert et al. also reveal that quaternized methacrylate polymers transfected poorly as compared to methacrylate polymers that contain secondary amine DNA-binding centers (21). These studies indicate that although quat-based polyplexes produce efficient intranuclear transcription following injection into *Xenopus* oocytes, the lack of transfection could be attributed to the absence of pH responsiveness of the quaternized polycation. In addition, van de Wetering et al. also observed low transfection efficiency from a quaternized methacrylate polymer (14). The inability of the quaternized derivatives to escape from the endosomes was confirmed by an experiment in where they added an endosome-disruptive agent (adenovirus) during the transfection experiment that led to a substantial increase in transfection efficiency.

In conclusion, a series of quaternary ammonium polymers containing *N,N,N,N*-tetramethyl-1,6-hexanediamine, D-trehalose, and  $\beta$ -cyclodextrin were synthesized and studied for their ability to bind pDNA and to deliver pDNA to BHK-21 cells. The results obtained indicate that the charge center type does not considerably influence the toxicity since no significant difference in toxicity was noted between the polycation families (quaternary ammonium versus amidine). However, it was found that the charge center type does have a significant influence on gene delivery efficiency since the amidine polycations consistently exhibit higher gene expression than their quaternary ammonium analogues. This result may be due in part to the inability of quat-based polyplexes to escape from endosomes since the addition of chloroquine to transfection experiments increased gene expression for QP3 but not with AP3.

#### ACKNOWLEDGMENT

We thank Insert Therapeutics, Inc. for partial support of this project. T.M.R. would like to thank the NIH for a National Research Service Award (1-F32 GM64919-01). We are grateful to Jeremy Heidel for his help with some of the chloroquine transfection experiments and Swaroop Mishra for amplifying the pDNA.

#### LITERATURE CITED

- (1) Reineke, T. M., and Davis, M. E. (2003) Structural effects of carbohydrate-containing polycations on gene delivery. Carbohydrate size and its distance from charge centers. *Bioconjugate Chem.* 14, 247–254.
- (2) Rubanyi, G. M. (2001) The future of human gene therapy. *Mol. Aspects Med.* 22, 113–142.
- (3) Li, S., and Ma, Z. (2001) Nonviral gene therapy. *Curr. Gene Ther.* 1, 201–226.
- (4) Han, S., Mahato, R. I., Sung, Y. K., and Kim, S. W. (2000) Development of biomaterials for gene therapy. *Mol. Ther.* 2, 302–317.
- (5) Ma, H., and Diamond, S. L. (2001) Nonviral gene therapy and its delivery systems. *Curr. Pharm. Biotechnol.* 2, 1–17.
- (6) De Smedt, S. C., Demeester, J., and Hennink, W. E. (2000) Cationic polymer based gene delivery systems. *Pharm. Res.* 17, 113–126.
- (7) Gonzalez, H., Hwang, S. J., and Davis, M. E. (1999) New class of polymers for the delivery of macromolecular therapeutics. *Bioconjugate Chem.* 10, 1068–1074.
- (8) Hwang, S. J., Bellocq, N. C., and Davis, M. E. (2001) Effects of structure of  $\beta$ -cyclodextrin-containing polymers on gene delivery. *Bioconjugate Chem.* 12, 280–290.
- (9) Hwang, S. J. and Davis, M. E. (2001) Cationic polymers for gene delivery: Designs for overcoming barriers to systematic administration. *Curr. Opin. Mol. Ther.* 3, 183–191.
- (10) Jones, N. A., Hill, I. R. C., Stolnik, S., Bignotti, F., Davis, S. S., and Garnett, M. C. (2000) Polymer chemical structure is a key determinant of physicochemical and colloidal properties of polymer-DNA complexes for gene delivery. *Biochim. Biophys. Acta* 1517, 1–18.
- (11) Neiman, Z., and Quinn, F. R. (1981) Quantitative structure–activity relationships of purines I: Choice of parameters and prediction of  $pK_a$  values. *J. Pharm. Sci.* 70, 425–430.
- (12) Tang, M., and Szoka, F. (1997) The influence of polymer structure on the interactions of cationic polymers with DNA and the morphology of the resulting complexes. *Gene Ther.* 4, 823–832.
- (13) Wadhwa, M. S., Collard, W. T., Adami, R. C., McKenzie, D. L., and Rice, K. G. (1997) Peptide-mediated gene delivery: Influence of peptide structure on gene expression. *Bioconjugate Chem.* 8, 81–88.
- (14) van de Wetering, P., Moret, E. E., Schuurmans-Nieuwenbroek, N. M. E., van Steenberg, M. J., and Hennink, W. E. (1999) Structure–activity relationships of water-soluble cationic methacrylate/methacrylamide polymers for nonviral gene delivery. *Bioconjugate Chem.* 10, 589–597.
- (15) Murphy, J. E., Uno, T., Hamer, J. D., Cohen, F. E., Dwarki, V., and Zuckerman, R. N. (1998) A combinatorial approach to the discovery of efficient cationic peptoid reagents for gene delivery. *Proc. Natl. Acad. Sci. U.S.A.* 95, 1517–1522.
- (16) Fischer, D., Bieber, T., Li, Y., Elsasser, H.-P., and Kissel, K. (1999) A novel nonviral vector for DNA delivery based on low molecular weight, branched polyethylenimine: Effect of molecular weight on transfection efficiency and cytotoxicity. *Pharm. Res.* 16, 1273–1279.
- (17) Ferruti, P., Manzoni, S., Richardson, S. C. W., Duncan, R., Patrick, N. G., Mendichi, R., and Casolaro, M. (2000) Amphoteric linear poly(amido-amines)s as endosomolytic polymers: Correlation between physicochemical and biological properties. *Macromolecules* 33, 7793–7800.
- (18) Godbey, W. T., Wu, K. K., and Mikos, A. G. (1999) Size matters: Molecular weight affects the efficiency of poly(ethylenimine) as a gene delivery vehicle. *J. Biomed. Mater. Res.* 45, 268–275.
- (19) Plank, C., Tang, M. X., Wolf, A. R., and Szoka, F. C. (1999) Branched cationic peptides for gene delivery: Role of type and number of cationic residues in formation and in vitro activity of DNA polyplexes. *Hum. Gene Ther.* 10, 319–332.
- (20) Wagner, E., Cotten, M., Foisner, R., and Birnstiel, M. L. (1991) Transferrin-polycation–DNA complexes: The effect of polycations on the structure of the complex and DNA delivery to cells. *Proc. Natl. Acad. Sci. U.S.A.* 88, 4255–4259.
- (21) Wolfert, M. A., Dash, P. R., Nazarova, O., Oupicky, D., Seymour, L. W., Smart, S., Strohalm, J., and Ulbrich, K. (1999) Polyelectrolyte vectors for gene delivery: Influence of cationic polymer on biophysical properties of complexes formed with DNA. *Bioconjugate Chem.* 10, 993–1004.
- (22) Rembaum, A., Rile, H., and Somoano, R. (1970) V. Kinetics of formation of high charge density ionene polymers. *Polym. Lett.* 8, 457–466.
- (23) Mislick, K. A., and Baldeschwieler, J. D. (1996) Evidence for the role of proteoglycans in cation-mediated gene transfer. *Proc. Natl. Acad. Sci. U.S.A.* 93, 12349–12354.
- (24) Rodal, S. K., Skretting, G., Garred, O., Vilhardt, F., van Deurs, B., and Sandvig, K. (1999) Extraction of cholesterol with methyl- $\beta$ -cyclodextrin perturbs formation of clathrin-coated endocytic vesicles. *Mol. Biol. Cell* 10, 961–974.

# A Concise Synthesis of the 3-*O*- $\beta$ -D- and 4'-*O*- $\beta$ -D-Glucuronide Conjugates of *trans*-Resveratrol

David A. Learmonth\*

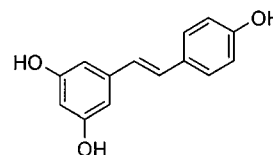
Laboratory of Chemistry, Department of Research & Development, BIAL, À Avenida da Siderurgia Nacional, 4745-457 S. Mamede do Coronado, Portugal. Received July 22, 2002;  
Revised Manuscript Received October 7, 2002

*trans*-Resveratrol ((*E*)-3,4',5-trihydroxystilbene, **1**) is a phytoalexin produced naturally in plants and grape skins as a stress metabolite protecting against fungal attack. Widespread interest in this apparently structurally simple molecule and synthetic stilbene analogues has arisen in recent years due to the discovery of its antioxidant, antiinflammatory, and anti-carcinogenic activities, among others. Although *O*-conjugation with glucuronic acid in vivo is known to represent a significant metabolic pathway for polyphenolic compounds in general and **1** in particular, preclinical studies have been hampered by the lack of chemically pure, completely characterized reference standards of both regioisomeric 3-*O*- $\beta$ -D- and 4'-*O*- $\beta$ -D-glucuronide conjugates of **1** for adequate identification and quantification of these significant metabolites. The present work describes a concise, convergent synthesis of both 3-*O*- $\beta$ -D- and 4'-*O*- $\beta$ -D-glucuronide conjugates of **1** using a strategy based on a novel Heck coupling of iodoaryl-*O*- $\beta$ -D-glucuronate esters with appropriately substituted styrenes, such that highly pure multimilligram to gram quantities of both the 3-*O*- $\beta$ -D- and 4'-*O*- $\beta$ -D-glucuronide conjugates of **1** can now be conveniently synthesized.

## INTRODUCTION

*trans*-Resveratrol ((*E*)-3,4',5-trihydroxystilbene, **1**) (Figure 1) is an intriguing polyhydroxy-stilbene derivative of apparent structural simplicity that has been detected in several plants (1), peanuts (2), and most abundantly in the skins of red grapes (3), where it is produced as a phytoalexin (plant antibiotic) as part of the defense mechanism against attack by the fungal grapevine pathogen *Bortrytis cinerea* (4). Widespread interest concerning resveratrol is manifested by an increasing number of reports describing its broad range of biological activities. Indeed, initial motivation behind research into **1** began with the discovery of its presence in appreciable (pharmacologically significant) concentrations in red wines, which was upheld as an explanation for the so-called "French Paradox" (5, 6), where despite a diet rich in fat and alcohol, the expected increase in coronary heart disease among the wine-drinking French population is not observed. Consequently, a series of sensitive chromatographic methods have been developed to quantify its concentration in red wines from various regions (7–10). To date, **1** has been shown to exhibit an impressive array of antioxidative (11), anticarcinogenic (12), anti-inflammatory (13), and cardioprotective (5) properties. For example, studies have shown that **1** inhibits the initiation, promotion, and progression of cancer (13), inhibits platelet aggregation and coagulation (14), and acts as a vasorelaxant by inhibiting the contractile response of the aorta to noradrenaline (15). The various relevant physiological properties of **1** have been reviewed and summarized in considerable depth (16).

Despite the enthusiastic push toward reaching clearer assessment of resveratrol's potential health protecting properties in humans, studies of its in vivo metabolism



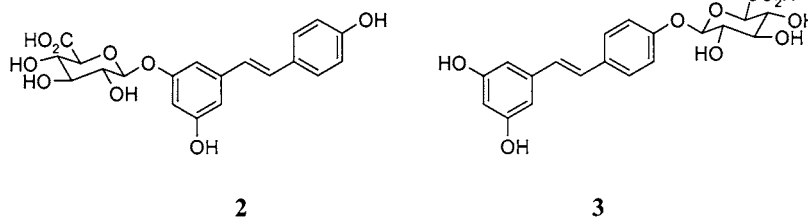
**1**

**Figure 1.** Chemical structure of resveratrol **1**.

have left doubts remaining as to the exact nature of its metabolic profile. Although *O*-conjugation of structurally related polyhydroxylic substrates, such as for example the flavanoids, with glucuronic acid is known to represent a major metabolic pathway for such compounds (17), it was somewhat surprising therefore to fail to discover suitable literature precedent for the chemical synthesis of the regioisomeric 3-*O*- $\beta$ -D- and 4'-*O*- $\beta$ -D-glucuronide conjugates (**2** and **3**, respectively) (Figure 2) of **1** for unequivocal identification and quantification of these conjugates in preclinical metabolic studies. Indeed, two distinct *O*-glucuronide conjugates were detected in a bioavailability study of **1** in the rat, but it was not possible to elucidate the exact position of conjugation or clearly ascertain the relative extent of conjugation at each position. Consequently, enzymatic deconjugation with a  $\beta$ -glucuronidase was required to liberate free **1** for more exact quantification (18). Although chemical synthesis of the naturally occurring 3-*O*- $\beta$ -glycoside (piceid) of **1** has been previously reported (19, 20), two drawbacks of this synthesis are apparent from the outset. The traditional Wittig phosphorus ylid chemistry employed therein to install the central carbon–carbon double bond gave predominantly what would be in this case, the unwanted *cis*-isomer (*cis*/*trans*, 2.3:1 ratio), and equally unfortunately, chromatographic separation of the *cis*/*trans* geometric isomers was difficult, contributing to diminish the overall yield of the desired *trans*-stilbene even

\* Tel: 351-22-9866104. Fax: 351-22-9866192. E-mail: david.learmonth@bial.com.





**Figure 2.** Chemical structures of resveratrol-3-*O*- $\beta$ -D-glucuronide **2** and resveratrol-4'-*O*- $\beta$ -D-glucuronide **3**.

**Table 1. Analytical Data (Combustion Analyses, New Compounds)**

no.	formula	calculated % (C, H)	found % (C, H)
6	C <sub>19</sub> H <sub>21</sub> IO <sub>10</sub>	C, 42.55; H, 3.95	C, 42.85; H, 3.95
8	C <sub>31</sub> H <sub>32</sub> O <sub>14</sub>	C, 59.23; H, 5.13	C, 59.03; H, 4.82
3	C <sub>20</sub> H <sub>20</sub> O <sub>9</sub>	C, 59.40; H, 4.98	C, 59.12; H, 5.29
10	C <sub>19</sub> H <sub>21</sub> IO <sub>11</sub>	C, 41.32; H, 3.83	C, 41.76; H, 4.08
11	C <sub>21</sub> H <sub>23</sub> IO <sub>12</sub>	C, 42.44; H, 3.90	C, 42.86; H, 4.08
13	C <sub>31</sub> H <sub>32</sub> O <sub>14</sub>	C, 59.23; H, 5.13	C, 59.23; H, 5.15
2	C <sub>20</sub> H <sub>20</sub> O <sub>9</sub>	C, 59.40; H, 4.98	C, 59.09; H, 5.26

further. Second, the deprotection procedure described for cleavage of a methoxyl protecting group in the last step (large excess of sodium ethanethiolate in DMF at 140 °C for 10 h) was considered incompatible with the presence of the rather sensitive *O*- $\beta$ -glucuronide substituent. Elsewhere, despite the considerable number of reported methods for chemical synthesis of **1** itself and related derivatives (21–24), there has appeared to date only a single recent report of enzymatic glucuronidation of **1** and its *cis*-isomer using human liver microsomes (25). Unfortunately, this enzymatic method allows for the preparation of only very low quantities of the required glucuronide conjugates, and this lack of appropriate methodology rendered necessary the development of efficient regio- and stereoselective chemical synthesis of both the 3-*O*- $\beta$ - and 4'-*O*- $\beta$ -D-glucuronide conjugates of **1** using a strategy based on a novel Heck coupling of iodoaryl-*O*- $\beta$ -D-glucuronate esters with appropriately substituted styrenes.

#### EXPERIMENTAL PROCEDURES

**Chemistry.** Melting points were measured in open capillary tubes on an Electrothermal Model 9100 hot stage apparatus and are uncorrected. NMR spectra were recorded on a Bruker Avance DPX (400 MHz) Spectrometer with solvent used as internal standard, and data are reported in the following order: chemical shift (ppm), multiplicity (s, singlet; d, doublet; t, triplet; m, multiplet; dd, double doublet; br, broad), number of protons, and approximate coupling constant in Hertz. IR spectra were measured with a Bomem Hartmann & Braun MB Series FTIR spectrometer using KBr tablets (see Table 1). Analytical HPLC was performed on an automated Agilent 1100 Series HPLC, using LiChrospher 100 RP-18 (5 $\mu$ m) LiChroCart 250–4 Cartridges (Merck) in combination with acetonitrile/water (1% formic acid) mixtures. Analytical TLC was performed on precoated silica gel plates (either Merck 60 Kieselgel F<sub>254</sub> or Merck RP-18 F<sub>254s</sub>) and visualized with UV light. Preparative chromatography was done on Merck 60 Kieselgel (0.063–0.2 mm). Elemental analyses were performed on a Fisons EA 1110 CHNS instrument and all analyses are consistent with theoretical values to within  $\pm 0.4\%$  unless otherwise indicated. Solvents and reagents were purchased from Aldrich, E. Merck, and Fluka. 3,5-Diacetoxystyrene **7** was prepared as previously reported by Guiso et al (26) from commercially available 3,5-dihydroxybenzaldehyde. 4-Ac-

etoxystyrene **12** was purchased from Aldrich and used as received. 3,5-Dihydroxyiodobenzene **9** was prepared from commercially available 3,5-dimethoxyaniline via Sandmeyer reaction (59% yield) and demethylation (57% HI, 90% yield) as previously described by Deboves et al (27). The trichloroacetimidate **5** was prepared according to the procedure of Fischer et al. (28).

**4-Iodo-*O*-2,3,4-triacetyl- $\beta$ -D-glucuronopyranosidobenzene Methyl Ester (6).** To a stirred and cooled (ice–water bath) solution of 4-iodophenol **4** (0.66 g, 2.98 mmol) and trichloroacetimidate **5** (2.0 g, 4.18 mmol) in dry dichloromethane (20 mL) under argon was added anhydrous boron trifluoride diethyl etherate (0.59 g, 4.18 mmol) dropwise. The resulting solution was allowed to stir at room temperature for 1 h and then poured onto ice–water (30 mL). The phases were separated, and the aqueous phase was extracted by dichloromethane (10 mL). The combined organic layers were washed by water (40 mL) and brine (40 mL), dried over anhydrous magnesium sulfate, filtered, and evaporated (40 °C, water aspirator pressure) to leave a pale orange residue that solidified on standing. Recrystallization (dichloromethane/2-propanol) afforded colorless crystals (1.30 g, 66%) of mp 161–162 °C. Anal. (C<sub>19</sub>H<sub>21</sub>IO<sub>10</sub>) C, H.

IR (KBr) 1756 cm<sup>−1</sup> (broad, C=O).

<sup>1</sup>H NMR (CDCl<sub>3</sub>)  $\delta$  7.61 (d, 2H, *J* = 8.9 Hz), 6.79 (d, 2H, *J* = 8.9 Hz), 5.40–5.25 (m, 3H), 5.12 (d, 1H, *J* = 7.3 Hz), 4.18 (m, 1H), 3.75 (s, 3H), 2.08 (s, 3H), 2.07 (s, 3H), 2.06 (s, 3H). <sup>13</sup>C NMR (CDCl<sub>3</sub>)  $\delta$  170.7, 169.9, 169.8, 167.3, 157.1, 139.1, 119.9, 99.5, 73.2, 72.2, 71.6, 69.5, 53.6, 21.2, 21.1.

**(*E*)-1-(3,5-Diacetoxyphenyl)-2-(4'-*O*-2,3,4-triacetyl- $\beta$ -D-glucuronopyranosidophenyl)ethene Methyl Ester (8).** To a stirred solution of 3,5-diacetoxystyrene **7** (0.31 g, 1.42 mmol) and the iodoaryl-*O*- $\beta$ -D-glucuronate ester **6** (1.14 g, 1.74 mmol) in dimethylformamide (15 mL) at room temperature under argon were added benzyltriethylammonium chloride (0.32 g, 1.42 mmol), tributylamine (0.69 g, 3.73 mmol), and palladium (II) acetate (15.3 mg, 0.068 mmol). The resulting pale orange solution was stirred at 110 °C for 30 min and then allowed to cool to room temperature. The mixture was poured into water (50 mL) with stirring causing formation of a pale yellow precipitate, which was filtered off and washed with water (5 mL). The precipitate was dissolved in dichloromethane (20 mL), and the organic layer was washed by water (20 mL), 2N HCl (10 mL), water again (10 mL), and brine (20 mL), then dried over anhydrous magnesium sulfate, filtered, and evaporated (40 °C, water aspirator pressure) to leave an orange/brown foam. Chromatography over silica gel (petroleum ether/ethyl acetate, 1:1) afforded the major product as an off-white solid that was triturated with diethyl ether to afford a white powder (0.49 g, 55%) of mp 152–154 °C. Anal. (C<sub>31</sub>H<sub>32</sub>O<sub>14</sub>) C, H.

IR (KBr) 1759 cm<sup>−1</sup> (broad, C=O).

<sup>1</sup>H NMR (DMSO-*d*<sub>6</sub>)  $\delta$  7.58 (d, 2H, *J* = 8.7 Hz), 7.29 (d, 1H, *J* = 16.4 Hz), 7.26 (d, 2H, *J* = 2.1 Hz), 7.14 (d, 1H, *J* = 16.4 Hz), 7.02 (d, 2H, *J* = 8.7 Hz), 6.88 (t, 1H, *J*

= 2.1 Hz), 5.7 (d, 1H,  $J$  = 8.0 Hz), 5.47 (t, 1H,  $J$  = 9.7 Hz), 5.11 (dd, 1H,  $J$  = 8.0 and 9.7 Hz), 5.07 (t, 1H,  $J$  = 9.7 Hz), 4.72 (d, 1H,  $J$  = 9.7 Hz), 3.64 (s, 3H), 2.28 (s, 6H), 2.02 (s, 3H), 2.01 (s, 3H), 2.00 (s, 3H).  $^{13}\text{C}$  NMR (DMSO- $d_6$ )  $\delta$  170.6, 170.4, 170.1, 170.1, 168.1, 157.1, 152.2, 140.5, 132.6, 130.6, 129.2, 126.6, 118.0, 117.6, 97.8, 72.1, 72.0, 71.5, 70.0, 53.7, 21.8, 21.3, 21.2.

**(E)-1-(3,5-Dihydroxyphenyl)-2-(4'-O- $\beta$ -D-glucuronopyranosidophenyl)ethene (3), (trans-Resveratrol-4'-O- $\beta$ -D-glucuronide).** To a stirred and cooled (ice–water bath) suspension of the glucuronate ester **8** (0.39 g, 0.61 mmol) in methanol (9 mL) was added dropwise aqueous 1 N sodium hydroxide solution (9 mL, 9 mmol). The resulting mixture was stirred in the cold for 30 min and then at room temperature for 15 min. The resulting solution was diluted with water (6 mL), and sufficient Amberlyst 15 ion-exchange resin was added with stirring to maintain pH  $\sim$ 2–3. The resin was then filtered off and washed with water (3 mL). The combined filtrate was evaporated (60 °C, water aspirator pressure). Toluene (5 mL) was added to the residue and re-evaporated. The residue was dried at room temperature over phosphorus pentoxide under high vacuum overnight. The resulting solid was triturated with diethyl ether (3 mL) and filtered to give a pale beige solid (0.21 g, 84%), which decomposed without melting above 230 °C. Anal. ( $\text{C}_{20}\text{H}_{20}\text{O}_9$ ) C,H.

IR (KBr) 3383 (very broad, OH) and 1730  $\text{cm}^{-1}$  (C=O).

$^1\text{H}$  NMR (DMSO- $d_6$ )  $\delta$  9.22 (br s, 2H), 7.52 (d, 2H,  $J$  = 8.7 Hz), 7.00 (d, 2H,  $J$  = 8.7 Hz), 6.99 (d, 1H,  $J$  = 16.4 Hz), 6.92 (d, 1H,  $J$  = 16.4 Hz), 6.41 (d, 2H,  $J$  = 1.7 Hz), 6.13 (t, 1H,  $J$  = 1.7 Hz), 5.46 (d, 1H,  $J$  = 3.75 Hz), 5.25 (br, 1H), 5.07 (d, 1H,  $J$  = 7.5 Hz), 3.90 (d, 1H,  $J$  = 9.6 Hz).  $^{13}\text{C}$  NMR (DMSO- $d_6$ )  $\delta$  171.2, 159.5, 157.5, 140.0, 132.1, 128.7, 128.3, 128.3, 117.3, 105.5, 103.1, 100.8, 76.8, 76.4, 74.0, 72.4.

**3-Hydroxy-5-iodo-O-2,3,4-triacetyl- $\beta$ -D-glucuronopyranosidobenzene Methyl Ester (10).** To a stirred and cooled (ice–water bath) solution of 3,5-dihydroxyiodobenzene **9** (2.36 g, 10 mmol) and the trichloroacetimidate **5** (4.79 g, 10 mmol) in dry dichloromethane (50 mL) under argon was added boron trifluoride diethyl etherate (1.42 g, 10 mmol) dropwise. The resulting mixture was allowed to stir at room temperature for forty minutes and then poured onto ice–water (30 mL). The phases were separated and the aqueous phase was extracted by dichloromethane (10 mL). The combined organic layers were washed by water (40 mL) and brine (40 mL), dried over anhydrous magnesium sulfate, filtered, and evaporated (40 °C, water aspirator pressure) to leave a pale yellow foam. Chromatography over silica gel (petroleum ether/ethyl acetate 2:1) afforded the major product as a white solid, (1.93 g, 35%) of mp 186–188 °C. Anal. ( $\text{C}_{19}\text{H}_{21}\text{IO}_{11}$ ) C,H.

IR (KBr) 3332 (OH) and 1748  $\text{cm}^{-1}$  (broad, C=O).

$^1\text{H}$  NMR ( $\text{CDCl}_3$ )  $\delta$  6.97 (dd, 1H,  $J$  = 1.4 and 2.1 Hz), 6.91 (dd, 1H,  $J$  = 1.4 and 2.1 Hz), 6.53 (t, 1H,  $J$  = 2.1 Hz), 6.23 (br, 1H), 5.45–5.20 (m, 3H), 5.15 (d, 1H,  $J$  = 7.5 Hz), 4.25 (d, 1H,  $J$  = 9.6 Hz), 3.76 (s, 3H), 2.09 (s, 3H), 2.08 (s, 3H), 2.07 (s, 3H).  $^{13}\text{C}$  NMR ( $\text{CDCl}_3$ )  $\delta$  171.0, 170.4, 169.9, 167.7, 158.3, 158.0, 120.8, 119.2, 105.3, 99.4, 94.3, 73.0, 72.3, 71.5, 69.7, 53.7, 21.2, 21.2, 21.1.

**3-Acetoxy-5-iodo-O-2,3,4-triacetyl- $\beta$ -D-glucuronopyranosidobenzene methyl ester (11)**

To a cooled (ice–water bath) stirred solution of the phenol **10** (1.81 g, 3.28 mmol) in dry dichloromethane (50 mL) was added pyridine (0.39 g, 4.92 mmol), 4-(dimethylamino)pyridine (10 mg) followed by acetic anhydride

(0.50 g, 4.92 mmol) dropwise. The resulting mixture was stirred in the cold for 30 min and then washed by 2N HCl (20 mL), water (20 mL), and brine (20 mL), then dried over anhydrous magnesium sulfate, filtered, and evaporated (40 °C, water aspirator pressure). Toluene (15 mL) was added to the residue and re-evaporated. The residue was recrystallized (dichloromethane/petroleum ether) to give a white solid, (1.63 g, 83%) of mp 126–128 °C. Anal. ( $\text{C}_{21}\text{H}_{23}\text{IO}_{12}$ ) C,H.

IR (KBr) 1757  $\text{cm}^{-1}$  (broad, C=O).

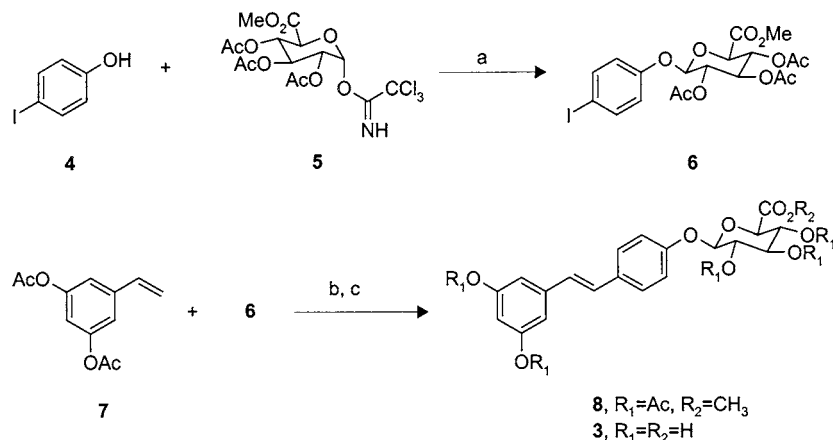
$^1\text{H}$  NMR ( $\text{CDCl}_3$ )  $\delta$  7.25 (dd, 1H,  $J$  = 1.4 and 2.1 Hz), 7.21 (dd, 1H,  $J$  = 1.4 and 2.1 Hz), 6.75 (t, 1H,  $J$  = 2.1 Hz), 5.45 (m, 3H), 5.15 (d, 1H,  $J$  = 7.0 Hz), 4.22 (d, 1H,  $J$  = 9.1 Hz), 3.75 (s, 3H), 2.30 (s, 3H), 2.08 (s, 3H), 2.06 (s, 3H).  $^{13}\text{C}$  NMR ( $\text{CDCl}_3$ )  $\delta$  170.6, 169.9, 169.8, 169.4, 167.3, 157.8, 152.0, 126.7, 124.2, 111.4, 99.3, 93.6, 73.2, 72.2, 71.5, 69.4, 53.6, 21.6, 21.2, 21.1.

**(E)-1-(3-Acetoxy-5-O-2,3,4-triacetyl- $\beta$ -D-glucuronopyranosidophenyl)-2-(4'-acetoxyphenyl)ethene Methyl Ester (13).** To a stirred solution of the iodophenyl-O- $\beta$ -D-glucuronate ester **11** (1.60 g, 2.69 mmol) and 4-acetoxystyrene **12** (0.40 g, 2.45 mmol) in dimethylformamide (40 mL) at room temperature under argon were added benzyltriethylammonium chloride (0.56 g, 2.45 mmol), tributylamine (1.19 g, 6.44 mmol), and palladium (II) acetate (27 mg, 0.122 mmol). The resulting pale orange solution was stirred at 120 °C for 40 min and then allowed to cool to room temperature. The mixture was poured onto water (50 mL) and extracted by dichloromethane (2  $\times$  30 mL). The organic extracts were washed by 2N HCl (20 mL), water (20 mL), and brine (20 mL), dried over anhydrous magnesium sulfate, filtered, and evaporated (40 °C, water aspirator pressure) to leave a brown oil. Chromatography over silica gel (petroleum ether/ethyl acetate, 2:1) afforded the major product as a pale yellow foam that was recrystallized (dichloromethane/diethyl ether) to give a white solid (0.69 g, 45%) of mp 153–154 °C. Anal. ( $\text{C}_{31}\text{H}_{32}\text{O}_{14}$ ) C,H.

IR (KBr) 1761  $\text{cm}^{-1}$  (broad, C=O).

$^1\text{H}$  NMR ( $\text{CDCl}_3$ )  $\delta$  7.51 (d, 2H,  $J$  = 8.7), 7.11 (d, 2H,  $J$  = 8.7 Hz), 7.07 (d, 1H,  $J$  = 16.4 Hz), 7.01 (m, 1H), 6.99 (m, 1H), 6.97 (d, 1H,  $J$  = 16.4 Hz), 6.66 (t, 1H,  $J$  = 2.1 Hz), 5.45–5.25 (m, 3H), 5.21 (d, 1H,  $J$  = 7.2 Hz), 4.24 (d, 1H,  $J$  = 9.2 Hz), 3.75 (s, 3H), 2.33 (s, 3H), 2.33 (s, 3H), 2.10 (s, 3H), 2.08 (s, 3H), 2.07 (s, 3H).  $^{13}\text{C}$  NMR ( $\text{CDCl}_3$ )  $\delta$  170.7, 170.0, 169.9, 169.8, 169.8, 167.4, 158.0, 152.2, 151.0, 140.3, 135.0, 130.1, 128.2, 127.9, 122.5, 115.2, 113.3, 110.2, 99.5, 73.3, 72.3, 71.6, 69.5, 53.6, 21.7, 21.2, 21.2, 21.1.

**(E)-1-(5-Hydroxy-3-O- $\beta$ -D-glucuronopyranosidophenyl)-2-(4'-hydroxyphenyl)ethene (2), (trans-resveratrol-3-O- $\beta$ -D-glucuronide).** To a stirred and cooled (ice–water bath) suspension of the glucuronate ester **13** (0.56 g, 0.89 mmol) in methanol (13 mL) was added dropwise aqueous 1 N sodium hydroxide solution (13 mL, 13 mmol). The resulting mixture was stirred in the cold for 30 min and then at room temperature for 40 min. The mixture was then gently warmed to 45 °C for 30 min to aid dissolution and then stirred at room temperature for a further hour. The resulting solution was diluted with water (12 mL), and sufficient Amberlyst 15 ion-exchange resin was added with stirring to maintain pH  $\sim$ 2–3. The resin was then filtered off and washed with water (10 mL). The combined filtrate was evaporated (60 °C, water aspirator pressure). Toluene (10 mL) was added to the residue and re-evaporated. The residue was dried at room temperature over phosphorus pentoxide under high vacuum overnight. The resulting solid was triturated with diethyl ether (3 mL) and filtered to give a pale beige

**Scheme 1. Synthesis of Resveratrol-4'-*O*- $\beta$ -D-glucuronide **3**<sup>a</sup>**

<sup>a</sup> Reagents: (a)  $\text{BF}_3 \cdot \text{OEt}_2$ ,  $\text{CH}_2\text{Cl}_2$ , 0  $^\circ\text{C}$  to room temperature, 1h, (66%); (b)  $\text{Pd}(\text{OAc})_2$ ,  $\text{BnEt}_3\text{N}^+\text{Cl}^-$ ,  $\text{Bu}_3\text{N}$ , DMF, 110  $^\circ\text{C}$ , 30 min, (55%); (c) (i) 1N NaOH (aq), MeOH, 0  $^\circ\text{C}$ , 30 min, (ii) Amberlyst 15 ion-exchange resin (84%).

solid (0.33 g, 92%), which decomposed without melting above 210  $^\circ\text{C}$ . Anal. ( $\text{C}_{20}\text{H}_{20}\text{O}_9$ ) C,H.

IR (KBr) 3372 (very broad, OH) and 1749  $\text{cm}^{-1}$  (C=O).

$^1\text{H}$  NMR ( $\text{DMSO}-d_6$ )  $\delta$  9.54 (br, 2H), 7.41 (d, 2H,  $J = 8.5$  Hz), 7.02 (d, 1H,  $J = 16.4$  Hz), 6.87 (d, 1H,  $J = 16.4$  Hz), 6.76 (d, 2H,  $J = 8.5$  Hz), 6.66 (t, 1H), 6.58 (t, 1H), 6.32 (t, 1H), 4.99 (d, 1H,  $J = 7.3$  Hz), 3.89 (d, 1H,  $J = 9.6$  Hz), 3.40 (t, 1H,  $J = 9.1$  Hz), 3.31 (t, 1H,  $J = 8.7$  Hz), 3.25 (t, 1H,  $J = 8.4$  Hz).  $^{13}\text{C}$  NMR ( $\text{DMSO}-d_6$ )  $\delta$  171.2, 159.5, 159.4, 158.4, 140.4, 129.6, 129.0, 126.1, 116.6, 108.2, 105.8, 103.6, 101.1, 76.8, 76.5, 74.0, 72.4.

**RESULTS AND DISCUSSION**

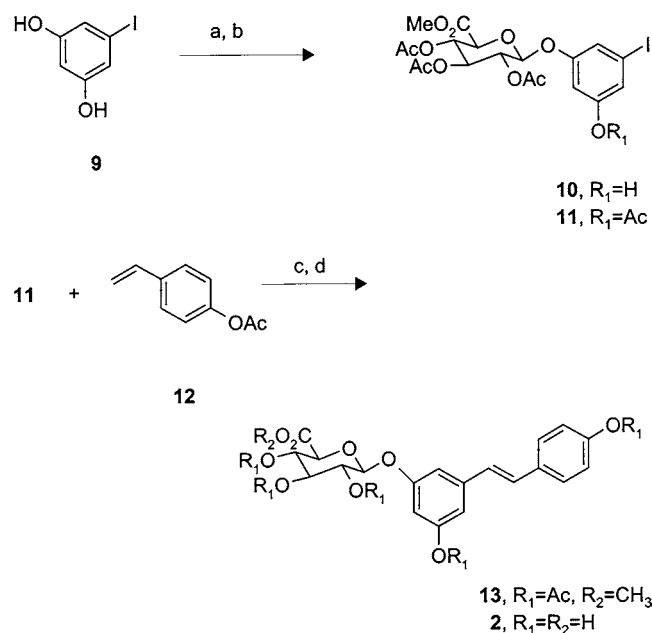
It has been previously shown that *O*-glucuronidation of **1** is a major metabolic pathway in the rat, giving rise to two *O*-conjugated glucuronide metabolites, which unfortunately could not be unambiguously characterized (18). Of course, *O*-glucuronidation of **1** is certainly expected to represent a major metabolic pathway in other species, including humans and hence synthesis of the individually pure *O*-glucuronide standards would greatly assist metabolic and pharmacokinetic studies of **1**. Although a number of chemical methods exist for preparation of *O*-glucuronide conjugates (29), synthesis of the individual resveratrol 3-*O*- $\beta$ -D- and 4'-*O*- $\beta$ -D-conjugates **2** and **3** represents a particular challenge, due to the presence of three equally reactive hydroxyl groups shared between two phenyl rings, separated by a highly conjugated central carbon-carbon double bond, structural features which effectively combine to complicate many protection/deprotection strategies. As such, direct methods of selective mono-*O*-glucuronidation of **1** were not considered. Alternatively, a convergent strategy was devised, where the two phenyl constituents of the stilbenic skeleton of glucuronides **2** and **3** were to be constructed separately, i.e a phenyl ring of the molecule containing the acetyl protected *O*- $\beta$ -D-glucuronide moiety and an appropriately *O*-substituted styrene, giving rise to two suitably functionalized synthons which could then theoretically be cross-coupled via a palladium catalyzed olefinic arylation, more commonly known as the Heck reaction (30, 31).

Starting with synthesis of resveratrol-4'-*O*- $\beta$ -D-glucuronide **3**, preference for the use of the aryl iodide was based on generally enhanced reactivity over bromides in the Heck reaction thereby also providing the possibility to employ phosphine-free conditions. Accordingly, the

reaction of commercially available 4-iodophenol **4** with Schmidt's trichloroacetimidate **5** proceeded smoothly under boron trifluoride catalysis to give in a completely stereoselective fashion (exclusive  $\beta$ -anomer formation) the acetyl protected *O*- $\beta$ -D-glucuronate ester **6** in good yield (66%). Preparation of the required diacetoxy olefin **7** was achieved as described (26) without incident. This olefin was in fact used in a Heck-mediated synthesis of **1** with 4-acetoxyiodobenzene (26), although when investigating this same reaction in this laboratory, the long reaction time and conditions (17 h at reflux) caused extensive deacetylation and decomposition, and the overall yield of **1** was rather low. In accordance, initial attempts to couple the glucuronate ester **6** with the olefin **7** under similar Heck conditions ( $\text{Pd}(\text{OAc})_2$ ,  $\text{Et}_3\text{N}$  or  $\text{Bu}_3\text{N}$ , DMF or  $\text{CH}_3\text{CN}$ , 100–120  $^\circ\text{C}$ ) were frankly disappointing, giving rise to mostly decomposition products (possibly again through extensive deacetylation) and eventually furnishing the desired protected stilbene derivative **8** in rather unsatisfactory yields (12–20%). The use of tetraalkylammonium halides (in particular chlorides) has been found to significantly accelerate certain Heck reactions (32) (Jeffery modification), and it was therefore extremely gratifying to find that the addition of one molar equivalent of benzyltriethylammonium chloride (used instead of the standard additive, tetrabutylammonium chloride) relative to the olefin greatly improved the situation; in fact, after only 30 min at 110  $^\circ\text{C}$ , the reaction had proceeded cleanly, and the desired protected (*E*)-stilbene **8** could be obtained exclusively in considerably improved yield (55%). To the best of the author's knowledge, this is the first reported example of the successful use of this type of aryl-*O*- $\beta$ -D-glucuronate ester in a Heck coupling reaction. Thereafter, deprotection of the acetyl protecting groups of the both the glucuronide and phenolic hydroxyl groups was easily achieved using aqueous 1 N sodium hydroxide in methanol. Acidic workup (Amberlyst 15 ion-exchange resin) and evaporation of the solvents afforded resveratrol-4-*O*- $\beta$ -D-glucuronide **3** in both good yield (84%) and excellent purity (HPLC, >99%) with minimum purification necessary (Scheme 1).

Thus, for the synthesis of resveratrol-3-*O*- $\beta$ -D-glucuronide **2**, 3,5-dihydroxyiodobenzene **9** and commercially available 4-acetoxystyrene **12** were considered suitably convenient starting materials. Aryl iodide **9** was prepared from commercially available 3,5-dimethoxyaniline as previously described (27) (attempts to convert another readily available precursor, 3,5-dimethoxychlorobenzene,



**Scheme 2. Synthesis of Resveratrol-3-*O*- $\beta$ -D-glucuronide **2**<sup>a</sup>**

<sup>a</sup> Reagents: (a) **5**, BF<sub>3</sub>·OEt<sub>2</sub>, CH<sub>2</sub>Cl<sub>2</sub>, 0 °C to room temperature, 40 min (35%); (b) Ac<sub>2</sub>O, pyridine, DMAP, CH<sub>2</sub>Cl<sub>2</sub>, 0 °C, 30 min, (83%); (c) Pd(OAc)<sub>2</sub>, BnEt<sub>3</sub>N<sup>+</sup>Cl<sup>-</sup>, Bu<sub>3</sub>N, DMF, 120 °C, 40 min, (45%); (d) (i) 1N NaOH (aq), MeOH, 0 °C for 30 min, room temperature for 40 min, 45 °C for 30 min, (ii) Amberlyst 15 ion-exchange resin (92%).

into the corresponding iodide by reaction with magnesium and iodine gave inconsistent results in agreement with observations made by another group (33). Attempted mono-acetylation of **9** (1 equiv Ac<sub>2</sub>O, Py, DMAP, CH<sub>2</sub>Cl<sub>2</sub>) gave a three-component mixture, containing predominantly diacetylated product and starting material rather than the desired mono-acetate. More encouraging however, was the completely stereoselective reaction of **9** with 1 equiv of Schmidt's trichloroacetimidate **5**, again under boron trifluoride catalysis, which allowed isolation of the mono-*O*- $\beta$ -D-glucuronate ester **10** in moderate yield (35%). Some unreacted **9** (~25%) could be recovered by chromatography and recycled. Since the presence of free hydroxyl groups is preferably avoided in the Heck reaction, **10** was *O*-acetylated to give fully protected **11**. Heck coupling of **11** with the styrene **12** under similar conditions used beforehand (Pd(OAc)<sub>2</sub>, Bu<sub>3</sub>N, BnEt<sub>3</sub>NCl, DMF, 120 °C) proceeded rapidly (40 min) and without significant decomposition, affording exclusively the protected (*E*)-stilbene **13** in now quite acceptable yield (45%). Subsequent acetyl-group deprotection of **13** was achieved under similar basic conditions as before, and the free glucuronide **2** could be isolated in excellent yield (92%) and purity (>99% homogeneous by HPLC) again with minimal purification (Scheme 2).

**CONCLUSIONS**

Short, efficient chemical methods suitable for the stereo- and regioselective, multimilligram to gram scale synthesis of highly pure individual 3-*O*- $\beta$ -D- and 4'-*O*- $\beta$ -D-glucuronide conjugates **2** and **3** of resveratrol **1** have been developed, based on a novel Heck coupling of iodoaryl-*O*- $\beta$ -D-glucuronate esters with *O*-protected styrenes. These compounds will find use in the more accurate determination of the metabolic and pharmacokinetic profile of **1** in several species, including humans. It is further hoped that the methodology herein described

will be found useful for the synthesis of *O*- $\beta$ -D-glucuronide conjugates of related polyhydroxy stilbenes.

**ACKNOWLEDGMENT**

The author wishes to thank Ana Paula Freitas for providing <sup>1</sup>H, <sup>13</sup>C NMR spectra and microanalytical data.

**LITERATURE CITED**

- (1) Mannila, E., Talvitie, A., and Kolehmainen, E. (1993) Antileukemic compounds derived from stilbenes in *Picea abies* bark. *Phytochemistry* 33 (4), 813–816.
- (2) Sobolev, V. S., Cole, R. J., Dorner, J. W., and Yagen, B. (1995) Isolation, purification and liquid chromatographic determination of stilbene phtoalexins in peanuts. *J. AOAC Int.* 78 (5), 1177–1182; *Chem. Abstr.* 123, 337690.
- (3) Celott, E., Ferrarini, R., Zironi, R., and Conte, L. S. (1996) Resveratrol content of some wines from dried Valpolicella grapes: Recioto and Amarone. *J. Chromatogr., A* 730, 47–52.
- (4) Schultz, T. P., Boldin, W. D., Fisher, T. H., Nicholas, D. D., McMurtrey, K. D., and Pobanz, K. (1992) Structure-fungicidal properties of some 3- and 4-hydroxylated stilbenes and bibenzyl analogues. *Phytochemistry* 31 (11), 3801–3806.
- (5) Kopp, P. (1998) Resveratrol, a phytoestrogen found in red wine. A possible explanation for the conundrum of the 'French Paradox'? *Eur. J. Endocrinol.* 138 (6), 619–620.
- (6) Das, D. K., Sato, M., Ray, P. S., Maulik, G., Engelman, R. M., Bertelli, A. A. E., and Bertelli, A. (1999) Cardioprotection of red wine. Role of polyphenolic antioxidants. *Drugs Exp. Clin. Res.* 25 (2/3), 115–120.
- (7) Vinas, P., López-Erroz, C., Marín-Hernández, J. J., and Hernández-Córdoba, M. (2000) Determination of phenols in wines by liquid chromatography with photodiode array and fluorescence detection. *J. Chromatogr., A* 871, 85–93.
- (8) Gu, X., Chu, Q., O'Dwyer, M., and Zeece, M. (2000) Analysis of resveratrol in wine by capillary electrophoresis. *J. Chromatogr., A* 881, 471–481.
- (9) Revilla, E., and Ryan, J. M. (2000) Analysis of several phenolic compounds with potential antioxidant properties in grape extracts and wines by high-performance liquid chromatography-photodiode array detection without sample preparation. *J. Chromatogr., A* 881, 461–469.
- (10) López, M., Martínez, F., Del Valle, C., Orte, C., and Miró, M. (2001) Analysis of phenolic constituents of biological interest in red wines by high-performance liquid chromatography. *J. Chromatogr., A* 922, 359–363.
- (11) Soleas, G. J., Tomlinson, G., Diamandis, E. P., and Goldberg, D. M. (1997) Relative contributions of polyphenolic constituents to the antioxidant status of wines: Development of a predictive model. *J. Agric. Food Chem.* 45 (10), 3995–4003.
- (12) Jang, M., and Pezzuto, J. M. (1999) Cancer chemopreventive activity of resveratrol. *Drugs Exp. Clin. Res.* 25 (2/3), 65–77.
- (13) Jang, M., Cai, L., Udeani, G. O., Slowing, K. V., Thomas, C. F., Beecher, C. W. W., Fong, H. H. S., Farnsworth, N. R., Kinghorn, A. D., Mehta, R. G., Moon, R. C., and Pezzuto, J. M. (1997) Cancer chemopreventive activity of resveratrol, a natural product derived from grapes. *Science* 275 (5297), 218–220.
- (14) Pace-Asciak, C. R., Hahn, S., Diamandis, E. P., Soleas, G., and Golberg, D. M. (1995) The red wine phenolics *trans*-resveratrol and quercetin block human platelet aggregation and eicosanoid synthesis: Implications for protection against coronary heart disease. *Clin. Chim. Acta* 235 (2), 207–219.
- (15) Chen, C. K., and Pace-Asciak, C. R. (1996) Vasorelaxing activity of resveratrol and quercetin in isolated rat aorta. *Gen. Pharmacol.* 27 (2), 363–366.
- (16) Soleas, G. J., Diamandis, E. P., and Goldberg, D. M. (1997) Resveratrol: a molecule whose time has come? And gone? *Clin. Biochem.* 30 (2), 91–113.
- (17) Walle, T., Otake, J. A., Brubaker, A., Walle, U.K., and Halushka, P. V. (2001) Disposition and metabolism of the

- flavanoid chrysin in normal volunteers. *Br. J. Clin. Pharmacol.* 51, 143–146.
- (18) Andlauer, W., Kolb, J., Siebert, K., and Furst, P. (2000) Assessment of resveratrol bioavailability in the perfused small intestine of the rat. *Drugs Exptl. Clin. Res.* 26 (2), 47–55.
- (19) Orsini, F., Pelizzoni, F., Bellini, B., and Miglierini, G. (1997) Synthesis of biologically active polyphenolic glycosides (combrestatin and resveratrol series). *Carbohydrate Res.* 301, 95–109.
- (20) Orsini, F., Pelizzoni, F., Verotta, L., and Aburjai, T. (1997) Isolation, synthesis and antiplatelet aggregation activity of resveratrol 3-*O*- $\beta$ -D-glucopyranoside and related compounds. *J. Nat. Prod.* 60, 1082–1087.
- (21) Alonso, E., Ramón, D. J., and Yus, M. (1997) Simple synthesis of 5-substituted resorcinols: a revisited family of interesting bioactive molecules. *J. Org. Chem.* 62, 417–421.
- (22) Cardona, M. L., Fernandez, M. I., Garcia, M. B., and Pedro, J. R. (1986) Synthesis of natural polyhydroxystilbenes. *Tetrahedron* 42 (10), 2725–2730.
- (23) Ali, M. A., Kondo, K., and Tsuda, Y. (1992) Synthesis and nematocidal activity of hydroxystilbenes. *Chem. Pharm. Bull.* 40 (5), 1130–1136.
- (24) Andrus, M and Meredith, E. (2001) The synthesis of resveratrol. *WO 01/60774 A1*; *Chem. Abstr.* 135, 180660.
- (25) Aumont, V., Krisa, S., Battaglia, E., Netter, P., Richard, T., Merillon, J. P., Magdalou, J., and Sabolovic, N. (2001) Regioselective and stereoselective glucuronidation of trans- and cis-resveratrol in human. *Arch. Biochem. Biophys.* 393 (2), 281–289.
- (26) Guiso, M., Marra, C., and Farina, A. (2002) A new efficient resveratrol synthesis. *Tetrahedron Lett.* 43 (4), 597–598.
- (27) Deboves, H. J. C., Montalbetti, C. A. G. N., and Jackson, R. F. W. (2001) Direct synthesis of Fmoc-protected amino acids using organozinc chemistry: application to polymethoxylated phenylalanines and 4-oxoamino acids. *J. Chem. Soc., Perkin Trans. 1*, 1876–1884.
- (28) Fischer, B., Nudelman, A., Ruse, M., Herzig, J., Gottlieb, H. E., and Keinan, E. (1984) A novel method for stereoselective glucuronidation. *J. Org. Chem.* 49 (25), 4988–4993.
- (29) Stachulski, A. V., and Jenkins, G. N. (1998) The synthesis of *O*-glucuronides. *Nat. Prod. Rep.* 15 (2), 173–186.
- (30) Heck, R. F., and Nolley, J. P. (1972) Palladium-catalysed vinylic hydrogen substitution reactions with aryl, benzyl and styryl halides. *J. Org. Chem.* 37 (14), 2320–2322.
- (31) Ziegler, C. B. Jr., and Heck, R. F. (1978) palladium-catalysed vinylic substitution with highly activated aryl halides. *J. Org. Chem.* 43 (15), 2941–2946.
- (32) Jeffery, T. (1996) On the efficiency of tetraalkylammonium salts in Heck-type reactions. *Tetrahedron* 52 (30), 10113–10130.
- (33) Dol, G. C., Kamer, P. C.J and van Leeuwen, P. W. N. M. (1998) Synthesis of 5-substituted resorcinol derivatives via cross-coupling reactions. *Eur. J. Org. Chem.* (2), 359–364.

BC020048X

# Biohydrogen Production from Sucrose Using the Visible Light Sensitization of Artificial Zn Chlorophyll-*a*

Yumi Takeuchi and Yutaka Amao\*

Department of Applied Chemistry, Oita University, Dannoharu 700, Oita 870-1192, Japan.

Received July 24, 2002; Revised Manuscript Received November 1, 2002

A photoinduced hydrogen production system that couples sucrose degradation with invertase and glucose dehydrogenase (GDH) and hydrogen production with colloidal platinum as a catalyst using visible light-induced photosensitization of artificial Zn chlorophyll-*a* (Zn Chl-*a*) has been developed. Continuous hydrogen gas production over more than 240 min was observed when the reaction mixture containing sucrose, invertase, GDH, nicotinamide adenine dinucleotide (NAD<sup>+</sup>), Zn Chl-*a*, methyl viologen (MV<sup>2+</sup>, an electron relay reagent), and colloidal platinum was irradiated by visible light. Zn Chl-*a* was superior to that of Mg Chl-*a* in photostability and photosensitization activity.

## INTRODUCTION

Hydrogen production systems from bioresources is important in environmental and energy development research (1–5). Some renewable biomass resources are starch, cellulose, sucrose, and lactose. These polysaccharides are hydrolyzed to form monosaccharides such as glucose. Thus, the conversion of glucose to hydrogen would be a useful new enzymatic pathway. Some studies on hydrogen production from glucose using an enzymatic pathway have been reported (6–10). Hydrogen production from glucose utilizing a combination of glucose dehydrogenase (GDH) and hydrogenase has been reported (11, 12). However, enzymatic photoinduced hydrogen production from other monosaccharides oligosaccharides or polysaccharides has received little attention. Glucose was obtained from sucrose by using invertase enzymatically. Thus, hydrogen production from oligosaccharides, such as sucrose, can be attained using a combination of invertase, GDH, and hydrogenase or some other hydrogen-evolving catalyst.

On the other hand, some photoinduced hydrogen production systems consist of electron donor, photosensitizer, electron carrier, and catalyst. (13–19). For hydrogen-evolving catalyst, colloidal platinum (17–19) and hydrogenase from *Desulfovibrio vulgaris* (Miyazaki) (13–16) are widely used in hydrogen production systems. Especially, colloidal platinum is stable against long-term irradiation. In photoinduced hydrogen production systems with visible light, as water-soluble zinc porphyrins have an absorption band in the visible light region (380–600 nm), these porphyrins have been widely used as an effective photosensitizer (13, 14). Especially, zinc tetraphenylporphyrin tetrasulfonate (ZnTPPS) is useful as a photosensitizer (13, 14). However, the molar absorption coefficient of zinc porphyrins in the visible light region (500–600 nm) was lower than that in the near ultraviolet light region (380–400 nm). On the other hand, Mg chlorophyll-*a* (Mg Chl-*a*), which acts as the effective photosensitizer in the photosynthesis of green plants (20), has an absorption maximum at 670 nm. Thus, Mg Chl-*a*

is attractive as a visible photosensitizer. So far, photoinduced hydrogen production systems with chemically modified chlorophyll and hydrogenase (21, 22), and chlorophyll derivatives (23–25), were reported previously. However, Mg Chl-*a* purified from green plants is unstable to irradiation. On the other hand, zinc bacteriochlorophyll *a* was found in an aerobic bacterium, *Acidiphilium rubrum* (26). As zinc porphyrins are stable to irradiation and effective photosensitizers, zinc chlorophylls are attractive as stable visible photosensitizers. Some studies on the preparation and characterization of the zinc chlorophyll and bacteriochlorophylls have been reported (20, 27).

In photoinduced hydrogen production with systems consisting of an electron donor, photosensitizer, electron relay, and catalyst, photoexcited photosensitizer reacts with the electron relay to form the reduced electron relay, hydrogen evolves by the proton reduction with the catalyst, and then the oxidized photosensitizer is reduced by the electron-donating reagent such as reduced nicotinamide adenine dinucleotide (NADH). Thus, the electron donor, NADH is the sacrificial reagent, and the oxidized electron donor, NAD<sup>+</sup> is consumed in the reaction system. If NADH is regenerated, the photoinduced hydrogen production system is accomplished without NAD<sup>+</sup> consumption. As GDH uses NAD<sup>+</sup> as a cofactor, photoinduced hydrogen production with GDH, electron donor, photosensitizer, electron relay reagent, and catalyst can be attained. We previously reported visible light-induced hydrogen production from sucrose using the photosensitization of Mg Chl-*a* (28). Thus, an effective photoinduced hydrogen production can be accomplished using Zn Chl-*a* as photosensitizer instead of Mg Chl-*a*.

In this work, we describe the visible light-induced hydrogen production system coupling sucrose degradation with invertase and GDH, and hydrogen production with colloidal platinum using the photosensitization of artificial Zn Chl-*a* in the presence of methyl viologen (MV<sup>2+</sup>) as an electron relay reagent as shown in Scheme 1.

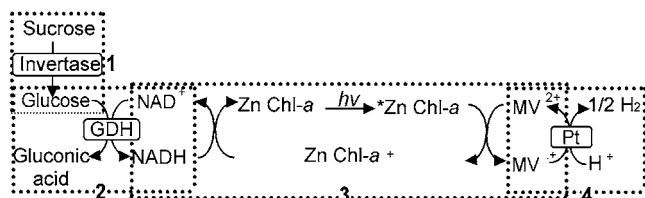
## EXPERIMENTAL PROCEDURES

**General.** Mg Chl-*a* from *spirulina*, invertase from yeast, and GDH from *Bacillus* sp. were purchased from Wako Pure Chemical Industries Ltd. (Osaka, Japan).

\* To whom correspondence should be addressed. Phone: +81-97-554-7972. Fax: +81-97-554-7972. E-mail: amao@cc.oita-u.ac.jp.



**Scheme 1. Visible Light-Induced Hydrogen Production System Coupling the Sucrose Degradation with Invertase and GDH and Hydrogen Production with Colloidal Platinum Using the Photosensitization of Zn Chl-*a* in the Presence of MV<sup>2+</sup>**

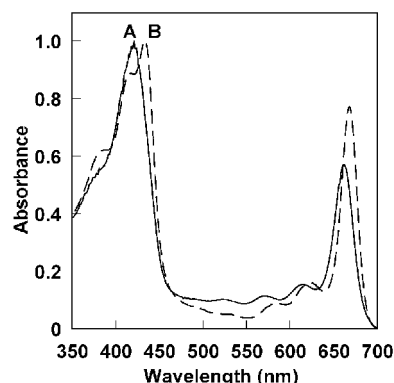


NAD<sup>+</sup> and NADH were purchased from Oriental Yeast Co. Ltd. MV<sup>2+</sup> dichloride and cetyltrimethylammonium bromide (CTAB) were purchased from Tokyo Kasei Co. Ltd (Tokyo, Japan). Hydrogen hexachloroplatinate hexahydrate and sodium citrate dihydrate were obtained from Kanto Chemical Co. Ltd (Tokyo, Japan). The other chemicals were analytical grade or the highest grade available. One unit of GDH activity was defined as the amount of enzyme that reduced 1.0  $\mu\text{mol}$  of NAD<sup>+</sup> to NADH by glucose per minute. One unit of invertase activity was defined as the amount of enzyme that produced 1.0  $\mu\text{mol}$  of glucose by sucrose per minute.

**Preparation of Zn Chl-*a*.** Zn Chl-*a* was synthesized by refluxing Mg Chl-*a* (50 mg, 56  $\mu\text{mol}$ ) with about 10 mol equiv of zinc acetate in 100 mL of methanol at 80 °C for 5 h. The insertion of zinc ion into the porphyrin ring of Chl-*a* was monitored by visible absorption spectroscopy. During the reaction, the characteristic absorption bands of Zn Chl-*a* at 421 and 662 nm increased and the absorbance bands at 433 and 668 nm of Mg Chl-*a* decreased gradually. After the mixture was cooled to room temperature, the solvent was removed by rotary evaporation, and then the reaction mixture was washed with water to remove the unreacted zinc acetate. Finally, Zn Chl-*a* was precipitated in water. Zn Chl-*a* was collected by filtration and washed with water. The purification was performed by recrystallization (water–methanol). Zn Chl-*a* and Mg Chl-*a* were solubilized with 10 mmol dm<sup>-3</sup> of CTAB, since Zn Chl-*a* and Mg Chl-*a* are insoluble in aqueous solution.

**Preparation of Colloidal Platinum.** Colloidal platinum was prepared by reduction of hexachloroplatinate solution with sodium citrate. The reduction procedure was similar to the previously reported method (17). A solution of 400 mL of water containing 30 mg of hydrogen hexachloroplatinate hexahydrate was refluxed using a mantle heater and magnetic stirrer for 1.5 h, and then a solution of 30 mL of water containing 600 mg of sodium citrate dihydrate was added and refluxed with a magnetic stirrer at 100 °C for 4 h. The particle size of colloidal platinum prepared was estimated to be 1.5 nm. In general, the colloidal platinum activity decreased with increase the particle size (more than 2.0 nm) (17). The prepared colloidal platinum has the ability to release 0.7  $\mu\text{mol}$  of hydrogen in the reaction system of 10  $\mu\text{L}$  of colloidal platinum,  $1.2 \times 10^{-5}$  mmol of methyl viologen, and  $7.7 \times 10^{-5}$  mmol of sodium dithionite in 4.0 mL of 50 mmol dm<sup>-3</sup> Tris-HCl buffer (pH 7.4) at 30 °C for 10 min. One unit of colloidal platinum activity was defined as the release of 1.0  $\mu\text{mol}$  of hydrogen per minute.

**Spectroscopic Measurements.** The UV–vis absorption spectrum of Zn Chl-*a* was recorded using a spectrophotometer (Multispec-1500 Shimadzu). The molar coefficients at the absorption maxima of Zn Chl-*a* were determined by the linear plot of absorbance versus Zn



**Figure 1.** UV–vis absorption spectra of Zn Chl-*a* (solid line) and Mg Chl-*a* (dashed line) in methanol solution. The concentrations of Zn Chl-*a* and Mg Chl-*a* were 79 and 16  $\mu\text{mol dm}^{-3}$ , respectively.

Chl-*a* concentration. The fluorescence emission spectrum of Zn Chl-*a* was measured using a spectrofluorophotometer with a 150 W xenon lamp as a visible excitation light source (RF-5300PC Shimadzu). The excitation and emission band-passes were 5.0 nm, respectively. The excitation wavelength was 600 nm. In these experiments, the absorbance at the excitation wavelength was kept constant at 0.2 for all the sample solutions.

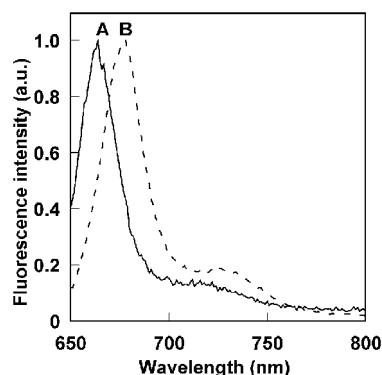
**NADH Formation with Sucrose, Invertase, and GDH.** The reaction was started by addition of NAD<sup>+</sup> (0.80  $\mu\text{mol}$ ) solution to the sample solution containing sucrose (16  $\mu\text{mol}$ ), invertase (4.0 units), and GDH (5.0 units) in 3.0 mL of 10 mmol dm<sup>-3</sup> potassium phosphate buffer (pH 7.0). The reduction of NAD<sup>+</sup> to NADH by GDH was monitored using a UV–vis spectrophotometer at 340 nm, with a molar extinction coefficient of  $6.3 \times 10^3$  mol dm<sup>3</sup> cm<sup>-1</sup>.

**Photoreduction of MV<sup>2+</sup>.** Photoreduction of MV<sup>2+</sup> was tested in the reaction mixture containing NAD<sup>+</sup>, sucrose, Zn Chl-*a*, MV<sup>2+</sup>, invertase, and GDH. The reaction system consisted of NAD<sup>+</sup> (15  $\mu\text{mol}$ ), sucrose (0.30 mmol), Zn Chl-*a* (4.5 nmol), MV<sup>2+</sup> (1.2  $\mu\text{mol}$ ), invertase (4.0 units), and GDH (5.0 units) in 3.0 mL of 10 mmol dm<sup>-3</sup> potassium phosphate buffer (pH 7.0). The sample solution was deaerated by repeated freeze–pump–thaw cycles and irradiated with a 200 W tungsten lamp at a distance of 3.0 cm, with a light intensity of 200 J m<sup>-2</sup> s<sup>-1</sup>, at 30 °C. The light of the wavelength less than 390 nm was removed by a Toshiba L-39 cutoff filter (Tokyo, Japan). The reduction of MV<sup>2+</sup> was monitored using a UV–vis spectrophotometer at 605 nm, with the molar extinction coefficient of  $1.3 \times 10^4$  mol dm<sup>3</sup> cm<sup>-1</sup> (29).

**Visible Light-Induced Hydrogen Production.** The photoinduced hydrogen production from sucrose was carried out as follows. The sample solution containing NAD<sup>+</sup> (15  $\mu\text{mol}$ ), sucrose (0.30 mmol), Zn Chl-*a* (4.5 nmol), MV<sup>2+</sup> (1.2  $\mu\text{mol}$ ), colloidal platinum (0.5 units), invertase (4.0 units), and GDH (5.0 units) in 3.0 mL of 10 mmol dm<sup>-3</sup> potassium phosphate buffer (pH 7.0) was deaerated by freeze–pump–thaw cycle six times, and substituted by argon gas. The amount of hydrogen evolved was measured by a Shimadzu GC-14B gas chromatograph (detector: TCD, column temperature: 40 °C, column: active charcoal with the particle size 60–80 mesh, carrier gas: nitrogen gas, carrier gas flow rate: 24 mL min<sup>-1</sup>).

## RESULTS AND DISCUSSION

**UV–vis Absorption Spectrum of Zn Chl-*a*.** Figure 1 shows the UV–vis absorption spectra of Zn Chl-*a* and Mg Chl-*a* in methanol solution. The absorption bands of



**Figure 2.** Fluorescence emission spectra of Zn Chl-*a* (solid line) and Mg Chl-*a* (dashed line) in methanol solution. The excitation wavelength was 600 nm. The concentrations of Zn Chl-*a* and Mg Chl-*a* were 0.6 and 0.4 mmol dm<sup>-3</sup>, respectively.

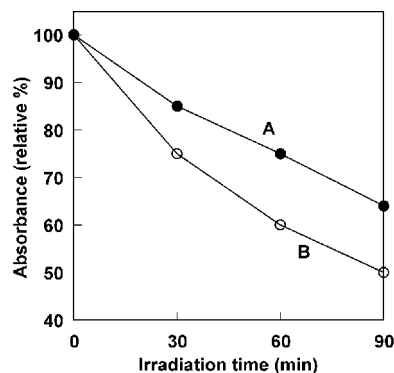
Zn Chl-*a* were 421 nm attributed to Soret band and 662 nm attributed to Q-band. On the other hand, the absorption bands of Mg Chl-*a* were 433 nm attributed to Soret band and 668 nm attributed to Q-band. In comparison of the absorption spectra of Zn Chl-*a* and Mg Chl-*a*, a blue-shift in the absorption bands of Zn Chl-*a* was observed.

#### Fluorescence Emission Spectrum of Zn Chl-*a*.

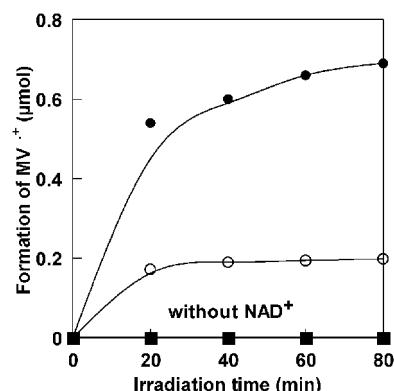
Figure 2 shows fluorescence emission spectra of Zn Chl-*a* and Mg Chl-*a* in methanol solution. The fluorescence emission peak of Zn Chl-*a* and Mg Chl-*a* were 664 and 678 nm, respectively. In comparison of the fluorescence emission spectra of Zn Chl-*a* and Mg Chl-*a*, the blue-shift in the emission peak of Zn Chl-*a* was observed as well as that in the absorption spectra. The energies of the first excited singlet states of Zn Chl-*a* and Mg Chl-*a* were calculated from the average value of the frequencies of the longest wavelength of absorption maxima and the shortest wavelength of the fluorescence emission maxima. The energies of the first excited singlet states of Zn Chl-*a* and Mg Chl-*a* were 1.50 and 1.47 eV, respectively.

**NADH Formation with Sucrose, Invertase, and GDH System.** When the sample solution containing sucrose, invertase, GDH, and NAD<sup>+</sup> was incubated, the initial rate of NADH formation, which was determined by the amount of NADH with incubation for 15 min, was estimated to be  $(3.4 \pm 0.1) \times 10^{-8}$  mol min<sup>-1</sup>. After 80 min incubation,  $0.77 \pm 0.03$  μmol of NADH was formed. The yield of conversion of NAD<sup>+</sup> to NADH in this system was ca. 100%. When the sample solution containing glucose (16 μmol), GDH, and NAD<sup>+</sup> (without sucrose and invertase) was incubated, the initial rate of NADH formation was estimated to be  $(4.2 \pm 0.1) \times 10^{-8}$  mol min<sup>-1</sup>. After 80 min incubation,  $0.77 \pm 0.02$  μmol NADH was formed, and the yield of conversion of NAD<sup>+</sup> to NADH in this system also was ca. 100%. These results show that glucose formation from sucrose (process 1 in Scheme 1) with invertase proceeded rapidly.

**Stability of Zn Chl-*a* against Irradiation.** The photostability of Zn Chl-*a* in the reaction mixture was investigated. The photostability was tested by irradiation with visible light using a 200 W tungsten lamp (light intensity of 200 J m<sup>-2</sup> s<sup>-1</sup>). Figure 3 shows the absorbance changes at 662 nm attributed to the absorption maximum of Zn Chl-*a* (A) and at 670 nm attributed to the absorption maximum of Mg Chl-*a* (B) with irradiation time. The absorbance decrease of Zn Chl-*a* was slower than that of Mg Chl-*a* in solution as shown in curves A and B, indicating that the degradation rate of Zn Chl-*a* was suppressed compared with that of Mg Chl-*a* against



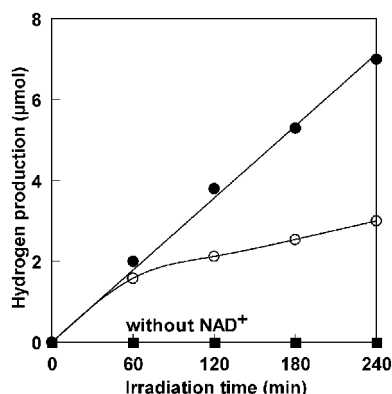
**Figure 3.** Photostability of Zn Chl-*a* solution under anaerobic conditions. Curves A and B are CTAB solubilized Zn Chl-*a* and Mg Chl-*a* aqueous solution, respectively. Samples were irradiated with visible light using 200 W tungsten lamp at a distance of 3.0 cm (light intensity of 200 J m<sup>-2</sup> s<sup>-1</sup>).



**Figure 4.** The time dependence of the MV<sup>2+</sup> concentration under steady-state irradiation with visible light using 200 W tungsten lamp at a distance of 3.0 cm (light intensity of 200 J m<sup>-2</sup> s<sup>-1</sup>). (Closed circle): The sample solution consisting of invertase (4.0 units), GDH (5.0 units), NAD<sup>+</sup> (15 μmol), sucrose (0.30 mmol), Zn Chl-*a* (4.5 nmol), and MV<sup>2+</sup> (1.2 μmol) in 3.0 mL of 10 mmol dm<sup>-3</sup> potassium phosphate buffer (pH = 7.0). (Open circle): Mg Chl-*a* (3.0 nmol) was used as photosensitizer instead of Zn Chl-*a*. (Closed square): In the absence of NAD<sup>+</sup>.

irradiation. Thus, Zn Chl-*a* was superior to Mg Chl-*a* in photostability.

**Photoreduction of MV<sup>2+</sup>.** Figure 4 shows the time dependence of the MV<sup>2+</sup> concentration in the system containing NAD<sup>+</sup>, sucrose, Zn Chl-*a*, MV<sup>2+</sup>, invertase, and GDH with visible light irradiation (closed circle). The absorbance at 605 nm, absorption band of MV<sup>2+</sup>, increased with irradiation time. After 80 min irradiation, 0.69 μmol of reduced MV<sup>2+</sup> was produced, and the yield of MV<sup>2+</sup> to MV<sup>+</sup> was estimated to be ca. 58%. The photoreduction rate was independent of the concentrations of NAD<sup>+</sup>, sucrose, invertase, and GDH. On the other hand, the reduction rate depends on the concentrations of Zn Chl-*a* and MV<sup>2+</sup>. Thus, the rate-limiting step in the MV<sup>2+</sup> reduction (processes 1, 2, and 3 in Scheme 1) is the photoinduced electron-transfer process from the photoexcited Zn Chl-*a* (\*Zn Chl-*a*) to MV<sup>2+</sup> (process 3 in Scheme 1). For the system using Mg Chl-*a*, 0.21 μmol of reduced MV<sup>2+</sup> was produced, and the yield of MV<sup>2+</sup> to MV<sup>+</sup> was estimated to be ca. 33% after 80 min irradiation (open circle). Thus, the photosensitization activity of Zn Chl-*a* was superior to that of Mg Chl-*a*. On the other hand, MV<sup>2+</sup> was not reduced without NAD<sup>+</sup> in the above system (closed square). There is no direct electron transfer between sucrose or glucose formed with invertase and MV<sup>2+</sup>, and between Zn Chl-*a* and MV<sup>2+</sup>. Thus, the visible light-induced MV<sup>2+</sup> reduction proceeded by



**Figure 5.** Time dependence of hydrogen production under steady-state irradiation with visible light using 200 W tungsten lamp at a distance of 3.0 cm (light intensity of  $200 \text{ J m}^{-2} \text{ s}^{-1}$ ). (Closed circle): The sample solution consisting of invertase (4.0 units), GDH (5.0 units)  $\text{NAD}^+$  (15  $\mu\text{mol}$ ), sucrose (0.30 mmol), Zn Chl-*a* (4.5 nmol),  $\text{MV}^{2+}$  (1.2  $\mu\text{mol}$ ), and colloidal platinum (0.5 unit) in 3.0 mL of 10 mmol  $\text{dm}^{-3}$  potassium phosphate buffer (pH = 7.0). (Open circle): Mg Chl-*a* (3.0 nmol) was used as photosensitizer instead of Zn Chl-*a*. (Closed square): In the absence of  $\text{NAD}^+$ .

coupling the sucrose degradation with invertase and GDH (processes 1 and 2 in Scheme 1) and  $\text{MV}^{2+}$  reduction using the photosensitization of Zn Chl-*a* (process 3 in Scheme 1).

**Visible Light-Induced Hydrogen Production.** As the  $\text{MV}^{2+}$  photoreduction system containing  $\text{NAD}^+$ , sucrose, Zn Chl-*a*,  $\text{MV}^{2+}$ , invertase and GDH was achieved, the photoinduced hydrogen production system was investigated. Figure 5 shows the time dependence of the photoinduced hydrogen production in the system containing  $\text{NAD}^+$ , sucrose, Zn Chl-*a*,  $\text{MV}^{2+}$ , colloidal platinum, invertase, and GDH by the visible light. By irradiation, hydrogen evolved continuously over more than 240 min. The amount of hydrogen production was estimated to be 7.0  $\mu\text{mol}$  after 240 min irradiation. It indicated that 14  $\mu\text{mol}$  of proton, that was 3111 times the amount of Zn Chl-*a* (4.5 nmol) in the sample solution, was reduced to hydrogen molecules. Therefore, the Zn Chl-*a* appeared to serve as the system for transferring electrons from  $\text{NADH}$ , which was formed from sucrose, to a more reductive hydrogen molecule. On the other hand, the hydrogen also was not evolved in the absence of  $\text{NAD}^+$  in the above system (closed square). There is no direct electron transfer between sucrose or glucose formed with invertase and colloidal platinum, and among Zn Chl-*a*,  $\text{MV}^{2+}$  and colloidal platinum. These results suggest that visible light-induced hydrogen production proceeded by coupling the sucrose degradation with invertase and GDH (processes 1 and 2 in Scheme 1) and the hydrogen production with colloidal platinum using the photosensitization of Zn Chl-*a* (processes 3 and 4 in Scheme 1). For the system using Mg Chl-*a*, the amount of hydrogen production was estimated to be 3.0  $\mu\text{mol}$  after 240 min irradiation. It indicated that 6.0  $\mu\text{mol}$  of proton, that was 2000 times the amount of Mg Chl-*a* (3.0 nmol) in the sample solution, was reduced to hydrogen molecules. Thus, the Zn Chl-*a* has a high activity of photosensitization compared with that of Mg Chl-*a* in the photoinduced hydrogen production system.

Next let us focus on the relationship between the photoreduction of  $\text{MV}^{2+}$  and the photoinduced hydrogen production using Zn Chl-*a* and colloidal platinum. The formation of  $\text{MV}^{+}$  reached a constant after 20 min irradiation as shown in Figure 4. This result suggests that the cycle of  $\text{MV}^{2+}$  and  $\text{MV}^{+}$  was stable. As shown

in Figure 5, on the other hand, the photoinduced hydrogen production was proportional to irradiation time. As indicated from Figures 4 and 5, an efficient hydrogen or electron relay in the system may lead to efficient hydrogen production.

In conclusion, a hydrogen production system that couples sucrose degradation with invertase and GDH and hydrogen production with colloidal platinum using visible light-induced photosensitization of artificial Zn Chl-*a* was developed, and continuous hydrogen gas was gained. Moreover, Zn Chl-*a* was superior to Mg Chl-*a* in photo-stability and photosensitization activity. Renewable biomass resources are effectively used to produce an environmentally clean energy source, hydrogen gas. However, since sucrose is expensive as a renewable biomass or clean energy source, hydrogen production from cellulose, which is an inexpensive renewable biomass, is desirable. Further research will be directed toward a photoinduced hydrogen production system that utilizes cellulose and cellulase instead of sucrose and invertase in process 1 of Scheme 1.

#### ACKNOWLEDGMENT

This work is partially supported by The Thermal & Electric Energy Technology (TEET) Foundation.

#### LITERATURE CITED

- Helena, L. C., and Overend, R. P. (2001) Biomass and renewable fuels. *Fuel Process. Technol.* 71, 187–195.
- Barbosa, M. J., Rocha, J. M., Tramper, J., and Wijffels, R. H. (2001) Acetate as a carbon source for hydrogen production by photosynthetic bacteria. *J. Biotechnol.* 85, 25–33.
- Garcia, L., French, R., Czernik, S., and Chornet, E. (2000) Catalytic steam reforming of bio-oils for the production of hydrogen: effects of catalyst composition. *Appl. Catal. A: Gen.* 201, 225–239.
- Wang, D. (1998) Production of hydrogen from biomass by catalytic steam reforming of fast pyrolysis oils. *Fuel Energy Abstr.* 39, 188.
- Minowa, T., and Inoue, S. (1999) Hydrogen production from biomass by catalytic gasification in hot compressed water. *Renew. Energy* 16, 1114–1117.
- Rustamov, V. R., Abdullayev, K. M., Aliyev, F. G., and Kerimov, V. K. (1998) Hydrogen formation from biomass using solar energy. *Int. J. Hydrogen Energy* 23, 649–652.
- Woodward, J., Orr, M., Cordray, K., and Greenbaum, E. (2000) Enzymatic biohydrogen production. *Nature* 405, 1014–1015.
- Mizuno, O., Dinsdale, R., Hawkes, F. R., Hawkes, D. L., and Noike, T. (2000) Enhancement of hydrogen production from glucose by nitrogen gas sparging. *Bioresour. Technol.* 73, 59–65.
- Akashah, M., Yoshida, M., Watanabe, M., Nakamura, M., and Matsumoto, J. (1997) Hydrogen gas production from glucose and its microbial kinetics in anaerobic systems. *Water Sci., Technol.* 36, 279–286.
- Ma, K., and Adams, M. W. (1994) Sulfide dehydrogenase from the hyperthermophilic archaeon *Pyrococcus furiosus*: a new multifunctional enzyme involved in the reduction of elemental sulfur. *J. Bacteriol.* 176, 6509–6517.
- Woodard, J., Mattingly, S. M., Danson, M., Hough, D., Ward, N., and Adams, M. (1996) In vitro hydrogen production by glucose dehydrogenase and hydrogenase. *Nature Biotechnol.* 14, 872–874.
- Inoue, T., Kumar, S. N., Kamachi, T., and Okura, I. (1999) Hydrogen evolution from glucose with the combination of glucose dehydrogenase and hydrogenase from *A. eutrophus* H16. *Chem. Lett.* 147–148.
- Okura, I. (1985) Hydrogenase and its application for photoinduced hydrogen evolution. *Coord. Chem. Rev.* 68, 53–99.



- (14) Okura, I. (1986) Application of hydrogenase for photoinduced hydrogen evolution. *Biochimie* 68, 189–199.
- (15) Okura, I., Aono, S., and Kusunoki, S. (1983) Photoreduction of viologens and hydrogen evolution with hydrogenase. *Inorg. Chim. Acta* 71, 77–80.
- (16) Okura, I., and Kim-Thuan, N. (1981) Kinetic studies of photoinduced methyl viologen reduction with ruthenium complexes and hydrogen evolution from water by hydrogenase. *J. Chem. Soc., Faraday Trans. 1* 77, 1411–1416.
- (17) Darwent, J. R., Douglas, P., Harriman, A., Porter, G., and Richoux, M. C. (1982) Metal phthalocyanines and porphyrins as photosensitizers for reduction of water to hydrogen. *Coord. Chem. Rev.* 44, 93–126.
- (18) Brugger, P. A., Cuendet, P., Grätzel, M. (1981) Ultrafine and specific catalysts affording efficient hydrogen evolution from water under visible light illumination. *J. Am. Chem. Soc.* 103, 2923–2927.
- (19) Kiwi, J., and Grätzel, M. (1979) Protection size factors, and reaction dynamics of colloidal redox catalysis mediating light induced hydrogen evolution from water. *J. Am. Chem. Soc.* 101, 7214–7217.
- (20) Scheer, H. (1991) *Chlorophylls*, CRC Press, London.
- (21) Itoh, T., Ishii, A., Kodera, Y., Matsushima, A., Hiroto, M., Nishimura, H., Tsuzuki, T., Kamachi, T., Okura, I., and Inada, Y. (1998) Photostable chlorophyll *a* with poly(vinylpyrrolidone)-smectite catalyzes photoreduction and hydrogen gas evolution by visible light. *Bioconjugate Chem.* 9, 409–412.
- (22) Itoh, T., Asada, H., Tobioka, K., Kodera, Y., Matsushima, A., Hiroto, M., Nishimura, H., Kamachi, T., Okura, I., and Inada, Y. (2000) Hydrogen gas evolution and carbon dioxide fixation with visible light by chlorophyllin coupled with poly(ethylene glycol). *Bioconjugate Chem.* 11, 8–13.
- (23) Koiso, T., Okuyama, M., Sakata, T., and Kawai, T. (1982) Efficient photoreduction of methyl viologen sensitized by chlorophyll derivatives and hydrogen evolution by visible light. *Bull. Chem. Soc. Jpn.* 55, 2659–2660.
- (24) Krasnovski, A. A., Chan-van-Ni, Nikandrov, V. V., and Brin, G. P. (1980) Conditions for effective hydrogen photoevolution by chloroplasts in the presence of bacterial hydrogenase. *Mol. Biol.* 14, 287–298.
- (25) Kiwi, J., and Grätzel, M. (1980) Chlorophyll a sensitized redox processes in microemulsion systems. *J. Phys. Chem.* 84, 1503–1507.
- (26) Kobayashi, M., Yamamura, M., Akiyama, M., Kise, H., Inoue, K., Hara, M., Wakao, N., Yahara, K., and Watanabe, T. (1998) Acid resistance of Zn-bacteriochlorophyll *a* from an acidophilic bacterium. *Acidiphilium rubrum*. *Anal. Sci.* 14, 1149–1152.
- (27) Wakao, N., Yokoi, N., Isoyama, N., Hiraishi, A., Shimada, K., Kobayashi, M., Kise, H., Iwaki, M., Itoh, S., Takaichi, S., and Sakurai, Y. (1996) Discovery of natural photosynthesis using Zn-containing bacteriochlorophyll in an aerobic bacterium *Acidiphilium rubrum*. *Plant Cell Physiol.* 37, 889–893.
- (28) Saiki, Y., and Amao, Y. (2002) Visible light induced biohydrogen production from sucrose using the photosensitization of Mg chlorophyll-*a*. *Bioconjugate Chem.* 13, 898–901.
- (29) Watanabe, T., and Honda, K. (1982) Measurement of the extinction coefficient of the methyl viologen cation radical and the efficiency of its formation by semiconductor photocatalysis. *J. Phys. Chem.* 86, 2617–2619.

BC0255844

## In Memoriam: Claude Hélène

One of the fathers of triple helix antigene targeting has died. Just a week after his 65th birthday and a few days after a grand symposium celebrating this occasion, held in Paris, in the Natural History Museum that also hosts his laboratory, Claude Hélène is no longer with us. Those of us who knew Claude will remember him as a very generous scientist and human being. Claude Hélène started out as a photobio-physicist but very early turned his attention to the properties and function of nucleic acids. Claude Hélène's scientific contributions are numerous, but there are two that particularly stand out. His first major contribution was the discovery that a tripeptide (LysTrpLys) binds to abasic sites in DNA by intercalation and catalyzes strand scission (*Nature* **1981**, 292, 858–859). Some years later he entered the emerging field of gene targeting by antisense oligonucleotides and was a central player in shaping this field. However, the finding in 1987 (in parallel with Peter Dervan) that short homopyrimidine oligonucleotides via triple helix formation can sequence specifically target double-stranded DNA (*Nucleic Acids Res.* **1987**, 15, 7749–7760) had the most impact on the fields of bioorganic chemistry, DNA recognition, and gene therapeutic drug discovery. The follow-up studies in the Hélène lab of this seminal discovery during the past 15 years showed that this process could be improved by chemical design to a stage where “proof of principle” in cells was obtained. Claude Hélène's impact on the field of gene targeting has been tremendous. He and his laboratory constantly sought the key experiments to rigorously show the path to the final goal: controlling gene function by design. Through a large number of international collaborations he was always very alert to implement the newest and most promising technologies to reach this goal, and he defined the forefront of the field.

Many of us will remember the special atmosphere when visiting Claude Hélène in his laboratory in the unique setting at the Museum of Natural History with plants and exotic animals “in the backyard”. Being with Claude Hélène and discussing science was always an inspiring experience, and at the numerous meetings he attended, Claude Hélène was always ready with penetrating and visionary questions. The discovery of the sequence-specific triple helix recognition of duplex DNA had very profound influence on my own research, as this demonstrated for the first time a way to digitally read the sequence of double-stranded DNA in the major groove. The triple helix principle was the direct inspiration that triggered us to consider alternative ways of chemically connecting the sequence-reading nucleobases in the major groove of the DNA, that eventually lead to the discovery of PNA. From that point on much of our research was paralleling that of Claude Hélène's group, including several collaborative projects. As in an ideal world, to Claude, science was not a competition but a universal effort toward a common goal.

I feel privileged to have known Claude Hélène and fortunate to have been able to pay tribute to a unique scientist at his 65th birthday symposium, a symposium that duly reflected the impact of the field he was instrumental in giving birth to.

A great scientist and human being is no longer among us: A grave loss for the scientific community. His wisdom, great spirit, foresight, and warmth will be deeply missed.

Peter E. Nielsen

Center for Biomolecular Recognition,  
Department of Medical Biochemistry and Genetics,  
The Panum Institute, University of Copenhagen,  
Blegdamsvej 3c, DK-2200, Copenhagen, Denmark

BC0300091

# CORRESPONDENCE

## Comment on "In Vitro and in Vivo Evaluation of a Technetium-99m-Labeled Cyclic RGD Peptide as a Specific Marker of $\alpha_v\beta_3$ Integrin for Tumor Imaging"

*Sir:* In the article by Zi-Fen Su et al. recently published in *Bioconjugate Chemistry* (1), a technetium-99m-labeled RGD-4C peptide was introduced as a radioactive tracer for imaging  $\alpha_v\beta_3$  expression. However, in two tumor models this compound showed only marginal accumulation in tumor bearing nude mice. We have recently developed two radiolabeled RGD-peptides (2, 3) that demonstrated a markedly higher and receptor-specific accumulation in tumor-bearing animals (tumor/blood ratio greater 8 compared to less than 2 in the study by Su et al.). These tracers have been successfully used to image noninvasively  $\alpha_v\beta_3$ -positive tumors in vivo. Therefore, our findings differ significantly from the data reported by Su et al. Thus, the statement of the authors (page 568) that their work confirms and explains our previous findings is obviously not correct.

Su et al. determined an association constant of  $7 \times 10^{-6} \text{ M}^{-1}$  for binding of Tc-99m-RGD to the  $\alpha_v\beta_3$  integrin. Because of this low affinity it is not surprising that uptake of Tc99m-RGD by  $\alpha_v\beta_3$ -positive tumors was only marginal in vivo. However, it is important to note that other radiolabeled  $\alpha_v\beta_3$ -specific ligands have shown markedly higher affinity. For example the association constant of an iodine-labeled DTPA RGD has been reported as  $10 \times 10^{-9} \text{ M}^{-1}$  (4). The  $\text{IC}_{50}$  values of Galacto-RGD and Gluco-RGD developed by our group are  $5 \times 10^{-9} \text{ M}$  and  $40 \times 10^{-9} \text{ M}$ , respectively. Therefore, the conclusion of the authors (abstract, last sentence) that RGD peptides generally bind with low affinity to  $\alpha_v\beta_3$  is not correct. The in vitro data of the study by Su et al. only indicate that labeling of RDG-4C with technetium-99m using HYNIC as a chelator results in peptides with only modest affinity that appear not suitable for in vivo imaging.

In addition, the results of the in vivo experiments are difficult to interpret because the expression of  $\alpha_v\beta_3$  by

the tumor or endothelial cells was not evaluated by immunohistochemistry or Western blotting. Thus, it is unclear whether the low accumulation in the tumor is due to the low affinity of the tracer or due to low expression of  $\alpha_v\beta_3$  in the tumor tissue.

### LITERATURE CITED

- (1) Su, Z.-F., Liu, G., Gupta, S., Zhu, Z., Rusckowski, M., and Hnatowich, D. J. (2002) In Vitro and in Vivo Evaluation of a Technetium-99m-Labeled Cyclic RGD Peptide as a Specific Marker of  $\alpha_v\beta_3$  Integrin for Tumor Imaging. *Bioconjugate Chem.* 13, 561–570.
- (2) Haubner, R., Wester, H., Weber, W., Ziegler, S., Senekowitsch-Schmidtke, R., Kessler, H., et al. (2001) Noninvasive imaging of  $\alpha_v\beta_3$  integrin expression using a  $^{18}\text{F}$ -labeled RGD-containing glycopeptide and positron emission tomography. *Cancer Res.* 61, 1781–1785.
- (3) Haubner, R., Wester, H. J., Burkhart, F., Senekowitsch-Schmidtke, R., Weber, W., Goodman, S. L., et al. (2001) Glycosylated RGD-containing peptides: tracer for tumor targeting and angiogenesis imaging with improved biokinetics. *J. Nucl. Med.* 42, 326–336.
- (4) van Hagen, P. M., Breeman, W. A., Bernard, H. F., Schaar, M., Mooij, C. M., Srinivasan, A., et al. (2000) Evaluation of a radiolabeled cyclic DTPA-RGD analogue for tumour imaging and radionuclide therapy. *Int. J. Cancer* 90, 186–198.

### Roland Haubner\* and Wolfgang Weber

Nuklearmedizinische Klinik und Poliklinik  
Technische Universität München  
Ismaninger Strasse 22,  
81675 München, Germany

E-mail: R.Haubner@lrz.tum.de

BC020084W



## Response to Comment on "In Vitro and in Vivo Evaluation of a Technetium-99m-Labeled Cyclic RGD Peptide as a Specific Marker of $\alpha_v\beta_3$ Integrin for Tumor Imaging"

*Sir:* The report in question (1) describes an investigation into the properties of  $^{99m}\text{Tc}$ -RGD-4C for tumor imaging. As is evident therein, our results were disappointing in that unsatisfactory tumor targeting was observed in two xenografts (LS174T and ACHN) in nude mice. In the conclusion of that report, we state that other investigators imaging the same receptor with cyclic RGD peptides have also experienced "marginal" results and, as an example, we cited the work of Dr. Haubner et al. (2). In retrospect, it was somewhat unfair to do so since the peptides are quite different. Whereas the RGD-4C used in our investigation was cyclized via two disulfide bridges, the RGD of Haubner et al. was cyclized via an amide bond. While Haubner et al. labeled with radioiodine via an attached tyrosine, we radiolabeled with  $^{99m}\text{Tc}$  via hynic/tricine. Furthermore, the RGD of Haubner et al. was glycosylated to improve pharmacokinetics. Finally, the tumor models used by Haubner et al. are reported to show a high expression of the receptor whereas the receptor concentration of the LS174T and ACHN tumors are unknown and were not measured by us. Under these conditions, the tumor uptake reported by Haubner et al. was decidedly superior at about 3%ID/g and could be inhibited vs about 0.7% ID/g in our case with no difference from control. But whether both studies are "marginal" is best left to the readership to decide.

In the final sentence of our abstract, we conclude that "RGD peptides may have limitations as tumor imaging

agents" because of low receptor numbers or low binding affinities. We recognize that binding affinities considerably higher than the micromolar value of our radiolabeled RGD-4C have been reported for other RGD peptides. Whether due to higher affinities or higher receptor numbers, we would be delighted to be proven wrong.

### LITERATURE CITED

- (1) Su, Z. F., Liu, G., Gupta, S., Zhu, Z., Rusckowski, M., and Hnatowich, D. J. In Vitro and in Vivo Evaluation of a Technetium-99m-Labeled Cyclic RGD Peptide as a Specific Marker of  $\alpha_v\beta_3$  Integrin for Tumor Imaging. *Bioconjugate Chem.* 13, 561–570.
- (2) Haubner, R., Wester, H. J., Burkhart, F., Senekowitsch-Schmidtke, R., Weber, W., Goodman, S. L., et al. (2001) Glycosylated RGD-containing peptides: tracer for tumor targeting and angiogenesis imaging with improved biokinetics. *J. Nucl. Med.* 42, 326–336.

### Donald Hnatowich

University of Massachusetts Medical Center  
Nuclear Medicine Department  
55 Lake Avenue  
North Worcester, Massachusetts 01655

E-mail: Donald.Hnatowich@umassmed.edu

BC020085O

# COMMUNICATIONS

## An Efficient and Versatile Synthesis of BisPNA–Peptide Conjugates Based on Chemoselective Oxime Formation

Philippe Neuner,<sup>†</sup> Pasquale Gallo,<sup>†</sup> Laura Orsatti,<sup>‡</sup> Laura Fontana,<sup>†</sup> and Paolo Monaci<sup>\*,†</sup>

Department of Molecular & Cell Biology and Department of Pharmacology, I.R.B.M. P. Angeletti, Pomezia (Roma), Italy. Received September 25, 2002

Oligomers with two identical peptide nucleic acid sequences joined by a flexible hairpin linker (bisPNA) can stably bind to specific DNA sequences without altering plasmid supercoiling, thus offering a unique opportunity to attach various functional entities to high molecular weight DNA. Current synthetic approaches, however, severely limit the possibility to link peptides or other chemical moieties (i.e., sugars, oligonucleotides, etc.) to bisPNA. Here we report a novel strategy for the synthesis of bisPNA–peptide conjugates in which chemoselective ligation of bisPNA to peptides was accomplished through oxime formation between an oxy-amine-containing peptide and a bisPNA–methyl ketone (complementary modifications can also be used). The described synthesis is highly efficient, does not require a protection strategy, and is carried out under mild aqueous conditions. Through this methodology long peptide sequences in either C to N or N to C polarity can be linked to bisPNA. In addition, this protocol makes the conjugation of cysteine-containing peptides feasible and allows disulfide bond formation to be controlled. This same approach can be exploited to link oligonucleotides, sugars, or other chemical entities to bisPNA.

### INTRODUCTION

Plasmid-based, nonviral gene delivery systems are a promising therapeutic approach for gene therapy and genetic immunization protocols (1–3). However, the poor efficiency and specificity of gene transduction obtained in vivo hampers the full exploitation of their potential in clinical settings. Several key steps can be identified along the route leading to gene expression: DNA condensation, efficient and specific targeting of cell surface receptors, cellular uptake, escape from the endosome/lysosome, stability against nucleases, intracellular distribution, efficient recruitment of transcription factors, etc. In many cases specific peptide sequences have been shown to increase the efficiency of one or more of these steps (4–8). However, conjugating peptides to DNA is not a straightforward procedure. A stable modification of plasmid DNA in its supercoiled form is often required, multiple copies of the peptides with defined polarity need to be conjugated, and the modification must not interfere with plasmid transcriptional activity.

Peptide nucleic acid (PNA) is a DNA analogue in which repeating *N*-(2-aminoethyl)glycine units replace the deoxyribose-phosphate backbone (9, 10). Due to the neutral charge of its backbone, PNA hybridizes to complementary DNA with affinity and specificity higher than the corre-

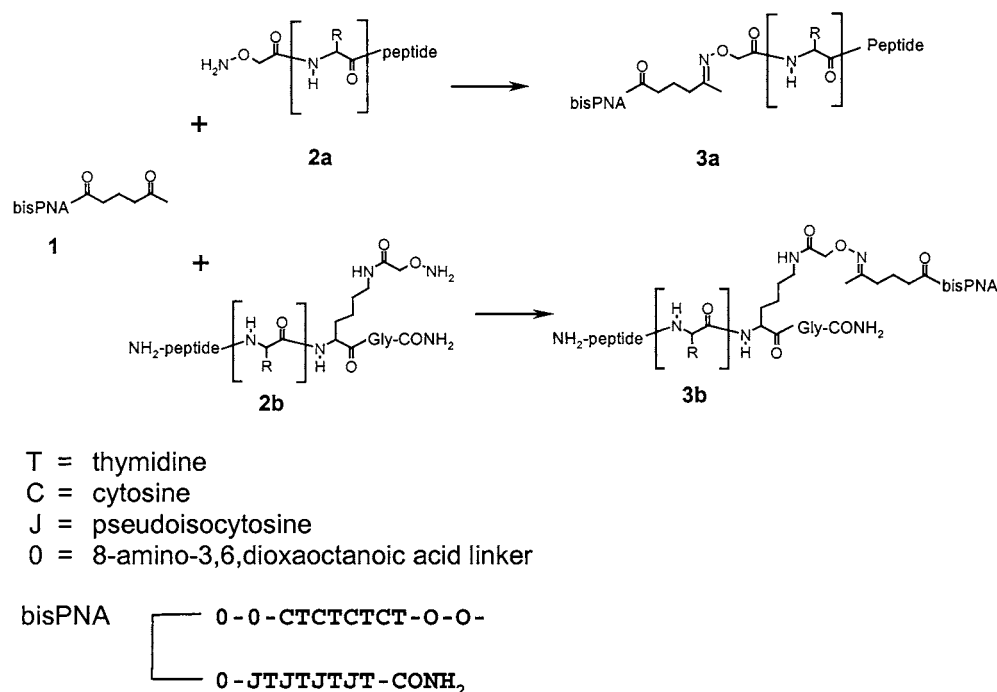
sponding DNA–DNA hybrid (11). A bisPNA molecule is an oligomer with two identical PNA sequences joined by a flexible hairpin linker (11–13). Binding of bisPNA to its DNA target is sequence-specific, stoichiometric, extremely stable, and essentially irreversible under physiological conditions (11, 14). Of note is that a bisPNA molecule targets a specific site on DNA, invades duplex DNA, and displaces the complementary DNA strand to form a stable PNA:DNA:PNA triplex hybrid, without affecting the supercoiled form of plasmid DNA (11). These properties identify bisPNA as a preferential method to efficiently link molecules with various functional properties at specific sites on supercoiled plasmid DNA. For example, fluorescein or rhodamine can be linked to bisPNA and the ensuing conjugate used to bind irreversibly and specifically to a binding site cloned into a plasmid to track distribution in vivo (14).

With the aim of improving plasmid-mediated gene transduction, peptides emerge as the most interesting class of molecules to link to bisPNA. Current methods for preparing bisPNA–peptide conjugates are based on collinear synthesis of the hybrid molecule, which present some drawbacks to its general application (15). For instance, synthesis is limited to C to N polarity of the peptide and is rather inefficient for long peptide sequences. In addition, the collinear synthesis of peptides containing cysteine residues is not feasible, since formation of disulfide bridges cannot be controlled. Finally, linking to bisPNA chemical moieties other than peptides, such as carbohydrates or oligonucleotide, clearly require alternative synthesis protocols.

\* Corresponding author: Paolo Monaci, IRBM P. Angeletti, Via Pontina km 30.600, 00040 – Pomezia (Roma), Italy. Tel. +39–06–91093–242, fax +39–06–91093–654, e-mail: paolo\_monaci@merck.com.

<sup>†</sup> Department of Molecular & Cell Biology.

<sup>‡</sup> Department of Pharmacology.



**Figure 1.** Ligation of amino-oxy peptide to bisPNA–methyl ketone through oxime linkage.

**Table 1. Peptides Linked to BisPNA<sup>a</sup>**

peptide	length	polarity	sequence
NL1.1	37 aa	C to N	NH <sub>2</sub> -AEGEFMYWGDSHWLQYWYEGDPAKGGSGGGSGGGK(aox)G-CONH <sub>2</sub>
NL4c	35 aa	C to N	NH <sub>2</sub> -AEGEFFCVSSGGSSCWDPAPAKGGSGGGSGGGK(aox)G-CONH <sub>2</sub>
(VP16) <sub>2</sub>	28 aa	N to C	(aox)NH-GGPADALDDFDLMDLPADALDDFDLMDL-CONH <sub>2</sub>
(VP16) <sub>3</sub>	41 aa	N to C	(aox)NH-GGPADALDDFDLMDLPADALDDFDLMDLPADALDDFDLMDL-CONH <sub>2</sub>

<sup>a</sup> aox, amino-oxyacetyl.

Recently, Felgner and co-workers described an approach in which sulfhydryl-containing peptides are conjugated to streptavidin maleimide, and the resulting streptavidin conjugates are then bound to a biotin–bisPNA-labeled plasmid (16). Alternatively, the same peptides can be directly coupled to a maleimide–bisPNA conjugate bound to plasmid DNA. This approach can also be extended to oligonucleotides containing free SH groups, but not to peptides containing cysteine residues.

As a further step toward broadening the applications of bisPNA conjugates, we describe an alternative and more versatile synthetic approach to conjugate peptides and other molecules to bisPNA based on chemoselective ligation of an amino-oxy peptide to a bisPNA–methyl ketone which circumvents the limitations listed above.

## RESULTS AND DISCUSSION

We adopted a novel synthesis approach to link peptides to bisPNA. An amino-oxy peptide was conjugated to bisPNA–methyl ketone through an oxime forming ligation (Figure 1). The amino-oxy group could be displayed either at the C or at the N terminus of the peptide. Complementary modifications (i.e., amino-oxy group at the N-terminus of the bisPNA and methyl ketone group at the N or C terminus of the peptide) can also be used.

**Solid-Phase Synthesis of the Amino-oxy Peptides.** Four different peptides were linked to a bisPNA molecule (Table 1). We chose peptides with specific biological properties, which differed in length, presence of cysteine residues, and polarity of conjugation to bisPNA. NL1.1 and NL4c are 24 and 22 aa long peptides, respectively, which specifically bind to HER2/neu, a tyrosine-kinase

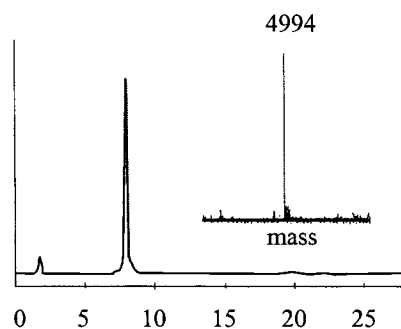
receptor which is overexpressed in 30–50% of human breast, gastric, and colon tumors (17, 18). These peptides have been identified by screening phage-displayed random peptide libraries (19, unpublished data). Of note, NL4c contains two cysteine residues forming a disulfide bridge. Both peptides must be linked C to N to bisPNA. VP16 is 13 aa minimal transcription activator domain derived from herpes simplex virus protein 16 (20). Just two VP16 peptides bound to DNA through a GAL4 DNA binding domain are sufficient to activate transcription from a downstream promoter (20).

We thus attempted to generate a minimal transcription activator by linking two or three VP16 peptides with the N to C polarity to bisPNA. Binding of this bisPNA chimera to plasmid DNA could enhance transcription from a downstream promoter without requiring the recruitment of intracellular transcription activators.

Peptides NL1.1, NL4c, VP16<sub>2</sub>, and VP16<sub>3</sub> were synthesized by standard Fmoc chemistry. GGG linker sequences were added to the C-terminus of NL1.1 (11 residues) and NL4c (12 residues) to facilitate the interaction of the peptides with the target promoter (21). An amino-oxy group was incorporated at the C terminus of NL1.1 and NL4c peptide by coupling the (amino-oxy) acetyl functionality at the  $\epsilon$ -amine side chain of an extra C-terminal Lys residue, as described by Canne et al. (15). Similarly, an amino-oxy group was incorporated at the N terminus of peptide VP16<sub>2</sub> and VP16<sub>3</sub>. Peptides were purified by HPLC and their structure verified by mass spectroscopy.

**Solid-Phase Synthesis of the BisPNA–Methyl Ketone.** All reagents including Boc-PNA-C(Z), Boc-PNA-T, Boc-AEEA-ODCHA spacer (L = 2-aminoethoxy-2-





**Figure 2.** HPLC and mass analysis of the purified bisPNA-methyl ketone.

ethoxyacetic acid), and HBTU were obtained from PerSeptive Biosystems (Framingham, MA). MBHA-resin was obtained from Calbiochem-Novabiochem AG (Laufelfingen, Switzerland). A bisPNA-methyl ketone oligomer (mKetone-NH-LL-TCTCTCTC-LLL-JTJTJT-CONH<sub>2</sub>) designed to bind the DNA sequence 5'-GAGAGAGAGA-3' was synthesized by hand on MBHA-resin (215 mg; substitution = 45.5  $\mu$ mol/g; 10  $\mu$ mol scale) essentially as described (22). Pseudoisocytosine J, an analogue of C which encourages a pH-independent specific formation of the Hoogsteen triplex hybrid, was synthesized as described by Egholm et al. (11).

In a typical procedure, 40  $\mu$ mol of monomers (4 equiv), *N,N*-diisopropylethylamine (6 equiv/monomer) and HBTU (0.9 equiv/monomer) were dissolved in 800  $\mu$ L of a mixture *N*-methylpyrrolidinone/pyridine (1:1). After 3 min of preactivation, the reaction mixture was applied to the resin, coupling was allowed to proceed for 4 h, and resin was washed with DMF/DCM (twice for 3 min each). Prior to the next coupling step, the Boc-protected amino terminus was deprotected with a mixture of TFA/*m*-cresol (95:5; twice for 4 min each). After completion of the bisPNA sequence, the methyl ketone moiety was introduced by activating 4-acetylbutyric acid (100  $\mu$ mol) as symmetric anhydride with DIC (50  $\mu$ mol) in DCM. After

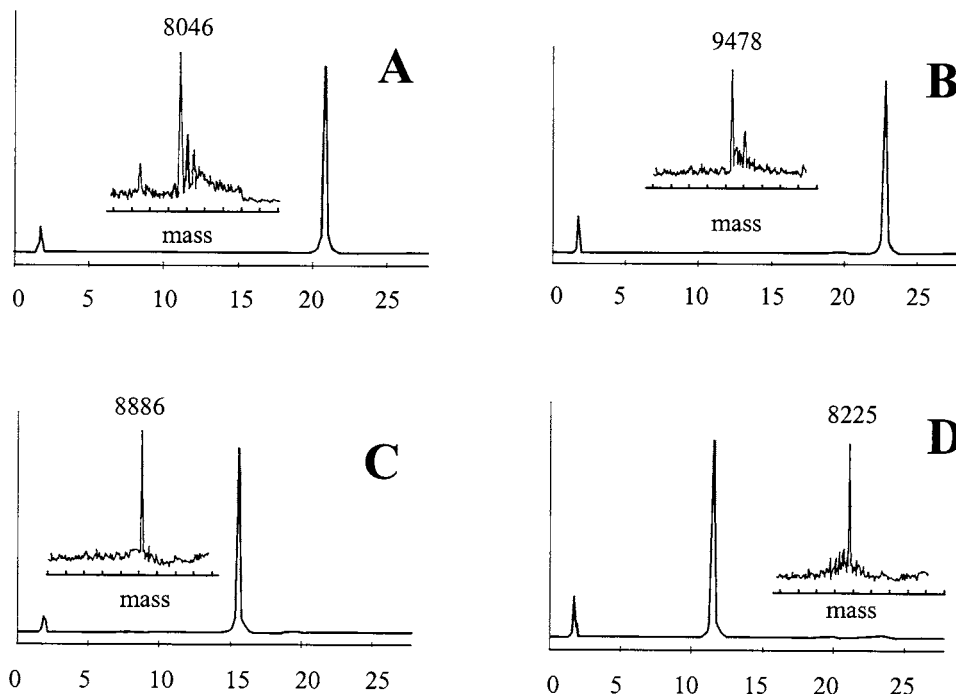
**Table 2.** Experimental and Calculated Mass for the BisPNA-Peptide Chimera

	M (experimental)	M (calculated)
BisPNA-NL1.1	8886.00	8887.65
BisPNA-NL4	8225.00	8227.27
BisPNA-VP16 <sub>2</sub>	8046.00	8047.32
BisPNA-VP16 <sub>3</sub>	9478.00	9479.91

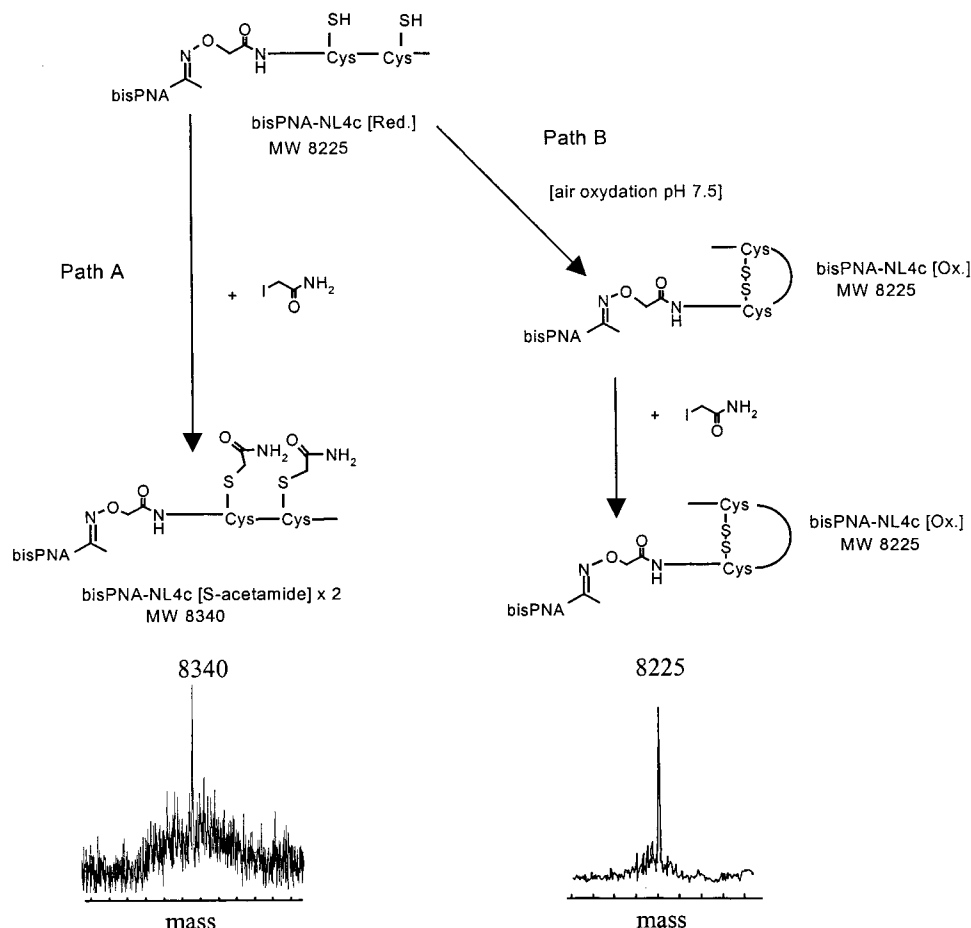
activation for 15 min, the mixture was diluted with DMF (1 mL), added to the PNA-resin, and coupled for 60 min. The resin was washed with DMF/DCM, dried, and transferred to a screw cap vial. The product bisPNA was deprotected and concomitantly cleaved from the resin by treatment with a mixture of TFMSA/TFA/*m*-cresol (18:73:9; 1 mL) for 2 h at 0 °C. The solid was separated by filtration and the filtrate poured into 10 volumes of ice cold Et<sub>2</sub>O. Centrifugation yielded a pellet, which was purified by HPLC. M (calculated) for C<sub>204</sub>H<sub>282</sub>N<sub>78</sub>O<sub>73</sub> = 4995.00; M (experimental) = 4994.00 (Figure 2).

**Synthesis of the BisPNA-Peptide Conjugate: Oxime-Forming Ligation.** Purified bisPNA-methyl ketone was mixed with the amino-oxy peptide to generate the oxime-linked bisPNA-peptide conjugate. The amino-oxy group was displayed either at the C (NL1.1 and NL4c) or at the N terminus (VP16<sub>2</sub> and VP16<sub>3</sub>) of the peptide (Figure 1).

In a typical experiment, bisPNA-methyl ketone **1** was coupled to the amino-oxy peptide **2** via oxime ligation (15). The bisPNA-methyl ketone (0.2  $\mu$ mol) was dissolved in 250  $\mu$ L of 0.1 M sodium acetate buffer (pH 4.2). Two equivalents (0.4  $\mu$ mol) of the amino-oxy peptide and 20  $\mu$ L of DMF were added to the resulting solution. Coupling reaction was allowed to proceed for 12 h, and the resulting conjugate was readily purified by semipreparative reverse-phase HPLC and lyophilized to give a white solid. Preparative RP C18 HPLC purification was performed using a SymmetryPrep C18 (7.8  $\times$  150 mm) reverse-phase column (Waters, Milford, MA). Eluant A: 99.9% water, 0.1% TFA; eluant B: 10% water, 89.9% acetonitrile, 0.1% TFA; a linear gradient of 5%-30%



**Figure 3.** HPLC and mass analysis of the purified bisPNA-peptide chimeras. BisPNA-VP16<sub>2</sub> (A), bisPNA-VP16<sub>3</sub> (B), bisPNA-NL1.1 (C), and bisPNA-NL4c (D).



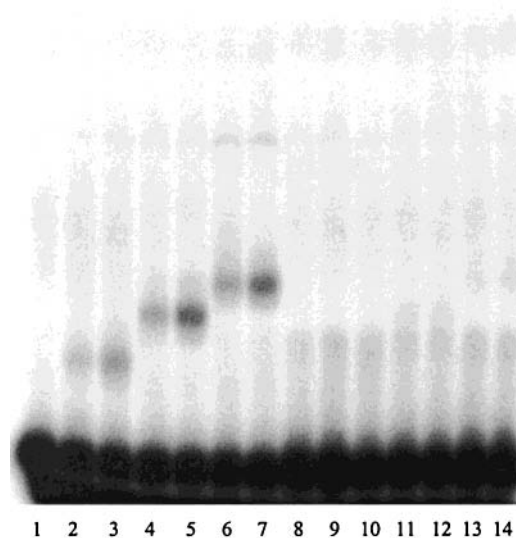
**Figure 4.** Iodoacetamide test reaction with reduced (path A) and oxidized (path B) bisPNA-NL4c chimera.

**Table 3. Nucleotides Sequence of Oligonucleotides Harboring BisPNA Binding Site**

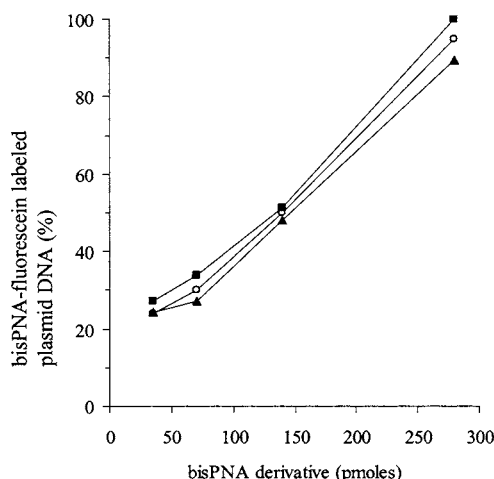
Target	GGGGGTCTCTCTCTCCCCC CCCCAGAGAGAGAGGGGGG
Control	GGGGGTCTCAATCTCCCCC CCCCAGAGTTAGAGGGGGG

eluant B over 25 min at a flow rate of 3.0 mL/min monitored at 260 nm. The average yield was usually 15–20% of purified chimeras. Final product was analyzed for purity by mass determination by LC/Quadrupole ion trap mass spectrometer Finnigan-MAT (San Jose, CA, Figure 3). Experimentally derived and calculated mass for the four bisPNA-peptides products are listed in Table 2.

As for the bisPNA-NL4c chimera, the crude product was purified by HPLC after oxime ligation, and the desired fractions were lyophilized. The resulting solid was resuspended at a concentration of 1 mg/mL in distilled water and air-oxidized overnight to allow intramolecular disulfide bridge formation. Oxidation of the NL4c peptide cysteine residues was assessed by adding a small excess of iodoacetamide to an aliquot of the purified bisPNA-NL4c chimera before and after air oxidation (Figure 4, paths A and B, respectively). Mass analysis of the iodoacetamide reaction product derived from path A showed an increase in mass of 114 (2 × 57), corresponding to the two acetamide adducts of the reduced bisPNA-NL4c chimera, whereas no mass variation was detected for the oxidized bisPNA-NL4c.



**Figure 5.** Specific binding of bisPNA-VP16 chimeras to target sequence. Three and six pmoles of bisPNA-methyl ketone (lanes 2, 3 and 9, 10), bisPNA-VP16<sub>2</sub> (lanes 4, 5 and 11, 12) or bisPNA-VP16<sub>3</sub> (lanes 6, 7 and 13, 14) were incubated at 37 °C for 15 min with approximately 1.5 pmol of the [ $\alpha$ -<sup>32</sup>P]-labeled double stranded oligonucleotide in 20  $\mu$ L of HBS buffer (10 mM Hepes, 50 mM NaCl, pH 7.0). Lanes 2–7 and lanes 9–14 refer to reactions with target or control oligonucleotide, respectively. Additional control reactions were included in the absence of bisPNA (lanes 1 and 8, with target and control oligo, respectively). Five microliters of 20% glycerol was added, and the samples were fractionated on a 5% polyacrylamide gel in TBE buffer (45 mM Tris-borate, 1 mM EDTA, pH = 7.5) at 10 V/cm for 3–4 h at 4 °C. Gel was dried and autoradiographed on Kodak XR5 film with intensifying screen.



**Figure 6.** BisPNA-peptide chimeras bind the target sequence within supercoiled plasmid DNA. Increasing amounts (35, 70, 140, and 280 pmol) of bisPNA-methyl ketone (empty circles, lanes 4–7), bisPNA-VP16<sub>2</sub> (filled squares; lanes 8–11), or bisPNA-VP16<sub>3</sub> (filled triangles; lanes 12–15) were incubated with 1.12 pmol of pGGLuc plasmid DNA in 40  $\mu$ L of HBS buffer for 45 min. The binding of these bisPNA derivatives was challenged, adding 32 pmol of bisPNA-fluorescein to the reaction and incubating for additional 20 min. Control reactions with bisPNA fluorescein (lane 1), pGGLuc (lane 2), or bisPNA-fluorescein conjugated with pGGLuc (lane 3) were also included. Seven microliters of 20% glycerol were added, and the samples were fractionated on a 0.8% agarose gel in TBE buffer (90 mM Tris-borate, 2 mM EDTA, pH 7.5). The incubations were performed at 37 °C and the samples run at room temperature. Gels were scanned using a GS-700 Imaging Densitometer BIORAD (Hercules, CA). Quantitation of the PNA-fluorescein conjugated was performed with a MacIntosh G3 computer using the program Molecular Analyst.

**Characterization of the BisPNA-Peptide Conjugates.** We wanted to assess the DNA-binding properties of these bisPNA-peptide chimeras. To this end we synthesized two double-stranded oligonucleotides containing the bisPNA binding sequence (target oligo) and the same sequence with two mutations (control oligo) (Table 3; binding sequence is indicated in bold and mutation are underlined). Two different amounts of bisPNA-methyl ketone, bisPNA-VP16<sub>2</sub>, or bisPNA-VP16<sub>3</sub> were incubated with target or control oligonucleotide (2 and 4 molar ratios).

Formation of the DNA:bisPNA-VP16 complex was detected by a gel mobility shift assay (Figure 5). Both bisPNA-VP16<sub>2</sub> and bisPNA-VP16<sub>3</sub> chimeras bound the target oligonucleotide in a manner indistinguishable from that of the reference bisPNA-methyl ketone molecule (Figure 5, lanes 2–7). By contrast, no binding could be detected to control oligonucleotide in the same conditions (Figure 5, lanes 9–14).

Next, we tested the ability of the same chimeras to bind the target binding sequence in the context of a supercoiled plasmid DNA. We used plasmid pGGLuc (Gene Therapy Systems, San Diego, CA) which bears a CMV immediate early promoter driving the expression of a luciferase reporter gene. This plasmid contains 10 binding sites for bisPNA molecule immediately after the translational termination site. We preincubated pGGLuc plasmid DNA with increasing amounts of bisPNA-methyl ketone, bisPNA-VP16<sub>2</sub>, or bisPNA-VP16<sub>3</sub>. Then, a fixed amount of bisPNA-fluorescein was allowed to bind plasmid DNA. Increasing the amount of either bisPNA derivatives reduced fluorescence-labeling of the plasmid (Figure 6).

These results indicate that bisPNA-VP16<sub>2</sub> or bisPNA-VP16<sub>3</sub> retains the binding properties of the reference bisPNA-methyl ketone and similarly prevented bisPNA-fluorescein binding to its target site on supercoiled plasmid DNA.

#### ACKNOWLEDGMENT

In summary, the data we report in this paper demonstrate that bisPNA-peptide conjugate can be prepared by post-assembly conjugation of an amino-oxy peptide with a bisPNA-methyl ketone molecule. The reaction is simple, efficient, and versatile, since it can be applied to linking long peptides, with or without cysteine residues, in both polarities, to bisPNA. The same approach can be extended to linking other chemical moieties to bisPNA, namely to oligonucleotides. The synthetic approach we describe makes generating several different bisPNA-peptide conjugates limited only by the efficiency of synthesis of the individual components. Indeed, bisPNA-peptide chimeras appear particularly suited for providing plasmid DNA with new functions (e.g., targeting specific cell types, subcellular localization, transcription activating domain, etc.) which could improve the efficiency of gene expression, *in vitro* and *in vivo*.

#### ACKNOWLEDGMENT

We wish to thank Antonello Pessi for useful discussion, Marco Finotto for the synthesis of the modified peptides, and Janet Clench for proofreading the manuscript.

#### LITERATURE CITED

- (1) Spack E. G., and Sorgi, F. L. (2001) Developing nonviral DNA delivery systems for cancer and infectious disease. *Drug Discov. Today* 6, 186–197.
- (2) Luo, D., and Saltzman, W. M. (2000) Synthetic DNA delivery systems. *Nat. Biotechnol.* 18, 33–37.
- (3) Donnelly, J. J., Ulmer, J. B., Shiver, J. W., and Liu, M. A. (1997) DNA vaccines. *Annu. Rev. Immunol.* 15, 617–648.
- (4) Branden, L. J., Christensson, B., and Smith, C. I. (2001) *In vivo* nuclear delivery of oligonucleotides via hybridizing bifunctional peptides. *Gene Ther.* 8, 84–87.
- (5) Good, L., Awasthi, S. K., Dryselius, R., Larsson, O., Nielsen, P. E. (2001) Bactericidal antisense effects of peptide-PNA conjugates. *Nat. Biotechnol.* 19, 360–364.
- (6) Cutrona, G., Carpaneto, E. M., Ulivi, M., Roncella, S., Landt, O., Ferrarini, M., and Boffa, L. C. (2000) Effects in live cells of a c-myc anti-gene PNA linked to a nuclear localization signal. *Nat. Biotechnol.* 18, 300–303.
- (7) Scarfi, S., Giovine, M., Gasparini, A., Damonte, G., Millo, E., Pozzolini, M., and Benatti, U. (1999) Modified peptide nucleic acids are internalized in mouse macrophages RAW 264.7 and inhibit inducible nitric oxide synthase. *FEBS Lett.* 451, 264–268.
- (8) Pooga, M., Soomets, U., Hallbrink, M., Valkna, A., Saar, K., Rezaei, K., Kahl, U., Hao, J. X., Xu, X. J., Wiesenfeld-Hallin, Z., et al. (1998) Cell penetrating PNA constructs regulate galanin receptor levels and modify pain transmission *in vivo*. *Nat. Biotechnol.* 16, 857–861.
- (9) Nielsen, P. E., Egholm, M., Berg, R. H., and Buchardt, O. (1991) Sequence-selective recognition of DNA by strand displacement with a thymine-substituted polyamide. *Science* 254, 1497–1500.
- (10) Egholm, M., Buchardt, O., Christensen, L., Behrens, C., Freier, S. M., Driver, D. A., Berg, R. H., Kim, S. K., Norden, B., and Nielsen, P. E. (1993) PNA hybridizes to complementary oligonucleotides obeying the Watson-Crick hydrogen-bonding rules. *Nature* 365, 566–568.
- (11) Egholm, M., Christensen, L., Dueholm, K. L., Buchardt, O., Coull, J., and Nielsen, P. E. (1995) Efficient pH-independent sequence-specific DNA binding by pseudoisocytosine-containing bis-PNA. *Nucleic Acids Res.* 23, 217–22.



- (12) Vickers, T. A., Griffith, M. C., Ramasamy, K., Risen, L. M., and Freier, S. M. (1995) Inhibition of NF-kappa B specific transcriptional activation by PNA strand invasion. *Nucleic Acids Res.* **23**, 3003–3008.
- (13) Kuhn, H., Demidov, V. V., Nielsen, P. E., and Frank-Kamenetskii, M. D. (1999) An experimental study of mechanism and specificity of peptide nucleic acid (PNA) binding to duplex DNA. *J. Mol. Biol.* **286**, 1337–45.
- (14) Zelphati, O., Liang, X., Hobart, P., and Felgner, P. L. (1999) Gene chemistry: functionally and conformationally intact fluorescent plasmid DNA. *Hum. Gene Ther.* **10**, 15–24.
- (15) Canne, L. E., Ferre-D'Amare, A. R., Burley, S. K., and Kent, S. B. H. (1995) Total Chemical Synthesis of a Unique Transcription Factor-Related Protein: cMyc-Max. *J. Am. Chem. Soc.* **117**, 2998–3007.
- (16) Zelphati, O., Liang, X., Nguyen, C., Barlow, S., Sheng, S., Shao, Z., and Felgner, P. L. (2000) PNA-dependent gene chemistry: stable coupling of peptides and oligonucleotides to plasmid DNA. *Biotechniques* **28**, 304–310, 12–14, 16.
- (17) Slamon, D. J., and Clark, G. M. (1988) Amplification of c-erbB-2 and aggressive human breast tumors? *Science* **240**, 1795–1798.
- (18) Klapper, L. N., Kirschbaum, M. H., Sela, M., and Yarden, Y. (2000) Biochemical and clinical implications of the ErbB/HER signaling network of growth factor receptors. *Adv. Cancer Res.* **77**, 25–79.
- (19) Urbanelli, L., Ronchini, C., Fontana, L., Menard, S., Orlandi, R., and Monaci, P. (2001) Targeted gene transduction of mammalian cells expressing the HER2/neu receptor by filamentous phage. *J. Mol. Biol.* **313**, 965–76.
- (20) Seipel, K., Georgiev, O., and Schaffner, W. (1992) Different activation domains stimulate transcription from remote ('enhancer') and proximal ('promoter') positions. *EMBO J.* **11**, 4961–8.
- (21) Argos, P. (1990) An investigation of oligopeptides linking domains in protein tertiary structures and possible candidates for general gene fusion. *J. Mol. Biol.* **211**, 943–58.
- (22) Christensen, L., Fitzpatrick, R., Gildea, B., Petersen, K. H., Hansen, H. F., Koch, T., Egholm, M., Buchardt, O., Nielsen, P. E., et al. (1995) Solid-phase synthesis of peptide nucleic acids. *J. Pept. Sci.* **1**, 185–83.

BC020060P

# ARTICLES

## Can Nuclear Localization Signals Enhance Nuclear Localization of Plasmid DNA?

Takeshi Nagasaki,<sup>\*,†</sup> Teruhiko Myohoji,<sup>†</sup> Taro Tachibana,<sup>†</sup> Shiroh Futaki,<sup>‡</sup> and Seizo Tamagaki<sup>†</sup>

Department of Applied and Bioapplied Chemistry, Graduate School of Engineering, Osaka City University, SORST (JST), Osaka, 558-8585, Japan, and Institute for Chemical Research, Kyoto University, Uji, Kyoto 611-0011, Japan. Received September 9, 2002; Revised Manuscript Received November 22, 2002

Nonviral vectors are safer and more cost-effective than viral vectors but are significantly less efficient, and thus, increasing the efficiency of nonviral vectors remains an important objective. One way to overcome this problem is by stimulating the nuclear localization of exogenous genes. Nuclear localization signals (NLSs) are known to be involved in the active transport of exogenous proteins and probes into the nucleus. However, stimulation of nuclear localization of plasmid DNA has yet to be confirmed completely. In the present study, we prepared plasmid DNA–NLS peptide conjugates and adjusted spacer length and number introduced in an attempt to increase transfection efficiency. In comparison to conjugates with unmodified plasmid DNA and short spacers, we found that NLS–plasmid DNA conjugates with covalent bonding by diazo coupling through PEG chain (MW 3400) stimulated complexation with the nuclear transport proteins importin  $\alpha$  and importin  $\beta$ . Evaluation of transfection showed higher expression efficiency with plasmid DNA–NLS peptide conjugates than with unmodified plasmids. However, evaluation of intracellular trafficking after microinjection into the cytoplasm showed plasmid DNA–NLS peptide conjugates only within the cytoplasm; there was no NLS–plasmid stimulation of nuclear localization. Our findings suggest that stimulation of plasmid nuclear localization cannot be achieved merely by changing spacer length or chemically modifying plasmid DNA–NLS peptide conjugates. An additional mechanism must be involved.

### INTRODUCTION

Gene therapy has been seriously investigated in the United States as a clinical treatment for genetic diseases such as adenosine deaminase (ADA) deficiency since 1990. Numerous studies have subsequently investigated the use of gene therapy for treatment of cancer, infections (such as AIDS), and other lifestyle-related diseases. The key to efficient transfection and expression of exogenous genes into cells is the use of “vectors” (gene carriers). Retrovirus and adenovirus vectors have conventionally been used because of their high efficiency. However, reports of a patient death due to an adenovirus vector in the United States in 1999 led to renewed interest in developing nonviral vectors to further increase safety (1). The increasing use of gene therapy in clinical practice also makes the development of nonviral vectors important with regard to cost and availability.

Nonviral vectors can broadly be divided into lipoplexes (lipid/DNA complexes) and polyplexes (polymer/DNA complexes) (2). However, the transfection and expression efficiencies of these nonviral vectors are much lower than those of viral vectors. The low efficiency of these vectors is also the most significant problem when they are used

for gene therapy. This necessitates research and development of nonviral vectors with higher efficiency by using nanoparticles consisting of complexes of nucleic acids and polycations such as dendrimer polymers or lipid aggregates (liposomes).

Nonviral vectors must overcome several intracellular barriers before mRNA transcription (3–5). The greatest barrier facing both polyplexes and lipoplexes is the nuclear membrane (6–9). Nuclear localization efficiency significantly influences expression efficiency.

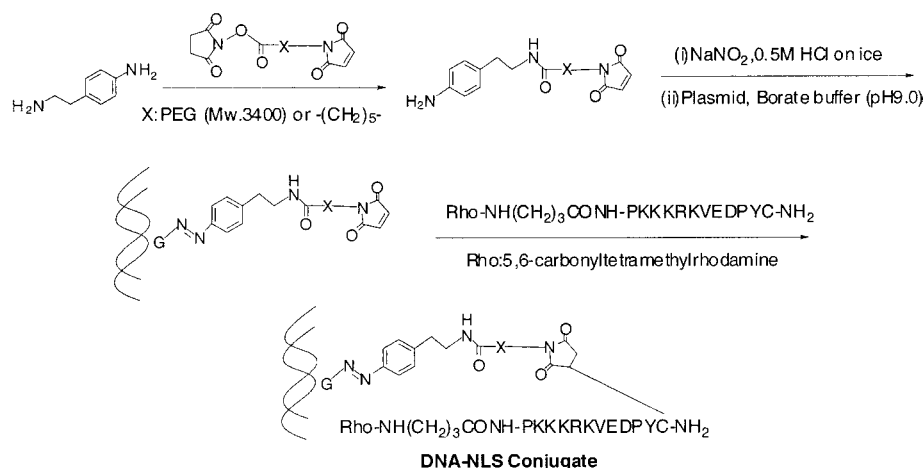
Recent studies have shown that intranuclear transport of large molecules such as proteins and nucleic acids is a selective process through nuclear pore complexes that involves energy dependent carrier proteins (10–15). Several investigations have focused on the nuclear-cytoplasm transport system used by biological organisms as a means of stimulating nuclear localization of exogenous genes (16, 17). Some studies have reported dramatic increases in expression efficiency using NLS modified linear DNA (18, 19), but similar results with plasmid DNA have not been reported to date (20–22).

The clinical application of gene therapy requires the development of highly efficient plasmid DNA delivery systems that can be synthesized both easily and in large quantities. The availability of plasmid DNA–NLS peptide conjugates providing reliable intranuclear transport would be of enormous benefit. In this regard, we must first consider why previous research has failed to achieve these goals. In plasmid DNA–NLS peptide conjugates

\* To whom correspondence should be addressed. Phone: 81 6 6605 2696. Fax: 81 6 6605 2785. E-mail: nagasaki@bioa.eng.osaka-cu.ac.jp.

<sup>†</sup> Osaka City University.

<sup>‡</sup> Kyoto University.

**Scheme 1. Syntheses of Plasmid DNA–NLS Peptide Conjugates<sup>a</sup>**

<sup>a</sup> The Spacer (X) Contains Either the Long PEG or Short Pentamethylene Chain.

designed to date (20–22), suboptimal spacer lengths between the cationic NLS and anionic DNA have resulted in a strong interaction between the NLS and plasmid and burying of the NLS within the negative charges. This interferes with recognition of transport proteins. Furthermore, the localization of large plasmid molecules may require insertion of multiple NLSs, whereas overfull chemical modification cause the inhibition of the transcriptional process. Therefore, our research has focused on developing a convenient method to produce plasmid DNA–NLS peptide conjugates with a more optimum spacer length and where the number of insertions can be regulated. The objective is the development of a highly efficient nonviral gene delivery system.

**EXPERIMENTAL METHODS**

**Materials.** 5(and 6)-Carboxyltetramethylrhodamine *N*-hydroxysuccinimide ester was purchased from Molecular Probes (Eugene, OR). *N*-(6-Maleimidocaproyloxy)-succinimide was purchased from Dojindo Lab. (Kumamoto, Japan). Maleimido-peg-carboxylic acid *N*-hydroxysuccinimide<sup>1</sup> ester was purchased from Shearwater (Huntsville, AL). Di-*tert*-Butyl dicarbonate and *N*-(9-fluorenylmethyloxy-carbonyloxy)succinimide were purchased from Peptide Lab. (Osaka, Japan). Recombinant GST fusion Importin  $\alpha$  and importin  $\beta$  were prepared as reported previously (12). Lipofectin was purchased from Invitrogen Corp. (Carlsbad, CA). Other reagents and solvents were purchased from Aldrich.

**Plasmids.** pGL3-control (pGL3) was purchased from Promega (Madison, WI). pEGFP-N1 (pGFP) was purchased from Clontech (Palo Alto, CA). Plasmid DNAs were amplified in *Escherichia coli* and purified by Endo-Free Plasmid Kit (Qiagen, Hilden, Germany).

**Rhodamine-Labeled NLS Peptide.** The NLS peptide, from SV-40 large T antigen, used in this study was manually synthesized by the Fmoc solid-phase method on a Rink amide resin as reported previously (23). After the elongation of the NLS sequence PKKKRKVEDPYC, 4-amino butyric acid was introduced as a spacer between the NLS and a fluorescent residue. Finally, the amino

group was labeled with 5(and 6)-carboxyltetramethylrhodamine succinimidyl ester. The protecting groups and the resin were removed with TFA in the presence of H<sub>2</sub>O (10%), phenol (5%), ethanedithiol (5%), and thioanisole (5%) at room temperature for 3 h. After addition of diethyl ether, the crude product was precipitated and then purified by RP-HPLC.

**Preparation of Plasmid DNA–NLS Peptide Conjugates.** Diazocoupling (24–26) and photoactivation (27–32) have been reported as the covalent modifications of DNA. In this study plasmid DNA–NLS peptide conjugates were prepared by the diazo coupling method according with Scheme 1. Synthesized conjugates were purified with ultrafiltration (Centricon Plus-10; nominal molecular weight limit = 10 kDa, Millipore, Bedford, MA). The number of NLS linked to one plasmid was determined by absorbance at 260 nm and fluorescent intensity (ex = 546 nm, em = 576 nm). The fluorescence polarization of rhodamine linked to the NLS was measured by BEACON 2000 spectrometer (Pan Vera, Madison, WI) in order to estimate the type of binding of the NLS to plasmid. PEGylated NLS (NLS-peg) prepared with the NLS peptide and PEG-maleimide (Mw. 5000, Shearwater, Huntsville, AL) was also examined for the fluorescence polarization method as a comparison.

**Importin Binding Assay.** Binding to importin  $\alpha$  in the presence of importin  $\beta$  was performed according to Wils et al. (22), with the following method: all assays were performed in binding buffer (20 mM HEPES, pH 7.0, 110 mM potassium acetate, 2 mM magnesium acetate, and 0.1 mg/mL bovine serum albumin). The GST fusion importin  $\alpha$  with and without importin  $\beta$  (1 mg per 10 mL of beads, respectively) was incubated with 0.25 mL of glutathione-sepharose beads (Amasham, Piscataway, NJ) in binding buffer (0.25 mL) for 30 min at room temperature. The beads were collected by centrifugation at 2000*g* for 30 s and washed five times with binding buffer (0.25 mL). The beads slurry (80  $\mu$ L) was incubated with 2  $\mu$ g of plasmid DNA–NLS peptide conjugate for 30 min at room temperature. The beads were collected by centrifugation at 2000*g* for 30 s. The supernatant was removed, and 30  $\mu$ L was used to analyze the presence of unbound DNA (this fraction is called the unbound fraction). The beads were washed five times with 0.25 mL of binding buffer and centrifuged at 2000*g* for 30 s. Finally, beads were resuspended with 50  $\mu$ L of the dissociation solution (0.1 M EDTA, 10% sodium lauryl sulfate) and vortexed deliberately at room temperature

<sup>1</sup> Abbreviations: PEG, poly(ethylene glycol); GST, glutathione *S*-transferase; GFP, green fluorescent protein; SV, simian virus; Fmoc, 9-fluorenylmethoxycarbonyl; TFA, trifluoroacetic acid; RP-HPLC, reversed-phase high performance liquid chromatography; DMEM, Dulbecco's modified Eagle's medium; FBS, fetal bovine serum; PBS, phosphate buffered saline; DAPI, 4',6-diamidino-2-phenylindole.



**Table 1. Synthesized NLS–Plasmid DNA Conjugates**

conjugate	used plasmid	ratio of reactants diazonium salt/ plasmid (mol/mol)	no. of insertions
2.8 NLS–peg–pGFP	pEGFP–N1	3.0	2.8
3.8 NLS–peg–pGFP	pEGFP–N1	10	3.8
1.9 NLS–C5–pGFP	pEGFP–N1	3.0	1.9
2.4 NLS–peg–pGL3	pGL3–control	3.0	2.4
5.1 NLS–peg–pGL3	pGL3–control	15	5.1
1.7 NLS–C5–pGL3	pGL3–control	3.0	1.7

for 1 h. After centrifugation at 2000*g* for 30 s, the supernatant was removed as the bound fraction. The bound and unbound fractions were analyzed by electrophoresis on 0.6% agarose gel, and DNA was stained with ethidium bromide.

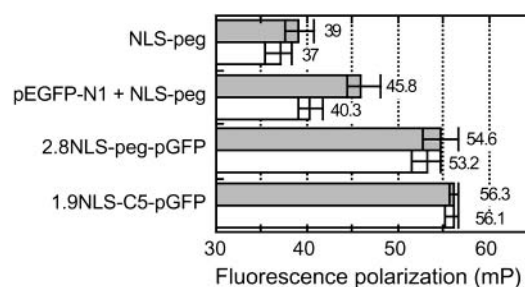
**Transfection.** COS-1 cells ( $3\text{--}4 \times 10^4$  cells for an each well) were grown to just before confluence in a 24-wells culture plates in DMEM with 10% FBS and 100 U/mL penicillin and 100  $\mu\text{g}/\text{mL}$  streptomycin in an atmosphere of 5%  $\text{CO}_2$  at 37 °C and washed twice with 0.5 mL of PBS. Complexation and transfection were performed as described in the protocol of Lipofectin with 1  $\mu\text{g}$  of plasmid DNA (pGL3–control)–NLS peptide conjugate for each well. Luciferase assays were performed as described in the protocol of Steady-Glo Luciferase Assay System (Promega, Madison, WI). Luciferase relative light units (RLU) were analyzed by luminometer (Fluoroskan Ascent-FL, Thermo Labsystems, Finland). The protein concentrations of the cell lysates were measured as described in the protocol of NanoOrange Protein Quantitation Kit (Molecular Probes, Eugene, OR) using bovine serum albumin as a standard. The light unit values shown in the table represent the specific luciferase activity (RLU/mg protein) which is standardized for total protein content of the cell lysate. The measurement of transfection efficiency was performed in triplicate.

**Microinjection.** COS-7 cells were grown at 37 °C in a 5%  $\text{CO}_2$  incubator on coverslips. The solutions of 1 mg/mL plasmid DNA–NLS peptide conjugates were injected into the cytoplasm via glass micropipets. Injections were carried out under visual control on a fixed stage of an inverted phase contrast microscope (Diaphoto, Nikon, Tokyo, Japan) using a micromanipulator MMO-220N and a microinjector IM-16 (Narishige, Tokyo, Japan). Following injection, the cells were incubated for 20 min to 6 h at 37 °C in a 5%  $\text{CO}_2$  incubator. The cells were then washed with PBS, fixed with 5% HCHO, and examined by fluorescence microscopy. Images of the samples were collected by fluorescence microscopy on an Olympus IX-70 (Tokyo, Japan) attaching a confocal scan unit CSU-10 (Yokogawa, Tokyo, Japan) with ORCA-ER CCD Camera (Hamamatsu Photonics, Hamamatsu, Japan) using a 40  $\times$  Uapo/340 objective with NA 0.9.

## RESULT

### Preparation of Plasmid DNA–NLS Conjugates.

For synthesis of the conjugates, we used a C<sub>5</sub> alkyl chain as a short spacer and poly(ethylene glycol) (PEG; 71 units, 3400 Da) as a long spacer. We also adjusted the equivalents of diazonium salt reacted per molecule of plasmid. Table 1 lists the synthesized plasmid DNA–NLS peptide conjugates with their spacers and number of insertions. The number introduced could easily be adjusted by changing the ratio of reactants. Appended NLSs were limited to a maximum of five introductions to prevent decreased expression due to interference with transcription.

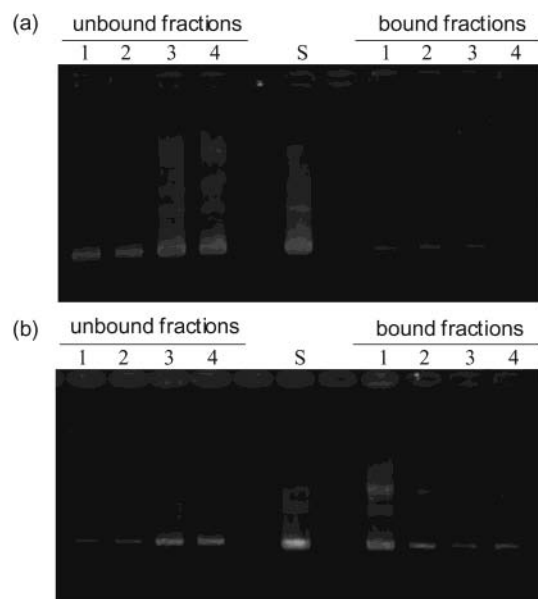


**Figure 1.** Measurement of fluorescence polarization of plasmid DNA–NLS peptide conjugates in the absence (gray bar) and presence (white bar) of excess PEI. To estimate the type of binding of the NLS to plasmid, the fluorescence polarization (ex = 546 nm, em = 576 nm) of rhodamine linked to the NLS was measured in 10 mM Tris-HCl buffer (pH 7.5) at room temperature.

**Characterization of Conjugates.** The introduced NLSs were basic peptides, and thus, in addition to conjugation by covalent bonding, it was also possible for complexes to be formed by noncovalent bonding through polyionic complexation (33). To confirm the type of bonding, we measured fluorescence polarization of rhodamine linked to the NLS upon addition of PEI (polyethylenimine), which has a higher affinity for plasmid DNA. Figure 1 shows the fluorescence polarization in the presence and absence of PEI. The parameter utilized in this method is the fluorescence polarization value (*P*). The *P* value, being a ratio of light intensities, is a dimensionless number. Polarization values are also expressed in millipolarization units (1 polarization unit = 1000 mp units). The *P* value was greatest for rhodamine-linked 1.9 NLS–C5–pGFP. The difference of the *P* value between 1.9 NLS–C5–pGFP and 2.8 NLS–peg–pGFP was nonsignificantly small. Even in the presence of PEI, there was almost no change in fluorescence polarization of these NLS-conjugated plasmids (decrease of <5%). However, when NLS–peg and pEGFP–N1 were combined, the fluorescence polarization obviously decreased. In the presence of PEI, the decrease in fluorescence polarization was greater than that observed with 2.8 NLS–peg–pGFP.

**Importin Protein Binding Assay.** We adsorbed GST-fused importin  $\alpha$  and importin  $\beta$  on glutathione beads and then evaluated the binding affinity of NLS-conjugated plasmid to the beads. The unbound supernatant fraction and bound plasmid were recovered from the beads after the treatment in the presence of surfactant and then electrophoresed on 0.6% agarose gel (Figure 2). We had done in the presence and absence of both importins  $\alpha$  and  $\beta$  in order to confirm nonspecific binding of NLS conjugates to a glutathione-sepharose gel. The amount of bound plasmid was greater with the presence versus absence of GST-fused importin  $\alpha$  and importin  $\beta$ . As the amount bound decreased with the presence of only GST-fused importin  $\alpha$  (data not shown), we could confirm the importance of ternary complex with importin  $\alpha$ , importin  $\beta$ , and NLS. The amount of bound plasmid with 5.1 NLS–peg–pGL3 was obviously greater compared with 2.4 NLS–peg–pGL3. When compared to the short spacer, the long peg spacer slightly increased the affinity of the conjugate to importin proteins.

**Transfection.** NLS–peg–pGL3 was also transfected to COS-1 cells to evaluate the influence of NLS on expression efficiency (Table 2). When compared to intact plasmid, the NLS–plasmid conjugate increased expression efficiency. Furthermore, similar to the results for binding of NLS-conjugated plasmid to beads, a higher



**Figure 2.** Interaction between glutathione-sepharose beads and plasmid DNA–NLS peptide conjugates in the absence (a) and presence (b) of GST-fused importin  $\alpha$  and  $\beta$ . Glutathione-sepharose beads (80  $\mu$ L) were incubated for 30 min at room temperature with plasmid DNA–NLS peptide conjugates (2  $\mu$ g) in the presence and absence of GST-fused importin  $\alpha$  and  $\beta$  (8  $\mu$ g, respectively). Bound and unbound fractions were analyzed by 0.6% agarose gel electrophoresis and ethidium bromide staining. (1) 5.1 NLS–peg–pGL3, (2) 2.4 NLS–peg–pGL3, (3) intact pGL3, (4) 1.7 NLS–C5–pGL3, and (5) unfractionated pGL3 control.

**Table 2. Transgene Expression after Transfection of NLS–Plasmid DNA Conjugates<sup>a</sup>**

used plasmid	transfection efficiency (RLU/mg protein)
pGL3 control	$(4.02 \pm 0.33) \times 10^5$
1.7 NLS–C5–pGL3	$(5.44 \pm 0.50) \times 10^5$
2.4 NLS–peg–pGL3	$(1.32 \pm 0.22) \times 10^6$
5.1 NLS–peg–pGL3	$(1.69 \pm 0.36) \times 10^6$

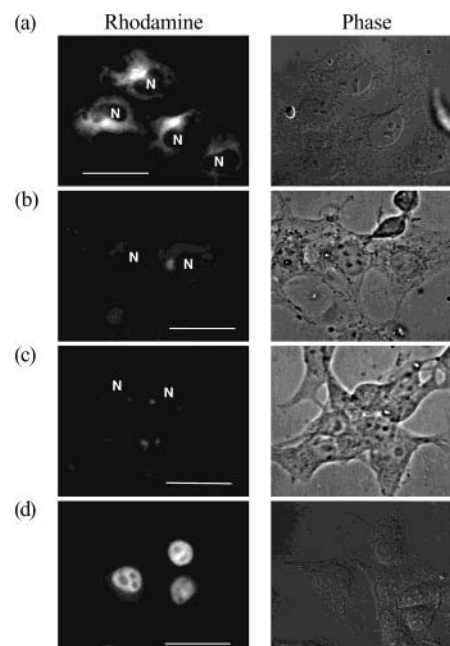
<sup>a</sup> Nonmodified plasmid and NLS–plasmid DNA conjugates were used for transfecting COS-1 cells with Lipofectin. The luciferase expression was estimated after 48 h of incubation.

number introduced and longer spacer increased expression efficiency. However, the rate of increase was insignificant compared to the  $\geq 150$ -fold increases in efficiency reported when one NLS is inserted into linear DNA (19).

**Cytoplasmic Microinjection.** The effects of NLS on stimulation of nuclear localization of NLS–plasmid were also evaluated with microinjection of plasmid DNA–NLS peptide conjugates (2.8 NLS–peg–pGFP and 3.8 NLS–peg–pGFP) into the cytoplasm of COS-7 cells. Cells were fixed with 5% HCHO after 20 min, 2 h, or 6 h. However, no relationship between the number of NLS insertions and spacer length or time was observed. Rhodamine-labeled NLS–plasmid was observed only in the cytoplasm (Figure 3a–c). There was no NLS–plasmid stimulation of nuclear localization.

## DISCUSSION

In comparison to conjugates with unmodified plasmid DNA and short spacers, we found that plasmid DNA–NLS peptide conjugates with covalent bonding by diazo coupling through PEG-chain-stimulated complexation with the nuclear transport proteins importin  $\alpha$  and importin  $\beta$  using importin proteins binding assay. Higher number introduced and longer spacers led to more



**Figure 3.** Cytoplasmic microinjection of plasmid DNA–NLS peptide conjugate. COS-7 cells were cytoplasmically microinjected with plasmid DNA–NLS peptide conjugate (3.8 NLS–peg–pGFP) and fixed after 20 min (a), 2 h (b), or 6 h (c). PEGylated NLS–peptide localized in nuclei (d). N indicates nucleus. Bar indicates 25  $\mu$ m.

favorable complex formation. Our findings confirmed that sufficient spacing from the anionic surface of the plasmid (a large molecule) and separation of the cationic peptide increased recognition of transport proteins.

Evaluation of transfection showed higher expression efficiency with plasmid DNA–NLS peptide conjugates than with unmodified plasmids. Furthermore, it was confirmed that a higher number introduced and longer spacer increased expression efficiency similar to the results for binding of NLS–conjugated plasmid to beads. However, evaluation of intracellular trafficking after microinjection into the cytoplasm showed NLS–plasmid only within the cytoplasm; there was no NLS–plasmid stimulation of nuclear localization.

In agreement with previous studies, our findings showed that plasmid DNA–NLS peptide conjugates increased the expression efficiency of plasmid DNA using nonviral vectors. The rate of increase correlated with the number of NLS insertions and the use of a longer PEG spacer. We also observed similar findings for complexation with the transport proteins importin  $\alpha$  and importin  $\beta$ . However, the rate of increase in expression efficiency was unremarkable. Microinjection of the plasmid DNA–NLS peptide conjugates, even with use of a long PEG spacer, did not produce nuclear localization of the plasmid. In conclusion, our findings suggest that because of the interaction of large molecules such as plasmids with nuclear pore complexes, efforts to stimulate nuclear localization by modifications using NLSs may not be successful, regardless of number of insertions or spacer length. On the basis of this knowledge, our efforts will now be directed at improving nuclear localization by direct conjugation of plasmids and transport proteins.

## ACKNOWLEDGMENT

This study was supported by a Grant-in-Aid for Scientific Research on Priority Area (No. 14030080) from the Ministry for Education, Culture, Sports, Science, and

Technology, Japan, and a Scholarship for Engineering Research from Graduate School of Engineering, Osaka City University.

# LITERATURE CITED

- (1) Lehrman, S. (1999) Virus treatment questioned after gene therapy death. *Nature* 401, 517–518.
- (2) Felgner, P. L., Barenholz, Y., Behr, J. P., Cheng, S. H., Cullis, P., Huang, L., Jessee, J. A., Seymour, L., Szoka, F., Thierry, A. R., Wagner, E., and Wu, G. (1997) Nomenclature for synthetic gene delivery systems. *Hum. Gene Ther.* 8, 511–512.
- (3) Zabner, J., Fasbender, A. J., Moninger, T., Poellinger, K. A., and Welsh, M. J. (1995) Cellular and molecular barriers to gene transfer by a cationic lipid. *J. Biol. Chem.* 270, 18997–19007.
- (4) Wattiaux, R., Laurent, N., Coninck, S. W., and Jadot, M. (2000) Endosomes, lysosomes: their implication in gene transfer. *Adv. Drug Deliv. Rev.* 41, 201–208.
- (5) Nishikawa, M., and Huang, L. (2001) Nonviral vectors in the new millennium: delivery barriers in gene transfer. *Hum. Gene Ther.* 12, 861–870.
- (6) Mirzayans, R., Remy, A. A., and Malcolm, P. C. (1992) Differential expression and stability of foreign genes introduced into human fibroblasts by nuclear versus cytoplasmic microinjection. *Mutat. Res.* 281, 115–122.
- (7) Dowty, M. E., Williams, P., Zhang, G., Hagstrom, J. E., and Wolff, J. A. (1995) Plasmid DNA entry into postmitotic nuclei of primary rat myotubes. *Proc. Natl. Acad. Sci. U.S.A.* 92, 4572–4576.
- (8) Escriou, V., Ciolina, C., Helbling-Leclerc, A., Wils, P., and Scherman, D. (1998) Cationic lipid-mediated gene transfer: analysis of cellular uptake and nuclear import of plasmid DNA. *Cell Biol. Toxicol.* 14, 95–104.
- (9) Schaffer, D. V., Fidelman, N. A., Dan, N., and Lauffenburger, D. A. (2000) Vector unpacking as a potential barrier for receptor-mediated polyplex gene delivery. *Biotechnol. Bioeng.* 67, 598–606.
- (10) Garcia-Bustos, J., Heitman, J., and Hall, M. N. (1991) Nuclear protein localization. *Biochim. Biophys. Acta* 1071, 83–101.
- (11) Adam, S. A., Sterne-Marr, R., and Gerace, L. (1992) Nuclear protein import using digitonin-permeabilized cells. *Methods Enzymol.* 219, 97–110.
- (12) Imamoto, N., Shimamoto, T., Takao, T., Tachibana, T., Kose, S., Matsubae, M., Sekimoto, T., Shimonishi, Y., and Yoneda, Y. (1995) In vivo evidence for involvement of 58 kDa component of nuclear pore-targeting complex in nuclear protein import. *EMBO J.* 14, 3617–3626.
- (13) Görlich, D., Vogel, F., Mills, A. D., Hartmann, E., and Laskey, R. A. (1995) Distinct functions for the two importin subunits in nuclear protein import. (1995) *Nature* 377, 246–248.
- (14) Rexach, M., and Blobel, G. (1995) Protein import into nuclei: association and dissociation reactions involving transport substrate, transport factors, and nucleoporins. *Cell* 83, 683–692.
- (15) Yoneda, Y. (1996) How proteins are transported from cytoplasm to the nucleus. *J. Biochem. Tokyo* 121, 811–817.
- (16) Tachibana, R., Harashima, H., Shinohara, Y., and Kiwada, H. (2001) Quantitative studies on the nuclear transport of plasmid DNA and gene expression employing nonviral vectors. *Adv. Drug Deliv. Rev.* 52, 219–226.
- (17) Cartier, R., and Reszka, R. (2002) Utilization of synthetic peptides containing nuclear localization signals for nonviral gene transfer systems. *Gene Ther.* 9, 157–167.
- (18) Ludtke, J. J., Zhang, G., Sebestyén, M. G., and Wolff, J. A. (1999) A nuclear localization signal can enhance both the nuclear transport and expression of 1kb DNA. *J. Cell Sci.* 112, 2033–2041.
- (19) Zanta, M. A., Belguise-Valladier, P., and Behr, J. P. (1999) Gene delivery: A single nuclear localization signal peptide is sufficient to carry DNA to the cell nucleus. *Proc. Natl. Acad. Sci. U.S.A.* 96, 91–96.
- (20) Sebestyén, M. G., Ludtke, J. J., Bassik, M. C., Zhang, G., Budker, V., Lukhtanov, E. A., Hagstrom, J. E., and Wolff, J. A. (1998) DNA vector chemistry: The covalent attachment of signal peptides to plasmid DNA. *Nat. Biotech.* 16, 80–85.
- (21) Neves, C., Escriou, V., Byk, G., Scherman, D., and Wils, P. (1999) Intracellular fate and nuclear targeting of plasmid DNA. *Cell Biol. Toxicol.* 15, 193–202.
- (22) Ciolina, C., V., Byk, Blanche, F., Thuillier, V., Scherman, D., and Wils, P. (1999) Coupling of nuclear localization signals to plasmid DNA and specific interaction of the conjugate with Importin  $\alpha$ . *Bioconjugate Chem.* 10, 49–55.
- (23) Futaki, S., Ishikawa, T., Niwa, M., Kitagawa, K., and Yagami, T. (1997) Embodying a stable alpha-helical protein structure through efficient chemical ligation via thioether formation. *Bioorg. Med. Chem.* 5, 1883–1891.
- (24) Akasaka, T., Matsuura, K., Emi, N., and Kobayashi, K. (1999) Conjugation of plasmid DNAs with lactose via diazo-coupling enhances resistance to restriction enzymes and acquires binding affinity to galactose-specific lectin. *Biochem. Biophys. Res. Commun.* 260, 323–328.
- (25) Matsuura, K., Akasaka, T., Hibino, M., and Kobayashi, K. (1999) Synthesis of DNA-carbohydrate conjugate via diazo-coupling: A new class of modified DNA with enhanced stability and lectin-recognition ability. *Chem. Lett.* 247–248.
- (26) Ishii, T., Okahata, Y., and Sato, T. (2000) Facile preparation of a fluorescence-labeled plasmid. *Chem. Lett.* 386–387.
- (27) Forster, A. C., McInnes, J. L., Skingle, D. C., and Symons, R. H. (1985) Nonradioactive hybridization probes prepared by the chemical labeling of DNA and RNA with a novel reagents, photobiotin. *Nucleic Acids Res.* 13, 745–761.
- (28) Geselowitz, D. A., and Neumann, R. D. (1995) Quantitation of triple-helix formation using a photocross-linkable aryl azide/biotin/oligonucleotide conjugate. *Bioconjugate Chem.* 6, 502–506.
- (29) Levina, A. S., Tabatadze, D. R., Dobrikov, M. I., Shishkin, G. H., Khalimskaya, L. M., and Zarytova, V. P. (1996) Site-specific photomodification of single-stranded DNA targets by aryl azide and perfluoroaryl azide derivatives f oligonucleotide. *Antisense Nucleic Acid Drug Dev.* 6, 119–126.
- (30) Levina, A. S., Tabatadze, D. R., Dobrikov, M. I., Shishkin, G. H., and Zarytova, V. P. (1996) Sequence-specific photomodification of single-stranded and double-stranded DNA fragments by oligonucleotide perfluoroazide derivative. *Antisense Nucleic Acid Drug Dev.* 6, 127–132.
- (31) Tseng, W., Purvis, N. B., Haselton, F. R., and Giorgio, T. D. (1996) Cationic liposomal delivery of plasmid to endothelial cells measured by quantitative flow cytometry. *Biotechnol. Bioeng.* 50, 548–554.
- (32) Neves, C., Byk, G., Scherman, D., and Wils, P. (1999) Coupling of a targeting peptide to plasmid DNA by covalent triple helix formation. *FEBS Lett.* 453, 41–45.
- (33) Aronsohn, A. I., and Hughes, J. A. (1997) Nuclear localization signal peptide enhance cationic liposome-mediated gene therapy. *J. Drug Target.* 5, 163–169.
- (34) Maeda, H. (1979) Assay of Proteolytic-Enzymes by the Fluorescence Polarization Technique. *Anal. Biochem.* 92, 222–227.

BC025602H



# Synthesis of Structurally Identical Fluorine-18 and Iodine Isotope Labeling Compounds for Comparative Imaging

Zizhong Li,<sup>\*,†</sup> Yu-Shin Ding,<sup>†,‡</sup> Andrew Gifford,<sup>†</sup> Joanna S. Fowler,<sup>‡</sup> and John S. Gatlley<sup>†</sup>

Medical Department and Chemistry Department, Brookhaven National Laboratory, Upton, New York 11978.  
Received September 30, 2002; Revised Manuscript Received December 9, 2002

The synthesis of a benzophenone-based labeling compound designed for comparative imaging studies with both in vivo positron emission tomograph (PET) and single-photon computed tomography (SPECT) and ex vivo autoradiography is described. The new compound can be labeled with either F-18 or iodine radioisotopes to give two different radioisotopomers: *N*-[2-fluoro-5-(3-[I-131]iodobenzoyl)benzyl]-2-bromoacetamide (**1**) and *N*-[2-[F-18]fluoro-5-(3-iodobenzoyl)benzyl]-2-bromoacetamide (**2**). Compound **1** and **2** have a 2-bromoacetyl group, which can be used to conjugate with biomolecules through a nucleophilic substitution reaction. Compound **1** was synthesized from the corresponding tributyltin derivatives via an oxidative destannylation reaction, and compound **2** was prepared via a four-step radiosynthesis (nucleophilic aromatic substitution, reduction, oxidation, and alkylation) starting from 4-(*N,N,N*-trimethylammonio)-3-cyano-3'-iodobenzophenone triflate. A remarkably high radiochemical yield (>90%) was achieved for the F-18 nucleophilic aromatic substitution under mild conditions (room temperature in less than 10 min), indicating the structural advantage of the designed molecule to facilitate the F-18 for trimethylammonium substitution in the presence of two electron-withdrawing groups (nitrile and carbonyl). The overall radiosynthesis time for compound **2** is less than 3 h after end of bombardment (EOB) with an unoptimized radiochemical yield of about 2% (not decay corrected) and specific activity of 0.8 Ci/ $\mu$ mol at EOB. The radiolabeling precursors for compound **1** and **2** were synthesized via a carbon–carbon bond-forming reaction between 2-substituted-5-lithiobenzonitrile and 3-substituted benzaldehyde derivatives. Compounds **1** and **2** should allow us to label biomolecules with F-18 or iodine isotopes and gives structurally identical products, which are expected to have identical biological properties and should be useful for comparative imaging studies.

## INTRODUCTION

Antisense oligonucleotides represent a group of newly developed therapeutic agents (Tseng and Brown, 1994). They take advantage of highly specific base-pair interaction to inhibit expression of disease-related genes in a selective and sequence-specific manner (Zamecnik and Stephenson, 1978). Radioisotope-labeled antisense oligonucleotides (Kühnast et al., 2000; Kobori et al., 1999; Lange et al., 2002) are also being explored as radiotracers for imaging in tissue targeted by the antisense mechanism. In theory, almost any gene sequence could be selectively imaged with a labeled antisense oligonucleotide. However, in living systems, gene targeting in the nucleus is far more complex due to enzymatic oligonucleotide degradation and the difficulty for the naked oligonucleotide to penetrate the cellular barrier (Crooke et al., 2000; Mahato et al., 1997; Hass et al., 1998). Nevertheless, oligonucleotides have become more and more attractive as imaging probes, stimulated by the recent introduction of several therapeutic oligonucleotides into clinical trials (Lebedeva and Stein, 2001; Pawlak et al., 2000; Hnatowich, 2000 and 1999). Permeation peptides, such as Tat-peptides, are also important because of their ability to cross cell membranes and to deliver therapeutic or diagnostic agents into the cell (Schwarze and Dowdy, 2000; Schwarze et al., 1999; Lindgren et al., 2000). On

the basis of the fact that most permeation peptides contain arginine- and lysine-rich sequences and are highly basic, they were thought to enter the cell through a nonspecific “inverted micelles” mechanism (Prochiantz, 2000). A recent study of the permeable barrier of epithelial cells to Tat-peptides, however, suggests the existence of a cell-specific mechanism (Violini et al., 2002). Permeation peptides or their conjugates with other functional molecules such as oligonucleotides, fluorescent probes, and radionuclides are currently being developed as possible imaging probes (Bullok et al., 2002).

Positron emission tomography (PET) is a medical imaging method, which uses positron-emitting radioisotope-labeled compounds to trace biochemical transformations and the movement of drugs in living systems (Eckelman et al. 2000; Fowler et al. 1999; Burn et al. 1999). Since it is impossible to obtain subcellular distribution information directly from population-based PET imaging, comparative imaging studies are necessary for evaluating the bioavailability of drugs whose function depend on their ability to enter the cells. First the molecule is labeled with a positron-emitting radioisotopes, such as fluorine-18 or carbon-11 or  $\gamma$ -emitting radioisotopes to conduct in vivo PET or single-photon computed tomography (SPECT) studies. Then the same molecule is labeled with fluorescent probe to obtain ex vivo subcellular fluoresce imaging or low-energy isotopes such as Auger-emitters I-125 or Br-77 to obtain in vitro higher resolution autoradiography and relate these to PET or SPECT imaging. The nonlinear signals, aggregation, and quenching both in vivo and in vitro associated

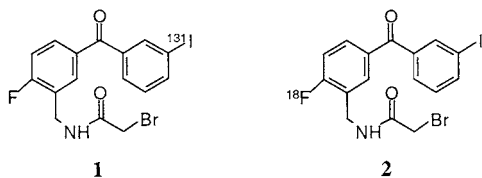
\* To whom correspondence should be addressed. E-mail: zizhong@bnl.gov, phone: 631 344 7161, fax 631 344 7902.

<sup>†</sup> Medical Department.

<sup>‡</sup> Chemistry Department.

with fluorescent probe-labeled biomolecules plus the potentially significant structural perturbation associated with a fluorescent probe to the parent compound makes radiolabeling method a better choice in terms of quantitative biochemical analysis. Labeling biomolecules with different radioisotopes is usually accomplished by linking them to different labeling compounds (Dolle et al., 1996; Bullok et al., 2002), result in molecules with different properties, and could compromise the biological properties of the parent biomolecules. For example, different chemical modification involved in the "tag on" labeling procedure may not interfere with the hybridization between the antisense oligonucleotide and target mRNA. Different labeling compounds, however, alter oligonucleotide cell membrane transport and its clearance from nontarget tissue (Hnatowich, 2000 and 1999), and oligonucleotides labeled with different labeling compounds may also have different cellular accumulation (Zhang et al., 2000). Different cellular uptake and similar subcellular localization were also observed between single-labeled and dual-labeled Tat-peptides (Bullok et al., 2002).

In this paper, we report, for the first time, the synthesis and radiolabeling of organic compounds: *N*-[2-fluoro-5-(3-[I-131]iodobenzoyl)benzyl]-2-bromoacetamide (**1**) and *N*-[2-[F-18]fluoro-5-(3-iodobenzoyl)benzyl]-2-bromoacetamide (**2**). The molecule contains a 2-bromoacetyl group,



which has been used previously to label oligonucleotides (Dolle et al., 1996) and peptides and proteins (Kilbourn et al., 1987) through a nucleophilic substitution reaction. Therefore, the pair of isotopomers should allow us to label biomolecules with F-18 or iodine isotopes and gives structurally identical products, which are expected to have identical biological properties and should be useful for comparative imaging studies.

## EXPERIMENTAL SECTION

**General.** All reactions were conducted under an argon atmosphere using glassware previously dried in an oven at 120 °C. Methylene chloride was freshly distilled from calcium hydride (CaH<sub>2</sub>) and tetrahydrofuran (THF) from benzophenone ketyl under an argon atmosphere. Hexane was dried over 4 Å molecular sieves. Flash column chromatography was performed using silica gel 60 Å (230–400 mesh). Silica gel thin-layer chromatography was done on plates (silica gel 60 Å, F254, 0.15 mm on glass). NMR spectra were recorded on a Bruker 400 MHz NMR instrument. Unless otherwise noted, samples were dissolved in chloroform-*d* (CDCl<sub>3</sub>) with tetramethylsilane (TMS) as an internal standard for proton NMR and the central peak of CDCl<sub>3</sub> signal at 77.0 ppm as the carbon-13 NMR reference.  $\delta$ : chemical shift in ppm; *J*: coupling constant in Hz. Mass spectra was measured by UCR Mass Spectrometry Facility, Department of Chemistry, UC Riverside.

**3-Tributyltinbenzaldehyde (11).** To a solution of 2-(3-bromophenyl)-1,3-dioxolane **9** (22.9 g, 100 mmol) in THF at –78 °C was added butyllithium (*n*-BuLi) (46 mL of 2.5 M in hexanes, 115 mmol) dropwise via syringe. After the mixture was stirred at –78 °C for 2 h,

tributyltin chloride (32 mL, 118 mmol) was added dropwise. After the mixture was stirred at –78 °C for 1.5 h, the reaction was slowly warmed to room temperature. Hydrochloric acid (1 N, 20 mL) was added. After the mixture was stirred at room temperature for 6 h, water (10 mL) and ether (30 mL) was added. The organic layer was washed with two additional portions of water (2 × 20 mL) and then dried over sodium sulfate, filtered, and concentrated. Flash chromatography (eluted with hexanes/ethyl acetate: 95/5, v/v) purification provided aldehyde **11** (32 g, 81%) as colorless oil: <sup>1</sup>H NMR (400 MHz, CDCl<sub>3</sub>)  $\delta$  7.93 (m, 1 H), 7.76 (td, *J* = 6.7, 1.0 Hz, 1 H), 7.70 (td, *J* = 7.2, 1.0 Hz, 1 H), 7.45 (t, *J* = 7.4 Hz, 1 H), 1.6 (m, 6H), 1.3 (m, 6 H), 1.0 (m, 6 H), 0.86 (t, *J* = 7.3 Hz, 9 H); <sup>13</sup>C NMR (100 MHz, CDCl<sub>3</sub>)  $\delta$  195.9, 146.3, 145.3, 140.4, 138.3, 132.2, 131.131.8, 30.3, 16.4, 12.4. MS (EI) *m/z* (%): 395 (M<sup>+</sup>, 1), 339 ([M – C<sub>4</sub>H<sub>9</sub>]<sup>+</sup>, 98), 283 ([M – C<sub>4</sub>H<sub>9</sub> – C<sub>4</sub>H<sub>9</sub>]<sup>+</sup>, 59), 225 ([M – C<sub>4</sub>H<sub>9</sub> – C<sub>4</sub>H<sub>9</sub> – C<sub>4</sub>H<sub>9</sub>]<sup>+</sup>, 100).

**4-Fluoro-3-cyano-3'-tributyltinbenzhydrol (5).** To a solution of 5-bromo-2-fluorobenzonitrile **3** (2.5 g, 12.5 mmol) in a mixture of THF (60 mL) and hexanes (20 mL) at –110 °C (ether, liquid nitrogen) was added *n*-BuLi (5.75 mL of 2.5 M in hexanes, 14.4 mmol) dropwise via syringe. After the mixture was stirred at –110 °C for 40 min, a solution of aldehyde **11** (5.0 g, 12.7 mmol) in THF (10 mL) was added. After the mixture was stirred at –110 °C for 1 h, the reaction was slowly warmed to room temperature. Hydrochloric acid (1 N, 20 mL) was added, the organic layer was washed with water (3 × 10 mL) and dried over sodium sulfate, filtered, and concentrated to yield an oil product, which was purified by flash chromatography (eluted with ethyl acetate/hexanes: 5/95 v/v) to give **5** (5.8 g, 89%) as colorless oil. <sup>1</sup>H NMR (400 MHz, CDCl<sub>3</sub>)  $\delta$  7.60 (dd, *J* = 6.0, 2.0 Hz, 1 H), 7.54 (m, 1 H), 7.35 (td, *J* = 6.6, 1.2 Hz, 1 H), 7.31 (d, *J* = 2.2 Hz, 1 H), 7.25 (t, *J* = 7.1 Hz, 1 H), 7.15 (td, *J* = 6.6, 1.2 Hz, 1 H), 7.09 (t, *J* = 7.0 Hz, 1 H). <sup>13</sup>C NMR (100 MHz, CDCl<sub>3</sub>)  $\delta$  165.0 (d, <sup>1</sup>*J*<sub>C–F</sub> = 164 Hz), 146.1, 143.7, 144.6, 139.4, 137.3, 135.8 (d, <sup>3</sup>*J*<sub>C–F</sub> = 8.3 Hz), 134.0, 131.1, 129.0, 119.0 (d, <sup>2</sup>*J*<sub>C–F</sub> = 19.6 Hz), 116.7, 104.0 (d, <sup>3</sup>*J*<sub>C–F</sub> = 16.0 Hz), 77.8, 31.8, 30.0, 16.4. HRMS (DCI): Calcd C<sub>26</sub>H<sub>36</sub>FNOSn (M – H) 516.1724, found 516.1715.

**4-Fluoro-3-aminomethyl-3'-tributyltinbenzhydrol (6).** To a suspension of lithium aluminum hydride (1.0 g, 26.4 mmol) in dry THF was added a solution of **5** (3.6 g, 7.0 mmol) in THF (10 mL) at 0 °C under argon. The disappearance of the starting material was monitored by TLC. After 16 h stirring, the reaction was quenched by the addition of water (2 mL), followed by sodium hydroxide solution (2 mL, 3 M) and water (2 mL). The resulting mixture was stirred at room temperature for 10 min, filtered, dried over sodium sulfate, and concentrated. The crude product was purified by a flash chromatography (eluted with ethyl acetate); yield 1.46 g (40%) of **6** as colorless oil. <sup>1</sup>H NMR (400 MHz, CDCl<sub>3</sub>)  $\delta$  7.41 (m, 1 H), 7.33 (m, 2 H), 7.24 (m, 2 H), 7.17 (m, 1 H), 6.93 (dd, *J* = 8.8, 9.6 Hz, 1 H), 1.51 (m, 6 H), 1.32 (m, 6 H), 1.05 (m, 6 H), 0.89 (t, *J* = 7.3 Hz, 9 H); <sup>13</sup>C NMR (100 MHz, CDCl<sub>3</sub>)  $\delta$  160.2 (d, <sup>1</sup>*J*<sub>C–F</sub> = 245 Hz), 143.3, 142.4, 140.3 (d, <sup>3</sup>*J*<sub>C–F</sub> = 3.8 Hz), 135.8, 134.7, 129.3 (d, <sup>2</sup>*J*<sub>C–F</sub> = 15.9 Hz), 128.1, 127.5 (d, <sup>3</sup>*J*<sub>C–F</sub> = 4.8 Hz), 127.0 (d, <sup>4</sup>*J*<sub>C–F</sub> = 8.3 Hz), 126.3, 115.2 (d, <sup>2</sup>*J*<sub>C–F</sub> = 22.0 Hz), 75.5, 40.5 (d, <sup>3</sup>*J*<sub>C–F</sub> = 4.1 Hz), 29.2, 27.4, 14.9, 9.9. HRMS (DCI): Calcd C<sub>26</sub>H<sub>39</sub>FNOSn (M – H) 520.2037, found 520.2051.

**4-Fluoro-3-aminomethyl-3'-tributyltinbenzophenone (7).** To a solution of **6** (1.3 g, 2.5 mmol) in methylene chloride (15 mL) was added pyridinium chlo-

rochromate (PCC) (1.08 g, 5 mmol) in small portions. The suspension was stirred at room temperature for 30 min. Aqueous sodium hydroxide (3 M) was added, and the aqueous layer was extracted with ether. The organics were combined, dried over sodium sulfate, filtered, and concentrated. Flash chromatography (eluted with ethyl acetate) provided **7** (1.14 g, 88%) as colorless oil.  $^1\text{H}$  NMR (400 MHz,  $\text{CDCl}_3$ )  $\delta$  7.88 (dd,  $J = 7.33, 2.20$  Hz, 1 H), 7.85 (m, 1 H), 7.66 (m, 2 H), 7.42 (t,  $J = 7.48$  Hz), 7.08 (dd,  $J = 8.57, 9.57$  Hz, 1 H), 1.5 (m, 6 H), 1.3 (m, 6 H), 1.1 (m, 6 H), 0.89 (t,  $J = 7.1$  Hz, 9 H);  $^{13}\text{C}$  NMR (100 MHz,  $\text{CDCl}_3$ )  $\delta$  196.0, 163.6 (d,  $^1J_{\text{C-F}} = 253$  Hz), 142.8, 140.59, 137.6, 136.8, 134.2, 131.5 (d,  $^3J_{\text{C-F}} = 6.36$  Hz), 131.1 (d,  $^3J_{\text{C-F}} = 9.26$  Hz), 130.7 (d,  $^2J_{\text{C-F}} = 15.8$  Hz), 129.6, 127.7, 115.2 (d,  $^2J_{\text{C-F}} = 22.62$  Hz), 40.5 (d,  $^3J_{\text{C-F}} = 3.2$  Hz), 29.1, 27.4, 14.9, 9.9, MS (EI)  $m/z$  (%): 504 ( $[\text{M} - \text{NH}_2]^+$ , 100), 462 ( $[\text{M} - \text{C}_4\text{H}_9]^+$ , 14), 229 ( $[\text{M} - \text{SnBu}_3]^+$ , 6).

**[N-[6-Fluoro-3-(3-tributyltinbenzoyl)benzyl]-2-bromoacetamide (8).** To a solution containing **7** (1.14 g, 2.2 mmol) and *N*-methylmorpholine (244 mg, 2.42 mmol) in dry methylene chloride was added dropwise bromoacetyl bromide (488 mg, 2.42 mmol) at 0 °C. The reaction mixture was stirred overnight. The reaction was quenched with ice. The organic layer was washed with water (2  $\times$  2 mL), dried over sodium sulfate, and concentrated to dryness, and the residue was chromatographed on silica gel (eluted with hexanes/ethyl acetate, 95:5, v/v) gave 1.1 g (yield 78%) of compound **8** as colorless oil, it solidified as a white waxlike solid upon storage in the refrigerator.  $^1\text{H}$  NMR (400 MHz,  $\text{CDCl}_3$ )  $\delta$  7.86 (dd,  $J = 7.33$  Hz,  $J = 2.20$  Hz, 1 H), 7.85 (m, 1 H), 7.73 (ddd,  $J = 2.20, 5.1, 7.4, 1$  H), 7.66 (td,  $J = 1.1, 7.2$  Hz), 7.61 (m, 1 H), 7.39 (t,  $J = 7.49$  Hz), 7.12 (dd,  $J = 8.63, 9.43$  Hz), 6.9 (broad t,  $J = 4.90$  Hz, 1 H), 4.55 (d,  $J = 6.0$  Hz, 2 H), 4.10 (s, 2 H), 1.5 (m, 6 H), 1.3 (m, 6 H), 1.1 (m, 6 H), 0.89 (t,  $J = 7.3$  Hz, 9 H);  $^{13}\text{C}$  NMR (100 MHz,  $\text{CDCl}_3$ )  $\delta$  195.7, 165.5, 163.5 (d,  $^1J_{\text{C-F}} = 253$  Hz), 143.0, 140.8, 137.6, 136.6, 134.4 (d,  $^3J_{\text{C-F}} = 3.1$  Hz), 132.2 (d,  $^3J_{\text{C-F}} = 5.40$  Hz), 132.1 (d,  $^3J_{\text{C-F}} = 4.50$  Hz), 129.7, 127.7, 125.0 (d,  $^2J_{\text{C-F}} = 15.50$  Hz), 115.4 (d,  $^2J_{\text{C-F}} = 22.0$  Hz), 40.5 (d,  $^3J_{\text{C-F}} = 3.6$  Hz), 29.1, 28.9, 27.4, 13.7, 9.8. HRMS (FAB): Calcd  $\text{C}_{28}\text{H}_{39}\text{BrFNO}_2\text{Sn}$  (M + H) 640.1248, found 640.1223.

**2-(*N,N*-Dimethylamino)-5-bromobenzonitrile (13).** To a 150 mL round-bottom flask was added 2-amino-5-bromobenzonitrile **12** (1.97 g, 10 mmol), *N,N*-dimethylformamide (DMF) (50 mL), iodomethane (10 mL), and sodium carbonate (2.11 g, 20 mmol). The reaction mixture was sealed off in the flask and kept in 110 °C oil bath for 24 h. After the mixture was cooled to room temperature, ethyl acetate (100 mL) was added and the mixture was washed with water (4  $\times$  20 mL) and dried over sodium sulfate. Filtration and removal of the solvent gave **13** as yellowish solid (1.9 g, 84%).  $^1\text{H}$  NMR (400 MHz,  $\text{CDCl}_3$ )  $\delta$  7.48 (d,  $J = 2.52$  Hz, 1 H), 7.38 (dd,  $J = 9.0$  Hz,  $J = 2.43$  Hz, 1 H), 6.69 (d,  $J = 9.0$  Hz, 1 H), 3.0 (s, 6 H);  $^{13}\text{C}$  NMR (100 MHz,  $\text{CDCl}_3$ )  $\delta$  153.90, 136.78, 136.42, 118.32, 109.92, 101.84, 42.95. MS (CI)  $m/z$  (%): 225 (M, 25), 145 (M - Br, 10).

**4-(*N,N*-Dimethylamino)-3-cyano-3'-iodobenzhy-drol (14).** To a solution of **13** in THF/hexanes (50 mL/15 mL) was added *n*-BuLi (1.17 mL, 1.2 eq, 2.5 M in hexanes) at -110 °C under argon. After the mixture was stirred at -110 °C for 1 h, a solution of 3-iodobenzylaldehyde (679 mg, 2.96 mmol) in THF (5 mL) was added via a glass syringe. TLC indicated complete reaction in 10 min. The resulting mixture was allowed to warm slowly to room temperature. Ether (20 mL) was added,

and the reaction mixture was washed with water (3  $\times$  10 mL), dried over sodium sulfate, filtered, and concentrated under reduced pressure on a rotary evaporator. The resulting oil was purified by flash column chromatography on silica gel (hexanes/ethyl acetate, 80/20 to 70/30 v/v) to give **14** as colorless oil (775 mg, 84%):  $^1\text{H}$  NMR (400 MHz,  $\text{CDCl}_3$ )  $\delta$  7.69 (m, 1 H), 7.58 (m, 1 H), 7.43 (d,  $J = 2.26$  Hz, 1 H), 7.31 (dd,  $J = 8.8$  Hz,  $J = 2.27$  Hz, 1 H), 7.26 (m, 1 H), 7.05 (t,  $J = 7.8$  Hz, 1 H), 6.80 (d,  $J = 8.8$  Hz, 1 H), 5.63 (s, 1 H), 3.02 (s, 6 H);  $^{13}\text{C}$  NMR (100 MHz,  $\text{CDCl}_3$ )  $\delta$  154.66, 145.65, 136.90, 135.35, 133.95, 133.17, 132.03, 130.44, 125.71, 119.72, 116.93, 100.36, 94.72, 43.00. HRMS (DEI): Calcd  $\text{C}_{16}\text{H}_{15}\text{IN}_2\text{O}$  378.0229, found 378.0230.

**4-(*N,N*-Dimethylamino)-3-cyano-3'-iodobenzophe-none (15b).** To a solution of 4-(*N,N*-dimethylamino)-3-cyano-3'-iodobenzhy-drol **14** (770 mg, 2 mmol) in methylene chloride (100 mL) was added PCC (878 mg, 4 mmol). TLC indicated the reaction was completed after stirring at room temperature for 2 h. The reaction mixture was filtered through a plug of silica gel. The product was eluted from the silica gel by hexanes/ethyl acetate (80/20: v/v). Evaporation of the solvent gave a mixture of **15a** and **15b** with a ratio of 2 to 8 from proton NMR analysis. The mixture was dissolved in DMF (100 mL) in a 250 mL round-bottom flask, and iodomethane (10 mL) and sodium carbonate (1.5 g) were added. The reaction mixture was sealed off in the flask and kept in a 110 °C oil bath overnight. After the mixture was cooled to room temperature, ethyl acetate (100 mL) was added and the organic phase was washed with water and dried over sodium sulfate. Filtration and removal of the solvent gave pure **15b** as yellowish solid (600 mg, 79% from **14**):  $^1\text{H}$  NMR (400 MHz,  $\text{CDCl}_3$ )  $\delta$  7.98 (t,  $J = 1.5$  Hz, 1 H), 7.91 (d,  $J = 2.23$  Hz, 1 H), 7.86 (ddd,  $J = 8.0$  Hz,  $J = 1.8$  Hz,  $J = 1.0$  Hz, 1 H), 7.82 (dd,  $J = 11.11$  Hz,  $J = 2.24$  Hz, 1 H), 7.59 (ddd,  $J = 7.6$  Hz,  $J = 1.5$  Hz,  $J = 1.0$  Hz, 1 H), 7.18 (t,  $J = 7.6$  Hz, 1 H), 6.81 (d,  $J = 9.0$  Hz, 1 H), 3.23 (s, 6 H);  $^{13}\text{C}$  NMR (100 MHz,  $\text{CDCl}_3$ )  $\delta$  191.70, 155.98, 140.88, 139.78, 139.52, 138.07, 135.05, 130.10, 128.53, 125.76, 119.55, 115.14, 96.51, 94.30, 42.60. HRMS (FAB): Calcd  $\text{C}_{16}\text{H}_{15}\text{IN}_2\text{O}$  378.0229, found 378.0230. HRMS (DEI): Calcd  $\text{C}_{16}\text{H}_{13}\text{IN}_2\text{O}$  376.0072, found 376.0072.

**4-(*N*-Methylamino)-3-cyano-3'-iodobenzophe-none (15a).** To a solution of the mixture of **15a** and **15b** (**15a/15b**: 2/8, 20 mg) in methylene chloride (10 mL) was added pyridinium chlorochromate (50 mg, 0.23 mmol). After being stirred at room temperature for 3 days, the reaction mixture was filtered through a plug of silica gel and the product was eluted from the silica gel by hexanes/ethyl acetate (80/20: v/v). Evaporation of the solvent under reduced pressure to give a yellowish solid which was purified on silica gel (hexanes/ethyl acetate: 70/30) to give pure **15a** (10 mg, 51%) as white solid:  $^1\text{H}$  NMR (400 MHz, acetone- $d_6$ )  $\delta$  7.99 (t,  $J = 1.5$  Hz, 1 H), 7.86 (m, 3 H), 7.60 (td,  $J = 7.7, 1.8$  Hz,  $J = 1.5$  Hz, 1 H), 7.23 (t,  $J = 7.7$  Hz, 1 H), 6.76 (d,  $J = 8.8$  Hz, 1 H), 6.1 (broad s, 1 H), 3.0 (d,  $J = 5.0$  Hz, 6 H).

**4-(*N,N,N*-Trimethylammonio)-3-cyano-3'-iodoben-zophenone Triflate (16).** To a solution of 4-(*N,N*-dimethylamino)-3-cyano-3'-iodobenzophenone **15b** (186 mg, 0.5 mmol) in dry methylenechloride (1 mL) was added methyl trifluoromethanesulfonate (283  $\mu\text{L}$ ,  $d = 1.45$ , 2.5 mmol, 5.0 equiv) via syringe. The reaction was stirred for 3 days at 80 °C. The solvent and the excess methyl trifluoromethanesulfonate were evaporated, and the residue was dried under vacuum and purified by C18 Cartridges (water/acetonitrile: 90/10 v/v), giving 65 mg (40%) of pure compound **16** as white solid.  $^1\text{H}$  NMR (400



MHz, acetone- $d_6$ )  $\delta$  8.56 (d,  $J$  = 9.0 Hz, 1 H), 8.53 (d,  $J$  = 2.1 Hz, 1 H), 8.34 (dd,  $J$  = 8.9 Hz, 2.1 Hz, 1 H), 8.15 (t,  $J$  = 1.3 Hz, 1 H), 8.11 (m, 1 H), 7.85 (m, 1 H), 7.41 (t,  $J$  = 7.88 Hz, 1 H), 4.21 (s, 9 H).  $^{13}\text{C}$  NMR (100 MHz,  $\text{CDCl}_3$ )  $\delta$  191.3, 148.5, 142.6, 139.6, 138.3, 137.8, 135.9, 130.9, 129.6, 123.8, 116.1, 106.4, 93.9, 57.3. HRMS (FAB/ACN/NBA): Calcd  $\text{C}_{17}\text{H}_{16}\text{IN}_2\text{O}$  391.0307, found 391.0325.

**4-Fluoro-3-cyano-3'-iodobenzhydrol (17).** To a solution of 5-bromo-2-fluorobenzonitrile **3** (2.0 g, 10 mmol) in THF (80 mL) was added butyllithium (4.4 mL, 2.5 M in hexanes, 11 mmol) at  $-110^\circ\text{C}$ . After the mixture was stirred at  $-110^\circ\text{C}$  for 1.5 h, a solution of 3-iodobenzaldehyde (2.55 g, 11 mmol) in THF (5 mL) was added dropwise via a syringe. The reaction mixture was stirred at  $-110^\circ\text{C}$  for 2 h and warmed slowly to room temperature. The resulting mixture was washed with water (3  $\times$  20 mL) and dried over sodium sulfate. The solvent was evaporated under reduced pressure on a rotary evaporator. The residual yellow oil was purified by silica gel column (elute: hexanes/ethyl acetate: 80/20 v/v) to offer 2.1 g (61%) expected product **17**.  $^1\text{H}$  NMR (400 MHz,  $\text{CDCl}_3$ )  $\delta$  7.5 to 7.7 (m, 4 H), 7.26 (d,  $J$  = 7.82 Hz, 1 H), 7.13 (t,  $J$  = 8.68 Hz, 1 H), 7.04 (t,  $J$  = 7.80 Hz, 1 H), 5.68 (s, 1 H), 4.0 (s, 1 H);  $^{13}\text{C}$  NMR (100 MHz,  $\text{CDCl}_3$ )  $\delta$  162.5 (d,  $J_{\text{C-F}}$  = 258.9 Hz), 145.3, 140.8, 137.2, 135.5, 133.6 (d,  $J_{\text{C-F}}$  = 8.5 Hz), 131.4, 130.7, 126.0, 116.6 (d,  $J_{\text{C-F}}$  = 19.8 Hz), 114.1, 109.7, 101.2 (d,  $J_{\text{C-F}}$  = 15.6 Hz), 94.89, 73.70. HRMS (DCI): Calcd  $\text{C}_{14}\text{H}_9\text{IFNO}$  352.9713, found 352.9718.

**4-Fluoro-3-cyano-3'-iodobenzophenone (18a).** To a solution of **17** (2.1 g, 5.9 mmol) in methylene chloride (100 mL) was added pyridinium chlorochromate (4.0 g, 18.6 mmol). After being stirred at room temperature for 2 h, the reaction mixture was filtered through a plug of silica gel. Removal of the solvent gave **18a** as white waxlike solid (1.8 g, 87%).  $^1\text{H}$  NMR (400 MHz,  $\text{CDCl}_3$ )  $\delta$  8.0 to 8.1 (m, 3 H), 7.98 (d,  $J$  = 7.8 Hz, 1 H), 7.68 (d,  $J$  = 8.8 Hz, 1 H), 7.38 (t,  $J$  = 8.0 Hz, 1 H), 7.27 (t,  $J$  = 7.8 Hz, 1 H);  $^{13}\text{C}$  NMR (100 MHz,  $\text{CDCl}_3$ )  $\delta$  191.86, 165.6 (d,  $J_{\text{C-F}}$  = 266.8 Hz), 142.4, 138.8, 138.4, 137.8 (d, 135.5,  $J_{\text{C-F}}$  = 9.0 Hz), 136.0, 134.3 (d,  $J_{\text{C-F}}$  = 3.6 Hz), 130.7, 129.3, 117.4 (d,  $J_{\text{C-F}}$  = 20.4 Hz), 113.2, 102.7 (d,  $J_{\text{C-F}}$  = 16.2 Hz), 94.9. HRMS (DEI): Calcd  $\text{C}_{14}\text{H}_7\text{IFNO}$  350.9556, found 350.9567.

**4-Fluoro-3-aminomethyl-3'-iodobenzhydrol (19a).** To a stirred solution of **18a** (351 mg, 1 mmol) in dry THF (10 mL) was added borane ( $\text{BH}_3$ ) (6 mL, 1 M in THF) using a glass syringe at room temperature. After the initial reaction subsided, the reaction mixture was refluxed for 8 h in a water bath. Excess  $\text{BH}_3$  was quenched by careful addition of ethanol (20 mL) to the cooled reaction mixture. The solvent was removed by rotary evaporation. The residue was dissolved in ethyl acetate and filtered through a plug of silica gel, and the plug was eluted with hexanes/ethyl acetate/methanol (80/20/5: v/v/v, 100 mL) followed by ethyl acetate (150 mL). The product was eluted from the silica gel with methanol (150 mL). Evaporation of methanol resulted in a waxlike solid (270 mg, 76%):  $^1\text{H}$  NMR (400 MHz,  $\text{CDCl}_3$ )  $\delta$  7.69 (t,  $J$  = 1.8 Hz, 1 H), 7.55 (td,  $J$  = 7.85, 1.2 Hz, 1 H), 7.24 (m, 1 H), 7.13 (m, 1 H), 7.01 (t,  $J$  = 7.64 Hz, 1 H), 6.96 (dd,  $J$  = 8.4, 6.5 Hz, 1 H), 5.55 (s, 1 H), 3.7 (s, 2 H), 3.0 (broad s, 3 H);  $^{13}\text{C}$  NMR (100 MHz,  $\text{CDCl}_3$ )  $\delta$  160.6 (d,  $J_{\text{C-F}}$  = 245.8 Hz), 147.0, 140.3 (d,  $J_{\text{C-F}}$  = 4.32 Hz), 136.8, 135.8, 130.62, 129.7 (d,  $J_{\text{C-F}}$  = 15.2 Hz), 127.9 (d,  $J_{\text{C-F}}$  = 5.0 Hz), 127.4 (d,  $J_{\text{C-F}}$  = 8.4 Hz), 126.15, 115.7 (d,  $J_{\text{C-F}}$  = 21.8 Hz), 95.0, 74.7, 40.5 (d,  $J_{\text{C-F}}$  = 3.5 Hz). HRMS (DEI): Calcd  $\text{C}_{14}\text{H}_9\text{IFNO}$  (M - H) 355.9947, found 355.9955.

**4-Fluoro-3-aminomethyl-3'-iodobenzophenone (20a).** To a solution of **19a** (270 mg, 0.75 mmol) in

methylene chloride (20 mL) was added pyridinium chlorochromate (326 mg, 0.87 mmol). After being stirred at room temperature for 1 h, the reaction mixture was washed with aqueous sodium hydroxide solution (3 M, 2  $\times$  1 mL) and dried over sodium sulfate. The organic layer was filtered through a plug of silica gel. The product was eluted from the silica gel with ethyl acetate (150 mL). Removal of the solvent provided **20a** as yellowish oil (180 mg, 67%).  $^1\text{H}$  NMR (400 MHz,  $\text{CDCl}_3$ )  $\delta$  8.10 (m, 1 H), 7.92 (m, 2 H), 7.69 (m, 2 H), 7.25 (t,  $J$  = 7.7 Hz, 1 H), 7.15 (t,  $J$  = 7.64 Hz, 1 H), 3.7 (s, 2 H);  $^{13}\text{C}$  NMR (100 MHz,  $\text{CDCl}_3$ )  $\delta$  193.8, 162.3 (d,  $J_{\text{C-F}}$  = 253.2 Hz), 141.3, 139.5, 138.5, 133.3, 131.5 (d,  $J_{\text{C-F}}$  = 6.3 Hz), 131.1 (d,  $J_{\text{C-F}}$  = 9.6 Hz), 130.1, 129.0, 115.5 (d,  $J_{\text{C-F}}$  = 22.3 Hz), 109.66, 94.22, 40.5 (d,  $J_{\text{C-F}}$  = 3.1 Hz). MS (CI)  $m/z$  (%): 355 (M, 20).

**N-[6-Fluoro-3-(3-iodobenzoyl)benzyl]-2-bromoacetamide (21).** To a solution of **20a** (36 mg, 0.1 mmol) in 4 mL of methylene chloride was added *N*-methylmorpholine (12  $\mu\text{L}$ , 0.12 mmol) and bromoacetyl bromide (9.5  $\mu\text{L}$ , 0.11 mmol). After being stirred at room temperature for 5 h, the reaction was quenched with water (0.5 mL). The organic layer was separated and washed with water (2  $\times$  0.5 mL) and dried over sodium sulfate. The solvent was removed under vacuum and the residue was chromatographed on silica gel (elute: hexanes/ethyl acetate: 80/20 to 70/30) to give **21** as white solid (38 mg, 80%):  $^1\text{H}$  NMR (400 MHz,  $\text{CDCl}_3$ )  $\delta$  7.80 (t,  $J$  = 1.7 Hz, 1 H), 7.65 (m, 1 H), 7.54 (dd,  $J$  = 2.3, 7.2, 1 H), 7.47 (ddd,  $J$  = 2.3, 5.0, 7.2 Hz, 1 H), 6.95 (t,  $J$  = 7.82 Hz), 6.92 (dd,  $J$  = 8.56, 9.45 Hz), 6.69 (broad, 1 H), 4.30 (d,  $J$  = 6.4 Hz, 2 H), 3.62 (s, 2 H);  $^{13}\text{C}$  NMR (100 MHz,  $\text{CDCl}_3$ )  $\delta$  193.5, 165.8, 163.5 (d,  $J_{\text{C-F}}$  = 255 Hz), 141.5, 139.2, 138.6, 133.4, 132.1 (d,  $J_{\text{C-F}}$  = 5.5 Hz), 132.0 (d,  $J_{\text{C-F}}$  = 9.3 Hz), 130.2, 129.1, 125.2 (d,  $J_{\text{C-F}}$  = 15.42 Hz), 115.9 (d,  $J_{\text{C-F}}$  = 22.1 Hz), 94.2, 38.1 (d,  $J_{\text{C-F}}$  = 3.6 Hz), 29.0. MS (CI)  $m/z$  (%): 475 (M, 5), 397 (M - Br, 40).

**Radiosynthesis. Analytical Methods.** TLC was done on plates (Sigma-Aldrich, highly purified silica gel, 60 Å, F254, 0.25 mm on polyester). HPLC analysis and purification were performed under following conditions: UV detection at 254 nm; radioactivity detectors Geiger Muller detector. Column A: C18  $\mu\text{Bondpak}$  Waters (300  $\times$  3.9 mm, 10  $\mu\text{m}$ ); Column B: semipreparative C18 Phenomenex phenosphere 5 (ODS-2 250  $\times$  10.00 mm, 5  $\mu\text{m}$ ). Solvent A: acetonitrile/aqueous ammonium acetate solution (40 mM): 50/50, v/v; Solvent B: acetonitrile/aqueous ammonium acetate solution (40 mM): 80/20, v/v. Flow rate: 1 mL/min for column A; 5 mL/min for column B.

**Preparation of N-[2-Fluoro-5-(3-iodo[ $I$ -131]benzoyl)benzyl]-1-bromoacetamide (1).** To a stock solution of sodium iodide[ $I$ -131] (Dupont-New England Nuclear) was added a solution of *N*-[6-fluoro-3-(3-tributyltinbenzoyl)benzyl]-2-bromoacetamide **8** (20  $\mu\text{L}$ , 1% in ethanol) followed by hydrochloric acid solution (10  $\mu\text{L}$ , 0.5 M) and a solution of chloramine-T (10  $\mu\text{L}$ , 2% solution in water). After 2 min reaction, the product **1** was purified by a Radio-RP-HPLC ( $t_R$  = 15 min, Column A, solvent A). The radiochemical yield varied from 86% to 99% and the radiochemical purity was >99%.

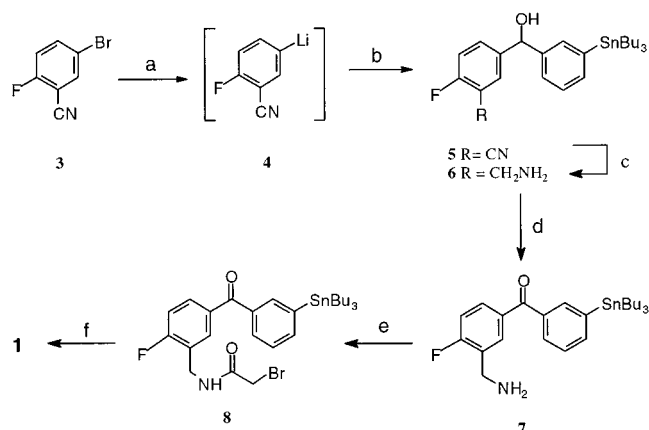
**Preparation of N-[2-Fluoro[ $F$ -18]-5-(3-iodobenzoyl)benzyl]-1-bromoacetamide (2).** [ $^{18}\text{F}$ ]Fluoride in 0.3 to 0.5 mL of aqueous 0.01 M potassium carbonate from the  $\text{H}_2^{18}\text{O}$  target was delivered to a silicon-coated glass tube charged with a stirring bar and a mixture of tetrabutylammonium hydroxide (40  $\mu\text{L}$ , 40% in water) and dry ice (1.0 to 2.0 g), and the water was azeotropically evaporated at  $120^\circ\text{C}$  under a argon stream and then

cooled to room temperature. 4-(*N,N,N*-Trimethylammonio)-3-cyano-3'-iodobenzophenone triflate **16** (2.0 mg) dissolved in acetonitrile (0.3 mL) was added. The solution was stirred at room temperature for 10 min to give compound **18b**. The radiochemical yield of the substitution is greater than 92% determined by radio-TLC ( $R_f = 0.4$ , eluant: ethyl acetate/hexanes: 8/92 v/v) and HPLC ( $t_R = 3.6$  min, Column B, Solvent B). The reaction mixture was then diluted with ethyl acetate (4 mL) and washed with water ( $2 \times 0.5$  mL) (less than 30% activity was lost in the water), dried over sodium sulfate, and filtered through a silica gel cartridge (17% of the total activity was lost on silica gel and dry agent). The resulting solution was concentrated to dryness at 120 °C with a stream of argon. The residue was dissolved in THF (0.2 mL), and borane (0.2 mL, 1.0 M in tetrahydrofuran) was added. The reaction vial was then tightly closed and heated at 120 °C for 10 min and then cooled to room temperature to give compound **19b**. The yield of the reduction varied from 60% to 78% as determined by radio RP-HPLC ( $t_R = 10.0$  min, column B, solvent B). The excess borane was quenched with ethanol (0.2 mL), and the solvent was evaporated with a stream of argon at room temperature. The residue was redissolved in methylene chloride (3 mL). The solution was washed with aqueous sodium hydroxide (0.2 mL, 1 N) and water (1 mL). The organic layer was loaded on a silica cartridge, and the product was eluted with methanol (6 mL). The resulting solution was evaporated to dryness, a solution of PCC (10 mg) in methylene chloride (1 mL) was added, and the mixture was stirred at room temperature for 15 min to give compound **20b**. The resulting yellow-brown reaction mixture was washed with aqueous sodium hydroxide and water. The yield of the oxidation varied from 65% to 90% as determined by radio RP-HPLC ( $t_R = 13.0$  min, column B, solvent B). The solvent was evaporated, and the residue was dissolved in methylene chloride. After addition of bromoacetyl bromide solution (100  $\mu$ L, 1.0 M in methylene chloride), the cloudy solution was stirred at room temperature for 2 min to give compound **2**, and the solvent was evaporated, the residue was dissolved in a mixture of acetonitrile and water (1/1, v/v) and purified by an RP-HPLC ( $t_R = 10.35$  min, column B, solvent A). In a typical run, 0.75 mCi compound **2** was obtained from 44 mCi [ $^{18}$ F]fluoride, in 2 h 45 min synthesis time with a specific activity of 0.74 Ci/ $\mu$ mol. The radiochemical purity of compound **2** was >99% from radio-TLC ( $R_f = 0.31$ , eluant: ethyl acetate/hexanes: 30/70 v/v) and HPLC ( $t_R = 10.35$  min, column B, solvent A).

## RESULTS AND DISCUSSION

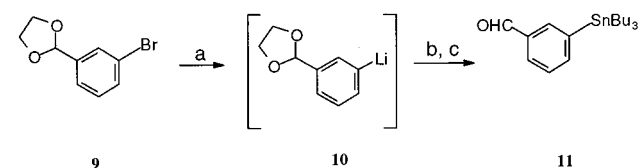
The synthesis of iodine labeling precursor, *N*-[2-fluoro-5-(3-tributyltinbenzoyl)benzyl]-2-bromoacetamide **8** is shown in Scheme 1. Tributyltin is a very useful functional group in iodine labeling since it allows us to introduce iodine isotopes in high radiochemical yields through an oxidative destannylation reaction (Arano et al., 1994; Zalutsky and Narula, 1987 and 1988). Moreover, an iodine atom at the meta position of a carbonyl group has higher resistance toward *in vivo* deiodination (Zalutsky and Narula, 1987) thus increasing the overall *in vivo* stability of radiolabel. 4-Fluoro-3-nitrile-3'-tributyltinbenzhydrol **5** was obtained at -110 °C in a mixture of tetrahydrofuran and hexanes (3:1, v/v) from a coupling reaction between 3-tributyltinbenzaldehyde **11** and 2-fluoro-5-lithiobenzonitrile **4**, which was generated from 5-bromo-2-fluorobenzonitrile **3** through a bromine-lithium exchange reaction (Ding et al., 1996; Parham and Lawrence,

**Scheme 1<sup>a</sup>**



<sup>a</sup> Key: (a) *n*-BuLi, THF/hexanes (3/1, v/v), -110 °C; (b) **11**, -110 °C to room temperature; (c) LiAlH<sub>4</sub>, THF, 0 °C to room temperature; (d) PCC, CH<sub>2</sub>Cl<sub>2</sub>, rt; (e) bromoacetyl bromide, *N*-methylmorpholine, CH<sub>2</sub>Cl<sub>2</sub>, 0 °C to room temperature; (f) Na<sup>131</sup>I, chloramine-T, rt, 2 min.

**Scheme 2<sup>a</sup>**

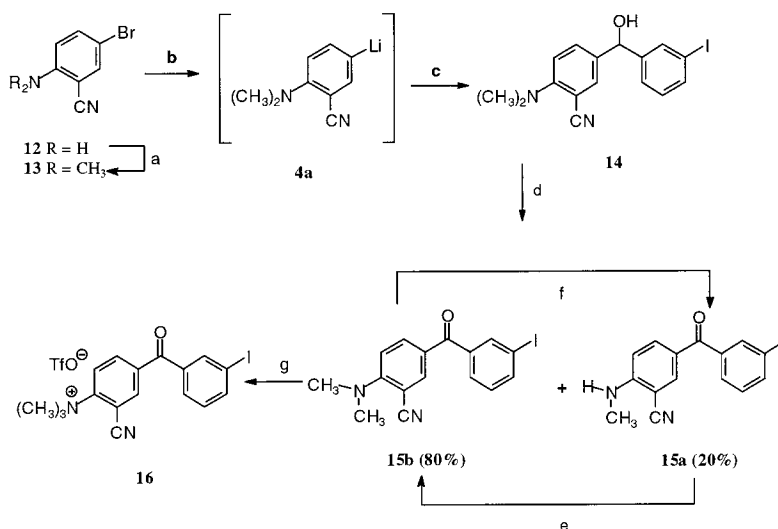


<sup>a</sup> Key: (a) *n*-BuLi, THF, -78 °C; (b) Bu<sub>3</sub>SnCl, -78 °C to room temperature; (c) 1 N HCl, rt.

1976). Compound **5** could not be synthesized at a temperature of -78 °C in THF due to a side reaction between the nitrile group and organometallic reagent. Parham (Parham and Lawrence, 1976) suggested that the *o*-lithiobenzonitrile generated at a reaction temperature of -78 °C by *n*-butyllithium is relatively stable; however, the side reaction between *o*-lithiobenzonitrile and *n*-butyl bromide and the reaction between nitrile group and *n*-butyllithium become significant at an elevated temperature. The nitrile group in compound **3** is presumably more vulnerable to nucleophilic reagents due to the electron-withdrawing property of the fluorine atom in the ortho position; therefore, compound **5** can only be synthesized at a lower temperature and in a less polar reaction medium. The aryllithium **10** (Scheme 2), on the other hand, is relatively stable and can be prepared at -78 °C by bromine-lithium exchange reaction. The reaction of **10** with tributyltin chloride followed by *in situ* deprotection with hydrochloric acid gave aldehyde **11** in 81% overall yield. Compound **11** can also be synthesized from 2-(3-bromophenyl)-1,3-dioxolane **9** through Grignard reaction (Al-Diab et al., 1982); the yield, however, was poor in our hands.

4-Fluorobenzonitrile can be rapidly reduced by lithium aluminum hydride at 120 °C to give a quantitative yield of corresponding amine (Dolle et al., 1996). No desired product, however, was isolated when the same conditions were applied to reduce compound **5**. At a lower temperature, starting from 0 °C to room temperature over 16 h, 4-fluoro-3-aminomethyl-3'-tributyltinbenzhydrol **6** was isolated in an acceptable yield (40%) (Scheme 1). The reduction at high temperature may cause the cleavage of the carbon-tin bond to produce an uncharacterizable mixture.

Pyridinium chlorochromate was used to oxidize benzhydrol **6** to the corresponding ketone **7** (Scheme 1). A

Scheme 3<sup>a</sup>

<sup>a</sup> Key: (a) MeI, DMF, 110 °C; (b) *n*-BuLi, -110 °C, THF/hexanes (3:1, v/v); (c) 3-iodobenzaldehyde in THF, -110 °C to room temperature; (d) PCC, CH<sub>2</sub>Cl<sub>2</sub>, rt, 30 min; (e) MeI, DMF, 110 °C; (f) PCC, CH<sub>2</sub>Cl<sub>2</sub>, rt, 3 days; (g) CF<sub>3</sub>SO<sub>3</sub>CH<sub>3</sub> (3–5 equiv), 80 °C, 3 days.

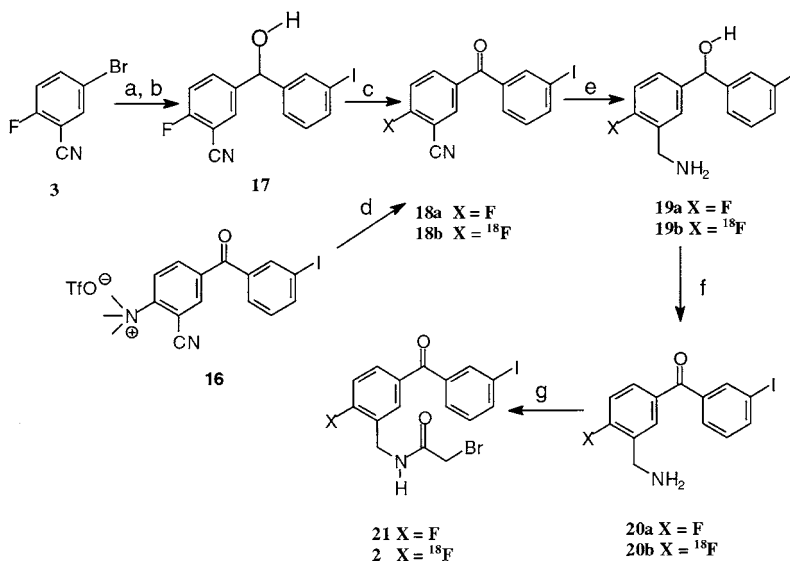
simple filtration through a plug of silica gel usually is a very efficient way to separate the product from the inorganic oxidizing reagent. Compound **7**, however, could not be isolated by this method, probably due to the formation of complexes between chlorochromate and aryl- and alkylamines (Kasmai et al., 1995). We found that compound **7** can be released from the complex by treating the reaction mixture with 3 M sodium hydroxide followed by purification by silica gel column chromatography. Compound **7** was then treated with bromoacetyl bromide in the presence of *N*-methylmorpholine to afford radioiodolabeling precursor **8** in 78% yield. Radioiodination was accomplished by treating compound **8** with sodium iodide (I-131) using chloramine-T as the oxidizing reagent followed by a reverse phase HPLC separation. Pure *N*-[2-fluoro-5-(3-[I-131]iodobenzoyl)benzyl]-2-bromoacetamide **1** was obtained in 86–99% radiochemical yield.

4-(*N,N,N*-Trimethylammonio)-3-cyano-3'-iodobenzophenone triflate **16** was synthesized as the precursor for F-18 labeling (Scheme 3) starting from 2-amino-5-bromobenzonitrile **12**. *N*-Methylation of **12** with iodomethane in the presence of sodium carbonate in DMF gave 2-(*N,N*-dimethylamino)-5-bromobenzonitrile **13** in 84% yield. Unlike compound **3**, the dimethylamino group in compound **13** stabilized the nitrile group toward the nucleophilic reaction, and metal halide exchange reaction of compound **13** with butyllithium proceeded at -78 °C in THF smoothly and produced stable 2-(*N,N*-dimethylamino)-5-lithiobenzonitrile which then reacted with 3-iodobenzylaldehyde to give 4-(*N,N*-dimethylamino)-3-cyano-3'-iodobenzhydrol **14** in 84% yield. Compound **14** was converted into a mixture of 4-(*N*-methylamino)-3-cyano-3'-iodobenzophenone **15a** and 4-(*N,N*-dimethylamino)-3-cyano-3'-iodobenzophenone **15b** in a ratio of about 20 to 80 by PCC oxidation. The ratio of the products depends on the reaction time; **15b** disappeared in 3 days, and pure **15a** was isolated using a silica gel column. The loss of a methyl group in the course of oxidation is due to a known oxidative demethylation reaction by chromate (Hostetler et al., 1999). The separation of **15a** from **15b** by silica gel column chromatography was not successful. Pure **15b** was obtained by remethylation **15a** in the mixture with iodomethane in DMF in the presence of sodium carbonate. Quaternization of *N,N*-dimethylaniline derivatives with methyl triflate usually proceeds

rapidly at room temperature to offer quantitative yield. However, prolonged heating was required for the methylation of compound **15b** (80 °C in a sealed ampule for 3 days) to yield 30 to 40% of product **16**. The electron-withdrawing carbonyl and nitrile groups and the unfavorable steric hindrance caused by the ortho position nitrile group appears to be responsible. The carbonyl or nitrile group, however, is routinely introduced into aryl-trimethylammonium to activate the aromatic ring for nucleophilic aromatic substitution by F-18 (Ding et al., 2000 and 1990). The presence of both in compound **16** makes the trimethylammonium group very labile toward fluoride substitution. In fact, quantitative fluoride substitution was accomplished in acetonitrile at room temperature in less than 5 min using 1.0 equiv of tetrabutylammonium fluoride as fluoride source to give compound **18a**, which can also be synthesized from **3** (Scheme 4). This efficient substitution reaction with fluoride is very unusual since fluoride ion is not a strong nucleophile. However, in this case the displacement of the trimethylammonium group is facilitated by the presence of the two electron-withdrawing groups (nitrile and carbonyl). Compound **18** can be reduced by borane in refluxing THF to give 4-fluoro-3-aminomethyl-3'-iodobenzhydrol **19a** in 76% yield. Upon PCC oxidation, 4-fluoro-3-aminomethyl-3'-iodobenzophenone **20a** was obtained in 67% and alkylation with bromoacetyl bromide to produce compound *N*-[6-fluoro-3-(3-iodobenzoyl)benzyl]-2-bromoacetamide **21** in 80% yield. Compound **21** is the parent compound for the radiolabeled compounds **1** and **2** and serves as a reference compound in the radiosynthesis.

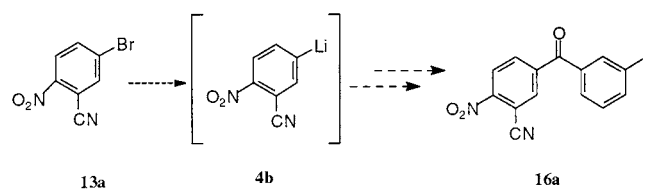
Initially, 4-nitro-3-cyano-3'-iodobenzophenone **16a** (Scheme 5) instead of **16** was proposed for the F-18 labeling precursor. However, we were not able to synthesize **16a** from 2-nitro-5-bromobenzonitrile **13a** under various temperature and solvent combinations. The nitrile group in 2-nitro-5-bromobenzonitrile **13a** was presumably activated by the ortho nitro group and very labile to nucleophilic reaction with *n*-butyllithium, and the 2-nitro-5-lithiobenzonitrile **4b** could not be generated through the bromine–lithium exchange reaction. Of course, the nitro group itself may also react with a strong base like butyllithium. On the basis of our results, it seems to be reasonable to conclude that the stability of the nitrile group in **3**, **13**, and **13a** toward the nucleophilic



Scheme 4<sup>a</sup>

<sup>a</sup> Key: For nonradiosynthesis: (a) *n*-BuLi, THF/hexanes (3/1, v/v), -110 °C, 45 min; (b) 3-iodobenzaldehyde, -110 °C to room temperature; (c) PCC, CH<sub>2</sub>Cl<sub>2</sub>, rt, 2 h; (d) 1.0 equiv of Bu<sub>4</sub>NF, acetonitrile, rt, 5 min; (e) BH<sub>3</sub>, THF, reflux, 8 h; (f) PCC, CH<sub>2</sub>Cl<sub>2</sub>, rt; (g) bromoacetyl bromide, N-methylmorpholine, CH<sub>2</sub>Cl<sub>2</sub>, rt. For radiosynthesis: (d) K<sub>2</sub>CO<sub>3</sub>, Bu<sub>4</sub>N(OH), dry ice, K<sup>18</sup>F, CH<sub>3</sub>CN, rt, 10 min; (e) BH<sub>3</sub>, THF, 120 °C, 10 min; (f) PCC, CH<sub>2</sub>Cl<sub>2</sub>, 15 min; (g) bromoacetyl bromide, CH<sub>2</sub>Cl<sub>2</sub>, 2 min.

Scheme 5



reaction is in the order of **13** > **3** > **13a**, which is consistent with the electron-withdrawing property of the amino, fluoro, and nitro group.

The F-18 labeling starting from compound **16** is shown in Scheme 4. The F-18 substitution reaction in acetonitrile at room temperature afforded **18b** in less than 10 min with a radiochemical yield (RCY) of 90 to 92%. To our best knowledge, this is the first example of a rapid room-temperature high yield F-18 substitute reaction, which makes compound **16** an ideal labeling precursor (Ding et al., 1990 and Fowler and Wolf, 1997). Borane reduction at 120 °C in 15 min yielded **19b** in 68% RCY. PCC oxidation at room temperature in 10 min gave **20b** in 68% RCY. Alkylation with bromoacetyl bromide at room temperature in 2 min followed by reverse phase HPLC purification afforded the F-18 labeled product **2**. The overall radiosynthesis from **16** takes less than 3 h after EOB with an unoptimized radiochemical yield of about 2% and specific activity of 0.8 Ci/μmol at EOB. The application of compound **2** to the F-18 labeling of oligonucleotides, peptides, and proteins is currently under investigation in our laboratory.

In summary, we have developed routes to synthesize novel precursor compounds, which can be used to label biomolecules with both F-18 and iodine radioisotopes and give structurally identical products. In the course of this project, we found that (1) nitrile and carbonyl groups at ortho and para positions in aryltrimethylammonium trifluoromethanesulfonate has an additive activation effect which facilitates the F-18 substitution reaction, and the F-18 labeling can proceed at room temperature. (2) The stability of nitrile group in 2-substitute-5-lithiobenzonitrile derivatives toward the nucleophilic agent de-

pends on the electronic properties of the 2-position substituent and in the order of dimethylamino > fluoro > nitro.

#### ACKNOWLEDGMENT

Financial support for this research was provided by the U.S. Department of Energy under the contract No. AC02-98CH10886. The assistance of C. Shea and V. Garza in the radiosynthesis, Y. Xu in the HPLC condition development, M. Schueller in the Cyclotron operation, and D. Schlyer and R. Ferrier in the radionuclides production is acknowledged.

#### LITERATURE CITED

- Al-Diab, S. S., Barcelon, M. A., Mark, J. E., and Zimmer, H. (1982) Synthesis and polymerization of some styrene-type monomers containing phenyl-tin-alkyl group. *Polym. Prepr. (Am. Chem. Soc., Div. Polym. Chem.)* 23 (1), 298–299.
- Arano, Y., Wakisaka, K., Ohmomo, Y., Uezono, T., Mukai, T., Motonari, H., Shiono, H., Sakahara, H., Konishi, J., Tanaka, C., et al. (1994) Maleimidoethyl 3-(tri-*n*-butylstannyl)hippurate: a useful radioiodination reagent for protein radiopharmaceuticals to enhance target selective radioactivity localization. *J. Med. Chem.* 37 (16), 2609–2618.
- Bullok, K. E., Dyszlewski, M., Prior, J. L., Pica, C. M., Sharma, V., and Piwnica-Worms, D. (2002) Characterization of novel histidine-tagged tat-Peptide complexes dual-labeled with (99m)Tc-tricarbonyl and fluorescein for scintigraphy and fluorescence microscopy. *Bioconjugate Chem.* 13 (6), 1226–1237.
- Burns, H. D., Hamill, T. G., Eng, W. S., Francis, B., Fioravanti, C., and Gibson, R. E. (1999) Positron emission tomography neuroreceptor imaging as a tool in drug discovery, research and development. *Curr. Opin. Chem. Biol.* 3 (4), 388–394.
- Crooke, R. M., Graham, M. J., Martin, M. J., Lemonidis, K. M., Wyrzykiewicz, T., and Cummins, L. L. (2000) Metabolism of antisense oligonucleotides in rat liver homogenates. *J. Pharmacol. Exp. Ther.* 292 (1), 140–149.
- Ding, Y. S., Liu, N., Wang, T., Marecek, J., Garza, V., Ojima, I., and Fowler, J. S. (2000) Synthesis and evaluation of 6-[<sup>18</sup>F]-fluoro-3-(2(s)-azetidylmethoxy)pyridine as a PET tracer for nicotinic acetylcholine receptors. *Nucl. Med. Biol.* 27, 381–389.
- Ding, Y. S., Shiue, C. Y., Fowler, J. S., Wolf, A. P., and Plenevaux, A. (1990) No-carrier-added (NCA) aryl[<sup>18</sup>F]-

- fluorides via the nucleophilic aromatic substitution of electron-rich aromatic rings. *J. Fluorine Chem.* **48**, 189–205.
- Ding, Y. S., Sugano, Y., Koomen, J., and Aggarwal, D. (1996) Synthesis of [ $^{18}\text{F}$ ]RO41–0960, a potent catechol-*o*-methyl-transfer inhibitor, for pet studies. *J. Labelled Compd. Radiopharm.* **39** (4), 303–318.
- Dolle, F., Ninnen, F., Vaufrey, F., Tavitian, B., and Crouzel, C. (1996) A general method for labeling oligodeoxynucleotides with  $^{18}\text{F}$  for in vivo imaging. *J. Labelled Compd. Radiopharm.* **34** (4), 319–330.
- Eckelman, W. C., Tatum, J. L., Kurdziel, K. A., and Croft, B. Y. (2000) Quantitative analysis of tumor biochemistry using PET and SPECT. *Nucl. Med. Biol.* **27** (7), 633–635.
- Fowler, J. S., Finn, R. D., Lambrecht, R. M., and Wolf, A. P. (1973) The synthesis of  $^{18}\text{F}$ -5-fluorouracil. VII. *J. Nucl. Med.* **14** (1), 63–64.
- Fowler, J. S., Volkow, N. D., Wang, G. J., Ding, Y. S., and Dewey, S. L. (1999) PET and drug research and development. *J. Nucl. Med.* **40** (7), 1154–1163.
- Fowler, J. S., and Wolf, A. P. (1997) Working against Time: Rapid Radiotracer Synthesis and Imaging the Human Brain. *Acc. Chem. Res.* **30** (4), 181–188.
- Hanss, B., Leal-Pinto, E., Bruggeman, L. A., Copeland, T. D., and Klotman, P. E. (1998) Identification and characterization of a cell membrane nucleic acid channel. *Proc. Natl. Acad. Sci. U. S. A.* **95** (4), 1921–1926.
- Hnatowich, D. J. (1999) Antisense and nuclear medicine. *J. Nucl. Med.* **40** (4), 693–703.
- Hnatowich, D. J. (2000) Antisense imaging: where are we now? *Cancer Biother. Radiopharm.* **15** (5), 447–457.
- Hostetler, E. D. J., S. D., Welch, M. J., and Katzenellenbogen, J. A. (1999) Synthesis of 2-[ $^{18}\text{F}$ ]Fluoroestradiol, a Potential Diagnostic Imaging Agent for Breast Cancer: Strategies to Achieve Nucleophilic Substitution of an Electron-Rich Aromatic Ring with [ $^{18}\text{F}$ ]F $^-$ . *J. Org. Chem.* **64** (1), 178–185.
- Kasmai, H. S., Mischke, S. J., and Blake, T. J. (1995) 18-Crown-6 Complexes of *n*-Butylammonium and Pyridinium Chlorochromates. Mild and Selective Oxidizing Agents for Alcohols. *J. Org. Chem.* **60** (7), 2267–2270.
- Kilbourn, M. R., Dence, C. S., Welch, M. J., and Mathias, C. J. (1987) Fluorine-18 labeling of proteins. *J. Nucl. Med.* **28** (4), 462–470.
- Kobori, N., Imahori, Y., Mineura, K., Ueda, S., and Fujii, R. (1999) Visualization of mRNA expression in CNS using  $^{11}\text{C}$ -labeled phosphorothioate oligodeoxynucleotide. *Neuroreport* **10** (14), 2971–2974.
- Kühnast, B., Dollé, F., Terrazzino, S., Rousseau, B., Loc'h, C., Vaufrey, F., Hinnen, F., Doignon, I., Pillon, F., David, C., Crouzel, C., and Tavitian, B. (2000) General method to label antisense oligonucleotides with radioactive halogens for pharmacological and imaging studies. *Bioconjugate Chem.* **11** (5), 627–636.
- Lange, C. W., VanBrocklin, H. F., and Taylor, S. E. (2002) Photoconjugation of 3-azido-5-nitrobenzyl[ $^{18}\text{F}$ ]fluoride to an oligonucleotide aptamer. *J. Labelled Compd. Radiopharm.* **45**, 257–268.
- Lebedeva, I., and Stein, C. A. (2001) Antisense oligonucleotides: promise and reality. *Annu. Rev. Pharmacol. Toxicol.* **41**, 403–19.
- Lindgren, M., Hallbrink, M., Prochiantz, A., and Langel, U. (2000) Cell-penetrating peptides. *Trends Pharmacol. Sci.* **21** (3), 99–103.
- Mahato, R. I., Takakura, Y., and Hashida, M. (1997). Development of targeted delivery systems for nucleic acid drugs. *J. Drug Target.* **4** (6), 337–357.
- Parham, W. E., and Lawrence, D. J. (1976) Elaboration of bromoarylnitriles. *J. Org. Chem.* **41** (7), 1187–1191.
- Pawlak, W., Zolnierrek, J., Sarosiek, T., and Szczylik, C. (2000) Antisense therapy in cancer. *Cancer Treat Rev.* **26** (5), 333–350.
- Prochiantz, A. (2000) Messenger proteins: homeoproteins, TAT and others. *Curr. Opin. Cell Biol.* **12** (4), 400–406.
- Schwarze, S. R., and Dowdy, S. F. (2000) In vivo protein transduction: intracellular delivery of biologically active proteins, compounds and DNA. *Trends Pharmacol. Sci.* **21** (2), 45–48.
- Schwarze, S. R., Ho, A., Vocero-Akbani, A., and Dowdy, S. F. (1999) In vivo protein transduction: delivery of a biologically active protein into the mouse. *Science* **285** (5433), 1569–1572.
- Tseng, B. Y., and Brown, K. D. (1994) Antisense oligonucleotide technology in the development of cancer therapeutics. *Cancer Gene Ther.* **1** (1), 65–71.
- Violini, S., Sharma, V., Prior, J. L., Dyszlewski, M., and Piwnicka-Worms, D. (2002) Evidence for a plasma membrane-mediated permeability barrier to tat basic domain in well-differentiated epithelial cells: lack of correlation with heparan sulfate. *Biochemistry* **41** (42), 12652–12661.
- Zalutsky, M. R., and Narula, A. S. (1987) A method for the radiohalogenation of proteins resulting in decreased thyroid uptake of radioiodine. *Appl. Radiat. Isot.* **38** (12), 1051–1055.
- Zalutsky, M. R., and Narula, A. S. (1988) Radiohalogenation of a monoclonal antibody using an *N*-succinimidyl 3-(tri-*n*-butylstannyl)benzoate intermediate. *Cancer Res.* **48** (6), 1446–1450.
- Zamecnik, P. C., and Stephenson, M. L. (1978) Inhibition of Rous sarcoma virus replication and cell transformation by a specific oligodeoxynucleotide. *Proc. Natl. Acad. Sci. U. S. A.* **75** (1), 280–284.
- Zhang, Y. M., Liu, N., Zhu, Z. H., Rusckowski, M., and Hnatowich, D. J. (2000) Influence of different chelators (HYNIC, MAG3 and DTPA) on tumor cell accumulation and mouse biodistribution of technetium-99m labeled to antisense DNA. *Eur. J. Nucl. Med.* **27** (11), 1700–1707.

BC025616N

# Conjugation of an Antisense Oligodeoxynucleotide to Ribonuclease H Results in Sequence-Specific Cleavage and Intracellular Inhibition of HCV Gene Expression

Toshiko Fukuma, Cherie M. Walton, Catherine H. Wu, and George Y. Wu\*

Department of Medicine, Division of Gastroenterology-Hepatology, University of Connecticut Health Center, Farmington, Connecticut. Received October 24, 2002; Revised Manuscript Received December 12, 2002

A recombinant *E. coli* ribonuclease H (RNase H) was chemically coupled to an antisense oligodeoxynucleotide (ODN) against the 5'-noncoding region (5'-NCR) of the hepatitis C virus. Purity of the conjugates was confirmed by sodium dodecyl sulfate-polyacrylamide gel electrophoresis (SDS-PAGE) as a band corresponding to approximately 23 kDa. Conjugate function was tested by the cleavage of a HCV RNA transcript including the 5'-NCR and core region and showed HCV sequence-specific cleavage by the appearance of an expected ~1000 nt fragment of RNA. Cleavage was not seen by RNase H alone, or ODN alone. Delivery studies using <sup>32</sup>P- and <sup>125</sup>I-labeling showed that while RNase H failed to enter cells, the conjugate was efficiently taken into the cells. To assess intracellular effects, a cell line, Huh-7/CMV-NCRCΔluc, which expresses HCV mRNA (nt 1–585) fused to a marker gene, was transfected with the conjugate. Reporter gene expression was suppressed by 51.2% with the conjugate compared to only 39.7% by ODN alone, 35.8% by a mixture of RNase H plus ODN, and not at all by RNase H alone. In conclusion, the RNase H-ODN conjugate effectively cleaved an HCV transcript in vitro and inhibited expression of an HCV-marker fusion construct in a liver-derived cell line.

## INTRODUCTION

Ribonuclease H (RNase H) is an endonuclease that cleaves only the RNA strand of RNA-DNA hybrids (1). However, it does not have sequence-specific properties. It has been isolated from *Escherichia coli* (2, 3) as well as human cells (4, 5). *E. coli* RNase H1 is composed of a single polypeptide chain with 155 amino acids, and its properties are well characterized (6–8).

Antisense oligodeoxynucleotides (ODNs) can hybridize with target RNA molecules in a sequence-specific manner, blocking translation and resulting in reduction of protein synthesis including that of several viruses (9–14). Antisense ODNs against the 5'-noncoding region (5'-NCR) and core region of hepatitis C virus (HCV) genome were used to inhibit the HCV-directed expression in vitro (15, 16) in human hepatoma cell lines (17–19) and in an animal model infected with an HCV-vaccinia virus recombinant (20).

Although endogenous RNase H is suggested to have a role in inhibition of gene expression by ODNs (21–24), the normal RNase H expression level in mammalian cells is low. To obtain high, intracellular concentrations of RNase H and to colocalize it with ODNs, we sought to link RNase H to ODN to form a conjugate. The aim was to synthesize an RNase H-ODN conjugate targeting HCV, test sequence-specific cleavage using HCV RNA transcript in vitro, and study its *intracellular* activity in a human liver cell line that expresses HCV mRNA.

## MATERIALS AND METHODS

**Purification of RNase H.** *E. coli* strain MIC1066 expressing a mutant RNase H (C63S, C133A) was a generous gift from Dr. Robert Crouch, NIH. RNase H was purified as previously described (25, 26).

**Antisense ODN Design.** A 14-mer HCV 5'-NCR sequence specific antisense ODN was designed against a target sequence based on the predicted secondary structure of the HCV genome, nt 325–338 (5'-CUCGUA-GACCGUGC-3'). A 12-base oligonucleotide (5'-GCAGGGT-GAAGC-3') specific for the DR1 site on HBV adw strain was prepared as a negative oligonucleotide control. The ODN was 5'-amino modified, and the backbone phosphorothioate was modified (HHMI/Keck Oligonucleotide Synthesis Facility, Yale University).

**RNase H-ODN Conjugate Synthesis.** RNase H-ODN conjugate was synthesized as previously described (25, 26). Briefly, 360 nM ODN and 50-fold molar excess water-soluble cross-linker, Sulfo-GMBS. RNase H-ODN conjugates were purified by anion exchange column, HiTrap Q (Amersham Pharmacia Biotech Inc., Piscataway, NJ). SDS-PAGE analysis was performed, and bands were visualized by Coomassie Brilliant Blue.

**<sup>32</sup>P-Labeling of ODN and <sup>125</sup>I-Labeling of RNase H.** DNA-labeling of RNase H-ODN conjugate and ODN were performed by 3'-OH end-labeling with α<sup>32</sup>P-ATP using terminal deoxynucleotidyl transferase according to manufacturer's instructions (Promega, Madison, WI). Labeled products were analyzed on SDS-polyacrylamide (15%)/urea (8 M) gels, followed by autoradiography. Protein-labeling of RNase H and RNase H-ODN conjugate were performed with <sup>125</sup>I by the chloramine-T method and analyzed by SDS-PAGE (15%) and autoradiography.

\* Address correspondence to: George Y. Wu, M. D., Ph.D., Department of Medicine, Division of Gastroenterology-Hepatology, University of Connecticut Health Center, Rm. AM-044, 263 Farmington Ave., Farmington, CT 06030-1845, (860) 679-3158, (860) 679-3159 (FAX), e-mail wu@nso.uchc.edu.



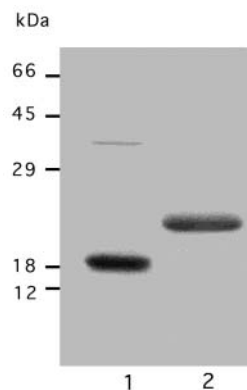
**Plasmids and in Vitro Transcription.** To evaluate the cleavage properties of RNase H-ODN conjugate, an in vitro cleavage substrate was prepared. The plasmid, p90/HCVFLong pU, containing a full length HCV cDNA (Genotype Ia, Dr. Charles M. Rice, Rockefeller University, NY), was digested with restriction enzymes Xba I/BamHI to generate a 1,357 bp fragment. This fragment was subcloned into pUC18, resulting in pUC18/T7-HCV (nt 1–1357). As a control, an HBV RNA template was also created from an adw R9 plasmid (Dr. T. J. Liang, NIH) resulting in a fragment of 1182 nt (26). In vitro transcription was performed using conventional T7 RNA polymerase reaction (Life Technologies, Grand Island, NY).

**In Vitro Transcript Cleavage Assay.** To assess cleavage, 0.5  $\mu$ M HCV RNA of in vitro transcript and varying concentrations of RNase H-ODN conjugate with ranging 6 nM–0.6  $\mu$ M, was incubated at 37 °C for 1 h in cleavage buffer [40 mM Tris-HCl, pH 7.4, 4 mM MgCl<sub>2</sub>, 1 mM DTT, 150 mM NaCl, 1  $\mu$ L anti-RNase (Ambion, Austin, TX)]. To RNase H-ODN conjugate samples, 25 mM *N*-ethylmaleimide (NEM) was added to prevent the nonspecific cleavage by unconjugated RNase H (27). The effect of the chelating agents EDTA and EGTA were also tested. Appearance of expected cleaved fragments was sought using 0.7% agarose 2.2 M formaldehyde gels. RNA bands were visualized by ethidium bromide staining.

**Cell Lines and RNase H-ODN Conjugate Transfection.** A cell line, Huh-7/CMV-NCRCLuc was used to test the inhibition of HCV mRNA. This cell line was established by transfecting the plasmid pRc/CMV-NCRCLuc that contains HCV cDNA nt 1–585 upstream of a firefly luciferase gene under the control of CMV promoter (28). Huh-7/CMV-luc, which expresses luciferase gene driven by a CMV promoter, was used as a control. These cell lines were cultured in DMEM supplemented with 10% FBS and 250  $\mu$ g/mL G418. HepG2 derived cells, HepG2 2.2.15, that produce unrelated HBV viral proteins, were also used as controls (29).

Transfections of ODN, RNase H, and RNase H-ODN conjugate into the cells were performed by a polycationic lipid method. Cells ( $2 \times 10^5$ ) were seeded on 24-well tissue culture dishes and incubated for 24 h prior to the transfection. Various amounts of RNase H-ODN conjugates ranging from 0  $\mu$ g to 1.6  $\mu$ g were mixed with LipofectAMINE (DOSPA plus DOPE, Invitrogen, Carlsbad, CA) in OPTI-MEM I (Life Technologies). Final protein concentrations ranged from 0  $\mu$ M to 0.3  $\mu$ M. Control samples of ODN alone, RNase H alone, and a mixture of RNase H and ODN were also prepared in the identical molar ratios as present in RNase H-ODN conjugate. Cells were incubated at 37 °C with 5% CO<sub>2</sub>. At 12 h after transfection, culture medium was replaced. Cells were harvested at 3, 6, 12, 24, and 48 h after transfection, and luciferase assays were performed.

**Delivery Studies.** <sup>32</sup>P-labeled ODN and <sup>125</sup>I-labeled RNase H were used to assess delivery of the conjugate, ODN and RNase H in Huh-7/CMV-NCRCLuc cells. Transfections were performed at 0.15  $\mu$ M using radiolabeled materials as described above. Cells were harvested at 3, 6, 12, 24, and 48 h after transfection. Tissue culture medium was collected and cell layers were washed three times with ice-cold PBS, stripping solution (PBS, pH 5, 10 mM EDTA) followed by lysis buffer. All solutions, and cell lysates were collected. <sup>32</sup>P-radioactivity was scintillation counted and <sup>125</sup>I-radioactivity was measured with gamma counter. Background cell-associated radioactivity was measured by binding assays incubating cells with radiolabeled materials at 4 °C for 2 h. The delivery was



**Figure 1.** SDS-PAGE analysis of the purified RNase H and RNase H-ODN (HCV) conjugate. Purified RNase H and RNase H-ODN (3  $\mu$ g) were separated by 15% SDS-PAGE and stained with Coomassie Brilliant Blue. Lane 1, RNase H; lane 2, RNase H-ODN (HCV) conjugate. Migration of the protein size markers is shown on the left.

assessed by intracellular accumulation, the sum of uptake and elimination from the cells. It was calculated by subtraction of background from total cell-associated amount. Results were expressed as means  $\pm$  SD ( $n = 6$ ).

**Reporter Gene Assays.** Luciferase assays were performed using a commercial kit (Promega) with a luminometer model, LB9501. Total cell protein was determined by Bio-Rad protein assay kit (Bio-Rad, Hercules, CA). Luciferase activity measurements were performed in duplicate, and normalized to the total protein concentration of each sample. Results are expressed as means  $\pm$  SD of four independent experiments. The HBs antigen was quantified by Abbott ELISA according to manufacturer's instructions (Abbott Laboratories, Abbott Park, IL).

**Statistical Analyses.** Statistical analyses were performed using Student's *t*-test with *p* values of  $<0.05$ .

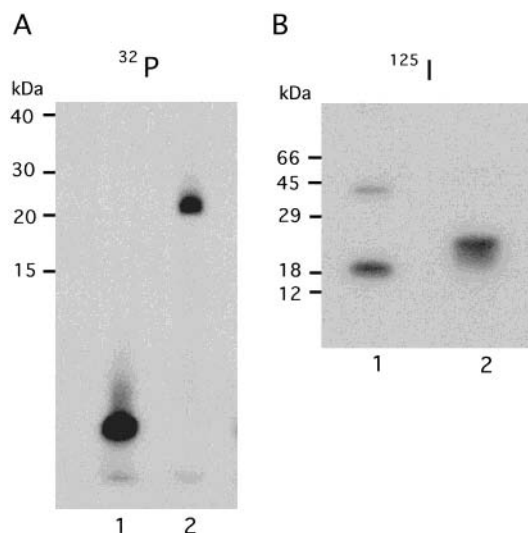
## RESULTS

**RNase H-ODN Conjugate Synthesis.** Figure 1 shows that recombinant mutant RNase H (C63S/C133A-RNase H) was generated from *E. coli* (lane 1). Recombinant RNase H mutant protein alone migrated at distance consistent with its known size of 18 kDa (lane 1). Chemical coupling of RNase H to ODN (HCV) was confirmed by SDS-PAGE analysis of the purified conjugate, showing a band with slower migration (lane 2). RNase H and ODN were found to be linked in a 1:1 molar ratio as calculated from spectrometer readings and Bio-Rad protein assays.

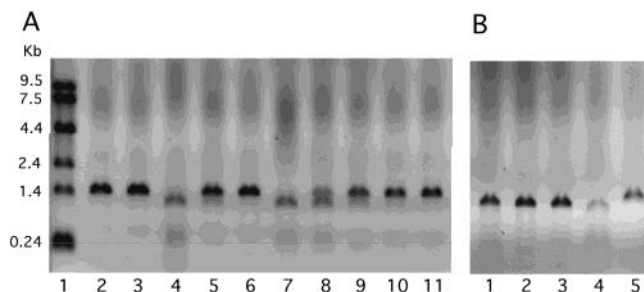
**Purity of <sup>32</sup>P-Labeled ODN and <sup>125</sup>I-Labeled RNase H.** Figure 2A shows an autoradiograph of SDS-polyacrylamide/urea gel analysis of the <sup>32</sup>P-ODN (HCV) and RNase H-(<sup>32</sup>P)ODN (HCV) conjugate. In lane 1, <sup>32</sup>P-ODN alone migrated rapidly due to its lower molecular weight. In contrast, lane 2 shows the slower migration of RNase H conjugate, with no free <sup>32</sup>P-ODN detectable in the purified conjugate.

Figure 2B shows an autoradiograph of SDS-PAGE analysis of the <sup>125</sup>I-RNase H and <sup>125</sup>I-RNase H-ODN (HCV) conjugate. <sup>125</sup>I-RNase H and <sup>125</sup>I-RNase H-ODN conjugate migrated differently with estimated molecular weights as shown in Figure 1. Unconjugated <sup>125</sup>I-RNase H contamination in <sup>125</sup>I-RNase H-ODN conjugate was not detectable.

**In Vitro Cleavage Assay.** Cleavage assay results using RNase H-ODN (HCV) conjugates are shown in Figure 3A and 3B. The untreated substrate (in vitro



**Figure 2.** SDS-PAGE analysis using radiolabeled materials. Migration of the protein size markers are shown on the left of both panels. (A)  $^{32}\text{P}$ -labeled ODN (HCV) and RNase H-ODN (HCV) conjugate with  $3 \times 10^5$  cpm radioactivity each were separated on a 15% polyacrylamide/8 M urea gel, and followed by autoradiography. Lane 1, ODN; lane 2, RNase H-ODN conjugate. (B)  $^{125}\text{I}$ -labeled RNase H and RNase H-ODN with  $1 \times 10^5$  cpm radioactivity each were separated on 15% SDS-PAGE and washed overnight, followed by autoradiography. Lane 1, RNase H; lane 2, RNase H-ODN conjugate.



**Figure 3.** Cleavage assay analyses on 2.2 M formaldehyde gels (0.7% agarose). (A) Cleavage assay with 1357 nt HCV transcripts using different RNase H-ODN (HCV) conjugate concentrations. Lane 1, RNA size marker; lane 2, RNase H 600 nM; lane 3, ODN 600 nM; lane 4, RNase H plus ODN 200 nM; lane 5, RNase H plus ODN 60 nM; lane 6, RNase H plus ODN 6 nM; lane 7, Conjugate 600 nM; lane 8, Conjugate 200 nM; lane 9, Conjugate 60 nM; lane 10, Conjugate 6 nM and lane 11, 1357 nt HCV transcript alone. (B) (Lane 1–3, 1182 nt HBV transcript; Lane 4 and 5, 1357 nt HCV transcript.) Lane 1, Conjugate 600 nM; lane 2, Conjugate 60 nM; lane 3, Conjugate 6 nM; lane 4, Conjugate 600 nM plus 25 mM EGTA and lane 5, Conjugate 600 nM plus 25 mM EDTA.

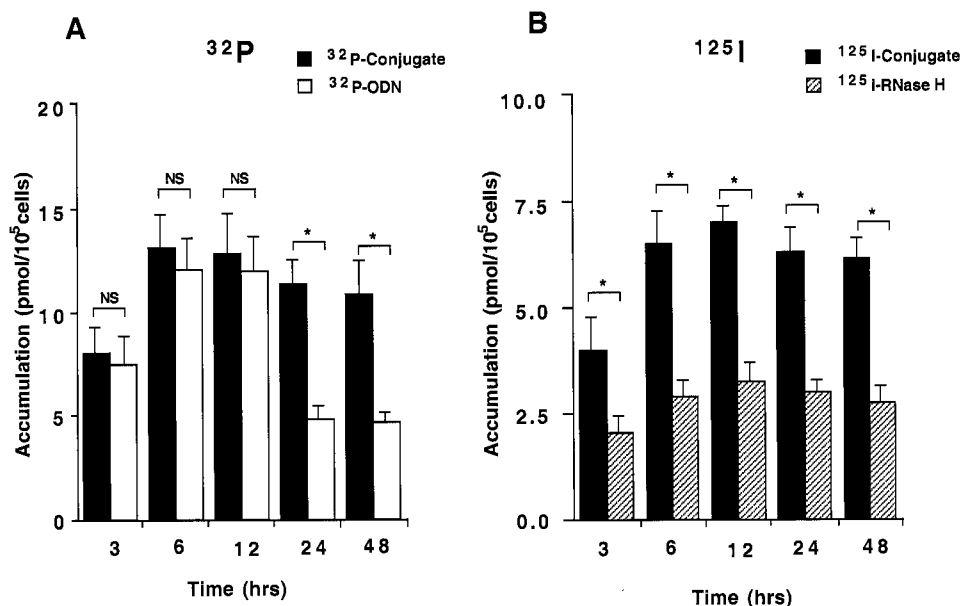
transcript) ran as an approximately 1400 nt band (panel A, lane 11). The reaction mixture incubated with RNase H-ODN conjugates showed HCV cleavage by the presence of an expected  $\sim 1000$  nt fragment. RNase H-ODN conjugate cleaved target transcript in a dose-dependent manner at conjugate concentrations between 60 nM and 600 nM (panel A, lanes 7–10). At concentrations higher than 600 nM, nonsequence-specific cleavage occurred (data not shown). Reaction mixtures containing RNase H plus ODN showed slightly higher cleavage activity than that of RNase H-ODNs conjugates with identical mole equivalents of components (panel A, lanes 4–6). Cleavage was not seen by RNase H alone (panel A, lane 2), or ODN alone (panel A, lane 3), confirming that the observed results with conjugated RNase H were not due to nonspecific RNase H activity or contamination with a nonspecific nuclease. A control HBV transcript of ap-

proximately 1200 nt, completely unrelated in sequence to HCV RNA, was also not cleaved by RNase H-ODN conjugate (panel B, lane 1–3), confirming the requirement for specific HCV sequences to obtain cleavage. The *in vitro* cleavage reaction of HCV transcript was inhibited by 25 mM EDTA (panel B lane 5), a  $\text{Mg}^{2+}$  chelator, but was not inhibited by 25 mM EGTA which binds  $\text{Ca}^{2+}$ , not  $\text{Mg}^{2+}$  (panel B, lane 4). This is consistent with the requirement of RNase H for only  $\text{Mg}^{2+}$ .

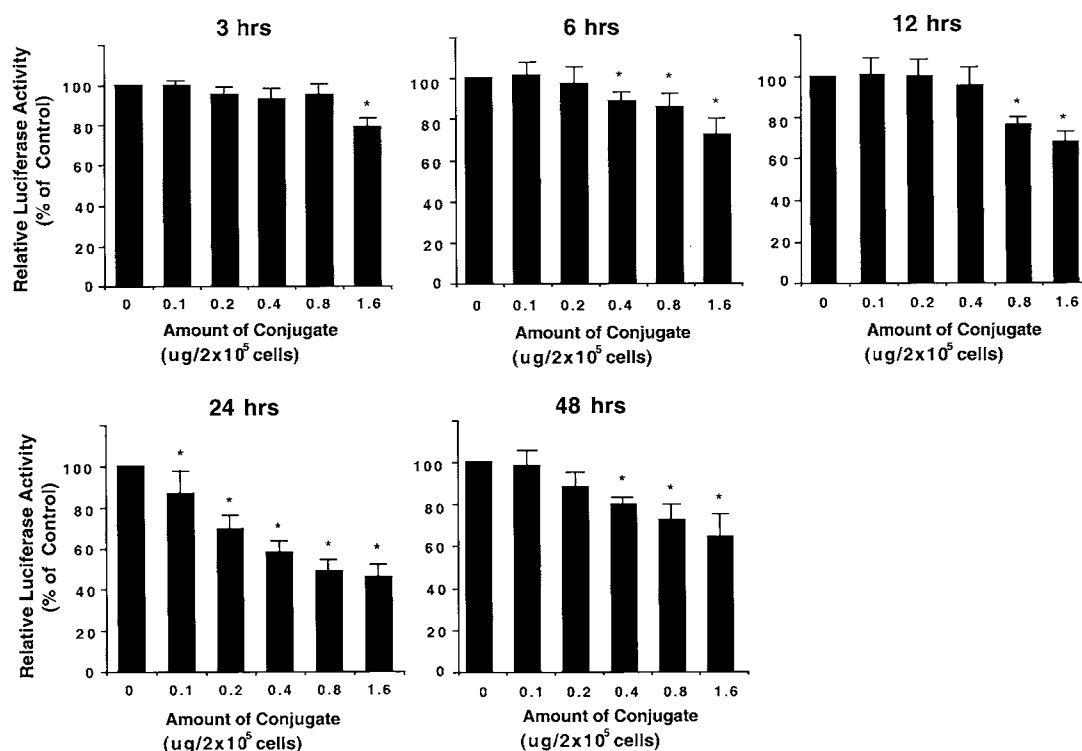
**Delivery of Radiolabeled RNase H-ODN Conjugates (HCV) into the Cells.** Delivery studies were performed to determine whether RNase H-ODN conjugate could be taken into the cells by polycationic lipid. Figure 4A shows the delivery of  $^{32}\text{P}$ -radiolabeled RNase H-ODN conjugate (HCV) and ODN (HCV) alone. Intracellular accumulation, subtraction of background from total cell-associated amount, was taken to represent the delivery of the conjugate or ODN. Background was less than 1.0 pmol/ $10^5$  cells in both groups. Peak accumulation of the conjugate, and ODN alone, were  $13.1 \pm 1.4$  pmol/ $10^5$  cells and  $12.0 \pm 1.3$  pmol/ $10^5$  cells, which correspond to 69.8% and 64.0% of total added amount, respectively, at 6 h after transfection. Thus, conjugated RNase H-ODN was transfected into cells as efficiently as ODN alone. The ODN alone treated cells showed a decline in accumulation to  $4.9 \pm 0.9$  pmol/ $10^5$  cells at 24 h, while conjugate levels remained at  $11.4 \pm 1.3$  pmol/ $10^5$  cells and relatively constant through 48 h, suggesting that more conjugated ODN survived longer than ODN alone in the cells. Figure 4B showed the delivery of  $^{125}\text{I}$ -labeled RNase H-ODN conjugate and RNase H alone. Both groups showed a maximum accumulation at 12 h, with values of  $7.0 \pm 0.58$  pmol/ $10^5$  cells for the conjugate and  $3.3 \pm 0.46$  pmol/ $10^5$  cells for RNase H alone. Beyond the 12 h point, accumulation was unchanged up to 48 h in both groups. These data indicate that intracellular accumulation of conjugated RNase H was more than twice as much as RNase H alone at all time points. At any time point, the differences between two groups were statistically significant ( $p < 0.05$ ).

**Reporter Luciferase Activity in Liver-Derived Cell Lines in the Presence of RNase H-ODN Conjugate (HCV).** A cell line, Huh-7/CMV-NCRC $\Delta$ luc, that expresses a fusion transcript of HCV nt 1–585/luciferase, was tested to investigate whether RNase H-ODN conjugate was functional in these cells. If the RNase H-ODN (HCV) conjugate was effective in cleaving the HCV target, the resulting recombinant HCV-luciferase activity should be inhibited to an extent greater than that amount of ODN alone. Figure 5 shows effects of reporter HCV-luciferase activity by RNase H-ODN conjugates (HCV) at varying times after transfection. RNase H-ODN conjugate inhibited HCV-luciferase expression in a dose dependent manner. The overall maximum suppression was seen at 24 h after transfection at all concentrations. With 1.6  $\mu\text{g}$  (0.3  $\mu\text{M}$ ), 0.8  $\mu\text{g}$  (0.15  $\mu\text{M}$ ), 0.4  $\mu\text{g}$  (0.075  $\mu\text{M}$ ), 0.2  $\mu\text{g}$  (37.5 nM), and 0.1  $\mu\text{g}$  (18.8 nM) of RNase H-ODN conjugate, reporter gene activity was suppressed by 52.0%, 51.2%, 42.0%, 30.6%, and 13.5%, respectively, relative to the lipid-treated control samples. At the 24 h point, suppression was statistically significant compared to the control samples at all conjugate concentrations ( $p < 0.05$ ).

**Effect of RNase H-ODN Conjugate (HCV) on HCV Reporter Gene Expression.** Figure 6 shows the effects of HCV-luciferase activity at 24 h after treatment with RNase H-ODN conjugate. With increasing RNase H-ODN conjugate (HCV) concentrations, inhibition was



**Figure 4.** Intracellular delivery of RNase H-ODN (HCV) Conjugate, ODN (HCV) alone and RNase H alone in Huh-7/CMV-NCR $\Delta$ luc cells. Intracellular accumulation was determined by the subtraction of background from the total cell associated amount as described in Materials and Methods. Data represent means  $\pm$  SD ( $n = 6$ ). (A) Intracellular accumulation of RNase H-ODN conjugate and ODN by  $^{32}\text{P}$ -labeling. (B) Intracellular accumulation of RNase H-ODN conjugate and RNase H by  $^{125}\text{I}$ -labeling. \*,  $p < 0.05$ .

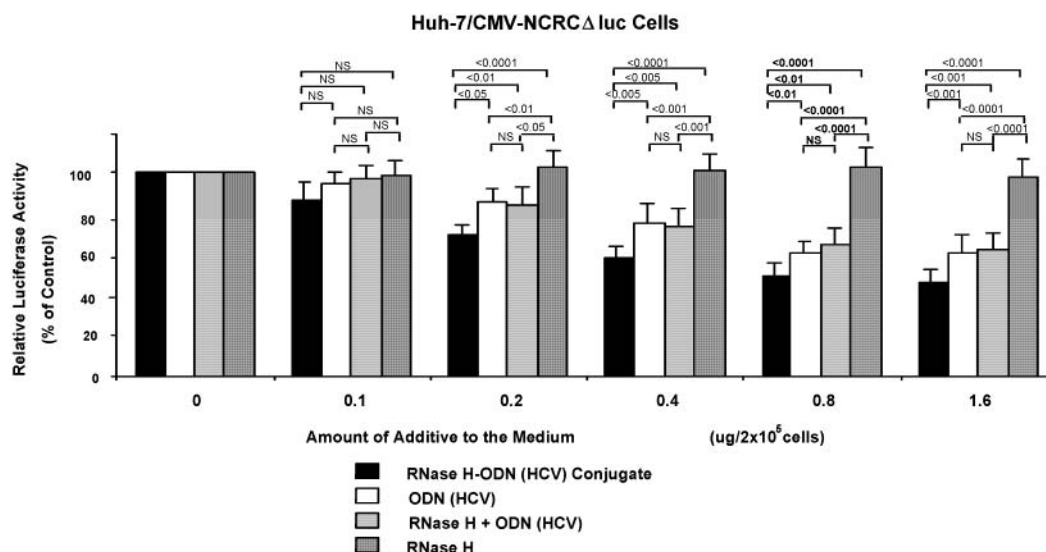


**Figure 5.** Effect on the reporter HCV-luciferase activity by RNase H-ODN (HCV) conjugates in Huh-7/CMV-NCR $\Delta$ luc cells. Cell lysates treated with RNase H-ODN (HCV) conjugate in six different concentrations were harvested at indicated times after transfection. Indicated RNase H-ODN conjugate amounts were added as shown on the horizontal axis, and corresponding concentrations are shown in parentheses: 0.16  $\mu\text{g}$  (0.3  $\mu\text{M}$ ), 0.8  $\mu\text{g}$  (0.15  $\mu\text{M}$ ), 0.4  $\mu\text{g}$  (0.075  $\mu\text{M}$ ), 0.2  $\mu\text{g}$  (37.5 nM), 0.1  $\mu\text{g}$  (18.8 nM), 0  $\mu\text{g}$  (0  $\mu\text{M}$ ) as described in Materials and Methods. Data represent means  $\pm$  SD ( $n = 4$ ). Each experiment was performed in duplicate. \*,  $p < 0.05$ .

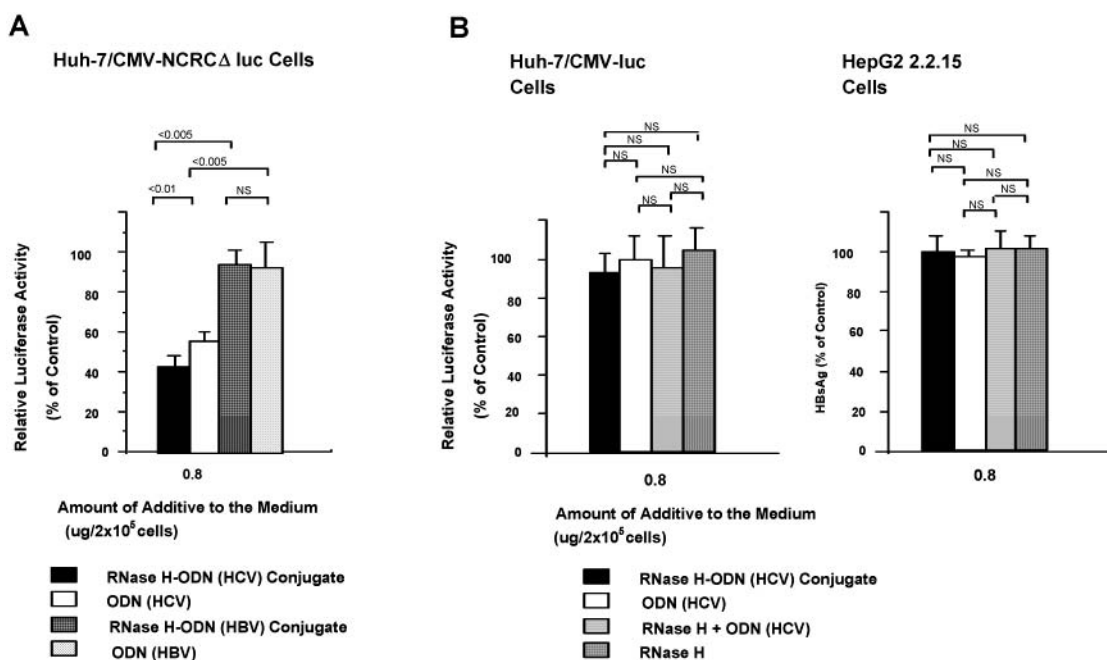
increased, but no further increase was seen above 0.8  $\mu\text{g}$  (0.15  $\mu\text{M}$ ) conjugate administration per  $2 \times 10^5$  cells. At this dose, RNase H-ODN conjugate suppressed reporter gene activity by 51.2% compared to lipid-treated controls, while ODN alone inhibited by 39.7%. Similarly, the mixture of RNase H plus ODN suppressed reporter gene expression by 35.8%, while RNase H alone failed to inhibit at all. ODN alone did show substantial inhibition

as expected, but less than that produced by conjugate. The mixture of RNase H and ODN did not show any additional effect above that of ODN alone, confirming the importance of the linkage of the 2 components to obtain increased efficiency. A control conjugate coupled to ODN (HBV) did not suppress the reporter gene expression (Figure 7A), or control cells lacking HCV sequences were not inhibited by the HCV conjugate (Figure 7B), confirm-





**Figure 6.** Effect of concentration of RNase H-ODN (HCV) conjugates and controls on the reporter HCV-luciferase activity at 24 h. Cells were harvested at 24 h after treatment. Assays using Huh-7/CMV-NCRC $\Delta$  luc cells. Data represent means  $\pm$  SD ( $n = 4$ ). Each experiment was performed in duplicate.  $p$  values are shown over each set of bars.



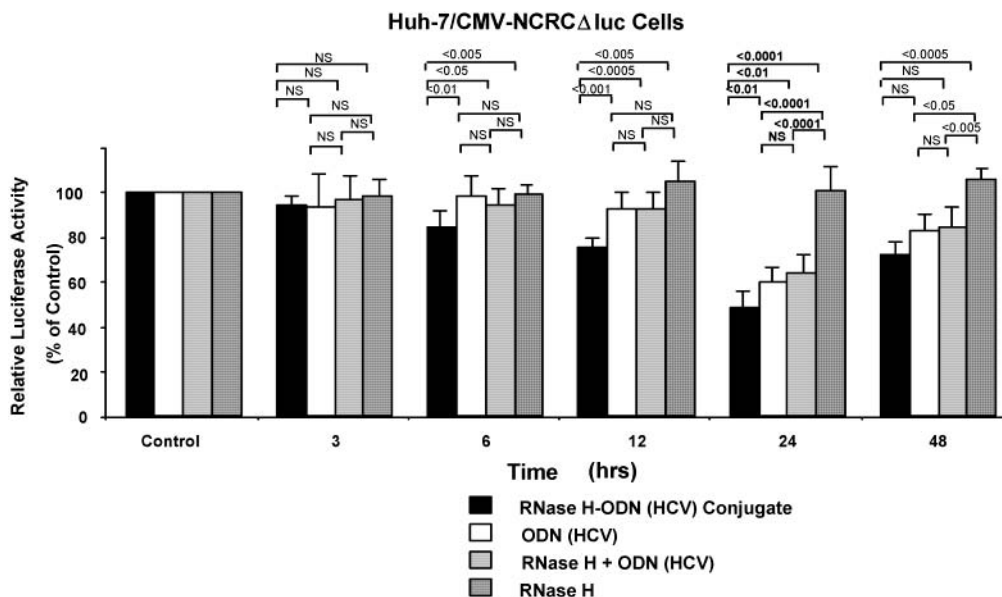
**Figure 7.** Assays using control cell lines and control conjugate coupled to HCV irrelevant ODN. (A) A control study using an ODN specific for HBV related sequence on Huh-7/CMV-NCRC $\Delta$  luc cells. (B) Huh-7/CMV-luc cells that contain luciferase, but lack HCV sequences, (left) and HepG2 2.2.15 cells (right) that both lack HCV and luciferase sequences. Data represent means  $\pm$  SD ( $n = 4$ ). Each experiment was performed in duplicate.  $p$  values are shown over each set of bars.

ing that the observed inhibition was not due to nonspecific effects. At  $0.15 \mu\text{M}$ , the conjugate suppressed reporter luciferase activity by only 6% in control Huh-7/CMV-luc cells (Figure 8), while at  $0.3 \mu\text{M}$ , twice the maximal effective dose, it caused considerable suppression by 18% (data not shown), suggesting nonspecific effects at the higher concentration. At  $0.15 \mu\text{M}$ , only RNase H-ODN (HCV) conjugate, but not ODN (HCV) alone, produced significant suppression at 6 and 12 h.

These results indicated that the suppression of HCV-luciferase expression was due to the presence of RNase H-ODN (HCV) conjugate. Inhibition of reporter gene activity by RNase H-ODN (HCV) conjugate was significantly greater than treatment with ODN (HCV) alone and had no evidence of nonspecific effects on expression of an unrelated gene.

## DISCUSSION

*E. coli* RNase H1 has been extensively studied regarding three-dimensional structure (30), and amino acid residues which are involved in catalytic and substrate-binding sites have been determined (8, 31). On the basis of the information, Kanaya et al. developed a mutant RNase H-conjugate having all cysteine residues replaced with alanine residues, and a newly introduced Cys-135. This cysteine was covalently linked to ODN resulting in sequence-specific RNA cleavage by the RNase H-ODN conjugate (32, 33). Ma et al. developed another mutant, C63S/C133A-RNase H, in which Cys-13 was available for the cross-linking with 5'-amino modified ODN. This mutant RNase H had 90% RNA cleavage activity compared to the wild-type RNase H. After the covalent linkage at Cys-13 with a mouse  $\beta$ -globin-specific 8-mer



**Figure 8.** Time course of the reporter HCV-luciferase activity in the presence of RNase H–ODN (HCV) conjugates and controls. Cells were treated with 0.8  $\mu$ g (0.15  $\mu$ M) conjugate or 0.15  $\mu$ M of each material and harvested at indicated time after transfection. Data represent means  $\pm$  SD ( $n = 4$ ). Each experiment was performed in duplicate.  $p$  values are shown over each set of bars.

antisense-ODN, they showed successful sequence-specific cleavage of murine  $\beta$ -globin mRNA in vitro. In their study, only 0.3% of original nonspecific cleavage activity was retained (25). We used the same mutant C63S/C133A-RNase H for conjugation of ODN against HCV. In our in vitro cleavage assay, the cleavage of target HCV RNA transcript in the presence of conjugate produced fragments consistent with sequence-specific recognition of the antisense ODN and RNA cleavage function by RNase H. Consistent with the previous report that the RNase H activity was decreased by the conjugation with ODN in vitro, our results showed that conjugate was less active than a combination of RNase H and ODN in test tube studies. The decrease of RNase H cleavage activity when conjugated to ODN may be due to change of exposure of active site residues to the target RNA by attachment of ODN to the enzyme in tertiary structure (25, 26, 32). Our results also confirmed  $Mg^{2+}$  dependency of the conjugate activity consistent with known properties of *E. coli* RNase H1 alone (2, 26).

Zabner et al. showed that COS cells took up approximately 60% of the fluorescence-labeled DNA added after 6 h exposure using cationic lipid. They also suggested that gold-labeled DNA was internalized by endocytosis (34). Intracellular ODN that had been introduced directly to the cytoplasm by microinjection was found to be eliminated gradually with time (35). However, in a pharmacokinetic study using polycationic lipid mediated delivery, the cell-associated amount of radiolabeled phosphorothioate ODN was found to increase up to 6 h (36), an observation that is consistent with our results. In contrast, Shi et al. showed that the cellular accumulation of phosphorothioate ODN increased up to 24 h. The difference may be due to different cell lines or labeling with FITC (37). In contrast to ODN alone, internalized RNase H–ODN conjugate was constant through 48 h. This may be due to decreased susceptibility of ODN to nuclease degradation when present in the form of a conjugate to RNase H. Our data further suggest that  $^{32}P$ -labeled RNase H–ODN conjugate had a higher accumulation over time compared to  $^{125}I$ -labeled conjugate and likely represents differences in the sum of uptake, degradation, and elimination of the 2 labeled forms in the cells. Our results also demonstrated that

the accumulation of RNase H–ODN conjugate was nearly twice as great as RNase H alone.

The expression level of two classes of RNase H, RNase H1 and H2, in mammalian cells is very low, and the enzyme is primarily localized in the nucleus (38, 39). Thus, RNA–ODN heteroduplexes are candidates for cleavage by RNase H, mostly in the nucleus. Because HCV replication occurs in the cytoplasm (40), it is reasonable to deliver an RNase H-antisense conjugate into the cytoplasm to inhibit HCV gene expression.

In conclusion, we have synthesized an RNase H–ODN conjugate which has substantial cleavage activity in vitro. When introduced into a liver-derived cell line, it resulted in specific suppression of HCV-directed marker gene expression and thus may be a useful tool in studying structure and function relationships of HCV RNA inside living cells.

#### ACKNOWLEDGMENT

This work was supported by grants from the NIDDK: DK-42182 (G.Y.W.) and the Herman Lopata Chair in Hepatitis Research (G.Y.W.).

#### LITERATURE CITED

- (1) Crouch, R. J., and Dirksen, M. L. (1982) Ribonuclease H. Nucleases (Linn, S. M., and Roberts, R. J., Ed.) pp 211–241, Cold Spring Harbor Laboratory, Cold Spring Harbor, NY.
- (2) Berkower, I., Leis, J., and Hurwitz, J. (1973) Isolation and characterization of an endonuclease from *Escherichia coli* specific for ribonucleic acid in ribonucleic acid–deoxyribonucleic acid hybrid structures. *J. Biol. Chem.* 248, 5914–5921.
- (3) Miller, H. I., Riggs, A. D., and Gill, G. N. (1973) Ribonuclease H (hybrid) in *Escherichia coli*. Identification and characterization. *J. Biol. Chem.* 248, 2621–2624.
- (4) Eder, P. S., and Walder, J. A. (1991) Ribonuclease H from K562 human erythroleukemia cells. Purification, characterization, and substrate specificity. *J. Biol. Chem.* 266, 6472–6479.
- (5) Frank, P., Braunshofer-Reiter, C., Wintersberger, U., Grimm, R., and Busen, W. (1998) Cloning of the cDNA encoding the large subunit of human RNase H1, a homologue of the prokaryotic RNase HII. *Proc. Natl. Acad. Sci. U.S.A.* 95, 12872–12877.

- (6) Kanaya, S., and Crouch, R. J. (1983) DNA sequence of the gene coding for *Escherichia coli* ribonuclease H. *J. Biol. Chem.* 258, 1276–1281.
- (7) Wu, H., Lima, W. F., and Crooke, S. T. (1999) Properties of cloned and expressed human RNase H1. *J. Biol. Chem.* 274, 28270–28278.
- (8) Kanaya, S., Kohara, A., Miura, Y., Sekiguchi, A., Iwai, S., Inoue, H., Ohtsuka, E., and Ikehara, M. (1990) Identification of the amino acid residues involved in an active site of *Escherichia coli* ribonuclease H by site-directed mutagenesis. *J. Biol. Chem.* 265, 4615–4621.
- (9) Mizuta, T., Fujiwara, M., Hatta, T., Abe, T., Miyano-Kurosaki, N., Shigeta, S., Yokota, T., and Takaku, H. (1999) Antisense oligonucleotides directed against the viral RNA polymerase gene enhance survival of mice infected with influenza A. *Nat. Biotechnol.* 17, 583–587.
- (10) Kulka, M., Wachsman, M., Miura, S., Fischelevich, R., Miller, P. S., Tso, P. O. P., and Aurelian, L. (1993) Antiviral effect of oligo(nucleoside methylphosphonates) complementary to the herpes simplex virus type 1 immediate early mRNAs 4 and 5. *Antiviral Res.* 20, 115–130.
- (11) Lisiewicz, J., Sun, D., Weichold, F. F., Thierry, A. R., Lusso, P., Tang, J., Gallo, R. C., and Agrawal, S. (1994) Antisense oligodeoxynucleotide phosphorothioate complementary to Gag mRNA blocks replication of human immunodeficiency virus type 1 in human peripheral blood cells. *Proc. Natl. Acad. Sci. U.S.A.* 91, 7942–7946.
- (12) Offensperger, W. B., Offensperger, S., Walter, E., Teubner, K., Igloi, G., Blum, H. E., and Gerok, W. (1993) In vivo inhibition of duck hepatitis B virus replication and gene expression by phosphorothioate modified antisense oligodeoxynucleotides. *EMBO J.* 12, 1257–1262.
- (13) Bartholomew, R. M., Carmichael, E. P., Findeis, M. A., Wu, C. H., and Wu, G. Y. (1995) Targeted delivery of antisense DNA in woodchuck hepatitis virus-infected woodchucks. *J. Viral. Hep.* 2, 273–278.
- (14) Robaczewska, M., Guerret, S., Remy, J. S., Chemin, I., Offensperger, W. B., Chevallier, M., Behr, J. P., Podhajska, A. J., Blum, H. E., Trepo, C., and Cova, L. (2001) Inhibition of hepadnaviral replication by polyethylenimine-based intravenous delivery of antisense phosphodiester oligodeoxynucleotides to the liver. *Gene Ther.* 8, 874–881.
- (15) Wakita, T., and Wands, J. R. (1994) Specific inhibition of hepatitis C virus expression by antisense oligodeoxynucleotides. In vitro model for selection of target sequence. *J. Biol. Chem.* 269, 14205–14210.
- (16) Lima, W. F., Brown-Driver, V., Fox, M., Hanecak, R., and Bruce, T. W. (1997) Combinatorial screening and rational optimization for hybridization to folded hepatitis C virus RNA of oligonucleotides with biological antisense activity. *J. Biol. Chem.* 272, 626–638.
- (17) Alt, M., Renz, R., Hofschneider, P. H., Paumgartner, G., and Caselmann, W. H. (1995) Specific inhibition of hepatitis C viral gene expression by antisense phosphorothioate oligodeoxynucleotides. *Hepatology* 22, 707–717.
- (18) Hanecak, R., Brown-Driver, V., Fox, M. C., Azad, R. F., Furusako, S., Nozaki, C., Ford, C., Sasmor, H., and Anderson, K. P. (1996) Antisense oligonucleotide inhibition of hepatitis C virus gene expression in transformed hepatocytes. *J. Virol.* 70, 5203–5212.
- (19) Wu, C. H., and Wu, G. Y. (1998) Targeted inhibition of hepatitis C virus-directed gene expression in human hepatoma cell lines. *Gastroenterology* 114, 1304–1312.
- (20) Zhang, H., Hanecak, R., Brown-Driver, V., Azad, R., Conklin, B., Fox, M. C., and Anderson, K. P. (1999) Antisense oligonucleotide inhibition of hepatitis C virus (HCV) gene expression in livers of mice infected with an HCV-vaccinia virus recombinant. *Antimicrob. Agents Chemother.* 43, 347–353.
- (21) Baertschi, A. J. (1994) Antisense oligonucleotide strategies in physiology. *Mol. Cell Endocrinol.* 101, R15–R24.
- (22) Veal, G. J., Agrawal, S., and Byrn, R. A. (1998) Sequence-specific RNase H cleavage of gag mRNA from HIV-1 infected cells by an antisense oligonucleotide in vitro. *Nucleic Acids Res.* 26, 5670–5675.
- (23) Baker, B. F., Condon, T. P., Koller, E., McKay, R. A., Siwkowski, A. M., Vickers, T. A., and Monia, B. P. (2001) Discovery and analysis of antisense oligonucleotide activity in cell culture. *Methods* 23, 191–198.
- (24) Crooke, S. T. (1999) Molecular mechanisms of action of antisense drugs. *Biochim. Biophys. Acta* 1489, 31–44.
- (25) Ma, W. P., Hamilton, S. E., Stowell, J. G., Byrn, S. R., and Davisson, V. J. (1994) Sequence specific cleavage of messenger RNA by a modified ribonuclease H. *Bioorg. Med. Chem.* 2, 169–179.
- (26) Walton, C. M., Wu, C. H., and Wu, G. Y. (2001) A ribonuclease H-oligo DNA conjugate that specifically cleaves hepatitis B viral messenger RNA. *Bioconjugate Chem.* 12, 770–775.
- (27) Kanaya, S., Kimura, S., Katsuda, C., and Ikehara, M. (1990) Role of cysteine residues in ribonuclease H from *Escherichia coli*. Site-directed mutagenesis and chemical modification. *Biochem. J.* 271, 59–66.
- (28) Sakamoto, N., Wu, C. H., and Wu, G. Y. (1996) Intracellular cleavage of hepatitis C virus RNA and inhibition of viral protein translation by hammerhead ribozymes. *J. Clin. Invest.* 98, 2720–2728.
- (29) Sells, M. A., Chen, M. L., and Acs, G. (1987) Production of hepatitis B virus particles in Hep G2 cells transfected with cloned hepatitis B virus DNA. *Proc. Natl. Acad. Sci. U.S.A.* 84, 1005–1009.
- (30) Katayanagi, K., Miyagawa, M., Matsushima, M., Ishikawa, M., Kanaya, S., Ikehara, M., Matsuzaki, T., and Morikawa, K. (1990) Three-dimensional structure of ribonuclease H from *E. coli*. *Nature* 347, 306–309.
- (31) Kanaya, S., Katsuda-Nakai, C., and Ikehara, M. (1991) Importance of the positive charge cluster in *Escherichia coli* ribonuclease HI for the effective binding of the substrate. *J. Biol. Chem.* 266, 11621–11627.
- (32) Kanaya, S., Nakai, C., Konishi, A., Inoue, H., Ohtsuka, E., and Ikehara, M. (1992) A hybrid ribonuclease H. A novel RNA cleaving enzyme with sequence-specific recognition. *J. Biol. Chem.* 267, 8492–8498.
- (33) Nakai, C., Konishi, A., Komatsu, Y., Inoue, H., Ohtsuka, E., and Kanaya, S. (1994) Sequence-specific cleavage of RNA by a hybrid ribonuclease H. *FEBS Lett.* 339, 67–72.
- (34) Zabner, J., Fasbender, A. J., Moninger, T., Poellinger, K. A., and Welsh, M. J. (1995) Cellular and molecular barriers to gene transfer by a cationic lipid. *J. Biol. Chem.* 270, 18997–19007.
- (35) Fisher, T. L., Terhorst, T., Xiaodong, C., and Wagner, R. W. (1993) Intracellular disposition and metabolism of fluorescently labeled unmodified and modified oligonucleotide microinjected into mammalian cells. *Nucleic Acids Res.* 21, 3857–3865.
- (36) Bennett, C. F., Chiang, M. Y., Chan, H., Shoemaker, J. E., and Mirabelli, C. K. (1992) Cationic lipids enhance cellular uptake and activity of phosphorothioate antisense oligonucleotides. *Mol. Pharmacol.* 41, 1023–1033.
- (37) Shi, F., Norden, A., Oberle, V., Engbert, J. B. F. N., and Hoekstra, D. (2001) Efficient cationic lipid-mediated delivery of antisense oligonucleotides into eukaryotic cells; down regulation of the corticotropin-releasing factor receptor. *Nucleic Acids Res.* 29, 2079–2087.
- (38) Sawai, Y., Kitahara, N., Thung, W. L., Yanokura, M., and Tsukada, K. (1981) Nuclear location of ribonuclease H and increased level of magnesium-dependent ribonuclease H in rat liver on thioacetamide treatment. *J. Biochem.* 90, 11–16.
- (39) Frank, P., Braunshofer-Reiter, C., Poltl, A., and Holzmann, K. (1998) Cloning, subcellular localization and functional expression of human RNase HIII. *Biol. Chem.* 379, 1407–1412.
- (40) Bartenschlager, R., and Lohmann, V. (2000) Replication of hepatitis C virus. *Gen. Virol.* 81, 1631–1648.



# Synthesis and Biological Evaluation of Paclitaxel–C225 Conjugate as a Model for Targeted Drug Delivery<sup>1</sup>

Ahmad Safavy,<sup>\*,†,||</sup> James A. Bonner,<sup>†,||</sup> Harlan W. Waksal,<sup>‡</sup> Donald J. Buchsbaum,<sup>†</sup> G. Yancey Gillespie,<sup>‡</sup> M.B. Khazaeli,<sup>†</sup> Ramin Arani,<sup>§</sup> Dung-Tsa Chen,<sup>§</sup> Mark Carpenter,<sup>§</sup> and Kevin P. Raisch<sup>†</sup>

Departments of Radiation Oncology and Surgery, Biostatistics Unit, and Comprehensive Cancer Center, University of Alabama at Birmingham, Birmingham, Alabama 35294, and ImClone Systems, Somerville, New Jersey 08876. Received April 24, 2002; Revised Manuscript Received October 1, 2002

Tumor-targeted drug delivery is an attractive strategy in cancer treatment. We have previously reported a paclitaxel model conjugate using a bombesin receptor-recognizing peptide in which the drug cytotoxicity against H1299 human nonsmall cell lung cancer was enhanced compared to unconjugated taxol. In an effort to expand the development of tumor-recognizing taxanes, paclitaxel (PTX, taxol) was conjugated to the *anti*-epidermal growth factor receptor (*anti*-EGFR) monoclonal antibody (MAb) Erbitux (C225) to serve as a model MAb-mediated drug delivery compound. Thus, paclitaxel was derivatized at its 2'-hydroxy function by introduction of a succinate linker, and the carboxyl group of the latter was covalently attached to C225 through amide bond formation. The final product conjugate (PTXC225) was analyzed mass spectrometrically for assessment of the drug-to-antibody ratios. Cytotoxicity screening of the drug-antibody conjugate against A431, UM-SCC-1, and UM-SCC-6 cells indicated an enhancement in cytotoxic effect of paclitaxel as compared to those of the free drug, the intact antibody, and a physical mixture of the two (*the controls*). In A431 cells, the conjugate showed  $25.2\% \pm 2.2\%$  of apoptosis induction as compared to little or no apoptosis caused by the controls. Biodistribution analysis of the PTXC225 in tumor-implanted nude mice and a tyrosine-kinase assay showed that conjugation of the drug did not interfere with the immunoreactivity of the antibody. The 24-h tumor uptake of C225 and PTXC225 were  $11.7\% \pm 6.0\%$  and  $7.1\% \pm 3.6\%$  of the injected dose per gram of tissue (%ID/g), respectively, which were not significantly different. Also, in A431-implanted nude mice, the conjugate and C225 showed tumor growth inhibition effects of 57.2% and 41.2%, respectively, against a saline-treated control, which were not significantly different from each other. This lack of difference in the *in vivo* antitumor activity of the MAb-delivered drug and free PTX may be due to either a relatively low dose of the antibody-delivered drug (346  $\mu\text{g/kg}$ ), or an untimely release of it, or both. The tumor growth inhibition pattern of the conjugate, however, was identical to that of C225, indicating that the attachment of PTX did not affect the antigen-binding and growth inhibitory features of the MAb. These preliminary results demonstrate the potential of tumor-targeted delivery of taxol as a promising strategy in cancer treatment and warrant further work to develop more suitable drug–MAb linkers as well as improved dosage and treatment protocols.

## INTRODUCTION

Although a powerful and important modality in cancer treatment, the effectiveness of chemotherapy is limited by the efficiency of the delivery of the drug to the tumor site(s), systemic toxicity, and side-effects of the agents used. The delicate balance between the toxicity and side-effects prevention, and producing the maximum therapeutic efficacy, is usually hard to achieve and requires long and tedious protocol development procedures which may jeopardize patient survival and quality of life. Development of antitumor drug delivery systems capable of tipping this balance in favor of a positive outcome of the therapy without worsening the side-effects would be highly desirable.

A potential strategy in achieving this goal may be drug delivery through a tumor-specific mechanism (1–3). Targeted treatment of neoplastic disease has advanced considerably in the last two decades, after the establishment of monoclonal antibody (MAb)<sup>2</sup> technology by Kohler and Milstein (4). An early realization of this technology was in the development of radiolabeled Mabs, which have reached clinical use for imaging and therapy

\* Corresponding author: Ahmad Safavy, Ph.D., 1824 6th Avenue South, WTI 674, Birmingham, AL 35294-6832. Telephone: (205) 934-7077; Fax: (205) 975-7060; e-mail: safavy@uab.edu.

<sup>†</sup> Department of Radiation Oncology.

<sup>‡</sup> Department of Surgery.

<sup>§</sup> Biostatistics Unit.

<sup>||</sup> Comprehensive Cancer Center.

<sup>±</sup> ImClone Systems.

<sup>1</sup> Presented in part at the Eighth Conference on Radioimmunodetection and Radioimmunotherapy of Cancer, Princeton, New Jersey, 12–14 October, 2000.

<sup>2</sup> Abbreviations: BSA, bovine serum albumin; DMEM, Dulbecco's modified Eagle medium; DMF, *N,N*-dimethylformamide; DPBS, Dulbecco's phosphate-buffered saline; EEDQ, 1-ethoxy-carbonyl-2-ethoxy-1,2-dihydroquinoline; EGFR, epidermal growth factor receptor; FBS, fetal bovine serum; HSR, hypersensitivity reaction; ip, intraperitoneal or intraperitoneally; iv, intravenous or intravenously; MAb, monoclonal antibody; MALDI-TOF, matrix-assisted laser desorption/ionization-time-of-flight; MS, mass spectrometry; MW, molecular weight; NHS, *N*-hydroxysuccinimide; PTX, paclitaxel; PTXSX, PTX-hemisuccinate; sc, subcutaneous or subcutaneously; SDM, standard deviation of the mean; TCC, targeted cancer chemotherapy.

(5, 6), with some still under study for future clinical applications (7). Drug-MAb conjugates have also been studied in cancer therapy, albeit to a lesser extent, and the field is still open to much improvement (8, 9). Conjugates of the widely used anticancer drug doxorubicin have been reported (8–12) in attempts to both ameliorate the significant toxicities of this drug and to enhance its efficacy. Hamann and co-workers have reported conjugates of the antitumor antibiotic calicheamicin with the anti-CD33 MAb P67.6 for treatment of acute myeloid leukemia (13, 14).

After our initial report on the synthesis and in vitro cytotoxicity evaluation of the first taxol-MAb conjugate (15), Correa and Pagé (16), and Guillemard and Saragovi (17), reported preparation and cell growth inhibition studies of PTX-BCM43/2E5 conjugate, and PTX-MC192 and PTX-5C3 conjugates, respectively. The latter report also included an in vivo tumor growth inhibition experiment for one conjugate (PTX-MC192). With the exception of two time-points and only in one cell line, the  $IC_{50}$  values of Correa and Pagé were close to or higher than those of free paclitaxel. In the other report, enhancement in cytotoxicity of roughly 26–33% against B104 rat neuroblastoma cells, with respect to free paclitaxel, were reported with only 9% improvement in in vivo tumor inhibition in a nude mice model bearing sc B104 xenografts (17).

The interest to develop tumor-targeting drug-MAB conjugates stems from a duality in character of most antitumor agents, that is, the ability to eradicate cancer cells and toxicity to normal tissue. Despite their potential and an impressive clinical record, taxane drugs also suffer from dose-limiting toxicities. An added drawback of the native taxol is its extremely low aqueous solubility, a mere 0.25 mg/mL. This has led to the currently used Taxol formulation (Bristol-Myers Squibb, Princeton, NJ) of this drug consisting of 30 mg of PTX in 5 mL of a 50/50 mixture of Cremophore EL (polyethoxylated castor oil, a solubilizing surfactant) and dehydrated ethanol, which yields a homogeneous parenteral preparation. Likewise, the clinical formulation of docetaxel (Taxotere, Rhone-Poulenc Rorer, Collegeville, PA) uses polysorbate 80 and 13% ethanol in water. Both formulations have been reported to cause medium to severe hypersensitivity reactions (HSRs). Cremophore EL has been reported to cause histamine release resulting in severe allergic reactions (18, 19). In fact, the early clinical trials of taxol were delayed due to the HSRs until an effective premedication regimen was developed (20). Because of these problems, the National Cancer Institute recommended a 24-h infusion protocol for taxol before which time the patient was premedicated with antiallergy drugs. In addition to HSRs, some major side effects are associated with the use of taxanes (21–25). A peripheral neuropathy is induced by PTX, which becomes more severe by cumulative dosing, and an arthralgia-myalgia syndrome resulting 2–5 days after administration of taxol which is more pronounced with shorter infusion schedules (26). Other systemic toxicities include cardiac arrhythmias, alopecia, mucositis, and fatigue (20). Skin and nail toxicities such as onycholysis, dermatitis, and reactive erythema (27, 28) and cardiac conduction disturbances (29) are among other side effects resulting from the toxicities of this drug. Research on the design and development of water-soluble and tumor-specific taxane drugs, which could be formulated without the use of allergenic excipients and possess higher therapeutic indices without increasing the effective dose, is therefore well justified.

We have reported the first PTXMAb and PTX-peptide conjugates designed for tumor-targeted delivery of this agent and have demonstrated the enhanced cytotoxic properties of the drug in controlled in vitro experiments (15, 30, 31). Here, we report accounts of synthesis, cytotoxicity, apoptosis induction, biodistribution, and a preliminary antitumor activity evaluation of a PTXMAb conjugate using the human-mouse chimeric anti-EGFR antibody C225 (32, 33).

## EXPERIMENTAL SECTION

**General Procedure for the Synthesis of PTXMAb Conjugates.** Paclitaxel (Hande Tech, Houston, TX) was derivatized according to the procedure of Deutsch et al., by succinic anhydride in pyridine, to paclitaxel-2'-succinate (PTXSX) (34). The carboxyl function of the PTXSX (2 mg, 2.1  $\mu$ mol) was activated by the addition of NHS (0.27 mg, 2.3  $\mu$ mol) and EEDQ (0.52 mg, 2.1  $\mu$ mol) in dry DMF (250  $\mu$ L) and at 0 °C for 1 h. The DMF solution of the activated ester (15.5  $\mu$ L, containing 0.13  $\mu$ mol of PTXNHS) was then added to a precooled (0 °C) solution of C225 (2 mg, 0.013  $\mu$ mol) in 600  $\mu$ L of PBS (25 mM, pH 8.1). The solution was stirred at this temperature for 1 h at which time the reaction progress was confirmed by MALDI-TOF MS and using BSA as a MW calibrator. The conjugate was purified by dialysis in DPBS (4  $\times$  2 L) at a MW cutoff of 50 kDa. The protein content of all samples were measured by the method of Lowry (35). The PTXC225 conjugates used in this work had a drug-to-MAb molar ratio of 1.6 or 2 by MALDI. In the following in vitro and in vivo experiments, the molar concentrations of the unconjugated PTX and C225 controls were adjusted according to these ratios as indicated.

**Tumor Cell Lines.** A431 human epidermoid cancer cells were obtained from the American Type Culture Collection (Manassas, VA). The A431 cell line was maintained in Dulbecco's modified Eagle's medium (DMEM): F12 (50:50) containing 7% FBS. The head and neck squamous cell carcinoma lines (UM-SCC-1 and UM-SCC-6) were maintained in DMEM containing 10% FBS. All cell lines were supplemented with L-glutamine, penicillin, and streptomycin and incubated at 37 °C in 5% CO<sub>2</sub>. The UM-SCC-1 and UM-SCC-6 lines were provided by Dr. Thomas Carey (University of Michigan).

**Assessment of EGFR Recognition and Receptor Phosphorylation.** A431 cells were plated in six-well plates at a density of 100 000 cells/well and allowed to grow for 48 h. The cells were treated with 1  $\mu$ g/mL each of C225 or PTXC225 conjugate for 24 h, after which time they were exposed to 10 nM EGF (Sigma Chemical Co., St. Louis, MO) for 5 min. Cell lysates were collected in lysis buffer (0.025 M Tris-HCl, pH 7.5, 0.25 M NaCl, 0.005 M EDTA, 1% (v/v) NP-40, 0.001 M phenylmethylsulfonyl fluoride, 2  $\mu$ g/mL aprotinin, 2  $\mu$ g/mL leupeptin, 0.001 M sodium orthovanadate, 0.05 M sodium fluoride and 0.03 M sodium pyrophosphate, as described previously (36). Equal amounts of protein (5  $\mu$ g) were loaded per lane and separated by 10% SDS-PAGE and transferred to Immobilon-P membrane (Millipore Corp., Bedford, MA).

The immunoblots were blocked in 10% milk/Tris-buffered saline with Tween-20 (TBS-T) (20 mM Tris-HCl, pH 7.5, 137 mM NaCl, 0.05% Tween-20) for 1 h at room temperature. The membrane was incubated with the primary antibody, anti-EGFR (Sigma Chemical Co.), or anti-phosphotyrosine (Santa Cruz Biotechnology Inc, Santa Cruz, CA) in 3% milk/TBS-T overnight at 4 °C.

The secondary *anti*-mouse IgG-HRP antibody (Sigma Chemical Co.) was incubated with the membrane at room temperature for 1 h. The blots were developed by chemiluminescence (Amersham Life Sciences Inc, Arlington Heights, IL).

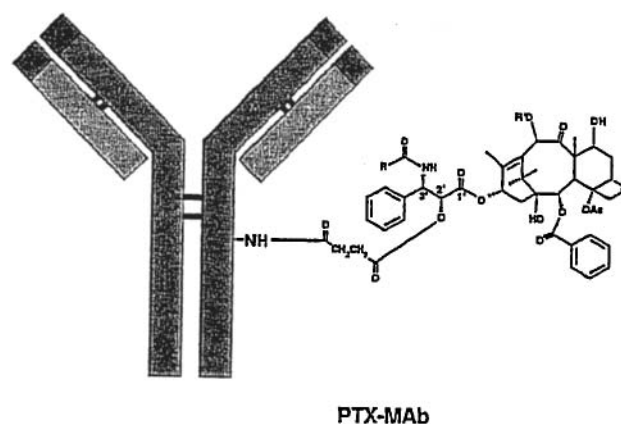
**In Vitro Cell Proliferation Assay.** The cells were plated in 24-well plates at a density of 10 000 cells/well and allowed to grow for 48 h, at which time (day 0) the cells were treated with C225 (3.2 nM), PTX (6.4 nM), C225 (3.2 nM) + PTX (6.4 nM), or PTXC225 conjugate (3.2 nM for a PTX:Mab of 2) for 24 h. The treatments were removed on day 1 and were replaced with drug-free medium. The cells were counted on day 4 and normalized to the percent of untreated cells. Each treatment was done in quadruplicate.

**Apoptosis-Induction Assay.** An Annexin V-FITC Apoptosis Detection kit (BioVision, Inc., Palo Alto, CA) was used to examine the induction of apoptosis. A431 cells were plated at a density of 40 000 cells per well in six-well plates. After 24 h, fresh culture medium was added to the appropriate wells containing the following agents: C225 (3.2 nM), PTX (6.4 nM), C225 (3.2 nM) + taxol (6.4 nM), or PTXC225 conjugate (3.2 nM for a PTX:C225 of 2). At 24 h posttreatment, the agents were removed and replaced with drug-free medium. The cells were collected 72 h later according to the manufacturer's protocol. Briefly, the trypsinized cells were pooled with the corresponding culture medium containing nonadherent cells. The cells were separated from the medium by centrifugation at 300*g* for 5 min. The cell pellets were suspended in 500  $\mu$ L ice-cold 1 $\times$  binding buffer. Annexin V FITC and propidium iodide were added to the cell suspension followed by a 10 min incubation at room temperature in the dark. The cells were collected by flow cytometry and analyzed by CellQuest v3.1 software (Becton Dickinson, San Jose, CA), and results are presented as percent average cell count  $\pm$  SD. All treatments were done in triplicate.

**<sup>125</sup>I-Labeling.** A standard iodogen radiolabeling method was used (37). Briefly, 10 mg of iodogen was dissolved in 1 mL of chloroform and 5 mL of this solution was dispensed into a vial containing a polystyrene bead. The bead was then dried under an argon flow. Sodium [<sup>125</sup>I]-iodide (5 mCi/bead) was added, followed by 5 $\times$  (v/v) of a pH 6 phosphate buffer. The C225 or PTXC225 was added, and the mixture was incubated for 15 min. The labeled MAb was purified on a PD-10 column (Pharmacia, Uppsala, Sweden) eluted with 0.1% HSA in DPBS.

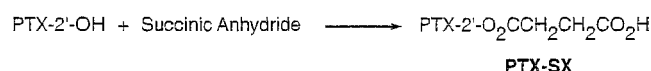
**Animal Model.** Athymic nude female *nu/nu* mice with a BALB/c background were obtained from the National Cancer Institute Frederick Research Laboratory (Frederick, MD) and were kept under sterile conditions. Procedures to minimize discomfort, pain, and distress were in accord with the Animal Resource Program at the University of Alabama at Birmingham, accredited by the American Association for Accreditation of Laboratory Animal Care. The A431 cells were harvested and suspended in sterile PBS at a concentration of  $7.5 \times 10^8$  viable cells/mL. Cell viability was determined by trypan blue dye exclusion. Viable cells ( $10^7$ ) in sterile PBS were injected sc into the right flank.

**Biodistribution of C225 and PTXC225.** Groups of mice (six per group) with established 7-day sc tumors received 5  $\mu$ Ci of the labeled antibody or conjugate as an iv bolus injection. At 4 and 24 h postinjection, the animals were exsanguinated after anesthesia and dissected. Samples of blood, heart, lung, liver, stomach, small intestine, spleen, kidney, skin, bone, muscle, uterus,



**Figure 1.** Schematic representation of a PTXMAB conjugate in which the linkage is through the 2'-hydroxy group of the drug.

#### Scheme 1



pancreas, and tumor were blotted dry, weighed, and counted for the uptake of radioactivity in a well-type gamma counter (Minaxi-gamma 5000 series, Packard, Chicago, IL). Results of biodistribution were expressed as mean  $\pm$  SD % ID/g (percent injected dose per gram of tissue) at 4 and 24 h postinjection.

**In Vivo Tumor Growth Inhibition Study.** Athymic nude female mice ( $n = 6$ , *nu/nu*, 19–22 g body weight) were implanted sc with A431 cells ( $5 \times 10^6$ ) on the right flank. At day 10, tumors were measured by vernier calipers, and tumor volumes were calculated and mice were sorted into three groups, evenly distributing tumors by volume size. The animals were injected ip with saline, C225 (894  $\mu$ g), and the PTXC225 (894  $\mu$ g) conjugate with a PTX:Mab of 1.6 (8.05  $\mu$ g PTX). Tumor sizes were monitored and increases in fractional tumor volumes (FTVs) were calculated from the following equation:

$$\text{FTV} = \text{Vol}_{\text{dn}} / \text{Vol}_{\text{d1}}$$

where  $\text{Vol}_{\text{dn}}$  and  $\text{Vol}_{\text{d1}}$  are volumes at days  $n$  and 1, respectively.

**Statistical Methods.** The %ID/g values were compared between the group with injection of C225 antibody and the group injected with the PTXC225. Group difference may indicate there exists interaction of C225 and PTX. Two sample  $t$  tests were used to detect the difference (38). If both groups have substantially different percentage of dose/gram, the  $p$  value produced by the  $t$  test will be small ( $<0.05$ ). The summary statistics of change in tumor size from baseline by group and assessment day are provided. Furthermore, regression analysis was utilized to compare the trend in change of tumor size relative to the baseline (i.e., initial time) tumor size across time.

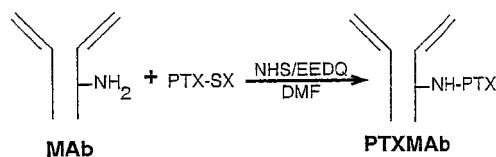
All statistical analyses were carried out using Statistical Analysis System, version 6.12 (38).

## RESULTS

**Synthesis of the Model PTX–C225 Conjugate.** The conjugates of PTX with C225 (Figure 1) were prepared by derivatizing the 2'-hydroxy function of the drug with succinic anhydride, according to the procedure of Deutch (Scheme 1) (34). The activated PTX was coupled to the MAb using NHS and EEDQ at a basic pH (Scheme 2).



Scheme 2



To develop a standard protocol for the conjugation reaction, the yields of product recovery and the number of substituted drugs per C225 (the PTX:Mab ratio) under different activation and coupling times, reactants molar ratios, buffers, and also at two different temperatures (0 °C and 25 °C) were studied. Molecular weight measurements and determination of the PTX:Mab ratio were carried out by MALDI-TOF MS. A typical increase in the MW of the MAb as a result of PTX conjugation is shown in Figure 2. The conjugate of Figure 2 (not used in this work) shows a measured molecular weight increase of 2925 Da by MALDI MS which refers to a PTX:C225 ratio of 3 using the equation of footnote a, Table 1. Reaction conditions and the experimentally measured drug-to-antibody molar ratios (PTX:C225) are shown in Table 1.

**Drug Cytotoxicity Studies.** To evaluate the effect of antibody attachment on the cytotoxicity of PTX, the conjugates were screened against three different cell lines: A human epidermoid carcinoma, A431, and two human head-and-neck carcinomas, UM-SCC1 and UM-SCC6. Each assay used the molar concentrations of antibody-conjugated drug, calculated from the MALDI-TOF MS analyses, and used this value to determine molar concentrations of the unconjugated drug, the C225, and their mixture.

**A431 Cell Line.** The C225 antibody is characterized as having the ability to block the ligand binding site of the EGFR, and thereby, blocking EGF-induced receptor tyrosine phosphorylation. Immunoblot analysis was performed to ensure that PTX conjugated to C225 antibody had no detrimental effect on its ability to bind to the EGF receptor. The A431 cells were treated with 1  $\mu$ g/mL concentrations of either the C225 or the PTXC225

**Table 1. Experimental<sup>a</sup> PTX:C225 Molar Ratios (MRs) for PTXC225 Conjugates Prepared at Different Reactant Molar Ratios and in Two Different Buffer Systems**

reaction	PTXSX:C225 <sup>b</sup>	MR (PBS) <sup>c</sup>	MR (carb) <sup>d</sup>
1	1:1	0	0
2	5:1	1.2 $\pm$ 0.6	0
3	10:1	2.2 $\pm$ 0.2	1.1 $\pm$ 0.3
4	20:1	4.5 $\pm$ 1.1	2.7 $\pm$ 1.7

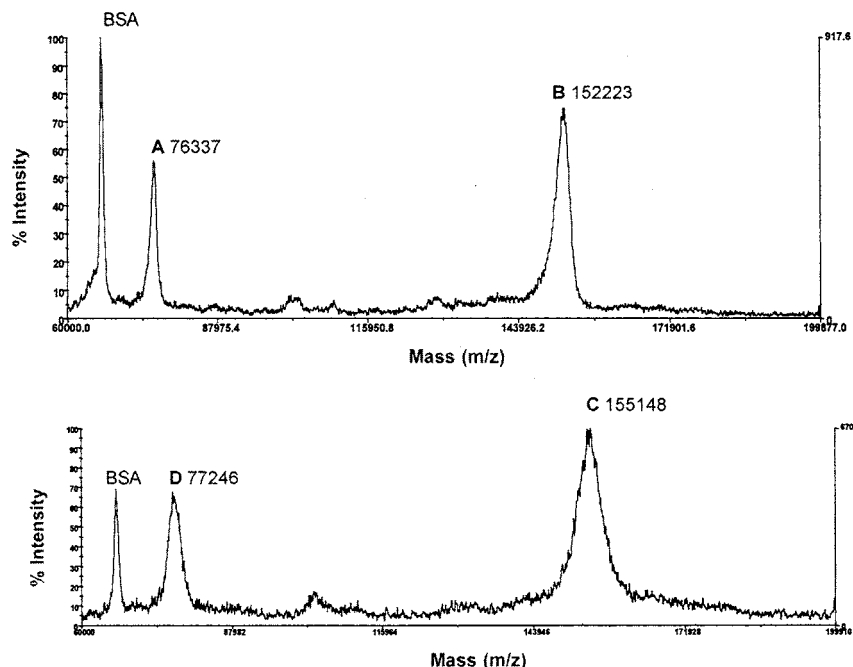
<sup>a</sup> Measured from  $MR = \frac{MW_{conjugate} - MW_{C225}}{MW_{PTXSX}}$  using MALDI-measured MWs. <sup>b</sup> Reactant molar ratios. <sup>c</sup> Phosphate-buffered saline, 25 mM, pH 8.1. <sup>d</sup> Carbonate buffer, 25 mM, pH 9.1.

conjugate for 24 h prior to EGF stimulation. Cell lysates were separated by SDS-PAGE and probed with *anti*-EGFR or *anti*-phosphotyrosine antibodies. Both the unconjugated C225 and PTXC225 prevented the phosphorylation of EGFRs as shown in Figure 3.

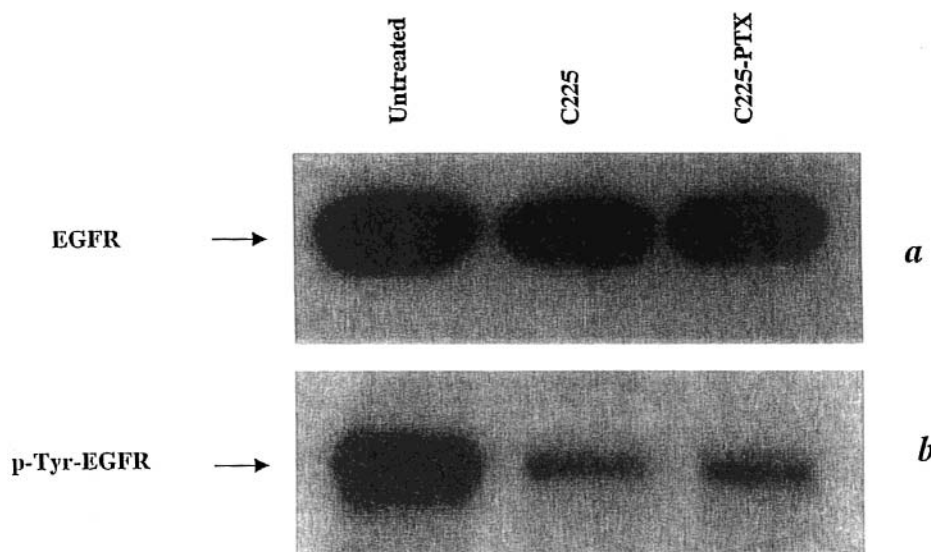
For the cytotoxicity screening, the cells were treated separately with equimolar amounts of the drug, the C225, the mixture of the two, and the PTXC225 conjugate, and the percent survival of the cells for each treatment was determined by counting the posttreatment populations. The percent cell survival of each treatment, as a measure of cytotoxicity, were  $81.0 \pm 3.5$ ,  $87.0 \pm 11.0$ ,  $68.0 \pm 8.0$ , and  $30.0 \pm 0.58$ , for paclitaxel, C225, the mixture, and the PTXC225 conjugate, respectively (Figure 4a).

**SCC1 and SCC6 Cell Lines.** This experiments was carried out to test the conjugate against other EGFR-positive cell lines. Squamous head-and-neck SCC1 and SCC6 cells were used in the screening assays through the same protocol as for A431 cells above. In SCC1 cells percent survival rates of  $78.0 \pm 9.5$ ,  $89.0 \pm 5.5$ ,  $64.0 \pm 6.5$ , and  $37.0 \pm 3.5$ , for PTX, C225, the mixture, and the PTXC225, respectively, were obtained as shown in Figure 4b. In SCC6 cells percent survival rates of  $76.0 \pm 8.5$ ,  $93.0 \pm 4.9$ ,  $73.0 \pm 5.8$ , and  $46.0 \pm 4.5$  were observed for the same order of treatment (Figure 4c).

**Apoptosis Induction Studies.** The apoptotic activity of the conjugated drug in A431 cells, both at mole-corrected fixed concentrations of the conjugate and PTX,



**Figure 2.** MALDI-TOF MS of C225 (B) and PTXC225 conjugate (C). The increase in the MW confirms addition of the drug. Numbers shown refer to the center of the peaks. BSA (MW 66 kDa) was used as a MW calibrator. Peaks A and D are the doubly charged molecular ions displaying the half-MWs of B and C, respectively.



**Figure 3.** Inhibition of EGFR kinase activity. (a) A 24-h exposure of A431 cells to C225 or PTXC225 did not alter the EGFR protein levels. (b) EGF-activated EGF tyrosine kinase activity was similarly reduced by both C225 and PTXC225. The cells were treated with C225 and PTXC225, followed by treatment with either *anti*-EGFR (a) or *anti*-phosphotyrosine (b) antibodies. Antibody-free cells were used as controls. Sample cells were treated with equimolar concentrations of C225 and PTXC225.

and at increasing concentrations of the latter, were investigated. The constant-concentration experiment evaluated the effect of 3.3 nM each of C225 and the conjugate, 6.6 nM of the unconjugated PTX, and a mixture of C225+PTX (3.3 nM and 6.6 nM, respectively, for a PTX:C225 of 2). Induction of apoptosis was observed by PTXC225 in  $25\% \pm 2.2\%$  of the cells. As shown in Figure 5a, little or no enhancement in apoptosis induction was noted by the unconjugated PTX, the C225, or their mixture. The variable-concentration assay showed approximately 16.5 nM of the free drug was needed to induce apoptosis to a similar extent as did the PTXC225 conjugate at 3.2 nM (Figure 5b).

**Biodistribution Studies.** To assess the effect of conjugation and the presence of the drug moiety on the C225 tumor and normal tissue uptake, the biodistribution of the  $^{125}\text{I}$ -labeled conjugate ( $^{125}\text{I}$ -PTXC225) was compared to that of the  $^{125}\text{I}$ -C225. Radioiodination of both proteins through a standard protocol (37) afforded the labeled molecules as evidenced by radio-detected size-exclusion HPLC. The labeled MAb and the conjugate were injected iv into athymic nude mice carrying sc A431 xenografts, tissues were removed at 4 and 24 h postinjection, and the radioactivity uptake, in %ID/g (Figure 6) were measured. For both C225 and PTXC225, the normal tissue uptake decreased from 4 to 24 h while tumor uptake increases. The tumor concentrations of  $^{125}\text{I}$ -C225 was  $7.0 \pm 2.1$  and  $11.7 \pm 6.0$  at 4 and 24 h after injection, while the corresponding values for  $^{125}\text{I}$ -PTXC225 were  $6.3 \pm 1.8$  and  $7.1 \pm 3.6$ . The tumor %ID/g values for the conjugate and C225 were not significantly different ( $p$  values of 0.563 and 0.131, for 4 and 24 h, respectively). The blood concentrations of  $^{125}\text{I}$ -C225 were  $28.7 \pm 2.8$  and  $15.7 \pm 4.1$  at 4 and 24 h after injections, and the corresponding values for  $^{125}\text{I}$ -PTXC225 were  $20.8 \pm 2.9$  and  $10.8 \pm 2.4$ .

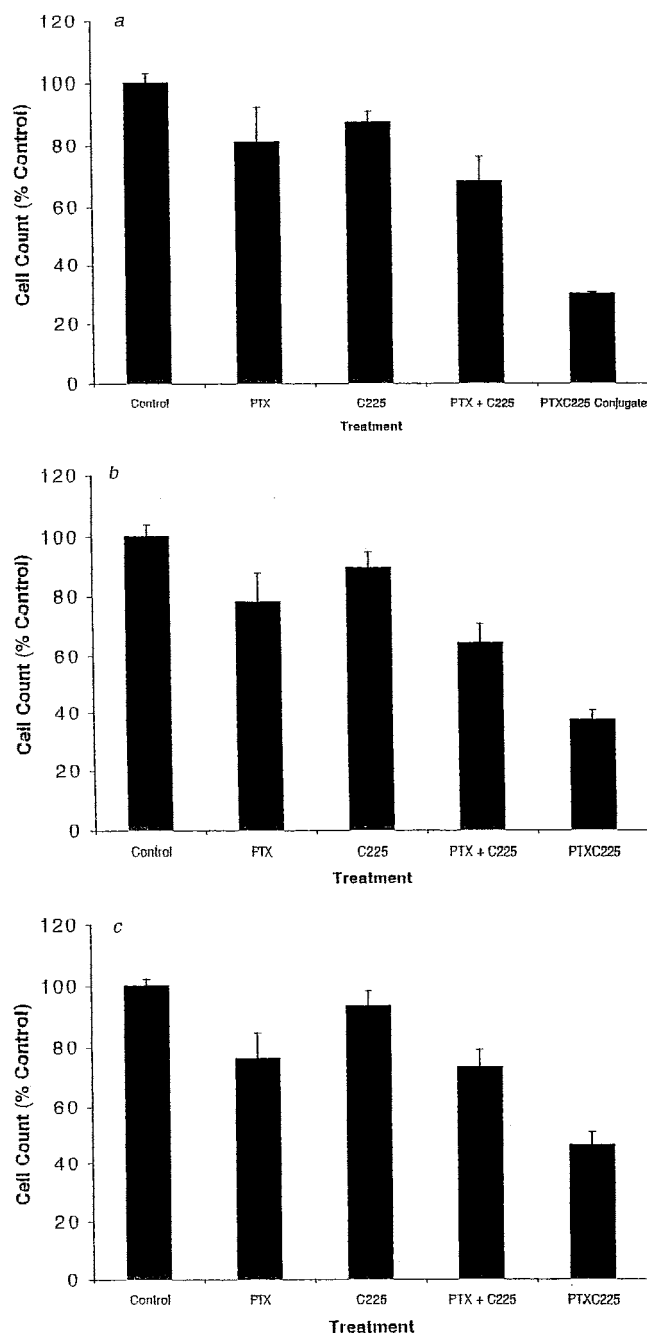
**Tumor Growth Inhibition Studies.** The tumor-inhibiting effect of the PTXC225 conjugate was examined in two groups of athymic nude female mice, implanted sc with A431 cells. The mice were treated with a single ip injection of saline, C225, or PTXC225 at equimolar amounts, and the tumor growth was monitored daily as shown in Figure 7. The summary statistics of change in tumor size from baseline by group and assessment day

are shown in Table 2. The trend in time for mean tumor size change in Group 1 was significantly larger than Group 3 ( $p = 0.0155$ ), but Group 2 was not significantly different from Group 3 ( $p = 0.720$ ).

## DISCUSSION

We report here a tumor-specific method of delivery of paclitaxel through covalent conjugation of the drug to a monoclonal antibody. The *anti*-EGFR MAb C225 used in this work is internalized into the cells after binding to EGFRs (39). We rationalized, therefore, that this clinically relevant MAb would be a suitable model in this study for internally delivering the drug which acts through a mitosis-directed mechanism. This conjugation also resulted in solubilization of the paclitaxel nucleus which suffers from an extremely low aqueous solubility ( $\approx 0.25$  mg/mL). It was found that conjugation of up to two PTX molecules per antibody keeps the drug completely solubilized in aqueous media at antibody concentrations usually used for in vitro and in vivo experiments. During the development of this work, we used conjugate solutions within a concentration range of 0.25–2.2 mg/mL. More recently, we have prepared completely soluble PTXC225 batches for therapy experiments in animal models with conjugate concentrations of up to 10 mg/mL (Safavy, A., unpublished results). Taxol solubility, however, seemed to be limited by the drug-to-antibody ratio, as a conjugate with a PTX:MAb ratio of more than 3, usually resulted in either immediate or delayed precipitation of the protein. On the other hand, a 2:1 molar ratio seemed to be sufficient for effective cell killing as demonstrated by the in vitro cytotoxicity experiments.

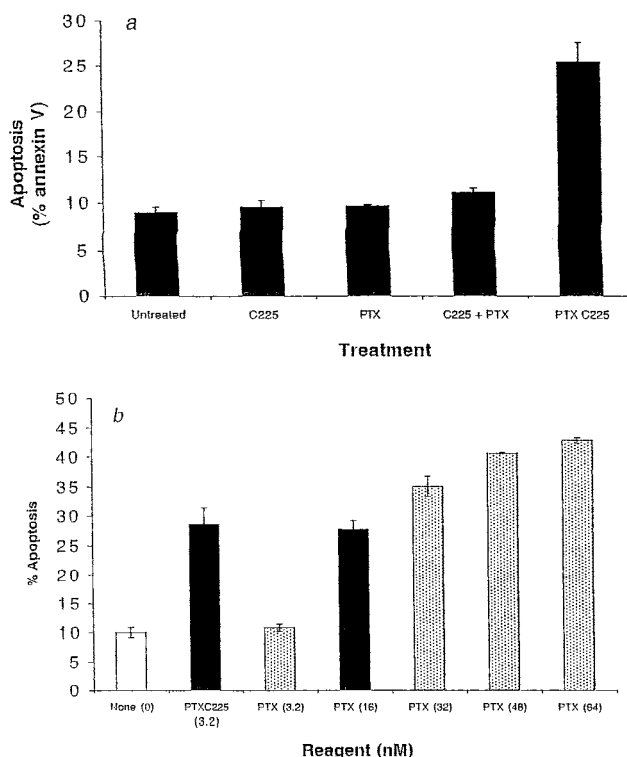
Because of reasons not clear at this time, the coupling of PTXSX to nucleophilic groups, such as amines, seemed to involve a highly reagent-selective mechanism. We examined several coupling reagents routinely used in peptide synthesis for amide bond formation (40), including DCC, DCC/HOBT, HBTU, BOP, and EEDQ, to couple this drug to the antibody. For each reagent, a two-step coupling reaction was carried out in which PTXSX was first activated and then added to C225 in basic buffer. The progress and the extent of the reaction were followed by MALDI MS (Figure 2), which from works reported



**Figure 4.** Inhibition of cell proliferation in (a) A431, (b) SCC-1, and (c) SCC-6. The cells were treated for 24 h with equimolar concentrations of PTX, C225, PTX + C225, and PTXC225. All cells were counted on day 4. Inhibition is represented as a measure of percent survival normalized against the untreated population. Each graph depicts three to four independent experiments done in quadruplicate with the mean  $\pm$  SEM plotted.

previously by our (41) and other (42) laboratories, is well established as a powerful, reliable, and most importantly, direct tool for the assessment of and monitoring reactions to attach small molecules to antibodies and other large proteins. With the exception of EEDQ, we could not detect a MW increase for C225 with any of the above coupling reagents. Since, at this time, only synthesis and biological evaluation of the PTXC225 were of interest, no in-depth mechanistic studies were carried out to uncover the reason for this observation at a molecular level.

Temperature did not seem to have any significant effect on the outcome of the PBS reaction. In the pH 9.1 carbonate, only small MW increases were observed



**Figure 5.** Induction of apoptosis by PTXC225. (a) Human A431 cells were treated with equimolar concentrations of PTX, C225, PTX+C225, and the PTXC225 for 24 h and analyzed on day 3. (b) To determine the approximate concentration of PTX which induces the same level of apoptosis as PTXC225, increasing concentrations of PTX were compared to a constant dose of PTXC225 within the same time frame as in part a.

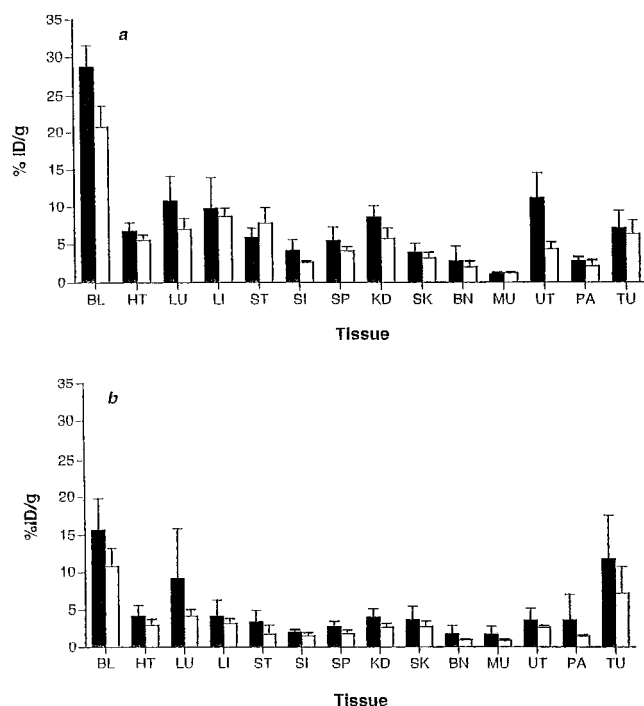
probably due to a fast decomposition of the PTX activated ester. The maximum increase in the MW occurred within 1 h from addition of the activated PTXSX and a longer reaction time did not have any effect on the extent of drug substitution.

On the basis of these observations, PTXSX-C225 coupling reactions in PBS (pH 8.1) and carbonate (pH 9.1) buffers, and at four PTXSX:C225 molar ratios, were studied (Table 1). When carried out at 0 °C and for 1 h, the 10:1 conjugation (Reaction 3, Table 1) showed a suitable drug-to-antibody ratio ( $2.2 \pm 0.2$ ). The criteria for selection of standard conditions (suitability) was based on the retention of the solubility of the antibody and preservation of its original antigen-binding properties. Later experiments determined that Reaction 3 (Table 1) could meet these criteria.

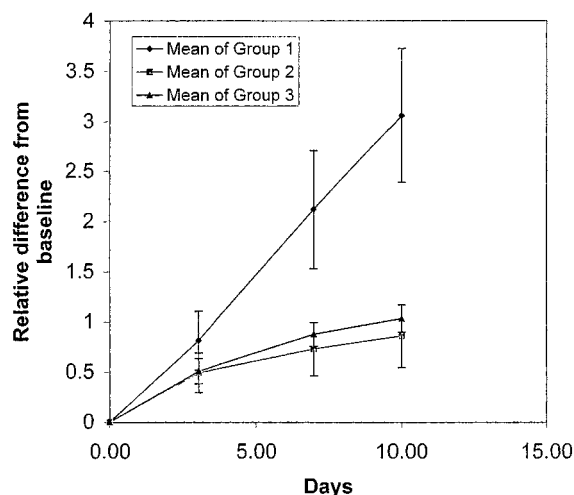
The physical identification of the drug–MAB conjugate is of critical importance, as an error in the measurement of the drug:MAB ratio will create errors in the calculation of the applied in vitro and in vivo doses, resulting in turn, in further complications such as low therapeutic indices or high toxicities. To this end, application of a direct method of measurement will have obvious advantages (42).

MALDI MS is a tool for direct MW analysis which yields a clear measure of substituent-to-MAB (S:A) ratio in real time (43) and has been used in the conjugation of small molecules to antibodies. In the development of a protocol for covalent attachment of unprotected hydroxamic acids to antibodies, we reported the application of this technique to optimize the reaction conditions and directly determine the S:A for the bifunctional chelating agent, trisuccin (41). Siegel et al. have used MALDI MS





**Figure 6.** Biodistribution of C225 (■) and PTXC225 (□) in nude mice bearing sc A431 xenografts. Bars show the uptake of each organ in %ID/g for  $^{125}\text{I}$ -C225 and  $^{125}\text{I}$ -PTXC225 at (a) 4 h, and (b) 24 h postinjection. Each tissue is abbreviated as follows: Blood, BL; heart, HT; lung, LU; liver, LI; stomach, ST; small intestine, SI; spleen, SP; kidney, KD; skin, SK; bone, BN; muscle, MU; uterus, UT; pancreas, PA; tumor, TU.



**Figure 7.** Tumor growth inhibition by a single injection of C225 and the PTXC225 conjugate. Female nude mice with sc A431 implants were given ip injections of saline, C225, or PTXC225 at a mg/kg body weight of 38.9 for C225 and 0.32 for PTX. Tumor sizes were monitored daily.

to determine the carbohydrate content as well as the S:A for metal chelators and anticancer drugs mitoxantrone, calicheamicin, and doxorubicin (42). It was shown in the present work also that MALDI MS was an unambiguous and efficient technique to evaluate the conditions for PTX-C225 conjugation and to directly measure the PTX:C225 ratios.

The efficiency of a drug-MAb conjugate in targeted drug delivery is, among other factors, determined by the preservation of antigen recognition of the MAb. The fact that the PTXC225 conjugate prepared by this method induced EGFR phosphorylation in A431 cells (Figure 3) and showed biodistribution patterns similar to that of

**Table 2.** Summary Statistics of Relative Change from Baseline for Tumor Size

group	day 3	day 7	day 10
1, saline ( $n = 6$ )	$0.8(\pm 0.3)^{ab}$	$2.1(\pm 0.6)$	$3.1(\pm 0.7)$
2, C225 ( $n = 6$ )	$0.5(\pm 0.2)$	$0.7(\pm 0.3)$	$0.9(\pm 0.3)$
3, PTXC225 ( $n = 5$ )	$0.5(\pm 0.1)$	$0.9(\pm 0.1)$	$1.0(\pm 0.1)$

<sup>a</sup> Entries refer to mean( $\pm$ standard error). <sup>b</sup> At day 3 for saline group, the summary statistics are based on  $n = 7$ .

the unconjugated C225 (Figures 6a and 6b) demonstrated that conjugation of up to two molecules of PTX per MAb did not affect the antibody-antigen binding site and that the conjugate was still capable of targeting PTX to EGFR-overexpressing tumors.

The in vitro cell proliferation of conjugated taxol was enhanced compared to the free drug. The fact that the enhancement in efficacy was due to a targeted delivery mechanism, and not from a synergistic interaction between paclitaxel and the MAb, was demonstrated by inclusion of a mixture of unconjugated paclitaxel and C225 which showed 56%, 42%, and 37% less growth inhibition against A431, SCC1, and SCC6 cells, respectively (Figures 4a-c).

Induction of apoptosis has been reported for taxanes and is another important feature of these drugs (44). It was demonstrated that the apoptosis-inducing effect of PTX is amplified by the antibody-mediated delivery of the drug whereas the unconjugated PTX, the C225, or their mixture, induced apoptosis in a negligibly small fraction of the cells (Figure 5a). Furthermore, to estimate the concentration of the free drug to produce the same apoptotic effect, a variable-concentration assay was also carried out. This experiment demonstrated that about a 5-fold molar increase in the concentration of PTX was required to induce apoptosis to the same extent as did the PTXC225 conjugate (Figure 5b).

As mentioned above, an important issue in the design of any tumor-directed drug conjugate is preservation of the receptor-recognizing ability of the targeting moiety and the effect of the drug conjugation on the in vivo biodistribution pattern of the molecule. These are important variables as a reduced receptor affinity will result in therapeutically insignificant tumor localization of the drug. At the same time, an impaired receptor recognition of the conjugate may increase the possibility of high normal tissue uptake, and thereby, high systemic toxicity.

To comply with these considerations, the biodistribution of radiolabeled C225 and PTXC225, in mice implanted sc with A431 cells, were studied at two time points (4 and 24 h). The conjugate displayed the same tissue uptake pattern as did C225, indicating that the chemistry of conjugation and the attachment of PTX to the MAb molecule did not significantly alter the biodistribution of the antibody (Figure 6).

The growth of A431 subcutaneous tumors was inhibited by both C225 and the conjugate (Figure 7). On day 10 postinjection the C225-treated mice (group 2) showed a growth inhibition of 41.2%, as compared to the saline-treated control (group 1), whereas the PTXC225-treated mice (group 3) showed an inhibition of 57%. Although growth inhibition induced by the conjugate was significant against the control group ( $p = 0.015$ ), it was not significantly different from that of the C225 group ( $p = 0.720$ ). Since the in vitro results clearly show an advantage for the antibody-mediated delivery of PTX, the lack of a significant difference between C225 and the conjugate in the in vivo model may be explained by either an insufficient dose of the drug, or an untimely release of

it, or both. It is also important to note that the equivalent dosage of PTX in the conjugate was only 346  $\mu\text{g}$  per kg of body weight which was administered in one single injection. This amount is far less than the usual therapeutic dosage ( $\approx 40$ –200 mg/kg) of other conjugates of this drug which are not tumor-directed (45–48). Furthermore, based on our earlier results, the succinate ester used here to link the PTX nucleus to C225, was anticipated to have suitable drug release kinetics; a PTX–PEG–peptide conjugate had shown a drug release half-life of about 113 min at 37 °C and in the presence of human plasma (30). It is possible, however, that this half-life is not long enough to survive the tumor localization time of C225. That is, by the time the PTXC225 conjugate, with a relatively large molecular weight, is localized in the tumor, a significant portion of the drug will have been already cleaved and lost. To this end, new linkers with expected improved release features have been designed and are under investigation. At this time, the tumor growth inhibition results reinforce those of the cytotoxicity and biodistribution experiments, in that the covalent attachment of PTX to the antibody does not remove its tumor binding and cytotoxicity properties.

The work reported in this article demonstrates the potential of tumor-directed drug delivery for the important taxane drugs, represented here by paclitaxel, and warrants further research toward the improvement of these conjugates. Such a strategy may imply the following benefits for this treatment modality: (1) Specific, therefore more efficient, delivery of the drug to primary, as well as micrometastatic tumors, (2) reduction of the administered doses due to the tumor-specific drug delivery, and thereby, lowering drug toxicity and side effects, (3) elimination of allergenic surfactants and excipients used in the current clinical formulations of taxanes, (4) a high-impact first-line therapy through targeted delivery of PTX may reduce the chances of drug resistance formation, spread of metastases, and side effects resulting from prolonged exposure of the patient to the drug, and (5) more economic formulation of the taxane drugs due to a lowered effective dose.

#### ACKNOWLEDGMENT

Assistance of the Department of Radiation Oncology, UAB, in the form of a Seed Grant is acknowledged. We would also like to thank Lori Coward and Marion Kirk (UAB Comprehensive Cancer Center Mass Spectroscopy Shared Facility) for their assistance in MW determinations. The assistance of Susanne H. Randall (tumor growth experiments) and Soneshia McMillan (manuscript preparation) are also acknowledged.

#### NOTE ADDED AFTER ASAP POSTING

The version of this paper posted January 28, 2003, had corrections omitted. These corrections are as follows: The contributing departments from the University of Alabama at Birmingham are the Departments of Radiation Oncology and Surgery. The value on line 13 of the abstract is  $25.2 \pm 2.2\%$ . The abbreviation for standard deviation of the mean is SDM. In the Experimental Section, under Animal Model, the number of viable cells is  $10^7$ . Also in the Experimental Section, under In Vivo Tumor Growth Inhibition Study, the units are micrograms: C225 (894  $\mu\text{g}$ ), PTXC225 (894  $\mu\text{g}$ ), (8.05  $\mu\text{g}$  PTX). In the caption of Figure 7, line 4, PTXC225 is actually PTX. On the same page, last paragraph, the text is changed to "...Figure 7). On day 10 postinjection, the C225-treated...". In Literature Cited, the authors of

reference 4 are Kohler, G., and Milstein, C. In reference 37, the compound name in the title is 1,3,4,6-tetrachloro-3 $\alpha$ ,6 $\alpha$ -diphenylglycouril. The corrected version of this paper was posted on February 5, 2003.

#### LITERATURE CITED

- (1) Arap, W., Pasqualini, R., and Ruoslahti, E. (1998) Cancer treatment by targeted drug delivery to tumor vasculature in a mouse model. *Science* 279, 377–380.
- (2) Arap, W., Pasqualini, R., and Ruoslahti, E. (1998) Chemotherapy targeted to tumor vasculature. *Curr. Opin. Oncol.* 10, 560–565.
- (3) Hong, F. D., and Clayman, G. L. (2000) Isolation of a peptide for targeted drug delivery into human head and neck solid tumors. *Cancer Res.* 60, 6551–6556.
- (4) Kohler, G. M., and Milstein, C. (1975) Continuous cultures of fused cells secreting antibody of predefined specificity. *Nature* 256, 495–497.
- (5) Kousparou, C. A., Deonarain, M. P., and Epenetos, A. A. (2000) Advances in tumour targeting. *J. Int. Soc. Tumour Target.* 1, 55–69.
- (6) Buchsbaum, D. J., and Lawrence, T. S. (1991) Tumor therapy with radiolabeled monoclonal antibodies. *Antibody Immunoconjugate Radiopharm.* 4, 245–272.
- (7) Safavy, A., and Buchsbaum, D. J. (2002) in *Drug Targeting in Cancer Therapy* (M. Pagé, Ed.) pp 257–275, The Human Press Inc., Totowa, NJ.
- (8) Stan, A. C., Radu, D. L., Casares, S., Bona, C. A., and Brumeanu, T. D. (1999) Antineoplastic efficacy of doxorubicin enzymatically assembled on galactose residues of a monoclonal antibody specific for the carcinoembryonic antigen. *Cancer Res.* 59, 115–121.
- (9) Florent, J. C., Dong, X., Gaudel, G., Mitaku, S., Monneret, C., Gesson, J. P., Jacquesy, J. C., Mondon, M., Renoux, B., Andrianomenjanahary, S., Michel, S., Koch, M., Tillequin, F., Gerken, M., Czech, J., Straub, R., and Bosslet, K. (1998) Prodrugs of anthracyclines for use in antibody-directed enzyme prodrug therapy. *J. Med. Chem.* 41, 3572–3581.
- (10) Shouval, D., Adler, R., Wands, J. R., Hurwitz, E., Isselbacher, K. J., and Sela, M. (1988) Doxorubicin conjugates of monoclonal antibodies to hepatoma-associated antigens. *Proc. Natl. Acad. Sci. U.S.A.* 85, 8276–8280.
- (11) Shih, L. B., Goldenberg, D. M., Xuan, H., Lu, H. W., Mattes, M. J., and Hall, T. C. (1994) Internalization of an intact doxorubicin immunoconjugate. *Cancer Immunol. Immunother.* 38, 92–98.
- (12) Rihova, B., Jelinkova, M., Strohalm, J., St'astny, M., Hovorka, O., Plocova, D., Kovar, M., Draberova, L., and Ulbrich, K. (2000) Antiproliferative effect of a lectin- and anti-Thy-1.2 antibody-targeted HPMA copolymer-bound doxorubicin on primary and metastatic human colorectal carcinoma and on human colorectal carcinoma transfected with the mouse Thy-1.2 gene. *Bioconjugate Chem.* 11, 664–673.
- (13) Hamann, P. R., Hinman, L. M., Hollander, I., Beyer, C. F., Lindh, D., Holcomb, R., Hallett, W., Tsou, H. R., Upešlaciš, J., Shochat, D., Mountain, A., Flowers, D. A., and Bernstein, I. (2002) Gemtuzumab ozogamicin, a potent and selective anti-CD33 antibody-calicheamicin conjugate for treatment of acute myeloid leukemia. *Bioconjugate Chem.* 13, 47–58.
- (14) Hamann, P. R., Hinman, L. M., Beyer, C. F., Lindh, D., Upešlaciš, J., Flowers, D. A., and Bernstein, I. (2002) An anti-CD33 antibody-calicheamicin conjugate for treatment of acute myeloid leukemia. Choice of linker. *Bioconjugate Chem.* 13, 40–46.
- (15) Safavy, A., Raisch, K. P., Waksal, H. W., Khazaeli, M. B., Buchsbaum, D. J., and Bonner, J. A. (2000) Synthesis, cytotoxicity evaluation, and biodistribution studies of a novel paclitaxel-MAb C225 conjugate. Proceedings of the Eighth Conference on Radioimmunodetection and Radioimmunotherapy of Cancer. *Cancer Biother. Radiopharm.* 15, 396.
- (16) Correa, J. J., and Pagé, M. (2002) Synthesis and evaluation of paclitaxel immunoconjugate with antitumor activity *in vitro*. *Tumor Targeting in Cancer Therapy* (M. Pagé, Ed.) pp 165–178, Humana Press, Totowa, NJ.

- (17) Guillemard, V., and Saragovi, H. U. (2001) Taxane-antibody conjugates afford potent cytotoxicity, enhanced solubility, and tumor target selectivity. *Cancer Res.* **61**, 694–699.
- (18) Dorr, R. T. (1994) Pharmacology and toxicology of Cremophor EL diluent. *Ann. Pharmacother.* **28**, S11–S14.
- (19) Sharma, A., Mayhew, E., Bolcsak, L., Cavanaugh, C., Harmon, P., Janoff, A., and Bernacki, R. J. (1997) Activity of paclitaxel liposome formulations against human ovarian tumor xenografts. *Int. J. Cancer* **71**, 103–107.
- (20) Rowinsky, E. K., and Donehower, R. C. (1995) Paclitaxel (taxol). *N. Engl. J. Med.* **332**, 1004–1014.
- (21) Roland, P. Y., Barnes, M. N., Niwas, S., Robertson, M. W., Alvarez, R., Austin, J. M., Kilgore, L. C., and Partridge, E. E. (1998) Response to salvage treatment in recurrent ovarian cancer treated initially with paclitaxel and platinum-based combination regimens. *Gynecol. Oncol.* **68**, 178–182.
- (22) Preston, N. J. (1996) Paclitaxel (Taxol): A guide to administration. *Eur. J. Cancer Care* **5**, 147–152.
- (23) Hajek, R., Vorlicek, J., and Slavik, M. (1996) Paclitaxel (Taxol): A review of its antitumor activity in clinical studies, Minireview. *Neoplasma* **43**, 141–154.
- (24) Postma, T. J., Vermorken, J. B., Liefting, A. J., Pinedo, H. M., and Heimans, J. J. (1995) Paclitaxel-induced neuropathy. *Ann. Oncol.* **6**, 489–494.
- (25) Maier-Lenz, H., Hauns, B., Haering, B., Koetting, J., Mross, K., Unger, C., Bauknecht, T., du Bois, A., Meerpohl, H. G., Hollaender, N., and Diergarten, K. (1997) Phase I study of paclitaxel administered as a 1-hour infusion: Toxicity and pharmacokinetics. *Semin. Oncol.* **24**, S19–16–S19–19.
- (26) Payne, J. Y., Holmes, F., Cohen, P. R., Gagel, R., Buzdar, A., and Dhingra, K. (1996) Paclitaxel: Severe mucocutaneous toxicity in a patient with hyperbilirubinemia. *South. Med. J.* **89**, 542–545.
- (27) Zimmerman, G. C., Keeling, J. H., Burris, H. A., Cook, G., Irvin, R., Kuhn, J., McCollough, M. L., and Von Hoff, D. D. (1995) Acute cutaneous reactions to docetaxel, a new chemotherapeutic agent. *Arch. Dermatol.* **131**, 202–206.
- (28) Llombart-Cussac, A., Pivot, X., and Spielmann, M. (1997) Docetaxel chemotherapy induces transverse superficial loss of the nail plate. *Arch. Dermatol.* **133**, 1466–1467.
- (29) Cortes, J. E., and Pazdur, R. (1995) Docetaxel. *J. Clin. Oncol.* **13**, 2643–2655.
- (30) Safavy, A., Raisch, K. P., Khazaeli, M. B., Buchsbaum, D. J., and Bonner, J. A. (1999) Paclitaxel derivatives for targeted therapy of cancer: Toward the development of smart taxanes. *J. Med. Chem.* **42**, 4919–4924.
- (31) Safavy, A. (2001), Taxane Derivatives for Targeted Therapy of Cancer. U.S. Patent 6191290.
- (32) Goldstein, N. I., Prewett, M., Zuklys, K., Rockwell, P., and Mendelsohn, J. (1995) Biological efficacy of a chimeric antibody to the epidermal growth factor receptor in a human tumor xenograft model. *Clin. Cancer Res.* **1**, 1311–1318.
- (33) Naramura, M., Gillies, S. D., Mendelsohn, J., Reisfeld, R. A., and Mueller, B. M. (1993) Therapeutic potential of chimeric and murine anti-(epidermal growth factor receptor) antibodies in a metastasis model for human melanoma. *Cancer Immunol. Immunother.* **37**, 343–349.
- (34) Deutsch, H., Glinski, J., Hernandez, M., Haugwitz, R., Narayanan, V., Suffness, M., and Zalkow, L. (1989) Synthesis of congeners and prodrugs: Water soluble prodrugs of taxol with potent antitumor activity. *J. Med. Chem.* **32**, 788–792.
- (35) Lowry, O. H., Rosebrough, N. J., Farr, A. L., and Randall, R. J. (1951) Protein measurement with the folin phenol reagent. *J. Biol. Chem.* **193**, 265–275.
- (36) Saleh, M. N., Raisch, K. P., Stackhouse, M. A., Grizzle, W. E., Bonner, J. A., Mayo, M. S., Kim, H.-G., Meredith, R. F., Wheeler, R. H., and Buchsbaum, D. J. (1999) Combined modality therapy of A431 human epidermoid cancer using anti-EGFR antibody C225 and radiation. *Cancer Biother. Radiopharm.* **14**, 451–463.
- (37) Fraker, P. J., and Speck, J. C. (1978) Protein and cell membrane iodinations with a sparingly soluble chloroamide, 1,3,4,6-tetrachloro-3 $\alpha$ ,6 $\alpha$ -diphenylglycoluril. *Biochem. Biophys. Res. Commun.* **80**, 849–857.
- (38) SAS Institute Inc., SAS User's Guide, Version 8, Cary, NC, 1999.
- (39) Fan, Z., Lu, Y., Wu, X., and Mendelsohn, J. (1994) Antibody-induced epidermal growth factor receptor dimerization mediates inhibition of autocrine proliferation of A431 squamous carcinoma cells. *J. Biol. Chem.* **269**, 27595–27602.
- (40) Lloyd-Williams, P., Albericio, F., and Giralt, E. (1997) *Chemical approaches to the synthesis of peptides*, CRC Press, Boca Raton, FL.
- (41) Safavy, A., Khazaeli, M. B., Kirk, M., Coward, L., and Buchsbaum, D. J. (1999) Further studies on the protein conjugation of hydroxamic acid bifunctional chelating agents: Group-specific conjugation at two different loci. *Bioconjugate Chem.* **10**, 18–23.
- (42) Siegel, M. M., Hollander, I. J., Hamann, P. R., James, J. P., Hinman, L., Smith, B. J., Farnsworth, A. P. H., Phipps, A., King, D. J., Karas, M., Ingendoh, A., and Hillenkamp, F. (1991) Matrix-assisted UV-laser desorption/ionization mass spectrometric analysis of monoclonal antibodies for the determination of carbohydrate, conjugated chelator, and conjugated drug content. *Anal. Chem.* **63**, 2470–2481.
- (43) Fenselau, C. (1997) MALDI MS and strategies for protein analysis. *Anal. Chem.* **69**, 661A–665A.
- (44) Wang, T. H., Wang, H. S., and Soong, Y. K. (2000) Paclitaxel-induced cell death: where the cell cycle and apoptosis come together. *Cancer* **88**, 2619–2628.
- (45) Li, C., Yu, D., Inoue, T., Yang, D. J., Milas, L., Hunter, N. R., Kim, E. E., and Wallace, S. (1996) Synthesis and evaluation of water-soluble poly(ethylene glycol)-paclitaxel conjugate as a paclitaxel prodrug. *Anticancer Drugs* **7**, 642–648.
- (46) Pendri, A., Conover, C. D., and Greenwald, R. B. (1998) Antitumor activity of paclitaxel-2'-glycinate conjugated to poly(ethylene glycol): a water-soluble prodrug. *Anticancer Drug Des.* **13**, 387–395.
- (47) Li, C., Yu, D. F., Newman, R. A., Cabral, F., Stephens, L. C., Hunter, N., Milas, L., and Wallace, S. (1998) Complete regression of well-established tumors using a novel water-soluble poly(L-glutamic acid)-paclitaxel conjugate. *Cancer Res.* **58**, 2404–2409.
- (48) Rose, W. C., Clark, J. L., Lee, F. Y., and Casazza, A. M. (1997) Preclinical antitumor activity of water-soluble paclitaxel derivatives. *Cancer Chemother. Pharmacol.* **39**, 486–492.



# Nanoparticulate DNA Packaging Using Terpolymers of Poly(lysine-*g*-(lactide-*b*-ethylene glycol))

Susan Park<sup>†,‡</sup> and Kevin E. Healy<sup>\*,†</sup>

University of California at Berkeley, Departments of Bioengineering and Materials Science and Engineering, 459 Evans Hall, Berkeley, California 94720-1762, and Northwestern University, Department of Biomedical Engineering, McCormick School of Engineering and Applied Science, 2145 Sheridan Rd., Tech E310, Evanston, Illinois 60208. Received October 8, 2002; Revised Manuscript Received January 9, 2003

Terpolymers of poly(lysine-*g*-(lactide-*b*-ethylene glycol)) (pK-pLL-pEG) were synthesized by using ring-opening polymerization and functional end-group grafting. Synthesis was characterized with gel permeation chromatography, proton nuclear magnetic resonance spectroscopy, and a trinitrobenzene sulfonic acid binding assay. Polymer association behavior with DNA was investigated using an ethidium bromide exclusion assay, static light scattering, and scanning electron microscopy. Polylactide molecular weight was varied to investigate its impact on DNA association and resulting complex characteristics. Polylysine ( $M_w = 8800$ , DP = 42) modified with either 7400 or 10 870  $M_w$  pLL-pEG reduced the minimum amount of primary amines necessary for complete condensation by 23% and 48%, respectively, compared to unmodified polylysine (pK42). Complexes formed with the highest molecular weight terpolymer demonstrated significantly ( $p < 0.1$ ) greater resistance to DNase I than lyophilized pK42-DNA particles. This study suggests that modification of pK42 with pLL-pEG diblock copolymers impacts polylysine's associative and binding behavior to DNA and resulting particle characteristics. Modulation of terpolymer composition in complexes can enable control over intracellular plasmid dissociation rates to improve transfection efficiency.

## INTRODUCTION

Gene therapy is one field that has exploited spontaneous polycation assembly with DNA as an alternative to packaging plasmids within either viral vectors or liposomes. Some of these systems include those based on polyamidoamines (dendrimer), polyacrylates, polyamino acids, and polyethyleneimine (1–4). Recent investigations have found that the gross morphology of condensates is surprisingly insensitive to large variances in polymer microarchitecture as well as DNA size, within 400 to 1 million base pairs (1, 5, 6). However, there is some evidence that polycation associative behavior can vary according to the form of DNA present (7). Free DNA that has a hydrodynamic radius on the order of microns can be condensed into complexes by highly branched polymers (e.g., polyethyleneimine) as well as more simple multivalent cations (e.g.,  $\text{Co}(\text{NH}_3)_6^{3+}$ ). The resulting particles are consistently on the order of 50–300 nm in diameter and can often appear as torroids, rods, and large aggregates; however, the predominance of each is affected by condensation parameters as well as polymer composition (1, 8).

The type of polycation used can have a dramatic effect on cytotoxicity, cellular response, and intracellular trafficking of the complexes (9–11). Two polymers that have generated the most publications in the literature are polyethyleneimine (pEI) and polylysine (pK). Polyethyleneimine is a polymer that can be found in linear or in hyperbranched form. The latter contains 1°, 2°, and 3° amines at a respective ratio of 1:2:1. The different  $pK_a$ 's

of the amines on branched pEI give it an usually high buffering capacity across a wide pH range as well as the ability to effectively condense DNA employing its protonated amines (1). Both forms of pEI have been shown to exhibit high levels of transfection (4, 11–14). It has been hypothesized that pEI's high transfection efficiency can be attributed to its large buffering capacity that neutralizes lysosomal pH and induces lysis via the resulting change in ionic osmolarity (14, 15). Unfortunately, pEI's membrane permeabilizing ability has raised concern about its cytotoxicity under conditions necessary for transfection (16, 17). Even though pEI is considerably less toxic when associated with DNA, it is not degradable, and its intracellular fate, as well as any other long-term implications on normal cellular transcriptive processes, is not yet known.

Polylysine (pK) is a polyamino acid that possesses side chains with terminal amines, which are protonated at physiological pH. It is an attractive option for gene therapy techniques since it is synthesized from a non-cytotoxic, naturally occurring monomer. The molecular weight of pK has some effect on particle diameter, with the smallest pK (DP = 19) forming particles of about 30 nm in diameter and the largest (DP = 1075) forming complexes about 120–300 nm (18). However, time-resolved static light scattering investigation of high molecular weight pK-DNA complexes revealed that they can aggregate into supramolecular particles of several micrometers in diameter (19). Furthermore, the molecular weight of polylysine used can have a significant effect on cell toxicity, transfection efficiency, and biodistribution (20).

The tenacity of electrostatic association between DNA and polycations should be considered when developing synthetic vectors for gene therapy. It has been shown that

\* To whom correspondence should be addressed. kehealy@scriates.berkeley.edu.

<sup>†</sup> University of California at Berkeley.

<sup>‡</sup> Northwestern University.

increasing pK molecular weight interfered with in vitro RNA transcription and was associated with a decrease in plasmid unpackaging rates as well as a protracted reporter expression (21, 22). In addition, higher transfection efficiencies were observed when 40% of the  $\epsilon$ -amines on pK were neutralized with sugar residues when compared to unsubstituted pK (23, 24).

Overall, pK has been shown to be a less effective transfection vehicle compared to PEI. Observations on intracellular trafficking of pK-plasmid complexes indicate that they are sequestered into endosomes and nuclear localization is not as prevalent when compared to complexes formed with PEI (9, 21). However, functionalization of pK with targeting ligands that induce receptor-mediated endocytosis can improve transfection efficiency significantly (22, 25, 26). In addition, reporter expression levels can be increased dramatically by conjugating fusogenic peptides derived from virus glycoproteins. These pH responsive peptides undergo a conformational change in acidic pH and then can disrupt lysosomal membranes (27–29). Other agents that combat endosomal degradation, such as chloroquine or hemolytic polymers, can be added to abet transfection (2, 30).

Block or graft copolymers have also been investigated with respect to their interaction with DNA and have often employed hydrophilic moieties to disguise complexes from recognition and subsequent sequestration by the reticuloendothelial system. When poly(ethylene glycol) (pEG) was bound to various polycations, the resulting complexes demonstrated improved colloidal stability and extended in vivo circulation lifetimes (17, 25, 31–34). The benefit of coupling pEG is not only due to greater particle hydrophilicity, but also diminished protein adsorption that activates phagocytosis.

To address some of the aforementioned issues, we have developed a polylysine-based ( $M_w = 8800$ , DP = 42) terpolymer grafted with diblock polymer components. A terminal pEG segment ( $M_w = 3400$ ) was employed to improve complex stability as well as to provide end-group functionality for conjugation of bioactive molecules, such as targeting ligands and fusogenic peptides that increase transfection specificity and efficiency. The intermediate segment of our terpolymer is a hydrolytically labile poly-L-lactide (pLL) block, which is intended to aid in protection of DNA from intracellular degradation as well as to promote premature DNA condensation through hydrophobic interactions. We hypothesize that a reduction in the amount of lysine moieties required for complete condensation will increase the rate of DNA unpackaging that is necessary for plasmid transcription. DNA release will also be contingent on the rate of pLL degradation and could possibly enable tailoring of transfection profiles by modulating the molecular weight of the pLL and/or pK segments. This investigation focuses on the synthesis and characterization of pK-pLL-pEG terpolymers as well as its interaction with plasmid DNA. The molecular weight of the pLL segment was varied to assess its impact on terpolymer association and complex characteristics.

## MATERIALS AND METHODS

A heterofunctional poly(ethylene glycol) ( $\text{NH}_2$ -pEG-OH,  $M_w = 3400$ ) bearing a terminal amino and hydroxyl group was purchased from Shearwater Corporation (Huntsville, AL). All other chemicals were purchased from Sigma-Aldrich (St. Louis, MO) and were used as received unless otherwise noted. The DNA used was

supercoiled  $\Phi$ X174 RF DNA (5386 bp) from Promega (Madison, WI).

**PEG Functionalization.** The amino end of 3400  $M_w$   $\text{NH}_2$ -pEG-OH was protected by reaction with a 6 molar excess of *N*-(9-fluorenylmethoxycarbonyloxy)succinimide (osu-fmoc) in dioxane for 4 h. The resulting fmoc-pEG was purified by repeated precipitation into cold ether until the characteristic succinimidyl proton peak at 2.82 ppm (in  $\text{CDCl}_3$ ) was undetectable by proton nuclear magnetic resonance spectroscopy ( $^1\text{H}$  NMR, Bruker AMX300). Percent substitution was calculated using the ratio of the fmoc doublet at 7.88–7.90 ppm with respect to the pEG peak at 3.63 ppm (in  $\text{CDCl}_3$ ). The polymer was dried under vacuum overnight.

**Diblock Copolymer Synthesis and Characterization.** L-Lactide was purified by recrystallization from toluene and dried under vacuum for 1 h immediately before use. A 0.5M stock solution of stannous octoate in anhydrous toluene was prepared and used at a constant lactide monomer:initiator ratio (M/I) of 300. The L-lactide and fmoc-pEG were reacted at monomer:hydroxyl (M/OH) ratios of 40 and 75 to control pLL molecular weight. To produce the diblock copolymer of lowest molecular weight, a M/OH of 75 was used and the reaction stopped after 2 h. A 20% w/v solution of the above reactants in anhydrous toluene was prepared in a sealed reaction vessel in a dry nitrogen atmosphere. Polymerization of L-lactide proceeded under refluxing toluene at 100 °C under a gentle flow of dry nitrogen for 6 h. The copolymer (pLL-pEG-fmoc) was purified by repeated dissolution in dioxane and precipitation into cold ether. Molecular weight characterization by size exclusion chromatography with multiangle laser light scattering (SEC-MALLS) was performed using an Agilent 1100 HPLC with 2 Polymer Laboratories mixed E columns in series and methylene chloride as the mobile phase. The detectors used included a multi-angle light scattering detector, refractive interferometer (Wyatt Technology Corporation, Santa Barbara, CA) and a photodiode array detector (Agilent Technologies, Mountainview, CA). The  $dn/dc$  values for each copolymer in methylene chloride were determined experimentally using a refractive interferometer (Wyatt). For comparison, proton nuclear magnetic resonance spectroscopy ( $^1\text{H}$  NMR) was also used to calculate molecular weight by using the known molecular weight of pEG as an internal standard.

The hydroxyl on the polylactide end of the diblock copolymer was then functionalized to be amine reactive (su-pLL-pEG-fmoc). Disuccinimidyl carbonate (DSC) (0.5M) and 4-dimethyl aminopyridine (DMAP) (0.5M) at a 6 molar excess in anhydrous dimethylformamide was added to the copolymer dissolved in anhydrous dioxane. The solution was stirred for 6 h under a dry nitrogen atmosphere and purified by precipitation into cold ether until the aromatic DMAP protons (in  $\text{CDCl}_3$ ) at 6.45 and 8.20 ppm disappeared. Percent substitution was calculated using the ratio of the reappeared succinimidyl peak area at 2.82 ppm to that of pEG at 3.63 ppm (in  $\text{CDCl}_3$ ).

**Terpolymer Synthesis and Characterization.** The terpolymer of poly(lysine-*g*-(lactide-*b*-ethylene glycol)) was synthesized by coupling of su-pLL-pEG-fmoc to the  $\epsilon$ -amines on poly-L-lysine (pK) ( $M_w = 8800$ , DP 42) at a 1:1 molar ratio in dimethyl sulfoxide. The nomenclature for the resulting terpolymers is pK42-Xk, where pK with a degree of polymerization of 42 has been grafted to a pLL-pEG diblock copolymer with a combined molecular weight of approximately X000.

Proton NMR in DMSO- $d_6$  was used to determine the amount of pK present in each terpolymer. For comparison, a binding assay using trinitrobenzyl sulfonic acid (TNBS) was performed using a modified standard protocol (35). In short, the copolymer was dissolved in DMSO (1 or 2 mg/mL) and reacted with an excess of TNBS in an overall reaction solution of 75% DMSO and 25% sodium bicarbonate buffer (pH 8.5). The reaction was performed at 37 °C for 1 h, after which 6M HCl was immediately added. The solution absorbance was then read at 436 nm and the amount of  $\epsilon$ -amines per milligram of polymer was calculated using a calibration curve made with known amounts of pK42.

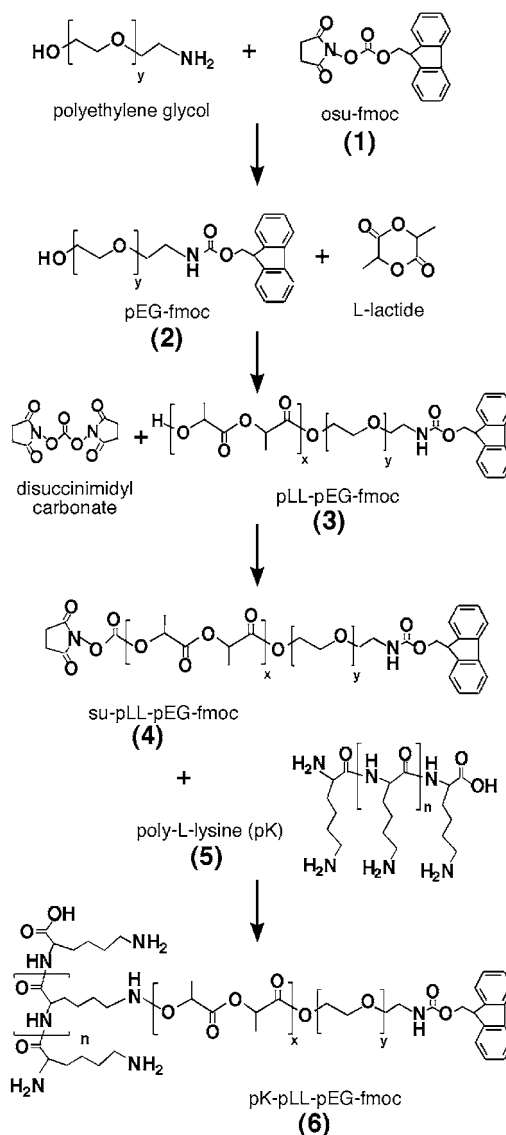
**Particle Formation and Characterization.** *Complex Formation.* Complexes were formed by adding a pK or pK–pLL–pEG in DMSO to approximately 5  $\mu$ g of DNA in ultrapure water (UPW, 18 M $\Omega$  cm) in Teflon vials. The total volume of DMSO used was kept below 10% v/v to minimize solvent effects on condensation (8). After 20 min, an additional volume of water was added, and the solutions were lyophilized. Complexes were resuspended in UPW for further characterization unless otherwise noted.

*Degree of Condensation.* Ethidium bromide (EB) was used as an indicator of condensation since it becomes intensely fluorescent upon intercalating with free DNA but cannot bind to condensed DNA (36). Particles were made and resuspended as described above, mixed with 1mM EB, and read in a black 96 well plate using a microplate fluorimeter (Molecular Devices, Sunnyvale, CA) (ex: 339 nm, em: 610 nm, cutoff: 515 nm). The autofluorescence of free EB was subtracted from each sample value and then normalized to the maximum fluorescence obtained for DNA with no polymer added. DNA condensation was considered to be complete when the percent relative fluorescence units (RFU) reached background levels.

*Determination of complex apparent  $M_w^*$  and  $r_g^*$ .* Static light scattering of complexes was performed using a multiangle light scattering detector (Wyatt) in microbatch mode to assess particle apparent molecular weight ( $M_w^*$ ) and apparent radius of gyration ( $r_g^*$ ). The UPW mobile phase was filtered with 0.02  $\mu$ m syringe filters, and light scattering measurements were obtained every 2 s using a flow rate of 0.2 mL/min. Sample dilutions were carefully made by weight, and the final concentration was considered to be the total amount of DNA plus polymer. The data used for analysis was limited to that from seven low-angle detectors (36–90°), since these low angles are the most critical to obtain the apparent molecular weight and  $r_g^*$  of complexes. The lowest measurable angles at 14° and 26° were excluded since low-angle detectors were the most sensitive to contaminating particles and were easily saturated. Samples were run in triplicate, and each run produced at least 20 data points. Only those data with a Debye fit of less than 10% error were used for further analysis. Complexes were also visualized by cold field emission scanning electron microscopy (Hitachi S-5000) using an accelerating voltage of 5kV. Samples were prepared by depositing drops of resuspended particles onto silicon wafers, freeze-drying and coating with 8–10 nm of carbon.

*Resistance to DNase Degradation.* The ability of particles to resist degradation by bovine pancreatic DNase I was assessed by agarose gel electrophoresis. Particles were made as described above except at a 5-fold increase in concentration and then evenly aliquoted into microvials before lyophilization. Dulbecco's complete phosphate buffered saline (PBS, Gibco BRL) was used for

# Scheme 1. Synthesis of pK–pLL–pEG Terpolymers

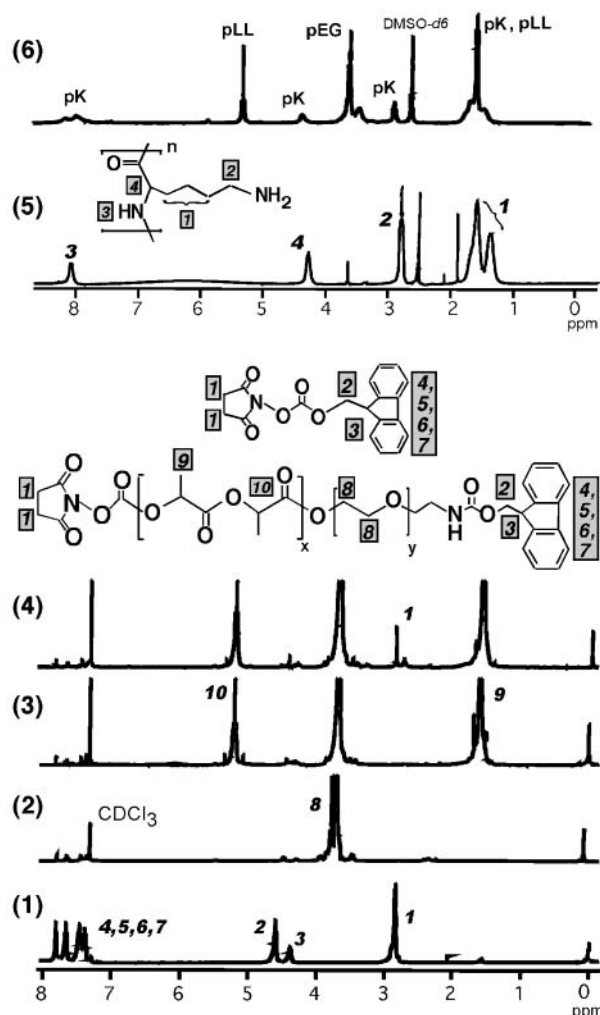


resuspension, and 2.5 units of DNase I (Pharmacia, Piscataway, NJ) were added for varying amounts of time. The reaction was stopped with 2 or 3  $\mu$ L of 6N NaOH/0.5M EDTA and run on a 0.8% agarose gel for 40 min at 4.0V/cm. The running buffer was an alkaline 20mM tris-acetate solution with 1mM EDTA (pH 12). The DNA was visualized by staining with 0.5 $\mu$ g/mL ethidium bromide in 1X TAE buffer for 20 min and subsequent destaining for 15 min. The gels were then stained with 0.1% Coomassie Brilliant Blue in UPW, methanol, glacial acetic acid (5:4:1 v/v/v) for 4 min and destained overnight in a solution mixed at a ratio of 15:4:1, respectively. Scanalytics gel analysis software was used on digital gel images to determine the extent of DNA degradation for each well. Since DNA concentration is proportional to fluorescence intensity, the amount of intact DNA was considered to be the intensity area that did not migrate past the negative control (0 min.). The value was then normalized to the total intensity in the lane (intact + degraded) in order to compensate for unavoidable fluctuations in sample loading concentration.

## RESULTS

**Synthesis Characterization.** The synthesis is depicted in Scheme 1, and its progression and purification

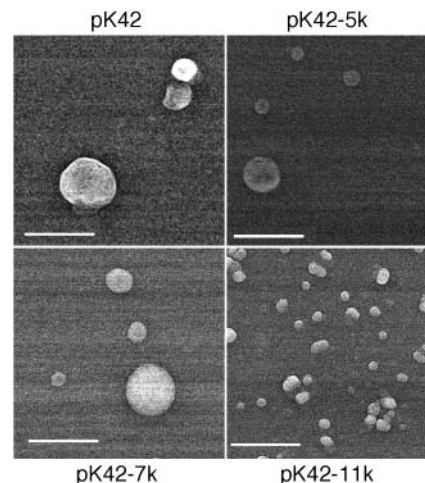




**Figure 1.** Representative proton nuclear magnetic resonance spectra of pK42-7k used to monitor the progression, purification and degree of end-group substitution after each reaction step. Spectra 1-6 correspond to the molecules numbered in Scheme 1. Peak shifts for spectra 1-4 ( $\text{CDCl}_3$ ): 1, 2.82 (s, 4H); 2, 4.56 (d, 2H); 3, 4.33 (t, 1H); 4, 7.77 (d, 2H); 5, 7.62 (d, 2H); 6, 7.42 (t, 2H); 7, 7.35 (t, 2H); 8, 3.63 (s, 4H); 9, 1.56 (d, 3H); 10, 5.13 (q, 1H). Peak shifts for spectrum 5 ( $\text{DMSO}-d_6$ ): 1, 1.56 (s, 4H) & 1.33 (s, 2H); 2, 2.76 (s, 2H); 3, 8.05 (d, 1H); 4, 4.25 (s, 1H).

was monitored primarily by proton NMR characterization after each step (Figure 1). The characteristic proton peaks for osu-fmoc are shown in spectrum 1, and after coupling to the terminal amine of  $\text{NH}_2\text{-pEG-OH}$ , the characteristic ether peak appeared at 3.63 ppm (spectrum 2, peak #8). The disappearance of the succinimidyl peak at 2.82 ppm indicated that unreacted osu-fmoc was removed and the degree of fmoc substitution on pEG was assessed to be above 85% (data not shown). Varying the lactide monomer:pEG hydroxyl ratio for ring opening polymerization or the reaction time easily enabled control over the pLL segment length. Lactide polymerization was indicated by shifts in its methine (from 5.02 to 5.13 ppm) and methyl (from 1.62 to 1.56 ppm) groups (spectrum 3). Succinimidyl functionalization of pLL-pEG-fmoc resulted in the reappearance of a peak at 2.82 ppm (spectrum 4, peak #1). Spectra of the final terpolymer after grafting su-pLL-pEG to pK revealed all relevant peaks after purification (spectrum 6).

There was good corroboration between molecular weight data obtained by  $^1\text{H}$  NMR using the known molecular weight of pEG as an internal standard and SEC-MALLS



**Figure 2.** Cold field emission scanning electron microscopy on complexes coated with  $\sim 10$  nm carbon. Complexes were made at an amine to phosphate charge ratio (N:P) of 1.0. The scale bars equal 500 nm in all images.

**Table 1. Diblock Mw Results**

pLL-pEG	$^1\text{H}$ NMR (g/mol)	MALLS (g/mol)	PDI
5k	3692	5800	1.02
7k	7648	7628	1.02
11k	11094	10440	1.06

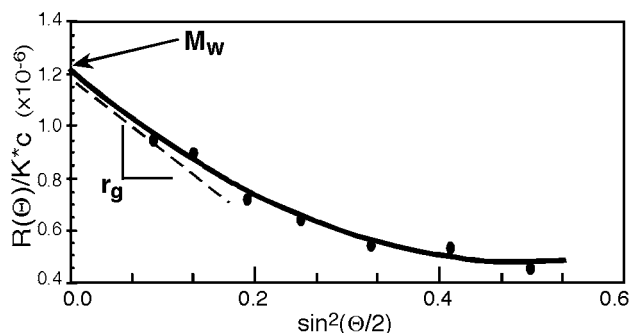
**Table 2.  $1^\circ$  Amine Content and Ethidium Bromide Assay Results**

	$\mu\text{mol NH}_2/\text{mg polymer}$ [% subst]		
	TNBS	$^1\text{N}$ NMR	N:P <sub>min</sub>
pK42	—	—	0.81
pK42-5k	$3.55 \pm 0.20$	3.20 [1.8%]	0.91
pK42-7k	$1.99 \pm 0.15$	1.81 [4.3%]	0.62
pK42-11k	$1.00 \pm 0.09$	1.05 [6.7%]	0.42

(Table 1). Polydispersity indices for all pLL-pEG diblocks were below 1.1, and a peak corresponding to unreacted pEG-fmoc was not revealed by any of the three detectors (data not shown). The TNBS binding assay, developed to determine the amount of amines present in the pK-pLL-pEG terpolymer, agreed very well with data obtained with  $^1\text{H}$  NMR (Table 2). Results from  $^1\text{H}$  NMR were used to calculate the amount of amines added for all subsequent DNA condensation experiments.

**Minimum Amine:Phosphate Charge Ratio Determination.** The progression of DNA condensation was studied by measuring the relative EB fluorescence. The minimum polymer amine:DNA phosphate charge ratio (N:P<sub>min</sub>) necessary for complete condensation is summarized in Table 2. Polylysine (pK42) was able to condense DNA at a N:P<sub>min</sub> of 0.81, while pK42-5k required a slightly higher N:P<sub>min</sub> of 0.91. However, when larger pLL segments were present in pK42-7k and pK42-11k, the N:P<sub>min</sub> decreased substantially to 0.62 and 0.42, respectively. Scanning electron micrographs revealed heterogeneous submicron complexes where the population size varied between 50 and 500 nm (Figure 2). The carbon coating did not seem to severely obstruct morphology since samples with thinner ( $\sim 1$  nm) platinum coatings showed similar images with a backscattering detector (not shown).

**Static Light Scattering of Complexes.** Static light scattering investigation of complexes provided information about the apparent  $M_w^*$  and radius of gyration ( $r_g^*$ ) by measuring the excess Rayleigh ratio ( $R_e$ ) values



**Figure 3.** A representative Debye fit to static light scattering data used to calculate apparent  $M_w^*$  and  $r_g^*$  of complexes. This plot is for pK42–11k complexes (N:P = 0.5) where  $M_w^* = (1.216 \pm 0.064) \times 10^6$  g/mol and  $r_g^* = 112.5 \pm 9.3$  nm.

scattered from particle solutions and fitting a second-order Debye curve at zero concentration limits according to the following relation:

$$\frac{R_\theta}{K^*c} = M_w P(\theta) \quad (1)$$

where

$$K^* = \frac{4\pi^2 n^2 \left(\frac{dn}{dc}\right)^2}{\lambda^4 N_A}$$

The particle scattering function,  $P(\theta)$ , is defined by

$$P(\theta) = 1 - \alpha_1 \left(\frac{4\pi}{\lambda} \sin \theta/2\right)^2 + \alpha_2 \left(\frac{4\pi}{\lambda} \sin \theta/2\right)^4 - \dots \quad (2)$$

where the coefficient  $\alpha_x$  is proportional to  $\int r^{2x} dM$  and is relevant to particle shape. The root-mean-square radius ( $\langle r_g^2 \rangle$  or rms) of the molecule can be derived from

$$\langle r_g^2 \rangle = 3\alpha_1$$

The concentration ( $c$ ) and angle of measurement ( $\theta$ ) are known parameters, while  $K^*$  contains constants for incident light wavelength ( $\lambda$ ), solvent refractive index ( $n$ ) and Avogadro's number ( $N_A$ ). The refractive index increment ( $dn/dc$ ) for each component in UPW was measured experimentally, except for pLL, which was estimated to have a  $dn/dc$  value approximately equal to that of pEG due to their similar indices of refraction (data not shown). The overall  $dn/dc$  values for particles of varying compositions were calculated using the relation:  $dn/dc_{\text{total}} = \sum x_i (dn/dc)_i$  where  $x_i$  denotes the weight percent of species  $i$ . When eq 1 is plotted as  $R_\theta/K^*c$  versus  $\sin^2(\theta/2)$ , the molecular weight ( $M_w$  or  $M_w^*$ ) can be calculated by extrapolation of the curve to zero angle, and the radius of gyration ( $r_g$  or  $r_g^*$ ) is determined by the initial slope. Figure 3 illustrates a typical Debye plot for pK42–11k (N:P = 0.5) used to determine the apparent  $M_w^*$  and  $r_g^*$ .

Analysis of the naked  $\Phi$ X174 plasmid resulted in values of 135 nm for  $r_g^*$  and  $3.57 \times 10^6$  D for  $M_w^*$ , which agreed extremely well with the theoretical value of  $3.55 \times 10^6$  D when using the common conversion of  $6.6 \times 10^5$  D = 1 kbp (37). Particles made with pK42 showed an order of magnitude increase in apparent  $M_w^*$  at low charge ratios (Figure 4a). When condensation was complete, as indicated by the accompanying EB curve (% RFU), the apparent  $M_w^*$  decreased dramatically. Values for  $r_g^*$  generally remained stable despite the fact that a decrease was expected. Particles made with each of the terpolymers did not show as extreme an increase in

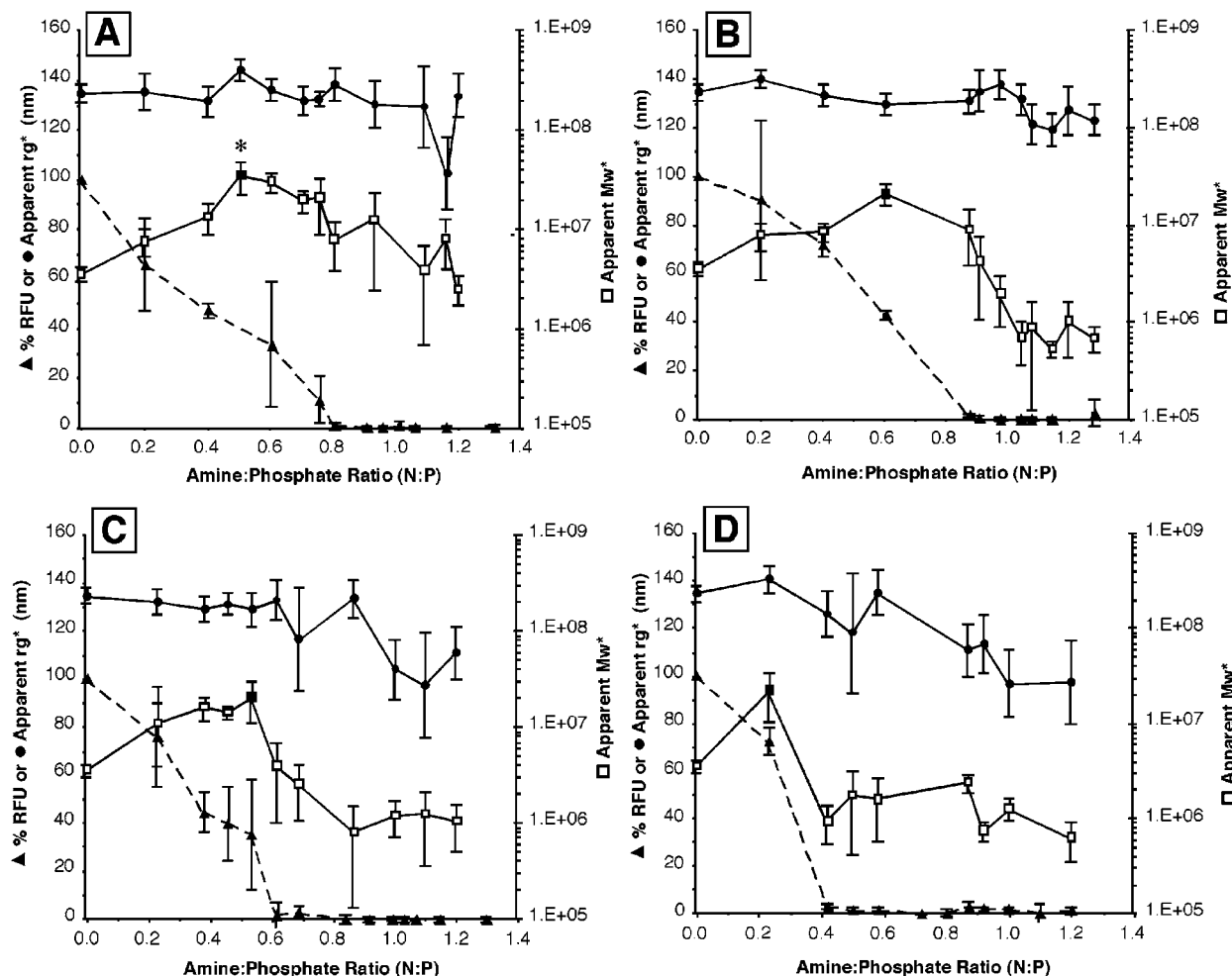
apparent  $M_w^*$  at N:P < N:P<sub>min</sub>, but showed similar overall trends with respect to the relative degree of condensation (Figure 4b–d). At charge ratios greater than N:P<sub>min</sub>, the  $M_w^*$  for each of the three terpolymers decreased more significantly than seen for pK42 and stabilized at approximately  $1 \times 10^6$  g/mol. Only complexes made with pK42–7k and pK42–11k displayed the expected decrease in  $r_g^*$  when DNA condensation was complete ( $p < 0.001$  at N:P = 1.2, ANOVA, Tukey HSD). The SEM images supported that there were many particles on the order of less than 100 nm; however, the large variance in the  $r_g^*$  is the result of heterogeneity in the particle size distribution.

**Degradation by DNase I.** Figure 5 shows the electrophoretic migration of free DNA and pK42–DNA complexes after exposure to DNase I and subsequent dissociation from polycations. Polymer staining with Coomassie Blue indicated that complex dissociation by NaOH was complete and maintained by the alkaline running buffer, since all staining was localized around the well, apart from the migrating DNA. At a pH of 12, the primary amines were largely deprotonated and, therefore, did not migrate toward the anode. Ethidium bromide staining of DNA revealed that simply making pK42–DNA complexes in the same manner as the triblock copolymer complexes dramatically decreased the extent of degradation by DNase I. Particles made with all pK–pLL–pEG triblock copolymers also showed improved DNA resistance to degradation over free DNA and freshly made pK42 particles (Figure 6). At 15 min, the percentage of intact DNA from particles made with the highest polylactide segment, pK42–11k, was significantly ( $p < 0.1$ , ANOVA, Tukey HSD) higher than that from similarly made (lyophilized) pK42–DNA particles.

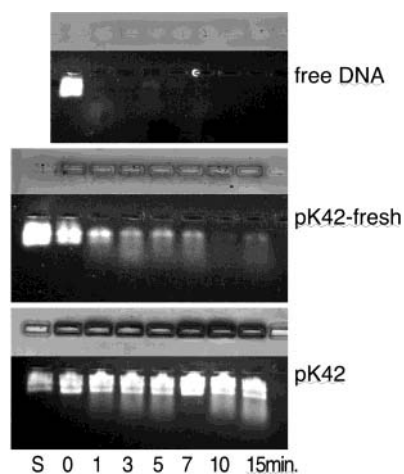
## DISCUSSION

Ring-opening polymerization of L-lactide from poly(ethylene glycol) has been widely documented regarding the effect of monomer-to-initiator ratio as well as monomer-to-hydroxyl ratio (38–40). A survey of the literature enabled predictable control over pLL molecular weight in the terpolymer by adjusting the M/OH ratio. There was some difficulty in producing the lowest molecular weight pLL–pEG (5, 800), perhaps due to slight impurities in the system that helped consume the small amount of monomer. However, the polymerization rates were monitored as a function of reaction time (data not shown) and the desirable pLL molecular weight was obtainable simply by adjusting the stop time. Size exclusion chromatography for all copolymers revealed single peaks attributable to pLL–pEG–fmoc diblock copolymers that eluted earlier than pEG–fmoc alone, indicating that there was no unreacted pEG remaining. Polydispersities calculated by multiangle light scattering for all synthesized diblocks were below 1.1, and there was good agreement between molecular weights assessed by  $^1\text{H}$  NMR and static light scattering. Prior knowledge of the pEG molecular weight (3400) was useful in providing an internal standard for  $^1\text{H}$  NMR in calculating the degree of polymerization of other polymer segments as well as degree of substitution of functional end groups (Figure 1). In these experiments, the fmoc group limited reactivity to just the hydroxyl end of pEG during pLL polymerization. In the future, a cross-linker will be substituted for fmoc to enable conjugation of bioactive moieties to the end of the pEG chains.

The amount of pK present in each terpolymer was assessed by  $^1\text{H}$  NMR in DMSO- $d_6$  as well as indirectly

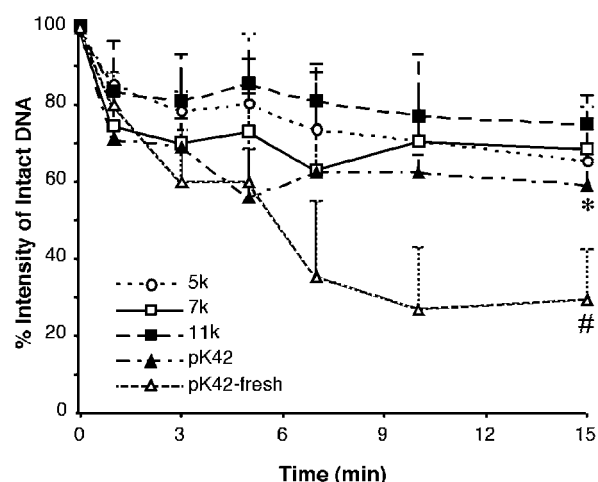


**Figure 4.** Static light scattering results of complexes made with (A) pK42, (B) pK42-5k, (C) pK42-7k, and (D) pK42-11k. The ethidium bromide fluorescence curves are overlaid as reference to correlate the degree of condensation to  $M_w^*$  and  $r_g$  trends. The peak  $M_w^*$  (indicated on each graph by the solid squares) for pK42 complexes (\*) were statistically greater than the peak  $M_w^*$  for all other samples ( $p < 0.001$ , ANOVA).



**Figure 5.** Alkaline agarose gel electrophoresis of free DNA, fresh pK42 complexes and lyophilized pK42 complexes after incubation with DNase I for varying time points. The top rows show coomassie blue staining of the dissociated polycation while the bottom rows reveal DNA stained by ethidium bromide.

by using a TNBS binding assay. A standard of pK42 was used to create the assay calibration curve since the binding efficiency was anticipated to be similar to that of the terpolymers. The amount of amines per milligram of terpolymer decreased with increasing pLL length since



**Figure 6.** Quantitative analysis of DNA degradation by DNase I. Complexes were made with pK42-5k (○), pK42-7k (□), pK42-11k (■), pK42 (▲) or pK42 without lyophilization (△) at a N:P = 1. At 15 min, degradation of fresh pK42 complexes (#) was significantly greater ( $p < 0.05$ ) than all other groups. Degradation of lyophilized pK42 complexes (\*) was significantly greater ( $p < 0.1$ ) than pK42-11k samples. ANOVA statistics and Tukey HSD post-hoc comparisons were used on triplicate samples.

the weight percent of the pLL-pEG diblock became more significant. Although pK and pLL-pEG were reacted at



1:1 molar ratios for all terpolymer synthesis, the degree of substitution increased with increasing pLL–pEG  $M_w$  possibly due to differences in purification efficiencies. The proton NMR results closely supported that from the TNBS assay (Table 2). SEC-MALLS data were not obtainable for the synthesized terpolymers due to solubility problems. Attempts at using several binary solvent mixtures resulted in very high and inconsistent  $dn/dc$  measurements due to preferential solvation of solvent components with the hydrophilic and hydrophobic polymer segments. To obtain accurate measurements, extensive dialysis and preequilibration would have been required, which could have reduced the molecular weight of the hydrolytically degradable copolymer (41, 42). The terpolymers were soluble in dimethyl sulfoxide, but aggregation and adsorption onto the column matrix occurred at the relatively high sample concentrations required for sufficient light scattering signal.

Figure 4 shows how the apparent  $M_w^*$  and apparent  $r_g^*$  changes with respect to the amine to phosphate charge ratio (N:P) can be used to characterize particle formation. For pK42, the  $M_w^*$  showed an initial dramatic increase at a N:P < 1 and decreased upon complete condensation. When there was excess DNA, each pK strand had the opportunity to interact with many DNA molecules, and the large increases in  $M_w^*$  most likely reflect that several DNA were linked together. Independent atomic force microscopy investigations have shown that partially condensed DNA on mica surfaces by spermidine, lipospermine, polyethyleneimine, and pK–pEG are multimolecular and possess centralized flowerlike conformations with highly overlapping crossover points (12, 43, 44). These observations would explain why  $r_g^*$  did not increase with corresponding  $M_w^*$  in our system. At high N:P ratios, condensation is complete and complex  $M_w^*$  decreases. For complexes made with pK42–7k and pK42–11k, a large decrease  $r_g^*$  was observed ( $p < 0.001$  between N:P = 0 and N:P = 1.2, ANOVA, Tukey HSD) despite large variances associated with those data due to the heterogeneous size population (Figure 2).

As the electrostatic repulsion is locally neutralized, other factors, including hydration, counterion, and hydrophobic forces, become more significant and are hypothesized to be the cause of complete condensation at less than electroneutral charge (45, 46). It is possible that the pLL segments of pK42–7k and pK42–11k were significant enough to aid condensation by hydrophobic interactions, as reflected in the lower N:P<sub>min</sub>. Our observations are supported by other theoretical and experimental investigations of the effect of surfactant hydrophobicity on its interaction with DNA (47, 48). In both studies, increasing the amount of hydrophobic moieties increased the surfactants' activity in associating with DNA. Corresponding analysis shows that at low N:P, the initial increase in particle  $M_w^*$  for pK42–7k and pK42–11k was not as dramatic as that for unmodified pK and was attributed to the presence of pLL and/or pEG. Since pEG is known to possess a large excluded volume, it is possible that it hindered the approach of other DNA molecules and reduced multi-molecular complex formation. In addition, if pLL participated in DNA condensation, it could have also constrained cationic counterion mobility and secondary DNA strand reorganization through hydrophobic interactions with neutralized pK and/or DNA (49, 50).

The complexes developed in this system deviated slightly from those predicted by traditional charge inversion and reentrance models (51, 52). The hydrophilic pEG

**Table 3.** Effect of Concentration Assumption on  $M_w$

	DNA+polymer ( $\times 10^{-6}$ g/mol)	DNA ( $\times 10^{-6}$ g/mol)
pK42	2.51 $\pm$ 0.80	5.13 $\pm$ 1.56
pK42–5k	1.03 $\pm$ 0.60	2.71 $\pm$ 1.36
pK42–7k	1.04 $\pm$ 0.54	3.47 $\pm$ 1.66
pK42–11k	0.64 $\pm$ 0.28	2.88 $\pm$ 1.17

segment aids in solubilizing complexes in aqueous media, thereby circumventing precipitation of charge neutralized particles. In addition, the relatively small variances in  $r_g^*$  at low N:P indicates that the polycation was distributed throughout the DNA instead of generating a mixed population of condensed and free DNA. The coexistence of condensed complexes and free DNA has been shown to be at least partially contingent on a large polycation charge density. Polyethyleneimine at low N:P ratios was shown to produce a mixed population of free and condensed DNA at a pH of 5; however, at pH 7 only partially condensed DNA was formed due to the reduced ionization of its amines (7). Another point of departure from theory was observed regarding  $M_w^*$  trends. It was expected that complex  $M_w^*$  should increase as the N:P ratio approached 1 since, electrostatic repulsion between partially neutralized DNA decreased. At N:P ratios greater than 1, excess polycation imparts a net positive charge that discourages intercomplex interactions and reduces complex  $M_w^*$ . While this trend on a similar system of pK and DNA was reported previously, our samples demonstrated a peak  $M_w^*$  at approximately  $1/2$  the N:P<sub>min</sub> instead of a N:P ratio near 1 (19).

For all complex systems, the  $M_w^*$  unexpectedly decreased below that of free DNA at high N:P ratios. This result is attributable to the fact the calculations of  $M_w^*$  and  $r_g^*$  are apparent rather than true values. At high N:P ratios, the condensing polycation is present in a large weight fraction but is small in size relative to DNA. Therefore, the assumption that sample concentration is a summation of both terpolymer and DNA overestimates sample concentrations at high N:P ratios. Equation 1 shows that  $R_\Theta$  is proportional to  $M_w^*$  and  $c$ , and if other parameters are held constant, then an overestimation in concentration would result in an artificially low  $M_w^*$  for a given  $R_\Theta$ . However, concentration did not affect calculations for  $r_g^*$  since they were determined from angle-dependent scattering and not overall light scattering signal. Table 3 illustrates this point by showing the  $M_w^*$  dependence using both concentration assumptions for each complex system at an N:P of 1.2. If it is assumed that DNA is the predominant scattering center due to its considerably larger size, then the concentration of condensing polymer is negligible with respect to its light scattering contribution (the effect on  $dn/dc$  is still considered significant), the recalculated  $M_w^*$  increases. For pK42, the difference in  $M_w^*$  is minimized, since pK42 contributes a small weight fraction. For pK42–11k, the adjustment for concentration is the largest due to the large weight fraction of pLL–pEG, which results in the largest percent increase in  $M_w^*$ . However, even after the concentration adjustment, the  $M_w^*$  of pK42 complexes remains statistically different from those made with the terpolymers ( $p < 0.001$ ). With such a system, it is difficult to definitively conclude which of the two assumptions to use for calculations. At high N:P charge ratios, the polymer contribution to the light scattering signal becomes significant and should be factored into the overall concentration in some capacity. The impact of system complexity, polydispersity, and particle inhomogeneity on other parameters, such as  $dn/dc$ , needs to be consid-

ered before specific physical interpretation can be extracted from these values (53, 54).

It has been shown that intracellular trafficking of plasmids condensed with polylysine involves endosomal compartmentalization and so plasmid degradation by nucleases is a concern (9). Condensation of DNA causes gross conformational changes that can hinder binding of nucleases, such as DNase I, whose activity is dependent on the insertion of its active loop into the minor groove. Figure 5 shows that freshly made pK42–DNA complexes slightly improve resistance to DNase I compared to naked DNA. However, lyophilized pK42–DNA complexes displayed even greater resistance to DNase I over those made and used immediately. DNase I has been shown to act as a catalyst that enables water to initiate a nucleophilic attack on the phosphodiester backbone (55). Lyophilization helped protect DNA in these complexes most likely by disrupting molecularly bound water that was not completely restored by resuspension. Since other differences in resistance to DNase I were not definitive by casual inspection of the electrophoresis gels, image analysis elucidated differences in the degree of plasmid degradation found in each lane. Figure 6 is a plot of the percentage of DNA remaining intact after various incubation times with DNase I. Complexes made with pK42–11k showed the greatest amount of intact DNA after 15 min of exposure. This observation could be the result of pLL interfering with DNase I binding either by further altering the backbone structure of condensed DNA or physically blocking binding sites. The ability of pLL to protect against nuclease degradation could extend the intracellular lifetime of plasmids and increase the likelihood of transcription. Ideally, a system can be developed where modulation over the pLL and pK molecular weights can be used to optimize DNA unpacking rates and, perhaps, temporal expression profiles. Future work will be performed in this direction using complexes functionalized with moieties for cell-specific targeting and endosomal escape.

## CONCLUSIONS

We have described the synthesis and characterization of poly(lysine-*g*-(lactide-*b*-ethylene glycol)) terpolymers that are capable of self-assembling with plasmid DNA. Static light scattering of complexed DNA was useful in characterizing differences in apparent  $M_w^*$  and  $r_g^*$  trends, which suggested that there were subtle changes in molecular association dynamics when pK was modified with pLL–pEG. In addition, terpolymers of pK–pLL–pEG demonstrated the ability to fully condense DNA at lower amine-to-phosphate ratios when compared to unmodified pK, while also improving upon pK's poor ability to protect condensed DNA from intracellular nucleases. These efforts to minimize the amount of pK necessary for complete plasmid condensation may improve transfection efficiency and reduce overall cytotoxicity.

## ACKNOWLEDGMENT

We are grateful for the support from NIDR T32 DE07042-25.

## LITERATURE CITED

- (1) Tang, M. X., and Szoka, F. C. (1997) The influence of polymer structure on the interactions of cationic polymers with DNA and morphology of the resulting complexes. *Gene Ther.* 4, 823–832.
- (2) Kyriakides, T. R., Cheung, C. Y., Murthy, N., Bornstein, P., Stayton, P. S., and Hoffman, A. S. (2002) pH-sensitive polymers that enhance intracellular drug delivery in vivo. *J. Controlled Release* 78, 295–303.
- (3) Dekie, L., Toncheva, V., Dubruel, P., Schacht, E. H., Barrett, L., and Seymour, L. W. (2000) Poly-L-glutamic acid derivatives as vectors for gene therapy. *J. Controlled Release* 65, 187–202.
- (4) Godbey, W. T., Wu, K. K., and Mikos, A. G. (1999) Poly(ethylenimine) and its role in gene delivery. *J. Controlled Release* 60, 149–160.
- (5) Chen, Q. R., Zhang, L., Stass, S. A., and Mixson, A. J. (2001) Branched copolymers of histidine and lysine are efficient carriers of plasmids. *Nucleic Acids Res.* 29, 1334–1340.
- (6) Widom, J., and Baldwin, R. L. (1980) Cation-induced toroidal condensation of DNA studies with  $\text{Co}^{3+}(\text{NH}_3)_6$ . *J. Mol. Biol.* 144, 431–453.
- (7) Bronich, T. K., Nguyen, H. K., Eisenberg, A., and Kabanov, A. V. (2000) Recognition of DNA topology in reactions between plasmid DNA and cationic copolymers. *J. Am. Chem. Soc.* 122, 8339–8343.
- (8) Arcsott, P. G., Ma, C., Wenner, J. R., and Bloomfield, V. A. (1995) DNA condensation by cobalt hexaammine (III) in alcohol-water mixtures: dielectric constant and other solvent effects. *Biopolymers* 36, 345–364.
- (9) Godbey, W. T., Barry, M. A., Saggau, P., Wu, K. K., and Mikos, A. G. (2000) Poly(ethylenimine)-mediated transfection: a new paradigm for gene delivery. *J. Biomed. Mater. Res.* 51, 321–328.
- (10) Godbey, W. T., Wu, K. K., and Mikos, A. G. (1999) Tracking the intracellular path of poly(ethylenimine)/DNA complexes for gene delivery. *Proc. Natl. Acad. Sci. U.S.A.* 96, 5177–5181.
- (11) Pollard, H., Remy, J. S., Loussouarn, G., Demolombe, S., Behr, J. P., and Escande, D. (1998) Polyethylenimine but not cationic lipids promotes transgene delivery to the nucleus in mammalian cells. *J. Biol. Chem.* 273, 7507–7511.
- (12) Dunlap, D. D., Maggi, A., Soria, M. R., and Monaco, L. (1997) Nanoscopic structure of DNA condensed for gene delivery. *Nucleic Acids Res.* 25, 3095–3101.
- (13) Boussif, O., Lezoualch, F., Zanta, M. A., Mergny, M. D., Scherman, D., Demeneix, B., and Behr, J. P. (1995) A versatile vector for gene and oligonucleotide transfer into cells in culture and in vivo: polyethylenimine. *Proc. Natl. Acad. Sci. U.S.A.* 92, 7297–7301.
- (14) Erbacher, P., Remy, J. S., and Behr, J. P. (1999) Gene transfer with synthetic virus-like particles via the integrin-mediated endocytosis pathway. *Gene Ther.* 6, 138–145.
- (15) Remy, J. S., Abdallah, B., Zanta, M. A., Boussif, O., Behr, J. P., and Demeneix, B. (1998) Gene transfer with lipospermines and polyethylenimines. *Adv. Drug Delivery Rev.* 30, 85–95.
- (16) Godbey, W. T., Wu, K. K., and Mikos, A. G. (2001) Poly(ethylenimine)-mediated gene delivery affects endothelial cell function and viability. *Biomaterials* 22, 471–480.
- (17) Ogris, M., Brunner, S., Schuller, S., Kircheis, R., and Wagner, E. (1999) PEGylated DNA/transferrin-PEI complexes: reduced interaction with blood components, extended circulation in blood and potential for systemic gene delivery. *Gene Ther.* 6, 595–605.
- (18) Wolfert, M. A., and Seymour, L. W. (1996) Atomic force microscopic analysis of the influence of the molecular weight of poly(L)lysine on the size of polyelectrolyte complexes formed with DNA. *Gene Ther.* 3, 269–273.
- (19) Lai, E., and van Zanten, J. H. (2001) Monitoring DNA/poly-L-lysine polyplex formation with time-resolved multi-angle laser light scattering. *Biophys. J.* 80, 864–873.
- (20) Ward, C. M., Read, M. L., and Seymour, L. W. (2001) Systemic circulation of poly(L-lysine)/DNA vectors is influenced by polycation molecular weight and type of DNA: differential circulation in mice and rats and the implications for human gene therapy. *Blood* 97, 2221–2229.
- (21) Schaffer, D. V., Fidelman, N. A., Dan, N., and Lauffenburger, D. A. (2000) Vector unpacking as a potential barrier for receptor-mediated polyplex gene delivery. *Biotechnol. Bioengineering* 67, 598–606.



- (22) Ziady, A. G., Ferkol, T., Dawson, D. V., Perlmutter, D. H., and Davis, P. B. (1999) Chain length of the polylysine in receptor-targeted gene transfer complexes affects duration of reporter gene expression both in vitro and in vivo. *J. Biol. Chem.* 274, 4908–4916.
- (23) Erbacher, P., Roche, A. C., Monsigny, M., and Midoux, P. (1995) Glycosylated polylysine/DNA complexes: gene transfer efficiency in relation with the size and the sugar substitution level of glycosylated polylysines and with the plasmid size. *Bioconjugate Chem.* 6, 401–410.
- (24) Erbacher, P., Roche, A. C., Monsigny, M., and Midoux, P. (1997) The reduction of the positive charges of polylysine by partial gluconoylation increases the transfection efficiency of polylysine/DNA complexes. *Biochim. Biophys. Acta* 1324, 27–36.
- (25) Choi, Y. H., Liu, F., Park, J. S., and Kim, S. W. (1998) Lactose-poly(ethylene glycol)-grafted poly-L-lysine as hepatoma cell-targeted gene carrier. *Bioconjugate Chem.* 9, 708–718.
- (26) Schaffer, D. V., and Lauffenburger, D. A. (1998) Optimization of cell surface binding enhances efficiency and specificity of molecular conjugate gene delivery. *J. Biol. Chem.* 273, 28004–28009.
- (27) Midoux, P., Kichler, A., Boutin, V., Maurizot, J. C., and Monsigny, M. (1998) Membrane permeabilization and efficient gene transfer by a peptide containing several histidines. *Bioconjugate Chem.* 9, 260–267.
- (28) Duguid, J. G., Li, C., Shi, M., Logan, M. J., Alila, H., Rolland, A., Tomlinson, E., Sparrow, J. T., and Smith, L. C. (1998) A physicochemical approach for predicting the effectiveness of peptide-based gene delivery systems for use in plasmid-based gene therapy. *Biophys. J.* 74, 2802–2814.
- (29) Wagner, E., Plank, C., Zatloukal, K., Cotten, M., and Birnstiel, M. L. (1992) Influenza virus hemagglutinin HA-2 N-terminal fusogenic peptides augment gene transfer by transferrin-polylysine-DNA complexes: toward a synthetic virus-like gene-transfer vehicle. *Proc. Natl. Acad. Sci. U.S.A.* 89, 7934–7938.
- (30) Erbacher, P., Roche, A. C., Monsigny, M., and Midoux, P. (1996) Putative role of chloroquine in gene transfer into a human hepatoma cell line by DNA/lactosylated polylysine complexes. *Exp. Cell Res.* 225, 186–194.
- (31) Toncheva, V., Wolfert, M. A., Dash, P. R., Oupicky, D., Ulbrich, K., Seymour, L. W., and Schacht, E. H. (1998) Novel vectors for gene delivery formed by self-assembly of DNA with poly(L-lysine) grafted with hydrophilic polymers. *Biochim. Biophys. Acta* 1380, 354–368.
- (32) Katayose, S., and Kataoka, K. (1997) Water-soluble polyion complex associates of DNA and poly(ethylene glycol)-poly(L-lysine) block copolymer. *Bioconjugate Chem.* 8, 702–707.
- (33) Blessing, T., Kurs, M., Holzhauser, R., Kircheis, R., and Wagner, E. (2001) Different strategies for formation of pegylated EGF-conjugated PEI/DNA complexes for targeted gene delivery. *Bioconjugate Chem.* 12, 529–537.
- (34) Kircheis, R., Blessing, T., Brunner, S., Wightman, L., and Wagner, E. (2001) Tumor targeting with surface-shielded ligand-polycation DNA complexes. *J. Controlled Release* 72, 165–170.
- (35) Hermanson, G. T. (1996) *Bioconjugate Techniques*, San Diego, Academic Press.
- (36) Waring, M. J. (1965) Complex formation between ethidium bromide and nucleic acids. *J. Mol. Biol.* 13, 269–282.
- (37) Sambrook, J., and Russell, D. W. (2001) *Molecular Cloning. A Laboratory Manual*, Cold Spring Harbor Laboratory Press, Cold Spring Harbor, NY.
- (38) Quellec, P., Gref, R., Perrin, I., Dellacherie, E., Sommer, F., Verbavatz, J., and Alonso, M. (1998) Protein encapsulation within poly(ethylene glycol)-coated nanospheres. I. Physicochemical characterization. *J. Biomed. Mater. Res.* 42, 45–54.
- (39) Stevels, W., Bernard, A., Witte, P. V. d., Dijkstra, P., and Feijen, J. (1996) Block copolymers of poly(L-lactide) and poly(e-caprolactone) or poly(ethylene glycol) prepared by reactive extrusion. *J. Appl. Polym. Sci.* 62, 1295–1301.
- (40) Zhang, X., Macdonald, D. A., Goosen, M. F. A., and Mcauley, K. B. (1994) Mechanism of lactide polymerization in the presence of stannous octoate: the effect of hydroxy and carboxylic acid substances. *J. Polym. Sci., Part A: Polym. Chem.* 32, 2965–2970.
- (41) Nordmeier, E., and Lechner, M. D. (1991) Light scattering from polymer-mixed solvent systems. 1. Selective adsorption phenomena of poly(N-vinylpyrrolidone). *Macromolecules* 24, 2529–2537.
- (42) Tuzar, Z., and Kratochvil, P. (1977) Extremely high refractive index increments in polymer/mixed solvent systems. *Macromolecules* 10, 1108–1110.
- (43) Fang, Y., and Hoh, J. H. (1998) Early intermediates in spermidine-induced DNA condensation on the surface of mica. *J. Am. Chem. Soc.* 120, 8903–8909.
- (44) Wolfert, M. A., Schacht, E. H., Toncheva, V., Ulbrich, K., Nazarova, O., and Seymour, L. W. (1996) Characterization of vectors for gene therapy formed by self-assembly of DNA with synthetic block copolymers. *Hum. Genet. Ther.* 7, 2123–2133.
- (45) Bloomfield, V. A. (1997) DNA condensation by multivalent cations. *Biopolymers* 44, 269–282.
- (46) Rau, D. C., and Parsegian, A. (1992) Direct measurement of the intermolecular forces between counterion-condensed DNA double helices. *Biophys. J.* 61, 246–259.
- (47) Bhattacharya, S., and Mandal, S. S. (1997) Interaction of surfactants with DNA. Role of hydrophobicity and surface charge on intercalation and DNA melting. *Biochim. Biophys. Acta* 1323, 29–44.
- (48) Kuhn, P. S., Barbosa, M. C., and Levin, Y. (2000) Effects of hydrophobicity in DNA surfactant complexation. *Physica A* 283, 113–118.
- (49) Ono, M. Y., and Spain, E. M. (1999) Dynamics of DNA condensates at the solid–liquid interface by atomic force microscopy. *J. Am. Chem. Soc.* 121, 7330–7334.
- (50) Fenley, M. O., Manning, G. S., and Olson, W. K. (1990) Approach to the limit of counterion condensation. *Biopolymers* 30, 1191–1203.
- (51) Nguyen, T. T., Rouzina, I., and Shklovskii, B. I. (2000) Reentrant condensation of DNA induced by multivalent counterions. *J. Chem. Phys.* 112, 2562–2568.
- (52) Nguyen, T. T., and Shklovskii, B. I. (2001) Complexation of DNA with positive spheres: Phase diagram of charge inversion and reentrant condensation. *J. Chem. Phys.* 115, 7298–7308.
- (53) Huglin, M. B. (1972) *Light Scattering from Polymer Solutions*, Academic Press, London.
- (54) Talingting, M. R., Voigt, U., Munk, P., and Webber, S. E. (2000) Observation of massive overcompensation in the complexation of sodium poly(styrenesulfonate) with cationic polymer micelles. *Macromolecules* 33, 9612–9619.
- (55) Suck, D., and Oefner, C. (1986) Structure of DNase I at 2.0 Å resolution suggests a mechanism for binding to and cutting DNA. *Nature* 321, 620–625.

BC025623B



# 4-(2-Aminooxyethoxy)-2-(ethylureido)quinoline–Oligonucleotide Conjugates: Synthesis, Binding Interactions, and Derivatization with Peptides

Tomoko Hamma<sup>†</sup> and Paul S. Miller\*

Department of Biochemistry and Molecular Biology, Bloomberg School of Public Health, Johns Hopkins University, 615 North Wolfe Street, Baltimore, Maryland 21205. Received November 13, 2002; Revised Manuscript Received January 9, 2003

Oligo-2'-*O*-methylribonucleotides conjugated with 4-(2-aminooxyethoxy)-2-(ethylureido)quinoline (AOQ) and 4-ethoxy-2-(ethylureido)quinoline (EOQ) were prepared by reaction of the AOQ or EOQ phosphoramidite with the protected oligonucleotide on a controlled pore glass support. Deprotection with ethylenediamine enabled successful isolation and purification of the highly reactive AOQ-conjugated oligomer. Polyacrylamide gel electrophoresis mobility shift experiments showed that the dissociation constants of complexes formed between an AOQ- or EOQ-conjugated 8-mer and complementary RNA or 2'-*O*-methyl-RNA targets (9- and 10-mers) were in the low nM concentration range at 37 °C, whereas no binding was observed for the corresponding nonconjugated oligomer, even at a concentration of 500 nM. Fluorescence studies suggested that this enhanced affinity is most likely due to the ability of the quinoline ring of the AOQ or EOQ group to stack on the last base pair formed between the oligomer and target, thus stabilizing the duplex. The binding affinity of a 2'-*O*-methyl RNA 15-mer, which contained an alternating methylphosphonate/phosphodiester backbone, for a 59-nucleotide stem-loop HIV TAR RNA target, increased 2.3 times as a consequence of conjugation with EOQ. The aminooxy group of AOQ-conjugated oligomers is a highly reactive nucleophile, which reacts readily with aldehydes and ketones to form stable oxime derivatives. This feature was used to couple an AOQ-oligomer with leupeptin, a tripeptide that contains a C-terminus aldehyde group. A simple method was developed to introduce a ketone functionality into peptides that contain a cysteine residue by reacting the peptide with bromoacetone. The resulting keto-peptide was then coupled to the AOQ-oligomer. This procedure was used to prepare oligonucleotide conjugates of a tetrapeptide, RGDC, and a derivative of HIV tat peptide having a C-terminus cysteine. The combination of the unique reactivity of the aminooxy group and enhanced binding affinity conferred by its quinoline ring suggests that AOQ may serve as a useful platform for the preparation of novel oligonucleotide conjugates.

## INTRODUCTION

Recent advances in chemical syntheses of modified oligonucleotides have enabled broad applications of antisense oligonucleotides as research tools in molecular biology; as diagnostic agents; and as potential therapeutics (see recent reviews in refs 1 and 2). The efficacy of antisense oligonucleotides relies on stable and specific hybridization with their RNA targets and on effective internalization by cells. A considerable amount of research has been devoted to synthesizing oligonucleotides that possess unique sugar, phosphate, or base moieties or with chemically reactive functional groups in an effort to enhance the binding affinities of the oligonucleotides for their targets. Furthermore, efforts have also been made to conjugate antisense oligonucleotides to small ligands, peptides, or proteins to facilitate their uptake by cells.

Chemically reactive functional groups such as psoralen (3, 4), dimethylanthraquinone (5), mitomycin (6), and 2-amino-6-vinylpurine (7) have been conjugated to oligonucleotides to achieve oligomer-target cross-linking.

However, these agents require photoactivation, reduction, or acidic conditions to trigger the cross-linking reaction. In contrast, groups such as aromatic 2-chloroethylamine (8, 9), cyclopropapyrroloindole (10), transplatin (11), and 5-methyl-N<sup>4</sup>, N<sup>4</sup>-ethanocytosine (12), when incorporated into oligonucleotides, can carry out alkylation when the oligonucleotide hybridizes to its target. Efficient covalent bond formation between an oligonucleotide and its target has been shown to correlate with the antisense efficacy in the cell (6, 11, 13).

The aminooxy group reacts readily with a variety of electrophiles. The high nucleophilicity of this group is attributed to the unshared pair of electrons on the oxygen atom adjacent to the amino nucleophilic center, inducing the so-called alpha effect (14). The high reactivity of the aminooxy group toward aldehydes and ketones (15–17) has been utilized for chemoselective conjugation of peptides (18, 19), proteins (20), carbohydrates (21–23), and oligonucleotides (15, 23–26), resulting in formation of a highly stable oxime linkage (15, 27). Alkoxyamines have also been shown to react with the 5–6 double bonds of cytosine and uracil to form covalent Michael adducts (28–31). It thus appeared possible that an aminooxy group, when appended to an oligonucleotide, might increase the binding affinity between the oligomer and its target as a result of covalent Michael adduct formation with a cytosine residue in the target.

\* Corresponding author. Phone: 410-955-3489. Fax: 410-955-2926. E-mail: pmiller@jhsp.h.edu.

<sup>†</sup> Current address: Division of Basic Science, Fred Hutchinson Cancer Research Center, 1100 Fairview Avenue North Mail Stop A3-015, Seattle, WA 98109.

To explore these possibilities, we have designed an antisense oligonucleotide bearing a 5'-4-(2-aminoxy-ethoxy)-2-(ethylureido)quinoline (AOQ) group. The interactions between this AOQ-derivatized oligonucleotide and complementary RNA and 2'-*O*-methyl-RNA targets were characterized by gel mobility shift assays and steady state fluorescence measurements. In addition, a novel, simple method was developed to conjugate the AOQ-derivatized oligonucleotide with small peptides. The increased binding of the AOQ-derivatized oligonucleotide to its target and its successful conjugation with biologically active peptides suggests that the AOQ group may be a useful modification for enhancing the efficacy of antisense oligonucleotides.

## EXPERIMENTAL PROCEDURES

**Materials.** 2-Amino-4-hydroxyquinoline hydrate (97%, Lancaster), 2-cyanoethyl diisopropyl chlorophosphoramidite (Chemgenes Corp.), bromoethane (98%, Acros Organics), and bromoacetone (1-bromo-2-propanone) (95%, Chem Service Inc.) were commercial products. Protected 2'-*O*-methylribonucleoside-3'-*O*-( $\beta$ -cyanoethyl-*N,N*-diisopropyl)phosphoramidites, ribonucleoside-3'-*O*-( $\beta$ -cyanoethyl-*N,N*-diisopropyl)-phosphoramidites, controlled pore glass supports, 4,5-dicyanoimidazole, 5-ethylthio-1*H*-tetrazole, and oligonucleotide synthesis reagents were purchased from Glen Research, Inc. Protected 2'-*O*-methylribonucleoside-3'-*O*-(*N,N*-diisopropyl)methylphosphoramidites were obtained from Chemgenes Corp. Ethyl acetate, dichloromethane, diisopropylethylamine, and triethylamine were stored over calcium hydride, whereas pyridine, chloroform, and *N,N*-dimethylformamide were stored over Linde-type 4 Å molecular sieves. Silica gel thin-layer chromatography (TLC) was carried out using Whatman aluminum-backed sheets that contained fluorescent indicator. Column chromatography was performed on Davisil-grade 634-type 60 Å silica gel, 100–200 mesh, obtained from Fisher Scientific. DEAE Sephadex A-25 columns were purchased from Sigma. Snake venom phosphodiesterase (SVP) from *Crotalus durissus* was purchased from Boehringer Mannheim, and calf intestinal alkaline phosphatase (CIP) and T4 polynucleotide kinase (PNK) were obtained from New England Biolabs. Synthetic leupeptin, H-Leu-Leu-Arg-H and synthetic tetrapeptide, H-Arg-Gly-Asp-Cys-OH, were obtained from Alexis Biochemicals and American Peptide Company, respectively. The derivative of HIV Tat peptide H-Gly-Arg-Lys-Lys-Arg-Gln-Arg-Arg-Arg-Pro-Gln-Cys-OH was synthesized and purified by the Protein/Peptide Sequencing Core Facility at Johns Hopkins University.

**General Methods.**  $^1\text{H}$  NMR spectra were acquired on a Bruker AMX 300 MHz spectrometer. Samples were prepared in dimethyl sulfoxide, and the chemical shifts were reported in ppm relative to the internal residual solvent peaks (DMSO: 2.5 ppm). MALDI-TOF mass spectrometry was carried out at the Johns Hopkins University Mass Spectrometry Facility and ESI mass spectrometry by the Scripps Research Institute. Reversed-phase (RP) HPLC was carried out on a Microsorb C-18 column ( $0.46 \times 15$  cm, C18, 10  $\mu\text{m}$ ) purchased from Varian Analytical using a flow rate of 1.0 mL/min. Strong anion exchange (SAX) HPLC was carried out on a Dynamax II column ( $0.46 \times 25$  cm) purchased from Rainin Instruments Co. using a flow rate of 0.6 mL/min. For the oligonucleotides, the columns were monitored at 260 and 290 nm for analytical runs and preparative runs, respectively. Peptides were analyzed and purified on the Microsorb C-18 column, monitored at 215 nm. Polyacryl-

amide gel electrophoresis was performed on  $20 \times 20 \times 0.75$  cm gels containing either 8% or 20% acrylamide in 1x TBE. Urea, 7 M, was added for denaturing gels. The gels were run in 1x TBE buffer, which contained 89 mM Tris, 89 mM boric acid, and 0.2 mM ethylenediamine-tetraacetate (EDTA) at pH 8.0.

**Oligonucleotides.** The sequences of the oligonucleotides are shown in Figure 1. They were synthesized on an Applied Biosystems Model 392 DNA/RNA synthesizer using commercially available phosphoramidites and phosphonamidites as described previously (32). The oligonucleotides were removed from the support and deprotected as described previously (32). Twenty  $A_{260}$  units of each crude oligomer, 1676, 1843, 1855, 1856, 1885, 1886, 1887, or 2016 were purified by SAX HPLC using a 30 min linear gradient of 0–0.4 M ammonium sulfate. RNA oligomer 1960 was purified on 20% polyacrylamide gels run under denaturing conditions (32). The oligomers were desalted using SEP PAK C-18 cartridges. The compositions of the oligomers were assessed by enzymatic digestion using SVP and CIP (33), and/or their molecular weights were determined by MALDI-TOF mass spectrometry. The extinction coefficients of the oligonucleotides were determined as described previously (33): 1676,  $1.3 \times 10^5$ ; 1843, AOQ-1843, EOQ-1843,  $6.23 \times 10^4$ ; 1855, 1856, 1885, 1886, 1887,  $7.67 \times 10^4$ ; 1960,  $1.0 \times 10^5$ ; and 2016,  $5.2 \times 10^4$ . HIV TAR RNA was prepared by in vitro transcription of a plasmid carrying a TAR RNA template (32). The 73 nucleotide run off transcript contained the 59 nucleotide TAR RNA sequence (underlined) 5'GAAUACUCAAGCUGGGUCUCUCUGGUUA-GAUUAGACUGAGCCUGGGAGCUCUCUGGCUAAC-UAGGGAACCCG.

**2-(2-Hydroxyethylureido)-4-hydroxyquinoline (2).** 2-Amino-4-hydroxyquinoline hydrate (**1**) (640 mg, 4 mmol, see Scheme 1) was coevaporated with anhydrous pyridine and dissolved in 40 mL of dry pyridine. To this stirred solution was added 10 equiv of 4-nitrophenylchloroformate (8.1 g, 40 mmol) dissolved in 20 mL dry chloroform (20 mL), and the reaction was allowed to stir for 60 min at room temperature. A thick orange suspension was obtained that was treated with 41 equiv of ethanolamine (10 mL, 164 mmol) and further stirred for 2 h at room temperature. The reaction was complete as determined by silica gel TLC [chloroform/methanol (4:1, v/v)], with conversion of the starting material ( $R_f = 0.25$ ) to a faster-moving product ( $R_f = 0.34$ ). The suspension was filtered through a 60 mL coarse sintered glass funnel, and the residue was washed briefly with 20% methanol in chloroform. The filtrate was concentrated under vacuum on a rotary evaporator to a syrup that was dissolved in a minimum amount of chloroform and applied to a column packed with a Davisil-grade 634-type 60 Å silica gel. The column was eluted using a gradient from 10% to 20% methanol in chloroform. Fractions containing the desired product were combined and concentrated to yield **2** as a brown syrup (1.2 g or 4 mmol, quantitative yield).  $^1\text{H}$  NMR ( $d_6$ -DMSO)  $\delta$  (ppm): 4.82 (s; 1H, ureido-NH), 4.64 (s; 1H, ureido-NH), 7.98–7.24 (m; 4H, quinoline H5–8), 7.00 (t; 1H, quinoline H3), 5.44 (s; 1H, quinoline –OH), 3.91–3.87 (t; 1H, –NHCH<sub>2</sub>CH<sub>2</sub>OH), 3.54–3–3.48 (t; 2H, –NHCH<sub>2</sub>CH<sub>2</sub>OH), 3.20–3.16 (t; 2H, –NHCH<sub>2</sub>CH<sub>2</sub>OH).

**2-(2-*O*-Monomethoxytritylureido)-4-hydroxyquinoline (3).** A solution of compound **2** (1.2 g, 4 mmol) in 40 mL of dry pyridine was treated with 5 equiv of monomethoxytrityl chloride (6.2 g, 20 mmol) for 4 h at room temperature. The clear orange solution was cooled in an ice bath, diluted with 10 mL of methanol and 2 mL of triethylamine, and then concentrated under vacuum

AOQ		EOQ	
AOQ or EOQ conjugated oligonucleotides			
1843	X-mr GpCpUpCpCpCpApG		
1676	X-mr CpUpCpCpCpApGpGpCpUpCpApGpApU		
2106	X-mr GpApUpCpU		
Target oligonucleotides			
2'-O-Me	1855	mr ACUGGGAGCU	
	1856	mr ACUGGGAGCC	
	1885	mr ACUGGGAGCG	
	1886	mr ACUGGGAGCA	
	1887	mr ACUGGGAGC	
RNA	1960	r ACUGGGAGCC	

TAR RNA	Alternating Methylphosphonate Backbone

**Figure 1.** Sequences of antisense oligonucleotides and their targets. **X** is AOQ, EOQ, or no modification. The symbols mr and r indicate 2'-O-methylribonucleoside or ribonucleotide respectively; p is a phosphodiester linkage, and  $\underline{p}$  a methylphosphonate linkage.

on a rotary evaporator. The product, **3**, which was purified by silica gel column chromatography using a gradient of 0–10% methanol in chloroform, was obtained as a brown syrup (1.4 g or 2.69 mmol, 67%).  $R_f$ : 0.54 [chloroform/methanol (9:1, v/v)].

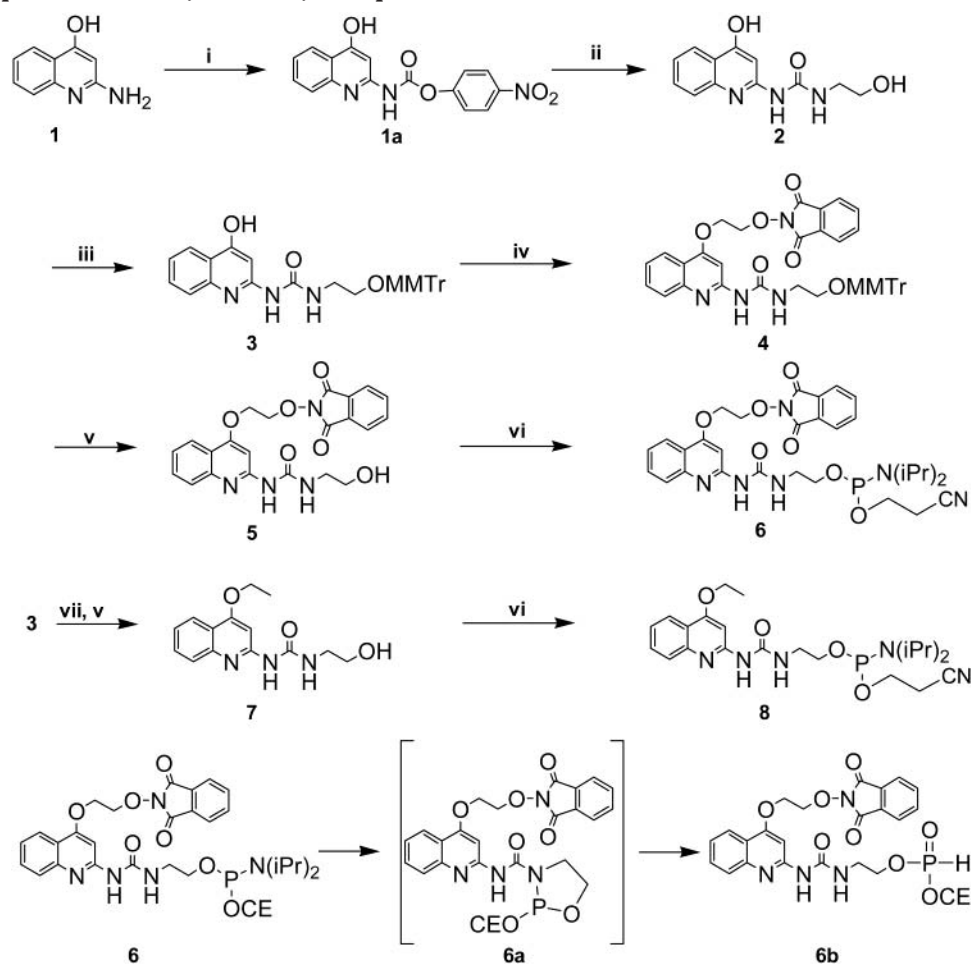
**2-(2-O-Monomethoxyltritylethylureido)-4-(2-phthalimidooxyethoxy)quinoline (4).** Compound **3** (1.4 g, 2.7 mmol) and 3 equiv of 2-phthalimidooxyethyl bromide (2.2 g, 8.1 mmol) were dissolved in dry *N,N*-dimethylformamide (10.8 mL), and the solution was treated with 3 equiv of dry powdered potassium carbonate (1.1 g, 8.1 mmol) overnight at room temperature. The potassium carbonate was removed by filtration, and the filtrate was concentrated under vacuum. The product, **4**, which was purified by silica gel column chromatography using a gradient of 0–5% methanol in chloroform, was obtained as a yellow syrup (1.4 g or 1.8 mmol, 67%).  $R_f$ : 0.28 [methanol:chloroform (1:19, v/v)].

**2-(2-Hydroxyethylureido)-4-(2-phthalimidooxyethoxy)quinoline (5).** Compound **4** (1.4 g, 1.8 mmol) was dissolved in 80% aqueous acetic acid (46 mL), and the solution was incubated at 37 °C for 45 min. The acetic acid was removed by coevaporation with 95% ethanol, and the product, **5**, was precipitated by addition of

absolute ethanol. The precipitate was collected on a fine porosity sintered glass funnel and dried under vacuum in a desiccator overnight to yield a light yellow powder (483 mg or 0.90 mmol, 50%).  $R_f$ : 0.1 [methanol:chloroform (1:4 v/v)]. The overall yield starting from **1** was 22%. The molecular weight of **5** was confirmed by ESI mass spectrometry ( $MH^+$ : calcd 437.4, found 437).  $^1H$  NMR ( $d_6$ -DMSO)  $\delta$  (ppm): 9.60 (s; 1H, ureido-NH), 9.53 (s; 1H, ureido-NH), 7.83 (s; 4H, phthalimide), 7.78–7.14 (m; 4H, quinoline H5–8), 6.77 (s; 1H, quinoline H3), 4.86–4.83 (t; 1H,  $-NHCH_2CH_2OH$ ), 4.67–4.45 (t; 4H,  $-OCH_2CH_2O-$ ), 3.58–3–3.30 (m; 4H,  $-NHCH_2CH_2OH$ ).

**2-[(2-Ureido)-4-(2-phthalimidooxyethoxy)quinoline]-ethyl-1-O- $\beta$ -cyanoethyl-*N,N*-diisopropylphosphoramidite (6).** Compound **5** (15 mg, 0.03 mmol) was dissolved in dry dichloromethane (600  $\mu$ L). Diisopropylethylamine (104.5  $\mu$ L, 0.60 mmol) and 2-cyanoethyl diisopropyl chlorophosphoramidite (41.7  $\mu$ L, 0.19 mmol) were added via syringe to the stirred solution, and the reaction was allowed to proceed at room temperature for 1 h. The product **6**, whose  $R_f$  was 0.21 on silica gel TLC [ethyl acetate:triethylamine, (95.5:0.5, v/v)], was purified by silica gel column chromatography using ethyl acetate/triethylamine (95.5:0.5, v/v). Fractions containing **6** were



**Scheme 1. Preparation of AOQ and EOQ Phosphoramidites<sup>a</sup>**

<sup>a</sup> Reagents: (i) 4-nitrophenyl chloroformate in chloroform and pyridine; (ii) ethanolamine; (iii) monomethoxytrityl chloride in pyridine; (iv) 2-phthalimidooxyethyl bromide, dimethylformamide, and potassium carbonate; (v) 80% acetic acid; (vi) 2-cyanoethyl-chlorodiisopropylphosphoramidite and diisopropylethylamine in dichloromethane. CE is 2-cyanoethyl.

combined and evaporated under vacuum to yield a clear light yellow syrup, which was dissolved in a minimum volume of dry dichloromethane (~300  $\mu$ L), and the solution was added dropwise with stirring to hexane at room temperature. The resulting precipitate was collected by centrifugation and dried under vacuum to yield a white solid (10.9 mg or 0.017 mmol, 57%). <sup>1</sup>H NMR (*d*<sub>6</sub>-DMSO)  $\delta$  (ppm): 9.70 (s; 1H, ureido-NH), 9.58 (s; 1H, ureido-NH), 7.83 (s; 4H, phthalimide), 7.79–7.15 (m, 4H; quinoline H5–8), 6.73 (s; 1H, quinoline H3), 4.68–4.46 (m, 4H, –OCH<sub>2</sub>CH<sub>2</sub>O–), 4.03–3.40 (m; –NHCH<sub>2</sub>–CH<sub>2</sub>O–), 2.91–2.73 (t; 4H, cyanoethyl), 1.23–1.12 (m; 24H, diisopropyl), 1.09–1.05 (m; 14H, diisopropyl). The MALDI-TOF mass spectrum was consistent for C<sub>25</sub>H<sub>24</sub>N<sub>5</sub>O<sub>8</sub>P (*m/z*: calc. 553.5, found 554.4), indicating that **6** had converted to its H-phosphonate derivative during analysis.

**2-(2-Hydroxyethylureido)-4-ethoxyquinoline (7).** Compound **3** (1.52 g, 2.9 mmol) and bromoethane (873  $\mu$ L, 12 mmol) were dissolved in 11.7 mL of dry dimethylformamide, and the solution was treated with dry, powdered potassium carbonate (1.6 g, 12 mmol) for 14 h at room temperature to give a new product whose *R<sub>f</sub>* was 0.75 [methanol: chloroform, (1:19 v/v)] on silica gel TLC. The potassium carbonate was removed by filtration and washed with several portions of dichloromethane. The filtrate was evaporated under vacuum, and the residue was treated with 58 mL of 80% aqueous acetic acid at 37 °C for 90 min. The acetic acid was removed by

coevaporation with 95% ethanol, and the resulting compound **7** was purified by silica gel column chromatography using 0–5% methanol in chloroform. Fractions containing **7** were combined and concentrated under vacuum to give an oil, *R<sub>f</sub>* = 0.18 [methanol: chloroform, (1:19 v/v)]. The oil was dissolved in a minimum volume of methanol, and heated water (50 °C) was added dropwise with stirring until the solution became turbid. This solution was heated until everything dissolved. The solution was then cooled slowly to 4 °C. The resulting solid was collected by filtration, washed several times with ice-cold water, and dried under vacuum. The product was obtained as a white powder (18 mg or 0.67 mmol, 17%), *R<sub>f</sub>* = 0.32 [ethyl acetate:triethylamine, (99.5:0.5, v/v)]. MALDI-TOF mass spectrometry (*m/z*: calcd 275.3, found 276.1).

**2-[(2-Ureido)-4-ethoxyquinoline]-ethyl-1-*O*- $\beta$ -cyanoethy-*N,N*-diisopropyl-phosphoramidite (8).** The synthesis of phosphoramidite **8** was identical to that of phosphoramidite **6** described above with the following modifications. After phosphitylation, the crude phosphoramidite was applied to a silica gel column using a mixture of petroleum ether and ethyl acetate (2:1 v/v), and the column was eluted with 0.5% triethylamine in ethyl acetate. The purified phosphoramidite was not precipitated in hexane. Rather, the oily product was transferred to an autosampler vial, evaporated under vacuum for 30 min, and the resulting oily residue was

used immediately for conjugation to the oligonucleotide as described below.

**Preparation of AOQ- and EOQ-Conjugated Oligonucleotides.** AOQ-1843, AOQ-2106, EOQ-1843, and EOQ-1676 were synthesized as follows. The oligo 2'-*O*-methylribonucleotides were synthesized as described above, and the 5'-DMT group was removed on the synthesizer. The oligonucleotide-CPG (10 mg) was mixed with AOQ phosphoramidite **6** in a 1.5 mL centrifuge tube or EOQ phosphoramidite **8** in a 4 mL autosampler vial. A 0.4 M solution of tetrazole in anhydrous acetonitrile was added, and the final concentration of the phosphoramidite was adjusted to 0.2 M by addition of anhydrous acetonitrile. The reaction mixture was incubated for 10 min at room temperature. The CPG was transferred to a synthesis cartridge and washed with 10 mL of acetonitrile, after which the oxidation and capping reactions were performed on the DNA synthesizer.

AOQ-1843 and AOQ-2106 were deprotected and purified as follows. The oligonucleotide-CPG, 10 mg, was treated with 30  $\mu$ L of a solution containing ethylenediamine, acetonitrile, 95% ethanol, and water (20:9:9:2 v/v) for 6 h at room temperature. The reaction mixture was cooled in an ice-water bath and neutralized by addition of 120  $\mu$ L of ice-cold 2 N hydrochloric acid. The deprotected oligomer was purified immediately by C-18 reversed phase HPLC using a 20 mL linear gradient of 0–50% acetonitrile in 50 mM sodium phosphate, pH 5.8. The oligomer was then desalted using a C-18 SEP PAK cartridge. The 50% aqueous acetonitrile solution containing the oligomer (9.9  $A_{260}$  units AOQ-1843; 0.34  $A_{260}$  units of AOQ-2106) was evaporated to dryness, and the dry residue was stored at  $-20^{\circ}\text{C}$ . The oligomers were analyzed by MALDI-TOF mass spectrometry: AOQ-1843 ( $m/z$ : calcd +  $\text{K}^+$  3001.8, found 3006.1); AOQ-2106 ( $m/z$ : calcd 1966.8, found 1967.1).

The EOQ-derivatized oligonucleotides were each deprotected and purified as follows. The oligonucleotide-CPG was treated with 400  $\mu$ L of concentrated ammonium hydroxide at  $65^{\circ}\text{C}$  for 5 h. After evaporation of solvents, the EOQ-oligonucleotide was purified by C-18 reversed-phase HPLC using a 20 mL linear gradient of 2–50% acetonitrile in 50 mM sodium phosphate, pH 7.8. Each purified EOQ-oligonucleotide was desalted on a C-18 SEP PAK cartridge and stored as a solution in 50% aqueous acetonitrile at  $4^{\circ}\text{C}$ . The oligonucleotides were analyzed by MALDI-TOF mass spectrometry: EOQ-1843 ( $m/z$ : calcd 2934.1, found 2935); EOQ-1676 ( $m/z$ : calcd +  $\text{K}^+$  5283.8, found 5279.0).

**Gel Mobility Shift Experiments.** Electrophoretic gel mobility shift assays were carried out as described previously (32). Oligonucleotide solutions with concentrations ranging from 0.5 nM to 100  $\mu$ M were prepared in binding buffer that contained 100 mM sodium chloride, 10 mM Tris, pH 7.5, and 0.5 mM EDTA in diethylpyrrolidone treated water. Solutions containing 0.2 nM of 5'-[ $^{32}\text{P}$ ]-end-labeled 1855, 1856, 1885, 1886, 1887, 1960, or TAR RNA (specific activity, 1000 Ci/mmol) were prepared in the same buffer. Equal volumes of oligomer and target solution (total volume, 10  $\mu$ L) were mixed in 0.5 mL centrifuge tubes, and 1  $\mu$ L of autoclaved 80% glycerol was added. Duplexes formed between 10-mer targets 1855, 1856, 1885, 1886, 1887, 1960, and 8-mer oligomers 1843, AOQ-1843, EOQ-1843, were incubated at  $37^{\circ}\text{C}$  for 1 h. Duplexes formed between TAR RNA and 15-mer oligomers 1676 or EOQ-1676 were incubated for 24 h at  $37^{\circ}\text{C}$ . The solutions were loaded onto a polyacrylamide gel using a 20  $\mu$ L syringe. Complexes formed with the short targets 1855, 1856, 1885, 1856, 1857, or

1960 were separated on a 20% nondenaturing acrylamide gel run at 500–600 V for 1.5 h at the same temperature at which the sample was incubated. In the case of the TAR RNA target, electrophoresis was carried out in a similar manner on an 8% nondenaturing polyacrylamide gel at 200–300 V for 2 h. The wet gels were visualized by phosphorimaging and quantitated using the phosphorimager software package. The apparent dissociation constants were determined as the half-maximal point on a plot of percent complex versus the log of oligomer concentration. Averages were obtained from at least three separate experiments.

**AOQ-1843–Leupeptin Conjugate.** Leupeptin (1.25  $\mu$ mol) was mixed with 5  $A_{260}$  units (0.8  $\mu$ mol) of AOQ-1843 in 54  $\mu$ L of 50% aqueous acetonitrile solution, and the solution was incubated for 60 min at room temperature. The AOQ-1843–leupeptin conjugate was purified by C-18 reversed-phase HPLC using a 20 mL linear gradient of 2–50% acetonitrile in 50 mM sodium phosphate, pH 5.8. The conjugate, which was obtained in quantitative yield, was desalted on a SEP PAK C-18 cartridge and analyzed by MALDI-TOF mass spectrometry ( $m/z$ : calcd 3373.4, found 3372.4).

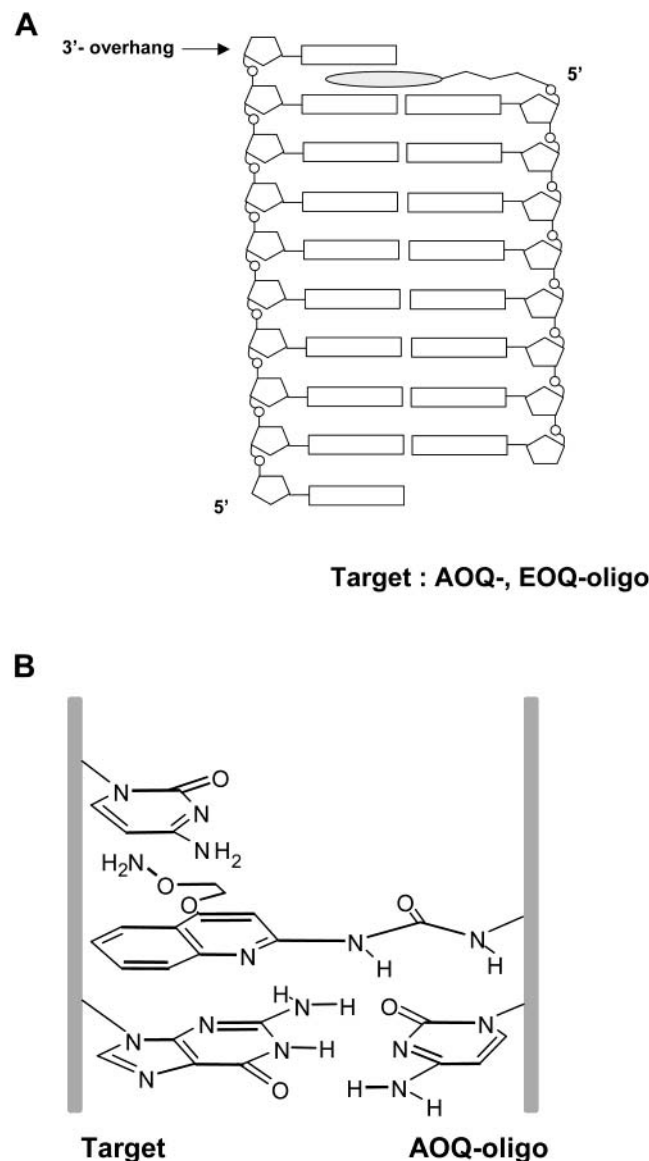
**AOQ-2106–RGDC or –Tat Conjugate.** A 0.2 M solution of bromoacetone in 50  $\mu$ L of 50% aqueous acetonitrile was added to either RGDC peptide (0.5 mg, 1.0  $\mu$ mol) or Tat peptide (0.5 mg, 0.3  $\mu$ mol) in a 1.5 mL centrifuge tube and the solution incubated for 1 h at room temperature. The reaction was shielded from light by covering the tube with aluminum foil during the incubation period. The resulting keto-peptide was purified by C-18 reversed phase HPLC using a 20 mL linear gradient of 2–50% acetonitrile in 0.1% trifluoroacetic acid. The fraction containing the keto-peptide was evaporated to dryness and redissolved in 50% aqueous acetonitrile. The keto-peptides were analyzed by MALDI-TOF mass spectrometry: keto-RDGC ( $m/z$ : calcd 506, found 506); keto-tat ( $m/z$ : calcd 1879, found 1880).

Keto-RDGC (19.5 nmol) was reacted with 0.1  $A_{260}$  unit (1.95 nmol) of AOQ-2106 in 53  $\mu$ L of 50% aqueous acetonitrile 1 h at room temperature. The resulting AOQ-2106–RDGC conjugate was purified by C-18 reversed-phase HPLC using a 20 mL linear gradient of 2–50% acetonitrile in 0.1% trifluoroacetic acid. Two peaks were observed that corresponded to the two oxime isomers. The conjugate was analyzed by MALDI-TOF mass spectrometry ( $m/z$ : calcd 2455, found 2457 for peaks 1 and 2, see Figure 6).

Keto-tat peptide (2.5 nmol) and 1.0  $A_{260}$  unit of AOQ-2106 (19.5 nmol) were incubated in 25  $\mu$ L of 50% aqueous acetonitrile for 1 h at room temperature. The resulting AOQ-2106–tat conjugate was separated from the unreacted AOQ-2106 by ion exchange chromatography. The reaction mixture was diluted with 75  $\mu$ L of 50% aqueous acetonitrile, and the solution was applied to a small (0.6  $\times$  1.2 cm) DEAE Sephadex A-25 column which had been preequilibrated with 50% aqueous acetonitrile. The column was washed with 50% aqueous acetonitrile, and the AOQ-2106–tat conjugate (1 nmol) was collected. The conjugate was analyzed by MALDI-TOF mass spectrometry: ( $m/z$ : calcd 3828, found 3829).

## RESULTS AND DISCUSSION

**AOQ- and EOQ-Conjugated Oligonucleotides.** The structures of the 4-(2-aminooxyethoxy)-2-(ethylureido)-quinoline (AOQ) and 4-ethoxy-2-(ethylureido)quinoline (EOQ) groups are shown in Figure 1. EOQ lacks an aminooxy group and thus is a nonreactive analogue of



**Figure 2.** Binding model. (A) The oval indicates either the AOQ or the EOQ group. (B) Possible stacking interaction between quinoline ring and neighboring bases. Left, target strand; right, antisense oligonucleotide strand.

AOQ. When bound to its target, the quinoline ring of an AOQ- or EOQ-conjugated oligonucleotide can potentially stack on the last base pair formed between the oligomer and the target as shown in Figure 2A. In this binding mode, the aminooxy group of the AOQ-oligomer could form a Michael adduct by reacting with the 5,6 double bond of a cytosine residue in the target as shown schematically in Figure 2B. Although such adduct formation would be expected to be transient, it could decrease the dissociation rate of the duplex, and consequently enhance the binding affinity of the AOQ-oligomer. In addition, the highly reactive aminooxy group can serve as a site for conjugation with other molecules that bear an aldehyde or ketone function.

To test these possibilities, AOQ or EOQ was conjugated via a phosphodiester linkage to the 5'-ends of oligo-2'-*O*-methylribonucleotides as shown in Figure 1. The sequences of these oligomers, with the exception of oligomer 2106, are complementary to the apical stem loop of HIV TAR RNA. Oligomer 1843 is complementary to nucleotides 31–38 of TAR RNA. Oligomer 1676, which contains alternating methylphosphonate/phosphodiester in-

ternucleotide linkages, is complementary to nucleotides 21–38 of TAR RNA.

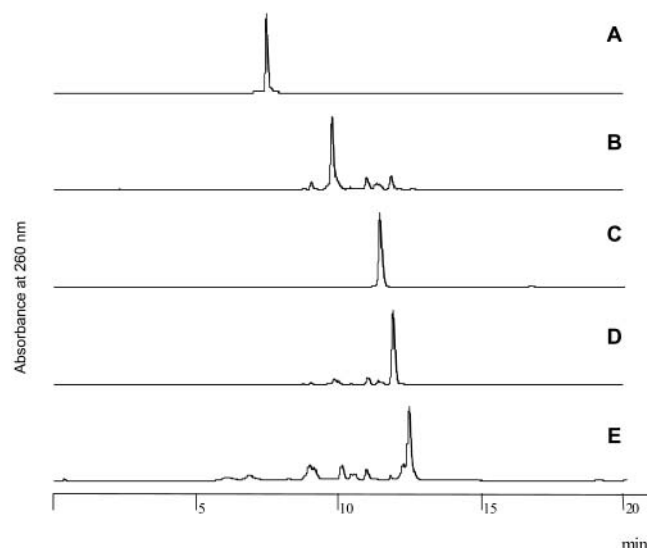
AOQ- and EOQ-phosphoramidites were prepared as shown in Scheme 1. 2-Amino-4-hydroxyquinoline, **1**, was converted to its *p*-nitrophenylcarbamate derivative, **1a**, by reaction with *p*-nitrophenylchloroformate. Compound **1a** was not isolated but was converted to the hydroxyethylureido derivative, **2**, by treatment with ethanolamine. The primary hydroxyl group of **2** was selectively protected by reaction with monomethoxytrityl chloride to give **3**. The 4-hydroxy group of **3** was then alkylated with 2-phthalimidooxyethyl bromide in the presence of potassium carbonate to give the protected AOQ derivative **4**. Treatment of **4** with 80% acetic acid removed the monomethoxytrityl group to produce compound **5**. The corresponding EOQ derivative **7** was prepared by alkylation of **3** with bromoethane in the presence of potassium carbonate followed by removal of the monomethoxytrityl group. AOQ and EOQ derivatives **5** and **7** were each converted to their phosphoramidite derivatives, **6** and **8**, respectively, by reaction with 2-cyanoethyl chlorodiisopropylphosphoramidite. The phosphoramidites were purified by silica gel column chromatography. The AOQ phosphoramidite, **6**, was precipitated from hexane and was obtained as a white powder. In contrast the EOQ phosphoramidite, **8**, failed to precipitate and was obtained as an oil.

Both phosphoramidites were very reactive and under some conditions appeared to be susceptible to conversion to their H-phosphonate derivatives. For example, mass spectrometric analysis of AOQ phosphoramidite **6** gave a mass consistent with that of the H-phosphonate of AOQ (**6b**). This species most likely arose from intramolecular displacement of the phosphorus *N,N*-diisopropylamino group by the nitrogen of the ureido linkage to produce a five-member cyclic phosphoramidite (**6a**). The cyclic phosphoramidite would be expected to be very reactive and readily react with traces of water in the solvent to give the H-phosphonate derivative. Consistent with this explanation is the observation that acetonitrile solutions of the AOQ or EOQ phosphoramidite showed conversion to a slower migrating product when monitored by silica gel TLC. The formation of this new compound correlated with a decrease in coupling efficiency to the oligonucleotides, indicating the formation of an inactive species.

The AOQ- and EOQ-conjugated oligonucleotides were prepared by first synthesizing the oligomers on controlled pore glass supports and removing the 5'-terminal dimethoxytrityl group. The supports were then transferred to an eppendorf tube or a glass autosampler vial that contained the dry phosphoramidite. A solution of tetrazole in dry acetonitrile was then added via a syringe and the coupling reaction was allowed to proceed for 10 min. The support was then returned to the DNA synthesis column, and capping and oxidation were carried out on the DNA synthesizer.

We initially tried deprotecting the AOQ-conjugated oligonucleotide by standard treatment with concentrated ammonium hydroxide solution at 65 °C for 5 h. However, a multitude of peaks were observed when the reaction mixture was analyzed by reversed phase HPLC (data not shown). Many of these peaks were detected at both 260 and 320 nm, indicating the presence of the AOQ group. However, among the AOQ containing peaks, only one possessed a reactive aminooxy group, as assessed by its ability to react with acetone to form the dimethylloxime derivative. Thus, it appeared that most of the AOQ-containing oligomers represented species where the aminooxy group had reacted with some component in the





**Figure 3.** Reverse-phase HPLC profile of (A) unmodified oligomer 1843, (B) AOQ-1843, (C) EOQ-1843, (D) dimethylloxime derivative of AOQ-1843, (E) leupeptin conjugated AOQ-1843. A 20 mL linear gradient of 2–50% acetonitrile (1 mL/min) in 50 mM sodium phosphate buffer (pH 5.8) was used.

deprotection reaction solution. This observation is in agreement with that of Salo et al., who reported that attempts to purify aminoxy containing oligomers were unsuccessful when concentrated ammonium hydroxide was used for deprotection (16). To circumvent this problem, an alternate deprotection method was developed which involved treatment of the oligonucleotide with ethylenediamine (EDA) at room temperature (34). To preclude generation of side products resulting from transamination of C by EDA during deprotection,  $N^4$ -acetyl-C or  $N^4$ -isobutryl-C protected phosphoramidite and methylphosphonamidite, respectively, were used to synthesize the oligonucleotides (34, 35). In separate experiments, we confirmed that no transamination occurred when acetyl- or isobutryl-protected C was treated with ethylenediamine under these conditions.

The AOQ-oligo was cleaved from the support, and all the protecting groups, including the phthalimide group, were completely removed after treatment with ethylenediamine for 6 h at room temperature. For example, as shown in Figure 3B for AOQ-1843, essentially a single peak was observed when the reaction mixture was analyzed by C-18 reversed phase HPLC. This peak, which adsorbed at both 260 and 320 nm, had a longer retention time than that of nonconjugated oligomer, 1843, which did not absorb at 320 nm. As shown in Figure 3D, AOQ-1843 reacted readily with acetone to give the dimethylloxime derivative, whose retention time was greater than that of AOQ-1843. The deprotected AOQ-oligo was immediately purified by C-18 reversed-phase HPLC. Storage of the purified AOQ-oligo in aqueous acetonitrile over time resulted in the generation of additional compounds as observed by C-18 reversed phase HPLC (data not shown). These compounds most likely result from reaction of the aminoxy group with minute amounts of aldehydes and/or ketones present in the solution as previously observed by others (15, 17). To prevent these unwanted reactions, the solution containing the AOQ-oligo after desalting was immediately evaporated to dryness and stored at  $-20^{\circ}\text{C}$ . Under these conditions, the dry AOQ-oligo proved to be stable, and the aminoxy function remained active.

In contrast to the AOQ-oligomers, the EOQ-oligonucleotides were successfully deprotected by treatment

**Table 1.** Apparent Dissociation Constant of Duplexes Formed between AOQ- or EOQ-1843 and Various Targets

target	$K_d$ (nM) <sup>a</sup>		
	1843	EOQ-1843	AOQ-1843
2'-O-Me 1855	mrACUGGGAGCU >500 <sup>b</sup>	4.6 ± 2.5	9.2 ± 1.0
1856	mrACUGGGAGCC >500	5.8 ± 1.7	8.2 ± 2.4
1885	mrACUGGGAGCG >500	1.9 ± 0.4	5.5 ± 4.1
1886	mrACUGGGAGCA >500	1.6 ± 0.4	5.2 ± 0.9
1887	mrACUGGGAGC >500	15.3 ± 0.1	19.6 ± 3.5
RNA 1960	rACUGGGAGCC >500	5.7 ± 1.2	7.1 ± 1.6

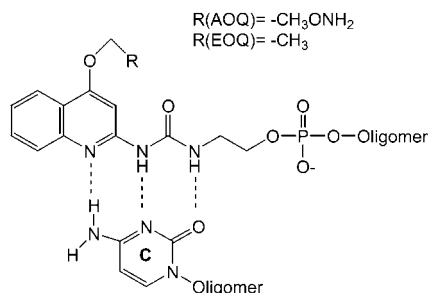
<sup>a</sup> Apparent dissociation constants were determined at  $37^{\circ}\text{C}$  in a buffer containing 100 mM sodium chloride, 10 mM Tris pH 7.5, 0.5 mM EDTA. <sup>b</sup>The highest concentration used for the measurements.

with concentrated ammonium hydroxide at  $65^{\circ}\text{C}$ . As shown in Figure 3C, EOQ-1843 gave a single peak whose retention time on C-18 reversed phase HPLC was approximately 6 min longer than that of unconjugated 1843. As was the case for the AOQ-oligomers, the EOQ-oligonucleotides absorbed at both 260 and 320 nm. MALDI-TOF mass spectrometric analyses of both the AOQ- and EOQ oligomers gave molecular weights consistent with the structures of the derivatized oligomers.

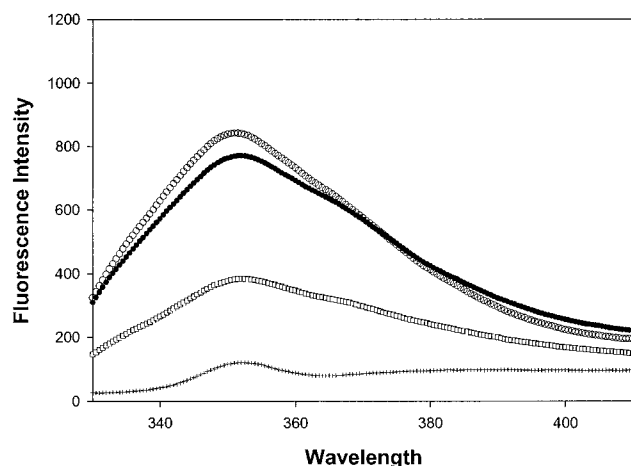
**Interactions of AOQ- and EOQ-Conjugated Oligonucleotides with Complementary Oligonucleotide Targets.** The interactions of AOQ-1843 and EOQ-1843 with oligo-2'-O-methylribonucleotides 1855, 1856, 1885, 1886, and 1887 and with oligoribonucleotide 1960 were studied by gel electrophoretic mobility shift assays at  $37^{\circ}\text{C}$ . The sequences of the target oligonucleotides are shown Figure 1. AOQ- and EOQ-1843 are each complementary to nucleotides 2–9 of the target oligomers. Hybridization of AOQ- or EOQ-1843 to targets 1855, 1856, 1885, 1886, or 1960 gives a duplex with a 3'-overhanging end, whereas hybridization to 1887 produces a duplex that lacks a 3'-overhanging base. Most of the binding studies were carried out using the oligo-2'-O-methylribonucleotide targets because these oligomers are easier to synthesize and handle than are RNA targets. Duplexes formed between AOQ- or EOQ-1843 and either the 2'-O-methylribonucleotide or RNA target are predicted to be in the A-type conformation, and thus the binding affinities of the oligomers for either target were expected to be the same.

As shown in Table 1, conjugation of oligomer 1843 with either AOQ or EOQ dramatically increased its binding affinity to all the targets studied at  $37^{\circ}\text{C}$ . Thus, the dissociation constants,  $K_d$ , of AOQ- or EOQ-1843 to these targets are in the low nanomolar range, whereas no binding was observed between 1843 and any of the targets, even at a concentration of 500 nM, which was the highest concentration of oligomer tested. As expected, the  $K_d$  values of duplexes formed with 2'-O-methylribonucleotide target 1856 or RNA target 1960, which have identical sequences, are almost identical. This result confirms that the 2'-O-methylribonucleotide targets are good models for the RNA target in these binding studies.

Targets 1855, 1856, 1885, 1886, and 1960 each have a 3'-overhanging base adjacent to the oligomer binding site. Removal of this base to give target 1887 results in approximately 3–10 times increase in the  $K_d$  of the duplex. This suggests that to some extent binding involves the 3'-base residue. Saito et al. have demonstrated that 2-amino-1,8-naphthyridine can bind to guanine via formation of specific hydrogen bonds (36). The ureidoquinoline moiety of AOQ or EOQ is structurally similar to 2-amino-1,8-naphthyridine and thus could potentially form similar hydrogen bonds with the 3'-C



**Figure 4.** Potential hydrogen bond formation between the AQO or EOQ group and a cytosine in the target strand.



**Figure 5.** Emission spectra of EOQ-1843 with its complementary target. Emission spectra were measured in a buffer containing 100 mM sodium chloride, 10 mM Tris pH 7.5, and 0.5 mM ethylenediaminetetraacetate at room temperature. 1843 only (+), EOQ-1843 only (O), EOQ-1843:1843 duplex (●), and EOQ-1843:1855 duplex (□).

residue of targets 1856 or 1960, as illustrated in Figure 4. However, as shown in Table 1, the  $K_d$ s of the duplexes formed with 1855, 1856, 1885, or 1886, each of which has a different 3'-base residue, are very similar, and thus it is unlikely that such hydrogen bonding interactions are the source of enhanced binding exhibited by AOQ- or EOQ-1843.

Both AOQ- and EOQ-1843 showed increased binding affinities compared to that of 1843, suggesting that the common aromatic quinoline ring of AOQ and EOQ contributes significantly to the binding interaction. Steady-state fluorescence experiments at room temperature were used to further investigate the binding mode. Because there were no significant differences in the  $K_d$ s of AOQ- or EOQ-1843, EOQ-1843 was used in these studies. The quinoline ring of the EOQ group absorbs UV light at 310 and 322 nm and fluoresces at 351 nm when excited at 314 nm. This fluorescence was used to study the interaction of the quinoline fluorophore with neighboring bases in the duplexes. Strong quenching and a concomitant red shift of the emission maximum have been observed upon the intercalative binding of polycyclic aromatic hydrocarbon-derivatized oligonucleotides with complementary targets (37, 38, and references therein). On the other hand, moderate quenching and very little or no red shift of the emission maximum has been interpreted as pi-stacking of the fluorophore to the exterior of the last base pair of the duplex (38–40).

As shown in Figure 5, the emission maximum of EOQ-1843 was clearly observed at 351 nm when excited at 314 nm, whereas 1843 did not show such emission. Duplexes formed between EOQ-1843 and targets 1855, 1856, 1885,

1886, or 1887 all showed a moderate decrease in fluorescence intensity and no shift in the emission maximum. As expected, there was no change in fluorescence intensity when equal amounts of EOQ-1843 and 1843 were mixed because these two oligomers do not form a duplex. These results are consistent with stacking of the quinoline ring on the end of the duplex rather than full intercalation between the last two base pairs of the duplex. In this binding mode, further stabilization could occur if the quinoline ring interacts with a 3'-overhanging base as shown in Figure 2A. The observation that 1855 and 1856, which have a pyrimidine overhang, have slightly higher  $K_d$ s than 1885 and 1886, which have a purine overhang, is consistent with this model. Thus, the quinoline ring may stack more effectively with the purine overhang leading to a lower  $K_d$ . In essence, the AOQ and EOQ groups may serve as "caps" to prevent fraying of terminal bases on the duplexes (39, 41–43).

The  $K_d$ s of duplexes formed by EOQ-1843 are 1.2–3.2 times lower than those of duplexes formed by AOQ-1843. This result suggests that Michael adduct formation by AOQ-1843 either does not take place, or if it does, that such formation does not contribute to the overall stability of the duplex. Deuterium exchange experiments were carried out to directly investigate the possible formation of Michael adducts. Equal amounts of AOQ-1843 and RNA target 1960 were incubated at room temperature overnight in buffer prepared with deuterated water. RNA 1960, which contains two cytosines in proximity to the AOQ binding site, was then digested with a combination of snake venom phosphodiesterase and calf intestinal phosphatase, and the resulting cytidine was isolated by C-18 reversed phase HPLC. The molecular weight of the cytidine was then determined by EIS mass spectrometry. If a Michael adduct formed, deuterium from the buffer would be incorporated at the 5 position of cytidine, resulting in a 1 mass unit increase in the molecular weight. No mass increase was observed for the recovered cytidine, suggesting that the aminoxy group of AOQ-1843 does not participate to any significant extent in Michael adduct formation with the C residues of target RNA. A control experiment using 1-(2-aminoxyethyl) cytosine, which undergoes intramolecular Michael adduct formation (44), showed that adduct formation could be detected by both NMR and mass spectrometry (data not shown). The inability of AOQ-1843 to form a Michael adduct may be due to unfavorable positioning of the aminoxy group when AOQ-1843 is bound to its target.

AOQ- or EOQ-1843 shows at least a 2 orders of magnitude increased binding affinity for the short, linear RNA target, 1960, compared to the nonconjugated oligomer, 1843. To determine if an EOQ-conjugated oligomer could also bind to a longer, structured RNA target, we studied the interaction between EOQ-1676 and HIV TAR RNA. This RNA target, whose sequence and secondary structure are shown in Figure 1, consists of two stems, 20 base pairs and 4 base pairs in length, joined by a 3 base bulge and capped with a 6 base loop. We have shown previously that 1676, which contains a nuclease resistant alternating methylphosphonate/phosphodiester backbone, binds with high affinity to this target at 37 °C (32). The interactions of 1676 and EOQ-1676 with TAR RNA were analyzed by gel mobility shift experiments. As shown in Table 2, EOQ-conjugated 1676 forms a duplex with TAR RNA whose apparent  $K_d$  is approximately 2.3 times less than that of the duplex formed by nonconjugated 1676. These results demonstrate that conjugation

**Table 2. Apparent Dissociation Constants of TAR RNA Duplexes**

oligomer	$K_d$ (nM) <sup>a</sup>
1676	101 ± 19
EOQ-1676	43 ± 7.4

<sup>a</sup> Apparent dissociation constants were determined at 37 °C in a buffer containing 100 mM sodium chloride, 10 mM Tris pH 7.5, 0.5 mM EDTA.

with EOQ can also enhance the binding affinity of oligonucleotides for targets with extensive secondary structure.

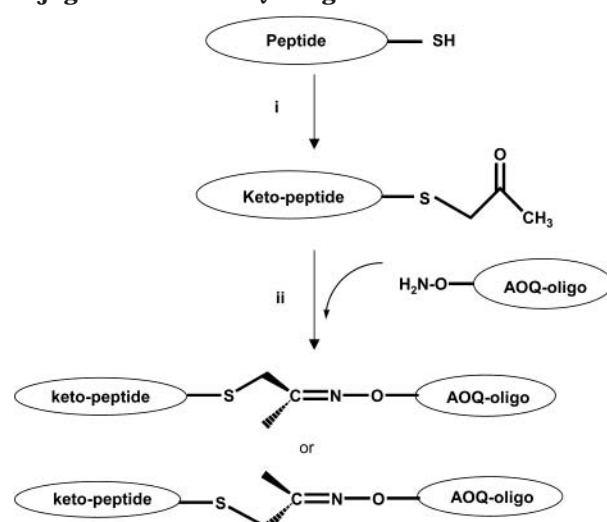
**Conjugation of AOQ-Derivatized Oligonucleotide with Peptides.** The aminooxy group reacts readily with aldehydes and ketones (15–17), and the resulting oxime linkage is very stable under physiological conditions (15, 27). This chemistry has been widely utilized for chemoselective ligation of a variety of compounds. In particular, Forget et al. have recently reported the successful preparation of peptide–oligonucleotide conjugates in which aldehyde containing peptides are conjugated with aminooxy-derivatized oligonucleotides or vice versa (15).

We have explored oxime formation to conjugate AOQ–oligonucleotides to small peptides. The AOQ group may be advantageous for this purpose because as shown above, AOQ-derivatized oligonucleotides have increased binding affinity for their RNA targets. Thus, the AOQ group could provide a duplex-stabilizing platform for chemoselective ligation of AOQ–oligonucleotides to a variety of compounds.

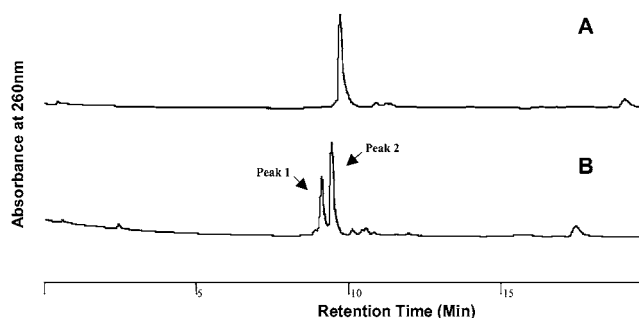
Initially, we conjugated commercially available, synthetic leupeptin to AOQ-1843. This tripeptide has a unique aldehyde group at its C-terminus that can react selectively with the aminooxy group of AOQ-1843 to form an oxime. As shown in the chromatogram in Figure 2E, the conjugation reaction was complete within 60 min at room temperature when carried out in 50% aqueous acetonitrile. The peptide–oligo conjugate was purified by C-18 reversed phase HPLC and its structure was confirmed by MALDI-TOF mass spectrometry analysis.

Conjugations between an oligonucleotide aminooxy group and a peptide aldehyde group are very efficient. Introduction of aldehyde groups into peptides can be accomplished by periodate oxidation of an N-terminus serine or threonine (27, 45), or by use of specific linker resins during solid-phase peptide synthesis (46, 47). An alternative approach would be to introduce into the peptide postsynthetically, a reactive functional group that could be conjugated with an aminooxy group of the oligonucleotide. To this end we developed a method to introduce a ketone functional group into a peptide by alkylating a cysteine residue in the peptide with bromoacetone, as illustrated in Scheme 2. The ketone functionality could be introduced anywhere in a peptide that already contains a cysteine residue or the peptide could be synthesized with a cysteine residue at its N terminus. The carbonyl group of the resulting keto-peptide then serves as a reactive site for conjugation with the aminooxy group of the oligonucleotide. This procedure is in some ways analogous to the recently reported procedure in which ketone modified DNA is conjugated with aminooxy-derivatized compounds (48).

We tested this procedure on a commercially available tetrapeptide, RGDC, and on a cysteine-modified 14 amino acid peptide derived from the transduction domain of HIV Tat protein. The RGD peptide motif has been used for cell targeting and gene delivery (49, 50), and the Tat peptide has been shown to promote the delivery of macromolecules into cells (51–53).

**Scheme 2. Synthesis of a Keto-Peptide and Conjugation to an AOQ–Oligo<sup>a</sup>**

<sup>a</sup> (i) Bromoacetone in 50% acetonitrile/water for 1 h at room temperature. (ii) 50% acetonitrile/water for 1 h at room temperature.



**Figure 6.** Reversed-phase (RP) HPLC profile of the reaction of keto-RGDC peptide and AOQ-2106 in 50% acetonitrile/water at room temperature. A 20 min linear gradient of 2–50% acetonitrile in 50 mM sodium phosphate (pH 5.8) was used. (A)  $T = 0$  h, (B)  $T = 1$  h.

The C-terminus cysteine residue of each peptide was first reacted with a 10–33-fold excess of bromoacetone to give the keto-peptide. The reaction was complete within 1 h as assayed by C-18 reversed phase HPLC. Three major peaks were observed in the chromatogram. The first peak was the unreacted bromoacetone, the second peak was the desired keto-peptide, and the third peak was the disulfide-linked peptide dimer. The keto-peptide was obtained in 50% yield for each peptide after purification by HPLC.

The keto-peptides were then reacted with the short oligo-2'-*O*-methylribonucleotide, AOQ-2106. As shown by the chromatograms in Figure 6, the conjugation reaction between keto-RGD and AOQ-2106 was complete within 1 h at room temperature. The peptide–oligonucleotide conjugate appeared as two peaks in the chromatogram. Subsequent characterization of each peak by MALDI-TOF mass spectrometry showed that they had identical molecular weights. Thus these two peaks are attributed to the two isomeric oximes shown in Scheme 2.

Keto-derivatized Tat peptide was reacted with AOQ-2016 in 50% acetonitrile/water at room temperature. Reactions were run using a 5-fold excess of keto-peptide to oligonucleotide or with a 8-fold excess of oligonucleotide to keto-peptide. Examination of the reaction mixtures by MALDI-TOF mass spectrometry showed the presence of a compound whose molecular weight was consistent with



the composition of the AOQ-2016-Tat conjugate. In addition to the conjugate, AOQ-2106 or keto-Tat peptide was also detected in the mass spectrum, depending on whether the reaction was run using an excess of oligonucleotide or an excess of keto-peptide.

Although we were able to detect the oligonucleotide–peptide conjugate by mass spectrometry, we were unable to detect the conjugate by C-18 reversed phase HPLC. A variety of solvent systems and columns were tested including those previously reported to be effective in eluting oligonucleotide–Tat conjugates (54, 55). This apparent irreversible absorption to the C-18 column appears to be a property of the conjugate because when unmodified 2106 and Tat peptide were mixed, both compounds could be detected by C-18 reversed phase HPLC.

We found that the Tat-2106 conjugate could be purified by DEAE Sephadex chromatography. The keto-Tat peptide has a net positive charge of +9, whereas AOQ-2106 has net negative charge of –4. Thus, the AOQ-2106–Tat conjugate would be expected to have a net positive charge of +5. We exploited this charge difference to purify the conjugate. Mass spectrometry showed that all of the keto-Tat could be converted to conjugate by carrying out the reaction in the presence of excess AOQ-2106. The excess AOQ-2106 was removed by simply passing the reaction mixture through a DEAE Sephadex column. The negatively charged AOQ-2106 was retained on the column, while the AOQ-2106–Tat conjugate, which is positively charged, passed through the column. The molecular weight of the purified oligo–Tat conjugate was confirmed by MALDI-TOF mass spectrometry analysis. Using this procedure, pure AOQ-2106–Tat conjugate was obtained at 39% yield.

## CONCLUSIONS

AOQ- and EOQ-conjugated oligo-2'-O-methylribonucleotides show enhanced binding affinities for complementary RNA targets. This most likely results from favorable stacking interactions between the quinoline ring and the terminal base pair of the duplex formed by the oligomer and the target. Although we could find no evidence that the aminoxy group of AOQ reacts with 5,6 double bond of cytosines in the target RNA, this functional group does provide a site for efficient conjugation of AOQ–oligonucleotides to peptides or other moieties that bear an aldehyde or ketone group. The combination of the unique reactivity of the aminoxy group and enhanced binding affinity conferred by its quinoline ring suggest that AOQ may serve as a useful platform for the preparation of novel oligonucleotide conjugates.

## ACKNOWLEDGMENT

The authors thank Dr. Eric Hildebrand for assistance with the fluorescence experiments, Dr. Anne Noronha for help obtaining the mass spectra, and Dr. David Noll for helpful comments and suggestions. This research was supported by a grant from the National Institutes of Health (GM57140).

## LITERATURE CITED

- (1) Gewirtz, A. M., Sokol, D. L., and Ratajczak, M. Z. (1998) Nucleic acid therapeutics: state of the art and future prospects. *Blood* 92, 712–736.
- (2) Bennett, C. F., and Cowsett, L. M. (1999) Application of antisense oligonucleotides for gene functionalization and target validation. *Curr. Opin. Mol. Ther.* 1, 359–371.
- (3) Bhan, P., and Miller, P. S. (1990) Photo-cross-linking of psoralen-derivatized oligonucleoside methylphosphonates to single-stranded DNA. *Bioconjugate Chem.* 1, 82–88.
- (4) Piele, U., and Englisch, U. (1989) Psoralen covalently linked to oligodeoxyribonucleotides: synthesis, sequence specific recognition of DNA and photo-cross-linking to pyrimidine residues of DNA. *Nucleic Acids Res.* 17, 285–299.
- (5) Kang, H., and Rokita, S. E. (1996) Site-specific and photo-induced alkylation of DNA by a dimethylantraquinone-oligodeoxynucleotide conjugate. *Nucleic Acids Res.* 24, 3896–3902.
- (6) Huh, N., Rege, A. A., Yoo, B., Kogan, T. P., and Kohn, H. (1996) Design, synthesis, and evaluation of mitomycin-tethered phosphorothioate oligodeoxynucleotides. *Bioconjugate Chem.* 7, 659–669.
- (7) Nagatsugi, F., Kawasaki, T., Tokuda, N., Maeda, M., and Sasaki, S. (2001) Site-directed alkylation to cytidine within duplex by the oligonucleotides containing functional nucleobases. *Nucleosides Nucleotides Nucleic Acids* 20, 915–919.
- (8) Knorre, D. G., and Vlassov, V. V. (1985) Complementary-addressed (sequence-specific) modification of nucleic acids. *Prog. Nucleic Acid Res. Mol. Biol.* 32, 291–320.
- (9) Tabone, J. C., Stamm, M. R., Gamper, H. B., and Meyer, R. B., Jr. (1994) Factors influencing the extent and regioselectivity of cross-link formation between single-stranded DNA and reactive complementary oligodeoxynucleotides. *Biochemistry* 33, 375–383.
- (10) Lukhtanov, E. A., Podyminogin, M. A., Kutuyavin, I. V., Meyer, R. B., and Gamper, H. B. (1996) Rapid and efficient hybridization-triggered cross-linking within a DNA duplex by an oligodeoxyribonucleotide bearing a conjugated cyclopropylpyrroloindole. *Nucleic Acids Res.* 24, 683–687.
- (11) Boudvillain, M., Guerin, M., Dalbès, R., Saison-Behmoaras, T., and Leng, M. (1997) Transplatin-modified oligo-(2'-O-methyl ribonucleotide)s: a new tool for selective modulation of gene expression. *Biochemistry* 36, 2925–2931.
- (12) Webb, T. R., and Matteucci, M. D. (1986) Hybridization triggered cross-linking of deoxyligoligonucleotides. *Nucleic Acids Res.* 14, 7661–7674.
- (13) Kulka, M., Wachsmann, M., Miura, S., Fischelevich, R., Miller, P. S., Ts'o, P. O., and Aurelian, L. (1993) Antiviral effect of oligo(nucleoside methylphosphonates) complementary to the herpes simplex virus type 1 immediate early mRNAs 4 and 5. *Antiviral Res.* 20, 115–130.
- (14) Um, I. H., and Buncel, E. (2000) The origin of the alpha-effect: dissection of ground-state and transition-state contributions. *J. Org. Chem.* 65, 577–582.
- (15) Forget, D., Boturyn, D., Defrancq, E., Lhomme, J., and Dumy, P. (2001) Highly efficient synthesis of peptide–oligonucleotide conjugates: chemoselective oxime and thiazolidine formation. *Chemistry* 7, 3976–3984.
- (16) Salo, H., Virta, P., Hakala, H., Prakash, T. P., Kawasaki, A. M., Manoharan, M., and Lonnberg, H. (1999) Aminoxy functionalized oligonucleotides: preparation, on-support derivatization, and postsynthetic attachment to polymer support. *Bioconjugate Chem.* 10, 815–823.
- (17) Bure, C., Lelievre, D., and Delmas, A. (2000) Identification of by-products from an orthogonal peptide ligation by oxime bonds using mass spectrometry and tandem mass spectrometry. *Rapid Commun. Mass. Spectrom.* 14, 2158–2164.
- (18) Shao, J., and Tam, J. P. (1995) Unprotected peptides as building blocks for the synthesis of peptide dendrimers with oxime, hydrazone, and thiazolidine linkages. *J. Am. Chem. Soc.* 117, 3893–3899.
- (19) Adamczyk, M., Gebler, J. C., Reddy, R. E., and Yu, Z. (2001) A chemoselective method for site-specific immobilization of peptides via aminoxy group. *Bioconjugate Chem.* 12, 139–142.
- (20) Canne, L. E., Feeré-D'Amaré, A. R., Burley, S. K., and Kent, S. B. H. (1995) Total chemical synthesis of a unique transcription factor-related protein: cmc-max. *J. Am. Chem. Soc.* 117, 2998–3007.
- (21) Rodriguez, E. C., Marcaurelle, L. A., and Bertozzi, C. R. (1998) Aminoxy-, hydrazide-, and thiosemicarbazide-functionalized saccharides: versatile reagents for glycoconjugate synthesis. *J. Org. Chem.* 63, 7134–7135.
- (22) Brask, J., and Jensen, K. J. (2000) Carbopeptides: chemoselective ligation of peptide aldehydes to an aminoxy-functionalized D-galactose template. *J. Pept. Sci.* 6, 290–299.

- (23) Forget, D., Renaudet, O., Defrancq, E., and Dumy, P. (2001) Efficient preparation of carbohydrate-oligonucleotide conjugates (COCs) using oxime bond formation. *Tetrahedron Lett.* 42, 7829–7832.
- (24) Trevisiol, E., Renard, A., Defrancq, E., and Lhomme, J. (1997) The oxyamino-aldehyde coupling reactions: an efficient method for the derivatization of oligonucleotides. *Tetrahedron Lett.* 38, 8687–8690.
- (25) Trevisiol, E., Renard, A., Defrancq, E., and Lhomme, J. (2000) Fluorescent labeling of oligodeoxyribonucleotides by the oxyamino-aldehyde coupling reaction. *Nucleosides Nucleotides Nucleic Acids* 19, 1427–1439.
- (26) Defrancq, E., and Lhomme, J. (2001) Use of an aminoxy linker for the functionalization of oligodeoxyribonucleotides. *Bioorg. Med. Chem. Lett.* 11, 931–933.
- (27) Rose, K. (1994) Facile synthesis of homogeneous artificial proteins. *J. Am. Chem. Soc.* 116, 30–33.
- (28) Brown, D. M. (1974) in *Basic Principles in Nucleic Acid Chemistry* (P. O. P. Ts'o, Ed.) pp 2–90, Academic Press, New York.
- (29) Brown, D. M., and Schell, P. (1965) Nucleotides. Part XLVIII. The reaction of hydroxylamine with cytosine and related compounds. *J. Chem. Soc.*, 208–215.
- (30) Brown, D. M., and Schell, P. (1961) The reaction of hydroxylamine with cytosine and related compounds. *J. Mol. Biol.* 3, 709–710.
- (31) Schalke, P. M., and Hall, C. D. (1975) Reactions of cytosine and cytidine with *O*-substituted hydroxylamines. *J. Chem. Soc., Perkin Trans. 1*, 2417–2422.
- (32) Hamma, T., and Miller, P. S. (1999) Syntheses of alternating oligo-2'-*O*-methylribonucleoside methylphosphonates and their interactions with HIV TAR RNA. *Biochemistry* 38, 15333–15342.
- (33) Miller, P. S., and Cushman, C. D. (1993) Triplex formation by oligodeoxyribonucleotides involving the formation of X.U.A. triads. *Biochemistry* 32, 2999–3004.
- (34) Miller, P. S., Reddy, M. P., Murakami, A., Blake, K. R., Lin, S. B., and Agris, C. H. (1986) Solid-phase syntheses of oligodeoxyribonucleoside methylphosphonates. *Biochemistry* 25, 5092–5097.
- (35) Reddy, M. P., Hanna, N. B., Farroqui, F. (1994) Fast cleavage and deprotection of oligonucleotides. *Tetrahedron Lett.* 35, 4311–4314.
- (36) Nakatani, K., Sando, S., Kumasawa, H., Kikuchi, J., and Saito, I. (2001) Recognition of guanine-guanine mismatches by the dimeric form of 2-amino-1,8-naphthyridine. *J. Am. Chem. Soc.* 123, 12650–12657.
- (37) Asseline, U., Toulme, F., Thuong, N. T., Delarue, M., Montenay-Garestier, T., and Helene, C. (1984) Oligodeoxynucleotides covalently linked to intercalating dyes as base sequence-specific ligands. Influence of dye attachment site. *Embo. J.* 3, 795–800.
- (38) Casale, R., and McLaughlin, L. W. (1990) Synthesis and properties of an oligodeoxynucleotide containing a polycyclic aromatic hydrocarbon site specifically bound to the N<sup>2</sup> amino group of a 2'-deoxyguanosine residue. *J. Am. Chem. Soc.* 112, 5264–5271.
- (39) Okamoto, A., Tanabe, K., and Saito, I. (2001) Synthesis and properties of peptide nucleic acids containing a psoralen unit. *Org. Lett.* 3, 925–927.
- (40) Nishimura, Y., Takahashi, S., Yamamoto, T., Tsuboi, M., Hattori, M., Miura, K., Yamaguchi, K., Ohtani, S., and Hata, T. (1980) On the base-stacking in the 5'-terminal cap structure of mRNA: a fluorescence study. *Nucleic Acids Res.* 8, 1107–1119.
- (41) Guckian, K. M., Schweitzer, B. A., Ren, R. X.-F., Sheils, C. J., Paris, P. L., Tahmassebi, D. C., Kool, E. T. (1996) Experimental measurement of aromatic stacking affinities in the context of duplex DNA. *J. Am. Chem. Soc.* 118, 8182–8183.
- (42) Ho, W. C., Steinbeck, C., and Richert, C. (1999) Solution structure of the aminoacyl-capped oligodeoxyribonucleotide duplex (W-TGCGCAC)(2). *Biochemistry* 38, 12597–12606.
- (43) Okamoto, A., Tanabe, K., Dohno, C., and Saito, I. (2002) Modulation of remote DNA oxidation by hybridization with peptide nucleic acids (PNA). *Bioorg. Med. Chem.* 10, 713–718.
- (44) Brown, D. M., Coe, P. F., and Green, D. P. L. (1971) The synthesis and some properties of 1-(2-amino-oxethyl)cytosines. *J. Chem. Soc.* 867–869.
- (45) Geoghegan, K. F., and Stroh, J. G. (1992) Site-directed conjugation of nonpeptide groups to peptides and proteins via periodate oxidation of a 2-amino alcohol. Application to modification at N-terminal serine. *Bioconjugate Chem.* 3, 138–146.
- (46) Fehrentz, J. A., Paris, M., Heitz, A., Velek, J., Winternitz, F., and Martinez, J. (1997) Solid-phase synthesis of C-terminal peptide aldehydes. *J. Org. Chem.* 62, 6792–6796.
- (47) Lelievre, D., Chabane, H., and Delmas, A. (1998) Simple and efficient solid-phase synthesis of unprotected peptide aldehyde for peptide segment ligation. *Tetrahedron Lett.* 39, 9675–9678.
- (48) Dey, S., and Sheppard, T. L. (2001) Ketone-DNA: a versatile postsynthetic DNA decoration platform. *Org. Lett.* 3, 3983–3986.
- (49) Aris, A., and Villaverde, A. (2000) Molecular organization of protein-DNA complexes for cell-targeted DNA delivery. *Biochem. Biophys. Res. Commun.* 278, 455–461.
- (50) Koizumi, N., Mizuguchi, H., Hosono, T., Ishii-Watabe, A., Uchida, E., Utoguchi, N., Watanabe, Y., and Hayakawa, T. (2001) Efficient gene transfer by fiber-mutant adenoviral vectors containing RGD peptide. *Biochim. Biophys. Acta* 1568, 13–20.
- (51) Snyder, E. L., and Dowdy, S. F. (2001) Protein/peptide transduction domains: potential to deliver large DNA molecules into cells. *Curr. Opin. Mol. Ther.* 3, 147–152.
- (52) Morris, M. C., Depollier, J., Mery, J., Heitz, F., and Divita, G. (2001) A peptide carrier for the delivery of biologically active proteins into mammalian cells. *Nat. Biotechnol.* 19, 1173–1176.
- (53) Schwarze, S. R., and Dowdy, S. F. (2000) In vivo protein transduction: intracellular delivery of biologically active proteins, compounds and DNA. *Trends Pharmacol. Sci.* 21, 45–48.
- (54) Stetsenko, D. A., and Gait, M. J. (2000) Efficient conjugation of peptides to oligonucleotides by "native ligation". *J. Org. Chem.* 65, 4900–4908.
- (55) Tung, C. H., Wang, J., Leibowitz, M. J., and Stein, S. (1995) Dual-specificity interaction of HIV-1 TAR RNA with Tat peptide-oligonucleotide conjugates. *Bioconjugate Chem.* 6, 292–295.

BC025638+

# ***N*-Succinimidyl 3-[<sup>131</sup>I]Iodo-4-phosphonomethylbenzoate ([<sup>131</sup>I]SIPMB), a Negatively Charged Substituent-Bearing Acylation Agent for the Radioiodination of Peptides and mAbs**

Sriram Shankar, Ganesan Vaidyanathan,\* Donna Affleck, Phillip C. Welsh, and Michael R. Zalutsky

Department of Radiology, Duke University Medical Center, Box 3808, Durham, North Carolina 27710.  
Received November 5, 2002; Revised Manuscript Received January 3, 2003

An important criterion in design of acylation agents for the radioiodination of internalizing monoclonal antibodies (mAbs) is to maximize the retention of radioiodine in the tumor following mAb intracellular processing. We have previously shown that labeling methods that generate positively charged catabolites have enhanced tumor retention. Herein we have extended this strategy to investigate the potential utility of labeling internalizing mAbs with an acylation agent that yielded labeled catabolites that would be negatively charged at lysosomal pH. The negatively charged acylation agent, *N*-succinimidyl 3-[<sup>131</sup>I]iodo-4-phosphonomethylbenzoate ([<sup>131</sup>I]SIPMB), was prepared from its tin precursor, *N*-succinimidyl 4-di-*tert*-butylphosphonomethyl-3-trimethylstannylbenzoate (*t*Bu-SPMTB), in 40% radiochemical yield. The free acid, 3-[<sup>131</sup>I]iodo-4-phosphonomethylbenzoic acid ([<sup>131</sup>I]IPMBA), was also prepared from the corresponding precursor, 4-di-*tert*-butylphosphonomethyl-3-trimethylstannylbenzoic acid (*t*Bu-PMTBA), in 80% radiochemical yield. The rapidly internalizing mAb L8A4 was conjugated to [<sup>131</sup>I]SIPMB in 25–40% yield with preservation of its immunoreactivity. Internalization and processing in the U87ΔEGFR glioma cell line was studied in a paired label format with L8A4 labeled with <sup>125</sup>I using the Iodogen method. Retention of initially bound radioactivity in these cells at 24 h from [<sup>131</sup>I]SIPMB-labeled mAb was approximately 6-fold higher than that for directly labeled mAb. Catabolite analysis demonstrated that this difference reflected an order of magnitude higher retention of low molecular weight species in these cells. The [<sup>131</sup>I]SIPMB-L8A4 conjugate was intact over the first 2 h; thereafter, lysine-[<sup>131</sup>I]SIPMB was the predominant catabolite. In contrast, L8A4 labeled using Iodogen rapidly gave rise to mono-[<sup>125</sup>I]iodotyrosine within 2 h, which then cleared rapidly from the cells. These results suggest that SIPMB could be a potent candidate for labeling internalizing mAbs and warrant further study.

## INTRODUCTION

Radiolabeled monoclonal antibodies (mAbs),<sup>1</sup> genetically derived mAb fragments, and peptides are attractive approaches for the targeted radiotherapy of tumors (Goel et al., 2001; Murray, 2000; Illidge and Brock, 2000; de Jong et al., 2002). Many of these potential radiotherapeutics are rapidly internalized in tumor cells after binding to their receptor or antigenic target (Zalutsky,

1997). Therefore, it is important to utilize labeling methods that result in a high degree of retention of the radionuclide in the tumor cell after intracellular processing of the labeled molecule. Conventional radioiodination methods yield molecules that are susceptible to the action of endogenous deiodinases; furthermore, the monoiodotyrosine arising from the lysosomal degradation of internalizing mAbs are rapidly eliminated from the tumor cells (Geisler et al., 1992; Press et al., 1996).

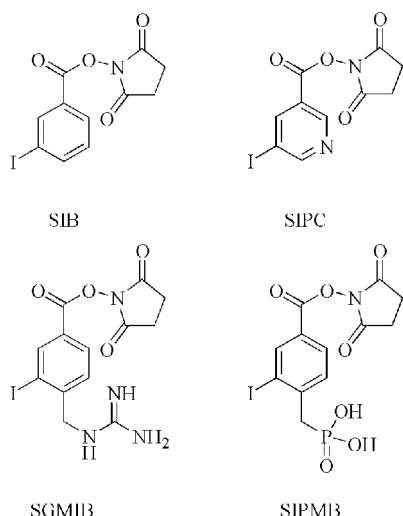
To overcome this problem, residualizing labels have been developed, so named because the catabolites generated from labeled internalizing proteins are trapped within the lysosomes. The first strategy investigated was the use of radioiodinated nonmetabolized disaccharide–tyramine conjugates (Ali et al., 1990; Thorpe et al., 1993; Stein et al., 1995). Although enhanced intracellular retention could be achieved, unacceptably low labeling yields and higher spleen and liver uptake due to aggregate formation during labeling were deterrents to their clinical application. Other approaches that are being pursued include the use of radioiodinated proteolytically inert D-amino acid prosthetic groups, either alone (Foulon et al., 2000; 2001) or conjugated to DTPA (Govindan et al., 1999).

Another approach is the use of labeled templates with basic functionalities in their structure with the rationale that radiolabeled catabolites bearing such moieties will be protonated at lysosomal pH of ~5 and hence will be trapped within the lysosomes (Chart 1). The usefulness

\* To whom correspondence should be addressed. Telephone: (919) 684-7811, FAX: (919) 684-7122, e-mail: ganesan.v@duke.edu.

<sup>1</sup> Abbreviations: CMC, 1-cyclohexyl-3-(2-morpholinoethyl)-carbodiimide metho-*p*-toluenesulfonate; DTPA, diethylenetriamine pentaacetic acid; EGFRvIII, epidermal growth factor receptor variant III; GMIBA, 4-guanidinomethyl-3-iodobenzoic acid; INA, 5-iodo-3-nicotinic acid; IPMBA, 3-iodo-4-phosphonomethylbenzoic acid; IR, immunoreactive fraction; kDa, kilo-Dalton; mAb, monoclonal antibody; PMSF, phenylmethylsulfonyl fluoride; ScFv, single chain fragment; SGMIB, *N*-succinimidyl 4-guanidinomethyl-3-iodobenzoate; SIB, *N*-succinimidyl 3-iodobenzoate; SIPC, *N*-succinimidyl 5-iodopyridine-3-carboxylate; SIPMB, *N*-succinimidyl 3-iodo-4-phosphonomethylbenzoate; *t*Bu-IPMBA, 3-iodo-4-di-*tert*-butylphosphonomethylbenzoic acid; *t*Bu-PMTBA, 4-di-*tert*-butylphosphonomethyl-3-trimethylstannylbenzoic acid; *t*Bu-SIPMB, *N*-succinimidyl 3-iodo-4-di-*tert*-butylphosphonomethylbenzoate; *t*Bu-SPMTB, *N*-succinimidyl 4-di-*tert*-butylphosphonomethyl-3-trimethylstannylbenzoate; TCA, trichloroacetic acid; TFA, trifluoroacetic acid; TMSE, 2-(trimethylsilyl)ethyl.



**Chart 1. Commonly Used Acyl-Transfer Agents for Labeling Monoclonal Antibodies.**

of this approach has been corroborated by work done in our laboratory using the mAb L8A4, which reacts with the tumor specific epidermal growth factor receptor deletion mutant, EGFRvIII (Wikstrand et al., 1995, 1997). The intracellular retention in vitro of L8A4 labeled with *N*-succinimidyl 3- $^{131}\text{I}$ iodopyridine-5-carboxylate ( $^{131}\text{I}$ SIPC) increased by up to 65% compared to the same mAb radioiodinated via Iodogen or using *N*-succinimidyl 3- $^{131}\text{I}$ iodobenzoate ( $^{131}\text{I}$ SIB) (Reist et al., 1996; 1997). Even higher tumor retention (300–400% higher than directly labeled mAb) was achieved both in vitro and in vivo for L8A4 labeled with *N*-succinimidyl 4-guanidinomethyl-3- $^{131}\text{I}$ iodobenzoate ( $^{131}\text{I}$ SGMIB), an acylation agent containing a more basic guanidine moiety (Vaidyanathan et al., 2001; 2002).

Selection of catabolites that would be positively charged in order for residualization of radioactivity was based on the well-known trapping of cationic dyes such as chloroquine in lysosomes (Holtzman, 1989). If the mechanism of retention is inhibition of exocytosis of labeled catabolites by passive transport across lysosomal and/or cell membranes due to their charge, then labeling methods that generate negatively charged catabolites should work as well. To test this hypothesis, we sought a phosphonic acid group-containing derivative of SIB, the prototypical acylation agent developed in our laboratory for the radioiodination of mAbs (Zalutsky and Narula, 1987). Herein, we present the no-carrier-added synthesis of *N*-succinimidyl 3- $^{131}\text{I}$ iodo-4-(phosphonomethyl)benzoate ( $^{131}\text{I}$ SIPMB) from a tin precursor and its conjugation to the anti-EGFRvIII mAb L8A4. Internalization assays and radiolabeled catabolite analyses were performed to determine the potential utility of  $^{131}\text{I}$ SIPMB for labeling internalizing mAbs.

## MATERIALS AND METHODS

**General.** All chemicals were purchased from Aldrich unless otherwise noted. Sodium  $^{125}\text{I}$ iodide and sodium  $^{131}\text{I}$ iodide with specific activities of 1200 Ci/mmol and 2200 Ci/mmol, respectively, were obtained from Perkin-Elmer Life Sciences. Commercially available 3-iodotyrosine (Sigma) was used as an HPLC standard in the catabolite assays.

Melting points were determined on a Haake Buchler apparatus and were uncorrected. High-pressure liquid chromatography was performed using one of three systems: (1) a Beckman System Gold HPLC equipped with

a Model 126 programmable solvent module, a Model 166 NM variable wavelength detector, a Model 170 radioisotope detector, and Beckman System Gold remote interface module SS420X, using a 32 karat software (3.1 build 22) run on an IBM NetVista computer with Windows NT v 4.00.1381 workstation and Intel Pentium III processor with SSE; (2) a Waters Delta 600 semipreparative HPLC equipped with Millennium software, a Delta 600 dual injector option, a 600 Pump, a 600E controller, and a 2487 dual  $\lambda$  absorbance detector; or (3) a Perkin-Elmer Series 4 Liquid Chromatograph connected to a Perkin-Elmer LC-95 UV/visible spectrophotometer detector and a Perkin-Elmer LCI-100 Laboratory Computing Integrator. Methods were programmed using a Perkin-Elmer 6312 display terminal. For reversed-phase chromatography, a Waters  $\mu$  Bondapak C18 (10  $\mu\text{m}$ ,  $3.9 \times 300$  mm) column, a Waters XTerra RP<sub>18</sub> column (5  $\mu\text{m}$ ,  $4.6 \times 250$  mm), or a Bondclone 10 C18 column (10  $\mu\text{m}$ ,  $3.9 \times 300$  mm, Phenomenex, Torrance, CA) was used. Preparative reversed-phase HPLC was performed using a Waters XTerra RP<sub>18</sub> (7  $\mu\text{m}$ ,  $19 \times 150$  mm) column. Normal-phase HPLC was done using a  $4.6 \times 250$  mm Partisil (10  $\mu$ ) silica column (Alltech, Deerfield, IL). Size-exclusion HPLC was performed using a  $7.5 \times 600$  mm Tosohaas TSK gel G3000 SW (10  $\mu\text{m}$ ) gel filtration column (Montgomeryville, PA) eluted with PBS at 1 mL/min. Analytical TLC utilized aluminum-backed sheets (Silica gel 60 F<sub>254</sub>), and normal-phase column chromatography was performed using silica gel 60, both obtained from EM Science (Gibbstown, NJ). Column chromatographic fractions were collected either manually or using a Gilson model 203 micro fraction collector (Middleton, WI) or an ISCO Foxy 200 fraction collector (Lincoln, NE), and products were identified by TLC. In some cases, an ISCO UA-6 UV-Vis detector was placed between the column outlet and the fraction collector to identify fractions. Preparative thick layer chromatography was done using  $20 \times 20$  cm, 1000  $\mu$  plates (Whatman, Clifton, NJ). Before applying the sample, the plates were run in ethyl acetate to clean the plates of any adsorbed impurities and then air-dried for 15–20 min. Radio-TLC was initially analyzed using a System 200 Imaging Scanner (BioScan, Washington, D.C.) and then cut into strips and counted on an automated gamma counter (LKB 1282, Wallac, Finland). Proton and carbon NMR spectra were obtained on either a Varian Mercury 300 spectrometer or a Varian Mercury 400 spectrometer. Chemical shifts are reported in  $\delta$  units; solvent peaks were referenced appropriately. Mass spectra were obtained on a Hewlett-Packard GC/MS/DS Model HP-5988A instrument, or an Applied Biosystems DE Pro, or on a JEOL SX-102 high-resolution mass spectrometer.

**Cells, mAb, and Culture Conditions.** The U87 $\Delta$ EGFR cell line was established from U87 MG glioblastoma cells transfected with EGFRvIII cDNA (Nishikawa et al., 1994). Cells were grown in zinc option media (Life Technologies, Inc., Grand Island, NY). On the basis of quantitative flow cytometry and Scatchard analyses, this line expresses an average of  $4\text{--}13 \times 10^5$  EGFRvIII molecules per cell in cell culture (Wikstrand et al., 1997). The purification and characterization of mAb L8A4, a murine IgG<sub>1</sub>, have been reported (Wikstrand et al., 1995). It reacts specifically with and has high affinity for the 145-kDa deletion mutant EGFRvIII molecule present on many human malignancies including breast, lung, and ovarian carcinomas, as well as on malignant gliomas (Wikstrand et al., 1997).

**4-Bromomethyl-3-iodobenzoic Acid (2).** Photolytic benzyl bromination of 3-iodo-4-methylbenzoic acid (1,

1.31 g, 5 mmol) was performed by refluxing with *N*-bromosuccinimide (890 mg, 5.0 mmol) and catalytic azo-*N,N*-biscyclohexylcarbonitrile (122 mg, 0.5 mmol) in 50 mL of 1,2-dichloroethane for 5 h under argon in the presence of an incandescent lamp. The reaction mixture was diluted with 50 mL of CH<sub>2</sub>Cl<sub>2</sub>, washed with 100 mL of water, and 50 mL of brine, dried, and concentrated to give 2.17 g of the crude product mixture as a yellow oil. Column chromatographic purification using a stepwise gradient of 10 to 50% EtOAc/hexane containing 1% AcOH gave 1.06 g (62%) of **2** as a white solid: mp 199–202 °C. <sup>1</sup>H NMR (CD<sub>3</sub>OD, 400 MHz) δ 8.45 (d, *J* = 1.54 Hz), 7.98 (dd, 1H, *J* = 7.86, 1.54 Hz), 7.61 (d, 1H, *J* = 8.03 Hz), 4.68 (s, 2H). MS (DIPCI) *m/z* 341 (MH<sup>+</sup>), 261 (MH<sup>+</sup> – Br). HRMS (FAB<sup>–</sup>) Calcd for C<sub>8</sub>H<sub>5</sub><sup>79</sup>BrIO<sub>2</sub> (M – H)<sup>–</sup>: 338.8518, Found 338.8518.

**3-Iodo-4-di-*tert*-butylphosphonomethylbenzoic Acid (tBu-IPMBA, 3).** Di-*tert*-butyl phosphite (740 mg, 3.8 mmol) in 0.5 mL of anhydrous THF was reacted with 3.8 mL of potassium *tert*-butoxide (1.0 M in THF) at 0 °C for 1 h under argon. To this homogeneous solution was added a solution of **2** (260 mg, 0.75 mmol) in 5 mL of THF, and the reaction mixture was stirred under argon at reflux temperature for 1 h. Excess unreacted base was decomposed by reaction with ca. 2 mL of MeOH. All solvents were removed by rotary evaporation, and the residue was adsorbed on silica and directly chromatographed using a stepwise gradient of 40 to 75% EtOAc/hexane containing 1% AcOH to give 183 mg (57%) of the product as an off-white solid: mp 163–165 °C. <sup>1</sup>H NMR (CD<sub>3</sub>OD, 300 MHz) δ 8.46 (s, 1H), 7.52 (dd, 1H, *J* = 8.0, 2.9 Hz), 7.04 (dd, 1H, *J* = 8.1, 1.0 Hz), 3.41 (d, 2H, *J* = 22.4 Hz), 1.46 (s, 18H). <sup>13</sup>C NMR (CD<sub>3</sub>OD, 75 MHz) δ 168.0, 143.2, 141.9, 132.1, 131.7, 130.1, 101.8, 84.8, 43.8, 30.7. MS (FAB<sup>+</sup>) *m/z* 455.04 (MH<sup>+</sup>). HRMS (FAB<sup>+</sup>) Calcd for C<sub>16</sub>H<sub>25</sub>IO<sub>5</sub>P (MH<sup>+</sup>): 455.0484, Found 455.0497.

**4-Di-*tert*-butylphosphonomethyl-3-trimethylstannylbenzoic Acid (tBu-PMTBA, 4).** To a solution of **3** (80 mg, 0.16 mmol) in 2 mL of dioxane were added hexamethylditin (272 mg, 0.83 mmol) and bis(triphenylphosphine)palladium(II) chloride (12 mg, 0.016 mmol), and the heterogeneous mixture was stirred at reflux temperature under argon for 1 h. The insolubles were filtered over Celite, and unreacted tin reagent and other highly nonpolar components were eluted over a short column of silica gel using hexane. The polar components were eluted with neat EtOAc and concentrated and were subjected to preparative TLC purification with 35% EtOAc/hexane containing 1% AcOH to give 11 mg (13%) of **4** as a pale yellow oil: <sup>1</sup>H NMR (CDCl<sub>3</sub>, 300 MHz) δ 8.13 (s, 1H), 7.96 (d, 1H, *J* = 7.8 Hz), 7.58 (s, 1H, *J* = 6.5 Hz), 3.16 (d, 2H, *J* = 22.3 Hz), 1.38 (s, 18H), 0.38 (s, 9H, *J*<sub>Sn–H</sub> = 26.5 Hz). MS (FAB<sup>–</sup>) *m/z* 491.04 (M – H)<sup>–</sup>, 434.98 (M – C<sub>4</sub>H<sub>9</sub>). HRMS (FAB<sup>+</sup>) Calcd for C<sub>18</sub>H<sub>30</sub>O<sub>5</sub>P<sup>116</sup>Sn (M – CH<sub>3</sub>)<sup>+</sup>: 473.0848, Found 473.0861.

**N-Succinimidyl 3-Iodo-4-di-*tert*-butylphosphonomethylbenzoate (tBu-SIPMB, 5).** To a solution of **3** (70 mg, 0.165 mmol) in 1 mL of anhydrous THF were added *N*-hydroxysuccinimide (96 mg, 0.83 mmol) and 1-cyclohexyl-3-(2-morpholinoethyl)carbodiimide metho-*p*-toluenesulfonate (CMC; 354 mg, 0.83 mmol), and the heterogeneous mixture was stirred for 3 h at ambient temperature under a flow of argon. The product mixture was filtered through a sintered glass funnel, the residue was washed with EtOAc, and the filtrate was concentrated to give 189 mg of the crude product. Preparative TLC purification using 40% EtOAc/1% AcOH/hexane afforded 84 mg (93% yield) of **5** as an oil: <sup>1</sup>H NMR (CDCl<sub>3</sub>, 400 MHz) δ 8.6 (d, 1H, *J* = 1.4 Hz), 8.03 (dd,

1H, *J* = 8.2, 1.0 Hz), 7.62 (dd, 1H, *J* = 8.2, 2.7 Hz), 3.36 (d, 2H, *J* = 22.6 Hz), 2.91 (br s, 4H), 1.46 (s, 18H). <sup>13</sup>C NMR (CDCl<sub>3</sub>, 100 MHz) δ 169.1, 160.3, 144.9, 141.2, 130.9, 129.7, 124.6, 101.2, 83.3, 30.4, 25.6, 20.7. MS (FAB) *m/z* 552.1 (M)<sup>+</sup>, 496.0 (M – isobutylene)<sup>+</sup>. HRMS (EI) Calcd for C<sub>20</sub>H<sub>28</sub>O<sub>7</sub>INP (M)<sup>+</sup>: 552.0648, Found 552.0649.

**N-Succinimidyl 4-Di-*tert*-butylphosphonomethyl-3-trimethylstannylbenzoate (tBu-SPMTB, 6).** To a solution of **5** (27 mg, 0.05 mmol) in 0.5 mL of anhydrous dioxane were added hexamethylditin (65 mg, 0.2 mmol) and catalytic Pd(TPP)<sub>2</sub>Cl<sub>2</sub> (8 mg, 0.01 mmol), and the heterogeneous reaction mixture was stirred at reflux temperature for 45 min. The reaction mixture turned black almost instantly upon commencing reflux. The Pd catalyst and inorganic salts were filtered over Celite. The tin reagent and other nonpolar byproducts were removed by elution over a short column of silica using hexane following which the stannylated product and other polar components were eluted with EtOAc. Preparative TLC purification of this product mixture using 100% EtOAc afforded 21 mg (70%) of **6** as a pale yellow oil: <sup>1</sup>H NMR (CDCl<sub>3</sub>, 300 MHz) δ 8.14 (s, 1H), 8.0 (dd, 1H, *J* = 8.24, 1.65 Hz), 7.65 (dd, 1H, *J* = 8.24, 2.40 Hz), 3.16 (d, 2H, *J* = 23.4 Hz), 2.91 (s, 4H), 1.40 (s, 18H), 0.39 (s, 9H, *J*<sub>Sn–H</sub> = 27.5 Hz). <sup>13</sup>C NMR (CDCl<sub>3</sub>, 75 MHz, selected peaks) δ 169.4, 148.1, 144.9, 138.2, 129.8, 82.7, 30.4, 30.3, 25.8. MS (FAB<sup>+</sup>) *m/z* 588.0 (M<sup>+</sup>), 532.0 (M – C<sub>4</sub>H<sub>8</sub>)<sup>+</sup>, 491 (M – succinimide). HRMS (FAB<sup>+</sup>) Calcd for C<sub>23</sub>H<sub>36</sub>NO<sub>7</sub>P<sup>116</sup>Sn (M<sup>+</sup>): 586.1172, Found 586.1170; Calcd for C<sub>23</sub>H<sub>36</sub>NO<sub>7</sub>P<sup>114</sup>-Sn: 584.1169, Found 584.1170.

**N-Succinimidyl 3-iodo-4-phosphonomethylbenzoate (SIPMB, 7).** A sample of **7** for a HPLC standard was obtained by deprotection of **5** (10 mg, 0.02 mmol) with 100 μL each TFA and CH<sub>2</sub>Cl<sub>2</sub> for 10 min. Excess TFA and other volatiles were removed under a stream of argon, and traces of the acid were removed by repeated coevaporation with CH<sub>2</sub>Cl<sub>2</sub> and hexane. <sup>1</sup>H NMR (CD<sub>3</sub>CN, 300 MHz) δ 8.54 (s, 1H), 8.05 (d, 1H, *J* = 7.83 Hz), 7.60 (m, 1H), 3.47 (d, 2H, *J* = 22.25 Hz), 2.83 (s, 4H). MS (FAB<sup>–</sup>) *m/z* 437.98 (M – H)<sup>–</sup>. HRMS (FAB<sup>–</sup>) Calcd for C<sub>12</sub>H<sub>10</sub>INO<sub>7</sub>P (M – H)<sup>–</sup>: 437.9240, Found 437.9245.

**3-Iodo-4-phosphonomethylbenzoic Acid (IPMBA, 8).** A sample of **8** for a HPLC standard was obtained as above by deprotection of **3** (8 mg, 0.02 mmol) for 15 min in 0.5 mL of TFA. Excess TFA was removed under a flow of argon and the residue coevaporated with CH<sub>2</sub>Cl<sub>2</sub> and hexane to give 6.5 mg (100%) of a white solid: mp 218–221 °C. <sup>1</sup>H NMR (CD<sub>3</sub>OD, 300 MHz) δ 8.45 (s, 1H), 7.94 (dd, 1H, *J* = 7.76, 1.44 Hz), 7.56 (dd, 1H, *J* = 7.96, 2.47 Hz), 3.43 (d, 2H, *J* = 22.4 Hz). MS (FAB<sup>–</sup>) *m/z* 340.81 (M – H)<sup>–</sup>. HRMS (FAB<sup>–</sup>) Calcd for C<sub>8</sub>H<sub>7</sub>IO<sub>5</sub>P (M – H)<sup>–</sup>: 340.9076, Found 340.9081. Analytical reversed-phase HPLC was performed to assay the purity of the sample using 0.1% TFA/water (A) and 0.1% TFA/CH<sub>3</sub>CN (B) using the following gradient: 95% A held for 10 min and ramped over 10 min to 95% B, held at 95% B for 5 min. *t*<sub>R</sub> = 19 min, with >95% purity.

**3-[<sup>131</sup>I]Iodo-4-di-*tert*-butylphosphonomethylbenzoic Acid (<sup>131</sup>I-3).** The radioiodination of tBu-PMTBA **4** was performed using a variation of conditions previously reported for other compounds (Vaidyanathan et al., 1998). Typically, to a vial containing 2–3 mCi of [<sup>131</sup>I]-iodide in 1–3 μL of NaOH was added ca. 0.4 mg of *N*-chlorosuccinimide in 10 μL of AcOH. The vial was vortexed and 0.2–0.3 mg of the tin precursor **4** in 10 μL of AcOH was added. The reaction mixture was vortexed again and maintained at room temperature for 30–45 min. The product (*t*<sub>R</sub> = 15 min) was isolated in ~80%



radiochemical yield from a normal-phase HPLC column eluted in isocratic mode with 50:50:0.1 EtOAc/hexane/AcOH.

**N-Succinimidyl 3- $^{131}\text{I}$ Iodo-4-di-*tert*-butylphosphonomethylbenzoate ( $^{131}\text{I}$ -5).** 1) Using the procedure outlined above,  $^t\text{Bu}$ -SPMTB **6** was radioiodinated to give  $^{131}\text{I}$ -5 in 40% radiochemical yield. The product ( $t_{\text{R}} = 33.0$  min) was isolated from a normal-phase HPLC column eluted at 1 mL/min with isocratic 50:50:0.1 EtOAc/hexane/AcOH. 2) Alternatively,  $^{131}\text{I}$ -3 synthesized as described earlier was reacted with 25  $\mu\text{L}$  each of 0.1 M disuccinimidyl carbonate (DSC) and pyridine in  $\text{CH}_3\text{CN}$  for 15 min at 75  $^\circ\text{C}$  (Vaidyanathan and Zalutsky, 1994). The reaction mixture was injected on a normal-phase HPLC column eluted with isocratic 50:50:0.1 EtOAc/hexane/AcOH to afford the product ( $t_{\text{R}} = 33.0$  min) in ~80% radiochemical yield.

**N-Succinimidyl 3- $^{131}\text{I}$ Iodo-4-phosphonomethylbenzoate ( $^{131}\text{I}$ -7).** Deprotection of the *tert*-butyl groups of  $^{131}\text{I}$ -5 was achieved readily by reaction with 100  $\mu\text{L}$  of TFA for 15 min at room temperature. All volatiles were removed by evaporation under a stream of argon. Persistent traces of TFA were removed by repeated coevaporation with EtOAc before coupling to mAb.

**3- $^{131}\text{I}$ Iodo-4-phosphonomethylbenzoic Acid ( $^{131}\text{I}$ -8).** Deprotection of [ $^{131}\text{I}$ ]-3 to [ $^{131}\text{I}$ ]-8 was performed as outlined above. Trace amounts of TFA were removed likewise by repeated coevaporation with EtOAc under a stream of argon.

**Glycine and Lysine Conjugate Synthesis.** These were prepared on a micromolar scale to be used principally as HPLC standards. The products were isolated by semipreparative reversed-phase HPLC and were characterized by mass spectrometry. The conditions for HPLC were as follows; a RP XTerra column was eluted with the following gradient consisting of 0.2% (v/v) HOAc in water (A) and 0.2% (v/v) HOAc in methanol (B) at 10 mL/min: Initial concentration of 5% B for 15 min was increased to 70% B over 10 min, maintained at 70% B for 5 min, and then increased to 100% B over 5 min.

**L-Lysine Conjugate of 4-Phosphonomethyl-3-iodobenzoic Acid.** To a solution of **5** (5.5 mg, 10.0  $\mu\text{mol}$ ) in 60  $\mu\text{L}$  of THF was added a solution of *N*- $\epsilon$ -Boc-L-lysine in 5  $\mu\text{L}$  of 0.1 M borate buffer, pH 8.5 (11.1 mg in 5  $\mu\text{L}$ , 45.0  $\mu\text{mol}$ ), and the mixture was stirred overnight at room temperature. THF was evaporated, and the residue was treated at room temperature for 15 min with 100  $\mu\text{L}$  of TFA. Excess TFA was evaporated under a stream of argon and residual traces of TFA were removed by coevaporation with methanol. The product ( $t_{\text{R}} = 28$  min) was isolated by semipreparative reversed-phase HPLC. MS (FAB $^-$ )  $m/z$  469.20 ( $\text{M} - \text{H}$ ) $^-$ .

**Glycine Conjugate of 4-Phosphonomethyl-3-iodobenzoic Acid.** To a solution of **5** (5.5 mg, 10.0  $\mu\text{mol}$ ) in 60  $\mu\text{L}$  of anhydrous THF was added a solution of glycine (3.5 mg, 50  $\mu\text{mol}$ ) in 5  $\mu\text{L}$  of 0.1 M borate pH 8.5, and the heterogeneous reaction mixture was stirred overnight at room temperature. The THF was evaporated, and the residue was treated at room temperature for 15 min with 100  $\mu\text{L}$  of TFA. Excess TFA was evaporated under a stream of argon, and residual traces of TFA were removed by coevaporation with methanol. The product ( $t_{\text{R}} = 32.5$  min) was isolated by semipreparative reversed-phase HPLC. MS (FAB $^-$ )  $m/z$  397.92 ( $\text{M} - \text{H}$ ) $^-$ . HRMS (FAB $^-$ ) Calcd for  $\text{C}_{10}\text{H}_{10}\text{INO}_6\text{P}$  ( $\text{M} - \text{H}$ ) $^-$ : 397.9291, Found 397.9295.

**Radiolabeling of the mAb L8A4.** 1. *Iodogen method.* To a  $1/2$ -dram vial coated with 10  $\mu\text{g}$  of Iodogen was added a solution of L8A4 in phosphate buffer, pH 7.14 (100  $\mu\text{L}$ ,

~2 mg/mL) and 1–2  $\mu\text{L}$  of  $^{125}\text{I}$  (0.5–1.0 mCi) in 0.1 N NaOH. The mixture was incubated at room temperature for 20 min, and the labeled mAb was isolated by gel filtration over a PD10 column (Amersham Biosciences, Piscataway, NJ) eluted with PBS.

2. *Using [ $^{131}\text{I}$ ]-SIPMB.*  $^{131}\text{I}$ -7 was coupled with ca. 150  $\mu\text{g}$  of mAb (1.5–2.9 mg/mL) in borate buffer (pH 8.5) for 30 min at room temperature. The radiolabeled mAb conjugate was isolated by filtration over a PD10 column eluted with PBS affording the acylated mAb in 25–40% yield.

**Octanol–Water Partition Coefficient.** The partition coefficient for  $^{131}\text{I}$ -8 was determined at two different pH values using PBS of pH 7.40 and 4.75. The buffer and *n*-octanol were each presaturated with the other prior to the experiment. About 250 000 CPM of [ $^{131}\text{I}$ ]-8 in 5–10  $\mu\text{L}$  of PBS were added in triplicate to a mixture of 1 mL each of *n*-octanol and buffer, and the contents were mixed thoroughly by vortexing for 1–2 min. The layers were separated by centrifugation. A 50  $\mu\text{L}$  aliquot of each layer in duplicate from each tube was withdrawn and counted for radioactivity, and the ratios of activities in *n*-octanol and buffer were calculated. The entire experiment was repeated twice.

#### Evaluation of Immunoreactivity of Labeled mAbs.

The assays were conducted using magnetic beads whose surfaces were coated with the extracellular domain of EGFRvIII or, as a negative control, BSA (Foulon et al., 2000). Specific binding was taken as the difference between the values obtained for the positive and the negative controls. The immunoreactive fraction of the mAb was determined according to the method of Lindmo (Lindmo et al., 1984).

**Internalization Assays.** Assays were performed in a paired-label format with U87 $\Delta$ EGFR cells at a density of  $5 \times 10^5$  cells per well as described (Vaidyanathan et al., 2001). Briefly, medium containing 1  $\mu\text{Ci}$  (0.5–1.0  $\mu\text{g}$  each, mAb excess) of the labeled mAbs was added, and the cells were incubated for 1 h at 4  $^\circ\text{C}$ . After washing, the cells were brought to 37  $^\circ\text{C}$ , and processed in triplicate at 0, 1, 2, 4, 8–10, 16, and 24 h as follows: The surface-bound radioactivity was removed by washing the cells with pH 2 Zinc Option medium, and the cells were solubilized in 0.5 mL of 0.5 N NaOH to determine internalized activity. Counts in the cell culture supernatants, acid washes (cell surface-bound), and the cell lysates (internalized) were expressed as the percentage of activity initially bound to the cells after the 1 h incubation at 4  $^\circ\text{C}$ .

**Paired-Label in Vitro Catabolism of L8A4 Labeled via SIPMB and Iodogen Methods.** To compare the in vitro catabolism of mAbs labeled using SIPMB (7) and Iodogen, an internalization assay was performed as above using about 1–3  $\mu\text{Ci}$  of each labeled mAb. After the surface-bound radioactivity was removed with acid washing, the cell pellets were lysed for 10 min at room temperature with 200  $\mu\text{L}$  of 0.5% NP40 in PBS containing the protease inhibitors aprotinin (0.02 mg/mL), leupeptin (0.05 mg/mL), PMSF (4 mM), and pepstatin (0.07 mg/mL). The cell debris was pelleted by centrifugation, and the cell lysates were isolated. High molecular weight components in cell lysates and initial cell culture supernatants, coinjected with gel filtration standards (BioRad) for comparison, were analyzed by size-exclusion HPLC. Fractions of 0.25 mL were collected and counted for  $^{125}\text{I}$  and  $^{131}\text{I}$  in an automated gamma counter, and the radioactivity was plotted versus time. To determine the low molecular weight catabolites, cell lysates, and cell culture supernatants at each time point were filtered at



4 °C for 240 min through Centricon-10 tubes (Amicon; 10 kDa cut off). The filtrates and the cartridges were counted for radioactivity prior to HPLC analyses of the filtrates to determine the fraction of low and high molecular weight components. The components of the filtrates were analyzed by reversed-phase chromatography. A C18 column (Bondclone) was eluted with a mobile phase gradient as described earlier in the Experimental Section. Fractions of 0.25 mL were collected and counted for radioactivity. Under these HPLC conditions, the retention times of the IPMBA, IPMBA-glycine, and IPMBA-lysine standards were 23.5, 32.5, and 28 min, respectively.

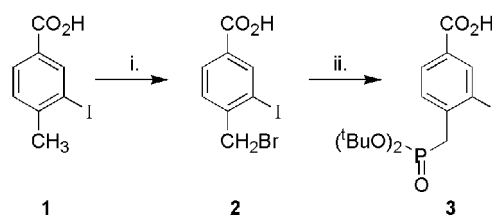
## RESULTS AND DISCUSSION

There is strong evidence that acylation agents for internalizing mAbs that generate positively charged catabolites increase the retention of radioiodine activity in tumor cells (Reist, 1996, 1997; Foulon, 2001; Vaidyanathan, 2001). The goal of these experiments was to develop an acylation agent bearing a negatively charged substituent to determine whether reagents of this type would offer similar advantages for labeling internalizing biomolecules. A practical motivation of the work is that use of negatively charged radioiodinated templates may be an approach for minimizing normal tissue accumulation, a problem noted particularly in the kidneys when the polycationic D-KRYRR peptide was used for mAb labeling (Foulon et al., 2000). Studies with both glycolated Fab fragments (Kobayashi et al., 2000) and copper complexes (Jones-Wilson et al., 1998; Sun et al., 2002) suggest that molecules bearing a negative charge are less avidly retained by the kidney and other normal tissues, presumably due to the negative charge on renal proximal tubules (Maack et al., 1992).

A benzyl phosphonic acid analogue was selected for this purpose for the following reasons. Phosphate esters and anhydrides are the most common functional groups present in nature's repertoire, and phosphonates have been extensively explored as phosphate surrogates in biology and medicine (Engel, 1977). Phosphonic acids are very polar compounds and, owing to their low first *pK<sub>a</sub>* of ca. 2–3 (Franz, 2001; Moe and Butler, 1983; Van Wazer, 1958), they are expected to exist in the anionic form even at a pH of 5. Thus, it can be expected that, after the degradation of the mAbs or oligopeptides, the catabolites bearing the radiolabeled phosphonic acid moiety will be negatively charged, which should impede their transport across lysosomal and cell membranes.

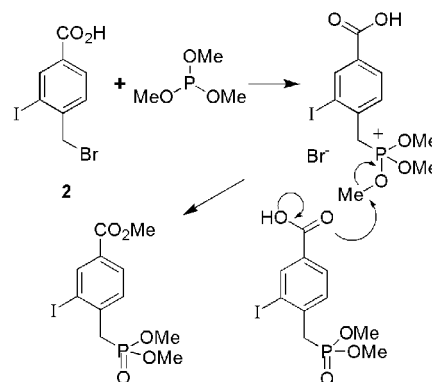
A methyl phosphonic acid derivative of 3-iodobenzoate was chosen as the target compound, which may be synthesized from 4-bromomethyl-3-iodobenzoic acid **2**. Commercially available 3-iodo-4-methylbenzoic acid **1** was brominated under free radical conditions. Initially, benzyl bromination utilizing the conventional conditions using *N*-bromosuccinimide (NBS) in CCl<sub>4</sub> and catalytic benzoyl peroxide was studied. However, the benzoic acid precursor remained mostly insoluble in the nonpolar solvent, even at reflux temperature, leading to largely heterogeneous reaction conditions that resulted in poor product yields even under prolonged refluxing conditions. This led us to attempt the bromination using NBS and the initiator azobiscyclohexylnitrile (Keck, 1987) in a higher boiling solvent, 1,2-dichloroethane (Sneath et al., 1976) (Scheme 1). The reaction mixture was homogeneous at reflux, but the reaction was still incomplete, and it afforded a mixture of the mono- and dibromo derivatives regardless of the stoichiometry of NBS employed.

**Scheme 1<sup>a</sup>**



<sup>a</sup> i. NBS, azo-*N,N*-biscyclohexyl nitrile (ABCN); ii. HPO(O<sup>t</sup>Bu)<sub>2</sub>, KO<sup>t</sup>Bu.

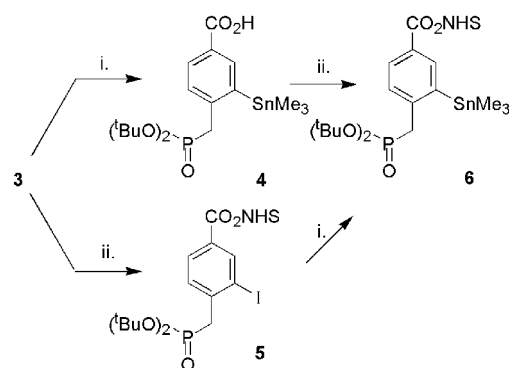
**Scheme 2. Proposed Mechanism of the Origin of Methyl (3-Iodo-4-dimethylphosphonomethyl)benzoate from a Michaelis-Arbuzov Reaction**



However, when compared to the conventional procedure, these reaction conditions gave higher yields of the monobrominated product **2**. Column chromatographic isolation of **2** from the reaction mixture using a MeOH/EtOAc solvent system was cumbersome owing to "streaking" of the very polar benzoic acid derivatives on silica gel. A modified EtOAc/hex/AcOH system proved to be much more effective in separating the components of the reactions. The monobrominated derivative **2** was isolated in ca. 60% yield by gravity column chromatography of the reaction mixture using a stepwise gradient of 20–50% EtOAc/hexane containing 1% AcOH.

Benzyl phosphorylation of **2** was first attempted by Arbuzov reaction (Bhattacharya and Thyagarajan, 1981) with trimethyl phosphite. There were several drawbacks to this approach, foremost among which was the lack of mild conditions in removing the methyl protecting group to reveal the free phosphonic acid, penultimate to labeling the mAb, without affecting the sensitive *N*-succinimidyl carboxylate ester. Besides, the reaction of **2** with trimethyl phosphite afforded an ester, methyl (3-iodo-4-dimethylphosphonomethyl)benzoate, as the primary product in ca. 40–50% yield. This unexpected and unprecedented product may result from the nucleophilic displacement of a methyl group from the intermediate quaternary phosphonate of the Arbuzov reaction (Scheme 2) by the benzoic acid moiety. This approach was not successful, and the mechanism of the reaction was not explored further.

The synthesis of 2-trimethylsilylethyl (3-iodo-4-bromomethyl)benzoate (TMSE-**2**, structure not shown) has been reported earlier by our laboratory (Vaidyanathan et al., 2001). To preempt methyl esterification of the free carboxylic acid moiety, the Arbuzov reaction of TMSE-**2** was attempted. However, removal of the methyl groups of the dimethylphosphonate to give free phosphonic acid, prior to coupling to the mAb, involves stringent conditions (heating with TMSBr/CH<sub>3</sub>CN, Qian et al., 1996), and two additional steps of protection and deprotection

Scheme 3<sup>a</sup>

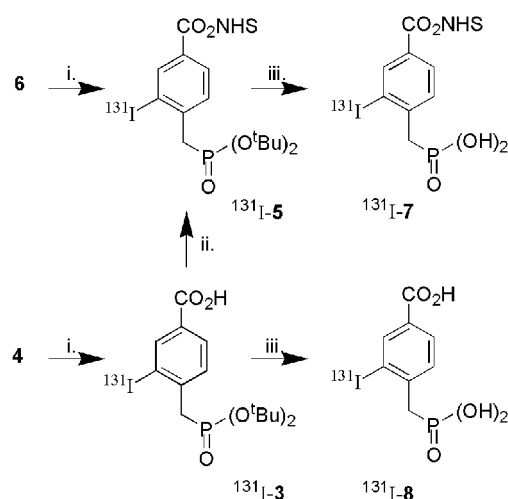
<sup>a</sup> i.  $(\text{Me}_3\text{Sn})_2$ ,  $\text{Pd}(\text{TPP})_2\text{Cl}_2$ , dioxane, reflux. ii. *N*-hydroxysuccinimide, CMC, THF.

of the carboxylic group were involved. Therefore, this route was replaced by the more direct route outlined in Scheme 1.

The *tert*-butyl group has been extensively used in peptide synthesis and total synthesis. It is renowned for its lability to acidic conditions and its ease of removal and has been used widely as a protecting group (Greene, 1991). The *tert*-butyl protecting group is removed easily under protic, e.g. TFA, and aprotic, e.g. TMSOTf, conditions alike (Greene, 1991). In fact, Burke et al. (1991) have utilized a *tert*-butyl protecting group in the synthesis of the aromatic  $\alpha$ -hydroxyphosphonate inhibitors of tyrosine kinases. The conditions for conversion of a benzyl di-*tert*-butylphosphonate to the free benzyl phosphonic acid (Burke et al., 1991) are known to be much milder compared to those for deprotection of the dimethylphosphonates (Qian, 1996). Therefore, we attempted to convert **2** to the di-*tert*-butylphosphonomethyl derivative **3** by its reaction with deprotonated di-*tert*-butyl phosphite (Baczko et al, 1996; Burke et al., 1991; Yao et al, 1999) (Scheme 1). A 5-fold excess of the phosphite reagent was deprotonated with  $\text{KO}^t\text{Bu}$  in THF at 0 °C and allowed to react with **2** in refluxing THF whereby the reaction proceeded cleanly to afford **3** in 57% yield.

Esterification of **3** to *N*-succinimidyl (3-iodo-4-di-*tert*-butylphosphonomethyl)benzoate **5** (*t*Bu-SIPMB) was achieved in high yield by reaction with *N*-hydroxysuccinimide and the water-soluble DCC-analogue, 1-cyclohexyl-3-(2-morpholinoethyl)carbodiimide metho-*p*-toluenesulfonate (CMC) (Scheme 3). The reaction was completed within 3 h, and the byproducts were simply filtered to afford, after chromatographic purification, **5** in 93% yield. Trimethylstannylation of **5** to **6** (*t*Bu-SPMTB) was accomplished by palladium-catalyzed coupling of the iodo precursor with hexamethylditin in refluxing dioxane (Scheme 3) (Wigerinck et al., 1993). It is imperative that anhydrous dioxane be utilized because residual moisture can lead to hydrolysis of the active ester under refluxing conditions. The stannylation reaction proceeded in 70% yield. Alternatively, stannylation of the free-acid **3** under the same conditions to give **4** followed by esterification to give **6** may also be performed (Scheme 3). The yield of the Pd-catalyzed stannylation reaction of **3** was very low ( $\approx 15\%$ ). Therefore, the former procedure was the approach of choice for the synthesis of **6**. However, the tin precursor **4** used to prepare  $^{131}\text{I}$ -**3** was synthesized using the latter method.

Radioiodination of **6** to  $^{131}\text{I}$ -**5** was accomplished employing *N*-chlorosuccinimide (NCS) in acetic acid as the oxidizing source as described (Vaidyanathan et al., 1998)

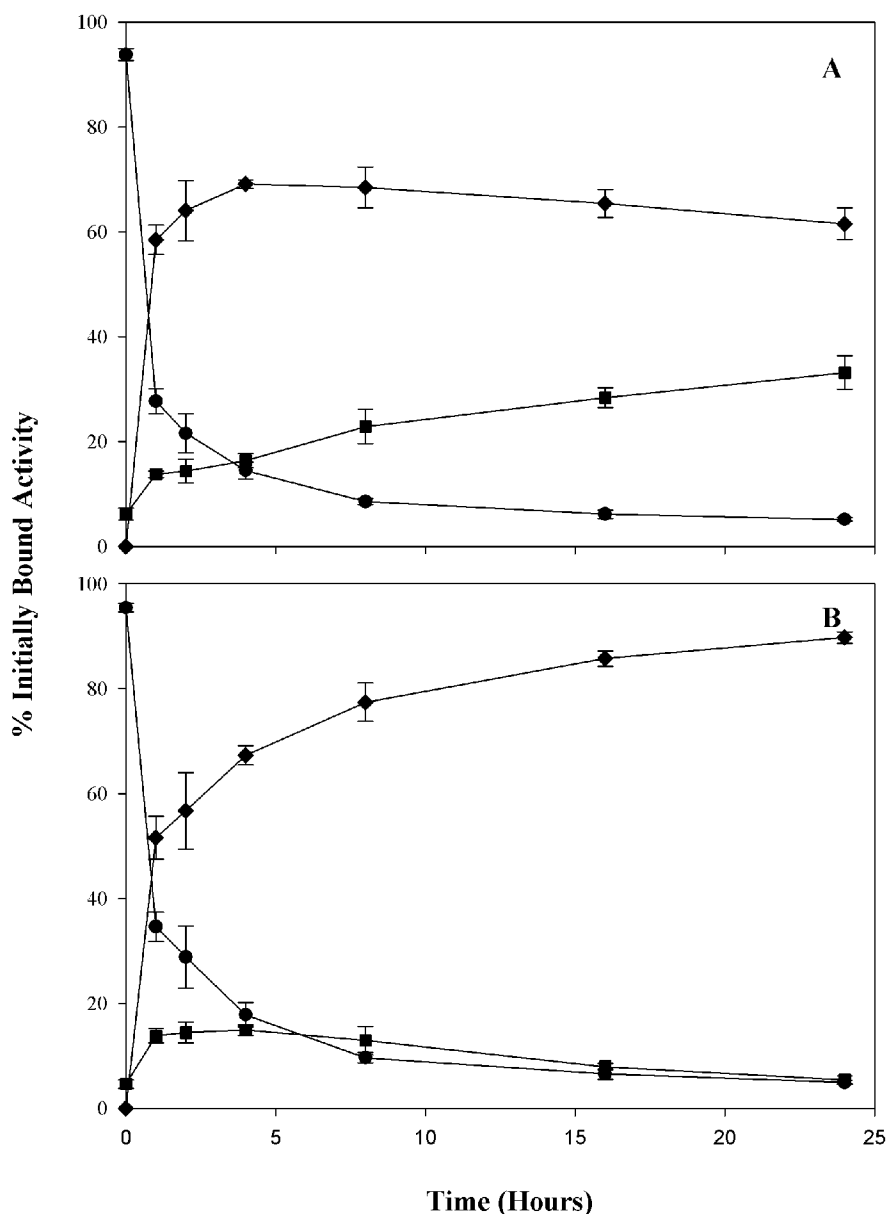
Scheme 4<sup>a</sup>

<sup>a</sup> i.  $^{131}\text{I}^-$ , NCS/AcOH; ii. Pyr, disuccinimidyl carbonate,  $\text{CH}_3\text{CN}$ ; iii. TFA.

and shown in Scheme 4. Alternatively, following an indirect route, **4** was radioiodinated to give  $^{131}\text{I}$ -**3** and converted to its active ester  $^{131}\text{I}$ -**5** by heating it with disuccinimidyl carbonate (DSC) and pyridine in  $\text{CH}_3\text{CN}$  (Vaidyanathan and Zalutsky, 1994) (Scheme 4). Although the two-step procedure resulted in a higher overall yield of  $^{131}\text{I}$ -**7** (ca. 80%), it was more labor and time intensive, involving two HPLC purification steps and evaporation of solvents, and therefore deemed less preferable to the one-step procedure. Furthermore, using the two-step procedure, the mAb coupling reaction often failed, with a maximum coupling yield of only 22% obtained. The immunoreactive fraction of the mAb conjugated with  $^{131}\text{I}$ -**7** synthesized in this fashion was low ( $\sim 20\%$ ) as well. We speculate that both problems might be attributable to the conjugation of an unidentified nonradioactive compound to the mAb that coeluted with  $^{131}\text{I}$ -**7**. As a consequence, the use of the one-step procedure for  $^{131}\text{I}$ -**5** is recommended.

Facile deprotection of  $^{131}\text{I}$ -**5** to give  $^{131}\text{I}$ -**7** was accomplished by treatment with anhydrous trifluoroacetic acid. Deprotection of  $^{131}\text{I}$ -**3** (*t*Bu- $^{131}\text{I}$ IPMBA) was carried out similarly to give  $^{131}\text{I}$ -**8** (Scheme 4). Excess trifluoroacetic acid usually was removed under a stream of argon. The effect of trace amounts of TFA on the pH of borate buffer used in the mAb coupling reaction was tested. Not surprisingly, even insignificant amounts of the strong acid caused considerable disruption of the pH of the buffer. To prevent damage to the mAb due to residual acid, traces of TFA were removed by repeated coevaporation with EtOAc. The pH of a borate buffer solution of  $^{131}\text{I}$ -**7**, coevaporated with EtOAc as described above, remained the same as that of the original buffer.

The  $^{131}\text{I}$ -**7** was coupled to mAb L8A4 with a yield of 25–40%, a value lower than reported for conjugation of mAbs with other acylation agents of this type (Vaidyanathan et al., 2001; Zalutsky and Narula, 1987). Coupling yields are affected by many factors including protein concentration (Vaidyanathan and Zalutsky, 1990), and the protein concentrations used in the current study were only in the range of 1.5–2.9 mg/mL. When  $^{131}\text{I}$ -**7** was conjugated with another mAb (murine 81C6) at  $\sim 16$  mg/mL concentration, a 75% coupling yield was obtained, which is consistent with previous results with other acylation agents at similar concentrations.



**Figure 1.** Paired-label in vitro internalization of L8A4 by U87ΔEGFR cells. L8A4 radioiodinated with [<sup>131</sup>I]SIPMB (A) and with <sup>125</sup>I using Iodogen (B). Percentage of radioactivity initially bound to cells that was surface-bound (●), internalized (■), and found in supernatant (◆) is shown.

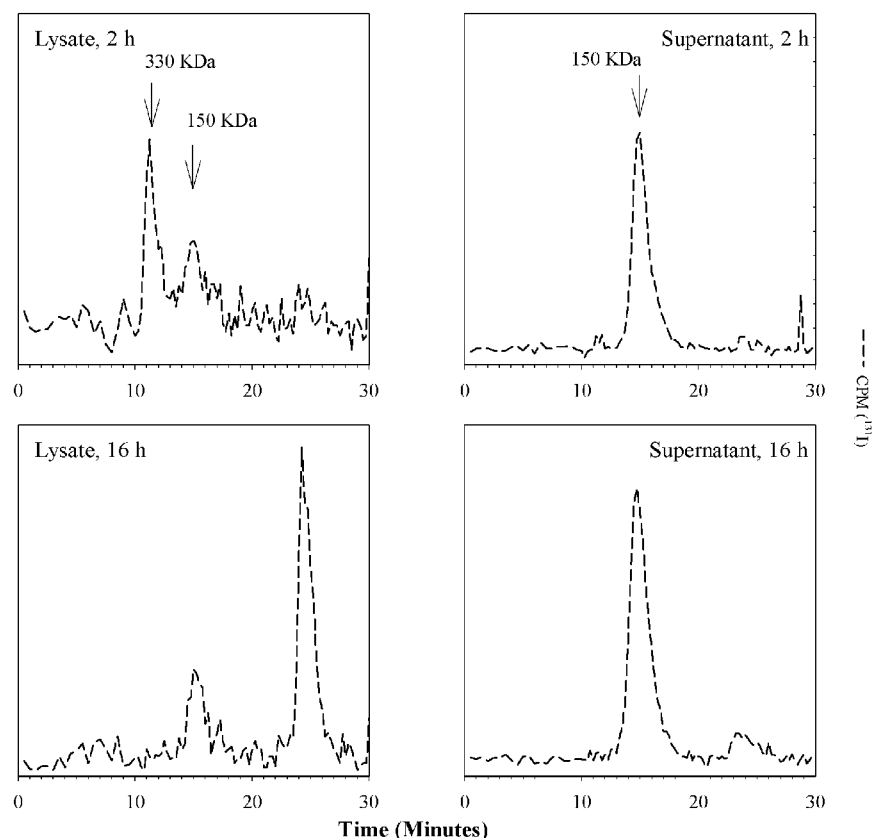
The % IR fraction was determined each time before internalization and metabolism studies to ensure the integrity of the radiolabeled mAb. The IR fraction of the mAb L8A4 labeled with [<sup>131</sup>I]SIPMB determined by the Lindmo method (Lindmo et al., 1984) was  $71 \pm 4.4\%$ . In comparison, the immunoreactive fraction for this batch of L8A4 labeled with <sup>125</sup>I using Iodogen was only  $50.7 \pm 9.5\%$ . TCA precipitation values of  $\geq 97.5\%$  for [<sup>131</sup>I]-SIPMB-labeled L8A4 were obtained for all preparations. Finally, no detectable high-molecular weight aggregates were seen by size-exclusion HPLC, with  $>95\%$  of injected radioactivity eluting with a retention time corresponding to the 150 kDa gel filtration standard, confirming mAb integrity postlabeling.

An internalization assay was performed in paired-label format on the EGFRvIII-expressing U87ΔEGFR cell line to determine whether labeling mAb L8A4 using [<sup>131</sup>I]-SIPMB increased the intracellular retention of radioiodine activity compared with a conventional radioiodination method (Iodogen). Typical results from one of three experiments are presented in Figure 1. Internalized

counts for the two labeling methods were similar from 0 h through 4 h; however, by the 10 h time point, there was an approximately 2-fold increase in intracellular counts for mAb labeled using [<sup>131</sup>I]SIPMB (SIPMB,  $22.9 \pm 3.4\%$ ; Iodogen,  $12.9 \pm 2.7\%$ ;  $P < 0.05$ , paired *t*-test). The enhancement in intracellular activity for mAb labeled using [<sup>131</sup>I]SIPMB compared with Iodogen increased with time, reaching a 6-fold advantage at 24 h (SIPMB,  $32.2 \pm 4.3\%$ ; Iodogen,  $5.4 \pm 0.8\%$ ;  $P < 0.05$ ). A corresponding increase in radioactivity in the supernatant was observed for mAb labeled using Iodogen. The degree of enhancement in intracellular counts for L8A4 labeled with negatively charged SIPMB compared with Iodogen is similar to that observed on this cell line when the positively charged SGMIB reagent was used for labeling this mAb (Vaidyanathan et al., 2001).

A catabolism study was undertaken next in order to determine whether the increased intracellular retention of radioiodine was related to the nature of the labeled species generated during the processing of mAbs labeled using [<sup>131</sup>I]SGMIB. Because of the well-known lysosomal





**Figure 2.** Radiochromatogram obtained from the size-exclusion HPLC of cell lysates and cell culture supernatants at 4 and 16 h from the paired-label in vitro metabolism study of L8A4 labeled with  $^{131}\text{I}$  using  $^{131}\text{I}$ SIPMB by U87EGFR cells.

**Table 1. Percentage of Low Molecular Weight Catabolites Retained by U87EGFR Cells Following Intracellular Processing of L8A4 Labeled with  $^{131}\text{I}$ SIPMB and with  $^{125}\text{I}$  Using Iodogen**

time (h)	low molecular weight catabolites retained in the cell (percent of total)		
	$^{131}\text{I}$ SIPMB-L8A4	$^{125}\text{I}$	$^{131}\text{I}$ SGMIB-L8A4 <sup>a</sup>
1	11.0	1.6	12.6
2	19.9	0.8	40.0
8	50.6	0.5	58.9
16	36.1	n.d.	29.3

<sup>a</sup> Vaidyanathan et al., 2001.

proteolysis of internalizing mAbs, differences in the distribution of low molecular weight catabolites were initially investigated. Table 1 summarizes the percentage of the total low molecular weight catabolites (defined as labeled species that passed through a 10 kDa filter) that were found in the cell lysates following the binding of L8A4 labeled using the SIPMB and Iodogen methods. The fraction of low molecular weight catabolites that were cell-associated was considerably higher for SIPMB at all time points with a greater than 100-fold difference seen at 8 h. The results with the positively charged SGMIB acylation agent, performed under identical assay conditions (Vaidyanathan et al., 2001), also are shown in Table 1, and are qualitatively similar to those obtained with SIPMB.

The percentage of radioiodine activity present as low molecular weight species in tumor cell lysates and in the cell culture supernatant was calculated and the results are presented in Table 2; again, data for SGMIB are provided for comparison. With directly labeled mAb, less than 2% of the radioiodine activity in cell lysates was in the form of low molecular weight molecules, while for SIPMB, 28–32% of the activity was in the form of low

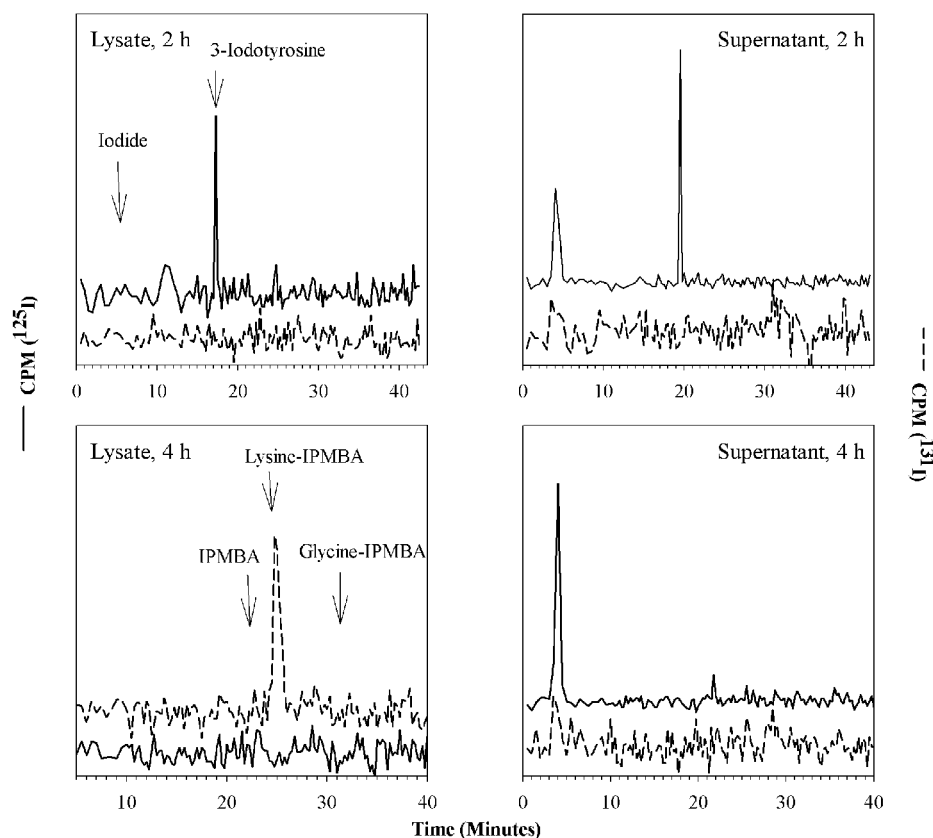
**Table 2. Percent of Total Activity Associated with Low Molecular Weight Catabolites in Cell Lysate and Cell Culture Supernatant**

time (h)	cell culture supernatant <sup>a</sup> (%)			cell lysate (%)		
	$^{131}\text{I}$ SIPMB	$^{125}\text{I}$	SGMIB <sup>b</sup>	$^{131}\text{I}$ SIPMB	$^{125}\text{I}$	SGMIB <sup>b</sup>
1	6.6	8.0	1.4	5.2	1.6	3.5
2	7.1	16.0	1.4	28.4	0.8	11.4
8	9.8	9.2	5.1	28.9	0.5	45.4
16	11.7	n.d.	17.4	32.3	n.d.	64.2

<sup>a</sup> (Activity in the low mw fraction  $\times$  100)/(activity in the low mw fraction + activity in the high mw fraction). <sup>b</sup> Vaidyanathan et al., 2001.

molecular weight species. Again, results for SGMIB were qualitatively similar to those observed in this study for mAb labeled using the SIPMB method. This suggests that, as with SGMIB-labeled mAb, the higher intracellular retention of activity observed with  $^{131}\text{I}$ SIPMB-labeled L8A4 is due to the increased presence of low molecular weight catabolites.

These data demonstrate that methods that involve coupling labeled templates bearing either a positive or a negative substituent to the mAb increase the retention of low molecular weight catabolites in tumor cells compared with directly labeled mAb. For radioiodination agents containing a benzoyl moiety, such as those used in this study, the chief low molecular weight catabolites are the free acid as well as its lysine and glycine conjugates (Garg et al., 1995). As an indication of its polarity, we determined the *n*-octanol:water partition coefficient for the free acid that would be generated from SIPMB-labeled mAbs, IPMBA, at physiological and lysosomal pH. The partition coefficient determined for IPMBA was  $0.02 \pm 0.01$  at pH 7.4 and  $0.03 \pm 0.00$  at pH 4.75. In comparison, those reported for GMIBA were  $0.02 \pm 0.00$  and  $0.06 \pm 0.00$  at pH 7.4 and 4.75, respectively



**Figure 3.** Radiochromatogram obtained from the reversed-phase HPLC of cell lysates and cell culture supernatants at 2 and 4 h from the paired-label in vitro metabolism study of L8A4 labeled with <sup>131</sup>I using [<sup>131</sup>I]SIPMB (short dashes) and with <sup>125</sup>I using Iodogen (solid line) by U87ΔEGFR cells.

(Vaidyanathan et al., 2001). Because of the high polarity of both acids at lysosomal pH, catabolites containing these groups should be retained in lysosomes, consistent with the results of internalization assays with L8A4 mAb labeled using SIPMB and SGMIB.

A catabolite analysis study was undertaken to determine the nature of the labeled species present in the cells and cell culture supernatants following exposure of mAb L8A4 to U87ΔEGFR cells in vitro. Size-exclusion HPLC of the [<sup>131</sup>I]SIPMB-L8A4 conjugate revealed that the majority of the radioiodine activity in the cell culture supernatant at all time points had a retention time corresponding to intact IgG (Figure 2). At 1 and 2 h, the predominant high molecular weight radioactive peak in the cell lysate coeluted with the 330 kDa molecular weight marker, which likely corresponds to a complex between the mAb and the 145 kDa EGFRvIII molecule. A peak corresponding to intact IgG also was seen. At 16 h, the mAb-EGFRvIII complex was absent and low molecular weight species predominated. These results were similar to those observed previously for the in vitro catabolism of L8A4 mAb labeled using the Iodogen, SGMIB, and SIPC methods (Reist et al., 1996; Vaidyanathan et al., 2001).

Reversed-phase HPLC was utilized to investigate the nature of the low molecular weight species generated after exposure of mAb L8A4 to U87ΔEGFR cells. To facilitate chromatogram interpretation, potential catabolites from the SIPMB template, namely IPMBA, lysine-IPMBA, and glycine-IPMBA conjugates, were prepared independently, isolated, and characterized by mass spectrometry. Analysis of the cell lysate indicated that the predominant low molecular weight catabolite of [<sup>131</sup>I]-SIPMB-L8A4 was the lysine-IPMBA conjugate (Figure 3); the free amine and carboxylate in the lysine adduct

being zwitterionic, the net charge of this catabolite retains a net negative charge. The peak corresponding to lysine-IPMBA was first seen at 4 h, and increased in quantity at the 8 and 16 h time points. Lysine conjugates can arise from the proteolytic cleavage of the acylated lysine from mAbs labeled using acylation agents (Arano et al., 1995; Duncan and Welch, 1993; Rogers et al., 1995). Consistent with the current results, the major catabolite of L8A4 labeled with [<sup>125</sup>I]SIPC was the lysine conjugate of [<sup>125</sup>I]iodonicotinic acid (Reist et al., 1996; Vaidyanathan et al., 2001).

Definitive levels of glycine-IPMBA were not observed following the degradation of [<sup>131</sup>I]SIPMB-L8A4. One of the pathways of aromatic carboxylic acid metabolism involves their conjugation with endogenous glycine, resulting in hippuric acid derivatives (Bridges et al., 1970; Hutt and Caldwell, 1990). If free benzoic acid derivatives are generated from the catabolism of mAbs labeled using benzoate templates, they can be subjected to similar metabolic process. For example, ex vivo and in vivo experiments have documented the formation of 3-[<sup>131</sup>I]iodobenzoyl-glycine from mAbs radioiodinated using [<sup>131</sup>I]SIB (Garg et al., 1995). Furthermore, when L8A4 was labeled with [<sup>131</sup>I]SGMIB, the glycine conjugate of the acid was the exclusive metabolite (Vaidyanathan et al., 2001). It appears that the metabolite that is preferentially formed, i.e., the lysine or the glycine conjugate, is dictated by the susceptibility of the amido group, formed between the mAb lysine ε-amino group and the acylation agent, toward proteolytic hydrolysis. Hence, it is reasonable to infer that the amide bond formed between SIPMB and the lysine ε-amino group is proteolytically inert, and therefore no free acid or glycine conjugate was generated under the in vitro assay conditions.

The major catabolite of L8A4 labeled using Iodogen that was observed previously was 3-[<sup>125</sup>I]iodotyrosine (Reist et al., 1996). The peak corresponding to iodotyrosine appeared in the reversed-phase HPLC radiochromatogram of the cell lysate at 1 and 2 h but was absent between the 4 and 16 h time points (Figure 2). This indicates that the iodotyrosine is formed and cleared rapidly from the cells after proteolysis of the protein. It is notable that no free iodide was seen in the lysate of L8A4 labeled by the Iodogen method at any time point. On the other hand, the predominant peak in the radiochromatogram of the cell culture supernatant for Iodogen-labeled L8A4 at all time points was free iodide. Significant levels of free iodide were not observed from L8A4 labeled using [<sup>131</sup>I]SIPMB in either the cell lysate or supernatant samples, except at a low level in the 1 h supernatant sample. This suggests that under these in vitro conditions, the IPMB template does not undergo appreciable levels of deiodination.

In conclusion, a method has been developed for the preparation of [<sup>131</sup>I]SIPMB, a radioiodination agent containing a negatively charged moiety. When labeled with this template, the anti-EGFRvIII mAb L8A4 retained immunoreactivity. Compared with mAb labeled using the Iodogen method, labeling L8A4 using SIPMB resulted in significantly enhanced retention of radioiodine activity in EGFRvIII-expressing tumor cells after mAb internalization. Our results suggest that this behavior likely reflects the generation of low molecular weight, polar catabolites that are retained intracellularly. Studies in animals bearing EGFRvIII-expressing xenografts are planned to further evaluate the potential utility of [<sup>131</sup>I]-SIPMB as a reagent for the radioiodination of internalizing mAbs.

#### ACKNOWLEDGMENT

This work was supported by Grants CA78417, CA42324, CA 91927, and NS20023 from the National Institutes of Health, and Grant 95ER62021 from the Department of Energy. We thank Dr. Darell Bigner, Department of Pathology, Duke University, for providing the L8A4 mAb and the U87ΔEGFR cell line.

#### LITERATURE CITED

- Ali, S., Eary, J. F., Warren, S. D., Badger, C. C., and Krohn, K. A. (1988) Synthesis and radioiodination of tyramine cellobiose for labeling monoclonal antibodies. *Nucl. Med. Biol.* 15, 557–561.
- Arano, Y., Mukai, T., Akizawa, H., Ueno, T., Montonari, H., Wakisaka, K., Kairiyama, C., and Yokoyama, A. (1995) Radiolabeled metabolites of proteins play a critical role in radioactivity elimination from the liver. *Nucl. Med. Biol.* 22, 555–564.
- Baczko, K., Liu, W.-Q., Roques, B. P., and Garbay-Jauregui, C. (1996) New synthesis of D, L-Fmoc protected 4-phosphonomethylphenylalanine derivatives and their enzymatic resolution. *Tetrahedron* 52, 2021–2030.
- Bhattacharya, A. K., and Thyagarajan, G. (1981) The Michaelis-Arbuzov Rearrangement. *Chem. Rev.* 81, 415–430.
- Bray, H. G., Thorpe, W. V., and White, K. (1951) Kinetic studies of the metabolism of foreign organic compounds. I. Formation of benzoic acid from benzamide, toluene, benzyl alcohol, and benzaldehyde and its conjugation with glucuronic acid in the rabbit. *Biochem. J.* 48, 88–96.
- Bridges, J. W., French, M. R., Smith, R. L., and Williams, R. T. (1970) The fate of benzoic acid in various species. *Biochem. J.* 118, 47–51.
- Burke, T. R., Li, Z.-H., Bolen, J. B., and Marquez, V. E. (1991) Phosphonate-containing inhibitors of tyrosine-specific protein kinases. *J. Med. Chem.* 34, 1577–1581.
- Crofts, P. C., and Kosolapoff, G. M. (1953) Preparation and determination of apparent dissociation constants of some alkylphosphonic and dialkylphosphonic acids. *J. Am. Chem. Soc.* 75, 3379–3383.
- de Jong, M., Valkema, R., Jamar, F., Kvols, L. K., Kwekkeboom, D. J., Breeman, W. A. P., Bakker, W. H., Smith, C., Pauwels, S., and Krenning, E. P. (2002) Somatostatin receptor-targeted radionuclide therapy of tumors: Preclinical and clinical findings. *Sem. Nuc. Med.* 32, 133–140.
- Duncan, J. R., and Welch, M. J. (1993) Intracellular metabolism of indium-111-DTPA-labeled receptor targeted proteins. *J. Nuc. Med.* 34, 1728–1738.
- Engel, R. (1977) Phosphonates as analogues of natural phosphates. *Chem. Rev.* 77, 349–367.
- Eumme, J. T., Gibbs, B. S., Zahn, T. J., Sebolt-Leopold, J. S., and Gibbs, R. A. (1999) Novel limonene phosphonate and farnesyl diphosphonate analogues: Design, synthesis, and evaluation as potential protein-farnesyl transferase inhibitors. *Bioorg. Med. Chem.* 7, 241–250.
- Foulon, C. F., Reist, C. J., Bigner, D. D., and Zalutsky, M. R. (2000) Radioiodination via D-amino acid peptide enhances cellular retention and tumor xenograft targeting of an internalizing anti-epidermal growth factor receptor variant III monoclonal antibody. *Cancer Res.* 60, 4453–4460.
- Foulon, C. F., Welsh, P. C., Bigner, D. D., and Zalutsky, M. R. (2001) Positively charged templates for labeling internalizing antibodies: Comparison of *N*-succinimidyl 5-iodo-3-pyridinecarboxylate and the D-amino acid peptide KRYRR. *Nucl. Med. Biol.* 28, 769–777.
- Franz, R. G. (2001) Comparisons of *pK<sub>a</sub>* and log *P* values of some carboxylic and phosphonic acids: Synthesis and measurement. *AAPS Pharm. Sci.* 3, E10.
- Geissler, F., Anderson, S. K., Venkatesan, P., and Press, O. (1992) Intracellular catabolism of radiolabeled anti-μ antibodies by malignant B-cells. *Cancer Res.* 52, 2907–2915.
- Goel, A., Augustine, S., Baranowska-Kortylewicz, J., Colcher, D., Booth, B. J., Pavlinkova, G., Tempero, M., and Batra, S. K. (2001) Single-dose versus fractionated radioimmunotherapy of human colon carcinoma xenografts using <sup>131</sup>I-labeled multivalent CC49 single-chain FVS. *Clin. Cancer Res.* 7, 175–184.
- Govindan, S. V., Mattes, M. J., Stein, R., McBride, B. J., Karacay, H., Goldenberg, D. M., Hansen, H. J., and Griffiths, G. L. (1999) Labeling of monoclonal antibodies with diethylenetriaminepentaacetic acid-appended radioiodinated peptides containing D-amino acids. *Bioconjugate Chem.* 10, 231–240.
- Green, T. W., and Wuts, P. G. M. (1991) *Protecting Groups in Organic Synthesis*, 2nd ed., John Wiley & Sons, Inc., New York.
- Gregus, Z., Fekete, T., Halasz, E., and Klaassen, C. D. (1996) Lipoic acid impairs glycine conjugation of benzoic acid and renal excretion of benzoylglycine. *Drug Metab. Dispos.* 24, 682–688.
- Hirrom, P. C., Millburn, P., and Smith, R. L. (1976) Bile and urine as complementary pathways for the excretion of foreign compounds. *Xenobiotica* 6, 55–64.
- Holtzman, E. (1989) *Lysosomes*, pp 95–100, Plenum Press, New York.
- Hutt, A. J., and Caldwell, J. (1990) Amino Acid Conjugation. *Conjugation Reactions in Drug Metabolism* (G. J. Mulder, Ed.) pp 273–305, Taylor and Francis Ltd., London.
- Illidge, T. M., and Brock, S. (2000) Radioimmunotherapy of cancer: Using monoclonal antibodies to target radiotherapy. *Curr. Pharm. Des.* 6, 1399–1418.
- Jones-Wilson, T. M., Deal, K. A., Anderson, C. J., McCarthy, D. W., Kovacs, Z., Motekaitis, R. J., Sherry, A. D., Martell, A. E., and Welch, M. J. (1998) The in vivo behavior of Copper-64-labeled azamacrocyclic complexes. *Nuc. Med. Biol.* 25, 523–530.
- Keck, G. E., and Burnett, D. A. (1987) β-Stannyl enones as radical traps: A very direct route to PGF<sub>2α</sub>. *J. Org. Chem.* 52, 2958.
- Kobayashi, H., Le, N., Kim, I.-S., Kim, M.-K., Pie, J.-E., Drumm, D., Paik, D. S., Waldmann, T. A., Paik, C. H., and Carasquillo, J. A. (1999) The pharmacokinetic characteristics



- of glycolated humanized anti-Tac Fabs are determined by their isoelectric points. *Cancer Res.* 59, 422–430.
- (28) Lindmo, T., Boven, E., Cuttitta, F., Fedorko, J., and Bunn, P. A., Jr. (1984) Determination of the immunoreactive fraction of radiolabeled monoclonal antibodies by linear extrapolation to binding at infinite antigen excess. *J. Immunol. Methods* 72, 77–89.
- (29) Maack, T., Park, C. H., and Camargo, M. J. (1992) Filtration, transport, and metabolism of proteins. *The Kidney: Physiology and Pathophysiology* (D. W. Seldin, and G. Giebisch, Eds.) pp 3005–3038, New York: Raven Press.
- (30) Maxwell, J. L., Baynes, J. W., and Thorpe, S. R. (1988) Inulin-<sup>125</sup>I-tyramine, an improved residualizing label for studies on sites of catabolism of circulating proteins. *J. Biol. Chem.* 263, 14122–14127.
- (31) Moe, Jr., O. A. and Butler, L. (1983) The catalytic mechanism of bovine intestinal 5'-nucleotide phosphodiesterase. *J. Biol. Chem.* 258, 6941–6946.
- (32) Murray, J. L. (2000) Monoclonal antibody treatment of solid tumors: a coming of age. *Sem. Oncol.* 27, 64–70.
- (33) Nishikawa, R., Ji, X. D., Harmon, R. C., Lazar, C. S., Gill, G. N., Cavenee, W. K., and Huang, H. J. (1994) A mutant epidermal growth factor receptor common in human glioma confers enhanced tumorigenicity. *Proc. Natl. Acad. Sci. U. S. A.* 91, 7727–7731.
- (34) Pittman, R., Carew, T. E., Glass, C. K., Green, S. R., Taylor, C. A., Jr., and Attie, A. D. (1983) A radioiodinated, intracellularly trapped ligand for determining the sites of plasma protein degradation in vivo. *Biochem. J.* 212, 791–800.
- (35) Press, O. W., Shan, D., Howell-Clark, J., Eary, J., Appelbaum, F. R., Matthews, D., King, D. J., Haines, A. M., Hamann, L., Shochat, D., and Bernsetin, I. D. (1996) Comparative metabolism and retention of iodine-125, yttrium-90, and indium-111 radioimmunoconjugates by cancer cells. *Cancer Res.* 56, 2123–2129.
- (36) Qian, Y., Vogt, A., Sebt, S. M., and Hamilton, A. D. (1996) Design and Synthesis of Non-Peptide Ras CAAAX Mimetics as Potent Farnesyltransferase Inhibitors. *J. Med. Chem.* 39, 217.
- (37) Reist, C. J., Archer, G. E., Kurpad, S. N., Wikstrand, C. J., Vaidyanathan, G., Willingham, M. C., Moscatello, D. K., Wong, A. J., Bigner, D. D., and Zalutsky, M. R. (1995) Tumor-specific anti-epidermal growth factor receptor variant III monoclonal antibodies: Use of the tyramine-cellobiose radioiodination method enhances cellular retention and uptake in tumor xenografts. *Cancer Res.* 55, 4375–82.
- (38) Reist, C. J., Garg, P. K., Alston, K. L., Bigner, D. D., and Zalutsky, M. R. (1996) Radioiodination of internalizing monoclonal antibodies using N-succinimidyl 5-iodo-3-pyridinecarboxylate. *Cancer Res.* 56, 4970–4977.
- (39) Reist, C. J., Archer, G. E., Wikstrand, C. J., Bigner, D. D., and Zalutsky, M. R. (1997) Improved targeting of an anti-epidermal growth factor receptor variant III monoclonal antibody in tumor xenografts after labeling using N-succinimidyl 5-iodo-3-pyridinecarboxylate. *Cancer Res.* 57, 1510–1515.
- (40) Rogers, B. E., Franano, F. N., Duncan, J. R., Edwards, W. B., Anderson, C. J., Connet, J. M., and Welch, M. J. (1995) Identification of metabolites of <sup>111</sup>In-diethylenetriaminepentaacetic acid-monoclonal antibodies and antibody fragments in vivo. *Cancer Res.* 55, 5714s–5720s.
- (41) Sneath, R. L., Jr., Wright, J. E., Soloway, A. H., O'Keefe, S. M., Dey, A. S., and Smolnycki, W. D. (1976) Protein-binding polyhedral boranes. 3. *J. Med. Chem.* 19 (11), 1290–1294.
- (42) Sun, X., Wuest, M., Weisman, G. R., Wong, E. H., Reed, D. P., Boswell, C. A., Motekaitis, R., Martell, A. E., Welch, M. J., and Anderson, C. J. (2002) Radiolabeling and in vivo behavior of Copper-64-labeled cross-bridged cyclam ligands. *J. Med. Chem.* 45, 469–477.
- (43) Thorpe, S. R., Baynes, J. W., and Chroneos, Z. C. (1993) The design and application of residualizing labels for studies of protein catabolism. *FASEB J.* 7, 399–405.
- (44) Vaidyanathan, G., and Zalutsky, M. R. (1990) Protein radiohalogenation: Observations on the design of N-succinimidyl ester acylation agents. *Bioconjugate Chem.* 1, 269–273.
- (45) Vaidyanathan, G., and Zalutsky, M. R. (1994) Improved synthesis of N-succinimidyl 4-[<sup>18</sup>F]fluorobenzoate and its application to the labeling of a monoclonal antibody fragment. *Bioconjugate Chem.* 5, 352–356.
- (46) Vaidyanathan, G., Affleck, D. J., and Zalutsky, M. R. (1997) Method for radioiodination of proteins using N-succinimidyl 3-hydroxy-4-iodobenzoate. *Bioconjugate Chem.* 8, 724–729.
- (47) Vaidyanathan, G., Zalutsky, M. R., and DeGrado, T. R. (1998) Iodopyridine-for-iodobenzene substitution for use with low molecular weight radiopharmaceuticals: application to m-iodobenzylguanidine. *Bioconjugate Chem.* 9, 758–764.
- (48) Vaidyanathan, G., Affleck, D. J., Li, J., Welsh, P., and Zalutsky, M. R. (2001) A polar substituent-containing acylation agent for the radioiodination of internalizing monoclonal antibodies: N-succinimidyl 4-guanidinomethyl-3-[<sup>131</sup>I]iodobenzoate ([<sup>131</sup>I]SGMIB). *Bioconjugate Chem.* 12, 428–438.
- (49) Vaidyanathan, G., Affleck, D. J., Bigner, D. D., and Zalutsky, M. R. (2002) Improved xenograft targeting of tumor-specific anti-epidermal growth factor receptor variant III antibody labeled using N-succinimidyl 4-guanidinomethyl-3-iodobenzoate. *Nucl. Med. Biol.* 29, 1–11.
- (50) Van Wazer, J. R. (1958) *Phosphorus and Its Compounds*, pp 384–386, Volume 1, Interscience, New York.
- (51) Wan, S. H., and Riegelman, S. (1972) Renal contribution to overall metabolism of drugs. I. Conversion of benzoic acid to hippuric acid. *J. Pharm. Sci.* 61, 1278–1284.
- (52) Wigerinck, P., Kerremans, L., Claes, P., Snoeck, R., Maudgal, P., Declercq, E., and Herdewijn, P. (1993) Synthesis and antiviral activity of 5-thien-2-yl-2'-deoxyuridine analogues. *J. Med. Chem.* 36, 538–543.
- (53) Wikstrand, C. J., Hale, L. P., Batra, S. K., Hill, M. L., Humphrey, P. A., Kurpad, S. N., McLendon, R. E., Moscatello, D., Pegram, C. N., Reist, C. J., Traweek, T., Wong, A. J., Zalutsky, M. R., and Bigner, D. D. (1995) Monoclonal antibodies against EGFRvIII are tumor specific and react with breast and lung carcinomas and malignant gliomas. *Cancer Res.* 55, 3140–3148.
- (54) Wikstrand, C. J., McLendon, R. E., Friedman, A. H., and Bigner, D. D. (1997) Cell surface localization and density of the tumor-associated variant of the epidermal growth factor receptor EGFRvIII. *Cancer Res.* 57, 4130–4140.
- (55) Wikstrand, C. J., Reist, C. J., Archer, G. E., Zalutsky, M. R., and Bigner, D. D. (1998) The class III variant of the epidermal growth factor receptor (EGFRvIII): Characterization and utilization as an immunotherapeutic target. *J. Neurol. Virol.* 4, 148–158.
- (56) Yao, Z.-J., Gao, Y., and Burke, T. R., Jr. (1999) Preparation of L-N<sup>α</sup>-Fmoc-4-[di-(tert-butyl)-phosphonomethyl]phenylalanine from L-tyrosine. *Tetrahedron Asymmetry* 19, 3727–3734.
- (57) Zalutsky, M. R. (1997) Growth factor receptors as molecular targets for cancer diagnosis and therapy. *Quart. J. Nucl. Med.* 41, 71–78.

# In Vitro and In Vivo Gene Transfer by an Optimized $\alpha$ -Cyclodextrin Conjugate with Polyamidoamine Dendrimer

Fumihiko Kihara, Hidetoshi Arima, Toshihito Tsutsumi, Fumitoshi Hirayama, and Kaneto Uekama\*

Faculty of Pharmaceutical Sciences, Kumamoto University, 5-1 Oe-honmachi, Kumamoto 862-0973, Japan.  
Received September 24, 2002; Revised Manuscript Received January 11, 2003

The purpose of the present study is to optimize the structure of the polyamidoamine starburst dendrimer (dendrimer) conjugate with  $\alpha$ -cyclodextrin ( $\alpha$ -CDE conjugate) as a nonviral vector.  $\alpha$ -CDE conjugates of dendrimer (generation 3, G3) with various average degrees of substitution (DS) of  $\alpha$ -CyD of 1.1, 2.4, and 5.4 were prepared.  $\alpha$ -CDE conjugates formed the complexes with pDNA, resulting in a change of the particle sizes of pDNA complexes, but the distinction of physicochemical properties among their vector/pDNA complexes was only very slight. The membrane-disruptive ability of  $\alpha$ -CDE conjugates on liposomes encapsulating calcein and their cytotoxicity to NIH3T3 and HepG2 increased with an increase in the DS value of  $\alpha$ -CyD. In vitro gene transfer activity of  $\alpha$ -CDE conjugates in both NIH3T3 and HepG2 cells augmented as the charge ratio (vector/pDNA) increased, and the activity of  $\alpha$ -CDE conjugate (DS 2.4) was the highest at higher charge ratios among dendrimer (G3), the three  $\alpha$ -CDE conjugates, and TransFast. After intravenous administration of pDNA complexes in mice,  $\alpha$ -CDE conjugate (DS 2.4) delivered pDNA more efficiently in spleen, liver, and kidney, compared with dendrimer and other  $\alpha$ -CDE conjugates (DS 1.1 and 5.4). The potential use of  $\alpha$ -CDE conjugate (G3, DS 2.4) could be expected as a nonviral vector in vitro and in vivo, and these data may be useful for design of  $\alpha$ -CyD conjugates with other nonviral vectors.

## INTRODUCTION

Gene therapy may be one of the most important therapies for the next generation (1). The following four methods may be available for gene transfer, i.e., viral vector, nonviral vector, and physical methods as well as naked plasmid DNA (pDNA) method without vectors (2, 3). While nonviral vectors are currently not as effective as viral vectors, they do have certain advantages: they are easily prepared, are not limited by gene size, and can be vested through structural modification with the ability to carry pDNA to the target cells (4, 5). For these reasons, improvement in gene transfer activity of nonviral vectors is of utmost importance in the present study. Thereby the following four barriers should be targeted for improvement of transfection efficiency: an entrance to the cell, a release from the endosomes, an entrance to the nucleus, and a demining of the gene silencing (6, 7).

Cyclodextrins (CyDs) are cyclic ( $\alpha$ -1,4)-linked oligosaccharides of  $\alpha$ -D-glucopyranose containing a hydrophobic central cavity and hydrophilic outer surface (8, 9). The most common CyDs are  $\alpha$ -,  $\beta$ -, and  $\gamma$ -CyDs, which consist of six-, seven-, and eight-D-glucopyranose units, respectively. CyDs are known to form inclusion complexes with

a variety of guest molecules both in solution and in a solid state (10, 11). The solubilizing effect of CyDs on lipophilic compounds has many uses in the pharmaceutical field (12, 13), while CyDs at higher concentrations release membrane components such as phospholipids and cholesterol from plasma membranes of various cells including erythrocytes, leading to hemolysis and a change in membrane permeability of hydrophilic compounds (14–16). CyDs have recently been applied to gene transfer (17–19) and oligonucleotide delivery (20–23). Notably, Davis and his colleagues (24, 25) reported that of cationic  $\beta$ -CyD polymers, a water soluble  $\beta$ -CyD polymer with 6<sup>A</sup>,6<sup>D</sup>-dideoxy-6<sup>A</sup>,6<sup>D</sup>-di-(2-aminoethanethio)- $\beta$ -CyD and dimethylsuberimidate ( $\beta$ CDP6) resulted in much higher gene transfer activity than Superfect and poly-L-lysine in BHK-21 and CHO-K1 with less cytotoxicity. In addition, they recently reported that the ternary complex of  $\beta$ CDP6, galactosylated poly(ethylene glycol) conjugate with adamantane, and pDNA possesses higher transfection efficiency in hepatoma cells through receptor-mediated endocytosis (26).

We previously revealed that polyamidoamine (PAM-AM) dendrimer (dendrimer, generation 2, G2) conjugates with  $\alpha$ -,  $\beta$ -, and  $\gamma$ -CyD (CDE conjugates) improve gene transfer activity, and especially dendrimer conjugate (G2) with  $\alpha$ -CyD ( $\alpha$ -CDE conjugate (G2)) possesses the greatest gene transfer activity (27). Of the  $\alpha$ -CDE conjugates with a distinct generation (G2–G4) of dendrimer,  $\alpha$ -CDE conjugate (G3) elicits the greatest gene transfer activity (28). However, it remains unclear whether  $\alpha$ -CDE conjugates (G3) with several  $\alpha$ -CyD molecules possess more gene transfer activity in vitro as well as in vivo. In the present study, we prepared  $\alpha$ -CDE conjugates with several  $\alpha$ -CyD molecules (the average degree of substitution (DS), 1.1, 2.4, and 5.4) and investigated the physicochemical properties, membrane-disruptive ability, cyto-

\* To whom correspondence should be addressed. Telephone: (81)-96-371-4160. Fax: (81)-96-371-4420. E-mail: uekama@gpo.kumamoto-u.ac.jp.

<sup>1</sup> Abbreviations: CyDs, cyclodextrins; dendrimer, polyamidoamine starburst dendrimer; G, generation;  $\alpha$ -CyD,  $\alpha$ -cyclodextrin; CDE conjugate, dendrimer conjugate with cyclodextrin;  $\alpha$ -CDE conjugate, dendrimer conjugate with  $\alpha$ -cyclodextrin; pDNA, plasmid DNA; DS, the average degree of substitution; FCS, fetal calf serum; DMEM, Dulbecco's modified Eagle's medium; PBS, phosphate-buffered saline; HBSS, Hanks' balanced salt solution; TBE buffer, Tris/borate/EDTA buffer; eggPC, egg phosphatidylcholine; GFP, green fluorescent protein; RLU, relative light unit; FITC, fluorescein isothiocyanate.

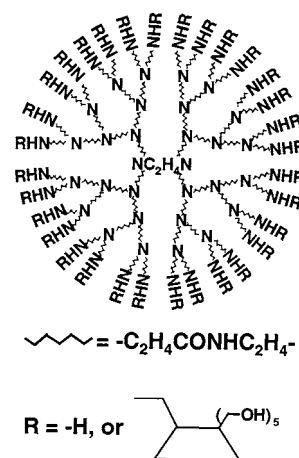
toxicity, and in vitro and in vivo gene transfer activity of the  $\alpha$ -CDE conjugates, in comparison with dendrimer and TransFast.

## EXPERIMENTAL SECTION

**Materials.**  $\alpha$ -CyD was donated by Nihon Shokuhin Kako (Tokyo, Japan) and recrystallized from water. Dendrimers (ethylenediamine core, G3, the terminal amino groups = 32, molecular weight = 6909) were purchased from Aldrich Chemical (Tokyo, Japan). *p*-Toluenesulfonyl chloride was purchased from Nakalai Tesque (Kyoto, Japan). Fetal calf serum (FCS) and Dulbecco's modified Eagle's medium (DMEM) were purchased from Nichirei (Tokyo, Japan) and Nissui Pharmaceuticals (Tokyo, Japan), respectively. TransFast transfection reagent, plasmid pGL3 control vector encoding firefly luciferase and plasmid pRL-CMV-Luc vector encoding Renilla luciferase were obtained from Promega (Tokyo, Japan). pEGFP-N1 vector encoding green fluorescent protein (GFP) was purchased from Clontech (Tokyo, Japan). The purification of pDNA amplified in bacteria was carried out using QIAGEN EndoFree plasmid maxi kit (<0.1 EU/ $\mu$ g endotoxin). Other chemicals and solvents were of analytical reagent grade.

**Preparation of  $\alpha$ -CDE Conjugates.**  $\alpha$ -CyDs were attached to primary amino residues of dendrimer (G3) according to the method of Suh et al. (29). Monotosyl- $\alpha$ -CyD was prepared according to the method of Melton et al. (30). The methanol solution containing dendrimer ( $2.6 \times 10^{-5}$  mol) was added to a flask and evaporated under reduced pressure. Monotosyl- $\alpha$ -CyD (DS 1.1, 25 mg ( $2.6 \times 10^{-5}$  mol); DS 2.4, 100 mg ( $1.0 \times 10^{-4}$  mol); DS 5.4, 200 mg ( $2.0 \times 10^{-4}$  mol)); and dimethyl sulfoxide (DMSO, 1.0 mL) were added into the flask. Under nitrogen atmosphere, the mixture was stirred at 60 °C for 24 h.  $\alpha$ -CDE conjugates were purified by gel-filtration (TOSOH TSKGel HW-40S, Tokyo, Japan) and then precipitated with methanol to remove the free dendrimer.  $^1\text{H}$  NMR spectra of the  $\alpha$ -CDE conjugates were measured, and the molar ratio of dendrimer and  $\alpha$ -CyD was calculated from the peak areas of anomeric proton of  $\alpha$ -CyD and ethylene protons of the dendrimer.  $\alpha$ -CDE conjugate (DS 1.1): yield, 15%;  $^1\text{H}$  NMR (500 MHz,  $\text{D}_2\text{O}$ )  $\delta$  (from TMS) 4.95 (H1,  $\alpha$ -CyD), 3.90–3.65 (H3, H5, H6,  $\alpha$ -CyD), 3.59–3.46 (H2, H4,  $\alpha$ -CyD), 3.38–3.15 (dendrimer methylene), 3.05–2.91 (dendrimer methylene), 2.95–2.60 (dendrimer methylene), 2.60–2.42 (dendrimer methylene), 2.20–2.18 (dendrimer methylene).  $\alpha$ -CDE conjugate (DS 2.4): yield, 18%;  $^1\text{H}$  NMR (500 MHz,  $\text{D}_2\text{O}$ )  $\delta$  (from TMS) 4.94 (H1,  $\alpha$ -CyD), 3.86–3.74 (H3, H5, H6,  $\alpha$ -CyD), 3.53–3.47 (H2, H4,  $\alpha$ -CyD), 3.27–3.13 (dendrimer methylene), 3.05–2.81 (dendrimer methylene), 2.72–2.51 (dendrimer methylene), 2.36–2.31 (dendrimer methylene).  $\alpha$ -CDE conjugate (DS 5.4): yield, 23%;  $^1\text{H}$  NMR (500 MHz,  $\text{D}_2\text{O}$ )  $\delta$  (from TMS) 5.30–4.96 (H1,  $\alpha$ -CyD), 3.88–3.75 (H3, H5, H6,  $\alpha$ -CyD), 3.55–3.47 (H2, H4,  $\alpha$ -CyD), 3.40–3.12 (dendrimer methylene), 3.07–2.98 (dendrimer methylene), 2.74–2.54 (dendrimer methylene), 2.36–2.33 (dendrimer methylene). The chemical structure of  $\alpha$ -CDE conjugates is shown in Figure 1.

**Gel Electrophoresis.** Electrophoretic mobility of the complexes of pDNA/dendrimers or pDNA/ $\alpha$ -CDE conjugates was measured using a gel electrophoresis system. Various amounts of dendrimers or  $\alpha$ -CDE conjugates were mixed with 0.2  $\mu$ g of pDNA (pGL3 control vector) in Hanks's balanced salt solution (HBSS, pH 7.4). Gel electrophoresis was carried out at room temperature in TBE buffer (45 mM tris-borate, 1 mM EDTA, pH 8.0) in



**Figure 1.** Chemical Structure of  $\alpha$ -CDE conjugates (G3, DS 1.1, 2.4, and 5.4).

1% (w/v) agarose gel (include 0.1  $\mu$ g/mL ethidium bromide) using Mupid system (Cosmo Bio, Tokyo, Japan) at 100 V for 50 min. The pDNA bands were visualized using an UV illuminator.

**Measurements of Particle Size.** Dendrimer- or  $\alpha$ -CDE conjugate (G3)-containing solutions (0.1 mL in HBSS) at various charge ratios were added to pDNA (pGL3 control vector) solution (4  $\mu$ g/1.5 mL in HBSS) and incubated for 15 min. Immediately, particle sizes of the complexes of pDNA/dendrimer and pDNA/ $\alpha$ -CDE conjugates were determined by quasielastic (dynamic) light scattering using a Beckman Coulter N4 Plus machine (Fullerton, CA). The wavelength of the He-Ne laser used was 632.8 nm. The measurement was carried out at a fixed angle of 62.6°, and the measuring time was 102 s at 25 °C. The measurements were carried out at least in triplicates.

**Liposome Leakage Assay.** Liposomes were prepared from egg phosphatidylcholine (eggPC) by reverse phase evaporation (31) with an aqueous phase of 100 mM calcein which was dissolved by the addition of 3.75 equiv of sodium hydroxide and 50 mM NaCl, extruded through a 0.22  $\mu$ m cellulose acetate membrane and purified by centrifugation with an iso-osmotic buffer (200 mM NaCl, 25 mM HEPES, pH 7.3). The liposomal suspension (6.0  $\mu$ M eggPC) was prepared using 10 mM phosphate buffer (pH 12). Fifty microliters of  $\alpha$ -CDE conjugate solution adjusted at the appropriate concentration using 10 mM phosphate buffer (pH 12) was added to 5  $\mu$ L of the liposomal suspension, and then the resulting suspension was agitated with vial mixer for 30 min at room temperature. Nine hundred microliters of phosphate buffer (pH 12) was further added to the suspension. The intensity of fluorescence of the suspension was finally measured with a fluorophotometer (Hitachi F-4500, Tokyo, Japan) at 25 °C; excitation and emission wavelengths were 495 and 515 nm, respectively. The value for 100% leakage was further obtained by the addition of 1  $\mu$ L of Triton X-100 to the suspension.

**Cell Culture.** NIH3T3 cells, a mouse fibroblast cell line, and HepG2 cells, a human hepatocarcinoma cell line, were obtained from the Japan Health Sciences Foundation (Osaka, Japan) and American Type culture collection (Rockville, MD), respectively. NIH3T3 and HepG2 cells were grown in DMEM containing  $1 \times 10^5$  mU/mL of penicillin, and 0.1 mg/mL of streptomycin supplemented with 10% (v/v) FCS at 37 °C in a humidified 5%  $\text{CO}_2$  and 95% air atmosphere.



**Cytotoxicity.** The cell viability was assayed by using a Cell Counting Kit (WST-1 method) from Wako Pure Chemical Industries (Osaka, Japan) (32). In brief, NIH3T3 and HepG2 cells were seeded at  $2 \times 10^5$  cells onto 35-mm dishes (Iwaki, Tokyo, Japan) and incubated for 18 h in a humidified atmosphere containing 5% CO<sub>2</sub> and 95% air at 37 °C. Cells were washed twice with serum free medium and then incubated for 1 h with 800  $\mu$ L of serum-free medium containing pDNA or the complexes with various vectors. The culture medium (1.5 mL) supplemented with 10% (v/v) FCS was added to each well, and the cells were incubated for 24 h in a humidified atmosphere containing 5% CO<sub>2</sub> and 95% air at 37 °C. After washing twice with HBSS (pH 7.4) to remove pDNA and/or various vectors, 0.5 mL of fresh HBSS and 50  $\mu$ L of WST-1 reagent were added to the plates and incubated for 4 h at 37 °C. The absorbance of aliquot (100  $\mu$ L) of the solution was measured at 405 nm, with a reference of the absorbance at 630 nm, with a microplate reader (Bio-Rad Model 550, Tokyo, Japan).

**In Vitro Gene Transfer.** In vitro transfection of the complexes of pDNA/dendrimers, pDNA/ $\alpha$ -CDE conjugates, or pDNA/TransFast was performed utilizing the expression of pDNA encoding firefly luciferase gene (pGL3 control vector) and pDNA encoding GFP (pEGFP-N1 vector) in NIH3T3 and HepG2 cells. The pDNA (2.0  $\mu$ g) was mixed with dendrimer or  $\alpha$ -CDE conjugates at various charge ratios. The pDNA complexes with dendrimers or  $\alpha$ -CDE conjugates were then allowed to stand for 15 min at room temperature. The cells ( $2 \times 10^5$  per 35 mm culture dish) were seeded 18 h before transfection and then washed twice with serum-free medium. Eight hundred microliters of serum-free medium containing pDNA or the complexes with various vectors was added to each dish and then incubated at 37 °C for 1 h. The culture medium (1.5 mL) supplemented with 10% (v/v) FCS was added to each dish. Control transfection was performed with TransFast in the same manner described above. The charge ratio of pDNA/TransFast was 1/1, at which an optimal gene transfer activity was obtained under the present experimental conditions. After transfection for 25 h, the gene expression was measured as follows: when pGL3 control vector was used, firefly luciferase content in the cell lysate was quantified using the Promega luciferase assay reagent (Tokyo, Japan) and a luminometer (Lumat LB9506, EG&G Berthold Japan, Tokyo, Japan). Absolute light emission generated from the luciferase enzyme reaction was determined. It was confirmed that  $\alpha$ -CyD and  $\alpha$ -CDE conjugates have no influence on the luciferase assay under the experimental conditions. Total protein content of the supernatant was determined by BCA protein assay kit (Pierce, Rockford, IL). One million relative light units correspond approximately to 1.6 ng of firefly luciferase. When pEGFP-N1 vector was used, NIH3T3 and HepG2 cells after transfection for 25 h were washed three times with PBS and then immediately scraped with 1 mL of PBS. The cells were collected and filtered through nylon mesh. Data were collected for  $2 \times 10^5$  cells on a FACS-Calibur flow cytometer using CellQuest software (Becton-Dickinson, Mountain View, CA).

**In Vivo Gene Transfer.** Four-weeks-old BALB/c female mice were intravenously injected in the tail vein with 500  $\mu$ L of a suspension containing the complex of pDNA/dendrimer (pRL-CMV-Luc) and that of pDNA/ $\alpha$ -CDE conjugates in 5% (w/v) mannitol at the amount of 50  $\mu$ g of pDNA in 1 min under anesthesia with ether. Twelve and 24 h after administration, the mice were sacrificed, and lung, heart, liver, spleen, and kidney were

isolated. The organs were washed twice with ice-cold saline and were added to 1 mL of the Promega cell lysis buffer (Tokyo, Japan) containing the Roche protease inhibitor, Complete (Tokyo, Japan). The organs were homogenized with a Polytron tissue grinder. After three cycles of freezing and thawing, the homogenate was centrifuged for 10 min at 10 000g (4 °C), and 20  $\mu$ L of the supernatant was added to 100  $\mu$ L of the Promega Renilla luciferase assay buffer (Tokyo, Japan). Luminescence was immediately measured for 10 s (Lumat LB9506, EG&G Berthold Japan, Tokyo, Japan). Total protein content of the supernatant was determined by BIO-RAD DC protein assay kit (Tokyo, Japan). One million relative light units correspond approximately to 0.4 ng of Renilla luciferase.

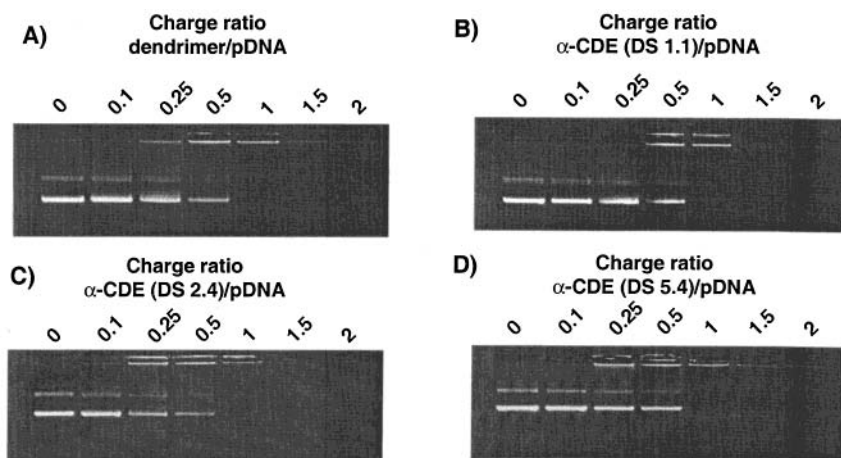
**Data Analysis.** Data are given as the mean  $\pm$  SEM. Statistical significance of mean coefficients for the studies was performed by analysis of variance followed by Scheffe's test. *p*-Values for significance were set at 0.05.

## RESULTS

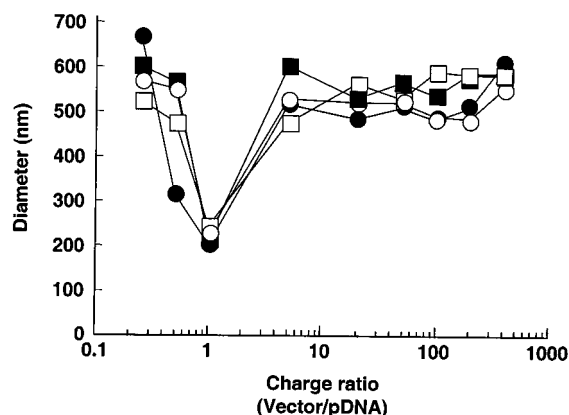
**Physicochemical Properties of pDNA Complexes with  $\alpha$ -CDE Conjugates.** We first studied the complexations between pDNA/dendrimer (G3) or pDNA/ $\alpha$ -CDE conjugate (DS 1.1, 2.4 and 5.4) using agarose electrophoresis. As shown in Figure 2A, the intensity of the band derived from pDNA decreased as the charge ratio of pDNA/dendrimer increased, and at the charge ratio of 1/1 the band disappeared. Similar patterns were observed in the pDNA/ $\alpha$ -CDE conjugates (DS 1.1, 2.4, and 5.4) systems (Figure 2B–D). CyDs alone did not change the electrophoretic band pattern of pDNA (data not shown). These results suggest that  $\alpha$ -CDE conjugates form the complexes with pDNA in a manner similar to dendrimer.

Next, the particle sizes of the complexes of pDNA/dendrimers and pDNA/ $\alpha$ -CDE conjugates were measured by quasielastic (dynamic) light scattering. As shown in Figure 3, the particle sizes of the complexes of pDNA/dendrimer or pDNA/ $\alpha$ -CDE conjugates were smallest at a charge ratio of 1/1, which was consistent with the ratio that the band disappeared (Figure 3). These results suggest that  $\alpha$ -CDE conjugates (DS 1.1, 2.4, and 5.4) form the most compact complexes (approximately 200 nm) at a charge ratio of 1/1, and at higher charge ratios the particle sizes of these complexes of pDNA/vectors were almost comparable (approximately 550 nm). Thus, it is evident that physicochemical properties of the pDNA complexes with  $\alpha$ -CDE conjugates differ only very slightly for that with dendrimer.

**Liposome Leakage Assay.** CyDs are known to induce hemolysis and to enhance the permeation of water-soluble drugs through biological membranes of epithelial cells via the release of membrane components such as phospholipids and cholesterol as described above (13, 14). In addition, we proposed the possibility that the enhancing mechanism by which  $\alpha$ -CDE conjugates augment the release of pDNA from endosomes to cytoplasm after cellular uptakes (25, 26). To confirm the membrane-disruptive ability of  $\alpha$ -CDE conjugates, we examined the effects of  $\alpha$ -CDE conjugates on the release of calcein from eggPC liposomes. As shown in Figure 4, dendrimer (G3) and  $\alpha$ -CDE conjugates (DS 1.1) did not release calcein from liposomes, whereas  $\alpha$ -CDE conjugates (DS 2.4 and 5.4) released it, indicating that  $\alpha$ -CDE conjugates possess membrane-disruptive ability. These results suggest that  $\alpha$ -CDE conjugates might increase the release of pDNA or the pDNA complex from endosomes following cellular uptake.



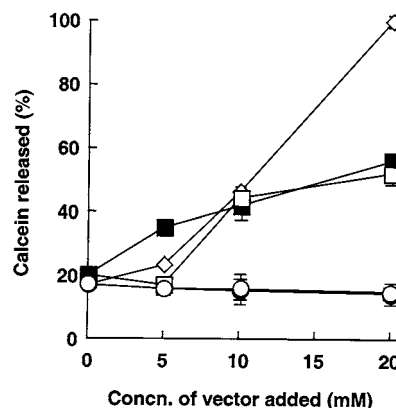
**Figure 2.** Agarose gel electrophoretic analysis of the complexes of pDNA/dendrimer (G3) and pDNA/ $\alpha$ -CDE conjugates (DS 1.1, 2.4, or 5.4) using TBE buffer (pH 8.0). The solutions containing the complexes of pDNA/dendrimer or pDNA/ $\alpha$ -CDE were incubated for 15 min at room temperature after slight agitation. The electrophoresis was performed at 100 V for about 50 min. A, dendrimer (G3); B,  $\alpha$ -CDE conjugate (DS 1.1); C,  $\alpha$ -CDE conjugate (DS 2.4); D,  $\alpha$ -CDE conjugate (DS 5.4).



**Figure 3.** Particle sizes of the complexes with pDNA/dendrimer (G3) or pDNA/ $\alpha$ -CDE conjugate (DS 1.1, 2.4, or 5.4). Dendrimer- or  $\alpha$ -CDE conjugate (DS 1.1, 2.4, or 5.4)-containing solutions at various charge ratios were added to pDNA solution and then incubated for 15 min. Particle sizes of the pDNA complexes with dendrimer and  $\alpha$ -CDE conjugates were determined by quasielastic (dynamic) light scattering: open circle, dendrimer (G3); closed circle,  $\alpha$ -CDE conjugate (DS 1.1); open square,  $\alpha$ -CDE conjugate (DS 2.4); closed square,  $\alpha$ -CDE conjugate (DS 5.4).

**Cytotoxicity.** Figure 5 shows cytotoxicity of dendrimer and  $\alpha$ -CDE conjugates in NIH3T3 and HepG2 cells. In both cells, cytotoxicity of dendrimer and  $\alpha$ -CDE conjugates was negligible up to a charge ratio of 100/1 (vector/pDNA), and slight cytotoxicity of  $\alpha$ -CDE conjugate (DS 5.4) was observed at a charge ratio of 200/1 (vector/pDNA). Above the charge ratio, the cytotoxic activity increased in the order of  $\alpha$ -CDE conjugate (DS 1.1) < (DS 2.4) < (DS 5.4) in NIH3T3 cells (Figure 5A). Likewise,  $\alpha$ -CDE conjugate (DS 5.4) provoked cytotoxicity to HepG2 cells in a concentration-dependent manner, but other  $\alpha$ -CDE conjugates showed only slight cytotoxicity (Figure 5B), suggesting that HepG2 cells are more resistant to the cytotoxic effect of  $\alpha$ -CDE conjugates than NIH3T3 cells. These results indicate that cytotoxicity of  $\alpha$ -CDE conjugates depends on the DS value of  $\alpha$ -CyD.

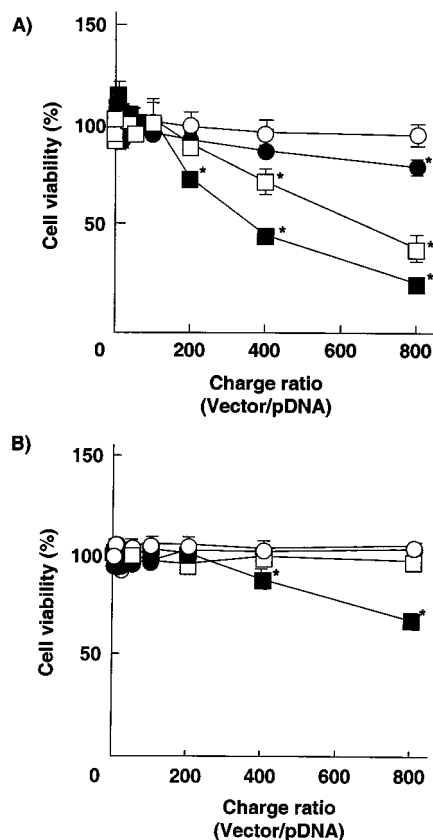
**In Vitro Transfection.** The in vitro gene transfer activity of dendrimer (G3) and  $\alpha$ -CDE conjugates (G3, DS 1.1, 2.4, and 5.4) was examined and compared with that of TransFast, which was employed as a positive control. Figures 6A and 6B show gene transfer activity of dendrimer and  $\alpha$ -CDE conjugates in NIH3T3 and HepG2 cells, respectively. When pDNA alone in the



**Figure 4.** Membrane-disruptive activity of dendrimer and  $\alpha$ -CDE conjugates (DS 1.1, 2.4, or 5.4) to liposomes. The solutions containing dendrimer and  $\alpha$ -CDE conjugates at various concentrations were added to the suspension containing egg phosphatidylcholine liposomes encapsulated calcein and mixed for 30 min at room temperature. The intensity of fluorescence of liposomal suspension was measured with fluorophotometer: open diamond,  $\alpha$ -CyD; open circle, dendrimer (G3); closed circle,  $\alpha$ -CDE conjugate (DS 1.1); open square,  $\alpha$ -CDE conjugate (DS 2.4); closed square,  $\alpha$ -CDE conjugate (DS 5.4). Each point represents the mean  $\pm$  SEM of four experiments.

absence and presence of  $\alpha$ -CyD was transfected to cells, no luciferase activity was observed (data not shown). Gene transfer activity of dendrimer and  $\alpha$ -CDE conjugates (DS 1.1 and 2.4) increased as the charge ratio (vector/pDNA) increased up to the charge ratio of 400/1 in NIH3T3 cells, and the activity of  $\alpha$ -CDE conjugate (DS 5.4) was greatest up to a charge ratio of 50/1. Of the three  $\alpha$ -CDE conjugates,  $\alpha$ -CDE conjugate (DS 2.4) provided the highest gene transfer activity at the charge ratios of 200/1 and 400/1. The enhancing effect of  $\alpha$ -CDE conjugate (DS 2.4) on gene transfer activity was approximately 3 times higher than that of TransFast in NIH3T3 cells (Figure 6A). The effects of the charge ratio on the activity in HepG2 cells were similar to those in NIH3T3 cells, the greatest gene transfer activity of  $\alpha$ -CDE conjugate (DS 2.4) was elicited at the charge ratio of 400/1. These results indicate that  $\alpha$ -CDE conjugate (DS 2.4) possesses superior gene transfer activity to dendrimer and  $\alpha$ -CDE conjugate (DS 1.1 and 5.4) at the higher charge ratios.

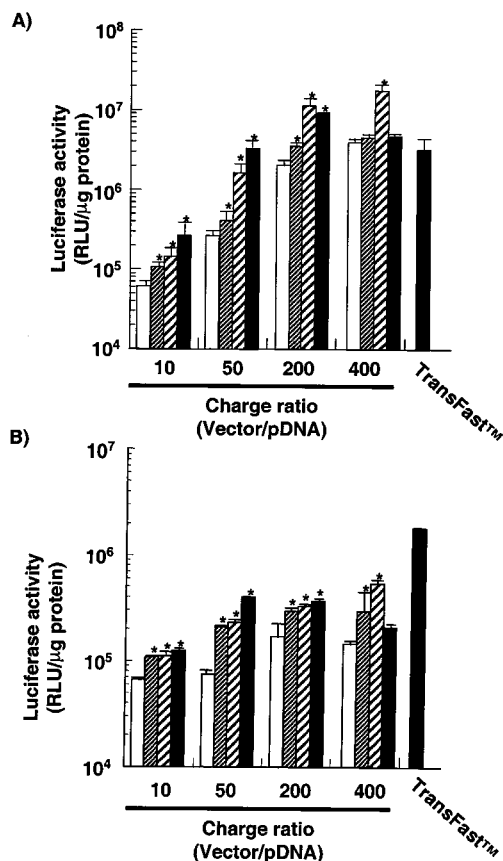
Next, we studied transfection efficiency of dendrimer or  $\alpha$ -CDE conjugates (DS 1.1, 2.4 and 5.4) using GFP by flow cytometer. Here pDNA complexes with dendrimer



**Figure 5.** Cytotoxicity of the complexes of pDNA/dendrimer or pDNA/ $\alpha$ -CDE conjugate (DS 1.1, 2.4, and 5.4) at various charge ratios in NIH3T3 cells (A) and HepG2 cells (B). The cell viability was assayed by WST-1 method as described in the Experimental Section. Open circle, dendrimer (G3); closed circle,  $\alpha$ -CDE conjugate (DS 1.1); open square,  $\alpha$ -CDE conjugate (DS 2.4); closed square,  $\alpha$ -CDE conjugate (DS 5.4). Each point represents the mean  $\pm$  SEM of four experiments. \* $p < 0.05$ , compared with dendrimer (G3).

or  $\alpha$ -CDE conjugates formed at charge ratios of 50/1 and 200/1 (vector/pDNA) were used. As shown in Figure 7A, the curve shifted to right-hand as the DS value of  $\alpha$ -CDE conjugates increased at a charge ratio of 50/1 in NIH3T3 cells. At a charge ratio of 200/1 the curves corresponding to  $\alpha$ -CDE conjugates (DS 2.4 and 5.4) overlapped and were shifted to the right of those of the dendrimer and  $\alpha$ -CDE conjugate (DS 1.1) in NIH3T3 cells (Figure 7B). In addition, a similar pattern was observed in HepG2 cells (Figures 7C and 7D). These results clearly indicate that  $\alpha$ -CDE conjugates (DS 2.4 and 5.4) provide superior gene transfer activity to dendrimer and  $\alpha$ -CDE conjugate (DS 1.1), and  $\alpha$ -CDE conjugate (DS 2.4) possesses almost comparable gene transfer efficiency of  $\alpha$ -CDE conjugate (DS 5.4) at a charge ratio of 200/1. On the other hand, when the complex of pDNA/TransFast was transfected at a charge ratio of 1/1, the corresponding curve showed a different pattern from that of pDNA/ $\alpha$ -CDE conjugates (Figure 7). These results suggest that of the three  $\alpha$ -CDE conjugates,  $\alpha$ -CDE conjugate (DS 2.4) possesses superior gene transfer activity at higher charge ratios of more than 200/1 to dendrimer,  $\alpha$ -CDE conjugates (DS 1.1 and 5.4), and TransFast, although gene transfer efficiency of  $\alpha$ -CDE conjugate (DS 2.4) was comparable to  $\alpha$ -CDE conjugate (DS 5.4). In addition, the gene transfer mode of  $\alpha$ -CDE conjugate (DS 2.4) may be somewhat different from that of TransFast.

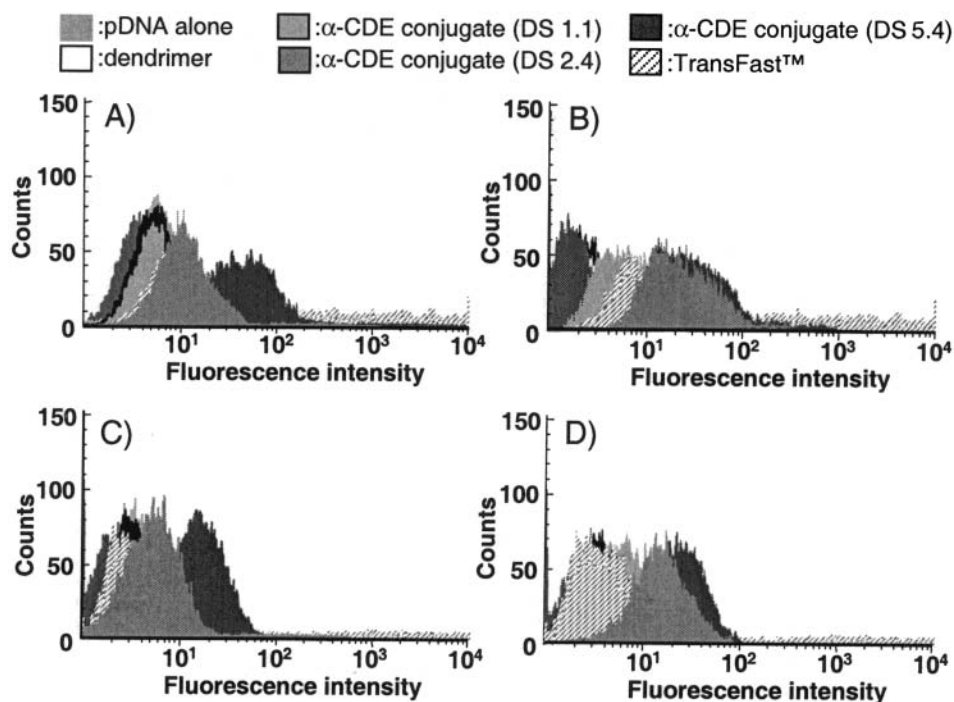
**In Vivo Transfection.** Figure 8 shows gene transfer activity 12 and 24 h after intravenous administration of



**Figure 6.** Gene transfer activity of the complexes of pDNA/dendrimer (G3) or pDNA/ $\alpha$ -CDE conjugates (DS 1.1, 2.4, and 5.4) at various charge ratios in NIH3T3 cells (A) and HepG2 cells (B). The luciferase activity in cell lysates was determined 25 h after incubation with pDNA alone or various complexes. The charge ratio of pDNA and TransFast is 1/1. Open column, dendrimer (G3); dark hatched column,  $\alpha$ -CDE conjugate (DS 1.1); light hatched column,  $\alpha$ -CDE conjugate (DS 2.4); closed column,  $\alpha$ -CDE conjugate (DS 5.4). One million relative light units correspond approximately to 1.6 ng of firefly luciferase. Each value represents the mean  $\pm$  SEM of four experiments. \* $p < 0.05$ , compared with dendrimer (G3).

the suspension containing the complexes of pDNA/dendrimer and pDNA/ $\alpha$ -CDE conjugates to tail vein of mice. Here we used pRL-CMV-Luc as plasmid DNA due to preferable gene expression in vivo. In the present study, we chose a charge ratio of pDNA/ $\alpha$ -CDE conjugate of 10/1 (vector/pDNA) because intravenous administration of the suspension containing pDNA complex with  $\alpha$ -CDE conjugate (DS 5.4), not  $\alpha$ -CDE conjugates (DS 1.1 and 2.4), at a charge ratio of 20/1 was fatal to mice (data not shown). Luciferase activity was much higher in the spleen than in other tissues, followed by the liver at 12 h after administration. The activity was higher in liver rather than spleen at 24 h, although the gene expression markedly lowered to less than one-hundredth (Figure 8). When the magnitude of gene transfer activity between nonviral vectors used here was compared,  $\alpha$ -CDE conjugate (DS 2.4) provided gene transfer activity higher than dendrimer and other  $\alpha$ -CDE conjugates in spleen at 12 h and in liver and kidney at 24 h following administration, respectively. In addition,  $\alpha$ -CDE conjugate (DS 5.4) significantly increased gene transfer activity compare to both dendrimer and other  $\alpha$ -CDE conjugates in liver at 12 h, but not in other tissues. These results indicate that  $\alpha$ -CDE conjugate (DS 2.4) possesses the preferable gene transfer activity in vivo.





**Figure 7.** Transfection efficiency of the complexes of pDNA/dendrimer (G3) or pDNA/ $\alpha$ -CDE conjugates (DS 1.1, 2.4, and 5.4) at various charge ratios in NIH3T3 cells (A, B) and HepG2 cells (C, D). pEGFP-N1 vector encoding GFP was used. The charge ratios of the complexes of dendrimer/pDNA,  $\alpha$ -CDE conjugates/pDNA were 50/1 (A, C) and 200/1 (B, D) and the charge ratio of and TransFast™ expression in the cells was measured with a flow cytometer.

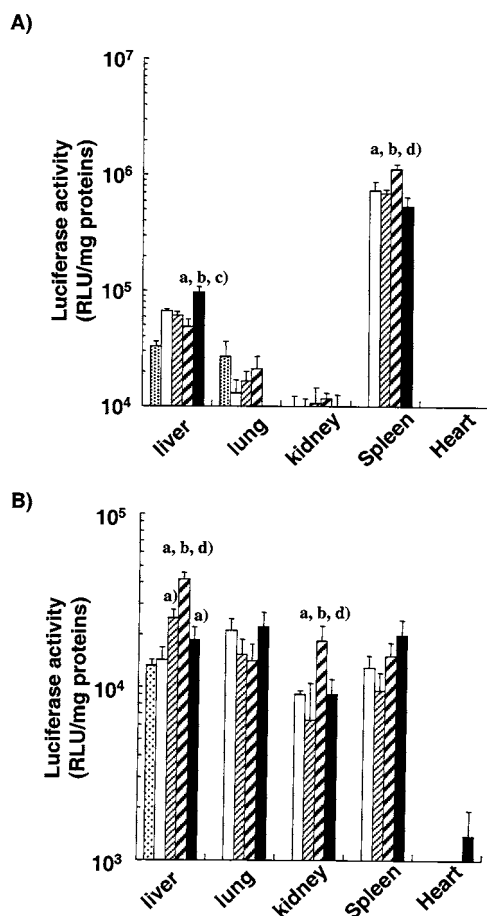
## DISCUSSION

In the present study, we clarified that gene transfer activity of  $\alpha$ -CDE conjugates is markedly affected by the DS values of  $\alpha$ -CyD in the conjugate, and of the three conjugates,  $\alpha$ -CDE conjugate (DS 2.4) possesses high gene transfer activity in vitro and in vivo with less cytotoxicity.

The physicochemical properties of polyplexes such as the particle size and net charge markedly affect gene transfer efficiency (6). From the molecular structure's point of view, the primary amino groups of  $\alpha$ -CDE conjugates apparently decrease with an increase in the DS value of  $\alpha$ -CyD; therefore, the interaction between  $\alpha$ -CDE conjugates and pDNA was expected to decrease. Contrary to our expectation,  $\alpha$ -CDE conjugates (DS 1.1, 2.4, and 5.4) formed the polyplexes in a similar way (Figures 2 and 3). This similarity of the complexation can be due to more than 28 residual free primary amino groups because dendrimer (G3) possesses terminal 32 amino groups in a molecule and the calculated values of the numbers of charge centers in dendrimer (G3) and  $\alpha$ -CDE conjugates (DS 1.1, 2.4, and 5.4) at physiological pH were 32, 30.9, 28.6, and 26.6, respectively (33). Thus, it is apparent that physicochemical properties are almost identical among the pDNA complexes with three  $\alpha$ -CDE conjugates. Regarding the particle size, it may be unreasonable that  $\alpha$ -CDE conjugates (DS 1.1, 2.4, and 5.4) form the most compact complexes (approximately 200 nm) at a charge ratio of 1/1 because neutral particles tend to aggregate. However, the lack of aggregation was observed up to 15 min after mixing pDNA and  $\alpha$ -CDE conjugates, at which the particle sizes were determined. This restricted aggregation may be preferable to prepare the injection containing pDNA/ $\alpha$ -CDE conjugates. Unfortunately, we could not show the morphological data of the polyplexes with dendrimer and  $\alpha$ -CDE conjugates here, but their morphology might be independent of the charge

ratio at the higher charge ratios because of the almost identical particle size of their polyplexes (Figure 3).

Polyplex-mediated transfection should overcome at least one of the major barriers for transfection, that is, the escape of pDNA from endosomes (34). We previously proposed the possibility that  $\alpha$ -CDE conjugate (DS 1.1) may enhance the release of pDNA or the pDNA complexes with  $\alpha$ -CDE conjugates from the endosomal compartment after the cellular uptake into NIH3T3 cells (27, 28). In the present study, we indeed revealed that  $\alpha$ -CDE conjugates are efficiently capable of releasing calcein from liposomes, depending on the DS value of  $\alpha$ -CDE conjugates, suggesting that  $\alpha$ -CDE conjugates (DS 2.4 and 5.4) potentially possess endosomal membrane-disruptive ability through the interaction between  $\alpha$ -CyD moiety and the membrane components after endocytosis into the cells. This inference may be supported by the findings that the disruption of liposomal membranes was not observed by adding dendrimer (G3) (Figure 4). However, it should be noted that the concentrations of  $\alpha$ -CDE conjugates acquired for liposomal disruption were higher than those under the in vitro transfection condition (approximately 20  $\mu$ M at a charge ratio of 200/1); thereby, it is possible that an endosomal disruption by  $\alpha$ -CDE conjugates hardly takes place after transfection. At the same time, we demonstrated that  $\alpha$ -CyD induces hemolysis through the extraction of membrane components from the erythrocyte membranes (14), and  $\alpha$ -CDE conjugates include fluorescent guest molecule, 2-(*p*-toluidinyl)naphthalene-6-sulfonate potassium salt (28), supporting the possible membrane-disruptive activity of  $\alpha$ -CDE conjugates. In addition, we observed more fluorescence in cytoplasm after transfection of fluorescein isothiocyanate (FITC)-labeled pDNA with  $\alpha$ -CDE conjugate (DS 2.4) compared to that with dendrimer in NIH3T3 cells (data not shown). Therefore, these results imply that  $\alpha$ -CDE conjugates might increase the release



**Figure 8.** In vivo gene transfer activity of the complexes of DNA/dendrimer or  $\alpha$ -CDE (DS 1.1, 2.4, 5.4). pRL-CMV-Luc encoding Renilla luciferase was used as pDNA. The solution containing pDNA and the suspensions containing the complexes of pDNA/dendrimer or with pDNA/ $\alpha$ -CDE conjugate were injected to tail vein of BALB/c mice. Twelve (A) and 24 h (B) after administration, the mice were sacrificed, and then lung, heart, liver, spleen, and kidney were isolated. The organs were washed and homogenized. After centrifugation of the homogenate, the supernatant was taken and added to Promega Renilla luciferase assay buffer. The luciferase activity in the solution was measured using a luminometer. Dotted column, pDNA alone; open column, dendrimer (G3); dark hatched column,  $\alpha$ -CDE conjugate (DS 1.1); light hatched column,  $\alpha$ -CDE conjugate (DS 2.4); closed column,  $\alpha$ -CDE conjugate (DS 5.4). One million relative light units correspond approximately to 0.4 ng of Renilla luciferase. Each value represents the mean  $\pm$  SEM of 4–9 mice. Four, six, six, nine, and six mice at 12 h were used in pDNA alone, pDNA/dendrimer, pDNA/ $\alpha$ -CDE conjugate (DS 1.1), pDNA/ $\alpha$ -CDE conjugate (DS 2.4), and pDNA/ $\alpha$ -CDE conjugate (DS 5.4) groups, and nine mice at 24 h were used in all of the groups. (a)  $p < 0.05$  compared with dendrimer (G3), (b)  $p < 0.05$  compared with  $\alpha$ -CDE conjugate (DS 1.1), (c)  $p < 0.05$  compared with  $\alpha$ -CDE conjugate (DS 2.4), (d)  $p < 0.05$  compared with  $\alpha$ -CDE conjugate (DS 5.4).

of pDNA or the pDNA complex from endosomes following cellular uptake, although it remains unclear to what extent the membrane disruptive ability of  $\alpha$ -CDE conjugates contributes to the enhancing effect on gene transfer activity. Further experiments should be performed to clarify the enhancing effect of  $\alpha$ -CDE conjugate on an endosomal escape of pDNA using FITC-labeled BSA with nuclear localization signal peptide. In addition,  $\alpha$ -CDE conjugate (DS 1.1), whose endosomal membrane-disruptive ability in the cells we proposed (27), did not release calcein from liposomes (Figure 4). This inconsistency may be due to the difference of the experimental conditions between cellular and liposomal systems.

From a safety point of view,  $\alpha$ -CDE conjugate (DS 5.4) may be inferior to  $\alpha$ -CDE conjugate (DS 2.4) because  $\alpha$ -CDE conjugate (DS 5.4) showed more cytotoxicity in vitro (Figure 5) and in vivo as mentioned above. In addition, the concentrations of dedrimer and  $\alpha$ -CDE conjugate (DS 1.1, 2.4, and 5.4) at a charge ratio of 100/1 were 24.38, 25.25, 26.36, and 29.33  $\mu$ M, respectively, under the present experimental condition regarding cytotoxicity. The cytotoxic effect of  $\alpha$ -CDE conjugate (DS 5.4) may allow transfection efficiency to attenuate at the higher charge ratios (Figure 5). So far, CyDs have been reported to fail to enter into the cells because of their hydrophilicity and high molecular weight (14). On the other hand, our preliminary results demonstrated that  $\alpha$ -CDE conjugates enter into the cells in terms of the adsorptive endocytotic machinery as other cationic non-viral vectors (35, 36). Therefore, the cytotoxic effect of  $\alpha$ -CDE conjugates might be exerted by an intracellular event such as an endosomal disruption. The results that the physical mixture of  $\alpha$ -CyD and pDNA complex with dendrimer (G3) showed neither cytotoxic nor an enhancing effect on gene transfer activity (27, 28) may also support the cellular uptake of  $\alpha$ -CDE conjugates. There are still some critical issues, however, as to the intracellular trafficking of pDNA complexes with  $\alpha$ -CDE conjugates after cellular uptake, i.e., (1) whether the pDNA complexes can enter into nucleus; (2) where the pDNA complexes with  $\alpha$ -CDE conjugates dissociate into each component; (3) how  $\alpha$ -CDE conjugates are released from the cells. Elaborate studies are further required to address these issues.

The introduction of  $\alpha$ -CyD to dendrimer (G3) is likely to increase not only the net luciferase activity but also the number of cells expressing GFP (Figure 7), indicating that  $\alpha$ -CDE conjugates improved both net gene transfer activity and transfection efficiency to each cell. In addition, the gene transfer activity of  $\alpha$ -CDE conjugate (G3, DS 2.4) was 3 or 4 times higher than that of TransFast at the charge ratios of 200/1 and 400/1 in NIH3T3 cells. The improving effect of  $\alpha$ -CDE conjugates on gene transfer activity may also be due to the distinct mechanism for the endosomal escape of pDNA or its complex:  $\alpha$ -CDE conjugates, and TransFast may allow pDNA to escape from the endosomes through the lipid extraction from the endosomal membranes and the membrane fusion with L-dioleoyl phosphatidyl-ethanolamine, a constituent of TransFast, respectively. However, the prominent gene transfer activity of  $\alpha$ -CDE conjugates compared with TransFast was not observed in HepG2 cells. The reason for this difference in the gene transfer activity between the cells remains unknown, but the different sensitivity between NIH3T3 and HepG2 cells to the cytotoxic effects of  $\alpha$ -CDE conjugates and TransFast may be involved.

The free  $\alpha$ -CDE conjugate may play a critical role for gene transfer activity. In the agarose gel electrophoretic study, the bands disappeared at a charge ratio of 1/1, suggesting that  $\alpha$ -CDE conjugates sufficiently form the complexes with pDNA at the charge ratio, where the calculated molar ratio of the pDNA complexes with  $\alpha$ -CDE conjugates (DS 1.1, 2.4, and 5.4) were 351, 363, and 404 ( $\alpha$ -CDE conjugate/pDNA), respectively. Thus, the free extent of  $\alpha$ -CDE conjugates must be raised, when the charge ratio increases in the range of 1/1–400/1, because the molar ratios were so high that  $\alpha$ -CDE conjugates may be unable to bind to pDNA. Therefore, the enhancement of gene transfer activity may be due to the additional free  $\alpha$ -CDE conjugates at the higher

charge ratios, although the precise extent of free fraction was unknown.

$\alpha$ -CDE conjugates, especially  $\alpha$ -CDE conjugate (G3, DS 2.4), may be used as in vivo gene transfer agents. As mentioned in the Experimental Section, 500  $\mu$ L of test solutions or suspensions were injected to the tail vein in a minute in the present study, suggesting that in vivo gene transfer activity could not be attributed to a hydrodynamics-based gene transfer because of low volume and injection rate (37). The gene expression was observed in several tissues after intravenous administration of the pDNA complexes with  $\alpha$ -CDE conjugates (DS 1.1, 2.4, and 5.4) (Figure 8). It should be noted that the luciferase activity in spleen at 12 h after administration of pDNA complex with  $\alpha$ -CDE conjugate (DS 2.4) was over  $1 \times 10^6$  RLU/mg proteins and the values in liver, lung, and kidney at 24 h were even over  $1.5 \times 10^4$  RLU/mg proteins. In addition, the high gene transfer activity of  $\alpha$ -CDE conjugates, especially  $\alpha$ -CDE conjugate (DS 2.4) may result from a change in an intracellular trafficking of pDNA in various organs, at least in part, after intravenous administration in mice. In vivo luciferase activities 24 h after intravenous administration of the complex of pDNA/ $\alpha$ -CDE conjugate (DS 2.4) at a charge ratio of 20/1 were  $13759 \pm 1062$ ,  $10220 \pm 935$ ,  $23831 \pm 7820$ ,  $9566 \pm 768$ , and  $10019 \pm 1962$  RLU/mg proteins in liver, lung, kidney, spleen, and heart, respectively. Thus, in vivo gene transfer activity of  $\alpha$ -CDE conjugates at the charge ratio of 20/1 was lower than that at 10/1, inconsistent with the in vitro results. This inconsistency could be attributed to a distinct sensitivity to cytotoxicity of nonviral vector between in vitro and in vivo, because intravenous administration of  $\alpha$ -CDE conjugate (DS 5.4) was fatal at the charge ratio of 20/1 in mice, but not in vitro. Taken together, these results suggest that  $\alpha$ -CDE conjugate (DS 2.4) possesses a promising in vivo gene transfer activity.

The in vivo luciferase activity elicited by  $\alpha$ -CDE conjugates in spleen was significantly lower below one-hundredth at 24 h compared with at 12 h after administration. This may not be, however, due to the cytotoxic effect of  $\alpha$ -CDE conjugates because the pDNA complex with dendrimer provided a similar pattern of gene transfer activity in spleen to that of  $\alpha$ -CDE conjugates (Figure 8). It is possible that the rapid impairment of gene expression could not be attributed to the epigenetic effects such as methylation of pDNA and histone deacetylation because the administration of DNA methyltransferase inhibitor, 5-azacytidine, and a histone deacetylase inhibitor, trichostatin A, did not increase the gene expression (data not shown), despite the fact that these inhibitors have been reported to enhance and prolong the expression of transgenes (38–41). It may be possible that a degradation of pDNA and/or unknown mechanisms play a critical role in this impairment. Further investigation regarding the extension as well as the modulation of in vivo gene expression elicited by  $\alpha$ -CDE conjugates is necessary.

In conclusion,  $\alpha$ -CDE conjugate (G3, DS 2.4) was shown to be the best  $\alpha$ -CDE conjugate among the  $\alpha$ -CDE conjugates prepared in a series of the studies, because it provided good gene transfer activity in vitro and in vivo with low cytotoxicity. Consequently, the potential use of  $\alpha$ -CDE conjugate (G3, DS 2.4) could be expected as a nonviral vector to deliver gene in vitro and in vivo and these data may be useful for design of  $\alpha$ -CyD conjugates with other nonviral vectors.

## ACKNOWLEDGMENT

We thank Dr. Makoto Uemura for assistance with the light scattering experiments using a Beckman Coulter N4 Plus machine at the Kumamoto Industrial Research Institute. This work was partially supported by a Grant-in-Aid from Tokyo Biochemical Research Foundation, a Grant-in-Aid from the Research Foundation for Pharmaceutical Sciences, a Grant-in-Aid for Encouragement of Young Scientists from the Ministry of Education, Science and Culture of Japan (12771464) and a Grant-in-Aid for Scientific Research (C) from Japan Society for the Promotion of Science (14572158).

## LITERATURE CITED

- (1) Pfeifer, A., and Verma, I. M. (2001) Gene Therapy: promises and problems. *Annu. Rev. Genomics. Hum. Genet.* 2, 177–211.
- (2) Grosshans, H. (2000) Gene therapy—when a simple concept meets a complex reality. Review on gene therapy. *Funct. Integr. Genomics* 1, 142–145.
- (3) Rolland, A. P. (1998) From genes to gene medicines: recent advances in nonviral gene delivery. *Crit. Rev. Ther. Drug Carrier Syst.* 15, 143–198.
- (4) Ledly, F. D. (1995) Nonviral gene therapy: the promise of genes as pharmaceutical products. *Hum. Gene Ther.* 6, 1129–1144.
- (5) Nishikawa, M., and Huang, L. (2001) Nonviral vectors in the new millennium: delivery barriers in gene transfer. *Hum. Gene Ther.* 12, 861–870.
- (6) Ma, H., and Diamond, S. L. (2001) Nonviral gene therapy and its delivery systems. *Curr. Pharm. Biotechnol.* 2, 1–17.
- (7) Lechardeur, D., and Lukacs, G. L. (2002) Intracellular barriers to nonviral gene transfer. *Curr. Gene Ther.* 2, 183–194.
- (8) Saenger, W. (1980) Cyclodextrin inclusion compound as research and industry. *Angew. Chem., Int. Ed. Engl.* 19, 344–362.
- (9) Szejtli, J. (1982) *Cyclodextrins and their inclusion complexes*, Akadémiai Kiadó, Budapest.
- (10) Szejtli, J. (1988) *Cyclodextrin technology*, Kluwer, Dordrecht, The Netherlands.
- (11) Uekama, K., Hirayama, F., and Irie, T. (1998) Cyclodextrin drug carrier systems. *Chem. Rev.* 5, 2045–2076.
- (12) Thompson, D. O. (1997) Cyclodextrins-enabling excipients: their present and future use in pharmaceuticals. *Crit. Rev. Ther. Drug Carrier Syst.* 14, 1–104.
- (13) Albers, E., and Müller, B. W. (1995) Cyclodextrin derivatives in pharmaceuticals. *Crit. Rev. Ther. Drug Carrier Syst.* 12, 311–337.
- (14) Irie, T., and Uekama, K. (1997) Pharmaceutical application of cyclodextrin. III. Toxicological issues and safety evaluation. *J. Pharm. Sci.* 86, 147–162.
- (15) Irie, T., and Uekama, K. (1999) Cyclodextrins in peptide and protein delivery. *Adv. Drug Deliv. Rev.* 36, 101–123.
- (16) Marttin, E., Verhoef, J. C., and Merkus, F. W. (1998) Efficacy, safety and mechanism of cyclodextrins as absorption enhancers in nasal delivery of peptide and protein drugs. *J. Drug Target.* 6, 17–36.
- (17) Roessler, B. J., Bielinska, A. U., Janczak, K., Lee, I., and Baker, J. R., Jr. (2001) Substituted  $\beta$ -cyclodextrins interact with PAMAM dendrimer-DNA complexes and modify transfection efficiency. *Biochem. Biophys. Res. Commun.* 283, 124–129.
- (18) Croyle, M. A., Rossler, B. J., Hsu, C. P., Sun, R., and Amidon, G. L. (1998)  $\beta$ -Cyclodextrins enhance adenoviral-mediated gene delivery to the intestine. *Pharm. Res.* 15, 1348–1355.
- (19) Frean, D. J., and Niven, R. W. (1996) The influence of sodium glycolate and other additives on the in vivo transfection of plasmid DNA in the lungs. *Pharm. Res.* 13, 202–209.
- (20) Dass, C. R. (2002) Vehicles for oligonucleotide delivery to tumours. *J. Pharm. Pharmacol.* 54, 3–27.
- (21) Redenti, E., Pietra, C., Gerloczy, A., and Szente, L. (2001) Cyclodextrins in oligonucleotide delivery. *Adv. Drug Deliv. Rev.* 53, 235–244.



- (22) Zhao, Q., Temsamani, J., and Agrawal, S. (1995) Use of cyclodextrin and its derivatives as carriers for oligonucleotide delivery. *Antisense Res. Dev.* 5, 185–192.
- (23) Abdou, S., Collomb, J., Sallas, F., Marsura, A., and Finance, C. (1997)  $\beta$ -Cyclodextrin derivatives as carriers to enhance the antiviral activity of an antisense oligonucleotide directed toward a coronavirus intergenetic consensus sequence. *Arch. Virol.* 142, 1585–1602.
- (24) Gonzalez, H., Hwang, S. J., and Davis, M. E. (1999) New class of polymers for the delivery of macromolecular therapeutics. *Bioconjugate Chem.* 10, 1068–1074.
- (25) Hwang, S. J., Bellocq, N. C., and Davis, M. E. (2001) Effects of structure of  $\beta$ -cyclodextrin-containing polymers on gene delivery. *Bioconjugate Chem.* 12, 280–290.
- (26) Pun, S. H., and Davis, M. E. (2002) Development of a nonviral gene delivery vehicle for systemic application. *Bioconjugate Chem.* 13, 630–639.
- (27) Arima, H., Kihara, F., Hirayama, F., and Uekama, K. (2001) Enhancement of gene expression by polyamidoamine dendrimer conjugates with  $\alpha$ -,  $\beta$ -, and  $\gamma$ -cyclodextrins. *Bioconjugate Chem.* 12, 476–484.
- (28) Kihara, F., Arima, H., Hirayama, F., and Uekama, K. (2002) Effects of Structure of Polyamidoamine Dendrimer on Gene Transfer Efficiency of the Dendrimer Conjugate with  $\alpha$ -Cyclodextrin. *Bioconjugate Chem.* 13, 1211–1219.
- (29) Suh, J., Lee, S. H., and Zoh, K. D. (1992) A novel host containing both binding site and nucleophilic prepared by attachment of  $\beta$ -cyclodextrin to poly(ethylenimine). *J. Am. Chem. Soc.* 114, 7916–7917.
- (30) Melton, L. D., and Slessor, K. N. (1971) Synthesis of monosubstituted cyclohexaamyloses. *Carbohydrate Res.* 18, 29–37.
- (31) Szoka, F., Jacobson, K., Derzko, Z., and Papahadjopoulos, D. (1980) Fluorescence studies on the mechanism of liposome-cell interactions in vitro. *Biochim. Biophys. Acta* 600, 1–18.
- (32) Ishiyama, M., Tominaga, H., Shiga, M., Sasamoto, K., Ohkura, Y., and Ueno, K. (1996) A combined assay of cell viability and in vitro cytotoxicity with a highly water-soluble tetrazolium salt, neutral red and crystal violet. *Biol. Pharm. Bull.* 19, 1518–1520.
- (33) Haensler, J., and Szoka, F. C., Jr. (1993) Polyamidoamine cascade polymers mediate efficient transfection of cells in culture. *Bioconjugate Chem.* 4, 372–379.
- (34) Pouton, C. W., and Seymour, L. W. (2001) Key issues in nonviral gene delivery. *Adv. Drug Deliv. Rev.* 46, 187–203.
- (35) Kircheis, R., Wightman, L., and Wagner, E. (2001) Design and gene delivery activity of modified polyethylenimines. *Adv. Drug Deliv. Rev.* 53, 341–358.
- (36) Mounkes, L. C., Zhong, W., Cipres-Palacin, G., Heath, T. D., and Debs, R. J. (1998) Proteoglycans mediate cationic liposome-DNA complex-based gene delivery in vitro and in vivo. *J. Biol. Chem.* 273, 26164–26170.
- (37) Song, Y. K., Liu, F., Zhang, G., and Liu, D. (2002) Hydrodynamics-based transfection: simple and efficient method for introducing and expressing transgenes in animals by intravenous injection of DNA. *Methods Enzymol.* 346, 92–105.
- (38) Chen, W. Y., Bailey, E. C., McCune, S. L., Dong, J. Y., and Townes, T. M. (1997) Reactivation of silenced, virally transduced genes by inhibitors of histone deacetylase. *Proc. Natl. Acad. Sci. U.S.A.* 94, 5798–5803.
- (39) Di Ianni, M., Terenzi, A., Perruccio, K., Ciurnelli, R., Lucheroni, F., Benedetti, R., Martelli, M. F., and Tabilio, A. (1999) 5-Azacytidine prevents transgene methylation in vivo. *Gene Ther.* 6, 703–707.
- (40) Gaetano, C., Catalano, A., Palumbo, R., Illi, B., Orlando, G., Ventrone, G., Serino, F., and Capogrossi, M. C. (2000) Transcriptionally active drugs improve adenovirus vector performance in vitro and in vivo. *Gene Ther.* 7, 1624–1630.
- (41) Hong, K., Sherley, J., and Lauffenburger, D. A. (2001) Methylation of episomal plasmids as a barrier to transient gene expression via a synthetic delivery vector. *Biomol. Eng.* 18, 185–192.

BC025613A

# S-Peptide as a Potent Peptidyl Linker for Protein Cross-Linking by Microbial Transglutaminase from *Streptomyces mobaraensis*

Noriho Kamiya,<sup>†</sup> Tsutomu Tanaka,<sup>†</sup> Tsutomu Suzuki,<sup>§</sup> Takeshi Takazawa,<sup>†</sup> Shuji Takeda,<sup>†</sup> Kimitsuna Watanabe,<sup>§</sup> and Teruyuki Nagamune<sup>\*,†</sup>

Department of Chemistry and Biotechnology, Graduate School of Engineering, The University of Tokyo, 7-3-1 Hongo, Bunkyo-ku, Tokyo 113-8656, Japan and Department of Integrated Biosciences, Graduate School of Frontier Sciences, The University of Tokyo, 5-1-5 Kashiwanoha, Kashiwa-shi, Chiba 277-8562, Japan. Received September 21, 2002; Revised Manuscript Received January 15, 2003

We have found that ribonuclease S-peptide can work as a novel peptidyl substrate in protein cross-linking reactions catalyzed by microbial transglutaminase (MTG) from *Streptomyces mobaraensis*. Enhanced green fluorescent protein tethered to S-peptide at its N-terminus (S-tag-EGFP) appeared to be efficiently cross-linked by MTG. As wild-type EGFP was not susceptible to cross-linking, the S-peptide moiety is likely to be responsible for the cross-linking. A site-directed mutation study assigned Gln15 in the S-peptide sequence as the sole acyl donor. Mass spectrometric analysis showed that two Lys residues (Lys5 and Lys11) in the S-peptide sequence functioned as acyl acceptors. We also succeeded in direct monitoring of the cross-linking process by virtue of fluorescence resonance energy transfer (FRET) between S-tag-EGFP and its blue fluorescent color variant (S-tag-EBFP). The protein cross-linking was tunable by either engineering S-peptide sequence or capping the S-peptide moiety with S-protein, the partner protein of S-peptide for the formation of ribonuclease A. The latter indicates that S-protein can be used as a specific inhibitor of S-peptide-directed protein cross-linking by MTG. The controllable protein cross-linking of S-peptide as a potent substrate of MTG will shed new light on biomolecule conjugation.

## INTRODUCTION

The major choice for conjugation or covalent modification of functional proteins with an organic molecule (including peptides and proteins) has basically been chemical manipulation because of their simplicity and variety (1). Although choosing the correct reagent systems can afford successful modification, one of the critical shortcomings in the chemical modification of proteins is the lack of specificity because of a number of functional groups on the protein surface that compete for a target molecule. Genetic manipulation, in which gene fragments encoding different kinds of peptides and/or proteins are fused onto a plasmid vector, has also been widely employed to prepare recombinant fusion proteins. However, this approach is often hampered by the poor yield of the target chimeric proteins, mainly due to the formation of inclusion bodies in the host cells of foreign origins. Transglutaminase (TG), which strictly catalyzes the acyl-transfer reaction between the  $\gamma$ -carboxamide group of a Gln residue (acyl donor) and the  $\epsilon$ -amino group of a Lys residue (acyl acceptor) of proteins and peptides, is conceptually applicable to Gln- or Lys-specific covalent modification or cross-linking of target proteins via an  $\epsilon$ -( $\gamma$ -glutamyl)lysine bridge (2, 3). However, this concept was demonstrated to only be applicable to a limited number of proteins by the use of guinea pig TG due to its strict substrate specificity (4, 5).

Microbial transglutaminase (MTG) from *Streptomyces mobaraensis* (6, 7) was found to be a powerful industrial catalyst owing to the rather broader substrate specificity for acyl acceptors than other TGs (8), the handling feasibility, such as  $\text{Ca}^{2+}$ -independence, and the availability originating from mass production by the microorganism. In the past decade, MTG has been an ideal enzyme for food processing (9), but there have been few reports on the application of MTG in other fields (10). Recently, the utilization of MTG has attracted much attention for either the modification or conjugation of functional proteins. Simple incorporation of organic molecules into target proteins was demonstrated in the preparation of a hapten–protein conjugate (11), a biotinylated monoclonal antibody (12), and a poly(ethylene-glycol)-modified human interleukin 2 (8). The conjugation of functional proteins (13) yielded a bifunctional protein. Site-specific modification of a peptide (14) or a protein (15) was directed to obtain an artificial nutrient. The stabilization of enzymes by MTG has also been studied by immobilization (16) and the elimination of deleterious factors (17). These studies clearly showed that MTG can be applicable to the modification of protein function and production of a new protein conjugate. However, most studies have been carried out with intact proteins (10–13) and little information is yet available on the substrate specificity of MTG (6, 18–21). As claimed by Sato et al. (5), the capability of posttranslational modification by TG offers a new choice for site-specific modification of target proteins when a specific peptide sequence can be introduced to proteins of interest by genetic engineering. More attention should thus be paid to the substrate requirements of MTG, which is superior to other TGs from a

\* To whom correspondence should be addressed. Tel: +81-3-5841-7328; Fax: +81-3-5841-8657; E-mail: nagamune@bio.t.u-tokyo.ac.jp.

<sup>†</sup> Department of Chemistry and Biotechnology.

<sup>§</sup> Department of Integrated Biosciences.

practical standpoint, to generalize TG-directed enzymatic protein conjugation in the field of protein engineering.

The aim of this study was to demonstrate that ribonuclease S-peptide can be a novel candidate as a tunable peptide tag that enables the site-specific cross-linking of functional proteins. Enhanced green fluorescent protein carrying an additional S-peptide sequence in its N-terminus (S-tag-EGFP) was employed as a model protein. The reactive cross-linking sites of dimerized S-tag-EGFP were explored by either site-directed mutagenesis or mass spectrometric analysis of S-tag-EGFP. Direct spectroscopic measurement of the cross-linking reaction was successfully monitored by the use of fluorescence resonance energy transfer (FRET) between cross-linked S-tag-EGFP and S-tag-EBFP (a fluorescent color variant of EGFP). Finally, as we succeeded in either the alteration of the reactivity of S-peptide by site-directed mutagenesis or the inhibition of the cross-linking by capping the S-peptide moiety with S-protein, this report shows, for the first time, controllable protein cross-linking by TG.

## MATERIALS AND METHODS

**Materials.** MTG was generously provided by Ajinomoto Co. Inc. (Japan) in a semipurified form. Carbobenzoyl-L-glutamylglycine (Z-QG) was obtained from Tokyo Chemical Industry Co. Ltd (Japan). S-Protein was purchased from Sigma-Aldrich. All other reagents used in this study were of the highest purity commercially available.

**Sample Preparation.** Purification of MTG was conducted with a Blue Sepharose CL-6B affinity column (Amersham Pharmacia Biotech Co.) as reported previously (6). The catalytic activity of purified MTG was measured by a colorimetric procedure described elsewhere (22). S-tag-EGFP and S-tag-EBFP were prepared as follows. DNA fragments encoding EGFP (enhanced GFP) and EBFP (enhanced blue fluorescent protein) were prepared from plasmids pEGFP and pEBFP-N1 (Clontech), respectively, and subcloned into pET32b(+) (Novagen) with *Nco*I/*Not*I double digestion. Both proteins were expressed in *Escherichia coli* strain BL21(DE3)-pLysS (Novagen) as *E. coli* thioredoxin fusion proteins according to a previously described procedure (23). The fusion proteins were purified by metal affinity chromatography through His-tag (Clontech). The purified proteins were subjected to site-specific cleavage with thrombin (Novagen) to eliminate the thioredoxin and His-tag in the N-terminus of the fusion proteins. The resultant proteins were employed as S-tag-EGFP and S-tag-EBFP, respectively. The N-terminal extended peptide sequence of S-tag-EG(B)FP in comparison with wild-type EG(B)FP was **GSGMKETA****AKFERQHMDSPDLGTDDDDKA** (the S-peptide sequence is shown in bold letters). Site-directed mutagenesis of Gln15 to Ala of S-tag-EGFP was performed using QuikChange mutagenesis kit (Stratagene) and the resultant protein was abbreviated as Q15A-tag-EGFP. The primer nucleotide sequences used for the mutagenesis of Gln15 to Ala were 5'-GCT GCT GCT AAA TTC GAA CGC GCG CAC ATG GAC AGC-3' and 5'-GCT GTC CAT GTG CGC GCG TTC GAA TTT AGC AGC AGC-3'. Site-directed mutagenesis of Lys5 to Ala of S-tag-EGFP, which yielded K5A-tag-EGFP, was also performed by the same procedure. The primer nucleotide sequences used for the mutagenesis of Lys5 to Ala were 5'-GAA ACC GCT GCT GCT GCA TTC GAA CGC CAG CAC-3' and 5'-GTG CTG GCG TTC GAA TGC AGC AGC AGC GGT TTC-3'. The homogeneity of the purified proteins was

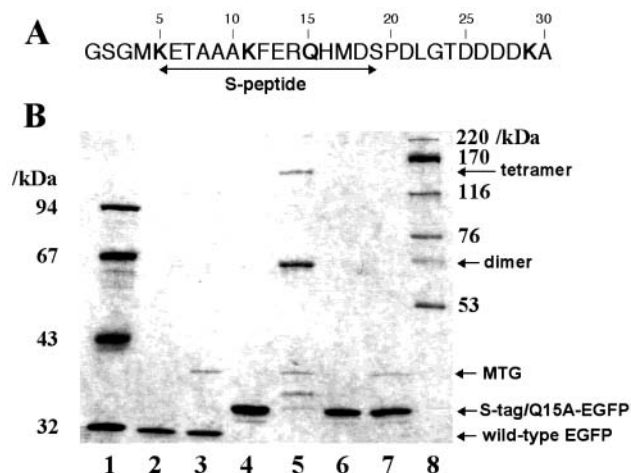
verified by sodium dodecyl sulfate–polyacrylamide gel electrophoresis (SDS–PAGE). The protein concentration was determined using the BCA assay Kit (Pierce). In the case of S-tag-EGFP and S-tag-EBFP, the protein concentrations were adjusted based on the absorbance of chromophores by assuming millimolar extinction coefficients of  $55 \text{ mM}^{-1} \text{ cm}^{-1}$  at 488 nm and  $31 \text{ mM}^{-1} \text{ cm}^{-1}$  at 380 nm, respectively (24).

**Cross-Linking of S-tag-EGFP by MTG.** In preliminary experiments, wild-type EGFP or S-tag-EGFP ( $1.2 \mu\text{M}$ ) was dissolved in 10 mM sodium phosphate buffer at pH 7.5. The cross-linking reaction was initiated by the addition of MTG (0.25 U/mL) at 4 °C. After incubation for 2 h, the reaction products were analyzed by SDS–PAGE. Image analysis of the result of SDS–PAGE was performed on a Macintosh computer using the public domain NIH Image program (developed at the U.S. National Institutes of Health and available on the Internet at <http://rsb.info.nih.gov/nih-image/>).

**Identification of Cross-Linking Sites of S-tag-EGFP by Mass Spectroscopy.** Z-QG was used as an acyl donor to identify the cross-linking sites of Lys residues working as acyl acceptors in S-tag-EGFP. Incorporation of Z-QG into S-tag-EGFP was carried out using the same protocol described above except for the presence of an excess amount of Z-QG ( $250 \mu\text{M}$ ) in the reaction mixture. The complete suppression of dimerization of S-tag-EGFP molecules by Z-QG was confirmed by SDS–PAGE. The reaction products on SDS–PAGE were visualized by CBB staining. The protein spot was excised and the gel piece was soaked in a buffer containing 0.2 M  $\text{NH}_4\text{HCO}_3$  with 50% acetonitrile and incubated at 30 °C for 30 min to remove SDS from the proteins. To ensure the complete removal of SDS, the step was repeated twice. The gel pieces were dried in a speedvac and then rehydrated with 5–10  $\mu\text{L}$  of trypsin digestion solution [0.2 M  $\text{NH}_4\text{HCO}_3$ , 15 ng/ $\mu\text{L}$  TPCK-trypsin (Pierce)]. After the gel pieces had absorbed the liquid, 10–20  $\mu\text{L}$  of 0.2 M  $\text{NH}_4\text{HCO}_3$  was added to the gel. Complete digestion was carried out overnight at 30 °C. The digested peptides were extracted from the gel by shaking in 200  $\mu\text{L}$  of 60% acetonitrile and 0.1% TFA solution for 20 min. This step was repeated twice more. The collected fractions containing each peptide were pooled together and dried in a speedvac, and the obtained sample was dissolved in 80  $\mu\text{L}$  of 0.1% formic acid. Twenty microliters of the collected peptide was subjected to LC/MS analysis to obtain the peptide mass map. A Finnigan LCQ ion trap mass spectrometer (ThermoQuest) equipped with an electrospray ionization source was used for the peptide analysis. The LC/MS analysis was performed using an ODS reverse-phase column (Magic C18,  $0.1 \times 15 \text{ cm}$ ; Michrom BioResource) connected on-line to the electrospray interface. A solvent system consisting of 0.1% formic acid in  $\text{H}_2\text{O}$  (A) and acetonitrile (B) was developed from 0% B to 70% B in 35 min at a flow rate of 50 mL/min using the Magic 2002 HPLC system (Michrom BioResource). The flow rate of sheath gas and the capillary temperature were kept at 55 arb and 235 °C, respectively. The zoom scan analysis and MS/MS experiment by collision-induced dissociation using the data dependent scan (triple play) were performed in the range of 300–2000  $m/z$  throughout the separation (25, 26).

**Monitoring the Cross-Linking Reaction of S-tag-EGFP and S-tag-EBFP by FRET.** When the MTG-catalyzed cross-linking process by FRET was monitored, S-tag-EBFP ( $1.2 \mu\text{M}$ ) and S-tag-EGFP ( $1.2 \mu\text{M}$ ) were mixed in a quartz cell at 15 °C. The cross-linking reaction was initiated by the addition of MTG (0.25 U/mL) to the





**Figure 1.** (A) Extra N-terminal peptide sequence of S-tag-EGFP. (B) SDS-PAGE analysis of the reaction products after MTG treatment of wild-type EGFP, S-tag-EGFP and Q15A-tag-EGFP (lane 1, low molecular weight markers; lane 2, wild-type EGFP; lane 3, wild-type EGFP treated with MTG; lane 4, S-tag-EGFP; lane 5, S-tag-EGFP treated with MTG; lane 6, Q15A-tag-EGFP; lane 7, Q15A-tag-EGFP treated with MTG; lane 8, high molecular weight markers).

reaction mixture. The change in fluorescence spectra (excited at 380 nm) was recorded at a certain time-interval after the addition of MTG using an F-2000 fluorescence spectrophotometer (Hitachi, Japan). The ratio of fluorescence emission intensity at 508 nm to that at 444 nm ( $I_{508}/I_{444}$ ) was normalized by the value at time zero (i.e., without MTG) and used as the FRET signal. When the cross-linking was followed by SDS-PAGE, an aliquot was periodically withdrawn and immediately mixed with SDS-PAGE sample buffer (50 mM Tris, 2% SDS, 6% 2-mercaptoethanol) to terminate the cross-linking reaction. When investigating the effect of S-protein on the cross-linking, S-protein (3.6  $\mu$ M) was mixed with the solution containing both S-tag-EBFP and S-tag-EGFP described above. After the mixture was incubated for 1 h on ice, the cross-linking reaction was initiated by the addition of MTG to the mixture at 15  $^{\circ}$ C.

## RESULTS AND DISCUSSION

**Cross-Linking of S-tag-EGFP by MTG.** The primal aim of this study was to search for a potent peptide linker that enabled site-specific cross-linking of functional proteins by MTG. During the preliminary exploration, we found that recombinantly expressed EGFP protein in *E. coli* was efficiently cross-linked by MTG. The protein is a fusion protein of EGFP, the N-terminus of which has thioredoxin, His-tag, a thrombin site and S-tag attached. Since wild-type EGFP was not susceptible to cross-linking by MTG (Figure 1B), similarly to guinea pig liver transglutaminase (27), the target peptide of MTG should be found in this fused peptide sequence. The removal of the N-terminal thioredoxin and His-tag portion by thrombin cleavage showed no effect on the cross-linking by MTG, indicating that the thioredoxin moiety did not participate in the transglutamination (data not shown). This fact prompted us to identify the extra N-terminal S-tag peptide of EGFP as a key peptide for protein cross-linking by MTG.

Interestingly, selective oligomeric, but no polymeric, forms of S-tag-EGFP were observed after the treatment with MTG in addition to the residual band around the monomeric form (Figure 1B, lane 5). The oligomeric

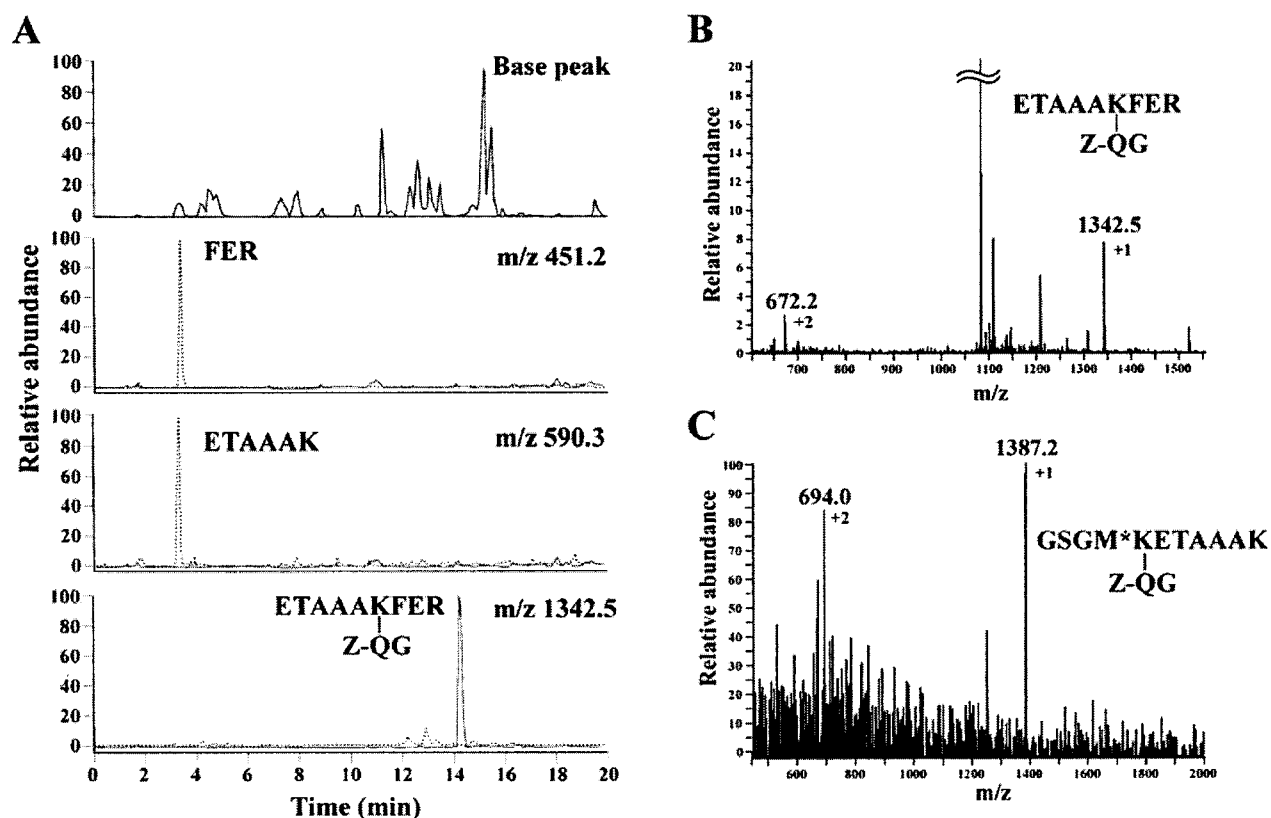
products may correspond to the dimer and the tetramer based on the molecular weight of S-tag-EGFP. The residual fraction around the monomeric form showed a slight shift in mobility in the SDS-PAGE compared to the intact monomer. This behavior may be ascribed to alteration of the charge distribution caused by the competitive hydrolysis of Gln to Glu (28) or the intramolecular cross-linking previously observed with guinea pig transglutaminase (27). It is worth noting that the trimer was not detectable by SDS-PAGE, suggesting poor reactivity between the monomer and dimer in the cross-linking reaction.

**Identification of Cross-Linking Sites in Oligomeric S-tag-EGFP.** Since Gln15 is the sole glutamine residue in the S-tag sequence, we substituted this residue with Ala (Q15A-tag-EGFP) by site-directed mutagenesis to confirm Gln15 as an acyl donor for the transglutamination. As shown in Figure 1B (lane 7), the Q15A-tag-EGFP remained intact even after the MTG treatment, indicating that Gln15 was the sole acyl donor in this system. With regard to the acyl acceptor for the transglutamination, there are three Lys residues (K5, K11, and K29) in the extra N-terminal sequence of S-tag-EGFP (Figure 1A). S-tag-EGFP was conjugated with Z-QG as a small acyl donor by MTG to determine the reactive Lys residues for cross-linking. The product was then digested with trypsin and subjected to mass spectrometric analysis to identify the Z-QG incorporated peptides. The peptide mass map of Z-QG treated-S-tag-EGFP was compared to that of nontreated S-tag-EGFP (Figure 2).

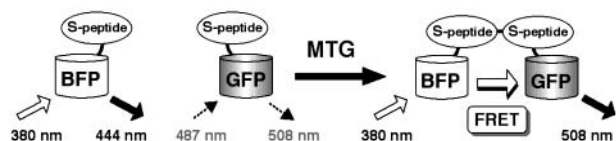
We found the absence of specific peptides, FER and ETAAAK, both of which were derived from the N-terminal S-tag sequence in the Z-QG treated-S-tag-EGFP (Figure 2A). No difference was observed in the other detectable peptides, including the K29-containing peptide. In the place of these missing peptides, we could identify two Z-QG-incorporated peptides derived from the N-terminal S-tag sequence, ETAAAK(zQG)FER (Figure 2B) and GSGMK(zQG)ETAAAK (Figure 2C). Thus, K5 and K11 were determined to be the acyl acceptors for the cross-linking by MTG. We can conclude that the possible cross-linking sites in oligomeric S-tag-EGFP are Gln15-Lys5 or Gln15-Lys11. Since relative intensity of GSGMK(zQG)ETAAAK was lower than that of ETAAAK(zQG)FER, it can be assumed that Lys5 is a minor site for the cross-linking reaction. However, we could not rule out other possible acyl acceptors, because Z-QG conjugation may not exactly reflect the protein cross-linking reaction. It should be noted that both the reactive Lys residues are located in the S-peptide sequence, indicating that MTG strictly recognizes a flexible region of the target protein.

**Direct Monitoring of the Protein Cross-Linking Process Using FRET.** The fluorescent intensity of S-tag-EGFP appeared to be virtually identical to the original one even after the transglutamination [more than 95% of fluorescence remained intact (data not shown)]. These observation encouraged us to carry out real-time spectroscopic measurement of the MTG-catalyzed cross-linking reaction using FRET (Figure 3).

The blue fluorescent color variant, S-tag-EBFP, was prepared for this purpose and the fluorescent spectral change was monitored in the presence of an equimolar amount of S-tag-EGFP. It was confirmed that wild-type EBFP was not cross-linked by MTG as well as wild-type EGFP (data not shown). As shown in Figure 4, the increase of fluorescent intensity at 508 nm was successfully monitored in the presence of MTG, while no



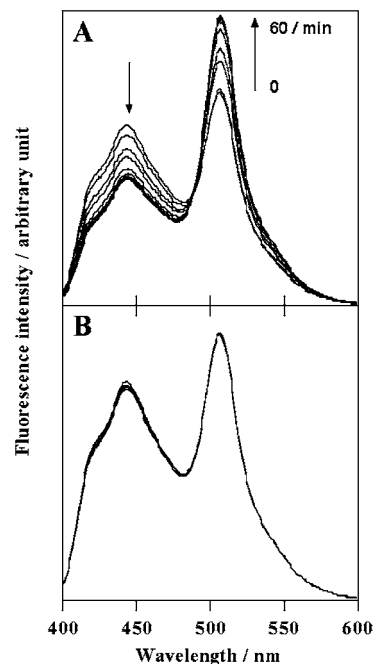
**Figure 2.** Liquid chromatography mass spectrometric analysis to identify Z-QG incorporated peptides. (A) Mass chromatograms for tryptic digests of Z-QG-treated and nontreated S-tag EGFP. Top column: peptide mass mapping of nontreated S-tag EGFP (base peak presentation). second-bottom columns: mass chromatograms for specific peptides, FER, ETAAAK and ETAAAK(Z-QG)FER, the  $m/z$  values of which are 451.2, 590.3, and 1342.5, respectively, showing the analyses of Z-QG-treated S-tag EGFP (solid lines) and nontreated S-tag EGFP (dotted lines). The relative ratio of peptide peak intensity for each analysis was adjusted using a common peptide, FEGLTLVNR [ $m/z$  1051.1 (+1)]. (B and C) Mass spectra for ETAAAK(Z-QG)FER and GSGM\*K(Z-QG)ETAAAK, respectively, with indication of singly and doubly charged ions. Met was identified in the oxidized form (M\*).



**Figure 3.** Principle of the direct monitoring of MTG-catalyzed cross-linking of S-tag-EBFP and S-tag-EGFP through their N-terminal extra S-peptide sequence using FRET.

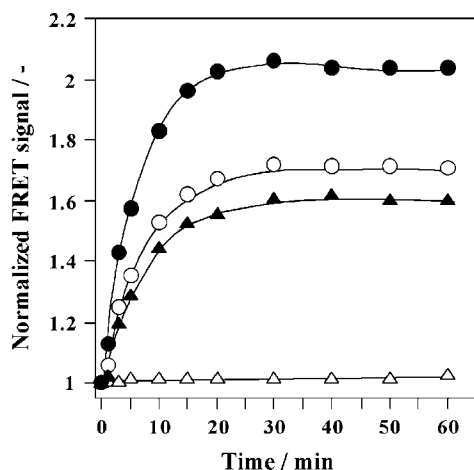
significant increase was observed without MTG, indicating the formation of a heterodimer between S-tag-EGFP and S-tag-EBFP, which permits us to detect the FRET signal in accordance with the cross-linking reaction.

With respect to the kinetics of the TG-catalyzed reaction, competitive hydrolysis of Gln to Glu should be taken into account (28, 29) and it makes analysis of the reaction somewhat complicated. Since the FRET signal solely reflects the productive cross-linking reaction, our strategy offers a simple way to evaluate transglutamination without considering nonproductive hydrolysis. To verify the applicability of the FRET signal for following the cross-linking process of target proteins, we designed simple experiments by focusing our attention on the heterodimerization. If the molar ratio of S-tag-EBFP to the partner EGFP protein is changed from 1/1 to 4/1 or 1/4 while keeping the total protein concentration constant, the composition of the heterodimer will be theoretically altered from 50% to 32%. Consequently, the FRET signal is expected to level off at a lower saturation level than that of the equimolar mixture. As shown in Figure 5, the FRET signal obtained at the 4/1 or 1/4 ratios



**Figure 4.** Fluorescent spectral change in the presence (A) or the absence (B) of MTG with an equimolar mixture of S-tag-EBFP and S-tag-EGFP.

was saturated at a lower level compared to that in the 1/1 ratio as we anticipated. Furthermore, the rate of FRET signal increase at the 4/1 or 1/4 ratios was about

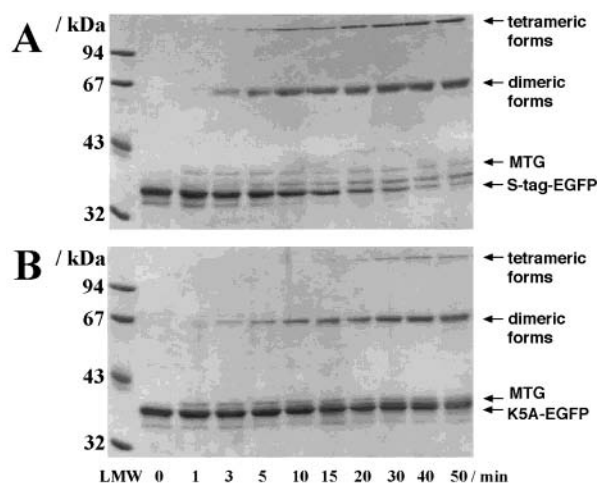


**Figure 5.** Time course of the cross-linking reaction between S-tag-EBFP and S-tag-EGFP followed by the change in FRET signal. The cross-linking reaction was carried out by varying the molar ratio of S-tag-EBFP to S-tag-EGFP at 1/1 (closed circles, with MTG; open triangles, without MTG), 1/4 (open circles, with MTG) and 4/1 (closed triangles, with MTG).

60–70% of that at the 1/1 ratio, being almost consistent with the theoretical value (64%). These results ensure that the signal increase reflected the cross-linking reaction between S-tag-EGFP and S-tag-EBFP catalyzed by MTG, indicating the feasibility of FRET-based evaluation of a protein cross-linking reaction. It seemed that the level of saturation of the FRET signal at the 4/1 ratio was slightly lower than that at the 1/4 ratio. This might be explained by the reabsorption of photons in the presence of an excess amount of S-tag-EBFP, which resulted in a decrease in the apparent number of S-tag-EBFP that participated in the generation of the FRET signal.

**Controlling the Protein Cross-Linking by Engineering S-Peptide.** The limited conjugation through an extra peptidyl linker of proteins of interest could lead us a stoichiometric preparation of dimeric proteins. As shown in Figure 1B (lane 5), a small portion of the tetrameric form of S-tag-EGFP was evident, suggesting that MTG catalyzes the subsequent cross-linking reaction of two dimers to a tetramer. As we identified two acyl acceptors, K5 and K11 (Figure 2), the formation of the tetramer could be ascribed to the presence of at least two types of dimeric forms of S-tag-EGFP, being distinctly cross-linked through Gln15-Lys5 or Gln15-Lys11. To gain further information on the tetramer formation, we prepared an engineered S-peptide of which Lys5, one of the previously identified acyl acceptors, was replaced by Ala, which results in the reduction of either the combination or the number of free Lys residues in dimeric forms of S-tag-EGFP. Then the cross-linking behavior of K5A-tag-EGFP by MTG was compared with that of S-tag-EGFP (Figure 6).

In both cases, the cross-linking reaction seemed to reach the equilibrium after 40 min based on SDS-PAGE analyses because no further change was observed in all protein bands. Figure 6A shows the accumulation of tetrameric forms of S-tag-EGFP concomitant with the formation of dimeric forms. On the other hand, in the case of K5A-tag-EGFP, the tetramer formation was significantly reduced by eliminating the possibility of Gln15-Lys5 cross-link (Figure 6B), suggesting that engineering S-peptide would facilitate the limited conjugation of target proteins approaching 1 to 1 stoichiometry. We attempted to estimate the relative portion of the



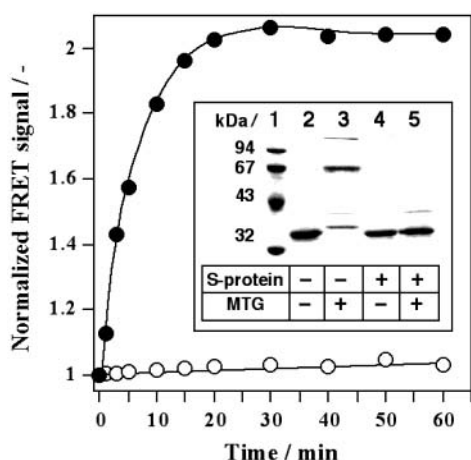
**Figure 6.** Time course of the cross-linking reaction of S-tag-EGFP (A) and K5A-tag-EGFP (B) followed by the SDS-PAGE analysis. Time zero indicates the intact samples without MTG in both cases.

tetramer to the dimer by the image analysis of Figure 6. The portion of the tetramer relative to the dimer was changed from approximately 3/7 with S-tag-EGFP to 1/9 with K5A-tag-EGFP, suggesting the selective dimer formation. However, slower cross-linking and more portion of the residual monomeric forms (due to the competitive hydrolysis of Gln to Glu (28) or the intramolecular cross-linking previously observed with guinea pig transglutaminase (27) as shown in Figure 1) were evident with K5A-tag-EGFP compared to S-tag-EGFP, implying the reduction of cross-linkability of the engineered S-peptide. More sophisticated protein cross-linking reaction requires further improvements of the peptidyl linker with regard to both the reactivity and the selectivity.

It should be noted that only the dimeric and the tetrameric forms were observed with no detectable formation of the trimer in both cases, suggesting that a monomer reacted with a higher activity with another monomer than with a dimer. This might be explained if a monomer experiences greater steric constraint around the cross-linking site of a dimer. However, it is hard to imagine that the reactivity between dimers would exceed that between a monomer and a dimer by simply taking steric aspects into account. MTG might have an inherent property that prefers cross-linked polymeric products. Although we have not had clear answers for this phenomenon yet, on the basis of the results obtained here, one can at least conclude that the protein cross-linking by MTG can be controlled by manipulating a peptidyl linker.

**Controlling the Protein Cross-Linking by S-Protein.** Protection and deprotection steps are common in multistep organic syntheses when target molecules have several reactive functional groups. For instance, a number of protective groups are employed in solid-phase peptide synthesis. When considering the TG-mediated conjugation of more than two proteins that possess several peptide linkers or susceptible sites for TG, there may be the possibility of temporal protection of a specific peptide tag for TG. S-protein, the partner protein of S-peptide for the formation of ribonuclease A (30), could be a perfect fit for this purpose. We thus examined the capability of S-protein for the suppression of the reactivity of the S-peptide for MTG. The effect of S-protein on the cross-linking reaction was evaluated by two means: the change in FRET signal and SDS-PAGE analysis.





**Figure 7.** Suppression of the cross-linking reaction by capping S-peptide with S-protein confirmed by the FRET signal and SDS-PAGE analysis (closed circles, with MTG; open circles, with both MTG and S-protein). Inset: lane 1, low molecular weight markers; lane 2, S-tag-EGFP; lane 3, S-tag-EGFP treated with MTG; lane 4, S-tag-EGFP treated with S-protein; lane 5, S-tag-EGFP treated with S-protein and MTG.

Figure 7 clearly demonstrates that S-protein completely abolished the ability of S-peptide to act as a peptidyl substrate, suggesting for the first time controllable protein cross-linking of a target protein by TG. In this sense, S-protein is thus a potent candidate as a protective group in the protein conjugation by MTG through S-peptide.

The next step should be directed at the modulation of the specific interaction (i.e., deprotection). In fact, it has been reported that the affinity of S-peptide for S-protein could be tunable by site-directed mutagenesis (30). In our case, the effect of amino acid substitution on the reactivity toward MTG should be taken into account as well.

In conclusion, our results demonstrate the potential of S-peptide as a novel peptidyl linker for tunable protein cross-linking by MTG. A new strategy that allows direct monitoring of the MTG-catalyzed protein cross-linking reaction using FRET enables us to optimize such a peptidyl linker. Our concept and experimental technique are promising for TG-directed enzymatic manipulation of recombinant proteins. Further studies are underway in our laboratory.

#### ACKNOWLEDGMENT

We are grateful to Ajinomoto Co., Inc., for providing the MTG sample. We would also like to thank Drs. Naoto Tonouchi, Yoshiyuki Fujishima and Yoshiyuki Kumazawa (Ajinomoto Co. Inc.) for helpful discussion on the characteristics of MTG. The present work was supported by the Grant-in-Aid for Exploratory Research (13875156) from the Ministry of Education, Culture, Science, Sports and Technology of Japan.

#### LITERATURE CITED

- (1) Hermanson, G. T. (1996) Functional targets. *Bioconjugate Techniques*, pp 3–23, Academic Press, San Diego.
- (2) Folk, E. J. (1983) Mechanism and basis for substrate specificity of transglutaminase-catalyzed  $\epsilon$ -( $\gamma$ -glutamyl)lysine bond formation. *Adv. Enzymol. Relat. Areas Mol. Biol.* 54, 1–56.
- (3) Wold, F. (1985) Reactions of the amide side-chains of glutamine and asparagine in vivo. *Trends Biochem. Sci.* 10, 4–6.
- (4) Coussons, P. J., Kelly, S. M., Price, N. C., Johnson, C. M., Smith, B., and Sawyer, L. (1991) Selective modification by

- transglutaminase of a glutamine side chain in the hinge region of the histidine-388  $\rightarrow$  glutamine mutant of yeast phosphoglycerate kinase. *Biochem. J.* 273, 73–78.
- (5) Sato, H., Ikeda, M., Suzuki, K., and Hirayama, K. (1996) Site-specific modification of interleukin-2 by the combined use of genetic engineering technique and transglutaminase. *Biochemistry* 35, 13072–13080.
- (6) Ando H., Adachi M., Umeda K., Matsuura A., Nonaka M., Uchio R., Tanaka H., and Motoki M. (1989) Purification and characteristics of novel transglutaminase derived from microorganisms. *Agric. Biol. Chem.* 53, 2613–2617.
- (7) Kanaji, T., Ozaki, H., Takao, T., Kawajiri, H., Ide, H., Motoki, M., and Shimonishi, Y. (1993) Primary structure of microbial transglutaminase from *Streptovorticillium* sp. strain s-8112. *J. Biol. Chem.* 268, 11565–11572.
- (8) Sato, H., Hayashi, E., Yamada, N., Yatagai, M., Takahara, Y. (2001) Further studies on the site-specific protein modification by microbial transglutaminase. *Bioconjugate Chem.* 12, 701–710.
- (9) Motoki, M., and Seguro, K. (1998) Transglutaminase and its use for food processing. *Trends Food Sci. Technol.* 9, 204–210.
- (10) Kamata, Y., Ishikawa, E., and Motoki, M. (1992) Enzyme immobilization on ion exchangers by forming an enzyme coating with transglutaminase as a crosslinker. *Biosci. Biotech. Biochem.* 56, 1323–1324.
- (11) Josten, A., Meusel, M., and Spener, F. (1998) Microbial transglutaminase-mediated synthesis of hapten-protein conjugates for immunoassays. *Anal. Biochem.* 258, 202–208.
- (12) Josten, A., Haalk, L., Spener, F., and Meusel, M. (2000) Use of microbial transglutaminase for the enzymatic biotinylation of antibody. *J. Immunol. Methods* 240, 47–54.
- (13) Bechtold, U., Otterbach, J. T., Pasternack, R., and Fuchs-bauer, H.-L. (2000) Enzymic preparation of protein G-peroxidase conjugates catalysed by transglutaminase. *J. Biochem.* 127, 239–245.
- (14) Ota, M., Sawa, A., Nio, N., and Ariyoshi, Y. (1999) Enzymatic ligation for synthesis of single-chain analogue of monellin by transglutaminase. *Biopolymers* 50, 193–200.
- (15) Wada, E., Matsuda, H., Imamura, K., Sakiyama, T., Adachi, S., Matsuno, R., Nakanishi, K. (2001) Enzymatic modification of  $\beta$ -lactoglobulin with N-fatty-acyl-dipeptide by transglutaminase from *Streptomyces mobaraensis*. *Biotechnol. Lett.* 23, 1367–1372.
- (16) Josten, A., Meusel, M., Spencer, F., and Haalk, L. (1999) Enzyme immobilization via microbial transglutaminase: a method for the generation of stable sensing surface. *J. Mol. Catal. B. Enzymol.* 7, 58–66.
- (17) Kamiya, N., Ogawa, T., Nagamune, T. (2001) Enhancement of apparent thermostability of lipase from *Rhizopus* sp. by the treatment with microbial transglutaminase. *Biotechnol. Lett.* 23, 1629–1632.
- (18) Nonaka, M., Matsuura, Y., and Motoki, M. (1996) Incorporation of lysine- and lysine-dipeptides into as1-casein by  $\text{Ca}^{2+}$ -independent microbial transglutaminase. *Biosci. Biotech. Biochem.* 60, 131–133.
- (19) Matsumura, Y., Chanyongvorakul, Y., Kumazawa, Y., Ohtsuka, T., and Mori, T. (1996) Enhanced susceptibility to transglutaminase reaction of  $\alpha$ -lactalbumin in the molten globule state. *Biochim. Biophys. Acta* 1292, 69–76.
- (20) Taguchi, S., Nishiyama, K., Igi, K., Ito, K., Taira, H., Motoki, M., and Momose, H. (2000) Substrate specificity analysis of microbial transglutaminase using proteinaceous protease inhibitors as natural model substrates. *J. Biochem.* 128, 415–425.
- (21) Seitz, A., Schneider, F., Pasternack, R., Fuchs-bauer, H.-L., and Hampp, N. (2001) Enzymatic cross-linking of purple membranes catalyzed by bacterial transglutaminase. *Bio-macromolecules* 2, 233–238.
- (22) Folk, J. E. and Cole, P. W. (1966) Mechanism of action of guinea pig liver transglutaminase. I. Purification and properties of the enzyme: identification of a functional cysteine essential for activity. *J. Biol. Chem.* 241, 5518–5525.
- (23) Arai, R., Ueda, H., Tsumoto, K., Mahoney, W. C., Kumagai, I., Nagamune, T. (2000) Fluorolabeling of antibody variable domains with green fluorescent protein variants: application

- to an energy transfer-based homogeneous immunoassay. *Protein Eng.* 13, 369–376.
- (24) Tsien, R. Y. (1998) The green fluorescent protein. *Annu. Rev. Biochem.* 67, 509–544.
- (25) Suzuki, T., Terasaki, M., Takemoto-Hori, C., Hanada, T., Ueda, T., Wada, A. and Watanabe, K. (2001) Structural compensation for deficit of rRNA with proteins in mammalian mitochondrial ribosome; systematic analysis of protein components of the large ribosomal subunit from mammalian mitochondria. *J. Biol. Chem.* 276, 21724–21736.
- (26) Suzuki, T., Terasaki, M., Takemoto-Hori, C., Hanada, T., Ueda, T., Wada, A. and Watanabe, K. (2001) Proteomic analysis of the mammalian mitochondrial ribosome; Identification of protein components in the 28S small subunit. *J. Biol. Chem.* 276, 33181–33195.
- (27) Furutani, Y., Kato, A., Notoya, M., Ghoneim, M. A., Hirose, S. (2001) A simple assay and histochemical localization of transglutaminase activity using a derivative of green fluorescent protein as substrate. *J. Histochem. Cytochem.* 49, 247–258.
- (28) Gross, M., Whetzel, N. K., Folk, J. E. (1975) The extended active site of guinea pig liver transglutaminase. *J. Biol. Chem.* 250, 4648–4655.
- (29) Day, N., Keillor, J. W. (1999) A continuous spectrophotometric linked enzyme assay for transglutaminase activity. *Anal. Biochem.* 274, 141–144.
- (30) Kim, J.-S., Raines, R. T. (1993) Ribonuclease S-peptide as a carrier in fusion proteins. *Protein Sci.* 2, 348–356.

BC025610Y

# Novel Galactosylated Polyamine Bolaamphiphiles for Gene Delivery

Karine Fabio, Jérôme Gaucheron, Christophe Di Giorgio, and Pierre Vierling\*

Laboratoire de Chimie Bioorganique, UMR 6001 CNRS-Université de Nice Sophia-Antipolis, Faculté des Sciences, 06108 Nice Cédex 2, France. Received November 26, 2002; Revised Manuscript Received January 29, 2003

We describe the synthesis of a series of  $\alpha$ -galacto- $\omega$ -polyamine double-chain bolaamphiphiles (Gal-CL) and report on the gene transfer mediated with lipoplexes they form either when used in conjunction with DOPE or with pcTG90:DOPE. Lipofection was investigated with human HepG2 and murine BNL-CL2 hepatocytes expressing the asialoglycoprotein (ASGP) receptor which displays a high affinity for galactosyl residues, and with A549 cells which do not express ASGP. Our results show that cationic  $N/P = 5$  and 2.5 Gal-CL lipoplexes constitute very efficient nonspecific gene transfer systems. Lipofection experiments performed in the presence of asialofetuin (a high affinity ligand of ASGP) led us to evidence also the involvement of a specific receptor-mediated endocytosis pathway for the transfection of the ASGP(+) HepG2 or BNL-CL2 hepatocytes with some Gal-CL formulations. This work suggests that targetable lipopolyamines presenting a single galactose residue appear as promising synthetic vectors for specific gene delivery to ASGP(+) cells.

## INTRODUCTION

Successful *in vivo* gene therapy will depend on the efficient delivery of genetic material to specific cells and its effective expression within these cells. Aiming at these goals, various cell-targeting ligands (for a recent review see ref 1), including galactosylated residues (2–14), were conjugated to the DNA complexes in order to trigger receptor-mediated gene delivery. As part of our contribution into this field, our laboratory has reported on the single alkyl chain  $\alpha$ -galacto- $\omega$ -spermine bolaamphiphile (GalSper in Scheme 1), which appeared as a promising synthetic vector for specific gene delivery to asialoglycoprotein(ASGP)-expressing cells (2). In continuation of this work, we elaborated novel galacto-polyamine bolaamphiphiles as specific gene transfer agents into ASGP(+) cells, such as hepatocytes. Their design combines a hydrophilic galactosyl residue (which serves as a molecular signal for cell targeting) linked through a long spacer to various hydrophilic linear or branched polyamine polar heads (for the interactions with DNA and its compaction) and to a hydrophobic tail constituted by two long alkyl chains (for increasing their hydrophobic character, preventing from DNA decondensation, and reducing the detergent effect and cell toxicity of the GalSper head molecule (2)). As a high density of galactose residues (which is important for effective receptor-mediated gene transfer (3)) can be provided on the cationized gene particle surface with such bolaamphiphiles (15), the sugar moieties are likely to provide a hydrophilic uncharged shield preventing these cationic lipoplexes from aggregation (15, 16), coating with serum proteins (14), and/or binding to the anionic proteoglycans of the extracellular matrix (14, 17, 18).

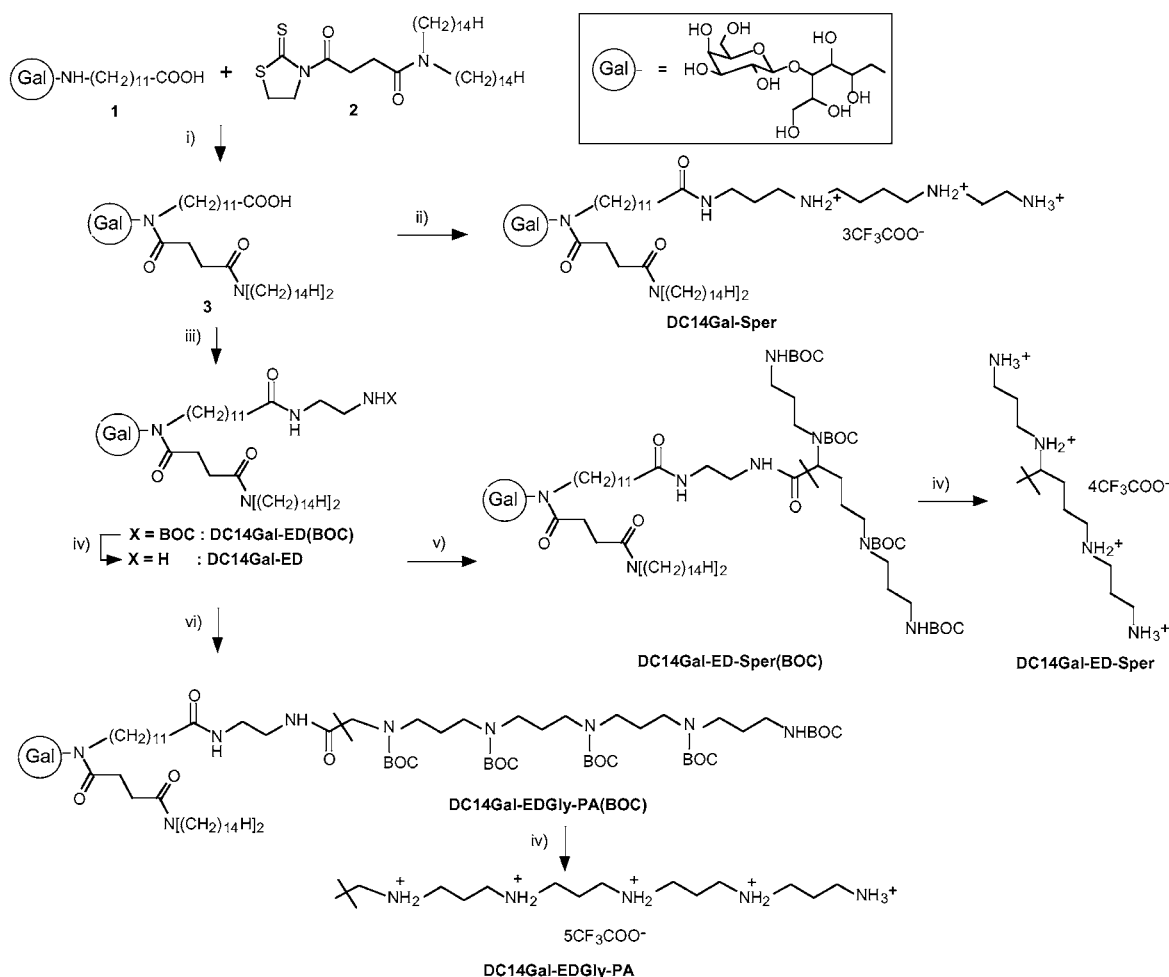
We describe here the synthesis of three new  $\alpha$ -galacto- $\omega$ -polycationic lipids (Gal-CLs) (Scheme 1) and report on their ability to mediate, *in vitro*, a specific gene transfer into cells expressing ASGP (human HepG2 and murine BNL-CL2 hepatocytes) (3–9). As cationized gene particles provide also receptor-independent gene transfer to cells, and more particularly to adherent cells, owing to their binding to the anionic proteoglycans which are expressed on their cell surface, we report also on the ability of the

cationic Gal-CLs to mediate, *in vitro*, a nonspecific gene transfer into the adherent ASGP(–) A549 cells. This study was further aimed at determining the conditions under which a specific gene transfer into adherent ASGP(+) cells could be evidenced with the cationic Gal-CLs. The Gal-CL-based lipoplexes were formulated in conjunction with DOPE, which, as helper lipid, was found to enhance markedly the transfection activity of GalSper (2). As co-formulation of nonlabeled lipoplexes with Gal-CL could also constitute a mean to obtain specific cell interactions and gene transfer, we report also on transfection experiments that were performed with Gal-CL used in combination with pcTG90:DOPE (which is known to be a very efficient nonspecific lipofection system (19, 20)). All these assays were performed in the absence or presence of an excess of asialofetuin (ASF), which is a high-affinity ligand of ASGP (3, 4), with the aim at demonstrating a specific receptor-mediated transfection process. These experiments were also intended to highlight the effects of this protein (that might result from coating of the lipoplexes and/or from its adsorption onto the cells) on the nonspecific transfection (i) of control ASGP(–) cells with Gal-CL-labeled lipoplexes and (ii) of ASGP(+) cells with control nontargeted pcTG90:DOPE lipoplexes. They were also performed in the absence of serum, to avoid the effects on lipoplexes and, consequently, on lipoplex-cell interactions and/or on ligand–receptor interactions that might be due to the serum constituents, and to facilitate the interpretation of the transfection results. Serum was indeed shown to inhibit transfection of HepG2 cells with galactosylated-labeled polyplexes, but to a lesser extent than with the nonlabeled ones (14).

## MATERIALS AND METHODS

**General Experiment and Analytical Conditions.** All the reactions were performed in anhydrous solvents under dry and oxygen-free nitrogen. Column chromatographies were performed with Merck silica gel 60 (mesh 70–230) or Sephadex LH 20 gel (Aldrich). *N*-[11-(Oxy-carbonyl)undecyl]-1-amino-1-deoxylactitol (1) was obtained from sodium 12-aminododecanoate and lactose



**Scheme 1 . Synthetic Routes to the  $\alpha$ -galacto- $\omega$ -polyamine Gal-CL Bolaamphiphiles<sup>a</sup>**

<sup>a</sup> (i) DMF,  $\text{NEt}_3$ , 60 °C, 5 days, (40%); (ii) BOP, spermine, DMF,  $\text{NEt}_3$ , rt, 2h, (63%); (iii) BOP,  $\text{BOCNH}(\text{CH}_2)_2\text{NH}_2$ , DMF,  $\text{NEt}_3$ , rt, 2h, (86%); (iv) excess TFA/ $\text{CH}_2\text{Cl}_2$ , rt 1h, (100%); (v) BOP,  $\text{BOCNH}(\text{CH}_2)_3\text{N}(\text{BOC})\text{CH}(\text{COOH})(\text{CH}_2)_3\text{N}(\text{BOC})(\text{CH}_2)_3\text{NHBOC}$ , DMF,  $\text{NEt}_3$ , 0 °C 2h (47%); (vi) BOP,  $\text{BOCNH}[(\text{CH}_2)_3\text{N}(\text{BOC})]_4\text{N}(\text{BOC})\text{CH}_2\text{COOH}$ , DMF,  $\text{NEt}_3$ , 0 °C, 1h (58%).

according to the procedure described in the literature (2). *N,N*-Ditetradecylamine and L-5-carboxytetradecyloxycarbonylspermine ( $\text{BOC}_4\text{SperCOOH}$ ) were prepared according to procedures described in ref 20.  $\text{BOCNH}[(\text{CH}_2)_3\text{N}(\text{BOC})]_4\text{CH}_2\text{COOH}$  and pcTG90, whose syntheses are described in ref 21, were gifts from Transgène, SA (Strasbourg, France). DOPE was purchased from Sigma. Reactions were monitored by thin-layer chromatography (TLC) using silica plate F<sub>254</sub> (SDS) and visualized by UV light (254 nm) and by charring with ninhydrine and 50%  $\text{MeOH}/\text{H}_2\text{SO}_4$ .  $^1\text{H}$  and  $^{13}\text{C}$  NMR spectra were recorded at 200 and 50.3 MHz, respectively, on a Bruker AC200. Chemical shifts ( $\delta$ ) were measured relative to  $\text{CDCl}_3$  (7.26 ppm),  $\text{CD}_3\text{OD}$  (3.31 ppm), or  $\text{D}_2\text{O}$  (4.79 ppm) for  $^1\text{H}$  and to  $\text{CDCl}_3$  (77.2 ppm) or  $\text{CD}_3\text{OD}$  (49.0 ppm) for  $^{13}\text{C}$  and expressed in parts per million indirectly in relation to TMS. The following abbreviations are used to describe the signal multiplicities: s (singlet), d (doublet), t (triplet), q (quadruplet), and m (multiplet). Chemical shifts are listed as follows: shift in parts per million (multiplicity, coupling, integration, and attribution). The doubling of some signals indicates the presence of conformational isomers due to restricted rotation of the amide bond. Electrospray ionization mass spectrometry (ESI-MS) in positive and negative mode was performed on a Finnigan MAT LCQ (TSQ 7000 FINNIGAN MAT) equipped with an atmospheric pressure ionization (API) source.

**Chemistry.** *Synthesis of 12-((3-Ditetradecylcarbamoyl-propionyl)-[2,3,5,6-tetrahydroxy-4-(3,4,5-trihydroxy-6-hydroxymethyl-tetrahydro-pyran-2-yloxy)-hexyl]-amino)-dodecanoic Acid, 3.* *Synthesis of 4-oxo-N,N-Ditetradecyl-4-(2-thioxo-thiazolidin-3-yl)-butyramide (2).* A solution of *N,N*-ditetradecylamine (1.3 g, 3.2 mmol), succinic anhydride (640 mg, 6.4 mmol; Aldrich), and  $\text{NEt}_3$  (0.9 mL, 6.4 mmol) in 50 mL of  $\text{CHCl}_3$  was stirred under reflux during 24 h. The organic phase was then washed with 5% citric acid, water, dried over  $\text{Na}_2\text{SO}_4$ , and evaporated. Chromatography of the residue over a silica gel column (35 g,  $\text{CHCl}_3$  to  $\text{CHCl}_3/\text{MeOH}$ : 98/2: v/v) afforded 735 mg (1.45 mmol; 45%) of *N,N*-ditetradecylsuccinamic acid as a white powder.  $^1\text{H}$  NMR ( $\text{CDCl}_3$ ):  $\delta$  0.86 (t,  $J = 6.0$  Hz, 6H,  $\text{CH}_3$ ); 1.24 (broad s, 44H,  $(\text{CH}_2)_{11}\text{CH}_3$ ); 1.53 (m, 4H,  $\text{CH}_2\text{CH}_2\text{N}$ ); 2.66 (broad s, 4H,  $\text{C}(\text{O})\text{CH}_2$ ); 3.25 (m, 4H,  $\text{CH}_2\text{N}$ ).  $^{13}\text{C}$  NMR ( $\text{CDCl}_3$ ):  $\delta$  14.1 ( $\text{CH}_3$ ); 22.7 ( $\text{CH}_2\text{CH}_3$ ); 26.9, 27.0 ( $\text{CH}_2(\text{CH}_2)_2\text{N}$ ); 27.7, 28.0 ( $\text{CH}_2\text{CH}_2\text{N}$ ); 28.8 ( $\text{C}(\text{O})\text{CH}_2$ ); 29.3, 29.5, 29.6, 29.7 ( $(\text{CH}_2)_9(\text{CH}_2)_2\text{CH}_3$ ); 30.1 ( $\text{CH}_2\text{C}(\text{O})$ ); 31.9 ( $\text{CH}_2\text{CH}_2\text{CH}_3$ ); 46.6, 48.2 ( $\text{CH}_2\text{N}$ ); 171.8 ( $\text{C}(\text{O})\text{N}$ ); 176.0 ( $\text{C}(\text{O})\text{O}$ ).

To 730 mg (1.44 mmol) of *N,N*-ditetradecylsuccinamic acid in 14 mL of DMF were added 242 mg (2.16 mmol) of 4-(dimethylamino)pyridine (DMAP; Aldrich), 413 mg (2.16 mmol) of 1-(3-dimethylaminopropyl)-3-ethylcarbodiimide hydrochloride (EDC; Aldrich), and 257 mg of 2-thiazolidine-2-thiol (2.16 mmol; Fluka). After 1 h at 0 °C and 48 h at room temperature, DMF was removed

under vacuum. The residue was solubilized in 80 mL of  $\text{CH}_2\text{Cl}_2$  and washed with 5% citric acid, 5% sodium carbonate, and water. The organic phase was dried over  $\text{Na}_2\text{SO}_4$  and evaporated. Chromatography of the residue over a silica gel column (20 g, hexane to hexane/ $\text{CHCl}_3$  4/6 v/v) afforded 506 mg (0.83 mmol; 57%) of **2** as a yellow oil.  $^1\text{H}$  NMR ( $\text{CDCl}_3$ ):  $\delta$  0.69 (t,  $J = 5.9$  Hz, 6H,  $\text{CH}_3$ ); 1.07 (broad s, 44H,  $(\text{CH}_2)_{11}\text{CH}_3$ ); 1.38 (m, 4H,  $\text{CH}_2\text{CH}_2\text{N}$ ); 2.52 (t,  $J = 6.1$  Hz, 2H,  $\text{C}(\text{O})\text{CH}_2$ ); 3.08 (m, 6H,  $\text{CH}_2\text{NC}$ ,  $\text{CH}_2\text{S}$ ); 3.31 (t,  $J = 5.5$  Hz,  $\text{CH}_2\text{NC}(\text{O})\text{C}(\text{S})$ ); 4.75 (t,  $J = 7.5$  Hz, 2H,  $\text{NCH}_2\text{CH}_2\text{S}$ ).  $^{13}\text{C}$  NMR ( $\text{CDCl}_3$ ):  $\delta$  14.5 ( $\text{CH}_3$ ); 23.0 ( $\text{CH}_2\text{CH}_3$ ); 27.3, 27.4 ( $\text{CH}_2(\text{CH}_2)_2\text{NC}(\text{O})$ ); 28.2, 28.4 ( $\text{CH}_2\text{CH}_2\text{NC}(\text{O})$ ); 28.8 ( $\text{NCH}_2\text{CH}_2\text{S}$ ); 29.3 ( $\text{CH}_2\text{C}(\text{O})\text{N}$ ); 29.7, 29.8, 29.9, 30.9 ( $(\text{CH}_2)_9(\text{CH}_2)_2\text{CH}_3$ ); 32.3 ( $\text{CH}_2\text{CH}_2\text{CH}_3$ ); 34.8 ( $\text{CH}_2\text{C}(\text{O})\text{NC}(\text{S})$ ); 46.6, 48.3 ( $\text{CH}_2\text{NC}(\text{O})$ ); 56.4 ( $\text{NCH}_2\text{CH}_2\text{S}$ ); 170.8, 174.9 ( $\text{C}=\text{O}$ ); 201.7 ( $\text{C}=\text{S}$ ).

**Synthesis of Compound 3.** To a solution of **2** (506 mg, 0.83 mmol) and  $\text{NEt}_3$  (0.2 mL, 1.5 mmol) in 25 mL of DMF was added 388 mg of **1** (0.75 mmol). After 5 days at 60 °C, DMF was removed under vacuum. The residue was solubilized in 100 mL of  $\text{CHCl}_3$  and washed with 5% citric acid and water. The organic phase was dried over  $\text{Na}_2\text{SO}_4$  and evaporated. Chromatography of the residue over a silica gel column (25 g,  $\text{CHCl}_3$  to  $\text{CHCl}_3/\text{MeOH}$  9/1 v/v) led to 320 mg (40%) of **3** as colorless oil.  $^1\text{H}$  NMR ( $\text{MeOD}$ ):  $\delta$  0.90 (t,  $J = 6.0$  Hz, 6H,  $\text{CH}_3$ ); 1.29 (s large, 58H,  $(\text{CH}_2)_{11}\text{CH}_3$ ,  $(\text{CH}_2)_7(\text{CH}_2)_2\text{C}(\text{O})$ ); 1.62 (m, 8H,  $\text{CH}_2\text{CH}_2\text{C}(\text{O})\text{O}$ ,  $\text{CH}_2\text{CH}_2\text{NC}(\text{O})$ ); 2.29 (t,  $J = 7.3$  Hz, 2H,  $\text{CH}_2\text{C}(\text{O})\text{O}$ ); 2.84 (m, 4H,  $\text{C}(\text{O})\text{CH}_2\text{CH}_2\text{C}(\text{O})$ ); 3.29–4.07 (m, 20 H,  $\text{CH}_2\text{NC}(\text{O})$ ,  $\text{CHOH}$ ,  $\text{CH}_2\text{OH}$ ); 4.47 (d,  $J = 7.1$  Hz, 1H, Gal H1).  $^{13}\text{C}$  NMR ( $\text{MeOD}$ ):  $\delta$  15.3 ( $\text{CH}_3$ ); 24.3 ( $\text{CH}_2\text{CH}_3$ ); 26.6 ( $\text{CH}_2\text{CH}_2\text{C}(\text{O})\text{O}$ ); 28.5, 28.6 ( $\text{CH}_2(\text{CH}_2)_2\text{NC}(\text{O})$ ); 29.8, 29.9 ( $\text{CH}_2\text{CH}_2\text{NC}(\text{O})$ ); 28.6, 29.3, 30.2, 30.4, 30.4, 30.8, 31.0, 31.1, 31.2, 31.3 ( $(\text{CH}_2)_8\text{CH}_2\text{C}(\text{O})\text{O}$ ,  $(\text{CH}_2)_8(\text{CH}_2)_2\text{CH}_3$ ); 30.4 ( $\text{C}(\text{O})\text{CH}_2\text{CH}_2\text{C}(\text{O})$ ); 33.6 ( $\text{CH}_2\text{CH}_2\text{CH}_3$ ); 35.8 ( $\text{CH}_2\text{C}(\text{O})\text{O}$ ); 48.1, 51.4, 52.2 ( $\text{CH}_2\text{NC}(\text{O})$ ); 63.1, 63.2 ( $\text{CH}_2\text{OH}$ ); 64.1 (Gal C6); 70.7, 70.8, 71.1, 71.4 ( $\text{CHOH}$ ); 72.3 (Gal C4); 73.3, 73.5 (Gal C2); 75.2 (Gal C3); 77.5 (Gal C5); 84.4, 84.6 ( $\text{OCH}(\text{CHOH})_2$ ); 106.1 (Gal C1); 173.9, 174.3, 175.0, 175.2 ( $\text{C}(\text{O})\text{N}$ ); 178.5 ( $\text{C}(\text{O})\text{O}$ ). ESI(–)-MS:  $m/z = 1031.7$ , in agreement with the calculated mass for  $[\text{M} - \text{H}]^- = \text{C}_{52}\text{H}_{103}\text{N}_5\text{O}_{12}$ .

**Synthesis of N-[11-(2-Amino-ethylcarbamoyl)-undecyl]-N,N'-ditetradecyl-N-[2,3,5,6-tetrahydroxy-4-(3,4,5-trihydroxy-6-hydroxymethyl-tetrahydro-pyran-2-yloxy)-hexyl]-succinamide, DC14Gal-ED.** To a solution of **3** (133 mg, 0.13 mmol) and 0.05 mL of  $\text{NEt}_3$  (0.36 mmol) in 7 mL of DMF were added 30  $\mu\text{L}$  of *N*-BOC-ethylenediamine (0.19 mmol) and 19 mg of BOP (0.04 mmol; Novabiochem). After 2 h at room temperature, evaporation under vacuum, and exclusion chromatography over a Sephadex LH20 column (4 g, MeOH), 125 mg (86%) of DC14Gal-ED(BOC) as a colorless oil was obtained.  $^1\text{H}$  NMR ( $\text{CD}_3\text{OD}$ ):  $\delta$  0.90 (t,  $J = 6.5$  Hz, 6H,  $\text{CH}_3$ ); 1.29 (broad s, 58H,  $(\text{CH}_2)_{11}\text{CH}_3$ ,  $(\text{CH}_2)_7(\text{CH}_2)_2\text{C}(\text{O})$ ); 1.43–1.60 (m, 17H,  $\text{CH}_3$  (BOC),  $\text{CH}_2\text{CH}_2\text{C}(\text{O})\text{NH}$ ,  $\text{CH}_2\text{CH}_2\text{NC}(\text{O})$ ); 2.17 (t,  $J = 7.2$  Hz, 2H,  $\text{CH}_2\text{C}(\text{O})\text{NH}$ ); 2.66 (m, 4H,  $\text{C}(\text{O})\text{CH}_2\text{CH}_2\text{C}(\text{O})$ ); 3.14–4.07 (m, 24 H,  $\text{CH}_2\text{NC}(\text{O})$ ,  $\text{C}(\text{O})\text{NH}(\text{CH}_2)_2$ ,  $\text{CHOH}$ ,  $\text{CH}_2\text{OH}$ ); 4.46 (d,  $J = 7.0$  Hz, 1H, Gal H1).  $^{13}\text{C}$  NMR ( $\text{CD}_3\text{OD}$ ):  $\delta$  14.1 ( $\text{CH}_3$ ); 23.3 ( $\text{CH}_2\text{CH}_3$ ); 26.5 ( $\text{CH}_2\text{CH}_2\text{C}(\text{O})\text{NH}$ ); 27.5, 27.6 ( $\text{CH}_2(\text{CH}_2)_2\text{NC}(\text{O})$ ); 28.4 ( $\text{CH}_3$ , BOC); 28.8, 29.0 ( $\text{CH}_2\text{CH}_2\text{NC}(\text{O})$ ); 27.9, 28.3, 29.2, 29.9, 30.0, 30.2, 30.3 ( $(\text{CH}_2)_8\text{CH}_2\text{C}(\text{O})\text{NH}$ ,  $(\text{CH}_2)_8(\text{CH}_2)_2\text{CH}_3$ ); 29.4 ( $\text{C}(\text{O})\text{CH}_2\text{CH}_2\text{C}(\text{O})$ ); 32.6 ( $\text{CH}_2\text{CH}_2\text{CH}_3$ ); 36.8 ( $\text{CH}_2\text{C}(\text{O})\text{NH}$ ); 40.1, 40.5 ( $\text{NH}(\text{CH}_2)_2\text{NHBOC}$ ); 47.1, 47.2, 50.4, 51.3 ( $\text{CH}_2\text{NC}(\text{O})$ ); 62.1, 62.2 ( $\text{CH}_2\text{OH}$ ); 63.2 (Gal C6); 69.8, 69.9, 70.2, 70.6 ( $\text{CHOH}$ ); 71.4 (Gal C4); 72.4, 72.6 (Gal C2); 74.4 (Gal C3); 76.6 (Gal C5); 79.9 ( $\text{C}(\text{CH}_3)_3$ ); 83.3, 83.4 ( $\text{OCH}(\text{CHOH})_2$ ); 105.1, 105.3 (Gal C1); 158.0 ( $\text{C}(\text{O})$ , BOC);

173.2, 173.5, 174.3, 174.3, 176.1 ( $\text{C}(\text{O})\text{N}$ ). ESI-MS:  $m/z = 1197.8$ , in agreement with the calculated mass for  $[\text{M} + \text{Na}]^+ = \text{C}_{52}\text{H}_{103}\text{N}_5\text{O}_{12}$ .

The *N*-BOC deprotection was quantitatively achieved by dissolving and keeping compound **4**(BOC) in a large excess of  $\text{TFA}:\text{CH}_2\text{Cl}_2$  (1:1, v/v) at room temperature for 2 h. The excess of TFA was removed by evaporation in the presence of  $\text{CH}_2\text{Cl}_2/\text{cyclohexane}$  and by gel permeation on a Sephadex LH20. Derivative **4**, as its TFA salt, was obtained in the form of a colorless resin. The presence of the TFA anion is confirmed by  $^{19}\text{F}$  NMR ( $\delta -75.7$  in  $\text{CD}_3\text{OD}$ ).

**Synthesis of DC14-GalSper.** To a solution of **3** (40 mg, 0.038 mmol), spermine (78 mg, 0.38 mmol), and  $\text{NEt}_3$  (0.05 mL, 0.36 mmol) in 2 mL of DMF was added 19 mg of BOP (0.04 mmol; Novabiochem). After 2 h at room temperature, evaporation under vacuum, and exclusion chromatography over a Sephadex LH20 column (3 g, MeOH), 29 mg of DC14GalSper (63%) was isolated as a yellow oil.  $^1\text{H}$  NMR ( $\text{CD}_3\text{OD}$ ):  $\delta$  0.80 (t,  $J = 5.9$  Hz, 6H,  $\text{CH}_3$ ); 1.19 (broad s, 58H,  $(\text{CH}_2)_{11}\text{CH}_3$ ,  $(\text{CH}_2)_7(\text{CH}_2)_2\text{C}(\text{O})$ ); 1.50 (m, 8H,  $\text{CH}_2\text{CH}_2\text{NC}(\text{O})$ ,  $\text{CH}_2\text{CH}_2\text{C}(\text{O})\text{NH}$ ); 1.70 (m, 6H,  $\text{CH}_2\text{CH}_2\text{NH}$ ); 2.02 (m,  $\text{CH}_2\text{CH}_2\text{NH}_2$ ); 2.12 (t,  $J = 7.2$  Hz,  $\text{CH}_2\text{C}(\text{O})\text{NH}$ ); 2.57 (m, 4H,  $\text{C}(\text{O})\text{CH}_2\text{CH}_2\text{C}(\text{O})$ ); 2.94 (m, 10H,  $\text{CH}_2\text{NH}$ ,  $\text{CH}_2\text{NH}_2$ ); 3.20–3.97 (m, 22 H,  $\text{CH}_2\text{NC}(\text{O})$ ,  $\text{C}(\text{O})\text{NHCH}_2$ ,  $\text{CHOH}$ ,  $\text{CH}_2\text{OH}$ ); 4.38 (d,  $J = 4.8$  Hz, 1H, Gal H1).  $^{13}\text{C}$  NMR ( $\text{CD}_3\text{OD}$ ):  $\delta$  14.8 ( $\text{CH}_3$ ); 24.1 ( $\text{CH}_2\text{CH}_3$ ); 24.6, 24.7 ( $\text{CH}_2\text{CH}_2\text{NH}_2$ ); 25.7 ( $\text{CH}_2\text{CH}_2\text{C}(\text{O})\text{NH}$ ); 27.1, 27.3, 27.7 ( $\text{CH}_2\text{CH}_2\text{NH}$ ); 28.3, 28.4, 28.4, 28.8, 29.1, 29.7, 29.9, 30.3, 30.8, 30.9, 31.0, 31.1, 31.2 ( $(\text{CH}_2)_{10}\text{CH}_2\text{C}(\text{O})(\text{CH}_2)_2\text{C}(\text{O})$ ,  $(\text{CH}_2)_8(\text{CH}_2)_2\text{C}(\text{O})$ ); 33.5 ( $\text{CH}_2\text{CH}_2\text{CH}_3$ ); 37.1, 37.4 ( $\text{CH}_2\text{C}(\text{O})\text{NH}$ ,  $\text{C}(\text{O})\text{NHCH}_2$ ); 38.2 ( $\text{CH}_2\text{NH}_2$ ); 46.2, 46.7 ( $\text{CH}_2\text{NH}$ ); 48.5, 48.6, 51.2, 51.2 ( $\text{CH}_2\text{NC}(\text{O})$ ); 62.9 ( $\text{CH}_2\text{OH}$ ); 64.0 (Gal C6); 70.7, 70.8, 71.1, 71.4 ( $\text{CHOH}$ ); 72.3 (Gal C4); 72.3, 73.5 (Gal C2); 75.2 (Gal C3); 77.5 (Gal C5); 84.0, 84.2 ( $\text{OCH}(\text{CHOH})_2$ ); 106.0, 106.2 (Gal C1); 174.2, 174.4, 175.3, 175.4, 177.9 ( $\text{C}(\text{O})\text{N}$ ). ESI-MS:  $m/z = 1217.9$ , in agreement with the calculated mass for  $[\text{M} + \text{H}]^+ = \text{C}_{52}\text{H}_{103}\text{N}_5\text{O}_{12}$ .

**Synthesis of DC14Gal-ED-Sper.** BOP (31 mg, 0.069 mmol) was added, at 0 °C, to a solution of DC14Gal-ED (62 mg, 0.058 mmol),  $\text{NEt}_3$  (0.02 mL, 0.014 mmol), and  $\text{BOC}_4\text{SperCOOH}$  (45 mg, 0.069 mmol) in 3.5 mL DMF. After 2 h at 0 °C, DMF was removed under vacuum. The residue was solubilized in 50 mL of  $\text{CH}_2\text{Cl}_2$ . The organic phase was washed with  $\text{Na}_2\text{CO}_3$  (5%) and then with water, dried over  $\text{Na}_2\text{SO}_4$ , and evaporated. Chromatography of the residue over a silica gel column (7 g  $\text{CH}_2\text{Cl}_2$  to  $\text{CH}_2\text{Cl}_2/\text{MeOH}$ , 8/2 v/v) led to 47 mg (47%) of DC14Gal-ED-Sper(BOC) as a colorless oil.  $^1\text{H}$  NMR ( $\text{CD}_3\text{OD}$ ):  $\delta$  0.80 (t,  $J = 5.9$  Hz, 6H,  $\text{CH}_3$ ); 1.19 (broad s, 58H,  $(\text{CH}_2)_{11}\text{CH}_3$ ,  $(\text{CH}_2)_7(\text{CH}_2)_2\text{C}(\text{O})$ ); 1.33–1.55 (m, 52H,  $\text{CH}_2\text{CH}_2\text{NHBOC}$ ,  $\text{CH}(\text{CH}_2)_2$ ,  $\text{CH}_2\text{CH}_2\text{NC}(\text{O})$ ,  $\text{CH}_2\text{CH}_2\text{C}(\text{O})\text{NH}$ ); 2.07 (t,  $J = 7.3$  Hz, 2H,  $\text{CH}_2\text{C}(\text{O})\text{NH}$ ); 2.57 (m, 4H,  $\text{C}(\text{O})\text{CH}_2\text{CH}_2\text{C}(\text{O})$ ); 2.93 (t,  $J = 6.7$  Hz, 4H,  $\text{CH}_2\text{NHBOC}$ ); 3.18 (m, 18H,  $\text{CH}_2\text{NC}(\text{O})$ ,  $\text{CH}_2\text{NHC}(\text{O})$ ,  $\text{CH}_2\text{NBOC}$ ); 3.33–3.97 (m, 13 H,  $\text{CHOH}$ ,  $\text{CH}_2\text{OH}$ ,  $\text{C}(\text{O})\text{CH}$ ); 4.36 (d,  $J = 7.0$  Hz, 1H, Gal H1).  $^{13}\text{C}$  NMR ( $\text{CD}_3\text{OD}$ ):  $\delta$  15.3 ( $\text{CH}_3$ ); 24.6 ( $\text{CH}_2\text{CH}_3$ ); 27.8 ( $\text{CH}_2\text{CH}_2\text{C}(\text{O})\text{NH}$ ); 28.8, 28.9 ( $\text{CH}_2(\text{CH}_2)_2\text{NC}(\text{O})$ ); 29.3, 30.2, 30.3, 30.4, 30.7, 31.3, 31.5, 31.6 ( $(\text{CH}_2)_8\text{CH}_2\text{CH}_2\text{CH}_2\text{C}(\text{O})(\text{CH}_2)_2\text{C}(\text{O})$ ,  $(\text{CH}_2)_8(\text{CH}_2)_2\text{C}(\text{O})\text{NH}$ ,  $\text{CH}_2\text{CH}_2\text{NHBOC}$ ); 33.9 ( $\text{CH}_2\text{CH}_2\text{CH}_3$ ); 38.1 ( $\text{CH}_2\text{C}(\text{O})\text{NH}$ ); 39.7, 40.1, 40.8, 41.2 ( $\text{CH}_2\text{NHBOC}$ ,  $\text{NH}(\text{CH}_2)_2\text{NH}$ ,  $\text{CH}_2\text{NBOC}$ ); 48.3, 51.7, 52.6 ( $\text{CH}_2\text{NC}(\text{O})$ ); 63.4 ( $\text{CH}_2\text{OH}$ ); 64.5 (Gal C6); 67.7 ( $\text{CHNHBOC}$ ); 71.1, 71.2, 71.4, 71.5, 71.8, 71.8 ( $\text{CHOH}$ ); 72.7 (Gal C4); 73.7, 74.0 (Gal C2); 75.7 (Gal C3); 78.0 (Gal C5); 80.3, 80.7, 82.6 ( $\text{C}(\text{CH}_3)_3$ ); 84.4, 84.6 ( $\text{OCH}$ -



(CHOH)<sub>2</sub>; 106.4, 106.6 (Gal C1); 158.2, 159.2 (C(O), BOC); 174.5, 174.6, 174.8 (C(O)NH); 175.7, 175.7, 177.4 (C(O)N).

The *N*-BOC deprotection of DC14Gal-ED-Sper(BOC) was performed as described for DC14Gal-ED(BOC) and led quantitatively to DC14Gal-ED-Sper (as its tetra-TFA salt) in the form of a white powder. <sup>1</sup>H NMR (MeOD): δ 0.79 (t, *J* = 5.9 Hz, 6H, CH<sub>3</sub>); 1.19 (s large, 58H, (CH<sub>2</sub>)<sub>11</sub>-CH<sub>3</sub>, (CH<sub>2</sub>)<sub>7</sub>(CH<sub>2</sub>)<sub>2</sub>C(O)); 1.49 (m, 8H, CH<sub>2</sub>CH<sub>2</sub>NC(O), CH<sub>2</sub>CH<sub>2</sub>C(O)NH); 1.63–2.06 (m, 8H, CH<sub>2</sub>CH<sub>2</sub>CH, CH<sub>2</sub>-CH<sub>2</sub>NH<sub>2</sub>); 2.10 (t, *J* = 6.9 Hz, 2H, CH<sub>2</sub>C(O)NH); 2.58 (m, 4H, C(O)(CH<sub>2</sub>)<sub>2</sub>C(O)); 2.96 (m, 10H, CH<sub>2</sub>NH, CH<sub>2</sub>NH<sub>2</sub>); 3.32–4.04 (m, 25H, CH<sub>2</sub>NC(O), NH(CH<sub>2</sub>)<sub>2</sub>NH, C(O)CH, CHOH, CH<sub>2</sub>OH); 4.39 (d, *J* = 5.6 Hz, 1H, Gal H1). <sup>13</sup>C NMR (MeOD): δ 14.8 (CH<sub>3</sub>); 23.3, 29.4 (CH(CH<sub>2</sub>)<sub>2</sub>); 24.1 (CH<sub>2</sub>CH<sub>3</sub>); 25.7, 26.2 (CH<sub>2</sub>CH<sub>2</sub>NH<sub>2</sub>); 27.4 (CH<sub>2</sub>CH<sub>2</sub>C(O)-NH); 28.3, 28.4, 28.8, 29.2, 29.4, 29.7, 29.9, 30.0, 30.2, 30.9, 31.2, 31.2 ((CH<sub>2</sub>)<sub>10</sub>CH<sub>2</sub>C(O)(CH<sub>2</sub>)<sub>2</sub>C(O), (CH<sub>2</sub>)<sub>8</sub>-(CH<sub>2</sub>)<sub>2</sub>C(O)); 33.5 (CH<sub>2</sub>CH<sub>2</sub>CH<sub>3</sub>); 37.7 (CH<sub>2</sub>C(O)NH); 38.2, 38.6, 45.6, 46.3 (CH<sub>2</sub>NH, CH<sub>2</sub>NH<sub>2</sub>); 40.0, 40.1 (NH(CH<sub>2</sub>)<sub>2</sub>-NH); 47.9, 48.0, 51.1, 51.2 (CH<sub>2</sub>NC(O)); 62.0 (C(O)CHNH); 63.0 (CH<sub>2</sub>OH); 64.0 (Gal C6); 70.7, 70.8, 70.8, 71.2, 71.4, 71.4 (CHOH); 72.2, 72.3 (Gal C4); 73.3, 73.5 (Gal C2); 75.2 (Gal C3); 77.5 (Gal C5); 84.0, 84.1 (OCH(CHOH)<sub>2</sub>); 106.0, 106.1 (Gal C1); 174.2, 174.4 (C(O)NH); 175.3, 175.4, 177.2 (C(O)N). ESI-MS: *m/z* = 1303.9, in agreement with the calculated mass for [M + H]<sup>+</sup> = C<sub>52</sub>H<sub>103</sub>N<sub>5</sub>O<sub>12</sub> + H<sup>+</sup>.

**Synthesis of DC14Gal-EDGly-PA.** The same procedure as described for the synthesis of DC14Gal-ED-Sper(BOC), when applied to DC14Gal-ED(51 mg, 0.047 mmol), Net<sub>3</sub> (0.03 mL, 0.019 mmol) and BOCNH-[(CH<sub>2</sub>)<sub>3</sub>N(BOC)]<sub>4</sub>CH<sub>2</sub>-COOH (19) (46 mg, 0.057 mmol) and to 25.3 mg of BOP (0.057 mmol), afforded 52.4 mg (58%) of DC14Gal-EDGly-PA(BOC) as a colorless oil. <sup>1</sup>H NMR (CD<sub>3</sub>OD): δ 0.79 (t, *J* = 5.9 Hz, 6H, CH<sub>3</sub>); 1.18 (broad s, 58H, (CH<sub>2</sub>)<sub>11</sub>CH<sub>3</sub>, (CH<sub>2</sub>)<sub>7</sub>(CH<sub>2</sub>)<sub>2</sub>C(O)); 1.37–1.67 (m, 61H, CH<sub>2</sub>CH<sub>2</sub>NBOC, CH(CH<sub>2</sub>)<sub>2</sub>, CH<sub>2</sub>CH<sub>2</sub>NC(O), CH<sub>2</sub>CH<sub>2</sub>C(O)NH); 2.08 (t, *J* = 7.2 Hz, 2H, CH<sub>2</sub>C(O)NH); 2.57 (m, 4H, C(O)(CH<sub>2</sub>)<sub>2</sub>C(O)); 2.40–3.29 (m, 30H, CH<sub>2</sub>NC(O), CH<sub>2</sub>NHC(O), CH<sub>2</sub>NBOC, CH<sub>2</sub>NHBOC, C(O)CH<sub>2</sub>NH); 3.29–3.97 (m, 12H, CHOH, CH<sub>2</sub>OH); 4.36 (d, *J* = 5.4 Hz, 1H, Gal H1). <sup>13</sup>C NMR (CD<sub>3</sub>OD): δ 14.3 (CH<sub>3</sub>); 23.1 (CH<sub>2</sub>CH<sub>3</sub>); 26.2 (CH<sub>2</sub>CH<sub>2</sub>C(O)-NH); 27.4, 27.5 (CH<sub>2</sub>(CH<sub>2</sub>)<sub>2</sub>NC(O)); 27.8, 27.8, 28.1, 29.2, 29.8, 30.1 ((CH<sub>2</sub>)<sub>8</sub>CH<sub>2</sub>CH<sub>2</sub>CH<sub>2</sub>C(O)(CH<sub>2</sub>)<sub>2</sub>C(O), ((CH<sub>2</sub>)<sub>8</sub>-(CH<sub>2</sub>)<sub>2</sub>C(O)NH, CH<sub>2</sub>CH<sub>2</sub>NHBOC); 32.3 (CH<sub>2</sub>CH<sub>2</sub>CH<sub>3</sub>); 36.8 (CH<sub>2</sub>C(O)NH); 38.1 (CH<sub>2</sub>NHBOC); 39.6 (NH(CH<sub>2</sub>)<sub>2</sub>-NH); 45.3 (CH<sub>2</sub>NBOC, C(O)CH<sub>2</sub>NBOC); 46.9, 47.0, 50.9, 51.0 (CH<sub>2</sub>NC(O)); 62.1 (CH<sub>2</sub>OH); 63.0 (Gal C6); 69.7, 69.8, 70.2, 70.8, 70.8 (CHOH); 72.1 (Gal C4); 72.3 (Gal C2); 74.0 (Gal C3); 76.2 (Gal C5); 80.4, 80.5 (C(CH<sub>3</sub>)<sub>3</sub>); 81.2 (OCH(CHOH)<sub>2</sub>); 104.8, 104.9 (Gal C1); 156.3, 156.4, 157.3 (C(O)BOC); 173.2, 174.0, 175.8 (C(O)N).

The *N*-BOC deprotection procedure as described above for the deprotection of DC14Gal-ED(BOC) when applied to DC14Gal-EDGly-PA(BOC) led quantitatively to DC14Gal-EDGly-PA (as its penta-TFA salt), as a white powder. <sup>1</sup>H NMR (D<sub>2</sub>O): δ 0.85 (m, 6H, CH<sub>3</sub>); 1.25 (broad s, 58H, (CH<sub>2</sub>)<sub>11</sub>CH<sub>3</sub>, (CH<sub>2</sub>)<sub>7</sub>(CH<sub>2</sub>)<sub>2</sub>C(O)); 1.52 (m, 8H, CH<sub>2</sub>CH<sub>2</sub>NC(O), CH<sub>2</sub>CH<sub>2</sub>C(O)NH); 2.08 (m, 10H, CH<sub>2</sub>CH<sub>2</sub>NH, CH<sub>2</sub>-CH<sub>2</sub>NH<sub>2</sub>, CH<sub>2</sub>C(O)NH); 2.68 (m, 4H, C(O)(CH<sub>2</sub>)<sub>2</sub>C(O)); 3.04–4.07 (m, 42H, CH<sub>2</sub>NH, CH<sub>2</sub>NH<sub>2</sub>, CH<sub>2</sub>NC(O), C(O)-CH<sub>2</sub>NH, CHOH, CH<sub>2</sub>OH); 4.51 (m, 1H, Gal H1). <sup>13</sup>C NMR (D<sub>2</sub>O): δ 15.3 (CH<sub>3</sub>); 24.3 (CH<sub>2</sub>CH<sub>3</sub>); 25.1 (CH<sub>2</sub>CH<sub>2</sub>NH<sub>2</sub>); 26.8 (CH<sub>2</sub>CH<sub>2</sub>C(O)NH); 27.9, 28.1, 28.4, 29.0, 29.3, 29.8, 30.2, 30.3, 30.5, 30.7, 30.8, 30.9, 31.1 ((CH<sub>2</sub>)<sub>10</sub>CH<sub>2</sub>C(O)-(CH<sub>2</sub>)<sub>2</sub>C(O), (CH<sub>2</sub>)<sub>8</sub>(CH<sub>2</sub>)<sub>2</sub>C(O), CH<sub>2</sub>CH<sub>2</sub>NH); 33.5 (CH<sub>2</sub>-CH<sub>2</sub>CH<sub>3</sub>); 36.3 (CH<sub>2</sub>C(O)NH); 37.0, 39.3, 45.2, 48.7 (CH<sub>2</sub>-NH, CH<sub>2</sub>NH<sub>2</sub>); 38.7 (NH(CH<sub>2</sub>)<sub>2</sub>NH); 42.1 (C(O)CH<sub>2</sub>NH);

47.5, 49.4, 50.0 (CH<sub>2</sub>NC(O)); 60.9 (CH<sub>2</sub>OH); 61.4, 62.6 (Gal C6); 69.1, 70.0, 70.3, 70.6 (CHOH); 71.4 (Gal C4); 72.2 (Gal C2); 73.2 (Gal C3); 75.8 (Gal C5); 81.9, 82.2 (OCH(CHOH)<sub>2</sub>); 104.9 (Gal C1); 167.4 (NH(C(O)CH<sub>2</sub>NH)); 173.8, 174.7, 175.2, 177.7 (C(O)N). ESI-MS: *m/z* = 1361.0, in agreement with the calculated mass for [M + H]<sup>+</sup> = C<sub>52</sub>H<sub>103</sub>N<sub>5</sub>O<sub>12</sub> + H<sup>+</sup>.

**Lipoplex Preparation.** The lipoplexes were prepared using plasmid pTG11236 (pCMV-SV40pA, 5739 bp) which was produced by Transgène SA (Strasbourg, France). Its endotoxin content (<1 endotoxin unit/mg of plasmid) was checked using Limulus Amebocyte Lysat kit (Biogenic, France). The quantities of compound used were calculated according to the desired DNA concentration of 0.1 mg/mL, the *N/P* ratio, the molar weight, and the number of positive charges in the selected Gal-CL and, if need be, of pcTG90. The *N/P* ratio of 5 for example corresponds to the molar amount of Gal-CL (or Gal-CL and pcTG90) necessary to have a ratio of 5 amino group nitrogens (for 1 mole of Gal-CL or for 0.5 mol of Gal-CL and 0.5 mol of pcTG90) per phosphate in the DNA (330 Da mean MW), as described elsewhere (2, 4).

The Gal-CL:DOPE (1:1 mol) and Gal-CL:pcTG90:DOPE (0.5:0.5:1 mol) lipoplexes are formulated by adding a desired volume of the Gal-CL:DOPE and Gal-CL:pcTG90:DOPE liposomal preparation (sizes between 50 and 100 nm) at a Gal-CL concentration of 10 mg/mL (in 5% glucose), respectively, to the desired volume of DNA solution to reach the desired DNA concentration of 0.1 mg/mL. Thus, for the preparation of the Gal-CL:DOPE (1:1 mol) *N/P* = 5 lipoplexes and 0.1 mg/mL DNA, 50 μL of the Gal-CL:DOPE solution (10 mg/mL of Gal-CL in MeOH) was transferred to a borosilicate glass tube (16 × 100 mm). The solvent was evaporated in a Rotavap evaporation system (45 °C, 30 pm, 0.2 bar, 40 min). Fifty microliters (50 μL) of 5% glucose was added to the film obtained. The preparation was vortexed for 12 h and further sonicated during 5 min (Branson sonifier 450 W at 50% duty cycle equipped with a micro tips sond) in order to obtain average particle sizes in the 50–100 nm range (measured by photon correlation spectroscopy using a Coulter N4Plus particle size analyzer). Then, 47.9 μL of this preparation was added to 952.1 μL DNA solution [100 μL DNA (1 mg/mL) diluted with 852.1 μL 5% glucose]. This preparation was used for the following experiments.

**Characterization.** Each sample (0.5 μg of plasmid) was electrophoresed for about 90 min under 75 V, through a 0.8% agarose gel in TAE 1 × (Tris-acetate-EDTA) buffer and stained by spreading an ethidium bromide (EtBr, Sigma) solution in TAE buffer (20 μL ethidium bromide of a 10 mg/mL solution) in 200 mL TAE). The DNA was then visualized after photographing on a UV transilluminator. The plasmid integrity in each sample (0.25 μg) was confirmed by electrophoresis after decomplexing the lipoplexes (10 μL of a plasmid 0.05 mg/mL) with sodium dodecyl sulfate (10 μL, 80 g/L).

**In Vitro Transfection.** Cell cultures were analyzed for detecting mycoplasma contaminants using a mycoplasma stain kit (Aldrich). Twenty-four hours before transfection, A549 cells (from human pulmonary carcinoma), human hepatoma HepG2 cells, or murine embryo BNL-CL2 cells were grown at a density of 2 × 10<sup>4</sup> cells/well in a 96-well plates in Dulbecco-modified Eagle culture medium (DMEM; Gibco-BRL) containing 10% fetal calf serum (FCS; Sigma), in a wet (37 °C) and 5% CO<sub>2</sub>/95% air atmosphere. Five microliters (5 μL) of lipoplex formulation were diluted to 100 μL in DMEM supplemented with 10% FCS in order to have 0.5 μg of DNA in the



**Table 1. Mean Sizes Determined by Light Scattering Spectroscopy of the Lipoplexes Formed between Plasmid pTG11033 and Gal-CL:DOPE (1:1), Gal-CL:pcTG90:DOPE (1:1:2), or pcTG90:DOPE (1:1) and Prepared in 5% Glucose**

formulation	mean size (standard deviation) in nm		
	<i>N/P</i> <sup>a</sup> (5)	<i>N/P</i> <sup>a</sup> (2.5)	<i>N/P</i> <sup>a</sup> (1.25)
GalSper:DOPE	210 (120)	170 (60)	p <sup>b</sup>
GalSper:pcTG90:DOPE	110 (50)	140 (50)	p <sup>b</sup>
DC14-GalSper:DOPE	140 (50)	220 (80)	210 (70)
DC14-GalSper:pcTG90:DOPE	180 (120)	140 (50)	p <sup>b</sup>
DC14-Gal-ED-Sper:DOPE	150 (90)	140 (50)	160 (50)
DC14-Gal-ED-Sper:pcTG90:DOPE	150 (90)	140 (50)	160 (50)
DC14-Gal-EDGly-PA:DOPE	120 (50)	120 (40)	p <sup>b</sup>
DC14-Gal-EDGly-PA: pcTG90:DOPE	210 (70)	300 (50)	280 (100)

<sup>a</sup> *N* = amine equivalents; *P* = plasmid phosphate equivalents. <sup>c</sup> p = precipitate.

preparation. The culture medium was removed and replaced by these 100  $\mu$ L of lipoplex/DMEM/FCS solution. For the transfection experiments performed in the presence of ASF, ASF (1 mg in 50  $\mu$ L DMEM) was added to the cells 10 min before the addition of the lipoplex preparation diluted to 50  $\mu$ L in DMEM supplemented with 10% FCS. After 4 and 24 h, 50 and 100  $\mu$ L of DMEM supplemented with 30% and 10% FCS, respectively, were added. After 48 h, the transfection was stopped, the culture medium was discarded, and the cells washed twice with 100  $\mu$ L of PBS and lysed with 50  $\mu$ L of lysis buffer (Promega, Charbonnières, France). The lysates were frozen at  $-32^{\circ}\text{C}$ , awaiting analysis of luciferase activity. This measurement was performed in a LB96P luminometer (Berthold, France) in dynamic mode, for 10 s on 10  $\mu$ L on the lysis mixture and using the "luciferase" determination system (Promega) in 96-well plates. The total protein concentration per well was determined by the BCA test (Pierce, Montluçon, France). For cells grown in the absence of lipoplexes, a well contains around 30–60  $\mu$ g of proteins. Luciferase activity was calculated as femtograms (fg) of luciferase per mg of protein. The percentage of cell viability of the lipoplexes was calculated as the ratio of the total protein amount per well of the transfected cells relative to that measured for untreated cells  $\times 100\%$ . The given means  $\pm$  SEMs were calculated from three or four repetitions in two independent experiments. Statistical analyses were performed using a Student *t* test. The difference between two means was considered as statistically significant when *p* is  $\leq 0.05$ .

## RESULTS AND DISCUSSION

**Synthesis.** The syntheses of the galacto-polyamino bolaamphiphiles were performed according to the procedures outlined in Scheme 1. Acylation of the galactosylated amine **1** (whose synthesis is described in ref 2) with the ditetradecylmercaptothiazolidine derivative **2** afforded compound **3**. Mercaptothiazolidine derivatives are mild acylating agents which are selective for amino groups and obviate the need for protection of the sugar hydroxyls (22). The low reactivity of the acylating agent and the starting secondary amine **1**, combined with the highly amphiphilic nature of compound **3** (which complicates its purification), are likely to be responsible for the low yields of the synthesis of **3**.

Bolaamphiphile DC14GalSper, which bears a "linear" spermine polar head, was obtained by condensing spermine onto the free acid function of **3** (63% yield) in the same way as that described for the synthesis of GalSper (2). This step was performed in the presence of BOP as coupling agent and a large excess of spermine in order to avoid the coupling of activated acid onto the two primary amino groups of spermine. DC14GalSper was

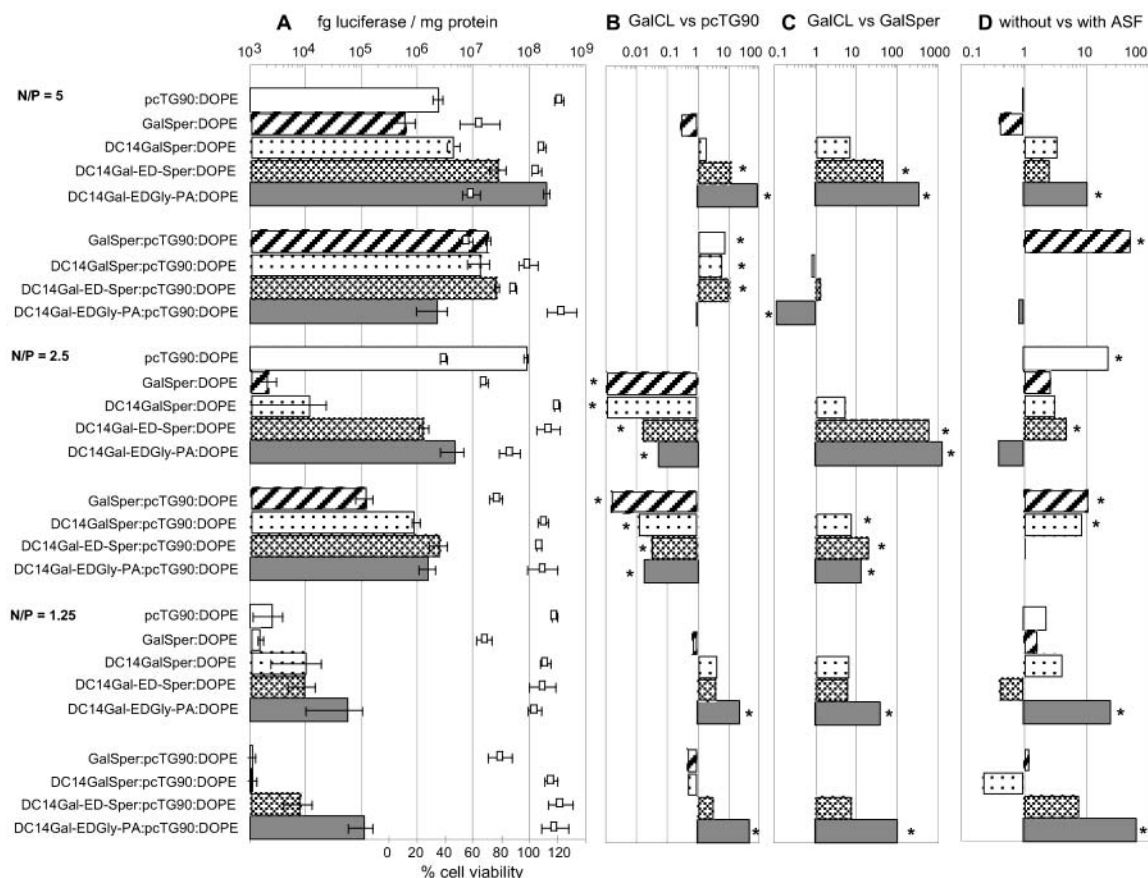
purified by size-exclusion chromatography on Sephadex LH-20.

The syntheses of the "branched" spermine DC14Gal-ED-Sper and "linear" pentamine DC14Gal-EDGly-PA derivatives were both performed from DC14-Gal-ED synthon. This derivative was obtained by condensing *N*-BOC-ethylenediamine onto acid **3** in the presence of BOP as coupling agent (86% yield), followed by quantitative BOC-deprotection using a large excess of TFA in  $\text{CH}_2\text{Cl}_2$ . When this two-step procedure (coupling and deprotection) was applied to DC14Gal-ED and to the BOC-protected carboxy-spermine derivative **5** (23) or glycine-pentamino derivative **6** (21), we respectively obtained DC14Gal-ED-Sper and DC14Gal-EDGly-PA (50–60% overall yields). Purification of these two compounds was best performed by silica gel chromatography on their respective BOC-protected form, and by size-exclusion chromatography on Sephadex LH-20 when deprotected.

The chemical structure of the three galacto-polyamino bolaamphiphiles was unambiguously confirmed by  $^1\text{H}$  and  $^{13}\text{C}$  NMR spectroscopy and by electrospray ionization mass spectrometry in positive and negative modes.

**Lipoplex Formation and Characterization.** The capability of Gal-CL to condense DNA and to form lipoplexes was analyzed with (i) an equimolar amount of DOPE or (ii) with an equimolar amount of pcTG90 and two equimolar amounts of DOPE. The lipoplexes were further formulated using *N/P* ratios of 5, 2.5, and 1.25 (*N* = number of lipid amines; *P* = number of DNA phosphates). Their average sizes were measured by light scattering spectroscopy. These studies were performed with pTG11033 plasmid, also used for the in vitro transfection screening assays (see below). The procedure applied for the lipoplex preparation relies on the dilution from Gal-CL:DOPE (1:1) or Gal-CL:pcTG90:DOPE (1:1:2) liposomes in 5% glucose. Table 1 collects the mean particle sizes measured for the different lipoplexes. These formulations were also analyzed by gel electrophoresis (data not shown). These analyses indicated the presence of "fully" complexed plasmid (not accessible to ethidium bromide) for *N/P* = 5 and 2.5 and for the *N/P* = 1.25 GalSper-based lipoplexes. Complexed plasmid but accessible to ethidium bromide, however, was detected for the *N/P* = 2.5 DC14Gal-ED-Sper and DC14Gal-EDGly-PA formulations. This was also the case for most of the *N/P* = 1.25 preparations, except for the GalSper-based ones.

When used with an equimolar amount of DOPE, the Gal-CLs were able to condense DNA into lipoplexes with mean particle sizes in the 120–220 nm range (Table 1). However, a precipitate was observed for the *N/P* = 1.25 GalSper and DC14Gal-EDGly-PA formulations. When the lipoplexes were formulated using a Gal-CL:pcTG90:DOPE (1:1:2 mol) mixture, polydispersed preparations of particles in the 110–300 nm range were measured and



**Figure 1.** A: Luciferase expression (bars) and cell viability (squares) in A549 cells of the lipoplexes prepared in 5% glucose and made of Gal-CL:DOPE (1:1) or Gal-CL:pcTG90:DOPE (1:1:2) and plasmid pTG11033 (DNA) for various *N/P* ratios, as compared to control pcTG90:DOPE (1:1). The transfection experiments were performed in DMEM and a DNA concentration of 0.5  $\mu$ g/well. The given means  $\pm$  SEM were calculated from three or four repetitions in two independent experiments. B: Transfection efficiency of the Gal-CL-based lipoplexes vs that of their corresponding pcTG90:DOPE controls. The luciferase level ratio LLR is the ratio of luciferase amount measured for the Gal-CL-based formulation vs that measured for its corresponding pcTG90:DOPE control. C: Transfection efficiency of the Gal-CL-based lipoplexes vs that of their corresponding GalSper:DOPE (or GalSper:pcTG90:DOPE). The luciferase level ratio LLR is the ratio of luciferase amount measured for the Gal-CL-based formulation vs that measured for its corresponding GalSper-based one. D: Transfection efficiency of the Gal-CL-based and control lipoplexes in the absence or presence of ASF. The luciferase level ratio LLR is the ratio of luciferase amount measured for the Gal-CL-based formulation in the absence of ASF vs that measured in the presence of ASF. For the transfection experiments performed in the presence of ASF, these were performed in DMEM supplemented with 1 mg/well of ASF which was added to the cells 10 min before addition of the lipoplexes. For panels B–D, \*  $p < 0.05$  was carried out in a pairwise comparison; if not specified, comparison is not significant.

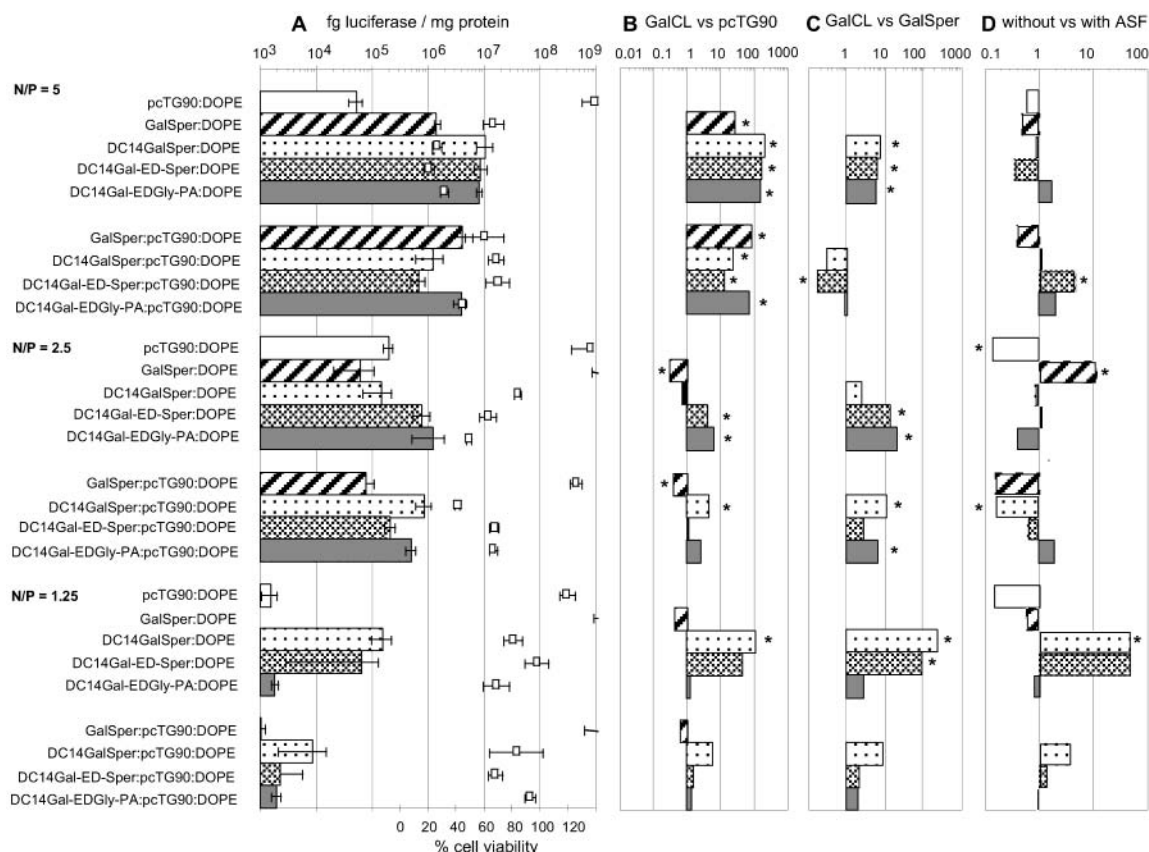
precipitates were observed only for GalSper:pcTG90:DOPE *N/P* = 1.25.

It is further noticeable that the Gal-CLs with DOPE or with pcTG90:DOPE form lipoplexes that do not precipitate at a *N/P* ratio of 2.5 and even 1.25 for some formulations, while most often precipitates were formed with (poly)cationic lipids for *N/P* = 2.5 or 1.25 (20, 24, 25). These results are indeed worth being noted if *in vivo* uses of such formulations are contemplated.

**In Vitro Transfection.** Our main objective was to demonstrate that targeted lipoplexes formulated with the cationic Gal-CL bolaamphiphiles (used as condensing and targeting components in the Gal-CL:DOPE lipoplexes, or as targeting component in the Gal:CL:pcTG90:DOPE lipoplexes) were able to deliver specifically genes to cells expressing ASGP receptors. However, cationic lipids provide also receptor-independent gene transfer to cells (and more particularly to adherent cells), which involves electrostatic interactions between the cationized-DNA particles and the anionic cell proteoglycans expressed on the cell surface (17, 18). It was therefore necessary to determine the conditions under which a nonspecific gene transfer process into adherent ASGP(–) or ASGP(+) cells can occur with the cationic Gal-CL-based lipoplexes.

Aiming at these goals, the potential of the various above-described Gal-CL:DOPE and Gal-CL:pcTG90:DOPE pTG11033 lipoplexes for mediating a nonspecific or a specific transfection was screened *in vitro* on control ASGP(–) A549 cells and on ASGP(+) BNL-CL2 and HepG2 cells, respectively. Control experiments were also realized with pcTG90:DOPE lipoplexes as nontargeted galactose lipoplexes. The transfection efficiency of the lipoplexes (expressed in femtograms (fg) of luciferase/mg of protein) was evaluated (i) in the absence or presence of ASF (1 mg/well), (ii) for *N/P* ratio of 1.25, 2.5, and 5, (iii) for a DNA amount of 0.5  $\mu$ g/well, and (iii) in the absence of serum for the reasons stated in the Introduction. Control transfection experiments performed with naked DNA under equivalent conditions led to expression levels of 10<sup>2–3</sup> fg luciferase/mg of protein. The cell viability of the lipoplexes was also checked by determining the total protein amount per well of the transfected cells relative to that measured for untreated cells (for which the total protein amount per well is in a 30–50  $\mu$ g/well range).

The transfection and cell viability results concerning the ASGP(–) A549 cells are illustrated in Figure 1A. These results indicate that Gal-CL:DOPE and Gal-CL:



**Figure 2.** A: Luciferase expression (bars) and cell viability (squares) in ASGP(+) HepG2 cells of the lipoplexes prepared in 5% glucose and made of Gal-CL:DOPE (1:1) or Gal-CL:pcTG90:DOPE (1:1:2) and plasmid pTG11033 (DNA) for various  $N/P$  ratios, as compared to control pcTG90:DOPE (1:1). B: Transfection efficiency of the Gal-CL-based lipoplexes vs that of their corresponding pcTG90:DOPE controls. C: Transfection efficiency of the Gal-CL-based lipoplexes vs that of their corresponding GalSper:DOPE (or GalSper:pcTG90:DOPE). D: Transfection efficiency of the Gal-CL-based and control lipoplexes in the absence or presence of ASF. For more details concerning panels A–D and the pairwise comparison, see caption of Figure 1.

pcTG90:DOPE mixtures are efficient gene transfer systems for mediating nonspecific transfection when used more particularly at a  $N/P$  ratio of 5 and 2.5. Luciferase expression levels in the  $10^6$ – $10^8$  fg/mg protein were indeed measured while much lower levels ( $10^3$ – $10^5$  fg/mg protein) were obtained for a  $N/P$  ratio of 1.25. They indicate also that an enhancement of transfection through a receptor-mediated endocytosis process can more likely be detected for  $N/P = 1.25$  Gal-CL lipoplexes for which the nonspecific electrostatic pathway is the less favoured. It is further noticeable that all these Gal-CL-based formulations were rather well tolerated (cell viability between 60 and 110%) while the very efficient control  $N/P = 2.5$  pcTG90:DOPE formulation was found to be more toxic (30% cell viability).

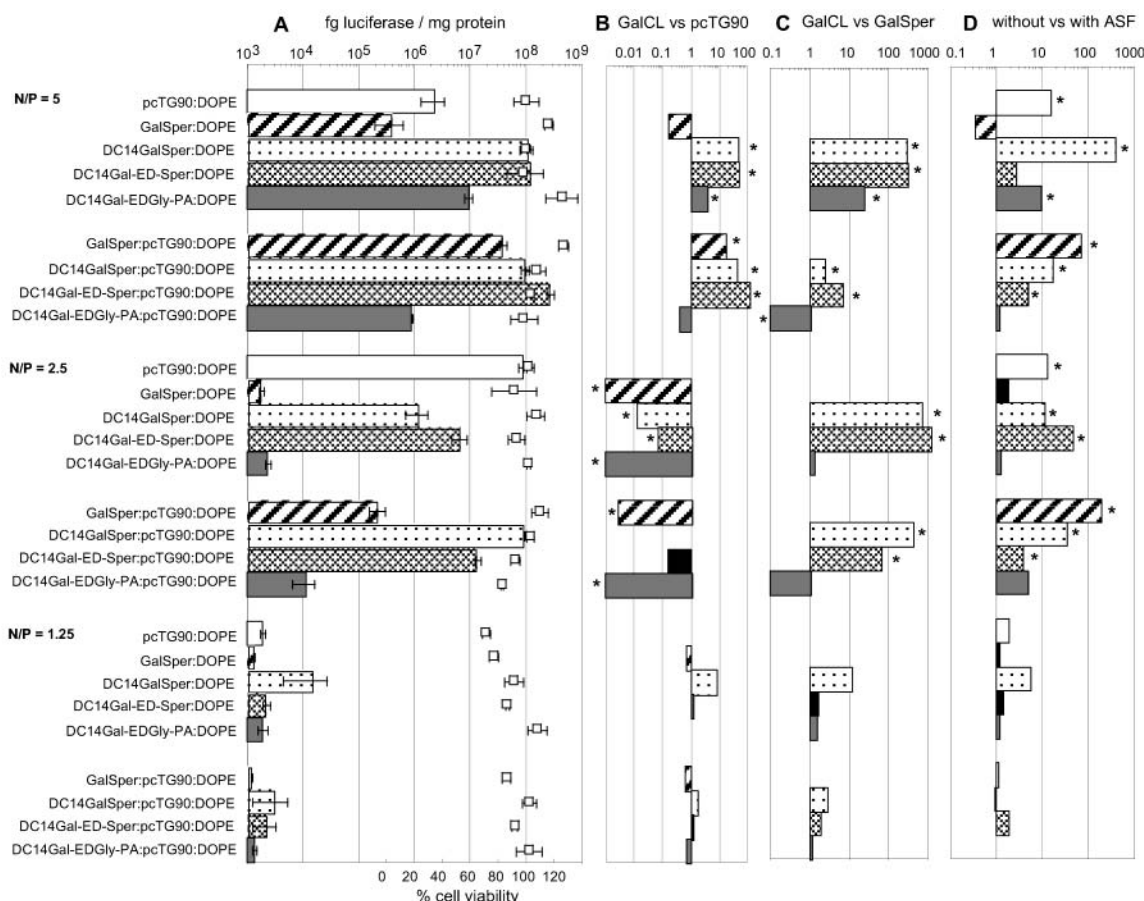
As compared with control pcTG90:DOPE lipoplexes which are among the most efficient lipid formulations known for transfecting A549 cells (19, 20), contrasting and unexpected results were obtained with the Gal-CL ones depending upon the  $N/P$  ratio and the nature of Gal-CL (see Figure 1B). As observed with other glycosylated DNA complexes (4, 5, 7, 14), one expects that the galactosyl coating of the lipoplexes provides a shielding effect which interferes with the binding of the cationic particles to the anionic cell surface, therefore inhibiting their entry into the cells. This is indeed what we have obtained for the GalSper formulations, whatever the  $N/P$  ratio, and for any of the Gal-CL  $N/P = 2.5$  formulations. However, comparable and even higher luciferase expression levels were measured for the DC14GalSper, DC14Gal-

ED-Sper and DC14Gal-ED-PA  $N/P = 5$  formulations than for the pcTG90:DOPE lipoplexes.

As compared with GalSper (which constituted the head compound of the Gal-CL bifunctional gene transfer agent series) and as illustrated in Figure 1C, the new DC14GalSper, DC14Gal-ED-Sper, and DC14Gal-ED-PA bolaamphiphiles, whether used with DOPE or with pcTG90:DOPE, were found statistically to lead to more efficient nonspecific gene transfer systems. This can be attributed to the increased hydrophobic character of the second generation of Gal-CL bolaamphiphiles owing to the presence of the two long alkyl chains. This is supported by the much higher transfection efficiency found for double-chain cationic lipids as compared with their single-chain analogues (23). It should be noted that the three new Gal-CLs behave very similarly, indicating that the number of amine functions (3, 4, and 5, respectively) and the "linear" or "branched" nature of the polar head have no major impact on transfection.

Concerning the effects of ASF on nonspecific-mediated transfection with these Gal-CL lipids (Figure 1D), the control experiments performed on ASGP(–) A549 cells in the presence of ASF (40-, 20-, and 10-fold molar excess over galactose for the  $N/P = 1.25$ , 2.5, and 5 formulations, respectively) showed likely that ASF does most frequently not interfere with the nonspecific transfection process, as expected. Although a substantial but surprising transfection inhibition was observed for some formulations (one-third of the 24 formulations tested), no systematic trend with the  $N/P$  ratio value nor with the Gal-CL nature could be evidenced. The unpredictability





**Figure 3.** A: Luciferase expression (bars) and cell viability (squares) in ASGP(+) BNL-CL2 cells of the lipoplexes prepared in 5% glucose and made of Gal-CL:DOPE (1:1) or Gal-CL:pcTG90:DOPE (1:1:2) and plasmid pTG11033 (DNA) for various *N/P* ratios, as compared to control pcTG90:DOPE (1:1). B: Transfection efficiency of the Gal-CL-based lipoplexes vs that of their corresponding pcTG90:DOPE controls. C: Transfection efficiency of the Gal-CL-based lipoplexes vs that of their corresponding GalSper:DOPE (or GalSper:pcTG90:DOPE). D: Transfection efficiency of the Gal-CL-based and control lipoplexes in the absence or presence of ASF. For more details concerning panels A–D and the pairwise comparison, see caption of Figure 1.

of such an issue is rather puzzling and indicates likely that to be unambiguously interpreted as a receptor-mediated transfection process, competition experiments with ASF should be analyzed with great care.

To evidence a receptor-mediated process of the transfection of ASGP expressing cells (HepG2 and BNL-CL2) with Gal-CL-based lipoplexes, we performed a series of experiments in the absence and in the presence of an excess of asialofetuin.

Before interpreting unambiguously the transfection results on ASGP(+) cells with Gal-CL-based lipoplexes, it was essential to estimate the effects of ASF on their nonspecific mediated transfection with the control pcTG90:DOPE lipoplexes. Although one expects that ASF has no determinant influence on transfection of ASGP(+) cells mediated with such nongalactosyl-labeled lipoplexes, the interactions of ASF with the cell surface, and/or with positively charged lipoplexes are likely to interfere with the transfection process. Our control experiments with the pcTG90:DOPE lipoplexes did not evidenced any systematic effect of ASF on nonspecific mediated transfection, these effects being rather cell-type-dependent. Indeed, the presence of ASF resulted at most into a 10-fold increase of luciferase expression for the HepG2 cells (Figure 2D). Providing that the comparison of the luciferase levels measured with and without ASF is statistically significant, any transfection inhibition of the HepG2 cells can thus be unambiguously interpreted as an inhibition of the receptor-mediated transfection pro-

cess. By contrast and as illustrated in Figure 3D, the presence of ASF decreased the nonspecific transfection of the BNL-CL2 cells with the pcTG90:DOPE lipoplexes by a factor of 15 (ASF was also found to inhibit the transfection of BNL-CL2 cells by PEI polyplexes (4)). These data are taken to indicate that transfection of the BNL-CL2 cells with the Gal-CL-based lipoplexes proceeded through a receptor-mediated process providing the competition experiments with ASF inhibited transfection by a statistically significant factor at least larger than 15.

Concerning transfection of the ASGP(+) cells with the less-cationic charged Gal-CL-based *N/P* = 1.25 lipoplexes (for which the electrostatic interactions with the cell proteoglycans are expected to be reduced), only the DC14GalSper:DOPE and DC14Gal-ED-Sper:DOPE formulations and in the case of HepG2 cells (Figure 2A) led to a moderate level of luciferase expression which was further inhibited significantly in the presence of ASF (Figure 2D). This likely indicates the participation of a receptor-mediated endocytosis pathway for the HepG2-cell transfection with these two *N/P* = 1.25 formulations. This is further supported by the low ability of these DC14GalSper:DOPE and DC14Gal-ED-Sper:DOPE *N/P* = 1.25 lipoplexes to transfect the control A549 cells through a receptor-independent process (Figure 1). Unfortunately, such a receptor-mediated endocytosis pathway could not be evidenced for the BNL-CL2 cells. Indeed, the transfection decrease observed in the pres-

ence of ASF for the sole  $N/P = 1.25$  Gal-CL formulation (i.e. DC14GalSper:DOPE) that was able to transfect these cells (Figures 3A,D) was too low to be significantly attributed to the inhibition of such a process.

Concerning transfection of the HepG2 cells with the cationic Gal-CL:DOPE and Gal-CL:pcTG90:DOPE  $N/P = 5$  and  $2.5$  lipoplexes, these formulations led to much higher luciferase expression levels than the control pcTG90:DOPE  $N/P = 5$  and  $2.5$  ones (Figure 2B). This is more particularly the case for the second generation of galactosylated bolaamphiphiles DC14Gal-EDGly-PA, DC14GalSper and DC14Gal-ED-Sper, whether used with DOPE alone or with pcTG90:DOPE. These new galactosylated polyamines are overall more efficient than GalSper (Figure 2C). However, expression of luciferase was found for most of these formulations not to be affected or even increased in the presence of ASF (Figure 2D). These results indicate likely a receptor-independent mechanism of transfection. They could also indicate that these cationic  $N/P = 5$  and  $2.5$  Gal-CL-based lipoplexes can transfect HepG2 cells through a receptor-dependent mechanism, and when this cell entry pathway is blocked, the receptor-independent mechanism takes then over.

For the transfection of the BNL-CL2 cells, markedly higher but lower levels of luciferase expression with the Gal-CL-based  $N/P = 5$  and  $2.5$  lipoplexes were measured as compared with their analogous control pcTG90:DOPE  $N/P = 5$  and  $2.5$  ones, respectively (Figure 3B). As compared with the GalSper head compound, the second generation of galactosylated bolaamphiphiles DC14GalSper and DC14Gal-ED-Sper, whether used with DOPE alone or with pcTG90:DOPE, were found to be overall more efficient (Figure 3C). Moreover, for most of these Gal-CL formulations, the presence of ASF did not decrease the expression of luciferase to a significantly larger extent than that for the control pcTG90:DOPE (Figure 3D), indicating likely, as for the transfection of the Hep-G2 cells, a receptor-independent mechanism of transfection. Interestingly, however, ASF was found to inhibit transfection by a factor significantly larger than 15 in the case of formulations DC14GalSper:DOPE  $N/P = 5$  ( $>300$ -fold), DC14Gal-ED-Sper:DOPE  $N/P = 2.5$  (48-fold), DC14GalSper:pcTG90:DOPE  $N/P = 2.5$  (33-fold), and GalSper:pcTG90:DOPE  $N/P = 5$  (68-fold) and  $2.5$  (180-fold) (see Figure 3D). This inhibition could be attributed to partial blockade by ASF of the targeted cell entry of the plasmid. It indicates nevertheless that transfection of these ASGP(+) cells with such highly cationic complexes is still dominated by the nonspecific electrostatic-mediated endocytosis pathway. If a systematic and significant inhibition by ASF is observed for the GalSper:pcTG90:DOPE formulations, there is, however, no such obvious trend for the formulations based on the three new Gal-CL.

Altogether, our results show that cationic  $N/P = 5$  and  $2.5$  Gal-CL lipoplexes constitute very efficient nonspecific gene transfer systems. The three new double-chain bolaamphiphiles (i.e., DC14GalSper, DC14Gal-ED-Sper, and DC14Gal-ED-PA), whether used with DOPE or with pcTG90:DOPE, were found to be more efficient nonspecific gene transfer agents than the single-chain head GalSper compound. They proved at least as or even more potent than the reference pcTG90:DOPE, which belongs to the most efficient lipofection systems. Interestingly, specific receptor-mediated endocytosis of DNA could be achieved in some instances with some formulations based on these targeted cationic Gal-CL bolaamphiphiles presenting a single galactose residue. These targetable Gal-CL lipopolyamines appear thus as promising synthetic

vectors for specific in vivo gene delivery to hepatocytes, providing, however, that Gal-CL-based lipoplexes of much lower particle sizes ( $\leq 50$  nm) than those found here could be formulated for enabling their penetration into the liver parenchyma across the fenestrated blood-vessel capillaries. Although encouraging, the transfection efficiencies and, more particularly, the transfection specificities obtained with these compounds should also be improved.

#### ACKNOWLEDGMENT

We wish to thank Transgène SA (Strasbourg, France), Drs. S. Braun, O. Meyer, and B. Cavallini (from Transgène) for their interest into this project and for supplying with BOCNH-[(CH<sub>2</sub>)<sub>3</sub>N(BOC)]<sub>4</sub>CH<sub>2</sub>COOH, pcTG90 and plasmid.

#### LITERATURE CITED

- (1) Anwer, K., Bailey, A., and Sullivan, S. M. (2000) Targeted gene delivery: a two-pronged approach. *Crit. Rev. Ther. Drug Carrier Syst.* 17, 377–424.
- (2) Gaucheron, J., Santaella, C., and Vierling, P. (2000) In vitro gene transfer with a novel galactosylated spermine bolaamphiphile. *Bioconjugate Chem.* 12, 569–575 (2001).
- (3) Remy, J. S., Kichler, A., Mordvinov, V., Schuber, F., and Behr, J. P. (1995) Targeted gene transfer into hepatoma cells with lipopolyamine-condensed DNA particles presenting galactose ligands: a stage toward artificial viruses. *Proc. Natl. Acad. Sci. U.S.A.* 92, 1744–1748.
- (4) Zanta, M. A., Boussif, O., Adib, A., and Behr, J. P. (1997) In vitro gene delivery to hepatocytes with galactosylated polyethylenimine. *Bioconjugate Chem.* 8, 839–844.
- (5) Hashida, M., Takemura, S., Nishikawa, M., and Takakura, Y. (1998) Targeted delivery of plasmid DNA complexed with galactosylated poly(L-lysine). *J. Controlled Release* 53, 301–310.
- (6) Kawakami, S., Yamashita, F., Nishikawa, M., Takakura, Y., and Hashida, M. (1998) Asialoglycoprotein receptor-mediated gene transfer using novel galactosylated cationic liposomes. *Biochem. Biophys. Res. Commun.* 252, 78–83.
- (7) Erbacher, P., Bettinger, T., Belguise-Valladier, P., Zou, S., Coll, J. L., Behr, J. P., and Remy, J. S. (1999) Transfection and physical properties of various saccharide, poly(ethylene glycol), and antibody-derivatized polyethylenimines (PEI). *J. Gene Med.* 1, 210–222.
- (8) Bettinger, T., Remy, J. S., and Erbacher, P. (1999) Size reduction of galactosylated PEI/DNA complexes improves lectin-mediated gene transfer into hepatocytes. *Bioconjugate Chem.* 10, 558–561.
- (9) Kawakami, S., Fumoto, S., Nishikawa, M., Yamashita, F., and Hashida, M. (2000) In vivo gene delivery to the liver using novel galactosylated cationic liposomes. *Pharm. Res.* 17, 306–313.
- (10) Ren, T., and Liu, D. (1999) Synthesis of targetable cationic amphiphiles. *Tetrahedron Lett.* 40, 7621–7625.
- (11) Ren, T., Zhang, G., and Liu, D. (2001) Synthesis of galactosyl compounds for targeted gene delivery. *Bioorg. Med. Chem.* 9, 2969–2978.
- (12) Banerjee, R., Mahidhar, Y. V., and Chaudhuri, A. (2001) Design, synthesis and transfection biology of novel cationic glycolipids for use in liposomal gene delivery. *J. Med. Chem.* 44, 4176–4185.
- (13) Jacopin, C., Hofland, H., Scherman, D., and Herscovici, J. (2001) Synthesis and transfecting properties of a glycosylated polycationic DNA vector. *Bioorg. Med. Chem. Lett.* 11, 419–422.
- (14) Lim, D. W., Yeom, Y. I., and Park, T. G. (2000) Poly-(DMAEMA-NVP)-b-PEG-galactose as gene delivery vector for hepatocytes. *Bioconjugate Chem.* 11, 688–95.
- (15) Jacopin, C., Egron, M.-J., Scherman, D., and Herscovici, J. (2002) Glycosidation of alkylamino-alkan-1-ol. A simple and convenient synthesis of glycosylated cationic lipids. *Bioorg. Med. Chem. Lett.* 12, 1447–1450.

- (16) Fuhrhop, J. H., and Tank, H. (1987) Bolaamphiphiles with mannose- and tetraalkylammonium headgroups as coatings for nucleic acids and possible reagents for transfections. *Chem. Phys. Lipids* 43, 193–213.
- (17) Mislick, K. A., and Baldeschwieler, J. D. (1996) Evidence for the role of proteoglycans in cation-mediated gene transfer. *Proc. Natl. Acad. Sci. U.S.A.* 93, 12349–12354.
- (18) Mounkes, L. C., Zhong, W., Cipres-Palacin, G., Heath, T. D., and Debs, R. J. (1998) Proteoglycans mediate cationic liposome-DNA complex-based gene delivery in vitro and in vivo. *J. Biol. Chem.* 273, 26164–26170.
- (19) Schughart, K., Bischoff, R., Hadji, D. A., Boussif, O., Perraud, F., Accart, N., Rasmussen, U. B., Pavirani, A., Van Rooijen, N., and Kolbe, H. V. (1999) Effect of liposome-encapsulated clodronate pretreatment on synthetic vector-mediated gene expression in mice. *Gene Ther.* 6, 448–453.
- (20) Gaucheron, J., Santaella, C., and Vierling, P. (2001) Highly fluorinated lipospermines for gene transfer: synthesis and evaluation of their in vitro transfection efficiency. *Bioconjugate Chem.* 12, 114–128.
- (21) Nazih, A., Cordier, Y., Bischoff, R., Kolbe, H. V., and Heissler, D. (1999) Synthesis and stability study of the new pentammonio lipid pcTG90, a gene transfer agent. *Tetrahedron Lett.* 40, 8089–8091.
- (22) Rico-Lattes, I., Garrigues, J. C., Perez, E., André-Barrès, C., Madelaine-Dupuich, C., Lattes, A., Linas, M. D., and Aubertin, A. M. (1995) A short route to analogues of galactosphingolipids possessing anti-HIV and anti-aspergillus activity. *New J. Chem.* 19, 341–344.
- (23) Remy, J. S., Sirlin, C., Vierling, P., and Behr, J. P. (1994) Gene transfer with a series of lipophilic DNA-binding molecules. *Bioconjugate Chem.* 5, 647–654.
- (24) Byk, G., Dubertret, C., Escriou, V., Frederic, M., Jaslin, G., Rangara, R., Pitard, B., Crouzet, J., Wils, P., Schwartz, B., and Scherman, D. (1998) Synthesis, activity, and structure–activity relationship studies of novel cationic lipids for DNA transfer. *J. Med. Chem.* 41, 224–235.
- (25) Pitard, B., Aguerre, O., Airiau, M., Lachagès, A.-M., Boukhnikachvili, T., Byk, G., Dubertret, C., Herviou, C., Scherman, D., Mayaux, J.-F., and Crouzet, J. (1997) Virus-sized self-assembling lamellar complexes between plasmid DNA and cationic micelles promote gene transfer. *Proc Natl. Acad. Sci. U.S.A.* 94, 14412–14417.

BC025645Y



# Quantitative Analysis of Permeation Peptide Complexes Labeled with Technetium-99m: Chiral and Sequence-Specific Effects on Net Cell Uptake

Seth T. Gammon, Victor M. Villalobos, Julie L. Prior, Vijay Sharma, and David Piwnica-Worms\*

Molecular Imaging Center, Mallinckrodt Institute of Radiology, and Department of Molecular Biology and Pharmacology, Washington University Medical School, Saint Louis, Missouri 63110 Received October 22, 2002; Revised Manuscript Received December 21, 2002

This study investigated sequence-specific cell uptake characteristics of Tat basic domain and related permeation peptides with an emphasis on residue chirality, length, and modified side chains. Effects on cell permeation of defined basic domain sequences within a library of 42 different peptides were evaluated using transport of radiolabeled peptides into human Jurkat leukemia cells. All other factors being equal, when the chirality of the peptide sequence was changed from L to D, uptake values increased up to 13-fold. Control experiments showed that the quantitative difference in uptake could not be attributed to increased decomposition of an L- versus a D-peptide by cellular or serum proteases. Furthermore, length, sequence, and type of chelation domain impacted peptide uptake into cells. The highest level of uptake was found with the following peptides: **(23)** D-Tat-Orn [Ac-rkkrr-orn-rrr-AHA-kgc-amide] and **(33)** D-poly-Arg<sub>9</sub> [Ac-rrrrrrrrr-AHA-kgc-amide]. The best of these peptide sequences could be employed as in vivo imaging and drug delivery agents to translocate substrates into cells.

## INTRODUCTION

Cell membranes typically are impermeable to charged molecules and peptides, thereby confounding delivery of these compounds into cytosolic and nuclear compartments (1). However, certain proteins (2, 3) and polypeptide sequences of charged amino acids known as permeation peptide domains have been found to enhance delivery of impermeant molecules into intracellular compartments (4). Permeation peptides are generally highly cationic at physiologic pH, contain between 8 and 12 amino acid residues, are often rich in Arg and Lys residues, and translocate rapidly across the plasma membrane into the cytosol and nucleus of most types of cells (4, 5). Among the best characterized of these permeation peptides are basic domains of transcription factors (e.g., HIV-1 Tat<sub>49–57</sub>), signal transducers, and other structural proteins as well as polycationic peptides (2, 3, 5–11). The utility of these membrane permeable sequences is evident upon conjugation to molecular cargoes, thereby enabling transmembrane transport and localization of impermeant compounds into cytoplasmic and nucleolar compartments of cells (4, 6, 12–14). Transported molecules include full-length proteins (12, 15–17), DNA (5), other small organics (6), and radiopharmaceuticals and imaging contrast agents (13, 14, 18).

The mechanism(s) of permeability remain unknown. It has been postulated that these permeation peptides enter cells via a reverse micelle mechanism (19) wherein internalization occurs as the peptides traverse the plasma membrane within a hydrophilic pocket. Alternatively, a putative transporter protein or channel has been proposed to mediate permeation. This is supported by the

observations that permeation is cell-type specific (20) and still occurs with little reduction in uptake into selected cells at 4 °C (21, 22), despite the tendency at cold temperatures for lipid bilayers to exhibit more rigidity and reduced permeability to standard solutes and drugs (23–25). In addition, inhibitors of cytoskeletal function, including endocytosis, or drugs that inhibit microtubule-mediated processes, such as colchicine and taxol, show no effect on the uptake of Tat permeation peptides (10, 22). Overall, these observations favor an uncharacterized mediated permeation process over a membrane diffusive mechanism.

A few studies have explored structure–activity relationships of Tat basic domain and related permeation peptides. Peptide constructs in general are positively charged at physiologic pH and the higher the  $pK_a$  values of the side groups, the more permeant the peptide (5). However, while most prior studies use fluorescence intensity of peptides conjugated to fluorophores for determination of cell accumulation and analysis of differences between cell types or conditions, fluorescence intensity is modulated by many factors other than cell content (26). In contrast, use of radionuclides enables unequivocal quantitative analysis of peptide content associated with target cells. Herein, we further explore sequence-specific cell uptake relationships for Tat basic domain and related peptides with a focus on residue chirality, length, and modified side chains in regard to transport of radiolabeled peptides into cells.

## EXPERIMENTAL PROCEDURES

**Peptide Synthesis.** Peptide conjugates were prepared by solid-phase peptide synthesis using L- or D-N- $\alpha$ -Fmoc-protected amino acids as indicated and standard BOP/HOBt coupling chemistry as previously described (13, 14), except for use of N- $\epsilon$ -Fmoc-protected Lys (\*K) in the chelation sequence to direct orthogonal peptide coupling and free the  $\alpha$ -amino for coordination with the incoming

\* Corresponding author. Address: Molecular Imaging Center, Mallinckrodt Institute of Radiology, Washington University Medical School, 510 S. Kingshighway Blvd., Box 8225, St. Louis, MO 63110. Tel: 314-362-9356. Fax: 314-362-0152. E-mail: piwnica-wormsd@mir.wustl.edu.

metal. Peptides were purified (>94%) by preparative C<sub>18</sub> reverse-phase HPLC, and single HPLC peaks were observed for each peptide conjugate. The identity of all peptides was confirmed by amino acid analysis and electrospray mass spectrometry.

**Preparation of Radiolabeled [<sup>99m</sup>Tc<sup>v</sup>O]Peptides.** Peptide conjugates containing a C-terminus Lys-Gly-Cys sequence were labeled with <sup>99m</sup>Tc by ligand exchange using [<sup>99m</sup>Tc]glucoheptonate and analyzed through radio-TLC and RP-HPLC as described previously (13, 14, 20). Specific activities were estimated to be  $\sim 2 \times 10^8$  mCi/mol.

**Preparation of [<sup>99m</sup>Tc(CO)<sub>3</sub>]Peptides.** N-terminus His tagged peptide conjugates were labeled with [<sup>99m</sup>Tc(CO)<sub>3</sub>] for the series 39, 40, 41, and 42 using a commercially available tricarbonyl radiopharmaceutical kit (K<sub>2</sub>BH<sub>3</sub>CO<sub>2</sub>, 4 mg; K<sub>2</sub>B<sub>4</sub>O<sub>7</sub>·H<sub>2</sub>O, 10 mg; NaK tartrate, 10 mg; pH 10; Mallinckrodt, Inc., St. Louis, MO) (14, 27). Kits were reconstituted with 1.0 mL of [<sup>99m</sup>Tc]Na(TcO<sub>4</sub>) (20–40 mCi) in isotonic saline obtained by eluting a commercial <sup>99</sup>Mo/<sup>99m</sup>Tc generator, and allowed to react in a 100 °C oil bath for 10–15 min. Following neutralization with 80 μL of 1N HCl, 90 μL of the [<sup>99m</sup>Tc(CO)<sub>3</sub>·(H<sub>2</sub>O)<sub>3</sub>]<sup>+</sup> solution was added to 10 μL of a stock peptide solution and allowed to react for 20 min at 85–90 °C. Radiochemical yields (>95%) of [<sup>99m</sup>Tc(CO)<sub>3</sub>]Tat-peptide complexes were determined by TLC using silica gel developed with either 68% MeOH/30% saline/2% TFA or H<sub>2</sub>O and scanning radiometric detection. Radiochemical purity (>90%) was determined by radiometric RP-HPLC using the solvent gradient system described above.

**Cell Culture.** Human Jurkat leukemia cells were maintained in RPMI supplemented with L-glutamine, penicillin/streptomycin, and 10% fetal calf serum at 37 °C in an atmosphere of 5% CO<sub>2</sub> (28).

**Cellular Uptake of [<sup>99m</sup>Tc]Peptide Conjugates.** Control solution for tracer uptake experiments was a modified Earle's balanced salt solution (MEBSS) containing (mM): 145 Na<sup>+</sup>, 5.4 K<sup>+</sup>, 1.2 Ca<sup>2+</sup>, 0.8 Mg<sup>2+</sup>, 152 Cl<sup>-</sup>, 0.8 H<sub>2</sub>PO<sub>4</sub><sup>-</sup>, 0.8 SO<sub>4</sub><sup>2-</sup>, 5.6 dextrose, 4.0 HEPES, and 1% bovine calf serum (vol/vol), pH 7.4 ± 0.05.

Cell uptake experiments with [<sup>99m</sup>Tc]peptide complexes were performed in Jurkat leukemia cells suspended in MEBSS with minor modifications of methods described in the literature (13, 29). These uptake experiments were performed in siliconized microfuge tubes and initiated by addition of 740 μL cells ( $5 \times 10^6$  cells/mL) in MEBSS to 10 μL of saline containing [<sup>99m</sup>Tc]peptide complex. Unless stated otherwise, [<sup>99m</sup>Tc]peptide complex was accompanied by molar excess unlabeled peptide as obtained directly from the labeling procedure; final total peptide concentration was typically 0.5–1 μM (10 μCi/mL). Tubes were incubated for 20 min in a 37 °C water bath with occasional mixing. The reaction was terminated by spinning 250 μL aliquots from the reaction for 10 s through 800 μL of a 75:25 mixture of silicon oil (density = 1.050; Aldrich) and mineral oil (density = 0.875; Acros). One aliquot of the aqueous phase was obtained to normalize extracellular concentration of the [Tc]peptide to cell-associated activity; then the oil and aqueous phases were aspirated and the cell pellet extracted in 0.5 mL of 1% SDS in sodium borate (10 mM). All cell extracts were assayed for protein by BCA analysis (Pierce Chemical Co.) using bovine serum albumin as the protein standard. Cell extracts, stock solutions, and extracellular buffer samples were assayed for gamma activity in a well-type sodium iodide gamma counter (Cobra II, Beckman; 130–165 keV window). Absolute concentration of total [Tc]Tat-peptide complex in solu-

tion was determined from the specific activity of <sup>99m</sup>Tc, based on equations of Mo/Tc generator equilibrium (30). Transport data are reported as (fmol of peptide)<sub>i</sub> (mg protein)<sub>i</sub><sup>-1</sup> (nM<sub>o</sub>)<sup>-1</sup>, wherein peptide<sub>i</sub> represents total peptide within the cells and (μM<sub>o</sub>)<sup>-1</sup> represents the concentration of total peptide in the extracellular buffer (31). Data are generally reported as mean ± SEM.

**Decomposition of [<sup>99m</sup>Tc]Peptide Conjugates.** One 10 μL aliquot of a stock solution of 32 or 33 (10 mg/mL) was mixed with water and [<sup>99m</sup>Tc]glucoheptonate (1–8 mCi) to a final peptide concentration of 1 mg/mL. This reaction mixture was incubated for 30 min in a water bath at 37 °C. Upon completion, radio-TLC on silica plates was developed in H<sub>2</sub>O or 68% MeOH/30% saline/2% TFA and analyzed by scanning radiometric detection (14). Radiometric RP-HPLC also was used to characterize each reaction using a 30 min linear gradient of 7% acetonitrile/0.1% TFA to 30% acetonitrile/0.1% TFA at a flow rate of 1 mL/min.

One 10.5 μL aliquot of [<sup>99m</sup>Tc]peptide was added to 740 μL of Jurkat cells ( $5 \times 10^6$  cells/mL) in MEBSS to yield a final peptide concentration of 7.1 μM. The cell suspension was incubated at 37 °C for 20 min, and then cells were pelleted by centrifugation in a tabletop centrifuge (4000 rpm for 4 min). One 400 μL aliquot of the supernatant was collected and combined with 100 μL of 25% acetonitrile for radio-RP-HPLC analysis. Furthermore, one 3 μL aliquot of the supernatant was spotted for radio-TLC analysis. Throughout analysis, samples were stored on ice to retard degradation of radiolabeled species. Both radio-TLC and radio RP-HPLC were performed on each sample as above.

TLC and RP-HPLC data processing programs were used to select regions of interest on the chromatograms and calculate percent of total counts in each region of interest (% ROI). This analysis was performed on radiolabeled peptides both before (% ROI<sub>in</sub>) and after (% ROI<sub>fin</sub>) incubation with the cells. The ratio of % ROI<sub>fin</sub>/ % ROI<sub>in</sub> × 100 yielded the percent intact peptide. This calculation corrected for scalar processes such as column retention, changes in specific activity between experiments, and decay of <sup>99m</sup>Tc between radio RP-HPLC runs. Errors introduced into the ROI analysis by radioactive decay of <sup>99m</sup>Tc over the time course of the RP-HPLC gradient were calculated to be <9%.

**Statistical Analysis.** Values are presented as mean ± SEM. When comparing pairs of peptides the Students *t*-test was applied. When groups of peptides were studied, an ANOVA procedure was first applied to determine whether there was significant variation, then the Bonferroni test was applied for comparison of two peptides within a group (32). For determining the direction of a trend, a linear model was applied to the data and the slope tested for a significant difference from zero (SigmaPlot 5.0).

## RESULTS

The purpose of this study was to quantitatively evaluate sequence-specific effects of permeation peptides on uptake into human cells. To accomplish this goal, 42 peptides were synthesized (Table 1), characterized through mass spectrometry, radiolabeled with <sup>99m</sup>Tc, and cell tracer studies performed with human Jurkat leukemia cells.

**Peptide Class.** Cell uptakes of representative permeation peptides from four classes were examined. As presented in Figure 1, there were significant differences between these peptides. The poly-Arg peptide (33) showed

**Table 1. Table of All Peptide Sequences with Molecular Weight (MW), Permeation Sequence Chirality, Chelation Moiety Chirality, and 20 min Jurkat Cell Uptake Values of the <sup>99m</sup>Tc Labeled Peptide (Mean ± SEM; fmol Peptide; (mg protein)<sup>-1</sup> (nM<sub>0</sub>)<sup>-1</sup>)<sup>a</sup>**

peptide #	MW	sequence	chirality		Jurkat cell uptake
			permeation sequence	chelation moiety	
1	1839.0	Ac-GRKKRRQRRR-AHA-K*GC-amide	L	L	92.90 ± 21.17
2	1839.3	Ac-GRKKRRQRRR-AHA-k*gc-amide	L	D	50.39 ± 25.73
3	1839.3	Ac-grkrrqrrr-AHA-k*gc-amide	D	D	256.97 ± 86.20
4	1782.2	Ac-RKKRRQRRR-AHA-K*GC-amide	L	L	90.75 ± 41.04
5	1782.2	Ac-RKKRRQRRR-AHA-k*gc-amide	L	D	48.81 ± 2.91
6	1782.2	Ac-rkrrrqrrr-AHA-K*GC-amide	D	L	300.10 ± 38.04
7	1782.2	Ac-rkrrrqrrr-AHA-k*gc-amide	D	D	340.35 ± 164.68
8	1740.2	RKKRRQRRR-AHA-k*gc-amide	L	D	64.35 ± 1.63
9	1740.2	rkrrrqrrr-AHA-k*gc-amide	D	D	236.81 ± 13.37
10	1797.2	GRKKRRQRRR-AHA-k*gc-amide	L	D	106.96 ± 1.55
11	1797.2	grkrrrqrrr-AHA-k*gc-amide	D	D	314.02 ± 61.48
12	1965.5	biotin-RKKRRQRRR-AHA-K*GC-amide	L	L	51.07 ± 11.78
13	1965.5	biotin-rkrrrqrrr-AHA-K*GC-amide	D	L	426.26 ± 96.33
14	1809.3	biotin-krrrqrrr-AHA-K*GC-amide	D	L	221.38 ± 27.51
15	1681.1	biotin-krrrqrrr-AHA-K*GC-amide	D	L	129.57 ± 24.99
16	1552.9	biotin-kkqrrr-AHA-K*GC-amide	D	L	76.57 ± 3.30
17	1396.7	biotin-rqrrr-AHA-K*GC-amide	D	L	51.37 ± 15.08
18	1297.6	biotin-rraarr-k*gc-amide	D	D	71.48 ± 10.32
19	1368.7	biotin-arraarr-k*gc-amide	D	D	51.19 ± 20.69
20	1439.8	biotin-aarraarr-k*gc-amide	D	D	49.98 ± 13.36
21	1595.9	biotin-raarraarr-k*gc-amide	D	D	66.48 ± 10.85
22	1768.2	Ac-rkkrr-n-rrr-AHA-k*gc-amide	D	D	528.64 ± 157.11
23	1768.2	Ac-rkkrr-orn-rrr-AHA-k*gc-amide	D	D	942.24 ± 102.99
24	1783.2	Ac-rkkrr-e-rrr-AHA-k*gc-amide	D	D	252.80 ± 62.26
25	1767.2	Ac-rkkrr-norleu-rrr-AHA-k*gc-amide	D	D	609.21 ± 39.36
26	1397.7	Ac-RRRRRRR-AHA-k*gc-amide	L	D	28.03 ± 18.97
27	1397.7	Ac-rrrrrrr-AHA-k*gc-amide	D	D	130.32 ± 29.01
28	1553.9	Ac-RRRRRRRR-AHA-k*gc-amide	L	D	34.73 ± 6.99
29	1553.9	Ac-rrrrrrrr-AHA-k*gc-amide	D	D	307.95 ± 34.80
30	1710.1	Ac-RRRRRRRRR-AHA-k*gc-amide	L	D	59.02 ± 5.52
31	1710.1	Ac-rrrrrrrrr-AHA-k*gc-amide	D	D	781.60 ± 266.98
32	1866.3	Ac-RRRRRRRRRR-AHA-k*gc-amide	L	D	129.11 ± 69.01
33	1866.3	Ac-rrrrrrrrrr-AHA-k*gc-amide	D	D	861.68 ± 349.61
34	1668.0	Ac-rrrr-n-rrr-AHA-k*gc-amide	D	D	297.72 ± 119.04
35	1668.0	Ac-rrrr-orn-rrr-AHA-k*gc-amide	D	D	532.24 ± 43.18
36	1683.0	Ac-rrrr-e-rrr-AHA-k*gc-amide	D	D	215.38 ± 16.00
37	1667.1	Ac-rrrr-norleu-rrr-AHA-k*gc-amide	D	D	324.24 ± 31.95
38	1731.1	Ac-plssifsrigdp-AHA-k*gc-amide	D	D	21.26 ± 0.72
39	1532.8	hg-rkrrrqrrr-amide	D	D	888.71 ± 54.81
40	1636.0	hg-rkrrrqrrr-amide	D	D	472.19 ± 59.06
41	1693.0	hg-rkrrrqrrr-gc-amide	D	D	542.76 ± 4.07
42	1882.3	hg-rkrrrqrrr-gk(Dde)-amide	D	D	607.21 ± 12.77

<sup>a</sup> Abbreviations: \*, K,ε-amino peptide coupling; AHA, amino hexanoic acid; Ac, N-terminus acetyl modified; biotin, N-terminus biotinylated; amide, C-terminus amido modified; Orn, ornithine; Norleu, norleucine; Dde, 1-(4,4-dimethyl-2,6-dioxocyclohexylidene)ethyl. Upper case denotes L-amino acids, while lower case denotes D-amino acids.

the highest overall uptake, followed by the Tat-basic domain peptide (**11**), an amphipathic polycationic peptide (**21**), and finally the viral permeation peptide (**38**), respectively. The viral permeation peptide was not further studied due to the relatively low uptake compared to other peptides.

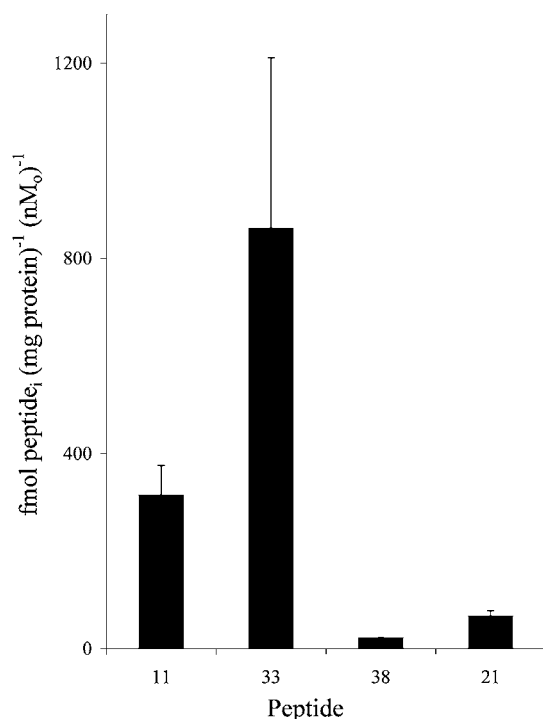
**Residue Number.** The effect of peptide length on cell uptake was determined for several classes of permeation peptide (Figure 2). For example, to generate the sequence consisting of **13**–**17**, one amino acid was removed from the N-terminus of the longest Tat basic domain sequence (**rkrrrqrrr**), while all other aspects of the peptide remained the same. From these data, a correlation between decreasing length and decreasing uptake of Tat basic domain peptide was observed (Figure 2). Similarly, there was an overall decrease in net cell uptake of the L-poly-Arg peptide as the length shortened from poly-Arg<sub>9</sub> to poly-Arg<sub>7</sub> and of D-poly-Arg peptide as length shortened from poly-Arg<sub>8</sub> to poly-Arg<sub>6</sub>. However, for the series **18**–**21** (**raarraarr**), a putative amphipathic sequence with α-helical properties (**33**), there was a relatively modest uptake and no change with decreasing length (Figure 2).

**Chirality.** Several series of peptides were tested to determine the independent contributions of chirality of the permeation sequences and chelate moiety on net cell uptake. In the first series, the permeation sequence of the peptide was either D- or L-amino acids, while all other aspects of the peptide, chelation moiety and N-terminus were identical. For example, the full sequence in **8** was **RKKRRQRRR-AHA-k\*gc-amide**, but in **9**, it was **rkrrrqrrr-AHA-k\*gc-amide**. Note that while both contained a D-chelation moiety, the permeation sequence was L or D, respectively.

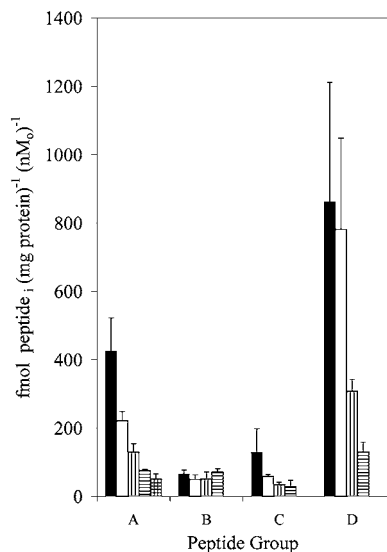
As shown in Figure 3, uptake of the D-permeation sequences into Jurkat cells was consistently greater than L-permeation sequences for all pairs. The uptake ratios ranged from a 2.9-fold (**10** vs **11**) to 13.2-fold (**30** vs **31**) greater uptake for D-stereoisomers. Thus, a D-peptide backbone increased cell uptake for any Tat basic domain sequence, poly-Arg peptide, or derivative thereof.

The contribution of the chirality of the chelation moiety to uptake was studied as well. For these studies, the stereoconfiguration of the chelation moiety was reversed, while the stereoconfiguration of the permeation sequence





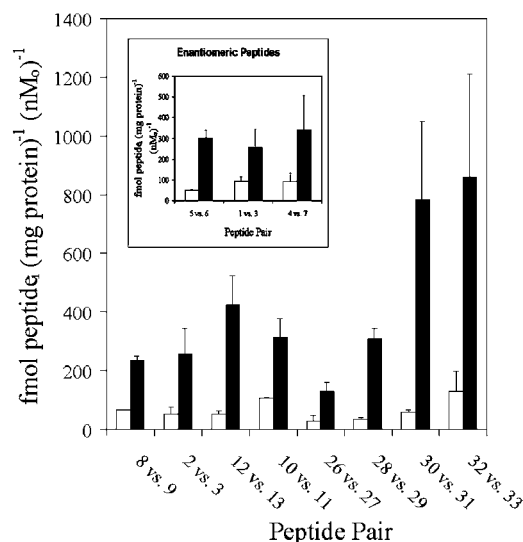
**Figure 1.** Net cell uptake of representative radiolabeled permeation peptides. Human Jurkat leukemia cells were incubated in MEBSS at 37 °C for 20 min with the indicated representative permeation peptides: **11**, Tat basic domain; **33**, poly-Arg<sub>n</sub>; **38**, viral permeation peptide; and **21**, amphipathic polycation (see Table 1). Final concentration of permeation peptide in solution was 0.5–1  $\mu$ M. Cells were then pelleted and counted, and uptake values were normalized to cellular protein and extracellular peptide concentration.



**Figure 2.** Net cell uptake of permeation peptides with varying lengths of the permeation sequence. Radiolabeled peptides were incubated with Jurkat cells as described in Figure 1 and Experimental Procedures. **A** = D-Tat basic domain (**13–17**), **B** = D-amphipathic cationic peptide (**18–21**), **C** = L-poly-Arg peptide (**26, 28, 30, 32**), **D** = D-poly-Arg peptide (**27, 29, 31, 33**); (■) 9 residues in permeation sequence, (□) 8 residues, (square with vertical lines) 7 residues, (square with horizontal lines) 6 residues, (square with checkered lines) 5 residues.

was held constant. Unlike chirality of the backbone, there was no significant difference between D and L-chelates on cell uptake (Table 1: 1 vs 2; 4 vs 5; 6 vs 7;  $p > 0.2$ ).

Because the pairs of peptides compared above were diastereomers, they could have intrinsically different



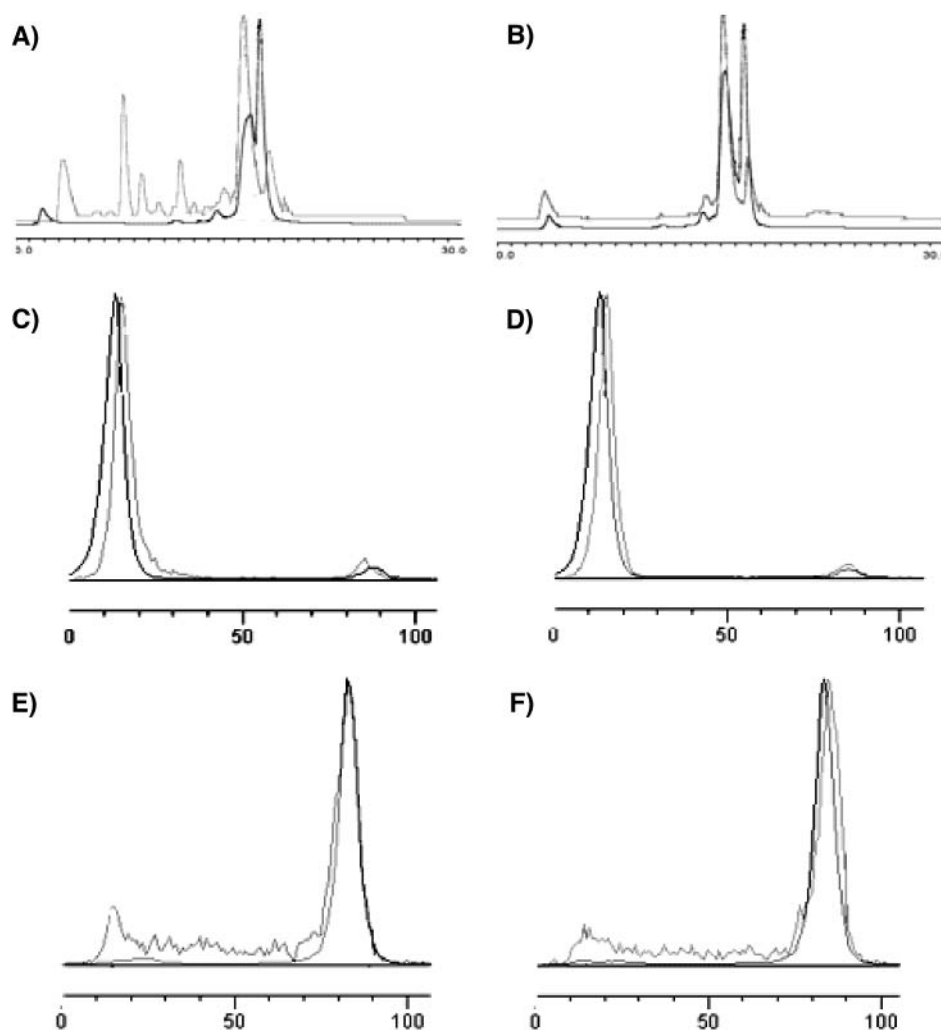
**Figure 3.** Effect of chirality of the permeation sequence on net cell uptake. Each pair represents an identical radiolabeled peptide except for the chirality of the permeation sequence. Inset: Enantiomeric pairs. (□) L-Permeation sequences, (■) D-permeation sequences.

physical properties. To determine whether a chiral entity mediates cell uptake of Tat basic domain, enantiomeric pairs of permeation peptides were studied. As illustrated in the inset of Figure 3, enantiomeric pairs were significantly different from each other with the D-permeation sequence always showing the highest uptake. This strongly suggested that peptide uptake was mediated by a chiral process and confirmed the permeation sequence as the source of the stereospecificity.

**Decomposition.** One alternative explanation for the markedly greater cellular accumulation of D-permeation sequences was degradation of L-permeation sequences by serum or cellular proteases. To test this hypothesis, peptides **32** and **33** were incubated with Jurkat cells, and the supernatant was analyzed by radio-TLC and radio-metric RP-HPLC to determine any differences in the degradation patterns of the peptides. By radio-TLC analysis, no significant differences were identified between **32** and **33**. By contrast, radio HPLC showed a significant difference in the pattern of peptide degradation products between **32** and **33** (Figure 4). On average, while D-peptide **33** showed minimal degradation over the course of the experiment ( $76 \pm 4.8\%$  intact), L-peptide **32** ( $48 \pm 6\%$  intact) showed 1.6-fold greater degradation over **33**. However, importantly, the fold-increase in degradation of the L-peptide was significantly less than the fold-decrease in cell uptake observed relative to the D-peptide (Figure 3).

**Substitution at Position –4 from the C-Terminus.** Residue 55 (Gln) of the Tat basic domain has been hypothesized to confer binding to TAR RNA (34). Several different amino acids were substituted in the corresponding residue in the D-Tat basic domain (**rkkrxr**) to determine the contribution of Gln to net cellular uptake. As shown in Figure 5A, significant differences in net cell uptakes were observed with single amino acid substitutions at this position. The substitutions lead to enhanced cell uptake in the following order: Glu < Gln < Asn < NorLeu < Orn. When a similar series of substitutions was performed on the D-poly-Arg<sub>8</sub> peptide at the analogous position, all substitutions decreased cellular uptake (Figure 5B).

**N-Terminus and C-Terminus Modifications and Chelation Strategies.** Avidin/biotin binding has been



**Figure 4.** Analysis of the supernatant of cells incubated with radiolabeled peptide **32** or **33**. Human Jurkat leukemia cells were incubated with peptides at 37 °C for 20 min, and then cells were pelleted and the supernatant collected for radio-TLC and radio-RP-HPLC analysis. (A, B) Radio-RP-HPLC chromatographs; (C, D) radio-TLC chromatographs developed in water; (E, F) radio-TLC chromatographs developed in methanol:saline:TFA (68:30:2); (A, C, E) analysis of L-peptide **32**; (B, D, F) analysis of D-peptide **33**. For all panels, the control peptide (dark line) and peptide collected from cell supernatant (gray line) were analyzed by identical methods. The vertical axes represent signal intensity corresponding to radioactivity detected in each sample and the horizontal axes represent retention time (min) for RP-HPLC or distance (mm) for radio-TLC. The vertical scale has been adjusted for ease of comparison between each run. Scale differences were irrelevant, as the ratio of the area under the curve was used for analysis.

used for conjugating cargoes to peptides (35). Thus, we thought it relevant to determine whether the biotin moiety itself impacted cell uptake of permeation peptides. Two sets of peptides were examined, each pair having an acetylated peptide and either an N-terminus biotinylated or unmodified peptide. Overall, there was no significant difference between acetylated and biotinylated peptides (Figure 6 inset). However, while two pairs of acetylated peptides were similar to their unmodified partners, in two other pairs of peptides (**5** vs **8** and **2** vs **10**), acetylation resulted in a statistically significant decrease of 1.3-fold and 2.1-fold in cell uptake, respectively, when compared to an unmodified N terminus (Figure 6). Nonetheless, N-terminus modifications overall impacted net cell uptake to a far lesser degree than changes in the permeation sequence.

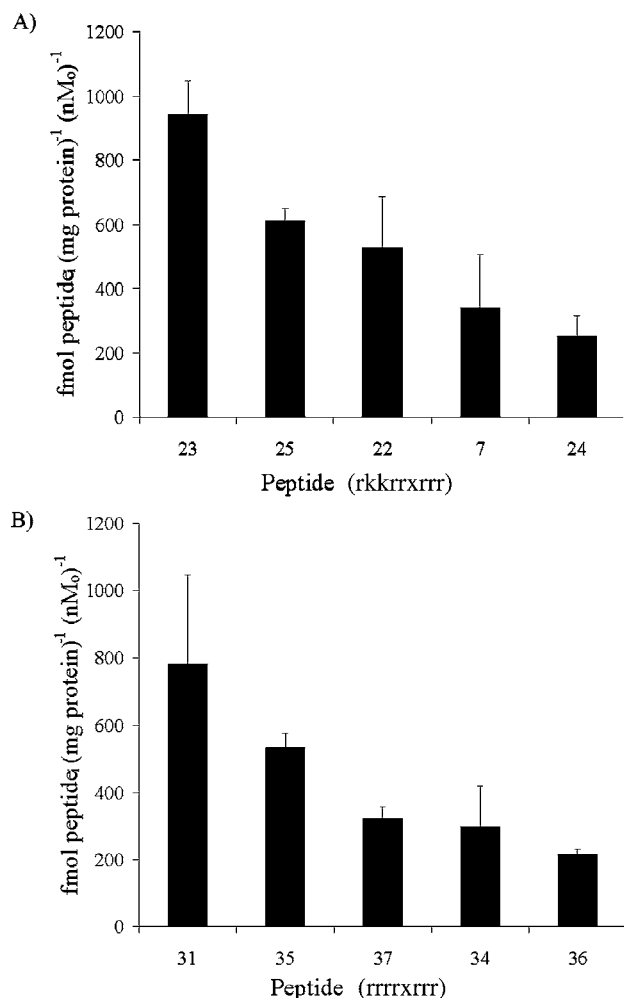
In addition, the impact of an alternative method of chelating  $^{99m}\text{Tc}$  by use of a  $^{99m}\text{Tc}$ -carbonyl species ( $^{99m}\text{Tc}(\text{CO})_3$ ) (14, 36) and a His-Gly chelation moiety on the N-terminus of Tat basic domain (peptide **39**) was examined. Furthermore, to determine the impact of an additional Cys on chelation and cell uptake, peptides **40** and **41** were synthesized and examined. Finally, peptide **42** was evaluated to determine whether bulky functional-

ity could be tolerated on the  $\epsilon$ -amine of a C-terminus Lys. For this analysis, peptide **7** was designed to act as a reference for comparing the  $^{99m}\text{Tc}$ -carbonyl labeled peptides to the Lys-Gly-Cys series of peptides. As a group, the  $^{99m}\text{Tc}(\text{CO})_3$  chelation method was significantly different by ANOVA analysis (Figure 7). As shown, the  $^{99m}\text{Tc}$ -carbonyl chelation strategy for labeling Tat basic domain modestly enhanced cell permeation or binding of these peptides.

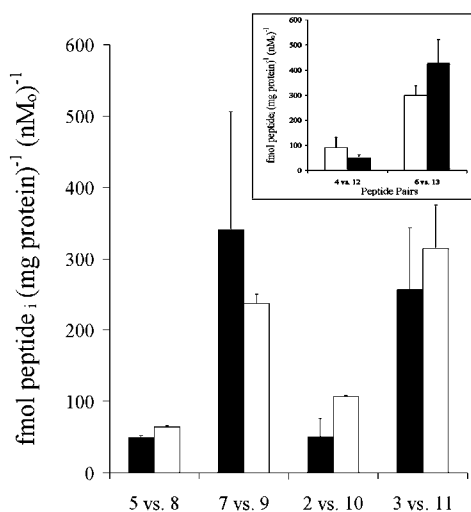
## DISCUSSION

This study was undertaken to determine quantitative sequence–cell uptake relationships for various permeation peptide sequences. Optimization of the permeation sequence for uptake would aid applications directed at the use of permeation peptides for delivery of imaging or therapeutic compounds. This investigation sought to identify optimal sequences from several classes of permeation peptides. In addition, characteristics necessary and important for permeation peptides to enter cells efficiently were examined.

Previous SAR studies have demonstrated several factors that affect peptide permeation of HIV-1 Tat basic

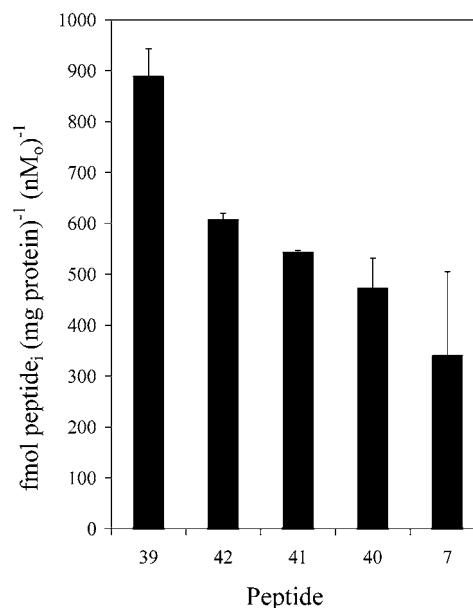


**Figure 5.** Substitution at position -4 from C-terminus. (A) Effect on Jurkat cell uptake of substituting different amino acids for Gln in Tat basic domain (rkkrrxrrr); X = Glu, **24**; Gln, **7**; Asn, **22**; Norleu, **25**; and Orn, **23**. (B) Effect on Jurkat cell uptake of a single substitution in poly-Arg<sub>8</sub> peptide (rrrrxrrr); X = Arg, **31**; Orn, **35**; Norleu, **37**; Asn, **34**; Glu, **36**.



**Figure 6.** Effects of N-terminal modification. Effect on Jurkat cell uptake of acetylation of permeation peptides. For each pair of peptides, the N-terminus of one peptide was acetylated (■) and the other remained unmodified (□). Inset: For each pair of peptides, the N-terminus of one peptide was acetylated (□), and the other was biotinylated (■).

domain and poly-cation sequences. For example, by FACS analysis of fluorescein-conjugated polypeptides, poly-Arg



**Figure 7.** Effect on Jurkat cell uptake of His-Gly chelation of <sup>99m</sup>Tc carbonyl. The indicated all D-His-Gly-tagged Tat basic domain peptides were compared to **7**, a Lys-Gly-Cys reference peptide.

(pK<sub>a</sub> = 12.5) constructs showed the highest uptake, followed by poly-Lys (pK<sub>a</sub> = 10.5) and poly-Orn (pK<sub>a</sub> ≈ 10.5), while poly-His (pK<sub>a</sub> = 6.1) showed the lowest relative permeation (37). However, toxicity of HIV-1 Tat peptide determined by MTT assay was far less than toxicity of the other simple, polycationic peptides (5, 6). In the toxicity experiments, use of retro-inverso Tat and Antennapedia peptides did not alter uptake into cells (5). Also, disruption of amphipathicity has not been shown to abrogate uptake. For example, when modified with proline or amino acids that prevent formation of amphipathic structures, uptake was not greatly affected as long as there were sufficient basic residues (21). To compound this fact, circular dichroism spectra in methanol of HIV-1 Tat<sub>48–60</sub>, FHV coat protein<sub>35–49</sub>, and Arg<sub>9</sub>-Tat peptides showed no significant secondary structure, whereas the only peptide that showed secondary α-helical structure was the HIV-1 Rev peptide (5). It has also been shown that uptake of certain peptides with seven Arg in the sequence have uptake comparable to Tat, but other peptides with five Arg or fewer showed much lower uptake into cells (5). Uptake of full-length Tat protein involves interaction with cell surface heparan sulfate proteoglycans (38). However, accumulation of Tat<sub>46–60</sub> basic domain is not affected by the presence or absence of heparan sulfate in the media (39), suggesting a different mechanism of cell uptake (20). Historically, Tat basic domain peptides were thought to enter all cells in mammals (40); however, certain types of cells were later shown impermeable to Tat basic domain peptide, including renal epithelial MDCK and intestinal epithelial CaCo-2 cells (20).

To further characterize and quantitatively analyze properties of permeation peptides, we radiolabeled the peptides and assayed for net cell uptake into human Jurkat leukemia cells, a well validated cell line for these experiments, thereby allowing comparison to the existing literature (11, 13, 33). By γ-counting the activity associated with cells, calculating the specific activity of each labeled peptide, and assaying cell protein in each sample, one can quantify precisely the permeation peptide content



associated with the cells. One caveat for use of radio-labeled peptides was that one could not discern peptide residing within the cell interior (cytosol and nucleus) versus peptide adsorbing on the membrane. However, peptides from all these classes, when labeled with fluorophores, have been shown to penetrate into the interior of cells by fluorescence microscopy (6, 11, 13, 14, 20, 33). Nonetheless, the ability to quantify net uptake of these peptides offered clear advantages when ranking peptides between different experiments and evaluating potential mechanisms of peptide uptake.

Several different classes of permeation peptide have been reported in the literature, and we chose to investigate four representative classes: Tat basic domain (11), poly-Arg (33), amphipathic polycationic (21), viral permeation sequences (38), and variants thereof (6, 10, 11, 33). By comparing the peptides as a class in Figure 1, the following trends were apparent: poly-Arg peptides had the highest cell uptake value, followed by Tat basic domain sequences, and then amphipathic polycationic peptides. In contrast, the viral permeation sequence showed cell uptake values only slightly above background. By FACS analysis, the poly-Arg peptides had already been shown to have a significantly enhanced cell uptake over Tat basic domain (33). However, an amphipathic polycationic sequence (YARAARRAARR) similar to 21 was reported to be superior by FACS analysis to Tat basic domain by 8-fold (33). In the present study, using the D-peptide backbone, this increase was not observed, and in fact, cell uptake was lower for the amphipathic peptide.

As a drug delivery vehicle, the minimal functional size of the permeation peptide could improve pharmacokinetics and reduce production costs. It was therefore deemed important to study the effects of length on cell uptake of permeation peptides. As noted by Wender et al. (11), there was a clear uptake dependence of the poly-Arg peptide on the number of residues and the present study also identified a similar relationship for the Tat basic domain. By both inspection and statistical analysis, Tat basic domain (series 12–17) had a clear length dependence, and net cell uptake declined as peptides were shortened. This trend also was observed in the D- or L-poly-Arg peptides. However, when amphipathic polycationic peptides (series 18–21) were studied, no length dependence was identified for these peptides. This suggested a different mechanism of translocation for the Tat basic domain and poly-Arg peptides when compared to amphipathic polycationic peptides.

The proposed conformations of these peptides may relate to differences in peptide uptake. Tat basic domain (Tat<sub>47–57</sub>) has been modeled as being  $\alpha$ -helical, and published NMR data suggested that Tat basic domain (Tat<sub>48–57</sub>) is helical when fused to the E1AV domain, a known helical polypeptide (33, 41). However, when free in solution, Tat<sub>32–72</sub> was shown to lack any secondary structure by CD measurements, until bound to TAR RNA (42). Thus, it may not be necessary to possess  $\alpha$ -helical conformation in solution to be efficiently transduced across membranes, since peptides which were designed to be  $\alpha$ -helical, such as 18–21, in fact showed a quantitatively lower uptake than did the poly-Arg and Tat basic domain sequences, which may exist in a coil conformation. While the helical content of Tat peptide remains in question, amphipathicity was certainly not required for transduction as Tat basic domain and poly-Arg peptides were not amphipathic, but showed both higher net uptake values and length-dependent transduction pathways.

Further sequence permutations were explored for the poly-Arg peptide and Tat basic domain sequences. Our permeation peptides conjugates consisted of two domains: the permeation sequence and the metal chelation moiety. First, the relationship between the chirality of amino acids in the peptide permeation sequence and uptake of the peptides was studied. D-Permeation peptides showed a 2.9–13.2-fold greater uptake in all variants of the poly-Arg and Tat basic domains compared with L-peptides. Because the chirality of the peptide backbone impacted cell uptake, the chirality of the amino acids in the chelation group was independently evaluated. In contrast to the permeation sequence, peptides with a D-amino acid chelation moiety, Lys-Gly-Cys, showed no significant difference in uptake compared to L-peptides.

The observed increased permeation for D-peptides has literature precedence. Increased uptake of D-amino acids in permeation peptides has been found with other permeation peptides such as transportan (35). Furthermore, increased uptake of D-peptides also has been seen by FACS analysis of FITC labeled Tat basic domains and poly-Arg peptides (11). The enhanced uptake observed in the present study and in the literature could be due to a change in physical chemical properties. Strictly speaking, all of the peptides compared in this phase of the analysis (Figure 3) were diastereomers of each other (e.g., D-permeation/D-chelate vs L-permeation/D-chelate), and perhaps simply possessed different physical properties, including cellular uptake. However, enantiomers cannot have different physical properties, and in fact, all enantiomers with D-amino acids in the permeation sequence backbone showed higher net uptake into cells (Figure 3 inset), independent of the stereoconfiguration of the peptide chelate moiety.

As expected, serum and cellular proteases preferentially degraded L-peptides more than D-peptides, and hypothetically, this preference could account for the apparent increase in uptake of D-peptides. While this hypothesis has been proposed previously, little data have been published to support this position (11, 35). To quantitatively determine the impact of protease activity on stereoselective peptide uptake, radiometabolites present after incubating radiolabeled peptides 32 and 33 with Jurkat cells were examined by both radio-TLC and radiometric RP-HPLC. On the basis of the regular pattern of the RP-HPLC trace in Figure 4 and the fact that 32 is a poly-Arg<sub>9</sub> peptide, one might hypothesize that the more mobile peaks were peptides which have been sequentially shortened by one residue with the fastest of the peaks being the shortest. Radio-TLC developed in H<sub>2</sub>O showed no increase in [<sup>99m</sup>Tc]glucoheptonate or <sup>99m</sup>TcO<sub>4</sub><sup>−</sup>, and the radio-TLC developed in methanol/saline/TFA showed no difference in the formation of <sup>99m</sup>TcO<sub>2</sub> species. However, even by radiometric RP-HPLC, a significant portion of the parent peptide remained after the 20 min incubation period, and the ratio of the percent intact peptide of 33/32 (D/L) was 1.57. Because of the ability of the radiotracer method to quantify peptide uptake, an estimate of the role that metabolism played in uptake could be calculated. The ratio of cell tracer uptake for 33/32 (D/L) was 6.7. Thus, after comparing this to the radio-HPLC data, and assuming a linear relationship between peptide concentration and cell uptake (13), metabolism only accounted for 23% of the enhanced uptake of D-peptides. Furthermore, the degradation experiment was actually biased toward finding a higher percentage degradation than was actually present during the uptake experiment. As shown in Figure 2,

shorter peptides would not permeate as readily, so they would have remained in the supernatant while intact full length species would have entered cells. Thus, the supernatant would be enriched with metabolites. These data support the hypothesis that a chiral mechanism enhanced cell uptake of D-permeation peptides, perhaps mediated by a blocked efflux transporter/channel, an enhanced influx transporter/channel, preferential intracellular binding of D-peptides, or interactions with a chiral structure within the membrane.

To explore additional parameters that contributed to the uptake mechanism of Tat basic domain, several substitutions were made for the Gln at position -4 from the C-terminus. Gln has been shown to enhance binding of Tat basic domain to its natural substrate, TAR RNA (34) and has been reported to increase binding of peptides to RNA in general through hydrogen bonding (43). Also, Asn has been shown to be important in binding HIV Rev to RNA (44). These data, in conjunction with the observation that these Tat peptides localize to the nucleolus (13, 20), a region rich in RNA species, suggested that Gln might participate in binding to RNA and therefore increase the observed cell retention of the peptide. However, as seen in Figure 5, when NorLeu was substituted to ablate the ability of the side chain to H-bond, uptake actually increased. Furthermore, changing the side chain to highly basic Orn revealed cell uptake values no different from poly-Arg<sub>9</sub> (33). In addition, substituting the negatively charged Glu gave the lowest uptake values. Given that changing the amino acid in position -4 of Tat basic domain could increase cell uptake, analogous substitutions were made for poly-Arg peptides. However, all substitutions decreased cell uptake from the already high levels observed for the positively charged poly-Arg sequence. Therefore, this supported the hypothesis that sequence specific effects as well as overall positive charge on the peptide, rather than putative binding of Gln to RNA, assisted translocation and intracellular localization of permeation peptides.

To examine effects of commonly used modifications on cellular uptake, the N terminus of Tat basic domain was either biotinylated or acetylated. Biotin already has been used as a linker in conjugate chemistry with permeation peptides (35). Addition of biotin to the N-terminus of several peptides in the present study did not result in a significant change in net cell uptake. This was in contrast to previous reports indicating that biotinylation may have a small effect on uptake of L-Tat basic domain (13). Nonetheless, Tat basic domain should tolerate linkage to biotin without significantly altering its cellular uptake, opening the door for avidin/streptavidin linkage strategies for Tat peptide-mediated delivery.

Effects of different metal chelates on Jurkat cell uptake were also studied. The previously discussed peptides were based on the ability of the Lys-Gly-Cys sequence to chelate <sup>99m</sup>Tc efficiently (45). Changing the chelation moiety imparted modest, but statistically significant changes in Tat basic domain cellular uptake. Using the His-Gly chelation sequence with <sup>99m</sup>Tc(CO)<sub>3</sub>, 39 showed a significant increase in cell uptake of the peptide. The His-Gly chelation moiety would also allow for radiolabeling of the N-terminus and further conjugation at the C-terminus via an additional Cys (14). Another point of conjugation strategy involved addition of a lysine at the C terminus and orthogonally conjugating cargo to the ε-amine of this lysine. When the 1-(4,4-dimethyl-2,6-dioxocyclohexylidene)ethyl (Dde) group, as a model for hydrophobic cargo, was added to the ε-amine, the peptide (42) showed a significant reduction in uptake. Nonethe-

less, peptide 42 still retained the second highest uptake of the sequences in this group. Of note, both of these strategies enable double or triple labeling of peptides for multimodality imaging or functionality (14).

## CONCLUSION

Several structural and sequence determinants of importance for net cell uptake of permeation peptides have been evaluated. D-Peptides show enhanced cell uptake quantitatively greater than L-peptides, and the difference cannot be attributed to preferential metabolism of L-peptides. Thus, some other mechanism, such as a chiral transporter, channel, receptor, or membrane structure must account for the stereoselectivity demonstrated by the cell uptake assays. Furthermore, eight amino acids would appear to optimize the permeation sequence for both Tat basic domain and poly-Arg peptides. Finally, after considering all of the peptide properties presented in this study, the two showing the greatest cell uptake were the D-peptides 23 and 33. These data may assist the design and optimization of permeation sequences for delivery of drugs and cargo in vivo.

## ACKNOWLEDGMENT

This work was supported by grants from the National Institutes of Health (RO1 CA82841 and P50 CA94056). S.G. is supported in part by a Department of Energy Training Grant (DE F0101 NE23051).

## LITERATURE CITED

- (1) Lebleu, B. (1996) Delivering information-rich drugs – prospects and challenges. *Trends Biotechnol.* 14, 109–110.
- (2) Frankel, A., and Pabo, C. (1988) Cellular uptake of the tat protein from human immunodeficiency virus. *Cell* 55, 1189–1193.
- (3) Green, M., and Loewenstein, P. (1988) Autonomous functional domains of chemically synthesized human immunodeficiency virus tat trans-activator protein. *Cell* 55, 1179–1188.
- (4) Schwarze, S., Hruska, K., and Dowdy, S. (2000) Protein transduction: unrestricted delivery into all cells? *Trends Cell Biol.* 10, 290–295.
- (5) Futaki, S., Suzuki, T., Ohashi, W., Yagami, T., S, T., Ueda, K., and Sugiura, Y. (2001) Arginine-rich Peptides: an abundant source of membrane-permeable peptides having potential as carriers for intracellular protein delivery. *J. Biol. Chem.* 276, 5836–5840.
- (6) Vives, E., Brodin, P., and Lebleu, B. (1997) A truncated HIV-1 Tat protein basic domain rapidly translocates through the plasma membrane and accumulates in the cell nucleus. *J. Biol. Chem.* 272, 16010–16017.
- (7) Derossi, D., Joliet, A., Chassaing, G., and Prochiantz, A. (1994) The third helix of the Antennapedia homeodomain translocates through biological membranes. *J. Biol. Chem.* 269, 10444–10450.
- (8) Lin, Y., Yao, S., Veach, R., Torgenson, T., and Hawiger, J. (1995) Inhibition of nuclear translocation of transcription factor NF-κB by a synthetic peptide containing a cell membrane-permeable motif and nuclear localization sequence. *J. Biol. Chem.* 270, 14255–14258.
- (9) Pooga, M., Hallbrink, M., Zorko, M., and Langel, U. (1998) Cell penetration by transportan. *FASEB J.* 12, 67–77.
- (10) Elliot, G., and O'Hare, P. (1997) Intercellular trafficking and protein delivery by a Herpesvirus structural protein. *Cell* 88, 223–233.
- (11) Wender, P., Mitchell, D., Pattabiraman, K., Pelkey, E., Steinman, L., and Rothbard, J. (2000) The design, synthesis, and evaluation of molecules that enable or enhance cellular uptake: peptoid molecular transporters. *Proc. Natl. Acad. Sci. U.S.A.* 97, 13003–13008.
- (12) Schwarze, S., Ho, A., Vocero-Akbani, A., and Dowdy, S. (1999) In vivo protein transduction: delivery of a biologically active protein into the mouse. *Science* 285, 1569–1572.

- (13) Polyakov, V., Sharma, V., Dahlheimer, J., Pica, C., Luker, G., and Piwnica-Worms, D. (2000) Novel Tat-peptide chelates for direct transduction of technetium-99m and rhenium into human cells for imaging and radiotherapy. *Bioconjugate Chem.* 11, 762–771.
- (14) Bullok, K., Dyszlewski, M., Prior, J., Pica, C., Sharma, V., and Piwnica-Worms, D. (2002) Characterization of novel histidine-tagged Tat-peptide complexes dual labeled with <sup>99m</sup>Tc-tricarbonyl and fluorescein for scintigraphy and fluorescence microscopy. *Bioconjugate Chem.* 13, 1226–1237.
- (15) Kim, D., Mitchell, D., Brockstedt, D., Fong, L., Nolan, G., Fathman, C., Engelman, E., and Rothbard, J. (1997) Introduction of soluble proteins into MHC class I pathways by conjugation to an HIV tat peptide. *J. Immunol.* 159, 1666–1668.
- (16) Nagahara, H., Vocero-Akbani, A., Synder, E., Ho, A., Latham, D., Lissy, N., Becker-Hapak, M., Ezhevsky, S., and Dowdy, S. (1998) Transduction of full-length TAT fusion proteins directly into mammalian cells: TAT-p27<sup>Kip1</sup> induces cell migration. *Nat. Med.* 4, 1449–1452.
- (17) Gius, D., Ezhevsky, S., Becker-Hapak, M., Nagahara, H., Wei, M., and Dowdy, S. (1999) Transduced p16INK4a peptides inhibit hypophosphorylation of retinoblastoma protein and cell cycle progression prior to activation of Cdk2 complexes in late G1. *Cancer Res.* 59, 2577–2580.
- (18) Lewin, M., McCarlesso, N., Tung, C., Tang, X., Cory, D., Scadden, D., and Weissleder, R. (2000) Tat peptide-derivatized magnetic nanoparticles allow in vivo tracking and recovery of progenitor cells. *Nat. Biotechnol.* 18, 410–414.
- (19) Prochiantz, A. (1999) Homeodomain-Derived Peptides: In and Out of the Cells. *Ann. N.Y. Acad. Sci.* 886, 172–179.
- (20) Violini, S., Sharma, V., Prior, J., Dyszlewski, M., and Piwnica-Worms, D. (2002) Evidence for a plasma membrane-mediated permeability barrier to Tat basic domain in well-differentiated epithelial cells: lack of correlation with heparan sulfate. *Biochemistry* 41, 12652–12661.
- (21) Scheller, A., Wiesner, B., Melzig, M., Bienert, M., and Oehlke, J. (2000) Evidence for an amphipathicity independent cellular uptake of amphipathic cell-penetrating peptides. *Eur. J. Biochem.* 267, 6043–6049.
- (22) Polyakov, V., Sharma, V., Dahlheimer, J., and Piwnica-Worms, D. (1999) Synthesis and characterization in vitro of membrane permeant peptide conjugates for imaging and radiotherapy. *J. Labeled Compd. Radiopharm.* 42, S4–S6.
- (23) Cullis, P., Hope, M., Bally, M., Madden, T., Mayer, L., and Fenske, D. (1997) Influence of pH gradients on the transbilayer transport of drugs, lipids, peptides and metal ions into large unilamellar vesicles. *Biochim. Biophys. Acta* 1331, 187–211.
- (24) Isenman, L., Liebow, C., and Rothman, S. (1995) Transport of proteins across membranes – a paradigm in transition. *Biochim. Biophys. Acta* 1241, 341–370.
- (25) Nagle, J., and Tristram-Nagle, S. (2000) Structure of lipid bilayers. *Biochim. Biophys. Acta* 1469, 159–195.
- (26) Chance, B. (1994) Noninvasive approaches to tissue bioenergetics. *Biochem. Soc. Trans.* 22, 983–987.
- (27) Alberto, R., Schibli, R., and Schubiger, A. P. (1999) First application of *fac*-[<sup>99m</sup>Tc(OH)<sub>2</sub>(CO)<sub>3</sub>]<sup>+</sup> in bioorganometallic chemistry: design, structure, and in vitro affinity of a 5-HT<sub>1A</sub> receptor ligand labeled with <sup>99m</sup>Tc. *J. Am. Chem. Soc.* 121, 6076–6077.
- (28) Peng, C., Graves, P., Thoma, R., Wu, Z., Shaw, A., and Piwnica-Worms, H. (1997) Mitotic and G2 checkpoint control: regulation of 14-3-3 protein binding by phosphorylation of Cdc25C on serine-216. *Science* 277, 1501–1505.
- (29) Bosch, I., Crankshaw, C., Piwnica-Worms, D., and Croop, J. (1997) Characterization of functional assays of P-glycoprotein transport activity. *Leukemia* 11, 1131–1137.
- (30) Lamson, M., Kirscher, A., Hotte, C., Lipsitz, E., and Ice, R. (1975) Generator-produced <sup>99m</sup>Tc–TcO<sub>4</sub><sup>–</sup>: carrier free? *J. Nucl. Med.* 16, 639–641.
- (31) Piwnica-Worms, D., Kronauge, J., and Chiu, M. (1990) Uptake and retention of hexakis (2-methoxy isobutyl isonitrile) technetium(I) in cultured chick myocardial cells: mitochondrial and plasma membrane potential dependence. *Circulation* 82, 1826–1838.
- (32) Glantz, S. A. (1987) *Primer of Biostatistics*, 2nd ed., p 379, McGraw-Hill, Inc., New York.
- (33) Ho, A., Schwarze, S. R., Mermelstein, S. J., Waksman, G., and Dowdy, S. (2001) Synthetic protein transduction domains: enhanced transduction potential in vitro and in vivo. *Cancer Res.* 61, 474–477.
- (34) Subramanian, T., Govindarajan, R., and Chinnadurai, G. (1991) Heterologous basic domain substitutions in the HIV-1 Tat protein reveal an arginine-rich motif required for transactivation. *EMBO J.* 10, 2311–2318.
- (35) Lindgren, M., Hallbrink, M., Prochiantz, A., and Langel, U. (2000) Cell-penetrating peptides. *Trends Pharmacol. Sci.* 21, 99–103.
- (36) Waibel, R., Alberto, R., Willuda, J., Finnnern, R., Schibli, R., Stichelberger, A., Egli, A., Abram, U., Mach, J.-P., Pluckthun, A. et al. (1999) Stable one-step technetium-99m labeling of His-tagged recombinant proteins with a novel Tc(I)-carbonyl complex. *Nat. Biotechnol.* 17, 897–901.
- (37) Buschle, M., Schmidt, W., Auner, W., Mechtler, K., Trska, B., Kirlappos, H., and Birnstiel, M. (1997) Translocation of tumor antigen-derived peptides into antigen-presenting cells. *Proc. Natl. Acad. Sci. U.S.A.* 94, 3256–3261.
- (38) Tyagi, M., Rusnati, M., Presta, M., and Giacca, M. (2001) Internalization of HIV-1 tat requires cell surface heparan sulfate proteoglycans. *J. Biol. Chem.* 276, 3254–3261.
- (39) Silhol, M., Tyagy, M., Giacca, M., Lebleu, B., and Vives, E. (2002) Different mechanisms for cellular internalization of the HIV-1 Tat-derived cell penetrating peptide and recombinant proteins fused to Tat. *Eur. J. Biochem.* 269, 494–501.
- (40) Vocero-Akbani, A., Lissy, N., and Dowdy, S. (2000) Transduction of Full-Length Tat Fusion Proteins Directly into Mammalian Cells: Analysis of T Cell Receptor Activation-Induced Cell Death. *Methods Enzymol.* 322, 508–521.
- (41) Mujeib, A., Bishop, K., Peterline, M. B., Christoph, T., Parslow, T. G., and James, T. L. (1994) NMR structure of a biologically active peptide containing the RNA-binding domain of human immunodeficiency virus type 1 Tat. *Proc. Natl. Acad. Sciences U.S.A.* 91, 8248–8252.
- (42) Metzger, A. U., Schindler, T., Willbold, D., Kraft, M., Steegborn, C., Volkmann, A., Frank, R. W., and Rosch, P. (1996) Structural rearrangements on HIV-1 Tat (32–72) TAR complex formation. *FEBS Lett.* 384, 255–259.
- (43) Rould, M., Perona, J., Soll, D., and Steitz, T. (1989) *Science* 246, 1135–1142.
- (44) Ye, X., Gorin, A., Ellington, A. D., and Patel, D. J. (1996) Deep penetration of an alpha-helix into a widened RNA major groove in the HIV-1 rev peptide-RNA aptamer complex. *Nat. Struct. Biol.* 3, 1026–1033.
- (45) Jurisson, S., and Lydon, J. (1999) Potential technetium small molecule radiopharmaceuticals. *Chem. Rev.* 99, 2205–2218.

BC0256291



# Maleimide-oligo(ethylene glycol) Derivatives of Camptothecin as Albumin-Binding Prodrugs: Synthesis and Antitumor Efficacy

André Warnecke and Felix Kratz\*

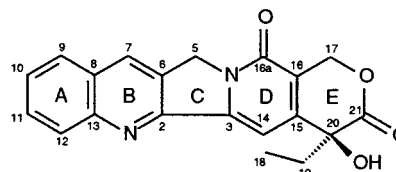
Tumor Biology Center, Breisacher Strasse 117, 79106 Freiburg, Germany. Received October 17, 2002;  
Revised Manuscript Received January 22, 2003

In situ binding of thiol-reactive prodrugs to the cysteine-34 position of circulating albumin is a new approach in drug delivery. Therefore, five maleimide-bearing derivatives of the anticancer drug camptothecin (CPT) were developed as albumin-binding prodrugs. These compounds were synthesized by reacting heterobifunctional cross-linkers based on oligo(ethylene glycols) [3–6 (O–CH<sub>2</sub>–CH<sub>2</sub>) units] bearing a maleimide group on one end and a carboxylic acid group on the other with camptothecin 20-*O*-glycinate. Incorporating oligo(ethylene glycol) chains into the prodrugs enhanced their water-solubility when compared to the parent compound (up to 27-fold). HPLC studies showed that the prodrugs react almost quantitatively with the cysteine-34 position of endogenous albumin within a few minutes after incubation of the CPT derivatives with human blood plasma. The therapeutic potential of two of the prodrugs was assessed in nude mice bearing a colon xenograft (HT-29). Both albumin-binding derivatives of camptothecin were well-tolerated and showed enhanced antitumor efficacy when compared to CPT.

## INTRODUCTION

Camptothecin (CPT,<sup>1</sup> **1**, see Figure 1), an alkaloid from the chinese tree *Camptotheca acuminata* first isolated by Wall and co-workers, shows strong cytotoxic activity (1). Due to its poor water solubility (2.5 µg/mL) (2), first clinical trials in the early seventies were performed using CPT as its sodium salt (hydroxycarboxylate form, open E-ring) (3). However, severe and unpredictable side effects hindered a further clinical development (4). A renewed interest in CPT and CPT derivatives succeeded the elucidation of the mechanism of action, i.e., the inhibition of the nuclear enzyme topoisomerase I (5). Whereas CPT did not gain any clinical importance, the water-soluble derivatives topotecan and irinotecan bearing tertiary amino groups have meanwhile been approved for the therapy of colorectal, ovarian, and lung cancer (6, 7). The clinical application of these low-molecular weight drugs is, however, limited by their toxic dose-related side effects, such as myelosuppression, gastrointestinal disorders, and stomatitis. To circumvent these limitations and to improve the therapeutic potential of anticancer drugs, several synthetic polymers and proteins are being investigated as drug carriers (8, 9).

Recently, three polymeric derivatives of camptothecin have entered clinical trials: two HPMA copolymer-bound camptothecin drugs (10, 11) and Prothecan, a PEG-based CPT prodrug (12). In all cases, binding CPT to polymers leads to highly water-soluble formulations which release the drug in a controlled fashion due to the incorporation of a hydrolyzable or enzymatically degradable amino acid spacers.



**Figure 1.** Chemical structure of 20(*S*)-camptothecin (**1**).

In our group, anticancer drugs have been successfully coupled to serum proteins such as human serum albumin or transferrin leading to well-tolerated and efficacious protein conjugates (13). In particular, we have focused our work on a prodrug strategy that exploits endogenous albumin as a drug carrier. In this approach, a maleimide-bearing prodrug is selectively bound to the cysteine-34 position of circulating albumin after intravenous administration (14).

Recently, we could demonstrate that a 6-maleimidocaproyl hydrazone derivative of doxorubicin fulfills essential requirements for use as an albumin-binding prodrug: The compound is sufficiently water soluble for intravenous administration, it binds rapidly and selectively to the cysteine-34 position of endogenous HSA, and proved distinctly superior to the parent compound in a number of animal models (15).

In the present work, we wanted to extend our prodrug approach to other anticancer agents and set out to develop albumin-binding derivatives of CPT in which the drug is bound through a glycine spacer to maleimide-bearing cross-linking reagents. We assumed that employing linkers with an oligo(ethylene glycol) backbone would enhance the water solubility of the drug. Further objectives of this work were to study the albumin-binding properties of the target compounds, the plasma stability of the respective drug–albumin conjugates, and their in vivo antitumor activity in comparison to free CPT.

\* To whom correspondence should be addressed. Tel.: +49-761-2062930. Fax.: +49-761-2061899. E-mail: felix@tumorbio.uni-freiburg.de.

<sup>1</sup> Abbreviations: CPT, camptothecin; DIAD, diisopropyl azodicarboxylate; Et<sub>2</sub>O, diethyl ether; EtOAc, ethyl acetate; EtOH, ethanol; HSA, human serum albumin; MeCN, acetonitrile; MeOH, methanol; THF, tetrahydrofuran.

## EXPERIMENTAL PROCEDURES

**General.** Chemicals and solvents were purchased from Sigma-Aldrich, Fluka, and Merck and were used without further purification except for methylene chloride, which was dried over calcium hydride and freshly distilled prior to use. Camptothecin was purchased from Hande Tech Development, Inc. (USA). Chemical reactions were carried out under a nitrogen atmosphere.

**Spectral Analyses.**  $^1\text{H}$  and  $^{13}\text{C}$  NMR spectra were recorded on a Bruker ARX 300. Chemical shifts are expressed as parts per million using tetramethylsilane as the internal standard ( $\delta = 0.0$  ppm). Mass spectra were obtained on a Finnigan MAT 312 with associated MAT SS 200 data system using electron spray ionization at 4.0 kV.

**Chromatography.** All reactions were monitored by TLC. Column chromatographic separations were carried out as flash chromatography using silica gel 60 from Merck with a particle size of 0.040–0.063 mm. HPLC for the determination of purity of the compounds was performed on a Nucleosil C18 column (100–5, 250  $\times$  4 mm) from Macherey-Nagel using a HPLC pump 590 from Waters (flow: 1 mL/min) and a LKB Bromma UV Detector ( $\lambda = 370$  nm). For incubation and stability studies, HPLC was performed with a Waters System (pump, Waters 616; detector, Waters 996 Photodiode Array Detector; controller, Waters 600S; auto sampler, Waters 717; software, Millenium Vers. 2.10). Column: Waters Symmetry C18 (300–5, 250  $\times$  4.6 mm) with precolumn; chromatographic conditions. Flow: 1.2–1.8 mL/min. Mobile phase A: 70% MeCN, 30% 200 mM potassium phosphate (pH 7.0). Mobile phase B: 27.5% MeCN, 72.5% 200 mM potassium phosphate (pH 7.0). Gradient: 0–26 min 100% mobile phase B; 26–41 min increase to 100% mobile phase A; 41–50 min 100% mobile phase A; 50–60 min decrease to 100% mobile phase B. Injection volume: 50  $\mu\text{L}$ .

***tert*-Butyl 11-Hydroxy-3,6,9-trioxaundecanoate (2).** Sodium hydride (60% suspension in mineral oil, 2.72 g, 68.0 mmol) was added in small portions to a solution of triethylene glycol (51.1 g, 0.34 mol) in 100 mL of anhydrous THF at 0  $^\circ\text{C}$ . After stirring for 30 min, *tert*-butyl bromoacetate (13.26 g, 68.0 mmol) was added dropwise to the reaction mixture within 10 min at 0  $^\circ\text{C}$ , and stirring was continued for 16 h. The volatiles were removed in vacuo, the oily residue was taken up in 100 mL of brine and extracted with 3  $\times$  100 mL  $\text{CH}_2\text{Cl}_2$ . The combined organic layers were dried over  $\text{MgSO}_4$ , and the volatiles were removed in vacuo. Purification of the crude product by silica column chromatography (EtOAc) yielded 5.25 g (29%) of **2** as a colorless oil.  $^1\text{H}$  NMR ( $\text{CDCl}_3$ ):  $\delta$  1.48 (s, 9H,  $\text{C}(\text{CH}_3)_3$ ), 2.93 (bs, 1H, OH), 3.58–3.75 (m, 12H,  $\text{OCH}_2$ ), 4.03 (s, 2H,  $\text{CH}_2\text{C}(\text{O})\text{O}^t\text{Bu}$ ).  $^{13}\text{C}$  NMR ( $\text{CDCl}_3$ ):  $\delta$  28.11 ( $\text{C}(\text{CH}_3)_3$ ), 61.74 ( $\text{HOCH}_2$ ), 69.03, 70.35, 70.58, 70.64, 70.70, 72.55 ( $\text{OCH}_2$ ), 81.63 ( $\text{C}(\text{CH}_3)_3$ ), 169.68 ( $\text{CH}_2\text{C}(\text{O})\text{O}^t\text{Bu}$ ).

***tert*-Butyl 20-Hydroxy-3,6,9,12,15,18-hexaoaeicosanoate (3).** Hexaethylene glycol (25.44 g, 90.1 mmol) was added dropwise within 5 min to a suspension of potassium hydride (35% suspension in mineral oil, 5.17 g, 45.1 mmol) in 500 mL of anhydrous THF at 0  $^\circ\text{C}$ . After stirring at room temperature for 1 h, *tert*-butyl bromoacetate (8.7 g, 45.1 mmol) was added, and the reaction mixture was stirred under reflux for 16 h. The solids were filtered off, and the volatiles were removed in vacuo. Silica column chromatography of the crude product ( $\text{CH}_2\text{Cl}_2/\text{MeOH}$  100:1  $\rightarrow$  40:1) yielded 12.16 g (68%) of **3** as a colorless oil.  $^1\text{H}$  NMR ( $\text{CDCl}_3$ ):  $\delta$  1.48 (s, 9H,  $\text{C}(\text{CH}_3)_3$ ), 2.75 (bs,

1H, OH), 3.57–3.75 (m, 24H,  $\text{OCH}_2$ ), 4.02 (s, 2H,  $\text{CH}_2\text{C}(\text{O})\text{O}^t\text{Bu}$ ).  $^{13}\text{C}$  NMR ( $\text{CDCl}_3$ ):  $\delta$  28.12 ( $\text{C}(\text{CH}_3)_3$ ), 61.75 ( $\text{HOCH}_2$ ), 69.06, 70.36, 70.60, 70.74, 72.55 ( $\text{OCH}_2$ ), 81.52 ( $\text{C}(\text{CH}_3)_3$ ), 169.69 ( $\text{CH}_2\text{C}(\text{O})\text{O}^t\text{Bu}$ ).

**General Procedure for the Monoalkylation of Oligo(ethylene glycols) with *tert*-Butyl Acrylate.** To a solution of the oligo(ethylene glycol) (0.30 mol) and a catalytic amount of potassium *tert*-butoxide (100 mg) in 150 mL of anhydrous THF was added dropwise *tert*-butyl acrylate (13.49 g, 105 mmol) dissolved in 150 mL THF. The reaction mixture was stirred at room temperature for 16 h and neutralized with 1 M HCl. The volatiles were removed in vacuo; the oily residue was taken up in 150 mL of brine and extracted three times with 75 mL of EtOAc. The combined organic layers were washed with 90 mL of brine and dried over  $\text{MgSO}_4$ . The solvent was removed in vacuo, and the residue was purified as described below.

***tert*-Butyl 12-Hydroxy-4,7,10-trioxadodecanoate (4)** (from the reaction with triethylene glycol). Silica column chromatography of the crude product (EtOAc) yielded 21.33 g (73%) of **4** as a colorless oil.  $^1\text{H}$  NMR ( $\text{CDCl}_3$ ):  $\delta$  1.45 (s, 9H,  $\text{C}(\text{CH}_3)_3$ ), 2.51 (t,  $J = 6.6$  Hz, 2H,  $\text{CH}_2\text{C}(\text{O})\text{O}^t\text{Bu}$ ), 2.72 (bs, 1H, OH), 3.58–3.75 (m, 14H,  $\text{OCH}_2$ ).  $^{13}\text{C}$  NMR ( $\text{CDCl}_3$ ):  $\delta$  28.10 ( $\text{C}(\text{CH}_3)_3$ ), 36.24 ( $\text{CH}_2\text{C}(\text{O})\text{O}^t\text{Bu}$ ), 61.74 ( $\text{HOCH}_2$ ), 66.92, 70.36, 70.39, 70.51, 70.64, 72.52 ( $\text{OCH}_2$ ), 80.53 ( $\text{C}(\text{CH}_3)_3$ ), 170.93 ( $\text{CH}_2\text{C}(\text{O})\text{O}^t\text{Bu}$ ).

***tert*-Butyl 15-Hydroxy-4,7,10,13-tetroxapentadecanoate (5)** (from the reaction with tetraethylene glycol). Silica column chromatography of the crude product (EtOAc/MeOH 10:1  $\rightarrow$  3:1) yielded 21.66 g (64%) of **5** as a colorless oil.  $^1\text{H}$  NMR ( $\text{CDCl}_3$ ):  $\delta$  1.45 (s, 9H,  $\text{C}(\text{CH}_3)_3$ ), 2.50 (t,  $J = 6.4$  Hz, 2H,  $\text{CH}_2\text{C}(\text{O})\text{O}^t\text{Bu}$ ), 2.72 (bs, 1H, OH), 3.58–3.75 (m, 18H,  $\text{OCH}_2$ ).  $^{13}\text{C}$  NMR ( $\text{CDCl}_3$ ):  $\delta$  28.10 ( $\text{C}(\text{CH}_3)_3$ ), 36.27 ( $\text{CH}_2\text{C}(\text{O})\text{O}^t\text{Bu}$ ), 61.74 ( $\text{HOCH}_2$ ), 66.90, 70.38, 70.52, 70.59, 70.64, 72.52 ( $\text{OCH}_2$ ), 80.50 ( $\text{C}(\text{CH}_3)_3$ ), 170.92 ( $\text{CH}_2\text{C}(\text{O})\text{O}^t\text{Bu}$ ).

***tert*-Butyl 21-Hydroxy-4,7,10,13,16,19-hexoxapentadecanoate (6)** (from the reaction with hexaethylene glycol). Silica column chromatography of the crude product (EtOAc/MeOH 5:1) yielded 34.48 g (80%) of **6** as a colorless oil.  $^1\text{H}$  NMR ( $\text{CDCl}_3$ ):  $\delta$  1.45 (s, 9H,  $\text{C}(\text{CH}_3)_3$ ), 2.50 (t,  $J = 6.6$  Hz, 2H,  $\text{CH}_2\text{C}(\text{O})\text{O}^t\text{Bu}$ ), 2.91 (s, 1H, OH), 3.58–3.74 (m, 26H,  $\text{OCH}_2$ ).  $^{13}\text{C}$  NMR ( $\text{CDCl}_3$ ):  $\delta$  28.09 ( $\text{C}(\text{CH}_3)_3$ ), 36.26 ( $\text{CH}_2\text{C}(\text{O})\text{O}^t\text{Bu}$ ), 61.68 ( $\text{HOCH}_2$ ), 66.88, 70.36, 70.49, 70.58, 70.61, 72.55 ( $\text{OCH}_2$ ), 80.46 ( $\text{C}(\text{CH}_3)_3$ ), 170.89 ( $\text{CH}_2\text{C}(\text{O})\text{O}^t\text{Bu}$ ).

**1-Benzylxy-3,6-dioxaoctan-8-ol (23).** To triethylene glycol (80.96 g, 0.54 mol) was added sodium (1.86 g, 80.9 mmol) in small portions. The mixture was heated until the sodium dissolved completely. After cooling to room temperature, benzyl bromide (6.40 mL, 53.9 mmol) was added dropwise to the reaction mixture within 10 min, and stirring was continued for 1 h. The mixture was poured into 50 mL water, neutralized with 1 M HCl, and extracted with 3  $\times$  100 mL  $\text{CH}_2\text{Cl}_2$ . The combined organic layers were dried over  $\text{MgSO}_4$ , and the solvent was removed in vacuo. Silica column chromatography of the crude product (EtOAc) yielded 10.06 g (78%) of **23** as a colorless oil.  $^1\text{H}$  NMR ( $\text{CDCl}_3$ ):  $\delta$  2.84 (bs, 1H, OH), 3.56–3.74 (m, 12H,  $\text{OCH}_2\text{CH}_2\text{O}$ ), 4.56 (s, 2H,  $\text{CH}_2\text{Ar}$ ), 7.23–7.34 (m, 5H, Ar-*H*).  $^{13}\text{C}$  NMR ( $\text{CDCl}_3$ ):  $\delta$  61.71 ( $\text{HOCH}_2$ ), 69.38, 70.37, 70.61, 70.66, 72.53, 73.25 ( $\text{OCH}_2$ ), 127.63 (Ar), 127.77 (Ar), 128.37 (Ar), 138.16 (Ar).

***tert*-Butyl 12-Benzylxy-4,7,10-trioxadodecanoate (24).** *tert*-Butyl acrylate (9.06 g, 70.7 mmol) dissolved in 100 mL THF was added dropwise within 20 min to a solution of **23** (11.33 g, 47.15 mmol) and a catalytic



amount of potassium *tert*-butoxide (100 mg) in 150 mL of anhydrous THF. The reaction mixture was stirred overnight, neutralized with 1 M HCl, and the solvent was removed in vacuo. Silica column chromatography of the crude product (EtOAc/isohexane 1:2) yielded 9.95 g (57%) of **24** as a colorless oil.  $^1\text{H}$  NMR ( $\text{CDCl}_3$ ):  $\delta$  1.44 (s, 9H,  $\text{C}(\text{CH}_3)_3$ ), 2.50 (t,  $J = 6.6$  Hz, 2H,  $\text{CH}_2\text{C}(\text{O})\text{O}^t\text{Bu}$ ), 3.57–3.75 (m, 14H,  $\text{OCH}_2$ ), 4.57 (s, 2H,  $\text{CH}_2\text{Ar}$ ), 7.23–7.37 (m, 5H, Ar-H).  $^{13}\text{C}$  NMR ( $\text{CDCl}_3$ ):  $\delta$  28.10 ( $\text{C}(\text{CH}_3)_3$ ), 36.28 ( $\text{CH}_2\text{C}(\text{O})\text{O}^t\text{Bu}$ ), 66.91, 69.44, 70.39, 70.54, 70.64, 70.67, 73.24 ( $\text{OCH}_2$ ), 80.49 ( $\text{C}(\text{CH}_3)_3$ ), 127.58 (Ar), 127.75 (Ar), 128.36 (Ar), 138.30 (Ar), 170.92 ( $\text{CH}_2\text{C}(\text{O})\text{O}^t\text{Bu}$ ).

**General Procedures for the Mitsunobu Alkylation of Maleimide with the Alcohols 2–6. Method A.** In a three-necked round-bottom flask with an internal thermometer and a dropping funnel, triphenyl phosphine (5.00 g, 19.1 mmol) was dissolved in 100 mL of anhydrous THF and cooled to  $-78^\circ\text{C}$ . DIAD (3.86 g, 19.1 mmol) was added within 5 min, and the resulting bright yellow solution was stirred for further 5 min. A solution of the alcohol (19.1 mmol) in 20 mL THF was added dropwise to the reaction mixture within 5 min. After stirring for 5 min, neopentyl alcohol (0.84 g, 9.6 mmol) dissolved in 10 mL THF and finely ground maleimide (1.52 g, 15.7 mmol) were added, and the mixture was kept for 5 min at  $-78^\circ\text{C}$ . The cooling bath was then removed and the solution was allowed to warm up to ambient temperature overnight. The volatiles were removed in vacuo, and the residue was purified as described below.

**Method B.** A carefully stirred suspension of the alcohol (10.1 mmol), neopentyl alcohol (404 mg, 4.59 mmol), and polymer-bound triphenyl phosphine (3 mmol  $\text{PhP}_3$  per g polymer, 3.36 g, 10.1 mmol) in 100 mL of anhydrous THF was cooled to  $0^\circ\text{C}$ . Finely ground maleimide (890 mg, 9.17 mmol) followed by DIAD (1.85 g, 9.17 mmol) were added, and the mixture was kept for 5 min at  $0^\circ\text{C}$ . The cooling bath was removed, and stirring was continued for 3 h at room temperature. The solids were filtered off over Celite and the volatiles were removed in vacuo. The oily residue was purified as described below.

**Method C.** A stirred solution of the alcohol (11.3 mmol), neopentyl alcohol (454 mg, 5.20 mmol), and triphenyl phosphine (2.70 g, 10.3 mmol) in 70 mL of anhydrous THF was cooled to  $0^\circ\text{C}$ . Finely ground maleimide (1000 mg, 10.3 mmol) followed by DIAD (2.08 g, 10.3 mmol) were added, and the mixture was kept for 5 min at  $0^\circ\text{C}$ . The cooling bath was removed, and stirring was continued for 3 h at room temperature. The volatiles were removed in vacuo, and the oily residue was purified as described below.

***tert*-Butyl 11-Maleimido-3,6,9-trioxaundecanoate (7) (Method A, from the Reaction with 2).** Silica column chromatography of the crude product ( $\text{Et}_2\text{O}/\text{isohexane}/\text{EtOAc}$  2:1:1) yielded 2.44 g (37%) of **7** as a colorless oil.  $^1\text{H}$  NMR ( $\text{CDCl}_3$ ):  $\delta$  1.48 (s, 9H,  $\text{C}(\text{CH}_3)_3$ ), 3.59–3.76 (m, 12H,  $\text{NCH}_2$ ,  $\text{OCH}_2$ ), 4.02 (s, 2H,  $\text{CH}_2\text{C}(\text{O})\text{O}^t\text{Bu}$ ), 6.71 (s, 2H,  $\text{CH}=\text{CH}$ ).  $^{13}\text{C}$  NMR ( $\text{CDCl}_3$ ):  $\delta$  28.12 ( $\text{C}(\text{CH}_3)_3$ ), 37.13 ( $\text{NCH}_2$ ), 67.83, 69.05, 70.04, 70.58, 70.64, 70.71 ( $\text{OCH}_2$ ), 81.52 ( $\text{C}(\text{CH}_3)_3$ ), 134.17 ( $\text{CH}=\text{CH}$ ), 169.69 ( $\text{CH}_2\text{C}(\text{O})\text{O}^t\text{Bu}$ ), 170.67 ( $\text{C}(\text{O})\text{CH}=\text{CHCO}$ ).

***tert*-Butyl 20-Maleimido-3,6,9,12,15,18-hexoxaeicosanoate (8) (Method B, from the Reaction with 3).** Silica column chromatography of the crude product (1,  $\text{Et}_2\text{O}/\text{EtOH}$  15:1; 2, chloroform/MeOH 50:1) yielded 1.37 g (31%) of **8** as a colorless oil.  $^1\text{H}$  NMR ( $\text{CDCl}_3$ ):  $\delta$  1.47 (s, 9H,  $\text{C}(\text{CH}_3)_3$ ), 3.58–3.74 (m, 24H,  $\text{NCH}_2$ ,  $\text{OCH}_2$ ), 4.02 (s, 2H,  $\text{CH}_2\text{C}(\text{O})\text{O}^t\text{Bu}$ ), 6.70 (s, 2H,  $\text{CH}=\text{CH}$ ).  $^{13}\text{C}$  NMR ( $\text{CDCl}_3$ ):  $\delta$  28.13 ( $\text{C}(\text{CH}_3)_3$ ), 37.15 ( $\text{NCH}_2$ ), 67.83, 69.06, 70.08, 70.60, 70.74 ( $\text{OCH}_2$ ), 81.52 ( $\text{C}(\text{CH}_3)_3$ ),

134.17 ( $\text{CH}=\text{CH}$ ), 169.69 ( $\text{CH}_2\text{C}(\text{O})\text{O}^t\text{Bu}$ ), 170.66 ( $\text{C}(\text{O})\text{CH}=\text{CHCO}$ ).

***tert*-Butyl 12-Maleimido-4,7,10-trioxadodecanoate (9) (Method A, from the Reaction with 4).** Silica column chromatography of the crude product ( $\text{Et}_2\text{O}/\text{isohexane}$  3:1) yielded 3.98 g (58%) of **9** as a colorless oil.  $^1\text{H}$  NMR ( $\text{CDCl}_3$ ):  $\delta$  1.45 (s, 9H,  $\text{C}(\text{CH}_3)_3$ ), 2.50 (t,  $J = 6.6$  Hz, 2H,  $\text{CH}_2\text{C}(\text{O})\text{O}^t\text{Bu}$ ), 3.57–3.76 (m, 14H,  $\text{NCH}_2$ ,  $\text{OCH}_2$ ), 6.71 (s, 2H,  $\text{CH}=\text{CH}$ ).  $^{13}\text{C}$  NMR ( $\text{CDCl}_3$ ):  $\delta$  28.10 ( $\text{C}(\text{CH}_3)_3$ ), 36.26 ( $\text{CH}_2\text{C}(\text{O})\text{O}^t\text{Bu}$ ), 37.12 ( $\text{NCH}_2$ ), 66.89, 67.81, 70.05, 70.35, 70.54, 70.56 ( $\text{OCH}_2$ ), 80.48 ( $\text{C}(\text{CH}_3)_3$ ), 134.16 ( $\text{CH}=\text{CH}$ ), 170.64 ( $\text{C}(\text{O})\text{CH}=\text{CHCO}$ ), 170.91 ( $\text{CH}_2\text{C}(\text{O})\text{O}^t\text{Bu}$ ).

***tert*-Butyl 15-Maleimido-4,7,10,13-tetroxapentadecanoate (10) (Method C, from the Reaction with 5).** Silica column chromatography of the crude product ( $\text{Et}_2\text{O}$ ) yielded 2.79 g (68%) of **10** as a colorless oil.  $^1\text{H}$  NMR ( $\text{CDCl}_3$ ):  $\delta$  1.45 (s, 9H,  $\text{C}(\text{CH}_3)_3$ ), 2.50 (t,  $J = 6.6$  Hz, 2H,  $\text{CH}_2\text{C}(\text{O})\text{O}^t\text{Bu}$ ), 3.57–3.76 (m, 18H,  $\text{NCH}_2$ ,  $\text{OCH}_2$ ), 6.71 (s, 2H,  $\text{CH}=\text{CH}$ ).  $^{13}\text{C}$  NMR ( $\text{CDCl}_3$ ):  $\delta$  28.11 ( $\text{C}(\text{CH}_3)_3$ ), 36.30 ( $\text{CH}_2\text{C}(\text{O})\text{O}^t\text{Bu}$ ), 37.15 ( $\text{NCH}_2$ ), 66.91, 67.81, 70.08, 70.39, 70.52, 70.57, 70.60, 70.65 ( $\text{OCH}_2$ ), 80.48 ( $\text{C}(\text{CH}_3)_3$ ), 134.17 ( $\text{CH}=\text{CH}$ ), 170.64 ( $\text{C}(\text{O})\text{CH}=\text{CHCO}$ ), 170.90 ( $\text{CH}_2\text{C}(\text{O})\text{O}^t\text{Bu}$ ).

***tert*-Butyl 21-Maleimido-4,7,10,13,16,19-hexoxaeicosanoate (11) (Method B, from the Reaction with 6).** Silica column chromatography of the crude product (1,  $\text{Et}_2\text{O}/\text{EtOH}$  15:1; 2, chloroform/MeOH 50:1) yielded 1.24 g (25%) of **11** as a colorless oil.  $^1\text{H}$  NMR ( $\text{CDCl}_3$ ):  $\delta$  1.45 (s, 9H,  $\text{C}(\text{CH}_3)_3$ ), 2.50 (t,  $J = 6.6$  Hz, 2H,  $\text{CH}_2\text{C}(\text{O})\text{O}^t\text{Bu}$ ), 3.57–3.75 (m, 26H,  $\text{NCH}_2$ ,  $\text{OCH}_2$ ), 6.71 (s, 2H,  $\text{CH}=\text{CH}$ ).  $^{13}\text{C}$  NMR ( $\text{CDCl}_3$ ):  $\delta$  28.11 ( $\text{C}(\text{CH}_3)_3$ ), 36.29 ( $\text{CH}_2\text{C}(\text{O})\text{O}^t\text{Bu}$ ), 37.15 ( $\text{NCH}_2$ ), 66.91, 67.81, 70.08, 70.38, 70.52, 70.59 ( $\text{OCH}_2$ ), 80.48 ( $\text{C}(\text{CH}_3)_3$ ), 134.17 ( $\text{CH}=\text{CH}$ ), 170.65 ( $\text{C}(\text{O})\text{CH}=\text{CHCO}$ ), 170.90 ( $\text{CH}_2\text{C}(\text{O})\text{O}^t\text{Bu}$ ).

**General Procedure for the Cleavage of the *tert*-Butyl Protective Groups of 7–11 and 24.** To a solution of 3 mmol of the *tert*-butyl esters in 5 mL of anhydrous  $\text{CH}_2\text{Cl}_2$  was added 5 mL of TFA. After stirring at room temperature for 1 h, the volatiles were removed in vacuo. The oily residue was dissolved in 30 mL of anhydrous  $\text{CH}_2\text{Cl}_2$  and treated with 4 g of Amberlyst A-21. After stirring at room temperature for 1 h, the solids were filtered off. The solvent was removed in vacuo to yield the carboxylic acids **12–16** and **25** in quantitative yields which were used in the next step without further purification.

**11-Maleimido-3,6,9-trioxaundecanoic Acid (12) (from the Reaction with 7).**  $^1\text{H}$  NMR ( $\text{CDCl}_3$ ):  $\delta$  3.58–3.80 (m, 12H,  $\text{NCH}_2$ ,  $\text{OCH}_2$ ), 4.18 (s, 2H,  $\text{CH}_2\text{COOH}$ ), 6.72 (s, 2H,  $\text{CH}=\text{CH}$ ), 7.21 (bs, 1H,  $\text{COOH}$ ).  $^{13}\text{C}$  NMR ( $\text{CDCl}_3$ ):  $\delta$  37.19 ( $\text{NCH}_2$ ), 68.02, 69.87, 70.27, 70.56, 71.28 ( $\text{OCH}_2$ ), 134.21 ( $\text{CH}=\text{CH}$ ), 170.67 ( $\text{C}(\text{O})\text{CH}=\text{CHCO}$ ), 172.84 ( $\text{COOH}$ ).

**20-Maleimido-3,6,9,12,15,18-hexoxaeicosanoic Acid (13) (from the Reaction with 8).**  $^1\text{H}$  NMR ( $\text{CDCl}_3$ ):  $\delta$  3.35–3.88 (m, 24H,  $\text{NCH}_2$ ,  $\text{OCH}_2$ ), 4.16 (s, 2H,  $\text{CH}_2\text{COOH}$ ), 5.92 (bs, 1H,  $\text{COOH}$ ), 6.71 (s, 2H,  $\text{CH}=\text{CH}$ ).  $^{13}\text{C}$  NMR ( $\text{CDCl}_3$ ):  $\delta$  37.16 ( $\text{NCH}_2$ ), 67.82, 69.14, 70.02, 70.26, 70.35, 70.39, 70.48, 70.58, 71.11 ( $\text{OCH}_2$ ), 134.19 ( $\text{CH}=\text{CH}$ ), 170.74 ( $\text{C}(\text{O})\text{CH}=\text{CHCO}$ ), 171.97 ( $\text{COOH}$ ).

**12-Maleimido-4,7,10-trioxadodecanoic Acid (14) (from the Reaction with 9).**  $^1\text{H}$  NMR ( $\text{CDCl}_3$ ):  $\delta$  2.64 (t,  $J = 6.2$  Hz, 2H,  $\text{CH}_2\text{COOH}$ ), 3.58–3.81 (m, 14H,  $\text{NCH}_2$ ,  $\text{OCH}_2$ ), 6.72 (s, 2H,  $\text{CH}=\text{CH}$ ), 9.76 (bs, 1H,  $\text{COOH}$ ).  $^{13}\text{C}$  NMR ( $\text{CDCl}_3$ ):  $\delta$  34.78 ( $\text{CH}_2\text{COOH}$ ), 37.14 ( $\text{NCH}_2$ ), 66.32, 67.86, 70.00, 70.37, 70.38, 70.52 ( $\text{OCH}_2$ ), 134.20 ( $\text{CH}=\text{CH}$ ), 170.79 ( $\text{C}(\text{O})\text{CH}=\text{CHCO}$ ), 176.32 ( $\text{COOH}$ ).



**15-Maleimido-4,7,10,13-tetroxapentadecanoic Acid (15) (from the Reaction with 10).**  $^1\text{H}$  NMR ( $\text{CDCl}_3$ ):  $\delta$  2.62 (t,  $J$  = 6.2 Hz, 2H,  $\text{CH}_2\text{COOH}$ ), 3.55–3.80 (m, 18H,  $\text{NCH}_2$ ,  $\text{OCH}_2$ ), 6.71 (s, 2H,  $\text{CH}=\text{CH}$ ), 8.75 (bs, 1H,  $\text{COOH}$ ).  $^{13}\text{C}$  NMR ( $\text{CDCl}_3$ ):  $\delta$  34.86 ( $\text{CH}_2\text{COOH}$ ), 37.11 ( $\text{NCH}_2$ ), 66.40, 67.79, 70.03, 70.32, 70.44, 70.47, 70.56, 70.60 ( $\text{OCH}_2$ ), 134.18 ( $\text{CH}=\text{CH}$ ), 170.75 ( $\text{C}(\text{O})\text{CH}=\text{CHCO}$ ), 175.65 ( $\text{COOH}$ ).

**21-Maleimido-4,7,10,13,16,19-hexoxauncosanoic Acid (16) (from the Reaction with 11).**  $^1\text{H}$  NMR ( $\text{CDCl}_3$ ):  $\delta$  2.62 (t,  $J$  = 6.2 Hz, 2H,  $\text{CH}_2\text{COOH}$ ), 3.56–3.81 (m, 26H,  $\text{NCH}_2$ ,  $\text{OCH}_2$ ), 6.71 (s, 2H,  $\text{CH}=\text{CH}$ ), 7.50 (bs, 1H,  $\text{COOH}$ ).  $^{13}\text{C}$  NMR ( $\text{CDCl}_3$ ):  $\delta$  34.93 ( $\text{CH}_2\text{COOH}$ ), 37.16 ( $\text{NCH}_2$ ), 66.50, 67.81, 70.04, 70.32, 70.49, 70.58, 70.65 ( $\text{OCH}_2$ ), 134.19 ( $\text{CH}=\text{CH}$ ), 170.72 ( $\text{C}(\text{O})\text{CH}=\text{CHCO}$ ), 174.87 ( $\text{COOH}$ ).

**12-Benzoyloxy-4,7,10-trioxadodecanoic Acid (25) (from the Reaction with 24).**  $^1\text{H}$  NMR ( $\text{CDCl}_3$ ):  $\delta$  2.61 (t,  $J$  = 6.2 Hz, 2H,  $\text{CH}_2\text{C}(\text{O})\text{O}^t\text{Bu}$ ), 3.59–3.71 (m, 12H,  $\text{OCH}_2$ ), 3.76 (t,  $J$  = 6.2 Hz, 2H,  $\text{CH}_2\text{CH}_2\text{C}(\text{O})\text{O}^t\text{Bu}$ ), 4.58 (s, 2H,  $\text{CH}_2\text{Ar}$ ), 7.24–7.37 (m, 5H, Ar-H), 8.72 (bs, 1H,  $\text{COOH}$ ).  $^{13}\text{C}$  NMR ( $\text{CDCl}_3$ ):  $\delta$  34.90 ( $\text{CH}_2\text{COOH}$ ), 66.39, 69.37, 70.30, 70.47, 70.53, 70.62, 73.21 ( $\text{OCH}_2$ ), 127.67 (Ar), 127.84 (Ar), 128.38 (Ar), 138.06 (Ar), 175.66 ( $\text{COOH}$ ).

**Camptothecin-20-O-glycinate Trifluoroacetate (17).** This compound was prepared from camptothecin using a two-step procedure as previously described (16).

**General Procedure for the Reaction of 17 with the Carboxylic Acids 18–22.** To a suspension of 17 (318 mg, 0.613 mmol), 0.919 mmol of the carboxylic acid, and triethylamine (256  $\mu\text{L}$ , 1.838 mmol) in 5 mL of anhydrous  $\text{CH}_2\text{Cl}_2$  was added 2-chloro-1-methylpyridinium iodide (Mukaiyama reagent) (235 mg, 0.919 mmol) as a finely ground solid. Stirring was continued for 2 h at room temperature during which the initially cloudy mixture turned into a yellow solution. The mixture was diluted with 50 mL of  $\text{CH}_2\text{Cl}_2$  and washed with 2  $\times$  20 mL of 1 M HCl and 2  $\times$  20 mL of water. The organic layer was dried over  $\text{MgSO}_4$ , and the solvent was removed in vacuo. The residue was purified as described below.

**Camptothecin-20-O-[(11-maleimido-3,6,9-trioxaundecanoyl)glycinate] (18) (from the reaction with 12).** Recrystallization of the crude product from MeOH yielded 223 mg (54%) of 18 as a pale yellow powder.  $^1\text{H}$  NMR ( $\text{DMSO}-d_6$ ):  $\delta$  0.94 (t,  $J$  = 7.4 Hz, 3H, C18-H), 2.17 (q,  $J$  = 7.4 Hz, 2H, C19-H), 3.38–3.58 (m, 12H,  $\text{NCH}_2\text{CH}_2\text{O}$ ,  $\text{OCH}_2\text{CH}_2\text{O}$ ), 3.93 (s', 2H,  $\text{CH}_2\text{C}(\text{O})\text{NH}$ ), 4.08/4.22 (dd,  $J_{\text{AB}}$  = 17.3 Hz,  $J_{\text{AX}}$  = 6.2 Hz, 2H,  $\text{NHCH}_2\text{CO}$ ), 5.22 (s, 2H, C5-H), 5.50 (s, 2H, C17-H), 6.97 (s, 2H,  $\text{C}(\text{O})\text{CH}=\text{CHCO}$ ), 7.16 (s, 1H, C14-H), 7.69 (t',  $J$  = 8.1 Hz, 1H, C10-H), 7.85 (t',  $J$  = 7.2 Hz, 1H, C11-H), 8.08 (d,  $J$  = 7.5 Hz, 1H, C9-H), 8.15 (d,  $J$  = 8.3 Hz, 1H, C12-H), 8.22 (t,  $J$  = 6.2 Hz, 1H, NH), 8.64 (s, 1H, C7-H).  $^{13}\text{C}$  NMR ( $\text{DMSO}-d_6$ ):  $\delta$  7.41 (C18), 30.35 (C19), 36.64 ( $\text{NCH}_2\text{CH}_2\text{O}$ ), 50.04 (C5), 66.22 (C17), 66.78, 69.24, 69.37, 69.48, 69.67, 70.15 ( $\text{OCH}_2$ ,  $\text{CH}_2\text{NH}$ ), 76.19 (C20), 95.10, 118.86, 127.57, 127.81, 128.38, 128.78, 129.56, 130.31, 131.43, 134.38 ( $\text{C}(\text{O})\text{CH}=\text{CHCO}$ ), 144.94, 145.82, 147.74, 152.18, 156.37 (C2,3,6–16,16a), 166.91, 168.79, 169.86, 170.76 (C21,  $\text{C}(\text{O})\text{CH}=\text{CHCO}$ ,  $\text{C}(\text{O})\text{OC20}$ ,  $\text{C}(\text{O})\text{NH}$ ). ESI-MS (4.4 kV, MeOH):  $m/z$  (%) 697.1 ( $[\text{M} + \text{Na}]^+$ , 100). Purity determined by HPLC (MeOH/water 70:30) >94%.

**Camptothecin-20-O-[(20-maleimido-3,6,9,12,15,18-hexoxaeicosanoyl)glycinate] (19) (from the Reaction with 13).** Silica column chromatography of the crude product (chloroform/MeOH 30:1) yielded 391 mg (79%) of 19 as a pale yellow waxy solid.  $^1\text{H}$  NMR ( $\text{DMSO}-d_6$ ):  $\delta$  0.92 (t,  $J$  = 7.3 Hz, 3H, C18-H), 2.16 (q,  $J$  = 7.3

Hz, 2H, C19-H), 3.35–3.61 (m, 24H,  $\text{NCH}_2\text{CH}_2\text{O}$ ,  $\text{OCH}_2\text{CH}_2\text{O}$ ), 3.93 (s', 2H,  $\text{CH}_2\text{C}(\text{O})\text{NH}$ ), 4.08/4.22 (dd,  $J_{\text{AB}}$  = 17.9 Hz,  $J_{\text{AX}}$  = 6.0 Hz, 2H,  $\text{NHCH}_2\text{CO}$ ), 5.28 (s, 2H, C5-H), 5.50 (s, 2H, C17-H), 7.00 (s, 2H,  $\text{C}(\text{O})\text{CH}=\text{CHCO}$ ), 7.17 (s, 1H, C14-H), 7.71 (t',  $J$  = 7.5 Hz, 1H, C10-H), 7.87 (t',  $J$  = 7.2 Hz, 1H, C11-H), 8.12 (d,  $J$  = 7.7 Hz, 1H, C9-H), 8.17 (d,  $J$  = 8.6 Hz, 1H, C12-H), 8.21 (t,  $J$  = 6.0 Hz, 1H, NH), 8.68 (s, 1H, C7-H).  $^{13}\text{C}$  NMR ( $\text{DMSO}-d_6$ ):  $\delta$  7.39 (C18), 30.36 (C19), 36.70 ( $\text{NCH}_2\text{CH}_2\text{O}$ ), 50.08 (C5), 66.23 (C17), 66.82, 69.31, 69.53, 69.62, 70.20 ( $\text{OCH}_2$ ,  $\text{CH}_2\text{NH}$ ), 76.15 (C20), 95.11, 118.89, 127.61, 127.87, 128.43, 128.82, 129.65, 130.33, 131.46, 134.43 ( $\text{C}(\text{O})\text{CH}=\text{CHCO}$ ), 144.93, 145.85, 147.80, 152.26, 156.40 (C2,3,6–16,16a), 166.88, 168.78, 169.86, 170.79 (C21,  $\text{C}(\text{O})\text{CH}=\text{CHCO}$ ,  $\text{C}(\text{O})\text{OC20}$ ,  $\text{C}(\text{O})\text{NH}$ ). ESI-MS (4.0 kV, MeOH):  $m/z$  (%) 829.3 ( $[\text{M} + \text{Na}]^+$ , 100). Purity determined by HPLC (MeOH/water 70:30) >96%.

**Camptothecin-20-O-[(12-maleimido-4,7,10-trioxadodecanoyl)glycinate] (20) (from the Reaction with 14).** Recrystallization of the crude product from EtOH yielded 279 mg (66%) of 20 as a pale yellow powder.  $^1\text{H}$  NMR ( $\text{DMSO}-d_6$ ):  $\delta$  0.93 (t,  $J$  = 7.4 Hz, 3H, C18-H), 2.17 (q,  $J$  = 7.4 Hz, 2H, C19-H), 2.38 (t',  $J$  = 6.4 Hz, 2H,  $\text{CH}_2\text{C}(\text{O})\text{NH}$ ), 3.36–3.68 (m, 14H,  $\text{NCH}_2\text{CH}_2\text{O}$ ,  $\text{OCH}_2\text{CH}_2\text{O}$ ), 4.02/4.21 (dd,  $J_{\text{AB}}$  = 17.4 Hz,  $J_{\text{AX}}$  = 5.9 Hz, 2H,  $\text{NHCH}_2\text{CO}$ ), 5.24 (s, 2H, C5-H), 5.50 (s, 2H, C17-H), 6.99 (s, 2H,  $\text{C}(\text{O})\text{CH}=\text{CHCO}$ ), 7.16 (s, 1H, C14-H), 7.70 (t',  $J$  = 7.5 Hz, 1H, C10-H), 7.86 (t',  $J$  = 7.7 Hz, 1H, C11-H), 8.10 (d,  $J$  = 7.5 Hz, 1H, C9-H), 8.16 (d,  $J$  = 8.7 Hz, 1H, C12-H), 8.43 (t,  $J$  = 5.9 Hz, 1H, NH), 8.65 (s, 1H, C7-H).  $^{13}\text{C}$  NMR ( $\text{DMSO}-d_6$ ):  $\delta$  7.42 (C18), 30.29 (C19), 35.61 ( $\text{CH}_2\text{C}(\text{O})\text{NH}$ ), 36.65 ( $\text{NCH}_2\text{CH}_2\text{O}$ ), 50.05 (C5), 66.20 (C17), 66.42, 66.78, 69.36, 69.47, 69.50, ( $\text{OCH}_2$ ,  $\text{CH}_2\text{NH}$ ), 76.10 (C20), 95.15, 118.83, 127.58, 127.82, 128.39, 128.80, 129.58, 130.31, 131.42, 134.41 ( $\text{C}(\text{O})\text{CH}=\text{CHCO}$ ), 144.98, 145.82, 147.75, 152.20, 156.37 (C2,3,6–16,16a), 166.98, 169.02, 170.58, 170.78 (C21,  $\text{C}(\text{O})\text{CH}=\text{CHCO}$ ,  $\text{C}(\text{O})\text{OC20}$ ,  $\text{C}(\text{O})\text{NH}$ ). ESI-MS (4.0 kV, MeOH):  $m/z$  (%) 711.1 ( $[\text{M} + \text{Na}]^+$ , 100). Purity determined by HPLC (MeOH/water 70:30) >95%.

**Camptothecin-20-O-[(15-maleimido-4,7,10,13-tetroxapentadecanoyl)glycinate] (21) (from the Reaction with 15).** Recrystallization of the crude product from EtOH yielded 392 mg (80%) of 21 as a pale yellow powder.  $^1\text{H}$  NMR ( $\text{DMSO}-d_6$ ):  $\delta$  0.94 (t,  $J$  = 7.3 Hz, 3H, C18-H), 2.17 (q,  $J$  = 7.3 Hz, 2H, C19-H), 2.39 (t',  $J$  = 6.4 Hz, 2H,  $\text{CH}_2\text{C}(\text{O})\text{NH}$ ), 3.31–3.70 (m, 18H,  $\text{NCH}_2\text{CH}_2\text{O}$ ,  $\text{OCH}_2\text{CH}_2\text{O}$ ), 4.02/4.21 (dd,  $J_{\text{AB}}$  = 17.9 Hz,  $J_{\text{AX}}$  = 5.8 Hz, 2H,  $\text{NHCH}_2\text{CO}$ ), 5.23 (s, 2H, C5-H), 5.50 (s, 2H, C17-H), 7.00 (s, 2H,  $\text{C}(\text{O})\text{CH}=\text{CHCO}$ ), 7.15 (s, 1H, C14-H), 7.69 (t',  $J$  = 7.5 Hz, 1H, C10-H), 7.86 (t',  $J$  = 7.5 Hz, 1H, C11-H), 8.09 (d,  $J$  = 7.5 Hz, 1H, C9-H), 8.16 (d,  $J$  = 7.5 Hz, 1H, C12-H), 8.43 (t,  $J$  = 5.8 Hz, 1H, NH), 8.64 (s, 1H, C7-H).  $^{13}\text{C}$  NMR ( $\text{DMSO}-d_6$ ):  $\delta$  7.41 (C18), 30.29 (C19), 35.62 ( $\text{CH}_2\text{C}(\text{O})\text{NH}$ ), 36.68 ( $\text{NCH}_2\text{CH}_2\text{O}$ ), 50.02 (C5), 66.20 (C17), 66.42, 66.80, 69.26, 69.38, 69.48, 69.58, 69.63 ( $\text{OCH}_2$ ,  $\text{CH}_2\text{NH}$ ), 76.09 (C20), 95.15, 118.82, 127.55, 127.80, 128.37, 128.79, 129.55, 130.30, 131.41, 134.41 ( $\text{C}(\text{O})\text{CH}=\text{CHCO}$ ), 144.98, 145.80, 147.74, 152.17, 156.36 (C2,3,6–16,16a), 166.96, 169.00, 170.57, 170.78 (C21,  $\text{C}(\text{O})\text{CH}=\text{CHCO}$ ,  $\text{C}(\text{O})\text{OC20}$ ,  $\text{C}(\text{O})\text{NH}$ ). ESI-MS (4.0 kV, MeOH):  $m/z$  (%) 755.2 ( $[\text{M} + \text{Na}]^+$ , 100). Purity determined by HPLC (MeOH/water 70:30) >97%.

**Camptothecin-20-O-[(21-maleimido-4,7,10,13,16,19-hexoxaeicosanoyl)glycinate] (22) (from the Reaction with 16).** Silica column chromatography of the crude product (chloroform/MeOH 30:1) yielded 448 mg (89%) of 22 as a pale yellow waxy solid.  $^1\text{H}$  NMR ( $\text{DMSO}-d_6$ ):  $\delta$  0.93 (t,  $J$  = 7.3 Hz, 3H, C18-H), 2.16 (q,  $J$  = 7.3

Hz, 2H, C19-H), 2.38 (t',  $J = 6.4$  Hz, 2H,  $\text{CH}_2\text{C}(\text{O})\text{NH}$ ), 3.29–3.66 (m, 26H,  $\text{NCH}_2\text{CH}_2\text{O}$ ,  $\text{OCH}_2\text{CH}_2\text{O}$ ), 4.01/4.20 (dd,  $J_{\text{AB}} = 18.3$  Hz,  $J_{\text{AX}} = 5.8$  Hz, 2H,  $\text{NHCH}_2\text{CO}$ ), 5.26 (s, 2H, C5-H), 5.50 (s, 2H, C17-H), 7.01 (s, 2H,  $\text{C}(\text{O})\text{-CH=CHCO}$ ), 7.16 (s, 1H, C14-H), 7.70 (t',  $J = 7.5$  Hz, 1H, C10-H), 7.87 (t',  $J = 7.8$  Hz, 1H, C11-H), 8.11 (d,  $J = 7.5$  Hz, 1H, C9-H), 8.17 (d,  $J = 8.7$  Hz, 1H, C12-H), 8.41 (t,  $J = 5.8$  Hz, 1H, NH), 8.67 (s, 1H, C7-H).  $^{13}\text{C}$  NMR ( $\text{DMSO}-d_6$ ):  $\delta$  7.42 (C18), 30.32 (C19), 35.63 ( $\text{CH}_2\text{C}(\text{O})\text{NH}$ ), 36.60 ( $\text{NCH}_2\text{CH}_2\text{O}$ ), 50.06 (C5), 66.22 (C17), 66.44, 66.83, 69.30, 69.40, 69.53, 69.63 ( $\text{OCH}_2$ ,  $\text{CH}_2\text{NH}$ ), 76.10 (C20), 95.14, 118.85, 127.58, 127.84, 128.41, 128.82, 129.59, 130.31, 131.43, 134.44 ( $\text{C}(\text{O})\text{CH=CHCO}$ ), 144.98, 145.84, 147.78, 152.22, 156.38 (C2,3,6–16,16a), 166.96, 169.00, 170.57, 170.80 (C21,  $\text{C}(\text{O})\text{CH=CHCO}$ ,  $\text{C}(\text{O})\text{OC20}$ ,  $\text{C}(\text{O})\text{NH}$ ). ESI-MS (4.0 kV, MeOH):  $m/z$  (%) 843.2 ( $[\text{M} + \text{Na}]^+$ , 100). Purity determined by HPLC (MeOH/water 70:30): >97%.

**Camptothecin-20-[(12-benzyloxy-4,7,10-trioxadodecanoyl)glycinate] (26) (from the Reaction with 25).** Recrystallization of the crude product from EtOH yielded 257 mg (60%) of **26** as a pale yellow powder.  $^1\text{H}$  NMR ( $\text{DMSO}-d_6$ ):  $\delta$  0.93 (t,  $J = 7.5$  Hz, 3H, C18-H), 2.16 (q,  $J = 7.5$  Hz, 2H, C19-H), 2.34–2.43 (m, 2H,  $\text{CH}_2\text{C}(\text{O})\text{-NH}$ ), 3.39–3.66 (m, 14H,  $\text{NCH}_2\text{CH}_2\text{O}$ ,  $\text{OCH}_2\text{CH}_2\text{O}$ ), 4.01/4.20 (dd,  $J_{\text{AB}} = 17.9$  Hz,  $J_{\text{AX}} = 5.8$  Hz, 2H,  $\text{NHCH}_2\text{CO}$ ), 4.45 (s, 2H,  $\text{CH}_2\text{Ar}$ ), 5.24 (s, 2H, C5-H), 5.50 (s, 2H, C17-H), 7.16 (s, 1H, C14-H), 7.21–7.38 (m, 6H, Ar-H, C10-H), 7.81–7.91 (m, 1H, C11-H), 8.10 (d,  $J = 7.5$  Hz, 1H, C9-H), 8.17 (d,  $J = 8.3$  Hz, 1H, C12-H), 8.42 (t,  $J = 5.8$  Hz, 1H, NH), 8.66 (s, 1H, C7-H).  $^{13}\text{C}$  NMR ( $\text{DMSO}-d_6$ ):  $\delta$  7.41 (C18), 30.30 (C19), 35.63 ( $\text{CH}_2\text{C}(\text{O})\text{NH}$ ), 50.07 (C5), 66.21 (C17), 66.43, 69.00, 69.40, 69.52, 69.63, 69.68, 71.89 ( $\text{OCH}_2$ ,  $\text{CH}_2\text{NH}$ ), 76.10 (C20), 95.16, 118.84, 127.24, 127.36, 127.59, 127.84, 128.09, 128.42, 128.82, 129.61, 130.32, 131.44, 138.36, 144.98, 145.84, 147.78, 152.23, 156.38 (C2,3,6–16,16a, Ar), 166.97, 169.00, 170.56 (C21,  $\text{C}(\text{O})\text{OC20}$ ,  $\text{C}(\text{O})\text{NH}$ ). ESI-MS (4.0 kV, MeOH):  $m/z$  (%) 722.3 ( $[\text{M} + \text{Na}]^+$ , 100).

**Camptothecin-20-[(12-hydroxy-4,7,10-trioxadodecanoyl)glycinate] (27).** To a suspension of **26** (218 mg, 0.312 mmol) and 200 mg Pd/C (10% Pd) in 20 mL of ethanol (abs.) was added 1 mL of cyclohexene. After heating under reflux for 16 h, the hot reaction mixture was filtered over Celite, and the solids were washed with a total amount of 50 mL  $\text{CH}_2\text{Cl}_2$ . The solvent was removed in vacuo, and the crude product was recrystallized from ethanol to yield 116 mg (61%) of **27** as a pale yellow powder.  $^1\text{H}$  NMR ( $\text{DMSO}-d_6$ ):  $\delta$  0.94 (t,  $J = 7.5$  Hz, 3H, C18-H), 2.17 (q,  $J = 7.5$  Hz, 2H, C19-H), 2.32–2.45 (m, 2H,  $\text{CH}_2\text{C}(\text{O})\text{NH}$ ), 3.29–3.71 (m, 14H,  $\text{NCH}_2\text{CH}_2\text{O}$ ,  $\text{OCH}_2\text{CH}_2\text{O}$ ), 4.02/4.21 (dd,  $J_{\text{AB}} = 18.1$  Hz,  $J_{\text{AX}} = 5.8$  Hz, 2H,  $\text{NHCH}_2\text{CO}$ ), 4.56 (t,  $J = 5.5$  Hz, 1H, OH), 5.23 (s, 2H, C5-H), 5.50 (s, 2H, C17-H), 7.15 (s, 1H, C14-H), 7.70 (t',  $J = 7.0$  Hz, C10-H), 7.80–7.91 (m, 1H, C11-H), 8.09 (d,  $J = 7.5$  Hz, 1H, C9-H), 8.16 (d,  $J = 8.3$  Hz, 1H, C12-H), 8.43 (t,  $J = 5.8$  Hz, 1H, NH), 8.65 (s, 1H, C7-H).  $^{13}\text{C}$  NMR ( $\text{DMSO}-d_6$ ):  $\delta$  7.43 (C18), 30.30 (C19), 35.62 ( $\text{CH}_2\text{C}(\text{O})\text{NH}$ ), 50.05 (C5), 66.21 (C17), 66.43, 69.40, 69.51, 69.61, 69.66, 72.21 ( $\text{OCH}_2$ ,  $\text{CH}_2\text{NH}$ ), 76.10 (C20), 95.15, 118.84, 127.57, 127.82, 128.39, 128.80, 129.58, 130.31, 131.43, 144.98, 145.82, 147.76, 152.20, 156.37 (C2,3,6–16,16a), 166.97, 169.00, 170.58 (C21,  $\text{C}(\text{O})\text{OC20}$ ,  $\text{C}(\text{O})\text{NH}$ ). ESI-MS (4.0 kV, MeOH):  $m/z$  (%) 632.3 ( $[\text{M} + \text{Na}]^+$ , 100). Purity determined by HPLC (MeOH/water 70:30), >97%.

**Determination of the Water Solubility of Compounds 20–22 and CPT.** A stock solution of the most water-soluble compound (**22**) in isotonic NaCl solution

(200  $\mu\text{g/mL}$ ) was diluted to concentrations of 50, 100, and 150  $\mu\text{g/mL}$ . The UV absorptions of all four concentrations were determined at 370 nm, and a calibration curve was generated from these results. Subsequently, compounds **20–22** and CPT were suspended in isotonic NaCl solution. After sonification in an ultrasound bath for 10 min at 25 °C, the samples were centrifuged, and the UV absorptions of the supernatants were measured at 370 nm. Finally, the concentrations of the saturated solutions were calculated by comparing the UV absorptions with the calibration curve of **22**.

#### Incubation Studies with Human Blood Plasma.

A stock solution of **19**, **20**, **22**, or **27** in MeOH (4 mM) or **22** in saline/Tween 80 9:1 was added to a 20-fold volume of human blood plasma (EDTA stabilized) preincubated at 37 °C, and the samples were incubated for 3–5 min at 37 °C; a 50  $\mu\text{L}$  sample was analyzed by HPLC. To study the stability of the albumin conjugates of **19** and **22**, the solutions were incubated at 37 °C for further 48 h. Samples were collected after 4, 20, 28, and 48 h and analyzed by HPLC. The decrease in the peak area of the conjugate at 370 nm with time was used to determine the half-lives.

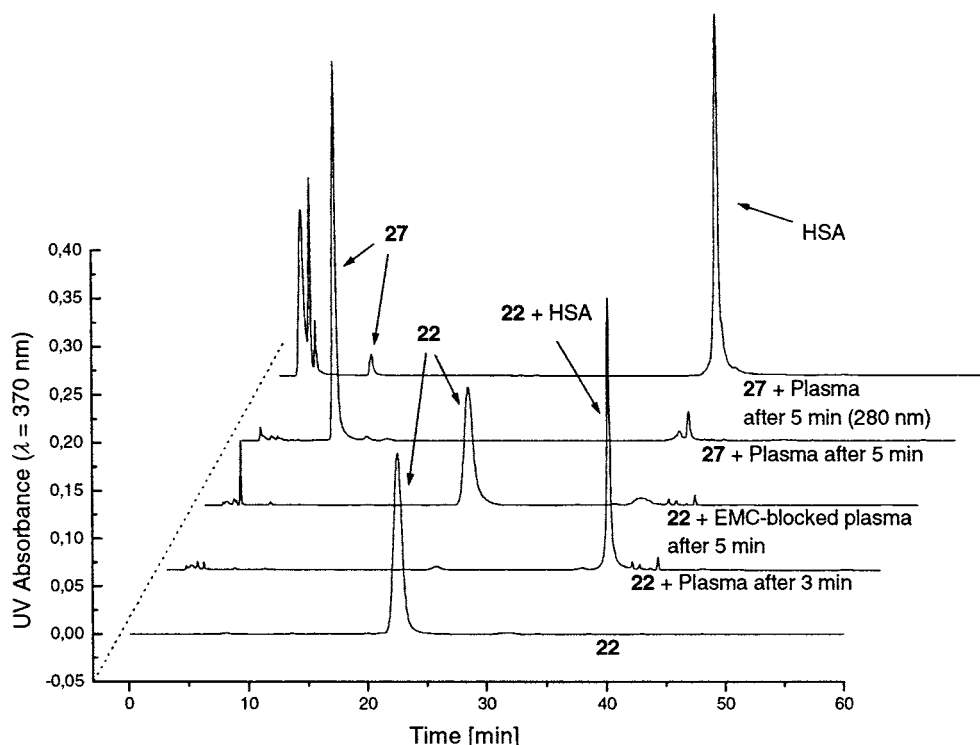
**In vivo Efficacy of 19 and 22.** For the in vivo testing of **19** and **22** in comparison with CPT female Ncr, nu/nu mice (Taconic breeding facility, Germantown, PA) were used. The mice were held in laminar flow shelves under sterile and standardized environmental conditions ( $25 \pm 2$  °C room temperature,  $50\% \pm 10\%$  relative humidity, 12 h light-dark-rhythm). They received autoclaved food and bedding (ssniff, Soest, Germany) and acidified (pH 4.0) drinking water ad libitum. All animal experiments were performed under the auspices of the German Animal Protection Law.

Aproximately  $10^7$  cells of HT-29 tumor tissue were transplanted subcutaneously (s.c.) into the left flank region of anaesthetized (40 mg/kg i.p. Radenarkon, Asta Medica, Frankfurt, Germany) mice on day zero. Mice were randomly distributed to the experimental groups (eight mice per group). When the tumors were grown to a palpable size (90–130 mm<sup>2</sup>), treatment was initiated (see Figure 3). Mice were treated intravenously at day 13, 17, 21, and 24 with either saline/Tween 80 9:1, camptothecin, **19** or **22** (compounds were administered as microsuspensions in saline/Tween 80 9:1); for doses, see corresponding tables and figures. The volume of administration was 0.15–0.3 mL/25 g body weight.

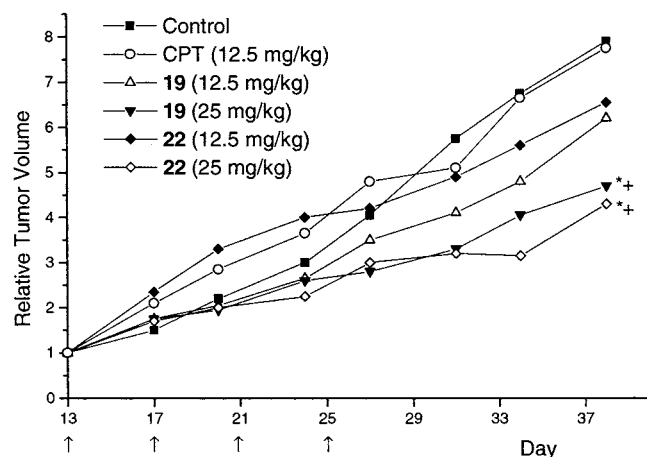
Tumor size was measured twice weekly with a calliper-like instrument in two dimensions. Individual tumor volumes ( $V$ ) were calculated by the formula  $V = (\text{length} + [\text{width}]^2)/2$  and related to the values on the first day of treatment (relative tumor volume, RTV). At each measurement day, treated/control values ( $T/C$ ) were calculated as percentage for each experimental group; the optimum (lowest) values obtained within two weeks after treatment were used for evaluating the efficacy of the compounds, and optimum  $T/C$  values are presented in the respective tables. Statistical analysis was performed with the U-test (Mann and Whitney) with  $p < 0.05$ . The body weight of mice was determined every 3–4 days and is depicted in Figure 5, Supporting Information. The maximum change in body weight (BWC) after initiation of treatment is presented in the respective tables.

## RESULTS

**Preparation of the Heterobifunctional Cross-Linkers 12–16.** The synthetic approach for obtaining compounds **12–16** was performed as a three-step proce-



**Figure 2.** Chromatograms of incubation studies of human plasma [and human plasma preincubated with 6-maleimidocaproic acid (EMC)] with methanolic solutions of **22** and **27** at 37 °C. Concentration of the CPT derivatives was 200  $\mu$ M. Chromatographic conditions: see Experimental Procedures.



**Figure 3.** Curves Depicting Tumor Growth Inhibition of Subcutaneously HT-29 Xenografts under Therapy with Camptothecin, **19**, and **22**. \*, significant to saline/Tween 80; +, significant to camptothecin.

cedure that included a monoalkylation of the oligo(ethylene glycol) to introduce a *tert*-butyl protected carboxylic group in the first step, followed by a Mitsunobu reaction introducing the maleimide group, and a cleavage of the *tert*-butyl ester in the final step (see Schemes 1–4). For the cross-linkers **12** and **13**, the synthetic route starts with a monoalkylation of tri- and hexaethylene glycol, respectively, as depicted in Scheme 1. Treatment of *tert*-butyl bromoacetate with an excess of the deprotonated oligo(ethylene glycol) afforded the *tert*-butyl esters **2** and **3** in low to moderate yields. It was found that method B (KH, heating under reflux) produced significantly higher yields than method A (NaH, stirring at room temperature). Compounds **4–6** with an additional methylene group were obtained using a modification of a published procedure (see Scheme 2) (17). Michael-addition of an

excess of the oligo(ethylene glycol) to *tert*-butyl acrylate in the presence of a catalytic amount of potassium *tert*-butoxide provided the *tert*-butyl esters **4–6** in moderate to good yields.

For introducing the maleimide group, the Mitsunobu reaction has proven useful as reported by Walker (18, 19). Hence, the alcohols **2–6** were treated with  $\text{Ph}_3\text{P}$ /DIAD, neopentyl alcohol, and maleimide to yield the compounds **7–12**; three methods were used which differ in reaction temperature, order of addition, and the use of polymer-bound  $\text{Ph}_3\text{P}$  (Scheme 3):

(a) Method A denotes the procedure originally described by Walker<sup>2</sup> (–78 °C, order of addition: 1,  $\text{Ph}_3\text{P}$ ; 2, DIAD; 3, alcohol/neopentyl alcohol; 4, maleimide) (19).

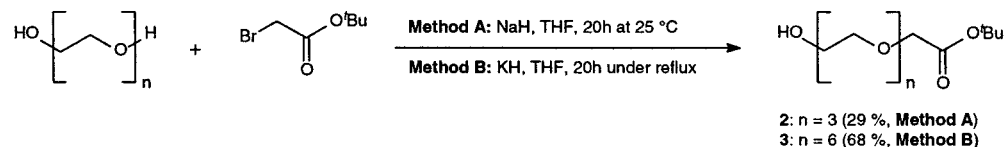
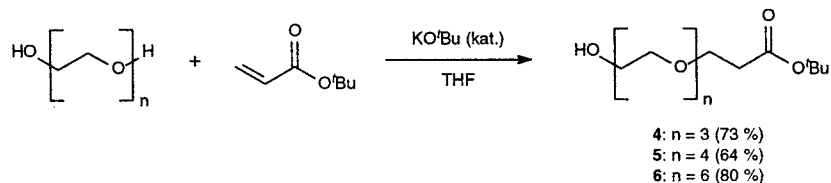
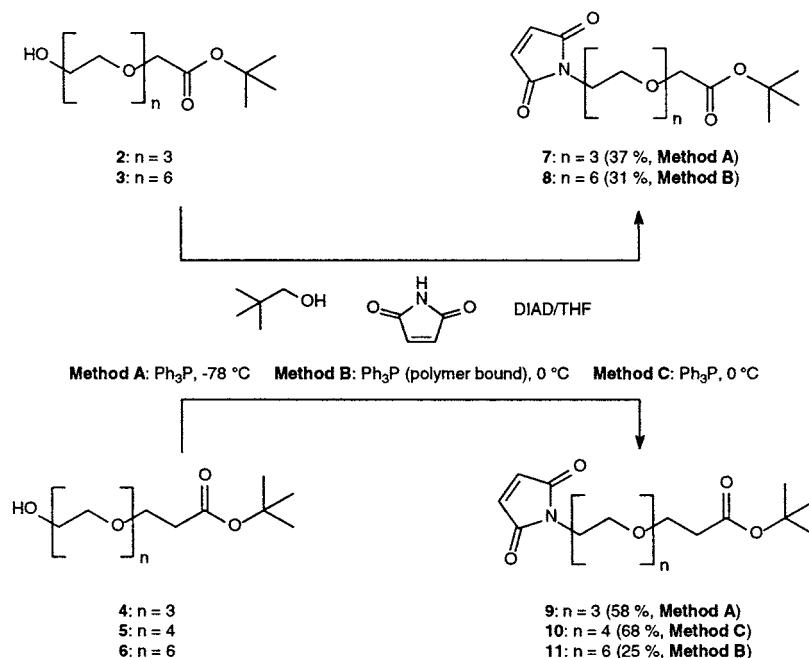
b) Method B uses polymer-bound  $\text{Ph}_3\text{P}$ .

c) Method C is the procedure typically utilized for the Mitsunobu esterification (0 °C, order of addition: 1,  $\text{Ph}_3\text{P}$ /alcohol/neopentyl alcohol/maleimide; 2, DIAD).

The obtained yields were poor to moderate when applying method A (compounds **7** and **9**). In contrast to Walker's results, we found that neither the order of addition of the reactants nor the reaction temperature had a significant influence on yield. Therefore, the preparation of **8**, **10**, and **11** was carried out more conveniently using the reaction conditions of the Mitsunobu esterification (methods B and C). The use of polymer-bound  $\text{Ph}_3\text{P}$  in the case of the hexaethylene glycol derivatives **8** and **12** (method B) turned out to be necessary since  $\text{Ph}_3\text{P}$  reacts to  $\text{Ph}_3\text{P}=\text{O}$  as a byproduct which proved to be difficult to separate from the products. In contrast, polymer-bound  $\text{Ph}_3\text{P}=\text{O}$  was removed by simple filtration.

<sup>2</sup> Instead of the hazardous and no longer commercially available diethyl azodicarboxylate (DEAD), diisopropyl azodicarboxylate (DIAD) was used. Walker reported slightly lower yields when employing DIAD (19).



**Scheme 1. Synthesis of Compounds 2 and 3****Scheme 2. Synthesis of Compounds 4–6****Scheme 3. Synthesis of Compounds 7–11**

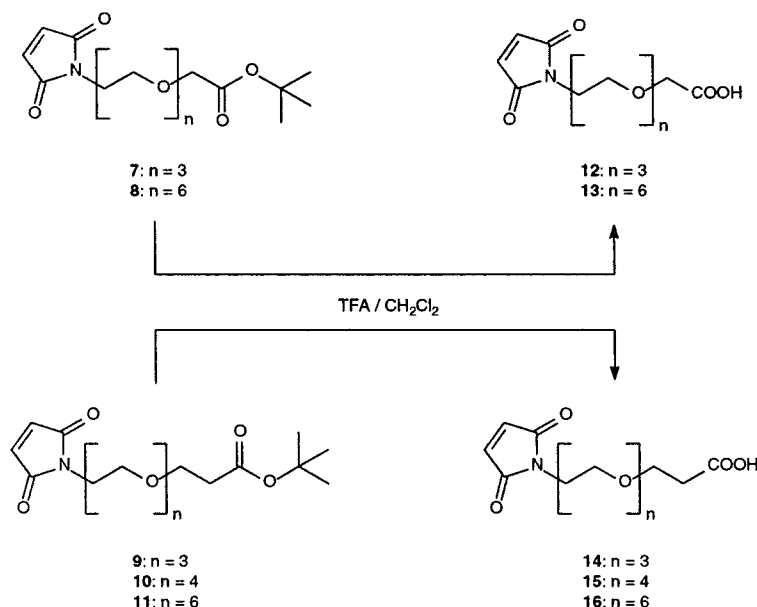
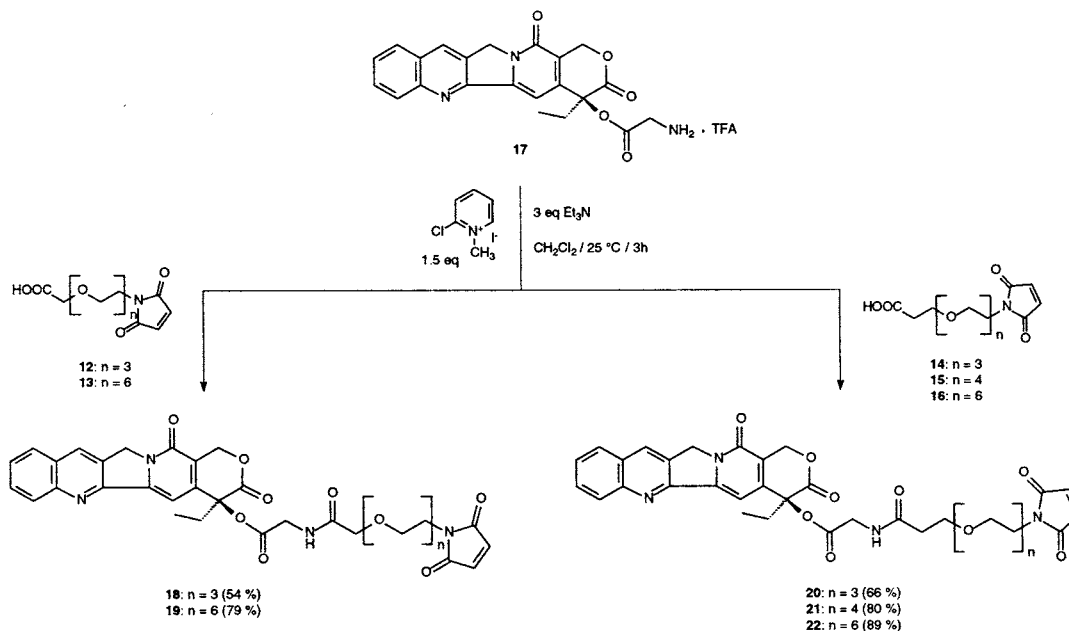
In the last step, quantitative cleavage of the *tert*-butyl esters was achieved by treatment of compounds 7–11 with trifluoroacetic acid (Scheme 4). Since complete removal of the latter under high vacuum could not be achieved, Amberlyst A-21 was successfully employed to scavenge excessive TFA. The heterobifunctional cross-linkers 12–16 were characterized by  $^1\text{H}$  and  $^{13}\text{C}$  NMR spectroscopy. They are oily substances which tend to polymerize at room temperature, but can be stored at  $-20^\circ\text{C}$  for several weeks without decomposition.

**Preparation of the Albumin-Binding Prodrugs 18–22.** For the synthesis of the albumin-binding prodrugs, 12–16 were reacted with camptothecin-20-*O*-glycinate trifluoroacetate (17) prepared according to a two-step procedure (16). Treatment of 17 with compounds 12–16 in the presence of the Mukaiyama reagent, 2-chloro-1-methylpyridinium iodide, and triethylamine afforded the prodrugs 18–22 in good yields (Scheme 5). The pale yellow crystalline to waxy solids were characterized by  $^1\text{H}$  and  $^{13}\text{C}$  NMR spectroscopy as well as mass spectrometry, and purity was determined by HPLC (see Experimental Section).

**Preparation of a Non-Albumin-Binding Camptothecin Derivative 27.** A compound with a structure analogous to 20, but with a hydroxy group instead of the maleimide moiety, was synthesized as a potential non-

albumin-binding camptothecin derivative. Scheme 6 shows the synthesis consisting of five steps starting with triethylene glycol. In the first step, the diol was mono-protected with benzyl bromide, followed by a Michael-addition of *tert*-butyl acrylate. In steps three and four, the *tert*-butyl ester was cleaved, and the resulting carboxylic acid (25) was then reacted with 17 to yield a benzyl-protected analogue of 20. To enhance water solubility, 26 was deprotected to afford 27 which was characterized using  $^1\text{H}$  and  $^{13}\text{C}$  NMR spectroscopy, mass spectrometry, and HPLC.

**Water Solubility of the Prodrugs 20–22.** Ideally, 18–22 should be sufficiently water soluble for intravenous application as albumin-binding prodrugs. Water solubility of compounds 20–22 and CPT was determined by measuring the UV absorbance of a saturated solution of the respective compound in isotonic NaCl-solution. The results are shown in Table 1. While the observed solubility of CPT was in the range of the published value ( $2.5\ \mu\text{g/mL}$ ) (2), water solubility of 20–22 improved with increasing numbers of internalized ether bonds. Compound 22 which incorporated the longest oligo(ethylene glycol) spacer, turned out to be 27-fold more water soluble than CPT. Furthermore, 19 had a nearly identical water solubility compared to 22 due to the same number of incorporated ethylene glycol units.

**Scheme 4. Synthesis of the Heterobifunctional Cross-Linkers 12–16****Scheme 5. Synthesis of the Albumin-Binding CPT Prodrugs 18–22**

**Albumin-Binding Properties of Compounds 19, 20, 22, and 27.** To determine that 18–22 bind rapidly and selectively to the cysteine-34 group of endogenous HSA, HPLC-studies with human plasma were performed at  $\lambda = 370$  nm, the maximum absorbance of CPT derivatives in the near UV-region. Figure 2 shows the chromatographic profile on a reversed phase system of 22 incubated with human blood plasma for 3 min. While the unbound compound elutes at  $\sim 22$  min, the signal disappears almost completely after incubation with human plasma, and a single peak eluting at the retention time of HSA (36–37 min) is observed. The coupling behavior was independent of whether 22 was dissolved in methanol or in saline/Tween 80 9:1. Very similar results were obtained with compounds 19 and 20 (not depicted).

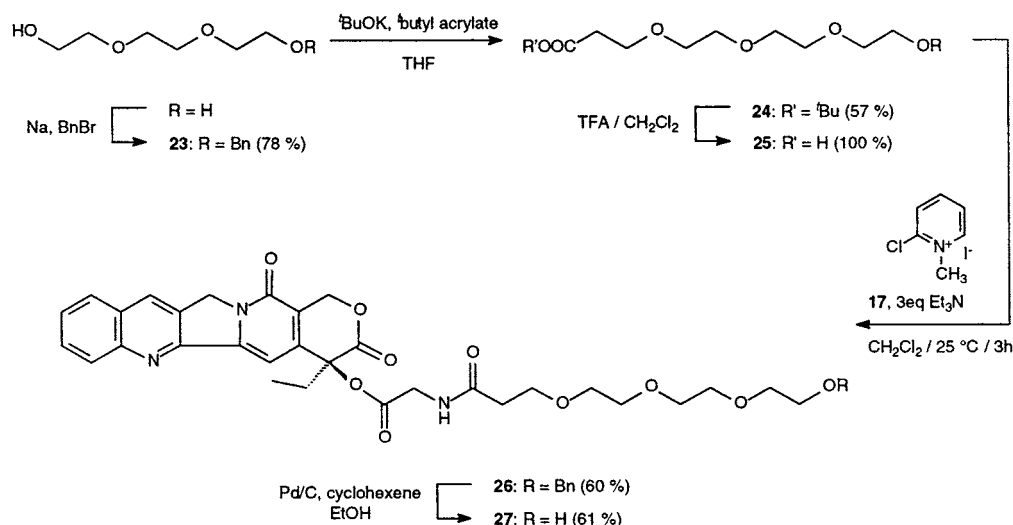
To prove that the fast binding result from a Michael-addition of the sulfhydryl group of HSA with the maleimide group of the prodrug, analogous HPLC experiments were carried out in which the cysteine-34 position of

endogenous HSA was blocked with an excess of  $\epsilon$ -maleimidocaproic acid prior to incubation with 22 (see Figure 2). In this case, marginal binding to HSA was observed after incubating plasma with 22 for 5 min. In an additional experiment with compound 27 which contains a hydroxy group instead of the maleimide ring, negligible binding to HSA could be detected after incubating 27 with plasma for 5 min (see Figure 2).

**Stability of 19 and 22 Bound to the Cysteine-34 Position of HSA in Human Plasma.** To determine the plasma stability of the two compounds that were tested *in vivo* (19 and 22, see below), the respective albumin conjugates were generated by incubation of the CPT derivatives with human blood plasma for 3 min at  $37^\circ\text{C}$  and subsequently analyzing samples after 3 min, 4, 20, 28, and 48 h through HPLC. From the decrease of the peak areas, the half-lives of the conjugates of 19 and 22 were calculated: 19,  $t_{1/2} = 9$  h; 22,  $t_{1/2} = 15$  h.

**In Vivo Activity of 19 and 22 Compared with CPT.** The *in vivo* efficacy of the most water-soluble compounds

## Scheme 6. Synthesis of the Non-Albumin-Binding CPT Derivative 27



**Table 1. Water-Solubilities of the Prodrugs 20–22 and Camptothecin Determined by UV Measurement ( $\lambda = 370$  nm) of Saturated Solutions (0.9% NaCl Solution)**

compound	MW [g/mol]	<i>n</i>	solubility	
			[ $\mu$ mol/L]	[ $\mu$ g/mL]
CPT	348.36	—	11 ( $\pm$ 1)	3.8 ( $\pm$ 0.3)
<b>20</b>	688.69	3	120 ( $\pm$ 2)	83 ( $\pm$ 2)
<b>21</b>	732.74	4	185 ( $\pm$ 3)	135 ( $\pm$ 2)
<b>22</b>	820.85	6	296 ( $\pm$ 7)	243 ( $\pm$ 6)

**Table 2. Antitumor Activity against Human Colorectal Xenografts (HT-29) in Vivo<sup>a</sup>**

compound	dose <sup>b</sup> [mg/kg]	total mortality	body weight change [%] (day 13–17)	<i>T/C</i> [%] maximal
CPT	12.5	0/8	+4	89 (day 31)
<b>19</b>	12.5	0/8	+2	71 (day 34)
<b>19</b>	25	0/8	0	57** (day 31)
<b>22</b>	12.5	0/8	+4	83 (day 38)
<b>22</b>	25	0/8	+1	47** (day 34)

<sup>a</sup> \*, significant to saline/Tween 80; +, significant to camptothecin. <sup>b</sup> Dose refers to CPT equivalents.

**19** and **22** and of CPT was assessed in xenografted nude mice using a human HT-29 colorectal cell line. CPT was evaluated at a dose of  $4 \times 12.5$  mg/kg (i.v.), which was reported to be the maximum tolerated dose (MTD) for camptothecin in nude mice (11). Both prodrugs were tested at the same dose and at a dose of  $4 \times 25$  mg/kg (i.v.) CPT equivalents. Table 2 and Figure 3 show the results of this experiment. In general, all compounds were well-tolerated since only marginal body weight changes were observed [see Table 2 and Figure 5, Supporting Information]. Whereas CPT ( $4 \times 12.5$  mg/kg) was completely inactive, both prodrugs exhibited a moderate antitumor activity at the same dose. Mice treated with **19** and **22** at the higher dose ( $4 \times 25$  mg/kg CPT equivalents) showed a clear response (*T/C* max.: 57% and 47%, respectively).

## DISCUSSION

The pathophysiology of tumor tissue, characterized by angiogenesis, hypervascularity, a defective vascular architecture, and an impaired lymphatic drainage, seems to be a universal feature of solid tumors that can be exploited for tumor-selective drug delivery using macromolecules as drug carriers (described in the literature

as the EPR effect) (20). In recent work, it was shown that the anticancer drug camptothecin is suitable for developing drug delivery systems by conjugating the 20-OH position of CPT through a glycine spacer to synthetic polymers such as PEG, HPMA copolymers, and poly(glutamic acid) (16, 21, 22). Besides a drug-targeting effect resulting from the macromolecular character of these drug–polymer conjugates, three further advantages were apparent:

(i) esterifying the 20-hydroxy group of CPT stabilizes the drug in its active lactone form (closed E-ring), which otherwise tends to hydrolyze under physiological conditions leading to the inactive and toxic hydroxycarboxylic acid form (23);

(ii) the incorporation of a glycine spacer ensures a controlled release of the drug (16);

(iii) the use of hydrophilic polymers leads to highly water-soluble formulations of CPT.

Due to our interest in the potential of circulating albumin as a drug carrier, we developed thiol-binding prodrugs of camptothecin in this work. To enhance the water solubility of CPT prodrugs, heterobifunctional cross-linkers based on oligo(ethylene glycols) (**12–16**) were prepared in a three-step procedure.

**12–16** were further reacted with camptothecin 20-O-glycidate to yield the thiol-binding prodrugs **18–22** that differ in the length of the oligo(ethylene glycol) chain and number of methylene groups adjacent to the amide bond [ $(\text{CH}_2)_n$ ,  $n = 1$  or 2]. Determination of the solubility of compounds **20–22** in saline (see Table 1) revealed that water solubility improves with the number of incorporated ether-bonds, the hexa(ethylene glycol) derivative (**22**) being 27-fold more soluble than CPT. A plot illustrating the relation between the number of oxygen atoms of the linker and the molar solubility of the respective prodrug is depicted in Figure 4, Supporting Information. In the range of 3–6 oxygen atoms, a linearity was observed. Assuming that linearity is also valid for more than six oxygen atoms, the required number of ethylene glycol-units for achieving a water solubility of 1 mg/mL (CPT equivalents) that was considered to be feasible for i.v. administration was estimated to be approximately 50 by extrapolating the linear-fitted curve. This means that following our strategy, a poly(ethylene glycol) linker with a molecular weight  $>2000$  Da [ $(\text{CH}_2-\text{CH}_2-\text{O})_n$ ,  $n \geq 50$ ] would have been needed, which is not practicable bearing in mind that our



aim was to develop well-defined low-molecular weight drugs. Although our approach to water-soluble CPT prodrugs employing oligo(ethylene glycol)-based linkers was not optimal, the same strategy has recently proven very successful when developing albumin-binding derivatives of the anticancer drugs doxorubicin (24) and carboplatin (25).

The CPT prodrugs were, however, sufficiently water soluble to assess their albumin-binding properties in human plasma. **18–22** bind quantitatively and selectively to the cysteine-34 position of HSA within 3 min of incubation in human blood plasma at 37 °C, whereas binding to other serum proteins was negligible. Furthermore, we found that the length of the cross-linker does not substantially influence the binding rate.

Plasma stabilities of the albumin conjugates of compounds **19** and **22** that were tested in vivo were determined by HPLC. We expected that the amide bond of **19** with an electron-withdrawing alkoxy group in the  $\alpha$ -position would be cleaved more rapidly than that of **22** incorporating an additional methylene group. The obtained results confirmed our presumption: The half-lives of the albumin conjugate of **19** and **22** determined at 37 °C were 9 and 15 h, respectively, showing a clear effect of the additional methylene group. Compared to the plasma stability of an analogous CPT-gly-PEG conjugate ( $t_{1/2}$  = 4 h) (26), the half-life of the albumin conjugate of **19** increased approximately 2-fold. This difference is probably due to a stabilizing effect of the protein environment. In our HPLC studies a number of degradation products including CPT as well as CPT-20-*O*-glycinate were noted over time which could be either due to hydrolysis or enzymatic cleavage (27).

The antitumor activity of **19**, **22**, and CPT was studied in HT-29 xenografted nude mice in order to obtain a first proof of concept in vivo. Due to insufficient water solubility, all compounds were administered as microsuspensions using a saline/Tween 80 mixture. The results showed no antitumor effect for CPT at the reported MTD of  $4 \times 2.5$  mg/kg (11) whereas the same dose induced a moderate activity in case of both prodrugs. A clear response was observed when applying twice the dose ( $4 \times 25$  mg/kg). In all cases the compounds were well-tolerated, showing no body weight reductions indicating that the MTDs of all compounds were not reached in this experiment. Interestingly, **19** and **22** showed comparable antitumor activity although they differ in their plasma stabilities.

In summary, we have prepared first examples of maleimide-containing prodrugs of the anticancer drug camptothecin that bind rapidly and selectively to the cysteine-34 position of endogenous serum albumin and were superior to the parent compound in a HT-29 colorectal model. Our next steps will focus on the development of highly water-soluble albumin-binding CPT prodrugs by incorporating other hydrophilic moieties such as ionic groups or glycosides.

#### ACKNOWLEDGMENT

The support of the Dr. Mildred-Scheel Stiftung der Deutschen Krebshilfe is gratefully acknowledged. Furthermore, we like to thank Cornelia Stockmar, Peter Lazar, and Karin Scheuermann for their technical assistance and Dr. Iduna Fichtner from Max-Delbrück Centrum Berlin for performing in vivo studies.

**Supporting Information Available:** Curves depicting water solubility and weight change. This material is

available free of charge via the Internet at <http://pubs.acs.org>.

#### LITERATURE CITED

- (1) Wall, M. E., Wani, M. C., Cook, C. E., and Palmer, K. H. (1966) Plant antitumor agents. I. The isolation and structure of camptothecin, a novel alkaloidal leukemia and tumor inhibitor from *camptotheca acuminata*. *J. Am. Chem. Soc.* **88**, 3888–3890.
- (2) Kingsbury, W., Boehm, J., Jakas, D., Holden, K., Hecht, S., Gallagher, G., Caranfa, M., McCabe, F., Faucette, L., Johnson, R., and Hertzberg, R. (1991) Synthesis of water-soluble (aminoalkyl)camptothecin analogues: inhibition of topoisomerase I and antitumor activity. *J. Med. Chem.* **34**, 98–107.
- (3) Gottlieb, J. A., Guarino, A. M., and Call, J. B. (1970) Preliminary pharmacologic and clinical evaluation of camptothecin sodium (NSC-100880). *Cancer Chemother. Rep.* **54**, 461–470.
- (4) Schaeppi, U., Fleischman, R. W., and Cooney, D. A. (1974) Toxicity of camptothecin (NSC-100880). *Cancer Chemother. Rep.* **3**, 5, 25–36.
- (5) Hsiang, Y.-H., Hertzberg, R., Hecht, S., and Liu, L. F. (1985) Camptothecin induces protein-linked DNA breaks via mammalian DNA topoisomerase I. *J. Biol. Chem.* **260**, 14873–14878.
- (6) Kollmannsberger, C., Mross, K., Jakob, A., Kanz, L., and Bokemeyer, C. (1999) Topotecan – a novel topoisomerase I inhibitor: pharmacology and clinical experience. *Oncology* **56**, 1–12.
- (7) Rothenberg, M. L. (2001) Irinotecan (CPT-11): recent developments and future directions – colorectal cancer and beyond. *Oncologist* **6**, 66–80.
- (8) Kratz, F., Warnecke, A., Rodrigues, P. C. A., and Riebesell, K. (2001) Anticancer drug conjugates with macromolecular carriers. In *Polymeric Biomaterials*, 2 ed. (S. Dumitriu, Ed.) pp 851–894, Marcel Dekker, New York.
- (9) Putnam, D., and Kopecek, J. (1995) Polymer conjugates with anticancer activity. *Adv. Polym. Sci.* **122**, 55–123.
- (10) Schoemaker, N. E., van Kesteren, C., Rosing, H., Jansen, S., Swart, M., Lieverst, J., Fraier, D., Breda, M., Pellizzoni, C., Spinelli, R., Grazia Porro, M., Beijnen, J. H., Schellens, J. H., and ten Bokkel Huinink, W. W. (2002) A phase I and pharmacokinetic study of MAG-CPT, a water-soluble polymer conjugate of camptothecin. *Br. J. Cancer* **87**, 608–614.
- (11) Caiolfa, V. R., Zama, M., Fiorino, A., Frigerio, E., Pellizzoni, C., d'Argy, R., Ghiglieri, A., Castelli, M. G., Farao, M., Pesenti, E., Gigli, M., Angelucci, F., and Suarato, A. (2000) Polymer-bound camptothecin: initial biodistribution and antitumor activity studies. *J. Controlled Release* **65**, 105–119.
- (12) Greenwald, R. B. (2001) PEG drugs: an overview. *J. Controlled Release* **74**, 159–171.
- (13) Kratz, F., Roth, T., Fichtner, I., Schumacher, P., Fiebig, H. H., and Unger, C. (2000) In vitro and in vivo efficacy of acid-sensitive transferrin and albumin doxorubicin conjugates in a human xenograft panel and in the MDA-MB-435 mammary carcinoma model. *J. Drug Targeting* **8**, 305–318.
- (14) Kratz, F., Mueller-Driver, R., Hofmann, I., Dreves, J., and Unger, C. (2000) A novel macromolecular prodrug concept exploiting endogenous serum albumin as a drug carrier for cancer chemotherapy. *J. Med. Chem.* **43**, 1253–1256.
- (15) Kratz, F., Warnecke, A., Scheuermann, K., Stockmar, C., Schwab, J., Lazar, P., Drückes, P., Esser, N., Dreves, J., Rognan, D., Bissantz, C., Hinderling, C., Folkers, G., Fichtner, I., and Unger, C. (2002) Probing the cysteine-34 position of endogenous serum albumin with thiol-binding doxorubicin derivatives: improved efficacy of an acid-sensitive doxorubicin derivative with specific albumin-binding properties compared to the parent compound. *J. Med. Chem.* **45**, 5523–5533.
- (16) Greenwald, R. B., Pendri, A., Conover, C. D., Lee, C., Choe, Y. H., Gilbert, C., Martinez, A., Xia, Y., Wu, D., and Hsue, M. (1998) Camptothecin-20-PEG ester transport forms: the effect of spacer groups on antitumor activity. *Bioorg. Med. Chem.* **6**, 551–562.

- (17) Seitz, O., and Kunz, H. (1997) HYCRON, an allylic anchor for high-efficiency solid-phase synthesis of protected peptides and glycopeptides. *J. Org. Chem.* **62**, 813–826.
- (18) Walker, M. A. (1994) The Mitsunobu reaction: a novel method for the synthesis of bifunctional maleimide linkers. *Tetrahedron Lett.* **35**, 665–668.
- (19) Walker, M. A. (1995) A high yielding synthesis of *N*-alkyl maleimides using a novel modification of the Mitsunobu reaction. *J. Org. Chem.* **60**, 5352–5355.
- (20) Maeda, H., Wu, J., Sawa, T., Matsumura, Y., and Hori, K. (2000) Tumor vascular permeability and the EPR effect in macromolecular therapeutics: a review. *J. Controlled Release* **65**, 271–284.
- (21) Fraier, D., Frigerio, E., Brianceschi, G., Casati, M., Benecchi, A., and James, C. (2000) Determination of MAG-camptothecin, a new polymer-bound camptothecin derivative, and free camptothecin in dog plasma by HPLC with fluorimetric detection. *J. Pharm. Biomed. Anal.* **22**, 505–514.
- (22) Singer, J. W., Bhatt, R., Tulinsky, J., Buhler, K. R., Heasley, E., Klein, P., and de Vries, P. (2001) Water-soluble poly-(L-glutamic acid)-glycamptothecin conjugates enhance camptothecin stability and efficacy in vivo. *J. Controlled Release* **74**, 243–247.
- (23) Zhao, H., Lee, C., Sai, P., Choe, Y. H., Boro, M., Pendri, A., Guan, S., and Greenwald, R. B. (2000) 20-*O*-Acylcamptothecin derivatives: evidence for lactone stabilization. *J. Org. Chem.* **65**, 4601–4606.
- (24) Mansour, A. M., Dreves, J., Esser, N., Hamada, F. M., Badary, O. A., Unger, C., Fichtner, I., and Kratz, F. A new approach for the treatment of malignant melanoma: enhanced antitumor efficacy of an albumin-binding doxorubicin prodrug that is cleaved by matrix metalloproteinase 2. *Cancer Res.*, submitted.
- (25) Warnecke, A., and Kratz, F. Highly water-soluble derivatives of the anticancer drug carboplatin as albumin-binding prodrugs. Manuscript in preparation.
- (26) Conover, C. D., Greenwald, R. B., Pendri, A., and Shum, K. L. (1999) Camptothecin delivery systems: the utility of amino acid spacers for the conjugation of camptothecin with polyethylene glycol to create prodrugs. *Anti-Cancer Drug Des.* **14**, 499–506.
- (27) Conover, C. D., Greenwald, R. B., Pendri, A., Gilbert, C. W., and Shum, K. L. (1998) Camptothecin delivery systems: enhanced efficacy and tumor accumulation of camptothecin following its conjugation to polyethylene glycol via a glycine linker. *Cancer Chemother. Pharmacol.* **42**, 407–414.

BC0256289

# Macromolecular MRI Contrast Agents with Small Dendrimers: Pharmacokinetic Differences between Sizes and Cores

Hisataka Kobayashi,<sup>\*,†</sup> Satomi Kawamoto,<sup>‡</sup> Sang-Kyung Jo,<sup>§</sup> Henry L. Bryant Jr.,<sup>||</sup> Martin W. Brechbiel,<sup>⊥</sup> and Robert A. Star<sup>§</sup>

Metabolism Branch, Center for Cancer Research, National Cancer Institute, National Institutes of Health, Bethesda, Maryland, Department of Radiology, School of Medicine, Johns Hopkins University, Baltimore, Maryland, Laboratory of Diagnostic Radiology Research, Warren Grant Magnuson Clinical Center, National Institutes of Health, Bethesda, Maryland, Radioimmune & Inorganic Chemistry Section, Radiation Oncology Branch, National Cancer Institute, National Institutes of Health, Bethesda, Maryland, and Renal Diagnostics and Therapeutics Unit, National Institutes of Diabetes and Digestive and Kidney Diseases, National Institutes of Health, Bethesda, Maryland. Received October 28, 2002; Revised Manuscript Received January 29, 2003

Large macromolecular MRI contrast agents with albumin or dendrimer cores are useful for imaging blood vessels. However, their prolonged retention is a major limitation for clinical use. Although smaller dendrimer-based MRI contrast agents are more quickly excreted by the kidneys, they are also able to visualize vascular structures better than Gd-DTPA due to less extravasation. Additionally, unlike Gd-DTPA, they transiently accumulate in renal tubules and thus also can be used to visualize renal structural and functional damage. However, these dendrimer agents are retained in the body for a prolonged time. The purpose of this study was to obtain information from which a macromolecular dendrimer-based MRI contrast agents feasible for use in further clinical studies could be chosen. Six small dendrimer-based MRI contrast agents were synthesized, and their pharmacokinetics, whole-body retention, and dynamic MRI were evaluated in mice to determine an optimal agent in comparison to Gd-[DTPA]-dimeglumine. Diaminobutane (DAB) dendrimer-based agents cleared more rapidly from the body than polyamidoamine (PAMAM) dendrimer-based agents with the same numbers of branches. Smaller dendrimer conjugates were more rapidly excreted from the body than the larger dendrimer conjugates. Since PAMAM-G2, DAB-G3, and DAB-G2 dendrimer-based contrast agents showed relatively rapid excretion, these three conjugates might be acceptable for use in further clinical applications.

## INTRODUCTION

Large macromolecular MRI contrast agents with either albumin or dendrimer cores were initially developed for imaging blood vessels because of their prolonged retention in the circulation compared with Gd-[DTPA] and their enhanced relaxivities (1–3). Smaller PAMAM-based macromolecular MRI contrast agents are not optimal vascular agents because they are rapidly cleared from the blood by glomerular filtration and subsequently excreted by the kidneys without significant retention (3–5). However, one of the relatively small dendrimer-based contrast agents with a generation-4 polyamidoamine (PAMAM) core [PAMAMG4-(1B4M-Gd)<sub>64</sub>] (termed herein as PAMAM-G4) transiently accumulated in renal tubules and allowed visualization of renal structural and functional damage in the mouse (6).

Unfortunately, many of the previously described dendrimer-based MR contrast agents are retained for lengthy

times in the body. Theoretical risk of increased toxicity from unstable Gd(III) chelation potentially releasing toxic Gd(III) ions might prevent their clinical use. For example, only 20% of injected dose (%ID) of the PAMAM-G4 based contrast agent was excreted from the body during the first 2 days (4, 5). In contrast, the liver MRI contrast agent based on a four-generation diaminobutane (DAB) dendrimer core [DAB-G4] was excreted from the body faster than PAMAM-G4 (7) despite its considerable accumulation in the liver. Yet, as previously demonstrated, smaller molecular weight dendrimer-based contrast agents consistently are more readily excreted from the body than are larger agents of similar architecture (3, 4). Therefore, small (MW < 60 kD) macromolecular MRI contrast agents with both PAMAM and DAB dendrimer cores were synthesized and their pharmacokinetic characteristics studied with respect to whole-body clearance rates, renal accumulation, and quality of MRI images that could be obtained.

## EXPERIMENTAL PROCEDURES

**Dendrimers.** A brief description of dendrimer terminology has been published by Tomalia (8). Polypropylenimine diaminobutyl (DAB) dendrimers [DAB-Am16, polypropylenimine hexadecaamine dendrimer, generation-2 (DAB-G2), DAB-Am32, polypropylenimine dotriacontamine dendrimer, generation-3 (DAB-G3), and DAB-Am64, polypropylenimine tetrahexacontamine dendrimer generation-4 (DAB-G4) (Aldrich Chemical Co., Milwau-

\* Corresponding author. Address: Metabolism Branch, Center for Cancer Research, National Cancer Institute, National Institutes of Health, Building 10, Room 4N109, 10 Center Drive, Bethesda, MD 20892-1374. Tel.: 1-301-435-8344. Fax: 301-496-9956. E-mail: Kobayash@mail.nih.gov.

† Center for Cancer Research, National Cancer Institute.

‡ Johns Hopkins University.

§ National Institutes of Diabetes and Digestive and Kidney Diseases.

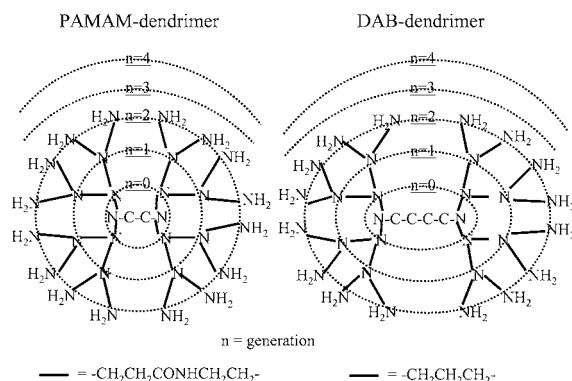
|| Warren Grant Magnuson Clinical Center.

⊥ Radiation Oncology Branch, National Cancer Institute.



**Table 1. Contrast Agents Used in the Current Study<sup>a</sup>**

name	MW (kD)	Gd atoms	core MW (kD)	R1 relaxivity (mM <sup>-1</sup> s <sup>-1</sup> )	commercial name
PAMAM-G4	59	64	14.2	28	PAMAM G <sup>a</sup> 4
PAMAM-G3	29	32	6.9	25	PAMAM G <sup>a</sup> 3
PAMAM-G2	14	16	3.5	20	PAMAM G <sup>a</sup> 2
DAB-G4	51	64	7.1	29	DAB-Am64 (G <sup>a</sup> 5)
DAB-G3	25	32	3.5	17	DAB-Am32 (G <sup>a</sup> 4)
DAB-G2	12	16	1.7	12	DAB-Am16 (G <sup>a</sup> 3)
Gd-[DTPA]-dimeglumine	0.8	1	N/A	5.5	Magnevist

<sup>a</sup> G: generation.**Figure 1.** Schematic representation of the two core types of dendrimers. The third- and fourth-generation dendrimer shells are not explicitly illustrated.

kee, WI) were used possessing a diaminobutane core and 16, 32, or 64 terminal primary amino groups, respectively (Table 1; note that Aldrich defines the DAB-Am16, -Am32, and -Am64 dendrimers as generations -3, -4, and -5, respectively. However, in this paper these are defined to be DAB generations -2, -3, and -4 to parallel the naming convention of the PAMAM dendrimers, thereby allowing for direct comparison of the number of surface amines). Generations -2, -3, and -4 (PAMAM-G2, -G3, and -G4) PAMAM dendrimers (Aldrich Chemical Co., Milwaukee, WI) were used possessing an ethylenediamine core and 16, 32, or 64 terminal primary amino groups (8), respectively (Figure 1, Table 1).

**Conjugation of the Chelating Agent to Dendrimers.** The dendrimers were concentrated to 10 mg/mL and diafiltered against 0.1 M pH 9 sodium phosphate buffer and reacted at 40 °C with a 16-, 32-, or 64-fold molar excess of 2-(*p*-isothiocyanatobenzyl)-6-methyl-diethylenetriaminepentaacetic acid (1B4M) for the generation-2, -3, and -4 dendrimers, respectively. The reaction solutions were maintained at pH 9 with 1 M NaOH over the reaction time of 48 h. Additional 1B4M equal to the initial amount was added as a solid after 24 h to each reaction. The resulting preparation was purified by diafiltration using a Centricon 30 (Amicon Co., Beverly, MA) for the generation-4 dendrimers and a Centricon 10 (Amicon Co.) for the generation-2 and -3 dendrimers. Over 98% of the amine groups on the dendrimers were reacted with the 1B4M as well as found not to contain free 1B4M chelates as determined by both a <sup>153</sup>Gd-labeling assay as previously described (9) and an analysis by size-exclusion HPLC (SE-HPLC) using a TSK G3000 SW column (TosoHaas, Philadelphia, PA; 0.1 M PBS; 0.01 M KCl; pH 7.4; 1 mL/min) using a UV detector at 280 nm absorbance.

**Radiolabeling of Dendrimer-1B4M.** <sup>153</sup>GdCl<sub>3</sub> containing no other stable isotope of Gd(III) was purchased from NEN DuPont (Boston, MA). Approximately 1500 μg of each dendrimer (containing 2 μmol of 1B4M) was reacted with 1.11 MBq (30 μCi) of <sup>153</sup>Gd citrate (46 pmol)

in 0.3 M citrate buffer at pH 5 for 30 min at room temperature. The preparation was then mixed with a 3-fold molar excess of nonradiolabeled Gd(III) citrate (6 μmol) to conjugate 1B4M to fully saturate the chelating groups with Gd(III). This reaction was incubated for 30 min before the addition of ethylenediaminetetraacetic acid (EDTA) and subsequent column purification. To remove any nonincorporated free metal, 10 μL of 0.5 M EDTA (Sigma, St. Louis, MO) was added to minimize formation of Gd(OH)<sub>3</sub> precipitate. The product was purified using a PD-10 column (Pharmacia, Uppsala, Sweden), eluting with pH 7.4 PBS. The radiopurity of the preparations was analyzed by SE-HPLC using a TSK G3000SW column (TosoHaas, Philadelphia, PA; 0.1 M PBS; 0.01 M KCl; pH 7.4; 1 mL/min). DTPA (Sigma) was also labeled with <sup>153</sup>Gd in 0.3 M citrate buffer for 30 min at room temperature.

**Preparation of Contrast Agents for MRI with Nonradioactive Gd(III).** The dendrimer-1B4M conjugates (containing 4 μmol of 1B4M) were mixed with 6.5 μmol of Gd(III) citrate (Sigma) in 0.3 M citrate buffer for 2 h at 40 °C. The excess Gd(III) in each preparation was removed by diafiltration using a Centricon 30 (Amicon Co., Beverly, MA) for generation-4 dendrimers and a Centricon 10 (Amicon Co.) for the generation-2 and -3 dendrimers while simultaneously changing the buffer to 0.05 M PBS. In short, conjugated samples were applied onto either a Centricon 30 or 10 and centrifuged at ~3000g for 45 min. Thereafter, 0.05 M PBS (2 mL) was added to 20 μL of the concentrated samples. The samples were again centrifuged at ~3000g for 45 min. The purified samples were diluted to 1 mL with 0.05 M PBS, and 100 μL of this final solution was used per mouse. A replacement assay using <sup>153</sup>Gd showed that the number of 1B4M chelators of the dendrimer-1B4M conjugates chelating Gd(III) atoms ranged from 77% to 87%. In brief, approximately 500 000 counts per min (9.3 kBq [0.25 μCi]) of <sup>153</sup>Gd citrate (0.38 pmol) were added with 0.1 μmol of nonradioactive Gd(III) to 5 μL of the injected samples and incubated in 0.5 M citrate buffer for 2 h at 40 °C. After this time, the bound and unbound fractions were separated as described above using a PD-10 column (Pharmacia).

The R1 relaxivities of the agents were approximately calculated from the T1 data obtained from all samples of 5, 10, and 20 μmolGd/mL and PBS. We used an inversion recovery spin-echo imaging sequence with various TI 50, 100, 200, and 400 ms and TR/TE: 6000/15 ms, using a 1.5-tesla superconductive magnet unit (Signa LX, General Electric Medical System, Milwaukee, WI) with a high-resolution wrist coils (General Electric Medical System) (Table 1). All images were obtained three slices with an 8 cm field of view and a 2 mm slice thickness, 256 × 256 matrix, and two excitations were averaged. The best slice was selected, and the data obtained from 12 mm<sup>2</sup> areas at the center of the tubes were averaged and used to calculate R1 values.

**The Biodistribution and Whole-Body Retention of  $^{153}\text{Gd}$ -Labeled Dendrimer-1B4M-Gd Conjugates.** Seven groups of nude mice ( $n = 4$  in each group) were injected with 37 kBq (1  $\mu\text{Ci}$ )/ 200  $\mu\text{L}$  of  $^{153}\text{Gd}$ -labeled dendrimer-1B4M-Gd conjugates or  $^{153}\text{Gd}$ -DTPA. The injected samples were added to nonradioactive preparations, and the total Gd(III) dose was adjusted to 0.02 mmolGd/kg, 20% of the dose of Gd-[DTPA]-dimeglumine used clinically. The mice were sacrificed 15 min postinjection of the  $^{153}\text{Gd}$ -labeled preparations, and biodistribution studies were performed. The data were expressed as the percentage of the injected dose per gram (%ID/g) of tissue and as the blood-to-normal tissue ratio. Bone marrow was included in bone accretion assessment. The carcasses of mice were also counted to calculate the whole-body retention (%ID). The urine radioactivity was not included in the whole-body retention amount, principally due to the mice urinating when they were sacrificed with inhalation of carbon dioxide.

**Contrast-Enhanced Dynamic 3D-Micro-MRI of Mice.** To evaluate the whole-body pharmacokinetics of the contrast agents, seven groups of 8-week-old female nude mice ( $n = 4$  or 5 in each group) (NCI, Frederick, MD) were used to obtain contrast-enhanced dynamic 3D-micro-MR images. In short, either 0.03 mmolGd/kg (30% of clinical dose) of dendrimer-1B4M-Gd conjugates or 0.1 mmolGd/kg of Gd-[DTPA]-dimeglumine (Magnevist, Schering, Berlin, Germany) were intravenously injected into the left tail vein. All images were obtained using the high-resolution wrist coil (General Electric Medical System) with a custom mouse holder using a Signa LX (General Electric Medical System). The mice were anesthetized with 1.15 mg of sodium pentobarbital (Dainabot, Osaka, Japan) and placed in the center of the coils. The fast spoiled gradient echo technique (FSPGR; TR/TE 19.4/4.2; flip angle 60°; scan time 1'40"; phase encoding steps 256  $\times$  256; 3 number of excitations; slab thickness 12) with chemical fat-suppression technique and serial 3D data acquisition was used to acquire images every 2 min from 0 (immediately after injection) to 14 min after injection of the contrast agents for all mice studies. The coronal images for dynamic MRI were reconstructed with 2 mm section thickness without gap reconstruction. In addition, slice data were processed into 3D images with the maximum intensity protection (MIP) method (Advantage Windows, General Electric Medical System).

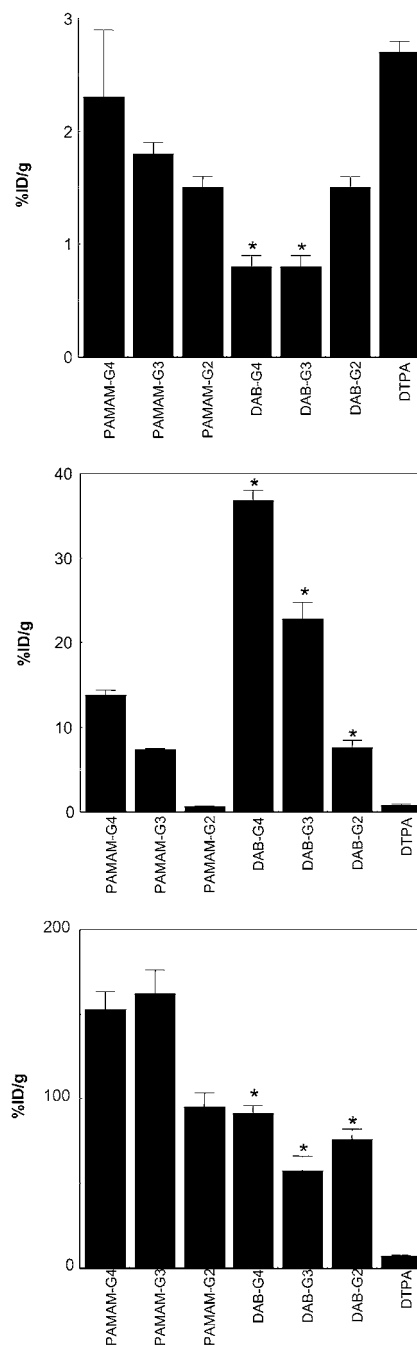
All studies were approved by the Animal Care Committee of National Institutes of Health.

**Statistical Analysis.** Statistical analysis was performed using Student's *t*-test (StatView, SAS Institute Inc., Cary, NC).

## RESULTS

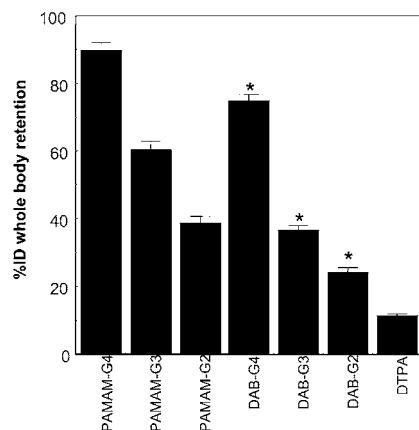
**Quality Control Study.** The radiolabeling yields of all preparations before purification ranged from 95% to 98%. The radiopurity of all preparations analyzed by SE-HPLC was greater than 97%. The retention times of the PAMAM-G4, -G3, and -G2 agents were 19.8, 20.7, and 21.5 min with a TSK G3000SW column, respectively. In addition, the retention times for the DAB-G4, -G3, and -G2 agents were 20.4, 21.0, and 21.6 min with the TSK G3000SW column, respectively. Therefore, by this method the physical sizes of the DAB agents at physiological pH were found to be smaller than those of the PAMAM agents of the same dendrimer generation.

**The Biodistribution and Whole-Body Retention of  $^{153}\text{Gd}$ -Labeled Dendrimer-1B4M-Gd Conjugates.** The amount of the  $^{153}\text{Gd}$ -labeled DAB-based agents



**Figure 2.** Retention of  $^{153}\text{Gd}$ -labeled dendrimer-1B4M-Gd conjugates or  $^{153}\text{Gd}$ -DTPA in the blood (a), liver (b), and kidney (c) in a normal nude mice ( $n = 4$ ) at 15 min after injection. Values are expressed as the mean percentages of the injected dose per gram of normal tissues and standard deviation. The asterisks indicate significant differences ( $p < 0.01$ ) between PAMAM and DAB of the same dendrimer generation.

remaining in the blood increased as molecular weight decreased (Figure 2a). In contrast, the amount of  $^{153}\text{Gd}$ -labeled PAMAM-based agents remaining in the blood increased as molecular weight increased (Figure 2a). However, all conjugates cleared from the circulation more rapidly than Gd-[DTPA]. The  $^{153}\text{Gd}$ -labeled DAB-based agents as a whole accumulated significantly greater in the liver (Figure 2b) and less in the kidney (Figure 2c) than the  $^{153}\text{Gd}$ -labeled PAMAM-based agents ( $p < 0.01$ ; for all values DAB versus PAMAM). The whole-body retention of the DAB-based agents was less than that of the PAMAM-based agents of the same dendrimer generation (Figure 3). Greater than 60% of the injected doses



**Figure 3.** Whole-body retention of  $^{153}\text{Gd}$ -labeled dendrimer-1B4M-Gd conjugates or  $^{153}\text{Gd}$ -DTPA in a normal nude mice ( $n = 4$ ) at 15 min after injection. Values are expressed as the mean percentages of the injected dose of mice and standard deviation. The asterisks indicate significant differences ( $p < 0.01$ ) between PAMAM and DAB of the same dendrimer generation.

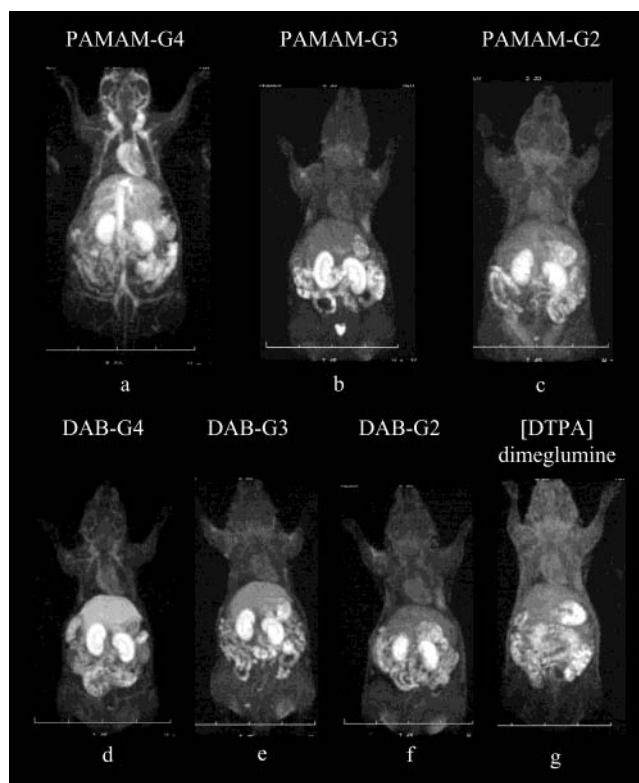
of the DAB-G3-, DAB-G2-, or PAMAM-G2-based contrast agents were cleared from the body within 15 min after injection.

**Contrast-Enhanced Dynamic 3D-Micro-MRI of Mice.** The 3D-micro-MR images were obtained using the MIP method following intravenous injection of 0.03 mmolGd/kg of dendrimers. Brighter liver images were obtained with DAB-based agents than PAMAM-based agents or Gd-[DTPA]-dimeglumine (Figure 4). The blood signal-intensity values were significantly higher with generation-4 PAMAM-based agents than with DAB-based agents ( $p < 0.01$ ) at time points later than 2 min after injection (Figure 5a). The blood signal-intensity values were significantly higher with generation-2 DAB-based agents than with PAMAM-based agents ( $p < 0.01$ ) at all time points examined (Figure 5c). The liver signal-intensity values were significantly higher with generation-3 and -4 DAB-based agents than with PAMAM-based agents of the same dendrimer generation ( $p < 0.01$ ) at all time points examined (Figure 5d,e). The kidney signal-intensity values obtained from generation-2 and -4 DAB-based agents were also significantly higher than those obtained with the PAMAM-based agents of the same dendrimer generation ( $p < 0.01$ ) at most of time points examined (Figure 5g,i).

## DISCUSSION

Dendrimers are a class of highly branched spherical polymers. Two types of dendrimers, the polyamidoamine (PAMAM) (8) and diaminobutane core polyaminoamine (DAB), are commercially available (10). Both types are highly soluble in aqueous solutions and possess a unique surface covered by primary amino groups (8, 11) (Figure 1). Almost all the amino groups are uncharged at pH above 9.0, and the defined structure and large number of available surface amino groups of these dendrimers serve as convenient attachment sites for chelating agents or single antibody molecules (11–15). These dendrimers have also been employed for the preparation of MRI contrast agents (1–3, 9, 16). Several studies that focus on the relationship between dendrimer generation and relaxivity of dendrimer-based contrast agents have been previously reported (1, 2).

This general class of organ-specific MRI agents showing different pharmacokinetics from Gd-[DTPA] has been actively investigated for years (17, 18), and the first

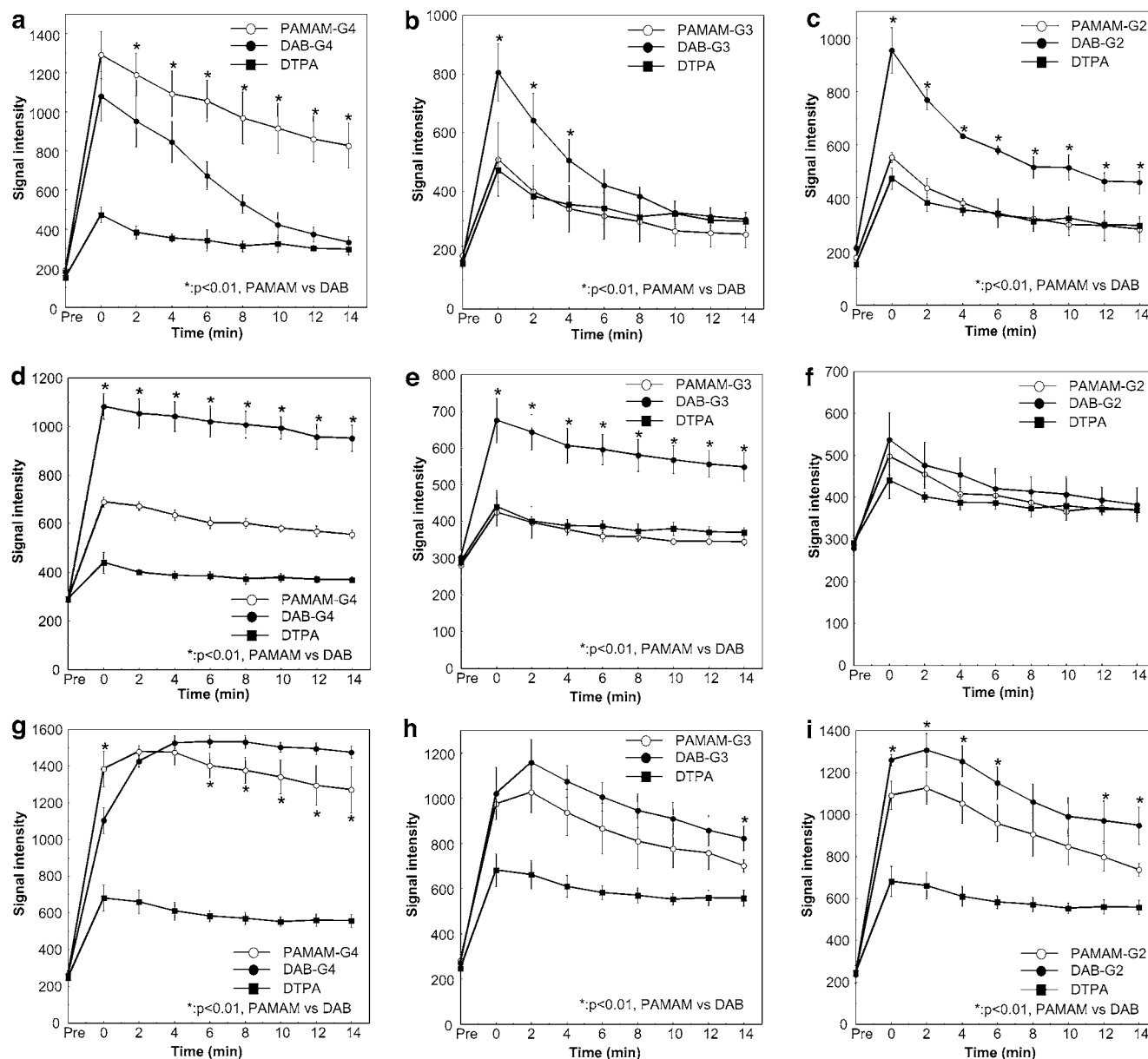


**Figure 4.** Whole-body 3D-micro-MR-imaging of mice injected with 0.03 mmol Gd/kg of dendrimer-1B4M-Gd conjugates or 0.1 mmol Gd/kg Gd-[DTPA]-dimeglumine [PAMAM-G4 (a), PAMAM-G3 (b), PAMAM-G2 (c), DAB-G4 (d), DAB-G3 (e), DAB-G2 (f), Gd-[DTPA]-dimeglumine (g)]. Images were obtained immediately after injection. Maximum intensity projections are shown.

gadolinium-based liver agent,  $[\text{Gd}(\text{BOPTA})(\text{H}_2\text{O})]^{2-}$  (MultiHance, Bracco-BYK Gulden, Germany), was approved in Europe in October 1998 (19–22). The composition and size of dendrimer-based MR imaging agents influences their behavior and, hence, the proposed clinical indications. For example, the presence of hydrophobic groups on metal chelates causes hepatocellular uptake and excretion into the bile ducts, gall bladder, and intestines. Actual physical size is also an important factor. Large macromolecular MRI contrast agents with albumin or dendrimer cores are useful for vascular imaging (1, 3, 23, 24). Smaller macromolecular MRI contrast agents are excreted by the kidneys; however, unlike Gd-[DTPA], they are concentrated in renal tubules and can visualize renal structural and functional damage (6).

In the current studies, optimization of the performance of dendrimer-based MRI agents was an objective. Size and internal structure were found to have important effects on whole-body retention and MRI imaging characteristics. A significantly larger amount of DAB-based agents accumulated in the liver as compared to the same generation PAMAM-based agents by pharmacokinetic studies with  $^{153}\text{Gd}$  as shown on Figure 2b. That reflected well to the intensity-time curves obtained by the MRI studies as shown in Figure 5d–f. In contrast, a significantly smaller amount of DAB-based agents accumulated in the kidney as compared to the same generation of PAMAM-based agents in the pharmacokinetic studies as shown on Figure 2c. However, DAB-based agents exhibited higher signal intensity than the same generation of PAMAM-based agents in the kidney as shown on Figure 5g–i. DAB-based agents, generation-2 and -3 of which





**Figure 5.** Plots of the signal intensity of the blood in the left ventricle of the heart (G4, a; G3, b; G2, c), the liver (G4, d; G3, e; G2, f), and the kidney (G4, g; G3, h; G2, i) obtained from the contrast-enhanced dynamic MRI of mice with 0.03 mmol/kg of dendrimer–1B4M–Gd conjugates (PAMAM, open circles; DAB, closed circles) or 0.1 mmol Gd/kg Gd-[DTPA]-dimeglumine (DTPA, closed square) are shown. A single most appropriate region of interest was set in each organ in each mouse ( $n = 4$  or 5). Data are expressed as the mean signal intensity and standard deviation. The asterisks indicate significant differences ( $p < 0.01$ ) between PAMAM and DAB of the same dendrimer generation.

showed smaller R1 relaxivity values than PAMAM-based agents of the same generation as shown in Table 1, were excreted into the urine more efficiently than PAMAM-based agents, which showed prolonged retention (14) and possible internalization into renal tubular cells. The high T1-weighted MRI signal obtained with DAB agents may be results of both high accessibility of water to Gd(III) ions and large proportion of DAB agents located in the free water (urine) rather than in the lipid vesicles (tubular cells) (25).

Although the MRI imaging characteristics of PAMAM (3, 4, 24) and DAB (7, 26) based contrast agents have been well studied, their toxicity profile remains uncertain. Malik et al. reported that the difference between terminal groups on the surface of the various dendrimer molecules could alter their biological characteristics, especially with respect to their cellular toxicity (10). However, although the internal repeat unit structures

of the dendrimers altered the *in vivo* pharmacokinetics in these studies, the biological toxicity characteristics were not measurably different (10, 26, 27). For use in clinical practice, macromolecular MR contrast agents must be efficiently and rapidly excreted to minimize the potential toxicity of these agents, mostly caused by free Gd(III). Renal filtration and excretion is usually considered to be the optimal route to remove circulating molecules from the body because they can be eliminated intact without cellular metabolism or processing. However, the filtered macromolecules could then be reabsorbed by the proximal tubules and retained within the cell. Even if the molecules could be catabolized and excreted, most of the chelated metal ions are retained in the cell (28, 29). If free Gd(III) is liberated in the cell, this could contribute to toxicity. Smaller MR contrast agents are generally considered to be safer, because they are more rapidly cleared, and have less cellular uptake,

although even in case of DAB-G2, 8% of the injected dose retained in the body at 48 h postinjection, which is much more than that of Gd-DTPA (>2% at 48 h postinjection). In the present study, the smaller dendrimer-Gd conjugates demonstrated lower retention in the whole body and thus could be used to obtain detailed renal structural information.

An elegant study has recently been reported with a series of synthetic peglated linear copolymer with molecular weight ranging 30–120 kD (30). The molecular weights of the agents were close to the larger size of the dendrimer-based agents in the current study. However, the excretion rate of the copolymer-based agents appeared to be much slower than that of both classes of dendrimer-based agents. The rapid excretion of the dendrimer-based agents was related to their small molecular sizes induced by their inherent spherical shape. Linear polymers might behave as larger molecules in the body than the spherical polymers of similar molecular weight.

Protein molecules with small molecular weights such as  $\beta 2$  microglobulin of the single-chain Fv fragment of antibody (Fv) were quickly filtered through glomerulus mostly at the first pass (31). In case disulfide-stabilized Fv, which has larger molecular weight (25kD) than PAMAM-G2, DAB-G3, and DAB-G2, was examined with the same method as we used in this study: around 80% of its injected dose into mice was stuck or passed through kidney within 15 min after injection (31). Therefore, the quick excretion rates of these contrast agents were reasonable for molecules with sizes in this range, although the excretion might be much slower in human than in mice because of their four times as much heart rates and quick catabolism of drugs.

In conclusion, although the dendrimer-1B4M-Gd conjugates with smaller molecular weight exhibited a more rapid excretion from the whole body, all of the dendrimer-1B4M-Gd conjugates visualized the proximal straight tubule in the kidney. Since the PAMAM-G2-, DAB-G3-, and DAB-G2-based contrast agents showed relatively rapid excretion from the body, these three conjugates may be acceptable for use in clinical practice as either blood-pool or functional kidney MRI contrast agents. Further investigations will be required to ascertain any resolution between these three agents in order to choose a final candidate for clinical evaluations.

#### LITERATURE CITED

- (1) Wiener, E. C., Brechbiel, M. W., Brothers, H., Magin, R. L., Gansow, O. A., Tomalia, D. A., and Lauterbur, P. C. (1994) Dendrimer-based metal chelates: a new class of magnetic resonance imaging contrast agents. *Magn. Reson. Med.* 31, 1–8.
- (2) Bryant, L. H., Jr., Brechbiel, M. W., Wu, C., Bulte, J. W., Herynek, V., and Frank, J. A. (1999) Synthesis and relaxometry of high-generation ( $G = 5, 7, 9$ , and  $10$ ) PAMAM dendrimer-DOTA-gadolinium chelates. *J. Magn. Reson. Imaging* 9, 348–352.
- (3) Kobayashi, H., Sato, N., Hiraga, A., Saga, T., Nakamoto, Y., Ueda, H., Konishi, J., Togashi, K., and Brechbiel, M. W. (2001) 3D-micro-MR angiography of mice using macromolecular MR contrast agents with polyamidoamine dendrimer core with references to their pharmacokinetic properties. *Magn. Reson. Med.* 45, 454–460.
- (4) Sato, N., Kobayashi, H., Hiraga, A., Saga, T., Togashi, K., Konishi, J., and Brechbiel, M. W. (2001) Pharmacokinetics and enhancement patterns of macromolecular MR contrast agents with various sizes of polyamidoamine dendrimer cores. *Magn. Reson. Med.* 46, 1169–1173.
- (5) Kobayashi, H., Sato, N., Kawamoto, S., Saga, T., Hiraga, A., Haque, T. L., Ishimori, T., Konishi, J., Togashi, K., and Brechbiel, M. W. (2001) A novel intravascular macromolecular MR contrast agent with generation-4 polyamidoamine dendrimer core: Accelerated renal excretion with co-injection of lysine. *Magn. Reson. Med.* 46, 457–464.
- (6) Kobayashi, H., Kawamoto, S., Jo, S., Sato, N., Saga, T., Hiraga, A., Konishi, J., Hu, S., Togashi, K., Brechbiel, M. W., and Star, R. A. (2002) Renal tubular damage detected by dynamic micro-MRI with a dendrimer-based MR contrast agent. *Kidney Int.* 61, 1980–1985.
- (7) Kobayashi, H., Kawamoto, S., Saga, T., Sato, N., Hiraga, A., Ishimori, T., Akita, Y., Mamede, M. H., Konishi, J., Togashi, K., and Brechbiel, M. W. (2001) Novel liver macromolecular MR contrast agent with a polypropylenimine diaminobutyl dendrimer core: comparison to the vascular MR contrast agent with the polyamidoamine dendrimer core. *Magn. Reson. Med.* 46, 795–802.
- (8) Tomalia, D. A., Naylor, A. M., and Goddard III, W. A. (1990) Starburst dendrimers: Molecular-level control of size, shape, surface chemistry, topology, and flexibility from atoms to macroscopic matter. *Angew. Chem., Int. Ed. Engl.* 29, 138–175.
- (9) Kobayashi, H., Sato, N., Kawamoto, S., Saga, T., Hiraga, A., Haque, T. L., Ishimori, T., Konishi, J., Togashi, K., and Brechbiel, M. W. (2001) Comparison of the macromolecular MR contrast agents with ethylenediamine-core versus ammonia-core generation-6 polyamidoamine dendrimer. *Bioconjugate Chem.* 12, 100–107.
- (10) Malik, N., Wiwattanapatapee, R., Klopsch, R., Lorenz, K., Frey, H., Weener, J. W., Meijer, E. W., Paulus, W., and Duncan, R. (2000) Dendrimers: relationship between structure and biocompatibility in vitro, and preliminary studies on the biodistribution of 125I-labeled polyamidoamine dendrimers in vivo. *J. Control Release* 65, 133–148.
- (11) Wu, C., Brechbiel, M. W., Kozak, R. W., and Gansow, O. A. (1994) Metal-chelate-dendrimer-antibody constructs for use in radioimmunotherapy and imaging. *Bioorg. Med. Chem. Lett.* 4, 449–454.
- (12) Singh, P., Moll, F., III, Lin, S. H., Ferzli, C., Yu, K. S., Koski, R. K., Saul, R. G., and Cronin, P. (1994) Starburst dendrimers: enhanced performance and flexibility for immunoassays. *Clin. Chem.* 40, 1845–1849.
- (13) Barth, R. F., Adams, D. M., Soloway, A. H., Alam, F., and Darby, M. V. (1994) Boronated starburst dendrimer-mono-clonal antibody immunoconjugates: evaluation as a potential delivery system for neutron capture therapy. *Bioconjugate Chem.* 5, 58–66.
- (14) Kobayashi, H., Wu, C., Kim, M. K., Paik, C. H., Carasquillo, J. A., and Brechbiel, M. W. (1999) Evaluation of the in vivo biodistribution of indium-111 and yttrium-88 labeled dendrimer-1B4M-DTPA and its conjugation with anti-Tac monoclonal antibody. *Bioconjugate Chem.* 10, 103–111.
- (15) Kobayashi, H., Sato, N., Saga, T., Nakamoto, Y., Ishimori, T., Toyama, S., Togashi, K., Konishi, J., and Brechbiel, M. W. (2000) Monoclonal antibody-dendrimer conjugates enable radiolabeling of antibody with markedly high specific activity with minimal loss of immunoreactivity. *Eur. J. Nucl. Med.* 27, 1334–1339.
- (16) Bourne, M. W., Margerun, L., Hylton, N., Campion, B., Lai, J. J., Derugin, N., and Higgins, C. B. (1996) Evaluation of the effects of intravascular MR contrast media (gadolinium dendrimer) on 3D time-of-flight magnetic resonance angiography of the body. *J. Magn. Reson. Imaging* 6, 305–310.
- (17) Schuhmann-Giampieri, G., Schmitt-Willich, H., Frenzel, T., and Schitt-Willich, H. (1993) Biliary excretion and pharmacokinetics of a gadolinium chelate used as a liver-specific contrast agent for magnetic resonance imaging in the rat. *J. Pharm. Sci.* 82, 799–803.
- (18) Schuhmann-Giampieri, G., Schmitt-Willich, H., Press, W. R., Negishi, C., Weinmann, H. J., and Speck, U. (1992) Preclinical evaluation of Gd-EOB-DTPA as a contrast agent in MR imaging of the hepatobiliary system. *Radiology* 183, 59–64.
- (19) Vogl, T. J., Pegios, W., Waitzinger, J., Pirovano, G., Balzer, J., and Lissner, J. (1992) NMR tomography of the liver with

- the new contrast agent Gd-BOPTA. The results of an in-vivo phase-I test. *Rofo Fortschr. Geb. Rontgenstr. Neuen Bildgeb. Verfahr.* 156, 465–470.
- (20) Caudana, R., Morana, G., Pirovano, G. P., Nicoli, N., Portuese, A., Spinazzi, A., Di Rito, R., and Pistolesi, G. F. (1996) Focal malignant hepatic lesions: MR imaging enhanced with gadolinium benzyloxypropionictetraacetate (BOPTA)—preliminary results of phase II clinical application. *Radiology* 199, 513–520.
- (21) Spinazzi, A., Lorusso, V., Pirovano, G., Taroni, P., Kirchin, M., and Davies, A. (1998) Multihance clinical pharmacology: biodistribution and MR enhancement of the liver. *Acad. Radiol.* 5 Suppl 1, S86–89; discussion S93–84.
- (22) Manfredi, R., Maresca, G., Baron, R. L., De Franco, A., De Gaetano, A. M., Cotroneo, A. R., Pirovano, G., Spinazzi, A., and Marano, P. (1998) Gadobenate dimeglumine (BOPTA) enhanced MR imaging: patterns of enhancement in normal liver and cirrhosis. *J. Magn. Reson. Imaging* 8, 862–867.
- (23) Schmiedl, U., Ogan, M. D., Moseley, M. E., and Brasch, R. C. (1986) Comparison of the contrast-enhancing properties of albumin-(Gd-DTPA) and Gd-DTPA at 2.0 T: and experimental study in rats. *AJR Am. J. Roentgenol.* 147, 1263–1270.
- (24) Kobayashi, H., Kawamoto, S., Saga, T., Sato, N., Hiraga, A., Konishi, J., Togashi, K., and Brechbiel, M. W. (2001) Micro-MR angiography of normal and intratumoral vessels in mice using dedicated intravascular MR contrast agents with high generation of polyamidoamine dendrimer core: reference to pharmacokinetic properties of dendrimer-based MR contrast agents. *J. Magn. Reson. Imaging* 14, 705–713.
- (25) Kobayashi, H., Kawamoto, S., Saga, T., Sato, N., Ishimori, T., Konishi, J., Ono, K., Togashi, K., and Brechbiel, M. W. (2001) Avidin-dendrimer-(1B4M-Gd)(254): a tumor-targeting therapeutic agent for gadolinium neutron capture therapy of intraperitoneal disseminated tumor which can be monitored by MRI. *Bioconjugate Chem.* 12, 587–593.
- (26) Kobayashi, H., Saga, T., Kawamoto, S., Sato, N., Hiraga, A., Ishimori, T., Konishi, J., Togashi, K., and Brechbiel, M. W. (2001) Dynamic micro-magnetic resonance imaging of liver micrometastasis in mice with a novel liver macromolecular magnetic resonance contrast agent DAB-Am64-(1B4M-Gd)-(64). *Cancer Res.* 61, 4966–4970.
- (27) Kobayashi, H., Sato, N., Kawamoto, S., Saga, T., Hiraga, A., Ishimori, T., Konishi, J., Togashi, K., and Brechbiel, M. W. (2001) 3D MR angiography of intratumoral vasculature using a novel macromolecular MR contrast agent. *Magn. Reson. Med.* 46, 579–585.
- (28) Kobayashi, H., Kao, C. H., Kreitman, R. J., Le, N., Kim, M. K., Brechbiel, M. W., Paik, C. H., Pastan, I., and Carrasquillo, J. A. (2000) Pharmacokinetics of  $^{111}\text{In}$ - and  $^{125}\text{I}$ -labeled antiTac single-chain Fv recombinant immunotoxin. *J. Nucl. Med.* 41, 755–762.
- (29) Naruki, Y., Carrasquillo, J. A., Reynolds, J. C., Maloney, P. J., Frincke, J. M., Neumann, R. D., and Larson, S. M. (1990) Differential cellular catabolism of  $^{111}\text{In}$ ,  $^{90}\text{Y}$  and  $^{125}\text{I}$  radiolabeled T101 anti-CD5 monoclonal antibody. *Int. J. Rad. Appl. Instrum., B* 17, 201–207.
- (30) Weissleder, R., Bogdanov, A., Jr., Tung, C. H., and Weimann, H. J. (2001) Size optimization of synthetic graft copolymers for in vivo angiogenesis imaging. *Bioconjugate Chem.* 12, 213–219.
- (31) Kobayashi, H., Yoo, T. M., Kim, I. S., Kim, M.-K., Le, N., Webber, K. O., Pastan, I., Paik, C. H., Eckelman, W. C., and Carrasquillo, J. A. (1996) L-lysine effectively blocks renal uptake of  $^{125}\text{I}$ - or  $^{99\text{m}}\text{Tc}$ -labeled anti-Tac dsFv. *Cancer Res.* 56, 3788–3795.

BC025633C



# Controlled Release of Proteins from Their Poly(Ethylene Glycol) Conjugates: Drug Delivery Systems Employing 1,6-Elimination

Richard B. Greenwald,\* Karen Yang, Hong Zhao, Charles D. Conover, Stanford Lee, and David Filpula

Enzon Pharmaceuticals Inc, 20 Kingsbridge Road, Piscataway, New Jersey, 08854. Received December 12, 2002; Revised Manuscript Received February 3, 2003

Several tripartate releasable PEG linkers (rPEG) that can provide anchimeric assistance to hydrolysis (cyclization prodrugs) were prepared and, after conjugation to lysozyme demonstrated rapid cleavage in rat plasma compared to nonassisted, permanently bound PEG. By varying the chemical structure and adding steric hindrance, the half-life of the protein conjugates can be adjusted from slow to very fast. The pharmacokinetics (PK) of regeneration of native protein, from various rPEG conjugates can, for the first time, be easily followed in the rat using green fluorescent protein. The PK in mice was also determined for rPEG–Interleukin 2 (rPEG–IL-2) conjugates in vivo using an ELISA assay. Thus, a systematic study of rPEGylated proteins, either in vivo or in vitro during processing, has been investigated based on regeneration of native protein. The employment of releasable PEG polymers substantially broadens the applications of PEGylation drug delivery technology by introducing the benefits of controlled release of native protein therapeutics.

## INTRODUCTION

Using lysozyme as the protein model, we recently synthesized a releasable PEG linker (rPEG) (1) that predictably releases native protein from its conjugate. Exhaustive analyses were performed in order to demonstrate that only native protein is released from the conjugate when the linker bond between rPEG and the protein is cleaved. Thus, these rPEG conjugates are prodrugs (or proproteins) and are based on a classical tripartate system (2). The three-component system which composes the tripartate proprotein contains an mPEG substituent on a trigger such as an ester, carbamate, or carbonate attached to a linker (*p*-substituted benzyl alcohol), which in turn connects to amino groups of the protein through a labile carbamate attachment. By using various combinations of ortho substituents on the benzene ring of the linker and bulky substituents at the  $\alpha$ -position of a given trigger, a host of measured hydrolysis rates based on  $t_{1/2}$ , which point to usable trends, can be established. It was clear from this first work (1) that not only the trigger of the linker employed affected in vitro and in vivo hydrolysis, but that the number of PEG strands also affected the rate of hydrolysis: increasing the PEG number from 1 to 2 more than doubled the stability of the conjugate.

The optimization of kinetics is important for practical applications, and therefore, for rapidly releasing rPEG linkers a more heavily conjugated protein may lend itself to in vivo implementation. Also the multistrand rPEG conjugate produces a higher molecular weight species that requires a simpler purification resulting in higher yields of the protein conjugate. Additionally, to carry out site-directed permanent PEGylation by further reaction of the rPEG conjugate with a permanent linker using SC–PEG (3) or T–PEG (4) (i.e., formation of a hybrid-PEG species), it would ultimately be necessary to remove

rPEG more rapidly, probably during in vitro processing. In this regard rPEG is being used as a protecting group for the  $\epsilon$ -amino group of lysine. Its use can be distinguished from employing small organic molecules for blocking amino moieties by the important property of water solubility, which allows protein conjugation to occur easily in buffer solution.

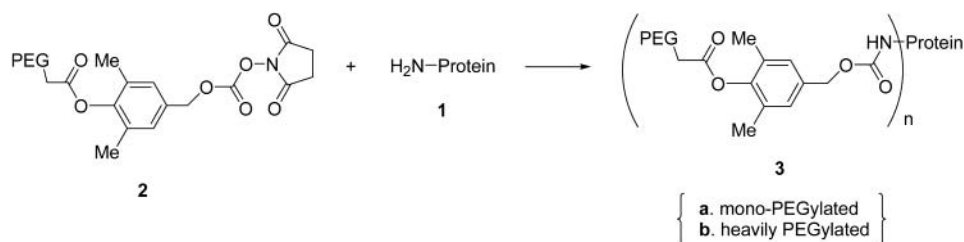
This work describes the development of PEG linkers that are more rapidly hydrolyzed, in vitro and in vivo, and thus are more uniquely suited for actual development of PEGylated candidate therapeutics. In addition, the determination of the effect of PEG number on the rates of hydrolysis has also been done for these rPEG linkers in our continuing efforts to understand the factors which need to be addressed to achieve site-directed permanent PEGylation. Furthermore, we examined the green fluorescent protein (GFP) and IL-2 conjugates of these linkers by carrying out rodent pharmacokinetics (PK) studies in order to verify the in vitro findings determined for the model rPEG–lysozyme conjugates prepared in this study.

## CHEMISTRY

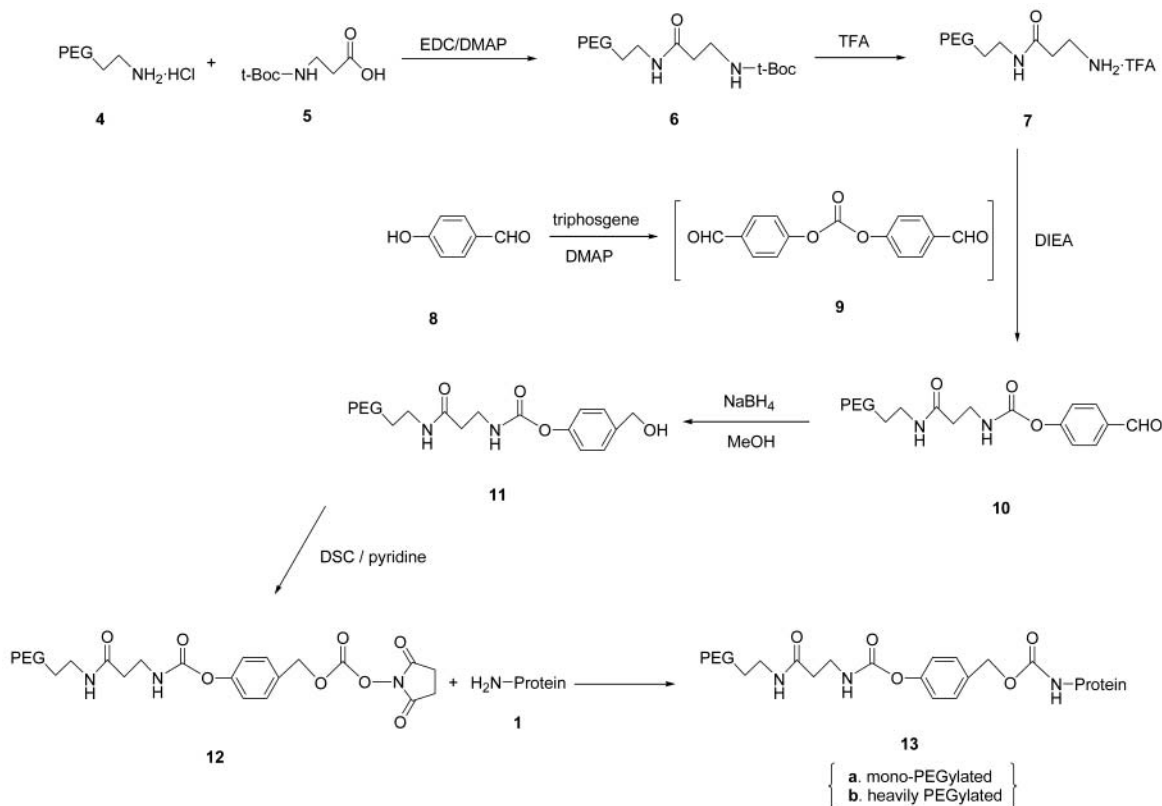
Five linkers were used for the conjugation of proteins in this study. All were N-hydroxy succinimidyl (NHS) carbonates and resulted in carbamate derivatives of the protein. SC–PEG produced a permanent bonded species that was used as a control. Compound 2 (Scheme 1) was prepared by previously described methods (5). Linker 12 was synthesized as shown in Scheme 2. For this particular sequence of reactions, it was found to be advantageous to employ the reactive species 9 in order to obtain higher yields and greater purity of the final linker. Linkers 22 and 23 were prepared from diglycolic anhydride as depicted in Scheme 3. These two linkers were designed to produce conjugates that were hydrolyzed rapidly by virtue of their ability to provide anchimeric assistance (intramolecular assistance to hydrolysis) (6). Linker 22 is an ester of a 1° alcohol and provides protein conjugates that are susceptible to general esterase hydrolysis. This

\* To whom correspondence should be addressed. Phone: (732) 980-4924. E-mail: richard.greenwald@enzon.com.

## Scheme 1



## Scheme 2



provides a carboxylate anion, which in turn causes rapid hydrolysis of the distal hindered ester link of the trigger via a six-membered ring transition state. Because of the less nucleophilic nature of the amide moiety, compound **23** shows more variation, but nonetheless assists in increasing the rate of hydrolysis (**7**). Another linker which has an accelerated rate of hydrolysis, but which is not dependent on an initial hydrolysis, was also explored. The mechanism of breakdown of conjugate **13a** (see Table 1) in rats should be similar to that of simpler phenolic carbamates, which is based on a proton removal from N-H and is about 4.6 h for small molecules (**5**). It should be noted that a six-membered ring transition state is possible for **13**, and this can further accelerate hydrolysis. This was observed in the case of the small molecule amphotericin, where  $t_{1/2}$  in rat plasma is only 1.5 h (**8**), and also in **13a** (4 h), which is equivalent to **24a** and **25a**. Ester linker **2**, is sterically hindered by the flanking *o*-methyl groups and has no avenue available for anchimeric assistance and shows the slowest rate of release. In general the synthetic techniques used to prepare rPEG linkers are so well defined (**5**) that virtually any  $t_{1/2}$  can be designed to release a particular protein. This can be of great value not only in preventing spiking by allowing the controlled release of native protein, but in the processing of "hybrid" types of PEG

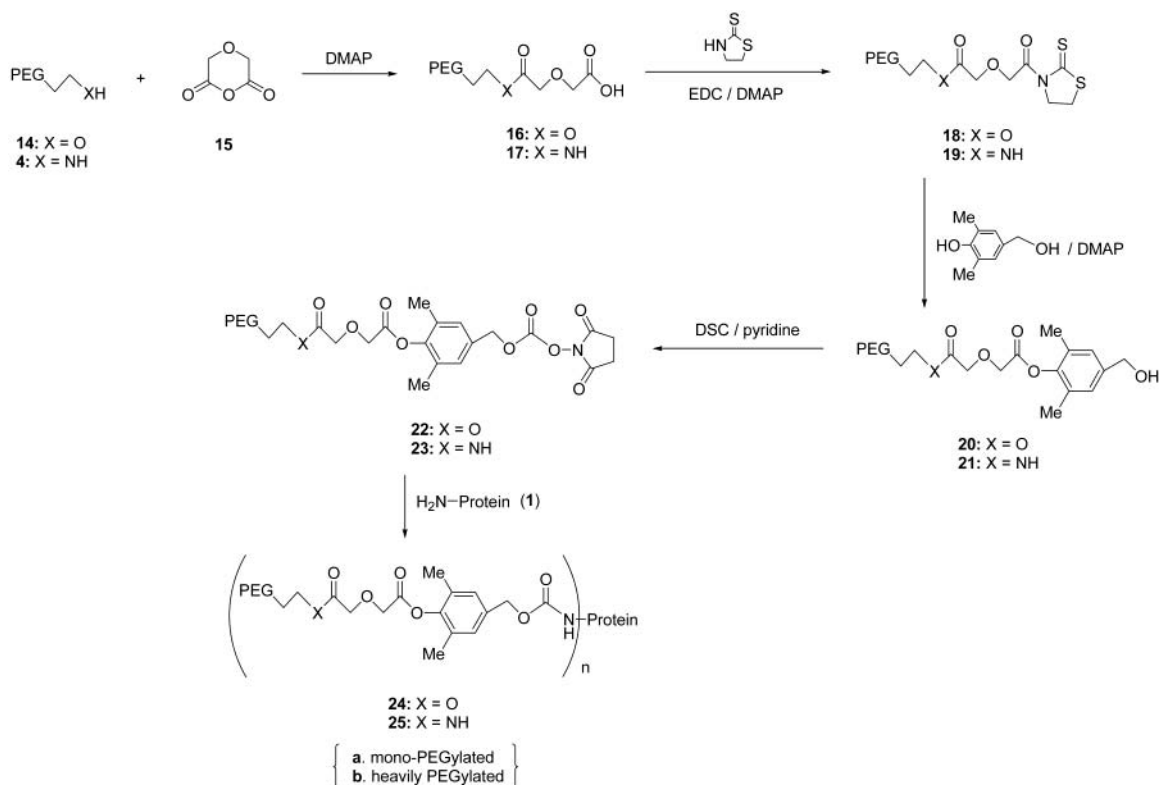
conjugates, it may be advantageous to have a rapid release in order to minimize manufacturing times.

## EXPERIMENTAL SECTION

**Procedures for the Synthesis of Releasable PEG Linkers.** *General.* All reactions were run under an atmosphere of dry nitrogen or argon. Commercial reagents were used without further purification. All PEG compounds were dried under vacuum or by azeotropic distillation from toluene prior to use. NMR spectra were obtained using a Varian Mercury 300 NMR spectrometer and deuterated chloroform as the solvent unless otherwise specified. Chemical shifts ( $\delta$ ) are reported in parts per million (ppm) downfield from tetramethylsilane (TMS).

**Compound 6.** To a solution of 12 kDa methoxypoly(ethylene glycol) (mPEG) amine hydrochloride (**4**, 32.0 g, 2.66 mmol) in anhydrous methylene chloride (DCM, 400 mL) was added *N*-*t*-Boc  $\beta$ -alanine (2.06 g, 10.63 mmol), 1-[3-(dimethylamino)propyl]-3-ethylcarbodiimide hydrochloride (EDC, 2.00 g, 10.63 mmol), and 4-(dimethylamino)pyridine (DMAP, 1.30 g, 10.66 mmol). The reaction was stirred for 18 h at room temperature, followed by partial removal of the solvent under reduced pressure. The product was precipitated with ethyl ether, filtered, and crystallized from 2-propanol (IPA) to give **6**

Scheme 3



(31.0 g, 2.55 mmol, 96%).  $^{13}\text{C}$  NMR (67.8 MHz,  $\text{CDCl}_3$ )  $\delta$  171.06, 155.38, 71.31–69.09 (PEG), 58.43, 38.59, 36.12, 35.27, 27.87.

**Compound 7.** A solution of **6** (30.0 g, 2.47 mmol) in DCM (300 mL) and trifluoroacetic acid (150 mL) was stirred at room temperature for 2 h, followed by partial removal of the solvent under reduced pressure. The product was precipitated by the addition of ethyl ether, filtered, and washed with more ether to yield 29.0 g, 2.37 mmol, 96% of **7**.  $^{13}\text{C}$  NMR (67.8 MHz,  $\text{CDCl}_3$ )  $\delta$  170.07, 161(q), 116(q), 71.40–68.15 (PEG), 58.50, 37.94, 36.96, 33.11.

**Compound 9.** To a solution of 4-hydroxybenzaldehyde (**8**, 1.0 g, 8.2 mmol) and triphosgene (0.34 g, 1.14 mmol) in anhydrous DCM (20 mL) cooled to 15 °C was added diisopropylethylamine (DIEA, 1.2 mL, 6.87 mmol) dropwise over 5 min, and the mixture was stirred at room temperature for 1 h. The solution was washed with 0.1 N HCl, and the organic layer was dried (anhydrous sodium sulfate) and filtered and the solvent removed from the filtrate under reduced pressure to give **9** (0.8 g, 2.99 mmol, 73%).  $^{13}\text{C}$  NMR (67.8 MHz,  $\text{CDCl}_3$ )  $\delta$  190.49, 154.82, 150.37, 134.36, 131.27, 121.42.

**Compound 10.** To a solution of **8** (0.71 g, 5.82 mmol) and triphosgene (0.246 g, 0.83 mmol) in anhydrous DCM (75 mL) cooled to 15 °C was added dropwise DIEA (1.2 mL, 6.87 mmol) over 5 min, and the reaction was stirred at room temperature for 1 h. To the mixture were then added **7** (5.0 g, 0.41 mmol) and DIEA (0.072 mL, 0.41 mmol), and the mixture was stirred for an additional 18 h at room temperature. The solvent was partially removed under reduced pressure, and the product was precipitated by the addition of ethyl ether, filtered, and crystallized from IPA to give **10** (4.6 g, 0.377 mmol, 92%).  $^{13}\text{C}$  NMR (67.8 MHz,  $\text{CDCl}_3$ )  $\delta$  190.43, 170.88, 155.54, 153.02, 132.72, 130.55, 121.45, 71.38–69.09 (PEG), 58.46, 38.71, 36.95, 34.66.

**Compound 11.** Sodium borohydride (0.032 g, 0.83

mmol) was added to a solution of **10** (6.1 g, 0.499 mmol) in methanol (60 mL) cooled to 15 °C. The reaction was allowed to warm to room temperature over a period of 2 h, followed by adjusting the pH to 6.5 with 1N HCl. The solvent was evaporated under reduced pressure and the residue taken up in water. The pH was lowered to 2.0 with 0.5 N HCl and the product extracted with DCM, dried (anhydrous sodium sulfate), and filtered. After partial removal of the solvent in vacuo, the product was precipitated with ethyl ether, filtered, and washed with additional solvent to give **11** (5.8 g, 0.474 mmol, 95%).  $^{13}\text{C}$  NMR (67.8 MHz,  $\text{CDCl}_3$ )  $\delta$  171.03, 154.25, 149.85, 138.02, 127.29, 121.03, 72.136–8.50 (PEG), 63.74, 58.57, 38.80, 36.96, 35.02.

**Compound 12.** To a solution of **11** (5.3 g, 0.434 mmol), disuccinimidyl carbonate (DSC, 0.89 g, 3.47 mmol) in a mixture of anhydrous DCM (50 mL), and dimethylformamide (DMF, 5 mL) cooled to 0 °C in an ice bath was added pyridine (0.274 g, 3.47 mmol), and the resulting mixture was allowed to warm to room temperature overnight. The solvent was partially removed under reduced pressure, and the product was precipitated by addition of ethyl ether, filtered, and crystallized from DCM/ethyl ether (20:80) to give **12** (4.7 g, 0.378 mmol, 87%).  $^{13}\text{C}$  NMR (67.8 MHz,  $\text{CDCl}_3$ )  $\delta$  171.04, 168.32, 153.87, 151.47, 151.16, 129.65, 129.43, 121.55, 71.78–69.26 (PEG), 58.62, 38.86, 37.03, 34.98, 25.05.

**Compound 16.** To a solution of 12 kDa mPEG (**14**, 50.0 g, 4.17 mmol) in DCM (500 mL) were added diglycolic anhydride, **15**, (3.87 g, 33.3 mmol) and DMAP (4.1 g, 33.3 mmol), and the reaction was stirred at room temperature for 12 h. The mixture was washed with 0.1 N HCl, dried (sodium sulfate), and filtered. After partial removal of the solvent in vacuo, the product was precipitated with addition of ethyl ether, filtered, and crystallized from IPA to give **16** (40.1 g, 3.29 mmol, 79%).  $^{13}\text{C}$  NMR (67.8 MHz,  $\text{CDCl}_3$ )  $\delta$  170.16, 169.41, 71.37–67.48 (PEG), 63.42, 58.43.



**Compound 17.** A solution of **4** (33.0 g, 2.74 mmol), **15** (1.3 g, 11.0 mmol), and DMAP (1.7 g, 13.7 mmol) in anhydrous DCM (40 mL) was stirred at room temperature for 12 h, followed by washing with 0.1 N HCl. The organic layer was dried (sodium sulfate) and filtered and the solvent partially removed under reduced pressure. The product was precipitated with ethyl ether, filtered, and crystallized from IPA to give **17** (28.2 g, 2.33 mmol, 85%).  $^{13}\text{C}$  NMR (67.8 MHz,  $\text{CDCl}_3$ )  $\delta$  170.68, 169.16, 71.52–68.81 (PEG), 58.62, 38.36.

**Compound 18.** To a solution of **16** (39.0 g, 3.22 mmol), 2-mercaptothiazoline (2-MT, 1.15 g, 9.66 mmol), and DMAP (1.18 g, 9.66 mmol) in anhydrous DCM (400 mL) cooled to 0 °C was added EDC (1.86 g, 9.66 mmol), and the reaction mixture was allowed to warm to room temperature after the addition and stirred for 12 h, followed by partial removal of the solvent under reduced pressure. The product was precipitated by the addition of ethyl ether, filtered, and crystallized from IPA to give **18** (37.5 g, 3.06 mmol, 95%).  $^{13}\text{C}$  NMR (67.8 MHz,  $\text{CDCl}_3$ )  $\delta$  200.73, 170.38, 169.09, 72.39–67.42 (PEG), 63.31, 58.35, 54.95, 28.90.

**Compound 19.** To a solution of **17** (20.0 g, 3.95 mmol), 2-MT (0.94 g, 7.91 mmol), and DMAP (0.96 g, 7.9 mmol) in anhydrous DCM (250 mL) cooled to 0 °C was added EDC (1.52 g, 7.91 mmol), and the reaction mixture was allowed to warm to room temperature. Stirring was continued for 12 h followed by partial removal of the solvent under reduced pressure. The product was precipitated with ethyl ether, filtered, and crystallized from IPA to give **19** (19.1 g, 3.71 mmol, 94%).  $^{13}\text{C}$  NMR (67.8 MHz,  $\text{CDCl}_3$ )  $\delta$  200.66, 171.30, 72.98–69.60 (PEG), 58.38, 54.96, 28.84.

**Compound 20.** A solution of **18** (36.0 g, 2.95 mmol), 3,5-dimethyl-4-hydroxybenzyl alcohol (2.7 g, 17.7 mmol), and DMAP (2.16 g, 17.7 mmol) in anhydrous DCM (350 mL) was refluxed for 12 h followed by partial removal of the solvent under reduced pressure. The product was precipitated by addition of ethyl ether, filtered, and crystallized from IPA to give **20** (33.6 g, 2.74 mmol, 93%).  $^{13}\text{C}$  NMR (67.8 MHz,  $\text{CDCl}_3$ )  $\delta$  168.99, 167.00, 146.03, 138.91, 129.25, 128.58, 71.38–67.14 (PEG), 63.49, 58.43, 15.82.

**Compound 21.** A solution of **19** (25.0 g, 2.05 mmol), 3,5-dimethyl-4-hydroxybenzyl alcohol (1.87 g, 12.28 mmol), and DMAP (1.5 g, 12.26 mmol) in anhydrous DCM (300 mL) was refluxed for 12 h, followed by partial removal of the solvent under reduced pressure. The product was precipitated by addition of ethyl ether, filtered, and crystallized from IPA to give **21** (24.1 g, 1.97 mmol, 96%).  $^{13}\text{C}$  NMR (67.8 MHz,  $\text{CDCl}_3$ )  $\delta$  168.56, 167.58, 139.46, 129.67, 127.13, 71.87–68.15 (PEG), 64.02, 58.93, 38.65, 16.32.

**Compound 22.** To a solution of **20** (9.0 g, 0.73 mmol) and DSC (0.75 g, 2.92 mmol) in anhydrous DCM (95 mL) and DMF (40 mL) was added pyridine (0.23 g, 2.91 mmol) and the reaction mixture stirred for 12 h at room temperature. Partial removal of the solvent was done under reduced pressure, and the product precipitated with ethyl ether, filtered, and crystallized from DCM/ethyl ether to give **22** (8.4 g, 0.68 mmol, 93%).  $^{13}\text{C}$  NMR (67.8 MHz,  $\text{CDCl}_3$ )  $\delta$  168.95, 168.23, 166.79, 151.02, 147.57, 130.65, 130.15, 128.39, 71.51–67.08 (PEG), 63.48, 58.42, 24.88, 15.79.

**Compound 23.** To a solution of **21** (10.0 g, 0.815 mmol) and DSC (1.67 g, 6.52 mmol) in a mixture of anhydrous DCM (100 mL) and DMF (10 mL) cooled to 0 °C was added pyridine (0.52 g, 6.58 mmol), and the resulting mixture was stirred at room temperature for 12 h. The

solvent was partially removed under reduced pressure and the product precipitated by the addition of ethyl ether, filtered, and crystallized from DCM/ethyl ether to yield **23** (9.6 g, 0.77 mmol, 95%).  $^{13}\text{C}$  NMR (67.8 MHz,  $\text{CDCl}_3$ )  $\delta$  168.45, 167.29, 151.49, 148.02, 131.18, 130.57, 128.97, 72.01–68.05 (PEG), 58.93, 38.64, 25.36, 16.26.

**Protein Conjugation and Analysis.** *Materials and Methods.* Chicken egg white lysozyme (EC 3.2.1.17), lysozyme substrate bacteria (*Micrococcus lysodeikticus*), and PBS buffer (10 mM phosphate, pH 7.4, 138 mM NaCl, and 2.7 mM KCl) were purchased from Sigma Inc. (St. Louis, MO). Pre-cast Tris-glycine SDS electrophoresis gel and the gel running buffer were obtained from Invitrogen (Carlsbad, CA). Rat plasma used to measure in vitro hydrolyses of the conjugates was processed in EDTA and stored frozen. IL-2 was purchased from PeproTech (Princeton, NJ), and GFP was obtained from Clontech (Palo Alto, CA). All in vivo measurements were done in triplicate, and a standard deviation of  $\pm 5\%$  was found for in vitro measurements.

*Preparation of Single PEG–Lysozyme Conjugates.* Lysozyme from chicken eggs has a molecular weight of 14 500 and 6 lysine residues. With fast stirring, the activated PEG powder, at a reaction molar ratio of 1:1 (PEG:lysozyme), was added to a lysozyme solution of 5 mg/mL in 0.1 M phosphate buffer, pH 7.3. After stirring for 45 min at 25 °C, the reaction was treated with 0.2 M sodium phosphate (pH 5.1) to a final pH of 6.5. The reaction mixture was dialyzed against 20 mM sodium phosphate, pH 5.1, at 4 °C, using 6000–8000 MW cutoff membrane. The sample conductivity after dialysis should be less than 2 mS. The isolation of single PEG–lysozyme was performed on a cation exchange column (Poros, HS) using a solvent system of 20 mM sodium phosphate at pH 5.1 with a NaCl gradient. The peak of single PEG–lysozyme was collected and concentrated using the ultrafree centrifugal filter device with 10k NMWL membrane (Millipore Corp., Bedford, MA). The yield of the purified single PEG–lysozyme was about 20–30%.

*Preparation of Multi PEG–Lysozyme Conjugates.* With fast stirring, the activated PEG linker at a reaction molar ratio of 30:1 (PEG:lysozyme) was added to a lysozyme solution of 5 mg/mL in 0.1 M phosphate buffer, pH 7.3. After stirring 45 min at room temperature, the reaction was treated with 0.2 M sodium phosphate (pH 5.1) to final pH of 6.5. The reaction mixture was diluted with  $\text{H}_2\text{O}$  and separated on Hiload Superdex 200 column at 1 mL/min. The column buffer contains 20 mM sodium phosphate (pH 6.8) and 140 mM NaCl. The fractions of the peak were pooled and concentrated using the ultrafree centrifugal filter device with 30k NMWL membrane (Millipore Corp., Bedford, MA). The yield of the purified multi PEG–lysozyme was about 85%, and the PEG number per lysozyme molecule as analyzed by fluorimetric assay (**9**) was found to be 5–6.

*Concentration Determination.* PEG–lysozyme conjugate concentration was determined by UV using an extinction coefficient of  $2.39 \text{ mL mg}^{-1} \text{ cm}^{-1}$  at 280 nm in 0.1 M sodium phosphate, pH 7.3.

*Enzyme Activity Assay for Lysozyme.* Under the reaction conditions mentioned above, lysozyme activity disappeared after conjugation with only a single PEG. The release of the lysozyme was indicated by regeneration of the lysozyme activity under various release conditions and confirmed on SDS electrophoresis gel.

In a typical lysozyme activity assay, 0.2 mL of 0.02% (w/v) *M. lysodeikticus* (substrate) was added to 0.12–0.24  $\mu\text{g}$  of lysozyme in 50  $\mu\text{L}$  66 mM potassium phosphate, pH 6.2, containing 0.01% BSA, in a 96-well titer plate.

The absorbance at 450 nm was followed for 5 min. The rate of decrease in absorbance was used as a measure of enzyme activity. One unit of enzyme activity produces a change of 0.001 absorbance/min at 25 °C at 450 nm.

**Release of Lysozyme in Rat Plasma and in Chemical Buffer.** PEG–lysozyme conjugates in phosphate buffer, pH 6.5, underwent buffer exchange with PBS, pH 7.4, to monitor release in rat plasma. The stability in PBS at 37 °C was measured. The conjugates also underwent buffer exchange with H<sub>2</sub>O for the release in Tris buffer, pH 8.5. CentriCon 10 K centrifuge tube (Millipore Corp., Bedford, MA) was used for the single PEG–lysozyme conjugates, while CentriCon 30K was used for the multi PEG–lysozyme conjugates. The release of lysozyme from single or multi PEG–lysozyme conjugates was conducted at 0.15 mg/mL, under N<sub>2</sub>. At the time indicated, 1 aliquot was withdrawn, neutralized with 0.2 M phosphate (pH 5.1) to pH 6.5, and stored at –20 °C until further analysis.

**Preparation of PEG–IL-2 Conjugates.** Recombinant human IL-2 is a protein containing 134 amino acid residues, 11 of which are lysines, and has a molecular weight of 15 400. IL-2 suspended in 0.1 M HOAc was added to a solution containing the appropriate PEG linker and 5 mM HOAc at pH 3. The final concentration of IL-2 was 1 mg/mL with a reaction molar ratio of 1:60 (IL-2:PEG). With fast stirring, 0.5 M sodium dibasic phosphate was added to raise pH from 3 to 7.3. (The final concentration of sodium phosphate was 94 mM). After a 1 h reaction at 25 °C, under nitrogen, the reaction pH was lowered to 6.6 with 0.5 M sodium monobasic phosphate. PEG–IL-2 conjugates were isolated on a Superdex 200 size exclusion column using 10 mM sodium phosphate, pH 6.6, and 140 mM NaCl.

**Enzyme-Linked Immunosorbent Assay (ELISA) of IL-2 and PEG–IL-2 Compounds.** Retention of IL-2 and PEG–IL-2 in Balb-C mice (1 mg/Kg, i.v. and collected at time points shown in Figure 7) was determined by an ELISA assay using the antibodies from R&D Systems (Minneapolis, MN). To obtain consistent results and high sensitivity, rPEG–IL-2 conjugates in plasma were hydrolyzed to native IL-2 prior to the ELISA assay. The hydrolysis was conducted in 0.2 M NH<sub>4</sub>OH under nitrogen, at 37 °C for 2 h, and then acidified with 0.1 M HOAc to pH 5–6.

**Conjugation of PEG to GFP and Purification of GFP–PEG Compounds.** In a typical reaction, activated PEG linker was added to a solution of GFP (2 mg/mL) in 0.05 M HEPES, pH 7.8, with a molar ratio of 30:1 (PEG:GFP; also see Discussion Section for references to GFP). The solution was stirred at 25 °C under N<sub>2</sub> for 45 min. After 45 min, the pH of the solution was lowered by adding sodium phosphate buffer, pH 6.4, to a final concentration of 50 mM. The free PEG was removed on a Superdex 200 Hiload 16/60 column (Amersham Pharmacia Biotech, Piscataway, NJ) using the Biocad Perfusion Chromatography Workstation. The elution buffer was comprised of 10 mM sodium phosphate, pH 6.8 and 150 mM NaCl. The fractions that exhibited both absorbance at 280 nm and fluorescence were pooled and concentrated using ultrafree-15 centrifugal filter device with 30k NMWL membrane (Millipore Corp., Bedford, MA). The PEG–GFP concentration was determined by UV at 489 nm using an extinction coefficient of 55 000 cm<sup>–1</sup> M<sup>–1</sup>.

**Pharmacokinetics of GFP and PEG–GFP Conjugates in Rats.** Conscious rats (three rats per compound) were restrained and injected intravenously via the tail vein with either GFP or PEG–GFP compound at 5 mg/kg. Following compound administration, sampling of blood

**Table 1. Release Rate of Mono PEGylated Lysozyme in Rat Plasma and in Buffer<sup>a</sup>**

compound	plasma	PBS, 37 °C	pH 8.5, 37 °C
<b>24a</b>	4	23	1
<b>25a</b>	4	12	0.6
<b>13a</b>	4	15	0.8
<b>3a</b>	17	>168	5.6
<b>SC</b>	N/R	N/R	N/R

<sup>a</sup> The data are expressed as *t*<sub>1/2</sub> in hours. The release in plasma was monitored for 3 days, the release in pH 8.5 buffer for 5 days, and the release in PBS for 7 days. PBS contains 138 mM NaCl, 2.7 mM KCl, and 10 mM phosphate, pH 7.4. The release of lysozyme was detected by regeneration of lysozyme activity and confirmed by gel electrophoresis. N/R stands for “no release”. Time points collected are shown in Figure 1.

**Table 2. Release Rate of Multi PEGylated Lysozyme in Rat Plasma and in Buffer<sup>a</sup>**

compound	plasma	PBS, 37 °C	pH 8.5, 37 °C
<b>24b</b>	64	>168	22
<b>25b</b>	21	65	7
<b>3b</b>	>72	N/R	>120
<b>SC</b>	N/R	N/R	N/R

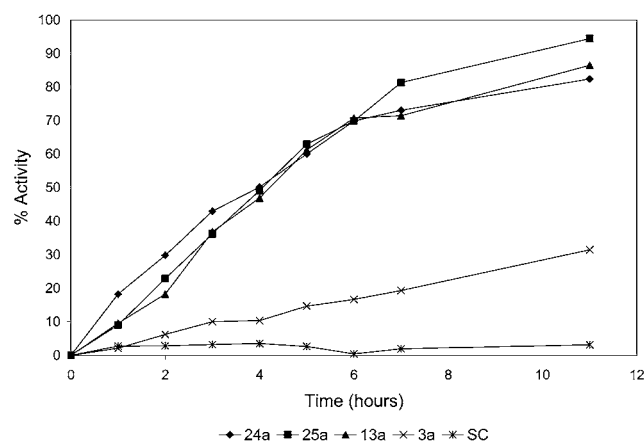
<sup>a</sup> The data are expressed as *t*<sub>1/2</sub> in hours. The release in plasma was monitored for 3 days, the release in pH 8.5 buffer for 5 days, and the release in PBS for 7 days. PBS contains 138 mM NaCl, 2.7 mM KCl, and 10 mM phosphate, pH 7.4. The release of lysozyme was detected by regeneration of lysozyme activity. N/R stands for “no release”.

began at various time points. Rats were lightly anesthetized with a 30% oxygen 70% carbon dioxide mixture and bled for 0.5 mL of whole blood via their retroorbital sinus. Whole blood was collected within an EDTA microtube and immediately processed for plasma. Plasma samples were snap frozen on dry ice and stored at –20 °C until analysis. A 10 µL aliquot of plasma containing GFP or PEG–GFP compound was diluted with 1 mL of 15 mM of Tris buffer, pH 7.4. After thorough mixing, the fluorescence intensity was measured using a HITACHI F-2000 Fluorescence Spectrophotometer. The autofluorescence generated from plasma alone was subtracted from all the samples, using 15 mM Tris, pH 7.4 buffer as a blank. Pharmacokinetic parameters were calculated using a one compartment i.v. bolus model (WinNonlin, Pharsight Corp., Mountainview, CA).

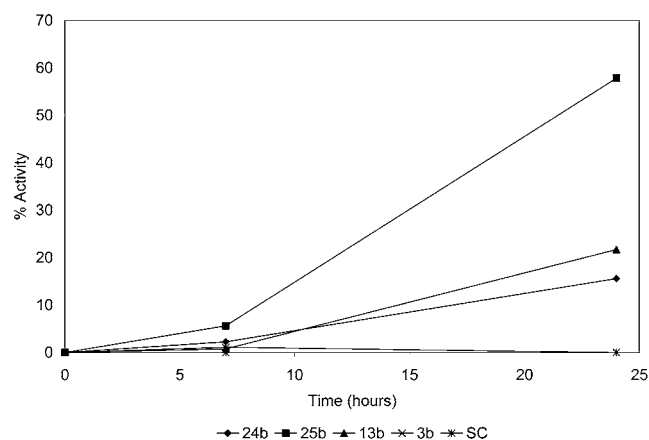
For analysis of the release profile in vivo, samples collected at different time points were diluted with PBS and analyzed on Superdex 75 HR 10/30 column (Amersham Pharmacia Biotech, Piscataway, NJ) using a Biocad Perfusion Chromatography Workstation. Specifically, a 20 µL plasma sample was diluted with 0.6 mL PBS, and 0.5 mL of the diluted sample was loaded on a Superdex 75 HR 10/30 column that had been equilibrated with PBS (Amersham Pharmacia Biotech, Piscataway, NJ). The fluorescence intensity of GFP and the PEG–GFP conjugates eluted from the column was measured using an on-line Waters 470 Scanning Fluorescence Detector set at *E*<sub>x</sub> = 489 nm, *E*<sub>m</sub> = 510 nm.

## RESULTS AND DISCUSSION

The various linkers designed for this study were conjugated to lysozyme not only to compare and validate the kinetics of hydrolysis determined from our first study of rPEG, but also to make a facile measurement of loss of activity: even a single 12 kDa PEG attachment eliminates the activity of lysozyme under standard reaction conditions (1). Our hypothesis that anchimeric assisted hydrolysis of PEG conjugates is born out by the data in Tables 1 and 2. Regardless of which rPEG linker



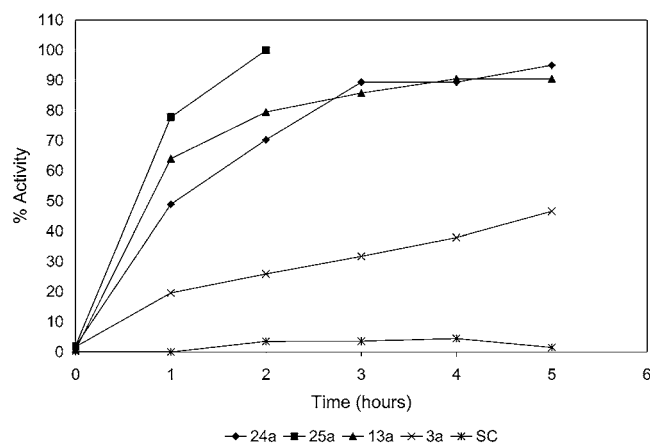
**Figure 1.** Regeneration of lysozyme activity from mono PEG-lysozyme conjugates in rat plasma. Mono PEG-lysozyme conjugates (0.15 mg/mL) were incubated in rat plasma at 37 °C under N<sub>2</sub>. At the time indicated, 1 aliquot was withdrawn and analyzed for lysozyme activity.



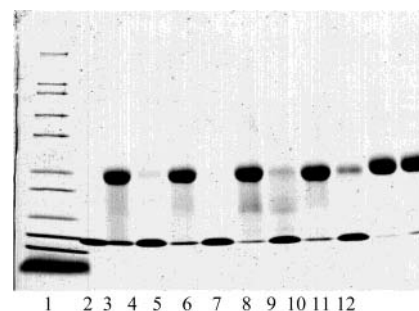
**Figure 2.** Regeneration of lysozyme activity from multi PEG-lysozyme conjugates in rat plasma. Multi PEG-lysozyme conjugates (0.15 mg/mL) were incubated in rat plasma at 37 °C under N<sub>2</sub>. At the time indicated, 1 aliquot was withdrawn and analyzed for lysozyme activity.

is employed, measurements of single strand conjugates can be seen to always hydrolyze more rapidly than multistrand (5–6 unit) PEG conjugates either in PBS buffer or rat plasma. In vitro rat plasma studies for the single strand conjugates all show a  $t_{1/2}$  of 4 h, with the exception of **3a** which, as expected, is 17 h (Table 1), and is consistent with our original findings (1), while for 5–6 multistrand conjugate **3b**, a  $t_{1/2} > 72$  h was obtained.

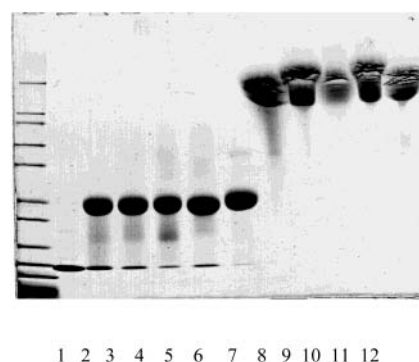
Having demonstrated the reproducibility of the lysozyme model, the three other linkers (**13**, **24**, and **25**) selected for this study were conjugated in the same, i.e., single versus multistrand rPEG. Accelerated hydrolysis was clearly observed for all three new rPEG-lysozyme conjugates and was several times more rapid than conjugate **3a** in both PBS and rat plasma (Figures 1 and 2). However, when stored at 4 °C in PBS, all the conjugates in this study showed no breakdown after 1 week. In PBS buffer at 37 °C,  $t_{1/2}$  for the mono conjugate **24a** was 23 h, while for **25a** and **13a** mono conjugates were 12 and 15 h, respectively (Table 1). Hydrolysis of these three monoconjugates of lysozyme was essentially complete in 2–3 h when the pH was raised to 8.5, while conjugate **3a** again was slower with only about 50% cleaved after 6 h (Table 1, Figures 3 and 4). This substantial increase in hydrolysis with slight shift in pH should enable rapid



**Figure 3.** Release of lysozyme from mono PEG-lysozyme conjugates at pH 8.5. Mono PEG-lysozyme conjugates (0.15 mg/mL) were incubated in 50 mM Tris buffer, pH 8.5, at 37 °C. At the time indicated, 1 aliquot was withdrawn and analyzed for lysozyme activity. The release was also confirmed by SDS-PAGE, as shown in Figure 4.



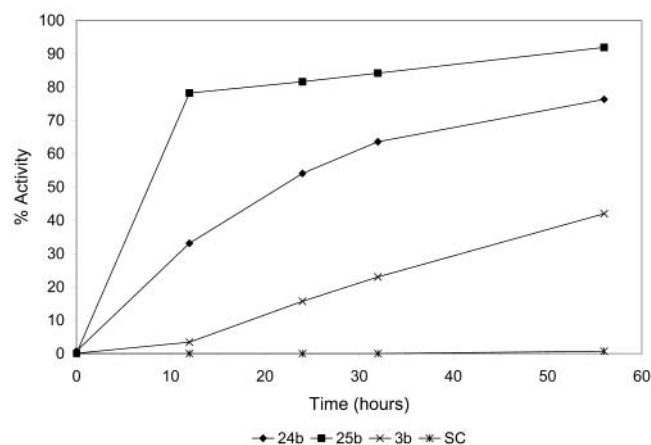
**Figure 4.** 4–20% SDS-PAGE analysis of release of lysozyme from mono PEG-lysozyme conjugates at pH 8.5. The hydrolysis was conducted at 37 °C under N<sub>2</sub> for 24 h. Lane 1, molecular markers (200, 116.3, 97.4, 66.3, 55.4, 36.5, 31, 21.5, 14.4, and 6 kDa); lane 2, lysozyme; lane 3 and 4, **24a** before and after hydrolysis; lane 5 and 6, **25a** before and after hydrolysis; lane 7 and 8, **13a** before and after hydrolysis; lane 9 and 10, **3a** before and after hydrolysis; lane 11 and 12, **SC** before and after hydrolysis.



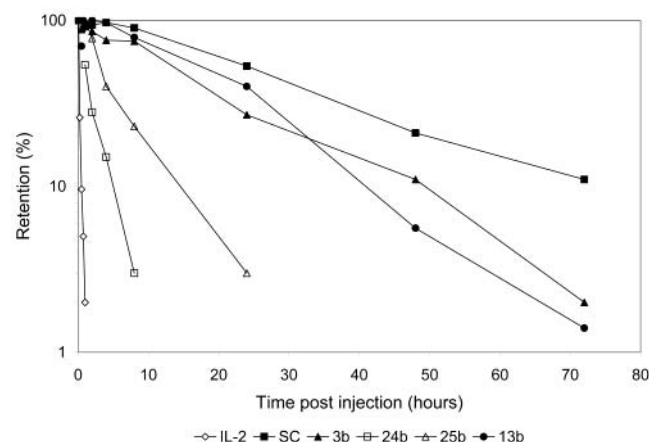
**Figure 5.** 4–20% SDS-PAGE analysis of mono and multi PEGylated lysozyme conjugates. Lane 1, molecular markers (200, 116.3, 97.4, 66.3, 55.4, 36.5, 31, 21.5, 14.4, and 6 kDa); lane 2, lysozyme; lane 3–7, **24a**, **25a**, **13a**, **3a**, and mono **SC** conjugates; lane 8–12, **24b**, **25b**, **13b**, **3b**, and multi **SC** conjugates.

processing of mixed PEGylated species (i.e., hybrids of rPEG and mPEG). We will report on this effect in future work. Generally, for binding proteins (e.g., interferon- $\alpha$ ) mono-PEGylation is preferred in order to maintain the highest possible specific activity. On the other hand for enzymes (e.g., L-asparaginase), multi-PEGylation is acceptable because a high specific activity can be obtained.





**Figure 6.** Release of lysozyme from multi PEG-lysozyme conjugates at pH 8.5. Multi PEG-lysozyme conjugates (0.15 mg/mL) were incubated in 50 mM Tris buffer, pH 8.5, at 37 °C. At the time indicated, 1 aliquot was withdrawn and analyzed for lysozyme activity.



**Figure 7.** Pharmacokinetics of IL-2 and PEG-IL-2 conjugates in mice after intravenous injection at 1 mg/kg dose, as determined by ELISA assay.

We therefore examined more highly PEGylated species of lysozyme as representative of the type of PEGylated enzymes usually encountered: these consisted of about 5–6 rPEG strands (Figure 5). The results obtained for the multi-PEGylated species indicate that the trends have changed compared to the single strand conjugates and exhibit an overall shift to longer half-lives (Table 2). This is expected for sterically more hindered conjugates as was pointed out in our previous work (1). However, in these cases a greater separation of half-lives still could be observed. In PBS buffer at 37 °C,  $t_{1/2}$  for conjugate **25b** was 65 h, while **24b** and **3b** were all >120 h (Table 2).

Raising the pH to 8.5 allowed the removal of two of the rPEGs in rapid fashion, but only **25b** with a  $t_{1/2}$  of 7

**Table 3. Pharmacokinetic Parameters of IL-2 and PEG-IL-2 Conjugates in Mice<sup>a</sup>**

compound	circulating half-life (h)	area under the curve (h dose %)
IL-2	0.2	0.18
<b>24b</b>	1.2	1.96
<b>25b</b>	3.5	6.33
<b>13b</b>	20	23.0
<b>3b</b>	16	20.7
SC	26	31.6

<sup>a</sup> Circulating half-life was determined from Figure 7 and area under the curve was estimated using trapezoidal rule. The dose at 5 min after injection was taken as a 100% control.

h would be practical in the case of lysozyme (Figure 6). As was the case for monopegylated species in rat plasma, both of the conjugates (**24b** and **25b**) have the most rapid  $t_{1/2}$ : 21 and 64 h respectively (Table 2). It is apparent that with the exception of **25b** (and possibly **24b**), the other conjugate prepared from nonanchimerically assisted linkers offers little usefulness in the way of rapid rPEG removal. However, the current data provides a convenient starting point for choosing a particular linker. For example the long-term continuous release of lysozyme from **3b** in vivo has been pointed out (1). All the rPEG multiconjugates of lysozyme are stable in PBS buffer at 4 °C, thus enabling long storage times before processing or purification. It should be noted that after 6 days at 25 °C in PBS buffer, only the **25b** conjugate shows about 10% breakdown (data not presented).

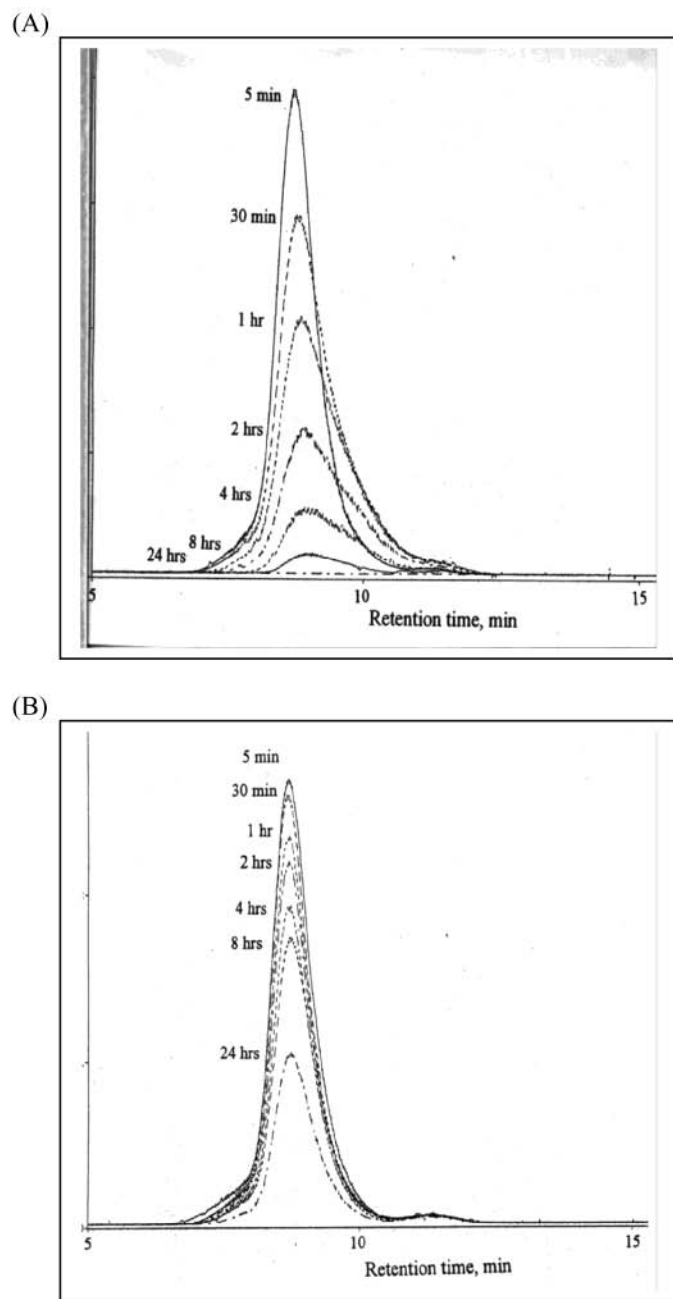
Multi-rPEGylation of IL-2 produced a conjugate with approximately 8–10 rPEG units. PK studies of this conjugate were performed in the usual manner (ELISA assay), resulting in release of rPEG over different time spans which is qualitatively similar to those produced by lysozyme (Table 3, Figure 7). Even though the in vitro  $t_{1/2}$  for multi rPEG-protein conjugates are in general >24 h (Table 2), in vivo they were released much more rapidly:  $t_{1/2}$  is now found to be 1–20 h (Table 3). Good use can be made of this property when rapid removal of rPEG is desired such as in the application of site-directed hybrids that can be generated in vivo.

In vivo (PK) results require substantial effort, so any additional rapid and accurate methods with which to study in vivo hydrolysis of rPEGylated proteins would be a valuable tool. Green fluorescent protein (GFP) from the jellyfish *Aequorea victoria* has received widespread utilization as a natural fluorescent marker for gene expression, localization of gene products, and identification of protein interaction and function. GFP is a protein consisting of 238 amino acids with a molecular mass of 27 000. The intrinsic fluorophore is a *p*-hydroxybenzylidene imidazolidine derivative. When illuminated by blue or UV light, GFP produces a bright green fluorescence that is species independent and does not require cofactors or substrates. A recent comprehensive review on GFP has summarized the pertinent details of this

**Table 4. Pharmacokinetic Parameters of GFP and PEG-GFP Conjugates in Rats<sup>a</sup>**

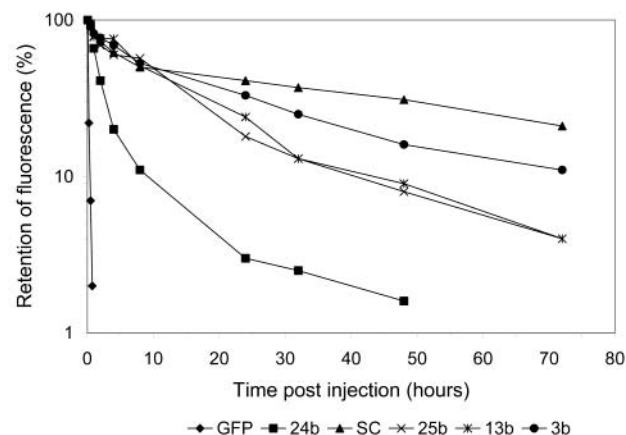
compound	circulating half-life of fluorescence (h)	area under the curve (h dose %)	mean residence time (h)
GFP	0.15	0.15	0.22
<b>24b</b>	1.78	1.78	2.57
<b>25b</b>	10.61	14.82	15.31
<b>13b</b>	11.71	13.77	16.89
<b>3b</b>	17.23	18.78	24.86
SC	24.62	29.19	35.52

<sup>a</sup> Data are average of three independent measurements with a standard deviation of less than 15%. Percent retention was calculated by dividing compound in the plasma at 2 min by the compound in the plasma at subsequent time.



**Figure 8.** Release profile of GFP from PEG-GFP conjugates in rats. Plasma samples collected at various time points were fractionated on SEC. The fluorescence intensity of GFP and PEG-GFP conjugates eluted from the column was measured using an on-line fluorescence detector. The release profile of **24b** was shown in panel A and **SC** in panel B.

fascinating protein (10). This protein is ideal for monitoring pharmacokinetics, since rPEG-GFP concentrations in plasma can simply be determined by measuring the total plasma fluorescence intensity regardless of the number of PEG molecules on GFP or the presence of other plasma proteins. In addition, the use of a size exclusion column allows detection of different species during the release process. Using various rPEG linkers reaction with free amino groups of GFP produces the expected carbamate bond. It was found that modification of GFP with rPEG (12 000) at a molar ratio of 30:1 (rPEG:GFP) did not affect  $\lambda$  max or GFP fluorescence intensity. This unique property of the GFP can now be used as a general tool in which to study the effect of PEG variation on protein conjugation.



**Figure 9.** Pharmacokinetics of GFP and PEG-GFP conjugates in rats after intravenous injection at 5 mg/kg dose. Percent retention was calculated by dividing total fluorescence in the plasma at 2 min by total fluorescence in the plasma at subsequent time. Fluorescence of plasma without compounds was subtracted from all samples.

All purified rPEG-GFP conjugates used in this study had an estimated PEG number of 8–10 PEGs per GFP by gel analysis. The objective of this study was therefore to prepare a series of rPEGylated GFP protein and determine if it would be possible to detect the release of various rPEGs from the native protein by a simple fluorescent measurement (Figure 8). This technique would demonstrate that modification of structure results in predictable release of native protein, at different rates, in vivo. A great separation of  $t_{1/2}$  values can be seen for the series of GFP conjugates in vivo, with **24b** being the most rapid (Table 4, Figure 9). Notice that the half-life of GFP in the rat was only 9.0 min, while the  $t_{1/2}$  of rPEG-GFP conjugates ranged from 1.8 to 17.2 h. As expected, the permanent PEG-GFP conjugate had the longest  $t_{1/2}$  of (25 h).

The stability profile of the GFP conjugate **24b** at 4 °C in PBS buffer (pH 7.4) however, was relatively good thus enabling long-term storage if necessary (data not shown). The results of a pharmacokinetic (PK) study are given in Table 4 and plotted in Figure 9, where it can be seen that for these multistrand rPEG-GFP conjugates there is again a separation of function (i.e. release of rPEG) compared to the permanent SC-GFP conjugate. Using this model it was seen that free GFP was released over a defined time period and that this release occurred before complete in vivo clearance: as the rate of release increased, the clearance also increased. Interestingly, in the case of GFP, conjugate **24b** is the most rapidly cleared (Figure 9,  $t_{1/2}$  = 2 h), again demonstrating that for specific applications the most desirable linker may have to be determined empirically.

## CONCLUSION

Three new rPEG linkers were synthesized and compared to permanently bonded PEG. These new rPEG linkers are rapidly released from their protein conjugates by anchimeric assistance to hydrolysis or proton removal or a combination of both. rPEG linkers that do not demonstrate anchimeric assistance to hydrolysis are predictably slower. Once again the rate of recovery of activity when PEG is attached to a protein typically was shown to depend on the number of PEG strands attached to the protein. It is clear from the lysozyme model that single strand conjugates hydrolyze more rapidly than multistrand conjugates.

This loss of activity after PEGylation also depends on the site of PEGylation, the protein structure, and the protein charge (11). A high PEG number may produce a longer plasma half-life, but often at the expense of protein activity. Releasable PEG, exemplified by the linkers **13a**, **24a**, and **25a**, allows a high degree of PEGylation of protein with the temporary masking of activity, followed by restoration of activity by a defined mechanism in a prescribed time frame, which can now be predicted with a greater degree of confidence. Modification of proteins may interrupt binding interactions with its substrate, thus reducing or eliminating the fundamental activity. Using rPEGylation, the rPEG conjugate can be transported to the site of activity where native protein is predictably released. Thus, rPEG provides a unique opportunity for the controlled release of native proteins, an unmet need in many cases of protein therapy.

In addition, we have shown that, for the first time, GFP conjugated to rPEG can be used as an informative, easily handled protein model to determine rates of PEG release by performing in vivo PK studies in the rat. This model is closely in agreement with the results obtained using the standard ELISA method for rPEG-IL-2. The implications of these findings are suggestive that broad applications of the rPEG methodology for the assessment of native protein delivery is probable.

#### ACKNOWLEDGMENT

We wish to thank Anthony Martinez, Haleema Janjua, and the Pharm/Tox group of Enzon for their important contributions to this work.

#### LITERATURE CITED

- (1) Lee, S., Greenwald, R. B., McGuire, J., Yang, K., and Shi, C. (2001) Drug Delivery Systems Employing 1,6-Elimination: Releasable Poly(ethylene glycol) Conjugates of Proteins. *Bioconjugate Chem.* 12, 163–169.
- (2) Carl, P. L., Chakravarty, P. K., and Katzenellenbogen, J. A. (1981) A Novel Connector Linkage Applicable in Prodrug Design. *J. Med. Chem.* 24, 479–480.
- (3) Miron, T., and Wilchek, M. (1993) Simplified Method for the Preparation of Succinimidyl Carbonate Polyethylene Glycol for Coupling to Proteins. *Bioconjugate Chem.* 4, 568–569.
- (4) Greenwald, R. B., Pendri, A., Martinez, A., Gilbert, C., and Bradley, P. (1996) PEG Thiazolidine-2-thione, a Novel Reagent for Facile Protein Modification of Bovine Hemoglobin. *Bioconjugate Chem.* 7, 638–641.
- (5) Greenwald, R. B., Pendri, A., Conover, C. D., Zhao, H., Choe, Y. H., Martinez, A., Shum, K., and Guan, S. (1999) Drug Delivery Systems Employing 1,4- or 1,6-Elimination: Poly(ethylene glycol) Prodrugs of Amine-Containing Compounds. *J. Med. Chem.* 42, 3657–3667.
- (6) See Greenwald, R. B., Pendri, A., Conover, C. D., Lee, C., Choe, Y. H., Gilbert, C., Martinez, A., Xia, J., Wu, D., and Hsue, M. (1998) Camptothecin-20-PEG Ester Transport Forms: The Effect of Spacer Groups on Antitumor Activity. *Bioorg. Med. Chem.* 6, 551–562, and references cited for other examples of anchimeric assistance.
- (7) Cremin, D. J., and Hegarty, A. F. (1977) Amide Group Catalysis of Ester Hydrolysis *Tetrahedron* 33, 1823–1826.
- (8) Conover, C. D., Zhao, H., Longley, C. B., Shum, K. L., and Greenwald, R. B. (2003) *Bioconjugate Chem.*, in press.
- (9) Stocks, S. J., Jones, A. J. M., Ramey, C. W., and Brooks, D. E. (1986) A Fluorometric Assay of the Degree of Modification of Protein Primary Amines with Polyethylene Glycol. *Anal. Biochem.* 154, 232–234.
- (10) Tsien, R. Y. (1998) The Green Fluorescent Protein. *Annu. Rev. Biochem.* 67, 509–544.
- (11) Harris, J. M., Martin, N. E., and Modi, M. (2001) Pegylation: A Novel Process for Modifying Pharmacokinetics. *Clin. Pharmacokinet.* 40, 539–551.

BC025652M



# Specific Association of Thiamine-Coated Gadolinium Nanoparticles with Human Breast Cancer Cells Expressing Thiamine Transporters

Moses O. Oyewumi,<sup>†</sup> Shuqian Liu,<sup>‡</sup> Jeffrey A. Moscow,<sup>‡</sup> and Russell J. Mumper<sup>\*,†</sup>

Division of Pharmaceutical Sciences, College of Pharmacy, and Department of Pediatrics, Chandler Medical Center, University of Kentucky, Lexington, Kentucky 40536-0082. Received January 2, 2003; Revised Manuscript Received January 28, 2003

Thiamine (vitamin B<sub>1</sub>) was investigated as a tumor-specific ligand for gadolinium nanoparticles. Solid nanoparticles containing gadolinium hexanediol (1.5 mg/mL) were engineered from oil-in-water microemulsion templates and coated with thiamine ligands. Thiamine ligands were synthesized by conjugating thiamine to either distearoylphosphatidylethanolamine (DSPE) or fluorescein via a poly-(ethylene glycol) (PEG) spacer (Mw 3350). The efficiency of thiamine ligand attachment to nanoparticles was evaluated using gel permeation chromatography (GPC). Cell association studies were carried out using a methotrexate-resistant breast cancer cell line, MTX<sup>R</sup>ZR75, transfected with thiamine transporter genes (THTR1 and THTR2). Thiamine-coated nanoparticle association with THTR1 and THTR2 cells was significantly greater than that with control breast cancer cells (MTX<sup>R</sup>ZR75 transfected with the empty expression vector pREP4) ( $p < 0.01$ ;  $t$ -test). The nanoparticle cell association was significantly dependent on the extent of thiamine ligand coating on nanoparticles, expression of thiamine transporters in cells, temperature of incubation, and the concentration of competitive inhibitor (free thiamine). Further studies are warranted to assess the potential of the engineered thiamine-coated gadolinium (Gd) nanoparticles in neutron capture therapy of tumors.

## INTRODUCTION

The application of nanoparticles as drug delivery systems has received increasing attention due to the opportunities of achieving drug targeting and controlled release (Cho et al., 2001). As such, nanoparticles have been widely applied in the delivery of drugs, genes, and vaccines to specific cells and tissues of interest with potential reduction of toxicity as well as increased therapeutic effects (Allen et al., 1995; Kreuter, 1995). Various types of targeting ligands that have been employed in cell specific nanoparticle formulations include antibodies, peptides, and vitamins (Vyas et al., 2001; Wang and Low, 1998). The utilization of vitamins in targeted delivery has been based on the fact that all eukaryotic cells have specific uptake mechanisms for essential vitamins such as folic acid, vitamin B<sub>12</sub>, and biotin (Russell-Jones et al., 1999). In particular, many studies carried out on folate receptors indicated that folate-conjugated macromolecules can be specifically taken up by folate receptor-bearing tumor cells (Lee and Low, 1995; Atkinson et al., 2001). Based on the previous work with folate, the present study has been designed to investigate the feasibility of engineering thiamine-coated nanoparticles and to determine the extent to which the presence of thiamine coating on nanoparticles could confer specificity to cells that overexpress thiamine transporters. To our knowledge, no previous work has

been done on the feasibility of thiamine as a cell specific ligand.

Thiamine is a member of the vitamin B family and is a water soluble micronutrient that is essential for normal cell function, growth, and development. Like other vitamin B family members, such as folic acid, thiamine has specified transport mechanisms in all eukaryotic cells (Said et al., 1999; Zhao et al., 2002). Earlier studies using gene mapping techniques have identified the genes for thiamine transporters THTR1 and THTR2 (Rajgoal et al., 2001; Lo and Wang, 2002). In its coenzyme form, thiamine pyrophosphate plays a critical role in carbohydrate metabolism (Said et al., 2001; Singleton and Martin, 2001). Specifically, thiamine pyrophosphate participates in the carboxylation of pyruvic and  $\alpha$ -ketoglutaric acids as well as in the utilization of pentose. Thiamine deficiency in humans leads to a variety of clinical abnormalities such as cardiovascular and neurological disorders (Seligmann et al., 2001; Lee et al., 1998). In addition, the importance of thiamine in the biosynthesis of many cell constituents, including neurotransmitters and nucleic acid precursors, has been shown to be the basis for the observed increased thiamine utilization in tumor cells (Singleton and Martin, 2001). Additional studies conducted in animals and humans showed that tumor growth might be related to the depletion of tissue thiamine stores, apparently because of the increased thiamine utilization (Lee et al., 1998; Weng et al., 1999; Cascante et al., 2000). Further studies carried out using radiolabeled glucose indicated that tumor cells rely heavily on nonoxidative transketolase (TK) pathway for ribose synthesis to build nucleic acids (Comin-Aduix et al., 2001). As such, antithiamine compounds have been employed in several tumor models to inhibit nucleic acid synthesis and tumor proliferation (Boros et al., 1997).

\* Corresponding author: Russell J. Mumper, Ph.D., Assistant Professor of Pharmaceutical Sciences, Assistant Director, Center for Pharmaceutical Science and Technology, College of Pharmacy, University of Kentucky, 907 Rose St., Lexington, KY 40536-0082. Tel: (859) 257-2300 ext. 258, Fax: (859) 323-5985, E-mail: rjmump2@email.uky.edu.

<sup>†</sup> Division of Pharmaceutical Sciences.

<sup>‡</sup> Department of Pediatrics.

Therefore, in the present study, gadolinium nanoparticles coated with thiamine were engineered, and selective cell association was evaluated using cells that overexpress thiamine transporters. We earlier reported on the engineering of nanoparticles from oil-in-water microemulsion templates (Oyewumi and Mumper, 2002a; Oyewumi and Mumper, 2002b). Nanoparticle formulations contained a final concentration of gadolinium hexanedione (GdH) of 1.5 mg/mL. Gadolinium is a potential anticancer agent for neutron capture therapy (NCT) (Shih and Brugger, 1992). To obtain thiamine-coated nanoparticles, thiamine ligands synthesized to contain either DSPE or fluorescein groups were added to preformed nanoparticle suspensions. Cell specificity of the engineered thiamine-coated nanoparticles was assessed on the basis of the rate and extent of cell association with human breast cancer cells transfected with thiamine transporter genes THTR1 and THTR2. Cells transfected with the empty expression vector pREP4 were used as controls in all experiments. The feasibility of engineering thiamine-coated gadolinium nanoparticles was evaluated as well as the potential of achieving cell specific association due to the thiamine coating.

#### EXPERIMENTAL PROCEDURES

**Materials.** Emulsifying wax was obtained from Spectrum Chemicals (New Brunswick, NJ), and polyoxyl 20 stearyl ether (Brij 78) was purchased from Uniqema (Wilmington, DE). Distearoylphosphatidylethanolamine (DSPE)–PEG–NHS and fluorescein (FL)–PEG–NHS were purchased from Shearwater Polymers (Huntsville, AL). Thiamine hydrochloride was obtained from Aldrich Chemicals (Milwaukee, WI). Sephadex G-75, Sepharose CL-4B, and potassium ferricyanide were purchased from Sigma Chemicals (St. Louis, MO). Fluorescein-DOPE was purchased from Avanti Polar Lipids (Alabaster, AL). Gadolinium hexanedione was synthesized as previously described (Oyewumi and Mumper, 2002b).

**Preparation of Nanoparticles from Microemulsion Templates.** Solid nanoparticles were engineered from oil-in-water microemulsion templates using emulsifying wax as the oil phase (matrix material). Briefly, 2 mg of emulsifying wax accurately weighed into a glass vial was melted together with 1.5 mg of gadolinium hexanedione (GdH) on a hotplate. Various volumes of polyoxyl 20 stearyl ether (Brij 78; 100 mM) were added to the melted mixture at 55 °C under magnetic stirring. Water (0.22  $\mu$ m filtered) was added to make the final volume of 1 mL. The formation of an oil-in-water microemulsion was verified by the clarity of the mixture and by photon correlation spectroscopy (PCS) using a Coulter N4 Plus Submicron Particle Sizer at 55 °C. Using optimal microemulsion templates, nanoparticles were prepared by simply cooling the stirring microemulsions to room temperature. The properties and characteristics of nanoparticles cured in each preparation were investigated as described below.

**Synthesis of Thiamine Ligands.** Thiamine ligands were synthesized by chemically linking thiamine to either DSPE or fluorescein via a PEG spacer (Mw 3350). The procedure was based on the modified method of Jayamani and Low (1992). Briefly, 2.0 mg of thiamine was reacted at room temperature for 2 h with 10 mg of either DSPE–PEG–NHS or Fluorescein–PEG–NHS in 1 mL of phosphate buffered saline (pH 7.4). Afterward, unreacted thiamine was removed from reaction mixture by dialysis in deionized water since free (unreacted) thiamine will

interfere in cell targeting. The conjugated thiamine was purified further by passing the reaction mixture through a gel permeation column (2.5 cm  $\times$  5.0 cm; Sephadex G-75) with phosphate buffer, pH 5.0 as the mobile phase. Thiamine conjugated to either DSPE or fluorescein was eluted at the void volume of the GPC column as determined by a thiochrome assay. The procedure of the thiochrome assay involved oxidizing thiamine in each GPC fraction to thiochrome and subsequently measuring fluorescence intensity at 365 nm (excitation) and 445 nm (emission). The efficiency of thiamine conjugation to either DSPE-PEG or Fluorescein-PEG was 40% and 18%, respectively. The conjugate was verified by IR spectroscopy.

**Addition of Thiamine Ligands to Nanoparticle Preparations.** Using a stock aqueous solution of thiamine ligand (0.5 mg/mL), various amounts of thiamine ligand were added to cured nanoparticle suspensions at 25 °C. The mixture was then gently stirred for 4 h at 25 °C. The efficiency of thiamine attachment/adsorption was assessed by gel permeation chromatography (GPC) elution profiles using a Sepharose CL-4B column. Briefly, 80  $\mu$ L of thiamine-coated nanoparticle suspensions were passed down the Sepharose CL-4B column (1.5 cm  $\times$  8 cm) using deionized water (0.22  $\mu$ m filtered) as the mobile phase. The elution of thiamine-coated nanoparticles and free thiamine ligand in all the GPC fractions was detected by laser light scattering counts per second (CPS) and the thiochrome assay method as mentioned above. In a separate study, the GPC elution profiles of control nanoparticles (without thiamine) and free thiamine ligand were obtained to serve as references. Based on the GPC elution profiles, the efficiency of thiamine ligand coating was calculated as the percentage of the ratio of the area under thiamine-coated nanoparticle profiles to the area under the total elution profiles. Calculation of the concentration of thiamine and total number of thiamine molecules used in coating nanoparticles was based on the coating efficiency data.

**Photon Correlation Spectroscopy (PCS).** The particle sizes of thiamine-coated nanoparticles were determined using an N4 Plus Submicron Particle Sizer at 20 °C by scattering light at angle 90° for 180 s (Beckman Coulter Corporation, Miami, FL). Prior to particle size measurements, the nanoparticles were diluted (1:10 v/v) with water (0.22  $\mu$ m filtered), to ensure that the light scattering signal as indicated by the particle counts per second (CPS) was within the sensitivity range of the instrument.

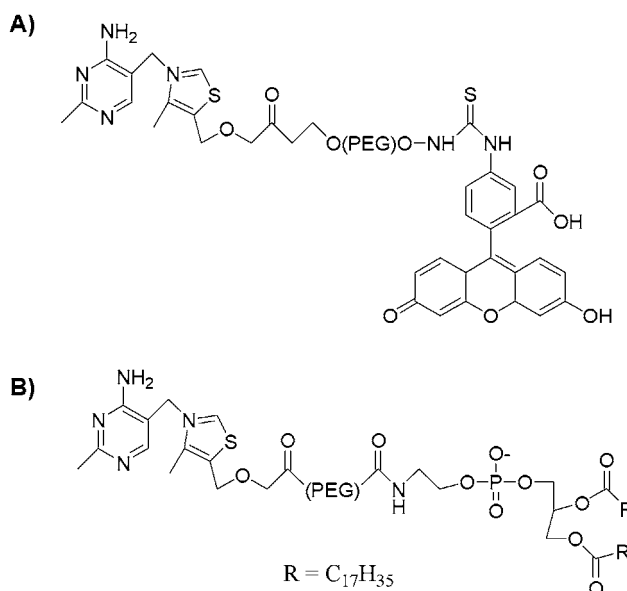
**Gel Permeation Chromatography (GPC).** To obtain the GPC elution profiles of nanoparticles, 80  $\mu$ L of nanoparticle suspensions was passed down a Sephadex G-75 column (1.5 cm  $\times$  8 cm) using deionized water (0.22  $\mu$ m filtered) as the mobile phase. The elution of thiamine-coated nanoparticles was detected by laser light scattering counts per second and thiochrome assay using fluorescence spectroscopy (Hitachi Model F-2000).

**Transmission Electron Microscopy (TEM).** The size and morphology of nanoparticles were observed using a JEOL Electron Microscope in the Imaging Facility Unit of the University of Kentucky. A carbon-coated 200-mesh copper specimen grid was glow-discharged for 1.5 min. One drop of nanoparticle suspension was deposited on the grid and allowed to stand for 1.5 min after which any excess fluid was removed with filter paper. The grid was later stained with 1 drop of 1% uranyl acetate (0.22  $\mu$ m filtered) for 30 s, and any excess stain was removed. The grids were allowed to dry for an additional 10 min before examination under the electron microscope.

**Transfection and Expression of THTR1 and THTR2 Genes in Human Breast Cancer Cells.** The transfection and expression of THTR1 and THTR2 thiamine transporter genes in breast cancer cells (MTX<sup>R</sup>ZR75 cells) was previously described (Liu et al., 2003). Briefly, the characteristics of THTR1 and THTR2 were defined in the host cell line of MTX<sup>R</sup>ZR75 cells because these cells have no detectable specific reduced folate carrier activity (Dixon et al., 1991; Dixon et al., 1994) which can transport thiamine pyrophosphate (Zhao et al., 2002). First, the THTR1 cDNA was cloned by RT-PCR using skeletal muscle RNA as a template, with primers which span the putative open reading frame: THTR1-U1 5'-CAGTTGGCGGAGGAGGAGAAGGAAG-3' and at the 3' end THTR1-L2 5'-AAGGTATTAGTCAAGTGGCTGCTGT-3'. For THTR2, the cDNA was cloned by RT-PCR using placenta RNA as a template, with the primers which span the putative open reading frame. The primers used were: THTR2-U1 5'-GGG GTA CCT AGT GAG CGA TTT GGT GAA CAG AC-3' and THTR2-L2 5'-CCG CTC GAG TAT GCC ACC CAT CTC AAA ATC TTT-3'. Unique restriction enzyme sites for directional cloning into the multiple cloning site of the episomal expression vector were added to the 5' ends of these primers. MTX<sup>R</sup>ZR75 cells were transfected with pREP4/THTR1, pREP4/THTR2, or pREP4 alone using LipofectAMINE reagent (Invitrogen, Carlsbad CA). Quantitative RT-PCR for measuring RNA levels was performed by using a Roche LightCycler, which uses real time fluorescence detection for quantitative measurement of PCR products. The quantitative measurement of each gene in each cell line was normalized to the relative amount of actin RNA in each cell line, as a control for equivalent cDNA loading in each sample.

Thiamine uptake studies were performed in a manner similar to previous studies of MTX uptake (Moscow et al., 1995). [<sup>3</sup>H]-Labeled thiamine was obtained from American Radiolabeled Chemicals (St. Louis, MO), and its purity was assayed by the manufacturer. For the initial thiamine uptake studies, cells were plated at a density of  $1 \times 10^5$  in 6-well Linbro dishes in medium containing 10% fetal bovine serum. After 48–72 h of growth, cells were washed three times in transport medium (125 mM NaCl, 4.8 mM KCl, 5.6 mM D-glucose, 1.2 mM CaCl<sub>2</sub>, 1.2 mM KH<sub>2</sub>PO<sub>4</sub>, 1.2 mM MgSO<sub>4</sub>, and 25 mM HEPES, pH 7.4) without [<sup>3</sup>H]-labeled thiamine and then exposed to 20 nM [<sup>3</sup>H]-labeled thiamine in transport medium. At specified intervals, the transport medium was aspirated, and the plates immersed in three successive washes of ice-cold 1X Dulbecco's phosphate-buffered saline containing Mg<sup>2+</sup> and Ca<sup>2+</sup> (D-PBS). The cells were then solubilized by overnight incubation in 0.2 N NaOH and neutralized with 0.2 N HCl, and the radioactivity was determined by liquid scintillation counting as previously described (Moscow et al., 1997). Protein concentrations were determined by the Bradford assay according to manufacturer's instructions (BioRad) using a spectrophotometer (Beckman). Nonspecific binding was determined by exposure of cells to transport medium for less than 5 s and was subtracted from measured values to indicate specific uptake.

**Cell Culture.** Cells were maintained and grown at 37 °C in Improved MEM Zinc Option (IMEM) (Gibco BRL, Gaithersburg, MD) supplemented with 10% fetal bovine serum (FBS) and 250 µg/mL hygromycin B. Medium was changed into Improved MEM Zinc Option (IMEM) without thiamine (Gibco BRL, Gaithersburg, MD) before the cell association studies of thiamine-coated nanoparticles.



**Figure 1.** Chemical structures of thiamine ligands synthesized by chemically linking thiamine to either distearylphosphatidylethanolamine (DSPE) or fluorescein (FL) via a PEG spacer: (A) thiamine-PEG-fluorescein, (B) thiamine-PEG-DSPE.

**Nanoparticle Cell Association Studies.** The cells were seeded in 24-well plates at a density of  $10^5$  cells/mL in 1 mL of medium and incubated at 37 °C in a humidified 5% CO<sub>2</sub>/air incubator for 24 h. To determine the effect of nanoparticle concentration on cell association, various dilutions of thiamine-coated nanoparticles or control nanoparticles (without thiamine) in cell growth medium were made in the concentration range of 20 to 360 µg/mL. After replacing the medium in each well with nanoparticles suspended in medium, the plates were incubated at 37 °C or 4 °C for various times. Prior to the cell association study at 4 °C, a 10 min equilibration time was allowed for nanoparticle suspensions and cells. In a separate experiment, nanoparticle suspensions (180 µg/mL) were incubated in the presence of various concentrations of free thiamine to serve as a competitive inhibitor. At the end of the incubation time, nanoparticle suspensions were removed from the wells, and the cell monolayers were rinsed three times with cold PBS and lysed using 1x lysis buffer (Promega). Cell associated fluorescence was measured using a fluorometer (Hitachi Model F-2000). Fluorescein-DOPE was used as a fluorescence marker in the studies. Initial experiments showed that fluorescein-DOPE (0.25%) could be entrapped in nanoparticles with ~100% efficiency. The amount of fluorescent-labeled nanoparticles associated with cells was measured by quantifying the intensity of internalized fluorescence at 521 nm (emission) with excitation at 497 nm. The percentage of nanoparticle cell association was calculated from the ratio of the observed cell associated fluorescence to the total fluorescence added to the cells. Additional control experiments were carried out to compare the total cell protein content of cells incubated with various concentrations of thiamine-coated nanoparticles ranging from 0 to 360 µg/mL. The total cell protein content in the cell lysate from each well was determined using the Coomassie Plus assay protocol (Pierce, Rockford, IL).

## RESULTS AND DISCUSSION

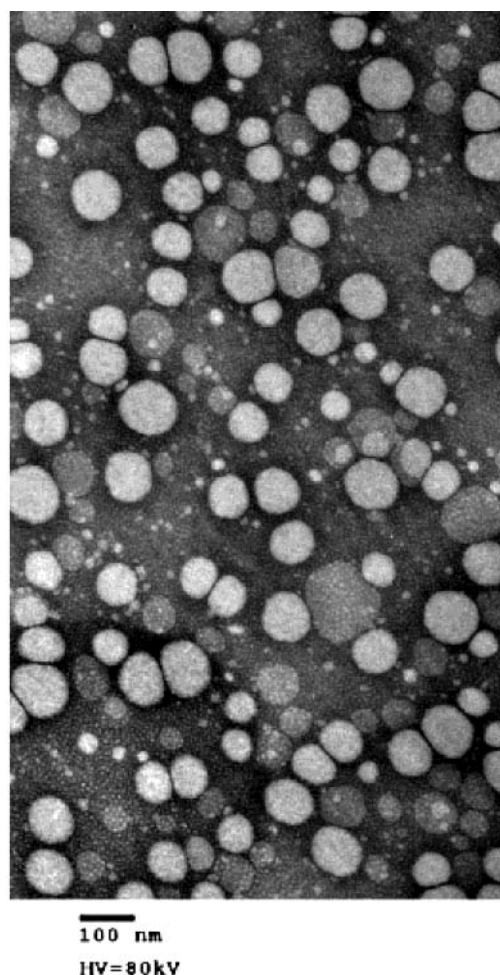
**Synthesis of Thiamine Ligands.** The chemical structures of the thiamine ligands are shown in Figure 1. The



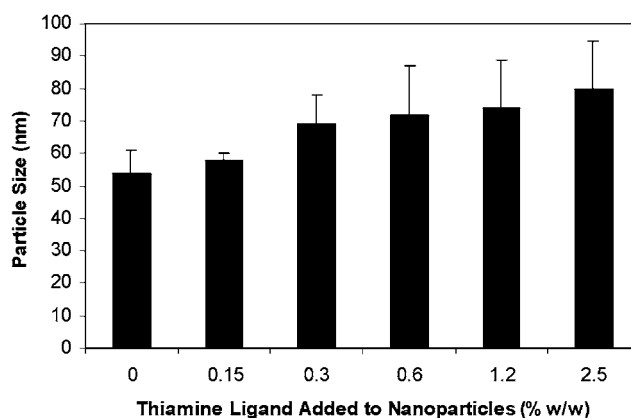
thiamine ligands were synthesized based on the nucleophilic attack of the hydroxyl group of thiamine on the electrophilic group of either DSPE-PEG-NHS or FL-PEG-NHS. The purpose of the synthesis was to chemically link thiamine to hydrophobic groups such as DSPE or fluorescein via a PEG spacer. The presence of the hydrophobic groups on the thiamine ligand was particularly necessary to ensure attachment to nanoparticles. Since the thiamine ligand was added to nanoparticle suspension by physical mixing, adsorption/insertion of the ligand on nanoparticles was facilitated by the presence of hydrophobic anchors. In addition, the PEG spacer theoretically facilitated cell recognition of the thiamine ligand on nanoparticles. Previous studies have demonstrated the importance of PEG spacers in targeted delivery systems (Lee and Low, 1995; Goren et al., 2000).

**Engineering Thiamine-Coated Nanoparticles.** The nanoparticle engineering process was based on the formation of oil-in-water microemulsions that were prepared at 55 °C, which upon cooling in one vessel resulted in the production of nanoparticles. Emulsifying wax was used as nanoparticle matrix material and Brij 78 (polyoxyl 20 stearyl ether) as the surfactant. The procedure of engineering nanoparticles from oil-in-water microemulsion templates was reported earlier (Oyewumi and Mumper, 2002a). Emulsifying wax is a nonionic wax comprised of cetostearyl alcohol and a polyethylene derivative of a fatty acid in a molar ratio of about 20:1. GdH was incorporated in nanoparticles by the addition to the oil phase (matrix materials) of the microemulsion templates. GdH is a gadolinium compound, synthesized by the complexation of  $Gd^{3+}$  with 2,4-hexanedione (Oyewumi and Mumper, 2002b). In addition to having a relatively higher weight percentage of Gd compared to other complexes of Gd (such as Gd-DTPA, Gd-DOTA, Gd-EDTA), GdH possesses other suitable properties such as lower melting point (55 °C) and increased hydrophobicity that could facilitate entrapment in nanoparticles. The final nanoparticle preparation was made with emulsifying wax (2 mg/mL) containing 1.5 mg of GdH using 3.0 mM Brij 78 as the surfactant. The choice and concentration of Brij 78 was based on results from earlier studies (Oyewumi and Mumper, 2002a). Solid nanoparticles containing GdH were engineered using the ternary system: melted oil, surfactant, and water. To obtain thiamine-coated nanoparticles, various concentrations of thiamine ligand were added to nanoparticle suspensions at 25 °C. The mixture of nanoparticles and ligand was gently stirred at room temperature to ensure complete adsorption/insertion of thiamine ligand on the nanoparticles. A TEM micrograph of thiamine-coated nanoparticles is shown in Figure 2. The engineered nanoparticles had a uniform particle size of about 100 nm. Although the addition of increasing amounts of thiamine ligand (0.15% w/w to 2.5% w/w) resulted in a slight increase in nanoparticle size, the average nanoparticle size was maintained below 100 nm (Figure 3). Further, the polydispersity index ranged from 0.2 to 0.4 with the addition of thiamine ligand at concentrations below 2.5% w/w, indicating uniformity of the coated nanoparticles. In particular, the nanoparticle size of about 100 nm is considered to be suitable for cell targeting since several other groups using liposomes and other macromolecules have shown that particles with small size (less than 400 nm and ideally less than 150 nm) are more efficient in cell targeting than larger particles (Desai et al., 1996; Jain, 1997).

The extent of thiamine ligand attachment to nanoparticles was determined by gel permeation chromatography

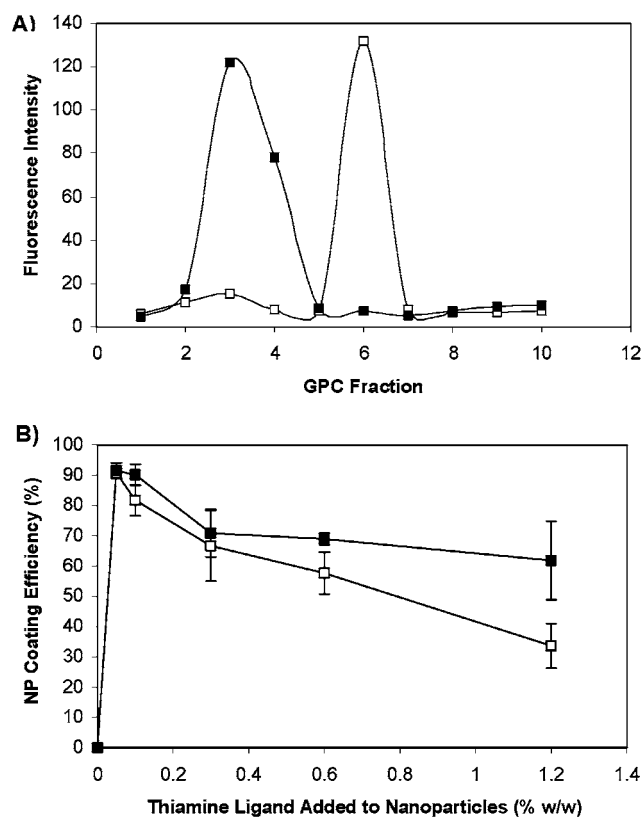


**Figure 2.** Transmission electron micrograph (TEM) showing the size and morphology of thiamine-coated emulsifying wax (2 mg/mL) nanoparticles containing gadolinium hexanedione (1.5 mg).



**Figure 3.** The average nanoparticle size after the addition of various concentrations of thiamine-PEG-DSPE (0–2.5% w/w). The particle size of each sample (after GPC purification) was determined by laser light scattering at 25 °C. Each value represents the mean  $\pm$  SD ( $n = 3$ ).

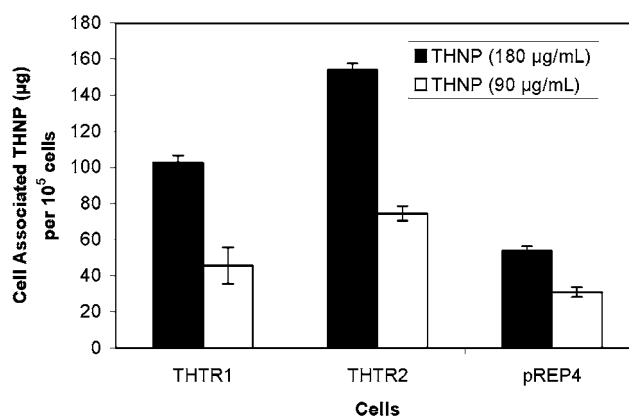
(GPC) based on the elution of free thiamine and thiamine-coated nanoparticles. Thiamine elution as free thiamine ligand or thiamine ligand attached to nanoparticles was monitored by the thiochrome assay. To calculate the coating efficiency of the ligand, both the elution of control nanoparticles (without thiamine) and free thiamine ligand were obtained and used as references. GPC elution of nanoparticles occurred at fraction 3 (void volume) as



**Figure 4.** (A) Gel permeation chromatography (GPC) elution profiles demonstrating that the elution of free thiamine ligand (□) was separated from that of thiamine-coated nanoparticles (■). Thiamine-coated nanoparticles were obtained by adding 0.2% w/w thiamine-PEG-DSPE to nanoparticle suspensions at 25 °C. The elution of thiamine from GPC column (Sephacrose CL-4B) was detected. The amount of thiamine in each GPC fraction was determined by fluorescence intensity at 445 nm (emission) and 365 nm (excitation) using a thiochrome assay. (B) Efficiency of thiamine ligand coating on nanoparticles (NP). Various concentrations (0–1.2% w/w) of either thiamine-PEG-DSPE (■) or thiamine-PEG-fluorescein (□) were added to nanoparticle suspensions at 25 °C. Each value represents the mean  $\pm$  SD ( $n = 3$ ).

monitored by laser light scattering counts per second (CPS) while the elution of free thiamine ligand occurred later than fraction 3 (Figure 4A). The coating efficiencies of various concentrations of thiamine-PEG-DSPE and thiamine-PEG-FL are shown in Figure 4B. At thiamine ligand concentrations below 0.2% w/w, comparable results were obtained for the two ligands indicating high coating efficiencies. The observed decrease in thiamine ligand coating efficiency at high concentrations was, however, pronounced with thiamine-PEG-FL. The difference in the trend observed for the two ligands indicates that hydrophobic groups on the ligand are necessary for optimal ligand attachment to the nanoparticles. Compared to DSPE, fluorescein is more hydrophilic due to the many hydroxyl groups that most likely participated in hydrogen bonding with the water continuous phase.

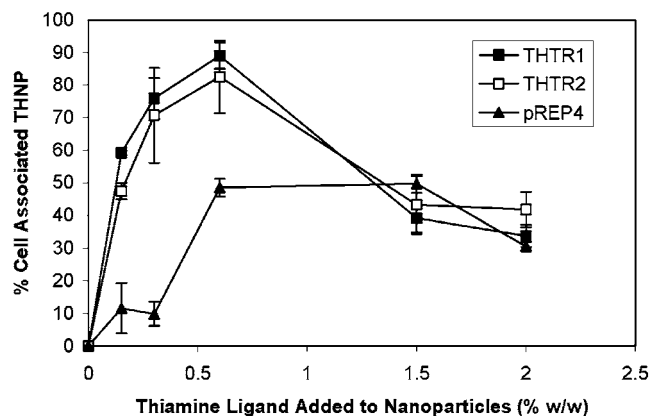
**Nanoparticle Cell Association Studies.** MTX<sup>R</sup>ZR75 cells transfected with THTR1 and THTR2 genes were referred to as simply THTR1 and THTR2 cells, respectively, while the same cell line transfected with the empty expression vector (pREP4) was referred to as pREP4 cells. The presence of THTR1 and THTR2 transgenes in MTX<sup>R</sup>ZR75 cells was confirmed by PCR reactions. Also, the MTX<sup>R</sup>ZR75 cells transfected with the cDNAs for THTR1 and THTR2 showed an increase in initial thiamine uptake relative to the control cell line. At 4 min,



**Figure 5.** Association of thiamine-coated nanoparticle (THNP) with THTR1, THTR2, and pREP4 cells as a function of nanoparticle concentrations. Cell-associated fluorescence after 15 min was measured at 497 nm (excitation) and 521 nm (emission) using fluorescein-DOPE as the marker. Each data point represents the mean  $\pm$  SD ( $n = 4$ ).

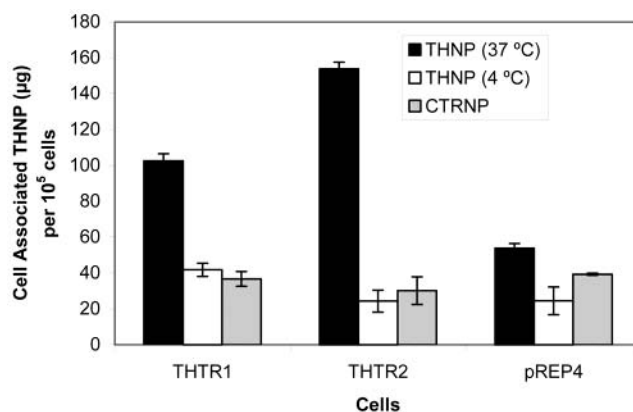
uptake of radiolabeled thiamine at an extracellular concentration of 20 nM was 47% greater in the THTR1-transfected cells than control cells, and 133% greater in the THTR2-transfected cells than in the control cells. Additional initial studies were carried out using thiamine-coated nanoparticles. After incubation with cells, the total protein in all the wells was measured and did not show any significant difference between different concentrations of nanoparticles (0–360 μg/mL) ( $p > 0.05$ ;  $t$ -test) (data not shown). It was also observed that thiamine-coated nanoparticles were stable (based on nanoparticle size and thiamine coating efficiency) when incubated at 37 °C (for 120 min) in either fetal bovine serum (10%) or PBS (pH 7.4).

Results obtained on thiamine-coated nanoparticle cell association as a function of nanoparticle concentration are shown in Figure 5. The extent of cell association of thiamine-coated nanoparticles was viewed as a reflection of thiamine transport activity present in all the cells. In comparison to pREP4 cells, nanoparticle cell association was greater with THTR1 and THTR2 cells most likely due to the higher level of expression of thiamine transport genes in these cells. For instance, at a nanoparticle concentration of 180 μg/mL, the concentration of nanoparticles in association with THTR1 and THTR2 cells was 90% and 185% higher than with control cells (pREP4), respectively (Figure 5). The enhanced nanoparticle association in transfected cells was expressed further by calculating the number of nanoparticles (~100 nm diameter) that associated with THTR1, THTR2, and control cells. Using the data in Figure 5 (at a nanoparticle concentration of 180 μg/mL), the number of nanoparticles that associated with a single THTR1, THTR2, and pREP4 cell was calculated. The analysis estimated that a single THTR1 and THTR2 cell had approximately 30 000 to 70 000 more nanoparticles associated than a single pREP4 cell at the same test condition. Further experiments were carried out to demonstrate the involvement of thiamine transporter genes in nanoparticle cell association. The effects of various concentrations of thiamine ligand used in coating nanoparticles were studied. As shown in Figure 6, at concentrations of thiamine ligand from 0.1 to 0.6% w/w, nanoparticle cell association with THTR1 and THTR2 cells was significantly greater ( $p < 0.01$ ;  $t$ -test) than with control cells (pREP4), probably due to the less expression of thiamine transporters in control cells. However, at concentrations of thiamine

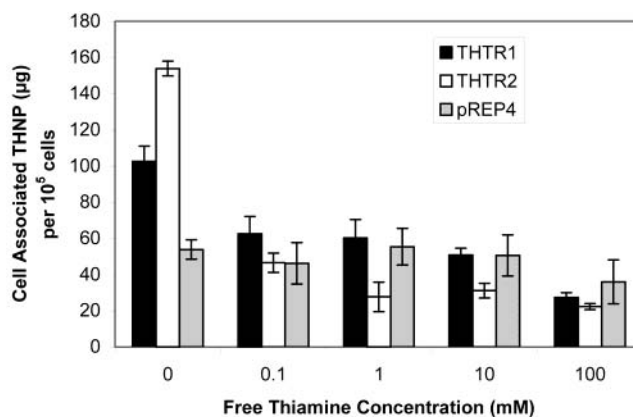


**Figure 6.** The effect of thiamine ligand concentration added to nanoparticle formulations on cell association. Results were expressed as percentage of the ratio of cell-associated fluorescence and total fluorescence added to cells. Cell-associated fluorescence was measured at 521 nm (emission) and 497 nm (excitation) after 15 min incubation of thiamine-coated nanoparticles (THNP) (180  $\mu$ g/mL) with either THTR1, THTR2, and pREP4 cells. Values represent mean  $\pm$  SD ( $n = 4$ ).

ligand above 1% w/w, nanoparticle association with THTR1- and THTR2-transfected cells decreased significantly to such a level that was comparable to pREP4 cells ( $p < 0.11$ ;  $t$ -test). This decrease in nanoparticle association with increased concentration of thiamine ligand can be attributed to the expected increase in the amount of free thiamine ligand in nanoparticle preparations. Since the nanoparticle preparations were applied in the study without GPC purification, the free thiamine ligand (unattached to nanoparticles) most likely competed with thiamine-coated nanoparticles for binding to the transporters. Subsequent experiments were carried out using nanoparticles coated with 0.2% w/w thiamine ligand containing 10  $\mu$ M of thiamine (as determined by thiochrome assay). The incubation time of 15 min was used in all the cases. Experiments conducted at various incubation time intervals (ranging from 5 to 60 min), showed that nanoparticle cell association (at 37  $^{\circ}$ C) occurred rapidly within 5 min and resulted in a plateau at 15 min (data not shown). The involvement of thiamine transporters in nanoparticle cell association was investigated further by using thiamine-coated nanoparticles and control nanoparticles (without thiamine ligand). As shown in Figure 7, association of thiamine-coated nanoparticles with THTR1- and THTR2-transfected cells was observed to be significantly higher than control nanoparticles ( $p < 0.05$ ). The possibility of thiamine transporters mediating nanoparticle cell association was reflected from the results obtained in pREP4 cells. Compared with THTR1- and THTR2-transfected cells, thiamine-coated nanoparticle association occurred to a lower extent in pREP4 cells and the effect was comparable to control nanoparticles ( $p > 0.11$ ;  $t$ -test). In contrast to the data obtained at 37  $^{\circ}$ C, studies conducted at 4  $^{\circ}$ C showed reduction ( $p < 0.005$ ;  $t$ -test) in association of thiamine-coated nanoparticles in all the cells (Figure 7). The reduction in nanoparticle cell association could be due to the expected reduced activity of thiamine transporter at 4  $^{\circ}$ C. Earlier studies have shown that ligand binding, association and endocytic activities are suppressed significantly at 4  $^{\circ}$ C (Shikata et al., 2002). As such, cell association at 4  $^{\circ}$ C will most likely be due to simple adhesion of nanoparticles to the cell surfaces. Since, adhesion alone did not fully account for the extent of cell association observed at 37  $^{\circ}$ C, the trend thus suggests



**Figure 7.** Cell association of (180  $\mu$ g/mL) of thiamine-coated nanoparticles (THNP) or control nanoparticles (CTRNP) after incubation at 37  $^{\circ}$ C or 4  $^{\circ}$ C for 15 min with THTR1, THTR2, and pREP4 cells. Control nanoparticles (CTRNP) had no thiamine ligand coating. After the incubation, cell-associated fluorescence was measured at 521 nm (emission) and 497 nm (excitation). Each data point represents the mean  $\pm$  SD ( $n = 4$ ).



**Figure 8.** The effect of coincubation of free thiamine on thiamine-coated nanoparticles (THNP) (180  $\mu$ g/mL). Cell-associated fluorescence after incubation at 37  $^{\circ}$ C for 15 min was measured at 521 nm (emission) and 497 nm (excitation). Each value represents the mean  $\pm$  SD ( $n = 3$ ).

the involvement of thiamine transporters in nanoparticle cell association. The specificity of nanoparticle association to the transporters was investigated by coincubation of free thiamine with thiamine-coated nanoparticles. The result showed that free thiamine inhibited cell association of thiamine-coated nanoparticles (Figure 8). The competitive effect of free thiamine was most evident in THTR1- and THTR2-transfected cells and at the highest concentration of free thiamine studied. For instance, coincubation of 100 mM free thiamine resulted in reduction of nanoparticle cell association to 31%, 15%, and 72% of its initial value (0 mM free thiamine) in THTR1, THTR2, and control cells, respectively, indicating that the reduction of nanoparticle cell association due to free thiamine competition was more pronounced in THTR1- and THTR2-transfected cells. In fact, at concentrations of free thiamine that were 10-fold to 100-fold higher than the concentration of thiamine ligand on nanoparticles, significant reduction of nanoparticle association was observed only with THTR1- and THTR2-transfected cells ( $p < 0.005$ ,  $t$ -test), and not with the control cells ( $p > 0.2$ ;  $t$ -test) (Figure 8). The studies demonstrated higher specificity of thiamine-coated nanoparticle association with THTR1- and THTR2-transfected cells compared with the control cells and dependence on the extent of expression of thiamine transporter genes in these cells.



The specific mechanism of nanoparticle cell association (involving either binding to the transporters alone and/or cell uptake) is yet to be investigated. Regardless of the mechanism of nanoparticle cell association, achieving tumor cell specificity of thiamine-coated gadolinium nanoparticles may potentially be employed in Gd neutron capture therapy (NCT) of tumors. GdNCT is a potential cancer therapy that utilizes a stable, nonradioactive Gd-157 nuclide delivered to tumor cells which upon irradiation by thermal or epithermal neutrons produces localized cytotoxic radiations. The tumor killing effect of GdNCT is due to the emission of prompt gamma rays followed by a series of low-energy conversion and Auger electrons. A favorable characteristic of GdNCT is that the cytotoxic emissions are deposited at long ranges within the target tumor site (Allen et al., 1989); as such, the location of Gd within the target tumor cell is not critical to the therapeutic effectiveness.

In general, thiamine-coated Gd nanoparticles have been engineered and characterized. The potential of using thiamine as a cell specific ligand has been investigated. Results showed that nanoparticle cell specific association was dependent on the extent of expression of thiamine transporters genes. Additional studies are warranted to determine the extent of expression of thiamine transporters in various human tumors compared to normal tissues and to assess the potential of the thiamine-coated Gd nanoparticles in neutron capture therapy.

#### LITERATURE CITED

- (1) Allen, B. J., McGregor, B. J., and Martin, R. F. (1989) Neutron capture therapy with gadolinium-157. *Stahlether Onkol.* 165, 156–158.
- (2) Allen, T. M., Brandeis, E., Hansen, C. B., Kao, G. Y., and Zaplisky, S. (1995) A new strategy for attachment of antibodies to sterically stabilized liposomes resulting in efficient targeting to cancer cells. *Biochim. Biophys. Acta* 1237, 99–108.
- (3) Atkinson, S. F., Bettinger, T., Seymour, L. W., Behr, J., and Ward, C. (2001) Conjugation of folate via gelonin carbohydrate residues retains ribosomal-inactivating properties of the toxin and permits targeting to folate receptor positive cells. *J. Biol. Chem.* 276, 27930–27935.
- (4) Boros, L. G., Puigjaner, J., Cascante, M., Lee, W. N. P., Brandeis, J. L., Bassilian, S., Yusuf, F. I., Williams, R. D., Muscarella, P., Melvin, W. S., and Schirmer, W. J. (1997) Oxythiamine and dehydroepiandrosterone inhibit the non-oxidative synthesis of ribose and cancer cell proliferation. *Cancer Res.* 57, 4242–4248.
- (5) Cascante, M., Centelles, J. J., Veech, R. L., Lee, W. N., and Boros, L. G. (2000) Role of thiamine (vitamin B-1) and transketolase in tumor cell proliferation. *Nutr. Cancer* 2, 150–154.
- (6) Cho, C. S., Cho, K. Y., Park, I. K., Kim, S. H., Sasagawa, T., Uchiyama, M., and Akaike, T. (2001) Receptor-mediated delivery of trans-retinoic acid to hepatocyte using poly (L-lactic acid) nanoparticles coated with galactose-carrying polystyrene. *J. Controlled Release* 77, 7–15.
- (7) Comin-Aduix, B., Boren, J., Martonez, S., Moro, C., Centelles, J. J., Trebukhina, R., Petushok, N., Lee, W. P., Boros, L. G., and Cascante, M. (2001) The effect of thiamine supplementation on tumour proliferation. A metabolic control analysis study. *Eur. J. Biochem.* 268, 4177–4182.
- (8) Desai, M. P., Labhasetwar, V., Amidon, G. L., and Levy, R. J. (1996) Gastrointestinal uptake of biodegradable microparticles in Caco-2 cells is size dependent. *Pharm. Res.* 14, 1568–1573.
- (9) Dixon, K. H., Trepel, J. B., Eng, S. C., and Cowan, K. H. (1991) Folate transport and the modulation of antifolate sensitivity in a methotrexate-resistant human breast cancer cell line. *Cancer Commun.* 3, 357–365.
- (10) Dixon, K. H., Lanpher, B. C., Chiu, J., Kelley, K., and Cowan, K. H. (1994) A novel cDNA restores reduced folate carrier activity and methotrexate sensitivity to transport deficient cells. *J. Biol. Chem.* 269, 17–20.
- (11) Goren, D., Horowitz, A. T., Tzemach, D., Tarshish, M. M., Zalipsky, S., and Gabizon, A. (2000) Nuclear delivery of doxorubicin via folate-targeted liposomes with bypass of multidrug-resistance efflux pump. *Clin. Cancer Res.* 6, 1949–1957.
- (12) Jayamani, M., and Low, P. S. (1992) An efficient method for conjugation of thiamine to proteins. *Biorg. Med. Chem. Lett.* 2, 1007–1012.
- (13) Jain, R. K. (1997) Delivery of molecular and cellular medicine to solid tumors. *Adv. Drug Deliv. Rev.* 26, 71–90.
- (14) Kreuter, J. (1995) Nanoparticles as adjuvants for vaccines. *Pharma. Biotechnol.* 6, 463–472.
- (15) Lee, W. N. P., Boros, L. G., Puigjaner, J., Bassilian, S., Lim, S., and Cascante, M. (1998) Mass isotopomer study of nonoxidative pathways of the pentose cycle with [1, 2 <sup>13</sup>C<sub>2</sub>] glucose. *Am. J. Physiol.* 274, E843–E851.
- (16) Lee, R. J., and Low P. S. (1995). Folate-mediated tumor cell targeting of liposome-entrapped doxorubicin in-vitro. *Biochim. Biophys. Acta* 1233, 134–144.
- (17) Liu, S., Huang, H. Lu, X., Golinski, M., Comesse, S., Watt, D., Grossman, R., and Moscow, J. (2003). Down-regulation of thiamine transporter THTR2 gene expression in breast cancer and its association with resistance to apoptosis. *Mol. Cancer Res.*, submitted.
- (18) Lo, P., Wang, F. (2002) Identification of transcriptional start sites and splicing of mouse thiamine transporter gene THTR-1 (Slc19a2). *Biochim. Biophys. Acta* 1576, 209–213.
- (19) Moscow, J. A., Gong, M., He, R., Sgagias, M. K., Dixon, K. H., Anzick, S. L., Meltzer, P. S., and Cowan, K. H. (1995) Isolation of gene encoding a human reduced folate carrier (RFC1) and analysis of its expression in transport-deficient, methotrexate-resistant human breast cancer cells. *Cancer Res.* 55, 3790–3794.
- (20) Moscow, J. A., Connolly, T., Myers, T., Paull, K., Cheng, C. C., and Cowan, K. H. (1997) Reduced folate carrier gene expression in transfected and nonselected cell lines. *Int. J. Cancer.* 72, 184–190.
- (21) Oyewumi, M. O., and Mumper, R. J. (2002a) Gadolinium-loaded nanoparticles engineered from microemulsions templates. *Drug Dev. Ind. Pharm.* 28, 317–328.
- (22) Oyewumi, M. O., and Mumper, R. J. (2002b) Engineering tumor-targeted gadolinium hexanedione nanoparticles for potential application in neutron capture therapy. *Bioconjugate Chem.* 13, 1328–1335.
- (23) Rajgoal, A., Edmondson, A., Goldman, D. I., and Zhao, R. (2001) SLC19A3 encodes a second thiamine transporter THTR2. *Biochim. Biophys. Acta* 1537, 175–178.
- (24) Russell-Jones, G. L., Arthur, L., and Walker, H. (1999). Vitamin B12-mediated transport of nanoparticles across Caco-2 cells. *Int. J. Pharm.* 179, 247–255.
- (25) Said, H. S., Orbitz, A., Kumar, C. K., Chatterjee, N., Dudeja, P. K., and Rubin, S. (1999) Transport of thiamine in human intestine: mechanism and regulation in intestinal epithelial cell model caco-2. *Am. J. Physiol.* 277, C645–C651.
- (26) Said, H. M., Orbitz, A., Subramanian, V. S., Neufeld, E. J., Moyer, M. P., and Dudeja, P. K. (2001) Mechanism of thiamine uptake by human colonocytes: studies with cultured colonic epithelial cell line NCM 460. *Am. J. Physiol. Gastrointest. Liver Physiol.* 284, G144–G150.
- (27) Seligmann, H. M., Levi, R., Konijn, A. M., and Prokocimer, M. (2001) Thiamine deficiency in patients with B-chronic lymphocytic leukaemia: a pilot study. *Postgrad. Med. J.* 77, 582–585.
- (28) Shih, J., and Brugger, R. M. (1992) Gadolinium as a neutron capture agent. *Med. Phys.* 3, 733–744.
- (29) Shikata, F., Tokumitsu, H., Ichikawa, H., and Fukumori, Y. (2002). In-vitro-cellular accumulation of gadolinium incorporated into chitosan nanoparticles designed for neutron-capture therapy of cancer. *Eur. J. Pharm. Biopharm.* 53, 57–63.

- (30) Singleton, C. K., and Martin, P. R. (2001) Molecular mechanisms of thiamine utilization. *Curr. Mol. Med.* 2, 197–207.
- (31) Vyas, S. P., Singh, A., and Sihorkar, V. (2001) Ligand–receptor mediated drug delivery: an emerging paradigm in cellular drug targeting. *Crit. Rev. Ther. Drug Carrier Syst.* 18, 1–76.
- (32) Wang, S., and Low, P. S. (1998) Folate-mediated targeting of antineoplastic drugs, imaging agents and nucleic acids to cancer cells. *J. Controlled Release* 53, 39–48.
- (33) Weng, G., Bhalla, U. S., and Iyenyar, R. (1999) Complexity in biological signaling systems. *Science* 284, 92–96.
- (34) Zhao, R., Gao, F., and Goldman, D. (2002) Reduced folate carrier transports thiamine monophosphate: an alternative route for thiamine delivery into mammalian cells. *Am. J. Physiol. Cell Physiol.* 282, C1512–C1517.

BC0340013

# Bioinspired pH-Responsive Polymers for the Intracellular Delivery of Biomolecular Drugs

Niren Murthy,<sup>†</sup> Jean Campbell,<sup>‡</sup> Nelson Fausto,<sup>‡</sup> Allan S. Hoffman,<sup>\*,†</sup> and Patrick S. Stayton<sup>\*,†</sup>

Department of Bioengineering and Department of Pathology, University of Washington, Seattle, Washington 98195. Received July 12, 2002; Revised Manuscript Received October 14, 2002

The biotechnology and pharmaceutical industries have developed a wide variety of potential therapeutics based on the molecules of biology: DNA, RNA, and proteins. While these therapeutics have tremendous potential, effectively formulating and delivering them have also been a widely recognized challenge. A variety of viruses and toxins have evolved multi-functional biomolecules to solve this problem by directing cellular uptake and enhancing biomolecular transport to the cytoplasm from the low pH endosomal compartment. In the study reported here, we have designed and synthesized bio-inspired, pH-responsive polymeric carriers, which we call "encrypted polymers", that mimic the multi-functional design of biology. These encrypted polymers target and direct cellular uptake, as well as enhance cytosolic delivery by disrupting endosomal membranes in a pH-dependent fashion. We show that the encrypted polymeric carriers significantly enhance the delivery of oligonucleotides and peptides to the cytoplasm of cultured macrophages, demonstrating the potential of this approach for delivery of biotherapeutics and vaccines.

## INTRODUCTION

The exciting potential of biomolecular therapeutics is well established, but numerous biological barriers to these relatively fragile drugs have proven to represent significant delivery challenges. The bioavailability of proteins and nucleic acids are typically low compared to traditional small molecule therapeutics, due to factors such as poor stability and susceptibility to enzymes. A widespread barrier for the activity of vaccines and biomolecular drugs that function intracellularly is cytoplasmic delivery. Proteins, peptides, and nucleic acids usually enter cells through the process of fluid-phase or receptor-mediated endocytosis and are initially localized in the endosomal compartment. A high percentage of these biomolecules are subsequently trafficked to lysosomes, where they are degraded. For example, the percentage of pinocytosed protein molecules released to the cytoplasm of cultured mouse fibroblast cells has been estimated to be less than 5% (1) and that of oligonucleotides to be less than 20% (2).

Thus, there is a significant need to design and synthesize carriers that can enhance the intracellular delivery of biotherapeutics, in particular to overcome the important barrier of lysosomal trafficking (3–8). The

issue of cytoplasmic delivery is particularly important for vaccine development, where antigenic proteins/peptides must reach the cytoplasm of antigen-presenting cells to enter the MHC1 pathway for subsequent stimulation of CD8<sup>+</sup> lymphocytes. Other biomolecular drugs or vaccine components such as plasmid DNA, antisense oligonucleotides, ribozymes, and immunotoxins must also be transported to the cytoplasm to reach their eventual intracellular molecular targets and compartments. The use of endosomal releasing proteins and peptides in gene and protein delivery systems has been widely investigated (9, 10), but potential limitations of cost, stability, and immunogenicity make alternative synthetic carrier systems desirable.

In this report we describe a new strategy for the design and synthesis of polymeric drug carriers that enhance the cytoplasmic delivery of biomolecules into macrophages by disrupting the endosomal membrane at the acidic pHs of the endosome. We have termed these polymers "encrypted" by analogy to encrypted domains in biological proteins that become exposed and activated by proteolytic processing at controlled timepoints (11). The challenge of intracellular delivery varies with cell type, and the macrophage is a particularly difficult model because of the high degradative activities of the endosomal/phagosome compartment. Macrophages are an important medical target because they play a key role in many inflammatory diseases as well as in the foreign body response to implants. Macrophages are also efficient antigen-presenting cells, where they play a role in the development of memory T and B cells, as well as the activation of naïve CD8<sup>+</sup> T-cells. There is considerable interest in developing delivery vehicles that can enhance cytoplasmic entry in macrophages of biotherapeutics such as antisense oligonucleotides and antigenic proteins and peptides.

## EXPERIMENTAL METHODS

**Materials.** The peptide FITC-(His)<sub>6</sub>-(Gly)<sub>4</sub>-Cys was purchased from the SynPep Corporation. The phospho-

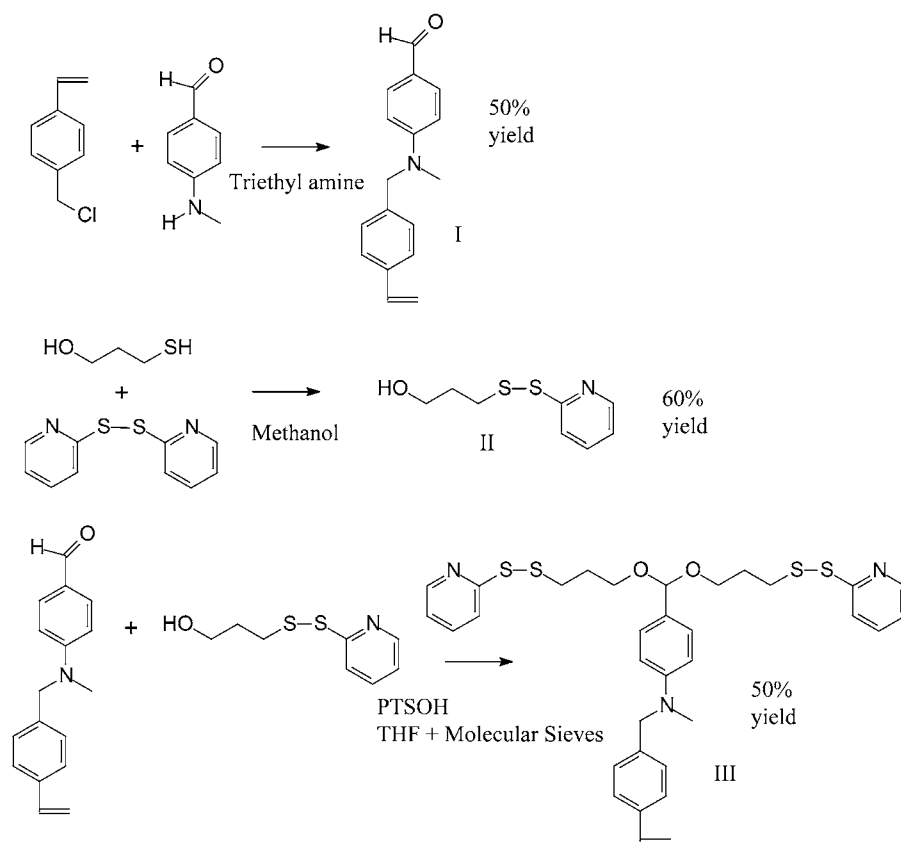
\* Corresponding authors. Address: Department of Bioengineering, Box 352255, University of Washington Seattle, WA 98195. A.S.H.: telephone 206-543-9423, fax 206-543-6124, e-mail: hoffman@u.washington.edu. P.S.S.: telephone 206-685-8148, fax: 206-685-8256, e-mail: stayton@u.washington.edu.

<sup>†</sup> Department of Bioengineering, University of Washington.

<sup>‡</sup> Department of Pathology, University of Washington.

<sup>1</sup> Abbreviations: DMAEMA, dimethylaminoethyl methacrylate; BMA, butyl methacrylate; BA, butyl acrylate; SBA, styrene benzaldehyde monomer; SA, styrene acetal monomer; AIBN, azobisisobutyronitrile; ODN, oligodeoxynucleotide; AS-ODN, antisense oligodeoxynucleotide; DMEM, Dulbecco's modified eagle's medium; iNOS, inducible nitric oxide synthetase; NO, nitric oxide; LPS, lipopolysaccharide; PTSOH, *p*-toluene sulfonic acid.



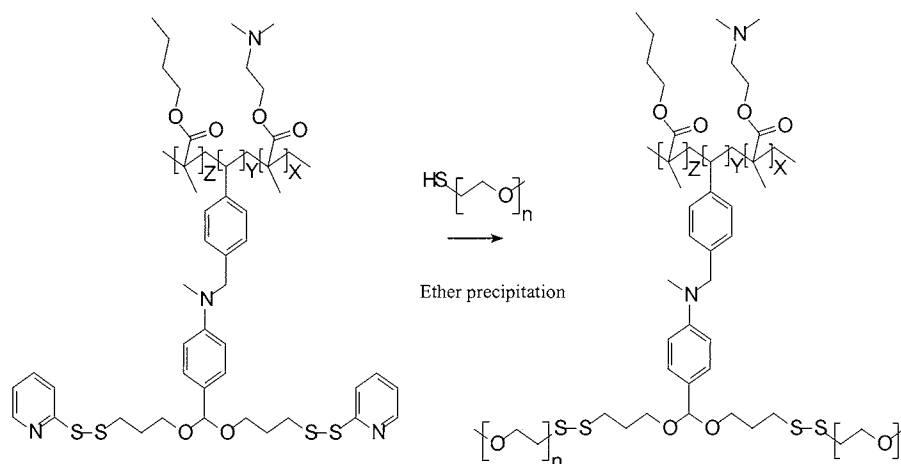
**Scheme 1. Synthesis of the Styrene Acetal Monomer (III)**

rothioate oligonucleotides (ODNs), antisense for inducible nitric oxide synthase (iNOS) (CCA-GGG-GCA-AGC-CAT-GTC-TG) (12), and scrambled iNOS (GAC-GTG-CG-AGT-CAG-CAC-TGC) (12) used in this study were purchased from Integrated DNA Technologies. Chemicals and solvents used for the synthesis of monomers and polymers were obtained from Aldrich, unless otherwise indicated. Mannopyranosylphenyl-isothiocyanate was purchased from Sigma. THF was distilled from sodium/benzophenone under a nitrogen atmosphere immediately before use. H NMRs of monomers were taken on a Bruker 200MHz machine, and H NMRs of copolymers were taken on a AM-400MHz machine. UV spectroscopy was performed on a Shimadzu 480 machine. Gel permeation chromatography was performed on a Waters GPC system using Styragel columns. The cell line Raw 264.7 was obtained from the ATCC.

**Styrene Aminobenzaldehyde (I).** A solution containing methyl amino benzaldehyde (2 mmol), chloromethyl styrene (5 mmol) and triethylamine (2 mmol) was prepared in a 10 mL round-bottom flask, fitted with a stir bar. The reaction was heated to 68 °C, with stirring for 10 h. The reaction was then purified by column chromatography on a column containing 30 g of silica gel. The column was eluted with 50 mL of 20/80 ethyl acetate/hexane, 75 mL of 30/70 ethyl acetate/hexane, and then 75 mL of 35/65 ethyl acetate/hexane. The yield was 50%. H NMR in CDCl<sub>3</sub> gave the following: 3.2 singlet 3H C–N–CH<sub>3</sub>, 4.7 singlet 2H CH<sub>2</sub>–N–C, 5.25 doublet 1H Ar–C=C–H, 5.8 doublet 1 H Ar–C=C–H, 6.7–6.9 multiplet 3H one hydrogen from Ar–CH=C and two aromatic hydrogens ortho to amino group, 7.2–7.5 two doublets 4H aromatic hydrogens on styrene ring, 7.8 doublet 2H aromatic hydrogens meta to amino group and ortho to aldehyde, 9.9 singlet 1H Ar–CH=O. UV analysis of the product gave a  $\epsilon_{346}$  of  $4.1 \times 10^4 \text{ M}^{-1} \text{ cm}^{-1}$  in DMF.

**Hydroxypropyl-mercaptopyridine (II).** A solution containing 2,2 dithiopyridine (0.109 mol), 1.6 mL of glacial acetic acid, and 125 mL of methanol was prepared in a 250 mL round-bottom flask with stir bar. Mercaptopropanol (0.054 mol) was dissolved in 20 mL of methanol and added to the dithiopyridine solution from a dropping funnel (Scheme 1). After 3 h of reacting at room temperature, the reaction was concentrated under vacuum, giving a green oil. This oil was then purified by flash chromatography over 200 g of silica gel. The column was eluted with 600 mL of 40/60 ethyl acetate/hexane and then 600 mL of 50/50 ethyl acetate/hexane. After one column purification, the product still contained impurities from unreacted 2,2-dithiopyridine and was again purified over 150 g of silica gel, eluting this time with 1 L of 1/2 ethyl acetate/hexane and then one liter of 1/1 ethyl acetate/hexane. The yield was 60%. H NMR in CDCl<sub>3</sub> gave the following: 1.9 pentet 2H C–CH<sub>2</sub>–C–O, 2.9 broad singlet 1H O–H, 3.0 triplet 2H S–S–CH<sub>2</sub>, 3.8 triplet 2H C–CH<sub>2</sub>–O, 7.1 multiplet 1H aromatic hydrogen meta to nitrogen, 7.7 multiplet 2H aromatic hydrogens para to nitrogen and ortho to thiol derivatized carbon, 8.5 quartet 1H aromatic hydrogen ortho to nitrogen. UV analysis of the product gave a  $\epsilon_{372}$  of  $5.8 \times 10^3 \text{ M}^{-1} \text{ cm}^{-1}$  in DMF, after reduction with DTT.

**Styrene Acetal Monomer (III).** A 100 mL round-bottom flask was fitted with stir bar and hydroxypropyl-mercaptopyridine (10 mmol), styrene aminobenzaldehyde (2 mmol), and *para*-toluenesulfonic acid (PTSOH) (1 millimole), and 5 Å molecular sieves (5 g) were placed inside the flask. Approximately 20 mL of THF was distilled from sodium benzophenone directly into this 100 mL flask. The reaction was then placed in an ice bath, under a nitrogen atmosphere, for 12 h. The reaction was quenched with 3 mL of triethylamine and filtered using methylene chloride as the rinsing solvent. The filtrate

**Scheme 2. PEGylation of Polymer Backbone E1**

was then concentrated under vacuum and loaded onto 30 g of basic alumina (Brockman's activity I). The column was eluted with 250 mL of 20/80 ethyl acetate/hexane stabilized with 2 mL of TEA. The yield was 50%. <sup>1</sup>H NMR in deuterated benzene gave the following: 2.0 pentet 4H O-C-CH<sub>2</sub>-C-S-S-, 2.75 singlet 3H C-N-CH<sub>3</sub>, 2.9 triplet 4H C-CH<sub>2</sub>-S-S-, 3.6 multiplet 4H O-CH<sub>2</sub>-C-, 4.4 singlet 2H CH<sub>2</sub>-N-C-, 5.2 doublet 1H Ar-C=C-H, 5.6 singlet 1H acetal hydrogen, 5.7 doublet 1H Ar-C=C-H, 6.6–6.9 multiplet 3H one hydrogen from Ar-CH=C and two aromatic hydrogens ortho to amino group, 7.1 multiplet 2H aromatic hydrogens meta to nitrogen on pyridal ring, 7.2–7.4 multiplet 4H aromatic hydrogens from styrene ring, 7.5–7.7 multiplet 6H; two aromatic hydrogens are meta to the methoxy group and four aromatic hydrogens from the pyridal ring, 8.4 doublet 2H aromatic protons ortho to nitrogen on pyridal ring. The presence of the acetal and thiopyridal groups were further confirmed by UV analysis. The acetal had a  $\epsilon_{346}$  of  $4.4 \times 10^3 \text{ M}^{-1} \text{ cm}^{-1}$  in DMF, which increased to  $4.1 \times 10^4 \text{ M}^{-1} \text{ cm}^{-1}$  upon hydrolysis to the benzaldehyde form with 1 N HCl. UV analysis of the product after reduction with DTT in DMF gave a  $\epsilon_{372}$  of  $1.2 \times 10^4 \text{ M}^{-1} \text{ cm}^{-1}$ , indicating the presence of the thiopyridone.

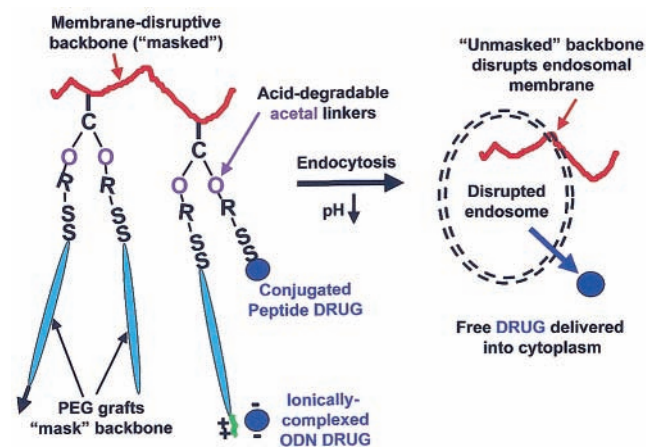
**Synthesis and Characterization of Encrypted Polymer E1.** A 150 mg (0.23 mmol) sample of the styrene-acetal monomer (III), 250 mg (1.5 mmol) of dimethylaminoethyl methacrylate (DMAEMA), 300 mg (2.1 mmol) of butyl methacrylate (BMA), and 20 mg (0.12 mmol) of 2,2-azobisisobutyronitrile (AIBN) were placed in a 5 mL round-bottom flask, fitted with a stopcock and stir bar. The reaction was subjected to three freeze–thaw–vacuum cycles and polymerized at 60 °C for 10 h. The polymer was isolated by dissolving the reaction in 3 mL of THF and precipitating it into 40 mL of ice cold hexane; the resulting solid was filtered and vacuum-dried. The molecular weight of the polymer was determined by GPC in THF (Styragel gel columns) with poly(methyl methacrylate) (PMMA) standards; the Mw of the polymer was 100 kD and the Mn was 44 kD. The composition of this terpolymer was determined by <sup>1</sup>H NMR, and UV spectroscopy to be DMAEMA/BMA/SA = 47/48/5. The mole ratio of the monomers DMAEMA/BMA was determined by <sup>1</sup>H NMR to be 4.7/4.8 (<sup>1</sup>H NMR in deuterated chloroform AM-400). The mole percent of III was determined by quantifying the thiopyridal groups in the polymer, after reduction with dithiothreitol (DTT) (372 nm in DMF). The polymer backbone E1 was PEGylated (see Scheme 2) by reacting, in an Eppendorf tube, 25 mg (15  $\mu\text{mol}$  of thiopyridal groups) with 130 mg (26

$\mu\text{mol}$ ) of PEG-thiol (5 kD) in 1 mL of DMF, containing 10  $\mu\text{L}$  of triethylamine (TEA). The PEGylation reaction was monitored by UV spectroscopy at 372 nm, for the released thiopyridone; after 12 h the reaction had gone to completion. The reaction mixture was precipitated in 20 mL of ice cold ether, filtered, and vacuum-dried; the yield was 80% (see Figure 2a for chemical structure).

**Synthesis of Thiol-PEG-Lys<sub>6</sub>.** A 2.10 g (0.61 mmoles) sample of Dithiol PEG (MW = 3400) was slowly added to a solution of 128 mg of maleimido-caproic acid (0.61 mmoles), 60  $\mu\text{L}$  of TEA, in 10 mL of DMF and stirred for 2 h. Ellmans analysis of the product indicated that 50% of the thiol groups of the dithiol-PEG had reacted with maleimido-caproic acid. The reaction was then added to 0.53 g of 2,2-dithiopyridine (2.2 mmoles) in 2 mL of DMF, stirred for 30 min, precipitated into cold ether, filtered, and vacuum-dried. A 2.10 g sample of thiopyridal-PEG-caproic acid, 190 mg of N-hydroxysuccinimide (NHS), and 190 mg of dicyclohexylcarbodiimide (DCC) were dissolved in 4 mL of dry methylene chloride, stirred for 4 h, filtered, and rotavapped down to a solid and then crystallized twice from ethyl acetate. The product was characterized by UV spectroscopy, and reduction of the thiopyridal group with DTT and hydrolysis of the NHS group indicated a 1:1 ratio of NHS groups to thiopyridal groups; the yield was 20%.

An 8.2 mg sample of hexalysine, 8 mg of thiopyridal-PEG-NHS, and 5  $\mu\text{L}$  of triethylamine were dissolved in 50  $\mu\text{L}$  of dry DMF and reacted overnight. The reaction was then diluted in 2.5 mL of deionized water and run through a PD-10 column to remove unreacted hexalysine. The high-MW fractions of the PD-10 column were lyophilized for 2 days. The recovered white solid was dissolved in 1 mL of 10 mM pH 7.4 phosphate buffer and loaded onto a high trap ion exchange column, equilibrated with 10 mM pH 7.4 phosphate buffer. The column was washed with 5 mL of 10 mM pH 7.4 phosphate buffer, and the product was eluted with 2.5 mL of 3 M NaCl. The product was run through a PD-10 column, and deionized water was used as the eluent. The high-MW fractions of the PD-10 column were lyophilized; the yield was 25%. The product had a thiopyridal/amine ratio of 1:5, the thiopyridal content was determined by reducing the product with DTT and UV analysis at 372 nm (DMF), and the amine content was determined by the 2,4,6-trinitrobenzene sulfonic acid (TNBS) assay.

**Synthesis of (Man)<sub>3</sub>-(Lys)<sub>3</sub>-PEG-SH.** A 50 mg sample of thiopyridal-PEG-(Lys)<sub>6</sub> (0.01 mmol) was mixed with 10 mg of mannopyranosylphenyl-isothiocyanate (0.03 mmol) in 0.5 mL of DMSO with 3  $\mu\text{L}$  of TEA. The reaction

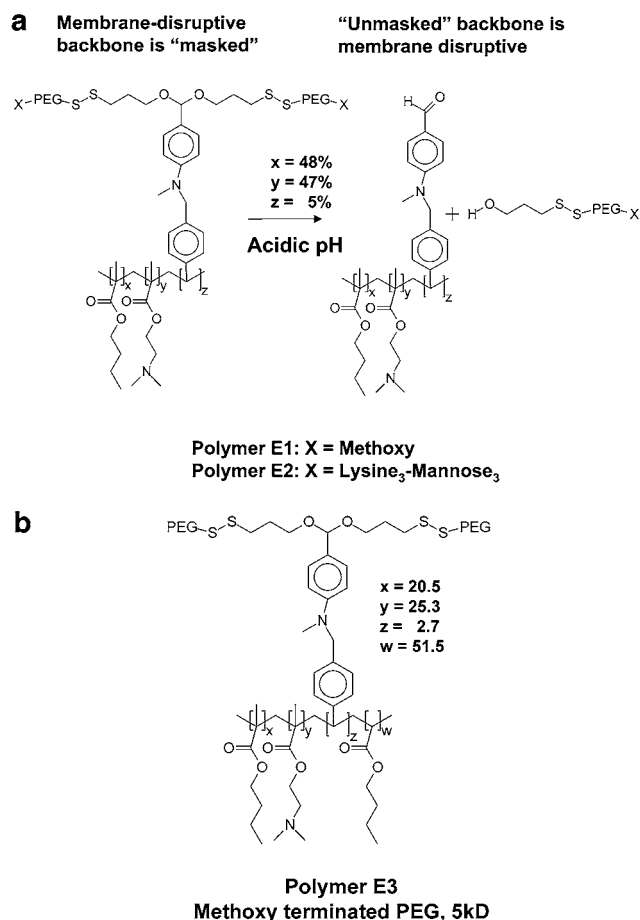


**Figure 1.** Schematic diagram of the encrypted polymer design. The polymers are designed to be PEGylated and serum stable at pH 7.4, but to be disruptive to the endosomal membrane at the acidic pHs within the endosome. The polymers have the following components: a membrane-disruptive backbone (red line), acid-degradable linkers (purple circle), PEG grafts (aqua ellipsoid), conjugated or ionically complexed drug molecules (blue circle), hexalysine peptide (green line), and targeting ligands (black arrow). At pH 7.4 the polymers are PEGylated ("masked"); however, after endocytosis the acid-degradable linker hydrolyzes and the polymer backbone becomes de-PEGylated ("unmasked") and membrane-disruptive, causing endosomal disruption. The PEGs may be conjugated to the backbone via both acid-degradable linkages and disulfide bonds. The latter are reduced in the cytoplasm to release the free drug. In the study reported here, two examples are presented. In the first case, a model peptide drug with a terminal cysteine is conjugated to the backbone via  $-S-S-$  bonds, and in the second case an antisense oligonucleotide (AS-ODN) is ionically complexed to cationic lysine groups that have been linked to the terminal ends of the PEG molecules. In the latter case, mannose groups have been linked along with the lysine groups to the ends of the PEGs for targeting the ODN to the RAW cells.

was allowed to proceed overnight and was then dialyzed against water in a Pierce Slidealyzer. The thiol content was quantified by reducing the thiopyridal group, and the mannose content was determined by performing the resorcinol/sulfuric acid assay. The mannose to thiol content was 3:1, leading to a lysine/mannose ratio of 1/1. The product was reduced with DTT, purified with a PD-10 column, and lyophilized.

**Synthesis of Encrypted Polymer E2.** A 1.6 mg sample of (Man)<sub>3</sub>-(Lys)<sub>3</sub>-PEG-SH (0.26  $\mu$ mol) was mixed with 353  $\mu$ g of the polymer backbone E1 (0.21  $\mu$ mol of thiopyridal groups) in 40  $\mu$ L of DMF, and allowed to react overnight. UV analysis of the released thiopyridone (372 nm DMF) indicated that 84% of the thiopyridal groups on the polymer backbone E1 had reacted with (Man)<sub>3</sub>-(Lys)<sub>3</sub>-PEG-SH.

**Synthesis of Encrypted Polymer E3.** A 200 mg (1.4 mmol) sample of BMA, 250 mg (1.5 mmol) of DMAEMA, 400 mg (3.0 mmol) of butyl acrylate (BA), 100 mg (0.153 mmol) of III, and 35 mg (0.21 mmol) of AIBN were placed in a 5 mL round-bottom flask fitted with a stir bar and stopcock. The reaction flask was subjected to three freeze-thaw-vacuum cycles and heated to 60  $^{\circ}$ C for 1.5 h. The reaction was then dissolved in 3 mL of THF with 1% TEA and precipitated in 20 mL of ice-cold hexane, decanted, and vacuum-dried. A white solid was recovered, which was precipitated again from THF into hexane, decanted, and vacuum-dried. GPC of the polymer (Styragel gel columns, with PMMA standards in THF) gave a MW of 58 kD and an Mn of 38 kD. The monomer composition of the E3 backbone was determined by H



**Figure 2.** Chemical structures of the "encrypted" polymeric carriers. (a) The membrane-disruptive backbone for polymer E1 is a terpolymer of three monomers: BMA, DMAEMA, and SBA. The acid-degradable linker is an acetal, specifically, *para*-aminobenzaldehyde-acetal. The PEG grafts have a molecular weight of 5 kD and in this study have been terminated with various functional groups. Polymer E1 has its PEG grafts terminated with methoxy groups. Polymer E2 has its PEG grafts terminated with Lysine<sub>3</sub>-Mannose<sub>3</sub>. (b) The membrane-disruptive backbone for polymer E3 is a copolymer of four monomers: BMA, BA, DMAEMA, and SBA. Polymer E3 has its PEG grafts terminated with methoxy groups.

NMR and UV spectroscopy, giving DMAEMA/BMA/BA/SA = 25.3/20.5/51.5/2.7. The molar ratios of the three main monomers of the E3 backbone, DMAEMA/BMA/BA, were determined by H NMR to be 2.5/2.0/5.0 (H NMR deuterated chloroform AM-400). The molar content of III was determined by reducing the polymer backbone with DTT, in DMF, and measuring the UV absorption at 372 nm. The polymer backbone E3 was PEGylated by reacting 15 mg of the polymer backbone (4.6  $\mu$ mol of thiopyridal groups) with 160 mg (16  $\mu$ mol) of PEG-thiol (5kD) in 1.5 mL of a 2/3 mixture of THF/DMF. The reaction was allowed to proceed overnight, and analysis of the released thiopyridone indicated that 100% of the thiopyridal groups had reacted. The reaction was precipitated in 20 mL of cold ether, filtered, and vacuum-dried overnight (see Figure 2b for structure).

**Synthesis of Cys-(Gly)<sub>4</sub>-(His)<sub>6</sub>-FITC-Polymer E3 Conjugate.** A 4.5 mg sample of the polymer backbone E3 (1.4  $\mu$ mol of thiopyridal groups) was dissolved in 270  $\mu$ L of 1/1 THF-DMF and added to 1 mg of PEG-thiol (5kD) (0.2  $\mu$ moles) dissolved in 170  $\mu$ L DMF. The PEGylation reaction was allowed to proceed for 4 h, and UV analysis indicated quantitative reaction of the PEG-thiol. Following this, 12.5 mg of the peptide Cys-(Gly)<sub>4</sub>-(His)<sub>6</sub>-



FITC (1.2  $\mu$ moles) was added to the reaction (Figure 2c) and allowed to proceed overnight. UV analysis of the reaction indicated quantitative reaction of the peptide with the polymer backbone. The Cys-(Gly)<sub>4</sub>-(His)<sub>6</sub>-FITC-polymer E3 conjugate was used directly for cell culture experiments.

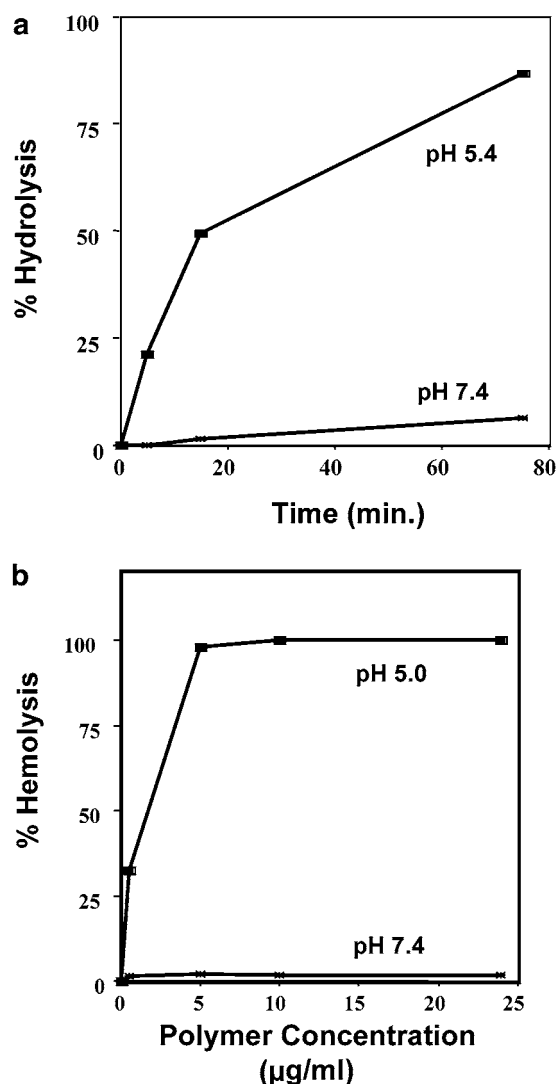
**Fluorescence Microscopy of Macrophages.** RAW cells were split onto #1 Gold coverslips in a 35 mm dish and allowed to grow for 16 h, reaching approximately 50% confluency. The cells were washed once with DMEM high-glucose media and incubated with either the peptide Cys-(Gly)<sub>4</sub>-(His)<sub>6</sub>-FITC, at a 40  $\mu$ g/mL concentration, in DMEM high glucose media, or the Cys-(Gly)<sub>4</sub>-(His)<sub>6</sub>-FITC-polymer E3 conjugate (40  $\mu$ g/mL peptide concentration), in a 1.5 mL volume for 12 h. The cells were washed once with DMEM high-glucose media and allowed to grow for 4 h in DMEM high-glucose media with 10% fetal bovine serum. The cells were then washed 6 times with PBS and fixed for 5 min with 3% paraformaldehyde and observed with a Zeiss digital fluorescent microscope at a 40 $\times$  magnification.

**iNOS Assay.** RAW cells were split onto a 96 well plate, at  $4 \times 10^5$  cells per well, and grown for 16 h in DMEM high glucose media with 10% fetal bovine serum (FBS). The RAW cell media was then removed and the appropriate polymer/ODN sample was added to the cells, in serum free media, the cells were incubated with polymer/ODN samples for 16 h. The media was then aspirated off, and the cells were stimulated with 10 units/mL of  $\gamma$  interferon and 10  $\mu$ g/mL of lipopolysaccharide (LPS) for 8 h in serum containing media (to stimulate iNOS) production). The cell medium was isolated, and the concentration of nitric oxide (NO) was determined with the Griess reagent (1% sulfanilamide, 0.1% naphthylethylene-diamine hydrochloride, and 5% phosphoric acid), a 1:1 mixture of the cell medium with the Griess reagent was made, incubated for 10 min at room temperature, and its absorbance at 540 nm was measured.

## RESULTS AND DISCUSSION

**Polymer Design.** The encrypted polymers are designed as multifunctional carriers that incorporate three primary functionalities of viruses and toxins: (a) a targeting agent that directs receptor-mediated endocytosis, (b) a pH-responsive element that selectively disrupts the endosomal membrane, and (c) the biomolecular therapeutic component which is delivered as a free and active agent into the cytoplasm. Our encrypted polymers contain a masked, membrane-disruptive backbone that is unmasked and activated in the low pH environment of the endosome. This design is shown schematically in Figure 1, and three specific compositions that we have synthesized are presented in Figure 2a,b (see Schemes 1 and 2 for synthesis). Copolymers of dimethylaminoethyl methacrylate (DMAEMA) with hydrophobic alkyl methacrylates (BMA) and alkylacrylates (BA) were chosen for the membrane-disruptive backbone, based on our previous work on endosomolytic polymers (13, 14). PEG was chosen as the solubilizing hydrophilic graft to "mask" the backbone because of its established ability to improve the stability, solubility, circulation lifetime, and biodistribution properties of a wide variety of drugs and delivery systems (15). The pH sensitivity of the encrypted polymer is provided through acid-degradable acetal bonds that link the PEGs and PEGylated drugs or targeting ligands to the polymer backbone.

**Hydrolysis Kinetics of PEG Grafts.** The encrypted polymer carrier system is designed to remain PEGylated



**Figure 3.** The pH-dependent hydrolysis and hemolytic properties of the polymer carriers. (a) The hydrolysis of polymer E1 was measured at 37  $^{\circ}$ C, in phosphate buffer, at either pH 5.4 or 7.4, by observing the change in UV absorbance at 340 nm. The experiments were done in triplicate and the standard deviation was under 5% for all samples. (b) pH-dependent hemolysis by polymer E1. The ability of the polymer E1 to disrupt red blood cell membranes was measured at either pH 5.0 or 7.4. In each hemolysis experiment,  $10^8$  RBCs were suspended in 1 mL of phosphate buffer saline. The incubation time was 20 min at 37  $^{\circ}$ C. The experiments were done in triplicate. The protocol used to isolate and purify the red blood cells and to quantitate hemolysis is described in (13, 14).

during circulation at pH 7.4, but then to be rapidly de-PEGylated after endocytosis, as the pH drops within the endosome to ca. 5.0. Endocytosed macromolecules are typically trafficked to lysosomes within 30–60 min after endocytosis, and therefore, we designed the linkage between the PEG and the membrane-disruptive backbone to hydrolyze within 30–60 min at pHs between 5 and 5.5. The hydrolysis kinetics of the PEG grafts from the polymer E1 are strongly pH-dependent, as expected, with a half-life of 15 min at pH 5.4 (Figure 3a). In contrast, at pH 7.4 less than 10% of the PEG grafts are hydrolyzed after 75 min, and only 38% are hydrolyzed after 12 h. The PEG grafts are released from the encrypted polymer backbone about 2 orders of magnitude faster at pH 5.4 than at pH 7.4. This 100-fold increase in hydrolysis kinetics agrees with the enhancement expected due to the 100-fold increase in the hydronium ion concentration

between pH 5.4 and 7.4. The hydrolysis rates of acetals can be manipulated over a wide range of time scales by changing the substituent group in the para position of the benzene ring to stabilize or destabilize the carbocation intermediate formed during hydrolysis (16). For example, by changing the para substituent from a nitrogen to an oxygen in polymer E1, the rate constant for hydrolysis is decreased by a factor of ca. 60 (data not shown). The ability to control the hydrolysis kinetics of the acid degradable linker is a critical design element of the encrypted polymer carrier system.

**Membrane Disruption by Polymer E1.** The pH-dependent membrane disruption properties of polymer E1 were characterized in a red blood cell (RBC) hemolysis assay at pH 5.0 and 7.4 (Figure 3b). After 20 min at pH 5.0, less than 5  $\mu\text{g/mL}$  of the polymer E1 caused almost 60% hemolysis of  $10^8$  cells/mL, while in contrast there was no significant hemolysis at pH 7.4 under those same conditions. These kinetic properties match the time frame of vesicular evolution in macrophages from endosomes to lysosomes, which has been estimated to occur on the order of 30 min (18). The ability of the encrypted polymers to avoid degradative lysosomal trafficking was first tested with antisense oligonucleotides (AS-ODNs) in a cultured macrophage cell line. The antisense ODN was designed to inhibit secretion of NO by macrophages by blocking the expression of inducible nitric oxide synthetase (iNOS). Several phosphorothioate AS-ODNs have been developed which selectively inhibit iNOS; however, they require high extracellular concentrations, where toxicity can become significant (19–22).

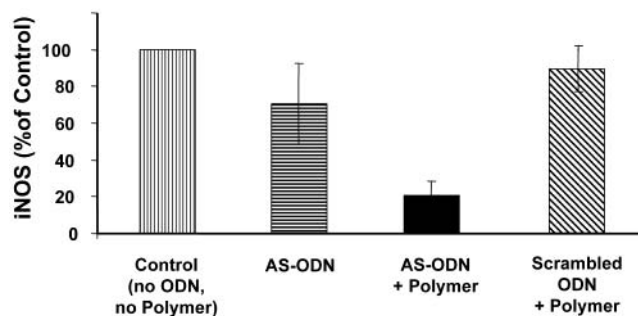
**AS-ODN Delivery.** The membrane-disruptive polymer backbone E1 was conjugated with heterobifunctional PEGs that were terminated with thiol groups at one end and with lysine<sub>3</sub>–mannose<sub>3</sub> groups at the other end. To synthesize this derivatized PEG, a hexalysine peptide was first conjugated to a carboxyl derivatized PEG, and then three of the six lysines groups were statistically reacted with mannose-isothiocyanate, generating a heterobifunctional PEG with three residual lysine groups. This graft copolymer is called “encrypted polymer E2”. These lysine-grafted polymers ionically complexed AS-ODNs efficiently, as determined in a gel shift assay (see Figure 4). At low pHs, the acetal groups linking the PEG–lysine<sub>3</sub>–mannose<sub>3</sub> graft to the backbone should be hydrolyzed, and since the PEG–lysine<sub>3</sub>–mannose<sub>3</sub> has no membrane-disruptive activity by itself, polymers E2 and E1 should therefore have very similar membrane disruptive activities. Polymer E2 was complexed with AS-ODNs at various charge ratios and their ability to inhibit the iNOS catalyzed synthesis of NO in the RAW cells was measured. As a control, the encrypted polymers were complexed with a scrambled ODN and incubated under the same conditions. As shown in Figure 5, the polymer E2 is able to significantly enhance the delivery into macrophages of AS-ODNs at a 1/1  $\pm$  charge ratio. At this charge ratio, the AS-ODN complexed to polymer E2 caused approximately 80% inhibition of iNOS, whereas by itself the iNOS AS-ODN causes only 25% inhibition. In addition, in another control experiment, when the scrambled ODN was complexed to the encrypted polymer, there was no significant inhibition of iNOS activity.

**Peptide Delivery with Polymer E3.** To test the ability of the encrypted polymers to enhance endosomal escape of polypeptides, the labeled peptide, FITC-(His)<sub>6</sub>-(Gly)<sub>4</sub>-Cys, was conjugated to the encrypted polymer E1 backbone through its thiopyridyl groups. A methoxy-PEG-thiol was also grafted through the thiopyridyl groups in order to enhance the solubility of the backbone

Lane 1: ODN  
Lane 2: ODN/Polymer E2 1/3  $\pm$  charge ratio  
Lane 3: ODN/Polymer E2 1/6  $\pm$  charge ratio  
Lane 4: ODN/Polymer E2 1/9  $\pm$  charge ratio  
Lane 5: ODN/Polymer E2 1/1.2  $\pm$  charge ratio

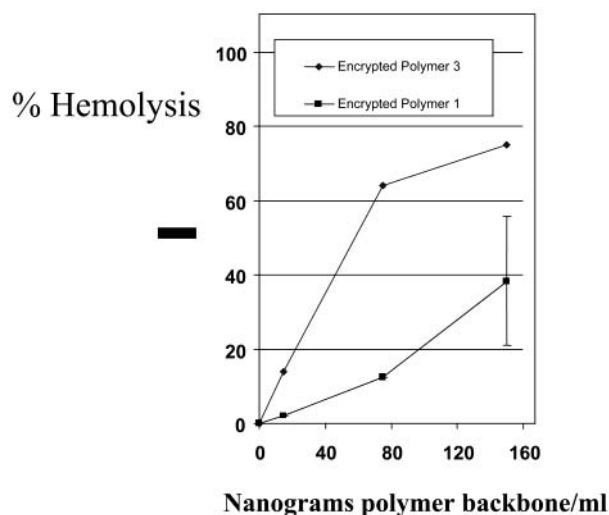


**Figure 4.** Gel Shift assay with polymer E2. The polymer E2 was incubated at various charge ratios with 2  $\mu\text{g}$  of the phosphorothioate oligonucleotide thiol-CCA-GGG-GCA-AGC-CAT-GTC-TG in a 20  $\mu\text{L}$  volume of 1X TAE buffer. The charge ratios indicated on the gel refer to the number of lysine residues from the grafts of polymer E2 vs the number of phosphate groups on the oligonucleotide backbone. The complexes were run on a 2% agarose gel at a 100 V for 45 min and then stained with ethidium bromide



**Figure 5.** AS-ODN delivery with polymer E2. Diagonal hatched lines: 104  $\mu\text{g/mL}$  of polymer E2 mixed with 10  $\mu\text{g/mL}$  of “scrambled” ODN. Dark filling: 104  $\mu\text{g/mL}$  of polymer E2 mixed with 10  $\mu\text{g/mL}$  of AS-ODN targeted against iNOS. Horizontal hatched lines: 10  $\mu\text{g/mL}$  of AS-ODN targeted against iNOS. Vertical hatched lines: A control in which cells were incubated with 10 mg/mL of LPS and 10 units/mL of  $\gamma$  interferon. This sample was used as the 100% reference. After incubation with the appropriate ODN formulation, each of the samples was stimulated with 10  $\mu\text{g/mL}$  of LPS and 10 units/mL of  $\gamma$  interferon. The cell supernatants were harvested after 8 h of stimulation and assayed for NO content. (See Materials and Methods for details.)

polymer. Initial delivery to the macrophage RAW cells of the peptide conjugated to the polymer backbone E1 was inefficient and resulted in lysosomal localization (as suggested by the punctate localization seen in fluorescence micrographs). However, a key aspect of the encrypted polymer strategy is the flexibility in polymer



**Figure 6.** Hemolysis by polymer E3 vs polymer E1. The membrane disruptive activities of polymer E3 and E1 were compared using a hemolysis assay at pH 5.0. In each hemolysis experiment,  $10^8$  RBCs were suspended in 1 mL of phosphate buffer saline. The incubation time was 20 min at 37 °C. The experiments were done in triplicate. The protocol used to isolate and purify the red blood cells and to quantitate hemolysis is described in (13, 14). The quantities of polymer indicated on the x axis refer to the mass of the polymer backbone generated after the PEG grafts are hydrolyzed from PEGylated polymers E1 and E3. The quantity of polymer backbone (x axis) was determined by estimating the weight percent of PEG in the polymers E3 and E1 and then subtracting it from the actual mass of polymer E1 and E3 used for the hemolysis assay.

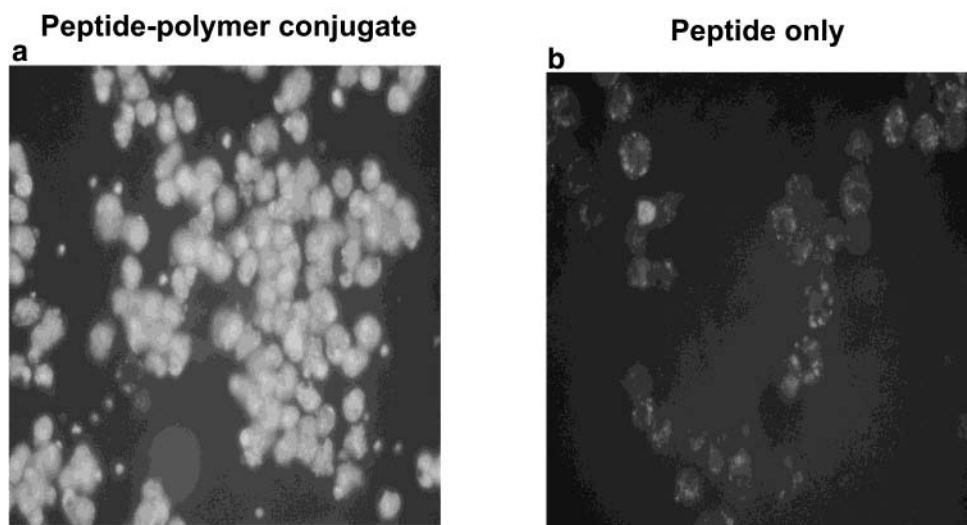
design it allows, and therefore, we subsequently designed and synthesized a new backbone, E3, which contained an additional monomer, butyl acrylate (BA). This polymer backbone is significantly more hydrophobic than the E1 or E2 backbones (compare panels a and b of Figure 2). We chose to add BA to the polymer composition because it copolymerizes exceptionally well with the other methacrylate-based monomers. The copolymer E3 is strikingly more effective at RBC hemolysis than the encrypted polymer E1 (see Figure 6). For example, the copolymer backbone E3 is hemolytically active at nanogram per milliliter concentrations, making it approximately 2–3 orders of magnitude more efficient at membrane disruption

on a molar basis than the best known peptides (9, 10) or the polycarboxylic polymers (e.g., poly[propylacrylic acid]) that we have previously studied (13, 14). Importantly, polymer E3 has no membrane disruptive activity at pH 7.4 at 25  $\mu\text{g/mL}$  (highest concentration tested).

The peptide FITC-(His)<sub>6</sub>-(Gly)<sub>4</sub>-Cys and methoxy-PEG-SH (5kD) were conjugated via disulfide linkages to the polymer backbone E3. This conjugate was incubated with RAW cells, and the intracellular location of the FITC-labeled peptide was determined by fluorescence microscopy. Figure 7b demonstrates that the peptide by itself was taken up by RAW cells but sequestered in punctate organelles, presumably lysosomes. The intracellular location of the peptide was dramatically altered after being conjugated to the PEGylated E3 backbone (Figure 7a) and was spread diffusely through the cytoplasm. This demonstrates that the conjugated E3 polymers were able to direct transport out of the macrophage endosomal compartments and release endocytosed peptides into the cytoplasm.

## CONCLUSIONS

In this report we describe a novel strategy for the design and synthesis of pH-responsive polymers as carriers that enhance the cytosolic delivery of fragile drugs, thus avoiding lysosomal degradation of the drugs. This strategy combines a relatively hydrophobic, membrane-disruptive polymer backbone that is “masked” at pH 7.4 by grafted PEG chains. The PEG grafts are linked to the backbones through two key linkers, first disulfide groups and then acid degradable acetal linkages. The acetal groups are designed to degrade in the acidic environment of the endosome, which then unmasks the membrane-disruptive backbone. This leads to disruption of the endosomal membrane and release into the cytosol of the grafted side chains, where the disulfide groups are reduced and release the drug. Peptide, protein, or anti-sense ODN therapeutics can be conjugated to the backbone of the polymer via the disulfide bonds. In the case of highly negative ODNs, they may also be electrostatically complexed to cationic groups that are either conjugated to the terminal ends of the grafted PEGs or included as a monomeric component of the polymer backbone. Targeting ligands may also be conjugated to the terminal ends of the PEGs.



**Figure 7.** Cytoplasmic delivery of peptides with polymer E3. (a) Fluorescence microscopy (40X magnification) of RAW cells treated overnight with the peptide Cys-(Gly)<sub>4</sub>-(His)<sub>6</sub>-FITC conjugated to polymer E3. (b) Lysosomal localization of the peptide Cys-(Gly)<sub>4</sub>-(His)<sub>6</sub>-FITC. The peptide Cys-(Gly)<sub>4</sub>-(His)<sub>6</sub>-FITC was incubated with RAW cells overnight and visualized by fluorescence microscopy at 40 $\times$  magnification.



This new type of pH-responsive polymer is at least 2–3 orders of magnitude more efficient at RBC membrane disruption than existing endosomal-disruptive polymers and peptides. We have shown that the encrypted polymers provide efficient endosomal escape in a model macrophage cell line, and are able to deliver functional antisense ODNs and peptides into the cytoplasm. This encrypted polymer strategy should therefore have broad applications in the design of peptide vaccine delivery systems for CD8<sup>+</sup> T cells and in the development of antisense ODN delivery systems. These multifunctional polymeric carriers mimic the sophisticated protein complexes of viruses and toxins that direct uptake and enhance cytosolic transport of DNA or proteins. Like the biological systems, they combine targeting elements that direct cellular uptake, together with the sensing of pH changes within the endosome to activate membrane destabilization and cytosolic delivery. Their intrinsic modular design makes it possible to tailor the targeting and membrane destabilizing activities for a wide range of biotherapeutics and vaccine applications.

#### ACKNOWLEDGMENT

The authors gratefully acknowledge the NIH (Grant No. GM-53771-02 to -04), University of Washington Office of Technology Transfer, Washington Research Foundation, and Center for Nanotechnology (fellowship to N.M.). We would also like to thank the University of Washington Engineered Biomaterials Research Center (UWEB) (NSF Grant No. EEC-9529161) for use of their cell culture facilities and the UWEB Optical Microscopy and Image Analysis Shared Resource (NSF Grant Nos. EEC-9872882 and EEC 9529161).

#### LITERATURE CITED

- (1) Berg, K., et al. (1999) Photochemical internalization: A novel technology for delivery of macromolecules into cytosol. *Cancer Res.* 59, 1180.
- (2) Bijsterboch, M. et al. (1997) In vivo fate of phosphorothioate antisense oligodeoxynucleotides: predominant uptake by scavenger receptors on endothelial liver cells. *Nucleic Acids Res.* 25, 3290.
- (3) Haensler, J., and Szoka, F. C. (1993) Polyamidoamine cascade polymers mediate efficient transfection of cells in culture. *Bioconjugate Chem.* 4, 312.
- (4) Choi, Y. H., Lui, F., Choi, J. S., Kim, S. W., and Park, J. S. (1999) Characterization of a targeted gene carrier, lactose-polyethylene glycol-grafted poly-L-lysine and its complex with plasmid DNA. *Hum. Gene Ther.* 10, 2657.
- (5) Richardson, S., Ferruti, S., and Duncan, R. (1994) Poly-(amidoamine)s as potential endosomolytic polymers: evaluation in vitro and body distribution in normal and tumour bearing animals. *J. Drug Target.* 6, 391.
- (6) Vinogradov, S. V., Bronich, T. K., and Kabanov, A. V. (1998) Self-assembly of polyamine-poly(ethylene glycol) copolymers with phosphorothioate oligonucleotides. *Bioconjugate Chem.* 9, 805.
- (7) Wetering, P., et al. (1997) Structure-activity relationships of water soluble cationic methacrylate/methacrylamide polymers for nonviral gene therapy. *Bioconjugate Chem.* 4, 687.
- (8) Boussif, O., Lezoualch, F., Zanta, F., Mergny, M. D., Scherman, D., Demeneix, B., and Behr, J. P. (1995) A versatile vector for gene and oligonucleotide transfer into cells in culture and in vivo. *Proc. Natl. Acad. Sci. U.S.A.* 92, 797.
- (9) Subbarao, N., Parente, R., Szoka, F., Nadasdi, L., and Pongracz, K. (1987) pH dependent bilayer destabilization by an amphiphatic peptide. *Biochemistry* 26, 2964.
- (10) Plank, C., Oberhauser, B., Mechtler, K., Koch, C., and Wagner, E. (1994) The influence of Endosome-disruptive peptides on gene transfer using synthetic virus such as gene transfer systems. *J. Biol. Chem.* 269, 12918.
- (11) Kaplan, F., and Shore, E. (1998) Encrypted morphogens of skeletogenesis: biological errors and pharmacologic potentials. *Biochem. Pharmacol.* 55, 373.
- (12) Bilecki, W., Okruszek, A., and Przewlocki, R. (1997) The Effect of Antisense Oligodeoxynucleotides on Nitric Oxide Secretion from Macrophages-Like Cells. *Antisense Nucleic Acid Drug Dev.* 7, 531–537.
- (13) Murthy, N., Robichaud, J. R., Tirrell, D. A., Stayton, P. S., and Hoffman, A. S. (1999) The design and synthesis of polymers for eukaryotic membrane disruption. *J. Controlled Release* 61, 137.
- (14) Murthy, N., Chang, I., Stayton, P. S., and Hoffman, A. S. (2001) pH-sensitive hemolysis by random copolymers of alkyl acrylates and acrylic acid. *Macromol. Symp.* 172, 149–155.
- (15) Woodle, M. C. In *Poly(ethylene-glycol) Chemistry and Biological Applications* (J. M. Harris and S. Zalipsky, Eds.) pp 60–77, American Chemical Society, Washington, DC.
- (16) Taft, R. W., and Kreevoy, M. M. (1955) The evaluation of inductive and resonance effects on reactivity. I hydrolysis rates of acetals and nonconjugated aldehydes and ketones. *J. Am. Chem. Soc.* 77, 5590.
- (17) Fife, T. H., and Jao, L. K. (1965) Substituent effects in acetal hydrolysis. *J. Am. Chem. Soc.* 87, 1492.
- (18) Mellman, I. (1996) Endocytosis and molecular sorting. *Annu. Rev. Cell Dev. Biol.* 12, 575.
- (19) Arima, H., et al. (1997) Specific Inhibition of Nitric Oxide Production in Macrophages by Phosphorothioate Antisense Oligonucleotides. *J. Pharm. Sci.* 86, 1079–1084.
- (20) Ding, M., et al. (1996) Antisense Blockade of Inducible Nitric Oxide Synthase in Glial Cells Derived From Adult SJL Mice. *Neurosci. Lett.* 220, 89–92.
- (21) Wood, L., et al. (1999) Enhancement of Methylcholanthrene-induced Neoplastic Transformation in Murine C3H 10T1/2 Fibroblasts by Antisense Phosphorothioate Oligodeoxynucleotide Sequences. *Cancer Lett.* 147, 163–173.
- (22) Ding, M., et al. (1998) Antisense Knockdown of Inducible Nitric Oxide Synthase Inhibits Induction of Experimental Autoimmune Encephalomyelitis in SJL/J Mice. *J. Immunol.* 160, 2560–2564.

BC020056D

# Low-pH-Sensitive PEG-Stabilized Plasmid–Lipid Nanoparticles: Preparation and Characterization

Joon Sig Choi,<sup>†</sup> J. Andrew MacKay,<sup>‡</sup> and Francis C. Szoka, Jr.\*<sup>†,‡</sup>

Department of Biopharmaceutical Sciences and Pharmaceutical Chemistry,  
University of California at San Francisco, San Francisco, California 94143-0446, and  
Joint Graduate Group in Bioengineering, University of California at San Francisco and Berkeley,  
San Francisco, California 94143-0446. Received October 9, 2002; Revised Manuscript Received December 2, 2002

The acid-labile poly(ethyleneglycol)-diorthoester-distearoylglycerol lipid (POD), was used with a cationic lipid–phosphatidylethanolamine mixture to prepare stabilized plasmid–lipid nanoparticles (POD SPLP) that could mediate gene transfer in vitro by a pH triggered escape from the endosome. Nanoparticles of 60 nm diameter were prepared at pH 8.5 using a detergent dialysis method. The DNA encapsulation efficiency in the nanoparticles was optimal between 10 and 13 mol % ratio of cationic lipid and at a POD content of 20 mol %. The apparent  $\zeta$  potential of the nanoparticles at 1 mM salt and pH 7.5 was positive, indicating cationic lipid on the external surface. However, the external layer of the nanoparticles was depleted in the cationic component compared to the starting mole ratio. Low pH sensitivity of the POD SPLP was characterized by a lag phase followed by a rapid collapse; at pH 5.3 the nanoparticles collapsed in 100 min. Nanoparticles prepared from a pH-insensitive PEG–lipid, PEG–distearoylglycerol had similar physicochemical characteristics as the POD SPLP but did not collapse at low pH. The POD SPLP had up to 3 orders of magnitude greater gene transfer activity than did the pH-insensitive nanoparticles. Both the pH-sensitive and pH-insensitive nanoparticles were internalized to a qualitatively similar extent in a punctate pattern into cultured cells within 2 h of incubation with the cells; thus, increased gene transfer of the POD SPLP was due to a more rapid escape from the endosome rather than to greater cell association of these nanoparticles. These results suggest that the pH-sensitive stabilized plasmid–lipid nanoparticles may be a useful component of a synthetic vector for parenterally administered gene therapy.

## INTRODUCTION

Gene therapy has attracted considerable scientific and pharmaceutical interest as a platform for unique therapies in the postgenomic era. Therapeutic genes have been delivered by either viral or synthetic vectors, such as cationic liposomes or cationic polymers. Viral vectors are considered more efficient and usually result in higher gene expression than do synthetic vectors. However, in human trials, viral vectors have been plagued with immunoreactivity, inflammatory issues leading to death as well as certain other unexpected results such as the appearance of the vectors in semen (Marshall, 2001). Nonviral synthetic vectors have been developed over the past decade (Henry, 2001; Ogris and Wagner, 2002) and in animal models can express sufficient amounts of therapeutically active compounds in solid tumors, resulting in reduced tumor growth (Hood et al., 2002; Ogris and Wagner, 2002).

The successful application of such synthetic nonviral vectors is dependent on several factors, such as the diameter, the surface charge of the complex, the DNA-to-particle ratio, the lipid composition or the polymer

structure, and other experimental conditions, for example, the presence of serum. The modification of a detergent dialysis method for preparing stable cationic lipid–DNA particles (Hofland et al., 1996) to create a liposomal system known as a stabilized plasmid–lipid particle (SPLP) has provided the field with a technique to create a synthetic vector with useful properties for parenteral gene delivery (Mok et al., 2001; Tam et al., 2000; Wheeler et al., 1999; Zhang et al., 1999). First, the SPLPs are water-soluble nanoparticles smaller than 100 nm. Second, the incorporated PEG–lipid functions as a masking agent to permit a longer circulation of the particles in the bloodstream than for unshielded particles. The long circulation permits a greater fraction of injected particles to extravasate through the leaky blood vessels and reach the tumor. Third, the particles deliver genes when the PEG coat is removed.

Our group has recently reported the synthesis of the acid-labile PEG<sup>1</sup> lipid, POD, and the use of this lipid to create a pH-sensitive liposome composed of POD/DOPE that circulated for a reasonable time after intravenous administration but could very rapidly release the encapsulated contents when the pH was reduced to 5.0, the pH found in the endosome (Guo and Szoka, 2001; Guo et

\* Corresponding author. Address: Department of Biopharmaceutical Sciences, HSE 1145, 513 Parnassus Avenue, University of California at San Francisco, San Francisco, CA 94143-0446. E-mail: szoka@cgl.ucsf.edu. Fax: (415) 476-0688. Tel: (415) 476-3895.

<sup>†</sup> Department of Biopharmaceutical Sciences and Pharmaceutical Chemistry, University of California at San Francisco.

<sup>‡</sup> Joint Graduate Group in Bioengineering, University of California at San Francisco and Berkeley.

<sup>1</sup> Abbreviations: DOPE, 1,2-dioleoyl-*sn*-glycero-3-phosphatidylethanolamine; DOTAP, 1,2-dioleoyl-3-trimethylammonium-propane; PEG–DSG, PEG–distearoylglycerol; OGP, *n*-octyl- $\beta$ -D-glucopyranoside; ONPG, *o*-nitrophenyl- $\beta$ -D-galactopyranoside; PEI, polyethylenimine; POD, poly(ethyleneglycol)-diorthoester-distearoylglycerol lipid; PEG, poly(ethylene glycol); Rh–PE, 1,2-dioleoyl-*sn*-glycero-3-phosphatidylethanolamine-*N*-lissamine rhodamine B; SPLP, stabilized plasmid–lipid particles.

al., 2003). The goal of this current study was to determine the characteristics of SPLP that incorporated POD as the masking component and to learn if POD SPLPs exhibit superior transfection activity than do 6 pH-insensitive SPLPs. Herein, we document that the acid-sensitive SPLP nanoparticles could be prepared with a good DNA encapsulation yield using basic conditions (pH 8.5), and they rapidly collapsed at low pH and efficiently delivered genes to cells in culture.

#### EXPERIMENTAL PROCEDURES

**Materials.** The diketene acetal, 3,9-diethylidene-2,4,8,10-tetraoxaspiro [5,5] undecane was a generous gift from Dr. Jorge Heller at Advanced Polymer Systems (Redwood City, CA). Monomethyl ether PEG (mPEG, MW 2000) was purchased from Shearwater Polymers, Inc (Huntsville, AL). 1,2-Distearoyl glycerol was obtained from Genzyme (Cambridge, MA). 1,2-Dioleoyl-*sn*-glycero-3-phosphatidylethanolamine (DOPE), 1,2-dioleoyl-3-trimethylammonium-propane (DOTAP), and 1,2-dioleoyl-*sn*-glycero-3-phosphatidylethanolamine-N-lissamine rhodamine B (Rh-PE) were purchased from Avanti Polar Lipids (Alabaster, AL). PEG-DSG (Sunbright DSG-20H) was a generous gift from Dr. A. Suganaka (NOF Corp., Tokyo, Japan). Plasmids (pCMV-Gal, pCMV-Luc, pCMV-GFP) were obtained from Valantis, Inc (Burlingame, CA). DME H-21 medium, fetal bovine serum (FBS), phosphate-buffered saline (PBS), and antibiotics were obtained from the UCSF Cell Culture Facility. All other chemicals were purchased from Aldrich, Sigma, or Fisher.

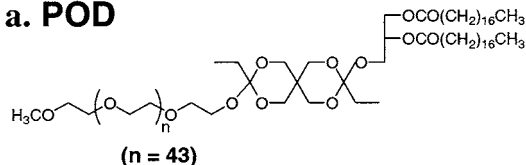
**POD Synthesis.** POD was synthesized as reported previously. In short, 1 g of mPEG (MW 2000, 0.5 mmol) and 312.5 mg of distearoyl glycerol (0.5 mmol) were dissolved in anhydrous THF under argon. A 100  $\mu$ L (110 mg, 0.5 mmol) sample of heat-melted 3,9-diethylidene-2,4,8,10-tetraoxaspiro[5,5]undecane was injected into the solution, and the reaction was initiated by adding 1 drop of 0.6 mg/mL *p*-toluenesulfonic acid in THF and stirring the mixture at 40 °C under argon for 2 h. The reaction was stopped by adding 200  $\mu$ L of triethylamine (TEA) followed by the addition of 30-fold volume excess of 1% TEA/MeOH. The reaction mixture was loaded onto silica column and eluted with chloroform/TEA using MeOH gradient, and fractions corresponding to the product were pooled, evaporated, and dried in high vacuum to give a white product with the correct mass and NMR spectrum (Guo and Szoka, 2001).

**Encapsulation of Plasmid DNA.** Plasmid DNA was encapsulated in SPLP by the detergent dialysis method (Hofland et al., 1996; Mok et al., 1999). In the typical preparation, 10  $\mu$ mol of total lipid was mixed at appropriate mole ratio in chloroform, dried under a stream of argon, and further dried under high vacuum for 2 h. The dried lipids were solubilized in 5 mM Tris/acetate, 150 mM NaCl, pH 8.5 (TBS) containing 0.2 M *n*-octyl- $\beta$ -D-glucopyranoside (OGP). A 200  $\mu$ g sample of DNA was added and incubated for 1 h at room temperature. The solution was transferred to a Slide-A-Lyzer dialysis cassette (MWCO 10 K, Pierce, Rockford, IL) and dialyzed for 2 days with three changes of 4 L TBS.

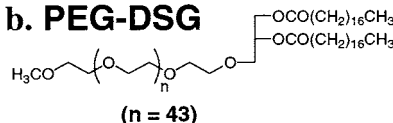
**DEAE-Sepharose CL-6B Column Chromatography.** Nonencapsulated DNA was removed by anion exchange chromatography on a DEAE-Sepharose CL-6B column (1  $\times$  4 cm, Sigma). The dialyzed SPLP solution (0.5–1.5 mL) was applied to the column and eluted using TBS. Free plasmid DNA bound to the column was eluted by application of 1 M NaCl. The UV absorbance of each fraction was measured at 260 nm.

**Sucrose Gradient Ultracentrifugation.** A stepwise sucrose gradient was formed in a tube (Beckman Ultra-

#### a. POD



#### b. PEG-DSG



**Figure 1.** Structure of PEG lipids used in this study ( $n = 43$ ). (a) POD and (b) PEG-DSG.

Clear tubes) using 3 mL of 1%/3 mL of 2.5%/3 mL of 10% sucrose in TBS (w/v). The sample was slowly loaded onto the top of the gradient and centrifuged using a swinging bucket rotor (SW-41Ti) in an ultracentrifuge (Beckman L2-65B). Ultracentrifugation was performed for 20 h at 36000 rpm (160 000g) at 4 °C. Aliquots (0.4 mL) were removed from top to bottom, and absorbance was measured at 260 nm. When the volume of the SPLP suspension was reduced, the suspension in a Slide-A-Lyzer was subject to incubation with Slide-A-Lyzer Concentrating Solution (Pierce, Rockford, IL) followed by dialysis overnight against TBS to adjust salt concentration to 150 mM.

**DNA Encapsulation Efficiency Assay.** After the separation of the nanoparticles from the DNA by the DEAE-Sepharose CL-6B column chromatography, DNA concentration was quantitated with the PicoGreen reagent (Molecular Probes, Inc., Junction City, OR). Encapsulation was calculated as  $I(\%) = (F^o - F)/F^o \times 100$ , where  $F^o$  and  $F$  is the respective fluorescence value in the presence or absence of 0.4% Triton X-100. DNA was considered to be encapsulated in the nanoparticle if it could not react with the PicoGreen dye in the absence of Triton X-100. The fractions containing SPLP were pooled together, and the total amount of DNA encapsulated in the particles was measured to compute the DNA encapsulation efficiency by comparing the recovered amount to the starting amount.

**Particle Size Measurements.** The diameter of the SPLP was measured using a Malvern Zeta 1000 Dynamic Light Scattering Instrument (Malvern Instruments Ltd., Worcestershire, U.K.) using the PCS 1.32a software. For pH-dependent collapse experiments, cuvettes containing POD SPLP or PEG-DSG SPLP (PEG lipid/DOTAP/DOPE = 20/ $x$ /80- $x$ , where  $x = 11, 12$ , and 13; total 10  $\mu$ mol of lipids with 200  $\mu$ g of pCMV-Gal DNA) were incubated at 37 °C at various pH conditions (pH 5.3, 6.3, 7.0, and 7.5 for POD SPLP; 5.2, 6.3, and 7.1 for PEG-DSG SPLP) for the indicated time and measured for the mean diameter. Photon correlation spectrometry of each sample was measured using the automatic algorithm mode in the Malvern software package for data analysis. To determine apparent pH shifts, nonlinear regression was performed by Microcal Origin version 6.0 (Northampton, MA).

**Zeta Potential.** To calibrate the correlation between positive charge on the SPLP surface and the electrophoretic mobility, two standard liposomes were prepared, one with 0% charge (PEG-DSG/DOPE = 20/80) and the other with 12% charge (DOTAP/PEG-DSG/DOPE = 12/20/68). Lipids were dissolved in chloroform, dried on glass under a stream of argon, and then hydrated in TBS. Liposomes were then extruded 21 times through a 50 nm polycarbonate membrane. The resulting liposomes were



**Table 1. Effect of Lipid Composition on DNA Encapsulation Efficiency and Mean Diameter of SPLP**

PEG-DSG <sup>a</sup>	POD <sup>b</sup>	DOTAP	DOPE	DNA protection (%) <sup>c</sup>	DNA encapsulation efficiency (%) <sup>d</sup>	diameter (nm) <sup>e</sup>
20	—	8	72	ND	0.25	ND <sup>f</sup>
20	—	10	70	99.1	32.4	52.8 ± 0.8
20	—	11	69	98.7	42.3	56.5 ± 1.2
20	—	12	68	98.8	36.1	56.2 ± 1.7
20	—	13	67	98.2	35.4	54.6 ± 0.7
20	—	14	66	98.1	21.6	53.9 ± 1.0
20	—	15	65	97.6	10.3	54.3 ± 2.1
—	20	8	72	ND	0.51	ND
—	20	10	70	99.1	44.2	52.8 ± 1.0
—	20	11	69	99.0	46.4	55.0 ± 1.0
—	20	12	68	98.7	41.6	54.4 ± 0.8
—	20	13	67	98.8	38.0	55.6 ± 0.7
—	20	14	66	97.8	25.4	60.3 ± 2.2
—	20	15	65	97.0	16.9	55.3 ± 0.8

<sup>a</sup> pH-insensitive PEG-lipid. <sup>b</sup> pH-sensitive PEG-lipid. <sup>c</sup> Protected DNA was determined by  $I$  (%) =  $(F^o - F)/F^o \times 100$  (see Materials and Methods). <sup>d</sup> DNA encapsulation efficiency was calculated by comparing the input DNA to the amount recovered in the SPLP. <sup>e</sup> Mean diameter ± standard deviation ( $n = 3$ ) was measured after DEAE-Sepharose CL-6B column chromatography. <sup>f</sup> ND, not determined.

between 50 and 60 nm in diameter by dynamic light scattering and had comparable diameters to the SPLP (Table 1).

The electrophoretic mobility was measured on a Zeta-sizer 3000 (Malvern Instruments; Worcestershire, U.K.) at various ionic strengths. Since the positive charge was located at the bilayer surface and buried under a coating of PEG, it was necessary to use very low concentrations of salt to detect electrophoretic mobility. Measurements were carried out by diluting the liposomes into a pH 7.5 HEPES buffered salt solution. The neutral and positive standards were measured at final salt concentrations of 1, 3.75, and 20 mM NaCl with final HEPES concentrations of 1, 1, and 10 mM, respectively. To achieve 1 mM NaCl, the liposomes were buffer exchanged on Micro Bio-spin 6 Chromatography Columns (Bio-Rad laboratories, Hercules CA) equilibrated with the 1 mM NaCl, 1 mM HEPES, pH 7.5. The electrophoretic mobility was converted into a  $\zeta$  potential using the modified Booth equations as described by Deshiikan and Papadopoulos (1998). This adjustment was needed because neither the Helmholtz–Smoluchowski, Hückel, nor Henry approximations are appropriate for 60 nm particles under low salt with high surface potentials.

$\zeta$  potential was tested for two SPLP preparations, PEG–DSG SPLP (DOTAP/PEG–DSG/DOPE = 12/20/68) and POD SPLP (DOTAP/POD/DOPE = 12/20/68). The SPLPs were measured using identical lipid composition, particle size, particle concentration, and buffer concentrations as the empty liposome standards. Using the  $\zeta$  potentials from the standards, a calibration curve was obtained by linear regression. The SPLP  $\zeta$  potential was then used to predict the external percentage of DOTAP on SPLP.

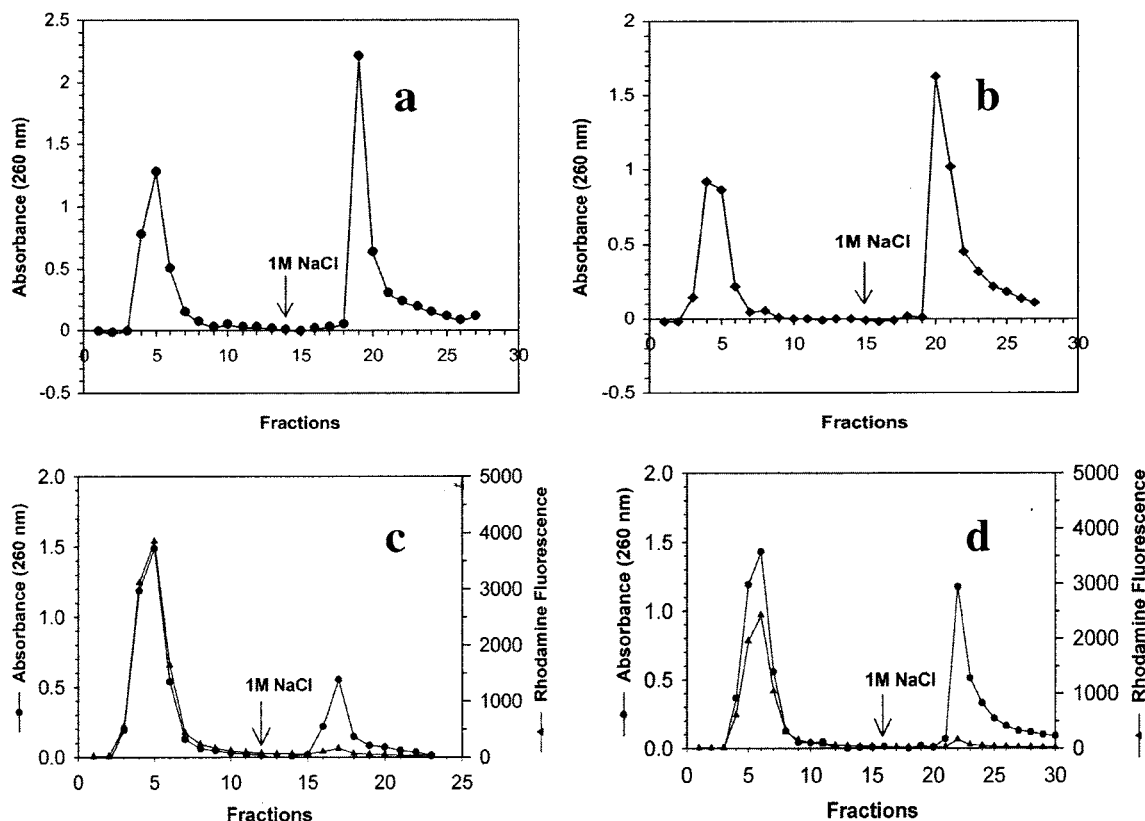
**Cell Culture and Transfection Experiments.** CV-1 cells (monkey fibroblasts) were provided by the UCSF Cell Culture Facility. Cells were grown in DME H-21 medium containing 10% fetal bovine serum and antibiotics (100 units/mL penicillin and 0.1 mg/mL streptomycin). Cells were maintained on plastic tissue culture dishes (Falcon) at 37 °C in an incubator (5% CO<sub>2</sub>/95% air). For transfection,  $1 \times 10^5$  cells/well were seeded in 24 well plates and incubated 1 day prior to transfection. Polyethylenimine (PEI) or DOTAP/DOPE liposome were mixed with plasmid DNA at charge ratio ( $\pm$ ) of 7:1 in FBS-free medium and incubated for 30–60 min at room temperature. If not stated otherwise, POD SPLP and PEG–DSG SPLPs were purified by anion exchange

chromatography, and the encapsulated DNA was assayed using PicoGreen reagent in the presence of 0.4% Triton X-100. When stated, both SPLPs were further purified by sucrose gradient ultracentrifugation after anion exchange chromatography. Appropriate amounts of PEI polyplex (Remy et al., 1998), DOTAP/DOPE lipoplex (Felgner et al., 1994), POD SPLP, or PEG–DSG SPLP were introduced to cells at time zero and incubated in media with 10% FBS.

**Expression Assays.** The expressed  $\beta$ -galactosidase activity was measured by a standard method as recommended by the manufacturer (Promega, Madison, WI, Technical Bulletin 097). In short, cells in 24 well plates were washed with PBS, lysed with Reporter Lysis Buffer (Promega), and centrifuged at 10 000 rpm for 5 min. The supernatant of the cell lysates were taken and analyzed for  $\beta$ -galactosidase activity using the colorimetric *o*-nitrophenyl- $\beta$ -D-galactopyranoside (ONPG) assay. Protein concentration was measured using the Pierce Micro BCA Protein Assay Reagent Kit.  $\beta$ -Galactosidase activity is expressed in total milliunits per milligram of protein. The standard curve was prepared using  $\beta$ -galactosidase (Grade X from *E. coli*, Sigma, St. Louis, MO), and 1 mu was defined as the amount of  $\beta$ -galactosidase that hydrolyzes 1 nmol of ONPG/min at pH 7.3 at 37 °C. To measure luciferase activity, cells were lysed and centrifuged as described above, and then 10  $\mu$ L of the lysate was used to measure the luciferase activity according to the recommendations of the manufacturer (Promega, Luciferase Assay System, E1501) using an Optocomp I Luminometer (MGM Inc., Hamden, CT). Protein concentration was measured as described above.

**Confocal Microscopy.** Confocal images were obtained using LaserSharp software installed on a BioRad (Hercules, CA) krypton–argon laser scanning confocal microscope (MRC-1024) outfitted with a Nikon Diaphot 200 microscope using a 60  $\times$  objective lens. Sections of 1024  $\times$  1024 pixels were taken every 2  $\mu$ m using all laser lines, 10% laser power, slow scan, and Kalman averaging of three scans. One pixel had the dimensions of 0.167  $\mu$ m  $\times$  0.167  $\mu$ m.

Cells ( $3.1 \times 10^4$ /2 mL medium) were seeded on WillCo dishes (World Precision Instrument, Sarasota, FL) and incubated overnight. After incubation, Rhodamine-labeled SPLPs containing 10  $\mu$ g of pCMV-GFP plasmid were added to the medium, and images were monitored as a time function. Images were analyzed using Confocal Assistant 4.02 software.



**Figure 2.** Separation of SPLP from non-entrapped DNA by DEAE-Sepharose CL-6B column chromatography. POD SPLP (a), PEG-DSG SPLP (b), rhodamine (Rh)-labeled POD SPLP (c), and Rh PEG-DSG SPLP (d). The SPLP (POD or PEG-DSG/DOTAP/DOPE = 20/12/68, total 10  $\mu$ mol of lipids with 200  $\mu$ g of pCMV-Gal) was prepared by the detergent dialysis method. The UV absorbance at 260 nm was measured for each fraction. To make fluorescent SPLP, 0.1 mol % of Rh-PE was added to total 10  $\mu$ mol of lipids (POD or PEG-DSG/DOTAP/DOPE/Rh-PE = 20/11/69/0.1), and 200  $\mu$ g pCMV-GFP plasmid per mL was used. The UV absorbance at 260 nm (●) and rhodamine fluorescence (▲) were measured for the fractions.

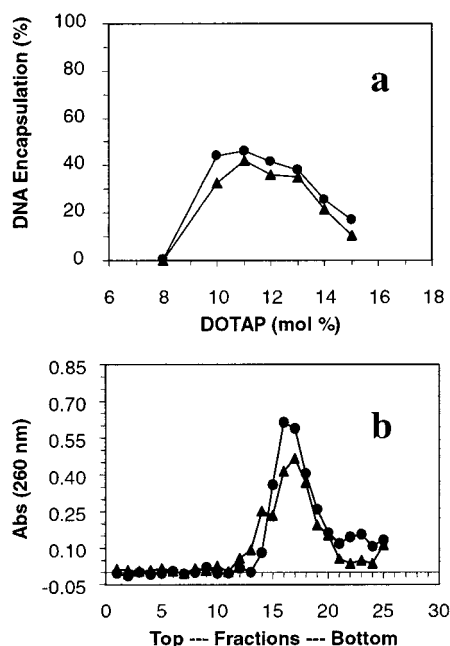
## RESULTS

**Preparation of Stabilized Plasmid-Lipid Particles (SPLPs) at Basic Condition.** Recently, it was reported that plasmid DNA can be encapsulated in SPLPs by a detergent dialysis procedure using octylglucoside (OGP) at pH 7.4 (Mok et al., 1999; Wheeler et al., 1999). We adopted this method to prepare pH-sensitive SPLPs employing POD, DOTAP, and DOPE. A control nanoparticle was prepared using a pH-insensitive PEG-lipid, PEG-distearoylglycerol (PEG-DSG). The structures of the PEG-lipids used in this study are shown in Figure 1. The two PEG lipids have a similar molecular weight PEG and acyl chain components. They differ only in the linker between the PEG and the distearoylglycerol.

It was of interest to determine whether SPLPs can be formed using basic solutions because an alkaline environment is required to minimize the degradation of POD. We based our initial conditions on the extensive prior work on detergent dialysis for DNA encapsulation (Hofland et al., 1996; Mok et al., 1999; Wheeler et al., 1999). SPLPs were prepared using mPEG-Ceramide C16 at pH 7.4 and 8.5. As reported by Mok et al. (1999), DNA encapsulation was optimal at a DOTAP mol % of between 7 and 8 at pH 7.4, whereas optimal DNA encapsulation at pH 8.5 required a DOTAP mol % of between 11 and 13 mol % (data not shown). To determine the compositions required for optimal DNA encapsulation by SPLPs prepared from POD or PEG-DSG, the DOTAP content was varied between 8 and 15 mol % range, and the PEG lipid content was maintained at 20 mol % (Table 1). At pH 8.5 nanoparticles were formed with diameters ranging between 53 and 60 nm (Table 1) regardless of the PEG derivatives employed.

Nanoparticles prepared from POD (Figure 2a,c) and from PEG-DSG (Figure 2b,d) behaved in a similar manner when separated from nonencapsulated DNA on anion exchange chromatography. Nanoparticles incorporating a fluorescent lipid analogue, rhodamine-phosphatidylethanolamine (Rh-PE), were not retained on the column (Figure 2c,d). Nonentrapped DNA was eluted from the column using a 1 M NaCl solution. Encapsulation efficiencies were optimal (approximately 40% of initial DNA) at a cationic lipid mole % between 10 and 13 mol % (Table 1, Figure 3a). The nanoparticles prepared with the pH-sensitive and pH-insensitive PEG lipid had similar DNA encapsulation properties and diameters (Table 1). Moreover, DNA in the separated SPLP was not accessible to the DNA stain Picogreen unless Triton X-100 was added to disrupt the bilayer, indicating that the DNA was encapsulated (Table 1). The PEG-stabilized nanoparticles were not retained when chromatographed on a cationic exchange resin using a pH 7.0 elution buffer containing 150 mM NaCl (data not shown). This indicates the PEG coat effectively masks any cationic charge that remained on the surface of the SPLP.

**Sucrose Gradient Ultracentrifugation of the SPLP Nanoparticles.** To separate the SPLP particles containing DNA from empty liposomes, the SPLPs were further purified using ultracentrifugation on a discontinuous sucrose gradient. After centrifugation at 160 000g for 20 h, both the POD SPLP and the PEG-DSG SPLPs were observed as a major band between fractions 14 and 20. This corresponds to the interface between 2.5% and 10% sucrose gradient (Figure 3b). In addition, the POD SPLPs showed one minor band between fractions 22 and 24,



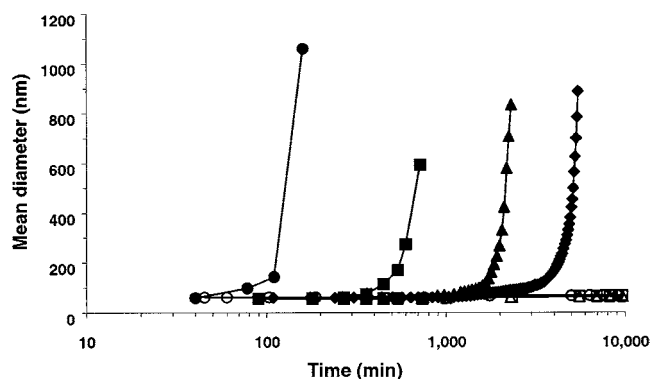
**Figure 3.** (a) Plasmid DNA encapsulation efficiency as a function of DOTAP amount. SPLP were prepared using 25  $\mu$ g pCMV-Gal plasmid with 5  $\mu$ mol total of lipid consisting of 20 mol % PEG-DSG or POD/ $x$  mol % DOTAP/ $80-x$  mol % DOPE. Encapsulation efficiency was measured by measuring DNA recovery in SPLP after eluting the dialysate through a DEAE Sepharose CL-6B column. (b) Fractionation of SPLP on sucrose density gradient ultracentrifugation. The UV absorbance of individual fractions was measured at 260 nm for SPLP (●) and PEG-DSG SPLP (▲). The profile was obtained by removing 0.4 mL fractions from top to bottom.

below the major SPLP band which was not further investigated.

**pH- and Time-Dependent Collapse of SPLP.** To determine whether the SPLPs prepared from the various compositions collapsed in response to a decrease in pH, we measured the mean diameter of the particles by dynamic light scattering as a function of time in various pH buffers. POD SPLP collapse was pH-dependent (Figure 4). The collapse exhibited a lag phase followed by a burst phase. There was a modest increase in particle diameter at a period slightly prior to collapse. Collapse was defined as the last time point before the  $\zeta$  size exceeded 150 nm. POD SPLPs at 37 °C and pH 5.3, 6.3, 7.0, and 7.5 collapse at 110, 450, 1720, and 3852 min respectively (Figure 4). POD SPLPs stored at 4 °C and pH 8.5 showed no change in nanoparticle diameter for 2 months but precipitated by the end of four months.

When the analogous pH-insensitive PEG-DSG SPLPs were prepared and subjected to identical acid conditions, nanoparticle growth and collapse was not observed at any pH tested. In fact, PEG-DSG SPLPs showed no change in diameter at 37 °C for more than 3 months (data not shown). One interesting aspect of the POD SPLP is that the low pH sensitivity was slower than observed in POD stabilized DOPE liposomes (Guo and Szoka, 2001). In fact, SPLP collapse time was increased by almost 1 order of magnitude compared with POD liposomes.

**Determination of External Surface Charge.** Two possible factors could account for the altered pH sensitivity of the POD SPLPs compared to POD/DOPE liposomes (Guo and Szoka, 2001). First, if the entire POD in the lipid mixture became situated on the outer membrane during SPLP formation, then the collapse time would increase modestly. Second, if some cationic lipid remained



**Figure 4.** pH- and time-dependent collapse profile of SPLP. The mean diameter of POD SPLP and PEG-DSG SPLP incubated at different pH conditions at 37 °C was measured as a function of time. The lipid composition for POD SPLP was POD/DOTAP/DOPE = 20/ $x$ /80- $x$  where  $x$  = 11 (pH 7.5), 12 (7.0, 6.3), 13 (5.3). For PEG-DSG SPLP, PEG-DSG/DOTAP/DOPE = 20/ $y$ /80- $y$  where  $y$  = 12 (pH 7.1, 6.3), 13 (5.2). 50 mM HEPES buffer pH 7.4 and 100 mM MES buffer, pH 4.9, were used to adjust the pH. The POD SPLP are filled symbols and the PEG-DSG SPLP are the open symbols. pH 5.3 (●), 5.2 (○); pH 6.3 (■), pH 7.0 (▲), 7.1 (△); pH 7.5 (◆).

on the outer membrane, then the interfacial pH would be increased. This would decrease the hydrolysis rate of POD by raising the interfacial pH above the bulk pH.

To determine the external charge on the SPLP, we measured the electrophoretic mobility at low ionic strength. At 20 mM NaCl and higher salt concentrations, the Debye length is reduced, and PEG effectively shields the surface charge; thus, electrophoretic mobility was barely detectable (Table 2). At lower ionic strengths (1 mM and 3.75 mM), the 0% and 12% DOTAP standards were easily differentiated ( $P < 0.05$ ) by  $\zeta$  potential measurements. At 1 mM NaCl, the percentage of DOTAP was a significant predictor of  $\zeta$  potential explaining 99.8% of the variance in  $\zeta$  potential ( $r^2 = 0.998$ ,  $P < 0.0001$ ). A best-fit line was determined through 0% DOTAP ( $n = 18$ ) and 12% DOTAP ( $n = 20$ ) with a slope of 5.805 mV/% DOTAP and an intercept of -25.95 mV. The lower and upper 95% confidence intervals for the SPLP  $\zeta$  potentials were used to obtain an upper and lower bound for the surface density of positive charge. The lowest salt concentration gave the highest resolution. At 1 mM NaCl the predicted external percentage of DOTAP was 5.5–5.6% for the PEG-DSG SPLP and 6.2–6.4% DOTAP for the POD SPLP.

**Transfection Mediated by the SPLP.** The transfection efficiencies in the presence of serum for the SPLP prepared by chromatography or ultracentrifugation are shown in Figure 5a. The POD SPLP mediated significant levels of gene transfer regardless of the method used to purify the nanoparticles. Transfection activity of the POD SPLP was compared to two standard transfection reagents, PEI polyplexes or DOTAP/DOPE lipoplexes. The transfection activity of the POD nanoparticle was about 20% of that achieved by these widely used procedures. However, the activity of  $\beta$ -galactosidase of cells transfected with the pH-insensitive SPLP was hardly detectable (Figure 5a).

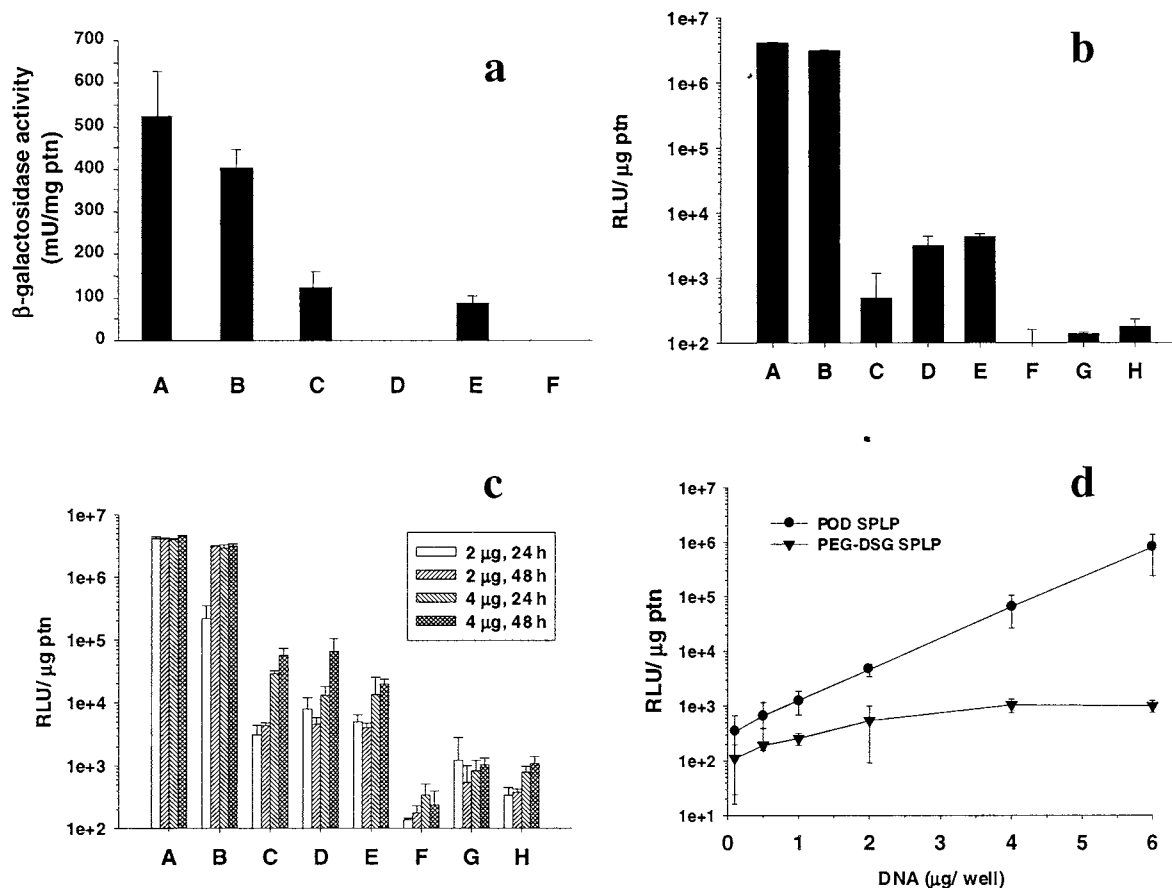
To better compare the relative gene transfer activity of the two SPLP, pCMV-Luc plasmid DNA was used to increase the assay sensitivity. For the POD SPLP, the efficiency was improved if the cells were exposed to the nanoparticles for 24 and 48 h rather than for 6 h. The PEG-DSG SPLP mediated a very low level of expression (Figure 5b). The relative transfection efficiencies of POD



**Table 2. Determination of Surface Charge by Electrophoretic Mobility at Low Ionic Strength**

		salt concentration		
		1 mM NaCl	3.75 mM NaCl	20 mM NaCl
measured $\zeta$	0% DOTAP (mV) <sup>a</sup>	-26.3 to -25.6	-10.4 to -9.4	-1.8 to -0.8
	12% DOTAP (mV) <sup>a</sup>	43.0-44.4	10.1-10.9	-0.8 to -0.2
	PEG-DSG SPLP (mV) <sup>a</sup>	6.1-6.6	-2.2 to -0.2	ND
	POD SPLP (mV) <sup>a</sup>	10.0-11.1	1.6-3.2	ND
linear regression parameters between 0% and 12% surface DOTAP	$r^2$	0.998	0.980	0.216
	$P$	<0.0001	<0.0001	0.181
	slope (mV/%) <sup>a</sup>	5.7-5.9	1.6-1.8	-0.03 to 0.16
predicted external percentage DOTAP	intercept (V) <sup>a</sup>	-27.0 to -24.9	-10.9 to -8.9	-2.13 to -0.49
	PEG-DSG SPLP (%) <sup>a</sup>	5.5-5.6	4.5-5.9	ND
	POD SPLP (%) <sup>a</sup>	6.2-6.4	6.8-7.7	ND

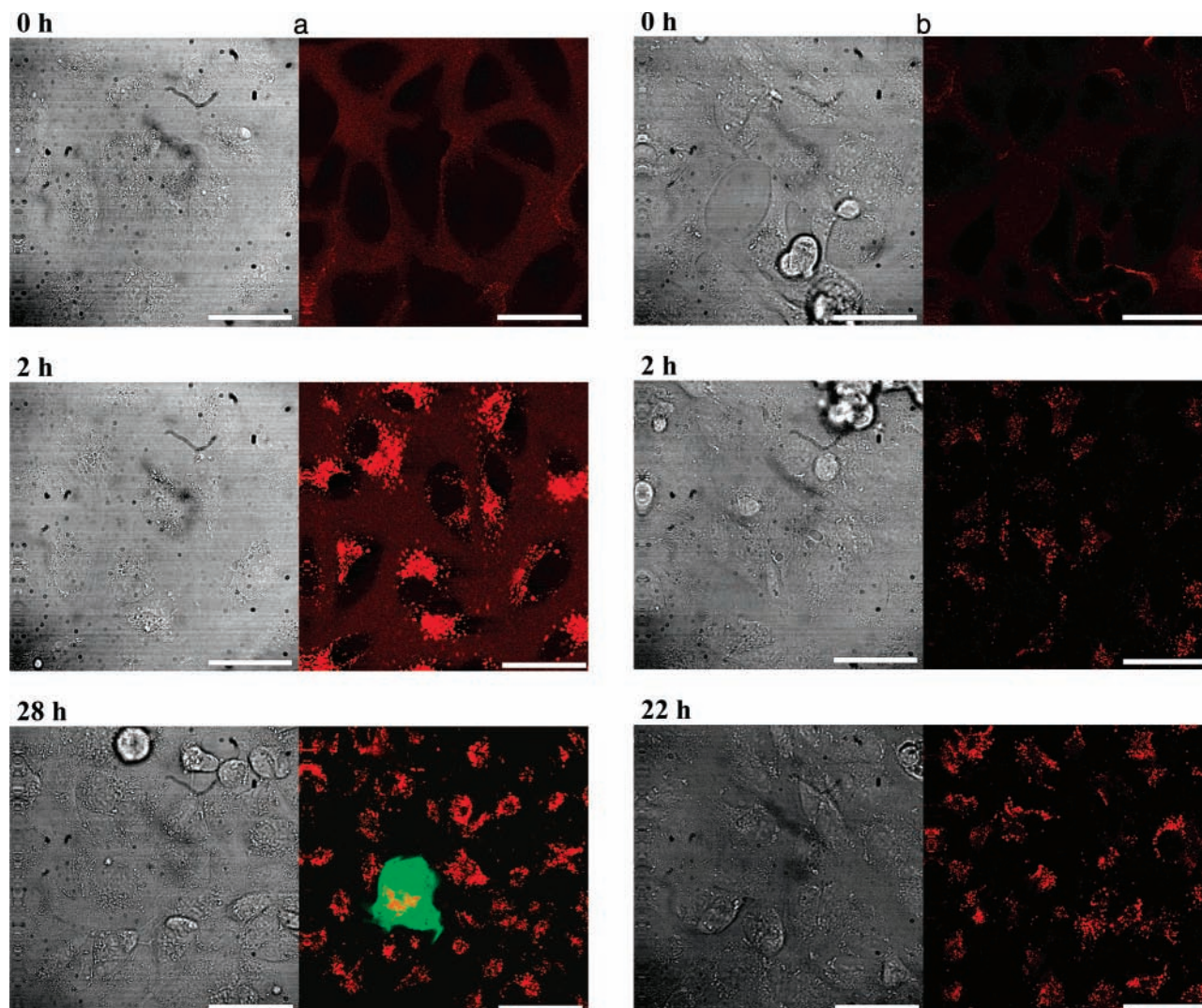
<sup>a</sup> values indicated in 95% confidence range ( $n = 18-20$  for measurements,  $n = 38-40$  for regressions).



**Figure 5.** Transfection efficiencies of SPLP on CV-1 cells. (a)  $\beta$ -Gal expression was assayed following incubation with PEI, DOTAP/DOPE, POD SPLP, PEG-DSG SPLP containing 2.0  $\mu$ g pCMV-Gal for 48 h in the presence of 10% FBS. PEI (A); DOTAP/DOPE (B); SPLP purified by anion exchange chromatography, POD (C) and PEG-DSG (D); SPLP purified further by sucrose gradient ultracentrifugation, POD (E) and PEG-DSG (F). (b) Transfection efficiencies as a function of transfection time. Luciferase expression was measured using 2.0  $\mu$ g pCMV-Luc plasmid per well. Transfection experiments were performed in the presence of serum for the indicated time. PEI 48 h (A); DOTAP/DOPE 48 h (B); POD SPLP for 6h (C), 24h (D), 48h (E); PEG-DSG SPLP for 6h (F), 24h (G), 48h (H). (c) Effect of DOTAP mole percent, time, and amount of DNA in luciferase expression. The amount of pCMV-Luc plasmid DNA was 2 or 4  $\mu$ g per well, and transfection was performed for 24 or 48 h in the presence of 10% serum. PEI (A); DOTAP/DOPE (B); POD SPLP (POD/DOTAP/DOPE = 20/ $x$ /80- $x$ ),  $x = 11$  (C), 12 (D), 13 (E); PEG-DSG SPLP (PEG-DSG/DOTAP/DOPE = 20/ $y$ /80- $y$ ),  $y = 11$  (F), 12 (G), 13 (H). (d) DNA dose dependence of luciferase expression by POD SPLP and PEG-DSG SPLP. The expressed luciferase activity was measured after the incubation of POD SPLP or PEG-DSG SPLP with CV-1 cells for 48 h in the presence of serum. Each point indicates the average and standard deviation from triplicates.

SPLP and PEG-DSG SPLP prepared with different amounts of DOTAP were compared as a function of incubation time at two different DNA levels. Transfection activity for the POD or PEG-DSG SPLP showed little dependency on the amount of cationic lipid used to form the particles (Figure 5c). The level of expression of POD SPLP was much higher than that of PEG-DSG SPLP (Figure 5c). Expression of luciferase delivered by POD SPLP increased in a large-linear fashion up the highest

DNA amount applied (Figure 5d), whereas expression reached a plateau at a very lower level when the plasmid was delivered in the PEG-DSG SPLP (Figure 5d). At the highest amount of DNA added, the POD SPLP mediated almost 3 orders of magnitude more activity than did the PEG-DSG SPLP. Compared to the PEI polyplex or the DOTAP/DOPE lipoplex, both SPLP nanoparticles were considerably better tolerated on the cultured cells.



**Figure 6.** Confocal microscopy images of CV-1 cells incubated with rhodamine-labeled POD SPLP (a) or PEG-DSG SPLP (b) for the indicated time. The images shown in the left panel are the respective transmitted light images of the same field.

**Confocal Microscopy Studies.** SPLP were prepared with a fluorescent lipid (Figure 2c,d) to enable the detection of the nanoparticles in cultured cells. The intracellular localization of Rh SPLP as a function of time is shown in Figure 6a,b. Both POD and PEG-DSG SPLPs were internalized by cells. There appeared little difference in either the extent of uptake or the intracellular location of either POD or PEG-DSG SPLP. The uptake occurred within 2 h and the SPLP particles were located in the cytoplasm in a punctate pattern (Figure 6). This cytoplasmic punctate pattern persisted in cells at later times (Figure 6). When the SPLPs were formed using a plasmid containing the gene for the green fluorescent protein (GFP), GFP expression was observed in about 1–3% of the cells treated with the POD SPLP (Figure 6f) but in only a few cells treated with the PEG-DSG SPLP. When all of the gene expression data ( $\beta$ -galactosidase, luciferase and GFP) are taken into account, the POD SPLPs were substantially more efficient at gene transfer than were the PEG-DSG SPLPs even though they had similar diameters, surface charge, and cell-association characteristics.

#### DISCUSSION

The quest for a suitable nonviral vector for systemic gene therapy has not yet achieved the goal of a system with a prolonged circulation time in blood that can

mediate high gene expression at the target. To improve circulation time, a number of groups have devised nano-systems that are coated with PEG (Kabanov et al., 1995; Kai et al., 1999; Choi et al., 1999, 2000; Collard et al., 2000; Lee et al., 2001; Kakizawa and Kataoka, 2002; Ogris and Wagner, 2002). While this tactic can enable DNA encapsulation in nanoparticles and enhance the circulation time, it significantly decreases gene transfer.

The SPLP system is a good example of the benefits and disadvantages of a PEG coat (Mok et al., 1999; Wheeler et al., 1999; Tam et al., 2000; Fenske et al., 2001). Nanoparticles can be formed with ceramides of various acyl chain lengths but SPLP formed only from the C8 chain ceramide mediate significant transfection in culture (Mok et al., 1999; Zhang et al., 1999), whereas SPLPs formed only from the C20 chain ceramide provide detectable transfection in animals (Tam et al., 2000). It has been speculated that the PEG reduces cellular uptake of the particles and interferes with membrane destabilization; PEG must be removed to enable transfection, but if removed too quickly, the system is then eliminated from circulation (Tam et al., 2000). One solution to this conundrum is to increase the uptake of a PEG-coated system by the incorporation of a ligand, beyond the PEG layer, that interacts with a cell surface receptor (Fenske et al., 2001). An alternative approach is to synthesize



intelligent materials that can undergo a transition and release the PEG from the surface when the nanoparticle is on, or in, the target cell. In this report we have taken the latter tack and incorporated a low pH-sensitive PEG lipid (Guo and Szoka, 2001) into the SPLP that leads to release of the PEG from the particle after the particle was placed in an acidic environment.

Such pH-sensitive triggers have been used extensively in drug and gene delivery with liposomes, polymers, and antibodies (Dillman et al., 1988; Legendre and Szoka, 1992; Heller, 1993; Boomer and Thompson, 1999; Drummond et al., 2000; Zhu et al., 2000; Asokan and Cho, 2002). There are a number of low pH-sensitive PEG-detergents or PEG-lipids (Yue et al., 1996; Budker et al., 1996; Hellberg et al., 2000; Guo and Szoka, 2001) that might be suitable for this purpose. The one introduced by our group is an acid-sensitive PEG orthoester diacyl chain lipid (POD) which confers a low pH-mediated collapse on PEG stabilized DOPE liposome (Guo and Szoka, 2001). The match between the pH collapse profile of the POD and the pH of the endosome trafficking pathway was quite good, in that collapse of a liposome containing 10% POD occurred within 10 min of lowering the pH to 5.5. Such a pH collapse profile in a gene transfer system could result in DNA delivery from the early endosome into the cytoplasm, perhaps minimizing delivery of the DNA to the lysosome.

Encapsulation of plasmid DNA into acid-sensitive SPLP using POD, DOTAP, DOPE, and plasmid DNA by the detergent dialysis method resulted in the formation of 60 nm SPLP with 40–45% DNA entrapping efficiency. To increase the stability of the POD SPLP, the detergent was removed by dialyzing against a pH 8.5 buffer. Using the pH 8.5 buffer, the optimum DOTAP percentage in the lipid mixture was about 10–13 mol % (Table 1). This is a higher cationic lipid content than that reported in the original publication (7 mol % of cationic lipid) (Mok et al., 1999). The requirement for an increased mole percent of the cationic lipid for optimal DNA entrapment could be due to an interaction between the quaternary amine of DOTAP with the phosphate anion of DOPE at pH 8.5. The basic condition used for the preparation of the POD SPLP leads to an increased negative charge on the DOPE. Hence, more DOTAP needs to be incorporated in the initial mixture to effectively complex DNA. The explanation for the decline in DNA encapsulation below 10 mol % DOTAP is that there is insufficient positive charge in the system to compact the plasmid.

The resulting low pH-sensitive POD SPLP collapse at pH 5.3, whereas the pH-insensitive PEG-DSG SPLP do not collapse at any observed pH (Figure 4). The time to collapse, at any pH, for the POD SPLP is longer than the time to collapse observed in the POD DOPE liposomes (Guo and Szoka, 2001; Guo et al., 2003). Part of the increased time to collapse can be accounted for by the fact that there is twice the amount of POD in the SPLP compared to the POD DOPE liposomes. However, this difference in starting composition would account for at most a 2-fold increase (even if all POD is situated on the external surface of the SPLP) in the collapse time of the POD SPLP not the 10 fold difference. Later in the discussion, we propose an explanation for the difference in the collapse time between the POD SPLP and the POD DOPE.

Most significantly the POD SPLPs mediate high levels of gene expression, but the PEG-DSG SPLPs do not (Figure 5). The levels of expression obtained with the POD SPLP are as good as observed with the C8 ceramide SPLP (Mok et al., 1999). POD SPLPs are less effective

at gene transfer compared to previously described PEI polyplexes (Remy et al., 1998) and optimized cationic lipoplexes (Felgner et al., 1994), but like the pH-insensitive SPLP (Tam et al., 2000), they are also less cytotoxic. Moreover, both the POD SPLP and PEG-DSG SPLP containing fluorescent phospholipids interact with cells in culture to a similar extent and are internalized into the cytoplasm (Figure 6). Cells exposed to the fluorescent SPLP exhibited a punctate fluorescent pattern that suggested a vesicular location for the internalized particles.

We were interested in better defining the surface characteristics of the particles to understand their structure, cell-association characteristics, and pH collapse properties.  $\zeta$  potential is a measure of the potential at the shear plane and can be used to determine the amount of charge on the "surface" of a particle as well as how steric stabilizing molecules, such as PEG-diaclylglycerols, can alter the observed  $\zeta$  potential (Shimada et al., 1995). The SPLPs have been formulated with 12% DOTAP to promote the encapsulation of negatively charged DNA. For extruded liposomes, such a lipid mixture would essentially distribute so that both monolayers have a similar composition. However, in the case of the SPLP, the DOTAP is probably not equally distributed on both monolayers; rather, the DOTAP will bind to the DNA and thus could be preferentially sequestered on the inside of the particle. In the extreme case, all of the DOTAP in the particle could be the inner face of the bilayer, in contact with DNA and the POD SPLP would have a  $\zeta$  potential similar to the neutral liposome standard.

Locating the DOTAP in the SPLP is made difficult because any positive charge is buried beneath a several nanometer thick layer of PEG (2000 MW) (Shimada et al., 1995). This means that the shear plane is appreciably beyond the location of the DOTAP, which is near the bilayer-aqueous interface. To detect the buried positive charge using  $\zeta$  potential, it is necessary to extend the electrostatic potential beyond the PEG layer. One method for increasing the potential is to lower the ionic strength of the solution, which effectively increases the Debye length (McLaughlin, 1989). This effect is readily observed in measurements of the  $\zeta$  potential of extruded liposomes with known surface percentages of DOTAP at low ionic strength. At 1 mM NaCl we obtained excellent resolution (70 mV difference) (Table 2) between liposomes compositions containing no DOTAP and those containing with 12% DOTAP. Upon measuring the  $\zeta$  potential of the PEG-DSG and POD SPLP at the same ionic strength, the electrophoretic mobility was clearly midway between the two reference liposome containing either 0% or 12% DOTAP (Table 2). To estimate the external DOTAP percentage on the SPLP surface, we used a linear interpolation between the standards. Both SPLP preparations have about 6% positive charge on their surface. Thus, there is a substantial amount of DOTAP on the external surface of both the POD SPLP and PEG-DSG SPLP.

The DOTAP on the exterior surface of the SPLP can account for the observed cell association of the nanoparticles (Figure 6). Even though the PEG shields the positively charged surface at physiological levels of salt, the flexibility of the PEG and fluidity of the bilayer can allow SPLP binding to the cell surface (Miller et al., 1998).

A second implication of the presence of DOTAP on the liposome surface is an increase in the interfacial pH (Kraayenhoff et al., 1993; Zuidam, and Barenholz, 1997; Banerjee et al., 1998). The presence of a high positive



surface charge density reduces hydronium ion concentration at the surface; thus, the interfacial pH becomes more basic than the bulk pH. In low ionic strength media (10 to 20 mM), a surface density of 50% DOTAP increases the interfacial pH by as much as 3 pH units measured either using a fluorescent probe (Fernandez and Fromherz, 1977; Krayenhoff et al., 1993; Zuidam and Barenholz, 1997) or a pH-sensitive reaction (Banerjee et al., 1998). The increased interfacial pH could be a major factor resulting in the increased time for the SPLP to collapse at low pH compared to the POD DOPE liposomes (Guo and Szoka, 2001; Guo et al., 2003).

The Gouy Chapman equation can predict the surface potential,  $\psi_0$ , as a function of the charge density of the DOTAP on the surface using the following equation (Tocanne and Tessie, 1990):

$$\psi_0 = \left( \frac{2kT}{ze} \right) \sinh^{-1} \left( \frac{ze\sigma\kappa^{-1}}{2\epsilon_0\epsilon_r kT} \right)$$

where  $k$  is the Boltzman constant,  $1.38 \times 10^{23}$  (J K<sup>-1</sup>),  $T$  is the absolute temperature (K),  $z$  is the ion valence,  $e$  is the charge of one electron,  $1.6 \times 10^{-19}$  (C),  $\sigma$  is the surface charge density (C m<sup>-2</sup>),  $\kappa^{-1}$  (m) is the Debye length computed as given below (McLaughlin, 1989),  $\epsilon_0$  is the relative permittivity of free space,  $8.85 \times 10^{-12}$  (C<sup>2</sup>J<sup>-1</sup>m<sup>-1</sup>),  $\epsilon_0$  is the dielectric constant in solution, and  $\epsilon_r$  is the dielectric constant at the membrane surface, here assumed to be about 8. In calculating the surface charge density, DOTAP, DOPE, PEG-DSG, and POD are assumed to have an area of 0.65 nm<sup>2</sup> per molecule (Zuidam and Barenholz, 1997).

The Debye length,  $\kappa^{-1}$ , is given by the following equation (Tocanne and Tessie, 1990):

$$\kappa^{-1} = \sqrt{\frac{\epsilon_0\epsilon_r kT}{N_A e^2 \sum c_i z_i^2}}$$

Where  $N_A$  is Avogadro's number,  $6.023 \times 10^{23}$  (molecules mol<sup>-1</sup>) and  $\sum c_i z_i^2$  is the total ion concentration (mol m<sup>-3</sup>).

The interfacial or surface pH is then a function of the bulk pH plus a pH shift (Tocanne and Tessie, 1990):

$$\text{pH}_{\text{surface}} = \text{pH}_{\text{bulk}} + \frac{\psi_0 e}{kT \ln(10)}$$

To calculate the surface pH under the physiological-like conditions used to measure the pH collapse (Figure 4), several assumptions are required: first that at 310 °K and 150 mM NaCl, the interfacial dielectric constant at the pH sensitive orthoester linker is significantly less than that in water (Fernandez and Fromherz, 1977; Zuidam and Barenholz, 1997). The dielectric constant rises rapidly within several nanometers of distance from the bilayer core (~3) to free water (~80). The pH-sensitive orthoester is most likely situated in the ester region of the bilayer rather than in the hydrocarbon region or outside the aqueous shell, so as elsewhere a dielectric of 8 is assumed (Zuidam and Barenholz, 1997). Using these assumptions we compute a pH shift of 0.8 units between the bulk pH and the interfacial pH for a 6 mol % DOTAP surface.

Guo and Szoka (2001) suggested that the log of the lag time to POD vesicle collapse is directly proportional to the pH, so an increase of pH by 0.8 units from a bulk pH would result in an 6.3-fold increase ( $10^{0.8} = 6.3$ ) in the lag time for collapse of a POD SPLP with 6 mol % DOTAP on its surface compared to one with no DOTAP on its

surface. Thus a neutral POD stabilized liposome might collapse in 5 min, but the presence of only 6% positive charge near the pH sensitive linker would increase the lag time to over 30 min.

The kinetic parameters implied by the "minimum shielding model" of Guo and Szoka (2001) were recently determined quantitatively (Guo et al., 2003). In this model the time to SPLP collapse can be predicted by the following equation:

$$t_{\text{collapse}} = \frac{\ln(A_{\text{initial}}/A_{\text{critical}})10^{\text{pH}}}{k}$$

Where  $A_{\text{initial}}$  is the starting surface percentage of POD,  $A_{\text{critical}} = 2.3\%$  is the minimum percentage shielding before collapse begins, and  $k = 1390 \text{ M}^{-1} \text{ s}^{-1}$  is a kinetic rate constant (Guo et al., 2003). Assuming that there is an interfacial pH shift,  $\Delta\text{pH}$ , from the bulk solution, the above equation can be rewritten as follows:

$$t_{\text{collapse}} = \frac{\ln(A_{\text{initial}}/A_{\text{critical}})10^{\text{pH}}10^{\Delta\text{pH}}}{k}$$

Using the pH-dependent collapse times of POD SPLP (Figure 4),  $A_{\text{initial}} = 20\%$ , and the parameters determined previously by Guo et al. (2003), nonlinear regression was used to determine ( $R^2 = 0.968$ ) that  $\Delta\text{pH} = 0.68 \pm 0.03$ . Thus, the detected surface DOTAP suggests a 0.8 pH unit shift, and independent measurement of the collapse kinetics suggest a similar 0.7 pH upward shift of the interfacial pH from the bulk solution. We think that a combination of the increased starting concentration of POD and an approximately 0.7 unit increase of interfacial pH in the POD SPLP accounts for the altered collapse times observed in our studies.

Although the mechanism of how DNA is introduced into the cell from the SPLP particles has not been established in this manuscript, the fact that only the pH sensitive system has appreciable transfection activity and the particles are observed in the cytoplasm suggests that the POD SPLP utilizes an endocytotic pathway to enter the cell. Hence understanding the factors that control the rate of collapse for the POD SPLP is critical so the time of collapse can occur between endocytosis and lysosomal degradation, a window of perhaps 10 min. A POD SPLP might have excellent endosomal escape and transfection with a neutrally charged surface; however, surface DOTAP, often used to enhance cell binding and transfection, may be deleterious to endosomal escape and transfection in these particles.

We have previously shown that the POD modified PE liposomes have an extended circulation half-life after intravenous injection in mice (Guo and Szoka, 2001); hence, we think that this approach holds forth the promise of a long circulating nonviral DNA delivery with good potency. The POD SPLP can be further engineered to obtain improved transfection by varying the amount of PEG-lipids, changing the molecular weight of the attached PEG, altering the hydrophobic anchor lipid, or employing different cationic lipids. In addition, adding to the POD SPLP a targeting moiety that can be recognized and internalized by a specific target cells might be a useful platform technology for systemic gene therapy.

## CONCLUSION

In this work, we have successfully implemented the concept of a low pH-sensitive SPLP nanoparticle for gene delivery. The POD SPLP rapidly collapse at low pH

conditions while remaining stable at higher pH conditions. The POD SPLP produced substantially superior in vitro gene transfection compared to a pH-insensitive SPLP. These data suggest that utilizing the pH-sensitive POD SPLP may offer a potential advantage for parenteral in vivo gene therapy.

#### ACKNOWLEDGMENT

This work was supported by NIH DK 46052 and GM61851. J. Andrew MacKay is a recipient of a Howard Hughes Medical Institute Predoctoral Fellowship. We gratefully acknowledge the helpful assistance of Dr. Xin Guo in the synthesis of POD, and the gifts of 3,9-diethylidene-2,4,8,10-tetraoxaspiro [5,5] undecane from J. Heller and Sunbright DSG-20H from A. Suginaka.

#### LITERATURE CITED

- (1) Asokan, A., and Cho, M. J. (2002) Exploitation of Intracellular pH Gradients in the Cellular Delivery of Macromolecules. *J. Pharm. Sci.* 91, 903–913.
- (2) Banerjee, R., Das, P. K., and Chaudhuri, A. (1988) Interfacial indazolization: novel chemical evidence for remarkably high exo-surface pH of cationic liposomes used in gene transfection. *Biochim. Biophys. Acta* 1373, 299–308.
- (3) Boomer, J. A., and Thompson, D. H. (1999) Synthesis of Acid-labile Diplasmeryl Lipids for Drug and Gene Delivery Applications. *Chem. Phys. Lipids* 99, 145–153.
- (4) Budker, V., Gurevich, V., Hagstrom, J. E., Bortzov, F., and Wolff, J. A. (1996) pH-sensitive, cationic liposomes: A new synthetic virus-like vector. *Nat. Biotech.* 14, 760–764.
- (5) Choi, J. S., Lee, E. J., Choi, Y. H., Jeong, Y. J., and Park, J. S. (1999) Poly(ethylene glycol)-block-poly(L-lysine) Dendrimer: Novel Linear Polymer/Dendrimer Block Copolymer Forming a Spherical Water-Soluble Polyionic Complex with DNA. *Bioconjugate Chem.* 10, 62–65.
- (6) Choi, J. S., Joo, D. K., Kim, C. H., Kim, K., and Park, J. S. (2000) Synthesis of a barbell-like triblock copolymer, poly(L-lysine) dendrimer-block-poly(ethylene glycol)-block-poly(L-lysine) dendrimer, and its self-assembly with plasmid DNA. *J. Am. Chem. Soc.* 122, 474–480.
- (7) Deshiikan, S. R., and Papadopoulos, K. D. (1998) Modified Booth equation for the calculation of zeta potential. *Colloid Polym. Sci.* 276, 117–124.
- (8) Dillman, R. O., Johnson, D. E., Shawler, D. L., and Koziol, J. A. (1988) Superiority of an Acid-labile Daunorubicin-Monoclonal Antibody Immunoconjugate Compared to Free Drug. *Cancer Res.* 48, 6097–6102.
- (9) Drummond D. C., Zignani, M., and Leroux, J. (2000) Current Status of pH-Sensitive Liposomes in Drug Delivery. *Prog. Lipid Res.* 39, 409–460.
- (10) Felgner, J. H., Kumar, R., Sridhar, C. N., Wheeler, C. J., Tsai, Y. J., Border, R., Ramsey, P., Martin, M., and Felgner, P. L. (1994) Enhanced gene delivery and mechanism studies with a novel series of cationic lipid formulations. *J. Biol. Chem.* 269, 2550–2561.
- (11) Fenske, D. B., Palmer, L. R., Chen, T., Wong, K. F., and Cullis, P. R. (2001) Cationic Poly(ethyleneglycol) Lipids Incorporated into Preformed Vesicles Enhance Binding and Uptake to BHK Cells. *Biochim. Biophys. Acta* 1512, 259–272.
- (12) Fernandez, M. S., and Fromherz, P. (1977) Lipid pH Indicators as Probes of Electrical Potential and Polarity in Micelles. *J. Phys. Chem.* 81, 1755–1761.
- (13) Guo, X., and Szoka, F. C., Jr. (2001) Steric Stabilization of Fusogenic Liposomes by a Low-pH Sensitive PEG-Diortho Ester-Lipid Conjugate. *Bioconj. Chem.* 12, 291–300.
- (14) Guo, X., MacKay, J. A., and Szoka, F. C., Jr. (2003) Mechanism of pH-Triggered Collapse of Phosphatidylethanolamine Liposomes Stabilized by an Orthoester Poly(ethylene glycol) Lipid. *Biophys. J.* 84, in press.
- (15) Hellberg, P., Bergström, K., and Juberg, M. (2000) Nonionic Cleavable Ortho Ester Surfactants. *J. Surfactants Deterg.* 3, 369–379.
- (16) Heller, J. (1993) Polymers for Controlled Parenteral Delivery of Peptides and Proteins. *Adv. Drug Deliv. Rev.* 10, 163–204.
- (17) Henry, C. M. (2001) Gene Delivery – without Viruses. *Chem. Eng. News* 79, 35–41.
- (18) Hofland, H. E., Shephard, L., and Sullivan, S. M. (1996) Formation of Stable Cationic Lipid/DNA Complexes for Gene Transfer. *Proc. Natl. Acad. Sci. U.S.A.* 93, 7305–7309.
- (19) Hood, J. D., Bednarski, M., Frausto, R., Guccione, S., Reisfeld, R. A., Xiang, R., and Cheresch, D. A. (2002) Tumor Regression by Targeted Gene Delivery to the Neovasculature. *Science* 296, 2404–2407.
- (20) Kakizawa, Y., and Kataoka, K. (2002) Block copolymer micelles for delivery of gene and related compounds. *Adv. Drug Deliv. Rev.* 54, 203–222.
- (21) Kraayenhof, R., Sterk, G. J., and Wong Fong Sang, H. W. (1993) Probing Biomembrane Interfacial Potential and pH Profiles with a New Type of Float-like Fluorophores Positioned at Varying Distance from the Membrane Surface. *Biochemistry* 32, 10057–10066.
- (22) Legendre, J., and Szoka, F. C., Jr. (1992) Delivery of Plasmid DNA into Mammalian Cell Lines Using pH-Sensitive Liposomes: Comparison with Cationic Liposomes. *Pharm. Res.* 9, 1235–1242.
- (23) Marshall, E. (2001) Viral Vectors Still Pack Surprises. *Science* 294, 1640.
- (24) McLaughlin, S. (1989) The electrostatic properties of membranes. *Annu. Rev. Biophys. Biophys. Chem.* 18, 113–36.
- (25) Miller, C. R., Bondurant, B., McLean, S. D., McGovern, K. A., and O'Brien, D. F. (1998) Liposome-cell interactions in vitro: effect of liposome surface charge on the binding and endocytosis of conventional and sterically stabilized liposomes. *Biochemistry* 37, 12875–83.
- (26) Mok, K. W. C., Lam, A. M. I., and Cullis, P. R. (1999) Stabilized Plasmid-Lipid Particles: Factors Influencing Plasmid Entrapment and Transfection Properties. *Biochim. Biophys. Acta* 1419, 137–150.
- (27) Ogris, M., and Wagner, E. (2002) Targeting Tumors with Nonviral Gene Delivery Systems. *Drug Discov. Today* 7, 479–485.
- (28) Remy, J., Abdallah, B., Zanta, M. A., Boussif, O., Behr, J., and Demeneix, B. (1998) Gene transfer with lipospermines and polyethylenimines. *Adv. Drug. Del. Rev.* 30, 85–95.
- (29) Shimada, K., Miyagishima, A., Sadzuka, Y., Nozawa, Y., Mochizuki, Y., Ohshima, H., and Hirota, S. (1995) Determination of the Thickness of the Fixed Aqueous Layer Around Polyethyleneglycol-coated Liposomes. *J. Drug Targeting* 3, 283–289.
- (30) Tam, P., Monck, M., Lee, D., Ludkovski, O., Leng, E. C., Clow, K., Stark, H., Scherrer, P., Graham, R. W., and Cullis, P. R. (2000) Stabilized Plasmid-Lipid Particles for Systemic Gene Therapy. *Gene Ther.* 7, 1867–1874.
- (31) Tocanne, J. F., and Tessie, J. (1990) Ionization of phospholipids and phospholipids-supported interfacial lateral diffusion of protons in membrane model systems. *Biochim. Biophys. Acta* 1031, 111–142.
- (32) Wheeler, J. J., Palmer, L., Ossanlou, M., MacLachlan, I., Graham, R. W., Zhang, Y. P., Hope, M. J., Scherrer, P., and Cullis, P. R. (1999) Stabilized Plasmid-Lipid Particles: Construction and Characterization. *Gene Ther.* 6, 271–281.
- (33) Yue, C., Harris, J. M., Hellberg, P., and Bergstrom, K. (1996) Synthesis and Characterization of Cleavable Surfactants Derived from Poly(ethylene glycol) Monomethyl Ether. *J. Am. Oil Chem. Soc.* 73, 841–845.
- (34) Zhang, Y. P., Sekirov, L., Saravolac, E. G., Wheeler, J. J., Tardi, P., Clow, K., Leng, E., Sun, R., and Cullis, P. R. (1999) Stabilized Plasmid-Lipid Particles for Regional Gene Therapy: Formulation and Transfection Properties. *Gene Ther.* 6, 1438–1447.
- (35) Zhu, J., Munn, R. J., and Nantz, M. H. (2000) Self-Cleaving Ortho Ester Lipids: A New Class of pH-Vulnerable Amphiphiles. *J. Am. Chem. Soc.* 122, 2645–2646.
- (36) Zuidam, N. J., and Barenholz, Y. (1997) Electrostatic parameters of cationic liposomes commonly used for gene delivery as determined by 4-heptadecyl-7-hydroxycoumarin. *Biochim. Biophys. Acta* 1329, 211–222.

# $\alpha$ -Oxo Semicarbazone Peptide or Oligodeoxynucleotide Microarrays

Christophe Olivier,<sup>†</sup> David Hot,<sup>‡</sup> Ludovic Huot,<sup>‡</sup> Nathalie Ollivier,<sup>†</sup> Ouafâa El-Mahdi,<sup>†</sup> Catherine Gouyette,<sup>§</sup> Tam Huynh-Dinh,<sup>§</sup> Hélène Gras-Masse,<sup>†</sup> Yves Lemoine,<sup>‡</sup> and Oleg Melnyk\*,<sup>†</sup>

UMR CNRS 8525, Biological Institute of Lille, 1 rue du Pr Calmette 59021 Lille France, Laboratoire des Biopuces, Pasteur Institute of Lille, 1 rue du Pr Calmette 59019 Cedex Lille France, and Pasteur Institute, URA 2128, 75724 Paris, France. Received July 10, 2002; Revised Manuscript Received December 9, 2002

We describe in this paper the preparation and characterization of semicarbazide glass slides and their use for the fabrication of microarrays using site-specific  $\alpha$ -oxo semicarbazone ligation. The functional density and homogeneity of the semicarbazide glass slides were optimized by analyzing the reactivity of the layer toward a synthetic glyoxylyl fluorescent probe. Oligonucleotide microarrays were prepared by site-specific immobilization of glyoxylyl oligodeoxynucleotides. The slides were directly used in the hybridization assays using fluorescence detection and displayed a significant gain in sensibility as compared to the aldehyde glass slide/amino oligodeoxynucleotide chemistry. Semicarbazide slides were also used for the immobilization of a biotinylated peptide  $\alpha$ -oxo aldehyde. The peptide microarrays allowed model interaction studies with streptavidin or an anti-biotin antibody.

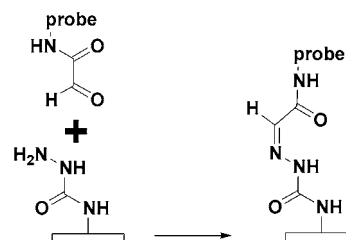
## INTRODUCTION

Today, the miniaturization of biological assays is at the origin of crucial biological research and medical advances. Over the past decade, the trends toward miniaturization of high-throughput screening systems have generated a great deal of interest in the scientific community. DNA microarrays have been applied for the monitoring of gene expression (1, 2), the genome-wide analysis of DNA copy-number changes (3), the screening of single-nucleotide polymorphism (4), and the diagnostics of mutations (5), as well as many other analytical purposes (6, 7). Micro-fabricated analytical devices have also found applications in the large-scale functional analysis of peptides (8–10) or proteins (11–13).

One of the most widely used strategy for microarray fabrication is to attach characterized and purified synthetic probes to a surface. In this case, the performances of the arrays, besides the selection of the probes and their mode of immobilization, rely mainly upon the chemical and physicochemical properties of the array.

Glass slides are now widely used for the preparation of DNA or polypeptide arrays. Indeed, glass is an inexpensive support medium which has a low intrinsic fluorescence and a relatively homogeneous chemical surface. Its properties have been studied in detail, and a diverse silanization chemistry is available for derivatization. The ideal glass surface for microarray fabrication must respond to several specifications: the glass coating must be (1) homogeneous, (2) stable upon storage, (3) chemically inert toward biomolecules such as nucleic acids or proteins but should allow the covalent and dense immobilization of functionalized probes so as to reach high signal-to-noise ratios, (4) minimize the adsorption of biomolecules so as to avoid the use of a blocking procedure following the printing step. On the other hand, the modified probes must be (1) stable upon storage and

## Scheme 1. $\alpha$ -Oxo Semicarbazone Immobilization Chemistry



(2) highly reactive toward the surface. Finally, the overall procedure for microarray fabrication must be robust to guarantee a high level of reproducibility, and importantly, a great advantage could be to use the same methodology for either oligodeoxynucleotide (ODN) or polypeptide microarray fabrication.

In search for a novel immobilization chemistry which would respond to these specifications, we have explored the interest of  $\alpha$ -oxo semicarbazone ligation of glyoxylyl-probes onto semicarbazide glass slides for microarray fabrication (Scheme 1).

We report in this article the fabrication and characterization of semicarbazide glass slides using either a multistep procedure or a direct silanization with a semicarbazide silane (14–17). Importantly, the slides were optimized owing to their ability to react site-specifically with a fluorescently labeled glyoxylyl dipeptide. This mode of visualization of surface semicarbazide groups constitutes a good quality control of the functional density and homogeneity of the glass surface. We describe the site-specific immobilization of 5'-glyoxylyl-ODNs through the formation of an  $\alpha$ -oxo semicarbazone bond and the use of these ODN arrays in model hybridization experiments using fluorescence detection. A comparative study with the widely used aldehyde glass slide/amino-ODN chemistry revealed a gain in sensibility of about 18-fold for the novel chemistry described here, due to both a higher signal intensity and a reduced background noise. We report also the synthesis of a glyoxylyl peptide labeled with biotin, its immobilization on semicarbazide slides,

\* Corresponding author. Tel: 33(0)3 20 87 12 15, Fax: 33-(0)3 20 87 12 35. E-mail: oleg.melnyk@ibl.fr.

<sup>†</sup> Biological Institute of Lille.

<sup>‡</sup> Pasteur Institute of Lille.

<sup>§</sup> Pasteur Institute.



and model interaction studies with streptavidin or an anti-biotin antibody. The stability of the  $\alpha$ -oxo semicarbazone linkage toward hydrolysis was examined.

## MATERIALS AND METHODS

**Buffers and Oligonucleotides.** Chemical reagents were obtained from commercial suppliers and were used without further purification: saline sodium citrate (SSC, Quantum Biotechnologies Inc.);  $20\times = 3\text{ M NaCl} + 0.3\text{ M sodium citrate pH } 7.0$ . Sodium borohydride ( $\text{NaBH}_4$ , Sigma); phosphate-buffered saline (PBS, Gibco Life Technology); 2-(*N*-morpholino)ethanesulfonic acid (MES, Sigma); dimethyl sulfoxide (DMSO, Sigma). Water was deionized using a Milli-Q purification system (Millipore).

**P1 5'-GTCCAAGCTCAGCTAATT-3', P1-NH<sub>2</sub> NH<sub>2</sub>C<sub>6</sub>H<sub>12</sub>OPO<sub>2</sub>-GTCCAAGCTCAGCTAATT, P2 5'-GCAGGACTCTAGAGGATC-3', P2-NH<sub>2</sub> NH<sub>2</sub>C<sub>6</sub>H<sub>12</sub>OPO<sub>2</sub>-GCAGGACTCTAGAGGATC** were from Eurogentech.

**P1c-Cy3 5'-Cy3-AATTAGCTGAGCTTGGAC-3', P1-PEG-NH<sub>2</sub> NH<sub>2</sub>C<sub>6</sub>H<sub>12</sub>OPO<sub>2</sub>[(OCH<sub>2</sub>CH<sub>2</sub>)<sub>6</sub>OPO<sub>2</sub>]<sub>2</sub>-5'-GTC-CAAGCTCAGCTAATT-3', P2-PEG-NH<sub>2</sub> NH<sub>2</sub>C<sub>6</sub>H<sub>12</sub>OPO<sub>2</sub>[(OCH<sub>2</sub>CH<sub>2</sub>)<sub>6</sub>OPO<sub>2</sub>]<sub>2</sub>-5'-GCAGGACTCTAGAGGATC-3' and P2c-Cy3 5'-Cy3-GATCCTCTAGAGTCCTGC-3'** were synthesized using standard phosphoramidite chemistry and were purified by RP-HPLC.

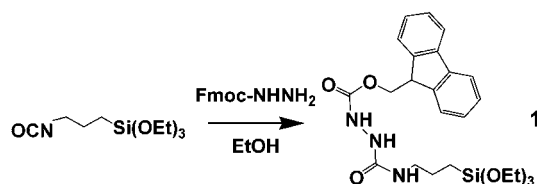
**Synthesis of P1-PEG-tar and P2-PEG-tar.** ODNs were assembled using standard phosphoramidite protocols on controlled pore glass solid support (1  $\mu\text{mol scale}$ ) (18). The terminal amino group was incorporated using 6-(4-monomethoxytritylamino)hexyl 2-cyanoethyl *N,N*-diisopropylphosphoramidite as usual. Monomethoxytrityl protecting group was deprotected using 3% trichloroacetic acid in  $\text{CH}_2\text{Cl}_2$  (6 min). The solid support was washed three times with acetonitrile, dried rapidly with argon. The solid support was treated with 5% by vol of 2,6-lutidine in THF (410  $\mu\text{L}$ ) containing 10 mg of (+)-diacetyl-L-tartaric anhydride (twice, 5 and 10 min). Aminolysis was performed as usual. **P1-PEG-tar** and **P2-PEG-tar** ODNs were isolated with about 30% yield following purification by C18-RP-HPLC (acetonitrile/pH = 6.5 triethylamine acetate). MALDI-TOF: **P1-PEG-tar** [ $\text{M} + \text{H}$ ]<sup>+</sup> calcd. 6459.48, found 6460.06; **P2-PEG-tar** [ $\text{M} + \text{H}$ ]<sup>+</sup> calcd. 6549.53, found 6550.53.

**Synthesis of P1-PEG-COCHO and P2-PEG-COCHO.** The periodate oxidation was performed on a 0.2  $\mu\text{mol scale}$  using 1.7 equiv of  $\text{NaIO}_4$  in a pH 6.6 0.1 M phosphate buffer (1 h). ODN concentration was 0.1–1 mM. Glyoxylyl-ODNs were purified by C18 RP-HPLC (acetonitrile/pH = 6.5 triethylamine acetate). (*n*-Bu)<sub>3</sub>P (0.005% by vol) and mannitol (6.67  $\mu\text{g}/1\text{ }\mu\text{g ODN}$ ) were added to the pure RP-HPLC fractions before lyophilization (85% yield). MALDI-TOF: **P1-PEG-COCHO** [ $\text{M} + \text{H}$ ]<sup>+</sup> calcd 6383.43, found 6385.55; **P2-PEG-COCHO** [ $\text{M} + \text{H}$ ]<sup>+</sup> calcd. 6473.48, found 6475.71.

**Semicarbazide-Functionalized Glass Slides Preparation.** (a) *Typical Multistep Procedure.* The preparation of the slides was performed using Wheaton racks for 20 slides (75  $\times$  25 mm), staining dish, and staining dish lid purchased from Merck. The slides were placed back to back, so that one rack contained 40 slides. Sonication was performed in B-5510 (9.5 L, 40 kHz) Branson sonicators. Typically, syntheses were done using simultaneously two sonicators (two racks per sonicator, 160 slides).

Microscope slides (ESCO Precleaned Micro slide Frosted) were cleaned using 10% aqueous NaOH (10 min under sonication and then overnight), water (3  $\times$  3 min), and aqueous 3.7% HCl (4 h). Alternatively, the use of a

## Scheme 2. Synthesis of Silane 1



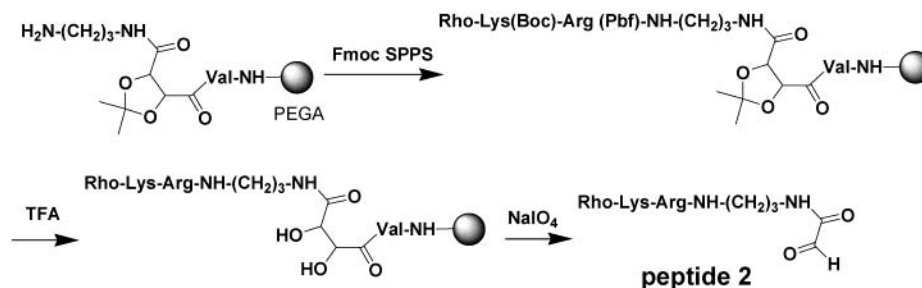
freshly prepared piranha solution ( $\text{H}_2\text{SO}_4/\text{H}_2\text{O}_2$ : 1/1 by vol) was found to be equally useful. The slides were washed with water (3  $\times$  3 min) and methanol (3 min) and treated with 3% 3-aminopropyltrimethoxysilane in methanol/water: 95/5 by vol (30 min, under sonication). The slides were then washed with methanol, water (two times), and methanol and cured 15 min at 110  $^\circ\text{C}$ . The slides were treated with 0.1 M triphosgene/0.8 M diisopropylethylamine solution in 1,2-dichloroethane (2 h, sonication) and then with a 22 mM Fmoc-NHNH<sub>2</sub> (19) solution in DMF containing 1% of ethanol (2 h, sonication). Deprotection was performed with 0.2% piperidine and 2% 1,8-diazabicyclo[5.4.0]undec-7-ene in DMF (30 min). The slides were washed with DMF, water (two times), and methanol and dried under reduced pressure. They were stored at room temperature for months in a dust-proof container.

(b) *One-Step Procedure.* Silane 1 (Scheme 2) was prepared by reacting 515 mg (2.03 mmol) of Fmoc-NHNH<sub>2</sub> with 570  $\mu\text{L}$  (2.28 mmol) of 3-isocyanatopropyltriethoxysilane in 15 mL of absolute EtOH at room temperature (rt). After 1 h, EtOH was removed under reduced pressure. The solid was redissolved in the minimal volume of dry  $\text{CH}_2\text{Cl}_2$ , precipitated with dry pentane, filtered, and dried. 841 mg (83% yield). <sup>1</sup>H NMR (300 MHz,  $\text{CDCl}_3$ ): 0.66 (t, 2H,  $J = 8.1\text{ Hz}$ ), 1.24 (t, 9H,  $J = 6.7\text{ Hz}$ ), 1.6 (m, 2H,  $J = 6.7\text{ Hz}$ ), 3.26 (q, 2H,  $J = 6.6\text{ Hz}$ ), 3.82 (q, 6H,  $J = 7\text{ Hz}$ ), 4.25 (t, 1H,  $J = 6.82\text{ Hz}$ ), 4.51 (d, 2H,  $J = 6.79\text{ Hz}$ ), 5.46 (m, 1H), 6.46 (s, 1H), 6.71 (s, 1H), 7.34 (t, 2H,  $J = 7.61\text{ Hz}$ ), 7.43 (t, 2H,  $J = 7.01\text{ Hz}$ ), 7.61 (d, 2H,  $J = 7.28\text{ Hz}$ ), 7.79 (d, 2H,  $J = 7.39\text{ Hz}$ ).

Microscope slides (ESCO Precleaned Micro slide Frosted) were immersed overnight in a freshly prepared piranha solution ( $\text{H}_2\text{SO}_4/\text{H}_2\text{O}_2$ : 1/1 by vol), washed with water (three times) and methanol and then treated at 47  $^\circ\text{C}$  with silane 1 in toluene/THF: 90/10 by vol (30 min, under sonication). The slides were then washed with toluene (2  $\times$  3 min) and dried at 120  $^\circ\text{C}$  during 15 min. Deprotection was performed as before.

**Slides Quality Control.** (a) *Synthesis of Glyoxylyl-peptide 2.* Synthesis of glyoxylyl-peptide 2 was performed on a 0.1 mmol scale using the Fmoc/*tert*-butyl strategy (20) on poly(ethylene glycol) polyacrylamide copolymer (PEGA resin (21)) modified by an isopropylidene tartrate-based linker as shown in Scheme 3 (see refs 24, 25).

Following peptide elongation, (5)-6-carboxytetramethylrhodamine (47.3 mg, 0.11 mmol) was coupled to the peptidyl-resin using HBTU/HOBt/DIEA activation (41.7 mg 0.11 mmol/14.9 mg 0.11 mmol/57.5  $\mu\text{L}$  0.33 mmol) in NMP (2 h). The resin was washed with NMP (3  $\times$  2 min) and  $\text{CH}_2\text{Cl}_2$  (2  $\times$  2 min) and dried under reduced pressure. The peptidyl-resin was deprotected using TFA/thioanisole/phenol/water/ethanedithiol/triisopropylsilane: 5 mL/307  $\mu\text{L}$ /306 mg/307  $\mu\text{L}$ /154  $\mu\text{L}$ /61  $\mu\text{L}$  (2 h). The resin was washed with  $\text{CH}_2\text{Cl}_2$  (3  $\times$  2 min), MeOH (2  $\times$  2 min), and AcOH/water: 1/3 by vol (2  $\times$  5 min). The periodate oxidation was performed in 5 mL of AcOH/water: 1/3 by vol containing 128 mg (0.6 mmol) of  $\text{NaIO}_4$ . After 2 min, the reaction was quenched with 145  $\mu\text{L}$  (2.4

**Scheme 3. Synthesis of Glyoxylyl-peptide 2**

mmol) of ethanolamine. The resin was filtered and washed twice with 6 mL of water. The combined filtrates were purified by RP-HPLC on a C18 15 × 300 mm Hyperprep column (linear water/acetonitrile gradient containing 0.05% TFA by vol) to give 56.4 mg (53% yield) of peptide **2**. MALDI-TOF:  $[M + H]^+$  monoisotopic calcd 827.4, found 827.6.

(b) *Synthesis of Peptide Amide 3*. Synthesis of peptide amide **3** Rho-Lys-Arg-NH<sub>2</sub> was performed on a 0.1 mmol scale using the Fmoc/*tert*-butyl strategy on a Rink amide AMPS 1% DVB resin (Senn Chemicals). (5)-6-carboxytetramethylrhodamine was coupled as described before. The peptide was deprotected and cleaved using TFA/thioanisole/phenol/water/ethanedithiol/triisopropylsilane: 5 mL/307  $\mu$ L/306 mg/307  $\mu$ L/154  $\mu$ L/61  $\mu$ L (1h30). The peptide was precipitated in diethyl ether/*n*-heptane: 1/1 by vol and purified as before to give 54 mg (57% yield) of peptide **3**. MALDI-TOF:  $[M + H]^+$  monoisotopic calcd 714.4, found 714.4.

(c) *Quality Control Procedure*. Two slides were used for the quality control. The slides were immersed 1 h at 37 °C in a 0.1 mM solution of peptide **2** or **3** dissolved in 0.1 M pH 5.5 sodium acetate buffer. The slides were washed rapidly with water and then successively with 5% aqueous K<sub>2</sub>HPO<sub>4</sub> (2 h under sonication), 0.1 M tris-(hydroxymethyl)aminomethane-acetate buffer containing 0.1% Tween 20 (30 min, under sonication), water, and MeOH. The slides were analyzed using the Cy3 channel of an Affymetrix 418 Array Scanner (Affymetrix Inc., 3380 Central Exwy Santa Clara, CA 95051). Quantification of fluorescence intensity and homogeneity was performed using 320 measurements covering all the surface of the slide (ScanAnalyze program written by M. Eisen, Stanford University; <http://rana.stanford.edu/software>).

**Preparation of ODN Arrays on Semicarbazide Glass Slides.** ODNs were dissolved in 3× SSC pH 5.5 to obtain 100, 50, 10, 1, and 0.1  $\mu$ M concentrations. Solutions were spotted on the slides using an Affymetrix 417 Arrayer (Affymetrix, Inc.). The printed slides were incubated 14 h at 30 °C in a water-saturated atmosphere. The slides were then washed 5 min at room temperature with 0.1% SDS in water and dried by centrifugation.

**Preparation of ODN Arrays on Aldehyde Slides.** Aldehyde slides (Cel Associates, Genpack Ltd.) were printed using solutions of ODNs in 0.1 M MES buffer/DMSO: 4/1 by vol using the same conditions as for semicarbazide slides. The printed slides were incubated 14 h at 30 °C in a water-saturated atmosphere and then treated 6 h at 42 °C with 0.13 M NaBH<sub>4</sub> in 1× PBS/EtOH: 3/1 by vol. The slides were washed at 42 °C with 0.2% SDS in water and water (twice) and dried by centrifugation.

**Radioactivity Measurements.** ODNs **P1**, **P1-PEG-COCHO**, **P1-PEG-NH<sub>2</sub>**, and **P1-NH<sub>2</sub>** were radiolabeled at the 3' terminus using  $[\alpha\text{-}^{32}\text{P}]\text{ddATP}$  (Amersham

Biosciences) and terminal deoxynucleotidyl transferase (Promega). Two hundred picomoles of ODN and 33 pmol of radiolabeled triphosphate (100  $\mu$ Ci) were reacted using condition specified by the manufacturer. The labeled probe was purified using the dNTP removal kit (Qiagen) and eluted in sterile water (pH 7.0). 10<sup>6</sup> cpm of the labeled probe was diluted in different quantities of unlabeled ODN (2, 1, 0.2, and 0.02 nmol) in 20  $\mu$ L to get final ODN concentrations of 100, 50, 10, or 1  $\mu$ M. The different samples were dried under vacuum and redissolved in 3× SSC pH 5.5 (**P1** or **P1-PEG-COCHO** for spotting on semicarbazide slides) or in 0.1 M MES +10% DMSO (**P1**, **P1-PEG-NH<sub>2</sub>**, or **P1-NH<sub>2</sub>** for spotting on aldehyde slides). Immobilized ODNs were quantified by phosphorimaging using Packard Cyclone storage phosphor system. The data from the phosphorimager were converted to fmol/spot by comparing with standard curves generated from serial dilutions of known amount of a labeled ODN spotted on the slide and dried without washing.

**Hybridization, Washing, and Fluorescence Analysis.** Hybridizations were performed using a 22 × 22 mm glass cover slip (Esco, Erie Scientific) in a CMT-hybridization chamber (Corning). Slides were hybridized 1 h at 42 °C with **P1c-Cy3** 4.5  $\mu$ M in 50% formamide, 6× SSC, 0.4% SDS, 4× Denhardt's mix (the solution was heated 5 min at 95 °C before use). After hybridization, the slides were washed successively with 0.1× SSC, 0.1% SDS (5 min) and 0.1× SSC (5 min, twice). The slides were dried by centrifugation before fluorescence quantification (Affymetrix 418 Array Scanner). Images were acquired at a resolution of 10  $\mu$ m per pixel using the 532 nm channel (Cy3 channel). The average fluorescence intensity for each spot was determined using ScanAnalyze program. The background fluorescence, determined as the mean fluorescence around each spot, was subtracted from the fluorescence values.

**Synthesis of Peptide 4.** Peptide **4** was elaborated on Novasyn TGR resin (0.1 mmol, 0.2 mmol/g, Novabiochem) using the procedure described for the preparation of the corresponding isopropylidene tartrate based linker on PEGA resin (22). Deprotection and cleavage from the solid support was performed at room temperature with TFA/H<sub>2</sub>O/Me<sub>2</sub>S: 9.25 mL/0.25 mL/0.5 mL (2 h). The peptide was precipitated in 200 mL of cold diethyl ether/heptane: 1/1 by vol. The peptide was centrifuged, redissolved in water/acetic acid: 5/1 by vol and lyophilized. The crude peptide (70 mg) was purified by RP-HPLC on a C18 nucleosil column (15 × 300 mm) (linear water/acetonitrile gradient containing 0.05% TFA by vol) to give 51 mg (32% yield) of the tartaramide precursor. MALDI-TOF:  $[M + H]^+$  monoisotopic calcd 1493.82, found 1493.92.

Periodate oxidation was performed on 20 mg (0.012 mmol) of tartaramide dissolved in 20 mL of MeOH/pH 6.54 0.1 M phosphate buffer: 1/1 by vol in the presence

of 14.3 mg of methionine. A 15.4 mg amount of  $\text{NaIO}_4$  dissolved in 5 mL of water was added in one portion. After 15 min, the reaction was stopped with 10  $\mu\text{L}$  of ethanolamine. Purification by RP-HPLC as above permitted the isolation of 8.8 mg (50% yield) of peptide **4** and 2 mg (12%) of peptide **5**. Peptide **4** was found to aggregate during lyophilization. Peptide **4**, MALDI-TOF  $[\text{M} + \text{H}]^+$  monoisotopic calcd 1319.52, found 1319.72. Peptide **5**,  $[\text{M} + \text{H}]^+$  monoisotopic calcd 1335.70, found 1335.68.

**Biotin–Streptavidin or Anti-Biotin Antibody Interactions.** Peptide **4** was printed on the slides using an Affymetrix 417 Arrayer. Each concentration (see Tables 2–4) was printed six times. Incubations were performed under cover glass (24  $\times$  60 mm) using 150  $\mu\text{L}$  of labeled streptavidin (streptavidin tetramethyl rhodamine conjugate, Molecular Probes, Oregon) or antibody (tetramethyl rhodamine conjugated affinity purified goat anti-biotin, Rockland, Gilbertsville, PA) diluted in PBS 0.01 M pH 7.2 at the concentrations indicated in Tables 2–4. The slides were incubated 2 h at 37  $^\circ\text{C}$  in a humid chamber, washed four times with PBS 0.05% Tween 20, deionized water, and ethanol/water: 95/5 by vol, and then dried 15 min at room temperature on the bench. Quantification of the fluorescence was performed with an Affymetrix 418 Array Scanner (L35/PMT50).

**Stability Studies.** Glyoxylyl-peptide **6** was obtained by periodate oxidation of the corresponding seryl precursor H-SILKEPVHGV-NH<sub>2</sub> using standard protocols (20% overall yield starting from a Novasyn TGR resin, Novabiochem, 0.29 mmol/g, 0.1 mmol scale, continuous flow Pioneer synthesizer) (23).

A 0.87 mg amount of glyoxylyl-peptide **6** dissolved in 4.35 mL of 100 mM pH = 5.3 sodium acetate buffer were treated with 20  $\mu\text{L}$  of a 1.18 M aqueous solution of semicarbazide hydrochloride. The reaction was agitated overnight at 37  $^\circ\text{C}$ . RP-HPLC of the reaction demonstrated the complete conversion of the  $\alpha$ -oxo aldehyde into the semicarbazone **7**. The product was desalted by RP-HPLC on a C18 hyperprep column (15  $\times$  250 mm), buffer A: water containing 0.05% TFA by vol; buffer B: acetonitrile/water: 4/1 containing 0.05% TFA by vol, 0–100% B in 90 min, flow rate 3 mL/min, 220 nm, 22  $^\circ\text{C}$ . MALDI-TOF monoisotopic  $[\text{M} + \text{H}]^+$  calcd 1103.0; found 1103.6.

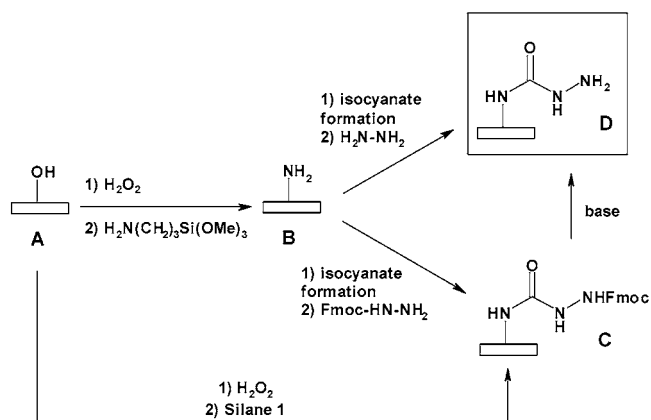
Conjugate **7** 0.1 mM in 100 mM HEPES (pH = 7.5) buffer was incubated at 65  $^\circ\text{C}$ . Aliquots at 0, 4 and 24 h were analyzed by RP-HPLC on a C18 nucleosil column (4.6  $\times$  150 mm), eluents as above, 0–100% B in 30 min, flow rate 1 mL/min, 215 nm, 30  $^\circ\text{C}$ . MALDI-TOF analysis of the major peak in the chromatogram confirmed the stability of the semicarbazone. Similar results were obtained at pH 7.1 or 8.0 (data not shown).

## RESULTS AND DISCUSSION

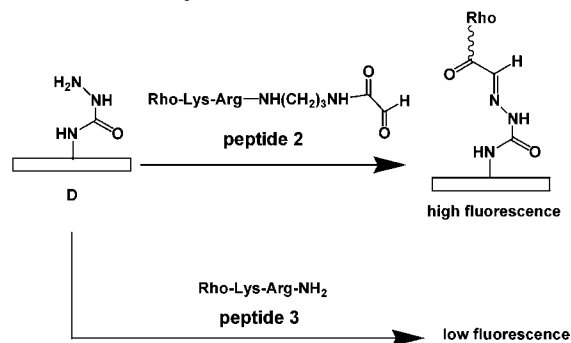
**Support Chemistry.** Two strategies were selected to install the semicarbazide layer (Scheme 4). The first one involves the silanization of the microscope glass slides with 3-aminopropyltrimethoxysilane to form an amine layer and the conversion of amino groups into isocyanate groups followed by their reaction with hydrazine or a protected form of hydrazine. The second strategy is more direct and is based upon the utilization of silane Fmoc-NHNHCONH(CH<sub>2</sub>)<sub>3</sub>Si(OEt)<sub>3</sub> **1** (Scheme 2).

The optimization of semicarbazide glass slides and the quality control of the different batches required a robust method for the qualitative evaluation of the surface density and homogeneity of semicarbazide groups. This

### Scheme 4. Synthesis of the Semicarbazide Glass Slides



### Scheme 5. Quality Control of Semicarbazide Slides

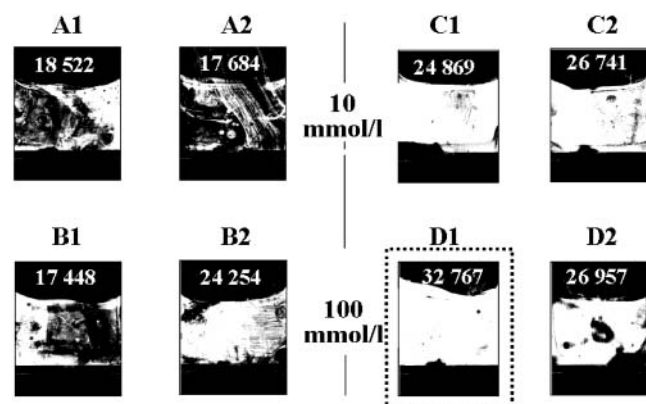


characterization was performed as described in Scheme 5 and required two slides and labeled dipeptides **2** and **3**. C-terminal glyoxylyl dipeptide Rho-Lys-Arg-NH(CH<sub>2</sub>)<sub>3</sub>NHCOCHO **2**, where Rho is (5)-6-carboxytetramethylrhodamine, was synthesized on the solid phase using an isopropylidene tartrate linker (24, 25). Dipeptide amide **3** Rho-Lys-Arg-NH<sub>2</sub> was elaborated on a Rink amide resin using standard protocols. One slide was immersed in a solution of glyoxylyl peptide **2**, whereas the other slide was treated with the control dipeptide amide **3**. The slides were washed to remove adsorbed peptide and analyzed using the Cy3 channel of the microarray fluorescence scanner. The mean fluorescence intensity of the slides and its standard deviation were determined using a grid of 320 virtual spots distributed upon all the surface. If the glass surface is densely covered by accessible semicarbazide groups, the difference in fluorescence intensity between the two slides must be high. The mean fluorescence intensity and its standard deviation is a good measure of the glass slide quality.

**Multistep Procedure A  $\rightarrow$  B  $\rightarrow$  C or D.** The silanization of silica materials with aminopropyltrialkoxysilanes have been studied in detail, and the resulting solid supports have been extensively used for the immobilization of biomolecules, either by simple adsorption or following activation with various reagents (27).

The slides were cleaned and silanized with 3-aminopropyltrimethoxysilane using an aqueous methanol mixture. The physicochemical properties of amine groups on a glass surface are known to differ significantly from those found in solution experiments (27). Thus, several reagents (CDI, triphosgene), solvents (1,2-dichloroethane, CH<sub>2</sub>Cl<sub>2</sub>, toluene, *t*BuOMe), concentrations (10 to 100 mmol/L), and reaction times with or without sonication were examined for isocyanate formation. Following treatment with 1% aqueous hydrazine in DMF, the slides were





**Figure 1.** Optimization of isocyanate formation. The numbers in the top of each slide represents the mean fluorescence (L35/PMT50). A: CDI 10 mM in DMF 2 h. B: CDI 100 mM in DMF 2 h. C: triphosgene 10 mM/DIEA 80 mM in 1,2-dichloroethane. D: triphosgene 100 mM/DIEA 800 mM in 1,2-dichloroethane. (1) With sonication. (2) Without sonication. D1 corresponds to the best experimental conditions.

analyzed using dipeptides **2** and **3** as described before. Some slides are shown in Figure 1. D1 corresponded to the best experimental conditions in term of fluorescence intensity and homogeneity.

We then examined the impact of the hydrazine derivative upon the quality of semicarbazide slides (B  $\rightarrow$  C for hydrazine or B  $\rightarrow$  D for Fmoc-NHNH<sub>2</sub>). Fmoc-NHNH<sub>2</sub> was always found to be superior to hydrazine hydrate. Removal of the Fmoc group was performed easily using either piperidine or piperidine/DBU in DMF. Semicarbazide slides prepared using the optimal protocol and treated with labeled peptides **2** or **3** are shown in Figure 2. The mean fluorescence and the standard deviation of 320 measurements distributed upon all the surface (ScanAlyse software) are collected in Table 1. The data presented in Table 1 show that the fluorescence intensity

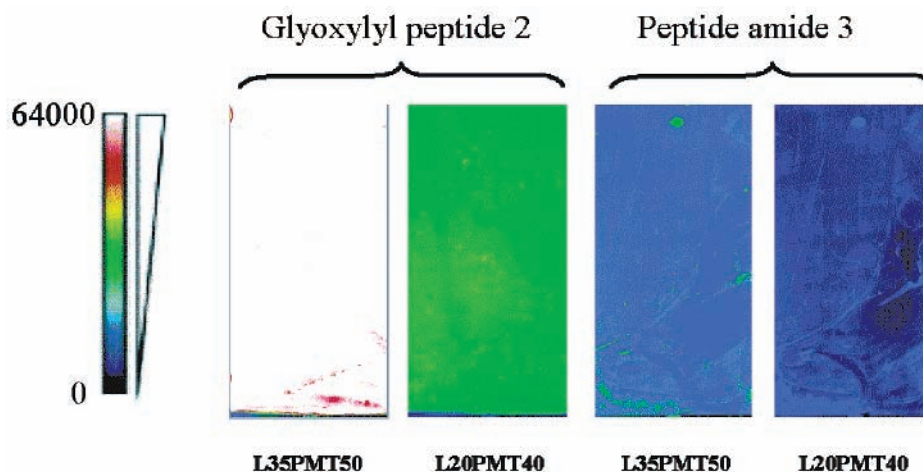
of semicarbazide slides was 10-fold higher with glyoxylyl dipeptide **2** than with peptide amide **3**. This large difference in fluorescence intensity was not observed with untreated slides. These data demonstrate the presence of semicarbazide groups upon the surface and the site-specific attachment of glyoxylyl dipeptide **2** through  $\alpha$ -oxo semicarbazone formation. The standard deviation, which reflects the level of homogeneity, represented about 10% of the mean fluorescence.

**Silanisation with Silane 1 and Comparison with the Stepwise Approach.** Preparation of semicarbazide slides using a more direct route was evaluated (path A  $\rightarrow$  C  $\rightarrow$  D). This method involves the preparation of silane **1**, by addition of Fmoc-NHNH<sub>2</sub> to commercially available 3-isocyanatopropyltriethoxysilane. This reagent was easily precipitated in a pure form from the reaction mixture and could be prepared in large quantities (50 g scale).

Piranha treated slides were silanized with silane **1** in a THF/toluene: 1/9 mixture at 50 °C, deprotected, and characterized as above (see Table 1). The mean fluorescence intensities and standard deviations collected in Table 1 show that the direct silanization method, in our hands, was found to be less efficient than the multistep procedure, both in term of surface semicarbazide group density and homogeneity. Further work is in progress to improve these results since the simple silanization protocol is best suited for large scale preparation.

In the rest of the study we have used the best protocol for semicarbazide glass slide preparation, i.e., the multistep procedure A  $\rightarrow$  B  $\rightarrow$  C or D.

**Synthesis of Glyoxylyl-ODNs.** The glyoxylyl group has been extensively employed in protein engineering (28, 29). This function reacts with hydrazines, hydroxylamines, and  $\beta$ -amino thiols to give the corresponding hydrazones, oximes, or thiazolidines in high yield. The glyoxylyl group is stable, does not form easily imine bonds

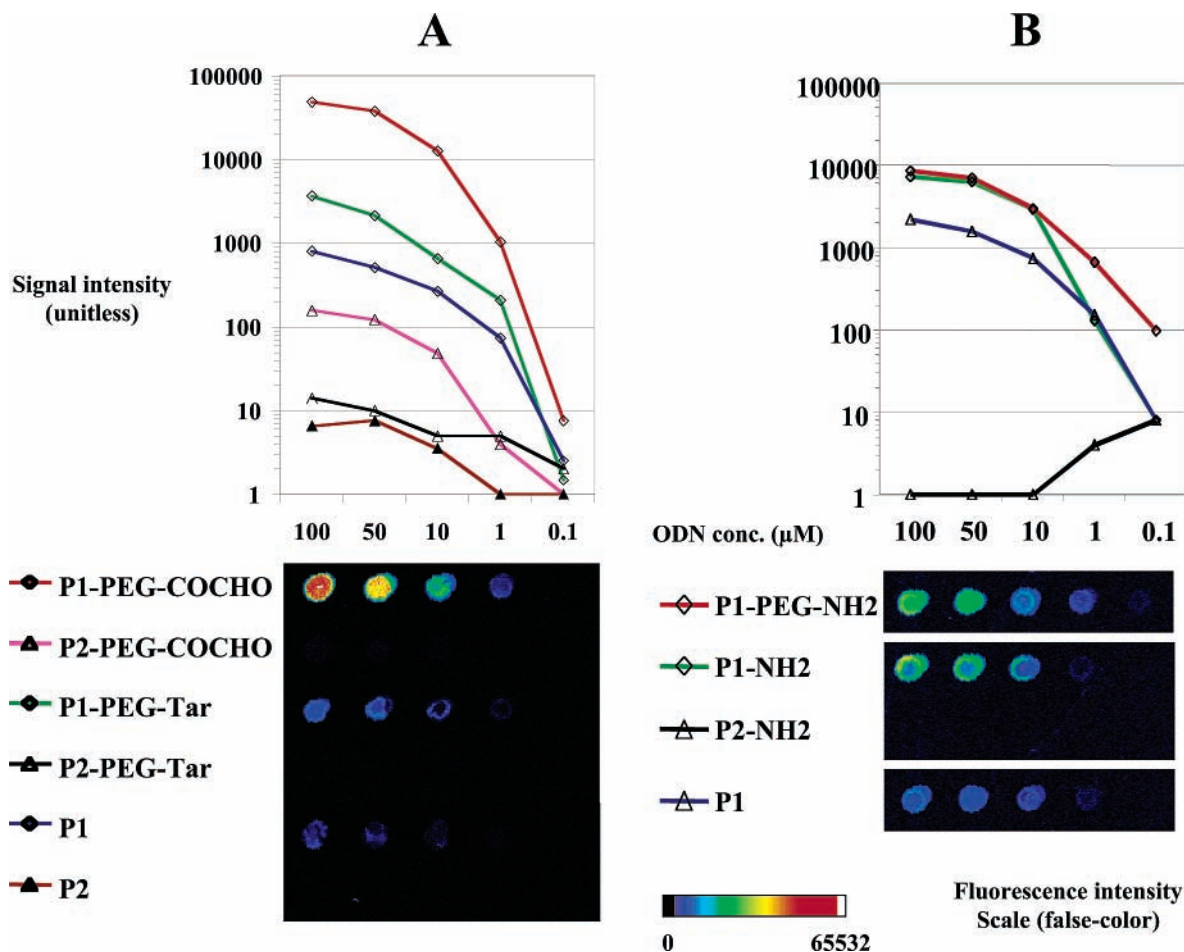


**Figure 2.** Optimized semicarbazide slides (stepwise approach). Quality control using glyoxylyl-peptide **2** and peptide amide **3**. The slides were scanned at L35PMT50 or L20PMT40 sensitivity.

**Table 1.** Characterization of Semicarbazide Glass Slides Using Dipeptides **2** and **3** Labeled with (5)-6-Carboxytetramethylrhodamine

	semicarbazide glass slides					
	multistep procedure: A $\rightarrow$ B $\rightarrow$ C $\rightarrow$ D		silane <b>1</b>		untreated slides	
	glyoxylyl peptide <b>2</b>	peptide amide <b>3</b>	glyoxylyl peptide <b>2</b>	peptide amide <b>3</b>	glyoxylyl peptide <b>2</b>	peptide amide <b>3</b>
mean fluorescence <sup>a</sup>	36260	3450	28882	1732	4489	5270
SD	3939	486	3427	91	671	934

<sup>a</sup> The mean fluorescence was determined using the ScanAlyse software and a grid of 320 virtual spots distributed upon all the surface of the glass slide. Analysis was performed at L30PMT45 scanner sensitivity.



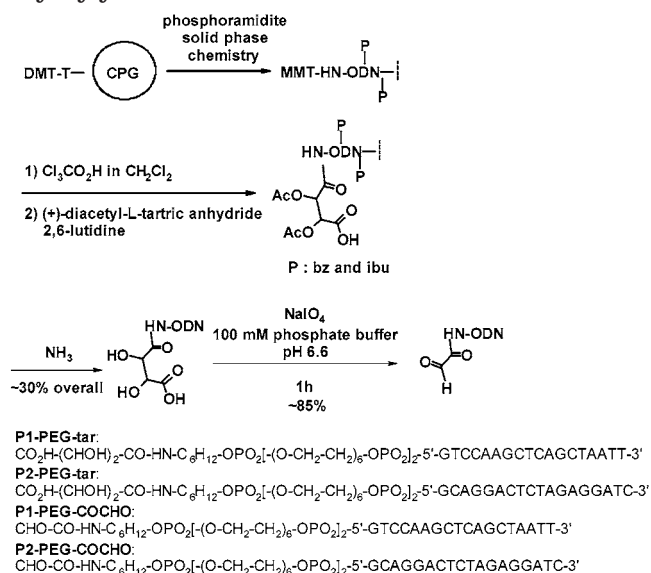
**Figure 3.** (A) Immobilization of glyoxylyl-ODNs **P1-PEG-COCHO** and **P2-PEG-COCHO**, tartaramide-ODNs **P1-PEG-Tar** and **P2-PEG-Tar**, and unmodified ODNs **P1** and **P2** on semicarbazide glass slides using concentrations from 100  $\mu$ M to 0.1  $\mu$ M followed by hybridization with **P1c-Cy3** (4.5  $\mu$ M). (B) Immobilization of amino-ODNs **P1-PEG-NH<sub>2</sub>**, **P1-NH<sub>2</sub>**, and **P2-NH<sub>2</sub>** and unmodified ODN **P1** on aldehyde slides (Cel Associates) using concentrations from 100  $\mu$ M to 0.1  $\mu$ M followed by hybridization with **P1c-Cy3** (4.5  $\mu$ M). The slides were scanned at L20PMT40. Quantification was performed using the ScanAlyse software (the negative and <1 values were replaced by 1 for graphic representation).

with aliphatic or aromatic amines, and importantly, the fluorescence of the corresponding semicarbazones is negligible.

The synthesis of glyoxylyl-ODNs was reported recently by our group (30). These ODN derivatives were found to react rapidly with  $\alpha$ -hydrazino acetyl peptides to give peptide-ODN conjugates assembled by an  $\alpha$ -oxo hydrazone link. Rapidly, glyoxylyl-ODNs **P1-PEG-COCHO** and **P2-PEG-COCHO** used in this study were synthesized as shown in Scheme 6. Tartaramides precursors **P1-PEG-tar** and **P2-PEG-tar** were obtained using standard solid-phase phosphoramidite chemistry on controlled pore glass. After the elongation step, a protected amino phosphoramidite was coupled to the 5' end. Deprotection of the amino group was followed by acylation with an excess of (+)-diacetyl-L-tartric anhydride in the presence of 2,6-lutidine. The tartaramide group was found to be fully stable during the aminolysis. The tartaramide moieties were then converted into  $\alpha$ -oxo aldehyde groups by a mild periodate oxidation at pH 6.6. The glyoxylyl-ODNs were stored at  $-20$   $^{\circ}$ C following lyophilization.

**Selection of the Spotting Buffer and of the Washing Solution.** In this study, all the slides were printed using a pin-and-ring type robot. The shape and homogeneity of the spots is known to be highly dependent upon the physicochemical properties of both the glass surface and of the ODN solution using this printing technology.

#### Scheme 6. Synthesis of Tartaramide and Glyoxylyl-ODNs



**P1c-Cy3** was used to screen various spotting buffers, with or without an organic cosolvent (DMSO, formamide). The best results, in term of shape and signal homogeneity was obtained using 3 $\times$  SSC pH 5.5. The addition of DMSO or formamide was found to be detrimental. The

same ODN was used to optimize the washing step allowing the elimination of adsorbed oligodeoxynucleotide. Washing 5 min in 0.1% SDS at room-temperature permitted removal of about 90% of adsorbed **P1c-Cy3** ODN. These washing conditions were found to remove 99% of unlabeled ODN **P1** (see the following paragraph).

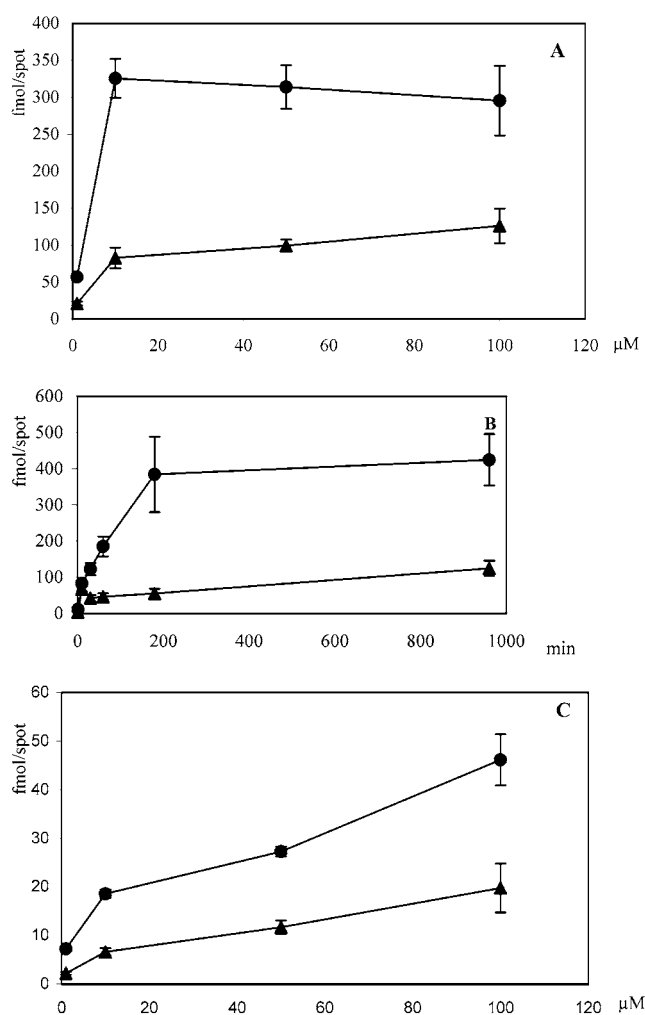
**Immobilization of Glyoxylyl-ODNs onto Semicarbazide Glass Slides or of Amine-ODNs on Aldehyde Slides and Hybridization with a Cy3-Labeled ODN Complementary to the P1 Sequence.** **P1** and **P2** ODNs modified by a glyoxylyl group (**P1-PEG-COCHO**, **P2-PEG-COCHO**) or a tartaramide moiety (**P1-PEG-tar**, **P2-PEG-tar**) or unmodified (**P1**, **P2**) were printed at various concentrations on semicarbazide-functionalized glass slides. The slides were washed as described above to remove adsorbed ODN. Printed slides were used directly in hybridization experiments with **P1c-Cy3** ODN complementary to the **P1** sequence. Figure 3A shows the scanned image of the slide (false-color scale). The fluorescence of the spots is plotted as a function of ODN concentration. For all the hybridization experiments, the concentration of **P1c-Cy3** (4.5  $\mu\text{M}$ ) was chosen above the minimal concentration (2–3  $\mu\text{M}$ ) permitting the saturation of the immobilized probes. With these experimental conditions, the measured fluorescence reflects the amount of immobilized probes and allows the comparison of the spots on the same slide or on different slides.

First of all, the signal associated with **P1-PEG-COCHO** at 100  $\mu\text{M}$  was found to be 15 or 100 fold greater than those associated with **P1-PEG-tar** or **P1** respectively, in accordance with the site-specific immobilization of glyoxylyl-ODNs through  $\alpha$ -oxo semicarbazone formation. Hybridization was found to be highly specific, since fluorescence associated with the **P2** ODNs was barely detectable. Similar results in term of specificity and sensitivity were obtained for hybridization experiments using **P2c-Cy3** ODN (data not shown).

In addition, the background of the slide was found to be very low, typically  $33 \pm 8$  at medium scanner sensitivity (L20PMT40), resulting in very high signal-to-noise ratios (about 1500 for **P1-PEG-COCHO** spotted at 100  $\mu\text{M}$ ). Interestingly, the capping of remaining semicarbazide groups present on the surface following the printing process was found to be unnecessary. Most of the existing site-specific immobilization chemistries require a capping step following the printing of the targets to avoid both the migration of unreacted functionalized ODNs to neighboring sites and the nonspecific adsorption of DNA during hybridization. For example, in the case of amino-ODN/aldehyde slide chemistry, reduction of remaining aldehyde groups with sodium borohydride is necessary. In the recent report of Podyminogin et al., who described the site-specific anchoring of benzaldehyde-ODNs on semicarbazide slides, the use of a blocking solution composed of 5-formyl-1,3-benzenedisulfonic acid disodium salt was also found to be necessary.

**Comparison of the  $\alpha$ -Oxo Aldehyde/Semicarbazide Immobilization Method with Amine/Aldehyde Chemistry.** To document the utility of the novel  $\alpha$ -oxo aldehyde/semicarbazide immobilization method relative to well-known immobilization chemistries,  $\alpha$ -oxo semicarbazone ODN arrays were compared to ODN arrays obtained by printing amino-ODNs onto aldehyde slides.

For aldehyde slide and for the highest concentrations (>10  $\mu\text{M}$ ), the signal displayed by **P1-PEG-NH<sub>2</sub>** ODN was found to be comparable to those given by **P1-NH<sub>2</sub>**, showing in this case a minor effect of the spacer on the immobilization and hybridization efficiencies. Importantly, the fluorescence associated with **P1** ODN suggests



**Figure 4.** (A) Immobilization of **P1-PEG-COCHO** (circle) and **P1** (triangle) onto semicarbazide slides, effect of concentration of printed ODN. (B) As in A, effect of incubation time at 100  $\mu\text{M}$ . (C) Immobilization of **P1-PEG-NH<sub>2</sub>** (circle) and **P1** (triangle) onto aldehyde slides. Standard deviation was calculated using four spots.

that a high proportion of the signal given by **P1-PEG-NH<sub>2</sub>** is due to adsorbed ODN (about 25%). On the other hand on  $\alpha$ -oxo semicarbazone arrays, the signal displayed by **P1** ODN at 100  $\mu\text{M}$  represented only 1.7% of those given by the corresponding glyoxylyl derivative. These data suggest that adsorption of nucleic acids on the semicarbazide surface is significantly lower than on aldehyde slides. Not surprisingly, the same trend was observed for the background level. Indeed, the mean background of semicarbazide arrays following the hybridization experiment ( $33 \pm 8$  at L20PMT40) was found to be about 3 times lower than those of aldehyde slides ( $113 \pm 6$  at L20PMT40). The possibility to reach a low background noise is of prime importance for the detection of weak signals or for the analysis of small variations.

If we compare now the signal intensities, a large difference was observed between semicarbazide arrays and aldehyde arrays. Indeed for the three highest concentrations (100–50–10  $\mu\text{M}$ ) the signal given by **P1-PEG-COCHO** on semicarbazide glass slides was found to be 5.6 times greater than those displayed by the corresponding **P1-PEG-NH<sub>2</sub>** on aldehyde slide, highlighting the efficiency of this immobilization chemistry. These data combined with the background levels resulted in a gain in sensibility of about 18.





**Table 3. Competition Experiments with Biotin**

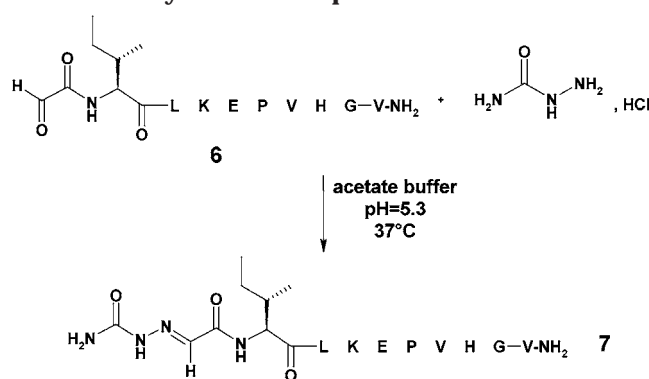
entry	peptide <b>4</b> (mol/L)	biotin (mol/L)									
		0		$10^{-7}$		$10^{-5}$		$10^{-4}$		$10^{-3}$	
		MF <sup>a</sup>	SD <sup>b</sup>	M	SD	M	SD	M	SD	M	SD
1	$10^{-3}$	29836	1515	17132	7141	16683	1615	2237	394	376	78
2	$10^{-4}$	24666	2886	12178	4067	9414	686	961	65	207	25
3	$10^{-5}$	20902	2554	6129	1701	3588	840	322	42	107	10
4	$10^{-6}$	10737	887	2611	441	2350	496	189	8	78	13
5	background	580	337	116	15	146	8	95	7	75	6

<sup>a</sup> Mean fluorescence calculated using six spots. <sup>b</sup> Standard deviation.

**Table 4. Microarray Experiments Using Peptide 4 and Tetramethyl Rhodamine Goat Anti-Biotin Antibody**

entry	peptide <b>4</b> (mol/L)	goat anti-biotin antibody tetramethyl rhodamine (mg/mL)							
		$10^{-1}$		$10^{-2}$		$10^{-3}$		$10^{-4}$	
		MF <sup>a</sup>	SD <sup>b</sup>	MF	SD	MF	SD	MF	SD
1	$10^{-3}$	15350	1172	13113	637	6828	883	2271	348
2	$10^{-4}$	14721	1443	9121	1974	4981	1065	1535	511
3	$10^{-5}$	10932	1475	6849	933	3377	292	1249	67
4	$10^{-6}$	6606	125	2947	825	791	87	385	39
5	background	1424	109	243	13	167	19	170	12

<sup>a</sup> Mean fluorescence calculated using six spots. <sup>b</sup> Standard deviation.

**Scheme 8. Synthesis of Peptide 7**

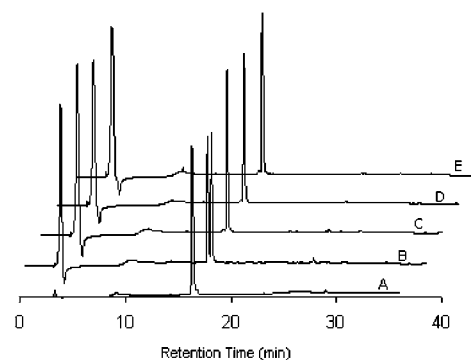
immobilization of streptavidin occurred through a specific interaction.

Incubation of the slides with an anti-biotin antibody labeled with tetramethylrhodamine led to the data collected in Table 4. Again, the biotin antibody interaction was correctly detected at low peptide concentration (Table 4, entry 4). The fluorescence of the spots resulted from a specific interaction, since the spots were found to be indistinguishable from the background following an incubation with a control antibody (goat anti-human Ig G-A-M labeled with tetramethylrhodamine, data not shown).

These results, obtained using model biomolecular interactions with biotin suggest that  $\alpha$ -oxo semicarbazone microarrays may be useful for the large scale study of ligand–protein interactions.

**Stability Study of the  $\alpha$ -Oxo Semicarbazone Linkage.** Among all the criteria considered for the selection of an immobilization chemistry for microarray fabrication, the stability of the bond linking the probe to the surface is perhaps the most important. The linkage has to survive to the different incubations and washings.

We have examined the stability of the  $\alpha$ -oxo semicarbazone bond to hydrolysis using peptide 7, synthesized as shown in Scheme 8 by reaction of glyoxylyl-peptide 6 with semicarbazide.  $\alpha$ -Oxo semicarbazone 7 was dissolved in pH 7.5 HEPES buffer using the experimental conditions described by Podymnugin et al. and incubated



**Figure 5.** Stability of  $\alpha$ -oxo semicarbazone 7 toward hydrolysis. RP-HPLC chromatograms (C18 nucleosil column (4.6  $\times$  150 mm), eluent A: water containing 0.05% TFA by vol; eluent B: acetonitrile/water: 4/1 containing 0.05% TFA by vol, 0–100% B in 30 min, flow rate 1 mL/min, 215 nm, 30  $^{\circ}$ C) of (A)  $\alpha$ -oxo aldehyde peptide 6; (B) coelution of peptide 6 with conjugate 7; (C)  $\alpha$ -oxo semicarbazone 7 in 100 mM HEPES, pH = 7.5 at  $t$  = 0; (D)  $\alpha$ -oxo semicarbazone 7 in 100 mM HEPES, pH = 7.5, 4 h at 65  $^{\circ}$ C, and (E) 24 h at 65  $^{\circ}$ C.

24 h at 65  $^{\circ}$ C. Figure 5 shows that the starting glyoxylyl-peptide 6 was separated by RP-HPLC from semicarbazone 7. Interestingly, no decomposition nor hydrolysis occurred following 24h of incubation at 65  $^{\circ}$ C, whereas Podymnugin reported about 40% of hydrolysis for a semicarbazone formed by reaction of benzyl semicarbazide with benzaldehyde–ODNs. The same resistance to hydrolysis was observed at pH 7.1 or 8.0, highlighting the good stability of the  $\alpha$ -oxo semicarbazone bond and the utility of this immobilization chemistry for microarray fabrication.

**CONCLUSION**

We show in this article that  $\alpha$ -oxo semicarbazone site-specific immobilization chemistry allows the preparation of high quality microarrays. The same chemistry could be used for the fabrication of either oligonucleotide or peptide microarrays. The  $\alpha$ -oxo semicarbazone linkage was found to be very resistant to hydrolysis. The efficiency of  $\alpha$ -oxo semicarbazone ligation and the unique properties of the semicarbazide surface led to high signal-to-noise ratios in different detection experiments.

## ACKNOWLEDGMENT

We acknowledge financial support from CNRS, University de Lille 2, Institut Pasteur de Lille, Institut Pasteur and Sedac-Therapeutics. We thank Jean-Olivier Durand for the preparation of silane **1** and useful discussions. We thank Samia Far for a generous gift of peptide **6**. This project was supported by Interreg II and CNRS fundings (ACI biopuces ADN).

## LITERATURE CITED

- (1) Schena, M., Shalon, D., Davis, R. W., and Brown, P. O. (1995) Quantitative monitoring of gene expression patterns with a complementary DNA microarray. *Science* 270, 467–470.
- (2) Lockhart, D. J., Dong, H., Byrne, M. C., Follettie, M. T., Gallo, M. V., Chee, M. S., Mittmann, C., Wang, C., Kobayashi, M., Horton, H., and Brown, E. L. (1996) Expression monitoring by hybridization to high-density oligonucleotide arrays. *Nat. Biotechnol.* 14, 1675–1680.
- (3) Pollack, J. R., Perou, C. M., Alizadeh, A. A., Eisen, M. B., Pergamenschikov, A., Williams, C. F., Jeffrey, S. S., Botstein, D., and Brown, P. O. (1999) Genome-wide analysis of DNA copy-number changes using cDNA microarrays. *Nature Genet.* 23, 41–46.
- (4) Sosnowski, R. E., Tu, E., Butler, W., O'Connell, J., and Heller, M. (1997) Rapid determination of single base mismatch mutations in DNA hybrids by direct electric field control. *Proc. Natl. Acad. Sci. U.S.A.* 94, 1119–1123.
- (5) Drobyshev, A. N., Mologina, N., Shick, V., Pobedinskaya, D., Yershov, G., and Mirzabekov, A. (1997) Sequence analysis by hybridisation with oligonucleotide microchip: identification of  $\beta$ -thalassaemia mutations. *Gene* 188, 45–52.
- (6) Bulyk, M., Gentalen, E., Lockhart, D. J., and Church, G. M. (1999) Quantifying DNA-protein interactions by double-stranded DNA arrays. *Nat. Biotechnol.* 17, 573–577.
- (7) Sturniolo, T., Bono, E., Ding, J., Radrizzani, L., Tuercio, O., Sahin, U., Braxenthaler, M., Gallazzi, F., Protti, M. P., Sinigaglia, F., and Hammer, J. (1999) Generation of tissue-specific and promiscuous HLA ligand databases using DNA microarrays and virtual HLA class II matrixes. *Nat. Biotechnol.* 17, 555–561.
- (8) Emili, A. Q., and Cagney, G. (2000) Large-scale functional analysis using peptide or protein arrays. *Nat. Biotechnol.* 18, 393–397.
- (9) Fodor, S. P. A., Read, J. L., Pirroung, M. C., Stryer, L., Tsai, Lu, A., and Solas, D. (1991) Light-directed, spatially addressable parallel chemical synthesis. *Science* 251, 767–773.
- (10) Falsey, J. R., Renil, M., Park, S., Li, S., and Lam, K. S. (2001) Peptide and small molecule microarray for high throughput cell adhesion and functional assays. *Bioconjugate Chem.* 12, 346–353.
- (11) Irwing, R. A., and Hudson, P. J. (2000) Proteins emerge from disarray. *Nat. Biotechnol.* 18, 932–933.
- (12) MacBeath, G., and Schreiber, S. L. (2000) Printing proteins as microarrays for high-throughput function determination. *Science* 289, 1760–1763.
- (13) Zhu, H., and Snyder, M. (2001) Protein arrays and microarrays. *Curr. Opin. Chem. Biol.* 5, 40–45.
- (14) During this project, Podymingogin et al. have described the fabrication of ODN microarrays by attachment of benzaldehyde-modified oligodeoxynucleotides to semicarbazide-coated glass. Podymingogin, M. A., Lukhtanov, E. A., and Reed, M. (2001) Attachment of benzaldehyde-modified oligodeoxynucleotide probes to semicarbazide-coated glass. *Nucleic Acids Res.* 29, 5090–5098.
- (15) Olivier, C., Ollivier, N., Hot, D., Huot, L., Lemoine, Y., Huynh-Dinh, T., Gouyette, C., Gras-Masse, H., and Melnyk, O. (2001) A novel generation of DNA microarrays fabricated using semicarbazone ligation. Seventh International Symposium on Solid-Phase Synthesis & Combinatorial Chemical Libraries, poster P22.
- (16) Gras-Masse, H., Lemoine, Y., and Melnyk, O. Patent Application FR 99 15392, publication number 2 801 904, Dec 7, 1999.
- (17) Melnyk, O., Olivier, C., Ollivier, N., Hot, D., Huot, L., Lemoine, Y., Huynh-Dinh, T., Gouyette, C., and Gras-Masse, H. Patent Application WO 01/42495, June 14, 2001.
- (18) Gait, M. J. (1984) An introduction to modern methods of DNA synthesis. In *Oligonucleotide Synthesis: A Practical Approach*; Gait, M. J., Ed., IRL Press: Oxford, pp 1–22.
- (19) Zhang, R. E., Cao, Y. L., and Hearn, M. W. (1991) Synthesis and application of Fmoc-hydrazine for the quantitative determination of saccharides by reversed-phase high-performance liquid chromatography in the low and subpicomole range. *Anal. Biochem.* 195, 160–167.
- (20) Fields, G. B., and Noble, R. L. (1990) Solid-phase peptide synthesis utilizing 9-fluorenylmethoxycarbonyl amino acids. *Int. J. Pept. Protein Res.* 35, 161–214.
- (21) Meldal, M. (1993) In *Peptides 1992, Proceedings of the European Peptide Symposium*; Schneider, C. H., Eberle, A. N., Eds.; ESCOM: Leiden; p 61.
- (22) Urbès, F., Fruchart, J. S., Gras-Masse, H., and Melnyk, O. (2002) C-terminal glyoxylyl peptides for sensitive enzyme-linked immunosorbent assays. *L. I. P. S.* 8, 253–258.
- (23) Geoghegan, K. F., and Stroh, J. G. (1992) Site-directed conjugation of nonpeptide groups to peptides and proteins via periodate oxidation of a 2-amino alcohol. Application to modification at N-terminal serine. *Bioconjugate Chem.* 3, 138–146.
- (24) Fruchart, J. S., Gras-Masse, H., and Melnyk, O. (1999) A new linker for the synthesis of C-terminal peptide  $\alpha$ -oxo aldehydes. *Tetrahedron Lett.* 40, 6225–6228.
- (25) Melnyk, O., Fruchart, J. S., Grandjean, C., and Gras-Masse, H. (2001) Tartric acid-based linker for the solid-phase synthesis of C-terminal peptide  $\alpha$ -oxo aldehydes. *J. Org. Chem.* 66, 4153–4160.
- (26) Ballardur, V., Theretz, A., and Mandrand, B. (1997) Determination of the main forces driving DNA oligonucleotide adsorption onto aminated silica wafers. *J. Colloid Interface Sci.* 194, 408–418.
- (27) Tertykh, V. A., and Yanishpolskii, V. V. (2000) Adsorption and chemisorption of enzymes and other natural macromolecules on silicas. *Surf. Sci. Ser.* 90, 523–564.
- (28) Melnyk, O., Fehrentz, J. A., Martinez, J., and Gras-Masse, H. (2000) Fonctionnalisation of peptides and proteins by aldehyde or keto groups. *Biopolymers (Pept. Sci.)* 55, 165–186.
- (29) Tam, J. P., and Spetzler, J. C. (1995) Chemoselective approaches to the preparation of peptide dendrimers and branched artificial proteins using unprotected peptides as building blocks. *Biomed. Pep. Prot. Nucl. Acids* 1, 123–132.
- (30) Ollivier, N., Olivier, C., Gouyette, C., Huynh-Dinh, T., Gras-Masse, H., and Melnyk, O. (2002) Synthesis of oligonucleotide–peptide conjugates using hydrazone chemical ligation. *Tetrahedron Lett.* 43, 997–999.
- (31) Shchepinov, M. V., Case-Green, S. C., and Southern, E. M. (1997) Steric factors influencing hybridisation of nucleic acids to oligonucleotide arrays. *Nucleic Acids Res.* 25, 1155–1162.
- (32) Melnyk, O., Duburcq, X., Olivier, C., Urbès, F., Auriault, C., and Gras-Masse, H. (2002) Peptide arrays for highly sensitive and specific antibody-binding fluorescence assays. *Bioconjugate Chem.* 13, 713–720.
- (33) Pérez-Luna, V. H., O'Brien, M. J., Opperman, K. A., Hampton, P. D., Lopez, G. P., Klumb, L. A., and Stayton, P. S. (1999) Molecular Recognition between genetically engineered streptavidin and surface-bound biotin. *J. Am. Chem. Soc.* 121, 6469–6478.



# Generation of a Functional Monomolecular Protein Lattice Consisting of an S-Layer Fusion Protein Comprising the Variable Domain of a Camel Heavy Chain Antibody

Magdalena Pleschberger,<sup>†,‡</sup> Angela Neubauer,<sup>‡</sup> Eva M. Egelseer,<sup>†,‡</sup> Stefan Weigert,<sup>‡</sup> Brigitte Lindner,<sup>‡</sup> Uwe B. Sleytr,<sup>†</sup> Serge Muyldermans,<sup>§</sup> and Margit Sára\*,<sup>†,‡</sup>

BMT-Biomolecular Therapeutics GmbH, Brunnerstrasse 59, A-1235 Vienna, Austria, Center for Ultrastructure Research and Ludwig Boltzmann-Institute for Molecular Nanotechnology, University of Agricultural Sciences Vienna, A-1180 Vienna, Austria, and Vrije Universiteit Brussel, Vlaams Interuniversitair Instituut voor Biotechnologie, Paardenstraat 65, B-1640 Sint Genesius Rode, Belgium. Received September 9, 2002; Revised Manuscript Received December 18, 2002

Crystalline bacterial cell surface layer (S-layer) proteins are composed of a single protein or glycoprotein species. Isolated S-layer subunits frequently recrystallize into monomolecular protein lattices on various types of solid supports. For generating a functional protein lattice, a chimeric protein was constructed, which comprised the secondary cell wall polymer-binding region and the self-assembly domain of the S-layer protein SbpA from *Bacillus sphaericus* CCM 2177, and a single variable region of a heavy chain camel antibody (cAb-Lys3) recognizing lysozyme as antigen. For construction of the S-layer fusion protein, the 3'-end of the sequence encoding the C-terminally truncated form rSbpA<sub>31–1068</sub> was fused via a short linker to the 5'-end of the sequence encoding cAb-Lys3. The functionality of the fused cAb-Lys3 in the S-layer fusion protein was proved by surface plasmon resonance measurements. Dot blot assays revealed that the accessibility of the fused functional sequence for the antigen was independent of the use of soluble or assembled S-layer fusion protein. Recrystallization of the S-layer fusion protein into the square lattice structure was observed on peptidoglycan-containing sacculi of *B. sphaericus* CCM 2177, on polystyrene or on gold chips precoated with thiolated secondary cell wall polymer, which is the natural anchoring molecule for the S-layer protein in the bacterial cell wall. Thereby, the fused cAb-Lys3 remained located on the outer S-layer surface and accessible for lysozyme binding. Together with solid supports precoated with secondary cell wall polymers, S-layer fusion proteins comprising rSbpA<sub>31–1068</sub> and cAbs directed against various antigens shall be exploited for building up monomolecular functional protein lattices as required for applications in nanobiotechnology.

## INTRODUCTION

Crystalline bacterial cell surface layers (S-layers) represent the outermost cell envelope component of many bacteria and archaea. S-Layer lattices completely cover the cell surface during all stages of bacterial growth and division, and they are mostly composed of a single protein or glycoprotein species. S-Layers exhibit either oblique, square, or hexagonal lattice symmetry (1–3). Depending on the type of S-layer protein, the subunits show a molecular mass of 40 000 to 200 000 Da. In bacteria, the S-layer subunits are linked to each other and to the underlying cell envelope layer by noncovalent interactions. In the case of *Bacillaceae*, the N-terminal part is involved in anchoring the S-layer subunits to the rigid cell wall layer via a distinct type of glycan, termed secondary cell wall polymer (1, 4–8).

Isolated S-layer subunits frequently possess the ability to recrystallize in suspension. This process leads to self-assembly products, which can have the shape of flat sheets or open-ended cylinders (2). The S-layer subunits

may also recrystallize into monomolecular protein lattices on solid supports, such as gold chips, silicon wafers, or plastics, at the air/water interface, on lipid films or liposomes. The properties of the underlying material allow prediction of the orientation of the S-layer subunits that attach either with their outer or inner surface (3, 9–11).

The cell surface of *Bacillus sphaericus* CCM 2177 is completely covered with a square S-layer lattice, which is composed of identical subunits with a molecular mass of 127 000 Da. The gene encoding this S-layer protein, termed SbpA, had been sequenced, cloned in plasmid pET28a and expressed in *Escherichia coli* HMS174(DE3) (12). The protein precursor includes a 30 amino acid long typical Gram-positive signal sequence peptide and consists of a total of 1 268 amino acids. Studies on the structure–function relationship of SbpA revealed that 200 C-terminal amino acids could be deleted without interfering with the self-assembly process or the formation of the square lattice structure (12). Furthermore, amino acid position 1 068 was found to be located on the outer S-layer surface and was therefore exploited as fusion site for the production of a chimeric S-layer protein comprising the sequence of the major birch pollen allergen (12). The S-layer protein SbpA recognizes a distinct type of secondary cell wall polymer as the proper anchoring structure in the rigid cell wall layer (13). The polymer chains, which are covalently linked to the

\* To whom correspondence should be addressed: University of Agricultural Sciences Vienna, Gregor Mendelstrasse 33, A-1180 Vienna, Austria. Tel.: +43-1-47 654 2208. Fax: +43-1-47 89 112. e-mail: sara@edv1.boku.ac.at.

<sup>†</sup> BMT-Biomolecular Therapeutics GmbH.

<sup>‡</sup> University of Agricultural Sciences Vienna.

<sup>§</sup> Vrije Universiteit Brussel.

peptidoglycan, consist of 8 to 9 disaccharide repeating units with the structure  $\rightarrow 3$ -[4,6-*O*-(1-carboxyethylidene)]- $\alpha$ -D-ManpNAc-(1 $\rightarrow$ 4)- $\beta$ -D-GlcpNAc-(1 $\rightarrow$ ). The formation of self-assembly products by SbpA or rSbpA strongly depends on the presence of bivalent cations (13).

Camel antibodies are part of the humoral immune response of camels and llamas. One group of antibodies of *Camelidae* are heavy chain dimers, in which the light chains are totally absent. This unique antibody species interacts with the antigen by virtue of a single variable domain, termed VHH (variable domain of a heavy chain of a camel heavy chain antibody). A single VHH domain has a molecular mass of only 15 000 Da and is the smallest known complete antigen binding fragment from a functional immunoglobulin. Despite the absence of the combinatorial diversity of conventional heterodimeric antibodies caused by the VH (variable domain of the heavy chain)-VL (variable domain of the light chain) parts, these heavy chain antibodies exhibit a broad antigen binding repertoire by having enlarged their variable region CDR3 (14, 15). Recombinant VHHs that were selected from VHH libraries are well expressed in *E. coli*, highly soluble in aqueous environments, and very resistant against denaturation and display high affinity and specificity toward their antigens. Because of their smaller size, VHHs can interact with epitopes that are not recognized by conventional antibody fragments. Due to these properties, VHHs clearly offer an improvement over conventional, more complex, antibody fragments, e. g., in diagnostic applications or as immunoadsorbents, where the stability of the biomolecular probes is critical. Moreover, VHHs constitute ideal modular building blocks for manifold molecular constructs (14, 15).

To explore the potential advantages of camel single domain antibodies and to gain insight into how they recognize their target, Desmyter et al. (16) solved the crystal structure of a camel VHH complexed with hen's egg lysozyme. Lysozyme was chosen as immunogen, because its 3-D structure is well-known and complexes with various antibody fragments have been analyzed before (17–24). Two VHHs that were cloned and expressed in *E. coli* (25, 26) bound lysozyme in a 1 to 1 stoichiometry with affinity constants of  $5 \times 10^{-8}$  M and  $5 \times 10^{-7}$  M, respectively. These VHHs were termed cAb-Lys2 and cAb-Lys3.

In the present study, an S-layer fusion protein comprising the sequence of cAb-Lys3 was constructed. For this purpose, the 3'-end of the gene encoding the C-terminally truncated form of the S-layer protein SbpA, termed rSbpA<sub>31–1068</sub>, was fused via a short linker to the 5'-end of the gene encoding the VHH fragment of the camel antibody cAb-Lys3 directed against lysozyme. The obtained S-layer fusion protein (theoretical molecular mass of 123 947 Da) represents a model system for the construction of further chimeric proteins, that comprise rSbpA<sub>31–1068</sub> and cAbs for generating monomolecular functional protein lattices on solid supports, as required for many applications in nanobiotechnology including biochip development.

## MATERIAL AND METHODS

**Cloning of the Genes Encoding rSbpA<sub>31–1068</sub>/cAb-Lys3.** All PCR reactions were performed as described in (27). For amplification of the gene encoding rSbpA<sub>31–1068</sub>, chromosomal DNA of *B. sphaericus* CCM 2177 was used as template. The oligonucleotide primers *sbpA*/*NcoI* [5'-CG GAT TCC ATG GCG CAA GTA AAC GAC TAT AAC AAA ATC-3'], which introduced the restriction site (bold)

*NcoI*, and the reverse primer *sbpA*/*NheI* [5'-GAC CGC GCT AGC TTC TGA ATA TGC AGT AGT TGC TGC C-3'], which introduced the *NheI* restriction site at the 3'-end, were constructed. The *cAb-Lys3* gene was amplified from plasmid *cAb-Lys3*-pHen6 (16). For this purpose, the oligonucleotide primers *cAb*/*NheI* [5'-CGG ATT GCT AGC GAT GTG CAG CTG CAG GCG-3'] and *cAb*/*XhoI* [5'-GAC CGC TCG AGT TAT GAG GAG ACG GTG ACC TGG G-3'], which introduced the restriction sites *NheI* and *XhoI*, were used. Because of the GC-rich sequence of *cAb-Lys3*, betaine was added to a final concentration of 1.5 M to the PCR mixture. To obtain the plasmid pET28a-*sbpA*<sub>(93–3204)</sub>, the gel-purified PCR product *sbpA*<sub>(93–3204)</sub>, encoding the truncated form of the S-layer protein, was ligated into the corresponding restriction sites of plasmid pET28a, which was established in *E. coli* TG1. For generating the chimeric *sbpA*<sub>(93–3204)</sub>/*cAb-Lys3* gene, the gel-purified PCR product *cAb-Lys3*, encoding the VHH domain of the camel antibody directed against lysozyme, was ligated into the corresponding restriction sites of plasmid pET28a-*sbpA*<sub>(93–3204)</sub>, which was used for transformation of *E. coli* TG1.

**Expression of the Chimeric *sbpA*<sub>(93–3204)</sub>/*cAb-Lys3* Gene.** The plasmid stability test and heterologous expression of the *sbpA*<sub>(93–3204)</sub>/*cAb-Lys3* gene in *E. coli* HMS174(DE3) were performed as described in (27). Samples of the *E. coli* HMS174(DE3) cultures were taken 1 to 5 h after induction of *sbpA*<sub>(93–3204)</sub>/*cAb-Lys3* gene expression by the addition of 1 mM isopropyl  $\beta$ -D-thiogalactopyranoside (IPTG, GEBRU). Preparation of samples for SDS-PAGE analysis was carried out as described by Laemmli (28). For electron microscopic investigation, whole cells of *E. coli* HMS174(DE3) were prepared as described in ref 29. Electron microscopic investigations were done with a Philips CM 100 transmission electron microscope (TEM).

**Isolation of the S-Layer Fusion Protein from the Host Cells and Purification.** Isolation of rSbpA<sub>31–1068</sub>/cAb-Lys3 from *E. coli* HMS174(DE3) was performed as described in a previous study (30). After lysis of the host cells, 100 mg wet pellet, obtained by centrifugation at 30 000g for 15 min at 4 °C, was suspended in 4 mL of 5 M guanidine hydrochloride in 50 mM Tris-HCl buffer (pH 7.2). Then the suspension was centrifuged at 36 000g for 30 min at 4 °C, the supernatant containing the S-layer fusion protein was diluted 1:2.5 with 50 mM Tris-HCl buffer (pH 7.2), and the clear solution was subjected to gel permeation chromatography using a Superdex 200 column (Pharmacia) equilibrated in 2 M guanidine hydrochloride in 50 mM Tris-HCl buffer (pH 7.2). Fractions belonging to the first peak were pooled and dialyzed against MilliQ-water for 18 h at 4 °C, lyophilized, and stored at -20 °C. All guanidine hydrochloride solutions and buffers used during the isolation and purification procedure contained 150 mM NaCl. Immunoblotting using a polyclonal rabbit antiserum raised against the S-layer protein of *B. sphaericus* CCM 2177 was performed as described (31). The presence of the cAb-Lys3 moiety in the S-layer fusion protein was checked by immunoreactivity with a polyclonal rabbit anti-camel antiserum (Sigma C7540).

**Investigation of the Self-Assembly Properties of the S-Layer Fusion Protein and Recrystallization on Peptidoglycan-Containing Sacculi.** Two milligrams of the gel permeation chromatography-purified and lyophilized S-layer fusion protein were dissolved in 1 mL 5 M guanidine hydrochloride in 50 mM Tris-HCl buffer (pH 7.2) and the solution was dialyzed against 10 mM CaCl<sub>2</sub> in MilliQ-water containing 1 mM 1,4-dithio-



DL-threitol (DTT) for 18 h at 4 °C. For recrystallization of the S-layer fusion protein on peptidoglycan-containing sacculi, 2 mg rSbpA<sub>31–1068</sub>/cAb-Lys3 was dissolved in 1 mL of 5 M guanidine hydrochloride in 50 mM Tris-HCl buffer (pH 7.2) and 2 mg of lyophilized peptidoglycan-containing sacculi of *B. sphaericus* CCM 2177, which was prepared according to (12, 13), was added. The suspension was dialyzed under conditions described above. Peptidoglycan-containing sacculi carrying a monolayer of recrystallized S-layer fusion protein are referred to as recrystallization products in all further experiments. To keep the S-layer fusion protein water soluble, the guanidine hydrochloride-extract was dialyzed against 1 mM DTT in MilliQ-water.

**Localization of the Fused cAb-Lys3 by Immunogold-Labeling of Self-Assembly and Recrystallization Products.** Self-assembly and recrystallization products obtained with rSbpA<sub>31–1068</sub>/cAb-Lys3 were incubated with a polyclonal rabbit antiserum raised against camel antibodies [Sigma C7540; diluted 1:2 with 50 mM Tris-HCl buffer (pH 7.2)] at 20 °C for 1 h. After centrifugation of the suspensions at  $16\,000 \times g$  for 20 min at 4 °C and two washing steps with TBS (50 mM Tris-HCl, pH 7.2, containing 0.15 M NaCl), the pellets were resuspended in 100  $\mu$ L solution of a Protein A-colloidal gold conjugate (10 nm, Sigma P1039) and incubated at 20 °C for 2 h. All further steps were carried out as described in ref 12.

**Surface Plasmon Resonance (SPR) Studies for Investigation of the Functionality of the Fused cAb-Lys3.** SPR experiments were performed with a Biacore 2000 system (BIAcore, Sweden). Lysozyme was immobilized on a CM5 chip on flow cell 1 (FC1). For this purpose the carboxylic acid groups on the sensor chip were activated by injecting 35  $\mu$ L of a solution of 400 mM 1-ethyl-3-(3-diaminopropyl)carbodiimide (EDC; Sigma E7750) and 100 mM *N*-hydroxysuccinimide in MilliQ-water. Thereafter, 50  $\mu$ L of a solution of 0.5 mg/mL lysozyme (Sigma L6876) in MilliQ-water was injected. The immobilization procedure was completed by blocking with 35  $\mu$ L of 1 M ethanolamine hydrochloride, dissolved in MilliQ-water at pH 8.5. Continuous flow buffer was HBS (10 mM HEPES, pH 7.2, containing 0.15 M NaCl and 0.005% Tween 20). The amount of immobilized lysozyme was expressed in terms of resonance units (RU; 1000 RU correspond to approximately 1 ng/mm<sup>2</sup>). Untreated carboxymethylated dextran on flow cell 2 (FC2) was used as reference surface. For interaction studies, gel permeation-chromatography purified, lyophilized rSbpA and rSbpA<sub>31–1068</sub>/cAb-Lys3 were dissolved in HBS buffer at a concentration of 0.8  $\mu$ mol/mL. During the reaction time, a continuous flow of HBS buffer (10  $\mu$ L/min) was maintained over the sensor surface. The contact and dissociation time of rSbpA<sub>31–1068</sub>/cAb-Lys3 with the surface was 20 min and 800 s, respectively.

**Dot Blot Assays for Investigating the Accessibility of the Fused cAb-Lys3.** To investigate the accessibility of the fused cAb-Lys3 in the water soluble, self-assembled, or recrystallized S-layer fusion protein, 5  $\mu$ L samples with an S-layer protein content of 1 mg/mL were dried onto a nitrocellulose membrane. After blocking with 2% Top Block (Fluka) in TBS and incubating in 20 mL of lysozyme solution (250  $\mu$ g/mL TBS containing 2% Top Block) for 1 h at 20 °C, the membrane was washed three times with washing buffer (TBS containing 0.5% Tween) and finally incubated in a polyclonal rabbit antiserum raised against lysozyme (Rockland 200–4172; diluted 1:4000 in washing buffer containing 2% Top Block). After further washing, the membrane was incubated with a

solution of anti-rabbit IgG alkaline phosphatase-conjugate (Sigma A3687; diluted 1:5000 in blocking solution) for 1 h at 20 °C. Bound antibody was finally visualized by using BCIP/NBT (Roche 1681451) as substrate for the alkaline phosphatase.

**Recrystallization of the S-Layer Fusion Protein on Polystyrene and Comparison of the Ability of the Formed Monolayer To Bind Lysozyme with That of a Monolayer Generated by Recrystallization of rSbpA and Chemical Coupling of cAb-Lys3 by Means of ELISA.** Lyophilized S-layer fusion protein (2 mg) was dissolved in 1.2 mL of 5 M guanidine hydrochloride in 50 mM Tris-HCl buffer (pH 7.2) and dialyzed against 1 mM DTT in MilliQ-water for 18 h at 4 °C. After centrifugation at 30 000g for 15 min at 4 °C, the clear supernatant was diluted to a final protein concentration of 100  $\mu$ g/mL with 50 mM Tris-HCl buffer (pH 9.0) containing 10 mM CaCl<sub>2</sub>. The wells of a polystyrene ELISA plate (Greiner Austria, 665101) were filled with 300  $\mu$ L aliquots of the protein solution and incubated for 18 h at 4 °C for recrystallization. After rinsing with MilliQ-water, samples were taken for AFM analysis.

Recrystallization of rSbpA was performed under the same conditions. After cross-linking the S-layer lattice with glutaraldehyde (1% in TBS), activation of free carboxylic acid groups with EDC (32), and washing with ice cold MilliQ-water, 100  $\mu$ L of a cAb-Lys3 solution (10  $\mu$ g/mL MilliQ-water, pH adjusted to 9.0 with 0.1 M NaOH) was added and incubated for 18 h at 4 °C. Unbound protein was removed by washing with TBS containing 0.1% TRITON X-100.

To investigate the ability to bind lysozyme, both types of monolayers were incubated with various concentrations of biotinylated lysozyme (3, 6, or 12 ng in TBS containing 1% TRITON X-100 per well) for 1 h at 20 °C. After rinsing with MilliQ-water and TBS containing 1% TRITON X-100, 100  $\mu$ L of a streptavidin–peroxidase conjugate (Amersham RPN 4401; diluted 1:5 000 in TBS containing 1% TRITON X-100) was transferred into the wells, and the plates were incubated for 1 h at 20 °C. Bound streptavidin–peroxidase conjugate was visualized by using 3,3',5,5'-tetramethylbenzidine (TMB; Sigma T3405) as substrate for peroxidase. Absorption was measured at 450 nm in an ELISA reader (E-Liza Mat-3000, DRG). As a reference, the ELISA was performed on plain rSbpA.

For determination of the amount of cAb-Lys3 that could be covalently bound to the rSbpA monolayer, the S-layer protein was recrystallized on polystyrene beads with a diameter of 1  $\mu$ m (Bangs Laboratories PC03N) under the same conditions as described for the ELISA wells. After cross-linking the S-layer lattice with glutaraldehyde and activation of free carboxylic acid groups with carbodiimide, cAb-Lys3 was immobilized under conditions described above. The amount of covalently bound cAb-Lys3 was determined as described in previous studies (32–34). The presence of the square lattice structure was checked by freeze-etching of the polystyrene beads and TEM analysis (29).

**Binding of Thiolated Secondary Cell Wall Polymer to Plain Gold Chips and Recrystallization of rSbpA and the S-Layer Fusion Protein.** Secondary cell wall polymer was isolated from peptidoglycan-containing sacculi of *B. sphaericus* CCM 2177 and purified (13). Chemical modification of the reducing end on the polymer chains and introduction of a terminal sulfhydryl group by modification with 2-iminothiolane was performed (35). Gold chips (silicon <100>, coated with 1



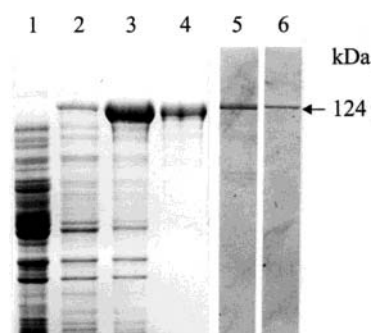
nm Ti and 60 nm Au) with an area of 1 cm<sup>2</sup> were cleaned by incubation in a solution containing 50 mM KOH and 15% H<sub>2</sub>O<sub>2</sub> for 30 min at 60 °C, extensive rinsing with MilliQ-water and drying in an oven at 150 °C for 1 h. The clean gold chips were incubated in a solution containing 100 ng of thiolated secondary cell wall polymer in 1 mL MilliQ-water (pH adjusted to 3.5 with 10 mM HCl) at 20 °C for 1 h and washed five times with MilliQ-water. Recrystallization of rSbpA and rSbpA<sub>31–1068</sub>/cAb-Lys3 on plain gold chips or on gold chips precoated with thiolated secondary cell wall polymer was performed under the same conditions as described for polystyrene.

**Atomic Force Microscope (AFM) Analysis.** A Nano-scope III AFM (Digital Instruments, Santa Barbara, CA) equipped with a liquid cell and a 120  $\mu$ m scanner and oxide-sharpened Si<sub>3</sub>N<sub>4</sub> tips (Nanoprobes, Digital Instruments, Santa Barbara, CA) with a nominal spring constant of 0.06 N/m was used for all AFM investigations. Imaging of rSbpA or rSbpA<sub>31–1068</sub>/cAb-Lys3 after recrystallization on solid supports was carried out in contact mode under liquid (100 mM NaCl). Height and deflection signals were recorded simultaneously (error signal mode). The applied force was kept at about 1 nN and the scan rate was 5.1 Hz at a scan size of 1 by 1  $\mu$ m. Particular care was taken to avoid dewetting of the samples when mounting them in the fluid cell. Force versus distance curves on plain gold chips or gold chips precoated with thiolated secondary cell wall polymer were recorded at 1 Hz. Measurements were carried out in the following electrolytes: 1 and 100 mM NaCl in 1 mM glycine-HCl buffer (pH 3.5), 1 mM Tris-HCl buffer (pH 7.2), or 1 mM Tris-HCl buffer (pH 9.0). Evaluation of force data was carried out using SPIP software (Image Metrology, Lyngby, Denmark).

## RESULTS

**Cloning and Expression of the Gene Encoding rSbpA<sub>31–1068</sub>/cAb-Lys3.** The PCR product which was obtained by amplification of the *sbpA* gene using the primers *sbpA/NcoI* and *sbpA/NheI* and which encoded the truncated form of the S-layer protein SbpA (rSbpA<sub>31–1068</sub>) was ligated into the pET28a vector. After cloning in *E. coli* TG1, amplification, and isolation of the plasmid pET28a-*sbpA*(<sub>93–3204</sub>), the gene encoding a single VHH domain of a camel antibody recognizing lysozyme, termed cAb-Lys3, was ligated via the corresponding restriction sites into this plasmid. The resulting vector pET28a-*sbpA*(<sub>93–3204</sub>)/cAb-Lys3 was established in *E. coli* HMS174(DE3). After induction of expression by the addition of IPTG, biomass samples of *E. coli* HMS174(DE3) were harvested at various points of time and subjected to SDS-PAGE analysis and ultrathin sectioning. In comparison to *E. coli* HMS174(DE3) cells harvested before the addition of IPTG (Figure 1; lane 1), an additional high molecular mass protein band was observed on SDS-gels in samples from *E. coli* HMS174(DE3) cultures induced to express the chimeric *sbpA*(<sub>93–3204</sub>)/cAb-Lys3 gene (Figure 1; lanes 2 and 3). This additional protein band had an apparent molecular mass of 124 000 Da.

**Isolation, Purification, and Characterization of the S-Layer Fusion Protein.** As derived from SDS-PAGE analysis, the recombinant S-layer fusion protein had accumulated in the insoluble fraction of the lysed *E. coli* HMS174(DE3) cells (data not shown). This was in agreement with data from ultrathin-sectioned preparations of whole cells, which revealed the presence of inclusion bodies in the cytoplasm of the host cells, as it was observed in a previous study for rSbpA (12). The



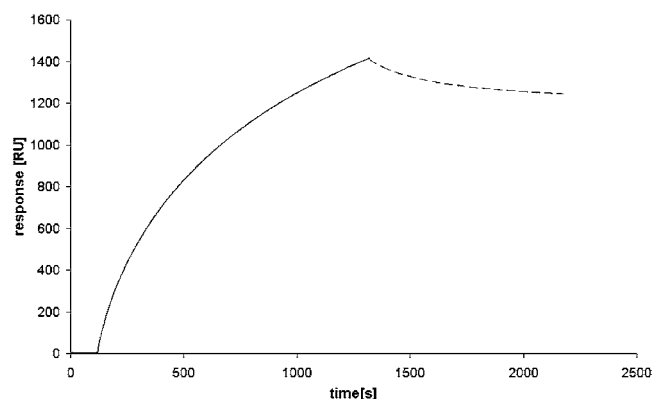
**Figure 1.** SDS PAGE analysis patterns (lanes 1–3) of SDS-extracts of whole cells of *E. coli* HMS174(DE3) harboring the pET28a-*sbpA*(<sub>93–3204</sub>)/cAb-Lys3 gene construct before (lane 1) and 2 h (lane 2) and 5 h (lane 3) after induction of *sbpA*(<sub>93–3204</sub>)/cAb-Lys3 expression. Lane 4: SDS-extracts of gel permeation chromatography purified rSbpA<sub>31–1068</sub>/cAb-Lys3. Immunoblot analysis of SDS-extracts of gel permeation chromatography purified rSbpA<sub>31–1068</sub>/cAb-Lys3 (lanes 5 and 6). The presence of the SbpA-portion was checked with anti-SbpA antiserum and anti-rabbit IgG-alkaline phosphatase conjugate (lane 5). The presence of the cAb-Lys3 moiety was checked with anti-camel antiserum and anti-rabbit IgG-alkaline phosphatase conjugate (lane 6).

insoluble fraction of the lysed *E. coli* HMS174(DE3) cells was extracted with guanidine hydrochloride and subjected to gel permeation chromatography. After unifying the fractions from the first peak and removing guanidine hydrochloride by dialysis, only a single major protein band with an apparent molecular mass of 124 000 Da was observed on SDS-gels (Figure 1; lane 4). On immunoblots, a strong cross reaction was observed between the high molecular mass protein band and the polyclonal rabbit antiserum raised against the S-layer protein SbpA of *B. sphaericus* CCM 2177, as well as with the polyclonal rabbit antiserum raised against camel serum (Figure 1; lanes 5 and 6). The identification of the high molecular mass protein band as the S-layer fusion protein rSbpA<sub>31–1068</sub>/cAb-Lys3 was finally accomplished by N-terminal sequencing. The first five amino acids (AQVND) were identical to those of the S-layer protein SbpA (12). To investigate the self-assembly properties, purified and lyophilized S-layer fusion protein was denatured in 2 M guanidine hydrochloride, and the solution was subsequently dialyzed against 10 mM CaCl<sub>2</sub> in 1 mM DTT. As shown by negative-staining, the S-layer fusion protein reassembled into flat sheets, which clearly exhibited the square lattice structure (not shown). Self-assembly products were mostly double layers, but also multilayers were observed. The S-layer fusion protein recognized peptidoglycan-containing sacculi of *B. sphaericus* CCM 2177 as binding site and recrystallized into the square lattice (Figure 2A).

**Localization of the Fused cAb-Lys3 by Immuno-gold-Labeling of Self-Assembly and Recrystallization Products.** Self-assembly and recrystallization products obtained with rSbpA<sub>31–1068</sub>/cAb-Lys3 were labeled with a polyclonal rabbit anti-camel antiserum and bound antibodies were visualized with a Protein A-colloidal gold conjugate. Negatively stained preparations of self-assembly products (not shown) and recrystallization products (Figure 2B) prepared with rSbpA<sub>31–1068</sub>/cAb-Lys3 were densely labeled with the Protein A-colloidal gold conjugate, while self-assembly and recrystallization products formed by rSbpA remained completely unlabeled (not shown). Because of the specific orientation of the S-layer fusion protein in recrystallization products, the inner S-layer surface was blocked, while the outer face was exposed to the environment. This finally confirmed



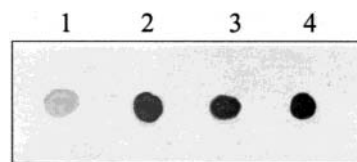
**Figure 2.** Electron micrographs of negatively stained preparations of recrystallization products formed by rSbpA<sub>31-1068</sub>/cAb-Lys3, (A) before and (B) after binding of anti-camel antibodies and labeling with a Protein A-colloidal gold conjugate. Bars, 100 nm.



**Figure 3.** Sensorgram showing the association (—) and dissociation (---) between lysozyme immobilized on the CM5 sensor chip surface and water soluble rSbpA<sub>31-1068</sub>/cAb-Lys3. The sensorgram indicates specific affinity of rSbpA<sub>31-1068</sub>/cAb-Lys3 to lysozyme.

that the cAb-Lys3-portion was located on the outer surface of the S-layer lattice (Figure 2 B).

**Surface Plasmon Resonance (SPR) Studies for Investigation of the Functionality of the Fused cAb-Lys3.** To investigate the functionality of the fused cAb-Lys3 by means of SPR measurements, a solution of rSbpA<sub>31-1068</sub>/cAb-Lys3 in HBS buffer was conducted over a CM5 sensor chip on which 900 RU of lysozyme had been covalently bound. In Figure 3, the untreated CM5 sensor surface which was used as a reference surface was subtracted from the sensorgram obtained with rSbpA<sub>31-1068</sub>/cAb-Lys3. The two separate sensorgrams clearly showed that the water soluble rSbpA<sub>31-1068</sub>/cAb-Lys3 exhibited affinity toward lysozyme, but did not bind



**Figure 4.** Dot Blots assays indicating the accessibility of cAb-Lys3 in the water soluble, self-assembled, and recrystallized S-layer fusion protein. Spot 1: rSbpA; spot 2: water soluble rSbpA<sub>31-1068</sub>/cAb-Lys3; spot 3: self-assembly products formed by rSbpA<sub>31-1068</sub>/cAb-Lys3; spot 4: recrystallization products obtained with rSbpA<sub>31-1068</sub>/cAb-Lys3.

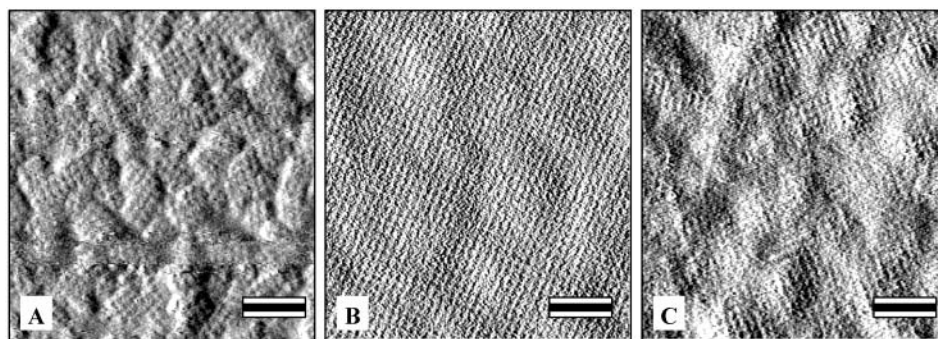
to the plain CM5 surface at all. To exclude the possibility of nonspecific interactions between the S-layer protein moiety and lysozyme, a solution of rSbpA was used in an additional experiment. Since rSbpA showed absolutely no affinity to lysozyme (curve not shown), it was confirmed that binding of the S-layer fusion protein had occurred due to specific interactions between the cAb-Lys3-moiety and the immobilized antigen.

**Dot Blot Assays for Investigating the Accessibility of the Fused cAb-Lys3.** Dot blot assays were performed to investigate the accessibility of the fused cAb-Lys3 in the water soluble, self-assembled, and recrystallized state of the S-layer fusion protein. As shown in Figure 4, the reaction toward lysozyme was comparable for all samples, independent of the state of the S-layer fusion protein. Assuming an identical functionality of cAb-Lys3 in all S-layer fusion protein samples, these findings indicated that the accessibility of the fused functional sequence for the antigen was not reduced in the self-assembled or recrystallized S-layer fusion protein.

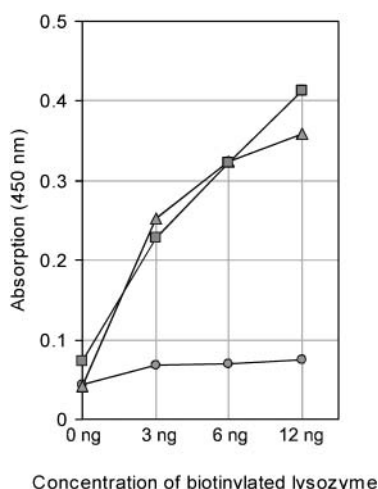
**Recrystallization of the S-Layer Fusion Protein on Polystyrene and Comparison of the Ability of the Formed Monolayer To Bind Lysozyme with That of a Monolayer Generated by Recrystallization of rSbpA and Chemical Coupling of cAb-Lys3 by Means of ELISA.** AFM analysis revealed that rSbpA and the S-layer fusion protein were capable of recrystallizing into the square lattice structure on polystyrene, which was the material of the ELISA wells. Both types of S-layer monolayers consisted of numerous randomly orientated monocrystalline patches with an average size of 100 nm (Figure 5A). The patches clearly displayed the square lattice structure with a center to center spacing of the morphological units of 13.1 nm, which is characteristic of the S-layer protein SbpA from *B. sphaericus* CCM 2177 (12).

For quantification of the amount of cAb-Lys3 that could be chemically coupled to the rSbpA monolayer, the S-layer protein was recrystallized on polystyrene beads with a diameter of 1  $\mu$ m. Freeze-etching revealed that the beads were completely covered with the square S-layer lattice (not shown). On all beads, the smooth outer S-layer surface was exposed, indicating that the subunits had attached with their more corrugated inner surface (9). After cross linking the S-layer protein with glutaraldehyde and activation of free carboxylic acid groups with carbodiimide, 130 ng cAb-Lys3 could be immobilized per cm<sup>2</sup> monomolecular S-layer lattice. Considering that the molecular mass of cAb-Lys3 is 15 000 Da, this amount corresponds to 8–9 cAb-Lys3 molecules per morphological unit or to at least 2 cAb-Lys3 molecules per S-layer subunit. For comparison, only 4 cAb-Lys3 residues were available per morphological unit in the case of the S-layer fusion protein. Despite this difference, both types of monolayers gave comparable





**Figure 5.** AFM images of (A) rSbpA recrystallized on polystyrene and (B) rSbpA and (C) rSbpA<sub>31-106</sub>/cAb-Lys3 recrystallized on gold chips precoated with thiolated secondary cell wall polymer. In B and C, spherical clusters of ~50 nm diameter resembling the topography of the sputtered gold surfaces are visible underneath the S-layer lattice. Images were recorded with simultaneous acquisition of the deflection signal and height signal (not shown). Bars, 100 nm.



**Figure 6.** ELISA curves to compare the ability of the monolayer formed by the S-layer fusion protein (■) and the monolayer generated by recrystallization of rSbpA and chemical coupling of cAb-Lys3 (▲) to bind biotinylated lysozyme (concentration in ng/well). rSbpA (●) was used as a blank.

signals in the ELISA to detect lysozyme. No binding of lysozyme was observed on the rSbpA monolayer used as reference substrate (Figure 6).

**Binding of Thiolated Secondary Cell Wall Polymer to Plain Gold Chips and AFM Analysis.** To exploit the specific interactions between the S-layer protein and its natural anchoring molecule in the bacterial cell wall (12, 13) and to favor recrystallization under in vivo like conditions in order to minimize the number of grain boundaries as observed on polystyrene, the gold chips were precoated with thiolated secondary cell wall polymer. Successful binding of the secondary cell wall polymer was confirmed by comparing force versus distance curves measured on plain gold chips with those obtained on gold chips precoated with thiolated secondary cell wall polymer. On clean gold chips, force versus distance curves typically displayed a clear jump-to-surface by van der Waals forces upon approach and some adhesion upon retraction of the tip independent of the ionic strength or pH of the electrolyte (Figure 7a). This was the expected behavior of a Si<sub>3</sub>N<sub>4</sub> tip and a clean, hard, hydrophobic surface in the absence of long-range interactions. In contrast, approach curves recorded on gold chips precoated with thiolated secondary cell wall polymer displayed a smooth, exponentially increasing, long range repulsive force (Figure 7b) with a decay length between 6 and 20 nm depending on the pH and the ionic strength of the electrolyte. A curve morphology like that is either caused by repulsive electrostatic forces (36, 37)

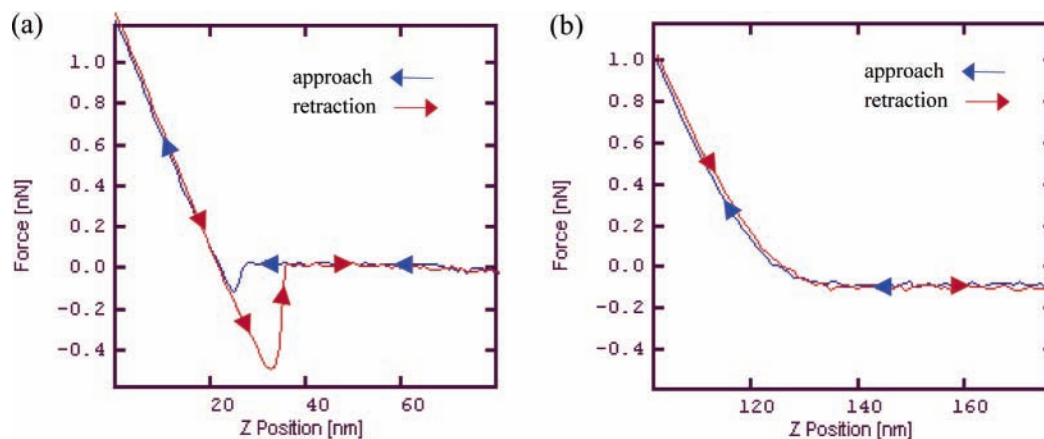
or by polymer brushes grafted to a surface (38, 39). Since in the case of the secondary cell wall polymer net negatively charged carbohydrate chains (13) were bound to the gold surface, force versus distance curves were most likely effected by both of the above-mentioned types of long-range forces. The Si<sub>3</sub>N<sub>4</sub> tip used also had a negative charge at pH > 6 (37, 40). The decay length of the repulsive force observed in the approach curves increased significantly from 6 to 20 nm, when the pH was increased from 3.5 to 7.2, reflecting the increase in charge density on both, the tip and polymer chains at higher pH. At the same time, there was only a moderate dependence of the decay length on the ionic strength. At pH 7.2, this was 20 nm in 1 mM NaCl and 15 nm in 100 mM NaCl. Since the range of electrostatic double layer forces is limited (~1 nm) in 100 mM NaCl, these findings indicated a significant impact of polymer brush forces to the observed repulsion. Thus it became obvious that under physiological conditions, the carbohydrate chains actually formed the expected structure with the individual chains reaching into the aqueous phase on the gold chip. The lack of adhesion in the retraction curves on gold chips precoated with thiolated secondary cell wall polymer was attributed to the hydrophilic nature of the coated surface.

**Recrystallization of rSbpA and the S-Layer Fusion Protein on Plain Gold Chips and Gold Chips Precoated with Thiolated Secondary Cell Wall Polymer and AFM Analyses.** The recombinant S-layer protein rSbpA was capable of recrystallizing into the square lattice structure on plain gold chips. As shown for polystyrene (Figure 5A), the S-layer monolayer consisted of randomly aligned monocrystalline S-layer patches with a size of approximately 200 nm, which clearly exhibited the square lattice structure. In contrast, a regularly structured protein lattice with significantly improved long range order was generated, when gold chips precoated with thiolated secondary cell wall polymer were used for recrystallization of rSbpA (Figure 5B). The S-layer fusion protein did not recrystallize on plain gold chips at all (not shown), but a monomolecular protein array consisting of extended patches of crystalline domains with square lattice symmetry was formed on gold chips precoated with thiolated secondary cell wall polymer (Figure 5 C).

## DISCUSSION

Studies on the structure–function relationship of the S-layer protein SbpA of *B. sphaericus* CCM 2177 were considered as presupposition for the construction of S-layer fusion proteins, which retained the specific self-





**Figure 7.** AFM analysis. Force versus distance curves measured on (a) plain gold and on (b) gold chips precoated with thiolated secondary cell wall polymer. The curves shown here were obtained in an electrolyte solution consisting of 100 mM NaCl in 1 mM Tris-HCl buffer (pH 7.2) using oxide-sharpened silicon nitride tips. Curves shown here were selected from the whole set of data collected in different electrolytes (curve morphologies are typical of the respective surfaces). The decay lengths of the repulsive force recorded on gold chips precoated with thiolated secondary cell wall polymer were evaluated after correction of the curves for the additional distance due to cantilever deflection. The approach and retraction parts of the curves are indicated by arrows.

assembly properties of the S-layer protein moiety, as well as the functionality of the fused peptide sequence. These studies revealed that the N-terminal part of SbpA located on the inner S-layer surface was required for anchoring the S-layer subunits via a pyruvylated secondary cell wall polymer to the rigid cell wall layer (13). Furthermore, it could be demonstrated that the deletion of 200 C-terminal amino acids had no influence on the self-assembly properties of this S-layer protein (12). For screening an amino acid position in the C-terminal part that is located on the outer S-layer surface and therefore well-suited for the fusion of functional peptide sequences, the sequence encoding the affinity peptide *Strep*-tag I was linked to the 3'-end of the sequence encoding rSbpA<sub>31–1268</sub> or rSbpA<sub>31–1068</sub>. Binding of streptavidin to rSbpA<sub>31–1268</sub>/*Strep*-tag I and rSbpA<sub>31–1068</sub>/*Strep*-tag I, which were either provided in water soluble form, as self-assembly or recrystallization products, revealed that *Strep*-tag I was accessible to a significantly higher extent in the C-terminally truncated form. Within the different rSbpA<sub>31–1068</sub>/*Strep*-tag I samples, the amount of bound streptavidin was independent of the use of soluble or assembled S-layer protein, which indicated that *Strep*-tag I was not located on the contact sites of adjacent S-layer subunits. Since *Strep*-tag I was found to be exposed on the outer S-layer surface, rSbpA<sub>31–1068</sub> was used in a previous study as base form for the construction of an S-layer fusion protein, which carried the sequence of the major birch pollen allergen (Bet v1) at the C-terminal end (12).

In the present study, the C-terminally truncated rSbpA form was also selected as base form for the construction of an S-layer fusion protein comprising the sequence of a single variable region of a camel heavy chain antibody directed against lysozyme (cAb-Lys3). The obtained S-layer fusion protein, termed rSbpA<sub>31–1068</sub>/cAb-Lys3, can be considered as a model system for the construction of further chimeric proteins, which comprise rSbpA<sub>31–1068</sub> and cAbs directed against various antigens.

The S-layer fusion protein was capable of self-assembling *in vitro* into flat sheets, which clearly resembled the square lattice structure of the native S-layer. To prove whether the fused cAb-Lys3 sequence was located on the outer S-layer surface, the S-layer fusion protein was recrystallized on peptidoglycan-containing sacculi of *B. sphaericus* CCM 2177, to which the S-layer subunits attach with their inner surface. Immunogold-labeling

using an anti-camel antiserum and a colloidal gold–Protein A conjugate confirmed the location of cAb-Lys3 on the outer S-layer surface. Dot blot assays were performed to compare the accessibility of cAb-Lys3 in the soluble, self-assembled, and recrystallized S-layer fusion protein. According to the data obtained with rSbpA<sub>31–1068</sub>/*Strep*-tag I and streptavidin (12, 41), the accessibility of the fused functional sequence for lysozyme was independent of the soluble or assembled state of the S-layer fusion protein.

As shown by AFM analysis, the S-layer fusion protein was capable of recrystallizing into the square lattice structure on polystyrene. The ability of cAb-Lys3 in the formed monolayer to bind lysozyme was investigated and compared with that of a monolayer generated by recrystallization of rSbpA and chemical coupling of cAb-Lys3. Although in the case of the S-layer fusion protein only 4 cAb-Lys3 residues were available per tetrameric morphological unit of the square S-layer lattice, the signal in the assay to detect lysozyme was similar to that for the rSbpA monolayer carrying 8–9 chemically coupled cAb-Lys3 molecules per morphological unit. Since lysozyme has a molecular mass of 14 600 Da, which is comparable to the molecular mass of cAb-Lys3 of ~15 000 Da, it is not likely that the reduced signal in relation to the number of chemically coupled cAb-Lys3 molecules is due to steric hindrance of the antigen. An important factor that has to be considered is the procedure applied to detect lysozyme, in which a streptavidin peroxidase–conjugate was used to bind to the biotinylated antigen and where steric factors may have played a role. Due to the presence of at least 2 chemically coupled cAb-Lys3 molecules per S-layer subunit, the large molecular mass of the streptavidin–peroxidase conjugate, the tetrameric nature of streptavidin and the size of one morphological unit of the S-layer lattice consisting of 4 subunits, it is feasible that a single streptavidin–peroxidase conjugate molecule could bind to two lysozyme molecules. In the case of the S-layer fusion protein, a single cAb-Lys3 residue was available per S-layer subunit, which due to steric reasons could most probably react with the streptavidin–peroxidase conjugate in a 1 to 1 stoichiometry. This may explain why despite the different numbers of cAb-Lys3 residues available, both types of monolayers gave comparable signals in the assay to detect lysozyme.

The cAb-Lys3 sequence was linked to an amino acid position in the S-layer protein, which in a previous study

(12) was found to be located on the outer S-layer surface. This should ensure that the fused functional sequence remained accessible for binding of target molecules, provided that the S-layer subunits attached with their inner surface to the supporting layer, which was the case when polystyrene was used as solid support. To achieve oriented binding and recrystallization of the S-layer fusion protein on gold chips, the specific interactions between the S-layer protein and its natural anchoring molecule in the bacterial cell wall, the secondary cell wall polymer (13), were exploited. For this purpose, the latent aldehyde group at the reducing end of the polymer chains was converted into a thiol group (35). By applying this modification procedure, each polymer chain carried a single thiol group, which was capable of binding to the gold surface and guaranteed that the polymer chains attached in uniform orientation.

To summarize, S-layer fusion proteins consisting of rSbpA<sub>31–1068</sub> and cAbs directed against various antigens shall be exploited for recrystallization on solid supports to generate functional monomolecular protein lattices, as required for applications in nanobiotechnology including biochip development. Due to the selected fusion site, the functional sequence remained located on the outer S-layer surface and was accessible for binding of target molecules, provided that the S-layer subunits attached with their inner surface. To ensure this, secondary cell wall polymers shall be exploited as S-layer specific biomimetic linker to the solid support in future developments. Because of the crystalline structure of the S-layer lattice, the fused functional sequences are arranged at well-defined distance and orientation to each other in the nanometer range.

#### ACKNOWLEDGMENT

This work was supported by the Austrian Science Foundation, project P14689-MOB, by the Competence Center "Biomolecular Therapeutics" and by the EU project PAMELA.

#### LITERATURE CITED

- (1) Sára, M., and Sleytr, U. B. (2000) S-Layer proteins. *J. Bacteriol.* 182, 859–868.
- (2) Sleytr, U. B., and Beveridge, T. J. (1999) Bacterial S-layers. *Trends Microbiol.* 7, 253–260.
- (3) Sleytr, U. B., Messner, P., Pum, D., and Sára, M. (1999) Crystalline bacterial cell surface layers (S-layers): from supramolecular cell structure to biomimetics and nanotechnology. *Angew. Chem., Int. Ed.* 38, 1034–1054.
- (4) Brechtel, E., and Bahl, H. (1999) In *Thermoanaerobacterium thermosulfurigenes* EM1 S-layer homology domains do not attach to peptidoglycan. *J. Bacteriol.* 181, 5017–5023.
- (5) Chauvaux, S., Matuschek, M., and Beguin, P. (1999) Distinct affinity of binding sites for S-layer homologous domains in *Clostridium thermocellum* and *Bacillus anthracis* cell envelopes. *J. Bacteriol.* 181, 2455–2458.
- (6) Lemaire, M., Miras, I., Gounon, P., and Beguin, P. (1998) Identification of a region responsible for binding to the cell wall within the S-layer protein of *Clostridium thermocellum*. *Microbiology* 144, 211–217.
- (7) Mesnage, S., Fontaine, T., Mignot, T., Delepierre, M., Mock, M., and Fouet, A. (2000) Bacterial SLH domain proteins are noncovalently anchored to the cell surface via a conserved mechanism involving wall polysaccharide pyruvylation. *EMBO J.* 19, 4473–4484.
- (8) Sára, M. (2001) Conserved anchoring mechanisms between crystalline cell surface S-layer proteins and secondary cell wall polymers in Gram-positive bacteria? *Trends Microbiol.* 9, 47–49.
- (9) Pum, D., Neubauer, A., Györfy, E., Sára, M., and Sleytr, U. B. (2000) S-layer proteins as basic building blocks in a biomolecular construction kit. *Nanotechnology* 11, 100–107.
- (10) Sleytr, U. B., Sára, M., and Pum, D. (2000) Crystalline bacterial cell surface layers (S-layers): a versatile self-assembly system. In *Supramolecular Polymers* (A. Ciferri, Ed.) pp 177–213, Marcel Dekker, Inc., New York – Basel.
- (11) Sleytr, U. B., Sára, M., Pum, D., and Schuster, B. (2002) Molecular nanotechnology and nanobiotechnology with two-dimensional protein crystals (S-layers). In *Nano-Surface Chemistry* (M. Rosoff, Ed.) pp 333–389, Marcel Dekker, Inc., New York – Basel.
- (12) Ilk, N., Völlenkne, C., Egelseer, E. M., Breitwieser, A., Sleytr, U. B., and Sára, M. (2002) Molecular Characterization of the S-Layer Gene, sbpA, of *Bacillus sphaericus* CCM 2177 and Production of a Functional S-Layer Fusion Protein with the Ability To Recrystallize in a Defined Orientation while Presenting the Fused Allergen. *Appl. Environ. Microbiol.* 68, 3251–3260.
- (13) Ilk, N., Kosma, P., Puchberger, M., Egelseer, E. M., Mayer, H. F., Sleytr, U. B., and Sára, M. (1999) Structural and functional analyses of the secondary cell wall polymer of *Bacillus sphaericus* CCM 2177 that serves as an S-layer-specific anchor. *J. Bacteriol.* 181, 7643–7646.
- (14) Muyldermans, S. (2001) Single domain camel antibodies: current status. *Mol. Biotechnol.* 74, 277–302.
- (15) Nguyen, V. K., Desmyter, A., and Muyldermans, S. (2001) Functional heavy-chain antibodies in *Camelidae*. *Adv. Immunol.* 79, 261–296.
- (16) Desmyter, A., Transue, T. R., Ghahroudi, M. A., Thi, M. H., Poortmans, F., Hamers, R., Muyldermans, S., and Wyns, L. (1996) Crystal structure of a camel single-domain VH antibody fragment in complex with lysozyme. *Nat. Struct. Biol.* 3, 803–811.
- (17) Sheriff, S., Silverton, E. W., Padlan, E. A., Cohen, G. H., Smith-Gill, S. J., Finzel, B. C., and Davies, D. R. (1987) Three-dimensional structure of an antibody–antigen complex. *Proc. Natl. Acad. Sci. U.S.A.* 84, 8075–8079.
- (18) Padlan, E. A., Silverton, E. W., Sheriff, S., Cohen, G. H., Smith-Gill, S. J., and Davies, D. R. (1989) Structure of an antibody–antigen complex: crystal structure of the HyHEL-10 Fab-lysozyme complex. *Proc. Natl. Acad. Sci. U.S.A.* 86, 5938–5942.
- (19) Amit, A. G., Mariuzza, R. A., Phillips, S. E., and Poljak, R. J. (1986) Three-dimensional structure of an antigen–antibody complex at 2.8 Å resolution. *Science* 233, 747–753.
- (20) Bhat, T. N., Bentley, G. A., Boulot, G., Greene, M. I., Tello, D., Dall'Acqua, W., Souchon, H., Schwarz, F. P., Mariuzza, R. A., and Poljak, R. J. (1994) Bound water molecules and conformational stabilization help mediate an antigen–antibody association. *Proc. Natl. Acad. Sci. U.S.A.* 91, 1089–1093.
- (21) Chitarra, V., Alzari, P. M., Bentley, G. A., Bhat, T. N., Eisele, J. L., Houdusse, A., Lescar, J., Souchon, H., and Poljak, R. J. (1993) Three-dimensional structure of a heteroclit antigen–antibody cross-reaction complex. *Proc. Natl. Acad. Sci. U.S.A.* 90, 7711–7715.
- (22) Braden, B. C., Souchon, H., Eisele, J. L., Bentley, G. A., Bhat, T. N., Navaza, J., and Poljak, R. J. (1994) Three-dimensional structures of the free and the antigen-complexed Fab from monoclonal anti-lysozyme antibody D44.1. *J. Mol. Biol.* 243, 767–781.
- (23) Davies, D. R., Padlan, E. A., and Sheriff, S. (1990) Antibody–antigen complexes. *Annu. Rev. Biochem.* 59, 439–473.
- (24) Lescar, J., Pellegrini, M., Souchon, H., Tello, D., Poljak, R. J., Peterson, N., Greene, M., and Alzari, P. M. (1995) Crystal structure of a cross-reaction complex between Fab F9.13.7 and guinea fowl lysozyme. *J. Biol. Chem.* 270, 18067–18076.
- (25) Hoogenboom, H. R., Griffiths, A. D., Johnson, K. S., Chiswell, D. J., Hudson, P., and Winter, G. (1991) Multi-subunit proteins on the surface of filamentous phage: methodologies for displaying antibody (Fab) heavy and light chains. *Nucleic Acids Res.* 19, 4133–4137.

- (26) Winter, G., Griffiths, A. D., Hawkins, R. E., and Hoogenboom, H. R. (1994) Making antibodies by phage display technology. *Annu. Rev. Immunol.* **12**, 433–455.
- (27) Jarosch, M., Egelseer, E. M., Mattanovich, D., Sleytr, U. B., and Sára, M. (2000) S-layer gene *sbsC* of *Bacillus stearothermophilus* ATCC 12980: molecular characterization and heterologous expression in *Escherichia coli*. *Microbiology* **146**, 273–281.
- (28) Laemmli, U. K. (1970) Cleavage of structural proteins during the assembly of the head of bacteriophage T4. *Nature* **227**, 680–685.
- (29) Messner P., Hollaus F., and Sleytr, U. B. (1984) Paracrystalline cell wall surface layers of different *Bacillus stearothermophilus* strains. *Int. J. Syst. Bacteriol.* **34**, 202–210.
- (30) Jarosch, M., Egelseer, E. M., Huber, C., Moll, D., Mattanovich, D., Sleytr, U. B., and Sára, M. (2001) Analysis of the structure–function relationship of the S-layer protein SbsC of *Bacillus stearothermophilus* ATCC 12980 by producing truncated forms. *Microbiology* **147**, 1353–1363.
- (31) Egelseer, E. M., Schocher, I., Sleytr, U. B., and Sára, M. (1996) Evidence that an N-terminal S-layer protein fragment triggers the release of a cell-associated high-molecular-weight amylase in *Bacillus stearothermophilus* ATCC 12980. *J. Bacteriol.* **178**, 5602–5609.
- (32) Breitwieser, A., Küpcü, S., Howorka, S., Weigert, S., Langer, C., Hoffmann-Sommergruber, K., Scheiner, O., Sleytr, U. B., and Sára, M. (1996) 2-D protein crystals as an immobilization matrix for producing reaction zones in dipstick-style immunoassays. *Biotechniques* **21**, 918–925.
- (33) Breitwieser, A., Mader, C., Schocher, I., Hoffmann-Sommergruber, K., Aberer, W., Scheiner, O., Sleytr, U. B., and Sára, M. (1998) A novel dipstick developed for rapid Bet v 1-specific IgE detection: recombinant allergen immobilized via a monoclonal antibody to crystalline bacterial cell-surface layers. *Allergy* **53**, 786–793.
- (34) Weiner C., Sára M., and Sleytr UB. (1994) Novel protein A affinity matrix prepared from two-dimensional protein crystals. *Biotechnol. Bioeng.* **43**, 321–330.
- (35) Mader, C., Moll, D., Hotzy, C., and Sára, M. (2002) Real-time monitoring of the interaction between a crystalline bacterial cell surface (S-) and a secondary cell wall polymer serving as attachment site in the cell wall sacculus using surface plasmon resonance biosensor technology. Unpublished results.
- (36) Butt, H.-J. (1991) Measuring electrostatic, van der Waals, and hydration forces in electrolyte solutions with an atomic force microscope. *Biophys. J.* **60**, 1438–1444.
- (37) Butt, H.-J. (1992) Measuring local surface charge densities in electrolyte solutions with a scanning force microscope. *Biophys. J.* **63**, 578–582.
- (38) Kelley, T. W., Schorr, P. A., Johnson, K. D., Tirrell, M., and Frisbie, C. D. (1998) Direct Force Measurements at Polymer Brush Surfaces by Atomic Force Microscopy. *Macromolecules* **31**, 4297–4300.
- (39) Overney, R. M., Leta, D. P., Pictroski, C. F., Rafailovich, M., Liu, Y., Quinn, J., Sokolov, J., Eisenberg, A., and Overney, G. (1996) Compliance measurements of confined polystyrene solutions by atomic force microscopy. *Phys. Rev. Lett.* **76**, 1272–1275.
- (40) Abendroth, R. P. (1970) Behaviour of pyrogenic silica in simple electrolytes. *J. Colloid Interface Sci.* **34**, 591–596.
- (41) Schmidt, T. G., and Skerra, A. (1994) One-step affinity purification of bacterially produced proteins by means of the “Strep tag” and immobilized recombinant core streptavidin. *J. Chromatogr. A* **676**, 337–345.

BC025603+



# Differential Gene Expression Profile between PC-14 Cells Treated with Free Cisplatin and Cisplatin-Incorporated Polymeric Micelles

Nobuhiro Nishiyama,<sup>†</sup> Fumiaki Koizumi,<sup>‡</sup> Soichiro Okazaki,<sup>†</sup> Yasuhiro Matsumura,<sup>§</sup> Kazuto Nishio,<sup>‡</sup> and Kazunori Kataoka<sup>\*,†</sup>

Department of Materials Science and Engineering, Graduate School of Engineering, The University of Tokyo, 7-3-1 Hongo, Bunkyo-ku, Tokyo 113-8656, Japan, Pharmacology Division, National Cancer Center Research Institute, 5-1-1 Tsukiji, Chuo-ku, Tokyo 104-0045, Japan, and Investigative Treatment Division, National Cancer Center Research Institute East, 6-5-1 Kashiwanoha, Kashiwa, Chiba 277-8577, Japan  
Received June 2, 2002; Revised Manuscript Received November 17, 2002

Cisplatin (CDDP)-incorporated polymeric micelles (CDDP/m) are a macromolecular carrier system possessing a time-modulated decaying property accompanied by sustained release of free drug. The gene expression profiles in nonsmall cell lung cancer PC-14 cells treated with free CDDP and CDDP/m were evaluated by a cDNA expression array for 807 genes. Although the total gene expression profile of the cells treated with CDDP/m approximated that of free CDDP in the hierarchical clustering analysis, a number of genes showed differential expression according to whether the cells had been treated with CDDP or CDDP/m. Ultimately, 50 genes with significant differential expression between cells treated with CDDP and CDDP/m were selected by principal component (PC) analysis and the unpaired *t*-test. The genes selected, including genes related to cell cycle regulation, apoptosis-related proteins, detoxification, and DNA repair enzymes, were considered to be related to CDDP-induced cytotoxicity. Interestingly, CDDP/m down-regulated the genes encoding integrins and matrix metalloproteinases (MMPs), which play an integral role in tumor invasion, metastasis, and angiogenesis, whereas free CDDP up-regulated them. The results suggest that use of the macromolecular carriers may yield additional therapeutic effects over free drug.

## INTRODUCTION

A variety of macromolecular carrier systems have been developed for the use in the diverse field of chemotherapy, particularly for cancer treatment, and this technology will continue to receive growing attention as a key to the development of novel therapeutic agents (1–4). Macromolecular carriers that provide increased accumulation at target sites and reduced accumulation at side effect sites should yield maximal therapeutic efficacy. Polymer–drug conjugates and colloidal drug carrier systems, such as liposomes and micelles, in particular, have been attracting great interest in tumor targeting therapy because of their preferential accumulation in solid tumors (5, 6). The preferential tumor accumulation of macromolecular drug carrier systems is explained by the so-called “enhanced permeability and retention (EPR)” effect, which accounts for the unique characteristics of solid tumors with enhanced permeability in tumor vasculature (7). Hence, some formulations have yielded remarkable antitumor activity and are being assessed in clinical studies (8, 9).

In addition to controlled biodistribution, macromolecular carrier systems allow controlled drug release and

alteration of the internalization routes and subcellular localization of drugs. The control of drug release and internalization routes by macromolecular carriers may lead additional or better therapeutic effects. Indeed, there is benefit of macromolecular drugs that will circumvent drug efflux, e.g., resistance against P-glycoprotein dependent efflux in multidrug resistant cells (10–12). In addition, we hypothesized that alteration of the modality of cell entry, leading to different subcellular drug localization, drug-concentration gradients, and controlled drug release, will regulate gene and protein expression in a manner different from exposure to the free drug, resulting in additional or better therapeutic effects. Indeed, Kopecek et al. have suggested that *N*-(2-hydroxypropyl) methacrylamide (HPMA) copolymer-doxorubicin (Dox) conjugates (PK-1), which are internalized via endocytosis, and whose entry into cells is followed by lysosomal enzyme-specific drug release, regulates different genes from free Dox and thereby overcomes the Dox-resistance of tumor cells both in vitro and in vivo (13, 14). In this study, we used cDNA expression array techniques (15, 16) to evaluate differences in gene expression between human nonsmall cell lung cancer (NSCLC) cells treated with cisplatin (CDDP) and CDDP-incorporated polymeric micelles (CDDP/m).

CDDP-incorporated micelles formed via a ligand exchange reaction of CDDP from the chloride to the carboxylate side chain of poly(ethylene glycol)-poly(amino acid) block copolymer was found to be very stable when diluted with distilled water, whereas they dissociated into unimers with sustained release of the regenerated CDDP via an inverse ligand exchange from carboxylate to

\* To whom correspondence should be addressed. Kazunori Kataoka, Ph.D., Department of Materials Science and Engineering, Graduate School of Engineering, The University of Tokyo, 7-3-1 Hongo, Bunkyo-ku, Tokyo 113-8656, Japan. Phone: +81-3-5841-7138. Fax: +81-3-5841-7139. E-mail: kataoka@bmw.t.u-tokyo.ac.jp.

<sup>†</sup> The University of Tokyo.

<sup>‡</sup> National Cancer Center Research Institute.

<sup>§</sup> National Cancer Center Research Institute East.

chloride in physiological saline at 37 °C (17). CDDP-incorporated micelles also yielded prolonged blood levels in murine Lewis lung carcinoma (LLC)-bearing mice, resulting in preferential and enhanced accumulation in tumors (18). These CDDP-incorporated micelles are also expected to allow different internalization into cells and subcellular drug distribution, and they can be expected to exert the novel biological actions.

## MATERIALS AND METHODS

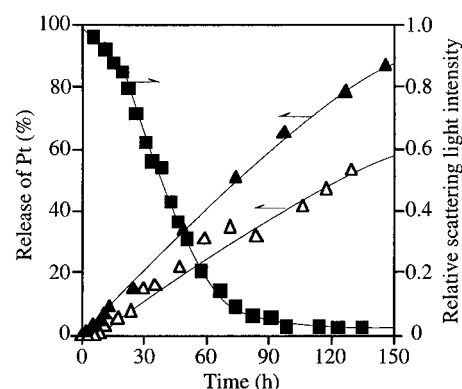
**Materials.** CDDP [*cis*-diamminedichloroplatinum(II): CDDP] was purchased from Aldrich Chemical Co., Inc., Milwaukee, WI.  $\alpha$ -Methoxy- $\omega$ -aminopoly(ethylene glycol) (CH<sub>3</sub>O-PEG-NH<sub>2</sub>;  $M_w$  = 12 000) was donated by Nippon Oil Fats Co., Ltd., Tokyo, Japan. 3-(4,5-Dimethylthiazol-2-yl)-2,5-diphenyltetrazolium bromide (MTT) and Isogen were obtained from Wako Pure Chemical Industries, Co., Ltd., Osaka, Japan, and Nippon Gene Co., Ltd., Tokyo, Japan, respectively. An Atlas Pure Total RNA Labeling System and Atlas cDNA Expression Array were purchased from BD Bioscience Clontech Co., Inc., (Palo Alto, CA.). [ $\alpha$ -<sup>32</sup>P]dATP (110 TBq/mmol) was obtained from Amersham Biosciences Co., Tokyo, Japan.

**Preparation of CDDP-Incorporated Micelles.** A micelle-forming poly(ethylene glycol)-poly(glutamic acid) block copolymer [PEG-P(Glu)] was prepared according to a previously reported procedure (19). Briefly, poly(ethylene glycol)-poly( $\beta$ -benzyl L-glutamate) block copolymer (PEG-PBLG) was synthesized by ring-opening polymerization of the *N*-carboxy anhydride of  $\beta$ -benzyl L-glutamate (BLG-NCA) initiated by CH<sub>3</sub>O-PEG-NH<sub>2</sub> in dimethylformamide (DMF), followed by alkali hydrolysis of  $\beta$ -benzyl group to prepare PEG-P(Glu). The degree of polymerization of P(Glu) segment was determined to be 35 by <sup>1</sup>H NMR measurement, and a narrow distribution of the obtained block copolymer was confirmed by gel-permeation chromatography (GPC) measurements ( $M_w/M_n \sim 1.06$ ).

CDDP-incorporated micelles were prepared by simple mixing of CDDP and PEG-P(Glu) in distilled water at a mixing molar ratio of CDDP to Glu residue of 1. Purification of CDDP-incorporated micelles was carried out by ultrafiltration (MWCO: 100 000, membrane: Millipore PT series).

**Characterization of CDDP-Incorporated Micelles.** The size of the CDDP-incorporated micelles and their CDDP content were determined by dynamic light scattering (DLS) and atomic absorption spectroscopy (AAS) measurements, respectively. The release of CDDP from CDDP-incorporated micelles in physiological saline at 37 °C (pH 5.2 and 7.4, 150 mM NaCl) was evaluated by the dialysis method (Spectra/Por-6 (MWCO: 1000), Spectrum Laboratories, Inc. Rnacho Dominguez, CA), and concomitant decay of the micellar structure was estimated by static light scattering (SLS) based on a change in the Rayleigh ratio at a scattering angle of 90° ( $R(90^\circ)$ ) (17). The  $R(90^\circ)$  value should decrease with micelle dissociation in tandem with a decrease in apparent molecular weight of the micelles ( $M_{w,app}$ ) and in micelle concentration. The  $R(90^\circ)$  value of the micelles in distilled water at 37 °C was used as the control in this measurement.

**MTT Assay.** The growth-inhibitory activity of free CDDP and CDDP-incorporated micelles on human non-small cell lung cancer cell line PC-14 was evaluated by MTT assay (20). PC-14 cells (5000 cells) were cultured in RPMI 1640 medium (Sigma Biosciences Co.) containing 10% fetal bovine serum in 96-well multiplate. The cells were then exposed to each preparation (free CDDP



**Figure 1.** Release of Pt from CDDP-incorporated micelles (CDDP/m) at pH 5.2 (closed triangle) and pH 7.4 (open triangle) and change in relative scattering light intensity of CDDP/m (closed square) in physiological saline at 37 °C.

or CDDP-incorporated micelles) for 72 h, and MTT solution was added. Cell viability was estimated by formazan absorbance at 570 nm.

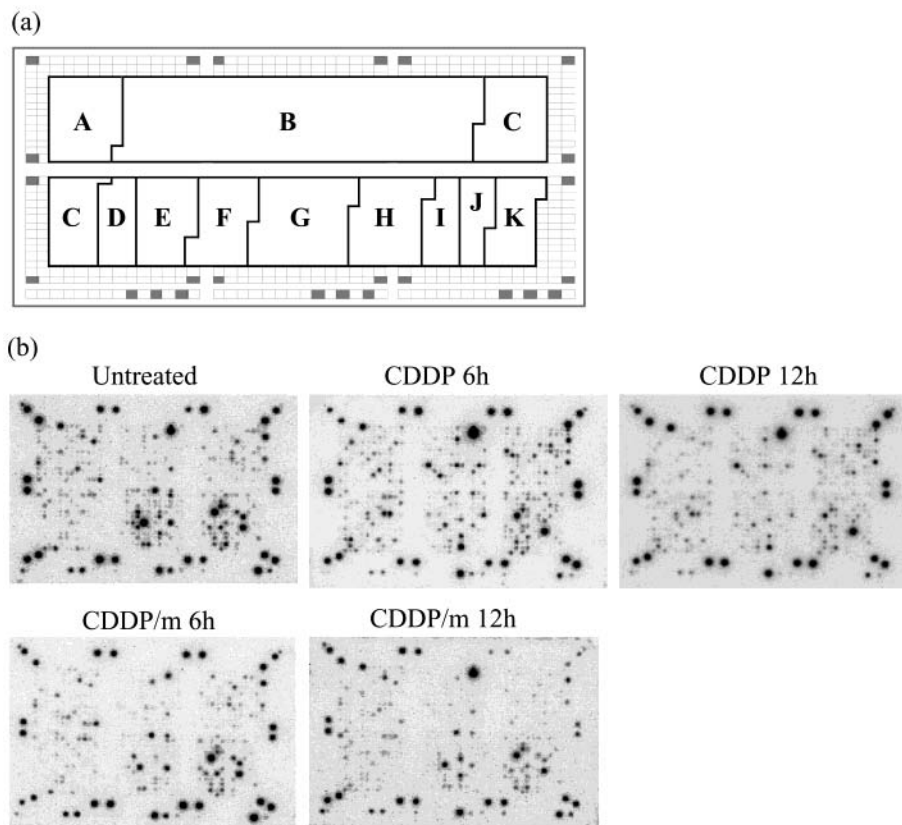
**RNA Isolation.** PC-14 cells were exposed to each preparation at the 90% cell growth-inhibitory concentration (IC<sub>90</sub>), which was estimated based on MTT assay after 72 h incubation. Following 6- or 12-h drug exposure, total RNA was isolated with Isogen based on phenol-chloroform extraction. mRNA was prepared with an Atlas Pure Total RNA Labeling System according to the manufacturer's protocol.

**cDNA Expression Array.** cDNA expression array analysis was carried out by using an Atlas cDNA expression array customized in our laboratory. The customized array consists of 807 genes including genes related to cell cycle regulation, signal/oncogenes, angiogenesis/adhesion/cell-cell interaction, growth factors, cytokines, apoptosis-related, DNA transcription factors/damage response/repair, and recombination, metabolism, translation/protein turnover/detoxification enzymes, transporters/nucleocytoplasmic transporters/symporter, and antiporters/cytoskeletal proteins (see Figure 2a). The experiment was performed according to the manufacturer's protocol.

**Data Analysis.** The image on the imaging plate (BAS-III2040; Fuji Film Co., Tokyo, Japan) that was exposed to the cDNA-hybridized membranes for 3–4 days was scanned with a BAS-2000II image scanner (Fuji Film Co.). The signal density of each spot was quantified by Array Gauge ver. 1.2 software (Fuji Film Co.), and the data were subjected to background adjustment by using the minimum density value of all spots and the global median normalization. The expression ratio ( $\log_2$  (drug-treated)/(drug untreated)) was used for further analysis. The hierarchical clustering analysis was carried out by using Web-available software, "Cluster" and "Tree View," provided by M. Eisen (<http://rana.lbl.gov/>). Principal component (PC) analysis with Simca-P ver. 8.0 (Umetrics Co. Ume, Sweden) followed by the unpaired *t*-test was performed to select genes differentially expressed by cells treated with CDDP and CDDP-incorporated micelles.

## RESULTS

Formation of CDDP-incorporated micelles (CDDP/m) having a diameter of 27.9 nm and a narrow size distribution was confirmed by DLS measurement. AAS measurement yielded a CDDP content of CDDP/m of 31% (w/w), which corresponds to a [CDDP]/[Glu] ratio of 0.61. Since CDDP/m showed a decrease in relative scattering light intensity and sustained release of CDDP in physiological saline (150 mM NaCl), as previously reported (Figure 1)



**Figure 2.** (a) Coordinates of the customized Atlas gene expression array composed of 807 genes including (A) genes encoding factors related to cell cycle regulation, (B) signal/oncogenes, (C) angiogenesis/adhesion/cell–cell interaction, (D) growth factors, (E) cytokines, (F) apoptosis-related genes, (G) DNA transcription factors/damage response/repair and recombination, (H) metabolism, (I) translation/protein turnover/detoxification enzymes, (J) transporters/nucleocytoplasmic transporters/symporter & antiporters/cytoskeletal proteins, (K) other genes. (b) gene expression images of untreated, CDDP 6 h-, CDDP 12 h-, CDDP/m 6 h-, CDDP 12 h-treated PC-14 cells.

**Table 1. Cytotoxic Activity of CDDP and CDDP/m against PC-14 Cells**

	IC <sub>50</sub> <sup>a</sup>		IC <sub>90</sub> <sup>b</sup>	
	48 h	72 h	48 h	72 h
CDDP	1.88	1.45	25.3	10.8
CDDP/m	5.49	4.82	48.7	28.3

<sup>a,b</sup> 50% and 90% cell growth-inhibitory concentration determined by MTT assay (unit:  $\mu\text{g/mL}$ ).

(17), CDDP/m is a novel type macromolecular carrier system exhibiting time-modulated decay of carrier as well as sustained drug release (18). Interestingly, the release of CDDP was accelerated by decreasing the pH of the media from 7.4 to 5.2, suggesting accelerated drug release from CDDP/m in the endosomal/lysosomal environment when whole CDDP/m is internalized into a cell.

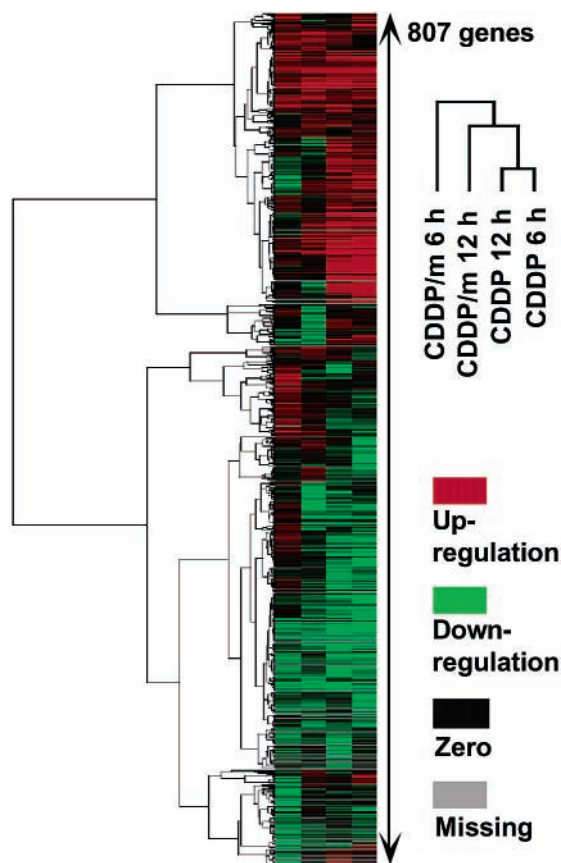
The growth-inhibitory effect of CDDP and CDDP/m on PC-14 cells was evaluated by MTT assay. The 50% and 90% cell growth-inhibitory concentrations (IC<sub>50</sub> and IC<sub>90</sub>) after 48 and 72 h drug exposure are shown in Table 1. The increased IC<sub>50</sub> value of CDDP/m may be consistent with the hypothesis that the CDDP released from the micelles is mainly responsible for the cytotoxic activity of CDDP/m. Indeed, we previously reported that preincubation of CDDP/m in physiological saline disrupting the micellar structure displayed comparable cytotoxicity to free CDDP (18). In this study, PC-14 cells were exposed to each drug at the IC<sub>90</sub>, which was estimated based on 72 h drug exposure (Table 1) to isolate total RNA.

The gene expression profiles of PC-14 cells were examined by using the customized Atlas cDNA expression array. The customized array consists of 807 genes,

and their coordinates are shown in Figure 2a. To investigate time-dependent gene expression, total RNA was isolated after 6 and 12 h of drug-exposure and followed by mRNA isolation and synthesis of <sup>32</sup>P-labeled cDNA. The array images after hybridization of cDNA from untreated, CDDP 6 h-, CDDP 12 h-, CDDP/m 6h-, and CDDP/m 12 h-treated PC-14 cells are shown in Figure 2b. The signal intensity of each spot was quantified by Array Gauge ver. 1.1, followed by background adjustment and global median normalization. The expression ratio [ $\log_2$  (drug-treated)/(drug untreated)] was used for further analysis. Hierarchical clustering of all 807 genes was performed and is shown in Figure 3. Although CDDP 6 and 12 h showed clustering into the closest branch, as expected, CDDP/m 12 h was clustered into the branch closer to CDDP 6 and 12 h rather than to CDDP/m 6 h. The clustering results suggest that regulation of total gene expression by CDDP/m may approximate that of free CDDP. This seems to be consistent with the aforementioned hypothesis that the CDDP released from micelles plays a major role of the cytotoxic activity of CDDP/m. Nevertheless, it is of great interest that a number of genes were differentially expressed by cells treated with CDDP/m in comparison to CDDP (Figure 3).

Principal component (PC) analysis by Simca-P 8.0 was performed to investigate the relation between important sets of variables (samples). PC modeling in Simca-P is programmed to calculate two or three score vectors for genes that summarize all the variables entered into the analysis and plot them against each other (score plot: Figure 4(B)). PC analysis by Simca-P also provides values





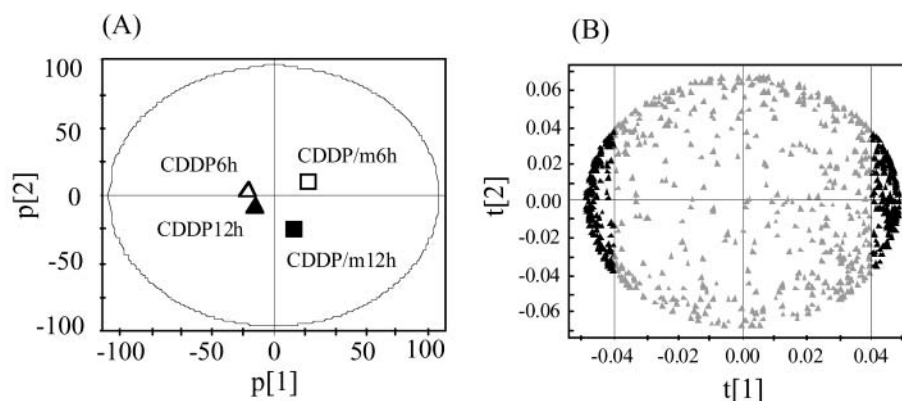
**Figure 3.** Hierarchical cluster analysis of the expression of all genes (807 genes) on the Atlas gene expression array.

for so-called loading vectors, showing how the variables are combined to form the scores. The plot of loading vectors (loading plot: Figure 4A) indicates which of the variables are important and corresponds to the directions in the score plot. Importantly, the opposite direction of the loading vector  $p[1]$ , the first principal component, was observed between CDDP and CDDP/m treatment. It is worth noting that the first principal component possessed a clearly larger fraction of sum of squares (SS) (0.526), which is also computed by Simca-P, than the next component (0.274). Since the position of an observation in a score plot is influenced by genes lying in the same direction in the loading plot, genes with an absolute score vector value ( $|t[1]|$ ) above 0.04 were extracted to select genes differentially regulated in cells treated with CDDP and CDDP/m. As a result, we selected 105 candidate genes.

The unpaired  $t$ -test between CDDP- and CDDP/m-treatment was further carried out for the aforementioned 105 candidate genes, and 50 significant genes were selected as a result ( $P < 0.05$ ) (Table 2). The 50 genes include the most important genes for the action of CDDP, such as the genes encoding check point kinase 1 (*Chk1*), phospholipase C delta (PLC-delta), p53-binding mouse double minute 2 homologue (MDM2), caspase-9 precursor, glutathione S-transferase (GST), glutathione reductase (GSR), and damage response and repair-related proteins, as well as interesting genes involved in angiogenesis and cell adhesion factors, such as integrins and matrix metalloproteinases (MMPs). The results of re-clustering the 50 genes selected are shown in Figure 5 and provide easy-to-follow graphical profiles of differential gene expression by genes treated with CDDP and CDDP/m.

## DISCUSSION

CDDP is one of the most important antitumor drugs in clinical use and is widely used for the treatment of many malignancies, including testicular, ovarian, bladder, head and neck, stomach, esophagus, and small-cell and non-small-cell lung cancers (21). However, it is well-known that CDDP has significant toxic side effects, such as nephrotoxicity and neurotoxicity, limiting its therapeutic window (22). Since intravenously administered CDDP is rapidly eliminated from the blood circulation by glomerular excretion (23), a large number of macromolecular carriers for CDDP have been developed with the aim of increasing its bioavailability and achieving selective targeting of solid tumors (24–27). We also prepared CDDP-incorporated polymeric micelles (CDDP/m) via polymer–metal complex formation between CDDP and PEG-poly (amino acid) block copolymers containing a carboxyl group and found that CDDP/m is a promising formulation for macromolecular carrier systems with both prolonged blood circulation and preferential accumulation in solid tumors (17, 18). In addition, CDDP/m exhibited the time-modulated decaying of a carrier and the sustained drug release at an increased rate in an acidic environment (Figure 1), which may lead to accelerated drug release from CDDP/m in the endosomal/lysosomal environment after internalization via an endocytic pathway. We hypothesized that the aforementioned characteristics of CDDP/m alter the pharmacological effect of free CDDP in addition to improving its biodistribution. In this study, we used cDNA expression array techniques to evaluate the biological effect of CDDP/m on PC-14 cells from the standpoint of the gene expression profiles.



**Figure 4.** Loading plot (A) and score plot (B) in the principal component (PC) analysis computed by Simca-P 8.0. The 105 genes most likely to influence the loading vector  $p[1]$  were selected in the Score plot.

**Table 2. List of Genes Differentially Expressed between CDDP- and CDDP/m-Treatment in PC-14 Cells (50 genes)**

coordinate	GenBank assoc. no.	GENES	CDDP 6 h <sup>a</sup>	CDDP 12 h <sup>a</sup>	CDDP/m 6 h <sup>a</sup>	CDDP/m 12 h <sup>a</sup>	P value
A04j	AF016582	checkpoint kinase 1 (CHK1)	0.2526	0.3589	-0.5818	-0.5492	0.0254
A04k	L25676	cell division protein kinase 9 (CDK9); serine/threonine protein kinase PITALRE	0.8879	0.9808	0.0236	-0.0425	0.0056
A05m	Z12020; M92424	p53-binding mouse double minute 2 homologue (MDM2)	-0.4768	-0.3122	0.7938	0.7725	0.0413
A13j	L36870	mitogen-activated protein kinase kinase 4 (MAP kinase kinase 4; MKK4; PRKMK4); c-jun N-terminal kinase kinase 1 (JNKK1); JNK-activating kinase 1; SAPK/ERK kinase 1 (SERK1; SEK1)	-0.4867	-0.2272	-1.3349	-1.0977	0.0400
B03k	M65066	cAMP-dependent protein kinase type I beta regulatory subunit (PRKAR1B)	4.1849	4.1084	-0.5778	-0.1806	0.0229
B04f	D10495	protein kinase C delta (PKC-delta)	0.8123	1.1251	-1.1035	-0.9485	0.0209
B04m	M22430; J04704	membrane-associated phospholipase A2 group 2A precursor (PLA2G2A); PLA2B; PLA2L; synovial group II phospholipase A2; phosphatidylcholine 2-acylhydrolase; RASFA	1.7693	1.4086	-0.0236	0.3154	0.0284
B05h	U09117	phospholipase C delta-1 (PLC-delta 1; PLCD1); PLC-III; 1-phosphatidylinositol-4,5-bisphosphate phosphodiesterase delta 1	1.3815	1.0711	-1.2880	-1.5894	0.0065
B09g	X60957; S89716	tyrosine kinase receptor tie-1 precursor	1.2182	1.0839	0.5231	0.6724	0.0322
C02h	M15042	carcinoembryonic antigen precursor (CEA); meconium antigen 100; CD66E antigen	2.3447	2.0317	-0.5250	0.0159	0.0290
C02i	M35296	Abelson murine leukemia viral oncogene homologue 2 (ABL2); Abelson-related gene (ARG)	4.0238	3.9180	0.2762	0.0546	0.0053
C03g	X95456	Rho7 protein	1.1885	0.9857	-0.2615	-0.5891	0.0260
C03h	X61587	rho-related GTP-binding protein (RHOG); ARHG	1.1718	1.6974	-1.5768	-1.0904	0.0166
C03k	L20688	rho GDP dissociation inhibitor 2 (RHO GDI2; RHO-GDI beta); LY-GDI; ARHGDIB; GDID4	2.1443	2.0033	0.1056	0.3166	0.0078
C08l	L36531	integrin alpha 8 (ITGA8)	1.4232	1.8722	-0.0612	-0.3279	0.0328
C08m	D25303; L24158	integrin alpha 9 (ITGA9); integrin alpha-RLC	1.0698	1.2810	-0.3565	-0.2194	0.0124
C09d	M34189	integrin beta 1 (ITGB1)	2.1738	2.1555	0.1417	0.0746	0.0061
C09g	M62880; S80335	integrin beta 7 precursor (ITGB7)	3.8544	4.4260	0.6540	-0.0444	0.0152
C09h	M73780	integrin beta 8 precursor (ITGB8)	3.8738	3.5687	0.1551	-0.2853	0.0078
C10i	X89576	matrix metalloproteinase 17 (MMP17); membrane-type matrix metalloproteinase 4 (MT-MMP4)	0.9206	0.7022	-1.3248	-0.8462	0.0449
C10k	J03210; J05471	matrix metalloproteinase 2 (MMP2); 72-kDa gelatinase A; 72-kDa type IV collagenase precursor (CLG4A); H-ras-transformed bronchial epithelial cells protein (TBE1)	1.4994	1.9333	-0.9108	-0.7919	0.0401
C12h	U14394	tissue inhibitor of metalloproteinase 3 precursor (TIMP3)	2.2666	1.6132	-0.0050	-0.5752	0.0372
D07e	M62403	insulin-like growth factor binding protein 4 precursor (IGF-binding protein 4; IGFBP4; IBP4)	-1.0697	-0.9829	0.6220	0.3936	0.0267
D09b	X63454	fibroblast growth factor 6 precursor (FGF6); HBGf6; HST2	1.1213	1.1856	0.3042	0.2158	0.0054
D10j	U31628	interleukin 15 receptor alpha subunit precursor	2.6822	2.2810	-0.2602	0.4647	0.0495
D11k	X01394	tumor necrosis factor alpha precursor (TNF-alpha; TNFA); cachectin	2.5606	2.1371	0.6883	1.0533	0.0355
D13j	X01992; M29383	interferon gamma precursor (IFN-gamma; IFNG); immune interferon	5.0160	4.7192	2.2839	2.0270	0.0056
E02i	X86779	fas-activated serine/threonine kinase (FAST)	-2.2257	-1.7354	0.2259	-0.3990	0.0459
E03e	U56390; U60521	caspase 9 precursor (CASP9); MCH6; ICE-like apoptotic protease 6 (ICE-LAP6); apoptotic protease activating factor 3 (APAF3)	1.7003	2.3393	-0.6017	-0.1793	0.0341
E04f	U18321 + x83544	ionizing radiation resistance-conferring protein + death-associated protein 3 (DAP3)	-3.4638	-3.2228	-1.6241	-1.6746	0.0374
E05g	X65372	polypyrimidine tract-binding protein (PTB); heterogeneous nuclear ribonucleoprotein I (HNRNP I); 57-kDa RNA-binding protein PPTB-1	-3.1025	-3.2089	-1.5117	-1.2152	0.0322
E06g	L16785; M36981	nucleoside diphosphate kinase B (NDP kinase B; NDKB); expressed in nonmetastatic cells 2 protein (NME2); myc purine-binding transcription factor (PUF); NM23B	-3.8504	-4.2303	-1.6370	-2.2779	0.0474
E06h	M58603	nuclear factor kappa-B DNA binding subunit (NF-kappaB; NFKB)	-1.9854	-2.1616	-0.9785	-0.8970	0.0225
E07g	M11722; K01919	DNA nucleotidyltransferase; terminal addition enzyme; terminal deoxynucleotidyltransferase (DNNT; TDT)	-2.1594	-2.3056	-1.3909	-1.1817	0.0239
E07h	M29971	6-O-methylguanine-DNA methyltransferase (MGMT); methylated-DNA-protein-cysteine methyltransferase	-2.3814	-2.5830	-1.2392	-1.2036	0.0447
E09e	X02308	thymidylate synthase (TYMS; TS)	-2.1649	-2.0495	-0.3644	-0.2277	0.0028
E09k	AF005482	histone deacetylase 3C (HD3C)	4.0119	3.3157	0.0742	0.3781	0.0347
E10b	X98743	RNA helicase	-2.3798	-1.7416	0.1599	-0.2631	0.0460
E10c	X95694	AP-2 BETA TRANSCRIPTION FACTOR	-1.4885	-1.2814	0.1142	-0.1966	0.0269
E10i	X16135	heterogeneous nuclear ribonucleoprotein L (HNRNPL)	-1.2177	-1.3347	-0.1598	-0.3418	0.0178
F01d	U39487	xanthine dehydrogenase/oxidase	-0.3445	-0.4636	0.5293	0.5462	0.0367
F02f	U89507	UDP-glucuronosyltransferase 1A7	-0.2770	-0.4710	0.4563	0.3379	0.0336
F02j	D29013	DNA polymerase beta (POLB)	-0.4463	-0.3087	0.5213	0.4079	0.0124
F02l	M81882	glutamate decarboxylase 65-kDa isoform; 65-kDa glutamic acid decarboxylase (GAD-65); GAD2	4.3263	3.8605	1.6765	1.2696	0.0144
F05g	X68676; S01719	glutathione S-transferase mu1 (GSTM1; GST1); HB subunit 4; GTH4	-0.8445	-1.0977	0.2464	0.0912	0.0274
F05l	X15722	glutathione reductase (GRase; GSR; GR)	-0.6048	-0.3911	0.4085	0.5739	0.0214
F06i	AF098951	ATP-binding cassette subfamily G (white) member 2 (ABCG2); breast cancer resistance protein (BCRP); mitoxantrone resistance protein 1 (MXR1)	0.0774	0.1956	0.7054	0.5973	0.0238
F07h	L06237	microtubule-associated protein 1B	1.0748	1.3015	0.2454	0.0838	0.0236
F08d	X03212	cytoskeletal keratin 7 (KRT7); cytokeratin 7 (CK7)	1.6226	1.7168	0.6525	0.8723	0.0450
F10i	AF007567	insulin receptor substrate 4	1.1887	1.3401	0.4567	0.3861	0.0274

<sup>a</sup> log-transformed gene expression ratio (log<sub>2</sub> (drug-treated)/(drug untreated)).



Figure 5. Hierarchical cluster analysis of the expression of 50 genes selected by PC analysis followed by the unpaired *t*-test ( $P < 0.05$ ).



It is well-known that CDDP is a DNA-damaging agent that reacts with genome DNA to form interstrand and intrastrand DNA cross-links and DNA-protein cross-links, and that the formation of CDDP-DNA adducts is essential to its cytotoxic activity (28, 29). Although the mechanism whereby the CDDP-induced DNA damage leads to cell death is not fully understood, there is evidence that an intrastrand cross-link between adjacent guanines (1,2-d(GpG)-CDDP adduct) forms more frequently and is more refractory to excision repair (29). The use of the macromolecular carriers might not change this essential subcellular target of CDDP (i.e., 1,2-d(GpG)), but may change the drug's modality of cellular uptake, its subcellular localization and concentration gradient, and interaction with subcellular molecules, such as lipids and proteins. It has been suggested that approximately one-half of free CDDP enters cells by passive diffusion and the other half by an unidentified pump (29). The internalized CDDP may interact with many cellular components with nucleophilic sites, especially being inactivated by binding to glutathione ( $\gamma$ -glutamylcysteinylglycine, GSH), and only approximately 1% of the internalized CDDP may interact with genomic DNA (28, 29). CDDP/m, on the other hand, is internalized via endocytosis, allowing intracellular drug release. Actually, the results of the hierarchical clustering analysis suggested that the total gene expression profile of CDDP/m may approximate that of free CDDP with free drug release from the micelles (Figure 3). Nevertheless, a large number of genes were found to be differentially expressed by cells treated with CDDP and CDDP/m (Figure 3). Indeed, the first principal component in the PC analysis was most likely to discriminate between CDDP and CDDP/m (Figure 4). As a result, 50 genes that significantly differed between cells treated with CDDP and CDDP/m were selected ( $P < 0.05$ ) (Table 2).

It is generally accepted that CDDP-induced DNA damage is detected by several families of DNA excision and mismatch repair proteins, leading to cell cycle arrest or induction of apoptosis depending on the level of CDDP-DNA adducts (28, 29). If the level of CDDP-DNA adducts is high enough to be irreparable during the  $G_2$  phase, apoptosis is triggered. *Chk1* has been proposed to constitute signaling pathways that respond to structures characteristic of DNA damage and/or incomplete DNA replication and regulate the  $G_2$  checkpoint (30, 31). The p53 tumor suppressor protein is also thought to influence CDDP-induced apoptosis (32). In response to DNA damage, p53 is activated and functions as a transcription factor to up-regulate gene products necessary for  $G_1$  phase cell cycle arrest or apoptosis (33). One of the genes up-regulated by p53, is *mdm2*, and MDM2 protein shuttles p53 through MDM2-p53 complex formation, promoting the degradation of p53 via polyubiquitination (34, 35). Thus, MDM2 constitutes a negative autoregulatory feedback of p53, preventing p53-dependent apoptosis. The caspase family was activated by CDDP treatment (28). Procaspace-9 is transformed into caspase-9 through the association initiated by binding of the apoptotic protease-activating factor-1 (Apaf-1) in the presence of ATP and cytochrome *c*, and activated caspase-9 sequentially activates caspase-3 leading to apoptosis (36, 37). Indeed, it has been suggested that the mitochondrial release of cytochrome *c* may be involved in CDDP-induced apoptosis (38). On the other hand, CDDP treatment may activate JNK kinase activity and induce c-jun expression (39, 40). Depending on the cell type, c-jun has been shown to act either as an effector of apoptosis or as an antiapoptotic factor after stress induced injury (41). c-Abl is a

nonreceptor tyrosine kinase that may be translated in response to CDDP-induced DNA damage (29) and may promote CDDP-induced apoptosis by unknown mechanism involving the DNA-dependent protein kinase and ataxia telangiectasia mutated (ATM) gene product (42, 43). *Abl2* is a null mutation of c-Abl with an almost identical phenotype (44). Although genomic DNA is generally accepted as the critical target for CDDP-induced cytotoxicity, there is evidence that other cellular targets may be involved in the cytotoxicity (28). The phosphatidylcholine-specific phospholipase C (PC-PLC) may be activated prior to DNA-CDDP adduct formation during CDDP treatment, and this early event may play an important role in CDDP-induced cytotoxicity (45). The data in Table 2 suggest that CDDP/m activates the aforementioned genes toward anti-apoptosis, whereas CDDP seems to activate them toward apoptosis.

Glutathione S-transferase (GST) and glutathione reductase (GSR) are responsible for detoxification of intracellular CDDP in a cell defense mechanism against CDDP toxicity, while several families of nucleotide excision repair enzymes function in removal of the platinum adducts from DNA (28, 29). We observed several differences in the expression of such genes between cells treated with CDDP and CDDP/m (Table 2).

Interestingly, CDDP/m down-regulated the gene expression of integrin and matrix metalloproteases (MMPs) families, whereas free CDDP up-regulated them (Table 2), and it has been suggested that the cell adhesion status and composition of cytoskeletal components may be associated with the antitumor effect of CDDP/m. The family of integrins, heterodimeric transmembrane glycoproteins, links the intracellular skeleton to the extracellular matrix (ECM) proteins, affecting cell adhesion and migratory activity. Some members of the integrin family have been reported to be overexpressed or differently expressed in chemotherapeutic agent-resistant cells compared with the sensitive parental cells (46–48). MMPs, a family of enzymes contributing to the degradation of ECM, play an integral role in tumor invasion, metastasis, and angiogenesis. MMPs are possible targets related to angiogenesis and metastasis for cancer treatment (49, 50). The down-regulation of integrin and MMPs genes by CDDP/m may lead to additional therapeutic effects.

In this study, cDNA expression array techniques revealed differential gene expression between PC-14 cells treated with CDDP and CDDP/m. These results may involve the effect of the delayed cellular response to the sustained release of free drug from the micelles leading to a lag in gene expression. In addition, it will be necessary to investigate the transcriptional and translational levels of the selected genes by conventional techniques, such as Northern blotting and Western blotting, respectively.

Furthermore, the hypothesized mechanism of CDDP/m needs to be confirmed by in vivo animal model experiment in the future work. Nevertheless, it is of a great interest that the expression of important sets of genes significantly differed between cells treated with CDDP and CDDP/m, and the difference in expression may affect the pharmacological effects of the drug. For example, we have often observed that macromolecular carriers containing antitumor drugs did not parallel with an equimolar dose of free drug in vitro (18, 51, 52) and in vivo (18, 53) that cannot be completely explained based on its pharmacodynamic and pharmacokinetic properties, and gene expression altered by macromolecular carrier systems may be involved in this unexplained cytotoxic

activity. On the other hand, since integrin and MMP family genes were down-regulated by CDDP/m, gene expression altered by macromolecular carrier systems may confer additional therapeutic effect. Thus, macromolecular carrier systems may provide technology that modulates not only pharmacokinetics in the body but therapeutic effects at diseased sites, and it may be necessary to take the latter effect into consideration in addition to optimization of pharmacokinetics when designing novel macromolecular carriers. In the future, more information regarding the relationships between structural, physicochemical, and functional properties of macromolecular carriers affecting drug release, cell entry, and subcellular localization and their pharmacological effects, including transcriptional and translational regulation, as well as interaction with intracellular molecules will provide better understanding of the signaling pathways specific to macromolecular carrier systems, leading to the design of clinically useful macromolecular carrier systems. Advanced bioinformatics technologies, such as gene expression and proteome analysis, will shed new light on such studies.

#### ACKNOWLEDGMENT

The authors would like to acknowledge a Grand-in-Aid for Scientific Research on Priority Area (A) (Molecular Synchronization for Design of New Materials System), and the Special Coordination Funds for Promoting Science and Technology from Ministry of Education, Science, Sports, and Culture, Japan.

#### LITERATURE CITED

- (1) Ringsdorf, H. (1975) Structure and properties of pharmacologically active polymers. *J. Polym. Sci. Polym. Symp.* 51, 135–153.
- (2) Kataoka, K. (1996) Targetable polymeric drugs. *Controlled drug delivery: the next generation* (K. Park, Ed.) Chapt. 4, American Chemical Society, Washington D. C.
- (3) Kopecek J., Kopeckova, P., Minko, T., and Lu, Z.-R. (2000) HPMa copolymer-anticancer drug conjugate: design, activity, and mechanism of action. *Eur. J. Pharm. Biopharm.* 50, 61–81.
- (4) Gabizon, A. A. (2001) Stealth liposomes and tumor targeting: one step further in the quest for the magic bullet. *Clin. Cancer Res.* 7, 223–225.
- (5) Maruyama, K., Ishida, O., Takizawa, T., and Moribe, (1999) K. Possibility and active targeting to tumor tissues with liposome. *Adv. Drug Deliv. Rev.* 40, 89–102.
- (6) Kwon, G., Suwa, S., Yokoyama, M., Okano, T., Sakurai, Y., and Kataoka, K. (1994) Enhanced tumor accumulation and prolonged circulation times of micelle-forming poly(ethylene oxide-aspartate) block copolymer-adriamycin conjugates. *J. Controlled Release* 29, 17–23.
- (7) Matsumura, Y., and Maeda, H. (1986) A new concept for macromolecular therapeutics in cancer chemotherapy: mechanism of tumoritropic accumulation of proteins and the antitumor agent Smancs. *Cancer Res.* 46, 6387–6392.
- (8) Matsumura, Y. (2001) Liposomes and micelles in cancer chemotherapy. *Drug Delivery Syst.* 16, 401–408.
- (9) Vasey, P. A., Kaye, S. B., Morrison, R., Twelves, C., Wilson, P., Duncan, R., Thomson, A. H., Murray, L. S., Hilditch, T. E., Murray, T., Burtles, S., Fraier, D., Frigerio, E., and Cassidy, J. (1999) Phase I clinical and pharmacokinetic study of PK-1 [N-(2-hydroxypropyl)methacrylamide copolymer doxorubicin]: first member of a new class of chemotherapeutic agents- drug-polymer conjugates. *Clin. Cancer Res.* 5, 83–94.
- (10) Miyamoto, Y., and Maeda, H. (1990) Comparison of the cytotoxic effects of the high- and low-molecular weight anticancer agents on multidrug-resistant Chinese hamster ovary cells in vitro. *Cancer Res.* 50, 1571–1575.
- (11) Miyamoto, Y., and Maeda, H. (1991) Enhancement by verapamil of neocarzinostatin action on multidrug-resistant Chinese hamster ovary cells: possible release of nonprotein chromophore in cells. *Jpn. J. Cancer Res.* 82, 351–356.
- (12) Omelyanenko, V., Kopeckova, P., Gentry, C., and Kopecek, J. (1998) Targetable HPMa copolymer-adriamycin conjugates. Recognition, internalization, and subcellular fate. *J. Controlled Release* 53, 25–37.
- (13) Minko, T., Kopeckova, P., and Kopecek, J. (1999) Comparison of the anticancer effect of free and HPMa copolymer-bound adriamycin in human ovarian carcinoma cells. *Pharm. Res.* 16, 986–996.
- (14) Minko, T., Kopeckova, P., and Kopecek, J. (2000) Efficacy of the chemotherapeutic action of HPMa copolymer-bound doxorubicin in a solid tumor model of ovarian carcinoma. *Int. J. Cancer* 86, 108–117.
- (15) Huang, P., Feng, L., Oldham, E. A., Keating, M. J., and Plunkett, W. (2000) Superoxide dismutase as a target for the selective killing of cancer cells. *Nature* 407, 390–395.
- (16) Kumar, A., Soprano, D. R., and Parekh, H. K. (2001) Cross-resistance to the synthetic retinoid CD437 in a paclitaxel-resistant human ovarian carcinoma cell line is independent of the overexpression of retinoic acid receptor- $\gamma^1$ . *Cancer Res.* 61, 7552–7555.
- (17) Nishiyama, N., Yokoyama, Y., Aoyagi, T., Okano, T., Sakurai, Y., and Kataoka, K. (1999) Preparation and characterization of self-assembled polymer-metal complex micelle from cis-dichlorodiammineplatinum(II) and poly(ethylene glycol)-poly( $\alpha$ ,  $\beta$ -aspartic acid) block copolymer in an aqueous medium. *Langmuir* 15, 377–383.
- (18) Nishiyama, N., Kato, Y., Sugiyama, Y., and Kataoka, K. (2001) Cisplatin-loaded polymer-metal complex micelle with time-modulated decaying property as a novel drug delivery system. *Pharm. Res.* 18, 1035–1041.
- (19) Harada, A., and Kataoka, K. (1995) Formation of polyion complex micelles in aqueous milieu from a pair of oppositely charged block copolymers with poly(ethylene glycol) segments. *Macromolecules* 28, 5294–5299.
- (20) Mosmann, T. (1983) Rapid colorimetric assay for cellular growth and survival: application to proliferation and cytotoxicity assays. *J. Immunological Methods* 65, 55–63.
- (21) Rosenberg, B. (1978) Platinum complexes for the treatment of cancer. *Interdiscip. Sci. Rev.* 3, 134–147.
- (22) Ponzani, V., Bressolle, F., Haug, I. J., Galtier, M., and Blayac, J. P. (1994) Cisplatin-induced renal toxicity and toxicity-modulating strategies: review *Cancer Chemother. Pharmacol.* 35, 1–9.
- (23) Siddik, Z. H., Newell, D. R., Boxall, F. E., and Harrap, K. R. (1987) The comparative pharmacokinetics of carboplatin and cisplatin in mice and rats. *Biochem. Pharmacol.* 36, 1925–1932.
- (24) Avichechter, D., Schechter, B., and Arnon, R. (1998) Functional polymers in drug delivery: carrier-supported CDDP (cis-platin) complexes of polycarboxylates – effect on human ovarian carcinoma. *React. Funct. Polym.* 36, 59–69.
- (25) Bogdanov Jr., A., Wright, S. C., Marecos, E. M., Bogdanova, A., Martin, C., Petherick, P., and Weissleder, R. (1997) A long-circulating copolymer in “passive targeting” to solid tumors. *J. Drug Targeting* 4, 321–330.
- (26) Perez-Soler, R., Han, I., Al-Baker, S., and Khokhar, A. R. (1994) Lipophilic platinum complexes entrapped in liposomes: improved stability and preserved antitumor activity with complexes containing linear alkyl carboxylate leaving groups. *Cancer Chemother. Pharmacol.* 33, 378–384.
- (27) Gianasi, E., Wasil, M., Evagarou, E. G., Kedde, A., Wilson, G., and Duncan, R. (1999) HPMa copolymer platinates as novel antitumor agents: in vitro properties, pharmacokinetics and antitumor activity in vivo. *Eur. J. Cancer* 35, 994–1002.
- (28) Gonzalez, V. M., Fuertes, M. A., Alonso, C., and Perez, J. M. (2001) Is cisplatin-induced cell death always produced by apoptosis? *Mol. Pharmacol.* 59, 657–663.
- (29) Kartalou, M., and Essigmann, J. M. (2001) Mechanism of resistance to cisplatin. *Mutation Res.* 478, 23–43.

- (30) Sanchez, Y., Wong, C., Thoma, R. S., Richman, R., Wu, Z., Piwnica-Worms, H., and Elledge, S. J. (1997) Conservation of the *Chk1* checkpoint pathway in mammals: linkage of DNA damage to Cdk regulation through Cdc25. *Science* 277, 1497–1501.
- (31) Zhao, H., and Piwnica-Worms, H. (2001) ATR-mediated checkpoint pathway regulate phosphorylation and activation of human *Chk1*. *Mol. Cell. Biol.* 21, 4129–4139.
- (32) Reed, E. (1999) *Cisplatin, in Cancer Chemotherapy and Biological Response Modifiers* (H. M. Pinedo, D. L. Longo, and B. A. Chabner, Eds.) pp 144–151, Elsevier Science BV, Amsterdam.
- (33) Fisher, D. E. (1994) Apoptosis in cancer therapy: Crossing the threshold. *Cell* 78, 539–542.
- (34) Gottifredi, V., and Prives, C. (2001) Getting p53 out of the nucleus. *Science* 292, 1851–1852.
- (35) Momand, J., Wu, H.-H., and Dasgupta, G. (2000) MDM2-master regulator of the p53 tumor suppressor protein. *Gene* 242, 15–29.
- (36) Li, P., Nijhawan, D., Budihardjo, I., Srinivasula, S. M., Ahmad, M., Alnemri, E. S., and Wang, X. (1997) Cytochrome *c* and dATP-dependent formation of Apaf-1/caspase 9 complex initiates an apoptotic protease cascade. *Cell* 91, 479–489.
- (37) Srinivasula, S. M., Ahmad, M., Fernandes-Alnemri, T., and Alnemri, E. S. (1998) Autoactivation of procaspase-9 by Apaf-1 mediated oligomerization. *Mol. Cell* 1, 949–957.
- (38) Kojima, H., Endo, K., Moriyama, H., Tanaka, Y., Alnemri, E. S., Slapak, C. A., Teicher, B., Kufe, D., and Datta, R. (1998) Abrogation of mitochondrial cytochrome *c* release and caspase-3 activation in acquired multidrug resistance. *J. Biol. Chem.* 273, 16647–16650.
- (39) Delmastro, D. A., Li, J., Vaisman, A., Solle, M., and Chaney, S. G. (1997) DNA damage inducible-gene expression following platinum treatment in human ovarian carcinoma cell lines. *Cancer Chemother. Pharmacol.* 39, 245–253.
- (40) Rubin, E., Kharbanda, S., Gunji, H., Weichselbaum, R., and Kunze, D. (1992) Cis-diamminedichloroplatinum(II) induces c-jun expression in human myeloid leukemia cells: potential involvement of a protein kinase c-dependent signaling pathway. *Cancer Res.* 52, 878–882.
- (41) Leppa, S., and Bohmann, D. (1999) Diverse functions of JNK signaling and c-Jun in stress response and apoptosis. *Oncogene* 18, 6158–6162.
- (42) Kharbanda, S., Yuan, Z. M., Weichselbaum, R., and Kufe, D. (1998) Determination of cell fate by c-Abl activation in the response to DNA damage. *Oncogene* 17, 3309–3318.
- (43) Agami, R., Blandino, G., Oren, M., and Shaul, Y. (1999) Interaction of c-Abl and p73a and their collaboration to induce apoptosis. *Nature* 399, 809–813.
- (44) Hardin, J. D., Boast, S., Schwartzberg, P. L., Lee, G., Alt, F. W., Stall, A. M., and Goff, S. P. (1996) Abnormal peripheral lymphocyte function in c-abl mutant mice. *Cell. Immunol.* 172, 100–107.
- (45) Nishio, K., Sugimoto, Y., Fujiwara, Y., Ohmori, T., Morikage, T., Takeda, Y., Ohata, M., and Saijo, N. (1992) Phospholipase c-mediated hydrolysis of phosphatidylcholine is activated by cis-diamminedichloroplatinum(II). *J. Clin. Invest.* 89, 1622–1628.
- (46) Maubant, S., Cruet-Hennequart, S., Poulain, L., Carreiras, F., Sichel, F., Luis, J., Staedel, C., and Gauduchon, P. (2002) Altered adhesion properties and alpha V integrin expression in a cisplatin-resistant human carcinoma cell line. *Int. J. Cancer* 97, 186–194.
- (47) Nista, A., Leonetti, C., Bernardini, G., Mattioni, M., and Santoni, A. (1997) Functional role of  $\alpha 4\beta 1$  and  $\alpha 5\beta 1$  integrin fibronectin receptors expressed on adriamycin-resistant MCF-7 human mammary carcinoma cells. *Int. J. Cancer* 72, 133–141.
- (48) Hoyt, D. G., Rusnak, J. M., Mannix, R. J., Modzelewski, R. A., Johnson, C. S., and Lazo, J. S. (1996) Integrin activation suppresses etoposide-induced DNA strand breakage in cultured murine tumour-derived endothelial cells. *Cancer Res.* 56, 4146–4149.
- (49) Zucker, S., Cao, J., and Chen, W.-T. (2000) Critical appraisal of the use of matrix metalloproteinase inhibitors in cancer treatment. *Oncogene* 19, 6642–6650.
- (50) Heath, E. I., and Grochow, L. B. (2000) Clinical potential of matrix metalloproteinase inhibitors in cancer therapy. *Drugs* 59, 1043–1055.
- (51) Rihova, B., Jelinkova, M., Strohalm, J., St'astny, M., Hovorka, O., Plocova, D., Kovar, M., Draberova, L., and Ulbrich, K. (2000) Antiproliferative effect of a lectin- and anti-Thy-1, 2 antibody-targeted HPMA copolymer-bound doxorubicin on primary and metastatic human colorectal carcinoma and on human colorectal carcinoma transfected with mouse Thy-1.2 gene. *Bioconjugate Chem.* 11, 664–673.
- (52) Kasuya, Y., Lu, Z.-R., Kopeckova, P., Minko, T., Tabibi, S. E., and Kopecek, J. (2001) Synthesis and characterization of HPMA copolymer-aminopropylgeldanamycin conjugates. *J. Controlled Release* 74, 203–211.
- (53) Parr, M. J., Masin, D., Cullis, P. R., and Bally, M. B. (1997) Accumulation of liposomal lipid and encapsulated doxorubicin in murine Lewis Lung Carcinoma: the lack of beneficial effects by coating liposomes with poly(ethylene glycol). *J. Pharmacol. Exp. Ther.* 280, 1319–1327.

BC025555T



# ***N*-Ac-DEVD-*N*-(Polyfluorobenzoyl)-R110: Novel Cell-Permeable Fluorogenic Caspase Substrates for the Detection of Caspase Activity and Apoptosis**

Han-Zhong Zhang, Shailaja Kasibhatla, John Guastella, Ben Tseng, John Drewe, and Sui Xiong Cai\*

Maxim Pharmaceuticals, 6650 Nancy Ridge Drive, San Diego, California 92121. Received October 1, 2002; Revised Manuscript Received January 13, 2003

*N*-Pentafluorobenzoyl-R110 (**1a**) and *N*-(2,3,4,5-tetrafluorobenzoyl)-R110 (**1b**) with enhanced cell retention properties, were prepared from rhodamine 110 (R-110) and the corresponding polyfluorobenzoyl chloride. *N*-Ac-DEVD-*N*-pentafluorobenzoyl-R110 (**3a**) and *N*-Ac-DEVD-*N*-(2,3,4,5-tetrafluorobenzoyl)-R110 (**3b**) were prepared as tetrapeptide substrates for caspases. Substrate **3b** was efficiently cleaved by human recombinant caspase-3 in an enzyme assay. Substrate **3b** also was efficiently cleaved in cell-based apoptosis assays. After cleavage in apoptotic cells by activated caspases, the substrate becomes fluorescent as measured by flow cytometry. These substrates should prove useful in cell-based assays for studying apoptosis inducers and inhibitors.

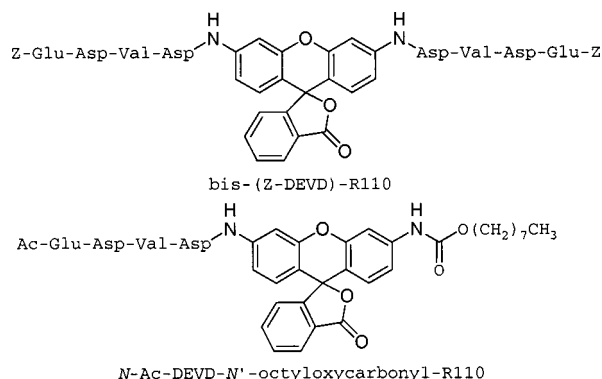
## INTRODUCTION

Apoptosis is a normal physiological process that occurs during embryonic development, as well as in the maintenance of tissue homeostasis. However, improperly regulated apoptosis can lead to several pathological conditions, including cancer and neurodegenerative diseases (1–5). Apoptosis is regulated through the activation of caspases (6), which cleave protein substrates and lead to apoptotic cell death. Caspase-3 has been identified as a key member of the caspases (7).

Coumarin-based fluorogenic substrates, such as Ac-DEVD-AFC and Z-DEVD-AMC, are useful for determining caspase activity from cellular lysates (8). However, due to their short wavelength, high background, and low extinction coefficient, they are not very suitable for high-throughput screening (HTS). The synthesis of bis-(Z-DEVD)rhodamine 110 (Chart 1) as a caspase substrate has been reported (9). Compared to coumarin, the advantages of a rhodamine-based substrate are as follows: (1) it has longer excitation and emission wavelengths, which reduced interference from testing compounds in HTS; (2) the uncleaved substrate is nonfluorescent, thus has a very low background signal; and (3) rhodamine is highly fluorescent. Interestingly, it was reported that the requirement of both peptide groups to be cleaved from this bis-peptide substrate in order to generate maximal signal limits its linear dynamic range, and the authors suggested that it is desirable to develop a rhodamine-based substrate with only one protease-cleavable amide bond (9).

Recently, we reported the design and synthesis of *N*-octyloxycarbonylrhodamine 110 as a novel fluorescent dye with enhanced cell penetration and retention properties, as well as the preparation of *N*-Ac-DEVD-*N*-octyloxycarbonyl-R110 (Chart 1) as a novel cell-permeable and pro-fluorescent caspase-3 substrate useful for cell-based caspase assays (10). It is known that the fluorine atom in a polyfluorobenzoyl group can be replaced by

Chart 1



nucleophiles (11). For examples, pentafluorobenzamide reacted with a nucleophile such as NaN<sub>3</sub> to produce 4-azido-2,3,5,6-tetrafluorobenzamide (11), while methyl 2,3,4,5-tetrafluorobenzoate reacted with NaN<sub>3</sub> to produce methyl 4-azido-2,3,5-trifluorobenzoate (12). We therefore hypothesized that R110, with one of its amino group modified with a polyfluorobenzoyl group, should react with nucleophiles inside the cells, thereby resulting in the covalent attachment of the R110 derivative to cellular proteins. This should prevent the diffusion of the fluorescent molecule out of the cells and increase its retention. Herein we report the synthesis and characterization of R110 derivatives, *N*-pentafluorobenzoyl rhodamine 110 (**1a**, *N*-PFB-R110) and *N*-(2,3,4,5-tetrafluorobenzoyl) rhodamine 110 (**1b**, *N*-TFB-R110), as well as *N*-Ac-DEVD-*N*-pentafluorobenzoyl rhodamine 110 (**3a**, *N*-Ac-DEVD-*N*-PFB-R110) and *N*-Ac-DEVD-*N*-(2,3,4,5-tetrafluorobenzoyl) rhodamine 110 (**3b**, *N*-Ac-DEVD-*N*-TFB-R110), as novel substrates for caspase-3.

## EXPERIMENTAL PROCEDURES

**General Methods and Materials.** The <sup>1</sup>H NMR spectra were recorded at 300 MHz. Chemical shifts are reported in parts per million (δ), and *J* coupling constants are reported in Hz. Rhodamine 110 was obtained from Acros, and pentafluorobenzoyl chloride and 2,3,4,5-tetra-

\* Corresponding author. Tel: 858-202-4006. Fax: 858-202-4000. E-mail: scai@maxim.com.

fluorobenzoyl chloride were obtained from Aldrich and were used as received. Tetrapeptide Ac-Asp(OBu-*t*)-Glu(OBu-*t*)-Val-Asp(OBu-*t*)-CO<sub>2</sub>H was obtained from Phoenix Pharmaceuticals, Inc. (Belmont, CA). Reagent-grade solvents were used without further purification unless otherwise specified. Elemental analyses were performed by Numega Resonance Labs, Inc. (San Diego, CA). Column chromatography was performed on Merck silica gel 60 (230–400 mesh) using reagent grade solvents. HL-60 cells and Jurkat T leukemia cells were obtained from American Type Culture Collection (Manassas, VA). Human recombinant caspase-3 enzyme was obtained from Calbiochem (San Diego, CA). Flow cytometry analyses were performed on FACScalibur (Becton Dickinson) using CellQuest analysis software.

***N*-Pentafluorobenzoylrhodamine 110 (1a).** To a solution of rhodamine 110 (1.5 g, 4.1 mmol) and *N,N*-diisopropylethylamine (0.63 g, 4.9 mmol) in dimethylformamide (40 mL) at –42 °C was added pentafluorobenzoyl chloride (1.1 g, 4.9 mmol) dropwise. The solution was stirred for 10 min at –42 °C; then it was warmed to room temperature and stirred at room temperature for 2 h. It was diluted with ice water (200 mL) and extracted with ethyl acetate (3 × 50 mL). The extracts were washed with brine (3 × 50 mL), dried over Na<sub>2</sub>SO<sub>4</sub>, and concentrated to give crude product, which was purified by column chromatography (hexane:EtOAc 1:1), and yielded 0.42 g (21%) of **1a** as a solid. <sup>1</sup>H NMR (CDCl<sub>3</sub>): 8.00 (s, 1H), 7.98 (d, *J* = 8.1, 1H), 7.80 (s, 1H), 7.71–7.59 (m, 2H), 7.20 (d, *J* = 6.9, 1H), 6.99 (d, *J* = 8.7, 1H), 6.71 (d, *J* = 8.7, 1H), 6.53–6.35 (m, 3H), 3.95 (brs, 2H). Anal. Calcd for C<sub>27</sub>H<sub>13</sub>F<sub>5</sub>N<sub>2</sub>O<sub>4</sub> 1.5 H<sub>2</sub>O: C, 58.85; H, 2.90; N, 5.08. Found: C, 58.27; H, 2.69; N, 4.63.

***N*-(2,3,4,5-Tetrafluorobenzoyl)rhodamine 110 (1b).** Compound **1b** was prepared from rhodamine 110 and 2,3,4,5-tetrafluorobenzoyl chloride by a method similar to that described for the preparation of **1a** (18%). <sup>1</sup>H NMR (CDCl<sub>3</sub>): 8.40 (d, *J* = 12.9, 1H), 8.01 (d, *J* = 7.5, 1H), 7.81 (s, 1H), 7.71–7.59 (m, 3H), 7.16 (d, *J* = 7.2, 1H), 7.01 (dd, *J* = 9.0, 2.4, 1H), 6.76 (d, *J* = 8.7, 1H), 6.50–6.45 (m, 2H), 6.34 (dd, *J* = 8.4, 2.1, 1H), 3.93 (brs, 2H). Anal. Calcd. for C<sub>27</sub>H<sub>14</sub>F<sub>4</sub>N<sub>2</sub>O<sub>4</sub>: C, 64.04; H, 2.79; N, 5.53. Found: C, 63.64; H, 3.26; N, 5.20.

***N*-[Ac-Asp(OBu-*t*)-Glu(OBu-*t*)-Val-Asp(OBu-*t*)]-*N*-pentafluorobenzoylrhodamine 110 (2a).** To a solution of Ac-Asp(OBu-*t*)-Glu(OBu-*t*)-Val-Asp(OBu-*t*)-CO<sub>2</sub>H (206 mg, 0.30 mmol) in an anhydrous 1:1 mixture of dimethylformamide and pyridine (2 mL) at 0 °C was added 1-[3-(dimethylamino)propyl]-3-ethylcarbodiimide hydrochloride (57 mg, 0.30 mmol). The solution was stirred for 20 min, and then *N*-pentafluorobenzoylrhodamine 110 (52 mg, 0.10 mmol) was added. It was stirred at room temperature for 5 days, then diluted with water (10 mL) and extracted with ethyl acetate (3 × 10 mL). The extracts were washed with 1N HCl (2 × 10 mL) and water (2 × 10 mL), dried over Na<sub>2</sub>SO<sub>4</sub>, and concentrated to give crude product, which was purified by column chromatography (EtOAc:CH<sub>2</sub>Cl<sub>2</sub> = 2:3), and yielded 63 mg (53%) of **2a** as a solid. <sup>1</sup>H NMR (CDCl<sub>3</sub>): 9.80–9.06 (m, 1H), 8.82–8.42 (m, 1H), 8.03–6.64 (m, 10H), 5.00–3.90 (m, 4H), 3.22–2.42 (m, 6H), 2.30–2.00 (m, 2H), 2.06 (s, 3H), 1.49–1.35 (m, 27H). Anal. Calcd for C<sub>59</sub>H<sub>65</sub>F<sub>5</sub>N<sub>6</sub>O<sub>15</sub> 2.0 H<sub>2</sub>O: C, 57.64; H, 5.61; N, 6.83. Found: C, 57.64; H, 5.45; N, 7.13.

***N*-[Ac-Asp(OBu-*t*)-Glu(OBu-*t*)-Val-Asp(OBu-*t*)]-*N*-(2,3,4,5-tetrafluorobenzoyl)rhodamine 110 (2b).** Compound **2b** was prepared from Ac-Asp(OBu-*t*)-Glu(OBu-*t*)-Val-Asp(OBu-*t*)-CO<sub>2</sub>H and *N*-(2,3,4,5-tetrafluorobenzoyl)rhodamine 110 (**1b**) by a method similar to that

described for the preparation of **2a** (27%). <sup>1</sup>H NMR (CDCl<sub>3</sub>): 9.80–9.06 (m, 1H), 8.82–8.42 (m, 2H), 8.03–6.64 (m, 10H), 5.00–3.90 (m, 4H), 3.22–2.42 (m, 6H), 2.30–2.00 (m, 2H), 2.06 (s, 3H), 1.49–1.35 (m, 27H), 1.11–1.00 (m, 6H). Anal. Calcd for C<sub>59</sub>H<sub>66</sub>F<sub>4</sub>N<sub>6</sub>O<sub>15</sub>: C, 60.30; H, 6.47; N, 7.15. Found: C, 60.03; H, 5.92; N, 7.20.

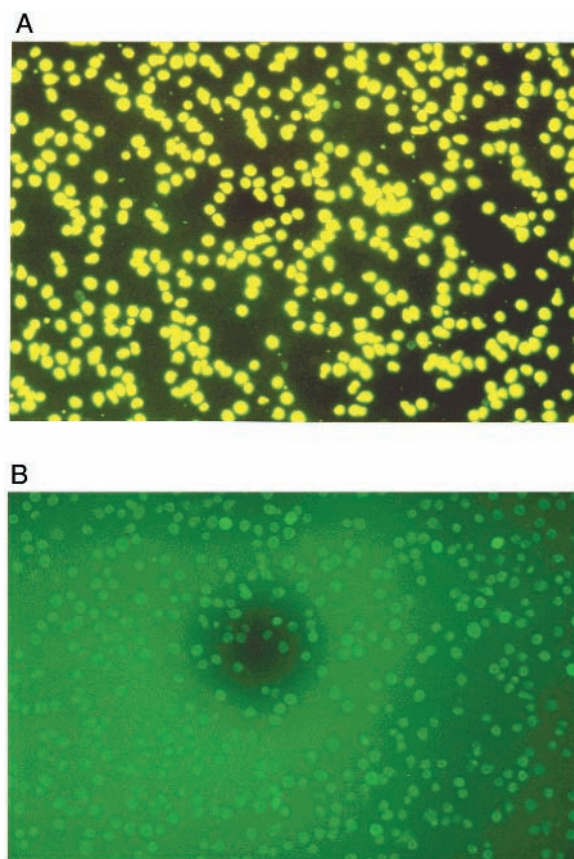
***N*-(Ac-Asp-Glu-Val-Asp)-*N*-pentafluorobenzoylrhodamine 110 (3a).** To a cooled solution (0 °C) of *N*-[Ac-Asp(OBu-*t*)-Glu(OBu-*t*)-Val-Asp(OBu-*t*)]-*N*-pentafluorobenzoylrhodamine 110 (40 mg, 0.034 mmol) in methylene chloride (2 mL) was added 50% trifluoroacetic acid in methylene chloride (1 mL). The solution turned orange and was stirred at room temperature for 4 h. The solvent was removed, and the residue was redissolved in a mixture solvent of EtOAc:MeOH (4:1; 0.25 mL). The solution was added dropwise into hexane (10 mL) to give a precipitate, which was filtered and dried to yield 31 mg (89%) of **3a**. <sup>1</sup>H NMR (CD<sub>3</sub>OD) 8.08–7.68 (m, 8H), 6.83–6.74 (m, 2H), 4.70–4.65 (m, 1H), 3.94 (m, 1H), 4.42–4.30 (m, 1H), 4.12–4.04 (m, 1H), 3.98–3.92 (m, 1H), 3.08–2.72 (m, 4H), 2.38 (m, 2H), 2.12 (m, 2H), 1.98–1.94 (m, 3H), 1.30 (s, 1H), 1.04–0.96 (m, 6H). Anal. Calcd for C<sub>47</sub>H<sub>41</sub>F<sub>5</sub>N<sub>6</sub>O<sub>15</sub> 3H<sub>2</sub>O: C, 52.36; H, 4.36; N, 7.79. Found: C, 52.36; H, 4.64; N, 7.58.

***N*-(Ac-Asp-Glu-Val-Asp)-*N*-(2,3,4,5-tetrafluorobenzoyl)rhodamine 110 (3b).** Compound **3b** was prepared from *N*-[Ac-Asp(OBu-*t*)-Glu(OBu-*t*)-Val-Asp(OBu-*t*)]-*N*-(2,3,4,5-tetrafluorobenzoyl)rhodamine 110 (**2b**) by a method similar to that described for the preparation of **3a** (94%). <sup>1</sup>H NMR (CD<sub>3</sub>OD): 8.40–7.40 (m, 9H), 6.92–6.72 (d, *J* = 7.8, 2H), 4.87 (m, 2H), 4.30–4.15 (m, 1H), 3.94 (m, 1H), 3.15–2.70 (m, 6H), 2.58 (m, 2H), 2.32 (m, 2H), 2.17–2.14 (m, 3H), 1.05–0.97 (m, 6H). Anal. Calcd for C<sub>47</sub>H<sub>42</sub>F<sub>4</sub>N<sub>6</sub>O<sub>15</sub> 4H<sub>2</sub>O: C, 52.32; H, 4.63; N, 7.78. Found: C, 51.99; H, 4.05; N, 7.72.

**Reaction of *N*-Pentafluorobenzoylrhodamine 110 1a with a Nucleophile 1-Dodecanethiol.** A solution of **1a** (26.2 mg, 0.05 mmol), 1-dodecanethiol (12.1 mg, 0.06 mmol), and diisopropylethylamine (8.4 mg, 0.065 mmol) in dimethylformamide (2 mL) was stirred at 25 °C for 16 h. TLC showed no more **1a**, and two new spots were observed. The solution was diluted with water (10 mL) and extracted with EtOAc (3 × 10 mL). The extracts were washed with water (3 × 10 mL), dried over Na<sub>2</sub>SO<sub>4</sub>, and concentrated to give crude product, which was purified by column chromatography (EtOAc/hexane = 1:2) to give two products. Compound I, 15 mg (42%), *R<sub>f</sub>* = 0.59 (EtOAc/hexane = 1:1), was identified as the monoadduct of 1-dodecanethiol with **1a**. <sup>1</sup>H NMR (CDCl<sub>3</sub>): 8.01–7.59 (m, 6H), 7.15 (d, *J* = 7.5 Hz, 1H), 7.02 (d, *J* = 8.4 Hz, 1H), 6.74 (d, *J* = 8.7 Hz, 1H), 6.54–6.32 (m, 2H), 3.93 (s, 2H), 2.89 (t, *J* = 7.2 Hz, 2H), 1.54 (m, 2H), 1.23 (bs, 18H), 0.88 (t, *J* = 6.0 Hz, 3H). MS. 707 (M + 1), 705 (M – 1). Compound II, 2.5 mg (5.6%), *R<sub>f</sub>* = 0.76 (EtOAc/hexane = 1:1), was identified as the bis-adduct of 1-dodecanethiol with **1a**. <sup>1</sup>H NMR (CDCl<sub>3</sub>): 8.00–7.58 (m, 6H), 7.18–7.639 (m, 5H), 3.93 (s, 2H), 2.95 (bs, 2H), 2.86 (t, *J* = 7.5 Hz, 2H), 1.58 (s, 4H), 1.62–1.50 (m, 4H), 1.38–1.20 (m, 36H), 0.88 (t, *J* = 0.57 Hz, 6H). MS. 889 (M + 1), 887 (M – 1).

**Staining of Cells with *N*-Pentafluorobenzoylrhodamine 110 and Rhodamine 110.** HL-60 cells were grown in RPMI 1640 media (Life Technologies, Inc.) + 10% FCS (Sigma Chemical Company) in a 5% CO<sub>2</sub> –95% humidity incubator at 37 °C. The cells (about 2 × 10<sup>6</sup>) were placed in 50 μL of Iscove's medium, without serum or phenol-red, containing 10 μM *N*-pentafluorobenzoylrhodamine 110 **1a**. A parallel sample was placed in the same medium containing 10 μM rhodamine 110. The cells

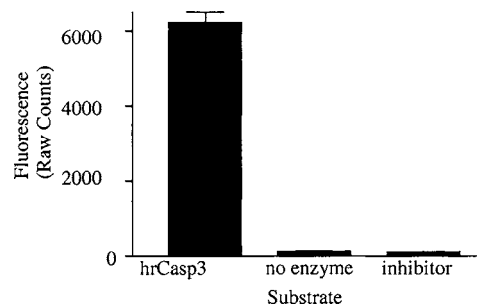




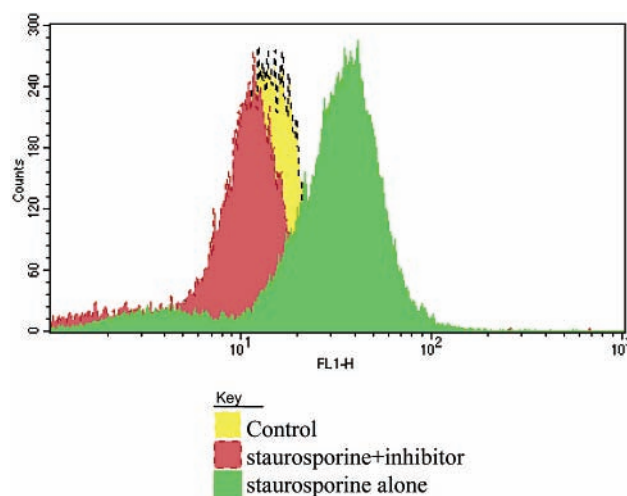
**Figure 1.** Staining of HL-60 cells by (A) *N*-PFB-R110 and (B) R110. The pictures were taken 15 min after the cells were placed in microslides.

were incubated for 2 h at 37 °C in a CO<sub>2</sub> incubator, recovered by centrifugation, and resuspended in 50  $\mu$ L of fresh medium without **1a**, or rhodamine 110. Aliquots of each cell suspension were placed in microslides and viewed on a Nikon inverted microscope with epifluorescent illumination (excitation wavelength of 490 nm). Cells incubated with rhodamine 110 initially emitted a strong yellowish-green fluorescent signal, but this signal faded rapidly with time as the dye leaked out of the cells into the surrounding medium (Figure 1B, 15 min after placed in microslides). In contrast, cells incubated with *N*-pentafluorobenzoylrhodamine 110 **1a** emitted a strong yellowish-green fluorescent signal, which remained constant in intensity during viewing periods of at least 15 min. The *N*-pentafluorobenzoylrhodamine 110 **1a** was well retained by the cells, as shown by the lack of fluorescence from the surrounding medium (Figure 1A, 15 min after placed in microslides).

**Cleavage of *N*-(Ac-DEVD)-*N*-(2,3,4,5-tetrafluorobenzoyl)-R110 by Recombinant Caspase-3.** The cleavage of *N*-Ac-DEVD-*N*-TFB-R110 by caspase-3 was tested in a cell-free assay using recombinant enzyme in a standard fluorometric microplate assay (13). In short, 1 unit of recombinant caspase-3 enzyme (Calbiochem, San Diego) was incubated with 10  $\mu$ M of substrate in a caspase assay buffer (40 mM PIPES; pH 7.2; 100 mM NaCl; 10% sucrose; 0.1% CHAPS; 1 mM EDTA; 10 mM DTT) for 3 h at 37 °C, as recommended by the supplier. Control reactions included one sample with no enzyme, which gave the background signal of the substrate, and one sample incubated in the presence of 10  $\mu$ M of the caspase-3 inhibitor, Ac-DEVD-CHO (14). Figure 2 shows that *N*-Ac-DEVD-*N*-TFB-R110 was readily cleaved by recombinant caspase-3, resulting in an approximate 50-



**Figure 2.** The cleavage of *N*-Ac-DEVD-*N*-TFB-R110 by hrCasp3 after 3 h incubation and its inhibition by caspase inhibitor Ac-DEVD-CHO.

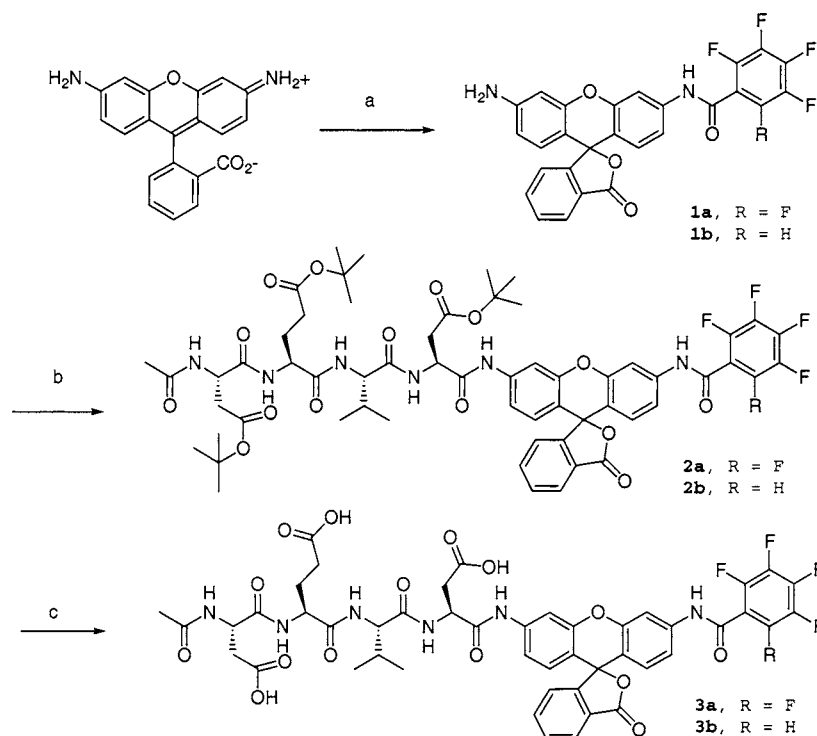


**Figure 3.** The cleavage of *N*-Ac-DEVD-*N*-TFB-R110 in staurosporine-treated apoptotic Jurkat T leukemia cells and its inhibition by a broad-spectrum caspase inhibitor Z-VD-fmk as measured by flow cytometric analysis. The *x*-axis is the fluorescence intensity, and the *y*-axis is the number of cells with that fluorescence intensity.

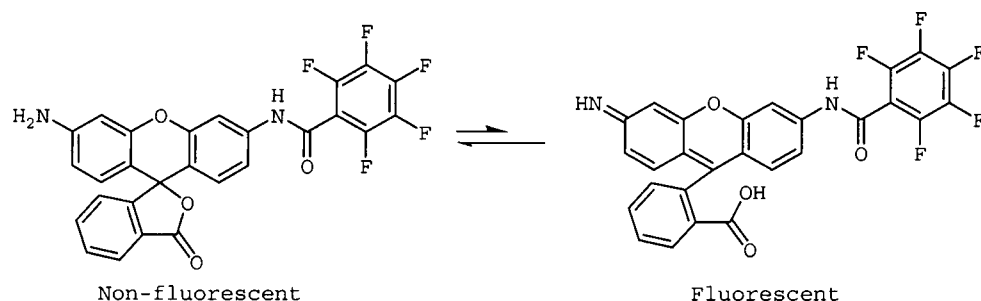
fold increase in fluorescence over background. In the presence of the caspase-3 inhibitor, Ac-DEVD-CHO, the cleavage of *N*-Ac-DEVD-*N*-TFB-R110 was completely inhibited and resulted in the reduction of the fluorescent signal to the background level.

**Induction of Apoptosis with Staurosporine Leads to Cleavage of *N*-Ac-DEVD-*N*-TFB-R110 in a Whole Cell Assay.** Jurkat T leukemia cells were grown in RPMI 1640 media (Life Technologies, Inc.) + 10% FCS (Sigma Chemical Company) in a 5% CO<sub>2</sub>–95% humidity incubator at 37 °C and maintained at a cell density between 4 and 8  $\times$  10<sup>5</sup> cells/mL. Cells were harvested at 200g and resuspended at 1  $\times$  10<sup>6</sup> cells/mL into RPMI 1640 media containing 10% FCS, and 1 mL each was dispensed in a 6-well plate. The apoptosis inducer, staurosporine (15), was added at 0.5  $\mu$ g/mL concentration, and the plate was incubated for 2 h at 37 °C in a 5% CO<sub>2</sub>–95% humidity incubator. In a separate well, the apoptosis inducer, staurosporine, was added in the presence of 10  $\mu$ M of a broad-spectrum caspase inhibitor, Cbz-Val-Asp-FMK (16), which inhibits all the caspases. Cells were pelleted and incubated with 50  $\mu$ M of substrate *N*-Ac-DEVD-*N*-TFB-R110 for 2 h at 37 °C in a serum-free RPMI medium. 500  $\mu$ L PBS was added, and samples were analyzed by flow cytometry. Figure 3 shows that induction of apoptosis in Jurkat cells by staurosporine leads to cleavage of the caspase-3 substrate, *N*-Ac-DEVD-*N*-TFB-R110, under whole cell assay conditions. Figure 3 also shows that the cleavage of the caspase substrate, *N*-Ac-DEVD-*N*-TFB-R110 in the apoptotic cells, can be inhibited by



**Scheme 1. Synthesis of *N*-PFB-R110 (**1a**), *N*-TFB-R110 (**1b**), *N*-Ac-DEVD-*N*-PFB-R110 (**3a**), and *N*-Ac-DEVD-*N*-TFB-R110 (**3b**)<sup>a</sup>**

<sup>a</sup> (a) C<sub>6</sub>F<sub>5</sub>COCl or C<sub>6</sub>F<sub>4</sub>HCOCl/(*i*-Pr)<sub>2</sub>NEt/DMF; (b) Ac-Asp(OBu-*t*)-Glu(OBu-*t*)-Val-Asp(OBu-*t*)/EDC/pyridine/DMF; (c) TFA/CH<sub>2</sub>Cl<sub>2</sub>.

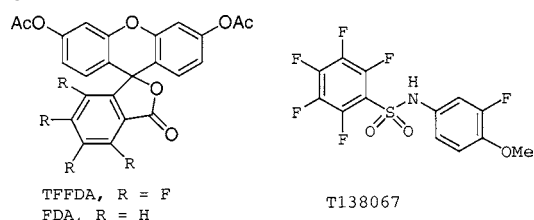
**Scheme 2. Equilibration of *N*-PFB-R110**

a broad-spectrum caspase inhibitor, Cbz-Val-Asp-FMK, under the same conditions.

**RESULTS AND DISCUSSION**

*N*-PFB-R110 (**1a**) and *N*-TFB-R110 (**1b**) were prepared by reaction of R110 with pentafluorobenzoyl chloride and 2,3,4,5-tetrafluorobenzoyl chloride (Scheme 1). The polyfluorobenzoyl-R110s were found to be fluorescent at a similar wavelength as that of R110 (excitation at 485 nm and emission at 525 nm). However, the polyfluorobenzoyl-R110s were found to be less fluorescent than that of R110. The relative fluorescence of *N*-PFB-R110 (**1a**) was only approximately 5% of R110. In comparison, *N*-octyloxycarbonyl-R110 had a relative fluorescence of approximately 16% of R110 (10). This suggests that the strong electron-withdrawing pentafluorobenzoyl group might make the rhodamine favor the nonfluorescent closed ring form when equilibrated in aqueous solution (Scheme 2).

The cell penetration and retention properties of the polyfluorobenzoyl-R110 **1a** were tested in HL-60 cells. Cells incubated with *N*-PFB-R110 (**1a**) were found to be highly fluorescent (Figure 1A), the signal remained strong, and no leakage of the fluorescent dye to the medium was observed. In comparison, cells incubated

**Chart 2**

with R110 initially showed a strong cellular fluorescent signal, but the signal faded quickly due to leakage of the dye from the cells, and the culture medium became highly fluorescent (Figure 1B). This experiment demonstrates that, although *N*-PFB-R110 is less fluorescent than R110, it can stain cells to a signal intensity as high as rhodamine 110, and unlike rhodamine 110, the *N*-PFB-R110 signal remains strong over time. These data suggest that *N*-PFB-R110 is retained better by the cells than R110, probably due to reaction of the pentafluorobenzoyl group with nucleophiles inside the cells. This is similar to what has been reported for a polyfluorinated fluorescein, 4,5,6,7-tetrafluorofluorescein diacetate (TFFDA, Chart 2), which reacted with intracellular components, including glutathione and proteins, and has better cell retention properties than that of fluorescein diacetate

(FDA, Chart 2) (17). 4,5,6,7-Tetrafluorofluorescein diacetate treated cells were found to show significantly higher fluorescence than those cells treated with fluorescein diacetate. The fluorescent dyes also were not transferred to other cells when cells labeled with TFFDA were mixed with unlabeled cells, suggesting that the polyfluorinated fluorescein TFFDA were trapped inside the cells by covalent attachment to intracellular components (17). Similarly, it also has been reported that incubation of T138067 (Chart 2), an anticancer agent, with MCF7 tumor cells resulted in the covalent attachment of T138067 to  $\beta$ -tubulin. This was found to be due to the replacement of the *p*-F in the pentafluorophenyl group by the thiol group in Cys-239 of  $\beta$ -tubulin (18).

To confirm that *N*-PFB-R110 (**1a**) can react with nucleophiles, *N*-PFB-R110 (**1a**) was treated with a thiol nucleophile 1-dodecanethiol. The reaction came to completion within 16 h at 25 °C. The products, as identified by <sup>1</sup>H NMR and MS, were found to be the adducts of **1a** with 1-dodecanethiol, confirming that the pentafluorobenzoyl group in **1a** can react with a nucleophile, similar to what has been observed for pentafluorobenzamide (11) and 4,5,6,7-tetrafluorofluorescein diacetate (17).

The caspase-3 substrates, *N*-Ac-DEVD-*N*-PFB-R110 (**3a**) and *N*-Ac-DEVD-*N*-TFB-R110 (**3b**), were prepared by coupling a *t*-Bu protected tetrapeptide, Ac-DEVD-CO<sub>2</sub>H, with **1a** and **1b** to give **2a** and **2b**, followed by deprotection of the *t*-Bu groups (Scheme 1). In comparison, due to the large size of the tetrapeptide, difficulties were encountered in the coupling of the tetrapeptide with R110 for the preparation of the bis(Z-DEVD)-R110 substrate, and the compound was prepared by sequential coupling of amino acids to R110 in a multistep reaction (9). Therefore, by blocking one of the amino group in R110, the preparation of a mono-peptide-R110 substrate such as **3a** is simplified compared to the preparation of bis(Z-DEVD)-R110. Another potential advantage of mono-DEVD-R110 substrates is that they are smaller and have three carboxylic acid groups versus six carboxylic acid groups in the bis-peptide substrate, which might improve its cell penetration properties. As expected, both compounds **3a** and **3b** are nonfluorescent.

The cleavage of the substrate *N*-Ac-DEVD-*N*-TFB-R110 (**3b**) by caspase-3 was tested first in a cell-free assay using human recombinant caspase-3 (hrCasp3). As seen in Figure 2, *N*-Ac-DEVD-*N*-TFB-R110 was readily cleaved by caspase-3, resulting in an approximate 50-fold increase in fluorescence over background after 3 h incubation, and the cleavage of **3b** by hrCasp3 was inhibited completely by the caspase-3 inhibitor, Ac-DEVD-CHO. These experiments show that *N*-Ac-DEVD-*N*-TFB-R110 is a suitable fluorogenic substrate for caspase-3, with low background fluorescence and a strong fluorescent signal in the cleaved state.

*N*-Ac-DEVD-*N*-TFB-R110 (**3b**) was tested as a substrate for the measurement of apoptosis in a whole cell assay using flow cytometry. Jurkat T leukemia cells were treated with the apoptosis inducer, staurosporine, incubated with *N*-Ac-DEVD-*N*-TFB-R110, and the samples were analyzed by flow cytometry. Figure 3 shows that induction of apoptosis in Jurkat cells by staurosporine leads to cleavage of the caspase-3 substrate *N*-Ac-DEVD-*N*-TFB-R110 under whole cell assay conditions. The presence of a broad spectrum caspase inhibitor, Z-Val-Asp-fmk (18), resulted in a shift in the fluorescent signal to a value slightly lower than the signal from the control cells, indicating that the cleavage of **3b** in staurosporine-treated cells was due to caspases. Since multicaspases can be activated in cells by an apoptosis inducer such as

staurosporine (19) and DEVD is known to be an optimal sequence for caspase-3 but also can be cleaved by other caspases such as caspase-7 (20), a broad spectrum caspase inhibitor can provide better inhibition of the caspases in cell based assays.

In conclusion, we have prepared polyfluorobenzoyl-derived R110 fluorescent dyes, *N*-pentafluorobenzoyl-R110 (**1a**) and *N*-(2,3,4,5-tetrafluorobenzoyl)-R110 (**1b**). Although these derivatives of R110 are much less fluorescent than R110, they are more cell-permeable and have much better cell retention properties than R110. Using **1a** and **1b**, the novel fluorogenic caspase-3 substrates, *N*-Ac-DEVD-*N*-PFB-R110 (**3a**) and *N*-Ac-DEVD-*N*-TFB-R110 (**3b**), have been prepared. Substrate **3b** has been shown to be a substrate for hrCasp3 and has been found to be useful for the measurement of apoptosis in staurosporine-treated, apoptotic Jurkat cells using flow cytometry. These substrates should be useful for the measurement of apoptosis in whole cell assays and for cell-based high throughput screening of apoptosis inhibitors or inducers. We have successfully used a mono-(Ac-DEVD)-R110 substrate for our cell-based high-throughput screening of apoptosis inducers, and the results will be reported elsewhere (21).

#### LITERATURE CITED

- (1) Reed, J. C., and Tomaselli, K. J. (2000) Drug discovery opportunities from apoptosis research. *Curr. Opin. Biotechnol.* **11**, 586–592.
- (2) Leung, D., Abbenante, G., and Fairlie, D. P. (2000) Protease inhibitors: current status and future prospects. *J. Med. Chem.* **43**, 305–341.
- (3) Keppler-Hafkemeyer, A., Brinkmann, U., and Pastan, I. (1998) Role of caspases in immunotoxin-induced apoptosis of cancer cells. *Biochemistry* **37**, 16934–16942.
- (4) Wellington, C. L., and Hayden, M. R. (2000) Caspases and neurodegeneration: on the cutting edge of new therapeutic approaches. *Clin. Genet.* **57**, 1–10.
- (5) Lowe, S. W., and Lin, A. W. (2000) Apoptosis in cancer. *Carcinogenesis* **21**, 485–495.
- (6) Thornberry, N. A. (1998) Caspases: key mediators of apoptosis. *Chem. Biol.* **5**, R97–R103.
- (7) Kumar, S. (1999) Regulation of caspase activation in apoptosis: implications in pathogenesis and treatment of disease. *Clin. Exp. Pharmacol. Physiol.* **26**, 295–303.
- (8) Stennicke, H. R., and Salvesen, G. S. J. (1997) Biochemical characteristics of caspases-3, -6, -7, and -8. *Biol. Chem.* **272**, 25719–25723.
- (9) Liu, J., Bhalgat, M., Zhang, C., Diwu, Z., Hoyland, B., and Klaubert, D. H. (1999) Fluorescent molecular probes V: a sensitive caspase-3 substrate for fluorometric assays. *Bioorg. Med. Chem. Lett.* **9**, 3231–3236.
- (10) Cai, S., Zhang, H., Guastella, J., Drewe, J., Yang, W., and Weber, E. (2001) Design and synthesis of rhodamine 110 derivative and caspase-3 substrate for enzyme- and cell-based fluorescent assay. *Bioorg. Med. Chem. Lett.* **11**, 39–42.
- (11) Keana, J. F. W., and Cai, S. X. (1990) New reagents for photoaffinity labeling: Synthesis and photolysis of functionalized perfluorophenyl azides. *J. Org. Chem.* **55**, 3640–3647.
- (12) Cai, S. X., Glenn, D. J., and Keana, J. F. W. (1992) Toward the development of radiolabeled fluorophenyl azide-based photolabeling reagents: synthesis and photolysis of iodinated 4-azido-perfluorobenzoates and 4-azido-3,5,6-trifluorobenzoates. *J. Org. Chem.* **57**, 1299–1304.
- (13) Thornberry, N. A. (1994) Interleukin-1 beta converting enzyme. *Methods Enzymol.* **244**, 615–631.
- (14) Casciola-Rosen, L., Nicholson, D. W., Chong, T., Rowan, K. R., Thornberry, N. A., Miller, D. K., and Rosen, A. (1996) Apopain/CPP32 cleaves proteins that are essential for cellular repair: a fundamental principle of apoptotic death. *J. Exp. Med.* **183**, 1957–64.

- (15) Falcieri, E., Martelli, A. M., Bareggi, R., Cataldi, A., and Cocco, L. (1993) The protein kinase inhibitor staurosporine induces morphological changes typical of apoptosis in MOLT-4 cells without concomitant DNA fragmentation. *Biochem. Biophys. Res. Commun.* 193, 19–25.
- (16) Jaeschke, H., Farhood, A., Cai, S. X., Tseng, B. Y., and Bajt, M. L. (2000) Protection against TNF-induced liver parenchymal cell apoptosis during endotoxemia by a novel caspase inhibitor in mice. *Tox. App. Pharm.* 169, 77–83.
- (17) Gee, K. R., Poot, M., Klaubert, D. H., Sun, W.-C., Haugland, R. P., and Mao, F. Fluorinated xanthene derivatives. US patent 6,162,931, column 76, example 132 and 133.
- (18) Shan, B., Medina, J. C., Santha, E., Frankmoelle, W. P., Chou, T. C., Learned, R. M., Narbut, M. R., Stott, D., Wu, P., Jaen, J. C., Rosen, T., Timmermans, P. B., and Beckmann, H. (1999) Selective covalent modification of beta-tubulin residue Cys-239 by T138067, an antitumor agent with in vivo efficacy against multidrug-resistant tumors. *Proc. Natl. Acad. Sci. U.S.A.* 96, 5686–5691.
- (19) Meller, R., Skradski, S. L., Simon, R. P., and Henshall, D. C. (2002) Expression, proteolysis and activation of caspases 6 and 7 during rat C<sub>6</sub> glioma cell apoptosis. *Neurosci. Lett.* 324, 33–36.
- (20) Thornberry, N. A., Rano, T. A., Peterson, E. P., Rasper, D. M., Timkey, T., Garcia-Calvo, M., Houtzager, V. M., Nordstrom, P. A., Roy, S., Vaillancourt, J. P., Chapman, K. T., and Nicholson, D. W. (1997) A combinatorial approach defines specificities of members of the caspase family and granzyme B. Functional relationships established for key mediators of apoptosis. *J. Biol. Chem.* 272, 17907–17911.
- (21) Cai, S. X., Nguyen, B., Jia, S., Guastella, J., Reddy, S., Tseng, B., Drewe, J., and Kasibhatla, S. Discovery of substituted *N*-phenyl nicotinamides as potent inducers of apoptosis using a cell and caspase based high throughput screening assay. *J. Med. Chem.*, submitted.

BC0256188



# Site-Specific PEGylation of Hemoglobin at Cys-93( $\beta$ ): Correlation between the Colligative Properties of the PEGylated Protein and the Length of the Conjugated PEG Chain

B. N. Manjula,<sup>\*,†</sup> A. Tsai,<sup>‡</sup> R. Upadhyay,<sup>†</sup> K. Perumalsamy,<sup>†</sup> P. K. Smith,<sup>§</sup> A. Malavalli,<sup>||</sup> K. Vandegriff,<sup>||</sup> R. M. Winslow,<sup>||</sup> M. Intaglietta,<sup>‡</sup> M. Prabhakaran,<sup>⊥</sup> J. M. Friedman,<sup>†</sup> and A. S. Acharya<sup>†</sup>

Albert Einstein College of Medicine, Bronx, New York, University of California—San Diego, La Jolla, California, BioAffinity Systems, Rockford, Illinois, Sangart, Inc., San Diego, California, and Structural BioInformatics, San Diego, California. Received September 5, 2002; Revised Manuscript Received December 13, 2002

Increasing the molecular size of acellular hemoglobin (Hb) has been proposed as an approach to reduce its undesirable vasoactive properties. The finding that bovine Hb surface decorated with about 10 copies of PEG5K per tetramer is vasoactive provides support for this concept. The PEGylated bovine Hb has a strikingly larger molecular radius than HbA (1). The colligative properties of the PEGylated bovine Hb are distinct from those of HbA and even polymerized Hb, suggesting a role for the colligative properties of PEGylated Hb in neutralizing the vasoactivity of acellular Hb. To correlate the colligative properties of surface-decorated Hb with the mass of the PEG attached and also its vasoactivity, we have developed a new maleimide-based protocol for the site-specific conjugation of PEG to Hb, taking advantage of the unusually high reactivity of Cys-93( $\beta$ ) of oxy HbA and the high reactivity of the maleimide to protein thiols. PEG chains of 5, 10, and 20 kDa have been functionalized at one of their hydroxyl groups with a maleidophenyl moiety through a carbamate linkage and used to conjugate the PEG chains at the  $\beta$ -93 Cys of HbA to generate PEGylated Hbs carrying two copies of PEG (of varying chain length) per tetramer. Homogeneous preparations of (SP-PEG5K)<sub>2</sub>-HbA, (SP-PEG10K)<sub>2</sub>-HbA, and (SP-PEG20K)<sub>2</sub>-HbA have been isolated by ion exchange chromatography. The oxygen affinity of Hb is increased slightly on PEGylation, but the length of the PEG-chain had very little additional influence on the O<sub>2</sub> affinity. Both the hydrodynamic volume and the molecular radius of the Hb increased on surface decoration with PEG and exhibited a linear correlation with the mass of the PEG chain attached. On the other hand, both the viscosity and the colloidal osmotic pressure (COP) of the PEGylated Hbs exhibited an exponential increase with the increase in PEG chain length. In contrast to the molecular volume, viscosity, and COP, the vasoactivity of the PEGylated Hbs was not a direct correlate of the PEG chain length. There appeared to be a threshold for the PEG chain length beyond which the protection against vasoactivity is decreased. These results suggest that the modulation of the vasoactivity of Hb by PEG could be a function of the surface shielding afforded by the PEG, the latter being a function of the disposition of the PEG chain on the protein surface, which in turn is a function of the length of the PEG chain. Thus, the biochemically homogeneous PEGylated Hbs described in the present study, surface-decorated with PEG chains of appropriate size, could serve as potential candidates for Hb-based oxygen carriers.

## INTRODUCTION

Several chemically and genetically modified acellular hemoglobins (Hbs)<sup>1</sup> have been investigated to date as oxygen carrying therapeutic agents (2–4). One of the two major toxicities of Hb, namely, nephrotoxicity, has been overcome by intramolecular cross-linking (2, 5). The current major focus in the field is to overcome the vasoactivity of Hb (6, 7). The vasoactivity of acellular Hb has been attributed to its extravasation into the interstitial spaces and subsequent scavenging of nitric oxide (6–16) and may involve a second mechanism related to

the autoregulation of capillary blood flow (17). Increasing the molecular size of Hb has been advocated as one of the approaches to prevent the extravasation of acellular Hb into the interstitial spaces. Intertetrameric cross-linking and conjugation to monofunctional PEG have been sought as approaches to increase the molecular size of Hb. PEGylation of proteins and peptides has been shown to increase their molecular size, resulting in an increased circulatory half-life and also to eliminate or reduce their antigenicity (18, 19). Recent studies by Winslow and co-workers (17, 20, 21) employing intratetramerically cross-linked Hbs, polymerized Hbs, and PEGylated Hbs have shown that, despite similar in vitro NO binding activity, the modified Hbs differ significantly

\* Corresponding author. Address: Department of Physiology and Biophysics, Albert Einstein College of Medicine, 1300 Morris Park Avenue, Bronx, NY 10461. Phone: 718-430-2062. Fax: 718-430-8819. E-mail: manjula@aeom.yu.edu.

<sup>†</sup> Albert Einstein College of Medicine.

<sup>‡</sup> UCSD.

<sup>§</sup> BioAffinity Systems.

<sup>||</sup> Sangart.

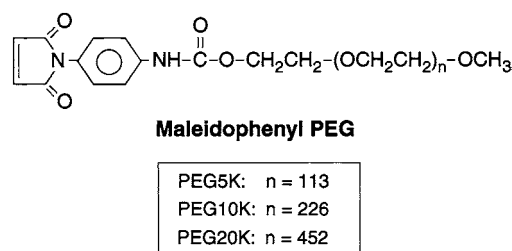
<sup>⊥</sup> Structural BioInformatics.

<sup>1</sup> Abbreviations: Hb, hemoglobin; PEG, poly(ethyleneglycol); SP, succinimidophenyl; IEF, isoelectric focusing; SEC, size exclusion chromatography; RPHPLC, reverse-phase high-performance liquid chromatography; PBS, phosphate-buffered saline; Tris, tris(hydroxymethyl) amino methane; COP, colloidal osmotic pressure; FCD, functional capillary density.

in their extent and duration of induced vasoactivity in a rat model. All hemoglobin tetramers studied were found to be vasoactive to different degrees, depending upon their oxygen affinity. Hemoglobin oligomers were less vasoactive, and their effect was transient. Of the two PEGylated Hbs examined, PEG-Hb (bovine Hb carrying ~10 copies of PEG5000 per tetramer - Enzon product) exhibited no pressor response, whereas PHP-Hb (PEGylated pyridoxalated Hb carrying ~10 copies of PEG3000 per tetramer-Ajinomoto product) exhibited a reduced and transient pressor response. Although the viscosity of the two PEGylated Hbs were nearly the same, PEG-Hb had a much higher colloidal osmotic pressure than PHP-Hb and a much higher molecular volume. Thus, the pressor effect of the PEGylated Hbs exhibited a correlation with their molecular size and solution properties. Thus, these studies suggested that PEGylation of Hb is an efficient way to reduce its vasoactivity.

The PEG-Hbs described above are generated by attachment of PEG to the surface amino groups of the protein using the succinimidyl chemistry. The activated PEG reagent is labile and reacts with lysine in competition with hydrolysis, necessitating the use of a large excess of reagent for the reaction. Hence, specificity of this reaction is low. Furthermore, the amino groups of Hb are randomly located on its surface. Thus, the stoichiometry of the PEG conjugated to the protein and the sites of conjugation cannot be precisely controlled, resulting in products that are not biochemically homogeneous. In addition, the linkage of the PEG to the Hb is through isopeptide bonds. As a result, the original positive charge of the surface amino group is lost during this modification. Thus, the altered surface electrostatic potential of the PEGylated Hb may also be contributing for the neutralization of the vasoactivity.

We have been exploring new and novel, site-specific chemical strategies which could overcome these limitations and enable the generation of chemically well-defined, molecularly homogeneous preparations of PEGylated-Hbs with varying colligative properties (controllable by the synthetic protocol) so that the same could be used for understanding the relation between the colligative properties of acellular Hb and its vasoactivity (22, 23). In the present study, we have taken advantage of the unusual chemical reactivity of Cys-93( $\beta$ ) of oxy-HbA and the high specificity of maleimide for the protein-SH groups for the surface decoration of HbA with PEG chains. A new series of maleimide based monofunctional PEG reagents have been developed for these studies. In the commercially available PEG-maleimide reagents, the maleimide moiety is linked to the terminal -OH of the PEG either through an ethylene linker or through an amide bond with a flexible aliphatic linker. In contrast, in our PEG maleimide reagents, we have introduced a rigid phenyl ring coupled to the PEG via a polar carbamate linkage, as the spacer between the maleimide and the PEG chain of the desired length (Figure 1). The choice of this stereochemistry for the PEG-maleimide reagent is based on our observation on the unusually high quantitative intramolecular cross-linking of HbA by bis-maleidophenyl PEG2000 (23). Reaction of HbA with monofunctional maleidophenyl PEG results in the conjugation of the PEG chains on to the intrinsic  $\beta$ 93 -SH groups of Hb via a succinimidophenyl linkage (2 PEG chains/Hb tetramer). The molecular size of Hb has been varied by varying the chain length of the PEG used for conjugation. The physical and functional properties of these PEGylated Hbs have been compared to understand the relationship of their colli-



**Figure 1.** Structure of the poly(ethylene glycol)-based monofunctional maleimide reagents.

gative properties and vasoactivity with the mass and chain length of PEG conjugated on Cy-93( $\beta$ ).

## MATERIALS AND METHODS

**Hemoglobin.** Human HbA was purified from the erythrocyte lysate as described earlier (24).

**Synthesis of Maleidophenyl Polyethylene Glycol (MalPhePEG) Reagents.** Mono functional maleidophenyl derivatives of PEG5000, PEG10000, and PEG20000 were synthesized according to the procedures described earlier (22). The synthesis essentially involves condensation of *p*-maleimidophenylisocyanate (PMPI) with methoxy PEG. The PMPI is generated by thermal Curtius rearrangement of *p*-maleimidobenzoylazide, which is synthesized from *p*-maleimidobenzoic acid essentially by procedures described by Yoshitake et al. (25) and Annunziato et al. (26). The acyl azide is stable and may be stored indefinitely with minimal precaution. Work in our laboratories is in agreement with the observation (26) that thermal, Curtius rearrangement of *p*-maleimidobenzoylazide to the isocyanate is quantitative. Since the resulting isocyanate is difficult to isolate and store without degradation, we have found it convenient to derivatize the hydroxyl containing PEG compounds by generating PMPI in the presence of the PEG. The in situ generation and consumption of PMPI thus obviates the need to isolate and store this sensitive compound.

Typically, 500 g of methoxy poly(ethylene glycol) (methoxy PEG5000 of low, <1%, diol content, MW 5000, Shearwater Polymers, Inc., Huntsville, AL) was dissolved in 2 L of dry toluene and refluxed with a Dean-Stark trap to remove water associated with the solvent, m-PEG or glassware. The contents were cooled under a dry nitrogen pad to a temperature of <50 °C. *p*-Maleimidobenzoylazide (24.2 g) of was added as a solid all at one time through a side port of the reaction flask. Heating was resumed and maintained at reflux (~104 °C) for 2 h. At the end of the 2 h reflux period, heating was discontinued, and the contents were allowed to stand at room temperature overnight. The next morning, the flask and contents were warmed briefly (~30 °C) to dissolve Mal-Phe-PEG carbamate crystals that had formed during the night. The warm solution was transferred to a rotary evaporator flask with the aid of fresh toluene rinses and concentrated under vacuum at 65 °C until a thick, syrupy, yellow-gold residue remained. The syrupy residue was cooled and triturated with approximately 1 L of diethyl ether in order to induce crystallization of the reaction product. A significant heat of crystallization accompanies the precipitation of PEG in ether. The ether/reaction product mixture is allowed to cool and stand until crystallization of product is complete (2–4 h). By means of a plastic rod, chunks of yellow PEG derivative are crushed under the ether, filtered, washed with fresh ether, and dried. The dry, crude PEG derivative is further purified by dissolving in a minimum volume of 0.5 M

NaCl, at room temperature. The resulting cloudy solution is allowed to stand for 1 h, then filtered through 0.2  $\mu$  glass filter mats repeatedly until the light yellow filtrate is sparkling clear. The entire clarified filtrate is extracted with 3  $\times$  1 L methylene chloride. The combined methylene chloride extracts (yellow) are dried with anhydrous magnesium sulfate, rotary evaporated to a syrup, and precipitated with ether as described above. Drying (vacuum) affords very pale yellow crystals of Mal-Phe-PEG-5K. Yield, 500–515 g.

The foregoing protocol may be used for the preparation of activated methoxy PEGs of MW 10 000 or 20 000 by adjusting the weights of the mPEG and *p*-maleimido-benzylazide to achieve equimolar ratios of the two reactants. Smaller-scale reactions, i.e., utilizing 25, 50, or 100 g amounts of mPEG, yield results nearly identical to those described here if proportions of solvents, and reactants are maintained along with adherence to reaction times and conditions described here.

The structure of the maleidophenyl PEG reagent is illustrated in Figure 1.

**Reaction of HbA with the MalPhePEG Reagents.** Hemoglobin A (0.5 mM) in PBS, pH 7.4, was reacted with a 10-fold molar excess of MalPhePEG of desired chain length either at 4 °C or at room temperature for overnight. Modification of HbA by PEG was monitored by reverse phase high-pressure liquid chromatography (RPHPLC) and size exclusion chromatography (SEC). The reaction product was dialyzed against 50 mM Tris-acetate buffer, pH 8.5, and subjected to purification by ion exchange chromatography.

**Purification of PEGylated Hbs.** The PEGylated Hbs were purified by ion exchange chromatography on Amersham Biosciences Q-Sepharose High Performance resin, using an AKTA Explorer 10 Protein Purification System. The Q-Sepharose High Performance column (2.6 cm  $\times$  62 cm) was equilibrated with 50 mM Tris-acetate buffer, pH 8.5, and the protein was eluted with a linear decreasing pH gradient consisting of 50 mM Tris-acetate, pH 8.5, and 50 mM Tris-acetate, pH 7.0, over 8 column volumes. The column effluent was monitored at 240 and 540 nm.

**Oxygen Affinity Measurements.** Oxygen equilibrium curves were measured at 37 °C using a Hem-O-Scan (Aminco) in PBS, pH 7.4, at a hemoglobin tetramer concentration of 1 mM.

**Viscosity Measurements.** The viscosity of the PEGylated Hbs was measured in a Rheometer, at a protein concentration of 4 g/dL, in PBS buffer, pH 7.4, and at 37 °C. The instrument was calibrated with deionized water prior to measurements of the viscosity of the Hb samples.

**Colloidal Osmotic Pressure Measurements.** The colloidal osmotic pressure of the PEGylated hemoglobins was determined using a Wescor 4420 Colloidal Osmometer. All measurements were done using 2 g/dL hemoglobin samples in PBS, pH 7.4, at room temperature. A 30 kDa cutoff membrane was used. The instrument was tested with Osmocoll reference standards prior to measurements of the samples.

**Analytical Methods.** The globin chains of the various PEGylated Hbs were analyzed by RPHPLC, by methods previously described (23). In short, the separation was carried out on a Vydac C4 (4.6  $\times$  250 mm) column, employing a linear gradient of 35–50% ACN containing 0.1% TFA in 100 min. The column effluent was monitored at 210 nm. The apparent molecular mass of the PEGylated Hbs was analyzed by size exclusion chromatography on a Superose 12 column (Amersham-Pharmacia Biotech) eluted with PBS, pH 7.4. SDS-PAGE analysis was carried out as previously described (27).

**Animal Model.** Investigations were carried out in a hamster skin fold window microcirculation model, essentially according to the procedures previously described (28, 29). Studies were performed on male Golden Syrian Hamsters (Charles Rivers) of 55–70 g body weight. All animal studies were approved by the Animal Subject Committee of University of California, San Diego, and performed according to NIH guidelines for the care and use of laboratory animals (NIH publication #85-23 Rev. 1985).

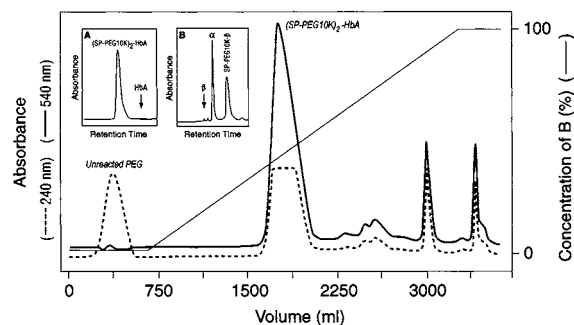
Each animal served as its own baseline. A 10% hypervolemic infusion was made at a rate of 0.20 mL/min into the animal via the jugular vein catheter using a microinfusion pump (CMA 100 Microinjection Pump; CMA, Sweden). The blood pressure, the arteriolar diameter, and the functional capillary density were measured immediately following the infusion and 30 min after the infusion.

**Computer Modeling.** The phenyl ring is attached to the nitrogen of the pyrroline ring, and the ethyl chains are added to the phenyl ring at its 4th position through an oxygen atom. The continuous N-(4-polyethoxy) phenyl pyrrolidine PEG chain contains 113, 226, and 452 ethoxy groups for 5000, 10 000, and 20 000 Da chains. These chains were coalesced together by means of molecular dynamics simulations at various temperatures (from 300 to 600 K and back to 300 K) followed by minimization at each cycle. The whole simulation package was carried out using INSIGHT II graphics and Discover simulation package with fairly large cut off radius (12 Å). Then these chains were attached to the two Cys-93( $\beta$ )s of hemoglobin. The covalent connection between the sulfur atom of the protein and C3 of the pyrroline ring is made without any van der Waals overlap between the PEG chain and protein. Many models were built and minimized. During the complex buildup, better packaging of the PEG 5000 chain and protein is found in comparison to with the other two. The complete minimization of the whole complex with the PEG 10 000 and PEG 20 000 chains was difficult due to memory limitations.

## RESULTS

**Preparation and Chromatographic Purification of Maleidophenyl Poly(Ethylene Glycol) (MalPhe-PEG) Derivatives of HbA.** The high reactivity of the thiol group of Cys-93( $\beta$ ) of the oxy HbA at pH 7.4 and the high reaction specificity of the maleimide group toward thiol groups has been exploited to chemically link the linear poly(ethylene glycol) chains of 5, 10, and 20 kDa on to HbA via the Cys-93( $\beta$ ). HbA (0.5 mM) in PBS, pH 7.4, was reacted with PEG-maleimides of varying PEG chain length, and the resulting products were subjected to ion-exchange chromatographic purification to separate the PEGylated Hb from unreacted PEG as well as side products of the reaction. A representative chromatographic profile of the purification of MalPhe-PEG10K-reacted HbA on a Q-Sepharose High Performance column is illustrated in Figure 2. Due to the presence of the phenyl ring, the maleidophenyl PEG reagent exhibits absorbance at 240 nm. Therefore, the chromatographic profile was monitored simultaneously at 240 and 540 nm to enable the detection of unreacted PEG in the reaction mixture. As can be seen, the material eluting unabsorbed from the column exhibits absorbance only at 240 nm, but not at 540 nm (region of heme absorbance). Thus, this material represents unreacted PEG reagent and is well separated from the 540 nm absorbing peaks. It is also apparent from the 540 nm



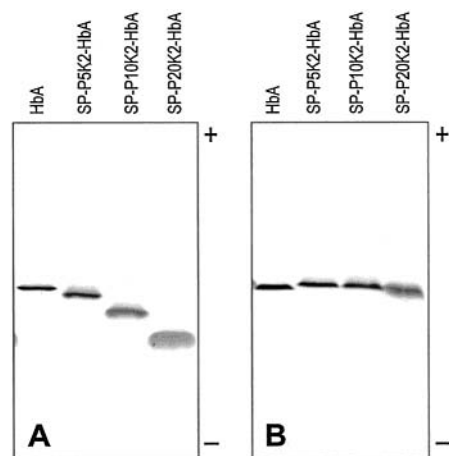


**Figure 2.** Purification of Mal-Phe-PEG10K-reacted HbA on Q-Sepharose high-performance column ( $2.6 \times 62$  cm), using an Amersham Biosciences AKTA Explorer 10 Protein Purification System. The column was equilibrated with 50 mM Tris-Ac, pH 8.5. The protein was eluted with a decreasing pH gradient consisting of 50 mM Tris-Ac, pH 8.5, and 50 mM Tris-Ac, pH 7.0, over 8 column volumes. Protein load: 1 g. The effluent was monitored at 240 nm and at 540 nm. The positions of unreacted PEG and (SP-PEG10K) $_2$ -HbA are indicated. Unreacted HbA elutes around 2930 mL on this column. Inset A: size exclusion chromatographic analysis of (SP-PEG10K) $_2$ -HbA on a Superose-12 column in PBS, pH 7.4. Inset B: RPHPLC analysis of (SP-PEG10K) $_2$ -HbA. The globin chains were separated on a Vydac C4 column ( $4.6 \times 250$  mm, 300 Å) using a linear gradient of 35–50% acetonitrile containing 0.1% TFA. The effluent was monitored at 210 nm.

profile that the MalPhePEG10K-reacted HbA contains one major and two minor modified components. The major peak, designated (SP-PEG10K) $_2$ -HbA, was isolated for further studies. The purity of the major peak was further confirmed by SEC and RPHPLC analyses (Figure 2, insets A and B, respectively). The modified protein elutes significantly earlier than the parent HbA from the size exclusion column, indicating an increase in its apparent molecular size. This may be a reflection of the increase in the hydrodynamic volume of HbA on surface decoration with PEG chains. RPHPLC analysis of (SP-PEG10K) $_2$ -HbA revealed the presence of unmodified  $\alpha$ -globin and the complete absence of  $\beta$ -globin and a new peak eluting after the  $\alpha$ -globin. Thus, it is apparent that in (SP-PEG10K) $_2$ -HbA, the  $\alpha$ -chains are unmodified and the  $\beta$ -chains are modified. HbA modified with Mal-Phe-PEG5K and Mal-Phe-PEG20K were also purified by similar ion exchange chromatographic procedures. HbA modified with PEG5K, PEG10K, and PEG20K are designated as (SP-PEG5K) $_2$ -HbA, (SP-PEG10K) $_2$ -HbA, and (SP-PEG20K) $_2$ -HbA, respectively.

#### Isoelectric Focusing Analysis of PEGylated HbA.

The isoelectric focusing pattern of (SP-PEG5K) $_2$ -HbA, (SP-PEG10K) $_2$ -HbA, and (SP-PEG20K) $_2$ -HbA is shown in Figure 3A,B. The results of the IEF analysis under the standard conditions used for HbA (45 min focusing time) are presented in Figure 3A. As can be seen, the anodic mobility of HbA is decreased upon conjugation with PEG. This decrease is directly related to the PEG chain length. At the outset, it appeared that this phenomenon may be either due to an influence of the attached PEG chain on the ionization behavior of one or more charged surface functional groups of HbA, the net effect of which depends on the length of the PEG chain attached or due to the increased molecular size of the surface-decorated HbA or a combination of both. However, when the focusing time was increased to 1  $\frac{1}{2}$  h, all the three PEGylated Hbs focused as sharp bands in much the same way as the control Hb and displayed a slight but noticeably higher anodic mobility than HbA (Figure 3B). Thus, the decreased anodic mobility of the PEGylating Hbs observed during the standard focusing condi-



**Figure 3.** Isoelectric focusing pattern of PEGylated Hbs. Isoelectric focusing was carried out on a Resolve precast Agarose pH 6–8 IEF gel (Isolab) for (A) 45 min at 10 W and (B) for 90 min at 10 W. Samples were applied closer to the cathode.

**Table 1.** Oxygen Affinity of PEGylated HbAs<sup>a</sup>

sample	$P_{50}$ (mm Hg)	Hill coefficient ( $n$ )
HbA	15.0	2.3
(SP-PEG5K) $_2$ -HbA	11.8	2.3
(SP-PEG10K) $_2$ -HbA	11.5	2.2
(SP-PEG20K) $_2$ -HbA	10.5	2.1

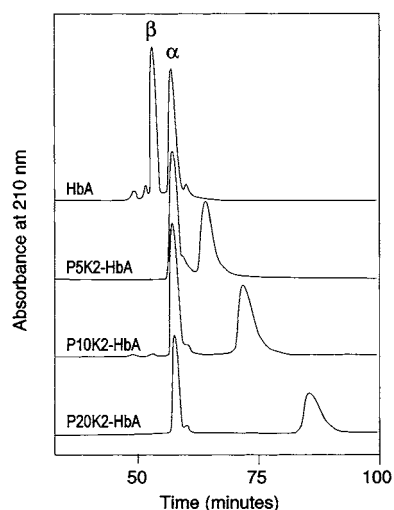
<sup>a</sup> The O<sub>2</sub> equilibrium curve was determined in a Hem-O-Scan in PBS, pH 7.4 at 37 °C.

tions (45 min of focusing) appears to be due to a hindrance of the mobility of the protein through the agarose gel by the attached PEG chain.

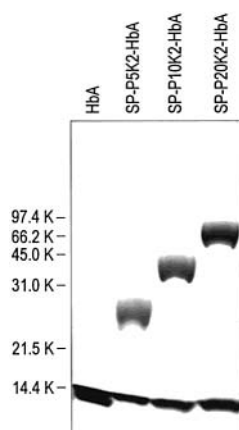
**Oxygen Affinity of PEGylated HbAs.** The results of the oxygen affinity measurements of the PEGylated Hbs in PBS, pH 7.4, are shown in Table 1. As can be seen, the PEGylated Hbs exhibit an increased oxygen affinity relative to control HbA. However, the increase in oxygen affinity (or decrease in the  $P_{50}$  values) is nearly the same for all the three PEGylated Hbs. Furthermore, calculation of the Hill coefficients indicated that conjugation of PEG chains on to the surface of Hb does not significantly influence its cooperativity for O<sub>2</sub> binding. These results suggest that the observed change in the oxygen affinity of HbA on PEGylation is a consequence of the modification of the Cys-93( $\beta$ ) with maleidophenyl PEG and is not significantly influenced by the length of the PEG chain.

**Globin Chain Analysis of HbA Surface Decorated with PEG of Varying Chain Length.** Globin chain analysis of the three purified PEGylated HbAs, (SP-PEG5K) $_2$ -HbA, (SP-PEG10K) $_2$ -HbA, and (SP-PEG20K) $_2$ -HbA, by RPHPLC analysis is shown in Figure 4. As can be seen, all the three PEGylated Hbs contain only two peaks, and in each case, the modification is specific to the  $\beta$ -chain. The retention time of the modified  $\beta$ -globin increases with the increase in the PEG chain length, which may be due to the increased molecular size and hydrophobicity of the modified chain.

**SDS-PAGE Analysis of PEGylated Hbs.** The results of the SDS-PAGE analysis of the PEGylated Hbs are shown in Figure 5. Unmodified HbA revealed the presence of two closely moving bands, consistent with the near identical sizes of its  $\alpha$ - and the  $\beta$ -globins. All the PEGylated Hbs also showed the presence of two bands, one in the region of the unmodified  $\alpha/\beta$  globin and a new band with a significantly slower mobility. In conjunction



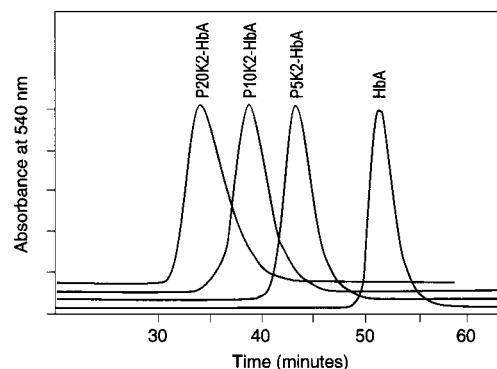
**Figure 4.** Comparison of the globin chain analysis of HbA PEGylated with PEG5K, PEG 10K, and PEG20K maleimide. The RPHPLC analysis was carried out as described under Figure 2, inset B.



**Figure 5.** SDS-PAGE analysis of PEGylated Hbs. The SDS-PAGE analysis was carried out on a precast 10% tris-glycine gel from the Invitrogen Corporation. The numbers on the left indicate the mass of the molecular weight markers.

with the results of the globin chain analysis, it is apparent that the band with the slower mobility is the modified  $\beta$ -globin. The presence of only one modified band indicates the mass homogeneity of the modified  $\beta$ -globin. Like the RPHPLC analysis, the decrease in the mobility of the  $\beta$ -globin is a function of the length (mass) of the attached PEG chain. However, the mass of the PEGylated  $\beta$ -globins determined by SDS-PAGE analysis is significantly higher than that estimated based on the actual mass of the PEG attached. Thus, the PEGylated  $\beta$ -globins exhibit an anomalous behavior by the SDS-PAGE analysis.

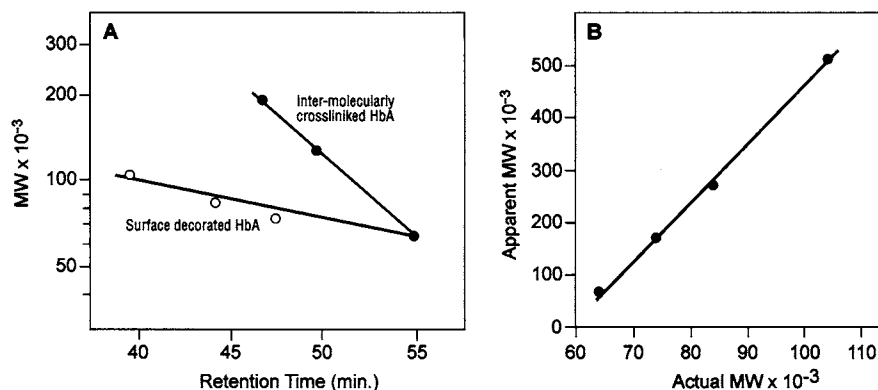
**Size Exclusion Chromatographic Analysis of PEGylated Hbs.** *Correlation of the Retention Time of HbA as a Function of the Chain Length of the Attached PEG.* The results of the SEC analysis of the PEGylated HbAs [(SP-PEG5K)<sub>2</sub>-HbA, (SP-PEG10K)<sub>2</sub>-HbA, and (SP-PEG20K)<sub>2</sub>-HbA] are presented in Figure 6. All the three PEGylated Hbs elute earlier from the Superose-12 column compared to the parent HbA. The actual molecular mass of the three surface-decorated HbAs carrying 2 PEG chains of 5, 10, and 20 kDa is 74, 84, and 104 kDa, respectively. Thus, no resolution among the three surface-decorated HbAs can be expected on the Superose-12 column based on the differences in their actual mass.



**Figure 6.** Comparison of the size exclusion chromatographic behavior of PEGylated Hbs. The purified PEGylated Hbs were gel filtered on a Superose 12 column eluted with PBS, pH 7.4. Two Amersham Biosciences HR 10/30 (1 cm  $\times$  30 cm) Superose 12 columns connected in series were used to obtain better resolution of the PEGylated Hbs. The column was eluted at a flow rate of 0.5 mL/min, and the effluent was monitored at 540 nm.

Nevertheless, the three PEGylated HbAs are well resolved from each other on the Superose12 column. The elution volume of the surface-decorated HbA decreased as the chain length of the reagent increased, indicating a progressive increase in the apparent size of HbA on surface decoration with PEG molecule of increasing chain length. A plot of the log MW vs retention time revealed that the retention time of the surface-decorated HbAs exhibit a linear relationship with their calculated molecular mass (MW of HbA + MW of 2 PEG chains) (Figure 7A, open circles).

**Size Enhancement of HbA on PEGylation.** To understand the influence of increasing the size of HbA by surface decoration with PEG as compared with that of increasing its size by oligomerization (i.e., increase of protein mass), we also studied the SEC behavior of oligomeric forms of HbA. The oligomeric forms of HbA were generated by intertetrameric cross-linking of  $\beta\beta$ -sebacyl Hb (i.e., HbA intramolecularly cross-linked at its  $\beta$ -82 lysines with bis-dibromo salicyl sebacate) with the bifunctional reagent Bis-maleidophenyl-PEG600. This cross-linking results in the formation of defined oligomeric forms of HbA with molecular weights that are multiples of 64 kDa. The octameric (128 kDa) and dodecameric (192 kDa) forms of HbA generated by this intertetrameric cross-linking were purified by size exclusion chromatography and used along with unmodified HbA (64 kDa) to calibrate the analytical Superose 12 column. As expected, the SEC retention times of the oligomeric HbAs exhibited a linear relationship with their molecular mass (Figure 7A, closed circles). However, as can be seen, the slope of the line generated by the PEGylated Hbs (Figure 7A, open circles) is much shallower than that of the oligomerized HbAs, indicating that the increase in the apparent mass of Hb on surface decoration with PEG is much higher than its actual mass. The apparent molecular mass of the PEGylated Hbs based on their retention times was calculated from the standard curve generated from the intermolecularly cross-linked Hbs. A linear correlation was observed between the apparent mass of the different PEGylated species and their calculated mass (Figure 7B). The slope of the correlation curve is  $\sim 10$ . If the measured molecular size is the same as the actual mass, then the slope of the line will be 1. Thus, the apparent molecular size of the PEGylated HbA is increased by nearly 8–10 times that



**Figure 7.** (A) Relation between the retention time and the molecular mass of oligomerized and surface-decorated Hbs. (B) Correlation between the actual and the apparent molecular mass of PEG Hbs.

**Table 2. Molecular Parameters of Surface Decorated Hemoglobins<sup>a</sup>**

hemoglobins	calculated mass (kDa)	radius (nm)	volume (nm <sup>3</sup> )
HbA	64	3.12	127
(SP-PEG5K) <sub>2</sub> -HbA	74	4.20	310
(SP-PEG10K) <sub>2</sub> -HbA	84	5.54	712
(SP-PEG20K) <sub>2</sub> -HbA	104	7.04	1436
HbA-octamer	128	4.12	293
HbA-dodecamer	192	5.56	720

<sup>a</sup> Molecular radius measurements were made using a DynaPro Dynamic Light Scattering Instrument from Protein Solutions, Lakewood, NJ. The radii of the octameric and dodecameric HbA are shown for comparison. The volumes calculated are for spheres, based on the respective molecular radii.

anticipated based on the actual molecular size of the attached PEG chain.

**Correlation between the Molecular Mass and the Molecular Radius of the PEGylated Hbs.** The molecular radii of the three PEGylated Hbs determined by dynamic light scattering measurements is shown in Table 2. The increase in the radius of Hb on PEGylation exhibited a fairly linear relation with the mass of the added PEG chain. A comparison of the molecular radius of the PEGylated Hbs with those of the oligomerized Hbs and the calculated molecular volumes of these proteins is also shown in Table 2. It may also be seen from the data in Table 2 that the oligomerized Hbs and the PEGylated Hbs of dissimilar molecular mass exhibit similar molecular radius and hydrodynamic volume. As can be seen, (SP-PEG5K)<sub>2</sub>-HbA with a calculated mass of 74 kDa exhibits a radius close to that of octameric HbA with a mass of 128 kDa. Similarly, (SP-PEG10K)<sub>2</sub>-HbA (MW 84 kDa) exhibits a radius similar to that of dodecameric HbA (MW, 192 kDa). A unique property of PEG is its ability to interact with water. Thus, the similarity of the molecular radius and the hydrodynamic volume of oligomerized Hb and surface-decorated Hb of dissimilar molecular mass apparently reflects the difference in the degree of hydration of these samples.

**Viscosity of the PEGylated HbA Solutions.** The viscosity of the PEGylated HbA solutions as a function of the mass of the PEG attached is shown in Figure 8A. As can be seen, the viscosity of Hb increases with the increase in the PEG chain length and hence the mass of the attached PEG. However, unlike the molecular radius, the increase in viscosity exhibits an exponential rather than a linear relation with the mass of the PEG. Thus, whereas the attachment of two PEG5000 chains brings about only a moderate increase in viscosity, increasing the length of the attached PEG chain to 10 000 and

20 000 Da brings about a significantly higher increase in viscosity.

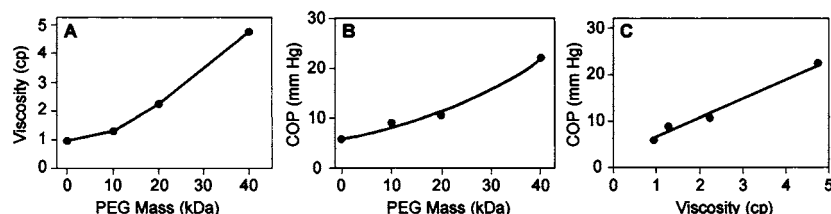
**Colloidal Osmotic Pressure of the PEGylated HbA Solutions.** The colloidal osmotic pressure (COP) of the PEGylated HbA solutions as a function of the mass of the PEG attached is shown in Figure 8B. As can be seen, like the viscosity, the colloidal osmotic pressure of Hb also increased with the increase in the PEG chain length and exhibited an exponential relation with the mass of the PEG attached. Furthermore, the COP of the PEGylated Hbs exhibited a linear correlation with their viscosity (Figure 8C).

**Vasoactivity of PEGylated Hbs.** Changes in mean arterial blood pressure, arteriolar diameter and functional capillary density (FCD) after infusion of the PEGylated Hb solutions (1.8 g/dL Hb concentrations) at 10% top loads were measured in the awake hamster skin fold model. The results are presented in Table 3. Changes are the averages relative to the baseline values for the individual animals in each group. No significant differences were observed in the MAP response and the arteriolar diameter among the three PEGylated Hbs. However, whereas there was no significant decrease in the FCD on infusion with the (SP-PEG5K)<sub>2</sub>-HbA and (SP-PEG10K)<sub>2</sub>-HbA, infusion of (SP-PEG20K)<sub>2</sub>-HbA resulted in a significant decrease in FCD. FCD is a measure of open capillaries, thus a measure of tissue perfusion and hence a more sensitive indicator of vasoactivity. Furthermore, previous studies of Intaglietta and co-workers (28, 29) have demonstrated that increased vasoactivity corresponds to a decrease in FCD.

## DISCUSSION

The results of the present study have demonstrated that site-specific conjugation of linear chains of PEG onto the surface of Hb can be achieved by a simple maleimide based chemistry by exploiting the unusually high reactivity of Cys-93( $\beta$ ) of oxy HbA around neutral pH. Our recent studies (30, 31) have demonstrated that the structure/conformation of PEGylated Hb is determined by the chemistry of attachment of PEG to Hb, the linker chemistry (i.e., the linker between the maleimide and the PEG), and the size of PEG. Accordingly, in the present study, we have conserved the chemistry of attachment and the linker chemistry and altered only the size of the PEG chain, to evaluate the correlation between the colligative properties of the PEGylated Hbs and the length of the attached PEG chain. Biochemically homogeneous preparations of three PEGylated Hbs carrying two PEG chains of varying chain length per tetramer have been obtained by ion exchange chromatography.





**Figure 8.** (A) Relation between the viscosity of the PEGylated Hb and the mass of the attached PEG. (B) Relation between the colloidal osmotic pressure of the PEGylated Hb and the mass of the attached PEG. (C) Correlation between viscosity and the colloidal osmotic pressure of the PEGylated Hbs.

**Table 3. Changes in Systemic Mean Arterial Pressure, Arteriolar Diameter, and Functional Capillary Density after Infusion with PEGylated Hemoglobins: Relationship to PEG Mass<sup>a</sup>**

PEGylated Hb	total PEG mass (kDa)	mean arterial blood pressure (mmHg)	arteriolar diameter ( $\mu$ m)	FCD % of baseline	n
(SP-PEG5K) <sub>2</sub> -HbA	10	113 $\pm$ 6 <sup>b</sup>	95 $\pm$ 9 <sup>c</sup>	91 $\pm$ 8 <sup>d</sup>	5
(SP-PEG10K) <sub>2</sub> -HbA	20	111 $\pm$ 10	92 $\pm$ 8	94 $\pm$ 4	5
(SP-PEG20K) <sub>2</sub> -HbA	40	115 $\pm$ 6	90 $\pm$ 16	80 $\pm$ 30	3

<sup>a</sup> The PEG-Hb solutions were tested at a protein concentration of 1.8 g/dL, at 10% top loads (estimated as 0.7% of the body weight). The experimental protocol consisted of infusing the test Hb solutions into the animal via indwelled jugular vein catheter over a period of 2 min. Significant  $p < 5\%$ . <sup>b</sup> Values of mean arterial blood pressure are normalized relative to control at 100 mm Hg. Average blood pressure at control: 94.8  $\pm$  8.3 mm Hg. <sup>c</sup> Arterial diameters are normalized relative to control at 100  $\mu$ m. Average arteriolar diameter: 57.7  $\pm$  20.9  $\mu$ m. <sup>d</sup> Functional capillary density normalized relative to control at 100%.

The molecular size of HbA is significantly enhanced by surface decoration with PEG and exhibits a linear correlation with the length of the attached PEG chain. The isoelectric focusing behavior of the PEGylated Hb molecule is also significantly influenced by the mass of the PEG chain, with an apparent decrease in the anodic mobility that correlated with the PEG chain length. However, it is apparent from the results of the IEF analysis wherein the run time of the focusing is extended, that the isoelectric pH of HbA is not significantly affected by PEGylation. Thus, the attachment of PEG on to HbA through its Cys-93( $\beta$ ) has no significant influence on the net charge of the protein. The longer duration needed to focus the PEGylated Hbs suggests that the attached PEG chain causes a hindrance for the mobility of the protein through the cross-linked agarose matrix of the isoelectric focusing gel.

The covalent attachment of PEG to the  $\beta$ -chains of HbA increases its molecular size as a function of the PEG size, as reflected by the SDS-PAGE analysis. However, the estimated mass points to an anomalous behavior of the PEGylated  $\beta$ -globin, a phenomenon similar to that observed with glycosylated proteins. The attachment of PEG also increased the hydrophobicity of the  $\beta$ -globin, the hydrophobicity correlating with the length of the attached PEG chain.

Surface decoration of Hb with PEG increased its oxygen affinity slightly, without significant effect on the cooperativity of oxygen binding. Moreover, the chain length of the attached PEG had very little influence on the oxygen affinity.

Whereas the hydrodynamic radius of the PEGylated Hb, and hence its molecular size/volume, increased almost linearly with the length of the attached PEG, the viscosity as well as the colloidal osmotic pressure of the PEGylated HbA solutions exhibited an exponential increase with the length of the conjugated PEG chain. In addition, there was a linear correlation between the viscosity and the COP of the PEGylated Hbs. Furthermore, the viscosity of PEGylated Hb appears to be a correlate of the total mass of the attached PEG. For example, at a protein concentration of 4 g/dL, the viscosity of (SP-PEG20K)<sub>2</sub>-HbA, carrying a mass of  $\sim$ 40

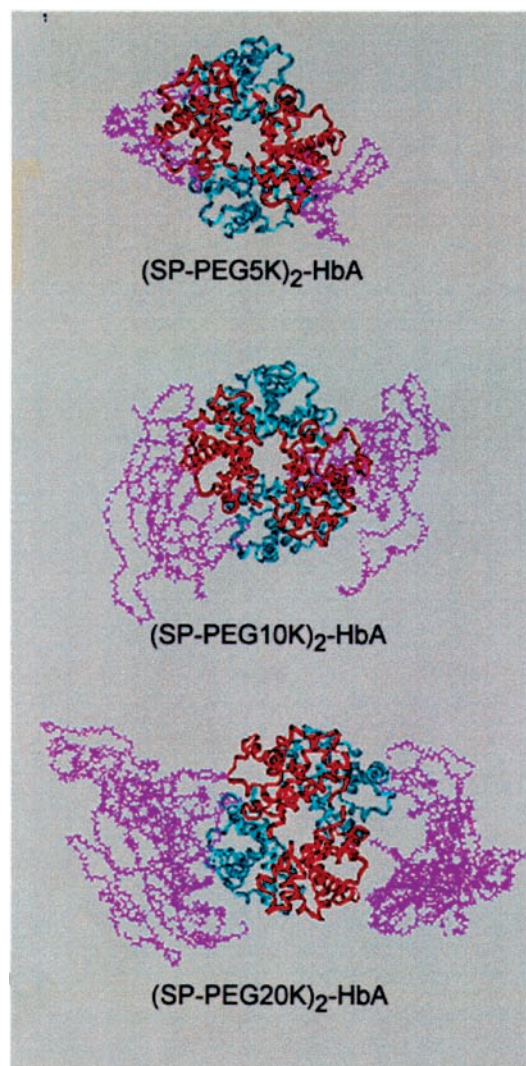
kDa PEG, is comparable to that reported for PEG-Hb (Enzon product), carrying about 10 copies of PEG5000 (32). Similarly, we have observed that the viscosity of one of our preparations of PEGylated Hbs, (PEG5K)<sub>6</sub>-HbA (prepared by thiolation mediated PEGylation and carrying 6–8 copies of PEG5000, i.e.,  $\sim$ 30–40 kDa PEG; Acharya et al., unpublished reports) is comparable to that of (SP-PEG20K)<sub>2</sub>-HbA.

Several assay systems have been used in the literature to evaluate the intrinsic vasoactivity of acellular Hb preparations. We have obtained consistent results in a hamster microcirculation model, measuring the mean arterial pressure of the microvasculature, arteriolar diameter as well as functional capillary density with 10% top loads of 2–4 g/dL Hb solutions. The results of this assay revealed that the reduction in vasoactivity afforded by the conjugation of PEG chains to Hb is not a direct correlate of the PEG chain length. Among the three PEGylated Hbs studied, (SP-PEG20K)<sub>2</sub>-HbA is clearly vasoactive. Thus, increasing the PEG chain length beyond 10 000 Da appears to decrease the protection against vasoactivity. The vasoactivity of (SP-PEG20K)<sub>2</sub>-HbA, however, cannot be due to its extravasation, since being the largest of the three PEGylated Hbs, (SP-PEG20K)<sub>2</sub>-HbA should extravasate the least and thus have had the least vasoactivity.

Computer modeling of the PEG chains on the surface of the Hb molecule suggested that the PEG is not passively extending on the surface of the protein. Rather, the PEG chain appears to fold upon itself to form a distinct loosely folded domain on the surface of the protein (Figure 9). Thus, it appears that although the surface of Hb covered by the PEG increases with an increase in PEG size, it is not directly proportional to the length of the PEG chains.

PEGylation has been shown to reduce the “stickiness” of the proteins with respect to their interaction with other biopolymers. Thus, reduced interactions of the PEGylated Hb with the endothelium could be one of the factors contributing for the reduction of its vasoactivity.

Recent studies by Winslow et al. (17), Intaglietta et al. (33), and others (34–36) have suggested a significant role of viscosity in maintaining adequate microvascular



**Figure 9.** Computer models of the PEGylated Hbs. The models were generated as described under Materials and Methods.

function as well as facilitated diffusion of oxygen. However, since the plasma Hb concentration is  $<0.18\%$  in the present top load experiments, the viscosity of the PEGylated Hb is unlikely to play any major role in dictating its vasoactivity under these conditions. The role of viscosity of the PEGylated Hbs in maintaining the optimum FCD needs to be evaluated in more detailed exchange transfusion models. Whereas the Hb tetramer exhibits a linear dependence of viscosity on protein concentration, PEGylated Hbs exhibit an exponential relationship. Thus, the level of viscosity desired could be controlled by the protein concentration and the size of the PEG attached to the surface of Hb. Thus, the approach described in the present study (i.e., the attachment of varying size PEG at a given site) provides a means of generating biochemically homogeneous PEGylated Hbs with varying viscosities that could be used for evaluating the role of viscosity for the vasoactivity of Hb. Thus, this new class of PEGylated Hbs could serve as potential blood substitute candidates.

#### ACKNOWLEDGMENT

This research was supported by a grant-in-aid from the American Heart Association Heritage Affiliate, the National Institutes of Health Grant HL58247, and USPHS NIH Bioengineering Partnership Grant 1 R24 HL 64395.

#### LITERATURE CITED

- (1) Rohlfes, R. J., Bruner, E., Chiu, A., Gonzales, A., Gonzales, M. L., Magde, M. D., Vandegriff, K. D., and Winslow, R. M. (1998) Arterial blood pressure responses to cell-free hemoglobin solutions and the reaction with nitric oxide. *J. Biol. Chem.* 273, 12128–12134.
- (2) Winslow, R. M. (1996) Blood substitute oxygen carriers designed for clinical applications. In *Blood Substitutes: New challenges* (R. M. Winslow, K. D. Vandegriff, and M. Intaglietta, Eds.) pp 60–73, Birkhauser, Boston.
- (3) Klein, H. G. (2000) The prospects for red-cell substitutes. *New Engl. J. Med.* 342, 1666–1668.
- (4) Riess, J. G. (2001) Oxygen Carriers ("Blood Substitutes") – Raison d'Etre, Chemistry and Some Physiology. *Chem. Rev.* 101, 2797–2920.
- (5) Winslow, R. M. (1992) *Hemoglobin-Based Red Cell Substitutes*, Johns Hopkins University Press, Baltimore.
- (6) Hess, J. R., Macdonald, V. W., and Brinkley, W. W. (1993) Systemic and pulmonary hypertension after resuscitation with cell free hemoglobin. *J. Appl. Physiol.* 74, 1769–1778.
- (7) Thomson, A., McGarry, A. E., Valeri, C. R., and Lieberthal, W. (1994) Stroma-free hemoglobin increases blood pressure and GFR in the hypotensive rat: role of nitric oxide. *J. Appl. Physiol.* 77, 2348–2354.
- (8) Muldoon, S. M., Ledvina, M. A., Hart, J. L., and Macdonald, V. W. (1996) Hemoglobin-induced contraction of pig pulmonary veins. *J. Lab. Clin. Med.* 128, 579–584.
- (9) Macdonald, V. W., and Motterlini, R. (1994) Vasoconstrictor effects in isolated rabbit heart perfused with bis(3,5-dibromosalicyl) fumarate crosslinked hemoglobin. *Artif. Cells, Blood Substitutes, Immobilization Biotechnol.* 22, 565–575.
- (10) Furchgott, R. (1984) The role of endothelium in the responses of vascular smooth muscle to drugs. *Annu. Rev. Pharmacol.* 24, 175–197.
- (11) Kilbourn, R., Ghislaine, J., Cashon, B., DeAngelo, J., and Bonaventura, J. (1994) Cell-free hemoglobin reverses the endotoxin mediated hyporesponsivity of rat aortic rings to  $\alpha$ -adrenergic agents. *Biochem. Biophys. Res. Commun.* 199, 155–162.
- (12) Martin, W., Smith, J., and White, D. (1986) The mechanisms by which hemoglobin inhibits the relaxation of rabbit aorta induced by nitrovasodilators, nitric oxide or bovine retractor penis inhibitory factor. *Br. J. Pharmacol.* 89, 563–571.
- (13) Motterlini, R., Vandegriff, K. D., and Winslow, R. M. (1996) Hemoglobin-nitric oxide interactions and its implications. *Transfusion Med. Rev.* 10, 77–84.
- (14) Wennmalm, A., Benthin, G., and Peterson, A. (1992) Dependence of the metabolism of nitric oxide by human whole blood on the oxygenation of its red cell hemoglobin. *Br. J. Pharmacol.* 106, 507–508.
- (15) Sharma, A. C., and Gulati, A. (1995) Yohimbine modulates dapsirin crosslinked hemoglobin-induced systemic hemodynamics and regional circulatory effects. *Crit. Care Med.* 23, 874–884.
- (16) Freas, W., Llave, R., Jing, M., Hart, J., MaQuillan, P., and Muldoon, S. (1995) Contractile effects of dapsirin cross-linked hemoglobin (DCLHb) on isolated porcine blood vessels. *J. Lab. Med.* 125, 762–767.
- (17) Winslow, R. M., Gonzales, A., Gonzales, M. L., Magde, M. D., McCarthy, M., Rohlfes, R. J., and Vandegriff, K. D. (1998) Vascular resistance and efficacy of red cell substitutes in a rat hemorrhage model. *J. Appl. Physiol.* 85, 993–1003.
- (18) Lee, L. S., Conover, C., Shi, C., Whitlow, M., and Filpula, D. (1999) Prolonged circulating lives of single-chain  $F_v$  proteins conjugated with polyethylene glycol: a comparison of conjugation chemistries and compounds. *Bioconjugate Chem.* 6, 973–981.
- (19) Davis, S., Abuchowski, A., Park, Y. K., and Davis, F. F. (1981) Alteration of the circulating life and antigenic properties of bovine adenosine deaminase in mice by attachment of polyethylene glycol. *Clin. Exp. Immunol.* 46, 649–652.
- (20) Rohlfes, R. J., Vandegriff, K. D., and Winslow, R. M. (1997) The reaction of nitric oxide with cell-free hemoglobin-based oxygen carriers: Physiological implications. In *Advances in*

- Blood Substitutes: Industrial Opportunities and Medical Challenges* (R. M. Winslow, K. D. Vandegriff, and M. Intaglietta, Eds.) pp298–323, Birkhauser, Boston.
- (21) Vandegriff, K. D., Rohlf, R. J., and Winslow, R. M. (1997) Colloid osmotic effects of hemoglobin-based oxygen carriers. In *Advances in Blood Substitutes: Industrial Opportunities and Medical Challenges* (R. M. Winslow, K. D. Vandegriff, and M. Intaglietta, Eds.) pp 207–227, Birkhauser, Boston.
- (22) Acharya, A. S., Manjula, B. N., and Smith, P. K. (1996) Hemoglobin crosslinkers, US Patent 5,585, 484.
- (23) Manjula, B. N., Malavalli, A., Smith P. K., Chan, N.-L., Arnone, A., Friedman, J. M., and Acharya, A. S. (2000) Cys-93- $\beta$ -succinimidophenyl polyethylene glycol 2000 hemoglobin A. *J. Biol. Chem.* 275, 5527–5534.
- (24) Acharya A. S., and Manning J. M. (1983) Reaction of glycolaldehyde with proteins: Latent cross-linking potential of  $\alpha$ -hydroxy aldehydes. *Proc. Natl. Acad. Sci. U.S.A.* 80, 3590–3594.
- (25) Yoshitake, S., Yamada, Y., Ishikawa, E., and Masseyeff, R. (1979) Conjugation of glucose oxidase from *Aspergillus niger* and rabbit antibodies using N-hydroxysuccinimide ester of N-(4-carboxycyclohexylmethyl)-maleimide *Eur. J. Biochem.* 101, 395–399.
- (26) Annunziato, M. E., Patel, U. S., Ranade, M., and Palumbo, P. S. (1993) p-Maleidophenyl isocyanate: A novel heterobifunctional linker for hydroxyl to thiol coupling. *Bioconjugate Chem.* 4, 212–218.
- (27) O'Donnel, J. K., Birch, P., Parsons, C. T., White, S. P., Okabe, J. F., Martin, M. J., Adams, C., Sundarapandian, K., Manjula, B. N., Acharya, A. S., Logan, J. S., and Kumar, R. A. (1994) Influence of the chemical nature of side chain at  $\beta$ 108 of hemoglobin A on the modulation of the oxygen affinity by chloride ions. *J. Biol. Chem.* 269, 27692–27699.
- (28) Mirhashemi, S., Breit, G. A., Chavez, R. H., and Intaglietta, M. (1988) Effects of hemodilution on skin microcirculation. *Am. J. Physiol. (Heart Circ. Physiol.)* 254, H411–H416.
- (29) Tsai, A., Kerger, H., and Intaglietta, M. (1996) Microvascular oxygen distribution: Effects due to free hemoglobin in plasma. In *Blood Substitutes New Challenges* (R. M. Winslow, K. D. Vandegriff, and M. Intaglietta, Eds.) pp 124–131, Birkhauser, Boston.
- (30) Juszczak, L. J., Manjula B. N., Bonaventura, C., Acharya A. S., and Friedman, J. M. (2002) UV Resonance Raman study of  $\beta$ 93-modified hemoglobin A: Chemical modifier-specific effects and added influences of attached poly(ethylene glycol) chains. *Biochemistry* 41, 376–385.
- (31) Khan, I., Dansker, D., Samuni, U., Friedman, A. J., Bonaventura, C., Manjula B. N., Acharya, A. S., and Friedman, J. M. (2001) Cys-93( $\beta$ ) modified hemoglobin: Kinetic and conformational consequences. *Biochemistry* 40, 7581–7592.
- (32) Vandegriff, K. D., McCarthy, M., Rohlf, R. J., and Winslow, R. M. (1997) Colloid osmotic properties of modified hemoglobins: chemically cross-linked versus polyethylene glycol surface-conjugated. *Biophys. Chem.* 69, 23–30.
- (33) Sakai, H., Hara, H., Yuasa, M., Tsai, A., Takeoka, S., Tushida, E., and Intaglietta, M. (2000) Molecular dimensions of Hb-based O<sub>2</sub> carriers determine constriction of resistance arteries and hypertension. *Am. J. Physiol. (Heart Circ. Physiol.)* 279, H908–H915.
- (34) de Wit C., Schafer, C., von Bismark, P., Bolz, S., and Pohl, U. (1997) Elevation of plasma viscosity induces sustained NO-mediated dilation in the hamster cremaster microcirculation in vivo. *Pflügers Arch.* 434, 354–361.
- (35) Waschke, K. F., Krieter, H., Hagen, G., Albrecht, D. M., Van Ackern, K., and Kuschinsky, W. (1994) Lack of dependence of cerebral flow on blood viscosity after blood exchange with a Newtonian O<sub>2</sub> carrier. *J. Cereb. Blood Flow Metab.* 14, 871–976.
- (36) Kuchan, M. J., Jo, H., and Frangos, J. (1994) Role of G proteins in shear stress-mediated nitric oxide production by endothelial cells. *Am. J. Physiol.* 267, C753–758.

BC0200733



# Novel Intracellular Delivery System of Antisense Oligonucleotide by Self-Assembled Hybrid Micelles Composed of DNA/PEG Conjugate and Cationic Fusogenic Peptide

Ji Hoon Jeong,<sup>†</sup> Sung Wan Kim,<sup>‡</sup> and Tae Gwan Park<sup>\*,†</sup>

Department of Biological Sciences, Korea Advanced Institute of Science and Technology, Taejeon 305-701, South Korea and CCCD/Department of Pharmaceutics and Pharmaceutical Chemistry, University of Utah, Salt Lake City, Utah 84112. Received October 27, 2002; Revised Manuscript Received January 13, 2003

An antisense oligonucleotide (ODN), *c-myb*, was covalently conjugated to poly(ethylene glycol) (PEG) via an acid-cleavable phosphoramidate linkage to form a diblock copolymer-like structure. The phosphoramidate linkage between ODN and PEG was completely cleaved within 5 h in an endosomal acidic condition (pH 4.7). When complexed with a cationic fusogenic peptide, KALA, the ODN/PEG conjugate self-associated to form polyelectrolyte complex micelles in an aqueous solution. The anionic ODN segments were ionically interacted with cationic KALA peptide to form an inner polyelectrolyte complex core, while the PEG segments constituted a surrounding corona. Effective hydrodynamic volume of the micelles was ca. 70 nm with a very narrow size distribution. The polyelectrolyte complex micelles, composed of *c-myb* ODN–PEG conjugate and KALA, were transported into cells far more efficiently than *c-myb* ODN itself. They also exhibited higher antiproliferative activity against smooth muscle cells. This study demonstrates that the DNA/PEG hybrid micelles system can be applied for the delivery of antisense oligonucleotide.

## INTRODUCTION

A wide variety of antisense oligonucleotides (ODN) have drawn much attention due to their specific interaction with cytoplasmic mRNA to block specific gene expression (1–4). Modulating the expression of a target gene by ODN has considerable potential for diverse therapeutic applications (5–8). Practical applications of antisense ODN as therapeutic chemical entities, however, have two inherent problems: susceptibility to enzymatic hydrolysis and poor cellular uptake (9, 10). The enzyme stability problem can be partly improved by synthesizing chemically modified ODN derivatives such as phosphorothioates and peptide nucleic acids. The modified ODN derivatives showed resistant to the enzymatic digestion by nucleases (11, 12). The limited cellular uptake of antisense ODN has yet been fully solved. Since ODN is a negatively charged macromolecular drug having a very low permeability across cell membrane, high dose of ODN is generally required to achieve the desired antisense effect. To increase the cellular uptake of ODN, antisense ODN was formulated with liposomes (13, 14), cationic lipids (15), and cationic polymers (16). These formulations are based on the formation of polyelectrolyte complex nanoparticles that can be more readily taken up by cells via an endocytosis pathway rather than a passive diffusion route. Significantly improved extent of cellular uptake as well as enhanced stability of ODN can be achieved using these nanoscale and nonviral vector formulations.

We recently reported a new DNA/polymer hybrid micelle structure as an ODN carrier. An antisense ODN

was covalently conjugated to the terminal end of a biodegradable polymer, poly(D,L-lactic-co-glycolic acid) (PLGA). The ODN/PLGA conjugate has an amphiphatic diblock copolymer structure composed of a hydrophilic ODN segment and a hydrophobic PLGA segment. The ODN/PLGA conjugate self-assembled to form micelles in an aqueous medium. The PLGA segment in the conjugate constituted an inner core while the ODN segment, highly hydrophilic and ionized, formed a surrounding corona (10). These ODN/PLGA micelles could be more efficiently transported within cells, suggesting that the micelle-type carriers could be an efficient alternative carrier for ODN delivery.

In the present study, antisense ODN, *c-myb*, was chemically conjugated with PEG via an acid cleavable linkage to produce an ODN–PEG conjugate. It was hypothesized that the ODN–PEG conjugate could self-assemble to form polyelectrolyte complex micelles by formulating with various cationic peptides and polymers. Ionic interaction between anionic ODN segments and cationic counterparts was expected to drive the formation of a polyelectrolyte complex inner core, whereas PEG segments constitute a surrounding corona. The entrapment of nucleic acids in the core of polyelectrolyte complex micelles could significantly improve the nuclease resistance of antisense ODN from enzymatic attack (17–19). The surrounding hydrophilic PEG segments not only improve the solubility of the nanoparticulate in aqueous milieu (20, 21), but also protect ODN from serum protein binding, owing to the steric hindrance effect of the flexible PEG chains (22–24). Physical properties of the polyelectrolyte complex micelles were characterized. Cellular uptake behaviors and antiproliferation effect of *c-myb* antisense ODN on smooth muscle cells were also investigated.

\* Corresponding author. Tel: +82-42-869-2621, fax: +82-42-869-2610, e-mail: tgpark@mail.kaist.ac.kr.

<sup>†</sup> Korea Advanced Institute of Science and Technology.

<sup>‡</sup> University of Utah.

## MATERIALS AND METHODS

**Materials.** Oligonucleotide (antisense *c-myb* ODN, 5'-GTG-TCG-GGG-TCT-CCG-GGC-3' and mis-matched ODN, 5'-GTC-TCC-GGC-TCA-CCC-GGG-3'), which has a terminal phosphate group at its 5' end, was synthesized and purified by Bioneer (Taejon, Korea). Cationic peptide, KALA (WEAKLAKALAKALAKHLAKA LAKALKACEA) was synthesized and purified by Peptron (Taejon, Korea). 1-Ethyl-3,3-dimethylaminopropylcarbodiimide (EDC), imidazole, ethylenediamine, protamine, and (3-(4,5-dimethylthiazolyl-2)-2,5-diphenyltetrazolium bromide) (MTT) were purchased from Sigma (St. Louis, MO). *N*-Hydroxyl-succinimide-derivatized poly(ethylene glycol) (SPA-PEG, MW 2000) was obtained from Shearwater (Huntsville, AL). Sephadex G-50 resin was purchased from Sigma (St. Louis, MO). Polyethylenimine (branched PEI, MW 25000) was purchased from Aldrich (Milwaukee, WI). Dulbecco's modified Eagle's medium (DMEM), Dulbecco's modified phosphate-buffered saline (DPBS), and fetal bovine serum (FBS) were purchased from Gibco BRL (Grand Island, NY). All other chemicals were of analytical grade.

**Synthesis of ODN-PEG Conjugate.** To form an active ODN-phosphorimidazolidine intermediate, ODN (1 mg, 180 nmol) and EDC (3.5 mg, 18  $\mu$ mol) were dissolved in 0.5 mL of 0.1 M imidazole (pH 6.0). The reaction mixture was incubated for 1 h at room temperature. The ODN having an imidazolidine group at its 5' position was isolated from the mixture by Sephadex G-50 spin-column chromatography and collected in 100  $\mu$ L of 10 mM phosphate buffer containing 100 mM NaCl and 1 mM EDTA, pH 7.5. One hundred microliters of 0.5 M ethylenediamine (pH 7.7) was added to the solution containing 5'-imidazolidine ODN. The reaction was carried out for 1 h at 50 °C. The ODN was then isolated by Sephadex G-50 spun-column chromatography. The conjugation of 5'-ethylenediamine-ODN to PEG was performed by adding NHS-derivatized PEG. The stoichiometric molar ratio (ODN/PEG) of the conjugation reaction was 1:5. The reaction mixture was incubated for 3 h at room temperature and dialyzed against deionized water to remove unreacted PEG (MWCO 3500).

**Reversed-Phase Chromatography Analysis.** The product from each reaction step was analyzed by an HPLC system (Waters 486, Waters, Milford, MA) equipped with UV detector (UV486, Waters, Milford, MA). The chromatography was performed on Hipore RP304 column (250  $\times$  4.6 mm, Biorad, Hercules, CA) with detection at 260 nm using a linear gradient elution of 100 mM ammonium acetate/acetonitrile from 5/95 (v/v) to 50/50 (v/v) with a flow rate of 1 mL/min. The eluate was monitored by UV absorption measurement at 260 nm.

To observe the acid-cleavage profile of ODN-PEG conjugate, the samples were incubated at either pH 4.7 (10 mM citric acid/sodium citrate buffer, pH 4.7) or pH 7.4 (10 mM phosphate buffer, pH 7.4). The samples were incubated at 37 °C. After 5 h, the sample incubated in pH 4.7 was neutralized by adding 0.1 N NaOH and then injected to the HPLC system for analysis. Free ODN was also analyzed in the same HPLC system to identify its retention time.

**Formation and Characterization of Polyelectrolyte Complex Micelles.** Desired amounts of ODN-PEG conjugate and KALA were separately diluted in PBS and filtered through a 0.2  $\mu$ m filter (Millipore, Bedford, MA). The diluted KALA solution was added to the ODN-PEG conjugate solution and mixed to form polyelectrolyte complex micelles, in which the stoichiometric molar ratio between the number of phosphate in ODN and the

number of lysine residues in KALA was adjusted at 1:1.57. The micelles were left for 30 min prior to use. Hydrodynamic volume and surface charge of the polyelectrolyte complex micelles were measured by dynamic light scattering at 25 °C using a dynamic light scattering photometer (Zeta Plus, Brookhaven Instrument Co., NY) equipped with He-Ne laser at a wavelength of 632 nm.

**Cell Culture.** A murine smooth muscle cell line, A7R5, was purchased from American Type Cell Culture (ATCC, Rockville, MD) and was maintained in DMEM supplemented with 10% FBS, streptomycin at 100  $\mu$ g/mL, penicillin at 100 IU/mL, and 2 mM L-glutamine at 37 °C in a humidified 5% CO<sub>2</sub> atmosphere.

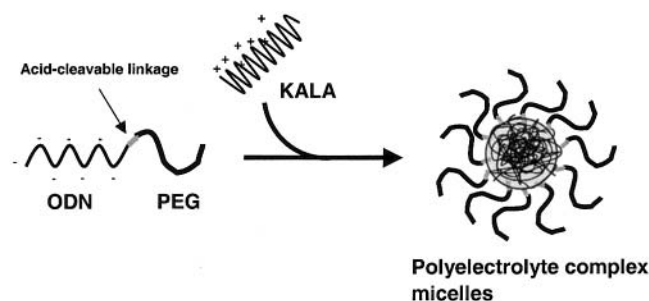
**Fluorescence Labeling of ODN-PEG Conjugate.** A FITC-labeled ODN having a complementary sequence to antisense *c-myb* ODN (sense *c-myb* ODN) was hybridized with either antisense *c-myb* ODN or antisense *c-myb* ODN-PEG conjugate. The mixture was then heated at 65 °C for 5 min and cooled in ice.

**Confocal Microscopy.** Confluent cells were trypsinized and 10000 cells per well were plated in a six-well plate (35 mm diameter, Nunc) containing collagen-coated cover-glass in 1.5 mL of DMEM with 10% FBS and incubated for 24 h before further experiments. After the replacement of the medium with fresh serum-free medium, the FITC-labeled ODN-PEG/KALA polyelectrolyte complex micelles were added to make an equivalent antisense ODN concentration of 20  $\mu$ g/mL. Unconjugated antisense *c-myb* ODN, which was also hybridized with the FITC-labeled ODN (sense strand), was used as a control. After 3 h incubation, the medium was discarded, and the cells were extensively washed with DPBS. The cells were submerged in a fixing solution (0.2% glutaraldehyde, 0.5% formaldehyde in DPBS) and stored at 4 °C for 30 min. The cells were then washed once with PBS and visualized by an LSM 510 confocal microscope (Carl Zeiss, Germany). An argon/krypton mixed gas laser with excitation line at 495 nm was used to induce FITC fluorescence.

**Cell Proliferation Studies.** Antiproliferative effect of *c-myb* antisense ODN was investigated using two types of methods, direct cell counting and MTT colorimetric assay (25–27). Cells were seeded at a density of 4000 cells per cm<sup>2</sup> in DMEM supplemented with 10% FBS. After 24 h, the medium was replaced with a medium with 0.5% FBS. The cells were maintained in the medium containing 0.5% FBS for 48 h (day 0). The cells were then supplemented with a medium with 10% FBS alone or with indicated amount of ODN formulations. For direct cell counting, the cells were trypsinized and counted by trypan blue exclusion on hemocytometer at appropriate time point. Degree of cell proliferation was also determined by using MTT assay after additional 72 h culture.

## RESULTS AND DISCUSSION

Polyelectrolyte complex micelles have been reported to be formed by complexing negatively charged ODN or plasmid DNA with a block or graft copolymer consisting of a cationic polymer and poly(ethylene glycol) (PEG). Poly(L-lysine)-PEG diblock copolymer (17–20) and PEG-grafted PEI copolymer (21) were reported to form self-assembled micellar associates when complexed with plasmid DNA or ODN. Electrostatic interactions between anionic ODN molecules and cationic polymer segments are responsible for the formation of charge-neutralized inner core, while PEG segments constitute a surrounding corona. In this study, ODN was conjugated to PEG via an acid cleavable linkage, phosphoramidate. The ODN–



**Figure 1.** A schematic illustration of the formation of polyelectrolyte complex micelles self-assembled from ODN-PEG conjugate and KALA.

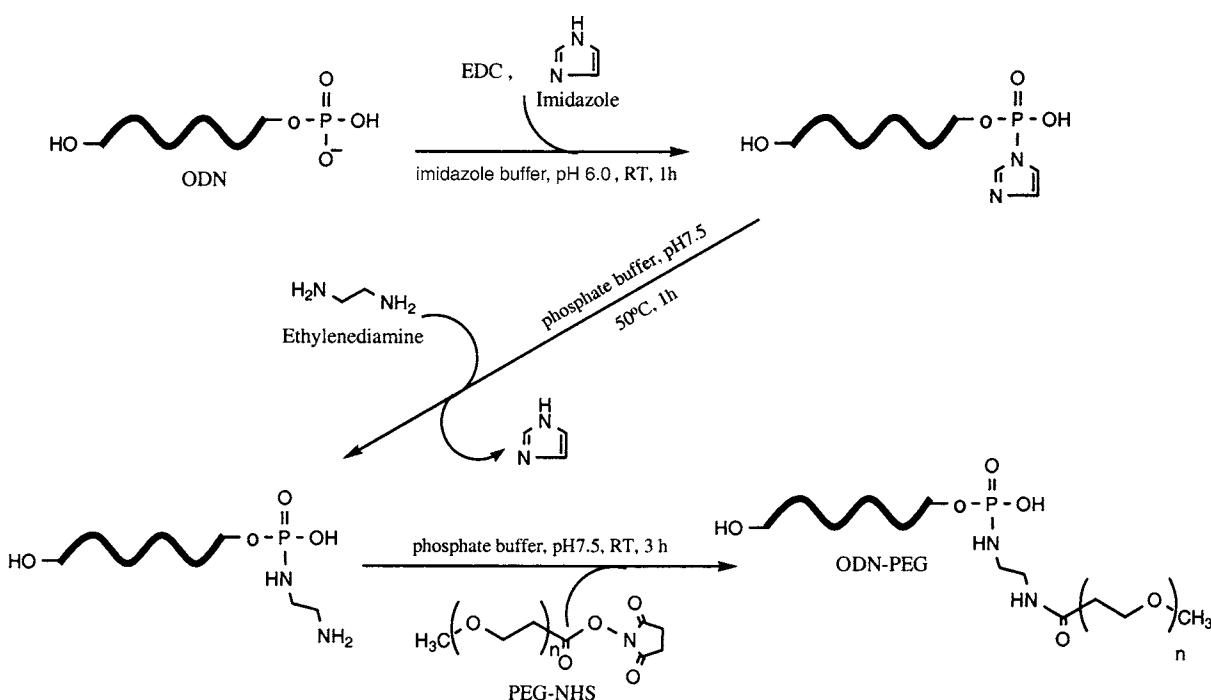
PEG conjugate, having a diblock copolymer structure, has two hydrophilic segments, but is expected to form polyelectrolyte complex micelles via charge-to-charge interaction between oppositely charged species of ODN segments and externally added cationic peptides. A fusogenic cationic peptide, KALA, was used in this study as a charge-neutralizing counterpart against ODN as schematically shown in Figure 1.

The covalent conjugation between oligonucleotide (ODN, antisense *c-myc*) having a 5' terminal phosphate group and PEG was carried out via a three-step reaction (Figure 2). The acid-labile linkage, phosphoramidate, was introduced between ODN and PEG. Coupling agents, EDC and imidazole, were used to form an active intermediate, ODN-phosphoimidazolide, which was then reacted with ethylenediamine via a phosphoramidate linkage. The resultant ethylenediamino-ODN was then coupled with a PEG derivative. The intermediate from each reaction were analyzed by HPLC, confirming the progress of conjugation reaction (data not shown). The conversion yield of ethylenediamino-ODN was ca. 90%, which is well agreed with previously published data (28). The ODN-PEG conjugate had small portion of unconjugated ODN impurities ( $\leq 1\%$ ) as determined by HPLC.

To enhance the antisense activity of ODN, an acid-cleavable phosphoramidate linkage was introduced be-

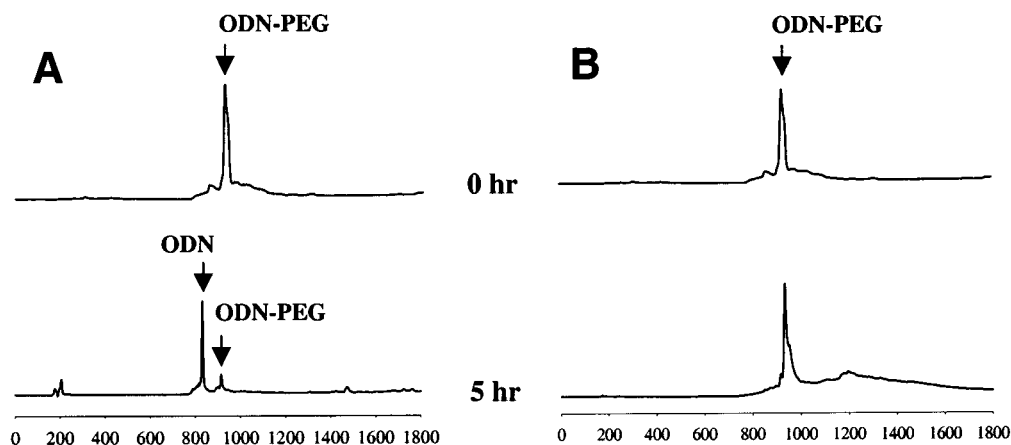
tween ODN and PEG. It was postulated that intracellularly delivered antisense ODN should be in a PEG-cleaved form to avoid the steric hindrance effect of PEG segment, which might hinder the interaction between the ODN and a target RNA sequence. The phosphoramidate linkage was reported to be labile in acidic environment, but relatively stable at neutral pH (29, 30). Considering that ODN-PEG/KALA complex micelles were first located in an acidic endosomal compartment after the endocytic cellular uptake, the acid-labile property of the phosphoramidate bond can trigger the cleavage of ODN from the ODN-PEG conjugate in the endosome compartment. The released ODN would diffuse into the cytoplasmic region where it can hybridize with its counterpart mRNA, without steric-hindrance of conjugated PEG, to block specific gene expression. Figure 3 shows cleavage profiles of ODN from ODN-PEG conjugate at different pH values. To observe the acid-sensitive cleavage profile of the phosphoramidate linkage, the ODN-PEG conjugate was incubated at pH 4.7 and pH 7.4 as a function of time. ODN was hardly cleaved when incubated at physiological pH (pH 7.4), but it was readily cleaved at pH 4.7. The cleavage of the phosphoramidate linkage at the acidic condition was completed within 5 h.

The ODN-PEG conjugates could self-assemble to form polyelectrolyte complex micelles by interacting with either cationic peptides or cationic polymers as schematically illustrated in Figure 1. Since this study aims at an efficient cellular delivery system of ODN in the form of micellar nanoparticles, ODN would be preferentially transported within cells by an endocytosis mechanism, not by a passive diffusion mechanism. In this case, rapid escape of ODN from an acidic endosomal compartment to cytoplasm region is essentially needed to avoid further chemical and enzymatic degradations of ODN in later endosome and lysosomal compartments. To facilitate the escape from endosomes, ODN-PEG conjugate was complexed with a cationic fusogenic peptide, KALA, which is known to disrupt the endosomal membrane. KALA has been widely used for enhancing the transfection efficien-

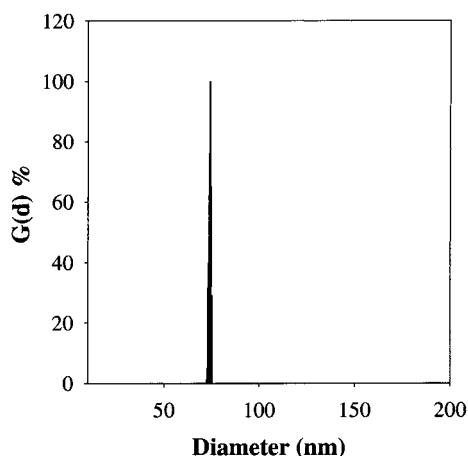


**Figure 2.** Synthetic scheme of ODN-PEG conjugate having an acid-cleavable linkage, phosphoramidate.



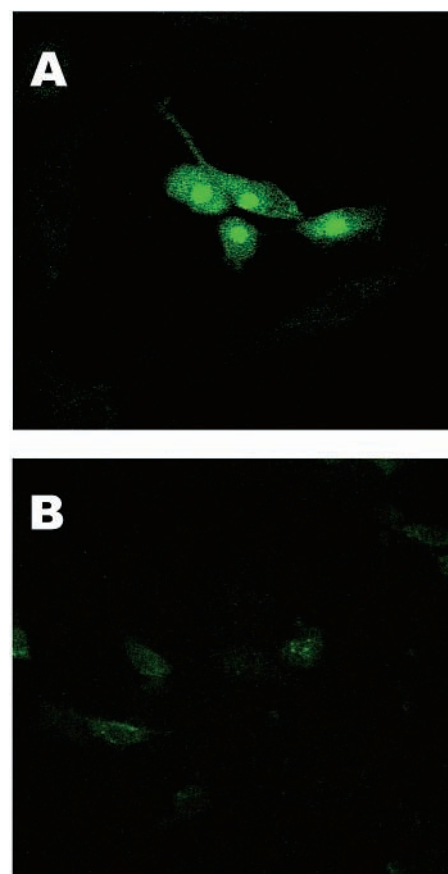


**Figure 3.** Cleavage profiles of ODN-PEG conjugate at pH 4.7 (A) and pH 7.4 (B). The ODN-PEG conjugate was incubated at indicated pH and analyzed by reversed-phase HPLC as described in Materials and Methods.



**Figure 4.** Size distribution of ODN-PEG/KALA polyelectrolyte complex micelles as determined by dynamic light scattering.

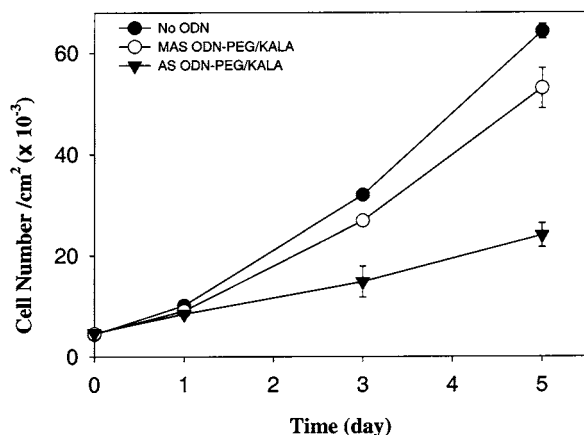
cies of various foreign plasmid genes (23, 24). KALA itself has been used as a DNA carrier for delivering plasmid DNA into cells (30, 31). To form polyelectrolyte complex micelles, stoichiometric molar ratio of the anionic phosphate group in ODN to the cationic lysine group in KALA was adjusted at 1:1.57, since KALA also contains two glutamic acid residues, which can neutralize the same number of counterions of lysine residue. The surface charge of the complex was almost neutral as determined by light scattering method (data not shown). The polyelectrolyte complex micelles generated between ODN-PEG and KALA showed a hydrodynamic diameter of ca. 74 nm with a very narrow size distribution (Figure 4). The resulting uniform size of micelles suggested that ODN segments were interacted with KALA to form an inner core of the micelles by the neutralization of the two oppositely charged polyelectrolytes. PEG segments composed of a surrounding corona play an important role in stabilizing the micellar structure, which not only prevents aggregation between the micelles, but also enhances their solubility in aqueous milieu (20, 21). In contrast, the formulation of KALA with free ODN resulted in the formation of nanoparticles with about 200 nm in diameter, of which surface charge values varies depending on the molar ratio of KALA and ODN (data not shown). It is of particular interest to note that the size distribution of ODN-PEG/KALA is very narrow, which can be attributed to the monodisperse molecular weight distributions of ODN and KALA. In contrast to synthetic polymers, ODN and KALA have fixed and



**Figure 5.** Confocal microscopic images of smooth muscle cells treated with (A) ODN-PEG/KALA polyelectrolyte complex micelles and (B) ODN alone. The ODN-PEG conjugate and the unmodified ODN were hybridized with FITC-labeled ODN having complementary sequence with the ODN for the visualization.

monodisperse molecular weight values. Thus, stoichiometrically balanced charge-to-charge interactions between ODN and KALA within the micellar core may occur in a well-defined fashion.

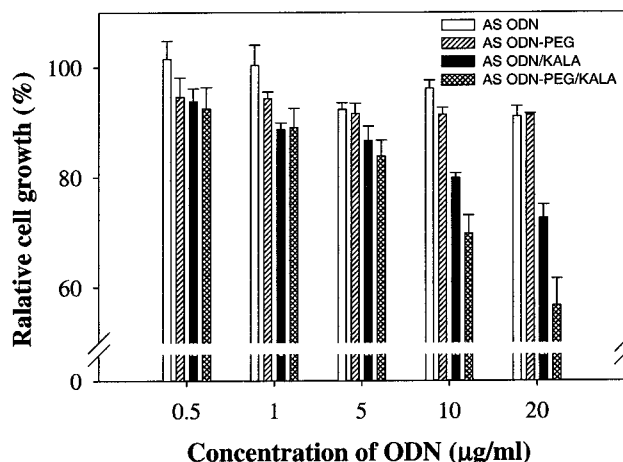
Uptake of ODN-PEG/KALA polyelectrolyte complex micelles by smooth muscle cells (A7R5) was visualized under confocal microscope (Figure 5). For visualization, fluorescent dye (FITC) labeled ODN having a complementary sequence to antisense *c-myb* (sense strand) was hybridized with the antisense *c-myb* ODN-PEG conjugates before forming the complex with KALA. The FITC-labeled hybrid complex (antisense-ODN-PEG/sense-



**Figure 6.** Proliferation rates of smooth muscle cells treated with no ODN (closed circle, ●), mismatched antisense ODN (MAS)-PEG/KALA micelles (open circle, ○), and antisense ODN (AS)-PEG/KALA micelles (inverted triangle, ▼). The concentration of the antisense ODN used in each formulation was 20  $\mu\text{g/mL}$ . The experiment was carried out in triplicate.

ODN-FITC/KALA) was showed similar size and distribution to those of ODN-PEG/KALA formulation (data not shown). It can be seen that the FITC-labeled micelles were distributed over entire cytoplasm region of smooth muscle cells (Figure 5A). In contrast, the cells treated with FITC-labeled ODN showed only negligible fluorescence in cytoplasmic region, suggesting that only small fraction of ODN should be transported within the cells most likely due to its limited passive diffusion through plasma membrane (Figure 5B). This result reveals that ODN could be delivered within cells more efficiently by forming a micellar nanoparticulate structure that was more readily taken up by cells via an endocytosis mechanism. This was also in good agreement with the previous results obtained ODN-PLGA conjugate micelles (10) and PEO-PBLA[poly( $\beta$ -benzyl L-aspartate)]-FITC micelles (33). The confocal image also suggests that ODN was likely to be released from endosomal compartments. This postulation was based on the observation that there were no localized fluorescent droplets scattered in the cytoplasm area, which indicate the presence of endosomes containing ODN-PEG/KALA micelles. This was possibly due to the fusogenic action of KALA that was incorporated to form an inner core of micelles.

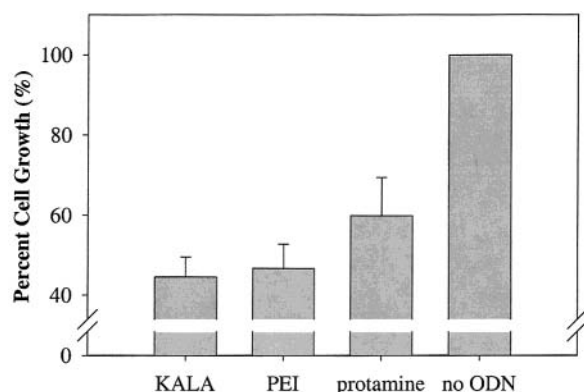
To test the efficiency of the ODN delivery system using the polyelectrolyte complex micelles, antisense ODN directed to *c-myb* was selected as a therapeutic ODN. Proto-oncogene *c-myb* is thought to play a major role in mitogen-induced proliferation of smooth muscle cells (34). An antisense *c-myb* has been attempted to use for the suppression of smooth muscle cell proliferation in coronary artery after a balloon angioplasty surgery procedure (35). The antisense *c-myb* was also reported to inhibit the proliferation of smooth muscle cells in vitro (36) and in vivo (33). Figure 6 shows the proliferation rate of smooth muscle cells (A7R5) for mismatched antisense and antisense ODN-PEG/KALA formulations at 20  $\mu\text{g/mL}$  of the antisense ODN concentration. The polyelectrolyte complex micelles containing antisense *c-myb* ODN showed about 70% inhibition in proliferation of the smooth muscle cells in comparison to mock-treated cells (no ODN), whereas those containing mismatched ODN exhibited no significant inhibition of proliferation (Figure 6). The 70% inhibition of the proliferation was achieved after 5 days at the concentration of 20  $\mu\text{g/mL}$  of the antisense ODN in the presence of 10% FBS. This also



**Figure 7.** Dose-dependent proliferation rate of smooth muscle cells treated with antisense ODN (open), antisense ODN-PEG conjugate (hatched), antisense ODN/KALA complexes (closed), and antisense ODN-PEG/KALA complex micelles (cross-hatched). Degree of cell proliferation was determined by using MTT assay after 72 h from the time of addition of the formulations. The experiment was carried out in the presence of 10% FBS.

suggests the possibility that the ODN delivery system using the ODN-PEG/KALA polyelectrolyte complex micelles could protect the ODN from digestion attack by enzymes abundant in serum. It is also noted that the significant reduction of the proliferation could be achieved at relatively lower concentration (20  $\mu\text{g/mL}$ ) compared to previous results using antisense *c-myb* (36) or *c-myc* (37) phosphothioate ODN, in which 50% inhibition of proliferation of smooth muscle cells could be achieved only at the concentration of higher than 90  $\mu\text{g/mL}$ . Figure 7 shows inhibition of proliferation of the smooth muscle cells as a function of the antisense ODN concentration for various ODN formulations. The relative proliferation rate of the cells was determined after 72 h incubation with the formulations using MTT assay and calculated as a percent cellular metabolic activity compared to mock-treated control cells (no ODN). The proliferation rate of the cells treated with the antisense ODN-PEG/KALA was significantly reduced relative to that of antisense ODN alone or the micelles containing mismatched ODN in the presence of serum. antisense ODN complexed with KALA (AS ODN/KALA) showed less extent of inhibition activity than the antisense micelle formulation (AS ODN-PEG/KALA), suggesting that PEG shell of the micelles not only enhanced the solubility of the polyelectrolyte complexes but efficiently stabilized the micelles in the presence of serum. Our previous studies also showed that the polyelectrolyte complexes between DNA and PEG-modified cationic polymers exhibited increased transfection efficiency compared to the complexes with unmodified polymer in the presence of serum (23, 24). This is probably because the flexible PEG chain can reduce the protein adsorption that induces interparticle aggregation. The same experiment set with mismatched ODN was also carried out but showed no significant effect on smooth muscle cell proliferation (data not shown).

To study the effect of different core forming cationic polymers on the antiproliferation activity of the polyelectrolyte complex micelles, different cationic polymers including KALA, polyethylenimine (branched-PEI, MW25000), and protamine were used as counter polyions. As shown in Figure 8, all of the polycations demonstrated desired inhibition activities on the proliferation of smooth muscle cells. The polyelectrolyte complex micelles gener-



**Figure 8.** Proliferation rate of smooth muscle cells treated with various polyelectrolyte complex micelles prepared by antisense *c-myc* ODN/PEG conjugate with different polycations, KALA, polyethylenimine (PEI), and protamine. The size and surface zeta-potential values of the different micellar formulations were similar to those of the ODN-PEG/KALA formulation. The experiment was performed under the same conditions as in Figure 7. The concentration of antisense ODN used in each formulation was 20  $\mu\text{g/mL}$ . The experiment was carried out in triplicate.

ated by using protamine showed slightly lower inhibition activity, suggesting that either fusogenic activity of KALA or the endosomal disruption property of PEI could improve antisense activity of ODN. This result also demonstrated that any type of cationic polymers with or without functionality could be applied to the formulation of ODN-PEG/polycation complex micelle systems.

In conclusion, this study demonstrates a novel formulation of antisense ODN for enhanced cellular uptake. ODN was conjugated to PEG to form a diblock copolymer-like structure via an acid-cleavable linkage, phosphoramidate. By combining the ODN-PEG conjugate with a fusogenic cationic peptide in aqueous solution, stable ODN-PEG/KALA micelles were produced. They were more readily transported within cells than ODN itself, which occurred probably by an endocytosis process. A therapeutic ODN, *c-myc*, exhibited far greater antiproliferation effect on smooth muscle cells when formulated the current micelle formulation. It can be envisioned that this novel formulation has a wide range of applications in intracellular delivery of ODN that has been the most challenging barrier for ODN therapeutics.

#### ACKNOWLEDGMENT

This work was supported by the grants from the Ministry of Information and Communication (IMT-2000-B3-2) and National Cancer Center (02-3-150), Republic of Korea.

#### LITERATURE CITED

- (1) Stein, C. A., and Cheng, Y. C. (1993) Antisense oligonucleotides as therapeutic agents—is the bullet really magical? *Science* 261, 1004–12.
- (2) Crooke, S. T. (1993) Progress toward oligonucleotide therapeutics: Pharmacodynamic properties. *FASEB J.* 7, 533–539.
- (3) Gewirtz, A. M., Sokol, D. L., and Ratajczak, M. Z. (1998) Nucleic acid therapeutics: State of the art and future prospects. *Blood* 92, 712–736.
- (4) Bennett, C. F. (1998) Antisense oligonucleotides: Is the glass half full or half empty? *Biochem. Pharmacol.* 55, 9–19.
- (5) Calabretta, B., Skorski, T., Ratajczak, M. Z., and Gewirtz, A. M. (1996) antisense strategies in the treatment of leukemias. *Semin Oncol* 23, 78–87.
- (6) Skorski, T., Nieborowska-Skorska, M., Wlodarski, P., Zon, G., Iozzo, R. V., and Calabretta B. (1996) antisense oligodeoxynucleotide combination therapy of primary chronic myelogenous leukemia blast crisis in SCID mice. *Blood* 88, 1005–1012.
- (7) Bennett, M. R., Anglin, S., McEwan, J. R., Jagoe, R., Newby, A. C., and Evan, G. I. (1994) Inhibition of vascular smooth muscle cell proliferation *in vitro* and *in vivo* by *c-myc* antisense oligodeoxynucleotides. *J. Clin. Invest.* 93, 820–828.
- (8) Simons, M., Edelman, E. R., DeKeyser, J. L., Langer, R., and Rogenberg, R. D. (1992) antisense *c-myc* oligonucleotides inhibit intimal arterial smooth muscle cell accumulation *in vivo*. *Nature* 359, 67–70.
- (9) Wagner, R. W. (1994) Gene inhibition using antisense oligodeoxynucleotides. *Nature* 372, 333–335.
- (10) Jeong, J. H., and Park, T. G., (2001) Novel polymer-DNA hybrid polymeric micelles composed of hydrophobic poly(D,L-lactic-co-glycolic acid) and hydrophilic oligonucleotides. *Bioconjugate Chem.* 12, 917–923.
- (11) Agrawal, S., Goodchild, J., Civeira, M. P., Thornton, A. H., Sarin, P. S., and Zamecnik, P. C. (1988) Oligodeoxy-nucleoside phosphoramidates and phosphorothioates as inhibitors of human immunodeficiency virus. *Proc. Natl. Acad. Sci. U.S.A.* 85, 7079–83.
- (12) Egholm, M., Buchardt, O., Christensen, L., Behrens, C., Frier, S. M., Driver, D. A., Berg, R. H., Kim, S. K., Norde'n, B., and Nielsen, P. E. (1993) PNA hybridizes to complementary oligo-nucleotides obeying the Watson-Crick hydrogen bonding rules. *Nature (London)* 365, 566–568.
- (13) Pagnan, G., Stuart, D. D., Pastorino, F., Raffaghello, L., Montaldo, P. G., Allen, T. M., Calabretta, B., and Ponzoni, M. (2000) Delivery of *c-myc* antisense oligodeoxynucleotides to human neuroblastoma cells via disialoganglioside GD 2-targeted immunoliposomes: antitumor effects. *J. Natl. Cancer Inst.* 92, 253–61.
- (14) Juliano, R. L., and Akhtar, S. (1992) Liposomes as a drug delivery system for antisense oligonucleotides. *antisense Res. Dev.* 2, 165–76.
- (15) Meyer, O., Kirpotin, D., Hong, K., Sternberg, B., Park, J. W., Woodley, M. C., and Papahadjopoulos, D. (1998) Cationic liposomes coated with poly(ethylene glycol) as carriers for oligonucleotides. *J. Biol. Chem.* 273, 15621–15627.
- (16) Kim, J. S., Kim, B.-I., Maruyama, A., Akaike, T., and Kim, S. W. (1998) A new nonviral DNA delivery vector: the terplex system. *J. Controlled Release* 53, 175–182.
- (17) Katayose, S., and Kataoka, K. (1997) Water-soluble polyion complex associates of DNA and poly(ethyleneglycol)-poly(L-lysine) block copolymer. *Bioconjugate Chem.* 8, 702–707.
- (18) Katayose, S., and Kataoka, K. (1998) Remarkable increase in nuclease resistance of plasmid DNA through supra-molecular assembly with poly(ethyleneglycol)-poly(L-lysine) block copolymer. *J. Pharm. Sci.* 87, 160–163.
- (19) Harada, A., Togawa, H., and Kataoka, K. (2001) Physico-chemical properties and nuclease resistance of antisense-oligonucleotides entrapped in the core of polyion complex micelles composed of poly(ethyleneglycol)-poly(L-lysine) block copolymer. *Eur. J. Pharm. Sci.* 13, 35–42.
- (20) Kataoka, K., Togawa, H., Harada, A., Yasugi, K., Matsumoto, T., and Katoyose, S. (1996) Spontaneous formation of polyion complex micelles with narrow distribution from antisense oligonucleotide and cationic block copolymer in physiological saline. *Macromolecules* 29, 8556–8557.
- (21) Vinogradov, S., Batrakova, E., Li, S., and Kabanov, A. (1999) Polyion complex micelles with protein-modified corona for receptor-mediated delivery of oligonucleotides into cells. *Bioconjugate Chem.* 10, 851–860.
- (22) Choi, Y. H., Liu, F., Choi, J. S., Kim, S. W., and Park, J. S. (1999) Characterization of a targeted gene carrier, lactose-poly(ethylene glycol)-grafted poly-L-lysine, and its complex with plasmid DNA. *Hum. Gene Ther.* 10, 2657–2665.
- (23) Lee, H., Jeong, J. H., and Park, T. G. (2002) PEG grafted polylysine with fusogenic peptide for gene delivery: high transfection efficiency with low cytotoxicity, *J. Controlled Release* 79, 283–291.



- (24) Lee, H., Jeong, J. H., and Park, T. G. A New Gene Delivery Formulation of polyethyleneimine/DNA complexes coated with PEG conjugated fusogenic peptide, *J. Controlled Release* 76, 138–192.
- (25) Mosmann, T. (1983) Rapid colorimetric assay for cellular growth and survival: application to proliferation and cytotoxicity assay, *J. Immunol. Methods* 65, 55–63.
- (26) Leonardi, A., DeFranchis, G., Fregona, I. A., Violato, D., Plebani, M., and Secchi, A. G. (2001) Effects of Cyclosporin A on Human Conjunctival Fibroblasts. *Arch. Ophthalmol.* 119, 1512–1517.
- (27) Stewart, D. A., Thomas, S. D., Mayfield, C. A., and Miller, D. M. (2001) Psoralen-modified clamp-forming antisense oligonucleotides reduce cellular c-Myc protein expression and B16-F0 proliferation. *Nucleic Acid Res.* 19, 4052–4061.
- (28) Chu, B. C. F., Wahl, G. M., and Orgel, L. E. (1983) Derivatization of unprotected polynucleotides. *Nucleic Acid Res.* 11, 6513–6529.
- (29) Rahil, J., and Haake, P. (1981) Reactivity and mechanism of hydrolysis of phosphoramidates. *J. Am. Chem. Soc.* 103, 1723–1734.
- (30) de Vruhe, R. L. A., Rump, E. T., Sliedregt, L. A. J. M., Biessen, E. A. L., van Berkel, T. J. C., and Bijsterbosch, M. K. (1999) Synthesis of a lipophilic prodrug of 9-(2-phosphorylmethoxyethyl)adenine (PMEA) and its incorporation into a hepatocyte-specific lipidic carrier. *Pharm. Res.* 16, 1179–1185.
- (31) Wyman, T. B., Nicol, F., Zephalti, O., Scaria, P. V., Plank, C., and Szoka, F. C. (1997) Design, Synthesis, and Characterization of a cationic peptide that binds to nucleic acids and permeabilizes bilayers, *Biochemistry* 36, 3008–3017.
- (32) Lim, D. W., Yeom, Y. I., and Park, T. G. (2000) Poly-(DMAEMA-NVP)-*b*-PEG-galactose as Gene Delivery Vector for Hepatocytes. *Bioconjugate Chem.* 11, 688–695.
- (33) Liaw, J., Aoyagi, T., Kataoka, K., Sakurai, Y., and Okano, T. (1999) Permeation of PEO-PBLA-FITC polymeric micelles in aortic endothelial cells. *Pharm. Res.* 16, 213–220.
- (34) Ross, R. (1986) The pathogenesis of atherosclerosis-an update. *N. Engl. J. Med.* 314, 488–500.
- (35) Simons, M., Edelman, E. R., DeKeyser, J. L., Langer, R., and Rogenberg, R. D. (1992) antisense *c-myc* oligonucleotides inhibit intimal arterial smooth muscle cell accumulation *in vivo*. *Nature* 359, 67–70.
- (36) Villa, A. E., Guzman, L. A., Poptic, E. J., Labhasetwar, V., D'Souza, S., Farrell, C. L., Plow, E. F., Levy, R. J., DiCorleto, P. E., and Topol, E. J. (1995) Effect of antisense *c-myc* oligonucleotides on vascular smooth muscle cell proliferation and response to vessel wall injury. *Circ. Res.* 76, 505–513.
- (37) Biro, S., Fu, Y.-M., Yu, Z.-X., and Epstein, S. E. (1993) Inhibitory effects of antisense oligodeoxynucleotide targeting *c-myc* mRNA on smooth muscle cell proliferation and migration. *Proc. Natl. Acad. Sci. U.S.A.* 90, 654–658.

BC025632K

# Mutants of Immunotoxin Anti-Tac(dsFv)-PE38 with Variable Number of Lysine Residues as Candidates for Site-Specific Chemical Modification. 1. Properties of Mutant Molecules

Masanori Onda, James J. Vincent, Byungkook Lee, and Ira Pastan\*

Laboratory of Molecular Biology, Center for Cancer Research, National Cancer Institute, National Institutes of Health, 37 Convent Drive, Room 5106, Bethesda, Maryland 20892-4264

Received August 8, 2002; Revised Manuscript Received December 15, 2002

Chemical modification of proteins with substances such as poly(ethylene glycol) can add useful properties to proteins. Currently PEGylation is done in a random manner utilizing amino residues dispersed throughout a protein. For proteins such as immunotoxins, which have several different functional domains, random modification leads to inactivation. To determine if we could produce an immunotoxin with a diminished number of lysine residues so that chemical modification could be restricted to certain regions of the protein, we chose the recombinant immunotoxin anti-Tac(dsFv)-PE38 that has 13 lysine residues in the Fv portion and 3 in the toxin. We prepared a series of mutants with 0–12 lysines in the Fv and 0 or 3 in the toxin. Almost all of these molecules retain full biological activity. Our data indicate that replacement of lysine residues can be achieved without loss of biological potency. These molecules are a useful starting point to carry out site-specific PEGylation experiments.

## INTRODUCTION

Recombinant immunotoxins are chimeric proteins in which a truncated toxin is fused to the Fv domain of an antibody. We have produced many different recombinant immunotoxins in which the Fv portion of an antibody against a tumor related antigen is fused to a 38 kDa mutant form of *Pseudomonas* exotoxin A (PE)<sup>1</sup> that has a deletion of its cell binding domain (Bera et al., 1998; Brinkmann et al., 1991; Chowdhury et al., 1998; Mansfield et al., 1997; Onda et al., 2001b; Pastan, 1997; Reiter et al., 1994). Five of these immunotoxins, anti-Tac(Fv)-PE38 (LMB2), B3(Fv)-PE38 (LMB7), B3(dsFv)-PE38 (LMB9), RFB4(dsFv)-PE38 (BL22), and e23(dsFv)-PE38 (erb38), have been evaluated in phase I trials in patients with cancer (Kreitman et al., 2000, 2001; Pai-Scherf et al., 1999).

Anti-Tac(Fv)-PE38, also called LMB2, contains the Fv fragment of the anti-Tac MAb that binds to the IL-2 receptor  $\alpha$  subunit. Treatment of patients with LMB2 has produced major clinical responses in several different hematologic malignancies (Kreitman et al., 1999, 2000). LMB2 was administered to 35 patients with CD25 positive tumors who had failed standard therapies. One patient had a complete remission, lasting 2 years, and seven others had partial responses of variable durations.

The toxic side effects of recombinant immunotoxins are of two types. One type results from specific targeting of normal cells that have the same antigen as the cancer cells. The second type is nonspecific and usually is characterized by damage to liver cells in mice and a fall in serum albumin, weight gain, and evidence of renal or liver toxicity in humans (Kreitman and Pastan, 1995;

Onda et al., 2000). We recently described a new strategy designed to decrease the side effects of LMB2 in which mutations were introduced into the framework region of the Fv to lower its isoelectric point (Onda et al., 1999, 2001a). These mutant immunotoxins are less toxic to mice. We also found that a tumor necrosis factor (TNF) binding protein and/or a cyclooxygenase inhibitor were useful in reducing liver toxicity because TNF $\alpha$  was identified as a major cause of liver toxicity (Onda et al., 2000). Administration of either of these two molecules allowed us to use higher doses of immunotoxin to treat animals with tumors. However, liver damage was still the dose limiting toxicity. Also, this approach is not designed to decrease immunogenicity of the immunotoxin.

PEG-conjugated proteins are frequently more effective than their corresponding unmodified parent molecules as therapeutic agents. Many pharmaceutical proteins have been PEGylated and shown to have an improvement in their properties (Chaffee et al., 1992; Katre et al., 1987; Kitamura et al., 1990; Pyatak et al., 1980; Wang et al., 1993). These improved clinical properties include better physical and thermal stability, protection against susceptibility to enzymatic degradation, increased solubility, longer in vivo circulating half-life, decreased clearance, enhanced potency, reduced immunogenicity and antigenicity, and reduced animal toxicity (Bailon and Berthold, 1998). We previously reported that a PEGylated chimeric toxin composed of transforming growth factor (TGF)- $\alpha$  and PE showed an improvement in blood residency time and a decrease in its immunogenicity (Wang et al., 1993). However, PEGylation was accompanied by a significant loss of cytotoxic activity of the TGF $\alpha$ -PE fusion protein. Decreased activity was attributed to a decrease in binding to the TGF $\alpha$  receptor and a consequent decreased ability of the toxin to kill the cell.

Every chemical modification or conjugation process involves the formation of a covalent bond. Reactive groups that couple with amine-containing molecules are

\* To whom correspondence should be addressed. Tel: (301) 496-4797. Fax: (301) 402-1344. E-mail: pasta@helix.nih.gov.

<sup>1</sup> Abbreviations: ASA, accessible surface area; CDR, complementarity determining regions; DTE, dithioerythritol; PE, *Pseudomonas* exotoxin A; PEG, poly(ethylene glycol); TGF, transforming growth factor; TNF, tumor necrosis factor.

by far the most common functional groups present on cross-linking or modification reagents. An amine-coupling method is most often used to couple protein or peptide molecules to each other as well as to other macromolecules. The primary coupling chemical reactions for modification of amines is proceeded by acylation or alkylation. Most of these reactions are rapid and occur in high yield to give stable amide or secondary amine bonds (Hermanson, 1996). In most cases, PEGylation of proteins is nonspecific and may target all of the lysine residues in the protein, some of which may be in or near the active site of the protein. To overcome this drawback, we previously performed site-specific PEGylation of an immunotoxin in the peptide connector that attaches the Fv to the toxin using site directed mutagenesis to insert a cysteine residue in the connector (Tsutsumi et al., 2000). The PEGylated molecule retained full in vitro specific cytotoxicity. Stability, plasma half-life, antitumor activity, immunogenicity, and animal toxicity were greatly improved. Thus, thiol chemistry is useful for the attachment of PEG to a cysteine residue at a specific site. Modification of thiol residues has certain difficulties. It is difficult to produce large amounts of recombinant immunotoxins with one free thiol and very difficult if two or more are present because of refolding problems. To overcome these problems, we have chosen to carry out modification of lysine residues by making immunotoxins with a limited number of lysine residues.

In the current study, we have used site directed mutagenesis to change the lysine residues of a recombinant immunotoxin to other residues to make site-specific chemical modification possible. A series of molecules containing 0–13 lysines in the Fv and 0 or 3 lysines in the toxin was prepared. Molecular modeling was used to locate exposed amino acids that are remote from the complementarity determining regions (CDRs) of the Fv and could be mutated to lysine residues. We find that all of these mutant molecules retain specific binding and cytotoxic activities.

Our studies indicate that controlling the number and location of lysine residues in a protein can be accomplished successfully and could be a useful approach to allow specific chemical modification using lysine chemistries.

## EXPERIMENTAL PROCEDURES

**Molecular Models and Calculation of Accessible Surface Area (ASA) of Lysine Residues.** Molecular models of anti-Tac(dsFv) were created using SWISS-MODEL (Peitsch, 1996). These models were used to compute the ASA of lysines. The algorithm of Shrake and Rupley (1973), as implemented in GRASP (Nicholls et al., 1991), was used for all ASA calculations.

**Mutagenesis of Anti-Tac(dsFv)-PE38.** Mutagenesis of M1(dsFv)-PE38 was done by Kunkel's method with some modifications (Kunkel, 1985). CJ236 cells were transformed with pOND9-1 and pOND9-2 (Onda et al., 1999, 2001a). The transformants were grown in 2× YT medium containing 100 µg/mL ampicillin at 37 °C. At an OD<sub>600</sub> of 0.36, the cells were infected with the helper phage M13 at a multiplicity of infection of 5. After incubation at 37°C/110 rpm for 1 h, the culture was maintained at 37°C/300 rpm for another 6 h. The bacterial cells then were precipitated by centrifugation, and the phage from the supernatant was precipitated with poly(ethylene glycol). The single-stranded, uracil-containing DNA from the purified phage was extracted with phenol and chloroform and precipitated with sodium

chloride and ethanol. This single-stranded DNA codes for the sense strand of M1(dsFv)-PE38. The following primers were used for mutagenesis: VL 18, 5'-GGCACTG-CAGGTTATGGTGACTTGCTCCCCTGGAGATG-CAGACAT-3'; VL39, 5'-CCATAGCTGGGGAGAAGTGC-CAGGCCTCTGCTGGAACCACTGCATGTA-3'; VL 45, 5'-GGATGTGGTATAAATCCATAGCTGGGGAGAAGT-GCCTGGCTT-3'; VL 77, 5'-GGCAGCATCTTCAGCCT-CCATATTCGAAATTGTGAGAGAGTAATCGGT-3'; VL 103–107, 5'-GTTAGCAGCCGAATTCTATTCCAGTTTC-CAGCTCGGTCCCGCAACCGAACGTAG-3'; VH 13, 5'-CATCTTCACTGAGGCCCCAGGTTCTGCTA-GCTCAGCCCCAGA-3'; VH 19–22–23, 5'-AGTAAAG-GTGTAGCCAGAAGCTGCGCAGGACAGCTG-CACTGAGGCCCCAGGTTCTGC-3'; VH23, 5'-AAAGGT-GTAGCCAGAAGCTGCGCAGGACATCTTCACTGA-3'; VH 38–40, 5'-AATCCATTCCAGCACTGTTTCAGGTGTC-TGTCTTACCCAGTGCATCTGTAG-3'; VH 62–64, 5'-GGAGGAATCGTCTGCAGTTAACGTGGCCT-TGTCTCTGAATCTCTGATTGTATTCACTATA-3'; VH62–64–66–67, 5'-GGAGGAATCGTCTGCAGTTAACGTGAA-TCTGTCTCTGAATCTCTGATTGTATTCACTATA-3'; VH 73, 5'-GCTCAGTTGCATGTAGGCAGTACTGGAG-GAATCGTCTGCAGTCAA-3'; PE604K, 5'-CAGGTCCCTC-GCGCGCGGTTGGCCGGGCCACCTTTCCCA-CCCTGGCTGGCGTAGTCCGGCAG-3'.

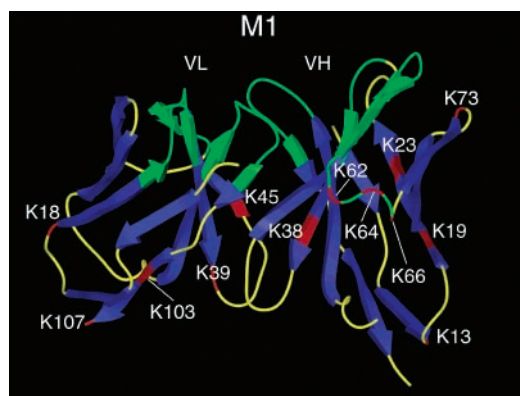
The primers were phosphorylated using polynucleotide kinase and T4 DNA ligase buffer from Boehringer Mannheim (Indianapolis, IN). These phosphorylated primers were used to introduce mutations in the uracil template of pOND9-1 and pOND9-2 using the Bio-Rad (Richmond, CA) Muta-Gene kit. The product at the end of the mutagenesis reaction was used to directly transform DH5α competent cells. Mutations in the clones were confirmed by automated DNA sequencing.

**Production of Recombinant Immunotoxin.** The two components of the recombinant immunotoxins were expressed in *Escherichia coli* BL21 (λDE3) and accumulated in inclusion bodies as previously described (Onda et al., 1999). Inclusion bodies were solubilized in Guanidine hydrochloride solution, reduced with dithioerythritol (DTE) and refolded by dilution in a refolding buffer containing arginine to prevent aggregation, and oxidized and reduced glutathione to facilitate redox shuffling. Active monomeric protein was purified from the refolding solution by ion exchange and size exclusion chromatography (Onda et al., 1999). Protein concentrations were determined by a Bradford assay (Coomassie Plus; Pierce, Rockford, IL).

**Cytotoxicity Assays.** The specific cytotoxicity of each immunotoxin was assessed by protein synthesis inhibition assays (inhibition of incorporation of tritium-labeled leucine into cellular protein) in 96-well plates as previously described (Onda et al., 1999). The activity of the molecule is defined by the IC<sub>50</sub>, the toxin concentration that reduced incorporation of radioactivity by 50% compared with cells that were not treated with toxin.

**Binding Assays.** Binding of anti-Tac(dsFv)-PE38 and its derivatives to the human adult T cell leukemia cell line, HUT102, was analyzed in a displacement assay. Human anti-Tac(HAT)-IgG (Queen et al., 1989) was modified by Bolton-Hunter reagent (Amersham Pharmacia Biotech, Piscataway, NJ) and purified by gel filtration on a PD-10 column (Amersham Pharmacia Biotech). HUT102 cells were plated at 2 × 10<sup>5</sup> cells/well in 96-well plates. Cells were washed with binding buffer (DMEM containing 0.2% BSA). An initial experiment showed that the binding of <sup>125</sup>I-HAT-IgG (specific activity 0.97 mCi/mg) to HUT102 cells reached equilibrium





**Figure 1.** Structural model of anti-Tac(dsFv). The structure was generated by homology modeling. The antigen binding site is located at the top center in this model and is colored green. Lysine residues of anti-Tac(dsFv) are colored red in the ribbon structure and have white labels indicating Kabat numbering.

**Table 1. Accessible Surface Area (ASA) of Lysine Residues in Modeled Anti-Tac Fv**

position	ASA (Å <sup>2</sup> )
VH K13	160.6
VH K19	127.6
VH K23	98.7
VH K38	0.9
VH K62	69.9
VH K64	83.5
VH K66	44.3
VH K73	125.2
VL K18	153.9
VL K39	59.6
VL K45	112.2
VL K103	120.7
VL K107	144.3

by 1.5 h. In the competition studies, various concentrations of unlabeled MAb or immunotoxins were added to these cells in the presence of a fixed concentration of labeled HAT-IgG (1.2 nM). Bound radioactivity was measured in an automated gamma counter.

**Statistical Analysis.** Values are expressed as mean  $\pm$  SD. For comparison between the two experimental groups Student's *t* test was used.  $p < 0.05$  was considered statistically significant.

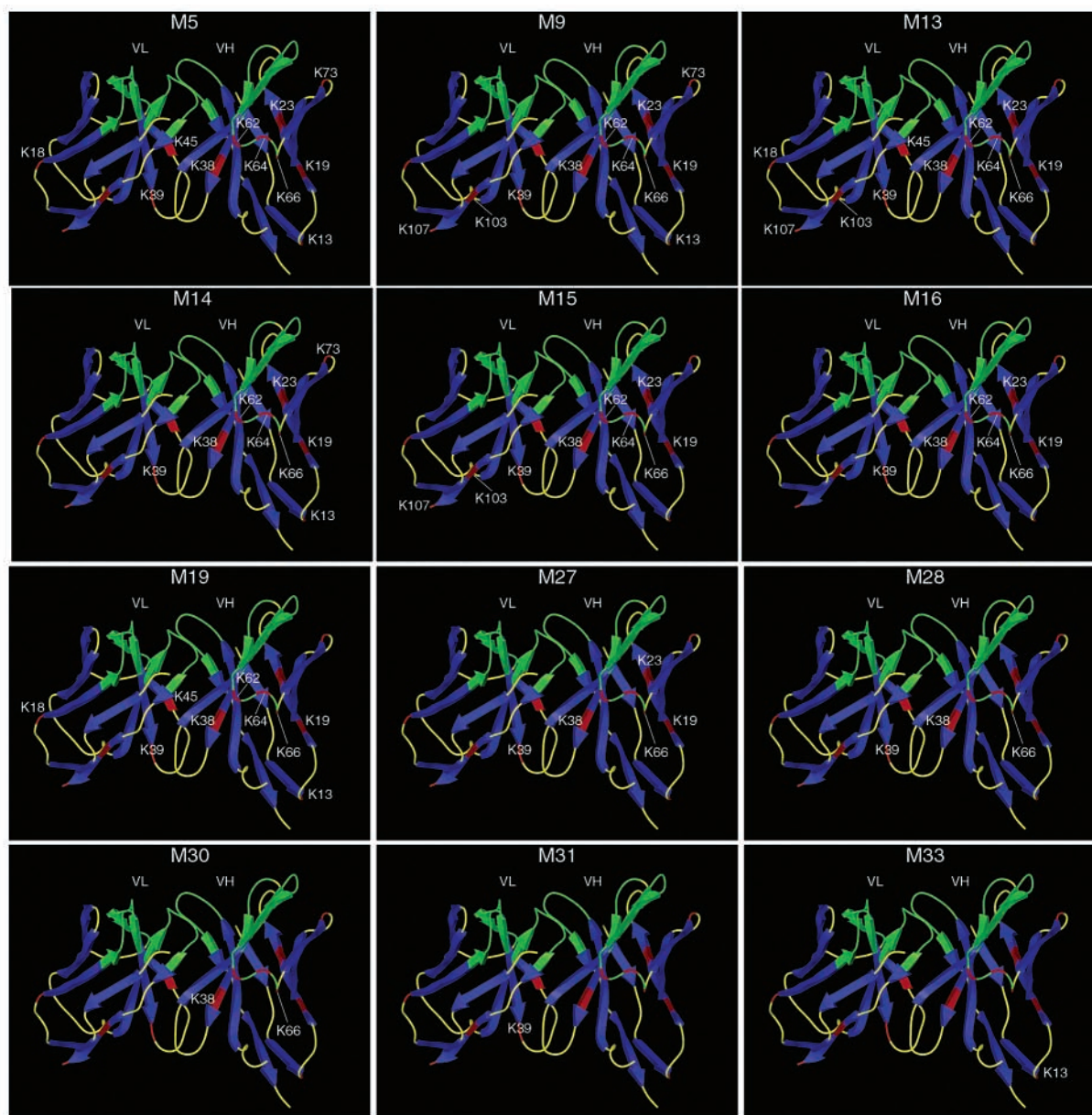
## RESULTS

**Identification of Mutation Sites in the Fv.** To identify residues that could be mutated without affecting protein stability, we have calculated the frequencies at which various amino acids occur at each position of the Fv using the Kabat database, reasoning that replacement of a lysine with an amino acid that also occurs frequently at that position would not decrease protein stability. M1-(dsFv)-PE38 is a mutant of anti-Tac(Fv)-PE38 in which the pI has been lowered from 10.2 to 6.82 by selective mutations of surface residues (Onda et al., 1999). It is less toxic to mice than anti-Tac(Fv)-PE38. Therefore, we decided to use this molecule as a starting point to perform the modifications. M1(dsFv)-PE38 has 16 lysine residues (K): 13 in the Fv and 3 in PE38. We replaced exposed lysines in a stepwise manner. The location of lysine residues in selected mutants is shown in Figures 1 and 2. Because residues on the surface of antibodies tend to be hydrophilic (Chothia et al., 1998), we chose to replace the selected residues with hydrophilic residues using the frequency table shown in Figure 3. For example, K103 in VL is an exposed hydrophilic residue (Table 1).

Because a lysine residue is highly conserved at this position, the frequency table did not suggest a good replacement candidate. In this case, we chose glutamic acid (E), which is hydrophilic. This choice also lowered the pI, which is likely to diminish nonspecific toxicity (Onda et al., 1999). This molecule is named M3(dsFv)-PE38. For the same reasons, we replaced the lysine at position 107 in VL with glutamic acid, producing mutant M4. We then combined the mutations of M3 and M4 into one molecule, which is called M5 (Figure 2). In a similar fashion, M6, M7, and M8 were made by the mutations VL K18Q (glutamine), VL K45Q, and VL R77N (asparagine), respectively. These mutations also reduced the pI of each molecule. Combining the mutations in M6, M7 and M8 produced M9. K13 was the most exposed residue in VH. M10 was made by replacing K13 in VH with E even though E is not common at this position. The change was made to lower the pI. M11 was produced by replacing K73 in VH with aspartic acid (D). K73 in VH was also replaced with N, which is more common than D at this position, to produce M12. All the mutants produced by this approach had full cytotoxic activity (Table 2). M13 contained the mutations present in M10 and M11. M14 contained the mutations present in M3, M4, M6, M7, and M8. We also combined the mutations in M6, M7, M8, M10, and M11 to make M15. M16 contained the mutations in M3, M4, M6, M7, M8, M10, and M11. In M16, the number of lysine residues in the Fv is reduced to 7, and there is no loss of cytotoxic activity (Onda et al., 2001a). To produce M18, K23 in the VH of M1 was replaced with alanine (A), the next most common amino acid at that position. Because M18 and M12 were fully active, we combined their mutations to produce M19.

PE38QQR is a 38 kDa toxin molecule in which lysines 590 and 606 have been replaced with glutamines and lysine 613 with arginine (Debinski and Pastan, 1994). Although PE38QQR does not contain lysine residues, it is still fully active. We combined PE38QQR with M16 Fv, which has seven lysine residues in the Fv, to produce M16(dsFv)-PE38QQR. This molecule retained full cytotoxic activity. Because the pI of M16 Fv is very low (pI = 4.42), we did not select negatively charged residues to replace K. Instead, we replaced K with Q or R to retain hydrophilicity.

K62 and K64 in VH are in the CDR2 of VH. Because these residues could potentially react with antigen, we replaced them with arginines to maintain the positive charge in the M1 background. Both mutants were fully active (Table 2). We then made these mutations in M16-(dsFv)-PE38QQR to make M27, which has five lysines and is fully active. To make M28, we replaced K19 with Q, K23 with A and methionine (M) 20 with leucine (L). Leucine is much more common than methionine at position 20 in the VH, and we speculated this mutation would help stability. M28 has three lysines and is fully active. We then proceeded stepwise to make M30 with two lysines, M31 with one lysine, and M32 with no lysine residues. All were fully active. When we replaced K38 in VH with R, we replaced R40 with T to help the stability of the Fv. Of 669 mouse Fv VH sequences with K at position 38, 62.5% have R at position 40. Of the 727 sequences with R at position 38, none has R at position 40. However, when R occurs at position 38, T occurs 20.9% of the time at position 40. Crystal structures of Fvs containing K38 and R40 show K38 is buried and R40 is partially buried. The side chains of these two residues are in close proximity and are parallel to each other. Replacing K38 with R would cause unfavorable interactions. Therefore, we replaced R40 with T. Also, when we



**Figure 2.** Structural models of anti-Tac(dsFv) mutants. Lysine labels indicate which lysine residues are present in each mutant.

replaced K66 in VH with R, we replaced A67 with F, using similar logic. We restored the lysine residue at position 13 in the VH distant from the CDRs. Presumably K13 might be PEGylated without affecting its ability to bind to CD25 on the cell surface. This molecule is M33-(dsFv)-PE38QQR. Finally, we placed a lysine residue at position 604 of PE38 to make M32(dsFv)-PE38QQR-(604K). This would allow us to PEGylate the carboxyl region of PE38, which is reported to have many B cell epitopes (Roscoe et al., 1994, 1997).

**Expression and Purification of Disulfide Bond-Stabilized Fv Recombinant Immunotoxins.** Mutations were confirmed by DNA sequencing. Recombinant proteins were expressed in *Escherichia coli*, BL21 ( $\lambda$ DE3), where they all accumulated in inclusion bodies. The immunotoxins were purified by our standard protocol, which consists of ion exchange and size exclusion chromatography using renatured inclusion body protein (Onda et al., 1999). Each immunotoxin eluted as a monomer upon TSK gel-filtration chromatography, and each migrated as a single major band of about 63 kDa in SDS-PAGE (Figure 4).

**Cytotoxicity Studies.** The data in Table 2 show the activity of each of the mutant molecules tested on ATAC4 cells, which contain the CD25 antigen. All but two of the mutant immunotoxins had similar cytotoxic activity on target cells. For example, the  $IC_{50}$ s of M1(dsFv)-PE38 and M16(dsFv)-PE38 are  $0.05 \pm 0.01$  and  $0.04 \pm 0.01$  ng/mL, respectively. The  $IC_{50}$ s of M13(dsFv)-PE38 and M15-(dsFv)-PE38 are 0.12 and 0.13 ng/mL, respectively. We have not investigated the reason for the decreased activity of these two molecules. Replacement of the lysine residues in VH CDR2 with arginine did not cause a loss of cytotoxic activity in immunotoxins M27, M28, M30, M31, M32, and M33. Typical cytotoxicity curves from which the  $IC_{50}$ s were calculated are shown in Figure 5A.

Figure 5B shows the activity of each of the mutant molecules tested on OHS cells, which do not express CD25. Each of the mutant molecules tested had no cytotoxic activity on these antigen negative cells, whereas immunotoxin TP3(dsFv)-PE38, which targets an antigen on these cells, is active (Onda et al., 2001b).

**Binding Activity of Immunotoxins.** Figure 6 shows a binding assay in which several different mutant im-



VL	FR1		CDR1	FR2		CDR2	FR3		CDR3	FR4	
	1	2	3	4	5	6	7	8	9	10	
Kabat	12345678901234567890123	456789012345678901234	456789012345678901234	5678901234567890123456	01234567	78901234567					

**Figure 3.** Sequences of Fvs aligned with frequency table. Top, the first sequence is VL of anti-Tac(dsFv). Numbering is according to Kabat. The remaining sequences are the anti-Tac Fv mutants constructed in our laboratory. Below is a table of amino acids sorted into bins according to their frequency in the Kabat database for each position in the framework region. Bottom, corresponding alignments for VHs. Residues shaded in gray indicate mutations made from anti-Tac(dsFv).

munotoxins were analyzed. All the immunotoxins displaced  $^{125}\text{I}$ -labeled human anti-Tac antibody in a similar manner with 50% displacement at 2 nM. This shows that the mutations did not affect binding to CD25. As expected, the bivalent antibody competed somewhat better than the monovalent immunotoxins with 50% displacement at 1 nM. Thus, substituting lysine residues with

other amino acids does not affect binding of the immunotoxin to CD25 positive cells.

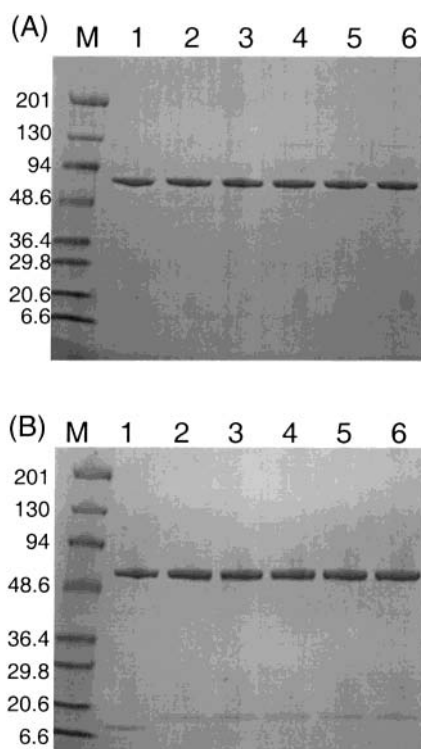
## DISCUSSION

In this work, we describe the design, production, and cytotoxic properties of mutants of recombinant immunotoxin derived from anti-Tac(dsFv)-PE38. These mutants

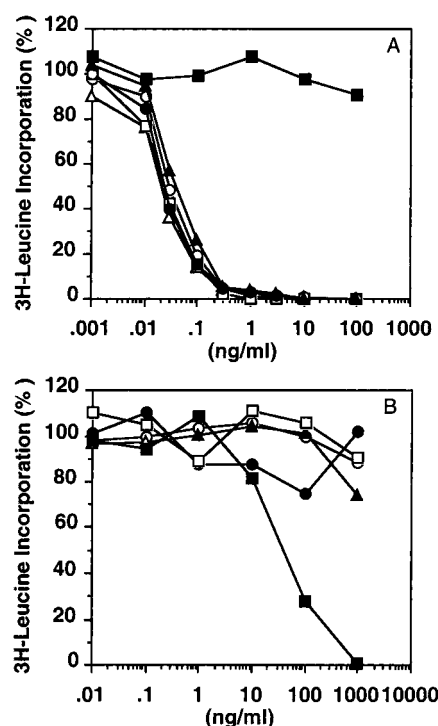


**Table 2. Mutations and Biological Activity of Anti-Tac Immunotoxins**

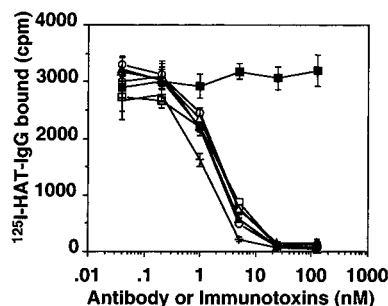
anti-Tac immunotoxin	residues mutated	number of lysine in Fv	number of lysine in whole ITs	IC50 (ng/mL)
M1(dsFv)-PE38		13	16	0.05 ± 0.01
M3(dsFv)-PE38	VL: K103	12	15	0.05 ± 0.01
M4(dsFv)-PE38	VL: K107	12	15	0.05 ± 0.01
M5(dsFv)-PE38	VL: K103, K107	11	14	0.05 ± 0.01
M6(dsFv)-PE38	VL: K18	12	15	0.05 ± 0.01
M7(dsFv)-PE38	VL: K45	12	15	0.05 ± 0.01
M9(dsFv)-PE38	VL: K18, K45, R77	11	14	0.05 ± 0.01
M10(dsFv)-PE38	VH: K13	12	15	0.05 ± 0.01
M11(dsFv)-PE38	VH: K73	12	15	0.05 ± 0.01
M12(dsFv)-PE38	VH: K73	12	15	0.05 ± 0.01
M13(dsFv)-PE38	VH: K13, K73	11	14	0.12 ± 0.03
M14(dsFv)-PE38	VL: K18, K45, K103, K107	9	12	0.06 ± 0.01
M15(dsFv)-PE38	VL: K18, K45, R77 VH: K13, K73	9	12	0.13 ± 0.02
M16(dsFv)-PE38	VL: K18, K45, R77, K103, K107 VH: K13, K73	7	10	0.04 ± 0.01
M16(dsFv)-PE38QQR	VL: K18, K45, R77, K103, K107 VH: K13, K73	7	7	0.04 ± 0.01
M18(dsFv)-PE38	VH: K23	12	15	0.05 ± 0.01
M19(dsFv)-PE38	VL: K103, K107 VH: K23, K73	11	14	0.05 ± 0.01
M27(dsFv)-PE38QQR	VL: K18, K45, R77, K103, K107 VH: K13, K62, K64, K73	5	5	0.04 ± 0.007
M28(dsFv)-PE38QQR	VL: K18, K45, R77, K103, K107 VH: K13, K19, M20, K23, K62, K64, K73	3	3	0.04 ± 0.01
M30(dsFv)-PE38QQR	VL: K18, K39, K45, R77, K103, K107 VH: K13, K19, M20, K23, K62, K64, K73	2	2	0.05 ± 0.01
M31(dsFv)-PE38QQR	VL: K18, K45, R77, K103, K107 VH: K13, K19, M20, K23, K38, R40, K62, K64, K66, A67, K73	1	1	0.03 ± 0.02
M32(dsFv)-PE38QQR	VL: K18, K39, K45, R77, K103, K107 VH: K13, K19, M20, K23, K38, R40, K62, K64, K66, A67, K73	0	0	0.04 ± 0.01
M32(dsFv)-PE38QQR(604K)	VL: K18, K39, K45, R77, K103, K107 VH: K13, K19, M20, K23, K38, R40, K62, K64, K66, A67, K73 PE: 604	0	1	0.05 ± 0.02
M33(dsFv)-PE38QQR	VL: K18, K39, K45, R77, K103, K107 VH: K19, M20, K23, K38, R40, K62, K64, K66, A67, K73	1	1	0.05 ± 0.02



**Figure 4.** SDS-PAGE analysis of purified immunotoxins. The purified proteins were run on 4–20% gradient SDS-PAGE under nonreducing conditions (A) and under reducing conditions (B). The gels were stained with Coomassie Blue. Lane 1, M1-(dsFv)-PE38; lane 2, M16(dsFv)-PE38QQR; lane 3, M27(dsFv)-PE38QQR; lane 4, M32(dsFv)-PE38QQR; lane 5, M32(dsFv)-PE38QQR(604K); lane 6, M33(dsFv)-PE38QQR; M, molecular mass standards are (top to bottom) 201, 130, 94, 48.6, 36.4, 29.8, 20.6, and 6.6 kDa, respectively.



**Figure 5.** In vitro specific cytotoxicity of anti-Tac(dsFv) immunotoxins and TP-3(dsFv)-PE38 on ATAC4 cells (A) and the human osteosarcoma cell line, OHS (B). Various immunotoxins were diluted with 0.2% BSA in DPBS. ATAC4 cells were seeded at  $1.6 \times 10^4$  cells/well in 96-well plates 24 h before the addition of immunotoxin, then incubated at 37 °C for 20 h, and assayed by measuring inhibition of incorporation of  $^3\text{H}$ -Leucine. M1-(dsFv)-PE38 (○), M16(dsFv)-PE38QQR (△), M32(dsFv)-PE38QQR (□), M33(dsFv)-PE38QQR (●), M32(dsFv)-PE38QQR(604K) (▲), and TP3(dsFv)-PE38 (■).



**Figure 6.** Displacement of  $^{125}\text{I}$ -HAT-IgG with anti-Tac(dsFv)-immunotoxins and TP-3(dsFv)-PE38 using HUT102 cell line, which expresses CD25 but not TP-3 antigen. Triplicate sample values were averaged and the standard deviation was calculated for each data point. M1(dsFv)-PE38 (○), M16(dsFv)-PE38QQR (△), M32(dsFv)-PE38QQR (□), M33(dsFv)-PE38QQR (■), M32(dsFv)-PE38QQR(604K) (▲), TP3(dsFv)-PE38 (●), and HAT-IgG (+).

differ in the number of lysines they contain. Almost all the immunotoxins were fully cytotoxic to ATAC4 cells and retained their affinity for CD25. The aim of this study was to show it was possible to diminish the number of lysine residues without losing biological function. Anti-Tac(dsFv)-PE38 has a total of 16 lysines. There are three lysines in PE38. The other 13 are in the Fv (Figure 1). Two of these lysines are in CDR2 of VH and could contribute to binding. We used the frequencies of residues at specific locations in the Fv to construct these mutants. For replacement, we chose hydrophilic residues because these are frequently present on the surface of proteins (Debinski and Pastan, 1994). The final molecule is M32-(dsFv)-PE38QQR. It has no lysine residues yet has completely retained its cytotoxic activity and antigen-binding activity.

Having established that we could produce an active immunotoxin without lysines and that it is fully active, we inserted lysine residues at positions that should minimally interfere with immunotoxin function. One is at VH K13, which is distant from the CDRs of the Fv. The other is at position 604 of PE38, a region previously shown to be highly immunogenic (Roscoe et al., 1994).

We applied our strategy to another molecule. We could remove all lysine residues from SS1(dsFv)-PE38 without losing biological activity (Beers et al., unpublished data). We are also trying to apply our strategy to another protein. We believe that our approach has an ability to be generalized.

In summary, we show that all lysine residues can be removed from anti-Tac(dsFv)-PE38 and that lysine residues can be introduced at new and potentially useful sites in the immunotoxin without loss of activity. The next paper in this series will describe the properties of immunotoxins modified by site specific PEGylation.

#### ACKNOWLEDGMENT

We especially thank Drs. Satoshi Nagata and Kenneth Santora for helpful discussions. We also thank Anna Mazzuca for expert editorial assistance.

#### LITERATURE CITED

- (1) Bailon, P., and Berthold, W. (1998) Polyethylene glycol-conjugated pharmaceutical proteins. *Pharm. Sci. Technol. Tox.* 1, 352–356.
- (2) Bera, T. K., Kennedy, P. E., Berger, E. A., Barbas, C. F. III and Pastan, I. (1998) Specific killing of HIV infected lymphocytes by a recombinant immunotoxins directed against the HIV1 envelope glycoprotein. *Mol. Med.* 4, 384–391.

- (3) Brinkmann, U., Pai, L. H., FitzGerald, D. J., Willingham, M., and Pastan, I. (1991) B3(Fv)-PE38KDEL, a single chain immunotoxins that causes complete regression of a human carcinoma in mice. *Proc. Natl. Acad. Sci. U.S.A.* 88, 8616–8620.
- (4) Chaffee, S., Mary, A., Stiehm, E. R., Girault, D., Fischer, A., and Hershfield, M. S. (1992) IgG antibody response to polyethylene glycol-modified adenosine deaminase in patients with adenosine deaminase deficiency. *J. Clin. Invest.* 89, 1643–1651.
- (5) Chothia, C., Gelfand, I., and Kister, A. (1998) Structural determinants in the sequences of immunoglobulin variable domain. *J. Mol. Biol.* 278, 457–479.
- (6) Chowdhury, P. S., Viner, J. L., Beers, R., and Pastan, I. (1998) Isolation of a high affinity stable single chain Fv specific for mesothelin from DNA-immunized mice by phage display and construction of a recombinant immunotoxin with anti-tumor activity. *Proc. Natl. Acad. Sci. U.S.A.* 95, 669–674.
- (7) Debinski, W., and Pastan, I. (1994) An immunotoxin with increased activity and homogeneity produced by reducing the number of lysine residues in recombinant *Pseudomonas* exotoxin. *Bioconjugate Chem.* 5, 40–46.
- (8) Hermanson, G. T. (1996) The chemistry of reactive groups. In *Bioconjugate Techniques*, pp 137–168, Academic Press, San Diego.
- (9) Katre, N. V., Knauf, M. J., and Laird, W. J. (1987) Chemical modification of recombinant interleukin 2 by polyethylene glycol increases its potency in the murine Meth A sarcoma model. *Proc. Natl. Acad. Sci. U.S.A.* 84, 1487–1491.
- (10) Kitamura, K., Takahashi, T., Takashina, K., Yamaguchi, T., Noguchi, A., Tsurumi, H., Toyokuni, T., and Hakomori, S. (1990) Polyethylene glycol modification of the monoclonal antibody A7 enhances its tumor localization. *Biochem. Biophys. Res. Commun.* 171, 1387–1394.
- (11) Kreitman, R. J., and Pastan, I. (1995) Targeting *Pseudomonas* exotoxin to hematologic malignancies. *Semin. Cancer Biol.* 6, 297–306.
- (12) Kreitman, R. J., Wilson, W. H., Robbins, D., Margulies, I., Stetler-Stevenson, M., Waldmann, T. A., and Pastan, I. (1999) Responses in refractory hairy cell leukemia to a recombinant immunotoxins. *Blood* 94, 3340–3348.
- (13) Kreitman, R. J., Wilson, W. H., White, J. D., Stetler-Stevenson, M., Jaffe, E. S., Giardina, S., Waldmann, T. A., and Pastan, I. (2000) Phase I trial of recombinant immunotoxins anti-Tac(Fv)-PE38 (LMB-2) in patients with hematologic malignancies. *J. Clin. Oncol.* 18, 1622–1636.
- (14) Kreitman, R. J., Wilson, W. H., Bergeron, K., Raggio, M., Stetler-Stevenson, M., FitzGerald, D. J., and Pastan, I. (2001) Efficacy of the anti-CD22 recombinant immunotoxins BL22 in chemotherapy-resistant Hairy-cell leukemia. *N. Engl. J. Med.* 345, 241–247.
- (15) Kunkel, T. A. (1985) Rapid and efficient site-specific mutagenesis without phenotypic selection. *Proc. Natl. Acad. Sci. U.S.A.* 82, 488–492.
- (16) Mansfield, E., Amlot, P., Pastan, I., and FitzGerald, P. (1997) Recombinant RFB4 immunotoxins exhibit potent cytotoxic activity for CD22-bearing cells and tumors. *Blood* 80, 2020–2026.
- (17) Nicholls, A., Sharp, K., and Honig, B. (1991) Protein folding and association: insights from the interfacial and thermodynamic properties of hydrocarbons. *Proteins: Struct. Funct. Genet.* 11, 281–296.
- (18) Onda, M., Kreitman, R. J., Vasmatzis, G., Lee, B., and Pastan, I. (1999) Reduction of the nonspecific animal toxicity of anti-Tac(Fv)-PE38 by mutations in the framework regions of the Fv which lower the isoelectric point. *J. Immunol.* 163, 6072–6077.
- (19) Onda, M., Willingham, M., Wang, Q. C., Kreitman, R. J., Tsutsumi, Y., Nagata, S., and Pastan, I. (2000) Inhibition of TNF- $\alpha$  produced by Kupffer cells protects against the non-specific liver toxicity of immunotoxins anti-Tac(Fv)-PE38, LMB-2. *J. Immunol.* 165, 7150–7156.
- (20) Onda, M., Nagata, S., Tsutsumi, Y., Vincent, J. J., Wang, Q., Kreitman, R. J., Lee, B., and Pastan, I. (2001a) Lowering the isoelectric point of the Fv portion of recombinant immu-

- notoxins leads to decreased nonspecific animal toxicity without affecting antitumor activity. *Cancer Res.* 61, 5070–5077.
- (21) Onda, M., Olafsen, T., Tsutsumi, Y., Bruland, Ø. S., and Pastan, I. (2001b) Cytotoxicity of antiosteosarcoma recombinant immunotoxins composed of TP-3 Fv fragments and a truncated *Pseudomonas* exotoxin A. *J. Immunother.* 24, 144–150.
- (22) Pai-Scherf, L., Villa, J., Pearson, D., Watson, T., Liu, E., Willingham, M. C., and Pastan, I. (1999) Hepatotoxicity in cancer patients receiving erb-38 a recombinant immunotoxins that targets the erbB2 receptor. *Clin. Cancer Res.* 5, 2311–2315.
- (23) Pastan, I. (1997) Targeted therapy of cancer with recombinant immunotoxins. *Biochim. Biophys. Acta: Rev. Cancer* 1333, C1–C6.
- (24) Peitsch, M. C. (1996) ProMod and Swiss-Model: Internet-based tools for automated comparative protein modeling. *Biochem. Soc. Trans.* 24, 274–279.
- (25) Pyatak, P. S., Abuchowski, A., and Davis, F. F. (1980) Preparation of a polyethylene glycol:superoxide dismutase adduct, and an examination of its blood circulation life and anti-inflammatory activity. *Res. Commun. Chem. Pathol. Pharmacol.* 29, 113–127.
- (26) Queen, C., Schneider, W. P., Slick, H. E., Payne, P. W., Landolfi, N. F., Duncan, J. F., Avdalovic, N. M., Levitt, M., Junghans, R. P., and Waldmann, T. A. (1989) A humanized antibody that binds to the interleukin 2 receptor. *Proc. Natl. Acad. Sci. U.S.A.* 86, 10029–10033.
- (27) Reiter, Y., Brinkmann, U., Jung, S. H., Lee, B., Kasprzyk, P. G., King, C. R., and Pastan, I. (1994) Improved binding and antitumor activity of a recombinant anti-erbB2 immunotoxins by disulfide stabilization of the Fv fragment. *J. Biol. Chem.* 269, 18327–18331.
- (28) Roscoe, D. M., Jung, S. H., Benhar, I., Pai, L., Lee, B. K., and Pastan, I. (1994) Primate antibody response to immunotoxins: serological and computer-aided analysis of epitopes on a truncated form of *Pseudomonas* exotoxin. *Infect. Immunol.* 62, 5055–5065.
- (29) Roscoe, D. M., Pai, L. H., and Pastan, I. (1997) Identification of epitopes on a mutant form of *Pseudomonas* exotoxin using serum from humans treated with *Pseudomonas* exotoxin containing immunotoxins. *Eur. J. Immunol.* 27, 1459–1468.
- (30) Shraake, A., and Rupley, J. (1973) Environment and exposure to solvent of protein atoms. Lysozyme and insulin. *J. Mol. Biol.* 79, 351–371.
- (31) Tsutsumi, Y., Onda, M., Nagata, S., Lee, B., Kreitman, R. J., and Pastan, I. (2000) Site-specific chemical modification with polyethylene glycol of recombinant immunotoxins anti-Tac(Fv)-PE38 (LMB-2) improves antitumor activity and reduces animal toxicity and immunogenicity. *Proc. Natl. Acad. Sci. U.S.A.* 97, 8548–8553.
- (32) Wang, Q. C., Pai, L. H., Debinski, W., FitzGerald, D. J., and Pastan, I. (1993) Polyethyleneglycol-modified chimeric toxin composed of transforming growth factor alpha and *Pseudomonas* exotoxin. *Cancer Res.* 53, 4588–4594.

BC020069R



# TECHNICAL NOTES

## Synthesis and Characterization of Covalently Linked Single-Stranded DNA Oligonucleotide–Dendron Conjugates

Stephen A. Bell,<sup>†</sup> Megan E. McLean,<sup>†</sup> Sang-Keun Oh,<sup>†</sup> Shane E. Tichy,<sup>†</sup> Wen Zhang,<sup>†</sup> Robert M. Corn,<sup>‡</sup> Richard M. Crooks,<sup>\*,†,§</sup> and Eric E. Simanek<sup>\*,†,||</sup>

Department of Chemistry, Texas A&M University, P.O. Box 30012, College Station, Texas 77842-3012 and Department of Chemistry, University of Wisconsin, Madison, Wisconsin 53706. Received September 25, 2002; Revised Manuscript Received November 14, 2002

A solution-phase synthesis and characterization of covalent DNA–dendron conjugates is presented. Thiol-terminated 12-base oligonucleotides were added to second- and third-generation triazine-based dendrons via thiol/disulfide exchange chemistry. Single-stranded DNA oligonucleotides were successfully attached to dendrons at the core, the periphery, and both. Proof of structure for these architectures is derived primarily from mass spectrometry and polyacrylamide gel electrophoresis and complemented by labeling analysis using Ellman's reagent and degradation analysis using a reducing agent.

### INTRODUCTION

We report the solution-phase synthesis and characterization of covalent DNA–dendron conjugates. Using thiol/disulfide exchange chemistry, thiol-terminated 12-base oligonucleotide sequences were added to second- and third-generation triazine-based dendrons. The synthesis permits either one or two single-stranded DNA (ssDNA) oligonucleotides to be covalently attached to the dendron at the core, the periphery, or both (Scheme 1). Proof of structure for these architectures is derived primarily from mass spectrometry, polyacrylamide gel electrophoresis, labeling analysis using Ellman's reagent (1), and degradation analysis with a reducing agent.

The use of DNA constructs in DNA-machines (2–5), DNA-computing (6), antisense therapy (7–9), and biosensors (4, 10, 11) has fueled intense research into suitable methods for immobilizing DNA on surfaces (12, 13) and preparing soluble DNA–nanoparticle assemblies (7, 14–17). Most of the latter applications rely on nanoparticle modification with multiple copies of ssDNA oligonucleotides of a particular sequence. For example, multiple ssDNA oligonucleotides have been attached to soluble organic polymers (18) and gold nanoparticles (19). However, methods for covalent attachment of individual ssDNA oligonucleotides to soluble nanoparticles are surprisingly rare (7). Synthetic methods that provide a means for conjugating precise numbers of identical or different ssDNA oligonucleotides to particular locations on nanoparticles could allow for simultaneous probing of multiple target oligonucleotides or for constructing interesting, new recursive materials. If such materials

also provide a means for attaching additional active components, such as fluorescent or electrochemical tags, their usefulness would be further increased.

The scaffolds used for these experiments were derived from melamine-based dendrimers, which were synthesized using methods similar to those we previously reported (20). These dendrimers offer opportunities for appending precise numbers of reactive groups to the periphery and the core. For the present work, dendrons incorporate reactive thiopyridyl groups (Scheme 2), which could subsequently undergo exchange with appropriately functionalized DNA oligonucleotides. Disulfide-terminated oligonucleotides were reduced to yield thiol-terminated ssDNA.

### EXPERIMENTAL SECTION

**Chemicals.** Reagent grade chloroform, dichloromethane, methanol, and ethyl acetate were used without further purification during dendrimer synthesis. Tetrahydrofuran (THF) was dried over 4 Å molecular sieves prior to use. Deuterated solvents were used as supplied by Cambridge Isotope Laboratories (Cambridge, MA). Cyanuric chloride (98%), diisopropylethylamine (DIPEA, 99%), and piperazine (99+%) were used as received from Acros (Pittsburgh, PA). Immobilized tris(carboxyethyl)-phosphine (TCEP) and succinimidyl 3-(2-pyridylthio)-propionate (SPDP) were used as purchased from Pierce Chemical (Rockford, IL). Electrophoresis grade acrylamide:bisacrylamide (29:1), ethidium bromide (1% solution), and coomassie blue R250 were used as received from FisherBiotech (Pittsburgh, PA). Trisborate EDTA (0.45 M) and 10× DNA gel loading buffer were purchased from Eppendorf (Hamburg, Germany). Molecule 7 (20) and cysteamine hydrochloride (21) were synthesized according to literature procedures.

**Synthesis of 1.** BOC-NHCH<sub>2</sub>(CH<sub>2</sub>OCH<sub>2</sub>)<sub>3</sub>CH<sub>2</sub>NH<sub>2</sub> (1.77 g, 6.05 mmol) in THF (15 mL) was added dropwise to a cooled (–6 °C), stirred THF solution (30 mL) of cyanuric

\* To whom correspondence should be addressed.

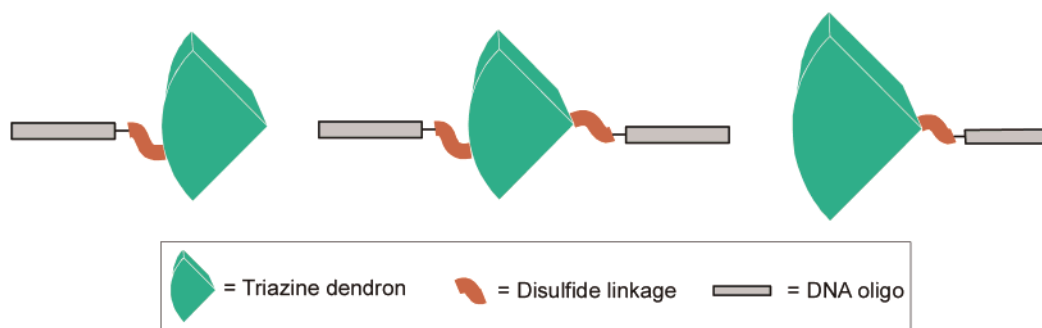
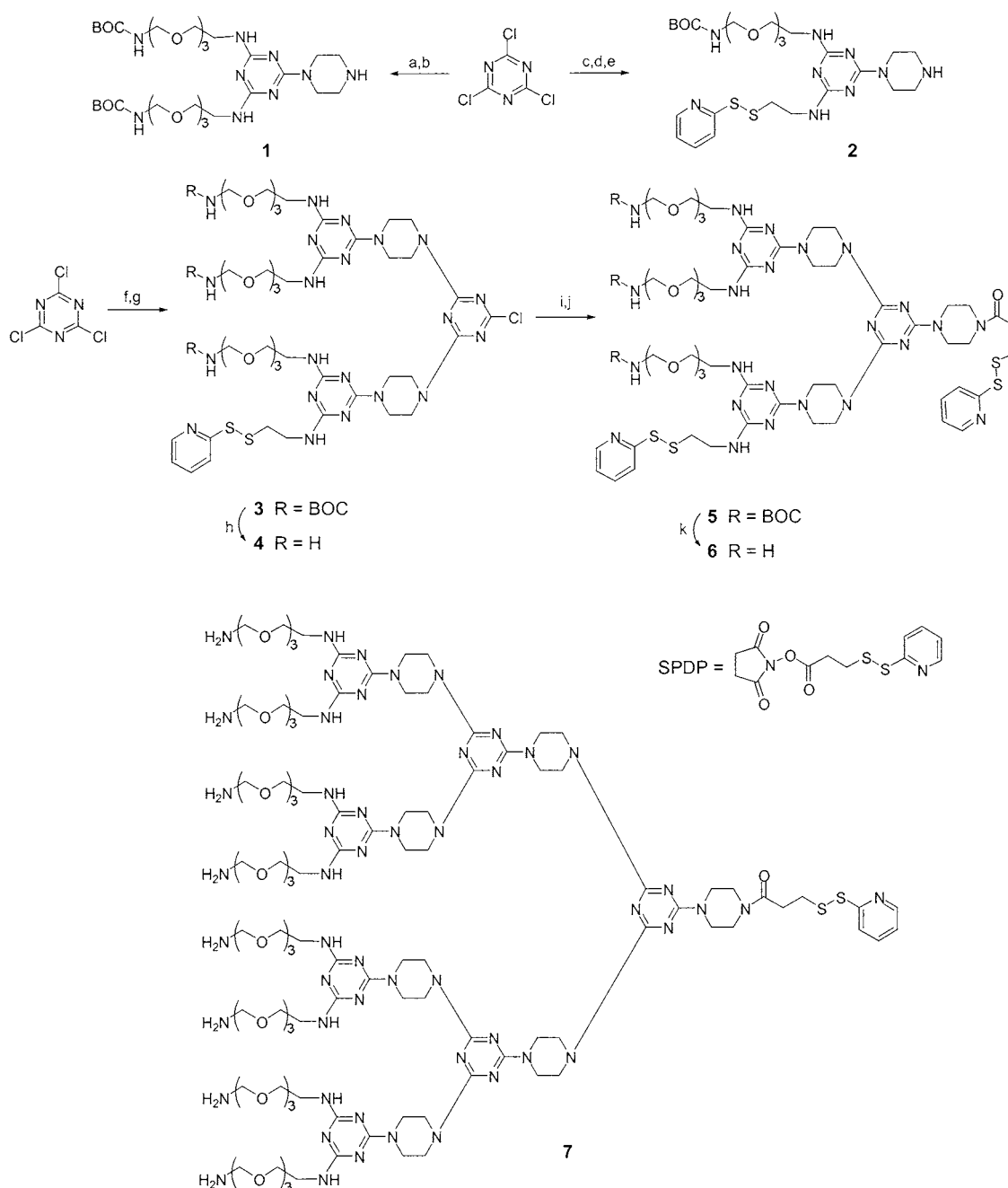
<sup>†</sup> Texas A&M University.

<sup>‡</sup> University of Wisconsin.

<sup>§</sup> Phone 979-845-5629; fax 979-845-1399; e-mail crooks@tamu.edu.

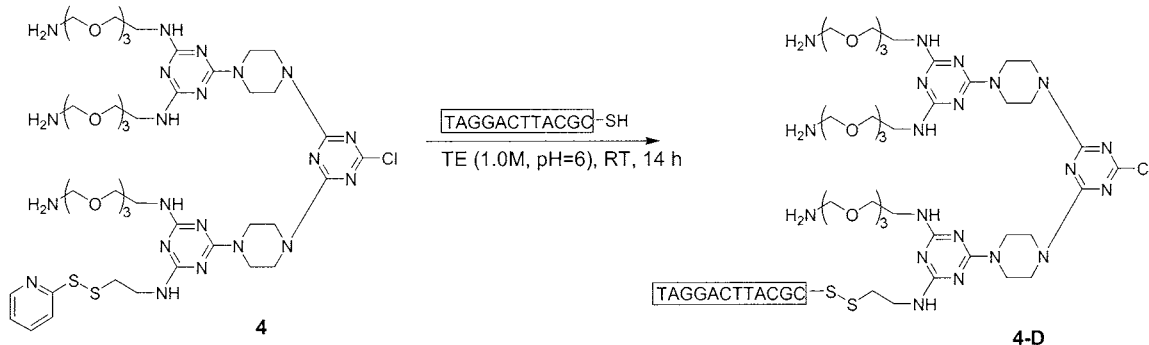
<sup>||</sup> Phone 979-845-4242; fax 979-845-9452; e-mail simanek@tamu.edu.

Scheme 1


 Scheme 2<sup>a</sup>


<sup>a</sup> (a) 2 equiv of BocNHCH<sub>2</sub>(CH<sub>2</sub>OCH<sub>2</sub>)<sub>3</sub>CH<sub>2</sub>NH<sub>2</sub>, DIPEA, THF, RT, 14 h; (b) piperazine, DIPEA, RT, 14 h; (c) BocNHCH<sub>2</sub>(CH<sub>2</sub>OCH<sub>2</sub>)<sub>3</sub>CH<sub>2</sub>NH<sub>2</sub>, DIPEA, THF, -6 °C, 2 h; (d) pyridyl-S-S-CH<sub>2</sub>CH<sub>2</sub>-NH<sub>2</sub>, DIPEA, THF, RT, 14 h; (e) piperazine, DIPEA, RT, 14 h; (f) **1**, DIPEA, THF, -6 °C; (g) **2**, DIPEA, THF, RT, 14 h; (h) trifluoroacetic acid (TFA), CH<sub>2</sub>Cl<sub>2</sub> (1:1), 10 h, RT; (i) piperazine, DIPEA, RT, 14 h; (j) SPDP, DIPEA, THF, RT, 24 h; (k) TFA:CH<sub>2</sub>Cl<sub>2</sub> (1:1), 10 h, RT.

## Scheme 3



chloride (0.581 g, 3.17 mmol) and DIPEA (1.5 mL, 4.84 mmol). After 2 h the reaction mixture was warmed to room temperature, and more DIPEA (1.5 mL, 4.84 mmol) was added. Stirring for 14 h at room-temperature resulted in a pale yellow solution with white precipitate, yielding a single TLC spot ( $R_f = 0.65$ .) Piperazine (1.64 g, 19.02 mmol) and DIPEA (1.5 mL, 4.84 mmol) were added, and the mixture was stirred for 14 h at room temperature. After removal of solvent, the residue was partitioned between  $\text{CH}_2\text{Cl}_2$  and water. The organic phases were concentrated to yield a pale yellow oil which was purified via silica gel column chromatography (100:3,  $\text{CH}_2\text{Cl}_2$ :MeOH eluent). A pale yellow oil was obtained (0.123 g, 82.3%).  $^1\text{H}$  NMR (300 MHz,  $\text{CD}_3\text{OD}$ )  $\delta$  3.72 (tr, 4H,  $\text{NCH}_2$ ), 3.62 (m, 24H,  $\text{CH}_2\text{OCH}_2$ ), 3.49 (tr, 4H,  $\text{C}(\text{O})\text{NHCH}_2\text{CH}_2$ ), 3.20 (tr, 4H,  $\text{NHCH}_2\text{CH}_2$ ), 2.79 (br, 4H,  $\text{HNCH}_2$ ), 1.42 (s, 18H,  $\text{OC}(\text{CH}_3)_3$ ).  $^{13}\text{C}$  NMR (75 MHz,  $\text{CD}_3\text{OD}$ )  $\delta$  166.2, 165.0, 157.1, 78.9, 70.4, 53.9, 43.7, 43.0, 40.4, 27.8; MALDI-TOF ( $m/z$ ):  $[\text{M} + \text{H}]^+$  calcd. for  $\text{C}_{33}\text{H}_{63}\text{N}_9\text{O}_{10}$ , 746.5; found, 746.8.

**Synthesis of 2.** BOC-NHCH<sub>2</sub>(CH<sub>2</sub>OCH<sub>2</sub>)<sub>3</sub>CH<sub>2</sub>NH<sub>2</sub> (1.39 g, 4.75 mmol) in THF (10 mL) was added dropwise to a cooled ( $-6^\circ\text{C}$ ), stirred solution of cyanuric chloride (0.908 g, 4.95 mmol) and DIPEA (3.3 mL, 9.82 mmol) in THF (30 mL). After 2 h the reaction mixture was warmed to room temperature, and more DIPEA (1.5 mL, 4.84 mmol) was added, followed by a THF solution (15 mL) of neutralized pyridyl cysteamine hydrochloride (1.10 g, 4.95 mmol). Stirring for 14 h at room-temperature resulted in a pale yellow solution with white precipitate, yielding a single TLC spot ( $R_f = 0.58$ .) A 6-fold excess of piperazine (2.55 g, 29.7 mmol) and DIPEA (1.5 mL, 4.84 mmol) was added, and the mixture was stirred for 14 h at room temperature. After removal of solvent, the residue was partitioned between  $\text{CH}_2\text{Cl}_2$  and water. The organic phases were concentrated to yield a pale yellow oil which was purified via silica gel column chromatography (100:3,  $\text{CH}_2\text{Cl}_2$ :MeOH eluent). A pale yellow oil was obtained (1.56 g, 49%).  $^1\text{H}$  NMR (300 MHz,  $\text{CD}_3\text{OD}$ )  $\delta$  8.2 (tr, 1H,  $\alpha\text{-CH}$ ), 7.75 (m, 2H,  $m\text{-CH}$ ), 7.2 (tr, 1H,  $p\text{-CH}$ ), 3.75 (br, 4H,  $\text{NCH}_2$ ), 3.63 (m, 12H,  $\text{CH}_2\text{OCH}_2$ ), 3.50 (tr, 4H,  $\text{C}(\text{O})\text{NHCH}_2\text{CH}_2$  and  $\text{NCH}_2\text{CH}_2\text{S}$ ), 3.21 (tr, 2H,  $\text{NHCH}_2\text{CH}_2$ ), 3.02 (tr, 2H,  $\text{NCH}_2\text{CH}_2\text{S}$ ), 2.82 (br, 4H,  $\text{NHCH}_2$ ), 1.43 (s, 9H,  $\text{OC}(\text{CH}_3)_3$ ).  $^{13}\text{C}$  NMR (75 MHz,  $\text{CD}_3\text{OD}$ )  $\delta$  167.6, 166.1, 161.2, 150.1, 139.2, 122.6, 121.2, 80.2, 71.4, 49.9, 46.3, 44.5, 41.4, 40.8, 39.6, 28.9; MALDI-TOF ( $m/z$ ):  $[\text{M} + \text{H}]^+$  calcd for  $\text{C}_{27}\text{H}_{45}\text{N}_9\text{O}_5\text{S}_2$ , 640.3; found, 640.4.

**Synthesis of 3.** Dendron 1 (0.601 g, 0.807 mmol) was dissolved in 15 mL of THF and added dropwise to a cooled ( $-6^\circ\text{C}$ ), stirred solution THF solution (30 mL) of cyanuric chloride (0.148 g, 0.807 mmol) and DIPEA (1.5 mL, 4.84 mmol). After 2 h the reaction mixture was warmed to room temperature, and more DIPEA (1.5 mL, 4.84 mmol)

was added, followed by a THF solution (15 mL) of **2** (0.505 g, 0.807 mmol). Stirring for 14 h at room-temperature resulted in a pale yellow solution with white precipitate. After removal of solvent, the residue was partitioned between  $\text{CH}_2\text{Cl}_2$  and water. The organic phases were concentrated to yield a pale yellow oil which was purified via silica gel column chromatography (100:3,  $\text{CH}_2\text{Cl}_2$ :MeOH eluent). A white, sticky solid was obtained (0.86 g, 71.2% yield).  $^1\text{H}$  NMR (300 MHz,  $\text{CD}_3\text{OD}$ )  $\delta$  8.2 (m, 1H,  $\alpha\text{-CH}$ ), 7.78 (m, 2H,  $m\text{-CH}$ ), 7.19 (tr, 1H,  $p\text{-CH}$ ), 3.75 (br, 16H,  $\text{NCH}_2$ ), 3.62 (m, 36H,  $\text{CH}_2\text{OCH}_2$ ), 3.50 (br, 8H,  $\text{C}(\text{O})\text{NHCH}_2\text{CH}_2$  and  $\text{NCH}_2\text{CH}_2\text{S}$ ), 3.22 (m, 6H,  $\text{NCH}_2$ ), 3.04 (tr, 2H,  $\text{NCH}_2\text{CH}_2\text{S}$ ), 1.43 (s, 27H,  $\text{OC}(\text{CH}_3)_3$ );  $^{13}\text{C}$  NMR (75 MHz,  $\text{CD}_3\text{OD}$ )  $\delta$  169.5, 166.1, 165.0, 164.4, 160.0, 157.0, 150.0, 137.8, 121.1, 119.8, 78.9, 71.2, 70.2, 43.5, 42.9, 40.3, 27.9. MALDI-TOF ( $m/z$ ):  $[\text{M} + \text{H}]^+$  calcd for  $\text{C}_{63}\text{H}_{10}\text{N}_{21}\text{O}_9\text{S}_2$ , 1495.5; found, 1495.8.

**Synthesis of 4.** Dendron 3 (0.86 g, 0.57 mmol) was reacted with 85% trifluoroacetic acid (TFA, 3 mL) for 14 h (1:1 TFA: $\text{CH}_2\text{Cl}_2$ ). A pale yellow oil was obtained after solvent evaporation (0.81 g, 94.2%).  $^1\text{H}$  NMR (300 MHz,  $\text{CD}_3\text{OD}$ )  $\delta$  8.12 (m, 1H,  $\alpha\text{-CH}$ ), 7.82 (m, 2H,  $m\text{-CH}$ ), 7.45 (tr, 1H,  $p\text{-CH}$ ), 3.84 (br, 14H,  $\text{NCH}_2$ ), 3.78 (br, 6H,  $\text{NH}_2\text{CH}_2\text{CH}_2$ ), 3.65 (m, 36H,  $\text{CH}_2\text{OCH}_2$ ), 3.22 (m, 6H,  $\text{N-CH}_2$ ), 3.04 (tr, 2H,  $\text{NHCH}_2\text{CH}_2\text{S}$ );  $^{13}\text{C}$  NMR (75 MHz,  $\text{CD}_3\text{OD}$ )  $\delta$  166.1, 165.0, 164.4, 157.0, 150.0, 137.8, 121.1, 119.8, 71.2, 70.2, 43.5, 42.9, 40.3. NMR Spectra are in Supporting Information. MALDI-TOF ( $m/z$ ):  $[\text{M} + \text{H}]^+$  calcd for  $\text{C}_{48}\text{H}_{82}\text{ClN}_{21}\text{O}_9\text{S}_2$ , 1196.6; found, 1196.6.

**Synthesis of 5.** Dendron 3 (0.100 g, 0.17 mmol), piperazine (0.072 g, 1.40 mmol), DIPEA (0.160 mL, 1.4 mmol), and THF (15 mL) were heated at  $70^\circ\text{C}$  for 14 h in a sealed, thick-walled reaction vessel. After removal of solvent, the residue was partitioned between  $\text{CH}_2\text{Cl}_2$  and water. The organic phases were concentrated to yield a pale yellow oil which was purified via silica gel column chromatography (20:1,  $\text{CH}_2\text{Cl}_2$ :MeOH eluent). A pale yellow oil was obtained (42 mg, 35.3%). The oil was stirred at room temperature with THF (10 mL), DIPEA (0.25 mL, 0.807 mmol), and SPDP (9.0 mg, 0.029 mmol). After removal of solvent, the residue was partitioned between  $\text{CH}_2\text{Cl}_2$  and water. The organic phases were concentrated to yield a pale, yellow oil which was purified via column chromatography (100:5,  $\text{CH}_2\text{Cl}_2$ :MeOH eluent) yielded an off-white viscous oil.  $^1\text{H}$  NMR (300 MHz,  $\text{CD}_3\text{OD}$ )  $\delta$  8.37 (m, 2H,  $\alpha\text{-CH}$ ), 7.77 (m, 4H,  $\text{meta-CH}$ ), 7.16 (tr, 2H,  $p\text{-CH}$ ), 3.68 (br, 24H,  $\text{NCH}_2$ ), 3.59 (m, 48H,  $\text{CH}_2\text{OCH}_2$ ), 3.48 (tr, 2H,  $\text{C}(\text{O})\text{NHCH}_2\text{CH}_2\text{S}$ ), 3.21 (tr, 10H,  $\text{NHCH}_2$ ), 3.04 (tr, 2H,  $\text{C}(\text{O})\text{NHCH}_2\text{CH}_2\text{S}$ ), 1.41 (s, 27H,  $\text{OC}(\text{CH}_3)_3$ ).  $^{13}\text{C}$  NMR (75 MHz,  $\text{CD}_3\text{OD}$ )  $\delta$  171.2, 166.2, 165.9, 161.6, 158.0, 149.8, 122.1, 120.9, 119.2, 80.1, 71.5, 71.2, 71.1, 44.2, 41.3, 36.2, 33.8, 31.9, 28.9. MALDI-TOF ( $m/z$ ):  $[\text{M} + \text{H}]^+$  calcd for  $\text{C}_{75}\text{H}_{122}\text{N}_{24}\text{O}_{16}\text{S}_4$ , 1743.7; found, 1743.7.

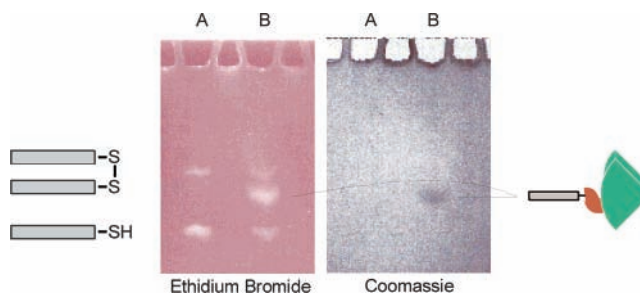


**Synthesis of 6.** Dendron 5 (100 mg, 0.069 mmol) was deprotected with TFA (1:1 TFA:CH<sub>2</sub>Cl<sub>2</sub>), yielding a sticky yellow oil (32 mg, 75.6%). <sup>1</sup>H NMR (300 MHz, CD<sub>3</sub>OD)  $\delta$  8.48 (d, 1H, *o*-CH<sub>a</sub>), 8.40 (d, 1H, *o*-CH<sub>b</sub>), 7.98 (m, 2H, *m*-CH<sub>a</sub>), 7.88 (m, 2H, *m*-CH<sub>b</sub>), 7.39 (tr, 1H, *p*-CH<sub>a</sub>), 7.25 (tr, 1H, *p*-CH<sub>b</sub>), 3.85 (br, 24H, N-CH<sub>2</sub>), 3.67 (m, 48H, CH<sub>2</sub>OCH<sub>2</sub>), 3.56 (tr, 2H, C(O)NHCH<sub>2</sub>CH<sub>2</sub>), 3.13 (tr, 10H, NHCH<sub>2</sub>), 2.92 (tr, 2H, C(O)CH<sub>2</sub>CH<sub>2</sub>S); <sup>13</sup>C NMR (75 MHz, CD<sub>3</sub>OD)  $\delta$  170.5, 165.5, 162.4, 158.0, 149.4, 138.0, 121.1, 120.0, 119.9, 115.1, 70.3, 70.2, 70.0, 68.7, 66.7, 43.9, 42.8, 40.4, 39.4, 34.1, 32.2. NMR spectra are in Supporting Information. MALDI-TOF (*m/z*): [M + H]<sup>+</sup> calcd for C<sub>60</sub>H<sub>98</sub>N<sub>24</sub>O<sub>10</sub>S<sub>4</sub>, 1443.5; found, 1443.7.

**DNA Conjugation.** All solvents and reagents used in DNA reactions were spectroscopic grade. Water, methanol, and acetonitrile were further purified by filtration through a 0.22  $\mu$ m filter. Disulfide-modified oligonucleotides were purchased from Trilink Biotechnologies (San Diego, CA). The lyophilized powders were dissolved in UV/UF purified (Barnstead) water [0.1 OD/ $\mu$ L]. The fluorescently labeled oligo 5'-(Oregon Green 514)-TAGGACTTACGC-(C3-thiol), and nonlabeled 12mer 5'-TAGGACTTACGC-(C3-thiol) (referred to as DNA<sub>a</sub>), were deprotected on immobilized TCEP (2-carboxyethylphosphine) for 15 min at room temperature and eluted with two volumes of TBE (45 mM Tris-borate, 1 mM EDTA) pH 8.3 buffer. The use of other buffers, including tris(hydroxymethyl) aminomethane buffer at pH 6.0 and 7.4, did not elute the DNA from the resin. In a typical conjugation, deprotected Oregon-Green labeled 12-mer [2.5 OD, 25  $\mu$ L H<sub>2</sub>O] was incubated with thiopyridyl-containing dendron 7 (41.8 nmol, 0.05 mg). After 12 h at room temperature the reaction was stopped, yielding the corresponding disulfide conjugated DNA-dendrimer. MALDI-TOF (*m/z*): [M + H]<sup>+</sup> calcd for DNA-dendron, 7-D, 7227.4; found, 7227.6.

**MALDI-TOF.** An overlayer preparation was used with a 2,4,6-trihydroxyacetophenone (THAP) matrix (22). A 1:1:1 mixture of 1  $\mu$ M aqueous reaction mixture, 10 mg/mL THAP matrix in methanol, and 15 mg/mL aqueous ammonium citrate was spotted in 1  $\mu$ L aliquots on a bed of THAP matrix. The analyte-doped matrix crystals were washed repeatedly (~5–15 times) with 5  $\mu$ L of cold water to remove alkali metals. MALDI-TOF mass spectra were acquired in positive- and negative-ion mode on a Voyager-DE STR mass spectrometer (Applied Biosystems, Framingham, MA) equipped with a pulsed nitrogen laser emitting at 337 nm. Samples were analyzed in linear mode using a delayed extraction time of 550 ns and an accelerating voltage of 20 kV. The laser light intensity was adjusted to provide the optimal signal-to-noise ratio. All spectra were the result of signal averaging 50–100 laser shots. Positive-ion mass calibrations were performed internally with the [M + 2H]<sup>2+</sup>, [M + H]<sup>+</sup>, and [2M + H]<sup>+</sup> ions of insulin (bovine). Negative-ion calibrations were performed externally with the [M - H]<sup>-</sup> and the [2M - H]<sup>-</sup> ions of DNA<sub>a</sub>. Mass spectra for 4, 6, 7, 6-D, 6-D<sub>2</sub>, and 7-D can be found in the Supporting Information.

**Gel Electrophoresis.** Polyacrylamide gels (20%) were prepared according to a standard protocol (23). Gels were run between 70 and 80 V for 2–3 h. The sample buffer was 0.25% bromophenol blue and 40% (w/v) sucrose in water. Samples were prepared by adding 0.1 volume of running buffer to each dendron and conjugate solution. The running buffer was TBE (90 mM Tris-Borate, 2 mM EDTA). Ethidium bromide and Coomassie Brilliant Blue R250 were used for staining and visualization.



**Figure 1.** PAGE gels visualized by differential staining with ethidium bromide and Coomassie Brilliant Blue R-250. Lanes A contain DNA-thiol only, and lanes B covalently linked 4-D. Removal of ethidium bromide, followed by staining with Coomassie Brilliant Blue R250 resulted in the second gel.

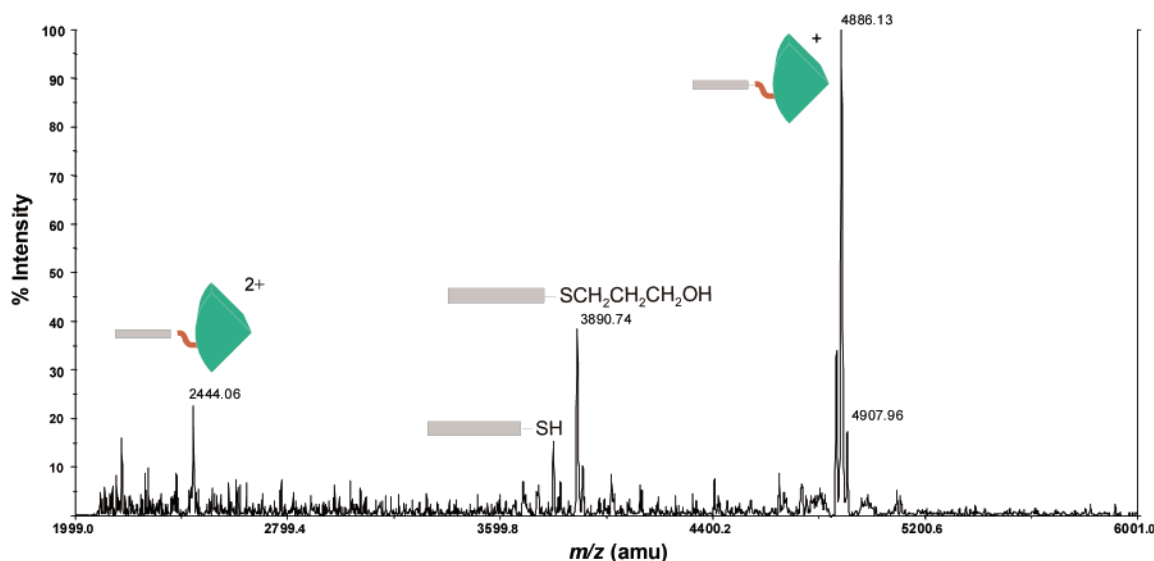
## RESULTS AND DISCUSSION

The objectives of this paper are to present a synthetic approach for synthesizing DNA-dendrimer constructs and then to prove unambiguously that the DNA linkage to the dendrimer is covalent rather than electrostatic. Electrostatic complexes between DNA and dendrimers have been reported previously (16). The motivation for using cationic dendrimers stems from both the high water solubility that these groups afford, and the opportunity for electrostatic binding between the DNA and dendrimeric reactants, which may be useful for enhancing the rate of covalent bond formation between the two species.

Dendron synthesis reactions proceed cleanly and in high yields to give products that are readily purified by chromatography. All intermediates and products give satisfactory <sup>1</sup>H and <sup>13</sup>C NMR spectra and the appropriate parent ion by mass spectrometry. The two disulfides of 6 are not spectroscopically equivalent, as evidenced by the five relevant pyridyl peaks in the <sup>1</sup>H NMR (Supporting Information), indicating a subtle difference in the chemical environment of these groups.


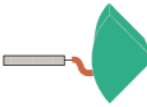



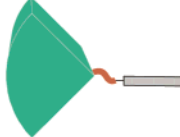
To conjugate DNA to the dendrons, the disulfide-terminated oligonucleotides were first reduced using tris(2-carboxyethyl)phosphine (TCEP) in a trisborate EDTA (TBE) buffer (pH 8.3) to yield thiol-terminated ssDNA. Addition of this DNA to aqueous solutions of dendrons yielded the DNA-dendron conjugates upon thiol-disulfide exchange (Scheme 3).

To distinguish between covalent attachment and electrostatic association (16), the products were characterized using polyacrylamide gel electrophoresis (PAGE) and matrix-assisted laser desorption/ionization – time-of-flight (MALDI-TOF) mass spectrometry (24). These DNA-dendron architectures (and the associated ssDNA starting materials) proved to be too small for agarose gel analysis. Instead, 20% polyacrylamide gels allowed successful separation of the initial G2-dendron, the ssDNA, and the DNA-dendron products (Figure 1). Column B of the gel shown in Figure 1 corresponds to the reaction of 4 with a deprotected 12-base oligonucleotide, in which we expect to make 4-D. This gel was stained with ethidium bromide, which stains DNA but not the dendrons used in this study. Starting from the bottom of the gel in column B, the three bands correspond to unreacted DNA-thiol, DNA-dendron conjugate (4-D, Scheme 1), and a disulfide-coupled DNA dimer. To confirm these assignments, we ran a gel using a solution nominally containing only DNA-thiol (Column A). The two bands present in this control experiment correspond to DNA-thiol and the anticipated DNA dimer, which is produced by oxidation of two DNA-thiol oligonucleotides to a DNA-S-S-DNA disulfide.



**Figure 2.** MALDI-TOF mass spectrum of **4-D**. Peaks at 4886.13 and 2444.06 correspond to the  $[M + H]^+$  and  $[M + 2H]^{2+}$  ions of **4-D**, and 3890.7 is the  $[M + H]^+$  for DNA not deprotected by TCEP but with subsequent loss of the dimethoxytrityl ether.

**Table 1**

Reagents	Mass <sup>a</sup>	Products	Mass
 <b>4</b>	1196.6 (1196.6)	 <b>4-D</b>	5561.76 (5561.97) <sup>b</sup> 4886.1 (4886.1) <sup>c</sup>
 <b>6</b>	1443.7 (1443.7)	 <b>6-D<sub>2</sub></b>	10172.8 (10171.1)
 <b>7</b>	2862.7 (2862.6)	 <b>7-D</b>	7227.4 (7227.6)

<sup>a</sup> Expected parent ion masses ( $m/z$ ) shown (observed molecular weight in parentheses); <sup>b</sup> Internal calibration shows only a 36 ppm error in mass accuracy. <sup>c</sup> Same oligonucleotide sequence, but not functionalized with Oregon-Green dye.

The band assignments were further confirmed by staining with Coomassie Brilliant Blue R250, which stains the dendrons used in this study but not DNA (25). As shown in Column B, only the middle band, corresponding to the DNA-dendron, is visible. In contrast, the bands in Column A, corresponding to the DNA-thiol control experiment, are not stained. The data in Figure 2 shows the presence of the DNA-dendron conjugate,  $[M + H]^+ = 4886.1$  and  $[M + H]^{2+} = 2444.1$ , along with a small amount of  $[M + H]^+ = 3890.7$ , which corresponds to DNA not deprotected by the original TCEP reduction with subsequent loss of dimethoxytrityl ether. We at-

tribute the absence of a band corresponding to the cationic dendron to the inability of these charged species to enter the polyacrylamide gel (they would migrate toward the cathode).

Table 1 provides MALDI-TOF mass spectrometry data for the key reagents and products prepared for this study. Importantly, the molecular weights for **4-D**, **6-D**, **6-D<sub>2</sub>**, and **7-D** correspond with the calculated masses for these DNA-dendron conjugates. As indicated previously, there are two potential linking motifs for the DNA-dendrons: electrostatic and covalent. The mass difference between these two adducts is only 2 Da. Nevertheless, it was

possible to distinguish between these two possible products using accurate-mass mass analysis. With bovine insulin as an internal calibrant ( $[M + H]^+ = 5734.39$ ), the measured molecular weight of **4-D** was 5561.97. This compared with the expected  $[M + H]^+$  of 5561.76, corresponding to an error of only 36 ppm. An electrostatic adduct ( $[M + H]^+ = 5563.85$ ) would have a much larger mass error of 200 ppm. The same mass spectrometry technique was used to confirm the covalent addition of one and two ssDNA oligonucleotides to **6** to yield **6-D** and **6-D<sub>2</sub>**, respectively.

In addition to mass spectrometry, Ellman's test (for free thiol) was used to distinguish between covalent and electrostatic attachment of DNA to the dendrons. Ellman's reagent oxidizes free thiols to mixed nitrobenzyl disulfides, which are easily identifiable by mass spectrometry. No Ellman's adduct was observed for **4-D**. Addition of a reducing agent, TCEP, to **4-D** led to disappearance of the mass spectral signal for the DNA-dendron conjugate, confirming covalent addition of DNA to the dendron.

## SUMMARY AND CONCLUSIONS

In summary, we have outlined a general synthesis for covalent DNA-dendron conjugates. These materials were subjected to rigorous characterization. We are currently investigating hybridization and enzymatic manipulation of these DNA-dendron conjugates.

## ACKNOWLEDGMENT

We gratefully acknowledge DARPA (Contract No. F30602-01-2-0555) for full financial support of this work. We also thank our collaborators Prof. Anne Condon (U. British Columbia), Prof. Robert Hamers (U. Wisconsin), and Prof. Lloyd Smith (U. Wisconsin) for stimulating discussions.

**Supporting Information Available:** NMR spectra and MALDI-TOF mass spectra. This material is available free of charge via the Internet at <http://pubs.acs.org>.

## LITERATURE CITED

- (1) Kuwata, K., Uebori, M., Yamada, K., and Yamazaki, K. (1982) Liquid chromatographic determination of alkylthiols via derivatization with Ellman's reagent. *Anal. Chem.* **54**, 1082–1087.
- (2) Shchepinov, M. S., Mir, K. U., Elder, J. K., Frank-Kamenetskii, M. D., and Southern, E. M. (1999) Oligonucleotide dendrimers: stable nano-structures. *Nucl. Acid. Res.* **27**, 3035–3041.
- (3) Nilsen, T. W., Grayzel, J., and Prenskey, W. (1997) Dendritic nucleic acid structures. *J. Theor. Biol.* **187**, 273–284.
- (4) Capaldi, S., Getts, R. C., and Jayasena, S. D. (2000) Signal amplification through nucleotide extension and excision on a dendritic DNA platform. *Nucl. Acid. Res.* **28**, e21.
- (5) Yan, H., Zhang, X. P., Shen, X. Y., and Seeman, N. C. (2002) A robust DNA mechanical device controlled by hybridization topology. *Nature* **415**, 62–65.
- (6) Frutos, A. G., Smith, L. M., and Corn, R. M. (1998) Enzymatic ligation reactions of DNA "words" on surfaces for DNA computing. *J. Am. Chem. Soc.* **120**, 10277–10282.
- (7) Francis, M. B., Goh, S. L., Prasad, D., Padilla De Jesus, O. L. P., and Fréchet, J. M. J. (2001) DNA-dendrimer conjugates for drug delivery. *Polym. Mater. Sci. Eng.* **84**, 12–13.
- (8) Bielinska, A. U., Chen, C., Johnson, J., and Baker, J. R., Jr. (1999) DNA complexing with polyamidoamine dendrimers: Implication for transfection. *Bioconjugate Chem.* **10**, 843–850.
- (9) Gebhart, C. L., and Kabanov, A. V. (2001) Evaluation of polyplexes as gene transfer agents. *J. Controlled Release* **73**, 401–416.
- (10) Taton, T. A., Mirkin, C. A., and Letsinger, R. L. (2000) Scanometric DNA array detection with nanoparticle probes. *Science* **289**, 1757–1760.
- (11) Stears, R. L., Getts, R. C., and Gullans, S. R. (2000) A novel, sensitive detection system for high-density microarrays using dendrimer technology. *Physiol. Genom.* **3**, 93–99.
- (12) Smith, E. A., Wanat, M. J., Cheng, Y. F., Barreira, S. V. P., Frutos, A. G., and Corn, R. M. (2001) Formation, spectroscopic characterization, and application of sulfhydryl-terminated alkanethiol monolayers for the chemical attachment of DNA onto gold surfaces. *Langmuir* **17**, 2502–2507.
- (13) Frutos, A. G., Brockman, J. M., and Corn, R. M. (2000) Reversible protection and reactive patterning of amine- and hydroxyl-terminated self-assembled monolayers on gold surfaces for the fabrication of biopolymer arrays. *Langmuir* **16**, 2192–2197.
- (14) Kabanov, V. A., Sergeyev, V. G., Pyshkina, O. A., Zinchenko, A. A., Zevin, A. B., Joosten, J. G. H., Brackman, J., and Yoshikawa, K. (2000) Interpolyelectrolyte complexes formed by DNA and Astramol poly(propylene imine) dendrimers. *Macromolecules* **33**, 9587–9593.
- (15) Choi, J. S., Joo, D. K., Kim, C. H., Kim, K., and Park, J. S. (2000) Synthesis of a barbell-like triblock copolymer, poly(l-lysine) dendrimer-*block*-poly(ethylene glycol)-*block*-poly(l-lysine) dendrimer, and its self-assembly with plasmid DNA. *J. Am. Chem. Soc.* **122**, 474–480.
- (16) Ottaviani, M. F., Furini, F., Casini, A., Turro, N. J., Jockuch, S., Tomalia, D. A., and Messori, L. (2000) Formation of supramolecular structures between DNA and starburst dendrimers studied by EPR, CD, UV, and melting profiles. *Macromolecules* **33**, 7842–7851.
- (17) Reynolds, R. A., III, Mirkin, C. A., and Letsinger, R. L. (2000) Homogeneous, nanoparticle-based quantitative colorimetric detection of oligonucleotides. *J. Am. Chem. Soc.* **122**, 3795–3796.
- (18) Watson, K. J., Park, S.-J., Im, J.-H., Nguyen, S. T., and Mirkin, C. A. (2001) DNA-block copolymer conjugates. *J. Am. Chem. Soc.* **123**, 5592–5593.
- (19) Niemeyer, C. M. (2001) Nanoparticles, proteins, and nucleic acids: biotechnology meets material science. *Angew. Chem., Int. Ed.* **40**, 4128–4158.
- (20) Zhang, W., Nowlan, D. T., III, Thomson, L. M., Lackowski, W. M., and Simanek, E. E. (2001) Orthogonal, convergent syntheses of dendrimers based on melamine with one or two unique surface sites for manipulation. *J. Am. Chem. Soc.* **123**, 8914–8922.
- (21) Ebright, Y. W., Chen, Y., Pendergast, P. S., and Ebright, R. H. (1992) Incorporation of an EDTA-metal complex at a rationally selected site within a protein – application to EDTA-iron DNA affinity cleaving with catabolite gene activator protein (CAP) and CRO. *Biochemistry* **31**, 10664–10670.
- (22) Pielles, U., Zuercher, W., Schaer, M., and Moser, H. E. (1993) Matrix-assisted laser desorption ionization time-of-flight mass-spectrometry. A powerful tool for the mass and sequence-analysis of natural and modified oligonucleotides. *Nucl. Acid. Res.* **21**, 3191–3196.
- (23) Sambrook, J., Fritsch, E. F., and Maniatis, T. (1989) *Molecular Cloning*. Cold Spring Harbor Press, 2nd ed.; New York, Vol. 1.
- (24) Karas, M., and Hillenkamp, F. (1988) Laser desorption ionization of proteins with molecular masses exceeding 10000 Daltons. *Anal. Chem.*, **60**, 2299–2301.
- (25) Brothers, H. M., Piehler, L. T., and Tomalia, D. A. (1998) Slab-gel and capillary electrophoretic characterization of polyamidoamine dendrimers. *J. Chromatogr. A* **814**, 233–246.

BC020075N



# Simultaneous Lipidation of a Characterized Peptide Mixture by Chemoselective Ligation

Line Bourel-Bonnet,\* Dominique Bonnet, Frédéric Malingue, Hélène Gras-Masse, and Oleg Melnyk\*

UMR 8525 CNRS-Université de Lille 2-Institut Pasteur de Lille, Institut de Biologie de Lille,  
1 rue du Pr. Calmette, BP 245, 59021 Lille, France. Received September 24, 2002;  
Revised Manuscript Received November 12, 2002

The modification of a peptide antigen by a fatty acid such as palmitic acid is now recognized as a mean to induce cellular responses. Mixtures of lipopeptides, obtained by combining individually synthesized compounds, were shown to be promising synthetic vaccine candidates. Usually, in lipopeptide synthesis, the fatty acyl moiety is introduced on the crude peptide chain using solid-phase methods. The separation of the target compound from impurities by RP-HPLC is often complicated by the amphiphilic properties of lipopeptides and results in low overall yields. To overcome the difficulties associated with lipopeptide synthesis and mixture preparation, we have developed a method where the fatty acyl moiety is site-specifically and collectively introduced in solution onto a mixture of individually prepurified peptides. The lipidation is based on the quasistoichiometric and high-yielding ligation of a glyoxylyl lipid with hydrazinoacetyl peptides. The hydrazone constructs were prepared in a salt-free medium and could be isolated by direct lyophilization of the reaction mixture. This process is compatible with cysteinyl peptides, and no aggregation nor degradation could be observed.

## INTRODUCTION

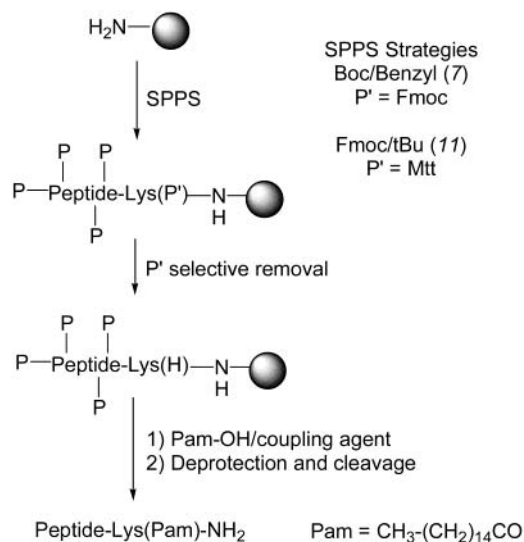
Synthetic vaccines composed of multiepitopic lipopeptides were found to induce virus-specific T-cell responses in primates (1–3) or in humans (4). Recently, the tolerance and the immunogenicity of 6 HIV-1-derived synthetic lipopeptides used in a phase I clinical trial confirmed the potential of this approach (5).

Peptides can be easily modified by a palmitoyl group using standard solid-phase protocols as shown in Scheme 1 (6–8). An orthogonally protected lysine residue is inserted during the peptide assembly. Selective removal of the protecting group P' is followed by acylation with a palmitic acid activated ester. Peptide deprotection and cleavage afford the crude lipopeptide which is then purified by preparative RP-HPLC.

The main limitation of this approach is the last RP-HPLC purification step, which is often tricky due to the generally low solubility of lipopeptides and to the line broadening induced by the fatty acid chain. Thus, not surprisingly, the major difficulty encountered during lipopeptides production is associated with the preparative RP-HPLC steps. Since the separation of the target compound from the byproducts can be achieved only with a limited column loading, a considerable part of the labor cost is devoted to the repetition of the chromatographic runs. The overall yields are generally modest for lab-scale productions (~10% at 10–100 mg scale) and much lower on a 1 g scale (<1%) (9).

In search for a novel process for the synthesis of lipopeptide mixtures, we premised that most of the above-mentioned problems could be overcome by setting the purification efforts before the lipidation step. The consequence of this strategy was to design a high-yielding

## Scheme 1. Lipopeptide Synthesis Using Standard SPPS



lipidation method, using stoichiometric conditions, compatible with diverse peptide structures, and in particular cysteine-containing peptides, so as to suppress the need for a second resolutive purification. Finally, a collective one-pot lipidation of all the vaccine constituents would skip the difficulties associated with the resolubilization and handling of each individual lipopeptide before the mixing step.

The lipidation strategy presented in scheme 2 and based on the formation of an  $\alpha$ -oxo hydrazone linkage between  $\alpha$ -hydrazinoacetyl peptides 1 and glyoxyl derivative 2 was found to fulfill all these specifications.

In this paper, we report the synthesis of several  $\alpha$ -hydrazinoacetyl peptides derived from the Simian immunodeficiency virus (SIV) and their collective conver-

\* Corresponding authors. E-mail: line.bourel@ibl.fr, oleg.melnik@ibl.fr. Telephone: 00 33 (0)3 20 87 12 18. Fax: 00 33 (0)3 20 87 12 33.

sion into lipopeptides using a salt-free medium and quasi-stoichiometric conditions. We show that the experimental conditions for  $\alpha$ -oxo hydrazone formation is compatible with cysteinyl peptides. The lipidation was found to be robust during scaling-up (from 15 to 150 mg) and easily followed by RP-HPLC.

## EXPERIMENTAL PROCEDURES

**Chemicals.** All Fmoc protected L-amino acids Asn(Trt), Asp(Ot-Bu), Arg(Pbf), Cys(Trt), Gln(Trt), Glu(Ot-Bu), His(Trt), Lys(Boc), Lys(Mtt), Ser(*t*-Bu), Thr(*t*-Bu), Trp(Boc), and Tyr(*t*-Bu) were purchased from Novabiochem (France Biochem, Meudon, France). HBTU<sup>1</sup> was from Senn Chemicals (Dielsdorf, Switzerland). PAL-PEG-PS resin was from Applied Biosystems (Warrington, UK). Amino-PEGA resin was from Novabiochem. Chemicals were from Sigma-Aldrich (St-Quentin Fallavier, France). *N,N,N*-tri(*tert*-butyloxycarbonyl)-hydrazinoacetic acid is commercially available at Novabiochem.

**Hydrazinoacetyl Peptide Synthesis.** Preparation of Resin **5**. 17.24 g (3.0 mmol) of Fmoc-PAL-PEG-PS resin (0.174 mmol/g) was deprotected using 20% piperidine in DMF. Fmoc-L-Lys(Mtt)-OH (7.5 g, 12 mmol) was coupled using 1 equiv/2 equiv PyBop/DIEA activation in 25 mL of NMP (1 h). After capping with 25 mL of 3/0.3/96.7 Ac<sub>2</sub>O/DIEA/DMF for 10 min, the Mtt group was removed with 1/99 TFA/CH<sub>2</sub>Cl<sub>2</sub> by vol as described elsewhere (16). *N,N,N*-Tri(*tert*-butyloxycarbonyl)-hydrazinoacetic acid **4** (1.41 g, 3.6 mmol) was coupled to the  $\epsilon$ -amino group using 1 equiv/2 equiv PyBop/DIEA in 10 mL of DMF (1 h) (10). The coupling was monitored using the TNBS test (11). The resin was washed successively with DMF, CH<sub>2</sub>Cl<sub>2</sub>, and Et<sub>2</sub>O and dried under vacuum. Loading (UV quantification of the dibenzofulvene-piperidine adduct): 0.153 mmol/g.

**Hydrazino Acetyl Peptide Synthesis 1a–h.** Syntheses were performed on a 0.1 mmol scale using standard Fmoc/*t*-Bu protocols (12–13) on a Pioneer synthesizer (Applied Biosystems, Warrington, U.K.). The couplings were performed using 10 equiv of amino acid and 10 equiv/10 equiv/30 equiv TBTU/HOBt/DIEA activation in DMF (simple couplings). Cleavage and deprotection by TFA in the presence of the appropriate scavengers (peptides **1a,b**, TFA/TIS/H<sub>2</sub>O (95/2.5/2.5 by vol); peptides **1c,d**, TFA/EDT/H<sub>2</sub>O (95/2.5/2.5 by vol); peptides **1e–g**, TFA/EDT/thioanisole/H<sub>2</sub>O/phenol (10/0.25/0.5/0.5/0.75 v/v/v/v/v)) for 2 h was followed by precipitation in cold Et<sub>2</sub>O. The crude materials were washed with Et<sub>2</sub>O, centrifuged, redissolved in aqueous acetic acid, and lyophilized. Purification was performed by preparative RP-HPLC, C3 Zorbax column, 15 × 350 mm. Eluent A, TFA 0.05% by vol in H<sub>2</sub>O; eluent B, 40/60/0.05 *n*-propanol/H<sub>2</sub>O/TFA by vol (peptides **1a–c** and **1f–h**) or 40/60/0.05 propan-2-ol/H<sub>2</sub>O/TFA by vol (peptides **1d–e**). Identity was controlled by ES-MS on a Micromass Quattro spectrometer (see Supporting Information). Purity was controlled by RP-HPLC (C18 Vydac column, 4.6 × 250 mm, same eluents as above) and CZE (Applied Biosystems 270A-HT: 30 kV, 200 nm, 45 °C, injection 1.5 s, citric acid 20 mM, pH 2.1 for peptides **1a–c** and **1g–h** or sodium borate 50 mM, pH 9.2 for **1d–f**). Quantitative amino acid analysis was performed after total acid hydrolysis in evacuated sealed tubes with 10/1 6N HCl/phenol by vol at 110 °C for 24 h (see Supporting Information).

**General Ligation Procedure.** Preparation of the  $\alpha$ -Hydrazinoacetyl Peptide **1a–g** Mixture. 55 mg of each peptide was solubilized separately in 3 mL of water. The solutions were pooled, and the resulting mixture was lyophilized (370.2 mg, 85.14  $\mu$ mol of total net hydrazinoacetyl peptides, calculated  $\alpha$ -hydrazinoacetyl net content of the mixture using the peptides net content of **1a–g** = 0.23 mmol/g).

**Ligation.** The reaction was performed under argon atmosphere at 30 °C in a 50 mL round-bottom flask containing Ø5 mm glass beads. 156 mg of the **1a–g** peptide mixture (35.8  $\mu$ mol) was moistened with 1.4 mL of degassed distilled water to give a viscous gel. 14.6 mg of **2** (39.5  $\mu$ mol) dissolved in 26.3 mL 2-methyl-propan-2-ol was added dropwise under vigorous stirring. After 6 h, the reaction was diluted with 73 mL of water and lyophilized. Mixture **3a–g** was obtained as a white powder.

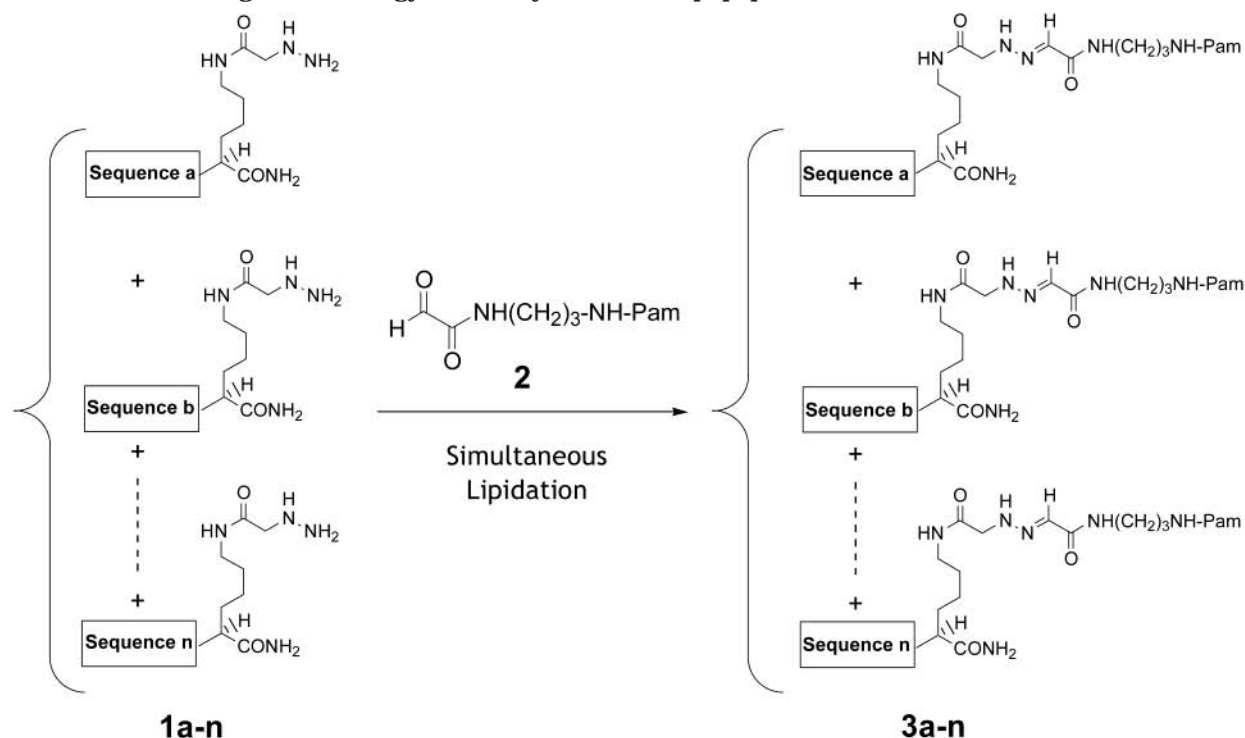
**RP-HPLC Monitoring.** The mixture was analyzed using a C3 Zorbax column (300 Å, 5  $\mu$ m, 4.6 × 300 mm), flow rate 1 mL/min, 50 °C. Eluent A: 0.05% TFA by vol in water; eluent B, *n*-propanol/H<sub>2</sub>O/TFA: 40/60/0.05 by vol Gradient: 0–100% B in 30 min, 100% B for 5 min, detection at 215 nm.

**LC-MS Analysis.** Under the same chromatographic conditions, with 1:5 effluent splitting to give a flow rate of about 40  $\mu$ L/min into the electrospray nebulizer, ion mass spectra were recorded on a simple-quadrupole mass spectrometer API I (Perkin-Elmer Sciex) equipped with an ion-spray source (Sciex, Toronto, Canada). Potential of the spray needle: +4.5 kV. Orifice voltage: 60 kV.

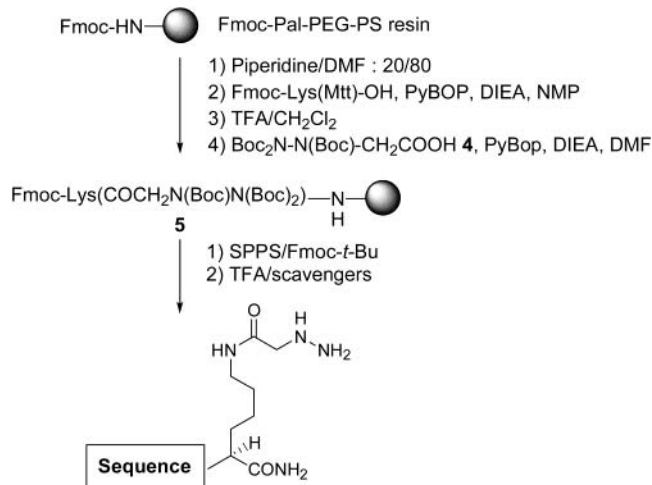
## RESULTS AND DISCUSSION

**Synthesis of  $\alpha$ -Hydrazinoacetyl Peptides.** The  $\alpha$ -hydrazinoacetyl peptides examined in this study were related to a project devoted to the development of a synthetic vaccine against HIV. We had to prepare a mixture of eight lipopeptides whose sequences are derived from the Nef and Gag proteins encoded by the Simian immunodeficiency virus (5) (sequences **a–g**) and a potent T-epitope derived from tetanus toxin (sequence **h**). In short, a strong and broad cross-clade cytotoxic T-lymphocytes recognition against highly conserved Gag-specific epitopes as well as multiple T-helper proliferate response have been well documented in both vaccinated animals and HIV-infected individuals (14–15). Epitopes from other nonstructural regulatory proteins, such as Nef, which is among the first to be expressed in the viral life, have been selected as important components of a candidate vaccine too.

<sup>1</sup>Abbreviations: BHT, 2,6-di-*tert*-butyl-4-methylphenol; Boc, *tert*-butyloxycarbonyl; BOP, benzotriazole-1-yl-oxy-tris-(dimethylamino)-phosphonium hexafluorophosphate; *Clt*, *Clostridium tetani*; CZE, capillary zone electrophoresis; DBU, 1,8-diazabicyclo[5.4.0]undec-7-ene; DIEA, diisopropylethylamine; DMAP, 4-*N,N*-(dimethylamino)pyridine; DMF, *N,N*-dimethylformamide; DMSO, dimethyl sulfoxide; EDT, ethanedithiol; ES-MS, electrospray mass spectrometry; equiv, equivalent; Fmoc, 9-fluorenylmethoxycarbonyl; HBTU, *N*-[1H-(benzotriazol-1-yl)-(dimethylamino)methylene]-*N*-methyl methanaminium hexafluorophosphate *N*-oxide; HOBt, *N*-hydroxybenzotriazole; IPT, isopropylidene tartrate; Mtt, 4-methyltrityl; NMP, *N*-methylpyrrolidone; Pam, palmitoyl; Pbf, 2,2,4,6,7-pentamethyldihydrobenzofuran-5-sulfonyl; PEGA, copolymer of *N,N*-dimethylacrylamide and mono-2-acrylamidoprop-1-yl-[2-aminoprop-1-yl]-poly(ethylene glycol) reticulated with bis 2-acrylamidoprop-1-yl poly(ethylene glycol); PyBop, benzotriazole-1-yl-oxy-tris-pyrrolidinophosphonium hexafluorophosphate; SIV, simian immunodeficiency virus; *t*-Bu, *tert*-butyl; TCEP, *tris*-(2-carboxyethyl)-phosphine hydrochloride; TBTU, *N*-[1H-(benzotriazol-1-yl)-(dimethylamino)methylene]-*N*-methyl methanaminium tetrafluoroborate *N*-oxide; TFA, trifluoroacetic acid; TIS, triisopropylsilane; TNBS, 2,4,6-trinitrobenzenesulfonic acid; TT, tetanus toxin.

**Scheme 2. Chemical Ligation Strategy for the Synthesis of Lipopeptide Mixtures****Table 1. Peptides 1a–h and Their Origin**

	peptide	origin
<b>1a</b>	H-SVRPKVPLRTMSYKLAIDMSHFKE-K(COCH <sub>2</sub> NHNH <sub>2</sub> )-NH <sub>2</sub>	SIV, Nef <sup>101–126</sup>
<b>1b</b>	H-EKGGLEGIYYSARRHRILDMYLE-K(COCH <sub>2</sub> NHNH <sub>2</sub> )-NH <sub>2</sub>	SIV, Nef <sup>125–147</sup>
<b>1c</b>	H-DWQDYTSQGIYRYPKTFGLWKLK-K(COCH <sub>2</sub> NHNH <sub>2</sub> )-NH <sub>2</sub>	SIV, Nef <sup>155–178</sup>
<b>1d</b>	H-SKWDDPWGEVLAWKFDPTLAYTYEA-K(COCH <sub>2</sub> NHNH <sub>2</sub> )-NH <sub>2</sub>	SIV, Nef <sup>201–225</sup>
<b>1e</b>	H-YTYEAYARYPEELEASQACQRKRLEEG-K(COCH <sub>2</sub> NHNH <sub>2</sub> )-NH <sub>2</sub>	SIV, Nef <sup>221–247</sup>
<b>1f</b>	H-KFGAEVVPGFQALSEGCTPYDINQMNLGVGD-K(COCH <sub>2</sub> NHNH <sub>2</sub> )-NH <sub>2</sub>	SIV, Gag <sup>165–195</sup>
<b>1g</b>	H-QIQWYRQQNPVGNIRRWIQLGLQKCVRMYNPTN-K(COCH <sub>2</sub> NHNH <sub>2</sub> )-NH <sub>2</sub>	SIV, Gag <sup>246–282</sup>
<b>1h</b>	Ac-QYIKANSKFIGITELKK-K(COCH <sub>2</sub> NHNH <sub>2</sub> )-NH <sub>2</sub>	Clf, TT <sup>830–846</sup>

**Scheme 3. Synthesis of  $\alpha$ -Hydrazinoacetyl Peptides**

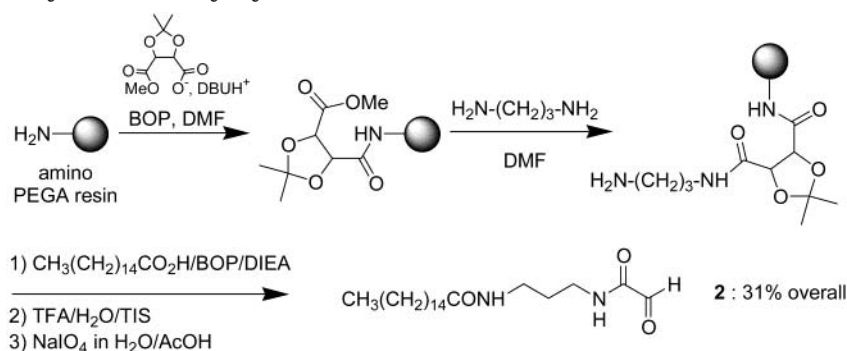
The strategy depicted in Scheme 2 required the synthesis of the corresponding  $\alpha$ -hydrazinoacetyl peptides **1a–h** (Table 1). Their solid-phase synthesis was performed as shown in Scheme 3 using the Fmoc/*t*-Bu strategy (12–13). The selective on-resin deprotection of a C-terminal Lys(Mtt) residue was performed by several washings with a 1% TFA/CH<sub>2</sub>Cl<sub>2</sub> and monitored by HPLC as described elsewhere (16). Incorporation of the  $\alpha$ -hydrazinoacetyl moiety was performed using a fully protected derivative of  $\alpha$ -hydrazinoacetic acid *N,N,N*-

tri(*tert*-butoxycarbonyl)-hydrazinoacetic acid **4** (10), which avoids the formation of polymeric side-products during the coupling step (17). The solid-phase assembly of the peptide chain was followed by a TFA treatment in the presence of scavengers to deprotect and cleave the peptides **1a–h** from the resin.

With the aim of setting most of the purification efforts before the lipidation step, the crude products were purified by RP-HPLC at pH 2 and lyophilized as their TFA salts. They were thoroughly characterized by amino acid analysis, HPLC, CZE, and ES-MS. The yields were in a range from 10% to 30%, and all analytical data confirmed the structure of the products. The net peptide content of the lyophilized powders was determined by amino acid analysis following total acid hydrolysis (see Supporting Information).

**Synthesis of Glyoxyl Derivative 2.** Glyoxyl lipid **2**, composed of a palmitoyl and glyoxyl group linked by a 1,3-diaminopropane moiety (Scheme 4), was prepared using an isopropylidene tartrate-based linker as described elsewhere (18) (19). In short, (+)-dimethyl-2,3-*O*-isopropylidene-D-tartrate was partially saponified with water and DBU, and anchored to amino PEGA resin using BOP in situ activation. The second ester moiety was displaced by 1,3-diamino-propane. Finally, the terminal amino group was acylated with palmitic acid using BOP activation. Unmasking of the 1,2-diol with concentrated TFA was followed by a periodic oxidation which permitted the formation of the  $\alpha$ -oxo aldehyde moiety and



**Scheme 4. Solid Phase Synthesis of Glyoxyl Derivative 2**

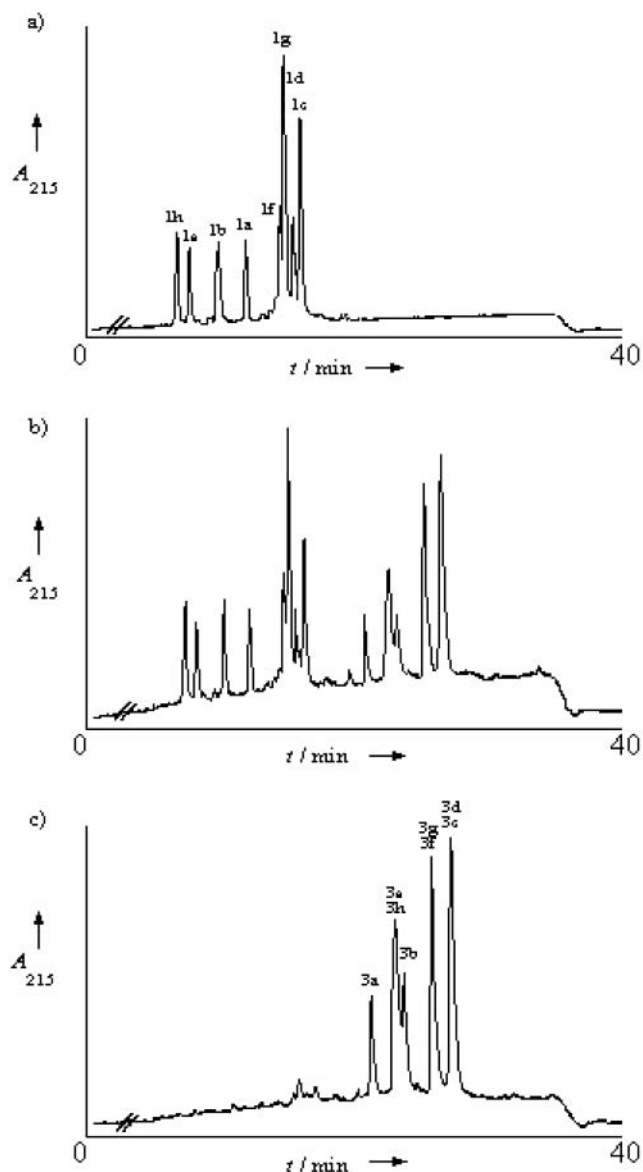
the separation of the compound from the solid support with an overall yield of 31%. A solution phase synthesis of compound **2** is available and will be reported in due course (20).

**Ligation.** We have recently demonstrated that a 38 amino acids  $\alpha$ -hydrazinoacetyl peptide could be reacted almost quantitatively with glyoxyl derivative **2** in a 95/5 2-methyl-propan-2-ol/water mixture. Interestingly, the  $\alpha$ -oxo hydrazone ligation proceeded in the absence of buffer. Thus, the reaction mixture could be lyophilized directly without purification and directly used for biological assays (18).

These results constituted a good starting point for the present work. Nevertheless, the application of this ligation method to the one-pot preparation of a lipopeptide mixture ready for immunization studies required that the  $\alpha$ -hydrazino peptide precursors could be collectively engaged in hydrazone formation as efficiently as a single peptide. In particular, the mixture had to be soluble in 2-methyl-propan-2-ol/ $\text{H}_2\text{O}$ , and the reactivity of the peptides had to be high and independent of the sequence. Importantly, the lipidated mixture had to remain in solution since precipitation could lead to the sequestration of unreacted **2** or starting hydrazino peptides. Premature precipitation of some lipopeptides could result also in the formation of a heterogeneous product. Finally, the propensity of cysteinyl peptides toward oxidation during the ligation had to be studied since some of the chosen epitopes, here **1e**, **1f**, and **1g**, contain one or two cysteinyl residues.

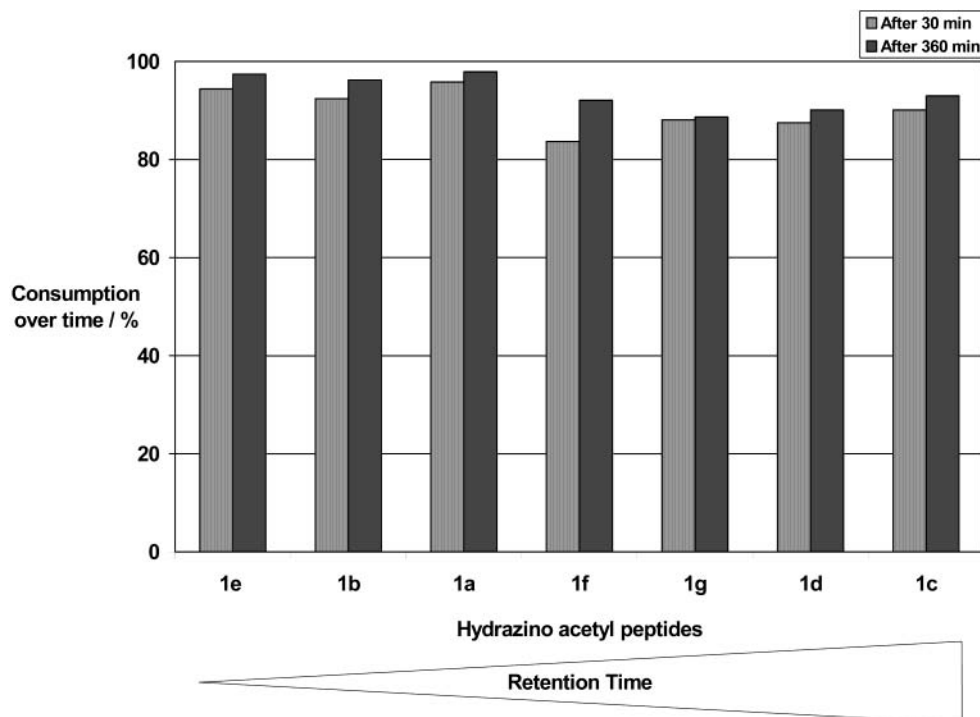
The air oxidation of thiols is known to be faster under basic conditions than in neutral or acidic media, as a consequence of the rapid electron transfer from thiolates to molecular oxygen. The hydrazone ligation occurred rapidly in the absence of buffer for peptides reacted as their TFA salts. Since these peptides give acidic aqueous solutions (for example, for peptides **1a** or **1h**, pH 4.1–4.3 at 0.25 mM), we hypothesized that the above experimental conditions for ligation would minimize this oxidation. Moreover, the addition of an organic cosolvent is known to increase the apparent  $\text{pK}_a$  of acids because the charge separation  $\text{AH} \rightarrow \text{A}^- + \text{H}^+$  is disfavored in media of low polarity (21–22). As a consequence, ligation in a 2-methyl-propan-2-ol-rich medium was expected to disfavor the formation of thiolate species, and thus the formation of disulfide bridges.

**Ligation of Cysteinyl Peptide 1e with 2.** Peptide **1e** was selected to document the stability of cysteinyl peptides during hydrazone formation. Reaction of **1e** with **2** in 95/5 2-methyl-propan-2-ol/water at 37 °C resulted in the clean and rapid formation of the corresponding hydrazone **3e** (see Supporting Information). A few seconds after addition of **2**, the conversion estimated by RP-HPLC was already as high as 75%. The reaction was



**Figure 1.** Hydrazone ligation of mixture **1a–h** with **2**. (a) RP-HPLC chromatogram of the starting  $\alpha$ -hydrazinoacetyl peptides **1a–h**, solubilized in 95/5 (by vol) 2-methyl-propan-2-ol/water at the concentration used for the ligation reaction. (b) RP-HPLC chromatogram of the ligation mixture, 20 min. (c) Ligation mixture, 6 h.

found to be complete after 1 h of reaction, and **3e** represented 95% of the total RP-HPLC detected area. The ligation mixture was found to be stable for at least 5 h at RT.



**Figure 2.** Conversion of hydrazinoacetyl peptides **1a–g** at 30 and 360 min. The conversion was calculated by comparing the RP-HPLC surfaces of each hydrazino acetyl peptide at a given time to the surfaces obtained with the control experiment (peptides **1a–g** in 95/5 2-methyl-propan-2-ol/water by vol without **2**).

Ligation product **3e** was submitted to air oxidation to force the formation of the corresponding dimer. Addition of ammonium bicarbonate in the ligation medium resulted in the disappearance of **3e** and in the formation of a new product eluting later in RP-HPLC. At this stage, the very low signal-to-noise ratio of the MALDI-TOF spectra precluded its characterization. However, this hydrophobic product could be converted again to **3e** by addition of reductive agent TCEP as shown by RP-HPLC and MALDI-TOF analyses, suggesting strongly that it corresponded to the dimer of **3e**.

Importantly, this oxidation product could not be detected in the ligation mixture by RP-HPLC, highlighting the compatibility of these experimental conditions with cysteinyl peptides. This result in hand, we next examined the simultaneous ligation reaction.

**Simultaneous Ligation, Mixture 1a–h.** The simultaneous lipidation was performed with lyophilized mixture **1a–h**. The  $\alpha$ -hydrazinoacetyl net content was calculated using the powder content of each peptide.

The first simultaneous lipidation involved 16 mg of mixture **1a–h**. A solution of **2** in 2-methyl-propan-2-ol (1.1 eq) was added under magnetic stirring to the gel formed by moistening the peptide powder with water. The reaction was monitored by RP-HPLC. The chromatographic conditions permitted a good separation of the starting  $\alpha$ -hydrazinoacetyl peptides (Figure 1a). Ligation resulted in the consumption of all starting  $\alpha$ -hydrazinoacetyl peptides and in the appearance of five new peaks at higher retention times (Figure 1b) which corresponded to hydrazones **3a–h** as shown by LC-MS analysis. **3e–h**, **3f,g**, and **3c,d** were found to coelute. Interestingly, starting peptides **1a–h** were well separated by RP-HPLC from the hydrazone products. Thus, the conversion rate could be estimated by comparison of the cumulated lipopeptide area with the total area. Hydrazone formation was found to be rapid, since the conversion was as high as 50% after 20 min (Figure 1b). Figure 1c corresponds to ligation mixture following 6 h of reaction, for which a

RP-HPLC conversion rate of about 90% could be measured. No significant evolution was observed after 6 h of reaction. Then, the mixture of crude lipopeptides was diluted with water and lyophilized directly. The lyophilized product was submitted to LC-MS analysis. No side product of high molecular weight resulting from disulfide bond formation could be observed.

**Scaleup of the Simultaneous Lipidation.** To document the viability of this methodology for lipopeptide vaccine production, the simultaneous lipidation of several  $\alpha$ -hydrazinoacetyl peptides was examined on a larger scale. 156 mg of lyophilized  $\alpha$ -hydrazinoacetyl peptides **1a–g** was engaged in a lipidation experiment. This quantity represented a scaling-up by a factor of 10 and corresponded to the preparation of 30 individual doses for immunization of *Rhesus* macaques according to previous studies on lipopeptide vaccines (1–3). During the first attempt, the moistened peptide powder was found to stick tightly to the flask, a phenomenon which led to an incomplete ligation. In a second attempt, introduction of glass beads in the flask permitted an efficient dispersion and a good solubilization of the solid, and no precipitation occurred during the ligation. The consumption of the starting hydrazinopeptides over time could be estimated by RP-HPLC. The data, classified according to the increasing retention time of the peptides, are presented in Figure 2 and show that the ligation kinetics are almost independent of the hydrophobicity of the starting hydrazinopeptides. Thus, the ligation process responded to our main specifications: the reaction mixture was found homogeneous, and the lipidation proceeded efficiently and similarly for all the hydrazinopeptides.

## CONCLUSION

We have shown in this article that hydrazone formation between  $\alpha$ -hydrazinoacetyl peptides and a glyoxylyl lipid can be used for the collective lipidation of peptidic antigens. The lipidation reaction was high yielding, rapid,

and occurred similarly for all the studied antigens. Ligation was performed in a salt-free 2-methyl-propan-2-ol-rich medium. Importantly, these experimental conditions were found to be compatible with cysteinyl peptides, since no degradation and/or oxidation was observed during the ligation. The salt-free and quasistoichiometric conditions permitted the direct lyophilisation of the lipopeptide mixture. The prepurification of the starting antigens combined to the high-yielding process permitted to end-up with a product of acceptable purity (~90%).

The preparation of vaccine doses still requires the exchange of trifluoroacetate ions (23) followed by a sterilizing filtration. This work is in progress and will be reported in due course together with the results of the immunizations.

#### ACKNOWLEDGMENT

This work was financially supported by the Agence Nationale de Recherche contre le SIDA, CNRS, Université de Lille 2, and Institut Pasteur de Lille. D.B. held a CNRS/Région Nord Pas-de-Calais grant. We are grateful to Dr. Cyrille Grandjean for fruitful discussions, P. Joly, A. Blanpain, and E. Diesis for technical assistance, and G. Ricart and B. Codeville for LC-MS and ES-MS experiments.

**Supporting Information Available:** Figure of ligation of cysteinyl peptide and tables of amino acid, LC-MS, and MALDI-TOF analyses. This material is available free of charge via the Internet at <http://pubs.acs.org>.

#### LITERATURE CITED

- (1) Bourgault-Villada, I., Mortara, L., Aubertin, A.-M., Gras-Masse, H., Lévy, J.-P., and Guillet, J.-G. (1997) Positive role of macaque cytotoxic T lymphocytes during SIV infection: decrease of cellular viremia and increase of asymptomatic clinical period. *FEMS Immunol. Med. Microbiol.* **19**, 81–87.
- (2) Mortara, L., Gras-Masse, H., Rommens, C., Venet, A., Guillet, J.-G., and Bourgault-Villada, I. (1999) Type 1 CD4(+) T-cell help is required for induction of antipeptide multi-specific cytotoxic T lymphocytes by a lipopeptidic vaccine in *Rhesus* macaques. *J. Virol.* **73**, 4447–4451.
- (3) Mortara, L., Letourneur, F., Villefroy, P., Beyer, C., Gras-Masse, H., Guillet, J.-G., and Bourgault-Villada, I. (2000) Temporal loss of Nef-epitope CTL recognition following macaque lipopeptide immunization and SIV challenge. *Virology* **278**, 551–561.
- (4) Gahéry-Ségard, H., Pialoux, G., Charmeteau, B., Sermet, S., Poncelet, H., Raux, M., Tartar, A., Lévy, J.-P., Gras-Masse, H., and Guillet, J.-G. (2000) Multi-epitopic B- and T-cell responses induced in humans by a human immunodeficiency virus type 1 lipopeptide vaccine. *J. Virol.* **74**, 1694–1703.
- (5) Pialoux, G., Gahéry-Ségard, H., Sermet, S., Poncelet, H., Fournier, S., Gérard, L., Tartar, A., Gras-Masse, H., Lévy, J.-P., and Guillet, J.-G. (2001) Lipopeptides induce cell-mediated anti-HIV immune responses in seronegative volunteers. *AIDS* **15**, 1239–1249.
- (6) Wiesmüller, K.-H., Bessler, W. G., and Jung, G. (1992) Solid-phase peptide synthesis of lipopeptide vaccines eliciting epitope-specific B-, T-helper and T-killer cell response. *Int. J. Pept. Protein Res.* **40**, 255–260.
- (7) Dépérez, B., Sauzet, J.-P., Boutillon, C., Martinon, F., Tartar, A., Sergheraert, C., Guillet, J.-G., Gomard, E., and Gras-Masse, H. (1996) Comparative efficiency of simple lipopeptide constructs for in vivo induction of virus-specific CTL. *Vaccine* **14**, 375–382.
- (8) Seitz, O., Heinemann, I., Mattes, A., and Waldmann, H. (2001) Synthetic conjugates. Tailor-made probes for the biology of protein modification and protein processing. *Tetrahedron* **57**, 2247–2277.
- (9) Gras-Masse, H. Unpublished results.
- (10) Bonnet, D., Ollivier, N., Gras-Masse, H., and Melnyk, O. (2001) Chemoselective acylation of fully deprotected hydrazinoacetyl peptides. Application to the synthesis of lipopeptides. *J. Org. Chem.* **66**, 443–446.
- (11) Hancock, W. S., and Battersby, J. E. (1976) A new micro-test for the detection of incomplete coupling reactions in solid-phase peptide synthesis using 2,4,6-trinitrobenzene-sulfonic acid. *Anal. Biochem.* **74**, 260–264.
- (12) Fields, G., and Noble, R. (1990) Solid-phase peptide synthesis utilizing 9-fluorenylmethoxycarbonyl amino acids. *Int. J. Pept. Protein Res.* **35**, 161–214.
- (13) W. C. Chan, and P. D. White (2000) *Fmoc Solid-Phase Synthesis, A Practical Approach*, Practical Approach Series, Oxford University Press, Oxford.
- (14) Betts, M. R., Krowka, J., Santamaria, C., Balsamo, K., Gao, F., Mulundu, G., Luo, C., N'Gandu, N., Sheppard, H., Allen, S., Hahn, B. H., Allen, S., and Frelinger, J. A. (1997) Cross-clade human immunodeficiency virus-specific cytotoxic T-lymphocyte responses in HIV-infected Zambians. *J. Virol.* **1**, 8908–8911.
- (15) Durali, D., Morvan, J., Letourneur, F., Schmitt, D., Guegan, N., Dalod, M., Saragosti, S., Sicard, D., Levy, J. P., and Gomard, E. (1998) Cross-reactions between the cytotoxic T-lymphocyte responses of human immunodeficiency virus-infected African and European patients. *J. Virol.* **2**, 3547–3553.
- (16) Bourel, L., Carion, O., Gras-Masse, H., and Melnyk, O. (2000) The deprotection of Lys(Mtt) revisited. *J. Pept. Sci.* **6**, 264–270.
- (17) Bonnet, D., Rommens, C., Gras-Masse, H., and Melnyk, O. (2000) Chemoselective acylation of hydrazino peptides: a novel and mild method for the derivatization of peptides with sensitive fatty acids. *Tetrahedron Lett.* **41**, 45–48.
- (18) Bonnet, D., Bourel, L., Gras-Masse, H., and Melnyk, O. (2000) A novel lipophilic glyoxylic acid derivative for the lipidation of peptides using salt-free hydrazone ligation. *Tetrahedron Lett.* **41**, 10003–10007.
- (19) Melnyk, O., Fruchart, J.-S., Grandjean, C., and Gras-Masse, H. (2001) A new tartaric-based linker for the solid-phase synthesis of C-terminal peptide  $\alpha$ -oxo aldehydes. *J. Org. Chem.* **66**, 4153–4160.
- (20) Bonnet, D., Grandjean, C., P., Joly, P., Fardel, N., Gras-Masse, H., and Melnyk, O. Manuscript in preparation.
- (21) Homandberg, G. A., Mattis, J. A., and Laskowski, M. Jr. (1978) Synthesis of peptides bonds by proteinases. addition of organic cosolvents shifts peptide bond equilibria toward synthesis. *Biochemistry* **17**, 5220–5227.
- (22) Mukerjee, P., and Ostrow, D. (1998) Effects of added dimethyl sulfoxide on  $pK_a$  values of uncharged Acids and pH values of aqueous buffers. *Tetrahedron Lett.* **39**, 423–426.
- (23) According to the ICH Q3C Guideline of the European Agency for the Evaluation of Medicinal products, trifluoroacetic acid (TFA) is an ICH class 4 solvent for which no adequate toxicological information are available.

BC0256143



# Synthesis and in Vivo Biodisposition of [ $^{14}\text{C}$ ]-Quaternary Ammonium–Melphalan Conjugate, a Potential Cartilage-Targeted Alkylating Drug

Maryse Rapp,\* Isabelle Giraud, Jean-Claude Maurizis, Marie-Josèphe Galmier, and Jean-Claude Madelmont

INSERM UMR 484, Rue Montalembert, BP 184, 63005 Clermont-Ferrand Cedex, France.

Received April 15, 2002; Revised Manuscript Received November 4, 2002

For the purpose of developing more selective anticancer drugs that would concentrate in the malignant cartilaginous tumors (chondrosarcomas), and so improve therapeutic index through a reduction of side effects, a quaternary ammonium (QA) conjugate of melphalan was synthesized and labeled with  $^{14}\text{C}$  by linking the QA moiety to nitrogen mustard via an amide bond. Comparative pharmacokinetic study of [ $^{14}\text{C}$ ]-melphalan and its [ $^{14}\text{C}$ ]-QA conjugate conducted on rats showed that the two compounds were principally excreted by the urinary way. The blood elimination of the QA conjugate was faster than that of the melphalan. In the other hand a higher rate of radioactivity derived of [ $^{14}\text{C}$ ]-MQA was found in feces. In the biodisposition for most organs, no striking differences were found between melphalan and its QA conjugate except for cartilages which exhibited more higher radioactivity level. Amounts of radioactivity derived from [ $^{14}\text{C}$ ]-QA conjugates measured in cartilaginous tissues until 1 h after injection demonstrate that the introduction of a QA moiety on melphalan allows the molecule to be carried selectively to cartilaginous tissues. As the [ $^{14}\text{C}$ ]-QA conjugate is radiolabeled on the chloroethyl alkylating moiety, levels of radioactivity measured in the cartilaginous tissues results from unchanged compound or metabolite having kept the active group.

## INTRODUCTION

Previous works developed in our laboratory have demonstrated that molecules owning quaternary ammonium moieties exhibited a high affinity for cartilage (1–5). As part of ongoing work on the targeting of cartilage, we are currently conducting research on the chemotherapy of malignant cartilaginous tumors (chondrosarcomas) (6). Indeed, chondrosarcoma is the second most common malignant tumor of bone after osteosarcomas (7–9). Such tumors are generally radio-resistant, and there is no effective treatment except by surgical excision (7, 9). In view of the problems encountered in the chemotherapy of chondrosarcomas, we set out to extend our cartilage targeting strategy, originally applied to the treatment of more usual cartilage disorders such as osteoarthritis or osteoarthritis, to this neoplastic context (3). Our objective was to develop more selective anticancer drugs that would concentrate in the malignant cartilaginous tissue and so improve therapeutic index through a reduction of side effects.

First we focused on the linkage of the QA carrier with one nitrogen mustard, melphalan. This bifunctional alkylating agent is a clinically important antitumor drug that express its cytotoxicity and antitumor effect by alkylation and cross-linking of DNA mainly on the N-7 position of deoxyguanosine residues (10). Melphalan was selected mainly for chemical reasons: its structure was (i) easy to a conjugate with our carrier system through the carboxylic acid function and (ii) easy to radiolabel via the chloroethyl alkylating moiety, the radiolabeling of the

QA derivative and its parent drugs being necessary for validation by biodistribution studies of the targeted cartilage.

Here, we describe the preparation of [ $^{14}\text{C}$ ]-melphalan and its [ $^{14}\text{C}$ ]-QA conjugate, where the QA entity was linked to the nitrogen mustard via the carboxylic function by an amide bond and their comparative pharmacokinetic studies in rats.

## EXPERIMENTAL PROCEDURES

**Syntheses.** *General.* All solvents and reagents obtained from commercial sources were used without further purification. Nuclear magnetic resonance spectra ( $^1\text{H}$  NMR and  $^{13}\text{C}$  NMR) were performed on a Bruker AM 200 (4.5 T) spectrometer. Chemical shifts are reported in parts per million relative to the internal tetramethylsilane standard for  $^1\text{H}$  NMR and the solvent for  $^{13}\text{C}$  NMR (DMSO- $d_6$ ,  $\delta$  = 39.5 ppm;  $\text{CDCl}_3$ ,  $\delta$  = 77.0 ppm). Coupling constants ( $J$  values) are given in Hertz. Infrared (IR) spectra were recorded on a Brüker Vector 22 FTIR system. Melting points (mp) were determined on an Electrothermal digital apparatus and are uncorrected. Analytical thin-layer chromatography (TLC) was conducted on precoated silica gel plates (SDS, 60 F $_{254}$ , 0.25 mm thick) or on precoated aluminum oxide plates (Merck, 60 F $_{254}$ , neutral type E, 0.20 mm thick) with both detection by ultraviolet light and visualization with iodine. Silica gel 60 (Chromagel, 35–60  $\mu\text{m}$ , SDS) was used for medium-pressure chromatography using the indicated solvent mixture expressed as volume/volume ratios. Radiochemical purity was determined by scanning the TLC plates with an Ambis 4000 detector. Specific activity of compounds was measured in a Wallac Winspectral 1414 liquid scintillation counter. Mass spectra were recorded on a Bruker Esquire-LC spectrometer.

\* To whom correspondence should be addressed. Phone: 33 4 73 15 08 12. Fax: 33 4 73 15 08 01. E-mail: rapp@inserm484.u-clermont1.fr.

Electrospray ionization mass spectrometry (ESI-MS) was used in positive or negative mode. L-Phenylalanine was purchased from Aldrich and [1,2-<sup>14</sup>C]ethylene oxide from NEN. 4-Nitro-L-phenylalanine (**1**) (ESI-MS mass calcd for C<sub>9</sub>H<sub>10</sub>N<sub>2</sub>O<sub>4</sub> (M+H)<sup>+</sup>, 211.07; found, 211.12) was prepared from L-phenylalanine as described in the literature (11, 12).

*N*-(*tert*-Butyloxycarbonyl)-4-nitro-L-phenylalanine (**2**). To a suspension of 4-nitro-L-phenylalanine (**1**) (4.01 g, 17.53 mmol) and triethylamine (2.45 mL, 17.53 mmol) in methanol (150 mL) was added di-*tert*-butyl dicarbonate (4.02 mL, 17.53 mmol). The mixture was stirred 10 min at 50 °C and then another 30 min at room temperature and finally evaporated under reduced pressure. The resulting oil was treated with cold 0.01 N hydrochloric acid (pH 2), and the solution was immediately extracted with ethyl acetate. The organic phase was dried over magnesium sulfate and evaporated under reduced pressure to afford **2** as a clear oil crystallizing from cyclohexane (5.06 g, 83%). mp 108–110 °C (dec); *R*<sub>f</sub> 0.35 (TLC silica, dichloromethane/ethanol 95/5), *R*<sub>f</sub> 0.46 (TLC silica, ethyl acetate); <sup>1</sup>H NMR (DMSO-*d*<sub>6</sub>) δ 1.38 (s, 9H, CH<sub>3</sub> Boc), 2.94 (dd, *J* = 13.6, *J* = 10.5, 1H, PhCH<sub>2</sub>a), 3.17 (dd, *J* = 13.6, *J* = 4.5, 1H, PhCH<sub>2</sub>b), 4.10–4.22 (m, 1H, PhCH<sub>2</sub>CH), 7.19 (d, *J* = 8.5, 1H, NHBoc), 7.52 (d, *J* = 8.7, 2H, aromatic H), 8.15 (d, *J* = 8.7, 2H, aromatic H), 12.71 (broad s, 1H, COOH); <sup>13</sup>C NMR (DMSO-*d*<sub>6</sub>) δ 28.09 (CH<sub>3</sub> Boc), 36.26 (PhCH<sub>2</sub>), 54.55 (PhCH<sub>2</sub>CH), 78.18 (C(CH<sub>3</sub>)<sub>3</sub> Boc), 123.21 130.52 146.25 146.54 (aromatic C), 155.37 173.11 (C=O); IR (KBr) ν cm<sup>-1</sup> 1729, 1688 (C=O). ESI-MS mass calcd for C<sub>14</sub>H<sub>18</sub>N<sub>2</sub>O<sub>6</sub> (M - H)<sup>-</sup>: 309.11. Found: 309.05.

1-([*N*-(*tert*-Butyloxycarbonyl)-4-nitro-L-phenylalanyl]-amino)-3-(dimethylamino)propane (**3**). To a solution of the Boc-amino acid **2** (4.50 g, 14.50 mmol), 1-hydroxy-1*H*-benzotriazole (1.96 g, 14.50 mmol) and 3-(dimethylamino)propylamine (1.83 mL, 14.50 mmol) in dichloromethane (20 mL) was added a solution of *N,N*-dicyclohexylcarbodiimide (3.01 g, 14.50 mmol) in the same solvent (30 mL). The mixture was stirred at room temperature for 5 h. After removing of the urea by filtration, the filtrate was extracted with 1 N sodium hydroxide and washed with water. The organic phase was dried over magnesium sulfate and evaporated under reduced pressure to afford **3** as a white solid (4.06 g, 71%). mp 134–135 °C (dec); *R*<sub>f</sub> 0.77 (TLC silica, dichloromethane/methanol/ammonium hydroxide 50/48/2), *R*<sub>f</sub> 0.79 (TLC aluminum oxide, ethanol); <sup>1</sup>H NMR (CDCl<sub>3</sub>) δ 1.40 (s, 9H, CH<sub>3</sub> Boc), 1.57 (qt, *J* = 6.1, 2H, CH<sub>2</sub>CH<sub>2</sub>CH<sub>2</sub>), 2.13 (s, 6H, N(CH<sub>3</sub>)<sub>2</sub>), 2.31 (t, *J* = 6.1, 2H, CH<sub>2</sub>CH<sub>2</sub>CH<sub>2</sub>N(CH<sub>3</sub>)<sub>2</sub>), 3.03–3.36 (m, 4H, PhCH<sub>2</sub> et CH<sub>2</sub>CH<sub>2</sub>CH<sub>2</sub>N(CH<sub>3</sub>)<sub>2</sub>), 4.30–4.38 (m, 1H, PhCH<sub>2</sub>CH), 5.09 (d, *J* = 8.9, 1H, NHBoc), 7.39 (d, *J* = 8.7, 2H, aromatic H), 7.73 (broad s, 1H, NH), 8.16 (d, *J* = 8.7, 2H, aromatic H); <sup>13</sup>C NMR (CDCl<sub>3</sub>) δ 25.15 (CH<sub>2</sub>CH<sub>2</sub>CH<sub>2</sub>), 28.24 (CH<sub>3</sub> Boc), 38.84 (PhCH<sub>2</sub>), 39.75 (CH<sub>2</sub>CH<sub>2</sub>CH<sub>2</sub>N(CH<sub>3</sub>)<sub>2</sub>), 45.10 (N(CH<sub>3</sub>)<sub>2</sub>), 55.50 (PhCH<sub>2</sub>CH), 58.70 (CH<sub>2</sub>CH<sub>2</sub>CH<sub>2</sub>N(CH<sub>3</sub>)<sub>2</sub>), 80.27 (C(CH<sub>3</sub>)<sub>3</sub> Boc), 123.60 130.31 144.98 146.96 (aromatic C), 155.08 170.00 (C=O); IR (KBr) ν cm<sup>-1</sup> 1687, 1652 (C=O). ESI-MS mass calcd for C<sub>19</sub>H<sub>30</sub>N<sub>4</sub>O<sub>5</sub> (M + H)<sup>+</sup>: 395.25. Found: 395.26.

1-([*N*-(*tert*-Butyloxycarbonyl)-4-amino-L-phenylalanyl]-amino)-3-(dimethylamino)propane (**4**). Compound **3** (3.81 g, 9.66 mmol) was hydrogenated at room temperature for 2 h in methanol (150 mL) over 10% Pd/C (0.4 g). The suspension was then filtered through a Celite pad, and the methanolic filtrate was evaporated under reduced pressure to afford the amino derivative **4** as a white solid (3.52 g, quantitative yield). mp 115–120 °C (dec); *R*<sub>f</sub> 0.60

(TLC silica, dichloromethane/methanol/ammonium hydroxide 50/48/2), *R*<sub>f</sub> 0.75 (TLC aluminum oxide, ethanol); <sup>1</sup>H NMR (CDCl<sub>3</sub>) δ 1.42 (s, 9H, CH<sub>3</sub> Boc), 1.58 (qt, *J* = 6.3, 2H, CH<sub>2</sub>CH<sub>2</sub>CH<sub>2</sub>), 2.17 (s, 6H, N(CH<sub>3</sub>)<sub>2</sub>), 2.31 (t, *J* = 6.3, 2H, CH<sub>2</sub>CH<sub>2</sub>CH<sub>2</sub>N(CH<sub>3</sub>)<sub>2</sub>), 2.90 (dd, *J* = 13.7, *J* = 7.3, 1H, PhCH<sub>2</sub>a), 3.01 (dd, *J* = 13.7, *J* = 5.8, 1H, PhCH<sub>2</sub>b), 3.27 (q, *J* = 6.3, 2H, CH<sub>2</sub>CH<sub>2</sub>CH<sub>2</sub>N(CH<sub>3</sub>)<sub>2</sub>), 3.60 (broad s, 2H, NH<sub>2</sub>), 4.14–4.23 (m, 1H, PhCH<sub>2</sub>CH), 5.00 (broad s, 1H, NHBoc), 6.61 (d, *J* = 8.4, 2H, aromatic H), 6.97 (d, *J* = 8.4, 2H, aromatic H), 7.26 (broad s, 1H, NH); <sup>13</sup>C NMR (CDCl<sub>3</sub>) δ 25.65 (CH<sub>2</sub>CH<sub>2</sub>CH<sub>2</sub>), 28.35 (CH<sub>3</sub> Boc), 38.09 (PhCH<sub>2</sub>), 39.26 (CH<sub>2</sub>CH<sub>2</sub>CH<sub>2</sub>N(CH<sub>3</sub>)<sub>2</sub>), 45.47 (N(CH<sub>3</sub>)<sub>2</sub>), 56.41 (PhCH<sub>2</sub>CH), 58.42 (CH<sub>2</sub>CH<sub>2</sub>CH<sub>2</sub>N(CH<sub>3</sub>)<sub>2</sub>), 79.80 (C(CH<sub>3</sub>)<sub>3</sub> Boc), 115.24 126.52 130.24 145.19 (aromatic C), 155.19 171.05 (C=O); IR (KBr) ν cm<sup>-1</sup> 1699, 1659 (C=O). ESI-MS mass calcd for C<sub>19</sub>H<sub>32</sub>N<sub>4</sub>O<sub>3</sub> (M + H)<sup>+</sup>: 365.26. Found: 365.24.

1-([*N*-(*tert*-Butyloxycarbonyl)-4-[bis(2-hydroxyethyl)-amino]-L-phenylalanyl]-amino)-3-(dimethylamino)propane (**5**). To a solution of the amino derivative **4** (3.03 g, 8.31 mmol) in acetic acid (20 mL) at 5 °C was added ethylene oxide (9.5 mL, 192 mmol). The mixture was stirred for 24 h at room temperature. After evaporation under reduced pressure, the residue was taken up in methanol and treated with a Dowex 1 × 2–400 resin (previously washed with 1 N sodium hydroxide and then water and methanol). After filtration of the resulting suspension, the methanolic filtrate was evaporated under reduced pressure and then purified by column chromatography on silica gel (eluent, dichloromethane/ethanol 50/50 and then dichloromethane/ethanol/ammonium hydroxide 50/49/1) to give the dihydroxy compound **5** as a white solid (2.82 g, 75%). mp 63–64 °C (dec); *R*<sub>f</sub> 0.70 (TLC silica, dichloromethane/methanol/ammonium hydroxide), *R*<sub>f</sub> 0.65 (TLC aluminum oxide, ethanol); <sup>1</sup>H NMR (DMSO-*d*<sub>6</sub>) δ 1.33 (s, 9H, CH<sub>3</sub> Boc), 1.50 (qt, *J* = 7.1, 2H, CH<sub>2</sub>CH<sub>2</sub>CH<sub>2</sub>), 2.14 (s, 6H, N(CH<sub>3</sub>)<sub>2</sub>), 2.21 (t, *J* = 7.1, 2H, CH<sub>2</sub>CH<sub>2</sub>CH<sub>2</sub>N(CH<sub>3</sub>)<sub>2</sub>), 2.50–2.85 (m, 2H, PhCH<sub>2</sub>), 3.07 (q, *J* = 5.5, 2H, CH<sub>2</sub>CH<sub>2</sub>CH<sub>2</sub>N(CH<sub>3</sub>)<sub>2</sub>), 3.35–3.54 (m, 8H, N(CH<sub>2</sub>CH<sub>2</sub>OH)<sub>2</sub>), 3.96–4.02 (m, 1H, PhCH<sub>2</sub>CH), 4.73 (broad s, 2H, OH), 6.56 (d, *J* = 8.6, 2H, aromatic H), 6.65 (d, *J* = 8.4, 1H, NHBoc), 6.98 (d, *J* = 8.6, 2H, aromatic H), 7.82 (t, *J* = 4.4, 1H, NH); <sup>13</sup>C NMR (DMSO-*d*<sub>6</sub>) δ 26.63 (CH<sub>2</sub>CH<sub>2</sub>CH<sub>2</sub>), 28.12 (CH<sub>3</sub> Boc), 36.71 (CH<sub>2</sub>CH<sub>2</sub>CH<sub>2</sub>N(CH<sub>3</sub>)<sub>2</sub>), 36.81 (PhCH<sub>2</sub>), 44.88 (N(CH<sub>3</sub>)<sub>2</sub>), 53.36 (N(CH<sub>2</sub>CH<sub>2</sub>OH)<sub>2</sub>), 56.12 (CH<sub>2</sub>CH<sub>2</sub>CH<sub>2</sub>N(CH<sub>3</sub>)<sub>2</sub>), 56.51 (PhCH<sub>2</sub>CH), 58.18 (N(CH<sub>2</sub>CH<sub>2</sub>OH)<sub>2</sub>), 77.83 (C(CH<sub>3</sub>)<sub>3</sub> Boc), 110.91 124.18 129.72 146.31 (aromatic C), 155.04 171.51 (C=O); IR (KBr) ν cm<sup>-1</sup> 1699, 1668 (C=O). ESI-MS mass calcd for C<sub>23</sub>H<sub>40</sub>N<sub>4</sub>O<sub>5</sub> (M + H)<sup>+</sup>: 453.31. Found: 453.31.

*N*-(*tert*-Butyloxycarbonyl)-4-[bis(2-hydroxy-[1,2-<sup>14</sup>C]ethyl)-amino]-L-phenylalanine Ethyl Ester (**7**). The reaction was performed in a vacuum manifold by the transfer of [1,2-<sup>14</sup>C]ethylene oxide (37 00 MBq (100.0 mCi), specific activity 503 MBq/mmol (13.6 mCi/mmol)) on a solution of *N*-(*tert*-butyloxycarbonyl)-4-amino-L-phenylalanine ethyl ester (**6**) (11, 13–16) (2.70 g, 8.76 mmol) in acetic acid (14 mL) cooled with liquid nitrogen. After completing the transfer, the reaction mixture was progressively warmed to 5 °C, stirred at this temperature for 1 h and for another 24 h at room temperature. Then, the solution was cooled again at 5 °C, treated with cold ethylene oxide (10 mL, 202 mmol), stirred for 24 h at room temperature, and then evaporated under reduced pressure. The resulting oil was dissolved into ethyl acetate, and this organic phase was washed with saturated sodium carbonate and water, dried over magnesium sulfate, and evaporated under reduced pressure. The residue was purified by column chromatography on silica gel (eluent: ethyl



acetate). Compound **7** was isolated as a clear oil with a radiochemical yield of 49% (2.13 g, 1828 MBq (49.4 mCi)) and a specific activity of 329 MBq/mmol (8.9 mCi/mmol). The radiochemical purity was 98.0%, as determined by TLC analysis (*R<sub>f</sub>* 0.40, TLC silica, ethyl acetate). Compound **7** was found by NMR and TLC to be identical to the unlabeled reference compound (**16**).

*N*-(*tert*-Butyloxycarbonyl)-4-[bis(2-chloro-[1,2-<sup>14</sup>C]ethyl)amino]-*L*-phenylalanine ethyl ester (**8**). To a stirred 0 °C solution of **7** (2.10 g, 5.30 mmol) in dichloromethane were added subsequently carbon tetrachloride (5 mL) and triphenylphosphine (3.92 g, 14.93 mmol) (**15**). The reaction mixture was stirred at room temperature for 16 h and then evaporated under reduced pressure. The resulting oil was purified by column chromatography on silica gel (eluent: gradient of diethyl ether in dichloromethane from 0% to 50%). Compound **8** was isolated as an oil in 60% yield (1.38 g, 1082 MBq (29.2 mCi)) with a specific activity of 340 MBq/mmol (9.2 mCi/mmol). The radiochemical purity was 98.8%, as determined by TLC analysis (*R<sub>f</sub>* 0.08, TLC silica, dichloromethane; *R<sub>f</sub>* 0.77, TLC silica, cyclohexane/ethyl acetate 6/4). Compound **8** was found by NMR and TLC to be identical to the unlabeled reference compound (**14**).

4-[Bis(2-chloro-[1,2-<sup>14</sup>C]ethyl)amino]-*L*-phenylalanine Hydrochloride ([<sup>14</sup>C]-Melphalan-HCl, [<sup>14</sup>C]-Mel-HCl). A solution of compound **8** (1.37 g, 3.16 mmol) in 6 N hydrochloric acid (20 mL) was heated to reflux for 3 h. Then, the reaction mixture was concentrated under reduced pressure until a white solid appeared. This resulting solid was washed with diethyl ether and dried. [<sup>14</sup>C]-Melphalan was isolated as its hydrochloride form in 89% yield (1.07 g, 958 MBq (25.9 mCi)) with a specific activity of 340 MBq/mmol (9.2 mCi/mmol). The radiochemical purity was 99.0%, as determined by TLC analysis (*R<sub>f</sub>* 0.30, TLC silica, chloroform/ethanol 1/1; *R<sub>f</sub>* 0.45, TLC silica, ethyl acetate/ethanol 2/6). [<sup>14</sup>C]-Mel-HCl was found by NMR and TLC to be identical to the unlabeled reference compound (**14**).

1-([*N*-(*tert*-Butyloxycarbonyl)-4-[bis(2-chloro-[1,2-<sup>14</sup>C]ethyl)amino]-*L*-phenylalanyl]-amino)-3-(dimethylamino)propane (**9**). To a stirred solution of [<sup>14</sup>C]-Mel-HCl (700 mg, 1.83 mmol) in methanol were successively added, at room temperature, triethylamine (1.02 mL, 7.34 mmol) and di-*tert*-butyl dicarbonate (0.83 mL, 3.66 mL). The mixture was stirred at room temperature for 30 min and then evaporated under reduced pressure. The resulting oily residue was treated with cold 0.01 N hydrochloric acid (pH 2) and extracted immediately with ethyl acetate. The organic extract was dried over magnesium sulfate and evaporated under reduced pressure. The resulting oil was dissolved in dichloromethane. To this solution were successively added 1-hydroxybenzotriazole (248 mg, 1.83 mmol), 3-(dimethylamino)propylamine (0.23 mL, 1.83 mmol) and then a solution of *N,N*-dicyclohexylcarbodiimide (378 mg, 1.83 mmol) in dichloromethane (8 mL). The mixture was stirred at room temperature for 5 h. The corresponding urea byproduct was isolated by filtration. The filtrate was then washed with 1 N sodium hydrogen carbonate and water. The organic extract was dried over magnesium sulfate and evaporated under reduced pressure. The resulting oil was purified by column chromatography on silica gel (eluent: dichloromethane/ethanol 50/50 and then dichloromethane/ethanol/ammonium hydroxide 50/48/2). Compound **9** was isolated as an oil in 62% yield (555 mg, 385 MBq (10.4 mCi)) with a specific activity of 340 MBq/mmol (9.2 mCi/mmol). The radiochemical purity was 98.1%, as determined by TLC analysis (*R<sub>f</sub>* 0.45, TLC silica, dichloro-

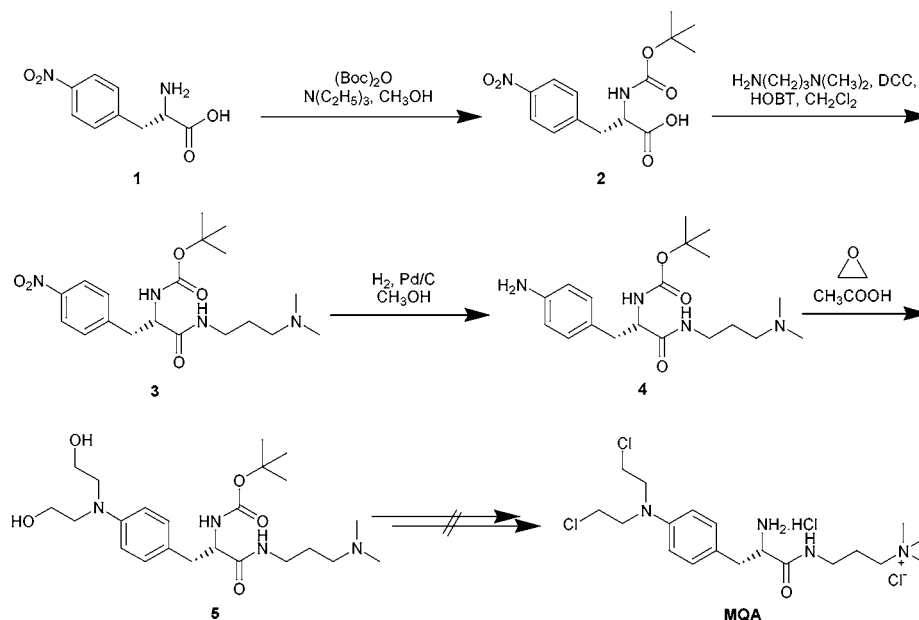
methane/ethanol/ammonium hydroxide 50/48/2; *R<sub>f</sub>* 0.30, TLC aluminum oxide, dichloromethane/ethanol 98/2). Compound **9** was found by NMR and TLC to be identical to the unlabeled reference compound (**6**).

[3-([*N*-(*tert*-Butyloxycarbonyl)-4-[bis(2-chloro-[1,2-<sup>14</sup>C]ethyl)amino]-*L*-phenylalanyl]-amino)propyl]trimethylammonium Iodide (**10**). To a solution of **9** (450 mg, 0.92 mmol) in ethanol (5 mL) was added, under an inert atmosphere, methyl iodide (86 µL, 1.38 mmol). The mixture was stirred at room temperature for 3 h and then evaporated under reduced pressure. The resulting oil was dissolved in the minimum amount of methanol and poured into diethyl ether (150 mL). The resulting precipitate was then filtered, washed with diethyl ether, and dried to afford **10** as a white solid (534 mg, 289 MBq (7.8 mCi), 92%) with a specific activity of 340 MBq/mmol (9.2 mCi/mmol). The radiochemical purity was 99.0% as determined by TLC analysis (*R<sub>f</sub>* 0.05, TLC silica, dichloromethane/ethanol/ammonium hydroxide 50/49/1; *R<sub>f</sub>* 0.45, TLC aluminum oxide, dichloromethane/ethanol 1/1). Compound **10** was found by NMR and TLC to be identical to the unlabeled reference compound (**6**).

[3-([4-[Bis(2-chloro-[1,2-<sup>14</sup>C]ethyl)amino]-*L*-phenylalanyl]amino)propyl]trimethylammonium Chloride (Hydrochloride Form) ([<sup>14</sup>C]-MAQ). Compound **10** (450 mg, 0.71 mmol) was treated with 2 N ethanolic hydrochloric acid at room temperature for 2 h. The solution was then evaporated under reduced pressure. The resulting oil was dissolved in methanol and poured into 2 N ethereal hydrochloric acid. The precipitate was filtered, washed with diethyl ether, and passed on a Dowex 1 × 2-400 ion-exchange resin (eluent: methanol). The methanolic fractions were evaporated under reduced pressure. The residue was dissolved again in methanol and poured into diethyl ether (200 mL). The resulting precipitate was then filtered, washed with diethyl ether, and dried to afford [<sup>14</sup>C]-MAQ as a white hygroscopic solid (350 mg, 222 MBq (6.0 mCi), 91%) with a specific activity of 340 MBq/mmol (9.2 mCi/mmol). The radiochemical purity was 99.0%, as determined by TLC analysis (*R<sub>f</sub>* 0.55, TLC silica, ethanol/ammonium hydroxide 1/1; *R<sub>f</sub>* 0.30, TLC aluminum oxide, dichloromethane/ethanol 9/1). [<sup>14</sup>C]-MAQ was found by NMR and TLC to be identical to the unlabeled reference compound (**6**).

**Pharmacokinetic Studies. Tissue Distribution Study.** For tissue distribution measurements, 4-week-old male Sprague Dawley rats weighing 80–100 g (Iffa-Credo, L'Arbresle, France) were intravenously dosed with each [<sup>14</sup>C]-labeled compound [27 µmol/kg, 1110 kBq (30 µCi) in 200 µL of physiological saline]. At times 2, 5, 10, 15, and 30 min and 1, 2, 6, and 24 h after injection, rats were rapidly frozen by immersion in liquid nitrogen after carbon dioxide inhalation. They were then embedded in a 2% gel of carboxymethyl cellulose. The resulting carboxyl methyl cellulose block was sagittally sectioned at –22 °C with a Reichert-Jung Cryopolytome cryomicrotome (Heidelberg, Germany). When section surfaces of interest appeared, the corresponding 40-µm-thick slices were taken using n° 810 Scotch band tape (3M, Saint Paul, MN) and dried for 48 h at –22 °C. These selected slices (*n* = 8 for each time studied) fixed on a hard-bound sheet were introduced into an Ambis 4000 detector (B.Braun Scientec) and subsequently analyzed. This detector is a computer-controlled multiwire proportional counter with an array of 3696 individual detector elements that simultaneously detect electronic emissions over the entire area by moving the sample through 288 positions beneath the detector array. Counts are recorded in 1 064 448 discrete detection points (data elements),



**Scheme 1. Synthesis of MAQ According to Route A**

from which the composite image is displayed on a high-resolution color monitor so that regions of interest may be quantified. The powerful image enhancement techniques include smoothing, sharpening, user-contoured variable gray scale, and selective back-ground filtration, allowing the investigator to increase image contrast and definition without affecting quantification. The quantification leads to a surface activity (cpm/mm<sup>2</sup>) which, thanks to a calibration, is directly converted into nCi per gram of tissue (17).

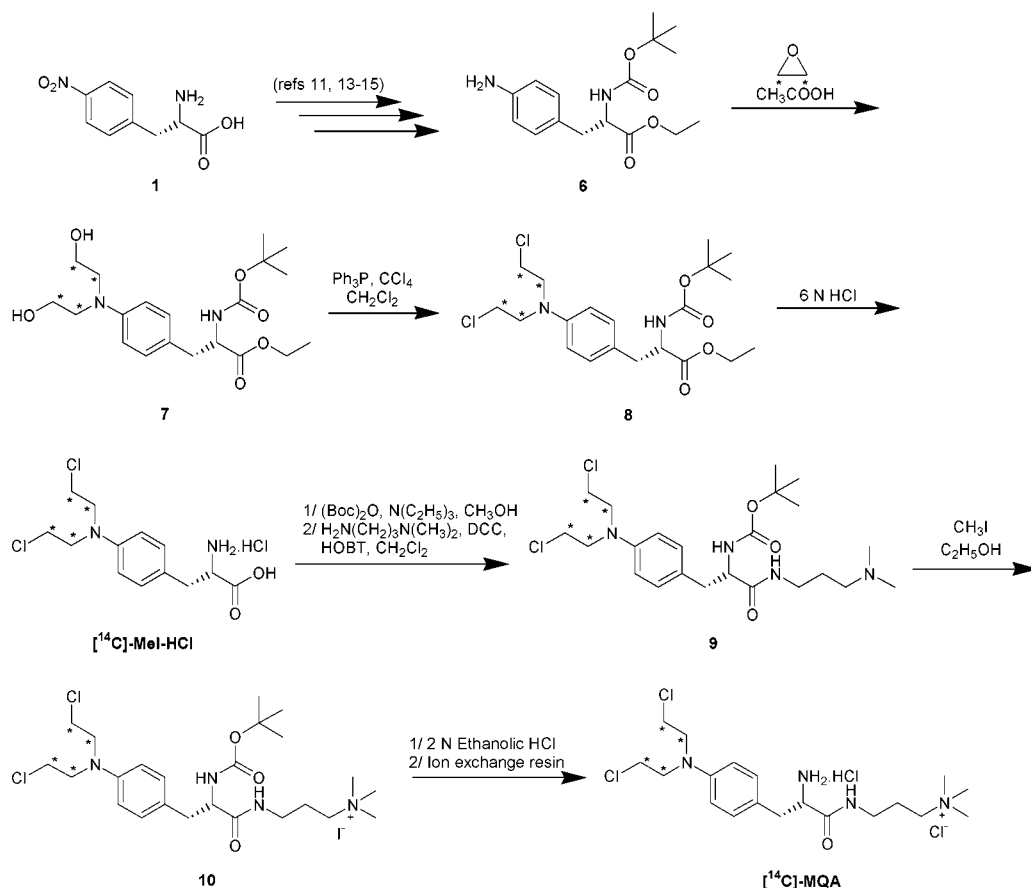
**Excretion Study.** In separate experiments, groups of five rats weighing 180–200 g given each [<sup>14</sup>C]-labeled test compound [27  $\mu\text{mol/kg}$ , 370 kBq (10  $\mu\text{Ci}$ )] were housed in metabolic cages (Iffa-Credo, l'Arbresle, France) enabling separate collection of feces and urine. Urine and feces were collected 6, 24, 48, and 72 h after administration. For the collection of expired [<sup>14</sup>C]-CO<sub>2</sub>, animal ( $n = 1$  for each test compound) was housed in an apparatus designed by us. Expired [<sup>14</sup>C]-CO<sub>2</sub> was trapped in a flask containing ethanolamine/methanol (20:80 v/v). Radioactivity of urine and ethanolamine/methanol samples was directly measured after addition of Packard Ultima Gold cocktail in a Wallac Winspectral 1414 liquid scintillation spectrometer. Radioactivity of dried feces was measured after combustion in a Packard 306 Oxidizer (Packard Instrument SA, Rungis, France).

**RESULTS**

**Preparation of [<sup>14</sup>C]-MQA.** The [<sup>14</sup>C]-radiolabeling was introduced in the chloroethyl groups for the following considerations: (i) In order to establish the cartilage targeting for the QA derivative, comparative biodistribution studies must be performed with MAQ and melphalan. Thus, the [<sup>14</sup>C]-radiosynthesis of MAQ and also that of melphalan had to be carried out. As both compounds were needed radiolabeled on the same position to allow the comparison of their biological results, [<sup>14</sup>C] was chosen to be incorporated into the mustard group. (ii) If the label was located in the alkylating portion of the molecule, the becoming of the biological active entity could be directly followed. On this basis, the radiolabeling was carried out by treatment of the adapted arylamine with [1,2-<sup>14</sup>C]-ethylene oxide, since 4-bis(2-hydroxyeth-

yl)aminoaryl derivatives can be converted readily into the corresponding 4-bis(2-chloroethyl)aminoaryl compounds.

To optimize the preparation of [<sup>14</sup>C]-MQA, two reversed synthetic approaches were investigated, both starting from 4-nitro-L-phenylalanine (**1**) (route A and route B, Scheme 1, and Scheme 2, respectively). Route A was based on the preliminary introduction of the spacer carrying the QA moiety and in the subsequent formation of the 2-chloroethyl entities. Inversely, according to route B, the formation of the nitrogen mustard group was performed before the introduction of the spacer: in fact, this sequence consisted in the synthesis of melphalan, and then in the preparation of MQA using melphalan as intermediate. These two reaction schemes were studied with unlabeled materials. Thus, according to route A, 4-nitro-L-phenylalanine (**1**) upon treatment with di-*tert*-butyl dicarbonate ((Boc)<sub>2</sub>O) and triethylamine in methanol afforded the *N*-*tert*-butyloxycarbonyl (t-Boc) derivative **2** in 83% yield. This *N*-protected intermediate **2** was then condensed with 3-(dimethylamino)propylamine in the presence of *N,N*-dicyclohexylcarbodiimide (DCC) and 1-hydroxybenzotriazole (HOBT) in dichloromethane to give the amide **3** in 71% yield after chromatographic purification. Then catalytic hydrogenation of compound **3** provided quantitatively the aminoaryl derivative **4** further converted to the dihydroxy compound **5** by reaction with ethylene oxide in acetic acid in 75% yield. Unfortunately, despite several attempts, the next to last step of route A based on the chlorination of **5** did not provide the desired compound. Consequently, the preparation of [<sup>14</sup>C]-MQA was performed using route B with melphalan as intermediate (Scheme 2). According to this route, *N*-t-Boc-4-amino-L-phenylalanine ethyl ester (**6**) was first prepared in three steps using published procedures (11, 14–16): esterification of **1** with ethanol, then protection of the amino group by a t-Boc group, and finally reduction of the nitro group to produce the amino derivative **6**. Then, [<sup>14</sup>C]-melphalan was synthesized from compound **6** according to a sequence slightly modified in comparison with the ones reported by literature and adapted to the use of radioactivity (11, 14, 16, 18). First, compound **6** was reacted with [1,2-<sup>14</sup>C]ethylene oxide in acetic acid to provide, after a purification by column

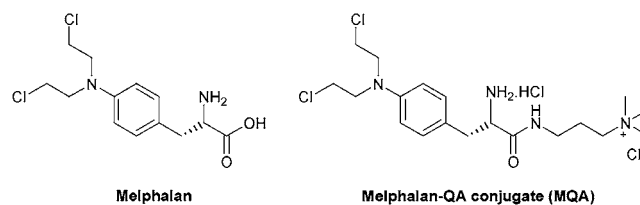
**Scheme 2. Synthesis of MAQ According to Route B**

chromatography on silica gel, the corresponding 4-[bis-(2-hydroxy-[1,2- $^{14}\text{C}$ ]ethyl)]amino-phenyl derivative (**7**) in 49% radiochemical yield. Chlorination of compound **7** with triphenylphosphine and carbon tetrachloride in dichloromethane gave the corresponding dichloro derivative **8** in 60% yield after chromatographic purification. Then, the *t*-Boc and ester protecting groups of compound **8** were removed with hydrochloric acid to provide [ $^{14}\text{C}$ ]-melphalan as its hydrochloride form ([ $^{14}\text{C}$ ]-Mel-HCl) in 89% yield. On the basis of this radiolabeled sequence, [ $^{14}\text{C}$ ]-Mel-HCl was isolated with a specific activity of 340 MBq/mmol (9.2 mCi/mmol) and a radiochemical purity of 99%, as determined by thin-layer chromatography analysis. For the preparation of [ $^{14}\text{C}$ ]-MQA from [ $^{14}\text{C}$ ]-Mel-HCl, the synthetic sequence was based on the syntheses developed for cold compounds (**6**). Thus, the amino group of [ $^{14}\text{C}$ ]-Mel-HCl was first protected again with a *t*-Boc group using  $(\text{Boc})_2\text{O}$  and triethylamine in methanol, and this *N*-protected melphalan was immediately coupled with 3-(dimethylamino)propylamine in the presence of DCC and HOBT to give the corresponding amide intermediate **9** in 62% overall yield after chromatographic purification. Quaternarization of the tertiary amine of **9** was carried out by condensation with methyl iodide to provide compound **10** in 92% yield. Treatment of **10** with ethanolic hydrochloric acid removed the Boc group and a chromatography over an ion-exchange resin (Dowex 1  $\times$  2-400) afforded the target quaternary ammonium derivative of melphalan ([ $^{14}\text{C}$ ]-MQA) in 91% yield. Finally, [ $^{14}\text{C}$ ]-MQA was isolated with a specific activity of 340 MBq/mmol (9.2 mCi/mmol) and a radiochemical purity of 99%, as determined by thin-layer chromatography analysis. The overall radiochemical yield of the labeling sequence was 13% based on [1,2- $^{14}\text{C}$ ]ethylene oxide.

**Table 1. Cumulative Radioactivity Excreted in Urine, Feces and Expired Air after Intravenous Administration of [ $^{14}\text{C}$ ]-Mel-HCl and [ $^{14}\text{C}$ ]-MQA in Male Sprague-Dawley Rats<sup>a</sup>**

	time (h)	urine	feces	[ $^{14}\text{C}$ ]-CO <sub>2</sub>	total excretion
Mel-HCl	0-6	47.01 $\pm$ 8.35	0.27 $\pm$ 0.37	3.85	75.78
	0-24	48.63 $\pm$ 7.97	12.25 $\pm$ 3.03	4.61	
	0-48	51.43 $\pm$ 8.07	16.35 $\pm$ 2.07	4.75	
	0-72	52.57 $\pm$ 8.09	16.97 $\pm$ 2.09	4.95	
	0-96	53.34 $\pm$ 8.08	17.49 $\pm$ 1.76		
MQA	0-6	45.24 $\pm$ 3.75	2.38 $\pm$ 4.21	1.86	89.14
	0-24	51.64 $\pm$ 3.49	23.27 $\pm$ 11.80	2.39	
	0-48	53.89 $\pm$ 3.95	29.40 $\pm$ 3.30	2.50	
	0-72	55.10 $\pm$ 3.81	30.38 $\pm$ 2.65	2.50	
	0-96	55.80 $\pm$ 3.89	30.84 $\pm$ 2.76		

<sup>a</sup> Results are expressed as the percentage of the injected dose and correspond to the mean  $\pm$  standard deviation for five animals for each point, except for [ $^{14}\text{C}$ ]-CO<sub>2</sub> (one rat studied).



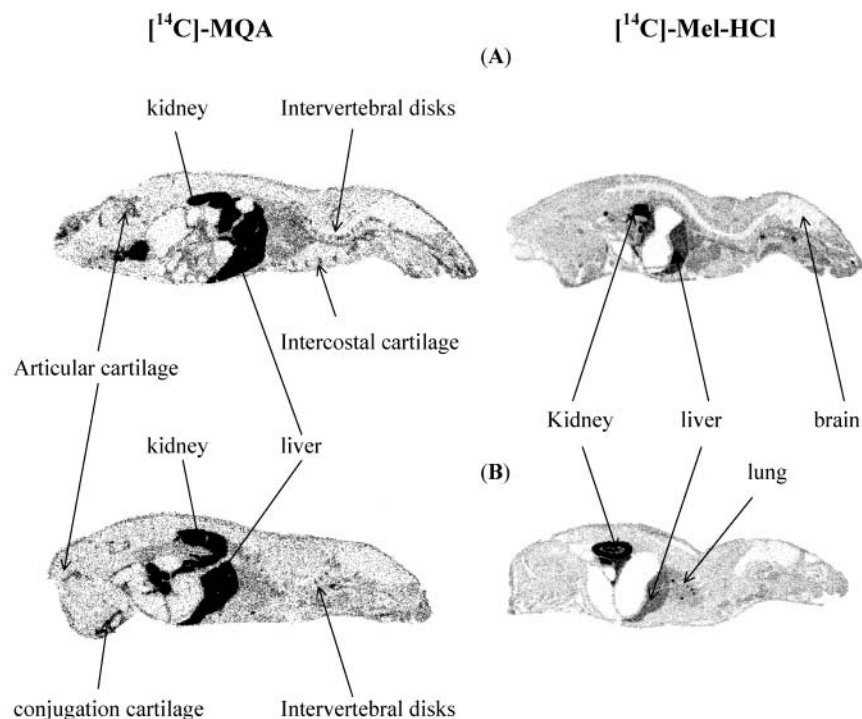
**Figure 1.** Structure of melphalan and its QA conjugate (MQA).

**Pharmacokinetic Studies. Radioactivity Excretion.** The cumulative excretion of the radioactivity in urine, feces and expired air of rats given iv a 27  $\mu\text{mol/kg}$  (10  $\mu\text{Ci}$ ) dose [ $^{14}\text{C}$ ]-Mel-HCl or its QA conjugate is shown in Table 1. These results showed that for both labeled species more than 50% of the radioactivity was excreted in the

**Table 2. Comparative Biodistribution of [<sup>14</sup>C]-Mel-HCl and [<sup>14</sup>C]-MQA in Male Sprague–Dawley Rats Following Intravenous Injection<sup>a</sup>**

tissue		liver	kidney	cartilage	blood	lung
2 min	Mel-HCl	142.4 ± 17.5	326.5 ± 55.9	<i>b</i>	116.9 ± 10.0	119.1 ± 13.6
	MQA	161.1 ± 16.6	457.3 ± 98.7	44.1 ± 5.4	69.7 ± 3.4	74.0 ± 5.2
5 min	Mel-HCl	120.5 ± 8.8	486.9 ± 174.9	<i>b</i>	70.4 ± 3.1	76.1 ± 10.0
	MQA	191.9 ± 30.4	379.4 ± 55.1	32.9 ± 6.7	24.2 ± 2.6	20.9 ± 4.3
10 min	Mel-HCl	80.8 ± 2.9	399.5 ± 182.6	<i>b</i>	48.6 ± 1.3	54.9 ± 4.2
	MQA	142.9 ± 12.1	264.6 ± 38.3	28.7 ± 5.3	15.1	15.8 ± 1.1
15 min	Mel-HCl	67.4 ± 3.5	403.6 ± 181.1	<i>b</i>	44.3 ± 2.7	45.7 ± 2.7
	MQA	108.8 ± 15.1	155.9 ± 30.2	15.8 ± 1.4	12.0	10.8 ± 1.5
30 min	Mel-HCl	45.3 ± 2.2	269.9 ± 120.9	<i>b</i>	26.0 ± 1.4	28.0 ± 1.1
	MQA	97.6 ± 9.2	190.7 ± 19.5	12.9 ± 3.2	9.1 ± 1.0	7.4 ± 0.5
1 h	Mel-HCl	53.3 ± 7.3	236.3 ± 63.1	<i>b</i>	22.2 ± 2.1	30.4 ± 4.4
	MQA	70.2 ± 3.8	191.3 ± 38.4	12.7	9.8 ± 0.7	11.6 ± 1.1
2 h	Mel-HCl	47.2 ± 6.2	184.6 ± 11.5	<i>b</i>	23.7 ± 3.4	23.8 ± 2.8
	MQA	33.2 ± 4.0	122.9 ± 36.5	<i>b</i>	<i>b</i>	<i>b</i>
6 h	Mel-HCl	21.6 ± 3.1	145.7 ± 42.2	<i>b</i>	14.5 ± 2.6	12.1 ± 2.9
	MQA	18.7 ± 2.4	74.8 ± 13.8	<i>b</i>	<i>b</i>	<i>b</i>
24 h	Mel-HCl	8.7 ± 0.5	63.9 ± 10.4	<i>b</i>	7.7	4.3 ± 0.4
	MQA	7.1 ± 2.0	41.5 ± 11.0	<i>b</i>	<i>b</i>	<i>b</i>

<sup>a</sup> Results are expressed as nanomoles drug equivalent per gram of tissue and correspond to the mean ± standard deviation for the quantification of eight whole-body sections of one animal for each point. <sup>b</sup> Non detectable.



**Figure 2.** Representative two-dimensional images obtained with Ambis 4000 detector of rat whole-body sections showing the tissue distribution of radioactivity 5 (A) and 15 min (B) following intravenous administration of each [<sup>14</sup>C]-labeled test compound: [<sup>14</sup>C]-Mel-HCl and [<sup>14</sup>C]-MQA. Each image is a screen printing, resulting from four different sheets which were contrasted differently. The images of cartilaginous tissues are only visualized on the slices of rats given [<sup>14</sup>C]-MQA.

urine and for [<sup>14</sup>C]-MQA fecal excretion was higher than for [<sup>14</sup>C]-Mel-HCl. Few radioactivity was found in expired CO<sub>2</sub> for the two compounds.

**Tissue Distribution.** Table 2 gives the radioactive tissue concentrations slices of rat given a 27 μmol/kg (30 μCi) of [<sup>14</sup>C]-Mel-HCl or [<sup>14</sup>C]-MQA determined by Ambis 4000 counting. Higher levels of each drug were found in the metabolizing and elimination organs, such as liver and kidney. Radioactivity rates in blood and lung of rats given [<sup>14</sup>C]-Mel-HCl were higher than in those of rats given [<sup>14</sup>C]-MQA. The radioactivity levels were quantified in cartilaginous tissue of rats as far as 1 h after injection of [<sup>14</sup>C]-MQA, while for [<sup>14</sup>C]-Mel-HCl, no cartilage quantification was possible because the cartilages of rat given [<sup>14</sup>C]-Mel-HCl are not visible despite the increase in contrast (Figure 2).

## DISCUSSION

The purpose of this work was to demonstrate the affinity of the melphalan QA conjugate for the cartilaginous tissues. This involved to perform pharmacokinetic studies in rats of the QA derivative, which consequently had to be radiolabeled. The tissue distribution study of [<sup>14</sup>C]-MQA was led with a new method of whole body autoradiography coupled with Ambis 4000 counting (17). Although melphalan was widely studied, to compare the behavior of both compounds, its pharmacokinetic study was also made with this method (19, 20).

Results of excretion of melphalan are consistent with those obtained in previous studies which showed that, although principally excreted by the urinary way, it was also eliminated by biliary and fecal ways. Urinary



excretion of [ $^{14}\text{C}$ ]-MQA was similar to that of its parent compound. On the other hand, a higher rate of radioactivity derived of [ $^{14}\text{C}$ ]-MQA was found in feces. [ $^{14}\text{C}$ ]-MQA was more eliminated than its parent compound. The amount of [ $^{14}\text{C}$ ]- $\text{CO}_2$  measured in the expired air for the two compounds suggests that a little part of two compounds was metabolized. The blood elimination of the QA conjugate was faster than that of melphalan. Indeed, 2 h after administration, radioactivity level in the blood of rats given [ $^{14}\text{C}$ ]-MQA was unquantifiable. For most organs no striking differences were found between melphalan and its QA conjugate except for cartilages. Amounts of radioactivity derived of [ $^{14}\text{C}$ ]-MQA were measured in cartilaginous tissues until 1 h after injection, whereas there were no images of cartilage on the slices of rat having received [ $^{14}\text{C}$ ]-Mel-HCl. As demonstrated in previous works, this study shows that the introduction of a QA moiety on melphalan allows the molecule to be carried selectively to cartilaginous tissues (1–4). As the label is located in the alkylating position of the molecule, the radioactivity due to [ $^{14}\text{C}$ ]-MQA and measured in the cartilaginous tissues results from unchanged compound or metabolite having kept the mustard group. In a previous work, we also demonstrated in cell culture that the QA functionalization does not affect the cytotoxic potency of melphalan, and even enhances it on a chondrosarcoma line, the effect being probably due to a binding to intracellular proteoglycans (5–6). On the basis of all these promising data, the next step will consist to evaluate the in vivo antitumor activity of the QA conjugate of melphalan on animals bearing chondrosarcoma.

#### ACKNOWLEDGMENT

This work was supported by Adir, Servier (France). We warmly thank Dr. Marie-France Moreau for helpful discussions.

#### LITERATURE CITED

- (1) Madelmont, J.-C., Giraud, I., Nicolas, C., Maurizis, J.-C., Rapp, M., Ollier, M., Renard, P., and Caignard, D.-H. French Patent 9,908,020, June 23, 1999, PCT/FR 00/01731, June 22, 2000.
- (2) Nicolas, C., Verny, M., Giraud, I., Ollier, M., Rapp, M., Maurizis, J.-C., and Madelmont, J.-C. (1999) New quaternary ammonium oxime derivatives targeted towards cartilage: synthesis, pharmacokinetic studies and anti-inflammatory potency. *J. Med. Chem.* 42, 5235–5240.
- (3) Giraud, I., Rapp, M., Maurizis, J.-C., and Madelmont, J.-C. (2000) Application to a cartilage targeting strategy: synthesis and in vivo biodistribution of [ $^{14}\text{C}$ ]-labeled quaternary ammonium-glucosamine conjugates. *Bioconjugate Chem.* 11, 212–218.
- (4) Maurizis, J.-C., Rapp, M., Nicolas, C., Ollier, M., Verny, M., and Madelmont, J.-C. (2000) Disposition in rats of *N*-pyridinium-propyl-cyclam, *N*-triethylammonium-propyl-cyclam, and *N*-[triethylammonium]-3-propyl-[15]ane-N5, potential cartilage imaging agents. *Drug Metab. Dispos.* 28, 418–422.
- (5) Maurizis, J.-C., Ollier, M., Nicolas, C., Madelmont, J.-C., Garrigue, H., and Veyre, A. (1992) In vitro binding of oxime acetylcholinesterase reactivators to proteoglycans synthesized by cultured chondrocytes and fibroblasts. *Biochem. Pharmacol.* 44, 1927–1933.
- (6) Giraud, I., Rapp, M., Maurizis, J.-C., and Madelmont, J.-C. (in press) Synthesis and in vitro evaluation of quaternary ammonium derivatives of chlorambucil and melphalan, anticancer drugs designed for the chemotherapy of chondrosarcoma. *J. Med. Chem.*
- (7) Dirix, L. Y., and Van Oosterom, A. T. (1991) Chondrosarcoma and other rare bone sarcomas. *Curr. Opin. Oncol.* 3, 694–699.
- (8) Lee, F. Y., Mankin, H. J., Fondren, G., Gebhardt, M. C., Springfield, D. S., Rosenberg, A. E., and Jennings, L. C. (1999) Chondrosarcoma of bone: an assessment of outcome. *J. Bone Joint Surgery Am.* 81, 326–338.
- (9) Springfield, D. S., Gebhardt, M. G., and McGuire, M. H. (1996) Chondrosarcoma: a review. *Intr. Course Lect.* 45, 417–424.
- (10) Chabner, B. A., Allegra, C. J., Curt, G. A., and Calabien, P. (1998) Anticancer Drugs. In *The Pharmacological Basis of Therapeutics*, 9th ed. (french version) (J. G. Hardman, L. E. Limbird, P. B. Molinoff, R. W. Ruddon, A. Goodman Gillman, A., Eds) pp 1225–1277, McGraw-Hill International (UK) Ltd., Berkshire, U.K.
- (11) Bergel, F., and Stock, J. A. (1954) Cyto-active amino-acid and peptide derivatives. Part I. Substituted Phenylalanines. *J. Chem. Soc.* 2409–2417.
- (12) Erlenmeyer, E., and Lipp, A. (1883) Synthese des tyrosins. *Anal. Chem.* 219, 161–233.
- (13) Compound (6) ESI-MS mass calcd for  $\text{C}_{16}\text{H}_{24}\text{N}_2\text{O}_4$  ( $\text{M}+\text{H}^+$ ): 309.18. Found: 309.16.
- (14) Nicolas, C., and Godenèche, D. (1978) Synthèse et marquage au  $^{14}\text{C}$  de la p-[bis(chloro-2-éthyl)amino]-L-phénylalanine ou melphalan. *J. Labeled Compd. Rad.* XIV, 205–214.
- (15) Verny, M., and Nicolas, C. (1988) [ $^3\text{H}$ ]-Labeling of hydroxyethyl groups – Synthesis of S-(2-hydroxy [2- $^3\text{H}$ ]ethyl) glutathione and of [ $^3\text{H}$ ]-melphalan. *J. Labeled Compound Radiat.* 25, 949–955.
- (16) Kupczyk-Subotkowska, L., Siahaan, T. J., Basile, A. S., Friedman, H. S., Higgins, P. E., Song, D., and Gallo, J. M. (1997) Modulation of melphalan resistance in glioma cells with a peripheral benzodiazepine receptor ligand–melphalan conjugate. *J. Med. Chem.* 40, 1726–1730.
- (17) Labarre P., Papon J., Moreau M. F., Madelmont, J.-C., and Veyre, A. (1998) A new quantitative method to evaluate the biodistribution of a radiolabeled tracer for melanoma using whole-body cryosectioning and a gaseous detector: comparison with conventional tissue combustion technology. *Eur. J. Nucl. Med.* 25, 109–114.
- (18) Soloway, A. H., and Nyilas, E. (1961) Synthesis of p-[di-(2- $^{14}\text{C}$ -chloroethyl)amino]-L-phenylalanine. A study of bis( $\beta$ -hydroxyethylation) of arylamines. *J. Org. Chem.* 26, 1091–1094.
- (19) Godenèche, D., Madelmont, J.-C., Moreau, M. F., Plagne, R., and Meyniel, G. (1980) Comparative physicochemical properties, biological effects and disposition in mice of four nitrogen mustards. *Cancer Chemother. Pharmacol.* 5, 1–9.
- (20) Byington, K. H., Bowe, C. C., and McKinsey, D. S. (1980) Biliary excretion of melphalan by control and anuric rats. *Biochem. Pharmacol.* 29, 2518–2520.

BC020031E

## COMMUNICATIONS

---

### A Rapid Method for the Construction of Oligonucleotide Arrays

P. Kumar and K. C. Gupta\*

Nucleic Acids Research Laboratory, Institute of Genomics and Integrative Biology  
(formerly Centre for Biochemical Technology), Mall Road, Delhi University Campus,  
Delhi-110 007, India . Received November 30, 2002

---

A simple method has been devised to construct oligonucleotide array on a variety of surfaces using commonly available reagents and chemistry with good efficiency and accuracy. The method involves the generation of hydroxyl functionalities on glass, polypropylene, polyethylene, and commonly used surfaces for construction of oligonucleotide arrays followed by their activation with trifluoroethane-sulfonyl chloride (tresyl chloride). The activated surface in the subsequent reaction is used to covalently immobilize oligonucleotides in regioselective fashion to create an oligonucleotide array. The surface bound tresyl sulfonate esters allow the immobilization of oligonucleotides specifically via their 3'- or 5'-end having mercaptohexyl- or aminohexyl functionalities. The constructed oligonucleotide arrays were successfully used to analyze oligonucleotides by hybridization technique.

---

#### INTRODUCTION

In recent years, the high-density oligonucleotide microarrays have emerged as an important tool for molecular biological studies. Arrays of short synthetic oligonucleotides have been used for various applications (1–4), viz., drug development, DNA sequencing, medical diagnostics, nucleic acid–ligand binding studies, DNA computing, etc. Basically, two approaches are being followed for the construction of oligonucleotide arrays. In one approach, the oligonucleotides are directly synthesized on the plane surface at a preselected position following conventional chemical methods or using photolithography or ink-jet methods (5). Though the photolithographic method is the most efficient method of constructing high-density oligonucleotide chips, it has

practical limitations in terms of flexibility and affordability. Another method, which is gaining popularity, is based on fixing prefabricated oligonucleotides on solid surface (6). The method offers great flexibility and can accommodate different chemistries as well as surfaces of choice. Two important factors which affect the quality of microarrays (microchip) fabricated by the latter method depend on the solid surface used and chemistry employed for fixing of oligonucleotides. A large number of chemical methods (7–10) and surfaces (11–13) have been reported for this purpose. We describe here a general method for the immobilization of presynthesized oligonucleotides on a variety of surfaces, e.g. glass, polypropylene, polyethylene, and polystyrene in regioselective fashion. The constructed oligonucleotide arrays were fully characterized and each spot spotted on different surfaces was visualized using labeled complementary oligonucleotides. The method employs a two-step process, viz., generation of hydroxyl functionalities on different surfaces followed

---

\* To whom correspondence should be addressed. Phone: 0091 11 2766 2491; Fax: 00 91 11 2766 7471. E-mail: kcgupta@igib.res.in.

**Table 1. Density of Hydroxyl Groups Generated via Photochemical Activation**

no.	polymer	loading
1.	polypropylene film	0.8 pmol/cm <sup>2</sup>
2.	polyethylene film	3.2 pmol/cm <sup>2</sup>
3.	polypropylene beads	11.6 $\mu$ mol/g
4.	polystyrene beads	16.3 $\mu$ mol/g
5.	controlled pore glass, 500 Å	9.7 $\mu$ mol/g

by activation with tresyl (2,2,2-trifluoroethanesulfonyl) chloride to have surface bound active sulfonate esters, which in the subsequent reaction with 3'- or 5'-mercapto- or aminohexyl-oligonucleotides result in surface bound oligonucleotides (microchip). Optimal concentration of oligonucleotide spots on the surface and other parameters were determined so that these microchips could be used effectively.

#### EXPERIMENTAL PROCEDURES

**Materials.** All the reagents were purified prior to their use. 2,2,2-Trifluoroethanesulfonyl chloride (tresyl chloride) and anthraquinone-2-methanol were procured from Aldrich Chemical Co., St. Louis, MO. Fluorescein-DMTr-dT-phosphoramidite (Fluorescein-dT) was obtained from Glen Research Inc., Sterling, VA. All the reactions were carried out in an inert atmosphere until unless it is specified. The synthesis of reagents, **1** and **2**, was carried out by reported procedures (14, 15). Polymer support, **3**, was prepared according to the published method (16) from this laboratory.

**Oligonucleotide Synthesis and Purification.** Oligonucleotides were synthesized on a 0.2  $\mu$ mol scale (Table 1) on a Pharmacia Gene Assembler Plus using the phosphoramidite approach following the manufacturer's protocol (17). After the synthesis of desired oligomers, the last coupling was performed with reagent **I** or **II** to generate 5'-amino- or 5'-mercaptohexyl groups, respectively. The coupling of these reagents was performed in an analogous manner to that of normal nucleoside-phosphoramidites. Similarly, the complementary labeled oligomers were synthesized with the last coupling performed with reagent **I**. After the deprotection reaction, the ammoniacal solutions in all the cases were concentrated in a speed vac and the residues dissolved in water (200  $\mu$ L) in each case and applied to a desalting column (reverse-phase C18 silica gel column). The oligomers were eluted with 30% acetonitrile in water, concentrated in a speed vac, and purified by anion-exchange chromatography on FPLC (Pharmacia) using buffer A (0.1 M NaCl, pH 12) and buffer B (1 M NaCl, pH 12) with a gradient 0–100 B in 35 min. These oligomers were then analyzed on reverse-phase high performance liquid chromatography (RP-HPLC) using a gradient of ammonium acetate (0.1 M, pH 7.1) and acetonitrile (0–50% B in 30 min). The complementary oligomers were then labeled with fluorescein isothiocyanate (FITC) following standard protocol (18) to obtain labeled oligomers for hybridization reactions.

Further, to study the concentration kinetics, an oligomer d(T<sup>F</sup>TT TTT TTT TTT TTT TTT–SH) (T<sup>F</sup> denotes fluorescein-dT) was synthesized on polymer support **III**. After d(T<sub>19</sub>) was synthesized on support **III**, the last coupling was performed with fluorescein-dT-phosphoramidite in an analogous manner to that of normal nucleoside-phosphoramidites except with an extended coupling time (5 min). Deprotection with aq ammonium hydroxide (30%) containing 0.1 M DTT yielded the desired fluorescein-labeled oligomer with a 3'-thiol group, which was desalted and purified as discussed above.

#### Generation of Hydroxyl Groups on Glass Slides.

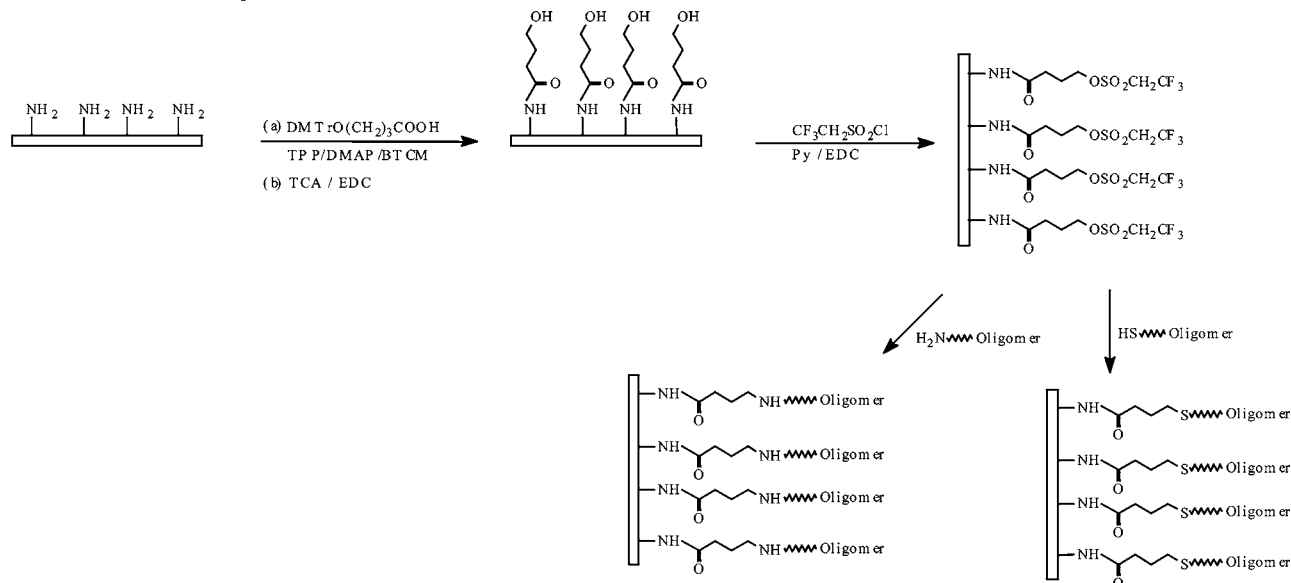
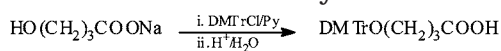
(i) *Preparation of O-(4,4'-Dimethoxytrityl)-4-hydroxybutyric Acid (DHBA).* 4-Hydroxybutyric acid sodium salt (10 mmol) was dried twice by coevaporation with anhydrous pyridine (25 mL) and finally suspended in pyridine (15 mL). To this suspension was added 4,4'-dimethoxytrityl chloride (10 mmol), and the mixture allowed to stir at room temperature for 5 h. After monitoring the completion of the reaction on TLC, it was quenched with the addition of methanol (1 mL). Pyridine was removed under vacuum on a rotary evaporator and the residue dissolved in ethyl acetate (150 mL). The organic layer was washed with 5% solution of sodium bicarbonate (2  $\times$  50 mL), citric acid (2  $\times$  50 mL), and water (1  $\times$  50 mL). The organic layer was collected and concentrated in vacuo to obtain the title compound in ~70% yield. <sup>1</sup>H NMR (CDCl<sub>3</sub>)  $\delta$ : 1.35 (m, 2H, CH<sub>2</sub>), 2.11 (t, 2H, CH<sub>2</sub>COO), 3.36 (t, 2H, OCH<sub>2</sub>), 3.78 (s, 6H, 2  $\times$  OCH<sub>3</sub>), 6.45–7.84 (m, 13H, Ar).

(ii) *Coupling of O-(4,4'-Dimethoxytrityl)-4-hydroxybutyric Acid with Aminated Glass Plates.* To a solution of O-(4,4'-dimethoxytrityl)-4-hydroxybutyric acid (1 mmol), 4-(dimethylamino)pyridine (2 mmol), and bromotrichloromethane (1 mmol) in *N,N*-dimethylformamide (5 mL) was added a solution of triphenylphosphine (1 mmol) in DMF (5 mL). The mixture was agitated for 30 s and added to a container with 3-aminopropylated glass plates. The reaction was allowed to stir for 1 h at room temperature. Then the plates were washed with DMF (2  $\times$  50 mL), methanol (1  $\times$  50 mL), and diethyl ether (2  $\times$  30 mL) and dried in air followed by under vacuum in a desiccator. The residual amino groups on the surface of glass slides were capped with a solution of acetic anhydride:triethylamine:1-methylimidazole:dichloromethane (1:1:0.4: 6, v/v/v/v) for 1 h at room temperature. Then the plates were washed with dichloromethane (3  $\times$  50 mL). After being dried in air, the plates were treated with a solution of 3% trichloroacetic acid in dichloromethane (3  $\times$  25 mL) to remove the DMTr group. Then the plates were washed with dichloromethane and dried under vacuum in a desiccator.

**Photochemical Functionalization of Polypropylene (PP) and Polyethylene (PE) Films.** To generate hydroxyl groups on the surface of inert polymers, e.g., polypropylene and polyethylene, the films were coated with a solution of anthraquinone-2-methanol (0.1 M) in acetonitrile:DMF (1:1, v/v) in a Petri dish. Then these films were exposed under UV irradiation (365 nm) for 30 min followed by washing of these films with DMF and methanol. To the dried films were added pyridine (5 mL), 4,4'-dimethoxytrityl chloride (1 mmol), and DMAP (0.1 mmol) separately. After 4 h of agitation, the solution was decanted off and washed with methanol (2  $\times$  10 mL) and diethyl ether (1  $\times$  10 mL) and dried. The extent of photochemical functionalization was determined by treating the measured pieces of films with a solution of 3% TCA in dichloromethane. The color released by this treatment was measured spectrophotometrically at 505 nm.

**Activation of Glass Slides and Polypropylene and Polyethylene Surfaces Using Tresyl Chloride.** Hydroxylated glass slide (or polypropylene or polyethylene film) was suspended in dry pyridine, and tresyl chloride (50 equiv) added dropwise over a period of 2–3 min. The contents were occasionally shaken for 1 h at room temperature. Subsequently, the solution was decanted off and washed with dry dichloromethane (3  $\times$  50 mL). Then the slides (or films) were dried under vacuum in a desiccator.



**Scheme 1. Chemical Pathway To Immobilize Oligonucleotides on the Tresylated Surface**

**Time Kinetics To Determine Optimal Time for Immobilization of Oligomers on the Preactivated Surface and their Efficiency of Immobilization.** To optimize the time required to fix the 5'-modified oligonucleotides on the tresylated surface as well as the extent of immobilization, an experiment was designed using controlled pore glass support (500 Å). The hydroxylated-CPG (200 mg, hydroxyl groups loading  $\sim 55 \mu\text{mol/g}$  of support) was activated with an excess of tresyl chloride (50 equiv) in anhydrous pyridine (4 mL). After 2 h, the support was washed with pyridine, acetonitrile, and dichloromethane (20 mL of each). In the subsequent steps, the activated support was divided into 14 parts, and the first seven parts were treated with 0.1 M solution of  $\text{DMTrO}(\text{CH}_2)_3\text{NH}_2$  and the other seven parts were treated with 0.1 M solution of  $\text{DMTrO}(\text{CH}_2)_6\text{SH}$  in the presence of triethylamine. The tubes were agitated at room temperature, and one tube from each set was withdrawn after a definite time interval (ca. 10 min). The support was washed with dichloromethane containing triethylamine (0.1%) and dried in a vacuum desiccator. Then the extent of reaction was determined by treating a weighed amount of support from each tube with 3% trichloroacetic acid in dichloromethane. The orange color of the DMTr cation released was measured spectrophotometrically, and the loading was determined in  $\mu\text{mol/g}$  of support. A graph was plotted between loading ( $\mu\text{mol/g}$ ) vs time (min). On the basis of calculation of loadings, the extent of reaction was determined.

**Concentration Kinetics To Determine Optimal Concentration of Oligonucleotide Spots on Surfaces for Fluorescent Detection.** To arrive at the optimal concentration required to visualize an oligomer immobilized on the glass surface, fluorescent oligomer  $\text{d}(\text{T}^{\text{F}}\text{TTT TTT TTT TTT TTT TT-SH})$  was diluted to four different concentrations (6, 10, 14, and  $20 \mu\text{M}$ ) in 0.1 M phosphate buffer containing 0.5 M NaCl, pH 8.0. The oligomer was spotted ( $0.5 \mu\text{L}$ ) manually in triplicates. After incubation for 30 min at room temperature, the slide was washed with 0.1 M phosphate buffer containing 0.5 M sodium chloride. After the slides were dried, the spots were visualized under laser scanner at 515 nm.

**Immobilization of 5'-Mercapto- or Aminoethyl-Oligonucleotides onto Tresylated Glass and Polypropylene and Polyethylene Surfaces.** The 5'-mercapto- and aminoethyl-oligonucleotides with concentration  $10 \mu\text{M}$  ( $0.5 \mu\text{L}$ ) were spotted on the tresylated surface in quadruplicate using a  $2 \mu\text{L}$  pipetman. After incubation for 30 and 60 min, respectively, for mercapto- and aminoethyl-oligonucleotides in a covered Petri dish at room temperature under inert atmosphere, the plates were washed with 0.1 M phosphate buffer followed by 0.5 M Tris buffer, pH 8.0, for 2 h in order to cap the unreacted tresyl groups. After washing with 0.1 M phosphate buffer ( $3 \times 20 \text{ mL}$ ), the plates were dried and used for hybridization experiment.

In a hybridization chamber, the spots on the plates were exposed to complementary oligomers labeled with fluorescein in a 0.1 M phosphate-saline buffer, pH 7.0. The solution was kept in contact with the immobilized oligomers for 2 h with gentle agitation at  $37^\circ\text{C}$ . After hybridization, the plates or surfaces were washed with the same buffer to remove excess complementary oligomers, and the spots on the plates were visualized under a laser scanner at 515 nm.

**RESULTS AND DISCUSSION**

In the present investigation, a method has been developed for covalent fixing of amino- and mercapto-hexylated-oligonucleotides. The strategy has been designed keeping the following points in mind, viz., (i) the method should be rapid, and (ii) it should not involve complex chemistry and reaction conditions as well as costly chemicals. Keeping these points into consideration, a rapid and clean method has been developed for immobilizing end-modified oligonucleotides.

**Chemical Method for the Generation of Hydroxyl Groups on 3-Aminopropylated Glass Slides.** The method begins with the generation of hydroxyl functionalities on glass microslides on which the oligomers are to be immobilized (Scheme 1). The reagent, *O*-(4,4'-dimethoxytrityl)-4-hydroxybutyric acid (DHBA), was prepared with the sodium salt of 4-hydroxybutyric acid and

**Table 2.** Oligonucleotide Sequences Synthesized, Their Deprotection Conditions, and Yields

no.	oligonucleotide sequence <sup>a</sup>	deprotection conditions	yield (A <sub>254</sub> nm, OD)
1	5'-H <sub>2</sub> N(CH <sub>2</sub> ) <sub>6</sub> OPO <sub>3</sub> (TTT TTT TTT TTT TTT TT)-3'	aq NH <sub>4</sub> OH, 16 h, 60 °C	28.8
2	5'-HS(CH <sub>2</sub> ) <sub>6</sub> OPO <sub>3</sub> (TTT TTT TTT TTT TTT TT)-3'	aq NH <sub>4</sub> OH containing 0.1 M DTT, 16 h, 60 °C	24.7
3	5'-H <sub>2</sub> N(CH <sub>2</sub> ) <sub>6</sub> OPO <sub>3</sub> (CTG CAT GCA TTA CCA CCT TT)-3'	aq NH <sub>4</sub> OH, 16 h, 60 °C	29.4
4	5'-HS(CH <sub>2</sub> ) <sub>6</sub> OPO <sub>3</sub> (CTG CAT GCA TTA CCA CCT TT)-3'	aq NH <sub>4</sub> OH containing 0.1 M DTT, 16 h, 60 °C	25.3
5	5'-Fluorescein-HN(CH <sub>2</sub> ) <sub>6</sub> OPO <sub>3</sub> (AAA AAA AAA AAA AAA AA)-3'	aq NH <sub>4</sub> OH, 16 h, 60 °C	23.1
6	5'-Fluorescein-HN(CH <sub>2</sub> ) <sub>6</sub> OPO <sub>3</sub> (AAA GGT GGT AAT GCA TGC AG)-3'	aq NH <sub>4</sub> OH, 16 h, 60 °C	24.2
7	5'-d(T <sup>F</sup> TT TTT TTT TTT TTT TT)O <sub>3</sub> PO(CH <sub>2</sub> ) <sub>5</sub> NHCO(CH <sub>2</sub> ) <sub>2</sub> SH-3'	aq NH <sub>4</sub> OH containing 0.1 M DTT, 16 h, 60 °C	23.6
8	5'-H <sub>2</sub> N(CH <sub>2</sub> ) <sub>6</sub> OPO <sub>3</sub> (ATG CTG ATT CCG TTC CTC AT)-3'	aq NH <sub>4</sub> OH, 16 h, 60 °C	28.6

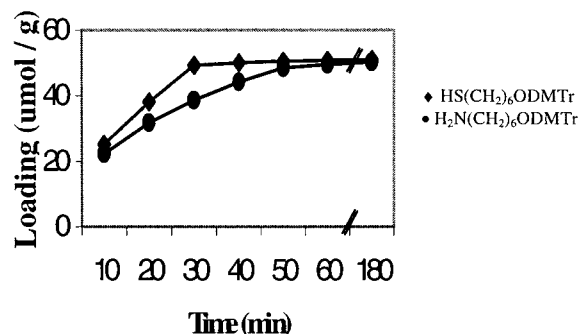
<sup>a</sup> T<sup>F</sup> denotes fluorescein-dT.

4,4'-dimethoxytrityl chloride in pyridine. To generate hydroxyl functionalities on glass microslides, commercially available 3-aminopropylated glass slides (Sigma, St. Louis, MO) were treated with this DHBA reagent using the oxidation–reduction condensation method as reported (19) earlier from this laboratory. The residual amino groups on the surface were blocked by acetic anhydride and triethylamine in anhydrous dichloromethane containing 1-methylimidazole. The hydroxyl groups were generated on treatment with 3% trichloroacetic acid (TCA) in dichloromethane for 10 min followed by washing with dichloromethane. The hydroxyl group bearing microslides were stored at room temperature under dry conditions.

**Photochemical Method for Generation of Hydroxyl Groups on a Variety of Inert Surfaces (polymers).** Basically, two protocols are being followed for the generation of functional groups in commonly used inert polymers, viz., polypropylene, polystyrene, polyethylene, etc. One method is based on generation of reactive functional groups by chemical methods either via free radical formation or by oxidation of the backbone of the polymer. The other one is based on photochemical activation, which involves the coating of a photoactivatable compound having functional groups on a polymer surface using organic solvent and a drying method. On exposure to ultraviolet light at 365 nm, the photochemically active group reacts with the polymer surface and the functional group is generated.

In this communication, hydroxyl groups were generated on the inert polymers with the help of photochemically active compound, anthraquinone-2-methanol. A solution of anthraquinone-2-methanol in acetonitrile-DMF (1:1, v/v) was coated on the polymer surface, viz., polypropylene (film and beads), polyethylene film, polystyrene beads, controlled pore glass beads, followed by irradiation under UV light (365 nm). The generated hydroxyl groups were reacted with DMTrCl, and the loading was determined after exposing a measured amount of beads or film to 3% TCA followed by spectrophotometric determination of DMTr cation released at 505 nm. The results are summarized in Table 1.

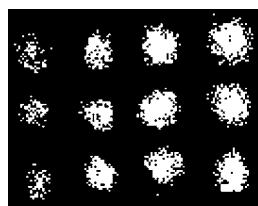
**Activation of Hydroxyl Groups.** To make the surface suitable for immobilization of amino- or mercaptoalkylated oligonucleotides, the hydroxyl groups on the polymer surfaces including glass slides were activated with tresyl chloride. It is well-known that mercaptoalkyl and aminoalkyl groups are the most reactive nucleophiles with sulfonate esters, with mercaptoalkyls showing the highest reactivity. Activation of glass slides with tresyl chloride was carried out in strictly anhydrous conditions (under Ar atmosphere). Tresyl chloride was added to glass slides and polymer films dipped in anhydrous

**Figure 1.** Time kinetics of the reaction of tresylated support with amino- and mercaptohexyl ligand.

pyridine. After washings with dry pyridine and diethyl ether, the plates were directly used for immobilization of oligonucleotides.

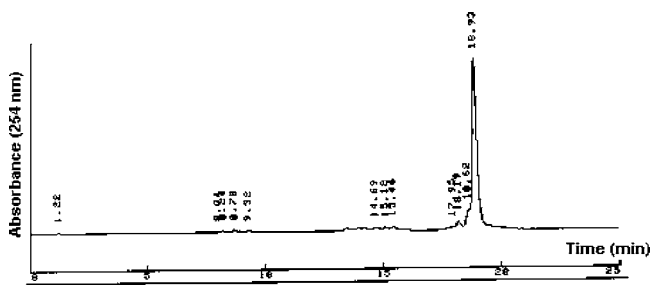
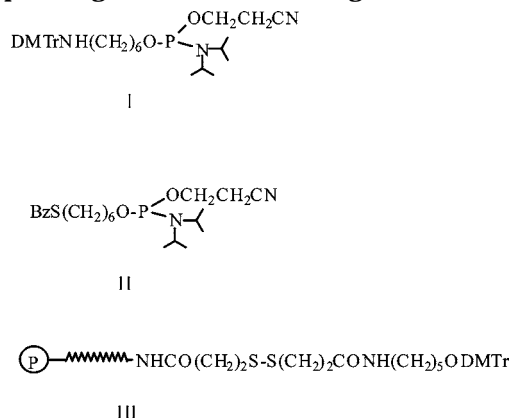
**Time Kinetics of the Reaction between Tresyl Activated Beads and Amino-/Mercaptoalkylated Ligand.** To arrive at the optimum time required for immobilization of modified oligonucleotides on the tresylated surface, the following experiment was designed. Tresylated-CPG (500A, 20 mg each) was taken up in seven vials and treated with 4,4'-dimethoxytrityloxy-5-amino-hexane. Vials were withdrawn at definite time intervals, and the contents were filtered, washed, and dried. The loading was determined and plotted against time (in minutes) as shown in Figure 1. Similarly, the reaction was carried out with 4,4'-dimethoxytrityloxy-6-mercaptohexane, and results are shown in Figure 1. The reaction completes in 30 and 60 min, respectively, in case of mercaptoalkyl- and aminoalkylated compounds. The extent of reactions were found to be ~89.4 and ~90.2%, respectively, in case of mercaptoalkyl- and aminoalkylated compounds. The same time period was used for the immobilization of oligonucleotides with 5'-mercaptohexyl and amino-hexyl groups.

**Concentration Kinetics To Determine Optimal Concentration of Oligonucleotide Spots on Surfaces for Fluorescent Detection.** Similarly, to calculate the optimal concentration required to visualize an oligomer immobilized on the glass surface, an oligomer d(T<sup>F</sup>TT TTT TTT TTT TTT T-SH) (entry 7, Table 2) was synthesized and diluted in four different concentrations (6, 10, 14, and 20 μM) in 0.1 M phosphate buffer containing 0.5 M NaCl, pH 8.0. The oligomer was spotted (0.5 μL) manually in triplicates. After incubation for 30 min at room temperature, the slide was washed with 0.1 M phosphate buffer containing 0.5 M sodium chloride. After drying the slides, the spots were visualized under laser scanner at 515 nm. Figure 2 shows the spots visualized under a laser scanner.

6  $\mu$ M 10  $\mu$ M 14  $\mu$ M 20  $\mu$ M

**Figure 2.** Immobilization of d(T<sup>18</sup>TTT TTT TTT TTT TTT TTT TTT)O<sub>3</sub>PO(CH<sub>2</sub>)<sub>5</sub>NHCO(CH<sub>2</sub>)<sub>2</sub>SH on a tresyl-activated surface in a concentration dependent manner in triplicates. Lane 1: 6  $\mu$ M; Lane 2: 10  $\mu$ M; Lane 3: 14  $\mu$ M; Lane 4: 20  $\mu$ M.

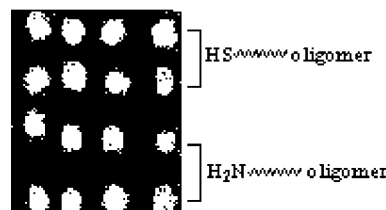
**Scheme 2. Reagents and Polymer Support Used for Incorporating Modifications in Oligonucleotides**



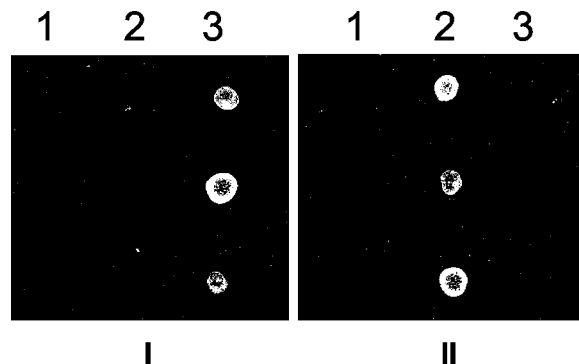
**Figure 3.** RP-HPLC elution profile of AEX-FPLC purified 5'-H<sub>2</sub>N(CH<sub>2</sub>)<sub>6</sub>OPO<sub>3</sub>(TTT TTT TTT TTT TTT TTT TT)-3'. Conditions: column, Lichrosphere RP-18 (Merck, Germany); buffer A, 0.1M NH<sub>4</sub>OAc, pH 7.1, solvent B, acetonitrile; flow rate, 1.0 mL/min; gradient, 0–50% B in 30 min; aufs, 0.05.

**Oligonucleotide Synthesis, Purification and Immobilization.** Oligomers were synthesized at 0.2  $\mu$ mol scale with desired modification (Table 2) on a Gene Assembler Plus (Scheme 2). After synthesis, the removal of protecting groups from nucleic bases and internucleotide phosphates and cleavage of oligomer chains from polymer support were effected by treatment of aq ammonium hydroxide (Table 2). The ammoniacal solution was removed under vacuum in a speed vac, and the residue was subjected to desalting on a reverse-phase silica gel column. The oligomers were purified by anion-exchange FPLC and analyzed on reverse-phase HPLC. Figure 3 shows an elution profile of an oligomer, 5'-H<sub>2</sub>N(CH<sub>2</sub>)<sub>6</sub>OPO<sub>3</sub>(TTT TTT TTT TTT TTT TTT TT)-3' on RP-HPLC after purification. Other oligomers used for immobilization purposes were of same quality.

Immobilization of 5'-aminoethyl- (entry 3, Table 2) and mercaptohexylated (entry 4, Table 2) oligomers was performed by dissolving these oligomers in 0.1 M phosphate buffer (pH 8.0) and spotted (0.5  $\mu$ L) with the help of a 2  $\mu$ L pipetman on the tresyl-activated surface. The



**Figure 4.** Immobilization of 5'-H<sub>2</sub>N(CH<sub>2</sub>)<sub>6</sub>OPO<sub>3</sub>(CTG CAT GCA TTA CCA CCT TT) and 5'-HS(CH<sub>2</sub>)<sub>6</sub>OPO<sub>3</sub>(CTG CAT GCA TTA CCA CCT TT) on tresylated surface followed by hybridization with labeled oligomer, 5'-fluorescein-HN(CH<sub>2</sub>)<sub>6</sub>OPO<sub>3</sub>(AAA GGT GGT AAT GCA TGC AG). Lane 1 and 2: Immobilization of 5'-H<sub>2</sub>N(CH<sub>2</sub>)<sub>6</sub>OPO<sub>3</sub>(CTG CAT GCA TTA CCA CCT TT); Lane 3, 4: Immobilization of 5'-HS(CH<sub>2</sub>)<sub>6</sub>OPO<sub>3</sub>(CTG CAT GCA TTA CCA CCT TT).



**Figure 5.** Specificity of labeled probes toward their targets. In both the slides, Lane 1: 5'-H<sub>2</sub>N(CH<sub>2</sub>)<sub>6</sub>OPO<sub>3</sub>(ATG CTG ATT CCG TTC CTC AT)-3'; Lane 2: 5'-H<sub>2</sub>N(CH<sub>2</sub>)<sub>6</sub>OPO<sub>3</sub>(CTG CAT GCA TTA CCA CCT TT)-3'; Lane 3: 5'-H<sub>2</sub>N(CH<sub>2</sub>)<sub>6</sub>OPO<sub>3</sub>(TTT TTT TTT TTT TTT TT)-3'. Slide I was hybridized with 5'-fluorescein-HN(CH<sub>2</sub>)<sub>6</sub>OPO<sub>3</sub>(AAA AAA AAA AAA AAA AAA AA) and slide II was with 5'-fluorescein-HN(CH<sub>2</sub>)<sub>6</sub>OPO<sub>3</sub>(AAA GGT GGT AAT GCA TGC AG).

spotted plates were kept in a humid Petri dish in an inert atmosphere for 30 and 60 min, respectively, in case of mercapto- and aminoethylated oligomers. After a stipulated time, the plates were washed and the residual active sites were blocked by Tris buffer.

**Hybridization of Microarray with Complementary Oligonucleotides.** The spotted plates were subjected to a hybridization experiment with complementary oligomers. The plates were covered with a solution of complementary fluorescent oligonucleotides (entry 6, Table 2) in a hybridization chamber. After being washed with phosphate buffer, the spots were visualized under a laser scanner at 515 nm as shown in Figure 4.

**Specificity of Labeled Probes.** To demonstrate the specificity of the labeled probes to their complementary targets, oligonucleotides, viz., 5'-H<sub>2</sub>N(CH<sub>2</sub>)<sub>6</sub>OPO<sub>3</sub>(TTT TTT TTT TTT TTT TT)-3', 5'-H<sub>2</sub>N(CH<sub>2</sub>)<sub>6</sub>OPO<sub>3</sub>(CTG CAT GCA TTA CCA CCT TT)-3', and 5'-H<sub>2</sub>N(CH<sub>2</sub>)<sub>6</sub>OPO<sub>3</sub>(ATG CTG ATT CCG TTC CTC AT)-3', were immobilized in triplicates on the activated glass slides as discussed above. On one slide, all the three immobilized oligonucleotides were hybridized with 5'-fluorescein-HN(CH<sub>2</sub>)<sub>6</sub>OPO<sub>3</sub>(AAA AAA AAA AAA AAA AAA AA), and on the second one, the immobilized targets were hybridized with 5'-fluorescein-HN(CH<sub>2</sub>)<sub>6</sub>OPO<sub>3</sub>(AAA GGT GGT AAT GCA TGC AG) in a hybridization chamber as discussed above. After being washed with phosphate buffer, the slides were scanned under a laser scanner at 515 nm. The first slide showed positive spots corresponding to d(T<sub>20</sub>), while the second slide showed positive spots corresponding to d(CTG CAT GCA TTA CCA CCT TT) as shown in Figure 5. Other spots were found invisible under laser scanner.



## CONCLUSION

A general method has been developed for the construction of an oligonucleotide array using presynthesized and end-modified oligonucleotides and employing a variety of inert surfaces. A photochemical method of generating functional groups on inert surfaces has also been developed, which allows one to have choices of solid surfaces for different applications. Since the method involves commonly used reagents, chemicals, and chemistry, it is hoped that this will enable individuals, particularly end users or nonchemists, an easy access to an oligonucleotide microarray for various studies.

## ACKNOWLEDGMENT

Authors gratefully thank Prof. S. K. Brahmachari, Director, IGIB, for his advice to initiate this project and also acknowledge the timely help of Dr. G. W. Rembhotkar for laser scanning the microslides.

## LITERATURE CITED

- (1) Drobyshev, A. N., Mologina, N., Shick, V., Pobedinskaya, D., Yershov, G., and Mirzabekov, A. D. (1997) Sequence analysis by hybridization with oligonucleotide chip: identification of  $\beta$ -thalassemia mutations. *Gene* 188, 45–52.
- (2) Hacia, J. G., Brody, L. C., Chee, M. S., Fodor, S. P. A., and Collins, F. S. (1996) Detection of heterozygous mutations in BRCA1 using high-density oligonucleotide arrays and two color fluorescence analysis. *Nat. Genet.* 14, 441–447.
- (3) Yershov, G., Barsky, V., Belgovskiy, A., Kirillov, E., Kreindlin, E., Ivanov, I., Parinov, S., and Guschin, D. (1996) DNA analysis and diagnostics on oligonucleotide microchips. *Proc. Natl. Acad. Sci. U.S.A.* 93, 4913–4918.
- (4) Cho, R. J., Fromont-Racine, M., Wodicka, L., Feierbach, B., Stearns, T., Legrain, P., Lockhart, D. J., and Davis, R. (1998) Parallel analysis of genetic selections using whole genome oligonucleotide arrays. *Proc. Natl. Acad. Sci. U.S.A.* 95, 3752–3757.
- (5) Schena, M. (2000) *Microarray Biochip Technology*, Eaton Publishing, Natick, MA.
- (6) Beier, M., and Hoheisel, J. D. (1999) Versatile derivatization of solid support media for covalent binding on DNA-microchips. *Nucleic Acids Res.* 27, 1970–1977.
- (7) Proudnikov, D., Timofeev, E., and Mirzabekov, A. D. (1998) Immobilization of DNA in polyacrylamide gel for the manufacture of DNA and DNA-oligonucleotide microchips. *Anal. Biochem.* 259, 34–41.
- (8) Rehman, F. N., Audeh, M., Abrams, E. S., Hammond, P. W., Kenney, M., and Christian Boles, T. (1999) Immobilization of acrylamide-modified oligonucleotides by copolymerization. *Nucleic Acids Res.* 27, 649–655.
- (9) Raddatz, S., Mueller-Ibeler, J., Kluge, J., Wab, L., Burdinski, G., Havens, J. R., Onofrey, T. J., Wang, D., and Schweitzer, M. (2002) Hydrazide oligonucleotides: new chemical modification for chip array attachment and conjugation. *Nucleic Acids Res.* 30, 4793–4802.
- (10) Kumar, A., Larsson, O., Parodi, D., and Liang, Z. (2000) Silanized nucleic acids: a general platform for DNA immobilization. *Nucleic Acids Res.* 28, e71.
- (11) Joos, B., Kuster, H., and Cone, R. (1997) Covalent attachment of hybridizable oligonucleotides to glass supports. *Anal. Biochem.* 247, 96–101.
- (12) Rasmussen, S. R., Larsen, M. R., and Rasmussen, S. (1991) covalent immobilization of DNA onto polystyrene microwells: the molecules are only bound at the 5'-end. *Anal. Biochem.* 198, 138–142.
- (13) Bader, R., Hinz, M., Schu, B., and Seliger, H. (1997) Oligonucleotide microsynthesis of a 200-mer and of one-dimensional arrays on a surface hydroxylated polypropylene tape. *Nucleosides Nucleotides* 16, 829–833.
- (14) Gaur, R. K., Sharma, P., and Gupta, K. C. (1989) A simple method for the introduction of thiol group at 5'-termini of oligonucleotides. *Nucleic Acids Res.* 17, 4404.
- (15) Kumar, P., Bhatia, D., Rastogi, R. C., and Gupta, K. C. (1996) Solid-phase synthesis and purification of 5'-mercaptoalkylated oligonucleotides. *BioMed. Chem. Lett.* 6, 683–688.
- (16) Gupta, K. C., Sharma, P., Sathyanarayana, S., and Kumar, P. (1990) A universal support for the synthesis of 3'-thiol group containing oligonucleotides. *Tetrahedron Lett.* 31, 247–250.
- (17) Pharmacia. LKB Gene Assembler Plus Manual, Upsala, Sweden.
- (18) Eckstein, F. (1991) *Oligonucleotides and Analogues: A Practical Approach*, IRL Press, Oxford.
- (19) Kumar, P., Sharma, A. K., Sharma, P., Garg, B. S., and Gupta, K. C. (1996) Express protocol for functionalization of polymer supports for oligonucleotide synthesis. *Nucleosides Nucleotides* 15, 879–888.

BC025646Q

# Photoenhancement of Transfection Efficiency Using Novel Cationic Lipids Having a Photocleavable Spacer

Takeshi Nagasaki,<sup>\*,†</sup> Akinobu Taniguchi, and Seizo Tamagaki

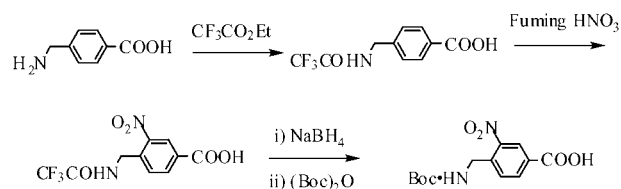
Department of Applied and Bioapplied Chemistry, Graduate School of Engineering, Osaka City University, SORST (JST), Osaka, 558-8585, Japan . Received December 26, 2002

New cationic lipids having an *o*-nitrobenzyl moiety as a photocleavable spacer between its hydrophilic and hydrophobic region were synthesized. To improve the efficiency of transfection with lipoplexes, after transfecting the cationic lipid aggregate/DNA complex, photoirradiation was performed. Photochemical decomposition of lipids would not only make the vector's membrane unstable to facilitate the fusion with endocytic vesicles, but also promote dissociation of cationic lipid–DNA complex, thus aiding the escape of DNA from the endocytic vesicles. Using a luciferase gene as a model, we show that UV irradiation of photoresponsive lipoplex-treated COS-1 cells induces a substantial increase in the efficiency of transfection. Herein, we show a novel photoresponsive gene delivery system.

In such techniques as gene therapy, when transducing and expressing exogenous genes in mammalian cells, viral vectors, which are natural DNA complex nanoparticles, are used in the overwhelming majority of the cases. The reason for this is their high efficiency, but their disadvantages include high cost, inability to transduce large genes, and safety issues. As a result, there is an urgent need to develop highly efficient nonviral vectors using artificial nanoparticles, such as liposome (lipid aggregate)/DNA complexes (lipoplexes) or polymer/DNA complexes (polyplexes) (*1*). To improve the transfection efficiency of nonviral vectors, it is necessary to improve several problems (*2–5*). With lipoplexes, one serious obstacle is the escape of DNA from endocytic vesicles after passing through the cell membrane by endocytosis (*6–10*). Factors affecting the endocytic pathway could either facilitate escape of plasmid DNA into the cytosol or protect these molecules from degradation by lysosomal nucleases, thereby influencing the efficiency of transfection (*11–15*). Prasmickaite et al. used a phthalocyanine derivative as a photosensitizer, and by destabilizing the membrane of endocytic vesicles with light irradiation, they successfully facilitated the escape of an exogenous gene and improved transfection efficiency (*16*). However, this method is highly toxic, and although the transfection efficiency of polyplexes is improved, the transfection efficiency of lipoplexes is reduced (*17*). With the exception of this type of photochemical internalization using photosensitizers, no studies have investigated the delivery of exogenous genes into the cytoplasm using the photoresponsive system.

In the hope of facilitating the escape of a gene from endocytic vesicles and improving transfection efficiency, we have investigated photoresponsive gene carriers and using UV irradiation during gene delivery to destabilize endocytic vesicle membranes and to facilitate membrane fusion. In the present study, to improve the efficiency of

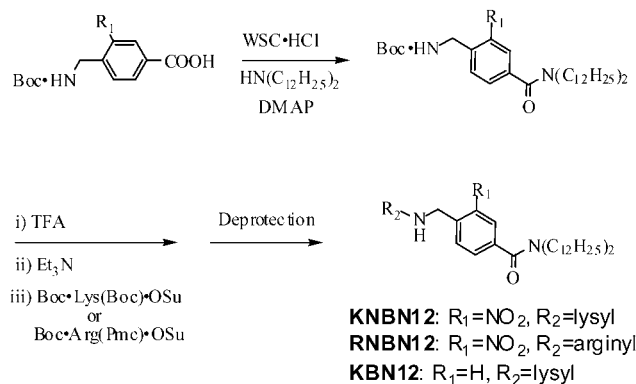
## Scheme 1. Synthesis of Boc-derivative of 3-Nitro-4-aminomethylbenzoic Acid



transfection with lipoplexes, after transfecting cationic lipid aggregate/DNA complexes including a photocleavable section in the lipid component, photoirradiation was performed. Photocleavage of cationic lipids would make vector's membranes unstable to facilitate the fusion with endocytic vesicles, thus resulting in the induction of the destabilization of vesicular membrane and aiding the escape of DNA from the endocytic vesicles. Key intermediate, Boc-derivative of 3-nitro-4-aminomethylbenzoic acid (*18*), was prepared in 43% total yield according with a modified synthetic route (Scheme 1). New photocleavable lipids, having an *o*-nitrobenzyl structure as a spacer, a lysine or arginine residue in its hydrophilic region, and a didodecyl tertiary amide structure in its hydrophobic region, were synthesized in the dark. New photocleavable lipids (**KNBN12** and **RNBN12**) were obtained in 36% and 41% total yield from Boc-derivative of 3-nitro-4-aminomethylbenzoic acid, respectively. Nonphotocleavable compound (**KBN12**) was also synthesized as control in 45% total yield (Scheme 2).<sup>1</sup> These lipids were dissolved in a chloroform/MeOH (50/50) solution, and through the use of an evaporator, a thin membrane was formed along the wall of a glass tube. Then, through the use of a vortex, the thin membrane was subjected to ultrasound at 50 °C and dispersed in a Tris buffer (pH 7.5) to attempt lipid aggregate formation. Then, complexes were formed using 1 mM lipid dispersion (7.7  $\mu$ L) and pGL3-control plasmid encoding luciferase (1  $\mu$ g). After that, transfection was carried out for 3 h using COS-1 cells in a 24-well plate, and the activity of luciferase in lysed cell solutions was measured 48 h later to assess transfection efficiency. The measurement of transfection efficiencies

<sup>\*</sup> To whom correspondence should be addressed. E-mail: nagasaki@bioa.eng.osaka-cu.ac.jp. Phone: 81 6 6605 2696. Fax: 81 6 6605 2785.

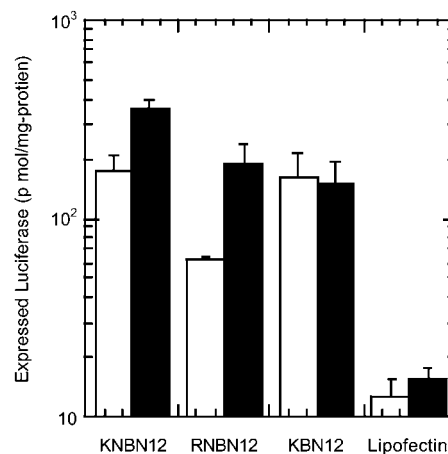
<sup>†</sup> SORST.

**Scheme 2. Syntheses of Cationic Lipids**

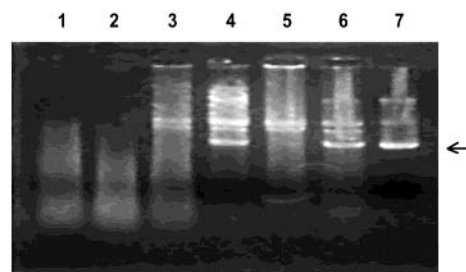
was performed in triplicate (Figure 1).<sup>2</sup> To investigate the effects of photoirradiation on transfection, after allowing cells to come in contact with complexes for 3 h, UV irradiation (365 nm, 3.5 mW/cm<sup>2</sup>) for 0 or 10 min was performed, and the results were compared. Transfection was performed using a prepared lipid aggregate solution consisting of photocleavable lipids: when compared to

<sup>1</sup> Selected data for **KNBN12**: mp 127–130 °C;  $\nu_{\text{max}}$  (KBr)/cm<sup>-1</sup> 2922, 2850 (C–H), 1701 (CONH), 1618 (ArCON), 1535 and 1340 (NO<sub>2</sub>);  $\delta$  (DMSO-*d*<sub>6</sub>, 25 °C, TMS) 0.85 (t,  $J$  = 6.8 Hz, 6H, CH<sub>3</sub>), 1.16–1.46 (m, 44H, CCH<sub>2</sub>C,  $\gamma$ - and  $\delta$ -CH<sub>2</sub> of lysyl), 1.55 and 1.71 (m  $\times$  2, 2H,  $\beta$ -CH<sub>2</sub> of lysyl), 3.13 and 3.40 (t, 4H, CONCH<sub>2</sub>C), 3.17 (m, 2H,  $\epsilon$ -CH<sub>2</sub> of lysyl), 3.81 (t,  $J$  = 6.2 Hz, 1H, CH), 4.66 (m, 2H, ArCH<sub>2</sub>NH), 7.64 (d,  $J$  = 8.0 Hz, 1H, *o*-ArH to CH<sub>2</sub>NH), 7.70 (d, 1H,  $J$  = 8.0 Hz, *m*-ArH to CH<sub>2</sub>NH), 7.85 (br s, 3H, NH), 7.97 (s, 1H, *o*-ArH to NO<sub>2</sub>); positive FAB-MS  $m/z$  660.6 ([M + H]<sup>+</sup>; calcd for C<sub>38</sub>H<sub>70</sub>N<sub>5</sub>O<sub>4</sub>, 660.5). Anal. Calcd for C<sub>38</sub>H<sub>69</sub>N<sub>5</sub>O<sub>4</sub>·2CF<sub>3</sub>CO<sub>2</sub>H: C, 56.81; H, 8.06; N, 7.89%. Found: C, 56.96; H, 8.23; N, 7.89. Data for **RNBN12**: mp 77–78 °C;  $\nu_{\text{max}}$  (KBr)/cm<sup>-1</sup> 2926, 2855 (C–H), 1675 (CONH), 1620 (ArCON), 1553 and 1367 (NO<sub>2</sub>);  $\delta$  (DMSO-*d*<sub>6</sub>, 20 °C, TMS) 0.85 (t,  $J$  = 6.4 Hz, 6H, CH<sub>2</sub>CH<sub>3</sub>), 1.16–1.30 (m, 40H, CCH<sub>2</sub>C), 1.5–1.8 (m, 4H,  $\beta$ - and  $\gamma$ -CH<sub>2</sub> of arginylyl), 3.13 and 3.44 (m, 4H, CONCH<sub>2</sub>C), 3.17 (m, 2H,  $\delta$ -CH<sub>2</sub> of arginylyl), 3.90 (s, 1H, CH), 4.67 (m, 2H, ArCH<sub>2</sub>NH), 7.33 (m, 4H, NH of guanidium), 7.67 (m, 2H, *o*-ArH and *m*-ArH to CH<sub>2</sub>NH), 7.98 (s, 1H, *o*-ArH to NO<sub>2</sub>), 9.17 (s, 1H, ArCH<sub>2</sub>NH); positive FAB-MS  $m/z$  688.6 ([M + H]<sup>+</sup>; calcd for C<sub>38</sub>H<sub>70</sub>N<sub>7</sub>O<sub>4</sub>, 688.6). Anal. Calcd for C<sub>38</sub>H<sub>69</sub>N<sub>7</sub>O<sub>4</sub>·2CF<sub>3</sub>CO<sub>2</sub>H: C, 55.07; H, 7.81; N, 10.70%. Found: C, 54.76; H, 7.90; N, 10.73. Data for **KBN12**: viscous oil;  $\nu_{\text{max}}$  (neat)/cm<sup>-1</sup> 2922, 2855 (C–H), 1680 (CONH), 1630 (ArCON);  $\delta$  (DMSO-*d*<sub>6</sub>, 25 °C, TMS) 0.86 (t,  $J$  = 6.8 Hz, 6H, CH<sub>3</sub>), 1.10–1.46 (m, 44H, CCH<sub>2</sub>C,  $\gamma$ - and  $\delta$ -CH<sub>2</sub> of lysyl), 1.59 and 1.77 (m  $\times$  2, 2H,  $\beta$ -CH<sub>2</sub> of lysyl), 2.75 and 3.41 (t  $\times$  2, 4H, CONCH<sub>2</sub>C), 3.12 (m, 2H,  $\epsilon$ -CH<sub>2</sub> of lysyl), 3.83 (t,  $J$  = 6.2 Hz, 1H, CH), 4.38 (m, 2H, ArCH<sub>2</sub>NH), 7.27 (d,  $J$  = 8.4 Hz, 2H, *o*-ArH to CH<sub>2</sub>NH), 7.35 (d,  $J$  = 8.4 Hz, 2H, *m*-ArH to CH<sub>2</sub>-3NH), 8.16 (br s, 6H, NH<sub>3</sub>), 9.18 (s, 1H, CONH); positive FAB-MS  $m/z$  615.2 ([M + H]<sup>+</sup>; calcd for C<sub>38</sub>H<sub>71</sub>N<sub>4</sub>O<sub>2</sub>, 615.6). Anal. Calcd for C<sub>38</sub>H<sub>69</sub>N<sub>4</sub>O<sub>2</sub>·2HCl·3.5H<sub>2</sub>O: C, 60.73; H, 10.52; N, 7.41%. Found: C, 60.64; H, 10.47; N, 7.41.

<sup>2</sup> COS-1 cells ((3–4)  $\times$  10<sup>4</sup> cells for each well) were grown to just before confluence in 24-well culture plates in DMEM with 10% FBS and 100 U/mL penicillin and 100 mg/mL streptomycin in an atmosphere of 5% CO<sub>2</sub> at 37 °C and washed twice with 0.5 mL of PBS. Transfection was performed with 1  $\mu$ g of plasmid DNA (pGL3-control) for each well. Luciferase assays were performed as described in the protocol of Steady-Glo Luciferase Assay System (Promega, Madison, WI). Luciferase relative light units (RLU) were analyzed by luminometer (Fluoroskan Ascent-FL, Thermo Labsystems, Finland). The protein concentrations of the cell lysates were measured as described in the protocol of NanoOrange Protein Quantitation Kit (Molecular Probes, Eugene, OR) using bovine serum albumin as a standard. The expressed luciferase shown in Figure 1 represent the amount (mole quantity) which is standardized for total protein content of the cell lysate.



**Figure 1.** Comparison of transfection efficiency of DNA complexes with cationic lipids. Open bars indicate the transfection efficiency in the dark conditions. Closed bars indicate that under UV irradiation.



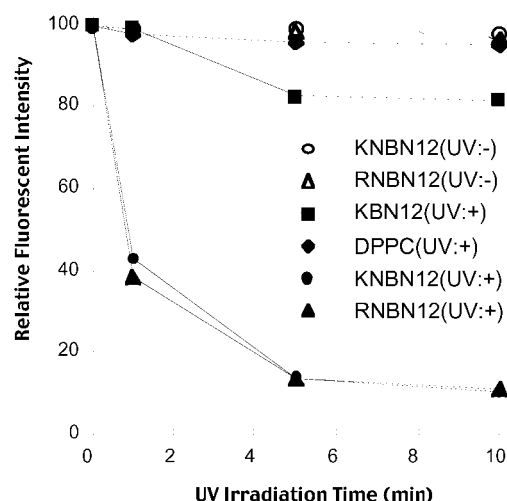
**Figure 2.** Complexes that protect pGL3-control against DNase I digestion. Lane 1, DNA (UV+); lane 2, DNA (UV-); lane 3, DNA recovered from **KNBN12** complex (UV+); lane 4, DNA recovered from **KNBN12** complex (UV-); lane 5, DNA recovered from **RNBN12** complex (UV+); lane 6, DNA recovered from **RNBN12** complex (UV-); lane 7, undigested DNA. Band marked by arrow mean intact supercoiled plasmid.

lipofectin (a commercially available tertiary ammonium lipid/DOPE, 1,2-dioleoyl-sn-glycero-3-phosphoethanolamine, mixture), the transfection efficiency of KNBN12 and RNBN12 was 13 and 3 times greater without the UV irradiation and more than 19 and 10 times greater with the UV irradiation, respectively. Also, since the photoirradiation did not increase the transfection efficiency of KBN12 (an analogue without a photocleavable structure), the decomposition of lipid structures must be involved in improved transfection efficiency. The higher basicity of RNBN12 than KNBN12 would result in lower efficiency due to less DNA release.

DNA protection is also an important factor involved in the high transfection efficiency for nonviral gene delivery (19). Therefore, to ascertain whether cationic lipids protect DNA from nuclease, the protection ability of KNBN12 and RNBN12 against the hydrolysis of DNase I was investigated (Figure 2).<sup>3</sup> Without UV irradiation to cationic lipid aggregate/DNA complexes the intact supercoiled plasmid DNA band was still observed

<sup>3</sup> Lipid/DNA (3  $\mu$ g of pGL3-control) complexes were prepared in 17  $\mu$ L of PBS (phosphate buffered saline) at a charge ratio of 5 with or without UV irradiation (365 nm, 5 min, 3.5 mW/cm<sup>2</sup>). The samples were incubated at 37 °C in the presence of DNase I (30 unit in 3  $\mu$ L, Wako Chemicals, Tokyo, Japan) for 15 min. The samples were mixed with 5  $\mu$ L of stop buffer (250 mM EDTA in PBS) under mild vortexing, followed by adding 5  $\mu$ L of 10% sodium dodecyl sulfate and incubated at room temperature for 1 h. Sample solutions (10  $\mu$ L) were analyzed by gel electrophoresis (0.8% agarose).





**Figure 3.** Photostimulation of membrane fusion. Fluorescent intensity of rhodamine in DPPC liposomes is quenched by cationic lipids when membrane fusion occurs.

after DNase I treatment (lane 4 and 6), although some nicking and decomposition of plasmid DNA occurred under recovering conditions with SDS (lane 7). On the other hand, intact band completely disappeared with UV irradiation (lane 3 and 5). Both **KNBN12** and **RNBN12** exhibited high protection ability, but 5-min UV irradiation (365 nm, 3.5 mW/cm<sup>2</sup>) lowered this ability. These findings suggest that photoirradiation lowers the affinity of lipids toward DNA and makes it easier for the nuclease to access to DNA. The hypothesis proposed by Szoka et al. (20) suggests that dissociation of transfecting DNA from lipidic vectors is an important step for the successful nuclear transport and final expression of a transgene. In the case of such photocleavable lipids, the photoenhanced DNA release also contributes to the increase of transfection efficiency.

Photoirradiation may improve transfection efficiency by facilitating the fusion between endocytic vesicles and unstable photocleaved lipids, thus making the endocytic vesicles unstable. Therefore, the ability of photoirradiation to facilitate membrane fusion was investigated: Liposomes, consisting solely of 1,2-dipalmitoyl-sn-glycero-3-phosphocholine (DPPC), were labeled using 1 mol % fluorescent rhodamine-modified phosphatidylethanolamine. Furthermore, a lipid dispersion consisting solely of photocleavable lipids was prepared and mixed with the above-mentioned liposomes. Then, the fluorescent intensity of rhodamine was measured after UV irradiation (365 nm, 3.5 mW/cm<sup>2</sup>) (Figure 3). The results showed that only when **KNBN12** or **RNBN12** was used and UV was irradiated was a large degree of decrease in fluorescent intensity seen because the fluorescence of rhodamine was quenched by the electron transfer from the amino group of uncleaved amino acid in the vicinity of fusion.

Furthermore, the intracellular trafficking of added lipids were examined by confocal fluorescence microscopy. First of all, COS-1 cells were transfected with the pEGFP-Endo gene (Clontech, Palo Alto, CA) which expresses a RhoB-fused green fluorescent protein. RhoB has been known to be an endosomal localization signaling protein (21). At transfected COS-1 cells, therefore, the lipid membrane of endocytic vesicles was visualized green. Next, lipid aggregate/DNA complexes, where photocleavable lipids were mixed with 1 mol % rhodamine-modified phosphatidylethanolamine, were prepared and added to cells. As was the case with the transfection, after

3 h of incubation, the cells were fixed and examined by confocal fluorescent microscopy. The result (data not shown) represented that the localization of the red fluorescence for administered lipids mostly matched the green fluorescence for the lipid membranes of cytoplasmic vesicles, such as endosomes. This finding confirms not only the internalization of the DNA complex by endocytosis, but also the existence of DNA complexes in endocytic vesicles when photoirradiation improves transfection efficiency.

In conclusion, we succeeded in developing a new transfection technique using cationic lipids having photocleavable spacer by irradiating UV after adding DNA complexes to cells. The transfection efficiency of this technique was substantially enhanced compared to non-irradiating transfection. The reason for this increased transfection efficiency would be that when lipoplexes enter cells, the photocleavage of lipids facilitates the escape of DNA from endocytic vesicles by not only the stimulated fusion with endocytic vesicles, but also enhanced dissociation of the cationic lipid–DNA complex.

#### ACKNOWLEDGMENT

This study was supported by a Grant from Osaka City University (Special Research Promotion Program) and a Health Sciences Research Grant for Human Genome, Tissue Engineering Food Biotechnology from the Ministry of Health, Labor and Welfare of Japan (13I-5).

#### LITERATURE CITED

- (1) Felgner, P. L., Barenholz, Y., Behr, J. P., Cheng, S. H., Cullis, P., Huang, L., Jessee, J. A., Seymour, L., Szoka, F., Thierry, A. R., Wagner, E., and Wu, G. (1997) Nomenclature for synthetic gene delivery systems. *Hum. Gene Ther.* 8, 511–512.
- (2) MacLachlan, I., Cullis, P., and Graham, R. W. (1999) Progress towards a synthetic virus for systemic gene therapy. *Curr. Opin. Mol. Ther.* 1, 252–259.
- (3) Brown, M. D., Schätzlein, A. G., and Uchegbu, I. F. (2001) Gene delivery with synthetic (non viral) carriers. *Int. J. Pharm.* 229, 1–21.
- (4) Nishikawa, M., and Huang, L. (2001) Nonviral vectors in the new millennium: delivery barriers in gene transfer. *Hum. Gene Ther.* 12, 861–870.
- (5) Harashima, H., Shinohara, Y., and Kiwada, H. (2001) Intracellular control of gene trafficking using liposomes as drug carriers. *Eur. J. Pharm. Sci.* 13, 85–89.
- (6) Zhou, X., and Huang, L. (1994) DNA transfection mediated by cationic liposomes containing lipopolylysine: characterization and mechanism of action. *Biochim. Biophys. Acta* 1189, 195–203.
- (7) Ouahabi, A. El, Thiry, M., Pector, V., Fuks, R., Ruyschaert, J. M., and Vandenbranden, M. (1997) The role of endosome destabilizing activity in the gene transfer process mediated by cationic lipids. *FEBS Lett.* 414, 187–192.
- (8) Noguchi, A., Furuno, T., Kawaura, C., and Nakanishi, M. (1998) Membrane fusion plays an important role in gene transfection mediated by cationic liposomes. *FEBS Lett.* 433, 169–173.
- (9) Mui, B., Ahkong, Q. F., Chow, L., and Hope, M. J. (2000) Membrane perturbation and the mechanism of lipid-mediated transfer of DNA into cells. *Biochim. Biophys. Acta* 1467, 281–292.
- (10) Wattiaux, R., Laurent, N., Coninck, S. W., and Jadot, M. (2000) Endosomes, lysosomes: their implication in gene transfer. *Adv. Drug Deliv. Rev.* 41, 201–208.
- (11) Farhood, H., Serbina, N., and Huang, L. (1995) The role of dioleoyl phosphatidylethanolamine in cationic liposome mediated gene transfer. *Biochim. Biophys. Acta* 1235, 289–295.

- (12) Budker, V., Gurevich, V., Hagstrom, J. E., Bortzov, F., and Wolff, J. A. (1996) pH-sensitive, cationic liposomes: A new synthetic virus-like vector. *Nature Biotech.* **14**, 760–764.
- (13) Wagner, E. (1999) Application of membrane-active peptides for nonviral gene delivery. *Adv. Drug Delv. Rev.* **38**, 279–289.
- (14) Simoes, S., Slepishkin, V., Pires, P., Gaspar, R., and de Lima, M. P. (1999) Mechanisms of gene transfer mediated by lipoplexes associated with targeting ligands or pH-sensitive peptides. *Gene Ther.* **6**, 1798–1807.
- (15) Kono, K., Torikoshi, Y., Mitsutomi, M., Itoh, T., Emi, N., Yanagie, H., and Takagishi, T. (2001) Novel gene delivery systems: complexes of fusogenic polymer-modified liposomes and lipoplexes. *Gene Ther.* **8**, 5–12.
- (16) Høgset, A., Prasmickaite, L., and Tjelle, T. E. (2000) Photochemical Transfection: A new technology for light-induced, site-directed gene delivery. *Hum. Gene Ther.* **11**, 869–880.
- (17) Prasmickaite, L., Høgset, A., Tjelle, T. E., Olsen, V. M., and Berg, K. (2000) Role of endosomes in gene transfection mediated by photochemical internalization (PCI). *J. Gene Med.* **2**, 477–488.
- (18) Rich, D. H., and Gurwara, S. K. (1975) Removal of C-terminal peptide amides from a 3-nitro-4-aminomethylbenzoyl amide resin by photolysis. *Tetrahedron Lett.* **5**, 301–304.
- (19) Lechardeur, D., Sohn, K. J., Haardt, M., Joshi, P. B., Monck, M., Graham R. W., Beatty, B., Squire, J., O'Brodovich, H., and Lukacs, G. L. (1999) Metabolic instability of plasmid DNA in the cytosol: a potential barrier to gene transfer. *Gene Ther.* **6**, 482–97.
- (20) Xu, Y. and Szoka, F. C. Jr. (1996) Mechanism of DNA release from cationic liposome/DNA complexes used in cell transfection. *Biochemistry* **35**, 5616–5623.
- (21) Ellis, S., and Mellor, H. (2000) Regulation of endocytic traffic by Rho family GTPases. *Trends Cell Biol.* **10**, 85–88.

BC0256603

# ARTICLES

## Temperature-Induced Switching of Enzyme Activity with Smart Polymer–Enzyme Conjugates

Tsuyoshi Shimoboji,<sup>†</sup> Edmund Larenas,<sup>‡</sup> Tim Fowler,<sup>‡</sup> Allan S. Hoffman,<sup>\*,†</sup> and Patrick S. Stayton<sup>\*,†</sup>

Department of Bioengineering, University of Washington, Seattle, Washington 98195, and Genencor International Inc., Palo Alto, California 94304. Received September 30, 2002;  
Revised Manuscript Received November 21, 2002

A method for thermally induced switching of enzyme activity has been developed, based on the site-directed conjugation of end-reactive temperature-responsive polymers to a unique cysteine (Cys) residue positioned near the enzyme active site. The reversible temperature-induced collapse of *N,N*-dimethylacrylamide (DMA)/*N*-4-phenylazo-phenylacrylamide (AZAAm) copolymers (DMAAm) has been used as a molecular switch to control the catalytic activity of endoglucanase 12A (EG 12A). The polymer was conjugated to the EG 12A site-directed mutant N55C, directly adjacent to the cellulose binding cleft, and to the S25C mutant, where the conjugation site is more distant. The N55C conjugate displayed a larger activity shutoff efficiency in the collapsed polymer state than the S25C conjugate. Increasing the polymer molecular weight was also shown to increase the shutoff efficiency of the switch. Related to these effects of conjugation site and polymer size, the switching efficiency was found to be strongly dependent on substrate size. With a small substrate, *o*-nitrophenyl- $\beta$ -D-cellobioside (ONPC), there was minimal blocking of enzyme activity when the polymer was in the expanded state. With a large substrate, hydroxyethyl cellulose (HEC), there was a large reduction of enzyme activity in the polymer expanded state, even with relatively small polymer chains, and a further reduction when the polymer was collapsed. Similar general trends for the interactive effects of conjugation site, polymer size, and substrate size were observed for immobilized conjugates. Kinetic studies demonstrated that the switching activity was due to the blocking of substrate association by the collapsed polymers. These investigations provide mechanistic insight that can be utilized to design molecular switches for a variety of stimuli-responsive polymer–protein conjugates.

### INTRODUCTION

The ability to reversibly control protein and enzyme activities with external stimuli could provide new opportunities for the development of molecular diagnostics, bioprocesses, affinity separations, lab assays, BioMEMS, bioelectronics, and biosensor technologies. We have been developing a new approach to molecular switches that utilizes site-specific conjugation of stimuli-responsive polymers near the active sites of proteins. These stimuli-responsive polymers undergo a large change in size and physical properties in response to external stimuli such as temperature, pH, or specific wavelengths of light. We have previously demonstrated that the change in physical properties can be used as a temperature-, pH-, or light-dependent activity switch to control ligand capture and release (1–5). We report here the first investigation of these smart polymer–protein conjugates for thermal-switching of enzyme activity.

Several interesting strategies have been investigated for regulating enzyme activity by external signals. The first has been to conjugate small, responsive molecules near the active sites or binding sites of proteins. For example, binding-site tyrosine residues in streptavidin and antibodies have been chemically modified with nitro groups to introduce a pH-dependent biotin binding (6, 7). Another important example involved the introduction of photoresponsive groups near protein recognition sites (8–10). A second general strategy has been to genetically engineer a “responsiveness” into the protein, in fashion similar to nature’s strategy of allostery (11–13).

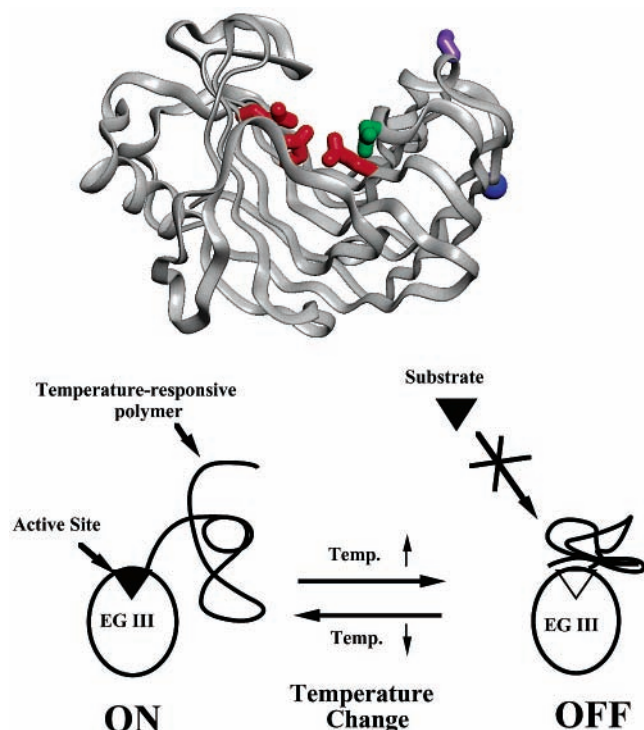
The endoglucanase EG 12A from *Trichoderma reesei* preferentially hydrolyzes the internal  $\beta(1\rightarrow4)$  linkages of amorphous cellulose (14). EG 12A is a single-domain cellulase that does not have a separate cellulose binding domain (15). EG 12A has been used in industrial textile processing, and the ability to finely regulate its activity could provide control over the degree of cellulose processing and fiber properties. Figure 1 shows the schematic design for constructing an enzyme that is thermally switched “on” and “off”. The smart polymer switch reversibly cycles between the expanded and collapsed states in response to temperature changes above and below the lower critical solution temperature (LCST).<sup>1</sup> In this paper, we demonstrate the striking activity of the thermally responsive enzyme switch, as well as a char-

\* Corresponding authors. A.S.H.: address, Department of Bioengineering, Box 352255, University of Washington, Seattle, WA 98195; telephone, 206-543-9423; fax, 206-543-6124; e-mail: hoffman@u.washington.edu. P.S.S.: address, Department of Bioengineering, Box 351721, University of Washington, Seattle, WA 98195; telephone, 206-685-8148; fax: 206-685-8256; e-mail, stayton@u.washington.edu.

<sup>†</sup> University of Washington.

<sup>‡</sup> Genencor International Inc.





**Figure 1.** Molecular model of endoglucanase 12A and schematic model of the DMAAm–enzyme molecular switch. The red residues represent the catalytic glutamic acid side chains at the active site of EG 12A, the green residue is the Asn 55 position, the purple residue is the Ser 25 position, and the N-terminus is represented as the blue circle.

acterization of the importance of the polymer conjugation site, the molecular weight of the conjugated polymer, the size of the substrate, and the role of free polymer. Although the polymer we have designed for these studies is both light- and temperature-responsive, this paper focuses primarily on the use of temperature to switch the enzyme activity.

## EXPERIMENTAL PROCEDURES

**Materials.** 4-Aminoazobenzene (Aldrich, Milwaukee, WI) was recrystallized from ethanol and water and dried in vacuo. *N,N*-Dimethyl acrylamide (DMA) (Fluka, Milwaukee, WI), diethyl ether, acryloyl chloride, triethylamine, and 2-mercaptoethanol (MEO) (Aldrich, Milwaukee, WI) were purified by distillation under reduced pressure. 2,2'-Azobisbutyronitrile (AIBN) (J. T. Baker, Phillipsburg, NJ) was recrystallized from methanol. Ethanol, dimethylformamide (DMF), tetrahydrofuran (THF), methylene chloride, potassium *tert*-butoxide, divinyl sulfone (DVS), and ethylenediamine tetraacetic acid (EDTA) (Aldrich, Milwaukee, WI) were used as received. Restriction

enzymes, *Xba*I and *Bgl*II, were purchased from New England Biolabs (Beverly, MA). QIA Prep Spin Plasmid Kit (QIAGEN, Santa Clarita, CA) and Quikchange Site-Directed Mutagenesis Kit (Stratagene, La Jolla, CA) were used as received. Butyl sepharose (Pharmacia, Piscataway, NJ), bis-tris propane, ammonium sulfate, *o*-nitrophenyl- $\beta$ -D-cellobioside (ONPC) (Sigma, St. Louis, MO), hydroxyethyl cellulose (HEC) medium Viscosity (Fluka, Ronkonkome, NY), tris(2-carboxyethyl)-phosphine hydrochloride (TCEP), BCA protein assay kit, Magna Bind Streptavidin, EZ-Link sulfo-NHS-LC-LC-biotin, 4'-hydroxyazobenzene-2-carboxylic acid (HABA), streptavidin magnetic beads (Pierce, Rockford, IL), Ultrafree Biomax (Millipore, Bedford, MA), Precast gel (Novex, San Diego, CA), and Kaleidoscope MW marker (Biorad, Hercules, CA) were used as received. All other reagents were of analytical-grade.

### Synthesis of Azobenzene-Containing Monomer.

An azobenzene-containing monomer, 4-phenylazophenylacrylamide (AZAAM), was synthesized as follows. 4-aminoazobenzene (0.2 mol) and triethylamine (0.26 mol) were dissolved in diethyl ether (200 mL). Acryloyl chloride (0.24 mol) dissolved in 80 mL of diethyl ether was added dropwise at 0 °C under nitrogen atmosphere with stirring. The reaction mixture was allowed to come to room temperature and stirred for 4 h. The reaction solution was filtered to remove triethylammonium chloride, washed with water, and evaporated. The product was recrystallized from ethanol–water mixture and dried in vacuo. The structures were confirmed by  $^1\text{H}$  NMR (d-DMSO):  $\delta$  = 5.7–6.7 (m, 3H), 7.4–7.8 (m, 5H), 7.8–8.2 (m, 4H).

### Synthesis of Temperature-Responsive Polymer.

The temperature responsive polymer DMA-*co*-AZAAM copolymer (DMAAm) was synthesized with a hydroxyl terminus by free-radical polymerization in DMF at 60 °C for 20 h, using MEO as a chain transfer reagent and AIBN as an initiator (monomer concentration = 2 mol/L). The ratios of DMA and AZAAM were varied to change the percentage of incorporated azobenzene moiety in the polymer. To vary  $M_n$ , the monomer/MEO/AIBN molar ratios were varied from 100/0.25/0.05 to 100/16.0/3.2. The product was purified by precipitation into diethyl ether three times and dried in vacuo.

The content of AZAAM incorporated in the copolymers was determined by  $^1\text{H}$  NMR (Spectrospin & Bruker, dpx200), comparing the ratio of aromatic and aliphatic hydrogens. The molecular weight ( $M_n$ ) of the polymer was determined by gel permeation chromatography (GPC, Water, Styragel HR3 and 4) in THF, using polystyrene as a standard.

The hydroxyl terminus of DMAAm was converted to a vinyl sulfone (VS) group for conjugation to a sulfhydryl group in the protein. DMAAm was dissolved in 20 mL of methylenechloride with 0.03 g of potassium *tert*-butoxide, and 100  $\mu\text{L}$  of divinyl sulfone (DVS) (DVS/OH = 10/1 molar ratio). The solution was stirred for 12 h at room temperature under nitrogen atmosphere. The polymer was precipitated and then washed in diethyl ether, and dried in vacuo. The LCST of the polymer was determined as the temperature at 10% of the maximum absorbance at 600 nm. The polymer concentration was 2 mg/mL in double-distilled water or 100 mM phosphate buffer (PB), pH 7.4.

**Site-Directed Mutagenesis of EG 12A.** The EG 12A S25C and N55C site-directed mutants were constructed using the Quikchange (Stratagene, CA) method. A 20 ng sample of the plasmid was mixed with 125 ng of the mutant primers (sense and antisense). The synthesis product was digested by Dpn I and transformed into

<sup>1</sup> Abbreviations: DMA, *N,N*-dimethylacrylamide; AZAAM, *N*-4-phenylazo-phenylacrylamide; DMAAm, DMA-*co*-AZAAM copolymer; EG 12A, endoglucanase 12A; N55C, Asn55Cys site-directed mutant; S25C, Ser25Cys site-directed mutant;  $M_n$ , number-averaged molecular weight; ONPC, *o*-nitrophenyl- $\beta$ -D-cellobioside; HEC, hydroxyethyl cellulose; LCST, lower critical solution temperature; MEO, 2-mercaptoethanol; AIBN, 2,2'-azobisbutyronitrile; DMF, dimethylformamide; THF, tetrahydrofuran; DVS, divinyl sulfone; EDTA, ethylenediamine tetraacetic acid; TCEP, tris(2-carboxyethyl)-phosphine hydrochloride; HABA, 4'-hydroxyazobenzene-2-carboxylic acid; RBB-CMC remazol brilliant blue carboxymethylcellulose; endo H, endoglycosidase H; AS, ammonium sulfate; PHBAH, *p*-hydroxybenzoic acid hydrazide.

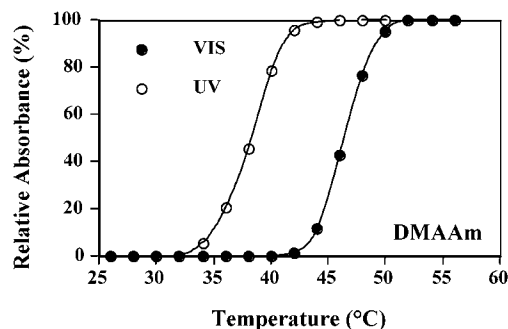
1. S25C 5'-p-CAACCTTTGGGGAGCA***TGTGCC***-  
GGCTCTGGATTGGG-3'  
5'-p-CCAAATCCAGAGCCGGC***ACA***-  
TGCTCCCCAAAGGTTG-3'

2. N55C 5'-p-GTGGTCCGGCGGCCAG***TGCAA***-  
CGTCAAGTCGTACC-3'  
5'-p-GGTACGACTTGACGTT***GCACT***-  
GGCCGCCGGACCAC-3'

**Conjugation of Temperature-Responsive Polymers to EG 12A Mutants.** Conjugations of EG 12A mutants to DMAAm-VS with different  $M_n$ 's were carried out by reacting the vinyl sulfone group of the polymer with the sulfhydryl-containing cysteine side chains of the EG 12A mutants in 50 mM PB, pH 8.0. The cysteine residues in the EG 12A mutants form disulfide bonds during purification and storage. To reduce these disulfide bonds to sulfhydryl groups, TCEP at 10-fold molar excess to the mutant was added and incubated for 20 min at room temperature. A 50-fold molar excess of the polymer to the mutant was added and reacted overnight at 4 °C to obtain high conjugation efficiency. The buffer was

**Catalytic Activity Assay.** The catalytic activity of the EG 12A conjugates was measured at 32 and 52 °C. The 32 °C temperature was chosen because it falls below the LCST transition, and 52 °C was chosen because it falls above the phase transition temperature of the polymer and EG 12A becomes unstable above 55 °C. To elucidate the mechanism of the stimuli-responses, the kinetic parameters  $K_m$  and  $k_{cat}$  of the conjugates were determined by Lineweaver–Burk plot assuming the Michaelis–Menten equation. Two substrates with different sizes, ONPC and HEC, were chosen to investigate the effect of the size of the substrate on the switching activity. ONPC is hydrolyzed by EG 12A to generate a nitrophenol dye that is detected at 405 nm. The assay was conducted in 50 mM sodium acetate buffer pH 5.5. ONPC (2–10 mM) and the conjugate (100 nM) solutions were preincubated at 32 and 52 °C. The reaction was initiated by addition of ONPC into EG 12A solution in a total volume of 1 mL, and it was incubated at each temperature. Samples were taken at 8–10 different time points in order to produce reliable values for the initial velocity determinations. A 100  $\mu$ L aliquot was taken from the reaction solution, and the reaction was terminated with the addition of 50  $\mu$ L of 200 mM glycine buffer pH10. The absorbance at 405 nm was measured in a microtiter plate reader (Benchmark, BioRad). The concentration of nitrophenol was calculated using the extinction coefficient at 405 nm.





**Figure 2.** The DMAAm LCST behavior under UV vs vis photoirradiation. The relative absorbance was measured at 600 nm for 2 mg/mL DMAAm (10 kDa) in 50 mM sodium acetate buffer, pH 5.5. The heating rate was 0.5 °C/min. The DMAAm solutions were photoirradiated with UV and vis light for 10 min and 3 h, respectively, before the LCST measurements.

HEC is a soluble cellulose derivative that is hydrolyzed by EG 12A to generate hydroxyethyl glucose. This product was subsequently quantitated by reaction with *p*-hydroxybenzoic acid hydrazide (PHBAH). PHBAH reacts with glucose to produce glucosazone, which is detected at 405 nm. In brief, the conjugate (100 nM) and HEC (Cellulose WP-40, Fluka-BioChemika) (0.25–2 w/v %) solutions in 50 mM sodium acetate buffer, pH 5.5, were preincubated in a microtube at each temperature. The reaction was initiated by addition of HEC into EG 12A solution in a total volume of 1 mL, and it was incubated at 32 and 52 °C. Samples were taken at 8–10 different time points in order to produce reliable values for the initial velocity determinations. A 100  $\mu$ L aliquot was taken from the reaction solution, and the reaction was stopped by addition of 50  $\mu$ L of 2% NaOH solution. A 20  $\mu$ L sample of the reaction solution was mixed with 400  $\mu$ L of PHBAH solution (1 w/v % in 0.3 N NaOH) in microtubes. The top of the cap of the microtube was punctured with syringe needle, and the tube was placed in boiling water for 10 min (for steam treatment). The solution was cooled, and 200  $\mu$ L of the solution was placed into microtiter wells. The absorbance at 405 nm was measured. The glucose concentration was calculated from the standard curve made by a series of concentration of glucose.

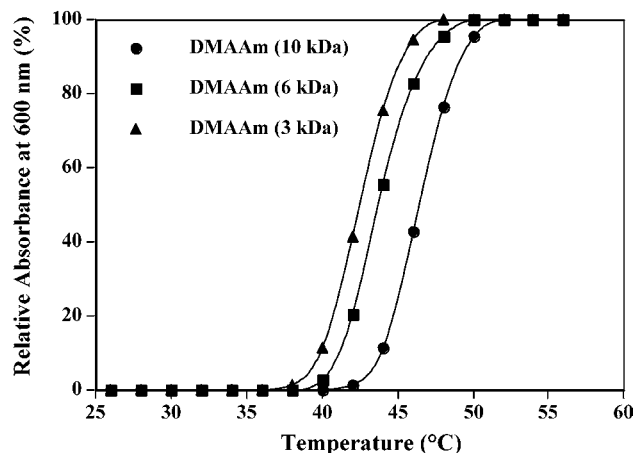
## RESULTS

**Synthesis and Characterization of Azobenzene and DMA Copolymers.** The DMAAm copolymers display dual temperature- and photo-responsive phase behavior (17, 18). The DMAAm copolymers exhibit a shift toward higher LCST values under vis illumination (Figure 2). The monomer ratios were selected so that the maximal difference in polymer expansion and collapse between the vis and UV states occurred in the range of 40–45 °C, where the enzyme exhibits an optimal balance between thermal stability and activity. For these studies focused on the development of a thermo-sensitive enzyme switch, three different DMAAm polymers with different  $M_n$ 's were synthesized in order to investigate the role of polymer size in the thermal switching activities for the polymer–EG 12A conjugates. The physical properties of the copolymers utilized in this study are summarized in Table 1. The thermally induced phase transition behaviors of the DMAAm polymers at three  $M_n$ 's (10, 6, 3 kDa) are shown in Figure 3. The LCST values fall between 37 and 43 °C. To create a thiol-reactive end group for conjugating to the genetically engineered cysteine on the

**Table 1. DMAAm Polymer Physical Properties**

polymer	MEO <sup>a</sup> (mol %)	AZAAM <sup>a</sup> (mol %)	$M_w^b$	$M_n^b$	$M_w/M_n^b$	yield (%)
M-10	0.25	5.5	14900	9600	1.55	31.6
M-6	1.0	8.0	9100	5700	1.59	48.5
M-3	2.0	9.0	5700	3200	1.79	74.1

<sup>a</sup> Molar ratio to total monomer in feed. <sup>b</sup> Determined by GPC.



**Figure 3.** The LCST behavior of DMAAm as a function of polymer  $M_n$ . The relative absorbance at 600 nm was measured for 10, 6, and 3 kDa polymer solutions (2 mg/mL) in 50 mM sodium acetate, pH 5.5. The heating rate was 0.5 °C/min.

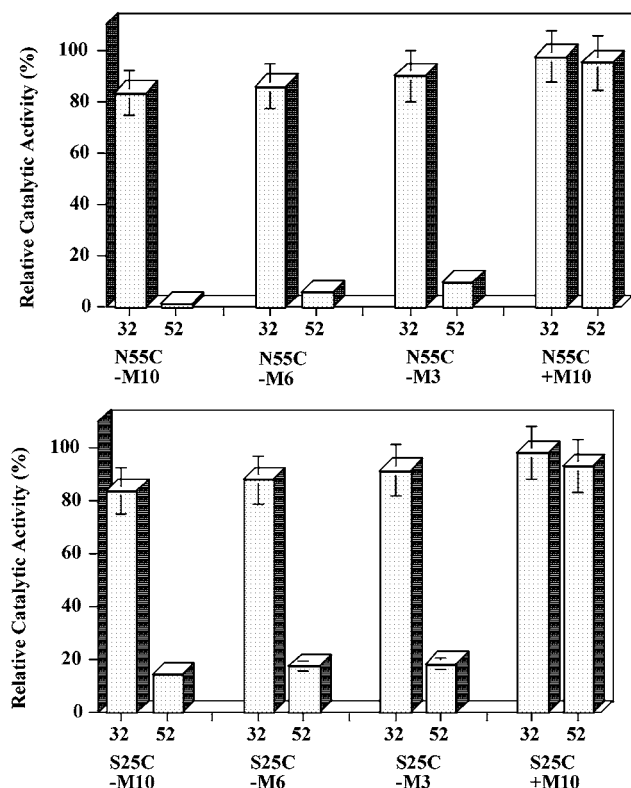
EG 12A enzymes, the hydroxyl termini of all the polymers were converted to a vinyl sulfone moiety by reaction with divinyl sulfone.

**Construction and Characterization of the Site-Directed EG 12A Mutants.** Figure 1 shows a 3-D schematic structure of EG 12A, with the site-directed mutation positions constructed for this study displayed in relation to the catalytic side chains at the active site. The criteria for selection of the Asn 55 and Ser 25 positions was that they be solvent exposed and on the outer edge of the concave cellulose binding cleft. The Ser 25 position was chosen to be more distant from the binding site cleft than Asn 55. The site-directed mutants were successfully constructed as demonstrated by DNA sequencing, and the mutant proteins were subsequently produced in an established *A. niger* expression system (16). The purities of the S25C and N55C mutants were determined to be 88.4% and 94.0%, respectively, by SDS–PAGE gel analysis. The N55C mutant displayed a small change in  $K_m$  of 33.9 versus 19.5 mM for wild-type with the model substrate, *o*-nitrophenyl  $\beta$ -D-cellobioside (ONPC) and no significant change in  $k_{cat}$  (13.6 vs 12.8 s<sup>–1</sup>). S25C exhibited a  $K_m$  of 20.8 mM and a  $k_{cat}$  of 14.5 s<sup>–1</sup>. The two mutants thus exhibited kinetic values that were largely unperturbed from the wild-type enzyme, and the subsequent smart polymer conjugates were normalized to the activity of the unconjugated mutants. Both mutants were conjugated to the DMAAm-VS in the presence of TCEP to reduce the interprotein dimers that formed during purification. The polymer–enzyme conjugates were separated from the unconjugated mutants by repeated thermally induced precipitation at 52 °C. Table 2 shows the overall yields of the conjugates. Control experiments showed that the EG 12A enzyme was not precipitated in physical mixtures of enzyme and polymer, demonstrating that only conjugated enzyme was purified by this technique. The S25C conjugates exhibited higher yields than the N55C conjugates, suggesting that the 25 position is more accessible and reactive than the 55 position.

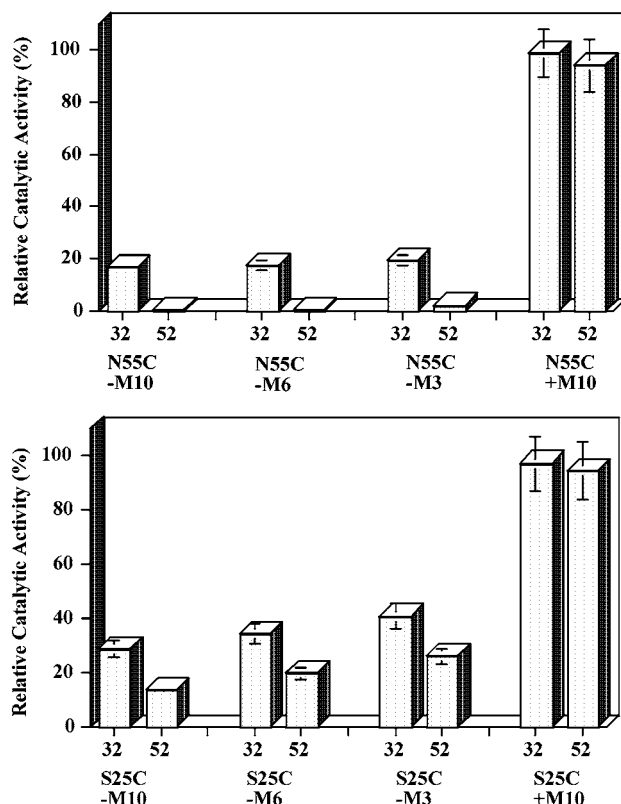


**Table 2. Conversion Efficiencies of the EG 12A–DMAAm Conjugations**

conjugate	total yield ( $\mu$ g)	%
S25C–DMAAm (10 kDa)	198	23.5
S25C–DMAAm (6 kDa)	292	34.6
S25C–DMAAm (3 kDa)	167	19.8
N55C–DMAAm (10 kDa)	141	19.4
N55C–DMAAm (6 kDa)	148	20.3
N55C–DMAAm (3 kDa)	144	19.8
WT + DMAAm (10 kDa)	0	0.0

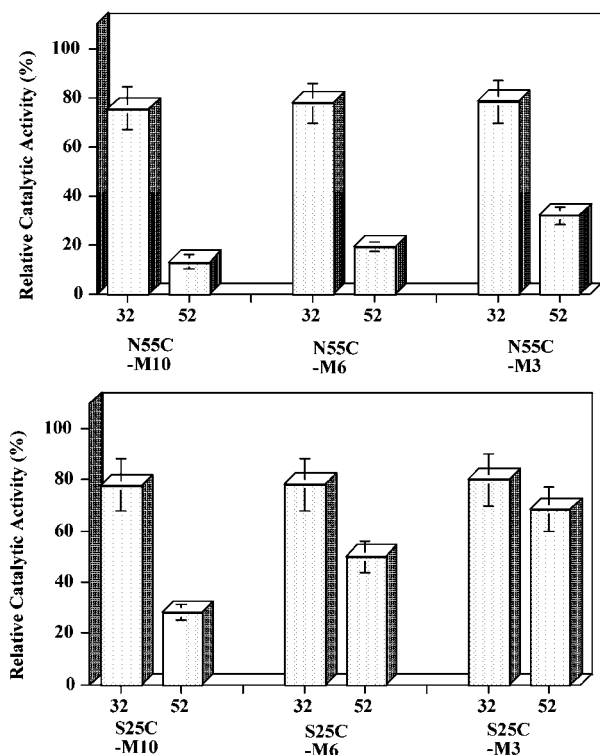
**Figure 4.** Characterization of ONPC enzyme activities for free DMAAm–EG 12A conjugates in solution at as function of polymer size and conjugation site. The enzyme activities were measured for 100 nM conjugates using ONPC (8mM) as a substrate and normalized to the activity of N55C or S25C EG12A controls as 100% at each temperature. EG 12A–M10, 10 kDa DMAAm–EG12A conjugate; EG 12A–M6, 6 kDa DMAAm–EG 12A conjugate; EG 12A–M3, 3 kDa DMAAm–EG 12A conjugate; and EG 12A + M10, physical mixture of enzyme plus 10 kDa DMAAm.

**Temperature-Responsive Properties of the Free EG 12A Conjugates in Solution.** *Switching Activities as a Function of Polymer Size and Conjugation Site.* The EG 12A conjugates were first characterized in solution with free polymer present. Figure 4 shows the comparison of the thermo-responsive activity changes of the N55C and S25C conjugates toward the small molecule substrate ONPC at 32 °C below the LCST and at 52 °C above the LCST. The activity of the conjugates was normalized to that of unconjugated N55C or S25C at each temperature. The physical mixtures of the mutants and the polymers were used as controls. While the physical mixtures did not show switching effects, both the N55C and S25C conjugates exhibited a sharp and reversible shutoff of the enzyme activities at 52 °C. In particular, the N55C–DMAAm of  $M_n$  10 kDa displayed a nearly complete switching of the enzyme activity at 52 °C. As the  $M_n$  of the conjugated polymer was decreased from 10 to 6 to 3 kDa, there was a concomitant decrease in

**Figure 5.** Characterization of HEC enzyme activities for free DMAAm–EG 12A conjugates in solution at as function of polymer size and conjugation site. The activities were measured for 100 nM conjugates with free polymer using HEC (20 mg/mL) as a substrate and normalized to the activity of N55C or S25C EG 12A controls as 100% at each temperature. EG 12A–M10, 10 kDa DMAAm–EG12A conjugate; EG 12A–M6, 6 kDa DMAAm–EG 12A conjugate; EG 12A–M3, 3 kDa DMAAm–EG 12A conjugate; and EG 12A + M10, physical mixture of enzyme plus 10 kDa DMAAm.

switch efficiency (Figure 4). For the S25C conjugates, a small but significant activity was retained, even with the 10 kDa DMAAm, when the conjugation site was moved to this more distant position relative to the active site carboxylate residues. Taken together, these results demonstrate that both the polymer  $M_n$  and the position of conjugation are critical for determining the magnitude of the switching effect.

*Switching Activities as a Function of Substrate Size.* The effect of substrate size on the switching activity was investigated by using the large HEC as a substrate. Figure 5 shows the results of the thermo-responsive switching activity measurements using HEC as a substrate for the N55C and S25C conjugates. At 32 °C, the enzyme activities were much lower than the unconjugated mutant EG 12A controls, and the physical mixtures of unconjugated enzyme and free polymer, while they were largely unchanged for the small molecule ONPC substrate. This suggests that the steric hindrance of the expanded, conjugated polymer interfered with the binding of the larger HEC to EG 12A. When the temperature was increased to 52 °C, the activity of the N55C and S25C conjugates toward HEC was shut off. This effect was observed not only with the 10 kDa N55C–DMAAm conjugate, but also with the 6 kDa polymer. This finding was in contrast to the incomplete shutoff of the smaller ONPC activity with the 6 kDa DMAAm polymer. When the conjugation site was moved to the more distant S25C position, the expanded polymer again blocked activity to a significant level at all three polymer sizes. The same



**Figure 6.** Characterization of ONPC switching activities for immobilized EG12A conjugates as a function of polymer molecular weight and conjugation site. The activities were measured using 8 mM ONPC as a substrate at 32 and 52 °C in 50 mM sodium acetate buffer, pH5.5, and normalized to the activity of WT EG 12A. DMAAm-EG12A conjugates of the following are shown for the N55C and S25C conjugates: 10 kDa  $M_n$ , M-10; 6 kDa  $M_n$ , M-6; and 3 kDa  $M_n$ , M-3.

**Table 3. Biotinylation Results for DMAAm-EG 12A Conjugates**

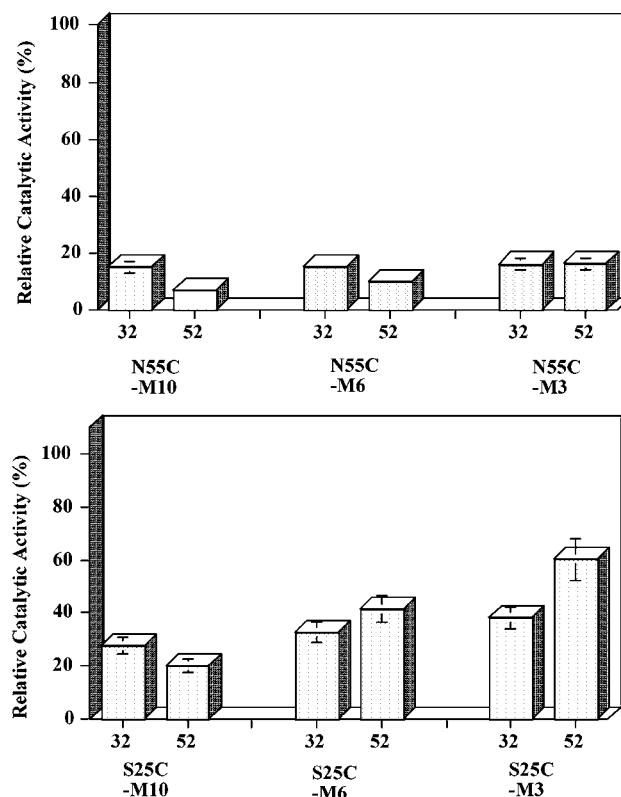
conjugate	number of biotins (#/EG 12A conjugate)
N55C-DMAAm (10 kDa)	1.4
N55C-DMAAm (6 kDa)	1.4
N55C-DMAAm (3 kDa)	1.5
S25C-DMAAm (10 kDa)	1.3
S25C-DMAAm (6 kDa)	1.4
S25C-DMAAm (3 kDa)	1.5

general trend was still found of a more complete shutoff effect as polymer  $M_n$  was increased, although the absolute magnitude of the off-state activities were consistently higher at the corresponding polymer sizes than for the N55C conjugates.

**Temperature-Responsive Activity Changes of Immobilized DMAAm-EG 12A Conjugates.** Immobilized enzymes are used in many applications and the switching properties were thus also investigated when the conjugates were bound to beads and free polymer was removed. The conjugates were biotinylated and immobilized onto streptavidin magnetic beads, followed by intensive washing to remove the free polymer chains. The degree of biotinylation was well controlled near a stoichiometry of one (Table 3). The quantities of the conjugates and the control WT EG 12A immobilized on the SA magnetic beads were controlled to equivalent levels (Table 4). A comparison of the catalytic activities of the immobilized and purified N55C and S25C conjugates toward ONPC and HEC at 32 and 52 °C is shown in Figures 6 and 7. The general trend of switching activity as a function of conjugation position, of polymer size, and of substrate size followed those of the conjugates in

**Table 4. Quantities of Immobilized Conjugates and WT EG 12A Control**

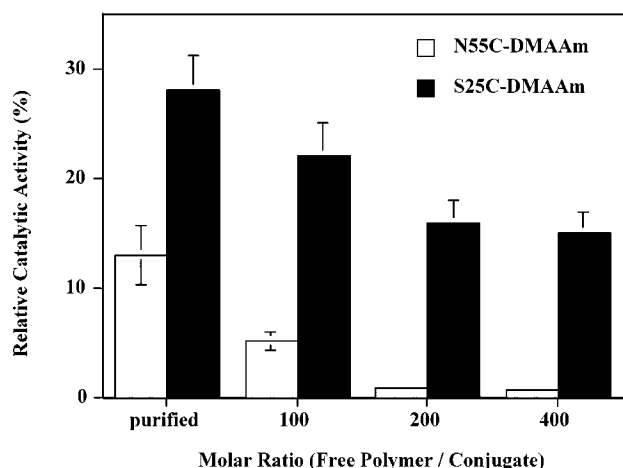
conjugate	immobilized quantity ( $\mu\text{g}/\text{mg}$ beads)
N55C-DMAAm (10 kDa)	18.8
N55C-DMAAm (6 kDa)	19.3
N55C-DMAAm (3 kDa)	19.5
S25C-DMAAm (10 kDa)	19.0
S25C-DMAAm (6 kDa)	19.5
S25C-DMAAm (3 kDa)	19.8
WT	19.8



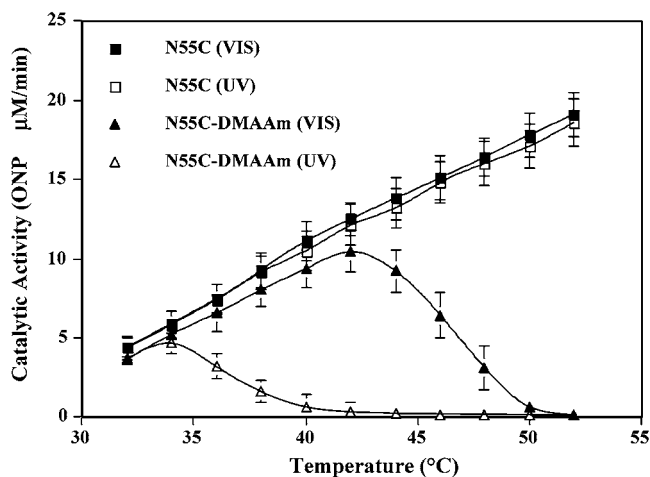
**Figure 7.** Characterization of HEC switching activities for immobilized EG12A conjugates as a function of polymer molecular weight and conjugation site. The activities were measured using 8 mM ONPC as a substrate at 32 and 52 °C in 50 mM sodium acetate buffer, pH5.5, and normalized to the activity of WT EG 12A. DMAAm-EG12A conjugates of the following are shown for the N55C and S25C conjugates: 10 kDa  $M_n$ , M-10; 6 kDa  $M_n$ , M-6; and 3 kDa  $M_n$ , M-3.

solution. The magnitude of the shutoff effects were generally good, although there was a significant residual activity in all samples at 52 °C, including with the 10 kDa conjugates. This residual activity was approximately 12% for the N55C-10 kDa DMAAm conjugate.

To investigate the effect of the free polymer on the switching activity of the immobilized conjugates, free DMAAm was added back to the beads at defined stoichiometries. The effect of free polymer addition on the activity of the immobilized conjugates at 52 °C is shown in Figure 8. The addition of free DMAAm polymer enhanced the shutoff effect for both S25C and N55C conjugates, with complete shutoff of enzyme activity for the N55C conjugates when 100–200 times excess of the free polymer was added. These results suggest that the conjugated polymer directs the aggregation of the free polymer to the conjugation site near the enzyme active site, where the higher effective size of the aggregate leads to more effective blocking of the substrate from the active site.



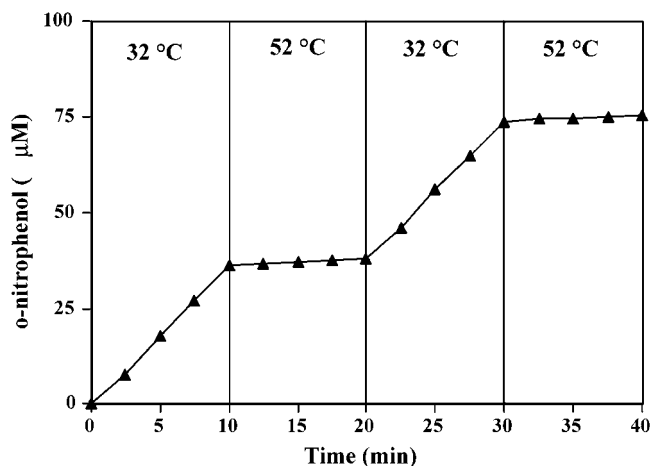
**Figure 8.** Effect of free polymer addition to immobilized EG 12A activities remaining above the LCST of the DMAAm. DMAAm of 10 kDa  $M_n$  was added to the immobilized N55C and S25C conjugates at the defined concentrations noted on the bar graph. The activities were measured for 100 nM conjugates using ONPC (8 mM) as a substrate at 52 °C in 50 mM sodium acetate buffer, pH 5.5, and normalized to the activity of immobilized WT EG 12A at each temperature.



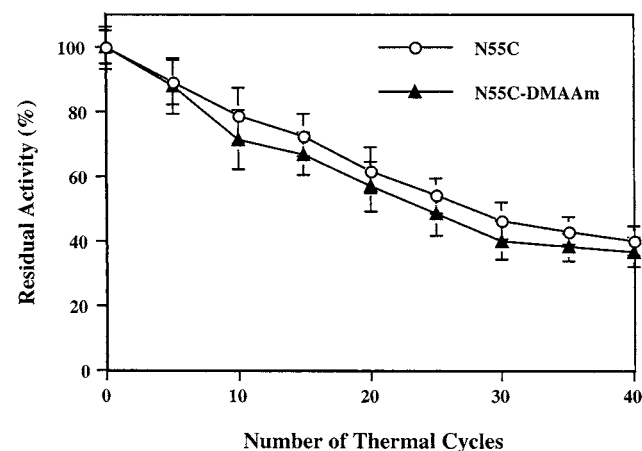
**Figure 9.** The complete activity profiles for the DMAAm–N55C EG 12A conjugate as a dual function of temperature and UV or Vis light irradiation. Initial velocities were determined for the 100 nM N55C–DMAAm (11 kDa) conjugate and the N55C control using 8 mM ONPC as the substrate in 50 mM sodium acetate buffer, pH 5.5. The samples were irradiated with either the UV or vis light for 10 min and 3 h, respectively, before the activity determinations.

#### Dual Photo- and Temperature Switching Activity Profiles.

The light-responsive enzyme switching has been described in a recent communication (18). The dual relationship between temperature and UV or vis irradiation on the activities of the N55C control and the N55C–DMAAm (10 kDa) conjugate are shown in Figure 9 with ONPC as substrate. The activity of the N55C increased with increasing temperature, and UV or vis irradiation did not influence the enzyme activity. The temperature response of the polymer switch generally follows the shift in LCST behavior under UV versus vis photoirradiation (Figure 2), confirming the action of the polymer as a switch between the expanded and collapsed states. The thermal cycling properties and reversibility of the DMAAm polymer switch are demonstrated in Figure 10. As the product accumulation profile demonstrates, the response time to turn on or off the enzyme activity was faster than the scale of seconds it took to switch between the two



**Figure 10.** Reversibility of the DMAAm–N55C EG 12A enzyme switch. The total product (*o*-nitrophenol) accumulation was measured for 100 nM conjugate using ONPC (8 mM) as a substrate in 50 mM sodium acetate buffer pH 5.5. The reaction vessel was transferred between 32 and 52 °C water baths with small aliquots removed to determine product accumulation as a function of time.



**Figure 11.** Thermal stability of the EG 12A enzyme switch. The temperature was cycled between 32 and 52 °C for 2 min each. The activities were measured for 100 nM N55C or the conjugates with free polymer using ONPC (8 mM) as a substrate at 32 °C after incubation for 20 min in 50 mM sodium acetate buffer pH 5.5.

temperature baths. There was some instability of the EG 12A to repeated thermal cyclings as shown in Figure 11, but the DMAAm conjugation did not significantly destabilize the enzyme further. The activities of both N55C and the conjugates decreased with increasing cycle number in equivalent fashion.

#### Kinetic Analysis of the Switching Mechanism.

Michaelis–Menton analysis of the catalytic activity data was conducted to provide mechanistic insight into the polymer switching activity. The effects of temperature changes under UV or vis photoirradiation on the Michaelis–Menton kinetic parameters  $k_{cat}$  and  $K_m$  for N55C and N55C–DMAAm (10 kDa) conjugates are shown in Table 5. These parameters were determined for both the small molecule ONPC substrate and the larger HEC substrate. The  $K_m$  values of the conjugates were increased substantially compared to those of unconjugated N55C at 52 °C compared to 32 °C. The  $k_{cat}$  values of the conjugates remained only slightly reduced in comparison to the N55C control. These results suggest that the shutoff effect is primarily due to the large decrease in substrate affinity upon polymer collapse above the LCST. The



**Table 5. Michaelis–Menton Analysis of Switching Mechanism**

	ONPC		HEC	
	$K_m$ [mM]	$k_{cat}$ [s <sup>-1</sup> ]	$K_m$ [m/mL]	$k_{cat}$ [s <sup>-1</sup> ]
	N55C			
32 °C	15.8	1.9	14.4	4.7
52 °C	33.9	13.6	29.2	12.7
	N55C–DMAAm			
32 °C	20.7	2.06	190	4.5
52 °C	1140	4.10	9660	9.3

switching is thus connected to the steric blocking of the active site by the collapsed DMAAm polymer when it is attached close to the active site. The activity of the DMAAm conjugates toward HEC is reduced at 32 °C, where the polymer exists in the expanded state. This reduced activity is also due to a large increase in  $K_m$ . The decrease in the affinity of the large HEC substrate, even when the DMAAm polymer is in the expanded state, is again consistent with a simple steric blocking mechanism, which is enhanced by the large size of the HEC substrate.

## DISCUSSION

A new approach has been developed for controlling enzyme activity using smart polymer switches that serve both as antennae and as actuators. We have previously shown that smart polymer collapse and expansion in response to small changes in temperature or pH can be used to control biotinylated-ligand binding to streptavidin (1–4). A similar general approach for controlling enzyme activity was investigated in this work, with a new family of dual temperature- and photo-responsive polymers. These polymers reversibly cycle between an expanded state, hydrated state, and a collapsed, hydrophobic state above and below their characteristic phase transition LCST. This LCST varies under UV versus vis irradiation, which provides the ability to use temperature and/or light to regulate polymer expansion and collapse. The EG12A enzyme has a distinctly different binding site compared to the previously studied streptavidin–biotin system. The binding site is a relatively broad and concave groove that is more open and accessible to the conjugated polymer chain than the nearly completely buried binding site of streptavidin. This likely plays an important role in the improved on and off reversibility of the enzyme switch compared to streptavidin, as well as the considerably faster substrate off-rate compared to that of biotin.

An important conclusion that can be drawn from these initial studies is that the polymer switch is largely acting by blocking substrate access when the chain is in the collapsed state, i.e., the off-state. In the expanded state below the LCST, i.e., the on-state, the hydrated polymer chain did not significantly alter the small substrate access as evidenced by the catalytic activities and  $K_m$  values. The key corollary is that the switch can be optimized by the interplay of conjugation site, polymer size, and substrate size. With a polymer of a given  $M_n$ , the efficiency of the off-state was reduced when the conjugation site was moved away from the active site. Consistent with this steric mechanistic model, the efficiency could be improved at the distant conjugation site by increasing the polymer chain length. These two design parameters of polymer  $M_n$  and conjugation site also trade off with respect to substrate size. In contrast to the small molecule ONPC substrate, we found significant blocking of the large HEC substrate by the expanded polymer

chain with even the 3 kDa DMAAm. Taken together, these findings suggest that the polymer switch approach should allow optimization for a given substrate through an appropriate choice of polymer size and conjugation site.

While it is clear that the blocking of substrate access is underlying the switching effects, the origins of this blocking mechanism could be different for the conjugates free in solution versus in the immobilized state on beads. From an applications standpoint, both are interesting as there are assay and microfluidic technologies where either or both of the systems might be useful. The immobilized conjugates were purified from free polymer and were found to possess strong switching activity. With these isolated conjugates, the mechanism should be close to the schematic model of polymer collapse and expansion in Figure 1. The remaining activity could be abrogated by the addition of free polymer, suggesting that larger polymer chains and/or a closer conjugation site could optimize the enzyme switch for the surface-immobilized enzymes.

On the other hand, the free conjugates in solution could be forming colloidal aggregates above the LCST, and the substrate blocking effects could be due to transport limitations to the active sites of the aggregated enzymes. These experiments were conducted at low concentrations ca. 100 nM, where there were no detectable changes in optical density (i.e., clouding) above the LCST and no aggregates could be pelleted. The time response in going from the collapsed off-state to the expanded on-state is at least as fast as seconds, consistent with very small aggregates that can dis-aggregate quickly. Finally, it should be noted that there is still a strong positional dependence of the conjugation site on the switching activity that follows the same trend as that of the immobilized system. Therefore the orientation of the enzyme active site relative to the polymer must be connected to the poor accessibility of substrate, which would only be possible in very small aggregates or isolated conjugates. Further experimentation with dynamic light scattering techniques will be necessary to determine the nature of the aggregates formed at these concentrations.

## ACKNOWLEDGMENT

We would like to thank Dr. J. Milton Harris of Shearwater Polymers for his advice on the addition of the polymer end hydroxyl groups to vinyl sulfone groups of DVS. We also wish to thank Dr. R. To for helping the construction of the EG 12A mutants and Dr. David Hyre for the molecular model of EG 12A. The NIH (Grant No.53771), UW Office of Technology Transfer, the Washington Research Foundation, and the Washington Technology Center are gratefully acknowledged for their support of this project.

## LITERATURE CITED

- (1) Stayton, P. S., Shimoboji, T., Long, C., Chilkoti, A., Chen, G., Harris, J. M., and Hoffman, A. S. (1995) Control of protein–ligand recognition using a stimuli-responsive polymer. *Nature* 378, 472–474.
- (2) Bulmus, E. V., Ding, Z., Long, C. J., Stayton, P. S., and Hoffman, A. S. (2000) A pH- and temperature-sensitive copolymer-streptavidin site-specific conjugate for pH-controlled binding and triggered release of biotin. *Bioconjugate Chem.* 11, 78–83.
- (3) Ding, Z. L., Long, C., Hayashi, Y., Bulmus, E. V., Hoffman, A. S., and Stayton, P. S. (1999) Temperature control of biotin

- binding and release with a streptavidin-poly(N-isopropylacrylamide) site-specific conjugate. *Bioconjugate Chem.* 10, 395–400.
- (4) Ding, Z., Fong, R. B., Long, C. J., Hoffman, A. S., and Stayton, P. S. (2001) Size-dependent control of the binding of biotinylated proteins to streptavidin using a polymer shield. *Nature* 411, 59–62.
- (5) Shimoboji, T., Ding, Z. L., Stayton, P. S., and Hoffman, A. S. (2002) Photoswitching of ligand association with a photoresponsive polymer-protein conjugate. *Bioconjugate Chem.* 13, 915–919.
- (6) Morag, E., Bayer, E. A., and Wilchek, M. (1996b) Immobilized nitro-avidin and nitro-streptavidin as reusable affinity matrixes for application in avidin–biotin technology. *Anal. Biochem.* 243, 257–263.
- (7) Tawfik, D. S., Chap, R., Eshhar, Z., and Green, B. S. (1994) pH on–off switching of antibody-hapten binding by site-specific chemical modification of tyrosine. *Protein Eng.* 7, 431–434.
- (8) Willner, I., Shai, R., and Riklin, A. (1991) Photoregulation of papain activity through anchoring photochromic azo groups to the enzyme backbone. *J. Am. Chem. Soc.*, 113, 3321–3325.
- (9) Bieth, J., Wasserman, N., Vratsanos, S. M., and Erlanger, B. F. (1970) Photoregulation of biological activity by photochromic reagents, IV. A model for diurnal variation of enzymic activity. *Proc. Natl. Acad. Sci. U.S.A.* 66, 850–854.
- (10) Namba, K., and Suzuki, S. (1975) Photocontrol of enzyme activity with a photochromic spiropyran compound-modification of  $\alpha$ -amylase with spiropyran compound. *Chem. Lett.* 9, 947–950.
- (11) Posey, K. L., and Gimble FS. (2002) Insertion of a reversible redox switch into a rare-cutting DNA endonuclease. *Biochemistry* 41, 2184–2190.
- (12) Seetharaman, S., Zivarts, M., Sudarsan, N., and Breaker, R. R. (2001) Immobilized RNA switches for the analysis of complex chemical and biological mixtures. *Nat. Biotechnol.* 19, 336–341.
- (13) Marvin, J. S., Corcoran, E. E., Hattangadi, N. A., Zhang, J. V., Gere, S. A., and Hellinga, H. W. (1997) The rational design of allosteric interactions in a monomeric protein and its applications to the construction of biosensors. *Proc. Natl. Acad. Sci. U.S.A.* 94, 4366–4371.
- (14) Hakansson, U., Fagerstam, L., Pettersson, G., and Andersson, L. (1978) Purification and characterization of a low molecular weight 1,4-beta-glucan glucanohydrolase from the cellulolytic fungus *Trichoderma viride* QM 9414. *Biochim. Biophys. Acta* 524, 385–392.
- (15) Ward, M., Wu, S., Darberman, J., Weiss, G., Larenas, E., Bower, B., Rey, M., Clarkson, K., and Bott, R. (1993) Cloning, sequence and preliminary structural analysis of a small, high pI endoglucanase (EG III) from *Trichoderma reesei*. *Found. Biotech. Ind. Ferment. Res.* 8, 153–158.
- (16) Sandgren, M., Shaw, A., Ropp, T. H., Wu, S., Bott, R., Cameron, A. D., Stahlberg, J., Mitchinson, C., and Jones, T. A. (2001) The X-ray crystal structure of the *Trichoderma reesei* family 12 endoglucanase 3, Cel12A, at 1.9 Å resolution. *J. Mol. Biol.* 308, 295–310.
- (17) Kroger, R., Menzel, H., and Hallensleben, M. L. (1994) Light controlled solubility change of polymers: copolymers of N,N-dimethylacrylamide and 4-phenylazophenyl acrylate. *Macromol. Chem. Phys.* 195, 2291–2298.
- (18) Shimoboji, T., Larenas, E., Fowler, T., Stayton, P. S., and Hoffman, A. S. (2002) Photoresponsive polymer-enzyme switches. *Proc. Natl. Acad. Sci. U.S.A.* 99, 16592–16596.

BC025615V

# Synthesis of Polymerized Thin Films for Immobilized Ligand Display in Proteomic Analysis

Susan K. Hobbs, Gongyi Shi, and Mark D. Bednarski\*

Stanford University School of Medicine, Lucas MRSI Research Center, 1201 Welch Road, Palo Alto, California 94304. Received November 8, 2002; Revised Manuscript Received January 24, 2003

We describe a new material for the display of biomolecular ligands for use in proteomic analysis. We report here on the construction of the first functionalized polymerized diacetylene thin films (PDTFs) for use in displaying immobilized ligands and their application in mass spectral proteomic analysis. Functionalized polymerized thin film surfaces were constructed with diacetylene-containing biotin lipid monomers designed for the capture of proteins (streptavidin) from a complex cellular lysate and detection with mass spectrometry (MS). These materials serve as a prototype for ligand-based spotted arrays amenable to high throughput screening. Functionalized PDTFs can be easily manufactured for customized microarrays and demonstrate high protein specificity and low nonspecific protein adsorption, and the resulting microarrays constructed from these materials are compatible with several different protein analysis platforms. Our results suggest that these materials have broad potential applications for use in mass spectral-based proteomic analysis.

## INTRODUCTION

We describe herein a new material for the construction of functionalized thin film-based microarrays and their use in protein capture and subsequent MS detection. This approach, termed Materials for Immobilized Ligand Display (MILD), is based on self-assembled polymerized diacetylene thin films (PDTFs) that are stable to the laser intensities employed in matrix-assisted laser desorption/ionization-mass spectrometry (MALDI-MS) and display ligands at the interface to capture proteins for MS detection. These materials are simple to construct, exhibit high specificity for different classes of proteins, and are amenable to high throughput data acquisition.

The current emphasis in proteomics is the development of materials for use in immobilized microarrays for protein detection similar to that of gene expression analysis (1). Currently, materials for microarray development have focused on arraying biomolecules in a manner that retains their biological activity. Antibodies, small molecules, peptide ligands, purified recombinant proteins, and whole tissue preparations have been non-specifically arrayed on different materials (2–11). A more difficult problem is to design materials that can capture specific proteins and limit nonspecific binding to the surface. So far, the investigation of small molecule or peptide arrays have been limited to model systems that contain only purified proteins binding to their respective ligands displayed on the material surface. An additional problem is that the captured biomolecule is often present at low concentrations and must be accurately detected and quantified (12). No materials have demonstrated the capability to both reproducibly capture specific proteins from complex protein mixtures and be amenable for rapid mass spectral analysis.

A potential solution to many of these problems is to chemically modify surfaces with organic monomolecular films such as self-assembled monolayers (SAMs) (13).

These films, which are formed on a platform surface by the spontaneous adsorption of molecules from solution, have important properties that can be utilized for proteomic analysis using a variety of detection methods including MALDI-MS. The films are chemically and physically flexible, thermodynamically and kinetically stable, and provide homogeneous surface coverage (14, 15). Polymerized diacetylene thin films (PDTFs) are unique SAMs with potential applications in microarrays because the polymerized films are stable to laser desorption and can appropriately display ligands for subsequent protein capture with low nonspecific protein binding (16). PDTFs can be arranged on a variety of platform surfaces and have been characterized using X-ray photoelectron spectroscopy (XPS), ellipsometry, fluorescent microscopy, contact angle measurement, atomic force microscopy, and scanning tunneling microscopy (17, 18). These studies demonstrated that PDTFs produce monolayers with the ligand functional groups directed toward the ambient surface, a property that is critical for proper binding of proteins (17). We have previously used PDTFs to present ligands on surfaces to study enzymatic reactions, as a model system to study cell adhesion, and as a detection system for protein–ligand binding (16, 19). We now describe the construction of polymerized diacetylene thin films that can be formulated into ligand-surface spotted arrays and assayed using currently available MALDI-TOF platforms.

## EXPERIMENTAL SECTION

**Preparation of Monomers.** *N*-(2-Hydroxyethyl)-10,12-pentacosadiynamide (EAPDA) was synthesized as previously described (17). Biotinylated-PEG-PDA was synthesized as previously described (20). The peptidomimetic integrin antagonist was synthesized as previously described (details included in the Supporting Information of ref 21).

**Film Formation.** Monomer mixtures (0.025–2.5 pmol functionalized biotin lipid monomer/layer and integrin antagonist functionalized lipid) were spread on a bead

\* To whom correspondence should be addressed. 650 723 7866 (phone), 650 723 5795 (fax), mark@s-word.stanford.edu.



of water covering a hydrophobic surface. The surface area of each spot was 3.14 mm<sup>2</sup>. Ultraviolet irradiation at 254 nm from a UV lamp (Model UVGL-55 Multiband 254/366 nm, UVP Inc, San Gabriel, CA) for approximately 15 min was used to polymerize the films. This was repeated twice. The polymerized films appeared slightly reddish in color. The surfaces were analyzed for fluorescence and birefringence for quality assurance. The surfaces were then cured at room temperature for at least 1.5 h.

**X-ray Photoelectron Spectroscopy (XPS).** Angle-resolved XPS measurements were performed in a Surface Science S-Probe XPS instrument using monochromatic Al K $\alpha$  radiation. Spectra in regions of interest were obtained as a function of takeoff angle. Rotation of the specimen holder allowed the takeoff angle to be varied from 75° to 15°. The angle between the incident X-rays and the electrons collected by the energy analyzer was fixed at 45° so that the angular dependence of the photoelectric emission cross section did not affect the angle-resolved XPS spectra.

**Cellular Lysate Preparation.** Human M21 melanoma cells (provided by Dr. D. Cheresch, Scripps) were pelleted (approximately 10<sup>7</sup> cells) and lysed in 500  $\mu$ L of 40 mM Tris (GibcoBRL Life Technologies, Rockville, MD), pH 8.5, in the presence of protease inhibitor cocktail (Roche, Germany) and sonicated at 4 °C for 30 s. The solution was centrifuged at 13 000 rpm for 10 min in a microcentrifuge (Centrifuge 5415, Eppendorf, Germany). Total protein concentration in the supernatant was determined by the bicinchonic acid (BCA) assay (Bio-Rad Laboratories, Hercules, CA).

**Streptavidin and  $\alpha_v\beta_3$  Integrin Mass Spectrometry Assay.** Five microliters of the following solutions was applied to the polymerized films: streptavidin (Sigma-Aldrich, St. Louis, MO) and purified  $\alpha_v\beta_3$  integrin (Chemicon, Temecula, CA) diluted in PBS, streptavidin and purified  $\alpha_v\beta_3$  integrin diluted into cellular lysate (determined to contain 1 mg/mL total protein), and streptavidin preincubated with free biotin. All were incubated at high humidity for 30 min at room temperature. Following incubation, the solutions were removed from the films and the surfaces were washed three times with PBS and one time with water. The surfaces were allowed to air-dry. Saturated sinnapinic acid (SPA, CIPHERGEN Biosystems, Fremont, CA) dissolved in 50% acetonitrile (Sigma-Aldrich, St. Louis, MO) containing 0.5% trifluoroacetic acid (Sigma-Aldrich, St. Louis MO) was placed onto the surface (0.5  $\mu$ L) and allowed to air-dry. The surfaces were then analyzed in a ProteinChip reader (Protein Biology System, CIPHERGEN Biosystems, Fremont, CA).

## RESULTS AND DISCUSSION

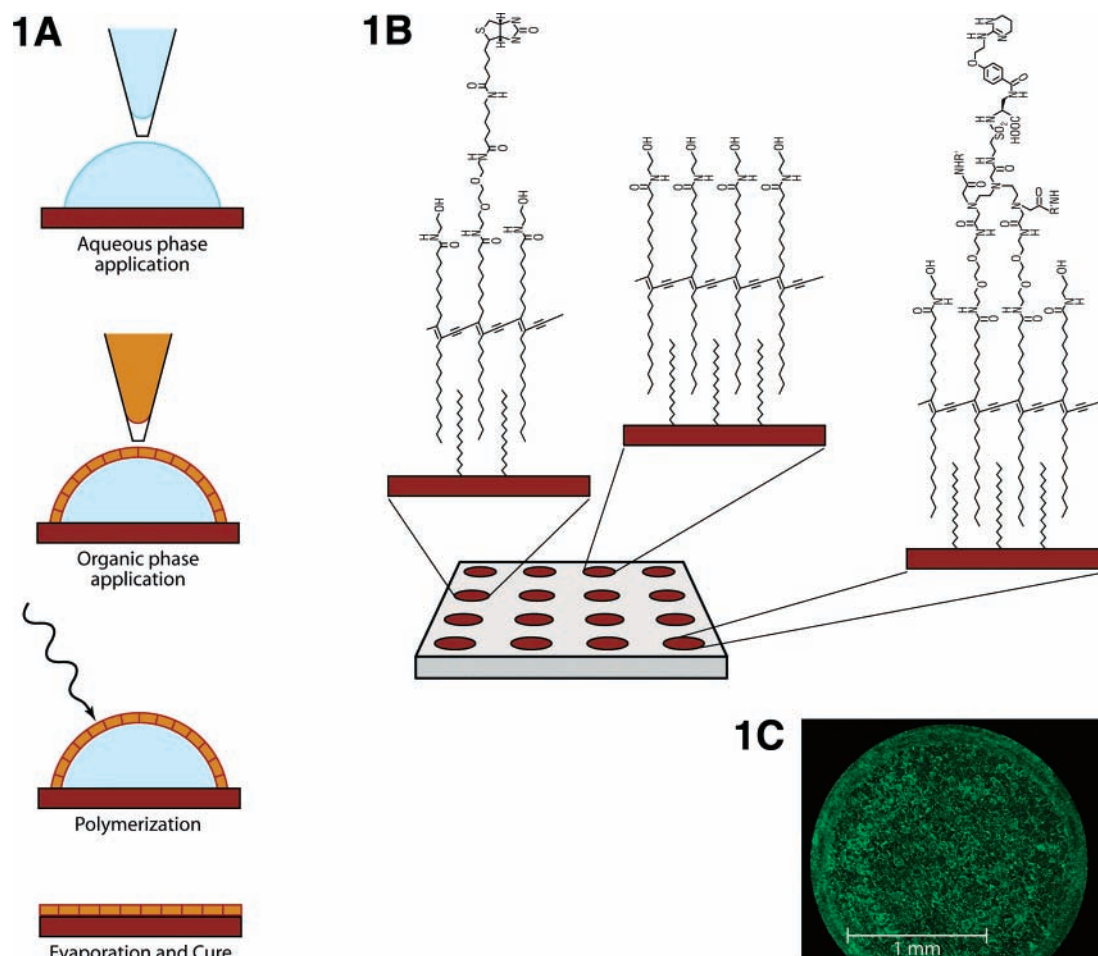
A modified hydrophobic aluminum oxide surface compatible with MALDI-MS or SELDI-MS was used as a platform surface for film deposition. An aqueous subphase was arrayed onto the hydrophobic surface (~2 mm diameter spot size), and next the polymerizable lipid (dissolved in chloroform) was transferred to the surface of the aqueous subphase (Figure 1A). Polymerization was achieved by ultraviolet light irradiation (254 nm) followed by curing at room temperature (see Methods). The chemical structure of the PDTFs (with hydroxyl, biotin, and peptidomimetic headgroup ligands) is shown in Figure 1B. The films were then evaluated with fluorescence microscopy and birefringence to determine the quality of surface coverage as well as crystalline struc-

ture. In general, using these techniques there was contiguous film coverage of the surface area as indicated by a high degree of fluorescence and crystalline structure (Figure 1C). Angle-resolved X-ray photoelectron spectroscopy (XPS) was performed to confirm that the biotin headgroups were localized at the film-ambient surface. The peak areas are plotted against the sine of the takeoff angle. Each peak area is scaled independently, and thus the relative areas do not reflect the actual elemental composition (Figure 2). The N 1s peak area, due to the amide nitrogens are nearly independent of takeoff angle indicating that the nitrogen atoms are localized in the interfacial region. This is similar to the findings of Wilson and Bednarski (17). The films are stable under standard MALDI-MS operating conditions as no interference from the monomer components of the PDTFs was detected as evidenced by the smooth baseline trace on all mass spectra. Therefore, we have established that stable PDTFs containing ligands can be arrayed on suitable surfaces for MALDI-MS analysis.

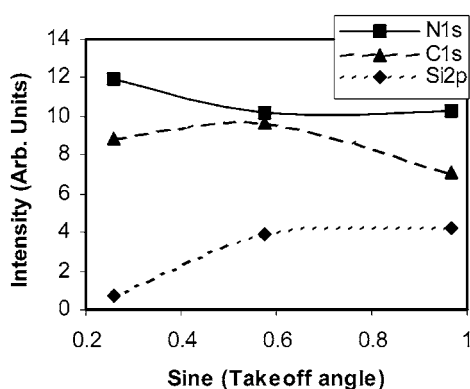
To demonstrate the feasibility of MILD-PDTFs in capturing and detecting specific proteins, we used a high affinity ligand-protein binding system (streptavidin-biotin) as a model. The streptavidin-biotin system also allows for future surface modifications with other biotinylated materials, such as antibodies. Streptavidin is a homotetrameric protein that contains four ~13 kDa biotin binding subunits (22). The remarkably strong biotin-streptavidin interaction ( $K_d \sim 10^{-15}$  M) (23) provides a ligand-protein binding model for the PDTF-MILD MALDI-MS protein detection approach.

We first constructed the MILD-PDTFs containing 0, 0.1, 1, and 10 mol % of a biotin-functionalized lipid within a matrix of EAPDA, a nonfunctionalized filler. All MILD-PDTF surfaces were incubated with the same amount of streptavidin (5  $\mu$ L of a 0.55  $\mu$ M solution, 2.75 pmol total protein). The surfaces were then washed with phosphate-buffered saline (PBS) to remove unbound proteins and analyzed by mass spectrometry. The streptavidin monomer (~13 kDa) was detected on the biotin surface in a ligand concentration dependent manner (Figure 3). Increasing the biotin concentration from 0.1 mol % to 10 mol % in the PDTFs led to an increased mass/charge ( $m/z$ ) area in a linear fashion through 1 mol % surface biotin concentration. The best signal intensity was observed on the PDTF containing 10 mol % biotin (or 2.5 pmol/monolayer). As a control, the same amount of streptavidin (2.75 pmol) was incubated on the EAPDA surface containing no biotin, but we were unable to detect significant streptavidin capture on the control surface. The low nonspecific protein binding property of these films is likely due to the preponderance of nonreactive hydroxyl groups of the EAPDA surface. The specific capture of streptavidin demonstrates that the biotin functional headgroups are biologically active at the interface of the films and that the ligand is structurally functional after PDTF formation and can be used in protein capture with MALDI-MS analysis.

To determine the specificity of protein capture on MILD-PDTFs we investigated streptavidin capture and detection from cellular lysate. Streptavidin was titrated into solutions containing a partially purified cellular lysate (1 mg/mL total protein) from 0.02% (0.2  $\mu$ g/mL streptavidin) to 2% (20  $\mu$ g/mL streptavidin) of total protein concentration, and the resulting mixtures were applied onto biotin MILD-PDTF surfaces to probe for presence of the protein. The high amount of protein contained in the cellular lysates was used to increase the amount of nonspecific proteins that were incubated on

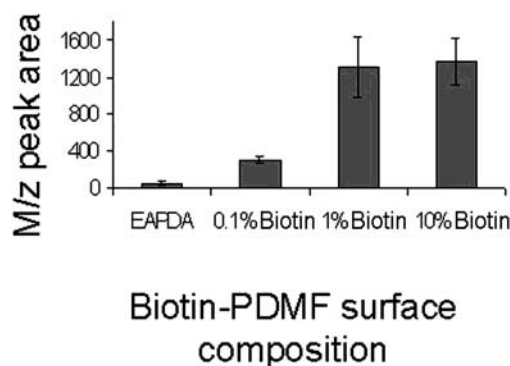


**Figure 1.** Materials for immobilized ligand display (MILD) array. (A) Method for constructing PDTFs. A modified hydrophobic aluminum oxide surface was used as a solid support for PDTF formation. An aqueous phase is applied to the base surface followed by an organic phase containing the diacetylene monomeric compounds. Polymerization is achieved through ultraviolet irradiation (254 nm for approximately 15 min). The materials are then cured at room temperature for 1.5 h. (B) Chemical structures of PDTFs. Schematic representation of biotin, hydroxyl, and integrin antagonist terminated headgroups. These ligands are immobilized and displayed within the PDTF backbone. (C) Fluorescent properties of PDTFs. Fluorescent micrograph obtained at 10 $\times$  magnification using FITC filters (PDTFs exhibit an excitation at 480 nm and emission at 525 nm) (16). Note the complete coverage and homogeneity of the film within the 2 mm spot size using the above arraying method.



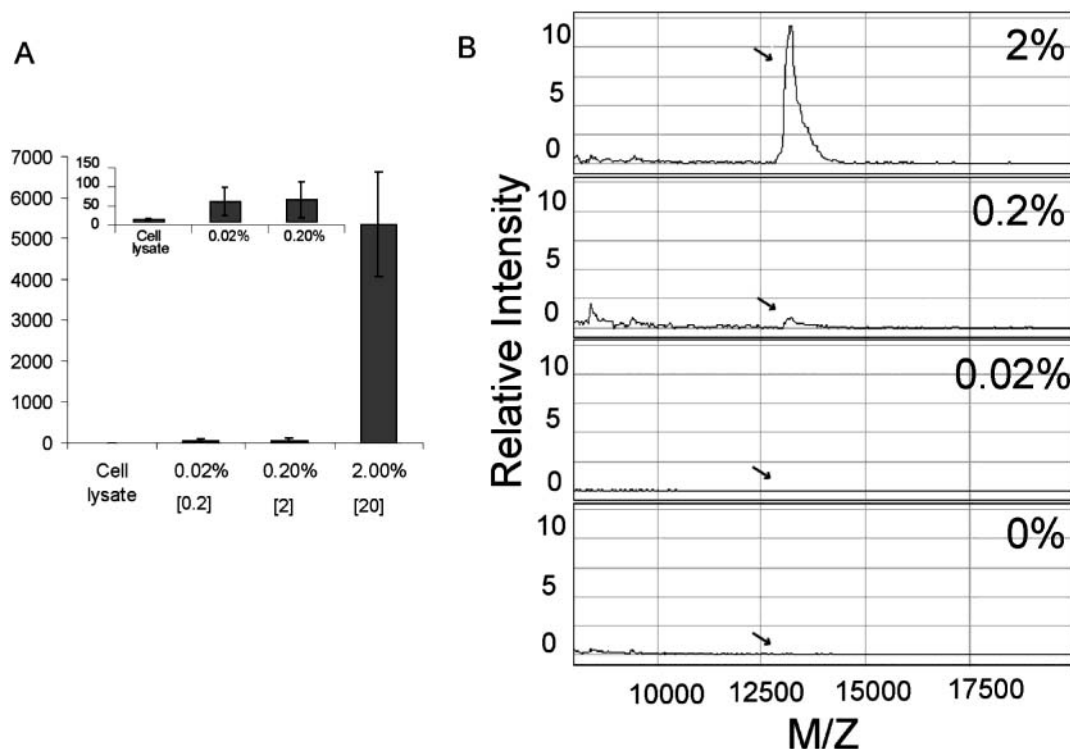
**Figure 2.** Composite presentation of the C 1s, N 1s, and Si 1s peak areas as a function of takeoff angle. The data are plotted as intensity versus sine of the takeoff angle. The larger values for the sine represent XPS sampling from deeper in the bulk. The N 1s signals due to the amide nitrogens are nearly independent of takeoff angle.

the PDTF surface. Interestingly, streptavidin capture was clearly identified even at a concentration as low as 0.02% (0.2  $\mu$ g streptavidin/mL) of total protein (Figure 4A). Increasing streptavidin capture and detection was related to increasing streptavidin application through 2% (20  $\mu$ g streptavidin/mL) of total protein concentration.

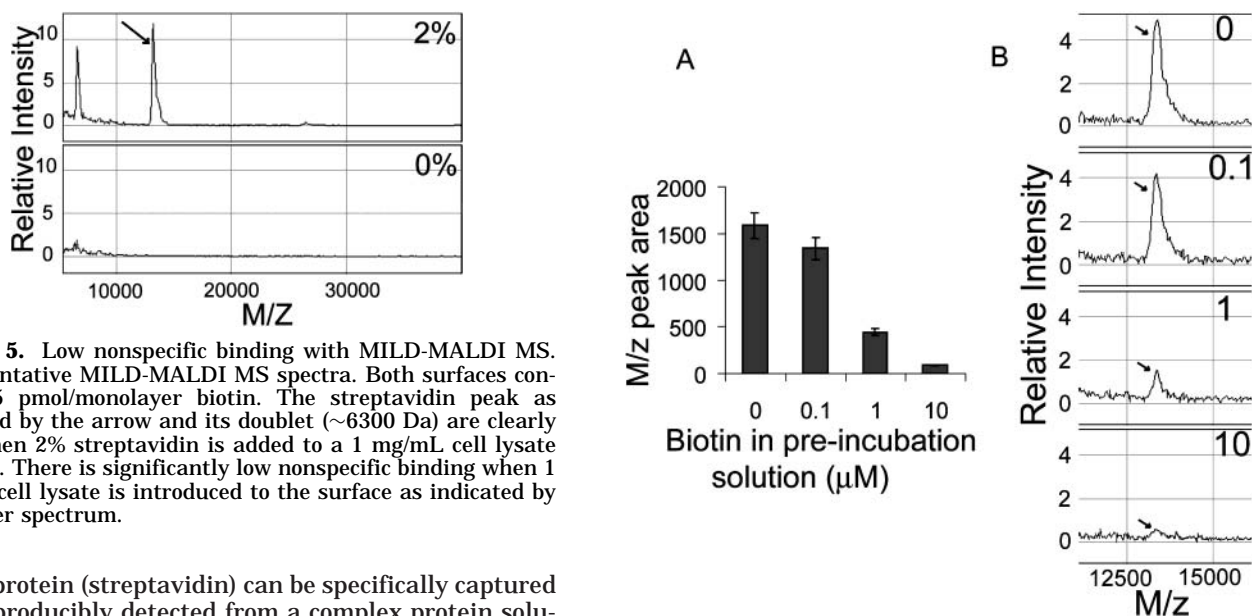


**Figure 3.** Streptavidin protein capture and detection with MILD-MALDI MS. The streptavidin mass/charge peak area was plotted against percentage of biotin contained in the PDTF. The mean and standard deviation of triplicate runs are shown. The PDTFs are EAPDA-PDTF, 0.1% (0.025 pmol/layer) biotin-PDTF, 1% (0.25 pmol/layer) biotin-PDTF, and 10% (2.5 pmol/layer) biotin-PDTF. All surfaces were incubated with the same amount of streptavidin (2.75 pmol).

Even with the complex cellular lysates containing a high concentration of nonspecific proteins (cellular lysates) in comparison to the streptavidin concentration, there was no significant nonspecific protein adsorption detected on the films (Figure 5). These results demonstrate that a



**Figure 4.** Sensitivity with MILD-MALDI MS. (A) The streptavidin mass/charge peak area was plotted against percentage of streptavidin contained in  $1 \mu\text{g/mL}$  total protein applied to the chip surface. The numbers in brackets refer to concentration of streptavidin ( $\mu\text{g/mL}$ ). The mean and standard deviation of triplicate runs are shown. All surfaces contain  $2.5 \text{ pmol/monolayer}$  biotin. (B) Representative MILD-MALDI MS spectra. All surfaces contain  $2.5 \text{ pmol/monolayer}$  biotin. Peak of streptavidin, as indicated by arrows, is detectable at 0.2% of total protein in solution in this example. Specific protein binding is demonstrated by the relative absence of other protein peaks.



**Figure 5.** Low nonspecific binding with MILD-MALDI MS. Representative MILD-MALDI MS spectra. Both surfaces contain  $2.5 \text{ pmol/monolayer}$  biotin. The streptavidin peak as indicated by the arrow and its doublet ( $\sim 6300 \text{ Da}$ ) are clearly seen when 2% streptavidin is added to a  $1 \text{ mg/mL}$  cell lysate solution. There is significantly low nonspecific binding when  $1 \text{ mg/mL}$  cell lysate is introduced to the surface as indicated by the lower spectrum.

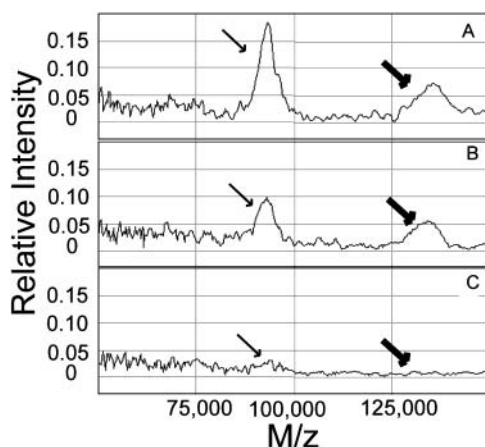
single protein (streptavidin) can be specifically captured and reproducibly detected from a complex protein solution such as cellular lysate via MILD-MALDI-MS.

To further demonstrate binding specificity, free biotin was incubated in solution with streptavidin prior to capture with the biotin-PDTF surface in a competitive inhibition experiment. Competition was achieved by increasing the amount of biotin in a constant streptavidin solution from 10 to 1000 mol % of the streptavidin. The effect of free biotin competition is clearly seen when the biotin concentration was 100-fold greater than that of streptavidin (Figure 6) with chip surfaces containing  $0.25 \text{ pmol/monolayer}$  biotin (1 mol % biotin-PDTF). The remaining free protein (in this case streptavidin) concentration in solution can then be estimated with the

**Figure 6.** Competitive inhibition. (A) The peak streptavidin area was plotted against the amount of biotin contained in the incubation solution prior to application to the MILD-PDTF surface. The mean and standard deviation of triplicate runs are shown. Streptavidin ( $0.01 \mu\text{M}$ ;  $50 \text{ fmol}$ ) was incubated with  $0.1 \mu\text{M}$ ,  $1 \mu\text{M}$ , or  $10 \mu\text{M}$  of free biotin for 30 min prior to incubation on the MILD-PDTF ( $0.25 \text{ pmol/monolayer}$  biotin) surface. (B) Representative MILD-MALDI MS spectra. Peak of streptavidin, indicated by arrows, decreases with increasing amount of biotin in solution.

MILD-MALDI-MS approach. These findings demonstrate a specific protein–ligand interaction between streptavidin and the immobilized biotin on the PDTF surface.





**Figure 7.** Integrin  $\alpha_v\beta_3$  protein capture and detection with MILD-MALDI-MS. (A) Purified  $\alpha_v\beta_3$  integrin (200 fmol) in PBS incubated on 30% integrin antagonist-PDTE. (B) Purified  $\alpha_v\beta_3$  (200 fmol) in cellular lysate (1 mg/mL) incubated on 30% integrin antagonist-PDTE. (C) Purified  $\alpha_v\beta_3$  (200 fmol) in cellular lysate (1 mg/mL) incubated on EAPDA-PDTE. Thin arrows indicate the expected mass peak of the integrin subunit  $\alpha_v$ ; thick arrows indicate peak of the  $\beta_3$  subunit.

The demonstrated binding specificity of MILD-PDTE using the biotin-streptavidin system encouraged us to extend its application to other biological interactions. Integrins are a family of transmembrane receptors that regulate cell adhesion, growth, and migration. They are also the targets of novel anticancer drugs in clinical trials (24). Integrin  $\alpha_v\beta_3$  is a heterodimeric complex of  $\alpha_v$  (~130 kDa) and  $\beta_3$  (~95 kDa) subunits (25, 26). We recently reported on the synthesis of high-avidity integrin  $\alpha_v\beta_3$  antagonist and its application as an integrin-targeting agent in vivo (21). A functionalized lipid containing this synthetic peptidomimetic was used as a MILD surface. PDTEs containing 30 mol % functionalized lipid in a matrix of EAPDA were incubated with 200 fmol of purified  $\alpha_v\beta_3$  integrin or  $\alpha_v\beta_3$  integrin solubilized in cellular lysate (1 mg/mL total protein). MILD-MS detected  $\alpha_v\beta_3$  integrin capture at this concentration (0.45% of the total protein in the incubation solution composed of  $\alpha_v\beta_3$  integrin or ~45 ng) in both the purified and the complex protein mixture systems as indicated by the presence of the  $\alpha_v$  and  $\beta_3$  subunits (Figure 7). This is comparable to other protein detection methods, such as silver staining. The exact physiological expression and distribution of the integrin depends on cell or tissue type and developmental or differentiation stage (27). The purpose of this study was to illustrate the feasibility of the system. Individuals using this system can tailor protein preparation methods to enrich for proteins of their interest and can use a ligand with appropriate affinity for the target protein. In addition, individuals may also investigate proteins of different molecular weights as the detection sensitivity of MALDI-MS decreases with increasing mass due to the increased number of multiple charges for larger proteins to improve detection sensitivity. Nevertheless, these results indicate that ligand-receptor interactions can be directly detected even from crude protein mixtures using a customized ligand surface, and with this demonstrated sensitivity we feel that MILD-MS could be applied in many physiological conditions.

Here we have described a material based on polymerized polydiacetylene thin films (PDTEs) that readily displays ligands to capture their binding molecules through molecular recognition that is compatible with MALDI-MS detection systems. The MILD-PDTE technol-

ogy has a number of advantages that allows it to take the challenging task of high throughput multiplexing analysis: (1) Specificity: our results indicate that proteins binding to ligands coupled to PDTE are highly specific. Washing conditions can be selected to preferentially remove nonspecific protein binding even further, (2) Quantification: mixing ligand-derived monomers with a monomer matrix prior to polymerization allows even distribution and proper display of the ligand at the material surface. This process also ensures the highly reproducible production of MILD-PDTEs that is essential for quantitative capture and subsequent detection of protein, (3) Versatility: Simple coupling chemistry can generate PDTEs functionalized with a wide variety of ligands. Combined with our simple film deposition technology, high-density custom-designed affinity surfaces can be rapidly constructed for substrate binding studies and deposited on a variety of base materials. The PDTEs are a new material that should find a use in the developing areas of proteomic analysis.

#### ACKNOWLEDGMENT

Supported by a grant from the Lucas Foundation, the Phil Allen trust, NIH P41 RR09784, and NIH CA86312-0. S. K. Hobbs is a NCI fellow supported by NIH T32 CA09696. We thank S. Narasimhan Danthi (National Institutes of Health) for a gift of integrin antagonist, and CIPHERgen Biosystems and Dan Lee for their input.

#### LITERATURE CITED

- (1) Williams, K., and Hochstrasse, D. (1997) Introduction to the Proteome. *Proteome Research: New frontiers in functional genomics* (Wilkins, M., Williams, K., Appel, R., Hochstrasse, D., Eds.) pp 1-12, Springer-Verlag, Berlin.
- (2) Haab, B., Dunham, M., and Brown, P. (2001) Protein microarrays for highly parallel detection and quantitation of specific proteins and antibodies in complex solutions. *Genome Biol.* 2, 1-13.
- (3) Kenseth, J., Harnisch, J., Jones, V., and Porter, M. (2001) Investigation of approaches for the fabrication of protein patterns by scanning probe lithography. *Langmuir* 17, 4105-4112.
- (4) de Wildt, R., Mundy, C., Gorick, B., and Tomlinson, I. (2000) Antibody arrays for high-throughput screening of antibody-antigen interactions. *Nature Biotechnol.* 18, 989-994.
- (5) MacBeath, G., Koehler, A., and Schreiber, S. (1999) Printing small molecules as microarrays and detecting protein-ligand interactions en masse. *J. Am. Chem. Soc.* 121, 7967-7968.
- (6) Houseman, B., Huh, J., Kron, S., and Mrksich, M. (2002) Peptide chips for the quantitative evaluation of protein kinase activity. *Nature Biotechnol.* 20, 270-274.
- (7) Martzen, M. (1999) A Biochemical genomics approach for identifying genes by the activity of their products. *Science* 286, 1153-1155.
- (8) Zhu, H., Bilgin, M., Bangham, R., Hall, D., Casamayor, A., Bertone, P., Lan, N., Jansen, R., Bidlingmaier, S., Houfek, T., Mitchell, T., Miller, P., Dean, R., Gerstein, M., and Snyder, M. (2001) Global analysis of protein activities using proteome chips. *Science* 293, 2101-2105.
- (9) Englert, C., Baibakov, G., and Emmert-Buck, M. (2000) Layered expression scanning: Rapid molecular profiling of tumor samples. *Cancer Res.* 60, 1526-1530.
- (10) Pawelcz, C., Charboneau, L., Bichsel, V., Simone, N., Chen, T., Gillespie, J., Emmert-Buck, M., Roth, M., Petricoin, E., and Liotta, L. (2001) Reverse phase protein microarrays which capture disease progression show activation of pro-survival pathways at the cancer invasion front. *Oncogene* 20, 1981-1989.
- (11) Stoeckli, M., Chaurand, P., Hallahan, D., Caprioli, R. (2001) Imaging mass spectrometry: A new technology for the analysis of protein expression in mammalian tissues. *Nature Med.* 7, 493-496.

- (12) Mitchell, P. (2002) A perspective on protein microarrays. *Nature Biotechnol.* 20, 225–229.
- (13) Mrksisch, M., and Whitesides, G. (1995) Patterning self-assembled monolayers using microcontact printing: a new technology for biosensors. *Trends Biotechnol.* 13, 228–235.
- (14) Bain, C., Troughton, E., Tao, Y., Evall, J., Whitesides, G., and Nuzzo, R. (1989) Formation of monolayer films by the spontaneous assembly of organic thiols from solution onto gold. *J. Am. Chem. Soc.* 111, 321–335.
- (15) Bain, C., and Whitesides, G. (1989) Formation of monolayers by the coadsorption of thiols on gold: Variation in the length of the alkyl chain. *J. Am. Chem. Soc.* 111, 7164–7175.
- (16) Charych, D. H., Nagy, J. O., Spevak, W., and Bednarski, M. D. (1993) Direct colorimetric detection of a receptor–ligand interaction by a polymerized bilayer assembly. *Science* 261, 585–588.
- (17) Wilson, T., and Bednarski, M. (1992) Polydiacetylene monolayers functionalized with amino acids. *Langmuir* 8, 2361–2364.
- (18) Wilson, T., Ogletree, D., Salmeron, M., and Bednarski, M. (1992) Evaluation of the structure of polydiacetylene monolayers using fluorescence microscopy and scanning tunneling microscopy. *Langmuir* 8, 2588–2590.
- (19) Tropper, F., and Bednarski, M. (1999) Models of cell surface carbohydrates and biological adhesion. *Bioorganic Chemistry: carbohydrates* (Hecht, S., Ed.) pp 335–369, Oxford University Press, New York.
- (20) Storrs, R. W., Tropper, F. D., Li, H. Y., Song, C. K., Kuniyoshi, J. K., Sipkins, D. A., Li, K. C. P., and Bednarski, M. D. (1995) Paramagnetic polymerized liposomes – Synthesis, characterization, and applications for magnetic-resonance-imaging. *J. Am. Chem. Soc.* 117, 7301–7306.
- (21) Hood, J., Bednarski, M., Frausto, R., Guccione, S., Reisfeld, R., Xiang, R., and Cheresch, D. A. (2002) Tumor regression by targeted gene delivery to the neovasculature. *Science* 296, 2404–2407.
- (22) Green, N. (1975) *Adv. Protein Chem.* 29, 85–113.
- (23) Chalet, L., and Wolf, E. (1964) The properties of streptavidin, a biotin-binding protein produced by *Streptomyces*. *Arch. Biochem. Biophys.* 108, 1–5.
- (24) Hood, J., and Cheresch, D. (2002) Role of Integrins in cell invasion and migration. *Nature Rev.-Cancer* 2, 91–100.
- (25) Cheresch, D. A., and Harper, J. (1987) Arg-Gly-Asp recognition by a cell adhesion receptor requires its 130 kDa alpha subunit. *J. Biol. Chem.* 262, 1434–1437.
- (26) Suzuki, S., Argraves, W., Pytela, R., Arai, H., Krusius, T., Pierschbacher, M., and Rouslahti, E. (1986) cDNA and amino acid sequences of the cell adhesion protein receptor recognizing vitronectin reveal a transmembrane domain and homologies with other adhesion protein receptors. *Proc. Natl. Acad. Sci.* 83, 8614–8618.
- (27) Rouslahti, E. (1999) Fibronectin and its integrin receptors in cancer. *Adv. Cancer Res.* 76, 1–20.

BC025637H

# A Concise Method for the Preparation of Peptide and Arginine-Rich Peptide-Conjugated Antisense Oligonucleotide

Chang-Po Chen,<sup>†</sup> Liang-Ren Zhang,<sup>†</sup> Yue-Feng Peng,<sup>‡</sup> Xiao-Bo Wang,<sup>§</sup> Sheng-Qi Wang,<sup>§</sup> and Li-He Zhang<sup>\*,†</sup>

School of Pharmaceutical Sciences, Peking University, Beijing 100083, China; School of Chemistry and Molecular Engineering, Peking University, Beijing 100871, China; and Beijing Institute of Radiation Medicine, Beijing, 100850, China. Received January 8, 2003; Revised Manuscript Received March 18, 2003

Peptide–oligonucleotide conjugates were synthesized using two strategies: a mimetic signal peptide-conjugated oligonucleotide was assembled stepwise on CPG by using 2,2-dimethyl-3-hydroxypropionic acid as a linker. To solve the precipitation problem in the coupling reaction caused by the electrostatic interaction of arginine-rich peptides and oligonucleotide, oligonucleotides were absorbed on an anion-exchange resin, and then the on-resin fragment was applied for the conjugation with arginine-rich peptide. The peptide–antisense oligonucleotides showed permeability to the cell membrane of HepG-2 cells.

## INTRODUCTION

Antisense oligonucleotides offer the possibility of highly selective pharmacological manipulation of gene expression. The rapid and specific inhibition of gene product expression makes antisense technology appealing for therapeutic applications and analysis of the function of newly discovered genes especially in the post-genome era (1, 2). Several requirements must be fulfilled by a potential antisense oligonucleotide including rapid penetration into cells and stability against the degradation by nuclease. Many methods were currently explored in order to realize efficient cell internalization and adequate intracellular targeting of oligonucleotides (3). The most attractive strategy is covalent binding of oligonucleotide to peptides able to pass through the cell membrane and to destabilize the endosomal membrane such as Antp peptide, Tat derived peptide, fusion peptide, and signal peptide (4–7).

Several strategies including solid-phase stepwise assembly, solution-phase fragment coupling, and solid-phase fragment coupling have been applied in the conjugation of peptide–oligonucleotide hybrids (8, 9). The major challenge for the conjugation of peptides and

nucleotides is the incompatibility of peptide chemistry and oligonucleotide chemistry. The difficulty of in-line synthesis is to find a combination of compatible protecting groups for the oligonucleotide and peptide moieties. Fragment conjugation in liquid medium requires the introduction of a suitable tether containing the reactive group to peptide or oligonucleotide motifs. Although the coupling reactions look straightforward, there are some limitations to this conjugation strategy, such as the solubility of peptide, the multistep purifications, and the electrostatic interaction of cationic peptides with nucleotides. In general, to synthesize the peptide–oligonucleotide conjugates, the N-terminus of peptide was coupled to a linker with a hydroxyl group which can be used for the formation of a phosphate diester bond connecting peptide and oligonucleotide by phosphoramidite chemistry. It was reported that the phosphate diester bond derived from the aliphatic hydroxyl function was unstable in concentrated aqueous ammonia; the breakage of the connection between peptide and oligonucleotide was caused by  $\beta$ -elimination (10). We had reported a synthetic signal peptide-conjugated oligonucleotide using *p*-hydroxybenzoic acid as the linker, and the conjugate was stable in basic condition (11). To avoid the  $\beta$ -elimination, in this paper, 2,2-dimethyl-3-hydroxypropionic acid was employed as the linker for the connection of peptide and oligonucleotide (Scheme 1).

Tat protein is the nuclear transcription activator of HIV containing 101 amino acids. It can efficiently cross the plasma membranes of cells in an apparent energy-dependent fashion. The sequence responsible for the cellular uptake of HIV Tat is amino residues 49–57 (RKKRRQRRR) (12, 13). The detailed mechanism for the cellular uptake remains unclear. The result of amino acid substitution shows that arginine residues play key roles in its cellular uptake. It would be interesting to investigate the properties of arginine-rich peptide-conjugated oligonucleotide. When we tried to conjugate arginine-rich peptides to an oligonucleotide, it was found that the solution-phase reaction could not be carried out because of serious precipitation. To overcome the precipitation problem caused by electrostatic interaction of the two

\* To whom correspondence should be addressed. Phone: 86-10-62091700. Fax: 86-10-62092724. E-mail: zdszlh@bjmu.edu.cn.

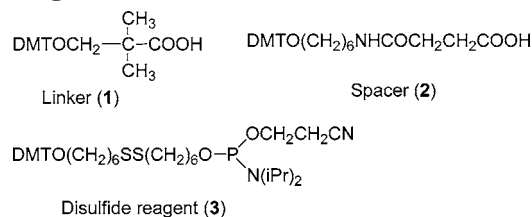
<sup>†</sup> School of Pharmaceutical Sciences, Peking University.

<sup>‡</sup> School of Chemistry and Molecular Engineering, Peking University.

<sup>§</sup> Beijing Institute of Radiation Medicine.

<sup>1</sup> Abbreviations: Boc, *tert*-butoxycarbonyl; CPG, controlled pore glass; DCM, dichloromethane; DIC, *N,N*-diisopropylcarbodiimide; DIPEA, diisopropylethylamine; DMAP, 4-(dimethylamino)pyridine; DMF, dimethylformamide; DMT, dimethoxytrityl; DTT, 1,4-dithiothreitol; FITC, fluorescein isothiocyanate; Fmoc, fluorenylmethoxycarbonyl; HBTU, *O*-benzotriazole-*N,N,N*-tetramethyluronium hexafluorophosphate; HOBT, 1-hydroxybenzotriazole; RP HPLC, reverse phase high performance liquid chromatography; MALDI, matrix-assisted laser desorption/ionization; MMT, monomethoxytrityl; OPC, oligonucleotide purification cartridge; PBS, phosphate-buffered saline; PNA, peptide nucleic acid; SDS, sodium dodecyl sulfate; TFA, trifluoroacetic acid; TOF MS, time-of-flight mass spectra; Pbf, 2,2,4,6,7-pentamethyldihydrobenzofuran-5-sulfonyl; Trt, trityl.



**Scheme 1. Structures of Spacer, Linker, and Disulfide Reagent**

moieties, we report here a concise method for this preparation. The oligonucleotide activated with a pyridinesulfonyl group was absorbed on an anion-exchange resin, and then the resin was reacted with a 3-fold excess of free sulfhydryl-containing arginine-rich peptide to give the designed conjugates.

Telomerase activity has been found in 85–90% of human tumors but not in adjacent normal cells. This makes telomerase as a target not only for cancer diagnosis but also for the development of novel therapeutic agents (14, 15). It has been reported that telomerase inhibition by peptide nucleic acids (PNA) occurred in a sequence-specific manner in a cell-free system (16). A 19mer antisense phosphorothioate oligonucleotide targeting telomerase RNA template encapsulated with transfection reagent decreased effectively the telomerase activity in HeLa cells (17). Wang et al. found that a 19mer oligonucleotide targeting telomerase mRNA could inhibit the proliferation of HepG2 cells (18). In this paper, we describe the inhibition by oligonucleotide carrying mimetic signal peptide of telomerase expression, and the cell membrane permeability of arginine-rich peptide-oligonucleotide conjugates in HepG-2 cells.

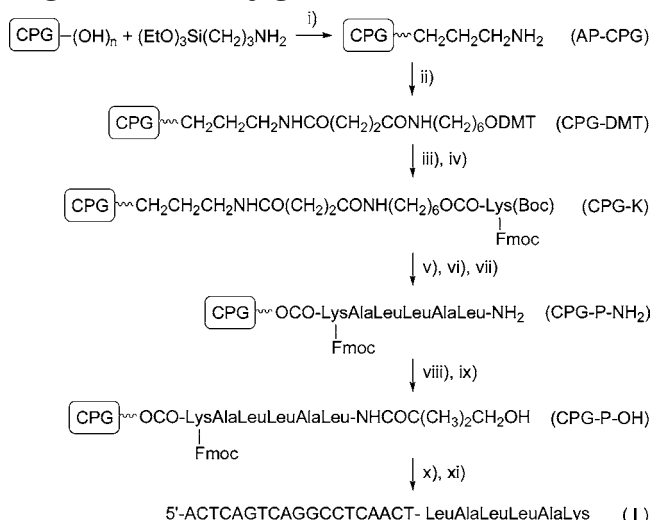
**EXPERIMENTAL SECTION**

**1. In-Line Synthesis of Mimetic Signal Peptide-Conjugated Oligonucleotide. a. 3-(6-*O*-Dimethoxytritylhexylcarbamoyl)propionic acid** (spacer, **2**) was synthesized by a known procedure (19).  $^1\text{H}$  NMR ( $\text{DMSO-}d_6$ ),  $\delta$  1.2–1.6 (m, 8H,  $\text{CH}_2$ ), 2.2–2.3 (m, 4H,  $\text{CH}_2$ ), 2.9 (m, 4H,  $\text{COCH}_2\text{CH}_2\text{CO}$ ), 3.7 (s, 6H,  $\text{OCH}_3$ ), 6.7–7.5 (m, 13H, ArH). MS (FAB+),  $m/z$  519.9.

**b. 2,2-Dimethyl-3-*O*-monomethoxytritylhydroxypropionic acid** (linker, **1**) was obtained by following the literature (20).  $^1\text{H}$  NMR ( $\text{DMSO-}d_6$ ),  $\delta$  1.2 (s, 6H,  $\text{CH}_3$ ), 3.1 (s, 2H,  $\text{CH}_2$ ), 3.8 (s, 3H,  $\text{OCH}_3$ ), 6.7–7.5 (m, 14H, ArH). MS (EI+),  $m/z$  390.0.

**c. Synthesis of Mimetic Signal Peptide LeuAla-LeuLeuAlaLys on CPG.** Spacer (**2** mmol), HOBt (10 mmol/g), and HBTU (2 mmol/g) were dissolved in 2 mL of DMF. To the solution was added 230  $\mu\text{L}$  of DIEA. The solution was stirred for 3 min at room temperature, aminopropyl-controlled pore glass (AP-CPG, PE product, pore size 500 Å, 0.5 g, amino group loading: 0.2 mmol/g) was added, and the mixture was placed in an incubator at 25 °C for 1 h under shaking to give the functional CPG-DMT (180  $\mu\text{mol/g}$ ). CPG-DMT was treated by 5% trichloroacetic acid in dichloromethane to remove the protecting group DMT. The deprotected CPG was drained and washed with dichloromethane, methanol, and dichloromethane.

$\alpha$ -Fmoc- $\epsilon$ -Boc-lysine (1.1 mmol) and diisopropylcarbodiimide (0.55 mmol) were dissolved in 2 mL of DMF and reacted for 30 min at room temperature. The solution and 0.22 mmol of DMAP were added to the deprotected CPG obtained in the previous step. The mixture was kept at room temperature for 30 min under shaking (90 rpm). The amino acid loading on the CPG was monitored by

**Scheme 2. Synthesis of Mimetic Signal Peptide Oligonucleotide Conjugates<sup>a</sup>**

<sup>a</sup> Reagents and conditions: (i) toluene, 90 °C; (ii) spacer **2**/HOBt/HBTU/DIEA, rt, 1 h; (iii) 5% TCA/DCM; (iv) AA/DIC/DMAP/DMF, rt, 4 h; (v) 33% TFA/DCM, 30 min; (vi) AA/HOBt/HBTU/DIEA, rt, 1 h; (vii) repeat v and vi; (viii) linker **1**/HOBt/HBTU/DIEA, rt, 1 h; (ix) 5% TCA/DCM; (x) standard DNA synthesis of PS oligonucleotide; (xi) concentrated aqueous ammonia, 55 °C, 10 h.

sampling the reaction mixture (ninhydrin assay). The CPG was washed with dichloromethane and MeOH alternately and finally with dichloromethane and then treated with acetic anhydride and triethylamine in dichloromethane (3 mL, 1:1:2, v/v/v) to cap the residual hydroxyl groups to give the CPG-K. The CPG-K was washed with dichloromethane and methanol for the next step.

The Boc group of the first amino acid on the CPG-K was removed by treatment with 33% TFA in dichloromethane (v/v) at room temperature for 30 min. The CPG-K was washed with dichloromethane and DMF. The assembly of peptide sequence (A, L, L, A, and L) was carried out on a manual peptide synthesizer using rapid in situ neutralization Boc chemistry (11, 12). After the last amino acid (Leu) was assembled, the CPG was treated with 33% TFA to free the terminal amino group (CPG-P-NH<sub>2</sub>).

2,2-Dimethyl-3-*O*-monomethoxytritylhydroxypropionic acid (linker) was coupled to the terminal amino group of CPG-P-NH<sub>2</sub> in the presence of HOBt/HBTU/DIEA as described in the peptide coupling reaction. The loading of the monomethoxytrityl group on the resulting CPG is 68  $\mu\text{mol/g}$ . To check the coupling reaction, part of the resulting CPG was treated by 33% TFA followed by concentrated ammonium hydroxide at 55 °C for 14 h. The functional peptide, LysAlaLeuLeuAlaLeu-NHCOC(CH<sub>3</sub>)<sub>2</sub>CO<sub>2</sub>H, was purified on HPLC and identified by MALDI-TOF MS,  $m/z$  728.48 ( $M + 1$ ), calculated for  $\text{C}_{35}\text{H}_{65}\text{N}_7\text{O}_9$   $m/z$  728.61.

**d. Assembly of Mimetic Signal Peptide Oligonucleotide Conjugate on CPG-P-OH.** The modified CPG obtained from the last step (15 mg, loading: 1.0  $\mu\text{mol}$ ) was treated with 5% TCA in dichloromethane to give CPG-P-OH for the oligonucleotide synthesis (Scheme 2). The synthesis of oligonucleotide was performed on AB891 Expedite synthesizer on 1  $\mu\text{mol}$  scale following phosphoramidite chemistry. The sequence was 5'-ACTCACTCAGGCCTCAGACT-3', which is complementary to telomerase mRNA. Stepwise thiolation was performed using 3-*H*-1,2-benzodithiol-3-one 1,1-dioxide. The synthe-

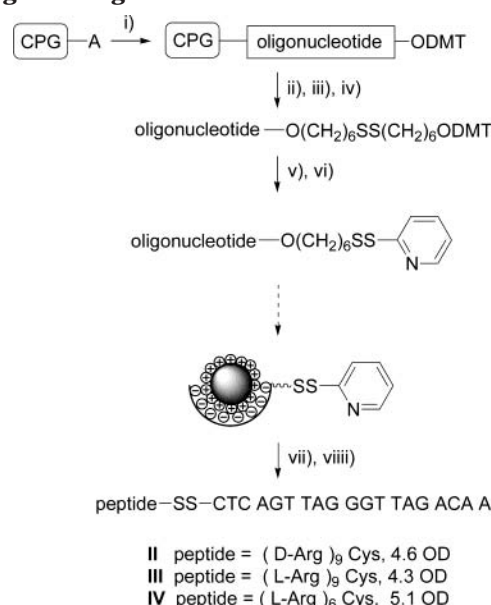
sis was completed by the DMT-on method, in which the dimethoxytrityl protecting group is retained on the last nucleotide. The solid support containing the oligonucleotide was treated with concentrated aqueous ammonia at 55 °C for 10 h. After filtration, the solution was vaporized in a vacuum to dryness, the residue was dissolved in water, and the conjugate was purified on HPLC using Delta-Pak C18 column (Waters, 100 Å, 15 µm, 7.8 × 300 mm); the gradient was 0–40% B for 25 min, 40–100% B for 15 min (mobile phase A was 0.1 M triethylammonium acetate (pH 7.0), and mobile phase B was acetonitrile.) The purified DMT-on conjugate was detritylated through an oligonucleotide purification cartridge (OPC). After concentration, conjugate **I** was further purified by HPLC using NUCLEOSIL C18 column (Phenomenex, 100 Å, 10 µm, 4.6 × 250 mm). The gradient was the same as above, but mobile phase A is 0.02 M triethylammonium acetate (pH 7.0) and mobile phase B is 50% acetonitrile in water. The conjugate **I** appeared as white powder (24 OD) after lyophilization. Conjugate **I** was identified by MALDI-TOF MS: calculated: 6803.67, found: 6800.00.

**2. The Inhibition by Conjugate I of the Expression of Telomerase in HepG-2 Cell.** HepG-2 cells were seeded in 96-well culture plate at a concentration of 5000 cells/well (40–50% confluence). After overnight culture in DMEM containing 10% fetal bovine serum, 100 units/mL of penicillin G sodium, and 100 µg/mL of streptomycin sulfate, the complete medium was removed, and the cells were washed by DMEM without antibiotics. Conjugate **I** was dissolved in DMEM, and the final concentrations were 0.2, 2.0, and 20 µM, respectively, which were then added to the well. After 5 h incubation at 37 °C in a humidified 5% CO<sub>2</sub> incubator, the plain medium was removed, and the cells were cultured in complete medium for 48 h.

After the medium was removed, the cells were scraped and washed with PBS. Total protein was extracted from the cells by lysing the cells with lysis buffer. Aliquots of cells extracts containing 30 µg of protein were resolved by 6% SDS-polyacrylamide gel electrophoresis and transferred to cellulose nitrate membrane, and the membrane was blocked by nonfat milk. Then, it was followed by rabbit anti-hTERT antibody (Santa Cruz corporation) and HRP-conjugated anti-rabbit (Zhongshan Company) secondary antibody. ECL was performed according to the manufacturer's instructions.

**3. Synthesis of Arginine-Rich Peptide-Conjugated Oligonucleotide on Resin.** **a. Synthesis of Oligonucleotide with Pyridine Sulfonyl-Activated Thiol Group at the 5' Terminus.** Oligonucleotide synthesis was carried out on a DNA synthesizer with standard phosphoramidite chemistry. The sequence was 5'-CT-CAGTTAGGGTTAGACAA-3', which is complementary to telomerase RNA template. After the final nucleotide was coupled, the oligomer was reacted with *O*-phosphoramidite-*O*-dimethoxytrityl-bis(6-hydroxyhexyl) disulfide (**3**) (**25**) (Scheme 3). The resulting oligonucleotide was cleaved from the solid support and deprotected in concentrated aqueous ammonia at 55 °C for 10 h. After the solid support was filtered, the filtrate was dried in a vacuum. The residue was purified by HPLC. The purified oligonucleotide (20 OD) was vaporized in a vacuum and then dissolved in 0.5 mL of 0.2 M phosphate buffer (pH 8.4), and DTT was added (the final concentration was 0.2 M) under the protection of argon. The mixture was kept at room temperature for 30 min. The oligonucleotide with a free sulfhydryl function at the 5' terminus was purified by HPLC. The eluent containing target oligomer was

**Scheme 3. Synthesis of Arginine-Rich Peptide-Conjugated Oligonucleotide<sup>a</sup>**



<sup>a</sup> Reagents and conditions: (i) standard DNA synthesis of PS oligonucleotide; (ii) disulfide reagent **3**/tetrazole/acetonitrile; (iii) thiolating reagent; (iv) concentrated aqueous ammonia, 55 °C, 10 h; (v) DTT/phosphate buffer, pH 8.2, rt, 30 min; (vi) 2,2'-dithiodipyridine/20% acetonitrile in 0.2 M phosphate buffer, pH 5.5, rt, 16 h; (vii) peptide/phosphate buffer, pH 7.0; (viii) 1 M NaCl.

dissolved in a solution (2 mL) of 20% acetonitrile in phosphate buffer (0.2 M, pH 5.5) containing 2 mg of 2,2'-bis(dipyridyl) disulfide, and the mixture was reacted for 12 h at room temperature under the protection of argon. The corresponding 2-pyridyl sulfide derivative was purified by RP HPLC and was vaporized in a vacuum to dryness. The dry powder was kept in refrigerator at –20 °C for further use.

**b. Synthesis of Arginine-Rich Peptide.** PAL resin (0.11 mmol/g) and rapid in situ neutralization protocols based on Fmoc/HBTU/HOBt/DIPEA chemistry were used in the peptide synthesis. The Fmoc amino acid derivatives were used as follows: Fmoc-L-Arg (Pbf), Fmoc-D-Arg (Pbf), Fmoc-Cys (Trt). The peptide synthesis was carried out in a manual synthesizer. Fmoc-amino acids were used in 2.5 mol equiv and activated with 2.5 mol equiv of HOBt, 2.38 mol equiv of HBTU, and 3 mol equiv of DIPEA in DMF for 3 min, followed by a 1 h coupling. Fmoc deprotection was performed in 20% piperidine in DMF. Cleavage and side chain deprotection were completed by treating the peptide with a mixture containing 82.5% TFA, 5% thioanisole, 5% phenol, 5% water, and 2.5% ethanedithiol (reagent K) overnight at room temperature under shaking. After the solid support was filtered, cold methyl *tert*-butyl ether was added to the filtrate. The precipitated peptide was purified by HPLC, which was carried out using a Waters column (7.8 × 300 mm). Samples were monitored at 225 nm. The gradient was 0–80% B in 30 min (mobile phase A was 0.1% TFA in water, and mobile phase B was 0.1% TFA in acetonitrile). The obtained arginine-rich peptide, (D-arginine)<sub>9</sub>cysteine, (L-arginine)<sub>9</sub>cysteine, and (L-arginine)<sub>6</sub>-cysteine were identified by MALDI-TOF MS, and the results of *m/z* were 1524.84, 1525.55, and 1057.53, respectively. The purified peptides were lyophilized and kept at –20 °C.

**c. Synthesis of Arginine-Rich Peptide-Oligonucleotide Conjugates (II, III, IV) on Resin.** Oligo-

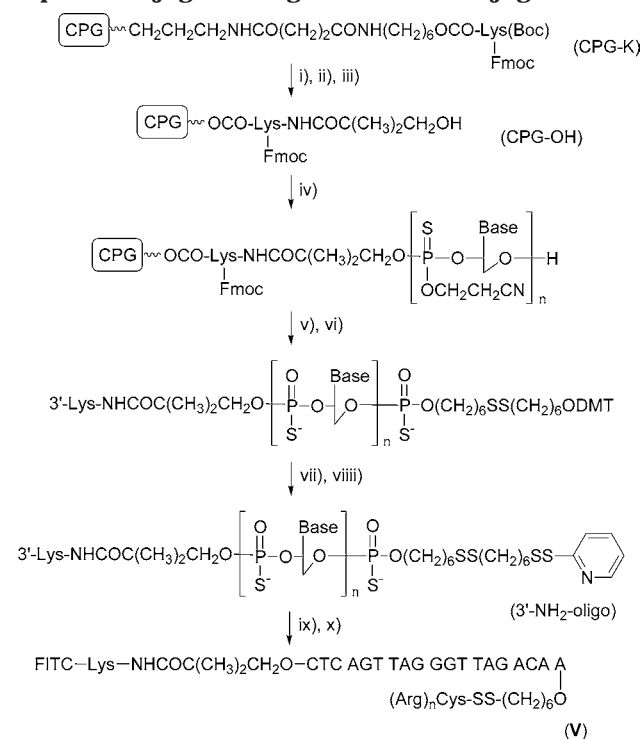
**Table 1. Retention Time and Molecular Weight of Free Oligonucleotide and Peptide–Oligonucleotide Conjugates**

compound	retention time (min)	MW	
		obsd	calcd
ODN	33.5	—	6446.37
D-R <sub>9</sub> C-ODN ( <b>II</b> )	28.3	7780.50	7782.06
L-R <sub>9</sub> C-ODN ( <b>III</b> )	28.1	7780.00	7782.06
L-R <sub>6</sub> C-ODN ( <b>IV</b> )	29.3	7311.00	7313.50

nucleotide with a pyridine sulfonyl-activated thiol function at the 5' terminus (10 OD) was dissolved in water, the solution was applied on 0.5 mL of anion-exchange resin (SOURCE, Amersham Pharmacia) contained in a column (diameter 4 mm), and the column was flushed by argon. The sulfhydryl group of the peptide was determined by its absorbance at 412 nm after reaction with 2,4-dithiobis(nitrobenzoic acid) (15). About 3 equiv of arginine-rich peptide dissolved in 20 mM phosphate buffer (pH 7.0) was added to the column under protection of argon. Eight hours later, the column was washed with water. The conjugates absorbed on the resin were eluted by 1 M NaCl. The collected solution was desalted through OPC and purified by HPLC using a DEAE column (column 8 × 100 mm, resin: SOURCE) with a linear gradient from 0 to 80% of 1 M NaCl in water in 30 min and recorded at 260 nm. After being desalted through OPC, the conjugate was dried in a vacuum. The conjugates **II**, **III**, and **IV** were further identified by ESI-TOF MS (Table 1).

**d. Synthesis of FITC-Labeled Conjugates.** The synthesis of FITC-labeled conjugates (**V**) was illustrated in Scheme 4. The preparation of CPG-K was the same as described above. After the Boc group in CPG-K was deprotected with 33% TFA, 2,2-dimethyl-3-*O*-(dimethoxytrityl)hydroxypropionic acid was coupled with CPG-K to give CPG-ODMT which was used for the oligonucleotide synthesis. The sequence was 5'-CTCAGTTAGGGT-TAGACAA-3', which is complementary to telomerase RNA template. After the final nucleotide was coupled, the oligonucleotide was modified by addition of the reagent, *O*-phosphoramidite-*O*-dimethoxytrityl-bis(6-hydroxyhexyl) disulfide. The resulting oligonucleotide was cleaved from the solid support and deprotected in concentrated aqueous ammonia at 55 °C for 10 h. After the solid support was filtered, the filtrate was dried in a vacuum. The residue was purified by HPLC. The synthesis of oligonucleotide (1 μmol) with pyridine sulfonyl-activated thiol group at the 5' terminus was performed as mentioned above to give 3'-amino-5'-pyridine sulfonyl-activated thiol oligonucleotide (3'-NH<sub>2</sub>-oligomer). The resulting 3'-NH<sub>2</sub>-oligomer (20 OD) was dissolved in 200 μL of 2 M sodium acetate, 0.2 M carbonate/bicarbonate buffer (pH 9.5) and 50 equiv of FITC (isomer I) was added, and then the mixture was allowed to stand overnight at 37 °C. The FITC-labeled oligonucleotide was precipitated by cold ethanol (−20 °C, 500 μL). The free FITC was removed by gel filtration on a Sephadex G-25 column. The FITC-labeled oligonucleotide was purified by HPLC. Labeled oligonucleotide (16.6 OD) was obtained. Part of FITC-labeled oligonucleotide was used for the control in the transmembrane test, and the conjugation of FITC-labeled oligonucleotide and arginine-rich peptide was carried out as described above to obtain the FITC-labeled arginine-rich peptide-conjugated oligonucleotide **V**. The labeled conjugate **V** was purified by HPLC, lyophilized, and kept at −20 °C for further use.

**c. Transmembrane Activity of Conjugate V.** The HepG-2 cells were grown in DMEM containing 10% fetal

**Scheme 4. Synthesis of FITC-Labeled Arginine-Rich Peptide-Conjugated Oligonucleotide Conjugates<sup>a</sup>**

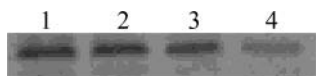
<sup>a</sup> Reagents and conditions: (i) 33%TFA/DCM; (ii) linker 1/HOBt/HBTU/DIEA, rt, 1 h; (iii) 5% TCA/DCM; (iv) standard DNA synthesis of PS oligonucleotide; (v) disulfide reagent 3/tetrazole/acetonitrile; (vi) concentrated aqueous ammonia, 55 °C, 10 h; (vii); (vii) DTT/phosphate buffer, pH 8.2, rt, 30 min; (viii) 2,2'-dithiodipyridine/20% acetonitrile in 0.2 M phosphate buffer, pH 5.5, rt, 16 h; (ix) FITC/phosphate buffer, pH 9.5, 37 °C, overnight; (x) peptide/phosphate buffer, pH 7.0, 8 h, rt; wash with 1 M NaCl.

bovine serum, 100 units/mL penicillin G sodium and 100 μg/mL streptomycin sulfate and kept at 37 °C in a humidified atmosphere of 5% CO<sub>2</sub>. For the transmembrane activity study, the cells were seeded on glass cover slips in 35 mm dishes at 5 × 10<sup>5</sup>/dish and incubated for 24 h. The cells were washed with PBS and cultivated in complete medium (without phenol red) containing 1 μM FITC labeled oligonucleotide or FITC labeled conjugate **V** for 6 h. Then the cells were washed with PBS. A Leica TCS SP2 confocal laser scanning microscope system (FITC, excitation wavelength: 488 nm, emission wavelength: 530 ± 15 nm; objective: 40 × 1.25 NA, oil) was employed to study the transmembrane activity of FITC labeled conjugate **V**.

## RESULTS AND DISCUSSIONS

**Mimetic Signal Peptide-Conjugated Oligonucleotide.** The preparation of mimetic signal peptide-conjugated oligonucleotide was shown in Scheme 2. Aminopropyl-controlled pore glass (AP-CPG) was selected as the solid support in the synthesis of peptide oligonucleotide conjugate. The AP-CPG was functionalized with a long chain molecule (Scheme 1) to increase the efficiency of peptide synthesis, the terminal dimethoxytrityl-protected hydroxyl group of the spacer (CPG-DMT) could be removed by acidic treatment and employed to form ester bond with the first protected amino acid. The ester bond could be cleaved under the basic condition after the oligonucleotide synthesis. The first loaded amino acid was α-Fmoc-ε-Boc-Lysine and the ε-amino group was used to couple the second amino acid.



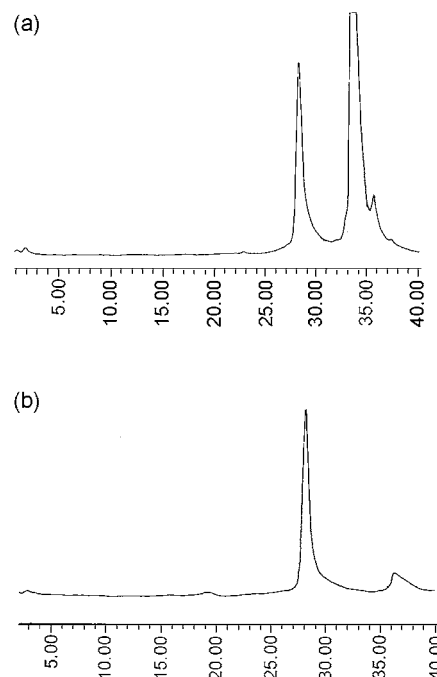


**Figure 1.** Western blot analysis of the effect of mimetic signal peptide-conjugated oligonucleotide on telomerase expression in HepG2 cells. Sense (lane 1), 0.2  $\mu$ M antisense (lane 2), 2  $\mu$ M antisense (lane 3), 20  $\mu$ M antisense (lane 4).

The assembly of peptide on CPG-K was carried out with in situ neutralization Boc chemistry, but the coupling time was reduced to less than 1 h and the neutralization step with triethylamine could be omitted comparing with the standard Boc chemistry. The modified strategy avoided the possible breakage of CPG under the long time of shaking. The coupling efficiency of every amino acid was over 99%. The N-terminal of last peptide on the CPG-P-NH<sub>2</sub> was coupled with 2,2-dimethyl-3-*O*-monomethoxytritylhydroxypropionic acid. The monomethoxytrityl (MMT)-protected linker was treated by acidic condition to give a hydroxyl group which can be used for the formation of the phosphate diester bond connecting peptide and oligonucleotide with phosphoramidite chemistry. It was reported that the phosphate diester bond derived from the aliphatic hydroxyl function was unstable in concentrated aqueous ammonia; the breakage of the connection between peptide and oligonucleotide was caused by  $\beta$ -elimination (10). We had synthesized mimetic signal peptide-conjugated oligonucleotide using *p*-hydroxybenzoic acid as the linker, and the conjugate was stable in basic condition (11). In this study, using 2,2-dimethyl-3-hydroxypropionic acid as a linker,  $\beta$ -elimination could be completely avoided. Therefore, the resultant CPG-P-OH was applied to DNA synthesizer, and the oligonucleotide sequence was synthesized by standard phosphoramidite chemistry using 3*H*-1,2-benzodithiol-3-one 1,1-dioxide as the thiolating agent. The complementary antisense sequence 5'-ACTCACTCAG-GCCTCAGACT-3' was designed to the telomerase mRNA. The stepwise coupling yield was over 99%. It was indicated that 2,2-dimethyl-3-hydroxypropionic acid as a linker in the solid DNA synthesis is easy to handle, and the phosphate diester bond is stable during the procedure. Standard cleavage and deprotection conditions were employed, and the Fmoc group was removed under the same conditions. The sequence of synthetic peptide-oligonucleotide conjugate **I** was identified by MALDI-TOF MS.

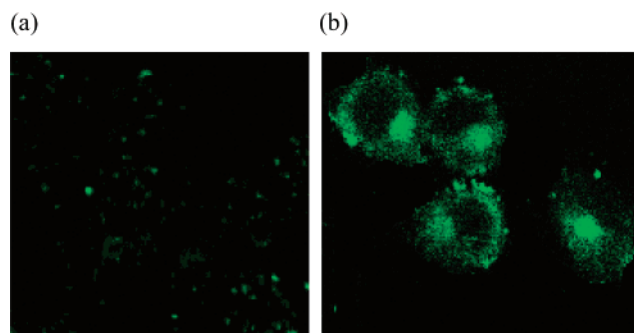
The mimetic signal peptide sequence LALLAK has the tendency to form  $\alpha$ -helix conformation (22, 23, 30). Previously, we have reported that this sequence peptide could direct the translocation of oligonucleotide through the cell membrane in HepG-2 and MCF-7 cells (11). The synthetic conjugate **I** showed inhibition of growth in HepG-2 cells, and the Western-blot results indicated that the antisense oligonucleotide-peptide conjugate reduced the expression of telomerase (Figure 1). These results proved that the mimetic signal peptide sequence could increase the cellular transportation of antisense oligonucleotide targeting to telomerase.

**Synthesis of Arginine-Rich Peptide-Conjugated Oligonucleotide.** The coupling protocols of Tat-derived peptide and oligonucleotide have been previously reported. These solution-phase conjugation reactions of an iodoacetylated oligonucleotide (25) or a pyridine sulfonyl-activated oligonucleotide (26) with an excess of a peptide with a cysteine residue lead to the formation of thioester or disulfide bonds. We designed and synthesized three arginine-rich peptides using rapid in situ neutralization Fmoc chemistry on PAL resin. Oligonucleotide targeting



**Figure 2.** HPLC chromatogram of arginine-rich peptide and oligonucleotide conjugation for 2 h (a) and 8 h (b).

to telomerase RNA template 5'-CTCAGTTAGGGTTA-GACAA-3' was synthesized using standard phosphoramidite chemistry. We tried to synthesize the arginine-rich peptide-conjugated oligonucleotide by these coupling reactions in solution. The 5'-end of oligonucleotide was coupled with the *O*-phosphoramidite-*O*-DMT-bis(6-hydroxyhexyl) disulfide, the disulfide bond at the end of the sequence was reduced by DTT, and the free sulfhydryl group was activated and protected through reaction with dithiodipyridine (27). The pyridine sulfonyl-activated thiol function at the 5'-end of the oligonucleotide allowed the disulfide bond formation of the oligonucleotide-peptide conjugate by the nucleophilic attack of the free sulfhydryl group at cysteine in the C-terminus of the arginine-rich peptide. However, the coupling reaction in solution encountered a serious precipitation problem caused by the electrostatic interaction between the arginine-rich peptide and the oligonucleotide. It was reported that the precipitation problem can be partially overcome by adding acetonitrile and salt to the conjugation mixture (28, 29). In our case, the precipitate did not dissolve in water, aqueous solution of 50% acetonitrile or DMF. The strong electrostatic interaction between the positive arginine-rich peptide and the negative oligonucleotide led to the formation of precipitate. To overcome the precipitation problem, the oligonucleotide activated with sulfonyl pyridine function was absorbed on an anion-exchange resin and then reacted with 3-fold excess of arginine-rich peptide (Scheme 3). In this manner, the coupling reaction between the arginine-rich peptides and oligonucleotide was carried out successfully in an aqueous solution containing 0.4 M KCl and 40% acetonitrile. Most of the negative charges in the oligonucleotide were neutralized by the electropositive centers on the resin, the pyridine sulfonyl group at the 5'-end of the oligonucleotide retains the activity to react with the arginine-rich peptide, and the precipitation problem is completely avoided. We followed the coupling reaction by HPLC (Figure 2). It showed that the coupling reaction was almost completed after 8 h.



**Figure 3.** Delivery of FITC-oligonucleotide (a) and (L-Arg)<sub>9</sub>Cys-conjugated FITC-labeled oligonucleotide (b) incubated with HepG-2 cells by confocal laser scanning microscopy.

Three conjugates of arginine-rich peptides and oligonucleotide were synthesized by the procedure, and the results are shown in Table 1.

FITC labeled arginine-rich peptide-oligonucleotide conjugate was prepared to study the localization of the hybrid molecules in HepG-2 cells. AP-CPG was functionalized with a long spacer and coupled with Fmoc-Lys-(Boc) to give CPG-K. After deprotection under 33% TFA, the amino group was reacted with 2,2-dimethyl-3-*O*-dimethoxytrityl-hydroxypropionic acid. After treatment with 5% TCA, CPG-OH was used for the oligonucleotide synthesis. 5'-Pyridine sulfonyl-activated thiol oligonucleotide was synthesized by standard protocol to obtain 3'-Lys-nucleotide-5'-pyridine disulfide. The amino group of Lys in 3'-Lys-oligonucleotide-5'-pyridine disulfide (3'-NH<sub>2</sub>-oligo) was used to label FITC, and the active pyridine sulfonyl group was conjugated with L-polyarginine using the on-resin coupling method (Scheme 4). The FITC-labeled arginine-rich peptide oligonucleotide conjugate **V** and the control sample, FITC-labeled oligonucleotide, were incubated with HepG-2 cells at 37 °C for 24 h, and the cells were observed by a Leica TCS SP2 confocal laser scanning microscope system. The scanning photos show that in both cases the fluorescent signal accumulates in endosomes of the cells, but compared to the control sample, the intensity of the fluorescence is greater for the arginine-rich peptide-conjugated FITC-labeled oligonucleotide **V** (Figure 3).

## CONCLUSION

A mimetic signal peptide-oligonucleotide conjugate targeting to telomerase mRNA was synthesized on AP-CPG by stepwise strategy. 2,2-Dimethyl-3-hydroxypropionic acid was used as a linker. This linker is stable in the procedures of deprotection and cleavage. To overcome the precipitation problem caused by the electrostatic interaction between the arginine-rich peptide and oligonucleotide, a novel on-resin fragmentation coupling method was developed. The transmembrane activity study showed that a short polyarginine peptide-conjugated oligonucleotide could penetrate the cell membrane and concentrate in the cells.

## ACKNOWLEDGMENT

This work was supported by National Natural Science Foundation of China and by National Key Project for Basic Research (G1998051103) awarded by The Ministry of Science and Technology, People's Republic of China.

## LITERATURE CITED

- (1) Tamm, I., Dorken, B., and Hartmann, G. (2001) Antisense therapy in oncology: new hope for an old idea? *Lancet* 358, 489–497.
- (2) Dean, N. M. (2001) Functional genomics and target validation approaches using antisense oligonucleotide technology. *Curr. Opin. Biotech.* 12, 622–625.
- (3) Garcia-Chaumont, C., Seksek, O., Grzybowski, J., Borowski, E., and Bolard, J. (2000) Delivery systems for antisense oligonucleotides. *J. Pharm. Ther.* 87, 255–277.
- (4) Allinquant, B., Hantraye, P., Mailleux, P., Moya, K., Bouillot, C., and Prochiantz, A. (1995) Down regulation of amyloid precursor protein inhibits neurite outgrowth in vitro. *J. Cell Biol.* 128, 919–927.
- (5) Vives, E., and Lebleu, B. (1997) Selective Coupling of a Highly Basic Peptide to an oligonucleotide. *Tetrahedron Lett.* 38, 1183–1186.
- (6) Bongartz, J. P., Aubertin, A. M., Milhaud, P. G., and Lebleu, B. (1994) Improved bioactivity of antisense oligonucleotides conjugated to a fusogenic peptide. *Nucleic Acids Res.* 22, 4681–4688.
- (7) Arar, K., Monsigny, M., and Mayer, R. (1993) Synthesis of oligonucleotide-peptide conjugates containing KDEL signal sequence. *Tetrahedron Lett.* 34, 8087–8090.
- (8) Chen, C. P., Min, J. M., and Zhang, L. H. (2001) Synthesis and properties of peptide-oligonucleotide conjugates. *Prog. Biochem. Biophys.* 28, 783–787.
- (9) Tung, C. H., and Stein, S. (2000) Preparation and applications of peptide-oligonucleotide conjugates. *Bioconjugate Chem.* 11, 605–618.
- (10) Waldmann, H., and Gabold, S. (1997) Chemoenzymatic synthesis of nucleopeptide. *Chem. Commun.* 19, 1861–1862.
- (11) Chen, C. P., Li, X. X., Zhang, L. R., Min, J. M., Chan, Y. W., Fung, K. P., Wang, S. Q., and Zhang, L. H. (2002) Synthesis of antisense oligonucleotide-peptide conjugate targeting to GLUT1 in HepG-2 and MCF-7 cells. *Bioconjugate Chem.* 13, 525–529.
- (12) Vives, E., Bodin, P., and Lebleu, B. (1997) A truncated HIV-1 Tat protein basic domain rapidly translocates through the plasma membrane and accumulates in the cell nucleus. *J. Biol. Chem.* 272, 16010–16017.
- (13) Wender, P. A., Mitchell, D. J., Pattabiraman, K., Pellkey, E. T., Steinman, L., and Rothbard, J. B. (2000) The design, synthesis, and evaluation of molecules that enable or enhance cellular uptake: peptoid molecular transporters. *Proc. Natl. Acad. Sci. U.S.A.* 97, 13003–13008.
- (14) Blackburn, E. H. (1991) Structure and function of telomeres. *Nature* 350, 569–573.
- (15) Kim, N. W., Piatyszek, M. A., Prowse, K. R., Harley, C. B., West, M. D., Ho, P. L. C., Coviello, G. M., Wright, W. E., Weinrich, S. L., and Shay, J. W. (1994) Specific association of human telomerase activity with immortal cells and cancers. *Science* 266, 2011–2015.
- (16) Norton, J. C., Piatyszek, M. A., Wright, W. E., Shay, J. W., and Corey, D. R. (1996) Inhibition of human telomerase activity by peptide nucleic acids. *Nature Biotech.* 14, 615–619.
- (17) Tamura, Y., Tao, M., Miyano-kurosaki, N., Takai, K., and Takaku, H. (2000) Inhibition of human telomerase activity by antisense phosphorothioate oligonucleotides encapsulated with the transfection reagent FuGENE6 in Hela cells. *Antisense Nucleic Acid Dev.* 10, 87–96.
- (18) Wang, S. Q., Lin, L., Chen, Z. B., Lin, R. X., Chen, S. H., Guan, W., and Wang, X. H. (2002) In vitro anticancer activity evaluation of antisense oligonucleotide targeting to hEST2 gene of telomerase. *Sin. Commun.* 47, 378–381.
- (19) Haralambidis, J., Duncan, L., Angus, K., and Tregear, G. W. (1990) The synthesis of polyamide-oligonucleotide conjugate molecules. *Nucleic Acid Res.* 18, 493–499.
- (20) Schwoppe, I., Bleczynski, C. F., and Richert, C. (1999) Synthesis of 3',5'-dipeptidyl oligonucleotides. *J. Org. Chem.* 64, 4749–4761.

- (21) Alewood, P., Alewood, D., and Miranda, L. (1997) Rapid in situ neutralization protocols for Boc and Fmoc solid-phase chemistries. *Methods Enzymol.* 289, 15–29.
- (22) Batenburg, A. M., Demel, R. A., Verkleij, A. J., de Kruijff, B. (1988) Penetration of the signal sequence of *Escherichia coli* PhoE protein into phospholipid model membranes leads to lipid-specific changes in signal peptide structure and alterations of lipid organization. *Biochemistry* 27, 5678–5685.
- (23) von Heijne, G. (1990) The signal peptide. *J. Membr. Biol.* 115, 195–201.
- (24) Gariepy, J., and Kawamura, K. (2001) Vectorial delivery of macromolecules into cells using peptide-based vehicles. *Trends Biotechnol.* 19, 21–28.
- (25) Wei, Z., Tung, C. H., Zhu, T., and Stein, S. (1994) Synthesis of oligoarginine-oligonucleotide conjugates and oligoarginine-bridged oligonucleotide pairs. *Bioconjugate Chem.* 5, 468–474.
- (26) Hughes, J. A., Astriab, A., Yoo, H., Alahari, S., Liang, E., and Juliano, R. L. (1999) In vitro transport and delivery of antisense oligonucleotides. *Methods Enzymol.* 313, 342–358.
- (27) Antopolsky, M., Azhayeva, E., Tengvall, U., Auriola, S., Jaaskelainen, I., Ronkko, S., Honkakoski, P., Urtti, A., Lonnberg, H., and Azhayev, A. (1999) Peptide-oligonucleotide phosphorothioate conjugates with membrane translocation and nuclear localization properties. *Bioconjugate Chem.* 10, 598–606.
- (28) Astriab-Fisher, A., Sergueev, D., S., Fisher, M., Shaw, B. R., and Juliano R. L. (2000) Antisense inhibition of P-glycoprotein expression using peptide-oligonucleotide conjugates. *Biochem. Pharm.* 60, 83–90.
- (29) Zhu, T., Wei, Z., Tung, C. H., Dickerhof, W. A., Breslauer, K. J., Georgopoulos, D. E., Leibowitz, M. J., and Stein, S. (1993) Oligonucleotide-poly-L-ornithine conjugates: binding to complementary DNA and RNA. *Antisense Res. Dev.* 3, 265–275.
- (30) Li, X., X., Zhang, L. R., Lu, J. F., Chen, Y. Z., Min, J. M., and Zhang, L. H. (2003), Signal Peptide Mimics Conjugated to Peptide Nucleic Acid: A Promising Solution for Improving Cell Membrane Permeability. *Bioconjugate Chem.* 14, 153–157.

BC034004F



# Enhanced Tumor Detection Using a Folate Receptor-Targeted Near-Infrared Fluorochrome Conjugate

Woo Kyung Moon,<sup>†</sup> Yuhui Lin, Terence O'Loughlin, Yi Tang, Dong-Eog Kim, Ralph Weissleder, and Ching-Hsuan Tung\*

Center for Molecular Imaging Research, Massachusetts General Hospital, Harvard Medical School, Charlestown, Massachusetts 02129. Received January 22, 2003; Revised Manuscript Received March 3, 2003

Fluorescence optical imaging technologies are currently being developed to image specific molecular targets in vivo. Detection technologies range from those providing microscopic detail to whole body imaging systems with potential clinical use. A number of target-specific near-infrared imaging probes have recently been developed to image receptors, antigens, and enzymes. The goal of the current study was to evaluate a new near-infrared (NIR) folate receptor (FR)-targeted imaging probe for its ability to improve detection of FR-positive cancers. We hypothesized that modification of folate would retain receptor affinity in vivo, despite the bulkier NIR fluorochrome, NIR2 ( $\epsilon_m = 682$  nm). Cellular uptake of the NIR conjugates was significantly higher in FR-positive nasopharyngeal epidermoid carcinoma, KB cells, compared to FR-negative human fibrosarcoma, HT1080 cells. When tumors were implanted in vivo, equal-sized KB tumors showed a 2.4-fold higher signal intensity compared to HT1080 tumors (24 h). The maximum signal-to-background ratio (3-fold) was observed at 24 h in KB tumor. Injection of the unmodified NIR2 fluorochrome did not result in persistent contrast increases under similar conditions. Furthermore, tumor enhancement with the NIR2–folate probe persisted over 48 h and was inhibitable in vivo by administration of unlabeled folate. These results indicate that folate-modified NIR fluorochrome conjugate can be used for improved detection of FR-positive tumors.

## INTRODUCTION

Light-based imaging technologies are routinely employed clinically (e.g., laparoscopy, colonoscopy, angiography, etc.), yet most applications rely on visual inspection of anatomic abnormalities. More recently the use of fluorescent imaging probes has been shown to significantly enhance tumor detection (1–4), facilitate identification of small preneoplastic lesions (5), enable in vivo characterization (6), improve the detection of metastatic spread (7), and allow objective assessment of new therapeutic paradigms (8) in animal studies. Potentially those in vivo optical imaging technologies can be translated into clinical applications. It has become clear that imaging in the near-infrared spectrum (700–900 nm) allows most efficient photon migration through the tissue, while autofluorescence is also minimized in this region (9). Despite these obvious opportunities, there is a paucity of near-infrared imaging agents with biocompatibility, stability, and conjugatability. We have previously shown that asymmetric cyanine dyes have ideal properties (10), and currently we are under the process of testing their preclinical utility by conjugating them to affinity ligands.

The goal of this study was to determine whether a fairly abundant receptor on tumor cells could serve as a target for near-infrared fluorescence (NIRF)-enhanced optical imaging. While other studies have successfully investigated the somatostatin receptor as a target for NIRF imaging (3, 4), we chose the folate receptor (FR), a

glycosylphosphatidylinositol-anchored protein. The FR is ideally suited for this studies because its was overexpressed in several cancers (including breast, lung, cervical, ovarian, colorectal, renal, and nasopharyngeal cancers) (11–13), low expression in normal tissues (14, 15), proven utility for MR and nuclear imaging (16–21), and cost-effectiveness for possible later clinical trials. We have recently described the synthesis of a folate-near-infrared fluorochrome conjugate (22). In the current study, we evaluate a FR-targeted conjugate for in vivo NIRF imaging, specifically on tumor enhancement characteristics as a function of time and comparison of the folate and NIRF conjugate to the NIR fluorochrome alone. Our results revealed that a folate-modified NIRF conjugate has potential applications in improved detection of FR positive tumors.

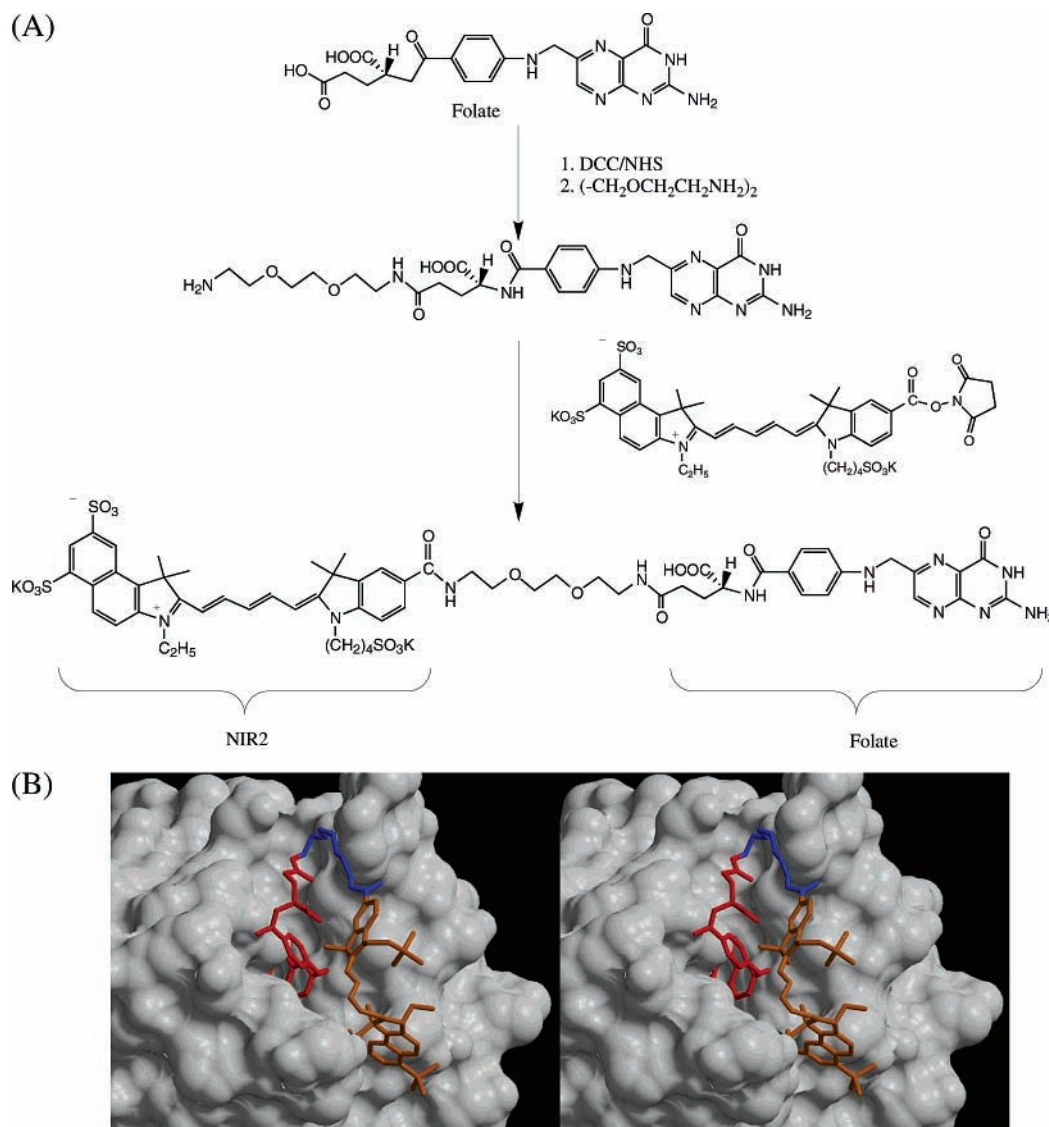
## MATERIALS AND METHODS

**Imaging Probe.** The folate-targeting optical probe (Figure 1), NIR2–folate, consisting of a near-infrared fluorochrome (10) and folic acid, was synthesized as previously described (22). Briefly, folic acid was first reacted with 2,2'-(ethylenedioxy)bis(ethylamine) using diisopropylcarbodiimide as the coupling agent in DMSO. The *N*-hydroxysuccinimide activated ester of near-infrared fluorochrome (NIR2) (10) was linked to the amino-derivatized folic acid in 0.1 M NaHCO<sub>3</sub>/DMF. The final conjugate was purified by C-18 reverse-phase HPLC and characterized by mass spectroscopic analysis. The NIR2–folate has an excitation maximum at 665 nm and an emission maximum at 686 nm.

**Modeling of Target Interaction.** Interaction of NIR2–folate and FR was studied using a model structure of riboflavin binding protein (RFBP) with bound riboflavin (23). The crystal structure of RFBP and riboflavin

\* Corresponding author: Ching H. Tung, Ph.D., Center for Molecular Imaging Research, Massachusetts General Hospital, 149 13th St., Rm. 5406, Charlestown, MA 02129. Tel: (617) 726-5779, Fax: (617) 726-5708, e-mail: tung@helix.mgh.harvard.edu.

<sup>†</sup> Current address: Department of Radiology and Clinical Research Institute, Seoul National University Hospital, Korea.



**Figure 1.** (A) Synthetic scheme of folate receptor (FR)-targeting near-infrared fluorescence probe (NIR2–folate). (B) Stereoview of computer modeling of NIR2–folate and its receptor analogue, riboflavin binding protein (RFBP). The RFBP is rendered in white as a vdw surface. Folic acid and NIR2 were colored in red and gold, respectively. The ring of folate is sandwiched between the planar residues tyr 75 and trp 156. The spacer (blue) extends from the binding pocket, allowing free rotation of NIR2.

was used to determine a model active site for simulated docking of NIR2–folate in the ligand fit module of Cerius<sup>2</sup> (Accelrys, San Diego, CA) (24). The docking algorithm performed  $10^6$  cycles of Monte Carlo simulations. First, a search using ligand torsion angles was used to generate random conformations. Docking scores were then determined by three algorithms, a softened Lennard–Jones 6–9 potential, the evaluation of buried polar surface area for attractive and repulsive interactions. The top 20 conformations placed the folate moiety of NIR2–folate in the binding pocket, in a parallel plane between trp156 and tyr75 of RFBP, which correspond to trp168 and tyr82 of FR. The RFBP van der Waals surface was generated using the program MSMS (25). All models were rendered with Raster3D (26).

**Characterization of Cell Lines.** A human nasopharyngeal epidermoid carcinoma, KB, and a human fibrosarcoma, HT1080, cell lines were purchased from American Type Culture Collection (ATCC, Manassas, VA). These cell lines were selected because of putative FR overexpression (KB) or lack of detectable FR expression (HT1080) (11). Both cell lines were cultured at 37 °C in a humidified atmosphere containing 5% CO<sub>2</sub> in folate-

deficient medium RPMI 1640 with 10% fetal calf serum (Gibco BRL/Life Technologies, Rockville, MD).

To confirm receptor expression levels, we first determined cellular binding/internalization using <sup>3</sup>H-folate. KB or HT1080 ( $10^6$  cells) grown in 12-well plates were incubated at 37 °C for different times (1, 10, 30, 60, 120 min) with 50 nM <sup>3</sup>H-folate (specific activity 34.5 Ci/mmol, American Radiolabeled Chemical Inc, St. Louis, MO). At the end of the incubation, cells were harvested using 0.1% Triton X-100, and the radioactivity (pmol/ $10^6$  cells) was determined using a scintillation counter. For competitive inhibition studies, KB cells were incubated with different amounts of folic acid or NIR2–folate probe (5, 50, 500, and 5000 nM).

**Cellular Uptake of the NIR2–Folate Probe.** Similar to previous uptake experiments, the NIR2–folate probe was tested in cell culture using KB and HT1080 cells grown at 70% confluency on glass cover slips. The culture medium was replaced with 0.5 mL of fresh medium containing 1  $\mu$ M NIR2–folate probe and incubated for 1 h at 37 °C. Cells were washed three times and fluorescence microscopy was performed using an

inverted epifluorescence microscope (Zeiss Axiovert, Thornwood, NY).

**Animal Preparation.** All animal studies were approved by the institutional animal care committee. Ketamine (90 mg per kilogram of body weight) and xylazine (10 mg/kg) given subcutaneously were used as anesthetics, and for euthanasia, pentobarbital (100 mg/kg) was administered intraperitoneally.

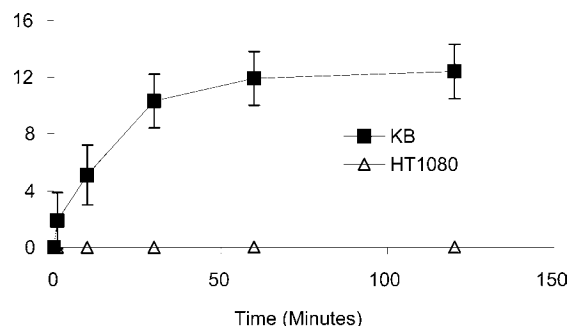
To induce solid tumors,  $10^6$  KB or HT1080 cells were injected subcutaneously into mammary fat pad and the lower abdomen of 36 nude mice (average weight 20 g). Within 7–17 days after implantations, each mouse developed 3–4 tumors of 1–14 mm (mean 4.1 mm) in size. To study tumor heterogeneity, the tumors with different size were included in the experiments. For dual-tumor experiments, six mice were injected with  $10^6$  of KB and HT1080 cells on the ipsilateral and contralateral side, respectively.

**Immunohistochemistry.** For immunohistochemical staining, tumors were frozen sectioned into 7  $\mu$ m thick slices and fixed with 4% paraformaldehyde for 5 min. Endogenous peroxidase activity was blocked with 0.3% hydrogen peroxide in 0.3% normal horse serum in phosphate-buffered saline for 5 min. The mouse immunoglobulin was blocked using M.O.M. immunodetection kit (Vector laboratories, Burlingame, CA), and sections were incubated with FR-recognizing MAb LK26 (15 to 20  $\mu$ g/mL immunoglobulin; Signet laboratories, Dedham, MA). Sections were washed and then incubated with biotinylated horse anti-mouse immunoglobulin for 30 min at room temperature, followed by avidin–biotin–horseradish peroxidase complex. The final reaction product was visualized with diaminobenzidine. Tissue sections were viewed using a Nikon Eclipse 800 microscope and images were digitally captured using a CCD-SPOT RT digital camera and compiled using Adobe Photoshop software (v5.5).

**In Vivo Studies.** Thirty-six mice bearing KB and/or HT1080 tumors ( $n = 60$  each) were divided into three groups so that each group had 12 mice with 40 tumors; five mice with 18 KB tumors, five mice with 18 HT1080 tumors, and two mice with both KB and HT1080 tumors. Group 1 was injected with the NIR2–folate probe (2 nmol/mouse), group 2 received free NIR2 fluorochrome (not conjugated to folate, 2 nmol/mouse), and group 3 was injected with the mixture of NIR2–folate probe (2 nmol/mouse) and free folic acid (600 nmol folate/mouse). NIRF imaging was performed before and 1, 4, 24, 48 h after tail vein injection of the probes. In two animals from each group, NIRF images were also acquired daily up to 7 days (168 h) to study the in vivo kinetics of the probe.

**Image and Data Analysis.** Imaging was performed using NIRF reflectance imaging system, which has been described in detail previously (27). Exposure time was 30 s per image, with maximum input photon flux delivered by the light source. Images were analyzed using commercially available software (Digital Science 1D software; Kodak). Regions of interest (300–320 pixels for each location) were placed manually within the visible tumor margins, the representative adjacent nontarget tissue (adjacent thigh), and a reference standard containing 10 nM free Cy5.5 fluorescent dye (Amersham Pharmacia, Piscataway, NJ). For determination of tumor contrast, mean fluorescence intensities of the tumor area ( $T$ ) and of the corresponding area at the ipsilateral thigh ( $N$ ) were calculated for each animal. Dividing  $T$  by  $N$  yielded the contrast between tumor tissue and normal tissue.

**Statistical Analysis.** Data are presented as means and standard error of the mean. Statistical analysis of



**Figure 2.** Cellular uptake of  $^3\text{H}$ -folate in the KB and HT1080 tumor cell lines. KB and HT1080 tumor cells were incubated with  $^3\text{H}$ -folate (50 nM) up to 120 min and cellular binding and uptake was quantitated by scintillation counting. The  $^3\text{H}$ -folate is internalized to significant amounts in the KB cells whereas the HT1080 cells show essentially no uptake of  $^3\text{H}$ -folate reflecting the receptor positive nature of the KB cells and the absence of receptors in the negative control cell line.

in vivo tumor fluorescence intensity (arbitrary unit) and the contrast between tumor and normal tissue was conducted by using a two-tailed paired Student  $t$  test. A  $P$  value of 0.05 or less was considered to indicate a statistically significant difference.

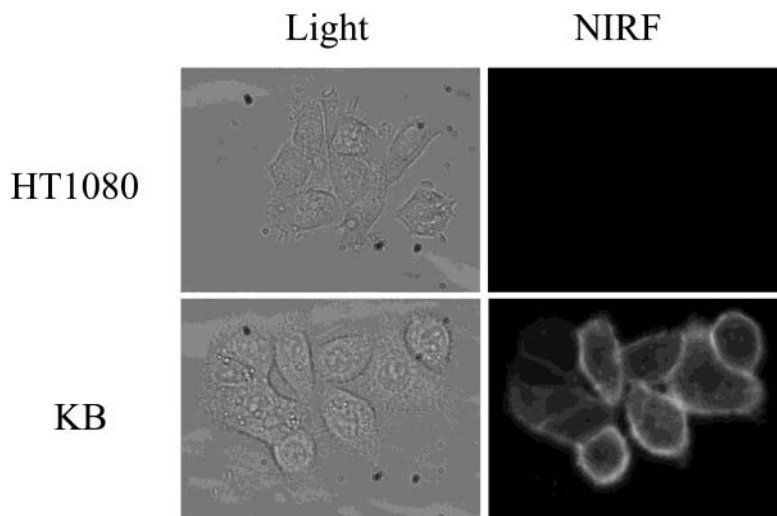
## RESULTS

**Modeling of NIR2–Folate and Receptor Interaction.** Before synthesizing the NIR2–folate probe, computer modeling was used to study the potential ligand and receptor interaction. The crystal structure of FR has not yet been solved, RFBP, a prototype protein for the riboflavin and folate binding protein family, was used instead (28). FR has approximately 30% sequence identity with RFBP, suggesting a high degree of structural homology. The binding site of RFBP contains a tryptophan, trp156, and a tyrosine, tyr75, oriented in parallel planes, forming a hydrophobic pocket. The isoalloxazine ring of riboflavin binds tightly between these two residues (23). Since FR also contains the same two residues, trp168 and tyr82, in its putative binding site, we used the crystal structure of RFBP to model the binding of a NIR2–folate conjugate.

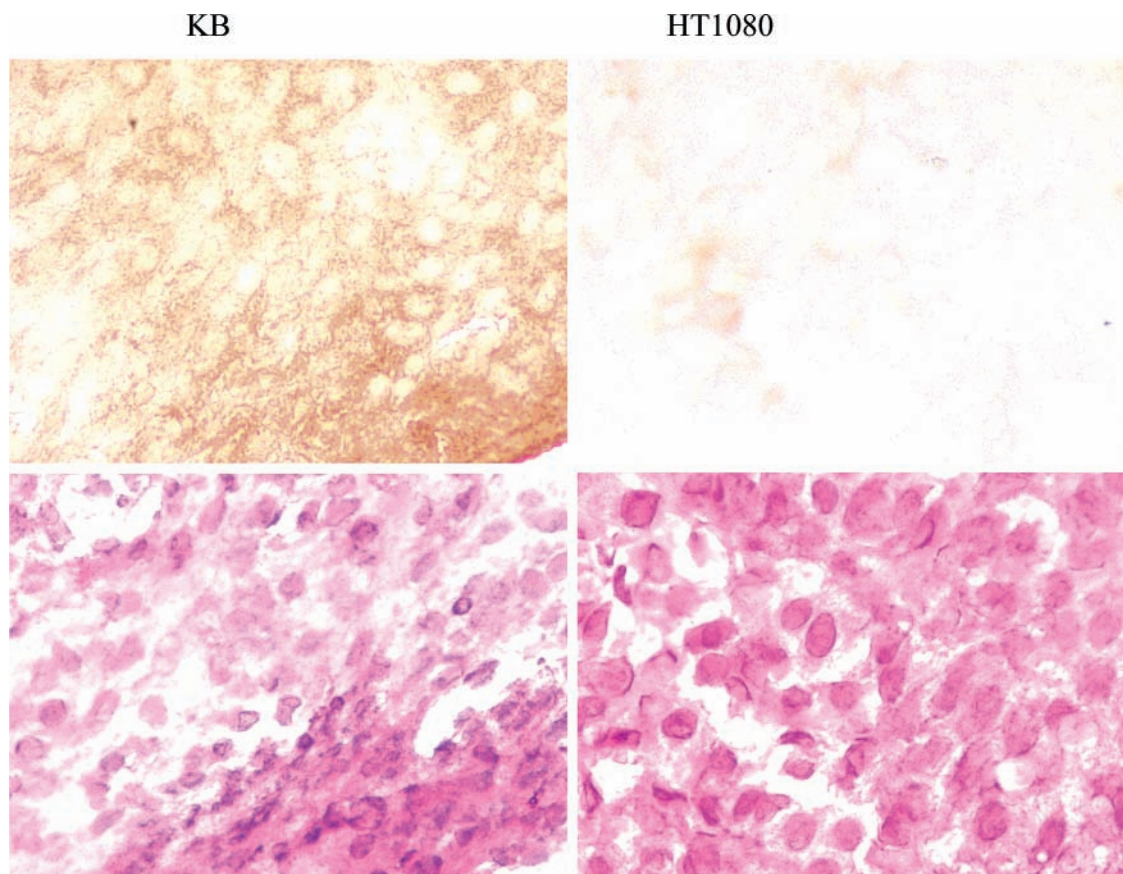
As expected, simulated docking experiments resulted in folate binding the active site of RFBP in an almost identical manner to riboflavin (Figure 1B). The binding pocket is deep and narrow, though it widens sufficiently at the protein surface to accommodate a long spacer for conjugation. On the basis of this, the 2,2'-(ethylenedioxy)-bis(ethylamine) was selected as the linking arm. Docking experiments with attachment of NIR2 directly to folate or with a shorter spacer arm resulted in poor binding because of steric hindrance. Additionally, there are 12 tryptophans in proximity to the active site in both RFBP and FR. These residues are likely responsible for the complete quenching of riboflavin fluorescence upon binding. The spacer forces NIR2 to remain at least 10 Å from these residues, minimizing any quenching effects.

**Validation of Tumor Model.** The HT1080 and KB cell lines were first characterized in terms of their putative capability of  $^3\text{H}$ -folate binding and uptake. Figure 2 summarizes the data showing significant uptake of  $^3\text{H}$ -folate by KB cells, but essentially no uptake by HT1080 cells. For KB cells, 50% of saturation of available FR by  $^3\text{H}$ -folate was reached in 20 min and uptake reached a plateau in 60 min. At peak maximum we observed 12 pmol of  $^3\text{H}$ -folate/ $10^6$  cells under the chosen experimental conditions. In competition assays, there was





**Figure 3.** Cellular uptake of NIR2-folate probe. KB and HT1080 tumor cells were incubated with NIR2-folate probe ( $0.1 \mu\text{M}$ ) for 30 min at  $37^\circ\text{C}$ , and cells were visualized by NIRF microscopy. Note strong fluorescence signals at the plasma membrane of KB cells suggesting the efficient binding of the NIR2-folate probe to FR present in the cell surface (magnification:  $20\times$ ).

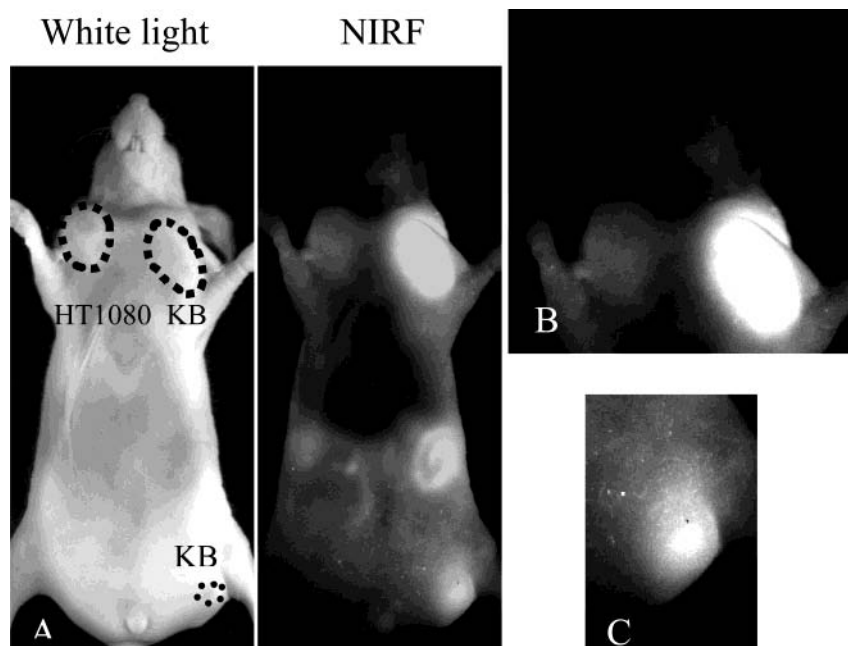


**Figure 4.** Immunohistochemical analysis of FR expression (top) and hematoxylin-eosin staining (bottom) of KB and HT1080 tumors. The staining of FR is strong positive in KB tumor cells whereas it is negative in HT1080. Note the localization of the LK26 antibody in the membrane and cytoplasm of the KB cells (original magnification,  $40\times$ ).

a 60% decrease in bound  $^3\text{H}$ -folate in the presence of an equimolar amount ( $50 \text{ nM}$ ) of the free folic acid ( $4.97 \text{ pmol}/10^6 \text{ cells}$ ) or NIR2-folate probe ( $5.01 \text{ pmol}/10^6 \text{ cells}$ ). As the concentration of the free folic acid or NIR2-folate probe was increased to  $5000 \text{ nM}$ , binding of  $^3\text{H}$ -folate also decreased to 15% of its initial value, free folic acid at  $1.86 \text{ pmol}/10^6 \text{ cells}$  or NIR2-folate probe at  $1.92 \text{ pmol}/10^6 \text{ cells}$ . Competition by the NIR2-folate probe was similar to that of unconjugated folic acid. These results confirmed that fluorochrome attachment does not interfere with FR binding.

To determine the localization of fluorescent folate within cells, fluorescence microscopy was performed on KB cells incubated with the NIR-2 folate probe. The cells showed extensive, bright fluorescence signal whereas there was essentially no binding or uptake of the NIR2-folate probe in the negative control, HT1080 cells (Figure 3). Fluorescence signal was seen primarily in the distribution of the plasma membrane of KB cells and in punctate vesicles in the interstitial compartment.

**FR Expression in Tumor.** Before testing the NIR2-folate probe in vivo, tumor expression of FR was further



**Figure 5.** In vivo imaging of folate receptor. (a) White light and NIRF images obtained 24 h after intravenous injection of the NIR2–folate probe in a representative animal. FR-positive KB tumors were implanted on the right of the chest and the low abdomen, and FR-negative HT1080 tumor on the left of the chest. (b) Enlarged NIRF images of the chest tumors. Note the strong fluorescence signal in the FR-positive KB tumors compared with the control HT1080 tumors. (The imaging shows 2.7-fold difference in signal). (c) Enlarged NIRF images of the low abdomen KB tumors (1 mm).

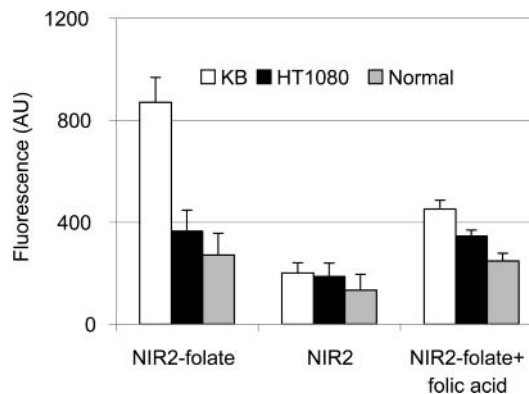
characterized by immunohistology with FR recognizing Mab LK26. The staining showed strong immunoprecipitation in KB tumor tissues, indicating that the receptor remains overexpressed following implantation (Figure 4). Antibody staining showed primarily membrane and cytoplasmic staining of the KB cells. In contrast, HT 1080 tumor sections were essentially negative for folate receptor. Hematoxylin-eosin staining revealed multiple mitotic figures present in the rapidly proliferating HT1080 fibrosarcoma, while relatively well differentiated epidermoid cells were seen in the KB tumors.

#### Tumor Detection with the Folate Conjugate.

Following intravenous administration of the NIRF–folate probe, KB tumors showed significantly higher fluorescence signal intensity compared to HT1080 tumors (Figure 5). Mice bearing KB tumors, tumoral fluorescence could be detected as early as 1 h after administration of the probe ( $728 \pm 109$  AU), which peaked at 4 h ( $1210$  AU  $\pm 127$ ) and then decreased ( $870$  AU  $\pm 98$  AU at 24 h,  $459$  AU  $\pm 48$  AU at 48 h, and  $255$  AU  $\pm 39$  at 72 h).

In tumors of equal size, there was a 2.4-fold ( $870$  AU  $\pm 98/366$  AU  $\pm 41$ ,  $P < 0.01$ ) higher fluorescence intensity in the FR-positive KB tumors compared with the control HT1080 tumors at 24-h images (Figure 6). In this set of experiments we also compared tumoral enhancement with the free NIR2 dye. At the 24 h time point, NIR-2 fluorochrome did not result in appreciably higher signal than background. Similarly, in competition studies, fluorescence signal of FR-positive KB tumor was reduced to that of FR-negative HT1080 tumors (Figure 6).

We next determined tumor to background contrast (an essential parameter for tumor detectability) and plotted these ratios as a function of time after injection for the three experimental groups (Figure 7). At 1 h time point, all agents had similar tumor/background ratios and these ratios were only moderately elevated in KB tumors. At 4 h after injection, a significantly higher tumor/background ratio for the NIR2–folate was observed when compared to the NIR2 compound. Importantly for clinical applications, tumor/background ratios remained elevated

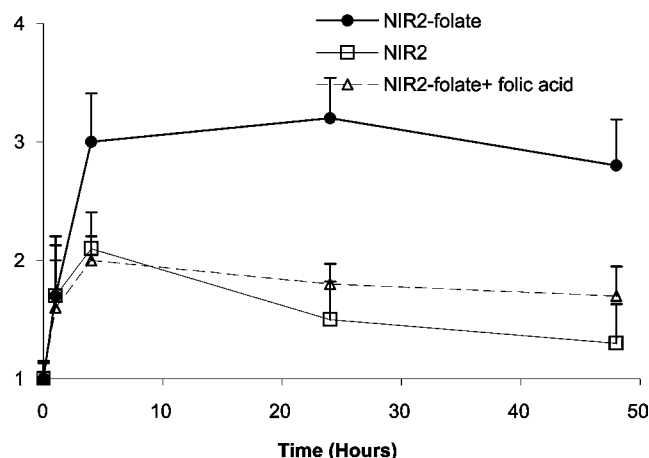


**Figure 6.** In vivo fluorescence signal of tumors and normal tissues. The fluorescence signal was obtained 24 h after intravenous injection of the NIR2–folate probes (2 nmol), the NIR2 compounds (2 nmol), and the NIR2–folate probes (2 nmol) with folic acid (600 nmol). Fluorescence intensity generated by the NIR2–folate probes in the FR-positive KB tumor is significantly higher than FR-negative HT1080 tumors whereas there is no significant difference between KB and HT1080 tumors after injection of the NIR2 compounds. In competition study performed with coinjection of the NIR2–folate probe and folic acid, fluorescence intensity of FR-positive tumors is reduced to that of FR-negative tumors.

with this probe for at least 24–48 h indicating its potential utility for endoscopic and intraoperative use (Figure 7). The tumoral fluorescence signal was reduced rapidly after 72 h ( $255$  AU  $\pm 39$ ) and returned to the baseline ( $115$  AU  $\pm 17$ ) in 5 days. Organ distribution of the probe was also examined after dissection. Highest fluorescence signal was observed in kidney because of high FR expression (29). Tumor, liver, lung, and intestine were at about the similar level.

#### DISCUSSION

The results show that in vivo receptor imaging is feasible using a NIR fluorochrome-labeled targeting ligand. After intravenous injection, the targeted probe



**Figure 7.** Time course of KB tumor with various probes. Tumor-to-normal contrast of FR-positive KB tumors after intravenous injection of the NIR2-folate probe, the NIR2 compounds and the NIR2-folate probe with folic acid was measured up to 48 h. Note the significantly higher tumor-to-normal contrast between 4 and 48 h after injection of the NIR2-folate probes compared with the NIR2 compounds injection or coinjection of the NIR2-folate probes and folic acid.

(NIR2-folate) was shown to significantly increase tumor fluorescence intensity and contrast to normal tissues in a nude mouse xenograft model compared to nontargeted fluorescence dye (NIR2). The specificity of this FR-targeted probe was confirmed in vitro and in vivo studies.

Our data indicate that the NIR2-folate probe has significant advantages over nonspecific fluorochromes for in vivo imaging, the latter often being used for nontargeted image enhancement (30, 31). Although NIR fluorochrome alone is capable of increasing tumor fluorescence, the actual contrast enhancement is typically lower. In KB tumors, the tumor contrast was about 3.0, 4 h after injection of the NIR2-folate probe. This is equivalent to 94% of maximum contrast value ( $3.2 \pm 0.41$ ) at 24 h. Rapid contrast enhancement of the tumor during the first few hours after injection is another major advantage of small molecular targeting agents (4).

Two additional experiments confirmed that the fluorescent probe uptake is receptor dependent. Compared to KB tumor, HT1080 tumor expressed significantly less FR, which was reflected by a 2.4-fold lower fluorescence signal. In addition, the in vivo competition assay showed that the availability of free folate was able to compete off the receptor binding to NIR2-folate probe. The results supported the hypothesis that fluorochrome-labeled folic acid can still be recognized by its receptor. Interestingly, the competition experiment also showed that folate probe binding was not completely blocked by 300-fold excess of free folic acid (Figure 6). It is speculated that short blood half-life of folic acid may cause incomplete blockage; however, more studies are needed.

Optical imaging is a noninvasive method and does not depend on radiolabeled contrast agents such as those in nuclear medicine; thus, there is no exposure of the patient to ionizing radiations. However, tissue penetration of near-infrared light in living tissue may limit the use of near-infrared contrast agents in tumor diagnostics to certain special applications, such as detection of superficial lesions, especially with endoscopic techniques and optical mammography (5, 32, 33). Recently, new imaging systems for deeper targets are under development to overcome these limitations. A tomographic reconstruction method has shown promise for in vivo imaging of fluorescent signal by surrounding the subject with photon sources and detectors (34).

In conclusion, in vivo tumor detection by optical imaging was feasible using a FR-targeted NIRF probe. Compared to nontargeted fluorescence dye (NIR2), intravenous injection of the targeting probe (NIR2-folate) was shown to significantly increase tumor contrast 4–48 h in a nude mouse xenograft model. These receptor-targeted imaging methods may facilitate both improved cancer diagnosis and staging, and early assessment of the effectiveness of treatment, by providing a more accurate in vivo characterization of tumor receptor status.

**Supporting Information Available:** Computer modeling of NIR2-folate and its receptor analogue, riboflavin binding protein. This material is available free of charge via the Internet at <http://pubs.acs.org>.

#### ACKNOWLEDGMENT

The authors would like to thank Dr. Philip Low for the technique suggestion. This research was supported by NIH P50-CA86355, NO1-CO17014, R33-CA88365, and NSF BES-0119382. W.K.M. was partly supported by the Korean Science & Engineering Foundation.

#### LITERATURE CITED

- Weissleder, R., Tung, C. H., Mahmood, U., and Bogdanov, A. (1999) In vivo imaging of tumors with protease-activated near-infrared fluorescent probes. *Nat. Biotech.* 17, 375–8.
- Tung, C. H., Mahmood, U., Bredow, S., and Weissleder, R. (2000) In vivo imaging of proteolytic enzyme activity using a novel molecular reporter. *Cancer Res.* 60, 4953–4958.
- Achilefu, S., Dorshow, R. B., Bugaj, J. E., and Rajagopalan, R. (2000) Novel receptor-targeted fluorescent contrast agents for in vivo tumor imaging. *Invest. Radiol.* 35, 479–85.
- Becker, A., Hensenius, C., Licha, K., Semmler, W., Wiedenmann, B., and Groetzing, C. (2001) Receptor targeted optical imaging of tumors with near-infrared fluorescent ligands. *Nat. Biotech.* 19, 327–31.
- Marten, K., Bremer, C., Khazaei, K., Sameni, M., Sloane, B., and Tung, C. H. et al. (2002) Detection of dysplastic intestinal adenomas using enzyme-sensing molecular beacons in mice. *Gastroenterology* 122, 406–14.
- Bremer, C., Tung, C. H., Bogdanov, A., Jr., and Weissleder, R. (2002) Imaging of differential protease expression in breast cancers for detection of aggressive tumor phenotypes. *Radiology* 222, 814–8.
- Bremer, C., Bredow, S., Mahmood, U., Weissleder, R., and Tung, C. H. (2001) Optical imaging of matrix metalloproteinase-2 activity in tumors: feasibility study in a mouse model. *Radiology* 221, 523–9.
- Bremer, C., Tung, C. H., and Weissleder, R. (2001) In vivo molecular target assessment of matrix metalloproteinase inhibition. *Nat. Med.* 7, 743–8.
- Weissleder, R., and Ntziachristos, V. (2003) Shedding light onto live molecular targets. *Nat. Med.* 9, 123–8.
- Lin, Y., Weissleder, R., and Tung, C. H. (2002) Novel near-infrared cyanine fluorochromes: synthesis, properties, and bioconjugation. *Bioconjugate Chem.* 13, 605–10.
- Ross, J. F., Chaudhuri, P. K., and Ratnam, M. (1994) Differential regulation of folate receptor isoforms in normal and malignant tissues in vivo and in established cell lines. Physiologic and clinical implications. *Cancer* 73, 2432–43.
- Miotti, S., Bagnoli, M., Ottone, F., Tomassetti, A., Colnaghi, M. I., and Canevari, S. (1997) Simultaneous activity of two different mechanisms of folate transport in ovarian carcinoma cell lines. *J. Cell Biochem.* 65, 479–91.
- Toffoli, G., Cernigoi, C., Russo, A., Gallo, A., Bagnoli, M., and Boiocchi, M. (1997) Overexpression of folate binding protein in ovarian cancers. *Int. J. Cancer* 74, 193–8.
- Leamon, C. P., DePrince, R. B., and Hendren, R. W. (1999) Folate-mediated drug delivery: effect of alternative conjugation chemistry. *J. Drug Target.* 7, 157–69.



- (15) Lu, Y., and Low, P. S. (2002) Folate-mediated delivery of macromolecular anticancer therapeutic agents. *Adv. Drug Deliv. Rev.* 54, 675–93.
- (16) Guo, W., Hinkle, G. H., and Lee, R. J. (1999) 99mTc–HYNIC-folate: a novel receptor-based targeted radiopharmaceutical for tumor imaging. *J. Nucl. Med.* 40, 1563–9.
- (17) Mathias, C. J., D. Hubers, Low, P. S., and Green, M. A. (2000) Synthesis of [(99m)Tc]DTPA-folate and its evaluation as a folate- receptor-targeted radiopharmaceutical. *Bioconjugate Chem.* 11, 253–7.
- (18) Mathias, C. J., Wang, S., Low, P. S., Waters, D. J., and Green, M. A. (1999) Receptor-mediated targeting of 67Ga-deferoxamine-folate to folate- receptor-positive human KB tumor xenografts. *Nucl. Med. Biol.* 26, 23–5.
- (19) Wang, S., J. Luo, D. A. Lantrip, Waters, D. J., C. J. Mathias, and Green, M. A. et al. (1997) Design and synthesis of [111In]DTPA-folate for use as a tumor-targeted radiopharmaceutical. *Bioconjugate Chem.* 8, 673–9.
- (20) Konda, S. D., M. Aref, S. Wang, M. Brechbiel, and E. C. Wiener (2001) Specific targeting of folate-dendrimer MRI contrast agents to the high affinity folate receptor expressed in ovarian tumor xenografts. *Magma* 12, 104–13.
- (21) Konda, S. D., S. Wang, M. Brechbiel, and E. C. Wiener (2002) Biodistribution of a 153 Gd-folate dendrimer, generation = 4, in mice with folate-receptor positive and negative ovarian tumor xenografts. *Invest. Radiol.* 37, 199–204.
- (22) Tung, C. H., Y. Lin, W. K. Moon, and Weissleder, R. (2002) A receptor-targeted near-infrared fluorescence probe for in vivo tumor imaging. *ChemBiochem* 3, 784–6.
- (23) Monaco, H. L. (1997) Crystal structure of chicken riboflavin-binding protein. *Embo J.* 16, 1475–83.
- (24) Bohm, H. J. (1998) Prediction of binding constants of protein ligands: a fast method for the prioritization of hits obtained from de novo design or 3D database search programs. *J. Comput.-Aided Mol. Des.* 12, 309–23.
- (25) Sanner, M. F., Olson, A. J., and Spehner, J. C. (1996) Reduced surface: an efficient way to compute molecular surfaces. *Biopolymers* 38, 305–20.
- (26) Merritt, E. A., and Bacon, D. J. (1997) Raster3D: Photo-realistic molecular graphics. *Methods Enzymol.* 277, 505–24.
- (27) Mahmood, U., Tung, C., Bogdanov, A., and Weissleder, R. (1999) Near-infrared optical imaging system to detect tumor protease activity. *Radiology* 213, 866–870.
- (28) Maziarz, K. M., Monaco, H. L., Shen, F., and Ratnam, M. (1999) Complete mapping of divergent amino acids responsible for differential ligand binding of folate receptors alpha and beta. *J. Biol. Chem.* 274, 11086–91.
- (29) Weitman, S. D., Lark, R. H., Coney, L. R., Fort, D. W., Frasca, V., and Zurawski, V. R., Jr., et al. (1992) Distribution of the folate receptor GP38 in normal and malignant cell lines and tissues. *Cancer Res.* 52, 3396–401.
- (30) Licha, K., Riefke, B., Ntziachristos, V., Becker, A., Chance, B., and Semmler, W. (2000) Hydrophilic cyanine dyes as contrast agents for near-infrared tumor imaging: synthesis, photophysical properties and spectroscopic in vivo characterization. *Photochem. Photobiol.* 72, 392–8.
- (31) Ntziachristos, V., Yodh, A. G., Schnall, M., and Chance, B. (2000) Concurrent MRI and diffuse optical tomography of breast after indocyanine green enhancement. *Proc. Natl. Acad. Sci. U.S.A.* 97, 2767–72.
- (32) Stepp, H., Sroka, R., and Baumgartner, R. (1998) Fluorescence endoscopy of gastrointestinal diseases: basic principles, techniques, and clinical experience. *Endoscopy* 30, 379–86.
- (33) Jiang, H., Iftimia, N. V., Xu, Y., Eggert, J. A., Fajardo, L. L., and Klove, K. L. (2002) Near-infrared optical imaging of the breast with model-based reconstruction. *Acad Radiol.* 9, 186–94.
- (34) Ntziachristos, V., Tung, C. H., Bremer, C., and Weissleder, R. (2002) Fluorescence molecular tomography resolves protease activity in vivo. *Nat. Med.* 8, 757–60.

BC0340114

# Monoclonal Antibody Radiopharmaceuticals: Cationization, Pegylation, Radiometal Chelation, Pharmacokinetics, and Tumor Imaging

Hwa Jeong Lee and William M. Pardridge\*

College of Pharmacy, Ewha Womans University, Seoul 120-750, South Korea and Department of Medicine, UCLA School of Medicine, Los Angeles, California 90024. Received December 31, 2002; Revised Manuscript Received February 20, 2003

The 528 murine monoclonal antibody (MAb) to the human epidermal growth factor receptor (EGFR) was sequentially cationized with hexamethylenediamine and conjugated with diethylenetriamine-pentaacetic acid (DTPA) as a potential antibody radiopharmaceutical for imaging EGFR-expressing cancer. The cationized 528 MAb was characterized with isoelectric focusing and electrophoresis, and an immunoradiometric assay, which showed the affinity of the 528 MAb for the human EGFR was retained following cationization. The native or cationized 528 MAb, labeled with  $^{111}\text{In}$ , was injected intravenously in scid mice bearing human U87 flank tumors, which express the EGFR, and tumor imaging was performed with both external detection in live animals and with whole body autoradiography. However, the tumor signal was not increased with the cationized MAb, relative to the native MAb, and this was due to a serum inhibition phenomenon that was confirmed by a pharmacokinetics analysis in control mice. In an attempt to block the serum inhibition, the cationized 528 MAb was pegylated with 2000 Da poly(ethylene glycol), and the cationized/pegylated MAb was conjugated with DTPA and labeled with  $^{111}\text{In}$ . However, a pharmacokinetics analysis showed the pegylation did not reverse the serum inhibition of the cationic charge on the MAb. These studies describe methods for reformulating monoclonal antibodies to develop improved radiopharmaceuticals, but show that radiolabeling a cationized MAb with DTPA produces a serum neutralization of the initial cationization modification.

## INTRODUCTION

Monoclonal antibody radiopharmaceuticals are potential diagnostic agents for the imaging of cancer and other regional disorders with standard imaging modalities such as single photon emission computed tomography. However, the initial promise of monoclonal antibody radiopharmaceuticals as tumor imaging agents has not been realized to date (1), because the intensity of the image over the tumor, relative to surrounding tissue, is generally not sufficiently high to allow for detection of small carcinomas. The single most important factor limiting imaging with monoclonal antibody radiopharmaceuticals is the poor transport of these large molecule drugs across the microvascular endothelial barrier of the capillaries perfusing the tumor or target end organ. The capillary wall of the tumor forms a blood–tumor barrier, and the poor transport of the antibody radiopharmaceutical across the microvascular barrier has two effects, both of which are deleterious to the tumor image. First, the slow exodus of the antibody from the vascular compartment within the tumor reduces the access of the antibody to the target antigen on the tumor cell, which reduces the imaging “signal”. Second, the slow exodus of the antibody from the vascular compartment results in the prolonged blood residence time, which increases the imaging “noise” from the tissue surrounding the tumor.

Monoclonal antibody radiopharmaceuticals could be new tumor imaging agents given the development of a technology that enhances monoclonal antibody transport across microvascular barriers. The antibody that is enabled to cross microvascular barriers must be reformulated in such a way that the affinity of the antibody for the target antigen is not compromised. These objectives may be accomplished with antibody cationization (2). In this approach, surface acidic amino acids on the monoclonal antibody are conjugated with amino group ligands, resulting in the conversion of surface carboxyl groups into extended amino groups on the modified antibody. Cationized proteins are generally taken up by cells via absorptive-mediated endocytosis (3, 4). This uptake is caused by electrostatic interactions between the cationic groups on the protein and anionic moieties on the plasma membrane of the cell (5). Native monoclonal antibodies are general excluded from the cell and it is necessary to physically inject an antibody into the cell to enable access of the antibody to an intracellular antigen (6). However, a cationized antibody is rapidly endocytosed by cells, and cationized antibodies rapidly undergo absorptive-mediated transcytosis across microvascular endothelial barriers in vivo (2).

The monoclonal antibody must be cationized in such a way that the affinity of the antibody for the target antigen is largely retained. Prior work has shown that monoclonal antibodies directed against a variety of antigens, including amyloid peptides (7), oncogenes (8, 9), or viral proteins (10), can be cationized with retention of antigen affinity. Pharmacokinetic analyses of cationized monoclonal antibody clearance from blood have

\* To whom correspondence should be addressed: Dr. William M. Pardridge, UCLA Warren Hall 13-164, 900 Veteran Ave., Los Angeles, CA 90024. Phone: (310) 825–8858. Fax: (310) 206-5163. E-mail: wpardridge@mednet.ucla.edu.

shown that the rate of exodus of the antibody from the blood is increased manyfold following cationization (7–9, 11). In these previous investigations of cationized antibodies, the cationized monoclonal antibody was radiolabeled with 125-iodine. However, the use of the 125-iodine radionuclide is not optimal for in vivo imaging, because the blood rapidly accumulates with low molecular weight, highly diffusible radioactive metabolites. These <sup>125</sup>I-labeled metabolites are generated by the rapid cellular metabolism of the <sup>125</sup>I-labeled cationized antibody, which occurs following the organ uptake of the antibody. The accumulation of the low molecular weight, diffusible <sup>125</sup>I-labeled metabolites in the organ diminishes the quality of the image.

An alternative radionuclide for labeling cationized monoclonal antibodies is 111-indium. The principal advantage of this radionuclide over <sup>125</sup>I is that <sup>111</sup>In labeled metabolites are retained in the peripheral tissues and do not return to the blood circulation (12). In contrast, the <sup>125</sup>I-labeled metabolites produced in peripheral tissues are exported back to blood to accumulate in the other organs. Labeling an antibody with <sup>111</sup>In requires the conjugation of the cationized antibody with a radio-metal chelating moiety, such as diethylenetriaminepentaacetic acid (DTPA).<sup>1</sup> The present studies report on the sequential cationization and DTPA conjugation of the 528 murine monoclonal antibody (MAb) to the human epidermal growth factor receptor (EGFR). The EGFR is overexpressed in the majority of solid cancers (13), and a radiolabeled, cationized anti-EGFR MAb is a potential new radiopharmaceutical for the imaging of cancer. In the course of the present studies, a serum inhibition phenomenon was observed in which the beneficial effects of the antibody cationization were neutralized in vivo in the circulation. Therefore, the present studies evaluated the triple conjugated 528 MAb, in which the antibody is sequentially cationized, conjugated with poly(ethylene glycol), and conjugated with DTPA, followed by labeling with <sup>111</sup>In and in vivo pharmacokinetic analysis.

## EXPERIMENTAL PROCEDURES

**Materials.** U87 human brain glioma cells (ATCC HTB 14) and the 528 hybridoma (ATCC HB 8509) were supplied by the American Type Culture Collection (Rockville, MD). [<sup>111</sup>In]Cl<sub>3</sub> was purchased from NEN Life Science Products Inc. (Boston, MA). [<sup>125</sup>I]Na was obtained from Amersham (Arlington Heights, IL). Diethylenetriaminepentaacetic (DTPA) dianhydride and hexamethylenediamine (HMD) were supplied by Aldrich Chemical Co., Inc. (Milwaukee, WI). NHS-PEG<sup>2000</sup> was obtained from Shearwater Polymers (Huntsville, AL), where NHS = *N*-hydroxysuccinimide and PEG<sup>2000</sup> = poly(ethylene glycol) of 2000 Da molecular weight. Superose 12 HR 10/30 FPLC columns, ampholine polyacrylamide (PAG) plates (pH = 3.5–9.5) for isoelectric focusing (IEF), and

Broad pI standard kit (pH = 3–10) were purchased from Pharmacia Biotech (Piscataway, NJ). Sodium dodecyl sulfate polyacrylamide gel electrophoresis (SDS–PAGE) supplies were obtained from Bio-Rad Inc. (Richmond, CA). Chloramine-T was purchased from MCB Reagents (Cincinnati, OH). *N*-Ethyl-*N*-(3-(dimethylamino)propyl)-carbodiimide (EDC) and all other chemicals were obtained from Sigma Chemical Co. (St. Louis, MO). Female BALB/c mice and female severe combined immunodeficient (SCID) mice were supplied by Harlan/Sprague Dawley (San Diego, CA).

**Antibody Cationization and Pegylation.** The 528 MAb was cationized with 2 different reaction conditions designed to give a protein with increasing degrees of cationization. In the first reaction, 3.2 mL of 2 M HMD was added to 1.0 mL of native 528 MAb (8.3 mg/mL in 0.01 M PBS/7.4) and the pH was adjusted to 6.8. After mixing, 44 mg of fresh EDC was added to the mixture, and the pH was readjusted to 6.8. In the second reaction, the pH was changed to 7.4, and the amounts of HMD and EDC were reduced to 1.6 mL of 2 M HMD and 21 mg EDC, respectively. The mixtures were gently rocked end over end for 3 h at room temperature, and the reaction was stopped by the addition of 1 mL of 1 M glycine, followed by incubation for 30 min at room temperature. The mixtures were dialyzed against 10 L of 0.01 M PBS/7.4 overnight at 4 °C using a 12 kDa MW cut off dialysis tubing. The cationized 528 MAbs were stored at –20 °C.

The cationized 528 MAb prepared at pH 7.4 was pegylated with a 100-fold or 1000-fold molar excess of NHS-PEG<sup>2000</sup> as follows: 0.1 mL of 0.5 M NaHCO<sub>3</sub>/pH 8.5 was added to 0.9 mL of the cationized 528 MAb (1.1 mg/mL). Either 1.2 mg or 12 mg of NHS-PEG<sup>2000</sup> was directly added to the mixture. The mixture was gently rocked for 60 min at room temperature, and the reaction was quenched by the addition of 50 µL of 1 M glycine, followed by incubation for 60 min at room temperature.

The pI of the native or cationized 528 MAbs was determined with polyacrylamide gel IEF. Approximately 10–20 µg of either native 528 MAb, cationized 528 MAb/pH = 6.8 or cationized 528 MAb/pH = 7.4, was solubilized in 2% NP-40 and applied to the IEF gel in parallel with pI standards. IEF was performed as described previously (8), followed by staining of the gel with Coomassie blue.

**Antibody Radioiodination or DTPA Conjugation and Indium Chelation.** The native 528 MAb (83 µg, 0.55 nmol) was iodinated with [<sup>125</sup>I]Na (1 mCi, 0.53 nmol) and chloramine T (8.4 nmol) in 0.05 M PBW/pH 7.4 at room temperature for 2 min. After the addition of sodium metabisulfite (12.5 nmol) to quench the reaction, [<sup>125</sup>I]-native 528 MAb was purified by Sephadex G25 gel filtration chromatography (0.7 × 28 cm column) with an elution buffer of 0.01 M PBS/pH 7.4 containing 0.1% BSA (PBSB). The final specific activity and the TCA precipitability of [<sup>125</sup>I]-native 528 MAb were 4.9 µCi/µg and > 99%, respectively. The [<sup>125</sup>I]-native 528 MAb was used in the immunoradiometric assay described below.

For [<sup>111</sup>In] labeling of the native 528 MAb, DTPA dianhydride (6.72 nmol) was added in a 12:1 molar ratio to 83 µg of the native 528 MAb (0.55 nmol) in 0.1 M NaHCO<sub>3</sub>/pH 8.3, followed by incubation at room temperature for 90 min. The DTPA-native 528 MAb was radiolabeled with 0.75 mCi of [<sup>111</sup>In]Cl<sub>3</sub> in 0.05 M Na acetate/0.15 M NaCl (ABS)/pH 5.5, followed by incubation at room temperature for 30 min. [<sup>111</sup>In]-native 528 MAb was separated from free [<sup>111</sup>In] by Sephadex G25 gel filtration chromatography (0.7 × 28 cm column) in 0.01

<sup>1</sup> Abbreviations: MAb, monoclonal antibody; IEF isoelectric focusing; pI, isoelectric point; ID, injected dose; DTPA, diethylenetriaminepentaacetic acid; NHS, *N*-hydroxysuccinimide; PEG, poly(ethylene glycol); EGFR, epidermal growth factor receptor; HMD, hexamethylenediamine; EDC, *N*-ethyl-*N*-(3-(dimethylamino)propyl)carbodiimide; SDS–PAGE, sodium dodecyl sulfate polyacrylamide gel electrophoresis; SCID, severe combined immunodeficiency; NHS, *N*-hydroxysuccinimide; *B*<sub>max</sub>, maximal receptor binding; *K*<sub>D</sub>, receptor binding dissociation constant; *K*<sub>I</sub>, receptor binding inhibitory constant; NSB, non-specific binding; AUC, area under the plasma concentration curve; FPLC, fast protein liquid chromatography; IRMA, immunoradiometric assay; mIgG, mouse immunoglobulin G.; CMC, carboxymethyl cellulose.



M PBS/pH = 7.4. [ $^{111}\text{In}$ ]-native 528 MAb had a specific activity of 6.4  $\mu\text{Ci}/\mu\text{g}$ .

For [ $^{111}\text{In}$ ] labeling of the cationized 528 MAb, DTPA dianhydride (21 nmol) was added in a 30:1 molar ratio to 105  $\mu\text{g}$  of the cationized 528 MAb (0.7 nmol) in 0.1 M  $\text{NaHCO}_3$ /pH 8.3, followed by incubation at room temperature for 90 min. The 528 MAb cationized at pH = 7.4 was used for DTPA conjugation. The DTPA-cationized 528 MAb was radiolabeled with 0.75 mCi [ $^{111}\text{In}$ ] $\text{Cl}_3$  in 0.05 M ABS/pH 5.5, followed by incubation at room temperature for 30 min. [ $^{111}\text{In}$ ]-cationized 528 MAb was purified by Sephadex G25 size-exclusion chromatography (0.7  $\times$  28 cm column) in 0.05 M ABS/pH 5.5 containing 0.05% Tween 20 (ABST). The final specific activity of [ $^{111}\text{In}$ ]-cationized 528 MAb was 6.5  $\mu\text{Ci}/\mu\text{g}$ .

For [ $^{111}\text{In}$ ] labeling of the PEG<sup>2000</sup>-cationized 528 MAb, DTPA dianhydride (50.4 nmol) was added in a 100:1 molar ratio to 100  $\mu\text{g}$  of the PEG<sup>2000</sup>-cationized 528 MAb (0.5 nmol) in 0.1 M  $\text{NaHCO}_3$ /pH 8.3, followed by incubation at room temperature for 90 min. The PEG<sup>2000</sup>-DTPA-cationized 528 MAb was radiolabeled with 1 mCi [ $^{111}\text{In}$ ] $\text{Cl}_3$  in 0.05 M ABS/pH 5.5, followed by incubation at room temperature for 30 min. PEG<sup>2000</sup>-[ $^{111}\text{In}$ ]-cationized 528 MAb was separated from free [ $^{111}\text{In}$ ] by Sephadex G25 gel filtration chromatography (0.7  $\times$  28 cm column) with an elution buffer of 0.01 M PBS/pH 7.4 containing 0.05% Tween 20 (PBST). The PEG<sup>2000</sup>-[ $^{111}\text{In}$ ]-cationized 528 MAb had a specific activity of 9.3  $\mu\text{Ci}/\mu\text{g}$ .

**Immunoradiometric Assay (IRMA).** U87 human brain glioma cells ( $3 \times 10^4$  cells/well) were plated on sterile 96-well plate and grown to confluency. These cells express the EGFR on the plasma membrane in cell culture (14). The cells were fixed by ice-cold methanol at  $-20^\circ\text{C}$  for 10 min. Each well (100  $\mu\text{L}$ ) contained 0.04  $\mu\text{Ci}$  of [ $^{125}\text{I}$ ]-native 528 MAb and 1–300  $\mu\text{g}/\text{mL}$  of either unlabeled native 528 MAb, cationized 528 MAb (pI = 8.7 or pI = 9.2), native mouse IgG (mIgG), or cationized mIgG in PBSB. After incubation for 3 h at room temperature, the wells were washed three times with 180  $\mu\text{L}$  of cold 0.01 M PBS/pH 7.4. Then, 100  $\mu\text{L}$  of 1 N NaOH was added to each well to solubilize the cells at  $60^\circ\text{C}$  for 30 min, followed by rocking at room temperature for 30 min. The solubilized cells (80  $\mu\text{L}$ ) from each well were counted for [ $^{125}\text{I}$ ] radioactivity using a  $\gamma$ -counter (Beckman Instruments, Inc., Fullerton, CA).

The binding constants for native or cationized 528 MAb binding to the human EGFR expressed on the fixed U87 cells were determined by fitting the binding data to equations derived for a single saturable binding site plus a nonsaturable binding site. The saturation of [ $^{125}\text{I}$ ]-native 528 MAb binding by unlabeled native 528 was fit to a Scatchard plot:

$$B/F = [(B_{\text{max}})/(K_D + F)] + \text{NSB}$$

where  $B$  = bound MAb,  $F$  = free MAb,  $B_{\text{max}}$  = maximal binding at the saturable site,  $K_D$  = the saturable binding site dissociation constant, and NSB = nonsaturable binding. The saturation of [ $^{125}\text{I}$ ]-native 528 MAb binding by unlabeled cationized 528 MAb was fit to a modified Scatchard plot:

$$B/F = [(B_{\text{max}}/K_D)/(1 + I/K_I)] + \text{NSB}$$

where  $I$  = the concentration of cationized 528 MAb, and  $K_I$  = the concentration of 50% inhibition of native 528 MAb binding. All binding data were fit with a weighted least squares regression analysis described below.

**Pharmacokinetics.** The BALB/c mice were anesthetized with ketamine (100 mg/kg) and xylazine (2 mg/kg) intraperitoneally. Either 5  $\mu\text{Ci}$  of [ $^{111}\text{In}$ ]-native 528 MAb in 0.01 M PBS/pH 7.4, 6.7  $\mu\text{Ci}$  of [ $^{111}\text{In}$ ]-cationized 528 MAb in 0.05 M ABST/pH 7.4, or 6  $\mu\text{Ci}$  of PEG<sup>2000</sup>-[ $^{111}\text{In}$ ]-cationized 528 MAb in 0.01 M PBST/pH 7.4 was injected into the jugular vein of each mouse.

Arterial blood was removed from the aorta at 0.25, 2, 5, 15, and 60 min after intravenous injection of the isotope solution. The blood samples were centrifuged and serum was counted for [ $^{111}\text{In}$ ]-radioactivity using a  $\gamma$ -counter. At 60 min after isotope administration, the mice were sacrificed and liver, kidney, heart, and lung were removed for counting of [ $^{111}\text{In}$ ]-radioactivity.

Pharmacokinetic parameters were estimated by fitting the serum concentration–time data to a monoexponential equation with a derivative-free nonlinear regression analysis (PARBMDP, Biomedical Computer P-Series, developed at UCLA Health Science Computing Facilities), using a weighting factor of  $1/(\text{concentration})^2$ , where  $A(t)$ , % ID (injected dose)/mL serum, and  $k$ ,  $\text{min}^{-1}$ , are the intercept and slope, respectively, of the monoexponential equation. The area under the serum concentration–time curve at 60 min [ $\text{AUC}(t)$ ] and at steady state [ $\text{AUC}_{\text{ss}}$ ] were calculated from the injected dose (ID), the slope, and the intercept of the monoexponential equation. The  $\text{AUC}_{\text{ss}}$  is considered only an approximation because the pharmacokinetics analysis was extended to only 60 min. The organ uptake of each compound was determined as follows:

$$\% \text{ ID/g organ} = [V_d - V_0]C_p(60 \text{ min})$$

where  $C_p(60 \text{ min})$  is the terminal serum concentration (%ID/ $\mu\text{L}$ ),  $V_d$  is the organ volume of distribution ( $\mu\text{L}/\text{g}$ ), and  $V_0$  is the organ plasma volume, which was reported previously for mice (15).

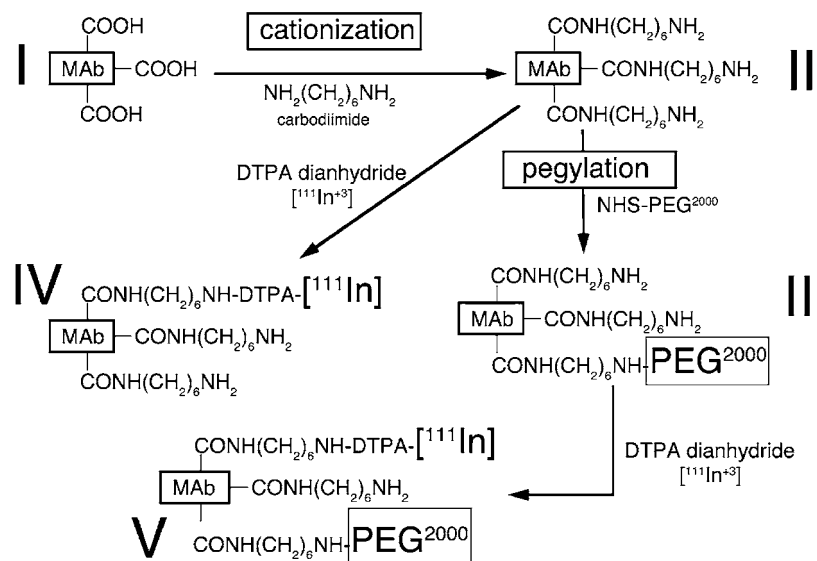
**Gel Filtration Fast Protein Liquid Chromatography (FPLC).** The metabolic stability of [ $^{111}\text{In}$ ]-native 528 MAb, [ $^{111}\text{In}$ ]-cationized 528 MAb, and PEG<sup>2000</sup>-[ $^{111}\text{In}$ ]-cationized 528 MAb was examined by injecting the pooled serum taken from 3 mice at 60 min on to a Superose 12 HR 10/30 FPLC column with elution at 0.5 mL/min in PBST for 60 min. The fractions (0.5 mL per each tube) were counted for [ $^{111}\text{In}$ ]-radioactivity using a  $\gamma$ -counter.

**External Detection Imaging and Whole Body Autoradiography of Flank Tumors.** U87 human glioma cells ( $10^6$  cells/mouse) were injected into right flank of female scid mice subcutaneously. U87 experimental tumors overexpress the human EGFR on the tumor cell membrane (14). Tumor sizes were measured twice a week and tumor volume was calculated by following equation:

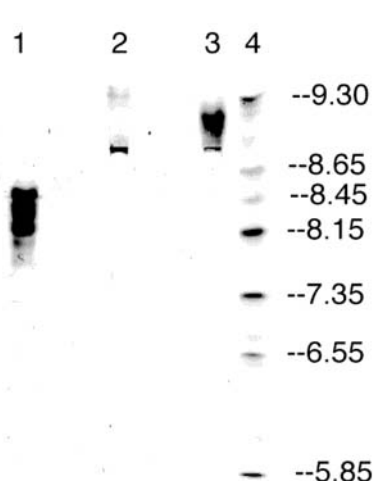
$$\text{tumor volume (mm}^3\text{)} = (4/3)\pi ab^2$$

where  $a$  = long radius and  $b$  = short radius. Tumor sizes ranged from 524 to 1600  $\text{mm}^2$  at 2 weeks after the injection of U87 cells. The tumors of the scid mice were imaged at 15 days after implantation.

The scid mice with flank tumors were divided into two groups and 50  $\mu\text{Ci}$  of either [ $^{111}\text{In}$ ]-native 528 MAb or [ $^{111}\text{In}$ ]-cationized 528 MAb was injected into the tail vein of each animal. At 24 h after the isotope injection, the mice were anesthetized with ketamine (100 mg/kg) and xylazine (2 mg/kg). The mice were placed on the plate in the prone position and were scanned with a stationary LFVO camera (Orbiter ZLC-7500, Siemens) at 247 keV or 172



**Figure 1.** Reaction schemes for reformulation of 528 MAb. The native MAb with surface carboxyl groups is shown as I. The native 528 MAb is cationized with hexamethylenediamine,  $\text{NH}_2(\text{CH}_2)_6\text{NH}_2$ , and EDC (also called carbodiimide) to form the cationized MAb, shown as II, and the surface carboxyl groups have now been converted to extended primary amine groups. The latter are pegylated with NHS-PEG<sup>2000</sup> to form the cationized, pegylated MAb as shown in III. Either II or III are reacted with DTPA dianhydride as shown in IV and V, respectively.



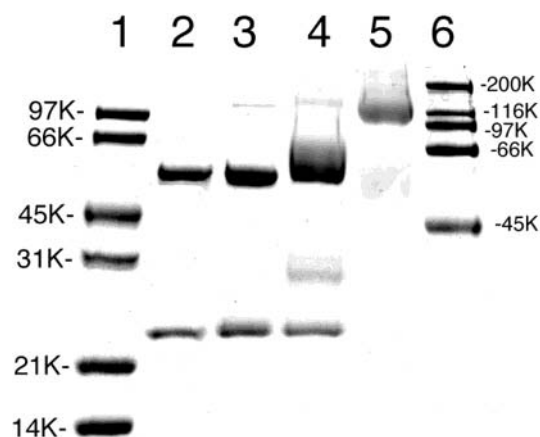
**Figure 2.** Isoelectric focusing of the native 528 MAb (lane 1) and the cationized 528 MAb (lanes 2 and 3); pI standards are shown in lane 4. The 528 MAb was cationized at either pH 7.4 or 6.8 to form the cationized MAb with a pI of 8.7 (lane 2) or 9.2 (lane 3), respectively. The gel was stained with Coomassie blue.

keV with 15% window width for 10 min. The scan data were saved on a Siemens ICON computer prior to generation of X-ray film images.

After  $\gamma$ -counter external detection, the mice were euthanized and placed on a Styrofoam board in the prone position and immersed in carboxymethyl cellulose (CMC) and dipped in liquid  $\text{N}_2$  for 10 min and stored at  $-20^\circ\text{C}$  overnight. The frozen CMC-mouse specimen was placed in a cryostat and  $50\text{ }\mu\text{m}$  thick sections were obtained. The frozen sections were placed in a Fuji-BAS cassette and exposed at  $-20^\circ\text{C}$  for 24 h. The plate was analyzed with a Fuji-BAS reader, saved as a MacBAS file with 100 micron resolution and 65 bit color, and converted to a pict file in Adobe Photoshop.

## RESULTS

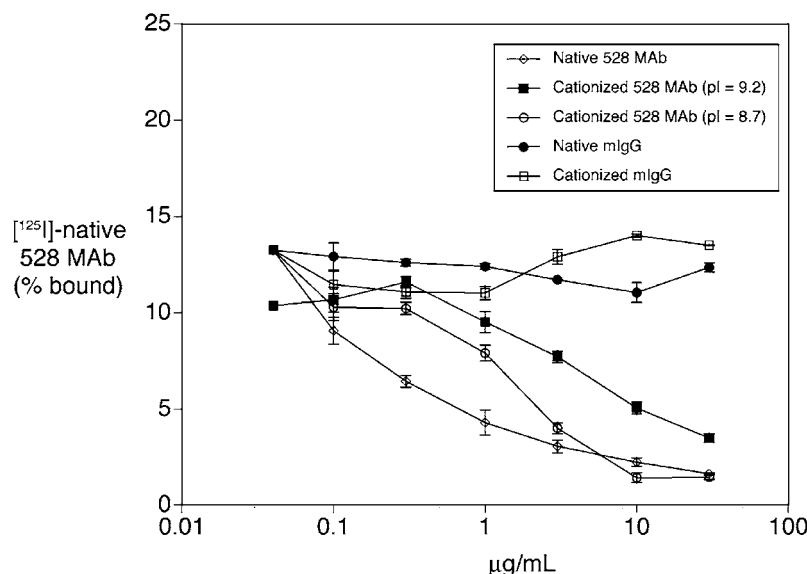
The native 528 MAb is shown as intermediate I in Figure 1 and the cationized 528 MAb is shown as II in



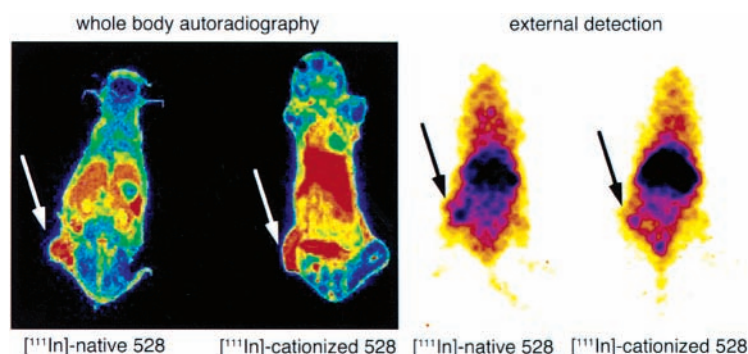
**Figure 3.** Sodium dodecyl sulfate polyacrylamide gel electrophoresis with Coomassie blue staining of molecular weight standards (lanes 1 and 6), native 528 MAb (lane 2), cationized 528 MAb/pI = 8.7 (lane 3), or PEG-cationized 528 MAb (lanes 4 and 5). The cationized 528 MAb pegylated with a 100-fold or 1000-fold molar excess of NHS-PEG<sup>2000</sup>:antibody is shown in lanes 4 and 5, respectively.

Figure 1. The 528 MAb that undergoes sequential cationization and DTPA conjugation followed by chelation with  $^{111}\text{In}$  is shown as IV in Figure 1. The 528 MAb was cationized at two different reaction pH's and the pI of the MAb following cationization at pH 7.4 is 8.7 and the pI of the antibody following cationization at pH 6.8 is 9.2 as shown by the IEF gel in Figure 2. The pI of the native 528 MAb ranges from 8.1 to 8.3 (lane 1, Figure 2). There was minimal formation of intramolecular bonds between antibody light or heavy chains following cationization as demonstrated by SDS-PAGE (Figure 3). The size of the light chain and heavy chain of the cationized 528 MAb (lane 3, Figure 3) is identical to the size of the light and heavy chains of the native 528 MAb (lane 2, Figure 3).

The affinity of the native or cationized 528 MAb for the target human EGFR was determined with the immunoradiometric assay. The binding of [ $^{125}\text{I}$ ] native 528 MAb to human U87 glioma cells was inhibited by increasing concentrations of unlabeled native 528 MAb



**Figure 4.** Immunoradiometric assay (IRMA) with methanol-fixed human U87 glioma cells as the solid-phase source of the human EGFR and [ $^{125}\text{I}$ ]-native 528 MAb as the tracer ligand. The competitive displacement of binding of the [ $^{125}\text{I}$ ]-native 528 MAb to the U87 cells was measured in the presence of 1–30  $\mu\text{g/mL}$  concentrations of native 528 MAb, cationized 528 MAb/pI = 9.2, cationized 528 MAb/pI = 8.7, native mouse IgG (mIgG), and cationized mIgG. Data are mean  $\pm$  SE ( $n = 3$ ). The affinity of the PEG<sup>2000</sup>-cationized 528 MAb for the EGFR was not measured.



**Figure 5.** Whole body autoradiography [left] or gamma counter external detection [right] of female scid mice implanted with U87 subcutaneous tumors in the right flank (arrows). Mice were injected with 50  $\mu\text{Ci}$  of either [ $^{111}\text{In}$ ]-native 528 MAb or [ $^{111}\text{In}$ ]-cationized 528 MAb. At 24 h after injection, the animals were anesthetized for external detection and then sacrificed for whole body autoradiography. The tumors were imaged 15 days after implantation.

**Table 1.** EGF Receptor Binding Constants<sup>a</sup>

monoclonal antibody	$K_D$ (nM)	$K_I$ (nM)	$B_{\text{max}}$ (fmol/dish)	NSB (fmol/dish)
native 528	$1.4 \pm 0.5$	-	$21.0 \pm 4.2$	$1.7 \pm 0.2$
cationized 528/pI = 8.7	-	$5.6 \pm 3.6$	-	$0.8 \pm 0.4$
cationized 528/pI = 9.2	-	$27 \pm 6$	-	$2.4 \pm 0.4$

<sup>a</sup> Parameters determined by nonlinear regression analysis of immunoradiometric assay (IRMA) shown in Figure 4.  $B_{\text{max}}$  = maximal binding; NSB = nonspecific binding.

but not by increasing concentrations of native or cationized preimmune mouse IgG (mIgG), shown in Figure 4. The binding curve for the native 528 MAb was analyzed by nonlinear regression analysis, which indicated the binding  $K_D$  was  $1.4 \pm 0.5$  nM for the native 528 MAb (Table 1). Increasing concentrations of both the cationized 528 MAb/pI = 8.7 and the cationized 528 MAb/pI = 9.2 decreased binding of [ $^{125}\text{I}$ ] native 528 MAb to the U87 cells (Figure 4). Nonlinear regression analysis demonstrated the  $K_I$  of the cationized 528/pI = 8.7 and the cationized 528/pI = 9.2 was  $5.6 \pm 2.6$  nM and  $27 \pm 6$  nM, respectively (Table 1). These findings indicated the affinity of the cationized 528/pI = 8.7 was comparable to that of the native 528 MAb, but that the affinity of the

cationized 528/pI = 9.2 was too low owing to the higher degree of cationization. Therefore, all subsequent work was performed with the cationized 528/pI = 8.7 MAb, which was cationized at pH = 7.4 (Methods).

The native or cationized 528 MAb was conjugated with DTPA anhydride (Figure 1) and radiolabeled with  $^{111}\text{In}$  and injected into tumor bearing SCID mice with unilateral U87 glioma flank tumors. The flank tumors could be detected with either the native or the cationized 528 MAb using either an external detection gamma camera or whole body autoradiography (Figure 5). Although there was increased hepatic uptake with the cationized 528 MAb, the uptake of the native or cationized 528 MAb over the tumor was comparable (Figure 5). The lack of an increased tumor signal with the cationized 528 suggested a possible serum inhibition phenomenon that neutralized the effects of the cationization modification of the antibody. This was confirmed with a series of pharmacokinetic studies in BALB/c mice.

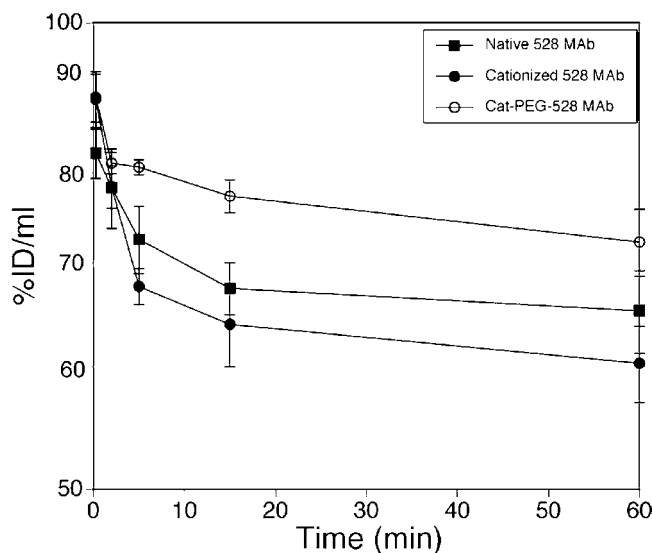
The [ $^{111}\text{In}$ ] native 528 MAb or the [ $^{111}\text{In}$ ] cationized 528 MAb was injected intravenously into mice, and serum radioactivity was measured over a 60 min period (Figure 6). The serum data were analyzed by nonlinear regres-



**Table 2. Pharmacokinetic Parameters<sup>a</sup>**

parameter	[ <sup>111</sup> In]-native 528 MAb	[ <sup>111</sup> In]-cationized 528 MAb	[ <sup>111</sup> In]-PEG <sup>2000</sup> -cationized 528 MAb
AUC (60 min) (%ID·min/mL)	4180 ± 210	3976 ± 192	4581 ± 45
AUC <sup>ss</sup> (%ID·min/mL)	25887 ± 3380	17770 ± 2301	43447 ± 9864
liver uptake (%ID/g)	11.0 ± 0.5	18.6 ± 0.8	0
kidney uptake (%ID/g)	0	4.8 ± 0.4	0
heart uptake (%ID/g)	0	0	0
lung uptake (%ID/g)	2.5 ± 1.6	4.9 ± 0.5	3.5 ± 0.5

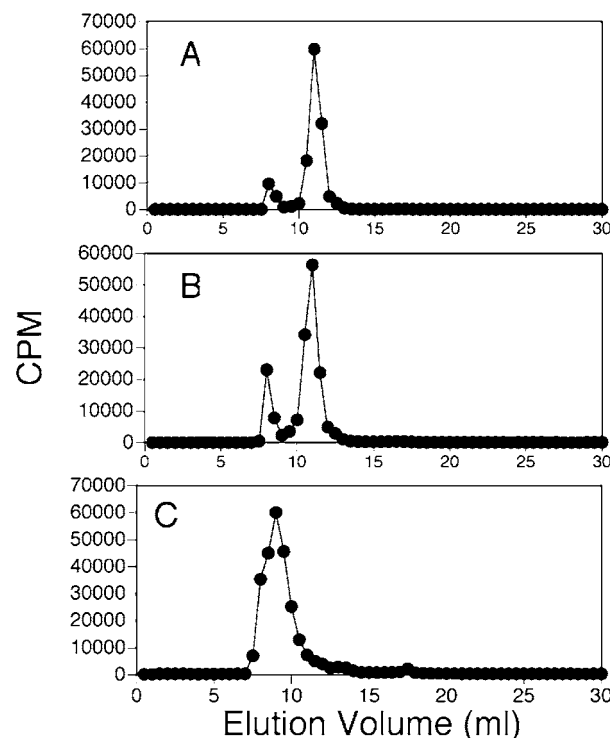
<sup>a</sup> AUC was calculated from data in Figure 6; organ %ID/gram are mean ± SE (*n* = 3 mice per group). An organ uptake (%ID/gram) of 0 indicates the organ volume of distribution was no greater than the organ blood volume in mice (15).



**Figure 6.** Serum concentration of [<sup>111</sup>In]-native 528 MAb, [<sup>111</sup>In]-cationized 528 MAb, and PEG<sup>2000</sup>-[<sup>111</sup>In]-cationized 528 MAb in mice at 0.25–60 min after a single intravenous injection. Data are mean ± SE (*n* = 3). The PEG<sup>2000</sup>-[<sup>111</sup>In]-cationized 528 MAb used in this study was prepared with a 1000:1 molar ratio of PEG:antibody (Methods).

sion analysis to yield the pharmacokinetic parameters shown in Table 2. Although the steady-state area under the plasma concentration curve (AUC<sup>ss</sup>) was reduced 31% following cationization, there was no difference in the 60 min AUC for cationized antibody as compared to the native antibody (Table 2). Cationization caused minor increases in the uptake of the MAb by organs such as liver, kidney, or lung, but had no effect on uptake by the heart. The 60 min serum from mice injected with either native or cationized 528 MAb was analyzed by gel filtration fast protein liquid chromatography (FPLC) as shown in Figure 7A and 7B, respectively. The data showed that the cationized 528 MAb migrated at the same elution volume as the native 528 MAb.

In an attempt to retard the serum inhibition of the cationized 528 MAb, this antibody was triple conjugated with sequential cationization, pegylation, and DTPA conjugation as outlined in Figure 1. The cationized 528 MAb was pegylated at two different molar ratios of PEG<sup>2000</sup>:antibody. Pegylation of the cationized 528 MAb at 100:1 molar ratio resulted in only minor increases in the size of the heavy or light chain of the antibody. However, with the 1000:1 molar ratio of PEG<sup>2000</sup>:antibody, the molecular weight of the cationized MAb was increased from 55K to approximately 110K (lane 5, Figure 3). Similarly, the molecular weight of the light chain was increased from 25K to approximately 55K (lane 5, Figure 3). The 528 MAb that was sequentially cationized, pegylated, and DTPA conjugated was radiolabeled with <sup>111</sup>In and injected into control mice for a pharmacokinetic analysis. The serum concentration profile over



**Figure 7.** Superose 12HR gel filtration fast protein liquid chromatography (FPLC) of pooled serum taken from 3 female BALB/c mice at 60 min after intravenous injection of [<sup>111</sup>In]-native 528 MAb (A), [<sup>111</sup>In]-cationized 528 MAb (B), and PEG<sup>2000</sup>-[<sup>111</sup>In]-cationized 528 MAb (C).

60 min is shown in Figure 6, and the pharmacokinetic parameters are shown in Table 2. Pegylation of the cationized 528 MAb resulted in a 10% increase in the plasma AUC at 60 min and a 68% increase in the steady-state plasma AUC (Table 2). Pegylation of the cationized 528 eliminated uptake of the antibody by liver or kidney and inhibited lung uptake of the cationized antibody (Table 2).

## DISCUSSION

These studies are consistent with the following conclusions. First, cationization of the murine 528 MAb to the human EGFR results in increased pI (Figure 2), stable heavy chain and light chain structure on SDS-PAGE (Figure 3), and high affinity binding to the EGFR in human U87 cells (Figure 4). Second, imaging EGFR expression in flank tumors in SCID mice in vivo does not result in increased tumor signal using the [<sup>111</sup>In]-cationized 528 MAb, as compared to the [<sup>111</sup>In] native 528 MAb (Figure 5). This correlates with a minimal increase in plasma clearance of the 528 MAb following cationization and radiolabeling with <sup>111</sup>In (Figure 6, Table 2). Third, the clearance of the [<sup>111</sup>In]-cationized 528 MAb is further

slowed by surface pegylation of the cationized MAb followed by radiolabeling with  $^{111}\text{In}$  (Figure 6, Table 2).

The mechanism of antibody cationization used in these studies is the conversion of surface carboxyl groups on aspartic acid and glutamic acid residues (intermediate I, Figure 1) to extended primary amino groups using hexamethylenediamine (intermediate II, Figure 1). The degree of cationization is enhanced with an increased molar ratio of hexamethylenediamine to antibody or with a decreased reactant pH (Figure 2). When the 528 MAb is cationized at pH = 7.4, there is minimal change in affinity of the cationized antibody for the target EGFR (Figure 4, Table 1). However, if the 528 MAb is cationized at pH 6.8, there is a 5-fold loss of affinity of the antibody for the target antigen (Figure 4, Table 1). By determining the optimal conditions of the cationization reaction, it is possible to cationize the monoclonal antibody without altering the structure of the heavy or light chains (Figure 3) and without substantially inhibiting the affinity of the antibody for the target antigen (Figure 4, Table 1).

Cationized monoclonal antibodies have been radiolabeled in previous work with 125-iodine. There is a profound increase in plasma clearance of the [ $^{125}\text{I}$ ]-antibody following cationization. Even if the native MAb has a net cationic charge, the cationization of the MAb has a marked effect on plasma clearance in vivo. For example, the native D146 MAb to the ras oncogene has an alkaline pI of 8.9, but this MAb is cleared slowly from plasma (8). Following cationization, the pI was raised to 9.5, and the plasma clearance in BALB/c mice was increased 58-fold compared to the plasma clearance of the [ $^{125}\text{I}$ ]-native D146 MAb (8). This change in pI of the native and cationized D146 MAb is comparable to that observed in the present study with the 528 MAb (Figure 2). The plasma clearance in scid mice of human immunoglobulins was increased >1000-fold following cationization and radiolabeling with 125-iodine (16). The plasma clearance in rats of the humanized HER2 antibody was increased 22-fold following cationization and radiolabeling with 125-iodine (9). The plasma clearance of the AMY33 murine monoclonal antibody to the A $\beta$  amyloid peptide was increased 29-fold in BALB/c mice following cationization and radiolabeling with 125-iodine (7). However, the plasma clearance of the AMY33 antibody in mice was increased only 4-fold following cationization and radiolabeling with  $^{111}\text{In}$  (7). In the dog, the plasma clearance of the [ $^{111}\text{In}$ ]-cationized AMY33 MAb was actually slower than the plasma clearance of the [ $^{111}\text{In}$ ]-native AMY33 MAb (7). The findings of the present study corroborate previous work in mice and dogs with AMY33 MAb and indicate that radiolabeling of a cationized MAb with  $^{111}\text{In}$  eliminates the ability of the antibody to rapidly cross microvascular barriers and undergo rapid exodus from the blood compartment. Prior work with isolated microvessels and in vitro binding assays with or without serum showed that the inhibition of plasma clearance of the [ $^{111}\text{In}$ ]-cationized MAb could be traced to inhibition by factors in serum (7). The serum inhibitory factors are low molecular weight since the elution of the cationized MAb on a gel filtration FPLC column is identical to that of the native MAb labeled with  $^{111}\text{In}$  (Figure 7B).

Pegylation of proteins inhibits the interaction of the protein with plasma constituents and thereby delays plasma clearance of the protein (17). The PEG moieties may be attached to either surface amino or carboxyl groups. In the present studies, the PEG was conjugated to amino groups on the cationized MAb (Figure 1), which would be expected to partially reverse the cationization,

which should reduce the plasma clearance of the cationized MAb. However, we hypothesized that pegylation of a cationized MAb may block the serum inhibition of the DTPA conjugated-cationized MAb and actually result in an increase in plasma clearance of the triply conjugated antibody following cationization, pegylation, and DTPA conjugation. The pharmacokinetic studies showed that pegylation of the cationized antibody that was subsequently DTPA conjugated was actually slower than the plasma clearance of the nonpegylated cationized antibody (Figure 6, Table 2). The cationized 528 MAb was effectively pegylated based on SDS-PAGE analysis (Figure 3). Pegylation at a 100:1 molar ratio of PEG:antibody resulted only in minor pegylation of the protein (lane 4, Figure 3). However, pegylation at 1000:1 molar ratio of PEG:antibody resulted in an increase in the size of the heavy chain from approximately 55 kDa to approximately 110 kDa (lane 5, Figure 3). This suggests that approximately 20–25 PEG $^{2000}$  moieties were attached to each heavy chain. The size of the light chain was increased from approximately 25 kDa to approximately 50–55 kDa (lane 5, Figure 3) indicating approximately 12–15 PEG $^{2000}$  moieties were conjugated to each light chain. However, pegylation of the cationized 528 antibody did not block the serum inhibition and actually caused a further slowing of the clearance of the antibody from the blood (Figure 6, Table 2).

In summary, these studies describe the reformulation of the 528 murine MAb to the human EGFR that involves sequential cationization, pegylation, and DTPA conjugation (Figure 1). Similar to previous studies with the AMY33 MAb to the amyloid peptide (7), the combined cationization and DTPA conjugation followed by radiolabeling with  $^{111}\text{In}$  resulted in an abrogation of the beneficial effects of cationization on plasma clearance of the MAb. The exodus of an antibody following cationization and radiolabeling with 125-iodine is increased from 20-fold to >1000-fold in mice and rats. However, the increased rate of exodus from blood of a cationized antibody is not observed when the antibody is radiolabeled with DTPA conjugation and  $^{111}\text{In}$  chelation, as described in these studies. Cationization of an MAb is a simple approach to antibody reformulation that causes rapid removal of the antibody from the blood compartment in vivo. This rapid clearance can result in increased signal and decreased noise in a tumor imaging modality in vivo. However, future work will be necessary to find the optimal method of radiolabeling the cationized monoclonal antibody that avoids the serum inhibition observed with DTPA conjugated cationized antibodies.

#### ACKNOWLEDGMENT

Supported by a grant 3IB-006 from the California Breast Cancer Research Program and by the U.S. Department of Energy. Dr. Sanjiv Gambhir's laboratory assisted with the whole body autoradiography.

#### LITERATURE CITED

- (1) Vriesendorp, H. M., and Quadri, S. M. (2001) Radiolabeled immunoglobulin therapy: Old barriers and new opportunities. *Expert Rev. Anticancer Ther.* 1, 461–478.
- (2) Triguero, D., Buciak, J. B., Yang, J., and Pardridge, W. M. (1989) Blood-brain barrier transport of cationized immunoglobulin G: Enhanced delivery compared to native protein. *Proc. Natl. Acad. Sci.* 86, 4761–4765.
- (3) Basu, S. K., Goldstein, J. L., Anderson, R. G. W., and Brown, M. S., (1976) Degradation of cationized low-density lipoprotein and regulation of cholesterol metabolism in homozygous

- familial hypercholesterolemia fibroblasts. *Proc. Natl. Acad. Sci. U.S.A.* 73, 1378–1382.
- (4) Shen, W.-C. and Ryser, H. J.-P. (1978) Conjugation of poly-L-lysine to albumin and horseradish peroxidase: A novel method of enhancing the cellular uptake of proteins. *Proc. Natl. Acad. Sci. U.S.A.* 75, 1872–1876.
- (5) Vorbrodt, A. W. (1989) Ultracytochemical characterization of anionic sites in the wall of brain capillaries. *J. Neurocytol.* 18, 359–368.
- (6) Riabowol, K. T., Vosatka, R. J., Ziff, E. B., Lamb, N. J., and Feramisco, J. R. (1998) Microinjection of fos-specific antibodies blocks DNA synthesis in fibroblast cells. *Mol. Cell. Biol.* 8, 1670–1676.
- (7) Bickel, U., Lee, V. M. Y., and Pardridge, W. M. (1995) Pharmacokinetic differences between  $^{111}\text{In}$ - and  $^{125}\text{I}$ -labeled cationized monoclonal antibody against  $\beta$ -amyloid in mouse and dog. *Drug Deliv.* 2, 128–135.
- (8) Pardridge, W. M., Kang, Y.-S., Yang, J., and Buciak, J. L. (1995) Enhanced cellular uptake and in vivo biodistribution of a monoclonal antibody following cationization. *J. Pharm. Sci.* 84, 943–948.
- (9) Pardridge, W. M., Buciak, J., Yang, J., and Wu, D. (1998) Enhanced endocytosis in cultured human breast carcinoma cells and in vivo biodistribution in rats of a humanized monoclonal antibody following cationization of the protein. *J. Pharmacol. Exp. Ther.* 286, 548–554.
- (10) Pardridge, W. M., Bickel, U., Buciak, J., Yang, J., Diagne, A., and Aepinus, C. (1994) Cationization of a monoclonal antibody to the human immunodeficiency virus rev protein enhances cellular uptake but does not impair antigen binding of the antibody. *Immunol. Lett.* 42, 191–195.
- (11) Hong, G., Bazin-Redureau, M. I., and Scherrmann, J. M. G. (1999) Pharmacokinetics and organ distribution of cationized colchicine-specific IgG and Fab fragments in rat. *J. Pharm. Sci.* 88, 147–153.
- (12) Kurihara, A., Deguchi, Y., and Pardridge, W. M. (1999) Epidermal growth factor radiopharmaceuticals:  $^{111}\text{In}$  chelation, conjugation to a blood-brain barrier delivery vector via a biotin-polyethylene linker, pharmacokinetics, and in vivo imaging of experimental brain tumors. *Bioconjugate Chem.* 10, 502–511.
- (13) Nicholson, R. I., Gee, J. M. W., and Harper, M. E. (2001) EGFR and cancer prognosis. *Eur. J. Cancer* 37, S9–S15.
- (14) Kurihara, A. and Pardridge, W. M. (1999) Imaging brain tumors by targeting peptide radiopharmaceuticals through the blood-brain barrier. *Cancer Res.* 54, 6159–6163.
- (15) Skarlatos, S. and Pardridge, W. M. (1995) Targeting of an anti-CR3 (CD11b/CD18) monoclonal antibody to spleen, but not brain, in vivo in mice. *J. Drug Targeting* 3, 9–14.
- (16) Pardridge, W. M., Kang, Y. S., Diagne, A., and Zack, J. A. (1996) Cationized hyperimmune immunoglobulins: Pharmacokinetics, toxicity evaluation, and treatment of HIV-infected scid-hu mice. *J. Pharmacol. Exp. Ther.* 276, 246–252.
- (17) Nucci, M. L., Shorr, R., and Abuchowski, A. (1991) The therapeutic value of poly(ethylene glycol)-modified proteins. *Adv. Drug Deliv. Rev.* 6, 133–151.

BC0256648



# A Cysteine-Linkable, Short Cleavable Photoprobe with Dual Functionality To Explore Protein–Protein Interfaces

Fatima Teixeira-Clerc,<sup>†</sup> Sophie Michalet,<sup>†</sup> André Ménez, and Pascal Kessler\*

CEA/Saclay, Département d'Ingénierie et d'Etudes des Protéines, 91191 Gif-sur-Yvette, France. Received December 11, 2002; Revised Manuscript Received February 28, 2003

We developed a bifunctional photoprobe with dual functionality, that can be specifically tethered to cysteinyl residues of peptides and proteins through a short cleavable disulfide bond. Thus, an aryldiazonium moiety is positioned at approximately 8.5 Å from the modified cysteinyl  $\alpha$ -carbon, leading to one of the shortest cleavable linkages. In a sodium azide-containing buffer, the aryldiazonium moiety is transformed into an aryl azide. Therefore, with one bifunctional photoprobe two types of photogenerated species can be obtained: a hydrophilic and positively charged arylation or a hydrophobic nitrene. We coupled the aryldiazonium probe, in a site-directed manner, to a nicotinic acetylcholine receptor competitive antagonist, obtained by chemical engineering of an analogue of a snake  $\alpha$ -neurotoxin. In this molecule, Arg33, which is known to interact with the receptor, was replaced by a cysteine residue, where the photoprobe could be attached. Under inactivating light, this novel photosensitive snake toxin behaved as a reversible ligand on the *Torpedo* acetylcholine receptor. However, when irradiated at 391 nm, it generated a highly reactive arylation which labeled mostly the receptor  $\alpha$ -subunit, confirming the location of the tip of the second toxic loop near this receptor subunit. Finally, we showed that reduction of the disulfide bond, linking the ligand to the photocoupled receptor, allowed introduction of radioactivity on the labeled residue(s), opening the way to further characterization and avoiding the synthesis of a radioactive bifunctional photoprobe.

## INTRODUCTION

Photoaffinity labeling is a widespread technique to study protein–ligand interactions and map ligand binding sites (for a review, see ref 1), especially for membrane proteins which resist crystallization. It often consists first in the introduction of a photoactivatable moiety on the ligand molecule. Under inactivating light, this modified ligand acts as a reversible probe on its receptor, allowing thus standard pharmacological studies. However, when irradiated under selected wavelengths, it generates a highly reactive species able to couple to proximal residues on the targeted receptor. To introduce a photoprobe on a peptidic ligand or a protein, lysinyl residues are usually modified with a bifunctional probe. However, this protocol precludes any choice of the modification site and implies purification of all the monomodified derivatives. Furthermore, after photocoupling, these ligands are most commonly covalently bound to their receptors by a noncleavable linkage, which greatly enhances the difficulty to isolate and to sequence the photolabeled peptides. Some cleavable bifunctional photoprobes are commercially available; however, most of them are coupled to the peptidic ligand through a long and flexible linker, hence decreasing the geometrical resolution around the site of cross-linking.

In this perspective, photoaffinity labeling of the nicotinic acetylcholine receptor (nAChR<sup>1</sup>) with modified snake curarimimetic toxins (2–12) represents a well-documented example of such a protein–ligand interaction

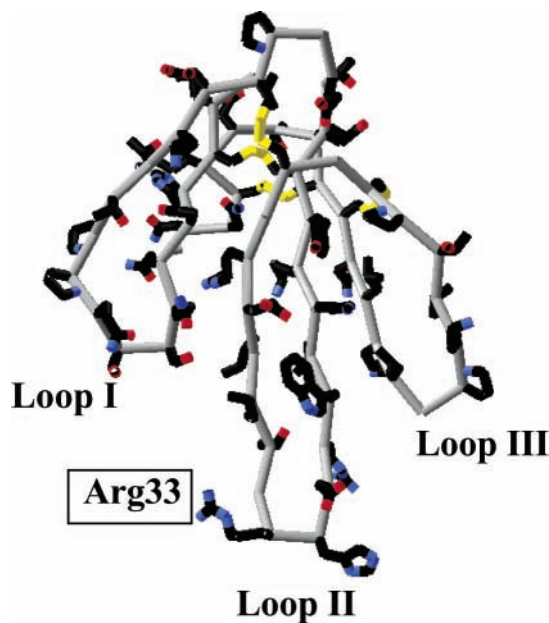
study, in which the ligand is itself a small protein. These competitive antagonists bind quasi-irreversibly to the acetylcholine receptor, with nano- to almost picomolar affinities. Their structure as three-fingered  $\beta$ -sheet proteins (Figure 1) has been well established (13), and mutagenesis studies showed that their binding site is shared by their three loops, on the concave side of the molecule (14–16). As some of these small proteins are commercially available and their structure well-known, they should have been valuable tools for the structural investigation of their binding site on the nAChR. However, none but one (9) of the past photolabeling experiments made with snake toxins led to the identification of the labeled residues on the receptor, while mapping of the neurotransmitter binding site was done quite extensively by (photo)affinity labeling with a number of small organic ligands (17–25). Many difficulties related to (i) low photolabeling yields, (ii) difficulties in labeled-subunits purification, (iii) loss of radioactivity during proteolysis of the labeled peptides, and mostly (iv) the presence of the toxin during all the isolation steps of the labeled residue(s) prevented the characterization of the labeled residues. The unique study which went to completion (9) used a photoprobe linked to the toxin through a cleavable disulfide bond, to get rid of the toxin after labeling. However, this commercial linker was too long to label residues located in close proximity to the toxin.

Therefore, with the view to overcome the past drawbacks and to facilitate the analysis, we have developed a novel short cleavable photoactivatable probe with dual

\* Corresponding author: Pascal Kessler, CEA/Saclay, Département d'Ingénierie et d'Etudes des Protéines, 91191 Gif-sur-Yvette, France. Tel.: 00-33-1-69-08-40-74. Fax: 00-33-1-69-08-90-71. E-mail: pascal.kessler@cea.fr.

<sup>†</sup> Both authors have equally contributed to this work.

<sup>1</sup> Abbreviations: nAChR, nicotinic acetylcholine receptor; DABD, 4-dimethylaminobenzenediazonium; DABD-Pys, 4-dimethylamino-3-(pyridin-2-yl)disulfenylmethyl)benzenediazonium; Pys, pyridin-2-ylsulfenyl; NaDodSO<sub>4</sub>, sodium dodecyl sulfate; DTT: dithiothreitol.



**Figure 1.** *Naja nigricollis*  $\alpha$ -neurotoxin. The structure has been taken from Zinn-Justin et al. (49). Only the backbone  $\alpha$ -carbons were shown (grey ribbon). Residues were drawn in cpk-colors. The four disulfide bonds were represented in yellow. Arg33, which was replaced by a cysteine residue in the R33C analogue, was highlighted on the tip of loop II. Note that the numbering of the residue corresponds to erabutoxin numbering.

functionality (DABD-Pys) which can be selectively linked to any natural or engineered cysteinyl residue in peptides or proteins through a disulfide bond. This paper describes the synthesis of the photoprobe, its coupling to a previously described chemically engineered  $\alpha$ -neurotoxin analogue (26), and the photolabeling experiment leading to the efficient photocoupling of the modified toxin essentially onto the  $\alpha$ -subunit of the nAChR, strengthening earlier reports about the location of the tip of the second loop of short curarimimetic toxins when interacting with nAChR (26, 27). We also showed that reduction of the photointroduced disulfide bond linking the toxin and the receptor allowed modification of the labeled residue(s) on the receptor with tritiated *N*-ethylmaleimide, which will facilitate identification. By eliminating the toxin, we now have a classical labeling experiment with a small radioactive organic molecule, which will simplify the characterization of nAChR-labeled residues.

#### EXPERIMENTAL PROCEDURES

Peptide synthesis was achieved on an Applied Biosystems 433 apparatus. The Fmoc-protected amino acids were obtained from Novabiochem or Advanced Chemtech. [ $^3\text{H}$ ]-*N*-Ethylmaleimide (51.7 Ci·mmol $^{-1}$ ) was from NEN-Dupont de Nemours and was isotopically diluted to 1 Ci·mmol $^{-1}$ . All the chemicals were of the highest purity commercially available. [ $^{125}\text{I}$ ]- $\alpha$ -Bgtx (200 Ci·mmol $^{-1}$ ) was obtained from Amersham. Live *Torpedo marmorata* were purchased from the Station Biologique d'Arcachon (France). mAb155 was a generous gift of Dr. Tzartos. Goat anti-rat (GAR-PO), Goat anti-mouse (GAM-PO), and rabbit anti-horse (RAH-PO) IgG peroxidase conjugates were purchased from Jackson ImmunoResearch Laboratories (West Grove, PA). Reverse phase HPLC purifications were achieved on a Vydac C4 semipreparative column (10  $\times$  250 mm; flow rate: 4 mL·min $^{-1}$ ; linear gradient: 5% B to 21% B in 6 min, then 21% to 27% B in 19 min; A: H $_2$ O–0.1% TFA, B: CH $_3$ CN). Electrospray mass spectrometry was achieved on a Quattro II from

Micromass. NMR spectra were recorded on a Bruker Avance 250 MHz. Melting points were taken on a Kofler device. The irradiating device was composed of a 1000 W mercury lamp (Osram), an aperture, and a series of lenses focusing the polychromatic light to a monochromator (Jobin-Yvon), after which a series of lenses focused the monochromatic light to a thermostated quartz cuvette containing the nAChR. The light intensity was measured with a radiometer IL1700 (International Light, Newburyport, MA). All the experiments involving aryl diazonium or aryl azide compounds were performed under inactinic light (Na light).

**2-Dimethylamino-5-nitrobenzoic Acid (2).** 2-Chloro-5-nitrobenzoic acid (**1**) (2.6 g, 13 mmol) was dissolved in dry THF (250 mL) saturated in dimethylamine and containing potassium carbonate (2 g, 1.1 equiv). The flask was sealed and heated to 120  $^{\circ}\text{C}$  overnight. The mixture was evaporated to dryness, solubilized in aqueous HCl, and extracted repeatedly with EtOAc. The organic layer was dried over MgSO $_4$ , filtered, evaporated to dryness, and yielded 2.5 g of yellow powder (92%). mp 167  $^{\circ}\text{C}$ .  $^1\text{H}$  NMR (DMSO- $d_6$ ):  $\delta$  (ppm) 3.00 (s, 6 H), 7.02 (d,  $J$  = 9.5 Hz, 1 H), 8.11 (dd,  $J_1$  = 9.5 Hz,  $J_2$  = 2.7 Hz, 1 H), 8.33 (d,  $J$  = 2.7 Hz, 1 H).  $^{13}\text{C}$  NMR (CDCl $_3$ ):  $\delta$  (ppm) 42.8, 115.2, 117.7, 127.0, 127.9, 135.8, 154.7, 168.1. C $_9$ H $_{10}$ N $_2$ O $_4$  (210.3) calcd %: C 51.43, H 4.80, N 13.33, found %: C 51.23, H 4.82, N 13.27.

**(2-(Dimethylamino)-5-nitrophenyl)methanol (3).** The acid compound **2** (2.7 g, 13 mmol) was selectively reduced with BH $_3$ –THF (2.2 equiv) in dry THF (150 mL), at reflux for 1 h. Dry MeOH was added to destroy the excess of borane and solvolyze the borates. The mixture was evaporated to dryness. The residue was then solubilized again in dry MeOH, evaporated to dryness, and finally purified by silica gel chromatography (eluent: *n*-hexane 7/EtOAc 3), yielding 2.2 g of a yellow oil (86%).  $^1\text{H}$  NMR (CDCl $_3$ ):  $\delta$  (ppm) 2.62 (s<sub>broad</sub>, 1 H), 2.87 (s, 6 H), 4.75 (s, 2 H), 6.97 (d,  $J$  = 8.9 Hz, 1 H), 8.03 (dd,  $J_1$  = 8.9 Hz,  $J_2$  = 2.0 Hz, 1 H), 8.24 (d,  $J$  = 2.0 Hz, 1 H).  $^{13}\text{C}$  NMR (CDCl $_3$ ):  $\delta$  (ppm) 43.7, 62.0, 117.4, 123.8, 124.8, 133.0, 141.4, 157.1. C $_9$ H $_{12}$ N $_2$ O $_3$  (196.2) calcd %: C 55.10, H 6.16, N 14.28, found %: C 54.43, H 6.27, N 14.11.

**(4-(Dimethylamino)-3-(hydroxymethyl)phenyl)-carbamic Acid *tert*-Butyl Ester (4).** The nitro compound **3** (2.1 g, 10.7 mmol) was reduced on Pd/C (10%) with H $_2$  (4 bar) in MeOH (100 mL), overnight, and protected in situ with di-*tert*-butyl dicarbonate (3.42 g, 1.2 equiv). The mixture was filtered, concentrated and purified by silica gel chromatography (eluent: *n*-hexane 6/EtOAc 4), yielding 2.3 g of a slightly yellow oil (80%).  $^1\text{H}$  NMR (CDCl $_3$ ):  $\delta$  (ppm) 1.50 (s, 9 H), 2.66 (s, 6 H), 4.76 (s, 2 H), 5.95 (s<sub>broad</sub>, 1 H), 6.84 (s<sub>broad</sub>, 1 H), 7.13 (d,  $J$  = 8.6 Hz, 1 H), 7.16 (d,  $J$  = 3.6 Hz, 1 H), 7.25 (dd,  $J_1$  = 8.6 Hz,  $J_2$  = 3.6 Hz, 1 H).  $^{13}\text{C}$  NMR (CDCl $_3$ ):  $\delta$  (ppm) 28.3, 44.8, 64.7, 80.3, 118.3, 118.6, 120.8, 135.0, 135.9, 147.0, 153.0. C $_{14}$ H $_{22}$ N $_2$ O $_3$  (266.3) calcd %: C 63.14, H 8.32, N 10.52, found %: C 62.51, H 8.44, N 10.12.

**Thioacetic Acid *S*-(5-(*tert*-Butoxycarbonylamino)-2-(dimethylamino)benzyl Ester (5).** Methanesulfonyl chloride (0.8 mL, 1.5 equiv) was added on a mixture of compound **4** (2 g, 7.5 mmol) and Et $_3$ N (1.6 mL, 1.5 equiv) in dry THF (40 mL) and stirred for 15 min. The solution was filtered, and the filtrate was evaporated. The residue was dried under vacuum overnight and resolubilized in anhydrous THF (40 mL). A mixture of thioacetic acid (1.3 mL, 2.5 equiv) and Et $_3$ N (2.6 mL, 2.5 equiv) in dry THF (20 mL) was added to the mesylate, and the solution was stirred for 3 h, at room temperature. After concentration, the residue was dissolved in EtOAc and washed with



water and brine, dried over  $\text{MgSO}_4$ , and purified by silica gel chromatography (eluent: *n*-hexane 85/EtOAc 15), yielding 1.3 g (53%) of a reddish oil.  $^1\text{H}$  NMR ( $\text{CDCl}_3$ ):  $\delta$  (ppm) 1.50 (s, 9 H), 2.34 (s, 3 H), 2.62 (s, 6 H), 4.22 (s, 2 H), 6.39 ( $S_{\text{broad}}$ , 1 H), 7.08 (d,  $J = 8.7$  Hz, 1 H), 7.18 (d,  $J = 2.6$  Hz, 1 H), 7.35 (dd,  $J_1 = 8.7$  Hz,  $J_2 = 2.6$  Hz, 1 H).  $^{13}\text{C}$  NMR ( $\text{CDCl}_3$ ):  $\delta$  (ppm) 28.2, 29.1, 30.2, 45.4, 80.2, 118.8, 120.7, 120.8, 133.3, 134.3, 148.4, 152.9, 196.0.  $\text{C}_{16}\text{H}_{24}\text{N}_2\text{O}_3\text{S}$  (324.4) calcd %: C 59.24, H 7.46, N 8.63, S 9.88, found %: C 58.63, H 7.40, N 8.35, S 9.80.

**Dithio-2-(dimethylamino)-5-(*tert*-butoxycarbonylamino)phenylmethane (6).** Thioacetate **5** (1.33 g, 4.1 mmol) was dissolved in dry MeOH (100 mL) and ethanolized with EtONa (327 mg, 1.1 equiv), at room temperature, overnight. The sulfhydryl was oxidized with  $\text{I}_2$ . The excess iodine was destroyed with a 10% sodium thiosulfate solution, and the mixture was concentrated. The residue was resuspended in EtOAc, washed with water and brine, and dried over  $\text{MgSO}_4$ . The product was purified by silica gel chromatography (eluent: *n*-hexane 9/EtOAc 1), yielding 707 mg (61%) of a slightly yellow wax.  $^1\text{H}$  NMR ( $\text{CDCl}_3$ ):  $\delta$  (ppm) 1.51 (s, 9 H), 2.64 (s, 6 H), 3.90 (s, 2 H), 6.64 ( $S_{\text{broad}}$ , 1 H), 7.07 (d,  $J = 8.9$  Hz, 1 H), 7.30 (dd,  $J_1 = 8.9$  Hz,  $J_2 = 2.6$  Hz, 1 H), 7.31 (d,  $J = 2.6$  Hz, 1 H).  $^{13}\text{C}$  NMR ( $\text{CDCl}_3$ ):  $\delta$  (ppm) 28.4, 39.3, 45.7, 80.3, 118.7, 120.8, 121.3, 133.6, 134.0, 148.5, 153.0.  $\text{C}_{28}\text{H}_{42}\text{N}_4\text{O}_4\text{S}_2$  (562.8) calcd %: C 59.76, H 7.52, N 9.96, S 11.39, found %: C 59.86, H 7.60, N 9.47, S 11.40.

**[4-(Dimethylamino)-3-(pyridin-2-yl)disulfanylmethyl]phenyl]carbamic Acid *tert*-Butyl Ester (7).** Disulfide **6** (707 mg, 1.25 mmol) was dissolved in dimethoxyethane (50 mL) containing water (2 mL) and tributylphosphine (1 equiv). This mixture was then added dropwise to a solution of 2,2'-dithiopyridine (551 mg, 2 equiv) in dimethoxyethane and stirred for 3 h. After evaporation, the residue was dissolved in EtOAc, washed with water and brine, and dried over  $\text{MgSO}_4$ . The product was purified by silica gel chromatography (eluent: *n*-hexane 8/EtOAc 2), yielding 456 mg (93%) of a slightly yellow oil. MS (ES-MS) 414.1 ( $\text{M} + \text{Na}^+$ ).  $^1\text{H}$  NMR ( $\text{CDCl}_3$ ):  $\delta$  (ppm) 1.50 (s, 9 H), 2.66 (s, 6 H), 4.13 (s, 2 H), 6.44 ( $S_{\text{broad}}$ , 1 H), 7.02 (dd,  $J_1 = 8.3$  Hz,  $J_2 = 2.5$  Hz, 1 H), 7.07 (d,  $J = 8.3$  Hz, 1 H), 7.22 (d,  $J = 2.5$  Hz, 1 H), 7.28 (m, 1 H), 7.56 (ddd,  $J_1 = 8.1$  Hz,  $J_2 = 7.3$  Hz,  $J_3 = 1.8$  Hz, 1 H), 7.67 (d,  $J = 8.1$  Hz), 8.43 (d,  $J = 4.7$  Hz, 1 H).  $^{13}\text{C}$  NMR ( $\text{CDCl}_3$ ):  $\delta$  (ppm) 28.3, 40.0, 45.7, 80.3, 119.1, 119.4, 120.3, 121.2, 132.7, 134.2, 136.8, 148.5, 149.2, 152.8, 160.7.  $\text{C}_{19}\text{H}_{25}\text{N}_3\text{O}_2\text{S}_2$  (391.5) calcd %: C 58.29, H 6.43, N 10.73, S 16.38, found %: C 58.47, H 6.55, N 10.18, S 15.92.

**4-(Dimethylamino)-3-(pyridin-2-yl)disulfanylmethyl]benzenediazonium (DABD-Pys) (8).** The aromatic amine of compound **7** (66 mg, 168  $\mu\text{mol}$ ) was deprotected in trifluoroacetic acid (2 mL) for 15 min. The mixture was cooled to  $-10^\circ\text{C}$  and sodium nitrite (1.1 equiv) dissolved in water (100  $\mu\text{L}$ ) was added dropwise. The solution was evaporated to dryness yielding aryl-diazonium **8**, which was further used without purification. MS (ES-MS):  $\text{M} = 303.1$  [ $\text{C}_{14}\text{H}_{15}\text{N}_4\text{S}_2$  (303.4)].  $^1\text{H}$  NMR ( $\text{CD}_3\text{OD}$ ):  $\delta$  (ppm) 3.33 (s, 6 H), 4.28 (s, 2 H), 6.86 (d,  $J = 9.6$  Hz), 7.22 (m, 1 H), 7.61 (d,  $J = 8.1$  Hz, 1 H), 7.74 (ddd,  $J_1 = 8.0$  Hz,  $J_2 = 7.46$  Hz,  $J_3 = 1.8$  Hz, 1 H), 7.92 (dd,  $J_1 = 9.6$  Hz,  $J_2 = 2.6$  Hz, 1 H), 8.08 (d,  $J = 2.6$  Hz, 1 H), 8.34 (d,  $J = 4.2$  Hz, 1 H).  $^{13}\text{C}$  NMR ( $\text{CD}_3\text{OD}$ ):  $\delta$  (ppm) 43.4, 44.4, 119.0, 122.7, 123.0, 126.0, 133.2, 138.6, 139.4, 150.2, 160.2, 160.6. UV:  $\lambda_{\text{max}} = 391$  nm,  $\epsilon = 25\,000$   $\text{M}^{-1}\cdot\text{cm}^{-1}$ .

**[4-Azido-2-(pyridin-2-yl)disulfanylmethyl]phenyl]-dimethylamine (9).** Sodium azide (1.1 equiv), in solu-

tion in water, was added to diazonium **8**, dissolved in water brought to pH 8 with sodium hydrogenocarbonate. The mixture was extracted with dichloromethane, and the organic phases were concentrated. Azido **9** was purified by silica gel chromatography (eluent: *n*-hexane 9/EtOAc 1) with an overall yield of 85%. MS (DCI):  $m/z = 318$  [ $\text{C}_9\text{H}_{10}\text{N}_2\text{O}_4$  (317.4)].  $^1\text{H}$  NMR ( $\text{CDCl}_3$ ):  $\delta$  (ppm) 2.67 (s, 6 H), 4.14 (s, 2 H), 6.84 (dd,  $J_{\text{ortho}} = 8.5$  Hz,  $J_{\text{meta}} = 2.5$  Hz, 1 H), 6.97 (d,  $J_{\text{meta}} = 2.5$  Hz, 1 H), 7.02–7.07 (m, 1 H), 7.10 (d,  $J_{\text{ortho}} = 8.5$  Hz, 1 H), 7.52–7.62 (m, 2 H), 8.44 (d,  $J = 4.6$  Hz).  $^{13}\text{C}$  NMR ( $\text{CDCl}_3$ ):  $\delta$  (ppm) 39.7, 45.5, 119.0, 119.5, 120.4, 121.2, 121.8, 133.8, 135.1, 136.7, 149.4, 150.2, 160.2. UV:  $\lambda_{\text{max}} = 253$  nm,  $\epsilon = 30\,000$   $\text{M}^{-1}\cdot\text{cm}^{-1}$ .

**Coupling of DABD-Pys (8) or Its Azido Derivative 9 to R33C.** A solution of 0.7 mg (0.1  $\mu\text{mol}$ ) of toxin analogue in 200  $\mu\text{L}$  of 500 mM sodium acetate buffer (pH 4.5)/EDTA 2.5 mM was mixed with 10 equiv of DABD-Pys (**8**) under rapid stirring. For the less water soluble azido derivative **9**, the coupling reaction was carried out in a 1:1 mixture of ethanol and sodium phosphate buffer (100 mM, pH 8). The mixture was allowed to stand at room temperature for 30 min. The toxin derivative was then purified according to the HPLC conditions described above and checked by electrospray mass spectrometry.  $M_{\text{calcd}}$  ( $\text{R33C} - \text{ArN}_2^+$ ) = 6926.01,  $M_{\text{found}} = 6897.65$  ( $M_{\text{calcd}} - \text{N}_2$ );  $M_{\text{calcd}}$  ( $\text{R33C} - \text{ArN}_3$ ) = 6940.02,  $M_{\text{found}} = 6939.36$ . UV:  $\lambda_{\text{max}}$  ( $\text{R33C} - \text{ArN}_2^+$ ) = 391 nm,  $\epsilon_{391}$  ( $\text{R33C} - \text{ArN}_2^+$ ) = 25 000  $\text{M}^{-1}\cdot\text{cm}^{-1}$ ;  $\lambda_{\text{max}}$  ( $\text{R33C} - \text{ArN}_3$ ) = 253 nm,  $\epsilon_{253}$  ( $\text{R33C} - \text{ArN}_3$ ) = 26 600  $\text{M}^{-1}\cdot\text{cm}^{-1}$ .

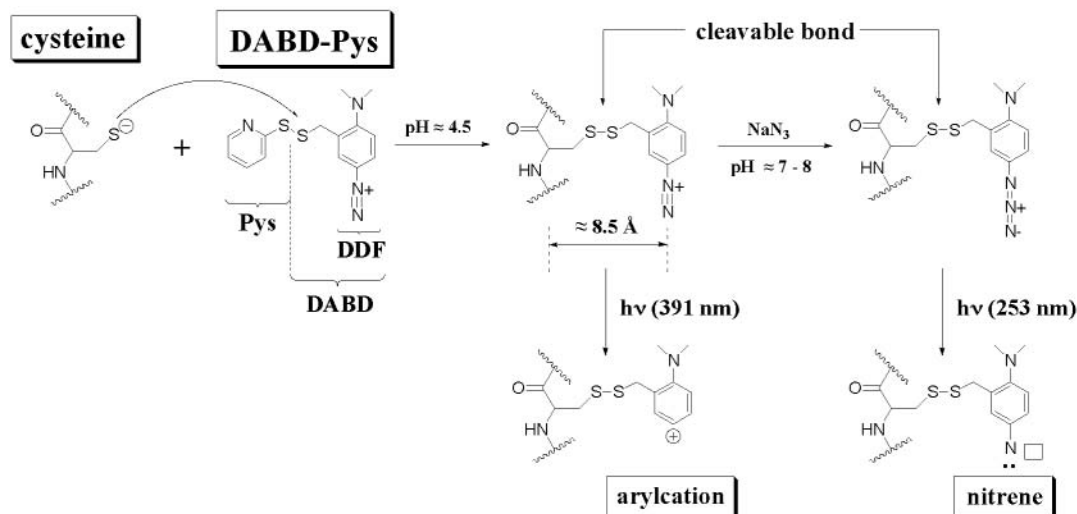
**Preparation of nAChR-Rich Membranes.** nAChR-rich membranes from the electric tissue of *Torpedo marmorata* were prepared as previously described (28) and were further purified by alkali treatment (29). The concentration of acetylcholine binding sites was typically between 2.5 and 3.5 nmol per mg of proteins.

**Binding Assay.** Competition experiments between  $\alpha$ -neurotoxin analogues and [ $^{125}\text{I}$ ]- $\alpha$ -bungarotoxin were performed as previously described (30). Equilibrium dissociation constants were determined according to Cheng and Prusoff (31).

**Photolabeling Experiment.** Alkali-treated membranes (2.4  $\mu\text{M}$   $\alpha$ -bungarotoxin sites) were incubated in Tris-HCl 10 mM, pH 7.6, NaCl 10 mM at  $4^\circ\text{C}$ , in the dark, for 2 h with 1 equiv of photoactivatable toxin analogue, or native  $\alpha$ -neurotoxin as a control. After equilibrium, the mixture was irradiated at 391 nm (10  $\mu\text{W}\cdot\text{cm}^{-2}$ ) for 30 min, at  $15^\circ\text{C}$ , under stirring in a quartz cuvette. The dimensions of the light beam were approximately 2 mm  $\times$  12 mm. For protection experiments, the membranes were incubated with 10 equiv of wild-type toxin, at room temperature for 1 h, before adding the photoactivatable probe. Following irradiation, the membrane suspension was centrifuged at 22 000g, for 15 min, at  $4^\circ\text{C}$ , and the pellets were solubilized in Na-DodSO<sub>4</sub> sample buffer, with or without  $\beta$ -mercaptoethanol, for gel electrophoresis (32).

**Modification of the Labeled Receptor Residue(s) with [ $^3\text{H}$ ]-*N*-Ethylmaleimide.** Alkali-treated *Torpedo* membranes (1.3 nmol of toxin binding sites) were first reduced with 5 mM DTT, for 30 min, at room temperature, under argon in degassed sodium phosphate buffer (100 mM, pH 7.8, 210  $\mu\text{L}$  final volume). The receptor was then incubated, under argon, in degassed sodium phosphate buffer (100 mM, pH 8, 420  $\mu\text{L}$  final volume) containing 20 mM iodoacetamide, for 1 h, at room temperature. The sample was centrifuged at 22 000g, for 15 min, at  $4^\circ\text{C}$ . The pellet was washed twice with buffer A (10 mM Tris/HCl pH 7.6, 10 mM NaCl; 420  $\mu\text{L}$



**Scheme 1. General Coupling Scheme of DABD-Pys with a Cysteinyll Residue**

final volume). For photolabeling experiments, the receptor (2.4  $\mu\text{M}$  of toxin binding sites) was mixed with 1 equiv of photoactivatable toxin analogue in buffer A, for 30 min, at room temperature, in the dark. After equilibrium, the mixture was irradiated at 391 nm (50  $\mu\text{W}\cdot\text{cm}^{-2}$ ) for 5 min, at 10 °C. For protection experiments, the membranes were first incubated with 10 equiv of wild-type toxin, at room temperature, for 1 h, before adding the photoactivatable probe. Following irradiation, the membrane suspension was centrifuged at 22 000g, for 15 min, at 4 °C, and the pellet solubilized in degassed sodium phosphate buffer (100 mM, pH 7.8, 1120  $\mu\text{L}$  final volume) containing 5 mM DTT. After 30 min at room temperature, the sample was centrifuged as described above. The supernatant was removed, and the pellet was washed with degassed buffer B (100 mM sodium phosphate buffer, pH 7). The reduced receptor was finally incubated with 20  $\mu\text{M}$  [<sup>3</sup>H]-*N*-ethylmaleimide (1 Ci·mmol<sup>-1</sup>) in buffer B (1120  $\mu\text{L}$  final volume), for 1 h, at room temperature. After centrifugation, the pellet was washed with buffer B to eliminate excess of [<sup>3</sup>H]-*N*-ethylmaleimide and finally resuspended in 560  $\mu\text{L}$  of Laemmli buffer containing 240 mM of  $\beta$ -mercaptoethanol.

**SDS-PAGE and Immunoblots.** SDS-PAGE and immunoblot experiments were achieved as previously described (26).

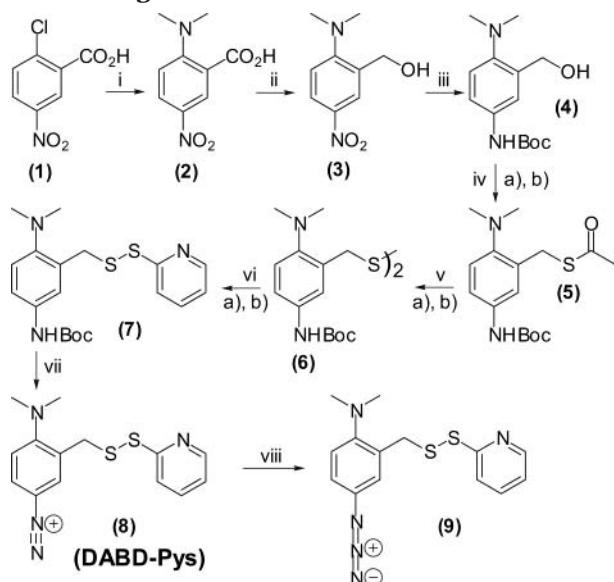
## RESULTS AND DISCUSSION

Many photoaffinity labeling experiments have been carried out during these past two decades, especially between nAChR and various photoactivatable snake curarimimetic toxins (2–12). However, the low yield of labeling, the difficulty to purify the labeled subunits on polyacrylamide gel electrophoresis, due to the overlay of some labeled subunits with other nonlabeled protein bands, the multiplicity of labeled peptides after proteolysis due to partial cleavages on the target protein times partial cleavages on the peptidic ligand, and some loss of radioactivity during proteolysis prevented almost always the characterization of the receptor labeled residues. To overcome some of these drawbacks and facilitate the analysis, we decided to develop a novel photoactivatable probe, belonging to a family of photosensitive moieties never coupled to peptides or proteins and which can be easily linked to a cysteine residue on a peptidic ligand through a short and cleavable disulfide bond. In this study, we used a previously described

analogue of *Naja nigricollis*  $\alpha$ -neurotoxin (26) as the cysteine-harboring ligand model (Figure 1).

**Choice of the Photoactivatable Probe.** Most of the photoactivatable probes that have been previously coupled to snake  $\alpha$ -neurotoxins were hydrophobic azido or diazirine moieties generating nitrenes, or carbenes, respectively (2–12). These derivatives were obtained by mono-modification of natural toxins on accessible lysinyl residues, leading to a loss of a positive charge for a hydrophobic entity and a lengthening of the amino acid side chain. Another drawback of this procedure is that it sets a priori the possible modification areas of the toxins. Up to now, the only experiment which led to the identification of the photolabeled residue on the nAChR was made with a photoprobe linked to the toxin through a cleavable disulfide bond (9). Therefore, following the automated synthesis of *Naja nigricollis*  $\alpha$ -neurotoxin analogues bearing a free cysteine (26), we decided to design a novel short bifunctional photoprobe (Scheme 1), which would be coupled to cysteinyl residues through a cleavable disulfide bond and which harbors a positive charge. We chose the aryldiazonium photosensitive moiety, used earlier in photolabeling experiments of cholinergic proteins with small organic molecules (18, 20, 33–39). Thus, it was previously shown that despite its low affinity for the nAChR ( $K_{\text{app}} = 1.5$  mM), the small antagonist DDF (*N*-dimethylaminobenzene diazonium fluoroborate) was the most efficient photoprobe (36), with a 60% specific covalent incorporation, never reached by any photoaffinity reagent on this receptor. Actually, the aryldiazonium moiety can be activated to a highly reactive arylation (lifetime < 0.5 ns) (40), under UV irradiation, which is safe for proteins (between 300 and 400 nm) (1).

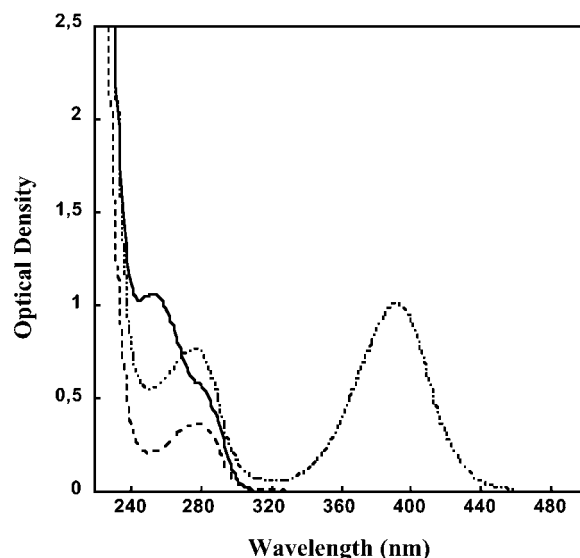
We therefore developed an analogue of DDF (Scheme 2) harboring a disulfide bond (DABD-Pys for 4-dimethylamino-3-(pyridin-2-yl)disulfenylmethyl)benzene diazonium), allowing modification of a site-specifically introduced cysteinyl residue on the toxin, by disulfide exchange (Scheme 1). After the photolabeling experiment, this linkage permits the release of the toxin at will, using a standard reducing treatment (DTT or  $\beta$ -mercaptoethanol), hence avoiding the “dilution” of the labeling in multiple overlapping peptides, related to partial cleavages of the toxin during proteolysis of the photolabeled subunit(s). This reduction introduced a free sulfhydryl on the labeled position(s), which may then be selectively

**Scheme 2. Synthetic Scheme of DABD-Pys and Its Azido Analogue<sup>a</sup>**

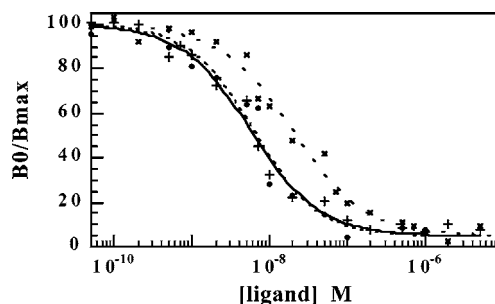
<sup>a</sup> Reagents and conditions: (i)  $\text{K}_2\text{CO}_3$ ,  $\text{HNMe}_2/\text{THF}$ ,  $120^\circ\text{C}$ ; (ii)  $\text{BH}_3\text{-THF}$ ; (iii)  $\text{H}_2$ ,  $\text{Pd/C}$ ,  $\text{Boc}_2\text{O}$ ,  $\text{MeOH}$ ; (iv) (a)  $\text{CH}_3\text{SO}_2\text{Cl}$ ,  $\text{Et}_3\text{N}$ ,  $\text{THF}$ , (b)  $\text{CH}_3\text{COSH}/\text{Et}_3\text{N}$ ,  $\text{THF}$ ; (v) (a)  $\text{NaOEt}$ ,  $\text{MeOH}$ , (b)  $\text{I}_2$ ,  $\text{MeOH}$ ; (vi) (a)  $\text{PBu}_3$ ,  $\text{DME}/\text{H}_2\text{O}$ , (b)  $\text{Pys}_2$ ; (vii)  $\text{TFA}$ ,  $\text{NaNO}_2$ ; (viii)  $\text{NaN}_3$ .

modified with commercially available thiol-reactive radioactive compounds. This advantage should avoid the synthesis of a radioactive bifunctional photoprobe. In contrast to previous toxin derivatizations (2–12), the replacement of a critical lysine or arginine residue by a cysteinyl-DABD moiety conserves the positive charge, at approximately the same distance from the toxin backbone (Scheme 1), leading to the shortest linker (8.5 Å) between the toxin and the photoactivatable moiety ever obtained. Moreover, a site-directed introduction of a photoprobe can be achieved anywhere on the ligand where the replacement of a native residue by a cysteine does not prevent proper folding of the toxin (30).

**Coupling of the Photoprobe to the Toxin Analogue.** Coupling of a cysteinyl residue to DABD-Pys must be accomplished at slightly acidic pH. This photoprobe possesses two electrophilic moieties, a sulfur atom coupled to the thiopyridyl group, introduced for the disulfide exchange, and a diazonium salt, which is known to react rapidly with thiolates (41). Nevertheless, no attack on the diazonium moiety occurred at pH 4.5, when using 1 equiv or less of sulfhydryl, only the expected disulfide exchange occurred. Increasing the pH reversed this tendency, and adding more than 1 equiv of thiol, destroyed the aryldiazonium salt (data not shown). Therefore, it is possible to introduce a short cleavable photoactivatable aryldiazonium group into proteins, providing that they harbor a free cysteine and that they are stable enough in moderately acidic conditions. In addition, the DABD moiety harbors a dual functionality because treatment of DABD-Pys, or the ligand-coupled probe, with sodium azide leads to the azido analogue (Scheme 1), which becomes thus a short, hydrophobic, cleavable, photoactivatable probe, precursor of a nitrene. Therefore, following the reaction of DABD-Pys with the ligand, both the charged hydrophilic aryldiazonium ion and the uncharged hydrophobic azido probe can easily be obtained (Scheme 1). Interestingly, arylazido compounds are more stable than aryldiazonium salts in the presence of thiols. Hence, the sulfhydryl exchange reaction with the peptidic ligand can be achieved at physiological pH,



**Figure 2.** UV/visible spectra of R33C, R33C-DABD, and its azido analogue. The spectra were taken in water. The derivatives were diluted at the same concentration (40  $\mu\text{M}$ ). R33C (dashed line), R33C-DABD (dotted line), azido analogue (continuous line).



**Figure 3.** Equilibrium binding of wild-type  $\alpha$ -neurotoxin and its analogues to muscular-type nAChR. Competition experiments with nAChR from *T. marmorata* (0.7 nM toxin-binding sites) were performed at equilibrium, using [ $^{125}\text{I}$ ]- $\alpha$ -bungarotoxin (9 nM) as a radioactive tracer. The lines correspond to theoretical concentration responses fitted through the data points using the nonlinear Hill equation. Wild-type toxin (+, continuous line), R33C (x, dashed line) and R33C-DABD (•, dotted line).

without any attack on the photosensitive moiety. Therefore, peptides or proteins, harboring a free sulfhydryl but unstable in mildly acidic media, may therefore be modified with the azido photoprobe (9) (Scheme 2).

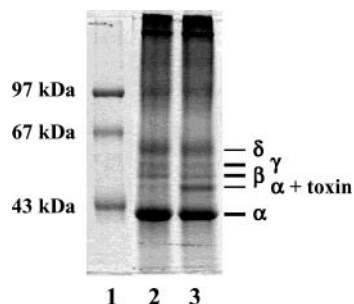
As  $\alpha$ -neurotoxins are fairly stable proteins, the R33C analogue of *Naja nigricollis* curarimimetic toxin (26) was coupled quantitatively to the DABD moiety at mildly acidic pH, leading to a photoactivatable toxin modified on a critical position (14) never explored before in photoaffinity labeling experiments (Figure 2). As expected, the maximum absorption wavelength (391 nm) of the coupled aryldiazonium salt is far above the protein absorption region, with a high molar extinction coefficient ( $25\,000\text{ M}^{-1}\cdot\text{cm}^{-1}$ ). Although we modified a critical residue of the toxic site, binding experiments showed that this new photosensitive toxin was a potent ligand of the nAChR under inactinic light, having a wild type-like affinity for the receptor (Figure 3, Table 1). Not unexpectedly, the presence of the aryldiazonium moiety increased the affinity of the R33C analogue, probably mimicking, at least for its positive charge, the native Arg33 residue which interacts in an aromatic pocket of the acetylcholine binding site (30, 42–44).

**Irradiation of the R33C-DABD/nAChR Complex.** To test the efficiency of this new photosensitive toxin

**Table 1. Inhibition Constants of *Naja nigricollis*  $\alpha$ -Neurotoxin Derivatives for *Torpedo marmorata* nAChR<sup>a</sup>**

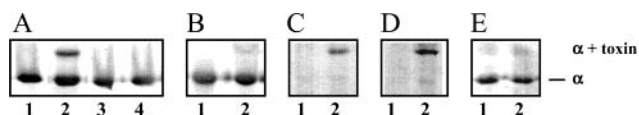
	K <sub>i</sub> (pM)	K <sub>i</sub> /K <sub>iwt</sub>
wild type	13 ± 2	1
R33C <sup>b</sup>	50 ± 13	3.8
R33C-DABD	14 ± 4	1

<sup>a</sup> Inhibition constants were obtained by competition at equilibrium against [<sup>125</sup>I]- $\alpha$ -bungarotoxin (9 nM) on *Torpedo marmorata* nAChR (0.7 nM toxin-binding sites). Values were estimated according to Cheng and Prusoff. Mean ± SE or standard errors for two or more measurements. K<sub>i</sub>: inhibition constant for toxin derivative; K<sub>iwt</sub>: inhibition constant for the wild-type toxin. <sup>b</sup> The numbering of the modified residue corresponds to erabutoxin numbering.



**Figure 4.** Coomassie-blue stained gel of nAChR after photolabeling with R33C-DABD. *Torpedo* membranes (2.4  $\mu$ M  $\alpha$ -bungarotoxin sites) were incubated with R33C-DABD (1 equiv) and irradiated at 391 nm for 30 min, at 15 °C (see Experimental Procedures). Following irradiation, the membrane suspension was centrifuged at 22 000g for 15 min at 4 °C, and the pellets were solubilized in NaDodSO<sub>4</sub> sample buffer and run on 10% SDS-PAGE. Lane 1: Weight markers; lane 2: nAChR irradiated in the absence of R33C-DABD; lane 3: nAChR irradiated in the presence of R33C-DABD.

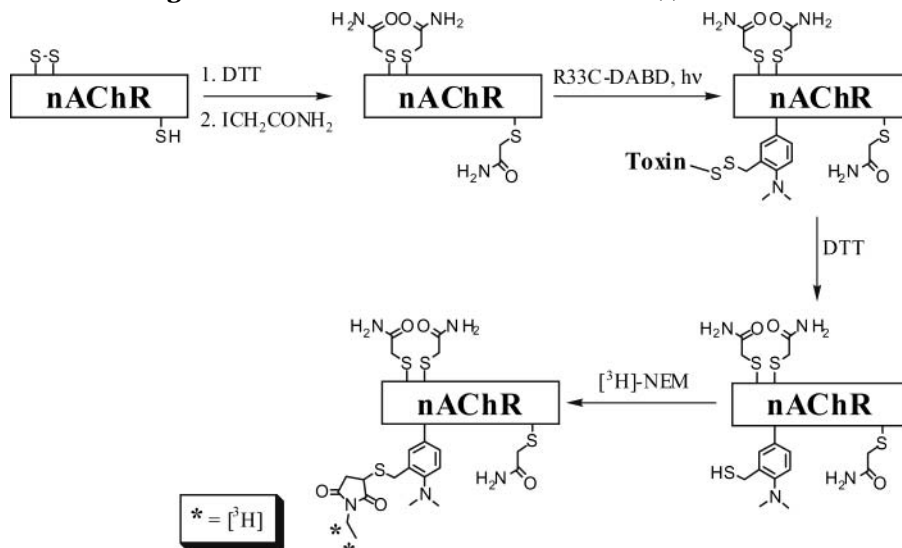
probe, we irradiated *Torpedo* membranes, at 391 nm, in the presence of the photoactivatable R33C-DABD ligand, and analyzed its covalent coupling to the  $\alpha$ -subunit of nAChR by polyacrylamide gel electrophoresis run in nonreducing conditions. A new band migrating close below the  $\beta$ -subunit, with a molecular weight of approximately 46 kDa can be observed on a Coomassie-blue stained gel (Figure 4). This apparent molecular weight fits with the sum of one  $\alpha$ -subunit (39 kDa) coupled to a toxin molecule (7 kDa). This band was not observed when



**Figure 5.** Specificity of labeling demonstrated by immunoblot experiments. SDS-PAGE experiment were run in nonreducing conditions in A and B (visualization of the receptor  $\alpha$ -subunit with mAb155), C (visualization of the toxin with a horse serum directed against the venom), and D (visualization of the toxin with the monoclonal antibody M $\alpha$ 1), and in reducing conditions in E (visualization of the receptor  $\alpha$ -subunit with mAb155). A: "protection experiment". Lane 1: nAChR irradiated in the absence of R33C-DABD; lane 2: nAChR irradiated in the presence of R33C-DABD (1 equiv); lane 3: nAChR preincubated with 10 equiv of wild-type toxin and irradiated in the absence of R33C-DABD; lane 4: nAChR preincubated with 10 equiv of wild-type toxin and irradiated in the presence of R33C-DABD (1 equiv). B: Nonirradiated control. Lane 1: nonirradiated nAChR without R33C-DABD; lane 2: nonirradiated nAChR incubated with R33C-DABD (1 equiv). C: lane 1: nAChR irradiated in the absence of R33C-DABD; lane 2: nAChR irradiated in the presence of R33C-DABD (1 equiv). D: lane 1: nAChR irradiated in the absence of R33C-DABD; lane 2: nAChR irradiated in the presence of R33C-DABD (1 equiv). E: Disulfide-bond-cleavage control (reducing conditions). Lane 1: nAChR irradiated in the absence of R33C-DABD; lane 2: nAChR irradiated in the presence of R33C-DABD (1 equiv).

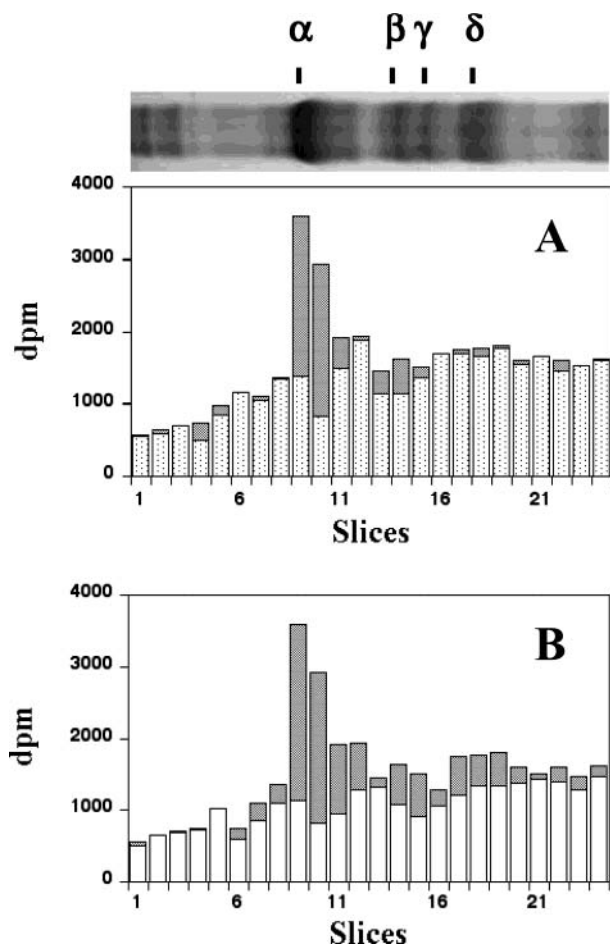
the receptor-toxin complex was not irradiated (Figure 5B). The labeling specificity was demonstrated by immunoblot experiments with (i) a specific antibody directed against the receptor  $\alpha$ -subunit (mAb155) (45) (Figure 5A), (ii) a horse serum directed against the whole venom (26) (Figure 5C), and (iii) a specific antibody directed against the  $\alpha$ -neurotoxin (M $\alpha$ 1) (46) (Figure 5D) which all revealed the presence of a 46 kDa band. This band disappeared also when the gel was run in reducing conditions (Figure 5E), as anticipated from the cleavage of the disulfide bond linking the toxin to the receptor through the irradiated DABD probe. Labeling of the receptor could be totally inhibited by prior incubation of the *Torpedo* membranes with an excess of wild-type toxin, further demonstrating the specificity of the photolabeling (Figure 5A). Interestingly, immunoblot experiments, with antibodies directed against each subunit, showed that labeling was restricted to the  $\alpha$ -subunit (data not shown), confirming previous reports, showing that Arg33 of short neurotoxins interacts with  $\alpha$ -Val188 (27), and was located close to  $\alpha$ -Cys192 and/or  $\alpha$ -Cys193

### Scheme 3. Radioactive Labeling Procedure of the Photolabeled Residue(s) of the nAChR<sup>a</sup>



<sup>a</sup> DTT: dithiothreitol; NEM: *N*-ethylmaleimide.





**Figure 6.** [ $^3\text{H}$ ]-*N*-Ethylmaleimide labeling pattern. The reduced photolabeled receptor was alkylated with [ $^3\text{H}$ ]-*N*-ethylmaleimide (20  $\mu\text{M}$ , 1 Ci $\cdot\text{mmol}^{-1}$ ) and run on a SDS-PAGE 10% gel, under reducing conditions. The gel was then cut in 1 mm slices which were counted on a rackbeta scintillation counter (Amersham). The sliced area of the gel is shown above the labeling histograms. Positions of the four subunits of the nAChR are indicated above the gel. A: Control experiment with native toxin. Grey bars: nAChR irradiated in the presence of R33C-DABD (1 equiv) before the reduction and radioactive labeling steps. Dotted bars: nAChR irradiated in the presence of wild-type toxin (1 equiv) before the reduction and radioactive labeling steps. B: Protection experiment. Grey bars: nAChR irradiated in the presence of R33C-DABD (1 equiv) before the reduction and radioactive labeling steps. White bars: nAChR preincubated with wild-type toxin (10 equiv) and irradiated in the presence of R33C-DABD (1 equiv) before the reduction and radioactive labeling steps.

(26). The coupling yield as assessed by gel densitometry on the Coomassie-blue stained gel was close to 10%. This is one of the highest yields obtained with photoactivatable toxin analogues, although it is still rather far from the 60% incorporation into the nAChR, observed with DDF. One major reason for this situation could be that the affinity of DDF for the nicotinic receptor was mainly due to the positive charge of the aryldiazonium. Since the nAChR/DDF complex was irradiated under tryptophan energy transfer conditions (36), the photoprobe was essentially activated in the tryptophanyl-rich acetylcholine binding site. Presumably, therefore, under these conditions, and due to the low affinity of DDF for the receptor, the medium was a huge reservoir of "fresh" photoprobe, which could replace the photoadduct that was not coupled to the nAChR, until total consumption of DDF. In contrast, the quasi-irreversible binding of snake curarimimetic toxins leads to a stoichiometric ratio of ligand to receptor, which is ideal for specific labeling,

but the probes which did not couple to the receptor could not be replaced by nonirradiated toxin analogues to further enhance the labeling yield, as did DDF.

To compare the ability of nitrenes and arylation to photolabel the nicotinic receptor, photolabeling experiments were also carried out with the azido derivative. In this case, labeling could only be detected by immunoblots (data not shown), indicating a lower efficiency of the azido moiety as compared to the aryldiazonium salt at least at position 33 of the toxin. Aryldiazonium salts are potentially able to couple to all types of amino acids. However, they show a clear preference for aromatic residues (1). In recent models of interaction between nAChR and  $\alpha$ -neurotoxins, it has been shown that the arginine residue in this position penetrates into an aromatic cage of the acetylcholine binding site (42–44). In contrast to the azido analogue, DABD could "mimick" the arginine residue, through its positive charge, and would then react in its preferred labeling environment.

**Radioactive Modification of the Labeled Residue(s).** A radioactive tag ( $^3\text{H}$  or  $^{125}\text{I}$ ) is mostly used to locate (i) the labeled peptide(s) after proteolysis of the photolabeled protein and (ii) the labeled residue(s) during sequencing of the isolated peptide(s). Since this radioactive tag is part of the photoprobe, it necessitates an adapted synthesis that allows introduction of tritium or  $^{125}\text{I}$ , preferably on the last step of the synthesis. Such a synthesis of a radioactive azido photoprobe, also tethered to cysteine residues through a disulfide bond, has been therefore described recently (47). However, the distance between the cysteine  $\alpha$ -carbon and the photoreactive atom in this compound ( $\sim 12 \text{ \AA}$ ) was longer than in our probe (8.5  $\text{\AA}$ ), decreasing the geometrical resolution around the site of cross-linking. We avoided the synthesis of a radioactive DABD molecule, taking advantage of the cleavable disulfide bond, present between the photolabeled nAChR and the toxin, to introduce a commercially available sulfhydryl-reactive tritiated label. This strategy was possible, since the nAChR could be reduced and alkylated without affecting afterward toxin binding (48). We thus pretreated *Torpedo* membranes, in the absence of toxin, with a low concentration of dithiothreitol and reacted thereafter all the sulfhydryls with iodoacetamide, alkylating thus all the free thiols and reducible disulfide bonds of the receptor (Scheme 3). Hence, following the photolabeling experiment made between this pretreated receptor and R33C-DABD, we could selectively reduce the toxin and the disulfide bond linking it to the receptor. The newly introduced thiol on the nAChR was then reacted with tritiated *N*-ethylmaleimide. We thus got rid of the toxin and introduced radioactivity on the receptor photolabeled residue(s). Even if this preliminary experiment still needs some improvement to lower the radioactive background by using for instance a highly purified receptor, or by adapting the various reducing and labeling conditions, it seems very promising as the  $\alpha$ -subunit represents, on the gel-slices, the main subunit which was specifically labeled by [ $^3\text{H}$ ]-*N*-ethylmaleimide (Figure 6), in agreement with immunoblot experiments (Figure 5). Furthermore, this specific labeling disappeared when native  $\alpha$ -neurotoxin was used in place of R33C-DABD (Figure 6A) or when the nAChR toxin-binding sites were already occupied by native  $\alpha$ -neurotoxin before photoirradiation in the presence of R33C-DABD (Figure 6B).

In conclusion, the novel short cleavable photoprobe, described in this paper, has been shown (i) to couple quantitatively to a cysteinyl residue of a protein, (ii) to efficiently link the peptidic ligand to its target through photoaffinity labeling, and (iii) to allow radioactive label-

ing of the photocoupled residue(s) with a commercially available molecule, avoiding chemical synthesis of a radioactive photoprobe. We have thus converted photolabeling of a membrane receptor with a soluble protein to a classical labeling with a small organic molecule, rendering the future identification of the labeled amino acid(s) easier. This photoprobe also allows photolabeling experiments with an azido derivative, which was however, in this case, less efficient than the aryldiazonium salt. We are currently trying to improve the radioactive labeling background, by developing a photoactivatable toxin harboring a biotinylated moiety on its N-terminus, which could help to prepurify the labeled subunits, before cleavage of the disulfide bond.

#### ACKNOWLEDGMENT

We thank Dr. Tzartos for a generous gift of monoclonal antibodies directed against each nAChR subunit, and Sébastien Vanneste for technical support.

#### LITERATURE CITED

- (1) Kotzby-Hibert, F., Kapfer, I., and Goeldner, M. (1995) Recent trends in photoaffinity labeling. *Angew. Chem., Int. Ed. Engl.* **34**, 1296–1312.
- (2) Hucho, F. (1979) Photoaffinity derivatives of  $\alpha$ -*Naja naja siamensis* toxin. *FEBS Lett.* **103**, 27–32.
- (3) Witzemann, V., Muchmore, D., and Raftery, M. A. (1979) Affinity-directed cross-linking of membrane-bound acetylcholine receptor polypeptides with photolabile  $\alpha$ -bungarotoxin derivatives. *Biochemistry* **18**, 5511–5518.
- (4) Ovchinnikov, Y., Grishin, E., and Tsetlin, V. (1984) Photoactivatable neurotoxins in studying membrane receptors. *Tetrahedron* **40**, 521–528.
- (5) Chatrenet, B., Trémeau, O., Bontemps, F., Goeldner, M. P., Hirth, C. G., and Ménez, A. (1990) Topography of toxin-acetylcholine receptor complexes by using photoactivatable toxin derivatives. *Proc. Natl. Acad. Sci. U.S.A.* **87**, 3378–3382.
- (6) Kreienkamp, H. J., Utkin, Y. N., Weise, C., Machold, J., Tsetlin, V. I., and Hucho, F. (1992) Investigation of ligand-binding sites of the acetylcholine receptor using photoactivatable derivatives of neurotoxin II from *Naja naja oxiana*. *Biochemistry* **31**, 8239–44.
- (7) Hervé, M., Pillet, L., Humbert, P., Trémeau, O., Ducancel, F., Hirth, C., and Ménez, A. (1992) Role and environment of the conserved Lys27 of snake curaremimetic toxins as probed by chemical modifications, site-directed mutagenesis and photolabeling experiments. *Eur. J. Biochem.* **208**, 125–131.
- (8) Machold, J., Weise, C., Utkin, Y., Tsetlin, V., and Hucho, F. (1995) The handedness of the subunit arrangement of the nicotinic acetylcholine receptor from *Torpedo californica*. *Eur. J. Biochem.* **234**, 427–430.
- (9) Machold, J., Utkin, Y., Kirsch, D., Kaufmann, R., Tsetlin, V., and Hucho, F. (1995) Photolabeling reveals the proximity of the  $\alpha$ -neurotoxin binding site to the M2 helix of the ion channel in the nicotinic acetylcholine receptor. *Proc. Natl. Acad. Sci. U.S.A.* **92**, 7282–7286.
- (10) Machold, J., Weise, C., Utkin, Y. N., Franke, P., Tsetlin, V. I., and Hucho, F. (1995) A new class of photoactivatable and cleavable derivatives of neurotoxin II from *Naja naja oxiana*. Synthesis, characterisation, and application for affinity labeling of the nicotinic acetylcholine receptor from *Torpedo californica*. *Eur. J. Biochem.* **228**, 947–954.
- (11) Utkin, Y. N., Krivoshein, A. V., Davydov, V. L., Kasheverov, I. E., Franke, P., Maslennikov, I. V., Arseniev, A. S., Hucho, F., and Tsetlin, V. I. (1998) Labeling of *Torpedo californica* nicotinic acetylcholine receptor subunits by cobratoxin derivatives with photoactivatable groups of different chemical nature at Lys23. *Eur. J. Biochem.* **253**, 229–235.
- (12) Kasheverov, I., Zhmak, M., Chivilyov, E., Saez-Brionez, P., Utkin, Y., Hucho, F., and Tsetlin, V. (1999) Benzophenone-type photoactivatable derivatives of alpha-neurotoxins and alpha-conotoxins in studies on *Torpedo* nicotinic acetylcholine receptor. *J. Recept. Signal Trans. Res.* **19**, 559–571.
- (13) Endo, T., and Tamiya, N. (1991) Structure–function relationships of postsynaptic neurotoxins from snake venoms in *Snake Toxins* (Harvey, A. L., Ed.) pp 165–222, Pergamon Press, Inc., New York.
- (14) Pillet, L., Trémeau, O., Ducancel, F., Drevet, P., Zinn Justin, S., Pinkasfeld, S., Boulain, J.-C., and Ménez, A. (1993) Genetic engineering of snake toxins. Role of invariant residues in the structural and functional properties of a curaremimetic toxin, as probed by site-directed mutagenesis. *J. Biol. Chem.* **268**, 909–916.
- (15) Trémeau, O., Lemaire, C., Drevet, P., Pinkasfeld, S., Ducancel, F., Boulain, J.-C., and Ménez, A. (1995) Genetic engineering of snake toxins. The functional site of Erabutoxin a, as delineated by site-directed mutagenesis, includes variant residues. *J. Biol. Chem.* **270**, 9362–9369.
- (16) Ackermann, E. J., and Taylor, P. (1997) Nonidentity of the alpha-neurotoxin binding sites on the nicotinic acetylcholine receptor revealed by modification in alpha-neurotoxin and receptor structures. *Biochemistry* **36**, 12836–12844.
- (17) Kao, P. N., Dwork, J. A., Kaldany, J. R. R., Wideman, S. J., Stein, S., and Karlin, A. (1984) Identification of the  $\alpha$ -subunit half-cystine specifically labeled by an affinity reagent for the acetylcholine receptor binding site. *J. Biol. Chem.* **259**, 11662–11665.
- (18) Dennis, M., Giraudat, J., Kotzby-Hibert, F., Goeldner, M., Hirth, C., Chang, J. Y., Lazure, C., Chrétien, M., and Changeux, J. P. (1988) Amino acids of the *Torpedo marmorata* acetylcholine receptor  $\alpha$ -subunit labeled by a photoaffinity ligand for the acetylcholine binding site. *Biochemistry* **27**, 2346–2357.
- (19) Abramson, S. N., Li, Y., Culver, P., and Taylor, P. (1989) An analogue of lophotoxin reacts covalently with Tyr<sup>190</sup> in the  $\alpha$ -subunit of the nicotinic acetylcholine receptor. *J. Biol. Chem.* **264**, 12666–12672.
- (20) Galzi, J. L., Revah, F., Black, D., Goeldner, M., Hirth, C., and Changeux, J. P. (1990) Identification of a novel amino acid  $\alpha$ -tyrosine 93 within the cholinergic ligands-binding sites of the acetylcholine receptor by photoaffinity labeling. *J. Biol. Chem.* **265**, 10430–10437.
- (21) Middleton, R. E., and Cohen, J. B. (1991) Mapping of the acetylcholine binding site of the nicotinic acetylcholine receptor: [<sup>3</sup>H]-nicotine as an agonist photoaffinity label. *Biochemistry* **30**, 6987–6997.
- (22) Cohen, J. B., Sharp, S. D., and Liu, W. S. (1991) Structure of the agonist-binding site of the nicotinic acetylcholine receptor. *J. Biol. Chem.* **266**, 23354–23364.
- (23) Czajkowski, C., and Karlin, A. (1995) Structure of the nicotinic receptor acetylcholine-binding site. Identification of acidic residues in the  $\delta$  subunit within 0.9 nm of the  $\alpha$  subunit-binding site disulfide. *J. Biol. Chem.* **270**, 3160–3164.
- (24) Chiara, D. C., and Cohen, J. B. (1997) Identification of amino acids contributing to high and low affinity d-tubocurarine sites in the *Torpedo* nicotinic acetylcholine receptor. *J. Biol. Chem.* **272**, 32940–32950.
- (25) Chiara, D. C., Middleton, R. E., and Cohen, J. B. (1998) Identification of tryptophan 55 as the primary site of [<sup>3</sup>H]-nicotine photoincorporation in the  $\gamma$ -subunit of the *Torpedo* nicotinic acetylcholine receptor. *FEBS Lett.* **423**, 223–226.
- (26) Michalet, S., Teixeira, F., Gilquin, B., Mourier, G., Servent, D., Drevet, P., Binder, P., Tzartos, S., Ménez, A., and Kessler, P. (2000) Relative spatial position of a snake neurotoxin and the reduced disulfide bond  $\alpha$ (Cys192–Cys193) at the  $\alpha\gamma$  interface of the nicotinic acetylcholine receptor. *J. Biol. Chem.* **275**, 25608–25615.
- (27) Ackermann, E. J., Ang, E. T. H., Kanter, J. R., Tsigelny, I., and Taylor, P. (1998) Identification of pairwise interactions in the  $\alpha$ -neurotoxin-nicotinic acetylcholine receptor complex through double mutant cycles. *J. Biol. Chem.* **273**, 10958–10964.
- (28) Saitoh, T., Oswald, R., Wennogle, L. D., and Changeux, J. P. (1980) Conditions for the selective labeling of the 66 000 Dalton chain of the acetylcholine receptor by the covalent noncompetitive blocker 5-azido-[<sup>3</sup>H]-Trimethisoquin. *FEBS Lett.* **116**, 30–36.

- (29) Neubig, R. R., Krodell, E. K., Boyd, N. D., and Cohen, J. B. (1979) Acetylcholine and local anesthetic binding to *Torpedo* nicotinic postsynaptic membranes after removal of nonreceptor peptides. *Proc. Natl. Acad. Sci. U.S.A.* 76, 690–694.
- (30) Teixeira-Clerc, F., Ménéz, A., and Kessler, P. (2002) How do short neurotoxins bind to a muscular-type nicotinic acetylcholine receptor? *J. Biol. Chem.* 277, 25741–25747.
- (31) Cheng, Y. C., and Prusoff, W. H. (1973) Relationship between the inhibition constant (KI) and the concentration of inhibitor which causes 50% inhibition (I50) of an enzymatic reaction. *Biochem. Pharmacol.* 22, 3099–3108.
- (32) Laemmli, U. K. (1970) Cleavage of structural proteins during the assembly of the head of bacteriophage T4. *Nature* 227, 680–685.
- (33) Goeldner, M., and Hirth, C. (1980) Specific photoaffinity labeling induced by energy transfer: Application to irreversible inhibition of acetylcholinesterase. *Proc. Natl. Acad. Sci. U.S.A.* 77, 6439–6442.
- (34) Kieffer, B., Goeldner, M., and Hirth, C. (1981) Aryldiazonium salts as photoaffinity labeling reagents for proteins. *J. Chem. Soc., Chem. Commun.* 398–399.
- (35) Kotzyba-Hibert, F., Lagenbuch-Cachat, J., Jaganathan, J., Goeldner, M., and Hirth, C. (1985) Aryldiazonium salts as photoaffinity labels of the nicotinic acetylcholine receptor PCP binding site. *FEBS Lett* 182, 297–301.
- (36) Lagenbuch-Cachat, J., Bon, C., Mulle, C., Goeldner, M., Hirth, C., and Changeux, J. P. (1988) Photoaffinity labeling of the acetylcholine binding sites on the nicotinic receptor by an aryldiazonium derivative. *Biochemistry* 27, 2337–2345.
- (37) Ehret-Sabatier, L., Schalk, I., Goeldner, M., and Hirth, C. (1992) Photoaffinity labeling of cholinesterases. Discrimination between active and peripheral sites [published erratum appears in *Eur. J. Biochem.* (1992) 206, 995]. *Eur. J. Biochem.* 203, 475–481.
- (38) Harel, M., Schalk, I., Ehret-Sabatier, L., Bouet, F., Goeldner, M., Hirth, C., Axelsen, P. H., Silman, I., and Sussman, J. L. (1993) Quaternary ligand binding to aromatic residues in the active-site gorge of acetylcholinesterase. *Proc. Natl. Acad. Sci. U.S.A.* 90, 9031–9035.
- (39) Schalk, I., Ehret-Sabatier, L., Bouet, F., Goeldner, M., and Hirth, C. (1994) Trp279 is involved in the binding of quaternary ammonium at the peripheral site of *Torpedo marmorata* acetylcholinesterase. *Eur. J. Biochem.* 219, 155–159.
- (40) Scaiano, J., and Nguyen, K. (1983) Diazonium salts in photochemistry. III: Attempts to characterize aryl cations. *J. Photochem.* 23, 269–276.
- (41) Pütter, R. (1965) *Aryldiazosulfide und deren Derivate*, 4th ed., Georg Thieme Verlag, Stuttgart.
- (42) Harel, M., Kasher, R., Nicolas, A., Guss, J. M., Balass, M., Fridkin, M., Smit, A. B., Brejc, K., Sixma, T. K., Katchalski-Katzir, E., Sussman, J. L., and Fuchs, S. (2001) The binding site of acetylcholine receptor as visualized in the X-ray structure of a complex between alpha-bungarotoxin and a mimotope peptide. *Neuron* 32, 265–275.
- (43) Fruchart-Gaillard, C., Gilquin, B., Antil-Delbeke, S., Le Novère, N., Tamiya, T., Corringier, P. J., Changeux, J. P., Menez, A., and Servent, D. (2002) Experimentally based model of a complex between a snake toxin and the alpha 7 nicotinic receptor. *Proc. Natl. Acad. Sci. U.S.A.* 99, 3216–3221.
- (44) Moise, L., Piserchio, A., Basus, V. J., and Hawrot, E. (2002) NMR structural analysis of  $\alpha$ -bungarotoxin and its complex with the principal  $\alpha$ -neurotoxin binding sequence on the  $\alpha 7$  subunit of a neuronal nicotinic acetylcholine receptor. *J. Biol. Chem.* 277, 12406–12417.
- (45) Tzartos, S. J., and Remoundos, M. S. (1992) Precise epitope mapping of monoclonal antibodies to the cytoplasmic side of the acetylcholine receptor alpha subunit. Dissecting a potentially myasthenogenic epitope. *Eur. J. Biochem.* 207, 915–922.
- (46) Boulain, J.-C., Ménéz, A., Couderc, J., Faure, G., Liacopoulos, P., and Fromageot, P. (1982) Neutralizing monoclonal antibody specific for *Naja nigricollis* toxin  $\alpha$ : preparation, characterization and localization of the antigenic binding site. *Biochemistry* 21, 2910–2915.
- (47) Masckauchan, N., Delfino, J., and Fernandez, H. (1998) A new photoactivatable reagent capable of transferring a radiolabel to target proteins. Application to the human growth hormone-rat liver prolactin receptor interaction. *Bioconjugate Chem.* 9, 507–511.
- (48) Barrantes, F. J. (1980) Modulation of acetylcholine receptor states by thiol modification. *Biochemistry* 19, 2957–2965.
- (49) Zinn Justin, S., Roumestand, C., Gilquin, B., Bontems, F., Ménéz, A., and Toma, F. (1992) Three-dimensional solution structure of a curaremimetic toxin from *Naja nigricollis* venom. A proton NMR and molecular modeling study. *Biochemistry* 31, 11335–11347.

BC0256502



# Folate-Targeted PEG as a Potential Carrier for Carboplatin Analogs. Synthesis and in Vitro Studies

Olga Aronov,<sup>†</sup> Aviva T. Horowitz,<sup>‡</sup> Alberto Gabizon,<sup>‡</sup> and Dan Gibson<sup>\*,†,§</sup>

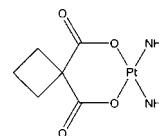
Department of Medicinal Chemistry and Natural Products, School of Pharmacy, P. O. Box 12065, The Hebrew University of Jerusalem, Jerusalem 91120, Israel, and Oncology Institute, Shaare Zedek Medical Center; Jerusalem, Israel. Received November 20, 2002; Revised Manuscript Received February 12, 2003

Like most low molecular weight drugs, carboplatin has a short blood circulation time, which reduces tumor uptake and intracellular DNA binding. Drugs conjugated to PEG carriers benefit from prolonged blood circulation, but suffer from reduced cell permeability. In this work we attempted to develop long-circulating PEGylated carboplatin analogues with improved cell permeation abilities, by conjugating the platinum moiety to folate-targeted PEG carriers capable of utilizing the folate receptor-mediated endocytosis (FRME). Two bifunctional FA-PEG conjugates, FA-PEG-Pt and FA-PEG-FITC, were prepared, and their cell uptake, DNA binding, and cytotoxicity were studied by fluorescent microscopy, FACS, and platinum analysis. Folate-targeted PEG conjugates enter the cells efficiently by the FRME pathway but form relatively few DNA adducts and have higher IC<sub>50</sub> values than carboplatin and their nontargeted analogues. Nontargeted PEG-Pt conjugates have a lower cellular uptake but produce higher levels of DNA binding and improved cytotoxicity. Carboplatin, used as a control, has the fastest cellular uptake, but after 16 h of postincubation a large percentage of the drug is excreted from the cells. The findings of this study suggest that folate-targeted conjugates such as FA-PEG-Pt, may not be an optimal prodrug for the carboplatin family compounds, because the conjugates or the active moieties are neutralized or blocked during the FRME process and do not manage to effectively reach the nuclear DNA.

## INTRODUCTION

Carboplatin [Pt(CBDCA-O,O')(NH<sub>3</sub>)<sub>2</sub>], where CBDCA is cyclobutane-1,1-dicarboxylate (Figure 1), is a second generation platinum anticancer drug, widely used for treatment of many types of cancer, including ovarian cancer, lung cancer, head and neck cancer, etc. (1–3). The antitumor effect of carboplatin is thought to be due to its interaction with DNA where the Pt(NH<sub>3</sub>)<sub>2</sub> moiety binds covalently to two adjacent guanines on the same strand (4). It is those Pt-DNA adducts that are believed to lead to the eventual death of the cancer cells. Due to the electrostatic effect and the chelate effect of the dicarboxylate ligand, the substitution kinetics of the Pt(II) complex are slow, rendering it quite inert. Therefore, the hydrolysis and direct platination of free DNA by carboplatin have been reported to be very slow (5, 6). Interestingly, when the level of DNA platination obtained upon exposure of Chinese hamster ovary cells to carboplatin was compared with platination levels of cell-free Salmon sperm DNA by carboplatin, it was reported that the former is 10 times more efficient (7). This indicates that carboplatin is more efficient in platinating DNA when exposed to some as yet unknown intracellular activation mechanisms.

Although carboplatin is highly efficient against many neoplasms, the drug has drawbacks that are related to its unfavorable pharmacokinetic properties. Like most



**Figure 1.** Carboplatin.

low molecular weight drugs, carboplatin has a short blood circulation time (8). The main route for the clearance of carboplatin from the body is through urinary excretion where 50% of the administered carboplatin is cleared within 24 h (9). This is a disadvantage especially due to the fact that the high intracellular levels of carboplatin, needed for efficient DNA platination, are difficult to obtain when carboplatin is rapidly cleared from the plasma.

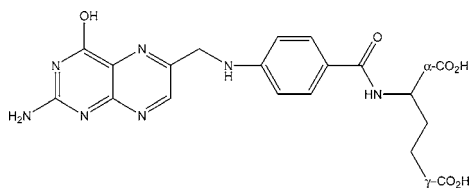
The use of water-soluble polymers as macromolecular carriers for low-molecular weight conventional drugs is a very promising recent strategy in anticancer therapy. In comparison with a native drug, a macromolecular prodrug exhibits improved body distribution and prolonged blood circulation, due to the dominant pharmacokinetic properties of the macromolecular carrier (10). Poly(ethylene glycol) (PEG) is a water soluble amphiphilic polymer showing excellent biocompatibility and is frequently used in biomedical applications (11). Drugs modified with PEG carriers also benefit from lowered immunogenicity and better tumor uptake (12–14). However, as a result of the increase in molecular weight, cell uptake and consequently biological activity of prodrug complexes may be reduced. Cell internalization ability is especially important for stable prodrugs, such as carboplatin analogues. Among numerous PEG-containing prodrugs, which were synthesized and tested recently, there is only one report about an attempt to modify

\* To whom correspondence should be addressed. Tel: +972-2-6758702. Fax: +972-2-6757076. E-mail: gibson@md.huji.ac.il.

<sup>†</sup> The Hebrew University of Jerusalem.

<sup>‡</sup> Shaare Zedek Medical Center.

<sup>§</sup> Affiliated with the David R. Bloom, Center for Pharmacy at The Hebrew University of Jerusalem, Israel.



**Figure 2.** Folic acid.

carboplatin by conjugation with PEG (15). Unfortunately, the lack of information about the cell uptake of the PEG–Pt conjugates and about DNA-platination levels precludes significant conclusions concerning the relationship between molecular weight, cell uptake, and biological activity of the complexes.

There are many examples for exploiting existing endocytosis pathways for specific targeting and delivery of macromolecules (16). Coupling of macromolecular carriers with a normally endocytosed ligand frequently improves intracellular accumulation of the prodrug. Folic acid (FA) is one of the most popular targeting ligands, which were utilized for this strategy. There are many reports that macromolecules and other carriers, conjugated to FA (Figure 2), were successfully recognized by FA receptors and internalized into cells via folate receptor-mediated endocytosis (FRME) (17, 18). The folate receptor is a glycosyl-phosphatidylinositol-anchored glycoprotein (19), with high affinity for the FA vitamin ( $K_d \sim 10^{-9}$ – $10^{-10}$  M).<sup>20</sup> It is located in caveolae and participates in the cellular accumulation of folate through the process of potocytosis. In this process, a ligand-bound receptor is sequestered in caveolae, followed by internalization into postcaveolar plasma vesicles, released from the receptor via an intravesicular reduction in pH, and subsequently transported into cytoplasm (for polyglutamation) (21, 22). In addition, cell surface receptors for folic acid are generally overexpressed in human cancer cells (23, 24). The combination of these facts with low immunogenicity and the relatively simple chemistry of FA make it a very useful tool in specific drug targeting.

In this study we prepared carboplatin-PEG conjugates (PEG–Pt) and their folic acid analogue (FA–PEG–Pt) and compared their cytotoxicities, cellular uptake, intracellular distribution and DNA platination levels.

## EXPERIMENTAL PROCEDURES

**Materials.** All reagents were purchased from Sigma-Aldrich Israel LTD, at least reagent grade and used without purification. Solvents for synthesis and for HPLC were synthesis and HPLC grade accordingly.

**NMR Spectroscopy.** NMR data were collected on a Varian Unity Inova 500 MHz spectrometer equipped with a 5-mm switchable probe for  $^1\text{H}$ ,  $^{13}\text{C}$ ,  $^{195}\text{Pt}$  NMR and 500 MHz  $^1\text{H}\{^{13}\text{C}/\text{X}\}$  5 mm PFG tunable triple inverse detection probe for 2D- $^1\text{H}$ ,  $^{15}\text{N}$  HSQC.

**$^{195}\text{Pt}$  NMR.** The platinum chemical shifts were measured relative to the external reference signal of  $\text{K}_2\text{PtCl}_4$ , set at  $-1624$  ppm. A line-broadening (lb) of 300 Hz was normally applied, and data were processed using the VNMR software.

**2D- $^1\text{H}$ ,  $^{15}\text{N}$  HSQC Spectroscopy.** The 2D spectra were recorded using a heteronuclear single quantum correlation (HSQC) with gradient selection and editing sequence according to Kay et al. (25).  $^{15}\text{N}$  spins were irradiated during the acquisition using the GARP-1 sequence.  $^{15}\text{N}$  chemical shifts were externally referenced to 1.5 M  $\text{NH}_4\text{Cl}$  in 1 M  $\text{HCl}$  ( $\delta_{\text{N}} = 0$  ppm,  $\delta_{\text{H}} = 7$  ppm);  $^1\text{H}$  chemical shifts were externally referenced to TSP ( $\text{Me}_3\text{Si}(\text{CD}_2)_2\text{CO}_2\text{Na}$ ) ( $\delta_{\text{H}} = 0$  ppm). Data were collected

at 25 °C. A total of 64 transients and 128 increments were collected over 6.5 h. All data were processed using the VNMR software, using the sinebell and sinebell shift functions in both dimensions. Data were zero filled to 4096 data points.

**RP HPLC.** Analytical monitoring of the products was conducted on a RP C-18 HPLC column (Merck 50833 Lichrosphere 250  $\times$  4.0 mm ID, 5  $\mu\text{M}$ ), using a Spectra Series P100 Gradient Pump and a Thermo Separation Products variable wavelength UV100 detector. The gradient running was 5% A/95% B to 100% A over 30 min at a flow rate of 1 mL/min with detection at 220 nm, where A is 0.1% TFA in acetonitrile and B is 0.1% TFA in water.

**Mass Spectrometry.** MALDI-TOF-MS of PEG conjugates was measured on Bruker REFLEX reflector time-of-flight instrument with SCOUT multiprobe (384) inlet and gridless delayed extraction ion source (Bruker, Bremen, Germany). All spectra were acquired in a positive-ion reflectron mode. For acquisition of mass spectrometric data, 0.5  $\mu\text{L}$  of sample (1:50 in water) was added to 0.5  $\mu\text{L}$  of 2,5-dihydroxybenzoic acid (0.1% TFA/acetonitrile 2:1) and dispensed onto the sample support. Angiotensin-2 and ACTH were used as external standards for MALDI-TOF MS spectra calibration. The spectra exhibited a bell-shaped distribution of 44-Da spaced lines. The shift in single mass peak of PEG conjugates spectra in comparison to the spectrum of the original PEG-3000 spectrum was detected.

**ESI-MS** was measured on a ThermoQuest Finnigan LCQ- Duo in the positive ion mode. Elution was in a mixture of 49:49:2 water:methanol:acetic acid at a flow rate of 15  $\mu\text{L}/\text{min}$ .

**UV Analysis.** The contents of folate and fluorescein in PEG conjugates were determined by quantitative UV spectrometry of the conjugates in PBS (pH = 7.4 solution). Using extinction coefficient values:  $\epsilon_{363} = 6197 \text{ M}^{-1}\text{cm}^{-1}$  for FA (26) and  $\epsilon_{490} = 67000 \text{ M}^{-1}\text{cm}^{-1}$  for FITC (27).

**Atomic absorption (AA)** measurements were performed on a Varian SpetraAA Zeeman 300 spectrometer. The platinum concentration was calculated according to a calibration curve of a known concentration of a  $\text{K}_2\text{PtCl}_4$  stock solution (250 ng/mL Pt).

**Inductively coupled plasma mass spectrometry (ICPMS)** measurements were performed on a Elan-DRC II, Perkin-Elmer Sciex spectrometer. The platinum concentration was calculated according to a known concentration of a  $\text{K}_2\text{PtCl}_4$  standard solution (10 ng/mL Pt).

**Synthesis and Characterization of PEG Conjugates.** *1, $\omega$ -Diaminopolyoxyethylene3000 (1).* Ten grams (3.3 mmol) of dry poly(ethylene)glycol 3000 was dissolved in 100 mL of dry  $\text{CH}_2\text{Cl}_2$ . Seven milliliters of triethylamine was added, the reaction was cooled in an ice-water bath, and 1 mL (13.3 mmol) of  $\text{CH}_3\text{SO}_2\text{Cl}$  was added dropwise with stirring. When all the  $\text{CH}_3\text{SO}_2\text{Cl}$  was added, the ice bath was removed, and the reaction was stirred overnight at room temperature. The reaction mixture was washed with 100 mL of 50 mM  $\text{NaHCO}_3$ . The organic fraction was dried over  $\text{MgSO}_4$  and filtered, and the solvent was evaporated to give 1, $\omega$ -dimethanesulfonypolyoxyethylene3000 that was immediately dissolved in 150 mL of a concentrated solution of aqueous ammonia and was left to stir for 48 h in a sealed flask. Then, the product was extracted twice with  $\text{CH}_2\text{Cl}_2$ , the organic fractions were combined, dried over  $\text{MgSO}_4$ , and filtered, and the solvent was removed under reduced pressure. The product was crystallized from  $\text{Et}_2\text{O}$ . The

yield was 80%.  $^1\text{H}$  NMR ( $\text{CDCl}_3$ )  $\delta$ (ppm): 3.68 (t, 2H,  $\text{NH}_2\text{CH}_2\text{CH}_2$ ), 3.6 (bs,  $\sim 280\text{H}$ ,  $\text{PEG}_{3000}$ ), 2.97 (t, 2H,  $\text{NH}_2\text{CH}_2$ ).

**1-FMOC, $\omega$ -aminopolyoxyethylene3000 (2).** Three grams (1 mmol) of (1) was dissolved in 150 mL of a 10 mM  $\text{NaHCO}_3$  solution and diluted with an additional 150 mL of  $\text{CH}_3\text{CN}$ , and 260 mg (1 mmol) of FMOC was dissolved in 50 mL of  $\text{CH}_3\text{CN}$  and added dropwise with stirring to the reaction. The mixture was left to react for an additional 1 h at room temperature, and then the mixture was acidified with HCl. The  $\text{CH}_3\text{CN}$  was evaporated, and the water was lyophilized. The mixture of products (unprotected, monoprotected, and bisprotected PEG-diamine) was desalted by dissolving the lyophilized sample in  $\text{CH}_2\text{Cl}_2$  followed by filtering out of the NaCl. The  $\text{CH}_2\text{Cl}_2$  was removed, and the mixture of products was dissolved in water and separated on Sephadex CM-25 cation exchange column. The monoprotected fraction was eluted with a 25 mM NaCl solution, collected, acidified with HCl, and lyophilized. The final product was desalted again by dissolving it in  $\text{CH}_2\text{Cl}_2$ , filtering out the solids, and evaporation of the solvent. The product was crystallized from  $\text{Et}_2\text{O}$ . The yield was 30%.  $^1\text{H}$  NMR ( $\text{DMSO}-d_6$ )  $\delta$ (ppm): 7.88 (d, 2H, fluor), 7.78 (d, 2H, fluor), 7.44–7.31 (dt, 4H, fluor), 4.28 (d, 2H, fluor- $\text{CH}_2\text{O}$ ), 4.22 (t, 1H, H-(C9)), 3.6 (bs,  $\sim 280\text{H}$ ,  $\text{PEG}_{3000}$ ), 3.14 (q, 2H, FMOC- $\text{NHCH}_2$ ), 2.95 (t, 2H,  $\text{CH}_2\text{NH}_2$ ).

**FA-PEG-FMOC (3).** Initially the active ester of the glutamic residue of the folic acid was prepared.

**FA-NHS Ester.** Folic acid (300 mg, 0.67 mmol) was dissolved in 12 mL of dry DMSO to which 93 mg (0.45 mmol) of DCC and 77 mg (0.67 mmol) of NHS were added. The reaction was left overnight at room temperature, in the dark. The DCU precipitate (a side product of the reaction) was filtered out, and 100 mL of 30% acetone in  $\text{Et}_2\text{O}$  was added with stirring. The yellow precipitate was collected on sintered glass and washed with acetone and ether and was used immediately in the next step of synthesis.

$\text{NH}_2$ -PEG-FMOC (500 mg, 0.15 mmol) was coevaporated with three 50 mL portions of dry pyridine and finally dissolved in 100 mL of dry pyridine. Then FA-NHS ester (2) obtained from the activation of 300 mg (0.67 mmol) of folic acid (see previous paragraph) was added to the solution and the reaction was left overnight stirring in the dark. Upon completion of the reaction (confirmed by the ninhydrine test) the pyridine was evaporated and the remaining solid was dissolved in 20 mL of 100 mM  $\text{NaHCO}_3$ . The reaction mixture was chromatographed on a Sephadex 25 column and lyophilized. The yield was 80%.  $^1\text{H}$  NMR ( $\text{D}_2\text{O}$ )  $\delta$ (ppm): 8.62 (s, 1H, folate-C(8)H), 7.85 (d, 2H, fluor), 7.78–7.65 (m, 4H, fluor/folate(PABA) $\text{H}_2$ ), 7.56–7.31 (dt, 4H, fluor), 6.81 (d, 2H, folate(PABA) $\text{H}_2$ ), 4.51 (s, 2H, folate( $\text{NH}-\text{CH}_2$ )), 4.38 (d, 2H, fluor- $\text{CH}_2\text{O}$ ), 4.32–4.22 (m, 2H, fluor(C9)-H/folate-(Glu) $\alpha$ -CH), 3.6 (bs,  $\sim 280\text{H}$ ,  $\text{PEG}_{3000}$ ), 3.14 (m, 4H, FMOC- $\text{NHCH}_2$ /folate- $\text{NHCH}_2$ ), 2.21–1.95 (bm, 4H, folate-(Glu) $\beta,\gamma$ - $\text{CH}_2$ ).

**HPLC Monitoring of CPG-Mediated Glutamic Acid Cleavage.** The experiment was carried out according to a published protocol:<sup>26</sup> 0.1 mL of 0.5 mg/mL solution of FA-PEG-FMOC was incubated with 2 units of CPG in a 150 mM, pH 7.3 Tris buffer, at 30 °C. After 4 h of incubation, the decrease in total peak area of the conjugate ( $t_R = 18.7$ , detection wavelength  $\lambda = 360$ ) was 65%. An additional 1 unit of CPG and prolonged incubation (up to 24 h) did not change this result.

**Cbz-PEG-FMOC (4).**  $\text{NH}_2$ -PEG-FMOC (500 mg, 0.15 mmol) was dissolved in 50 mL of a 10 mM  $\text{NaHCO}_3$

solution and diluted with an additional 50 mL of acetonitrile. Cbz-Cl (51 mg, 0.3 mmol) was dissolved in 10 mL of  $\text{CH}_3\text{CN}$  and added dropwise with stirring to the reaction, at room temperature. The mixture was left to react for an additional 1 h after the  $\text{CH}_3\text{CN}$ , water, and excess Cbz-Cl was removed by evaporation. The product was desalted, as described above. The yield was 90%.  $^1\text{H}$  NMR ( $\text{DMSO}-d_6$ )  $\delta$ (ppm): 7.88 (d, 2H, fluor), 7.78 (d, 2H, fluor), 7.65 (t, 1H, FMOC-NH), 7.44–7.31 (m, 9H, Ph, fluor), 7.23 (t, 1H, Cbz-NH), 4.99 (s, 2H,  $\text{PhCH}_2\text{O}$ ), 4.73 (bs,  $\sim 280\text{H}$ ,  $\text{PEG}_{3000}$ ), 4.28 (d, 2H, fluor- $\text{CH}_2\text{O}$ ), 4.22 (t, 1H, H-(C9)), 3.14 (q, 2H, Cbz- $\text{NHCH}_2$ ), 2.95 (t, 2H,  $\text{CH}_2\text{-NH}_2$ ).

**FA-PEG-FITC (5).** First, the FMOC protecting group was removed from FA-PEG-FMOC by piperidine treatment. FA-PEG-FMOC (400 mg) was dissolved in 50 mL of 25% aqueous piperidine. Then white precipitate was removed by filtration, and solvents were evaporated. To remove all traces of piperidine, the product was dissolved in water and evaporated again. The process was repeated twice.

FA-PEG- $\text{NH}_2$  (100 mg, 0.026 mmol) was dissolved in 5 mL of DMF, and 20 mg (0.05 mmol) of FITC was added in the dark to the reaction mixture which stood at room temperature. Ninhydrin test indicated that the reaction was complete after 20 h. Aminopropanol (0.01 mL) was added to deactivate the excess of FITC, and the solvent was removed by evaporation. The product was purified on a Sephadex-25 column and lyophilized. The yield was 90%. HPLC:  $t_R = 17.7$ ; UV (FA/FITC):  $[\text{FA}]/[\text{FITC}] = 0.94$ .

**Cbz-PEG-FITC (6).** The FMOC protecting group was selectively removed from Cbz-PEG-FMOC (4) as described above, and the primary amine was coupled to FITC as described in the previous section. The yield was 90%. HPLC:  $t_R = 16.8$ ; MALDI TOF: The shift in single mass peak (in comparison to original PEG) is 708 (calculated 691).

**Di-*tert*-butyl 2-(3-Phthalimidopropyl)malonate (7).** Di-*tert*-butyl malonate (2.2 mL, 10 mmol) was dissolved in 100 mL of dry THF, and 1.8 g (8 mmol) of KO $\text{t}$ -Bu was added to the reaction mixture with stirring and under dry  $\text{N}_2$ . The reaction mixture was slightly heated until the solution became clear, and then 3-bromopropylphthalimide was added. The reaction was left to stand overnight with stirring and under reflux. The end of the reaction was confirmed by TLC [95%  $\text{CHCl}_3$ /5% ethyl acetate;  $R_f$ (bromopropylphthalimide) = 0.6,  $R_f$ (7) = 0.4]. The THF was removed by evaporation, and the product was redissolved in  $\text{CH}_2\text{Cl}_2$  and washed with 5% aqueous acetic acid. The organic fractions were combined, dried over  $\text{MgSO}_4$ , and filtered, and the solvent was evaporated. The final product was isolated by silica column chromatography (95% chloroform, 5% ethyl acetate) and crystallized from petroleum ether. The yield was 60%.  $^1\text{H}$  NMR ( $\text{CDCl}_3$ )  $\delta$ (ppm): 7.82 (d, 2H, Ph), 7.68 (t, 2H, Ph), 3.69 (t, 2H, phthalimide- $\text{CH}_2$ ), 3.17 (t, 1H,  $\alpha$ -CH, malonate), 1.85 (m, 2H,  $\text{CH}_2\text{CH}$ ), 1.62 (m, 2H,  $\text{CH}_2\text{CH}_2\text{-CH}_2$ ), 1.48 (s, 18H, *t*-Bu).  $^{13}\text{C}$  NMR ( $\text{CDCl}_3$ )  $\delta$ (ppm): 168.90 (C(O)-*t*Bu), 168.31 (C(O), phthalimide), 133.87 (CH, phthalimide), 132.09 (C, phthalimide), 123.917 (CH, phthalimide), 81.81 (C quaternary, *t*Bu), 53.41 ( $\text{CH}_2\text{NH}$ ), 39.29 ( $\alpha$ -CH, malonate), 27.78 ( $\text{CH}_3$ , *t*Bu), 26.75 ( $\text{NHCH}_2\text{-CH}_2$ ), 25.69 ( $\text{CH}_2\text{CH}$ ).

**Di-*tert*-butyl 2-(3-Aminopropyl)malonate (8).** 7 (4 g, 10 mmol) was dissolved in 100 mL of absolute ethanol, and 0.8 mL (25 mmol) of hydrazine monohydrate was added. The reaction was refluxed for 3 h; after that the solvent and excess of hydrazine monohydrate were



evaporated under reduced pressure. The remaining solid was dissolved in methylene chloride and washed with 100 mL of 0.5 N NaOH. The aqueous phase was extracted with methylene chloride, the organic fractions were combined, dried over  $\text{MgSO}_4$ , and filtered, and the solvent was removed to yield the product. The yield was 80%.

$^1\text{H}$  NMR ( $\text{CDCl}_3$ )  $\delta$ (ppm): 3.17 (t, 1H,  $\alpha\text{-CH}$ ), 2.71 (t, 2H,  $\text{NH}_2\text{CH}_2$ ), 1.85 (m, 2H,  $\text{CH}_2\text{CH}$ ), 1.62 (m, 2H,  $\text{CH}_2\text{CH}_2\text{CH}_2$ ), 1.48 (s, 18H, *t*-Bu);  $^{13}\text{C}$  NMR ( $\text{CDCl}_3$ )  $\delta$ (ppm): 81.81 (*C* quaternary, *t*Bu), 53.41 ( $\text{CH}_2\text{NH}$ ), 39.29 ( $\alpha\text{-CH}$ , malonate), 27.78 ( $\text{CH}_3$ , *t*Bu), 26.75 ( $\text{NHCH}_2\text{CH}_2$ ), 25.69 ( $\text{CH}_2\text{CH}$ ). ESI MS: 274 (calculated 274).

**Di-*tert*-butyl 2-(3-Succinylaminopropyl)malonate (9).** 2 (2 g, 7.3 mmol) was dissolved in 100 mL of dry methylene chloride, and 1 g (10 mmol) of succinic anhydride was added with stirring to the reaction that was left overnight at room temperature. The end of reaction was confirmed by the ninhydrin test. Then, 50 mL of a 5% citric acid solution in water was added, and the reaction proceeded with stirring for an additional 60 min. The organic phase was separated and washed with an additional 50 mL portion of 5% citric acid solution. The organic fraction was dried under  $\text{MgSO}_4$  and filtered, and the solvent was evaporated. The product was crystallized from  $\text{Et}_2\text{O}$ . The yield was 90%.

$^1\text{H}$  NMR ( $\text{DMSO}-d_6$ )  $\delta$ (ppm): 7.84 (bt, 1H,  $\text{C}(\text{O})\text{NH}$ ), 3.16 (t, 1H,  $\alpha\text{-CH}$ ), 2.99 (q, 2H,  $\text{NHCH}_2$ ), 2.38 (t, 2H,  $\text{succ-CH}_2$ ), 2.29 (t, 2H,  $\text{succ-CH}_2$ ), 1.61 (m, 2H,  $\text{CH}_2\text{CH}$ ), 1.41 (bs, 20H,  $\text{CH}_2\text{CH}_2\text{CH}_2/t\text{-Bu}$ ).  $^{13}\text{C}$  NMR ( $\text{CDCl}_3$ )  $\delta$ (ppm): 175.76 ( $\text{COOH}$ ), 172.52 ( $\text{C}(\text{O})\text{NH}$ ), 168.90 ( $\text{C}(\text{O})\text{-tBu}$ ), 81.81 (*C* quaternary, *t*Bu), 53.41 ( $\text{CH}_2\text{NH}$ ), 39.29 ( $\alpha\text{-CH}$ , malonate), 30.75 ( $\text{HOOCCH}_2$ ), 29.91 ( $\text{CH}_2\text{C}(\text{O})\text{NH}$ ), 27.78 ( $\text{CH}_3$ , *t*Bu), 26.75 ( $\text{NHCH}_2\text{CH}_2$ ), 25.69 ( $\text{CH}_2\text{CH}$ ). ESI MS: 374.53 (calculated 373.44).

**FMOC-PEG-MAL(*t*Bu)<sub>2</sub> (10).**  $\text{NH}_2\text{-PEG-FMOC}$  (1.6 g, 0.5 mmol), di-*tert*-butyl 2-(3-succinylaminopropyl)malonate (9) (205 mg, 0.55 mmol), ECI (192 mg, 2 mmol), and DIEA (0.35 mL) were dissolved in 100 mL of dry methylene chloride at room temperature. The reaction was stirred for 3 h, and the completion of reaction was confirmed by the ninhydrin test. Then, the excess of ECI and DIEA was extracted with a 1% solution of citric acid. The organic fraction was dried over  $\text{MgSO}_4$  and filtered, and the solvent was evaporated. The product was crystallized from  $\text{Et}_2\text{O}$ . The yield was 85%.  $^1\text{H}$  NMR ( $\text{D}_2\text{O}$ )  $\delta$ (ppm): 7.88 (d, 2H, fluor), 7.78 (d, 2H, fluor), 7.44–7.31 (dt, 4H, fluor), 4.28 (d, 2H, fluor- $\text{CH}_2\text{O}$ ), 4.22 (t, 1H, H-(C9)), 3.6 (bs,  $\sim 280\text{H}$ ,  $\text{PEG}_{3000}$ ), 3.34 (m, 4H,  $\text{PEG-CH}_2\text{NH}$ ), 3.26 (t, 1H, Mal- $\alpha\text{-CH}$ ), 3.07 (t, 2H,  $\text{NHCH}_2$ ), 2.48 (m, 4H,  $\text{succ-CH}_2$ ), 1.61 (m, 2H,  $\text{CH}_2\text{CH}$ ), 1.46–1.38 (m+s, 20H,  $\text{CH}_2\text{CH}_2\text{CH}_2/t\text{-Bu}$ ).

**FA-PEG-MAL(*t*Bu)<sub>2</sub> (11).** First, the FMOC was removed from FMOC-PEG-MAL(*t*Bu)<sub>2</sub> as described above. Then, it was coupled to FA, as described above. The yield was 80%.  $^1\text{H}$  NMR ( $\text{D}_2\text{O}$ )  $\delta$ (ppm): 8.62 (s, 1H, folate-C(8)H), 7.65 (d, 2H, folate(PABA)H<sub>2</sub>), 6.81 (d, 2H, folate(PABA)H<sub>2</sub>), 4.51 (s, 2H, folate( $\text{NH-CH}_2$ )), 4.22 (m, 1H, folate( $\text{Glu}\alpha\text{-CH}$ )), 3.6 (bs,  $\sim 280\text{H}$ ,  $\text{PEG}_{3000}$ ), 3.34 (m, 4H,  $\text{PEG-CH}_2\text{NH}$ ), 3.26 (t, 1H, Mal- $\alpha\text{-CH}$ ), 3.07 (t, 2H,  $\text{NHCH}_2$ ), 2.48 (m, 4H,  $\text{succ-CH}_2$ ), 2.21–1.95 (bm, 4H, folate( $\text{Glu}\beta,\gamma\text{-CH}_2$ )), 1.61 (m, 2H,  $\text{CH}_2\text{CH}$ ), 1.46–1.38 (m+s, 20H,  $\text{CH}_2\text{CH}_2\text{CH}_2/t\text{-Bu}$ ).

**HPLC Monitoring of CPG-Mediated Cleavage.** The experiment was carried according to a published protocol (26), as described in the FA-PEG-FMOC preparation procedure. Integration area of the conjugate ( $t_R = 19.1$ ) was reduced to 35% of original size.

**Cbz-PEG-MAL(*t*Bu)<sub>2</sub> (12).** First, the FMOC group was removed from FMOC-PEG-MAL(*t*Bu)<sub>2</sub> as described

above and then the free amine coupled with Cbz, as described in above. The yield was 90%.  $^1\text{H}$  NMR ( $\text{DMSO}-d_6$ )  $\delta$ (ppm): 7.84 (dt, 2H,  $\text{CH}_2\text{C}(\text{O})\text{NH}$ ), 7.32 (m, 5H, CH(Ph)), 7.23 (t, 1H, Cbz-NH), 4.98 (s, 2H, Cbz), 3.6 (bs,  $\sim 280\text{H}$ ,  $\text{PEG}_{3000}$ ), 3.34 (m, 4H,  $\text{PEG-CH}_2\text{NH}$ ), 3.26 (t, 1H, Mal- $\alpha\text{-CH}$ ), 3.07 (t, 2H,  $\text{NHCH}_2$ ), 2.48 (m, 4H,  $\text{succ-CH}_2$ ), 1.61 (m, 2H,  $\text{CH}_2\text{CH}$ ), 1.41 (bs, 20H,  $\text{CH}_2\text{CH}_2\text{CH}_2/t\text{-Bu}$ ).

**FA-PEG-MAL(*Na*)<sub>2</sub> (13).** First, the *t*-Bu protecting group was removed from FA-PEG-MAL(*t*Bu)<sub>2</sub>, and then 500 mg (0.13 mmol) of FA-PEG-MAL(*t*Bu)<sub>2</sub> was dissolved in 30 mL of a 25% TFA solution in  $\text{CH}_2\text{Cl}_2$ . The reaction proceeded 2 h at room temperature, the  $\text{CH}_2\text{Cl}_2$  and THF were removed by evaporation, and the product was washed with  $\text{Et}_2\text{O}$  and dissolved in water. The pH of the solution was fixed at pH = 7, by titration with 1 M solution of NaOH.  $^1\text{H}$  NMR ( $\text{D}_2\text{O}$ )  $\delta$ (ppm): 8.62 (s, 1H, folate-C(8)H), 7.65 (d, 2H, folate(PABA)H<sub>2</sub>), 6.81 (d, 2H, folate(PABA)H<sub>2</sub>), 4.51 (s, 2H, folate( $\text{NHCH}_2$ )), 4.22 (m, 1H, folate( $\text{Glu}\alpha\text{-CH}$ )), 3.6 (bs,  $\sim 280\text{H}$ ,  $\text{PEG}_{3000}$ ), 3.34 (m, 4H,  $\text{PEG-CH}_2\text{NH}$ ), 3.07 (t, 2H,  $\text{NHCH}_2$ ), 2.92 (t, 1H, Mal- $\alpha\text{-CH}$ ), 2.48 (m, 4H,  $\text{succ-CH}_2$ ), 2.21–1.95 (bm, 4H, folate( $\text{Glu}\beta,\gamma\text{-CH}_2$ )), 1.73 (m, 2H,  $\text{CH}_2\text{CH}$ ), 1.44 (m, 2H,  $\text{CH}_2\text{CH}_2\text{CH}_2$ ). RP-HPLC:  $t_R = 15.8$ .

**Cbz-PEG-MAL(*Na*)<sub>2</sub> (14)** was prepared as described in the procedure for the preparation of FA-PEG-MAL(*Na*)<sub>2</sub>.  $^1\text{H}$  NMR ( $\text{D}_2\text{O}$ )  $\delta$ (ppm): 7.32 (m, 5H, CH(Ph)), 4.98 (s, 2H, Cbz), 3.6 (bs,  $\sim 280\text{H}$ ,  $\text{PEG}_{3000}$ ), 3.36 (t, 4H,  $\text{PEG-CH}_2\text{NH}$ ), 3.14 (t, 2H,  $\text{NHCH}_2$ ), 2.92 (t, 2H,  $\alpha\text{-CH}$ ), 2.48 (m, 4H,  $\text{succ-CH}_2$ ), 1.73 (m, 2H,  $\text{CH}_2\text{CH}$ ), 1.44 (m, 2H,  $\text{CH}_2\text{CH}_2\text{CH}_2$ ). HPLC:  $t_R = 14.7$ .

**FA-PEG-Pt (15).** Initially, *cis*-[Pt( $\text{NH}_3$ )<sub>2</sub>( $\text{D}_2\text{O}$ )<sub>2</sub>]<sup>2+</sup>-( $\text{NO}_3$ )<sub>2</sub> was synthesized. *cis*-PtI<sub>2</sub>( $\text{NH}_3$ )<sub>2</sub> (40 mg, 0.082 mmol) and  $\text{AgNO}_3$  (28 mg, 0.162 mmol) were stirred vigorously overnight, in the dark in 2 mL of  $\text{D}_2\text{O}$ . The yellow precipitate (AgI) was filtered out, and the filtrate was characterized by a single peak ( $\delta = -1580$  ppm) in the  $^{195}\text{Pt}$  NMR spectrum.

The solution of *cis*-[Pt( $\text{NH}_3$ )<sub>2</sub>( $\text{D}_2\text{O}$ )<sub>2</sub>]<sup>2+</sup>-( $\text{NO}_3$ )<sub>2</sub> was mixed with 152 mg (0.041 mmol) of FA-PEG-MAL(*Na*)<sub>2</sub> and stirred at room-temperature overnight. The end of reaction was confirmed by  $^1\text{H}$  NMR. The product was purified on a Sephadex-25 column and lyophilized.  $^1\text{H}$  NMR ( $\text{D}_2\text{O}$ )  $\delta$ (ppm): 3.6 (bs,  $\sim 280\text{H}$ ,  $\text{PEG}_{3000}$ ), 3.36 (t, 4H,  $\text{PEG-CH}_2\text{NH}$ ), 3.14 (t, 2H,  $\text{NHCH}_2$ ), 2.92 (t, 2H,  $\alpha\text{-CH}$ ), 2.48 (m, 4H,  $\text{succ-CH}_2$ ), 2.26 (m, 2H,  $\text{CH}_2\text{CH}$ ), 1.48 (m, 2H,  $\text{CH}_2\text{CH}_2\text{CH}_2$ ).  $^{195}\text{Pt}$  NMR ( $\text{D}_2\text{O}$ )  $\delta$ (ppm): -1698; HPLC:  $t_R = 17.8$ ; UV (FA): AA (Pt): [FA]/[Pt] = 1.13.

**Cbz-PEG-Pt (16)** was prepared as described in the procedure for the preparation of 15.  $^{15}\text{N}$ -Labeled Pt complexes were synthesized according to the published procedures for the synthesis of *cis*-DDP.<sup>27</sup>  $^1\text{H}$  NMR ( $\text{D}_2\text{O}$ )  $\delta$ (ppm): 7.32 (m, 5H, CH(Ph)), 4.98 (s, 2H, Cbz), 3.6 (bs,  $\sim 280\text{H}$ ,  $\text{PEG}_{3000}$ ), 3.36 (t, 4H,  $\text{PEG-CH}_2\text{NH}$ ), 3.14 (t, 2H,  $\text{NHCH}_2$ ), 2.92 (t, 2H,  $\alpha\text{-CH}$ ), 2.48 (m, 4H,  $\text{succ-CH}_2$ ), 2.26 (m, 2H,  $\text{CH}_2\text{CH}$ ), 1.48 (m, 2H,  $\text{CH}_2\text{CH}_2\text{CH}_2$ ).  $^{195}\text{Pt}$  NMR ( $\text{D}_2\text{O}$ )  $\delta$ (ppm): -1698; 2D- $^1\text{H}$ ,  $^{15}\text{N}$ ] HSQC (10%  $\text{D}_2\text{O}$ ) [4.15/–7.78] HPLC:  $t_R = 16.6$ ; MALDI TOF: The shift in single mass peak (in comparison to original PEG) is 767 (calculated 764).

**Cell Culture and Biological Studies. Medium.** Cells were cultured in FA-free RPMI medium (RPMI-1640, Biological Industries, Beyt Haemek, Israel), with 10% fetal bovine serum (GIBCO, Grand Island, NY), 2 mM glutamine, 50 units/mL penicillin, and 50  $\mu\text{g/mL}$  streptomycin. The concentration of FA in serum-containing FA-free medium is only 3 nM, as opposed to 2.26  $\mu\text{M}$  (1 mg/L) under normal culture conditions. Cells were routinely passed by treatment with a trypsin (0.05%)/EDTA

(0.02%) solution in calcium- and magnesium-free phosphate-buffered saline (PBS).

**Cell Lines.** M109 is a murine lung carcinoma line of BALB/c mice (28). By culturing these cells in FA-free medium for several passages, we obtained a subline expressing a high amount of FA receptors, named M109 HiFR, to emphasize the overexpression of folic acid receptors (26).

**Fluorescent Microscopy Studies.** Cells were grown on eight-well glass slides (Nunk). Forty-eight hours prior to the experiment,  $0.2 \times 10^5$  cells were seeded per each well of the slide. The cells were washed with FA, serum-free RPMI medium and incubated for 4 h at 37 °C with 0.2 mL of a 0.5  $\mu$ M solution of fluorescein-labeled PEG's in FA, serum-free RPMI medium. Free folate competition experiments were conducted under the same conditions, except that incubation solutions contained, in addition to fluorescein-labeled PEG, free folic acid at a concentration of 1 mM. After incubation, cells were washed three times with 0.5 mL of RPMI medium and fixed with 3% formaldehyde in PBS. The fluorescent images were obtained with an LSM410 invert Laser Scan Confocal Microscope, at the wavelength  $\lambda = 488$  nm.

**Fluorescent Flow Cytometry Studies.** Forty-eight hours prior to experiment,  $2 \times 10^6$  cells were seeded per each 60 mm dish. Then cells were washed with RPMI medium and incubated for 4 h at 37 °C with 2 mL of 0.5  $\mu$ M solution of fluorescein-labeled PEG's in RPMI medium. Free folate competition experiments were conducted under the same conditions, except that the incubation solutions contained, in addition to fluorescein-labeled PEG's, free folic acid at a concentration 1 mM. After incubation cells were washed three times with 0.5 mL of RPMI medium, released from plates with trypsin/EDTA treatment, centrifuged, and resuspended in 2 mL of PBS. The fluorescence scanning of the cells performed by FACScan (B&D Beckton-Dickinson) at the wavelength  $\lambda = 488$  nm.

**Cells Growth Inhibition Studies.** The cytotoxic effect of free carboplatin and two PEG–Pt conjugates (FA–PEG–Pt and PEG–Pt) was assayed colorimetrically by the MB staining method described previously (29). In our assays M109HiFR cells in 200  $\mu$ L aliquots were plated onto 96-well flat-bottom microtiter plates. Following 20 h in culture, 20  $\mu$ L of the tested drug was added to each well. For each 10-fold increase in drug concentration, five drug concentration points were tested. Each test was performed in triplicate wells and in two parallel plates. The cells were treated continuously for 72 h. The drug concentration which caused a 50% inhibition of the control growth rate ( $IC_{50}$ ) was calculated by interpolation of the two closest values of the growth inhibition curve.

**Pt Uptake Studies with Continuous Incubation.** The uptake of the Pt compounds was assayed through measurement of the level of cell-associated Pt. Forty-eight hours prior to an assay,  $2 \times 10^6$  cells were seeded per 60 mm dish, to obtain  $5 \times 10^6$  cells/plate. At the day of the assay, plates were washed twice with RPMI medium and incubated for 4 h at 37 °C with 2 mL of FA-free RPMI medium, containing three different concentrations (100, 200, and 500  $\mu$ M) of the platinum compound. Then the incubation solution was removed, and cells were washed with 2 mL of RPMI medium, released from plates with trypsin/EDTA treatment, washed three times with PBS, counted, and dried under reduced pressure. Cell-associated platinum was extracted with 0.1 mL of concentrated nitric acid for 15 min at 90 °C. Subsequently, solutions were diluted with water, and the Pt concentration was established using ICPMS.

**Pt Uptake Studies with Postincubation.** Six days prior to an assay,  $1 \times 10^6$  cells were seeded per 162 cm<sup>2</sup> flask, to obtain about  $40 \times 10^6$  cells/flask. At the day of the assay, plates were washed twice with 15 mL FA, serum-free RPMI medium and incubated for 4 h at 37 °C with 15 mL of FA, serum-free RPMI medium, containing 200  $\mu$ M of the platinum compound. Then, the incubation solution was removed and the cells were washed twice with 15 mL of FA, serum-free RPMI medium and were incubated in 15 mL of RPMI medium at 37 °C for an additional 16 h. After incubation cells washed with FA, serum-free RPMI medium and released from the flask by trypsin/EDTA treatment. Ten percent of cells were separated and taken to Pt uptake assay. Cells were counted, cell-associated platinum was extracted, and its content was established as described in previous section. The rest of the cell fraction (90%) was used for Pt–DNA binding measurement as detailed below.

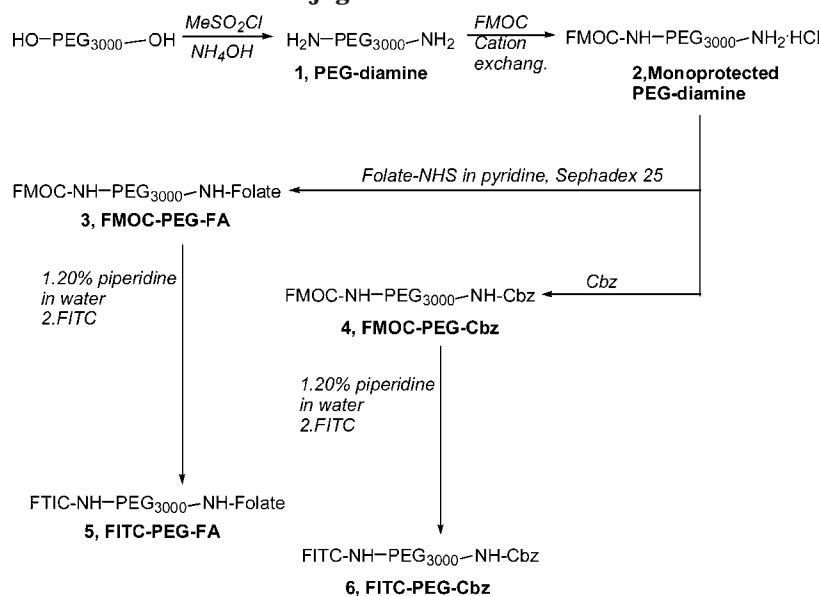
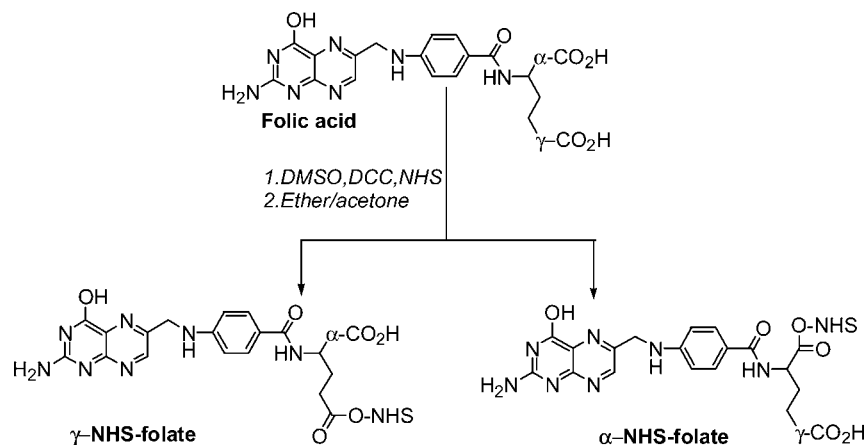
**Pt–DNA Binding.** Cells were centrifuged, and the DNA was extracted by the salting out procedure (30). Cells were resuspended in 10 mL of Nuclear Lysis buffer (10 mM Tris pH 8.2, 400 mM NaCl, 2mM EDTA). The cell lysates were digested for 4 h at 37 °C with 0.5 mL of 10% SDS and 0.1 mL of protease K solution (Sigma, 20  $\mu$ g/mL water solution). Then, 5.5 mL of a saturated NaCl solution was added to the lysates, and the mixture was shaken vigorously followed by centrifugation at  $g = 10000$  rpm for 15 min. The supernatant containing the DNA was transferred to another tube, containing 20 mL of absolute ethanol and mixed gently. DNA strands were removed, washed three times in water/ethanol mixture (1:1), and dissolved in 2 mL of distilled water. DNA concentration was established according to absorbance at 260 nm, and the samples were diluted with TE buffer (10 mM Tris pH 8, 1mM EDTA) buffer. DNA purity was determined by calculating the ratio of absorbance at 260 nm to absorbance at 280 nm. All samples showed the  $A_{260}/A_{280}$  ratio of 1.7–1.9, which indicates that we obtained pure DNA. The platinum content in the DNA solutions was determined by ICPMS measurements.

## RESULTS

**Synthesis and Characterization of FITC-Labeled PEG Conjugates.** FITC-labeled PEG conjugates were synthesized in order to evaluate, by fluorescence-sensitive techniques, whether the conjugated folate alters the PEGs accumulation in HiFR cells.

The general strategy of the synthesis is shown on Scheme 1. The synthesis of monoprotected PEG diamine (2) provided us a universal starting material for all subsequent syntheses. Through stable amide bonds, desirable functions can be easily attached to either end of the polymer. Because of the difficulty of separating modified and unmodified PEGs, we used an excess of the low molecular weight ligands in the conjugation reactions, to increase the yield and to simplify the purifications.

The next step was conjugation of FA to the unprotected primary amine. Folic acid has two carboxy groups, and in order to couple only one PEG–NH<sub>2</sub> to one folic acid, care must be taken to activate only one ester group per folic acid molecule prior to coupling. Thus, complete solubilization of the folic acid is imperative prior to the addition of 1 equiv of the coupling reagents (NHS and DCC). Folic acid suffers from low solubility in most organic solvents, and the only solvent in which folic acid is completely soluble is DMSO. Unfortunately, when the coupling reaction was carried out in DMSO, it was

**Scheme 1. Synthesis of FITC-Labeled PEG Conjugates****Scheme 2. Preparation of Activated Folate**

impossible to isolate the product from the reaction mixture. Thus, we decided to separate the ester activation and the coupling step, and we first prepared and isolated the *N*-hydroxysuccinimide activated FA derivative (Scheme 2), which precipitates readily from DMSO, when a mixture of acetone/ether mixture is added. The activated ester was immediately reacted with a pyridine solution of the monoprotected PEG diamine **2**. The excess of unreacted FA was easily removed by GPC (gel permeation chromatography). Since it was reported that only the folic acid conjugates that were attached through the  $\gamma$  carboxyl group possess biological activity (17), it was important to measure the percentage of the  $\gamma$ -isomer in the FA-PEG conjugates. For this purpose we used the carboxypeptidase G HPLC assay (26), that is based on the ability of CPG to cleave the glutamic residue of FA only if its  $\gamma$ -carboxyl is unconjugated. In view of the fact that 65% of the FA-PEG conjugate was enzymatically cleaved by CPG we assume that  $\gamma$ -isomer fraction is 65%. To prepare a nontargeted control conjugate, we blocked the free amine with a Cbz protective group, instead of folate (**4**). Cbz was chosen because of its relatively low weight and high stability in physiological conditions. After removal of the Fmoc-protecting group, it was easy to conjugate the free amine with FITC (**5**, **6**).

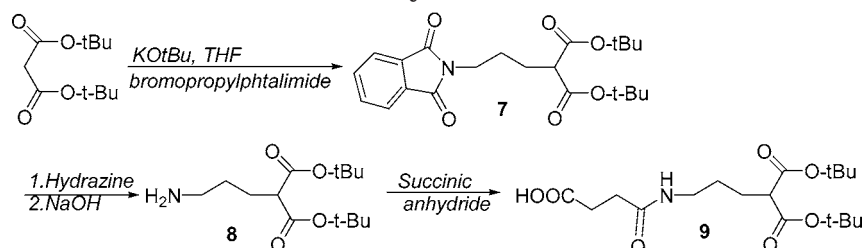
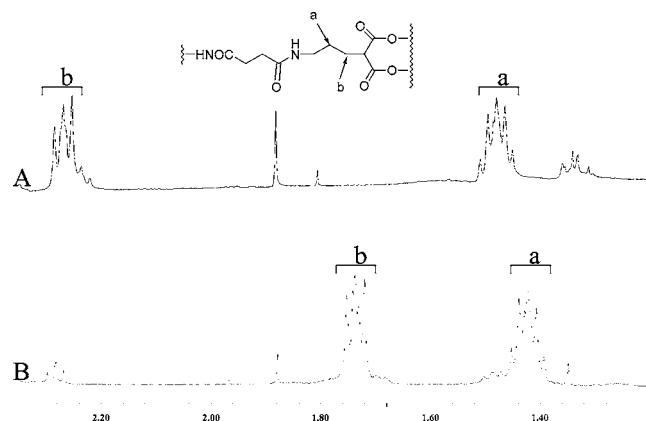
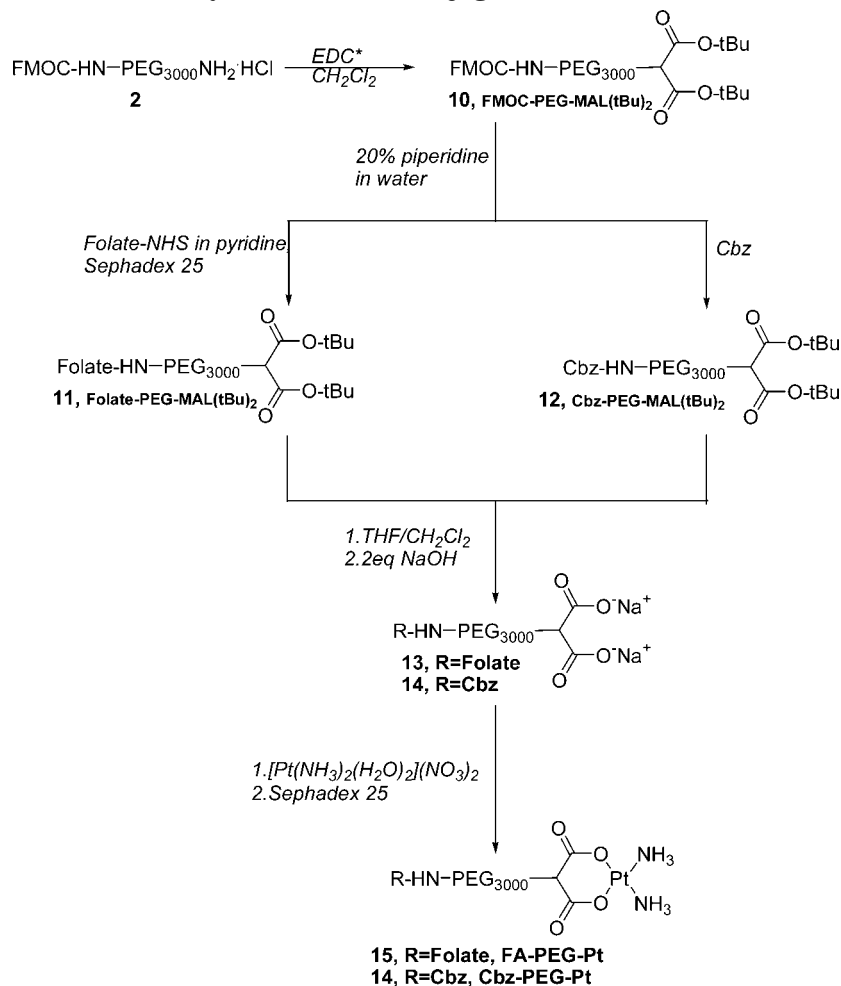
**Synthesis of Pt-PEG Conjugates.** To prepare PEG conjugates that can release the Pt from the carrier once inside the cells (analogues of carboplatin), the Pt moiety

was attached to the PEG through a modified dicarboxylate ligand. Malonic acid derivatives form bidentate chelates with Pt(II), through the binding of the two carboxylic groups. To enable easy conjugation of the dicarboxylate ligand to the PEG-amine carriers, we modified the protected malonate with short side chain, having free carboxylic acid at the end (Scheme 3). Compound **8** is a versatile synthon that allows for easy coupling of the protected malonate to any primary or secondary amine.

The subsequent stages of the synthesis, including the platination steps, are depicted in Scheme 4. The free amine of the monoprotected PEG-diamine **2** was coupled to the side-chain carboxylate of **7** using ECI as the coupling agent. Then amine group of **10** was deprotected and conjugated to either folate (**11**) or Cbz (**12**), as described in the previous section. According to the CPG assay the fraction of the  $\gamma$ -isomer in FA-PEG-MAL(tBu)<sub>2</sub> was ~65%.

After deprotection, the dicarboxylate was platinated using a standard procedure, in which an excess of the reactive diaqua Pt complex {Pt(NH<sub>3</sub>)<sub>2</sub>(H<sub>2</sub>O)<sub>2</sub>}<sup>2+</sup> was reacted with the carrier. Monitoring of the platination reaction was carried out by proton NMR. The chemical shifts of the two methylene groups adjacent to the malonate change significantly upon platination going from 1.73 and 1.44 ppm in the unplatinated carrier to 2.26 and 1.48 ppm, respectively, in the platinated con-



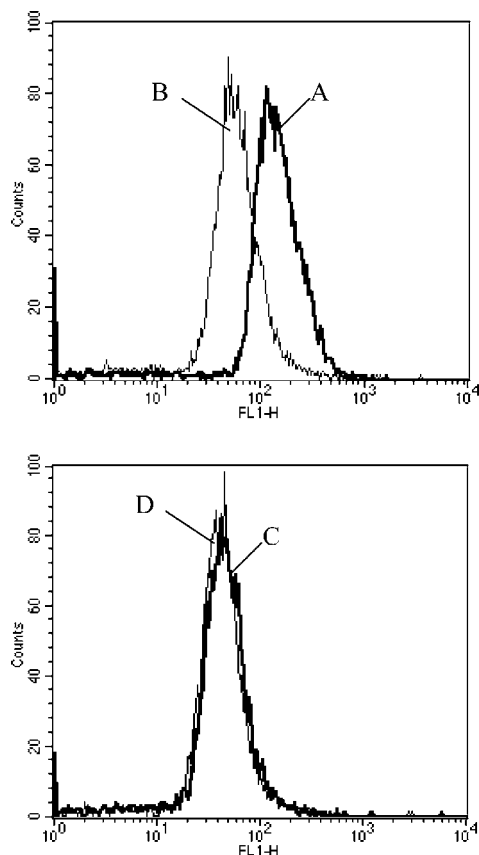
**Scheme 3. Synthesis of Functionalized Malonic Moiety****Scheme 4. Synthesis of PEG-dicarboxylato-Platinum Conjugates**

**Figure 3.**  $^1\text{H}$  NMR of platinated (A) and unplatinated (B) PEG-dicarboxylate ligand.

jugate (see Figure 3). Total disappearance of the peaks related to unplatinated ligand indicated that the reaction

was completed. The excess of the unreacted diaqua Pt complex was removed by gel permeation chromatography.  $^{195}\text{Pt}$  NMR spectroscopy was used to characterize the Pt complex.  $^{195}\text{Pt}$  NMR chemical shifts are sensitive to the nature of the first coordination sphere of Pt(II) and coupled with the fact that the chemical shift scale of  $^{195}\text{Pt}$  NMR is quite large (thousands of ppm), this technique allows us to establish the nature of the complex. The  $^{195}\text{Pt}$  chemical shift of the diaqua Pt complex in water is  $\delta = -1580$  ppm and the chemical shift of carboplatin is  $\delta = -1710$  ppm. Thus, the single peak at  $\delta = -1699$  ppm that was obtained for two products (15, 16) indicates that the desired platinum conjugate was obtained.

**Cell Uptake Studies of Fluorescent Labeled PEGs.** All biological experiments were carried out with the M109HiFR cell line, enriched with folate binding receptors. The cell uptake of FITC-PEGs was evaluated by two fluorescent sensitive techniques: FACS and direct fluorescent microscopy. FACS enables us to compare the



**Figure 4.** Flow cytometry profiles of fluorescence from cell-associated fluorescein. M109 HiFR cells were incubated with 50  $\mu$ M PEG-fluorescein conjugates for 4 h at 37  $^{\circ}$ C. Upper panel: cells treated with FA-PEG-FITC in folate-free RPMI (A) or 1 mM folate containing RPMI (B). Lower panel: cells treated with PEG-FITC in folate-free RPMI (C) or 1 mM folate containing RPMI (D).

uptake of folate targeted PEG and nontargeted PEG in low folate and free folate competition conditions.

The results summarized in Figure 4 clearly indicate that the uptake of folate-targeted PEG increases significantly in folate free medium (profile A) when compared with the uptake of the nontargeted PEG (profile C). The competition with free folate reduces the uptake of folate-targeted PEG (profile B), but does not influence the uptake of nontargeted PEG (profile D).

The FACS results were confirmed by direct fluorescence microscopy (Figure 5). Both targeted (image B) and nontargeted (image A) PEGs concentrated mainly in cytoplasm after 4 h of incubation, but there is a major increase in fluorescence intensity with the folate-targeted PEG (image B). As in the FACS experiment, free folate competition reduces the cell uptake of folate-PEG (image C). These results indicate that folate targeted PEG accumulates in M109-HiFR cells through the folate receptor endocytosis pathway.

**Cells Growth Inhibition Study.** To estimate the impact of folate targeting on the cytotoxicity of PEG-Pt conjugates, growth inhibition tests of M109 HiFR cell line were carried out. In this test we compared targeted PEG-Pt complex to the nontargeted one, and also we used free carboplatin as a general reference, since both complexes are structural analogues of carboplatin. The IC<sub>50</sub> values are presented in Table 1.

Surprisingly the folate-targeted complex was the least cytotoxic, among the three molecules tested. There are two possible explanations for this phenomenon: (a) for

some reason the PEG-Pt conjugates are not internalized by the FRME as is the case for the PEG-FITC conjugates; (b) folate-targeted PEG-Pt complexes do enter the cells through folate endocytosis, but this pathway prevents interaction with DNA and thereby reduces the cytotoxic potency of the PEG-Pt conjugates.

To clarify which one of two hypotheses is right, Pt uptake and DNA-Pt adducts measurements were performed.

**Platinum Cell Uptake.** We measured Pt content in M109 HiFR cells incubated with PEG-Pt conjugates or with free carboplatin. After a 4 h incubation at three different concentrations of each compound, Pt concentrations was measured by ICPMS technique. The results of the experiment are shown in Figure 6.

According to these results, the conjugated folate significantly elevates the uptake of PEG-Pt complex in HiFR cells. This indicates that FRME participates in the tumor cell uptake of folate-targeted PEG-Pt conjugate as in the case of folate PEG-FITC.

Another observation from Figure 6 is that, unlike PEG-Pt or carboplatin, the uptake of FA-PEG-Pt does not increase proportionally with the Pt-compound concentration. This is likely to result from saturation of the FR-mediated uptake. In contrast nontargeted PEG-Pt and carboplatin do not enter the cell through FR endocytosis pathway, and therefore their uptake increases proportionally to their concentration in incubation solution.

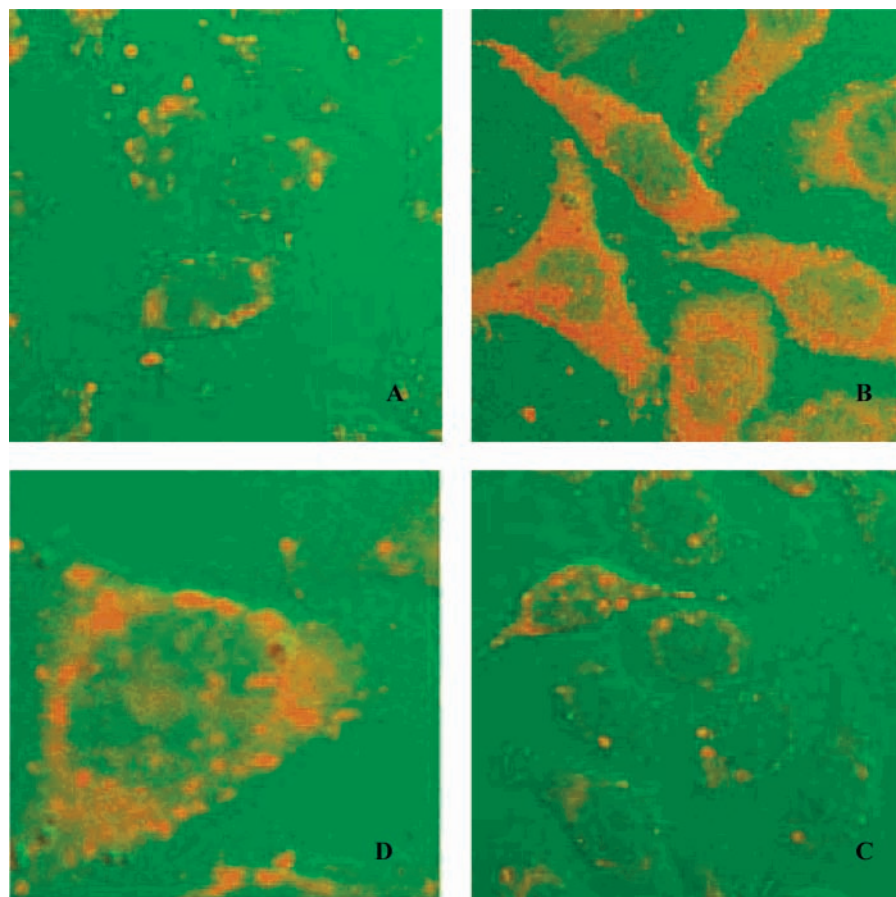
So, folate-containing PEG-Pt conjugates enter cells through the FR endocytosis pathway. Their efficient internalization should result in higher DNA platination levels.

**Pt-DNA Adducts.** Since carboplatin and its analogues exert their cytotoxicity by formation of adducts with DNA, one of the most important measures for the potency of carboplatin analogues is their ability to form Pt-DNA adducts. To allow more efficient platination of the DNA by the Pt complexes, we prolonged the incubation period till 20 h (7). Cells were incubated with the drugs (PEG-Pt, FA-PEG-Pt, and carboplatin) for only 4 h, the medium was changed and the experiment proceeded for an additional 16 h in the drug free medium. When the postincubation ended, 10% of cells were taken for Pt cell uptake studies and the remaining cell fraction was used for DNA extraction (30).

The results of DNA platination levels presented in Table 1 indicate that folate targeted FA-PEG-Pt produces less DNA adducts than the nontargeted PEG-Pt complex. This may explain its decreased cytotoxicity. More surprising was the fact that carboplatin yielded a very poor DNA platination level in comparison with PEG-Pt despite the fact that it displayed the highest Pt accumulation levels after 4 h of incubation.

The results of the Pt uptake experiments with and without postincubation (Table 1) point to massive efflux of carboplatin from the cells, during the postincubation period in contrast with the stable levels for the PEG conjugates. The elevated efflux of carboplatin during postincubation period provides at least a partial explanation for the phenomenon of reduced DNA-platination potency of carboplatin.

In fact, a collateral finding of this study is that nontargeted PEG-Pt causes more effective DNA platination than carboplatin itself. Pt-DNA adducts expressed as a fraction of whole cell drug uptake, were more than twice as high for PEG-Pt treated cells, than for carboplatin (Table 1).



**Figure 5.** Cellular accumulation of fluorescein-labeled PEG conjugates in M109 HiFR cells. Cells were incubated with 50  $\mu$ M substrates for 4 h at 37  $^{\circ}$ C followed by fixation. Panels A and B show fluorescence images of M109 HiFR cells incubated in folate-free RPMI medium with PEG-FITC (A) or FA-PEG-FITC (B). Panel C shows fluorescence images of M109 HiFR cells incubated with 50  $\mu$ M FA-PEG-FITC in RPMI medium containing 1 mM of free FA. Panel D shows zoomed image of panel B.

**Table 1. Biological Monitoring of PEG-Pt Compounds**

platinum compound	IC <sub>50</sub> <sup>a</sup> , $\mu$ M	cell uptake <sup>b</sup> (ng Pt/10 <sup>6</sup> cells)		Pt-DNA adducts ng Pt/mg DNA <sup>c</sup>	calculation of Pt-DNA adducts/whole cell uptake, <sup>d</sup> %	
		4 h incubation	20 h incubation		4 h incubation	20 h incubation
PEG-Pt	16.1 $\pm$ 2.7	6.7 $\pm$ 0.8	4.3 $\pm$ 0.3	9.7 $\pm$ 1.3	3.6	5.6
FA-PEG-Pt	27.7 $\pm$ 0.6	10.3 $\pm$ 0.4	6.7 $\pm$ 0.9	4.3 $\pm$ 0.8	1.0	1.6
Carboplatin	18.5 $\pm$ 1.2	25.2 $\pm$ 0.3	4.6 $\pm$ 0.4	3.7 $\pm$ 0.5	0.36	2

<sup>a</sup> The IC<sub>50</sub> values were calculated from the MB assay. The experiment was performed in two or more separate plates with triplicate cultures for each drug concentration. SD values refer to results from the separate plates. <sup>b</sup> The uptake values were obtained after incubation with 200  $\mu$ M of the platinum compound solution. SD values represent two independent experiments carried out in triplicate cultures. 4h incubation means 4 h continuous exposure to platinum compound. 20 h incubation means 4 h continuous exposure to platinum compound followed by 16 h of postincubation in free medium. <sup>c</sup> DNA-associated Pt was measured after 4 h continuous exposure to a 200  $\mu$ M platinum compound solution followed by 16 h of postincubation in drug-free medium. SD values represent two independent experiments carried out in triplicate cultures. <sup>d</sup> Pt-DNA adducts (see footnote c) expressed as a fraction of whole cell drug uptake (see footnote b). The calculations based on our data, that  $40 \times 10^6$  cells give approximately 1 mg of DNA.

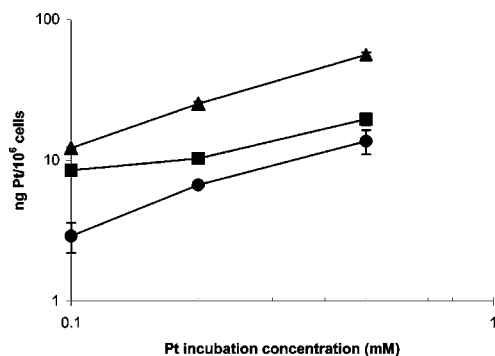
## DISCUSSION

Many attempts have been made to improve the therapeutic index of platinum anticancer agents by conjugating them to large polymeric carriers. Such modifications usually improve the pharmacokinetics and tissue distribution of the drug, but significantly reduce the cell permeability (due to the high molecular weight of the conjugate) (10). Although some macromolecular prodrugs of low molecular weight drugs such as mitomycin C can exert cytotoxicity by releasing the free drug in the extracellular medium (31), this may prove to be problematic in the case of platinum anticancer agents since they act as nonspecific electrophiles, and should the Pt moiety be released from the carrier prior to cellular internalization, the Pt will be rapidly inactivated by

extracellular nucleophiles. In this work we attempted to overcome this shortcoming by developing folate-targeted PEG carriers, for efficient, rapid, active transport of the platinum-carrier conjugate into cancer cells, utilizing folate receptor-mediated endocytosis, aimed at increasing cellular uptake and improving cytotoxicity.

To test our working hypothesis, we prepared two bifunctional FA-PEG conjugates: FA-PEG-Pt and FA-PEG-FITC (see Schemes 1–4). FA-PEG-FITC enabled us to visualize (by confocal microscopy) and to quantitate (by FACS) the effect of conjugating folate to the PEG polymer on the cellular uptake of the PEG. FA-PEG-Pt made possible to examine whether increased cellular uptake results in increased DNA platination and





**Figure 6.** Pt uptake of Pt-containing drugs by M109 HiFR cells. Cells were incubated with different concentration of carboplatin (▲), FA-PEG-Pt (■), or PEG-Pt (●) in folate-free RPMI solution for 4 h at 37 °C. Cell-associated platinum concentrations were measured using ICPMS technique. Each point represents the mean of at least three determinations; bars represent  $\pm$  SD when larger than the symbol.

improved cytotoxicity. The synthetic strategy that was employed in this study is depicted in Schemes 1–4.

Although somewhat tedious, the preparation of the FMOC-PEG-NH<sub>2</sub> lends flexibility to the design of the syntheses of the conjugates, and once the di-*tert*-butyl malonate is coupled to it, essentially any targeting or reporting groups can be attached to its other end. On the basis of this approach, any moiety terminating with a free carboxylate can now be attached to the monoprotected polymer by a simple condensation reaction. We find this method more convenient and more efficient than the previously reported approach of direct alkylation of the di-*tert* butyl malonate by a functionalized polymer (15). Because of the high efficiency and mild reaction conditions of the amine–carboxyl condensation reaction, our carboxyl-functionalized malonate ligand may be easily attached to any amine-containing molecule. NHS-activated folate was prepared as an efficient synthon for the conjugation of the FA moiety to PEG-NH<sub>2</sub>.

A major concern in the chemistry of PEG conjugates is the purification and characterization of the conjugates. All the Pt–PEG conjugates were analyzed by RP-HPLC, displaying a single peak in the chromatogram that attests to the purity of the conjugates. In addition, MALDI-TOF-MS served both to confirm the purity of the conjugates as well as to characterize them. The mode of platination was established by preparing the <sup>15</sup>N labeled analogues of the platinated conjugates and measuring the [<sup>1</sup>H,<sup>15</sup>N] inverse detection HSQC NMR spectra that showed a single peak corresponding to the diamminedicarboxylate coordination sphere. The identity of the coordination sphere of the platinum was also corroborated by <sup>195</sup>Pt analysis and by <sup>1</sup>H NMR. Thus, we also provide here, for the first time, a complete chemical characterization of PEG–Pt conjugates including <sup>1</sup>H NMR, <sup>195</sup>Pt NMR, [<sup>1</sup>H,<sup>15</sup>N] inverse detection HSQC and MALDI-TOF-MS.

Confocal microscopy and FACS were used to study the cellular uptake of the fluorescent PEG conjugates. In both techniques the intensity of cell-associated fluorescence provided the indication for cell uptake of the fluorescein-labeled PEG conjugates (FA-PEG-FITC and PEG-FITC). The data obtained by confocal microscopy (see Figure 5) and by FACS (see Figure 4) indicated that the folate targeted PEG (FA-PEG-FITC) is taken up by the folate receptor-enriched M109 cancer cells approximately three times more efficiently than the untargeted PEG (PEG-FITC). To prove that the FA-PEG conjugates entered the cell via the FR pathway, the uptake experiments were repeated in the presence of an excess of free folate. The

reduction of cellular uptake of the FA-PEG conjugates in the presence of the free folate (see Figures 4, 5) clearly indicates that free folate successfully competes with the conjugates for the folic acid receptor sites thereby reducing the cellular uptake of the conjugates. Additional evidence to support this claim comes from the observation that the cellular accumulation of FA-PEG-Pt does not linearly depend on the platinum concentration in the medium, but at higher platinum concentrations the uptake is less efficient probably due to saturation of the folate receptors (Figure 6). While the FACS provides the quantitative data, confocal microscopy demonstrated that the conjugates actually entered into cytoplasm and did not merely adhere to the exterior of the cell membrane.

Cytotoxicity studies were carried out on cancer cells enriched with folate receptors in order to evaluate the potency of the conjugates and to see whether higher cellular uptake indeed results in higher potency. Surprisingly, the cytotoxicity data showed that FA-PEG-Pt is less potent than PEG-Pt (see Table 1). The IC<sub>50</sub> value of FA-PEG-Pt is higher by factor 1.7, than that of PEG-Pt (Table 1). The cell-associated Pt levels measured by ICP-MS (see Figure 6) were greater for the folate-targeted conjugate, pointing to a lack of correlation between the cellular Pt levels and cytotoxicity.

These contrasting findings prompted us to measure the levels of Pt binding to cellular DNA. Surprisingly, it was found that PEG-Pt forms twice as many adducts with the cellular DNA than does FA-PEG-Pt despite the higher cellular uptake of the latter. One possible explanation for this unexpected phenomenon pertains to the nature of FRME process. In this process, the folate-targeted conjugates are not freely released into the cytosol but are directed to acidic cytoplasmic vesicles, such as endosomes and lysosomes. The release of FA-PEG-Pt from the vesicle to the cytoplasm may be slow and inefficient, reducing the cytotoxic activity of the delivered complex. Observations made by Rui et al. (32) and Qualls and Thompson (33) with folate-targeted pH-sensitive liposomes point to a major increase in cytosol delivery and biological activity of the encapsulated compounds when compared to stable liposomes. This supports the hypothesis that FRME leads to an acidic vesicular compartment with reduced access to other cell compartments unless the delivery system is unstable at low pH. Although our study deals with a polymer–drug complex, much smaller than a liposome, it is possible that these complexes remain to a large extent trapped in acidic vesicles following FRME, thus preventing their cytotoxic activity.

During the course of the study we noticed that despite its low cellular uptake, PEG-Pt is at least as cytotoxic as carboplatin. This was surprising since in the initial cell uptake studies (see Figure 6) carboplatin was internalized much more efficiently than PEG-Pt. To further explore this point, the cells were incubated with the Pt compounds for 4 h, the medium was replaced, and the cells were allowed to grow for an additional 16 h prior to measuring the cell-associated Pt levels. As can be seen from Table 1, the carboplatin levels after 4 h of incubation and 16 h of postincubation are dramatically lower than those measured without the postincubation, suggesting that carboplatin is being excreted from the cells while the PEG-Pt conjugate is retained in the cells once it is internalized. Since the IC<sub>50</sub> measurements were performed with continuous exposure of the cells to the drugs, and the cell uptake and DNA binding were performed with a 4 h exposure and a 16 h postincubation, we have also looked at cell survival using the latter conditions.

The results indicate that the PEG–Pt is one and a half times more effective in inhibition of cell growth than FA–PEG–Pt and four times more effective than carboplatin (data not shown). Both these facts indicate that the untargeted PEG–Pt conjugate is a potentially promising anticancer agent and deserves independent investigation.

The findings of this study suggest that folate-targeted conjugates such as FA–PEG–Pt, may be problematic as a prodrug for the carboplatin family, because the conjugates or the active moieties are neutralized or blocked during the FRME process. Thus, the attempt to increase the levels of Pt–DNA adducts by active targeting with FA resulted in a different kind of detoxification mechanism: entrapment of the prodrugs in certain cellular compartments.

#### ACKNOWLEDGMENT

This research was funded in part by the Israel Cancer Association through the Chaya and Naftali Bloch Memorial Fund.

#### ABBREVIATIONS

CBDCA, cyclobutane-1,1-dicarboxylate; PEG, poly(ethylene glycol); FA, folic acid; FRME, folate receptor-mediated endocytosis; Fmoc, fluorenylmethyl chloroformate; Cbz-Cl, benzyl chloroformate; FITC, fluorescein isothiocyanate; DCC, dicyclohexylcarbodiimide; DCU, dicyclohexylurea; ECI, 1-[3-(dimethylamino)propyl]-3-ethylcarbodiimide hydrochloride; DIEA, diisopropylethylamine; AA, atomic absorption; CPG, carboxypeptidase G; MALDI-TOFMS, matrix-assisted laser desorption ionization time-of-flight mass spectrometry; HiFr, high folate receptor; ICPMS, inductively coupled plasma mass spectrometry; FACS, fluorescence-assisted cell sorting; MB, methylene blue; PEG<sub>3000</sub>,  $-(\text{CH}_2\text{CH}_2\text{O})_{68}-$ ; NHS, *N*-hydroxysuccinimide.

#### LITERATURE CITED

- Calvert, A. H., Harland, S. J., Newell, D. R., Siddik, Z. H., Jones, A. C., McElwain, T. J., Raju, S., Wiltshaw, E., Smith, I. E., Baker, J. M., Peckham, M. J., and Harrap, K. R. (1982) Early clinical studies with cis-diammine-1,1-cyclobutane dicarboxylate platinum II. *Cancer Chemother. Pharmacol.* **9**, 140–147.
- Curt, G. A., Grygiel, J. J., Corden, B. J., Ozols, R. F., Weiss, R. B., Tell, D. T., Myers, C. E., and Collins, J. M. (1983) A phase I and pharmacokinetic study of diamminecyclobutanedicarboxylatoplatinum (NSC 241240). *Cancer Res.* **43**, 4470–4473.
- Wiltshaw, E. (1985) Ovarian trials at the Royal Marsden. *Cancer Treat. Rev.* **12 Suppl A**, 67–71.
- Micetich, K. C., Barnes, D., and Erickson, L. C. (1985) A comparative study of the cytotoxicity and DNA-damaging effects of cis-(diammine)(1,1-cyclobutanedicarboxylato)-platinum(II) and cis-diamminedichloroplatinum(II) on L1210 cells. *Cancer Res.* **45**, 4043–4047.
- Knox, R. J., Friedlos, F., Lydall, D. A., and Roberts, J. J. (1986) Mechanism of cytotoxicity of anticancer platinum drugs: evidence that cis-diamminedichloroplatinum(II) and cis-diammine-(1,1-cyclobutanedicarboxylato)platinum(II) differ only in the kinetics of their interaction with DNA. *Cancer Res.* **46**, 1972–1979.
- Frey, U., Ranford, J. D., and Sadler, P. J. (1993) Ring-Opening Reactions of the Anticancer Drug Carboplatin – NMR Characterization of Cis-[Pt(Nh3)2(Cbdca-O)(5'-Gmp-N7)] in Solution. *Inorg. Chem.* **32**, 1333–1340.
- Blommaert, F. A., van Dijk-Knijnenburg, H. C., Dijt, F. J., den Engelse, L., Baan, R. A., Berends, F., and Fichtinger-Schepman, A. M. (1995) Formation of DNA adducts by the anticancer drug carboplatin: different nucleotide sequence preferences in vitro and in cells. *Biochemistry* **34**, 8474–8480.
- Lokich, J., and Anderson, N. (1998) Carboplatin versus cisplatin in solid tumors: an analysis of the literature. *Ann. Oncol.* **9**, 13–21.
- Sancho, A. R., and Dowell, J. A.; Wolf, W. (1997) The effects of anesthesia on the biodistribution of drugs in rats: a carboplatin study. *Cancer Chemother. Pharmacol.* **40**, 521–525.
- Takakura, Y., and Hashida, M. (1996) Macromolecular carrier systems for targeted drug delivery: Pharmacokinetic considerations on biodistribution. *Pharm. Res.* **13**, 820–831.
- Zalipsky, S. (1995) Chemistry of Polyethylene-Glycol Conjugates with Biologically-Active Molecules. *Adv. Drug Delivery Rev.* **16**, 157–182.
- Sehon, A. H. (1991) Suppression of Antibody-Responses by Conjugates of Antigens and Monomethoxypoly(Ethylene Glycol). *Adv. Drug Delivery Rev.* **6**, 203–217.
- Delgado, C., Francis, G. E., and Fisher, D. (1992) The uses and properties of PEG-linked proteins. *Crit. Rev. Ther. Drug Carrier Syst.* **9**, 249–304.
- Zalipsky, S., Brandeis, E., Newman, M. S., and Woodle, M. C. (1994) Long circulating, cationic liposomes containing amino-PEG-phosphatidylethanolamine. *FEBS Lett.* **353**, 71–74.
- Ohya, Y. S., S., Matsumoto, M., and Ouchi, T. (2000) Design of poly(ethylene glycol) immobilizing platinum complex through chelate-type coordination bond. *Polym. Adv. Technol.* **11**, 635–641.
- Duncan, R., Connors, T. A., and Meada, H. (1996) Drug targeting in cancer therapy: the magic bullet, what next? *J. Drug Target.* **3**, 317–319.
- Wang, S., and Low, P. S. (1998) Folate-mediated targeting of antineoplastic drugs, imaging agents, and nucleic acids to cancer cells. *J. Controlled Release* **53**, 39–48.
- Sudimack, J., and Lee, R. J. (2000) Targeted drug delivery via the folate receptor. *Adv. Drug Delivery Rev.* **41**, 147–162.
- Elwood, P. C. (1989) Molecular cloning and characterization of the human folate-binding protein cDNA from placenta and malignant tissue culture (KB) cells. *J. Biol. Chem.* **264**, 14893–14901.
- McHugh, M., and Cheng, Y. C. (1979) Demonstration of a high affinity folate binder in human cell membranes and its characterization in cultured human KB cells. *J. Biol. Chem.* **254**, 11312–11318.
- Anderson, R. G., Kamen, B. A., Rothberg, K. G., and Lacey, S. W. (1992) Potocytosis: sequestration and transport of small molecules by caveolae. *Science* **255**, 410–411.
- Rothberg, K. G., Ying, Y. S., Kolhouse, J. F.; Kamen, B. A.; Anderson, R. G. (1990) The glycopospholipid-linked folate receptor internalizes folate without entering the clathrin-coated pit endocytic pathway. *J. Cell Biol.* **110**, 637–649.
- Mantovani, L. T., Miotti, S., Menard, S., Canevari, S., Raspagliesi, F., Bottini, C., Bottero, F., and Colnaghi, M. I. Folate binding protein distribution in normal tissues and biological fluids from ovarian carcinoma patients as detected by the monoclonal antibodies MOv18 and MOv19. (1994) *Eur. J. Cancer* **30A**, 363–369.
- Weitman, S. D., Lark, R. H., Coney, L. R., Fort, D. W., Frasca, V., Zurawski, V. R., Jr., and Kamen, B. A. (1992) Distribution of the folate receptor GP38 in normal and malignant cell lines and tissues. *Cancer Res.* **52**, 3396–3401.
- Kay, L. E., Keifer, P. A., and Saarinen, T. (1992) Pure Absorption Gradient Enhanced Heteronuclear Single Quantum Correlation Spectroscopy with Improved Sensitivity. *J. Am. Chem. Soc.* **114**, 10663–10665.
- Gabizon, A., Horowitz, A. T., Goren, D., Tzemach, D., Mandelbaum-Shavit, F., Qazen, M. M., and Zalipsky, S. (1999) Targeting folate receptor with folate linked to extremities of poly(ethylene glycol)-grafted liposomes: in vitro studies. *Bioconjugate Chem.* **10**, 289–298.
- Boreham, C. J., Broomhead, J. A., and Fairlie, D. P. A. (1995) Pt and <sup>15</sup>N N. M. R. (1981) Study of the Anticancer Drug, cis-Diamminedichloroplatinum(II), and its Hydrolysis and Oligomerization Products. *Aust. J. Chem.* **34**, 659–669.

- (28) Marks, T. A., Woodman, R. J., Geran, R. I., Billups, L. H., and Madison, R. M. (1977) Characterization and responsiveness of the Madison 109 lung carcinoma to various antitumor agents. *Cancer Treat. Rep.* 61, 1459–1470.
- (29) Horowitz, A. T., Barenholz, Y., and Gabizon, A. A. (1992) In vitro cytotoxicity of liposome-encapsulated doxorubicin: dependence on liposome composition and drug release. *Biochim. Biophys. Acta* 1109, 203–209.
- (30) Miller, S. A., Dykes, D. D., and Polesky, H. F. (1988) A simple salting out procedure for extracting DNA from human nucleated cells. *Nucleic Acids Res.* 16, 1215.
- (31) Senter, P. D., Wallace, P. M., Svensson, H. P., Vruthula, V. M., Kerr, D. E., Hellstrom, I., and Hellstrom, K. E. (1993) Generation of cytotoxic agents by targeted enzymes. *Bioconjugate Chem.* 4, 3–9.
- (32) Rui, Y. J., Wang, S., Low, P. S., and Thompson, D. H. (1998) Dipalmenylcholine-folate liposomes: an efficient vehicle for intracellular drug delivery. *J. Am. Chem. Soc.* 120, 11213–11218.
- (33) Qualls, M. M., and Thompson, D. H. (2001) Chloroaluminum phthalocyanine tetrasulfonate delivered via acid-labile dipalmenylcholine-folate liposomes: Intracellular localization and synergistic phototoxicity. *Int. J. Cancer* 93, 384–392.

BC025642L



# Affinity Thermoprecipitation and Recovery of Biotinylated Biomolecules via a Mutant Streptavidin–Smart Polymer Conjugate

Noah Malmstadt, David E. Hyre, Zhongli Ding, Allan S. Hoffman,\* and Patrick S. Stayton\*

Department of Bioengineering, University of Washington, Seattle Washington 98195. Received August 14, 2002

A system has been developed for reversibly binding and thermoprecipitating biotinylated macromolecules. A high off-rate Ser45Ala (S45A) streptavidin mutant has been covalently conjugated to poly(*N*-isopropylacrylamide) (PNIPAAm), a temperature-responsive polymer. The resulting conjugate is shown to coprecipitate biotinylated immunoglobulin G (IgG) and a biotinylated oligonucleotide in response to a thermal stimulus. Thermally precipitated biotinylated macromolecules can be released from the S45A–PNIPAAm conjugate by simple treatment with excess free biotin. This release step has been shown to be unique to the mutant streptavidin conjugate—a conjugate of wild type (WT) streptavidin and PNIPAAm does not release bound biotinylated molecules upon treatment with excess free biotin. The capture efficiency (fraction of target molecule precipitated from solution) of the S45A–PNIPAAm conjugate is similar to that of the WT–PNIPAAm conjugate for the biotinylated IgG target molecule (near 100%), but significantly smaller for the biotinylated oligonucleotide target (approximately 60% for the S45A–PNIPAAm conjugate compared to 80% for the WT–PNIPAAm conjugate). The release efficiency (fraction of originally precipitated target molecule released after treatment with free biotin) of the S45A–PNIPAAm conjugate is 70–80% for the biotinylated IgG target and nears 100% for the biotinylated oligonucleotide target. This system demonstrates the use of a high off-rate streptavidin mutant to add reversibility to a system based on smart-polymer–streptavidin conjugates.

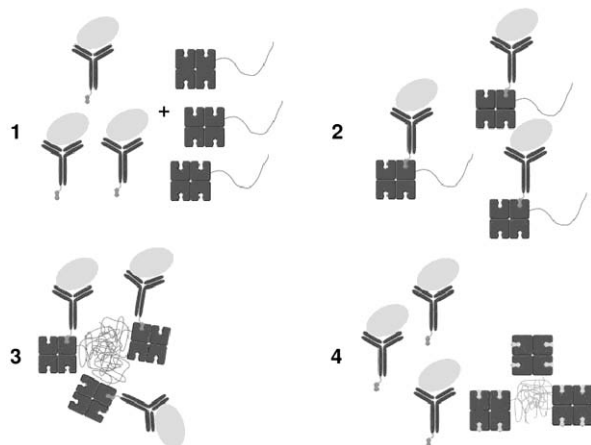
## INTRODUCTION

Streptavidin is a 53 kDa tetrameric protein produced in nature by the bacterium *Streptomyces avidinii* (1–3). Each of the four streptavidin monomers binds one molecule of the vitamin biotin with extraordinarily high affinity: one of the strongest known noncovalent interactions in biochemistry, with an association constant ( $K_a$ ) of  $10^{14}$ – $10^{15}$  M<sup>-1</sup> (3, 4). Because of this high affinity, the capacity of streptavidin to bind multiple biotin molecules, and the ease with which a great variety of molecules can be biotinylated, the biotin–streptavidin system has become a key component of many processes in biotechnology and the biomedical sciences (5, 6). The utility of the biotin–streptavidin system is limited, however, by the difficulty in releasing captured biotinylated targets. The half-life of the binding interaction between wild-type (WT) streptavidin and biotin at 25 °C is over 35 h (7, 8). The potential for utilizing site-directed streptavidin mutants to introduce reversibility has been shown previously by our group (9) and more recently by others (10, 11). In the work presented here, we show that a site-directed mutant of streptavidin that displays a relatively high biotin off-rate can be used in combination with “smart” polymers to create a reversible molecular separations systems for biotinylated targets. The mutant protein, in which residue 45 has been changed from serine to alanine via recombinant techniques, has a biotin off-rate of 0.05 s<sup>-1</sup> at 37 °C, corresponding to a binding half-

life of 14 s (12). Hence, when a complex of mutant (termed S45A) streptavidin bound to biotinylated macromolecule is treated with an excess of free biotin, the macromolecule should be completely displaced by the free biotin within minutes.

In the work presented here, this capacity for release has been investigated in the context of an affinity thermoprecipitation system, in which a conjugate of S45A streptavidin and thermoresponsive smart polymer serves as a bioseparation agent for a variety of biotinylated macromolecules. Affinity precipitation systems—bioseparation systems in which a target molecule is bound in solution to a species which can later be precipitated from solution along with the target—have been a subject of much recent interest (13–17). Since binding takes place in solution phase, affinity precipitation systems avoid the mass transport limitations inherent in affinity chromatography. Affinity precipitation technologies also result in smaller product volumes than affinity chromatography, simplifying downstream processing. One approach to affinity precipitation is to conjugate the affinity moiety to a “smart” polymer that undergoes a phase transition upon the application of a specific external stimulus (18–20). After binding to the affinity-modified polymer in solution, the target molecule is precipitated via the phase-change stimulus of the polymer. Here we make use of poly(*N*-isopropylacrylamide) (PNIPAAm), which is soluble at low temperatures but undergoes a hydrophobic transition, aggregation, and precipitation at temperatures above about a lower critical solution temperature (LCST) that is dependent upon polymer molecular weight and solution conditions (21–23). We have conjugated PNIPAAm to S45A streptavidin to facilitate the affinity thermoprecipitation of various biotinylated biomolecules. This separation was followed by a release

\* Corresponding authors. A.S.H.: (address) Department of Bioengineering, Box 352255, University of Washington, Seattle, WA 98195; (tel) 206-543-9423; (fax) 206-543-6124; (e-mail) hoffman@u.washington.edu. P.S.S.: (address) Department of Bioengineering, Box 351721, University of Washington, Seattle, WA 98195; (tel) 206-685-8148; (fax) 206-685-8256; (e-mail) stayton@u.washington.edu.



**Figure 1.** Diagram of a proposed application of mutant streptavidin-smart polymer thermoprecipitation. A target molecule is incubated with a biotinylated antibody to that molecule. Mutant streptavidin-smart polymer conjugate is added to the mixture (1). The biotinylated antibody, with bound target molecule, binds the streptavidin-smart polymer conjugate (2). The phase transition stimulus of the smart polymer is triggered, and the resulting aggregates are separated from bulk solution (3). Free biotin is added to the complex, releasing the biotinylated antibody. Antibody-target complex is separated from the aggregated streptavidin-smart polymer conjugates (4).

step, in which the target molecule was freed from the PNIPAAm-streptavidin complex by treatment with excess free biotin. This system demonstrates the flexibility that a reversible biotin-streptavidin linkage can add to technologies built on smart polymer-mediated affinity separations and the biotin-streptavidin system. A prospective application of this system to an immunoseparation is shown diagrammatically in Figure 1.

#### MATERIALS AND METHODS

**Preparation of PNIPAAm.** Linear PNIPAAm containing a single terminal N-hydroxysuccinimidyl (NHS) ester group was synthesized according to a previously published protocol (24). The number-averaged molecular weight ( $M_n$ ) of this polymer was determined to be 11 028 by vapor pressure osmometry (VPO, device model OSV111, Knauer, Germany). The polymer LCST in pure water was determined to be 32 °C. To generate free (unmodified) PNIPAAm matching the molecular weight distribution of this NHS-terminated polymer, the NHS-terminated polymer was dissolved in deionized water at 3.2 mg/mL and incubated at room temperature for 48 h to allow for hydrolysis of the NHS group.

**Preparation of S45A and WT streptavidin.** The S45A streptavidin gene was constructed from the recombinant WT core streptavidin gene by PCR mutagenesis as described by Hyre et al. (12). Recombinant S45A and WT streptavidin were expressed and purified according to a previously published protocol (25).

**PNIPAAm-Streptavidin conjugation.** A solution of 20–30 mg/mL streptavidin (WT or S45A) in pH 7.6 phosphate buffered saline (PBS, 20mM phosphate, 5mM sodium chloride) was prepared. To this solution 50  $\mu$ L of 140 mg/mL NHS-PNIPAAm solution in DMF was added. This reaction mixture was incubated with rotation at 4 °C overnight. Following reaction, the PNIPAAm-containing species were thermoprecipitated. Thermoprecipitation proceeded as follow: the reaction mixture was centrifuged for 10 minutes at 14 000 rpm in a microcentrifuge, which had been heated to 37 °C. The pellet was resolubilized by incubation in 150  $\mu$ L of pH 7.6 PBS (20mM

phosphate, 5mM sodium chloride) at 4 °C for 1 h followed by vortexing. The supernatant was subjected to heated centrifugation twice more, with resolubilization of each resultant pellet. The resolubilized pellets were pooled, and the supernatant was reserved. The supernatant contained a high concentration of unreacted streptavidin—to this solution was added a fresh volume of NHS-PNIPAAm solution, and the reaction and thermoprecipitation process was repeated. The reaction was repeated twice more, until most of the streptavidin in the supernatant had been reacted. The resolubilized pellets from each reaction were pooled and subjected to iminobiotin affinity chromatography (26), removing all unreacted polymer (iminobiotin-modified agarose beads were obtained from Pierce, Rockford, IL). Thermoprecipitation was repeated a final time with the resultant conjugate solution, to remove any unreacted streptavidin.

**Biotinylated IgG and Oligonucleotide Preparation.** Immunoglobulin G (IgG) was used as a model protein target molecule. Pooled bovine IgG was obtained from Sigma (St. Louis, MO) and dissolved at 15 mg/mL in pH 7.6 PBS (20 mM phosphate, 5 mM sodium chloride). To 800  $\mu$ L of this solution was added 20  $\mu$ L of 9 mg/mL NHS-LC-biotin (Pierce) in DMF. Following incubation on ice for 10 min, the reaction was quenched by the addition of 100  $\mu$ L 100 mM pH 7.6 Tris buffer. The reaction mixture was then dialyzed overnight across a 10,000 molecular weight cutoff (MWCO) membrane into pH 7.6 PBS, with one buffer exchange. This biotinylated IgG was then fluorescently labeled with Texas Red C2 maleimide (Molecular Probes, Eugene OR), a thiol-reactive label. The IgG solution was concentrated to 400  $\mu$ L, and 40  $\mu$ L of 20 mM tris(2-carboxyethyl) phosphine hydrochloride (TCEP-HCl, Pierce) solution was added to reduce disulfides. To this solution was added 40  $\mu$ L of 30 mg/mL Texas Red C2 maleimide in DMSO. This reaction mixture was rotated at 4 °C for 4 h and then dialyzed across a 10 000 MWCO membrane into pH 7.6 PBS for 48 h, with two buffer exchanges.

Biotinylated, fluorescently labeled oligonucleotide was obtained directly from Integrated DNA Technologies (IDT, Coralville, IA). The single-stranded oligonucleotide had the sequence GGACTCAGGCTTATAGCTGT and contained a 5' fluorescein modification and a 3' biotin modification (with a tri-(ethylene glycol) spacer).

**Analysis of Conjugation Products.** The conjugation products were assayed spectrophotometrically using a Hewlett-Packard model 8452A spectrophotometer (HP, Cupertino, CA). To determine the degree of biotinylation of the IgG-biotin conjugate, the 2-(4'-hydroxyazobenzene) benzoic acid (HABA) assay (27) was used. IgG concentration was monitored based on the optical density of the IgG solution at 280 nm, using an extinction coefficient of 210 000  $\text{cm}^{-1} \text{M}^{-1}$ . The fluorophore-labeling ratio for the IgG species was determined by measuring the optical density of the solution at 582 nm (the excitation maximum of Texas Red), using an extinction coefficient of 112 000  $\text{cm}^{-1} \text{M}^{-1}$ . PNIPAAm-streptavidin conjugation yield was determined by monitoring the optical density of the product solution at 280 nm, based on a streptavidin extinction coefficient of 139 000  $\text{cm}^{-1} \text{M}^{-1}$  for the tetramer.

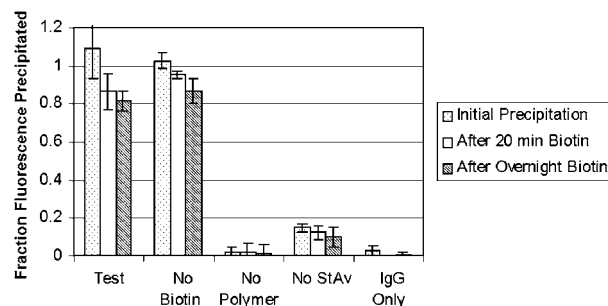
**Separation and Recovery of IgG Target.** Biotinylated, fluorescently labeled IgG (120 nM) was incubated with a 35 $\times$  molar excess (based on tetramer concentration) of either S45A-PNIPAAm conjugate or WT-PNIPAAm conjugate in 500  $\mu$ L of pH 7.6 PBS with 20 mM phosphate and 5 mM sodium chloride. To these IgG/streptavidin-PNIPAAm solutions were added bovine

serum albumin (BSA, Sigma) at 13  $\mu$ M to block nonspecific interactions and unconjugated 11 kDa PNIPAAm at 30  $\mu$ M to aid thermoprecipitation. The initial fluorescence of each solution was measured, and thermoprecipitation was performed in triplicate at 37  $^{\circ}$ C, as described above, with free PNIPAAm (to a concentration of 30  $\mu$ M) added to the supernatant after each centrifugation. The pellets were resolubilized in PBS and pooled such that the total volume of the pooled pellet solution was equal to the initial sample volume. BSA was added to each resolubilized pooled pellet solution to a concentration of 13  $\mu$ M. The fluorescence of the pooled resolubilized pellet solution was measured and a 25 $\times$  molar excess (relative to streptavidin binding sites) of free biotin (Sigma) was added. After incubating this solution at room temperature for 20 min, the thermoprecipitation process was repeated, and the fluorescence of the resulting pooled pellet solution was measured. To this resolubilized pellet solution was added a 25 $\times$  molar excess of free biotin, and the solution was then incubated at room temperature overnight. Following this incubation, the thermoprecipitation process was repeated a final time, and the fluorescence of the resulting pooled pellet solution was measured. Controls for this experiment included samples containing unconjugated streptavidin rather than streptavidin–PNIPAAm conjugate, samples containing free PNIPAAm but no streptavidin–PNIPAAm conjugate, samples containing neither streptavidin nor PNIPAAm, and samples to which no free biotin was added. All experiments were performed in triplicate. Fluorescence measurements were taken with a Hitachi F-4500 fluorescence spectrophotometer (Hitachi Instruments, Inc., Tokyo, Japan).

**Separation and Recovery of Oligonucleotide Target.** Experiments investigating the separation of the biotinylated oligonucleotide target via the streptavidin–PNIPAAm conjugates were performed in the same manner as the experiments investigating the separation of biotinylated IgG, with the following exceptions. Samples were prepared in 250  $\mu$ L pH 7.6 PBS with 20 mM phosphate and 100 mM sodium chloride. Samples contained a 120 nM concentration of biotinylated, fluorescently labeled oligonucleotide rather than IgG. In addition, samples that were thermoprecipitated at 28  $^{\circ}$ C contained 250 mM ammonium sulfate, which served to depress the LCST of PNIPAAm. Component concentrations were otherwise as described above. Thermoprecipitations were performed as described above, at either 37 or 28  $^{\circ}$ C. Biotin additions were as described above, maintaining a molar ratio of 25 $\times$  excess free biotin relative to available biotin-binding sites. Controls were similar to those described above. Fluorescence measurements for these experiments were performed on a Perkin-Elmer LS50B fluorescence spectrophotometer (Perkin-Elmer Instruments, Inc., Shelton, CT).

## RESULTS AND DISCUSSION

**Characterization of Conjugation Products.** The HABA assay of the IgG–biotin conjugate revealed an average of 1.5 biotin groups per IgG molecule and the ratio of IgG dye labeling was similar. For the complete streptavidin–PNIPAAm conjugation procedure (four reaction cycles), the overall yield of conjugate was approximately 20%. Similar results were observed for WT and S45A streptavidin. The low yield is likely due to the relative inaccessibility of primary amines on the surface of the streptavidin molecule, as well as hydrolysis of NHS groups during polymer storage.

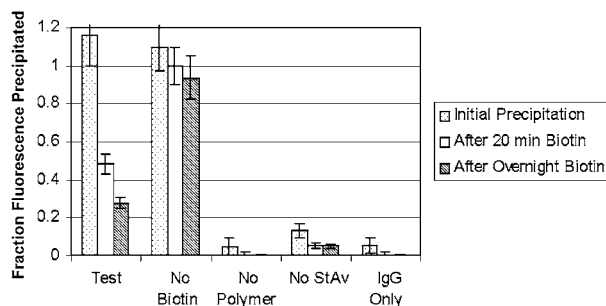


**Figure 2.** Data for thermoprecipitation and recovery of biotinylated IgG via WT streptavidin–PNIPAAm conjugate. Data are shown for the sample containing 120 nM biotinylated IgG and 4.2  $\mu$ M thermosensitive streptavidin–polymer conjugate in 500  $\mu$ L pH 7.6 PBS (labeled “Test”), as well as for four control samples. All data points describe the amount of fluorescence measured in a pellet formed by thermoprecipitation at 37  $^{\circ}$ C, normalized to the fluorescence measured in the sample prior to any thermoprecipitation. This fraction of initial fluorescence contained in the precipitate is shown for each sample at three points: after an initial thermoprecipitation; after a thermoprecipitation that followed a 20 min incubation with excess free biotin; and after a thermoprecipitation that followed an overnight incubation with excess free biotin. The exception to this is the “no biotin” control, to which no free biotin was added at any point; the three points shown for this sample are from three thermoprecipitations timed similarly to those for the other samples. Error bars are  $\pm 1$  standard deviation over three experiments.

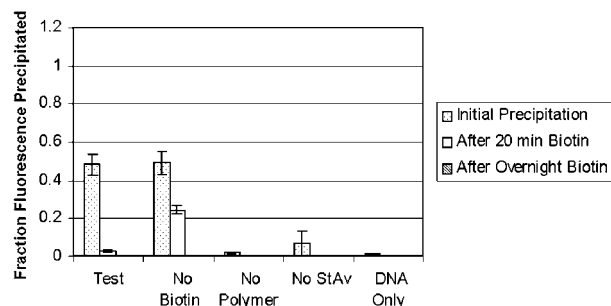
**Thermoprecipitation and Release of Biotinylated IgG.** Figure 2 shows the results of a separation/release experiment with biotinylated IgG and WT–PNIPAAm conjugate. The data shown are the fluorescent intensities of the resolubilized pellets at three points in the experiment—after an initial thermoprecipitation, after a thermoprecipitation which followed a 20 min incubation with biotin, and after a thermoprecipitation which followed an overnight incubation with biotin—normalized to the initial fluorescent intensity. The three bars corresponding to the experiment as described are on the far left. Also shown are data corresponding to the following controls: no biotin added in the release steps, no polymer present (only unconjugated streptavidin present), no streptavidin present (only unconjugated polymer present), and neither polymer nor streptavidin present. Error bars are plus and minus one standard deviation over a series of three experiments. Except for a small coprecipitation effect evident with the unconjugated polymer, there was no nonspecific IgG thermoprecipitation observed in the control experiments. The WT–PNIPAAm conjugate was an effective thermoprecipitation agent, capable of separating all initially present biotinylated IgG. Release, however, was not effective. Even after overnight incubation with free biotin, only about 10–20% of the fluorescence was freed from the conjugate. This negligible release effect was comparable to the control in which free biotin has not been added.

These results can be contrasted to the excellent reversibility observed for biotinylated IgG and the S45A–PNIPAAm conjugate, shown in Figure 3. The S45A–PNIPAAm conjugate proved to be as effective a thermoprecipitation agent as the WT–PNIPAAm complex. However, it did release biotinylated IgG upon treatment with free biotin. 50–60% of the initially precipitated fluorescence was freed after 20 min incubation at 20  $^{\circ}$ C with biotin and 70–80% of this fluorescence was freed after overnight incubation with biotin. This release effect was not seen in the biotin-free control. Even after overnight incubation with free biotin, some biotinylated





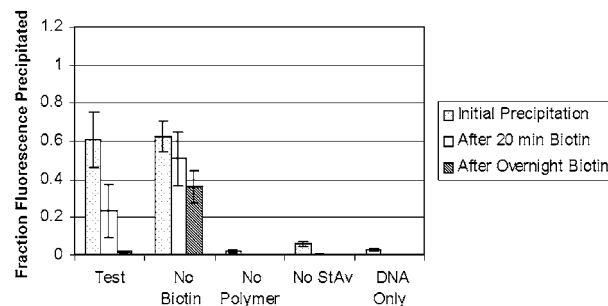
**Figure 3.** Thermoprecipitation and recovery of biotinylated IgG via S45A streptavidin–PNIPAAm conjugate. Samples are as described for Figure 2.



**Figure 4.** Thermoprecipitation and recovery of biotinylated oligonucleotide via S45A streptavidin–PNIPAAm conjugate at 37 °C. Data are shown for the sample containing 120 nM biotinylated oligonucleotide and 4.2  $\mu$ M thermosensitive streptavidin–polymer conjugate in 250  $\mu$ L of pH 7.6 PBS (labeled “Test”), as well as for four control samples. All data points describe the amount of fluorescence measured in a pellet formed by thermoprecipitation at 37 °C, normalized to the fluorescence measured in the sample prior to any thermoprecipitation. Data are organized as in Figure 2.

IgG remained bound to the S45A–PNIPAAm conjugate. This residually bound IgG might be explained by the fact that the IgG population contained some multiply biotinylated protein molecules. If multiple biotin moieties on a single IgG molecule bind to the same streptavidin molecule, an avidity effect is expected. It has been shown (28) that high off-rate streptavidin mutant molecules interacting with a biotinylated surface demonstrate a radically decreased apparent off-rate when allowed to bind bivalently. In the context of these thermoprecipitation experiments, this decreased off-rate was observed as a population of multiply biotinylated IgG molecules that did not dissociate from the S45A–PNIPAAm complex in the same time frame as the majority of the biotinylated IgG.

**Thermoprecipitation and Release of a Biotinylated Oligonucleotide.** To control for this effect, separation and release were investigated for a molecule containing only a single biotin moiety—a biotinylated oligonucleotide. The data for separation and release of the oligonucleotide target via the S45A–PNIPAAm conjugate at 37 °C are shown in Figure 4. There are two important features apparent in these data. The release of the biotinylated target after treatment with free biotin was rapid and nearly total, and a much smaller fraction of the initially present target molecule was precipitated than in the case of biotinylated IgG. The complete release demonstrates that a singly biotinylated molecule is not retained by the high off-rate conjugate in the presence of excess free biotin. The smaller fraction of initially precipitated oligonucleotide is indicative of a decrease in the equilibrium affinity of the S45A–PNIPAAm conju-

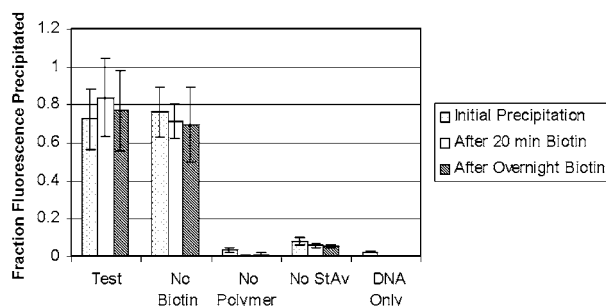


**Figure 5.** Thermoprecipitation and recovery of biotinylated oligonucleotide via S45A streptavidin–PNIPAAm conjugate at 28 °C. Data are shown for the sample containing 120 nM biotinylated oligonucleotide and 4.2  $\mu$ M thermosensitive streptavidin–polymer conjugate in 250  $\mu$ L of pH 7.6 PBS with 250 mM ammonium sulfate (labeled “Test”), as well as for four control samples. All data points describe the amount of fluorescence measured in a pellet formed by thermoprecipitation at 28 °C, normalized to the fluorescence measured in the sample prior to any thermoprecipitation. Data are organized as in Figure 2.

gate for biotinylated oligonucleotide relative to that for biotinylated IgG. This is further indicated by the data for the biotin-free control (second cluster of bars from the left, Figure 4), which show only a fraction of the initially precipitated oligonucleotide being captured in the second precipitation. This is consistent with a reequilibration of the streptavidin–biotin binding, at a lower-than-expected affinity, following the initial precipitation and removal of the unbound oligonucleotide in the supernatant. The affinity of biotinylated target will be dependent on the specific type of linker and connecting regions. This is an interesting demonstration of the fact that not all biotinylated targets bind at the same high-affinity, and this represents a challenge to the use of streptavidin or avidin affinity mutants.

To improve the separation of biotinylated oligonucleotide, the separation experiments were repeated at a lower temperature (28 °C), in the presence of a moderate concentration of ammonium sulfate, which lowers the LCST of PNIPAAm. Figure 5 shows the data for thermoprecipitation and recovery of a biotinylated oligonucleotide 20-mer via S45A–PNIPAAm conjugate at 28 °C. The fraction of biotin–DNA initially precipitated is higher than at 37 °C, and the biotin-free sample remains bound to a much higher fraction of biotin–DNA throughout the experiment. This indicates that the increase in the biotin–S45A affinity (and decrease in off rate) between 37 °C and 28 °C is large enough to significantly impact the utility of S45A as an affinity ligand. This is expected, given the strong temperature dependence of S45A biotin affinity and off-rate (12). The data for the S45A conjugate can be compared with those for the WT–PNIPAAm conjugate and biotinylated DNA (Figure 6). These data are similar to those for the experiments with WT–PNIPAAm and biotinylated IgG, revealing nearly complete and specific thermoprecipitation and no recovery in response to treatment with free biotin.

The measured  $K_a$  for S45A streptavidin at 37 °C is  $4.9 \times 10^9 \text{ M}^{-1}$  (12). At the concentrations of streptavidin and biotinylated DNA used in these experiments, over 99.99% of the biotinylated oligonucleotide originally present in solution should be bound to streptavidin–PNIPAAm conjugate molecules at equilibrium. In order for the binding fraction to decrease to 50% as observed, the  $K_a$  of the interaction must decrease by over four orders of magnitude. Since a shift in affinity is observable in the oligonucleotide separation experiments, but not in the IgG separation experiments, this effect is specific to the



**Figure 6.** Thermoprecipitation and recovery of biotinylated oligonucleotide via WT streptavidin-PNIPAAm conjugate at 28 °C. Samples are as described for Figure 5.

biotinylated oligonucleotide. Similar decreases in the affinity of the biotin-streptavidin system have been observed for various chemical modifications to the biotin tail (29); it is conceivable therefore that the conjugation of an oligonucleotide to biotin would decrease the affinity of the system. A 4-order magnitude decrease in the affinity of WT streptavidin for biotinylated oligonucleotide would not be expected to have as drastic an impact in these experiments, since the affinity of WT for unmodified biotin is nearly 4 orders of magnitude greater than that of S45A. The observed fraction of biotinylated oligonucleotide thermoprecipitated by the WT-PNIPAAm conjugate is therefore consistent with a general large decrease in the affinity of streptavidin for biotin conjugated to an oligonucleotide.

## CONCLUSIONS

We have demonstrated an affinity precipitation system in which the replacement of WT streptavidin with a high off-rate streptavidin mutant allows for the triggered release of biotinylated macromolecules from the smart polymer affinity precipitation agent. This release is a demonstration of the reversibility that high off-rate streptavidin mutants can impart to systems relying on the biotin-streptavidin interaction. The system developed here also demonstrates some potential pitfalls of relying on high off-rate streptavidin mutants. Binding to multiply biotinylated molecules can partially eliminate the reversibility of the system, and unexpected decreases in the off-rate due to biotin modification can have drastic effects since the baseline off-rate is already unusually high. However, the techniques presented here open a range of new possibilities for biotin-streptavidin technology and demonstrate the power of coupling protein engineering and smart polymer technologies to develop novel conjugate molecules with highly specified properties.

## ACKNOWLEDGMENT

The NIH (Grant No.53771 and Grant No. DKY9655), the UW Office of Technology Licensing, the Washington Research Foundation, and the Washington Technology Center are gratefully acknowledged for their support of this project.

## LITERATURE CITED

- (1) Chaliot, L., Miller, F. W., Tausig, F., and Wolf, F. J. (1963) Antibiotic MSD-235. 2. Separation and purification of synergistic components. *Antimicrob. Agents Chemother.* 3, 28–32.
- (2) Green, N. M. (1975) Avidin. *Adv. Protein Chem.* 29, 85–133.

- (3) Green, N. M. (1990) Avidin and streptavidin. *Methods Enzymol.* 184, 51–67.
- (4) Green, N. M. (1963) Avidin: 1. The Use of [14C]biotin for kinetic studies and for assay. *Biochem. J.* 89, 585–591.
- (5) Diamandis, E. P., and Christopoulos, T. K. (1991) The biotin (strept)avidin system – principles and applications in biotechnology. *Clin. Chem.* 37, 625–636.
- (6) Wilchek, M., and Bayer, E. A. (1990) Applications of avidin-biotin technology: literature survey. *Methods Enzymol.* 184, 14–45.
- (7) Chilkoti, A., and Stayton, P. S. (1995) Molecular-origins of the slow streptavidin-biotin dissociation kinetics. *J. Am. Chem. Soc.* 117, 10622–10628.
- (8) Piran, U., and Riordan, W. J. (1990) Dissociation rate constant of the biotin-streptavidin complex. *J. Immunol. Methods.* 133, 141–143.
- (9) Chilkoti, A., Schwartz, B. L., Smith, R. D., Long, C. J., and Stayton, P. S. (1995) Engineered chimeric streptavidin tetramers as novel tools for bioseparations and drug-delivery. *Biotechnology* 13, 1198–1204.
- (10) Qureshi, M. H., Yeung, J. C., Wu, S. C., and Wong, S. L. (2001) Development and characterization of a series of soluble tetrameric and monomeric streptavidin muteins with differential biotin binding affinities. *J. Biol. Chem.* 276, 46422–46428.
- (11) Reznik, G. O., Vajda, S., Sano, T., and Cantor, C. R. (1998) A streptavidin mutant with altered ligand-binding specificity. *Proc. Nat. Acad. Sci. U.S.A.* 95, 13525–13530.
- (12) Hyre, D. E., Le Trong, I., Freitag, S., Stenkamp, R. E., and Stayton, P. S. (2000) Ser45 plays an important role in managing both the equilibrium and transition state energetics of the streptavidin-biotin system. *Protein Sci.* 9, 878–885.
- (13) Eggert, M., Baltes, T., Garret-Flaudy, F., and Freitag, R. (1998) Affinity precipitation – an alternative to fluidized bed adsorption? *J. Chrom. A.* 827, 269–280.
- (14) Luong, J. H. T., and Nguyen, A.-L. (1992) Novel separations based on affinity interactions. In *Bioseparation* (Tsao GT, Belfort G, Eds.) pp 137–158, Springer-Verlag, Berlin.
- (15) Niederauer, M. Q., and Glatz, C. E. (1992) Selective Precipitation. In *Bioseparation* (Tsao GT, Belfort G, Eds.) pp 159–188, Springer-Verlag, Berlin.
- (16) Monji, N., and Hoffman, A. S. (1987) A novel immunoassay system and bioseparation process based on thermal phase separating polymers. *Appl. Biochem. Biotech.* 14, 107–120.
- (17) Chen, J. P., and Hoffman, A. S. (1990) Protein conjugates 2. Affinity precipitation of human immuno-gamma-globulin by a poly(N-isopropylacrylamide)-protein-A conjugate. *Biomaterials* 11, 631–634.
- (18) Anastase-Ravion, S., Ding, Z., Pelle, A., Hoffman, A. S., and Letourneur, D. (2001) New antibody purification procedure using a thermally responsive poly(N-isopropylacrylamide)-dextran derivative conjugate. *J. Chromatogr., B* 761, 247–254.
- (19) Fong, R. B., Ding, Z. L., Long, C. J., Hoffman, A. S., and Stayton, P. S. (1999) Thermoprecipitation of streptavidin via oligonucleotide-mediated self-assembly with poly (N-isopropylacrylamide). *Bioconj. Chem.* 10, 720–725.
- (20) Hoffman, A. S., Stayton, P. S., Bulmus, V., Chen, G. H., Chen, J. P., Cheung, C., et al. (2000) Really smart bioconjugates of smart polymers and receptor proteins. *J. Biomed. Mater. Res* 52, 577–586.
- (21) Heskins, M., and Guillet, J. E. (1968) Solution properties of poly(N-isopropylacrylamide). *J. Macromol. Sci.-Chem.* A2, 1441–1455.
- (22) Hoffman, A. S., and Monji, N. (1987) A novel immunoassay system and bioseparation process based on thermal phase separating polymers. *App. Biochem. Biotech.* 14, 107–120.
- (23) Takei, Y., Aoki, T., Sanui, K., Ogata, N., Okano, T., and Sakurai, Y. (1993) Temperature-responsive bioconjugates. 1. Synthesis of temperature-responsive oligomers with reactive end groups and their coupling to biomolecules. *Bioconjugate Chem.* 4, 42–46.
- (24) Ding, Z. L., Chen, G. H., and Hoffman, A. S. (1996)

- Synthesis and purification of thermally sensitive oligomer-enzyme conjugates of poly(N-isopropylacrylamide)-trypsin. *Bioconjugate Chem.* 7, 121–125.
- (25) Chilkoti, A., Tan, P. H., and Stayton, P. S. (1995) Site-directed mutagenesis studies of the high-affinity streptavidin–biotin complex—contributions of tryptophan residue-79, residue-108, and residue-120. *Proc. Nat. Acad. Sci. U.S.A.* 92, 1754–1758.
- (26) Heney, G., and Orr, G. A. (1981) The purification of avidin and its derivatives on 2-iminobiotin-6-aminoethyl-Sepharose 4B. *Anal. Biochem.* 114, 92–96.
- (27) Green, N. M. (1970) Spectrophotometric determination of avidin and biotin. *Methods Enzymol.*, 18, 418.
- (28) Perez-Luna, V. H., O'Brien, M. J., Opperman, K. A., Hampton, P. D., Lopez, G. P., Klumb, L. A., et al. (1999) Molecular recognition between genetically engineered streptavidin and surface-bound biotin. *J. Am. Chem. Soc.* 121, 6469–6478.
- (29) Wilbur, D. S., Chyan, M. K., Pathare, P. M., Hamlin, D. K., Frownfelter, M. B., and Kegley, B. B. (2000) Biotin reagents for antibody pretargeting. 4. Selection of biotin conjugates for in vivo application based on their dissociation rate from avidin and streptavidin. *Bioconjugate Chem.* 11, 569–583.

BC020055L



# Synthesis of Linear Polyethylenimine Derivatives for DNA Transfection

Blandine Brissault,<sup>†</sup> Antoine Kichler,<sup>‡</sup> Christine Guis,<sup>†</sup> Christian Leborgne,<sup>‡</sup> Olivier Danos,<sup>‡</sup> and Hervé Cheradame<sup>\*,†</sup>

Laboratory "Matériaux Polymères aux Interfaces", UMR CNRS 7581, University of Evry, Bld Mitterrand, 91025 Evry Cedex, France, and Généthon III-URA 1923 CNRS, 1 rue de l'Internationale, 91000 Evry, France. Received July 20, 2002; Revised Manuscript Received February 13, 2003

A series of linear polymers containing varying amounts of ethylenimine or *N*-propylethylenimine units were synthesized by hydrolysis and/or reduction of polyethyloxazolines. The  $pK_a$ s of the polyamines were determined potentiometrically. Gel mobility shift assay showed that the efficiency of DNA complexation was related to the fraction of amino groups that are protonated at neutral pH. The effects of cationic charge density and molar weight of the polymers on the transfection efficiency were evaluated on HepG2 cells. The results obtained with different copolymers show that the transfection efficiency primarily depends on the fraction of ethylenimine units included in the polymer albeit the molar weight is also of importance. On the basis of the results obtained with poly(*N*-propylethylenimines), we also demonstrate that the high transfection efficiency of polyethylenimines does not solely rely on their capacity to capture protons which are transferred into the endo-lysosomes during acidification.

## INTRODUCTION

The development in the past decade of vectors allowing delivery of genes into eukaryotic cells opened the possibility to treat genetic as well as acquired diseases by using DNA as a prodrug. Although nonviral vectors are significantly less efficient in mediating gene transfer than viral ones, they present several advantages such as ease of production and simplicity of handling. A large variety of cationic compounds, among them lipids, polymers, and peptides, were shown to be able to efficiently deliver nucleic acids into numerous cell lines. However, only a few of these vectors allow transgene expression after systemic administration of DNA complexes. One of the most powerful and versatile families of carriers are polyethylenimines (PEIs)<sup>1</sup> (1–5).

It was proposed that the high gene transfer efficiency of these polymers is due to their capacity to buffer endosomes (1). This hypothesis is based on the chemical structure of PEIs: they differ from other polymers such as polylysine in that only a fraction of the amino groups are protonated at physiological pH (6, 7). When the pH in the endo-lysosomal compartment becomes acidic, the capacity of PEIs to capture protons causes osmotic swelling and subsequent endosome disruption ("proton sponge effect"), thus permitting the release of endocytosed material into the cytosol. These findings have led

to the design of new polymers that, like PEIs, exploit the acidification of the endocytic vesicles. A polylysine, partially substituted with histidyl residues which become cationic upon protonation of the imidazole groups at pH below 6.0, has a transfection efficiency that is significantly higher compared to nonmodified polylysine (8). These and other results (9, 10) support the idea that the buffering capacities of PEIs play an important role during transfection. However, since the exact mechanism of PEI-mediated transfection remains to be elucidated, it is possible that additional properties are required to obtain high transfection efficiencies.

We report here the synthesis of linear cationic polymers of various molar weight containing different proportions of ethylenimine units. Additionally, the synthesis of polymers containing *N*-propylethylenimine units was realized, allowing the study of the influence of the class of the amine function on the biological activity of the polymers.

Our work concerns the transfection efficiency of the different copolymers in relation to the fraction of ethylenimine units contained in the molecule. Moreover, we investigate whether the capacity of a polymer to capture protons in an acidic environment is sufficient to obtain a highly efficient transfection agent.

## EXPERIMENTAL PROCEDURES

**Materials.** Methylene chloride, acetonitrile (sds), and 2-ethyl-2-oxazoline (Aldrich) were distilled over calcium hydride. Poly(2-ethyl-2-oxazoline) (50 kDa) (Aldrich), hydrochloric acid 37% (Aldrich), lithium aluminum chloride in THF 1 mol/L (Aldrich), methyl *p*-toluenesulfonate (Aldrich), and sodium hydroxide pellets (Aldrich) were used as received. The branched polyethylenimine of 25 kDa was from Aldrich. SMD2-LucDITR (7.6 kb) is an expression plasmid encoding the firefly luciferase gene under the control of the human cytomegalovirus (CMV) immediate-early promoter.

\* To whom correspondence should be addressed. E-mail: herve.cheradame@chimie.univ-evry.fr.

<sup>†</sup> University of Evry.

<sup>‡</sup> Généthon III-URA 1923 CNRS.

<sup>1</sup> Abbreviations: PEI, polyethylenimine; BPEI, branched polyethylenimine; LPEI, linear polyethylenimine; EtOXZ, ethyl-oxazoline; PEtOXZ, polyethyloxazoline; LPNPEI, poly(*N*-propylethylenimine); LP(EtOXZ-*co*-EI), poly(ethyl-oxazoline-*co*-ethylenimine); LP(EtOXZ-*co*-NPEI), poly(ethyl-oxazoline-*co*-*N*-propylethylenimine); LP(EI-*co*-NPEI), poly(ethylenimine-*co*-*N*-propylethylenimine); LMW, low molar weight; DP<sub>n</sub>, number polymerization degree.

**Polymer Characterization.** Polymer analysis was performed by NMR spectroscopy (Bruker 200 or 300 MHz, solvents:  $\text{CDCl}_3$  or  $\text{D}_2\text{O}$ ); small angle neutron scattering spectroscopy (PACE (Orphée reactor, LLB Saclay), polymer concentration: 10 wt % in 1 M NaCl).

**Synthesis of Poly(2-ethyl-2-oxazoline) (PEtOXZ) of 17.5 kDa.** To a solution of methyl *p*-toluenesulfonate (74 mg, 397  $\mu\text{mol}$ ) in acetonitrile (60 mL) was added 8 mL of 2-EtOXZ (79 mmol). The reaction mixture was stirred refluxing for 143 h. After evaporation, the crude product was dissolved in methylene chloride and precipitated in diethyl ether. After filtration, the product was dried in vacuo yielding 7.05 g (88%) of a yellow powder.  $^1\text{H}$  NMR ( $\text{CDCl}_3$ ):  $\delta$  (ppm) = 1.1 (s,  $\text{NCOCH}_2\text{CH}_3$ ); 2.3 (m,  $\text{NCOCH}_2\text{CH}_3$ ); 3.4 (s,  $\text{N}(\text{COEt})\text{CH}_2\text{CH}_2$ ); 7.1 and 7.6 (d,  $H_{\text{ar}}$ ).

**Synthesis of a Linear Polyethylenimine (LPEI) of 7.3 kDa.** One gram of poly(2-ethyl-2-oxazoline) ( $M_{\text{n(NMR)}} = 17.5$  kDa) was heated with a mixture of concentrated (37%) hydrochloric acid (11 mL) and water (8 mL) at  $110^\circ\text{C}$  for 3 h. After evaporation in vacuo of the solvent and the newly formed propionic acid, the product was dissolved in water, and NaOH pellets were added until pH 9–10 was reached. The aqueous layer was then evaporated and the residue washed with methylene chloride. After filtration, the organic layer was dried ( $\text{Na}_2\text{SO}_4$ ) and evaporated. Yield was 320 mg (71%).  $^1\text{H}$  NMR ( $\text{CDCl}_3$ ):  $\delta$  (ppm) = 1.7 (br m,  $\text{NHCH}_2\text{CH}_2$ ); 2.7 (s,  $\text{NHCH}_2\text{CH}_2$ ).

**Synthesis of Poly(ethyl-oxazoline-co-ethylenimine) Copolymers (LP(EtOXZ-co-EI)).** As a typical example, a copolymer was prepared as follows: to 4 g of PEtOXZ<sub>50kDa</sub> (0.08 mmol) dissolved in 80 mL of water was added 2.4 mL of hydrochloric acid (29 mmol), and the mixture was heated under reflux for 67 h. The aqueous layer was then evaporated to remove the propionic acid. The residue was dissolved in water, and NaOH pellets were added for neutralization. After evaporation, the product was dissolved in methylene chloride. After filtration of sodium chloride and propionate residue, the organic layer was dried ( $\text{Na}_2\text{SO}_4$ ) and evaporated in vacuo. Yield of copolymer was 2.83 g (96%), with a 60% hydrolysis content.  $^1\text{H}$  NMR ( $\text{D}_2\text{O}$ ):  $\delta$  (ppm) = 1.1 (t,  $\text{NCOCH}_2\text{CH}_3$ ); 2.4 (q,  $\text{NCOCH}_2\text{CH}_3$ ); 2.8 (m,  $\text{NHCH}_2\text{CH}_2$ ); 3.5 (m,  $\text{N}(\text{COEt})\text{CH}_2\text{CH}_2$ ).

**Synthesis of Poly(ethyl-oxazoline-co-N-propylethylenimine) (LP(EtOXZ-co-NPEI)) and Poly(N-propylethylenimine) (LPNPEI).** To a solution of poly(2-ethyl-2-oxazoline)<sub>50kDa</sub> (4 g, 0.08 mmol) in methylene chloride (400 mL) was added  $\text{LiAlH}_4$  (17 mL, 17 mmol). The reaction mixture was stirred refluxing for 14 h. After addition of water, the organic layer was filtered to remove  $\text{LiOH}$  and  $\text{Al}(\text{OH})_3$  and then the solvent was evaporated. Yield was 2.16 g (58%) with a 64% reduction content for polymer.  $^1\text{H}$  NMR ( $\text{CDCl}_3$ ):  $\delta$  (ppm) = 0.8 (t,  $\text{NCH}_2\text{CH}_2\text{CH}_3$ ); 1.1 (t,  $\text{NCOCH}_2\text{CH}_3$ ); 1.4 (q,  $\text{NCH}_2\text{CH}_2\text{CH}_3$ ); 2.3 (t,  $\text{NCOCH}_2\text{CH}_3$ ); 2.6 (m,  $\text{N}(\text{CH}_2\text{Et})\text{CH}_2\text{CH}_2$ ); 3.4 (m,  $\text{N}(\text{COEt})\text{CH}_2\text{CH}_2$ ).

For poly(*N*-propylethylenimine) synthesis, an excess of  $\text{LiAlH}_4$  ( $[\text{LiAlH}_4]/[\text{NCOEt}] \geq 2$ ) solution was used to reduce 1 equiv of *N*-propionylethylenimine monomer unit of poly(2-ethyl-2-oxazoline).

**Synthesis of Poly(ethylenimine-co-N-propylethylenimine) Copolymers (LP(EI-co-NPEI)).** Typically, 4 g of PEtOXZ<sub>50kDa</sub> (0.08 mmol) was hydrolyzed with HCl (4.3 mL, 52 mmol) as described above. The product (2 g) was isolated and then reduced by  $\text{LiAlH}_4$  (30 mL, 30 mmol). Yield was 1.94 g (93%).  $^1\text{H}$  NMR ( $\text{D}_2\text{O}$ ):  $\delta$  (ppm) = 0.9 (t,  $\text{NCH}_2\text{CH}_2\text{CH}_3$ ); 1.5 (m,  $\text{NCH}_2\text{CH}_2\text{CH}_3$ );

2.6 (m,  $\text{NCH}_2\text{CH}_2\text{CH}_3$ ); 2.8 (m,  $\text{N}(\text{nPr})\text{CH}_2\text{CH}_2$ ); 3.0 (s,  $\text{NHCH}_2\text{CH}_2$ ).

**Potentiometric Titrations.** To a solution of either LPEI<sub>22kDa</sub> (33 mg, 1.4 mmol), LP(EtOXZ<sub>20</sub>-co-EI<sub>270</sub>-co-NPEI<sub>210</sub>) (22 mg, 0.7 mmol), or LPNPEI<sub>42.5kDa</sub> (45 mg, 1  $\mu\text{mol}$ ) in water was added HCl (10 mL,  $1.0 \times 10^{-1}$  mol/L). After stirring, potentiometric titration of solution was measured with  $9.2 \times 10^{-2}$  M NaOH as a titrant by using the automatic titration system LogipH. The  $\text{pK}_a$  values of monomer units, respectively *N,N*-diethylethylenediamine, *N,N,N,N*-tetraethylethylenediamine, and pentaethylenamine hexamine were also determined by direct titration with LogipH using 0.1 M HCl.

**Cell Culture.** Dulbecco's modified Eagle medium (DMEM; Gibco-BRL) was supplemented with 2 mM L-glutamine, 100 units/mL penicillin, 100  $\mu\text{g/mL}$  streptomycin, and 10% of fetal calf serum (FCS; HyClone). Human hepatocarcinoma cells (HepG2 cells; American Type Culture Collection) were used for the transfection experiments.

**Preparation of Polycation/DNA Complexes.** Four micrograms of plasmid DNA and the desired amount of polymer (1 or 0.5 mg/mL solution, depending on the polymer) were each diluted in 100  $\mu\text{L}$  of 150 mM NaCl and gently mixed. After 15 min of incubation, the mixture was diluted with serum-free medium to a final volume of 1 mL.

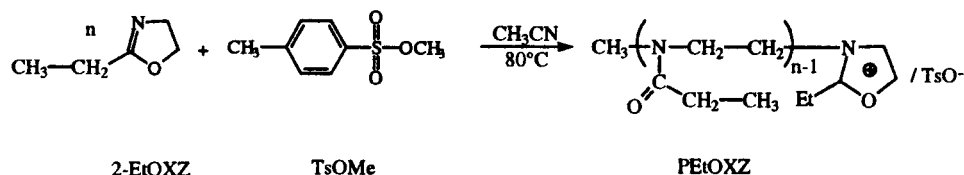
**DNA Retardation Assay.** DNA binding was studied by means of an agarose gel retardation assay. Plasmid DNA (1  $\mu\text{g}$ ) and increasing amounts of polymer were each diluted in 25  $\mu\text{L}$  of 150 mM NaCl and mixed. After 15 min, samples (20  $\mu\text{L}$ ) were electrophoresed through a 1% agarose gel using Tris-borate-EDTA buffer. The DNA was visualized after ethidium bromide staining.

**Transfection Experiments.** Cells plated in 24-well plates (Costar) were transfected once confluency reached 50–80%. For transfection, 0.5 mL of serum-free medium containing the DNA complexes were transferred into each well. After incubation for 2 h 30 to 4 h at  $37^\circ\text{C}$ , the medium was replaced with fresh one containing 10% FCS. Luciferase activity was measured 24–48 h after transfection. Each experiment was carried out several times; within a series, experiments were done in duplicate.

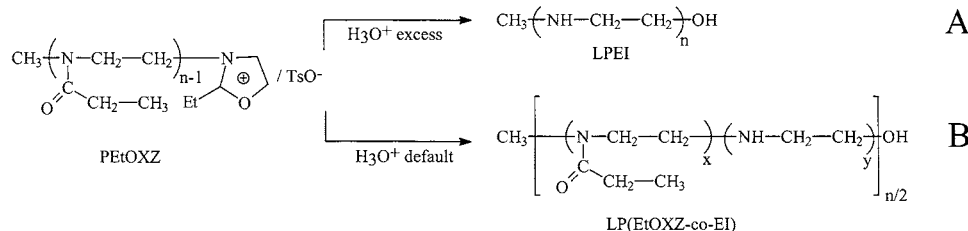
For luciferase activity, cells were harvested in 250  $\mu\text{L}$  of lysis buffer (8 mM  $\text{MgCl}_2$ , 1 mM dithiothreitol, 1 mM EDTA, 1% Triton X-100, 15% glycerol, and 25 mM Tris-phosphate buffer pH 7.8). The cell lysate was then transferred into Eppendorf tubes and centrifuged for 5 min at 10 000g to pellet debris. Luciferase light units were measured in a 96-well plate format with a PhL luminometer (Mediators Diagnostika) from an aliquot of the supernatant (50  $\mu\text{L}$ ). The measurement was done over 10 s after automatic injection of 100  $\mu\text{L}$  of assay buffer (lysis buffer without Triton X-100 supplemented with 2 mM ATP) and 100  $\mu\text{L}$  of luciferin solution (167  $\mu\text{M}$  in water; Molecular Probes). Luciferase background (about 300 light units) was subtracted from each value, and the transfection efficiency was expressed as total light units/10 s/well (with 1 light unit = 10 counts) and are the means of duplicates. The protein content of the transfected cells was measured by Bradford dye-binding using the BioRad protein assay.

## RESULTS AND DISCUSSION

**Synthesis of Linear Polyethylenimines (LPEIs).** High molar weight LPEI was obtained as described by hydrolysis of the commercial poly(2-ethyl-2-oxazoline)



**Figure 1.** Polymerization scheme of 2-EtOXZ initiated by TsOMe.



**Figure 2.** Scheme of acid hydrolysis of poly(2-ethyl-2-oxazoline) followed by neutralization (A) with an excess of HCl and (B) with a default of HCl.

**Table 1.**  $pK_a$  Values of the Polymers and Their Model Monomer Molecules

compd	TEDA <sup>a</sup>	DEDA <sup>b</sup>	PEHA <sup>c</sup>	LPNPEI 42.5 kDa	LPNPEI 170 kDa	LPEI 22 kDa	LP (EtOXZ <sub>20</sub> -co-EI <sub>270</sub> -co-NPEI <sub>210</sub> )
$pK_{a1}$	6.2	6.9					
$pK_{a2}$	9.5	9.9					
$pK_a^d$			8.2	7.2	7.2	7.9	7.7

<sup>a</sup> *N,N,N,N*-Tetraethylethylenediamine. <sup>b</sup> *N,N*-Diethylethylenediamine. <sup>c</sup> Pentaethylene hexamine. <sup>d</sup> Average  $pK_a$  values of the polymers.

(PEtOXZ) of 50 kDa in acidic aqueous medium under reflux (11). Oligomers of PEtOXZ, which are precursors of LPEIs of low molar mass, were synthesized by cationic polymerization of 2-ethyl-2-oxazoline (EtOXZ) initiated by methyl *p*-toluenesulfonate (TsOMe) in acetonitrile at 80°C, by varying the ratio [EtOXZ]<sub>0</sub>/[TsOMe]<sub>0</sub> (Figure 1). After workup and purification, two PEtOXZ of different molar mass were collected and analyzed by <sup>1</sup>H NMR spectroscopy. The spectra indicate the presence of peaks corresponding to the amide group at 1.1, 2.3, and 3.4 ppm, and the aromatic proton peaks corresponding to the tosylate counteranion of the ionic terminations of the polymer at 7.1 and 7.6 ppm (12). The peaks corresponding to the ethyl group of the oxazolinium ion and that of the initiating methyl group are hidden by other signals. As it was previously reported, polymerization of EtOXZ initiated by TsOMe proceeds according to a living process, all chains being under oxazolinium tosylate ends (12, 13). Consequently, the number average polymerization degrees (DP<sub>n</sub>) of polymers could be estimated by <sup>1</sup>H NMR spectroscopy from the determination of the ratio of the peak areas corresponding respectively to the propanoyl groups (1.1 ppm) to the aromatic part of tosylate ones (7.1 and 7.6 ppm). In these conditions, two PEtOXZ of 8 and 17.5 kDa were synthesized and characterized.

Acid hydrolysis of the poly(ethyl oxazoline)s was carried out using an excess of hydrochloric acid (Figure 2A). According to literature, the NMR spectra of the different LPEIs obtained (3.6, 7.3, and 22 kDa) confirmed the presence of methylene and NH groups by two peaks respectively at 2.7 and 1.7 ppm and the absence of signals corresponding to amide groups, showing thereby that the hydrolysis was complete (11). Of note, the disappearance of the signals corresponding to the tosylate counteranion of the precursors shows that the chain ends were hydrolyzed, producing a chain end of the type *N*-(2-hydroxyethyl)ethylenimine (Figure 2A). Neutron scattering of the protonated LPEI of 22 kDa showed that this polymer is a high molar mass rigid rod like structure,

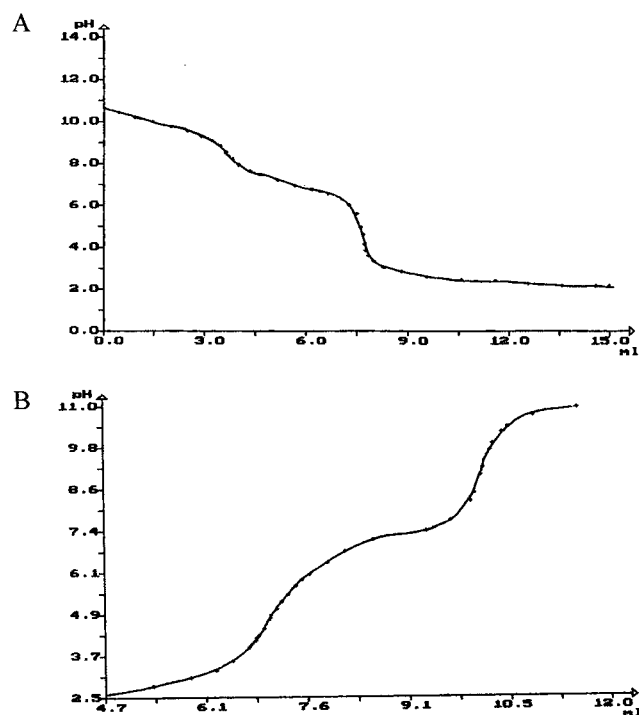
which is in tune with the repulsion effect of neighboring positive charges.

Potentiometric titration of this LPEI was then carried out. Neutral LPEI being insoluble in water, the titration requires the addition of an excess of hydrochloric acid and back-titration of this excess. The average  $pK_a$  is equal to 7.9 which shows that at a physiological pH more than 90% of the amino groups are protonated (Table 1). To check the relevancy of this  $pK_a$  determination, the titration of a model molecule, namely *N,N*-diethylethylenediamine, was also performed (Figure 3A). Two pH jumps can be seen on the curve corresponding to the two amino groups. This difference of basicity between two neighboring amino sites was already described in the literature (14). The protonation of one of the two sites on the same molecule influences the second one, thereby decreasing its basicity. The value of the acidity constants given by the pH at half equivalence ( $pK_{a1} = 9.9$  and  $pK_{a2} = 6.9$  respectively) allow to calculate an average  $pK_a$  of 8.4. The average  $pK_a$  of 7.9 of LPEI indicates a small decrease of the basicity of the amine functions in the polymer. This is due to the well-known polyelectrolyte effect and is in agreement with data reported in the literature (15).

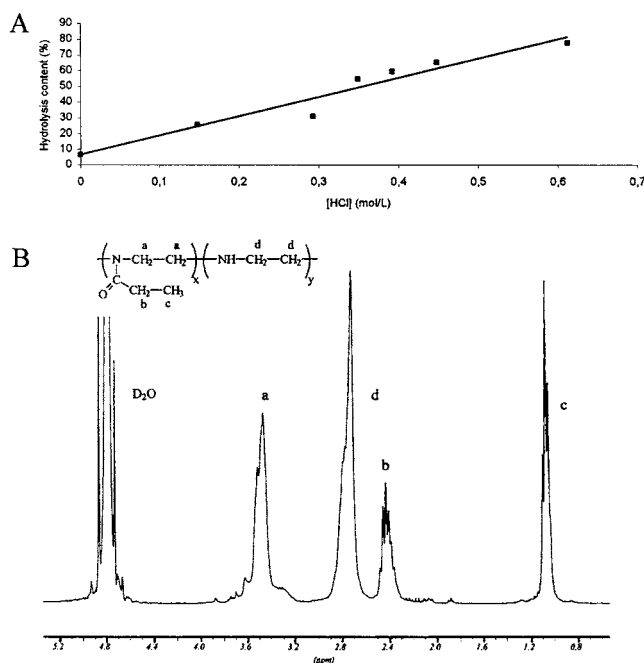
**Synthesis of Poly(2-ethyl-2-oxazoline-*co*-ethylenimine) Copolymers (LP(EtOXZ-*co*-EI)).** Incomplete acid hydrolysis of commercial samples of PEtOXZ<sub>50kDa</sub> was carried out by varying the acid concentration in the reaction medium (Figure 2B). Different random copolymers LP(EtOXZ-*co*-EI) were obtained corresponding to various hydrolysis ratios with a yield of about 90%. The linear relationship obtained by plotting the hydrolysis ratio versus the initial acid concentration (Figure 4A) indicates a good control of the hydrolysis. This plot also suggests that there is a small initial hydrolysis even in the absence of hydrochloric acid.

The <sup>1</sup>H NMR spectra of the products collected after medium neutralization show the peaks of various methylene groups which correspond respectively to ethylen-



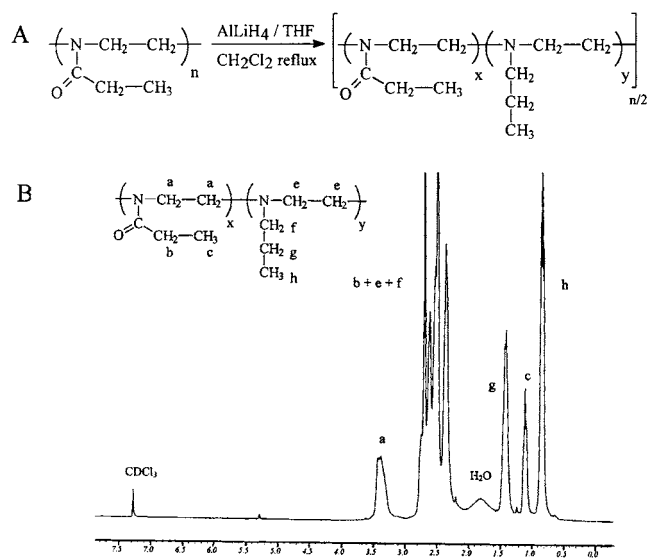


**Figure 3.** (A) Potentiometric titration of *N,N*-diethylethylenediamine. The titration was carried out by using 0.1 M HCl as titrant. (B) Potentiometric titration of acidic LPNPEI<sub>42.5kDa</sub> solution by using  $9.2 \times 10^{-2}$  M NaOH as titrant.



**Figure 4.** (A) Ethylenimine monomer unit content in copolymers obtained by partial hydrolysis of poly(2-ethyl-2-oxazoline) vs HCl concentration used. (B)  $^1\text{H}$  NMR spectrum (300 MHz) of LP(EtOXZ<sub>200</sub>-co-EI<sub>300</sub>) in D<sub>2</sub>O after neutralization.

imine units (2.8 ppm) and ethylenimine units substituted by the *N*-propanoyl side groups (3.5 ppm) (Figure 4B). The ratio of the areas of these peaks allowed the determination of the ethylenimine unit content in the different copolymers produced according to this method. However, in contrast to previously published results, no signals corresponding to propanoate residues were detected on the spectra (1.1 and 2.2 ppm) (16). This indicates, first, that the workup procedure applied at the



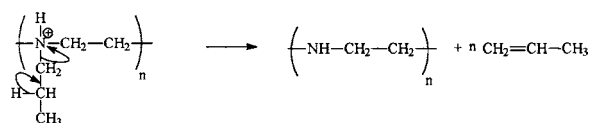
**Figure 5.** (A) Synthetic route of LP(EtOXZ-*co*-NPEI) and LPNPEI polymers by reduction of PEtOXZ using LiAlH<sub>4</sub>. (B)  $^1\text{H}$  NMR spectrum (300 MHz) of LP(EtOXZ-*co*-NPEI) with 81% reduction content in CDCl<sub>3</sub>.

end of reaction, i.e., neutralization followed by dichloromethane extraction, is a more efficient method than that used by Jeong et al. to get rid of the sodium propanoate produced by the neutralization reaction. Second, it shows that the propanoate groups eventually present on NMR spectra cannot be attributed to NH<sub>2</sub><sup>+</sup>/propanoate ion pairs (16).

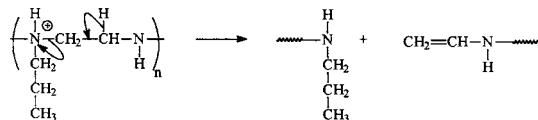
**Synthesis of Poly(2-ethyl-2-oxazoline-*co*-*N*-propylethylenimine) Copolymers (LP(EtOXZ-*co*-NPEI)).** The hydrogenation of poly(2-methyl-2-oxazoline) giving poly(*N*-ethylethylenimine) by LiAlH<sub>4</sub> or AlH<sub>3</sub> has been previously reported in the literature (17). We applied this to poly(2-ethyl-2-oxazoline)s of different polymerization degrees by using various quantities of LiAlH<sub>4</sub> in order to obtain fully or partially reduced polymers (Figure 5A). This technique applied to PEtOXZ<sub>50kDa</sub> allowed us to obtain poly(2-ethyl-2-oxazoline-*co*-*N*-propylethylenimine) (LP(EtOXZ-*co*-NPEI)) copolymers with a good control of the hydrogenation ratio. On the other hand, by using an excess of hydride, PEtOXZ of different DP<sub>n</sub> gave homopolymers LNPEIs with various molecular weights.  $^1\text{H}$  NMR spectroscopic analysis of LP(EtOXZ-*co*-NPEI) samples obtained by incomplete reduction of PEtOXZ<sub>50kDa</sub> showed the decrease of the signals corresponding to the propanoyl groups and the presence of signals corresponding to newly formed *N*-propyl groups at 0.8, 1.4, and 2.6 ppm (Figure 5B). The disappearance of the peaks in the aromatic range corresponding to the tosylate counteranions of the ionic termini on the starting polymers confirmed that the oxazolinium cycle was reduced into a *N*-(ethyl)propylamine chain end. The reduction content was determined from the ratio of the surface of the methyl resonance (CH<sub>3</sub>CH<sub>2</sub>CH<sub>2</sub>N) at 0.8 ppm to that of the total content of methyl groups of the polymer (0.8 + 1.1 ppm).

Potentiometric titration gave the average pK<sub>a</sub> of the tertiary polyamine LPNPEI<sub>42.5 kDa</sub> that was found equal to 7.2 (Figure 3B). This value which is lower than that of LPEI<sub>22 kDa</sub> is in agreement with the different pK<sub>a</sub> of the model molecule *N,N,N,N*-tetraethylethylenediamine which are respectively equal to 6.2 and 9.5, showing unambiguously that the tertiary amino sites are of lower basicity than the secondary ones (Table 1). Thus, LPN-

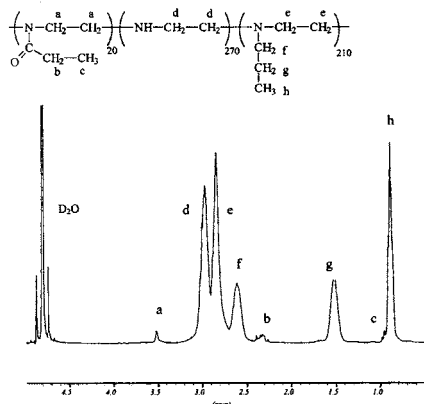
## A • On side chains



## • On main chain



## B



**Figure 6.** (A) Degradation process of LP(EtOXZ-*co*-NPEI) during acid hydrolysis. (B)  $^1\text{H}$  NMR spectrum (300 MHz) of LP(EtOXZ<sub>20</sub>-*co*-EI<sub>270</sub>-*co*-NPEI<sub>210</sub>) in  $\text{D}_2\text{O}$ .

PEI polymers are less protonated at a physiological pH (about 50%) than LPEIs.

**Synthesis of Poly(ethylenimine-*co*-*N*-propylethylenimine) (LP(EI-*co*-NPEI)).** The synthesis of poly(ethylenimine-*co*-*N*-propylethylenimine) (LP(EI-*co*-NPEI)) of different ratios using hydrolysis or reduction reactions was attempted starting from LP(EtOXZ-*co*-NPEI) and LP(EtOXZ-*co*-EI).

Hydrolysis was first carried out from LP(EtOXZ-*co*-NPEI) in hydrochloric medium under reflux for 18 h.  $^1\text{H}$  NMR analysis of the residue obtained at the end of reaction indicated the absence of the characteristic *N*-propylethylenimine units, suggesting that some degradation occurred. A possible explanation could be found in the Hoffman degradation, inducing the cleavage of the *N*-propyl groups by  $\beta$  elimination (Figure 6A).

Starting again from the same copolymers LP(EtOXZ-*co*-NPEI) of various reduction ratios, hydrolysis in basic medium was tested, using different sodium hydroxide concentrations under reflux for different reaction times. Table 2 shows that in all cases and whatever the NPEI unit content of starting polymers, there always remained 20% of amide units, even with the highest sodium hydroxide concentration or the longest reaction time. This observation can be explained by some repulsion induced by the presence of tertiary amino groups on the nucleophilic reactant.

Since the two types of hydrolysis failed to give access to the copolymer LP(EI-*co*-NPEI), we tested whether the reduction of the amide units of the copolymers LP(EtOXZ-*co*-EI) having different hydrolysis ratios would allow to obtain the desired compounds. The results are presented in Table 3. The determination of the NPEI unit content of the products was done by  $^1\text{H}$  NMR spectroscopy.

**Table 2. Hydrolysis of Poly(ethyl-oxazoline-*co*-*N*-propylethylenimine)s (LP(EtOXZ-*co*-NPEI)) in Basic Aqueous Solution**

starting polymer LP(EtOXZ- <i>co</i> -NPEI) <sup>a</sup>			
NPEI <sup>b</sup> content (%)	64	83	81
[NaOH]/[NCOEt] <sup>c</sup>	2	2.2	3.6
time (h)	17	17	67
EI <sup>d</sup> content (%)	17	0	0
resulting polymer composition	LP(EtOXZ <sub>95</sub> - <i>co</i> -EI <sub>85</sub> - <i>co</i> -NPEI <sub>320</sub> ) <sup>e</sup>	LP(EtOXZ <sub>85</sub> - <i>co</i> -NPEI <sub>415</sub> )	LP(EtOXZ <sub>95</sub> - <i>co</i> -NPEI <sub>405</sub> )

<sup>a</sup> Total number of monomer units = 500. <sup>b</sup> *N*-propylethylenimine monomer unit. <sup>c</sup> *N*-propanylethylenimine monomer unit concentration. <sup>d</sup> Ethylenimine monomer unit. <sup>e</sup> Polymer obtained from precursor LP(EtOXZ<sub>180</sub>-*co*-NPEI<sub>320</sub>). This polymer was not tested in transfection experiments.

**Table 3. Reduction of Poly(ethyl-oxazoline-*co*-ethylenimine)s (LP(EtOXZ-*co*-EI)) with  $\text{LiAlH}_4$  in  $\text{THF}/\text{CH}_2\text{Cl}_2$**

starting polymer LP(EtOXZ- <i>co</i> -EI) <sup>a</sup>			
EI <sup>b</sup> content (%)	26	54	76
[ $\text{LiAlH}_4$ ]/[NCOEt] <sup>c</sup>	2.2	2.1	3.3
time (h)	7.5	16.5	16.5
yield (%)	51	72	68
NPEI <sup>d</sup> content (%)	56	42	24
resulting polymer composition	LP(EtOXZ <sub>90</sub> - <i>co</i> -EI <sub>130</sub> - <i>co</i> -NPEI <sub>280</sub> )	LP(EtOXZ <sub>20</sub> - <i>co</i> -EI <sub>270</sub> - <i>co</i> -NPEI <sub>210</sub> )	LP(EI <sub>380</sub> - <i>co</i> -NPEI <sub>120</sub> )

<sup>a</sup> Total number of monomer units = 500. <sup>b</sup> Ethylenimine monomer unit. <sup>c</sup> *N*-propanylethylenimine monomer unit concentration. <sup>d</sup> *N*-propylethylenimine monomer unit.

copy. Using an excess of reducing agent, this method gave a total reduction of the amide sites, whatever the fraction of ethyloxazoline units in the starting copolymer. The nearly complete reduction was shown by the presence of residual signals corresponding to the amide group and characteristic peaks of the secondary and tertiary ethylenimine units respectively at 3.0 and 2.8 ppm (Figure 6B).

Of note, the low downfield shift of the methylene protons ( $\text{CH}_2\text{CH}_2\text{NH}$ ) of the ethylenimine units at 3.0 ppm of the copolymer LP(EI-*co*-NPEI), compared to that of the same protons of the copolymer LP(EtOXZ-*co*-EI) at 2.8 ppm, can be explained by the more electron-withdrawing effect of secondary amino groups in this case, due to the loss of hydrogen bonding between NH and propanoyl groups, which probably exists in the former copolymer.

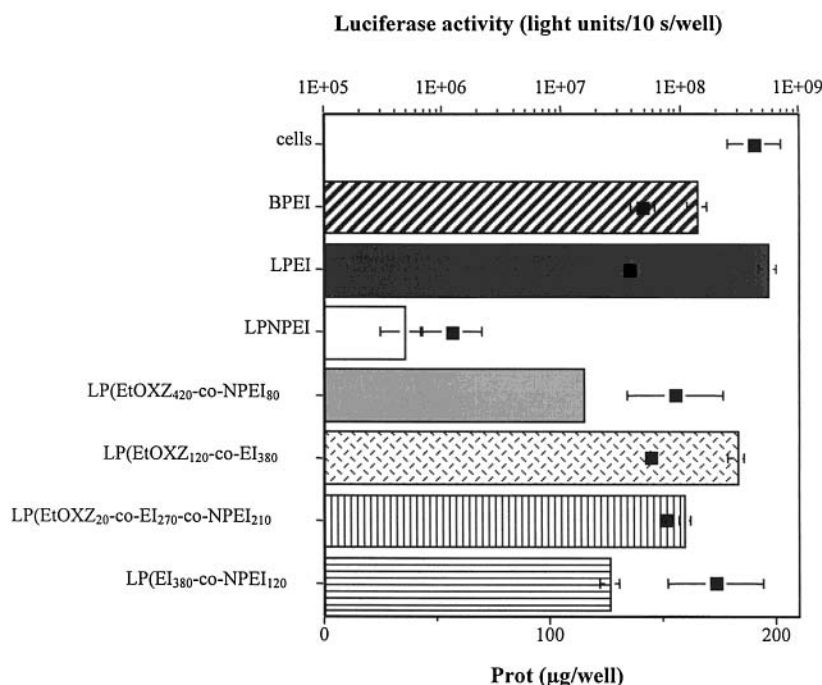
The determination of the average  $\text{pK}_a$  of the copolymer LP(EtOXZ<sub>20</sub>-*co*-EI<sub>270</sub>-*co*-NPEI<sub>210</sub>) is in tune with the weaker basicity of the tertiary amines (Table 1).

**DNA Retardation Assay.** The polymers were first tested for their capacity to interact with plasmid DNA. Therefore, increasing amounts of polymer were mixed with a constant amount of DNA, and the complexes were electrophoresed through an agarose gel. In this system, the polymer/DNA interactions are visualized by the retardation of the migration of DNA. As shown in Table 4, all the polymers except PEtOXZ were able to complex DNA. The LPEIs and the LP(EtOXZ<sub>120</sub>-*co*-EI<sub>380</sub>) copolymer were the most efficient in retarding DNA migration whereas the LPNPEIs of low molar weight and the LP(EtOXZ<sub>350</sub>-*co*-EI<sub>150</sub>) copolymer were the least efficient. It is interesting to note that homopolymers containing *N*-propylethylenimine units are weaker complexing agents than random LP(EtOXZ-*co*-NPEI) copolymers. The more efficient DNA complexation observed with the latter polymers may be due to the fact that the amino sites are partially isolated from each others by amide units, thereby increasing their basicity (see Table 1 for  $\text{pK}_a$  values). Moreover, our results show that the complex-

**Table 4. Efficiency of the Different Polymers**

polymer	DNA retardation ( $\mu\text{g}$ polymer) <sup>a</sup>	transfection efficiency <sup>b</sup>
LPEI (MW = 3600)	0.5	100
LPEI (MW = 7300)	0.5	500
LPEI (MW = 22000)	0.5	1000
LPNPEI (MW = 6100)	>4	0.1 <
LPNPEI (MW = 14400)	>4	0.1 <
LPNPEI (MW = 42500)	2.5	0.2
LPNPEI (MW = 171700)	2	1
LP(EI <sub>380</sub> -co-NPEI <sub>120</sub> ) (MW = 26600)	1	30
PEtOXZ (MW = 50000)	no retardation	-
LP(EtOXZ <sub>420</sub> -co-NPEI <sub>80</sub> ) (MW = 48900)	2	55
LP(EtOXZ <sub>90</sub> -co-NPEI <sub>90</sub> ) (MW = 16300)	2	50
LP(EtOXZ <sub>180</sub> -co-NPEI <sub>320</sub> ) (MW = 45500)	1	3
LP(EtOXZ <sub>350</sub> -co-EI <sub>150</sub> ) (MW = 41500)	15	0.2
LP(EtOXZ <sub>200</sub> -co-EI <sub>300</sub> ) (MW = 32700)	1	55
LP(EtOXZ <sub>120</sub> -co-EI <sub>380</sub> ) (MW = 28900)	0.5	450
LP(EtOXZ <sub>90</sub> -co-EI <sub>130</sub> -co-NPEI <sub>280</sub> ) (MW = 38800)	2.5	0.2
LP(EtOXZ <sub>20</sub> -co-EI <sub>270</sub> -co-NPEI <sub>210</sub> ) (MW = 31500)	2.5	150

<sup>a</sup> Approximative amount of polymer ( $\mu\text{g}$ ) needed for complete retardation of 1  $\mu\text{g}$  of DNA. <sup>b</sup> The activity of the polymers was evaluated on HepG2 cells by using the reporter gene luciferase. The value 1000 was given to the transfection efficiency of the LPEI of 22 kDa.



**Figure 7.** Evaluation of the transfection efficiency of PEI derivatives on HepG2 cells. Increasing amounts of polymer were mixed with a constant amount of reporter gene (4  $\mu\text{g}$  per duplicate). The complexes were incubated in serum-free culture medium for 3 h with HepG2 cells. The luciferase activity was measured 30 h thereafter. The transfection efficiency (bars) was expressed as total light units/10 s/well and is the mean of the duplicates. Only the optimal condition for each compound is shown. The protein content (filled squares) was determined by using the BioRad protein assay.

ation efficiency increased with an increase of the fraction of the secondary amine functions and consequently with the decrease of the proportion of tertiary amines.

Taken together, these results show that the efficiency of complexation is related to the fraction of amino groups that are protonated at neutral pH. Thus, the higher the  $pK_a$  of the amines, the more efficient is the neutralization of the phosphate groups of the DNA.

**Evaluation of the Transfection Activity.** The transfection activity of the different polymer series was tested on human hepatocarcinoma cells (HepG2). Increasing amounts of polymer were complexed with 4  $\mu\text{g}$  of a plasmid encoding a luciferase reporter gene under the control of the human cytomegalovirus (CMV) immediate-early promoter and applied to the cells for 3 h in the absence of serum. The luciferase activity and the protein content were measured 1 or 2 days thereafter. For comparison, we included in our assays the branched PEI

of 25 kDa (BPEI) and the linear PEI of 22 kDa (LPEI), both of which were shown to be among the most efficient *in vitro* transfection agents (1, 2, 5).

The results show that when all the amino nitrogens of LPEI are substituted with propyl groups as it is the case with the LPNPEI series, the transfection efficiency is strongly reduced compared to that of the LPEI of 22 kDa (Table 4 and Figure 7). The toxicity of the polymer/DNA complexes on HepG2 cells following transfection was evaluated by measuring the total amount of protein per well. The results indicate that the lower transfection efficiency of LPNPEIs when compared to PEIs is at least partially due to an increased cytotoxicity (Figure 7).

It should be noted that the transfection activity increased with the molar mass of the homopolymers. Interestingly, copolymers of PEtOXZ and LPNPEI are more efficient and less cytotoxic than LPNPEIs. The highest efficiency was obtained with copolymers having



the same or more EtOXZ than NPEI units. These results suggest that other parameters than density of amino nitrogens and buffer capacity are important for gene transfer. It is possible that EtOXZ ensures a higher solubility and/or flexibility of the polymer.

In contrast to the results obtained with LP(EtOXZ-co-NPEI) polymers, the most efficient LP(EtOXZ-co-EI) copolymers were those having more EI than EtOXZ units. In fact, the most efficient copolymer tested is the one which has a EI fraction of 75%. This proportion has been already found by Jeong and co-workers to be the most efficient on 3T3 cells among a series of random copolymers (16).

A comparison of the activity of LP(EtOXZ<sub>120</sub>-co-EI<sub>380</sub>) and LP(EI<sub>380</sub>-co-NPEI<sub>120</sub>) showed that the substitution of EtOXZ units by NPEIs induced a decrease of 20-fold of the level of luciferase expression, suggesting again that other parameters than the density in amino nitrogens are important. Among the two polymers containing EtOXZ, EI, and NPEI units, the most efficient was the one having the highest ratio of EI. This latter unit is thus the most important for efficient gene transfer. Of note, the activity of LP(EtOXZ<sub>20</sub>-co-EI<sub>270</sub>-co-NPEI<sub>210</sub>) is comparable to that of the copolymer LP(EtOXZ<sub>200</sub>-co-EI<sub>300</sub>). This can probably be assigned to the fact that they have in common approximately the same fraction of ethylenimine units (about 55%), which corresponds to the fraction of secondary amines of the branched PEI of 25 kDa.

Finally, Bieber and Elsässer recently showed that branched PEIs of low molar weight (LMW) are more efficient in vitro than branched PEIs having high MWs (18). We therefore asked whether linear polymers having low molar weights are more efficient than the LPEI<sub>22</sub> kDa. Thus, LPEIs of 3.6 and 7.3 kDa were synthesized and their transfection efficiency subsequently evaluated. The results show that the LMW LPEIs allowed expression of significant levels of luciferase, although lower than those obtained by the LPEI<sub>22</sub> kDa (Table 4). Of note, however, the LPEI of 3.6 kDa was as efficient as the branched PEI of 25 kDa (not shown).

These results show that, as it was the case for the LPNPEIs, the transfection activity increased with the molar weight of the LPEI.

In conclusion, this work shows that it is possible to include a fraction of EtOXZ units, which are not positively charged, without decreasing importantly the activity of linear PEIs. We also demonstrate that it is possible to synthesize linear copolymers having tertiary and secondary aziridine units. Polymers containing tertiary amines such as LPNPEIs were significantly less efficient in mediating gene transfer than PEIs, although these polymers contain more amino nitrogens which are not protonated at neutral pH. This result indicates that the capacity to buffer endo-lysosomes is not sufficient to make a molecule an efficient transfection agent. A similar finding was made by Tang and Szoka with starburst dendrimers (7, 19). They found that in contrast to fractured dendrimers, intact dendrimers are not very efficient in gene transfer although they present groups that can be protonated during acidification of endosomes. Taken together, our results show that the high transfection efficiency of PEIs is not solely based on their capacity to buffer endosomes. Other parameters such as flexibility of the polymer may be of importance.

#### ACKNOWLEDGMENT

Dr. L. Auvray is gratefully acknowledged for neutron scattering analysis. The biological part of this work was

performed with the financial support of the Association Française contre les Myopathies (AFM).

#### LITERATURE CITED

- (1) Boussif, O., Lezoualc'h, F., Zanta, M. A., Mergny, M. D., Scherman, D., Demeneix, B., and Behr, J.-P. (1995) A versatile vector for gene and oligonucleotide transfer into cells in culture and in vivo: polyethylenimine. *Proc. Natl. Acad. Sci. U.S.A.* 92, 7297–7301.
- (2) Boussif, O., Zanta, M. A., and Behr, J.-P. (1996) Optimized galenics improve in vitro gene transfer with cationic molecules up to 1000-fold. *Gene Ther.* 3, 1074–1080.
- (3) Goula, D., Benoist, C., Mantero, S., Merlo, G., Levi, G., and Demeneix, B. A. (1998) Polyethylenimine-based intravenous delivery of transgenes to mouse lung. *Gene Ther.* 5, 1291–1295.
- (4) Bragonzi, A., Boletta, A., Biffi, A., Muggia, A., Sersale, G., Cheng, S. H., Bordignon, C., Assael, B. M., and Conese, M. (1999) Comparison between cationic polymers and lipids in mediating systemic gene delivery to the lungs. *Gene Ther.* 6, 1995–2004.
- (5) Zou, S. M., Erbacher, P., Remy, J.-S., and Behr, J.-P. (2000) Systemic linear polyethylenimine (L-PEI)-mediated gene delivery in the mouse. *J. Gene Med.* 2, 128–134.
- (6) Suh, J., Paik, H. J., and Hwang, B. K. (1994) Ionization of polyethylenimine and polyallylamine at various pHs. *Bioorg. Chem.* 22, 318–327.
- (7) Tang, M. X., and Szoka, F. C. (1997) The influence of polymer structure on the interactions of cationic polymers with DNA and morphology of the resulting complexes. *Gene Ther.* 4, 823–832.
- (8) Midoux P., and Monsigny, M. (1999) Efficient gene transfer by histidylated polylysine/pDNA complexes. *Bioconjugate Chem.* 10, 406–411.
- (9) Kichler, A., Leborgne, C., Coeytaux, E., and Danos, O. (2001) Polyethylenimine-mediated gene delivery: a mechanistic study. *J. Gene Med.* 3, 135–144.
- (10) Thomas, M., and Klivanov, A. M. (2002) Enhancing polyethylenimine's delivery of plasmid DNA into mammalian cells. *Proc. Natl. Acad. Sci. U.S.A.* 23, 14640–14645.
- (11) Kem, K. M. (1979) Kinetics of the hydrolysis of linear poly[(acylimino)-ethylenes]. *J. Polym. Sci. Polym. Chem. Ed.* 17, 1977–1990.
- (12) McAlvin, J. E., Scott, S. B., Fraser, C. L. (2000) Synthesis of thermochromic iron II tris(bipyridine)-centered star-shaped polyoxazolines and their bipyridine-centered macroligand counterparts. *Macromolecules* 33, 6953–6964.
- (13) Miyamoto, M., Naka, K., Tokumizu, M., and Saegusa, T. (1989) End capping of growing species of poly(2-oxazoline) with carboxylic acid: a novel and convenient route to prepare vinyl- and carboxy-terminated macromonomers. *Macromolecules* 22, 1604–1607.
- (14) Pradny, M., and Sevcik, S. (1987) Precursors of hydrophilic polymers. 7: Potentiometric properties and structure of copolymers of 2-dimethylaminoethyl methacrylate. *Makromol. Chem.* 188, 227–238.
- (15) Van de Wetering, P., Moret, Ed E., Schuurmans-Nieuwenbrock, N. M. E., Van Steenberghe, M. J., and Hennink, W. E. (1999) Structure–activity relationships of water-soluble cationic methacrylamide polymers for nonviral gene delivery. *Bioconjugate Chem.* 10, 589–597.
- (16) Jeong, J. H., Song, S. H., Lim, D. W., Lee, H., and Park T. G. (2001) DNA transfection using linear poly(ethylenimine) prepared by controlled acid hydrolysis of poly(2-ethyl-2-oxazoline). *J. Controlled Release* 73, 391–399.
- (17) Saegusa, T., Yamada, A., Taoda, H., and Kobayashi, S. (1978) Linear poly(*N*-alkylethylenimine)s. *Macromolecules* 11, 435–436.
- (18) Bieber, T., and Elsässer, H. P. (2001) Preparation of a low molecular weight polyethylenimine for efficient cell transfection. *Biotechniques* 30, 74–77.
- (19) Tang, M. X., Redemann, C. T., and Szoka, F. C. (1996) In vitro gene delivery by degraded polyamidoamine dendrimers. *Bioconjugate Chem.* 7, 703–714.

# Synthesis and Properties of Ester-Linked Peptide Nucleic Acid Prodrug Conjugates

Nadia Bendifallah,<sup>†,§</sup> Edward Kristensen,<sup>‡</sup> Otto Dahl,<sup>§</sup> Uffe Koppelhus,<sup>†</sup> and Peter E. Nielsen<sup>\*,†,‡</sup>

Center for Biomolecular Recognition, Department of Medical Biochemistry and Genetics, University of Copenhagen, The Panum Institute, Blegdamsvej 3c, DK-2200 N Copenhagen, Denmark, Pantheco A/S, Bøge Allé 3, 2970 Hørsholm, Denmark, and Department of Chemistry, University of Copenhagen, Universitetsparken 5, DK-2100 Copenhagen Ø, Denmark. Received October 7, 2002; Revised Manuscript Received February 13, 2003

A Boc-protected amino acid containing an ester function, 2-([*N*-Boc-glycyl]oxymethyl)benzoic acid, has been synthesized and incorporated into peptide nucleic acid (PNA) oligomers. In model experiments it is found that the ester is fairly stable in aqueous solution at pH 7.4 and 37 °C ( $t_{1/2}$  = 6 h), whereas it is rapidly cleaved in mouse serum and in kidney and liver homogenates ( $t_{1/2}$  = 0.1–0.5 min). Furthermore, ester-linked fatty acid PNA conjugates targeted to an aberrant splice site in luciferase mRNA were prepared and shown to be twice as potent for inducing active luciferase as the corresponding conjugate not containing the linker. Thus, a PNA prodrug approach may be useful for both ex vivo as well as in vivo applications.

## INTRODUCTION

Esterases with highly relaxed substrate specificity are ubiquitous in mammalian cells and tissues as well as in the blood stream. Therefore ester-linkages are exploited with great success in the design of medical prodrugs (1, 2).

Peptide nucleic acids are pseudopeptide DNA mimics based on amide chemistry. High biological (and chemical) stability combined with very favorable RNA (and DNA) hybridization properties have made PNAs attractive candidates for development of gene therapeutic antisense (and antigene) drugs, and recently a wide range of results have reemphasized this potential (3, 4).

Cellular delivery of PNA is an area of active research, and several methods have been devised relying on conjugation to peptide transporters (5–8) or accomplished via cationic liposome carriers (9–11). In the latter case either PNA–DNA hybrids or PNA–fatty acid conjugates were employed.

We reasoned that it would be advantageous to develop chemistry that would enable incorporation of an enzyme cleavable ester function between the PNA and the carrier. For instance this should allow cellular (and animal) delivery of lipophilic PNA prodrugs that could transverse the lipid bilayer of the cell with subsequent intracellular enzymatic release of the free PNA.

However, PNA oligomerization (and especially cleavage from the resin) involves rather harsh acid and/or alkaline treatment, which is not a priori compatible with ester stability. Nonetheless, we now describe the synthesis of such an ester containing amino acid monomer and demonstrate that this is easily incorporated into PNA oligomers using standard solid-phase polymerization,

deprotection, and cleavage conditions. We also show that this ester is a substrate for enzymes (esterases) present in plasma and tissue extracts. Finally, we present preliminary cellular antisense data on ester-linked PNA–fatty acid conjugates.

## EXPERIMENTAL SECTION

<sup>1</sup>H and <sup>13</sup>C NMR spectra were obtained at either 250 MHz (Bruker AMX 250) or at 400 MHz (Varian Unity 400) in 5 mm tubes. FAB mass spectra were recorded on a JEOL Hx 110/110 mass spectrometer. MALDI-TOF mass spectra were recorded on a Kratos Compact Maldi II instrument operating in the positive ion mode, using 3,5-dimethoxy-4-hydroxycinnamic acid as the matrix.

Dichloromethane (LAB-SCAN) and diethyl ether (LAB-SCAN) were dried over molecular sieves. The following chemicals were used as received: phthalide (Aldrich), 1,3-dicyclohexylcarbodiimide (DCC, Aldrich), *N*-Boc-glycine (Sigma), 4-(dimethylamino)pyridine (DMAP, Aldrich), 4-(1-pyrenyl)butyric acid (Aldrich), decanoic acid (Aldrich), (1-adamantyl)acetic acid (Aldrich). TLC was performed on silica 60 (Merck 5554 aluminum sheet).

**2-(Hydroxymethyl)benzoic Acid.** A modification of the procedure of Gilman et al. (12) was used: Phthalide (5.0 g, 37.3 mmol) was dissolved in methanol (20 mL) and water (20 mL). NaOH (10 M, 8 mL) was added, and the mixture was refluxed for 90 min. The reaction mixture was then cooled to room temperature, and the free acid was precipitated with 4 M HCl (ca. 10 mL). The resulting precipitate was filtered off, washed with ice-cold water, and finally dried in vacuo to give a white crystalline product (5.03 g, 89%). Mp 101–105 °C (lit. 120.5–121.5 °C). <sup>1</sup>H NMR (DMSO-*d*<sub>6</sub>) δ 8.12 (dd, 1H), 7.61 (m, 1H), 7.47 (m, 2H), 4.86 (s, 2H), <sup>13</sup>C NMR (DMSO-*d*<sub>6</sub>) δ 133.79, 132.01, 130.32, 128.00, 64.61 (it was not possible to see the C=O signal because of the low sample concentration). FAB<sup>+</sup>MS: 153.12 (M + H<sup>+</sup>).

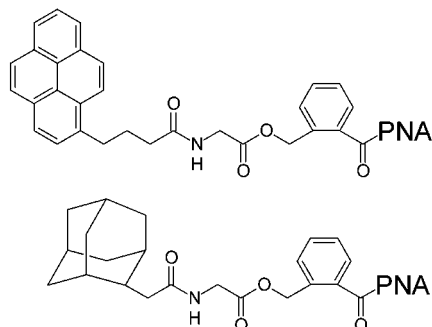
**2-([*N*-Boc-glycyl]oxymethyl)benzoic Acid.** A symmetrical anhydride was formed from *N*-Boc-glycine (7.72 g, 44.1 mmol) and DCC (4.55 g, 22.0 mmol) in dry

\* Corresponding author: E-mail: pen@imb.g.ku.dk; Fax: +4535396042.

<sup>†</sup> Department of Medical Biochemistry and Genetics, University of Copenhagen.

<sup>‡</sup> Pantheco A/S.

<sup>§</sup> Department of Chemistry, University of Copenhagen.

**Chart 1. Structures of Ester-Linked Pyrene and Adamantyl PNA Conjugates**

dichloromethane (25 mL). The mixture was stirred at 0 °C for 30 min. The resulting *N,N*-dicyclohexylurea (DCU) was filtered off, and the filtrate was added directly to a suspension of freshly prepared 2-(hydroxymethyl)benzoic acid (2.34 g, 15.4 mmol) in dry dichloromethane (30 mL). DMAP (0.19 g, 1.5 mmol) was added, and the mixture was refluxed overnight. The reaction mixture was washed with saturated aqueous  $\text{NaHCO}_3$  ( $3 \times 50$  mL). The combined aqueous extracts were acidified with 4 N HCl to pH 2, and the resulting precipitate was filtered off, washed with ice-cold water, and finally dried *in vacuo* to give a white crystalline product (2.98 g, 63%). Mp: 122–124 °C.  $^1\text{H}$  NMR ( $\text{DMSO}-d_6$ )  $\delta$  7.93 (d, 1H,  $J = 7.5$  Hz), 7.55 (m, 2H), 7.44 (m, 1H), 7.28 (t, 1H,  $J = 6.1$  Hz), 5.49 (s, 2H), 3.79 (d, 2H,  $J = 6.1$  Hz), 1.38 (s, 9H).  $^{13}\text{C}$  NMR ( $\text{DMSO}-d_6$ )  $\delta$  170.33, 168.0, 155.99, 137.38, 132.21, 130.60, 129.28, 127.83, 127.53, 78.38, 64.18, 42.12, 28.24. FAB<sup>+</sup>HRMS: 310.1265 ( $\text{M} + \text{H}^+$ , calc. for  $\text{C}_{15}\text{H}_{19}\text{NO}_6 + \text{H}^+$  310.1291).

**PNA Conjugates.** The following PNA conjugates were synthesized (cf. Chart 1):

**PNA-1:** Pyr-GMB2-TJ-eg1-eg1-eg1-CTTCTT-NH<sub>2</sub>\*

**PNA-2:** Deca-eg1-Fl<sub>Lys</sub>-eg1-CATAGTATAAGT-LysNH<sub>2</sub>

**PNA-3:** Ada-eg1-Fl<sub>Lys</sub>-eg1-CATAGTATAAGT-LysNH<sub>2</sub>

**PNA-4:** Deca-GMB2-eg1-Fl<sub>Lys</sub>-eg1-CATAGTATAAGT-LysNH<sub>2</sub>

**PNA-5:** Ada-GMB2-eg1-Fl<sub>Lys</sub>-eg1-CATAGTATAAGT-LysNH<sub>2</sub>

**PNA-6:** Deca-GMB2-eg1-CCTCTTACCTCAGTTACA-NH<sub>2</sub>

**PNA-7:** Deca-eg1-CCTCTTACCTCAGTTACA-NH<sub>2</sub>

**PNA-8:** Ada-GMB2-eg1-CCTCTTACCTCAGTTACA-NH<sub>2</sub>

**PNA-9:** Ada-eg1-CCTCTTACCTCAGTTACA-NH<sub>2</sub>

**PNA-10:** Deca-eg1-CTTCTAACCTCTGTTACA-NH<sub>2</sub>

**PNA-11:** Deca-GMB2-eg1-CTTCTAACCTCTGTTACA-NH<sub>2</sub>

\*[(ada: 1-adamantyl acetyl, GMB2: 2-(glycyl-oxymethyl)benzoyl, deca: decanoyl, eg1: 8-amino-3,6-dioxaoctanoyl ("ethyleneglycol linker"), Fl<sub>Lys</sub>: fluorescein-lysyl, pyr: 4-(1-pyrenyl)butanoyl, J: pseudoisocytosine].

**PNA-1** was synthesized on a Boc-T-4-methylbenzhydrylamine resin (loading 0.12 mmol/g) using the standard synthetic protocol (13). For the incorporation of 4-(1-pyrenyl)butyric acid and 2-([*N*-Boc-glycyl]oxymethyl)benzoic acid, the coupling was allowed to proceed for 60 min.

**PNAs 2 through 5** were synthesized on a Boc-L-Lys-(2-chlorobenzoyloxycarbonyl)-4-methylbenzhydrylamine resin (loading 0.15 mmol/g) using the standard synthesis protocol (13). **PNAs 6 through 11** were synthesized similarly on a Boc-A-4-methylbenzhydrylamine resin. For the incorporation of decanoic acid, 1-adamantylacetic acid, 2-([*N*-Boc-glycyl]oxymethyl)benzoic acid, and the

fluorescein-lysine monomer (6-*O*-[*N*-(5-Boc-amino-5-carboxypentyl)carbamoylmethyl]fluorescein ethyl ester) (14), the coupling was allowed to proceed for 60 min.

The resulting PNA conjugates were deprotected and cleaved from the resin with a cocktail composed of *m*-cresol/thioanisole/trifluoromethanesulfonic acid/TFA (1/1/2/6, v/v), and the crude material was precipitated and washed with anhydrous (crucial to ensure ester stability) diethyl ether. The PNA conjugates were then purified by reversed-phase high performance liquid chromatography (HPLC) using a C18 column and an acetonitrile gradient in 0.1% TFA in H<sub>2</sub>O and characterized by MALDI-TOF mass spectroscopy.

**Tissue Extracts and Stability Analyses.** The HPLC system (Waters) consisted of an Alliance 2690 (pump, autosampler, and degasser), a PDA UV absorbance detector Model 996 (195 nm – 600 nm), and Millennium<sup>32</sup> Chromatography software version 3.2. HPLC separation was performed on a Waters Symmetry 300 C18, 2.1 × 150 mm (3.5  $\mu\text{m}$  particles with 300 Å pore size) analytical column (Waters) equipped with a Zorbax Eclipse XDB-C18 (5  $\mu\text{m}$  particles with 80 Å pore size) guard column (Agilent) using a linear gradient of solvent A (0.1% TFA in water) and solvent B (0.1% TFA in acetonitrile) from 2% to 75% solvent B over 8 min. The column was operated at 50 °C. Samples were kept in the autosampler at 5 °C. Solvent flow was 0.4 mL/min. Polypropylene (PP) test tubes and containers (Sarsted) were generally used for all solutions containing the test PNA. Samples were centrifuged in a Hettich Rotina 46R centrifuge and evaporated to dryness in a SpeedVac AES 2010 from Savant.

NMRI mice (female, 25 g body weight) were obtained from M&B (Denmark). Plasma and tissue from sacrificed animals were used for *in vitro* stability/metabolism studies.

**Preparation of Tissue Homogenates for *in Vitro* Studies.** The animal was sacrificed and the relevant tissues (liver, kidneys) rapidly excised. The tissue was immediately placed in 0.25 M sucrose at 0 °C for rapid cooling and removal of external blood. After cooling (3–5 min), the tissue was dried by blotting with paper and subsequently weighed and transferred to clean polypropylene test tubes. To each tissue was added 0.25 M sucrose in water to a final concentration of 150 mg tissue/mL, using a density of 1 mg/mL for the tissue. The tissue was cut into pieces and homogenized for 1–5 min (depending on tissue) in an Ultra-Turrax T25 homogenizer (IKA) followed by centrifugation of the homogenate in a refrigerated centrifuge (4 °C) for 30 min at 3000 rpm (corresponding to approximately 1000 × *g*) to isolate subcellular fractions. The supernatant was carefully decanted (i.e., the postmitochondrial supernatant), transferred to polypropylene containers, and stored at –80 °C pending use.

***In Vitro* Metabolism Studies.** A mixture of 0.025 mL of 0.1 M Tris buffer pH 7.4, 0.135 mL of water, and 0.025 mL of the tissue homogenate (or plasma) was preincubated at 37 °C for 2 min; then 0.015 mL of the PNA stock solution (1 mg/mL) was added. After incubation for the desired time period, the enzymatic reactions were stopped by adding 0.300 mL of 16.6% acetonitrile in 0.1% TFA in water, and the sample immediately transferred to an ice–water bath (0 °C). The mixture was frozen at minus 18 °C for 30 min. For analysis, the homogenate mixtures were thawed at 4 °C and centrifuged at 3000 rpm for 10 min (approximately 1000 × *g*) at 4 °C. The supernatant (0.200 mL) was transferred directly to the HPLC autosampler vials, and 0.010 mL aliquots were injected into



the HPLC system. Blind samples were prepared by replacing the PNA test compound with water. The blind samples were incubated and analyzed as described for the test samples. Recovery in the incubated samples was calculated from the HPLC areas using a reference solution. To determine whether the ester monomer was in fact cleaved, a sample was analyzed by LC-MS, giving the intact PNA-1 ( $m/z$  3264.3 (calcd: 3266.9)) and the resulting PNA from which the pyrene was cleaved off ( $m/z$  2939.7 (calcd: 2939.5)).

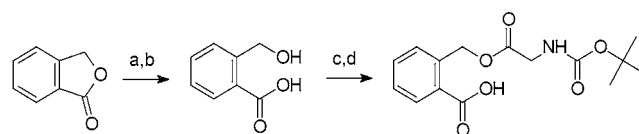
**Cellular Uptake.** The IMR-90 cell line (human fetal fibroblast) were obtained from American Type Culture Collection and grown in Dulbecco's modified Eagle's medium (DMEM) supplemented with penicillin/streptomycin (10  $\mu\text{g/mL}$ ) (antibiotics) and 10% fetal calf serum (Gibco, Invitrogen, Denmark). Cell cultures were maintained at 37 °C in a humidified atmosphere containing 5%  $\text{CO}_2$  (standard conditions).

For uptake analysis of the PNA conjugates, the cells were cultivated on four-well chamber slides (Nunc, Invitrogen, Denmark). The cells were seeded in a concentration of  $20 \times 10^3/\text{mL}$ . The next day the semiconfluent cells were prepared for transfection. This was done by washing the cells twice in fresh DMEM containing antibiotics and 2% fetal calf serum. After this procedure, to the cells was added fresh DMEM containing antibiotics and 2% fetal calf serum, and the slides were incubated 40 min at the standard conditions before subsequent replacement of the media with the transfection mixture. The transfection mixture was prepared as follows: 4  $\mu\text{L}$  of lipofectAMINE (2 mg/mL) (Life Technologies) was diluted in 46  $\mu\text{L}$  of DMEM (without serum) and left 5 min at room temperature. In a separate tube, PNA was diluted in 50  $\mu\text{L}$  of DMEM (without serum) to a final concentration of 4  $\mu\text{M}$  (approximately 18  $\mu\text{g/mL}$ ). Subsequently the lipofectAMINE dilution and the PNA dilution were gently mixed and left for equilibration at room temperature for 30 min. Thereafter, 400  $\mu\text{L}$  of DMEM containing antibiotics and 2% fetal calf serum was added to the combined PNA/lipofectAMINE solution. The resulting transfection mixture was then gently layered upon the cells. After 14–16 h of incubation at the standard conditions, the cells were washed thoroughly in phosphate-buffered saline (PBS) and fixed on ice for 30 min in 3.7% formaldehyde, washed once more in PBS, and mounted with Slowfade Antifade Kit (Molecular Probes, PoortGebouw, The Netherlands) according to the manufacturer's instructions. Counterstaining of the cells with propidium iodide (PI) (Sigma) was performed by adding PI to a final concentration of 5  $\mu\text{g/mL}$  to the cells for 15 min at the end of the incubation with the test substances. Counterstaining with Hoechst 33258 (Sigma) was performed, after formaldehyde fixation of the cells, by 20 min incubation at room temperature in PBS containing Hoechst 33258 (2.5  $\mu\text{g/mL}$ ). No detergent was used.

Cells were examined by fluorescence microscopy on an Olympus BX61 microscope. Image analysis was performed using MetaMorph 4.6 (Universal Imaging Corporation) and Adobe Photoshop 4.0 (Adobe Systems Inc.).

**Antisense Activation of Luciferase in the Reporter Cell Line, pLuc705 HeLa.** The pLuc705 HeLa cell line was purchased from Gene Tools (Philomath, Oregon). pLuc 705 HeLa cells are derived by stable integration of the pLuc705 plasmid into HeLa S2 cells as described in ref 15. The plasmid has luciferase downstream and out-of-frame with a dominant splice-mutation in the  $\beta$ -globin intron position 705. The recombinant luciferase gene is under control of the immediate

**Scheme 1<sup>a</sup>**



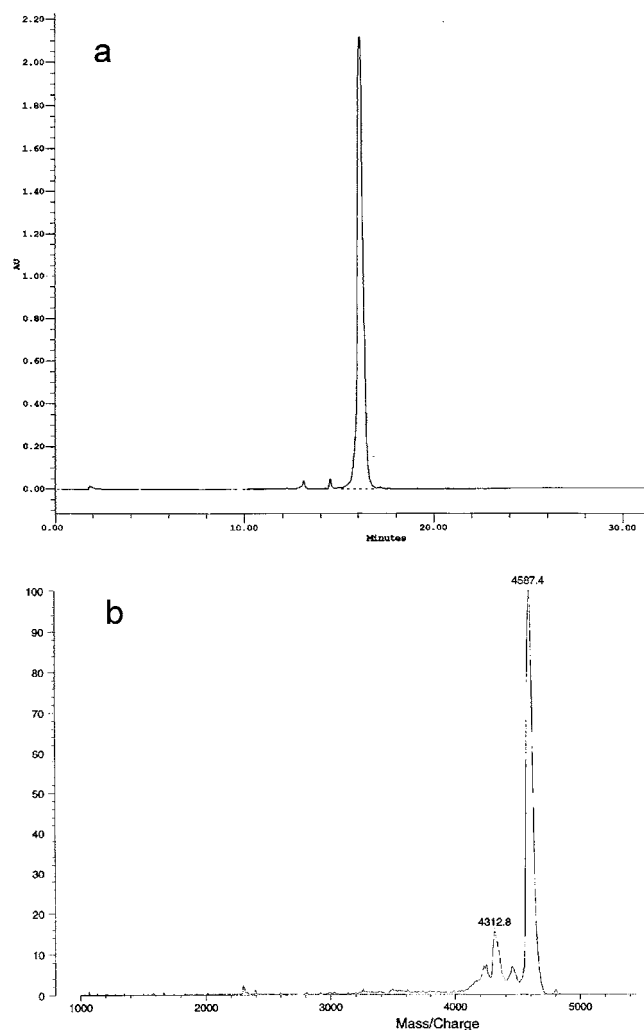
<sup>a</sup> (a) NaOH, MeOH aq,  $\Delta$ , 90 min; (b) 4N HCl (89%); (c) [Boc-Gly]<sub>2</sub>-O, DMAP, DCM,  $\Delta$ , overnight; (d) 4 N HCl (63%).

early cytomegalovirus promoter. Binding of PNA (of sequence H-CCT CTT ACC TCA GTT ACA-NH<sub>2</sub>) to a region covering the splice mutation results in restoration of wild-type splicing which generates a transcript with luciferase in-frame (15, 16).

pLuc 705 HeLa cells were grown in Dulbecco's modified Eagle's medium (DMEM) supplemented with penicillin/streptomycin (10  $\mu\text{g/mL}$ ) (antibiotics) and 10% fetal calf serum (Gibco, Invitrogen, Denmark). Cell cultures were maintained at 37 °C in a humidified atmosphere containing 5%  $\text{CO}_2$  (standard conditions). For transfection with the PNA conjugates, the cells were seeded in a 96-well microtiterplate (Nunc, Invitrogen, Denmark) in a volume of 200  $\mu\text{L}$  and a concentration of  $50\text{--}70 \times 10^3$  cells/mL. The next day the semiconfluent cells were prepared for transfection. This was performed by washing the cells once in fresh DMEM containing antibiotics but no serum (serum-free DMEM) and adding 200  $\mu\text{L}$  of the medium to the cells afterward. The cells were then incubated at standard conditions before subsequent replacement of the medium with the transfection mixture. The transfection mixture was prepared as follows: 0.5  $\mu\text{L}$  of lipofectAMINE (2 mg/mL) (Life Technologies) was diluted in 4.5  $\mu\text{L}$  of DMEM (without serum) and left 5 min at room temperature. In a separate tube, PNA was diluted in 18  $\mu\text{L}$  of DMEM (without serum) to a final concentration of 5.5  $\mu\text{M}$  (approximately 23  $\mu\text{g/mL}$ ). Subsequently the lipofectAMINE dilution and the PNA dilution was gently mixed and left for equilibration at room temperature for 30 min. Thereafter, 77  $\mu\text{L}$  of fresh DMEM (without serum) was added to the combined PNA/lipofectAMINE solution. The resulting transfection mixture was then gently layered upon the cells. After 2–4 h of incubation at the standard conditions, the transfection mixture was supplemented with 100  $\mu\text{L}$  of DMEM containing penicillin/streptomycin (10  $\mu\text{g/mL}$ ) and 20% fetal calf serum. Control experiments were performed exactly as described here with the exception that addition of PNA and lipofectAMINE or just PNA was omitted. After incubation at standard conditions for 14–18 h, the luciferase activity was measured by use of the Steady-Glo Luciferase Assay System (Promega, Ramcon A/S, Birkerød, Denmark) and a Victor<sup>2</sup> Multilabel Counter (Wallac, Perkin-Elmer Danmark A/S, Allerød, Denmark) according to the manufacturer's instructions.

## RESULTS AND DISCUSSION

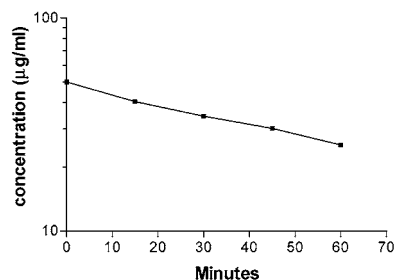
The ester-monomer, 2-([N-Boc-glycyl]oxymethyl)benzoic acid, was prepared as outlined in Scheme 1. A successful synthesis was dependent on preventing the intermediate 2-(hydroxymethyl)benzoic acid from reverting to phthalide. This occurred when 2-(hydroxymethyl)benzoic acid was kept in humid air or dissolved in solvents such as DMF or ethyl acetate. However, a suspension in dry dichloromethane worked well and gave the product in 63% yield. Analogously, we also prepared the 4-([N-Boc-glycyl]oxymethyl)benzoic acid.



**Figure 1.** HPLC (a) and MALDI-TOF mass spectrometric (b) analysis of **PNA-5**.

Incorporation of the 2-(glycyloxymethyl)benzoic acid ester-monomer into PNA oligomers proceeded under standard PNA oligomerization conditions and yielded products that were readily purified by reversed phase HPLC (Figure 1). The only necessary precaution taken was the employment of carefully dried ether for precipitation of the product after cleavage from the resin in order to avoid hydrolysis of the ester. (In contrast, we were not able to isolate correct oligomer products when using 4-([*N*-Boc-glycyl]oxymethyl)benzoic acid, presumably due to degradation during deprotection and/or cleavage from the resin.)

To assess the utility of the 2-([*N*-Boc-glycyl]oxymethyl)-benzoic acid monomer in a prodrug approach, we measured the stability of **PNA-1** in mouse plasma and in mouse kidney and liver homogenates. **PNA-1** was incubated with tissue homogenates at dilutions of the homogenates that resulted in convenient stability for analysis. The analysis was performed by reversed phase HPLC which resolved the intact **PNA-1**, the resulting PNA from which the pyrene was cleaved off as well as the released pyrene. Quantification was performed on the basis of peak area of the intact **PNA-1** as compared to a standard curve of **PNA-1**. Samples were taken at various time points, and  $t_{1/2}$  was calculated from the [**PNA-1**] versus time plots (Figure 2). Taking the homogenate dilution factor into account, the stability in undiluted tissue homogenates could be estimated (Table 1). These results



**Figure 2.** Kinetic plot of **PNA-1** stability in mouse liver homogenate.

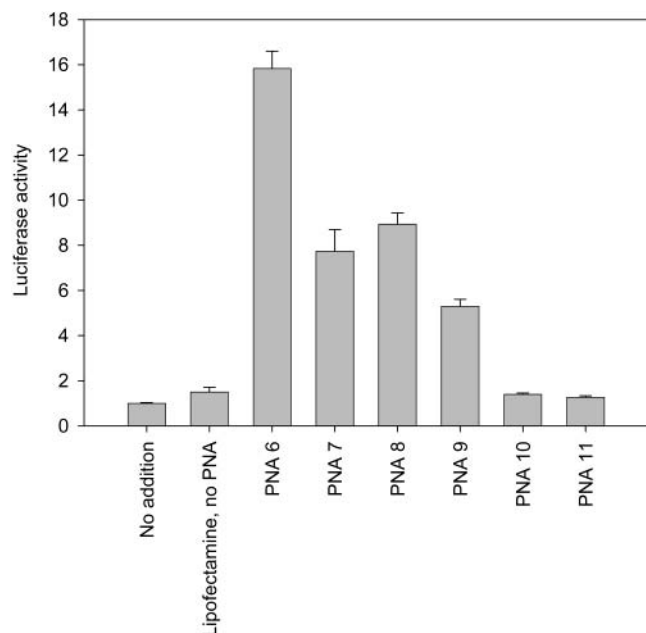
**Table 1.** Half-Lives of **PNA-1** in Various "Tissue Homogenates" As Determined by HPLC Analysis<sup>a</sup>

"tissue"	$t_{1/2}$ min	dilution	estimated $t_{1/2}$ in "tissue"
none (control)	363	—	360
plasma	100	1:1000	0.1
liver	61	1:140	0.5
kidney	37	1:280	0.15

<sup>a</sup> The half-life in "tissue" is extrapolated from the homogenate dilution factor.

clearly demonstrate that the ester is up to 2000–3000 times less stable in these tissue homogenates as compared to the stability in buffer, pH 7.4, at 37 °C. The results also show a reasonable although somewhat limited stability in buffer ( $t_{1/2}$  = 6 h) of this ester linkage.

We have previously found that fatty acid–PNA conjugates are more readily taken up by eukaryotic cells as compared to "naked" PNA (10). In particular, such PNA conjugates can be delivered via cationic liposomes (10, 11). However, it could be an advantage if the PNA oligomers were released from the fatty acid once inside the cell, especially because PNA–fatty acid conjugates have limited solubility in an aqueous environment. Thus, they may easily become entrapped in lipid compartments inside the cell, such as various (endosomal, nuclear, and other) membranes which could limit their access to the intended mRNA (or DNA) targets. We therefore synthesized the ester-containing PNA conjugates **PNA-4** and **PNA-5** and the corresponding nonester controls **PNA-2** and **PNA-3**. Preliminary studies of the uptake of these PNAs in IMR-90 cells indicated a different intracellular distribution of the ester linked conjugates (**PNA-4** and **PNA-5**) as compared to the noncleavable conjugates (**PNA-2** and **PNA-3**). The ester-linked PNA seemed to exhibit a less dispersed intracellular localization with a higher tendency to compartmentalize around the nuclei of the cells than their nonester-linked analogues. However, repeated experiments revealed that the differences were subtle and difficult to reproduce (results not shown). Although the cellular uptake experiments did not demonstrate a clear advantage of the ester-linked PNA conjugates, we designed a series of PNA conjugates for antisense experiments. We chose a PNA sequence (**PNAs 6–9**) that is known to up-regulate luciferase activity in a reporter cell line by restoring correct splicing through blockage of an intron–exon junction (for further details, see Experimental Section). The results presented in Figure 3 clearly demonstrate that the ester-linked decanoic acid PNA conjugate is twice as potent as the corresponding conjugate not containing the ester linkage, whereas only a smaller enhancement was seen for the adamantyl conjugates, and a two-base mismatch control (**PNA-10** and **PNA-11**) did not show any activity. Transfection of naked PNA as well as simple addition of the PNA conjugates resulted only in a slight increase in



**Figure 3.** Effect of lipofectamine mediated transfection of different PNA conjugates on the expression of luciferase in pLuc 705 HeLa cells. The transfections were performed as described in the methods section. All transfection were done in triplicates and error bars indicate the standard deviations. All results were normalized to the average value of the nontreated control cultures.

luciferase activity (approximately two times the background, results not shown).

Clearly we cannot at this stage ascribe the different uptake pattern of **PNA-4** and **PNA-5** and the improved cellular antisense potency of **PNA-6** (and **PNA-8**) to cleavage of the ester linkage, but the results do encourage further studies of this type of PNA prodrugs for both ex vivo cellular as well as for future in vivo animal applications. This new monomer can of course also be incorporated into other peptides in which an esterase sensitive linkage is desired.

#### ACKNOWLEDGMENT

This work was supported by Association for International Cancer Research (AICR), The Danish Cancer Society and the Lundbeck Foundation.

#### LITERATURE CITED

- (1) Mizen, L., and Burton, G. (1998) The use of esters as prodrugs for oral delivery of beta-lactam antibiotics. *Pharm. Biotechnol.* **11**, 345–365.
- (2) He, G., Massarella, J., and Ward, P. (1999) Clinical pharmacokinetics of the prodrug oseltamivir and its active metabolite Ro 64–0802. *Clin. Pharmacokinet.* **37**, 471–484.
- (3) Nielsen, P. E. (2000) Antisense peptide nucleic acids. *Current Opinion in Mol. Therapeutics* **2**, 282–287.
- (4) Braasch, D. A., and Corey, D. R. (2002) Novel antisense and peptide nucleic acid strategies for controlling gene expression. *Biochemistry* **41**, 4503–4510.
- (5) Aldrian-Herrada, G., Desarmenien, M. G., Orcel, H., Boissin-Agasse, L., Mery, J., Brugidou, J., and Rabie, A. (1998) A peptide nucleic acid (PNA) is more rapidly internalized in cultured neurons when coupled to a retro-inverso delivery peptide. The antisense activity depresses the target mRNA and protein in magnocellular oxytocin neurons. *Nucleic Acids Res.* **26**, 4910–4916.
- (6) Pooga, M., Soomets, U., Hallbrink, M., Valkna, A., Saar, K., Rezaei, K., Kahl, U., Hao, J. X., Xu, X. J., Wiesenfeld-Hallin, Z., Hokfelt, T., Bartfai, T., and Langel, U. (1998) Cell penetrating PNA constructs regulate galanin receptor levels and modify pain transmission in vivo. *Nat. Biotechnol.* **16**, 857–861.
- (7) Cutrona, G., Carpaneto, E. M., Ulivi, M., Roncella, S., Landt, O., Ferrarini, M., and Boffa, L. C. (2000) Effects in live cells of a c-myc anti-gene PNA linked to a nuclear localization signal. *Nat. Biotechnol.* **18**, 300–303.
- (8) Good, L., Awasthi, S. K., Dryselius, R., Larsson, O., and Nielsen, P. E. (2001) Bactericidal antisense effects of peptide-PNA conjugates. *Nat. Biotechnol.* **19**, 360–364.
- (9) Hamilton, S. E., Simmons, C. G., Kathiriyi, I. S., and Corey, D. R. (1999) Cellular delivery of peptide nucleic acids and inhibition of human telomerase. *Chemistry & Biology* **6**, 343–351.
- (10) Ljungström, T., Knudsen, H., and Nielsen, P. E. (1999) Cellular uptake of adamantyl conjugated peptide nucleic acids. *Bioconjugate Chem.* **10**, 965–972.
- (11) Mologni, L., Marchesi, E., Nielsen, P. E., and Gambacorti-Passerini, C. (2001) Inhibition of promyelocytic leukemia (PML)/retinoic acid receptor-alpha and PML expression in acute promyelocytic leukemia cells by anti-PML peptide nucleic acid. *Cancer Res.* **61**, 5468–5473.
- (12) Gilman, H., Brown, G. E., Webb, F. J., and Spatz, S. M. (1940) *J. Am. Chem. Soc.* **62**, 977.
- (13) Christensen, L., Fitzpatrick, R., Gildea, B., Petersen, K. H., Hansen, H. F., Koch, T., Egholm, M., Burchardt, O., Nielsen, P. E., Coull, J. and Berg, R. H. (1995) Solid-phase synthesis of peptide nucleic acids (PNA). *J. Peptide Sci.* **3**, 175–183.
- (14) Lohse, J., Nielsen, P. E., Harrit, N., and Dahl, O. (1997) Fluorescein-Conjugated Lysine Monomers for Solid-Phase Synthesis of Fluorescent Peptides and PNA Oligomers. *Bioconjugate Chem.* **8**, 503–509.
- (15) Schmajak, G., Sierakowska, H. and Kole, R. (1999) Antisense oligonucleotides with different backbones. Modification of splicing pathways and efficacy of uptake. *J. Biol. Chem.* **274**(31), 21783–21789.
- (16) Sazani, P., Kang, S. H., Maier, M. A., Wei, C., Dillman, J., Summerton, J., Manoharan, M., and Kole, R. (2001) Nuclear antisense effects of neutral, anionic and cationic oligonucleotide analogues. *Nucleic Acids Res.* **29**(19), 3965–3974.

BC025621R



# Atomic Force Microscopy of Liposomes Bearing Fibrinogen

Elisenda Casals,<sup>†</sup> Albert Verdaguer,<sup>‡</sup> Raúl Tonda,<sup>§</sup> Ana Galán,<sup>§</sup> Ginés Escolar,<sup>§</sup> and Joan Estelrich<sup>\*,†</sup>

Departament de Fisicoquímica, Facultat de Farmàcia, Universitat de Barcelona, Barcelona, Spain, Unitat de Tècniques Nanomètriques, Serveis Científic-Tècnics, Universitat de Barcelona, Barcelona, Spain, and Servei d'Hemoteràpia i Hemostàsia, Hospital Clínic, Facultat de Medicina, Universitat de Barcelona, Barcelona, Spain. Received November 18, 2002; Revised Manuscript Received February 4, 2003

Extruded liposomes formed from dipalmitoylphosphatidylcholine and cholesterol, with and without fibrinogen, were examined by atomic force microscopy (AFM). The sequence of events involved in the transition from attached liposomes to bilayer patches on mica supports was viewed by tapping mode in liquid. After adhesion to the mica surface, both liposomes without fibrinogen and liposomes with attached fibrinogen collapsed into patches. The fibrinogen layer attached to the liposomes was 2.6 nm thick. This implied that the protein was spread over the entire liposome and the protein characteristic trinodular structure disappeared. To check the type of bond between fibrinogen and liposome, sequential images were taken after the incubation of fibrinogen with liposomes with and without a chemical group for attaching the protein. The results clearly confirmed that fibrinogen bound covalently to liposomes.

## INTRODUCTION

Liposomes are lipid structures used as a model of biological membranes. They are also part of a drug-delivery system of well-defined physicochemical characteristics (1). The promotion by synthetic phospholipids of procoagulant activity in damaged vessels (2) and the fact that acidic phospholipids contribute to prothrombin activation (3, 4) have opened up new possibilities for the therapeutic use of liposomes. Liposomes can also be used as platelet substitutes in coagulant therapy. Along these lines, some authors have prepared liposomes to carry the domain of the platelet glycoprotein Ib $\alpha$  that binds the von Willebrand factor (5, 6).

Fibrinogen has a central function in the regulation of hemostasis and thrombosis. It coagulates blood and facilitates adhesion and aggregation of platelets (7). Fibrinogen is a 340 kDa dimeric molecule consisting of two sets of three intertwined polypeptide chains held together by 29 disulfide bonds, three of which connect the N-termini of the dimer subunits in an antiparallel arrangement (7–9). In thrombus formation on thrombogenic surfaces, platelet adhesion is successfully achieved by the surface-bound fibrinogen, while the dimeric structure of fibrinogen enables platelet–platelet bridging, which leads to macroscopic platelet aggregation (10). Thus, the binding of fibrinogen to liposomes favors the further adsorption of fibrinogen on a thrombogenic surface. When mixed with normal platelets, liposomes enhance platelet function. Therefore, when transfused in vivo, these liposomes are expected to adhere to suben-

dothelial matrix and to participate in the formation of platelet thrombi at the site of vascular injury, supporting hemostasis in thrombocytopenic patients. To check this hypothesis, we bound fibrinogen to neutral liposomes covalently. To investigate the location and structure of fibrinogen on the liposomes, we employed atomic force microscopy (AFM<sup>1</sup>). This technique has been successfully employed to study the dynamic change in surface topography during the adhesion of proteins (11) and polymers (12) to a solid surface. The development of AFM has allowed direct in situ examination of many biological materials, including phospholipid membranes (13). AFM images surfaces at very high resolution in aqueous environments. Liposomes are a great challenge for current AFM technology, since they are fluid and dynamic systems (14–20).

## MATERIALS AND METHODS

**Materials.** DL- $\alpha$ -Dipalmitoylphosphatidylcholine (DPPC), cholesterol (CHOL), and type-I fibrinogen (from human plasma) came from Sigma (St. Louis, MO); *N*-succinimidyl-*S*-acetylthioacetate (SATA) and Excellulose GF-5 desalting column were from Pierce (Rockford, IL); egg phosphatidylethanolamine (PE) and 1,1-dipalmitoyl-*sn*-glycero-3-phosphoethanolamine-*N*-[4-(*p*-maleimidophenyl)-butyramide] (N-MPB-PE) were from Avanti Polar Lipids (Alabaster, AL). The buffer used was 50 mM Hepes, pH 7.5 (with and without 1 mM EDTA for liposomes with and without fibrinogen). Other reagents used were of analytical grade. Water was distilled twice and deionized (Millipore, Molsheim, France).

**Preparation of Thiolated Fibrinogen.** The procedure for thiolating proteins with SATA is similar to that described by Heeremans et al. (21). Fibrinogen was

\* Corresponding author: Dr. Joan Estelrich, Departament de Fisicoquímica, Facultat de Farmàcia, Universitat de Barcelona, Avda. Joan XXIII s/n; 08028 Barcelona (Catalonia, Spain). Tel: + 34-93-4024559; fax: + 34-93-4035987; e-mail estelric@farmacia.far.ub.es.

<sup>†</sup> Departament de Fisicoquímica, Facultat de Farmàcia.

<sup>‡</sup> Unitat de Tècniques Nanomètriques, Serveis Científic-Tècnics.

<sup>§</sup> Servei d'Hemoteràpia i Hemostàsia, Hospital Clínic, Facultat de Medicina.

<sup>1</sup> Abbreviations: AFM, atomic force microscopy; CHOL, cholesterol; DPPC, DL- $\alpha$ -dipalmitoylphosphatidylcholine; EDTA, ethylenediaminetetraacetic acid; N-MPB-PE, 1,1-dipalmitoyl-*sn*-glycero-3-phosphoethanolamine-*N*-[4-(*p*-maleimidophenyl)-butyramide]; PE, phosphatidylethanolamine; SATA, *N*-succinimidyl-*S*-acetylthioacetate.

dissolved in saline solution (145 mM NaCl) at 60  $\mu$ M. Immediately before reaction, about 14 mg of SATA was dissolved in 1.0 mL of dimethyl sulfoxide. One milliliter of the fibrinogen solution was combined with 10  $\mu$ L of the SATA solution in a test tube. This corresponded to a SATA:fibrinogen molar ratio of 10. After mixing, the resulting solution was left to react at room temperature for 30 min. Fibrinogen was purified by size-exclusion chromatography by means of Excellulose GF-5 equilibrated with Hepes/EDTA buffer. The presence of fibrinogen in the eluates was checked by monitoring their absorbance at 278 nm. Fractions containing the protein were pooled. Acetylthioacetyl-protein (1 mL) was deacetylated by adding 100  $\mu$ L of a freshly prepared 0.5 M hydroxylamine-HCl solution containing 50 mM Hepes and 25 mM EDTA, pH 7.5. The incubation lasted for 2 h at room temperature. Then, thiolated protein was purified again by size-exclusion chromatography. The number of introduced thiol groups was assayed according to Ellman, using cysteine for the calibration curve (22). In this assay, the blank consisted of all components of the sample itself, the only difference being that, instead of thiolated fibrinogen, the same concentration of nonthiolated protein was used. According to this assay, the number of introduced thiol groups (expressed as mol SH per mol fibrinogen) was  $1.6 \pm 0.1$ .

**Liposome Preparation.** Phospholipids (DPPC:CHOL: N-MPB-PE and DPPC:CHOL:PE at the molar ratio 50:20:30) were dissolved in chloroform in a round-bottomed flask and dried in a rotary evaporator under reduced pressure at 50  $^{\circ}$ C to form a thin film on the flask. The film was hydrated with Hepes buffer to give a concentration of 20 mM. Multilamellar liposomes were formed by constant vortexing for 4 min on a vortex mixer and sonication in a bath for 4 min. Multilamellar liposomes were downsized to form uni- or oligolamellar vesicles by extrusion through polycarbonate membranes of a nominal size of 200 nm (Poretics, Livermore, CA) at 50  $^{\circ}$ C in an extruder device (LiposoFast, Avestin, Ottawa, Canada).

**Coupling of Thiolated Fibrinogen to Liposomes.** A volume of liposome suspension (DPPC:CHOL:N-MPB-PE) was combined with an equal volume of fibrinogen solution. The resulting suspension was left to react overnight at room temperature, while being shaken at 1000 rpm. The coupling reaction was stopped by adding 50  $\mu$ L of *N*-ethylmaleimide (8 mM in Hepes buffer), and the liposomes were separated from free protein by two centrifugation steps in a Centrikon T-1170 (Kontron Instruments, Milan, Italy) for 40 min at  $100\,000 \times g$  and at 7  $^{\circ}$ C.

**Liposome Characterization.** Phospholipid content was based on the phosphorus content (23), the fibrinogen concentration was determined by the Bradford's method (24) after liposome disruption in sodium dodecyl sulfate (10%), the vesicle size distribution was determined by photon correlation spectroscopy with an Autosizer IIc spectrometer (Malvern Instruments, Malvern, UK), and surface charge was determined as  $\zeta$  potential by Doppler microelectrophoresis in a Zetasizer 4 (Malvern Instruments, Malvern, UK) using the Henry correction of Smoluchowski's equation (25).

**Substrate Preparation and AFM Observation.** A Digital Instruments Nanoscope IIIa AFM (Santa Barbara, CA) with a 12  $\mu$ m scanner (E-scanner) and Tapping Mode liquid cell was employed. Before use, the liquid cell was cleaned with ultrapure water, then with ethanol, and was rinsed again with ultrapure water. A small square ( $\approx 5 \times 5$  mm) of muscovite mica was glued with water-insoluble glue to a Teflon disk with a supporting steel

disk, and 120- $\mu$ m-long V-shaped cantilevers from Olympus Ltd. (Tokyo, Japan) with  $\text{Si}_3\text{N}_4$  tips and a nominal force constant  $k = 0.1 \text{ N}\cdot\text{m}^{-1}$ , which minimized force during scans, were used. The scanning line speed was optimized to 2 Hz. Height and amplitude of the images of  $256 \times 256$  pixels were taken simultaneously. Height images were flattened and plane adjusted. All measurements were taken on the height images, but breadth images were also shown for easier viewing of the processes. Before the adsorption to freshly cleaved mica, the samples were diluted to a lipid concentration of 0.1 mM in buffer solution. To achieve a better interaction between mica and liposomes, 50  $\mu$ L of 0.5 M NaCl was deposited on a mica surface. After 10 min, the surface was rinsed gently with Hepes buffer. Then, 40–50  $\mu$ L of liposome sample was added. After 10–15 min of incubation, the surface was rinsed gently with Hepes buffer at room temperature, and the samples in buffer solution were examined directly. Heights of the images were determined by cross-sectional analysis of a software zoom of the image, and the results are expressed as mean  $\pm$  standard deviation,  $n$  being the number of liposomes measured.

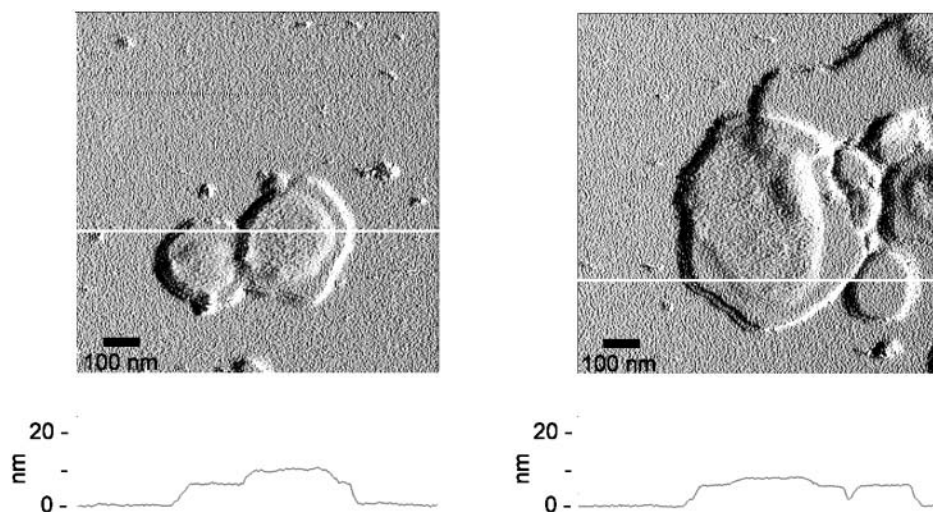
## RESULTS AND DISCUSSION

**Liposome Characterization.** The incubation ratio of SATA/fibrinogen of 10 (molar ratio) resulted in the introduction of 1.5–1.7 mol of thiol groups per mole of fibrinogen. For the different fibrinogen-liposome batches tested in this study, 33 to 53  $\mu$ g of fibrinogen per  $\mu$ mole of phospholipid were coupled, which corresponded with about 34–55 protein molecules per liposome, assuming unilamellarity, uniform particle size, spherical particle shape, and a phospholipid molecular area of 0.70 nm<sup>2</sup>. Photon correlation spectroscopy found that liposomes were monodisperse and monomodal in their distribution. Their average diameter was  $200 \pm 5$  nm for liposomes lacking protein, and  $250 \pm 20$  nm after the coupling procedure. As the average end-to-end length of fibrinogen is about 46 nm (26–28), the increase of vesicle diameter is coherent with the presence of the protein molecule on the liposomal surface. This effect has been described by other authors (29). The polydispersity index, which ranges from 0.0 for an entirely monodisperse sample to 1.0 for a highly polydisperse sample, was always less than 0.2. In this way, despite the presence of more than one thiol group per protein molecule, and that theoretically a multivalent interaction could exist, the results of vesicle size and polydispersity seem to rule out the possibility that fibrinogen had cross-linked more than one liposome.

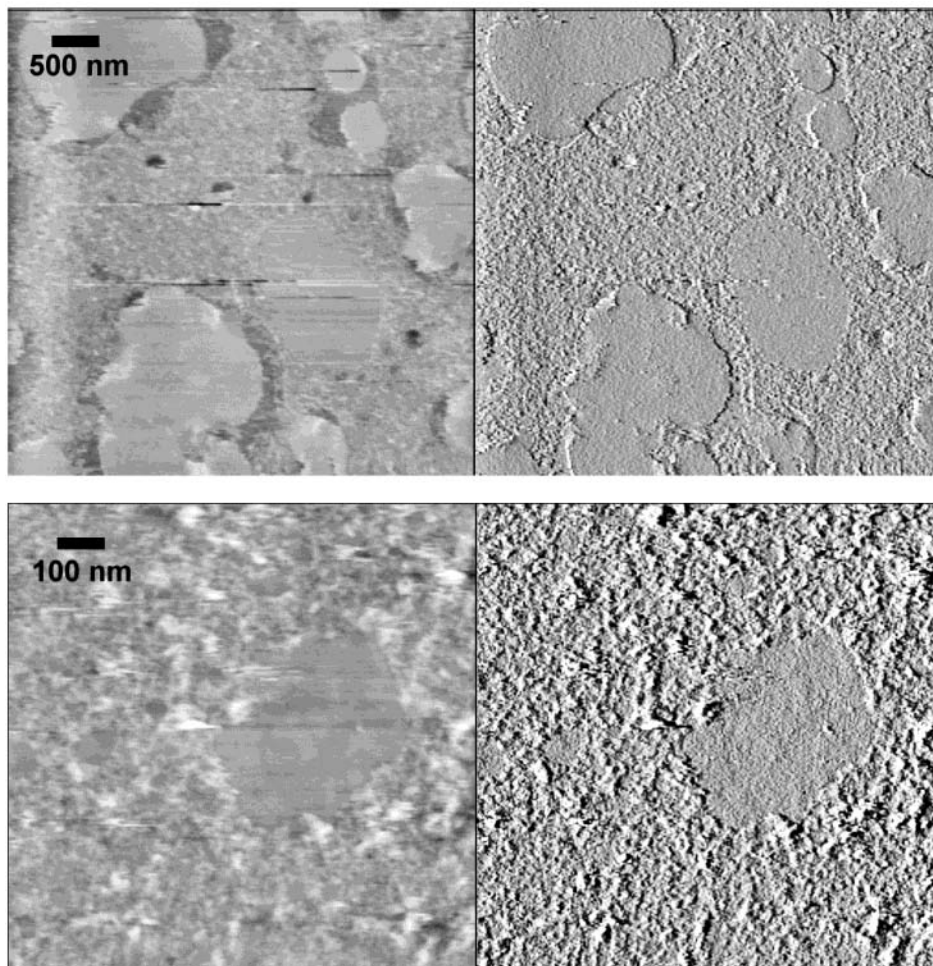
When the electrophoretic mobility of liposomes was determined by Doppler microelectrophoresis, an average value of  $-18$  mV was obtained for the composition DPPC:CHOL:PE. This figure corroborates previous values (30) for liposomes bearing the same percentage of the zwitterionic PE. However, in liposomes with the PE conjugated to the maleimide group (DPPC:CHOL:N-MPB-PE), the average  $\zeta$  potential is close to  $-1$  mV. In fibrinogen-bearing liposomes, the  $\zeta$  potential rose to  $-60$  mV. This was due to negative net charge on the protein at pH 7.5, since the isoelectric point of fibrinogen is 4.9.

The  $\zeta$  potential of the mica surface was determined by means of the plane interface technique (31), in which the velocity profile of a standard particle is extrapolated. On the basis of the electro-osmotic flow to the cell wall of the mica plate, this technique gave highly negative values. As the electrostatic interaction between liposomes





**Figure 1.** Amplitude tapping mode images in liquid of a mica surface after exposure to liposomes formed by DPPC:CHOL:PE (50:30:20, molar ratio) at 0.1 mM lipid concentration and bearing fibrinogen (30% of attachment sites, molar ratio). The images show flattened liposomes and liposomes with a second layer of rough surface. The cross-section of the areas identified by the line (measured from the height images) shows that the height of the flattened liposome is 5.9 nm, and of the liposome for the rough surface, 8.4 nm. The difference in height is due to the network that fibrinogen forms on the liposome surface.



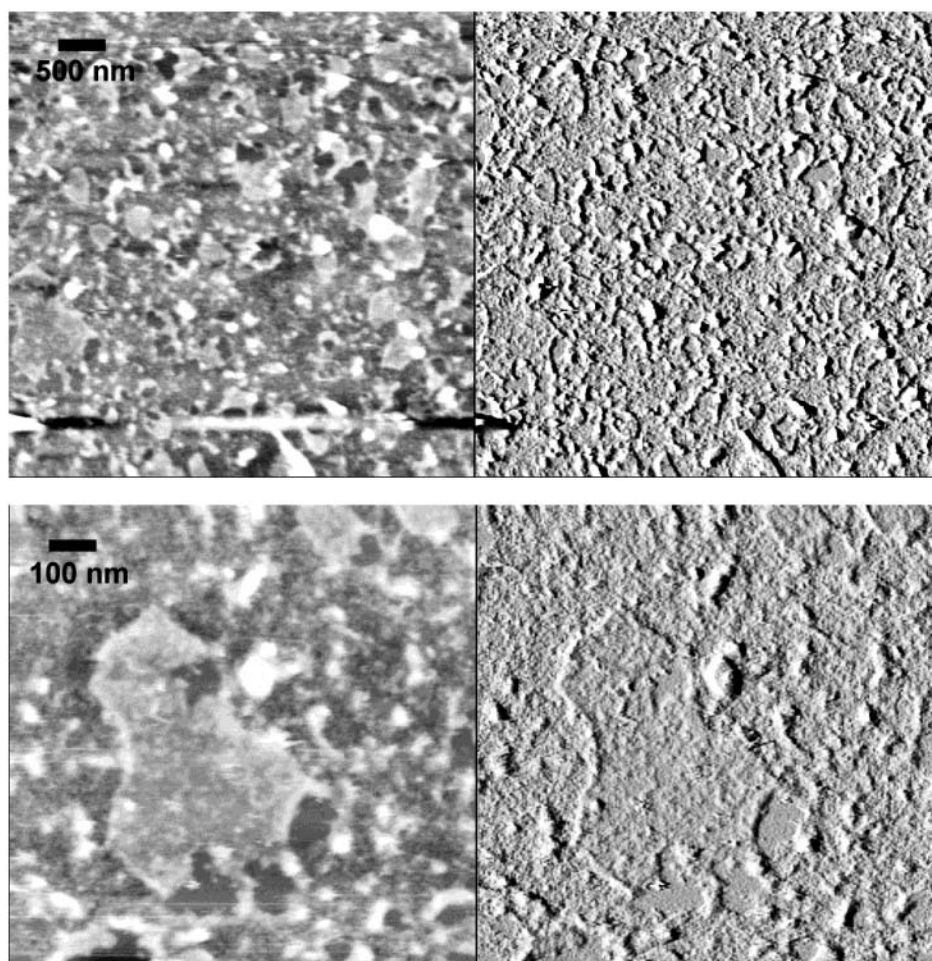
**Figure 2.** Images of height (left) and width (right) of liposomes formed by DPPC:CHOL:PE (50:30:20, molar ratio). The top images are  $5 \times 5 \mu\text{m}$ , and the bottom ones of a more detailed image of  $1 \times 1 \mu\text{m}$ . After incubation with  $5 \mu\text{L}$  of  $1.5 \mu\text{M}$  fibrinogen and further rinsing with HEPES buffer, the liposome surface is clean, whereas the mica surface is covered by fibrinogen. The stronger interaction between the mica and the fibrinogen avoids the sweeping of the protein.

and the mica surface is an important factor in determining the adhesion rate of liposomes to a mica surface, the interaction between two negative entities did not lead to adhesion. The incubation of the mica surface with NaCl reduces or even overcompensates the negative  $\zeta$  potential.

Therefore, in electrostatic terms, it can be assumed that mica treated with 0.5 M NaCl will adhere well to liposomes.

**AFM Imaging of Liposomes.** When liposomes not bearing fibrinogen were deposited on mica, the AFM





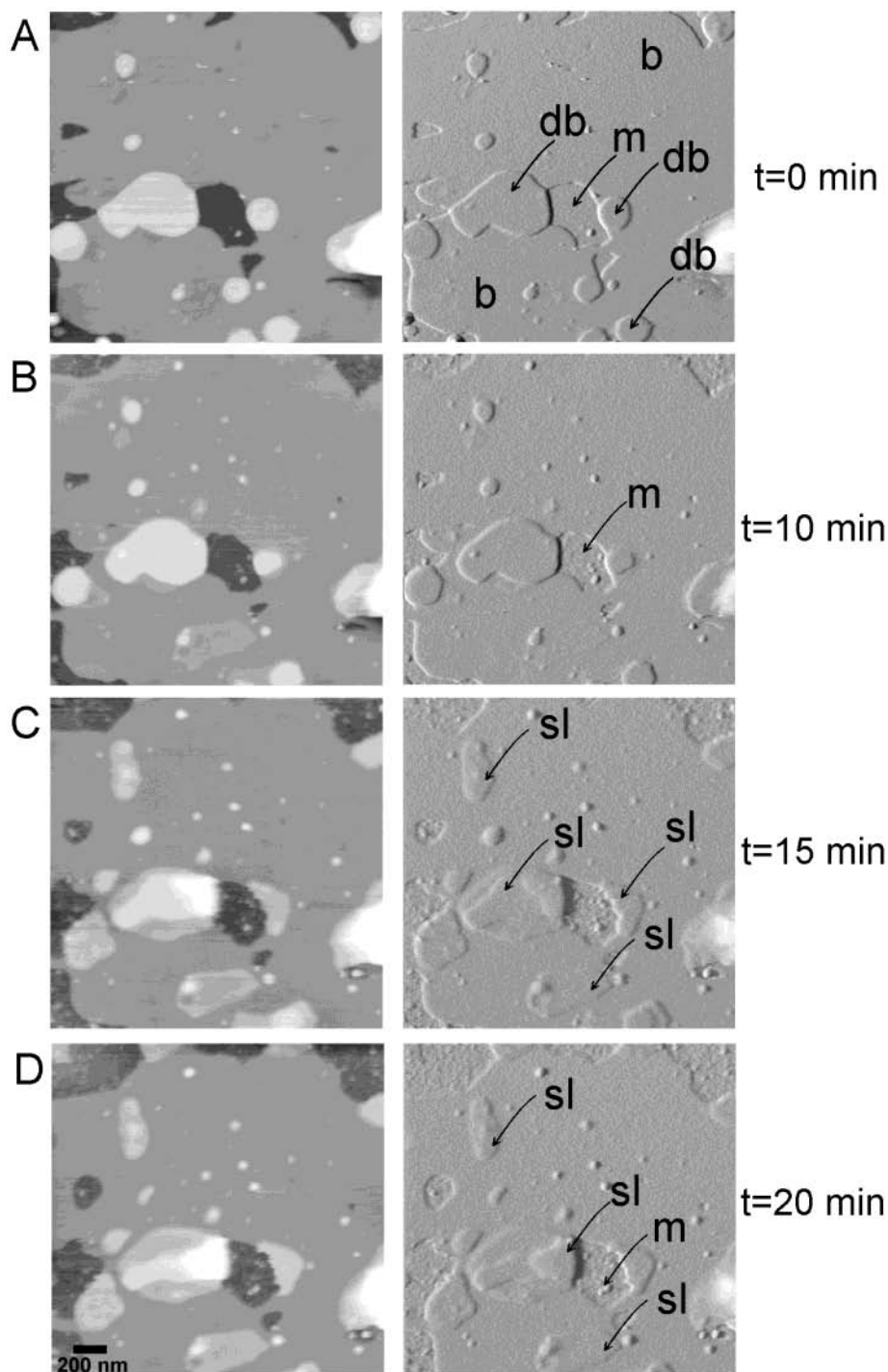
**Figure 3.** Images of height (left) and width (right) of liposomes formed by DPPC:CHOL:MPB-PE (50:30:20, molar ratio). The top images are  $5 \times 5 \mu\text{m}$ , and the bottom ones of a more detailed image of  $1 \times 1 \mu\text{m}$ . After incubation with  $5 \mu\text{L}$  of  $1.5 \mu\text{M}$  fibrinogen and further rinsing with Hepes buffer, the liposome surface is covered by fibrinogen in a way similar to the mica surface. The attachment of fibrinogen to the liposome is now strong enough to keep the protein bound to the vesicles.

imaging showed that larger areas of the surface were covered by liposomes (image not shown). However, only a few of these liposomes were attached intact to the surface or partly flattened. Most of them were completely flattened, forming layers of two different heights. The value of the higher layer was  $12.0 \pm 1.6 \text{ nm}$  ( $n = 5$ ). This may correspond to a double-bilayered structure. The lower layer, at  $5.9 \pm 0.7 \text{ nm}$  ( $n = 5$ ), is characteristic of a single bilayer. Sequential imaging (not shown) had the following steps: (1) adsorption to surface, (2) flattening and spreading; and (3) fusing and spreading of bilayers. More explicitly, the initially adsorbed liposomes seemed to collapse from the outer periphery toward the center of the liposome. The process continued until the whole liposome had produced two bilayers stacked one on top of the other. At this point the double-bilayer disk abruptly fused with already formed bilayer patches, and its thickness changed to that of a single bilayer. The absence of any elastic or restorative forces in this process indicates two main features. First, the fused bilayer fragments slide over each other in the aqueous layer that separates them, and, second, the relatively high energetic cost of exposing the hydrophobic inner membrane precludes the sliding of the tails over each other. This is the same pattern of liposome collapse as is described in the literature (18).

When the different stages of collapse of liposomes bearing fibrinogen were observed under the same conditions as those described above, the same smooth layer,

$5.9 \pm 0.8 \text{ nm}$  thick ( $n = 5$ ), that was observed in liposomes lacking fibrinogen was also appreciated (Figure 1). Sometimes an additional layer, with a rougher aspect,  $8.5 \pm 0.4 \text{ nm}$  thick ( $n = 5$ ), was found. The fibrinogen molecules may form a network over the whole surface, in which case the characteristic trinodular structure disappears.

According to the model of the transformation of the liposomes in a planar bilayer proposed by Jass et al. (18) the transition from a double bilayer to a single bilayer involves the movement of the upper bilayer from the lower one to unoccupied areas of the surface. This movement can occur by either sliding or rolling, leading in both cases to a single bilayered structure. As a consequence of such processes, much of the face viewed by AFM is the internal layer of the liposomes. Moreover, in the presence of fibrinogen, the strong interaction between the mica and the protein increases the proportion of the inner layer that can be seen. Therefore, the smooth bilayers displayed in Figures 1 and 2 correspond to the internal layer of the liposome, as the external bilayer is in contact with the mica. Occasionally, some fibrinogen fibers could be observed just at the edges of the lipid layers (not shown in the figures). As stated above, the height of the bilayer observed is, as a general rule, on average the same (5.9 nm), irrespective of the presence of fibrinogen. This implies that when fibrinogen is present, it is in contact with the mica and must be extremely compressed. In a few such cases, a rough layer



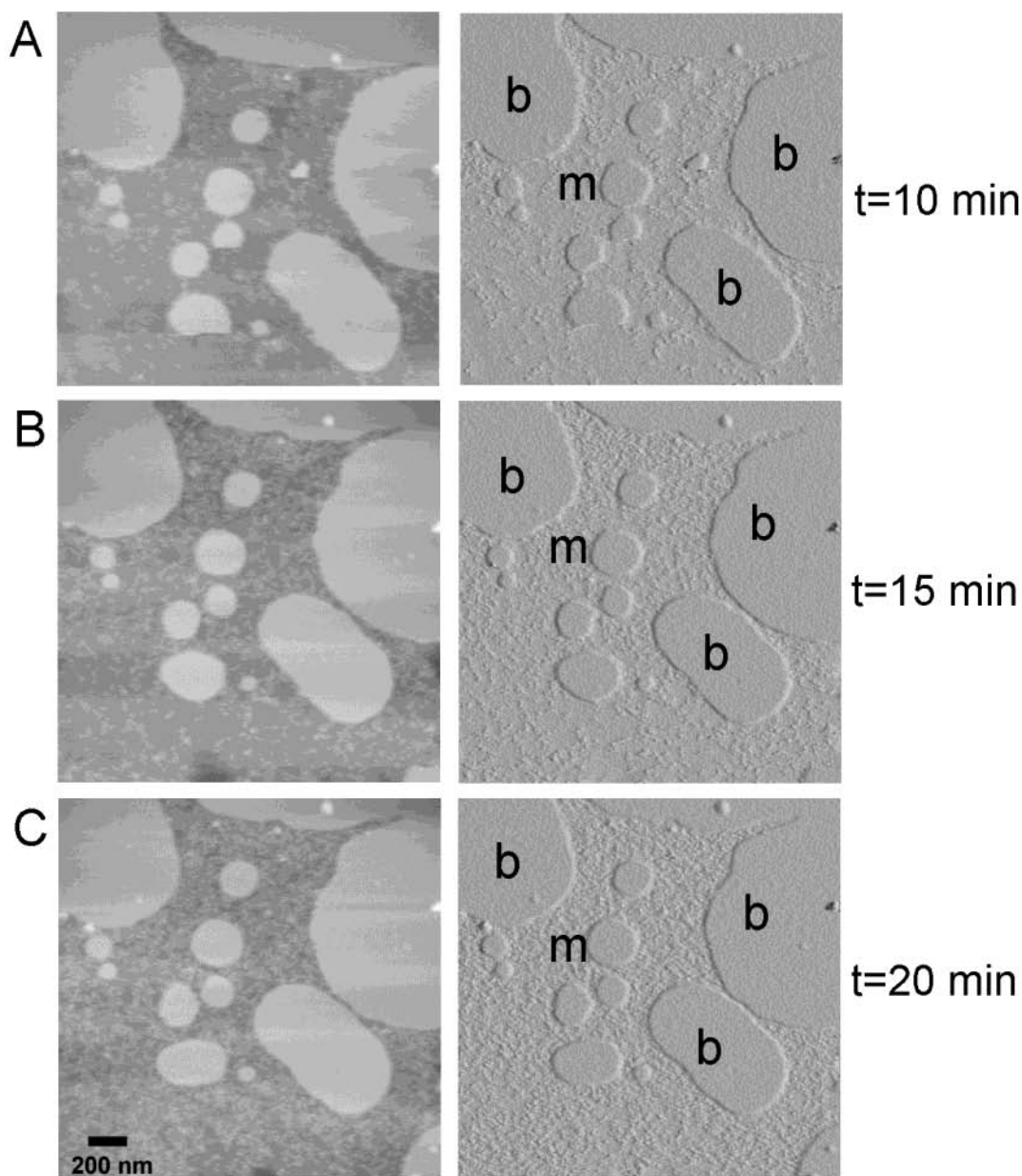
**Figure 4.** Series of height (left) and width (right) of  $2 \times 2 \mu\text{m}$  images in liquid taken to perform a kinetic experiment. After flattening DPPC:CHOL:MPB-PE liposomes at 0.1 mM lipid concentration on the mica surface,  $1.5 \mu\text{M}$  fibrinogen was injected directly until its presence on the mica surface was clear. This occurred at various times after fibrinogen incubation. (A) Image showing liposomes before the injection of fibrinogen, (db): double bilayer, (m): mica. (B) First stages of the deposition of fibrinogen on the mica surface (m). (C) In this image some changes can be appreciated on the lipid bilayers: apparition of a new smooth layer (sl) spread principally on double bilayers. (D) Most of the single bilayer is still unaltered, but the new smooth layer (sl) can be appreciated on some parts of the single bilayer. Mica (m) and double bilayers are now completely covered.

of 8.5 nm was observed, which should correspond to the external face of the liposome covered by fibrinogen. Thus, the layer of fibrinogen attached to the liposome was 2.6 nm thick. The value of the additional thickness found in the indicated liposomes confirms that the height of fibrinogen alone deposited on mica varies from 2.3 to 2.5 nm (31). As indicated above, the molecular length of fibrinogen is about 46 nm, and when the fibrinogen is in solution (aqueous buffers are good solvents for proteins),

the protein chains extend into the solution and gain conformational entropy. Under such conditions, the high degree of freedom of the protein molecule is favored by the covalent bond between liposome and protein. This can explain the difference of 50 nm between liposomes bearing fibrinogen and liposomes without it found by photon correlation spectroscopy.

Macroscopic and microscopic studies have shown that fibrinogen binds strongly and in high amount to most





**Figure 5.** The same kind of images as those in Figure 4, but now using liposomes without a specific binding-point for fibrinogen. (A) image showing some flattened liposomes (db) at the first stages of deposition of fibrinogen on mica surface (m). (B) After 15 min, the percentage of protein on mica has increased. (C) The mica surface is steadily covered by fibrinogen. No changes on the liposomal surface (b) can be appreciated.

surfaces (32). Ta et al. (33) have proposed a model for fibrinogen adsorption both on hydrophobic and hydrophilic surfaces. At the mica–buffer interface, fibrinogen forms a monolayer, and it lies flatter than on a hydrophobic surface. The external side of a liposome bilayer has hydrophilic properties, and, therefore, one can expect a similar liposome–fibrinogen interaction. Moreover, the flattening effect of the tip must be also considered.

At the moment, findings have shown only that fibrinogen is present on liposomes, but this does not ensure that the protein binds covalently to the liposome, since fibrinogen could be attached to the liposome by adsorption or by a hydrogen bridge. To determine how the protein is bound, two kinds of liposomes were prepared: liposomes composed of DPPC:CHOL:N-MPB-PE (50:20:30, molar ratio), i.e., liposomes with the point of attachment free, and liposomes composed of DPPC:CHOL:PE (50:20:30, molar ratio), which had no specific place for attaching the fibrinogen. Liposomes were deposited on

the mica. The tip imaging was left until most of the liposomes were completely flattened on the surface. At that point, 5  $\mu$ L of 1.5  $\mu$ M fibrinogen solution was added to the liposomal sample. After 10 min of incubation, the sample was rinsed with Hepes buffer. For reference images, the same procedure was applied to freshly cleaved mica to which only fibrinogen was added. Figure 2 shows that the flat surface of liposomes without MPB is clean, without fibrinogen, whereas the mica is fully covered by the protein. However, the surface of liposomes bearing MPB was also covered by the fibrinogen, just like the mica surface (Figure 3). In the latter case, multiple rinses of the surface were unable to clean the liposome surfaces. This confirms that fibrinogen is strongly attached to the liposome, since the washing procedure should have removed loosely bound material. To delve further into the process of fibrinogen binding to liposomes, an *in situ* kinetic experiment was performed. The liposomes bearing the group MPB adhered to the mica



surface. Images were taken periodically, and, after the flattening of liposomes, an area was chosen where the mica surface and the lipid bilayer could be examined in the same image. The tip scan was then left in the same position all the time, and images were taken. Fibrinogen (1.5  $\mu\text{M}$ ) in buffer was injected directly into the liquid cell. The process was repeated until the first molecules of fibrinogen became attached to the mica surface. At this moment, the injections were stopped, and the system was left to evolve. In Figure 4, this evolution can be followed in four different images. To show clearly all the changes on the mica surface, images of height and width are shown together. Figure 4A shows the liposome before the injection of fibrinogen. On the mica surface (m) there is a layer of about 6 nm, which may correspond to a lipid bilayer (b); and, in some places, layers with a height of 12 nm, which may logically correspond to a double bilayer (db) structure (see arrows). After 10 min of incubation, the first steps of the deposition can be observed. The existence of roughness on the mica is due to the attachment of the first molecules of fibrinogen (Figure 4B). After 15 min, some changes can be appreciated in the lipid bilayers (Figure 4C). In the places that exhibited a double bilayer, a new smooth layer (sl) spread over the surface. Similar new layers were found in those zones where only a single bilayer appeared before. The rest of the surface did not show any change. In the last image (time elapsed 25 min, Figure 4D) we can see that most of the liposome surface has still not changed. However, mica and the liposomal zones, which had been covered previously by fibrinogen, are now completely covered by a new layer. The liposomes have continued their evolution, and the edges of the single and double lipid bilayers have changed in comparison with the first image. The height of the new layer measured  $7.4 \pm 0.8$  ( $n = 5$ ) when it corresponded to the height difference between the mica and the lipid bilayer/fibrinogen layer. Note that this value had to be carefully borne in mind because of the difficulties involved in seeing a zone with clean mica. The direct measurement of the fibrinogen layer from the lipid bilayer gave a height of  $2.8 \pm 0.4$  nm ( $n = 4$ ). The difference of height between this second bilayer and the first bilayer was  $8.6 \pm 0.4$  nm.

The same in situ experiment was performed with liposomes without a specific site for attaching the fibrinogen. In Figure 5, a surface of mica (m) partially covered by a layer of liposomes can be seen (b). Image 5A was taken 10 min after the injection of the fibrinogen, and it was already possible to see some individual molecules of fibrinogen on the surface. Five minutes later, the number of protein molecules attached to the mica had increased (Figure 5B), and eventually, 20 min after the injection, the entire mica surface was covered by fibrinogen (Figure 5C). However, on the liposome surface no change can be appreciated, even on the small double bilayer that appears at the top of the image. It seems logical to suppose that fibrinogen has been swept off by the tip.

## CONCLUSIONS

AFM was used for in situ viewing of the dynamic morphological changes in liposome adhesion to a mica surface. The structure observed is strongly dependent upon the interaction between the liposomes and the mica surface. The AFM images display a spontaneous deformation from a spherical liposome to a flat bilayer. Liposomes without fibrinogen mainly formed two layers, of the thickness of one and two bilayers. In some liposomes with fibrinogen, an additional layer appeared. This was due to the fibrinogen spread on the surface.

Successful imaging of the covalent presence of fibrinogen in liposomes illustrates the potential of AFM for determining the degree to which macromolecules located on the liposome surface are natural or synthetic.

## ACKNOWLEDGMENT

This research was supported by funds from the FIS 99-0110 (Spain) and FEDER 2FD97-0778.

## LITERATURE CITED

- (1) Lasic, D. D. (1993) *Liposomes: From Physics to Applications*, Elsevier, Amsterdam.
- (2) Galán, A. M., Hernández, M. R., Bozzo, J., Reverter, J. C., Estelrich, J., Roy, M. T., Mazzara, R., Ordinas, A., and Escolar, G. (1998) Preparations of synthetic phospholipids promote procoagulant activity on damaged vessels: studies under flow conditions. *Transfusion* 38, 1004–1010.
- (3) Koppaka, V., Wang, J., Banerjee, M., and Lentz, B. R. (1996) Soluble phospholipids enhance factor Xa-catalyzed prothrombin activation in solution. *Biochemistry* 35, 7482–7491.
- (4) Koppaka, V., and Lentz, B. R. (1996) Binding of bovine factor Va to phosphatidylcholine membranes. *Biophys. J.* 70, 2930–2937.
- (5) Kitaguchi, T., Murata, M., Iijima, K., Kamide, K., Imagawa, T., and Ikeda, Y. (1999) Characterization of liposomes carrying von Willebrand factor-binding domain of platelet glycoprotein Ib $\alpha$ : A potential substitute for platelets transfusion. *Biochem. Biophys. Res. Commun.* 261, 784–789.
- (6) Nishiyama, T., Murata, M., Handa, M., and Ikeda, Y. (2000) Targeting of liposomes carrying recombinant fragments of platelet membrane glycoprotein Ib $\alpha$  to immobilized von Willebrand factor under flow conditions. *Biochem. Biophys. Res. Commun.* 270, 755–760.
- (7) Hantgan, R. R., Francis, C. W., and Marder, V. J. (1984) Fibrinogen structure and physiology. *Hemostasis and Thrombosis: Basic Principles and Clinical Practice*, 3rd ed. (Colman, R. W., Hirsch, J., Marder, V. J., and Salzman, E. W., Eds.) pp 277–300, J. B. Lippincott, Philadelphia.
- (8) Hoeprich, P. D., and Doolittle, R. F. (1983) Dimeric half molecules of human fibrinogen are joined through disulfide bonds in an antiparallel orientation. *Biochemistry* 22, 2049–2055.
- (9) Gärlund, B., Hessel, B., and Marguerie, G. (1977) Primary structure of human fibrinogen: characterizations of disulfide-containing cyanogen-bromide fragments. *Eur. J. Biochem.* 77, 595–610.
- (10) Savage, B., Saldivar, E., and Ruggeri, Z. M. (1996) Initiation of platelet adhesion by arrest onto fibrinogen or translocation on von Willebrand factor. *Cell* 84, 289–297.
- (11) Drake, B., Prater, C. B., Weisenborn, A. L., Gould, S. A. C., Albrecht, T. R., Quate, C. F., Cannell, D. S., Hansma, H. G., and Hansma, P. K. (1989) Imaging crystals, polymers, and processes in water with the atomic force microscope. *Science* 243, 1586–1589.
- (12) Stipp, S. L. S. (1996) In-situ, real-time observations of the adsorption and self-assembly of macromolecules from aqueous-solution onto an untreated, natural surface. *Langmuir* 12, 1884–1891.
- (13) Shao, Z., and Yang, J. (1995) Progress in high-resolution atomic force microscopy in biology. *Quart. Rev. Biophys.* 28, 195–251.
- (14) Iwamoto, H., and Wakayama, N. (1997) Structural studies on phosphatidylcholine liposomes in various phases using atomic force microscopy. *Jpn. J. Appl. Phys.* 36, 3913–3916.
- (15) Egawa, H., and Furusawa, K. (1999) Liposome adhesion on mica surface studied by atomic force microscopy. *Langmuir* 15, 1660–1666.
- (16) Thomson, N. H., Collin, I., Davies, M. C., Palin, K., Parkins, D., Roberts, C. J., Tendler, S. J. B., and Williams, P. M. (2000) Atomic force microscopy of cationic liposomes. *Langmuir* 16, 4813–4818.
- (17) Sideratou, Z., Tsiourvas, D., Paleos, C., Tsortos, A., Pypassopoulos, S., and Nounesis, G. (2002) Interaction of phosphatidyl choline based liposomes functionalized at the

- interface with adenine and barbituric acid moieties. *Langmuir* 18, 829–835.
- (18) Jass, J., Tjärnhage, T., and Puu, G. (2000) From liposomes to supported, planar bilayer structures on hydrophilic and hydrophobic surfaces: an atomic force microscopy study. *Biophys. J.* 79, 3153–3163.
- (19) Maeda, N., Senden, T. J., and di Meglio, J. M. (2002) Micromanipulation of phospholipid bilayers by atomic force microscopy. *Biochim. Biophys. Acta* 1564, 165–172.
- (20) Takiguchi, K., Nomura, F., Inaba, T., Takeda, S., Saitoh, A., and Hotani, H. (2002) Liposomes possess drastic capabilities for topological transformation. *Chem. Phys. Chem.* 3, 571–574.
- (21) Heeremans, J. L. M., Kraaijenga, J. J., Los, P., Kluft, C., and Crommelin, D. J. A. (1992) Development of a procedure for coupling the homing device glu-plasminogen to liposomes. *Biochim. Biophys. Acta* 1117, 258–264.
- (22) Ellman, G. L. (1959) Tissue sulphydryl groups. *Arch. Biochem. Biophys.* 82, 70–77.
- (23) Barlett, G. R. J. (1959) Phosphorus assay in column chromatography. *J. Biol. Chem.* 234, 466–468.
- (24) Bradford, M. M. (1976) A rapid and sensitive method for the quantitation of microgram quantities of protein utilizing the principle of protein-dye binding. *Anal. Biochem.* 72, 248–254.
- (25) Hunter, J. R. (1981) *Zeta Potential in Colloid Science*, Chapter 3, Academic Press, London.
- (26) Brown, J. H., Volkmann, N., Jun, G., Henschen-Edman, A. H., Cohen, C. (2000) The crystal structure of modified bovine fibrinogen. *Proc. Natl. Acad. Sci. U.S.A.* 97, 85–90.
- (27) Yang, Z., Mochalkin, I., Veerapandian, L., Riley, M., Doolittle, R. F. Crystal structure of native chicken fibrinogen at 5.5-Å resolution. *Proc. Natl. Acad. Sci. U.S.A.* 97, 3907–3912.
- (28) Sidney Sit, P., and Marchant, R. E. (1999) Surface-dependent conformations of human fibrinogen observed by atomic force microscopy under aqueous conditions. *Thromb. Haemostasis* 82, 1053–1060.
- (29) DeAnglis, P., Fox, M. D., and Retzinger, G. S. (1999) Accumulation of fibrinogen-coated microparticles at a fibrinogen-rich inflammatory site. *Biotechnol. Appl. Biochem.* 29, 251–261.
- (30) Roy, M. T., Gallardo, M., and Estelrich, J. (1998) Influence of size on electrokinetic behavior of phosphatidylserine and phosphatidylethanolamine lipid vesicles. *J. Colloid Interface Sci.* 206, 512–517.
- (31) Sasaki, H., Muramatsu, A., Arakatsu, A., and Usui, S. (1991) Zeta-potential measurement by means of the plane interface technique. *J. Colloid Interface Sci.* 142, 266–271.
- (32) Feng, L., and Andrade, J. D. (1995) *Proteins at Interfaces II: Fundamentals and Applications* (Brash, J. L., and Horbett, T. A., Eds.) Chapter 5, ACS Symposium Series No. 602; American Chemical Society, Washington, DC.
- (33) Ta, T. C., Sykes, M. T., and McDermott, M. T. (1998) Real-time observation of plasma protein film formation on well-defined surfaces with scanning force microscopy. *Langmuir* 14, 2435–2443.

BC025641T

# Interaction of a Ferrocenoyl-Modified Peptide with Papain: Toward Protein-Sensitive Electrochemical Probes

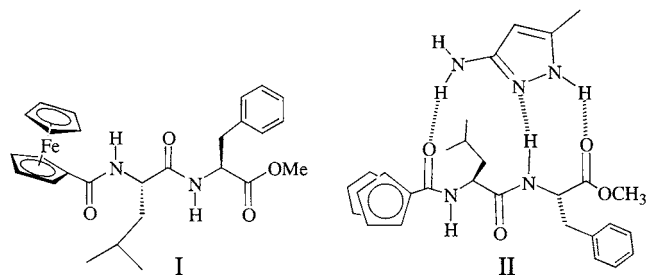
Kevin Plumb and Heinz-Bernhard Kraatz\*

Department of Chemistry, University of Saskatchewan, 110 Science Place, Saskatoon, SK S7N 5C9, Canada.  
Received November 25, 2002; Revised Manuscript Received March 16, 2003

A new ferrocenoyl tetrapeptide, Fc-Gly-Gly-Tyr-Arg-OH, has been synthesized, which acts as an effective competitive inhibitor to papain, with a  $K_i$  of 9  $\mu$ M at pH 6.2. The electrochemical potential of the ferrocenoyl moiety is influenced by papain binding, resulting in a small cathodic shift of 30 mV.

## INTRODUCTION

Molecular recognition of molecules and their electrochemical detection using receptors equipped with electrophores is a rapidly expanding research area and has resulted in the development of receptors selective for cations, anions, and neutral molecules (1, 2). A number of studies have made use of ferrocene derivatives having a podant group that will selectively bind to a substrate and will allow the binding to be monitored electrochemically (3, 4). Recently, we have developed a novel class of ferrocene (Fc)-peptide conjugates, such as Fc-Leu-Phe-OMe (I), which allow the electrochemical monitoring of the interaction of organic substrates, such as 3-aminopyrazole derivatives, with the podant peptide chain (5, 6) to give the corresponding adducts (II).



Upon ligand coordination to the peptide, the redox potential of the ferrocene group shifts significantly to lower potential, making it easier to oxidize the ferrocene electrophore. The magnitude of the shift has been related to the strength of the interaction. This observation led us to speculate that Fc-peptides, having a suitable peptide sequence attached to the electrophore, which will strongly and selectively interact with a protein, may be useful as highly selective and sensitive electrochemical sensors for the detection of large proteins (7). As a first step in this direction, we decided to develop a Fc-peptide for the detection of papain, a 212 amino acid proteolytic enzyme isolated from the papaya fruit. The structure of several papain/inhibitor complexes were reported in the literature (8–10). On the basis of earlier experiments by Blumberg, Schechter, and Berger (11, 12), Kaiser showed

that H-Gly-Gly-Tyr-Arg-OH has a high affinity for binding to papain at pH 6 and can be readily attached to a polymer resin without losing its binding affinity for papain (13). Thus we chose the *N*-Fc derivative of this tetrapeptide, Fc-Gly-Gly-Tyr-Arg-OH (7), as our synthetic target for our study. Here we report its synthesis, the results of a study of its interaction with papain, and the results of solution electrochemical studies.

## MATERIALS AND METHODS

**Materials and General Procedures.** 1-Ethyl-3-(3-dimethylaminopropyl)carbodiimide hydrochloride (EDAC·HCl) and 1-hydroxybenzotriazole hydrate (HOBt) were purchased from Quantum Technologies. Papain (2× crystallized), *N*-benzoylarginine ethyl ester hydrochloride (BAEE) and H-Gly-Gly-OH were purchased from Sigma-Aldrich. Boc-Tyr(OBzl)-OH and H-Arg(NO<sub>2</sub>)-OMe·HCl were obtained from Advanced ChemTech. Ferrocene monocarboxylic acid (Fc-OH) was purchased from Strem Chemicals. Unless otherwise stated, all starting materials were obtained from commercial sources and were used as received. Only L-amino acids were used in this study. CH<sub>2</sub>Cl<sub>2</sub> (ACS grade) was dried over CaH<sub>2</sub> and freshly distilled prior to use. Fc-OBt (4) was prepared as reported in the literature (14).

<sup>1</sup>H NMR spectra were recorded on a Bruker AMX-300, reported in ppm ( $\delta$ ) relative to tetramethylsilane, and referenced to the residual signals of either CHCl<sub>3</sub> ( $\delta$  7.27), DMSO ( $\delta$  2.62), or MeOH ( $\delta$  4.87). 2D-COSY experiments were used to assist in the spectral assignments. Splitting patterns are designated as follows: s, singlet; d, doublet; t, triplet; q, quartet; m, multiplet; br, broad. Analytical thin-layer chromatography was carried out on silica gel 60 F254 aluminum oxide plates (Merck). Preparative column chromatography was performed on silica gel 60 (Merck, 230–400 mesh). All reactions were performed at room temperature and pressure unless otherwise stated.

**Synthesis.** *Preparation of Boc-Gly-Gly-OH (1).* In a typical experiment, 1,4-dioxane (35 mL) and Et<sub>3</sub>N (11 mL) were added to a solution of H-Gly-Gly-OH (6.61 g, 50 mmol) in deionized water (35 mL), followed by Boc<sub>2</sub>O (55 mmol, 12.0 g). The solution was stirred for 16 h, followed by treatment with a solution of deionized water (75 mL) and EtOAc (120 mL). The aqueous layer was again washed with EtOAc (120 mL), followed by acidification with 10% citric acid (500 mL) to a pH of 2.0. The two EtOAc layers collected to this point were discarded.

\* To whom correspondence should be addressed. Fax: +1-306-966-4730; Tel: +1-306-966-4660. E-mail: kraatz@skyway.usask.ca.



The aqueous layer was extracted 3× with EtOAc (50 mL). The EtOAc layers were combined, dried over Na<sub>2</sub>SO<sub>4</sub>, and evaporated under reduced pressure, yielding a colorless wax. The product was dried under a reduced pressure for 3 days to give compound **1** as a white solid (yield: 9.01 g, 71%); mp 110–115 °C. FAB-MS 233.1 (M + 1)<sup>+</sup>. <sup>1</sup>H NMR (DMSO, 300 MHz) δ 8.05 (1H, t, *J* = 5.5 Hz, NH G<sub>2</sub>); 6.99 (1H, t, *J* = 5.7 Hz, NH G<sub>1</sub>); 3.76 (2H, d, *J* = 5.5 Hz, CH<sub>2</sub> G<sub>2</sub>); 3.56 (2H, d, *J* = 5.7 Hz, CH<sub>2</sub> G<sub>1</sub>); 1.38 (9H, s, carbamate).

**Preparation of Boc-Tyr(Bzl)-Arg(NO<sub>2</sub>)-OMe (2).** To a solution of Boc-Tyr(Bzl)-OBt, prepared in situ from Boc-Tyr(Bzl)-OH (20 mmol, 7.43 g), HOBT (22 mmol, 3.37 g), and EDAC·HCl (22 mmol, 4.22 g) in dry CH<sub>2</sub>Cl<sub>2</sub> (200 mL, 0 °C) was added and stirred overnight a solution of H-Arg(NO<sub>2</sub>)-OMe, obtained by treatment of H-Arg(NO<sub>2</sub>)-OMe·HCl (22 mmol, 5.93 g) with Et<sub>3</sub>N (24 mL) in dry CH<sub>2</sub>Cl<sub>2</sub> (120 mL). The reaction mixture was then treated consecutively with aqueous solutions of NaHCO<sub>3</sub> (sat.), citric acid (10%), and water, dried over Na<sub>2</sub>SO<sub>4</sub>, and evaporated to dryness under reduced pressure. The crude product was purified by flash column chromatography (SiO<sub>2</sub>, 1:1 EtOAc–ACN) to give compound **2** as a white crystalline solid (yield: 10.39 g, 89%); mp 75–80 °C. FAB-MS 587.3 (M + 1)<sup>+</sup>. <sup>1</sup>H NMR (CDCl<sub>3</sub>, 300 MHz) δ 8.72 (2H, br s, NHC(NH)NHNO<sub>2</sub>); 7.68 (1H, br s, NHC-(NH)NHNO<sub>2</sub>); 7.41 (5H, m, *m*-, *p*-, *o*-CH Bzl); 7.11 (2H, d, *J* = 8.6 Hz, *o*-CH Y); 6.91 (2H, d, *J* = 8.6 Hz, *m*-CH Y); 6.77 (1H, br s, NHR); 5.18 (1H, d, NH Y); 5.04 (2H, s, CH<sub>2</sub> Bzl); 4.57 (1H, m, CHR); 4.29 (1H, m, CH Y); 3.71 (3H, s, OCH<sub>3</sub>); 3.58 (1H, br s, 1H of the two diastereotopic CH<sub>2</sub> groups of CH<sub>2</sub>CH<sub>2</sub>CH<sub>2</sub>NH R); 3.24 (1H, br s, 1H of the two diastereotopic CH<sub>2</sub> groups of CH<sub>2</sub>CH<sub>2</sub>CH<sub>2</sub>NH R); 2.97 (2H, m, CH<sub>2</sub> Y); 1.87 (1H, br m, 1H of the two diastereotopic CH<sub>2</sub> groups of CH<sub>2</sub>CH<sub>2</sub>CH<sub>2</sub>NH); 1.65 (3H, br m, 2H of CH<sub>2</sub>CH<sub>2</sub>CH<sub>2</sub>NH and 1H of the two diastereotopic CH<sub>2</sub> groups of CH<sub>2</sub>CH<sub>2</sub>CH<sub>2</sub>NH); 1.38 (9H, s, Boc group).

**Preparation of Boc-Gly-Gly-Tyr(Bzl)-Arg(NO<sub>2</sub>)-OMe (3).** Boc-Tyr(Bzl)-Arg(NO<sub>2</sub>)-OMe (8.8 mmol, 5.16 g) was dissolved in CH<sub>2</sub>Cl<sub>2</sub> (6 mL) and treated with TFA (6 mL) for 30 min. The CH<sub>2</sub>Cl<sub>2</sub> and TFA were subsequently removed in vacuo. The resulting residue was redissolved in CH<sub>2</sub>Cl<sub>2</sub> (10 mL) and cooled in an ice bath prior to the dropwise addition of Et<sub>3</sub>N (2 mL). To this was added a solution of Boc-Gly-Gly-OBt, prepared in situ from Boc-Gly-Gly-OH (8 mmol, 1.86 g), HOBT (8.8 mmol, 1.35 g), and EDAC·HCl (8.8 mmol, 1.69 g) in dry CH<sub>2</sub>Cl<sub>2</sub> (25 mL, 0 °C). The reaction mixture was then warmed to room temperature and left to stir overnight. The resulting solution was then treated as per **2**. The product was purified by flash column chromatography (SiO<sub>2</sub>, 90:10 CHCl<sub>3</sub>:MeOH) and recrystallized in CHCl<sub>3</sub> to yield white crystalline compound **3** (yield: 3.47 g, 62%). IR (cm<sup>-1</sup>, KBr, film): 1656, 1740 (C=O); 861, 1250, 1511 NO<sub>2</sub>. FAB-MS 701.4 (M + 1)<sup>+</sup>. <sup>1</sup>H NMR (MeOH, 300 MHz) δ 7.36 (5H, m, CH Bzl); 7.14 (2H, d, *J* = 8.6 Hz, *o*-CH Y); 6.88 (2H, d, *J* = 8.7 Hz, *m*-CH Y); 5.02 (2H, s, CH<sub>2</sub> Bzl); 4.52 (1H, m, α-CHR); 4.41 (1H, m, α-CH Y); 3.80 (2H, s, CH<sub>2</sub> G<sub>2</sub>); 3.71 (2H, s, CH<sub>2</sub> G<sub>1</sub>); 3.65 (3H, s, OCH<sub>3</sub>); 3.25 (2H, m, CH<sub>2</sub> of CH<sub>2</sub>CH<sub>2</sub>CH<sub>2</sub>NH); 3.06 (1H, m, 1H of the two diastereotopic CH<sub>2</sub> groups of Y); 2.90 (1H, m, 1H of the two diastereotopic CH<sub>2</sub> of Y); 1.86 (1H, m, 1H of the two diastereotopic CH<sub>2</sub> groups of CH<sub>2</sub>CH<sub>2</sub>CH<sub>2</sub>NH); 1.73 (3H, m, 2H of CH<sub>2</sub> of CH<sub>2</sub>CH<sub>2</sub>CH<sub>2</sub>NH and 1H of the two diastereotopic CH<sub>2</sub> groups of CH<sub>2</sub>CH<sub>2</sub>CH<sub>2</sub>NH); 1.42 (9H, s, C(CH<sub>3</sub>)<sub>3</sub> Boc group).

**Preparation of Fc-Gly-Gly-Tyr(Bzl)-Arg(NO<sub>2</sub>)-OMe (5).** After the removal of the Boc group from **3** (1.1 mmol, 0.77

g) using TFA (1.5 mL), the excess acid was removed in vacuo and Et<sub>3</sub>N (1.0 mL) in CH<sub>2</sub>Cl<sub>2</sub> (10 mL) was added. This solution was added to a stirring solution of Fc-OBt (**14**) (1.0 mmol, 0.33 g) in CH<sub>2</sub>Cl<sub>2</sub> (20 mL) and allowed to react overnight. Purification was carried out by flash column chromatography (SiO<sub>2</sub>, 5:1 EtOAc:MeOH, *R<sub>f</sub>* = 0.5) to give **5** in 83% yield as an orange solid (0.67 g). Anal. Calcd for C<sub>38</sub>H<sub>44</sub>N<sub>8</sub>O<sub>9</sub>Fe: C, 56.16; H, 5.46; N, 13.79. Found: C, 56.35; H, 5.88; N, 13.42. IR (cm<sup>-1</sup>, KBr, film) 1653, 1741 (C=O); 1261, 1512 (NO<sub>2</sub>). FAB-MS 813.3 (M + 1)<sup>+</sup>. <sup>1</sup>H NMR (MeOH, 300 MHz) δ 7.38 (5H, m, CH Bzl); 7.17 (2H, d, *J* = 8.6 Hz, *o*-CH Y); 6.87 (2H, d, *J* = 8.6 Hz, *m*-CH Y); 5.01 (2H, s, CH<sub>2</sub> Bzl); 4.78 (2H, m, *o*-CH substituted Cp ring); 4.38 (1H, m, α-CHR); 4.26 (3H, m, *m*-CH substituted Cp and α-CH Y); 4.22 (5H, m, CH unsubstituted Cp ring); 3.95 (2H, s, CH<sub>2</sub> G<sub>2</sub>); 3.82 (2H, s, CH<sub>2</sub> G<sub>1</sub>); 3.64 (3H, s, OCH<sub>3</sub>); 3.16 (3H, m, 2H of CH<sub>2</sub>-CH<sub>2</sub>CH<sub>2</sub>NH and 1H of the two diastereotopic CH<sub>2</sub> groups of Y); 2.94 (1H, m, 1H of the two diastereotopic CH<sub>2</sub> groups of Y); 1.81 (1H, br m, 2H of CH<sub>2</sub>CH<sub>2</sub>CH<sub>2</sub>NH and 1H of the two diastereotopic CH<sub>2</sub> of CH<sub>2</sub>CH<sub>2</sub>CH<sub>2</sub>NH); 1.60 (3H, br m, CH<sub>2</sub> of CH<sub>2</sub>CH<sub>2</sub>CH<sub>2</sub>NH and CH<sub>2</sub>CH<sub>2</sub>CH<sub>2</sub>NH).

**Preparation of Fc-Gly-Gly-Tyr(Bzl)-Arg(NO<sub>2</sub>)-OH (6).** To a solution of **5** (0.500 g, 0.62 mmol) in MeOH (2.0 mL) was added 1 N NaOH (2.2 mL) with stirring. The reaction was stored at room temperature for 3 h after which 1 N HCl (1.0 mL) was added. The MeOH was then removed in vacuo followed by cooling of the solution in a ice bath prior to the dropwise addition of 1 N HCl (2.0 mL). The solution was then stored in the fridge for 2 h after which the precipitate was filtered off and washed 3× with cold, distilled water (50 mL) and dried under reduced pressure overnight to give **6** as a yellow solid in 85% yield (426 mg). FAB-MS 799.3 (M + 1)<sup>+</sup>. <sup>1</sup>H NMR (MeOH, 300 MHz) δ 7.32 (5H, m, CH Bzl); 7.17 (2H, d, *J* = 8.6 Hz, *o*-CH Y); 6.87 (2H, d, *J* = 8.7 Hz, *m*-CH Y); 5.00 (2H, s, CH<sub>2</sub> Bzl); 4.78 (2H, m, *o*-CH substituted Cp ring); 4.58 (1H, m, α-CHR); 4.35 (3H, m, *m*-CH substituted Cp and α-CH Y); 4.20 (5H, CH unsubstituted Cp ring); 3.95 (2H, s, CH<sub>2</sub> G<sub>2</sub>); 3.82 (2H, s, CH<sub>2</sub> G<sub>1</sub>); 3.20 (3H, m, 2H of CH<sub>2</sub>CH<sub>2</sub>-CH<sub>2</sub>NH and 1H of the two diastereotopic CH<sub>2</sub> groups of Y); 2.97 (1H, m, 1H of the two diastereotopic CH<sub>2</sub> groups of Y); 1.87 (1H, m, 1H of the two diastereotopic CH<sub>2</sub> groups of CH<sub>2</sub>CH<sub>2</sub>CH<sub>2</sub>NH); 1.65 (3H, m, 2H of CH<sub>2</sub>CH<sub>2</sub>-CH<sub>2</sub>NH and 1H of the two diastereotopic CH<sub>2</sub> groups of CH<sub>2</sub>CH<sub>2</sub>CH<sub>2</sub>NH).

**Preparation of Fc-Gly-Gly-Tyr-Arg-OH (7).** A solution of Fc-Gly-Gly-Tyr(Bzl)-Arg(NO<sub>2</sub>)-OH (100 mg, 0.13 mmol) in a 3:1 mixture of MeOH and distilled water (20 mL) was hydrogenated using 5% palladium on powdered charcoal (65 mg) as catalyst. The reduction was performed at room temperature in a Parr Apparatus at 60 psi for 20 h. The progress of the reaction was followed by TLC (60:40 CHCl<sub>3</sub>–MeOH). The reaction mixture was then filtered and evaporated to dryness under reduced pressure. The crude product was purified by column chromatography (SiO<sub>2</sub>, 1:1 MeCN:MeOH, *R<sub>f</sub>* = 0.3) to give **7** as an orange solid (yield: 58 mg, 70%). Anal. Calcd for C<sub>30</sub>H<sub>37</sub>N<sub>7</sub>O<sub>7</sub>Fe: C, 54.31; H, 5.62; N, 14.78. Found: C, 53.98; H, 5.70; N, 15.05. FAB-MS 664.1 (M + 1)<sup>+</sup>. IR (cm<sup>-1</sup>, KBr, film): 1650 (C=O amide); 1742 (C=O ester); <sup>1</sup>H NMR (MeOH, 300 MHz) δ 7.09 (2H, d, *J* = 8.5 Hz, *o*-CH Y); 6.69 (2H, d, *J* = 8.5 Hz, *m*-CH Y); 4.82 (2H, s, *o*-CH substituted Cp ring); 4.55 (1H, m, α-CH R); 4.41 (2H, m, *m*-CH substituted Cp); 4.25 (5H, s, CH unsubstituted Cp ring); 3.98 (2H, s, CH<sub>2</sub> G<sub>2</sub>); 3.87 (2H, q, CH<sub>2</sub> G<sub>1</sub>); 3.13 (3H, m, 2H of CH<sub>2</sub>CH<sub>2</sub>CH<sub>2</sub>NH and 1H of the two diastereotopic CH<sub>2</sub> groups of CH<sub>2</sub> Y); 2.91 (1H, m, 1H of the two diastereotopic CH<sub>2</sub> groups of Y); 1.87 (1H,

**Chart 1.**

- (a) enzyme diluent (activation buffer), 100 mL:
- (b) substrate solution, 50 mL:
- (c) substrate solution diluent, 50 mL:
- (d) inhibitor solution, 1.0 mL:
- (e) active enzyme solution, 5.0 mL:
- (f) 0.01 N NaOH, 50 mL

1.0 mM EDTA, 0.06 mM mercaptoethanol,  
5.0 mM cysteine·HCl  
41.4 mM BAEE, 0.38 mM disodium EDTA,  
1.90 mM cysteine·HCl  
0.38 mM disodium EDTA, 1.90 mM cysteine·HCl  
1 mg Fc-GGYR/mL substrate solution diluent  
0.05–1.0 mg papain/mL enzyme diluent

br m, 1H of the two diastereotopic CH<sub>2</sub> groups of CH<sub>2</sub>-CH<sub>2</sub>CH<sub>2</sub>NH); 1.70 (3H, m, 2H of CH<sub>2</sub>CH<sub>2</sub>CH<sub>2</sub>NH and CH<sub>2</sub>CH<sub>2</sub>CH<sub>2</sub>NH).

**Inhibitor Studies.** In preparation of the inhibitor studies the following solutions were prepared as shown in Chart 1. Into a series of seven sterile polypropylene sample tubes labeled A1–A7, also defined as series A, were added the following ascending volumes of substrate solution and a magnetic stir bar: 100  $\mu$ L, 130  $\mu$ L, 190  $\mu$ L, 280  $\mu$ L, 400  $\mu$ L, 550  $\mu$ L, 910  $\mu$ L. The volumes of the solutions were made up to 1000  $\mu$ L by adding the corresponding amounts of the substrate solution diluent. The same procedure was repeated to produce series B–F. A two-point calibration was performed on the pH electrode at the beginning of each set of experiments.

The titrimetric experiments for all six series were run one series at a time. Just prior to running each series, additions of 1000  $\mu$ L of 3.0 M NaCl and 1000  $\mu$ L of Millipore water were made. Immediately prior to the addition of the enzyme, the inhibitor was added and the pH of the solution was adjusted to  $6.240 \pm 0.010$  with 0.01 N NaOH. The following ratios of enzyme to inhibitor were used in determining the volume of inhibitor solution to add: 1:0, 1:50, 1:100, 1:250, 1:500, 1:750, 1:1000. Based on the desired ratio and the known concentration of the activated enzyme in solution determined by UV–vis spectrophotometry where  $\text{mg papain/mL} = A_{280} \times 0.4$ , the appropriate volume of inhibitor was added.

The active enzyme was then pipetted into the magnetically stirred solution, and the pH electrode was added in order to monitor the change in pH of the solution. Only the initial rate of change is useful in these types of experiments. Thus once the enzyme is added it is crucial to wait only a few seconds for the enzyme to mix with the other components of the solution and to allow the pH meter to stabilize. This occurred fairly quickly and generally between pH 6.22 and 6.20. The time was then measured for the pH to drop an additional 0.05 from the pH at which the meter was observed to have stabilized. This was observed to take between 1 min and 30 min depending on the concentrations of substrate and inhibitor present during the trial. The pH electrode was rinsed thoroughly with Millipore water between each trial.

**Electrochemical Studies.** All electrochemical experiments were carried out using a CV-50W Voltammetric Analyzer (BAS) at room temperature ( $20 \pm 2$  °C). No special precautions were taken to exclude oxygen. Borate buffer (pH 6.2) in Millipore water was used throughout the electrochemical studies. Sodium perchlorate was used as supporting electrolyte (0.1 M). For the cyclic voltammetry studies, a glassy carbon working electrode (BAS, diameter 2 mm) and a platinum wire counter electrode were used. The glassy carbon working electrode was polished with 3  $\mu$ m followed by 1  $\mu$ m and then 0.5  $\mu$ m alumina prior to use to remove any surface contaminants. The reference electrode was a Ag/AgCl electrode (BAS). iR compensation was applied. Backgrounds of the buffer containing 0.1 M NaClO<sub>4</sub> were collected before each set of experiments and then subtracted from the spectra. The experiment was repeated at least 10 times to get reliable

values for  $E_{1/2}$ . The heterogeneous electron-transfer rate constant was obtained by simulations using the DigiSim 2.1 software (BAS).

**RESULTS AND DISCUSSION**

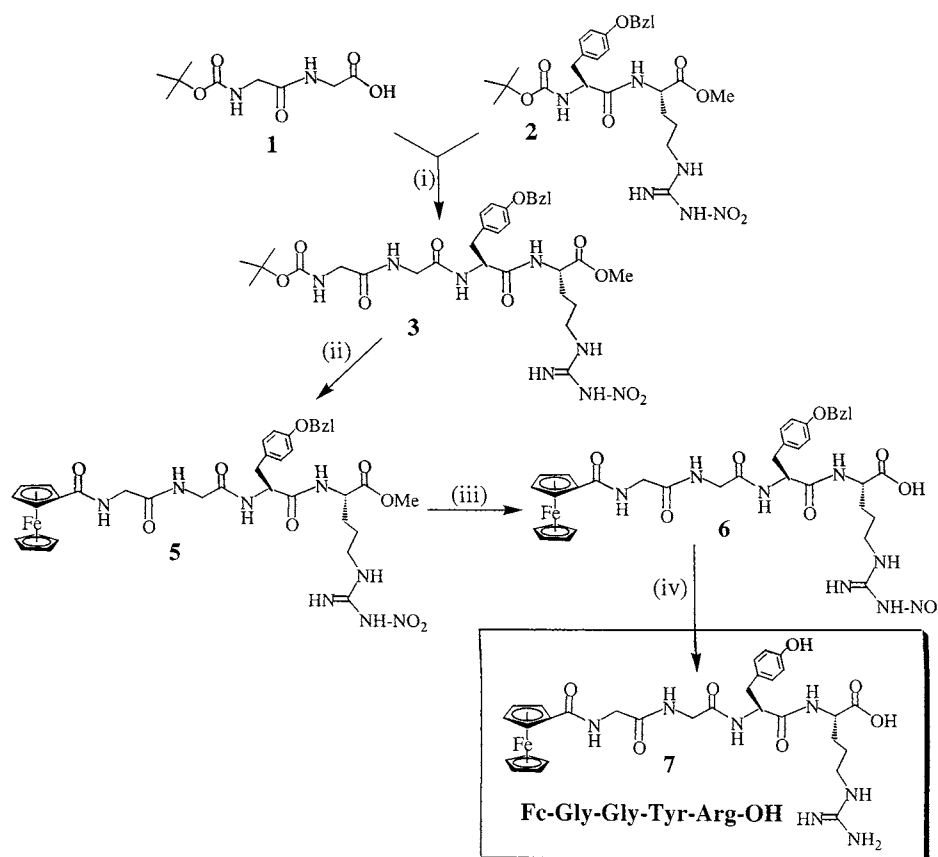
Compound **7** was synthesized in several steps by standard solution-phase carbodiimide coupling (15) according to Scheme 1.

After the deprotection of Boc-Tyr(Bzl)-Arg(NO<sub>2</sub>)-OMe (**2**) with trifluoroacetic acid in dichloromethane, the resulting free dipeptide ester was coupled with Boc-Gly<sub>2</sub>-OH (**1**) using EDC/HOBt to give the fully protected tetrapeptide Boc-Gly<sub>2</sub>-Tyr(Bzl)-Arg(NO<sub>2</sub>)-OMe (**3**). After removal of the Boc group, the *N*-deprotected tetrapeptide was then added to a solution of Fc-OBt (**14**). The desired fully protected Fc-tetrapeptide Fc-Gly<sub>2</sub>-Tyr(Bzl)-Arg(NO<sub>2</sub>)-OMe (**5**) was obtained as an orange solid.

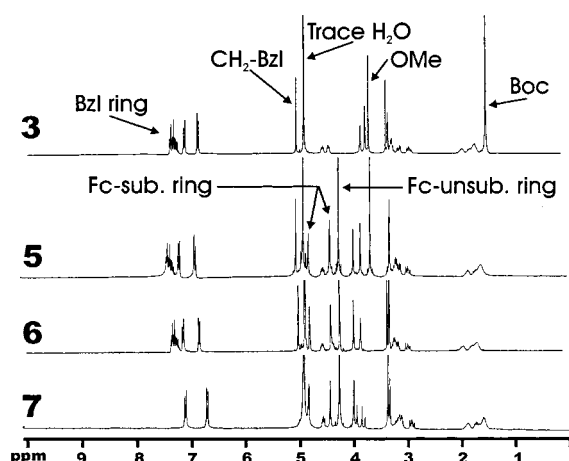
The <sup>1</sup>H NMR spectrum of compound **5** exhibited the expected 2:2:5 signal pattern for monosubstituted Fc-peptides (see Figure 1). Signals of the  $\alpha$ -Hs of Arg and Tyr were observed at  $\delta$  4.51 and 4.22, respectively. Base hydrolysis of the methyl ester group resulted in formation of the free acid **6**, which lacks the resonance due to the methoxy group at  $\delta$  3.67. As a last step, the desired fully deprotected Fc-tetrapeptide Fc-Gly-Gly-Tyr-Arg-OH (**7**) was obtained after hydrogenation of a methanol–water solution of **6** with 5% Pd on carbon. The progress of the Arg deprotection was conveniently followed by IR spectroscopy. Compound **7** lacks the strong absorption in the IR due to the NO<sub>2</sub> group at 1512 cm<sup>−1</sup>. The orange product was isolated by column chromatography and fully characterized by <sup>1</sup>H NMR, FT-IR, and FAB mass spectrometry. Its <sup>1</sup>H NMR spectrum lacks the benzylic protons present in compounds **5** and **6**. In addition, the aromatic region shows resonances only due to the Tyr aromatic.

To evaluate the ability of compound **7** to inhibit substrate hydrolysis and thus its ability to interact with papain, we carried out inhibition studies. The Michaelis–Menten constant ( $K_m$ ) for papain as well as the inhibition constant  $K_i$  for the ferrocenoyl tetrapeptide **7**, were determined using *N*-benzoylarginine ethyl ester hydrochloride (BAEE·HCl) as substrate (16). Initial hydrolysis rates were determined using a pH meter in a solution containing NaCl (1.0 mol L<sup>−1</sup>), Na<sub>2</sub>EDTA (0.1 mM), and cysteine·HCl (0.6 mM), at 23 °C. The enzyme was activated prior to use in a solution of mercaptoethanol (0.06 mM), Na<sub>2</sub>EDTA (1.0 mM), and cysteine·HCl (5.0 mM). Papain concentrations ranged between 0.33 and 0.66  $\mu$ g/mL determined by UV–vis spectroscopy given by  $\text{mg papain/mL} = A_{280} \times 0.4$ .

Figure 1 shows the Lineweaver–Burk plot indicating competitive inhibition, as was reported before for H-Gly-Gly-Tyr-Arg-OH (**13**). A  $K_m$  of 15 mM was determined for the substrate at pH 6.2, which compares well with a  $K_m$  reported by Blumberg et al. (11). The Dixon–Webb plot (Figure 2) clearly indicates competitive inhibition and thus indicates a direct interaction of the Fc-tetrapeptide with the substrate binding site of papain (17,

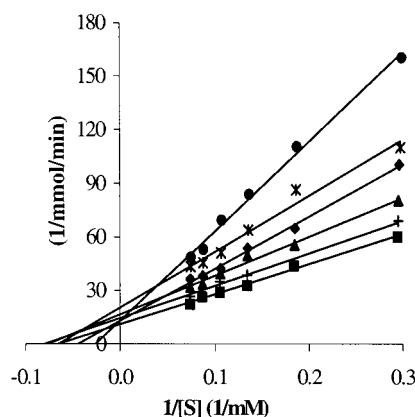
**Scheme 1: Synthesis of Fc-Gly<sub>2</sub>-Tyr-Arg-OH (7)<sup>a</sup>**

<sup>a</sup> (i) TFA deprotection of **2**, Et<sub>3</sub>N; HOBT, EDC, RT, 12 h; (ii) TFA deprotection of **3**, Et<sub>3</sub>N; CH<sub>2</sub>Cl<sub>2</sub>, Fc-OBt, RT; (iii) MeOH, NaOH (1 N); (iv) 5% Pd/C, MeOH:water 3:1, H<sub>2</sub> (60 psi), 20 h.



**Figure 1.** <sup>1</sup>H NMR spectra for compounds **3** and **5–7**. Note the sharp singlet for compound **3** at  $\delta$  1.4 due to the Boc group and the appearance of doublets at  $\delta$  4.8 and  $\delta$  4.3 in compounds **5–7** corresponding to the protons of the substituted cyclopentadienyl ring and the strong singlet at  $\delta$  4.2 due to the unsubstituted Cp ring of the Fc conjugates. Stepwise deprotection of the fully protected Fc-Gly-Gly-Tyr(Bzl)-Arg(NO<sub>2</sub>)-OMe (**5**) leads to the free acid **6**, which lacks the OMe resonance at  $\delta$  3.64, and finally to the target compound **7**, which lacks the multiplet at  $\delta$  7.4 of the benzyl group from the tyrosine residue.

18). A  $K_i$  was derived at pH 6.2 from plots of  $\nu_o/\nu$  versus  $[I]$ , while holding the substrate concentration constant, where  $\nu_o$  is the initial, uninhibited rate of hydrolysis and  $\nu$  is the initial rate in the presence of the inhibitor. The plot is linear, and the inhibition constant  $K_i$  was calculated from the slope (Figure 4) to be 9  $\mu$ M. This is

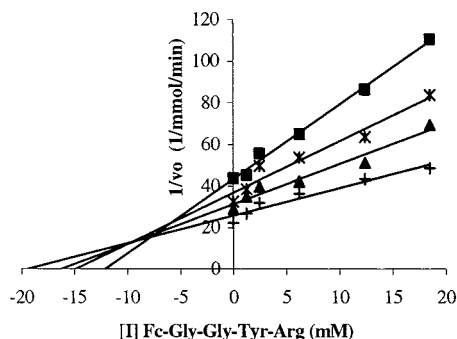


**Figure 2.** Double-reciprocal (Lineweaver-Burk) plots showing that Fc-Gly-Gly-Tyr-Arg-OH (**7**) behaves as a competitive papain inhibitor for BAEE hydrolysis.  $K_m$  calculated as 15 mM. Substrate:inhibitor ratio:  $\blacksquare$  = no inhibitor,  $+$  = 1: 50,  $\blacktriangle$  = 1:100,  $\blacklozenge$  = 1:250,  $*$  = 1:500,  $\bullet$  = 1:750.

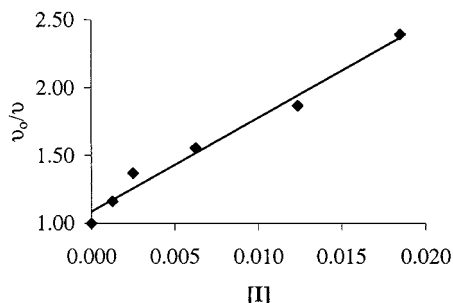
significantly better than for the related benzyl-protected derivative H-Gly-Gly-Tyr(Bzl)-Arg-OH (123  $\mu$ M at pH 6). Kaiser and co-workers noted that inhibition is enhanced by the presence of the aromatic group (13). Furthermore, *N*-conjugation increased the affinity for papain. The Fc group appears to enhance binding significantly. We are currently investigating this further and attempting to cocrystallize compound **7** with papain to get more insight into the nature of the interaction.

The electrochemical properties of compound **7** were investigated using cyclic voltammetry (CV) in borate buffer using NaClO<sub>4</sub> (0.1 M) as supporting electrolyte.





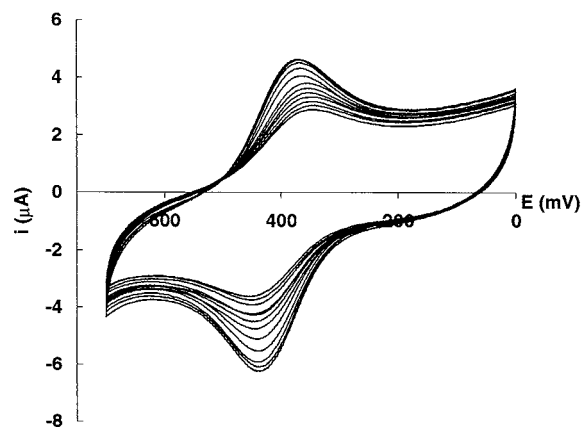
**Figure 3.** Dixon-Webb plot showing that Fc-Gly-Gly-Tyr-Arg-OH (**7**) is a competitive inhibitor to papain. Substrate:inhibitor ratio: ■ = 1:50, \* = 1:100, ▲ = 1:250, + = 1:750.



**Figure 4.** Plot of  $v_0/v$  vs  $[I]$  where  $v_0$  is the rate of hydrolysis in the absence of the inhibitor and  $v$  is the rate in the presence of the inhibitor. The  $K_i$  for Fc-Gly-Gly-Tyr-Arg-OH (**7**) was determined to be 9  $\mu$ M where  $1/K_i = \text{slope} (1 + [S]/K_m)$ .

Binding of papain to **7** is expected to be optimal at pH 6.2, thus making it necessary to control the pH of the solution during the electrochemical studies. Our experiments show that at  $\text{pH} \leq 7$ , the redox potential remains reversible and is experiencing reproducibly small anodic shifts of about 5 mV. At  $\text{pH} \geq 10$ , the oxidation wave irreversible due to the reaction of the  $\text{OH}^-$  with the ferrocenium cation, compatible with earlier reports of the decomposition of ferrocene derivatives in basic solutions by an EC mechanism, in which the oxidized species reacts with  $\text{OH}^-$  to give various decomposition products (19). A solution of **7** in borate buffer at pH 6.2 exhibits a fully reversible one-electron oxidation due to the ferrocene/ferrocenium redox couple at 430 mV (vs Ag/AgCl;  $E_{\text{pa}} - E_{\text{pc}} = 66$  mV).

Figure 5 shows the changes in the CVs for compound **7** upon addition of small aliquots (0.06 equiv per addition) of a solution of papain up to a maximum of 0.7 equivalents at pH 6.2, the optimum pH for papain binding. The addition of stoichiometric amounts of papain to a buffered solution of **7** led to a reduction of the oxidative and reductive peak current, as expected for a papain-**7** with a diffusion coefficient that is significantly smaller than that of **7**. Addition to a full 1 equivalent mixture resulted in the formation of a gelatinous precipitate. In addition to the decrease in current intensity, a cathodic shift of the half-wave potential of the  $7/7^+$ -redox couple of 30 mV to 400 mV is observed. In addition, the peak separation increases in the presence of papain to 87 mV, indicating a slowing of the electron-transfer process from the **7**-papain complex to the electrode surface ( $k_0 = 1.2 \times 10^{-3} \text{ cm s}^{-1}$  by simulation of the CV using DigiSim 2.1, BAS). The shift of the reduction peak potential is larger, indicating a stronger interaction of papain to  $7^+$ . No significant changes in the redox potential were observed outside the optimum pH for binding of papain to the tetrapeptide ( $7 \leq \text{pH} \leq 5$ ). The changes in the redox



**Figure 5.** Successive additions of papain to a 1 mM solution of Fc-Gly-Gly-Tyr-Arg-OH (**7**) in borate buffer (20 mM, pH 6.2). Glassy carbon, Pt counter, Ag/AgCl reference electrode, scan rate = 100  $\text{mV s}^{-1}$ , 0.1 M  $\text{NaClO}_4$ .

potential are modest but specific to the presence of papain in solution. No changes in the redox potential of compound **7** were observed in the presence of other enzymes, such as trypsin and pepsin.

## CONCLUSIONS

In conclusion, we have synthesized a ferrocenyl tetrapeptide receptor specifically designed to bind to papain. Binding of papain to the receptor molecule causes an electrochemical response. At present the electrochemical response is very modest. However, the response is in the presence of an equimolar amount of papain. Although, higher papain concentrations could not be evaluated due to the insolubility of the papain under these conditions, our results may significantly expand the applications of ferrocene modified receptors to include biomolecules. The next step in our work will be to bind the receptor to a surface and to develop a surface-bound protein sensor platform using ferrocenyl peptidylcystamines (20, 21). This will also solve the signal intensity since now the redox signal of the probe is not any longer diffusion dependent.

## ACKNOWLEDGMENT

We thank the Health Utilization and Research Commission (HSURC) of the Province of Saskatchewan for a Biomedical Establishment Grant to H.B.K. H.B.K. is Canada Research Chair in Biomaterials.

## LITERATURE CITED

- (1) Beer, P. D., Gale, P. A., and Chen, G. Z. (1999) Electrochemical molecular recognition: pathways between complexation and signaling. *J. Chem. Soc., Dalton Trans.* 1897–1909.
- (2) Beer, P. D., and Gale, P. A. (2001) Anion recognition and sensing: The state of the art and future perspectives. *Angew. Chem., Int. Ed.* 40, 486–516.
- (3) Carr, J. D., Lambert, L., Hibbs, D. E., Hursthouse, M. B., Abdul Malik, K. M., and Tucker, J. H. R. (1997) Novel electrochemical sensors for neutral molecules. *Chem. Commun.* 1649–1650.
- (4) Carr, J. D., Coles, S. J., Hassan, W. W., Hursthouse, M. B., Abdul Malik, K. M., and Tucker, J. H. R. (1999) The effect of protonation on the spectroscopic and redox properties of a series of ferrocenyl derivatives. *J. Chem. Soc., Dalton Trans.* 57–62.
- (5) Kraatz, H. B., Leek, D. M., Houmam, A., Enright, G. D., Luszyk, J., and Wayner, D. D. M. (1999) The ferrocene moiety as a structural probe: redox and structural properties

- of ferrocenoyl-oligoproline Fc-Pro<sub>n</sub>-OBzl ( $n = 1-4$ ) and Fc-Pro<sub>2</sub>-Phe-OBzl. *J. Organomet. Chem.* **589**, 38–49.
- (6) Saweczko, P., Enright, G. D., and Kraatz, H. B. (2001) Interaction of Ferrocenoyl-dipeptides with 3-aminopyrazole derivatives:  $\beta$ -sheet models? A synthetic, spectroscopic, structural, and electrochemical study. *Inorg. Chem.* **40**, 4409–4419.
- (7) Xu, Y., and Kraatz, H. B. (2001) Efficient synthesis of unsymmetrically disubstituted ferrocenes: towards electrochemical dipeptide-Fc-biosensors. *Tetrahedron Lett.* **42**, 2601–2603.
- (8) Yamamoto, D., Matsumoto, K., Ohishi, H., Ishida, T., Inoue, M., Kitamura, K., and Mizuna, H. (1991) Refined X-ray structure of papain·E-64-c complex at 2.1 Å resolution. *J. Biol. Chem.* **266**, 14771–14777.
- (9) Mastumoto, K., Murata, M., Sumiya, S., Kitamura, K., and Ishida, T. (1994) Clarification of substrate specificity of papain by crystal analyses of complexes with covalent-type inhibitors. *Biochim Biophys. Acta* **1208**, 268–276.
- (10) Mastumoto, K., Murata, M., Sumiya, S., Mizoue, K., Kitamura, K., and Ishida, T. (1998) X-ray crystal structure of papain complexed with cathepsin B-specific covalent-type inhibitor: substrate specificity and inhibitor activity. *Biochim Biophys. Acta* **1383**, 93–100.
- (11) Blumberg, S., Schechter, I., and Berger, A. (1970) The purification of papain by affinity chromatography. *Eur. J. Biochem.* **15**, 97–102.
- (12) Berger, A., and Schechter, I. (1970) Mapping the active site of papain with the aid of peptide substrates and inhibitors. *Philos. Trans. R. Soc. London, Ser. B* **257**, 249–264.
- (13) Funk, M. O., Nakagawa, Y., Skochdopole, J., and Kaiser, E. T. (1979) Affinity chromatographic purification of papain. A reinvestigation. *Int. J. Pept. Protein Res.* **13**, 296–303.
- (14) Kraatz, H.-B., Luszyk, J., and Enright, G. E. (1997) Ferrocenoyl Amino Acids: A Synthetic and Structural Study. *Inorg. Chem.* **36**, 2400–2405.
- (15) Bodansky, M., and Bodansky, A. (1984) *The Practice of Peptide Synthesis*, Springer-Verlag, Berlin.
- (16) <http://www.worthington-biochem.com/manual/P/PAP.html>.
- (17) Dixon, M. (1953) The determination of enzyme inhibitor constants. *Biochem. J.* **55**, 170–171.
- (18) Bornish-Bowden, A. (1974) A simple graphical method for determining the inhibition constants for mixed, uncompetitive and noncompetitive inhibitors. *Biochem. J.* **137**, 143–144.
- (19) Prins, R., Korswagen, A. R., and Kortbeek, A. G. T. G. (1972) Decomposition of the ferricenium cation by nucleophilic reagents. *J. Organomet. Chem.* **39**, 335–344.
- (20) Bediako-Amoa, I., Silerova, R., and Kraatz, H. B. (2002) Ferrocenoyl glycylcystamine: organization into a supramolecular helicate structure. *Chem. Commun.* 2430–2431.
- (21) Galka, M. M., and Kraatz, H. B. (2002) Electron-transfer studies on self-assembled monolayers of helical ferrocenoyl-oligoproline-cystamine bound to gold. *Chem. Phys. Chem.* **3**, 356–359.

BC0256446

## Nucleosides and Nucleotides. 218. Alternate-Strand Triple-Helix Formation by the 3'-3'-Linked Oligodeoxynucleotides Using a Purine Motif<sup>†</sup>

Shuichi Hoshika, Yoshihito Ueno,<sup>‡</sup> and Akira Matsuda\*

Graduate School of Pharmaceutical Sciences, Hokkaido University, Kita-12, Nishi-6, Kita-ku, Sapporo 060-0812, Japan. Received December 10, 2002

In this paper, we describe the synthesis of the 3'-3'-linked TFOs that can form the antiparallel triplexes with the duplex DNA target by reverse Hoogsteen hydrogen bonds. Stability of the alternate-strand triplexes between these TFOs and the target DNAs was investigated using the electrophoretic mobility shift assay (EMSA). It was found that the alternate-strand triplexes were significantly stabilized by linking the TFO fragments with the pentaerythritol linker. And, unlike the alternate-strand triplexes composed of the pyrimidine motif, the terminal ammonium ion of the aminobutyl-linker and the intercalator of the TFOs did not contribute to the stability of the alternate-strand triplex comprised of the purine motif. We also tested the ability of the 3'-3'-linked TFOs to inhibit cleavage of the duplex DNA target **17** by the restriction enzyme *Eco*T14I and found that the 3'-3'-linked TFOs **12** and **13** inhibited the cleavage by the enzyme more effectively than the unlinked decamer **8**. Thus, the TFOs linked with pentaerythritol may be useful as the antigene oligonucleotide to the DNA targets, which have alternating oligopyrimidine-oligopurine sequences.

### INTRODUCTION

Triple helix (triplex)-forming oligonucleotides (TFOs) have attracted a great deal of attention because of their ability to specifically bind double-stranded DNA and because of their potential use in gene therapy (i.e., in antigene strategy). A triplex is usually formed through sequence-specific interaction of a single-stranded oligopurine or oligopyrimidine TFO with a major groove of oligopurine/oligopyrimidine stretch in DNA duplex (*1*). In the pyrimidine motif triplex, an oligopyrimidine TFO binds parallel to the oligopurine strand of the target duplex by Hoogsteen hydrogen bonding to form T·AT and C<sup>+</sup>·GC base triplets (*2, 3*). On the other hand, in the purine motif triplex, an oligopurine TFO binds antiparallel to the oligopurine strand of the target by reverse Hoogsteen hydrogen bonding to form A·AT (or T·AT) and G·GC base triplets (*4, 5*). However, target sequences in the antigene strategy are very restricted. Since thermal stability of the triplexes is generally much lower than that of the duplexes under physiological conditions, an oligopurine cluster with long chain lengths is usually required for stable triplex formation. In addition, formation of the pyrimidine motif triplex needs conditions of low pH (pH < 6.0) because unmodified cytosine residues, if present in the TFO, must be protonated to bind with guanine of the G:C duplex (*2, 6*).

Several approaches have been attempted to expand the repertoire of potential DNA targets. If short oligopurine sequences appear adjacently and alternately on the two strands of the DNA target, the alternate sequences can

be recognized by TFOs that simultaneously and cooperatively bind to the adjacent oligopurine domains on alternate strands by crossover in the major groove (*7–24*). These so-called "alternate-strand triplex formations" are divided into two categories. A natural oligonucleotide such as 5'-oligopurine-oligopyrimidine-3' or 5'-oligopyrimidine-oligopurine-3' can be used as a TFO for alternate-strand triplex formation (*7–14*). In this case, the oligopyrimidine part of the TFO binds to the oligopurine domain on the DNA target by Hoogsteen hydrogen bonding, and the oligopurine part binds to the oligopurine domain by reverse Hoogsteen hydrogen bonding. In the second approach, only one set of motifs (i.e., Hoogsteen or reverse Hoogsteen motif) is employed (*15–24*). In this case, the 3'- and 3'- or 5'- and 5'-termini of the two oligonucleotide fragments have to be connected by using an appropriate linker to invert polarity. The different possibilities for alternate-strand triplex formations in the latter case are shown in Figure 1. When the oligopyrimidine sequence follows the oligopurine sequence, the 3'-3'-linked and the 5'-5'-linked TFOs can form the parallel (a) and antiparallel (b) triplexes with the duplex DNA target by Hoogsteen and reverse Hoogsteen hydrogen bonds, respectively. On the other hand, when the oligopurine sequence follows the oligopyrimidine sequence, the 5'-5'-linked and the 3'-3'-linked TFOs can form the parallel (c) and antiparallel (d) triplexes with the duplex DNA target by Hoogsteen and reverse Hoogsteen hydrogen bonds, respectively.

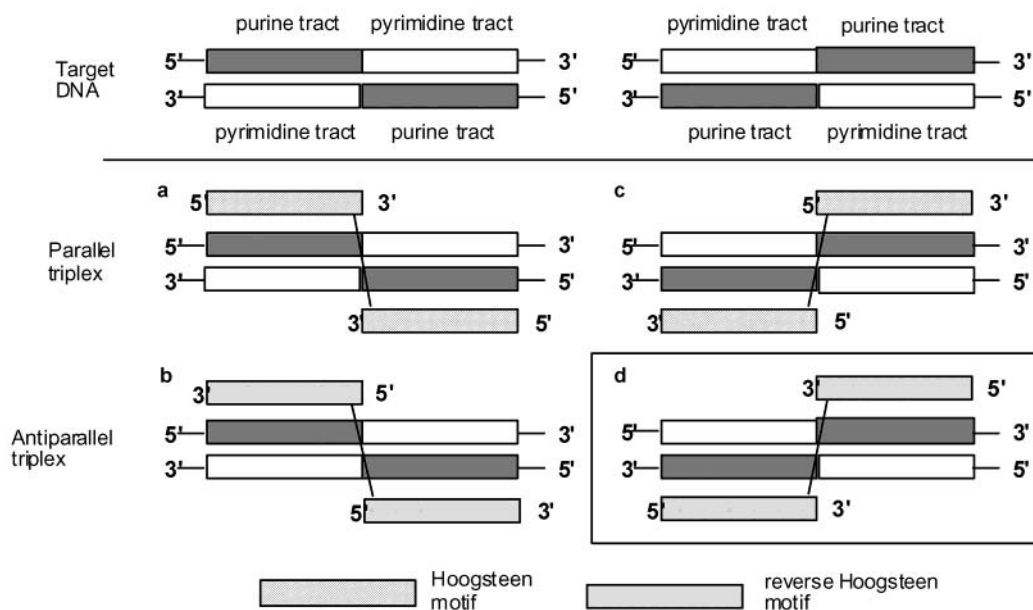
Recently, we reported the synthesis of the 3'-3'-linked TFOs with the 2-anthraquinonecarbonyl group at the junction point (*25*). We found that the 3'-3'-linked TFOs with the 2-anthraquinonecarbonyl group as an intercalator enhanced the thermal stability of the parallel type of triplex with a DNA target (Figure 1a) as compared with those without the intercalator and the unlinked nonamer. Moreover, we revealed that the 3'-3'-linked TFO with the anthraquinonyl group inhibits the cleavage by the restriction enzyme *Hind* III more effectively than the unlinked nonamer and the 3'-3'-linked TFO without

<sup>†</sup> For Part 217 in this series, see: Minakawa, N., Kato, Y., Uetake, K., Kaga, D., and Matsuda, A. (2003) An improved large scale synthesis of 1,4-anhydro-4-thio-D-ribitol. *Tetrahedron* **59**, 1699–1702.

\* Corresponding author. Phone: +81-11-706-3228. Fax: +81-11-706-4980. E-mail: matuda@pharm.hokudai.ac.jp.

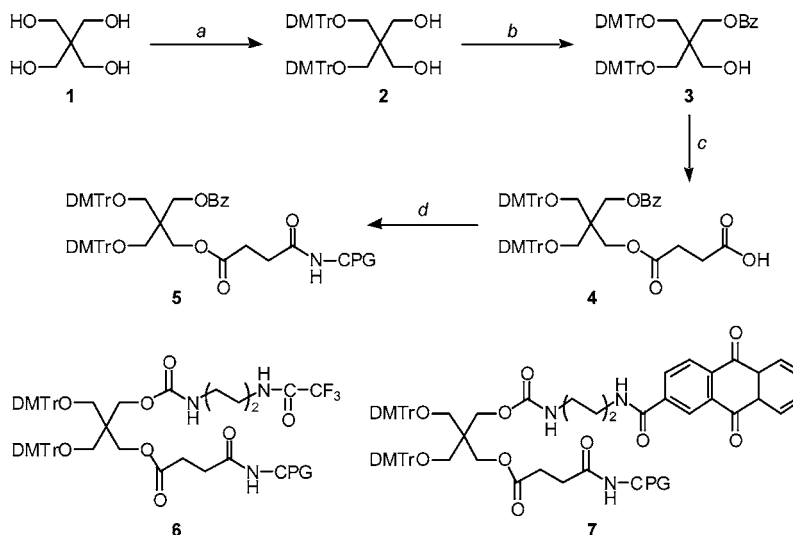
<sup>‡</sup> Present address: Faculty of Engineering, Gifu University, Yanagido, Gifu 501-1193, Japan.





**Figure 1.** Schematic presentation of "alternate-strand triplex" formation by the 3'-3' or 5'-5'-linked TFOs.

**Scheme 1**<sup>a</sup>



<sup>a</sup> (a) DMTrCl, pyridine, room temperature; (b) (1)  $\text{Bu}_2\text{SnO}$ , benzene, 80 °C; (2)  $\text{BzCl}$ , benzene, room temperature; (c) succinic anhydride,  $\text{Et}_3\text{N}$ , DMAP,  $\text{CH}_3\text{CN}$ , room temperature; (f) aminopropyl-controlled pore glass, 1-ethyl-3-(3-dimethylaminopropyl)carbodiimide hydrochloride, DMF, room temperature.

the intercalator. However, as mentioned above, because cytosines have to be protonated, the pyrimidine-rich motif requires a slightly acidic pH for stable triplex formation, thereby limiting its use under physiological conditions. In contrast, triplex formation by purine-rich TFOs is pH-independent, and for this reason they have been more frequently used in the antigene strategy (1, 26, 27).

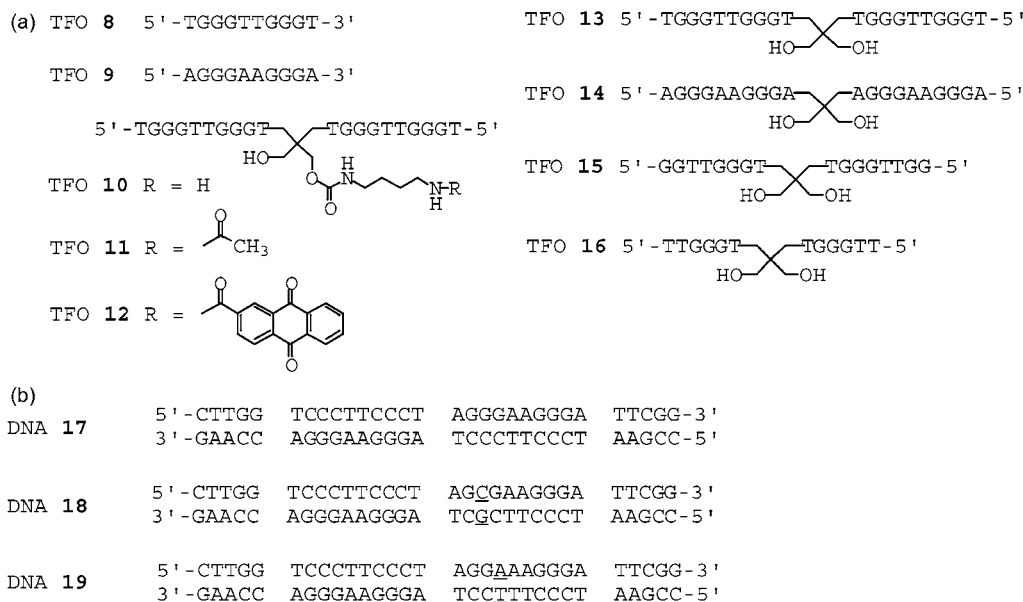
In this paper, we report the synthesis of the 3'-3'-linked TFOs that can form the antiparallel triplexes with the duplex DNA target by reverse Hoogsteen hydrogen bonds (Figure 1d). Stability of the alternate-strand triplexes between these TFOs and the target DNAs was investigated with the use of the electrophoretic mobility shift assay (EMSA). The ability of the 3'-3'-linked TFOs to inhibit cleavage of a target DNA by a restriction enzyme was also studied.

## RESULTS AND DISCUSSION

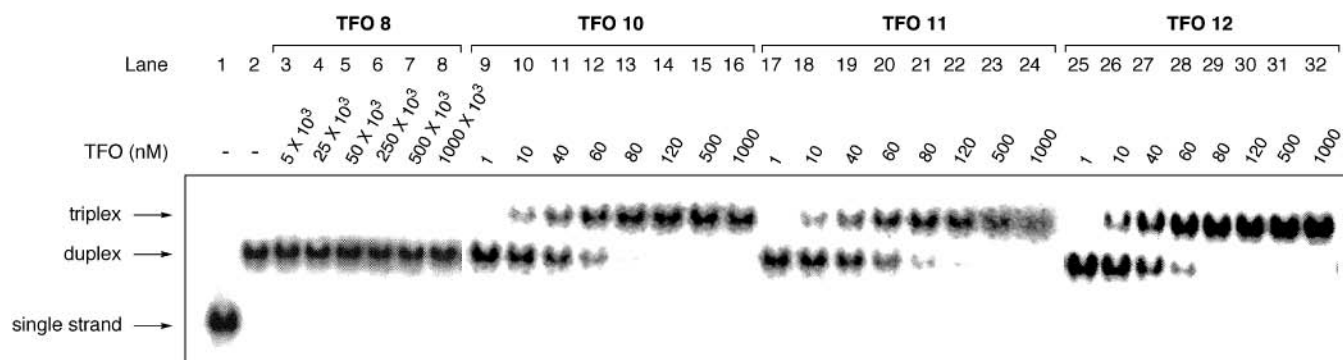
**Synthesis.** The controlled pore glass (CPG) with Pentaerythritol was synthesized as shown in Scheme 1.

First, pentaerythritol **1** was treated with two equivalents of 4,4'-dimethoxytrityl chloride (DMTrCl) in pyridine to give the *O*-bis(DMTr) derivative **2** in 27% yield. Compound **2** was treated with  $\text{Bu}_2\text{SnO}$  and then reacted with  $\text{BzCl}$  to produce the *O*-mono(Bz) derivative **3** in 98% yield. Compound **3** was succinated to give **4**, which was further reacted with CPG to afford a solid support **5** bearing **4** (25  $\mu\text{mol/g}$ ).

The 3'-3'-linked TFOs **13–16** (Figure 2a), which consist of 2'-deoxyguanosine (G) and thymidine (T) or G and 2'-deoxyadenosine (A), were synthesized on a DNA synthesizer using the CPG **5**. The fully protected TFOs (each 0.25  $\mu\text{mol}$ ) linked to the solid support were treated with concentrated  $\text{NH}_4\text{OH}$  at 55 °C for 16 h. The released TFOs were purified by denaturing with 20% polyacrylamide gel electrophoresis (20% PAGE) to give the deprotected TFOs **13–16**, in 6.6, 9.9, 6.7, and 7.1  $\text{OD}_{260}$  units, respectively. These TFOs were analyzed by matrix-assisted laser desorption/ionization time-of-flight mass spectrometry (MALDI-TOF/MS), and the observed mo-



**Figure 2.** Sequences of TFOs and the target duplexes.



**Figure 3.** Quantitative EMSA to detect binding of TFO **8** (lanes 3–8), TFO **10** (lanes 9–16), TFO **11** (lanes 17–24), and TFO **12** (lanes 25–32) to DNA target. DNA concentration: 10 nM. TFO concentrations are indicated.

lecular weights supported their structures. The TFO **10** with an aminobutyl-linker, the TFO **11** protected with an acetyl group, and the TFO **12** with a 2-anthraquinonecarbonyl group were also synthesized according to the reported method (25) using the CPGs **6** and **7** (Scheme 1).

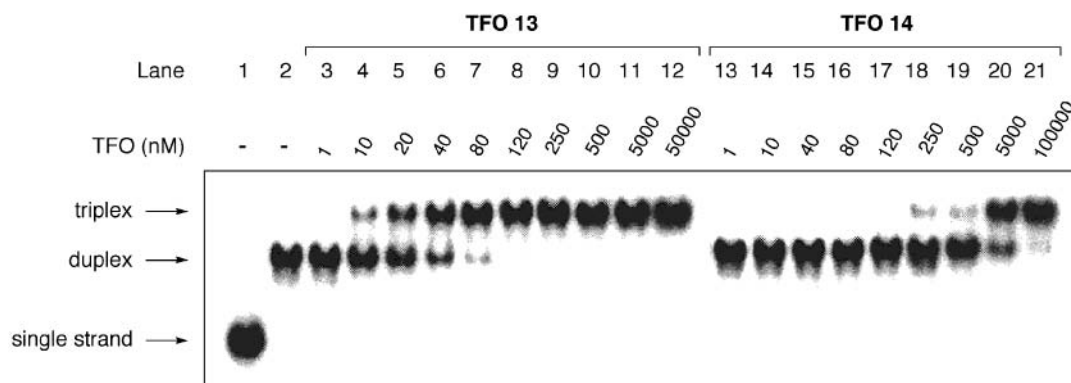
**Studies of Triplex Formation by the Electrophoretic Mobility Shift Assay.** The stability of the triplexes was investigated using the electrophoretic mobility shift assay (EMSA). The EMSA detects the difference in electrophoretic mobility of the double-stranded DNA and the triplex formed. First, we tested the ability of the unlinked decamers **8** and **9** and the 3'-3'-linked TFOs **10–12** to bind to the target DNA **17**, which has oligopurine sequences, one on each strand (Figure 2b). The sequences of the binding domains (each 10 mer length) are symmetrical.

The <sup>32</sup>P-labeled DNA **17** was incubated in the presence of increasing concentrations of the unlinked decamer **8** or **9** or the 3'-3'-linked TFO **10**, **11**, or **12** in a buffer of 20 mM Tris-HCl (pH 7.5) containing 10 mM MgCl<sub>2</sub>. The mixtures were then analyzed by nondenaturing 20% polyacrylamide gel electrophoresis (PAGE) at 4 °C. As shown in Figure 3, the retarded bands corresponding to the triplexes were observed for the TFOs **10**, **11**, and **12**, whereas the band corresponding to the triplex was not detected for the TFOs **8** and **9**. Table 1 summarizes the dissociation constants (*K<sub>d</sub>*) of the TFOs bound to the duplex DNA target. The *K<sub>d</sub>* values of the TFOs **10**, **11**,

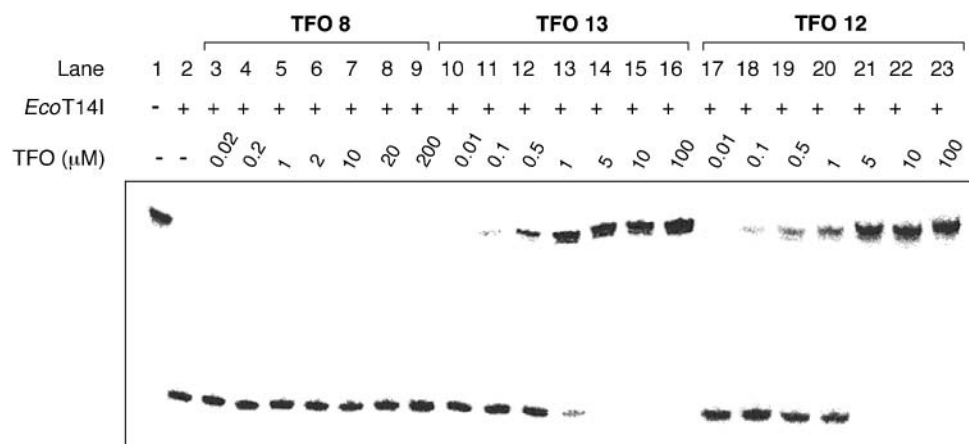
**Table 1. Summary of Dissociation Constants (*K<sub>d</sub>*) of the TFOs Bound to the DNA Targets**

TFO	duplex	<i>K<sub>d</sub></i> (nM)
TFO <b>8</b>	DNA <b>17</b>	>1 000 000
TFO <b>9</b>	DNA <b>17</b>	>1 000 000
TFO <b>10</b>	DNA <b>17</b>	33 (±12)
TFO <b>11</b>	DNA <b>17</b>	33 (±8)
TFO <b>12</b>	DNA <b>17</b>	38 (±22)
TFO <b>13</b>	DNA <b>17</b>	41 (±6)
TFO <b>14</b>	DNA <b>17</b>	17 000 (±3000)
TFO <b>15</b>	DNA <b>17</b>	340 (±10)
TFO <b>16</b>	DNA <b>17</b>	>100 000
TFO <b>13</b>	DNA <b>18</b>	>100 000

and **12** to the DNA **17** were 33 ± 12, 33 ± 8, and 38 ± 22 nM, respectively. On the other hand, the *K<sub>d</sub>* values of the unlinked decamers **8** and **9** to the DNA **17** were both more than 1 mM. It was found that the alternate-strand triplexes are significantly stabilized by linking the TFO fragments with the pentaerythritol linker. However, the *K<sub>d</sub>* values of TFO **10** with the aminobutyl-linker, **11** with *N*-acetylaminobutyl-linker, and **12** with the 2-anthraquinonecarbonyl group to the DNA **17** were almost the same. Thus, in contrast to the alternate-strand triplexes composed of the pyrimidine motif (25), the terminal ammonium ion of the aminobutyl-linker and the intercalator of the TFOs were found not to contribute to the stability of the alternate-strand triplex consisting of the purine motif under these conditions.



**Figure 4.** Quantitative EMSA to detect binding of TFO **13** (lanes 3–12) and TFO **14** (lanes 13–21) to DNA target. DNA concentration: 10 nM. TFO concentrations are indicated.



**Figure 5.** Specific inhibition of *EcoT14I* cleavage by the TFOs **8** (lanes 3–9), **13** (lanes 10–16), or **12** (lanes 17–23). Experimental conditions are described in Experimental Procedures.

To examine the effect of the composition and the length of a third strand on the alternate-strand triplex formation, the ability of the 3'-3'-linked TFO **13** consisting of T and G, the 3'-3'-linked TFO **14** comprised of A and G, the 3'-3'-linked TFO **15** composed of 16 bases, and the 3'-3'-linked TFO **16** consisting of 12 bases to bind to the DNA **17** was examined (Figure 4). The  $K_d$  of the TFO **13** to the DNA **17** was  $41 \pm 6$  nM, whereas that of the TFO **14** was  $17 \pm 3$   $\mu$ M. It has been reported that the sequences of the junction regions of the alternate-strand triplex critically influence the stabilities of the triplexes. It was found that the TFO consisting of T and G stabilizes the alternate-strand triplex more efficiently than that composed of A and G. It has been reported that the presence of a series of alternating d(GA) repeats within the sequence facilitates formation of parallel-stranded homoduplexes with G:G and A:A base pairs (28–30). Thus, the self-association of the 3'-3'-linked TFO **14** may be partially responsible for the difference of the  $K_d$  values between the TFO **13** and **14**. On the other hand, the  $K_d$  values of the TFOs **15** and **16** to the DNA **17** were  $340 \pm 10$  nM and more than 100  $\mu$ M, respectively. Thus, the TFO composed of more than 16 bases is required for the stable alternate-strand triplex formation by the purine motif.

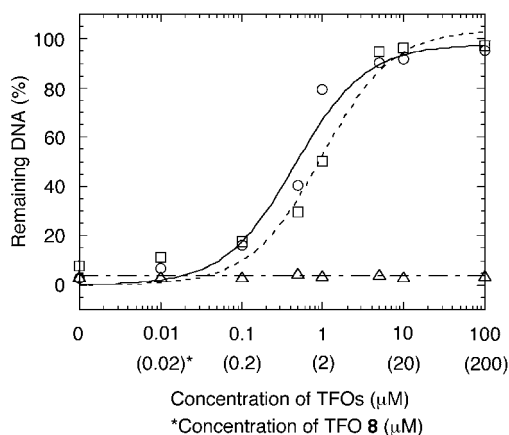
To investigate the base recognition ability of the 3'-3'-linked TFOs, we tested the ability of the 3'-3'-linked TFO **13** to bind to the DNA target **18** involving one C:G base pair that cannot form reverse Hoogsteen hydrogen bonding with the G residue in the TFO **13**. The  $K_d$  value of the TFO **13** to the DNA target **18** was more than 100  $\mu$ M. Thus, it was revealed that the 3'-3'-linked TFOs have high base recognition ability. This result also indicates

that the 3'-3'-linked TFO **13** binds simultaneously to both the adjacent oligopurine domains of the DNA target **17** to form the stable triplex.

**Inhibition of Restriction Endonuclease Cleavage via Triplex Formation.** We next tested the ability of the 3'-3'-linked TFOs to inhibit cleavage of a target DNA by a restriction endonuclease. The restriction enzyme *EcoT14I* recognizes the palindromic 6 bp sequence 5'-CCTAGG-3'/3'-GGATCC-5' and cleaves the two strands in a symmetric way (31). The DNA **17** contains the *EcoT14I* recognition site at its center and also involves oligopurine sequences, one on each strand, that can be recognized by the third strand. The unlinked decamer **8**, the 3'-3'-linked TFO **13**, and the 3'-3'-linked TFO **12** with the 2-anthraquinonecarbonyl group were used as the third strands.

A series of experiments was carried out at 37 °C in a 50 mM Tris-HCl buffer (pH 7.5) containing 25 mM  $MgCl_2$  and 1 mM DTT. Increasing amounts of the third strand were added to the DNA **17**, labeled at one 5'-end by  $^{32}P$ , and the solutions were preincubated at 37 °C for 30 min before addition of the restriction enzyme. After being incubated at 37 °C for 2 h, the products were analyzed by polyacrylamide gel electrophoresis under denaturing conditions (Figure 5). Densities of radioactivity of the gel were visualized by a Bio-imaging analyzer. As shown in Figure 6, the cleavage was inhibited in a dose-dependent manner when the 3'-3'-linked TFO **12** or **13** was used as the third strand. The 50% inhibitory concentrations ( $IC_{50}$ s) of the 3'-3'-linked TFOs **12** and **13** were 0.90 and 0.48  $\mu$ M, respectively. On the other hand, inhibition of the cleavage by the enzyme was not observed up to 200  $\mu$ M with the TFO **8** as the third strand.





**Figure 6.** Specific inhibition of *Eco*T14I cleavage by triplex formation: plots of percentage remaining DNA versus the concentration of TFO in the reaction mixture. The symbols on the plot indicate the TFOs **13** (○), **12** (△), and **8** (□).

To show that the inhibition was due to the interaction of the TFOs with the target DNA rather than with the restriction enzyme, a parallel experiment was carried out with the DNA **19**, which contains one restriction site for *Eco*T14I but no sequence fully complementary to that of the TFO **13**. It was found that the TFO **13** does not inhibit the cleavage of the DNA **19** by the enzyme at all (data not shown). Therefore, the inhibition of the cleavage was not due to the TFOs binding to the enzyme but to triplex formation at the binding site of the enzyme.

## CONCLUSION

In this paper, we describe the synthesis of the 3'-3'-linked TFOs that can form the antiparallel triplexes with the DNA target by reverse Hoogsteen hydrogen bonds. Stability of the alternate-strand triplexes between these TFOs and the target duplex DNAs was investigated by the EMSA. It was found that the alternate-strand triplexes were significantly stabilized by linking the TFO fragments with the pentaerythritol linker. To our knowledge, this is the first example of the alternate-strand triplex composed of only the purine motif. In addition, we found that in contrast to the alternate-strand triplexes composed of the pyrimidine motif, the terminal ammonium ion of the aminobutyl-linker and the intercalator of the TFOs did not contribute to the stability of the alternate-strand triplex comprised of the purine motif.

We tested the ability of the 3'-3'-linked TFOs to inhibit cleavage of the DNA target **17** by the restriction enzyme *Eco*T14I. It was revealed that the 3'-3'-linked TFO **12** and **13** inhibited the cleavage by the enzyme more effectively than the unlinked decamer **8**. Thus, the TFOs linked with pentaerythritol may be useful as antigene oligonucleotides to the duplex DNAs, which have the alternating oligopyrimidine-oligopurine sequences.

## EXPERIMENTAL PROCEDURES

**General Remarks.** NMR spectra were recorded at 270 MHz (<sup>1</sup>H) and at 100 MHz (<sup>13</sup>C). Chemical shifts (δ) and coupling constants (*J*) are reported in parts per million downfield from TMS and in Hz, respectively. Mass spectra were obtained by fast atom bombardment (FAB) method. Thin-layer chromatography was done on Merck coated plates 60F<sub>254</sub>. The silica gel used for column chromatography was Merck silica gel 5715.

**2,2-Bis-(4,4'-dimethoxytrityloxymethyl)-1,3-propanediol (2).** After successive coevaporation with dry pyridine, pentaerythritol **1** (2.7 g, 20 mmol) was dissolved

in dry pyridine (200 mL). DMTrCl (13.6 g, 40 mmol) was added in four portions, and stirred for 18 h at room temperature. EtOH (20 mL) was added to the solution, which was stirred at room temperature. After 30 min, the mixture was concentrated in vacuo and was taken in EtOAc, which was washed with aqueous NaHCO<sub>3</sub> (saturated) and brine, dried (Na<sub>2</sub>SO<sub>4</sub>), and concentrated. The residue was purified by column chromatography (SiO<sub>2</sub>, EtOAc) to give **2** (3.9 g, 27% as a yellow foam): <sup>1</sup>H NMR (CDCl<sub>3</sub>) δ 7.37–6.78 (m, 26H), 3.78 (s, 12H), 3.78–3.74 (m, 4H), 3.31 (s, 4H), 2.19–2.14 (t, 2H, *J* = 6.6). <sup>13</sup>C NMR (CDCl<sub>3</sub>) δ 45.4, 55.2, 63.2, 65.5, 86.2, 113.1, 126.7, 127.8, 128.0, 130.0, 135.5, 144.5, 158.3. HRMS calcd for C<sub>47</sub>H<sub>48</sub>O<sub>8</sub>Na (M + Na<sup>+</sup>), 763.3247; found, 763.3235. Anal. Calcd for C<sub>47</sub>H<sub>48</sub>O<sub>8</sub>: C, 76.19; H, 6.53. Found: C, 75.95; H, 6.65.

**2-Benzoyloxymethyl-1,3-bis-*O*-(4,4'-dimethoxytrityl)-2-hydroxymethyl-1,3-propanediol (3).** After successive coevaporation with dry benzene, **2** (400 mg, 0.54 mmol) was dissolved in dry benzene (20 mL). Bu<sub>2</sub>SnO (147 mg, 0.59 mmol) was added to the solution, which was heated under reflux for 6 h. The mixture was evaporated and dissolved in dry benzene (20 mL). BzCl (69 μL, 0.59 mmol) was added to the solution, which was stirred at room temperature. After 90 min, aqueous NaHCO<sub>3</sub> (10 mL, saturated) was added to the solution, which was stirred at room temperature. After 15 h, the mixture was diluted with EtOAc. The organic layer was washed with aqueous NaHCO<sub>3</sub> (saturated) and brine, dried (Na<sub>2</sub>SO<sub>4</sub>), and concentrated. The residue was purified by column chromatography (SiO<sub>2</sub>, 65% EtOAc in hexane) to give **3** (451 mg, 98% as a white foam): <sup>1</sup>H NMR (CDCl<sub>3</sub>) δ 7.76–6.71 (m, 31H), 4.45 (s, 2H), 3.72 (s, 12H), 3.72–3.64 (m, 2H), 3.33 (s, 4H), 2.34 (bs, 1H). <sup>13</sup>C NMR (CDCl<sub>3</sub>) δ 45.1, 55.1, 62.0, 63.8, 64.6, 86.2, 113.0, 126.6, 127.7, 127.9, 128.2, 129.6, 129.7, 130.0, 132.9, 135.5, 144.6, 158.3, 166.2. HRMS calcd for C<sub>54</sub>H<sub>52</sub>O<sub>9</sub>Na (M + Na<sup>+</sup>), 867.3509; found, 867.3486. Anal. Calcd for C<sub>54</sub>H<sub>52</sub>O<sub>9</sub>: C, 76.76; H, 6.20. Found: C, 76.67; H, 6.25.

**2-Benzoyloxymethyl-1,3-bis-*O*-(4,4'-dimethoxytrityl)-2-(*O*-succinyl)oxymethyl-1,3-propanediol (4).** Compound **3** (300 mg, 0.36 mmol) was dissolved in dry CH<sub>3</sub>CN (5 mL). DMAP (44 mg, 0.36 mmol), Et<sub>3</sub>N (176 μL, 1.26 mmol), and succinic anhydride (126 mg, 1.26 mmol) was added to the solution, which was stirred at room temperature. After 3 days, aqueous NaHCO<sub>3</sub> (5 mL, saturated) was added to the mixture, which was concentrated in vacuo. The residue was taken in EtOAc, which was washed with aqueous NaHCO<sub>3</sub> (saturated) and brine, dried (Na<sub>2</sub>SO<sub>4</sub>), and concentrated. The residue was purified by column chromatography (SiO<sub>2</sub>, EtOAc) to give **4** (257 mg, 75% as a white foam): <sup>1</sup>H NMR (CDCl<sub>3</sub>) δ 7.74–6.69 (m, 31H), 4.38 (s, 2H), 4.23 (s, 2H), 3.71 (s, 12H), 3.30 (s, 4H), 2.46–2.41 (m, 4H). <sup>13</sup>C NMR (CDCl<sub>3</sub>) δ 28.6, 28.7, 44.0, 55.1, 60.2, 63.1, 63.3, 85.9, 112.9, 126.5, 127.6, 128.0, 128.2, 129.5, 129.7, 130.0, 132.9, 135.5, 144.6, 158.2, 165.9, 171.4, 176.5. HRMS calcd for C<sub>58</sub>H<sub>56</sub>O<sub>12</sub>Na (M + Na<sup>+</sup>), 967.3669; found, 967.3650. Anal. Calcd for C<sub>58</sub>H<sub>56</sub>O<sub>12</sub>: C, 73.71; H, 5.97. Found: C, 73.49; H, 6.18.

**Synthesis of CPG 5.** Aminopropyl controlled pore glass (448 mg, 40 μmol, 90.4 μmol/g, CPG Inc.) was added to a solution of **4** (150 mg, 0.159 mmol) and 1-ethyl-3-(3-dimethylaminopropyl)carbodiimide hydrochloride (31 mg, 0.159 mmol) in dry DMF (4 mL), and the mixture was kept at room temperature for 3 days. After the resin was washed with pyridine, 5 mL of a capping solution (0.5 M DMAP in pyridine:Ac<sub>2</sub>O = 9:1) was added, and the whole was kept at room temperature for 15 h. The

resin was washed with EtOH and acetone and was dried under vacuum. The loaded **4** to the solid support is 25  $\mu\text{mol/g}$  from the calculation of released dimethoxytrityl cation by a solution of 70%  $\text{HClO}_4\text{:EtOH}$  (3:2, v/v).

**Synthesis of TFOs.** TFOs were synthesized on a DNA synthesizer (Applied Biosystem Model 392) by the phosphoramidite method. Each TFO linked to the resin was treated with concentrated  $\text{NH}_4\text{OH}$  at 55 °C for 16 h, and the released TFO was purified by denaturing 20% polyacrylamide gel electrophoresis (20% PAGE) with 7 M urea at 600 V for 8 h. The TFO was visualized by UV shadowing and eluted from crushed gel slices by incubation at room temperature in 0.1 M Tris buffer (pH 7.0) and 1 mM EDTA for 15 h. The TFO was purified on a Sep-Pak C18 cartridge to give the deprotected TFO **10** (13.6), **12** (10.8), **13** (6.6), **14** (9.9), **15** (6.7), and **16** (7.1). The yields are indicated in parentheses as OD units at 260 nm starting from 0.25  $\mu\text{mol}$  scale.

**Acetylation of TFO 10.** A solution containing TFO **10** (5.0 OD units at 260 nm) and  $\text{Ac}_2\text{O}$  (10  $\mu\text{L}$ ) in 0.2 M HEPES buffer (pH 7.2, 1.0 mL) was kept for 5 h at room temperature. Concentrated  $\text{NH}_4\text{OH}$  (2.0 mL) was added to the mixture, and the whole was kept overnight at 4 °C. The solvent was removed in vacuo, and the residue was purified by HPLC with a C18 column to give TFO **11** (3.7 OD units at 260 nm).

**Matrix-Assisted Laser Desorption/Ionization Time-of-Flight Mass Spectrometry.** Spectra were obtained on a Voyager Elite reflection time-of-flight mass spectrometry (PerSeptive Biosystems, Inc., Framingham, MA) equipped with a nitrogen laser (337 nm, 3 ns pulse). 3-Hydroxypicolinic acid (HPA), dissolved in  $\text{H}_2\text{O}$  to give a saturated solution at room temperature, was used as the matrix. TFO **10**: calculated mass, 6633.31; observed mass, 6634.87. TFO **11**: calculated mass, 6675.35; observed mass, 6675.85. TFO **12**: calculated mass, 6867.57; observed mass, 6868.89. TFO **13**: calculated mass, 6519.17; observed mass, 6520.42. TFO **14**: calculated mass, 6591.27; observed mass, 6592.76. TFO **15**: calculated mass, 5252.37; observed mass, 5252.74. TFO **16**: calculated mass, 3935.54; observed mass, 3936.74.

**Electrophoretic Mobility Shift Assays.** DNA (10 nM) labeled at one 5'-end by  $^{32}\text{P}$  was incubated in the presence of various amounts of TFO in a 20 mM Tris-HCl buffer (pH 7.5) containing 10 mM  $\text{MgCl}_2$  (total 20  $\mu\text{L}$ ) at 70 °C for 5 min and then gradually cooled to 4 °C. The reaction mixture was supplemented with 4  $\mu\text{L}$  of a 50% glycerol solution containing bromophenol blue. The reaction was analyzed by electrophoresis on 20% non-denaturing polyacrylamide gel (39:1 acrylamide:bisacrylamide) using a TB buffer (45 mM Tris borate, pH 8, 10 mM  $\text{MgCl}_2$ ) at 60–80 mV for 24–36 h at 4 °C. After drying, density of radioactivity of the gel was visualized by a Bio-imaging Analyzer (Bas 2000, Fuji, Co. Ltd.).

**Enzymatic Assays.** Enzymatic assays were performed in a 50 mM Tris-HCl buffer (pH 7.5) containing 25 mM  $\text{MgCl}_2$ , and 1 mM DTT. Various amounts of the third strands were added to the duplex (1 pmol), labeled at one 5'-end by  $^{32}\text{P}$ , and the solutions were preincubated at 37 °C for 30 min. Twenty units of *EcoT14I* (Takara Shuzo Co., Ltd.) was added to each solution, and the mixture (total 10  $\mu\text{L}$ ) was incubated at 37 °C for 2 h. One aliquot (1.5  $\mu\text{L}$ ) of the reaction mixture was separated and added to a loading solution (8 M urea, 0.1% xylene cyanol, 0.1% bromophenol blue, 5  $\mu\text{L}$ ). The solution was analyzed by electrophoresis on 20% polyacrylamide gel containing 7 M urea. Densities of radioactivity of the gel were visualized by a Bio-imaging analyzer (Bas 2000, Fuji Co., Ltd.).

## ACKNOWLEDGMENT

This work was supported in part by a Grant-in-Aid for Encouragement of Young Scientists from the Ministry of Education, Science, Sports, and Culture of Japan and a grant from the "Research for the Future" Program of the Japan Society for the Promotion of Science (JSPS-RFTF97I00301). We thank Y. Misawa (Hokkaido University) for technical assistance.

## LITERATURE CITED

- (1) Thuong, N. T., and Hélène, C. (1993) Sequence specific recognition and modification of double-helical DNA by oligonucleotides. *Angew. Chem., Int. Ed. Engl.* **32**, 666–690.
- (2) Moser, H. E., and Dervan, P. B. (1987) Sequence specific cleavage of double helical DNA by triple helix formation. *Science* **238**, 645–650.
- (3) Rajagopal, P., and Feigon, J. (1989) Triple-strand formation in the homopurine:homopyrimidine DNA oligonucleotides d(G-A)<sub>4</sub> and d(T-C)<sub>4</sub>. *Nature* **339**, 637–640.
- (4) Beal, P. A., and Dervan, P. B. (1991) Second structural motif for recognition of DNA by oligonucleotide-directed triple-helix formation. *Science* **251**, 1360–1363.
- (5) Pilch, D. S., Levenson, C., and Shafer, R. H. (1991) Structure, stability, and thermodynamics of a short intermolecular purine-purine-pyrimidine triple helix. *Biochemistry* **30**, 6081–6088.
- (6) Singleton, S. F., and Dervan, P. B. (1992) Influence of pH on the equilibrium association constants for oligodeoxyribonucleotide-directed triple helix formation at single DNA sites. *Biochemistry* **31**, 10995–11003.
- (7) Beal, P. A., and Dervan, P. B. (1992) Recognition of double helical DNA by alternate strand triple helix formation. *J. Am. Chem. Soc.* **114**, 4976–4982.
- (8) Jayasena, S. D., and Johnston, B. H. (1992) Oligonucleotide-directed triple helix formation at adjacent oligopurine and oligopyrimidine DNA tracts by alternate strand recognition. *Nucleic Acids Res.* **20**, 5279–5288.
- (9) Jayasena, S. D., and Johnston, B. H. (1992) Intramolecular triple-helix formation at (Pu<sub>n</sub>Py<sub>n</sub>)(Pu<sub>n</sub>Py<sub>n</sub>) tracts: recognition of alternate strands via Pu-PuPy and Py-PuPy base triplets. *Biochemistry* **31**, 320–327.
- (10) Balatskaya, S. V., Belotserkovskii, B. P., and Johnston, B. H. (1996) Alternate-strand triplex formation: modulation of binding to matched and mismatched duplexes by sequence choice in the Pu-Pu-Py Block. *Biochemistry* **35**, 13328–13337.
- (11) Washbrook, E., and Fox, K. R. (1994) Alternate-strand DNA triple-helix formation using short acridine-linked oligonucleotides. *Biochem. J.* **301**, 569–575.
- (12) Washbrook, E., and Fox, K. R. (1994) Comparison of antiparallel A-AT and T-AT triplets within an alternate strand DNA triple helix. *Nucleic Acids Res.* **22**, 3977–3982.
- (13) De Bizemont, T., Sun, J.-S., Garestier, T., and Hélène, C. (1998) New junction models for alternate-strand triple-helix formation. *Chem. Biol.* **5**, 755–762.
- (14) Brodin, P., Sun, J.-S., Mouscadet, J.-F., and Auclair, C. (1999) Optimization of alternate-strand triple helix formation at the 5'-TpA-3' and 5'-ApT-3' junctions. *Nucleic Acids Res.* **27**, 3029–3034.
- (15) Horne, D. A., and Dervan, P. B. (1990) Recognition of mixed-sequence duplex DNA by alternate-strand triple-helix formation. *J. Am. Chem. Soc.* **112**, 2435–2437.
- (16) Ono, A., Chen, C. N., and Kan, L. S. (1991) DNA triplex formation of oligonucleotide analogues consisting of linker groups and octamer segments that have opposite sugar-phosphate backbone polarities. *Biochemistry* **30**, 9914–9921.
- (17) McCurdy, S., Moulds, C., and Froehler, B. (1991) Deoxyoligonucleotides with inverted polarity: synthesis and use in triple-helix formation. *Nucleosides Nucleotides* **10**, 287–290.
- (18) Froehler, B. C., Terhorst, T., Shaw, J. P., and McCurdy, S. N. (1992) Triple-helix formation and cooperative binding by oligodeoxynucleotides with a 3'-3' internucleotide junction. *Biochemistry* **31**, 1603–1609.

- (19) Asseline, U., and Thuong, N. T. (1993) Oligonucleotides tethered via nucleic bases. A potential new set of compounds for alternate strand triple-helix formation. *Tetrahedron Lett.* 34, 4173–4176.
- (20) Asseline, U., and Thuong, N. T. (1994) 5'-5' Tethered oligonucleotides via nucleic bases: a potential new set of compounds for alternate strand triple-helix formation. *Tetrahedron Lett.* 35, 5221–5224.
- (21) Asseline, U., Roig, V., and Thuong, N. T. (1998) Modified oligonucleotides with 5'-5' interbase semirigid junction for alternate strand triplex formation. *Tetrahedron Lett.* 39, 8991–8994.
- (22) Zhou, B.-W., Marchand, C., Asseline, U., Thuong, N. T., Sun, J.-S., Garestier, T., and Hélène, C. (1995) Recognition of alternating oligopurine/oligopyrimidine tracts of DNA by oligonucleotides with base-to-base linkages. *Bioconjugate Chem.* 6, 516–523.
- (23) Ueno, Y., Ogawa, A., Nakagawa, A., and Matsuda, A. (1996) Nucleosides and nucleotides. 162. Facile synthesis of 5'-5'-linked oligodeoxyribonucleotides with the potential for triple-helix formation. *Bioorg. Med. Chem. Lett.* 23, 2817–2822.
- (24) De Napoli, L., Messere, A., Montesarchio, D., Pepe, A., Piccialli, G., and Varra, M. (1997) Synthesis and triple helix formation by alternate strand recognition of oligonucleotides containing 3'-3' phosphodiester bonds. *J. Org. Chem.* 62, 9024–9030.
- (25) Ueno, Y., Mikawa, M., Hoshika, S., and Matsuda, A. (2001) Alternate-strand triple-helix formation by the 3'-3'-linked oligodeoxynucleotides with the anthraquinonyl group at the junction point. *Bioconjugate Chem.* 12, 635–642.
- (26) Wang, G., Seidman, M. M., and Glazer, P. M. (1996) Mutagenesis in mammalian cells induced by triple helix formation and transcription-coupled repair. *Science* 271, 802–805.
- (27) Cogoi, S., Rapozzi, V., Quadrifoglio, F., and Xodo, L. (2001) Anti-gene effect in live cells of AG motif triplex-forming oligonucleotides containing an increasing number of phosphorothioate linkages. *Biochemistry* 40, 1135–1143.
- (28) Rippe, K., Fritsch, V., Westhof, E., and Jovin, T. M. (1992) Alternating d(G-A) sequences form a parallel-stranded DNA homoduplex. *EMBO J.* 11, 3777–3786.
- (29) Huertas, D., Bellolell, L., Casasnovas, J. M., Coll, M., and Azorin, F. (1993) Alternating d(GA)<sub>n</sub> DNA sequences form antiparallel stranded homoduplexes stabilized by the formation of G·A base pairs. *EMBO J.* 12, 4029–4038.
- (30) Noonberg, S. B., François, J.-C., Garestier, T., and Hélène, C. (1995) Effect of competing self-structure on triplex formation with purine-rich oligodeoxynucleotides containing GA repeats. *Nucleic Acids Res.* 23, 1956–1963.
- (31) Mise, K., and Nakajima, K. (1985) Purification of a new restriction endonuclease, StyI, from *Escherichia coli* carrying the hsd<sup>+</sup> miniplasmid. *Gene* 33, 357–61.

BC0256493



# A Novel Method for the Rational Construction of Well-Defined Immunogens: The Use of Oximation To Conjugate Cholera Toxin B Subunit to a Peptide–Polyoxime Complex

Jianhua Chen,<sup>†</sup> Weiguang Zeng,<sup>‡</sup> Robin Offord,<sup>†</sup> and Keith Rose<sup>\*,†</sup>

Department of Medical Biochemistry, University Medical Center, rue Michel-Servet 1, 1211 Geneva 4, Switzerland, and Cooperative Research Centre for Vaccine Technology, Department of Microbiology and Immunology, University of Melbourne, Parkville, Australia. Received December 12, 2002; Revised Manuscript Received February 11, 2003

Cholera toxin B subunit (CTB), capable of binding to all mucous membranes in its pentameric form, is a potential carrier of mucosal vaccines. In our previous work we reported that the N-terminus of CTB, a threonine, could in principle undergo oxidation and oximation to form conjugates with a cascade of immunogenic peptides. In this study, we set up a model by chemically coupling CTB to a polyoxime that possessed five copies of influenza virus-derived peptides displayed in comblike form. The construct was reconstituted into pentameric form when eluted from a Superdex column after conjugation, and the pentameric nature of this CTB–viral peptide complex was confirmed by SDS–PAGE. GM<sub>1</sub>-ELISA assay showed that the binding properties of CTB–viral peptide complex were increased 4–5-fold over native CTB.

## INTRODUCTION

Cholera toxin, an AB<sub>5</sub> hexameric protein, composed of five identical B subunits and a single A subunit, is the primary enterotoxin produced by *Vibrio cholerae* bacteria and is the causative agent of cholera infection. The B subunits of Cholera toxin (CTB) are the nontoxic binding components of the CT holotoxin (1) and function in pentameric form to specifically recognize the GM<sub>1</sub> ganglioside receptor present on the surface of mucous cells. It has been demonstrated in a large field trial that CTB afforded, when orally administered, protection against both cholera and enterotoxigenic *E. coli*-caused diarrhea (2), and when conjugated to a poor immunogen and given orally, CTB showed the ability to dramatically increase the mucosal immunogenicity (3, 4). This raised the possibility of using CTB as a potential carrier of mucosal vaccines. J. Holmgren et al. and other workers also reported that the physical coupling of foreign antigens to CTB is a very effective way of inducing such a mucosal immune response after oral vaccination (5, 6). In our previous work we reported that the N-terminus of CTB, a threonine, could in principle undergo oxidation and oximation to form conjugates with a cascade of immunogenic peptides (7). Here we explore a possible way to generate novel mucosal vaccines that are chemically coupled to peptide and reconstituted into a CTB–viral peptide complex in vitro. Since the mucosal immune response from oral vaccination is not restricted to the intestine but also partly disseminates to other mucosal tissues, this approach raises the prospect to use CTB as a vaccine carrier against infections in the intestinal as well as in any other mucosal tissues.

Synthetic peptides can serve as immunogens to induce antibodies, but a small linear peptide may not be effective as an immunogen because of the influence of protein conformation (8) and because of its lack of high molecular mass that is necessary for enhanced immunogenicity. One way to solve these problems is to create an artificial protein by coupling the antigenic peptide to protein carriers such as mucosal adhering proteins [e.g., CTB or LTB (*E. coli* heat-labile toxin B-subunit)]. In this way, a synthetic immunogenic peptide is attached to part of a protein carrier capable of localizing in a specific tissue (mucosa of gastrointestinal tract, for example). To enhance peptide immunogenicity further, it is possible to cross-link antigenic peptides to a synthetic core in a branched (radial or comb) manner. For instance, Tam (9) in 1988 designed an amide-linked branched artificial protein, a multiple antigenic peptide (MAP) system, to increase molecular weight. This is a macromolecule containing several copies of synthetic epitopes or protein antigens that are coupled to a peptide core matrix (based on lysine) by peptide bond formation. MAP directs the immune system to a specific response. As MAPs are entirely synthetic, they are in principle safer vaccines as they are free of replicative agents (viruses, DNA, prions) and endotoxin. Unfortunately, with this approach it is impossible to produce homogeneous artificial proteins due to inevitable side-reactions and coupling failures, and the desired material, when the peptide epitope is longer, cannot be purified from the many impurities present with similar structure. One solution is to couple the prepurified synthetic peptides to the MAP-core matrix by site-specific conjugation. Oximation chemistry is one of the mild and effective methods for such site-specific tagging that permits the modification of proteins without damaging their intricate structure (10).

In this study we set up a model by grafting a MAP system to the N-terminus of CTB. An antigenic peptide derived from hemagglutinin protein of influenza virus was selected (11, 12). We aim to use this model composed

\* To whom correspondence should be addressed: GeneProt, Inc., 2 Pré-de-la-Fontaine, CP125, CH-1217 Meyrin 2, Switzerland. Phone: +41 22 7193900, Fax: +41 22 7193970, E-mail: keith.rose@geneprot.com.

<sup>†</sup> University Medical Center.

<sup>‡</sup> University of Melbourne.

of polyoxime and mucosal carrier protein to study the possibility of attaching a cascade of immunogenic peptide to CTB and retaining or reconstituting its pentameric form.

## MATERIALS AND METHODS

**1. Reagents and Chemicals.** Unless otherwise specified, all solvents and reagents were obtained from Fluka, Buchs, Switzerland, were of analytical or higher grade, and were used without further purification. All amino acids were purchased from Peptide Institute Inc., Japan. The resins were from Applied Biosystems (Foster City, CA), Novabiochem (Laufelfingen, Switzerland), or Bachem (Bubendorf, Switzerland). CTB was from Swiss Serum & Vaccine Institute (Bern, Switzerland). Water was repurified using a Milli-Q system (Millipore, Inc., Bedford, MA).

**2. HPLC and MS.** Analytical RP-HPLC (reverse-phase high performance liquid chromatography) was performed using a column  $250 \times 4$  mm i.d. packed with Nucleosil 300-A  $5 \mu\text{m}$   $\text{C}_8$  particles at a flow rate of 0.6 mL/min, and effluent was monitored at 214 nm. Peptides were purified on a  $\text{C}_8$  semipreparative column ( $250 \times 10$  mm i.d. Nucleosil 300-A  $5 \mu\text{m}$  particle size) at a flow rate of 4 mL/min monitoring at 214 nm, or purified on a  $\text{C}_{18}$  preparative column ( $210 \times 25$  mm i.d. Novapak  $6 \mu\text{m}$  particle size) at 20 mL/min monitoring at 229 nm. Solvents used in RP-HPLC were as follows: A, 0.1% TFA (1 g TFA in 1 L  $\text{H}_2\text{O}$ ); B, 0.1% TFA in 90% acetonitrile (1 g of TFA mixed with 100 mL of  $\text{H}_2\text{O}$  and then brought to 1 L with acetonitrile). Generally, the conditions used in analytical work were 5 min isocratic at 100% A followed by a linear gradient 2% B/min to 100% B, and in preparative work a shallower linear gradient (usually 0.5% B/min) was used. All peptide components were collected manually at the detector exit, evaporated at room temperature and reduced pressure, frozen, and then recovered by lyophilization.

Electrospray ionization mass spectrometry (ESI-MS) was performed in positive ion mode on a Trio 2000 machine or a Platform-II instrument (both from Micromass, Manchester, England). Samples were introduced either at  $2 \mu\text{L}/\text{min}$  (Trio) in an acidified solvent acetonitrile/water/AcOH (49.5:49.5:1) or at  $10 \mu\text{L}/\text{min}$  (Platform) in solvent acetonitrile/water/formic acid (49.9:49.9:0.2). MALDI-TOF mass spectrometry was performed in linear mode using sinapinic acid as matrix on a Voyager Elite machine (Applied Biosystems) equipped with delayed extraction. External calibration was performed on the electrospray machines using a solution of horse heart apomyoglobin and on the MALDI-TOF machine using the mixture of peptides supplied by the manufacturer.

**3. Synthesis of Peptides.** The antigenic peptide sequences  $\text{NH}_2\text{OCH}_2\text{CO-KTYQRTRALV}$  derived from influenza virus (11, 12) were synthesized by Boc chemistry on 0.5 mmol of Boc-Val-PAM resin (phenylacetamidomethyl resin, Applied Biosystems) using an automated solid-phase synthesizer (model ABI 430A, Applied Biosystems). Italic type denotes linker residues not present in the corresponding protein sequences. Side-chain protection of Boc-protected amino acid was Lys-(2ClZ), Thr(Bzl), Arg(Tos). After chain elongation with Boc chemistry, the N-terminal Boc-protection of Lys was deprotected with TFA. The Boc-aminooxyacetyl (AOA) was attached to the Lys residue with an activated mixture solution (1.0 mmol of Boc-AOA-OSu, 2-fold excess over the substitution of the resin in 5 mL of DMSO, 1 mL of *N*-methylmorpholine) to form aminooxyacetyl precursor peptide.

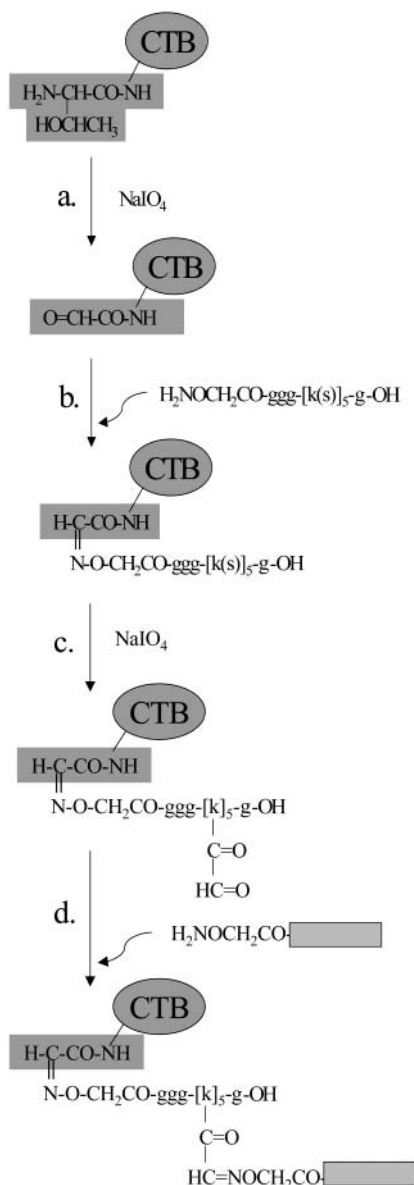
The linker  $\text{NH}_2\text{OCH}_2\text{CO-Gly}_3\text{-[Lys(Ser)]}_5\text{-Gly-OH}$  was synthesized manually on 0.5 mmol of Boc-Gly-PAM resin. After Boc deprotection, five cycles of coupling with Fmoc-Lys(Boc) and deprotection were performed by Fmoc-chemistry to form the linear polylysine core, followed by three cycles of Fmoc-Gly. The side-chain protection of Lys core was then removed, and Boc-Ser(Bzl) groups were attached to the core with an activated mixture solution (8 mmol Boc-Ser(Bzl)-OSu in 8 mL of DMSO and 2 mL of *N*-methylmorpholine), followed by Fmoc deprotection of the N-terminal amino group and attachment of a Boc-AOA group as above.

The resin and all other side-protection groups were cleaved with HF ( $0^\circ\text{C}$  for 1 h in the presence of 5% *p*-cresol). Peptides were precipitated with cold ether, extracted with 50% acetonitrile, filtered, and lyophilized. The crude peptides were purified by preparative HPLC and characterized by ESI-MS.

**4. Preparation of Polyoxime Conjugated to CTB.** A 1 mg amount of CTB, supplied as a lyophilized powder together with buffer salts, was dissolved in 1 mL water and isolated by gel filtration as the noncovalent pentamer on a Superdex 75 HR column (Amersham Pharmacia Biotech) at a flow rate of 0.4 mL/min. A phosphate buffer prepared by mixing  $\text{NaH}_2\text{PO}_4$  (0.25 M in  $\text{H}_2\text{O}$ ) with  $\text{Na}_2\text{-HPO}_4$  (0.25 M in  $\text{H}_2\text{O}$ ) to obtain pH 7.0 and containing EDTA (to a final concentration of 1 mM) was used as eluent solution. The protein was concentrated by ultrafiltration (Centricon, Amicon, Beverly, MA, 10000 MW cut off, precentrifuged twice with 1 mL of the phosphate buffer) to  $400 \mu\text{L}$ . Methionine ( $50 \mu\text{L}$ , 0.2 M in  $\text{H}_2\text{O}$ ) was added. N-Terminal threonine was then oxidized for 5 min by adding  $25 \mu\text{L}$  of sodium periodate (40 mM in  $\text{H}_2\text{O}$ ). The reaction was quenched with  $60 \mu\text{L}$  of ethylene glycol (0.5 M in  $\text{H}_2\text{O}$ ). After 4 min, 27.8 mg of aminooxyacetyl linker was added, followed by  $50 \mu\text{L}$  of acetic acid. Thirty minutes later,  $15 \mu\text{L}$  of the reaction solution was removed for HPLC and ESI-MS, while 500 mg of guanidine hydrochloride was added to the rest. After a reaction time of 16–18 h, the protein oxime was isolated by gel filtration and concentrated to  $400 \mu\text{L}$  as before.

The five Ser residues on the linker  $\text{NH}_2\text{OCH}_2\text{CO-Gly}_3\text{-[Lys(Ser)]}_5\text{-Gly-OH}$  ligated to CTB were oxidized for 5 min by addition of  $150 \mu\text{L}$  of methionine (0.2 M in  $\text{H}_2\text{O}$ ) and  $62.5 \mu\text{L}$  of sodium metaperiodate (80 mM in  $\text{H}_2\text{O}$ ). The reaction was quenched with  $300 \mu\text{L}$  of 1,3-diamino-2-propanol (0.5 M in  $\text{H}_2\text{O}$ , adjusted to pH 7.8 with acetic acid). Four minutes later, 500 mg of guanidine hydrochloride was added and the oxidized protein isolated again by gel filtration and concentrated by ultrafiltration to  $400 \mu\text{L}$ . A second  $400 \mu\text{L}$  of sample from a separate experiment was pooled at this stage. Then the powder of aminooxyacetyl influenza peptide (5.7 mg) was added to the pool ( $800 \mu\text{L}$ ), followed by acetic acid to a final concentration of 4%. The reaction was left overnight, the final product was isolated by gel filtration, and the CTB–viral peptide complex was isolated in pentameric form. An aliquot of the final product was analyzed by analytical HPLC and characterized by ESI-MS, and all the rest of the eluted protein solutions were frozen in liquid nitrogen and stored at  $-20^\circ\text{C}$ .

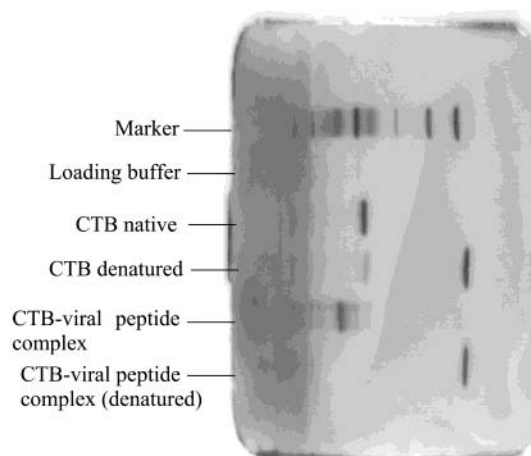
**5. Concentration Determination.** CTB–viral peptide complex was analyzed by UV spectrophotometry (Ultrospec III, Pharmacia Biotech) scanning the region 240–320 nm, and the concentration was calculated according to the formula  $\text{absorbance}_{280} = \sum I \times C$  [ $C$ , concentration of the product;  $\sum I$ , total of molar absorptivity ( $\epsilon$ ) of tryptophan and tyrosine in the CTB–viral peptide complex: absorptivity ( $\epsilon \times 10^{-3}$ ) of tryptophan

**Scheme 1. Schematic Chemical Reactions Involved in Constructing CTB–Immunogenic Peptide Complex<sup>a</sup>**


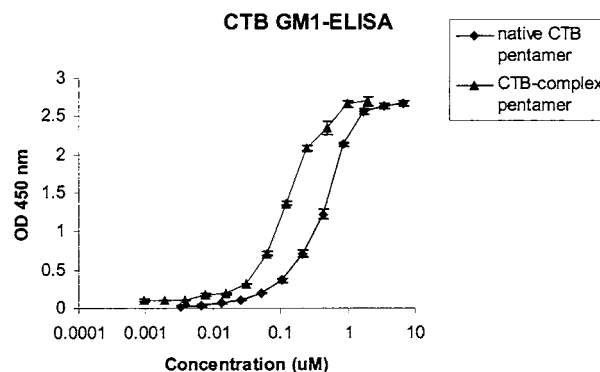
<sup>a</sup> (a, b) "One-pot" oxidation–oximation of CTB: oxidation of N-terminus (Thr) of CTB subunit, followed by direct oximation with linker,  $\text{H}_2\text{NOCH}_2\text{CO-ggg-[k(s)]}_5\text{-g-OH}$  without isolation of the aldehydic form. (c) Oxidation of CTB–linker complex to generate five aldehyde groups on the side chains of linker. (d) Oximation with aminooxyacetylated synthetic immunogenic peptide,  $\text{H}_2\text{NOCH}_2\text{CO-}$ .

at 279 nm is 5.6, and absorptivity ( $\epsilon \times 10^{-3}$ ) of tyrosine at 275 nm is 1.4.]

**6. SDS–PAGE.** A sample of CTB–viral peptide complex was heated in a boiling water bath prior to the electrophoresis. Three microliters of heated and unheated samples ( $1 \mu\text{g}/\mu\text{L}$ ) of CTB–viral peptide complex was then loaded and run on a Homogeneous-20 Phast gel using a PhastGel System (Amersham Pharmacia Biotech) for approximately 30 min using a standard method. Two samples of commercial CTB (one native, one heated) were used as positive controls for the pentamer and monomer of CTB, and SDS buffer served as negative control. A LMW calibration kit of protein standards was used as a marker. The gel was then developed with silver staining automatically on PhastGel system for 90 min.



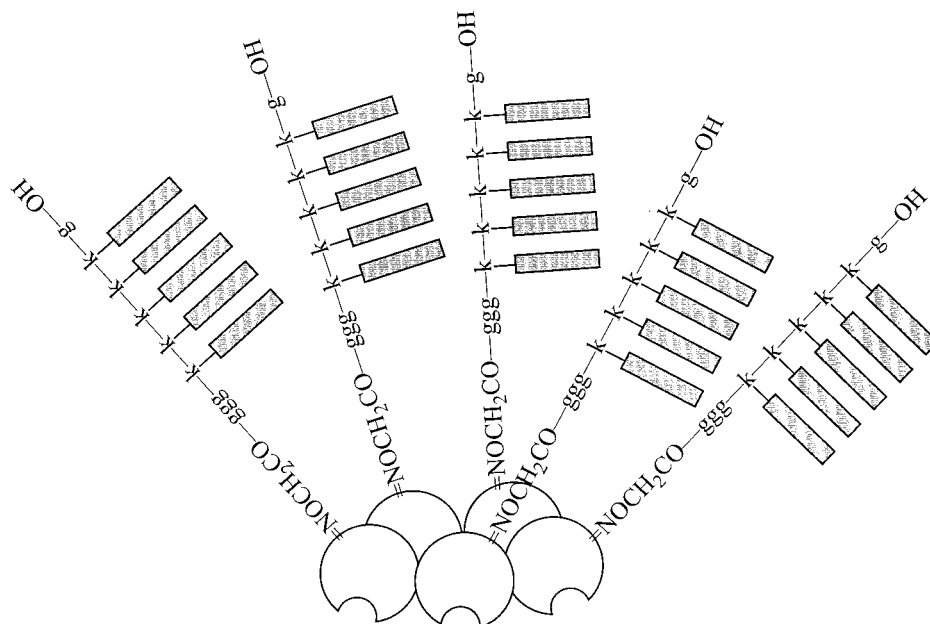
**Figure 1.** SDS–PAGE of commercial CTB and CTB–viral peptide complex. CTB–viral peptide complex ( $M_r$  64 690) is in noncovalent pentameric form like its control CTB native ( $M_r$  58 020), while CTB–viral peptide complex ( $M_r$  12 938) when denatured by heat runs close to monomeric CTB standard ( $M_r$  11 604) produced by denaturation of the native pentamer. Negative control (loading buffer) and molecular weight markers are shown in the figure.



**Figure 2.** GM<sub>1</sub>-ELISA of CTB ELISA plates were coated with  $1.5 \mu\text{M}$  Ganglioside GM<sub>1</sub> in PBS. Commercial CTB (native CTB pentamer) or CTB–viral peptide complex (CTB complex pentamer) were tested for their binding properties using a modified method from Svennerholm AM and Holmgren J (15). Result shows the avidity of CTB complex pentamer are 4–5-fold higher than commercial CTB pentamer.

**7. GM<sub>1</sub>-ELISA.** A polystyrene 96-well ELISA plate was coated by incubation at  $4^\circ\text{C}$  overnight with  $200 \mu\text{L}/\text{well}$  of  $1.5 \mu\text{M}$  Ganglioside GM<sub>1</sub> coating buffer (PBS). The plate was washed three times with PBS, and the additional binding sites were blocked by incubating plates with  $200 \mu\text{L}/\text{well}$  of a 2% (vol/vol) skim milk–PBS solution for 30–60 min at  $37^\circ\text{C}$  followed by washing three times with PBS. Test samples ( $100 \mu\text{L}$ ) were pipetted into wells immediately and the plates incubated at  $37^\circ\text{C}$  for 1 h. The plate was washed again with PBS buffer, and  $100 \mu\text{L}$  of 1:2000 goat anti-CTB was added to each well followed by incubation for 1 h at  $37^\circ\text{C}$ . After being washed with PBS buffer, each well received  $100 \mu\text{L}$  of a 1:24000 dilution of anti-Goat IgG (peroxidase), and the plate was incubated for 1 h at  $37^\circ\text{C}$ . The plate was washed,  $100 \mu\text{L}$  of the chromogenic reagent (POD substrate) was added, and the plate was incubated 3–5 min to obtain a blue coloration. The reaction was finally stopped by addition of  $100 \mu\text{L}$  of 1 N  $\text{H}_2\text{SO}_4$  (color change to yellow), and results were read at 450 nm using an ELISA reader.



**Scheme 2. Structure of CTB–Viral Peptide Complex in Pentameric Form<sup>a</sup>**

<sup>a</sup> Five copies of CTB–viral peptide complex were pentamerized uncovalently, and each subunit of CTB–viral peptide complex possesses a linear pentalysine linker and an antigenic peptide on the side chain of each lysine. Thus, the pentamer of CTB–viral peptide complex possesses  $5 \times 5$  copies of antigenic peptides.

## RESULTS AND DISCUSSION

### 1. “One Pot” Oxidation and Oximation of CTB.

Oxidation and oximation of CTB with the linker molecule  $\text{NH}_2\text{OCH}_2\text{CO-Gly}_3\text{-[Lys(Ser)]}_5\text{-Gly-OH}$  was performed under “one-pot” conditions as previously described (7). The expected oxime  $\text{CTB=NOCH}_2\text{CO-Gly}_3\text{-[Lys(Ser)]}_5\text{-Gly-OH}$  was purified by gel filtration, and one aliquot was analyzed by HPLC and characterized. Relative molecular mass found on ESI-MS was 12 938, close to the expected 12 937. Ser residues on the CTB–linker complex were oxidized, and the product was purified by gel filtration. The oxidized protein possessed five aldehyde groups which were then oximated with aminooxyacetyl influenza virus peptide  $\text{NH}_2\text{OCH}_2\text{CO-KTYQRTRALV}$  ( $\text{NH}_2\text{OCH}_2\text{CO-peptide}$ ) and isolated by gel filtration. One aliquot was analyzed by HPLC (five minutes at 30% B followed by a linear gradient to 50% B at 0.25% B per minute, retention time of the expected compound 50 min) and characterized by ESI-MS which showed this product (relative molecular mass found, 19 236; theoretical, 19 234) to be the expected branched hybrid  $\text{CTB=NOCH}_2\text{CO-Gly}_3\text{-[Lys(COCH=NOCH}_2\text{CO-peptide)]}_5\text{-Gly-OH}$ . Generally, there is an advantage to isolate an oxidized N-terminal threonyl or seryl polypeptide prior to oximation, to avoid the necessity to use an excess of aminoxy component over the aldehydes coproduced from the oxidation reaction (formaldehyde from Ser, acetaldehyde from Thr, and formaldehyde from oxidation of the quenching agent ethylene glycol). In our case, however, the N-terminal sequence of CTB is Thr-Pro (13). We demonstrated in our previous study that when N-terminal Thr-Pro is oxidized, the resulting aldehyde group  $\text{O=CHCO}$  can undergo a rapid cyclization and dehydration reaction through nucleophilic attack by the amide nitrogen of the third amino acid residue because of the rigidity of the proline ring which keeps the two reaction centers in proximity (7). “One pot” oxidation–oximation was adopted here so as to avoid possible formation of the cyclic isomer of the aldehyde.

The “one pot” oxidation–oximation also works with other different synthetic immunogenic peptides when

conjugated to the N-terminus of CTB. As we described previously (7), a different aminooxyacetyl peptide  $\text{CH}_3\text{CO-DC(CH}_2\text{CONH}_2\text{)TLIDALLGDPHK(COCH}_2\text{ONH}_2\text{)-NH}_2$  was conjugated in the same way to the CTB as above.

Scheme 1 shows all chemical reactions involved in constructing a CTB–immunogenic peptide complex and thus provides a generic method for preparing an immunogen in which any synthetic immunogenic peptide can be conjugated to the N-terminus of CTB to construct a CTB–immunogenic peptide complex.

### 2. CTB–Viral Peptide Complex in Pentameric Form.

CTB normally exists as a noncovalent pentamer which is necessary for CTB to specifically recognize the  $\text{GM}_1$  ganglioside receptor present on the surface of mucous cells, but treatment with acid and organic solvents leads to quantitative dissociation to the monomeric form. A stepwise denaturation–renaturation process has been reported which allows CTB to regain its active form (14). However, using this method in our previous study, most of the CTB complex could not be obtained in pentameric form. The protocol was thus modified to obtain  $\text{CTB=NOCH}_2\text{CO-Gly}_3\text{-[Lys(COCH=NOCH}_2\text{CO-peptide)]}_5\text{-Gly-OH}$  from gel filtration in pentameric form. An aliquot of the eluate was taken for HPLC analysis and characterization, and the rest was kept for concentration determination by UV spectrophotometry and then used directly for the immunization assay. A volume of 1.5 mL of such pentameric solution was obtained in this way, with an absorbance after pooling of  $\text{OD}_{280}$  0.068. Thus the concentration of CTB–viral peptide complex was determined as  $0.81 \mu\text{M}$  by use of the formula  $\text{OD}_{280} = \sum I \times C$  ( $\sum I = 84 \times 10^3 \text{ L/mol cm}$ , total of molar absorptivity ( $\epsilon$ ) of tryptophan and tyrosine in the CTB–viral peptide complex;  $C$ , concentration of the product).

The pentameric form of CTB–viral peptide complex was further confirmed by SDS–PAGE. This was done using the standard method on PhastGel System (Amersham Pharmacia Biotech). Two samples of CTB–viral peptide complex pentamer (one was heated in boiling

water for denaturation) obtained from gel filtration were detected on the electrophoresis gel, alongside two samples of commercial CTB (one was denatured) as positive control. The result (Figure 1) showed that the denatured CTB-viral peptide complex ( $M_r$  12 938) and its control, denatured commercial CTB ( $M_r$  11 604), were close to the molecular marker 14 400, while the CTB-viral peptide complex ( $M_r$  64 690) and native commercial CTB ( $M_r$  58 020) were close to molecular marker 67 000. This indicated that the CTB-viral peptide complex like native commercial CTB was its noncovalent pentameric form and when denatured it can be dissociated into its monomeric form. Moreover, there were several parallel bands for CTB-viral peptide complex on the electrophoresis gel, which might be due to CTB-viral peptide complex lacking a copy of aminooxyacetyl peptide on one or more subunits. An ESI mass spectrum of the complex consisting of a single CTB with five viral peptides showed no evidence of loss of such a peptide (results not shown), and we note that the loss could have occurred during gel electrophoresis. Our previous work (7) showed that the purified pentaoxime is not contaminated with species lacking a copy of aminooxyacetyl peptide.

**3. CTB-Viral Peptide Complex Shows Enhanced Binding to GM<sub>1</sub>.** To determine the ability of the CTB-viral peptide complex to bind to the cholera toxin receptor, GM<sub>1</sub> ganglioside was bound to the surface of plastic microtiter plates and reacted with the CTB-viral peptide complex. ELISA assay was performed using a modified method from Svennerholm AM and Holmgren J (15). Results were read at 450 nm using an ELISA reader, and a standard ELISA curve was obtained by testing the binding property of native CTB pentamer (Figure 2). The same GM<sub>1</sub>-ELISA experiment was also done on CTB-viral peptide complex, from which a ELISA curve was obtained (Figure 2). The curve of CTB-viral peptide complex was shifted to the left of the standard one, and its value at 1.5 (OD 450 nm) showed that the affinity of CTB-viral peptide complex was 4–5-fold higher than that of commercial CTB, which may result from favorable conformational change or stabilization of the CTB-viral peptide complex. This indicates that binding properties of the CTB-viral peptide complex are at least as strong as those of the native CTB, despite the conjugation of antigenic peptides to its N-terminus. Since CTB-viral peptide complex pentamer possesses 5 × 5 antigenic peptides (see Scheme 2) it represents a useful candidate immunogen. This approach is general and opens the way to create vaccine candidates using other immunogenic peptides.

## CONCLUSION

A polyoxime, employing influenza virus-derived peptides as building blocks, was successfully conjugated to the N-terminus of CTB, a potential carrier of mucosal vaccines, via a "one-pot" oxidation-oximation process. The construct was reconstituted into pentameric form when eluted from a Superdex column after conjugation, and this CTB-viral peptide complex was confirmed by SDS-PAGE. GM<sub>1</sub>-ELISA assay showed that the binding properties of CTB conjugate were improved 4–5-fold over native CTB. Although we have not studied the immunogenicity of the CTB conjugate, this general approach

opens an interesting approach to create vaccine candidates using other immunogenic peptides.

## ACKNOWLEDGMENT

We thank the Swiss National Foundation for financial support, and thank Irène Rossitto-Borlat and Pierre-Olivier Regamey for expert technical assistance.

## LITERATURE CITED

- (1) Sun, J. B., Holmgren, J., and Czerkinsky, C. (1994) Cholera toxin B subunit: an efficient transmucosal carrier-delivery system for induction of peripheral immunological tolerance. *Proc. Natl. Acad. Sci. U. S. A.* 91, 10795–10799.
- (2) Holmgren, J., Lycke, N., and Czerkinsky, C. (1993) Cholera toxin and cholera B subunit as oral-mucosal adjuvant and antigen vector systems. *Vaccine* 11, 1179–1184.
- (3) Rask, C., Fredriksson, M., Lindblad, M., Czerkinsky, C., and Holmgren, J. (2000) Mucosal and systemic antibody responses after peroral or intranasal immunization: effects of conjugation to enterotoxin B subunits and/or of co-administration with free toxin as adjuvant. *APMIS* 108, 178–186.
- (4) McKenzie, S. J., and Halsey, J. F. (1984) Cholera toxin B subunit as a carrier protein to stimulate a mucosal immune response. *J. Immunol.* 133, 1818–1824.
- (5) Yuki, Y., Byun, Y., Fujita, M., Izutani, W., Suzuki, T., Uda, S., Fujihashi, K., McGhee, J. R., and Kiyono, H. (2001) Production of a recombinant hybrid molecule of cholera toxin-B-subunit and proteolipid-protein-peptide for the treatment of experimental encephalomyelitis. *Biotechnol. Bioeng.* 74, 62–69.
- (6) Holmgren, J., Czerkinsky, C., Lycke, N., and Svennerholm, A. M. (1994) Strategies for the induction of immune responses at mucosal surfaces making use of cholera toxin B subunit as immunogen, carrier, and adjuvant. *Am. J. Trop. Med. Hyg.* 50 (5 Suppl), 42–54.
- (7) Rose, K., Chen, J., Dragovic, M., Zeng, W., Jeannerat, D., Kamalaprija, P., and Burger, U. (1999) A new cyclization reaction at the amino terminus of peptides and proteins. *Bioconjugate Chem.* 10, 1038–1043.
- (8) Janeway, C. A., Jr. (1999) Manipulation of the immune response: Synthetic peptides of protective antigens can elicit protective immunity. *Immuno Biology*, 4th ed. (P. Austin, and E. Lawrence, Eds.) pp 568–569, Elsevier Science Ltd.: London, U.K.
- (9) Tam, J. P. (1988) Synthetic peptide vaccine design: synthesis and properties of a high-density multiple antigenic peptide system. *Proc. Natl. Acad. Sci. U.S.A.* 85, 5409–5413.
- (10) Rose, K. (1994) Facile synthesis of artificial proteins. *J. Am. Chem. Soc.* 116, 30–33.
- (11) Bodmer, H. C., Pemberton, R. M., Rothbard, J. B., and Askonas, B. A. (1988) Enhanced recognition of a modified peptide antigen by cytotoxic T cells specific for influenza nucleoprotein. *Cell* 52, 253–258.
- (12) Sherman, L. A., Burke, T. A., and Biggs, J. A. (1992) Extracellular processing of peptide antigens that bind class I major histocompatibility molecules. *J. Exp. Med.* 175, 1221–1226.
- (13) Takao, T., Watanabe, H., and Shimonishi, Y. (1985) Facile identification of protein sequences by mass spectrometry: B subunit of *Vibrio cholerae* classical biotype Inaba 569B toxin. *Eur. J. Biochem.* 146, 503–508.
- (14) Hatic, S. O. 2nd, McCann, J. A., and Picking, W. D. (2001) In vitro assembly of novel cholera toxin-like complexes. *Anal. Biochem.* 292, 171–177.
- (15) Back, E., Svennerholm, A. M., Holmgren, J., and Mollby, R. (1979) Evaluation of a ganglioside immunosorbent assay for detection of *Escherichia coli* heat-labile enterotoxin. *J. Clin. Microbiol.* 10, 791–795.

BC025651U

# Site-Specific Quantitative Evaluation of the Protein Glycation Product *N*<sup>6</sup>-(2,3-Dihydroxy-5,6-dioxohexyl)-L-lysinate by LC–(ESI)MS Peptide Mapping: Evidence for Its Key Role in AGE Formation

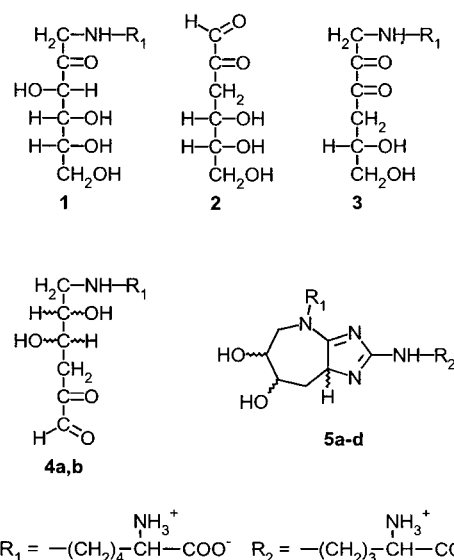
Klaus M. Biemel\* and Markus O. Lederer

Institut für Lebensmittelchemie (170), Universität Hohenheim, Garbenstrasse 28, D-70593 Stuttgart, Germany.  
Received December 13, 2002

Advanced glycation end products (AGEs) contribute to various pathologies associated with the general aging process and long-term complications of diabetes. Involvement of  $\alpha$ -dicarbonyl intermediates in the formation of such compounds is firmly established. We now report on the first unequivocal identification of the dideoxyosone *N*<sup>6</sup>-(2,3-dihydroxy-5,6-dioxohexyl)-L-lysinate (**4**) on lysozyme via its quinoxaline derivative *N*<sup>6</sup>-(2,3-dihydroxy-4-quinoxalin-2-ylbutyl)-L-lysinate (**6**), formed by reaction of **4** with *o*-phenylenediamine (OPD). For accurate quantification of the total content of **6** as well as of glucosepane **5** by LC–(ESI)MS, <sup>13</sup>C<sub>6</sub>-labeled reference compounds were independently synthesized; **5** so far is the only established follow-up product of **4**. With an overall lysine derivatization quota of 5%, compound **4** is shown to be a quantitatively important Maillard intermediate of which only about 8‰ are transformed into the cross-link **5**. Hence, the major follow-up products of the highly reactive intermediate **4** are yet unknown. The site-specific quantitative evaluation of aminoketose **1** and quinoxaline **6** by LC–(ESI)MS peptide mapping shows that all lysine moieties in lysozyme are in fact modified by these compounds. If an arginine side chain is adjacent to the lysine moiety, transformation of **1** into **4** seems to be favored. The efficient formation and high reactivity of **4** clearly points to its potential as exogenous or endogenous glycotoxin.

## INTRODUCTION

The spontaneous reaction of reducing carbohydrates with amino functions, preferentially the  $\epsilon$ -amino group of lysine moieties in peptides and proteins, is generally subsumed under the terms Maillard reaction or non-enzymatic browning (1, 2). The reaction is initiated by the formation of Schiff bases which, as a rule, rearrange to the more stable aminoketoses (Amadori products); in the course of this process the protein becomes 'glycated'. The first steps of the glycation reaction are reversible. After about 20–40 days, a steady state is reached for the Amadori product **1** (Figure 1), i.e., its concentration remains constant and is only dependent on the glucose concentration (3). During prolonged reaction, the aminoketoses are degraded to a plethora of compounds, designated 'advanced glycation end products' (AGEs).<sup>1</sup>  $\alpha$ -Dicarbonyl compounds such as 3-deoxyglucosone (3-DG, **2**; Figure 1), methylglyoxal (MG), and glyoxal (GO) are established key-intermediates in these complex reac-



**Figure 1.** Structural formulas of the Amadori compound **1**, the  $\alpha$ -dicarbonyl intermediates **2–4**, and the major protein cross-link glucosepane **5**. The dideoxyosone *N*<sup>6</sup>-(2,3-dihydroxy-5,6-dioxohexyl)-L-lysinate (**4a,b**) generally is incorporated into a protein and thus differs strikingly from 3-deoxyglucosone (**2**); compound **4** is the established precursor of glucosepane **5**. So far, formation of *N*<sup>6</sup>-(5,6-dihydroxy-2,3-dioxohexyl)lysinate (**3**) from glucose could not be proven.

tion cascades which proceed both in vitro and in vivo. Such compounds may be regarded as so-called 'glycotoxins', capable of modifying proteins and lipoproteins by AGE formation. The pathogenicity of endogenous, glucose-derived AGEs in human tissues has been subject of intense investigation and is now well established (4–7).

\* To whom correspondence should be addressed. Phone: +49 711 459 4095. Fax: +49 711 459 4096. E-mail: bipa@uni-hohenheim.de.

<sup>1</sup> Abbreviations used: AG, aminoguanidine; AGE, advanced glycation end product; *t*-Boc, *tert*-butoxycarbonyl; 3-DG, 3-deoxyglucosone; DTT, dithiothreitol; glucosepane **5**, 6-[2-[[[(4*S*)-4-ammonio-5-oxido-5-oxopentyl]amino]-6,7-dihydroxy-6,7,8,8a-tetrahydroimidazo[4,5-*b*]azepin-4(5*H*)-yl]-L-norleucinate; GO, glyoxal; HFBA, heptafluorobutyric acid; HPLC, high performance liquid chromatography; ISTD, internal standard; LC–(ESI)MS, coupled liquid chromatography – electrospray ionization mass spectrometry; MG, methylglyoxal; MWCO, molecular weight cutoff; OPD, *o*-phenylenediamine; SIM, selected ion monitoring; TFA, trifluoroacetic acid; TIC, total ion current; TLCK, *N*<sup>α</sup>-tosyl-L-lysine chloromethyl ketone; TPCK, *N*-*p*-tosyl-L-phenylalanine chloromethyl ketone.



As reported in the recent literature, the pluripotent effects of AGEs range from multiple gene activation to proatherosclerotic and glomerulosclerotic effects involving cytokine and growth factor modulation, lipid peroxidation, and albuminuria (6–10). Of particular significance is the finding that the process of degradation of tissue-bound AGEs exposes a new pool of previously internal, highly reactive AGE intermediates to circulation. Some of these serum AGE precursors have been found capable to react with proteins (e.g., LDL, collagen), propagating oxidative modifications or forming new AGE cross-links (11, 12). The formation of covalently cross-linked proteins is a major consequence of the advanced Maillard reaction. Especially in long-lived tissue proteins, the cross-links are supposed to be the most significant AGEs, as they are likely responsible, for example, for the decreased flexibility of collagen (13) and the high level of urea-insoluble proteins in human cataracts (14). Koschinsky et al. found that AGE precursors may not only be derived from endogenous processes but also from dietary uptake (15). This study confirmed the absorption of 10% of ingested AGEs and showed that only one-third of those resorbed are excreted within 48 h in the urine of patients with normal renal function. Exogenous glycotoxins, not cleared by the kidney, are supposed to remain biologically active and thus modify tissue proteins. Especially in case of nephropathy, exogenous as well as endogenous AGE precursors are of pathophysiological significance.

Since most of the structurally identified AGEs (e.g., CML (16), GOLD (17), CEL (18), MOLD (19), imidazolone A (20), pyralline (21)) are derived from  $\alpha$ -dicarbonyl intermediates, it seems reasonable to expect that glycotoxins liberated from glycosylated proteins incorporate a similar highly reactive building block. The only protein-linked dicarbonyl structure which so far has been considered in terms of AGE formation is  $N^6$ -(5,6-dihydroxy-2,3-dioxohexyl)lysinate (3, Amadori dione) (6, 22) even though it has not yet been identified in proteins, either in vitro or in vivo. Recently, we could show that the major protein cross-link glucosepane 5 is derived from the regioisomeric structure  $N^6$ -(2,3-Dihydroxy-5,6-dioxohexyl)-L-lysinate (4) (23, 24). In this dideoxyosone, being formed via the aminoketose 1, the lysine  $N^6$  is directly bonded to C-1 of the original sugar; generation of 4 requires carbonyl shifts along the entire carbohydrate backbone.

We now report on the site-specific quantitative evaluation of the aminoketose 1 and the lysine-linked dicarbonyl compound 4 in lysozyme by LC-(ESI)MS peptide mapping using several enzymes for proteolytic digestion. For quantification of the total content and unequivocal identification of 4 by LC-(ESI)MS, a  $^{13}\text{C}$ -labeled standard for its quinoxaline derivative 6 was synthesized independently and the structure definitely established. The effect of the concentration of the trapping reagent *o*-phenylenediamine (OPD) on glucosepane 5 suppression and quinoxaline 6 formation was also investigated.

## EXPERIMENTAL PROCEDURES

**Materials.** Milli-Q water (purified to  $18\text{ M}\Omega\cdot\text{cm}^{-2}$ ; Millipore, Eschborn, Germany) was used in the preparation of all solutions, and HPLC grade methanol and acetonitrile were employed for LC-MS. Propionic acid, 2-propanol, *o*-phenylenediamine (OPD),  $N^{\alpha}$ -*t*-Boc-L-lysine,  $N^{\epsilon}$ -*t*-Boc-L-lysine,  $N^{\alpha}$ -*t*-Boc-L-arginine, dithiothreitol (DTT), and iodoacetamide were purchased from Fluka (Neu-Ulm, Germany), *n*-heptafluorobutyric acid (HFBA) from

**Table 1.**  $^{13}\text{C}$  NMR Data for the Labeled Positions of the Quinoxaline 6a,b- $^{13}\text{C}_6$  ( $\text{D}_2\text{O}$ ,  $25^\circ\text{C}$ )

	$\delta$ (ppm) <sup>a</sup>		$J$ (Hz) <sup>b</sup>	
	6a	6b	6a	6b
C-1	50.3	49.9	$^1J_{1,2}$	39.5
C-2	69.3	70.2	$^1J_{2,3}$	40.5
C-3	72.2	73.0	$^1J_{3,4}$	38.0
C-4	39.6	39.6	$^1J_{4,5}$	50.5
C-5	155.1	155.1	$^1J_{5,6}$	35.5
C-6	146.9	146.9	$^2J_{4,6}$	7.0

<sup>a</sup>  $\delta$  (ppm), chemical shift for the indicated carbon. The NMR data of the unlabeled compounds 6a,b are given in ref 24. The numbering C-1 to C-6 refers to the original carbohydrate backbone and does not follow IUPAC rules. <sup>b</sup>  $J$  (Hz), coupling constant between the indicated carbons.

Aldrich (Steinheim, Germany), phosphate-buffered saline (PBS),  $\alpha$ -chymotrypsin (TLCK treated), endoproteinase Glu-C (V 8 strain), trypsin (TPCK treated), peptidase, and aminopeptidase M from Sigma (Steinheim, Germany), D-glucose, trifluoroacetic acid (TFA), and Pronase E from Merck (Darmstadt, Germany), and D-glucose- $^{13}\text{C}_6$  from Dr. Glaser AG (Basel, Switzerland). For a phosphate buffer salt mixture giving solutions with pH 7.4,  $\text{KH}_2\text{PO}_4$  (2.68 g, 20 mmol) and  $\text{Na}_2\text{HPO}_4\cdot 2\text{H}_2\text{O}$  (14.30 g, 80 mmol) were mixed vigorously.  $N^2$ -(*tert*-Butoxycarbonyl)- $N^6$ -(1-deoxy- $\beta$ -D-fructopyranos-1-yl)-L-lysine (*t*-Boc-1) was generously supplied by Marcus A. Glomb (Technical University of Berlin, Germany). Glucosepane- $^{13}\text{C}_6$ , was prepared according to ref 23.

**Preparation of  $N^6$ -(2,3-Dihydroxy-4-quinoxalin-2-ylbutyl)-L-lysinate (6a,b)- $^{13}\text{C}_6$ .** Synthesis with D-glucose- $^{13}\text{C}_6$  and isolation of the quinoxaline 6a,b- $^{13}\text{C}_6$  follows the procedure given in ref 24; for NMR data see Table 1.

**Incubations of  $N^{\alpha}$ -*t*-Boc-L-lysine and Glucose with OPD.** D-Glucose (90 mg, 0.5 mmol), was reacted with  $N^{\alpha}$ -*t*-Boc-L-lysine (8.6 mg, 35  $\mu\text{mol}$ ), OPD (2.7 mg, 25  $\mu\text{mol}$ , 10.8 mg, 100  $\mu\text{mol}$ , or 27 mg, 250  $\mu\text{mol}$ ), and DTPA (2 mg, 5  $\mu\text{mol}$ ) at pH 7.4 in phosphate buffer (5 mL, 0.1 M). The mixtures were flushed with argon and kept for 5 days at  $60^\circ\text{C}$ . Aliquots (100  $\mu\text{L}$ ) were taken, hydrochloric acid (6 N, 150  $\mu\text{L}$ ) was added, and the solution was kept at ambient temperature for 15 min. The volume was filled up to 0.5 mL, the pH adjusted to 7 by slowly adding solid  $\text{NaHCO}_3$ , and the mixture subjected to LC-(ESI)MS analysis (column A, full scan mode).

**D-Glucose-Hen Egg Lysozyme Incubations.** Lysozyme (1 g, 70  $\mu\text{mol}$ ) and D-glucose (1.8 g, 10 mmol) were dissolved in phosphate buffer (100 mL, 0.1 M, pH 7.4) containing DTPA (78 mg, 0.2 mmol) and passed through a  $0.45\text{ }\mu\text{m}$  membrane filter. To four aliquots (15 mL each) was added OPD (0 mg, 0 mmol; 8.1 mg, 75  $\mu\text{mol}$ ; 32.4 mg, 300  $\mu\text{mol}$ ; and 81.0 mg, 750  $\mu\text{mol}$ , respectively). The samples were filtered (sterile filter,  $0.2\text{ }\mu\text{m}$ ) into tubes, sealed tightly, and kept for 8 weeks at  $37^\circ\text{C}$  with gentle shaking. Each lysozyme incubation (equivalent to 150 mg of protein) was transferred to an Amicon 8050 (Witten, Germany) stirred cell, diluted to 30 mL, ultrafiltered

(Millipore PM 10 filter disks, MWCO 10 kDa) with water (0.6 L) by applying a pressure of 4.5 bar, and lyophilized.

**Total Enzymatic Hydrolysis of Lysozyme.** Aliquots of proteins (1 mg) were enzymatically hydrolyzed according to the procedure of Glomb et al., protocol C (25). A stock solution (20  $\mu$ L) containing **6a,b**- $^{13}\text{C}_6$  (10.7 mg/L) and **5a-d**- $^{13}\text{C}_6$  (4.5 mg/L) was added at the outset of the digestion procedure. The hydrolysates were ultrafiltered by centrifugation (Millipore Ultrafree MC, MWCO 5 kDa) and the filtrates (0.4 mL) subjected to LC-(ESI)MS analysis (column A, SIM mode).

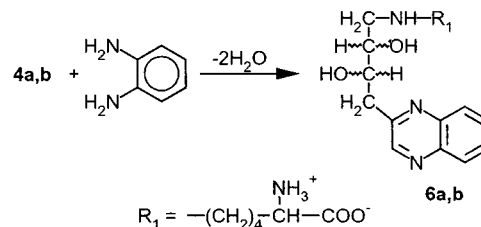
**Evaluation of the Relative Molar ESI<sup>+</sup> Responses of Lysine, 1, and 6.** To a solution (300  $\mu$ L) containing lysine, **1**, and **6** (14 mM each) was added hydrochloric acid (3 N, 2.7 mL) and the mixture kept at room temperature for 15 min. The pH was adjusted to 7 with solid  $\text{NaHCO}_3$ , and the solution was diluted 1:50 with water and immediately subjected to LC-(ESI)MS analysis (column A, SIM mode).

**Lysozyme Carbamidomethylation.** Native or incubated lysozyme (15 mg, 1.05  $\mu$ mol) was dissolved in Tris-HCl buffer (3 mL, 250 mM, pH 8.5) containing 8 M urea and 1 mM EDTA. A fresh solution of DTT (170  $\mu$ L, 100 mM) was added, the tubes were flushed with argon, and the reduction was allowed to proceed in the dark at 37 °C for 30 min. Iodoacetamide solution (75  $\mu$ L, 1 M) was added and the mixture kept at 37 °C for 30 min, followed by addition of precooled acetone (10 mL, -20 °C), vigorous shaking, and centrifugation (2500g, 0 °C). The resulting pellets were washed thrice with cold acetone/water (80:20 v/v), suspended in water (3 mL), and lyophilized.

**Trypsin, Chymotrypsin, and Endoproteinase Glu-C Peptide Mapping.** Three separate proteolytic digestions were performed for the carbamidomethyl derivatives of native lysozyme and lysozyme incubated in the presence of 100 mM D-glucose and 20 mM or 50 mM OPD. For the tryptic and chymotryptic digestion, the protein (2 mg) was dissolved in ammonium carbonate buffer (250  $\mu$ L, 100 mM, pH 8.5), aliquots (5  $\mu$ L) of TPCK-treated trypsin or TLCK-treated chymotrypsin (both 5 mg/mL, in 1 mM HCl containing 12 mM  $\text{CaCl}_2$ ) were added, and the mixture was kept at 37 °C for 2 h. For the endoproteinase Glu-C digestion, the protein (2 mg) was dissolved in 200  $\mu$ L phosphate buffer (50 mM, pH 8.7), endoproteinase Glu-C solution (16  $\mu$ L, 4 mg/mL) added, and the mixture kept at 37 °C for 18 h. The digestions were stopped by adjusting the pH to 5 with 10% formic acid. After incubation (30 min, 37 °C) with gentle shaking, the hydrolysates were adjusted to pH 3 and lyophilized. The residues were dissolved in the eluent for peptide mapping (80  $\mu$ L) and subjected to LC-(ESI)-MS analysis (column B, full scan mode).

**LC-(ESI)MS Analyses.** The LC-(ESI)MS analyses were run on an HP1100 (Hewlett-Packard, Waldbronn, Germany) HPLC system coupled to a Micromass (Manchester, UK) VG platform II quadrupole mass spectrometer equipped with an electrospray (ESI) interface. The HPLC system comprised an HP1100 autosampler, HP1100 gradient pump, HP1100 thermoregulator, and HP1100 diode array detector (DAD) module. Columns: (A) YMC - Pack Pro C18, 120 Å, 5  $\mu$ m, (guard column 10  $\times$  4.6 mm, column 150  $\times$  4.6 mm); column temperature 25 °C; flow rate 1.0 mL/min; (B) Waters (Eschborn, Germany) XTerra MS C18, 5  $\mu$ m (guard column 20  $\times$  3.0 mm, column 250  $\times$  3.0 mm); column temperature 25 °C; flow rate 0.5 mL/min. The following gradient % MeOH (*t* [min]) was applied for column A: 10 mM HFBA-MeOH, 5(0)-50(25)-95(30-35)-5(40-47). MS parameters: ESI<sup>+</sup>,

### Scheme 1. Transformation of Dideoxyosone **4** into the Quinoxaline **6a**<sup>a</sup>



<sup>a</sup> Intermediate **4** cannot directly be detected in complex incubation mixtures and thus is reacted with the efficient trapping reagent OPD to yield the stable derivative **6**.

source temperature 120 °C, capillary 3.5 kV, HV lens 0.5 kV; the system was operated either in full scan (*m/z* 150–1000, cone 40 V) or in SIM mode (span 0.5 Da; dwell time 0.2 s). The monitoring masses in the SIM mode were *m/z* 435.3, 429.3 (cone 65 V) and *m/z* 369.25, 363.25 (cone 45 V) for the quantification of **6**, or *m/z* 147.0, 309.1, and 363.2 (cone 40 V) for the evaluation of the relative molar response of lysine, **1**, and **6**. The separation of the lysozyme peptides from the digests was performed on column B with 0.1% aqueous TFA-MeCN/H<sub>2</sub>O/TFA (90:10:0.1, v/v/v) and the following gradient: % (MeCN/H<sub>2</sub>O/TFA (90:10:0.1, v/v/v)) (*t* [min]), 2(0)-44(35)-100(37-39)-2(42-48). The MS system was operated in the full scan mode (*m/z* 240–1500), cone voltage ramp 20–80 V. For the quantitative evaluation of modified peptides and acquisitions in the selected ion monitoring (SIM) mode, postcolumn addition of propionic acid/2-propanol (3:1, v/v) in a 1:3 ratio with the HPLC mobile phase was performed with a Knauer WellChrom Maxi-Star K-1000 HPLC pump. The eluent was finally split 1:20 before being introduced into the ion source.

**Nuclear Magnetic Resonance (NMR) Spectroscopy.** <sup>1</sup>H and <sup>13</sup>C spectra were recorded at 25 °C, in D<sub>2</sub>O, on a Varian (Darmstadt, Germany) Unity-plus 300 spectrometer (300 and 75 MHz nominal frequency, respectively).

**Lyophilization.** A Labconco Centrивap Concentrator (Kansas City, MO) was applied.

**Software.** In silico digestions were performed using the protein identification and analysis tools of the ExPASy Molecular Biology Server (<http://www.expasy.ch/>). LC-(ESI)MS data were processed with MassLynx 3.2 software. Positions of lysine residues and their local protein environment were determined by the Swiss-Pdb Viewer (<http://www.expasy.ch/spdbv/>).

## RESULTS

**Identification and Quantification of Lysozyme-Bound Quinoxaline **6** and Glucosepane **5** by LC-(ESI)MS.** Reactive  $\alpha$ -dicarbonyl intermediates such as **2** and **4** (Figure 1) usually cannot be detected in native form in complex reaction mixtures but only as stable derivatives. The most frequently employed trapping reagents are *o*-phenylenediamine (OPD) (26–28) and aminoguanidine (AG) (29); the relative reactivity of these two agents has recently been compared (30). As preliminary experiments have shown, the trapping capability of AG toward the dideoxyosone **4** is much lower than that of OPD which forms N<sup>6</sup>-(2,3-dihydroxy-4-quinoxalin-2-ylbutyl)-L-lysinate (**6**) (Scheme 1) in high yield. Compound **6** thus turned out to be the most suitable derivative for identification and quantification of **4**. The cross-link glucosepane **5**, which so far is the only known follow-up product of **4** (23, 24), was also monitored. The LC-

**Table 2. Peptides Obtained by Endoproteinase Glu C Digestion of Lysozyme Incubated with D-Glucose (100 mM) and OPD (50 mM)**

GluC peptide <sup>a</sup>	position	sequence <sup>a</sup>	calculated <i>m/z</i> <sup>b</sup>	observed <i>m/z</i> <sup>b</sup>	modification site
G1	1–7	KVFGRC	895.5	895.4	
G1*	1–7	K*VFGRCE	1111.5	1111.4	K1
G2	8–18	LAAAMKRHGLD	1182.6	1182.5	
G2+3	8–35	LAAAMKRHGLDNRYGYS LGNWVCAAKFE	3198.6	3198.4	
G2+3*	8–35	LAAAMKRHGLDNRYGYS LGNWVCAAK*FE	3414.6	3414.4	K13/ K33
G3	19–35	NYRGYS LGNWVCAAKFE	2035.0	2034.7	
G3*	19–35	NYRGYS LGNWVCAAK*FE	2251.0	2251.8	K33
G4	36–48	SNFNTQATNRNTD	1482.7	1482.4	
G4+5	36–52	SNFNTQATNRNTD GSTD	1842.8	1842.8	
G7	67–87	GRTPGSRNLCNIPCSALLSSD	2275.1	2275.0	
G8	88–101	ITASVNCAKKIVSD	1505.8	1505.6	
G10	120–129	VQAWIRGCR	1258.7	1258.5	

<sup>a</sup> Peptides modified with the quinoxaline **6** are marked with an asterisk. <sup>b</sup> Cysteine (C) moieties are carbamidomethylated. This derivatization has to be taken into account regarding *m/z* values of peptides containing C.

**Table 3. Peptides Obtained by Tryptic Digestion of Lysozyme Incubated with D-Glucose (100 mM) and OPD (50 mM)**

tryptic peptide <sup>a</sup>	position	sequence <sup>a</sup>	calculated <i>m/z</i> <sup>b</sup>	observed <i>m/z</i> <sup>b</sup>	modification site
T1+2	1–5	KVFGR	606.4	606.2	
T1+2*	1–5	K*VFGR	822.5	822.3	K1
T2	2–5	VFGR	478.3	478.3	
T3	6–13	CELAAAMK	893.4	893.3	
T3+4	6–14	CELAAAMKR	1049.5	1049.4	
T3+4*	6–14	CELAAAMK*R	1265.6	1265.4	K13
T5	15–21	HGLDNRY	874.4	874.3	
T6	22–33	GYS LGNWVCAAK	1325.6	1325.4	
T6+7*	22–45	GYS LGNWVCAAK*FESNFNTQATNR	2951.3	2951.1	K33
T7	34–45	FESNFNTQATNR	1428.6	1428.4	
T8	46–61	NTD GSTDY GILQINSR	1753.8	1753.8	
T9	62–68	WWCNDGR	993.4	993.3	
T10	69–73	TPGSR	517.3	517.3	
T11	74–96	NLCNIPCSALLSSDITASVNCAK	2508.2	2507.9	
T11+12*	74–97	NLCNIPCSALLSSDITASVNCAK*K	2852.4	2852.1	K96
T12+13	97–112	KLVS DGN GMNAWVAWR	1803.9	1803.8	
T12+13*	97–112	K*LVSDGN GMNAWVAWR	2020.0	2020.0	K97
T13	98–112	LVSDGN GMNAWVAWR	1675.8	1675.8	
T15+16	115–125	CKGTDVQAWIR	1333.7	1333.4	
T15+16*	115–125	CK*GTDVQAWIR	1549.8	1549.6	K116
T16	117–125	GTDVQAWIR	1045.5	1045.4	
T17+18	126–129	GCRI	505.2	505.2	

<sup>a</sup> Peptides modified with the quinoxaline **6** are marked with an asterisk. <sup>b</sup> Cysteine (C) moieties are carbamidomethylated. This derivatization has to be taken into account regarding *m/z* values of peptides containing C.

(ESI)MS system was calibrated with independently synthesized stable-isotope-labeled reference compounds in the range of 1.8–5480.0  $\mu\text{g}$  of **5**/L (ISTD 281.8  $\mu\text{g}$  of **5**-<sup>13</sup>C<sub>6</sub>/L) and 2.8–8888.0  $\mu\text{g}$  of **6**/L (ISTD 533.8  $\mu\text{g}$  of **6**-<sup>13</sup>C<sub>6</sub>/L), respectively. The linear calibration graphs are described by the equations  $\text{area} = (-53 \pm 294) + (1041 \pm 4)\text{L}/\mu\text{g} \times c(\mathbf{5})$  and  $\text{area} = (-1950 \pm 5319) + (755 \pm 29)\text{L}/\mu\text{g} \times c(\mathbf{6})$ , the values in brackets representing means  $\pm$  confidence intervals ( $P = 95\%$ ). Limits of detection 1.2 or 26.1  $\mu\text{g}/\text{L}$ , and limits of quantitation 1.8 or 39.0  $\mu\text{g}/\text{L}$  for **5** or **6**, were calculated according to the recommendations of the Deutsche Forschungsgemeinschaft (DFG) (34). With this ISTD method, glucosamine **5** and quinoxaline **6** were unequivocally identified and quantified in the lysozyme incubations by LC–(ESI)MS; analyses were performed directly from the total enzymatic digests. Since lysozyme has an N-terminal lysine (see Tables 2–4), the respective  $\alpha\text{-NH}_2$  group may also be involved in the formation of a dideoxyosone which would be a regioisomer of **4**. To test this hypothesis, N<sup>ε</sup>-(2,3-dihydroxy-4-quinoxalin-2-ylbutyl)-L-lysinate was independently synthesized from N<sup>ε</sup>-*t*-Boc-L-lysine and the chromatographic and spectroscopic data established (not shown). It could be clearly shown that the hydrolysates contained only minute amounts of the respective quinoxaline derivative. The N-terminal amino group thence is not an important glycation site. These findings agree

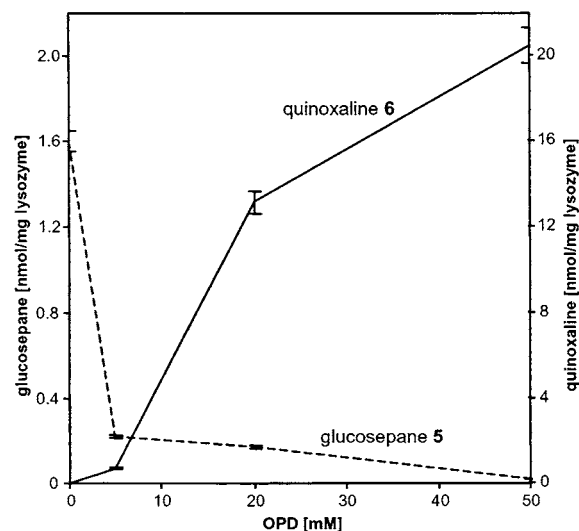
well with those reported by Tagami et al. who found the lysine N<sup>α</sup> in lysozyme not to be fructosylated (32). Figure 2 shows the quantitative results for 8-week incubations of lysozyme (37 °C, 0.7 mM) with 100 mM glucose in the presence of various OPD concentrations. Without OPD, the protein derivatization by glucosamine **5** reaches a level of 1.6 nmol/mg. As expected, the amount of **5** is reduced in the presence of OPD which traps the cross-link precursor **4**. Surprisingly, formation of **5** is already suppressed by 85% at 5 mM OPD while the concentration of quinoxaline **6** remains still rather low. The value for **6** increases dramatically at 20 mM OPD (18-fold compared to 5 mM OPD) and reaches a 'maximum' at 50 mM OPD; the concentration of 20.5 nmol/mg corresponds to an overall lysine derivatization quota of 4.9%. To test whether OPD has a catalytic effect on the formation of the dideoxyosone **4**, which might be expected due to the curve progression for **6**, N<sup>α</sup>-*t*-Boc-L-lysine and 100 mM glucose were incubated in the presence of 5, 20, or 50 mM OPD; the concentration of lysine residues was similar to that provided by the reaction with lysozyme. In this case, the amounts determined for **6** are almost identical for all OPD concentrations. Hence, formation of **4** was proven not to be significantly catalyzed by OPD which acts only as a trapping reagent. It can hardly be determined whether a true maximum is reached at 50 mM OPD (Figure 2) since the OPD concentration cannot



**Table 4. Peptides Obtained by Chymotryptic Digestion of Lysozyme Incubated with D-Glucose (100 mM) and OPD (50 mM)**

chymotryptic peptide <sup>a</sup>	position	sequence <sup>a</sup>	calculated $m/z$ <sup>b</sup>	observed $m/z$ <sup>b</sup>	modification site
C1	1–3	KVF	393.3	393.2	
C1*	1–3	K*VF	609.3	609.2	K1
C2	4–8	GRCEL	634.3	634.2	
C3	9–12	AAAM	363.2	363.2	
C4+5	13–20	KRHGLDNY	1002.5	1002.4	
C4+5*	13–20	K*RHGLDNY	1218.6	1218.4	K13
C6	21–23	RGY	395.2	395.2	
C7+8	24–28	SLGNW	576.3	576.2	
C9	29–34	VCAAKF	695.4	695.2	
C9*	29–34	VCAAK*F	911.4	911.4	K33
C10	35–38	ESNF	496.2	496.3	
C11	39–53	NTQATNRNTDGSTDY	1657.7	1657.5	
C12+13+14	54–63	GILQINSSRW	1272.7	1272.5	
C13+14	57–63	QINSSRW	989.5	989.5	
C15	64–75	CNDGRTGPSRL	1346.6	1346.4	
C16	76–83	CNIPCSAL	934.4	934.3	
C16+17	76–84	CNIPCSALL	1047.5	1047.4	
C18a	85–93	SSDITASVN	893.4	893.3	
C18b	94–105	CAKKIVSDGNGM	1279.6	1279.4	
C18b+19	94–108	CAKKIVSDGNGMNAW	1650.8	1650.7	
C18b+19*	94–108	CAK*KIVSDGNGMNAW	1866.8	1866.6	K96/K97
C18b+19**	94–108	CAK*K*IVSDGNGMNAW	2082.9	2082.7	K96+K97
C19	106–108	NAW	390.2	390.2	
C20	109–111	VAW	375.2	375.2	
C21	112–123	RNRCKGTDVQAW	1490.7	1490.5	
C21*	112–123	RNRCK*GTDVQAW	1706.8	1706.8	K116

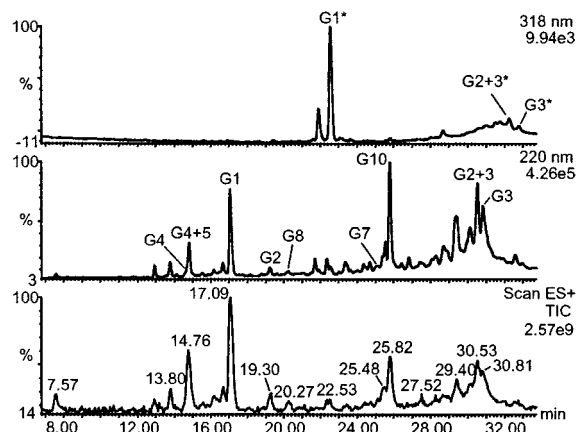
<sup>a</sup>Peptides modified with the quinoxaline **6** are marked with an asterisk. <sup>b</sup>Cysteine (C) moieties are carbamidomethylated. This derivatization has to be taken into account regarding  $m/z$  values of peptides containing C.



**Figure 2.** Effect of OPD concentration on glucosamine **5** suppression and quinoxaline **6** formation. Glucosamine **5** and quinoxaline **6** were quantified in incubations of lysozyme (10 g/L) with glucose (100 mM) and OPD (0, 5, 20, or 50 mM) after total enzymatic hydrolysis of the protein. Whereas formation of **5** is effectively suppressed (85%) at 5 mM OPD, the dideoxyosone **4** requires higher OPD concentrations for an efficient trapping in form of quinoxaline **6**.

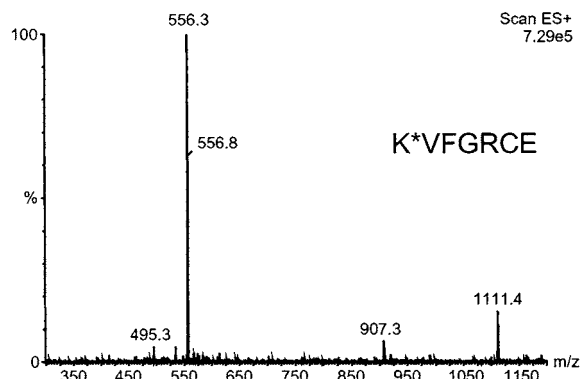
be raised much higher due to its limited solubility under the given conditions. Nevertheless, at 50 mM OPD, no glucosamine **5** is detected any more, indicating almost complete trapping of its precursor **4**. Hence, the following quantitative evaluations are based on reactions in the presence of 50 mM OPD.

**Localization and Quantitative Evaluation of Aminoketose **1** and Quinoxaline **6** by LC-(ESI)MS Peptide Mapping.** To obtain information about the site-specific modification of the lysine moieties, lysozyme incubated with 100 mM glucose and 50 mM OPD was reduced with dithiothreitol, carbamidomethylated, and

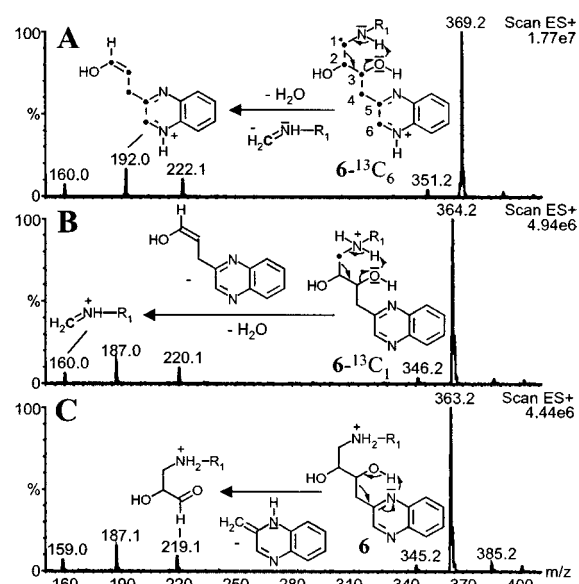


**Figure 3.** Endoproteinase Glu C peptide mapping. Lysozyme, incubated with glucose in the presence of 50 mM OPD for eight weeks, was digested with endoproteinase Glu C. TIC as well as UV traces at 220 and 318 nm of the LC-(ESI)MS analysis are displayed. In the 220 nm chromatogram, identified peptides are labeled with G and the corresponding numbers refer to the fragments and sequences listed in Table 2. Modified peptides bearing the quinoxaline **6** appear in the 318 nm trace and are marked with an asterisk.

partially digested by endoproteinase Glu C, trypsin, or chymotrypsin. Endoproteinase Glu C cleaves C-terminal E and D peptide bonds in phosphate-buffered medium. However, scission of D–X is less favored than that of E–X which thus yields the major fragments (33). In Table 2, the identified peptides are listed; the total ion current (TIC) and the UV traces at 220 and 318 nm from the respective LC-(ESI)MS run are displayed in Figure 3. Peptides modified with the quinoxaline **6** (marked with an asterisk) are easily detected in the 318 nm trace; this wavelength represents the longest-wavelength absorption band of the quinoxaline derivative **6**. The identity of both native and modified peptides was unequivocally established by comparing the  $m/z$  values of the quasimolecular ions  $[M + H]^+$  with those obtained by in silico digestion

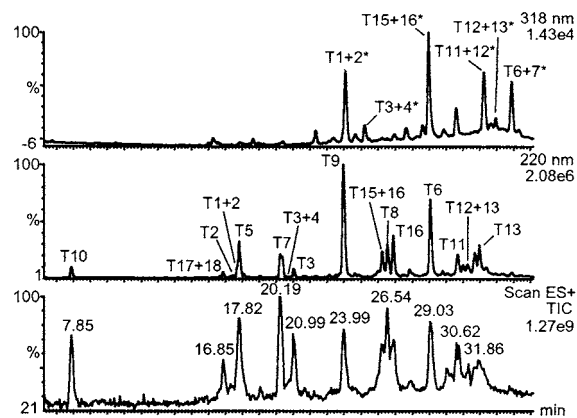


**Figure 4.** ESI<sup>+</sup> mass spectrum of G1\*. The spectrum shows the quasimolecular ions  $[M + H]^+$  at  $m/z$  1111.4 and  $[M + 2H]^{2+}$  at  $m/z$  556.3. The fragment ion at  $m/z$  907.3 results from the loss of H<sub>2</sub>O and 3-quinoxalin-2-ylprop-1-en-1-ol from  $[M + H]^+$  (cf. Figure 5B).



**Figure 5.** ESI<sup>+</sup> mass spectra of 6-<sup>13</sup>C<sub>6</sub>, 6-<sup>13</sup>C<sub>1</sub>, and 6. The ESI<sup>+</sup> fragmentation pattern of the quinoxaline **6** was investigated by analyzing the mass spectra of **6** (C) and its isotopomers 6-<sup>13</sup>C<sub>6</sub> (A) and 6-<sup>13</sup>C<sub>1</sub> (B); ● and C in the structural formulas mark <sup>13</sup>C atoms. From the relative fragment ion mass shifts of the isotopomers, it can clearly be deduced how many C atoms from the native carbohydrate backbone are eliminated in the course of the respective neutral loss. The fragmentation pathways thus could be established.

of lysozyme with the ExPASy Molecular Biology Server tools; this procedure was followed for all other investigations detailed below. In the 220 nm trace (cf. Figure 3), the only signals of sufficient intensity to allow for a detection of the respective species modified by **6** are those for G1, G2+3, G3, and G10. Only G1\* and, almost at the limit of detection, G2+3\* and G3\* could thus be identified (G10 contains no lysine residue). The ESI<sup>+</sup> mass spectrum of G1\* in Figure 4 shows  $[M + H]^+$  at  $m/z$  1111.4,  $[M + 2H]^{2+}$  at  $m/z$  556.3, and a daughter ion of  $m/z$  1111.4 at  $m/z$  907.3. This loss of 204 Da can be explained by fragmentation of the quinoxaline derivative and is characteristic for this modification. As detailed experiments on the ESI<sup>+</sup> fragmentation of native **6** and two <sup>13</sup>C-isotopomers have shown (Figure 5), the 204 Da loss results from elimination of H<sub>2</sub>O and 3-quinoxalin-2-ylprop-1-en-1-ol yielding a formiminium cation (Figure 5B). Analyses of various mass spectra of modified peptides have shown that the observability of this fragmen-



**Figure 6.** Trypsin peptide mapping. Lysozyme, incubated with glucose in the presence of 50 mM OPD for eight weeks, was digested with trypsin. TIC as well as UV traces at 220 and 318 nm of the LC-(ESI)MS analysis are displayed. In the 220 nm chromatogram, identified peptides are labeled with T, and the corresponding numbers refer to the fragments and sequences listed in Table 3. Modified peptides bearing the quinoxaline **6** appear in the 318 nm trace and are marked with an asterisk.

tation unfortunately seems to depend on the nature of the peptide to which the quinoxaline is linked, i.e., absence of the 204 Da loss does not necessarily provide negative evidence for this derivatization. Especially larger peptides primarily show conventional peptide fragmentation (a, b, y-series (34)) instead of the specific loss of 204 Da in collision-induced dissociation. Anyway, with endoproteinase Glu C digestion only modifications of the lysine residues K1, K13, and K33 can be detected (see Table 2 and Figure 3). Furthermore, the very low intensities of the signals for G2+3\* and G3\* prevent a reasonable quantitative evaluation of the respective glycation sites, and thus solely G1\* can be used for this purpose. Endoproteinase Glu C digestion thus is unsuitable for assessing all lysine glycation sites by LC-(ESI)-MS peptide mapping.

In the next step, trypsin was used for partial enzymatic hydrolysis of glycated lysozyme. This enzyme cleaves C-terminal K and R bonds, theoretically resulting in the formation of 18 peptide fragments. However, as can be taken from Table 3, the elimination of single amino acids could not be monitored because they show no retention under the given chromatographic conditions; e.g., T1, representing only K, was not detected. Contrary to the endoproteinase Glu C digestion, all lysine glycation sites (K1, K13, K33, K96, K97, and K116) can be clearly monitored. As already reported by Smales et al. (35) for fructosylated lysozyme (Amadori-lysozyme), trypsin does not cleave at the modified positions. This finding is confirmed by our results which show that lysine moieties bearing the quinoxaline derivative **6** are not recognized as cleavage sites by trypsin. Hence, K-modified lysozyme peptides are formed only from tryptic cleavage at R-X, as outlined in the 318 nm UV trace of Figure 6 and thus allow for a highly specific detection. In case of the adjacent lysine moieties K96 and K97, peptides were found which point to a derivatization at either K96 or K97. Detection of T11+12\* proves modification at K96 because the protein chain is cleaved at K97 which thus cannot be derivatized; the reverse is true for T12+13\*. A parallel modification of both positions would result in a T11-13\*\* fragment for which no signal above the limit of detection was observed. Formation of K96/K97\*\* thence cannot be a major glycation pathway. Although the intensities of the T\* peptides would allow for a site-





noaxaline **6** (Scheme 1), to be the only prominent lysine-linked  $\alpha$ -diketo compound formed from the reaction of glucose with lysozyme. The respective quinoxaline derivative of **3**, with the same molecular mass as **6**, was not detected. In general, the presence of further quantitatively important protein-bound quinoxalines should be visible in the 318 nm UV trace (cf. Figs. 4, 7, and 8). The identity of **6** was verified with independently synthesized stable-isotope-labeled reference material; formation of **4** on a protein thus was proven for the first time. As shown in Figure 2, presence of OPD in incubations of lysozyme with glucose results in a competition between arginine moieties of the protein and the trapping reagent OPD. Three out of six lysine residues in lysozyme (K33, K96, and K116) have an arginine side chain in a suitable distance for an intramolecular formation of the cross-link glucosepane **5** (R5, R21, and R112). Without OPD, about 8% of these arginine moieties are transformed into **5**. The average lysine derivatization quota by **4** at K33, K96, and K116 however is 6–7% (see Table 5); i.e., only 10–13% of **4** yield glucosepane **5**. These calculations rest on the reasonable assumption that at 50 mM OPD the dideoxyosone **4** is quantitatively trapped as quinoxaline **6**. The curve progression for the formation of **6** (Figure 2) and the fact that only a small amount of **4** is transformed into **5** both indicate **4** to be highly reactive and other reaction pathways to be operative. Investigations are currently in progress to identify further follow-up products of **4**. The high OPD concentration required for an efficient trapping of **4** may in part be traced back to a hampered diffusion of the reagent in the viscous protein solution. Rather, it seems that protein-linked **4** enters faster into consecutive reactions than the free compound. This conclusion is based on the observation that in comparable incubations of  $N^{\alpha}$ -*t*-Boc-L-lysine with glucose equal amounts of **6** are formed at different OPD levels. In this case, 5 mM OPD obviously suffice to efficiently trap the dideoxyosone **4** due to its 'extended lifetime'. The lifetime hypothesis is also supported by the fact that at 5 mM OPD the formation of glucosepane **5**, being characterized by a low reaction rate, is largely suppressed (cf. Figure 2). Even at low concentration, OPD effectively interferes with this slow reaction whereas trapping the bulk of **4**, which is susceptible to fast transformations, requires high OPD concentrations.

To get insight into the formation of the dideoxyosone **4** at specific lysine moieties with special attention to the local protein environment, we performed LC-(ESI)MS peptide mapping employing endoproteinase Glu C, trypsin, and chymotrypsin. As already addressed in the Results section, partial digestion with endoproteinase Glu C is unsuitable for assessing glycation of all six lysine moieties in lysozyme. For qualitative purposes, trypsin peptide mapping is the most suitable of the investigated procedures. To quantitatively evaluate the derivatization of specific lysine moieties, however, chymotryptic digestion is required. When addressing a specific modification problem, as in the case of K96/K97 in lysozyme (cf. Table 5), a combined analysis of the data from the tryptic and chymotryptic digest is obligatory. The term "quantitative evaluation" instead of "quantification" was chosen because the values determined rely on the presupposition that native peptides and peptides modified by the aminoketose **1** or the quinoxaline **6** have almost identical molar ESI<sup>+</sup> responses. The findings from LC-(ESI)MS experiments with lysine, **1**, and **6** strongly support this assumption. For a proper quantification, however, it would be necessary to synthesize peptides incorporating a stable-isotope-labeled derivative (e.g. **6**-<sup>13</sup>C<sub>6</sub>) of the

investigated glycation product to allow for stable-isotope dilution analysis. Due to the large number of lysine containing peptides monitored in the present study (see Tables 2–4), this time-consuming and expensive procedure appears not justified, especially in view of the fact that lysozyme serves only as a model to establish LC-(ESI)MS peptide mapping as a valuable tool for site-specific determination of glycation products, such as the dideoxyosone **4**. The stable-isotope dilution technique should be kept in mind, however, for the quantification of specific lysine modification sites in tissue or serum proteins which may point to their pathophysiological significance, e.g., the ability to form intra- or inter-molecular protein cross-links. Preferred glycation of certain lysine moieties has already been established in more complex proteins than lysozyme. Only nine of 55  $\epsilon$ -NH<sub>2</sub> groups in human serum albumin are measurably fructosylated, with K525 bearing 33% of the total fructosylation (42). Hence, accurate quantification by a stable-isotope dilution protocol can be limited to the analysis of a few peptides.

With an eight-week incubation period for the glycation of lysozyme by glucose, a steady-state concentration of the Amadori product **1** can be safely assumed (3). To compare the derivatization quota of accumulated **6** with that of its precursor **1**, quantitative evaluation of the aminoketose **1** was also performed. As the data in Table 5 show, lysine fructosylation is in the range of 9.5–14.5% for K13–K116, only K1 shows a considerably elevated value (23.5%). The ratio **1**:**6**, representing the effectivity of the respective transformation, ranges from 4.7 to 1.6. K33 and K116, as well as K96, show comparatively low ratios; the value for K96 is not explicitly given in Table 5, but is definitely below the average of 2.8 for K96/K97 as deduced from the results of the trypsin peptide mapping. Since the three lysine residues K33, K96, and K116 have an arginine side chain (R5, R21, and R112, respectively) at less than 5 Å distance, it seems likely that the guanidine group has a catalytic effect on the enolization reactions which transform **1** into **4**. This interesting correlation suggests that formation of glucosepane **5** is in part an autocatalytic process and underlines the role of **5** as quantitatively most important Maillard cross-link known to date (23). LC-(ESI)MS peptide mapping in principle should also be suitable for the site-specific determination of **5**. However, the low amounts formed (only about 8% of R5, R21, and R112 are transformed into **5**) hamper unequivocal identification of the corresponding cross-linked peptides due to sensitivity problems; investigations are currently in progress to overcome this analytical obstacle.

In conclusion, the present study has clearly established  $N^6$ -(2,3-dihydroxy-5,6-dioxohexyl)-L-lysinate (**4**) as a quantitatively important posttranslational protein modification, with the respective lysine derivatization quota ranging from 3 to 7.5%. Compound **4** is the first protein-linked  $\alpha$ -dicarbonyl moiety identified so far. The high yield and reactivity clearly point to the potential of **4** as exogenous or endogenous glycotxin and thus to its key role in AGE formation. Since only a small amount of **4** is involved in the formation of **5**, it must be concluded that the major follow-up products are yet unknown. Especially internal lysine residues of globular proteins modified by **4** may constitute significant glycotoxins, if they are exposed by gastrointestinal digestion from food proteins or by catabolic metabolism of tissue or plasma proteins. LC-(ESI)MS peptide mapping will be a very helpful tool to identify such glycation sites. Due to its carcinogenic properties, OPD cannot be used as trapping reagent for

in vivo investigations; the quinoxaline derivative **6** thus is ruled out as analytical in vivo-probe for **4**. Aminoguanidine, on the other hand, transforms **4** into a triazine, and is already used in diabetes therapy. Because of the low yield of this transformation, AG is a problematical agent for detecting or even quantifying **4**. We are currently testing new trapping reagents which exhibit both a good tolerance by the living organism and a high reaction rate for an efficient transformation of **4** into a stable derivative. Such compounds may at the same time represent novel antiglycation drugs.

#### ACKNOWLEDGMENT

This work was supported by grant LE 1152/2-2 of the Deutsche Forschungsgemeinschaft. We thank Priv.-Doz. Dr. P. Fischer, Institute of Organic Chemistry, University of Stuttgart, for many helpful discussions and Prof. Dr. W. Schwack, University of Hohenheim, for the excellent working conditions at the Institute of Food Chemistry. To S. Mika, Institute of Chemistry, University of Hohenheim, we are grateful for the recording of the NMR spectra.

#### LITERATURE CITED

- (1) Ledl, F., and Schleicher, E. (1990) New aspects of the Maillard reaction in foods and in the human body. *Angew. Chem., Int. Ed. Engl.* 29, 565–594.
- (2) Friedman, M. (1996) Food browning and its prevention – an overview. *J. Agric. Food Chem.* 44, 631–653.
- (3) Schleicher, E., and Wieland, O. H. (1986) Kinetic analysis of glycation as a tool for assessing the half-life of proteins. *Biochim. Biophys. Acta* 884, 199–205.
- (4) Vlassara, H., Bucala, R., and Striker, L. (1994) Pathogenic effects of advanced glycosylation – biochemical, biologic, and clinical implications for diabetes and aging. *Lab. Invest.* 70, 138–151.
- (5) Grandhee, S. K., and Monnier, V. M. (1991) Mechanism of formation of the Maillard protein cross-link pentosidine: glucose, fructose, and ascorbate as pentosidine precursors. *J. Biol. Chem.* 266, 11649–11653.
- (6) Ulrich, P., and Cerami, A. (2001) Protein glycation, diabetes, and aging. *Recent Prog. Horm. Res.* 56, 1–21.
- (7) Vlassara, H., and Palace, M. R. (2002) Diabetes and advanced glycation endproducts. *J. Intern. Med.* 251, 87–101.
- (8) Miyata, T., Oda, O., Inagi, R., Iida, Y., Araki, N., Yamada, N., Horiuchi, S., Taniguchi, N., Maeda, K., and Kinoshita, T. (1993)  $\beta$ 2-Microglobulin modified with advanced glycation end products is a major component of hemodialysis-associated amyloidosis. *J. Clin. Invest.* 92, 1243–1252.
- (9) Vlassara, H., Striker, L. J., Teichberg, S., Fuh, H., Li, Y. M., and Steffes, M. (1994) Advanced glycation end products induce glomerular sclerosis and albuminuria in normal rats. *Proc. Natl. Acad. Sci. U.S.A.* 91, 11704–11708.
- (10) Yang, C. W., Vlassara, H., Peten, E. P., He, C. J., Striker, G. E., and Striker, L. J. (1994) Advanced glycation end products up-regulate gene expression found in diabetic glomerular disease. *Proc. Natl. Acad. Sci. U.S.A.* 91, 9436–9440.
- (11) Makita, Z., Bucala, R., Rayfield, E. J., Friedman, E. A., Kaufman, A. M., Korbet, S. M., Barth, R. H., Winston, J. A., Fuh, H., Manogue, K. R., Cerami, A., and Vlassara, H. (1994) Reactive glycosylation endproducts in diabetic uraemia and treatment of renal failure. *Lancet* 343, 1519–1522.
- (12) Bucala, R., Makita, Z., Vega, G., Grundy, S., Koschinsky, T., Cerami, A., and Vlassara, H. (1994) Modification of low-density lipoprotein by advanced glycation end products contributes to the dyslipidemia of diabetes and renal insufficiency. *Proc. Natl. Acad. Sci. U.S.A.* 91, 9441–9445.
- (13) Reiser, K. M. (1998) Nonenzymatic glycation of collagen in aging and diabetes. *Proc. Soc. Exp. Biol. Med.* 218, 23–37.
- (14) Nagaraj, R. H., Sell, D. R., Prabhakaram, M., Ortwerth, B. J., and Monnier, V. M. (1991) High correlation between pentosidine protein cross-links and pigmentation implicates ascorbate oxidation in human lens senescence and cataractogenesis. *Proc. Natl. Acad. Sci. U.S.A.* 88, 10257–10261.
- (15) Koschinsky, T., He, C. J., Mitsuhashi, T., Bucala, R., Liu, C., Buening, C., Heitmann, K., and Vlassara, H. (1997) Orally absorbed reactive glycation products (glycotoxins) – an environmental risk factor in diabetic nephropathy. *Proc. Natl. Acad. Sci. U.S.A.* 94, 6474–6479.
- (16) Glomb, M. A., and Monnier, V. M. (1995) Mechanism of protein modification by glyoxal and glycolaldehyde, reactive intermediates of the maillard reaction. *J. Biol. Chem.* 270, 10017–10026.
- (17) Wells-Knecht, K. J., Brinkmann, E., and Baynes, J. W. (1995) Characterization of an imidazolium salt formed from glyoxal and *N*<sup>ε</sup>-hippuryllysine – a model for maillard reaction cross-links in proteins. *J. Org. Chem.* 60, 6246–6247.
- (18) Ahmed, M. U., Brinkmann-Frye, E., Degenhardt, T. P., Thorpe, S. R., and Baynes, J. W. (1997) *N*<sup>ε</sup>-(carboxyethyl)-lysine, a product of the chemical modification of proteins by methylglyoxal, increases with age in human lens proteins. *Biochem. J.* 324, 565–570.
- (19) Nagaraj, R. H., Shipanova, I. N., and Faust, F. M. (1996) Protein cross-linking by the maillard reaction – isolation, characterization, and in vivo detection of a lysine-lysine cross-link derived from methylglyoxal. *J. Biol. Chem.* 271, 19338–19345.
- (20) Niwa, T., Katsuzaki, T., Ishizaki, Y., Hayase, F., Miyazaki, T., Uematsu, T., Tatemichi, N., and Takei, Y. (1997) Imidazolone, a novel advanced glycation end product, is present at high levels in kidneys of rats with streptozotocin-induced diabetes. *FEBS Lett.* 407, 297–302.
- (21) Portero-Otin, M., Nagaraj, R. H., and Monnier, V. M. (1995) Chromatographic evidence for pyrraline formation during protein glycation in vitro and in vivo. *Biochim. Biophys. Acta* 1247, 74–80.
- (22) Vasan, S., Zhang, X., Kapurniotu, A., Bernhagen, J., Teichberg, S., Basgen, J., Wagle, D., Shih, D., Terlecky, I., Bucala, R., Cerami, A., Egan, J., and Ulrich, P. (1996) An agent cleaving glucose-derived protein cross-links in vitro and in vivo. *Nature* 382, 275–278.
- (23) Biemel, K. M., Friedl, D. A., and Lederer, M. O. (2002) Identification and quantification of major Maillard cross-links in human serum albumin and lens protein: evidence for glucosepane as the dominant compound. *J. Biol. Chem.* 277, 24907–24915.
- (24) Biemel, K. M., Conrad, J., and Lederer, M. O. (2002) Unexpected carbonyl mobility in aminoketoses: the key to major Maillard cross-links. *Angew. Chem., Int. Ed.* 41, 801–804.
- (25) Glomb, M. A., and Pfahler, C. (2001) Amides are novel protein modifications formed by physiological sugars. *J. Biol. Chem.* 276, 41638–41647.
- (26) Beck, J., Ledl, F., and Severin, T. (1988) Formation of 1-deoxy-D-erythro-2,3-hexodiulose from Amadori compounds. *Carbohydr. Res.* 177, 240–243.
- (27) Beck, J., Ledl, F., and Severin, T. (1989) Formation of glucosyl deoxyosones from Amadori compounds of maltose. *Z. Lebensm. Unters. Forsch.* 188, 118–121.
- (28) Huber, B., and Ledl, F. (1990) Formation of 1-amino-1,4-dideoxy-2,3-hexodiuloses and 2-aminoacetylfurans in the Maillard reaction. *Carbohydr. Res.* 204, 215–220.
- (29) Hirsch, J., Petrakova, E., and Feather, M. S. (1992) The reaction of some dicarbonyl sugars with aminoguanidine. *Carbohydr. Res.* 232, 125–130.
- (30) Glomb, M. A., and Tschirnich, R. (2001) Detection of  $\alpha$ -dicarbonyl compounds in Maillard reaction systems and in vivo. *J. Agric. Food Chem.* 49, 5543–5550.
- (31) Walter, H.-F., Holtz, K.-H., Frehse, H., Gorbach, S. G., and Thier, H.-P. (1991) Ableitung von Nachweis- und Bestimmungsgrenze nach dem Eichgeradenverfahren. *Rückstandsanalytik von Pflanzenschutzmitteln – Mitteilung VI der Senatskommission für Pflanzenschutz, Pflanzenbehandlungs-, und Vorratsschutzmittel – Methodensammlung der Arbeitsgruppe 'Analytik'* (Senatskommission der Deutschen Forschungsgemeinschaft, Ed.) Chapter XI-A, pp 1–22, VCH, Weinheim.

- (32) Tagami, U., Akashi, S., Mizukoshi, T., Suzuki, E., and Hirayama, K. (2000) Structural studies of the Maillard reaction products of a protein using ion trap mass spectrometry. *J. Mass Spectrom.* **35**, 131–138.
- (33) Humeny, A., Kislinger, T., Becker, C. M., and Pischetsrieder, M. (2002) Qualitative determination of specific protein glycation products by matrix-assisted laser desorption/ionization mass spectrometry peptide mapping. *J. Agric. Food Chem.* **50**, 2153–2160.
- (34) Roepstorff, P., and Fohlman, J. (1984) Proposal for a common nomenclature for sequence ions in mass spectra of peptides. *Biomed. Mass Spectrom.* **11**, 601.
- (35) Smales, C. M., Pepper, D. S., and James, D. C. (2000) Protein modification during antiviral heat bioprocessing. *Biotech. Bioeng.* **67**, 177–188.
- (36) Yeboah, F. K., and Yaylayan, V. A. (2001) Analysis of glycated proteins by mass spectrometric techniques: qualitative and quantitative aspects. *Nahrung-Food* **45**, 164–171.
- (37) Fountain, W. C., Requena, J. R., Jenkins, A. J., Lyons, T. J., Smyth, B., Baynes, J. W., and Thorpe, S. R. (1999) Quantification of *N*-(glucitol)ethanolamine and *N*-(carboxymethyl)serine: Two products of nonenzymatic modification of aminophospholipids formed in vivo. *Anal. Biochem.* **272**, 48–55.
- (38) Feather, M. S., Flynn, T. G., Munro, K. A., Kubiseski, T. J., and Walton, D. J. (1995) Catalysis of reduction of carbohydrate 2-oxoaldehydes (osones) by mammalian aldose reductase and aldehyde reductase. *Biochim. Biophys. Acta – Gen. Subj.* **1244**, 10–16.
- (39) Hayase, F., Liang, Z. Q., Suzuki, Y., Chuyen, N. V., Shinoda, T., and Kato, H. (1991) Enzymatic metabolism of 3-deoxyglucosone, a Maillard intermediate. *Amino Acids* **1**, 307–318.
- (40) Thornalley, P. J. (1994) Methylglyoxal, glyoxalases and the development of diabetic complications. *Amino Acids* **6**, 15–23.
- (41) Schoetter, C., Pischetsrieder, M., Lerche, H., and Severin, T. (1994) Formation of aminoreductones from maltose. *Tetrahedron Lett.* **35**, 7369–7370.
- (42) Iberg, N., and Flückiger, R. (1986) Nonenzymatic glycosylation of albumin in vivo. Identification of multiple glycosylated sites. *J. Biol. Chem.* **261**, 13542–13545.

BC025653E



# Synthesis and Biological Evaluation of Halogenated Naphthyridone Carboxamides as Potential Ligands for in Vivo Imaging Studies of Substance P Receptors

Caroline Bagot-Gu  ret,<sup>†</sup> Marie-Delphine Le Bas,<sup>‡</sup> Sylvie Tymciu,<sup>§</sup> Mircea Darabantu,<sup>‡</sup> Patrick Emond,<sup>||</sup> Denis Guilloteau,<sup>||</sup> Marie Claire Lasne,<sup>‡</sup> Anne Wijkhuisen,<sup>§</sup> Louisa Barr  ,\*<sup>†</sup> and C  cile Perrio\*<sup>‡</sup>

Groupe de D  veloppements M  thodologiques en Tomographie par   mission de Positons, UMR CEA, Universit   de Caen-Basse Normandie, Centre Cyceron, 15 Boulevard Henri Becquerel, 14070 Caen Cedex, France, Laboratoire de Chimie Mol  culaire et Thioorganique, CNRS UMR 6507, ENSICAEN, Universit   de Caen-Basse Normandie, 6 Boulevard Mar  chal Juin, 14050 Caen Cedex, France, CEA-Universit   Paris 7, DRM/SPI, CEA-Saclay, 91 191 Gif sur Yvette, France, and Laboratoire de Biophysique M  dicale et Pharmaceutique, INSERM U 316, Universit   Fran  ois Rabelais, 31 Avenue Monge, 37 200 Tours, France  
Received December 19, 2002; Revised Manuscript Received February 19, 2003

With the aim of developing new radioligands for in vivo studies of substance P receptors using positron emission tomography or single photon emission computed tomography, 2- and 3-halo naphthyridone-6-carboxamide derivatives were synthesized. Their affinities toward the target receptors were evaluated on CHO cells and compared to the unsubstituted analogue EP 00652218 ( $IC_{50} = 100 \text{ nM} \pm 20$ ). The  $IC_{50}$  value was not altered in the case of 2-chloro compound **1** ( $IC_{50} = 100 \text{ nM} \pm 15$ ) and only slightly reduced for the 2-fluoro and -iodo analogues **6** and **8** ( $IC_{50} = 500 \text{ nM} \pm 80$ ). A drastic reduction in binding ( $IC_{50} > 1000 \text{ nM}$ ) was observed for the halogenated compounds **2–5**, **7**, and **9**.

## INTRODUCTION

Substance P (SP) is an important neuropeptide of the mammalian tachykinin family besides neurokinin A (NKA) and neurokinin B (NKB) (*1*). These neurotransmitters share the common C-terminal amino acid sequence “-Phe-X-Gly-Leu-Met-NH<sub>2</sub>” and are involved in a wide variety of physiological activities both in the central (CNS) and peripheral (PNS) nervous system, such as contraction of muscles, vasodilatation, stimulation of salivary secretion, and activation of pain transmission and stress signals (*1, 2*). The biological responses induced by the tachykinins are mediated by three distinct receptors termed as NK1 (SP-preferring), NK2 (NKA-preferring), and NK3 (NKB-preferring). Characterization of these receptors, carried out by pharmacological studies and binding assays, has been finally supported by isolation and cloning of the three receptor proteins. The distribution of these latter has mainly been investigated by autoradiography or by in situ hybridization histochemistry and immunocytochemistry. NK1 receptors are widely distributed in various brain areas (*2–4*) and in PNS, while expression of NK2 and NK3 receptors is primarily confined in PNS and in CNS, respectively. Increasing interest in central NK receptors is based on reports describing their possible role in various pathological conditions. NK antagonists (*5, 6*) have been proposed for the treatment of migraine, inflammation, asth-

ma, emesis, cancer, and psychiatric disorders (depression, anxiety, schizophrenia). Their involvement in neurodegenerative diseases has also been suggested (*7–11*).

Positron emission tomography (PET) and single photon emission computed tomography (SPECT) are unique and complementary imaging techniques for in vivo assessment of drug distribution and interaction with biochemical target systems (*12–16*). They are well adapted for the exploration of brain function in healthy and disease conditions and crucial tools for clinical research and diagnosis. PET is a quantitative and very sensitive method, but it requires high cost facilities due to the use of tracers labeled with cyclotron-produced positron emitters (carbon-11,  $t_{1/2} = 20.4 \text{ min}$ ; fluorine-18,  $t_{1/2} = 109.7 \text{ min}$ ; bromine-76,  $t_{1/2} = 16 \text{ h}$ ). SPECT has coarser spatial and temporal resolution, reduced sensitivity and less quantification capability; however, it uses commercially available gamma emitter radionuclides of relatively long half-lives (iodine-123,  $t_{1/2} = 13.2 \text{ h}$ ; technetium-99m,  $t_{1/2} = 6 \text{ h}$ ) and thus is routinely employed in nuclear medicine centers. A few radioligands have been synthesized for PET or SPECT studies of NK1 receptors (Figure 1). The first ones had quinclidine {[<sup>11</sup>C]CP-96,345 (*17, 18*) and [<sup>125</sup>I]L 703606 (*19*)} or piperidine structures {[<sup>11</sup>C]CP-99,994 (*20*), [<sup>18</sup>F]FTP (*21*), [<sup>11</sup>C]GR 203040 (*22*), [<sup>11</sup>C]GR 205171 (*22*), [<sup>18</sup>F]L 829,165 (*23*), and [<sup>11</sup>C]CP-643,051 (*24*)}. More recently, a tryptophan derivative {[<sup>11</sup>C]LY 303870 (*25*)} and a substituted piperazine {[<sup>11</sup>C]R 116301 (*26*)} were also described. All radioligands, except [<sup>18</sup>F]L 829,165, for which biological studies in human are promising, suffer from low brain uptake, nonspecific binding, and extensive metabolism. The search for highly selective radioligands as well as the development of a unique tracer for PET and SPECT is still needed. This challenge requires the presence, in the same structure, of atoms (C, F, I, Br) that can be substituted for their positron (<sup>11</sup>C, <sup>18</sup>F, <sup>77</sup>Br) or gamma (<sup>123/125</sup>I) isotope.

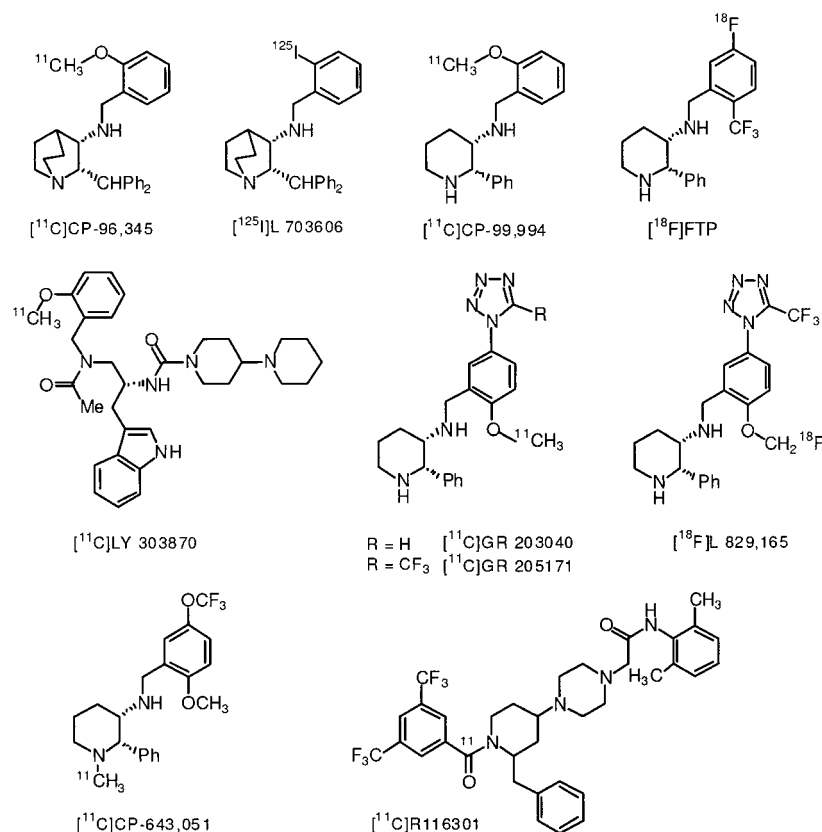
\* To whom correspondence should be addressed. E-mail: barre@cyceron.fr.

<sup>†</sup> Groupe de D  veloppements M  thodologiques en Tomographie par   mission de Positons, Universit   de Caen-Basse Normandie.

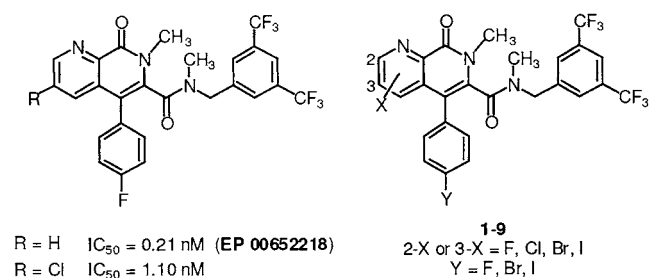
<sup>‡</sup> Laboratoire de Chimie Mol  culaire et Thioorganique, Universit   de Caen-Basse Normandie.

<sup>§</sup> CEA-Universit   Paris 7.

<sup>||</sup> Laboratoire de biophysique m  dicale et pharmaceutique INSERM U 316, Tours.



**Figure 1.** Radioligands for in vivo NK1 receptor imaging.



**Figure 2.** EP00652218 and target molecules.

In 1995, Takeda company described a series of 6-pyrido[3,4-*b*]pyridinecarboxamide derivatives as a novel class of highly potent, selective, and orally active NK1 receptor antagonists (Figure 2) (27–30). The lead compound, EP 00652218, was shown to exhibit subnanomolar affinity (IC<sub>50</sub>: 0.21 nM, in vitro inhibition of [<sup>125</sup>I]-(BH)-SP binding in human IM-9 cells) and selectivity toward the NK1 receptor (NK1/NK2 and NK1/NK3 > 1000). SAR studies demonstrated that the bis(trifluoromethylbenzyl) moiety was essential for the affinity and that structural modifications on the pyridine ring have a relatively small influence on this value. For instance, introduction of a chlorine atom on the pyridine ring in the 3-position maintained a nanomolar affinity and a good selectivity. This result, with the other reported data (28), suggested that halogenated derivatives of EP 00652218 could display a similar affinity toward the NK1 receptor. Herein we describe the synthesis and the in vitro evaluation of halogenated 6-pyrido[3,4-*b*]pyridinecarboxamide derivatives **1–9**.

#### EXPERIMENTAL SECTION

All reagents were purchased from ACROS, Aldrich, or Fluka and used without further purification. Solvents

were freshly distilled under nitrogen prior to use: 1,4-dioxane from sodium, *N,N*-dimethylformamide (DMF), and acetonitrile from calcium hydride, tetrahydrofuran (THF), from sodium benzophenone ketyl. Haloquinolinic acids **11–13** were prepared according to (31). [<sup>125</sup>I]-Bolton–Hunter (BH)-SP was purchased from Amersham France. CHO cells expressing the human NK1 receptor were a generous gift from Dr. L. Prodier, Rhône-Poulenc Rorer, Yvry, France. <sup>1</sup>H (200 MHz), <sup>13</sup>C (62.8 MHz), and <sup>19</sup>F (235.4 MHz) NMR spectra were recorded on a Bruker AC instrument. Chemical shifts (δ) are reported in parts per million downfield from internal tetramethylsilane (for <sup>1</sup>H and <sup>13</sup>C NMR) or from external freon (for <sup>19</sup>F NMR) and referenced from solvent resonances. NMR coupling constants are reported as absolute values in hertz. All the new structures were assigned by <sup>1</sup>H and <sup>13</sup>C NMR using heteronuclear correlation experiments. IR spectra were recorded on a Perkin-Elmer 684. Low resolution (EI or CI) mass spectra were recorded on a Nermag R 10 or a JEOL Gcmate instrument at 70 eV. Relative intensities are given in brackets. High resolution (HRMS, EI or FAB) mass spectra were obtained on a JEOL Gcmate instrument. Elemental analyses were performed using a ThermoQuest analyzer CHNS–O and were within ±0.4% of the calculated values. Melting points were determined using Koffler bank and are uncorrected.

Flash chromatography was performed using Merck silica gel Si 60 (0.040–0.063 mm) packing. Reverse phase chromatography was performed using C-18 silica gel Macherey-Nagel PolygoPrep 60–50. HPLC analysis was carried out by means of a Waters 501 pump, an UV detector set to 254 nm, and a Valco valve injector.

**General Procedure for the Synthesis of Quinolinic Anhydrides 14–16.** A solution of quinolinic acid (31) **11–13** (8–12 mmol) in thionyl chloride (10–20 mL)

was refluxed for 3 h. After concentration under vacuum, the residue was heated in chloroform for 0.5 h. The resulting suspension was filtered off, and the filtrate was concentrated to give the expected anhydride **14–16**.

**6-Chloroquinolinic Anhydride (14).** Anhydride **14** was obtained from **11** (2.54 g, 11.57 mmol): white solid, mp 127 °C; 93% (1.97 g).  $^1\text{H}$  NMR ( $\text{CDCl}_3$ )  $\delta$  7.97 (d,  $^3J_{\text{HH}} = 8.2$  Hz, 1H), 8.34 (d,  $^3J_{\text{HH}} = 8.2$  Hz, 1H).  $^{13}\text{C}$  NMR ( $\text{CDCl}_3$ )  $\delta$  125.5, 130.7, 135.5, 150.8, 159.2, 159.4, 161.2. IR (KBr) 1868, 1786.  $m/z$  (EI) 185 ( $\text{M}^+$ ,  $\text{C}_7\text{H}_2^{37}\text{ClNO}_3$ , 1), 183 ( $\text{M}^+$ ,  $\text{C}_7\text{H}_2^{35}\text{ClNO}_3$ , 4), 139 (100).

**5-Bromoquinolinic Anhydride (15).** Anhydride **15** was obtained from **12** (2.14 g, 8.7 mmol): white solid, mp 138–140 °C (lit. (32) 137–140 °C); 90% (1.8 g).  $^1\text{H}$  NMR ( $\text{CDCl}_3$ )  $\delta$  8.49 (d,  $^4J_{\text{HH}} = 2.0$  Hz, 1H), 9.22 (d,  $^4J_{\text{HH}} = 2.0$  Hz, 1H).  $^{13}\text{C}$  NMR ( $\text{CDCl}_3$ )  $\delta$  127.8, 128.1, 136.1, 148.2, 151.7, 159.1, 159.7. IR (KBr) 1870, 1774.

**5-Iodoquinolinic Anhydride (16).** Anhydride **16** was obtained from **13** (0.612 g, 2.1 mmol): white solid, mp 140 °C; 73% (0.422 g).  $^1\text{H}$  NMR ( $\text{CDCl}_3$ )  $\delta$  8.72 (d,  $^4J_{\text{HH}} = 2.0$  Hz, 1H), 9.44 (d,  $^4J_{\text{HH}} = 2.0$  Hz, 1H).  $^{13}\text{C}$  NMR ( $\text{CDCl}_3$ )  $\delta$  101.1, 128.4, 142.2, 149.1, 156.8, 160.5, 164.7. IR (KBr) 1750, 1718, 1684.  $m/z$  (EI) 275 ( $\text{M}^+$ , 19), 249 (100). HRMS (EI) ( $\text{M}^+$ ,  $\text{C}_7\text{H}_2\text{NO}_3\text{I}$ ) calcd 274.9083, found 274.9090. Anal. ( $\text{C}_7\text{H}_2\text{NO}_3\text{I}$ ) C, H, N.

**General Procedure for Friedel–Crafts Reactions.** Aluminum chloride (2.5 equiv) was added to anhydride **14–16** (1 equiv) in halobenzene or to a mixture of anhydride **14–16** (1 equiv) and halobenzene (1.5 equiv) in 1,2-dichloroethane. The solution was refluxed for 3 to 6 h or stirred at room temperature for 24 h. After cooling to room temperature, cold water (10 mL) and HCl 36% (10 mL) were added. The solution was stirred until precipitation (1 h to 3 d). The precipitate was filtered off, washed with water ( $2 \times 4$  mL), and dried under vacuum to give the expected acid **17–21**.

**3-(4-Bromobenzoyl)-6-chloropyridine-2-carboxylic Acid Hydrochloride (17).** Acid **17** was obtained from **14** (2.3 g, 12.53 mmol) and bromobenzene (2.0 mL, 18.7 mmol) after reaction in 1,2-dichloroethane (12 mL) for 4 h under reflux and recrystallization from methanol: beige solid, mp 178 °C; 65% (2.77 g).  $^1\text{H}$  NMR ( $\text{CDCl}_3$ )  $\delta$  7.54–7.61 (m, 4H), 7.72 (d,  $^3J_{\text{HH}} = 8.0$  Hz, 1H), 7.80 (d,  $^3J_{\text{HH}} = 8.0$  Hz, 1H).  $^{13}\text{C}$  NMR ( $\text{CDCl}_3$ )  $\delta$  127.4, 128.1, 130.9, 132.6, 134.9, 136.2, 138.2, 142.7, 150.0, 160.9, 190.8. IR (KBr) 3372, 1710, 1658.  $m/z$  (EI) 343 ( $\text{M}^+$ ,  $\text{C}_{13}\text{H}_7^{81}\text{Br}^{37}\text{ClNO}_3$ , 1), 341 ( $\text{M}^+$ ,  $\text{C}_{13}\text{H}_7^{79}\text{Br}^{37}\text{ClNO}_3$  and  $\text{C}_{13}\text{H}_7^{81}\text{Br}^{35}\text{ClNO}_3$ , 5), 339 ( $\text{M}^+$ ,  $\text{C}_{13}\text{H}_7^{79}\text{Br}^{35}\text{ClNO}_3$ , 4), 76 (100).

**6-Chloro-3-(4-fluorobenzoyl)pyridine-2-carboxylic Acid Hydrochloride (18).** Acid **18** was obtained from **14** (3.51 g, 19.1 mmol) and fluorobenzene (2.68 mL, 28.7 mmol) after reaction in 1,2-dichloroethane (50 mL) under reflux for 6 h: beige solid, mp 181 °C; 85% (5.12 g).  $^1\text{H}$  NMR ( $\text{DMSO}-d_6$ )  $\delta$  7.25 (t,  $^3J_{\text{HH}} = ^3J_{\text{HF}} = 8.7$  Hz, 2H), 7.69 (dd,  $^3J_{\text{HH}} = 8.7$  Hz,  $^4J_{\text{HF}} = 5.6$  Hz, 2H), 7.78 (d,  $^3J_{\text{HH}} = 8.2$  Hz, 1H), 7.97 (d,  $^3J_{\text{HH}} = 8.2$  Hz, 1H).  $^{13}\text{C}$  NMR ( $\text{CDCl}_3$ )  $\delta$  116.5 (d,  $^2J_{\text{CF}} = 22.2$  Hz), 129.1, 132.4 (d,  $^3J_{\text{CF}} = 9.6$  Hz), 132.9 (d,  $^4J_{\text{CF}} = 2.9$  Hz), 136.9, 140.0, 144.1, 151.6, 162.7, 166.6 (d,  $^1J_{\text{CF}} = 257.0$  Hz), 192.0.  $^{19}\text{F}$  NMR ( $\text{CDCl}_3$ )  $\delta$  –103.4.

**6-Chloro-3-(4-iodobenzoyl)pyridine-2-carboxylic Acid Hydrochloride (19).** Acid **19** was obtained in a mixture (0.34 g, 34%) with the deiodinated compound (**19**/deiodinated compound ratio of 75/25) from **14** (0.50 g, 2.94 mmol) and iodobenzene (0.46 mL, 4.08 mmol) after reaction in 1,2-dichloroethane (10 mL) for 24 h at room temperature and was used in the next step without further purification.  $^1\text{H}$  NMR ( $\text{CDCl}_3$ )  $\delta$  7.43 (d,  $^3J_{\text{HH}} =$

6.4 Hz, 2H), 7.61 (d,  $^3J_{\text{HH}} = 7.3$  Hz, 1H), 7.73–7.85 (m, 3H).  $^{13}\text{C}$  NMR ( $\text{CDCl}_3$ )  $\delta$  102.8, 129.2, 129.8, 130.9, 135.8, 138.6, 139.7, 144.2, 151.7, 162.4, 192.1.

**5-Bromo-3-(4-fluorobenzoyl)pyridine-2-carboxylic Acid Hydrochloride (20).** Acid **20** was obtained from **15** (1.80 g, 7.9 mmol) after reaction in fluorobenzene (20 mL) under reflux for 3 h: white solid, mp 190 °C; 100% (2.9 g).  $^1\text{H}$  NMR ( $\text{CDCl}_3$ )  $\delta$  7.06 (t,  $^3J_{\text{HH}} = ^3J_{\text{HF}} = 8.5$  Hz, 2H), 7.69 (dd,  $^3J_{\text{HH}} = 8.5$  Hz,  $^4J_{\text{HF}} = 5.4$  Hz, 2H), 7.89 (d,  $^4J_{\text{HH}} = 1.6$  Hz, 1H), 8.78 (d,  $^4J_{\text{HH}} = 1.6$  Hz, 1H).  $^{13}\text{C}$  NMR ( $\text{CDCl}_3$ )  $\delta$  115.1 (d,  $^2J_{\text{CF}} = 22.2$  Hz), 124.4, 131.1 (d,  $^3J_{\text{CF}} = 9.6$  Hz), 131.6, 137.7, 138.1, 141.5, 149.9, 162.1, 165.2 (d,  $^1J_{\text{CF}} = 257.0$  Hz), 189.8.  $^{19}\text{F}$  NMR ( $\text{CDCl}_3$ )  $\delta$  –103.6. IR (KBr) 1712, 1674.  $m/z$  (EI) 325 ( $\text{M}^+$ ,  $\text{C}_{13}\text{H}_7\text{NO}_3\text{F}^{81}\text{Br}$ , 12), 323 ( $\text{M}^+$ ,  $\text{C}_{13}\text{H}_7\text{NO}_3\text{F}^{79}\text{Br}$ , 13), 123 (100). HRMS (FAB $^+$ ) ( $\text{MH}^+$ ,  $\text{C}_{13}\text{H}_8\text{NO}_3\text{F}^{81}\text{Br}$ ) calcd 325.9670, found 325.9675, ( $\text{MH}^+$ ,  $\text{C}_{13}\text{H}_8\text{NO}_3\text{F}^{79}\text{Br}$ ) calcd 323.9671, found 325.9670. Anal. ( $\text{C}_{13}\text{H}_7\text{NO}_3\text{FBr}\cdot\text{HCl}$ ) C, H, N.

**3-(4-Fluorobenzoyl)-5-iodopyridine-2-carboxylic Acid Hydrochloride (21).** Acid **21** was obtained from **16** (1.0 g, 3.6 mmol) after reaction in fluorobenzene (15 mL) under reflux for 3 h: white solid, mp 176–177 °C; 55% (0.731 g).  $^1\text{H}$  NMR ( $\text{CDCl}_3$ )  $\delta$  7.14 (t,  $^3J_{\text{HH}} = ^3J_{\text{HF}} = 8.5$  Hz, 2H), 7.76 (dd,  $^3J_{\text{HH}} = 8.5$ ,  $^4J_{\text{HF}} = 5.3$  Hz, 2H), 8.18 (d,  $^4J_{\text{HH}} = 1.6$  Hz, 1H), 8.99 (d,  $^4J_{\text{HH}} = 1.6$  Hz, 1H).  $^{13}\text{C}$  NMR ( $\text{CDCl}_3$ )  $\delta$  98.7, 116.2 (d,  $^2J_{\text{CF}} = 22.6$  Hz), 132.1 (d,  $^3J_{\text{CF}} = 10.1$  Hz), 132.5 (d,  $^4J_{\text{CF}} = 3.1$  Hz), 138.7, 142.1, 144.9, 155.3, 162.9, 166.2 (d,  $^1J_{\text{CF}} = 268.6$  Hz), 190.7.  $^{19}\text{F}$  NMR ( $\text{CDCl}_3$ )  $\delta$  –103.3. IR (KBr) 1720, 1690, 1600, 1290.  $m/z$  (EI) 370 ( $\text{M}^+$ , 22), 50 (100). Anal. ( $\text{C}_{13}\text{H}_8\text{NO}_3\text{FI}\cdot\text{HCl}$ ) C, H, N.

**General Procedure for Amidation of Acids 17 and 20 with a *N*-Methylglycinate.** A mixture of acid **17** or **20** (1 equiv), oxalyl chloride (3–3.5 equiv), and DMF (0.1 equiv) in  $\text{CH}_2\text{Cl}_2$  (20 or 40 mL) was stirred at room temperature for 3 h and then concentrated under vacuum. The residue was diluted in  $\text{CH}_2\text{Cl}_2$  (25 or 50 mL), and sarcosine ester (1.8 equiv) and  $\text{Et}_3\text{N}$  (3 equiv) were added. The mixture was stirred at room temperature for 16 h and then concentrated under vacuum. After addition of ethyl acetate (30 mL) to the residue and filtration, the organic layer was washed with brine ( $2 \times 20$  mL), dried over  $\text{MgSO}_4$ , and concentrated under vacuum to give a crude oil which was purified by column chromatography.

***N*-Methyl-*N*[(methyloxycarbonyl)methyl]-3-(4-bromobenzoyl)-6-chloropyridine-2-carboxamide (22).** Amide **22** was obtained from **17** (1 g, 2.92 mmol) and sarcosine methyl ester hydrochloride (0.73 g, 5.25 mmol): white solid, mp 129 °C; 52% (0.65 g).  $R_f$  0.38 (AcOEt/pentane 30/70).  $^1\text{H}$  NMR ( $\text{CDCl}_3$ ) (2 rotamers in a 1/1 ratio)  $\delta$  3.04 and 3.13 (s, 3H), 3.66 and 3.77 (s, 3H), 4.10 and 4.17 (s, 2H), 7.38 and 7.40 (d,  $^3J_{\text{HH}} = 8.2$  Hz, 1H), 7.52–7.58 (m, 4H), 7.64 and 7.70 (d,  $^3J_{\text{HH}} = 8.2$  Hz, 1H).  $^{13}\text{C}$  NMR ( $\text{CDCl}_3$ ) (2 rotamers in a 1/1 ratio)  $\delta$  35.0 and 36.9, 48.2 and 51.3, 51.4 and 52.1, 123.3 and 123.7, 128.0 and 128.1, 130.2 and 130.3, 130.9 and 131.0, 132.5 and 133.9, 134.0 and 134.1, 137.8 and 138.1, 149.7 and 150.8, 152.0 and 153.2, 164.5 and 165.7, 167.6 and 168.4, 191.7 and 191.9. IR (KBr) 1746, 1670, 1654.  $m/z$  (EI) 428 ( $\text{M}^+$ ,  $\text{C}_{17}\text{H}_{14}^{81}\text{Br}^{37}\text{ClN}_2\text{O}_4$ , 4), 426 ( $\text{M}^+$ ,  $\text{C}_{17}\text{H}_{14}^{81}\text{Br}^{35}\text{ClN}_2\text{O}_4$  and  $\text{C}_{17}\text{H}_{14}^{79}\text{Br}^{37}\text{ClN}_2\text{O}_4$ , 13), 424 ( $\text{M}^+$ ,  $\text{C}_{17}\text{H}_{14}^{79}\text{Br}^{35}\text{ClN}_2\text{O}_4$ , 10), 102 (100).

***N*-Methyl-*N*[(ethyloxycarbonyl)methyl]-3-(4-bromobenzoyl)-6-chloropyridine-2-carboxamide (23).** Amide **23** was obtained from **17** (1 g, 2.92 mmol) and sarcosine ethyl ester hydrochloride (0.80 g, 5.25 mmol): yellow oil; 51% (0.65 g).  $R_f$  0.61 (AcOEt/pentane 30/70).  $^1\text{H}$  NMR ( $\text{CDCl}_3$ ) (2 rotamers in a 1/1 ratio)  $\delta$  1.17 and 1.23 (t,  $^3J_{\text{HH}} = 7.2$  Hz, 3H), 3.00 and 3.09 (s, 3H), 4.05



and 4.13 (s, 2H), 4.08 and 4.19 (q,  $^3J_{\text{HH}} = 7.2$  Hz, 2H), 7.36 and 7.37 (d,  $^3J_{\text{HH}} = 8.1$  Hz, 1H) 7.52–7.53 (m, 4H), 7.63 and 7.69 (d,  $^3J_{\text{HH}} = 8.1$  Hz, 1H).  $^{13}\text{C}$  NMR ( $\text{CDCl}_3$ ) (2 rotamers in a 1/1 ratio)  $\delta$  16.1 and 16.2, 38.0 and 39.9, 51.3 and 55.2, 63.3 and 63.5, 126.2 and 126.6, 131.0 and 131.1, 133.3 and 133.4, 134.0 and 134.1, 135.5 and 136.9, 137.0 and 137.1, 139.2 and 139.4, 151.2 and 152.2, 153.5 and 154.8, 165.9 and 167.1, 168.5 and 169.3, 193.1 and 193.3. IR (KBr) 1742, 1690, 1652.  $m/z$  (EI) 442 ( $\text{M}^+$ ,  $\text{C}_{18}\text{H}_{16}^{81}\text{Br}^{37}\text{ClN}_2\text{O}_4$ , 5), 440 ( $\text{M}^+$ ,  $\text{C}_{18}\text{H}_{16}^{81}\text{Br}^{35}\text{ClN}_2\text{O}_4$  and  $\text{C}_{18}\text{H}_{16}^{79}\text{Br}^{37}\text{ClN}_2\text{O}_4$ , 19), 438 ( $\text{M}^+$ ,  $\text{C}_{18}\text{H}_{16}^{79}\text{Br}^{35}\text{ClN}_2\text{O}_4$ , 12), 324 (100).

***N*-Methyl-*N*-[(*tert*-butyloxycarbonyl)methyl]-3-(4-bromobenzoyl)-6-chloropyridine-2-carboxamide (24).** Amide **24** was obtained from **17** (1 g, 2.92 mmol) and sarcosine *tert*-butyl ester hydrochloride (0.95 g, 5.25 mmol): beige solid, mp 104 °C; 54% (0.73 g).  $R_f$  0.80 (AcOEt/pentane 30/70).  $^1\text{H}$  NMR ( $\text{CDCl}_3$ ) (2 rotamers in a 1/1 ratio)  $\delta$  1.46 and 1.53 (s, 9H), 3.07 and 3.18 (s, 3H), 4.04 and 4.13 (s, 2H), 7.46 and 7.47 (d,  $^3J_{\text{HH}} = 8.1$  Hz, 1H), 7.58–7.66 (m, 4H), 7.73 and 7.79 (d,  $^3J_{\text{HH}} = 8.1$  Hz, 1H).  $^{13}\text{C}$  NMR ( $\text{CDCl}_3$ ) (2 rotamers in a 1/1 ratio)  $\delta$  26.0 and 26.1, 33.8 and 35.8, 48.0 and 51.7, 80.0 and 80.3, 122.2 and 122.6, 126.9 and 127.0, 129.3 and 129.9, 130.0 and 130.2, 131.5 and 132.8, 132.9 and 133.0, 136.8 and 137.0, 149.0 and 149.7, 151.5 and 152.3, 163.4 and 163.5, 165.1 and 165.7, 190.7 and 190.9. IR (KBr) 1718, 1684, 1646.  $m/z$  (EI) 470 ( $\text{M}^+$ ,  $\text{C}_{20}\text{H}_{20}^{81}\text{Br}^{37}\text{ClN}_2\text{O}_4$ , 1), 468 ( $\text{M}^+$ ,  $\text{C}_{20}\text{H}_{20}^{81}\text{Br}^{35}\text{ClN}_2\text{O}_4$  and  $\text{C}_{20}\text{H}_{20}^{79}\text{Br}^{37}\text{ClN}_2\text{O}_4$ , 3), 466 ( $\text{M}^+$ ,  $\text{C}_{20}\text{H}_{20}^{79}\text{Br}^{35}\text{ClN}_2\text{O}_4$ , 2), 44 (100). Anal. ( $\text{C}_{20}\text{H}_{20}\text{BrClN}_2\text{O}_4$ ) C, H, N.

***N*-Methyl-*N*-[(ethyloxycarbonyl)methyl]-5-bromo-3-(4-fluorobenzoyl)pyridine-2-carboxamide (25).** Amide **25** was obtained from **20** (4 g, 11.1 mmol) and sarcosine ethyl ester hydrochloride (3.0 g, 19.8 mmol): brown oil; 95% (4.46 g).  $R_f$  0.4 ( $\text{CH}_2\text{Cl}_2/\text{EtOH}/\text{H}_2\text{O}/\text{EtNH}_2$  95/4.7/0.1/0.2).  $^1\text{H}$  NMR ( $\text{CDCl}_3$ ) (2 rotamers)  $\delta$  1.27 (t,  $^3J_{\text{HH}} = 7.1$  Hz, 1.8H), 1.32 (t,  $^3J_{\text{HH}} = 7.1$  Hz, 1.2H), 3.09 (s, 1.2H), 3.19 (s, 1.8H), 4.16 (s, 1.2H), 4.26 (s, 0.8H), 4.19 (q,  $^3J_{\text{HH}} = 7.1$  Hz, 1.2H), 4.27 (q,  $^3J_{\text{HH}} = 7.1$  Hz, 0.8H), 7.15 (t,  $^3J_{\text{HH}} = ^3J_{\text{HF}} = 8.5$  Hz, 0.8H), 7.16 (t,  $^3J_{\text{HH}} = ^3J_{\text{HF}} = 8.5$  Hz, 1.2H), 7.82 (dd,  $^3J_{\text{HH}} = 8.8$  Hz,  $^4J_{\text{HF}} = 5.3$  Hz, 0.8H), 7.83 (dd,  $^3J_{\text{HH}} = 8.8$  Hz,  $^4J_{\text{HF}} = 5.3$  Hz, 1.2H), 7.87 (d,  $^4J_{\text{HH}} = 2.2$  Hz, 0.8H), 7.92 (d,  $^4J_{\text{HH}} = 2.2$  Hz, 1.2H), 8.66 (d,  $^4J_{\text{HH}} = 2.2$  Hz, 0.8H), 8.78 (d,  $^4J_{\text{HH}} = 2.2$  Hz, 1.2H).  $^{13}\text{C}$  NMR ( $\text{CDCl}_3$ ) (2 rotamers)  $\delta$  13.9 and 14.0, 35.6 and 37.7, 49.1 and 52.9, 61.0 and 61.1, 115.6 and 115.7 (d,  $^2J_{\text{CF}} = 22.6$  Hz), 120.4 and 120.9, 132.4 and 132.6 (d,  $^3J_{\text{CF}} = 7.5$  Hz), 136.4 and 137.8, 138.3 and 138.4, 149.6 and 150.6, 150.9 and 151.9, 165.8 and 165.9 (d,  $^1J_{\text{CF}} = 254.7$  Hz), 166.0 and 167.2, 167.9 and 168.7, 191.4 and 191.5.  $^{19}\text{F}$  NMR ( $\text{CDCl}_3$ )  $\delta$  -(103.7–104.0) (m).  $m/z$  (EI) 424 ( $\text{M}^+$ ,  $\text{C}_{18}\text{H}_{16}^{81}\text{BrFN}_2\text{O}_4$ , 8), 422 ( $\text{M}^+$ ,  $\text{C}_{18}\text{H}_{16}^{79}\text{BrFN}_2\text{O}_4$ , 9), 116 (100). HRMS (EI) ( $\text{M}^+$ ,  $\text{C}_{18}\text{H}_{16}^{81}\text{BrFN}_2\text{O}_4$ ) calcd 424.0253, found 424.0269 ( $\text{M}^+$ ,  $\text{C}_{18}\text{H}_{16}^{79}\text{BrFN}_2\text{O}_4$ ) calcd 422.0274, found 422.0267.

**General Procedure for the Cyclization-Dehydration of Pyridine Carboxamides 22–25.** A mixture of ester **22–25** (1 equiv) and DBU (2.3 equiv for esters **22–24** or 3.15 equiv for ester **25**) in toluene (90–100 mL) was refluxed for 4 h (for esters **22–24**) or for 20 h (for ester **25**). After cooling to room temperature, HCl 1 N (80 mL) was added until pH 1. The pH was then adjusted to 4–5 by addition of aqueous  $\text{Na}_2\text{CO}_3$  (10%). After extraction with ethyl acetate/THF 1/1 (2  $\times$  50 mL), the combined organic layers were washed with brine (2  $\times$  20 mL), dried over  $\text{MgSO}_4$ , and concentrated under vacuum to give a crude product which was purified by column chromatography.

**5-(4-Bromophenyl)-2-chloro-7-methyl-8-oxo-7,8-dihydro-[1,7]naphthyridine-6-carboxylic Methyl Ester (26).** Ester **26** was obtained from **22** (1.42 g, 3.43 mmol): white solid, mp 40–50 °C; 30% (0.40 g).  $R_f$  0.40 (AcOEt/pentane 50/50).  $^1\text{H}$  NMR ( $\text{CDCl}_3$ )  $\delta$  3.56 (s, 6H), 7.12 (d,  $^3J_{\text{HH}} = 8.4$  Hz, 2H), 7.42 (d,  $^3J_{\text{HH}} = 8.7$  Hz, 1H), 7.49 (d,  $^3J_{\text{HH}} = 8.7$  Hz, 1H), 7.56 (d,  $^3J_{\text{HH}} = 8.4$  Hz, 2H).  $^{13}\text{C}$  NMR ( $\text{CDCl}_3$ )  $\delta$  34.4, 53.4, 114.6, 123.7, 128.7, 131.7, 132.2, 132.5, 132.6, 135.9, 137.1, 141.5, 152.5, 159.5, 163.5. IR (KBr) 1736, 1672.  $m/z$  (EI) 410 ( $\text{M}^+$ ,  $\text{C}_{17}\text{H}_{12}^{81}\text{Br}^{37}\text{ClN}_2\text{O}_3$ , 22), 408 ( $\text{M}^+$ ,  $\text{C}_{17}\text{H}_{12}^{81}\text{Br}^{35}\text{ClN}_2\text{O}_3$  and  $\text{C}_{17}\text{H}_{12}^{79}\text{Br}^{37}\text{ClN}_2\text{O}_3$ , 100), 406 ( $\text{M}^+$ ,  $\text{C}_{17}\text{H}_{12}^{79}\text{Br}^{35}\text{ClN}_2\text{O}_3$ , 76). Anal. ( $\text{C}_{17}\text{H}_{12}\text{BrClN}_2\text{O}_3$ ) C, H, N.

**5-(4-Bromophenyl)-2-chloro-7-methyl-8-oxo-7,8-dihydro-[1,7]naphthyridine-6-carboxylic Ethyl Ester (27).** Ester **27** was obtained from **23** (1.47 g, 3.34 mmol): white solid, mp 30–40 °C; 49% (0.69 g).  $R_f$  0.46 (AcOEt/pentane 50/50).  $^1\text{H}$  NMR ( $\text{CDCl}_3$ )  $\delta$  1.03 (t,  $^3J_{\text{HH}} = 7.1$  Hz, 3H), 3.66 (s, 3H), 4.11 (q,  $^3J_{\text{HH}} = 7.1$  Hz, 2H), 7.19 (d,  $^3J_{\text{HH}} = 8.6$  Hz, 2H), 7.48 (d,  $^3J_{\text{HH}} = 8.4$  Hz, 1H), 7.54 (d,  $^3J_{\text{HH}} = 8.4$  Hz, 1H), 7.62 (d,  $^3J_{\text{HH}} = 8.6$  Hz, 2H).  $^{13}\text{C}$  NMR ( $\text{CDCl}_3$ )  $\delta$  12.5, 32.9, 61.7, 113.1, 122.2, 127.2, 128.4, 129.7, 130.4, 130.7, 134.7, 135.7, 140.0, 151.0, 158.2, 161.5. IR (KBr) 1730, 1670.  $m/z$  (EI) 424 ( $\text{M}^+$ ,  $\text{C}_{18}\text{H}_{14}^{81}\text{Br}^{37}\text{ClN}_2\text{O}_3$ , 26), 422 ( $\text{M}^+$ ,  $\text{C}_{18}\text{H}_{14}^{81}\text{Br}^{35}\text{ClN}_2\text{O}_3$  and  $\text{C}_{18}\text{H}_{14}^{79}\text{Br}^{37}\text{ClN}_2\text{O}_3$ , 100), 420 ( $\text{M}^+$ ,  $\text{C}_{18}\text{H}_{14}^{79}\text{Br}^{35}\text{ClN}_2\text{O}_3$ , 77).

**5-(4-Bromophenyl)-2-chloro-7-methyl-8-oxo-7,8-dihydro-[1,7]naphthyridine-6-carboxylic *tert*-Butyl Ester (28).** Ester **28** was obtained from **24** (1.56 g, 3.34 mmol): white solid, mp 160 °C; 45% (0.67 g).  $R_f$  0.53 (AcOEt/pentane 50/50).  $^1\text{H}$  NMR ( $\text{CDCl}_3$ )  $\delta$  1.27 (s, 9H), 3.67 (s, 3H), 7.22 (d,  $^3J_{\text{HH}} = 8.2$  Hz, 2H), 7.48 (d,  $^3J_{\text{HH}} = 8.6$  Hz, 1H), 7.53 (d,  $^3J_{\text{HH}} = 8.6$  Hz, 1H), 7.64 (d,  $^3J_{\text{HH}} = 8.2$  Hz, 2H).  $^{13}\text{C}$  NMR ( $\text{CDCl}_3$ )  $\delta$  28.5, 34.4, 85.8, 113.7, 123.9, 129.0, 132.4, 132.8, 132.9, 133.6, 137.3, 137.5, 141.6, 152.5, 160.0, 162.3; IR (KBr) 1728, 1672.  $m/z$  (EI) 452 ( $\text{M}^+$ ,  $\text{C}_{20}\text{H}_{18}^{81}\text{Br}^{37}\text{ClN}_2\text{O}_3$ , 0.1), 450 ( $\text{M}^+$ ,  $\text{C}_{20}\text{H}_{18}^{81}\text{Br}^{35}\text{ClN}_2\text{O}_3$  and  $\text{C}_{20}\text{H}_{18}^{79}\text{Br}^{37}\text{ClN}_2\text{O}_3$ , 0.4), 448 ( $\text{M}^+$ ,  $\text{C}_{20}\text{H}_{18}^{79}\text{Br}^{35}\text{ClN}_2\text{O}_3$ , 0.2), 56 (100).

**3-Bromo-5-(4-fluorophenyl)-7-methyl-8-oxo-7,8-dihydro-[1,7]naphthyridine-6-carboxylic Ethyl Ester (29).** Ester **29** was obtained from **25** (1.8 g, 4.25 mmol): white solid, mp 188 °C; 85% (1.45 g).  $R_f$  0.50 (AcOEt).  $^1\text{H}$  NMR ( $\text{CDCl}_3$ )  $\delta$  1.03 (t,  $^3J_{\text{HH}} = 7.1$  Hz, 3H), 3.67 (s, 3H), 4.11 (q,  $^3J_{\text{HH}} = 7.1$  Hz, 2H), 7.11 (dd,  $^3J_{\text{HH}} = 8.6$ ,  $^4J_{\text{HF}} = 5.4$  Hz, 2H), 7.21 (t,  $^3J_{\text{HH}} = ^3J_{\text{HF}} = 8.6$  Hz, 2H), 7.69 (d,  $^4J_{\text{HH}} = 2.0$  Hz, 1H), 8.93 (d,  $^4J_{\text{HH}} = 2.0$  Hz, 1H).  $^{13}\text{C}$  NMR ( $\text{CDCl}_3$ )  $\delta$  13.9, 34.2, 63.0, 114.0, 116.5 (d,  $^2J_{\text{CF}} = 21.6$  Hz), 125.1, 128.8 (d,  $^4J_{\text{CF}} = 3.6$  Hz), 133.0 (d,  $^3J_{\text{CF}} = 8.2$  Hz), 134.4, 135.9, 137.2, 140.0, 151.9, 160.4, 163.0, 163.4 (d,  $^1J_{\text{CF}} = 249.3$  Hz).  $^{19}\text{F}$  NMR ( $\text{CDCl}_3$ )  $\delta$  -(112.3–112.4) (m). IR (KBr) 1742, 1676, 1512, 1226.  $m/z$  (CI, isobutane) 407 ( $\text{MH}^+$ ,  $\text{C}_{18}\text{H}_{15}^{81}\text{BrFN}_2\text{O}_3$ , 92), 405 ( $\text{MH}^+$ ,  $\text{C}_{18}\text{H}_{15}^{79}\text{BrFN}_2\text{O}_3$ , 100). HRMS (CI, isobutane) ( $\text{MH}^+$ ,  $\text{C}_{18}\text{H}_{15}^{81}\text{BrFN}_2\text{O}_3$ ) calcd 407.0231, found 407.0229, ( $\text{MH}^+$ ,  $\text{C}_{18}\text{H}_{15}^{79}\text{BrFN}_2\text{O}_3$ ) calcd 405.0250, found 405.0212.

**Hydrolysis of Esters 26–29.** **5-(4-Bromophenyl)-6-carboxy-2-chloro-7-methyl-8-oxo-7,8-dihydro-[1,7]naphthyridinium Trifluoroacetate (34).** A mixture of ester **28** (1 g, 2.2 mmol) and trifluoroacetic acid (7 mL) in  $\text{CH}_2\text{Cl}_2$  (14 mL) was stirred at room temperature for 7 h. After concentration, acid **34** was obtained as a yellow solid, mp > 260 °C; 98% (1.1 g).  $^1\text{H}$  NMR ( $\text{DMSO}-d_6$ )  $\delta$  3.61 (s, 3H), 7.37 (d,  $^3J_{\text{HH}} = 8.3$  Hz, 2H), 7.65 (d,  $^3J_{\text{HH}} = 8.6$  Hz, 1H), 7.78 (d,  $^3J_{\text{HH}} = 8.3$  Hz, 2H), 7.80 (d,  $^3J_{\text{HH}} = 8.6$  Hz, 1H).  $^{13}\text{C}$  NMR ( $\text{DMSO}-d_6$ )  $\delta$  34.0, 111.9, 119.1 (q,  $^1J_{\text{CF}} = 295.5$  Hz), 122.5, 128.8, 132.0, 132.1, 132.7, 133.2, 137.9, 138.3, 140.3, 150.4, 158.6, 162.6 (q,  $^2J_{\text{CF}} = 32.3$

Hz), 170.6.  $^{19}\text{F}$  NMR (DMSO- $d_6$ )  $\delta$  -75.6 (s). IR (KBr) 1732, 1668, 1578.  $m/z$  (EI) 396 ( $\text{M}^+$ ,  $\text{C}_{16}\text{H}_{10}^{81}\text{Br}^{37}\text{ClN}_2\text{O}_3$ , 0.1), 394 ( $\text{M}^+$ ,  $\text{C}_{16}\text{H}_{10}^{81}\text{Br}^{35}\text{ClN}_2\text{O}_3$  and  $\text{C}_{16}\text{H}_{10}^{79}\text{Br}^{37}\text{ClN}_2\text{O}_3$ , 0.3), 392 ( $\text{M}^+$ ,  $\text{C}_{16}\text{H}_{10}^{79}\text{Br}^{35}\text{ClN}_2\text{O}_3$ , 0.2), 42 (100).

**3-Bromo-5-(4-fluorophenyl)-7-methyl-8-oxo-7,8-dihydro-[1,7]naphthyridine-6-carboxylic Acid (35).** Ester **29** (2.2 g, 5.4 mmol) in a mixture of EtOH/THF/aqueous NaOH 1 N 1/1/1 (84 mL) was refluxed for 5 h. The solvents were removed under vacuum, and the residue was dissolved in water. The aqueous layer was washed with ethyl acetate and acidified with HCl 36% to pH 1. After extraction with ethyl acetate (2  $\times$  20 mL), the organic layer was dried over  $\text{MgSO}_4$  and then concentrated under vacuum to give acid **35** as a yellow solid, mp 190–192  $^\circ\text{C}$ ; 72% (1.6 g).  $^1\text{H}$  NMR (DMSO- $d_6$ )  $\delta$  2.54 (s, 3H), 7.35 (t,  $^3J_{\text{HH}} = ^3J_{\text{HF}} = 8.6$  Hz, 2H), 7.40 (dd,  $^3J_{\text{HH}} = 8.6$  Hz,  $^4J_{\text{HF}} = 5.6$  Hz, 2H), 7.60 (d,  $^4J_{\text{HH}} = 2.1$  Hz, 1H), 8.93 (d,  $^4J_{\text{HH}} = 2.1$  Hz, 1H).  $^{13}\text{C}$  NMR (DMSO- $d_6$ )  $\delta$  34.4, 111.9, 116.6 (d,  $^2J_{\text{CF}} = 20.1$  Hz), 124.8, 128.7 (d,  $^4J_{\text{CF}} = 4.0$  Hz), 133.9 (d,  $^3J_{\text{CF}} = 8.0$  Hz), 134.9, 135.7, 139.1, 139.6, 151.3, 159.8, 163.0 (d,  $^1J_{\text{CF}} = 245.5$  Hz), 164.5.  $^{19}\text{F}$  NMR (DMSO- $d_6$ )  $\delta$  -113.5 (s). IR (KBr) 1734, 1662, 1636, 1574.  $m/z$  (EI) 334 ( $\text{C}_{16}\text{H}_{10}^{81}\text{BrFN}_2\text{O}_3 - \text{CO}_2$ , 49), 332 ( $\text{C}_{16}\text{H}_{10}^{79}\text{BrFN}_2\text{O}_3 - \text{CO}_2$ , 61), 42 (100). HRMS (EI) ( $\text{M}^+$ ,  $\text{C}_{16}\text{H}_{10}^{81}\text{BrFN}_2\text{O}_3$ ) calcd 377.9830, found 377.9841, ( $\text{M}^+$ ,  $\text{C}_{16}\text{H}_{10}^{79}\text{BrFN}_2\text{O}_3$ ) calcd 375.9859, found 375.9820.

**5-(4-Bromophenyl)-6-carboxy-2-ethoxy-7-methyl-8-oxo-7,8-dihydro-[1,7]naphthyridinium Chloride (36).** To ester **27** (0.5 g, 1.18 mmol) in a mixture of EtOH/THF 1/1 (100 mL) was added aqueous NaOH 5 N (5 mL). The mixture was heated under reflux for 2 h. After evaporation to dryness, HCl 5 N was added to the residue, and the final suspension was filtered off to give **36** as a yellow solid, mp 218  $^\circ\text{C}$ ; 64% (0.33 g).  $^1\text{H}$  NMR (DMSO- $d_6$ )  $\delta$  1.37 (t,  $^3J_{\text{HH}} = 7.0$  Hz, 3H), 3.54 (s, 3H), 4.47 (q,  $^3J_{\text{HH}} = 7.0$  Hz, 2H), 7.13 (d,  $^3J_{\text{HH}} = 8.9$  Hz, 1H), 7.29 (d,  $^3J_{\text{HH}} = 8.4$  Hz, 2H), 7.44 (d,  $^3J_{\text{HH}} = 8.9$  Hz, 1H), 7.70 (d,  $^3J_{\text{HH}} = 8.4$  Hz, 2H).  $^{13}\text{C}$  NMR (DMSO- $d_6$ )  $\delta$  14.7, 33.9, 62.3, 112.6, 117.5, 122.1, 127.8, 131.9, 133.2, 133.5, 137.1, 138.5, 159.1, 162.7, 164.4, 177.0. IR (KBr) 1724, 1636.  $m/z$  (EI) 404 ( $\text{M}^+$ ,  $\text{C}_{18}\text{H}_{15}^{81}\text{BrN}_2\text{O}_4$ , 89), 402 ( $\text{M}^+$ ,  $\text{C}_{18}\text{H}_{15}^{79}\text{BrN}_2\text{O}_4$ , 88), 126 (100).

**5-(4-Bromophenyl)-6-carboxy-2-hydroxy-7-methyl-8-oxo-7,8-dihydro-[1,7]naphthyridinium Chloride (37).** Acid **36** (0.13 g, 0.30 mmol) in HCl 6 N (6.5 mL) was refluxed for 2 h. After cooling to room temperature and filtration, acid **37** was isolated as a beige solid, mp > 265  $^\circ\text{C}$ ; 60% (0.073 g).  $^1\text{H}$  NMR (DMSO- $d_6$ )  $\delta$  3.56 (s, 3H), 6.69 (d,  $^3J_{\text{HH}} = 9.7$  Hz, 1H), 7.16 (d,  $^3J_{\text{HH}} = 9.7$  Hz, 1H), 7.27 (d,  $^3J_{\text{HH}} = 8.4$  Hz, 2H), 7.70 (d,  $^3J_{\text{HH}} = 8.4$  Hz, 2H).  $^{13}\text{C}$  NMR (DMSO- $d_6$ )  $\delta$  34.0, 113.7, 119.7, 122.3, 128.0, 130.0, 131.9, 133.0, 133.1, 136.9, 154.3, 161.2, 164.1, 177.2. IR (KBr) 3330, 1664, 1654.  $m/z$  (EI) 376 ( $\text{M}^+$ ,  $\text{C}_{16}\text{H}_{11}^{81}\text{BrN}_2\text{O}_4$ , 45), 374 ( $\text{M}^+$ ,  $\text{C}_{16}\text{H}_{11}^{79}\text{BrN}_2\text{O}_4$ , 45), 330 (100).

**5-(4-Bromophenyl)-2-hydroxy-7-methyl-8-oxo-7,8-dihydro-[1,7]naphthyridine-6-carboxylic Ethyl Ester (38).** Ester **27** (0.05 g, 0.11 mmol) and HCl (6 N, 1 mL) in 1,4-dioxane (1 mL) was refluxed for 24 h. After evaporation of solvent, water (3 mL) was added to the residue. The suspension was filtered off to give a mixture of compounds **37** and **38** in a 1/1 ratio.  $^1\text{H}$  NMR (DMSO- $d_6$ )  $\delta$  0.89 (t,  $^3J_{\text{HH}} = 7.0$  Hz, 3H), 3.53 (s, 3H), 4.04 (q,  $^3J_{\text{HH}} = 7.0$  Hz, 2H), 6.70 (d,  $^3J_{\text{HH}} = 9.7$  Hz, 1H), 7.18 (d,  $^3J_{\text{HH}} = 9.7$  Hz, 1H), 7.24 (d,  $^3J_{\text{HH}} = 8.0$  Hz, 2H), 7.68 (d,  $^3J_{\text{HH}} = 8.0$  Hz, 2H).

**Synthesis of *N*-Methylbenzylammonium Trifluoroacetate 41.** *N*-[3,5-Bis(trifluoromethyl)benzyl]car-

**bamic Acid *tert*-Butyl Ester (39).** To 3,5-bis(trifluoromethyl)benzylamine (10 g, 41.1 mmol) in  $\text{CH}_2\text{Cl}_2$  (125 mL) were added triethylamine (0.577 mL, 4.11 mmol) and di-*tert*-butyl dicarbonate (9.4 g, 43.2 mmol) at room temperature. The mixture was stirred for 4 h, and then aqueous saturated  $\text{NaHCO}_3$  (70 mL) was added. After extraction with  $\text{CH}_2\text{Cl}_2$  (2  $\times$  30 mL), the organic layers were combined, washed with HCl 1 N (50 mL) and then with water (2  $\times$  50 mL), dried over  $\text{MgSO}_4$ , and concentrated under vacuum to give a crude product which was recrystallized from pentane: white solid, mp 72–73  $^\circ\text{C}$ ; 95% (14 g).  $^1\text{H}$  NMR ( $\text{CDCl}_3$ )  $\delta$  1.46 (s, 9H), 4.42–4.44 (m, 2H), 5.30 (br s, 1H), 7.73 (s, 2H), 7.77 (s, 1H).  $^{13}\text{C}$  NMR ( $\text{CDCl}_3$ )  $\delta$  28.6, 44.1, 80.6, 121.2 (sept,  $^3J_{\text{CF}} = 3.8$  Hz), 123.2 (q,  $^1J_{\text{CF}} = 273.0$  Hz), 127.6–127.7 (m), 132.2 (q,  $^2J_{\text{CF}} = 33.1$  Hz), 142.3, 156.3.  $^{19}\text{F}$  NMR ( $\text{CDCl}_3$ )  $\delta$  -63.6 (s). IR (KBr) 1684, 1442, 1278.  $m/z$  (CI, isobutane) 344 ( $\text{MH}^+$ ,  $\text{C}_{14}\text{H}_{16}\text{F}_6\text{NO}_2$ , 100). HRMS (CI, isobutane) ( $\text{MH}^+$ ,  $\text{C}_{14}\text{H}_{16}\text{F}_6\text{NO}_2$ ) calcd 344.1091, found 344.1085. Anal. ( $\text{C}_{14}\text{H}_{16}\text{F}_6\text{NO}_2$ ) C, H, N.

***N*-[3,5-Bis(trifluoromethyl)benzyl]-*N*-methylcarbamate *tert*-Butyl Ester (40).** To a suspension of NaH (60% dispersion in mineral oil, 0.7 g, 17.5 mmol) in DMF (80 mL) was added carbamate **39** (3 g, 8.75 mmol). The mixture was stirred at room temperature for 1 h, and methyl iodide (1.1 mL, 17.5 mmol) was added. After stirring for 15 h, water (120 mL) and then ethyl acetate (180 mL) were added. The aqueous layer was extracted with ethyl acetate (3  $\times$  40 mL). The combined organic layers were washed successively with HCl 1 N (60 mL), aqueous saturated  $\text{NaHCO}_3$ , and water (60 mL), dried over  $\text{MgSO}_4$ , and concentrated under vacuum to give a crude product which was purified by column chromatography: yellow oil; 80% (2.45 g).  $R_f$  0.4 (AcOEt/pentane 1/9).  $^1\text{H}$  NMR ( $\text{CDCl}_3$ )  $\delta$  1.50 (s, 9H), 2.93 (s, 3H), 4.58 (s, 2H), 7.43 (s, 2H), 7.81 (s, 1H).  $^{13}\text{C}$  NMR ( $\text{CDCl}_3$ )  $\delta$  28.4, 34.6, 52.3, 80.6, 121.4 (sept,  $^3J_{\text{CF}} = 3.8$  Hz), 123.6 (q,  $^1J_{\text{CF}} = 267.5$  Hz), 127.6, 133.2 (q,  $^2J_{\text{CF}} = 33.1$  Hz), 141.5, 156.4.  $^{19}\text{F}$  NMR ( $\text{CDCl}_3$ )  $\delta$  -63.7 (s). IR (NaCl) 1698, 1394, 1136.  $m/z$  (CI, isobutane) 358 ( $\text{MH}^+$ ,  $\text{C}_{15}\text{H}_{18}\text{F}_6\text{NO}_2$ , 40), 302 (100). HRMS (CI, isobutane) ( $\text{MH}^+$ ,  $\text{C}_{15}\text{H}_{18}\text{F}_6\text{NO}_2$ ) calcd 358.1242, found 358.1246. Anal. ( $\text{C}_{15}\text{H}_{18}\text{F}_6\text{NO}_2$ ) C, H, N.

***N*-[3,5-Bis(trifluoromethyl)benzyl]-*N*-methylammonium Trifluoroacetate (41).** A mixture of *N*-methylcarbamate **40** (2.35 g, 6.58 mmol) and trifluoroacetic acid (9 mL, 116.7 mmol) in  $\text{CH}_2\text{Cl}_2$  was stirred at room temperature for 15 h. After concentration under vacuum, the crude product was recrystallized from  $\text{Et}_2\text{O}$ : white solid, mp 149–150  $^\circ\text{C}$ ; 87% (2.12 g).  $^1\text{H}$  NMR (DMSO- $d_6$ )  $\delta$  2.70 (s, 3H), 4.40 (s, 2H), 8.20 (s, 1H), 8.30 (s, 2H), 9.50 (br s, 2H).  $^{13}\text{C}$  NMR (DMSO- $d_6$ )  $\delta$  32.6, 50.4, 117.4 (q,  $^1J_{\text{CF}} = 298.1$  Hz), 122.9 (sept,  $^3J_{\text{CF}} = 3.8$  Hz), 123.5 (q,  $^1J_{\text{CF}} = 272.9$  Hz), 125.7, 131.0 (q,  $^2J_{\text{CF}} = 32.8$  Hz), 135.7, 159.2 (q,  $^2J_{\text{CF}} = 31.7$  Hz).  $^{19}\text{F}$  NMR (DMSO- $d_6$ )  $\delta$  -62.1 (s, 6F), -74.5 (s, 3F).  $m/z$  (EI) 371 ( $\text{M}^+$ ,  $\text{C}_{12}\text{H}_{10}\text{F}_9\text{NO}_2$ , 0.5), 257 (100). Anal. ( $\text{C}_{12}\text{H}_{10}\text{F}_9\text{NO}_2$ ) C, H, N.

**Synthesis of *N*-Methylglycine Amide 43.** *N*-[3,5-Bis(trifluoromethyl)benzyl]-*N*-methylcarbamoylmethyl]-*N*-methylcarbamate *tert*-Butyl Ester (**42**). To a mixture of DCC (0.66 g, 3.2 mmol), Boc-sarcosine (0.51 g, 2.7 mmol), and DMAP (0.03 g, 0.27 mmol) in chloroform (30 mL) were added benzylammonium trifluoroacetate **41** (1 g, 2.7 mmol) and diisopropylethylamine (0.56 mL, 3.2 mmol) in chloroform (10 mL). The mixture was stirred at room temperature for 15 h, and the precipitate was filtered off. The filtrate was washed successively with aqueous saturated  $\text{Na}_2\text{CO}_3$  (20 mL), HCl 1 M (20 mL), and water (20 mL), dried over  $\text{MgSO}_4$ , and then concentrated under vacuum. After



addition of Et<sub>2</sub>O (50 mL) to the residue, stirring for 10 min, and filtration of the resulting suspension, the organic layer was concentrated under vacuum to give a crude product which was recrystallized from pentane: white solid, mp 59–61 °C; 65% (0.75 g). <sup>1</sup>H NMR (CDCl<sub>3</sub>) (2 rotamers) δ 1.40 (s, 5.4H), 1.48 (s, 3.6H), 2.95 (s, 1.2H), 2.98 (s, 3H), 2.99 (s, 1.8H), 4.06 (s, 0.8H), 4.13 (s, 1.2H), 4.64 (s, 1.2H), 4.70 (s, 0.8H), 7.72 (s, 2H), 7.79 (s, 1H). <sup>13</sup>C NMR (CDCl<sub>3</sub>) δ 28.6, 34.6, 36.2, 52.9, 80.5, 122.0–122.1 (m), 123.5 (q, <sup>1</sup>J<sub>CF</sub> = 297.8 Hz), 128.4 (m), 132.4 (q, <sup>2</sup>J<sub>CF</sub> = 33.2 Hz), 140.2, 156.7, 169.8. <sup>19</sup>F NMR (CDCl<sub>3</sub>) δ –63.4 (s). IR (KBr) 1694, 1652, 1282, 1174, 1130. *m/z* (EI) 428 (M<sup>+</sup>, C<sub>18</sub>H<sub>22</sub>F<sub>6</sub>N<sub>2</sub>O<sub>3</sub>, 0.1), 372 (3), 44 (100). Anal. (C<sub>18</sub>H<sub>22</sub>F<sub>6</sub>N<sub>2</sub>O<sub>3</sub>) C, H, N.

**N-{N-[3,5-Bis(trifluoromethyl)benzyl]-N-methylcarbamoylmethyl}-N-methylammonium Trifluoroacetate (43).** To carbamate **42** (2.03 g, 4.74 mmol) in chloroform (6 mL) was added trifluoroacetic acid (5.5 mL, 71.1 mmol) at 0 °C. After stirring at room temperature for 15 h, the mixture was concentrated under vacuum to give a crude product which was recrystallized from Et<sub>2</sub>O: white solid, mp 100–101 °C; 66% (1.38 g). <sup>1</sup>H NMR (DMSO-*d*<sub>6</sub>) δ 2.55 (s, 3H), 2.94 (s, 3H), 4.13 (s, 2H), 4.70 (s, 2H), 6.83 (br s, 2H), 7.90 (s, 2H), 7.93 (s, 1H). <sup>13</sup>C NMR (DMSO-*d*<sub>6</sub>) δ 33.0, 34.5, 48.9, 50.1, 116.6 (q, <sup>1</sup>J<sub>CF</sub> = 292.5 Hz), 121.4–121.5 (m), 123.6 (q, <sup>1</sup>J<sub>CF</sub> = 270.6 Hz), 128.7–128.8 (m), 130.8 (q, <sup>2</sup>J<sub>CF</sub> = 32.5 Hz), 141.1, 158.9 (q, <sup>1</sup>J<sub>CF</sub> = 34.4 Hz), 166.7. <sup>19</sup>F NMR (DMSO-*d*<sub>6</sub>) δ –61.9 (s, 6F), –75.1 (s, 3F). IR (KBr) 1690, 1670, 1282, 1150. *m/z* (EI) 328 (M<sup>+</sup>, C<sub>13</sub>H<sub>14</sub>F<sub>6</sub>N<sub>2</sub>O, 0.5), 44 (100). HRMS (FAB<sup>+</sup>) (MH<sup>+</sup>, C<sub>13</sub>H<sub>15</sub>F<sub>6</sub>N<sub>2</sub>O) calcd 329.1089, found 329.1077. Anal. (C<sub>15</sub>H<sub>15</sub>F<sub>9</sub>N<sub>2</sub>O<sub>3</sub>) C, H, N.

**N-{N-[3,5-Bis(trifluoromethyl)benzyl]carbamoylmethyl}-N-methylcarbamic Acid *tert*-Butyl Ester (44).** To a mixture of 3,5-bis(trifluoromethyl)benzylamine (1.5 g, 6.17 mmol), Boc-sarcosine (1.17 g, 6.17 mmol), and DMAP (0.075 g, 0.62 mmol) in chloroform (30 mL) was added DCC (1.59 g, 7.71 mmol). The mixture was stirred at room temperature for 23 h, and the formed precipitate was filtered off. The filtrate was washed successively with aqueous saturated Na<sub>2</sub>CO<sub>3</sub> (40 mL), HCl 1 M (40 mL), and water (40 mL), dried over MgSO<sub>4</sub>, and then concentrated under vacuum. After addition of Et<sub>2</sub>O (50 mL) to the residue, stirring for 10 min, and filtration of the resulting suspension, the organic layer was concentrated under vacuum to give a crude product which was recrystallized from pentane: white solid, mp 103–104 °C; 78% (1.98 g). <sup>1</sup>H NMR (CDCl<sub>3</sub>) δ 1.41 (s, 9H), 2.97 (s, 3H), 3.92 (s, 2H), 4.58 (m, 2H), 7.00 (br s, 1H), 7.72 (s, 2H), 7.78 (s, 1H). <sup>13</sup>C NMR (CDCl<sub>3</sub>) δ 27.8, 35.6, 41.9, 52.9, 80.6, 121.3 (sept, <sup>3</sup>J<sub>CF</sub> = 3.7 Hz), 123.5 (q, <sup>1</sup>J<sub>CF</sub> = 272.4 Hz), 127.6, 132.0 (q, <sup>2</sup>J<sub>CF</sub> = 33.1 Hz), 141.5, 162.7. <sup>19</sup>F NMR (CDCl<sub>3</sub>) δ –63.3 (s, 6F). IR (KBr) 1696, 1654, 1278, 1134. *m/z* (EI) 414 (M<sup>+</sup>, C<sub>17</sub>H<sub>20</sub>F<sub>6</sub>N<sub>2</sub>O<sub>3</sub>, 0.2), 44 (100). Anal. (C<sub>17</sub>H<sub>20</sub>F<sub>6</sub>N<sub>2</sub>O<sub>3</sub>) C, H, N.

**3-[3,5-Bis(trifluoromethyl)benzyl]-1-methylimidazolidine-2,4-dione (45).** To a suspension of NaH (60% dispersion in mineral oil, 0.11 g, 2.75 mmol) in DMF (50 mL) was added carbamate **44** (1 g, 2.41 mmol) in DMF (3 mL). The mixture was stirred at room temperature for 1 h, and methyl iodide (0.165 mL, 2.65 mmol) was added. After stirring for 18 h, water (50 mL) and then ethyl acetate (50 mL) were added. The aqueous layer was extracted with ethyl acetate (3 × 20 mL). The combined organic layers were washed with water (2 × 25 mL), dried over MgSO<sub>4</sub>, and concentrated under vacuum to give a crude product which was purified by chromatography followed by recrystallization in pentane: white solid, mp

69–70 °C; 60% (0.48 g); *R*<sub>f</sub> 0.7 (pentane/AcOEt 2/1). <sup>1</sup>H NMR (CDCl<sub>3</sub>) δ 2.94 (s, 3H), 3.85 (s, 2H), 4.67 (s, 2H), 7.73 (s, 1H), 7.79 (s, 2H). <sup>13</sup>C NMR (CDCl<sub>3</sub>) δ 30.1, 42.1, 52.1, 122.5, 123.5 (q, <sup>1</sup>J<sub>CF</sub> = 271.3 Hz), 129.5, 132.4 (q, <sup>2</sup>J<sub>CF</sub> = 33.1 Hz), 138.8, 156.4, 169.7. <sup>19</sup>F NMR (CDCl<sub>3</sub>) δ –63.5 (s). IR (KBr) 1780, 1712, 1294, 1174, 1136. *m/z* (EI) 340 (M<sup>+</sup>, C<sub>13</sub>H<sub>10</sub>F<sub>6</sub>N<sub>2</sub>O<sub>2</sub>, 100). Anal. (C<sub>13</sub>H<sub>10</sub>F<sub>6</sub>N<sub>2</sub>O<sub>2</sub>) C, H, N.

**General Procedure for Amidation of Acids 17–21 with Sarcosine Amide 43.** A mixture of acid **17–21** (1 equiv), oxalyl chloride (3.3 equiv), and DMF (0.1 equiv) in CH<sub>2</sub>Cl<sub>2</sub> (10–40 mL) was stirred at room temperature for 2–4 h and then concentrated under vacuum. After dilution of the residue in CH<sub>2</sub>Cl<sub>2</sub> (20–60 mL), sarcosine amide **43** (1.0–1.8 equiv) and then Et<sub>3</sub>N (4 equiv) were added. The mixture was stirred at room temperature for 16 h and then concentrated under vacuum. After addition of ethyl acetate (30 mL) to the residue and filtration, the organic layer was washed with brine (2 × 20 mL), dried over MgSO<sub>4</sub>, and concentrated under vacuum to give a crude product which was purified by column chromatography.

**N-{N-[3,5-Bis(trifluoromethyl)benzyl]-N-methylcarbamoylmethyl}-N-methyl-3-(4-bromobenzoyl)-6-chloropyridine-2-carboxamide (46).** Diamide **46** was obtained from **17** (1.7 g, 5.0 mmol) and **43** (2.3 g, 5.10 mmol): yellow oil; 65% (2.1 g). *R*<sub>f</sub> 0.55 (CH<sub>2</sub>Cl<sub>2</sub>/Et<sub>2</sub>O 5.5/0.5). <sup>1</sup>H NMR (CDCl<sub>3</sub>) δ 2.96 (s, 3H), 3.38 (s, 3H), 4.28 (s, 2H), 4.69 (s, 2H), 7.08–7.78 (m, 6H), 7.65 (s, 2H), 7.86 (s, 1H). <sup>13</sup>C NMR (CDCl<sub>3</sub>) δ 35.8, 37.9, 45.2, 46.0, 115.4, 120.6, 122.3 (q, <sup>1</sup>J<sub>CF</sub> = 273.2 Hz), 122.4, 126.5, 126.9, 129.5 (q, <sup>2</sup>J<sub>CF</sub> = 32.7 Hz), 130.4, 132.4, 134.0, 135.3, 139.7, 141.5, 149.2, 157.0, 157.2, 171.6, 190.5. <sup>19</sup>F NMR (CDCl<sub>3</sub>) δ –61.4 (s).

**N-{N-[3,5-Bis(trifluoromethyl)benzyl]-N-methylcarbamoylmethyl}-N-methyl-6-chloro-3-(4-fluorobenzoyl)pyridine-2-carboxamide (47).** Diamide **47** was obtained from **18** (0.5 g, 1.58 mmol) and **43** (0.7 g, 1.60 mmol): yellow oil; 61% (0.57 g). *R*<sub>f</sub> 0.49 (CH<sub>2</sub>Cl<sub>2</sub>/Et<sub>2</sub>O 5/1). <sup>1</sup>H NMR (CDCl<sub>3</sub>) δ 3.05 (s, 3H), 3.31 (s, 3H), 4.30 (s, 2H), 4.73 (s, 2H), 7.12–7.80 (m, 6H), 7.69 (s, 2H), 7.82 (s, 1H). <sup>13</sup>C NMR (CDCl<sub>3</sub>) δ 35.7, 38.1, 45.0, 45.9, 115.3 (d, <sup>2</sup>J<sub>CF</sub> = 28.3 Hz), 120.5, 122.0 (q, <sup>1</sup>J<sub>CF</sub> = 273.3 Hz), 122.2, 126.8, 129.4 (q, <sup>2</sup>J<sub>CF</sub> = 33.1 Hz), 131.6, 133.8, 138.2, 139.7, 140.1, 149.3, 157.0, 157.2, 164.4 (d, <sup>1</sup>J<sub>CF</sub> = 261.2 Hz), 171.8, 190.7. <sup>19</sup>F NMR (CDCl<sub>3</sub>) δ –63.4 (s, 6F), –111.3 (s, 1F).

**N-{N-[3,5-Bis(trifluoromethyl)benzyl]-N-methylcarbamoylmethyl}-N-methyl-6-chloro-3-(4-iodobenzoyl)pyridine-2-carboxamide (48).** Diamide **48** was obtained from **19** (0.235 g, 0.54 mmol) and **43** (0.25 g, 0.55 mmol): yellow oil; 29% (0.11 g). *R*<sub>f</sub> 0.49 (CH<sub>2</sub>Cl<sub>2</sub>/Et<sub>2</sub>O 5/0.5). <sup>1</sup>H NMR (CDCl<sub>3</sub>) δ 3.00 (s, 3H), 3.22 (s, 3H), 4.28–4.75 (m, 4H), 7.41–7.85 (m, 9H). <sup>13</sup>C NMR (CDCl<sub>3</sub>) δ 35.7, 38.0, 45.2, 45.9, 100.8, 120.5, 122.2 (q, <sup>1</sup>J<sub>CF</sub> = 273.2 Hz), 122.4, 126.8, 129.4 (q, <sup>2</sup>J<sub>CF</sub> = 32.8 Hz), 131.6, 133.9, 135.3, 138.1, 139.7, 141.4, 149.2, 156.9, 157.0, 171.6, 190.6.

**N-{N-[3,5-Bis(trifluoromethyl)benzyl]-N-methylcarbamoylmethyl}-N-methyl-5-bromo-3-(4-fluorobenzoyl)pyridine-2-carboxamide (49).** Diamide **49** was obtained from **20** (1.26 g, 3.50 mmol) and **43** (1.65 g, 3.87 mmol): yellow solid, mp 59–64 °C; 81% (1.8 g). *R*<sub>f</sub> 0.50 (CH<sub>2</sub>Cl<sub>2</sub>/Et<sub>2</sub>O 5/1). <sup>1</sup>H NMR (CDCl<sub>3</sub>) (2 rotamers) δ 2.93 (s, 0.9H), 2.98 (s, 2.1H), 3.07 (s, 0.9H), 3.14 (s, 2.1H), 4.36 (s, 1.4H), 4.52 (s, 0.6H), 4.69 (s, 1.4H), 4.76 (s, 0.6H), 7.14 (t, <sup>3</sup>J<sub>HF</sub> = <sup>3</sup>J<sub>HH</sub> = 8.5 Hz, 2H), 7.62 (s, 1.4H), 7.71 (s, 0.6H), 7.78 (s, 0.3H), 7.79 (s, 0.7H), 7.82 (dd, <sup>3</sup>J<sub>HH</sub> = 8.5 Hz, <sup>4</sup>J<sub>HF</sub> = 5.5 Hz, 2H), 7.92 (d, <sup>4</sup>J<sub>HH</sub> = 2.2 Hz, 1H), 8.47 (d, <sup>4</sup>J<sub>HH</sub> = 2.2 Hz, 0.3H), 8.79 (d, <sup>4</sup>J<sub>HH</sub> = 2.2 Hz, 0.6H). <sup>13</sup>C NMR



(CDCl<sub>3</sub>) (2 rotamers)  $\delta$  34.7 and 35.1, 36.8 and 38.2, 49.6, 51.2, 116.3 and 116.4 (d,  $^2J_{CF}$  = 22.0 Hz), 120.9, 122.0 (sept,  $^3J_{CF}$  = 3.8 Hz), 123.6 (q,  $^1J_{CF}$  = 273.0 Hz), 128.5 (br s), 132.4 (q,  $^2J_{CF}$  = 33.1 Hz), 132.6, 133.1 and 133.2 (d,  $^3J_{CF}$  = 9.4 Hz), 136.5, 138.8 and 139.1, 140.2 and 140.3, 149.7 and 151.3, 152.9, 166.5 (d,  $^1J_{CF}$  = 257.3 Hz), 167.7, 168.2, 192.1. <sup>19</sup>F NMR (CDCl<sub>3</sub>)  $\delta$  -63.3 (s, 6F), -103.4 (s, 1F). IR (KBr) 1670, 1654, 1648, 1598, 1280. *m/z* (EI) 635 (M<sup>+</sup>, C<sub>26</sub>H<sub>19</sub><sup>81</sup>BrF<sub>7</sub>N<sub>3</sub>O<sub>3</sub>, 1), 633 (M<sup>+</sup>, C<sub>26</sub>H<sub>19</sub><sup>79</sup>BrF<sub>7</sub>N<sub>3</sub>O<sub>3</sub>, 4), 44 (100). Anal. (C<sub>26</sub>H<sub>19</sub>BrF<sub>7</sub>N<sub>3</sub>O<sub>3</sub>) C, H, N.

**N-[N-(3,5-Bis(trifluoromethyl)benzyl)-N-methyl-carbamoylmethyl]-N-methyl-3-(4-fluorobenzoyl)-5-iodopyridine-2-carboxamide (50).** Diamide **50** was obtained from **21** (0.33 g, 0.80 mmol) and **43** (0.64 g, 1.44 mmol): white solid, mp 67–68 °C; 35% (0.19 g). *R<sub>f</sub>* 0.60 (CH<sub>2</sub>Cl<sub>2</sub>/Et<sub>2</sub>O 5/1). <sup>1</sup>H NMR (CDCl<sub>3</sub>) (2 rotamers)  $\delta$  2.95 (s, 0.9H), 3.02 (s, 2.1H), 3.16 (s, 0.9H), 3.24 (s, 2.1H), 4.38 (s, 1.4H), 4.54 (s, 0.6H), 4.70 (s, 1.4H), 4.78 (s, 0.6H), 7.18 (t,  $^3J_{HH}$  =  $^3J_{HF}$  = 8.4 Hz, 2H), 7.73 (s, 2H), 7.83 (dd,  $^3J_{HH}$  = 8.8 Hz,  $^4J_{HF}$  = 5.6 Hz, 2H), 7.84 (s, 1H), 8.03 (d,  $^4J_{HH}$  = 2.0 Hz, 0.3H), 8.12 (d,  $^4J_{HH}$  = 2.0 Hz, 0.7H), 8.65 (d,  $^4J_{HH}$  = 2.0 Hz, 0.3H), 8.97 (d,  $^4J_{HH}$  = 2.0 Hz, 0.7H). <sup>13</sup>C NMR (CDCl<sub>3</sub>) (2 rotamers)  $\delta$  34.7 and 35.1, 36.6 and 38.1, 49.6, 51.3 and 53.3, 93.2, 116.3 and 116.4 (d,  $^2J_{CF}$  = 22.1 Hz), 122.2, 123.6 (q,  $^1J_{CF}$  = 276.7 Hz), 128.5, 132.4 (q,  $^2J_{CF}$  = 33.2 Hz), 132.6, 133.1 and 133.2 (d,  $^3J_{CF}$  = 9.1 Hz), 136.7, 140.2, 144.3 and 144.6, 151.7 and 153.3, 154.7 and 166.3, 167.6 (d,  $^1J_{CF}$  = 250.6 Hz), 167.8, 168.2, 192.4. <sup>19</sup>F NMR (CDCl<sub>3</sub>)  $\delta$  -63.3 (s, 6F), -103.7 (s, 1F). IR (KBr) 1670, 1650, 1280. *m/z* (EI) 681 (M<sup>+</sup>, C<sub>26</sub>H<sub>19</sub>FIN<sub>3</sub>O<sub>2</sub>, 37), 354 (100). Anal. (C<sub>26</sub>H<sub>19</sub>FIN<sub>3</sub>O<sub>2</sub>) C, H, N.

**Synthesis of Compounds 1–5. General Procedure for Amidation of Acids 34 and 35 with Benzylammonium Trifluoroacetate 41.** A mixture of acid **34** or **35** (1 equiv), oxalyl chloride (13.5 equiv), and DMF (0.1 equiv) in CH<sub>2</sub>Cl<sub>2</sub> (10–40 mL) was stirred at room temperature for 2.5 h and then concentrated under vacuum. To the residue were added CH<sub>2</sub>Cl<sub>2</sub> (20–60 mL), benzylammonium trifluoroacetate **41** (1.35 equiv), and Et<sub>3</sub>N (5.35 equiv). The mixture was stirred at room temperature for 16 h and then concentrated under vacuum. After addition of ethyl acetate (30 mL) to the residue and filtration of the suspension, the organic layer was washed successively with brine (50 mL), HCl 1 N (50 mL), brine (50 mL), saturated NaHCO<sub>3</sub> (50 mL), and brine (50 mL), dried over MgSO<sub>4</sub>, and concentrated under vacuum to give a crude oil which was purified by column chromatography.

**General Procedure for Cyclization-Dehydration of Polyamides 46–50 with DBU.** A mixture of polyamides **46–50** (1 equiv) and DBU (3.7 equiv) in toluene (90–100 mL) was refluxed for 8 days. After cooling to room temperature, the solution was acidified with HCl 1 N to pH 1 and then pH was adjusted to 4–5 by addition of aqueous Na<sub>2</sub>CO<sub>3</sub> (10%). After extraction with ethyl acetate (2 × 100 mL), the combined organic layers were washed with brine (2 × 20 mL), dried over MgSO<sub>4</sub>, and concentrated under vacuum to give a crude oil which was purified by chromatography.

**N-[3,5-Bis(trifluoromethyl)benzyl]-N-methyl-5-(4-bromophenyl)-2-chloro-7-methyl-8-oxo-7,8-dihydro-[1,7]naphthyridine-6-carboxamide (1).** Naphthyridone **1** was obtained from acid **34** (1 g, 1.97 mmol) and benzylamine **41** (0.99 g, 266 mmol): white solid, mp 187 °C; 66% (0.82 g). *R<sub>f</sub>* (2 rotamers) 0.72 (major) and 0.42 (minor) (AcOEt). <sup>1</sup>H NMR (CDCl<sub>3</sub>) (2 rotamers)  $\delta$  2.79 (s, 0.38H), 2.91 (s, 2.62H), 3.63 (s, 2.62H), 3.67 (s, 0.38H), 4.23 and 4.87 (AB,  $^2J_{AB}$  = 14.4 Hz, 0.24H), 4.41 and 4.69 (AB,  $^2J_{AB}$  = 14.4 Hz, 1.76H), 7.08–7.52 (m, 6H), 7.65 (s,

2H), 7.90 (s, 1H). <sup>13</sup>C NMR (CDCl<sub>3</sub>)  $\delta$  33.2, 35.9, 50.0, 112.4, 122.3, 122.5, 123.4 (q,  $^1J_{CF}$  = 273.0 Hz), 128.3, 130.9, 131.5, 131.9, 132.4 (q,  $^2J_{CF}$  = 32.8 Hz), 132.6, 132.9, 136.3, 136.4, 137.6, 140.8, 151.8, 159.4, 163.4. <sup>19</sup>F NMR (CDCl<sub>3</sub>)  $\delta$  -63.3 (s). IR (KBr) 1654, 1648. *m/z* (EI) 635 (M<sup>+</sup>, C<sub>26</sub>H<sub>17</sub><sup>81</sup>Br<sup>37</sup>ClF<sub>6</sub>N<sub>3</sub>O<sub>2</sub>, 28), 633 (M<sup>+</sup>, C<sub>26</sub>H<sub>17</sub><sup>81</sup>BrF<sub>6</sub><sup>35</sup>-ClN<sub>3</sub>O<sub>2</sub> and C<sub>26</sub>H<sub>17</sub><sup>79</sup>Br<sup>37</sup>ClF<sub>6</sub>N<sub>3</sub>O<sub>2</sub>, 100), 631 (M<sup>+</sup>, C<sub>26</sub>H<sub>17</sub><sup>79</sup>-Br<sup>35</sup>ClF<sub>6</sub>N<sub>3</sub>O<sub>2</sub>, 74). Anal. (C<sub>26</sub>H<sub>17</sub>BrClF<sub>6</sub>N<sub>3</sub>O<sub>2</sub>) C, H, N.

Naphthyridone **1** was also obtained from diamide **46** (2.1 g, 3.24 mmol) and DBU (1.8 mL, 12.0 mmol): 53% (1.1 g).

**N-[3,5-Bis(trifluoromethyl)benzyl]-N-methyl-3-bromo-5-(4-fluorophenyl)-7-methyl-8-oxo-7,8-dihydro-[1,7]naphthyridine-6-carboxamide (2).** Naphthyridone **2** was obtained from acid **35** (1 g, 2.42 mmol) and benzylamine **41** (0.75 g, 2.90 mmol): white solid, mp 206–208 °C; 86% (1.3 g). *R<sub>f</sub>* 0.1 (AcOEt). <sup>1</sup>H NMR (CDCl<sub>3</sub>)  $\delta$  2.82 (s, 3H), 3.64 (s, 3H), 4.23 and 4.83 (AB,  $^2J_{AB}$  = 15.0 Hz, 2H), 7.01 (t,  $^3J_{HH}$  =  $^3J_{HF}$  = 8.0 Hz, 1H), 7.03 (t,  $^3J_{HH}$  =  $^3J_{HF}$  = 8.0 Hz, 1H), 7.13 (dd,  $^3J_{HH}$  = 7.6 Hz,  $^4J_{HF}$  = 4.8 Hz, 1H), 7.35 (dd,  $^3J_{HH}$  = 8.0 Hz,  $^4J_{HF}$  = 5.2 Hz, 1H), 7.54 (s, 2H), 7.63 (d,  $^4J_{HH}$  = 2.1 Hz, 1H), 7.84 (s, 1H), 8.91 (d,  $^4J_{HH}$  = 2.1 Hz, 1H). <sup>13</sup>C NMR (CDCl<sub>3</sub>)  $\delta$  33.5, 36.2, 50.2, 112.5, 116.0 (d,  $^2J_{CF}$  = 21.2 Hz), 116.9 (d,  $^2J_{CF}$  = 21.2 Hz), 122.6–122.7 (m), 123.3 (q,  $^1J_{CF}$  = 272.8 Hz), 125.2, 127.7 (d,  $^4J_{CF}$  = 3.7 Hz), 129.3 (br s), 131.5 (d,  $^3J_{CF}$  = 8.2 Hz), 132.6 (q,  $^2J_{CF}$  = 33.6 Hz), 133.8 (d,  $^3J_{CF}$  = 8.2 Hz), 134.3, 135.5, 137.7, 137.8, 139.7, 151.8, 160.6, 163.1 (d,  $^1J_{CF}$  = 250.3 Hz), 163.7. <sup>19</sup>F NMR (CDCl<sub>3</sub>)  $\delta$  -63.3 (s, 6F), -111.1 (s, 1F). IR (KBr) 1672, 1650, 1616, 1282, 1162. *m/z* (EI) 618 (MH<sup>+</sup>, C<sub>26</sub>H<sub>17</sub><sup>81</sup>BrF<sub>7</sub>N<sub>3</sub>O<sub>2</sub>, 35), 617 (M<sup>+</sup>, C<sub>26</sub>H<sub>17</sub><sup>81</sup>BrF<sub>7</sub>N<sub>3</sub>O<sub>2</sub>, 100), 616 (MH<sup>+</sup>, C<sub>26</sub>H<sub>17</sub><sup>79</sup>BrF<sub>7</sub>N<sub>3</sub>O<sub>2</sub>, 33), 615 (M<sup>+</sup>, C<sub>26</sub>H<sub>17</sub><sup>79</sup>BrF<sub>7</sub>N<sub>3</sub>O<sub>2</sub>, 100). Anal. (C<sub>26</sub>H<sub>17</sub>-BrF<sub>7</sub>N<sub>3</sub>O<sub>2</sub>) C, H, N. Naphthyridone **2** was also obtained from diamide **49** (1.67 g, 2.6 mmol) and DBU (2.3 g, 15.6 mmol): 62% (1 g) or from diamide **49** and NaH according to the following procedure. To a suspension of NaH (60% dispersion in mineral oil, 1.9 mg, 0.08 mmol) in DMF (10 mL) was added dropwise, at 0 °C, a solution of diamide **49** (0.05 g, 0.08 mmol) in THF. The mixture was heated at 100 °C for 4 h, cooled to 0 °C, and then poured onto ice (5 g). After extraction with ethyl acetate (3 × 5 mL), the combined organic layers were washed with water (3 × 10 mL), dried over MgSO<sub>4</sub>, and concentrated under vacuum to give a crude product which was purified by column chromatography: 100% (0.051 g).

**N-[3,5-Bis(trifluoromethyl)benzyl]-N-methyl-5-(4-fluorophenyl)-3-iodo-7-methyl-8-oxo-7,8-dihydro-[1,7]naphthyridine-6-carboxamide (3).** Naphthyridone **3** was obtained from diamide **50** (0.9 g, 0.27 mmol) and DBU (0.25 mL, 1.70 mmol): white solid, mp 114–116 °C; 17% (0.03 g). *R<sub>f</sub>* 0.3 (AcOEt). <sup>1</sup>H NMR (CDCl<sub>3</sub>)  $\delta$  2.83 (s, 3H), 3.65 (s, 3H), 4.24 and 4.86 (AB,  $^2J_{AB}$  = 14.4 Hz, 2H), 7.02 (t,  $^3J_{HH}$  =  $^3J_{HF}$  = 8.5 Hz, 1H), 7.03 (t,  $^3J_{HH}$  =  $^3J_{HF}$  = 8.3 Hz, 1H), 7.13 (dd,  $^3J_{HH}$  = 9.0 Hz,  $^4J_{HF}$  = 5.7 Hz, 1H), 7.35 (dd,  $^3J_{HH}$  = 9.0 Hz,  $^4J_{HF}$  = 5.7 Hz, 1H), 7.55 (s, 2H), 7.86 (s, 1H), 7.86 (d,  $^4J_{HH}$  = 1.7 Hz, 1H), 9.08 (d,  $^4J_{HH}$  = 1.7 Hz, 1H). <sup>13</sup>C NMR (CDCl<sub>3</sub>)  $\delta$  33.6, 36.2, 50.2, 98.9, 112.5, 116.0 (d,  $^2J_{CF}$  = 22.0 Hz), 116.9 (d,  $^2J_{CF}$  = 21.2 Hz), 122.7–122.8 (m), 123.3 (q,  $^1J_{CF}$  = 272.0 Hz), 127.7 (d,  $^4J_{CF}$  = 3.4 Hz), 129.3–129.4 (m), 131.5 (d,  $^3J_{CF}$  = 8.2 Hz), 132.6 (q,  $^2J_{CF}$  = 33.5 Hz), 133.8 (d,  $^3J_{CF}$  = 8.1 Hz), 134.3, 137.5, 137.9, 140.0, 141.6, 156.5, 160.9, 163.1 (d,  $^1J_{CF}$  = 250.3 Hz), 163.7. <sup>19</sup>F NMR (CDCl<sub>3</sub>)  $\delta$  -63.3 (s, 6F), -111.1 (s, 1F). IR (KBr) 1680, 1650, 1500, 1280. *m/z* (EI) 663 (M<sup>+</sup>, C<sub>26</sub>H<sub>17</sub>F<sub>7</sub>IN<sub>3</sub>O<sub>2</sub>, 41), 91 (100). HRMS (EI) (M<sup>+</sup>, C<sub>26</sub>H<sub>17</sub>F<sub>7</sub>IN<sub>3</sub>O<sub>2</sub>) calcd 663.3255, found 663.3253. Anal. (C<sub>26</sub>H<sub>17</sub>F<sub>7</sub>IN<sub>3</sub>O<sub>2</sub>) C, H, N.

***N*-[3,5-Bis(trifluoromethyl)benzyl]-*N*-methyl-2-chloro-5-(4-fluorophenyl)-7-methyl-8-oxo-7,8-dihydro-[1,7]naphthyridine-6-carboxamide (4).** Naphthyridone 4 was obtained from diamide 47 (0.45 g, 0.76 mmol) and DBU (0.42 mL, 2.83 mmol): beige solid, mp 128–130 °C; 43% (0.19 g).  $R_f$  0.52 (AcOEt).  $^1\text{H}$  NMR ( $\text{CDCl}_3$ )  $\delta$  2.81 (s, 3H), 3.56 (s, 3H), 4.19 and 4.73 (AB,  $^2J_{AB}$  = 14.4 Hz, 2H), 6.87–7.25 (m, 6H), 7.48 (s, 2H), 7.77 (s, 1H).  $^{13}\text{C}$  NMR ( $\text{CDCl}_3$ )  $\delta$  33.6, 36.3, 50.2, 113.1, 116.7 (d,  $^2J_{CF}$  = 21.4 Hz), 122.3 (q,  $^1J_{CF}$  = 271.7 Hz), 128.0, 128.6, 129.3, 131.6, 132.4 (q,  $^2J_{CF}$  = 31.7 Hz), 132.7, 133.7, 136.9, 137.9, 139.2, 141.1, 159.8, 163.0 (d,  $^1J_{CF}$  = 250.1 Hz), 163.8, 169.2.  $^{19}\text{F}$  NMR ( $\text{CDCl}_3$ )  $\delta$  -63.3 (s, 6F), -111.3 (s, 1F). IR (KBr) 1654, 1648. HRMS (EI) ( $\text{M}^+$ ,  $\text{C}_{26}\text{H}_{17}\text{ClF}_7\text{N}_3\text{O}_2$ ) calcd 571.8742, found 571.8748. Anal. ( $\text{C}_{26}\text{H}_{17}\text{ClF}_7\text{N}_3\text{O}_2$ ) C, H, N.

***N*-[3,5-Bis(trifluoromethyl)benzyl]-*N*-methyl-2-chloro-5-(4-iodophenyl)-7-methyl-8-oxo-7,8-dihydro-[1,7]naphthyridine-6-carboxamide (5).** Naphthyridone 5 was obtained from diamide 48 (0.11 g, 0.16 mmol) and DBU (0.09 mL, 0.59 mmol): colorless oil; 64% (0.07 g).  $R_f$  0.43 (AcOEt/pentane 85/15).  $^1\text{H}$  NMR ( $\text{CDCl}_3$ )  $\delta$  2.77 (s, 3H), 3.53 (s, 3H), 4.38 and 4.52 (AB,  $^2J_{AB}$  = 14.6 Hz, 2H), 6.84–6.87 (m, 1H), 7.00–7.05 (m, 1H), 7.36–7.45 (m, 2H), 7.55–7.61 (m, 4H), 7.84 (s, 1H).  $^{13}\text{C}$  NMR ( $\text{CDCl}_3$ )  $\delta$  33.4, 35.9, 50.2, 95.4, 112.4, 122.1, 123.4 (q,  $^1J_{CF}$  = 273.1 Hz), 128.5, 130.8, 131.4, 132.5 (q,  $^2J_{CF}$  = 32.6 Hz), 132.7, 132.9, 136.3, 136.6, 137.7, 138.0, 140.8, 151.9, 159.6, 163.6. HRMS (EI) ( $\text{M}^+$ ,  $\text{C}_{26}\text{H}_{17}\text{ClF}_6\text{IN}_3\text{O}_2$ ) calcd 679.7804, found 679.7807. Anal. ( $\text{C}_{26}\text{H}_{17}\text{ClF}_6\text{IN}_3\text{O}_2$ ) C, H, N.

**Synthesis of Compounds 6–9: Halogen–Halogen Exchanges.** ***N*-[3,5-Bis(trifluoromethyl)benzyl]-*N*-methyl-5-(4-bromophenyl)-2-fluoro-7-methyl-8-oxo-7,8-dihydro-[1,7]naphthyridine-6-carboxamide (6).** A mixture of naphthyridone 1 (0.10 g, 0.16 mmol), potassium fluoride (0.027 g, 0.16 mmol), and Kryptofix 222 (0.060 g, 0.16 mmol) in DMSO (0.7 mL) was heated at 120 °C for 4 h. After cooling to room temperature, water (15 mL) was added and the mixture was extracted with ethyl acetate (40 mL). The organic layer was washed with water, dried over magnesium sulfate, filtered off, and concentrated under vacuum to give a crude product which was purified by chromatography: beige solid, mp 97–100 °C; 57% (0.055 g).  $R_f$  0.65 (AcOEt).  $^1\text{H}$  NMR ( $\text{CDCl}_3$ )  $\delta$  2.89 (s, 3H), 3.62 (s, 3H), 4.40 and 4.69 (AB,  $^2J_{AB}$  = 14.4 Hz, 2H), 7.07–7.27 (m, 3H), 7.40–7.48 (m, 2H), 7.61–7.68 (m, 3H), 7.88 (s, 1H).  $^{13}\text{C}$  NMR ( $\text{CDCl}_3$ )  $\delta$  33.2, 35.8, 50.0, 111.3 (d,  $^2J_{CF}$  = 28.4 Hz), 112.7, 122.3, 122.6, 123.3 (q,  $^1J_{CF}$  = 273.0 Hz), 128.4, 131.3, 131.7, 132.4 (q,  $^2J_{CF}$  = 32.8 Hz), 132.7, 132.8, 136.2, 136.4, 137.9, 141.2, 156.4 (d,  $^1J_{CF}$  = 255.2 Hz), 161.3, 163.4.  $^{19}\text{F}$  NMR ( $\text{CDCl}_3$ )  $\delta$  -62.1 (s, 1F), -63.3 (s, 6F). IR (KBr) 1654, 1648.  $m/z$  (EI) 617 ( $\text{M}^+$ ,  $\text{C}_{26}\text{H}_{17}^{81}\text{BrF}_7\text{N}_3\text{O}_2$ , 19), 615 ( $\text{M}^+$ ,  $\text{C}_{26}\text{H}_{17}^{79}\text{BrF}_7\text{N}_3\text{O}_2$ , 20), 334 (100). HRMS (EI) ( $\text{M}^+$ ,  $\text{C}_{26}\text{H}_{17}^{79}\text{BrF}_7\text{N}_3\text{O}_2$ ) calcd 615.0394, found 615.0392. Anal. ( $\text{C}_{26}\text{H}_{17}\text{BrF}_7\text{N}_3\text{O}_2$ ) C, H, N.

***N*-[3,5-Bis(trifluoromethyl)benzyl]-*N*-methyl-2-fluoro-5-(4-iodophenyl)-7-methyl-8-oxo-7,8-dihydro-[1,7]naphthyridine-6-carboxamide (7).** A mixture of naphthyridone 5 (0.07 g, 0.10 mmol) and potassium fluoride (0.018 g, 0.31 mmol) in DMSO (1 mL) was heated at 120 °C for 6 h. After cooling to room temperature, water (15 mL) was added and the mixture was extracted with ethyl acetate (40 mL). The organic layer was washed with water, dried over magnesium sulfate, filtered off, and concentrated under vacuum to give a crude product which was purified by chromatography: white solid, 47% (0.032 g).  $R_f$  0.46 (AcOEt).  $^1\text{H}$  NMR ( $\text{CDCl}_3$ )  $\delta$  2.90 (s, 3H), 3.60

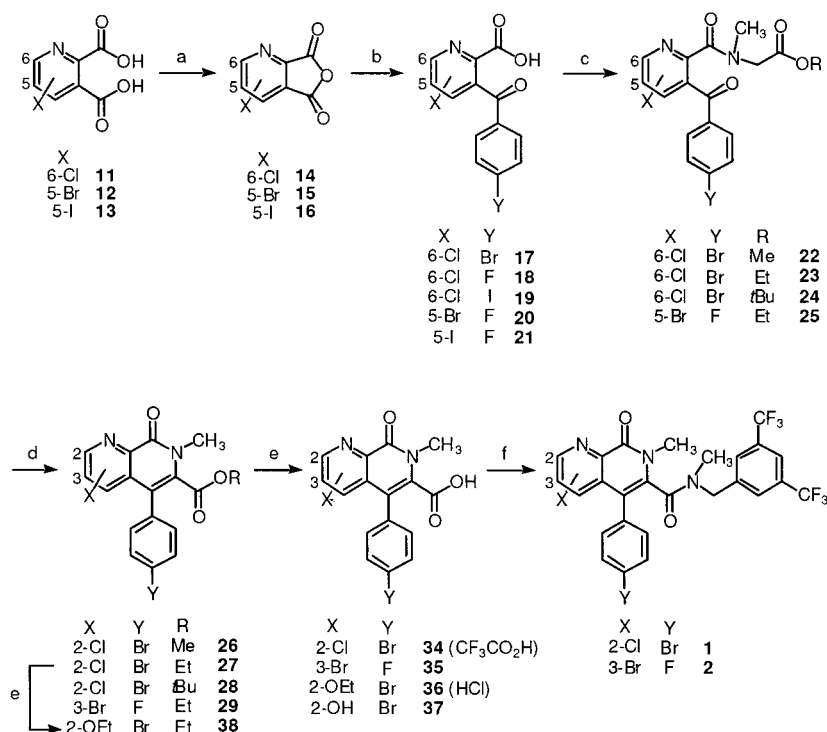
(s, 3H), 4.38 and 4.67 (AB,  $^2J_{AB}$  = 14.3 Hz, 2H), 7.07–7.22 (m, 3H), 7.42–7.49 (m, 2H), 7.54–7.68 (m, 3H), 7.86 (s, 1H).  $^{13}\text{C}$  NMR ( $\text{CDCl}_3$ )  $\delta$  33.4, 35.7, 50.0, 95.3, 112.4, 113.9 (d,  $^2J_{CF}$  = 28.4 Hz), 122.1, 123.6 (q,  $^1J_{CF}$  = 273.0 Hz), 128.5, 130.8, 131.3, 132.5 (q,  $^2J_{CF}$  = 32.6 Hz), 132.6, 136.3, 136.5, 137.6, 138.2, 140.8, 156.2 (d,  $^1J_{CF}$  = 255.1 Hz), 159.4, 163.9. HRMS (EI) ( $\text{M}^+$ ,  $\text{C}_{26}\text{H}_{17}\text{F}_7\text{IN}_3\text{O}_2$ ) calcd 663.3255, found 663.3257. Anal. ( $\text{C}_{26}\text{H}_{17}\text{F}_7\text{IN}_3\text{O}_2$ ) C, H, N.

***N*-[3,5-Bis(trifluoromethyl)benzyl]-*N*-methyl-5-(4-fluorophenyl)-2-iodo-7-methyl-8-oxo-7,8-dihydro-[1,7]naphthyridine-6-carboxamide (8).** A mixture of naphthyridone 4 (0.1 g, 0.18 mmol), acetyl chloride (97  $\mu\text{L}$ ), and sodium iodide (0.15 g, 0.91 mmol) in  $\text{CH}_3\text{CN}$  (2.5 mL) was stirred for 1 h at room temperature. After addition of aqueous  $\text{K}_2\text{CO}_3$  10% (10 mL) and  $\text{NaHSO}_3$  5% (10 mL), the mixture was extracted with  $\text{CH}_2\text{Cl}_2$  ( $3 \times 15$  mL). The combined organic layers were dried over  $\text{MgSO}_4$ , filtered off, and concentrated under vacuum to give a crude product which was purified by HPLC (column Waters Symmetry C18,  $300 \times 7.8$  mm i.d., size 7  $\mu\text{m}$ ;  $\lambda$  254 nm; flow rate 2 mL/min; mobile phase:  $\text{MeOH}/\text{H}_2\text{O}$ , 80/20,  $t_R$  13.8 min). After evaporation of the eluent, 8 was obtained as a yellow oil: 80% (0.097 g).  $^1\text{H}$  NMR ( $\text{CDCl}_3$ )  $\delta$  2.83 (s, 3H), 3.62 (s, 3H), 4.25 and 4.82 (AB,  $^2J_{AB}$  = 14.3 Hz, 2H), 6.87–7.33 (m, 6H), 7.54 (s, 2H), 7.80 (s, 1H).  $^{13}\text{C}$  NMR ( $\text{CDCl}_3$ )  $\delta$  33.6, 36.2, 50.2, 113.2, 116.7 (d,  $^2J_{CF}$  = 21.2 Hz), 122.5 (q,  $^1J_{CF}$  = 272.5 Hz), 128.0, 129.3, 131.6, 132.4 (q,  $^2J_{CF}$  = 31.6 Hz), 132.7, 134.9, 137.1, 133.7, 137.9, 138.7, 142.4, 159.7, 163.8, 163.1 (d,  $^1J_{CF}$  = 250.5 Hz), 169.1.  $^{19}\text{F}$  NMR ( $\text{CDCl}_3$ )  $\delta$  -63.3 (s, 6F), -111.4 (s, 1F). IR (KBr) 1654, 1648.  $m/z$  (EI) 664 ( $\text{MH}^+$ ,  $\text{C}_{26}\text{H}_{18}\text{F}_7\text{IN}_3\text{O}_2$ , 20), 663 ( $\text{M}^+$ ,  $\text{C}_{26}\text{H}_{17}\text{F}_7\text{IN}_3\text{O}_2$ , 36), 227 (100). HRMS (EI) ( $\text{M}^+$ ,  $\text{C}_{26}\text{H}_{17}\text{F}_7\text{IN}_3\text{O}_2$ ) calcd 663.3255, found 663.3259. Anal. ( $\text{C}_{26}\text{H}_{17}\text{F}_7\text{IN}_3\text{O}_2$ ) C, H, N.

***N*-[3,5-Bis(trifluoromethyl)benzyl]-*N*-methyl-5-(4-bromophenyl)-2-iodo-7-methyl-8-oxo-7,8-dihydro-[1,7]naphthyridine-6-carboxamide (9).** A mixture of naphthyridone 1 (0.05 g, 0.08 mmol), acetyl chloride (42  $\mu\text{L}$ ), 0.59 mmol), and sodium iodide (0.059 g, 0.4 mmol) in  $\text{CH}_3\text{CN}$  (2.5 mL) was stirred for 1 h at room temperature. After addition of aqueous  $\text{K}_2\text{CO}_3$  10% (10 mL) and  $\text{NaHSO}_3$  5% (10 mL), the mixture was extracted with  $\text{CH}_2\text{Cl}_2$  ( $3 \times 15$  mL). The combined organic layers were dried over magnesium sulfate, filtered off, and concentrated under vacuum to give a crude product which was purified by HPLC (column Waters  $\mu\text{Bondapak}$  C18,  $300 \times 7.8$  mm i.d., size 10  $\mu\text{m}$ ;  $\lambda$  254 nm; flow rate 3.5 mL/min; mobile phase:  $\text{MeOH}/\text{H}_2\text{O}$ , 70/30,  $t_R$  30.7 min). After evaporation of solvent, 9 was obtained as a yellow solid, mp 50–60 °C; 37% (0.021 g).  $^1\text{H}$  NMR ( $\text{CDCl}_3$ )  $\delta$  2.86 (s, 3H), 3.60 (s, 3H), 4.39 and 4.66 (AB,  $^2J_{AB}$  = 14.4 Hz, 2H), 7.03–7.07 (m, 1H), 7.13 (d,  $^3J_{HH}$  = 8.5 Hz, 1H), 7.18–7.26 (m, 1H), 7.40–7.48 (m, 2H), 7.63 (s, 2H), 7.81 (d,  $^3J_{HH}$  = 8.5 Hz, 1H), 7.89 (s, 1H).  $^{13}\text{C}$  NMR ( $\text{CDCl}_3$ )  $\delta$  33.1, 36.0, 50.2, 112.4, 118.8, 122.2, 122.4, 123.4 (q,  $^1J_{CF}$  = 273.0 Hz), 128.2, 131.5, 131.8, 132.3 (q,  $^2J_{CF}$  = 32.8 Hz), 132.6, 132.8, 135.7, 136.2, 136.4, 137.7, 140.7, 159.2, 163.4.  $^{19}\text{F}$  NMR ( $\text{CDCl}_3$ )  $\delta$  -63.4 (s). IR (KBr) 1654, 1648.  $m/z$  (EI) 726 ( $\text{MH}^+$ ,  $\text{C}_{26}\text{H}_{18}^{81}\text{BrF}_6\text{IN}_3\text{O}_2$ , 46), 725 ( $\text{M}^+$ ,  $\text{C}_{26}\text{H}_{17}^{81}\text{BrF}_6\text{IN}_3\text{O}_2$ , 100), 724 ( $\text{MH}^+$ ,  $\text{C}_{26}\text{H}_{18}^{79}\text{BrF}_6\text{IN}_3\text{O}_2$ , 48), 723 ( $\text{M}^+$ ,  $\text{C}_{26}\text{H}_{17}^{79}\text{BrF}_6\text{IN}_3\text{O}_2$ , 99). HRMS (EI) ( $\text{M}^+$ ,  $\text{C}_{26}\text{H}_{17}^{79}\text{BrF}_6\text{IN}_3\text{O}_2$ ) calcd 722.9453, found 722.9441. Anal. ( $\text{C}_{26}\text{H}_{17}\text{BrF}_6\text{IN}_3\text{O}_2$ ) C, H, N.

**Cell Culture and Membrane Preparation.** CHO cells expressing the human NK1 receptor were cultured in Ham's F-12 nutrient mixture supplemented with 10% fetal bovine serum and 1% penicillin–streptomycin. Cells were seeded and grown to confluence in 100 nm diameter



Scheme 1<sup>a</sup>

<sup>a</sup> Reagents: (a)  $\text{SOCl}_2$ ; (b)  $\text{YC}_6\text{H}_5$ ,  $\text{AlCl}_3$  (2.5 equiv); (c) (1)  $(\text{COCl})_2$ , DMF, (2) sarcosine ester,  $\text{Et}_3\text{N}$ ; (d) DBU; (e) for **34** from **28**,  $\text{CF}_3\text{CO}_2\text{H}$ ; for **35** from **29**,  $\text{KOH}_{\text{aq}}$  1 N; for **36**, **37**, or **38** from **26** or **27**, NaOH or HCl; (f) (1)  $(\text{COCl})_2$ , DMF, (2) 3,5-bis(trifluoromethyl)benzylamine,  $\text{Et}_3\text{N}$ .

culture dishes. Cells were first washed with 8 mL of 50 mM Tris/HCl, pH 7.4, 0.15 M NaCl and incubated until detachment with 50 mM Tris/HCl, pH 7.4, 0.15 M NaCl containing EDTA (2 mM). Detaching cells were collected in Falcon tubes and centrifuged for 15 min (1000*g*). The pellet was then resuspended at 4 °C in 0.5 mL (per dish) of 10 mM Tris/HCl, pH 7.4, containing 1 mM EDTA, 0.5 mM phenylmethylsulfonyl fluoride (PMSF), 40  $\mu\text{g}/\text{mL}$  bacitracin, 5  $\mu\text{g}/\text{mL}$  leupeptin, and 5  $\mu\text{g}/\text{mL}$  soybean trypsin inhibitor. After 30 min at 4 °C, the pellets were homogenized with a Potter-Elvehjem glass homogenizer (10–15 times) and centrifuged (1000*g*) to remove debris. The resulting supernatant was sedimented at 48000*g* for 30 min at 4 °C, the membrane pellet was stored at –80 °C in 50 mM Tris/HCl, pH 7.4, containing 1 mM EDTA, 10 mM  $\text{MgCl}_2$ , 35  $\mu\text{g}/\text{mL}$  phenylmethylsulfonyl fluoride (PMSF), 50  $\mu\text{g}/\text{mL}$  bacitracin, 2  $\mu\text{g}/\text{mL}$  leupeptin, 300  $\mu\text{g}/\text{mL}$  of benzamidine, 2  $\mu\text{g}/\text{mL}$  of chymostatin, at a concentration of 2 mg protein/ mL which was determined using the BCA protein assay reagent (Pierce).

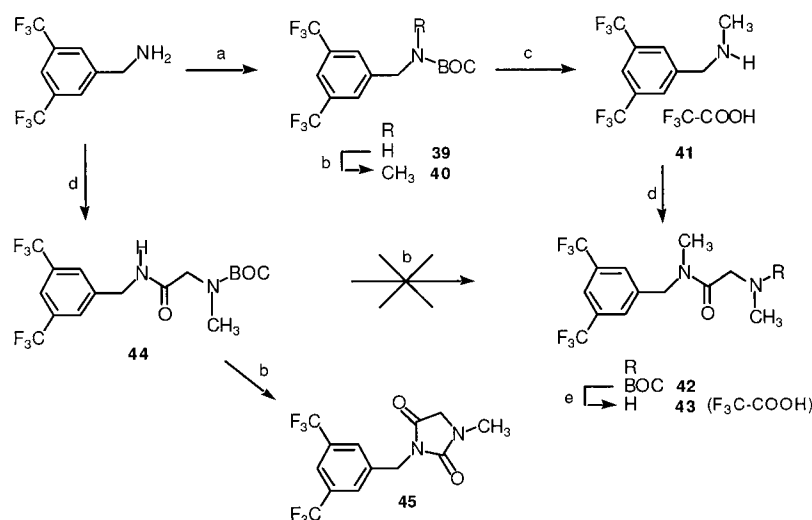
**Binding Assays.** CHO cell membranes (10  $\mu\text{g}$  of proteins) were preincubated for 90 min at room temperature in a binding buffer (50 mM TrisHCl, pH 7.4, containing 3 mM  $\text{MnCl}_2$ , 0.1% bovine serum albumin, 35  $\mu\text{g}/\text{mL}$  of phenylmethylsulfonyl fluoride, 50  $\mu\text{g}/\text{mL}$  of bacitracin, 2  $\mu\text{g}/\text{mL}$  of leupeptin, 300  $\mu\text{g}/\text{mL}$  of benzamidine, 2  $\mu\text{g}/\text{mL}$  of chymostatin). After centrifugation (4000*g*, 10 min) and removal of supernatants, the pellets were incubated for 3 h with [ $^{125}\text{I}$ ]-BH-SP (74 TBq/mmol, final concentration 6 pmol/tube) and with EP 00652218 or analogues **1–9** at different final concentrations ranged between  $10^{-5}$  M and  $10^{-11}$  M in a total assay volume of 200  $\mu\text{L}$ . The reaction was stopped by filtration on GF/C filters (Whatman International, Maidstone) previously saturated for 5 h in polyethylenimine 2% (w/v). After four washes with 4 mL of cold 50 mM Tris-HCl, pH 7.4, radioactivity was directly counted. Nonspecific binding was estimated by adding an excess of SP ( $10^{-6}$  M).

## RESULTS AND DISCUSSION

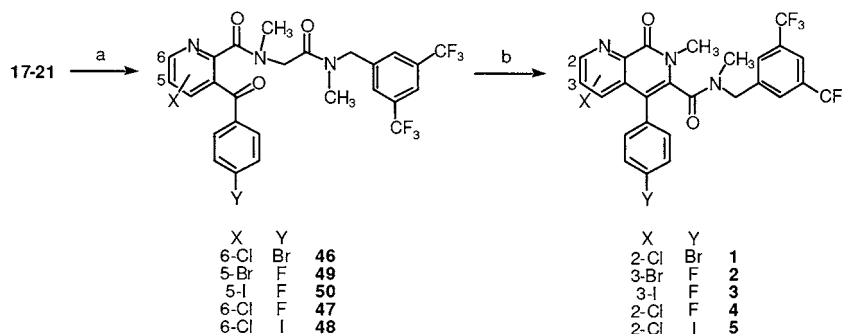
Syntheses of the target compounds **1–9** are shown in Schemes 1–4. The strategy was based on the described synthesis of EP 00652218 starting from quinolinic anhydride (**27–30**). Due to the presence of an halogen on the pyridine ring of the naphthyrindones **1–9**, this procedure required important modifications.

Halogenated quinolinic anhydrides **14–16**, not being commercially available, the corresponding quinolinic acids **11–13** were employed as starting material. These latter were obtained by oxidation of halogenoquinolines according to methods we previously developed (**31**). Acids **11–13** were transformed into anhydrides **14–16** by dehydration of the corresponding quinolinic acids. Thionyl chloride (**33**, **34**) was shown to be the reagent of choice compared to acetic anhydride (**32**, **35**) (overall yields: 73–93% versus 30–60%). Reaction of anhydrides **14–16** with 4-halobenzenes under Friedel–Crafts conditions (**27–30**, **32**) yielded the acids **17–21** with a total regioselectivity. The reaction conditions were set up with fluorobenzene. Initial attempts using stoichiometric amounts of reagents and substrate and no solvent failed (**36**). When fluorobenzene was the solvent of the reaction, the yields of **20** were strongly dependent on the amounts of aluminum chloride (42, 63, and 100%, respectively, with 1.67, 2, and 2.5 equiv). Under these conditions (haloarene as the solvent, 2.5 equiv of  $\text{AlCl}_3$ ), the bromo and fluoro compounds **17** and **21** were obtained in 46 and 55% yields, respectively. In 1,2-dichloroethane, the syntheses of **17** and **18** were achieved in 65 and 85% yields respectively whereas the iodo acid **19** was obtained in a low yield (25% from  $^1\text{H}$  NMR of the crude product) and was contaminated with its deiodinated analogue (**19**/byproduct: 75/25 ratio). Due to its instability, the iodo acid **19** was used without any purification.



Scheme 2<sup>a</sup>

<sup>a</sup> Reagents: (a) *t*-BuOCO<sub>2</sub>*t*-Bu, Et<sub>3</sub>N; (b) (1) NaH, (2) MeI; (c) CF<sub>3</sub>CO<sub>2</sub>H; (d) Boc-sarcosine, DCC, DMAP, <sup>3</sup>Pr<sub>2</sub>NEt; (e) CF<sub>3</sub>CO<sub>2</sub>H.

Scheme 3<sup>a</sup>

<sup>a</sup> Reagents: (a) (1) (COCl)<sub>2</sub>, DMF, (2) sarcosine amide 43, Et<sub>3</sub>N; (b) DBU.

Amidation of acids **17** and **20** with *N*-methylglycine ester (R = Et, Me, *t*-Bu) was carried out via the acid chlorides. The amides **22**–**25** were obtained in moderate to high yields (51–95%). Formation of the naphthyridone-esters **26**–**29** was achieved in 30–85% yield after purification by dehydration with DBU (1,8-diazabicyclo[5.4.0]-undec-7-ene) in refluxing toluene.

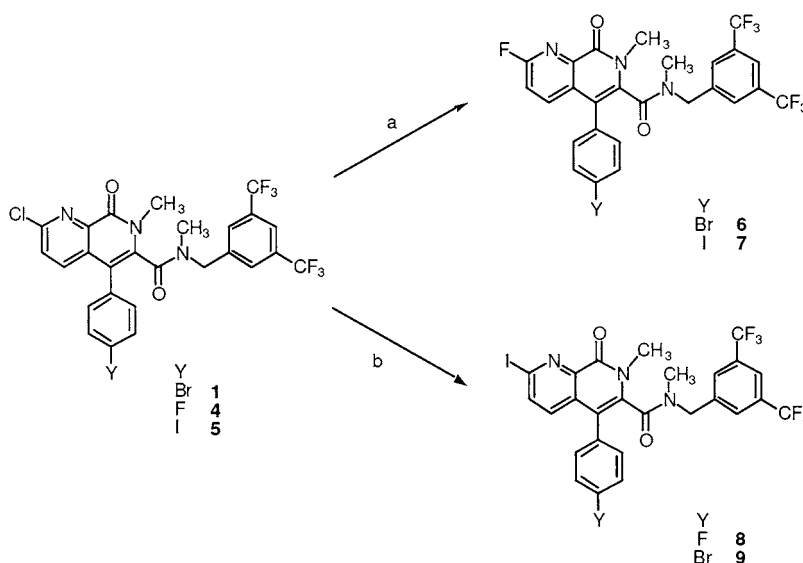
Hydrolysis of the 3-substituted ester **29** into the acid **35** was successfully carried out under basic conditions (27–30). These conditions as well as acidic ones (6 N HCl) (37) could not be used for the hydrolysis of the ethyl or methyl esters of 2-halo substituted pyridines **26** or **27** due to the competitive formation of the hydroxy- and alkoxynaphthyridones **36**–**38**. After several attempts, the *tert*-butyl ester **28** was found the best substrate for an efficient hydrolysis (38) into the acid **34** (98%).

Transformation of the acids **34** and **35** into the target compounds **1** and **2** required the preparation of the amine salt **41** (**39**, **40**) for which no synthesis was reported. Attempts of direct methylation of (bistrifluoromethyl)benzylamine, reductive amination with formaldehyde (**41**) or reduction of an intermediate carbamate (**42**), failed. In all cases, a mixture of products was obtained due to either a polyalkylation or a partial reduction of the CF<sub>3</sub> group. The amine salt **41** was obtained in 49% total yield in a three-step procedure from (bistrifluoromethyl)benzylamine (protection, methylation, and deprotection) (Scheme 2). Finally, its reaction with acids **34** and **35** afforded the compounds **1** and **2** in 10 and 15% overall yields, respectively, from the corresponding quinolinic acids **11** and **12**.

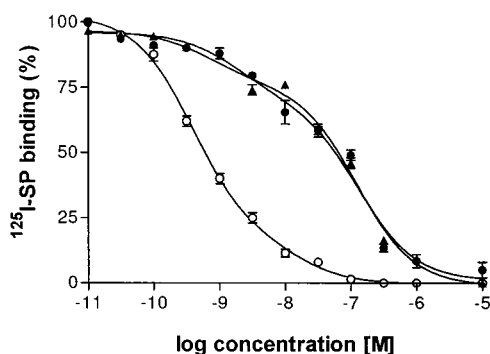
To shorten the synthesis and to improve the overall yield, the synthesis of amides **46**–**50** was envisaged. With this aim, a synthesis of the salt **43** was studied. Attempt to methylate (NaH and then MeI) the amino-amide **44** led to the cyclic compound **45**. To avoid this side-reaction, the salt **43** was prepared by amidation of **41** with Boc-sarcosine followed by deprotection of the amine (overall yield: 66%). Reaction of **43** with the pyridine carboxylic acids **17**–**21** as their acid chlorides led to the amides **46**–**50** in moderate to good yields (Scheme 3).

Transformation of amides **46**–**50** into the target compounds was first carried out with DBU in toluene as for esters **22**–**25**. Under these conditions, the cyclization required more than 8 days and naphthyridone carboxamides **1**–**5** were obtained in 17–64% yields from amides **46**–**50**. To improve both the yield and the time, the reaction parameters (solvent, base, temperature, and time) were studied. The cyclization–dehydration sequence was found slightly faster by using DMF instead of toluene and by adding calcium hydride as desiccant. No reaction was observed when this reagent was used without DBU. Attempts to use *t*-BuOK (**43**) provided compounds that could not be identified. Finally, sodium hydride (**44**) was found to be an ideal base and the naphthyridone **2** was obtained in quantitative yield when amide **49** was heated for 4 h in DMF at 100 °C. This route afforded the target compounds **1** and **2** in three steps from quinolinic acids **11** and **12** in double yields compared to those previously obtained.

Syntheses of compounds **6**–**9** were undertaken by direct halogen/halogen exchange reactions from the chlo-

Scheme 4<sup>a</sup>

<sup>a</sup> Reagents: (a) KF, K222, DMSO; (b) NaI, AcCl, CH<sub>3</sub>CN.



**Figure 3.** [<sup>125</sup>I]-(BH)-SP Displacement studies with SP(○), EP 00652218 (▲), and compound 1 (●) on membranes of human NK1 receptor-transfected CHO cells.

ronaphthyridones **1**, **4**, and **5** (Scheme 4). The fluoro compounds **6** and **7** were prepared in 57 and 47% yields, respectively, from **1** and **5** using anhydrous potassium fluoride in the presence of Kryptofix in DMSO (45), conditions easily adaptable to the introduction of a fluorine-18 atom on a pyridine ring (46). Sodium iodide in hydriodic acid (47, 48) was tested for the transformation of chloro-compound **1** to its iodo analogue **9** but poor conversion (35%) was observed. The couple sodium iodide/acetyl chloride (49) was shown to be more efficient. The exchange was quantitative (HPLC analysis), and the compound **9** was isolated in only 37% yield. This procedure, applied to the naphthyridone **4**, afforded its iodo analogue **8** in 80% yield.

Binding efficiency of naphthyridones **1–9** was evaluated by analyzing the specific displacement of iodine-labeled substance P ([<sup>125</sup>I]-(BH)-SP) on CHO cells stably transfected with the human recombinant NK1 receptor cDNA. This cellular model was chosen due to the large amounts of NK1 receptors expressed on their surface ( $5 \times 10^5$  receptors/cell) (50). Results were compared with those obtained with CP-96,345 and EP 00652218 used as references. As shown in Figure 3 and Table 1, compound **1** and EP 00652218 displayed similar affinities; this suggested that the introduction of a chlorine atom in position-2 on the pyridine ring and the substitution of a fluorine by a bromine on the phenyl ring exerted a small influence on the IC<sub>50</sub> value. The 2-fluoro and

**Table 1.** Affinities (IC<sub>50</sub>, nM; mean  $\pm$  SEM) of SP, CP-96,345, and Compounds **1–9**

compd	IM-9 <sup>a</sup>	CHO <sup>e</sup>
SP	0.6–0.7 <sup>b</sup>	0.8 $\pm$ 0.1
CP-96,345	0.4 $\pm$ 0.2 ( <i>K<sub>i</sub></i> ) <sup>c</sup>	3 $\pm$ 1.5 <sup>f</sup>
EP 00652218	0.21 $\pm$ 0.03 <sup>d</sup>	100 $\pm$ 20
<b>1</b>	-	100 $\pm$ 15
<b>2</b>	-	>1000
<b>3</b>	-	>1000
<b>4</b>	-	>1000
<b>5</b>	-	>1000
<b>6</b>	-	500 $\pm$ 60
<b>7</b>	-	>1000
<b>8</b>	-	500 $\pm$ 80
<b>9</b>	-	>1000

<sup>a</sup> Data from literature. <sup>b</sup> Reported in ref 52. <sup>c</sup> Reported in ref 51. <sup>d</sup> Reported in refs 27, 28. <sup>e</sup> Our results; see Experimental Section for details. <sup>f</sup> This value was comparable to that previously reported (8.6 nM  $\pm$  0.19) (53).

2-iodo derivatives **6** and **8** exhibited a 5-fold lower affinity whereas the IC<sub>50</sub> values for the 2-haloanalogues **4**, **5**, **7**, and **9** were drastically reduced. The replacement of the hydrogen by a bromine or a iodine in the 3-substituted series (compounds **2** and **3**) led to a drastic loss of the binding properties contrary to the reported results concerning the introduction of a chlorine atom (28). This could be attributed to the high disruption in the steric and electronic effects for the active site recognition (27).

Surprisingly, the binding affinity of EP 00652218 we determined on CHO cells was much lower than that originally reported by Takeda company (27–30) on IM-9 cells (IC<sub>50</sub>(CHO)/IC<sub>50</sub>(IM9) = 500), which naturally expressed the NK1 receptor (<10<sup>4</sup> receptors/cell) (51). However, IC<sub>50</sub> values we found for SP and CP 96345 were similar to those currently described in the literature (Table 1) (51–53). These differences of EP 00652218 affinity magnitude seemed to be due to the cellular model. Indeed, it is now admitted that the NK1 receptor exists under two different conformers, each of them being constitutively associated either with Gs or with Gq proteins under an inactive complex (54). These conformers could be expressed under different proportions depending on the cell type and EP 00652218 could exhibit strongly different affinities for each one in opposite to SP and CP 96345. To our knowledge, this is the only example where compound

binding affinity for the NK1 receptor was strongly affected by the cellular model used. In this context, it seems to be interesting to evaluate the in vivo recognition of the NK1 receptor by EP 00652218 itself and by its analogues.

## CONCLUSION

A series of 2- and 3-halonaphthyridone-6-carboxamide derivatives, analogues of EP 00652218, have been developed for in vivo imaging studies of the NK1 receptor by PET or SPECT. The affinities were found strongly dependent on the nature and on the position of the halogen. Moreover the IC<sub>50</sub> value obtained for EP 00652218 in our study on CHO cells expressing NK1 receptor was 500-fold lower than that originally determined by Natsugari et al. on IM9 cells. This discrepancy in affinities could be explained by the cellular model and by the occurrence of different conformers of the NK1 receptor expressed on these cell types. From these findings, the potentiality of EP 00652218 and haloanalogues **1**, **6**, and **8** as radiotracers for PET or SPECT imaging could not be predicted. In vivo studies with these compounds labeled either with a positron or a gamma emitter are in progress and will be reported in due course.

## ACKNOWLEDGMENT

This research has been supported through one grant from the CEA and one from the PUNCH Orga (Region Basse-Normandie), and fundings were provided in part from CNRS (Physique Chimie du Vivant 2000).

## LITERATURE CITED

- Regoli, D., Boudon, A., and Fauch  re, J.-C. (1994) Receptors and Antagonists for Substance P and Related Peptides. *Pharmacol. Rev.* **46**, 551–599.
- Quartara, L., and Maggi, C. A. (1998) The Tachykinin NK<sub>1</sub> Receptor. Part II: Distribution and Pathophysiological Roles. *Neuropeptides* **32**, 1–49.
- Maeno, H., Kiyama, H., and Tohyama, M. (1993) Distribution of the Substance P Receptor (NK-1 Receptor) in the Central Nervous System. *Mol. Brain Res.* **18**, 43–58.
- Yip, J., and Chahl, L. A. (2001) Localization of NK1 and NK3 Receptors in Guinea-Pig Brain. *Regul. Pept.* **98**, 55–62.
- Quartara, L., and Maggi, C. A. (1997) The Tachykinin NK<sub>1</sub> Receptor. Part I: Ligands and Mechanisms of Cellular Activation. *Neuropeptides* **31**, 537–563.
- Maggi, C. A., Patacchini, R., Rovero, P., and Giachetti, A. (1993) Tachykinin Receptors and Tachykinin Receptor Antagonists. *J. Auton. Pharmacol.* **13**, 23–93.
- von Sprecher, A., Gerspacher, M., and Anderson, G. P. (1998) Neurokinin Antagonists as Potential Therapies for Inflammation and Rheumatoid Arthritis. *R. I. Drugs Rev. Neurokinin Antagonists* **1**, 73–91.
- Varty, G. B., Cohen-Williams, M. E., Morgan, C. A., Pylak, U., Duffy, R. A., Lachowicz, J. E., Carey, G. J., and Coffin, V. L. (2002) The Gerbil Elevated Plus-maze. II. Anxiolytic-like Effects of Selective Neurokinin NK1 Receptor Antagonists. *Neuropsychopharmacology* **27**, 371–379.
- Argyropoulos, S. V., and Nutt, D. J. (2000) Substance P Antagonists: Novel Agents in the Treatment of Depression. *Expert Opin. Invest. Drugs* **9**, 1871–1875.
- Baker, R., Curtis, N. R., Elliott, J. M., Harrison, T., Hollingworth, G. J., Jackson, P. S., Kulagowski, J. J., Rupi  niak, N. M., Seward, E. M., Swain, C. J., and Williams, B. J. (2000) Use of NK-1 Receptor Antagonists for Treating Schizophrenic Disorders. US Pat. Appl. 6100256; *Chem. Abstr.* **133**, 144929.
- Burnet, P. W., and Harrison, P. J. (2000) Substance P (NK1) Receptors in the Cingulate Cortex in Unipolar and Bipolar Mood Disorder and Schizophrenia. *Biol. Psychiat.* **47**, 80–83.
- Fowler, J. S., and Wolf, A. P. (1997) Working Against Time: Rapid Radiotracer Synthesis and Imaging the Human Brain. *Acc. Chem. Res.* **30**, 181–188.
- Fowler, J. S., and Wolf, A. P. (1986) *Positron Emission Tomography and Autoradiography: Principles and Applications for the Brain and Heart* (M. Phelps, J. Mazziotta, and H. Schelbert, Eds.) pp 391–450, Raven Press, New York.
- Wagner, H. N., Jr. (1991) Clinical PET: its Time Has Come. *J. Nucl. Med.* **32**, 561–751.
- McCarthy, T. J., Schwarz, S. W., and Welch, M. J. (1994) Nuclear Medicine and Positron Emission Tomography: an Overview. *J. Chem. Educ.* **71**, 830–836.
- Gibson, R. E., Burns, H. D., Hamill, T. G., Eng, W., Francis, B. E., and Ryan, C. (2000) Non-Invasive Radiotracer Imaging as a Tool for Drug Development. *Curr. Pharm. Des.* **6**, 973–989.
- Mickala, P., Dauphin, F., Barr  , L., Debruyne, D., Young, A. R., Touzani, O., Roux, P., Camsonne, R., MacKenzie, E. T., and Baron, J. C. (1994) Regional Brain Distribution and Metabolism of [<sup>11</sup>C]CP96, 345, a Non-Peptide Substance P (NK-1) Receptor Antagonist, in the Anaesthetized Guinea-Pig. *Circ. M  tab. Cerveau* **11**, 367–376.
- Del Rosario, R. B., Mangner, T. J., Gildersleeve, D. L., Shervz, P. D., Wieland, D. M., Lowe, J. A., Drozda, S. E., and Snider, R. M. (1993) Synthesis of a Nonpeptide Carbon-11 Labeled Substance P Antagonist for PET Studies. *Nucl. Med. Biol.* **20**, 545–547.
- Francis, B. E., Swain, C., Sabin, V., and Burns, H. D. (1994) Radioiodinated L-703, 606: a Potent Selective Antagonist to the Human NK1 Receptor. *Appl. Radiat. Isot.* **45**, 97–103.
- Livni, E., Babich, J. W., Desai, M. C., Godek, D. M., Wilkinson, R. A., Rubin, R. H., and Fischman, A. (1995) Synthesis of a <sup>11</sup>C-Labeled NK1 Receptor Ligand for PET Studies. *Nucl. Med. Biol.* **22**, 31–36.
- Mishani, E., McCarthy, T. J., Brodbeck, R., Dence, C. S., Krause, J. E., and Welch, M. J. (1997) Synthesis and Evaluation of a Fluorine-18 Labeled NK-1 Antagonist. *J. Labelled Compd. Radiopharm.* **40**, 653–655.
- Berstr  m, M., Fasth, K. J., Kilpatrick, G., Ward, P., Cable, K. M., Wiperman, M. D., Sutherland, D. R., and Langstr  m, B. (2000) Brain Uptake and Receptor Binding of Two [<sup>11</sup>C]-Labeled Selective High Affinity NK1 Antagonists, GR203040 and GR205171 – PET Studies in Rhesus Monkey. *Neuropharmacology* **39**, 664–670.
- Burns, H. D., Gibson, R. E., and Hamill, T. G. (2000) PCT Int. Appl. WO 99-US22163 38; *Chem. Abstr.* **132**, 251079.
- Bender, D., Smith, D. F., Marthi, K., and Gjedde, A. (2001) Synthesis and in vivo Evaluation (Pig) of CP-643, 051, the N-[<sup>11</sup>C]Methyl Analogue of the NK1 Receptor Antagonist CP-122, 721. *J. Labelled Compd. Radiopharm.* **44**, S286–S288.
- Sandell, J., Thorell, J. O., Pauli, S., Halldin, C., Stone-Elander, S., Swahn, C. G., Ingvar, M., Farde L., Iyengar, S., Hipskin, P., and Sedvall, G. (1997) Carbon-11 Labelling of an NK-1 Receptor Antagonist, LY303870, and Evaluation with PET. *J. Labelled Compd. Radiopharm.* **40**, 648–650.
- van der Mey, M., Leysen J. E., Windhorst, A. D., and Herscheid, J. D. M. (2001) Radiosynthesis of [<sup>11</sup>C]R116301: a Potential PET Ligand for Central NK1 Receptors. *J. Labelled Compd. Radiopharm.* **51**, 277–279.
- Natsugari, H., Ikeura, Y., Kiyota, Y., Ishichi, Y., Ishimaru, T., Saga, O., Shirafuji, H., Tanaka, T., Kamo, I., Doi, T., and Otsuka, M. (1995) Novel, Potent, and Orally Active Substance P Antagonists: Synthesis and Antagonist Activity of N-Benzylcarboxamide Derivatives of Pyrido[3,4-b]pyridine. *J. Med. Chem.* **38**, 3106–3120.
- Natsugari, H., Ishimaru, T., and Doi, T. (1994) Eur. Pat. Appl. 652218A1; (1995) *Chem. Abstr.* **123**, 256684.
- Ikeura, Y., Tanaka, T., Kiyota, Y., Morimoto, S., Ogino, M., Ishimaru, T., Kamo, I., Doi, T., and Natsugari, H. (1997) Potent NK<sub>1</sub> Receptor Antagonists: Synthesis and Antagonistic Activity of Various Heterocycles with an N-[3,5-Bis-(trifluoromethyl)benzyl]-N-methylcarbamoyl Substituent. *Chem. Pharm. Bull.* **45**, 1642–1652.



- (30) Hosoki, R., Tanagisawa, M., Onishi, Y., Yoshioka, K., and Otsuka, M. (1998) Pharmacological Profiles of New Orally Active Nonpeptide Tachykinin NK1 Receptor Antagonists. *Eur. J. Pharmacol.* **341**, 235–241.
- (31) Le Bas, M.-D., Guéret, C., Perrio-Huard, C., Lasne, M.-C., and Barré, L. (2001) Oxidation of 2-or 3-Halogenated Quinolines: an Easy Access to 5-or 6-Halogeno-2,3-Pyridine Dicarboxylic Acids. *Synthesis* 2495–2500.
- (32) Cochran, J. C., and Little, W. F. (1961) Electrolytic Oxidation of Some Substituted Quinolines to Quinolinic Acids and Acylations with Substituted Quinolinic Anhydrides. *J. Org. Chem.* **26**, 808–811.
- (33) Norman, M. H., Kelley, J. L., and Hollignsworth, E. B. (1993) Conformationally Restricted Analogues of Remoxipride as Potential Antipsychotic Agents. *J. Med. Chem.* **36**, 3417–3423.
- (34) Gribble, G. W., Fletcher, G. L., Ketcha, D. M., and Rajopadhye, M. (1989) Metalated Heterocycles in the Synthesis of Ellipticine Analogues. A new Route to the 10H-Pyrido[2,3-b]Carbazole Ring System. *J. Org. Chem.* **54**, 3264–3269.
- (35) McMaster, L., and Ahmann, F. F. (1928) Action of Thionyl Chloride on Organic Acids. *J. Am. Chem. Soc.* **50**, 145–149.
- (36) Ghiaci, M., and Asghari, J. (1998) Friedel–Crafts Alkylation and Acylation in the Absence of Solvent. *Synth. Commun.* **28**, 2213–2220.
- (37) Vanbilloen, H. P., Cleynehen, B. J., and Verbruggen, A. M. (1998) Importance of the Two Ester Functions for the Brain Retention of  $^{99m}\text{Tc}$ -Labelled Ethylene Dicycysteine Diethyl Ester ( $^{99m}\text{Tc}$ -ECD). *Nucl. Med. Biol.* **25**, 569–575.
- (38) Barany, G., and Albericio, F. (1985) A Three-Dimensional Orthogonal Protection Scheme for Solid-Phase Peptide Synthesis Under Mild Conditions. *J. Am. Chem. Soc.* **107**, 4936–4942.
- (39) Alvaro, G., Di Fabio, R., Giovannini, R., Guercio, G. S. D. Y., and Ursini, A. (2001) PCT Int. Appl. WO 0125219A2; (2001) *Chem. Abstr.* **134**, 295839.
- (40) Qi, H., Shah, S. K., Cascieri, M. A., Sadowski, S. J., and MacCoss, M. L. (1998) Tryptophan Urea Amides as NK1/NK2 Dual Antagonists. *Bioorg. Med. Chem. Lett.* **8**, 2259–2262.
- (41) Abdel-Magid, A. F., Carson, K. G., Harris, B. D., Maryanoff, C. A., and Shah, R. D. (1996) Reductive Amination of Aldehydes and Ketones with Sodium Triacetoxyborohydride. Studies on Direct and Indirect Reductive Amination Procedures. *J. Org. Chem.* **61**, 3849–3862.
- (42) Micouin, L., Jullian, V., Quirion, J.-C., and Husson, H.-P. (1996) Origins of Diastereoselectivity in the Alkylation of *N*-Substituted Lactams and Amides Derived from Optically Active Aminoalcohols. *Tetrahedron: Asymmetry* **7**, 2839–2846.
- (43) Varnavas, A., Lassiani, L., Luxich, E., Zacchigna, M., Boccu, E., and Pichierri, F. (1996) Quinolone Derivatives: Synthesis and Binding Evaluation on Cholecystokinin Receptors. *Farmaco* **51**, 341–350.
- (44) Hirai, K., Ishiba, T., Sugimoto, H., and Fujishita, T. (1981) *N*-Substituted (Sarcosylamino)Benzophenones. Their Synthesis and Conversion into Heterocycles. *J. Org. Chem.* **46**, 4489–4493.
- (45) Hamer, J., Link, W. J., Jurjevich, A., and Vigo, T. L. (1962) Preparation of 2-Fluoroquinoline and 2,6-Difluoropyridine by Halogen Exchange. *Rec. Trav. Chim.* **81**, 1058–1060.
- (46) Lasne, M.-C., Perrio, C., Rouden, J., Barré, L., Roeda, D., Dollé, F., and Crouzel, C. (2002) Chemistry of  $\beta^+$ -Emitting Compounds Based on Fluorine-18. *Topics in Current Chemistry* (W. Krause, Ed.) Vol. 222, pp 239–240, Springer, Berlin, and references therein.
- (47) Narasimhan, N. S., Sunder, N. M., Ammanamanchi, R., and Bonde, B. D. (1990) Evidence in Favor of Lithium–Halogen Exchange Being Faster than Lithium–Acidic Hydrogen (Deuterium) Exchange. *J. Am. Chem. Soc.* **112**, 4431–4435.
- (48) Newkome, G. R., Moorfield, C. N., and Sabbaghian, B. (1986) Reductive Dehalogenation of Electron-Poor Heterocycles: Nicotinic Acid Derivatives. *J. Org. Chem.* **51**, 953–954.
- (49) Corcoran, R. C., and Bang, S. H. (1990) Iodopyridines from Bromo- and Chloropyridines. *Tetrahedron Lett.* **31**, 6757–6758.
- (50) Sagan, S., Chassaing, G., Pradier, L., and Lavielle, S. (1996) Tachykinin Peptides Affect Differently the Second Messenger Pathways after Binding to CHO-Expressed Human NK-1 Receptors. *J. Pharmacol. Exp. Ther.* **276**, 1039–1048.
- (51) Goso, C., Potier, E., Manzini, S., and Szallasi, A. (1994) Comparison of Tachykinin NK1 Receptors in Human IM9 and U373 MG Cells, using Antagonist (FK888, ( $\pm$ )-CP-96,345, and RP 67580) Binding. *Eur. J. Pharmacol.* **254**, 221–227.
- (52) Payan, D. G., Brewster, D. R., and Goetzl, E. J. (1984) Stereospecific Receptors for Substance P on Cultured Human IM-9 Lymphoblasts. *J. Immunol.* **133**, 3260–3265.
- (53) Lundstrom, K., Hawcock, A. B., Vargas, A., Ward, P., Thomas, P., and Naylor, A. (1997) Effect of Single Point Mutations of the Human Tachykinin NK1 Receptor on Antagonist Affinity. *Eur. J. Pharmacol.* **337**, 73–81.
- (54) Holst, B., Hastrup, H., Raffetseder, U., Martini, L., and Schwartz, T. W. (2001) Two Active Molecular Phenotypes of the Tachykinin NK1 Receptor Revealed by G-Protein Fusions and Mutagenesis. *J. Biol. Chem.* **276**, 19793–19799.

BC025656R

# New Reagents for the Introduction of Reactive Functional Groups into Chemically Synthesized DNA Probes

Zbigniew Skrzypczynski\* and Sarah Wayland

Third Wave Technologies, 502 S. Rosa Road, Madison, Wisconsin 53719. Received December 19, 2002; Revised Manuscript Received March 10, 2003

An efficient and versatile preparative approach is described, allowing for the preparation of DNA probes modified with an aldehyde group at the 3'- or 5'-end. The developed synthetic strategy allows for the preparation of a new family of phosphoramidites and solid supports compatible with the automated synthesis of modified oligonucleotide probes. These new reagents were prepared from intermediates **3** and **3a**, obtained from the commercially available aleuritic acid **1**. It was demonstrated that the new phosphoramidite reagents also could be used as new types of cleavable linkers. A new and efficient method for the production of 5' aldehyde-labeled DNA probes was developed.

## INTRODUCTION

The discovery of the phosphoramidite method, which enables automated synthesis of natural and modified DNA molecules (1–4), has stimulated the development of numerous reagents and methods to introduce a specific modification or functional group at a selected position within a synthesized oligonucleotide (5–19). Some phosphoramidite labeling reagents are commercially available. However, escalating interest in the use of chemically modified, synthetic oligonucleotides in the disciplines of biology, medicine, and biotechnology (20–30) has intensified the need for less expensive and more broadly applicable labeling reagents. Despite its popularity and efficiency, automated oligonucleotide synthesis does not always address all synthetic requirements. Efforts are focused increasingly on the development of new postsynthetic strategies for the preparation of oligonucleotide conjugates with other molecules and biological moieties, as well as on new protocols for immobilizing DNA onto solid surfaces. In our search for new options to address our synthesis goals, we focused on commercially available aleuritic acid (DL-erythro-9,10,16-trihydroxypalmitic acid) **1** (Figure 1) as a valuable starting material for the preparation of new versatile labeling reagents.

The structural features of aleuritic acid **1** offer ample opportunities for the preparation of new types of phosphoramidite reagents that can introduce both a carboxyl group and a masked aldehyde group into a synthesized DNA probe or can be used for the preparation of a new family of cleavable linkers. Carboxyl and aldehyde groups play particularly significant roles in the postsynthetic modification of oligonucleotide probes (31–47), the preparation of oligonucleotide conjugates (48–59), and the immobilization of DNA probes onto amino-modified solid surfaces (60–70).

Several recent papers highlighting the use of DNA probes modified with different functional groups at either their 3'- or 5'-terminus (60, 65, 68) demonstrate the superiority of the aldehyde group in postsynthetic conjugation and immobilization techniques compared to

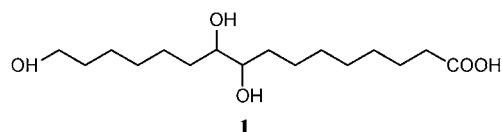


Figure 1. Structure of aleuritic acid **1**.

other functional groups. We outline an efficient and flexible synthetic strategy that leads to the preparation of new phosphoramidite reagents, new cleavable linkers, and a new type of solid support—all of which are useful in the preparation of DNA probes modified with an aldehyde group.

## MATERIALS AND METHODS

All new compounds, aldehyde-labeled DNA probes, and products of their conjugation with molecules containing a reactive primary amino group were characterized by HPLC and mass spectrometry (MS). HPLC analyses were performed with a Hitachi D-7000 Interface, L-7100 gradient pump, and L-7400 UV detector using a Varian Omnisphere 5 C18 column (250 × 4.6 mm) and 100 mM TEAA, pH 7/acetoneitrile. <sup>1</sup>H NMR spectra were recorded on a Varian UNITYINOVA instrument. MS analysis of all DNA-containing species was performed using a PerSeptive Biosystems Voyager-DE Biospectrometry Workstation V800520. MS analysis of small molecules was performed using an Applied Biosystems/MDS Sciex API 365 LC/MS/MS triple quadrupole with an electrospray ionization source. Automated oligonucleotide synthesis was performed using a PerSeptive Biosystems Expedite Nucleic Acid Synthesis System. Column chromatography purification used 70 × 230 mesh, 60 Å silica gel (Aldrich, Milwaukee, WI). Analytical TLC was carried out on EM Science F<sub>254</sub> glass-backed fluorescence indicator plates. DNA synthesis reagents and columns were purchased from Applied Biosystems (Foster City, CA). Unless otherwise noted, reagents were purchased from Aldrich and used without further purification. Solvents were dried over activated 3 Å molecular sieves. Nap-10 columns were purchased from Amersham Pharmacia Biotech (Uppsala, Sweden).

**Synthesis of 2.** A 250 mL round-bottom flask was charged with 2.2 g (7.2 mmol) aleuritic acid **1** (Lancaster

\* To whom correspondence should be addressed: [telephone (608) 273-8933; fax (608) 273-8618; e-mail zskrzypczynski@tw.com].

Synthesis Inc, Windham, NH) and 100 mL of pyridine. Solid 4,4'-dimethoxytrityl chloride (3.2 g, 9.4 mmol) was added slowly and mixed for 1 h. The reaction was concentrated by rotary evaporation, and column chromatography purification (5% methanol/5% triethylamine/methylene chloride) resulted in an off-white solid product with a yield of 4.0 g, 90%.  $R_f$  = 0.35 (10% methanol/5% triethylamine/methylene chloride).  $^1\text{H}$  NMR,  $\text{CD}_3\text{CN}$ , 400 MHz,  $\delta$  7.41 (m, 2H), 7.29 (m, 6H), 7.22 (t, 1H), 6.86 (m, 4H), 3.76 (s, 6H), 3.60 (m, 2H), 2.99 (t, 2H), 2.83 (m, 2H), 2.27 (t, 2H), 1.6–1.2 (aliphatic, 22H) ppm. ESI-MS for  $\text{C}_{37}\text{H}_{50}\text{O}_7$  ( $\text{M} + \text{K}$ ) $^+$ : calculated 646; found 646.

**Synthesis of 3.** Combined **2** (4.0 g, 6.6 mmol), *N,N*-diisopropylethylamine (8.5 g, 66 mmol), *N*-methylimidazole (1.6 g, 20 mmol), 60 mL of tetrahydrofuran, and 60 mL of pyridine in a 250 mL round-bottom flask. With stirring at 0 °C under argon flow, acetic anhydride (3.4 g, 33 mmol) was added via syringe. After 1 h, the reaction mixture was concentrated by rotary evaporation. The crude reaction material was dissolved in methylene chloride (100 mL), washed with saturated sodium chloride (100 mL), and purified by column chromatography (5% methanol/5% triethylamine/methylene chloride). Compound **3** was obtained as a yellow oil (3.7 g, 81%).  $R_f$  = 0.5 (5% methanol/5% triethylamine/methylene chloride).  $^1\text{H}$  NMR,  $\text{CD}_3\text{CN}$ , 400 MHz,  $\delta$  7.43 (m, 2H), 7.30 (m, 6H), 7.21 (t, 1H), 6.85 (m, 4H), 4.93 (m, 2H), 3.76 (s, 6H), 2.98 (t, 2H), 2.20 (t, 2H), 2.00 (s, 3H), 1.99 (s, 3H), 1.50 (m, 8H), 1.25 (m, 14H) ppm. ESI-MS for  $\text{C}_{41}\text{H}_{54}\text{O}_9$  ( $\text{M} + \text{K}$ ) $^+$ : calculated 730; found 730.

**Synthesis of 3a.** Dissolved **3** (see above, 1.6 g, 2.3 mmol) in 100 mL of tetrahydrofuran. Solid *N*-hydroxysuccinimide (0.30 g, 2.6 mmol) and 1,3-dicyclohexylcarbodiimide (0.72 g, 3.5 mmol) were added to the mixture, stirred at room temperature for 16 h under a drying tube, and concentrated by rotary evaporation. Crude material **3a** was purified by column chromatography (50% ethyl acetate/50% hexane), resulting in a white solid with a yield of 1.1 g, 60%.  $R_f$  = 0.62 (75% ethyl acetate/25% hexane).  $^1\text{H}$  NMR,  $\text{CD}_3\text{CN}$ , 400 MHz,  $\delta$  7.43 (m, 2H), 7.30 (m, 6H), 7.23 (m, 1H), 6.85 (m, 4H), 4.93 (m, 2H), 3.76 (s, 6H), 2.99 (t, 2H), 2.75 (s, 4H), 2.58 (t, 2H), 2.00 (s, 3H), 1.99 (s, 3H), 1.6–1.2 (aliphatic, 22H) ppm. ESI-MS for  $\text{C}_{45}\text{H}_{57}\text{NO}_{11}$  ( $\text{M} + \text{K}$ ) $^+$ : calculated 827; found 827.

**Synthesis of 4.** A 100 mL round-bottom flask was charged with compound **3** (0.92 g, 1.3 mmol), 4-(dimethylamino)pyridine (210 mg, 1.7 mmol), 1,6-hexanediol (1.6 g, 13 mmol), and 50 mL of tetrahydrofuran. Solid 1,3-dicyclohexylcarbodiimide (3.0 g, 14.3 mmol) was added, and the reaction mixture was stirred at room temperature under a drying tube for 16 h. Rotary evaporation and purification by column chromatography (2% triethylamine/49% ethyl acetate/49% hexane) yielded a white solid, 0.59 g, 59%.  $R_f$  = 0.58 (75% ethyl acetate/25% hexane).  $^1\text{H}$  NMR,  $\text{CD}_3\text{CN}$ , 400 MHz,  $\delta$  7.42 (m, 2H), 7.29 (m, 6H), 7.23 (t, 1H), 6.85 (m, 4H), 4.93 (m, 2H), 4.02 (t, 2H), 3.76 (s, 6H), 3.47 (q, 2H), 2.99 (t, 2H), 2.44 (t, 1H), 2.25 (t, 2H), 2.00 (s, 3H), 1.99 (s, 3H), 1.6–1.2 (aliphatic, 30H) ppm. ESI-MS for  $\text{C}_{47}\text{H}_{66}\text{O}_{10}$  ( $\text{M} + \text{K}$ ) $^+$ : calculated 830; found 830.

**Synthesis of 5.** **4** (0.59 g, 0.74 mmol), *N,N*-diisopropylethylamine (0.12 g, 0.89 mmol), and 4-(dimethylamino)pyridine (45 mg, 0.37 mmol) were combined in 50 mL of tetrahydrofuran. Solid diglycolic anhydride (0.13 g, 1.1 mmol) was added to the reaction mixture and stirred for 3.5 h under a drying tube. The solvent was evaporated, and purification by column chromatography (70  $\times$  230 mesh, 60A silica, 5% methanol/5% triethylamine/methylene chloride) yielded a pale yellow oil (0.44 g, 70%).

$R_f$  = 0.31 (5% methanol/5% triethylamine/methylene chloride). ESI-MS for  $\text{C}_{51}\text{H}_{70}\text{O}_{14}$  ( $\text{M} + \text{H}$ ) $^+$ : calculated 906; found 906.

**Synthesis of 6.** Four grams of lcaa-CPG (Glen Research, Sterling, VA, #20-0001, 1000A, 69  $\mu\text{mol/g}$ ) was added to a 50 mL round-bottom flask. Compound **5** (0.36 g, 0.36 mmol) was dissolved in 20 mL of pyridine and added to the CPG. 4-(Dimethylamino)pyridine (24 mg, 0.20 mmol), triethylamine (0.16 g, 1.6 mmol), *N*-hydroxysuccinimide (91 mg, 0.79 mmol), and 1-ethyl-(3-dimethylaminopropyl)carbodiimide hydrochloride (0.30 g, 1.6 mmol) were added, and the reaction mixture was vortexed at RT for 16 h. Additional aliquots of 1-ethyl-(3-dimethylaminopropyl)carbodiimide hydrochloride (total of 0.60 g, 3.2 mmol) and **5** (total of 0.10 g, 0.01 mmol) were added to the reaction slurry to achieve a final loading of at least 20  $\mu\text{mol}$  **5/g** CPG. The support was filtered, washed with acetonitrile, and dried with argon flow. The material was capped with an equal mixture of 6% 4-(dimethylamino)pyridine in acetonitrile and 2/3/5 (acetic anhydride/2,4,6-collidine/acetonitrile) (100 mL total volume) for 2 h. The support was filtered, washed with pyridine, methanol, and methylene chloride, and dried overnight under vacuum. By measuring the absorbance at 504 nm of a solution containing a known mass of CPG and a known volume of 3% dichloroacetic acid/methylene chloride, to determine the concentration of the released trityl cation, the amount of **5** conjugated to the CPG was calculated to be 22.8  $\mu\text{mol/g}$  CPG.

**Synthesis of 10a.** A 100 mL round-bottom flask was charged with material **3a** (0.52 g, 0.66 mmol), *N,N*-diisopropylethylamine (0.13 g, 0.99 mmol), 6-amino-1-hexanol (0.093 g, 0.80 mmol), and 50 mL of acetonitrile. The reaction mixture was stirred for 45 min at RT under a drying tube and concentrated by rotary evaporation. The reaction product was purified by column chromatography (5% methanol/5% triethylamine/methylene chloride), yielding a pale yellow oil, 0.44 g, 84%.  $R_f$  = 0.47 (5% methanol/5% triethylamine/methylene chloride).  $^1\text{H}$  NMR,  $\text{CD}_3\text{CN}$ , 400 MHz,  $\delta$  7.42 (m, 2H), 7.29 (m, 6H), 7.23 (t, 1H), 6.85 (m, 4H), 6.28 (s, broad, 1H), 4.93 (m, 2H), 3.76 (s, 6H), 3.47 (q, 2H), 3.10 (q, 2H), 2.98 (t, 2H), 2.51 (t, 1H), 2.05 (t, 2H), 2.00 (s, 3H), 1.99 (s, 3H), 1.6–1.2 (aliphatic, 30H) ppm. ESI-MS: calculated for  $\text{C}_{47}\text{H}_{67}\text{NO}_9$  ( $\text{M} + \text{K}$ ) $^+$  829; found 829.

**Synthesis of 11a.** Material **10a** (0.40 g, 0.51 mmol) was coevaporated three times with 20 mL of acetonitrile and dissolved in 4 mL of methylene chloride. 2-Cyanoethyl *N,N,N,N*-tetraisopropylphosphorodiamidite (0.19 g, 0.61 mmol) was added, followed by the addition of a solution of 1*H*-tetrazole in acetonitrile (28 mg, 0.40 mmol/2 mL) with vigorous swirling. The reaction mixture was vortexed at RT for 2 h. Methylene chloride (25 mL) was added to the reaction to increase the volume, and the crude solution was washed with 25 mL of 5% sodium bicarbonate/0.5% triethylamine. The organic layer was dried over magnesium sulfate for 10 min, filtered, concentrated, and coevaporated twice with (20 mL) acetonitrile. The residue was dissolved in acetonitrile (15 mL) and dried over several granules of calcium hydride. The product solution was aliquoted (five aliquots of 3 mL, 100  $\mu\text{mol}$ ) into amber Expedite bottles, concentrated by aspiration vacuum, then dried overnight under vacuum in a desiccator containing phosphorus pentoxide (0.49 g, 98%).  $R_f$  = 0.48 (5% triethylamine/dioxane).

**Synthesis of 10b.** The method for the synthesis of **10a** was followed using **3a** (0.18 g, 0.22 mmol), *N,N*-Diisopropylethylamine (0.04 g, 0.29 mmol), PEG<sub>3400</sub>-amine (Shearwater Corporation, Huntsville, AL, 0.50 g, 0.15



mmol), and 50 mL of acetonitrile. The crude product was purified by column chromatography (2% methanol/5% triethylamine/methylene chloride). Compound **10b** was obtained as a white solid with a yield higher than the theoretical value due to the hygroscopic character of the material.  $R_f = 0.29$  (5% methanol/5% triethylamine/methylene chloride). ESI-MS: calculated for  $C_{195}H_{363}NO_{85}$  ( $M + H$ )<sup>+</sup> 4080, product displayed a PEG mass dispersion centered around 4100.

**Synthesis of 11b.** The method for the synthesis of **11a** was followed using **10b** (0.40 g, 0.01 mmol), 2-Cyanoethyl *N,N,N,N*-tetraisopropylphosphorodiamidite (0.04 g, 0.12 mmol), and 1*H*-tetrazole in acetonitrile (5 mg, 0.08 mmol/1 mL). The product yield was 0.23 g, 56%.  $R_f = 0.69$  (5% triethylamine/dioxane).

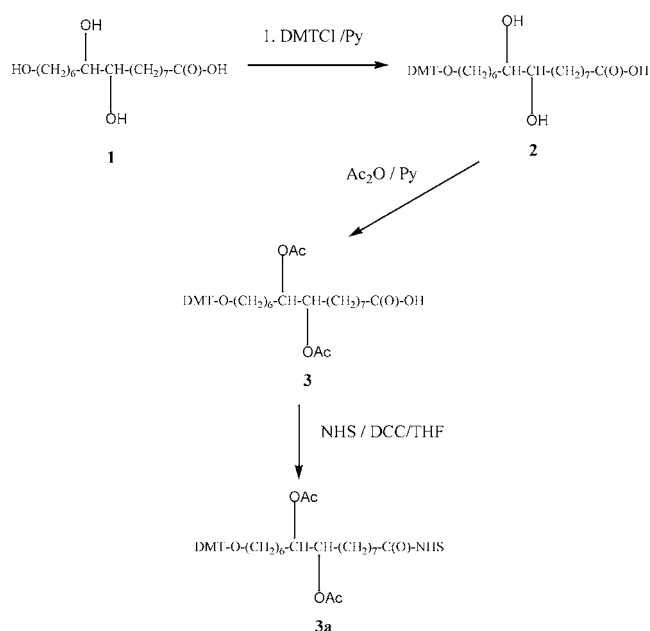
**Synthesis of Mono-dimethoxytrityl-1,12-dodecanediol.** Combined 1,12-dodecanediol (4 g, 20 mmol), *N,N*-diisopropylethylamine (1.3 g, 9.9 mmol), and 100 mL of THF. 4,4'-Dimethoxytrityl chloride (2.2 g, 6.6 mmol) was added slowly as a solid. After 1 h, the reaction was concentrated by rotary evaporation, and the product was purified by column chromatography (25% ethyl acetate/75% hexane), yielding a colorless oil, 3.3 g, 99%.  $R_f = 0.39$  (50% ethyl acetate/50% hexane). ESI-MS: calculated for  $C_{33}H_{44}O_4$  ( $M + K$ )<sup>+</sup> 543, found 543.

**Synthesis of Dodecanediol Phosphoramidite.** The method for the synthesis of **11a** was followed using mono-dimethoxytrityl-1,12-dodecanediol (0.60 g, 1.2 mmol), 2-cyanoethyl *N,N,N,N*-tetraisopropylphosphorodiamidite (0.43 g, 1.4 mmol), and 1*H*-tetrazole in acetonitrile (64 mg, 0.92 mmol/3 mL). The product yield was 0.80 g, 96%.  $R_f = 0.42$  (75% ethyl acetate/25% hexane).

**Cleavage and Deprotection of Aleuritic Acid-Conjugated Oligonucleotides Leading to the Formation of 7, 12a, and 12b.** After synthesis of the aleuritic acid DNA conjugate on a 1  $\mu$ mol scale, the product was cleaved and deprotected in a solution of 20% 0.4 M sodium hydroxide/methanol (1 mL) for 3 h at 55 °C. The slurry was filtered, and the filtrate was neutralized with 4  $\mu$ L of 80% acetic acid and desalted on a NAP-10 column.

**Oxidation of Aleuritic Acid-Conjugated Oligonucleotides (7, 12a, and 12b) Leading to the Preparation of Aldehyde-Modified Probes (8, 13a, and 13b).** A 1  $\mu$ mol synthesis of aleuritic acid-DNA conjugate was dissolved in 0.9 mL of 100 mM sodium phosphate buffer, pH 7.6, and 0.1 mL of 100 mM sodium periodate in 100 mM sodium phosphate buffer, pH 7.6. The reaction solution was incubated in the dark for 30 min at RT, then purified on a NAP-10 column.

**Coupling of Aldehyde-Modified Oligonucleotides to Amine-Containing Compounds. Preparation of 9a, 9b, and 15.** A solution of amine (25  $\mu$ mol) was prepared in 1 mL of reaction buffer (for synthesis of **9a**: 25 mM sodium borate, pH 9.5; for synthesis of **9b**: 8% DMSO/25% methanol/25 mM sodium borate buffer, pH 9.5; for synthesis of **15**: 10% methanol/30% acetonitrile/25 mM sodium borate buffer, pH 9.5). The aldehyde-labeled oligonucleotide (1  $\mu$ mol) was dissolved in the appropriate amine-containing reaction buffer, and 10  $\mu$ L of 5 M sodium cyanoborohydride in 1 N sodium hydroxide was added. The pH of the reaction solution was adjusted between 9 and 10 with either 80% acetic acid or 1 N sodium hydroxide, and the reaction solution was incubated at RT. The crude reactions were monitored by HPLC analysis and, upon completion (3 h), were purified on NAP-10 columns. The products (**9a**, **9b**, and **13a**) were analyzed by MS to confirm product formation.



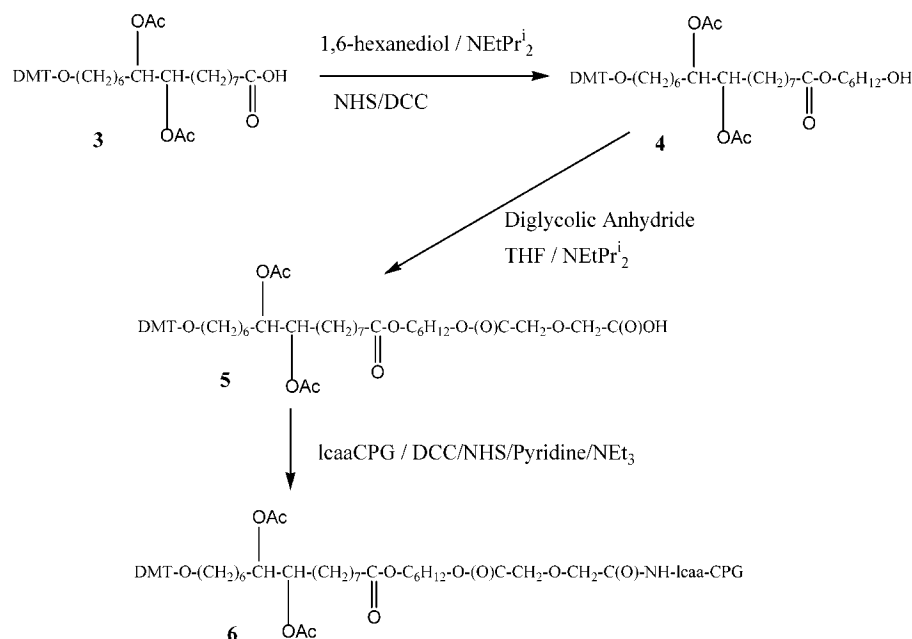
**Figure 2.** Synthesis of the NHS ester of the selectively protected aleuritic acid **3a**.

**Protocol for the Preparation of the 5'-Aldehyde-Modified DNA Probes using C18 Oligonucleotide Purification Cartridge.** The purification was performed using Supelco, Supelclean Envi-18, 1 g, 12 mL tubes. All additions were allowed to completely enter the gel bed before initiating the next step. The resin was equilibrated with one wash each of 5 mL of methanol, 5 mL of water, and 5 mL of 0.5 M sodium chloride. The DNA sample was loaded onto the column in an equal volume of water and 0.5 M sodium chloride (3 mL total volume). The column was washed with 5 mL of 0.5 M sodium chloride, followed by a 1 mL addition of 100 mM sodium periodate solution which was allowed to incubate on the column for 15 min. The column was washed with 5 mL of water, then 1.5 mL of 10% methanol/water to elute the cleaved fragments. The final product was eluted with 1.5 mL of methanol/water 1:1.

## RESULTS AND DISCUSSION

**Attachment of Aleuritic Acid Moiety to the 3'-Loci of the DNA Probes. Synthesis of the Aleuritic Acid CPG.** In recent years, the chemical literature has reported numerous methods for synthesizing different phosphoramidite reagents used to introduce single or multiple functional groups at the 3' or 5' terminus of a synthesized DNA oligonucleotide (5–19). In contrast, far fewer methods are reported for synthesizing 3'-modified oligonucleotides (13, 71–82), most likely due to the synthetic inconveniences associated with the preparation of such reagents. We found that the approach of synthesizing a solid support modified with an aleuritic acid moiety represents a very attractive way to introduce a carboxyl or masked aldehyde group into the 3'-end of a synthesized DNA oligonucleotide, leaving the 5'-terminus available for other modifications. In the first step of our synthetic strategy, we prepared selectively protected derivatives of aleuritic acid **3** and **3a** that can serve as intermediates for further preparations of modified solid supports or for the synthesis of new phosphoramidite reagents (Figure 2).

Known differences in the reactivity between the primary and secondary hydroxyl groups (83) facilitated the



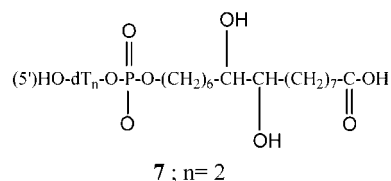
**Figure 3.** Preparation of the aleuritic acid CPG **6**.

synthesis and chromatographic isolation of the aleuritic acid derivative **2** with a DMT-protected primary hydroxyl group. In the subsequent step of the procedure, derivative **2** was treated with acetic anhydride in pyridine and converted into intermediate compound **3**, in which both the primary and the secondary hydroxyl groups were selectively protected with the DMT and the acetyl groups. In the next step, the fully protected compound **3** was converted into the *N*-hydroxysuccinimide (NHS) ester **3a**. Synthesized compounds **3** and **3a** can serve as a key intermediates for the synthesis of a variety of reagents used in the introduction of the modification into DNA probes. Figure 3 illustrates the use of the compound **3** in the preparation of a new CPG material modified with the aleuritic acid moiety.

In the initial step, compound **3** was converted into the 1,6-hexanediol monoester **4**. In the next step, the free hydroxyl group of the ester **4** was reacted with diglycolic anhydride (**85**) to form the diglycolic monoester **5**. Finally, the diglycolic monoester **5** was coupled to the lcaa-CPG support, yielding solid support **6** modified with the aleuritic acid moiety.

In all synthetic steps leading to the production of the solid support **6**, standard reaction conditions and coupling protocols were employed (*1, 2, 75, 84, 85*). The efficiency of the coupling reaction of the diglycolic monoester **5** to the lcaa-CPG solid support was estimated by measuring the concentration of the DMT cation released from the support **6** after treatment with 3% dichloroacetic acid in dichloromethane. Typically, the observed loading of the DMT-protected aleuritic acid on the synthesized solid support **6** was in the range of 22–26  $\mu\text{mol/g}$ .

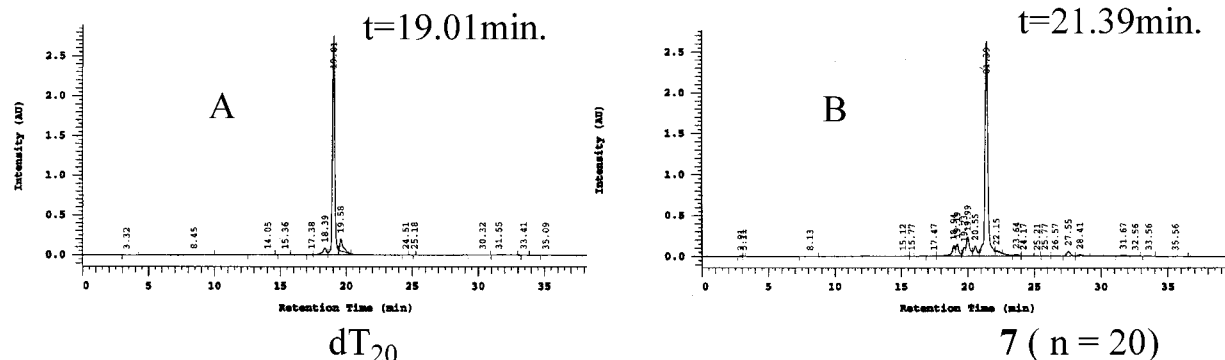
To examine the applicability of the prepared solid support **6** to the synthesis of 3'-modified DNA probes, we tested this material under the conditions of automated oligonucleotide synthesis. To perform the synthesis, an appropriate amount of the solid support **6**, containing 1  $\mu\text{mol}$  of the attached aleuritic acid, was loaded into cartridges compatible with the PerSeptive Biosystems Expedite automated DNA synthesizer. The standard phosphoramidite coupling protocol was applied for the synthesis of the DNA probes. In the first experiment, we synthesized a 3'-modified dinucleotide **7** ( $n = 2$ ) as a



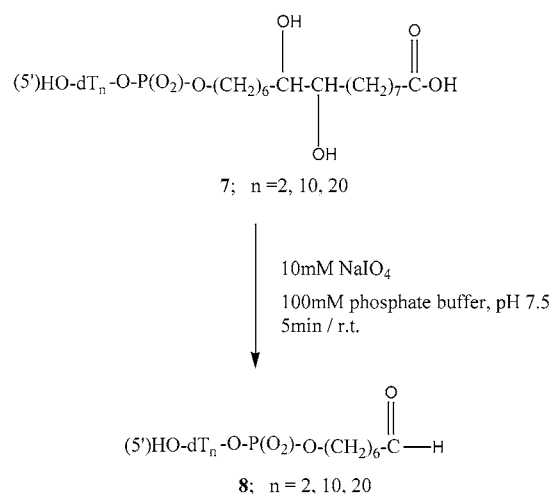
**Figure 4.** Structure of the dT dinucleotide **7** ( $n = 2$ ), modified at its 3'-end with the aleuritic acid moiety.

convenient model material for the study of cleavage and deprotection conditions that would lead to formation of a final product with a deprotected carboxyl group and fully deprotected vicinal hydroxyl groups (Figure 4).

We expected the relatively low molecular weight of compound **7** ( $n = 2$ ) to facilitate the reversed-phase (RP) HPLC analysis of the reaction product, given that any partially deprotected derivatives of the desired final product would be more easily separated and detected. In our initial experiments with compound **7** ( $n = 2$ ), we followed the standard protocol widely used for the cleavage and deprotection of chemically synthesized oligonucleotides (concentrated ammonia, 6 to 12 h at 55  $^{\circ}\text{C}$ ) (*1–4*). RP HPLC analysis (data not shown) of the generated reaction product revealed that such deprotection conditions yielded multiple compounds regardless of the length of contact of the synthesized material with concentrated ammonia. The disappearance of certain compounds by use of extended incubation in concentrated ammonia suggested that the crude product of the cleavage and deprotection reaction contained incompletely deprotected final material. The nature of other compounds present in the crude material was not studied. We achieved formation of a uniform and fully deprotected product **7** ( $n = 2$ ) by replacing the concentrated ammonia with a solution of 80% methanol/20% 0.2 M NaOH/ $\text{H}_2\text{O}$  and incubating the protected compound **7** ( $n = 2$ ) for 3 h at 55  $^{\circ}\text{C}$  (conditions recommended by GlenResearch to cleave and deprotect DNA probes synthesized on 3'-carboxylate photolabile CPG; see also ref 75). When this deprotection protocol was applied to the synthesis of longer, 3'-labeled oligonucleotides **7** ( $n = 10$  and  $n = 20$ ), we synthesized the desired products with efficiency and purity comparable to those achieved in the synthesis of



**Figure 5.** (A) RP HPLC of the crude unmodified  $\text{dT}_{20}$  cleaved from the solid support with concentrated ammonia. (B) RP HPLC of the 3'-modified probe **7** ( $n = 20$ ) cleaved from the solid support **6** with a solution of 80% methanol/20% 0.2 M NaOH/ $\text{H}_2\text{O}$  for 3 h at 55 °C.



**Figure 6.** Sodium periodate oxidation of the aleuritic acid moiety attached to the 3'-loci of the probes **7** ( $n = 2, 10, 20$ ).

unmodified dT oligomers of the same length. Figure 5 compares the RP-HPLC analytical profile of crude material **7** ( $n = 20$ ), synthesized on solid support **6** and deprotected with adapted protocol, to that of the crude 3'-unmodified dT-20-mer synthesized and deprotected according to the standard protocols.

All synthesized compounds **7** ( $n = 2, 10, 20$ ) labeled at the 3'-end with the aleuritic acid moiety were isolated by RP HPLC, and their identities were confirmed by MS. As mentioned above, the structural features of the aleuritic acid attached to the synthesized oligonucleotide probe allow for the efficient introduction not only of a carboxyl group, but also a masked aldehyde group. Vicinal diols can be readily oxidized by a solution of sodium periodate under very mild conditions. This reaction leads to the bond cleavage between carbon atoms bearing vicinal hydroxyl groups and to the formation of two molecules containing aldehyde functional groups (36, 40). The two newly formed molecules may be identical or different, depending on the symmetry of the oxidized vicinal diol. Such a synthetic approach was reported in a number of cases describing the preparations of aldehyde-modified DNA probes and oligonucleotide bioconjugates, as well as in the immobilization protocols of DNA probes onto solid surfaces (31–70). We selected previously synthesized compounds **7** ( $n = 2, 10$ , and 20) as models to study the conditions of the sodium periodate oxidation of vicinal hydroxyl groups present in the structure of aleuritic acid linked to the 3'-ends of the synthesized DNA probes **7** (Figure 6).

Oxidation of compounds **7** ( $n = 2, 10, 20$ ) was performed with 100 mM sodium periodate in 100 mM sodium phosphate buffer, pH 7.5, at room temperature (46, 97). The corresponding 3'-aldehyde labeled DNA probes **8** ( $n = 2, 10, 20$ ) were formed quickly and efficiently. Monitoring the progress of the oxidation reaction by RP HPLC revealed that the full conversion of compounds **7** ( $n = 10, 20$ ) into the corresponding 3'-aldehyde labeled derivatives **8** ( $n = 10, 20$ ) occurred in less than 5 min (Figure 7). The structure of the oxidation products **8** ( $n = 2, 10, 20$ ), isolated by RP HPLC, was confirmed by MS.

To demonstrate the utility of synthesized 3'-aldehyde-labeled probe **8** ( $n = 10$ ) as a starting material in the postsynthetic conjugation protocols, we used this material as a substrate in the reductive amination reaction with 1-pyrene methylamine and 4,7,10-trioxo-1,13-tridecanediamine (Figure 8).

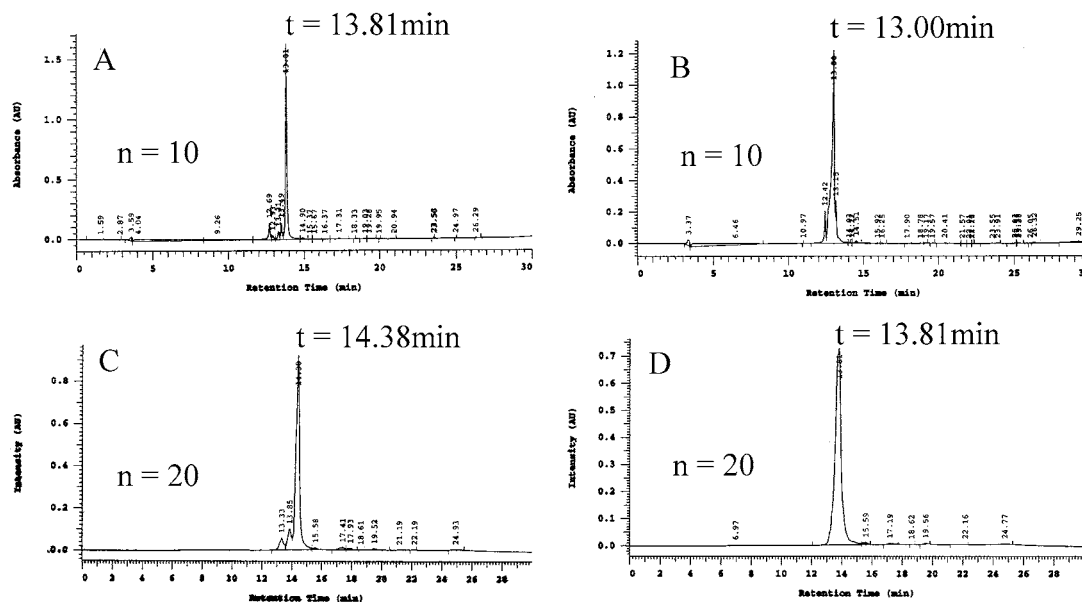
The conjugation of material **8** ( $n = 10$ ) to water soluble 4,7,10-trioxo-1,13-tridecanediamine proceeded with excellent yield under standard reaction conditions (97), producing conjugate **9a**. The conjugation reaction of the 1-pyrene methylamine to material **8** ( $n = 10$ ), leading to the formation of the conjugate **9b**, was, however, negatively affected by the low solubility of the 1-pyrene methylamine hydrochloride in aqueous media. The use of a solvent system containing 25% methanol and 8% of DMSO was necessary to achieve 60% coupling yield of the 1-pyrene methylamine to the 3'-aldehyde labeled probe **8** ( $n = 10$ ).

#### Phosphoramidites of Aleuritic Acid Derivatives.

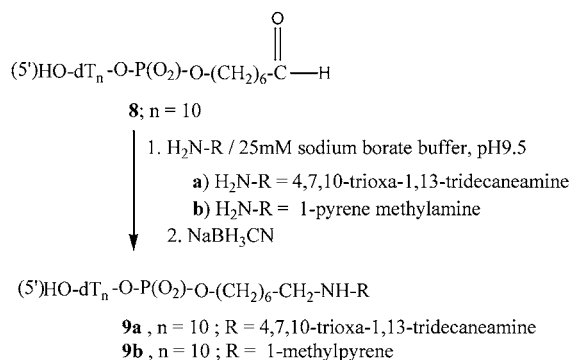
The synthesis of new reagents allowing for the introduction of an aldehyde group into DNA probes has been reported recently (40, 41, 43, 44, 55, 68). This research indicates a renewed interest in the synthesis and application of the aldehyde group not only in the preparation of modified DNA probes, but also in the immobilization of modified oligonucleotides onto solid surfaces (60, 63, 65, 68, 70). During the course of our study, we have found that the aleuritic acid intermediate **3a** serves as a convenient intermediate in the synthesis of a new family of structurally diverse phosphoramidites **11**, capable of introducing a masked aldehyde group into a synthesized DNA probe (Figure 9).

Group R in the synthesized phosphoramidites **11** can be selected from a variety of organic molecules, depending on the length of the linker or its desired chemical, physical or spectral properties (86–94). As an example, we synthesized two new phosphoramidites: phosphoramidite **11a**,  $\text{R} = \text{C}_6\text{H}_{12}$ , and phosphoramidite **11b**,  $\text{R} = \text{PEG}$ , MW 3400. Both phosphoramidites **11a** and **11b**





**Figure 7.** RP HPLC analysis of the 3'-aleuritic acid-labeled probes **7**: (A) compound **7** ( $n = 10$ ); (B) compound **8** ( $n = 10$ ); (C) compound **7** ( $n = 20$ ); and the RP HPLC analysis of the crude product of their oxidation with sodium periodate after 5 min; (D) compound **8** ( $n = 20$ ). All analytical runs were done using 2%/min acetonitrile gradient.

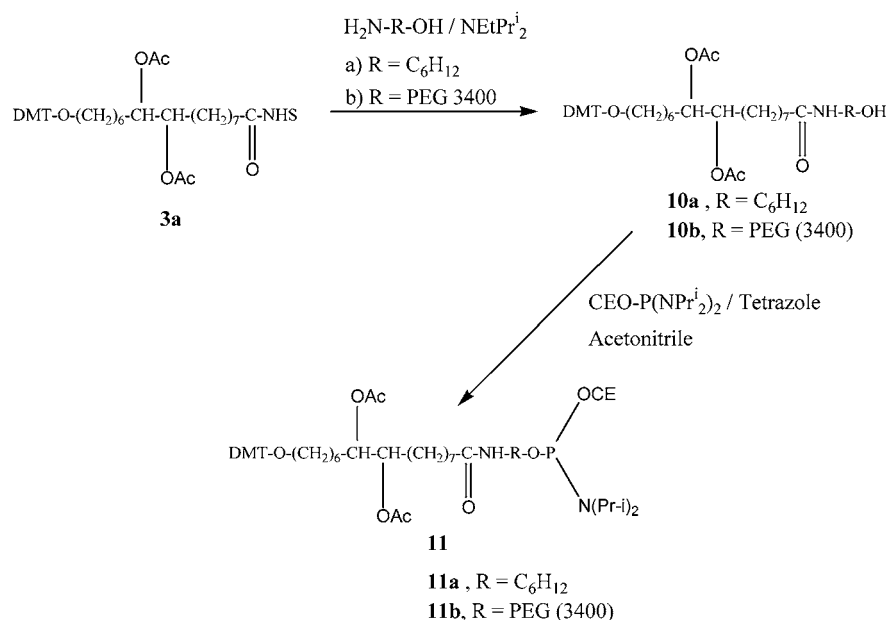


**Figure 8.** Reductive amination coupling reaction of the 3'-aldehyde-labeled probe **8** ( $n = 10$ ) to 4,7,10-trioxa-1,13-tridecanediamine and 1-pyrene methylamine.

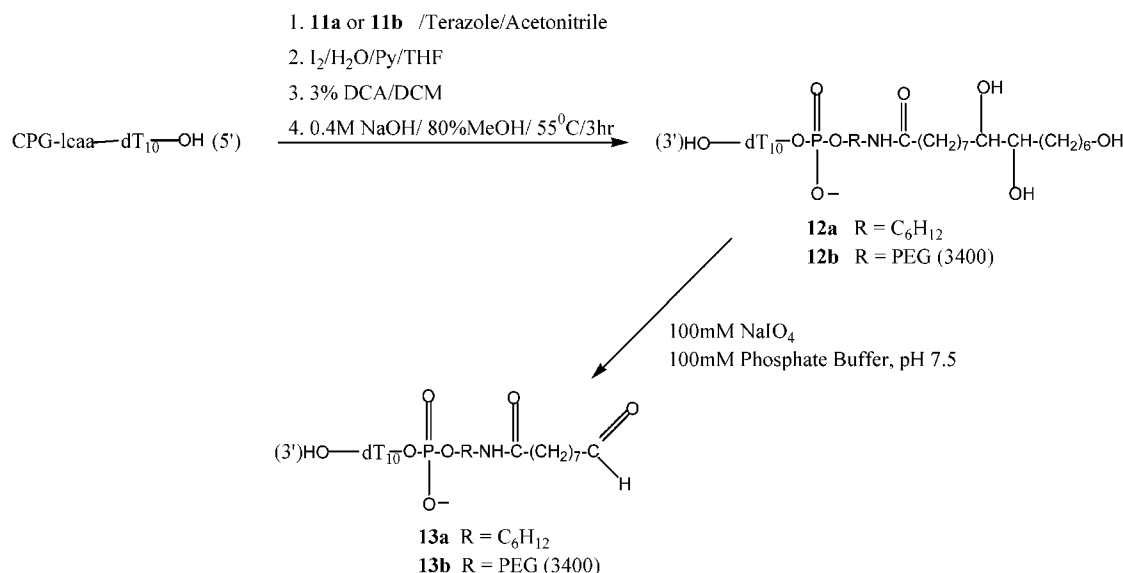
were successfully applied as reagents in the automated synthesis of two different 5'-modified DNA probes, **12a**

( $n = 2$ ), R = C<sub>6</sub>H<sub>12</sub> and **12b** ( $n = 10$ ), R = PEG, MW 3400. Both DNA probes **12a** and **12b** were subsequently oxidized to the 5'-aldehyde-modified probes **13a** and **13b** (Figure 10).

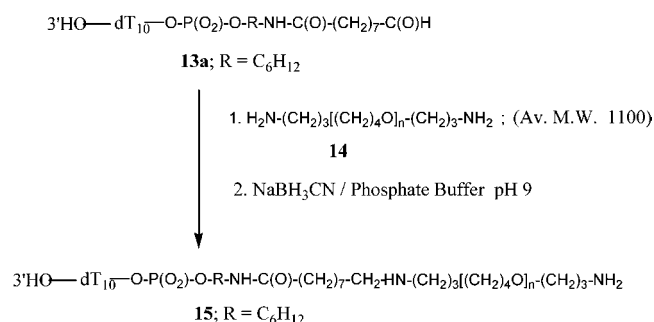
During the course of these experiments, phosphoramidites **11a** and **11b** were proven to be fully compatible with the standard phosphoramidite protocol for automated DNA synthesis. With phosphoramidite **11b**, however, a lower coupling yield was observed. Lower coupling efficiencies of phosphoramidite reagents used to introduce long linker molecules have been reported previously (86, 94). The synthesis of the phosphoramidite **11b** deserves special attention. Due to their chemical and physiological properties, conjugates of poly(ethylene glycol) (PEG) with other biologically active molecules (enzymes, peptides, and oligonucleotides) represent a very important class of bioconjugates (98). Recent chemical literature reports many synthetic efforts leading to the preparation of such



**Figure 9.** The synthesis of the phosphoramidites **11a** and **11b**.



**Figure 10.** Synthesis of the 5'-aldehyde-modified DNA probes **13a** and **13b**.



**Figure 11.** Reductive amination coupling of the 5'-aldehyde modified probe **13a** to the bis(3-aminopropyl)-terminated polytetrahydrofuran **14**.

molecules (**91–94**). In our experiments, we demonstrated that the PEG-modified oligonucleotide probe **12b**, containing a masked aldehyde group, could be synthesized using phosphoramidite **11b** in conjunction with the standard phosphoramidite protocol for automated oligonucleotide synthesis (Figure 10). The effectiveness of the reductive amination reaction, leading to the formation of the 3'-amino labeled compound **9a**, prompted us to test the efficiency of the reductive amination reaction between the 5'-aldehyde labeled compound **13a** and bis(3-aminopropyl)-terminated polytetrahydrofuran **14**, (Average *M<sub>n</sub>* ca. 1100) (Figure 11).

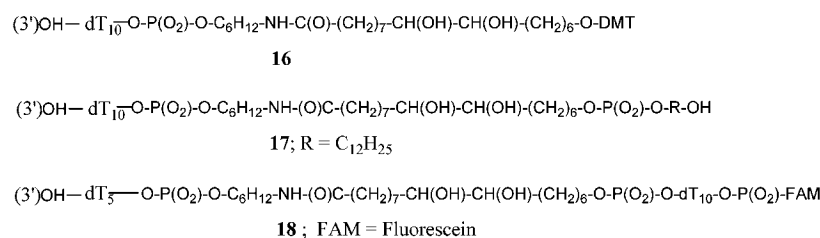
The desired reaction product **15**, in which the primary amino group was linked to the 5'-loci of the oligonucleotide by a long, nonlipophilic polymeric linker, was formed with excellent yield. MS analysis of the HPLC-purified material **15** revealed the presence of products with mass equal to the sum of the masses of the compounds **13a** and **14**. Synthetic flexibility in the preparation of struc-

turally different phosphoramidites **11** and the possibility of their combined use with phosphoramidites of other reagents opens new avenues allowing for the synthesis of structurally diverse DNA probes modified with the aldehyde group. Such probes can be used in the immobilization protocols of DNA probes onto solid surfaces (**60–70**) and in the preparation of specific DNA conjugates with performance dependent upon the character and the length of the linker attached the oligonucleotide moiety (**86, 88**).

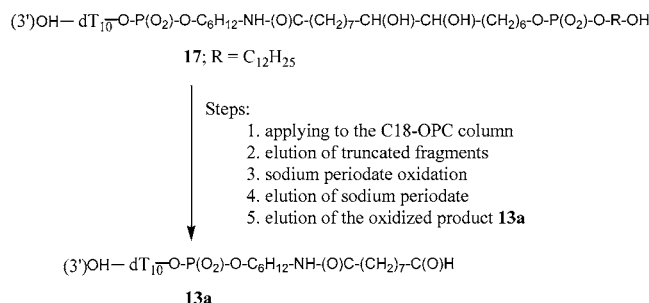
**Aleuritic Acid Phosphoramidites as Cleavable Linkers.** Synthesized phosphoramidite **11a** (R = C<sub>6</sub>H<sub>12</sub>) can be used not only as a reagent for the introduction of an aldehyde group into the 5'-end of the DNA probe, but also as a new type of cleavable linker (**95**), useful in the preparation of specific DNA probes or conjugates. We tested the efficiency of this approach by the synthesis of three model compounds **16–18**, each containing two units that were linked by phosphoramidite **11a** (R = C<sub>6</sub>H<sub>12</sub>) (Figure 12).

The difference in size and chemical character between compounds **16–18** and the products of their sodium periodate oxidation facilitated RP HPLC monitoring of the progress of cleaved product formation. At room temperature, the sodium periodate oxidation of the vicinal diols of the aleuritic acid linker in probes **16–18** was fast (less than 15 min) and led to the formation of the dT10 DNA probes modified with the aldehyde group at the 5'- or 3'-end.

Oligonucleotides modified with the aldehyde group and formed as products of the sodium periodate oxidation of compounds **16–18** were isolated by RP HPLC (data not shown), and their identity was confirmed by MS. The efficiency and ease with which the aleuritic acid linker



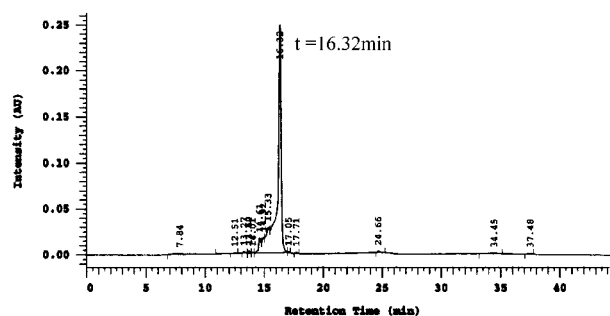
**Figure 12.** Synthesized compounds **16**, **17**, and **18**. 5'-Fluorescein phosphoramidite (FAM) was purchased from Glen Research (Sterling, VA).



**Figure 13.** Preparation of the 5'-aldehyde-modified probe **13a** via sodium periodate oxidation of the 5'-aleuritic acid-modified probe **17** absorbed on the C18-OPC cartridge.

was cleaved by the sodium periodate solution led us to the development of a new, efficient method for the production of DNA probes labeled with the aldehyde group at the 5' end, without time-consuming chromatographic purification of the final material. The method is conceptually similar to the "DMT-ON" purification protocol that is widely used in the separation of the "5'-DMT-ON," full-length DNA sequences from truncated fragments formed during the automated solid-phase synthesis of oligonucleotides (96). The "DMT-ON" purification method uses commercially available C18-oligonucleotide purification columns capable of retaining oligonucleotides modified with lipophilic (e.g., DMT) groups, while allowing elution of unmodified and truncated DNA fragments with an appropriate buffer. In the next step of the "DMT-ON" purification protocol, an acid solution is applied to the column, which leads to the cleavage of the DMT group from the retained full-length sequence. Subsequently, the full-length 5'-deprotected product is eluted from the column with another buffer addition. Generally, this purification protocol works well for 5'-DMT-protected oligonucleotides. However, the inherent instability of the DMT protecting group can occasionally cause its partial loss and, in consequence, the full-length product may be eluted along with shorter fragments in the initial step of the purification.

In our method, we adapted the "DMT-ON" purification protocol with a minor modification to the preparation and purification of the 5'-aldehyde-modified DNA probe synthesized with phosphoramidite **11a** (R = C<sub>6</sub>H<sub>12</sub>). To ensure the presence of the lipophilic group at the 5'-loci of the synthesized material, we used phosphoramidite of the DMT-protected 1-dodecanol to incorporate the desired, more stable (in comparison to the DMT group), moiety into the DNA probe **17**. In the initial step of the developed method, crude product **17** (R = C<sub>12</sub>H<sub>25</sub>) was applied to the C18-OPC cartridge (Supelco, Supelclean Envi-18), and all truncated and unmodified oligonucleotide fragments were eluted according to the standard purification protocol (see Experimental Section). Next, 1 mL of the 100 mM solution of sodium periodate was applied on the column. After the sodium periodate solution was fully absorbed, the column was left for 15 min at room temperature. This step led to the oxidation and cleavage of the aleuritic acid of the 5'-modified DNA probe **17** still retained on the column and to the formation of the 5'-aldehyde-modified DNA probe **13a**. Subsequently, the sodium periodate solution was removed by washing the column with deionized water. Finally, the desired 5'-aldehyde-labeled full-length product **13a** was efficiently eluted using a methanol:water (1:1) solution. An HPLC analysis of the eluted material **13a** demonstrated its high purity (Figure 13). MS analysis of the HPLC isolated material **13a** confirmed its structure.



**Figure 14.** RP HPLC of the material **13a** eluted from the C18-OPC column. All analytical runs were done using 2%/min acetonitrile gradient.

Figure 14 illustrates the RP HPLC analytical profile of the 5'-aldehyde-modified probe **13a** eluted from the C18-OPC cartridge.

In conclusion, we have presented an efficient and versatile synthetic strategy that allows for the preparation of a broad range of new reagents. These reagents can be used in the synthesis of aldehyde-modified DNA probes and for the preparation of new types of cleavable linkers. We demonstrated that the aldehyde-labeled DNA probes, synthesized according to the presented method, can serve as valuable starting materials in conjugation reactions with other organic moieties containing primary amino groups. The mild reaction conditions, leading to either the introduction of the aldehyde group in DNA probes or the cleavage of the aleuritic acid linker, facilitate the preparation of aldehyde-labeled materials, even in the presence of sensitive organic groups. A simple method to prepare DNA probes modified at their 5'-end with the aldehyde group has been developed.

#### ACKNOWLEDGMENT

We wish to thank Andrea Mast for her assistance in preparing this manuscript.

#### LITERATURE CITED

- (1) Letsinger, R. L., and Lunsdorf, W. B. (1976) Synthesis of thymidine oligonucleotides by phosphite triester intermediates. *J. Am. Chem. Soc.* 98, 3655-3661.
- (2) Caruthers, M. H., Barone, A. D., Beaucage, S. L., Dodds, D. R., Fisher, E. F., McBride, L. J., Matteucci, M., Stabinsky, Z., Tang, J. Y. (1987) Chemical synthesis of deoxyoligonucleotides by the phosphoramidite method. *Methods Enzymol.* 154, 287-313.
- (3) Beaucage, S. L., and Iyer, R. P. (1992) Advances in the synthesis of Oligonucleotides by the Phosphoramidite Approach. *Tetrahedron* 48, 2223-2311.
- (4) Agrawal, S., Ed. (1993) Protocols for Oligonucleotides and Analogues. *Methods in Molecular Biology, Vol. 20*, Humana Press, Totowa, NJ.
- (5) Gottikh, M., Asseline, U., and Thuong, N. (1990) Synthesis of Oligonucleotides Containing a Carboxyl Group at Either Their 5' End or Their 3' End and Their Subsequent Derivatization by an Intercalating Agent. *Tetrahedron Lett.* 31, 6657-6660.
- (6) Agrawal, S., and Zamecnik, P. (1990) Site Specific functionalization of oligonucleotides for attaching two different reporter groups. *Nucleic Acids Res.* 18, 5419-5423.
- (7) Pon, R. (1991) A Long Chain Phosphoramidite Reagent for the Automated Synthesis of 5'-Biotinylated Oligonucleotides. *Tetrahedron Lett.* 32, 1715-1718.
- (8) Thiesen, P., McCollum, C., Upadhyaya, K., Jacobson, K., Vu, H., Andrus, A. (1992) Fluorescent Dye Phosphoramidite Labeling of Oligonucleotides. *Tetrahedron Lett.* 33, 5033-5036.



- (9) Kumar, A. (1993) A Versatile Solid-Phase Method for the Synthesis of Masked 3'-Thiol Group Containing Oligonucleotides. *Nucleosides Nucleotides* 12, 1047-1059.
- (10) Beaucage, S. L., and Iyer, R. P. (1993) The Functionalization of Oligonucleotides Via Phosphoramidite Derivatives. *Tetrahedron* 49, 1925-1963.
- (11) Agrawal, S., Ed. (1994) Protocols for Oligonucleotide Conjugates. *Methods in Molecular Biology*, Vol. 26, Humana Press, Totowa, NJ.
- (12) Guzayev, A., Salo, H., Azhayev, A., and Lonnberg, H. (1995) A New Approach for Chemical Phosphorylation of Oligonucleotides at the 5'-Terminus. *Tetrahedron* 51, 9375-9384.
- (13) Matray, T. J., Yoo, D. J., McMinn, D. J., and Greenberg, M. M. (1997) Synthesis of Oligonucleotides Containing 3'-Alkylcarboxylic Acids Using a Palladium Labile Oligonucleotide Solid-Phase Synthesis Support. *Bioconjugate Chem.* 8, 99-102.
- (14) Huang, Z., and Szostak, J. (1996) A simple method for 3'-labeling of RNA. *Nucleic Acids Res.* 24, 4360-4361.
- (15) Lyttle, M., Adams, H., Hudson, D., and Cook, R. (1997) Versatile Linker Chemistry for Synthesis of 3'-Modified DNA. *Bioconjugate Chem.* 8, 193-198.
- (16) Hovinen, J., and Salo, H. (1997) C-Glycoside phosphoramidite building block for versatile functionalization of oligodeoxyribonucleotides. *J. Chem. Soc. Perkin Trans. 1* 3017-3020.
- (17) Bruck, R., Koppitz, M., Joyce, G., and Orgel, L. (1997) A simple procedure for constructing 5'-amino-terminated oligodeoxynucleotides in aqueous solution. *Nucleic Acids Res.* 25, 1309-1310.
- (18) Shepinov, M., and Stetsenko, D. (1997) A Facile Route to 3'-Modified Oligonucleotides. *Bioorg. Med. Chem. Lett.* 7, 1181-1184.
- (19) Smith, T. H., LaTout, J. V., Bokchariov, D., Chaga, G., and Nelson, P. S. (1999) Bifunctional phosphoramidite reagents for the introduction of histidyl and dihistidyl residues into oligonucleotides. *Bioconjugate Chem.* 10, 647-52.
- (20) Goodchild, J. (1990) Conjugates of Oligonucleotides and Modified Oligonucleotides: a Review of Their Synthesis and Properties. *Bioconjugate Chem.* 1, 165-187.
- (21) Cook, P. (1991) Medicinal Chemistry of Antisense Oligonucleotides. *Anti-Cancer Drug Des.* 6, 585-607.
- (22) Riordan, M., and Martin, J. (1991) Oligonucleotide-Based Therapeutics. *Nature* 350, 442-443.
- (23) Englisch, U., and Gauss, D. (1991) Chemically Modified Oligonucleotides as Probes and Inhibitors. *Angew. Chem., Int. Ed.* 30, 613-722.
- (24) Knorre, D., Vlassov, V. V., Zarytova, V. F., Lebedev, A. S., and Fedorova, S. O. (1994) *Design and Targeted Reactions of Oligonucleotide Derivatives*, CRC Press, Boca Raton, FL.
- (25) Agrawal, S., and Iyer, R. P. (1999) Modified Oligonucleotides as Therapeutic and Diagnostic Agents. *Curr. Opin. Biotechnol.* 6, 12-19.
- (26) Akhtar, S., Ed. (1995) Delivery Strategies for Antisense Oligonucleotide Therapeutics. CRC Press, Boca Raton, FL.
- (27) Matysiak, S., Frank, R., and Pfeleiderer, W. (1997) Acetal Oligonucleotide Conjugates in Antisense Strategy. *Nucleosides Nucleotides* 16, 855-861.
- (28) Wojcowski, C., Stolze, K., and Engels, J. W. (1999) Fluorescent Oligonucleotides - Versatile Tools as Probes and Primers for DNA and RNA Analysis. *Synlett* 10, 1667-1678.
- (29) Zhao, X., Nampali, S., Serino, A. J., and Kumar, S. (2001) Immobilization of oligodeoxyribonucleotides with multiple anchors to microchips. *Nucleic Acids Res.* 29, 955-959.
- (30) Yang, M., McGovern, M. E., and Thompson, M. (1997) Gensensor technology and the detection of interfacial nucleic acid chemistry. *Anal. Chim. Acta* 346, 259-275.
- (31) Agrawal, S., Christodoulou, C., and Gait, M. (1986) Efficient Methods for Attaching Non-Radioactive labels to the 5' ends of synthetic oligodeoxyribonucleotides. *Nucleic Acids Res.* 14, 6227-6245.
- (32) Ide, H., Akamatsu, K., Kimura, Y., Michiue, K., Makino, K., Asaeda, A., Takamori, Y., and Kubo, K. (1993) Synthesis and Damage Specificity of a Novel Probe for the Detection of Abasic Sites in DNA. *Biochemistry* 32, 8276-8283.
- (33) Dechamps, M., and Sonveaux, E. (1995) Aldehyde Functions in Synthetic Oligonucleotides. *Nucleosides Nucleotides* 14, 867-870.
- (34) Boutryn, D., Boudali, A., Constant, J. F., Defrancq, E., and Lhomme, J. (1997) Synthesis of Fluorescent Probes for the Detection of Abasic Sites in DNA. *Tetrahedron* 53, 5485-5492.
- (35) Trevisiol, E., Renard, A., Defrancq, E., and Lhomme, J. (1997) The Oxyamino-Aldehyde Coupling Reaction: An Efficient Method for the Derivatization of Oligonucleotides. *Tetrahedron Lett.* 38, 8687-8690.
- (36) Ermolinsky, B. C., and Mikhailov, S. N. (2000) Periodate Oxidation in Chemistry of Nucleic Acids: Dialdehyde Derivatives of Nucleosides, Nucleotides and Oligonucleotides (Review). *Russ. J. Bioorg. Chem.* 26, 429-449.
- (37) Trevisiol, E., Renard, A., Defrancq, E., and Lhomme, J. (2000) Fluorescent labeling of oligodeoxynucleotides by the oxyamino-aldehyde coupling reaction. *Nucleosides, Nucleotides Nucleic Acids* 19, 1427-1439.
- (38) Krotz, A. H., Gaus, H., Ravikumar, V. T., and Cole, D. L. (2001) Preparation of Oligonucleotides Without Aldehyde Abasic Sites. *Bioorg. Med. Chem. Lett.* 11, 1863-1867.
- (39) Defrancq, E., and Lhomme, J. (2001) Use of an aminoxyl linker for the functionalization of oligodeoxynucleotides. *Bioorg. Med. Chem. Lett.* 11, 931-3.
- (40) Tilquin, J. M., Dechamps, M., Sonveaux, E. (2001) Incorporation of an Aldehyde Function in Oligonucleotides. *Bioconjugate Chem.* 12, 451-457.
- (41) Karino, N., Ueno, Y., and Matsuda, A. (2001) Synthesis and properties of oligonucleotides containing 5-formyl 2'-deoxycytidine: in vitro DNA polymerase reactions on DNA templates containing 5-formyl-2'-deoxycytidine. *Nucleic Acids Res.* 29, 2456-2463.
- (42) Proudnikov, D., and Morzabekov, A. (1996) Chemical methods of DNA and RNA fluorescent labeling. *Nucleic Acids Res.* 24, 4535-4542.
- (43) Dechamps, M., and Sonveaux, E. (1998) Aldehyde-oligonucleotides for bioconjugation. *Nucleosides Nucleotides* 17, 697-708.
- (44) Greenberg, M. M., and Kahl, J. D. (2001) Template-Free Segmental Synthesis of Oligonucleotides Containing Nonnative Linkages. *J. Org. Chem.* 66, 7151-7154.
- (45) Bellon, L., Workman, C., Jarvis, T., and Wincott, F. (1997) Postsynthetically Ligated Ribozymes: An Alternative Approach to Iterative Solid-Phase Synthesis. *Bioconjugate Chem.* 8, 204-212.
- (46) Urata, H., and Akagi, M. (1993) A Convenient Synthesis of Oligonucleotides with a 3'-Phospho-glycolate and 3'-Phosphoglycaldehyde Terminus. *Tetrahedron Lett.* 34, 4015-4018.
- (47) Okamoto, A., Tainaka, K., and Saito, I. (2002) A facile incorporation of the aldehyde function into DNA: 3-formylindole nucleosides as an aldehyde-containing nucleoside. *Tetrahedron Lett.* 43, 4581-4583.
- (48) Ghosh, S. S., Kao, P. M., and Kwok, D. Y. (1989) Synthesis of 5'-Oligonucleotide Hyrazide Derivatives and Their Use in Preparation of Enzyme-Nucleic Acid Hybridization Probes. *Anal. Biochem.* 178, 43-51.
- (49) Chang, G., Shiao, M., Liaw, J., and Lee, H. (1989) Periodate-oxidized 3-Aminopyridine Adenine Dinucleotide Phosphate as a Fluorescent Affinity Label for Pigeon Malic Enzyme. *J. Biol. Chem.* 264, 289-287.
- (50) Cremer, G., Kalbas, M., Fasold, H., and Prochov, D. (1992) Covalent Attachment of Ribonucleic Acids to Proteins. *J. Protein Chem.* 11, 553-560.
- (51) Reyes, R. A., and Cockerell, G. L. (1993) Preparation of pure oligonucleotide-alkaline phosphatase conjugates. *Nucleic Acids Res.* 21, 5532-5533.
- (52) Lin, C. C., and Chang, G. G. (1993) Using Periodate-Oxidized Nucleotide as Affinity Label for the Nucleotide Site of Proteins. *J. Protein Chem.* 12, 627-632.
- (53) Ruth, J. (1994) Oligonucleotide-Enzyme Conjugates. *Methods Mol. Biol.* 26, 167-185.
- (54) Brevnov, M. G., Gritsenko, O. M., Mikhailov, S. N., Efimtseva, E. V., Ermolinsky, B. S., Van Aershot, A., Herdewijn, P., Repyk, A. V., Gromova, E. S. (1997) DNA duplexes

- with reactive dialdehyde groups as novel reagents for cross-linking to restriction-modification of enzymes. *Nucleic Acids Res.* 25, 3302–3309.
- (55) Czaplinski, J. L., and Sheppard, T. L. (2001) Nucleic Acid Template-Directed Assembly of Metallosalen-DNA Conjugates. *J. Am. Chem. Soc.* 123, 8618–8619.
- (56) Forget, D., Boutryn, D., Defrancq, E., Lhomme, J., and Dumy, P. (2001) Highly efficient synthesis of peptide–oligonucleotide conjugates: chemoselective oxime and thiazolidine formation. *Chem. Eur. J.* 7, 3976–3984.
- (57) Asseline, U., Thuong, N. T. (1997) Synthesis and properties of oligonucleotides covalently linked to intercalating agents. *New J. Chem.* 21, 5–17.
- (58) Zatsepin, T. S., Stetsenko, D. A., Arzumanov, A. A., Romanova, E. A., Gait, M. J., and Oretskaya, T. S. (2002) Synthesis of peptide–oligonucleotide conjugates with single and multiple peptides attached to 2'-aldehydes thorough thiazolidine, oxime and hydrazine linkages. *Bioconjugate Chem.* 13(4), 822–830.
- (59) Forget, D., Renaudet, O., Defrancq, E., and Dumy, P. (2001) Efficient preparation of carbohydrate-oligonucleotide conjugates (COCs) using oxime bond formation. *Tetrahedron Lett.* 42, 7829–7832.
- (60) Kremsky, J. W., Wooters, J. L., Dougherty, J. P., Meyers, R. E., Collins, M., and Brown, E. L. (1987) Immobilization of DNA via oligonucleotide containing aldehyde or carboxylic acid group at the 5'-terminus. *Nucleic Acids Res.* 15, 2891–2909.
- (61) Timofeev, E., Kochetkova, V., Mirzabekov, A. D., and Florentiev, V. L. (1996) Regioselective immobilization of short oligonucleotides to acrylic copolymer gels. *Nucleic Acids Res.* 24, 3142–3149.
- (62) Rogers, T. H., Jiang-Baucom, P., Huang, Z. J., Anderson, S., Boyce-Jacino, M. T. (1999) Immobilization of oligonucleotides onto a glass support via disulfide bonds: A method for preparation of DNA arrays. *Anal. Biochem.* 266, 23–30.
- (63) Salo, H., Virta, P., Hakala, H., Prakash, T. O., Kawasaki, A. M., Manoharan, M., and Lonnberg, H. (1999) Aminoxy functionalized oligonucleotides: preparation, on-support derivatization and postsynthetic attachment to polymer support. *Bioconjugate Chem.* 10, 815–823.
- (64) Schluep, T., and Cooney, C. (1999) Immobilization of oligonucleotides on a large pore support for plasmid purification by triplex affinity interaction. *Bioseparation* 7, 317–326.
- (65) Zammattéo, N., Jeanmart, L., Hamels, S., Courtois, S., Louette, P., Havesi, L., and Remacle, J. (2000) Comparison between Different Strategies of Covalent Attachment of DNA to Glass Surfaces to build DNA Micro-arrays. *Anal. Biochem.* 280, 143–150.
- (66) Afanassiev, V., Hanemann, V., Wolf, S. (2000) Preparation of DNA and protein micro arrays on glass slides coated with an agarose film. *Nucleic Acid Res.* 28, E66.
- (67) Strother, T., Hamers, R. J., and Smith, L. M. (2001) Covalent Attachment of oligodeoxyribonucleotides to amine-modified Si(001) surfaces. *Nucleic Acids Res.* 29, 3535–3541.
- (68) Podymnagin, M. A., Lukhtanov, E. A., and Reed, M. W. (2001) Attachment of benzaldehyde – modified oligonucleotide probes to semicarbazide coated glass. *Nucleic Acids Res.* 29, 5090–5098.
- (69) Lindroos, K., Liljedahl, U., Raitio, M., and Syvänen, A. S. (2001) Minisequencing on oligonucleotide microarrays: comparison of immobilization chemistries. *Nucleic Acids Res.* 29, e69.
- (70) Dombi, K. L., Griesang, N., and Richert, C. (2002) Oligonucleotide arrays from aldehyde-bearing glass with coated background. *Synthesis* 6, 816–824.
- (71) Gupta, K. C., Sharma, P., Sathyanarayana, S., and Kumar, P. (1990) A Universal Solid Support for the Synthesis of 3'-Thiol Group Containing Oligonucleotides. *Tetrahedron Lett.* 31, 2471–2474.
- (72) Gupta, K., Malhotra, V., Sharma, A., Sharma, P. (1992) One Pot General Method for the Derivatization of Polymer Support for Oligonucleotide Synthesis. *Nucleic Acids Res.* 20, 4100.
- (73) Kumar, A. (1993) A New Solid-Phase Method for the Synthesis of Oligonucleotides with Terminal-3'-Phosphate. *Nucleosides Nucleotides* 12, 441–447.
- (74) Hovinen, J., Guzaev, A., Azhayev, A., and Lonnberg, H. (1993) Synthesis of 3'-Functionalized Oligonucleotides on a Single Solid Support. *Tetrahedron Lett.* 34, 8169–8172.
- (75) Hovinen, J., Guzaev, A., Azhayev, A., and Lonnberg, H. (1993) A new method to prepare 3'-modified oligonucleotides. *Tetrahedron Lett.* 34, 5163–5166.
- (76) Guzaev, A., Hovinen, J., Azhayev, A., and Lonnberg, H. (1994) Novel Solid Supports for the Preparation of 3'-Derivatized Oligonucleotides: Introduction of 3'-Alkyl phosphate Tether Groups Bearing Amino, Carboxy, Carboxamido, and Mercapto Functionalities. *Tetrahedron* 50, 7203–7218.
- (77) Yoo, D. J., and Greenberg, M. (1995) Synthesis of Oligonucleotides Containing 3'-Alkyl Carboxylic Acids Using Universal, Photolabile Solid-Phase Synthesis Supports. *J. Org. Chem.* 60, 3358–3364.
- (78) Avino, A., Garcia, R., Albercio, F., Mann, M., Wilm, M., Neubauer, G., and Eritja, R. (1996) New Carbamate Supports for the Preparation of 3'-Amino-modified Oligonucleotides. *Bioorg. Med. Chem.* 4, 1649–1658.
- (79) Habus, I., Xie, J., Iyer, R. P., Zhou, W. Q., Shen, L. X., and Agrawal, S. (1998) A Mild and Efficient Solid-Support Synthesis of Novel Oligonucleotide Conjugates. *Bioconjugate Chem.* 9, 283–291.
- (80) Stetsenko, D., and Gait, M. (2001) A Convenient Solid-Phase Method for Synthesis of 3'-Conjugates of Oligonucleotides. *Bioconjugate Chem.* 12, 576–586.
- (81) Hausch, F., and Jäschke, A. (2001) Multifunctional dinucleotide analogues for the generation of complex RNA conjugates. *Tetrahedron* 57, 1261–1268.
- (82) Nelson, P. S., Muthini, S., Kent, M. A., and Smith, T. H. (1997) 3'-terminal modification of oligonucleotides using a universal solid support. *Nucleosides Nucleotides* 16, 1951–1959.
- (83) Greene, T. W., and Wuts, P. G. M. (1999) *Protective Groups in Organic Synthesis*, Chapter 2, John Wiley & Sons, Inc., New York.
- (84) Montserat, F. X., Grandas, A., Pedroso, E. (1993) Predictable and reproducible yields in the anchoring of DMT-nucleoside-succinate to highly loaded aminoalkyl-polystyrene resins. *Nucleosides Nucleotides* 12, 967–971.
- (85) Pon R. T., and Yu, S. (1997) Hydroquinone-O, O'-diacetic acid ('Q-linker') as a replacement for succinyl and oxalyl linker arms in solid-phase oligonucleotide synthesis. *Nucleic Acids Res.* 25, 3629–3635.
- (86) Shchepinov, M. S., Case-Green, S. C., and Southern, E. M. (1997) Steric Factors influencing hybridization of nucleic acids to oligonucleotide arrays. *Nucleic Acids Res.* 25, 1155–1161.
- (87) Watterson, J. H., Piumno, P. A. E., Wust, C. C., and Krull, U. J. (2000) Effects of oligonucleotide immobilization density on selectivity of quantitative transduction of hybridization on immobilized DNA. *Langmuir* 16, 4984–4992.
- (88) Steel, A. B., Levicky, R. L., Herne, T. M., and Tarlov, M. J. (2000) Immobilization of nucleic acids on solid surfaces: effect of oligonucleotide length on layer assembly. *Biophys. J.* 79, 975–81.
- (89) Guzenhauser, S., Biala, E., and Strazewski, P. (1999) Tetraethylene glycol-derived spacer for oligonucleotide synthesis. *Nucleosides Nucleotides* 18, 1223–1224.
- (90) Ozaki, H., Ogawa, Y., Mine, M., and Sawai, H. (1998) Effect of acridine with various linker arms attached to C5 position of 2'-deoxyuridine on the stability of DNA/DNA and DNA/RNA duplexes. *Nucleosides Nucleotides* 17, 911–923.
- (91) Bonora, G. M., Ivanova, E., Zarytova, V., Burcovich, B., and Veronese, F. M. (1997) Synthesis and Characterization of High-Molecular Mass Polyethylene Glycol-Conjugated Oligonucleotides. *Bioconjugate Chem.* 8, 793–797.
- (92) Jäschke, A., Furste, J. P., Nordhoff, E., Hillenkamp, F., Cech, D., and Erdmann, V. (1994) Synthesis and Properties of oligodeoxyribonucleotides-poly(ethylene glycol) conjugates. *Nucleic Acids Res.* 22, 4810–4817.

- (93) Jäschke, A., Bald, R., Nordhoff, E., Hillenkamp, F., Cech, D., Erdmann, V. A., and Fürste, J. P. (1996) Synthesis and analytical characterization of RNA – poly(ethylene glycol) conjugates. *Nucleosides Nucleotides* 15, 1519–1529.
- (94) Jäschke, A., Fürste, J., Cech, D., and Erdmann, V. (1993) Automated Incorporation of Polyethylene Glycol into Synthetic Oligonucleotides. *Tetrahedron Lett.* 34, 301–304.
- (95) Horn, T., Chang, C., and Urdea, M. (1997) Chemical synthesis and characterization of branched oligodeoxynucleotides (bDNA) for use as a signal amplifiers in nucleic acid quantification assays. *Nucleic Acids Res.* 25, 4842–4849.
- (96) McBride, L. J., McCollum, C., Davidson, S., Efcavitch, J. W., Andrus, A., and Lombardi, S. J. (1988) A new, reliable cartridge for the rapid purification of synthetic DNA. *Biotechniques* 6, 362–7.
- (97) Hermanson, G. T. (1996) *Bioconjugate Techniques*, pp 186–186, Academic Press, New York.
- (98) Greenwald, R. B., Conover, C. D., Choe, Y. H. (2000) Poly(ethylene glycol) conjugated drugs and prodrugs: a comprehensive review. *Crit. Rev. Ther. Drug Carrier Syst.* 17, 101–61.

BC025657J



# Extending the Applicability of Carboxyfluorescein in Solid-Phase Synthesis

Rainer Fischer,<sup>†</sup> Oliver Mader,<sup>†</sup> Günther Jung,<sup>§</sup> and Roland Brock<sup>\*,†</sup>

Institute for Cell Biology, University of Tübingen, Auf der Morgenstelle 15, 72076 Tübingen, Germany, and  
Institute of Organic Chemistry, University of Tübingen, Auf der Morgenstelle 18, 72076 Tübingen, Germany.  
Received December 20, 2002; Revised Manuscript Received March 4, 2003

Optimized coupling protocols are presented for the efficient and automated generation of carboxyfluorescein-labeled peptides. Side products, generated when applying earlier protocols for the in situ activation of carboxyfluorescein, were eliminated by a simple procedure, yielding highly pure fluorescent peptides and minimizing postsynthesis workup. For the cost-efficient labeling of large compound collections, coupling protocols were developed reducing the amount of coupling reagent and fluorophore. To enable further chemical derivatization of carboxyfluorescein-labeled peptides in solid-phase synthesis, the on-resin introduction of the trityl group was devised as a protecting group strategy for carboxyfluorescein. This protecting group strategy was exploited for the synthesis of peptides labeled with two different fluorescent dyes, essential tools for bioanalytical applications based on fluorescence resonance energy transfer (FRET). Tritylation and optimized labeling conditions led to the development of a fluorescein-preloaded resin for the automated synthesis of fluorescein-labeled compound collections with uniform labeling yields.

## INTRODUCTION

A growing number of applications in bioanalytical chemistry depend on fluorescently labeled molecules with biological activity (1). Carboxyfluorescein has remained a reagent of choice for the preparation of hydrolytically stable fluorescent peptides and protein conjugates (2, 3). Fluorescein owes this popularity to its biocompatibility, low price, and availability of instrumentation for the detection of its fluorescence. Fluorescein-labeled peptide derivatives have been employed as fluorescent markers in bioanalytical applications, such as confocal laser scanning microscopy (4), flow cytometry (5), and more recently fluorescence polarization measurements (6) and intracellular fluorescence correlation spectroscopy (7).

Moreover, carboxyfluorescein has been shown to be a useful educt for the synthesis of further fluorescent reagents (8–10).

Labeling of peptides with fluorescein can either be performed in solution or using side chain-protected polymer-bound peptides in solid-phase peptide synthesis (SPPS).<sup>1</sup> In most cases reported so far, labeling has been accomplished using activated reagents, namely fluorescein isothiocyanate (11) or carboxyfluorescein-*N*-succinimidyl ester (12). However, these activated fluorescein derivatives are rather expensive in comparison to 5(6)-carboxyfluorescein (2).

In solid-phase synthesis, coupling of carboxyfluorescein has been accomplished using in situ activation with different coupling reagents (2, 13). However, when applying the published protocols, we detected the formation of various side products. Here we present the elucidation of these side products and their removal by a simple procedure yielding highly pure carboxyfluorescein-labeled peptides.

When dealing with the synthesis of large peptide collections (14) and combinatorial compound libraries (14, 15), the use of a large excess of fluorophore is not economical. This is especially the case when isomerically pure carboxyfluorescein is desired (16). Thus we have established a protocol employing far less equivalents of carboxyfluorescein, which still results in complete turnover of the solid-phase bound peptides.

Peptides bearing two different fluorescent dyes extend the use of fluorescently labeled reporter molecules to fluorescence resonance energy transfer (FRET) experiments (17). These peptides can be used for various in vitro applications, e.g., the detection of metal ions (18), the investigation of protein–ligand interactions (19), and monitoring of transpeptidation reactions (20) or proteolytic activity (21). In combination with large genetically encoded libraries of protein variants, such com-

\* To whom correspondence should be addressed. Ph.: +49–7071–2977629. Fax: +49–7071–295891. E-mail: roland.brock@uni-tuebingen.de. rainer.fischer@uni-tuebingen.de.

<sup>†</sup> Institute for Cell Biology, University of Tübingen.

<sup>§</sup> Institute of Organic Chemistry, University of Tübingen.

<sup>1</sup> Abbreviations: ACN, acetonitrile; Ahx, 6-aminohexanoic acid; Boc, *tert*-butoxycarbonyl; DCM, dichloromethane; Dde, 1-(4,4-dimethyl-2,6-dioxocyclohexylidene)ethyl; DHAP, 2,5-dihydroxyacetophenone; DIC, *N,N*-diisopropyl carbodiimide; DIPEA, *N,N*-diisopropylethylamine; DMF, *N,N*-dimethylformamide; FITC, fluorescein isothiocyanate; Fluo, 5(6)-carboxyfluorescein, Fmoc, 9-fluorenylmethoxycarbonyl; FRET, fluorescence resonance energy transfer; FT-ATR-IR, Fourier transform attenuated total reflection infrared; HFIP, hexafluoro-2-propanol; HOBt, 1-hydroxybenzotriazol; HPLC, high-performance liquid chromatography; MALDI-MS, matrix-assisted laser desorption ionization mass spectrometry; MeOH, methanol; MHC, major histocompatibility complex; Mtt, 4-methyltrityl; NMR, nuclear magnetic resonance; Pamb, 4-aminomethyl benzoic acid; RP, reversed phase; RT, room temperature; SPPS, solid-phase peptide synthesis; SPS, solid-phase synthesis; Tamra, 5(6)-carboxytetramethylrhodamine; *t*Bu, *tert*-butyl; *t*BuOH, *tert*-butyl alcohol; TBTU, 2-(1*H*-benzotriazol-1-yl)-1,1,3,3-tetramethyluronium tetrafluoroborate; TFA, trifluoroacetic acid; TIS, triisopropylsilane; Trt, trityl.

pounds have been used as substrates in order to identify proteolytic enzymes with novel substrate specificities (22). For in vivo studies, such peptides have been employed for the analysis of cellular uptake and proteolytic processing of peptides (12, 23).

During solid-phase synthesis of such doubly labeled peptides, two complications are encountered. (i) The first fluorophore introduced must be chemically inert to the reaction conditions required for the selective deprotection of the second attachment site. (ii) Moreover, the first fluorophore may itself possess functional groups that may react with the activated second fluorophore.

Here a generally applicable strategy is presented in which carboxyfluorescein is introduced as the first fluorophore. By introducing an *O*-trityl-protecting group to polymer-bound carboxyfluorescein, the reaction of an activated second fluorophore with the phenolic hydroxy groups of the fluorescein moiety could be prevented. In addition, carboxyfluorescein was rendered chemically inert to the removal of the Dde-protecting group by hydrazine treatment enabling the orthogonal exposure of a second functional group. Trityl deprotection is achieved during the final TFA-cleavage of the peptide from the resin.

The ability to render carboxyfluorescein chemically inert to a broad range of conditions in SPPS led to the development of a carboxyfluorescein-preloaded resin. This resin is ideally suited for the automated synthesis of large collections of fluorescein-labeled peptides with uniform labeling efficiency, and for the generation of large numbers of doubly labeled peptides, bearing a fluorescein moiety at the C-terminus and a second dye of choice at the N-terminus.

## MATERIALS AND METHODS

**Peptide Synthesis.** Automated peptide synthesis was performed by solid-phase Fmoc/tBu-chemistry using an automated peptide synthesizer for multiple peptide synthesis (RSP5032, Tecan, Hombrechtikon, Switzerland) in 2 mL syringes. Fmoc-protected amino acids (twelve fold excess) were activated in situ by DIC/HOBt. After 90 min, the Fmoc protecting group was removed by treatment with piperidine/DMF (1:4, v/v) twice for 8 min. The resin was washed with DMF (6 $\times$ ) after each coupling and deprotection step. Side chains of Asp, Glu, Ser, Thr, and Tyr were tBu protected, side chains of His and Gln were Trt protected and the side chain of Lys was Boc protected. Fmoc-(4-aminomethyl)benzoic acid (Fmoc-Pamb-OH) was purchased from Neosystem (Strasbourg, France) and Fmoc-Lys(Dde)-OH from Novabiochem (Läufelfingen, Schweiz). 5(6)-Carboxyfluorescein (Fluo) and 5(6)-carboxytetramethylrhodamine (Tamra)-*N*-succinimidyl ester were from Fluka (Deisenhofen, Germany).

Derivatizations of peptides were performed manually in 2 mL syringes on a shaker at RT. Reactions were stopped by washing the resins three times each with DMF, MeOH, DCM, and diethyl ether. Completeness of amine acylation was confirmed using the Kaiser test (24). Manual Fmoc-deprotection was achieved by treating the resin with piperidine/DMF (1:4, v/v) twice for 10 min. Deprotection of the Dde protecting group was performed using 2% hydrazine monohydrate in DMF (v/v) twice for 3 min.

Unless otherwise stated, peptides were cleaved off the resin using TFA/TIS/H<sub>2</sub>O (95:2.5:2.5, v/v/v) for the indicated period of time. Crude peptides were precipitated by adding cold diethyl ether ( $-20^{\circ}\text{C}$ ). The precipitated

peptide was collected by centrifugation and resuspended in cold diethyl ether. This procedure was repeated twice. Finally peptides were dissolved in tBuOH/H<sub>2</sub>O (4:1, v/v) and lyophilized.

**FT-ATR-IR Spectroscopy.** On-bead FT-ATR-IR spectroscopy was performed on a Bruker IFS48 Spectrometer (Bremen, Germany). The intensities of the spectra were adjusted according to the intensity of the amide band at  $1670\text{ cm}^{-1}$ .

**HPLC.** Peptides and conjugates were analyzed using analytical RP-HPLC using a water (0.1% TFA)(solvent A)/ACN (0.1% TFA)(solvent B) gradient on a Waters 600 System (Eschborn, Germany) with detection at 214 nm. The samples were analyzed on an analytical column (Nucleosil 100,  $250 \times 2\text{ mm}$ , C18 column,  $5\text{ }\mu\text{m}$  particle diameter; Grom, Herrenberg, Germany), using a linear gradient from 10% B to 100% B within 30 min (flow rate:  $0.3\text{ mL/min}$ ).

Peptides were purified by preparative RP-HPLC (Nucleosil 300,  $250 \times 20\text{ mm}$ , C18 column,  $10\text{ }\mu\text{m}$  particle diameter; Grom, Herrenberg, Germany) on a Waters 600 Multisolvant Delivery System (flow rate:  $10\text{ mL/min}$ ). Gradient Systems were adjusted according to the elution profiles and peak profiles obtained from the analytical HPLC chromatograms.

**MALDI-MS.** One microliter of DHAP matrix (20 mg of DHAP, 5 mg of ammonium citrate in 1 mL of 80% isopropyl alcohol) was mixed with  $1\text{ }\mu\text{L}$  of each sample (dissolved in ACN/water (1:1) at a concentration of  $1\text{ mg/mL}$ ) on a gold target. Measurements were made using a laser-desorption time-of-flight system (G2025A, Hewlett-Packard, Waldbronn, Germany). For signal generation 20–50 laser shots were added up in the single shot mode.

**Labeling of Peptides with Carboxyfluorescein.** In all experiments, the isomeric mixture of 5- and 6-carboxyfluorescein (61:39 isomer ratio, purchased from Fluka) was used for labeling, unless otherwise stated. 5(6)-Carboxyfluorescein is also known as 4(5)-carboxyfluorescein (10, 16).

**Fluorescence Emission and Absorption Spectra.** Fluorescence emission spectra were recorded from 450 to 750 nm (excitation at 492 nm) at RT in 100 mM Tris/HCl (pH 8.8) using an LS50B spectrofluorometer (Perkin-Elmer, Norwalk, CT). The spectra were corrected for the sensitivity of the detection system. The excitation and emission bandwidths were set to 5 nm. Absorption spectra were acquired using an Ultrospec 2000 (Pharmacia Biotech, Cambridge, England) using 100 mM Tris/HCl (pH 8.8).

**Synthesis of Fluo-Phe-OH (1a and 1b) with High Excess of Carboxyfluorescein.** Fmoc-Phe-Wang resin (14 mg,  $10\text{ }\mu\text{mol}$ ) was Fmoc-deprotected and treated as described (2) for 1 h with 5(6)-carboxyfluorescein (37.6 mg,  $100\text{ }\mu\text{mol}$ ), DIC ( $15.5\text{ }\mu\text{L}$ ,  $100\text{ }\mu\text{mol}$ ), and HOBt (15.3 mg,  $100\text{ }\mu\text{mol}$ ) in DMF ( $130\text{ }\mu\text{L}$ ). The resin was then divided into two portions of  $5\text{ }\mu\text{mol}$  each (1a and 1b). 1a was treated with 20% piperidine/DMF (v/v) in a syringe until the solution was free of excess carboxyfluorescein (15 min). The products (1a and 1b) were cleaved off using TFA/H<sub>2</sub>O (97.5:2.5, v/v) over 4 h. After evaporation of the cleavage mixture to dryness, the products were dissolved in ACN/water (1:1), lyophilized, and analyzed by HPLC and MALDI-MS.

**Synthesis of Fluo-DYGIPADH (2a and 2b) with Low Excess of Carboxyfluorescein.** The peptide H-DYGIPADH-OH was synthesized automatically on 2-chlorotriethyl resin, which was preloaded with Fmoc-His(Trt)-OH. Resin-bound H-DYGIPADH-OH ( $6\text{ }\mu\text{mol}$ ) was allowed

to react with 5(6)-carboxyfluorescein (5.6 mg, 15  $\mu$ mol), DIC (2.3  $\mu$ L, 15  $\mu$ mol), and HOBt (2.3 mg, 15  $\mu$ mol) in DMF (150  $\mu$ L) for 16 h. After washing the resin as described above, the resin was divided into two portions of 3  $\mu$ mol each (**2a** and **2b**). **2a** was treated with 20% piperidine/DMF as described for **1a** (45 min).

The carboxyfluorescein-labeled peptides **2a** and **2b** were cleaved from the resin with TFA/TIS/H<sub>2</sub>O (95:2.5:2.5, v/v/v) for 4 h. After precipitation with diethyl ether, both peptides were dissolved in ACN/water, lyophilized, and analyzed by HPLC and MALDI-MS.

**On-Resin Introduction of the *O*-Trityl-Protecting Group to Carboxyfluorescein (**3**).** Fluo-Phe-Wang resin (10  $\mu$ mol) was prepared as described for **1**. The resin was then divided into two portions of 5  $\mu$ mol each (**3a** and **3b**). **3a** was treated twice with trityl chloride (16.7 mg, 60  $\mu$ mol) and DIPEA (10.3  $\mu$ L, 60  $\mu$ mol) in DCM for 16 h. Small amounts of resins **3a** and **3b** were vacuum-dried and analyzed by on-bead FT-ATR-IR spectroscopy.

**Treatment of **3a** and **3b** with Hydrazine.** Resins **3a** and **3b** were treated twice using 2% hydrazine hydrate in DMF for 3 min and washed thoroughly. Products were cleaved off using TFA/TIS/H<sub>2</sub>O (95:2.5:2.5, v/v/v) for 2 h. After evaporation of the cleavage mixture to dryness the products were dissolved in ACN/water, lyophilized, and analyzed by HPLC and MALDI-MS.

**Synthesis of Fluo-APPPEPPP-Pamb-Lys(Tamra) (**4**).** The peptide amide H-APPPEPPP-Pamb-Lys(Dde)-NH<sub>2</sub> was synthesized by automated solid-phase peptide synthesis on Rink amide resin. H-APPPEPPP-Pamb-Lys(Dde)-NH<sub>2</sub> Rink amide resin (14  $\mu$ mol) was labeled with 5(6)-carboxyfluorescein as described for **2a** and then treated twice with trityl chloride (168  $\mu$ mol, 46.8 mg) and DIPEA (168  $\mu$ mol, 28.8  $\mu$ L) in DCM for 16 h. Subsequently, Dde-deprotection of resin-bound Fluo(Trt)-APPPEPPP-Pamb-Lys(Dde)-NH<sub>2</sub> was performed as described. 5(6)-Carboxytetramethylrhodamine-*N*-succinimidyl ester (8  $\mu$ mol, 4.2 mg) was dissolved in DMF (150  $\mu$ L) containing DIPEA (20  $\mu$ mol, 3.4  $\mu$ L), and the solution was then added to resin loaded with 4  $\mu$ mol of peptide. After 16 h, the resin was thoroughly washed. Deprotection of the doubly labeled peptide amide was performed using TFA/TIS/H<sub>2</sub>O (95:2.5:2.5, v/v/v) for 4 h. Following ether precipitation, peptide **4** was dissolved in ACN/water, lyophilized, and analyzed by HPLC and MALDI-MS. The peptide was purified as described by preparative HPLC for spectroscopic characterization.

**Preparation of Fluo(Trt)-Lys-Rink Amide Resin (**5a**, **5b**).** Fmoc-Rink amide resin (200  $\mu$ mol, 270 mg) was deprotected and reacted with Fmoc-Lys(Dde)-OH (1 mmol, 533 mg), DIC (155  $\mu$ L, 1 mmol), and HOBt (153 mg, 1 mmol) in DMF for 16 h. After N $\alpha$ -Fmoc-deprotection, the N $\alpha$ -amino group was labeled with 5(6)-carboxyfluorescein as described for **2a**, yielding Fluo-Lys(Dde)-Rink amide resin. Immediately afterward, 50  $\mu$ mol of the Fluo-Lys(Dde)-Rink amide resin were Dde-deprotected (**5a**). In a parallel reaction 100  $\mu$ mol of the Fluo-Lys(Dde)-Rink amide resin was tritylated first as described for **3a** and then Dde deprotected (**5b**). A set of four peptides (as listed in Table 1) were synthesized by automated peptide synthesis on the  $\epsilon$ -lysine side chain of resins **5a** and **5b** for a comparative study.

## RESULTS

**Optimization of Reaction Conditions for Fluorescein Labeling.** The in situ generation of active esters in solid-phase peptide synthesis circumvents the need for

the synthesis, workup, and storage of water-labile amino acid active esters. Nevertheless the introduction of amine-reactive fluorescent reporter groups has mostly relied on the use of cost-intensive preformed active ester derivatives (12). We applied a protocol describing the introduction of 5(6)-carboxyfluorescein by in situ activation using 10 equiv of dye, DIC, and HOBt (1:1:1) and a reaction time of 1 h for the labeling of several peptides (2). Using this protocol, we detected several additional products by analytical HPLC and MALDI-MS. The molecular weights of the additional products differed from the masses of the carboxyfluorescein-labeled peptides by additional masses of *n* times 358.3 Da. These mass differences correspond to the masses of one, and several additional 5(6)-carboxyfluorescein groups.

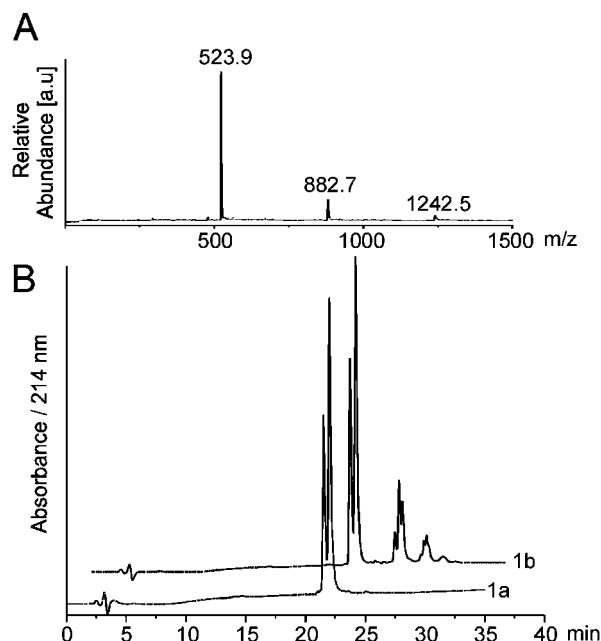
To analyze the identity of the side-products in more detail, Wang resin-bound L-phenylalanine was chosen as a model compound. The phenyl moiety enables the detection of unlabeled material by UV-spectroscopy. HPLC-MS analysis of the product (**1a**) formed by reacting Phe-Wang resin with excess 5(6)-carboxyfluorescein, as described (2), confirmed the formation of side products (29% according to HPLC-analysis [214 nm], Figure 1B). The two positional isomers of Fluo-Phe-OH showed retention times of 21.5 and 22 min ( $[M + H]^+ = 524.2$  Da). Three further products eluted at about 25.5 min ( $[M + H]^+ = 882.3$  Da) followed by further additional products eluting at about 27.7 min ( $[M + H]^+ = 1241.1$  Da). The masses of these side products corresponded to carboxyfluorescein-labeled phenylalanine, carrying two and three additional carboxyfluorescein molecules (Figure 1A). These side products could also be detected by MALDI-MS (Figure 1A). Treatment of resin **1** with piperidine/DMF (1:4, v/v) prior to TFA cleavage removed these side products, yielding highly pure Fluo-Phe-OH.

Even though complete turnover of the starting material was achieved in only 1 h, the use of 10 equiv of dye and coupling reagent is uneconomical. For this reason, fewer equivalents but longer reaction times were tested as an alternative coupling condition. Labeling of Phe-Wang resin with only 2.5 equiv of 5(6)-carboxyfluorescein, DIC, and HOBt (1:1:1) for 16 h resulted in complete acylation as monitored by Kaiser test. However, side products bearing additional carboxyfluorescein moieties were still formed. Again, the removal of these side products was achieved by piperidine treatment (data not shown).

Next, we validated this labeling procedure for the octapeptide DYGIADH, which has been shown to exhibit selective protein kinase C  $\epsilon$  isozyme agonist activity (25). Acylation with 2.5 equiv of 5(6)-carboxyfluorescein/DIC/HOBt (1:1:1) for 16 h again resulted in complete formation of the desired product Fluo-DYGIADH (Figure 2). Without piperidine/DMF treatment of the resin-bound carboxyfluorescein-labeled peptide, more than 40% (HPLC, [214 nm]) of the peptide was labeled with more than one molecule of 5(6)-carboxyfluorescein. These analytical data for an N-terminally labeled octapeptide again outline the importance of the piperidine treatment for the generation of carboxyfluorescein-labeled pure products.

The MHC class I-binding peptide ligand SIINFKEK(Fluo)L (26, 27) was synthesized in order to confirm that our strategy is also applicable to the labeling of peptides via a lysine side chain. Fmoc-Lys(Dde)-OH was incorporated by automated SPPS, yielding resin-bound SIINFKEK(Dde)L. After introducing the Boc protecting group at the N-terminus, the Dde protecting group was





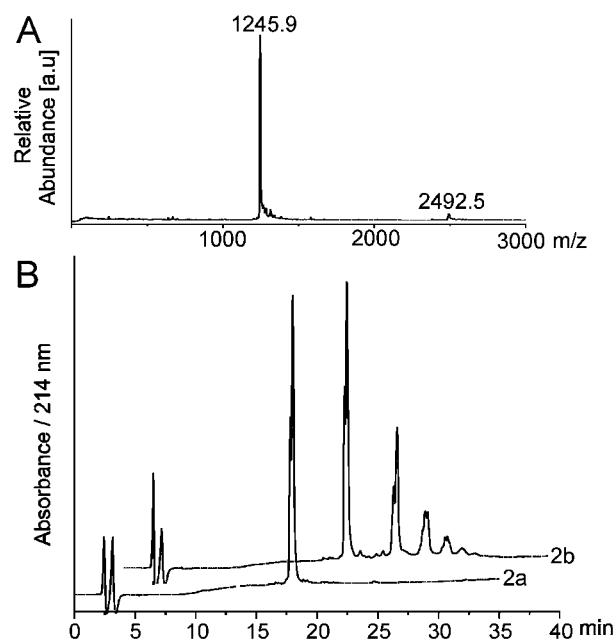
**Figure 1.** (A) MALDI mass spectrum of Fluo-Phe-OH (compound **1b**, theor.  $[M + H]^+ = 524.5$  Da) without piperidine treatment. The side products ( $[M + H]^+ = 882.7$  Da,  $[M + H]^+ = 1242.5$  Da) differ by mass differences corresponding to one and two additional fluorescein moieties. (B) HPLC elution profiles of Fluo-Phe-OH synthesized with (compound **1a**) and without (compound **1b**) subsequent piperidine treatment. LC-MS analysis revealed the following masses: products eluting at 21.5 and 22 min,  $[M + H]^+ = 524.2$  Da; three products at 25.5 min,  $[M + H]^+ = 882.3$  Da; several additional products at 27.7 min  $[M + H]^+ = 1241.1$  Da. The larger number of peaks for side products with higher molecular masses and eluting at later times may be explained by side products carrying different combinations of 5- and 6-carboxyfluorescein.

removed, and the free  $\epsilon$ -amino group was labeled with 5(6)-carboxyfluorescein according to our protocol, yielding a highly pure peptide.

#### On-Resin O-Tritylation of Carboxyfluorescein.

Peptides labeled with two different fluorescent dyes can either be generated in solution or using side chain-protected polymer-bound peptides in SPPS in combination with orthogonal protecting group strategies. The scope of solution phase labeling is severely limited to sequences with special side-chain characteristics (19, 28). Moreover, several laborious purification steps are often required for this approach. To explore and optimize the generation of doubly labeled peptides by an SPPS-based approach, Fmoc-Lys(Dde)-OH (29, 30) was selected as a building block for the introduction of a second fluorescent dye via a selectively deprotectable lysine side chain (12). The Dde-protecting group can be removed selectively by treatment of the resin-bound peptide with 2% hydrazine hydrate/DMF. We chose this strategy instead of the incorporation of Fmoc-Lys(Mtt)-OH (31). When working with Fmoc-Lys(Mtt)-OH in the presence of other trityl-based protecting groups, selective Mtt removal had been difficult to achieve (32). Our strategy, described here, is based on the introduction of carboxyfluorescein at the N-terminus of a solid phase bound peptide and of a second fluorophore via the selectively deprotectable lysine side chain.

However, exposure of carboxyfluorescein-labeled peptides to 2% hydrazine hydrate/DMF twice for 3 min resulted in the formation of side products eluting several minutes earlier in analytical HPLC and possessing a mass 14 Da higher than that of the desired product.

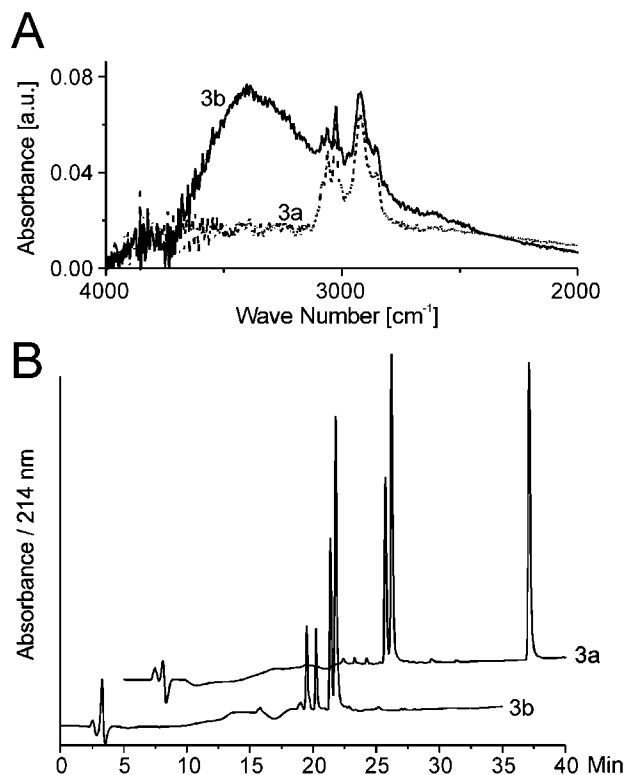


**Figure 2.** (A) MALDI mass spectrum of Fluo-DYGIPADH-OH synthesized with piperidine treatment following the coupling of carboxyfluorescein (compound **2a**) (theor  $[M + H]^+ = 1246.2$  Da). (B) HPLC elution profiles of Fluo-DYGIPADH-OH with (compound **2a**) and without (compound **2b**) piperidine treatment. The unlabeled peptide H-DYGIPADH-OH eluted at 13.5 min, the positional isomers of Fluo-DYGIPADH-OH at 17.8 and 18.0 min. In **2b** the side products eluting at 22.5, 24.7, and 26.6 min correspond to peptides carrying several molecules of carboxyfluorescein ( $[M + H]^+ = 1604.4$  Da,  $[M + H]^+ = 1963.0$  Da,  $[M + H]^+ = 2322.3$  Da, respectively).

To assess whether this side product was due to the fluorescein moiety, the Fluo-Phe-Wang resin was also treated with 2% hydrazine hydrate/DMF. Again the formation of a side product with a mass surplus of 14 Da decreased the purity of the Fluo-Phe-OH compound by 24% (Figure 3B). This mass difference is indicative of the formation of a hydrazone or a hydrazide with peptide-bound carboxyfluorescein.

At this point we realized that the phenolic hydroxy groups of carboxyfluorescein could be protected by treatment with anhydrides, such as acetic anhydride or trimethylacetic anhydride. These reactions lead to the conversion of carboxyfluorescein into the corresponding phenolic diesters of the lactone form (8, 9, 16). The conversion of the fluorescein moiety into its lactonic form can be monitored visually by the color change from orange to yellow and the loss of fluorescence. However, due to the lability of these phenolic esters to basic conditions, this protecting group strategy is incompatible with the conditions of hydrazine treatment. Instead, phenols can also be efficiently protected by base-stable trityl-based protecting groups (33) using trityl chloride for the introduction (14). Removal can be accomplished during TFA cleavage of the peptide from the resin.

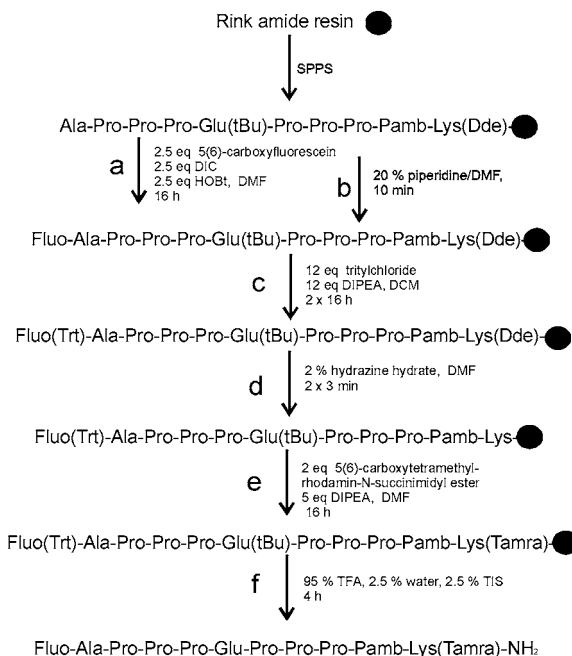
Fluo-Phe-Wang resin was treated with trityl chloride/DIPEA in DCM. Completeness of the tritylation was confirmed by the disappearance of the infrared band due to free hydroxy groups ( $3600\text{--}3200\text{ cm}^{-1}$ ) by on-bead FT-ATR-IR spectroscopy (Figure 3A). Moreover, consistent with a conversion of carboxyfluorescein from its acid into its lactone form, the color of the resin changed from orange to yellow. Subsequently, the Fluo(Trt)-Phe-Wang resin was treated with 2% hydrazine hydrate/DMF twice for 3 min. In this case, almost no side product with a mass difference of 14 Da was formed (Figure 3B). This



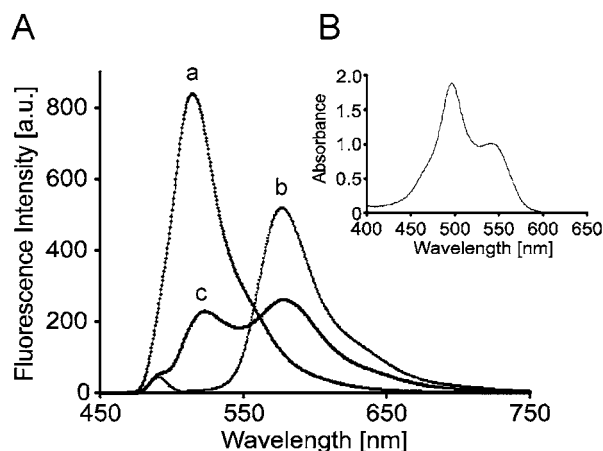
**Figure 3.** (A) Relevant regions of the on-bead FT-ATR-IR spectra of the Fluo(Trt)-Phe-Wang resin (**3a**) and of the Fluo-Phe-Wang resin (**3b**). The broad peak at 3300 cm<sup>-1</sup> indicates the presence of unprotected hydroxy groups of resin bound carboxyfluorescein (**3b**). For the Fluo(Trt)-Phe-Wang resin no such peak is detectable. The intensities of the two spectra were adjusted according to the intensity of the amide band at 1670 cm<sup>-1</sup>. (B) Analytical HPLC profile of Fluo-Phe-OH after treatment with 2% hydrazine/DMF, with (compound **3a**) and without (compound **3b**) prior tritylation. Apart from the two positional isomers of Fluo-Phe-OH ( $[M + H]^+ = 524.1$  Da) two side products of compound **3b** eluted at 19.5 and 20.2 min ( $[M + H]^+ = 538.1$  Da). In the upper HPLC trace (**3a**) triphenylmethane, originating from the trityl-protecting group, eluted at 32.1 min.

result clearly demonstrates that the trityl-protecting group renders resin-bound carboxyfluorescein stable to the modification by hydrazine.

**Synthesis of a Doubly Labeled Peptide.** To evaluate the trityl-protecting group strategy for the generation of doubly labeled peptides, the peptide amide Fluo-APPPEPPP-Pamb-Lys(Tamra)-NH<sub>2</sub> was synthesized using SPPS on Rink amide resin (Figure 4). Such L-proline oligomers had been presented as peptide-bridged fluorescence resonance energy transfer cassettes (*34*) in order to study FRET characteristics of different dye-pairs. After introducing carboxyfluorescein at the N-terminus of the resin-bound peptide amide APPPEPPP-Pamb-Lys(Dde), piperidine treatment and subsequent tritylation, the Dde-protecting group was removed by hydrazinolysis. The  $\epsilon$ -amino group of the C-terminal lysine was dye labeled using activated 5(6)-carboxytetramethylrhodamine-N-succinimidyl ester. According to analytical HPLC, the purity of the crude Fluo-APPPEPPP-Pamb-Lys(Tamra) peptide amide after cleavage was 85%, (calc.  $[M + H]^+ = 1833.0$  Da, exp.  $[M + H]^+ = 1833.2$  Da, determined by MALDI-MS). Figure 5 shows the fluorescence emission spectra of the doubly labeled peptide, of 5(6)-carboxytetramethylrhodamine and of 5(6)-carboxyfluorescein. When compared with the free fluorophores the fluorescence of both labels in this peptide was quenched significantly as



**Figure 4.** Synthesis of the doubly labeled peptide amide Fluo-APPPEPPP-Pamb-Lys(Tamra)-NH<sub>2</sub> (compound **4**). Optimized procedures include the introduction of 5(6)-carboxyfluorescein as the first fluorophore (a), cleavage of the phenolic ester (b), protection of the phenol (c), cleavage of the Dde-group (d), introduction of the second fluorophore (e), cleavage of the peptide (f).

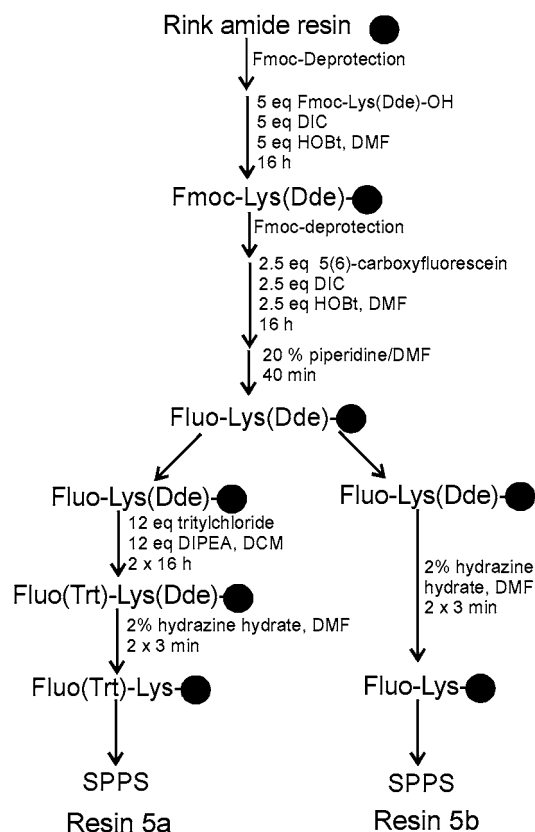


**Figure 5.** (A) Fluorescence emission spectra of 5(6)-carboxyfluorescein (500 nM, curve a), 5(6)-carboxytetramethylrhodamine (1  $\mu$ M, curve b), and the peptide amide Fluo-APPPEPPP-Pamb-Lys(Tamra)-NH<sub>2</sub> (1  $\mu$ M, curve c). Fluorescence was excited at 492 nm. (B) Absorption spectrum of the peptide Fluo-APPPEPPP-Pamb-Lys(Tamra)-NH<sub>2</sub>.

reported previously for other peptides carrying this combination of fluorophores (*12, 19, 28*).

**Generation of a Fluorescein-Preloaded Resin for the Automated Synthesis of C-Terminally Labeled Peptides.** The procedures described so far require the fluorescent derivatization of peptides after automated SPPS. To accelerate the generation of carboxyfluorescein-labeled peptides and guarantee uniform labeling yields for all peptides, we decided to establish a resin already carrying a fluorescein moiety. Such a preloaded resin should be compatible with automated parallel peptide synthesis.

Rink amide resin was loaded with Fmoc-Lys(Dde)-OH, followed by deprotection of the N $\alpha$ -amino group and coupling of 5(6)-carboxyfluorescein, as described. Follow-



**Figure 6.** Preparation of the  $N^{\epsilon}$ -carboxyfluorescein-labeled lysyl-Rink amide resins **5a** and **5b** with a free  $\epsilon$ -amino group for peptide assembly.

ing tritylation of the fluorescein moiety and removal of the Dde protecting group, the  $N_{\epsilon}$ -group was available for further peptide synthesis (Figure 6). A set of four peptides was synthesized by automated parallel peptide synthesis on this resin (resin **5a**, Fluo(Trt)-Lys-Rink amide resin) and compared with the peptides synthesized on a resin carrying a nontritylated carboxyfluorescein moiety (resin **5b**, Fluo-Lys-Rink amide resin). Tritylation of the fluorescein moiety increased the purity of all peptides significantly (Table 1). The purity was increased by about 20% for the two 9-mer peptides and by about 40% for the 16- and 13-mer peptides. For the nontritylated resin **5b** the  $\Delta M = +14$  Da side product (compound **3b**) was present, as well as an unidentified side product with a mass surplus of 68 Da (Table 1). The latter reduced the purity of the peptides most significantly. All peptides synthesized on resin **5b** did not exhibit the typical yellow color of fluorescein in aqueous solutions, but a slightly brown color.

## DISCUSSION

This contribution presents optimized coupling procedures and protocols for the generation of fluorescently labeled peptides and particularly doubly labeled peptides by SPPS. So far no investigator has addressed the chemistry of the introduction of 5(6)-carboxyfluorescein by in situ activation in detail. A large excess of fluorophore and coupling reagents for N-terminal labeling of solid phase-bound peptides led to the generation of side products with higher molecular masses which matched multiples of the carboxyfluorescein moiety. TBTU as an alternative in situ activation reagent did not affect the formation of these side products (data not shown). Considering the absence of any reactive functional group

in the chosen L-phenylalanine model compound, apart from the free  $\alpha$ -amino group, the phenolic hydroxy groups of fluorescein are the only available reactive functional groups. In organic solvents, like DMF, fluorescein exists predominantly in its lactonic form (35). Evidently, the phenolic hydroxy group of carboxyfluorescein can be acylated by in situ-activated carboxyfluorescein resulting in the formation of phenolic esters. Moreover, phenolic esters, in particular activated phenyl esters with electron-withdrawing groups, are well-known to be cleavable by nucleophiles, such as free amino groups of peptides or in basic media. Consistent with this hypothesis, treatment with piperidine readily removed these side products yielding highly pure carboxyfluorescein-labeled peptides.

Completion of removal of the ester-bound carboxyfluorescein could be confirmed by the absence of the red color of carboxyfluorescein in piperidine/DMF. It should be noted that using continuous flow-through, the removal of ester-bound carboxyfluorescein with 20% piperidine/DMF lasted between 10 and 45 min, depending on the peptide sequence. The use of piperidine for this crucial ester cleavage makes it possible to work with automated parallel SPPS, because piperidine is routinely used for Fmoc-removal during Fmoc/tBu-based SPPS. Moreover, peptide synthesizers are frequently equipped with UV-detectors in order to monitor Fmoc-removal, which makes it possible to monitor the removal of the ester-bound carboxyfluorescein molecules.

A considerable reduction of the equivalents of fluorophore and coupling reagents and the extension of the reaction times still ensured a quantitative turnover. This procedure is especially useful for applications in which the use of isomerically pure carboxyfluorescein is desired, which is far more expensive than the mixture of the two positional isomers (16). Fulop et al. presented the labeling of individual peptides with 1.5- and 3-fold excess and variable coupling times from 4 to 24 h. Here, we validated a 2.5-fold excess and a 16 h coupling time as a general approach yielding complete turn over and high purities of the crude products for a large number of different peptides.

Labeling of resin-bound L-phenylalanine with 5-carboxyfluorescein resulted in only one single product peak after piperidine treatment, consistent with a lack of reactivity of the carboxy group in the 2' position. Fluorescein derivatives are known to exist as lactones or free acid tautomers (36). The lack of reactivity of the 2' carboxy group is indicative of the fact, that fluorescein exists predominantly in its lactonic form in organic solvents, like DMF (35).

For further derivatization of fluorescein-labeled peptides, the phenolic hydroxy groups were protected by tritylation. O-Tritylation could be monitored by the change of color of the resin from orange to yellow, consistent with a conversion of carboxyfluorescein from the acid into its lactonic form. Completeness of the O-tritylation of the carboxyfluorescein moiety was deduced from on-bead FT-ATR-IR spectroscopy and the resulting chemical inertness. A direct structural confirmation by NMR was not possible due to the failure to release the protected compound from the resin without partial loss of the highly acid labile trityl protecting group.

The availability of a protecting group strategy for carboxyfluorescein compatible with Fmoc/tBu-SPPS and orthogonal side chain protecting groups, such as Dde, offers highly attractive options for the generation of biological probe molecules carrying a second dye or modification (e.g., a biotin or a lipid moiety) apart from



**Table 1. Analytical Data for the Peptides Synthesized on Resins 5a and 5b**

peptide sequence, calcd [M + H] <sup>+</sup>	resin <b>5a</b> purity, [M + H] <sup>+</sup>	resin <b>5b</b> purity	resin <b>5b</b> major side product, [M + H] <sup>+</sup>
Ahx-KGFKGVDAQGTLS-Ahx- $\epsilon$ Lys(Fluo), 2020.3 Da	90%, 2019.8 Da	49%	28%, 2087.2 Da
DYGIPADH- $\epsilon$ Lys(Fluo), 1373.4 Da	>95%, 1373.2 Da	76%	12%, 1441.0 Da
APPEPPP-Pamb- $\epsilon$ Lys(Fluo), 1420.6 Da	>95%, 1420.4 Da	75%	13%, 1488.1 Da
Ahx-EQKLISEEDL-Ahx- $\epsilon$ Lys(Fluo), 1916.2 Da	87%, 1917.1 Da	48%	29%, 1983.6 Da

N-terminal carboxyfluorescein. In the absence of tritylation, removal of Dde with hydrazine led to the formation of a side product with a 14 Da mass surplus. While the prevalence of the lactonic form of fluorescein favors the hydrazide as the side product, the formation of the hydrazone with the quinoid carbonyl C-atom of carboxyfluorescein in a residual fraction of the acid form may also be possible. Moreover, the tritylated resin-bound fluorescein is inert toward an activated second dye, which may by itself react with the fluorescein moiety.

Despite the O-tritylation of the Fluo-Phe-OH model compound, minor amounts of the side product were still formed, as shown in Figure 3B (trace **3a**). This residual formation of side product is probably caused by incomplete tritylation and not by the lability of the trityl group. In our hands O-tritylation of carboxyfluorescein has proven to be stable to various conditions of SPPS employing the Fluo(Trt)-Lys-Rink amide resin, i.e., repetitive steps of coupling, piperidine treatment, and washing. Methanol was omitted from the washing steps, however, because prolonged exposure to protic solvents led to partial removal of the trityl-protecting group.

Finally, the O-trityl-protecting group enabled the development of a Fluo(Trt)-Lys preloaded resin for the generation of C-terminally labeled peptides. This resin eliminates the problem of sequence dependent reaction times necessary for the cleavage of the phenolic esters. Using this resin, carboxyfluorescein-labeled peptides with uniform labeling yields could be obtained by automated procedures. In contrast to protocols published previously our procedure leads to a major improvement in the purity of the crude peptides and reduces the number of steps required for the generation of a doubly labeled peptide after automated peptide synthesis (12, 20).

Interestingly, when using a resin preloaded with a nontritylated carboxyfluorescein the major side product was not derived from hydrazine treatment. The major side product accumulated with increasing length of the assembled peptide and showed a mass surplus of 68 Da. This mass difference might be explained by the addition of piperidine under conditions of water condensation. The exact identity of this side product is under investigation.

The Fluo(Trt)-Lys-Rink amide resin is currently used in our laboratory for the parallel-automated synthesis of doubly labeled peptides, carrying carboxyfluorescein as the C-terminal fluorescent dye and a second fluorophore of choice at the N-terminus. Moreover, we expect that such a resin is of general use in solid-phase synthesis with applications in the generation of fluorescein-labeled combinatorial compound collections (15).

#### ACKNOWLEDGMENT

We thank Nicole Sessler for excellent technical assistance in peptide synthesis, Lisa Neumann for proof-reading the manuscript and Michael Barth for assisting in FT-ATR-IR spectroscopy. This work was supported by the German Science Council (DFG, Sonderforschungsbereich 510). We gratefully acknowledge financial support from the Volkswagen Foundation (Nachwuchsgruppen an Universitäten). O.M. was funded through a grant

in the focus area Conformational Control of Biomolecular Function from the Volkswagen Foundation.

#### LITERATURE CITED

- (1) Brand, L., and Johnson, M. L. (1997) Fluorescence spectroscopy. *Methods Enzymol.* 278.
- (2) Weber, P. J. A., Bader, J. E., Folkers, G., and Beck-Sickinger, A. G. (1998) A fast and inexpensive method for N-terminal fluorescein-labeling of peptides. *Bioorg. Med. Chem. Lett.* 8, 597–600.
- (3) Brinkley, M. (1992) A brief survey of methods for preparing protein conjugates dyes, haptens, and cross-linking reagents. *Bioconjugate Chem.* 3, 2–13.
- (4) Schmidt, M. C., Rothen-Rutishauser, B., Rist, B., Beck-Sickinger, A. G., Wunderli-Allenspach, H., Rubas, W., Sadee, W., and Merkle, H. P. (1998) Translocation of human calcitonin in respiratory nasal epithelium is associated with self-assembly in lipid membrane. *Biochemistry* 37, 16582–16590.
- (5) Owens, M. A., and Loken, M. T. (1995). In *Flow cytometry: Principles for clinical laboratory practice*, pp 28–29, Wiley-Liss, New York.
- (6) Dedier, S., Reinelt, S., Rion, S., Folkers, G., and Rognan, D. (2001) Use of fluorescence polarization to monitor MHC-peptide interactions in solution. *J. Immunol. Methods* 255, 57–66.
- (7) Waizenegger, T., Fischer, R., and Brock, R. (2002) Intracellular concentration measurements in adherent cells: A comparison of import efficiencies of cell-permeable peptides. *Biol. Chem* 383, 291–299.
- (8) Theisen, P., McCollum, C., Upadhy, K., Jacobson, K., Vu, H., and Andrus, A. (1992) Fluorescent dye phosphoramidite labelling of oligonucleotides. *Tetrahedron Lett.* 33, 5033–5036.
- (9) Mattingly, P. G. (1992) Preparation of 5- and 6-(aminomethyl)fluorescein. *Bioconjugate Chem.* 3, 430–431.
- (10) Adamczyk, M., Fishpaugh, J. R., and Heuser, K. J. (1997) Preparation of succinimidyl and pentafluorophenyl active esters of 5- and 6- carboxyfluorescein. *Bioconjugate Chem.* 8, 253–255.
- (11) Dettin, M., Scarinci, C., Zannotto, C., Cabrelle, A., de Rossi, A., and di Bello, C. (1998) Design, synthesis and CD4 binding studies of a fluorescent analogue of a peptide that enhances HIV-1 infectivity. *J. Pept. Res.* 51, 110–115.
- (12) Hoogerhout, P., Stittelaar, K. J., Brugghe, H. F., Timmermans, J. A. M., ten Hove, G. J., Jiskoot, W., Hoekman, J. H. G., and Roholl, P. J. M. (1999) Solid-phase synthesis and application of double-fluorescent-labeled lipopeptides, containing a CTL-epitope from the measles fusion protein. *J. Pept. Res.* 54, 436–443.
- (13) Fulop, L., Penke, B., and Zarandi, M. (2001) Synthesis and fluorescent labeling of beta-amyloid peptides. *J. Pept. Sci.* 7, 397–401.
- (14) Jung, G. (1996) *Combinatorial Peptide and Nonpeptide Libraries: A Handbook*, Wiley-VCH, Weinheim.
- (15) Jung, G. (1999) *Combinatorial Chemistry: Synthesis, Analysis, Screening*, Wiley-VCH, Weinheim.
- (16) Rossi, F. M., and Kao, J. P. Y. (1997) Practical method for the multigram separation of the 5- and 6 isomers of carboxyfluorescein. *Bioconjugate Chem.* 8, 495–497.
- (17) Clegg, R. M. (1995) Fluorescence resonance energy transfer. *Curr. Opin. Biotechnol.* 6, 429–435.
- (18) Pearce, D. A., Walkup, G. K., and Imperiali, B. (1998) Peptidyl chemosensors incorporating a FRET mechanism for detection of Ni(II). *Bioorg. Med. Chem. Lett.* 8, 1963–1968.
- (19) Wei, A.-P., Blumenthal, D. K., and Herron, J. N. (1994) Antibody-mediated fluorescence enhancement based on shift-

- ing the intramolecular dimer $\leftrightarrow$ monomer equilibrium of fluorescent dyes. *Anal. Chem.* **66**, 1500–1506.
- (20) Kruger, R. G., Dostal, P., and McCafferty, D. G. (2002) An economical and preparative orthogonal solid-phase synthesis of fluorescein and rhodamine derivatized peptides: FRET substrates for the *Staphylococcus aureus* sortase SrtA transpeptidase reaction. *Chem. Commun.* **18**, 2092–2093.
- (21) Cummings, R. T., Salowe, S. P., Cunningham, B. R., Wiltsie, J., Park, Y. W., Sonatore, L. M., Wisniewski, D., Douglas, C. D., Hermes, J. D., and Scolnick, E. M. (2002) A peptide-based fluorescence resonance energy transfer assay for *Bacillus anthracis* lethal factor protease. *Proc. Natl. Acad. Sci.* **99**, 6603–6606.
- (22) Olsen, M. J., Stephens, D., Griffiths, D., Daugherty, P., Georgiou, G., and Iverson, B. L. (2000) Function-based isolation of novel enzymes from a large library. *Nat. Biotechnol.* **18**, 1071–1074.
- (23) Bark, S. J., and Hahn, K. M. (2000) Fluorescent indicators of peptide cleavage in the trafficking compartments of living cells: Peptides site-specifically labeled with two dyes. *Methods* **20**, 429–435.
- (24) Sarin, V. K., Kent, S. B. H., Tam, J. P., and Merrifield, R. B. (1981) Quantitative monitoring of solid-phase peptide synthesis by the ninhydrin reaction. *Anal. Biochem.* **117**, 147–157.
- (25) Chen, L., Wright, L. R., Chen, C.-H., Oliver, S. F., Wender, P. A., and Mochly-Rosen, D. (2001) Molecular transporters for peptides: delivery of a cardioprotective epsilon PKC agonist peptide into cells and intact ischemic heart using a transport system, R-7. *Chem. Biol.* **8**, 1123–1129.
- (26) Röttschke, O., Falk, K., Stevanovic, S., Jung, G., Walden, P., and Rammensee, H.-G. (1991) Exact prediction of a natural T cell epitope. *Eur. J. Immunol.* **21**, 2891–2894.
- (27) Wiesmüller, K.-H., Brich, M., Jung, G., Sparbier, K., and Walden, P. (1995) Peptide binding to MHC class I molecules analyzed by confocal microscopy. *Eur. J. Cell Biol.* **66**, 389–393.
- (28) Geoghegan, K. F., Rosner, P. J., and Hoth, L. R. (2000) Dye-pair reporter systems for protein-peptide molecular interactions. *Bioconjugate Chem.* **11**, 71–77.
- (29) Bycroft, B. W., Chan, W. C., Chhabra, S. R., and Hone, N. D. (1993) A novel lysine-protecting procedure for continuous flow solid-phase synthesis of branched peptides. *J. Chem. Soc., Chem. Commun.* 778–779.
- (30) Augustyns, K., Kraas, W., and Jung, G. (1998) Investigation of the stability of the Dde protecting group used in peptide synthesis – migration to an unprotected lysine. *J. Pept. Res.* **51**, 127–133.
- (31) Aletras, A., Barlos, K., Gatos, D., Koutsogianni, S., and Mamos, P. (1995) Preparation of the very acid-sensitive Fmoc-Lys(Mtt)-OH. *Int. J. Pept. Protein Res.* **45**, 488–496.
- (32) Bourel, L., Carion, O., Gras-Masse, H., and Melnyk, O. (2000) The deprotection of Lys(Mtt) revisited. *J. Pept. Sci.* **6**, 264–270.
- (33) Barlos, K., Gatos, D., Koutsogianni, S., Schäfer, W., Stavropoulos, G., and Wenqing, Y. (1991) Darstellung und Einsatz von N-Fmoc-O-Trt-Hydroxyaminosäuren zur "Solid Phase" Synthese von Peptiden. *Tetrahedron Lett.* **21**, 471–474.
- (34) Li, Y., and Glazer, A. N. (1999) Design, synthesis, and spectroscopic properties of peptide-bridged fluorescence energy-transfer cassettes. *Bioconjugate Chem.* **10**, 241–245.
- (35) Fompeydie, D., and Levillain, P. (1980) Equilibre entre formes structurales de l'éosine et de la fluoresceine moléculaires. Influence des solvants. *Bull. Soc. Chim. Fr.* I-459–I-465.
- (36) Anthoni, U., Christophersen, C., Nielsen, P. H., Püschel, A., and Schaumburg, K. (1995) Structure of red and orange fluorescein. *Struct. Chem.* **6**, 161–165.

BC025658B

# Utility of Poly(ethylene glycol) Conjugation To Create Prodrugs of Amphotericin B

Charles D. Conover, Hong Zhao, Clifford B. Longley,\* Kwok L. Shum, and Richard B. Greenwald

Enzon Pharmaceutical, Inc., 20 Kingsbridge Road, Piscataway, New Jersey 08854-3998. Received December 23, 2002; Revised Manuscript Received February 6, 2003

This paper reports on the synthesis, safety, and efficacy of a series of water-soluble derivatives of poly(ethylene glycol) (PEG)-conjugated amphotericin B (AmB). PEG 40 000 attached to the sugar amino group of AmB via labile carbamate and carbonate linkages was examined. The synthetic program conducted for this investigation provided a series of disubstituted PEG–AmB derivatives which had in vitro PEG half-life of hydrolyses rates in rat plasma varying between 1 and 3 h. Importantly, all conjugates demonstrated less than 6% hydrolysis following 24 h incubation in pH 7.4 phosphate buffer at 25 °C and showed solubilities greater than 46 mg/mL in aqueous solutions. The solubility of AmB in the conjugates increased up to approximately 200 times compared to unmodified AmB in saline. As a major finding, this investigation demonstrated that conjugation of PEG to AmB could produce conjugates that were significantly (6×) less toxic than AmB-deoxycholate and maintained, or even had enhanced, in vivo antifungal activity.

## INTRODUCTION

Available since 1960, amphotericin B (AmB) is an amphoteric polyene antibiotic prepared from the soil microorganism, *Streptomyces nodosus*. It binds selectively to ergosterol in the cell membrane of susceptible fungi, inducing changes in permeability that can produce lethal cell injury. Because this fungicide has such broad-spectrum activity, it remains the gold standard agent for many life-threatening fungal infections. However, AmB is virtually insoluble in water and can only be formulated into a suspension. Intravenous administration of AmB formulated as a deoxycholate micellar suspension (Fungizone) is often complicated by both infusion-related adverse reactions (e.g., fever, chills, rigors, nausea, vomiting, and hypotension) and systemic toxicities (e.g., nephrotoxicity, acidosis, hypokalemia, hypomagnesemia, and anemia). To overcome the limitations of AmB, other modalities of AmB have been developed in which this agent is encapsulated in liposomes (20) or is bound to carriers (8). A number of the lipid carrier approaches have been successful in increasing the therapeutic index of AmB and a few have achieved clinical application (20).

One methodology that has received only sparse consideration is the conjugation of AmB to poly(ethylene glycol) (PEG) (24). PEG is a condensation product of ethylene oxide having the general formula  $\text{HO}(\text{CH}_2\text{CH}_2\text{O})_n\text{H}$ . It is a linear amphiphilic polymer that is nonbiodegradable, nontoxic, and nonimmunogenic and has been widely studied for both protein (10) and small molecule modification (15). PEG has been extensively utilized due to its ability to increase the solubility, circulating life, safety, and permeable tissue accumulation level of proteins, while decreasing their immunogenicity and renal excretion (16, 18, 22, 26). This technology has also been extended into small molecule prodrug platforms (15). The use of prodrug design has been applied to numerous therapeutic areas with the goal to improving the pharmacologic properties of drugs. A

prodrug is a biologically inactive derivative of a parent drug molecule that usually requires an enzymatic or chemical transformation within the body in order to release the active drug and has improved delivery properties over the parent molecule (25). Essential to drug delivery with a prodrug is the rate of release of the active drug. A rapid breakdown of the prodrug can result in spiking of the parent drug and possible toxicity, while too slow a release rate will compromise the drug's effectiveness. The linkages between the active drug and the carrier molecule can theoretically be chosen so that either pH or enzymatic degradation mediate prolonged drug release. Therefore, the effectiveness of prodrug delivery is dependent on the stability of the drug conjugate linkage and its potential for controlled degradation.

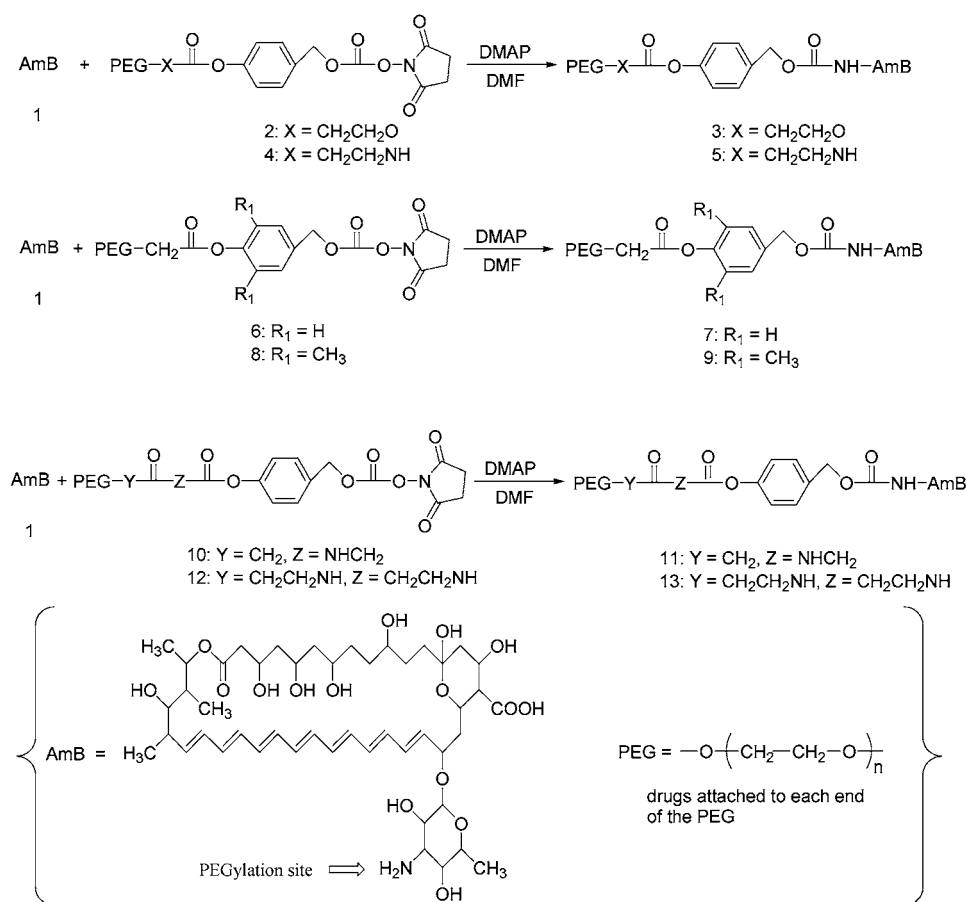
The amino group on the sugar moiety of AmB is essential for its antifungal activities (1, 21) and provides an ideal site for attachment of PEG. Recently we have developed two platform technologies for PEG conjugates through the controlled release of amino groups (13, 14). Both methods can be utilized for AmB; however, the 1,6-benzyl elimination system is more easily applied. The chemistry of these conjugations continues our exploration of delivery of insoluble bioactive agents using PEG, strategies first initiated with paclitaxel (11) and camptothecin (12). For these two agents, PEG modifications were shown to extend circulatory exposure, reduce toxicity, and increase the therapeutic index of the parent compounds (5, 23). The objective of the current study is to assess the use of PEG conjugation to the antifungal agent AmB and evaluate its in vitro and in vivo activity.

## MATERIALS AND METHODS

**Chemicals.** Amphotericin B was purchased from Fluka Chemie AG, Switzerland, and all other reagents and solvents were purchased from Aldrich Chemical Co. (Milwaukee, WI) and Advanced ChemTech (Louisville, KY). Unless stated otherwise, they were used without further purification. All the PEGs used in this study had a molecular weight of 40 kDa and were dried under vacuum or by azeotropic distillation from toluene prior

\* Corresponding author. Phone: 1-732-980-4832. Fax: 1-732-885-2950. E-mail: Clifford.longley@enzon.com.



**Scheme 1. Syntheses of PEGylated AmB Conjugates Using Bifunctional PEG**

to use. Organic solutions were dried over MgSO<sub>4</sub>. Solvents were removed by rotary evaporation. <sup>13</sup>C NMR spectra were obtained on a JEOL JNM-GSX270 FT NMR System. Deuterated chloroform or pyridine was used as solvents unless otherwise specified. Analytical HPLC was conducted on a ZORBAX 300 SB C8 RP column (150 × 4.6 mm) with a gradient of 30 to 80% acetonitrile in 0.1 M triethylamine acetate buffer (pH = 6.8) at a flow rate of 1 mL/min.

**Synthetic Approaches.** The preparation of the various PEG 1,6 benzyl elimination linkers was carried out according to published procedures (13). Conjugation of PEG linkers with AmB was done in anhydrous dimethylformamide (DMF) in the presence of 4-(dimethylamino)pyridine (DMAP) (Scheme 1). We observed that once AmB was conjugated through the sugar amino group, the glycosyl bond between the sugar moiety and the macrocyclic heptaene in PEG-AmB conjugates were very sensitive to acid. Therefore, pyridine was added to recrystallization solvents in order to maintain basicity and prevent the breakdown of this bond.

**Compound 3.** To a solution of PEG linker 2 (13) (4.0 g, 0.0983 mmol) in 40 mL anhydrous DMF were added AmB (0.272 g, 0.295 mmol) and DMAP (0.360 g, 2.95 mmol), and the mixture was stirred for 12 h at room temperature. Ethyl ether (100 mL) was added to the reaction solution with swirling and the PEG derivative precipitated. The mixture was stored at -20 °C for 12 h and filtered. The crude solid was recrystallized from a mixture of 100 mL of 2-propanol (IPA) and 1 mL of pyridine twice to give pure product 3 (3.80 g, 0.090 mmol, 91%). <sup>13</sup>C NMR (67.8 MHz, C<sub>5</sub>D<sub>5</sub>N) δ 176.21, 171.73, 157.35, 153.98, 151.20, 137.67, 137.21, 134.85, 134.57, 134.46, 134.10, 133.80, 133.27, 133.02, 132.94, 132.78,

132.69, 132.55, 129.47, 127.97, 121.51, 98.25, 97.93, 78.34, 76.37, 75.75, 74.91, 74.33, 73.50–69.20 (PEG), 68.89, 68.23, 66.73, 66.29, 65.55, 63.46, 61.55, 59.11, 58.26, 47.29, 45.76, 45.00, 43.59, 42.79, 40.79, 40.52, 38.08, 36.41, 31.77, 18.91, 18.59, 17.20, 12.63.

**Compounds 5, 7, 9, 11, and 13** were prepared in a manner similar to that of 3.

**Compound 5.** <sup>13</sup>C NMR (67.8 MHz, C<sub>5</sub>D<sub>5</sub>N) δ 176.14, 171.66, 157.35, 155.37, 133.03, 131.05, 129.33, 127.74, 121.45, 98.35, 78.00, 74.50–69.00 (PEG), 66.83, 65.93, 63.33, 61.65, 59.29, 58.37, 47.38, 45.95, 45.18, 43.72, 42.98, 41.70, 41.16, 40.05, 36.59, 31.90, 26.15, 19.10, 18.81, 17.43, 12.84.

**Compound 7.** <sup>13</sup>C NMR (67.8 MHz, C<sub>5</sub>D<sub>5</sub>N) δ 176.06, 171.67, 169.41, 157.25, 134.47, 133.20, 132.96, 132.75, 129.86, 127.93, 121.93, 98.15, 97.80, 78.29, 76.70, 74.79, 74.59, 73.50–69.00 (PEG), 68.63, 68.35, 66.60, 65.70, 58.96, 58.61, 47.00, 44.87, 43.56, 42.64, 36.33, 31.76, 18.88, 18.52, 17.16, 12.59.

**Compound 9.** <sup>13</sup>C NMR (67.8 MHz, C<sub>5</sub>D<sub>5</sub>N) 176.14, 171.63, 168.76, 157.43, 147.69, 137.67, 137.10, 134.07, 133.76, 132.99, 130.40, 129.57, 128.61, 127.29, 98.30, 97.96, 78.41, 76.50–66.50 (PEG), 66.84, 66.35, 65.88, 61.65, 59.13, 58.35, 47.46, 45.88, 45.14, 43.72, 42.94, 40.66, 36.56, 31.92, 19.09, 18.76, 17.40, 16.36, 12.84.

**Compound 11.** <sup>13</sup>C NMR (67.8 MHz, C<sub>5</sub>D<sub>5</sub>N) δ 176.13, 171.63, 171.02, 170.33, 161.67, 132.98, 129.45, 127.18, 98.30, 78.47, 76.47, 75.01, 74.41, 73.50–69.00 (PEG), 66.84, 64.49, 63.32, 61.67, 59.23, 58.42, 47.41, 45.88, 45.15, 43.72, 42.91, 41.45, 40.79, 40.52, 36.57, 31.98, 19.08, 18.82, 17.42, 12.84.

**Compound 13.** <sup>13</sup>C NMR (67.8 MHz, C<sub>5</sub>D<sub>5</sub>N) δ 176.11, 171.63, 171.20, 157.34, 133.74, 133.01, 129.29, 127.74, 98.30, 98.01, 78.42, 76.50–67.00 (PEG), 66.86, 65.93,

63.76, 61.61, 59.27, 58.36, 47.45, 45.90, 45.15, 43.72, 42.97, 40.71, 39.84, 38.34, 36.51, 31.93, 19.07, 18.79, 17.40, 12.84.

**In Vitro Solubility, Stability, and Dissociation Profile.** The solubility of the conjugates was determined by dissolution in saline. Briefly, a known amount of compound was added to 1 mL of 0.9% saline in a 4 mL glass vial. The mixture was vortexed for 5 min and left for 10 min. The mixture was filtered through a 0.45  $\mu$ m hydrophilic filter membrane, and the filtrate was lyophilized to dryness and weighed. Rates of hydrolysis (dissociation of PEG conjugate) of the PEG–AmB derivatives were determined in phosphate-buffered saline (PBS, pH 7.4) and fresh rat plasma as previously described (12).

**In Vitro Efficacy.** In vitro microbial proliferation was assessed by using an Alamar Blue based proliferation assay (11) to determine each conjugate's  $IC_{50}$  (drug concentration inhibiting growth of cells by 50%). Briefly 2-fold dilutions of PEG conjugates were made in yeast-peptone-dextrose (YPD) broth. A 50  $\mu$ L aliquot of *Saccharomyces cerevisiae* (ATCC 9763) was seeded into microwell plates at a final density of  $2 \times 10^3$  cells per well. Plates were incubated at 30 °C in a humidified incubator with 5%  $CO_2$  for 3 days. Cell growth was measured by the addition of 10  $\mu$ L/well of Alamar Blue (Alamar Biosciences, Inc., Sacramento, CA), and the plates were incubated further for 4 h at 30 °C. The  $IC_{50}$  values for each compound were determined from absorbance versus dilution factor plots. In addition, minimum inhibitory concentration (MIC) was determined by the broth dilution method (7). Constructs were dissolved and serially diluted in 100% DMSO. For each concentration tested, 0.01 mL of the aliquot was added to a 48-well plate containing 0.99 mL of potato dextrose broth (DIFCO, Detroit, MI) with  $10^3$  to  $10^4$  CFU/mL of *Aspergillus niger* (ATCC 8740). The final maximum concentration of DMSO was 1%, and the initial conjugate concentration was 100  $\mu$ g/mL. The plates were incubated at 24 °C for 48 h and then visually examined and scored positive for inhibition of growth or turbidity or negative for no effect upon growth or turbidity. Vehicle-control and an AmB reference were used as blank and positive controls, respectively. Each concentration was evaluated in duplicate.

**Erythrocyte Permeability.** Erythrocyte permeability was assessed by examining the effect of the conjugates on erythrocyte hemolysis (9). Rabbit erythrocytes were suspended in PBS and were washed twice in the same buffer by centrifugation ( $3000 \times g$  for 10 min). The hemolysis reaction was conducted in glass tubes containing 0.1 mL of the serially diluted compounds and 0.9 mL of erythrocytes. Tubes were incubated for either 30 min or 3 h at 37 °C and then placed into a refrigerator for 5 min to halt the reaction. Samples were then centrifuged, and the supernatant was measured in duplicate for hemoglobin concentration (OSM3 Hemoximeter, Radiometer, Copenhagen).

**Circulatory Retention.** Circulatory retention studies were performed in 260 g, non-tumor-bearing Sprague Dawley female rats (Charles River Laboratories, Stone Ridge, NY). Rats received an iv bolus of either 45.77 mg/kg of **3** (2 mg/kg AmB equivalents) in saline or 2 mg/kg of a deoxycholate micellar suspension of amphotericin B (Fungizone, Sigma, St. Louis, MO) via the tail vein at an injection rate of 0.5 mL/min. Rats were bled over a 48 h period (three rats/time point). Bleeding was conducted in unconscious (70%  $CO_2$ /30%  $O_2$ ) animals via retro-orbital plexus into a sterile EDTA containing tube. A minimum of 250  $\mu$ L of whole blood was collected and

centrifuged at 4 °C for 5 min at 5000 rpm. The plasma fraction was collected and frozen immediately at –80 °C on dry ice until analyzed. The plasma samples were thawed and analyzed by HPLC within 1 to 2 h of thawing using a modification of the method by Echevarria (6). Briefly, 10  $\mu$ L of a 2.5 mg/mL solution piroxicam (Sigma, St. Louis, MO) was added to 60  $\mu$ L of plasma as an internal standard. Compound **1** and **3** were extracted from the plasma by addition of 250  $\mu$ L of acetonitrile/methanol (1:1), incubating at room temperature for 5 min and then centrifuging the mixture at 14 000 rpm for 3 min in a microcentrifuge. The supernatant was transferred to a microcentrifuge tube. A 100  $\mu$ L aliquot of the extract was applied to a Jupiter C18 (4.6 mm  $\times$  250 mm, Phenomenex) column previously equilibrated with solvent A (41% acetonitrile, 4.3% acetic acid, 54.7% water). The HPLC was eluted for 12 min with solvent A and stepped to 100% acetonitrile for 5 min, and the column was reequilibrated with solvent A for 5 min. The eluted peaks were detected by UV absorbance using 357 nm for the initial 7.5 min of the elution and 290 nm for the final 14.5 min. The amount of **1** and **3** in the plasma was calculated from the linear regression analysis of **1** and **3** standard curves performed in rat plasma identical to the rat plasma samples. The area under the plasma curve (AUC), elimination half-life ( $t_{1/2}$ ), and peak or maximum concentration ( $C_{max}$ ), were calculated using a one compartment, iv bolus, first-order elimination model (Win-Nonlin, Pharsight Corp., Mountain View, CA).

**In Vivo Safety.** For in vivo administration, AmB solubilized in sodium deoxycholate (Fungizone, Gibco BRL, Life Technologies) was employed. AmB and PEG–AmB dosages were dissolved in sterile physiological saline prior to in vivo dosing. All PEG–AmB dosages were given as their AmB equivalents (absolute amount of AmB given). The maximum tolerated single dose (MTD) of selected PEG-conjugated AmB derivatives was estimated by body weight loss in female ICR mice (7–8 weeks old, Harlan Labs). The MTD was determined by administering different groups of mice ( $N = 4$ –5) ascending iv doses of between 4 and 12 mg (AmB content) at 1 to 2 mg/kg increments. Body weights were measured twice weekly for two weeks. The highest dose to cause a loss of less than 20% of initial weight within the time period was considered the MTD. All animals received humane care in compliance with the "Principles of Laboratory Animal Care" formulated by the National Society of Medical Research and the "Guide for the Care and Use of Laboratory Animals" published by the National Institute of Health. This animal facilities' Institutional Animal Care and Use Committee approved these experimental protocols.

**In Vivo Efficacy.** Antifungal animal testing (17) was conducted at MDS Pharma Services (Bothell, WA). Briefly, groups of 10 ICR-derived male mice (MDS Pharma Services- Taiwan Ltd.) weighing  $22 \pm 1$  g were used. Mice were inoculated iv with an  $LD_{90-100}$  of *Candida albicans* (ATCC 10231,  $1.1 \times 10^7$  CFU/mouse, American Type Culture Collection, Rockville MD) in 0.2 mL of PBS without mucin. Test substances and vehicle control, sterile saline, were administered iv (10 mL/kg) with doses ranging from 0.5 mg/kg to 6 mg/kg to test animals 1 h after the fungal inoculation. Mortality was recorded once daily for 10 days. An increased survival of 50% or more relative to the vehicle control group after the fungal inoculation was considered significant protective activity. All aspects of the study were performed according to the International Guiding Principles for

**Table 1. In Vitro Profile<sup>a</sup> of PEG-Conjugated Amphotericin B**

compd	solubility in saline (mg/mL) <sup>b</sup>	% buffer hydrolysis in 4 h <sup>c</sup>	% buffer hydrolysis in 24 h <sup>c</sup>	dissociation $t_{1/2}$ (h) rat plasma <sup>c</sup>	IC <sub>50</sub> <i>S. cerevisiae</i> ( $\mu$ M) <sup>d</sup>	MIC <i>A. niger</i> ( $\mu$ g/mL) <sup>d</sup>
<b>1</b>	<0.01	—	—	—	0.035	0.3
<b>3</b>	49.9 [2.2]	1.5	4.5	3.0	5.0	>100
<b>5</b>	66.3 [2.5]	1.0	3.4	1.3	2.0	ND <sup>e</sup>
<b>7</b>	46.0 [1.4]	1.4	6.3	1.0	0.297	30
<b>9</b>	60.3 [2.3]	0.5	4.6	3.0	6.0	ND
<b>11</b>	56.6 [2.5]	1.8	4.6	1.5	2.0	ND
<b>13</b>	56.3 [2.5]	1.0	4.4	1.5	4.0	100

<sup>a</sup> All experiments were conducted at least in duplicate. Standard deviation of measurements =  $\pm 10\%$ . <sup>b</sup> Solubility of AmB in conjugate (mg/mL) in brackets. <sup>c</sup> Rates of hydrolysis of the PEG–AmB derivatives were determined in phosphate-buffered saline (PBS, pH 7.4) at 25 °C and fresh rat plasma at 37 °C. <sup>d</sup> IC<sub>50</sub> and MIC were measured by an Alamar-blue-based cytotoxicity assay and the broth dilution method, respectively. Values express as AmB equivalence. <sup>e</sup> ND not determined.

Biomedical Research Involving Animals (CIOMS Publication No. ISBN 92 90360194, 1985).

## RESULTS

**In Vitro Solubility, Stability, and Dissociation Profile.** The in vitro profile of PEG-conjugated AmB derivatives are shown in Table 1. The solubility of the PEG-conjugated AmB compounds in saline ranged from 46.0 to 66.3 mg/mL, thus increasing AmB's solubility from less than 0.01 mg/mL to as high as 2.5 mg/mL when presented in the conjugate form. The rates of hydrolysis of the PEG conjugates were determined in phosphate-buffered saline, pH 7.4 (PBS) and fresh rat plasma. The PEG–AmB conjugates appeared quite stable in PBS at room temperature with less than 7% hydrolysis occurring within 24 h. The hydrolysis half-life ( $t_{1/2}$ ) of PEG–AmB conjugates in fresh rat plasma varied between 1 and 3 h.

**In Vitro Efficacy.** The in vitro antifungal activity of all the conjugates was tested using *Saccharomyces cerevisiae*. The inhibition of proliferation by AmB and the PEG–AmB conjugates are shown in Table 1. The IC<sub>50</sub> of AmB was 35 nM, which is within its reported range (2). In contrast, it appears to take roughly 100 times greater quantity of AmB within the slower releasing PEG conjugates to show the same level of inhibition produced with free AmB. The MIC of conjugates **3** and **13** were also assessed using *Aspergillus niger*. Again, based on an AmB content, the PEG conjugates were approximated 100 times less effective than free AmB.

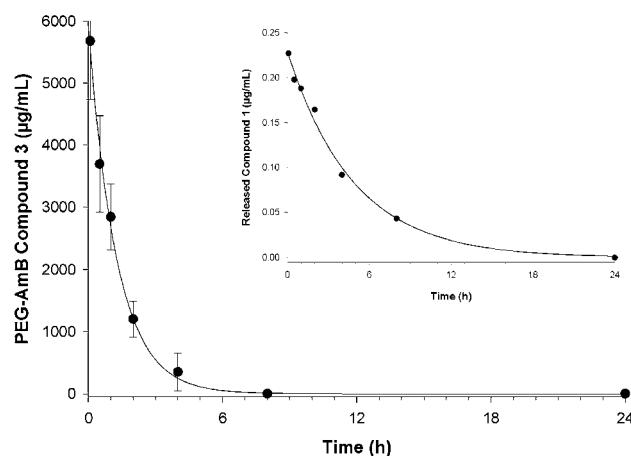
**Erythrocyte Membrane Permeability.** The effect of PEG–AmB on perturbing plasma membranes was determined by examining the hemolysis of rabbit erythrocytes using varying concentrations of PEG–AmB. The two PEG–AmB conjugates representing the slowest in vitro dissociation rates **3** and **9** were assessed after 30 min and 3 h for these effects on erythrocyte plasma membranes. After 30 min incubation, neither PEG–AmB conjugate showed any hemolysis at concentrations up to 1 mg/mL, the highest concentration examined. In contrast, free AmB in a deoxycholate micellar suspension was hemolytic at concentrations greater than 10  $\mu$ g/mL. The level of hemolysis for 1 mg/mL of AmB after a 30 min exposure was approximately 10% which increased to over 70% after the 3 h incubation. In contrast, the two PEG–AmB conjugates at 1 mg/mL (AmB content) showed less than 3% hemolysis after 3 h.

**Circulatory Retention.** The modeled pharmacokinetic parameters for both **1** and **3** are shown in Table 2. A plot of the plasma concentration–time curve for **3** administered iv in rats is shown in Figure 1. The correlation between observed and predicted model time point values for individual rats gave coefficients of determination ( $r^2$ ) of greater than 0.95. Compound **1**

**Table 2. Pharmacokinetic Parameters of Compound 1 and Compound 3**

compound	$C_{\max}$ ( $\mu$ g/mL) <sup>a,b</sup>	$t_{1/2}$ (h) <sup>b</sup>	AUC ( $\mu$ g/mL·h) <sup>a,b</sup>
AmB ( <b>1</b> )	0.26 $\pm$ 0.02	1.88 $\pm$ 1.73	0.68 $\pm$ 0.62
PEG–AmB ( <b>3</b> )	6254 $\pm$ 990 [273 $\pm$ 43]	0.41 $\pm$ 0.03	3715 $\pm$ 820 [162 $\pm$ 35.7]
AmB ( <b>1</b> ) released from <b>3</b>	0.31 $\pm$ 0.04	1.93 $\pm$ 1.22	0.83 $\pm$ 0.43

<sup>a</sup> AmB in conjugate ( $\mu$ g/mL) in brackets. <sup>b</sup> Each value represents the mean  $\pm$  standard deviation ( $n = 3$ ).

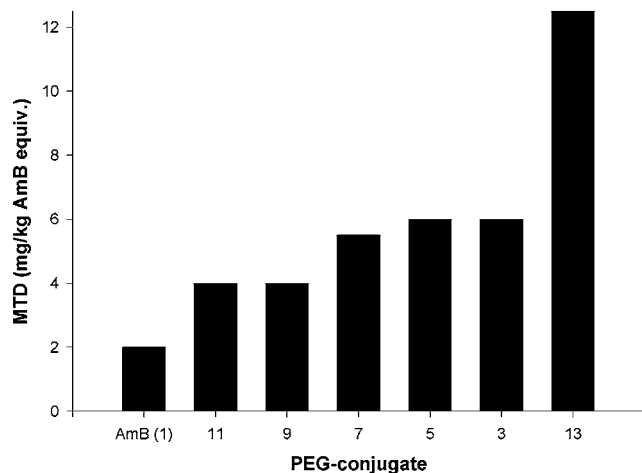


**Figure 1.** Mean plasma concentration–time profile for PEG–AmB conjugate **3** administered intravenously at 45.77 mg/kg, equaling 2 mg/kg AmB equivalents, to Sprague–Dawley rats ( $n = 3$ ). Inset indicates plasma concentration–time curve of released compound **1** (AmB) from compound **3**.

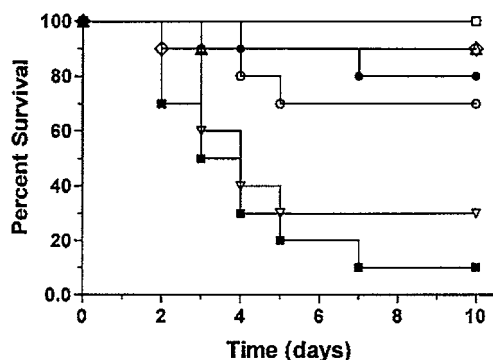
showed a  $C_{\max}$  of 0.26  $\pm$  0.02  $\mu$ g/mL with an elimination  $t_{1/2}$  of 1.88  $\pm$  1.73 h and an AUC of 0.68  $\pm$  0.62  $\mu$ g/mL·h. In contrast, **3** showed a  $C_{\max}$  of 273  $\pm$  43  $\mu$ g/mL AmB equivalents, a 1000-fold increase from that observed for **1** (AmB). The elimination  $t_{1/2}$  of **3** in the plasma was estimated to be 0.41  $\pm$  0.03 h with an area under the curve (AUC) of 3.71  $\pm$  0.82 mg/mL·h or 162.3  $\pm$  35.7  $\mu$ g/mL·h AmB equivalents, an almost 200-fold increase compared to **1**. The inset within Figure 1 shows the detected amount of **1** released in vivo from **3**. The correlation between observed and predicted model time point values gave a  $r^2$  of 0.97. The estimated pharmacokinetic parameters for AmB released from **3** were similar to those observed for **1**. The  $C_{\max}$  of released AmB was 0.31  $\pm$  0.03  $\mu$ g/mL with an estimated elimination  $t_{1/2}$  of 1.93  $\pm$  1.2 h and an AUC of 0.83  $\pm$  0.43  $\mu$ g/mL·h.

**In Vivo Safety.** The maximum tolerated single dose (MTD) of all the PEG–AmB conjugates was estimated by body weight loss in female ICR mice (Figure 2). After a single dose of the PEG–AmBs, animals tend to show toxic effects within 24 h with severe morbidity occurring within 3 days. Free AmB in a deoxycholate micellar





**Figure 2.** Acute toxicity of formulations. The maximum tolerated single dose (MTD) of selected PEG-conjugated AmB derivatives was estimated by body weight loss in female ICR mice. The MTD was determined following administration ascending iv doses of PEG-AmB to mice ( $n = 4-5$ ) at 1 to 2 mg/kg increments. Body weights were measured thrice weekly for two weeks. The highest dose to cause a loss of less than 20% of initial weight within the time period was considered the MTD.



**Figure 3.** In vivo efficacy of PEG-AmB conjugate 3. Survival of mice infected with *C. albicans* was determined for control mice and mice treated with either AmB (Fungizone) or doses of PEG-AmB compound 3 up to their MTD. Mortality was recorded once daily of 10 days. Untreated control (■); AmB 1 mg/kg (●); Compound 3: 6 mg/kg (□), 4 mg/kg (△), 2 mg/kg (◇), 1 mg/kg (○), 0.5 mg/kg (▽).

suspension had a MTD of 2 mg/kg, which is in line with the toxicity seen by others (4, 20). Within the PEG-AmB series, both 11 and 9 showed the lowest MTD at 4 mg/kg followed closely by 7, 5, and 3 which were within the 5 to 6 mg/kg range (based on AmB content). Compound 13 appeared to be the safest conjugate with a MTD of 12 mg/kg.

**In Vivo Efficacy.** The in vivo therapeutic efficacy of PEG-AmB conjugate 3, due to its comparatively elevated MTD and longer rat plasma half-life, and AmB [1] was studied with mice infected with *Candida albicans*. A dose/response with 3 is shown in Figure 3. Conjugate 3 when administered iv at its MTD (6 mg/kg) or at either 1/3 or 2/3 its MTD resulted in 100% and 90% survival, respectively. A dose of 1 mg/kg showed 80% survival, whereas, 0.5 mg/kg showed only 30% survival. Negative and positive controls showed 10% of the vehicle control mice survived as compared to 70% of mice treated with 1 mg/kg AmB. Noteworthy, was the observation that the deaths in the 1/3 to 2/3 MTD PEG-AmB treated mice occurred within the first 2 to 4 days, while AmB treated mice died more toward the middle of the 10-day monitoring period. Effective protection, as defined by a  $\geq 50\%$

survival rate, was observed for doses at 1 mg/kg and greater for PEG-AmB.

## DISCUSSION

PEG conjugated to amino prodrugs that function via a 1,4-benzyl or 1,6-benzyl elimination has been demonstrated to be a feasible methodology to deliver anticancer drugs (15). Now this technology also has been proven to be useful for the delivery of antifungal agents as exemplified by AmB. In this PEG-linker-drug tripartate system, alteration of PEG conjugate pharmacokinetics can be easily achieved by changing the PEG-linker, thereby, altering the linker-drug cleavability and the introduction of steric hindrance (13). Modification of these parameters, therefore, can promote greater drug efficacy.

The synthetic program conducted for this initial investigation of PEG-AmB prodrugs provided a series of disubstituted PEG-AmB, most of which demonstrated stability ( $>24$  h) in pH 7.4 phosphate buffer at 25 °C, thus, physically the conjugates have potential clinical utility as injectable agents. These PEG conjugates, which carried two AmB molecules, were highly soluble ( $>46$  mg/mL in saline) and were engineered to vary in their rate of in vitro hydrolysis (dissociation of PEG conjugate in plasma) from one to 3 h. As a major finding, this investigation demonstrated that conjugation of PEG to AmB could produce prodrugs that were significantly ( $6\times$ ) less toxic than AmB-deoxycholate but maintained or even enhanced their in vivo antifungal effectiveness. Concomitantly, the prodrug characteristic of these PEG conjugates was likewise exemplified by the lack of antifungal activity with *S. cerevisiae* and *A. niger* and the minimal protuberance of erythrocyte membranes in vitro, suggesting that hydrolysis of AmB from the PEG may be required.

In general, many small molecule drugs have poor solubility, including antifungal agents, like AmB, Nystatin, etc. By designing PEG conjugates of these insoluble molecules their water solubility can be greatly increased. In this study the water solubility of AmB increased from less than 0.01 mg/mL for the native AmB to 1.4 to 2.5 mg/mL as the PEG conjugate, an increase of approximately 150 to 250 times. The enhanced solubility of the PEG-AmB conjugate form makes it possible to use less of the drug to achieve the same level of efficacy, thereby reducing the side effects of the drug. As shown in this study, PEG-AmB conjugates were significantly less toxic than AmB-deoxycholate yet maintained their in vivo antifungal effectiveness. This study also demonstrates that the rate of hydrolysis can be decreased by not only changing the PEG hydrolytic linkage but also by introducing steric hindrance through the use of ortho substituents on the benzyl component of the prodrug. As expected, PEGylation of AmB increased in vivo plasma AmB concentration and the released AmB had an elimination  $t_{1/2}$  that was similar AmB. Future attempts to further increase plasma  $t_{1/2}$  of these conjugates by exploration of chemistries with different linker moieties are being considered.

## ACKNOWLEDGMENT

The authors wish to thank the following team members for their quality technical assistance on this project: Jenny Hsu, Ping Hu, Virna Browoski, and Mary Mehlig of the pharmacology and toxicology team, Prasanna Reddy, Anthony Martinez, and Shuiyun Guan of the medicinal and organic chemistry team, Michelle Boro and Dr. Chyi Lee of the analytical chemistry team.

## LITERATURE CITED

- (1) Brajtburg, J., Powderly, W. G., Kobayashi, G. S., and Medoff, G. (1990) Amphotericin B: Current understanding of mechanism of action. *Antimicrob. Agents Chemother.* **34**, 183–188.
- (2) Brajtburg, J., and Bolard, J. (1996) Carrier effects on biological activity of amphotericin B. *Clin. Microbiol. Rev.* **9**, 512–531.
- (3) Cheron M., Cybulska, B., Mazerski, J., Grzybowska, J., Czerwinski, A., and Borowski, E. (1988) Quantitative structure–activity relationships in amphotericin B derivatives. *Biochem. Pharmacol.* **37**, 827–836.
- (4) Clark, J. M., Whitney, R. R., Olsen, S. J., George, R. J., Swerdel, M. R., Kunselman, L., and Bonner, D. P. (1991) Amphotericin B lipid complex therapy of experimental fungal infections in mice. *Antimicrob. Agents Chemother.* **35**, 615–21.
- (5) Conover C. D., Pendri, A., Lee, C., Gilbert, C. W., Shum, K. L., and Greenwald, R. B. (1997) Camptothecin delivery systems: the antitumor activity of a camptothecin-20-poly(ethylene glycol) ester transport form. *Anticancer Res.* **17**, 3361–3368.
- (6) Echevarria, I., Barturen, C., Renedo, M. J., and Dios-Vieitez, M. C. (1998) High performance liquid chromatographic determination of amphotericin B in plasma and tissue: Application to pharmacokinetic and tissue distributions studies in rats. *J. Chromatogr. A* **819**, 171–176.
- (7) Edwards, J. R., Turner, P. J., Withnell, E. S., Grindy, A. J., and Nairn, K. (1989) In vitro antibacterial activity of SM-7338, a carbapenem antibiotic with stability to dehydropeptidase I. *Antimicrob. Agents Chemother.* **33**, 215–222.
- (8) Falk, R., Domb, A. J., and Polackeck, I. (1999) A novel injectable water-soluble amphotericin B-arabinogalactan conjugate. *Antimicrob. Agents Chemother.* **43**, 1975–1981.
- (9) Forster, D., Washington, C., and Davis, S. S. (1988) Toxicity of solubilized and colloidal amphotericin B formulations to human erythrocytes. *J. Pharm. Pharmacol.* **40**, 325–328.
- (10) Francis, G. E., Fisher, D., Delgado, C., Malik, F., Gardiner, A., and Neale, D. (1998) PEGylation of cytokines and other therapeutic proteins and peptides: the importance of biological optimization of coupling techniques. *Int. J. Hematol.* **68**, 1–18.
- (11) Greenwald, R. B., Gilbert, C. W., Pendri, A., Xia, J., and Martinez, A. (1996) Drug delivery systems: water soluble taxol 2'-poly(ethylene glycol) ester prodrugs-design and in vivo effectiveness. *J. Med. Chem.* **39**, 424–431.
- (12) Greenwald, R. B., Pendri, A., Conover, C. D., Lee, C., Choe, Y. H., Gilbert, C., Martinez, A., Xia, J., Wu, D., and Hsue, M. (1998) Camptothecin-20-PEG ester transport forms: the effect of spacer groups on antitumor activity. *Bioorg. Med. Chem.* **6**, 551–562.
- (13) Greenwald, R. B., Pendri, A., Conover, C. D., Zhao, H., Choe, Y. H., Martinez, A., Shum, K. L., and Guan, S. (2000) Drug delivery systems employing 1,4- or 1,6-elimination: poly(ethylene glycol) prodrugs of amino-containing compounds. *J. Med. Chem.* **42**, 18, 3657–3667.
- (14) Greenwald, R. B., Choe, Y. H., Conover, C. D., Shum, K. L., Wu, D., and Royzen, M. (2000) Drug Delivery systems based on trimethyl lock lactonization: poly(ethylene glycol) prodrugs of amino-containing compounds. *J. Med. Chem.* **43**, 475–487.
- (15) Greenwald, R. B., Conover, C. D., and Choe, Y. H. (2001) Poly(ethylene glycol) conjugated drugs and prodrugs: a comprehensive review. *Crit. Rev. Ther. Drug* **17**, 101–161.
- (16) Greenwald, R. B. (2001) PEG drugs: an overview. *J. Controlled Release* **74**, 159–171.
- (17) Hanson, L. H., Perlman, A. M., Clemons, K. V., and Stevens, D. A. (1991) Synergy between Cilofungin and amphotericin B in a murine model of candidiasis. *Antimicrob. Agents Chemother.* **35**, 1334–1337.
- (18) Jorgensen K. E., and Moller, J. V. (1979) Use of flexible polymers as probes of glomerular pore size. *Am. J. Physiol.* **236**, 103–111.
- (19) Keim, G. R., Poutsiaika, J. W., Kirpan, J., and Keysser, C. H. (1973) Amphotericin B methyl ester hydrochloride and amphotericin B: comparative acute toxicity. *Science* **179**, 584–585.
- (20) Leenders, A., and de Maria, S. (1996) The use of lipid formulations of amphotericin B for systemic fungal infections. *Leukemia* **10**, 1570–75.
- (21) Mechlinski, W., and Schaffner, C. P. (1972) Polyene Macrolide Derivatives. I.: N-Acylation and esterification reactions with amphotericin B. *J. Antibiot.* **25**, 256–258.
- (22) Nucci, M. L., Shorr, R., and Abuchowski, A. (1991) The therapeutic value of poly(ethylene glycol)-modified proteins. *Adv. Drug Delivery Rev.* **6**, 133–151.
- (23) Pendri, A., Conover, C. D., and Greenwald, R. B. (1998) Antitumor activity of paclitaxel-2'-glycinate conjugated to poly(ethylene glycol): a water soluble prodrug. *Anti-Cancer Drug Des.* **13**, 387–395.
- (24) Sedlak, M., Buchta, V., Kubicova, L., Simunek, P., Holcapek, M., and Kasparova, P. (2001) Synthesis and characterization of a new amphotericin B-methoxypoly(ethylene glycol) conjugate. *Bioorg. Med. Chem. Lett.* **11**, 2833–2835.
- (25) Stella, V. J., Charman, W. N., and Naringrekar, V. H. (1985) Prodrugs, Do they have advantages in clinical practice? *Drugs* **29**, 455–473.
- (26) Yamaoka, T., Tabata, Y., and Ikada, Y. (1995) Fate of water-soluble polymers administered via different routes. *J. Pharm. Sci.* **84**, 349–354.

BC0256594

# Enhanced Hydrolytic Stability and Water Solubility of an Aromatic Nitrogen Mustard by Conjugation with Molecular Umbrellas

Saketh Vijayaraghavan,<sup>‡</sup> Bingwen Jing,<sup>‡</sup> Tracy Vrablik,<sup>‡</sup> Ting-Chao Chou,<sup>†</sup> and Steven L. Regen<sup>\*,‡</sup>

Department of Chemistry, Lehigh University, Bethlehem, Pennsylvania 18015, and Laboratory of Preclinical Pharmacology, Memorial Sloan-Kettering Cancer Center, 1275 York Avenue, New York, New York, 10021  
Received January 16, 2003

Chlorambucil, an aromatic nitrogen mustard, has been conjugated to putrescine- and spermidine-based scaffolds bearing one, two, and four persulfated cholic acid units. Those conjugates bearing two or four sterols show improved hydrolytic stability and water solubility relative to chlorambucil. A similar conjugate that contained only one sterol unit shows negligible improvement in hydrolytic stability but a significant increase in water solubility. Qualitatively, the hydrolytic stability within this series of conjugates parallels the shielding effects that have previously been found for related conjugates bearing a pendant, hydrophobic fluorescent probe. In vitro studies indicate that these conjugates possess modest to moderate activity against certain human lymphoblastic leukemia and human colon carcinoma cells.

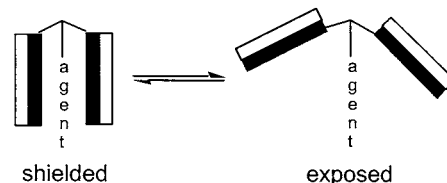
## INTRODUCTION

Molecular umbrellas are a unique class of amphiphiles that are capable of shielding an attached agent from an incompatible environment. Such molecules are composed of a central scaffold that bears two or more facially amphiphilic units (*1*). When a hydrophobic agent is bound to a molecular umbrella, immersion in water favors a *shielded* conformation whereby intramolecular hydrophobic interactions are maximized (*2*). A stylized illustration of shielded and exposed conformers of a molecular umbrella that contains two facially amphiphilic units and a hydrophobic agent is shown in Scheme 1. Here, the shaded rectangle represents a hydrophobic face.

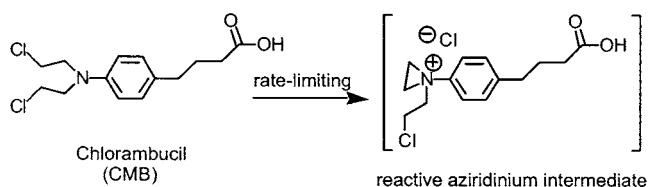
In previous studies, we have shown that certain molecular umbrellas are effective in shielding an attached hydrophobic fluorescent probe, 5-(dimethylamino)-1-naphthalenesulfonyl (Dansyl), from direct contact with an aqueous phase (*2*). On the basis of such findings, we hypothesized that molecular umbrellas should be capable of significantly altering the physical and chemical properties of attached hydrophobic agents. Specifically, we hypothesized that strong alkylating agents bound to molecular umbrellas should exhibit greater hydrolytic stability and water solubility. The primary aim of the work that is described herein was to test this hypothesis. For this purpose, chlorambucil (CMB) was chosen as a prototype due to its hydrolytic instability, its poor water-solubility, and its clinical importance as an anticancer agent (*3*).

Kinetic studies of nucleophilic substitution reactions of Chlorambucil support a mechanism in which intramolecular displacement, leading to an aziridinium ion, is rate-limiting (*4–7*). Subsequent reaction with water or other nucleophiles (e.g., DNA) then yields hydrolyzed and alkylated products (*8, 9*). Because charge is developed in the transition state leading to the aziridinium ion, one

Scheme 1



would expect that its rate of formation should be faster in a polar microenvironment. Conversely, a slower rate would be expected in a more hydrophobic microenvironment. Thus, a shielded conformation of a molecular umbrella–chlorambucil conjugate would be expected to result in a reduced rate of hydrolysis. At the same time, by exposing the hydrophilic face of the amphiphilic units to the aqueous phase, one would expect to observe a significant increase in water solubility. The present work explores these possibilities by use of a family of suitably designed conjugates.



## MATERIALS AND METHODS

**General Methods.** Unless stated otherwise, all reagents were obtained from commercial sources and used without further purification. House-deionized water was purified using a Millipore Milli-Q-filtering system containing one carbon and two ion-exchange stages. All <sup>1</sup>H NMR spectra were recorded on a Bruker AMX 360 MHz or a Bruker Avance 500 MHz instrument; chemical shifts are reported in ppm relative to residual solvent. All UV spectra were recorded using a Carey 300 Bio UV–Visible spectrophotometer operating at ambient temperature.

**N-(4-Aminobutyl)choleamide (4).** A mixture of 817 mg (2.0 mmol) of cholic acid, 253 mg (2.2 mmol) of

\* To whom correspondence should be addressed. E-mail: slr0@lehigh.edu.

<sup>†</sup> Memorial Sloan-Kettering Cancer Center.

<sup>‡</sup> Lehigh University.



*N*-hydroxysuccinimide, and 454 mg (2.2 mmol) of *N,N*-dicyclohexylcarbodiimide (DCC) in 10 mL of THF was stirred at room temperature for 6 h. The insoluble urea that was formed was removed by filtration. To the filtrate was added a solution made from 377 mg (2.0 mmol) of *N*-Boc-1,4-diaminobutane (Fluka Chemical Company) and 2 mL of THF, followed by addition of 697  $\mu$ L of *N,N*-diisopropyl-*N*-ethylamine (DIPEA). After stirring overnight at room temperature, the mixture was concentrated under reduced pressure, and the residue was dissolved in chloroform. Subsequent washing with dilute aqueous hydrochloride and brine, concentrating under reduced pressure, and purifying the residue via column chromatography (silica gel, CHCl<sub>3</sub>/CH<sub>3</sub>OH, 10/1, v/v) afforded 851 mg (73%) of 4-*N*-Boc-butylcholeamide having *R*<sub>f</sub> 0.41, and <sup>1</sup>H NMR (CDCl<sub>3</sub>, 50 °C, 500 MHz)  $\delta$ : 0.70 (s, 3 H), 0.90–2.25 (m, 43 H), 3.04 (m, 2 H), 3.16 (m, 2 H), 3.36 (m, 1 H), 3.78 (d, 1 H), 3.93 (d, 1 H).

To an ice-cold solution of 626 mg (1.081 mmol) of 4-*N*-Boc-butylcholeamide in 10 mL of methanol was added 4 mL of acetyl chloride over a 30 min period. The mixture was then allowed to stir at room temperature for 3 h. Subsequent purification by column chromatography (silica gel, CHCl<sub>3</sub>/CH<sub>3</sub>OH/NH<sub>4</sub>OH, 40/10/1, v/v/v) afforded 440 mg (85%) of **4** having *R*<sub>f</sub> 0.22 and <sup>1</sup>H NMR (CD<sub>3</sub>OD, 25 °C, 500 MHz)  $\delta$ : 0.70 (s, 3 H), 0.90–2.25 (m, 34 H), 2.94 (t, 2 H), 3.20 (m, 2 H), 3.37 (m, 1 H), 3.79 (d, 1 H), 3.94 (s, 1 H).

**Conjugate 5.** A mixture of 190 mg (0.625 mmol) of chlorambucil, 79 mg (0.686 mmol) of *N*-hydroxysuccinimide, and 132 mg (0.688 mmol) of *N*-(3-dimethylaminopropyl)-*N*-ethylcarbodiimide hydrochloride (EDC·HCl) in 4 mL of chloroform was stirred for 4 h at room temperature. To this solution was added 272 mg (0.568 mmol) of **4** followed by 198  $\mu$ L of DIPEA. After stirring for an additional 12 h, the mixture was washed with aqueous hydrochloride and brine. The organic layer was then concentrated under reduced pressure, and the residue was purified by column chromatography [silica, using, initially, CHCl<sub>3</sub>/CH<sub>3</sub>CO<sub>2</sub>CH<sub>2</sub>CH<sub>3</sub> (5/1, v/v) followed by CHCl<sub>3</sub>/CH<sub>3</sub>OH (9/1, v/v)] to give 283 mg (65%) of **5** having *R*<sub>f</sub> 0.33 and <sup>1</sup>H NMR (CD<sub>3</sub>OD, 25 °C, 500 MHz)  $\delta$ : 0.65 (s, 3 H), 0.85–2.25 (m, 38 H), 2.49 (t, 2 H), 3.13 (m, 4 H), 3.34 (m, 1 H), 3.57 (t, 4 H), 3.67 (t, 4 H), 3.77 (d, 1 H), 3.90 (s, 1 H), 6.60 (dt, 2 H), 7.03 (dd, 2 H). HRMS for C<sub>42</sub>H<sub>68</sub>Cl<sub>2</sub>N<sub>3</sub>O<sub>5</sub> (MH<sup>+</sup>): Calcd: 764.4536. Found: 764.4533.

**Conjugate 1.** To a solution of 196 mg (0.256 mmol) of **5** in 5 mL of DMF at 0 °C was added 367 mg (2.31 mmol) of Pyr·SO<sub>3</sub>. After stirring for 6 h at room temperature, the reaction mixture was cooled to 0 °C. The pH was then adjusted to ca. 9 via the addition of aqueous sodium bicarbonate, while maintaining the temperature of ca. 0 °C. Removal of solvent under reduced pressure (23 °C), followed by sequential column chromatographic purification of the residue (silica, CHCl<sub>3</sub>/CH<sub>3</sub>OH/H<sub>2</sub>O, 60/40/10, v/v/v) and preparative thin layer chromatograph (silica, CHCl<sub>3</sub>/CH<sub>3</sub>OH/H<sub>2</sub>O, 60/40/10, v/v/v), afforded 257 mg (93%) of **1** having *R*<sub>f</sub> 0.44 and <sup>1</sup>H NMR (CD<sub>3</sub>OD, 25 °C, 360 MHz)  $\delta$ : 0.74 (s, 3 H), 0.80–2.50 (m, 40 H), 3.16 (s, 4 H), 3.61–3.72 (m, 8 H), 4.12 (bs, 1 H), 4.43 (s, 1 H), 4.64 (s, 1 H), 6.66 (d, 2 H), 7.04 (d, 2 H).

**Chlorambucil Benzotriazinone Activated Ester.** To a solution of 393 mg (1.29 mmol) of chlorambucil and 232 mg (1.42 mmol) of 3-hydroxy-1,2,3-benzotriazin-4(3*H*)-one in 5 mL of chloroform was added 227 mg (1.42 mmol) of DCC. After being stirred for 9 h at room temperature, the mixture was filtered and concentrated under reduced pressure. Recrystallization of the residue with ethanol afforded 448 mg (77%) of the activated ester

of chlorambucil having <sup>1</sup>H NMR (CDCl<sub>3</sub>, 25 °C, 360 MHz)  $\delta$ : 2.10 (pent, 2 H), 2.72 (pent, 4 H), 3.61 (pent, 4 H), 3.69 (pent, 4 H), 6.65 (t, 2 H), 7.13 (t, 2 H), 7.83 (t, 1 H), 7.98 (q, 1 H), 8.20 (d, 1 H), 8.34 (q, 1 H).

**Conjugate 6.** To a solution, made from 305 mg (0.33 mmol) of *N*<sub>1</sub>,*N*<sub>3</sub>-spermidine-bis[choleic acid amide], 92  $\mu$ L of triethylamine, and 5 mL of DMF was added 178 mg (0.395 mmol) of chlorambucil benzotriazinone activated ester, and the mixture was allowed to stir overnight at room temperature. Subsequent removal of DMF under reduced pressure and purification of the residue by column chromatography (silica, CHCl<sub>3</sub>/CH<sub>3</sub>OH/H<sub>2</sub>O, 40/10/1, v/v/v) afforded 284 mg (77%) of **6** having *R*<sub>f</sub> 0.65 and <sup>1</sup>H NMR (CDCl<sub>3</sub>/CD<sub>3</sub>OD, 3/1, 45 °C, 500 MHz)  $\delta$ : 0.60 (s, 6 H), 0.81–2.24 (m, 70 H), 2.49 (m, 2 H), 3.06–3.35 (m, 10 H), 3.54 (m, 4 H), 3.63 (m, 4 H), 3.73 (s, 2 H), 3.85 (s, 2 H), 6.58 (d, 2 H), 6.99 (d, 2 H). HRMS for C<sub>69</sub>H<sub>112</sub>Cl<sub>2</sub>N<sub>4</sub>O<sub>9</sub> (MNa<sup>+</sup>): Calcd: 1233.7699. Found: 1233.7738.

**Conjugate 2.** To an ice-cold solution made from 253 mg (0.209 mmol) of **6** and 5 mL of DMF was added 598 mg (3.75 mmol) of Pyr·SO<sub>3</sub>. The resulting mixture was stirred for 3 h at 0 °C and then for 15 h at room temperature. The mixture was subsequently cooled to 0 °C and 5 mL of cold water added to it. The pH was adjusted to ca. 9 by addition of a sodium bicarbonate solution, while maintaining a temperature of 0 °C. After removal of the solvents under reduced pressure, the residue was dissolved in ca. 10 mL of methanol, and the solids were removed by filtration. Concentration of the filtrate under reduced pressure afforded a residue that was purified by column chromatography (silica, CHCl<sub>3</sub>/CH<sub>3</sub>OH/H<sub>2</sub>O, 60/40/10, v/v/v, *R*<sub>f</sub> 0.26). Additional purification was made by reverse phase preparative thin-layer chromatography (C-18 silica, CH<sub>3</sub>OH/H<sub>2</sub>O, 1/1, v/v, *R*<sub>f</sub> 0.37), followed by another regular phase preparative thin-layer chromatography (silica, CHCl<sub>3</sub>/CH<sub>3</sub>OH/H<sub>2</sub>O, 60/40/10, v/v/v, *R*<sub>f</sub> 0.26) to give 256 mg (67%) of **2** having, and <sup>1</sup>H NMR (CD<sub>3</sub>OD, 25 °C, 500 MHz)  $\delta$ : 0.74 (s, 6 H), 0.92–2.55 (m, 72 H), 3.10–3.34 (m, 8 H), 3.63–3.73 (m, 8 H), 4.12 (m, 2 H), 4.43 (s, 2 H), 4.64 (s, 2 H), 6.73 (d, 2 H), 7.05 (d, 2 H); <sup>13</sup>C NMR (CD<sub>3</sub>OD, 25 °C)  $\delta$ : 41.63 [N(CH<sub>2</sub>CH<sub>2</sub>Cl)<sub>2</sub>], 54.56 [N(CH<sub>2</sub>CH<sub>2</sub>Cl)<sub>2</sub>].<sup>3</sup>

**Conjugate 8.** To a solution made from 40 mg (0.13 mmol) of chlorambucil, 25 mg (0.15 mmol) of 3-hydroxy-1,2,3-benzotriazin-4(3*H*)-one, and 2 mL of chloroform was added 30 mg (0.15 mmol) of *N*-(3-dimethylaminopropyl)-*N*-ethylcarbodiimide hydrochloride (EDC·HCl). After the mixture was stirred for 4 h, 194 mg (0.10 mmol) of the tetrawalled molecular umbrella, **7**, was added along with 46  $\mu$ L (0.26 mmol) of DIPEA. Subsequently, ca. 1 mL of methanol was added, followed by stirring at room temperature for 12 h. Removal of solvent under reduced pressure, followed by column chromatography (silica, CHCl<sub>3</sub>/CH<sub>3</sub>OH/H<sub>2</sub>O, 35/10/1, v/v/v), afforded 182 mg (81%) of **8** having *R*<sub>f</sub> 0.39 and <sup>1</sup>H NMR (CD<sub>3</sub>OD, 25 °C, 500 MHz)  $\delta$ : 0.69 (d, 12 H), 0.90–2.25 (m, 136 H), 2.52 (t, 2 H), 3.10–3.29 (m, 10 H), 3.31–3.39 (m, 10 H), 3.66 (q, 4 H), 3.71 (q, 4 H), 3.78 (s, 4 H), 3.93 (s, 4 H), 4.23 (brs, 2 H), 4.34 (m, 2 H), 6.68 (d, 2 H), 7.06 (d, 2 H). HRMS for C<sub>128</sub>H<sub>210</sub>Cl<sub>2</sub>N<sub>8</sub>O<sub>19</sub> (MNa<sup>+</sup>): Calcd: 2256.4982. Found: 2256.5044.

**Conjugate 3.** To an ice-cold solution made from 161 mg (0.072 mmol) of **8** and 4 mL of DMF was added 825 mg (5.18 mmol) of Pyr·SO<sub>3</sub>. After the mixture was stirred overnight at room temperature, 2 mL of cold water was added to quench the reaction (maintaining the temperature of the mixture at ca. 0 °C), followed by addition of aqueous sodium bicarbonate to adjust the pH to ca. 9. The mixture was then concentrated under reduced pres-

sure (at 23 °C) and the residue purified by preparative thin-layer chromatography (silica,  $\text{CHCl}_3/\text{CH}_3\text{OH}/\text{H}_2\text{O}$ , 5/4/1, v/v/v,  $R_f$  0.23), followed by preparative reverse phase thin-layer chromatography (C-18 silica,  $\text{CH}_3\text{OH}/\text{H}_2\text{O}$ , 1/1, v/v  $R_f$  0.47) and one final regular phase preparative thin-layer chromatography (silica,  $\text{CHCl}_3/\text{CH}_3\text{OH}/\text{H}_2\text{O}$ , 5/4/1, v/v/v,  $R_f$  0.23) to give 135 mg (54%) of **3** having  $^1\text{H}$  NMR ( $\text{CD}_3\text{OD}$ , 25 °C, 360 MHz)  $\delta$ : 0.75 (d, 12 H), 0.90–2.50 (m, 138 H), 3.15 (m, 8 H), 3.35 (m, 8 H), 3.65–3.71 (m, 8 H), 4.12 (brs, 4 H), 4.22 (s, 2 H), 4.32 (s, 2 H), 4.43 (s, 4 H), 4.65 (s, 4 H), 6.65 (d, 2 H), 7.05 (d, 2 H).

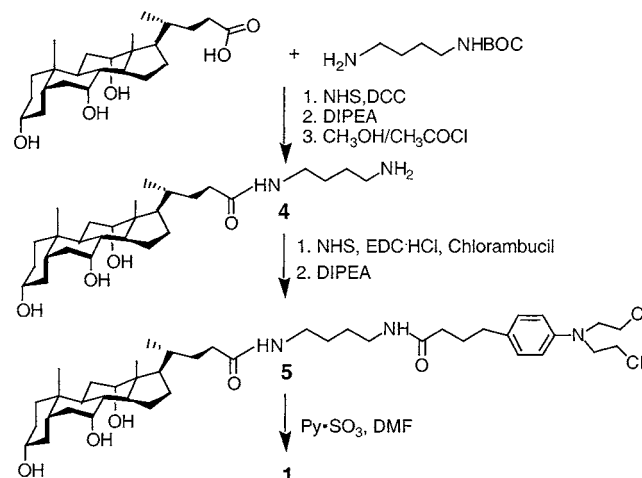
**Water Solubility.** Water solubilities were estimated at ambient temperature by adding ca. 1.0 mg of **1**, **2**, or **3** in a v-vial (microvial, Wheaton, NJ), and adding, incrementally, 1  $\mu\text{L}$  volumes of water. The mixture was shaken by hand, and a maximum solubility was recorded by visual inspection; that is, the minimum volume of water needed to obtain a clear solution was noted.

**Hydrolysis of the Nitrogen Mustards.** In a typical procedure, a vial was charged with 5.00 mL of a 0.1 M aqueous phosphate buffer (pH 7.4) and immersed in a temperature bath that was maintained at 37 °C. To this vial was added 50  $\mu\text{L}$  of a 10 mM acetone solution of chlorambucil. Aliquots (300  $\mu\text{L}$ ) were then withdrawn as a function of time and added to separate vials, which contained 3  $\mu\text{L}$  of a 0.5 M acetone solution of 4-(4-nitrobenzyl)pyridine (NBP). These vials were vigorously shaken for 0.25 min and then incubated at 37 °C for 2 h. The contents of these vials were then transferred to centrifuge tubes, which was followed by the sequential addition of 100  $\mu\text{L}$  of a 10 M aqueous NaOH solution and 600  $\mu\text{L}$  of 1-octanol. The mixture was quickly shaken and centrifuged (total time of 1 min), and the UV absorbance ( $\lambda_{\text{max}}$  534 nm) of the 1-octanol layer was immediately recorded.

A similar procedure was used in the case of **2**, except that the conjugate was directly added to the aqueous phosphate solution (maintained at 37 °C) as a solid, such that its final concentration was 100  $\mu\text{M}$ . Also, with **2**, the volume of the 0.5 M NBP solution was increased to 6  $\mu\text{L}$  and the time that was used for reaction with NBP increased to 3 h. It should be noted that due to the enhanced water solubility, UV absorption measurements ( $\lambda_{\text{max}}$  567 nm) were recorded using the aqueous phase, containing the violet-colored, alkylated product derived from **2**. In the case of **1** and **3**, 20  $\mu\text{L}$  of 20 mM solutions [made using  $\text{CH}_3\text{OH}$  and  $\text{H}_2\text{O}$ , respectively] were added to the aqueous phosphate buffer. These stock solutions were prepared at room temperature and used immediately (within 3 min) to minimize decomposition; with **1** and **3**, 9  $\mu\text{L}$  of the 0.5 M acetone solution of NBP was used for a reaction time of 2 h. Similar to **2**, the alkylated, violet-colored products in these cases were present in the aqueous phase.

**Biological Activity.** Activity for inhibiting cell growth in vitro were conducted in human lymphoblastic leukemia cells (CCRF-CEM) and its subline that was 80-fold resistant to vinblastine (CCRF-CEM/VBL), and in human colon carcinoma cells HCT-116. For the solid tumor cells, HCT-116, growing in a monolayer, cytotoxicity of the drug was determined in 96-well microtiter plates by using the sulforhodamine B (SRB) method described by Skehan et al. (10). For leukemia CCRF-CEM and its subline growth in suspension, cytotoxicity was measured by XTT-microculture method (11). Dose-effect relationship data were analyzed with the median-effect plot by using a previously described computer program (12, 13).

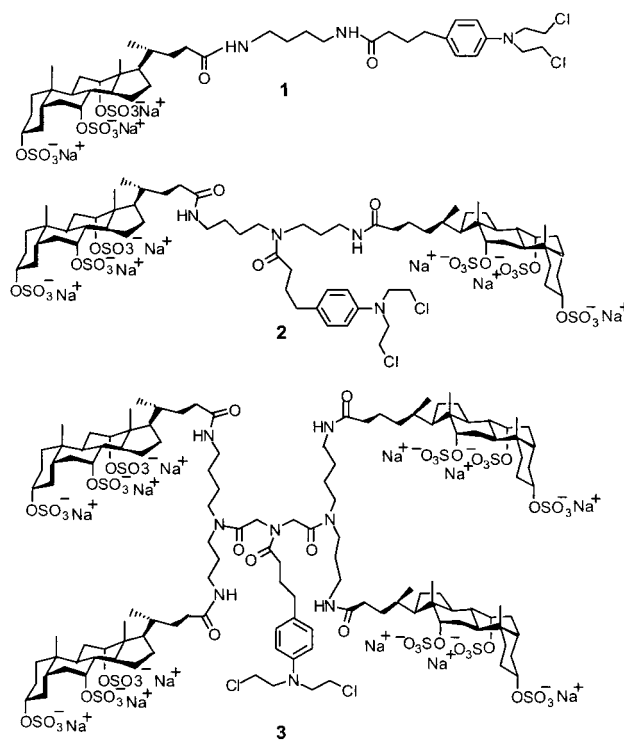
Scheme 2



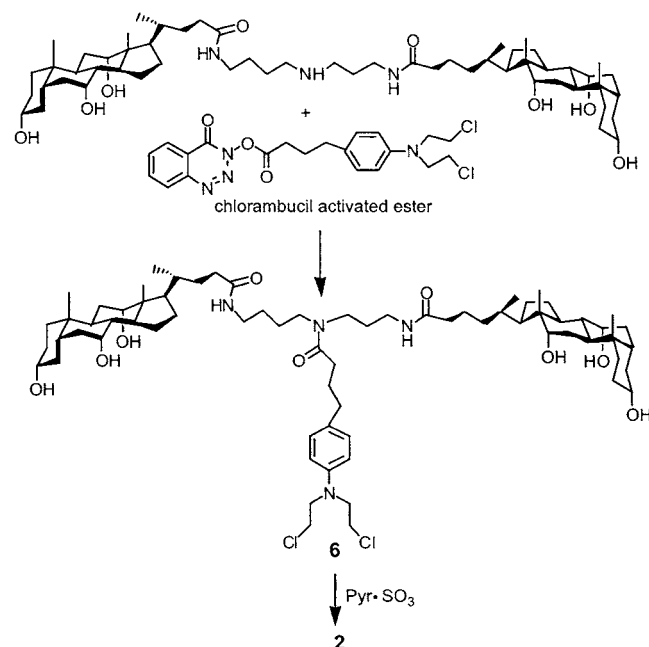
## RESULTS AND DISCUSSION

### Chlorambucil-Molecular Umbrella Conjugates.

Specific molecules that were chosen as targets for this study (**1**, **2**, and **3**) were conjugates derived from cholic acid, putrescine, spermidine, and chlorambucil. By analogy to related conjugates bearing a hydrophobic fluorescent probe, we expected that **2** would provide significant shielding of the nitrogen mustard, that **3** would provide even greater shielding, and that the shielding effects associated with **1** would be relatively modest. Thus, we predicted that the relative rates of hydrolysis would be chlorambucil  $\sim$  **1** > **2** > **3**. Because of the introduction of multiple sulfate groups, we further expected that the water solubility of **1**, **2**, and **3** would be substantially greater than that of chlorambucil.

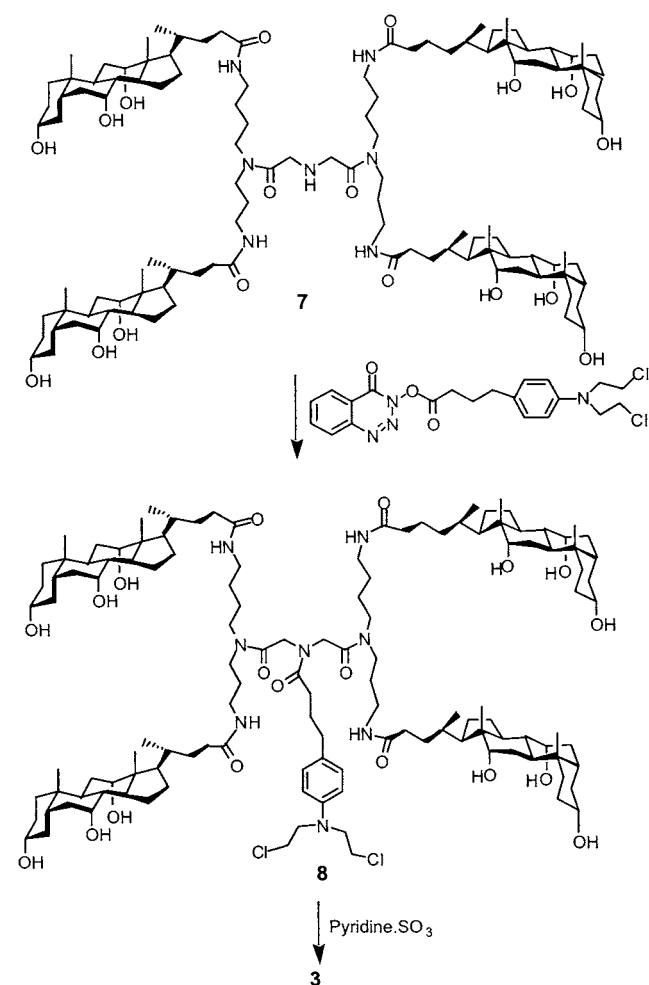


The synthetic route that was used to prepare **1** is summarized in Scheme 2. In brief, condensation of cholic acid with *N*-Boc-1,4-diaminobutane, followed by deprotection, coupling to chlorambucil, and sulfation afforded the requisite conjugate. Similarly, conjugate **2** was

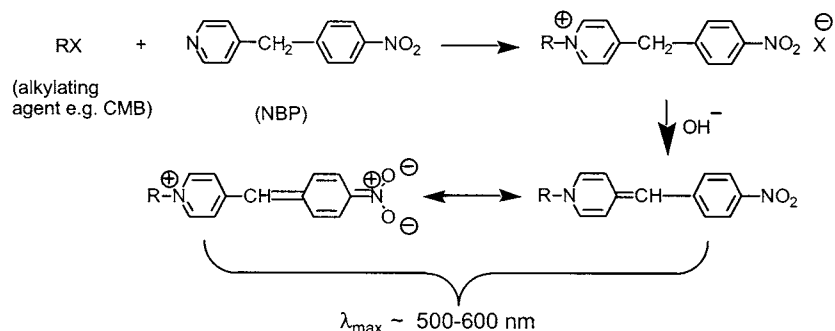
**Scheme 3**

prepared by acylation of *N*<sub>1</sub>,*N*<sub>3</sub>-spermidine-bis[choleic acid amide] with chlorambucil, followed by sulfation (Scheme 3). An analogous sequence of reactions (Scheme 4) was used to prepare **3**, starting from a tetrasterol conjugate (**7**), whose synthesis has previously been reported (*14*).

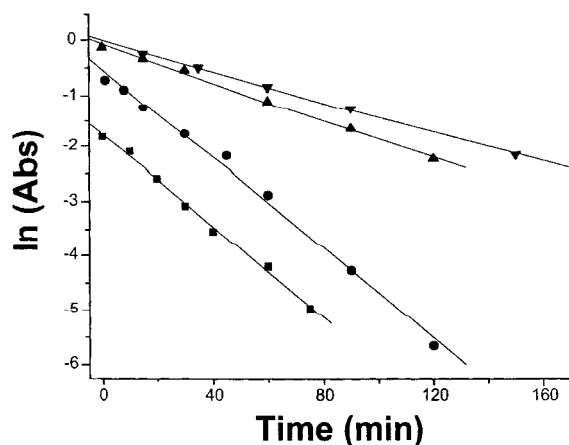
**Hydrolytic Stability.** To judge the hydrolytic stabilities of chlorambucil, **1**, **2**, and **3**, we used a simplified method in which reaction with 4-(4-nitrobenzyl)pyridine (NBP), and subsequent deprotonation affords intensely colored products (Scheme 5) (*3*). This method assumes that the reactivity of both chloroethyl groups within each nitrogen mustard are the same and also that the molar absorptivity of the alkylated NBP moieties in mono- and dialkylated products are the same (*8*). Experimentally, each nitrogen mustard was incubated in an aqueous phosphate buffer (pH 7.4) at 37 °C, and aliquots were withdrawn as a function of time. These aliquots were then immediately reacted with a 25-fold excess of NBP. Since UV absorbances should then be directly proportional to the concentration of unhydrolyzed chloroethyl groups, and since the rate disappearance of these groups is controlled by the formation of aziridinium ions, a first-order decrease in the UV absorbance is expected. As shown in Figure 1, such kinetic behavior has, in fact, been found for chlorambucil as well as for each of the chlorambucil conjugates. From the slopes of these plots, the observed first-order rate constants,  $k_{\text{obsd}}$ , were found to be  $7.03 \times 10^{-4}$ ,  $6.90 \times 10^{-4}$ ,  $2.95 \times 10^{-4}$ , and  $2.35 \times 10^{-4}$  s<sup>-1</sup>, for chlorambucil, **1**, **2** and **3**, respectively, which

**Scheme 4**

correspond to half-lives of 16.4, 16.7, 39.2, and 49.1 min, respectively. Additional evidence for enhanced hydrolytic stability was obtained by thin-layer chromatography. Specifically, an examination of an aqueous solution of chlorambucil by TLC (silica, CHCl<sub>3</sub>/CH<sub>3</sub>OH, 9/1, v/v) revealed the complete disappearance of the starting mustard ( $R_f$  0.41) after ca. 50 min of incubation; with **2**, complete loss of the starting material (silica, CHCl<sub>3</sub>/CH<sub>3</sub>OH/H<sub>2</sub>O, 30/20/5, v/v/v,  $R_f$  0.39) required ca. 3 h. In the case of **1**, the complete loss of the starting conjugate (silica, CHCl<sub>3</sub>/CH<sub>3</sub>OH/H<sub>2</sub>O, 30/20/5, v/v/v,  $R_f$  0.31) was apparent after ca. 70 min. Thus, as predicted, the relative rates of hydrolysis for chlorambucil, **1**, **2**, and **3** parallel the shielding efficiencies found for analogous conjugates bearing a hydrophobic fluorescent group.

**Scheme 5**





**Figure 1.** Plot of  $\ln(\text{abs})$  as a function of hydrolysis time for (■) chlorambucil, (●) **1**, (▲) **2**, and (▼) **3**. See Materials and Methods for experimental details.

**Table 1. Potency for Inhibiting Cancer Cell Growth in Vitro<sup>a</sup>**

mustard agent	human lymphoblastic leukemia cells		human colon carcinoma
	CCRF–CEM	CRF–CEM/VBL	HCT-116
CMB <sup>b</sup>	2.15	1.36	11.4
<b>1</b>	97.9	74.0	68.3
<b>2</b>	172.7	110.1	53.7
<b>3</b>	35.6	113.2	23.4

<sup>a</sup> IC<sub>50</sub> values represent the micromolar concentration needed to inhibit 50% growth. <sup>b</sup> Chlorambucil.

**Water Solubility.** The increase in the water solubility of chlorambucil, upon conjugation with one or more of these sulfated sterols, is dramatic. In particular, whereas chlorambucil was found to have a solubility in water that was less than 0.55 mg/mL, conjugates **1**, **2**, and **3** showed water solubilities corresponding to 560, 1210, and 1000 mg/mL. Thus, conjugation leads to increase in water-solubility by more than 3 orders of magnitude!

**In Vitro Anticancer Activity.** In preliminary studies, we have examined the activity of chlorambucil, **1**, **2**, and **3** in inhibiting the growth of human lymphoblastic leukemia cells, as well as human colon carcinoma cells. Table 1 summarizes our principal findings. When CCRF–CEM cells were used as targets, the conjugate that contained four sterol units (i.e., **3**), showed moderate activity and was ca. 16 times less active than chlorambucil. Decreasing the number of sterol units to two led to a decrease in activity. Further removal of one sterol (i.e., **1**) resulted in a modest increase in activity. While **1** also showed greater activity than **2** toward a subline that was 80-fold resistant to vinblastine (CCRF–CEM/VBL), the activity of **3** toward these target cells was similar to that of **2**. Perhaps the most striking aspect of the data shown in Table 1 is that whereas chlorambucil was more effective against leukemia cells than the human colon carcinoma cells, the conjugates showed exactly the reverse behavior. Also, in contrast to their activity against the leukemia cells, the conjugates showed a clear trend against the colon carcinoma cells such that the activity increased with increasing numbers of sterol units. It is noteworthy that the activity of **3** compared favorably with that of chlorambucil toward the colon carcinoma cells. Although we do not presently understand these differences from a mechanistic point of view, it would appear, nonetheless, that at least one of these conjugates (i.e., **3**) warrants in vivo testing.

## CONCLUSIONS

The covalent attachment of chlorambucil to molecules bearing one, two, or four persulfated cholic acid moieties increases its water solubility by more than 3 orders of magnitude. When two or four sterol units are included in the conjugate, a significant increase in hydrolytic stability is also observed. If only one sterol unit is present, the hydrolytic stability of the conjugate is essentially the same as that found for chlorambucil. These results closely parallel the shielding efficiencies that have previously been found for analogous cholic acid conjugates bearing a hydrophobic fluorescent probe.

In vitro studies have shown that conjugates **1**, **2**, and **3** exhibit modest to moderate anticancer activity against certain tumor cells. On the basis of an increase in water solubility by a more than 3 orders of magnitude, it is likely that the biodistribution of such conjugates, in vivo, would be very different from chlorambucil. Whether such differences would lead to an increase or decrease in the therapeutic efficacy, however, remains to be determined.

In a broader context, the present findings significantly extend the molecular umbrella concept by showing how a molecular umbrella can enhance the stability and water solubility of a hydrolytically sensitive agent.

## ACKNOWLEDGMENT

We are grateful to the National Institutes of Health (PHS Grant GM51814) for support of this research.

**Supporting Information Available:** <sup>1</sup>H NMR spectra for **1**, **2**, and **3**. This material is available free of charge via the Internet at <http://pubs.acs.org>.

## LITERATURE CITED

- (1) Janout, V., Lanier, M., and Regen, S. L. (1996) *J. Am. Chem. Soc.* **118**, 1573.
- (2) Janout, V., Lanier, M., and Regen, S. L. (1997) *J. Am. Chem. Soc.* **119**, 640.
- (3) Giraud, I., Rapp, M., Mauriziz, J. C., and Madelmont, J. C. (2002) *J. Med. Chem.* **45**, 2116.
- (4) Benn, M. H., Kazmaier, P., Watantada, C., and Owen, L. N. (1970) *J. Chem. Soc., Chem. Commun.* 1685.
- (5) Chatterji, C. C., Yeager, R. L., and Gallelli, J. F. (1982) *J. Pharm. Sci.* **71**, 50.
- (6) Ehrsson, H., Eksborg, S., Wallin, I., and Nilsson, S. O. (1980) *J. Pharm. Sci.* **69**, 1091.
- (7) Owen, W. R., and Steward, P. (1979) *J. Pharm. Sci.* **68**, 992.
- (8) Kudu, G. C., Schullek, J. R., and Wilson, I. B. (1994) *Pharmacol. Biochem. Behav.* **49**, 621.
- (9) O'Connor, C. J., Denny, W. A., Fan, J. Y., Gravatt, G. L., Grigor, B. A., and McLennan, D. J. (1991) *J. Chem. Soc., Perkin Trans. 2*, 1933.
- (10) Skehan, P., Storeng, R., Scudiero, D., Monks, A., McMahon, J., Vistica, D., Warren, J. T., Bokesch, H., Kenny, S., and Boyd, M. R. (1990) *J. Natl. Cancer Inst.* **82**, 1107.
- (11) Scudiero, D. A., Shoemaker, R. H., Paull, K. D., Monks, A., Tierney, S., Nofzieger, T. H., Currens, M. J., Sciff, D., and Boyd, M. R. (1988) *Cancer Res.* **48**, 4827.
- (12) Chou, T.-C., and Talalay, P. T. (1984) *Adv. Enzyme Regul.* **22**, 27.
- (13) Chou, T.-C., and Hayball, M. *CalcuSyn for Windows* (Biosoft, Cambridge, U.K.), 1997.
- (14) Shawaphun, S., Janout, V., and Regen, S. L. (1999) *J. Am. Chem. Soc.* **121**, 5860.

## Structural Effects of Carbohydrate-Containing Polycations on Gene Delivery. 3. Cyclodextrin Type and Functionalization

Stephen R. Popielarski, Swaroop Mishra, and Mark E. Davis\*

Chemical Engineering, California Institute of Technology, Pasadena, California 91125. Received January 21, 2003; Revised Manuscript Received February 13, 2003

Linear cationic  $\beta$ -cyclodextrin ( $\beta$ -CD)-based polymers can form polyplexes with plasmid DNA and transfect cultured cells. The effectiveness of the gene delivery and the cellular toxicity has been related to structural features in these polycations. Previous  $\beta$ -CD polycations were prepared from the cocondensation of 6<sup>A</sup>,6<sup>D</sup>-dideoxy-6<sup>A</sup>,6<sup>D</sup>-diamino- $\beta$ -CD monomers with other difunctionalized monomers such as dimethyl suberimide (DMS). Here, the type of CD and its functionalization are varied by synthesizing numerous 3<sup>A</sup>,3<sup>B</sup>-dideoxy-3<sup>A</sup>,3<sup>B</sup>-diamino- $\beta$ - and  $\gamma$ -CD monomers. Both alkyl- and alkoxy-diamines are prepared in order to vary the nature of the spacing between the CD and the primary amines in the monomers. These diamino-CD-monomers are polymerized with DMS to yield amidine-based polycations. The nature of the spacer between the CD-ring and the primary amines of each monomer is found to influence both molecular weight and polydispersity of the polycations. When these polycations are used to form polyplexes with plasmid DNA, longer alkyl regions between the CD and the charge centers in the polycation backbone increase transfection efficiency and toxicity in BHK-21 cells, while increasing hydrophilicity of the spacer (alkoxy versus alkyl) provides for lower toxicity. Further,  $\gamma$ -CD-based polycations are shown to be less toxic than otherwise identical  $\beta$ -CD-based polycations.

### INTRODUCTION

Numerous nonviral gene delivery studies are involved in elucidating the relationships between vector structure and transfection efficiency by modifying promising systems and assaying their performance. This ongoing research has demonstrated the significant influence of polycation structure on efficiency of gene delivery. Poly(ethyleneimine)s (PEIs) are a widely studied class of polycations for gene delivery. PEI molecular weight has been shown to affect both cytotoxicity and transfection efficiency (1, 2). The charge density (1) and degree of branching (3) in the PEI backbone also significantly alter transfection efficiency in vitro. Furthermore, substituents grafted onto PEI affect the interaction of PEI with DNA as well as PEI/DNA polyplex interactions with cells (4–6, and references therein). Ionenenes are another class of gene delivery vehicles whose structure has been related to stability of interaction with DNA (7) and to transfection efficiency (8). Structure–function studies have also been undertaken with systems based on chitosan (9), poly(L-lysine) (10), linear poly(amidoamine)s (11), polysaccharide–oligoamine conjugates (12), and others. It is clear from these reports that minor changes in structure of the gene delivery vehicle can have dramatic effects on the gene delivery efficiency and toxicity of the vector.

We have prepared families of linear,  $\beta$ -cyclodextrin-containing polycations ( $\beta$ CDPs) and have shown that these polymers can be used as gene delivery vectors (13, 14). Cyclodextrins (CDs) are cup-shaped molecules formed of cyclic oligomers of glucose. Cyclodextrins comprised of 6, 7, and 8 glucopyranose units are called  $\alpha$ -,  $\beta$ -, and  $\gamma$ -CD, respectively ( $\beta$ -CD is represented in Figure 1). There are three distinct hydroxyls per glucopyranose

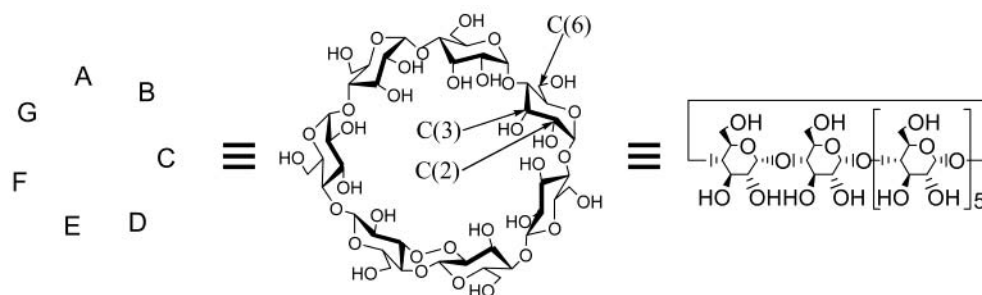
unit; two secondary carbons and one primary carbon bear these hydroxyls and they are labeled C(2), C(3), and C(6), respectively (Figure 1). The glucopyranose units are denoted alphabetically starting with 'A' and proceeding around the cyclodextrin ring (Figure 1).

Initial structure–function studies with  $\beta$ CDPs demonstrated the importance of interchange spacing to transfection efficiency and toxicity (14). Significant effects on transfection efficiency were observed when the inter-amidine distance was reduced by just 2 Å. Upon the basis of this finding, we initiated a more complete structure–function investigation using linear, cyclodextrin-containing polycations. In part 1 of our study, we showed that cellular toxicity was related to the distance of the charge center from the carbohydrate unit (whether it be a cyclodextrin or trehalose), and that increasing polycation hydrophilicity provides decreasing toxicity (15). Part 2 of our work revealed that the type of charge center can dramatically change the delivery efficiency (16). With the  $\beta$ CDPs, amidine charge centers give greater gene delivery than quaternary ammonium charge centers. Here, we vary the type of cyclodextrin ( $\beta$  and  $\gamma$ ) and the functionalization at the cyclodextrin, i.e., 3<sup>A</sup>,3<sup>B</sup>-dideoxy-3<sup>A</sup>,3<sup>B</sup>-diamino- $\beta$ - and  $\gamma$ -CD, as compared to the previously used 6<sup>A</sup>,6<sup>D</sup>-dideoxy-6<sup>A</sup>,6<sup>D</sup>-diamino- $\beta$ -CD, to prepare a distinct series of linear, cyclodextrin-containing polycations. Additionally, we report the effects of spacer length between the cyclodextrin and the charge center in order to make direct comparisons between otherwise identical  $\beta$ - and  $\gamma$ -CD-based polyamides. The polycations were characterized and assayed for plasmid DNA (pDNA) binding, polyplex size and  $\zeta$ -potential, and in vitro transfection efficiency and toxicity.

### MATERIALS AND METHODS

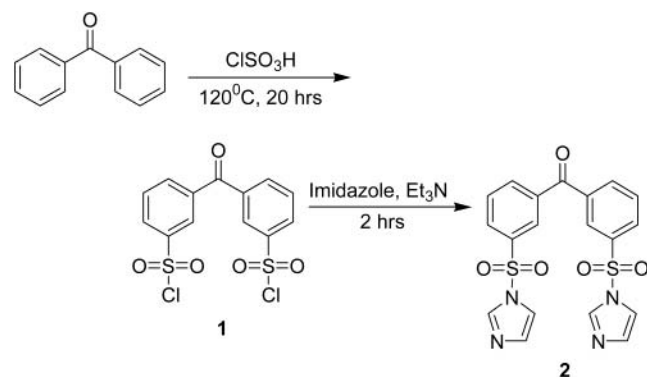
$\beta$ - and  $\gamma$ -Cyclodextrins were purchased from Wacker Biochem Corp. (Adrian, MI) and dried in vacuo at

\* To whom correspondence should be addressed. E-mail: mdavis@cheme.caltech.edu.



**Figure 1.** Representations and labeling of  $\beta$ -cyclodextrin.

**Scheme 1**



120 °C overnight before use. Chlorosulfonic acid (Alfa Aesar; Ward Hill, MA) was distilled before use. Dimethyl suberimidate $\cdot$ 2HCl (DMS) was purchased from Pierce Endogen (Rockford, IL) and used without further purification. All other reagents were obtained from commercial suppliers and were used as received. Ion-exchange chromatography was run on a Tosopearl SP-650M (TosoHaas; Montgomeryville, PA) column ( $\text{NH}_4^+$  form), and products were eluted with aqueous ammonium bicarbonate up to 0.4M. Thin-layer chromatography was performed on Silica Gel 60 F 254 plates (EM Separations Technology; Gibbstown, NJ) and the amino compounds were eluted with 5:3:3:1 *n*-PrOH:AcOEt:H<sub>2</sub>O:NH<sub>3</sub>(aq) and visualized by reaction with ninhydrin. Matrix-assisted, laser desorption/ionization time-of-flight mass spectrometry (MALDI-TOF-MS) was performed on a PerSeptive Biosystems Voyager DE PRO BioSpectrometry Workstation in the positive ion mode using a 2,5-dihydroxy benzoic acid matrix. NMR spectra were recorded on a Bruker AMX500 spectrometer as dilute solutions of either D<sub>2</sub>O or DMSO-*d*<sub>6</sub>. Dialysis was carried out using a 3500 molecular weight cutoff regenerated cellulose dialysis cassette (Pierce Endogen).

**Synthesis of Benzophenone-3,3'-disulfonyl Chloride (1, Scheme 1).** Benzophenone (26.06 g, 0.143 mol) was added in small portions to 190 mL (2.86 mol) of freshly distilled chlorosulfonic acid under an argon atmosphere. The solution was then heated to 120 °C with reflux. After 20 h at 120 °C, the cooled solution was added slowly to about 1000 g of ice in a 2 L Erlenmeyer flask. The slurry was poured into a separatory funnel then extracted with chloroform (350 mL then 300 mL) and washed with saturated NaHCO<sub>3</sub> (200 mL), water (200 mL), and saturated NaCl (200 mL, twice). The chloroform was removed under reduced pressure. The yellow solid obtained was recrystallized twice from chloroform/hexanes. First-crop yielded 30 g of off-white crystals; second-crop yielded 5.4 g. (65% yield). Anal. (C<sub>13</sub>H<sub>8</sub>Cl<sub>2</sub>O<sub>5</sub>S<sub>2</sub>) C, H, Cl, S.

**Synthesis of Benzophenone-3,3'-disulfonyl Imidazole (2, Scheme 1).** **1** (13 g, 34.3 mmol) was dissolved in 150 mL of chloroform. Imidazole (4.95 g, 72.7 mmol) and Et<sub>3</sub>N (10.2 mL, 73.2 mmol) were added. After about 30 min of stirring, 50 mL of dichloromethane was added to the slurry and allowed to stir for an additional 30 min. About 200 mL of dichloromethane was required to homogenize the reaction slurry, which was then washed with water (200 mL, twice) and dried with sodium sulfate. Benzophenone-3,3'-disulfonyl imidazole, **2**, was recrystallized from dichloromethane/ethyl acetate giving 13.9 g of colorless needles (92% yield). Anal. (C<sub>19</sub>H<sub>14</sub>N<sub>4</sub>O<sub>5</sub>S<sub>2</sub>) C, H, N, S. NMR data were in agreement with published chemical shifts (17).

**Synthesis of Cyclodextrin Polycations (6a–d and 7a–d, Scheme 2).** Syntheses of 2<sup>A</sup>,2<sup>B</sup>-disulfonated  $\beta$ -cyclodextrin (17) (**3a**) and 2<sup>A</sup>,2<sup>B</sup>-disulfonated  $\gamma$ -cyclodextrin (18) (**3b**) were carried out according to literature methods. NMR and mass spectra data were in agreement with published values (17, 18).

Syntheses of 3<sup>A</sup>,3<sup>B</sup>-di(aminoalkylamino)- $\beta$ - and 3<sup>A</sup>,3<sup>B</sup>-bis(aminoalkoxyamino)- $\gamma$ -cyclodextrins (**4a–d** and **5a–d**) were carried out as exemplified by the following procedure.

**Synthesis of 5c.** Hexamethylenediamine (5.89 g, 50.7 mmol) was dissolved in 35 mL of degassed water. **3b** (1.50 g, 0.88 mmol) was added at once and stirred at 37 °C under nitrogen for 19 h. The reaction was further carried out at 70 °C for 3 h then concentrated under reduced pressure. Cyclodextrins were precipitated with 11:1 acetone:methanol and collected by filtration. Ion-exchange chromatography yielded the pure product (855 mg, 54% yield). MALDI-TOF-MS [ $\text{M} + \text{H}$ ]<sup>+</sup> = 1493.7.

The polycations were prepared as exemplified by the following procedure.

**Synthesis of 7c.** **5c** (100 mg, 54.7  $\mu$ mol) and DMS (15.5 mg, 56.7  $\mu$ mol) were taken up in 108  $\mu$ L of 0.5 M Na<sub>2</sub>CO<sub>3</sub> and stirred for 13 h. Acidification with 1 N HCl to pH 2.0 followed by exhaustive dialysis yielded 58.4 mg of a white powder (56% yield).

**Light Scattering and Molecular Weight Determination.** The specific refractive index (RI) increment,  $\text{d}n/\text{dc}$ , of each polycation was determined by fitting a linear curve to plots of RI versus concentration (five data points per polycation). Polycations were then analyzed on a Hitachi D6000 HPLC system equipped with an ERC-7512 RI detector and a Precision Detectors PD2020/DLS light scattering detector using a PL aquagel-OH column (Polymer Laboratories, Amherst, MA). The eluent was 0.8 M ammonium acetate with 0.05% sodium azide, adjusted to pH 2.8 with phosphoric acid and flowing at 0.7 mL/min. RI values were measured on a Carl Zeiss refractometer (Max Erb Instrument Co., Burbank, CA) in the same eluent as used for HPLC analysis.

**Plasmid DNA.** Plasmid pGL3-CV (Promega; Madison, WI) was amplified with the DH5 $\alpha$  strain of *E. coli* (Gibco





**Table 1. Effect of Cyclodextrin Comonomer Structure on Polymerization**

polycation	polymerization yield (%)	dn/dc (mL/g)	M <sub>w</sub> (kDa)	M <sub>w</sub> /M <sub>n</sub>	average degree of polymerization
<b>6a</b>	32	0.1029	10.0	1.1	6
<b>6b</b>	44	0.1406	8.1	1.3	5
<b>6c</b>	61	0.1515	13.9	1.7	8
<b>6d</b>	74	0.1322	13.0	1.4	7
<b>7a</b>	32	0.1085	9.3	1.1	5
<b>7b</b>	47	0.1386	9.6	1.4	5
<b>7c</b>	56	0.1237	14.7	1.6	8
<b>7d</b>	58	0.1279	13.3	1.3	7

**Table 2. Particle Sizing and Zeta-Potential of Polycation/pDNA Complexes Formulated at Charge Ratio ( $\pm$ ) of 5**

polycation	particle diameter (nm)	zeta potential (mV)
<b>6a</b>	121.5 $\pm$ 1.3	12.5 $\pm$ 0.3
<b>6b</b>	96.4 $\pm$ 1.1	6.4 $\pm$ 1.1
<b>6c</b>	107.7 $\pm$ 0.9	16.7 $\pm$ 1.7
<b>6d</b>	88.2 $\pm$ 6.9	27.7 $\pm$ 1.0
<b>7a</b>	124.1 $\pm$ 1.6	23.3 $\pm$ 0.5
<b>7b</b>	118.6 $\pm$ 23.9	17.5 $\pm$ 3.0
<b>7c</b>	153.3 $\pm$ 1.7	9.6 $\pm$ 1.1
<b>7d</b>	102.9 $\pm$ 1.0	30.7 $\pm$ 1.4

fewer than four methylenes between the cyclodextrin and the primary amine yielded polycations with an average degree of polymerization (DOP) of 5 or 6, while those synthesized from monomers with over four spacer methylenes produced an average DOP of 7 or 8. An increase in polydispersity accompanied the increase in polycation length.

**Polyplex Formation and Characterization.** To demonstrate polycation interaction with pDNA, polyplexes were formulated and run on a 0.8% agarose gel at a range of charge ratios. Polycations **6a** and **7a** did not completely retard DNA below a charge ratio of 1.5, while **6b–d** and **7b–d** retarded DNA at charge ratios of 0.5 and above (Figure 2). The diameter of polycation/pDNA polyplexes varied between 100 and 150 nm, while the associated  $\zeta$ -potentials were all found to be positive (Table 2).

**In Vitro Transfection Efficiency.** In vitro transfection efficiency to BHK-21 cells was assessed in triplicate at charge ratios ( $\pm$ ) of 2, 4, 6, 8, 10, 15, and 20. Lysates of transfected cells were assessed for luciferase activity by measuring the relative light units (RLU) normalized by total protein content (Figure 3). Among the diaminoalkyl-CD analogues, **6a–c** and **7a–c**, increased spacer length produced greater transfection efficiency, with more pronounced enhancements between the **a** and **b** variants in each series. The diaminoalkoxy-CD analogues, **6d** and **7d**, demonstrated intermediate levels of luciferase expression, below that achieved with the **b** analogues. Generally speaking, the  $\beta$ -CD and  $\gamma$ -CD polycations with identical spacers produced similar luciferase gene expression.

**In Vitro Cellular Toxicity.** The total protein content of cell lysates was used as a measure of polyplex and/or polycation toxicity (Figures 4 and 5). The fractional cell survival of transfected cells was assessed by comparison to untransfected cells. Among the charge ratios investigated, polycations **6a–c** and **7a–c** demonstrated a marked decrease in cell viability with increased spacer length; **6d** and **7d** were essentially nontoxic at the concentrations employed. For the **b** and **c** analogues, cell viability decreased with increasing charge ratio and was worse for the  $\beta$ -CD polycations than for the  $\gamma$ -CD polycations. The toxicity of each polycation was independent

of the presence of pDNA, as determined by comparison of polyplex-transfected cells with those exposed to an equal amount of polycation alone (Figure 5).

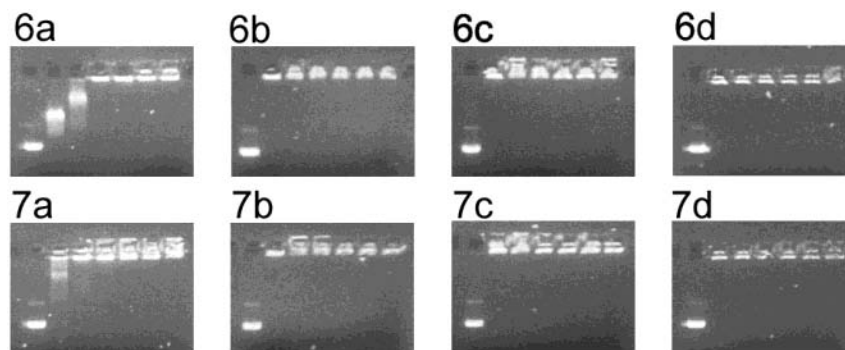
## DISCUSSION

Previous studies of  $\beta$ -cyclodextrin-containing polycations ( $\beta$ CDPs) have demonstrated the importance of polycation structure to cellular toxicity and in vitro transfection efficiency. The effect of interamidine distance (14) has been elucidated, as has the importance of using a bulky cyclodextrin instead of a smaller carbohydrate such as trehalose (15). Here, we investigated the relevance of cyclodextrin ring size by studying otherwise identical series of  $\beta$ - and  $\gamma$ -cyclodextrin polycations. Within each series, the length and character of the spacer between the cyclodextrin ring and the amidine charge center were varied to understand the importance of these additional variables in our system. Such an approach allows the direct evaluation of the effect of cyclodextrin-type on in vitro transfection efficiency and cellular toxicity as well as providing further insights into the role of charge spacing along the polycationic backbone. For in vivo application of the polycations described in this report, modifications are required to impart salt and serum stability. Methodologies for modifying similar cyclodextrin-based polycations for in vivo use are available in our earlier publication (20).

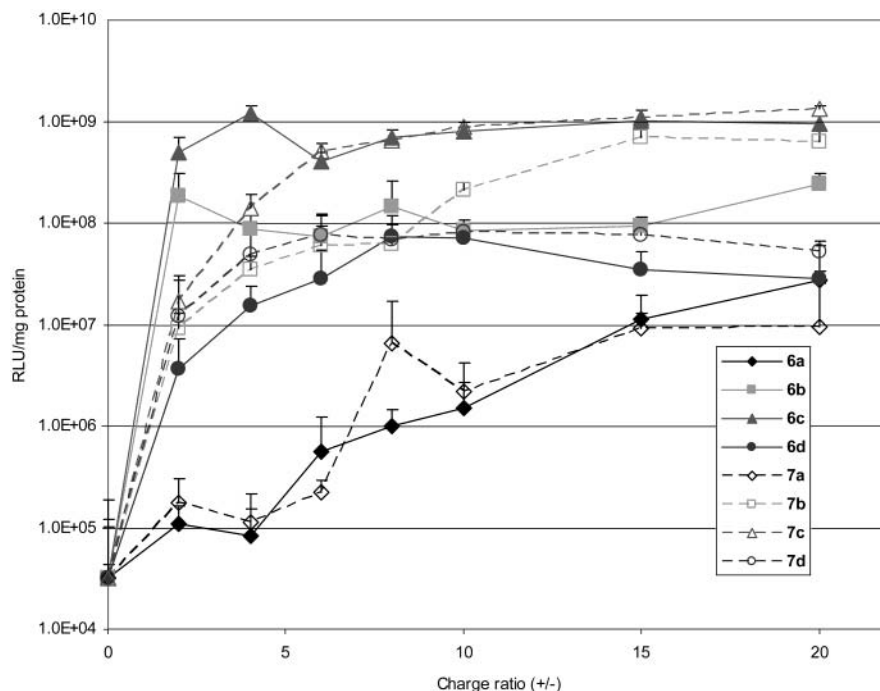
The  $\beta$ - and  $\gamma$ -CD-based series of polycations follow remarkably similar trends in the DOP. DOP is found to increase with distance between the reactive primary amines of the CD-monomers and the cyclodextrins themselves. As the number of methylenes between the cyclodextrin and primary amine increases, an increase in DOP is observed with an accompanying increase in polydispersity. All polycations shown here have an average DOP between 5 and 8, corresponding to an average of 10–16 amidine charge centers per polycation chain. Assuming these differences in DOP do not significantly affect polycation performance, a direct correlation may be made between polycation structure and the observed performance.

Previous work demonstrated that the transfection efficiency and toxicity achieved with CD-containing polycations is affected by the presence of cyclodextrins and by the alkyl chain length between charge centers (14, 15). Here, it is demonstrated that the transfection efficiency and toxicity of a related set of polycations is affected by the structure of the spacer separating the CD ring from the charge centers and, to a lesser degree, the type of CD used.

Diaminoalkyl-CD polycations **6a–c** and **7a–c** exhibit a marked increase in transfection efficiency as the spacer length increases, particularly with the increase from 2 to 4 methylene units. Dramatic differences between the **a** and **b** analogues are observed despite only a small change in polycation structure (a 2 Å increase in distance between the cyclodextrin and the amidine charge center). A smaller but significant increase in transfection efficiency is observed between the **b** and **c** analogues. Polycations **6a** and **7a** gave low levels of luciferase expression that gradually increased with increasing charge ratio. Optimum expression levels observed with these two polycations were of the same order as transfection efficiencies seen with polycations **6b**, **6c**, **7b**, and **7c** at the lowest charge ratios. Having reached relatively high transfection efficiencies at the lowest investigated charge ratios, polycations **6b**, **6c**, **7b**, and **7c** did not display the steady and marked increase with charge ratio



**Figure 2.** Agarose gel electrophoresis of polycation/pDNA complexes. For each polycation, complexes were formulated at charge ratios ( $\pm$ ) of 0, 0.5, 1.0, 1.5, 2.0, 2.5, and 3.0 and run in order of increasing charge ratio (left to right) on a 0.8% agarose gel.



**Figure 3.** Relative light units (RLU)/mg protein as a function of charge ratio for cyclodextrin-polycation/pDNA complexes. Complexes were formulated at various charge ratios and exposed to BHK cells in serum-free medium for 4 h. 48 h after exposure, the cells were assayed for luciferase activity. Charge ratio of 0 indicates naked pDNA.

seen with **6a** and **7a**. Beyond a charge ratio of  $6\pm$ , only **7b** demonstrated a significant increase in luciferase expression.

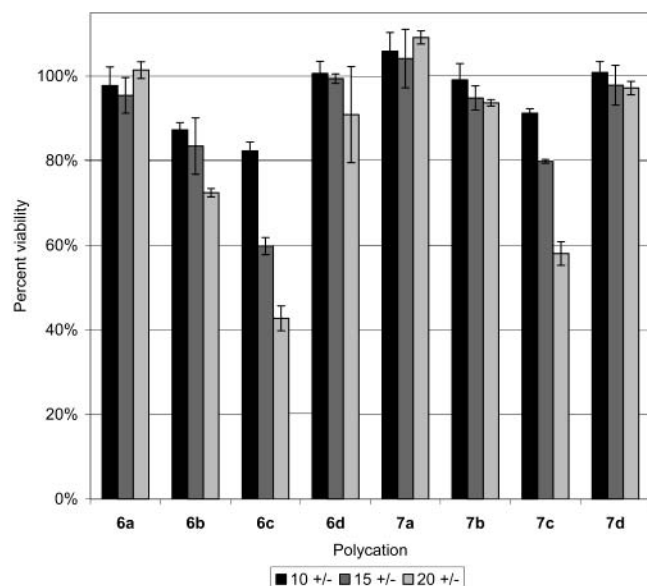
The least effective polycations, **6a** and **7a**, are also observed to require the highest charge ratio to completely retard pDNA in the electrophoresis assay. Previous work with CD-containing polycations has shown a correlation between relative binding efficiency and transfection efficiency (15). The reduced binding efficiency associated with decreased spacer length may result from the bulky cyclodextrins impeding the access of polycation amidines to pDNA phosphates.

The presence of CDs in the polycation backbone has been shown to produce a dramatic reduction in toxicity of  $\beta$ -CD-containing polycations (13–16). In part 1 of our study (15), 6<sup>A</sup>,6<sup>P</sup>-dideoxy-6<sup>A</sup>,6<sup>P</sup>-diamino- $\beta$ -CDs were studied, while 3<sup>A</sup>,3<sup>B</sup>-dideoxy-3<sup>A</sup>,3<sup>B</sup>-diamino- $\beta$ - and  $\gamma$ -CDs are investigated here. The transfection and toxicity assays employed in this series of papers do not indicate any advantages of functionalization of the CD at the C(3)-position over functionalization at the C(6)-position. In part 1 it was shown that longer spacer lengths between the CD and the charge center result in increased toxicity, that is in agreement with the result that polycations

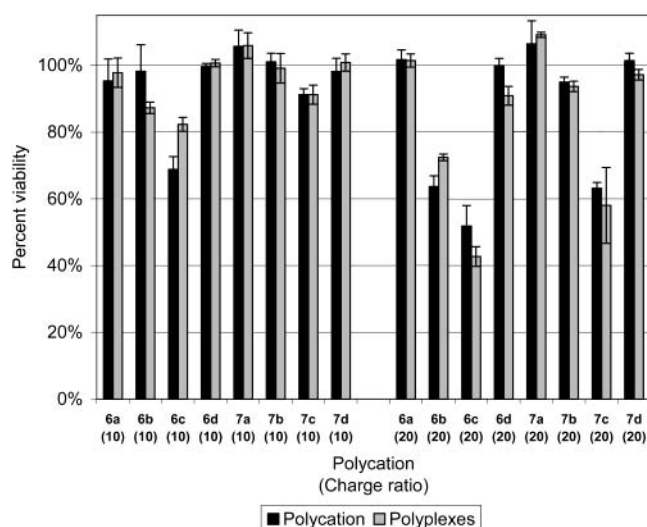
**6a–c** and **7a–c** demonstrate an increase in toxicity as the CD-amidine distance is increased. These results suggest that there is a toxicity-mitigating influence of the CD on the cationic center, regardless of the site of CD-derivatization. The CD may be affecting the interaction of the amidine charge centers with intracellular entities through its steric bulk and/or large sphere of hydration and thus lowering the toxicity of amidine-containing polycations. The bulkiness of the CD also hinders access of polycation amidines to pDNA phosphates. Since CD bulkiness and/or sphere of hydration correlate with the trends in both toxicity and transfection efficiency, the observation that decreases in toxicity are associated with decreases in transfection efficiency and effective pDNA binding strength are self-consistent.

The diaminoalkoxy-CD polycations **6d** and **7d** demonstrate an intermediate level of transfection efficiency and insignificant toxicity. Although this polycation pair provides the largest spacing between the CD and amidine residues among polycations in this study, the hydrophilic nature of the alkoxy spacer likely enlarges the effective hydration sphere around the cyclodextrin ring. In addition, the alkoxy spacer has more flexibility than alkyl spacers. These factors somehow mitigate the toxicity of





**Figure 4.** Cell viability to exposure of polycation/pDNA complexes at various charge ratios. Cells were assayed for viability 48 h after exposure to complexes; data were normalized with respect to untreated cells.



**Figure 5.** Comparison of the toxicity of polycation alone to polycation/pDNA complexes. Cells were exposed to polycation alone or to an equal amount of polycation complexed with pDNA; "charge ratio" for polycation alone merely represents amount of polycation. Total protein concentrations in cell lysates were used as measure of viability; data were normalized using values for untreated cells.

polycations **6d** and **7d**. The change in transfection efficiency as a function of charge ratio is also intermediate relative to the diaminoalkyl-CD polycations; RLU/mg protein readings with polycations **6d** and **7d** rose gradually up to a charge ratio of  $6 \pm$ , above which no increase is observed.

Each polycation produced measurable luciferase expression above background levels; the luciferase activities of untreated cells and cells treated with polycation alone are roughly  $5 \times 10^3$  RLU/mg protein (data not shown) while the luciferase activity of cells treated with pDNA alone is roughly  $5 \times 10^4$  RLU/mg protein. For comparison, BHK-21 cells were transfected with complexes of pDNA formulated with 25 kDa branched polyethylenimine or with  $\beta$ CDP6 (*14*). Polyethylenimine complexes at an N/P of 5 were found to give luciferase activity of  $5 \times 10^9$  RLU/

mg protein (data not shown).  $\beta$ CDP6 complexes produced  $2 \times 10^8$  RLU/mg protein at a charge ratio of  $10 \pm$  (data not shown).

Here, analogous  $\beta$ - and  $\gamma$ -CD-containing polycations produced similar levels of gene expression, with the exception that polycations **6b** and **6c** outperform their  $\gamma$ -CD-containing analogues **7b** and **7c** at charge ratios of two and four; however, these differences do not persist as the charge ratio is increased. At higher charge ratios, toxicity differences between the  $\beta$ -CD-containing polycations **6b** and **6c** and the  $\gamma$ -CD-containing analogues become apparent, with the  $\gamma$ -CD-containing polycations being less toxic. It is again interesting to note the correlation between enhanced transfection efficiency and increased toxicity.

The peripheral diameter of  $\gamma$ -CD is about 17.5 Å while that of  $\beta$ -CD is about 15.4 Å (*19*), highlighting the importance of even small variations in the CD-containing polycation system to in vitro performance. Since the polycation backbone goes through adjacent sugar residues of the cyclodextrin ring in the case of the  $\beta$ - and  $\gamma$ -CD polycations discussed in this report, the linear backbone structure varies minimally between the two. However, the remainder of the cyclodextrin-ring, which can be considered pendant to the backbone, is certainly larger in the case of  $\gamma$ - over  $\beta$ -CD.

In part 1, Reineke and Davis showed that trehalose-based polyamides are more toxic than those based on  $\beta$ -CD. Here, CD-containing polycations demonstrate an increase in toxicity with an increase in distance between the CD and the amidine charge center and with a decrease in the size of the CD-ring. Together, these results are consistent with the hypothesis that the size of the carbohydrate moiety and its associated sphere of hydration (overall increase in hydrophilicity) mitigate the toxicity of the amidine-based polycations.

We have described the synthesis and characterization of a family of cyclodextrin-containing polycations and demonstrated significant and clear effects of polycation structure on in vitro gene expression efficiency and cellular toxicity against BHK-21 cells. The structure of diaminated cyclodextrins was found to influence both the molecular weight and polydispersity of polycations resulting from reaction of these compounds with dimethyl suberimidate. Longer alkyl regions in the polycation backbone increased transfection efficiency and toxicity, while increasing hydrophilicity was toxicity-reducing. Further,  $\gamma$ -CD polycations were shown to be less toxic than otherwise identical  $\beta$ -CD polycations.

#### ACKNOWLEDGMENT

S.R.P. thanks the Department of Defense for an NDSEG fellowship. We would also like to thank Insert Therapeutics Inc. for partial support of this project. M.E.D. is a consultant to and has financial interest in Insert Therapeutics, Inc.

**Supporting Information Available:** MALDI-TOF spectra of CD-monomers **4a–d** and **5a–d**. This material is available free of charge via the Internet at <http://pubs.acs.org>.

#### LITERATURE CITED

- Jeong, J. H., Song, S. H., Lim, D. W., Lee, H., and Park, T. G. (2001) DNA transfection using linear poly(ethylenimine) prepared by controlled acid hydrolysis of poly(2-ethyl-2-oxazoline). *J. Controlled Release* 73, 391–399.
- Godbey, W. T., Wu, K. K., and Mikos, A. G. (1999) Size matters: Molecular weight affects the efficiency of poly-

- (ethylenimine) as a gene delivery vehicle. *J. Biomed. Mater. Res.* 45, 268–275.
- (3) Remy, J.-S., Abdallah, P., Zanta, M. A., Boussif, O., Behr, J.-P., and Demeneix, B. (1998) Gene transfer with lipospermines and polyethylenimines. *Adv. Drug Deliv. Rev.* 30, 85–95.
- (4) Fischer, D., von Harpe, A., Kunath, K., Petersen, H., Li, Y., and Kissel, T. (2002) Copolymers of ethylene imine and N-(2-hydroxyethyl)-ethylene imine as tools to study effects of polymer structure on physicochemical and biological properties of DNA complexes. *Bioconjugate Chem.* 13, 1124–1133.
- (5) Petersen, H., Fechner, P. M., Martin, A. L., Kunath, K., Stolnik, S., Roberts, C. J., Fischer, D., Davies, M. C., and Kissel, T. (2002) Polyethylenimine-graft-poly(ethylene glycol) copolymers: Influence of copolymer block structure on DNA complexation and biological activities as gene delivery system. *Bioconjugate Chem.* 13, 845–854.
- (6) Kircheis, R., Wightman, L., and Wagner E. (2001) Design and gene delivery activity of modified polyethylenimines. *Adv. Drug Deliv. Rev.* 53, 341–358.
- (7) Zelikin, A. N., and Izumrudov, V. A. (2002) Polyelectrolyte complexes formed by calf thymus DNA and aliphatic ionenes: Unexpected change in stability upon variation of chain length of ionenes of different charge density. *Macromol. Biosci.* 2, 78–81.
- (8) Zelikin, A. N., Putnam, D., Shastri, P., Langer, R., and Izumrudov, V. A. (2002) Aliphatic ionenes as gene delivery agents: Elucidation of structure–function relationship through modification of charge density and polymer length. *Bioconjugate Chem.* 13, 548–553.
- (9) Köping-Höggård, M., Tubulekas, I., Guan, H., Edwards, K., Nilsson, M., Vårum, K. M., and Artursson, P. (2001) Chitosan as a nonviral gene delivery system. Structure–property relationships and characteristics compared with polyethylenimine in vitro and after lung administration in vivo. *Gene Therapy* 8, 1108–1121.
- (10) Ohsaki, M., Okuda, T., Wada, A., Hirayama, T., Niidome, T., and Aoyagi, H. (2002) In vitro gene transfection using dendritic poly(L-lysine). *Bioconjugate Chem.* 13, 510–517.
- (11) Jones, N. A., Hill, I. R. C., Stolnik, S., Bignotti, F., Davis, S. S., and Garnett, M. C. (2000) Polymer chemical structure is a key determinant of physicochemical and colloidal properties of polymer-DNA complexes for gene delivery. *BBA – Gene Struct. Expr.* 1517, 1–18.
- (12) Azzam, T., Eliyahu, H., Shapira, L., Linial, M., Barenholz, Y., and Domb, A. J. (2002) Polysaccharide-oligoamine based conjugates for gene delivery. *J. Med. Chem.* 45, 1817–1824.
- (13) Gonzalez, H., Hwang, S. J., and Davis, M. E. (1999) New class of polymers for the delivery of macromolecular therapeutics. *Bioconjugate Chem.* 10, 1068–1074.
- (14) Hwang, S. J., Bellocq, N. C., and Davis, M. E. (2001) Effects of structure of  $\beta$ -cyclodextrin-containing polymers on gene delivery. *Bioconjugate Chem.* 12, 280–290.
- (15) Reineke, T. M., and Davis, M. E. (2003) Structural effects of carbohydrate-containing polycations on gene delivery. 1. Carbohydrate size and its distance from charge centers. *Bioconjugate Chem.* 14, 247–254.
- (16) Reineke, T. M., and Davis, M. E. (2003) Structural effects of carbohydrate-containing polycations on gene delivery. 2. Charge center type. *Bioconjugate Chem.* 14, 255–261.
- (17) Teranishi, K. (2000) Practicable regiospecific bifunctionalization on the secondary face of  $\alpha$ - and  $\beta$ -cyclodextrins. *Chem. Commun.* 14, 1255–1256.
- (18) Teranishi, K., Hisamatsu, M., and Yamada, T. (2000) Regiospecific synthesis of 2<sup>A</sup>, 2<sup>B</sup>-disulfonated  $\gamma$ -cyclodextrin. *Tetrahedron Lett.* 41, 933–936.
- (19) Szejtli, J., Ed. (1988) *Cyclodextrin Technology*, Kluwer Academic Publishers, Dordrecht.
- (20) Pun, S. H., and Davis, M. E. (2002) Development of a nonviral gene delivery vehicle for systemic application. *Bioconjugate Chem.* 13, 630–639.

BC034010B

# PNA-Based RNA-Triggered Drug-Releasing System

Zhaochun Ma and John-Stephen Taylor\*

Department of Chemistry, Washington University, St. Louis, Missouri 63130. Received January 30, 2003; Revised Manuscript Received March 26, 2003

A three-component sequence-specific RNA-triggered drug-releasing system is described that consists of an 8-mer PNA linked to a coumarin ester (the prodrug component) and a 14-mer PNA linked to histidine (the catalytic component) that are complementary to the C loop of *E. coli* 5S rRNA (the triggering component). Binding of the catalytic component to the RNA creates a prodrug-metabolizing enzyme that catalyzes a 60 000-fold acceleration in the rate of coumarin release from the prodrug compared to the rate of coumarin release from the ester subunit catalyzed by imidazole alone. RNA-triggered release of hydroxycoumarin is only slightly less efficient than that triggered by a short unfolded DNA sequence corresponding to the PNA binding sites. The lower efficiency results from a decrease in  $k_{\text{cat}}$  and an increase in  $K_{\text{M}}$ , presumably due to the bent nature of the RNA. The efficiency of DNA-triggered hydroxycoumarin release was found to depend on the distance between the catalytic and prodrug components.

## INTRODUCTION

Chemotherapeutic approaches to cancer and infectious disease involve drugs that are selectively toxic to the diseased cell or the disease-causing virus or organism. Most conventional anticancer drugs work by interfering with replication and cell division and owe their marginal selectivity for cancer cells to the fact that cancer cells divide more rapidly than normal cells. Current approaches to increasing drug selectivity involve antibody-, gene-, and bacterial-directed enzymatic activation of prodrugs inside or in the vicinity of a cancer cell (1, 2). Other approaches are based on interfering with cancer-specific biochemical pathways through small molecule or antisense- or antigene-based drugs (3–5). All these methods depend on detailed knowledge of the biochemistry of the cancer cells and how they differ from that of normal cells. Recent DNA array-based analyses of cancer cells from patients having the same type of cancer have revealed variations in their individual pattern of gene expression (6, 7). Consequently, a drug that works well on a cancer in one patient may not work well on the same type of cancer in another patient. Another problem is that cancer cells can become resistant to drugs due to mutations in the proteins involved in the mechanism of action by the drug. Unfortunately, it would be very difficult if not impossible to tailor biochemistry-based chemotherapeutic agents for an individual patient or respond to a mutagenic event because of the time involved in developing and approving the appropriate drug.

Recently, we proposed a new approach to the design of highly selective and patient-specific chemotherapeutic agents which in principle does not require any knowledge of the biochemistry of the diseased cell and could work against cancers, viruses, and other pathogenic organisms (8, 9). The idea is to use disease-specific genetic information (the signal) to trigger the release of a toxic agent within the diseased cell (signal transduction). One implementation of this idea is to use a unique or overexpressed

mRNA specific to the disease state to template the association of a prodrug and a catalytic component which releases the drug (Figure 1). We have previously demonstrated the feasibility of such approach with DNA-based model systems in which the prodrug was constructed by attaching *p*-nitrophenolate to an oligodeoxynucleotide (ODN) that is complementary to one-half of a triggering ODN via an ester linkage (8, 9). Hydrolysis of the nitrophenyl ester would release nitrophenolate which has been used by others to release cytotoxic drugs such as fluorouracil and daunorubicin that have been appended to the ortho or para position via a carbamoylmethyl linkage (10–12). The catalytic component was made by attaching imidazole, a well-known catalyst for ester hydrolysis, to an ODN complementary to the other half of the targeting ODN. When incubated together, the nitrophenolate was released with an approximately 1000-fold rate enhancement over that in the absence of the triggering ODN.

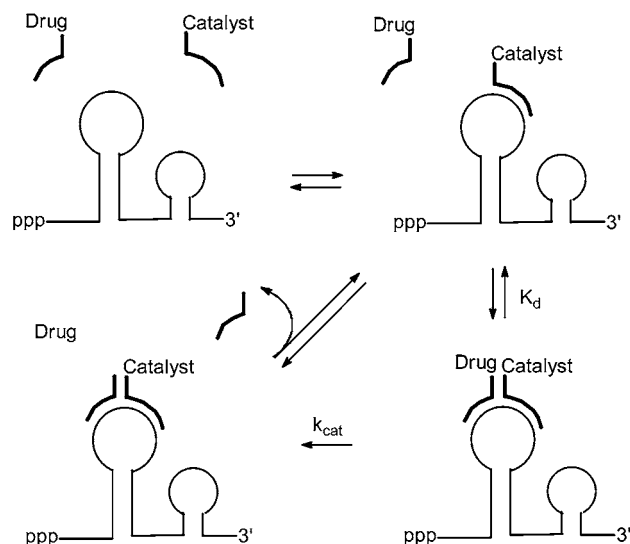
The DNA-based system used to initially test the concept of nucleic acid-triggered drug release in vitro is not suitable for RNA-triggered drug release in vivo. Use of a DNA-based system could cause depletion of the RNA triggering sequence through DNA-mediated cleavage by RNaseH. DNA itself is also degraded by enzymatic action within a cell and would therefore not be suitable for sustained activity of the catalytic and prodrug components. What is also unknown from the previous studies is how well a folded RNA structure will serve as a trigger. Herein, we describe a peptide nucleic acid (PNA)-based drug-releasing system, which should not suffer from the problems inherent with a DNA-based system, and show that it can be triggered by a folded RNA molecule almost equally well as an unfolded DNA molecule.

## EXPERIMENTAL PROCEDURES

**Materials and Methods.** Reagents for automatic PNA synthesis were purchased from PerSeptive Biosystems. Tris(2-carboxyethyl)phosphine hydrochloride (TCEP-HCl) was purchased from Pierce. ODNs were purchased from IDT (Coraville, IA) and purified by reversed-phase HPLC as triethylammonium salts. High-pressure liquid

\* To whom correspondence should be addressed. Telephone: (314) 935–6721. Fax: (314) 935–4481. E-mail: taylor@wuchem.wustl.edu.





**Figure 1.** General concept of mRNA-triggered catalytic drug release. The catalyst and cytotoxic drug are attached to nucleic acids or analogues that are complementary to an exposed loop of an mRNA specific to the disease state (the signal). The recognition sequence of the catalytic component is made sufficiently long enough to specifically recognize and bind tightly to the triggering sequence and thereby transform the mRNA into a prodrug-metabolizing enzyme. The recognition sequence of the prodrug component is made shorter so that it binds reversibly, thereby facilitating turnover of the prodrug and release of multiple cytotoxic drugs (signal transduction) which then kill the cell. In this system, the rate of drug release catalyzed by the catalytic component in the absence of the RNA trigger is very low.

chromatography was carried out on a Beckman HPLC system consisting of two 110B pumps, a 406 Analogue Interface, and a 166 variable wavelength detector, under control of an IBM PS/2 and System Gold software. PNA and ODNs were quantified by spectrophotometric A260 values. 5S rRNA was purchased from Sigma and renatured before use according to a literature procedure (13). UV spectral data were acquired on a Bausch and Lomb Spectronic 1001 spectrophotometer or Varian Cary 1E UV-vis spectrophotometer. Fluorescence measurements were carried out on a SPEX Fluoromax instrument. MALDI mass spectra of oligonucleotides and PNAs were acquired on a PerSeptive Voyager RP MALDI-TOF mass spectrometer using sinapinic acid as a matrix and calibrated versus insulin (average  $[M + H]^+$  = 5734.5) that was present as an internal standard.

**Synthesis of the 8-mer PNA and Catalytic Component.** The PNA-peptide conjugates  $\text{NH}_2\text{-Lys-CTGGGGTA-Cys-H}$  and  $\text{NH}_2\text{-His-CGGCTTGAGTCC-Lys-H}$  were synthesized on a 2  $\mu\text{mol}$  scale by standard Fmoc off chemistry on an Applied Biosystems (Foster City, CA) Expedite 8909 Synthesizer using trityl-histidine, Boc-lysine, trityl-cysteine, and Bhoc-protected PNA building blocks and the universal support XAL-PEG-PS (Applied Biosystems) using a standard protocol. The PNAs were purified by reversed phase HPLC on a Microsorb C18 column (300 Å pore, 5  $\mu\text{m}$  particle size,  $4.6 \times 250$  mm) using 1 mL/min linear gradients of solvent B [0.1% TFA in acetonitrile] in A [0.1% TFA in water]. The effluent was monitored by absorbance at 260 nm, and the major peaks were collected, concentrated to dryness in vacuo, and analyzed by MALDI-TOF mass spectrometry.  $\text{NH}_2\text{-His-CGGCTTGAGTCTTC-Lys-H}$  was purified using a 5% to 70% linear gradient of solvent B in A over 65 min to yield 180 nmol of purified product eluting at 22 min: calcd avg ( $M + H^+$ ) 4059.9, found 4061.5.  $\text{NH}_2\text{-}$

$\text{Lys-CTGGGGTA-Cys-H}$  was purified with a 5 min 5% solvent B in A, followed by a linear gradient of 5% B – 35% B in A over 30 min to yield 488 nmol of purified product eluting at 22 min: avg calcd ( $M + H^+$ ) 2473.4, found 2469.2.

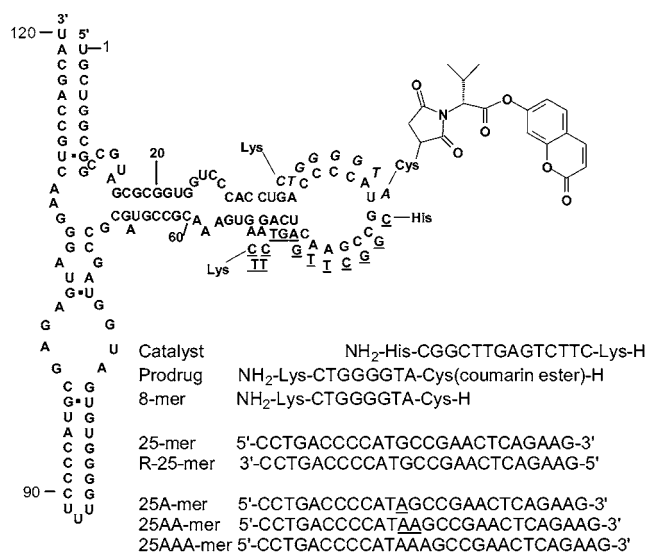
**Synthesis of the Prodrug Component.** The maleoyl coumarin ester was linked to the 8-mer PNA according to a general procedure (14). Thus, the PNA-peptide conjugate  $\text{NH}_2\text{-Lys-CTGGGGTA-Cys-H}$  (24.4 nmol) was treated with TCEP (110 nmol) in 500  $\mu\text{L}$  of 0.1 M sodium phosphate buffer, pH 7.0, for 2 h at room temperature under argon. *N*-Maleoyl-D-valine coumarin ester (9) (293 nmol in 10  $\mu\text{L}$  of acetonitrile) was then added and allowed to stir for an additional 1 h. The PNA conjugate was purified by reversed phase HPLC as described above with a linear gradient of 5% to 70% solvent B in solvent A in 65 min. The desired fraction eluting at 29 min was collected (9.7 nmol, 40% yield), concentrated to dryness in vacuo, and analyzed by MALDI-TOF mass spectrometry, calcd avg ( $M + H^+$ ) 2814.74, found 2812.9.

**Kinetics of Hydroxycoumarin Release.** A fluorescence calibration curve was obtained by plotting fluorescence intensity (cps) as a function of 7-hydroxycoumarin concentration in the buffer used for the kinetic experiments ( $\lambda_{\text{ex}}$  = 350 nm,  $\lambda_{\text{em}}$  = 452 nm). An equation relating concentration of 7-hydroxycoumarin to the observed fluorescence intensity was obtained by linear regression analysis of the calibration curve. The catalytic component (1  $\mu\text{M}$ ) was incubated with the trigger (1  $\mu\text{M}$  complementary DNA or 5S rRNA) and a given concentration of the prodrug component and the release of 7-hydroxycoumarin was monitored by fluorescence spectroscopy for 1 h. Michaelis-Menten  $k_{\text{cat}}$  and  $K_M$  parameters were obtained by measuring the rate of 7-hydroxycoumarin release as a function of prodrug concentration (0.2, 0.4, 0.8, 2.0, 5.0, and 20  $\mu\text{M}$ ). The initial rates of hydroxycoumarin release by linear regression and corrected for background hydrolysis. The initial rates were plotted against the prodrug concentration and fitted to the Michaelis-Menten equation using Kaleidagraph software.

## RESULTS AND DISCUSSION

PNA has a number of properties that make it ideal for a RNA-triggered drug-releasing system: (1) it binds to RNA with higher affinity than natural ODNs and can invade duplex regions (15), (2) it can bind RNA in vivo as judged by its ability to sequence-specifically inhibit translation (16–20), (3) it has much higher biological stability than ODNs in serum and in cells (21), (4) unlike ODNs it does not stimulate RNA degradation by RNaseH upon duplex formation with RNA (22), (5) it can be efficiently delivered into cells by conjugation with protein transduction domains (PTDs) such as HIV-1 TAT protein (23, 24), and (6) it can be easily synthesized together with amino acids by solid-phase peptide synthesis on commercially available DNA/PNA or peptide synthesizers (25, 26).

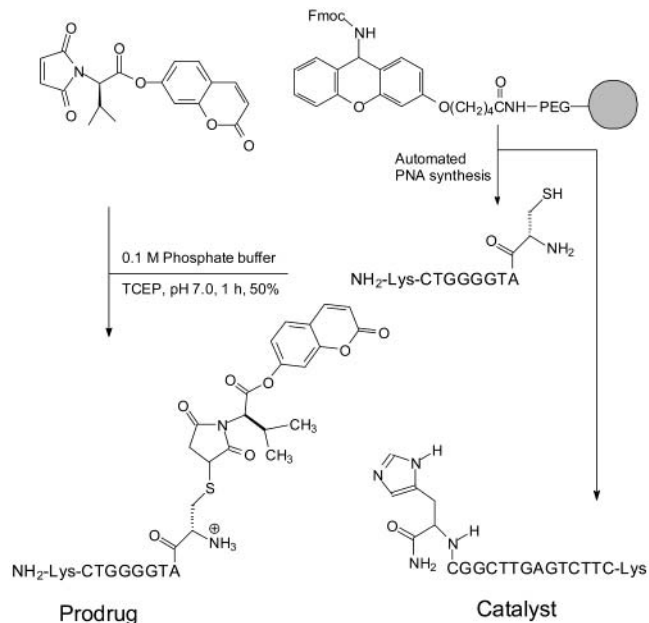
**Design and Synthesis of the PNA Components.** The three-component PNA-based RNA-triggered drug-releasing system used in this study is shown in Figure 2. The RNA trigger was chosen to be the 120 nt 5S rRNA of *E. coli* because its folded structure has been well established by a variety of methods (27, 28) and because its C region has been previously been shown to bind an antisense ODN (29). The catalytic component consists of a 14-mer PNA complementary to the C region that is linked on its carboxy end to histidine, which bears the imidazole functionality that was successfully used to



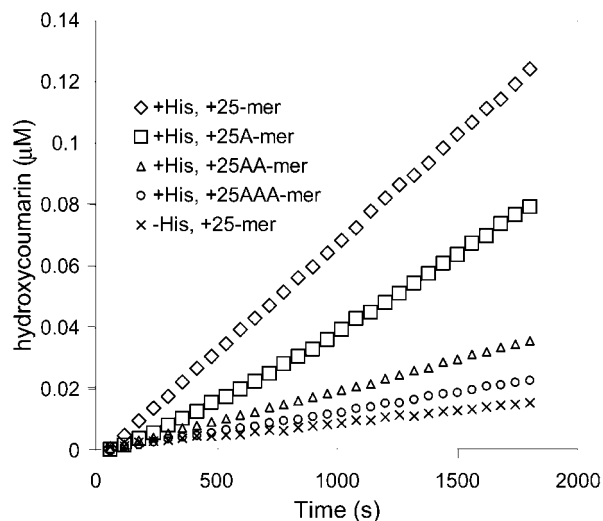
**Figure 2.** PNA-based drug-releasing system using *E. coli* 5S rRNA and ODNs as triggering sequences. The prodrug component is in italics, whereas the catalytic component is underlined. The 25-mer ODN corresponds to the 25-mer section of the 5S rRNA containing the C-loop used as the triggering sequence. The R-25-mer ODN is the same sequence but in reverse, and the 25A<sub>n</sub>-mer ODNs have *n* As between the binding sites for the prodrug and catalytic components. The carboxy terminal amide is indicated by NH<sub>2</sub> and the amino terminal amino group by H (see Figure 3 for a more detailed structure).

catalyze ester hydrolysis in the ODN-based systems (8, 9). The prodrug component consists of an 8-mer PNA complementary to the adjacent site on the C region that is linked to 7-hydroxy coumarin through an ester linkage which renders the hydroxycoumarin nonfluorescent. Coumarin has been previously used to monitor the stability of esterase-sensitive prodrugs of amines, peptides, and peptidomimetics (30). Both components are linked on their other ends to lysine to increase water solubility and facilitate HPLC purification. The required PNA-peptide hybrids, NH<sub>2</sub>-His-CGGCTTGAGTCC-Lys-H and NH<sub>2</sub>-Lys-CTGGGGTA-Cys-H, were synthesized by standard automated Fmoc-based PNA synthesis using trityl-protected histidine, Boc-lysine, trityl-cysteine, and Bhoc-protected PNA building blocks. The prodrug component was synthesized by coupling *N*-maleoyl-D-valine coumarin ester (9) at neutral pH to the sulphydryl of NH<sub>2</sub>-Lys-CTGGGGTA-Cys-H by a general procedure (14).

**Effect of Orientation and Spacing on DNA-Triggered Hydroxycoumarin Release.** We first examined the ability of a 25-mer ODN corresponding to the C loop region of 5S rRNA (nt 30–54) to trigger release of 7-hydroxycoumarin from the PNA-based system in 10 mM phosphate, 0.1 M NaCl, pH 7, at 37 °C (1 μM in all three substrates). In accord with the known orientation preference (31), coumarin was found to be released at a significantly higher rate in the presence of the antiparallel than the parallel 25-mer (taking the amino terminal end of the PNA to be equivalent to the 5'-end of DNA), which was no better than the background rate for the prodrug alone (7.1:1.0:0.8 × 10<sup>-5</sup> μM/s respectively). The background rate is much higher than previously seen with the *N*-maleoyl-D-valine coumarin ester used to form the prodrug component (9) and may be due to lactam formation with the free amino group of the terminal cysteine to which it is attached (Figure 3). As expected, the rate of 7-hydroxycoumarin release also depended on the distance between prodrug and catalytic component as evidenced by the decreasing rate of release upon



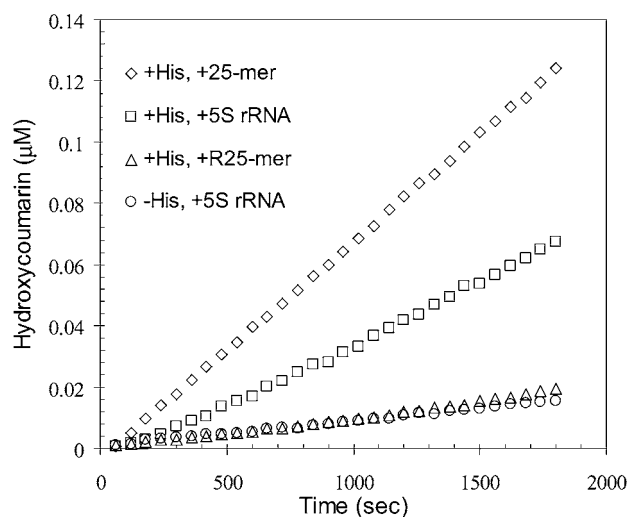
**Figure 3.** Synthetic scheme for the preparation of the catalytic and prodrug components.



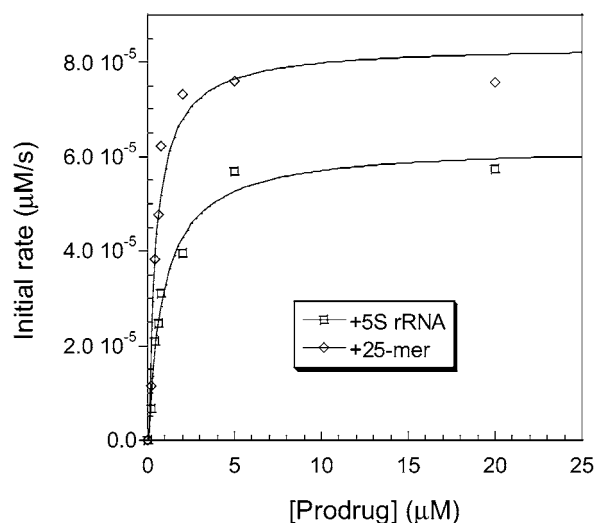
**Figure 4.** Effect of spacing between the prodrug and catalytic components on 7-hydroxycoumarin release. The prodrug component (1 μM) was incubated with 1 μM of catalytic component (+His) and 1 μM of the triggering ODN in 10 mM phosphate, 0.1 M NaCl, pH 7, at 37 °C. Also shown is the effect of removing the histidine from the catalytic component (–His).

increasing the number of A's between the two binding sites (1–3 A's: 5.7:2.0:1.3 × 10<sup>-5</sup> μM/s respectively) (Figure 4). This decrease in rate with increasing distance contrasts with a recent publication describing distance-independent rates of DNA-templated chemical reactions (32).

**RNA-Triggered Release of Hydroxycoumarin.** The rate of hydroxycoumarin release from the 5S rRNA was slightly slower (4.0 × 10<sup>-5</sup> μM/s) than that from the 25-mer ODN and is intermediate between the one and two nucleotide-gapped DNA triggers (5.7 and 2.0 × 10<sup>-5</sup> μM/s, respectively) (Figure 5). The lower rate could be due to reduced binding affinity of the drug component for a bent RNA sequence and/or to reduced catalytic efficiency due to a change in geometry. To gain further insight into the origin of the difference in rate between the ODN- and RNA-triggered reactions, drug release was examined as



**Figure 5.** Kinetics of RNA-triggered 7-hydroxycoumarin release. The prodrug component ( $1 \mu\text{M}$ ) was incubated in the presence of  $1 \mu\text{M}$  of the catalytic component (+His) and  $1 \mu\text{M}$  of the 5S rRNA in 10 mM phosphate, 0.1 M NaCl, pH 7, at  $37^\circ\text{C}$ . Hydroxycoumarin release was also measured with the catalytic component lacking the histidine (−His) and on the reversed DNA template (R25-mer).



**Figure 6.** Michaelis–Menten behavior of RNA- and ODN-triggered hydroxycoumarin release. Initial rate of 7-hydroxycoumarin release corrected for background hydrolysis plotted against the concentration of the prodrug component in the presence of  $1 \mu\text{M}$  catalytic component and  $1 \mu\text{M}$  25-mer ODN or 5S rRNA in 10 mM phosphate, 0.1 M NaCl, pH 7, at  $37^\circ\text{C}$ .

a function of the concentration of the prodrug component (Figure 6). In both cases, hydroxycoumarin release showed saturation kinetics as expected for the Michaelis–Menten mechanism which had previously been shown to operate for the ODN-based drug-releasing system (8, 9). The ODN-triggered system has a  $k_{\text{cat}}$  of  $8.4 \pm 0.6 \times 10^{-5} \text{ s}^{-1}$  and a  $K_{\text{M}}$  of  $0.46 \pm 0.12 \mu\text{M}$ , which corresponds to an effective rate acceleration of 160 000 over free imidazole ( $k_{\text{im}} = 1.13 \times 10^{-3} \text{ M}^{-1} \text{ s}^{-1}$ ) as calculated from  $(k_{\text{cat}}/K_{\text{M}})/k_{\text{im}}$ . The value of  $k_{\text{cat}}$  is almost twice that of  $4.4 \times 10^{-5} \text{ s}^{-1}$  previously observed for hydroxycoumarin release from a corresponding DNA-based system (9) and may be due to the more constrained nature of the linkers tethering the hydroxycoumarin ester and imidazole to the PNA. The value of  $K_{\text{M}}$  is almost 100-times lower than that of  $50 \mu\text{M}$  observed for a DNA-based 8-mer prodrug in a different sequence context and is responsible for

much of the large increase in rate acceleration on going from the DNA-based system to the PNA-based system. The significantly lower  $K_{\text{M}}$  for the PNA system may be due in part to the higher binding affinity of PNA for DNA (3f) and in part to elimination of unfavorable electrostatic interactions between the catalytic and prodrug components in the DNA-based system. The RNA-triggered system has a slightly lower  $k_{\text{cat}}$  of  $6.2 \pm 0.3 \times 10^{-5} \text{ s}^{-1}$  and a slightly higher  $K_{\text{M}}$  of  $0.91 \pm 0.14 \mu\text{M}$ , which is consistent with the idea that both the binding affinity and catalytic efficiency are reduced because of binding to a bent RNA sequence. In this case the apparent rate acceleration is 60 000.

## CONCLUSIONS

We have shown that a folded RNA molecule is capable of triggering the release of coumarin from a PNA-based drug-releasing system with a high rate of acceleration over free imidazole that can be attributed to the high binding affinity of the PNA-based prodrug component. We also show that the rate of folded RNA-triggered drug release is only slightly less efficient than the corresponding linear DNA template and is due to a drop in  $k_{\text{cat}}$  and a rise in  $K_{\text{M}}$ , probably as a result of the bent nature of the RNA trigger. Unlike a previous report, we have shown that the rate of nucleic acid-templated chemical reactions are distance dependent as would be expected. We are now trying to determine whether this PNA-based drug-releasing system can be made to work inside human cells.

## ACKNOWLEDGMENT

Supported by NIH (RO1-CA92477) and a Wheeler Fellowship for Z. Ma. The assistance of the Washington University Mass Spectrometry Resource, a NIH Research Resource (Grant No. P41RR0954), is also acknowledged.

**Supporting Information Available:** HPLC traces and ESI spectra of the catalytic component, the 8-mer PNA, and the prodrug component. This material is available free of charge via the Internet at <http://pubs.acs.org/BC>.

## LITERATURE CITED

- (1) Denny, W. A. (1996) The design of selectively activated prodrugs for cancer chemotherapy. *Curr. Pharm. Des.* 2, 281–294.
- (2) Dubowchik, G. M., and Walker, M. A. (1999) Receptor-mediated and enzyme-dependent targeting of cytotoxic anti-cancer drugs. *Pharmacol. Ther.* 83, 67–123.
- (3) Elayadi, A. N., and Corey, D. R. (2001) Application of PNA and LNA oligomers to chemotherapy. *Curr Opin Investig. Drugs* 2, 558–61.
- (4) Gottesfeld, J. M., Turner, J. M., and Dervan, P. B. (2000) Chemical approaches to control gene expression. *Gene Expr.* 9, 77–91.
- (5) Thurston, D. E. (1999) Nucleic acid targeting: therapeutic strategies for the 21st century. *Br. J. Cancer* 80, 65–85.
- (6) Notterman, D. A., Alon, U., Sierk, A. J., and Levine, A. J. (2001) Transcriptional gene expression profiles of colorectal adenoma, adenocarcinoma, and normal tissue examined by oligonucleotide arrays. *Cancer Res.* 61, 3124–30.
- (7) De Vos, J., Thykjaer, T., Tarte, K., Ensslen, M., Raynaud, P., Requirand, G., Pellet, F., Pantescio, V., Reme, T., Jourdan, M., Rossi, J. F., Orntoft, T., and Klein, B. (2002) Comparison of gene expression profiling between malignant and normal plasma cells with oligonucleotide arrays. *Oncogene* 21, 6848–57.
- (8) Ma, Z., and Taylor, J.-S. (2000) Nucleic Acid Triggered Catalytic Drug Release. *Proc. Natl. Acad. Sci. U.S.A.* 97, 11159–63.



- (9) Ma, Z., and Taylor, J. S. (2001) Nucleic acid triggered catalytic drug and probe release: a new concept for the design of chemotherapeutic and diagnostic agents. *Bioorg. Med. Chem.* 9, 2501–10.
- (10) Gesson, J. P., Jacquesy, J. C., Mondon, M., Petit, P., Renoux, B., Andrianomenjanahary, S., Dufat-Trinh Van, H., Koch, M., Michel, S., Tillequin, F., Florent, J. C., Monneret, C., Bosslet, K., Czech, J., and Hoffmann, D. (1994) Prodrugs of anthracyclines for chemotherapy via enzyme-monoclonal antibody conjugates. *Anticancer Drug Des.* 9, 409–23.
- (11) Lougerstay-Madec, R., Florent, J.-C., Monneret, C., Nemati, F., and Poupon, M. F. (1998) Synthesis of self-immolative glucuronide-based prodrugs of a phenol mustard. *Anti-Cancer Drug Des.* 13, 995–1007.
- (12) Madec-Lougerstay, R., Florent, J.-C., and Monneret, C. (1999) Synthesis of self-immolative glucuronide spacers based on aminomethylcarbamate. Application to 5-fluorouracil prodrugs for antibody-directed enzyme prodrug therapy. *J. Chem. Soc., Perkin Trans. 1* 1369–1376.
- (13) Goring, H. U., and Wagner, R. (1988) 5S RNA structure and function. *Methods Enzymol.* 164, 721–47.
- (14) Arar, K., Monsigny, M., and Mayer, R. (1993) Synthesis of oligonucleotide–peptide conjugates containing a KDEL signal sequence. *Tetrahedron Lett.* 34, 8087–90.
- (15) Pfeffer, N. J., Hanvey, J. C., Bisi, J. E., Thomson, S. A., Hassman, C. F., Noble, S. A., and Babiss, L. E. (1993) Strand-invasion of duplex DNA by peptide nucleic acid oligomers. *Proc. Natl. Acad. Sci. U.S.A.* 90, 10648–52.
- (16) Gambacorti-Passerini, C., Mologni, L., Bertazzoli, C., le Coutre, P., Marchesi, E., Grignani, F., and Nielsen, P. E. (1996) In vitro transcription and translation inhibition by anti-promyelocytic leukemia (PML)/retinoic acid receptor alpha and anti-PML peptide nucleic acid. *Blood* 88, 1411–7.
- (17) Nielsen, P. E. (1999) Peptide nucleic acids as therapeutic agents. *Curr. Opin. Struct. Biol.* 9, 353–7.
- (18) Larsen, H. J., Bentin, T., and Nielsen, P. E. (1999) Antisense properties of peptide nucleic acid. *Biochim. Biophys. Acta* 1489, 159–166.
- (19) Doyle, D. F., Braasch, D. A., Simmons, C. G., Janowski, B. A., and Corey, D. R. (2001) Inhibition of gene expression inside cells by peptide nucleic acids: effect of mRNA target sequence, mismatched bases, and PNA length. *Biochemistry* 40, 53–64.
- (20) Pooga, M., Land, T., Bartfai, T., and Langel, U. (2001) PNA oligomers as tools for specific modulation of gene expression. *Biomol. Eng.* 17, 183–92.
- (21) Uhlmann, E., and Peyman, A. (1990) Antisense oligonucleotides: A new therapeutic principle. *Chem. Rev.* 90, 543–584.
- (22) Gee, J. E., Robbins, I., Van Der Laan, A. C., Van Boom, J. H., Colombier, C., Leng, M., Raible, A. M., Nelson, J. S., and Lebleu, B. (1998) Assessment of high-affinity hybridization, RNase H cleavage, and covalent linkage in translation arrest by antisense oligonucleotides. *Antisense Nucleic Acid Drug Dev.* 8, 103–111.
- (23) Pooga, M., Soomets, U., Hallbrink, M., Valkna, A., Saar, K., Rezaei, K., Kahl, U., Hao, J. X., Xu, X. J., Wiesenfeld-Hallin, Z., Hokfelt, T., Bartfai, T., and Langel, U. (1998) Cell penetrating PNA constructs regulate galanin receptor levels and modify pain transmission in vivo. *Nat. Biotechnol.* 16, 857–61.
- (24) Schwarze, S. R., Hruska, K. A., and Dowdy, S. F. (2000) Protein transduction: unrestricted delivery into all cells? *Trends Cell Biol.* 10, 290–5.
- (25) Mayfield, L. D., and Corey, D. R. (1999) Automated synthesis of peptide nucleic acids and peptide nucleic acid-peptide conjugates. *Anal. Biochem.* 268, 401–4.
- (26) Christensen, L., Fitzpatrick, R., Gildea, B., Petersen, K. H., Hansen, H. F., Koch, T., Egholm, M., Buchardt, O., Nielsen, P. E., Coull, J., and et al. (1995) Solid-phase synthesis of peptide nucleic acids. *J. Pept. Sci.* 1, 175–83.
- (27) Noller, H. F. (1984) Structure of ribosomal RNA. *Annu. Rev. Biochem.* 53, 119–62.
- (28) Cannistraro, V. J., and Kennell, D. (1997) RNase YI\* and RNA structure studies. *Nucleic Acids Res.* 25, 1405–12.
- (29) Hines, J. V., Ammar, G. M., Buss, J., and Schmalbrock, P. (1999) Paramagnetic oligonucleotides: contrast agents for magnetic resonance imaging with proton relaxation enhancement effects. *Bioconjugate Chem.* 10, 155–8.
- (30) Liao, Y., Hendrata, S., Bae, S. Y., and Wang, B. (2000) The effect of phenyl substituents on the release rates of esterase-sensitive coumarin-based prodrugs. *Chem. Pharm. Bull.* 48, 1138–1147.
- (31) Egholm, M., Buchardt, O., Christensen, L., Behrens, C., Freier, S. M., Driver, D. A., Berg, R. H., Kim, S. K., Norden, B., and Nielsen, P. E. (1993) PNA hybridizes to complementary oligonucleotides obeying the Watson–Crick hydrogen bonding rules. *Nature* 365, 566–568.
- (32) Gartner, Z. J., and Liu, D. R. (2001) The generality of DNA-templated synthesis as a basis for evolving nonnatural small molecules. *J. Am. Chem. Soc.* 123, 6961–3.

BC0340130

# TECHNICAL NOTES

## Synthesis of 3'-3'-Linked Oligonucleotides Branched by a Pentaerythritol Linker and the Thermal Stabilities of the Triplexes with Single-Stranded DNA or RNA

Yoshihito Ueno,<sup>†</sup> Aya Shibata,<sup>†</sup> Akira Matsuda,<sup>‡</sup> and Yukio Kitade<sup>\*,†</sup>

Department of Biomolecular Science, Faculty of Engineering, Gifu University, Yanagido, Gifu 501-1193, Japan and Graduate School of Pharmaceutical Sciences, Hokkaido University, Kita-12, Nishi-6, Kita-ku, Sapporo 060-0812, Japan. Received August 17, 2002; Revised Manuscript Received February 6, 2003

Synthesis of 3'-3'-linked oligonucleotides branched by a pentaerythritol linker is described. The branched oligonucleotides were synthesized on a DNA/RNA synthesizer using a controlled pore glass (CPG) with a pentaerythritol linker carrying 4,4'-dimethoxytrityl (DMTr) and levulinyl (Lev) groups. The stability of the triplexes between the branched oligonucleotides and the target single-stranded DNA or RNA was studied by thermal denaturation. The oligonucleotides with the pentaerythritol linker formed thermally stable triplexes with the single-stranded DNA and RNA. Furthermore, the branched oligonucleotides containing 2'-*O*-methylribonucleosides, especially the oligonucleotide composed of 2'-deoxyribonucleosides and 2'-*O*-methylribonucleosides, stabilized the triplexes with the single-stranded DNA or RNA. Thus, the branched oligonucleotide containing 2'-*O*-methylribonucleosides may be a candidate for a novel antisense molecule by the triplex formation.

### INTRODUCTION

In the antisense strategy for controlling translation of mRNA, an oligonucleotide sequence-specifically binds to the mRNA by the Watson–Crick hydrogen bonds (1,2). On the other hand, in the antigene strategy for controlling gene transcription, an oligonucleotide binds to the major groove of the double-stranded DNA by Hoogsteen or reverse Hoogsteen hydrogen bonds and forms a local triple-helix (triplex) (3). Depending on the orientation of the third strand, two major classes of triplexes are identified. When the third strand mainly consists of pyrimidines, Hoogsteen type Py–PuPy base triplets (T•AT and C<sup>+</sup>•GC, where the first letter represents the pyrimidine Hoogsteen strand, the second is the purine central strand, and the third is the pyrimidine Watson–Crick complementary strand) are formed in which the third strand is parallel to the purine strand of the target duplex (4, 5). When the third strand is predominantly purines, reverse Hoogsteen type Pu–PuPy base triplets (G•GC and A•AT) are formed in which the third strand is antiparallel to the purine strand of the target duplex (6, 7).

Much attention is being given to the approach of targeting single-stranded DNA or RNA through the formation of triplexes (8–12). It was demonstrated that a single-stranded oligonucleotide consisting of two oligopyrimidine stretches linked by a poly(ethylene glycol) linker or an oligonucleotide sequence formed a thermally stable triplex with the target single-stranded DNA (8, 9). It was also reported that circular oligonucleotides

formed thermally and thermodynamically stable triplexes with the single-stranded DNA or RNA (10, 11).

Triplex structures have been shown to be highly sensitive to DNA versus RNA backbone; for example, the DNA•DNA•DNA (D•DD), RNA•DNA•DNA (R•DD), and R•DR-type triplexes are stable, while the D•RD and D•RR-type triplexes are reported not to be formed (13, 14). Shimizu et al. also showed that the triplex containing the oligonucleotide analogue composed of 2'-*O*-methylribonucleosides in the third strand was more thermally stable than that formed by DNA oligonucleotides (15).

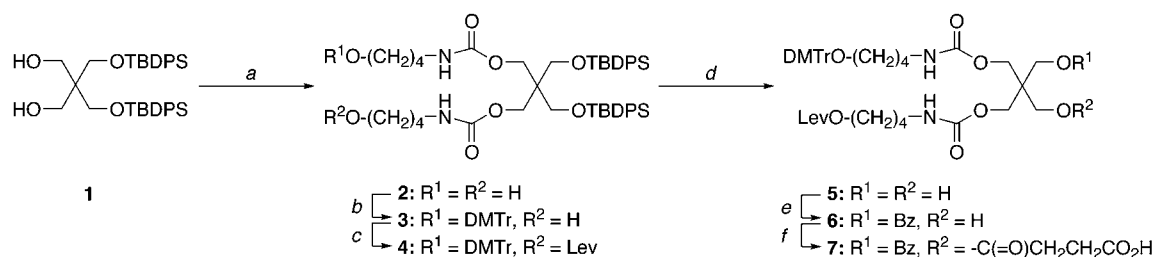
On the other hand, we recently reported the synthesis of branched oligonucleotides with a pentaerythritol at the junction point (16). We found that the oligonucleotides with a four-way junction formed the thermally stable parallel and antiparallel triplexes with the single-stranded DNAs. We also showed that the 3'-3'-linked oligonucleotides with intercalators at the junction point formed thermally stable triplexes with the duplexes composed of oligopurine–oligopyrimidine sequences (17). In the course of the investigation, we planned a synthesis of 3'-3'-linked oligonucleotides containing 2'-*O*-methylribonucleosides in the third and/or second strand of triplexes (Figure 1). We envisioned that the oligonucleotides would enhance the thermal stability of parallel-type of triplexes with the single-stranded DNA or RNA as compared with the *un*-linked oligonucleotides composed of 2'-deoxyribonucleosides.

In this paper, we report the synthesis of 3'-3'-linked oligonucleotides branched by the pentaerythritol linker and the thermal stability of the triplexes between these branched oligonucleotides and the target single-stranded DNA or RNA.

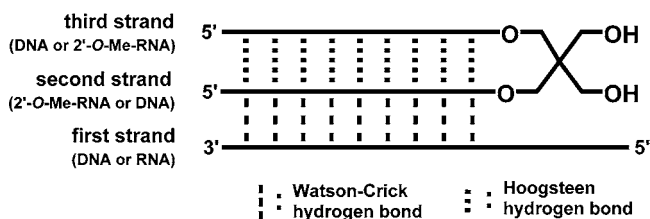
\* To whom reprint requests should be addressed. Phone and fax: +81-58-293-2640. E-mail: kitade@biomol.gifu-u.ac.jp.

<sup>†</sup> Gifu University.

<sup>‡</sup> Hokkaido University.

Scheme 1<sup>a</sup>

<sup>a</sup> (a) (1) *N,N'*-Carbonyldiimidazole, DMAP, DMF, room temperature; (2) H<sub>2</sub>N(CH<sub>2</sub>)<sub>4</sub>OH, DMF, room temperature; (b) DMTrCl, pyridine, room temperature; (c) Lev<sub>2</sub>O, DMAP, pyridine, room temperature; (d) TBAF, THF, room temperature; (e) BzCl, pyridine, room temperature; (f) succinic anhydride, DMAP, pyridine, room temperature.



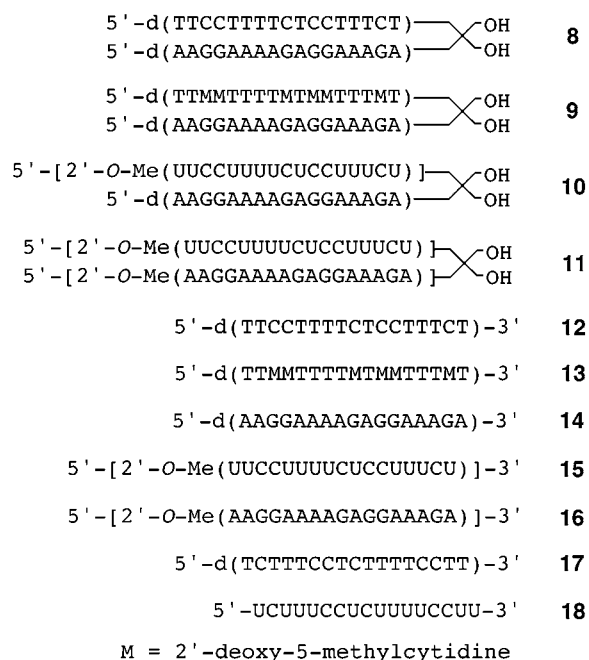
**Figure 1.** Schematic presentation of the triplex composed of the branched oligonucleotide and the single-stranded DNA or RNA.

## RESULTS AND DISCUSSION

**Synthesis.** To synthesize the branched oligonucleotides linked at the 3'-ends of each strand on a DNA/RNA synthesizer, we prepared a controlled pore glass (CPG) with pentaerythritol carrying two kinds of protective groups which could be deprotected under orthogonal conditions. We selected 4,4'-dimethoxytrityl (DMTr) and levulinyl (Lev) as such protective groups (18). A strategy for the synthesis of the CPG is shown in Scheme 1. First, 1,3-*O*-bis(*tert*-butyldiphenylsilyl)-2,2-bis(hydroxymethyl)-1,3-propanediol (**1**) (16) was treated with *N,N'*-carbonyldiimidazole in the presence of DMAP and then reacted with 4-amino-1-butanol to produce **2** in 75% yield. Compound **2** was treated with 1.2 equiv of DMTrCl to give the mono *O*-DMTr derivative **3** in 44% yield. After protection of the other hydroxyl group of **3** with a levulinyl group, the *tert*-butyldiphenylsilyl groups were removed by treating with tetrabutylammonium fluoride (TBAF) to give **5** in 48% yield. One of two hydroxyl groups of **5** was protected with a benzoyl (Bz) group to produce **6** in 30% yield. Compound **6** was modified to the corresponding 3'-succinate **7**, which was reacted with a CPG to give a solid support containing **7** (43 μmol/g).

The 3'-3'-linked oligonucleotides **8**–**11** were synthesized using a CPG on a DNA/RNA synthesizer (Figure 2). The oligonucleotide **8** consists of oligopyrimidine and oligopurine strands which are composed of natural 2'-deoxynucleosides. The oligonucleotide **9** is composed of an oligopyrimidine strand comprising thymidine (dT) and 5-methyl-2'-deoxycytidine (dM) and an oligopurine strand comprising 2'-deoxyadenosine (dA) and 2'-deoxyguanosine (dG). The oligonucleotide **10** is composed of an oligopyrimidine strand comprising 2'-*O*-methylribonucleosides and an oligopurine strand comprising dA and dG. On the other hand, the oligonucleotide **11** consists of oligopyrimidine and oligopurine strands which are composed of 2'-*O*-methylribonucleosides.

The oligonucleotides were synthesized by a phosphoramidite method. One strand was elongated in the usual manner. After capping the 5'-end of the strand and removing the Lev group, the other the strand was elongated. The fully protected oligonucleotides (each 1



**Figure 2.** Sequences of oligonucleotides used in this study.

μmol) linked to the solid support were treated with concentrated NH<sub>4</sub>OH at 55 °C for 16 h. The released oligonucleotides were purified by denaturing with 20% polyacrylamide gel electrophoresis (20% PAGE) to give the deprotected oligonucleotides **8**, **9**, **10**, and **11** in 4, 2, 8, and 5 OD<sub>260</sub> units, respectively. These oligonucleotides were analyzed by matrix-assisted laser desorption/ionization time-of-flight mass spectrometry (MALDI-TOF/MS). The observed molecular weights supported their structures.

**Study of Triplex and Duplex Formation by Thermal Denaturation.** The stability of the triplexes and the duplexes was studied by thermal denaturation in a buffer of 25 mM Tris-HCl (pH 7.0) containing 100 mM NaCl and 10 mM MgCl<sub>2</sub>. Sequences of control oligonucleotides **12**–**16**, target DNA **17**, and RNA **18** used in this study are shown in Figure 2.

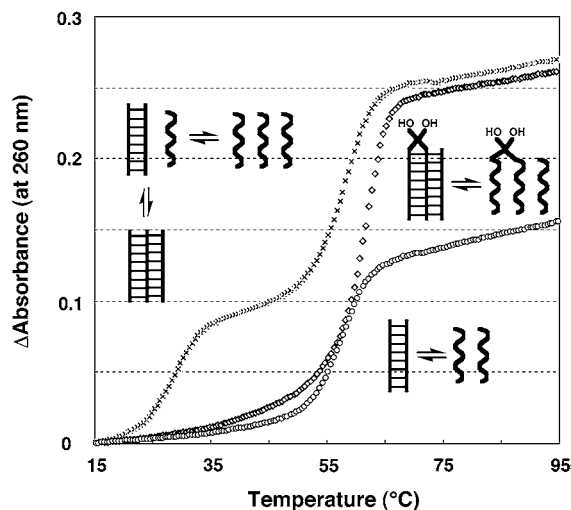
Figure 3 shows melting profiles of the triplexes between **12**, **14** and **17** (a square), and **8** and **17** (a diamond), and the duplex between **14** and **17** (a circle). The *T<sub>m</sub>* values are listed in Table 1. Two transitions were observed in the melting profile of the complex between **12**, **14**, and **17**: the transition with the lower *T<sub>m</sub>* (29.2 °C) was due to dissociation of the third strand from the triplex, and the transition with the higher *T<sub>m</sub>* (58.2 °C) corresponded to melting of the duplex between **14** and **17**. The *T<sub>m</sub>* of the duplex between **14** and **17** (Figure 3; a circle) was 57.8 °C in the same buffer. On the other hand,



**Table 1. Hybridization Data<sup>a</sup>**

complexes	pH 7.0	pH 6.0	complexes	pH 7.0	duplexes	pH 7.0	pH 6.0
<b>8•17</b>	62.2	64.1	<b>12•14•17</b>	29.3 (58.2)	<b>14•17</b>	57.8	57.1
<b>9•17</b>	67.4	68.6	<b>13•14•17</b>	46.3 (58.2)	<b>16•17</b>	68.2	68.1
<b>10•17</b>	71.8	72.6	<b>15•14•17</b>	58.0	<b>14•18</b>	47.8	47.6
<b>11•17</b>	70.9	71.1	<b>15•16•17</b>	68.0	<b>16•18</b>	78.7	79.5
<b>8•18</b>	51.8	57.2	<b>12•14•18</b>	30.3 (47.1)			
<b>9•18</b>	57.8	61.7	<b>13•14•18</b>	37.1 (46.5)			
<b>10•18</b>	71.1	73.6	<b>15•14•18</b>	68.3			
<b>11•18</b>	77.6	78.5	<b>15•16•18</b>	77.6			

<sup>a</sup> The  $T_m$  values of the duplexes are indicated in parentheses. Experimental conditions are described in the Experimental Procedures.

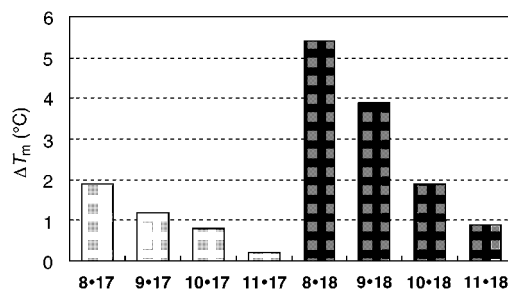


**Figure 3.** Melting profiles: the triplex between **12**, **14**, and **17** (x); the triplex between **8** and **17** (◇); the duplex between the **14** and **17** (○).

when the branched oligonucleotide **8** and DNA **17** were used, only one transition was observed in the melting profile. The increment in the absorbance in melting the complex was almost equal to that of the complex between **12**, **14**, and **17**. This means that the thermal denaturation from triplex to complete random coil occurred cooperatively in a single transition. The  $T_m$  value of the complex was 62.2 °C. It was 32.9 °C and 4 °C higher than those of dissociation of the third strand from the triplex between **12**, **14**, and **17** and melting of the duplex between **14** and **17**, respectively. Thus, it was found that the triplex was largely thermally stabilized by connecting the second and third strands with an appropriate linker.

The thermal stabilities of the complexes targeting the single-stranded DNA **17** were compared. When 2'-deoxy-5-methylcytidine was incorporated into the third strand instead of 2'-deoxycytidine, the  $T_m$  of the triplex consisting of **13**, **14**, and **17** increased 17.0 °C as compared with that of the triplex between **12**, **14**, and **17**. On the other hand, when 2'-deoxy-5-methylcythyridine was incorporated into the branched oligonucleotide, the  $T_m$  of the triplex consisting of **9** and **17** increased 5.2 °C as compared with that of the triplex between **8** and **17**. Thus, it was found that 2'-deoxy-5-methylcytidine stabilized the triplex composed of the branched oligonucleotide as well as the triplex composed of the *un*-branched oligonucleotides, although the increment of the  $T_m$  value for the triplex composed of the branched oligonucleotide was smaller than that for the triplex composed of the *un*-branched oligonucleotides.

When the oligonucleotides consisting of 2'-*O*-methyl-ribonucleosides were used as the second and third strands, a single transition was also observed for the complex between **15**, **16**, and **17**. The  $T_m$  (68.0 °C) of the complex was almost equal to that of the duplex between



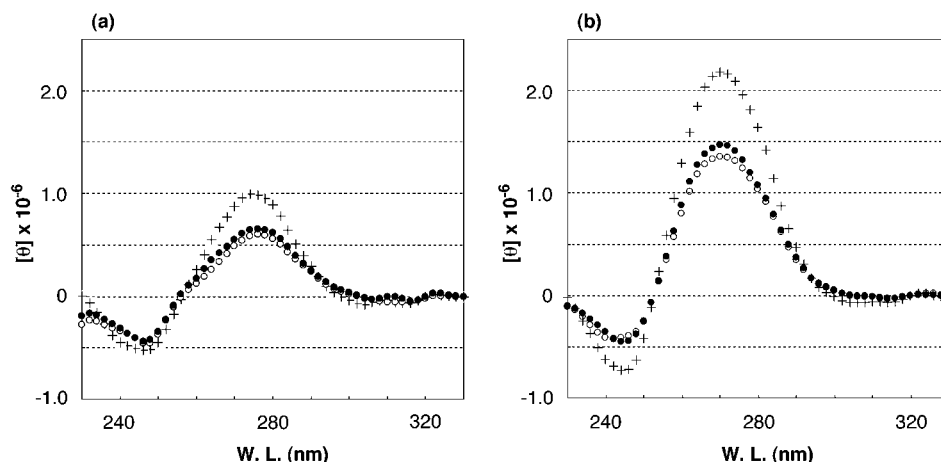
**Figure 4.**  $\Delta T_m$ s [ $T_m$  (at pH 6.0) –  $T_m$  (at pH 7.0)].

**16** and **17**. On the other hand, the  $T_m$  of the complex between **11** and **17** was 70.9 °C, which was 2.9 °C higher than that of the complex consisting of **15**, **16**, and **17**. Among the complexes targeting the single-stranded DNA **17**, the complex between **10** and **17**, which has the oligonucleotide consisting of 2'-*O*-methylribonucleosides as the third strand, showed the highest  $T_m$  value (71.8 °C). This was 13.8 °C higher than that of the complex composed of **15**, **14**, and **17**.

Next, we compared the thermal stabilities of the complexes targeting the single-stranded RNA **18**. The trend in the relative stabilities of the complexes was similar to that of the complexes targeting the single-stranded DNA **17**. When the oligonucleotide **15** consisting of 2'-*O*-methylribonucleosides was used as the third strand, the triplex was largely stabilized. The  $T_m$  of the triplex between **15**, **14**, and **18** was 20.5 °C higher than that of the duplex between **14** and **18** (47.8 °C). Furthermore, the  $T_m$  of the triplex composed of **10** and **18** was 3.4 °C higher than that of the triplex between **15**, **14**, and **18**.

**Thermal Denaturation Study at pH 6.0.** In parallel-type triplexes, the N-3 positions of the cytosine residues of the third strand must be protonated to form two hydrogen bonds with the C/G base pairs in the Watson–Crick duplex (2). It is reported that the parallel-type triplex containing cytosine residues in the third strand is thermally stabilized in slightly acidic solutions as compared with neutral or basic solutions (19–21). Thus, we compared the  $T_m$ s of triplexes composed of branched oligonucleotides in acidic solutions (pH 6.0) with the  $T_m$ s in neutral solutions. The complexes that show increased stabilities at the lower pH value are likely to be triple helical in structure, and the complexes that show no pH sensitivity are almost certainly not triple helical.

The  $T_m$  values in acidic solutions are summarized in Table 1.  $\Delta T_m$ s [ $T_m$  (at pH 6.0) –  $T_m$  (at pH 7.0)] for the branched oligonucleotides are shown graphically in Figure 4. The  $\Delta T_m$  value of the triplex between **8** and **17** was 1.9 °C whereas that of the triplex between **9**, containing 5-methylcytosine, and **17** was 1.2 °C. The electron-donating methyl substitute at the 5 position of the cytosine residue is thought to stabilize protonation at the N-3 position of the cytosine in the triplex although



**Figure 5.** CD spectra. (a) A **10:17** solution (○); a **15:14:17** solution (●); the normalized sum of an **15** plus **14:17** solutions (+). (b) A **10:18** solution (○); a **15:14:18** solution (●); the normalized sum of an **15** plus **14:18** solutions (+).

this stabilization is modest in the uncomplexed cytosine ( $pK_a$  values: 2'-deoxycytidine and 2'-deoxy-5-methylcytosine are 4.3 and 4.4, respectively) (22, 23). Thus, the difference in pH sensitivities of these triplexes would reflect the  $pK_a$ s of  $N3H^+$  of the cytosine residues in the triplexes. On the other hand, the  $\Delta T_m$  value of the triplex between **10**, composed of 2'-deoxyribonucleosides and 2'-*O*-methylribonucleosides, and **17** was 0.8 °C while that of the triplex between **11**, consisting of 2'-*O*-methylribonucleosides, and **17** was 0.2 °C. These results indicate that interaction between the third strand and second strand in the complex composed of **11** and **17** is weaker than those of other triplexes.

Next,  $\Delta T_m$ s of the triplexes targeting the single-stranded RNA were compared. As shown in Figure 4, although the values were greater than those for the single-stranded DNA, the trend in the relative  $\Delta T_m$  values was similar to that for DNA **17**. Thus, these results suggest that the complexes studied in this experiment are triple helical in structure although the Hoogsteen hydrogen bonds of the complex composed of **11** and **17** are weaker than those of other triplexes.

**Circular Dichroism.** To confirm the triplex formations, the circular dichroism (CD) spectrum of each complex was measured. The CD spectra of the mixtures of a 1:1 molar ratio of the branched oligonucleotide **10**:DNA **17** and a 1:1:1 molar ratio of **15:14**:DNA **17** in a buffer of 25 mM Tris-HCl (pH 7.0) containing 100 mM NaCl and 10 mM  $MgCl_2$  were compared with the appropriately normalized summed spectrum of the DNA **14**–DNA **17** duplex and the oligonucleotide **15**. As shown in Figure 5a, the CD spectrum of the branched oligonucleotide **10**:DNA **17** solution had a positive CD band at 276 nm, which was similar to that of the **15:14**:DNA **17** solution and different in intensity from that of the normalized summed spectrum of the DNA **14**–DNA **17** duplex.

Similarly, the CD spectra of the mixtures of a 1:1 molar ratio of the branched oligonucleotide **10**:RNA **18** and a 1:1:1 molar ratio of **15:14**:RNA **18** were compared with the appropriately normalized summed spectrum of the DNA **14**–RNA **18** duplex and the oligonucleotide **15**. As shown in Figure 5b, the CD spectrum of the branched oligonucleotide **10**:RNA **18** solution had a positive CD band at 271 nm, which was similar to that of the **15:14**:RNA **18** solution and different in intensity from that of the normalized summed spectrum of the DNA **14**–RNA **18** duplex and **15**. Therefore, these CD spectral data also

support the existence of the triplexes between branched oligonucleotide **10** and DNA **17** and between branched oligonucleotide **10** and DNA **18**.

## CONCLUSION

In this paper, we reported the synthesis of 3'-3'-linked oligonucleotides **8**–**11** branched by the pentaerythritol linker and the thermal stability of the triplexes between these branched oligonucleotides and the target single-stranded DNA **17** or RNA **18**. The oligonucleotides with the pentaerythritol linker formed thermally stable triplexes with single-stranded DNA **17** and RNA **18**. Furthermore, the branched oligonucleotides containing 2'-*O*-methylribonucleosides, especially the oligonucleotide **10** composed of 2'-deoxyribonucleosides and 2'-*O*-methylribonucleosides, stabilized the triplexes (R·DD and R·DR-type triplexes) with single-stranded DNA **17** or RNA **18**. Thus, the branched oligonucleotide containing 2'-*O*-methylribonucleosides may be a candidate for a novel antisense molecule by the triplex formation.

## EXPERIMENTAL PROCEDURES

**General Remarks.**  $^1H$  NMR spectra were recorded at 400 MHz. Chemical shifts ( $\delta$ ) and coupling constants ( $J$ ) are reported in ppm downfield from TMS and in Hz, respectively. Mass spectra were obtained by fast atom bombardment (FAB) method. Thin-layer chromatography was done on Merck coated plates 60F<sub>254</sub>. The silica gel used for column chromatography was Wakogel C-300.

**1,3-*O*-Bis(*tert*-butyldiphenylsilyl)-2,2-bis[*N*-(4-hydroxybutyl)carbamoyl]oxymethyl]-1,3-propanediol (**2**).** *N,N*-Carbonyldiimidazole (925 mg, 5.70 mmol) and DMAP (36 mg, 0.29 mmol) were added to a solution of 1,3-*O*-bis(*tert*-butyldiphenylsilyl)-2,2-bis(hydroxymethyl)-1,3-propanediol (**1**) (**16**) (874 mg, 1.43 mmol) in DMF (4.8 mL), and the mixture was stirred at room temperature. After 2 h, 4-amino-1-butanol (1.97 g, 22.1 mmol) was added to the mixture, which was stirred at room temperature. After 12 h, the mixture was partitioned between EtOAc and H<sub>2</sub>O. The organic layer was washed with brine, dried ( $Na_2SO_4$ ), and concentrated. The residue was purified by column chromatography ( $SiO_2$ , 0–4% MeOH in  $CHCl_3$ ) to give **2** (905 mg, 75% as a white solid): FAB-MS  $m/z$  843 ( $MH^+$ );  $^1H$  NMR ( $CDCl_3$ )  $\delta$  7.64–7.00 (m, 20H), 4.60 (br, 2H), 4.08 (s, 4H), 3.66–3.24 (m, 8H), 3.15 (m, 4H), 2.11 (br, 2H), 1.55 (m, 8H), 1.03 (s, 18H). Anal. Calcd for  $C_{47}H_{66}N_2O_8Si_2 \cdot 1/4 H_2O$ : C, 66.59; H, 7.91; N, 3.30. Found: C, 66.85; H, 8.20; N, 3.28.

**1,3-*O*-Bis(*tert*-butyldiphenylsilyl)-2-[*N*-(4,4'-dimethoxytrityl)oxybutyl]carbamoyl]oxymethyl-2-[*N*-(4-hydroxybutyl)carbamoyl]oxymethyl-1,3-propanediol (3).** A mixture of **2** (848 mg, 1.01 mmol) and DMTrCl (397 mg, 1.17 mmol) in pyridine (10 mL) was stirred at room temperature for 12 h. The mixture was partitioned between EtOAc and H<sub>2</sub>O. The organic layer was washed with brine, dried (Na<sub>2</sub>SO<sub>4</sub>), and evaporated under reduced pressure. The residue was purified by column chromatography (SiO<sub>2</sub>, 25–100% EtOAc in hexane) to give **3** (512 mg, 44% as a white foam): FAB-MS *m/z* 1145 (M<sup>+</sup>); <sup>1</sup>H NMR (CDCl<sub>3</sub>) δ 7.62–6.80 (m, 33H), 4.51 (br, 1H), 4.39 (br, 1H), 4.11 (m, 4H), 3.78 (s, 6H), 3.64 (m, 6H), 3.09 (m, 4H), 1.56 (m, 8H), 1.01 (s, 18H). Anal. Calcd for C<sub>68</sub>H<sub>84</sub>N<sub>2</sub>O<sub>10</sub>Si<sub>2</sub>·<sup>3</sup>/<sub>2</sub>H<sub>2</sub>O: C, 69.65; H, 7.48; N, 2.39. Found: C, 69.68; H, 7.57; N, 2.29.

**1,3-*O*-Bis(*tert*-butyldiphenylsilyl)-2-[*N*-(4,4'-dimethoxytrityloxy)butyl]carbamoyl]oxymethyl-2-[*N*-(4-levulinyloxy)butyl]carbamoyl]oxymethyl-1,3-propanediol (4).** A mixture of levulinic acid (326 mg, 2.81 mmol) and 1-ethyl-3-(3-dimethylaminopropyl)carbodiimide hydrochloride (WSCl) (275 mg, 1.43 mmol) in DMF (4.8 mL) was stirred at room temperature. After 24 h, the mixture was evaporated under reduced pressure, and the residue was dissolved in pyridine (2.5 mL). To the solution were added **3** (227 mg, 0.198 mmol) and DMAP (17 mg, 0.140 mmol), and the mixture was stirred at room temperature. After 12 h, the mixture was partitioned between EtOAc and H<sub>2</sub>O. The organic layer was washed with brine, dried (Na<sub>2</sub>SO<sub>4</sub>), and evaporated under reduced pressure. The residue was purified by column chromatography (SiO<sub>2</sub>, 33–50% EtOAc in hexane) to give **4** (148 mg, 60% as a white foam): FAB-MS *m/z* 1243 (MH<sup>+</sup>); <sup>1</sup>H NMR (CDCl<sub>3</sub>) δ 7.61–6.80 (m, 33H), 4.46 (br, 1H), 4.39 (br, 1H), 4.11 (m, 6H), 3.78 (s, 6H), 3.63 (s, 4H), 3.15–3.05 (m, 6H), 2.73 (m, 2H), 2.55 (m, 2H), 2.17 (s, 3H), 1.56 (m, 8H), 1.00 (s, 18H). Anal. Calcd for C<sub>73</sub>H<sub>90</sub>N<sub>2</sub>O<sub>12</sub>Si<sub>2</sub>·H<sub>2</sub>O: C, 69.49; H, 7.35; N, 2.22. Found: C, 69.35; H, 7.51; N, 2.11.

**2-[*N*-(4,4'-Dimethoxytrityloxy)butyl]carbamoyl]oxymethyl-2-[*N*-(4-levulinyloxy)butyl]carbamoyl]oxymethyl-1,3-propanediol (5).** A mixture of **4** (488 mg, 0.392 mmol) and TBAF (1 M in THF, 1.20 mL, 1.20 mmol) in THF (5 mL) was stirred at room temperature for 12 h. The mixture was evaporated under reduced pressure. The residue was purified by column chromatography (SiO<sub>2</sub>, 50–100% EtOAc in hexane) to give **5** (145 mg, 48% as an oil): FAB-MS *m/z* 766 (M<sup>+</sup>); <sup>1</sup>H NMR (CDCl<sub>3</sub>) δ 7.43–6.81 (m, 13H), 5.14 (br, 1H), 5.08 (br, 1H), 4.10 (m, 6H), 3.79 (s, 6H), 3.47 (m, 4H), 3.21 (m, 4H), 3.08 (t, *J* = 5.6, 2H), 2.76 (t, *J* = 6.4, 2H), 2.56 (t, *J* = 6.2, 2H), 2.18 (s, 3H), 1.59 (m, 8H). Anal. Calcd for C<sub>68</sub>H<sub>84</sub>N<sub>2</sub>O<sub>10</sub>Si<sub>2</sub>·<sup>1</sup>/<sub>2</sub>H<sub>2</sub>O: C, 63.47; H, 7.14; N, 3.61. Found: C, 63.51; H, 7.52; N, 3.43.

**1-*O*-Benzoyl-2-[*N*-(4,4'-dimethoxytrityloxy)butyl]carbamoyl]oxymethyl-2-[*N*-(4-levulinyloxy)butyl]carbamoyl]oxymethyl-1,3-propanediol (6).** A mixture of **5** (137 mg, 0.179 mmol) and BzCl (22 μL, 0.188 mmol) in pyridine (1.8 mL) was stirred at room temperature for 12 h. The mixture was partitioned between EtOAc and H<sub>2</sub>O. The organic layer was washed with aqueous NaHCO<sub>3</sub> (saturated) and brine, dried (Na<sub>2</sub>SO<sub>4</sub>), and evaporated under reduced pressure. The residue was purified by column chromatography (SiO<sub>2</sub>, 50–90% EtOAc in hexane) to give **6** (47 mg, 30% as an oil): FAB-MS *m/z* 871 (MH<sup>+</sup>); <sup>1</sup>H NMR (CDCl<sub>3</sub>) δ 8.02–6.81 (m, 18H), 4.89 (br, 2H), 4.32 (s, 2H), 4.18 (m, 6H), 3.78 (s, 6H), 3.53 (m, 4H), 3.21 (m, 4H), 3.08 (m, 2H), 2.75 (t, *J* = 6.4, 2H), 2.55 (t, *J* = 6.4, 2H), 2.18 (s, 3H), 1.59 (m, 8H). Anal.

Calcd for C<sub>48</sub>H<sub>58</sub>N<sub>2</sub>O<sub>13</sub>·3H<sub>2</sub>O: C, 62.32; H, 6.97; N, 3.03. Found: C, 62.59; H, 6.61; N, 2.85.

**Synthesis of the Controlled Pore Glass Support with 1-*O*-Benzoyl-2-[*N*-(4,4'-dimethoxytrityloxy)butyl]carbamoyl]oxymethyl-2-[*N*-(4-levulinyloxy)butyl]carbamoyl]oxymethyl-3-*O*-succinyl-1,3-propanediol (7).** A mixture of **6** (66 mg, 75 μmol), succinic anhydride (28 mg, 0.281 mmol), and DMAP (19 mg, 0.154 mmol) in pyridine (1 mL) was stirred at room temperature. After 2 days, the mixture was partitioned between EtOAc and H<sub>2</sub>O. The organic layer was washed with aqueous NaHCO<sub>3</sub> (saturated) and brine, dried (Na<sub>2</sub>SO<sub>4</sub>), and concentrated. The residue was dissolved in DMF (2 mL). To the solution were added aminopropyl controlled pore glass (279 mg, 25 μmol, 90.4 μmol/g, CPG Inc.) and WSCI (16 mg, 82 μmol), and the mixture was kept at room temperature for 2 days. After the resin was washed with pyridine, 2 mL of a capping solution (0.1 M DMAP in pyridine:Ac<sub>2</sub>O = 9:1, v/v) was added, and the whole was kept at room temperature for 2 days. The resin was washed with pyridine, MeOH, and acetone and was dried under vacuum. The amount of loaded **7** to the solid support is 43 μmol/g from the calculation of released dimethoxytrityl cation by a solution of 70% HClO<sub>4</sub>:EtOH (3:2, v/v).

**Synthesis of Oligonucleotides.** Branched oligonucleotides were synthesized on a DNA/RNA synthesizer (Applied Biosystems Model Expedite) by the phosphoramidite method. One strand was elongated by the usual manner. The resin was treated with 2 mL of 0.1 M DMAP in pyridine:Ac<sub>2</sub>O (9:1, v/v) for 1 h and then 2 mL of 0.5 M hydrazine in pyridine:CH<sub>3</sub>CO<sub>2</sub>H (4:1, v/v) for 20 min. Other strand was elongated by the usual manner. The oligonucleotides linked to the resins were treated with concentrated NH<sub>4</sub>OH at 55 °C for 16 h, and the released oligonucleotides were purified by denaturing 20% polyacrylamide gel electrophoresis (20% PAGE) run at 600 V for 8 h. The oligonucleotides were visualized by UV shadowing and eluted from crushed gel slices by incubation at room temperature in 0.1 M triethylammonium acetate (TEAA, pH 7.0) and 1 mM EDTA for 15 h. The oligonucleotides were further purified by a Sep-Pak C18 cartridge to give the deprotected oligonucleotides **8** (4), **9** (2), **10** (8), and **11** (5). The yields are indicated in parentheses as OD units at 260 nm starting from 1 μmol scale.

**Matrix-Assisted Laser Desorption/Ionization Time-of-Flight Mass Spectrometry.** Spectra were obtained on a Voyager Elite reflection time-of-flight mass spectrometry (PerSeptive Biosystems, Inc., Framingham, MA) equipped with a nitrogen laser (337 nm, 3-ns pulse). 3-Hydroxypicolinic acid (HPA), dissolved in H<sub>2</sub>O to give a saturated solution at room temperature, was used as the matrix. Time-to-mass conversion was achieved by calibration by using the peak representing the C<sup>+</sup> cation of the charged derivative to be analyzed. Oligonucleotide **8**: calculated mass, 10868.14; observed mass, 10869.00. Oligonucleotide **9**: calculated mass, 10952.30; observed mass, 10955.60. Oligonucleotide **10**: calculated mass, 11224.29; observed mass, 11227.70. Oligonucleotide **11**: calculated mass, 11734.73; observed mass, 11734.90.

**Thermal Denaturation and CD Spectroscopy.** The solution that contained the branched oligonucleotide (2 μM) and the target DNA **17** (2 μM) or RNA **18** (2 μM) in a buffer of 25 mM Tris-HCl (pH 7.0), 100 mM NaCl, and 10 mM MgCl<sub>2</sub> or 10 mM PIPES (pH 6.0), 100 mM NaCl, and 10 mM MgCl<sub>2</sub> was heated at 90 °C for 5 min, then cooled gradually to an appropriate temperature, and used for the thermal denaturation study. Thermal-induced



transitions of each mixture were monitored at 260 nm on a Beckman DU 650 spectrophotometer. Sample temperature was increased 0.5 °C/min. Extinction coefficients of the branched oligonucleotides were calculated from those of mononucleotides and dinucleotides according to the nearest-neighbor approximation (24). Samples for CD spectroscopy were prepared by the same procedure used in the thermal denaturation study, and spectra were measured at 20 °C. The ellipticities of triplexes were recorded from 200 to 350 nm in a cuvette with a path length 1 mm. CD data were converted into mdeg·mol of residues<sup>-1</sup>·cm<sup>-1</sup>.

#### ACKNOWLEDGMENT

This work was supported in part by a Grant-in-Aid for Encouragement of Young Scientists from the Ministry of Education, Science, Sports, and Culture of Japan.

#### LITERATURE CITED

- (1) Uhlmann, E., and Peyman, A. (1990) Antisense oligonucleotides: a new therapeutic principle. *Chem. Rev.* 90, 544–584.
- (2) Milligan, J. F., Matteucci, M. D., and Martin, J. C. (1993) Current concepts in antisense drug design. *J. Med. Chem.* 36, 1923–1937.
- (3) Thuong, N. T., and Hélène, C. (1993) Sequence specific recognition and modification of double-helical DNA by oligonucleotides. *Angew. Chem., Int. Ed. Engl.* 32, 666–690.
- (4) Moser, H. E., and Dervan, P. B. (1987) Sequence specific cleavage of double helical DNA by triple helix formation. *Science* 238, 645–650.
- (5) Rajagopal, P., and Feigon, J. (1989) Triple-strand formation in the homopurine: homopyrimidine DNA oligonucleotides d(G-A)<sub>4</sub> and d(T-C)<sub>4</sub>. *Nature* 339, 637–640.
- (6) Beal, P. A., and Dervan, P. B. (1991) Second structural motif for recognition of DNA by oligonucleotide-directed triple-helix formation. *Science* 251, 1360–1363.
- (7) Pilch, D. S., Levenson, C., and Shafer, R. H. (1991) Structure, stability, and thermodynamics of a short intermolecular purine–purine–pyrimidine triple helix. *Biochemistry* 30, 6081–6088.
- (8) Giovannangeli, C., Montenay-Garestier, T., Rougée, Chasignol, M., Thuong, N. T., and Hélène, C. (1991) Single-stranded DNA as a target for triple-helix formation. *J. Am. Chem. Soc.* 113, 7775–7777.
- (9) Giovannangeli, C., Thuong, N. T., and Hélène, C. (1993) Oligonucleotide clamps arrest DNA synthesis on a single-stranded DNA target. *Proc. Natl. Acad. Sci. U.S.A.* 90, 10013–10017.
- (10) Kool, E. T. (1997) Preorganization of DNA: Design principles for improving nucleic acid recognition by synthetic oligonucleotides. *Chem. Rev.* 97, 1473–1487.
- (11) Wang, S., and Kool, E. T. (1995) Relative stabilities of triple helices composed of combinations of DNA, RNA and 2'-O-methyl-RNA backbones: chimeric circular oligonucleotides as probes. *Nucleic Acids Res.* 23, 1157–1164.
- (12) Kandimalla, E. R., Agrawal, S., Venkataraman, G., and Sasisekharan, V. (1995) Single strand target triplex formation: parallel-stranded DNA hairpin duplexes for targeting pyrimidine strands. *J. Am. Chem. Soc.* 117, 6416–6417.
- (13) Roberts, R. W., and Crothers, D. M. (1992) Stability and properties of double and triple helices: Dramatic effects of RNA or DNA backbone composition. *Science* 258, 1463–1466.
- (14) Han, H., and Dervan, P. B. (1993) Sequence-specific recognition of double helical RNA and RNA·DNA by triple helix formation. *Proc. Natl. Acad. Sci. U.S.A.* 90, 3806–3810.
- (15) Shimizu, M., Konishi, A., Shimada, Y., Inoue, H., and Ohtsuka, E. (1992) Oligo(2'-O-methyl)ribonucleotides: Effective probes for duplex DNA. *FEBS Lett.* 302, 155–158.
- (16) Ueno, Y., Takeba, M., Mikawa, M., and Matsuda, A. (1999) Synthesis of branched oligodeoxynucleotides (branched ODNs) with pentaerythritol at the branch point and their thermal stabilization of triplex formation. *J. Org. Chem.* 64, 1211–1217.
- (17) Ueno, Y., Mikawa, M., Hoshika, S., and Matsuda, A. (2001) Alternate-strand triple-helix formation by the 3'-3'-linked oligodeoxynucleotides with the anthraquinonyl group at the junction point. *Bioconjugate Chem.* 12, 635–642.
- (18) Azhayev, A., Gouzaev, A., Hovinen, J., Azhayeva, E., and Lönnberg, H. (1993) Analogues of oligonucleotides containing 3'-deoxy-β-D-psicothymidine. *Tetrahedron Lett.* 34, 6435–6438.
- (19) Morgan, A. R., and Wells, R. D. (1968) Specificity of the three-stranded complex formation between double-stranded DNA and single-stranded RNA containing repeating nucleotides sequences. *J. Mol. Biol.* 37, 63–80.
- (20) Lee, J. S., Johnson, D. A., and Morgan, A. R. (1979) Complexes formed by (pyrimidine)<sub>n</sub>·(purine)<sub>n</sub> DNAs on lowering the pH are three-stranded. *Nucleic Acids Res.* 6, 3073–3091.
- (21) Singleton, S. F., and Dervan, P. B. (1992) Influence of pH on the equilibrium association constants for oligodeoxyribonucleotide-directed triple helix formation at single DNA sites. *Biochemistry* 31, 10995–11003.
- (22) Lee, J. S., Woodsworth, M. L., Latimer, L. J. P., and Morgan, A. R. (1984) Poly(pyrimidine)·poly(purine) synthetic DNAs containing 5-methylcytosine form stable triplexes at neutral pH. *Nucleic Acids Res.* 12, 6603–6614.
- (23) Povsic, T. J., and Dervan, P. B. (1989) Triple helix formation by oligonucleotides on DNA extended to the physiological pH range. *J. Am. Chem. Soc.* 111, 3059–3061.
- (24) Puglisi, J. D., Tinoco, I., Jr. In *Methods in Enzymology*; Dahlberg, J. E., Abelson, J. N., Eds.; Academic Press: San Diego, 1989; Vol. 180, pp 304–325.

BC020059Q

# Synthesis of Antisense Oligonucleotides Carrying Modified 2-5A Molecules at Their 5'-Termini and Their Properties

Yoshihito Ueno, Yoichiro Kato, Shusaku Okatani, Norihisa Ishida, Masayuki Nakanishi, and Yukio Kitade\*

Department of Biomolecular Science, Faculty of Engineering, Gifu University, Yanagido, Gifu 501-1193, Japan.  
Received September 25, 2002; Revised Manuscript Received February 6, 2003

The synthesis of 8-methyladenosine-substituted 2-5A tetramers with hydroxyalkyl groups at the 5'-phosphates and the corresponding 2-5A-antisense chimeras is described. These oligonucleotides were synthesized by the phosphoramidite method with a DNA/RNA synthesizer. These 2-5A tetramers with hydroxyethyl and hydroxybutyl groups at their 5'-phosphates were more resistant to hydrolysis by alkaline phosphatase than those without the hydroxyalkyl groups. Incorporation of the hydroxyethyl group into the 2-5A tetramer and 2-5A-antisense chimera slightly reduced the abilities of their analogues to activate recombinant human RNase L, but the abilities of the 2-5A tetramer and the 2-5A-antisense chimera both with the hydroxyethyl group and 8-methyladenosine returned to 80 and 50% relative to those of the oligonucleotides without the hydroxyethyl group and 8-methyladenosine, respectively. Furthermore, the enzyme activated by 8-methyladenosine-substituted 2-5A-antisense chimera with the hydroxyethyl group cleaved the complementary RNA as efficiently as that activated by 2-5A-antisense chimera without the hydroxyethyl group and 8-methyladenosine. Thus, the 2-5A-antisense chimera carrying the hydroxyethyl group and 8-methyladenosine will be a candidate for a novel antisense molecule.

## INTRODUCTION

Antisense oligonucleotides have been applied extensively for the regulation of cellular and viral gene expression. They hybridize to mRNA targets through Watson–Crick base-pairing and inhibit the translation of mRNA in a sequence-specific manner (1–3). One of the major problems encountered when using naturally occurring phosphodiester oligonucleotides as antisense molecules is their rapid degradation by nucleases present in cell culture media and inside cells. Therefore, several types of backbone-modified oligonucleotides such as phosphorothioates, methylphosphonates, phosphoramidates, and peptide nucleic acids (PNAs) have been synthesized and used for antisense studies (4). However, the benefits of such enzymatic stabilization are sometimes counteracted by the loss of important properties for antisense activity. RNase H, an enzyme that plays an important role in the conventional antisense mechanism of action, cannot cleave duplexes between RNA and methylphosphonate or phosphoramidate oligonucleotides, or PNA. Thus, inhibition of mRNA translation by these oligonucleotides is limited since it is based only on a secondary mechanism, the steric inhibition of translation (1, 2).

A small oligoadenylate containing unique 2',5'-phosphodiester bonds, known as 2-5A, plays a key role in mediating the antiviral effect of interferon (5). RNase L, an enzyme found in many eukaryotic cells, is allosterically activated by 2-5A. The activated RNase L cleaves single-stranded RNA preferentially on the 3'-side of UpN. Recently, an oligonucleotide modified with a 5'-mono-

phosphorylated 2-5A tetramer has been applied to antisense studies (6–13). The antisense moiety of a 2-5A-antisense chimera sequence-specifically binds to mRNA. The 2-5A moiety activates RNase L, and then the activated RNase L cleaves mRNA. Thus, even if a duplex between an antisense oligonucleotide and mRNA is not a substrate of RNase H, the 2-5A-antisense chimera can irreversibly inhibit the translation of mRNA.

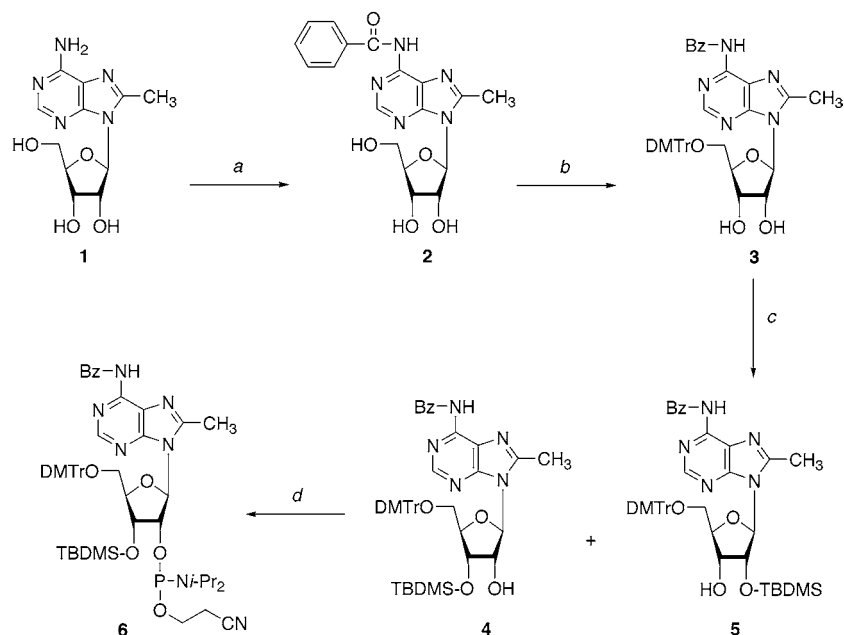
When 2-5A-antisense chimeras are applied to antisense studies, stabilization of the 2-5A-antisense chimeras against phosphatases is necessary since these enzymes are ubiquitous in biological systems (14). On the other hand, we previously reported that a 5'-triphosphorylated 2-5A trimer with 8-methyladenosine (**1**, Scheme 1) at the 2'-terminal position of the 2-5A trimer was significantly more effective as an activator of RNase L than the *un*-substituted 5'-triphosphorylated 2-5A trimer (15). Thus, we envisioned that modification of the 5'-phosphates with hydroxyalkyl groups and incorporation of **1** into the 2-5A moieties of the 2-5A-antisense chimeras would impart phosphatase-resistant property to the analogues without reducing their abilities to activate RNase L.

In this paper, we report the synthesis and phosphatase-resistant property of 8-methyladenosine-substituted 2-5A tetramers and the corresponding antisense chimeras with hydroxyalkyl groups at 5'-phosphates. The ability of the modified 2-5A tetramers and 2-5A-antisense chimeras to activate recombinant human RNase L was also studied.

## RESULTS AND DISCUSSION

**Synthesis.** 2-5A analogues and 2-5A-antisense chimeras were synthesized with a DNA/RNA synthesizer by the phosphoramidite method. The phosphoramidite unit of 8-methyladenosine was synthesized as follows: 8-methyladenosine (**1**), which was prepared by the re-

\* To whom correspondence should be addressed. Phone and fax: +81-58-293-2640. E-mail: kitade@biomol.gifu-u.ac.jp.

Scheme 1<sup>a</sup>


<sup>a</sup> (a) (1) TMSCl, pyridine, room temperature; (2) BzCl, pyridine, room temperature; (3) NH<sub>4</sub>OH, pyridine, room temperature; (b) DMTrCl, Et<sub>3</sub>N, DMAP, pyridine, room temperature; (c) TBDMS-Cl, imidazole, DMF, room temperature; (d) 2-cyanoethyl *N,N*-diisopropylchlorophosphoramidite, *N,N*-diisopropylethylamine, THF, room temperature.

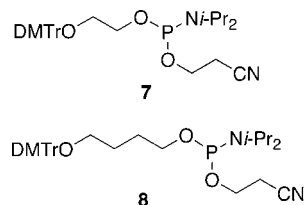


Figure 1. Structures of phosphoramidites.

ported method (16), was treated with TMSCl and then BzCl to produce *N*<sup>6</sup>-benzoyl-8-methyladenosine (**2**) in a 83% yield (Scheme 1). The 5'-hydroxyl group of **2** was protected with a DMTr group to give **3** in a 69% yield. 5'-O-DMTr derivative **3** was treated with a 1.2 equiv of TBDMS-Cl to afford 3'-O-TBDMS and 2'-O-TBDMS derivatives, **4** and **5**, in 50 and 23% yields, respectively. 3'-O-TBDMS derivative, **4**, was phosphitylated by a standard procedure to give the corresponding nucleoside phosphoramidite, **6**, in a 74% yield. The phosphoramidite

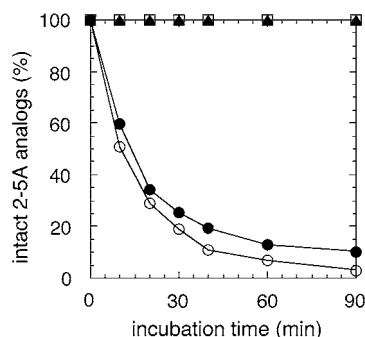
units of ethylene glycol, **7**, and 1,4-dihydroxybutane, **8**, were synthesized according to the reported method (6, 11) (Figure 1).

2-5A analogues **9–13** and 2-5A-antisense chimeras **14–17** were synthesized using phosphoramidite, **6**, **7**, and **8**, with a DNA/RNA synthesizer (Figure 2). It has been reported that oligonucleotides composed of 2'-O-methylnucleosides are more resistant to nucleolytic hydrolysis by nucleases than *un*-modified DNA or RNA, and increase the thermal stability of duplexes with complementary DNA or RNA (17). Thus, we chose oligonucleotides consisting of 2'-O-methylnucleosides as the antisense parts of the 2-5A-antisense chimeras. The fully protected oligonucleotides (1 μmol each) linked to the solid support were treated with concentrated NH<sub>4</sub>OH:EtOH (3:1, v/v) at 55 °C for 12 h and then 1 M TBAF/THF at room temperature for 12 h. The released oligonucleotides were purified by reversed phase HPLC or denaturing 20% polyacrylamide gel electrophoresis (20% PAGE) to give

(a)		(c)	
No.	2-5A analogs	No.	target RNAs
9	p5'ApApApA2'	18	5' [r(CCCCCCCCCCUCCCCC) dC] 3'
10	HO(CH <sub>2</sub> ) <sub>2</sub> O-p5'ApApApA2'	19	5' [r(GAUGACGGCGACCCUGAGACCCCCCUCCCCC) dT] 3'
11	HO(CH <sub>2</sub> ) <sub>4</sub> O-p5'ApApApA2'		
12	p5'ApAp(me <sup>8</sup> A)pA2'		
13	HO(CH <sub>2</sub> ) <sub>2</sub> O-p5'ApAp(me <sup>8</sup> A)pA2'		
(b)			
No.	2-5A-antisense chimeras		
14	p5'ApApApA2'-O(CH <sub>2</sub> ) <sub>4</sub> OpO(CH <sub>2</sub> ) <sub>4</sub> O-5' [2'-O-Me(CUCUCAGGGGUCGCCGUCAU) pdC] 3'		
15	HO(CH <sub>2</sub> ) <sub>2</sub> O-p5'ApApApA2'-O(CH <sub>2</sub> ) <sub>4</sub> OpO(CH <sub>2</sub> ) <sub>4</sub> O-5' [2'-O-Me(CUCUCAGGGGUCGCCGUCAU) pdC] 3'		
16	p5'ApAp(me <sup>8</sup> A)pA2'-O(CH <sub>2</sub> ) <sub>4</sub> OpO(CH <sub>2</sub> ) <sub>4</sub> O-5' [2'-O-Me(CUCUCAGGGGUCGCCGUCAU) pdC] 3'		
17	HO(CH <sub>2</sub> ) <sub>2</sub> O-p5'ApAp(me <sup>8</sup> A)pA2'-O(CH <sub>2</sub> ) <sub>4</sub> OpO(CH <sub>2</sub> ) <sub>4</sub> O-5' [2'-O-Me(CUCUCAGGGGUCGCCGUCAU) pdC] 3'		

Figure 2. Sequences of oligonucleotides.





**Figure 3.** Stabilities of 2-5A analogues toward alkaline phosphatase. **10** (□); **11** (▲); **9** (●); **12** (○). The experimental conditions are given in Experimental Procedures.

deprotected oligonucleotides, **9–13** and **14–17**, in 3–6 and 10–70 OD<sub>260</sub> units, respectively. These oligonucleotides were analyzed by matrix-assisted laser desorption/ionization time-of-flight mass spectrometry (MALDI-TOF/MS), and the observed molecular weights supported their structures.

**Phosphatase-Resistant Property.** First, the stability of modified 2-5A tetramers **10–12** as to hydrolysis by phosphatases was investigated. 2-5A tetramers **9–12** were incubated with alkaline phosphatase in a buffer comprising 10 mM tris-acetate (pH 8.8) containing 1 mM MgCl<sub>2</sub> at 37 °C, and the reactions were analyzed by reversed phase HPLC. 2-5A tetramers **9** and **12** were almost completely hydrolyzed on 90 min incubation (Figure 3). The half-lives of 2-5A tetramers **9** and **12** were 14 and 10 min, respectively. In contrast, 2-5A tetramers **10** and **11** modified with 2-hydroxyethyl and 4-hydroxybutyl groups were stable under the same conditions on 90 min incubation.

**Activation of Recombinant Human RNase L.** The ability of 2-5A analogues **9–13** and 2-5A-antisense chimeras **14–17** to activate RNase L was estimated by monitoring the cleavage of a synthetic RNA by the activated RNase L. In this study, 5'-r(C<sub>11</sub>U<sub>2</sub>C<sub>6</sub>)dC-3' (**18**) was used as a substrate. Carroll and co-workers reported that initial cleavage of RNA by RNase L occurs on the 3'-side of r(C<sub>11</sub>U<sub>2</sub>) to yield r(C<sub>11</sub>UpUp), and second cleavage occur on the 3'-side of r(C<sub>11</sub>U) to give r(C<sub>11</sub>Up) with a higher enzyme concentration or longer incubation time (*18*). The ability of 2-5A analogues **9–13** to activate the

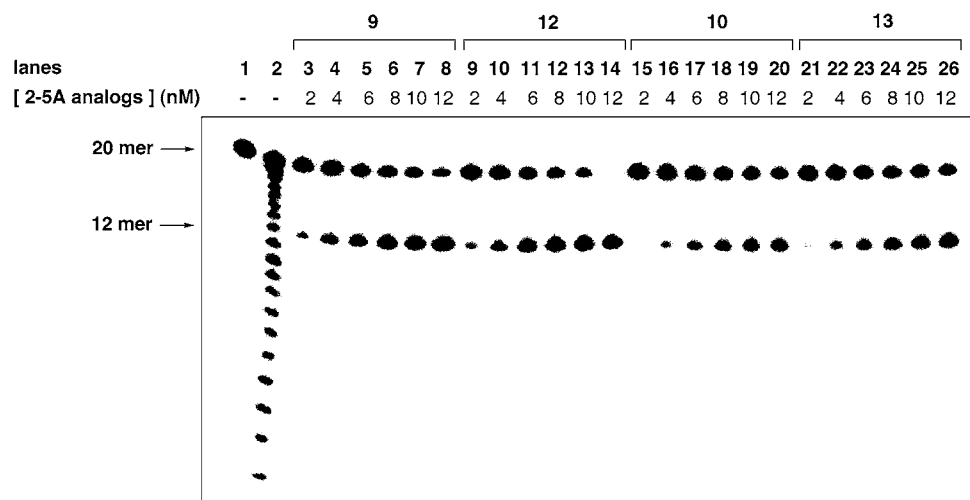
**Table 1.** Activities of 2-5A Analogues

oligonucleotide	EC <sub>50</sub> <sup>a</sup> (nM)	relative activity
<b>9</b>	7.5	1.00
<b>10</b>	11.6	0.64
<b>11</b>	17.4	0.43
<b>12</b>	6.3	1.19
<b>13</b>	9.1	0.82

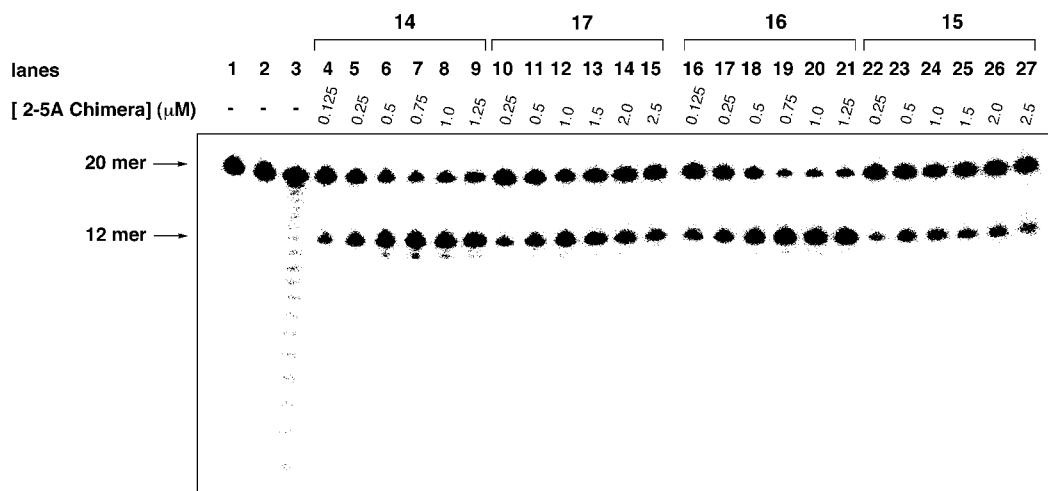
<sup>a</sup> Concentrations of 2-5A analogues required for cleavage of half target RNA.

enzyme was represented in terms of the concentrations of the analogues required to cleave half of the RNA (EC<sub>50</sub>). Recombinant human RNase L was expressed in *E. coli* and purified according to the reported procedure with a slight modification (*19*). The RNA labeled at the 5'-end with <sup>32</sup>P was incubated with the enzyme that had been preincubated with 2-5A analogues **9–13**. The reactions were analyzed by polyacrylamide gel electrophoresis under denaturing conditions. The densities of radioactive bands on the gel were determined with a bioimaging analyzer (Figure 4). The EC<sub>50</sub> values and relative activities of analogues **10–13** as to 2-5A **9** (EC<sub>50</sub> of **9**/EC<sub>50</sub> of each 2-5A analog) are summarized in Table 1. The EC<sub>50</sub> value of 2-5A **9** was 7.5 nM when 100 ng of RNase L was used. The relative activities of analogues **10** and **11** with the hydroxyethyl and hydroxybutyl groups at their 5'-phosphates were 0.64 and 0.43, respectively. Although the ability of **10** and **11** to activate RNase L was weaker than that of **9**, the EC<sub>50</sub> values of **10** and **11** were only 1.5- and 2.3-fold higher than that of **9**, respectively. When 8-methyladenosine **1** was introduced into 2-5A at the third position from the 5'-end, the ability of analogue **12** to elicit RNase L activity was increased as compared with that of **9**. The relative activity of 2-5A analogue **13**, which has the hydroxyethyl group and contains **1**, was 0.82. Thus, it was revealed that the hydroxyethyl group, which endows 2-5A analogue **13** with the phosphatase-resistant property, slightly reduces the ability of analogue **13** to activate RNase L. However, the ability of 2-5A analogue **13** to elicit RNase L activity returned to 80% relative to that of **9** on the incorporation of **1** into it.

Next, the ability of 2-5A-antisense chimeras **14–17** to activate RNase L was studied (Figure 5). The EC<sub>50</sub> value of antisense chimera **14** was 0.3 μM when 800 ng of RNase L was used. The EC<sub>50</sub> values and relative activities of antisense chimeras **15–17** as to antisense chimera



**Figure 4.** Polyacrylamide gel electrophoresis of 5'-<sup>32</sup>P-labeled RNA **18** hydrolyzed by recombinant human RNase L activated with 2-5A analogues **9–13**. Lane 1: 5'-<sup>32</sup>P-labeled RNA **18**; lane 2: limited alkaline hydrolysis of 5'-<sup>32</sup>P-labeled RNA **18**; lanes 3–26: 5'-<sup>32</sup>P-labeled RNA **18** + 2-5A analogues + recombinant human RNase L. The experimental conditions are given in Experimental Procedures.



**Figure 5.** Polyacrylamide gel electrophoresis of 5'-<sup>32</sup>P-labeled RNA **18** hydrolyzed by recombinant human RNase L activated with 2-5A-antisense chimeras **14–17**. Lane 1: 5'-<sup>32</sup>P-labeled RNA **18**; lane 2: 5'-<sup>32</sup>P-labeled RNA **18** + recombinant human RNase L; lane 3: limited alkaline hydrolysis of 5'-<sup>32</sup>P-labeled RNA **18**; lanes 4–27: 5'-<sup>32</sup>P-labeled RNA **18** + 2-5A-antisense chimeras + recombinant human RNase L. The experimental conditions are given under Experimental Procedures.

**Table 2. Activities of 2-5A-Antisense Chimeras**

oligonucleotide	EC <sub>50</sub> <sup>a</sup> (μM)	relative activity
<b>14</b>	0.30	1.00
<b>15</b>	0.90	0.34
<b>16</b>	0.28	1.11
<b>17</b>	0.65	0.48

<sup>a</sup> Concentration of 2-5A-antisense chimeras required for cleavage of half target RNA.

**14** (EC<sub>50</sub> of **14**/EC<sub>50</sub> of each antisense chimera) are listed in Table 2. Although the EC<sub>50</sub> values of antisense chimeras **14–17** were higher than those of 2-5A analogues **9–13**, the trend of the relative activities of antisense chimeras **14–17** was similar to that of 2-5A analogues **9–13**. Torrence et al. reported that 2-5A-antisense chimeras were 10–100 fold less potent than the parent 2-5A tetramer in the ability to activate RNase L (13). Our results are consistent with these data. They stated that the mechanism underlying the difference has not yet been investigated, but may involve steric interference by the antisense moiety in the interaction of 2-5A and the enzyme, or in the process of enzyme dimerization. However, it is noteworthy that antisense chimera **17** modified with the hydroxyethyl group at the 5'-phosphate was only 2-fold less potent than unmodified 2-5A-antisense chimera **14**.

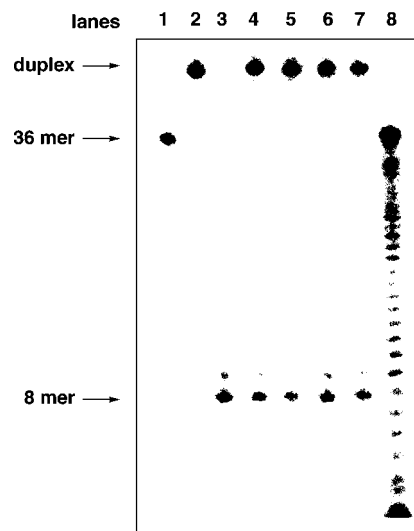
**Thermal Denaturation Studies.** The stability of duplexes composed of antisense chimeras **14–17** and a complementary RNA was studied by thermal denaturation in a buffer comprising 10 mM sodium phosphate (pH 7.0) containing 10 mM NaCl. RNA **19**, 5'-r(GAUG-ACG<sub>2</sub>CGAC<sub>4</sub>UGAGAGC<sub>6</sub>UUC<sub>6</sub>)dT-3', which contains a sequence complementary to the antisense moiety of 2-5A-antisense chimeras, was used in this study. One transition was observed in the melting profile of each duplex (data not shown). The melting temperatures (*T*<sub>m</sub>s) are listed in Table 3. The *T*<sub>m</sub> values of the 2-5A-antisense chimeras were all around 94 °C. Thus, it was revealed that 2-5A-antisense chimeras **14–17** had sufficient thermal stability for application to antisense studies.

**Cleavage of Complementary RNA by Recombinant Human RNase L activated with 2-5A antisense chimeras.** Finally, we studied the RNA cleavage by 2-5A-antisense chimeras **14–17** using synthetic RNA **19**, 5'-r(GAUGACG<sub>2</sub>CGAC<sub>4</sub>UGAGAGC<sub>6</sub>UUC<sub>6</sub>)dT-3', which contained a sequence complementary to the antisense

**Table 3. Hybridization Data<sup>a</sup>**

oligonucleotide	<i>T</i> <sub>m</sub> (°C)
<b>14</b>	93.9
<b>15</b>	93.5
<b>16</b>	93.1
<b>17</b>	93.4

<sup>a</sup> RNA **19** was used as the complementary oligonucleotide. The experimental conditions are given under Experimental Procedures.



**Figure 6.** Polyacrylamide gel electrophoresis of 3'-<sup>32</sup>pCp-labeled RNA **19** hydrolyzed by recombinant human RNase L activated with 2-5A-antisense chimeras **14–17**. Lane 1: 3'-<sup>32</sup>pCp-labeled RNA **19**; lane 2: 3'-<sup>32</sup>pCp-labeled RNA **19** + 2-5A-antisense chimera **14**; lane 3: 3'-<sup>32</sup>pCp-labeled RNA **19** + 2-5A tetramer **9** (4 nM) + recombinant human RNase L; lanes 4–7: 3'-<sup>32</sup>pCp-labeled RNA **19** + 2-5A-antisense chimeras + recombinant human RNase L; lane 8: limited alkaline hydrolysis of 3'-<sup>32</sup>pCp-labeled RNA **19**. The experimental conditions are given under Experimental Procedures.

moiety of the 2-5A-antisense chimeras. RNase L was activated by preincubation with each 2-5A-antisense chimera. The solution containing the activated RNase L was added to the solution containing the RNA labeled at the 3'-end with <sup>32</sup>pCp, followed by incubation at 37 °C for 30 min. The reactions were analyzed by polyacrylamide gel electrophoresis under denaturing conditions (Figure 6). Table 4 shows the percentages of the synthetic

**Table 4. Activities of 2-5A-Antisense Chimeras**

oligonucleotide	cleaved RNA (%)
<b>14</b>	20.6
<b>15</b>	8.8
<b>16</b>	33.2
<b>17</b>	18.0

RNA cleaved by the enzyme activated with 2-5A-antisense chimeras **14**–**17**. The RNA was chiefly cleaved on the 3'-side of 5'-r(GAUGACG<sub>2</sub>CGAC<sub>4</sub>UGAGAGC<sub>6</sub>UU)-3'. Except for the intact RNA, 5'-rC<sub>6</sub>dT<sup>32</sup>pCp was mainly observed. The enzyme activated with antisense chimera **14** cleaved 21% of the RNA under the conditions used. The activity of the enzyme slightly decreased on modification at the 5'-phosphate of the antisense chimera with a hydroxyethyl group. However, the activity of the enzyme activated by antisense chimera **17**, which had a hydroxyethyl group and contained 8-methyladenosine **1**, was almost equal to that activated by antisense chimera **14**.

## CONCLUSION

In this paper, we reported the synthesis of 8-methyladenosine-containing 2-5A tetramers and the corresponding antisense chimeras with hydroxyalkyl groups at 5'-phosphates. The phosphatase-resistant property and the ability of these oligonucleotides to activate recombinant human RNase L were studied. The 2-5A tetramers with hydroxyethyl and hydroxybutyl groups at their 5'-phosphates were more resistant to hydrolysis by alkaline phosphatase than those without the hydroxyalkyl groups. Incorporation of the hydroxyethyl group into the 2-5A tetramer and 2-5A-antisense chimera slightly reduced the abilities of the analogues to activate RNase L, but their abilities to activate the enzyme returned to 80 and 50% relative to those of *un*-modified oligonucleotides **9** and **14**, respectively, on the incorporation of **1** into them. Furthermore, the enzyme activated by the 2-5A-antisense chimera, which had the hydroxyethyl group and contained **1**, cleaved the complementary RNA as efficiently as that activated by the 2-5-antisense chimera without the hydroxyethyl group and **1**. Thus, the 2-5A-antisense chimera carrying the hydroxyethyl group and **1** will be a candidate for a novel antisense molecule.

## EXPERIMENTAL PROCEDURES

**General Remarks.** <sup>1</sup>H NMR spectra were recorded at 400 MHz. Chemical shifts ( $\delta$ ) and coupling constants (*J*) are reported in ppm downfield from TMS and in Hz, respectively. Mass spectra were obtained by the fast atom bombardment (FAB) method. Thin-layer chromatography was performed on Merck coated plates 60F<sub>254</sub>. The silica gel used for column chromatography was Wakogel C-300.

**6-*N*-Benzoyl-8-methyladenosine (2).** TMSCl (0.61 mL, 4.8 mmol) was added to a solution of 8-methyladenosine (**1**) (0.27 g, 0.96 mmol) in pyridine (9.5 mL), and then the mixture was stirred at room temperature. After 20 min, BzCl (0.56 mL, 4.8 mmol) was added to the mixture, which was stirred at room temperature. After 2 h, H<sub>2</sub>O (1 mL) and concentrated NH<sub>4</sub>OH (2 mL) were added to the mixture, which was stirred at room temperature. After 30 min, the mixture was partitioned between CHCl<sub>3</sub> and aqueous NaHCO<sub>3</sub> (saturated). The organic layer was washed with brine, dried (Na<sub>2</sub>SO<sub>4</sub>), and then concentrated. The residue was purified by column chromatography (SiO<sub>2</sub>, 5% MeOH in CHCl<sub>3</sub>) to give **2** (0.31 g, 83%): EI-MS *m/z* 385 (M<sup>+</sup>); <sup>1</sup>H NMR (CDCl<sub>3</sub>)  $\delta$  9.18 (s, 1H, NH-6), 8.31 (s, 1H, H-2), 7.99 (d, 2H, aromatic

H, *J* = 7.2), 7.61 (t, 1H, aromatic H, *J* = 7.2), 7.52 (t, 2H, aromatic H, *J* = 7.6), 6.30 (d, 1H, H-1', *J* = 10.4), 5.86 (d, 1H, HO-2', *J* = 8.0), 5.42 (d, 1H, HO-3', *J* = 6.0), 5.11 (q, 1H, H-2', *J* = 7.2), 4.40 (d, 1H, H-3', *J* = 4.8), 3.91 (d, 1H, H-4', *J* = 12.8), 3.71 (t, 2H, H-5', *J* = 8.0), 3.48 (d, 1H, HO-5', *J* = 3.2), 2.56 (s, 3H, CH<sub>3</sub>-8); HRMS calcd for C<sub>18</sub>H<sub>19</sub>O<sub>5</sub>N<sub>5</sub>: 385.1836. Found: 385.1379.

**6-*N*-Benzoyl-5'-*O*-(4,4'-dimethoxytrityl)-8-methyladenosine (3).** A mixture of **2** (0.30 g, 0.78 mmol), DMTrCl (0.47 g, 1.39 mmol), Et<sub>3</sub>N (0.20 mL, 2.69 mmol), and DMAP (6 mg, 50  $\mu$ mol) in pyridine (7.8 mL) was stirred at room temperature for 6 h. The mixture was partitioned between EtOAc and aqueous NaHCO<sub>3</sub> (saturated). The organic layer was washed with brine, dried (Na<sub>2</sub>SO<sub>4</sub>), and then evaporated under reduced pressure. The residue was purified by column chromatography (SiO<sub>2</sub>, 2% MeOH in CHCl<sub>3</sub>) to give **3** (0.37 g, 69%): FAB-MS *m/z* 688 (MH<sup>+</sup>); <sup>1</sup>H NMR (CDCl<sub>3</sub>)  $\delta$  8.99 (s, 1H, NH-6), 8.42 (s, 1H, H-2), 8.01 (d, 2H, aromatic H, *J* = 7.6), 7.62 (t, 1H, aromatic H, *J* = 7.6), 7.53 (t, 2H, aromatic H, *J* = 8.0), 7.35–7.17 (m, 9H, aromatic H), 6.73 (dd, 4H, aromatic H, *J* = 4.4, 8.8), 5.90 (d, 1H, H-1', *J* = 2.0), 5.51 (m, 1H, H-2'), 4.90 (m, 1H, HO-2'), 4.63 (m, 1H, H-3'), 4.29 (q, 1H, H-4', *J* = 3.6), 3.73 (s, 6H, CH<sub>3</sub>O), 3.45–3.31 (m, 3H, HO-3' and H-5'), 2.62 (s, 3H, CH<sub>3</sub>-8); HRMS calcd for C<sub>39</sub>H<sub>38</sub>O<sub>5</sub>N<sub>7</sub>: 688.2771. Found: 688.2760.

**6-*N*-Benzoyl-3'-*O*-*tert*-butyldimethylsilyl-5'-*O*-(4,4'-dimethoxytrityl)-8-methyladenosine (4) and 6-*N*-benzoyl-2'-*O*-*tert*-butyldimethylsilyl-5'-*O*-(4,4'-dimethoxytrityl)-8-methyladenosine (5).** A mixture of **3** (0.35 g, 0.50 mmol), TBDMSCl (0.10 g, 0.65 mmol), and imidazole (0.17 g, 2.5 mmol) in DMF (2.0 mL) was stirred at room temperature for 3 h. The mixture was partitioned between EtOAc and aqueous NaHCO<sub>3</sub> (saturated). The organic layer was washed with brine, dried (Na<sub>2</sub>SO<sub>4</sub>), and then evaporated under reduced pressure. The residue was purified by column chromatography (SiO<sub>2</sub>, 30–50% EtOAc in hexane) to give **4** (198 mg, 50%) and **5** (97 mg, 23%). Physical data of **4**: FAB-MS *m/z* 802 (MH<sup>+</sup>); <sup>1</sup>H NMR (CDCl<sub>3</sub>)  $\delta$  8.88 (s, 1H, NH-6), 8.68 (s, 1H, H-2), 8.00 (d, 2H, aromatic H, *J* = 6.8), 7.59 (t, 1H, aromatic H, *J* = 7.2), 7.51 (t, 2H, aromatic H, *J* = 7.2), 7.32–7.15 (m, 9H, aromatic H), 6.73 (d, 4H, aromatic H, *J* = 8.8), 5.90 (d, 1H, H-1', *J* = 3.6), 5.31 (q, 1H, H-2', *J* = 4.0), 5.03 (t, 1H, H-3', *J* = 5.6), 4.13 (m, 1H, H-4'), 3.77 (s, 6H, CH<sub>3</sub>O), 3.46 (m, 1H, H-5'), 3.13 (m, 1H, H-5'), 3.12 (d, 1H, HO-2', *J* = 4.8), 2.77 (s, 3H, CH<sub>3</sub>-8), 0.90 (s, 9H, *t*-Bu-Si), 0.15 (s, 3H, CH<sub>3</sub>Si), 0.04 (s, 3H, CH<sub>3</sub>Si); HRMS calcd for C<sub>45</sub>H<sub>52</sub>O<sub>7</sub>N<sub>5</sub>Si: 802.3636. Found: 802.3641. Physical data of **5**: <sup>1</sup>H NMR (CDCl<sub>3</sub>)  $\delta$  8.95 (s, 1H, NH-6), 8.52 (s, 1H, H-2), 8.02 (d, 2H, aromatic H, *J* = 7.2), 7.61 (t, 1H, aromatic H, *J* = 7.2), 7.53 (t, 2H, aromatic H, *J* = 7.2), 7.46–7.18 (m, 9H, aromatic H), 6.77 (d, 4H, aromatic H, *J* = 8.8), 5.83 (d, 1H, H-1', *J* = 6.0), 5.68 (t, 1H, H-2', *J* = 6.0), 4.41 (m, 1H, H-3'), 4.26 (m, 1H, H-4'), 3.77 (s, 6H, CH<sub>3</sub>O), 3.50 (dd, 1H, H-5', *J* = 4.8, 10.4), 3.35 (dd, 1H, H-5', *J* = 4.8, 10.4), 2.75 (d, 1H, HO-3', *J* = 2.8), 2.69 (s, 3H, CH<sub>3</sub>-8), 0.81 (s, 9H, *t*-Bu-Si), –0.05 (s, 3H, CH<sub>3</sub>Si), –0.30 (s, 3H, CH<sub>3</sub>Si); HRMS calcd for C<sub>45</sub>H<sub>52</sub>O<sub>7</sub>N<sub>5</sub>Si: 802.3636. Found: 802.3643.

**6-*N*-Benzoyl-3'-*O*-*tert*-butyldimethylsilyl-5'-*O*-(4,4'-dimethoxytrityl)-8-methyladenosine 2'-*O*-(2-cyanoethyl) *N,N*-diisopropylphosphoramidite (6).** A solution of **4** (0.19 g, 0.23 mmol), *N,N*-diisopropylethylamine (0.24 mL, 2.4 mmol), and chloro(2-cyanoethoxy)(*N,N*-diisopropylamino)phosphine (0.12 g, 0.48 mmol) in THF (2 mL) was stirred at room temperature for 1 h. The mixture was partitioned between EtOAc and aqueous



NaHCO<sub>3</sub> (saturated). The organic layer was washed with brine, dried (Na<sub>2</sub>SO<sub>4</sub>), and then evaporated under reduced pressure. The residue was purified by column chromatography (neutralized SiO<sub>2</sub>, 50% EtOAc in hexane) to give **6** (0.17 g, 74%): FAB-MS *m/z* 1002 (MH<sup>+</sup>); <sup>31</sup>P NMR (162 MHz, CDCl<sub>3</sub>)  $\delta$  152.05, 150.31.

**Synthesis of Oligonucleotides.** Oligonucleotides were synthesized with a DNA/RNA synthesizer (Applied Biosystems Model Expedite) by the phosphoramidite method. Each oligonucleotide linked to the resin was treated with 3 mL of concentrated NH<sub>4</sub>OH:EtOH (3:1, v/v) at 55 °C for 12 h. The resin was washed with 50% CH<sub>3</sub>CN several times, and then the combined washings were evaporated in a Speed-Vac apparatus. The resulting residue was treated with 1 mL of 1 M TBAF/THF at room temperature for 12 h. The reaction was quenched with 30 mL of sterile 0.1 M TEAA buffer (pH 7.0) and then applied directly to a Sep-Pak C18 cartridge. The compound was eluted with 50% CH<sub>3</sub>CN. The deprotected oligonucleotide was further purified by reversed-phase HPLC or 20% polyacrylamide gel electrophoresis (20% PAGE). Purification by reversed-phase HPLC: the oligonucleotide was purified by reversed-phase HPLC on a J'sphere ODN M80 column (4.6 × 150 mm, YMC) with a linear gradient of CH<sub>3</sub>CN (from 10 to 35% over 20 min) in 0.01 M TEAA buffer (pH 7.0) to give a highly purified oligonucleotide, **9** (4), **10** (6), **11** (6), **12** (3), or **13** (3). Purification by 20% PAGE: the deprotected oligonucleotide was purified by denaturing 20% PAGE with 7 M urea at 600 V for 8 h. The oligonucleotide was visualized by UV shadowing and eluted from crushed gel slices by incubation at room temperature in 0.1 M TEAA buffer (pH 7.0) and 1 mM EDTA for 15 h. The oligonucleotide was further purified on a Sep-Pak C18 cartridge to give the deprotected oligonucleotide, **14** (70), **15** (29), **16** (25), or **17** (10). The yields are indicated in parentheses as OD units at 260 nm starting from 1  $\mu$ mol scale.

**Matrix-Assisted Laser Desorption/Ionization Time-of-Flight Mass Spectrometry.** Spectra were obtained with a Voyager Elite reflection time-of-flight mass spectrometer (PerSeptive Biosystems, Inc., Framingham, MA) equipped with a nitrogen laser (337 nm, 3-ns pulse). 3-Hydroxypicolinic acid (HPA), dissolved in H<sub>2</sub>O to give a saturated solution at room temperature, was used as the matrix. Time-to-mass conversion was achieved by calibration using the peak representing the C<sup>+</sup> cation of the charged derivative to be analyzed. Oligonucleotide **9**: calculated mass, 1334.84; observed mass, 1333.50. Oligonucleotide **10**: calculated mass, 1378.89; observed mass, 1377.50. Oligonucleotide **11**: calculated mass, 1406.95; observed mass, 1405.45. Oligonucleotide **12**: calculated mass, 1348.87; observed mass, 1346.28. Oligonucleotide **13**: calculated mass, 1392.92; observed mass, 1389.76. Oligonucleotide **14**: calculated mass, 8605.47; observed mass, 8606.70. Oligonucleotide **15**: calculated mass, 8619.50; observed mass, 8620.07. Oligonucleotide **16**: calculated mass, 8649.52; observed mass, 8651.48. Oligonucleotide **17**: calculated mass, 8663.55; observed mass, 8661.11.

**Hydrolysis of 2-5A Analogues with Alkaline Phosphatase.** Each 2-5A analogue (2.4 nmol) was incubated with alkaline phosphatase (0.002 units) in a buffer comprising 10 mM Tris-acetate (pH 8.8) containing 1 mM MgCl<sub>2</sub> (total, 100  $\mu$ L) at 37 °C. At appropriate times, aliquots of the reaction mixture were taken and heated for 3 min at 90 °C. Then the solutions were analyzed by reversed-phase HPLC.

**Thermal Denaturation.** A solution containing a 2-5A-antisense chimera (2  $\mu$ M) and RNA **19** (2  $\mu$ M) in a buffer comprising 10 mM sodium phosphate (pH 7.0) and 10 mM NaCl was heated at 100 °C for 3 min, cooled gradually to an appropriate temperature, and then used for the thermal denaturation study. The thermal-induced transition of each mixture was monitored at 260 nm with a Beckman DU 650 spectrophotometer. The sample temperature was increased by 0.5 °C/min. The extinction coefficients of the oligonucleotides were calculated from those of mononucleotides and dinucleotides according to the nearest-neighbor approximation method (20).

**RNA Cleavage by Recombinant Human RNase L Activated with 2-5A Analogues.** Recombinant human RNase L was expressed and purified according to the reported procedure with a slight modification (19). The 2-5A analogues, **9–13** (final concentrations, 2 to 12 nM), were each mixed with 100 ng of recombinant human RNase L in a buffer comprising 20 mM Tris-HCl (pH 7.5), 10 mM magnesium acetate, 8 mM 2-mercaptoethanol, 90 mM KCl, and 0.1 mM ATP (total, 19  $\mu$ L), and then the mixtures were incubated on ice. After 30 min, 1  $\mu$ L of a solution containing 2  $\mu$ M RNA **18** labeled with <sup>32</sup>P at the 5'-end was added to each mixture (total, 20  $\mu$ L), and then the solution was incubated at 37 °C. After 30 min, an aliquot of the reaction mixture (5  $\mu$ L) was added to a loading solution (10  $\mu$ L) containing 7 M urea. The solution was analyzed by electrophoresis on a 20% polyacrylamide gel containing 7 M urea. The densities of radioactive bands on the gel were determined with a Bio-imaging Analyzer (Bas 2000, Fuji Co., Ltd.).

**RNA Cleavage by Recombinant Human RNase L Activated with 2-5A-Antisense Chimeras.** The 2-5A-antisense chimeras, **14–17** (final concentrations, 0.125 to 2.5  $\mu$ M), were each mixed with 800 ng of recombinant human RNase L in a buffer comprising 20 mM Tris-HCl (pH 7.5), 10 mM magnesium acetate, 8 mM 2-mercaptoethanol, 90 mM KCl, and 0.1 mM ATP (total, 19  $\mu$ L), and then the mixtures were incubated on ice. After 30 min, 1  $\mu$ L of a solution containing 2  $\mu$ M RNA **18** labeled with <sup>32</sup>P at the 5'-end was added to each mixture (total, 20  $\mu$ L), and then the solution was incubated at 37 °C. After 30 min, an aliquot of the reaction mixture (5  $\mu$ L) was added to a loading solution (10  $\mu$ L) containing 7 M urea. The solution was analyzed as described above.

**Cleavage of Complementary RNA by Recombinant Human RNase L Activated with 2-5A-Antisense Chimeras.** The 2-5A-antisense chimeras, **14–17** (final concentrations, 500 nM), were each mixed with 400 ng of recombinant human RNase L in a buffer comprising 20 mM Tris-HCl (pH 7.5), 10 mM magnesium acetate, 8 mM 2-mercaptoethanol, 90 mM KCl, and 0.1 mM ATP (total, 19  $\mu$ L), and then the mixtures were incubated on ice. After 30 min, 1  $\mu$ L of a solution containing 2  $\mu$ M RNA **19** labeled with <sup>32</sup>pCp at the 3'-end was added to each mixture (total, 20  $\mu$ L), and then the solution was incubated at 37 °C. After 30 min, an aliquot of the reaction mixture (5  $\mu$ L) was added to a loading solution (10  $\mu$ L) containing 7 M urea. The solution was analyzed as described above.

#### ACKNOWLEDGMENT

This work was supported in part by a Grant-in-Aid for the Encouragement of Young Scientists, No. 12771388 (to Y.U.), and a Grant-in-Aid for Scientific Research, No. 12672150 (to Y.K.), from the Ministry of Education, Science, Sports, and Culture of Japan.

## LITERATURE CITED

- (1) Uhlmann, E., and Peyman, A. (1990) Antisense oligonucleotides: a new therapeutic principle. *Chem. Rev.* **90**, 544–584.
- (2) Milligan, J. F., Matteucci, M. D., and Martin, J. C. (1993) Current concepts in antisense drug design. *J. Med. Chem.* **36**, 1923–1937.
- (3) Stein, C. A. (1999) Keeping the biotechnology of antisense in context. *Nat. Biotechnol.* **17**, 209.
- (4) Mesmaeker, A. D., Altmann, K.-H., Waldner, A., and Wendeborn, S. (1995) Backbone modifications in oligonucleotides and peptide nucleic acid systems. *Curr. Opin. Struct. Biol.* **5**, 343–355, and references therein.
- (5) Player, M., and Torrence, P. F. (1998) The 2-5A system: modulation of viral and cellular processes through acceleration of RNA degradation. *Pharmacol. Ther.* **78**, 55–113.
- (6) Lesiak, K., Khamnei, S., and Torrence, P. F. (1993) 2',5'-Oligoadenylate: antisense chimeras – synthesis and properties. *Bioconjugate Chem.* **4**, 467–472.
- (7) Maran, A., Maitra, R. K., Kumar, A., Dong, B., Xiao, W., Li, G., Williams, B. R. G., Torrence, P. F., and Silverman, R. H. (1994) Blockage of NF- $\kappa$ B signaling by selective ablation of an mRNA target by 2-5A antisense chimeras. *Science* **265**, 789–792.
- (8) Cirino, N. M., Li, G., Xiao, W., Torrence, P. F., and Silverman, R. H. (1997) Targeting RNA decay with 2',5' oligoadenylate-antisense in respiratory syncytial virus-infected cells. *Proc. Natl. Acad. Sci. U.S.A.* **94**, 1937–1942.
- (9) Player, M. R., Maitra, R. K., Silverman, R. H., and Torrence, P. F. (1998) Targeting RNase L to human immunodeficiency virus RNA with 2-5A-antisense. *Antivir. Chem., Chemother.* **9**, 225–231.
- (10) Xiao, W., Li, G., Player, M. R., Maitra, R. K., Waller, C. F., Silverman, R. H., and Torrence, P. F. (1998) Nuclease-resistant composite 2',5'-oligoadenylate-3',5'-oligonucleotides for the targeted destruction of RNA: 2-5A-iso-antisense. *J. Med. Chem.* **41**, 1531–1539.
- (11) Verheijen, J. C., van der Marel, G. A., van Boom, J. H., Bayly, S. F., Player, M. R., and Torrence, P. F. (1999) 2',5'-Oligoadenylate-peptide nucleic acids (2-5A-PNAs) activate RNase L. *Bioorg. Med. Chem.* **7**, 449–455.
- (12) Wang, Z., Chen, L., Bayly, S. F., and Torrence, P. F. (2000) Convergent synthesis of ribonuclease L-active 2',5'-oligoadenylate-peptide nucleic acids. *Bioorg. Med. Chem. Lett.* **10**, 1357–1360.
- (13) Adah, S. A., Bayly, S. F., Cramer, H., Silverman, R. H., and Torrence, P. F. (2001) Chemistry and biochemistry of 2',5'-oligoadenylate-based antisense strategy. *Curr. Med. Chem.* **8**, 1189–1212.
- (14) Xiao, W., Li, G., Lesiak, K., Dong, B., Silverman, R. H., and Torrence, P. F. (1994) Synthesis of a 5'-thiophosphate analogue of 2-5A, a phosphatase resistant activator of the 2-5A-dependent ribonuclease. *Bioorg. Med. Chem. Lett.* **4**, 2609–2614.
- (15) Kitade, Y., Nakata, Y., Hirota, K., Maki, Y., Pabuccuoglu, A., and Torrence, P. F. (1991) 8-Methyladenosine-substituted analogues of 2-5A: synthesis and their biological activities. *Nucleic Acids Res.* **19**, 4103–4108.
- (16) Hirota, K., Kitade, Y., Kanbe, Y., and Maki, Y. (1992) Convenient method for the synthesis of C-alkylated purine nucleosides: palladium-catalyzed cross-coupling reaction of halogenopurine nucleosides with trialkylaluminums. *J. Org. Chem.* **57**, 5268–5270.
- (17) Inoue, H., Hayase, Y., Imura, A., Iwai, S., Miura, K., and Ohtsuka, E. (1987) Synthesis and hybridization studies on two complementary nona(2'-O-methyl)ribonucleotides. *Nucleic Acids Res.* **15**, 6131–6148.
- (18) Carroll, S. S., Chen, E., Viscount, T., Geib, J., Sardana, M. K., Gehman, J., and Kuo, L. C. (1996) Cleavage of oligoribonucleotides by the 2',5'-oligoadenylate-dependent ribonuclease L. *J. Biol. Chem.* **271**, 4988–4992.
- (19) Yoshimura, A., Nakanishi, M., Yatome, C., and Kitade, Y. (2002) A comparative study on the biological properties of 2',5'-oligoadenylates with purified human RNase L expressed in *E. coli*. *J. Biochem.* **132**, 643–648.
- (20) Puglisi, J. D. and Tinoco, I., Jr. In *Methods in Enzymology*; Dahlberg, J. E., and Abelson, J. N., Eds.; Academic Press, Inc.: San Diego, 1989; Vol. 180, pp 304–325.

BC020072A

# Site-Specific Fluorescent Labeling of DNA Using Staudinger Ligation

Charles C.-Y. Wang,<sup>†,§</sup> Tae Seok Seo,<sup>†</sup> Zengmin Li, Hameer Ruparel, and Jingyue Ju\*

Columbia Genome Center, Columbia University College of Physicians and Surgeons, New York, New York 10032, and Department of Chemical Engineering, Columbia University, New York, New York 10027. Received November 13, 2002; Revised Manuscript Received February 26, 2003

We report the site-specific fluorescent labeling of DNA using Staudinger ligation with high efficiency and high selectivity. An oligonucleotide modified at its 5' end by an azido group was selectively reacted with 5-[(*N*-(3'-diphenylphosphinyl-4'-methoxycarbonyl)phenylcarbonyl)aminoacetamido]fluorescein (Fam) under aqueous conditions to produce a Fam-labeled oligonucleotide with a high yield (~90%). The fluorescent oligonucleotide was characterized by matrix-assisted laser desorption/ionization time-of-flight mass spectrometry (MALDI-TOF MS). Because of the relatively high yield of the Staudinger ligation, simple purification of the product by size-exclusion chromatography and desalting is sufficient for the resulting fluorescent oligonucleotide to be used as a primer in a Sanger dideoxy sequencing reaction to produce fluorescent DNA extension fragments, which are analyzed by a fluorescent electrophoresis DNA sequencer. The results indicate that the Staudinger ligation can be used successfully and site-specifically to prepare fluorescent oligonucleotides to produce DNA sequencing products, which are detected with single base resolution in a capillary electrophoresis DNA sequencer using laser-induced fluorescence detection.

## INTRODUCTION

Selective chemical coupling methods are widely used to synthesize modified oligonucleotides for use in fundamental and applied biological research. These oligonucleotides can be used as primers for DNA sequencing (1) and polymerase chain reaction (PCR) (2), antisense agents for therapeutic applications (3), molecular beacons for detecting genetic mutations (4), and probes for measuring gene expression in DNA microarrays and gene chips (5). Several methods have been developed to couple a variety of functional groups to oligonucleotides (6). The most common method is to first synthesize modified phosphoramidites (7–10) or phosphodiester residues (11) labeled with the desired functionality and then incorporate them into DNA sequences at precise sites during automated solid-phase DNA synthesis (12). Another approach involves postsynthetic DNA modification (13). In this method, a specific chemical functional group is inserted in the DNA molecule during solid-phase synthesis, and then the group is selectively reacted with a reporter of choice in solution coupling conditions. Fluorescent oligonucleotides are often synthesized using coupling chemistry between the succinimidyl ester of a fluorophore and a primary alkylamine-modified oligonucleotide (14). However, a limitation of this technique is the requirement of aqueous conditions for the coupling reaction which can hydrolyze the succinimidyl ester. A method to address this limitation involves the direct coupling of phosphoramidite derivatives of the fluoro-

phore to oligonucleotides during the solid-phase oligonucleotide synthesis (15). However, this approach is limited to functional groups that are stable to the basic deprotection condition used in the solid-phase DNA synthesis. Therefore, there is still a need to develop a very specific coupling chemistry to modify DNA which overcomes the above limitations. Recently, we have demonstrated the use of the "Click chemistry" 1,3-dipolar cycloaddition between an alkynyl 6-carboxyfluorescein (Fam) and an azido-labeled single-stranded (ss) DNA to synthesize fluorescent DNA with a high selectivity, stability, and yield (16). We also investigated an alternative coupling chemistry for DNA modification based on Staudinger ligation that was developed by Bertozzi et al. (17, 18). This reaction allows the chemoselective formation of amide-linked products from azides and triarylphosphines. The classical Staudinger reaction (19, 20) between a phosphine and an azide produces an unstable intermediate, aza-ylide, which hydrolyzes spontaneously to form a primary amine and the corresponding phosphine oxide. To produce a stable amide-linked product, Bertozzi et al. designed a specifically engineered triarylphosphine that allows rearrangement of the unstable aza-ylide to a stable covalent adduct by intramolecular cyclization (17). This chemical reaction is highly selective and efficient and proceeds rapidly at room temperature under physiological conditions. These characteristics enabled the Staudinger ligation to chemoselectively modify cell surface (17) and proteins (21). Here, we report the synthesis of fluorescent ssDNA using the Staudinger ligation and its application as a primer in a Sanger dideoxy chain termination reaction (22) to produce DNA sequencing fragments.

## EXPERIMENTAL SECTION

**Materials and General Procedures.** 5-(Aminoacetamido)fluorescein was purchased from Molecular Probe, Inc. Amino-linker-modified oligonucleotide (5'-amino-GTT

\* To whom correspondence should be addressed. J. Ju, Room 405A Russ Berrie Medical Science Pavilion, Columbia University, College of Physicians and Surgeons, 1150 St. Nicholas Ave., New York, NY 10032. Email: dj222@columbia.edu. Phone: 212-851-5172. Fax: 212-851-5215.

<sup>†</sup> Both contributed equally to this work.

<sup>§</sup> Current address: Department of Chemistry, The University of Hong Kong, Pokfulam Road, Hong Kong, SAR, China.



TTC CCA GTC ACG ACG-3'; M13-40 universal forward sequencing primer) and an internal standard oligonucleotide for mass measurement of DNA were obtained from Midland, Inc. PD-10 column and DNA sequencing reagents were obtained from Amersham Biosciences, and an oligonucleotide purification cartridge (OPC) was obtained from Applied Biosystems. All reagents for polymerase chain reaction (PCR) and chemicals for organic synthesis were purchased from Sigma-Aldrich. UV-vis spectra of DNA samples in acetonitrile/water (1:1, v/v) were recorded on a Perkin-Elmer Lambda 40 spectrophotometer. The  $^1\text{H}$ ,  $^{13}\text{C}$ , and  $^{31}\text{P}$  NMR spectra were recorded on Bruker 300, 400, and 500 MHz NMR spectrometers.  $^{31}\text{P}$  NMR spectra were measured using 85%  $\text{H}_3\text{PO}_4$  as an external standard. High-resolution mass spectrometry (HRMS) data were obtained using a JEOL JMS HX 110A mass spectrometer. Mass measurement of oligonucleotides was performed using an Applied Biosystems Voyager DE MALDI-TOF mass spectrometer.

**Succinimidyl 5-Azidovalerate, 1.** This compound was prepared by coupling 5-azidovaleric acid (**23**) with *N*-hydroxysuccinimide mediated by 1-(3-dimethylaminopropyl)-3-ethylcarbodiimide hydrochloride (EDC) as previously described (**16**).

**Synthesis of an Azido-Labeled DNA, 2.** To incorporate the azido group at the 5'-end of the oligonucleotide, 10 nmol of the amino-modified oligonucleotide in 40  $\mu\text{L}$  of 0.25 M  $\text{Na}_2\text{CO}_3/\text{NaHCO}_3$  buffer (pH 9.0) was incubated for 12 h at room temperature with 10  $\mu\text{mol}$  of succinimidyl 5-azidovalerate **1** in 12  $\mu\text{L}$  of dimethyl sulfoxide. The azido-labeled DNA was purified as described previously (**16**) with an isolated yield of 96%.

**Succinimidyl 3-Diphenylphosphino-4-methoxycarbonylbenzoate, 3.** 3-Diphenylphosphino-4-methoxycarbonylbenzoic acid (216 mg, 0.593 mmol) (**17**), dicyclohexylcarbodiimide (DCC) (129 mg, 0.623 mmol), and *N*-hydroxysuccinimide (NHS) (72 mg, 0.623 mmol) were dissolved in diethyl ether (20 mL) under Ar and stirred overnight at room temperature. After the diethyl ether solvent was evaporated, the yellow crystalline product was isolated by filtration. Recrystallization from 2-propanol (20 mL) yielded 164 mg (60%) of **3** as yellow crystals.  $^1\text{H}$  NMR ( $\text{CDCl}_3$ , 400 MHz)  $\delta$  8.15 (s, 2H), 7.67 (d, 1H,  $J = 3.2$  Hz), 7.39–7.22 (m, 10H), 3.75 (s, 3H), 2.82 (s, 4H,  $\text{COCH}_2\text{CH}_2\text{CO}$ );  $^{13}\text{C}$  NMR ( $\text{CDCl}_3$ , 75 MHz)  $\delta$  169.4 ( $\text{COCH}_2\text{CH}_2\text{CO}$ ), 166.7, 161.5, 143.0, 142.6, 140.1, 139.9, 137.0, 136.8, 136.6, 134.5, 134.2, 131.3, 130.2, 129.6, 129.2, 129.1, 128.1, 53.0, 26.0 ( $\text{COCH}_2\text{CH}_2\text{CO}$ );  $^{31}\text{P}$  NMR ( $\text{CDCl}_3$ , 121 MHz)  $\delta$  -3.05; HRMS ( $\text{FAB}^+$ ) Calcd for  $\text{C}_{25}\text{H}_{21}\text{O}_6\text{NP}$ , 462.1107 ( $\text{M} + \text{H}$ ) $^+$ ; found, 462.1093.

**5-[(*N*-(3'-Diphenylphosphinyl-4'-methoxycarbonyl)phenylcarbonyl)aminoacetamido]fluorescein, 4.** The FAM-tethered triphenylphosphine **4** was prepared by mixing a 1:0.8 ratio of 5-(aminoacetamido)fluorescein (5 mg, 12.3  $\mu\text{mol}$ ) and **3** (4.5 mg, 10  $\mu\text{mol}$ ) in 1 mL of DMF under argon at room temperature. After reacting for 12 h, the solvent was evaporated under vacuum. The residue was chromatographed on a silica gel plate in  $\text{CHCl}_3/\text{MeOH}$  (9:1), yielding **4** quantitatively.  $^1\text{H}$  NMR ( $\text{CD}_3\text{OD}$ , 500 MHz)  $\delta$  8.21 (d, 1H,  $J = 1.6$  Hz), 8.05 (dd, 1H,  $J = 3.4$ , 4.6 Hz), 7.85 (dd, 1H,  $J = 1.4$ , 6.5 Hz), 7.70 (dd, 1H,  $J = 1.9$ , 6.4 Hz), 7.48 (dd, 1H,  $J = 1.5$ , 2.1 Hz), 7.25–7.30 (m, 6H), 7.19–7.24 (m, 4H), 7.07 (d, 1H,  $J = 8.3$  Hz), 6.58–6.62 (m, 4H), 6.49 (d, 1H,  $J = 2.4$  Hz), 6.47 (d, 1H,  $J = 2.4$  Hz), 4.2 (s, 2H), 3.62 (s, 3H);  $^{13}\text{C}$  NMR ( $\text{CD}_3\text{OD}$ , 100 MHz)  $\delta$  175.0, 171.4, 169.9, 169.6, 168.4, 168.3, 154.5, 142.6, 142.3, 141.5, 138.7, 138.6, 138.5, 138.1, 135.2, 134.9, 134.7, 131.6, 131.5, 130.4, 130.1, 129.7, 129.5, 127.9, 127.6, 126.2, 116.6, 114.3, 111.8,

103.5, 52.6, 44.6, 26.7;  $^{31}\text{P}$  NMR ( $\text{CD}_3\text{OD}$ , 121 MHz)  $\delta$  -3.00; HRMS ( $\text{FAB}^+$ ) Calcd for  $\text{C}_{43}\text{H}_{32}\text{O}_9\text{N}_2\text{P}$ , 751.7088 ( $\text{M} + \text{H}$ ) $^+$ ; found, 751.7115.

**Fam-Labeled DNA, 5.** A DMF solution (30  $\mu\text{L}$ ) of **4** (0.4 mg, 0.5  $\mu\text{mol}$ ) was added to a solution of 2.4 nmol of the azido-labeled DNA **2** in 100  $\mu\text{L}$  of 0.25 M  $\text{Na}_2\text{CO}_3/\text{NaHCO}_3$  buffer (pH 9.0) solution in a 500  $\mu\text{L}$  Eppendorf tube. The tube was shaken for 12 h at room temperature on a shaker, and then the sample was purified by passing through a PD10 size-exclusion column followed by desalting with an OPC column. Calculation of concentration based on the absorbance at 260 nm indicated that DNA was collected with  $\sim 90\%$  yield. The sample was characterized by MALDI-TOF mass spectrometry, which showed that a majority of the sample gave a single peak at 6463 Da (calcd value for **5**: 6464 Da).

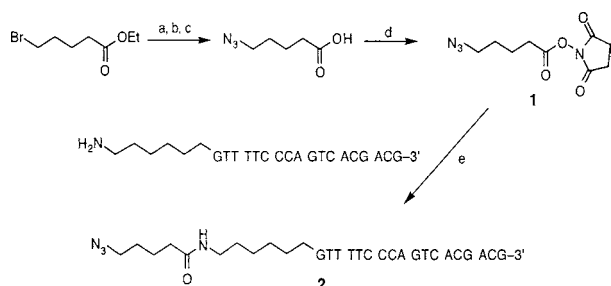
**Mass Spectrum of DNA.** 30 pmol of the DNA product was mixed with 10 pmol of the internal mass standard and the mixture was suspended in 2  $\mu\text{L}$  of 3-hydroxypicolinic acid matrix solution. 0.5  $\mu\text{L}$  of this mixture was spotted on a stainless steel sample plate, air-dried and analyzed. The measurement was taken using a positive ion mode with 25 kV accelerating voltage, 94% grid voltage, and a 350 ns delay time.

**PCR Amplification of DNA Template.** A PCR DNA product amplified from a pBluescript II SK(+) phagemid vector was used as a sequencing template, as it has a binding site for M13-40 universal primer. Amplification was carried out using the M13-40 universal forward and reverse primers in a 20  $\mu\text{L}$  reaction, which contained 1X Accutag LA Reaction Buffer, 250 pmol of each dNTP, 40 pmol of each primer, 0.5 units of Jumpstart Red Accutag LA DNA Polymerase, and 100 ng of the phagemid template. The reaction was performed in a DNA thermal cycler using an initial activation step of 96  $^\circ\text{C}$  for 1 min. This was followed by 30 cycles of 94  $^\circ\text{C}$  for 30 s, 50  $^\circ\text{C}$  for 30 s, and 72  $^\circ\text{C}$  for 2 min. At the end of the PCR reaction, 20  $\mu\text{L}$  of an enzymatic mixture containing 5 units of shrimp alkaline phosphatase (SAP), 4  $\mu\text{L}$  of 10X SAP buffer, 6 units of *E. coli* exonuclease I, and 10  $\mu\text{L}$  of water was added to the PCR reaction to degrade the excess primers and dNTPs. The reaction mixture was incubated at 37  $^\circ\text{C}$  for 90 min and then heated at 72  $^\circ\text{C}$  for 30 min to inactivate the enzymes.

**Generation and Detection of Sanger DNA Sequencing Fragments.** A Sanger DNA sequencing reaction was performed using the FAM-labeled DNA **5** as a primer and the above PCR product as a template. A 30  $\mu\text{L}$  reaction mixture was made, consisting of 2.22 nmol of each of the dNTPs (A, C, G, T), 37 pmol of Biotin-11-ddATP (Perkin-Elmer), 20 pmol of primer, 9 units of Thermo Sequenase DNA polymerase, 1X Thermo Sequenase Reaction Buffer, and 20  $\mu\text{L}$  of PCR product. The reaction consisted of 30 cycles of 94  $^\circ\text{C}$  for 20 s, 50  $^\circ\text{C}$  for 20 s, and 60  $^\circ\text{C}$  for 90 s. DNA fragments correctly terminated by Biotin-11-ddATP were purified from other reaction components using solid-phase capture according to the published method (**24**). The fluorescent DNA fragments in 8  $\mu\text{L}$  of formamide were electrokinetically injected at 3 kV into a capillary filled with linear polyacrylamide (LPA) gel in a capillary array fluorescent DNA sequencer (Amersham), and then separated at 8kV in LPA buffer to produce a fluorescence electropherogram.

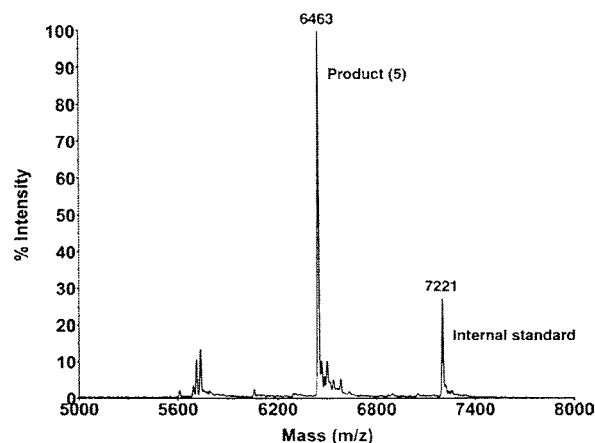
## RESULTS AND DISCUSSION

Succinimidyl 5-azidovalerate **1** was reacted with the amino-linker modified oligonucleotide (5'-amino-GTT

Scheme 1<sup>a</sup>

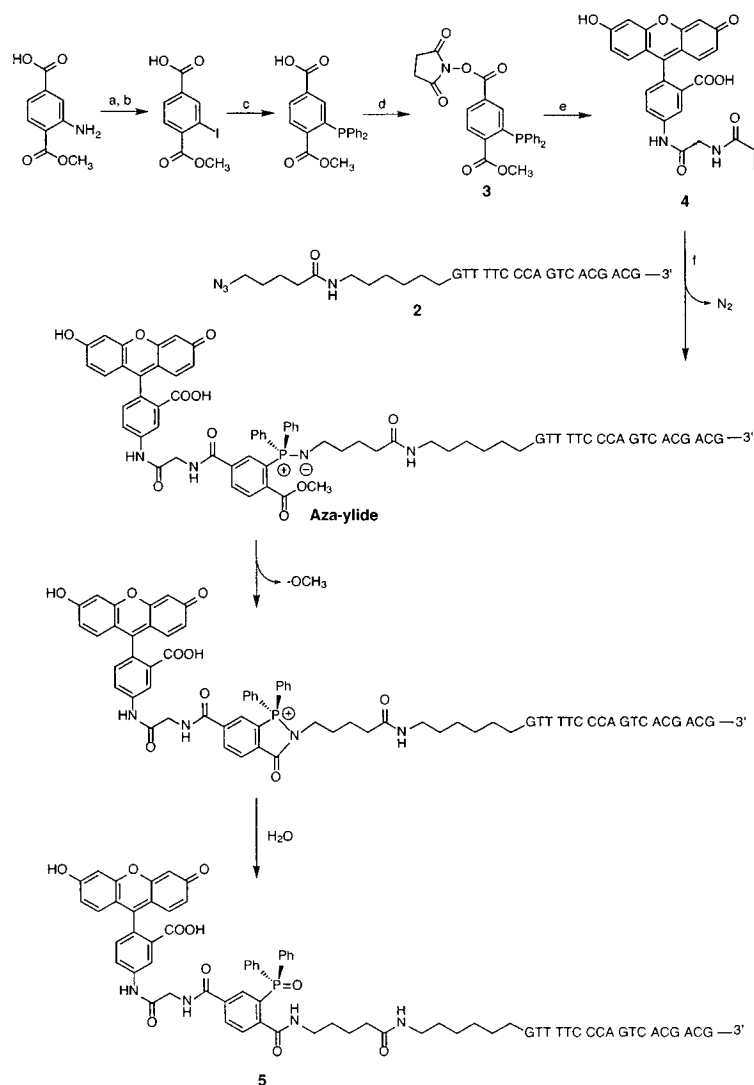
<sup>a</sup> Reagents: (a) NaN<sub>3</sub>, DMSO; (b) NaOH, MeOH, H<sub>2</sub>O; (c) HCl; (d) *N*-hydroxysuccinimide, 1-(3-dimethylaminopropyl)-3-ethylcarbodiimide hydrochloride, CH<sub>2</sub>Cl<sub>2</sub>; (e) Na<sub>2</sub>CO<sub>3</sub>/NaHCO<sub>3</sub> buffer (pH 9.0), DMSO.

TTC CCA GTC ACG ACG-3') to produce the azido-labeled DNA **2** with a 96% yield (Scheme 1) (16). The MALDI-TOF MS spectrum of **2** shows a single major peak at 5757 Da (calcd value for **2**: 5758 Da). 3-Diphenylphosphino-4-methoxycarbonylbenzoic acid was prepared according to the procedure described by Bertozzi et al. (17). Treatment of 3-diphenylphosphino-4-methoxycarbonylbenzoic acid with *N*-hydroxysuccinimide forms the corresponding NHS ester **3**. The reaction of **3** with 5-(aminoacetamido)-

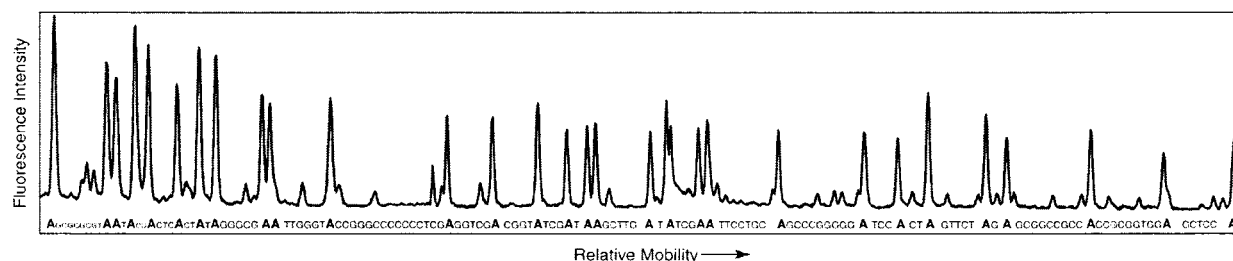


**Figure 1.** MALDI-TOF mass spectrum of **5**.

fluorescein produced FAM-tethered triphenylphosphine **4** which was then coupled with the azido-modified oligonucleotide **2** to form Fam-labeled DNA **5** (Scheme 2). During the Staudinger ligation between **2** and **4**, an azaylide intermediate was first formed by the nucleophilic attack of the phosphine on the azide accompanied by the release of N<sub>2</sub>. A methoxycarbonyl group situated on one

Scheme 2<sup>a</sup>

<sup>a</sup> Reagents: (a) NaNO<sub>2</sub>, HCl, H<sub>2</sub>O; (b) KI, H<sub>2</sub>O; (c) Ph<sub>2</sub>PH, Pd(AcO)<sub>2</sub>, triethylamine, MeOH; (d) *N*-hydroxysuccinimide, DCC; (e) 5-(aminoacetamido)fluorescein, DMF; (f) Na<sub>2</sub>CO<sub>3</sub>/NaHCO<sub>3</sub> buffer (pH 9.0), DMF.



**Figure 2.** Electropherogram of the DNA sequencing fragments generated with **5**.

of the aryl rings of the phosphine traps the aza-ylide in a five-membered ring intermediate, resulting in an amide-linked phosphine oxide **5** after hydrolysis (18). The Fam-labeled DNA **5** was purified by size-exclusion chromatography and then desalted with an OPC column. The collected DNA was examined by UV/Vis spectrophotometry, and the yield of the DNA **5** was found to be 90% based on the absorbance at 260 nm. In the UV/vis spectrum of **5**, in addition to the peak at 260 nm, there is a strong peak centered at 496 nm, indicating that the Fam moiety **4** was successfully coupled to the DNA by the Staudinger ligation. The product **5** was characterized by MALDI-TOF mass spectrometry, and the result is shown in Figure 1. In the presence of an internal mass standard (7221 Da), the mass spectrum of the modified DNA product revealed that a majority of the Staudinger ligation product had a mass value of 6463 Da, that matched well with the theoretical value of 6464 Da for **5**.

To demonstrate the utility of **5** for genetic analysis, we used the Fam-labeled oligonucleotide **5** as a primer in a Sanger dideoxy DNA sequencing reaction to produce DNA sequencing fragments terminated by biotinylated dideoxyadenine triphosphate (ddATP-biotin). The reaction mixture consisted of all four dNTPs (A, C, G, T) along with a biotinylated ddATP. Consequently, the resulting DNA sequencing fragments were all terminated with an 'A' at the 3' end and labeled with a fluorophore (Fam) at the 5' end. Solid-phase capture using streptavidin-coated magnetic beads allows the isolation of pure DNA extension fragments free from false terminations and other components of the sequencing reaction (24). The purified DNA fragments were separated in a capillary electrophoresis fluorescent DNA sequencer and resolved to produce an electropherogram as shown in Figure 2. The peaks represent the Fam fluorescence emission from each DNA fragment that was extended from **5** and terminated by ddATP. This "A" sequencing ladder shown in Figure 2 matched exactly with the sequence of the DNA template.

In conclusion, we have synthesized a fluorescent oligonucleotide by the Staudinger ligation with a high yield and selectivity. Without the requirement of conventional purification methods, such as gel electrophoresis or HPLC, simple purification by size-exclusion chromatography and desalting of the product is sufficient for the resulting fluorescent oligonucleotide to be used as a primer in a Sanger dideoxy sequencing reaction to produce fluorescent DNA extension fragments, which were subsequently analyzed by a fluorescent electrophoresis DNA sequencer. The results indicate that the Staudinger ligation can be used successfully and site-specifically to prepare fluorescent oligonucleotide to produce DNA sequencing products, which are detected with single base resolution in a capillary electrophoresis DNA sequencer using laser-induced fluorescence detection. Since the amide bond formed by the Staudinger

ligation that couples a fluorophore to the oligonucleotide is very stable, the relatively high temperature of 94 °C used in DNA cycle sequencing caused no degradation of the DNA. It is expected that the Staudinger ligation can also be used to site-specifically introduce other functional groups to DNA for PCR-based genetic analysis as well as for selective covalent attachment of DNA on a solid surface.

#### ACKNOWLEDGMENT

This research is supported by the National Science Foundation Biophotonics Partnership Initiative Grant 86933 and Sensing and Imaging Initiative Grant 97793.

#### LITERATURE CITED

- (1) (a) Smith, L. M., Sanders, J. Z., Kaiser, R. J., Hughes, P., Dodd, C., Connell, C. R., Heiner, C., Kent, S. B. H., and Hood, L. E. (1986) Fluorescence detection in automated DNA sequence analysis. *Nature* 321, 674–679. (b) Ju, J., Ruan, C., Fuller, C. W., Glazer, A. N., and Mathies, R. A. (1995) Fluorescence energy transfer dye-labeled primers for DNA sequencing and analysis. *Proc. Natl. Acad. Sci. U.S.A.* 92, 4347–4351.
- (2) Mullis, K. B., and Faloona, F. A. (1987) Specific synthesis of DNA in Vitro via a polymerase-catalyzed chain reaction. *Methods Enzymol.* 155, 335–350.
- (3) Uhlmann, E., and Peyman, A. (1990) Antisense oligonucleotides: A new therapeutic principle. *Chem. Rev.* 90, 543–584.
- (4) Tyagi, S., and Kramer, F. R. (1996) Molecular Beacons: probes that fluoresce upon hybridization. *Nat. Biotechnol.* 14, 303–308.
- (5) (a) Schena, M., Shalon, D., Davis, R. W., and Brown, P. O. (1995) Quantitative monitoring of gene expression patterns with a complementary DNA microarray. *Science* 270, 467–470. (b) Fodor, S. P., Read, J. L., Pirrung, M. C., Stryer, L., Lu, A. T., and Solas, D. (1991) Light-directed, spatially addressable parallel chemical synthesis. *Science* 251, 767–773.
- (6) (a) Goodchild, J. (1990) Conjugates of oligonucleotides and modified oligonucleotides: A review of their synthesis and properties. *Bioconjugate Chem.* 1, 165–187. (b) Verma, S., and Eckstein, F. (1998) Modified oligonucleotides: Synthesis and strategy for users. *Annu. Rev. Biochem.* 67, 99–134. (c) Beaucage, S. L., and Iyer, R. P. (1993) The functionalization of oligonucleotides via phosphoramidite derivatives. *Tetrahedron* 49, 1925–1963.
- (7) Khan, S. I., and Grinstaff, M. W. (1999) Palladium(0)-catalyzed modification of oligonucleotides during automated solid-phase synthesis. *J. Am. Chem. Soc.* 121, 4704–4705.
- (8) Kahl, J. D., and Greenberg, M. M. (1999) Introducing Structural Diversity in oligonucleotides via photolabile, convertible C5-substituted nucleotides. *J. Am. Chem. Soc.* 121, 597–604.
- (9) Xu, Y., Zheng, Q., and Swann, P. F. (1992) Synthesis of DNA containing modified bases by postsynthetic substitution. Synthesis of oligomers containing 4-substituted thymine: O4-Alkylthymine, 5-methylcytosine, N4-(dimethylamino)-5-methylcytosine, and 4-thiothymine. *J. Org. Chem.* 57, 3839–3845.



- (10) Hwang, J., and Greenberg, M. M. (2001) Synthesis of 2'-modified oligodeoxynucleotides via on-column conjugation. *J. Org. Chem.* **66**, 363–369.
- (11) Fidanza, J. A., Ozaki, H., and McLaughlin, L. W. (1992) Site-specific labeling of DNA sequences containing phosphorothioate diesters. *J. Am. Chem. Soc.* **114**, 5509–5517.
- (12) Caruthers, M. H. (1985) Gene synthesis machines: DNA chemistry and its use. *Science* **230**, 281–285.
- (13) Dey, S., and Sheppard, T. L. (2001) Ketone-DNA: A versatile postsynthetic DNA decoration platform. *Org. Lett.* **3**, 3983–3986.
- (14) Chehab, F. F., and Kan, Y. W. (1989) Detection of specific DNA sequences by fluorescence amplification: a color complementation assay. *Proc. Natl. Acad. Sci. U.S.A.* **86**, 9178–9182.
- (15) (a) Adamczyk, M., Chan, C. M., Fino, J. R., and Mattingly, P. G. (2000) Synthesis of 5- and 6-hydroxymethylfluorescein phosphoramidites. *J. Org. Chem.* **65**, 596–601. (b) Lyttle, M. H., Walton, T. A., Dick, D. J., Carter, T. G., Beckman, J. H., and Cook, R. M. (2002) New reagents and methods for the synthesis of internal and 3'-labeled DNA. *Bioconjugate Chem.* **13**, 1146–1154. (c) Theisen, P., McCollum, C., Upadhy, K., Jacobson, K., Vu, H., and Andrus, A. (1992) Fluorescent dye phosphoramidite labeling of oligonucleotides. *Tetrahedron Lett.* **33**, 5033–5036.
- (16) Seo, T. S., Li, Z., Ruparel, H., and Ju, J. (2003) Click chemistry to construct fluorescent oligonucleotides for DNA sequencing. *J. Org. Chem.* **68**, 609–612.
- (17) Saxon, E., and Bertozzi, C. R. (2000) Cell surface engineering by a modified Staudinger reaction. *Science* **287**, 2007–2010.
- (18) Saxon, E., Armstrong, J. I., and Bertozzi, C. R. (2000) A traceless Staudinger ligation for the chemoselective synthesis of amide bonds. *Org. Lett.* **2**, 2141–2143.
- (19) Staudinger, H., and Meyer, J. (1919) Über neue organische phosphorverbindungen III. Phosphinmethylenederivate und phosphinimine. *Helv. Chim. Acta* **2**, 635–646.
- (20) Gololobov, Y. G., and Kasukhin, L. F. (1992) Recent advances in the Staudinger reaction. *Tetrahedron* **48**, 1353–1406.
- (21) Kiick, K. L., Saxon, E., Tirrell, D. A., and Bertozzi, C. R. (2002) Incorporation of azides into recombinant proteins for chemoselective modification by the Staudinger ligation. *Proc. Natl. Acad. Sci. U.S.A.* **99**, 19–24.
- (22) Sanger, F., Nicklen, S., and Coulson, A. R. (1977) DNA sequencing with chain-terminating inhibitors. *Proc. Natl. Acad. Sci. U.S.A.* **74**, 5463–5467.
- (23) McGeary, R. P. (1998) Facile and chemoselective reduction of carboxylic acids to alcohols using BOP reagent and sodium borohydride. *Tetrahedron Lett.* **39**, 3319–3322.
- (24) Ju, J. (2002) DNA sequencing with solid-phase-capturable dideoxynucleotides and energy transfer primers. *Anal. Biochem.* **309**, 35–39.

BC0256392

## COMMUNICATIONS

---

### Fibronectin-Based Masking Molecule Blocks Platelet Adhesion

David H. Geho,<sup>\*,†</sup> William I. Smith, Jr.,<sup>§</sup> Lance A. Liotta,<sup>†,‡</sup> and David D. Roberts<sup>†,‡</sup>

Laboratory of Pathology, National Cancer Institute, National Institutes of Health, Bethesda, Maryland 20892, and Department of Pathology, Suburban Hospital, Bethesda, Maryland 20814. Received March 12, 2003

---

Vessel wall extracellular matrix, which underlies the endothelium, is a potent stimulator of platelet adhesion and activation. Exposure of this matrix can result from damage incurred by vascular interventions, such as saphenous vein bypass grafting and angioplasty. Fibrillar collagens are an important component of the thrombogenic extracellular matrix. Herein we describe a means of targeting poly(ethylene glycol) (PEG)-mediated blockade directly to platelet-binding ECM molecules, such as type I collagen, thereby selectively blocking platelet adhesion to vascular matrix. Purified fibronectin (FN), a matrix protein that interacts with fibrillar collagens and platelets, was selectively pegylated to generate a targeted molecular shielding reagent that masked ECM ligands from platelet recognition and adhesion. This approach protects the functions of other vascular proteins, including surface proteins on intact endothelium. To mask the platelet-binding site of FN, PEG-propyl moieties (5000 Da) were covalently appended to lysine residues on the surface of FN, generating FNPEG-5K. To preserve the collagen-binding function of FN, it was pegylated while bound to a gelatin agarose matrix. We demonstrate that FNPEG-5K blocks platelet adhesion to purified type I collagen. Moreover, the same preparation blocks platelet adhesion to vascular wall components, including collagens.

---

#### INTRODUCTION

Platelet adhesion to extracellular matrix (ECM)<sup>1</sup> proteins exposed by damage incurred during vascular pro-

cedures can lead to thrombotic occlusions at the intervention sites (1). A number of vascular ECM proteins contribute to platelet adhesion, including collagens and fibronectin (FN) (2, 3). Herein we describe a means of targeting poly(ethylene glycol) (PEG)-mediated blockade directly to platelet-binding ECM molecules, thereby selectively blocking platelet adhesion to vascular matrix. Purified FN, a matrix protein that interacts with fibrillar collagens and platelets, was selectively pegylated to generate a targeted molecular shielding reagent that masked ECM ligands from platelet recognition and adhesion<sup>2</sup> (3–5). This approach protects the functions of other vascular proteins, including surface proteins on intact endothelium.

---

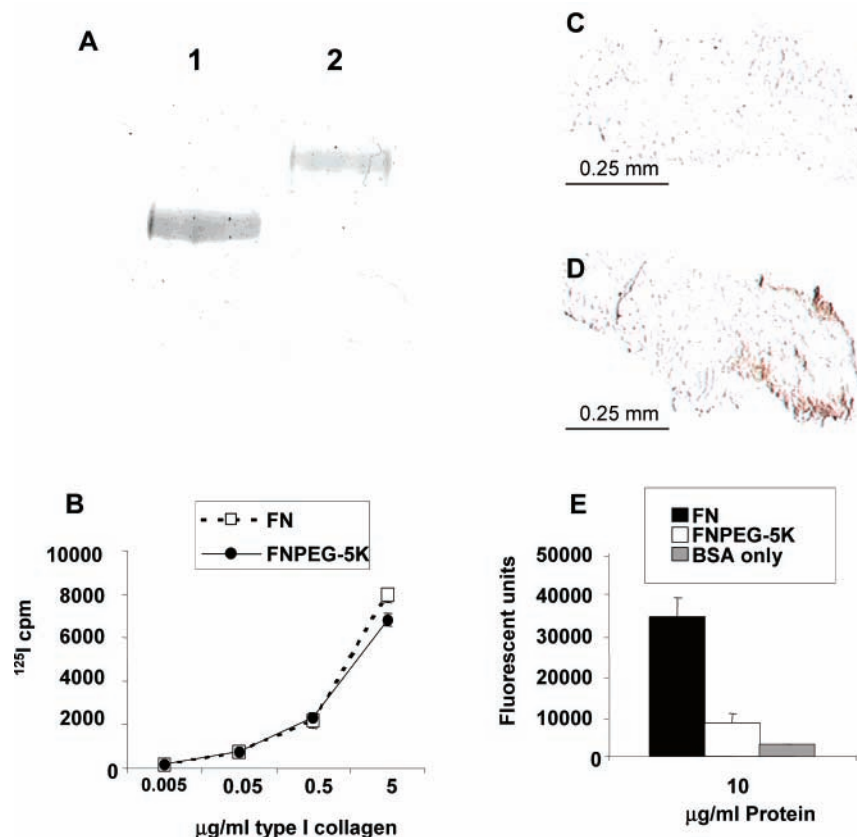
\* Correspondence: David Geho, Laboratory of Pathology, NCI, Building 10-2N212, 10 Center Drive, Bethesda, MD 20892. Telephone: 301-594-2944. Fax: 301-480-9488. E-mail: gehod@mail.nih.gov.

<sup>†</sup> National Institutes of Health.

<sup>§</sup> Suburban Hospital.

<sup>‡</sup> Both of these senior authors contributed equally to this investigation.

<sup>1</sup> Extracellular matrix (ECM), fibronectin (FN), phosphate buffer saline (PBS), poly(ethylene glycol) (PEG), bovine serum albumin (BSA), Tyrode's calcium-free buffer (TCFB), prostaglandin E<sub>1</sub> (PGE<sub>1</sub>).



**Figure 1.** FNPEG-5K binds collagen, lacks platelet binding properties, and binds to blood vessels. (A) FN (lane 1, 2  $\mu$ g) and FNPEG-5K (lane 2, 2  $\mu$ g) were run on a reducing 7.5% SDS-PAGE and stained with Coomassie blue. FN migrated at  $M_r$  220 000. (B) Binding of iodinated native (□) or modified FN (●) to type I collagen coated wells. (C and D) A human vein was incubated with FNPEG-5K that contained biotinylated PEG moieties, and biotin reactivity resulting from FNPEG-5K adherence was probed. (C) No FNPEG-5K added to tissue (negative control). (D) Biotinylated FNPEG-5K (10  $\mu$ g/mL). (E) Binding of fluorescently labeled platelets to plate bound FN and FNPEG-5K. The results shown for experiments B and E are representative of three similar experiments for each, mean  $\pm$  SD; C and D are representative of two similar experiments.

To derive an ECM-targeted masking molecule from FN, we neutralized its ability to bind platelets while protecting its collagen-binding properties (2, 3). Covalent addition of PEG residues to protein surfaces can inhibit undesirable interactions, such as stimulating an immune response (6). Accordingly, modification of lysines present on the surface of plasma FN with mPEG-propionaldehyde via reductive amination (7, 8) provided a means to neutralize its platelet adhesive function. In order for FNPEG-5K to be a targeted masking molecule, it needed

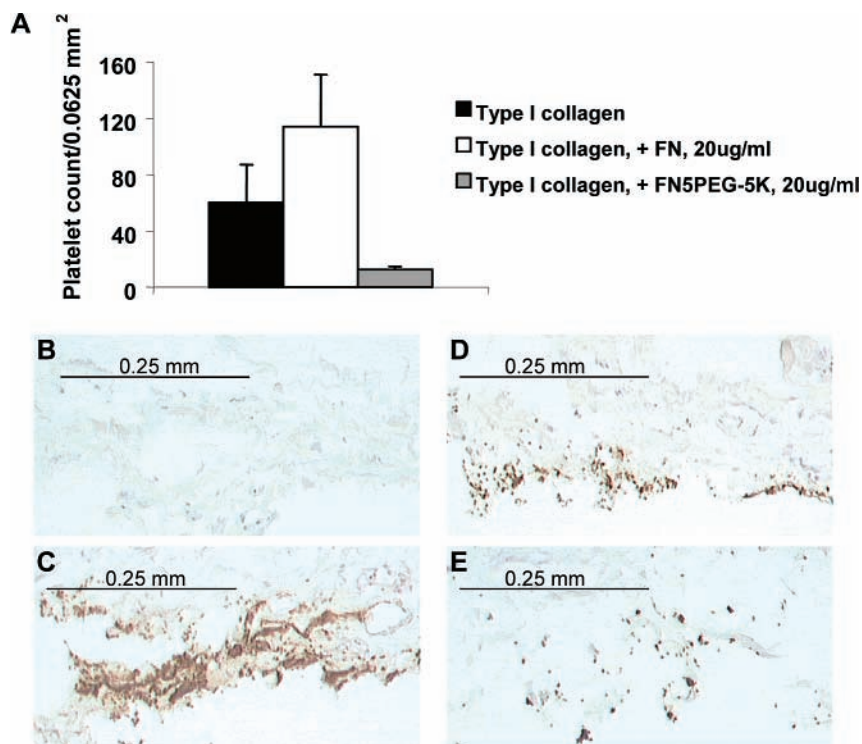
to retain its binding activity for fibrillar collagen in the subendothelial matrix. An immobilized substrate was used previously to protect enzyme active sites from modification during pegylation (9). Gelatin, which is a denatured form of type I collagen, binds FN with a higher affinity than native collagen (4). Purified plasma FN, therefore, was bound to a gelatin agarose affinity matrix during pegylation (5). SDS-PAGE assessment showed that FNPEG-5K prepared in this manner migrated more slowly than native FN, consistent with the addition of PEG moieties (Figure 1A).

Conditions for the pegylation of FN were optimized to minimize platelet adhesion and preserve collagen binding by varying the duration of derivatization and the concentrations of both mPEG-propionaldehyde and sodium cyanoborohydride. A fluorescamine assay indicated that 25–30% of available lysines were pegylated using optimal reaction conditions (10). In binding studies, iodinated FNPEG-5K bound plate-immobilized collagen in a manner similar to native FN (Figure 1B).<sup>3</sup> Thus, the key collagen-binding properties of FN were selectively protected by this targeted modification approach. A biotinylated form of FNPEG-5K was incubated with a human blood vessel that had been stretched to induce injury to confirm that FNPEG-5K retained binding to exposed blood vessel wall components (Figure 1C,D).<sup>4</sup>

Having FNPEG-5K in hand, we next tested whether the PEG moieties inhibited platelet adhesion (Figure 1E)<sup>5</sup> (11, 12). Unlike native FN, immobilized FNPEG-5K did not mediate adhesion of platelets. The cell-binding domain of FN contains an RGD sequence as well as a

<sup>2</sup> Human FN was purified from human plasma using a previously described protocol (see ref 5). Briefly, human plasma was applied to a sepharose CL-4B column and then directly applied to a gelatin agarose matrix that had been pretreated by washing with 4 M urea, 10 mM Tris-HCl, pH 7, followed by equilibration with phosphate-buffered saline (PBS). The column was then washed with 1 M NaCl in PBS followed by washing with plain PBS. FN was then eluted by using an acidic buffer (0.1 M NaCl, 0.05 M citric acid, pH 5.5) and neutralized by adding 1.0 M Na<sub>2</sub>HPO<sub>4</sub> at 1/20th volume. Protein concentrations were measured using a bicinchoninic acid kit. To make FNPEG-5K, purified FN was bound to gelatin agarose followed by the addition of 8 mg/mL sodium cyanoborohydride and 32 mg/mL of monomethyl poly(ethylene glycol) (PEG)-propionaldehyde 5 kDa (Shearwater, Huntsville, AL) in 0.1 M sodium phosphate buffer (pH 8.0). After at least 16 h, the protein was eluted. For biotinylated FNPEG-5K, biotin-PEG-NHS (3400 Da) (Shearwater) was incubated with gelatin-immobilized FN for 1 h followed by pegylation as above. To assess the extent of pegylation, FN and FNPEG-5K were compared by 7.5% Tris-HCl SDS-PAGE and a fluorescamine assay using a standard protocol (see ref 10).





**Figure 2.** FNPEG-5K inhibits platelet adhesion. (A) Soluble FN or FNPEG were bound to immobilized type I collagen. After being washed and blocked, platelets were incubated for 30 min. After repeated washings, adherent platelets were fixed with glutaraldehyde, stained, and counted. The level of background binding of platelets to blocked plastic was below 5% in the experiment shown. The result shown is representative of three similar experiments, mean  $\pm$  SD. (B, C, D, E) Human ileac artery autopsy specimens were coated with FNPEG-5K and then incubated with biotinylated platelets. After unbound platelets were washed away, frozen sections of the tissues were made, and biotin reactivity resulting from platelet adherence was probed. (B) No FNPEG-5K and no platelets added to tissue (negative control). (C) Only biotinylated platelets added (positive control). (D) FNPEG-5K (30  $\mu$ g/mL) and platelets added. (E) FNPEG-5K (60  $\mu$ g/mL) and platelets added. The results shown in B, C, D, and E are representative of two similar experiments.

number of residues that contribute to an electrostatic interaction with the platelet integrins (13). PEG residues attached to the cell-binding domain may sterically hinder

<sup>3</sup> **Fibronectin- $^{125}$ I Binding Assay.** Iodinated FN was added to gelatin agarose, equilibrated as above, and incubated, rotating for 1 h at room temperature. Following this incubation, the supernatant was removed and a reaction mixture containing 4 mg/mL NaCNBH<sub>3</sub> and 8 mg/mL of mPEG-propionaldehyde 5kDa diluted in 0.1 M Na<sub>2</sub>HPO<sub>4</sub> buffer, pH 8.0, was added and rotated overnight for 16 h at room temperature. Following this incubation, the protein was eluted as before. Equivalent counts of native Fn-I<sup>125</sup> and Fn-I<sup>125</sup> PEG-5K were added to Immulon 2 wells that had been precoated with type I collagen (Vitrogen 100, Collagen Corporation, Palo Alto, CA) overnight at 4 °C followed by 1 h blocking with 1% BSA in DPBS at room temperature. After an incubation at 4 °C for 3 h, the wells were washed and aspirated twice with 100  $\mu$ L of DPBS. The wells were then collected and counted in a gamma counter.

<sup>4</sup> **Binding Experiments with Blood Vessels.** Blood vessels were obtained from either autopsy specimens or anonymized samples from excess surgical material. The National Institutes of Health Office of Human Subjects Research deems these types of specimens exempt. The vessels were dissected, damaged by lightly stretching the vessel during handling, and incubated in 0.5% BSA. Depending on the experiment, FNPEG-5K or a biotinylated form of FNPEG-5K was added to the vessels. After an incubation of at least 30 min, the vessel pieces were washed three times with PBS. For vessels treated with nonbiotinylated FNPEG-5K, platelets that had been labeled with sulfo-succinimidyl-6-(biotinamido)hexanoate were then added to the vessels. After 30 minutes, the nonadhered platelets were removed by three washes. The vessels were fixed with glutaraldehyde and processed as frozen sections. The slides were rinsed and probed for biotin reactivity using Vectalabs Elite ABC and DAB kits (Vector Laboratories, Burlingame, CA).

these interactions between FNPEG-5K and platelet integrins, leading to a loss of platelet binding.

Since modified FNPEG-5K retained the collagen-binding properties of native FN while lacking its intrinsic platelet adhesive properties, the ability of FNPEG-5K

<sup>5</sup> **Plastic-based Platelet Adhesion Assays.** On the basis of a previously published protocol (see ref 11), Immulon 1B 96-well plates were coated with FN or FNPEG-5K and blocked with 100  $\mu$ L of Tyrode's calcium-free buffer (140 mM NaCl, 3 mM KCl, 12 mM NaHCO<sub>3</sub>, 0.4 mM NaH<sub>2</sub>PO<sub>4</sub>·H<sub>2</sub>O, 1 mM MgCl<sub>2</sub>·6 H<sub>2</sub>O, 0.35% BSA, 0.1% glucose, pH 7.33) (TCFB) with 3% BSA and 20 ng/mL prostaglandin E<sub>1</sub> (PGE<sub>1</sub>). The wells were then washed three times with TCFB. Platelets, approved for use under the National Institutes of Health IRB protocol 99CC0168, were retrieved from the blood bank and resuspended in TCFB (1  $\times$  10<sup>9</sup>/mL) with 24  $\mu$ g/mL of 5-(and-6)-carboxyfluorescein diacetate succinimidyl ester (Molecular Probes, Eugene, OR), 20 ng/mL PGE<sub>1</sub>, and 130  $\mu$ g/mL apyrase and incubated for at least 30 min at 37 °C (see ref 12). Another incubation followed for 10 min at 37 °C in TCFB with 20 ng/mL PGE<sub>1</sub>. After being washed, the platelets were incubated in FN-coated wells and then washed multiple times, and the plate was read using a spectrofluorimeter plate reader with excitation of 485 nm and emission of 535 nm. For platelet/collagen binding assays, Falcon 1008 plastic dishes were coated with 6  $\mu$ L drops of type I collagen. The plates were washed, and then FN or FNPEG-5K was added for at least 1 h at room temperature followed by aspiration and blocking with TCFB (1% BSA, 20ng/mL PGE<sub>1</sub>). Two mL of platelets (prepared as before except for fluorescent label) in TCFB (20 million/mL) were added to the dish and incubated for 30 to 40 min at room temperature. Unbound platelets were then washed away and the bound platelets were fixed with 1% glutaraldehyde. The bound platelets were stained with DiffQuick (Dade Behring AG, Dudenggen, Switzerland) and counted.

to inhibit platelet adherence to type I collagen, a key ECM component, was investigated (Figure 2A). Although native FN enhanced platelet adhesion to a collagen-coated substrate, FNPEG-5K potently and dramatically protected type I collagen from platelet binding. In a similar manner, the adventitia of blood vessels, a rich source of type I collagen, were incubated with FNPEG-5K, followed by incubation with biotinylated platelets (14). The platelets bound readily to adventitial vascular wall components (Figure 2C). In contrast, preincubation of FNPEG-5K with the blood vessel markedly decreased, in a dose-dependent manner, the number of platelets that adhered to the blood vessel wall (Figure 2D,E). Thus, coating with FNPEG-5K protects vessel wall components from platelet adhesion.

In this communication, we describe a method for transforming native FN from a platelet-binding protein into FNPEG-5K, a targeted molecular shielding reagent that masks ECM collagens from platelet recognition and adhesion. Such a reagent could potentially be used in vascular interventions. For example, during vessel harvesting for bypass procedures, the vessel could be bathed in FNPEG-5K prior to anastomosis. In so doing, sites of platelet adhesion could be masked with FNPEG-5K prior to reestablishment of blood flow through the vessel. This would leave nondamaged vascular cell surface proteins free to function normally. This represents a significant advance over a previously described method wherein function-attenuating PEG was added indiscriminately to vascular graft proteins (15). Moreover, platelet function would not be compromised, a noted side effect of integrin IIb/IIIa antagonists (16). Because PEG is not immunogenic, molecules such as FNPEG-5K should not be expected to generate antibody responses, even after repeated administrations. Thus, a multifunctional adhesion protein can be engineered through artificial post-translational modifications into a targeted masking molecule. Moreover, this provides an example of how PEG-mediated steric blocking can be selectively targeted to binding sites for specific ligands of therapeutic relevance. The next step in characterizing FNPEG-5K will involve testing whether this bioconjugate will block platelet binding in an animal-based vasculature intervention model.

In a broader sense, this technique represents a protein-based alternative to antisense oligonucleotides that have been envisioned as potential vessel wall therapeutics (17). By selectively binding and coating targeted molecules, one can neutralize undesired intermolecular interactions. Similar chimeras have the potential to be useful tools in cellular engineering and protein-based therapies (18).

#### ACKNOWLEDGMENT

We thank Dr. M. Pendrak for preparing iodinated FN and Ms. J. Cashel for preparing purified FN. We also thank Dr. William Pritchard for his helpful advice.

#### LITERATURE CITED

- (1) Motwani, J. G., and E. J. Topol. (1998) Aortocoronary saphenous vein graft disease: pathogenesis, predisposition, and prevention. *Circulation* 97, 916–931.
- (2) Sixma, J. J., G. H. van Zanten, E. U. Saelman, M. Verkleij, H. Lankhof, H. K. Nieuwenhuis, and P. G. de Groot. (1995) Platelet adhesion to collagen. *Thromb. Haemost.* 74, 454–459.
- (3) Houdijk, W. P., and J. J. Sixma. (1985) Fibronectin in artery subendothelium is important for platelet adhesion. *Blood* 65, 598–604.
- (4) Yamada, K. M. (1989) Fibronectin domains and receptors. *Fibronectin* (D. F. Mosher, Ed.) pp 47–121, Academic Press, San Diego.
- (5) Miekka, S. I., Ingham, K. C., and Menache, D. (1982) Rapid methods for isolation of human plasma fibronectin. *Thromb. Res.* 27, 1–14.
- (6) Abuchowski, A., van Es, T., Palczuk, N. C., and Davis, F. F. (1977) Alteration of immunological properties of bovine serum albumin by covalent attachment of poly(ethylene glycol). *J. Biol. Chem.* 252, 3578–3581.
- (7) Jentoft, N., and Dearborn, D. G. (1979) Labeling of proteins by reductive methylation using sodium cyanoborohydride. *J. Biol. Chem.* 254, 4359–4365.
- (8) Chamow, S. M., Kogan, T. P., Venuti, M., Gadek, T., Harris, R. J., Peers, D. H., Mordenti, J., Shak, S., and Ashkenazi, A. (1994) Modification of CD4 immunoadhesin with monomethoxypoly(ethylene glycol) aldehyde via reductive alkylation. *Bioconjugate Chem.* 5, 133–140.
- (9) Caliceti, P., Schiavon, O., Sartore, L., Monfardini, C., and Veronese, F. (1993) Active site protection of proteolytic enzymes by poly(ethylene glycol) surface modification. *J. Bioact. Compat. Polym.* 8, 41–50.
- (10) Stocks, S. J., Jones, A. J., Ramey, C. W., and Brooks, D. E. (1986) A fluorometric assay of the degree of modification of protein primary amines with poly(ethylene glycol). *Anal. Biochem.* 154, 232–234.
- (11) McGregor, J., Gayet, O., Mercier, N., McGregor, L., and Chignier, E. (1996) Identification, isolation, and characterization of platelet glycoproteins mediating platelet adhesion. *Platelets: a practical approach* (S. Watson, and K. Authi, Eds.) pp 132–133, Oxford University Press, New York.
- (12) Baker, G. R., Sullam, P. M., and Levin, J. (1997) A simple, fluorescent method to internally label platelets suitable for physiological measurements. *Am. J. Hematol.* 56, 17–25.
- (13) Kauf, A. C., Hough, S. M., and Bowditch, R. D. (2001) Recognition of fibronectin by the platelet integrin  $\alpha$ IIb  $\beta$ 3 involves an extended interface with multiple electrostatic interactions. *Biochemistry* 40, 9159–9166.
- (14) Rhodes, R. K. Blood Vessels. (1982) *Collagen in Health and Disease* (J. B. Weiss, and M. I. V. Jayson, Eds.) pp 376–387, Churchill Livingstone, New York.
- (15) Deible, C. R., Beckman, E. J., Russell, A. J., and Wagner, W. R. (1998) Creating molecular barriers to acute platelet deposition on damaged arteries with reactive poly(ethylene glycol). *J. Biomed. Mater. Res.* 41, 251–256.
- (16) Waters, J. H., Anthony, D. G., Gottlieb, A., and Sprung, J. (2001) Bleeding in a patient receiving platelet aggregation inhibitors. *Anesth. Analg.* 93, 878–882.
- (17) Simons, M., Edelman, E. R., DeKeyser, J. L., Langer, R., and Rosenberg, R. D. (1992) Antisense c-myc oligonucleotides inhibit intimal arterial smooth muscle cell accumulation in vivo. *Nature* 359, 67–70.
- (18) Tykocinski, M. L., Kaplan, D. R., and Medof, M. E. (1996) Antigen-presenting cell engineering. The molecular toolbox. *Am. J. Pathol.* 148, 1–16.

BC034037V

# High Transfection Efficiency of Poly(4-vinylimidazole) as a New Gene Carrier

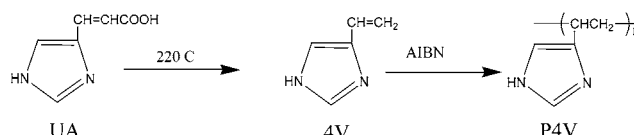
Jong-Eun Ihm,<sup>†</sup> Ki-Ok Han,<sup>‡</sup> In-Kwon Han,<sup>‡</sup> Kwang-Duk Ahn,<sup>§</sup> Dong-Keun Han,<sup>§</sup> and Chong-Su Cho<sup>\*,†</sup>

School of Agricultural Biotechnology, Seoul National University, Suwon 441-744, Korea, Department of Internal Medicine, School of Medicine, SungKyunkwan University, Seoul 100-380, Korea, and Biomaterials Research Center, Korea Institute of Science and Technology, P.O. Box 131, Seoul 130-650, Korea. Received September 23, 2002

Poly(4-vinylimidazole) (P4V) was obtained by free radical polymerization of 4-vinylimidazole (4V) prepared by decarboxylation of urocanic acid. P4V formed a complex with DNA that exhibited higher transfection efficiency on Hela cells than polyethylenimine (PEI), through the proton sponge mechanism of the imidazole groups in the side chain of the P4V, and low cell toxicity.

## INTRODUCTION

Gene therapy presents a promising approach for the treatment of genetic diseases (1) such as hemophilia, muscular dystrophy, or cystic fibrosis and acquired diseases such as HIV infection (2) or various cancers (3). An ideal gene transfer vector should be safe, stable, and cost-effective to treat clinically relevant quantities and capable of efficient and appropriate tissue-specific gene delivery. Recombinant viruses among many viruses have been the gene carriers of choice in the majority of clinical gene therapy trials undertaken (4). However, the recombinant viruses have the limitations on potential immunogenicity and/or oncogenicity, difficult production and purification, and target-cell specificities (5). Over the past decade there have been many attempts to design a nonviral vector to overcome the limitations of the viral vectors. Existing nonviral vectors consist of DNA complexes of cationic liposomes and/or cationic polymers which are able to compact DNA and mask its negative charges (6, 7). However, they are much less efficient than viruses, greatly limiting their practical applications. Among the nonviral vectors, polyethylenimine (PEI) has been shown to effectively condense plasmids into colloidal particle that effectively transfect DNA into a variety of cells both in vitro and in vivo (8). It was reported that this property has been attributed to the so-called "proton-sponge" effect in which unprotonated amino moieties on the polymer buffer the pH inside the endocytic vesicle (9). But the PEI/DNA complexes are very toxic to the cell and are prone to aggregation (8). We have explored poly(4-vinylimidazole) (P4V) as a new gene carrier for possible clinical application based on high transfection efficiency and low toxicity on cells. P4V was used as the polymeric catalyst because of the proton-donating property of the imidazole group in the side chain of P4V (10). Recently, Midoux et al. reported that histidylated poly(L-lysine) exhibited high transfection efficiency owing to pH-responsive endolysosome escape (11). It would be ex-



**Figure 1.** Synthetic scheme of P4V.

pected that P4V is a new gene carrier with high transfection because P4V has an imidazole side chain like that of polyhistidine.

## RESULTS AND DISCUSSION

4-Vinylimidazole (4V) was prepared by decarboxylation of urocanic acid (UA) (Aldrich Chemical Co.) at 220 °C, and polymerization of 4V was carried out using azobis(isobutyronitrile) (AIBN) (Aldrich Chemical Co.) as an initiator at 60 °C for 24 h, which were slightly modified methods to those previously reported (10). The synthetic scheme of P4V is shown in Figure 1. Yields of 4V from UA and P4V from 4V were 38.8 and 90 wt %, respectively. The obtained 4V and P4V were confirmed by <sup>1</sup>H NMR measurement (data not shown). The average molecular weight (*M<sub>w</sub>*) of prepared P4V determined by GPC was 26 200. Figure 2 shows agarose gel electrophoresis of P4V/DNA complexes according to the weight ratios. The movement of DNA was retarded and remained at the top of the gel for P4V/DNA weight ratios greater than 1, indicating that P4V forms a complex with DNA. Figure 3 shows particle sizes (a) and zeta potentials (b) of P4V/DNA complexes with various weight ratios. The particle sizes decreased with increasing weight ratio of P4V to DNA and had a minimum value around 110 nm at a weight ratio of 6. The zeta potentials of P4V/DNA increased with an increase of weight ratio of P4V to DNA. Figure 4 shows transfection of three kinds of cells with DNA, the PEI/DNA complex, and the P4V/DNA complex. The results indicated that transfection efficiency of P4V on HeLa and MC3T3-E1 cells was similar to that of PEI although the transfection efficiency of P4V on 293 cells was lower than that of PEI, indicating cell dependency for the transfection of P4V. Cell viability of PEI, the PEI/DNA complex, P4V, and the P4V/DNA complex is shown in Figure 5. It was found that the cell viability of PEI and the PEI/DNA complex rapidly decreased with an

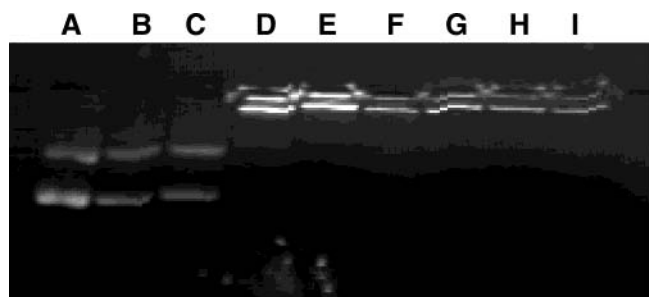
\* To whom correspondence should be addressed. E-mail: chocs@plaza.snu.ac.kr.

<sup>†</sup> Seoul National University.

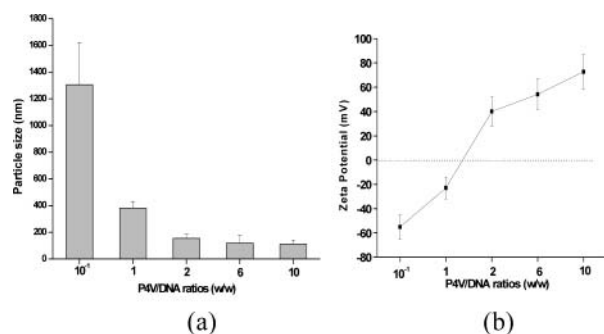
<sup>‡</sup> SungKyunkwan University.

<sup>§</sup> Korea Institute of Science and Technology.

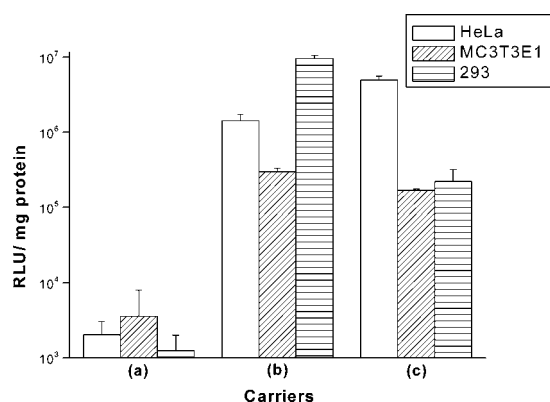




**Figure 2.** Agarose gel electrophoresis of P4V/DNA complexes according to weight ratios: lane A (0/1); lane B ( $10^{-2}/1$ ); lane C ( $10^{-1}/1$ ); lane D (1/1); lane E (2/1); lane F (4/1); lane G (6/1); lane H (8/1); lane I (10/1). The P4V/DNA complex was prepared by mixing DNA dissolved in phosphate-buffered saline (PBS, pH 7.4) with P4V diluted in PBS after dissolving P4V in 1 wt % acetic acid (final pH: 6.7~7.0). The complexes of P4V/DNA prepared with various weight ratios were incubated with the plasmid DNA, pGL3-control (Promega Co.) for 30 min at room temperature and followed by 1% agarose gel electrophoresis.

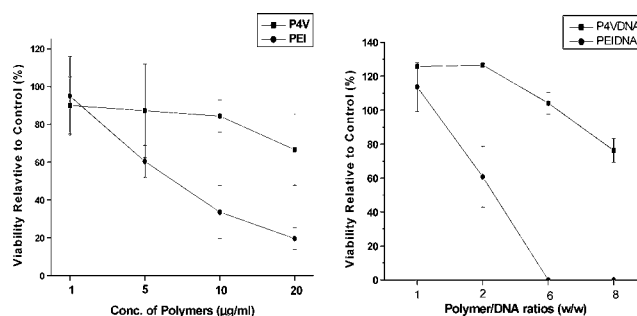


**Figure 3.** The particle sizes (a) and zeta potentials (b) of the P4V/DNA complex with various weight ratios (PBS, pH 6.7–7.0). The error bars represent standard deviation as mean  $\pm$  SD ( $n = 3$ ).



**Figure 4.** Transfection of various cells with DNA (a), PEI/DNA (b), and P4V/DNA (c) at polymer/DNA weight ratio (P/D) = 6. (DNA: 1  $\mu$ g of PGL3-control encoding for reporter gene luciferase; complex was transfected for 6 h in MEM- $\alpha$  without FBS and then incubated for an additional 24 h in fresh media with 10% FBS). The error bars represent standard deviation as mean  $\pm$  SD ( $n = 3$ ).

increase of polymer concentration whereas that of P4V and the P4V/DNA complex was not much changed with an increase of polymer concentration, indicating less toxicity than PEI and high transfection efficiency. It was already reported that the PEI/DNA complex has been shown to produce high level of gene expression in vitro and in vivo among the nonviral vectors (8) because the PEI may enhance intracellular trafficking by buffering the endosomal compartments, thus protecting the DNA



**Figure 5.** Cell viability of P4V, PEI, the P4V/DNA complex, and the PEI/DNA complex on HeLa cells as determined by cell proliferation assay. The error bars represent standard deviation as mean  $\pm$  SD ( $n = 4$ ).

from lysosomal disruption (12). Also, Bennis et al. reported that transfection efficiency into 293 T cells using the poly(L-histidine)(PLH)-graft-poly(L-lysine)/DNA complex was enhanced owing to endosomolytic property of PLH (13). Therefore, it can be said that high transfection efficiency of the P4V can be attributed to the “proton sponge” effect of the imidazole groups in the side chains in which unprotonated amino moieties on the polymer buffer the pH inside endosomal vesicle. A more detailed mechanism of the transfection of the P4V into cells will be reported.

Conclusively, this study shows that the P4V forms a complex with DNA, and that the P4V/DNA complex exhibited very high transfection efficiency, through the proton sponge mechanism of the imidazole groups, and low cell toxicity.

#### ACKNOWLEDGMENT

We thank the Korean Science and Engineering Foundation for support of this research (R01-2002-000-00414-0).

#### LITERATURE CITED

- (1) Anderson, W. F. (1998) *Nature* 392, 25.
- (2) Yu, M., Poeschla, E., and Wong-Staal, F. (1994) *Gene Ther.* 1, 13.
- (3) Folkman, J. (1998) *Proc. Natl. Acad. Sci. U.S.A.* 95, 9064.
- (4) Rosenfeld, M. A., Siegfried, K., Yoshimura, K., Fukayama, M., Stier, L. E., Paakko, P. K., Gilardi, P., Stratford-Perricaudet, L. D., Perricaudet, M., et al. (1991) *Science* 252, 431.
- (5) Mulligan, R. C. (1993) *Science* 260, 926.
- (6) Vogel, K., Wang, R. G., Lee, G., Chmielewski, G., and Low, P. S. (1996) *J. Am. Chem. Soc.* 118, 1581.
- (7) Bielinska, A. U.; Yen, A.; Wu, H. L.; Zahos, K. M.; Sun, R.; Weiner, N. D.; Baker, J. R., Jr.; Roessler, B. J. (2000) *Biomaterials* 21, 877.
- (8) Boussif, O., Lezoualc'h, F., Zanta, M., Mergny, M. D., Scherman, D., Demeneix, B., and Behr, J. P. (1995) *Proc. Natl. Acad. Sci. U.S.A.* 92, 7297.
- (9) Garnett, M. C. (1999) *Crit. Rev. Ther. Drug Carrier Syst.* 16, 147.
- (10) Overberger, C. G., and Vorchheimer, N. (1963) *J. Am. Chem. Soc.* 85, 951.
- (11) Midox, P., and Monsigny, M. (1999) *Bioconjugate Chem.* 10, 406.
- (12) Han, S. O., Mahato, R. I., Sung, Y. K., and Kim, S. W. (2000) *Mol. Ther.* 2, 302.
- (13) Bennis, J. M., Choi, J. S., Mahato, R. I., Park, J. S., and Kim, S. W. (2000) *Bioconjugate Chem.* 11, 637.

BC025611Q

# Pyropheophorbide 2-Deoxyglucosamide: A New Photosensitizer Targeting Glucose Transporters

Min Zhang,<sup>†,‡,▽</sup> Zhihong Zhang,<sup>†,§,▽</sup> Dana Blessington,<sup>‡</sup> Hui Li,<sup>†</sup> Theresa M. Busch,<sup>§</sup> Vanessa Madrak,<sup>||</sup> Jeremy Miles,<sup>§</sup> Britton Chance,<sup>‡</sup> Jerry D. Glickson,<sup>†</sup> and Gang Zheng<sup>\*,†</sup>

Departments of Radiology, Biochemistry and Biophysics, Radiation Oncology, and Physics, University of Pennsylvania, Philadelphia, Pennsylvania 19104; Department of Chemistry, Shanghai University, Shanghai 200436, China; and Key Laboratory of Biomedical Photonics of Minister of Education, Huazhong University of Science and Technology, Wuhan 430074, China. Received March 17, 2003

To prepare near-infrared fluorescence imaging and photodynamic therapy agents targeted at glucose transporters, pyropheophorbide 2-deoxyglucosamide (Pyro-2DG) was synthesized and evaluated in a 9L glioma rat model. Fluorescence imaging studies demonstrate that Pyro-2DG is selectively accumulated in the tumor. Upon its photoactivation, we demonstrate that this agent efficiently causes selective mitochondrial damage to the region of a tumor that was photoirradiated after administration of this agent, but does not affect tissues photoirradiated in the absence of the agent or tissues treated with the agent that are not photoirradiated. Preliminary confocal microscopy studies suggest that Pyro-2DG is delivered and trapped in tumor cells via the GLUT/hexokinase pathway and therefore is useful both as a tumor-targeted NIR fluorescence imaging probe and as a PDT agent for the destruction of cancer.

## INTRODUCTION

One of the biochemical “hallmarks” of malignancy is enhanced tumor glycolysis, which is primarily due to the overexpression of glucose transporters (GLUTs) and the increased activity of mitochondria-bound hexokinase in tumors (1). Utilizing these cancer signatures, [<sup>18</sup>F] 2-fluoro-2-deoxyglucose (<sup>18</sup>FDG)-based positron emission tomography (PET) has become a widely used molecular imaging modality in the detection of a wide range of human cancers (2).

<sup>18</sup>FDG is an analogue of glucose that enters cells via glucose transporters (GLUT) and is phosphorylated to <sup>18</sup>FDG-6-phosphate by hexokinase, the first enzyme in the glycolytic pathway. This enzyme converts glucose, 2-deoxyglucose or <sup>18</sup>FDG from a neutral membrane permeable form to an anionic membrane impermeable form. Reversal of this reaction requires glucose-6-phosphatase, which is generally not present at high enough concentration in most cells to mediate this reaction. Further metabolism of <sup>18</sup>FDG-6-phosphate by phosphoglucose isomerase, the next enzyme in the glycolytic pathway, or by enzymes in the glycogen or pentose shunt pathways does not occur (3). Therefore, <sup>18</sup>FDG-6-phosphate is trapped in the cell. The high affinity of <sup>18</sup>FDG

for tumors derives from the high levels of aerobic glycolysis (4) and overexpression of GLUTs exhibited by most, but not all (5), tumors.

The mechanism of action of <sup>18</sup>FDG could be exploited to deliver other diagnostic and therapeutic agents into tumors and other cells that express high levels of GLUTs and hexokinase. This approach was first employed by Speizer in 1985 (6), who used it to deliver a fluorescent analogue of glucose, 6-deoxy-*N*-(7-nitrobenz-2-oxa-1,3-diazol-4-yl)aminoglucose, into human erythrocytes. This is a derivative of 6-deoxyglucose containing a fluorophore on the 6-position. A fluorescent derivative of 2-deoxyglucose, 2-[*N*-(7-nitrobenz-2-oxa-1,3-diazol-4-yl)amino]-2-deoxy-D-glucose (2-NBDG) (Ex: 475 nm; Em: 550 nm), was introduced by Yoshioka et al. in 1996 (7), who demonstrated that localization of this agent in the yeast *Candida albicans* was inhibited by D-glucose, but not L-glucose. Similar D-glucose (but not L-glucose) inhibited uptake of 2-NBDG has been demonstrated in *E. coli* (7–9), yeast (10), vascular smooth muscle cells (11), and pancreatic  $\beta$ -cells transfected to overexpress Glut2 glucose transporters (12). Utilization of the glucose transport system was further supported by competitive inhibition of 2-NBDG uptake by the glucose analogues 3-*o*-methyl glucose and D-glucosamine (9). Internalization of 2-NBDG in isolated rabbit enterocytes was demonstrated by confocal microscopy (13). Conversion of 2-NBDG to 2-NBDG-6-phosphate in *E. coli* cells was confirmed by mass spectrometry and by demonstration that glucose-6-phosphatase regenerated 2-NBDG (8). Localization of 2-NBDG in rat 9L glioma has recently been reported by Baidoo et al. (14). They found that animals injected with 2-NBDG under fasting conditions (low serum glucose level) accumulated this probe in tumors, and uptake of 2-NBDG could be blocked under nonfasting conditions (high serum glucose level).

\* Address correspondence to Dr. Gang Zheng, University of Pennsylvania, Chemistry Building R310, Box 66, 231 South 34th Street, Philadelphia, PA 19104. Tel: +1-215-898-3105. Fax: +1-215-573-2159. E-mail: zheng@rad.upenn.edu.

<sup>†</sup> Department of Radiology, University of Pennsylvania.

<sup>‡</sup> Department of Biochemistry and Biophysics, University of Pennsylvania.

<sup>§</sup> Department of Radiation Oncology, University of Pennsylvania.

<sup>||</sup> Department of Physics, University of Pennsylvania.

<sup>±</sup> Shanghai University.

<sup>⊗</sup> Huazhong University of Science and Technology.

<sup>▽</sup> First two authors contributed equally to this work.

The evidence that 2-NBDG is internalized via glucose transporters and phosphorylated by hexokinase demonstrates that 2-deoxyglucose could be utilized to deliver probes larger than fluorine into tumors and other tissues that exhibit high levels of GLUT expression and hexokinase activity. The structural limitations on 2-DG derivatives that can be transported and trapped via the GLUT/hexokinase pathway remain to be elucidated. We hypothesize that this pathway can be used to deliver a number of other diagnostic and therapeutic agents that can be utilized in the clinical management and study of cancer.

Near-infrared (NIR) dyes are presently attracting considerable interest as fluorescence probes for detection of cancer (15) and as photosensitizers for cancer treatment by photodynamic therapy (PDT) (16). Since tissue is relatively transparent to NIR light, NIR fluorescence imaging (NIRF) and PDT are capable of detecting and treating, respectively, even subsurface tumors. Owing to the need to increase photosensitizer's water solubility and to increase their affinity for tumor tissues, a great deal of efforts have been devoted by many research groups to develop photosensitizers covalently linked with various carbohydrate moieties (17). However, none of them was intended to take advantage of the intracellular trapping mechanism for 2DG in tumor cells as it does for FDG. Thus, we have prepared a pyropheophorbide derivative of 2-deoxyglucose, Pyro-2DG, as a GLUT-targeted photosensitizer. Its fluorophore, pyropheophorbide *a* (1), has long wavelength absorption of 667 nm, fluorescence emission at 679 nm, and near-infrared (NIR) fluorescence emission at 720 nm (18). One of its derivatives, the hexyl ether analogue of pyropheophorbide (HPPH) (19), is currently in phase I/II clinical trial as a PDT agent. Another derivative, the HPPH carotenoid conjugate has been reported as an NIR imaging agent (20). Utilizing a low temperature 3D scanning fluorometer (21), we demonstrate that this agent efficiently causes selective mitochondrial damage to the region of a tumor that was photoirradiated after administration of this agent, but does not affect tissues photoirradiated in the absence of the agent or tissues treated with the agent that are not photoirradiated. Our confocal microscopy data are consistent with the hypothesis that Pyro-2-DG has been delivered and trapped in tumor cells via the GLUT/hexokinase pathway.

## EXPERIMENTAL PROCEDURES

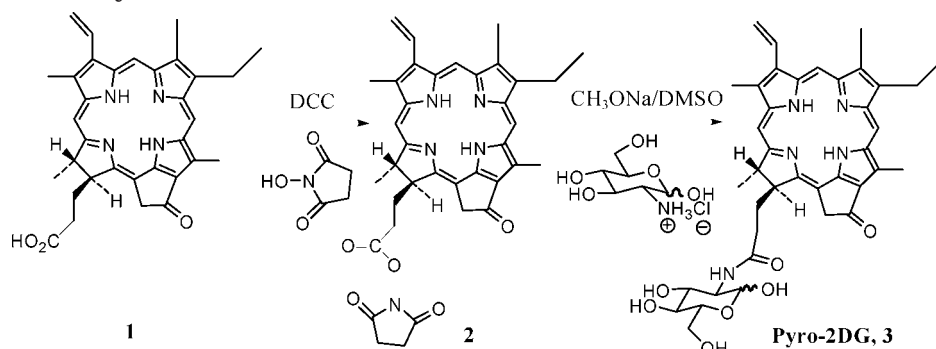
**Materials and General Methods.** Melting points are uncorrected. UV-vis spectra were recorded on a Beckman DU-600 spectrophotometer. Fluorescence emission was measured with a Perkin-Elmer LS-50B fluorometer.  $^1\text{H}$  NMR spectra were recorded on a Bruker ASPECT 360 MHz instrument. ESI-MS and HRMS spectrometric analysis were performed at the Mass Spectrometry Facility of the Department of Chemistry, University of Pennsylvania. Methyl pheophorbide *a* was isolated from *Spirulina pacifica* algae available from Cyanotech Corp., Hawaii. Pyropheophorbide (1) was synthesized from methyl pheophorbide according to literature procedures (18). Other chemicals were purchased from Aldrich. When necessary, solvents were dried before use. For TLC, EM Science TLC plates (silica gel 60 F<sub>254</sub>) were used. Reverse phase (RP) analytical HPLC was performed using a Zorbax RX-C8 (9.4 mm  $\times$  250 mm) column eluting at 1.0 mL/min with MeCN/phosphate buffer (0% to 99% MeCN gradient) with UV-vis detection at 414 nm.

**Pyropheophorbide Succinimidyl Ester (2).** Pyropheophorbide (1) (208 mg 0.39 mmol) was activated with DCC (80 mg 0.39 mmol) and *N*-hydroxysuccinimide (92 mg 0.8 mmol) in 10 mL of DMF. After stirring for 24 h, urea was filtered off, and solvents were removed. The crude product was purified by column chromatography (silica gel 60) and eluted with 5% methanol in  $\text{CH}_2\text{Cl}_2$ . The desired product was crystallized from  $\text{CH}_2\text{Cl}_2$ /hexane in 80% yield (195 mg 0.31 mmol). Mp: 200–202 °C. UV-vis in  $\text{CH}_2\text{Cl}_2$ : 413 nm ( $\epsilon$   $1.1 \times 10^5$ ), 509 ( $1.2 \times 10^4$ ), 538 ( $1.0 \times 10^4$ ), 609 ( $8.7 \times 10^3$ ), and 666 ( $5.0 \times 10^4$ ). Mass calculated for  $\text{C}_{37}\text{H}_{37}\text{N}_5\text{O}_5$ : 631.7; found by ESI-MS 632.7 ( $\text{MH}^+$ ) and 654.6 ( $\text{M} + \text{Na}^+$ ).  $^1\text{H}$  NMR ( $\text{CDCl}_3$ ,  $\delta$ ): 9.42, 9.31, and 8.56 (each s, 1H, 5-H, 10-H, and 20-H); 7.95 (dd,  $J$  = 17.8, 11.8 Hz, 1H, 3'-CH=CH<sub>2</sub>); 6.25 (d,  $J$  = 17.8 Hz, 1H, *trans*-3<sup>2</sup>-CH=CH<sub>2</sub>); 6.14 (d,  $J$  = 11.8 Hz, 1H, *cis*-3<sup>2</sup>-CH=CH<sub>2</sub>); 5.17 (ABX, 2H, 13<sup>2</sup>-CH<sub>2</sub>); 4.49 (d,  $J$  = 7.2 Hz, 1H for 18-H); 4.40 (m,  $J$  = 7.2 Hz, 1H for 17-H); 3.63 (s, 5H, 8-CH<sub>2</sub>CH<sub>3</sub>, 12-CH<sub>3</sub>); 3.40 and 3.18 (each s, 3H, 2-CH<sub>3</sub> and 7-CH<sub>3</sub>); 2.87 (br, 5H, 17<sup>1</sup>-H and succinimide-CH<sub>2</sub>CH<sub>2</sub>-); 2.62 and 2.27 (each m, 1H, for 2  $\times$  17<sup>2</sup>-H); 1.93 (m, 1H for 17<sup>1</sup>-H); 1.82 (d,  $J$  = 7.2 Hz, 3H, 18-CH<sub>3</sub>); 1.70 (t,  $J$  = 7.2 Hz, 3H, 8-CH<sub>2</sub>CH<sub>3</sub>); 1.33 and 1.12 (each brs, 1H, 2  $\times$  N-H).

**Pyropheophorbide-2-deoxyglucosamide (Pyro-2DG) (3).** D-Glucosamine hydrochloride (130 mg 0.6 mmol) was added to a solution of sodium methoxide (32.4 mg 0.6 mmol) in 7 mL of DMSO. The mixture was stirred for 2 h, and pyropheophorbide succinimide ester (2) (190 mg 0.3 mmol) was added. The reaction mixture was stirred under argon atmosphere for 20 h. After solvents were removed, the crude product was washed with dichloromethane and water and crystallized from methanol. The title compound was obtained in 102 mg yield. The filtrate was further concentrated and purified by silica gel plate chromatography (20% methanol in dichloromethane), and 30 mg more of Pyro-2DG was obtained. Thus, the total product yield is 63% (132 mg, 0.19 mmol). Mp: >200 °C. Analytical RP HPLC:  $t_R$  20.9 min, 99.5%. UV-vis in DMSO: 415 nm ( $\epsilon$   $1.2 \times 10^5$ ), 510 ( $1.2 \times 10^4$ ), 540 ( $1.0 \times 10^4$ ), 611 ( $8.6 \times 10^3$ ), and 668 ( $5.0 \times 10^4$ ). Mass calcd for  $\text{C}_{39}\text{H}_{45}\text{N}_5\text{O}_7$ : 718.3217 ( $\text{M} + \text{Na}^+$ ), found by HRMS: 718.3249 ( $\text{M} + \text{Na}^+$ ).  $^1\text{H}$  NMR ( $\text{DMSO}-d_6$ ): 8.97, 8.70, and 8.69 (each s, 1H, 5-H, 10-H, and 20-H); 7.97 (dd,  $J$  = 17.7, 11.8 Hz, 1H, 3<sup>1</sup>-CH=CH<sub>2</sub>); 6.15 (dd, 2H,  $J$  = 17.7 Hz, 1H, *trans*-3<sup>2</sup>-CH=CH<sub>2</sub>,  $J$  = 5.4 Hz,  $\alpha$ -H); 5.97 (d,  $J$  = 11.8 Hz, 1H, *cis*-3<sup>2</sup>-CH=CH<sub>2</sub>); 4.98 (ABX, 2H, 13<sup>2</sup>-CH<sub>2</sub>); 4.81–4.35 (each m, total 5H, sugar-H); 4.18 (br, 1H for 18-H); 4.11 (d,  $J$  = 7.2 Hz, 1H for 17-H); 3.68 (q,  $J$  = 7.4 Hz, 2H, 8-CH<sub>2</sub>CH<sub>3</sub>); 3.58, 3.43, and 3.16 (s, each 3H, 12-CH<sub>3</sub>, 2-CH<sub>3</sub> and 7-CH<sub>3</sub>); 2.59 (m, 1H, 17<sup>1</sup>-H); 2.50 (m, 2H, 17<sup>2</sup>-H); 2.12 (m, 1H, 17<sup>1</sup>-H); 1.80 (d,  $J$  = 7.2 Hz, 3H, 18-CH<sub>3</sub>); 1.59 (t,  $J$  = 7.2 Hz, 3H, 8-CH<sub>2</sub>CH<sub>3</sub>).

**Confocal Microscopic Studies.** 9L glioma cells were grown for 5 days in four-well Lab-Tek chamber slides (Naperville, IL). Before the cell experiments, the culture medium was replaced by preincubation medium (medium with 1% (w/v) BSA instead of FBS). The cells were washed three times with preincubation medium (for 15, 15, and 30 min) and cultured in this medium for a further 20 h. Experiments were started, after two quick washes with preincubation medium, by the addition of preincubation medium containing the indicated amounts of Pyro-2DG and/or D-glucose. After 30 min incubation at 37 °C, the cells were washed five times with ice-cold PBS containing 0.8% BSA and two times with PBS alone and fixed for 20 min with 2% formaldehyde in PBS at room temperature. Then the chamber slides were mounted and sealed for confocal microscopic analysis.



**Scheme 1. Synthesis of Pyro-2DG**

**Animals.** Rat 9L glioma was implanted on the flanks of male Fisher 344 rats (150–200 g) via subcutaneous injection of 0.1 mL,  $\sim 10^6$  9L glioma cells. Within 10 days, tumors grew to the desired size of 1 cm in diameter. After not feeding animals for 24 h, we anaesthetized the rats via intraperitoneal injection of Ketamine (75 mg/kg) and Xylazine (10 mg/kg). Pyro-2DG (2 mL, concentration: 0.25 mg/mL) was injected via tail vein infusion over a period of 1 h (dose: 2.5 mg/kg). Thirty minutes later, the rats were anesthetized again and subjected to PDT.

**PDT Protocol.** For proof-of-principle, we designed a “point treatment” protocol for evaluating PDT response of Pyro-2DG. PDT was carried out using a KTP YAG pumped dye module (Laserscope, San Jose, CA) tuned to produce 670 nm light. Light delivery was through a 1 mm fiber to create a treatment spot of 0.96 mm in diameter when the fiber was held closely adjacent to the tumor. The light field was fixed in position at the center of the tumor by mounting the fiber in the center of a circular plate which was glued to the anesthetized animal. The light was delivered at a fluence rate of 75 mW/cm<sup>2</sup> to a total dose of 175 J/cm<sup>2</sup>. Laser power output was measured with a power meter (Coherent, Auburn, CA).

**Fluorescence Imaging of Tumors** (21, 24–25). Immediately after PDT, animals were immersed in precooled isopentane (−150 °C) and transferred to liquid nitrogen (−196 °C) 5 min later. Tumors were then surgically excised, embedded in a mixture of ethanol–glycerol–water (freeze point: −30 °C), and mounted at low temperature for 3D surface fluorometric scanning. Thus, the frozen tumor sample was milled flat and imaged every 100  $\mu$ m from the top surface to the bottom of the tumor. The light guide (fused silica, 50  $\mu$ m core diameter) stepped across the tissue surface at a fixed distance from the tissue surface (70  $\mu$ m). The imaging resolution of the low-temperature scanning fluorometer was 80  $\mu$ m. The fluorescent signals of FP (filters: Ex: 440DF20, Em: 520DF40), PN (filters: Ex: 365HT25, Em: 455DF70), and Pyro-2DG (filters: Ex: 405DF40, Em: 700ALP) were imaged for each depth of tumor. The scanning was performed at 128  $\times$  128 steps that could cover 1.024  $\times$  1.024 cm<sup>2</sup>. The fluorescence signal was automatically digitized and recorded on a PC. The redox ratio of FP/(FP+PN) was calculated with MATLAB.

**RESULTS AND DISCUSSION**

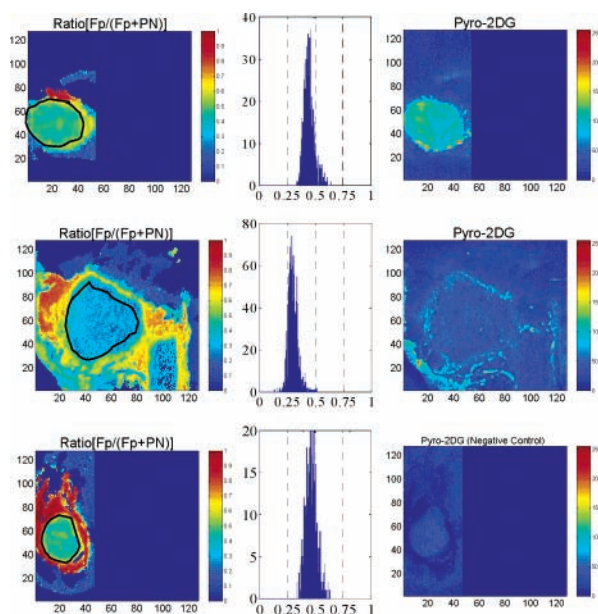
To synthesize the desired Pyro-2DG, we first treated the pyropheophorbide with *N*-hydroxysuccinimide in the presence of DCC. The pyropheophorbide succinimidyl ester **2** so obtained was reacted with D-glucosamine that was activated by treating D-glucosamine hydrochloride with sodium methoxide to yield the desired conjugate **3**

in 50% overall yield (see Scheme 1). The structures of all new compounds were confirmed by HRMS and NMR spectroscopy. The HPLC chromatograms of the final conjugate confirmed its homogeneity.

Despite containing the hydrophilic 2DG moiety, Pyro-2DG is only partially water-soluble due to the hydrophobic nature of the porphyrin macrocycle. Formulation with detergent (1% Tween 80) made it completely miscible with water and suitable for in vivo administration. For proof-of-principle, we designed a “point treatment” protocol for evaluating PDT response of Pyro-2DG. Instead of irradiating the whole tumor area (1 cm in diameter), only an area  $\sim 1$  mm in diameter at the center of the tumor was treated. The same laser power and light dose (75 mW/cm<sup>2</sup>, 175 J/cm<sup>2</sup>) were used throughout the experiments. On the basis of the absorption and emission maxima of Pyro-2DG ( $\lambda_{\text{ex}}$  = 665 nm;  $\lambda_{\text{em}}$  = 720 nm), the 9L tumor was treated with 670 nm laser light, and a 700 nm long pass filter was incorporated into the 3D fluorescence scanner for collecting the Pyro-2DG fluorescence at 720 nm. This point treatment procedure is designed for two purposes: (1) to allow the adjacent untreated tumor region along with the normal tissue region to serve as internal controls; and (2) to evaluate possible bystander effects.

The tumor specificity of Pyro-2DG is, of course, limited by uptake of glucose by various normal tissues; however, most tumors consume substantially more glucose than the surrounding normal tissues. Thus, all PDT experiments were carried out under fasting conditions. Low serum glucose levels were achieved by not feeding animals for 24 h before the experiments. Moreover, the animals were given low concentration Pyro-2DG via tail vein infusion over a period of 1 h to enhance the tumor uptake. Thirty minutes after injection, the animals were subjected to the PDT (75 mW/cm<sup>2</sup>, 175 J/cm<sup>2</sup>). After PDT, animals were rapidly frozen and kept in liquid nitrogen for fluorescence imaging studies using the low temperature 3D scanning fluorometer.

This fluorometer was designed originally to examine the redox state of in-vivo-freeze-trapped tissue (21). It detects the intrinsic fluorescence of oxidized flavoprotein (FP,  $\lambda_{\text{ex}}$ : 436 nm,  $\lambda_{\text{em}}$ : 560 nm) and reduced pyridine nucleotide (PN,  $\lambda_{\text{ex}}$ : 366 nm,  $\lambda_{\text{em}}$ : 450 nm) stemming from mitochondria. The PN signal indicates mainly NADH, whereas the FP signal originates from the flavins of dehydrolipoamide dehydrogenase component of pyruvate dehydrogenase and  $\alpha$ -ketoglutarate dehydrogenase. Because (1) the flavoproteins are coupled to the mitochondrial NAD/NADH redox system by pyruvate dehydrogenase and  $\alpha$ -ketoglutarate dehydrogenase reactions, and (2) only the reduced form of the PN system and the oxidized species of FP couple are strongly fluorescent, the



**Figure 1.** Fluorescence images of drug control (top row: tumor + Pyro-2DG), normal tissue control (middle row: normal tissue of the same animal), and tumor control (bottom row: tumor alone) in 9L glioma bearing animals. Note: The tumor and normal muscle margin are outlined with a black circle in the redox ratio images (the first column), the redox ratio histograms corresponding to the marked region (black circle) are also presented here (the second column).

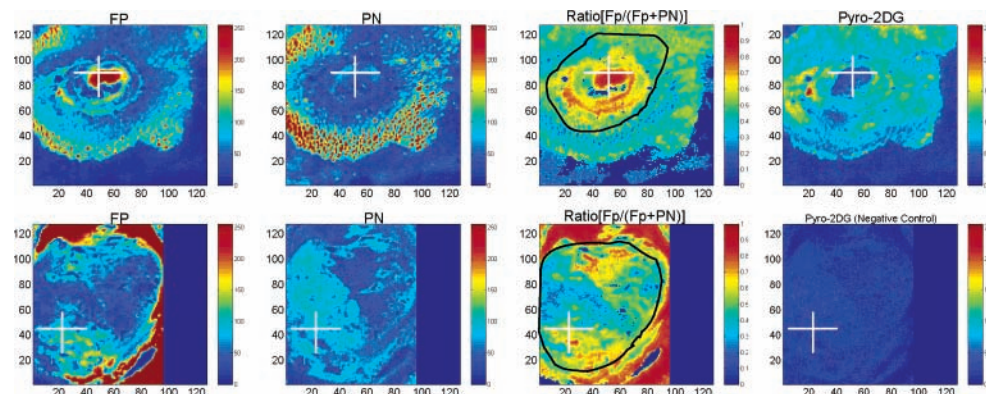
ratio of FP/(FP+PN) calculated from FP and PN signals accurately represents the redox state of the mitochondrial NAD/NADH redox couple (23). Thus, the redox ratio can be used to evaluate the PDT damage to the tumor mitochondria. In addition to monitoring the fluorescence of endogenous PN (NADH) and FP, this fluorometer is also useful in detecting any exogenous fluorophore (e.g., Pyro-2DG) that is present in the specimen.

There are some distinctive advantages of this freeze-quenching technique (21, 23). First, it stops metabolic processes, providing a "snapshot" of metabolism at the moment of freezing and also allowing a 3D analysis by means of reflectance spectrophotometric imaging of successive slices through the frozen tissue block. Furthermore, the fluorescence quantum yield is typically 5- to 10-fold higher at liquid nitrogen temperature, vastly improving the signal-to-noise ratio. Also, because of the complete arrest of metabolic processes, the time taken for the analysis is not of importance. This facilitates high-resolution scanning with signal/noise enhancement

through signal averaging. Using this technique, we have studied fluorescence images of FP, PN (NADH), and Pyro-2DG on animals with or without PDT treatment. The results are discussed below:

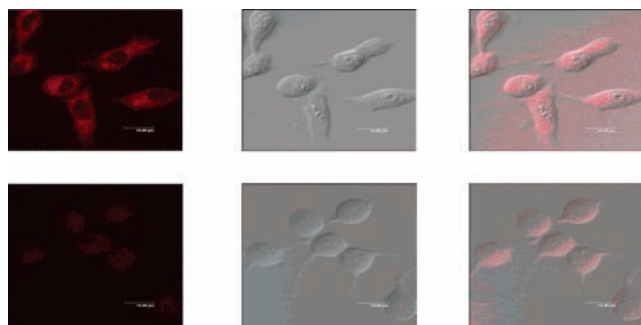
Figure 1 shows the redox ratio images (the first column), their corresponding histograms (the second column), and the Pyro-2DG fluorescence images (the third column) of 9L glioma and surrounding muscle tissue. The *x* and *y* axes of images represents the number of pixels scanned, whereas *x* and *y* axes of the histograms represents the relative redox ratio value and its corresponding pixel number, respectively. As shown in Figure 1, Pyro-2DG is selectively accumulated inside the tumor margin (top row images) compared to surrounding normal tissue such as muscle (middle row images), and there is no background fluorescence observed from the control experiment in which tumor is imaged in the absence of Pyro-2DG (bottom row images). This study also demonstrates that the tumor control (tumor alone) and the drug control (Pyro-2DG + tumor) exhibit similar redox states since similar FP and PN signals and similar FP/(FP+PN) ratios were detected in both instances. This indicates that the addition of Pyro-2DG has no effect on the mitochondrial activities of the tumor in the absence of light.

Upon PDT treatment, Pyro-2DG dramatically altered the redox state of the tumor. As shown in Figure 2, the irradiated spot (indicated by a cross) exhibited a marked increase in FP fluorescence (red region in the center of tumor, see the first image of the top row) and a significant decrease in NADH fluorescence (see the second image of the top row). This produced a dramatic increase in the redox ratio of the tumor [FP/(FP+PN), see the third image of the top row]. Since the ratio of FP/(FP+PN) represents the redox state of the mitochondrial NAD/NADH redox couple, the significant enhancement of this ratio clearly reflects the extensive mitochondrial damage (oxidation) experienced by the irradiated region of the tumor, but not the adjacent unirradiated region. Strikingly, the complete disappearance of the Pyro-2DG fluorescence signal was observed in the same region (there is a dark "hole" at the center of the tumor, see the last image of the top row), indicating selective photobleaching of the photosensitizer. Since PDT is mediated by the production of reactive oxygen species resulting in cell kill via oxidation (22), there is a direct correlation between the selective photobleaching of the Pyro-2DG and the selective tumor destruction stemming from the oxidation of tumor mitochondria. To verify that such tumor destruction is caused by the photodynamic action of the Pyro-2DG, a PDT control experiment was con-



**Figure 2.** Selective tumor destruction by PDT corresponds to a marked change in the intrinsic fluorescence of tumors (decreased NADH, increased FP) and the selective photobleaching of Pyro-2DG. (Top row: PDT of tumor with Pyro-2DG; bottom row: light control, PDT of tumor without Pyro-2DG). Note: The irradiated region is marked as a white cross, and the tumor margin is outlined with a black circle in both experiments.





**Figure 3.** Confocal microscopy images of 9L glioma cells incubated with 50  $\mu$ M Pyro-2DG for 30 min at 37  $^{\circ}$ C in the absence (upper) and presence (lower) of 50 mM D-glucose. Left hand: fluorescence images; middle: bright field images; right-hand: overlapping images.

ducted by not injecting the photosensitizer. As shown in Figure 2 (see the bottom row images), there is little or no change in the redox ratio in the absence of Pyro-2DG; this experiment, therefore, clearly demonstrates that the PDT response is due to Pyro-2DG' photosensitization.

To determine the specificity of Pyro-2DG toward GLUTs, we performed preliminary confocal fluorescence microscopy studies. As shown in Figure 3, Pyro-2DG localizes within 9L glioma cells at 37  $^{\circ}$ C and that localization was competitively inhibited by D-glucose. In contrast to Pyro-2DG, uptake of pyropheophorbide *a* in 9L glioma cells is concentration dependent and is not inhibited by D-glucose, indicating that its uptake is GLUT-independent (data not shown). This study suggests that Pyro-2DG is delivered and trapped in tumor cells via the GLUT/hexokinase pathway.

In conclusion, we have designed and synthesized a new photosensitizer targeted at the GLUT pathway to serve as both a targeted PDT agent and a NIR imaging agent. Following intravenous administration to 9L glioma-bearing animals, Pyro-2DG selectively accumulated in the tumor compared to the surrounding normal tissue as observed by measuring its NIR fluorescence at 720 nm using a low-temperature 3D fluorescence scanner. Upon PDT treatment of this tumor, we demonstrate that this agent efficiently causes selective mitochondrial damage to the region of a tumor that was photoirradiated after administration of this agent, but does not affect tissues photoirradiated in the absence of the agent or tissues treated with the agent that are not photoirradiated. Our confocal microscopy data are consistent with the hypothesis that Pyro-2DG has been delivered and trapped in tumor cells via the GLUT/hexokinase pathway, and therefore, Pyro-2DG is useful both as a tumor-selective NIR fluorescence imaging probe and as a PDT agent. This study could provide the basis for the design and synthesis of a large group of diagnostic/therapeutic agents that exploit a key pathway distinguishing most tumors from most (but not all) normal tissues—their high levels of GLUT and hexokinase activity.

#### ACKNOWLEDGMENT

This work was funded by NIH grants R21 CA95330 (G.Z.) and NO1-CM97065 (B.C.) and an Oncologic Foundation of Buffalo award (G.Z.). Partial support from NIH grants P20 CA86255 (J.D.G.), R24 CA83105 (J.D.G.), and RO1 CA85831 (T.M.B.) are also acknowledged. We are grateful to Dr. Ponzy Lu of the Chemistry Department for housing our organic chemistry lab and to Mr. David Nelson of the Department of Radiology for technical assistance.

**Supporting Information Available:** The absorption and fluorescence emission spectra of Pyro-2DG, the illustration of PDT treatment protocol, and the HPLC chromatograms of the Pyro-2DG. This material is available free of charge via the Internet at <http://pubs.acs.org>.

#### LITERATURE CITED

- (1) Medina, R. A., and Owen, G. I. (2002) Glucose transporters: expression, regulation and cancer. *Biol. Res.* **35**, 9–26.
- (2) Czernin, J., and Phelps, M. E. (2002) Positron emission tomography scanning: current and future applications. *Annu. Rev. Med.* **53**, 89–112.
- (3) Pauwels, E. K., Ribeiro, M. J., Stoot, J. H., McCready, V. R., Bourguignon, M., and Maziere, B. (1998) FDG accumulation and tumor biology. *Nuclear Med. Biol.* **25**, 317–322.
- (4) Vaupel, P., Kallinowski, F., and Okunieff, P. (1989) Blood flow, oxygen and nutrient supply, and metabolic microenvironment of human tumors: a review. *Cancer Res.* **49**, 6449–6465.
- (5) Weinhouse, S. (1976) The Warburg hypothesis fifty years later. *Z. fur Krebsforsch. Klin. Onkol.* **87**, 115–126.
- (6) Speizer, L., Haugland, R., and Kutchai, H. (1985) Asymmetric transport of a fluorescent glucose analogue by human erythrocytes. *Biochim. Biophys. Acta* **815**, 75–84.
- (7) Yoshioka, K., Takahashi, H., Homma, T., Saito, M., Oh, K. B., Nemoto, Y., and Matsuoka, H. (1996) A novel fluorescent derivative of glucose applicable to the assessment of glucose uptake activity of *Escherichia coli*. *Biochim. Biophys. Acta* **1289**, 5–9.
- (8) Yoshioka, K., Saito, M., Oh, K. B., Nemoto, Y., Matsuoka, H., Natsume, M., and Abe, H. (1996) Intracellular fate of 2-NBDG, a fluorescent probe for glucose uptake activity, in *Escherichia coli* cells. *Biosci. Biotech. Biochem.* **60**, 1899–1901.
- (9) Natarajan, A., and Srienc, F. (2000) Glucose uptake rates of single *E. coli* cells grown in glucose-limited chemostat cultures. *J. Microbiol. Methods* **42**, 87–96.
- (10) Oh, K. B., and Matsuoka, H. (2002) Rapid viability assessment of yeast cells using vital staining with 2-NBDG, a fluorescent derivative of glucose. *Int. J. Food Microbiol.* **76**, 47–53.
- (11) Lloyd, P. G., Hardin, C. D., and Sturek, M. (1999) Examining glucose transport in single vascular smooth muscle cells with a fluorescent glucose analogue. *Physiol. Res.* **48**, 401–410.
- (12) Yamada, K., Nakata, M., Horimoto, N., Saito, M., Matsuoka, H., and Inagaki, N. (2000) Measurement of glucose uptake and intracellular calcium concentration in single, living pancreatic beta-cells. *J. Biol. Chem.* **275**, 22278–22283.
- (13) Roman, Y., Alfonso, A., Louzao, M. C., Vieytes, M. R., and Botana, L. M. (2001) Confocal microscopy study of the different patterns of 2-NBDG uptake in rabbit enterocytes in the apical and basal zone. *Pflügers Arch. – Eur. J. Physiol.* **443**, 234–239.
- (14) Baidoo, K. E., Mathews, W., and Wagner, H. N. (2000) Fluorescent imaging of deoxyglucose. Presented at the 8th International Conference of Peace through Mind/Brain Science, Hamamatsu, Japan, February 2–4.
- (15) (a) Lin, Y., Weissleder, R., and Tung, C. H. (2002) Novel near-infrared cyanine fluorochromes: synthesis, properties, and bioconjugation. *Bioconjugate Chem.* **13**, 605–610. (b) Achilefu, S., Jimenez, H. N., Dorshow, R. B., Bugaj, J. E., Webb, E. G., Wilhelm, R. R., Rajagopalan, R., Johler, J., Erion, J. L. (2002) Synthesis, in vitro receptor binding, and in vivo evaluation of fluorescein and carbocyanine peptide-based optical contrast agents. *J. Med. Chem.* **45**, 2003–2015. (c) Mujumdar, S. R., Mujumdar, R. B., Grant, C. M., and Waggoner, A. S. (1996) Cyanine-labeling reagents: sulfobenzindocyanine succinimidyl esters. *Bioconjugate Chem.* **7**, 356–362.
- (16) Dougherty, T. J., Gomer, C. J., Henderson, B. W., Jori, G., Kessel, D., Korbek, M., Moan, J., and Peng, Q. (1998) Photodynamic therapy. *J. Natl. Cancer Inst.* **90**, 889–905.



- (17) (a) Sternberg, E. D., Dolphin, D., and Bruckner, C. (1998) Porphyrin-based photosensitizers for use in photodynamic therapy. *Tetrahedron* **54**, 4151–4202. (b) Licha, K. (2002) Contrast agents for optical imaging. *Top. Curr. Chem.* **222**, 1–29.
- (18) Zheng, G., Li, H., Zhang, M., Chance, B., and Glickson, J. D. (2002) Low-density Lipoprotein Reconstituted by Pyropheophorbide Cholesteryl Oleate as Target Specific Photosensitizer. *Bioconjugate Chem.* **13**, 392–396.
- (19) Henderson, B. W., Bellnier, D. A., Greco, W. R., Sharma, A., Pandey, R. K., Vaughan, L. A., Weishaupt, K. R., and Dougherty, T. J. (1997) An in vivo quantitative structure–activity relationship for a congeneric series of pyropheophorbide derivatives as photosensitizers for photodynamic therapy. *Cancer Res.* **57**, 4000–4007.
- (20) Gurfinkel, M., Thompson, A. B., Ralston, W., Troy, T. L., Moore, A. L., Moore, T. A., Gust, J. D., Tatman, D., Reynolds, J. S., Muggenburg, B., Nikula, K., Pandey, R., Mayer, R. H., Hawrysz, D. J., Sevick-Muraca, E. M. (2000) Pharmacokinetics of ICG and HPPH-car for the detection of normal and tumor tissue using fluorescence, near-infrared reflectance imaging: A case study. *Photochem. Photobiol.* **72**, 94–102.
- (21) Quistorff, B., Haselgrove, J. C., and Chance, B. (1985) High spatial resolution readout of 3-D metabolic organ structure: an automated, low-temperature redox ratio-scanning instrument. *Anal. Biochem.* **148**, 389–400.
- (22) Weishaupt, K. R., Gomer, C. J., and Dougherty, T. J. (1976) Identification of singlet oxygen as the cytotoxic agent in photoinactivation of a murine tumor. *Cancer Res.* **36**, 2326–2329.
- (23) Chance, B., Schoener, B., Oshino, R., Itshak, F., and Nadase, Y. (1979) Oxidation–Reduction Ratio Studies of Mitochondria in Freeze-Trapped Samples. *J. Biol. Chem.* **254**, 4764–4771.
- (24) Gu, Y. Q., Qian, Z. Y., Chen, J. X., Blessington, D., Ramanujam, N., and Chance, B. (2002) High-resolution three-dimensional scanning optical image system for intrinsic and extrinsic contrast agents in tissue. *Rev. Sci. Instrum.* **73**, 172–178.
- (25) Ramanujam, N., Richards-Kortum, R., Thomsen, S., Mahadevan-Jansen, A., Follen, M., and Chance, B. (2001) Low-temperature fluorescence imaging of freeze-trapped human cervical tissues. *Opt. Express* **8**, 335–343.

BC034038N

## **Pyropheophorbide 2-Deoxyglucosamide: A New Photosensitizer Targeting Glucose Transporters**

Min Zhang, Zhihong Zhang, Dana Blessington, Hui Li, Theresa M. Busch, Vanessa Madrak, Jeremy Miles, Britton Chance, Jerry D. Glickson, and Gang Zheng \*

### **Supporting Information**

Figure 1. Absorption and fluorescence emission spectra of Pyro-2DG

Figure 2. PDT Laser setup for evaluating Pyro-2DG in 9L glioma bearing rat

Figure 3. HPLC chromatograms of Pyro-2DG

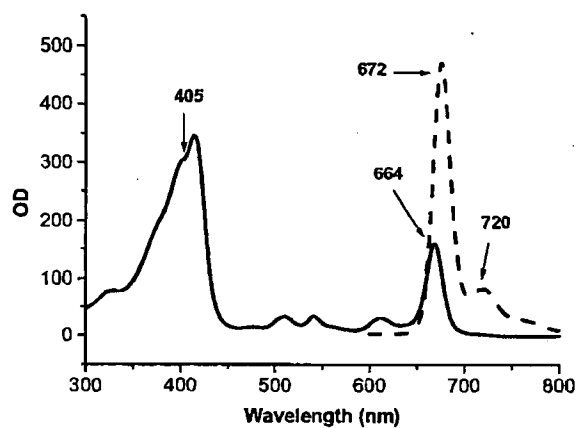


Figure 1. Spectroscopic properties of Pyro-2DG (solid line: absorption, dotted line: fluorescence).

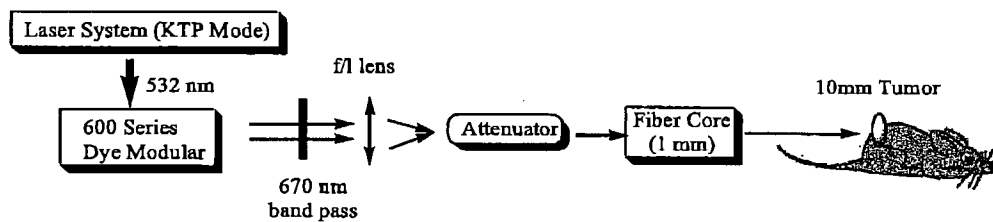


Figure 2. PDT Laser setup for evaluating Pyro-2DG in 9L glioma bearing rat.



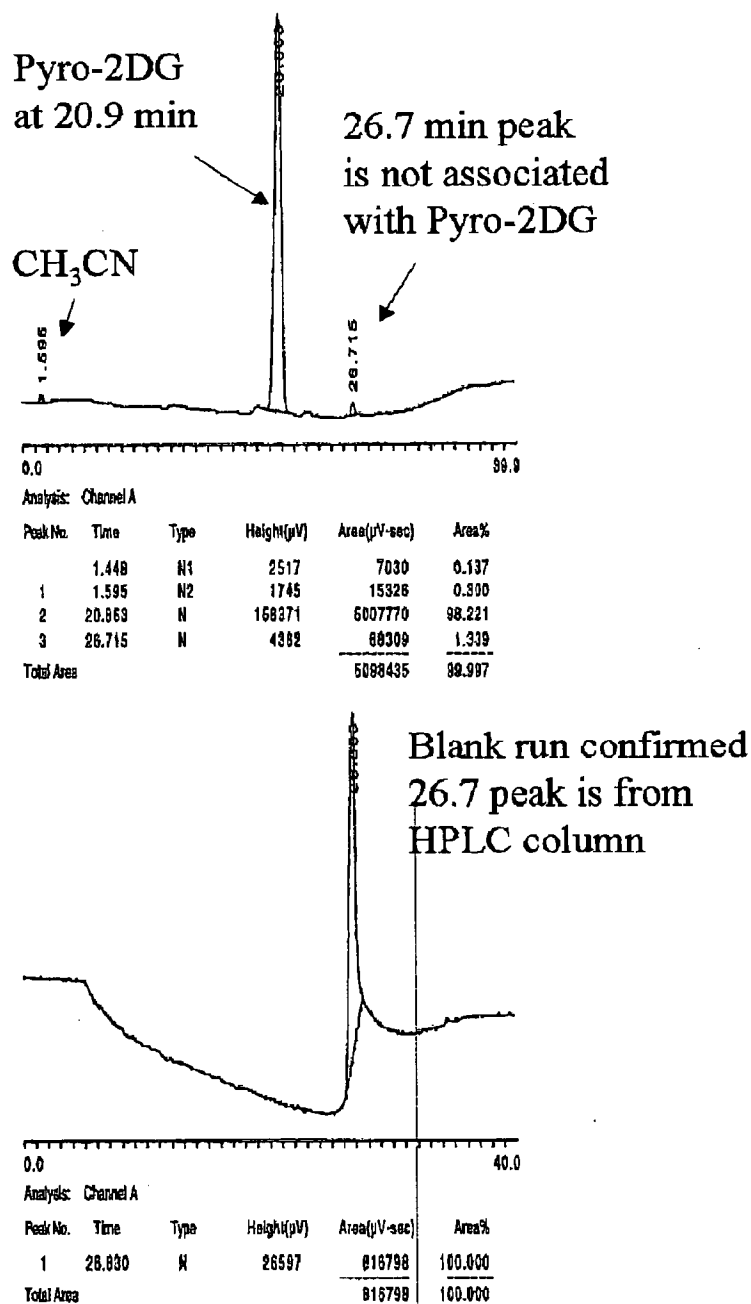


Figure 3. HPLC chromatograms of this compound that indicates its homogeneity. As shown in the top figure, the target compound is the major peak at 20.9 min (98.22%), however, the minor peak at 26.7 minute (1.34%) is not the impurity of our compound because blank run confirmed it is present in our HPLC column (see bottom figure). That makes purity of Pyro-2DG above 99.5%.

# **Pyropheophorbide 2-Deoxyglucosamide: A New Photosensitizer Targeting Glucose Transporters**

Min Zhang, Zhihong Zhang, Dana Blessington, Hui Li, Theresa M. Busch, Vanessa Madrak, Jeremy Miles, Britton Chance, Jerry D. Glickson, and Gang Zheng \*

## **Supporting Information**

Figure 1. Absorption and fluorescence emission spectra of Pyro-2DG

Figure 2. PDT Laser setup for evaluating Pyro-2DG in 9L glioma bearing rat

Figure 3. HPLC chromatograms of Pyro-2DG

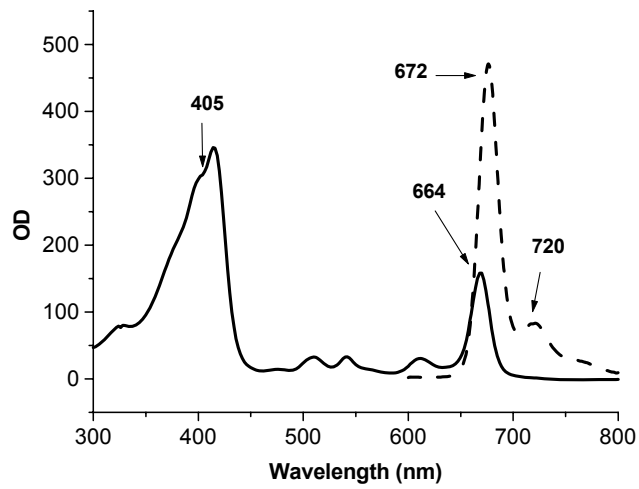


Figure 1. Spectroscopic properties of Pyro-2DG (solid line: absorption, dotted line: fluorescence).

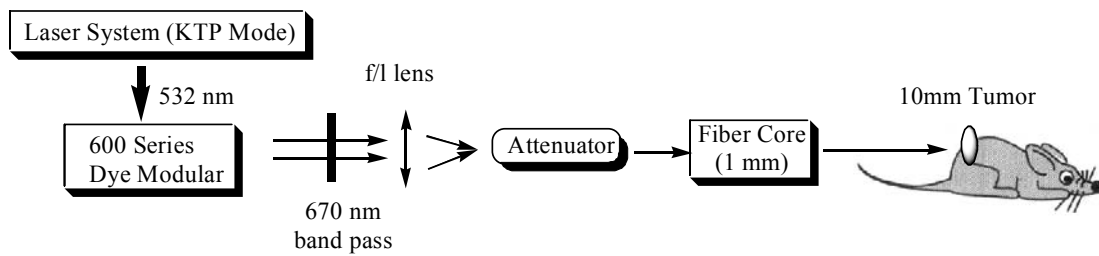


Figure 2. PDT Laser setup for evaluating Pyro-2DG in 9L glioma bearing rat.



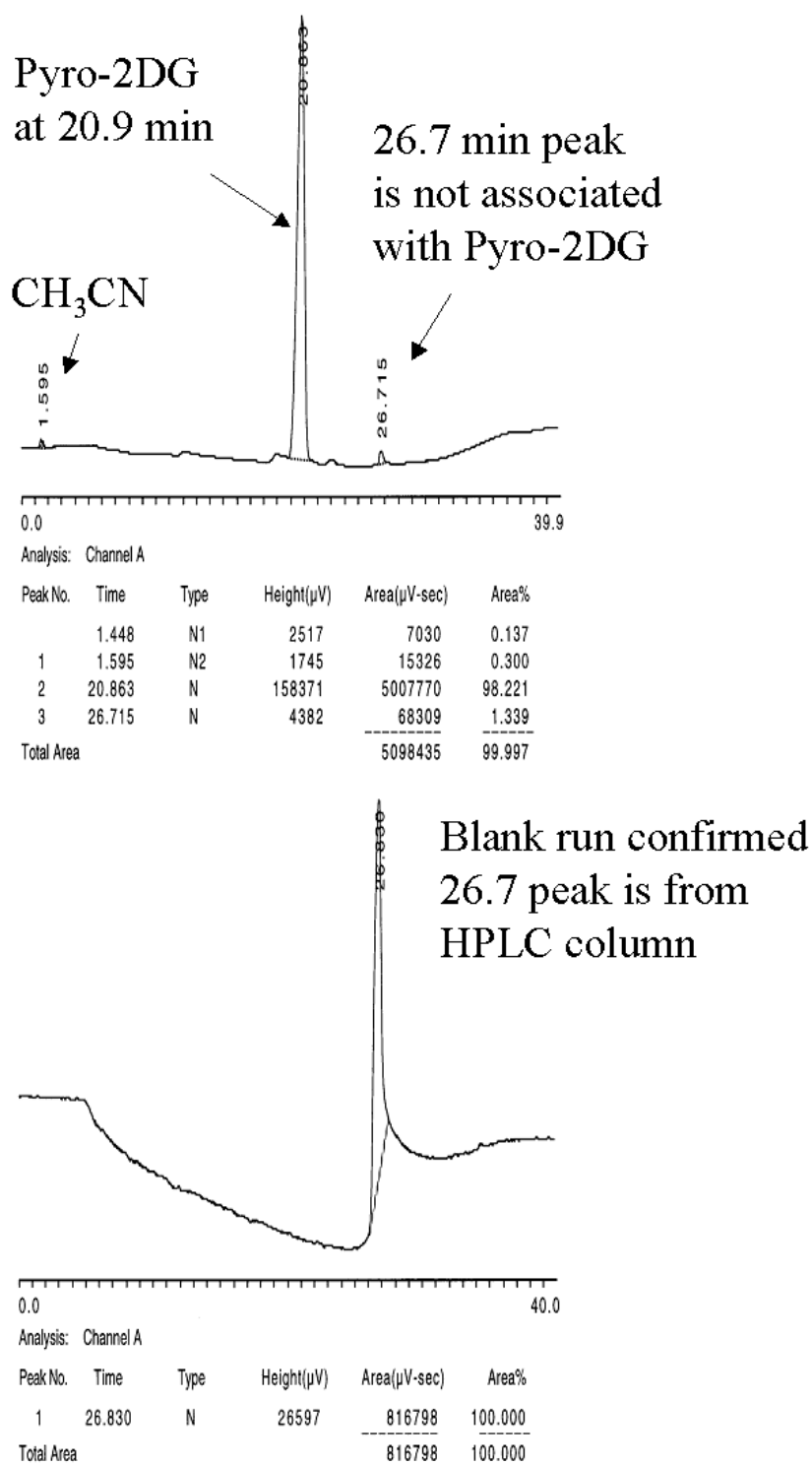


Figure 3. HPLC chromatograms of this compound that indicates its homogeneity. As shown in the top figure, the target compound is the major peak at 20.9 min (98.22%), however, the minor peak at 26.7 minute (1.34%) is not the impurity of our compound because blank run confirmed it is present in our HPLC column (see bottom figure). That makes purity of Pyro-2DG above 99.5%.

# Poly(L-glutamic acid) Gd(III)-DOTA Conjugate with a Degradable Spacer for Magnetic Resonance Imaging

Zheng-Rong Lu,<sup>\*,†</sup> Xinghe Wang,<sup>†</sup> Dennis L. Parker,<sup>‡</sup> K. Craig Goodrich,<sup>§</sup> and Henry R. Buswell<sup>‡</sup>

Department of Pharmaceutics and Pharmaceutical Chemistry, Department of Radiology, University of Utah, Salt Lake City, Utah 84108 and Department of Radiology, LDS Hospital, Salt Lake City, Utah 84102. Received March 26, 2003

The clinical application of macromolecular Gd(III) complexes as MRI contrast agents is impeded by their slow excretion and potential toxicity due to the release of Gd(III) ions caused by the metabolism of the agents. A polymer Gd(III) chelate conjugate with a cleavable spacer has been designed to solve this problem. Poly(L-glutamic acid)–cystamine–[Gd(III)-DOTA] was prepared by the conjugation of DOTA to PGA (MW = 50 000) via cystamine, a cleavable disulfide spacer, followed by the complexation with GdCl<sub>3</sub>. A Gd(III) DOTA chelate derivative was readily released from the polymer conjugate in the incubation with cysteine, an endogenous plasma thiol. The conjugate produced significant MRI blood pool contrast enhancement in nude mice bearing OVCAR-3 human ovarian carcinoma xenografts. Less significant contrast enhancement was observed for a small molecular contrast agent, Gd(DTPA-BMA). The pharmacokinetic MRI study showed that the Gd(III) chelate from the conjugate accumulated in the urinary bladder in a similar kinetic pattern to Gd(DTPA-BMA), suggesting that the chelate was released by the endogenous thiols and excreted through renal filtration. The preliminary results suggest that this novel design has a great potential to solve the safety problem of macromolecular MRI contrast agents.

Paramagnetic metal chelates Gd(III)-DTPA, Gd(III)-DOTA, and their derivatives increase the relaxation rate of surrounding water protons and are used as contrast agents for magnetic resonance imaging (MRI) (1). However, these low molecular weight contrast agents cannot effectively discriminate diseased tissue from normal tissues. Macromolecular Gd(III) complexes have been developed by conjugating these Gd(III) chelates to biomedical polymers, including poly(amino acids) (2, 3), polysaccharides (4, 5), dendrimers (6–8), proteins (9, 10), etc, to improve image contrast enhancement. These macromolecular agents have demonstrated superior contrast enhancement for blood pool imaging and cancer imaging in animal models. Unfortunately, the clinical application of macromolecular agents is limited by their slow excretion after MRI exams (11, 12) and potential toxicity of Gd(III) ions released by the metabolism of the agents (13–15). Recently, there have been some efforts to facilitate the clearance of macromolecular Gd(III) complexes. For example, lysine has been coinjected with dendrimer-based macromolecular agents to facilitate their renal clearance by blocking the renal tubular reabsorption (16). However, this approach cannot facilitate the clearance of macromolecules of relatively high molecular weights. Innovative design of macromolecular Gd(III) complexes is needed to accelerate the clearance

of Gd(III) complexes after the MRI examinations and to reduce the potential side effects of macromolecular contrast agents.

We hypothesize that the conjugation of Gd(III) chelates to biomedical polymers via biodegradable spacers can facilitate the excretion of Gd(III) chelates and result in safe, effective macromolecular MRI contrast agents. The macromolecular agents will be relatively intact during the imaging. The Gd(III) chelates can then be gradually released from the polymers by the cleavage of the spacers with endogenous biomolecules. The release of Gd(III) chelates from macromolecules can also be accelerated in a controllable way by administering exogenous substances after the imaging examination. Organic disulfide–thiol exchange reaction plays a crucial role in biological systems, and the disulfide bond can be readily released by the thiols present in the body. The disulfide bond appears to be an ideal cleavable spacer to conjugate Gd(III) chelates to biomedical polymers. Since macromolecular Gd(III) complexes are extracellular MRI contrast agents and the thiol concentration in the plasma is relatively low, approximately 15  $\mu$ M (17, 18), the cleavage rate of the disulfide spacer will be relatively slow in the plasma. The macromolecular agents will have an adequate plasma stability and provide an acceptable time window for effective contrast-enhanced diagnostic imaging. The rate of cleavage of the disulfide spacer and excretion of Gd(III) chelates can also be accelerated with exogenous thiols after the MRI examinations.

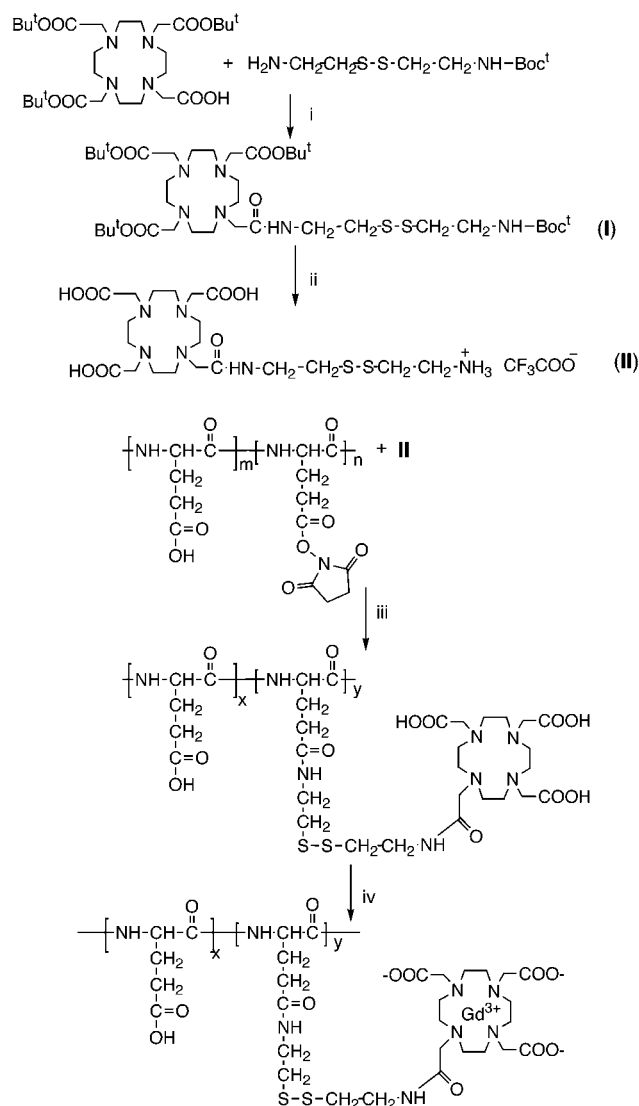
We report here the synthesis and preliminary evaluation of the first polymer–Gd(III) chelate conjugate with a degradable disulfide spacer. We used anionic poly(L-glutamic acid) (PGA) as the macromolecular carrier for Gd(III) chelates and cystamine as the cleavable spacer. Poly(L-glutamic acid) is an anionic biocompatible poly-

\* Address correspondence to this author. Dr. Zheng-Rong Lu, Assistant Professor, The University of Utah, Department of Pharmaceutics and Pharmaceutical Chemistry, 421 Wakara Way, Suite 318, Salt Lake City, UT 84108. Phone: 801 587-9450. Fax: 801 585-3614. E-mail: zhengrong.lu@utah.edu.

<sup>†</sup> Department of Pharmaceutics and Pharmaceutical Chemistry, University of Utah.

<sup>‡</sup> Department of Radiology, University of Utah.

<sup>§</sup> LDS Hospital.

**Scheme 1. Synthesis of PGA-Cystamine-[Gd(III)DOTA] Conjugate<sup>a</sup>**


<sup>a</sup> (i) TBTU, *N*-hydroxysuccinimide, DMF, rt, 3 h, 89%; (ii) trifluoroacetic acid, rt, 4.5 h, 86%; (iii) DMAP, DMF, rt, overnight, NaOH, 80%; (iv) GdCl<sub>3</sub>, Na<sub>2</sub>-EDTA, pH 5.0–5.5, rt, 24 h, 91%.

mer, which has been used as a macromolecular carrier for drug delivery (19). PGA is less cytotoxic than cationic polymers including polylysine and PAMAM dendrimer (20, 21). The carboxylic groups in PGA are suitable for the conjugation of a relatively large number of paramagnetic metal chelates per polymer chain, which is important for effective contrast enhanced MRI. Macrocyclic 1,4,7,10-tetraazacyclododecane-*N,N,N',N''*-tetraacetic acid (DOTA) gadolinium(III) chelate has a high thermodynamic and in vivo kinetic stability (22) and was conjugated to PGA via cystamine.

The synthesis of PGA-cystamine-[Gd(III)DOTA] conjugate is described in Scheme 1. Mono-Boc-cystamine was first prepared by reacting an excess of cystamine with di-*tert*-butyl dicarbonate similarly as described in the literature (23). 1,4,7,10-Tetraazacyclododecane-1,4,7-tris(acetic acid-*tert*-butyl ester)-10-acetic acid *N*-Boc-cystamine amide (I) was then prepared by the reaction of 1,4,7,10-tetraazacyclododecane-1,4,7-tris(acetic acid-*tert*-butyl ester)-10-acetic acid (TB-DOTA, Macrocyclics, Dallas, TX) with mono-Boc-cystamine in the presence of 2-(1*H*-benzotriazol-1-yl)-1,1,3,3-tetramethyluronium tet-

rafluoroborate (TBTU, Nova Chemicals) and *N*-hydroxysuccinimide in a high yield. The use of *N*-hydroxysuccinimide was crucial to minimize the side reactions. In the absence of *N*-hydroxysuccinimide, the reaction was complicated, and the yield of compound I was very low. The reaction mechanism may involve the formation of an *N*-hydroxysuccinimide active ester intermediate. Compound I was characterized by proton NMR and electrospray ionization mass spectrometry (*m/z*: 807.57 (*M*<sup>+</sup> + 1), calculated 807.46).

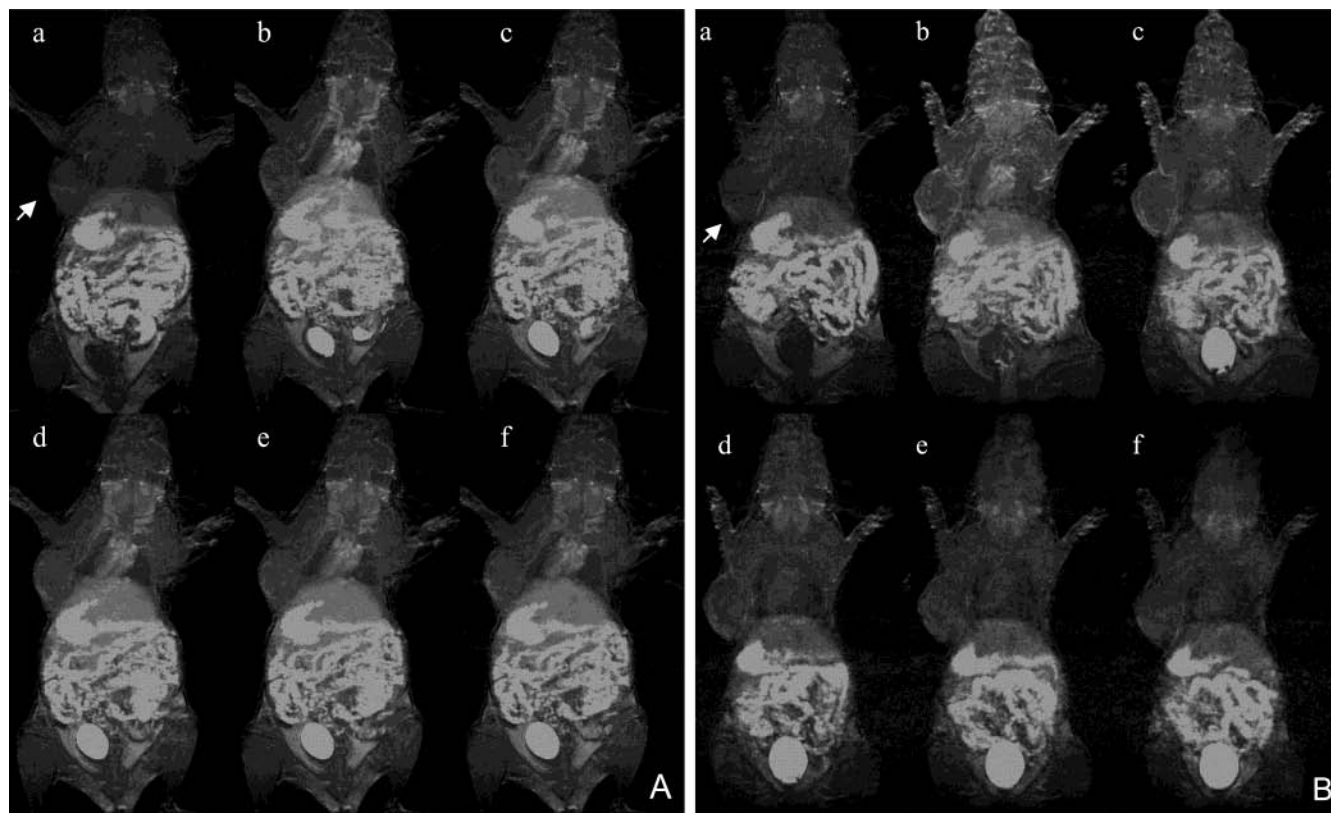
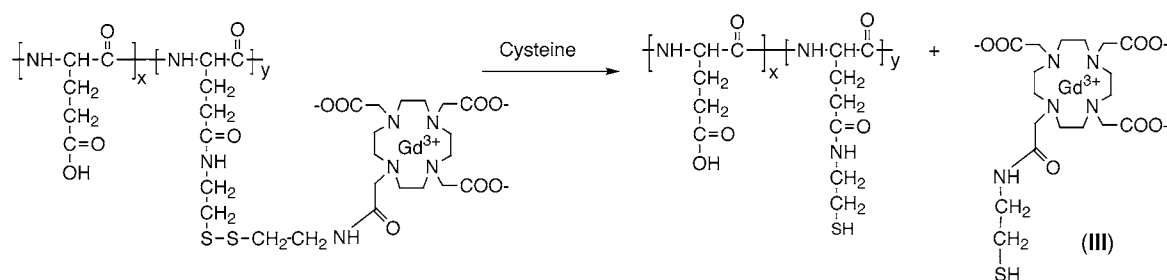
A cystamine-containing DOTA derivative (II) was prepared by the deprotection of compound I with trifluoroacetic acid in a high yield. The product was characterized by proton NMR and electrospray ionization mass spectrometry. The *m/z* (*M*<sup>+</sup> + 1) of the compound II was 539.1 (calculated 539.22). The *t*-Boc deprotection took a relatively long reaction time because *tert*-butyl ester was difficult to remove with trifluoroacetic acid. We attempted to conjugate TB-DOTA-cystamine to PGA after partial deprotection and found that it took longer to completely remove the *t*-Boc ester in the polymer conjugate.

Poly(L-glutamic acid)-cystamine-DOTA conjugate was prepared by the reaction of amino group of DOTA-cystamine with the PGA *N*-hydroxysuccinimide esters in the presence of (dimethylamino)pyridine. PGA *N*-hydroxysuccinimide esters were prepared by reaction of PGA (MW = 54 000 Da, Sigma, St. Louis, MO) with *N*-hydroxysuccinimide in the presence of 1-ethyl-3-(3-dimethylaminopropyl)carbodiimide hydrochloride (EDC) (24). When the conjugation reaction was complete, unreacted active esters in the polymer conjugate were hydrolyzed in NaOH aqueous solution. The PGA-cystamine-DOTA conjugate was purified by size exclusion chromatography (SEC) on a Sephadex G-25 column to remove unreacted DOTA-cystamine. The conjugate was characterized by proton NMR and signals corresponding to both DOTA and PGA were identified in the spectrum. The content of DOTA was approximately 10%-molar, as estimated from the signal intensities of NCH<sub>2</sub>CH<sub>2</sub>N of DOTA and CH<sub>2</sub> of PGA.

PGA-cystamine-[Gd(III)-DOTA] conjugate was prepared by the complexation PGA-cystamine-DOTA with GdCl<sub>3</sub>. An excess of GdCl<sub>3</sub>, based on DOTA content in the conjugate, was used to ensure complete complexation of DOTA in the conjugate. Precipitate was formed when GdCl<sub>3</sub> was added, possibly due to the complexation with carboxylic groups of PGA with Gd<sup>3+</sup> ions. EDTA disodium salt was used to remove the excess Gd(III) ions from the PGA, resulting in a clear reaction mixture at pH 5.0–5.5, adjusted with dilute NaOH. EDTA is a chelate ligand, forming complex with Gd<sup>3+</sup> ions of intermediate stability. It can readily strip off the Gd(III) ions stuck to PGA and will not affect the formation of more stable Gd(III)-DOTA complexes. The PGA-cystamine-[Gd(III)-DOTA] conjugate was purified by SEC on a Sephadex G-25 column to remove Gd(III)-EDTA complex. The gadolinium content was 0.50 mmol-Gd per gram of polymer conjugate as determined by ICP-OES after purification. The molar content was 10%, same as the content estimated from the proton NMR.

The *T*<sub>1</sub> of PGA-cystamine-[Gd(III)-DOTA] conjugate at various concentration in aqueous solution was measured using a B1 homogeneity corrected Look-Locker technique on a 1.5T GE NV/CVi scanner with the LX 8.4 operating system at room temperature (25). The *T*<sub>1</sub> relaxivity of the conjugate was 2.50 mM<sup>-1</sup> s<sup>-1</sup> per complexed Gd(III) ion, lower than that of Gd-DOTA (1). It may be attributed to the competitive coordination of carboxylic groups in PGA to the Gd(III) ions, which



**Scheme 2. Release of Gd(III)-DOTA from the Conjugate by Cysteine**

**Figure 1.** Contrast enhanced three-dimensional (MIP) MR images of mice bearing tumors using PGA-cystamine-(Gd-DOTA) (A) and Gd-(DTPA-BMA) (B). The images were taken before contrast (a), and 5 (b), 15 (c), 30 (d), 45 (e), and 60 (f) min postinjection. The arrow points to the tumor.

interfere the coordination of water molecules to its ninth coordination site in the polymer conjugate. The coordination of bulky water molecules is crucial for the relaxivity of Gd(III) complexes.

To verify the cleavage of the disulfide spacer and release of Gd(III)DOTA chelate, PGA-cystamine-[Gd(III)-DOTA] was incubated with cysteine. Disulfide-thiol exchange reaction between the disulfide spacer and cysteine resulted in the cleavage of the spacer and release of a Gd(III)DOTA chelate derivative (Scheme 2. Gd(III)-DOTA-cysteimine (**III**)) with gadolinium mass distribution pattern ( $m/z = 616.03\text{--}621.08$ ,  $M^+ + 1$ ;  $638.02\text{--}643.03$ ,  $M^+ + \text{Na}$ ) was identified in MALDI-TOF mass spectrum of the incubation mixture. The identification of compound **III** confirmed the degradability of disulfide spacer of PGA-cystamine-[Gd(III)DOTA] conjugate by disulfide-thiol exchange reaction.

The MRI contrast enhancement of the PGA-cystamine-(Gd-DOTA) conjugate was preliminarily evaluated in nude female mice bearing xenografts of OVCAR-3 human ovarian carcinoma (26) with Gd-(DTPA-BMA) as a control. The mice were anesthetized by intraperitoneal administration of a mixture of ketamine and telazol. The

contrast agents were injected intravenously in a tail vein at a dose of  $0.1 \text{ mmol-Gd/kg}$ . A three-dimensional spoiled gradient echo (SPGR) pulse sequence was used for MR imaging.

Figure 1 shows the three-dimensional MR images of mice bearing OVCAR-3 tumor xenografts before contrast and at various time points after the injection of the polymer conjugate and Gd-(DTPA-BMA), respectively. The low molecular weight control agent did not produce significant contrast enhancement of the blood vessels. It brightened the tumor tissue as well as surrounding normal tissue at the initial period after injection, and the image contrast enhancement of the tumor tissue was not significant. The polymer conjugate had a long blood pool retention time and resulted in much more significant contrast enhancement in the heart and blood vessels than the low molecular weight control. An angiogenic blood vessel to the tumor was clearly revealed by the polymer conjugate. The polymer conjugate also produced better image contrast between the tumor tissue and normal tissue. The signal intensity in the tumor gradually increased up to 45 min postinjection. The signal intensities in the heart and blood vessels gradually decreased

over time, but significant contrast enhancement was still visible 1 h postinjection with the conjugate. Most interestingly, the signal intensity of the urinary bladder of the mouse injected with the polymer conjugate increased in a similar pharmacokinetic pattern to that of mouse with the control agent. The increasing signal intensity suggests the accumulation of Gd(III) complexes in the urinary bladder. The result indicates that the Gd chelate was gradually released from the conjugate by the endogenous thiols, excreted through renal filtration, and accumulated in the urinary bladder similarly to the low molecular weight agent.

These preliminary results have shown that the disulfide spacer in PGA–cystamine–[Gd(III)DOTA] conjugate can be readily cleaved by cysteine, a plasma thiol, to release the Gd(III) chelate from the polymer carrier. Because the plasma thiol concentration is very low, approximately 15  $\mu$ M, in vivo cleavage of the disulfide spacer, release, and excretion of Gd(III) chelates would be a gradual process, as shown by the pharmacokinetic imaging study. The paramagnetic polymer conjugate was relatively stable with an acceptable time window for effective contrast enhanced MRI, especially for contrast-enhanced blood pool imaging. The Gd(III) chelates was gradually released from the polymer carrier by the endogenous thiols including cysteine and glutathione and excreted via renal filtration. The in vivo degradability of disulfide spacer can be adjusted with chemical modification around the spacer (27). The release and excretion of Gd(III) chelates can also be accelerated with administration of exogenous thiols after the MRI examinations. Currently, a number of thiols are approved for human uses. For example, glutathione is used as a nutritional supplement (28), and *N*-acetylcysteine was used in nuclear medicine to prevent contrast nephropathy (29).

The degradable disulfide spacer between Gd(III)DOTA and PGA is crucial for the release and excretion of Gd(III) chelates, although PGA is a biodegradable polymer. As matter of fact, the slow excretion of macromolecular contrast agents was mainly observed for the agents based on typical biodegradable polymers including polylysine (11, 12), protein (13), and polysaccharides (14). The degradation of these macromolecules is an enzymatic reaction, occurring in the subcellular compartments. Furthermore, the degradation rate often dramatically decreases with chemical modification (30). The cleavage of the disulfide spacer can readily occur in the plasma, which avoid the slow passive cellular internalization of macromolecules, resulting in more rapid excretion Gd(III) chelates.

In summary, the novel design of macromolecular Gd(III) chelate with a degradable disulfide spacer has a great promise to solve the safety problems suffered by macromolecular Gd(III) complexes due to their slow clearance and potential toxic side effects. The polymer conjugate will have application in contrast enhanced blood pool imaging and cancer imaging. Further evaluation of PGA–cystamine–[Gd(III)DOTA] conjugate is ongoing.

**Supporting Information Available:** Experimental details. This material is available free of charge via the Internet at <http://pubs.acs.org>.

#### LITERATURE CITED

- (1) Caravan, P., Ellison, J. J., McMurry, T. J., and Lauffer, R. B. (1999) Gadolinium (III) chelates as MRI contrast agents: Structure, dynamics, and applications. *Chem. Rev.* 99, 2293–2352.
- (2) Schuhmann-Giampieri, G., Schmitt-Willich, H., Frenzel, T., Press, W. R., and Weinmann, H. J. (1991) In vivo and in vitro evaluation of Gd-DTPA-polylysine as a macromolecular contrast agent for magnetic resonance imaging. *Invest. Radiol.* 26, 969–974.
- (3) Weissleder, R., Bogdanov, A., Jr., Tung, C. H., Weinmann, H. J. (2001) Size optimization of synthetic graft copolymers for in vivo angiogenesis imaging. *Bioconjugate Chem.* 12, 213–219.
- (4) Rongved, P., and Klaveness, J. (1991) Water-soluble polysaccharides as carriers of paramagnetic contrast agents for magnetic resonance imaging: synthesis and relaxation properties. *Carbohydr. Res.* 214, 315–323.
- (5) Gibby, W. A., Bogdan, A., and Ovitt, T. W., (1989) Cross-linked DTPA polysaccharides for magnetic resonance imaging. *Invest. Radiol.* 24, 302–309.
- (6) Wiener, E. C., Brechbiel, M. W., Brothers, H., Magin, R. L., Gansow, O. A., Tomalia, D. A., and Lauterbur, P. C. (1994) Dendrimer-based metal chelates: a new class of magnetic resonance imaging contrast agents. *Magn. Reson. Med.* 31, 1–8.
- (7) Bryant, L. H., Brechbiel, M. W., Wu, C., Bulte, J. W. M., Herynek, V., and Frank, J. A. (1999) Synthesis and relaxation of high generation ( $G = 5, 7, 9$  and  $10$ ) PAMAM dendrimer-DOTA-gadolinium chelates. *J. Magn. Reson. Imaging* 9, 348–352.
- (8) Kobayashi, H., Sato, N., Kawamoto, S., Saga, T., Hiraga, A., Haque, T. L., Ishimori, T., Konishi, J., Togashi, K., and Brechbiel, M. W. (2001) Comparison of the macromolecular MR contrast agents with ethylenediamine-core versus ammonia-core generation-6 polyamidoamine dendrimer. *Bioconjugate Chem.* 12, 100–107.
- (9) Lauffer, R., and Brady, T. J. (1985) Preparation and water relaxation properties of proteins labeled with paramagnetic metal chelates. *Magn. Reson. Imaging* 3, 11–16.
- (10) Roberts, H. C., Saeed, M., Roberts, T. P., Muhler, A., Shames, D. M., Mann, J. S., Stiskal, M., Demsar, F., and Brasch, R. C. (1997) Comparison of albumin-(Gd-DTPA)<sub>30</sub> and Gd-DTPA-24-cascade-polymer for measurements of normal and microvascular permeability. *J. Magn. Reson. Imaging* 7, 331–338.
- (11) Schuhmann-Giampieri G., Schmitt-Willich H., Frenzel T., Press W. R., and Weinmann H. J. (1991) In vivo and in vitro evaluation of Gd-DTPA-polylysine as a macromolecular contrast agent for magnetic resonance imaging. *Invest. Radiol.* 26, 969–974.
- (12) Bogdanov, A. A., Jr., Weissleder R., Frank H. W., Bogdanova A. V., Nossif N., Schaffer B. K., Tsai E., Papisov M. I., and Brady T. J. (1993) A new macromolecule as a contrast agent for MR angiography: preparation, properties, and animal studies. *Radiology* 187, 701–706.
- (13) Franano, F. N., Edwards, W. B., Welch, M. J., Brechbiel, M. W., Gansow, O. A., and Duncan, J. R. (1995) Biodistribution and metabolism of targeted and nontargeted protein-chelate-gadolinium complexes: evidence for gadolinium dissociation in vitro and in vivo. *Magn. Reson. Imaging* 13, 201–214.
- (14) Rebizak, R., Schaefer, M., and Dellacherie, E. (1998) Polymeric conjugates of Gd<sup>3+</sup>-diethylenetriaminepentaacetic acid and dextran. 2. Influence of spacer arm length and conjugate molecular mass on the paramagnetic properties and some biological parameters. *Bioconjugate Chem.* 9, 94–99.
- (15) Kobayashi, H., Kawamoto, S., Jo, S.-K., Bryant, H. L., Jr., Brechbiel M. W., and Star, R. A. Macromolecular MRI contrast agents with small dendrimers: pharmacokinetic differences between sizes and cores. *Bioconjugate Chem.*, in press.
- (16) Kobayashi, H., Sato, N., Kawamoto, S., Saga, T., Hiraga, A., Ishimori, T., Konishi, J., Togashi, K., and Brechbiel, M. W. (2001) Novel intravascular macromolecular MRI contrast agent with generation-4 polyamidoamine dendrimer core: accelerated renal excretion with co-injection of lysine. *Magn. Reson. Med.* 46, 457–464.

- (17) Andersson, A., Lindgren, A., and Hultberg, B. (1995) Effect of thiol oxidation and thiol export from erythrocytes on determination of redox status of homocysteine and other thiols in plasma from healthy subjects and patients with cerebral infarction. *Clin. Chem.* 41, 361–366.
- (18) Deneke, S. M. (2000) Thiol-based antioxidants. *Curr. Top. Cell Regul.* 36, 151–180.
- (19) Li, C. (2002) Poly(L-glutamic acid)-anticancer drug conjugates. *Adv. Drug Delivery Rev.* 54, 695–713.
- (20) Duncan, R., Bakoo, M., and Riley, M. L. (1991) Soluble drug carriers: haemocompatibility. In *Progress in Membrane Biotechnology* (J. C. Gomez-Fernandez, D. Chapman, and L. Packer, Eds.) pp 253–265, Birkhayser Verlag, Basel, Switzerland.
- (21) Malik, N., Wiwattanapatapee, R., Klopsch, R., Lorenz, K., Frey, H., Weener, J. W., Meijer, E. W., Paulus, W., and Duncan, R. (2000) Dendrimers: Relationship between structure and biocompatibility in vitro, and preliminary studies on the biodistribution of  $^{125}\text{I}$ -labeled PAMAM dendrimers in vivo. *J. Controlled Release* 65, 133–148.
- (22) Magerstadt, M., Gansow, O. A., Brechbiel, M. W., Colcher, D., Baltzer, L., Knop, R. H., Girton, M. E., and Naegele, M. (1986) Gd(DOTA): an alternative to Gd(DTPA) as a T1,2 relaxation agent for NMR imaging or spectroscopy. *Magn. Reson. Med.* 3, 808–812.
- (23) Callahan, J. F., Ashton-Shue, D., Bryan, H. G., Bryan, W. M., Kechman, G. D., Kinter, L. B., McDonald, J. E., Moore, M. L., Schmidt, D. B., Silvestri, J. S., Stassen, F. L., Sulat, L., Yim, N. C. F., and Hoffman, W. F. (1989) Structure–activity relationships of novel vasopressin antagonists containing C-terminal diaminoalkanes and (aminoalkyl)guanidines. *J. Med. Chem.* 32, 391–396.
- (24) Iwata, H., Matsuda, S., Mitsuhashi, K., Itoh E., and Ikada, Y. (1998) A novel surgical glue composed of gelatin and N-hydroxysuccinimide activated poly(L-glutamic acid): part 1. synthesis of activated poly(L-glutamic acid) and its gelation with gelatin. *Biomaterials* 19, 1869–1876.
- (25) Parker, D. L., Christian, B. A., Goodrich, K. C., Alexander, A. L., Buswell, H. R. and Yoon, C. Improved accuracy in T<sub>1</sub> measurements. *Proc. ISMRM*, Sydney, Australia, April, 1998; p 2171.
- (26) Lu, Z.-R., Shiah, J.-G., Kopeckova, P., and Kopecek, J. (2001) Preparation and biological evaluation of polymerizable antibody Fab' fragment targeted polymeric drug delivery system. *J. Controlled Release* 74, 263–268.
- (27) Thorpe, P. E., Wallace, P. M., Knwoles, P. P., Relf, M. G., Brown, A. N., Watson, G. J., Knyba, R. E., Wawrzynczak, E. J., and Blakey, D. C. (1987) New coupling agents for the synthesis of immunotoxins containing a hindered disulfide bond with improved stability in vivo. *Cancer Res.* 47, 5924–5931.
- (28) Valencia, E., and Hardy, G. (2002) Practicalities of glutathione supplementation in nutritional support. *Curr. Opin. Clin. Nutr. Metab. Care* 5, 321–326.
- (29) Tepel, M., and Zidek, W. (2002) Acetylcysteine and contrast media nephropathy. *Curr. Opin. Nephrol. Hypertens.* 11, 503–506.
- (30) Crepon, B., Jozefonvicz, J., Chytry, V., Rihova, B., and Kopecek, J. (1991) Enzymatic degradation and immunogenic properties of derivatized dextrans. *Biomaterials* 12, 550–554.

BC0340464



## Materials and Methods

Poly(*L*-glutamic acid) sodium salt (MW 54,000 Da) was purchased from Sigma, St. Louis, MO. 1,4,7,10-Tetraazacyclododecane-1,4,7-tris(acetic acid-*t*-butyl ester)-10-acetic acid (TB-DOTA) was purchased from Macrocyclics, Dallas, TX. 1-Ethyl-3-(3-dimethylaminopropyl)carbodiimide hydrochloride (EDC), 2-(1H-benzotriazole-1-yl)-1,1,3,3-tetramethyluronium tetrafluoroborate (TBTU) and di-*tert*-butyl dicarbonate were from Nova Chemicals. Cystamine dichloride was obtained from Fluka. Solvent and all other agents were reagent grade or better.

**Mono-Boc-cystamine.** Mono-Boc-cystamine was prepared similarly as described [21]. <sup>1</sup>H NMR(CDCl<sub>3</sub>, ppm): 1.42 (s, 9 H, *t*Bu), 2.77 (m, 6H, SCH<sub>2</sub>, NCH<sub>2</sub>), 2.98 (t, 2H, CONCH<sub>2</sub>), 3.42 (sh, 2H, NH<sub>2</sub>), 3.63 (sh, 1H, NH).

**1,4,7,10-Tetraazacyclododecane-1,4,7-tris(acetic acid-*t*-butyl ester)-10-acetic acid N'-Boc-cystamine amide (I).** TB-DOTA (200 mg, 0.35 mmol) and N-hydroxysuccinimide (HOSu, 100 mg, excess) were dissolved in 5 ml anhydrous DMF. HBTU (130 mg, excess) was added to above solution and the mixture was kept for 10 min. Mono-Boc-cystamine was then added and the mixture was stirred for 3 hours at r.t. The solvent was evaporated under vacuum and dilute NaOH was added to the residue. The mixture was extracted with CH<sub>2</sub>Cl<sub>2</sub> (30 ml x 3). The organic layers were combined and dried with anhydrous NaSO<sub>4</sub>. The solvent was evaporated under vacuum and the residue was recrystallized with CH<sub>2</sub>Cl<sub>2</sub> and hexane. Yield: 250 mg, 89%. <sup>1</sup>H-NMR (CDCl<sub>3</sub>, ppm): 1.43 (s, 36H, *t*Bu), 2.40 (t, 4H, SCH<sub>2</sub>), 2.49 (t, 4H, SCH<sub>2</sub>), 2.75 – 3.55 (m, 24 H, NCH<sub>2</sub>), 5.02 (sh, 1H, NH), 5.18 (sh, 1H, NH). MS (scan ES<sup>+</sup>, m/z): 807.57 (M<sup>+</sup>+1, calculated 806.46).

**1,4,7,10-Tetraazacyclododecane-1,4,7-tris(acetic acid)-10-acetic acid cystamine monoamide (II).** Compound **II** (250 mg) was dissolved in 3 ml trifluoroacetic acid, and the mixture was kept for 4.5 hours at r.t. Trifluoroacetic acid was evaporated undervacuum and the residue was treated with ether. A colorless solid was collected and washed with ether, dried under vacuum. Yield: 230 mg, 86% (calculated based on di-trifluoroacetate).  $^1\text{H-NMR}(\text{D}_2\text{O}, \text{ppm})$ : 2.74 (m, 4H,  $\text{SCH}_2$ ), 2.89 (m, 4H,  $\text{NCH}_2$  of cystamine), 3.0 – 3.40 (m, 16H,  $\text{NCH}_2$  of the ring), 3.42 (s, 2H,  $\text{CH}_2\text{CON}$ ), 3.50-3.70 (m, 6H,  $\text{CH}_2\text{COOH}$ ). MS (scan  $\text{ES}^+$ ,  $m/z$ ): 539.1 ( $\text{M}^++1$ , calculated 538.22).

**PGA-cystamine-DOTA conjugate.** PGA sodium salt (1.0 g) was dissolved in deionized water (50 ml) and acidified with dilute hydrochloric acid to pH 2.0. The solution was desalted by dialysis with a membrane of molecular weight cutoff 6,000 – 8,000 Da against deionized water. PGA was recovered after evaporating water under vacuum giving a colorless solid. PGA (250 mg), N-hydroxysuccinimide (250 mg) and EDC (250 mg) was dissolved in anhydrous DMF and stirred overnight at room r.t. The reaction mixture was then added dropwise to precipitate PGA-OSu active ester. The polymer was collected by filtration, washed with ether and dried under vacuum (yield: 90 %). PGA-OSu (150 mg), compound **II** (120 mg) and dimethylaminopyridine (100 mg) were dissolved in 20 ml DMF. The mixture was stirred overnight and then the solvent was evaporated under vacuum. The residue was dissolved in 1.0 N NaOH aqueous solution. The polymer conjugates was purified by size exclusion chromatography (SEC) with Pharmacia Sephadex G-25, eluted with deionized water. The polymer fraction was collected and lyophilized. Yield: 120 mg. The content of the conjugated DOTA was approximately 10 %-molar as estimated from the proton NMR

spectrum of PGA-cystamine-DOTA.

**PGA-cystamine-[Gd(III)-DOTA] conjugate.** PGA-cystamine-DOTA (120 mg) was dissolved in 2 ml deionized water and  $\text{GdCl}_3$  (80 mg) was added. EDTA disodium salt solution was added with stirring until a clear solution was obtained. The pH of the reaction mixture was adjusted to 5.0 – 5.5 with dilute NaOH. The reaction mixture was stirred for 24 hours at r.t. The polymer conjugate was isolated by SEC with Pharmacia G-25, eluted with deionized water. The polymer fraction was collected and lyophilized. Yield: 110 mg. The gadolinium content was determined at 342 nm by inductively coupled plasma optical emission spectroscopy (ICP-OES, Perkin Elmer Optima 3100XL). The  $T_1$  and  $T_2$  relaxivities of the conjugate were measured in water on a 1.5 T GE NV/CVi MRI scanner at room temperature.

**Release of Gd(III)DOTA chelate.** PGA-cystamine-[Gd(III)DOTA] (2 mg) and cysteine or N-acetylcysteine (1 mg) were dissolved in deionized water and the pH was adjusted to 7.0. The reaction mixture was kept at room temperature until mass spectrometric analysis. The reaction mixtures were characterized by MALDI-TOF mass spectrometry.

**MR imaging.** The MRI contrast enhancement of the PGA-cystamine-(Gd-DOTA) conjugates were preliminarily evaluated in nude mice bearing xenographs of OVCAR-3 human ovarian carcinoma with Omniscan® as a control. The mice were anesthetized by intraperitoneal administration of a mixture of ketamine and telazol. The contrast agents were injected intravenously in the tail vein at a dose of 0.1 mmol-Gd/kg. We used a 3-dimensional spoiled gradient echo (SPGR) pulse sequence. The system body coil was used for RF excitation and a phased array wrist coil was used for F



reception. Imaging parameters used were 2.2 ms echo time (TE), 9.5 ms repetition time (TR), 25 degree tip angle, 15.63 kHz receive bandwidth, 10 cm field of view, 1 average, 1.0 mm slice thickness (coronal orientation) and a 246x256x64 imaging matrix interpolated to 512x512x124. We used an inversion recovery prepped sequence with an inversion time of 300 ms.

# ARTICLES

## Phosphine-Containing HYNIC Derivatives as Potential Bifunctional Chelators for $^{99m}\text{Tc}$ -Labeling of Small Biomolecules

Ajay Purohit, Shuang Liu,<sup>\*,†</sup> Dave Casebier, and D. Scott Edwards

Discovery Chemistry, Bristol-Myers Squibb Medical Imaging, 331 Treble Cove Road, North Billerica, Massachusetts 01862. Received April 18, 2003

Two prototype phosphine-containing HYNIC chelators, HYNIC-Kp-DPPB and HYNIC-Ko-DPPB (HYNIC = 6-hydrazinonicotinamide; K = lysine; and DPPB = diphenylphosphine-benzoic acid), have been synthesized and characterized by NMR ( $^1\text{H}$ ,  $^{13}\text{C}$ , and  $^{31}\text{P}$ ) and LC-MS. Macrocyclic  $^{99m}\text{Tc}$  complexes, [ $^{99m}\text{Tc}(\text{HYNIC-Ko-TPPB})(\text{tricine})$ ] and [ $^{99m}\text{Tc}(\text{HYNIC-Kp-DPPB})(\text{tricine})$ ], were prepared by reacting the phosphine-containing HYNIC chelator with  $^{99m}\text{TcO}_4^-$  in the presence of excess tricine and stannous chloride. Results from this study clearly demonstrated that both HYNIC-Kp-DPPB and HYNIC-Ko-DPPB are able to form highly stable macrocyclic  $^{99m}\text{Tc}$  complexes, [ $^{99m}\text{Tc}(\text{HYNIC-Ko-TPPB})(\text{tricine})$ ] and [ $^{99m}\text{Tc}(\text{HYNIC-Kp-DPPB})(\text{tricine})$ ], when tricine is used as the coligand. Radio-HPLC data suggest that the complex [ $^{99m}\text{Tc}(\text{HYNIC-Kp-DPPB})(\text{tricine})$ ] exists as only one detectable isomer in solution while the complex [ $^{99m}\text{Tc}(\text{HYNIC-Ko-DPPB})(\text{tricine})$ ] has three isomers. It was also found that three isomers of [ $^{99m}\text{Tc}(\text{HYNIC-Ko-DPPB})(\text{tricine})$ ] interconvert at elevated temperatures, suggesting that the presence of these isomers might be due conformational changes in the macrocyclic Tc chelate. The LC-MS data for both macrocyclic  $^{99m}\text{Tc}$  complexes are completely consistent with the proposed composition. The phosphine-containing HYNIC chelators described in this study may have the potential as bifunctional chelators for  $^{99m}\text{Tc}$  labeling of small biomolecules.

### INTRODUCTION

Abrams and co-workers (1, 2) first reported the use of organic hydrazines, including 6-hydrazinonicotinamide (HYNIC), as bifunctional coupling agents (BFCs) for the  $^{99m}\text{Tc}$ -labeling of polyclonal IgG. Since then, HYNIC has successfully been used for the  $^{99m}\text{Tc}$ -labeling of antibodies (3, 4) and small biomolecules, including chemotactic peptides (5–8), somatostatin analogues (9–14), liposomes (15), antisense oligonucleotides (16, 17), a folate receptor ligand (18), and polypeptides (19, 20). The use of HYNIC for  $^{99m}\text{Tc}$ -labeling of small biomolecules has recently been reviewed (21–24). The advantage of HYNIC as a BFC is its high labeling efficiency (rapid and high yield radio-labeling) and the high in vivo stability of resulting  $^{99m}\text{Tc}$  complexes. Since HYNIC can only occupy one coordination site (Figure 1), a coligand such as tricine is needed to complete the coordination sphere of the Tc. The choice of coligands allows easy modification of the hydrophilicity and biological properties of the  $^{99m}\text{Tc}$ -labeled small biomolecules.

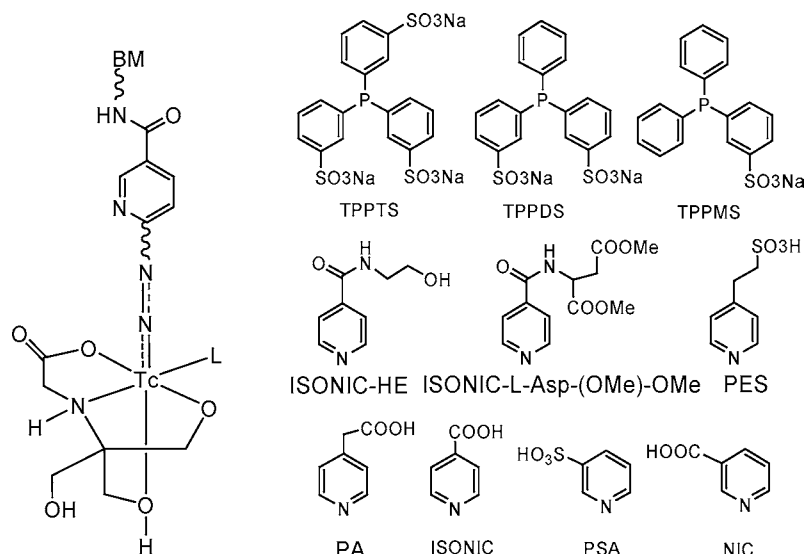
For the last several years, we have been using a ternary ligand system (Figure 1: HYNIC-BM, tricine, and TPPTS) for  $^{99m}\text{Tc}$ -labeling of small biomolecules. These include chemotactic peptides (25) and LTB<sub>4</sub> receptor antagonists (26, 27) for imaging infection and inflam-

mation, a vitronectin receptor antagonist for tumor imaging (28), and a GPIIb/IIIa receptor antagonist for imaging thrombosis (29–34). The combination of HYNIC-BM, tricine, and TPPTS results in a ternary ligand system that forms technetium complexes, [ $^{99m}\text{Tc}(\text{HYNIC-BM})(\text{tricine})(\text{TPPTS})$ ] (BM = peptide or nonpeptide receptor ligands) with extremely high specific activity. These ternary ligand  $^{99m}\text{Tc}$  complexes are stable in solution for >6 h and are formed as equal mixtures of two detectable isomers if the biomolecule has a chiral center. The composition of these  $^{99m}\text{Tc}$  complexes has been determined to be 1:1:1:1 for Tc:HYNIC-BM:tricine:TPPTS through a series of mixed ligand experiments and confirmed by LC-MS at both the macroscopic and tracer ( $^{99m}\text{Tc}$ ) levels (27, 28, 35, 36). Like phosphines, pyridine analogues (Figure 1) have also been used as coligands for the  $^{99m}\text{Tc}$ -labeling of small biomolecules (34). Compared to water-soluble phosphines, pyridine analogues are much smaller and more amenable for further derivatization.

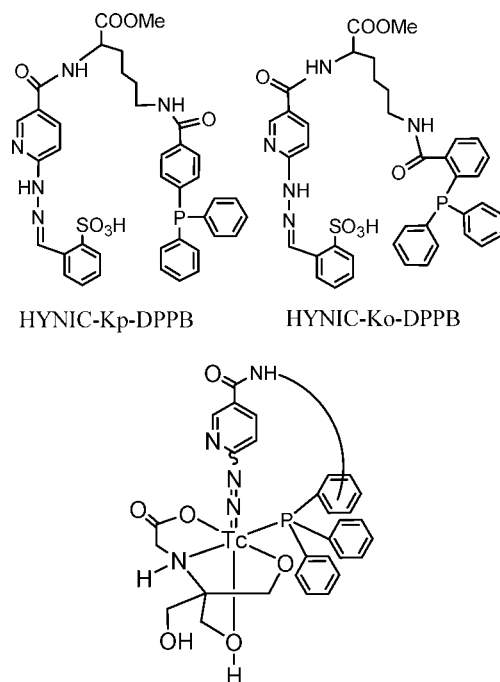
In principle, the ternary ligand system (HYNIC-BM, tricine, and TPPTS) can be used for  $^{99m}\text{Tc}$ -labeling of any HYNIC-conjugated biomolecules. However, problem may arise when it is used for  $^{99m}\text{Tc}$ -labeling of small biomolecules containing one or more disulfide linkages. The use of a large amount of TPPTS in combination with high temperature heating may destroy the S–S disulfide bonds, which are often vital to keep the rigid cyclic conformation of the small biomolecule and to maintain the high receptor binding affinity, and cause adverse effect on the biological properties of the  $^{99m}\text{Tc}$ -labeled biomolecule. Therefore, there is a continuing need for a

\* To whom correspondence should be addressed. Phone: 765-494-0236; fax 765-496-3367; e-mail: lius@pharmacy.purdue.edu.

† Present address: Department of Industrial and Physical Pharmacy, School of Pharmacy, Purdue University, 575 Stadium Dr., West Lafayette, IN 47907-2051.



**Figure 1.** Structures of coligands and their ternary ligand  $^{99m}\text{Tc}$  complexes.



**Figure 2.** Phosphine-containing HYNIC chelators and their macrocyclic Tc complexes.

better chelating system, which does not require the use of large amount of phosphine coligand.

One approach to minimize the use of large amount of phosphine coligand is to attach the phosphine coligand onto HYNIC via a linker to form the phosphine-containing HYNIC chelator. Figure 2 shows two prototype phosphine-containing HYNIC chelators, which are designed in such a way that when HYNIC binds to the Tc center, the "effective concentration" of the attached phosphine-P donor in the vicinity of the Tc will be increased dramatically. This makes it much easier for the phosphine-P donor to bond to the Tc and form a macrocyclic  $^{99m}\text{Tc}$  chelate. The linker between HYNIC and the triphenylphosphine moiety may be a polymethylene chain or a small peptide sequence. The attachment site for the linker may vary for the triphenylphosphine moiety. Lysine is selected as a linker to connect HYNIC with the triphenylphosphine moiety while the carboxylic group of the lysine linker can be used for conjugation of

biomolecules for the development of target-specific radiopharmaceuticals.

As a continuation of our interest in developing new  $^{99m}\text{Tc}$  chelating systems, we now report the synthesis of two prototype phosphine-containing HYNIC chelators (Figure 2: HYNIC-Ko-DPPB and HYNIC-Kp-DPPB). The combination of a phosphine-containing HYNIC chelator with tricine results in a unique chelating system that forms highly stable macrocyclic  $^{99m}\text{Tc}$  complexes with high specific activity. The phosphine-containing HYNIC chelators described in this study have the potential as BFCs for  $^{99m}\text{Tc}$ -labeling of small biomolecules.

## EXPERIMENTAL SECTION

*N*- $\epsilon$ -(*tert*-Butoxycarbonyl)lysine methyl ester hydrochloride, 2-(diphenylphosphino)benzoic acid (o-DPPB), 4-(diphenylphosphino)benzoic acid (p-DPPB), ethylenediamine-*N,N*-diacetic acid (EDDA), 1-hydroxybenzotriazole, 1-hydroxyazabenzotriazole, *N*-(2-hydroxyethyl)iminediacetic acid (HIDA), 4 M HCl in dioxane, 1-*O*-(*N,N,N',N''*-tetramethyluronium)benzotriazoloxyl hexafluorophosphate, and 1-*O*-(*N,N,N',N''*-tetramethyluronium)azabenzotriazoloxyl hexafluorophosphate were purchased from Aldrich or Sigma and were used as received.  $\text{Na}^{99m}\text{TcO}_4$  was obtained from a Technelite  $^{99}\text{Mo}/^{99m}\text{Tc}$  generator, Bristol-Myers Squibb Medical Imaging Inc., North Billerica, MA. Sodium succinimidyl 6-(2-(2-sulfonatobenzaldehyde)hydrazono)nicotinate (HYNIC-OSu) was prepared according to published procedure (37).

**Instruments.** NMR spectral data ( $^1\text{H}$  and  $^{13}\text{C}$ ) were recorded on a 600 MHz Bruker DRX FT NMR spectrometer. The  $^1\text{H}$  NMR data were reported as  $\delta$  (ppm) relative to TMS.  $^{31}\text{P}$  NMR were proton decoupled and with phosphoric acid as an internal standard. Electrospray MS analyses were performed using an IonSpec Ultima FT Mass Spectrometer in the positive ion mode. LC-MS spectral data were collected using a HP1100 LC/MSD system with an API-electrospray interface. The LC-MS method used a Zorbax  $\text{C}_{18}$  column (4.6 mm  $\times$  150 mm, 3.5  $\mu\text{m}$  particle size). The flow rate was 1 mL/min with a gradient mobile phase starting 80% solvent A (25 mM ammonium acetate buffer, pH 6.8) and 20% solvent B (acetonitrile) to 75% A and 25% solvent B at 20 min.

The HPLC method 1 used a Varian semiprep HPLC system equipped with an UV/visible detector ( $\lambda = 220$  nm) and a Varian Prep Star on the Jupiter C18 column



(15  $\mu\text{m}$ , 300  $\text{\AA}$ ,  $41.4 \times 250$  mm). The flow rate was 80 mL/min with the mobile phase starting with 20% solvent B (0.1%TFA in 90% acetonitrile) and 80% solvent A (0.1%TFA in water) to 90% solvent B and 10% solvent A at 40 min.

The radio-HPLC method 2 used a HP-1100 HPLC system with an UV/visible detector ( $\lambda = 215$  nm), an IN-US radiodetector and a Zorbax  $\text{C}_{18}$  column (4.6 mm  $\times$  250 mm, 3.5  $\mu\text{m}$  pore size). The flow rate was 1 mL/min with a gradient mobile phase starting 80% solvent A (25 mM ammonium acetate buffer, pH 6.8) and 20% solvent B (acetonitrile) to 75% A and 25% solvent B at 20 min. The ITLC method used Gelman Sciences silica gel paper strips and a 1:1 mixture of acetone and saline as eluant.

**Synthesis of *N*- $\epsilon$ -(*tert*-Butoxycarbonyl)-*N*- $\alpha$ -(6-(2-(2-sulfonatobenzaldehyde)hydrazono)nicotinyl)-lysine Methyl Ester.** To a 25 mL round-bottom flask was added HYNIC-OSu (250 mg, 0.567 mmol) followed by 3 mL of DMF. The solid was allowed to dissolve, and to the solution was then added *N*- $\epsilon$ -(*tert*-butoxycarbonyl)-lysine methyl ester hydrochloride (184 mg, 0.623 mmol) followed by diisopropylethylamine (0.32 mg, 0.434 mL). The resulting solution was stirred under a nitrogen atmosphere for 15 h. DMF was removed in vacuo and the crude oil subjected to HPLC purification (Method 1). The collected fractions were combined and were lyophilized to give a fluffy white powder. The yield was 239 mg (~75%). High-resolution MS (ESI):  $m/z = 564.2244$  for  $\text{C}_{25}\text{H}_{33}\text{N}_5\text{O}_8\text{S}$  ( $[\text{M} + \text{H}]^+$ ).  $^1\text{H}$  NMR (600 MHz,  $\text{DMSO}-d_6 + \text{DCl}$ ): 9.376 (s, 1H), 8.617 (s, 1H), 8.466 (dd, 1H,  $J = 2.4$  Hz), 7.8 (m, 1H), 7.4 (m, 2H), 7.25 (bd, 1H), 4.38 (t, 1H,  $J = 7.2$  Hz), 3.64 (s, 3H), 2.89 (m, 2H), 1.8 (q, 2H,  $J = 7.2$  Hz), 1.34–1.38 (13H).  $^{13}\text{C}$  NMR ( $\text{DMSO}-d_6 + \text{DCl}$ ): 172.4, 162.5, 155.5, 149.8, 147.5, 129.5, 120.2, 77.43, 52.84, 51.97, 31.25, 30.07, 29.6, 29, 28.2, 26.5, and 23.

**Synthesis of *N*- $\alpha$ -(6-(2-(2-Sulfonatobenzaldehyde)hydrazono)nicotinyl)lysine Methyl Ester Hydrochloride Salt.** To a 25 mL round-bottom flask was added *N*- $\epsilon$ -(*tert*-butoxycarbonyl)-*N*- $\alpha$ -(6-(2-(2-sulfonatobenzaldehyde)hydrazono)nicotinyl)lysine methyl ester (200 mg, 0.355 mmol). The flask cooled to 0  $^\circ\text{C}$ . Upon addition of 2.0 mL of 4 M HCl in dioxane, the fluffy white starting material immediately turned to a pale yellow solid. The reaction mixture was allowed to stand at 0  $^\circ\text{C}$  for 5 min and then at room temperature for 25 min with occasional shaking. The pale yellow solid was separated by filtration and dried under vacuum overnight. The product was used for the next reaction without further purification. The yield was 164 mg (~100%). High-resolution MS (ESI):  $m/z = 464.1526$  for  $\text{C}_{25}\text{H}_{33}\text{N}_5\text{O}_8\text{S}$  ( $[\text{M} + \text{H}]^+$ ).  $^1\text{H}$  NMR ( $\text{DMSO}-d_6 + \text{D}_2\text{O}$ ): 9.23 (s, 1H) 8.55 (d, 1H,  $J = 1.8$  Hz), 8.33 (br d, 1H), 8.23 (br d, 1H), 7.8 (d of d, 1H,  $J = 7.2$ , 1.8 Hz), 7.4 (m, 2H), 7.2 (d, 2H,  $J = 9.6$  Hz), 4.4 (m, 1H), 3.65 (s, 3H), 2.7 (t, 2H,  $J = 7.2$  Hz), 1.8 (m, 2H), 1.5 (m, 2H), 1.38–1.42 (m, 2H).

**Synthesis of *N*- $\epsilon$ -(4-(Diphenylphosphino)benzoyl)-*N*- $\alpha$ -(6-(2-(2-sulfonatobenzaldehyde)hydrazono)nicotinyl)lysine Methyl Ester (HYNIC-Kp-DPPB).** To a round-bottom flask were added 4-(diphenylphosphino)benzoic acid (22.94 mg, 0.074 mmol) and 3 mL of DMF. To the solution were added 1-*O*-(*N,N,N',N'*-tetramethyluronium)benzotriazoloxyl hexafluorophosphate (31.24 mg, 0.082 mmol), 1-hydroxybenzotriazole (11.11 mg, 0.082 mmol), and diisopropylethylamine (48.4 mg, 0.065 mL). After the reaction mixture was stirred for 7 min, *N*- $\alpha$ -(6-(2-(2-sulfonatobenzaldehyde)hydrazono)nicotinyl)lysine methyl ester hydrochloride (45 mg, 0.089 mmol) in 4 mL of DMF was added to the above

mixture. The reaction mixture was stirred for 2 h at room temperature. The solvent was removed in vacuo, and the resulting crude oil was subjected to HPLC purification (method 1). The collected fractions were combined and were lyophilized to give a pale yellow solid. The yield was 33 mg (~60%). High-resolution MS (ESI):  $m/z = 752.2302$  for  $\text{C}_{39}\text{H}_{38}\text{N}_5\text{O}_7\text{PS}$  ( $[\text{M} + \text{H}]^+$ ).  $^1\text{H}$  NMR ( $\text{CD}_3\text{OD}$ ): 9.32 (s, 1H), 8.56 (s, 1H), 8.4 (d of d, 1H), 8.3 (m, 1H), 8.0 (m, 1H), 7.7 (d of d, 2H,  $J = 1.2$ , 7.2 Hz), 7.5 (m, 2H), 7.38–7.28 (m, 12H), 4.6 (m, 1H), 3.76 (s, 3H), 3.4 (m, 2H), 2.0 & 1.9 (m, 2H), 1.7 (m, 2H), 1.55 (m, 2H).  $^{31}\text{P}$  NMR ( $\text{CD}_3\text{OD}$ ):  $-4.57$ .

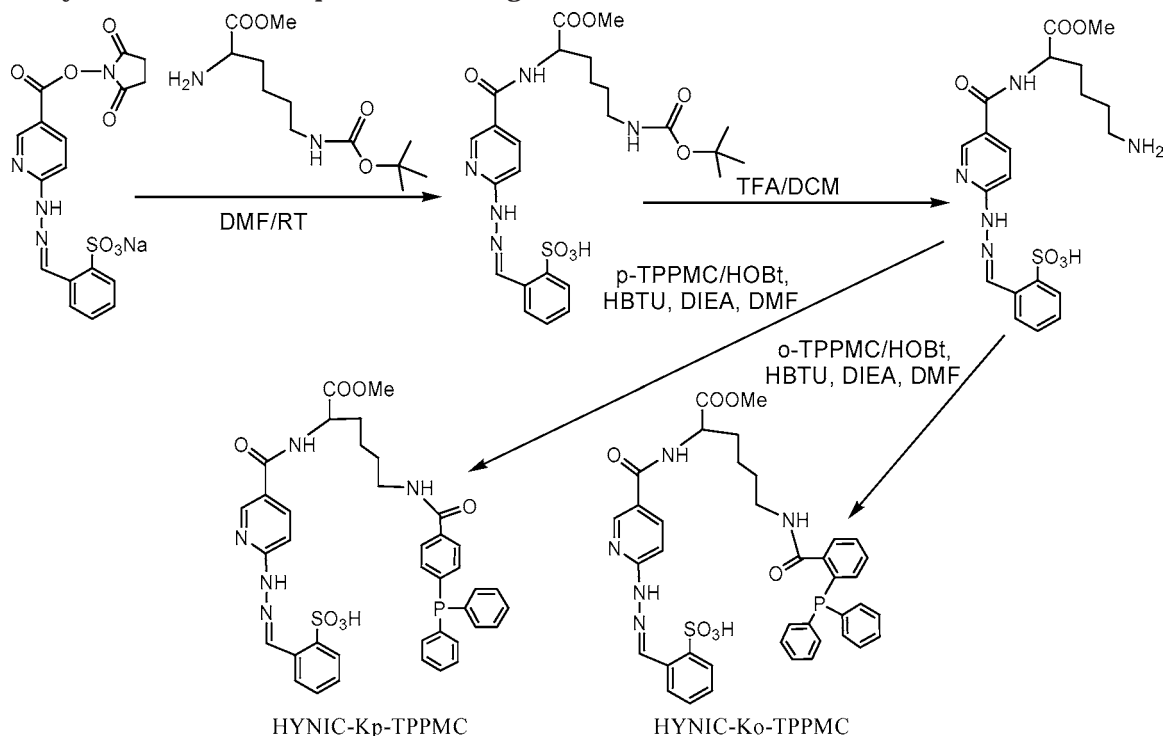
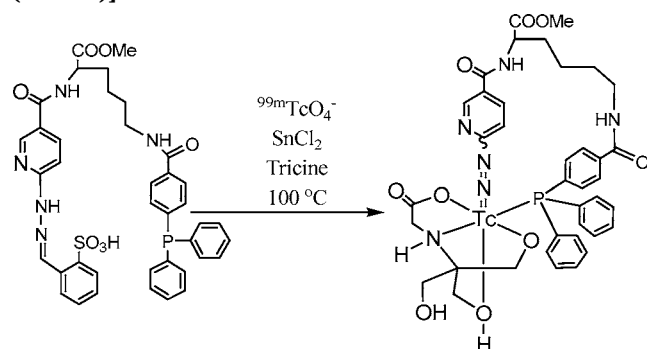
**Synthesis of *N*- $\epsilon$ -(2-(Diphenylphosphino)benzoyl)-*N*- $\alpha$ -(6-(2-(2-Sulfonatobenzaldehyde)hydrazono)nicotinyl)lysine Methyl Ester (HYNIC-Ko-DPPB).** To a round-bottom flask were added 2-(diphenylphosphino)benzoic acid (17.94 mg, 0.058 mmol) and 3 mL of DMF. To the solution were added 1-*O*-(*N,N,N',N'*-tetramethyluronium)azabenzotriazoloxyl hexafluorophosphate (26.73 mg, 0.070 mmol), 1-hydroxyazabenzotriazole (9.56 mg, 0.070 mmol), and diisopropylethylamine (45.4 mg, 0.061 mL). After the reaction mixture was stirred for 7 min, *N*- $\alpha$ -(6-(2-(2-sulfonatobenzaldehyde)hydrazono)nicotinyl)lysine methyl ester hydrochloride (35.2 mg, 0.070 mmol) dissolved in 4 mL of DMF was added to the above mixture. The reaction mixture was stirred for 2 h. The solvent was removed in vacuo, and the resulting crude oil was subjected to HPLC purification using the method described above. The collected fractions were combined and were lyophilized to give the product as a pale yellow solid. The yield was 29 mg (66%) after HPLC purification. High-resolution MS (ESI):  $m/z = 752.2302$  for  $\text{C}_{39}\text{H}_{38}\text{N}_5\text{O}_7\text{PS}$  ( $[\text{M} + \text{H}]^+$ ).  $^1\text{H}$  NMR ( $\text{CD}_3\text{OD}$ ): 9.37 (s, 1H), 8.6 (s, 1H), 8.4 (dd, 2H,  $J = 1.8$ , 7.2 Hz), 7.8 (m, 1H), 7.68–7.41 (m, 16H), 7.17 (bd, 1H), 4.3 (m, 1H), 3.66 (s, 3H), 2.7 (m, 2H), 1.8–1.75 (m, 2H), 1.35–1.26 (m, 4H).  $^{31}\text{P}$  ( $\text{CD}_3\text{OD}$ )  $\delta$ :  $-8.23$ .

**General Procedure for Preparation of Macro-cyclic  $^{99\text{m}}\text{Tc}$  Complexes.** To a sealed clean 5.0 mL vial were added the phosphine-containing HYNIC chelator (5–40  $\mu\text{g}$ ), 0.4 mL of in 0.25 M succinate buffer (pH = 5.0), 0.2 mL of ethanol, and 0.4 mL of tricine solution (25–100 mg/mL in 0.25 M succinate buffer, pH = 5.0). The mixture was immediately degassed under vacuum ( $<0.5$  mmHg) for 1–2 min. After addition of 0.5 mL of  $^{99\text{m}}\text{TcO}_4^-$  solution (40–80 mCi/mL in saline) and 25  $\mu\text{L}$  of  $\text{SnCl}_2 \cdot 2\text{H}_2\text{O}$  solution (1.0 mg/mL in 0.1 N HCl), the mixture was heated in a water-bath at 95–100  $^\circ\text{C}$  for 15 min. After being cooled to room temperature, a sample of the resulting solution was analyzed by radio-HPLC and ITLC to determine the radiochemical purity (RCP) of the resulting macrocyclic  $^{99\text{m}}\text{Tc}$  complex.

**Solution Stability Studies.** Macrocyclic  $^{99\text{m}}\text{Tc}$  complexes were first prepared, and samples of the resulting reaction were analyzed by HPLC (method 2) at  $t = 0$ , 1, 2, 3, and 4 h postlabeling. For solution stability of the HPLC-purified macrocyclic  $^{99\text{m}}\text{Tc}$  complexes, the peaks of interest were collected into a 25 mL round-bottom flask. Solvents were removed using a rotary evaporator. The residue was dissolved in saline, and samples of the resulting solution were analyzed by HPLC (method 2) at 0.5, 1.5, 2.5, 3.5, and 4.5 h postpurification.

## RESULTS AND DISCUSSION

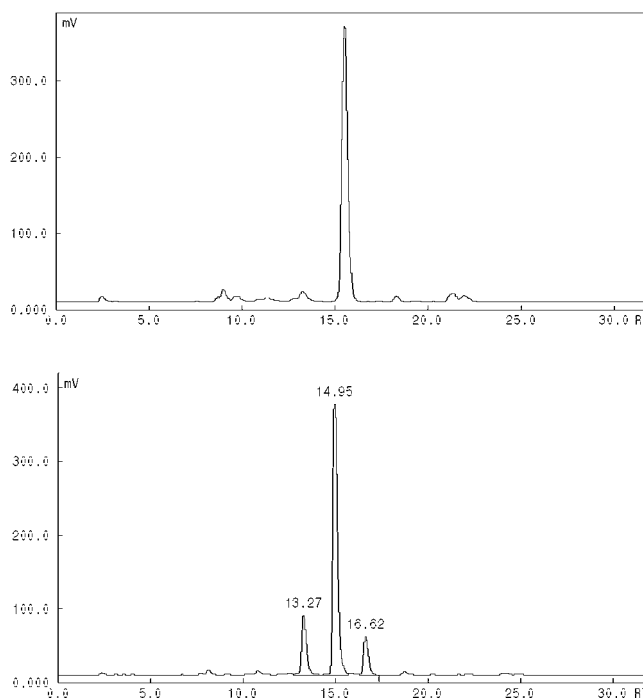
HYNIC-Ko-DPPB and HYNIC-Kp-DPPB were prepared according to Scheme 1. HYNIC-OSu was allowed to react with  $\omega$ -Boc-lysine methyl ester at room temperature to give HYNIC-( $\omega$ -Boc)K(OMe). The Boc-protecting

**Scheme 1. Synthesis of Two Phosphine-Containing HYNIC Chelators****Scheme 2. Synthesis of [<sup>99m</sup>Tc(HYNIC-Kp-TPPMC)-(tricine)]**

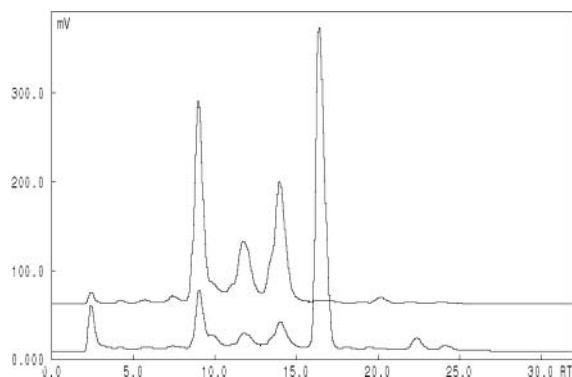
group in HYNIC-(*ω*-Boc)K(OMe) was readily removed in a 4 M HCl dioxane solution to give the intermediate HYNIC-K(OMe). Conjugation of HYNIC-K(OMe) with *o*-DPPB and *p*-DPPB afforded phosphine-containing HYNIC chelators (HYNIC-Ko-DPPB and HYNIC-Kp-DPPB, respectively) as their methyl esters. The <sup>1</sup>H, <sup>13</sup>C, and <sup>31</sup>P NMR data are completely consistent with the proposed structures. Since they are readily oxidized, HYNIC-Ko-DPPB and HYNIC-Kp-DPPB have to be stored under inert atmosphere.

The free hydrazine group in HYNIC is not stable to oxidation, particularly under basic conditions, and reacts readily with aldehydes or ketones, which makes it very difficult to maintain the purity and the stability of the hydrazine-containing chelators (37). Therefore, the 2-sulfonatobenzaldehyde hydrazone was used as the protecting group for the hydrazine group of HYNIC. However, the hydrazone-protecting group must hydrolyze to produce sufficient quantity of the free hydrazine moiety prior to bonding to the <sup>99m</sup>Tc (33). The higher the degree of hydrolysis is, the higher the yield would be for the macrocyclic <sup>99m</sup>Tc complex. The hydrolysis may not need to go to completion since there are typically 10–50 equivalents of hydrazone to the total Tc in the reaction mixture.

**Synthesis of Macrocyclic <sup>99m</sup>Tc Complexes.** Macrocyclic <sup>99m</sup>Tc complexes were prepared according to Scheme 2 using conditions similar to those described in our previous communications (30–34). The phosphine-containing HYNIC chelator was allowed to react directly with <sup>99m</sup>TcO<sub>4</sub><sup>-</sup> in the presence of stannous chloride and excess tricine. The radiolabeling was achieved by heating the reaction mixture at 100 °C for 10–15 min. Since the phosphine is readily oxidized, exclusion of oxygen in the reaction mixture is necessary before the addition of <sup>99m</sup>TcO<sub>4</sub><sup>-</sup>. After radiolabeling, an example of the resulting



**Figure 3.** Typical radio-HPLC chromatograms of macrocyclic <sup>99m</sup>Tc complexes [<sup>99m</sup>Tc(HYNIC-Kp-DPPB)(tricine)] (top) and [<sup>99m</sup>Tc(HYNIC-Ko-DPPB)(tricine)] (bottom).



**Figure 4.** Radio-HPLC chromatograms of  $[^{99m}\text{Tc}(\text{HYNIC-Kp-ODPPB})(\text{tricine})_2]$  (top) and  $[^{99m}\text{Tc}(\text{HYNIC-Kp-DPPB})(\text{tricine})]$  (bottom) prepared by using 20  $\mu\text{g}$  of HYNIC-Kp-DPPB for 40 mCi of  $[^{99m}\text{Tc}]\text{pertechnetate}$  in the presence of air.

solution was analyzed by radio-HPLC and TLC. The RCP was >85% for the complex  $[^{99m}\text{Tc}(\text{HYNIC-Kp-DPPB})(\text{tricine})]$  and >95% for  $[^{99m}\text{Tc}(\text{HYNIC-Ko-DPPB})(\text{tricine})]$ . In both cases, formation of  $[^{99m}\text{Tc}]\text{colloid}$  was minimal. The  $^{99m}\text{Tc}$ -labeling efficiency is extremely high for HYNIC-Kp-DPPB. The minimum amount of HYNIC-Kp-DPPB to achieve high yield  $^{99m}\text{Tc}$ -labeling is about 5  $\mu\text{g}$  for 20 mCi of  $^{99m}\text{TcO}_4^-$ , corresponding to a molar ratio of ~1:50 for Tc:HYNIC-Kp-DPPB.

We also tried to use other polydentate aminocarboxylates, such as nitrilotriacetic acid (NTA), *N*-(2-hydroxyethyl)iminodiacetic acid (HIDA), *N*-(2-hydroxyethyl)glycine (monocine), *N,N*-bis(2-hydroxymethyl)glycine (Bicine), ethylenediamine-*N,N*-diacetic acid (EDDA), and *N*-(hydroxyethyl)ethylenediamine triacetic acid (HEDTA), as coligands to replace tricine. The yields for their  $^{99m}\text{Tc}$  complexes are very low (<30%). Among various polydentate aminocarboxylate coligands, tricine remains to be the best coligand with respect to the yield and radiochemical purity, and the number of isomers of their macrocyclic  $^{99m}\text{Tc}$  complexes. The amounts of the tricine coligand used for preparation of macrocyclic  $^{99m}\text{Tc}$  complexes can range from 10 mg/mL to 100 mg/mL. If the tricine concentration is <10 mg/mL, the formation of  $[^{99m}\text{Tc}]\text{colloid}$  may become significant. If the tricine concentration is >100 mg/mL, the radiolabeling yields for macrocyclic  $^{99m}\text{Tc}$  complexes will decrease.

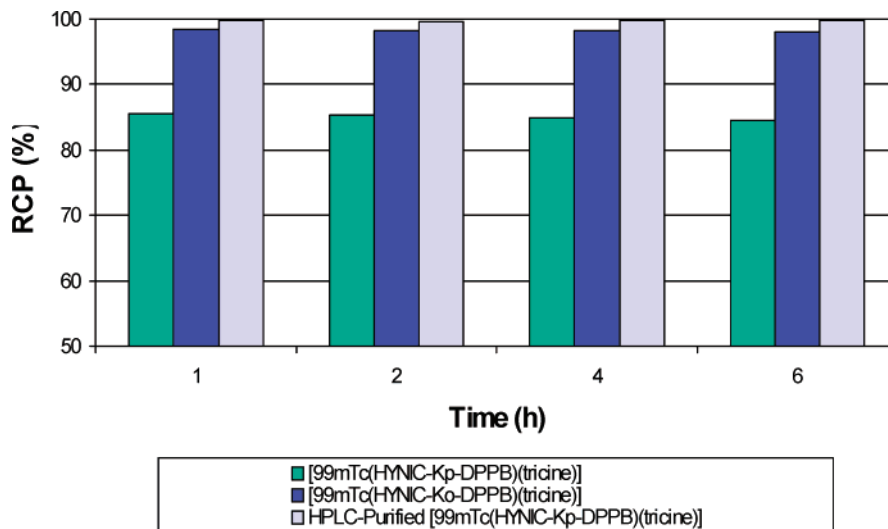
**HPLC Characterization of Macrocyclic  $^{99m}\text{Tc}$  Complexes.** A reverse phase HPLC method was used for

characterization of complexes  $[^{99m}\text{Tc}(\text{HYNIC-Kp-DPPB})(\text{tricine})]$  and  $[^{99m}\text{Tc}(\text{HYNIC-Ko-DPPB})(\text{tricine})]$ . Figure 3 shows typical radio-HPLC chromatograms for  $[^{99m}\text{Tc}(\text{HYNIC-Kp-DPPB})(\text{tricine})]$  (top) and  $[^{99m}\text{Tc}(\text{HYNIC-Ko-DPPB})(\text{tricine})]$  (bottom). Under almost isocratic conditions (20–25% AcCN over 20 min), the macrocyclic  $^{99m}\text{Tc}$  complex  $[^{99m}\text{Tc}(\text{HYNIC-Kp-DPPB})(\text{tricine})]$  shows only one radiometric peak in its radio-HPLC chromatogram while there are three radiometric peaks from  $[^{99m}\text{Tc}(\text{HYNIC-Ko-DPPB})(\text{tricine})]$ , and the peak ratios remained constant over 6 h post-labeling. There is less oxidized species in kit matrix containing the macrocyclic  $^{99m}\text{Tc}$  complex  $[^{99m}\text{Tc}(\text{HYNIC-Kp-DPPB})(\text{tricine})]$ , as evidenced by the disappearance of small peaks in the HPLC chromatogram (Figure 3). These results strongly suggest that the phosphine-P is bonded to the Tc to form an unprecedented macrocyclic Tc chelate ring.

In another experiment, the complex  $[^{99m}\text{Tc}(\text{HYNIC-Kp-DPPB})(\text{tricine})]$  was prepared using 20  $\mu\text{g}$  of HYNIC-Kp-DPPB for 40 mCi of  $^{99m}\text{TcO}_4^-$  in the presence of air. The radio-HPLC chromatogram (Figure 4) shows several major radioimpurity peaks, retention times of which match those due to the binary ligand  $^{99m}\text{Tc}$  complex  $[^{99m}\text{Tc}(\text{HYNIC-Kp-ODPPB})(\text{tricine})_2]$  prepared under identical conditions using 20  $\mu\text{g}$  of oxidized HYNIC-Kp-DPPB. We believe that the presence of these radioimpurities is most likely due to oxidation of HYNIC-Kp-DPPB by oxygen dissolved in the solution or free radicals produced during radiolabeling. These results provide further evidence that the phosphine-P is indeed bonded to the Tc in the macrocyclic  $^{99m}\text{Tc}$  complex  $[^{99m}\text{Tc}(\text{HYNIC-Kp-DPPB})(\text{tricine})]$ .

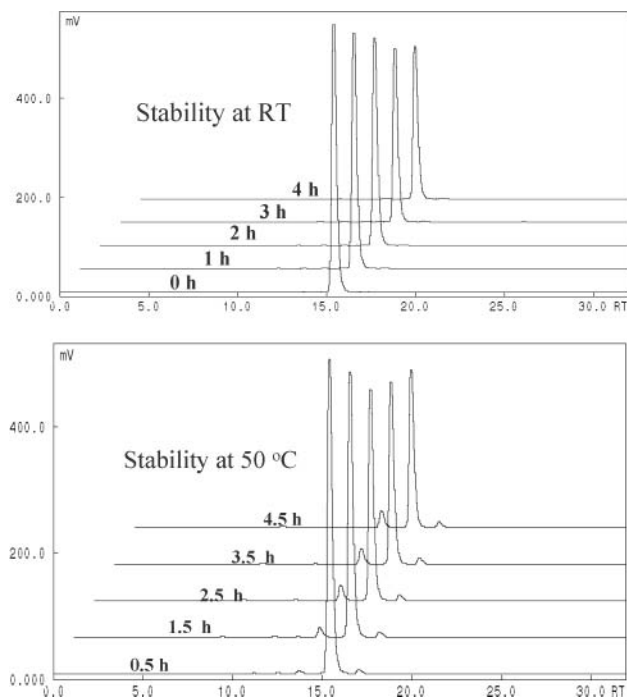
**Solution Stability of Macrocyclic  $^{99m}\text{Tc}$  Complexes.** We examined the solution stability of both  $[^{99m}\text{Tc}(\text{HYNIC-Kp-DPPB})(\text{tricine})]$  and  $[^{99m}\text{Tc}(\text{HYNIC-Ko-DPPB})(\text{tricine})]$  in the kit matrix. The stability was assessed by radio-HPLC (method 2) by performing six injections over 6 h. Figure 5 shows the plot of RCP vs time for macrocyclic  $^{99m}\text{Tc}$  complexes  $[^{99m}\text{Tc}(\text{HYNIC-Kp-DPPB})(\text{tricine})]$  and  $[^{99m}\text{Tc}(\text{HYNIC-Ko-DPPB})(\text{tricine})]$ . In both cases, there is no significant RCP change, suggesting that they are stable in the kit matrix for >6 h.

We also examined the solution stability of HPLC-purified macrocyclic  $^{99m}\text{Tc}$  complexes  $[^{99m}\text{Tc}(\text{HYNIC-Kp-DPPB})(\text{tricine})]$  and  $[^{99m}\text{Tc}(\text{HYNIC-Ko-DPPB})(\text{tricine})]$ . For the complex  $[^{99m}\text{Tc}(\text{HYNIC-Kp-DPPB})(\text{tricine})]$ , the peak at 15 min was collected. Volatiles were removed



**Figure 5.** Solution stability data for  $[^{99m}\text{Tc}(\text{HYNIC-Kp-TPPMC})(\text{tricine})]$  and  $[^{99m}\text{Tc}(\text{HYNIC-Kp-TPPMC})(\text{tricine})]$ .





**Figure 6.** Solution stability for the HPLC-purified  $[^{99m}\text{Tc}(\text{HYNIC-Ko-DPPB})(\text{tricine})]$ .

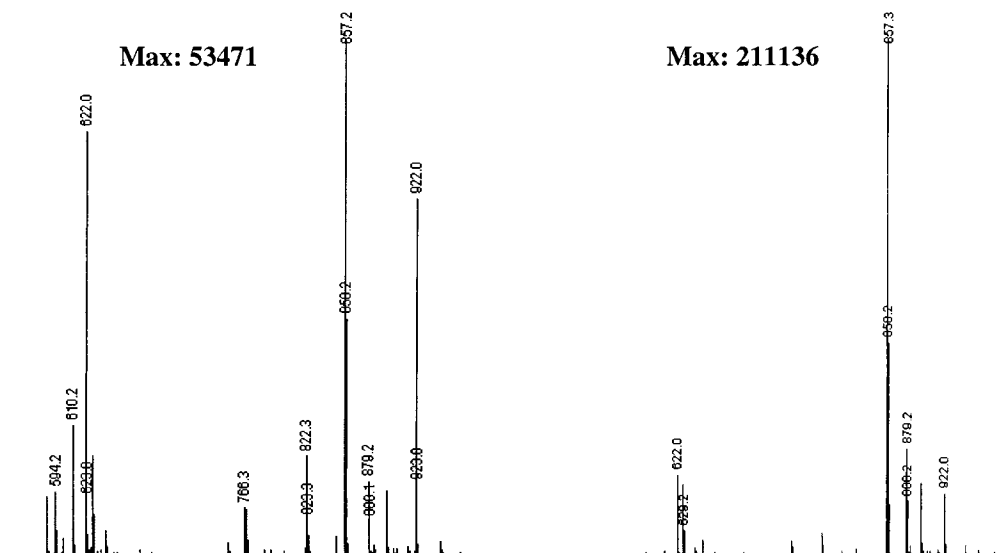
under vacuum. The residue was redissolved in saline to give a concentration of  $\sim 2$  mCi/mL. Since the HPLC mobile phase contains ammonium acetate buffer (pH = 6.8), no additional buffer was used for dilution. The solution was monitored by radio-HPLC (method 2). It was found that the macrocyclic complex  $[^{99m}\text{Tc}(\text{HYNIC-Kp-DPPB})(\text{tricine})]$  remains stable for  $>6$  h at room temperature after HPLC purification. There is no indication of any significant decomposition during this period of time. Addition of TPPTS (1 mg/mL:  $\sim 2 \times 10^{-3}$  M) into the solution above caused no significant change in the radio-HPLC chromatogram. The fact that the macrocyclic complex  $[^{99m}\text{Tc}(\text{HYNIC-Kp-DPPB})(\text{tricine})]$  remains intact in the presence of a large excess of TPPTS is significant. This suggests that the ligand exchange reaction is not dependent on the concentration of the entering ligand, and dissociation of the Tc–P bond is the rate-limiting step. Therefore, the high solution stability

of  $[^{99m}\text{Tc}(\text{HYNIC-Kp-DPPB})(\text{tricine})]$  is probably due to its kinetic inertness.

For the macrocyclic complex  $[^{99m}\text{Tc}(\text{HYNIC-Ko-DPPB})(\text{tricine})]$ , only the peak at  $\sim 15$  min was collected. Volatiles were removed under reduced pressure. The residue was redissolved in saline to give a concentration of  $\sim 2$  mCi/mL. Figure 6 shows staggered HPLC chromatograms for the HPLC-purified complex  $[^{99m}\text{Tc}(\text{HYNIC-Ko-DPPB})(\text{tricine})]$ . Obviously, the main species  $\sim 15$  min remains unchanged over 4 h at room temperature. At  $50^\circ\text{C}$ , however, it is slowly converted to the two minor components until it reaches equilibrium over  $\sim 6$  h. There is no indication of any significant decomposition during this period of time. These results clearly demonstrate the high solution stability of the complex  $[^{99m}\text{Tc}(\text{HYNIC-Ko-DPPB})(\text{tricine})]$ .

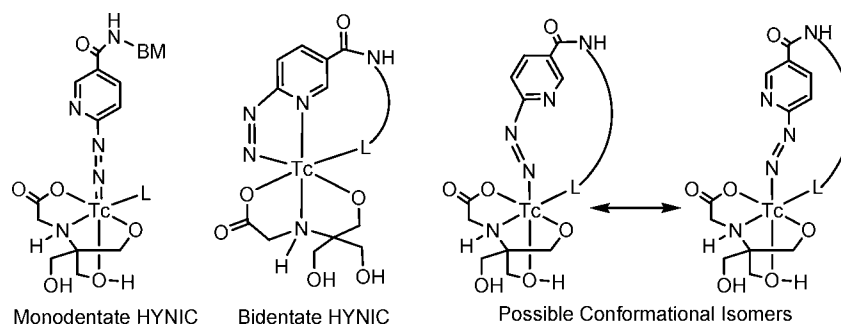
**LC-MS Data of Macrocyclic  $^{99m}\text{Tc}$  Complexes.** One of the important aspects of radiochemistry is to know the chemical composition of the radiopharmaceutical prepared in the radiolabeled kit. Since the total Tc ( $^{99m}\text{Tc}$  and  $^{99}\text{Tc}$ ) concentration in the generator eluant is very low ( $10^{-8}$  to  $10^{-6}$  M), it is impossible to use spectroscopic (IR, UV/vis, and NMR) methods to characterize  $^{99m}\text{Tc}$  radiopharmaceuticals at the tracer level. Recently, we reported the use of LC-MS for characterization of small molecule  $^{99m}\text{Tc}$  radiopharmaceuticals (36). It was found that the LC-MS is particularly useful for determining the composition of  $^{99m}\text{Tc}$  radiopharmaceuticals at the tracer ( $^{99m}\text{Tc}$ ) level.

In this study, we used a decayed generator eluant to prepare macrocyclic  $^{99m}\text{Tc}$  complexes  $[^{99m}\text{Tc}(\text{HYNIC-Kp-DPPB})(\text{tricine})]$  and  $[^{99m}\text{Tc}(\text{HYNIC-Ko-DPPB})(\text{tricine})]$ . We used LC-MS to analyze solutions containing macrocyclic  $^{99m}\text{Tc}$  complexes  $[^{99m}\text{Tc}(\text{HYNIC-Kp-DPPB})(\text{tricine})]$  and  $[^{99m}\text{Tc}(\text{HYNIC-Ko-DPPB})(\text{tricine})]$ . Figure 7 shows LC-MS spectra for  $[^{99m}\text{Tc}(\text{HYNIC-Kp-DPPB})(\text{tricine})]$  (top) and  $[^{99m}\text{Tc}(\text{HYNIC-Ko-DPPB})(\text{tricine})]$  (bottom). The LC-MS data is completely consistent with the proposed composition. The LC-MS data (Table 1) of  $[^{99m}\text{Tc}(\text{HYNIC-Kp-TPPMC})(\text{tricine})]$  also show that all three peaks have the same molecular weight with  $m/z = 857.3$  for  $[\text{M} + \text{H}]^+$ . These results clearly show that (1) the phosphine-P is indeed bonded to Tc in the macrocyclic complex  $[^{99m}\text{Tc}(\text{HYNIC-Ko-DPPB})(\text{tricine})]$ , (2) the presence of three radiometric peaks in its radio-HPLC chromatogram is due to resolution of three different isomers; and (3)



**Table 1.** LC-MS Data for Macrocylic  $^{99m}\text{Tc}$  Complexes

$^{99m}\text{Tc}$ complex	formula ( $[\text{M} + \text{H}]^+$ )	formula weight	found ( $[\text{M} + \text{H}]^+$ )
$[\text{}^{99m}\text{Tc}(\text{HYNIC-Kp-DPPB})(\text{tricine})]$	$\text{C}_{38}\text{H}_{24}\text{N}_6\text{PO}_9$	857.25	857.2
$[\text{}^{99m}\text{Tc}(\text{HYNIC-Ko-DPPB})(\text{tricine})]$ , peak A	$\text{C}_{38}\text{H}_{24}\text{N}_6\text{PO}_9$	857.25	857.3
$[\text{}^{99m}\text{Tc}(\text{HYNIC-Ko-DPPB})(\text{tricine})]$ , peak B	$\text{C}_{38}\text{H}_{24}\text{N}_6\text{PO}_9$	857.25	857.3
$[\text{}^{99m}\text{Tc}(\text{HYNIC-Ko-DPPB})(\text{tricine})]$ , peak C	$\text{C}_{38}\text{H}_{24}\text{N}_6\text{PO}_9$	857.25	857.3

**Figure 8.** Proposed structures for macrocylic  $^{99m}\text{Tc}$  complexes.

the attachment site of the linker has a significant impact on the coordination chemistry of the phosphine-containing HYNIC chelator.

## CONCLUSIONS

Our preliminary results clearly demonstrate that the phosphine-containing HYNIC chelators (HYNIC-Kp-DPPB and HYNIC-Ko-DPPB) described in this study are able to form highly stable macrocylic  $^{99m}\text{Tc}$  complexes when tricine is used as the coligand. The complex  $[\text{}^{99m}\text{Tc}(\text{HYNIC-Kp-TPPB})(\text{tricine})]$  shows only one detectable isomer in solution while the complex  $[\text{}^{99m}\text{Tc}(\text{HYNIC-Ko-TPPB})(\text{tricine})]$  has three isomers. The composition of the two macrocylic  $^{99m}\text{Tc}$  complexes has been determined by LC-MS at the tracer level. The LC-MS data is completely consistent with the proposed composition of the two macrocylic  $^{99m}\text{Tc}$  complexes. We also found that the triphenylphosphine moiety is sensitive to oxidation by the oxygen in the reaction mixture and free radicals produced during radiolabeling due to radiolysis.

Several questions remain unanswered. These include (1) the bonding modality of the HYNIC chelator and the coordinated tricine, (2) the identity of three isomers in the macrocylic  $^{99m}\text{Tc}$  complex  $[\text{}^{99m}\text{Tc}(\text{HYNIC-Ko-TPPB})(\text{tricine})]$ , (3) the reason that there are three isomers for the complex  $[\text{}^{99m}\text{Tc}(\text{HYNIC-Ko-TPPB})(\text{tricine})]$  while only one is detectable for the complex  $[\text{}^{99m}\text{Tc}(\text{HYNIC-Kp-TPPB})(\text{tricine})]$ , and (4) the impact of linker length and attachment site on the coordination chemistry of phosphine-containing HYNIC chelators.

In ternary ligand  $^{99m}\text{Tc}$  complexes,  $[\text{Tc}(\text{HYNIC-BM})(\text{tricine})(\text{TPPTS})]$ , the HYNIC group is monodentate due to the presence of the tetradentate tricine and monodentate phosphine coligands. The HYNIC group in macrocylic  $^{99m}\text{Tc}$  complexes,  $[\text{Tc}(\text{HYNIC-L})(\text{tricine})]$  ( $\text{L} = \text{o-TPPB}$  and  $\text{p-TPPB}$ ), may be forced to become bidentate (Figure 8) due to the bonding of the attached phosphine-P. The tridentate tricine are expected to result in formation of different isomers due to its asymmetric nature in bonding to the Tc. If HYNIC is monodentate in the macrocylic  $^{99m}\text{Tc}$  complex, conformational isomers may form due to the limited freedom of rotation in the macrocylic Tc chelate. This may explain the presence of three different isomers, which interconvert in solution at elevated temperatures, for  $[\text{}^{99m}\text{Tc}(\text{HYNIC-Ko-TPPB})(\text{tricine})]$ . However, in the absence of solid-state structure and variable temperature NMR studies, this ex-

planation remains a speculation. Studies on structures of macrocylic  $^{99m}\text{Tc}$  complexes will definitely help us to understand the fundamental coordination chemistry of HYNIC chelators in their macrocylic  $^{99m}\text{Tc}$  complexes.

## LITERATURE CITED

- (1) Abrams, M. J., Juweid, M., tenKate, C. I., Schwartz, D. A., Hauser, M. M., Gaul, F. E., Fuccello, A. J., Rubin, R. H., Strauss, H. W., and Fischman, A. J. (1990) Technetium-99m-human polyclonal IgG radiolabeled via the hydrazino nicotinamide derivative for imaging focal sites of infection in rats. *J. Nucl. Med.* **31**, 2022–2028.
- (2) Schwartz, D. A., Abrams, M. J., Hauser, M. M., Gaul, F. E., Larsen, S. K., Rauh, D., and Zubieta, J. (1991) Preparation of hydrazino-modified proteins and their use for the synthesis of  $^{99m}\text{Tc}$ -protein conjugates. *Bioconjugate Chem.* **2**, 333–336.
- (3) Ultee, M. E., Bridger, G. J., Abrams, M. J., Longley, C. B., Burton, C. A., Larsen, S., Henson, G. W., Padmanabhan, S., Gaul, F. E., and Schwartz, D. A. (1997) Tumour imaging with technetium-99m-labeled hydrazinonicotinamide-Fab' conjugates. *J. Nucl. Med.* **38**, 133–138.
- (4) Bridger, G. J., Abrams, M. J., Padmanabhan, S., Gaul, F. E., Larsen, S., Henson, G. W., Schwartz, D. A., Burton, C. A., and Ultee, M. E. (1996) A comparison of cleavable and noncleavable hydrazinopyridine linkers for the  $^{99m}\text{Tc}$ -labeling of Fab' monoclonal antibody fragments. *Bioconjugate Chem.* **7**, 255–264.
- (5) Babich, J. W., Solomon, H., Pike, M. C., Kroon, D., Graham, W., Abrams, M. J., Tompkins, R. G., Rubin, R. H., and Fischman, A. J. (1993) Technetium-99m labeled hydrazino nicotinamide derivatized chemotactic peptide analogues for imaging focal sites of bacterial infection. *J. Nucl. Med.* **34**, 1967–1974.
- (6) Babich, J. W., and Fischman, A. J. (1995) Effect of "coligand" on the biodistribution of  $^{99m}\text{Tc}$ -labeled hydrazino nicotinic acid derivatized chemotactic peptides. *Nucl. Med. Biol.* **22**, 25–30.
- (7) Babich, J. W., Graham, W., Barrow, S. A., and Fischman, A. J. (1993) Comparison of the infection imaging properties of a  $^{99m}\text{Tc}$  labeled chemotactic peptide with  $^{111}\text{In}$  IgG. *Nucl. Med. Biol.* **22**, 643–648.
- (8) Babich, J. W., Coco, W. G., Barrow, S. A., Fischman, A. J., Femia, F. J., and Zubieta, J. (2000)  $^{99m}\text{Tc}$ -labeled chemotactic peptides: influence of coligands on distribution of molecular species and infection imaging properties. Synthesis and structural characterization of model complexes with the  $\{\text{Re}(\eta^2\text{-HNNC}_5\text{H}_4\text{N})(\eta^1\text{-HNNC}_5\text{H}_4\text{N})\}$  core. *Inorg. Chim. Acta* **309**, 123–136.
- (9) Decristoforo, C., and Mather, S. J. (1999)  $^{99m}\text{Tc}$ -labeled peptide-HYNIC conjugates: effect of lipophilicity and stability on biodistribution. *Nucl. Med. Biol.* **26**, 389–396.

- (10) Decristoforo, C., and Mather, S. J. (1999) Preparation,  $^{99m}\text{Tc}$ -labeling, and in vitro characterization of HYNIC and  $\text{N}_3\text{S}$  modified RC-160 and  $[\text{Tyr}^3]\text{Octreotide}$ . *Bioconjugate Chem.* 10, 431–438.
- (11) Decristoforo, C., and Mather, S. J. (1999) Technetium-99m somatostatin analogues: effect of labeling methods and peptide sequence. *Eur. J. Nucl. Med.* 26, 869–876.
- (12) Decristoforo, C., Melendez, L., Sosabowski, J. K., and Mather, S. J. (2000)  $^{99m}\text{Tc}$ -HYNIC- $[\text{Tyr}^3]$ -octreotide for imaging somatostatin-receptor-positive tumors: preclinical evaluation and comparison with  $^{111}\text{In}$ -Octreotide. *J. Nucl. Med.* 41, 1114–1119.
- (13) Bangard, M., Béhé, M., Gohlke, S., Otte, R., Bender, H., Maecke, H. R., and Birsack, H. J. (2000) Detection of somatostatin receptor-positive tumours using the new  $^{99m}\text{Tc}$ -tricine-HYNIC-D-Phe<sup>1</sup>-Tyr<sup>3</sup>-octreotide: first results in patients and comparison with  $^{111}\text{In}$ -DTPA-D-Phe<sup>1</sup>-Tyr<sup>3</sup>-octreotide. *Eur. J. Nucl. Med.* 27, 628–637.
- (14) Decristoforo, C., Mather, S. J., Cholewinski, W., Donnemiller, E., Riccabona, G., and Moncayo, R. (2000)  $^{99m}\text{Tc}$ -EDDA/HYNIC-TOC: a new  $^{99m}\text{Tc}$ -labeled radiopharmaceutical for imaging somatostatin receptor-positive tumors: first clinical results and inpatient comparison with  $^{111}\text{In}$ -labeled octreotide derivatives. *Eur. J. Nucl. Med.* 27, 1318–1325.
- (15) Laverman, P., Dams, E. Th. M., Oyen, W. J. G., Storm, G., Koenders, E. B., Prevost, R., van der Meer, J. W. M., Corstens, F. H. M., and Boerman, O. C. (1999) A novel method to label liposomes with  $^{99m}\text{Tc}$  by the hydrazine nicotinyl derivative. *J. Nucl. Med.* 40, 192–197.
- (16) Zhang, Y.-M., Liu, N., Zhu, Z.-H., Rusckowski, M., and Hnatowich, D. J. (2000) Influence of different chelators (HYNIC,  $\text{MAG}_3$  and DTPA) on tumor cell accumulation and mouse biodistribution of technetium-99m labeled antisense DNA. *Eur. J. Nucl. Med.* 27, 1700–1707.
- (17) Hnatowich, D. J., Winnard, P., Jr., Virzi, F., Santo, T., Smith, C. L., Cantor, C. R., and Rusckowski, M. (1995) Technetium-99m labeling of DNA oligonucleotides. *J. Nucl. Med.* 36, 2036–2314.
- (18) Guo, W., Hinkle, G. H., and Lee, R. J. (1999)  $^{99m}\text{Tc}$ -HYNIC-folate: a novel receptor-based targeted radiopharmaceutical for tumor imaging. *J. Nucl. Med.* 40, 1563–1569.
- (19) Ono, M., Arano, Y., Mukai, T., Uehara, T., Fujioka, Y., Ogawa, K., Namba, S., Nakayama, M., Saga, T., Konishi, J., Horiuchi, K., Yokoyama, A., and Saji, H. (2001) Plasma protein binding of  $^{99m}\text{Tc}$ -labeled hydrazine nicotinamide derivatized polypeptides and peptides. *Nucl. Med. Biol.* 28, 155–164.
- (20) Ono, M., Arano, Y., Mukai, T., Fujioka, Y., Ogawa, K., Uehara, T., Namba, S., Saga, T., Konishi, J., and Saji, H. (2001)  $^{99m}\text{Tc}$ -HYNIC-derivatized ternary ligand complexes for  $^{99m}\text{Tc}$ -labeled peptides with low in vivo protein binding. *Nucl. Med. Biol.* 28, 215–224.
- (21) Liu, S., Edwards, D. S., and Barrett, J. A. (1997)  $^{99m}\text{Tc}$ -labeling of highly potent small peptides. *Bioconjugate Chem.* 8, 621–636.
- (22) Edwards, D. S., and Liu, S. (1997)  $^{99m}\text{Tc}$ -labeling of hydrazinonicotinamide modified highly potent small molecules: Problems and solutions. *Transition Metal Chem.* 22, 425–426.
- (23) Liu, S., and Edwards, D. S. (1999)  $^{99m}\text{Tc}$ -labeled small peptides as diagnostic radiopharmaceuticals. *Chem. Rev.* 99, 2235–2268.
- (24) Liu, S., and Edwards, D. S. (2001) New Radiopharmaceuticals for imaging infection and inflammation. *Drugs Future* 26, 375–382.
- (25) Edwards, D. S., Liu, S., Ziegler, M. C., Harris, A. R., Crocker, A. C., Heminway, S. J., Barrett, J. A., Bridger, G. J., Abrams, M. J., and Higgins, J. D. (1999) RP463: A stabilized technetium-99m complex of a hydrazino nicotinamide conjugated chemotactic peptide for infection imaging. *Bioconjugate Chem.* 10, 884–891.
- (26) Brouwers, A. H., Laverman, P., Boerman, O. C., Oyen, W. J. G., Barrett, J. A., Harris, T. D., Edwards, D. S., and Corstens, F. H. M. (2000) A  $^{99m}\text{Tc}$ -labeled leukotriene B4 receptor antagonist for scintigraphic detection of infection in rabbits. *Nucl. Med. Commun.* 21, 1043–1051.
- (27) Liu, S., Edwards, D. S., Ziegler, M. C., and Harris, A. R. (2002)  $^{99m}\text{Tc}$ -labeling of a hydrazinonicotinamide-conjugated  $\text{LTB}_4$  receptor antagonist useful for imaging infection. *Bioconjugate Chem.* 13, 881–886.
- (28) Liu, S., Edwards, D. S., Ziegler, M. C., Harris, A. R., Heminway, S. J., and Barrett, J. A. (2001)  $^{99m}\text{Tc}$ -Labeling of a hydrazinonicotinamide-conjugated vitronectin receptor antagonist. *Bioconjugate Chem.* 12, 624–629.
- (29) Liu, S., Edwards, D. S., Looby, R. J., Harris, A. R., Poirier, M. J., Barrett, J. A., Heminway, S. J., and Carroll, T. R. (1996) Labeling a hydrazinonicotinamide-modified cyclic IIb/IIIa receptor antagonist with  $^{99m}\text{Tc}$  using aminocarboxylates as co-ligands. *Bioconjugate Chem.* 7, 63–70.
- (30) Edwards, D. S., Liu, S., Barrett, J. A., Harris, A. R., Looby, R. J., Ziegler, M. C., Heminway, S. J., and Carroll, T. R. (1997) A new and versatile ternary ligand system for technetium radiopharmaceuticals: water soluble phosphines and tricine as coligands in labeling a hydrazino nicotinamide-modified cyclic glycoprotein IIb/IIIa receptor antagonist with  $^{99m}\text{Tc}$ . *Bioconjugate Chem.* 8, 146–154.
- (31) Edwards, D. S., Liu, S., Harris, A. R., and Ewels, B. A. (1999)  $^{99m}\text{Tc}$ -labeling hydrazones of a hydrazinonicotinamide conjugated cyclic peptide. *Bioconjugate Chem.* 10, 803–807.
- (32) Liu, S., Edwards, D. S., Harris, A. R., Ziegler, M. C., Poirier, M. J., Ewels, B. A., DiLuzio, W. R., and Hui, P. (2001) Towards developing a non- $\text{SnCl}_2$  formulation for DMP444: a new radiopharmaceutical for thrombus imaging. *J. Pharm. Sci.* 90, 114–123.
- (33) Edwards, D. S., Liu, S., Harris, A. R., and Ewels, B. A. (1999)  $^{99m}\text{Tc}$ -labeling hydrazones of a hydrazinonicotinamide conjugated cyclic peptide. *Bioconjugate Chem.* 10, 803–807.
- (34) Liu, S., Edwards, D. S., and Harris, A. R. (1998) A novel ternary ligand system for technetium radiopharmaceuticals: imine-N containing heterocycles as coligands in labeling a hydrazinonicotinamide-modified cyclic platelet glycoprotein IIb/IIIa receptor antagonist with  $^{99m}\text{Tc}$ . *Bioconjugate Chem.* 9, 583–595.
- (35) Liu, S., Edwards, D. S., Harris, A. R., Heminway, S. J., and Barrett, J. A. (1999) Technetium complexes of a hydrazinonicotinamide-conjugated cyclic peptide and 2-hydrazinopyridine: Synthesis and characterization. *Inorg. Chem.* 38, 1326–1335.
- (36) Liu, S., Ziegler, M. C., and Edwards, D. S. (2000) Radio-LC-MS for the characterization of  $^{99m}\text{Tc}$ -labeled bioconjugates. *Bioconjugate Chem.* 11, 113–117.
- (37) Harris, T. D., Sworin, M., Williams, N., Rajopadhye, M., Damphousse, P. R., Glowacka, D., Poirier, M. J., and Yu, K. (1998) Synthesis of stable hydrazones of a hydrazinonicotinyl-modified peptide for the preparation of  $^{99m}\text{Tc}$ -labeled radiopharmaceuticals. *Bioconjugate Chem.* 10, 808–814.

BC034059H



# Artificial Metalloglycoclusters: Compact Saccharide Shell to Induce High Lectin Affinity as Well as Strong Luminescence

Teruaki Hasegawa,<sup>†</sup> Takahiro Yonemura, Kazunori Matsuura,<sup>†</sup> and Kazukiyo Kobayashi\*

Department of Molecular Design and Department of Biotechnology, Graduate School of Engineering, Nagoya University, Chikusa, Nagoya 464-8603, Japan. Received March 28, 2002;  
Revised Manuscript Received December 13, 2002

Tris-bipyridine ferrous and ruthenium complexes carrying various saccharide appendages have been investigated to develop sensory systems for monitoring saccharide-binding phenomena. Ferrous *O*-glycoclusters having spacer moieties inserted between saccharide appendages and the complex core showed enhanced affinities to lectins, but ferrous *N*-glycoclusters, in which the saccharide-appendages are directly linked to the complex core via amide linkage, had low lectin-affinities. Molecular dynamics calculation indicated that the *O*-glycoclusters have flexible and densely packed saccharide clusters, in contrast to the octahedrally fixed saccharide arrays of *N*-glycoclusters. Flexibility of saccharide clusters is essential for their enhanced affinity, probably to induce conformational change to fit the recognition sites of lectins. According to these insights, ruthenium *O*-glycoclusters have been designed as luminescence biosensors. The ruthenium complexes carrying  $\alpha$ -manno clusters exhibited excellent affinities ( $IC_{min} = 9.0 \times 10^{-8}$  M) to concanavalin A (ConA). It is suggested from conformational analysis that densely packed mannoclusters can be fit properly to the recognition site of ConA. The binding was enthalpically driven ( $\Delta H^\circ = -21.8$  kcal/mol). This binding behavior is quite similar to that of 1–3/1–6 trimannoside to ConA. They have strongly amplified luminescence ( $\Phi_{em} = 0.15$ ), and their luminescence intensities were changed ( $\sim 40\%$ ) upon binding to the specific lectins. The ruthenium glycoclusters can be a suitable sensory system for saccharide-binding phenomena.

## INTRODUCTION

Saccharide chains are key substances that constitute major cell surface antigens, mediate cell adhesion and recognition, and control signal transductions through membranes (1). The saccharide chains on cell surfaces also function as receptors for various bacteria, viruses, and toxins in their first stage of infections. These functions are highly dependent on the density of the saccharide chains on the cell surfaces: clustered or multivalent saccharide chains are essential to induce strong and specific carbohydrate recognition events. Despite their critical importance, saccharide-initiated molecular recognition events and subsequent signal transduction processes have not been clearly understood, mainly owing to inherent heterogeneity and/or small quantity of saccharide fraction on cell surfaces.

Artificial glycoconjugates have received increasing interest in these days (2). Since these glycoconjugates carrying homogeneous saccharide clusters can be synthesized chemically or enzymatically in moderate quantity, they are one of the most prominent models to investigate the role of saccharide clusters on cell surfaces. Owing to their multivalent saccharide arrays, the artificial glycoclusters induce strong and specific carbohydrate recognition processes, and their applications have been expanded to vast research area, including carbohydrate-based therapeutics. Neutralization of fatal viruses and toxins, inhibition of inflammatory response, and cell-specific drug delivery could be achieved by the artificial

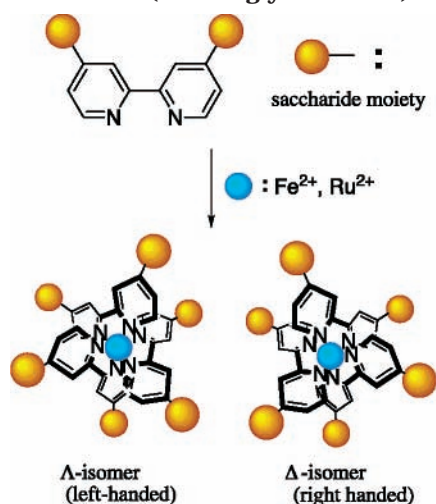
glycoclusters based on linear polymers (3), dendrimers (4), calixarenes (5, 6), cyclodextrins (6, 7), and porphyrins (8). Recently, C<sub>60</sub>-fullerene- (9) and DNAs-based (10) glycoclusters have been reported to be advantageous in therapeutic use such as cell-specific injury via active oxygen and cell-targeted gene therapy, respectively.

One of the most attractive applications of artificial glycoclusters is monitoring system for saccharide-binding phenomena. These glycoclusters would be useful as tools to study the saccharide-induced molecular recognition and signal transduction process on the cell surfaces as well as to detect fatal bacteria, viruses, and toxins in food and/or water. Polydiacetylene vesicle (11) and polythiophene (12)-based glycoclusters have been reported to be useful for colorimetric detection of bacteria, viruses, and toxins. Fluorophore-labeled oligosaccharide incorporated into bilayer system were advantageous for optical toxin sensor based on fluorescent resonance energy transfer mechanism (13). Quartz crystal microbalance (14) (QCM) and cyclic voltammetric (15) (CV)-based biosensors utilizing saccharide-modified Au surfaces have been also developed. In our research on glycoclusters, we are interested in redox and luminescence glycoclusters as a highly sensitive, selective, and reagent-free monitoring system for saccharide-recognition phenomena. To attain these glycoclusters, we have focused on tris-bipyridine transition metal complexes as sensing probes. Since they are redox-active and some are luminescent, various molecular sensors based on tris-bipyridine ferrous, ruthenium, and osmium complexes have been developed. Boronic acid-substituted tris-bipyridine ferrous complexes showed positive shift of their redox peak upon binding to carbohydrates (16). Guanidin (17) and crown ether- (18) functionalized tris-bipyridine ruthe-

\* Corresponding author. Telephone: +81-52-789-2488. Fax: +81-52-789-2528. E-mail: kobayash@mol.nagoya-u.ac.jp.

<sup>†</sup> Present address: Department of Applied Chemistry, Graduate School of Engineering, Kyushu University, Hakozaki, 6-10-1, Fukuoka 812-8581, Japan.

**Chart 1. Schematic Illustration of Glycosylated Bipyridines and Their Assembly into Tris-bipyridine Transition Metal Complexes Having Hexavalent Saccharide Clusters (Metalloglycoclusters)**



nium complexes were reported to detect their specific guests, phosphodiester and potassium chloride, respectively. However, tris-bipyridine transition metal-based glycoclusters have not been reported yet, except for one example, in which the trivalent glycoclusters based on tris-bipyridine ferrous complexes exhibited unique circular dichroism (CD) spectral change on binding to lectins (19).

Recently, we reported brief communications on the synthesis and enhanced lectin affinity of the tris-bipyridine ferrous and ruthenium complexes carrying hexavalent glycoclusters (20). The key step to access these glycoclusters is to assemble glyco-bipyridines onto ferrous and ruthenium ions as shown in Chart 1. Construction of both saccharide clusters and redox/luminescent cores has been achieved simultaneously in one-step procedure. In this paper, we will discuss their high lectin-affinity, especially that of ruthenium glycoclusters, on the basis of the stabilities, conformations, and thermodynamic aspects of their lectin-binding process. We will also describe the amplified luminescence of ruthenium glycoclusters and their application for luminescence-based sensory systems.

#### EXPERIMENTAL PROCEDURES

**General Methods.**  $^1\text{H}$  NMR and  $^{13}\text{C}$  NMR spectra were recorded on Varian Gemini-200 and Gemini-500 NMR spectrometers. The chemical shifts were reported in parts per million ( $\delta$ ) relative to  $\text{Me}_4\text{Si}$  or residual nondeuterated solvents. IR spectra were recorded on a JASCO FT/IR-230 Fourier transform infrared spectrometer. Optical rotations were determined with a JASCO DIP-1000 digital polarimeter using a water-jacketed 100 mm cell at 25 °C. Circular dichroism spectroscopy (CD) was carried out with a JASCO J-725 spectropolarimeter using a 10 mm cell. UV spectroscopy was carried out with a JASCO V-530 UV/vis spectrophotometer. Fast atom bombardment (FAB) mass spectra were obtained on a JEOL JMS-AX505HA mass spectrometer using the electron impact method operating in the positive mode. Electrospray ionization time-of-flight (ESI-TOF) mass spectra were recorded on a Micromass LCT spectrometer. Molecular mechanics and molecular dynamics calculations were carried out using Insight II/Discover program at Venture Business Laboratory of Nagoya University. Cyclic voltammograms were measured by CV-50W vol-

tammetric analyzer (BAS Co. Ltd.). Silica gel 60 (particle size 0.063–0.200 mm) for chromatography was purchased from Merck. Thin-layer chromatography (TLC) was carried out with Merck TLC plates precoated with silica gel 60. Lectin-binding assays were carried out by inhibition of hemagglutination using ConA and RCA<sub>120</sub> (Sigma).

**4,4'-Di{[N-(tetra-*O*-acetyl- $\beta$ -D-glucopyranosyl)]amido}-2,2'-bipyridine (Ac- $\beta$ -Glc-bpy).** Treatment of 2,2'-bipyridine 4,4'-dicarboxylic acid (105.2 mg, 0.43 mmol) with a boiling thionyl chloride (5 mL) for 20 h afforded 2,2'-bipyridine 4,4'-dicarbonyl chloride. Evaporation of excess thionyl chloride and drying in vacuo for 2 h gave 2,2'-bipyridine 4,4'-dicarbonyl chloride as a yellow solid. 2,3,4,6-Tetra-*O*-acetyl- $\beta$ -D-glucopyranosyl azide (0.93 g, 2.49 mmol) was dissolved in 50 mL of tetrahydrofuran and then 10% palladium on carbon (0.25 g) was added. The mixture was bubbled with hydrogen gas with stirring at room temperature for 30 min until TLC (chloroform: methanol = 4:1) indicated complete conversion of the substrate. The catalytic palladium on carbon was removed by filtration, and 2,2'-bipyridine 4,4'-dicarbonyl chloride in tetrahydrofuran was added. Stirring was continued for 1 h, and the resulting mixture was diluted with ethyl acetate and then washed with 0.5 N HCl aqueous solution and pure water several times. The organic layer was dried over anhydrous magnesium sulfate and evaporated to dryness. The product was purified by chromatography on a silica gel column (30 cm long; 3 cm i.d.; toluene-ethyl acetate = 1:1 in v/v) to give 0.36 g (93.1%) of Ac- $\beta$ -Glc-bpy in a colorless solid. mp 108–111 °C;  $[\alpha]_D^{25} -18.8^\circ$  ( $c = 1.0$ ,  $\text{CHCl}_3$ );  $^1\text{H}$  NMR (500 MHz,  $\text{CDCl}_3$ )  $\delta$  8.49 (d,  $J = 5.0$  Hz, 2H, bpy-6), 8.34 (s, 2H, bpy-3), 8.12 (br d,  $J = 9.5$  Hz, 2H, amide), 7.67 (dd,  $J = 1.5$  and 5.0 Hz, 2H, bpy-5), 5.65 (t,  $J = 9.0$  Hz, 2H, Glc-1), 5.48 (t,  $J = 9.0$  Hz, 2H, Glc-3), 5.43 (t,  $J = 9.0$  Hz, 2H, Glc-2), 5.09 (t,  $J = 9.5$  Hz, 2H, Glc-4), 4.25–4.15 (m, 4H, Glc-6), 3.98–3.94 (m, 2H, Glc-5), and 2.19, 2.14, 2.08, and 2.07 (s  $\times$  4, 24H, acetyl);  $^{13}\text{C}$  NMR (500 MHz,  $\text{CDCl}_3$ )  $\delta$  171.95, 170.46, 169.94, and 169.44 (C=O, acetyl), 164.80 (C=O, amide), 155.77 (bpy-4), 149.76 (bpy-6), 140.58 (bpy-2), 122.35 (bpy-5), 117.55 (bpy-3), 78.46 (Glc-1), 73.78 (Glc-5), 72.74 (Glc-3), 71.19 (Glc-2), 68.40 (Glc-4), and 62.09 (Glc-6), and 20.81, 20.65, 20.50, and 20.48 ( $\text{CH}_3$ , acetyl); IR (KBr,  $\text{cm}^{-1}$ ) 1753 ( $\nu_{\text{C=O}}$  acetyl), 1685 ( $\nu_{\text{C=O}}$  amide), and 1537 ( $\delta_{\text{N-H}}$  amide).

**4,4'-Di{[N-( $\beta$ -D-glucopyranosyl)]amido}-2,2'-bipyridine ( $\beta$ -Glc-bpy).** Ac- $\beta$ -Glc-bpy (102.3 mg, 113.3 mmol) was added to a mixture of tetrahydrofuran/methanol (1/1 v/v, 100 mL), and then sodium methoxide was added. The resulting mixture was stirred until TLC (chloroform: methanol = 1:1) indicated complete conversion of the substrate. The resulting mixture was neutralized with Amberlist and evaporated to dryness to give 0.64 g (99.1%) of  $\beta$ -Glc-bpy in a colorless solid.  $^1\text{H}$  NMR (500 MHz,  $\text{D}_2\text{O}$ )  $\delta$  8.65 (d,  $J = 5.0$  Hz, 2H, bpy-6), 8.42 (s, 2H, bpy-3), 7.75 (d,  $J = 5.0$  Hz, 2H, bpy-5), 5.10 (d,  $J = 8.5$  Hz, 2H, Glc-1), 3.77 (dd,  $J = 2.5$  and 12.5 Hz, 2H, Glc-6), 3.63 (dd,  $J = 5.0$  and 12.5 Hz, 2H, Glc-6), 3.50–3.46 (m, 2H, Glc-3 and 5), 3.44 (t,  $J = 9.0$  Hz, 2H, Glc-2), 3.35 (t,  $J = 9.5$  Hz, 2H, Glc-4); IR (KBr,  $\text{cm}^{-1}$ ) 3400 ( $\nu_{\text{OH}}$ ), 1664 ( $\nu_{\text{C=O}}$ , amide), and 1537 ( $\delta_{\text{N-H}}$  amide); MS  $m/z$  567 ( $\text{M} + \text{H}^+$ ).

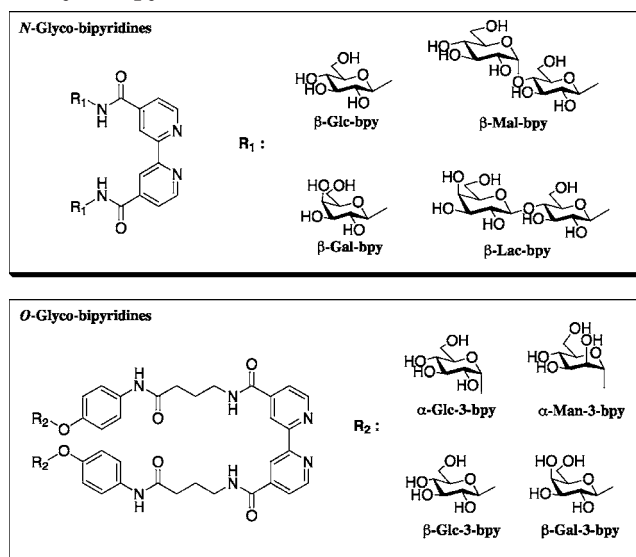
**1-{*p*-(4-Azidobutanamido)phenyl}-2,3,4,6-tetra-*O*-acetyl- $\alpha$ -D-glucopyranose (Ac- $\alpha$ -Glc-3- $\text{N}_3$ ).** *p*-Nitrophenyl 2,3,4,6-tetra-*O*-acetyl- $\alpha$ -D-glucopyranoside (0.83 g, 1.77 mmol) was dissolved in 50 mL of tetrahydrofuran and then 10% palladium on carbon (0.46 g) was added. The mixture was bubbled with hydrogen gas with stirring

at room temperature for 30 min until TLC (chloroform:methanol = 3:2) indicated complete conversion of the substrate. The catalytic palladium on carbon was removed by filtration and 4-azido butanoyl chloride in diethyl ether was added. Stirring was continued for 10 min, and the resulting solution was distilled with ethyl acetate and then washed with saturated sodium bicarbonate aqueous solution, 0.5 N HCl aqueous solution, and pure water. The organic layer was dried over anhydrous magnesium sulfate and evaporated to dryness. The product was purified by chromatography on a silica gel column (30 cm long; 3 cm i.d.; chloroform-methanol = 25:1 in v/v) to give 0.86 g (87.9%) of Ac-Glc( $\alpha$ )-3-N<sub>3</sub> as a colorless solid. mp 96–97 °C; <sup>1</sup>H NMR (500 MHz, CDCl<sub>3</sub>)  $\delta$  7.86 (s, 1H, amide), 7.46 (d,  $J$  = 9.0 Hz, 2H, benz), 7.03 (d,  $J$  = 9.0 Hz, 2H, benz), 5.69 (t,  $J$  = 10.0 Hz, 1H, Glc-3), 5.68 (d,  $J$  = 3.5 Hz, 1H, Glc-1), 5.16 (t,  $J$  = 10.0 Hz, 1H, Glc-4), 5.03 (dd,  $J$  = 3.5 and 10.0 Hz, 1H, Glc-2), 4.26 (dd,  $J$  = 5.0 and 12.0 Hz, 1H, Glc-6<sub>R</sub>), 4.15–4.11 (m, 1H, Glc-5), 4.06 (dd,  $J$  = 2.0 and 12.0 Hz, 1H, Glc-6<sub>S</sub>), 3.40 (t,  $J$  = 6.0 Hz, 2H, alkyl-4), 2.49 (t,  $J$  = 7.0 Hz, 2H, alkyl-2), 2.06, 2.06, 2.05, and 2.04 (s  $\times$  4, 12H, acetyl), and 1.99 (quintet,  $J$  = 6.5 Hz, 2H, alkyl-3); <sup>13</sup>C NMR (500 MHz, CDCl<sub>3</sub>)  $\delta$  170.48, 170.35, 170.11, 170.04, and 170.03 (C=O, acetyl), 169.46 (C=O, amide), 152.50, 133.13, 121.44, and 116.95 (phenyl), 94.47 (Glc-1), 70.28 (Glc-2), 69.85 (Glc-3), 68.14 (Glc-4), 67.81 (Glc-5), 61.45 (Glc-6), 50.55, 33.68, and 24.49 (alkyl spacer), and 20.53, 20.51, 20.44, and 20.41 (CH<sub>3</sub>-, acetyl); IR (KBr, cm<sup>-1</sup>) 2104 ( $\nu$ -N<sub>3</sub>), 1743 ( $\nu$ -C=O, acetyl), 1662 ( $\nu$ -C=O, amide), and 1521 ( $\delta$ -N-H amide); MS  $m/z$  551 (M + H<sup>+</sup>).

**4,4'-Di-*N*-[*N*-{*p*-O-(2,3,4,6-tetra-O-acetyl- $\alpha$ -D-glucopyranosyl)phenyl}amidopropyl]amido-2,2'-bipyridine (Ac- $\alpha$ -Glc-3-bpy).** Ac- $\alpha$ -Glc-3-N<sub>3</sub> (1.14 g, 2.07 mmol) was dissolved in 100 mL of tetrahydrofuran and then 10% palladium on carbon (0.48 g) was added. The mixture was bubbled with hydrogen gas with stirring at room temperature for 10 min. The catalytic palladium on carbon was removed by filtration, and 2,2'-bipyridine 4,4'-dicarbonyl chloride in tetrahydrofuran, and 2 mL of triethylamine was added. Stirring was continued for overnight, and the resulting solution was distilled with ethyl acetate and then washed with saturated sodium 0.5 N HCl aqueous solution, and pure water. The organic layer was dried over anhydrous magnesium sulfate and evaporated to dryness. The product was purified by chromatography on a silica gel column (30 cm long; 3 cm i.d.; chloroform-methanol = 25:1 ~ 9:1 in v/v, linear gradient) to give 0.59 g (90.0%) of Ac-Glc( $\alpha$ )-3-bpy as a colorless solid. mp 235–236 °C; <sup>1</sup>H NMR (500 MHz, CDCl<sub>3</sub>:CD<sub>3</sub>OD = 1:1, TMS)  $\delta$  8.78 (d,  $J$  = 5.0 Hz, 2H, bpy-6), 8.76 (s, 2H, bpy-3), 7.64 (d,  $J$  = 4.5 Hz, 2H, bpy-5), 7.52 (d,  $J$  = 9.0 Hz, 2H, benz), 7.03 (d,  $J$  = 9.0 Hz, 2H, benz), 5.68 (dd,  $J$  = 3.5 Hz, 1H, Glc-1), 5.66 (t,  $J$  = 9.5 Hz, 1H, Glc-3), 5.13 (t,  $J$  = 10.0 Hz, 1H, Glc-4), 5.03 (dd,  $J_{1,2}$  = 3.0 and 10.0 Hz, 1H, Glc-2), 4.25 (dd,  $J$  = 4.5 and 12.0 Hz, 1H, Glc-6<sub>R</sub>), 4.18–4.15 (m, 1H, Glc-5), 4.09 (dd,  $J$  = 2.0 and 12.0 Hz, 1H, Glc-6<sub>S</sub>), 3.55 (t,  $J$  = 6.0 Hz, 2H, alkyl-4), 2.50 (t,  $J$  = 7.0 Hz, 2H, alkyl-2), 2.09–2.03 (m, 14H, acetyl and alkyl-3); IR (KBr, cm<sup>-1</sup>) 3297 ( $\nu$ -N-H, amide), 1749 ( $\nu$ -C=O, acetyl), 1653 ( $\nu$ -C=O, amide), 1637 ( $\nu$ -C=O, amide), 1558 ( $\delta$ -N-H amide), and 1541 ( $\delta$ -N-H amide); MS  $m/z$  1258 (M + H<sup>+</sup>).

**4,4'-Di-*N*-[*N*-{*p*-O-( $\alpha$ -D-glucopyranosyl)phenyl}amidopropyl]amido-2,2'-bipyridine ( $\alpha$ -Glc-3-bpy).** Ac- $\alpha$ -Glc-3-bpy was added to 200 mL of a mixture of tetrahydrofuran/methanol (1/1 v/v) and then sodium methoxide was added. The resulting heterogeneous mixture was stirred until TLC (chloroform:methanol = 1:1)

**Chart 2. Structures and Abbreviations of *N*- and *O*-Glyco-bipyridines**



indicated complete conversion of the substrate and then pure water was added. The resulting homogeneous mixture was neutralized by Amberlist and evaporated to dryness to give  $\alpha$ -Glc-3-bpy in a colorless solid. <sup>1</sup>H NMR (500 MHz, DMSO-*d*<sub>6</sub> containing D<sub>2</sub>O, TMS)  $\delta$  8.85 (d,  $J$  = 5.0 Hz, 2H, bpy-6), 8.80 (s, 2H, bpy-3), 7.85 (dd,  $J$  = 1.5 and 5.0 Hz, 2H, bpy-5), 7.48 (d,  $J$  = 9.0 Hz, 4H, benz), 7.00 (d,  $J$  = 9.0 Hz, 4H, benz), 5.27 (d,  $J$  = 4.0 Hz, 2H, Glc-1), 3.61–3.05 (m, 16H, Glc-2, 3, 4, 5, 6, and alkyl), 2.36 (t,  $J$  = 7.0 Hz, 4H, alkyl), and 1.87 (quintet,  $J$  = 6.5 Hz, 4H, alkyl); IR (KBr, cm<sup>-1</sup>) 3288 ( $\nu$ -O-H), 1653 ( $\nu$ -C=O, amide), 1653 and 1625 ( $\nu$ -C=O, amide), 1541 and 1508 ( $\delta$ -N-H amide).

## RESULTS AND DISCUSSION

**Synthesis of Glyco-Bipyridines.** We have designed two types (*N*- and *O*-) of glyco-bipyridines, as shown in Chart 2. The *N*-glyco-bipyridines carrying two  $\beta$ -*N*-glycosides attached directly via amide linkage were synthesized from peracetyl glycosyl azides via hydrogenation, coupling of the resulting amino function with 2,2'-bipyridine 4,4'-dicarbonyl chloride, and the subsequent deacetylation. Bipyridines presenting *N*-linked  $\beta$ -glucoside ( $\beta$ -Glc-bpy),  $\beta$ -galactoside ( $\beta$ -Gal-bpy),  $\beta$ -maltoside ( $\beta$ -Mal-bpy), and  $\beta$ -lactoside ( $\beta$ -Lac-bpy) were obtained. The *O*-glyco-bipyridines carrying two *O*-glycoside terminals through flexible trimethylene spacers were synthesized from acetylated *p*-nitrophenyl D-glycopyranosides as starting materials. The nitro function was hydrogenated and the resulting amine was acylated with 4-azido-butanoyl chloride. The terminal azido group was hydrogenated and coupled with 2,2'-bipyridine 4,4'-dicarbonyl chloride, followed by deacetylation to afford glyco-bipyridines ( $\alpha$ -Glc-3-bpy,  $\beta$ -Glc-3-bpy,  $\alpha$ -Man-3-bpy, and  $\beta$ -Gal-3-bpy) in moderate total yields.

**Ferrous Glycoclusters: Preparation and Characterizations.** The *N*-glyco-bipyridines were well soluble in aqueous solution and hence the preparation of the corresponding glycoclusters could be performed in pure water. When the *N*-glyco-bipyridines were treated with 1/3 equiv of ferrous chloride in water at room temperature, the solution turned red gradually, indicating the formation of the corresponding hexavalent glycoclusters. On the other hand, the *O*-glyco-bipyridines were poorly soluble in pure water due to their hydrophobic phenyl



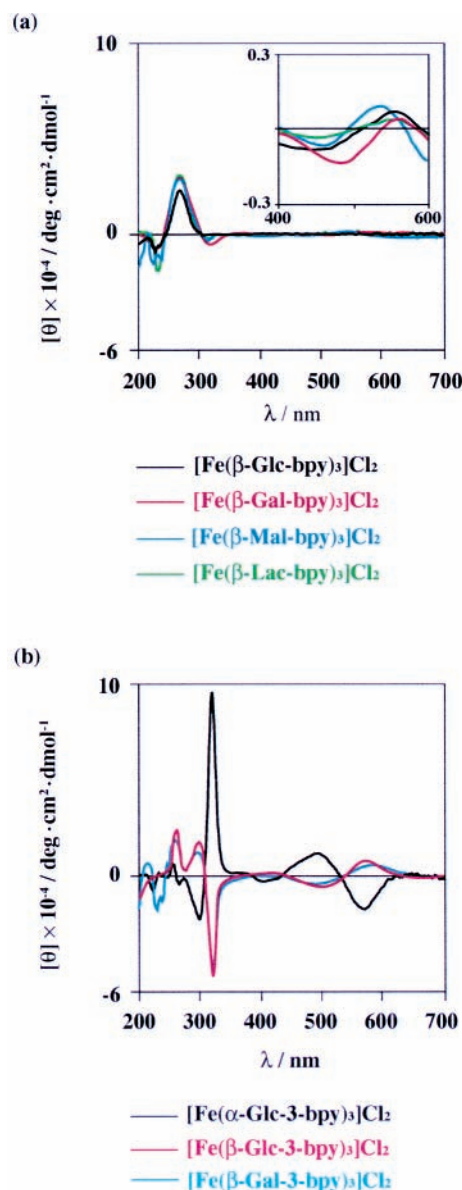
and trimethylene spacer. Therefore, preparation of the corresponding glycoclusters was performed in a water/methanol mixture (1/1 v/v) at room temperature. After treating the *O*-glyco-bipyridines with ferrous chloride, the solution turned red gradually, but the color change was slower than those of *N*-glyco-bipyridines due to low solubility. Lyophilization of the resulting red solutions afforded the ferrous glycoclusters in purple powders. The resulting glycoclusters were well soluble in pure water, owing to their dicationic charge on ferrous complex center.

The constitutions of the glycoclusters were proved as follows. (1) The UV spectra of glycoclusters showed metal-to-ligand charge transfer (MLCT) absorption band at around 544 nm that is characteristic for  $[\text{Fe}(\text{bpy})_3]^{2+}$ ; their MLCT absorptions were red-shifted from that (523 nm) of the  $[\text{Fe}(\text{bpy})_3]\text{Cl}_2$  (bpy: 2,2'-bipyridine), owing to the electron-withdrawing amide linkages. (2) The 3:1 stoichiometry of glyco-bipyridines and ferrous chloride was confirmed via UV spectrometric titration. (3) The dicationic molecular ions of these glycoclusters were detected by electrospray ionization time-of-flight mass spectrometry (ESI-TOF-MS). (4)  $^1\text{H}$  NMR showed only two distinct signals assignable to both  $\Delta$ - and  $\Lambda$ -stereoisomeric glycoclusters. Interestingly, the diastereo ( $\Delta$  and  $\Lambda$ )-excess (d.e.) of *O*-glycoclusters estimated from the  $^1\text{H}$  NMR was higher than that of *N*-glycoclusters:  $[\text{Fe}(\alpha\text{-Glc-3-bpy})_3]\text{Cl}_2$  (49% d.e.) >  $[\text{Fe}(\beta\text{-Glc-bpy})_3]\text{Cl}_2$  (18% d.e.), despite the spacers separating the saccharide appendages from the complex core. The high diastereo-excess in *O*-glycoclusters originates from the spatial proximity of their saccharide appendages to the complex-cores (described in the following section in detail).

The CD spectra of *N*-glycoclusters in Figure 1a are similar to each other and assignable to  $\Delta$ -isomer (21). The preferential formation of  $\Delta$ -isomers should be caused by their anomeric  $\beta$ -*N*-configuration. However, their peak intensities were smaller than that of enantio-pure  $\Delta$ - $[\text{Fe}(\text{bpy})_3]^{2+}$ , due to their low d.e. values. In *O*-glycoclusters (Figure 1b),  $[\text{Fe}(\alpha\text{-Glc-3-bpy})_3]\text{Cl}_2$  and  $[\text{Fe}(\beta\text{-Glc-3-bpy})_3]\text{Cl}_2$  gave almost symmetrical CD spectra that are assignable to  $\Lambda$ - and  $\Delta$ - $[\text{Fe}(\text{bpy})_3]^{2+}$ , respectively. On the other hand, the CD spectra of  $[\text{Fe}(\beta\text{-Gal-3-bpy})_3]\text{Cl}_2$  and  $[\text{Fe}(\beta\text{-Glc-3-bpy})_3]\text{Cl}_2$  were quite similar with each other. The stereochemistry of the metal complexes was induced mainly by the chirality at the anomeric positions of saccharide moieties. Both molar ellipticities due to  $\pi$ - $\pi^*$  transition (ca. 300 nm) and MLCT (ca. 540 nm) were smaller than those of enantio-pure  $[\text{Fe}(\text{bpy})_3]^{2+}$ , also indicative of the mixtures of  $\Lambda$ - and  $\Delta$ -stereoisomers of these glycoclusters. However, it is interesting to note that the *O*-glycoclusters have stronger CD intensities than those of the *N*-glycoclusters, reflecting their high diastereo-excesses.

$[\text{Fe}(\alpha\text{-Glc-3-bpy})_3]\text{Cl}_2$  and  $[\text{Fe}(\beta\text{-Glc-bpy})_3]\text{Cl}_2$  could be separated into diastereo  $\Delta$ - and  $\Lambda$ -isomers by reverse-phase high-performance liquid chromatography (HPLC), but the broadening of their peaks was observed. Since ferrous glycoclusters were labile, isomerization as well as dissociation may occur even in HPLC separation time-scale, resulting in the observed peak-broadening. The assignments of their major and minor peaks were based on their CD spectra. The  $\Lambda$ - $\Delta$  ratios estimated from their integration were 73:27 ( $[\text{Fe}(\alpha\text{-Glc-3-bpy})_3]\text{Cl}_2$ ) and 41:59 ( $[\text{Fe}(\beta\text{-Glc-bpy})_3]\text{Cl}_2$ ). The observed high d.e. value of *O*-glycocluster coincide with that estimated by  $^1\text{H}$  NMR spectra.

The stabilities of the *N*-glycoclusters could be estimated by the UV titration method using the absorbance



**Figure 1.** CD spectra of (a) *N*- and (b) *O*-ferrous glycoclusters in water at 25 °C.

**Table 1.** Dissociation Constants of the Conjugates<sup>a</sup>

Tris-bipyridine ferrous complexes	$K_d \times 10^6/\text{M}$
$[\text{Fe}(\beta\text{-Glc-bpy})_3]\text{Cl}_2$	43.4
$[\text{Fe}(\beta\text{-Gal-bpy})_3]\text{Cl}_2$	54.9
$[\text{Fe}(\beta\text{-Mal-bpy})_3]\text{Cl}_2$	73.9
$[\text{Fe}(\beta\text{-Lac-bpy})_3]\text{Cl}_2$	74.3
$[\text{Fe}(\text{bpy})_3]\text{Cl}_2$ <sup>b</sup>	1.8

<sup>a</sup> At 25 °C, in water. <sup>b</sup> Martell, A. E., et al. (ref 22).

at 544 nm ( $\text{Abs}_{544 \text{ nm}}$ ) of glyco-bipyridine ( $0$ – $5 \times 10^{-4}$  M) in an aqueous solutions containing  $\text{FeCl}_2$  ( $3 \times 10^{-6}$  M) and summarized in Table 1. The dissociation constants ( $K_d$ ) of the glycoclusters were on the order of  $10^{-5}$  and higher than that of  $[\text{Fe}(\text{bpy})_3]^{2+}$  by a factor of 24–41. Destabilization of glycocluster compared to  $[\text{Fe}(\text{bpy})_3]^{2+}$  arise from the electron-withdrawing amide linkage that reduces the electron density on bipyridine nitrogen atom and their coordination ability. Furthermore, the steric repulsion among their bulky saccharide moieties is also attributable to their low stabilities, as suggested by the lower dissociation constants of the disaccharide clusters than those of monosaccharide clusters. On

**Table 2.** Inhibition of ConA- and RCA<sub>120</sub>-Induced Hemagglutination by Ferrous Glycoclusters<sup>a</sup>

inhibitor	IC <sub>min</sub> <sup>b</sup> /M <sup>c</sup>	
	ConA	RCA <sub>120</sub>
<i>O</i> -Glycoclusters		
[Fe(α-Glc-3-bpy) <sub>3</sub> ]Cl <sub>2</sub> <sup>e</sup>	9.6 × 10 <sup>-6</sup>	n.i. <sup>d</sup>
[Fe(α-Man-3-bpy) <sub>3</sub> ]Cl <sub>2</sub> <sup>e</sup>	3.5 × 10 <sup>-7</sup>	n.i. <sup>d</sup>
[Fe(β-Gal-3-bpy) <sub>3</sub> ]Cl <sub>2</sub> <sup>e</sup>	n.i. <sup>d</sup>	4.4 × 10 <sup>-5</sup>
<i>N</i> -Glycoclusters		
[Fe(β-Glc-bpy) <sub>3</sub> ]Cl <sub>2</sub> <sup>e</sup>	9.5 × 10 <sup>-2</sup>	n.i. <sup>d</sup>
[Fe(β-Mal-bpy) <sub>3</sub> ]Cl <sub>2</sub> <sup>e</sup>	1.9 × 10 <sup>-3</sup>	n.i. <sup>d</sup>
[Fe(β-Gal-bpy) <sub>3</sub> ]Cl <sub>2</sub> <sup>e</sup>	n.i. <sup>d</sup>	2.5 × 10 <sup>-3</sup>
[Fe(β-Lac-bpy) <sub>3</sub> ]Cl <sub>2</sub> <sup>e</sup>	n.i. <sup>d</sup>	5.4 × 10 <sup>-4</sup>
Monovalent Saccharide		
α-Glc- <i>p</i> NP	1.9 × 10 <sup>-4</sup>	n.i. <sup>d</sup>
α-Man- <i>p</i> NP	2.1 × 10 <sup>-5</sup>	n.i. <sup>d</sup>
β-Gal- <i>p</i> NP	n.i. <sup>d</sup>	2.8 × 10 <sup>-4</sup>
glucose	7.3 × 10 <sup>-3</sup>	n.i. <sup>d</sup>
maltose	8.0 × 10 <sup>-4</sup>	n.i. <sup>d</sup>
galactose	n.i. <sup>d</sup>	1.9 × 10 <sup>-3</sup>
lactose	n.i. <sup>d</sup>	5.0 × 10 <sup>-4</sup>

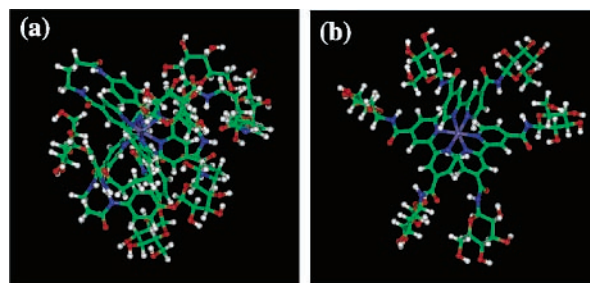
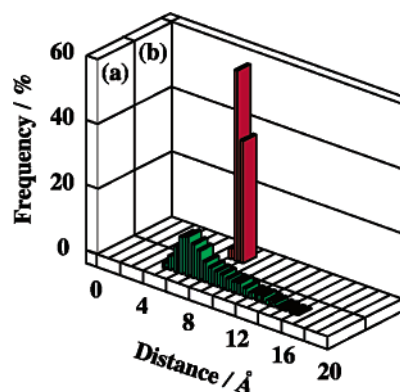
<sup>a</sup> [Lectin] = 8 × [minimum concentration required for hemagglutination]. <sup>b</sup> Minimum inhibition concentration. <sup>c</sup> Molarity of saccharide unit. <sup>d</sup> Not inhibited by 0.1 M. <sup>e</sup> Δ-Δ mixture.

the other hand, the dissociation constants of *O*-glycoclusters could not be determined because of their poor solubility in water.

**Ferrous Glycoclusters: Binding to Lectins.** Binding of the ferrous glycoclusters to lectins was investigated by hemagglutination inhibition assay using α-glucoside/mannoside-specific concanavalin A (ConA) and β-galactoside-specific *Ricinus communis* agglutinin (RCA<sub>120</sub>). Monovalent *p*-nitrophenyl glycosides and saccharides themselves were used as references to estimate saccharide cluster effects in these glycoclusters. The minimum concentrations of saccharide units to inhibit lectin-induced hemagglutination (IC<sub>min</sub>) are summarized in Table 2.

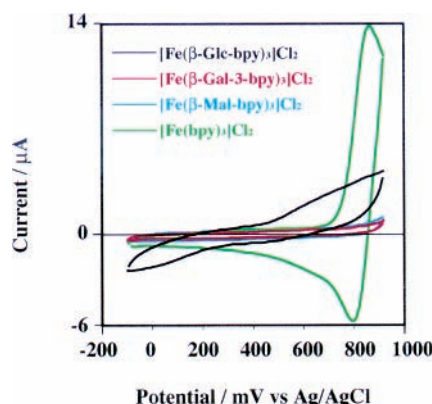
The *O*-glycoclusters inhibited lectin-induced hemagglutination more strongly than the corresponding monovalent *p*-nitrophenyl glycosides by a factor of 20 (gluco-), 60 (manno-), and 6 (galacto-). Together with the fact that [Fe(bpy)<sub>3</sub>]Cl<sub>2</sub> could not inhibit lectin-induced hemagglutination at all, the origin of the enhanced lectin-affinity was certainly assigned to their hexavalent glycoarrays. However, these IC<sub>min</sub> values were lower than we expected. In such a low concentration, some glycocluster complexes dissociate into the corresponding glyco-bipyridines. On the other hand, the situation was quite different in *N*-glycoclusters. No enhancement in lectin affinity of *N*-glycoclusters compared to the corresponding monovalent saccharide was observed. In particular, it is of interest to note that even [Fe(β-Mal-3-bpy)<sub>3</sub>]Cl<sub>2</sub> and [Fe(β-Lac-bpy)<sub>3</sub>]Cl<sub>2</sub> were not potent inhibitors for ConA- and RCA<sub>120</sub>-induced hemagglutination, respectively, despite their multivalent *O*-α-gluco- and *O*-β-galactoclusters.

To reveal the origin of the critical difference between *O*- and *N*-glycoclusters in their lectin-affinities, we investigated their spatial structure via molecular dynamics (MD) calculations using InsightII/Discover program and esff force field. After 400 ps equilibrium, 600 ps dynamics were performed at 300 K and ε = 80.0. The most stable conformations of Δ-[Fe(α-Glc-3-bpy)<sub>3</sub>]<sup>2+</sup> and Δ-[Fe(β-Glc-bpy)<sub>3</sub>]<sup>2+</sup> in MD calculation are shown in Figure 2. The *O*-glycocluster, Δ-[Fe(α-Glc-3-bpy)<sub>3</sub>]<sup>2+</sup>, has compact and densely packed saccharide arrays surrounding complex core despite the presence of spacers. On the other hand, the *N*-glycocluster, Δ-[Fe(β-Glc-bpy)<sub>3</sub>]<sup>2+</sup>, has

**Figure 2.** Most stable conformations of (a) Δ-[Fe(α-Glc-3-bpy)<sub>3</sub>]<sup>2+</sup> and (b) Δ-[Fe(β-Glc-bpy)<sub>3</sub>]<sup>2+</sup> given by MD calculations.**Figure 3.** The histogram of the distances between central ferrous atom and the anomeric carbons of (a) [Fe(α-Glc-3-bpy)<sub>3</sub>]<sup>2+</sup> and (b) [Fe(β-Glc-bpy)<sub>3</sub>]<sup>2+</sup> in the MD calculations.

octahedrally fixed saccharide arrays templated by complex core. Furthermore, the distances between their anomeric carbons and the ferrous atom in the MD calculation are quite different between *O*- and *N*-glycoclusters. The distance histogram (Figure 3) shows that the saccharide moieties in the *O*-glycoclusters were fluctuated within the wide range from 4.8 to 17.6 Å (ave. 7.4 Å), but those of *N*-glycoclusters were highly fixed at around 7.8 Å. Their critical difference in flexibility apparently arises from the existence of inserted spacers. The saccharide arrays of *N*-glycoclusters may be regulated in octahedral manner so tightly that they could not be accessible or induced-fit to the binding sites of lectins. The spatial compatibility as well as flexibility may be substantial factors for the high lectin-affinity of metalloglycoclusters, as previously reported for the helical glyco-arrays along a polyisocyanide template (23).

**Ferrous Glycoclusters: Electrochemical Properties.** Their electrochemical properties were investigated by using cyclic voltammetry in water containing 0.2 M sodium sulfate (Figure 4). Tris-bipyridine ferrous complex without any saccharide unit, [Fe(bpy)<sub>3</sub>]Cl<sub>2</sub>, gave clear redox peak at about +840 mV, assignable to the redox of metal center (Fe<sup>2+</sup>/Fe<sup>3+</sup>). However, the *N*-glycoclusters, [Fe(β-Glc-bpy)<sub>3</sub>]Cl<sub>2</sub> and [Fe(β-Mal-bpy)<sub>3</sub>]Cl<sub>2</sub>, exhibited weak and broadened redox peaks in the potential range from -100 to +920 mV. It is noteworthy that disaccharide-appended complex has more depressed redox peak than monosaccharide-appended one. Although it could not be excluded that the electron-withdrawing amide linkage may shift the redox peaks positively to out of our potential range, we assume that the bulky saccharide attachment may isolate the ferrous center from the outer circumstance and hinder electron transfer between the electrode and the redox core. The isolating effect of carbohydrate moieties was much clearly demonstrated by the flexible glycoclusters: [Fe(β-Gal-3-bpy)<sub>3</sub>]Cl<sub>2</sub> showed

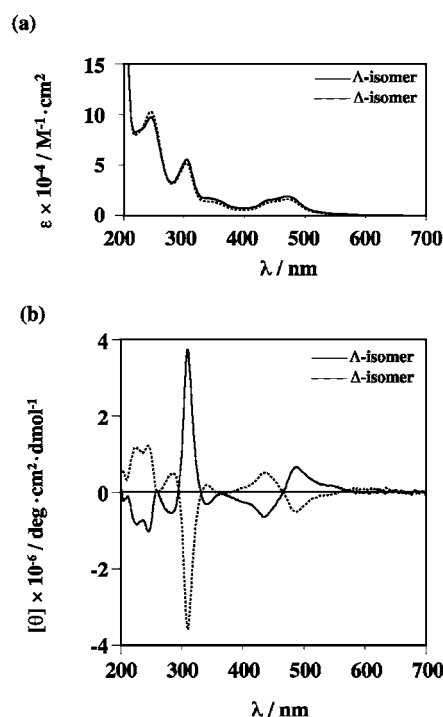


**Figure 4.** Cyclic voltammogram of ferrous glycoclusters ( $[\text{Fe}(\beta\text{-Gal-3-bpy})_3]\text{Cl}_2$ ,  $[\text{Fe}(\beta\text{-Glc-bpy})_3]\text{Cl}_2$ , and  $[\text{Fe}(\beta\text{-Mal-bpy})_3]\text{Cl}_2$ ) and  $[\text{Fe}(\text{bpy})_3]\text{Cl}_2$  at a gold electrode in 0.2 M  $\text{Na}_2\text{SO}_4$  aqueous solution. Scan rate is 200 mV/s; Pt counter electrode and Ag/AgCl (in 3 M NaCl) reference electrode.

no redox peak in our potential range. It is likely that, although its saccharide structure is small (monosaccharide), the densely packed glyco-arrays serve as “carbohydrate-shell” which completely isolate ferrous center. Recently, similar carbohydrate-shell effects to protect redox cores from solvent interactions were reported for ferrocene derivatives carrying saccharide-terminated dendrimers (24). These isolating phenomena were of interest in the light of mimicking the proteins that have an isolated redox unit embedded into a polypeptide framework. However, the present ferrous glycoclusters seem not to be suitable as redox biosensor owing to the disappearance of redox peak as well as instability in diluted solution.

**Ruthenium Glycoclusters: Preparation and Characterizations.** According to the insight obtained from ferrous glycoclusters, we have designed ruthenium-*O*-glycoclusters to develop more robust and luminescent sensory system for monitoring saccharide recognition phenomena. The following synthetic and separation procedures yielded each stereoisomeric  $\Lambda$ - and  $\Delta$ -type  $\alpha$ -mannocluster ( $\Lambda$ - and  $\Delta$ - $[\text{Ru}(\alpha\text{-Man-3-bpy})_3]\text{Cl}_2$ ) and the corresponding  $\alpha$ -glucoclusters, but the  $\beta$ -galactocluster as a  $\Lambda$ - and  $\Delta$ -type mixture. When 3 equiv of  $\alpha$ -Man-3-bpy were treated with  $\text{RuCl}_3$  in a boiling water/ethanol mixture, the solution turned orange gradually, suggesting the formation of the corresponding tris-bipyridine ruthenium complex. After 20 h boiling, the orange solution was filtered to remove the precipitate containing unreacted ligands and ruthenium and then chromatographed through Toyo-Pearl HW40-S gel using aqueous 0.03 M ammonium acetate as the eluent. The respective isomers were separated and lyophilized to afford pure  $\Lambda$ - and  $\Delta$ - $[\text{Ru}(\alpha\text{-Man-3-bpy})_3]\text{Cl}_2$  as orange powder. Neither isomerization nor dissociation was detected even in highly diluted aqueous solution at room temperature, suggestive of the robust  $[\text{Ru}(\text{bpy})_3]^{2+}$  core.

The assignment of  $\Lambda$ - and  $\Delta$ - $[\text{Ru}(\alpha\text{-Man-3-bpy})_3]\text{Cl}_2$  was based on the ESI-TOF-MS, UV, and CD spectra. The ESI-TOF-MS detected the dicationic molecular ion peak (1431.93) of  $[\text{Ru}(\alpha\text{-Man-3-bpy})_3]^{2+}$  (calc. 1431.97). Their UV-vis spectra gave MLCT absorption band at 466 nm characteristic of tris-bipyridine ruthenium complex, as shown in Figure 5a. Their MLCT bands were shifted to a longer wavelength ( $\sim 16$  nm) with slightly larger extinction coefficient than that of  $[\text{Ru}(\text{bpy})_3]\text{Cl}_2$  itself. Their CD spectra were almost symmetrical at the bipyridine  $\pi\text{-}\pi^*$  (ca. 300 nm) and MLCT absorption bands



**Figure 5.** (a) UV and (b) CD spectra of  $\Lambda$ - and  $\Delta$ - $[\text{Ru}(\alpha\text{-Man-3-bpy})_3]\text{Cl}_2$  in water at 25 °C.

**Table 3. Inhibition of ConA- and RCA<sub>120</sub>-Induced Hemagglutination by Ruthenium Glycoclusters<sup>a</sup>**

inhibitor	IC <sub>min</sub> <sup>b</sup> /M <sup>c</sup>	
	ConA	RCA <sub>120</sub>
Ruthenium Glycoclusters		
$\Lambda$ - $[\text{Ru}(\alpha\text{-Glc-3-bpy})_3]\text{Cl}_2$	$1.4 \times 10^{-5}$	n.i. <sup>d</sup>
$\Delta$ - $[\text{Ru}(\alpha\text{-Glc-3-bpy})_3]\text{Cl}_2$	$1.1 \times 10^{-5}$	n.i. <sup>d</sup>
$\Lambda$ - $[\text{Ru}(\alpha\text{-Man-3-bpy})_3]\text{Cl}_2$	$9.0 \times 10^{-8}$	n.i. <sup>d</sup>
$\Delta$ - $[\text{Ru}(\alpha\text{-Man-3-bpy})_3]\text{Cl}_2$	$1.5 \times 10^{-7}$	n.i. <sup>d</sup>
$[\text{Ru}(\alpha\text{-Gal-3-bpy})_3]\text{Cl}_2^e$	n.i. <sup>d</sup>	$2.5 \times 10^{-6}$
Monovalent Saccharide		
$\alpha$ -Glc- <i>p</i> NP	$1.9 \times 10^{-4}$	n.i. <sup>d</sup>
$\alpha$ -Man- <i>p</i> NP	$2.1 \times 10^{-5}$	n.i. <sup>d</sup>
$\beta$ -Gal- <i>p</i> NP	n.i. <sup>d</sup>	$2.8 \times 10^{-4}$

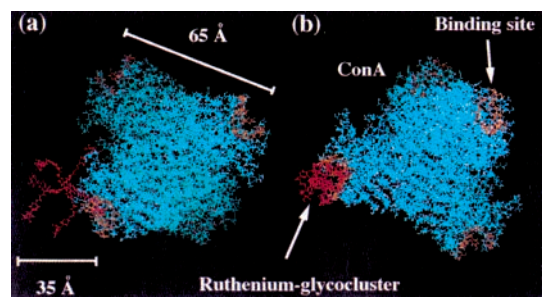
<sup>a</sup> [Lectin] =  $8 \times$  [Minimum concentration required for hemagglutination]. <sup>b</sup> Minimum inhibition concentration. <sup>c</sup> Molarity of saccharide unit. <sup>d</sup> Not inhibited by 0.1 M. <sup>e</sup>  $\Delta$ - $\Lambda$  mixture.

(ca. 460 nm) characteristic for  $\Lambda$ - and  $\Delta$ -configurations, as shown in Figure 5b (25).

**Ruthenium Glycoclusters: Binding to Lectins.** Hemagglutination inhibition assay of the ruthenium glycoclusters using ConA and RCA<sub>120</sub> is summarized in Table 3. The inhibitory potency of the ruthenium glycoclusters was dramatically enhanced, compared to the corresponding monovalent *p*-nitrophenyl glycosides as well as the corresponding ferrous glycoclusters. It is reasonable to assume that their high lectin-affinity is attributable to their robust structures that retain their hexavalent saccharide clusters even in the highly diluted solutions. It is of interest to note that the most remarkable enhancement (230-fold) in affinity was observed for mannoclusters.  $\Lambda$ - $[\text{Ru}(\alpha\text{-Man-3-bpy})_3]\text{Cl}_2$  inhibited lectin-induced hemagglutination at the low concentration of  $9 \times 10^{-8}$  M: the excellent affinity was comparable to those of polyvalent  $\alpha$ -mannosylated polymer (poly(*p*-N-acrylamidophenyl- $\alpha$ -D-mannopyranoside,  $M_n \sim 4 \times 10^{-7}$  M).

The difference in binding to lectins between the present glycoclusters and glycosylated polymers can be discussed as follows. Glycosylated polymers are capable of cross-





**Figure 6.** The superimpose of (a) the expanded and (b) the most stable conformation of  $\Lambda$ -isomer of  $\alpha$ -mannosylated complexes onto the crystallographic structure of ConA. The glycoclusters and the saccharide-binding sites of ConA are depicted in red and brown, respectively. ConA is depicted in blue and white.

linking the multiple binding sites on lectins, which must play substantial roles in their high affinity. On the other hand, the present glycoclusters could not bind to ConA in the cross-linking manner because the diameter ( $\sim 3.8$  nm) of the present glycoclusters is much smaller than the distance (6.8 nm) between the two binding sites on the adjacent subunits in ConA (Figure 6a). To the best of our knowledge, the reported small glycoclusters, such as glycosylated cyclodextrins and calixarenes, have relatively low lectin affinity compared to large glycopolymers. It is of interest why the lectin affinity of the present small mannocluster is as high as those of the polymer-based glycoclusters. The following discussion is made on their structural as well as thermodynamic aspect for the binding to lectins.

The densely packed saccharide arrays, or "saccharide shell", of these glycoclusters were confirmed by  $^1\text{H}$  NMR as well as MD. Nuclear Overhauser effect between the bipyridine and the anomeric protons of both  $\Lambda$ - and  $\Delta$ -stereoisomers of  $[\text{Ru}(\alpha\text{-Man-3-bpy})_3]\text{Cl}_2$  was observed in  $^1\text{H}$  NMR spectra, suggesting the spatial proximity of their saccharide appendages to their complex core through the trimethylene spacers. Similar nuclear Overhauser effects were also observed in the both stereoisomers of the corresponding  $\alpha$ -glucoclusters. These densely packed saccharide clusters surrounding the complex core may also arise from the hydrophobic interaction between the complex core and the phenyl ring of the aglycon. MD calculations (method and conditions were identical with those used for ferrous-based ones) revealed that the most stable conformations of  $\Lambda$ - and  $\Delta$ - $[\text{Ru}(\alpha\text{-Man-3-bpy})_3]^{2+}$  have densely packed saccharide clusters surrounding complex cores, similar to ferrous-*O*-glycoclusters. The distances between their anomeric carbons and the ruthenium center are distributed widely from 4.8 to 18.5 Å, suggestive of their flexible saccharide arrays. The average distance of  $\Delta$ -isomer (7.5 Å) was slightly shorter than that of the corresponding  $\Lambda$ -isomer (7.9 Å), indicating that the  $\Delta$ -isomer takes more compact conformation than the corresponding  $\Lambda$ -isomer. Furthermore, it is worthy to note that these mannoclusters have more densely packed saccharide arrays compared to the corresponding glucoclusters: the average distances of glucoclusters were estimated to 9.2 and 8.7 Å for  $\Lambda$ - and  $\Delta$ -isomers, respectively. Molecular mechanics (MM) calculation demonstrates that ruthenium-based mannocluster can be fit properly to the recognition site of ConA, which strongly recognizes 1-3/1-6 trimannosides (Figure 6b). We assume that the densely packed manno-

**Table 4.** Thermodynamic Parameters of the Ruthenium Glycoclusters, along with that of Monomannoside, Trimannoside, and Mannosylated Polymer-Functionalized Nanosphere<sup>a</sup>

	$K_a$ ( $\text{M}^{-1}$ )	$\text{kcal mol}^{-1}$		
		$\Delta G^\circ$	$\Delta H^\circ$	$T\Delta S^\circ$
Man $\alpha$ -OMe <sup>b</sup>	$8.2 \times 10^3$	-5.3	-8.2	-2.9
Man $\alpha$ -1-6(Man $\alpha$ -1-3)Man $\alpha$ -OMe <sup>b</sup>	$4.9 \times 10^5$	-7.8	-14.4	-6.6
$\Lambda$ - $[\text{Ru}(\alpha\text{-Man-3-bpy})_3]\text{Cl}_2$	$5.4 \times 10^6$	-9.7	-21.8	-12.1
$\Delta$ - $[\text{Ru}(\alpha\text{-Glc-3-bpy})_3]\text{Cl}_2$	$9.5 \times 10^5$	-8.4	-13.8	-5.4
DODA-PMEP Man (DP = 17) <sup>c</sup>	$3.0 \times 10^5$	-7.3	-3.6	3.7

<sup>a</sup> At 25 °C. <sup>b</sup> Mandal, D. K., et al. (ref 27). <sup>c</sup> Tagawa, K., et al. (ref 26).

arrays act as a trimannoside mimic and then bound to ConA with strong affinity comparable to those of glycopolymers.

The thermodynamic parameters ( $\Delta G^\circ$ ,  $\Delta H^\circ$ , and  $T\Delta S^\circ$ ) between  $\Lambda$ - $[\text{Ru}(\alpha\text{-Man-3-bpy})_3]\text{Cl}_2$  and ConA have been evaluated from the temperature dependence of the association constants as follows. A mixture of ruthenium glycoclusters ( $9.4 \times 10^{-7}$  M) and ConA ( $1.0 \times 10^{-6}$  to  $1.0 \times 10^{-7}$  M) in PBS (pH 6.5) was incubated at the temperature (15–35 °C). The glycoclusters-ConA aggregates were removed by ultrafiltration through a Millipore Ultrafree-MC membrane (cut off 30 000), and the concentrations of free glycoclusters in the resultant orange filtrate were determined by fluorometry. The association constants ( $K_a$ ) were calculated by using computational curve fitting. The remarkable affinity of ruthenium glycoclusters, especially  $\Lambda$ - $[\text{Ru}(\alpha\text{-Man-3-bpy})_3]\text{Cl}_2$ , to ConA below submicron concentration, has been again demonstrated and their temperature dependence was given as van't Hoff plots. Table 4 summarizes the association constants and thermodynamic parameters of the glycoclusters, along with those of methylmannoside, methyl 1-3/1-6 trimannoside, polymer-based saccharide cluster.

The origin of their high lectin affinity can be discussed on the basis of thermodynamic parameters. The  $\Delta H^\circ$  and  $\Delta S^\circ$  values for ruthenium glycoclusters were all negative, indicating that their interaction with ConA was favorable in enthalpy and unfavorable in entropy. The negative entropy value ( $\Delta S^\circ$ ) may be attributable mainly to suppression in molecular motion of glycoclusters embedding on saccharide-binding sites of lectins. Their flexibility arising from trimethylene spacer may be contributed to the large negative entropy value. This tendency is quite different from glycopolymer-functionalized liposome system, in which positive  $\Delta S^\circ$  value is suggestive that the glycoclusters can bind to four saccharide-recognition sites of tetrameric ConA lectin in multivalent and bridging manner (26).

It is of interest to note that the binding of  $\Lambda$ - $[\text{Ru}(\alpha\text{-Man-3-bpy})_3]\text{Cl}_2$  to ConA was enthalpically driven, similarly to that of 1-3/1-6 trimannoside. These thermodynamic character should support our assumption that the compactly packed mannocluster of  $\Lambda$ - $[\text{Ru}(\alpha\text{-Man-3-bpy})_3]\text{Cl}_2$  mimics 1-3/1-6 trimannoside to induce their excellent affinities. Furthermore, the electrostatic interaction between the dicationic complex center and the anionic protein residues may be taken into account. According to the crystal structure of ConA-trimannoside complex, some acidic protein residues (Asp16 and Asp208) are located closely to trimannoside (28). These acidic residues should possess anionic charges under neutral condition and also contribute to electrostatic interaction that induce large negative enthalpy value as well as strong bindings.

**Table 5. The Emission Wave Length and Luminescence Quantum Yield ( $\Phi_{em}$ ) of the Ruthenium-Based Glycoclusters<sup>a</sup>**

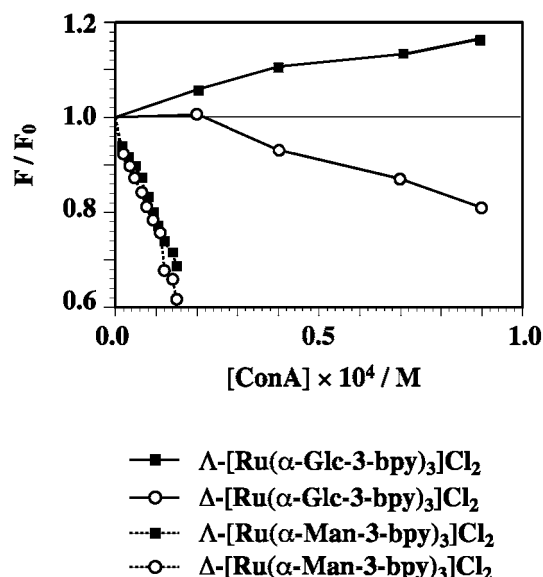
ruthenium-based complex	$\lambda_{em}/nm$	$\phi_{em}$
$\Lambda$ -[Ru( $\alpha$ -Glc-3-bpy) <sub>3</sub> ]Cl <sub>2</sub>	605.8	0.105
$\Delta$ -[Ru( $\alpha$ -Glc-3-bpy) <sub>3</sub> ]Cl <sub>2</sub>	604.4	0.086
$\Lambda$ -[Ru( $\alpha$ -Man-3-bpy) <sub>3</sub> ]Cl <sub>2</sub>	600.6	0.150
$\Delta$ -[Ru( $\alpha$ -Man-3-bpy) <sub>3</sub> ]Cl <sub>2</sub>	603.2	0.113
[Ru( $\alpha$ -Gal-3-bpy) <sub>3</sub> ]Cl <sub>2</sub> <sup>c</sup>	607.6	0.121
[Ru(bpy-OH) <sub>3</sub> ]Cl <sub>2</sub> <sup>c</sup>	604.0	0.047
[Ru(bpy) <sub>3</sub> ]Cl <sub>2</sub> <sup>b,c</sup>	588.2	0.042

<sup>a</sup> [Complex] =  $1.0 \times 10^{-5}$  M, 25 °C. <sup>b</sup> Houten, J. V., et al. (ref 29). <sup>c</sup>  $\Delta$ - $\Lambda$  mixture.

**Ruthenium Glycoclusters: Amplified Luminescence and Its Change upon Binding to Lectins.** The ruthenium glycoclusters exhibited intense emission in water with excitation of MLCT band as summarized in Table 5. The maximum emission bands were red-shifted, and the intensities were largely increased as compared with [Ru(bpy)<sub>3</sub>]Cl<sub>2</sub>. Since [Ru(bpy-OH)<sub>3</sub>]Cl<sub>2</sub> having spacer moieties without saccharide terminals (20b) induced the red shift of emission but no enhancement of luminescence, the enhancement of luminescence apparently arise from their saccharide-cluster structures. The luminescence lifetimes of  $\Lambda$ - and  $\Delta$ -isomeric  $\alpha$ -mannoclusters determined in aqueous solution at 25 °C were 1.33 and 1.21  $\mu$ s, respectively, which are much longer than that (0.43  $\mu$ s) of [Ru(bpy)<sub>3</sub>]Cl<sub>2</sub>. We assume that the densely packed saccharide arrays surrounding complex center should serve as "carbohydrate-shell" isolating the luminescence core from the outer aqueous circumstance to extend the luminescence lifetime and enhance the emission intensity. Furthermore, we have preliminary data to support carbohydrate-shell effect inducing amplified luminescence of glycoclusters: luminescence intensity of mannocluster in aqueous solution was decreased with increasing contents of organic cosolvent (methanol, acetonitrile, and tetrahydrofuran). These solvents may disrupt hydrophobic interaction between the complex core and the phenyl ring of the aglycon to destroy carbohydrate-shell structure.

The ruthenium glycoclusters have been found to exhibit high stability, strong lectin-affinity, and amplified luminescence. These characteristics are advantageous as sensitive monitoring systems for saccharide binding phenomena. To assess their potential as a luminescence-based biosensor, we investigated the change of luminescence intensities of the ruthenium glycoclusters on binding to lectins. Addition of small aliquots of lectin solution decreased the luminescent intensity of the ruthenium-based mannocluster without any shift of emission wavelength and also without any precipitates and aggregates. Aggregation was observed above the critical concentrations of ConA ( $1.0 \times 10^{-4}$  M for glucoclusters and  $2.0 \times 10^{-5}$  M for mannoclusters). The addition of bovine serum albumin (BSA) solution showed no effects on their luminescence properties. Their luminescence responses were induced by specific interactions with saccharide-binding proteins.

The luminescence responses of the ruthenium glycoclusters against ConA were shown in Figure 7. It is reasonable to assume that the luminescence responses of the mannoclusters for ConA are much sensitive than that of the corresponding glucoclusters, since ConA has the superior affinities to the mannoclusters over the glucoclusters. It is interesting that the response of the  $\Lambda$ - and  $\Delta$ -[Ru( $\alpha$ -Glc-3-bpy)<sub>3</sub>]Cl<sub>2</sub> against ConA depends on the stereochemistry of metal-complex centers ( $\Lambda$ :

**Figure 7.** Plots of maximum luminescence intensities of the ruthenium glycoclusters against the concentration of ConA.

increase,  $\Delta$ : decrease). Change of luminescence upon binding to lectins depends on many factors including molecular motion and hydration, and then, the origins of the change in luminescence intensities are too complicate to be determined. However, we assume that destruction of carbohydrate shell is one of the main factors of luminescence change of ruthenium glycoclusters upon binding to ConA.

## CONCLUSION

The tris-bipyridine ruthenium-based glycoclusters have been found to show excellent affinity to lectins. Despite their small saccharide clusters, their lectin affinity was comparable to those of polymer-based large saccharide clusters. Their flexible and densely packed saccharide arrays play critical role in their high lectin-affinity. In particular, the importance of flexibility was clearly demonstrated by a comparison with the *N*-glycoclusters. The flexibility should leave the saccharide cluster to induced-fit onto the saccharide-binding site of lectins, resulting in excellent affinity. Furthermore, we should underline the importance of densely packed saccharide cluster. To our best knowledge, small glycoclusters based on cyclodextrins and calixarenes have lower lectin-affinity than those based on large polymers and dendrimers. Since cyclodextrins and calixarenes are also rigid molecules, spacer moieties tethering saccharide appendages were essential to attain multivalent interaction. However, insertion of spacer moieties may have another side effect to separate each saccharide moieties to reduce saccharide density and their lectin-affinity. We assume that not dispersed saccharide moieties but densely packed saccharide cluster are essential to design small glycoclusters with excellent lectin-affinities.

The densely packed glycoarrays of metalloglycoclusters also play as a saccharide shell to isolate the complex cores and then enhance the luminescence. Furthermore, specific saccharide-binding phenomena could be easily monitored as the change of luminescence intensity of these ruthenium glycoclusters. Now, our investigations are focused on the preparation of the ruthenium-based glycocluster bearing complex oligosaccharide via enzymatic synthesis to develop the sensory system for influenza viruses.



Finally, the importance of the spatial compatibility between the glyco-arrays and saccharide-binding site that has been clearly demonstrated by the *N*-glycoclusters, should be emphasized. The carbohydrate-epitopes usually have loose specificity and the multiple saccharide-binding proteins often bind the same carbohydrate determinant, despite their critical role in human biology. It seems likely that the spatial arrays of saccharide units in the glycoclusters could serve as advanced information to overcome this cross-reactivity of saccharide determinant.

#### ACKNOWLEDGMENT

We are grateful to Professors Mitsuhiro Shionoya and Kentaro Tanaka, The University of Tokyo, for ESI-TOF-MS measurement and to Mr. Yuta Fukatsu and Professors Makoto Kimura and Yasuhiko Sawaki, Nagoya University, for luminescence lifetime measurement.

**Supporting Information Available:** Analytical data of the synthetic compounds and the procedures for molecular mechanics calculation, thermodynamic binding analysis, and binding assay by fluorometry. This material is available free of charge via the Internet at <http://pubs.acs.org>.

#### LITERATURE CITED

- (1) (a) Varki, A., Cummings, R., Esko, J., Freeze, H., Hart, G., and Marth, J. (1999) *Essentials of Glycobiology*, Cold Spring Harbor Laboratory Press, Cold Spring Harbor, NY. (b) Fukuda, M., and Hindsgaul, O. (2000) *Molecular and Cellular Glycobiology*, Oxford University Press, Oxford. (c) Dwek, R. A., (1996) Glycobiology: Toward Understanding the Function of Sugars. *Chem. Rev.* 96, 683. (d) Mammen, M., Choi, S.-K., and Whitesides, G. M. (1998) Polyvalent interactions in biological systems: Implication for design and use of multivalent ligands and inhibitors. *Angew. Chem., Int. Ed. Engl.* 37, 2754.
- (2) Davis, B. G. (1999) Recent developments in glycoconjugates. *J. Chem. Soc., Perkin Trans. 1*, 3215
- (3) (a) Bovin, N. V., and Gabius, H.-J. (1995) Polymer-immobilized Carbohydrate Ligands: Versatile Chemical Tools for Biochemistry and Medical Sciences. *Chem. Soc. Rev.* 24, 413. (b) Kiessling, L. L., and Pohl, N. L. (1996) Strength in numbers: nonnatural polyvalent carbohydrate derivatives. *Chem. Biol.* 3, 71.
- (4) (a) Zanini, D., and Roy, R. (1997) Synthesis of New  $\alpha$ -Thiosialodendrimers and Their Binding Properties to the Sialic Acid Specific Lectin from *Limax flavus*. *J. Am. Chem. Soc.* 119, 2088. (b) Aoi, K., Ito, K., and Okada, M. (1995) Globular Carbohydrate Macromolecules "Sugar balls". 1. Synthesis of Novel Sugar-Per-substituted Poly(amido amine) Dendrimers. *Macromolecules* 28, 5391.
- (5) Fujimoto, T., Shimizu, C., Hayashida, O., and Aoyama, Y. (1997) Solution-to-Surface Molecular-Delivery System Using a Macrocyclic Sugar Cluster. Sugar-Directed Adsorption of Guests in Water on Polar Solid Surfaces. *J. Am. Chem. Soc.* 119, 6676.
- (6) Fulton, D. A., and Stoddart, J. F. (2001) Neoglycoconjugates Based on Cyclodextrins and Calixarenes. *Bioconjugate Chem.* 12, 656.
- (7) (a) Ortega-Caballero, F., Gimenez-Martinez, J. J., Garcia-Fuentes, L., Ortiz-Salmeron E., Santoyo-Gonzalez, F., and Vargas-Berenguel, A. (2001) Binding Affinity Properties of Dendritic Glycosides Based on a  $\beta$ -Cyclodextrin Core toward Guest Molecules and Concanavalin A. *J. Org. Chem.* 66, 7786. (b) Yasuda, N., Aoki, N., Abe H., and Hattori, K. (2000) Per-C-6 Oligosaccharide-Branched Cyclodextrin Interacting with Both the Lectin and Drug. *Chem. Lett.* 706.
- (8) (a) Fujimoto, K., Miyata, T., and Aoyama, Y. (2000) Saccharide-Directed Cell Recognition and Molecular Delivery Using Macrocyclic Saccharide Clusters: Masking of Hydrophobicity to Enhance the Saccharide Specificity. *J. Am. Chem. Soc.* 122, 3558. (b) Tamaru, S., Nakamura M, Takeuchi, M., and Shinkai, S. (2001) Rational Design of a Sugar-Appended Porphyrin Gelator That Is Forced To Assemble into a One-Dimensional Aggregate. *Org. Lett.* 3, 3631
- (9) Yashiro, A., Nishida, Y., Ohno, M., Eguchi, S., Kobayashi, K. (1998) A General Synthetic Approach towards Fullerene Glycoconjugates via Cycloaddition of Per-O-Acetyl Glycosyl Azides to [60]Fullerene. *Tetrahedron Lett.* 39, 9031
- (10) (a) Akasaka, T., Matsuura, K., Emi, N., and Kobayashi, K. (1999) Conjugation of Plasmid DNA with Lactose via Diazo Coupling Enhances Resistance to Restriction Enzymes and Acquires Binding Affinity to Galactose Specific Lectin. *Biochem. Biophys. Res. Commun.* 260, 323. (b) Matsuura, K., Akasaka, T., Hibino M., and Kobayashi, K. (2000) Facile Synthesis of Stable and Lectin-recognizable DNA-Carbohydrate Conjugates via Diazo Coupling. *Bioconjugate Chem.* 11, 11202.
- (11) Okada, S., Peng, S., Spevak, W., and Charych, D. (1998) Color and Chromism of Polydiacetylene Vesicles. *Acc. Chem. Res.* 31, 229.
- (12) Beak, M.-G., Stevens, R. C., and Charych, D. H. (2000) Design and Synthesis of Novel Glycopolymers Assemblies for Colorimetric Detection of Influenza Virus and E. coli. *Bioconjugate Chem.* 11, 777
- (13) Song, X., and Swanson, B. I. (1999) Direct, Ultrasensitive, and Selective Optical Detection of Protein Toxins Using Multivalent Interactions. *Anal. Chem.* 71, 2097
- (14) (a) Ebara, Y., and Okahata, Y. (1994) A Kinetic Study of Concanavalin A Binding to Glycolipid Monolayers by Using a Quartz-Crystal Microbalance. *J. Am. Chem. Soc.* 116, 11209. (b) Uzawa, H., Kamiya, S., Minoura, N., Dohi, H. Nishida, Y., Taguchi, K., Yokoyama, S., Mori, H., Shimizu T., and Kobayashi K. (2002) A Quartz Crystal Microbalance (QCM) Method for Rapid Detection and Differentiation of Shiga Toxins, Stx-1 and Stx-2, Applying a Monoalkyl Globobioside as the Toxin Ligand. *Biomacromolecules* 3, 411.
- (15) Sugawara, K., Ueda, K., Kuramitz, H., Hoshi, S., Akatsuka, K., and Tanaka, S. (2000) Voltammetric Behaviors of Lectin-Sugar Binding Using An Electrode Modified with Galactosamine. *Chem. Lett.* 214.
- (16) Nicolas, M., Fabre, B., and Simonet, J. (2001) Electrochemical sensing of fluoride and sugar with a boronic acid-substituted bipyridine Fe(II) complex in solution and attached onto an electrode surface. *Electrochim. Acta.* 46, 1179.
- (17) Watanabe, S., Onogawa, O., Komatsu, Y., and Yoshida, K. (1998) Luminescent Metalloreceptor with a Neutral Bis-(Acylaminoimidazole) Binding Site: Optical Sensing of Anionic and Neutral Phosphodiester. *J. Am. Chem. Soc.* 120, 229.
- (18) Beer, P. D., and Dent, S. W. (1998) Potassium cation induced switch in anion selectivity exhibited by heteroditopic ruthenium(II) and rhenium(I) bipyridyl bis(benzo-15-crown-5) ion pair receptors. *Chem. Commun.* 825.
- (19) Sakai, S., Shigemasa, Y., and Sasaki, T. (1999) Iron(II)-Assisted Assembly of Trivalent GalNAc Clusters and Their Interactions with GalNAc-Specific Lectins. *Bull. Chem. Soc. Jpn.* 72, 1313.
- (20) (a) Hasegawa, T., Matsuura, K., and Kobayashi, K. (2000) Glucosylated Tris-bipyridine Ferrous Complexes: Construction of Hexavalent Saccharide Clusters via Self-assembly and Their Recognition by Lectin. *Chem. Lett.* 466. (b) Hasegawa, T., Yonemura, T., Matsuura, K., and Kobayashi, K. (2001) Tris-bipyridine Ruthenium Complex-based Glycoclusters: Amplified Luminescence and Enhanced Lectin-Affinities. *Tetrahedron Lett.* 42, 3989.
- (21) Milder, S. J., and Gold, J. S., and Kligler, D. S. (1986) Circular Dichroism of a Subnanosecond State:  $(\Delta)$ -Fe(bpy)<sub>3</sub><sup>2+</sup>. *J. Am. Chem. Soc.* 108, 8295.
- (22) Martell, A. E., and Smith, R. M. (1975) *Critical Stability Constants*, Plenum Press, New York.
- (23) (a) Hasegawa, T., Kondoh, S., Matsuura, K., and Kobayashi, K. (1999) Rigid Helical Poly(glyco-phenylisocyanide)s: Synthesis, Conformational Analysis, and Recognition by Lectins. *Macromolecules* 32, 6595. (b) Hasegawa, T.,



- Matsuura, K., Ariga, K., and Kobayashi, K. (2000) Multilayer Adsorption and Molecular Organization of Rigid Cylindrical Glycoconjugate Poly(phenylisocyanide) on Hydrophilic Surfaces. *Macromolecules* 33, 2772.
- (24) Ashton, P. R., Balzani, V., Clemente-Leon, M., Colonna, B., Credi, A., Jayaraman, N., Raymo, F. M., Stoddart, J. F., and Venturi, M. (2002) Ferrocene-Containing Carbohydrate Dendrimers. *Chem. Eur. J.* 8, 673.
- (25) Lippard, S. J. (1989) *Progress in Inorganic Chemistry*, John Wiley & Sons, New York.
- (26) Tagawa, K., Sendai, N., Ohno, K., Kawaguchi, T., and Kitano, H. (1999) Recognition of Novel Lipopolypeptide with Many Pendent Sugar Residues by Lectin. *Bioconjugate Chem.* 10, 354.
- (27) Mandal, D. K., N. Kishore, N., and Brewer, C. F. (1994) Thermodynamics of Lectin-Carbohydrate Interactions. Titration Microcalorimetry Measurements of Binding of N-Linked Carbohydrates and Ovalbumin to Concanavalin A. *Biochemistry* 33, 1149.
- (28) Naismith, J. H., and Field, R. A. (1996) Structural Basis of Trimannoside Recognition by Concanavalin A. *J. Biol. Chem.* 271, 972.
- (29) Houten, J. V., and Watts, R. J. (1976) Temperature Dependence of the Photophysical and Photochemical properties of the Tris(2,2'-bipyridyl)ruthenium(II) Ion in Aqueous solution. *J. Am. Chem. Soc.* 98, 4853.

BC020026A

**Manuscript number****Supporting Information:****BC0200026***Bioconjugate Chemistry***Artificial Metallo-glycoclusters: Compact Saccharide-shell to Induce High Lectin-affinity as well as Strong Luminescence**

Teruaki Hasegawa, Takahiro Yonemura, Kazunori Matsuura, and Kazukiyo Kobayashi\*

**4,4'-Di{N-(tetra-*O*-acetyl- $\beta$ -galactopyranosyl)amido}-2,2'-bipyridine (Ac- $\beta$ -Gal-bpy).**  $[\alpha]_D^{25} -27.3^\circ$  ( $c = 0.1$ ,  $\text{CHCl}_3$ );  $^1\text{H-NMR}$  (500 MHz,  $\text{CDCl}_3$ )  $\delta$  8.87 (d,  $J = 5.0$  Hz, 2H, bpy-6), 8.75 (s, 2H, bpy-3), 7.72 (dd,  $J = 1.5$  and 5.0 Hz, 2H, bpy-5), 7.32 (d,  $J = 9.0$  Hz, 2H, amide), 5.40 (d,  $J = 3.0$  Hz, 2H, Gal-4), 5.46 (t,  $J = 9.0$  Hz, 2H, Gal-1), 5.28 (dd,  $J = 9.0$  and 10.5 Hz, 2H, Gal-2), 5.23 (dd,  $J = 3.5$  and 10.5 Hz, 2H, Gal-3), 4.19-4.11 (m, 3H, Gal-5 and -6), and 2.19, 2.07, 2.06, and 2.03 (s  $\times$  4, 24H, acetyl);  $^{13}\text{C-NMR}$  (500 MHz,  $\text{CDCl}_3$ )  $\delta$  171.56, 170.35, 169.94, and 169.70 (C=O, acetyl), 165.32 (C=O, amide), 156.13 (bpy-4), 150.21 (bpy-6), 141.22 (bpy-2), 121.56 (bpy-5), 118.29 (bpy-3), 78.95 (Gal-1), 72.40 (Gal-5), 70.71 (Gal-3), 68.50 (Gal-2), 67.14 (Gal-4), 61.11 (Gal-6), and 20.68, 20.56, 20.49, and 20.43 ( $\text{CH}_3$ -, acetyl); IR (KBr,  $\text{cm}^{-1}$ ) 1753( $\nu_{\text{C=O}}$  acetyl), 1687( $\nu_{\text{C=O}}$  amide), and 1535( $\delta_{\text{N-H}}$  amide); MS  $m/z$  901 ( $\text{MH}^+$ ).

**4,4'-Di{N-(hepta-*O*-acetyl- $\beta$ -maltosyl)amido}-2,2'-bipyridine (Ac- $\beta$ -Mal-bpy).**  $^1\text{H-NMR}$  (500 MHz,  $\text{CDCl}_3$ )  $\delta$  8.53 (d,  $J = 5.0$  Hz, 2H, bpy-6), 8.35 (s, 2H, bpy-3), 7.92 (d,  $J = 8.5$  Hz, 2H, N-H), 7.64 (dd,  $J = 4.0$  Hz, 2H, bpy-5), 5.62 (t,  $J = 9.5$  Hz, 2H, Glc<sub>1</sub>-1), 5.50 (t,  $J = 9.0$  Hz, 4H, Glc<sub>1</sub>-3), 5.47 (d,  $J = 4.0$  Hz, 2H, Glc<sub>2</sub>-1), 5.40 (t,  $J = 10.0$  Hz, 2H, Glc<sub>2</sub>-3), 5.20 (t,  $J = 9.0$  Hz, 2H, Glc<sub>1</sub>-2), 5.11 (t,  $J = 10.0$  Hz, 2H, Glc<sub>2</sub>-4), 4.93 (dd,  $J =$

4.0 and 10.5 Hz, 2H, Glc<sub>2</sub>-2), 4.49-4.46 (m, 2H, Glc<sub>2</sub>-6S), 4.34-4.24 (m, 4H, Glc<sub>2</sub>-6R and Glc<sub>1</sub>-6S), 4.10-3.95 (m, 8H, Glc<sub>1</sub>-4, -5, -6R, and Glc<sub>2</sub>-5), and 2.14, 2.13, 2.09, 2.09, 2.07, 2.05, and 2.03 (s × 7, 42H, acetyl); IR (KBr, cm<sup>-1</sup>) 1751( $\nu_{\text{C=O}}$  acetyl), 1687( $\nu_{\text{C=O}}$  amide), and 1537( $\delta_{\text{N-H}}$  amide).

**4,4'-Di{N-(hepta-*O*-acetyl- $\beta$ -lactosyl)amido}-2,2'-bipyridine (Ac- $\beta$ -Lac-bpy).** mp 164-169 °C;  $[\alpha]_{\text{D}}^{25}$  -26.0 ° (c = 1.2, CHCl<sub>3</sub>); <sup>1</sup>H-NMR (500 MHz, CDCl<sub>3</sub>)  $\delta$  8.81 (d, *J* = 5.0 Hz, 2H, bpy-6), 8.67 (s, 2H, bpy-3), 7.69 (dd, *J* = 1.5 and 5.0 Hz, 2H, bpy-5), 7.42 (d, *J* = 8.5 Hz, 2H, N-H), 5.42 (t, *J* = 9.0 Hz, 2H, Glc-1), 5.37 (m, 4H, Glc-3 and Gal-4), 5.12 (dd, *J* = 8.0 and 10.5 Hz, 2H, Gal-2), 5.00 (t, *J* = 9.5 Hz, 2H, Glc-2), 4.96 (dd, *J* = 3.5 and 10.5 Hz, 2H, Gal-3), 4.50-4.45 (m, 2H, Glc-6S), 4.19-4.15 (m, 4H, Glc-6R and Gal-6S), 4.10-4.06 (m, 2H, Gal-6R), 3.89 (dd, *J* = 7.5 and 7.5 Hz, 2H, Gal-5), 3.86-3.81 (m, 4H, Glc-4 and Glc-5), and 2.16, 2.12, 2.08, 2.07, 2.05, 2.04, and 1.96 (s × 7, 21H, acetyl); <sup>13</sup>C-NMR (500 MHz, CDCl<sub>3</sub>)  $\delta$  171.60, 170.35, 170.32, 170.12, 170.06, 169.35, and 168.98 (C=O, acetyl), 165.31 (C=O, amide), 156.15 (bpy-4), 150.26 (bpy-6), 141.27 (bpy-2), 121.72 (bpy-5), 118.25 (bpy-3), 100.86 (Gal-1), 78.58 (Glc-4), 74.57 (Glc-5), 72.24 (Glc-3), 71.10 (Glc-2), 70.92 (Glc-3), 70.67 (Gal-5), 68.93 (Gal-2), 66.56 (Gal-4), 61.85 (Gal-6), 60.81 (Glc-6), and 20.83, 20.74, 20.70, 20.61, 20.60, 20.58, and 20.46 (CH<sub>3</sub>-, acetyl); IR (KBr, cm<sup>-1</sup>) 1751( $\nu_{\text{C=O}}$  acetyl), 1685( $\nu_{\text{C=O}}$  amide), and 1543( $\delta_{\text{N-H}}$  amide).

**4,4'-Di{N-( $\beta$ -galactopyranosyl)amido}-2,2'-bipyridine ( $\beta$ -Gal-bpy).** IR (KBr, cm<sup>-1</sup>) 3406( $\nu_{\text{O-H}}$ ), 1654( $\nu_{\text{C=O}}$  amide), and 1555( $\delta_{\text{N-H}}$  amide).

**4,4'-Di{N-( $\beta$ -maltosyl)amido}-2,2'-bipyridine ( $\beta$ -Mal-bpy).** <sup>1</sup>H-NMR (500 MHz, D<sub>2</sub>O)  $\delta$  8.55 (d, *J* = 5.0 Hz, 2H, bpy-6), 8.10 (s, 2H, bpy-3), 7.61 (dd, *J* = 2.0 and 5.0 Hz,



2H, bpy-5), 5.30 (d,  $J = 4.0$  Hz, 2H, Glc<sub>2</sub>-1), 5.09 (d,  $J = 9.5$  Hz, 2H, Glc<sub>1</sub>-1), 3.81-3.25 (m, 12H, sugar); IR (KBr, cm<sup>-1</sup>) 3365( $\nu_{\text{O-H}}$ ), 1674( $\nu_{\text{C=O}}$  amide), and 1558( $\delta_{\text{N-H}}$  amide).

**4,4'-Di{N-( $\beta$ -lactosyl)amido}-2,2'-bipyridine ( $\beta$ -Lac-bpy).** IR (KBr, cm<sup>-1</sup>) 3417( $\nu_{\text{O-H}}$ ), 1660( $\nu_{\text{C=O}}$  amide), and 1549( $\delta_{\text{N-H}}$  amide).

**Ethyl 4-azidobutanoate.** Ethyl 4-chlorobutanoate (23.2 g, 154.1 mmol) was dissolved in 100 ml of *N,N*-dimethylformamide and then sodium azide (20.6 g, 316.9 mmol) was added. The mixture was stirred at 60 °C for 6 h. The solution was diluted with ethyl acetate and washed with a saturated sodium chloride aqueous solutions. The organic layer was dried over anhydrous magnesium sulfate and concentrated to a viscous and colorless liquid. <sup>1</sup>H-NMR (200 MHz, CDCl<sub>3</sub>)  $\delta$  4.15 (q,  $J = 7.0$  Hz, 2H), 3.36 (t,  $J = 6.6$  Hz, 2H), 2.41 (t,  $J = 6.6$  Hz, 2H), 1.91 (q,  $J = 7.0$  Hz, 2H), 1.27 (t,  $J = 6.6$  Hz, 3H); IR (KBr, cm<sup>-1</sup>) 2102 ( $\nu_{\text{N}_3}$ ), 1736 ( $\nu_{\text{C=O}}$ ).

**4-Azidobutanoic acid.** Ethyl 4-azidobutanoate was dissolved in 200 ml of 1.0 N NaOH aqueous solution. The mixture was vigorously stirred at room temperature for 1 h and then acidified (pH 2~3) with 1.0 N HCl aqueous solution. The aqueous mixture was extracted with five 100 ml portions of chloroform. The combined organic layer was dried over anhydrous magnesium sulfate and concentrated to a viscous and colorless liquid. <sup>1</sup>H-NMR (200 MHz, CDCl<sub>3</sub>)  $\delta$  10.86 (br s, 1H), 3.39 (t,  $J = 6.6$  Hz, 2H), 2.48 (t,  $J = 7.2$  Hz, 2H), 1.92 (quintet,  $J = 7.0$  Hz, 2H); IR (KBr, cm<sup>-1</sup>) 2102 ( $\nu_{\text{N}_3}$ ), 1712 ( $\nu_{\text{C=O}}$ ).

**4-Azidobutanoyl chloride.** 4-Azidobutanoic acid was dissolved in 150 ml of thionylchloride and then refluxed for 3 h. The progress of the reaction was directly monitored by <sup>1</sup>H-NMR (200 MHz, CDCl<sub>3</sub>) in which the small portion from the reaction mixture was diluted in CDCl<sub>3</sub>. 4-Azidobutanoyl chloride was purified by vacuum

distillation. The resulting viscous colorless liquid was stored in a refrigerator as diethyl ether solution.  $^1\text{H-NMR}$  (200 MHz,  $\text{CDCl}_3$ )  $\delta$  3.41 (t,  $J = 6.4$  Hz, 2H), 3.03 (t,  $J = 7.0$  Hz, 2H), 1.97 (quintet,  $J = 6.6$  Hz, 2H); IR ( $\text{KBr}, \text{cm}^{-1}$ ) 2104 ( $-\text{N}_3$ ), 1711 ( $\nu_{\text{C=O}}$ ).

**1- $\{p$ -(4-Azidobutanamido)phenyl}-2,3,4,6-tetra- $O$ -acetyl- $\beta$ -glucopyranose (Ac- $\beta$ -Glc-3- $\text{N}_3$ ).**  $^1\text{H-NMR}$  (500 MHz,  $\text{CDCl}_3$ )  $\delta$  7.51 (s, 1H, amide), 7.43 (d,  $J = 9.0$  Hz, 2H, benz), 6.95 (d,  $J = 9.0$  Hz, 2H, benz), 5.30 (t,  $J = 9.5$  Hz, 1H, Glc-3), 5.25 (dd,  $J = 7.5$  and 9.0 Hz, 1H, Glc-2), 5.16 (t,  $J = 10.0$  Hz, 1H, Glc-4), 5.02 (d,  $J = 7.5$  Hz, 1H, Glc-1), 4.26 (dd,  $J = 5.0$  and 12.5 Hz, 1H, Glc-6<sub>R</sub>), 4.06 (dd,  $J = 2.5$  and 12.0 Hz, 1H, Glc-6<sub>S</sub>), 3.87-3.83 (m, 1H, Glc-5), 3.41 (t,  $J = 6.5$  Hz, 2H, alkyl), 2.45 (t,  $J = 6.5$  Hz, 2H, alkyl), 2.08, 2.07, 2.05, and 2.03 (s  $\times$  4, 12H, acetyl), and 2.00 (quintet,  $J = 6.5$  Hz, 2H, alkyl);  $^{13}\text{C-NMR}$  (500 MHz,  $\text{CDCl}_3$ )  $\delta$  170.55, 170.13, 170.03, and 169.36 ( $\text{C=O}$ , acetyl), 169.31 ( $\text{C=O}$ , amide), 153.36 (benz) 133.35 (benz), 121.42 (benz), 117.63 (benz), 99.37 (Glc-1), 72.57 (Glc-2), 71.93 (Glc-3), 71.07 (Glc-4), 68.23 (Glc-5), 61.83 (Glc-6), 50.62, 33.81, and 24.53 (alkyl spacer), and 20.72, 20.66, 20.61, and 20.42 ( $\text{CH}_3$ , acetyl); IR ( $\text{KBr}, \text{cm}^{-1}$ ) 3354 ( $\nu_{\text{N-H}}$ , amide), 2100 ( $-\text{N}_3$ ), 1749 ( $\nu_{\text{C=O}}$ , acetyl), 1676 ( $\nu_{\text{C=O}}$ , amide), and 1512 ( $\delta_{\text{N-H}}$  amide); MS  $m/z$  551 ( $\text{M}+\text{H}^+$ ); mp 106-107  $^\circ\text{C}$ .

**1- $\{p$ -(4-Azidobutanamido)phenyl}-2,3,4,6-tetra- $O$ -acetyl- $\beta$ -galactopyranose (Ac- $\beta$ -Gal-3- $\text{N}_3$ ).**  $[\alpha]_{\text{D}}^{25} +3.19^\circ$  ( $c = 1.37$ ,  $\text{CHCl}_3$ ); mp 194-196  $^\circ\text{C}$ ;  $^1\text{H-NMR}$  (500 MHz,  $\text{CDCl}_3$ )  $\delta$  7.43 (d,  $J = 9.0$  Hz, 2H, benz), 7.32 (s, 1H, amide), 6.97 (d,  $J = 9.0$  Hz, 2H, benz), 5.47 (dd,  $J = 8.0$  and 10.5 Hz, 1H, Glc-2), 5.45 (d,  $J = 1.0$  and 3.5 Hz, 1H, Glc-4), 5.10 (dd,  $J = 3.5$  and 10.5 Hz, 1H, Glc-3), 4.98 (dd,  $J = 8.0$  Hz, 1H, Glc-1), 4.22 (dd,  $J = 7.0$  and 11.5 Hz, 1H, Glc-6<sub>R</sub>), 4.16 (dd,  $J = 6.5$  and 11.5 Hz, 1H, Glc-6<sub>S</sub>), 4.06-4.03 (m, 1H, Glc-5), 3.42 (t,  $J = 6.5$  Hz, 2H, alkyl), 2.46 (t,  $J = 7.5$  Hz, 2H, alkyl), 2.18, 2.08,

2.06, and 2.01 (s  $\times$  4, 12H, acetyl), and 2.00 (quintet,  $J$  = 7.0 Hz, 2H, alkyl);  $^{13}\text{C}$ -NMR (500 MHz,  $\text{CDCl}_3$ )  $\delta$  170.34, 170.20, 170.08, and 169.89 (C=O, acetyl), 169.38 (C=O, amide), 153.58, 133.21, 121.44, and 117.61 (phenyl), 100.08 (Glc-1), 71.01 (Glc-2), 70.77 (Glc-3), 68.62 (Glc-4), 66.85 (Glc-5), 61.33 (Glc-6), 50.67, 33.93, and 24.59 (alkyl spacer), and 20.72, 20.64, 20.63, and 20.56 ( $\text{CH}_3$ -, acetyl); IR (KBr,  $\text{cm}^{-1}$ ) 2092 ( $-\text{N}_3$ ), 1753 ( $\nu_{\text{C=O}}$ , acetyl), 1657 ( $\nu_{\text{C=O}}$ , amide), and 1510 ( $\delta_{\text{N-H}}$  amide); MS  $m/z$  551 ( $\text{M}+\text{H}^+$ ).

**1- $\{p$ -(4-Azidobutanamido)phenyl}-2,3,4,6-tetra- $O$ -acetyl- $\alpha$ -mannopyranose (Ac- $\alpha$ -Man-3- $\text{N}_3$ ).**  $^1\text{H}$ -NMR (500 MHz,  $\text{CDCl}_3$ )  $\delta$  7.43 (d,  $J$  = 9.0 Hz, 2H, benz), 7.17 (s, 1H, amide), 7.05 (d,  $J$  = 9.0 Hz, 2H, benz), 5.55 (dd,  $J$  = 3.5 and 10.0 Hz, 1H, Man-3), 5.47 (d,  $J$  = 1.5 Hz, 1H, Man-1), 5.44 (dd,  $J$  = 1.5 and 3.5 Hz, 1H, Man-2), 5.36 (t,  $J$  = 10.0 Hz, 1H, Man-4), 4.30-4.05 (m, 3H, Man-5 and man-6), 3.43 (t,  $J$  = 6.5 Hz, 2H, alkyl-4), 2.46 (t,  $J$  = 7.0 Hz, 2H, alkyl-2), 2.05-2.04 (m, 12H, acetyl), and 2.02 (quintet,  $J$  = 6.5 Hz, 2H, alkyl-3).

**4,4'-Di- $N$ -[ $N$ - $\{p$ - $O$ -(2,3,4,6-tetra- $O$ -acetyl- $\beta$ -glucopyranosyl)phenyl]amidopropyl]amido-2,2'-bipyridine (Ac- $\beta$ -Glc-3-bpy).**  $[\alpha]_{\text{D}}^{25}$  -14.6  $^\circ$  ( $c$  = 1.01,  $\text{CDCl}_3$ ); mp 187-188  $^\circ\text{C}$ ; IR (KBr,  $\text{cm}^{-1}$ ) 3311 ( $\nu_{\text{N-H}}$ , amide), 1749 ( $\nu_{\text{C=O}}$ , acetyl), 1653 ( $\nu_{\text{C=O}}$ , amide), 1637 ( $\nu_{\text{C=O}}$ , amide), 1557 ( $\delta_{\text{N-H}}$  amide), and 1541 ( $\delta_{\text{N-H}}$  amide);  $^1\text{H}$ -NMR (500 MHz,  $\text{CDCl}_3$  :  $\text{CD}_3\text{OD}$  = 1 : 1, TMS)  $\delta$  8.70 (d,  $J$  = 5.0 Hz, 2H, bpy-6), 8.69 (s, 2H, bpy-3), 7.73 (d,  $J$  = 5.0 Hz, 2H, bpy-5), 7.40 (d,  $J$  = 9.5 Hz, 4H, phenyl), 6.84 (d,  $J$  = 9.5 Hz, 4H, phenyl), 5.25 (t,  $J$  = 9.5 Hz, 2H, Glc-3), 5.12 (t,  $J$  = 9.0 Hz, 2H, Glc-2), 5.06 (t,  $J$  = 10.0 Hz, 2H, Glc-4), 5.04 (d,  $J$  = 7.5 Hz, 2H, Glc-1), 4.23 (dd,  $J$  = 5.0 and 12.0 Hz, 2H, Glc-6<sub>R</sub>), 4.07 (dd,  $J$  = 2.5 and 12.5 Hz, 2H, Glc-6<sub>S</sub>), 3.89-3.87 (m, 2H, Glc-5), 3.45 (t,  $J$  = 6.5 Hz, 4H, alkyl-4), 2.40 (t,  $J$  = 7.0 Hz, 2H, alkyl-2),



1.99-1.95 (m, 14H, acetyl and alkyl-3);  $^{13}\text{C}$ -NMR (500 MHz,  $\text{CDCl}_3$  :  $\text{CD}_3\text{OD}$  = 1 : 1, TMS)  $\delta$  171.82, 170.68, 170.07, and 169.46 (C=O, acetyl), 169.43 and 165.86 (C=O, amide), 155.01 (bpy-4), 152.75, 133.57, 120.94, and 116.86 (phenyl), 149.22 (bpy-6), 142.89 (bpy-2), 121.68 (bpy-5), 118.69 (bpy-3), 98.86 (Glc-1), 72.35 (Glc-5), 70.89 (Glc-2), 67.88 (Glc-4), 61.49 (Glc-6), 39.17 (alkyl-4), 33.87 (alkyl-2), and 24.76 (alkyl-3), and 19.87, 19.84, 19.79, and 19.77 ( $\text{CH}_3$ -, acetyl); MS  $m/z$  1258 ( $\text{M}+\text{H}^+$ ).

**4,4'-Di-*N*-[*N*-(*p*-*O*-(2,3,4,6-tetra-*O*-acetyl- $\beta$ -galactopyranosyl)phenyl)amidopropyl]amido-2,2'-bipyridine (Ac- $\beta$ -Gal-3-bpy).**

$[\alpha]_{\text{D}}^{25}$  ( $c$  = 0.37,  $\text{CHCl}_3$  :  $\text{CH}_3\text{OH}$  = 1 : 1) +2.1  $^\circ$ ; mp 146-151  $^\circ\text{C}$ ; IR (KBr,  $\text{cm}^{-1}$ ) 3319 ( $\nu_{\text{N-H}}$ , amide), 1752 ( $\nu_{\text{C=O}}$ , acetyl), 1658 ( $\nu_{\text{C=O}}$ , amide), 1606 ( $\nu_{\text{C=O}}$ , amide), 1543 ( $\delta_{\text{N-H}}$  amide), 1508 ( $\delta_{\text{N-H}}$  amide) and 1219 ( $\nu_{\text{C-O}}$ , acetyl);  $^1\text{H}$ -NMR (300 MHz,  $\text{CDCl}_3$  :  $\text{CD}_3\text{OD}$  = 9 : 1, TMS)  $\delta$  8.76 (d,  $J$  = 5.1 Hz, 2H, bpy-6), 8.69 (s, 2H, bpy-3), 7.79 (dd,  $J$  = 1.5 and 5.1 Hz, 2H, bpy-5), 7.49 (d,  $J$  = 9.0 Hz, 4H, phenyl), 6.92 (d,  $J$  = 9.0 Hz, 4H, phenyl), 5.45 (dd,  $J$  = 1.2 and 3.3 Hz, 2H, Gal-4), 5.44 (dd,  $J$  = 8.1 and 10.2 Hz, 2H, Gal-2), 5.12 (dd,  $J$  = 3.3 and 10.2 Hz, 2H, Gal-3), 5.00 (d,  $J$  = 8.1 Hz, 2H, Gal-1), 4.26-4.12 (m, 4H, Gal-6), 4.11-4.06 (m, 2H, Gal-5), 3.55 (t,  $J$  = 6.0 Hz, 4H, alkyl), 2.47 (t,  $J$  = 6.9 Hz, 4H, alkyl), 2.19, 2.09, 2.06, and 2.02 (s  $\times$  4, 12H, acetyl);  $^{13}\text{C}$ -NMR (300 MHz,  $\text{CDCl}_3$  :  $\text{CD}_3\text{OD}$  = 9 : 1, TMS)  $\delta$  171.75, 170.43, 170.25, and 170.10 (C=O, acetyl), 169.50 and 166.16 (C=O, amide), 155.73 (bpy-4), 153.03, 133.66, 120.92, and 117.24 (phenyl), 149.70 (bpy-6), 142.65 (bpy-2), 121.70 (bpy-5), 118.53 (bpy-3), 99.92 (Gal-1), 70.85 (Gal-5), 68.73 (Gal-5), 66.98 (Gal-2), 66.81 (Gal-4), 61.29 (Gal-6), 39.48, 34.45, and 25.35 (alkyl), and 20.61, 20.56, 20.51, and 20.46 ( $\text{CH}_3$ -, acetyl); MS  $m/z$  1258 ( $\text{M}+\text{H}^+$ ).

**4,4'-Di-*N*-[*N*-{*p*-*O*-(2,3,4,6-tetra-*O*-acetyl- $\alpha$ -mannopyranosyl)phenyl]amidopropyl]amido-2,2'-bipyridine (Ac- $\alpha$ -Man-3-bpy).**  $^1\text{H}$ -NMR (500 MHz,  $\text{CDCl}_3$ :  $\text{CD}_3\text{OD}$  = 1 : 1, TMS)  $\delta$  8.67 (d,  $J$  = 5.0 Hz, 2H, bpy-6), 8.63 (s, 2H, bpy-3), 8.51 (s, 2H, amide), 7.70 (dd,  $J$  = 1.0 and 4.5 Hz, 2H, bpy-5), 7.55 (t,  $J$  = 5.5 Hz, 2H, amide), 7.48 (d,  $J$  = 9.0 Hz, 2H, benz), 6.86 (d,  $J$  = 9.0 Hz, 2H, benz), 5.50 (dd,  $J$  = 3.0 and 10.0 Hz, 2H, Man-3), 5.40-5.39 (m, 4H, Man-1 and 2), 5.36 (dd,  $J$  = 10.0 and 10.0 Hz, 1H, Man-4), 4.26 (dd,  $J$  = 5.5 and 12.5 Hz, 2H, Man-6), 4.08-4.03 (m, 4H, Man-5 and Man-6), 3.60 (m, 4H, alkyl), 2.51 (t,  $J$  = 6.5 Hz, 4H, alkyl), 2.21 (s, 6H, acetyl), 2.08 (q, 4H, alkyl), 2.05, 2.04, and 2.03 (s, 18H, acetyl and alkyl).

**4,4'-Di-*N*-[*N*-{*p*-*O*-( $\beta$ -glucopyranosyl)phenyl]amidopropyl]amido-2,2'-bipyridine ( $\beta$ -Glc-3-bpy).** mp 192-193 °C; IR (KBr,  $\text{cm}^{-1}$ ) 3298 ( $\nu_{\text{O-H}}$ ), 1651 and 1601 ( $\nu_{\text{C=O}}$ , amide), 1539 and 1510 ( $\delta_{\text{N-H}}$  amide).

**4,4'-Di-*N*-[*N*-{*p*-*O*-( $\beta$ -galactopyranosyl)phenyl]amidopropyl]amido-2,2'-bipyridine ( $\beta$ -Gal-3-bpy).** mp 223-238 °C; IR (KBr,  $\text{cm}^{-1}$ ) 3284 ( $\nu_{\text{O-H}}$ ), 2925 ( $\nu_{\text{N-H}}$ , amide), 1654 and 1595 ( $\nu_{\text{C=O}}$ , amide), 1539 and 1510 ( $\delta_{\text{N-H}}$  amide).

**4,4'-Di-*N*-[*N*-{*p*-*O*-( $\beta$ -mannopyranosyl)phenyl]amidopropyl]amido-2,2'-bipyridine ( $\alpha$ -Man-3-bpy).**  $^1\text{H}$ -NMR (500 MHz,  $\text{DMSO-d}_6$  containing  $\text{D}_2\text{O}$ )  $\delta$  8.84 (dd,  $J$  = 0.5 and 5.0 Hz, 2H, bpy-6), 8.77 (d,  $J$  = 0.5 Hz, 2H, bpy-3), 7.83 (dd,  $J$  = 2.0 and 5.0 Hz, 2H, bpy-5), 7.46 (d,  $J$  = 9.0 Hz, 2H, benz), 6.98 (d,  $J$  = 9.0 Hz, 2H, benz), 5.25 (d,  $J$  = 2.0 Hz, 2H, Man-1), 3.78 (dd,  $J$  = 2.0 and 3.5 Hz, 2H, Man-2), 3.78 (dd,  $J$  = 3.5 and 9.0 Hz, 2H, Man-3), 3.51-3.40 (m, 8H, Man-4, 5, and 6), 3.35 (t,  $J$  = 7.0 Hz, 4H, alkyl), 2.35 (t,  $J$  = 7.5 Hz, 4H, alkyl), 1.86 (q,  $J$  = 7.0 Hz, 4H, acetyl); IR (KBr,  $\text{cm}^{-1}$ ) 3311 ( $\nu_{\text{N-H}}$ ,

amide), 1652 ( $\nu_{\text{C=O}}$ , amide), 1612 ( $\nu_{\text{C=O}}$ , amide), 1545 ( $\delta_{\text{N-H}}$  amide), and 1512 ( $\delta_{\text{N-H}}$  amide).

**4,4'-Di-*N*-(2-hydroxyethyl)amido-2,2'-bipyridine (bpy-OH).** 2,2'-Bipyridine 4,4'-dicarbonyl chloride was prepared by chlorination of 2,2'-bipyridine 4,4'-dicarboxylic acid (219.0 mg, 0.90 mmol) under reflux in thionyl chloride (30 ml) for 20 h. Evaporation of excess thionyl chloride and drying in vacuo for 1 h resulted in 2,2'-bipyridine 4,4'-dicarbonyl chloride as a yellow solid. 2-Aminoethanol (450  $\mu\text{l}$ ) was dissolved in 100 ml of tetrahydrofurane and then 2,2'-bipyridine 4,4'-dicarbonyl chloride in THF (13 ml) and triethylamine (5 ml) were added. The mixture was stirred at room temperature for 2 days. The insoluble fraction was filtrated and washed with ice-cooled methanol. The methanol-insoluble fraction was recovered by washing with a mixture of chloroform/methanol (1/1 v/v) and dried in vacuo to give bpy-OH as a colorless solid.  $^1\text{H-NMR}$  (500 MHz,  $\text{DMSO-}d_6$ ):  $\delta$  8.93 (t,  $J = 5.5$  Hz, 2H, amide), 8.85 (d,  $J = 5.0$  Hz, 2H, bpy-6), 8.80 (s, 2H, bpy-3), 7.85 (dd,  $J = 2.0$  and 5.0 Hz, 2H, bpy-5), 4.78 (t,  $J = 5.5$  Hz, 2H, hydroxyl), 3.54 (quint,  $J = 5.5$  Hz, 4H, alkyl), and 3.37 (quint,  $J = 5.5$  Hz, 4H, alkyl).

**$[\text{Fe}(\beta\text{-Glc-bpy})_3]\text{Cl}_2$ .**  $\text{FeCl}_2 \cdot 4\text{H}_2\text{O}$  (15.0 mg, 75.4  $\mu\text{mol}$ ) was added to 10 ml of water and then  $\beta\text{-Glc-bpy}$  (128.1 mg, 226.1  $\mu\text{mol}$ ) was added. The mixture was stirred for 30 min and the resulting purple solution was evaporated to obtain the ferrous-based glycoconjugate in diastereo-mixture form.

**$[\text{Ru}(\alpha\text{-Glc-3-bpy})_3]\text{Cl}_2$ .**  $\text{RuCl}_3$  (5.2 mg, 24.9  $\mu\text{mol}$ ) dehydrated by heating under reduced pressure was added to 14 ml of a mixture of water/ethanol (1/1 v/v) and then  $\alpha\text{-Glc-3-bpy}$  (81.5 mg, 74.8  $\mu\text{mol}$ ) was added. The resulting mixture was refluxed for 18 h



until the solution turned to orange (indicative of the corresponding tris complex formation) and cooled to ambient temperature. The insoluble fraction containing unreacted bipyridine and  $\text{RuCl}_3$  was filtrated and the resulting filtrate was evaporated to dryness. The residue was chromatographed through Toyo-Pearl HW40-S gel with aqueous 0.1 M ammonium acetate as eluent to obtain the two isomeric products.  $^1\text{H}$ -NMR (500 MHz,  $\text{D}_2\text{O}$ ):  $\delta$  8.09 (s, 2H, bpy-3), 7.65 (br s, 4H, bpy-5 and 6), 7.03 (d,  $J$  = 8.5 Hz, 4H, benz), 6.55 (d,  $J$  = 8.5 Hz, 4H, benz), 4.41 (br s, 2H, Glc-1), 3.54-3.10 (m, 16H, Glc-2, 3, 4, 5, 6, and alkyl), 2.23 (br, 4H, alkyl), 2.00-1.86 (m, 4H, alkyl) ( $\Lambda$ -isomer) and  $\delta$  8.44 (s, 2H, bpy-3), 7.58 (m, 4H, bpy-5 and 6), 7.00 (d,  $J$  = 8.5 Hz, 4H, benz), 6.58 (d,  $J$  = 8.5 Hz, 4H, benz), 5.08 (d,  $J$  = 3.5 Hz, 2H, Glc-1), 3.58-3.22 (m, 16H, Glc-2, 3, 4, 5, 6, and alkyl), 2.27 (br, 4H, alkyl), 1.82 (s, 4H, alkyl) ( $\Delta$ -isomer).

**$[\text{Ru}(\alpha\text{-Man-3-bpy})_3]\text{Cl}_2$ .**  $^1\text{H}$ -NMR (500 MHz,  $\text{D}_2\text{O}$ ):  $\delta$  8.41 (s, 2H, bpy-3), 7.90 and 7.80 (dx2,  $J$  = 6.0 Hz, 2Hx2, bpy-5 and 6), 7.23 (d,  $J$  = 9.0 Hz, 4H, benz), 6.71 (d,  $J$  = 8.5 Hz, 4H, benz), 4.80 (br s, 2H, Man-1), 3.80-3.42 (m, 16H, Man-2, 3, 4, 5, 6, and alkyl), 2.57 (br, 4H, alkyl), 2.14 (br, 4H, alkyl) ( $\Lambda$ -isomer) and  $\delta$  8.65 (s, 2H, bpy-3), 7.84 and 7.80 (d $\times$ 2,  $J$  = 6.0 Hz, 2H $\times$ 2, bpy-5 and 6), 7.22 (d,  $J$  = 9.0 Hz, 4H, benz), 6.75 (d,  $J$  = 8.5 Hz, 4H, benz), 5.12 (br s, 2H, Man-1), 3.78-3.47 (m, 16H, Man-2, 3, 4, 5, 6, and alkyl), 2.51 (br, 4H, alkyl), 2.06 (br, 4H, alkyl) ( $\Delta$ -isomer).

**$[\text{Ru}(\text{bpy-OH})_3]\text{Cl}_2$ .**  $^1\text{H}$ -NMR (500 MHz,  $\text{DMSO-}d_6$ ):  $\delta$  8.97 (d,  $J$  = 2.0 Hz, 2H, bpy-3), 7.95 (d,  $J$  = 6.0 Hz, 2H, bpy-6), 7.74 (dd,  $J$  = 2.0 and 6.0 Hz, 2H, bpy-5), 3.78 (t,  $J$  = 5.5 Hz, 4H, alkyl), and 3.58 (t,  $J$  = 5.5 Hz, 4H, alkyl).

**Molecular mechanics calculation.** Mannocluster was manually fitted onto ConA binding site to take similar conformation to 1-3/1-6 trimannose in a complex with ConA

and then used as the initial structure for molecular mechanics calculation. MM calculation (20000 steps, esff) was carried out against mannocluster-ConA complex to reveal the most stable binding structure.

**Thermodynamic analysis of the glycoconjugate-lectin binding.** Aliquots of ruthenium-glycoconjugates ( $9.4 \times 10^{-7}$  M) in PBS (pH 6.5) were added to various concentrations ( $1.0 \times 10^{-6} \sim 1.0 \times 10^{-7}$  M) of ConA in PBS (pH 6.5) and incubated at temperatures of 15 to 35 °C (5 °C intervals) for 1h. The glycoconjugates-ConA aggregates were removed by the ultrafiltration through a Millipore Ultrafree®-MC membrane (cut off 30000), and the concentrations of free glycoconjugates in the resultant orange filtrates were determined from their luminescent intensity (Ex = 450 nm, Em = 600 nm, 25 °C). The association constants ( $K_a$ ), between glycoconjugates and lectins, were calculated by computational curve fitting on eq. 1. The thermodynamic parameters ( $\Delta G^\circ$ ,  $\Delta H^\circ$ , and  $T\Delta S^\circ$ ) were determined via van't Hoff analysis.

$$[\text{ConA} \cdot \text{Ru}] = \frac{4[\text{ConA}]_0 + [\text{Ru}]_0 + K_a^{-1} - \sqrt{(4[\text{ConA}]_0 + [\text{Ru}]_0 + K_a^{-1})^2 - 16[\text{ConA}]_0[\text{Ru}]_0}}{2}$$

(eq.1)

**Binding assay by fluorometry.** An aliquot of a stock solution of ConA or BSA was injected into ruthenium-based glycoconjugates in PBS (pH 6.5, 2 ml). After incubation for 20 min below 25 °C, the luminescent spectrum (Ex. = 450 nm) of the resulting mixture was measured.

# Folate-Liposome-Mediated Antisense Oligodeoxynucleotide Targeting to Cancer Cells: Evaluation in Vitro and in Vivo

Christopher P. Leamon,\* Scott R. Cooper, and Gregory E. Hardee

Department of Drug Delivery & Pharmaceutical Development, Isis Pharmaceuticals, 2292 Faraday Avenue, Carlsbad, California 92008. Received October 25, 2002; Revised Manuscript Received March 5, 2003

The objective of this study was to investigate the use of folate-targeted liposomes for the delivery of encapsulated oligonucleotides to folate receptor (FR)-positive tumor cells in vitro and in vivo. This project involved the synthesis and biological evaluation of many folate-PEG-lipid conjugates, where the chemical form of the folate moiety (pteroate) and the length of the PEG linker chain were varied widely. Folate-targeted oligonucleotide-containing liposomes were prepared using conventional methods, and the extent of cell uptake was evaluated using, among others, the FR positive KB cell line. Oligonucleotide-loaded folate-targeted liposomes were found to rapidly associate with the KB cells, and saturation was typically reached within the first hour of incubation at 37 °C. Nearly 100 000 liposomes per cell were bound or internalized at saturation. Importantly, cell association was blocked by a large excess folic acid, thus reflecting the FR-specific nature of the cell interaction. Full targeting potential was achieved with PEG linkers as low as 1000 in molecular weight, and pteroates bearing glycine or  $\gamma$ -aminobutyryl residues juxtaposed to the pteric acid moiety were also effective for targeting, provided that a terminal cysteine moiety was present at the distal end of the PEG chain for added hydrophilicity. When tested in vivo, folate-targeted liposomes were found to deliver ~1.8-fold more oligonucleotide to the livers of nude mice (relative to the nontargeted PEG-containing formulations); however, no improvement in KB tumor uptake was observed. We conclude from these results that folate liposomes can effectively deliver oligonucleotides into folate receptor-bearing cells in vitro, but additional barriers exist in vivo that prevent or decrease effective tumor uptake and retention.

## INTRODUCTION

Following a gene's transcription into mRNA, the transcript travels to the cytoplasm where ribosomes translate the mRNA into protein (1). If the expression of that gene plays a vital role in the abnormal cell growth and differentiation (as in the case of oncogenes), inhibition of its translation may lead to reduced cell growth or even cell death (2). Synthetic phosphorothioate antisense oligodeoxynucleotides (asODN) have been shown to effectively block the translation of mRNA via a sequence-specific hybridization-based mechanism by using endogenous RNase H to cleave the target mRNA of the mRNA: asODN duplex (3–5). Thus, asODN are considered as potential therapeutics for the treatment of cancers as well as viral infections or other pathological disorders (6–8).

When administered intravenously, asODN distribute broadly to all peripheral tissues. Liver, kidney, bone marrow, skeletal muscle, and skin accumulate the highest percentage of dose, but other tissues (including a variety of tumors) also accumulate measurable quantities of drug (9–11). The means by which antisense oligonucleotides are brought into individual cells is still not fully understood. However, there is some evidence that a cell surface receptor(s) may, in part, play a role in cell uptake (12). Indeed, antisense-specific pharmacological activity has been demonstrated in Kupffer, endothelial,

hepatocyte, and tumor cells, following in vivo administration of saline formulations of oligo (13, 14). Because of the high degree of asODN target specificity and proven safety in humans (15), uptake into nontarget tissues may prove to be biologically inconsequential. However, for the case of cancer chemotherapy, it is generally accepted that greater tumor-associated antisense activity may result if a larger fraction of total injected dose were to accumulate within the tumor tissue.

Of the many possible drug delivery approaches used for improving or enhancing pharmacological activity, liposomes are considered to be a viable option for the delivery of asODN. Indeed, a considerable improvement in pharmacokinetics for liposomal formulations of asODN can be achieved by encapsulating the asODNs within neutral liposomes (16–18). Since asODN are hydrophilic, they can be passively entrapped within the aqueous space of neutral phosphatidylcholine (PC)-based liposomes (19). Blood clearance rates can also be substantially decreased if the liposomes bear a small percentage of PEGylated lipid (20). This technique affords increased accumulation of the asODN-filled liposomes within diseased tissues

\* Current address and to whom correspondence should be addressed: Endocyte Inc., 1205 Kent Ave., West Lafayette, IN 47906. Phone (765) 463-7175; Fax (765) 463-9271; e-mail leamon@endocyte.com.

<sup>1</sup> Abbreviations: FFMEM, folate-free Dulbecco's modified Eagles medium; FR, folate receptor; asODN, phosphorothioate antisense oligodeoxynucleotide; NHS-PEG-MAL, *N*-hydroxysuccinimidyl-poly(ethylene glycol)-maleimide; PBS, phosphate-buffered saline; PEG, poly(ethylene glycol);  $\gamma$ Abu, 4-aminobutyric acid; Pte, pteric acid; Pte-Glu, folic acid; DSPE, distearylphosphatidylethanolamine; EggPC, egg phosphatidylcholine; Chol, cholesterol; PEG, poly(ethylene glycol); FITC, fluorescein isothiocyanate; SDS, sodium dodecyl sulfate.



(27). Unfortunately, the improvement in pharmacokinetics typically comes at the expense of reduced target cell binding and uptake. Thus, cell-specific targeting ligands have often been added to many liposome formulations with the intent of improving the cellular uptake and deposition of drug-encapsulated liposomes (22–25).

It is widely accepted that simple covalent attachment of the ligand, folic acid, to virtually any macromolecule produces a conjugate that can be internalized into folate receptor (FR)-bearing cells in an identical fashion to that of free folic acid (26). Numerous publications have surfaced to better elucidate the mechanism and to further define the advantages as well as limitations of this technology. To date, folate conjugates of radiopharmaceutical agents (27–32), MRI contrast agents (33), low molecular weight chemotherapeutic agents (34), antisense oligonucleotides and ribozymes (35–40), proteins and protein toxins (26, 41–45), immunotherapeutic agents (46–49), liposomes with entrapped drugs (23, 50–53), and plasmids (54–60) have all been successfully delivered to FR-expressing cancer cells. In this current investigation, we chose to examine the ability of the vitamin folate, and various pterate derivatives thereof, to target asODN-loaded neutral liposomes to KB cells both in vitro and in vivo.

#### EXPERIMENTAL PROCEDURES

**Materials.**  $N^{10}$ -Trifluoroacetylptericoic acid was purchased from Aldrich, or synthesized as previously described (61). Fmoc-Glu-OtBu, Fmoc-Glu(OtBu)-OH and Fmoc-Gly were purchased from NovaBiochem, and cysteine-modified *p*-hydroxymethylphenoxymethyl polystyrene resin was purchased from Applied Biosystems Inc.; [*O*-(7-azabenzotriazol-1-yl)-1,1,3,3-tetramethyluronium] hexafluorophosphate was obtained from PerSeptive Biosystems; lipids were obtained from Avanti, Inc. (Alabaster, AL); NHS-PEG-MAL powders were purchased from Shearwater polymers (Huntsville, AL); DC protein assay was obtained from BioRad, and Slowfade reagent from Molecular Probes; phosphorothioate oligonucleotides were synthesized by Isis Pharmaceuticals, and ISIS-2503 and ISIS-2302 were custom labeled with  $^{35}\text{S}$  by Moravsek, Inc. (Brea, CA). All other chemicals were of reagent grade from major suppliers.

**Preparation of Pterates.** Figure 5 lists the structures of the compounds synthesized for this study. Because all of the molecules listed have a common Pte moiety, we will generally refer to these compounds as pterates. Pte- $\gamma$ Glu-Cys was synthesized by a modified procedure to that previously described (62). Briefly, the compound was formed by the stepwise addition of [*O*-(7-azabenzotriazol-1-yl)-1,1,3,3-tetramethyluronium] hexafluorophosphate-activated Fmoc-Glu-OtBu followed by  $N^{10}$ -trifluoroacetylptericoic acid onto a cysteine-modified *p*-benzyloxybenzyl alcohol resin. Following a wash with excess dichloromethane, the resin was repeatedly treated with 0.1 M aqueous piperidine or ammonium hydroxide (to remove the  $N^{10}$ -trifluoroacetyl group) and then with a cleavage/deprotection cocktail consisting of 750 mg of phenol, 10 mL of trifluoroacetic acid, 0.5 mL of water, 0.25 mL of dithioethane, and 0.5 mL of thioanisole for 2 h at room temperature. The freely soluble compound was separated from the resin by filtration through a medium pore fritted funnel. The filtrate was then diluted with 4 volumes of diethyl ether to precipitate the Pte- $\gamma$ Glu-Cys product. Following multiple ether washes, the precipitate was dried in vacuo. Barring no further purification, Pte- $\gamma$ Glu-Cys produced in this manner was typically 80–90%

pure, as determined by the  $A_{280}$  peak area generated from  $\text{C}_{18}$  reversed phase HPLC analyses, with the primary impurity being the dimerized (disulfide-linked) species. An Ellman's assay (63) on the crude material confirmed that the solid contained 80–90% free thiols.

All other cysteine-containing pterate derivatives were synthesized using similar solid-phase synthetic procedures to that exemplified above for Pte- $\gamma$ Glu-Cys. Overall, mass spectrometric analysis (negative electrospray) clearly identified the  $\text{M} - \text{H}$  species for each pterate compound:  $m/z = 471, 499, 543,$  and  $543$  for Pte-Gly-Cys, Pte- $\gamma$ Abu-Cys, Pte- $\gamma$ Glu-Cys, and Pte- $\alpha$ Glu-Cys, respectively.

Pte- $\gamma$ Abu was synthesized by a slightly different procedure. Briefly, Fmoc- $\gamma$ Abu (preloaded on a *p*-benzyloxybenzyl alcohol resin) was first treated with piperidine, washed with excess DMF, and then coupled with [*O*-(7-azabenzotriazol-1-yl)-1,1,3,3-tetramethyluronium]hexafluorophosphate-activated  $N^{10}$ -trifluoroacetylptericoic acid. The resin was later treated with 0.1 M aqueous ammonium hydroxide, washed with dimethylformamide and dichloromethane, and then treated with the trifluoroacetic acid cleavage cocktail as described above. The final product was precipitated in ether, air-dried, and then analyzed by HPLC for purity. No further purification was necessary. Mass spectrometric analysis confirmed the ( $\text{M} - \text{H}$ )  $m/z = 396$ .

#### Preparation of Lipid-PEG-Pterate Conjugates.

Pterate-conjugated lipids were commonly produced on a 147 mmol scale. Briefly, 5.5 mL of distearylphosphatidylethanolamine (DSPE: 110 mg, 147 mmol) were placed in a 50 mL round-bottom flask plus 10 mL of  $\text{CHCl}_3$ . Two equivalents of triethylamine followed by 147 mmol of NHS-PEG-MAL powder (Shearwater polymers) was added next. Note, some preparations used PEGs of various sizes, as indicated. The reaction vessel was heated to 60 °C for 30 s to clear the solution followed by continual stirring for 2 h at room temperature. Reaction completion was confirmed by thin-layer chromatography using the solvent system 65:25:4  $\text{CHCl}_3/\text{CH}_3\text{OH}/\text{H}_2\text{O}$ . A 1.2-fold molar excess of a cysteine-containing pterate derivative was then directly added to the reaction vessel along with an additional 5 equiv of triethylamine. The reaction was left to stir overnight at room temperature in the absence of light. The solution was next filtered through a fine Buchner filter, and the filtrate was rotoevaporated to a minimal volume. The concentrated solution was then added dropwise to 100 mL of stirring ether and placed on ice for 10 min. The sample was centrifuged for 10 min at 4 °C 3000 rpm, and the supernatant was discarded. The ether wash step was repeated a total of three times. The final yellow pellet was dissolved in 30 mL of 2:1  $\text{CHCl}_3/\text{CH}_3\text{OH}$ , and purity was assessed by thin-layer chromatography (single spot,  $R_f = 0.25$ ). If present, residual unreacted PEG products ( $R_f > 0.6$ ) were separated from the DSPE-PEG-pterate compounds using standard flash chromatography methods (silica gel) and eluting with  $\text{CHCl}_3$  followed by  $\text{CHCl}_3/\text{CH}_3\text{OH}$  at stepwise increasing proportions.

For the preparation of Pte- $\gamma$ Abu-PEG<sub>3400</sub>-DSPE, DSPE was first reacted with NHS-PEG<sub>3400</sub>-NH-Fmoc (Shearwater Polymers) in  $\text{CHCl}_3$  along with 2 equiv of triethylamine. The reaction vessel was heated to 60 °C for 30 s to clear the solution followed by continual stirring for 2 h at room temperature. Reaction completion was confirmed by thin-layer chromatography using the solvent system 65:25:4  $\text{CHCl}_3/\text{CH}_3\text{OH}/\text{H}_2\text{O}$ . The Fmoc protecting group was easily removed by treating the crude product with 20% piperidine for 20 min, and the DSPE-PEG-NH<sub>2</sub>

product was purified by flash chromatography. A 1.2-fold molar excess of [*O*-(7-azabenzotriazol-1-yl)-1,1,3,3-tetramethyluronium] hexafluorophosphate-activated Pte- $\gamma$ Abu (in dimethylformamide) was added to the DSPE-PEG-NH<sub>2</sub> in CHCl<sub>3</sub> (1:1 v/v) along with 2 equiv of triethylamine. The reaction was left to stir overnight at room temperature in the absence of light, and it was then worked up and purified by procedures described above.

DPPE-Cys- $\gamma$ Glu-Pte was synthesized by the addition of 1.2 equiv Cys- $\gamma$ Glu-Pte (in dimethylformamide) to 1,2-dipalmitoyl-*sn*-glycero-3-phosphoethanolamine-*N*-[4-(*p*-maleimidomethyl)cyclohexanecarboxamide] (Avanti Inc.) in CHCl<sub>3</sub> containing 5 equiv of triethylamine. The reaction was left to stir overnight at room temperature in the absence of light, and it was then worked up and purified by procedures described above.

**Preparation of Oligonucleotide Liposome Formulations.** Egg phosphatidylcholine (eggPC) and cholesterol (Chol) solutions were prepared at 20 mg/mL in chloroform. DSPE-PEG- $\gamma$ phosphate solutions were prepared at 10 mg/mL in 2:1 CHCl<sub>3</sub>/CH<sub>3</sub>OH with ~0.5% deionized water. Lipids were dispensed into 30 mL round-bottom flasks at defined ratios. Unless otherwise stated, liposomes were composed of eggPC, Chol, and DSPE-PEG- $\gamma$ phosphate at a mole ratio of 59:40:1. Where noted, 50  $\mu$ Ci of <sup>3</sup>H-dipalmitoylphosphatidylcholine was included as a radiotracer. Organic solvents were removed in vacuo using a rotary evaporator at 60 °C. Phosphorothioate oligonucleotides were dissolved in deionized water at 10 to 100 mg/mL. Where indicated, tracer amounts of <sup>35</sup>S-labeled oligo were included in the hydration solution. Alternatively, a fluorescein-labeled oligonucleotide solution (FITC-ISIS-5132) was used for liposome samples intended for confocal microscopic evaluation (see below). The tonicity of the oligo solutions was adjusted to 310 mOsM with the addition of a small quantity of 5M NaCl. All asODN solutions were filtered through a 0.22  $\mu$ m polycarbonate membrane prior to use. Typically, 0.5 mL of the oligonucleotide solution was added to the flask containing the dry lipid film. The flask was rotated at 240 rpm, 60 °C for 5 min and then vortexed heavily. Following five cycles of freezing and thawing (60 °C water bath to dry ice/acetone bath), the crude liposomes were then repeatedly extruded through 100 nm polycarbonate membranes (21 strokes). Unencapsulated oligo was separated from the liposome formulation by passing down a Superdex-200 HR 10/30 FPLC column (Pharmacia) equilibrated in phosphate-buffered saline, pH 7.4 (PBS). Under normal operational conditions, baseline separation of the liposome-oligonucleotide formulations from the unencapsulated oligonucleotide occurred. Pooled liposome-oligonucleotide fractions were sterile filtered through 0.22  $\mu$ m membranes prior to characterization and use. Particle size was assessed by laser scattering techniques. All liposome samples were determined to be ~90 to 110 nm in average diameter.

**Cell Culture.** All cells were grown continuously as monolayers using folate-free RPMI media (FFRPMI) containing 10% heat-inactivated fetal calf serum and 2 mM L-glutamine at 37 °C in a 5% CO<sub>2</sub>/95% air-humidified atmosphere. The heat-inactivated serum contained its normal complement of endogenous folates which enabled the cells to sustain growth in this more physiologically relevant medium (26).

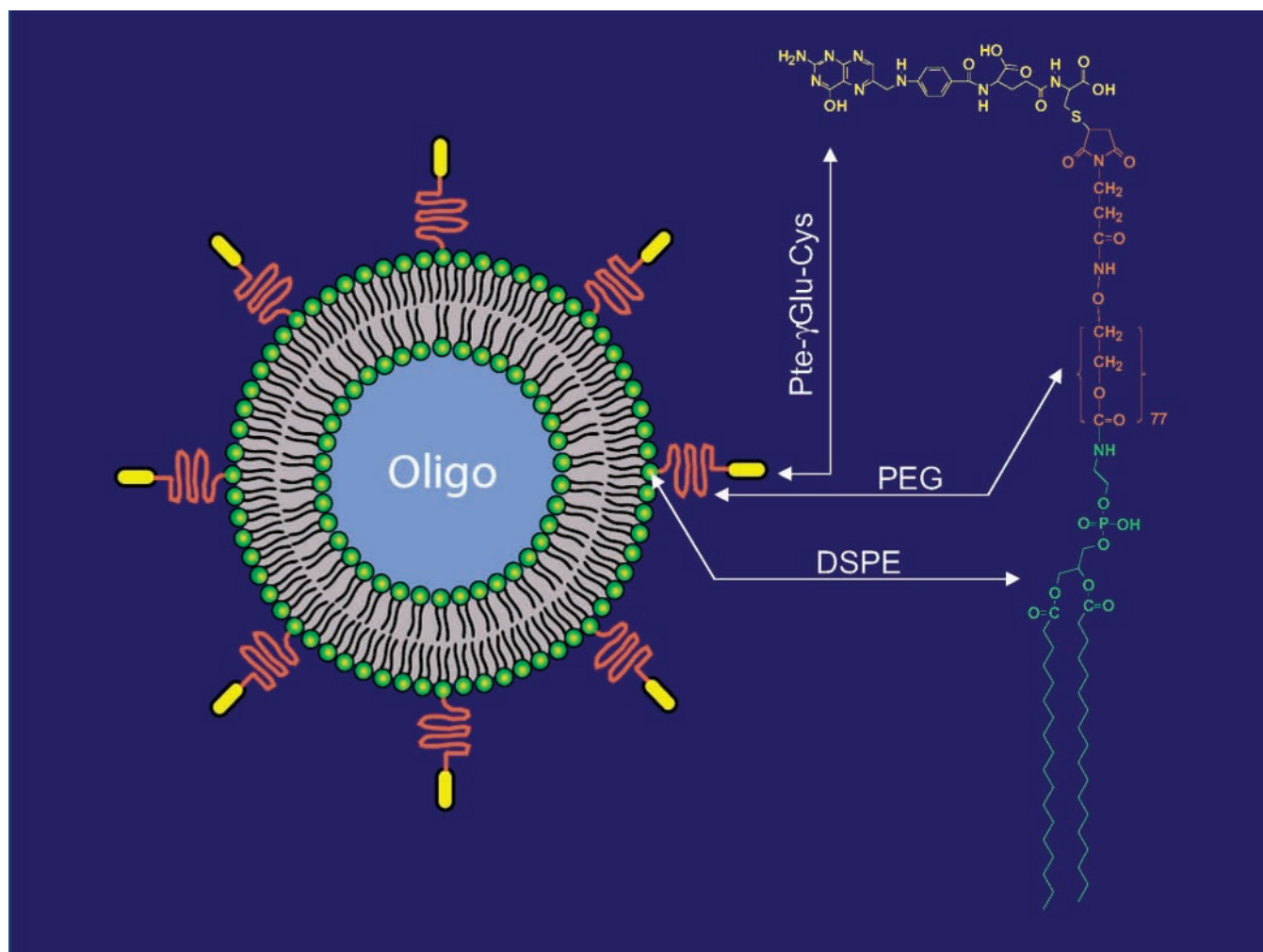
**Time-Dependent Uptake Study.** A suspension of approximately  $1 \times 10^5$  cells in 2 mL of growth medium was deposited per well in six-well Falcon plates. Cells were allowed to attach to the plates and grow for no longer than 3 days at 37 °C. Spent growth medium was

replaced with 2 mL of fresh serum-containing medium per well. Aliquots of <sup>35</sup>S-ISIS-2503 formulations were added to the wells, and the cells were incubated for increasing times at 37 °C. Each well was rinsed four times with 1 mL of ice-cold PBS to remove non-cell-associated material. The cell monolayers were then dissolved in 1 mL of 1% sodium dodecyl sulfate (SDS) in PBS, pH 7.4, for 30 min at room temperature. Cell lysate (800  $\mu$ L) was transferred to glass scintillation vials containing 10 mL of scintillation cocktail and then measured for radioactive content using a Packard scintillation counter. One hundred microliters of the remaining cell lysate was used to quantitate the amount of cell protein using a detergent-compatible protein assay (DC protein assay, BioRad). DPM values were normalized with respect to each sample's protein content. Final results are expressed as molecules of oligonucleotide per cell, as calculated using the known specific activity of the <sup>35</sup>S-ISIS-2503 and the conversion factor of  $2.23 \times 10^{-10}$  g of total protein per cell (64).

**Concentration-Dependent Uptake Studies.** Cells were deposited per well in six-well Falcon plates and incubated as described above. Spent growth medium was replaced with 2 mL of fresh serum-containing medium per well. Aliquots of free <sup>35</sup>S-labeled oligonucleotides or <sup>3</sup>H-DPPC-liposomes containing encapsulated ISIS 2302 were added to the wells, and the cells were incubated for 2 h at 37 °C. Sample wells were then handled exactly as described above. Final results are expressed as molecules of oligonucleotide per cell when <sup>35</sup>S-oligonucleotide was used, or as liposomes per cell when the <sup>3</sup>H-DPPC radiotracer was used. Note, the conversion factor for the latter calculation was  $3.39 \times 10^6$  liposomes per DPM.

**Confocal Microscopy.**  $5 \times 10^4$  cells in 1 mL of growth media were deposited into six-well Falcon plates. Each well contained one #1.5 glass coverslip. Cells were incubated for 2 days at 37 °C to encourage strong coverslip adherence and optimal subconfluent cell spreading. Spent incubation media was replaced with 1 mL of fresh serum-supplemented media containing either free FITC-ISIS-5132 oligonucleotide or liposome formulations thereof at the indicated concentrations. Following an 8 h 37 °C incubation, each dish was rinsed four times with 1 mL of PBS, pH 7.4, and then fixed in 2 mL of fresh 5% neutral-buffered formalin at 4 °C overnight. Coverslips were then mounted on top of 4.5  $\mu$ L of Slowfade reagent (Molecular Probes), sealed to the glass slide using nail polish, and then stored at 4 °C until examined. Cell-associated fluorescence was imaged within 2 days using a BioRad MRC1024 confocal laser-scanning microscope.

**Biodistribution Studies.** EggPC/Chol/DSPE-PEG<sub>3400</sub> and eggPC/Chol/DSPE-PEG<sub>3400</sub>-cys- $\gamma$ Glu-Pte liposome formulations (59:40:1) encapsulating <sup>35</sup>S-ISIS-2503 were used for the biodistribution studies. Fresh KB tumor slices of approximately 30 mm<sup>3</sup> size were surgically inserted subcutaneously in Taconic NCR *nu/nu* mice and allowed to grow to ~200 mm<sup>3</sup> volume. Mice were maintained on a folate-free rodent chow (Harlan) for three weeks prior to the study (28). Liposome formulations were injected intravenously via the lateral tail vein at 15 mg/kg relative to <sup>35</sup>S-ISIS-2503. Following a 24 h period, mice were sacrificed, and selected tissues were removed and weighed. Tissues were homogenized in 15 mL of water, and 1 mL was placed in a glass scintillation vial along with 3 mL of Soluene 350 (Packard). Tissues were allowed to dissolve overnight at room temperature. The solution was then neutralized with 1 mL of 2 N HCl and then mixed in 10 mL of scintillation cocktail.



**Figure 1.** Proposed model of pteroate-liposome formulation.

Samples were placed in the dark for 24 h (to reduce autofluorescence) and then counted for associated radioactivity.

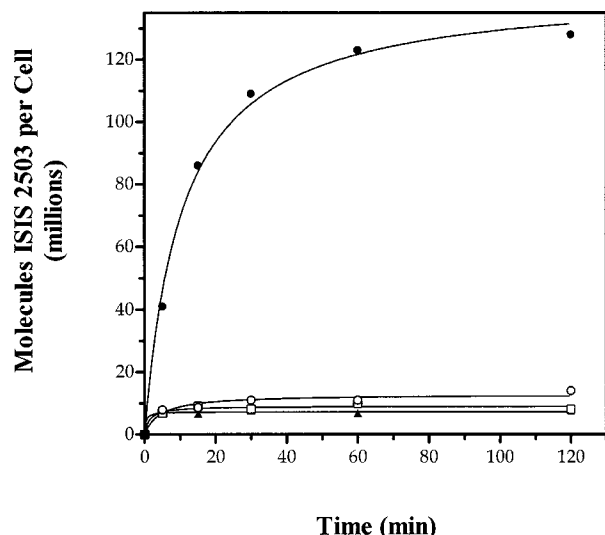
**Plasma and Serum Studies.** EggPC/Chol/DSPE-PEG<sub>3400</sub>-Cys- $\gamma$ Glu-Pte liposomes (59:40:1) containing the <sup>3</sup>H-DPPC radiotracer were prepared by hydrating with PBS, pH 7.4. Fresh *nu/nu* mouse plasma and serum (derived from mice fed a folate-free diet for three weeks) were prepared on the same day of study. Blood was collected by cardiac puncture under avertin anesthesia. The plasma was prepared by placing the blood in heparin-coated tubes before centrifugation. The serum was prepared by placing the blood in plasma collection tubes and allowing the blood to clot before centrifugation. Fresh plasma or serum was added at 50% concentration by volume to liposome formulations in FFRPMI. Following a 30 min 37 °C preincubation, increasing lipid concentrations (expressed as nM equivalents of DSPE-PEG<sub>3400</sub>-Cys- $\gamma$ Glu-Pte component) were then added to KB cells adherent to 12-well Falcon plates (approximately 80% confluent), and cells were incubated for 2 h at 37 °C. Each well was rinsed 4  $\times$  0.5 mL with ice-cold PBS and then dissolved in 0.5 mL of 1% SDS in PBS for a minimum of 30 min. Cell lysates were assayed for associated radioactivity and for cell protein according to the procedures described above.

## RESULTS

**Formulation Model.** Figure 1 depicts a proposed structure of a folate (pteroate)-targeted liposome. A small mole percentage of a DSPE-PEG-pteroate conjugate is included in the lipid formulation. Pte- $\gamma$ Glu-Cys is the pteroate shown for illustrative purposes. We have had success in introducing the lipid conjugate into the liposome membrane by a variety of techniques. For example, the DSPE-PEG-pteroate component can simply be added to the initial lipid mixture prior to evaporation of the organic solvents and subsequent lipid film hydration. However, we have also been successful inserting the targeting lipid into the bilayer by simply adding a micellar suspension of pure DSPE-PEG-pteroate to preformed liposomes (25).

**Time-Dependent Cell Association of <sup>35</sup>S-ISIS-2503 Liposome Formulations.** We began our investigation by examining the kinetics of <sup>35</sup>S-ISIS-2503 association with FR-positive KB cells when presented either alone or when encapsulated within a liposome formulation. As shown in Figure 2, approximately 10 million molecules of the free oligonucleotide had quickly associated with the KB cells; however, there was no significant change in this value over the course of 2 h at 37 °C. Nearly the same level of cell-associated oligo resulted when <sup>35</sup>S-ISIS-2503 was introduced to the cells as a nontargeted PEGylated liposome formulation. However, the addition of a small amount of DSPE-PEG<sub>3400</sub>-Cys- $\gamma$ Glu-Pte to

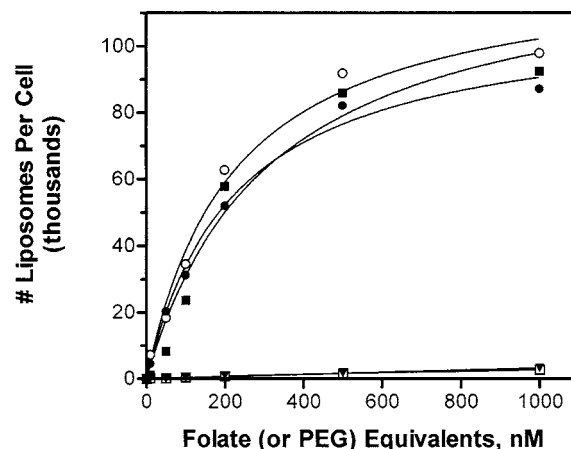




**Figure 2.** Time-dependence of folate-liposome cell uptake. KB cells were incubated for increasing times at 37 °C with 10  $\mu$ M  $^{35}$ S-ISIS-2503 ( $\blacktriangle$ ) or the same quantity of oligonucleotide encapsulated within liposomes comprised of eggPC/Chol/DSPE-PEG<sub>3400</sub>-Cys- $\gamma$ Glu-Pte ( $\bullet$ ) or eggPC/Chol/DSPE-PEG<sub>3400</sub> ( $\square$ ). As a control for specificity, some cells were incubated with eggPC/Chol/DSPE-PEG<sub>3400</sub>-Cys- $\gamma$ Glu-Pte liposomes in the presence of 0.1 mM folic acid ( $\circ$ ). Following a rinse to remove non-cell-associated material, cells were harvested and counted for associated radioactivity. DPM values were normalized with respect to a sample's protein content. Final results are expressed as molecules of oligonucleotide per cell, as described in Experimental Procedures. Points represent the average of duplicate values.

the liposome formulation manifested a dramatic increase in overall cell association of the formulated oligonucleotide. We observed a rapid uptake profile where >120 million molecules of  $^{35}$ S-ISIS-2503 associated with the KB cells after 1 h of incubation. Furthermore, the specificity of this high degree of cell association was demonstrated by the near complete inhibition of uptake when an excess of free folic acid was present in the culture media. Taken together, these data suggest that folate-targeted liposome formulations can enhance the cell uptake of oligonucleotides by >12-fold via a folate-specific, saturable uptake mechanism.

**Effect of PEG Spacer Length on Folate-Liposome Targeting.** In an effort to define and possibly optimize the folate-liposome targeting technique, a variety of folate-lipid constructs were prepared whereby the length of the intramolecular PEG linker was varied. Thus, constructs containing either no PEG or PEG up to 3400 in molecular weight were formulated into  $^3$ H-DPPC-labeled liposomes, and the extent of cell-association was measured. As shown in Figure 3, no more than 2000 folate-liposomes associated with the cells if the PEG linker was absent (i.e., with DSPE-Cys- $\gamma$ Glu-Pte). Interestingly, this is the same amount of cell association that nontargeted, PEG<sub>2000</sub>-containing liposomes display. In contrast, inclusion of a PEG<sub>1000</sub> spacer between the folate and lipid moieties fully restored the targeting activity, and virtually no difference in cell uptake was noted for PEG linkers ranging in size from 1000 to 3400 in molecular weight. Maximum liposome uptake was reached when ~90 000 liposomes became associated with the KB cells. Similar uptake studies performed with this formulation revealed that MiaPaCa, HeLa, and OV1063 cells each associated 49, 35, and 29 thousand liposomes per cell, respectively, at the point of saturation. Although it was not examined further, the differences in liposome



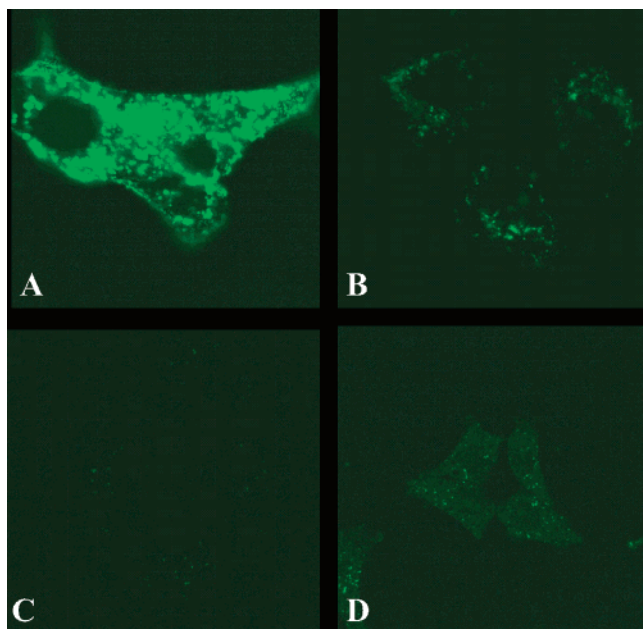
**Figure 3.** Effect of PEG spacer length. KB cells were incubated for 2 h at 37 °C with increasing concentrations of  $^3$ H-DPPC-labeled liposomes (plotted relative to the net liposome-associated folate or PEG concentration). Following a rinse to remove non-cell-associated material, cells were harvested and counted for associated radioactivity. DPM values were normalized with respect to a sample's protein content. Final results are expressed as the number of liposomes associated per cell, as described in Experimental Procedures. Points represent the average of duplicate values. EggPC/Cholesterol liposome formulations contained either 1 mol % of DSPE-PEG<sub>3400</sub>-Cys- $\gamma$ Glu-Pte ( $\blacksquare$ ), DSPE-PEG<sub>2000</sub>-Cys- $\gamma$ Glu-Pte ( $\circ$ ), DSPE-PEG<sub>1000</sub>-Cys- $\gamma$ Glu-Pte ( $\bullet$ ), DSPE-PEG<sub>2000</sub> alone ( $\square$ ), or DPPE-Cys- $\gamma$ Glu-Pte ( $\blacktriangledown$ ).

uptake among these four cell lines was likely due to their FR expression levels.

It is interesting to note that the KB cells used for these studies expressed approximately 4 million FR per cell. Since only 90 000 pterolate-targeted liposomes could maximally bind to these cells, it is likely that either (i) the liposomes bound to and occupied more than one FR (multivalency), and/or (ii) the steric hindrance among adjacent cell-bound liposomes prevented some of the surface FRs from binding individual folate-liposomes. For the remainder of our studies, we elected to use PEG<sub>3400</sub> as the linker for all targeted liposome preparations.

**Visualization of KB Cell Uptake of FITC-ISIS-5132 Formulations.** In an attempt to confirm our aforementioned quantitative observations, confocal microscopy was used to visually monitor the cell association of FITC-labeled ISIS-5132. As shown in Figure 4A, significant amounts of FITC-ISIS-5132 could clearly be seen associated with the KB cells when the asODN was encapsulated within folate-targeted liposomes. Large and numerous punctuate fluorescent structures (endosomes and multivesicular bodies) were found in all observed cells. And like the radiolabeled folate-liposome formulation, excess free folic acid in the culture media prevented the uptake of these fluorescent liposomes (Figure 4C). Furthermore, a dramatic reduction in cell association was observed for FITC-ISIS-5132 formulations that lacked the folate ligand (e.g., nontargeted PEGylated liposomes; Figure 4B). These data support our conclusion that folate-liposomes can efficiently target encapsulated oligonucleotides to FR-positive cells.

**Structural Activity of the Targeting Ligand.** All of the previous liposome work was conducted using Pte- $\gamma$ Glu-Cys as the targeting ligand. Because a recent report indicated that other pterolate forms of folate can be used for targeting exogenous molecules or formulations to FR-positive cells (62), we elected to synthesize a few alternative pterolates and test them for their ability to target liposomes. The pterolates used in this investigation are listed in Figure 5, and their respective targeting activities



**Figure 4.** Confocal microscopy. KB cells were plated onto #1.5 glass coverslips and incubated for 2 days at 37 °C to encourage strong coverslip adherence. FITC-ISIS-5132-containing formulations were incubated with the cells for 8 h at 37 °C. Following extensive rinsing, cells were fixed in fresh 5% neutral-buffered formalin at 4 °C overnight and then mounted. Cell-associated fluorescence was imaged within 2 days using a BioRad MRC1024 confocal laser-scanning microscope. Cells were treated with: Panel A, eggPC/Chol/DSPE-PEG<sub>3400</sub>-Cys-γGlu-Pte (59:40:1 mol ratio) liposomes encapsulating FITC-ISIS-5132; Panel B, nontargeted eggPC/Chol/DSPE-PEG<sub>3400</sub> (59:40:1 mol ratio) liposomes encapsulating FITC-ISIS-5132; Panel C, liposomes from Panel A in the presence of 0.1 mM folic acid; Panel D, free FITC-ISIS-5132.

are displayed in Figure 6. Similar to what was described for protein targeting (62), we found no difference in targeting potential for the Pte-αGlu-Cys, Pte-γGlu-Cys, or Pte-Gly-Cys ligands. Interestingly, removal of the α-carboxyl group from the Pte-γGlu-Cys to form Pte-γAbu-Cys manifested a slight reduction in targeting potential, but further removal of the terminal cysteine residue completely abolished the targeting activity. In other words, the cell-associative activity of the Pte-γAbu ligand was indistinguishable from the formulation that lacked a Pte group (i.e. PEGylated liposomes) or from the freely administered oligonucleotide itself. These results suggest that the cysteine residue of Pte-γAbu-Cys may be acting as an efficient spacer between the Pte moiety and the PEG<sub>3400</sub> linker. However, the more likely explanation is that the cysteine residue provides sufficient water solubility of the overall ligand to orient the Pte moiety outward where it can efficiently enter the binding pocket of the cell surface FR. For practical considerations, we chose to continue using the Pte-γGlu-Cys-PEG<sub>3400</sub>-DSPE conjugate for the remainder of our studies.

**Tissue Distribution of <sup>35</sup>S-ISIS-2503-Loaded Folate Liposomes.** Following our detailed in vitro examination of folate-liposome-mediated oligonucleotides delivery, we decided to examine the tissue distribution of <sup>35</sup>S-ISIS-2503-loaded liposomes formulated with either Pte-γGlu-Cys-PEG<sub>3400</sub>-DSPE (targeted), or PEG<sub>2000</sub>-DSPE (PEGylated liposome control). Importantly, the tissue distribution of the free oligonucleotide was also tested for comparison. Thus, formulations were injected intravenously into nude mice bearing large, established subcutaneous KB tumors. Twenty-four hours later, mice were

sacrificed, and the amount of <sup>35</sup>S-ISIS-2503 remaining in major organs was quantitated. As shown in Figure 7, the free oligonucleotide was found to effectively clear from the plasma and accumulate in the kidney, liver, and, to some extent, spleen; however, little uptake was noted in the lung, heart, intestines, muscle, or the KB tumor. When formulated within PEGylated liposomes, a significant amount of the oligonucleotide remained in the plasma, and enhanced uptake was noted in all tissues except for the kidney (which decreased) and the liver (which stayed constant). Notably, PEGylated liposomes enhanced the tumor uptake of <sup>35</sup>S-ISIS-2503 by ~3-fold.

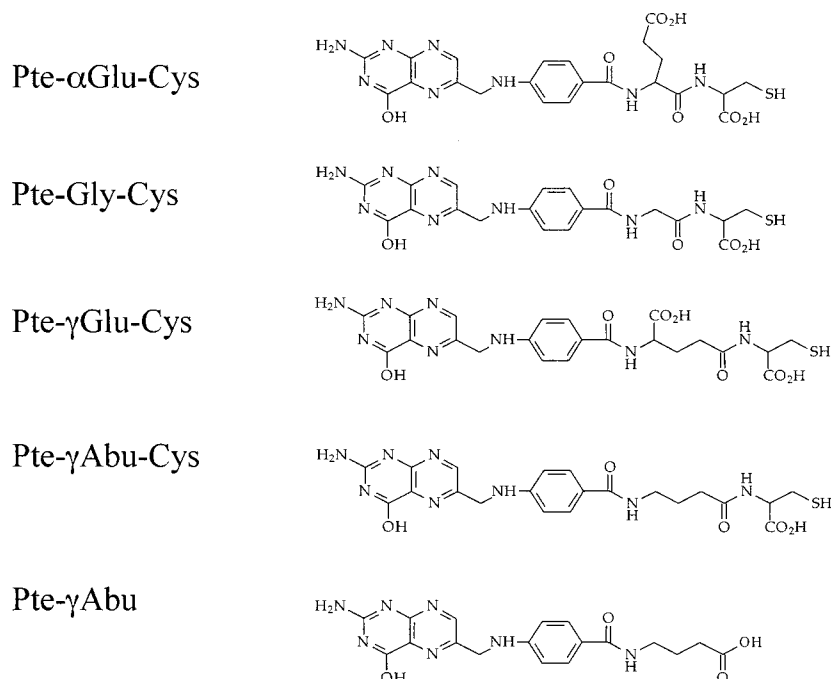
Oligonucleotides formulated within the folate-targeted liposomes had preferentially accumulated to the greatest extent within the liver. We measured a 1.8- to 2-fold increase in liver uptake relative to the PEGylated liposome or free oligonucleotide formulations, respectively (see Discussion). Similar to the PEGylated liposomes, though, uptake of folate-targeted liposomes was enhanced in all tissues except for the kidney and plasma. But, although a sizable folate receptor-positive KB tumor was present, no enhanced uptake of <sup>35</sup>S-ISIS-2503 was found, as compared to the PEGylated liposome formulation.

**Effect of Fresh Serum or Plasma on Folate-Liposome Targeting.** The disappointing tumor results prompted us to search for a possible explanation. It is known that the enzyme, γ-glutamyl hydrolase (EC 3.4.19.9), is present in the plasma of mammals (65). Since PEGylated liposomes circulate in the plasma for extended periods of time (20), we reasoned that the γGlu-Cys bond within the Pte-γGlu-Cys-PEG<sub>3400</sub>-DSPE conjugate or the targeted liposomes could have been a substrate for such an enzyme. Thus, in vivo enzyme hydrolysis of that bond would have resulted in the decimation of liposome targeting potential. To address this concern, we isolated fresh plasma and fresh serum from nude mice and then immediately mixed them with Pte-γGlu-Cys-PEG<sub>3400</sub>-DSPE-containing liposomes. Following 30 min of incubation at 37 °C, the samples were added to cultured KB cells, and the extent of liposome cell association was measured. As shown in Figure 8, preexposure of the folate-targeted liposomes to 50% of either fresh murine serum or plasma caused no reduction of liposome cell association. Notably, similar results were obtained with 50% fetal calf serum (data not shown). We conclude from these observations that plasma-derived γ-glutamyl hydrolase activity had no effect on the biodistribution of folate-targeted liposomes in KB tumor-bearing nude mice.

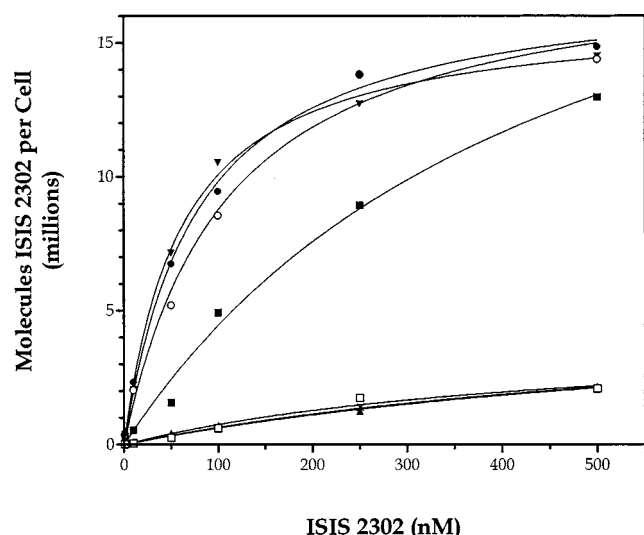
## DISCUSSION

The objective of this study was to investigate the use of folate-targeted liposomes for the delivery of encapsulated oligonucleotides to FR-positive tumor cells in vitro and in vivo. This project required the synthesis and biological evaluation of many folate-PEG-lipid conjugates, where the chemical form of the folate moiety (pterolate) and the length of the PEG linker chain were widely varied.

Folate-targeted oligonucleotide-containing liposomes were prepared using conventional methods, and the extent of cell uptake was evaluated in vitro. These liposomes were found to rapidly associate with FR-positive KB cells, and saturation was typically reached within the first hour of incubation. At this point, nearly 100 000 liposomes per cell were bound or internalized. The cell association was completely blocked by excess folic acid, thus reflecting the FR-specific nature of the cell interaction.



**Figure 5.** Structures of DSPE-PEG<sub>3400</sub>-pterolate conjugates.



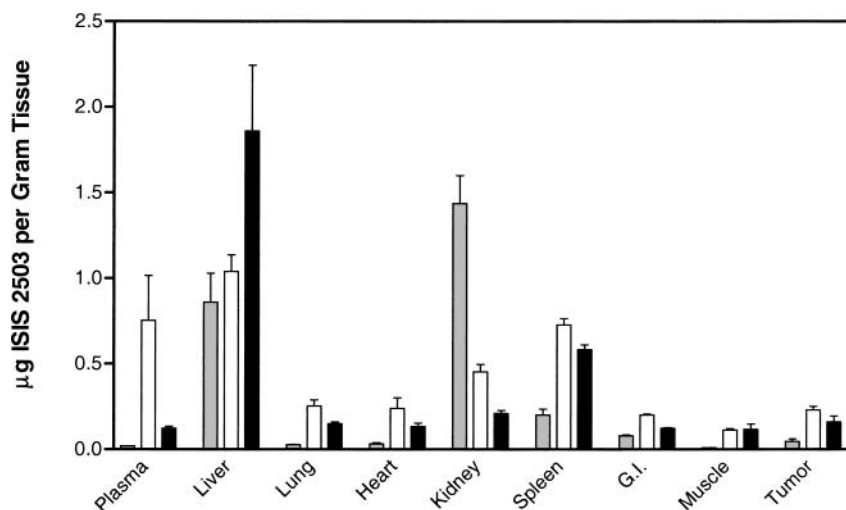
**Figure 6.** Concentration-dependent uptake of ISIS-2302 formulations. KB cells were incubated for 2 h at 37 °C with increasing concentrations of ISIS-2302 encapsulated within <sup>3</sup>H-DPPC-labeled liposomes. Following a rinse to remove non-cell-associated material, cells were harvested and counted for associated radioactivity. DPM values were normalized with respect to a sample's protein content. Final results are expressed as molecules of oligonucleotide per cell, as described in Experimental Procedures. Points represent the average of duplicate values. EggPC/Cholesterol liposome formulations contained 1 mol % of DSPE-PEG<sub>3400</sub> (×) or with the PEG terminus modified with Cys- $\gamma$ Glu-Pte (●), Cys- $\alpha$ Glu-Pte (○), Cys-Gly-Pte (▼), Cys- $\gamma$ Abu-Pte (■), or  $\gamma$ Abu-Pte (□). Cell association of free <sup>35</sup>S-ISIS-2302 is shown as (▲).

During our investigation, we attempted to optimize the targeting activity of these liposomes by modifying the length of the PEG linker. Lee et al. were the first to describe the dependence of folate-liposome targeting on the distance between the folate moiety and the lipid bilayer (23). This dependency is believed to be due to the need for folate to enter the binding pocket of the cell surface FR. These investigators demonstrated that a PEG<sub>3400</sub> linker was necessary for targeting, since no

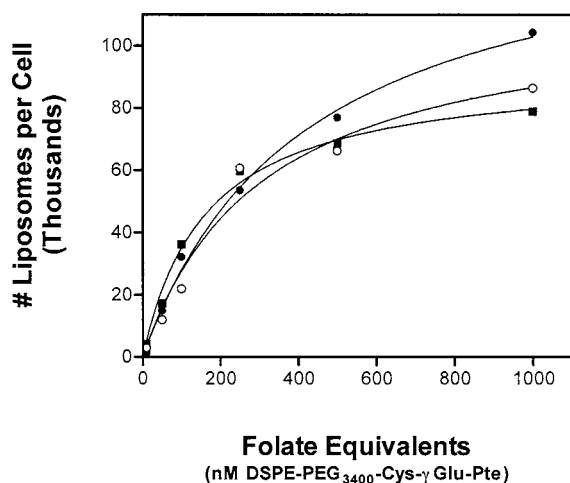
liposome cell association occurred when folate was attached either directly to the lipid head or with a single amino acid spacer. However, no additional information was given in regards to the minimal PEG length needed to restore full targeting potential. In our current study, we confirmed the result of Lee et al. and further found that PEGs as small as 1000 in molecular weight (or 25 Å root-mean-square distance; (66)) could also function as effective linkers. Unfortunately, the lower PEG threshold length was still not identified.

Additional optimization studies were performed on the targeting ligand. It was previously shown that proteins could efficiently be targeted to FR-bearing cells if tethered to folate via either its  $\alpha$ - or  $\gamma$ -glutamyl carboxylate (62). Furthermore, the distal glutamyl moiety of Pte-Glu could actually be replaced with a glycine residue, and this new pterolate retained maximum potential for targeting proteins to FR-bearing cells. It was concluded from these studies that (i) endocytosis-competent pterolates do not require a free carboxylic acid (juxtaposed to the *p*-aminobenzoic acid moiety) to effectively bind to and become internalized by the FR, and (ii) the spatial distance of the attached macromolecule from the *p*-aminobenzoic acid moiety of these pterolates is more likely the prominent factor governing the ability of a pterolate conjugate to interact with the FR. Using a similar structure-activity approach, we chose to repeat and expand upon those studies by investigating the liposome targeting potential of various pterolate ligands (see Figure 5). Our results confirmed that, similar to peptides, pteric acid was an effective liposome targeting ligand if it were conjugated to the PEG-DSPE construct via an  $\alpha$ - or  $\gamma$ -Glu-Cys, or Gly-Cys peptide linker. Interestingly, removal of the free  $\alpha$ -carboxyl group from the  $\gamma$ -Glu-Cys moiety produced Pte- $\gamma$ Abu-Cys, which did effectively target liposomes to the FR-positive cells (albeit at ~3.5-fold lower relative affinity). However, elimination of the terminal Cys residue produced Pte- $\gamma$ Abu, a pterolate that lacked effective targeting potential. Together with the previously published protein targeting data (62), we strongly believe that (i) the Glu residue of folate (Pte-Glu) is absolutely not needed for targeting attached





**Figure 7.** Tissue biodistribution of  $^{35}\text{S}$ -ISIS-2503 formulations. Free  $^{35}\text{S}$ -ISIS-2503 (gray bars) or encapsulated within eggPC/Chol/DSPE-PEG<sub>3400</sub> (open bars) or eggPC/Chol/DSPE-PEG<sub>3400</sub>-Cys- $\gamma$ Glu-Pte (black bars) liposome formulations were injected intravenously at 15 mg/kg (relative to ISIS-2503) into *nu/nu* mice bearing subcutaneous KB tumors. Following a 24 h period, mice were sacrificed and the quantity of tissue-associated radioactivity was measured. Bars represent the average  $\pm$  1 SD from three mice.



**Figure 8.** Effect of serum and plasma on folate-liposome cell uptake. EggPC/Chol/DSPE-PEG<sub>3400</sub>-cysFolate liposomes (59:40:1) containing the  $^3\text{H}$ -DPPC radiotracer were pretreated for 30 min at 37 °C with fresh *nu/nu* plasma or serum (50% concentration by volume). Liposome formulations were added to KB cells at increasing lipid concentrations (expressed as nM equivalents of DSPE-PEG<sub>3400</sub>-Cys- $\gamma$ Glu-Pte component), and cells were incubated for 2 h at 37 °C. Cell lysates were assayed for associated radioactivity and for cell protein according to the procedures described in Experimental Procedures. Points represent the average of duplicate values. (■), FFRPMI only; (○), 50% fresh mouse serum; (●), 50% fresh mouse plasma.

molecules to FR-positive cells, and (ii) targeting requires that the Pte residue be sufficiently soluble in water (or solvated) to be effectively presented to the FR for binding. The latter requirement can therefore be satisfied if a charged residue is nearby, such as that provided by the Cys residue in Pte- $\gamma$ Abu-Cys.

Despite our success in maximizing the targeting potential of folate-labeled liposomes *in vitro*, we were disappointed to find that the targeted liposomes accumulated poorly in KB tumor tissue. In fact, the folate liposomes delivered no higher amounts of encapsulated oligonucleotide into large KB tumors than did the non-targeted PEGylated formulation (see Figure 7). The folate-liposomes did manage to deliver  $\sim$ 1.8-fold higher levels of oligonucleotide to the liver and 2- and 6-fold less oligonucleotide to the kidney and plasma, respectively,

relative to the PEGylated formulation. Interestingly, it was recently discovered that activated liver-derived macrophages (Kupffer cells) in mice do express the FR (67). While it was beyond the scope of this investigation, it is possible that the Kupffer cells in the livers of our KB tumor-bearing mice were responsible for capturing and retaining the oligonucleotide-loaded folate-liposomes. But, further studies are warranted to fully understand the nature of folate-liposome accumulation in the liver.

#### ACKNOWLEDGMENT

We wish to thank Katy Trent for her excellent assistance with our animal study.

#### LITERATURE CITED

- (1) Toulme, J. J., and Helene, C. (1988) Antimessenger oligodeoxyribonucleotides: an alternative to antisense RNA for artificial regulation of gene expression—a review. *Gene* 72, 51–58.
- (2) Tonkinson, J. L., and Stein, C. A. (1996) Antisense oligodeoxynucleotides as clinical therapeutic agents. *Cancer Invest.* 14, 54–65.
- (3) Chiang, M. Y., Chan, H., Zounes, M. A., Freier, S. M., Lima, W. F., and Bennett, C. F. (1991) Antisense oligonucleotides inhibit intercellular adhesion molecule 1 expression by two distinct mechanisms. *J. Biol. Chem.* 266, 18162–18171.
- (4) Dean, N. M., McKay, R., Condon, T. P., and Bennett, C. F. (1994) Inhibition of protein kinase C- $\alpha$  expression in human A549 cells by antisense oligonucleotides inhibits induction of intercellular adhesion molecule 1 (ICAM-1) mRNA by phorbol esters. *J. Biol. Chem.* 269, 16416–16424.
- (5) Skorski, T., Nieborowska-Skorska, M., Nicolaidis, N. C., Szczylik, C., Iversen, P., Iozzo, R. V., Zon, G., and Calabretta, B. (1994) Suppression of Philadelphia1 leukemia cell growth in mice by BCR-ABL antisense oligodeoxynucleotide. *Proc. Natl. Acad. Sci. U.S.A.* 91, 4504–4508.
- (6) Cohen, J. S. (1991) Antisense oligodeoxynucleotides as antiviral agents. *Antiviral Res.* 16, 121–133.
- (7) Crooke, S. T. (1992) Therapeutic applications of oligonucleotides. *Annu. Rev. Pharmacol. Toxicol.* 32, 329–376.
- (8) Stein, C. A., and Cheng, Y. C. (1993) Antisense oligonucleotides as therapeutic agents—is the bullet really magical? *Science* 261, 1004–1012.
- (9) Cossam, P. A., Sasnor, H., Dellinger, D., Truong, L., Cummins, L., Owens, S. R., Markham, P. M., Shea, J. P., and Crooke, S. (1993) Disposition of the  $^{14}\text{C}$ -labeled phospho-

- rothioate oligonucleotide ISIS 2105 after intravenous administration to rats. *J. Pharmacol. Exp. Ther.* 267, 1181–1190.
- (10) Cossum, P. A., Truong, L., Owens, S. R., Markham, P. M., Shea, J. P., and Crooke, S. T. (1994) Pharmacokinetics of a  $^{14}\text{C}$ -labeled phosphorothioate oligonucleotide, ISIS 2105, after intradermal administration to rats. *J. Pharmacol. Exp. Ther.* 269, 89–94.
  - (11) Dewanjee, M. K., Ghafouripour, A. K., Kapadvanjwala, M., Dewanjee, S., Serafini, A. N., Lopez, D. M., and Sfakianakis, G. N. (1994) Noninvasive imaging of c-myc oncogene messenger RNA with indium-111-antisense probes in a mammary tumor-bearing mouse model. *J. Nucl. Med.* 35, 1054–1063.
  - (12) Yakubov, L. A., Deeva, E. A., Zarytova, V. F., Ivanova, E. M., Ryte, A. S., Yurchenko, L. V., and Vlassov, V. V. (1989) Mechanism of oligonucleotide uptake by cells: involvement of specific receptors? *Proc. Natl. Acad. Sci. U.S.A.* 86, 6454–6458.
  - (13) Graham, M. J., Crooke, S. T., Monteith, D. K., Cooper, S. R., Lemonidis, K. M., Stecker, K. K., Martin, M. J., and Crooke, R. M. (1998) In vivo distribution and metabolism of a phosphorothioate oligonucleotide within rat liver after intravenous administration. *J. Pharmacol. Exp. Ther.* 286, 447–458.
  - (14) Wang, H., Nan, L., Yu, D., Agrawal, S., and Zhang, R. (2001) Antisense anti-MDM2 oligonucleotides as a novel therapeutic approach to human breast cancer: in vitro and in vivo activities and mechanisms. *Clin. Cancer Res.* 7, 3613–3624.
  - (15) Crooke, S. T. (2000) Potential roles of antisense technology in cancer chemotherapy. *Oncogene* 19, 6651–6659.
  - (16) Stuart, D. D., and Allen, T. M. (2000) A new liposomal formulation for antisense oligodeoxynucleotides with small size, high incorporation efficiency and good stability. *Biochim. Biophys. Acta* 1463, 219–29.
  - (17) Nakamura, N., Timmermann, S. A., Hart, D. A., Kaneda, Y., Shrive, N. G., Shino, K., Ochi, T., and Frank, C. B. (1998) A comparison of in vivo gene delivery methods for antisense therapy in ligament healing. *Gene Ther.* 5, 1455–1461.
  - (18) Zelphati, O., Zon, G., and Leserman, L. (1993) Inhibition of HIV-1 replication in cultured cells with antisense oligonucleotides encapsulated in immunoliposomes. *Antisense Res. Dev.* 3, 323–338.
  - (19) Pastorino, F., Stuart, D., Ponzoni, M., and Allen, T. M. (2001) Targeted delivery of antisense oligonucleotides in cancer. *J. Controlled Release* 74, 69–75.
  - (20) Allen, T. M. (1994) The use of glycolipids and hydrophilic polymers in avoiding rapid uptake of liposomes by the mononuclear phagocyte system. *Adv. Drug Deliv. Rev.* 13, 285–309.
  - (21) Stuart, D. D., Kao, G. Y., and Allen, T. M. (2000) A novel, long-circulating, and functional liposomal formulation of antisense oligodeoxynucleotides targeted against MDR1. *Cancer Gene Ther.* 7, 466–475.
  - (22) Lopes de Menezes, D. E., Pilarski, L. M., and Allen, T. M. (1998) In vitro and in vivo targeting of immunoliposomal doxorubicin to human B-cell lymphoma. *Cancer Res.* 58, 3320–3330.
  - (23) Lee, R. J., and Low, P. S. (1994) Delivery of Liposomes into Cultured KB Cells via Folate Receptor-mediated Endocytosis. *J. Biol. Chem.* 269, 3198–3204.
  - (24) Pagnan, G., Montaldo, P. G., Pastorino, F., Raffaghello, L., Kirchmeier, M., Allen, T. M., and Ponzoni, M. (1999) GD2-mediated melanoma cell targeting and cytotoxicity of liposome-entrapped fenretinide. *Int. J. Cancer* 81, 268–274.
  - (25) Zalipsky, S., Mullah, N., Harding, J. A., Gittelman, J., Guo, L., and DeFrees, S. A. (1997) Poly(ethylene glycol)-grafted liposomes with oligopeptide or oligosaccharide ligands appended to the termini of the polymer chains. *Bioconjugate Chem.* 8, 111–118.
  - (26) Leamon, C. P., and Low, P. S. (1991) Delivery of Macromolecules into Living Cells: A Method that Exploits Folate Receptor Endocytosis. *Proc. Natl. Acad. Sci., U.S.A.* 88, 5572–5576.
  - (27) Wang, S., Lee, R. J., Mathias, C. J., Green, M. A., and Low, P. S. (1996) Synthesis, purification, and tumor cell uptake of  $^{67}\text{Ga}$ -deferoxamine-folate, a potential radiopharmaceutical for tumor imaging. *Bioconjugate Chem.* 7, 56–62.
  - (28) Mathias, C. J., Wang, S., Lee, R. J., Waters, D. J., Low, P. S., and Green, M. A. (1996) Tumor-selective radiopharmaceutical targeting via receptor-mediated endocytosis of Gallium-67-deferoxamine-folate. *J. Nucl. Med.* 37, 1003–1008.
  - (29) Mathias, C. J., Wang, S., Waters, D. J., Turek, J. J., Low, P. S., and Green, M. A. (1998) Indium-111-DTPA-folate as a potential folate-receptor-targeted radiopharmaceutical. *J. Nucl. Med.* 39, 1579–1585.
  - (30) Ilgan, S., Yang, D. J., Higuchi, T., Zareneyrizi, F., Bayham, H., Yu, D., Kim, E. E., and Podoloff, D. A. (1998)  $^{99\text{m}}\text{Tc}$ -Ethylenedicysteine-folate: A new tumor imaging agent. Synthesis, labeling and evaluation in animals. *Cancer Biother. Radiopharm.* 13, 427–435.
  - (31) Guo, W., Hinkle, G. H., and Lee, R. J. (1999)  $^{99\text{m}}\text{Tc}$ -HYNIC-folate: A novel receptor-based targeted radiopharmaceutical for tumor imaging. *J. Nucl. Med.* 40, 1563–1569.
  - (32) Linder, K. E., Wedeking, P., Ramalingam, K., Nunn, A. D., and Tweedle, M. F. (2000) In vitro & in vivo studies with  $\alpha$ - and  $\gamma$ -isomers of  $^{99\text{m}}\text{Tc}$ -OXA-Folate show uptake of both isomers in folate-receptor (+) KB cell lines. *Soc. Nucl. Med.; Proc. 47th Annu. Meet.* 41, 119P.
  - (33) Konda, S. D., Aref, M., Brechbiel, M., and Wiener, E. C. (2000) Development of a tumor-targeting MR contrast agent using the high-affinity folate receptor. *Investigative Radiology* 35, 50–57.
  - (34) Ladino, C. A., Chari, R. V. J., Bourret, L. A., Kedersha, N. L., and Goldmacher, V. S. (1997) Folate-maytansinoids: Target-selective drugs of low molecular weight. *Int. J. Cancer* 73, 859–864.
  - (35) Citro, G., Szczylik, C., Ginobbi, P., Zupi, G., and Calabretta, B. (1994) Inhibition of leukaemia cell proliferation by folic acid-polylysine-mediated introduction of c-myc antisense oligodeoxynucleotides into HL-60 cells. *Br. J. Cancer* 69, 463–467.
  - (36) Wang, S., Lee, R. J., Cauchon, G., Gorenstein, D. G., and Low, P. S. (1995) Delivery of antisense oligodeoxyribonucleotides against the human epidermal growth factor receptor into cultured KB cells with liposomes conjugated to folate via poly(ethylene glycol). *Proc. Natl. Acad. Sci., U.S.A.* 92, 3318–3322.
  - (37) Li, S., and Huang, L. (1997) Targeted delivery of antisense oligodeoxynucleotides by LPDII. *J. Liposome Res.* 7, 63–75.
  - (38) Li, S., and Huang, L. (1998) Targeted delivery of antisense oligodeoxynucleotides formulated in a novel lipidic vector. *J. Liposome Res.* 8, 239–250.
  - (39) Li, S., Deshmukh, H. M., and Huang, L. (1998) Folate-mediated targeting of antisense oligonucleotides to ovarian cancer cells. *Pharm. Res.* 15, 1540–1545.
  - (40) Leopold, L. H., Shore, S. K., Newkirk, T. A., Reddy, R. M., and Reddy, E. P. (1995) Multi-unit ribozyme-mediated cleavage of bcr-abl mRNA in myeloid leukemias. *Blood* 85, 2162–2170.
  - (41) Ward, C. M., Acheson, N., and Seymour, L. M. (2000) Folic acid targeting of protein conjugates into ascites tumor cells from ovarian cancer patients. *J. Drug Targeting* 8, 119–123.
  - (42) Lu, J. Y., Lowe, D. A., Kennedy, M. D., and Low, P. S. (1999) Folate-targeted enzyme prodrug cancer therapy utilizing penicillin-V amidase and a doxorubicin prodrug. *J. Drug Targeting* 7, 43–53.
  - (43) Leamon, C. P., and Low, P. S. (1992) Cytotoxicity of Momordin-Folate Conjugates in Cultured Human Cells. *J. Biol. Chem.* 267, 24966–24971.
  - (44) Leamon, C. P., Pastan, I., and Low, P. S. (1993) Cytotoxicity of Folate-Pseudomonas Exotoxin Conjugates Toward Tumor Cells. *J. Biol. Chem.* 268, 24847–24854.
  - (45) Leamon, C. P., and Low, P. S. (1994) Selective Targeting of Malignant Cells with Cytotoxin-Folate Conjugates. *J. Drug Targeting* 2, 101–112.
  - (46) Kranz, D. M., Patrick, T. A., Brigle, K. E., Spinella, M. J., and Roy, E. J. (1995) Conjugates of folate and anti-T-cell-receptor antibodies specifically target folate-receptor-positive tumor cells for lysis. *Proc. Natl. Acad. Sci., U.S.A.* 92, 9057–9061.

- (47) Cho, B. K., Roy, E. J., Patrick, T. A., and Kranz, D. M. (1997) Single-chain Fv/folate conjugates mediate efficient lysis of folate-receptor-positive tumor cells. *Bioconjugate Chem.* **8**, 338–346.
- (48) Kranz, D. M., Manning, T. C., Rund, L. A., Cho, B. K., Gruber, M. M., and Roy, E. J. (1998) Targeting tumor cells with bispecific antibodies and T cells. *J. Controlled Release* **53**, 77–84.
- (49) Rund, L. A., Cho, B. K., Manning, T. C., Holler, P. D., Roy, E. J., and Kranz, D. M. (1999) Bispecific agents target endogenous murine T cells against human tumor xenografts. *Int. J. Cancer* **83**, 141–149.
- (50) Lee, R. J., and Low, P. S. (1995) Folate-mediated tumor cell targeting of liposome-entrapped doxorubicin in vitro. *Biochim. Biophys. Acta* **1233**, 134–144.
- (51) Vogel, K., Wang, S., Lee, R. J., Chmielewski, J., and Low, P. S. (1996) Peptide-mediated release of folate-targeted liposome contents from endosomal compartments. *J. Am. Chem. Soc.* **118**, 1581–1586.
- (52) Rui, Y., Wang, S., Low, P. S., and Thompson, D. H. (1998) Dipalmitoylcholine-folate liposomes: An efficient vehicle for intracellular drug delivery. *J. Am. Chem. Soc.* **120**, 11213–11218.
- (53) Gabizon, A., Horowitz, A. T., Goren, D., Tzemach, D., Mandelbaum-Shavit, F., Qazen, M. M., and Zalipsky, S. (1999) Targeting folate receptor with folate linked to extremities of poly(ethylene glycol)-grafted liposomes: in vitro studies. *Bioconjugate Chem.* **10**, 289–298.
- (54) Gottschalk, S., Cristiano, R. J., Smith, L. C., and Woo, S. L. C. (1994) Folate receptor mediated DNA delivery into tumor cells: lysosomal disruption results in enhanced gene expression. *Gene Ther.* **1**, 185–191.
- (55) Mislick, K. A., Baldeschwieler, J. D., Kayyem, J. F., and Meade, T. J. (1995) Transfection of folate-polylysine DNA complexes: Evidence for lysosomal delivery. *Bioconjugate Chem.* **6**, 512–515.
- (56) Douglas, J. T., Rogers, B. E., Rosenfeld, M. E., Michael, S. I., Feng, M., and Curiel, D. T. (1996) Targeted gene delivery by tropism-modified adenoviral vectors. *Nature Biotech.* **14**, 1574–1578.
- (57) Leamon, C. P., Weigl, D., and Hendren, R. W. (1999) Folate copolymer-mediated transfection of cultured cells. *Bioconjugate Chem.* **10**, 947–957.
- (58) Guo, W., and Lee, R. J. (1999) Receptor-targeted gene delivery via folate-conjugated polyethylenimine. *PharmSci* **1**, article 19.
- (59) Reddy, J. A., Dean, D., Kennedy, M. D., and Low, P. S. (1999) Optimization of folate-conjugated liposomal vectors for folate receptor-mediated gene therapy. *J. Pharm. Sci.* **88**, 1112–1118.
- (60) Reddy, J. A., and Low, P. S. (2000) Enhanced folate receptor mediated gene therapy using a novel pH-sensitive lipid formulation. *J. Controlled Release* **64**, 27–37.
- (61) Godwin, H. A., Rosenberg, I. H., Ferenz, C. R., Jacobs, P. M., and Meienhofer, J. (1972) The synthesis of biologically active pteroyl oligo-L-glutamates (folic acid conjugates): evaluation of [3H]pteroyl heptaglutamate for metabolic studies. *J. Biol. Chem.* **247**, 2296–2271.
- (62) Leamon, C. P., DePrince, R. B., and Hendren, R. W. (1999) Folate-mediated drug delivery: Effect of alternative conjugation chemistry. *J. Drug Targeting* **7**, 157–169.
- (63) Riddles, P. W., Blakeley, R. L., and Zerner, B. (1979) Ellman's reagent: 5,5'-dithiobis(2-nitrobenzoic acid)- a reexamination. *Anal. Biochem.* **94**, 75–81.
- (64) Leamon, C. P., and Low, P. S. (1993) Membrane Folate-binding Proteins are Responsible for Folate- protein Conjugate Endocytosis into Cultured Cells. *Biochem. J.* **291**, 855–860.
- (65) Galivan, J., Ryan, T. J., Chave, K., Rhee, M., Yao, R., and Yin, D. (2000) Glutamyl hydrolase: pharmacological role and enzymatic characterization. *Pharmacol. Ther.* **85**, 207–215.
- (66) Knoll, D., and Hermans, J. (1983) Polymer-protein interactions. Comparison of experiment and excluded volume theory. *J. Biol. Chem.* **258**, 5710–5715.
- (67) Turk, M. J., Breur, G. J., Widmer, W. R., Paulos, C. M., Xu, L. C., Grote, L. A., and Low, P. S. (2002) Folate-targeted imaging of activated macrophages in rats with adjuvant-induced arthritis. *Arthr. Rheum.* **46**, 1947–1955.

BC020089T



# Enzymatic Modification of Self-Assembled Peptide Structures with Tissue Transglutaminase

Joel H. Collier and Phillip B. Messersmith\*

Northwestern University, Department of Biomedical Engineering, 2145 Sheridan Road, Room E310, Evanston, Illinois 60208 Received February 11, 2003; Revised Manuscript Received May 15, 2003

A de novo peptide that self-assembles into fibrillar structures and serves as a substrate for the cross-linking enzyme tissue transglutaminase was developed (Ac-QQKFQFQFEQQ-Am). Congo red staining, circular dichroism, and FTIR spectroscopy showed that this 11-amino acid peptide produced predominantly  $\beta$ -sheet structures. TEM with negative staining and quick-freeze deep etch (QFDE) TEM showed that the peptide structures were composed of a highly entangled fibrillar network. These  $\beta$ -sheet fibrillar nanostructures were then covalently coupled to pendant amine-containing biomolecules via tissue transglutaminase. MALDI-TOF mass spectrometry and HPLC were utilized to monitor the extent of the transglutaminase modification of the peptide, showing that as many as five glutamines in the peptide were reactive via transglutaminase for covalent conjugation. This strategy, based on the post-assembly modification of a self-assembling peptide, has potential applications for tailoring supramolecular structures for drug delivery, tissue engineering, or other biomedical applications.

## INTRODUCTION

Self-assembling systems based on peptides, lipids, or hybrid peptide–amphiphiles are currently being investigated as potential materials for biomedical applications such as controlled drug release matrixes and tissue engineering scaffolds (1–7). In these approaches, small molecules are designed such that they self-assemble into complex nanostructures, in many cases fibrillar networks or hydrogels. The assembly of these materials is highly dependent on solution conditions such as pH, temperature, solvent polarity, and the presence of salts. Because of this sensitivity to solution conditions, self-assembly can often be induced with small, physiologically benign perturbations of pH, salt content, or temperature, making these materials attractive candidates for new in situ gelling biomaterials (7, 8). Peptides are particularly attractive self-assembling molecules for such applications because they are easily synthesized, either by solid-phase chemical synthesis or by recombinant DNA technology, and self-assembly motifs can be based upon simple secondary structure elements such as  $\alpha$ -helices (9) and  $\beta$ -sheets (2, 4, 7, 10, 11).

Previous work in our laboratory and others has focused upon peptides with alternating hydrophilic/hydrophobic primary structures that self-assemble into  $\beta$ -sheet fibrillar structures (7, 10–13). At peptide concentrations in the 10–30 mM range, these fibrillar structures are sufficiently entangled to form gellike materials (3, 7, 11). These materials have recently been investigated as scaffolds for tissue engineering applications, and it has been found that they perform well as three-dimensional culture substrates for nerve cells (2) and chondrocytes (3). The propensity of these peptides to form  $\beta$ -sheet structures is conferred by their alternating primary structure, which positions all hydrophobic residues on one side of the  $\beta$ -sheet and all the hydrophilic residues on the other (15–18). Subsequent assembly into fibrillar

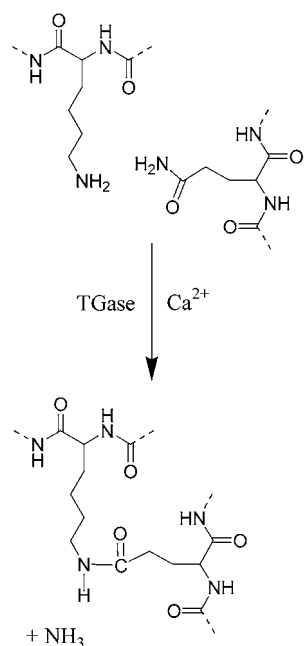
structures then proceeds, in part by association of the hydrophobic faces of the  $\beta$ -sheets under solution conditions that effectively shield the electrostatic repulsive forces that arise from charged side-chains (19). That is, in aqueous salt solutions, self-assembly rapidly progresses, whereas self-assembly is retarded or absent in pure aqueous solutions (12). This salt-sensitivity has been utilized to develop materials that rapidly gel in response to certain triggers, such as body temperature or near-infrared light exposure (7).

Tailoring these assemblies by covalently attaching pendant biomolecules would be useful in several scenarios, including covalently attaching drugs or growth factors for controlled release (20–22) or for attaching peptides for ligand-specific interactions with cells (23–25). Recently, factor XIII, a transglutaminase enzyme, has been utilized by Hubbell and co-workers to covalently link cell-attachment peptides or heparin-binding peptides to self-assembled fibrin matrixes (26–28). Transglutaminases (TGases) catalyze the formation of isopeptide bonds between glutamine and lysine residues of proteins and polypeptides (Figure 1, for review see ref 29) and are attractive for covalent modification of self-assembled scaffolds because they operate under benign reaction conditions, have a high specificity, and can be triggered from an inactive to active form by the introduction of  $\text{Ca}^{2+}$  ions. In the work presented here, we developed a de novo self-assembling peptide as a scaffold for the subsequent attachment of other amine-containing biomolecules via tissue transglutaminase (tTGase) (Figure 2).

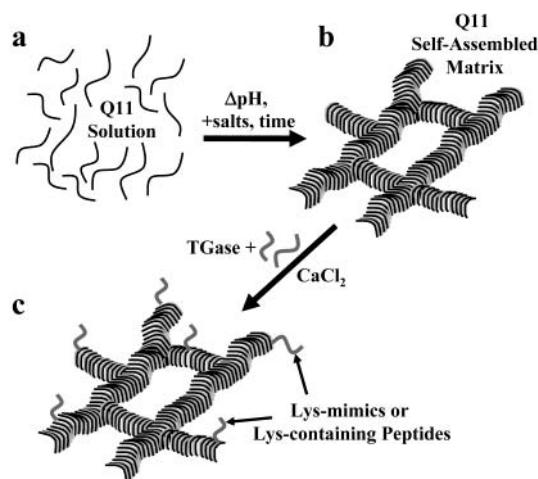
## EXPERIMENTAL PROCEDURES

**Chemicals.** Except as noted below, all chemicals and reagents were purchased from Aldrich or Fisher and used as provided. Protected amino acids were purchased from Peptides International. Rink amide-AM resin and benzotriazol-1-yloxytripyrrolidinophosphonium hexafluorophosphate (PyBOP) were purchased from Nova Biochem. *N*-Methylpyrrolidone (NMP), *O*-benzotriazole-*N,N,N,N*-tetramethyluronium hexafluorophosphate (HBTU), 1-

\* Corresponding author. Phone: 847-467-5273. Fax: 847-491-4928. E-mail: philm@northwestern.edu.



**Figure 1.** Transglutaminase-mediated coupling between lysine and glutamine residues.



**Figure 2.** Schematic of Q11 self-assembly and subsequent modification by Tase. A Q11 solution (a) is induced to self-assemble, either by the addition of salts, a pH change, or the passage of time. The resultant self-assembled matrix (b) then serves as a tase substrate for the immobilization of appropriate lysine-containing biomolecules (c).

hydroxybenzotriazole (HOBt), *N,N*-diisopropylethylamine (DIEA), and piperidine were purchased from Applied Biosystems. All water was purified with a Barnstead-Thermolyne Nanopure Infinity water purifier to a resistivity of 18.1 M $\Omega$ -cm or greater.

**Peptide Synthesis.** Peptides Ac-QQKFQFQFEQQ-Am (Q11) and n-dansyl-GLKGGRGDS-Am (RGD1) were synthesized on a 0.25 mmol scale with standard fluorenylmethoxycarbonyl solid-phase techniques using an Applied Biosystems 433A automated peptide synthesizer. Rink amide resin (0.6 mmol/g substitution, 200–400 mesh) was used to produce C-terminal amides, activation was performed with 0.45M HOBt/HBTU in DMF (Fast-Moc kit, Applied Biosystems cat#401132), and coupling reactions were monitored with ninhydrin. RGD1 was dansylated by the incorporation of dansyl-Gly-OH at the N-terminus. Q11 was acetylated on-resin using 10 equiv of acetic acid, 10 equiv of HOBt, 10 equiv of PyBOP, and 20 equiv of DIEA in 5 mL NMP for 1 h. After being rinsed

with NMP, dichloromethane (DCM), and 2-propanol, peptides were then cleaved from the resin and deprotected with 40 mL of 95% trifluoroacetic acid (TFA), 2.5% triisopropylsilane, and 2.5% water. After rotary evaporation of the cleavage cocktail to 3 mL, the peptides were precipitated and washed several times with cold ethyl ether. The cleaved peptides were then collected by centrifugation, dried overnight in vacuo, redissolved in water, lyophilized, and stored at  $-20^{\circ}\text{C}$ . The water solubility of lyophilized Q11 increased significantly after a second dissolution in TFA, precipitation from cold ether, resuspension in water, and re-lyophilization. It was presumed that this second dissolution in TFA enhanced Q11's water solubility by disaggregating any  $\beta$ -sheet aggregates (30). Identity of the peptides was confirmed with MALDI-TOF and ESI mass spectrometry. Q11  $[\text{M} + \text{H}]^{+}$  predicted  $m/z$ : 1527.69, observed: 1527.59. RGD1  $[\text{M} + \text{H}]^{+}$  predicted  $m/z$ : 1079.23, observed: 1079.20. Purity of peptides was estimated to be greater than 90% by HPLC (C4 reverse-phase column).

**Self-Assembly and Secondary Structure Evaluation.** To determine the solution conditions in which Q11 formed supramolecular aggregates, aqueous solutions of 2–30 mM Q11 were prepared. These solutions were then pipetted into either Dulbecco's phosphate-buffered saline (PBS), aqueous NaCl (1–100 mM), or aqueous  $\text{CaCl}_2$  (1–100 mM). Each solution contained 10  $\mu\text{M}$  Congo red, a dye that specifically binds  $\beta$ -sheet fibrillar aggregates (31). Alternatively, aqueous Q11 (2–30 mM) was pipetted onto the bottoms of multiwell dishes, allowed to dry, and then rehydrated with various solutions and buffers containing 10  $\mu\text{M}$  Congo red. Congo red staining was then observed with brightfield microscopy and under cross-polarizers.

Circular dichroism (CD) and FTIR spectroscopy were utilized to evaluate the secondary structure characteristics of Q11. For CD, peptides were dissolved in water, and concentrations were verified spectrophotometrically by measuring the absorption of the phenylalanine residues at 260 nm ( $\epsilon_{260}(\text{Phe}) = 187 \text{ M}^{-1} \text{ cm}^{-1}$ ). pH was not adjusted for the CD concentration studies, and the pH was slightly acidic (pH 4.7), most likely from residual TFA. A stock solution of 1 mM Q11 was diluted to concentrations between 20  $\mu\text{M}$  and 100  $\mu\text{M}$ , and CD measurements were made within 20 min of dilution. Measurements were made on a JASCO J-715 from 190 to 280 nm with a 1 nm step resolution, a scan speed of 100 nm/min, 10 accumulations, a 10s response time, a 1 nm bandwidth, and data smoothing (3rd order, 7 point smoothing). Quartz cuvettes with a 10 mm path length were used. To study the effects of NaCl on the assembly of Q11 in dilute aqueous solutions, a stock solution of 1mM Q11 and a stock solution of 1mM NaCl were prepared. These were mixed and diluted with water to achieve a peptide concentration of 30  $\mu\text{M}$  Q11 and 0–100 mM NaCl. CD measurements were then taken exactly 10 min after mixing.

FTIR spectroscopy was performed for concentrated Q11 (26 mM in 1:1  $\text{D}_2\text{O}:\text{H}_2\text{O}$ ) with a Biorad FTS-60 using a liquid cell with  $\text{BaF}_2$  windows and 10  $\mu\text{m}$  spacers. Q11 was water-soluble, but sparingly soluble in  $\text{D}_2\text{O}$ , so some precipitation was observed during analysis. Scans were performed between 1550 and 1750  $\text{cm}^{-1}$  to monitor the amide I vibration. Sixteen scans were summed. For second-derivative calculations, the Savitsky–Golay method was used (2nd degree, 40–50 points).

**Negative-Stained TEM and Quick-Freeze Deep-Etch (QFDE) TEM.** To evaluate the self-assembled morphology of Q11, two electron microscopic techniques

were utilized. For negative staining, fibrils were allowed to form from concentrated aqueous Q11 solutions (40 mg/mL in water for 3 days under a layer of PBS). The PBS was then removed, and the formed fibrils were diluted 1:100 in H<sub>2</sub>O, vortexed vigorously to disrupt the gellike self-assembled structure into small fragments, immediately applied to O<sub>2</sub> plasma-treated lacey carbon TEM grids, and stained with 1% uranyl acetate. Grids were then imaged directly on a JEOL JEM 1200-EX.

For QFDE TEM, Q11 was dissolved in water (40 mg/mL) and allowed to self-assemble for 3 days. The Q11 self-assembled structures were then rapidly frozen by slamming them against a copper block at -195 °C (Gentleman Jim device, Ted Pella, Inc., Irvine, CA). Fracture and deep etching were performed on a Cressington CFE 40. Fracture was performed at -186 °C, etching at -95 °C for 25 min, and replication at -125 °C with a ~2 nm layer of PtC at a 20° angle followed by a strengthening coat of C at a 90° angle. TEM was performed on the replicas with a JEOL 120 CX.

**Enzymatic Cross-Linking and Analysis.** For enzymatic cross-linking studies, tTGase from guinea pig liver was used (Sigma T-5398). The substrate properties of Q11 in both early and mature states of self-assembly were investigated. tTGase was aliquotted at 1.2–3 units/mL in buffer containing 1.33 mM ethylenediaminetetraacetic acid (EDTA), 20 mM dithiothreitol, and 50 mM Tris (pH 7.4 at 37 °C). Aliquotting was performed on ice, and aliquots were stored at -80 °C until use. To evaluate the amine acceptor properties of Q11, the lysine-mimic monodansylcadaverine (MDC) was used. MDC is a convenient model molecule for TGase studies, as its side-chain mimics that of lysine, and it has been utilized extensively in investigations of TGases and their substrates (32–35).

To investigate the tTGase reactivity of freshly solubilized Q11 in an early aggregation state (dilute Q11 solutions in water), aqueous solutions were prepared containing Q11 and MDC and immediately reacted with tTGase before any observable self-assembly had occurred. In a typical experiment, to a Q11 solution was added TGase, CaCl<sub>2</sub>, and MDC (final concentrations: 0.1–1.5 mM Q11, 0.1–2 mM MDC, 1.67–2.0 mM CaCl<sub>2</sub>, 0.4–1.0 U/mL TGase, and 50 mM Tris, pH 7.4–8). Control reactions lacked tTGase. These mixtures were then allowed to react for time periods from 2 min to several hours at either room temperature or at 37 °C. The reactions were quenched by the addition of TFA.

To study the tTGase reactivity of self-assembled Q11, Q11 was first self-assembled under the influence of dissolved ions and subsequently reacted via tTGase. In a typical experiment, Q11 was first dissolved in water at a concentration of 40 mg/mL (26 mM). Fifty microliters of PBS was then layered over 10  $\mu$ L of this Q11 solution to induce gelation. After 24 h of incubation at room temperature, the PBS layer was removed from the now gellike Q11 layer, and the self-assembled Q11 was reacted by adding tTGase, CaCl<sub>2</sub>, and MDC (final concentrations: 1.35 U/mL tTGase, 2.8 mM CaCl<sub>2</sub>, 1.35 mM MDC, 2.6 mM Q11, in self-assembled form, 45 mM Tris, pH 7.4 @ 37 °C). The mixture was vortexed vigorously to distribute the reactants among the self-assembled Q11 fibrils, and the reaction proceeded for 1 h at 37 °C. The Q11 fibrils were then collected by centrifugation. The reactions were quenched, and Q11 was disaggregated by the 10:1 dilution of the reacted fibrils in TFA. TFA addition solubilized and disassembled the Q11 fibrils, producing nonviscous fluids. It is known that TFA is an excellent solvent for disaggregating these and similar

$\beta$ -sheet fibril-forming peptides (30), and disaggregated Q11 produced single peaks in reverse phase-HPLC. To investigate the suitability of peptide substrates for tTGase-mediated cross-linking to Q11, the peptide RGD1 was reacted with unassembled and self-assembled Q11 in the same manner as with MDC described above.

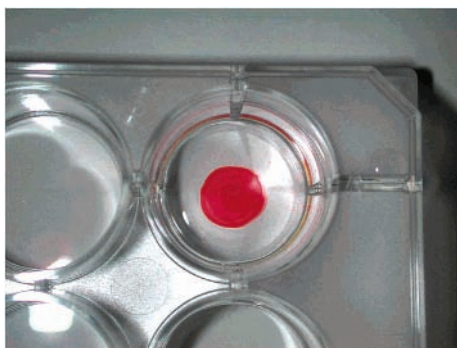
**Reverse-Phase HPLC.** To quantify the amount of MDC incorporation, a known quantity of an internal standard, dansyl- $\epsilon$ -aminocaproic acid, was dissolved in TFA and added to the TFA solutions containing disaggregated Q11 and its reaction products (dansyl- $\epsilon$ -aminocaproic acid standard curve  $R^2 = 0.987$ ). These solutions were then analyzed on a Waters HPLC system equipped with a photodiode array detector and a Vydak analytical C4 reverse-phase column, in a 10%–63% acetonitrile gradient over 30 min. The amount of dansylated product was then calculated by comparing the areas of dansylated Q11 reaction product peaks with those of the dansyl- $\epsilon$ -aminocaproic acid internal standard peak at 280 nm. Absorbance of the dansyl groups at 280 nm was utilized for the peak measurements, as no other species present in the reaction mixtures absorbed at this wavelength. It was not possible to perform LC/MS experiments on these samples, as the TFA necessary to disaggregate the peptide gels confounds LC/MS analysis, but the HPLC chromatograms were compared with MALDI mass spectrometry data. The number of product peaks shown by HPLC corresponded to those observed with mass spectrometry, and it was assumed that the sequence of product peaks observed in HPLC corresponded to sequential additions of MDC (which are expected to be sequentially more hydrophobic with each MDC addition). Calculations of product concentrations then took into account the fact that Q11–MDC<sub>x</sub> adducts had  $x$  times the dansyl fluorescence of singly labeled peptides.

**Mass Spectrometry.** To identify the tTGase-mediated cross-linking products of Q11, MALDI-TOF mass spectrometry was utilized (PE Biosystems Voyager DE-PRO System 6050). Quenched enzyme reactions were mixed 1:1 with a solution of saturated  $\alpha$ -cyano-4-hydroxycinnamic acid (CHCA) in 1:1 acetonitrile:H<sub>2</sub>O with 0.1% TFA. These mixtures were then spotted onto a 100-well MALDI plate and dried in ambient conditions. Peptides and peptide conjugates were analyzed both in positive and negative reflector mode with delayed extraction, typically with an accelerating voltage of 25 kV, a grid voltage of 75%, a mirror voltage ratio of 1.12, a guide wire voltage of 0.05%, and a delay time of 360 ns. Scans were averaged over 100 laser shots, and spectra were baseline-corrected and noise-filtered.

## RESULTS

**Q11 Self-Assembles in Aqueous Solutions.** Q11 was observed to have a high solubility in water, up to 50 mg/mL. Interestingly, it was observed that this solubility sometimes decreased upon extended storage as a lyophilized powder at -20 °C, but that maximal water solubility of the peptide could be restored by dissolving Q11 in TFA, precipitating in Et<sub>2</sub>O, and re-lyophilizing. It is suspected that this TFA treatment disaggregates  $\beta$ -sheet structures that render the peptide insoluble (30). From its water-soluble state, Q11 self-assembled into gellike materials in a variety of aqueous solutions. For example, Q11 rapidly formed Congo-red stainable structures in 1–100 mM NaCl, 1–100 mM CaCl<sub>2</sub>, and PBS (Figure 3). Also, when Q11 was incubated in concentrations from 10 to 30 mM in pure water at room temperature for time



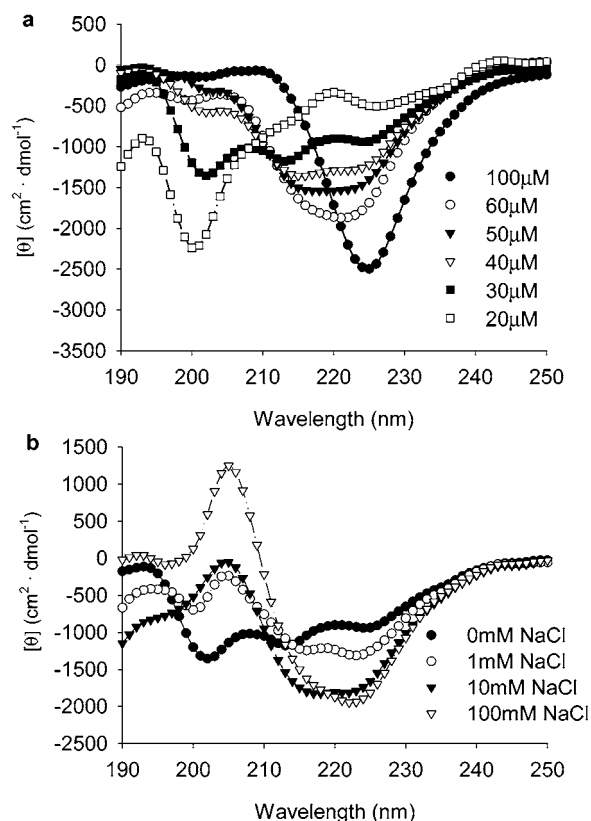


**Figure 3.** Congo red-stained Q11 in a 12-well polystyrene culture dish. An aqueous solution of 40 mg/mL Q11 was pipetted onto the bottom of the dish, dried in a fume hood, and then rehydrated with Dulbecco's PBS containing 30  $\mu$ M Congo red. The staining solution was removed after 3 days and replaced with fresh PBS.

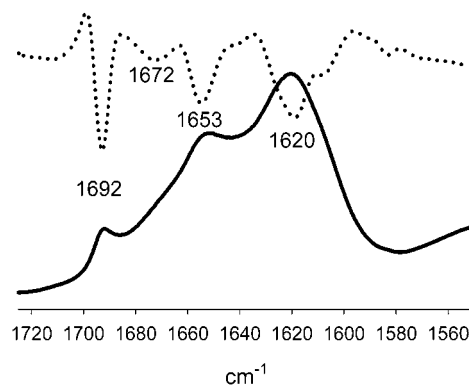
periods on the order of a few days, gellike materials were produced. This indicates that Q11 also self-assembles in pure water, albeit more slowly than in salt-containing solutions. Under cross-polarizers, Congo red-stained peptide aggregates possessed the characteristic apple-green birefringence that is a hallmark of Congo red-stained  $\beta$ -sheet fibrils (31).

**Q11 Forms a Predominantly  $\beta$ -Sheet Secondary Structure.** Using CD and FTIR spectroscopy, the secondary structure of Q11 was evaluated. CD spectra of very dilute solutions of Q11 (20–30  $\mu$ M) resembled those expected for unordered peptide conformations (36, 37). However, increasing the concentration of Q11 induced a conformational change to a structure that resembles an aggregated  $\beta$ -sheet (Figure 4a). The developing negative peak near 220 nm is a hallmark of  $\beta$ -sheet conformation (37). The addition of NaCl to dilute Q11 solutions (30  $\mu$ M) also induced a conformational change from a random coil to a conformation resembling an aggregated  $\beta$ -sheet (Figure 4b). This behavior of  $\beta$ -sheet formation in a salt- and concentration-dependent manner is consistent with other similar short  $\beta$ -sheet forming peptides (7, 10, 12, 19). FTIR spectra further supported that Q11 forms  $\beta$ -sheet secondary structures above the 0.1mM regime and in the presence of salts. For concentrated Q11 solutions (40 mg/mL in 1:1 D<sub>2</sub>O:H<sub>2</sub>O), major absorbances were seen at 1620  $\text{cm}^{-1}$  and 1692  $\text{cm}^{-1}$  (antiparallel  $\beta$ -sheet), and minor absorbances were seen at 1653  $\text{cm}^{-1}$  (helix) and 1672 (residual TFA) (Figure 5) (38). For Q11 in salt-containing solutions (40 mg/mL Q11 in 50 mM CaCl<sub>2</sub>, 1:1 D<sub>2</sub>O:H<sub>2</sub>O), major absorbances were seen at 1619  $\text{cm}^{-1}$  and 1692  $\text{cm}^{-1}$  (antiparallel  $\beta$ -sheet), and minor absorbances were seen at 1654  $\text{cm}^{-1}$  (helix) and 1672  $\text{cm}^{-1}$  (residual TFA) (data not shown). This indicates that while there is a small amount of helical structure,  $\beta$ -sheet structure predominates in concentrated Q11 solutions, both in the presence of salts and in pure aqueous solutions. Furthermore, these IR absorbances are similar to other previously studied  $\beta$ -sheet fibril-forming peptides (7).

**Electron Microscopy of Self-Assembled Nanostructures.** Quick-freeze deep etch (QFDE) TEM indicated that the self-assembly product of Q11 is a loosely entangled network of fibrils (Figure 6a). In QFDE images, fibril widths were on average about 20 nm, and the distance between entanglement points appeared to be about 100 nm. Uranyl acetate staining of fibrils that had been dried onto TEM grids showed that the structure of self-assembled Q11 appears to be a network of individual fibrils with widths of 4–8 nm (Figure 6b). Lateral

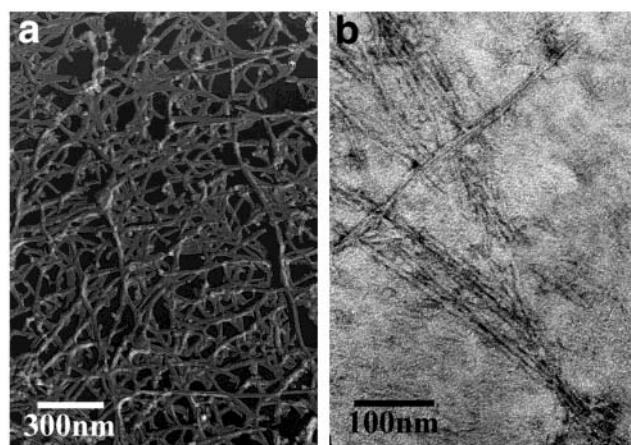


**Figure 4.** Circular Dichroism of Q11 in dilute solutions. Q11 in a range of concentrations in water (a) showed a conformational switch from an unordered conformation at low concentrations (20–30  $\mu$ M) to increasing amounts of  $\beta$ -sheet content above concentrations of 40  $\mu$ M. A similar transition can be induced in 30  $\mu$ M Q11 by the addition of salts, such as NaCl (b).



**Figure 5.** FTIR spectrum (solid) and second-derivative (dotted) for Q11, 40 mg/mL in 1:1 H<sub>2</sub>O:D<sub>2</sub>O. Major peaks at 1620  $\text{cm}^{-1}$  and 1692  $\text{cm}^{-1}$  indicate that Q11 is predominantly in a  $\beta$ -sheet structure, and the smaller peak at 1653  $\text{cm}^{-1}$  indicates that some helical structure is also present. The small absorbance at 1672  $\text{cm}^{-1}$  is a result of trace amounts of TFA.

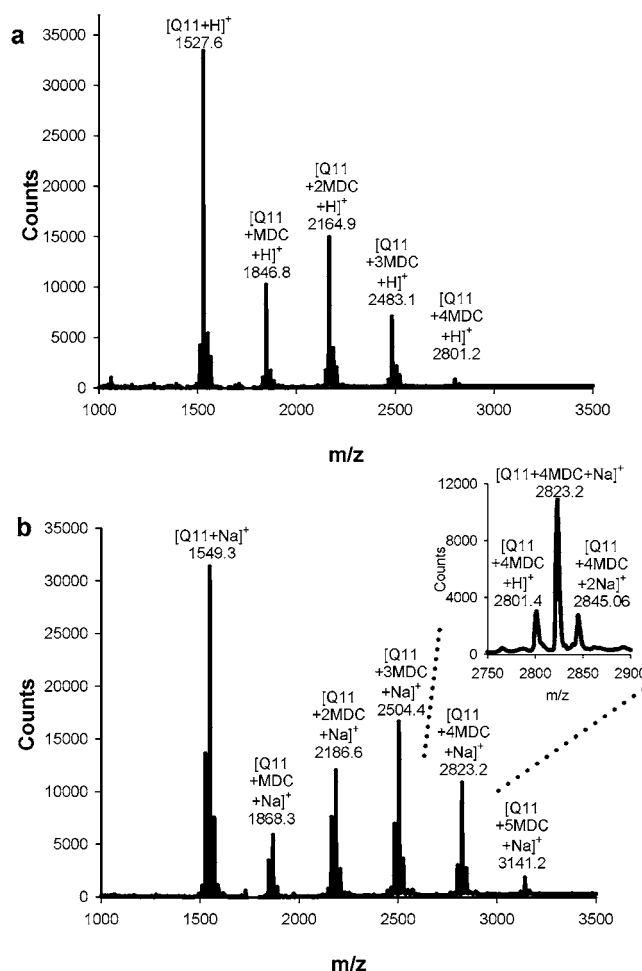
association of these fibrils was also observed, in some cases forming cables with overall widths of 15–30 nm. This self-assembled morphology is similar to that of several other well-known  $\beta$ -sheet fibril-forming peptides and proteins. For example, amyloids formed from a wide variety of natural peptides form fibrils of remarkably similar structure (39). Also, the alternating hydrophobic–hydrophilic peptides studied by Zhang and co-workers form similar 10–20 nm wide fibrils in loosely entangled networks (2, 12). Furthermore, other alternating peptides have been observed to first self-assemble into ~8 nm wide fibrils and subsequently aggregate into thicker bands of parallel fibrils (40).



**Figure 6.** QFDE (a) and negative stained (b) TEM images. QFDE showed that Q11 self-assembles into a highly entangled network of fibrils, with  $\sim 20$  nm diameter fibrils and  $\sim 100$  nm between entanglement points. Negative staining revealed smaller fibrils, about 8 nm in diameter, in entangled networks.

**MALDI-TOF Mass Spectrometry.** MALDI-TOF mass spectrometry was utilized to investigate the tTGase substrate properties of Q11 because other analysis techniques (such as gel electrophoresis) were hindered by the tendency of Q11 to aggregate in buffers, even in the presence of high concentrations of denaturing agents such as SDS, urea, or guanidinium chloride. In contrast, MALDI-TOF mass spectrometry accurately identified peptides and cross-linked species. Furthermore, because mass spectrometry has a much finer resolution ( $<1$  Da) than electrophoresis, the  $\text{NH}_3$  evolution that is a property of TGase cross-linking (Figure 1) was utilized as verification that the products observed were in fact tTGase-mediated cross-linking products rather than noncovalent aggregates. The substrate properties of Q11 were first evaluated with monodansylcadaverine (MDC), a lysine mimic that has been extensively utilized for the investigation of TGases and their substrates (32–35). With its lysine-mimicking side chain and dansyl fluorophore, MDC is a convenient label for identifying tTGase-mediated reaction products with mass spectrometry and UV spectrophotometry. After reaction of Q11 with tTGase in dilute solutions (below the concentration required to produce macroscopic gels), mass spectra showed the emergence of product peaks with  $m/z$  values corresponding to Q11–MDC adducts with up to four attached MDC molecules (Figure 7a). Strong positive  $m/z$  peaks were observed for unreacted Q11,  $[\text{Q11} + \text{H}]^+$  calcd: 1527.69, observed: 1527.59 and the Q11–MDC adducts (subtracting the mass of one  $\text{NH}_3$  per couple)  $[\text{Q11} + \text{MDC} + \text{H}]^+$  calcd: 1846.08, observed: 1846.77;  $[\text{Q11} + 2\text{MDC} + \text{H}]^+$  calcd: 2164.48, observed: 2164.91;  $[\text{Q11} + 3\text{MDC} + \text{H}]^+$  calcd: 2482.87, observed: 2483.11; and  $[\text{Q11} + 4\text{MDC} + \text{H}]^+$  calcd: 2801.27 observed: 2801.23. Control experiments (without tTGase) showed no evolution of any product peaks.

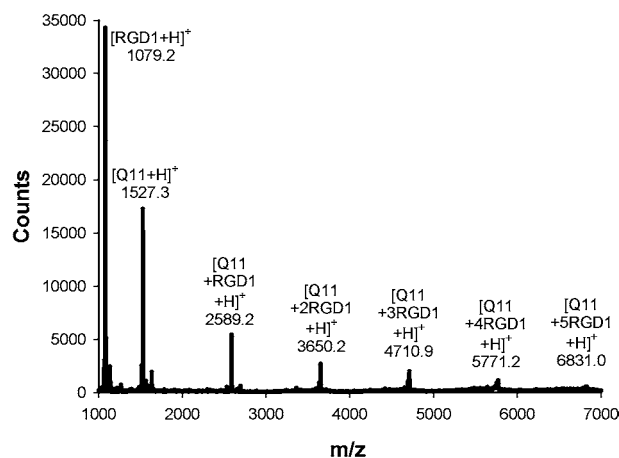
For Q11 that had self-assembled into a gellike material under the influence of salt ions, mass spectrometry showed that up to five glutamines were active, as there existed Q11 peptides with as many as five conjugated MDC molecules after 1 h of reaction (Figure 7b). In these mass spectra, most species were observed to be associated with one and sometimes two  $\text{Na}^+$  ions (22.99 Da), a result of using PBS to self-assemble the Q11 before tTGase reaction (Figure 7b, inset). Strong positive  $m/z$  peaks were observed for unreacted Q11,  $[\text{Q11} + \text{Na}]^+$  calcd: 1549.67, observed: 1549.27 and the Q11–MDC adducts



**Figure 7.** MALDI-TOF MS spectra of tTGase-mediated cross-linking reactions. (a) Soluble Q11 and MDC (reaction conditions: 1 U/mL tTGase, 2 mM  $\text{CaCl}_2$ , 1 mM MDC, 1 mM Q11 (unassembled, freshly dissolved), in 33.3 mM Tris, pH 7.4, for 1 h at  $37^\circ\text{C}$ ). (b) Self-assembled Q11 and MDC (reaction conditions: 1.35 U/mL tTGase, 2.81 mM  $\text{CaCl}_2$ , 1.35 mM MDC, 2.62 mM Q11 (previously assembled under a layer of PBS), 45 mM Tris, pH 7.4 for 1 h at  $37^\circ\text{C}$ . For Q11 that had been self-assembled under a layer of PBS,  $\text{Na}^+$  adducts were observed (b, inset).

(subtracting the mass of one  $\text{NH}_3$  per couple)  $[\text{Q11} + \text{MDC} + \text{Na}]^+$  calcd: 1868.06, observed: 1868.24;  $[\text{Q11} + 2\text{MDC} + \text{Na}]^+$  calcd: 2186.46, observed: 2186.65;  $[\text{Q11} + 3\text{MDC} + \text{Na}]^+$  calcd: 2504.85, observed: 2504.44;  $[\text{Q11} + 4\text{MDC} + \text{Na}]^+$  calcd: 2823.25, observed: 2823.21; and  $[\text{Q11} + 5\text{MDC} + \text{Na}]^+$  calcd: 3141.64, observed: 3141.18. These data clearly show that MDC is covalently coupled to the self-assembled Q11 at as many as five glutamine locations via tTGase.

MALDI-TOF mass spectrometry also showed that tTGase could be utilized to conjugate the bidomain peptide RGD1 to Q11. This peptide was designed such that the N-terminal end possessed a Leu-Lys sequence for tTGase substrate activity (41). The C-terminal end possessed an integrin-binding RGD sequence for future cell-attachment studies, and a diglycyl spacer separated the two domains. MALDI showed that up to five RGD1 peptides could be coupled to Q11 via transglutaminase in 1 h (Figure 8). Strong positive  $m/z$  peaks were observed for unreacted Q11,  $[\text{Q11} + \text{H}]^+$  calcd: 1527.7, observed: 1527.3; unreacted RGD1,  $[\text{RGD1} + \text{H}]^+$  calcd: 1079.2, observed: 1079.2 and the Q11–RGD1 adducts (subtracting the mass of one  $\text{NH}_3$  per couple)  $[\text{Q11} + \text{RGD1} + \text{H}]^+$  calcd: 2588.8, observed: 2589.2;  $[\text{Q11} + 2\text{RGD1} + \text{H}]^+$



**Figure 8.** MALDI-TOF MS spectrum of tTGase-mediated cross-linking reactions between Q11 and RGD1 peptides. Reaction conditions: 0.4 U/mL tTGase, 1.67 mM  $\text{CaCl}_2$ , 1 mM RGD1, 0.25 mM Q11 (unassembled, freshly dissolved), in 50 mM Tris, pH 7.4 at 37 °C for 70 min.

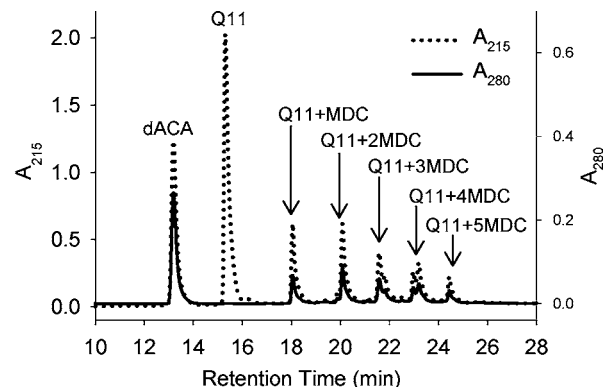
**Table 1. Quantification of Q11–MDC Cross-linking Products for Soluble and Self-Assembled Q11 (mean  $\pm$  one standard deviation).**

product	soluble Q11 <sup>a</sup> (% of total Q11)	self-assembled Q11 <sup>b</sup> (% of total Q11)
unconjugated Q11	85.5% $\pm$ 2.1%	93.7% $\pm$ 2.5%
Q11 + 1MDC	4.9% $\pm$ 0.67%	2.6% $\pm$ 0.9%
Q11 + 2MDC	4.0% $\pm$ 0.58%	1.7% $\pm$ 0.7%
Q11 + 3MDC	2.8% $\pm$ 0.57%	1.0% $\pm$ 0.4%
Q11 + 4MDC	2.2% $\pm$ 0.8%	0.7% $\pm$ 0.3%
Q11 + 5MDC	0.6% $\pm$ 0.23%	0.2% $\pm$ 0.07%

<sup>a</sup> Reaction conditions: 1 U/mL tTGase, 2 mM  $\text{CaCl}_2$ , 1 mM MDC, 1 mM Q11 (unassembled, freshly dissolved), in 33.3 mM Tris, pH 7.4, for 1 h at 37 °C. <sup>b</sup> Reaction conditions: 1.35 U/mL tTGase, 2.81 mM  $\text{CaCl}_2$ , 1.35 mM MDC, 2.62 mM Q11 (previously assembled under a layer of PBS), 45 mM Tris, pH 7.4 for 1 h at 37 °C.

calcd: 3649.9, observed: 3650.2; [Q11 + 3RGD1 + H]<sup>+</sup> calcd: 4711.0, observed: 4710.9; [Q11 + 4RGD1 + H]<sup>+</sup> calcd: 5772.1, observed: 5771.2; and [Q11 + 5RGD1 + H]<sup>+</sup> calcd: 6833.3, observed: 6831.0. These results indicate that lysine-containing peptides can be coupled to Q11 in the same way that MDC can be coupled.

**HPLC Quantification of Q11–MDC Cross-Linking.** Because the quantification of reaction products is difficult with MALDI due to the sensitivity of peak height to instrument parameters and ionization efficiencies, HPLC was utilized to quantify the tTGase-mediated cross-linking products between Q11 and the model lysine-mimic MDC. Chromatograms were collected at 280 nm (dansyl) and 215 nm (amide). Only product peaks (with their conjugated dansyl groups from MDC) absorbed at 280 nm, and their concentrations were calculated by comparing their peak areas at 280 nm to the area of the dansyl- $\epsilon$ -aminocaproic acid internal standard peak. The amount of each reaction product was then expressed as a percentage of total Q11 available in the original reaction mixture. HPLC analysis showed that in dilute reaction conditions, the amount of Q11 peptides that were conjugated to at least one MDC molecule was on average 14.5% at 1 h of reaction time. The distribution of Q11 reaction products is listed in Table 1. From these data it can be seen that Q11 with one conjugated MDC is the most common product, with each subsequent MDC addition occurring less frequently. For self-assembled Q11, HPLC showed that on average up to 6.3% of the available Q11 was coupled to at least one MDC molecule, with five



**Figure 9.** HPLC quantification of tTGase-mediated cross-linking between self-assembled Q11 and MDC. Quantities of reaction products are listed in Table 1.

product peaks observed (Figure 9). The quantities of each product are shown in Table 1. Again, Q11 with one grafted MDC is the most common product, with each subsequent MDC addition occurring less frequently. The reaction conditions for the data shown in Figure 9 and in Table 1 are the same as those described for the Q11–MDC cross-linking reactions that were analyzed by mass spectrometry (Figure 7). The reaction conditions varied slightly between the experiments performed on unassembled Q11 and self-assembled Q11 (for both the MALDI and HPLC experiments), so differences in substrate properties between self-assembled and unassembled Q11 are not easily from these data. However, it is clear that MDC can be coupled in significant amounts to both unassembled and self-assembled Q11 via tTGase.

## DISCUSSION

To produce a short peptide that both self-assembles into  $\beta$ -sheet fibrillar structures and acts as a transglutaminase substrate, a number of natural and synthetic peptides were considered. Common features between these peptides were then incorporated into the design of Q11. For example, a water-soluble peptide designed by Aggeli and co-workers (10, 42), Ac-QQR-FQWQFEQQ-Am (DN1), self-assembles into  $\beta$ -sheet fibrillar structures and has a high content of glutamine residues for possible TGase reactivity. Another peptide that possesses these properties is a sequence from an extracellular matrix protein, microfibril-associated glycoprotein-1 (MAGP-1, residues 57–80, PPEEQFQFQS-QQQVQQEVIPAPTL) (43). This fragment, possessing an alternating QFQFQ central sequence and many Gln residues, self-assembles into Congo-red stainable  $\beta$ -sheet structures. Interestingly, MAGP-1 is a transglutaminase substrate, though it is not yet known whether the glutamines within this  $\beta$ -sheet-forming domain are active (43). In other work involving alternating hydrophilic–hydrophobic peptides (which have a high propensity for forming  $\beta$ -sheet structures), Caplan and co-workers designed a  $\beta$ -sheet fibril-forming peptide, FKFQFK-FQFKFQ, from alternating glutamine, lysine, and phenylalanine residues (44, 45). Last, amyloidogenic peptides such as polyglutamines and the Alzheimers peptide A $\beta$  are well-known  $\beta$ -sheet fibril formers and can also act as transglutaminase substrates (46–48). Longer polyglutamines, however, are key pathological components of neurodegenerative disorders such as Huntington's disease, in which polyglutamines of 30–100 Gln residues (depending on severity of the disease) show a toxic gain of function (49). A $\beta$  is also a key pathological component



in Alzheimer's disease, though its specific role remains elusive (39, 50). As such, these potentially toxic natural peptides would be inappropriate for potential biomedical applications, but short, nontoxic Gln repeats still possess tTGase reactivity (46). Thus, the peptide described here, Q11, Ac-QQKFQFQFEQQ-Am, possesses key features of the peptides mentioned above, having 11 amino acids in an overall layout similar to Aggeli et al.'s DN1, an alternating FQFQF core, and short polyglutamine repeats. Furthermore, it is neutrally charged to avoid electrostatic repulsion in self-assembly.

It is interesting that Q11 was not found to be both an acyl acceptor (lysine substrate), as well as an acyl donor (glutamine substrate). Although Q11 possesses one potentially active lysine residue, experiments performed to specifically look for this cross-linking reaction showed no evidence of Q11–Q11 conjugation (data not shown). This result is particularly interesting because it is widely considered that the sequence specificity of tTGase is less stringent for amines than for glutamine residues (51). Perhaps Lys<sub>3</sub> in Q11 is buried within the  $\beta$ -sheet fibril in such a way as to render it inaccessible to the enzyme. It would be interesting to develop a  $\beta$ -sheet fibril-forming peptide that can be cross-linked to itself in a "covalent capture" approach (5, 52). In such a strategy, the strength or stiffness of the self-assembled matrix could be increased via the generation of intermolecular cross-links. Another interesting result was that both the self-assembled and unassembled Q11 possessed similar tTGase substrate characteristics. This could be because the "unassembled" Q11, even when freshly dissolved in low concentrations, most likely exists in some early state of self-assembly and not truly in a unimolecular state in solution. The CD data shows that even in the micromolar regime, Q11 exists in a  $\beta$ -sheet conformation, even without the presence of salts. This suggests that the Q11 is self-associating, at least into bimolecular or oligomolecular aggregates, as it is possible but unlikely that the Q11 adopts a unimolecular  $\beta$ -sheet conformation.

The potential utility of this approach includes applications in drug delivery, in tissue engineering, and as tissue glues. Recent investigations have focused on similar  $\beta$ -sheet fibril-forming peptides for tissue engineering (2, 3), demonstrating that similar  $\beta$ -sheet fibril-forming peptides appear to be nonimmunogenic (2) and are able to support the three-dimensional culture of chondrocytes (3) as well as nerve cells (2). Also, earlier studies showed that similar self-assembled scaffolds supported the culture of a wide variety of cell types (4). The approach presented here for tTGase-mediated decoration of these self-assembled scaffolds could lead to the tailoring such matrixes for the presentation of appropriate cell-binding ligands (27, 28) or even growth factors (26) to induce desired cellular functions. As a proof-of-concept, we have shown that fusion peptides of tTGase substrates and bioactive sequences (such as the integrin-binding RGD sequence) can be coupled to Q11 scaffolds with tTGase. Ongoing studies in our laboratory are investigating whether cell attachment to Q11 scaffolds can be modulated by the tTGase-mediated grafting of integrin-binding peptides to Q11.

## CONCLUSIONS

An 11-amino acid peptide, Q11, was synthesized and observed to self-assemble into  $\beta$ -sheet fibrillar structures. This peptide was also able to covalently couple to lysine mimics and lysine-containing peptides via tissue transglutaminase. This approach is potentially useful for the

covalent modification of self-assembling peptide systems for biomedical applications.

## ACKNOWLEDGMENT

We would like to thank Annelise Barron for use of the peptide synthesizer, Jiahn-Dar Huang for processing the QFDE samples, and Bi-Huang Hu for helpful discussions regarding peptide synthesis and characterization. This work was funded by NIH grants R01 DE 13030 and T32 DE 07042.

**Supporting Information Available:** HPLC chromatogram and MALDI-TOF mass spectrum of Q11. This material is available free of charge via the Internet at <http://pubs.acs.org>.

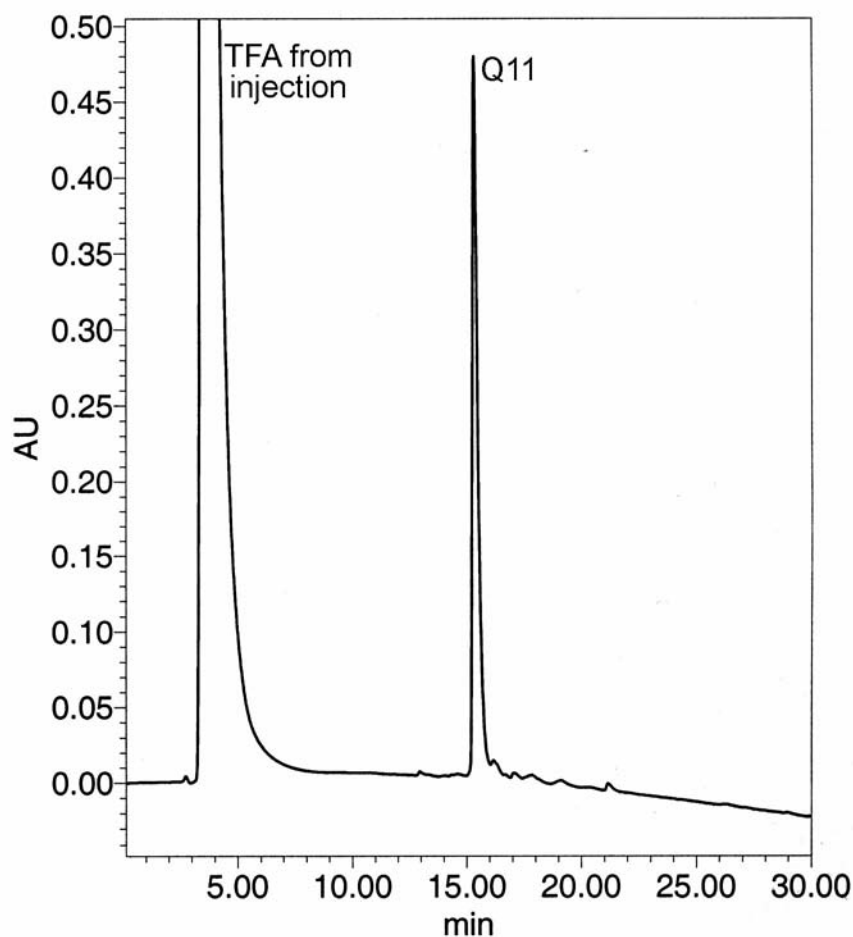
## LITERATURE CITED

- (1) Holmes, T. C. (2002) Novel peptide-based biomaterial scaffolds for tissue engineering. *Trends Biotechnol.* 20, 16–21.
- (2) Holmes, T. C., de Lacalle, S., Su, X., Liu, G. S., Rich, A., and Zhang, S. G. (2000) Extensive neurite outgrowth and active synapse formation on self-assembling peptide scaffolds. *Proc. Nat. Acad. Sci. U.S.A.* 97, 6728–6733.
- (3) Kisiday, J., Jin, M., Kurz, B., Hung, H., Semino, C., Zhang, S., and Grodzinsky, A. J. (2002) Self-assembling peptide hydrogel fosters chondrocyte extracellular matrix production and cell division: Implications for cartilage tissue repair. *Proc. Nat. Acad. Sci. U.S.A.* 99, 9996–10001.
- (4) Zhang, S. G., Holmes, T. C., DiPersio, C. M., Hynes, R. O., Su, X., and Rich, A. (1995) Self-complementary oligopeptide matrices support mammalian cell attachment. *Biomaterials* 16, 1385–1393.
- (5) Hartgerink, J. D., Beniash, E., and Stupp, S. I. (2001) Self-assembly and mineralization of peptide-amphiphile nanofibers. *Science* 294, 1684–1688.
- (6) Fields, G. B., Lauer, J. L., Dori, Y., Forns, P., Yu, Y. C., and Tirrell, M. (1998) Proteinlike molecular architecture: Biomaterial applications for inducing cellular receptor binding and signal transduction. *Biopolymers* 47, 143–151.
- (7) Collier, J. H., Hu, B. H., Ruberti, J. W., Zhang, J., Shum, P., Thompson, D. H., and Messersmith, P. B. (2001) Thermally and photochemically triggered self-assembly of peptide hydrogels. *J. Am. Chem. Soc.* 123, 9463–9464.
- (8) Caplan, M. R., and Lauffenburger, D. A. (2002) Nature's complex copolymers: Engineering design of oligopeptide materials. *Ind. Eng. Chem. Res.* 41, 403–412.
- (9) Petka, W. A., Harden, J. L., McGrath, K. P., Wirtz, D., and Tirrell, D. A. (1998) Reversible hydrogels from self-assembling artificial proteins. *Science* 281, 389–392.
- (10) Aggeli, A., Bell, M., Boden, N., Keen, J. N., Knowles, P. F., McLeish, T. C. B., Pitkeathly, M., and Radford, S. E. (1997) Responsive gels formed by the spontaneous self-assembly of peptides into polymeric  $\beta$ -sheet tapes. *Nature* 386, 259–262.
- (11) Schneider, J. P., Pochan, D. J., Ozbas, B., Rajagopal, K., Pakstis, L., and Kretsinger, J. (2002) Responsive hydrogels from the intramolecular folding and self-assembly of a designed peptide. *J. Am. Chem. Soc.* 124 15030–15037.
- (12) Zhang, S. G., Holmes, T., Lockshin, C., and Rich, A. (1993) Spontaneous assembly of a self-complementary oligopeptide to form a stable macroscopic membrane. *Proc. Nat. Acad. Sci. U.S.A.* 90, 3334–3338.
- (13) Lashuel, H. A., LaBrenz, S. R., Woo, L., Serpell, L. C., and Kelly, J. W. (2000) Protofilaments, filaments, ribbons, and fibrils from peptidomimetic self-assembly: Implications for amyloid formation and materials science. *J. Am. Chem. Soc.* 122, 5262–5277.
- (14) MacPhee, C. E., and Dobson, C. M. (2000) Formation of mixed fibrils demonstrates the generic nature and potential utility of amyloid nanostructures. *J. Am. Chem. Soc.* 122, 12707–12713.
- (15) West, M. W., Wang, W. X., Patterson, J., Mancias, J. D., Beasley, J. R., and Hecht, M. H. (1999) De novo amyloid

- proteins from designed combinatorial libraries. *Proc. Nat. Acad. Sci. U.S.A.* 96, 11211–11216.
- (16) West, M. W., and Hecht, M. H. (1995) Binary patterning of polar and nonpolar amino acids in the sequences and structures of native proteins. *Protein Sci.* 4, 2032–2039.
  - (17) Brack, A., and Orgel, L. E. (1975) Beta structures of alternating polypeptides and their possible prebiotic significance. *Nature* 256, 383–387.
  - (18) Xiong, H. Y., Buckwalter, B. L., Shieh, H. M., and Hecht, M. H. (1995) Periodicity of Polar and Nonpolar Amino-Acids Is the Major Determinant of Secondary Structure in Self-Assembling Oligomeric Peptides. *Proc. Nat. Acad. Sci. U.S.A.* 92, 6349–6353.
  - (19) Caplan, M. R., Moore, P. N., Zhang, S., Kamm, R. D., and Lauffenburger, D. A. (2000) Self-assembly of a beta-sheet protein governed by relief of electrostatic repulsion relative to van der Waals attraction. *Biomacromolecules* 1, 627–631.
  - (20) Mann, B. K., Schmedlen, R. H., and West, J. L. (2001) Tethered-TGF-beta increases extracellular matrix production of vascular smooth muscle cells. *Biomaterials* 22, 439–444.
  - (21) Kuhl, P. R., and Griffith-Cima, L. G. (1996) Tethered epidermal growth factor as a paradigm for growth factor-induced stimulation from the solid phase. *Nat. Med.* 2, 1022–1027.
  - (22) Bentz, H., Schroeder, J. A., and Estridge, T. D. (1998) Improved local delivery of TGF-beta 2 by binding to injectable fibrillar collagen via difunctional polyethylene glycol. *J. Biomed. Mater. Res.* 39, 539–548.
  - (23) Hubbell, J. A., Massia, S. P., Desai, N. P., and Drumheller, P. D. (1991) Endothelial Cell-Selective Materials for Tissue Engineering in the Vascular Graft Via a New Receptor. *Bio/Technology* 9, 568–572.
  - (24) Massia, S. P., and Hubbell, J. A. (1990) Covalently Attached GRGD on Polymer Surfaces Promotes Biospecific Adhesion of Mammalian-Cells. *Ann. N. Y. Acad. Sci.* 589, 261–270.
  - (25) Cook, A. D., Hrkach, J. S., Gao, N. N., Johnson, I. M., Pajvani, U. B., Cannizzaro, S. M., and Langer, R. (1997) Characterization and development of RGD-peptide-modified poly(lactic acid-co-lysine) as an interactive, resorbable biomaterial. *J. Biomed. Mater. Res.* 35, 513–523.
  - (26) Sakiyama-Elbert, S. E., and Hubbell, J. A. (2000) Development of fibrin derivatives for controlled release of heparin-binding growth factors. *J. Controlled Release* 65, 389–402.
  - (27) Schense, J. C., and Hubbell, J. A. (1999) Cross-linking exogenous bifunctional peptides into fibrin gels with factor XIIIa. *Bioconjugate Chem.* 10, 75–81.
  - (28) Schense, J. C., and Hubbell, J. A. (2000) Three-dimensional migration of neurites is mediated by adhesion site density and affinity. *J. Biol. Chem.* 275, 6813–6818.
  - (29) Lorand, L., and Conrad, S. M. (1984) Transglutaminases. *Mol. Cell Biochem.* 58, 9–35.
  - (30) Jao, S. C., Ma, K., Talafous, J., Orlando, R., and Zagorski, M. G. (1997) Trifluoroacetic acid pretreatment reproducibly disaggregates the amyloid beta-peptide. *Amyloid* 4, 240–252.
  - (31) Pears, A. G. E. (1960) *Histochemistry: Theoretical and Applied*, Little, Brown, Boston.
  - (32) Lorand, L., Sieftring, G. E., Tong, Y. S., Brunerlorand, J., and Gray, A. J. (1979) Dansylcadaverine Specific Staining for Transamidating Enzymes. *Anal. Biochem.* 93, 453–458.
  - (33) Jeitner, T. M., Fuchsbauer, H. L., Blass, J. P., and Cooper, A. J. L. (2001) A sensitive fluorometric assay for tissue transglutaminase. *Anal. Biochem.* 292, 198–206.
  - (34) Zhang, Z. Y., Shum, P., Yates, M., Messersmith, P. B., and Thompson, D. H. (2002) Formation of fibrinogen-based hydrogels using phototriggerable diplasmalogen liposomes. *Bioconjugate Chem.* 13, 640–646.
  - (35) Valnickova, Z., and Enghild, J. J. (1998) Human procarboxypeptidase U, or thrombin-activable fibrinolysis inhibitor, is a substrate for transglutaminases – Evidence for transglutaminase-catalyzed cross-linking to fibrin. *J. Biol. Chem.* 273, 27220–27224.
  - (36) Johnson, W. C. (1988) Secondary structure of proteins through circular dichroism spectroscopy. *Annu. Rev. Biophys. Biophys. Chem.* 17, 145–166.
  - (37) Greenfield, N., and Fasman, G. D. (1969) Computed Circular Dichroism Spectra for Evaluation of Protein Conformation. *Biochemistry* 8, 4108–4116.
  - (38) Haris, P. I., and Chapman, D. (1995) The conformational analysis of peptides using Fourier transform IR spectroscopy. *Biopolymers* 37, 251–263.
  - (39) Lynn, D. G., and Meredith, S. C. (2000) Review: Model peptides and the physicochemical approach to beta-amyloids. *J. Struct. Biol.* 130, 153–173.
  - (40) Marini, D. M., Hwang, W., Lauffenburger, D. A., Zhang, S. G., and Kamm, R. D. (2002) Left-handed helical ribbon intermediates in the self-assembly of a beta-sheet peptide. *Nano Lett.* 2, 295–299.
  - (41) Gross, M., Whetzel, N. K., and Folk, J. E. (1977) Amine Binding-Sites in Acyl Intermediates of Transglutaminases – Human-Blood Plasma Enzyme (Activated Coagulation Factor-XIII) and Guinea-Pig Liver-Enzyme. *J. Biol. Chem.* 252, 3752–3759.
  - (42) Aggeli, A., Bell, M., Boden, N., Keen, J. N., McLeish, T. C. B., Nyrkova, I., Radford, S. E., and Semenov, A. (1997) Engineering of peptide beta-sheet nanotapes. *J. Mater. Chem.* 7, 1135–1145.
  - (43) Trask, B. C., Broekelmann, T., Ritty, T. M., Trask, T. M., Tisdale, C., and Mecham, R. P. (2001) Posttranslational modifications of microfibril associated glycoprotein-1 (MAGP-1). *Biochemistry* 40, 4372–80.
  - (44) Caplan, M. R., Schwartzfarb, E. M., Zhang, S. G., Kamm, R. D., and Lauffenburger, D. A. (2002) Effects of systematic variation of amino acid sequence on the mechanical properties of a self-assembling, oligopeptide biomaterial. *J. Biomater. Sci. Polym. Ed.* 13, 225–236.
  - (45) Caplan, M. R., Schwartzfarb, E. M., Zhang, S. G., Kamm, R. D., and Lauffenburger, D. A. (2002) Control of self-assembling oligopeptide matrix formation through systematic variation of amino acid sequence. *Biomaterials* 23, 219–227.
  - (46) Kahlem, P., Terre, C., Green, H., and Djian, P. (1996) Peptides containing glutamine repeats as substrates for transglutaminase-catalyzed cross-linking: relevance to diseases of the nervous system. *Proc. Nat. Acad. Sci. U.S.A.* 93, 14580–5.
  - (47) Benzinger, T. L. S., Gregory, D. M., Burkoth, T. S., Miller-Auer, H., Lynn, D. G., Botto, R. E., and Meredith, S. C. (1998) Propagating structure of Alzheimer's beta-amyloid(10–35) is parallel beta-sheet with residues in exact register. *Proc. Nat. Acad. Sci. U.S.A.* 95, 13407–12.
  - (48) Dudek, S. M., and Johnson, G. V. W. (1994) Transglutaminase Facilitates the Formation of Polymers of the Beta-Amyloid Peptide. *Brain Res.* 651, 129–133.
  - (49) Zoghbi, H. Y., and Orr, H. T. (2000) Glutamine repeats and neurodegeneration. *Annu. Rev. Neurosci.* 23, 217–47.
  - (50) Koo, E. H., Lansbury, P. T., and Kelly, J. W. (1999) Amyloid diseases: abnormal protein aggregation in neurodegeneration. *Proc. Nat. Acad. Sci. U.S.A.* 96, 9989–90.
  - (51) Greenberg, C. S., Birckbichler, P. J., and Rice, R. H. (1991) Transglutaminases – Multifunctional Cross-Linking Enzymes That Stabilize Tissues. *FASEB J.* 5, 3071–3077.
  - (52) Clark, T. D., Kobayashi, K., and Ghadiri, M. R. (1999) Covalent capture and stabilization of cylindrical  $\beta$ -sheet peptide assemblies. *Chem. Eur. J.* 5, 782–792.

BC034017T

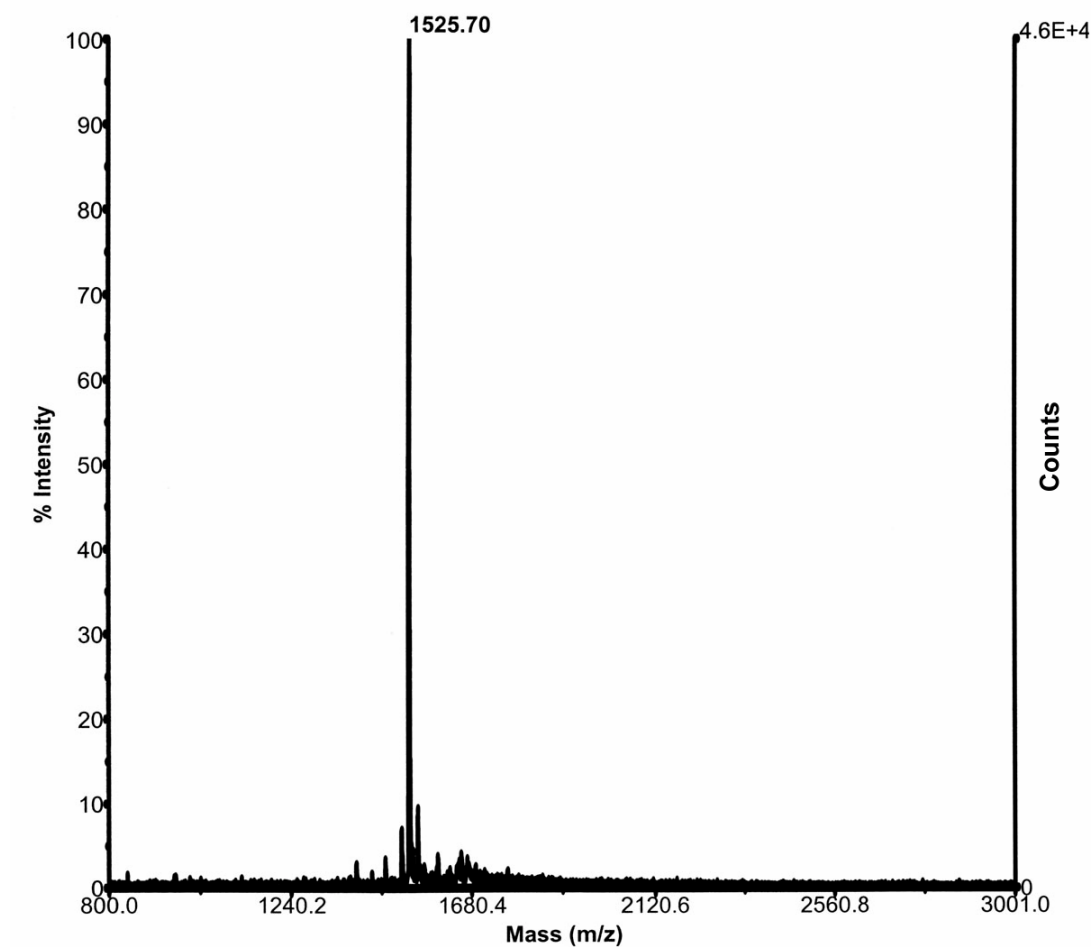
## Supplementary Information



**Supplementary Figure A:** HPLC chromatogram of Q11. 10 $\mu$ L of Q11 (1mg/mL in TFA) was injected into a Waters HPLC system equipped with a Waters 600 controller and pump system, a Waters 996 photodiode array detector, a Waters 717plus autosampler, and a Vydak C4 analytical column (Cat#214MS54). The gradient was 10% acetonitrile/0.1%TFA to 63% acetonitrile/0.1%TFA over 30minutes. Absorbance was monitored at 215nm. Q11 was dissolved in TFA for the injection because Q11 tended to aggregate slightly in water or acetonitrile. However, Q11 injected from TFA resulted in reproducible single peaks, as shown above. The TFA eluted quickly, producing a large peak upon injection due to its strong absorbance at 215nm.



## Supplementary Information



**Supplementary Figure B:** Negative mode MALDI-TOF mass spectrometry of Q11. Calculated  $m/z$  for Q11  $[M-H]^-$ : 1525.72, observed: 1525.70. Spectra were collected on a PE Biosystems Voyager DE-PRO System 6050 with delayed extraction, typically with an accelerating voltage of 25kV, a grid voltage of 75%, a mirror voltage ratio of 1.12, a guide wire voltage of 0.05%, and a delay time of 360nsec. Scans were averaged over 100 laser shots. The matrix material was  $\alpha$ -cyano-4-hydroxycinnamic acid.

# MicroPET Imaging of a Gastrin-Releasing Peptide Receptor-Positive Tumor in a Mouse Model of Human Prostate Cancer Using a $^{64}\text{Cu}$ -Labeled Bombesin Analogue

Buck E. Rogers,<sup>\*,†</sup> Heather M. Bigott,<sup>‡</sup> Deborah W. McCarthy,<sup>‡</sup> Debbie Della Manna,<sup>†</sup> Joonyoung Kim,<sup>‡</sup> Terry L. Sharp,<sup>‡</sup> and Michael J. Welch<sup>‡</sup>

Department of Radiation Oncology, University of Alabama at Birmingham, Birmingham, Alabama 35294 and Mallinckrodt Institute of Radiology, Washington University School of Medicine, St. Louis, Missouri 63110. Received February 12, 2003; Revised Manuscript Received May 1, 2003

The gastrin-releasing peptide receptor (GRPR) is overexpressed on a variety of carcinomas and has been the target for detection and treatment of these neoplasms in animals. In particular, analogues of the tetradecapeptide bombesin (BN) have been radiolabeled with  $^{99\text{m}}\text{Tc}$  and  $^{111}\text{In}$  for detection of GRPR-positive tumors by gamma ray scintigraphy. The goal of this study was to evaluate the potential of the bombesin analogue, DOTA-Aoc-BN(7–14), for positron-emission tomographic (PET) imaging after radiolabeling with the positron-emitter  $^{64}\text{Cu}$ . A saturation binding assay on PC-3 human prostate cancer cells showed that  $^{64}\text{Cu}$ -DOTA-Aoc-BN(7–14) had an equilibrium binding constant ( $K_d$ ) of  $6.1 \pm 2.5$  nM and a receptor concentration ( $B_{\text{max}}$ ) of  $2.7 \pm 0.6 \times 10^5$  receptors/cell. The radiolabeled analogue also showed rapid internalization with 18.2% internalized into  $10^5$  PC-3 cells by 2 h. The tumor localization of  $^{64}\text{Cu}$ -DOTA-Aoc-BN(7–14) was 5.5% injected dose per gram in athymic nude mice bearing PC-3 xenografts at 2 h postinjection. The tumor retention with respect to the 2 h value was 76% and 45% at 4 and 24 h, respectively, and was GRPR-mediated as shown by inhibition with a coinjection of excess peptide. MicroPET imaging of  $^{64}\text{Cu}$ -DOTA-Aoc-BN(7–14) in athymic nude mice bearing subcutaneous PC-3 tumors showed good tumor localization. Further studies with  $^{64}\text{Cu}$ -pyruvaldehyde-bis( $N^4$ -methylthiosemicarbazone) ( $^{64}\text{Cu}$ -PTSM) suggested that low blood flow to the PC-3 tumors may have limited the localization of  $^{64}\text{Cu}$ -DOTA-Aoc-BN(7–14). This study demonstrates that  $^{64}\text{Cu}$ -DOTA-Aoc-BN(7–14) can be used to detect GRPR-positive tumors by PET imaging.

## INTRODUCTION

The amphibian tetradecapeptide BN<sup>1</sup> and its mammalian counterpart, GRP, have been shown to produce a variety of biological responses including release of gastrointestinal hormones, effects on blood pressure, and thermoregulation (1, 2), as well as having a role in human cancer. In this regard, these peptides bind with high affinity to receptors that have been detected in various types of human carcinoma (3–7). Four BN receptor subtypes have been characterized including the BN- and GRP-preferring subtype (GRPR) (2), the neuromedin B-preferring subtype (8), and subtypes 3 and 4, which have lower affinities for both BN and GRP relative to GRPR (9, 10). BN-like peptides have been shown to function as growth stimulators in neoplastic tissues through autocrine mechanisms (3, 11). Therefore, several

BN antagonists have been synthesized and shown to be efficacious in animal cancer models and in nude mice bearing human xenografts (12–14). In addition, conjugation of BN antagonists to cytotoxic agents such as doxorubicin have been shown to be potent *in vitro* and in mice bearing human tumor xenografts (15).

Another strategy for detecting and treating GRPR-positive neoplasms is to radiolabel BN analogues with radioisotopes that can be used for noninvasive imaging and radiotherapy. In this regard, various BN analogues have been radiolabeled with radioactive iodine or radioactive metals. In particular,  $^{131}\text{I}$ ,  $^{149}\text{Pm}$ ,  $^{188}\text{Re}$ , and  $^{177}\text{Lu}$  have been used to radiolabel BN analogues for potential radiotherapy applications through their beta emissions (16–19), while  $^{99\text{m}}\text{Tc}$ - and  $^{111}\text{In}$ -labeled analogues have been used for detecting GRPR-positive tumors by gamma ray scintigraphy (20–28). Positron-emission tomography (PET) should have better resolution than gamma camera imaging at the sensitivity needed for imaging GRPR expression; therefore, a BN analogue radiolabeled with a positron-emitter would have advantages over a gamma ray emitting radioisotope for detecting GRPR-positive tumors.

Copper-64 ( $t_{1/2} = 12.7$  h) is a positron-emitter (19%,  $E_{\beta^+ \text{max}} = 656$  keV) that has been shown to have therapeutic potential (39%,  $E_{\beta^- \text{max}} = 573$  keV) when targeted to tumors using monoclonal antibodies or peptides (29, 30). It is readily produced on a medical cyclotron (31), and its intermediate half-life should be suitable for imaging the localization of  $^{64}\text{Cu}$ -labeled BN analogues. The macrocyclic chelate, 1,4,7,10-tetraazacyclododecane-

\* Current address of corresponding author: Buck E. Rogers, Ph.D., Department of Radiation Oncology, Radiation and Cancer Biology Division, Washington University in St. Louis, 4511 Forest Park Blvd., Suite 411, St. Louis, MO 63108. Phone: 314-362-9787. Fax: 314-362-9790. E-mail: rogers@radonc.wustl.edu.

<sup>†</sup> University of Alabama at Birmingham.

<sup>‡</sup> Washington University School of Medicine.

<sup>1</sup> Abbreviations used: BN, bombesin; GRP, gastrin-releasing peptide; GRPR, gastrin-releasing peptide receptor; PET, positron-emission tomography; DOTA, 1,4,7,10-tetraazacyclododecane-1,4,7,10-tetraacetic acid; Aoc, 8-amino-octanoic acid; TLC, thin-layer chromatography;  $^{64}\text{Cu}$ -PTSM,  $^{64}\text{Cu}$ -pyruvaldehyde-bis( $N^4$ -methylthiosemicarbazone);  $K_d$ , equilibrium binding constant;  $B_{\text{max}}$ , concentration of GRPR; % ID/g, percent injected dose per gram of tissue; PI, postinjection.

1,4,7,10-tetraacetic acid (DOTA), has been used to radiolabel antibodies and peptides with copper radioisotopes and has been conjugated to the N-terminus of a BN analogue for radiolabeling with  $^{177}\text{Lu}$  (18). This compound (DOTA-Aoc-BN(7–14)) consisted of an 8-aminooctanoic acid (Aoc) spacer between DOTA and the eight C-terminal amino acids of BN (BN(7–14)).

In the present study, we sought to evaluate DOTA-Aoc-BN(7–14) after radiolabeling with  $^{64}\text{Cu}$  in binding and internalization assays of PC-3 human prostate cancer cells overexpressing GRPR and in athymic nude mice bearing subcutaneous (sc) PC-3 xenografts. The *in vivo* tumor localization and specificity of  $^{64}\text{Cu}$ -DOTA-Aoc-BN(7–14) was demonstrated by tissue biodistribution and microPET imaging. Further studies were conducted with  $^{64}\text{Cu}$ -PTSM to compare the blood flow in the PC-3 tumors to that in other tissues.

## MATERIALS AND METHODS

### Radiolabeling of DOTA-Aoc-BN(7–14) with $^{64}\text{Cu}$ .

Copper-64 was produced on a CS-15 biomedical cyclotron at Washington University School of Medicine according to published procedures (31). 1,4,7,10-Tetraazacyclododecane-1,4,7-tris(acetic acid *tert*-butyl ester)-10-acetic acid (DOTA-tris(*tert*-butyl ester)) was purchased from Macrocyclics, Inc. (Dallas, TX) and 8-aminooctanoic acid was purchased from Advanced ChemTech (Louisville, KY). The DOTA-Aoc-BN(7–14) was synthesized using standard Fmoc chemistry by solid-phase peptide synthesis at the University of Alabama at Birmingham Comprehensive Cancer Center Peptide Synthesis and Analysis Shared Facility and shown to be >98% pure by high performance liquid chromatography. For radiolabeling,  $^{64}\text{CuCl}_2$  was diluted with a 10-fold excess of 0.1 M ammonium acetate ( $\text{NH}_4\text{OAc}$ ), pH = 5.5, and then added to DOTA-Aoc-BN(7–14). After incubating at room temperature for 30 min, radiochemical purity was determined by radio-thin-layer chromatography (radio-TLC). To increase the specific activity and prevent radiolysis for microPET studies, the radiolabeling was performed in the presence of 2,5-dihydroxybenzoic acid (gentisic acid) (4 mg/mL final concentration) (Sigma Chemical Co., St. Louis, MO). Samples were applied to Whatman MKC18F TLC plates, developed with 10%  $\text{NH}_4\text{OAc}$ :methanol (30:70), and analyzed using a BIOSCAN System 200 imaging scanner (Washington, DC).

**Saturation Binding Assays.** The PC-3 human prostate cancer cell line was obtained from the American Type Culture Collection (Rockville, MD) and cultured in Ham's F12K medium containing 10% fetal bovine serum (FBS) and 1% L-glutamine at 37 °C in a humidified atmosphere with 5%  $\text{CO}_2$ . For binding assays, the cells were harvested by incubating with 4 mM EDTA/0.05% KCl for 3 min, centrifuging and resuspending in cold PBS at a concentration of  $1 \times 10^7$  cells/mL. The cells were then aliquoted into polystyrene tubes in triplicate followed by the addition of various amounts of  $^{64}\text{Cu}$ -DOTA-Aoc-BN(7–14) such that the final concentration ranged between 0.1 and 500 nM. The cells were incubated for 1 h at 4 °C in the presence or absence of excess competitor (30  $\mu\text{M}$ , Tyr<sup>4</sup>-BN, Sigma Chemical Co., St. Louis, MO). The samples were then rinsed with PBS and centrifuged at 1700g for 10 min, the supernatant was removed, and the cells were measured for radioactivity in a gamma counter (Packard Auto Gamma 5000 Series, Chicago, IL) to determine the amount of bound radioactivity. The data were analyzed using the GraphPad Prism software (San Diego, CA).

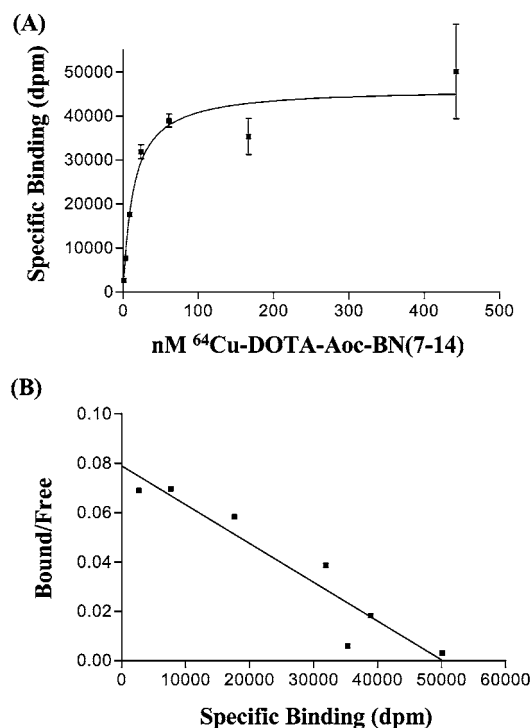
**Internalization Assays.** PC-3 cells were harvested and seeded in six-well plates at  $3 \times 10^5$  cells per well. Twenty-four hours later,  $^{64}\text{Cu}$ -DOTA-Aoc-BN(7–14) was added to the wells such that the final concentration was 1 nM and incubated at 37 °C for 30, 120, and 240 min. An excess (30  $\mu\text{M}$ ) of Tyr<sup>4</sup>-BN was added to half of the wells as a competitor. At the appropriate time point, a six-well plate was removed from the incubator, media was removed, and cells were rinsed with PBS. The cells were then rinsed twice with Hank's Balanced Salt Solution (HBSS) containing 20 mM NaOAc, pH 4.0, to remove surface bound radioactivity, and the cells were harvested by adding 1 N NaOH. The acid wash and the cells were measured for radioactivity in a gamma counter to determine the amount of surface bound and internalized radioactivity, respectively. These data were normalized as a percentage of the total amount of radioactivity added per cell.

**Biodistribution Studies.** Experiments were performed in 4–5 week old female athymic nude mice (National Cancer Institute Frederick Research Laboratory, Frederick, MD) implanted sc with  $2 \times 10^7$  PC-3 cells mixed 1:1 with Matrigel (Becton Dickinson, Bedford, MA). Three weeks later, the mice were injected with 2–5  $\mu\text{Ci}$  of  $^{64}\text{Cu}$ -DOTA-Aoc-BN(7–14) (specific activity = 60–130 mCi/mg) via the tail vein. Biodistribution was performed with groups of four to six mice sacrificed 2, 4, and 24 h postinjection (PI) of  $^{64}\text{Cu}$ -DOTA-Aoc-BN(7–14). Another group of mice were coinjected with  $^{64}\text{Cu}$ -DOTA-Aoc-BN(7–14) and 100  $\mu\text{g}$  of Tyr<sup>4</sup>-BN as a competitor and sacrificed 2 h PI. The blood, liver, small intestine, spleen, kidney, muscle, bone, pancreas, and tumor were removed and weighed, and the radioactivity was measured in a gamma counter to determine the percent injected dose per gram of tissue (% ID/g).

**MicroPET Imaging.** PET imaging was performed on a microPET-R4 system (Concorde Microsystems Inc, Knoxville, TN) which was based on the design of Cherry and colleagues (32). The microPET-R4 has a field-of-view of 8 cm axially by 11 cm transversally and is capable of a spatial resolution of 2.3 mm and an absolute sensitivity of 1020 cps/microcurie in the middle of the field-of-view. Images were generated from 3-dimensional sinogram data, rebinned to two-dimensional format by the FORE algorithm (33) followed by two-dimensional filtered-back projection. For imaging studies, the animal model described above was used followed by injection of 500  $\mu\text{Ci}$  of  $^{64}\text{Cu}$ -DOTA-Aoc-BN(7–14) (specific activity = 2000 mCi/mg) with or without 100  $\mu\text{g}$  Tyr<sup>4</sup>-BN via the tail vein. Two hours later, the mice were anesthetized with 1–2% isoflurane, positioned supine, and immobilized in a specially prepared scanner cradle. A total of four mice were imaged with two mice being imaged simultaneously (one with competitor, one without).

**Ex Vivo Determination of Receptor Density.** The pancreata (mean weight = ~130 mg) and PC-3 tumors (mean weight = ~270 mg) were harvested from two euthanized mice and processed according to a previously published procedure for cell membrane preparations (34) to determine the expression of GRPR on each. A competitive binding assay was performed by adding 25  $\mu\text{g}$  of membrane protein to Multiscreen Durapore filtration plates (type FB, 1.0  $\mu\text{m}$  borosilicate glass fiber over 1.2  $\mu\text{m}$  Durapore membrane; Millipore, Bedford, MA) and washed with buffer (10 mM HEPES, 5 mM  $\text{MgCl}_2$ , 1 mM EDTA, and 0.1% BSA, pH 7.4). One hundred microliters of  $^{125}\text{I}$ -Tyr<sup>4</sup>-BN (0.05 nM, DuPont/NEN Research Products, Boston, MA) in PBS was added to each well in triplicate along with various concentrations (0.2 pM to





**Figure 1.** Representative plots of <sup>64</sup>Cu-DOTA-Aoc-BN(7-14) saturation binding (A) and Scatchard transformation (B). PC-3 cells were incubated with increasing concentrations of <sup>64</sup>Cu-DOTA-Aoc-BN(7-14) in the presence or absence of excess competitor to determine nonspecific binding. Data represent the specific binding in dpm for the mean of triplicate measurements  $\pm$  standard deviation.

60  $\mu$ M) of unlabeled Tyr<sup>4</sup>-BN and incubated for 60 min at room temperature. The samples were rinsed twice with PBS and dried, and radioactivity was measured in a gamma counter. The data were analyzed using the GraphPad Prism software.

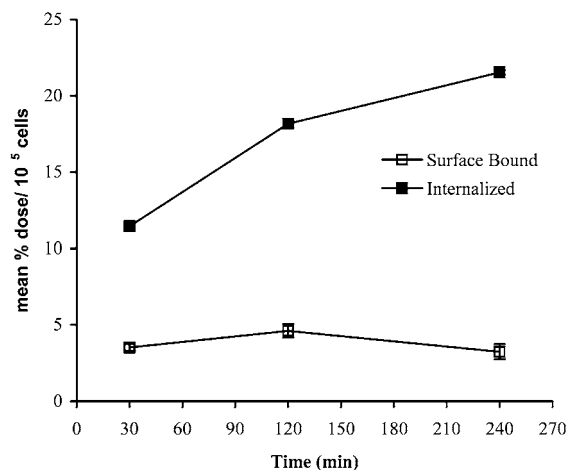
**In Vivo Determination of Blood Flow.** Mice ( $n = 3$ ) bearing established PC-3 tumors were injected iv with 10  $\mu$ Ci of <sup>64</sup>Cu-pyruvaldehyde-bis(*N*<sup>1</sup>-methylthiosemicarbazone) (<sup>64</sup>Cu-PTSM). <sup>64</sup>Cu-PTSM was synthesized and radiolabeled as previously described (35), and radiochemical purity was  $>98\%$  as determined by radio-TLC. Ten minutes after injection of <sup>64</sup>Cu-PTSM, the mice were sacrificed and biodistribution was performed as described above. The data are presented as % ID/g to determine the relative blood flow to each tissue.

**Statistical Analysis.** The Student's *t* test was used to determine statistical significance at the 95% confidence level with  $P < 0.05$  being considered significantly different.

## RESULTS

**Radiolabeling of DOTA-Aoc-BN(7-14) with <sup>64</sup>Cu.** Initial radiolabeling attempts of DOTA-Aoc-BN(7-14) with <sup>64</sup>Cu yielded maximum specific activities of 130 mCi/mg (199 Ci/mmol). Subsequent radiolabelings achieved specific activities of 2000 mCi/mg (3062 Ci/mmol) in the presence of gentisic acid to prevent radiolysis of the peptide. In all cases, the radiochemical purity was  $>98\%$  as determined by radio-TLC and the radiolabeled peptide was used immediately for both in vitro and in vivo assays.

**Saturation Binding Assays.** A representative saturation binding curve and scatchard transformation are shown in Figure 1. This shows that <sup>64</sup>Cu-DOTA-Aoc-BN(7-14) bound specifically to a single class of binding sites

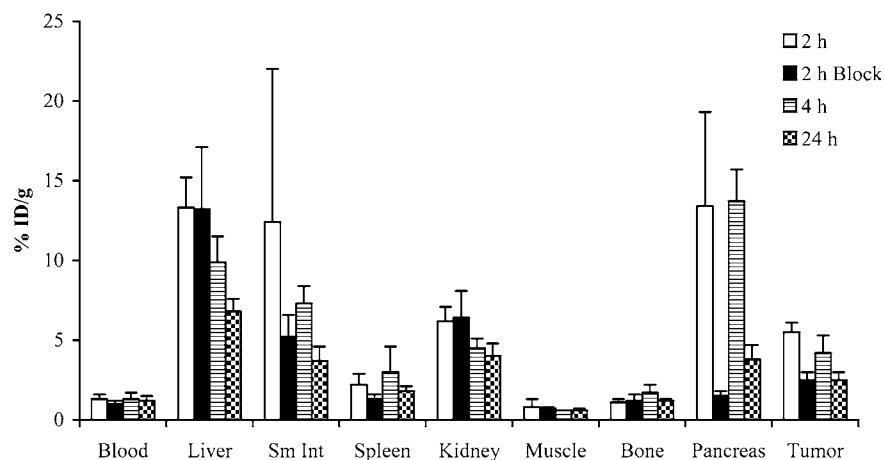


**Figure 2.** Internalization of <sup>64</sup>Cu-DOTA-Aoc-BN(7-14) into PC-3 cells. <sup>64</sup>Cu-DOTA-Aoc-BN(7-14) was added to the cells in the presence or absence of excess competitor and incubated at 37 °C. At various time points, the media was removed, the cells acid-washed to remove surface bound radioactivity, and harvested. The cell pellets (internalized) and acid wash (surface bound) were counted and the specific internalized and surface bound radioactivity determined. The data are presented as the mean  $\pm$  standard deviation of the % of total radioactivity added divided by the total number of cells in each well for triplicate measurements. Note that the error bars are contained within the symbols.

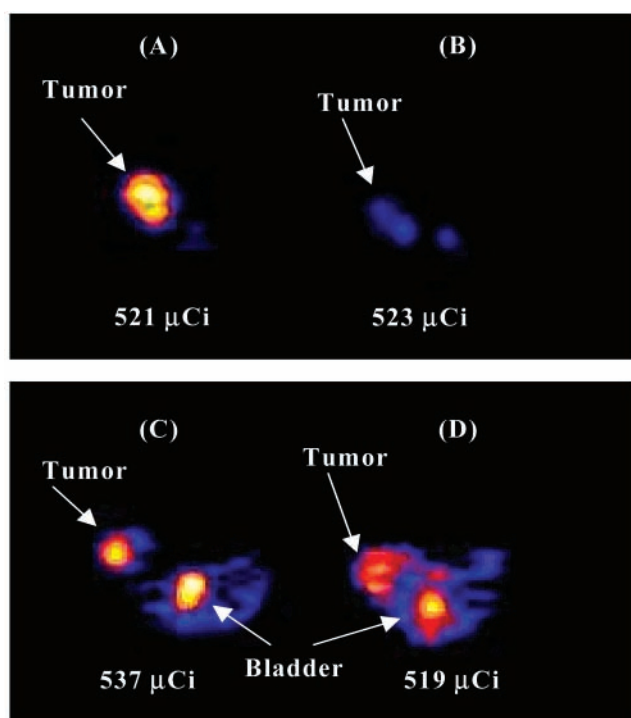
with high affinity. The mean equilibrium binding constant,  $K_d$ , of <sup>64</sup>Cu-DOTA-Aoc-BN(7-14) for GRPR from three independent experiments was  $6.1 \pm 2.5$  nM with a  $B_{max}$  of  $2.7 \pm 0.6 \times 10^5$  GRP receptors per PC-3 cell.

**Internalization Assays.** The internalization of <sup>64</sup>Cu-DOTA-Aoc-BN(7-14) into PC-3 cells is shown in Figure 2. The amount of specifically internalized (amount internalized without competitor minus the amount internalized with competitor) <sup>64</sup>Cu-DOTA-Aoc-BN(7-14) per  $10^5$  PC-3 cells was  $11.4 \pm 0.2\%$  after a 30 min incubation, which increased to  $18.2 \pm 0.4\%$  and  $21.5 \pm 0.5\%$  at 120 and 240 min, respectively. The amount of internalized <sup>64</sup>Cu-DOTA-Aoc-BN(7-14) was significantly greater ( $P < 0.05$ ) than the amount of surface bound <sup>64</sup>Cu-DOTA-Aoc-BN(7-14) at all time points, which ranged from 3.3 to 4.6%. The amount of <sup>64</sup>Cu-DOTA-Aoc-BN(7-14) internalized or surface bound in the presence of competitor was  $< 0.5\%$  at all time points.

**Biodistribution Studies.** The tissue and tumor localization of <sup>64</sup>Cu-DOTA-Aoc-BN(7-14) is shown in Figure 3. These studies were performed with 2–5  $\mu$ Ci (15–40 ng) of <sup>64</sup>Cu-DOTA-Aoc-BN(7-14) radiolabeled at a specific activity of 130 mCi/mg. These results show specific GRPR localization of <sup>64</sup>Cu-DOTA-Aoc-BN(7-14) in the tumor ( $P < 0.0001$ ), pancreas ( $P < 0.01$ ), and spleen ( $P < 0.05$ ) 2 h PI as the uptake in these tissues are inhibited upon co-injection of Tyr<sup>4</sup>-BN. The tumor localization was  $5.5 \pm 0.6\%$  ID/g at 2 h PI that decreased to  $4.2 \pm 1.1\%$  ID/g and  $2.5 \pm 0.5\%$  ID/g at 4 and 24 h PI, respectively. There was rapid blood clearance of <sup>64</sup>Cu-DOTA-Aoc-BN(7-14) as only  $1.3 \pm 0.3\%$  ID/g remained at 2 h, which was similar to the concentration at 4 and 24 h. The pancreas had a high localization of <sup>64</sup>Cu-DOTA-Aoc-BN(7-14) at 2 and 4 h ( $13.4 \pm 5.9\%$  ID/g and  $13.7 \pm 2.0\%$  ID/g, respectively) that decreased rapidly by 24 h ( $3.8 \pm 0.9$ ). The liver and pancreas were the only tissues to have significantly greater uptake ( $P < 0.05$ ) of <sup>64</sup>Cu-DOTA-Aoc-BN(7-14) than the tumor at all three time points. The tumor had significantly greater localization than the blood ( $P < 0.01$ ), bone ( $P < 0.01$ ), and muscle



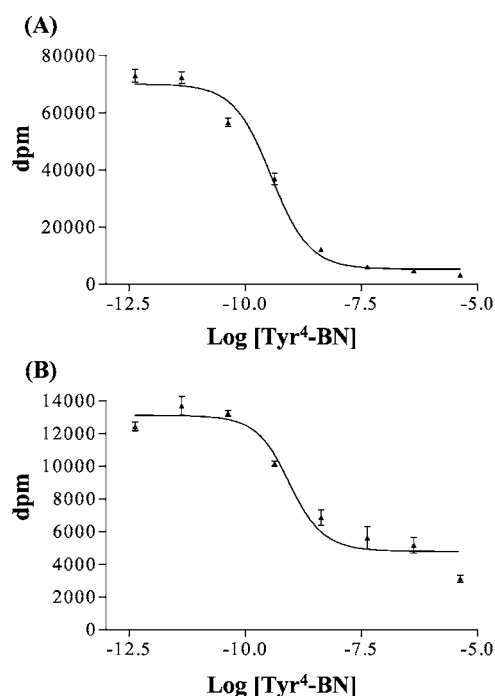
**Figure 3.** Biodistribution of  $^{64}\text{Cu}$ -DOTA-Aoc-BN(7-14) in athymic nude mice bearing sc. PC-3 tumors. Mice were administered  $^{64}\text{Cu}$ -DOTA-Aoc-BN(7-14) via the tail vein after tumors were established and the mice sacrificed 2, 4, and 24 h later. A coinjection of Tyr<sup>4</sup>-BN was administered to another group of mice to determine GRPR specific binding at the 2 h time point. The data are presented as the % ID/g for the mean  $\pm$  standard deviation of four to six mice per time point.



**Figure 4.** Transaxial microPET images of athymic nude mice bearing PC-3 tumors 2 h after tail vein injection of  $^{64}\text{Cu}$ -DOTA-Aoc-BN(7-14) in the absence (A,C) or presence (B,D) of a coinjection of Tyr<sup>4</sup>-BN.

( $P = 0.001$ ) at all time points and greater than the spleen at 2 and 24 h ( $P < 0.05$ ).

**MicroPET Imaging.** The localization of  $^{64}\text{Cu}$ -DOTA-Aoc-BN(7-14) in PC-3 tumors as determined by microPET imaging is shown in Figure 4. These studies were performed with 500  $\mu\text{Ci}$  (250 ng) of  $^{64}\text{Cu}$ -DOTA-Aoc-BN(7-14) radiolabeled at a specific activity of 2000 mCi/mg. Because of the high levels of radioactivity in normal tissues as shown in Figure 3, transaxial images were used to focus on the localization of  $^{64}\text{Cu}$ -DOTA-Aoc-BN(7-14) in the tumor. Representative transaxial images are shown of four mice (two mice without competitor (A and C), and two mice with competitor (B and D)) 2 h PI of  $^{64}\text{Cu}$ -DOTA-Aoc-BN(7-14). There is clear visualization of the PC-3 tumors in animals on the left (A and C) that did not receive competitor, along with clearance of  $^{64}\text{Cu}$ -DOTA-Aoc-BN(7-14) through the bladder. The mice on



**Figure 5.** Representative competitive binding assays on membrane preparations of PC-3 tumors (A) or pancreas (B). Established PC-3 tumors or pancreata were harvested from mice and used for membrane preparations. Various concentrations of Tyr<sup>4</sup>-BN were added to 25  $\mu\text{g}$  of the membranes to inhibit the binding of  $^{125}\text{I}$ -Tyr<sup>4</sup>-BN. The data are presented as the binding in dpm vs the log of the molar concentration of Tyr<sup>4</sup>-BN for the mean of triplicate measurements  $\pm$  standard deviation.

the right (B and D), which received the competitor, show a decrease in tumor localization of  $^{64}\text{Cu}$ -DOTA-Aoc-BN(7-14). It is likely that the decrease in tracer localization for mouse D was not as dramatic as the decrease for mouse B due to incomplete blocking as the tumor for mouse D was 2-fold larger than the others in the imaging studies.

**Ex Vivo Determination of Receptor Density.** The competitive binding studies used to determine the expression of GRPR on pancreas and tumor are shown in Figure 5. These data show that the expression of GRPR is about 14-fold greater on tumor ( $376 \pm 55$  fmol/mg of protein) than on the pancreas ( $27 \pm 13$  fmol/mg of

**Table 1. Blood Flow of Various Tissues as Determined by Sacrifice of Athymic Nude Mice Bearing PC-3 Tumors 10 min after Tail Vein Administration of  $^{64}\text{Cu}$ -PTSM. Data Are Presented as % ID/g for Three Mice**

tissue	10 min $^{64}\text{Cu}$ -PTSM (% ID/g)
blood	$2.51 \pm 0.28$
liver	$16.06 \pm 3.49$
sm int	$8.09 \pm 0.96$
spleen	$2.65 \pm 0.84$
kidney	$16.87 \pm 1.92$
muscle	$3.03 \pm 0.43$
pancreas	$6.00 \pm 0.84$
tumor	$2.29 \pm 0.70$

protein). Membranes were also made from PC-3 cells and these binding data show that they express about 15-fold more GRPR ( $5479 \pm 410$  fmol/mg) than the PC-3 tumors (data not shown). These results are similar to our earlier results with intact PC-3 cells, as 5479 fmol/mg is equal to approximately  $4.4 \times 10^5$  receptors/cell (based upon 7500 PC-3 cells per microgram of protein).

**In Vivo Determination of Blood Flow.** The results of  $^{64}\text{Cu}$ -PTSM blood flow studies in mice bearing PC-3 tumors are shown in Table 1. This demonstrates that the blood flow to the tumor is among the lowest of all of the tissues examined and is not significantly different from blood, spleen, or muscle ( $P > 0.05$ ). However, the blood flow to the tumor ( $2.3 \pm 0.7\%$  ID/g) is significantly lower ( $P < 0.01$ ) than the blood flow to the pancreas ( $6.0 \pm 0.8\%$  ID/g). The liver ( $16.1 \pm 3.5\%$  ID/g), kidney ( $16.9 \pm 1.9\%$  ID/g), and small intestine ( $8.1 \pm 1.1\%$  ID/g) are the tissues with the highest blood flow.

## DISCUSSION

A number of radiolabeled peptides have been successfully used for the noninvasive imaging of tumors overexpressing receptors that have high affinity for these peptides. In particular, peptides specific for somatostatin receptors, vasoactive intestinal peptide receptors, and melanocyte stimulating hormone receptors have been shown to be useful for scintigraphy of tumors overexpressing these receptors (36–38). The gastrin-releasing peptide receptor has also been the target for radiolabeled peptide imaging in recent years. In this regard, GRPR-avid peptides have been radiolabeled with  $^{111}\text{In}$  and  $^{99\text{m}}\text{Tc}$  and evaluated in animals and humans as potential imaging agents. Breeman et al. demonstrated GRPR-specific imaging of 7315b pituitary tumors in rats using a DTPA-BN analogue radiolabeled with  $^{111}\text{In}$  (22). Van de Wiele et al. evaluated the biodistribution and dosimetry of a  $^{99\text{m}}\text{Tc}$ -labeled BN agonist ( $^{99\text{m}}\text{Tc}$ -RP527) in healthy (26) and carcinoma bearing (24) volunteers by gamma camera imaging. These studies show the potential of radiolabeled BN analogues for imaging BN-positive tumors and use in humans.

Initial radiolabeling attempts of DOTA-Aoc-BN(7–14) with  $^{64}\text{Cu}$  achieved specific activities of 130 mCi/mg. Labeling at higher specific activities led to radiolysis of the peptide as determined by radio-TLC.  $^{64}\text{Cu}$ -DOTA-Aoc-BN(7–14) labeled at this specific activity was used for the in vitro assays and biodistribution studies. Further radiolabeling attempts achieved specific activities of 2000 mCi/mg by adding gentisic acid to prevent radiolysis.  $^{64}\text{Cu}$ -DOTA-Aoc-BN(7–14) labeled at this specific activity was used for the microPET studies and for a biodistribution study at 2 h to confirm the results of the lower specific activity biodistribution.

The  $^{64}\text{Cu}$ -DOTA-Aoc-BN(7–14) had a high affinity for GRPR ( $K_d = 6.1$  nM) as shown in Figure 1. This is similar

to other studies that demonstrated that chelate-BN analogues and metal-chelate-analogues had  $\text{IC}_{50}$  values that were similar to BN(7–14) (19, 20, 22, 27). The  $B_{\text{max}}$  value of  $2.7 \times 10^5$  receptors/cell is higher than the  $4.4 \times 10^4$  reported by Reile et al (39). This difference could be a function of the density of the cells when the assays were performed. For example, our cells were harvested in an exponential phase of growth, while harvesting a confluent monolayer may result in receptor down regulation. Figure 2 shows that  $^{64}\text{Cu}$ -DOTA-Aoc-BN(7–14) was rapidly internalized into PC-3 cells with 11.4% of the added radioactivity internalized after a 30 min incubation and 21.5% after 4 h. Breeman et al. demonstrated that radiolabeled BN agonists were internalized into GRPR-positive cells, but not radiolabeled antagonists (22). In general, BN analogues that maintain their amidated C-terminal methionine have been shown to be agonists (40), which have potential for tumor imaging when radiolabeled with various radioisotopes as discussed by Van de Wiele et al (25). Thus, although not explicitly demonstrated in these studies,  $^{64}\text{Cu}$ -DOTA-Aoc-BN(7–14) is presumed to be an agonist. This is in agreement with other radiolabeled BN(7–14) analogues that have also been demonstrated to undergo rapid in vitro internalization. For example, LaBella et al. showed that two  $^{99\text{m}}\text{Tc}$ -labeled BN(7–14) analogues reached 70% internalization into PC-3 cells by 15 min (27, 28). These studies are significant because internalization of radiolabeled peptides has been shown to be important for developing diagnostic and therapeutic agents (41).

In vivo biodistribution (Figure 3) showed good localization of  $^{64}\text{Cu}$ -DOTA-Aoc-BN(7–14) into PC-3 tumors that was specific for GRPR, as demonstrated by coinjection of an excess of unlabeled BN. These results are favorable to other studies using different BN analogues and different tumor models. In rats bearing 7315b rat pituitary tumors, Breeman et al. reported that an  $^{111}\text{In}$ -labeled BN agonist had a tumor localization of 0.05% ID/g at 24 h compared to 2.5% ID/g at 24 h in our mouse model (22). Using the same PC-3 tumor model in mice, La Bella et al. had 0.3–0.6% ID/g in tumor 1.5 h after injection for two  $^{99\text{m}}\text{Tc}$ -labeled BN analogues (27, 28). Smith et al. reported a tumor localization of 4.2% ID/g in the PC-3 mouse tumor model at 1 h for this same DOTA-Aoc-BN(7–14) radiolabeled with  $^{177}\text{Lu}$  (18). The localization of  $^{64}\text{Cu}$ -DOTA-Aoc-BN(7–14) in normal tissues, however, is higher than that reported in other studies. Normal tissue uptake (except for pancreas and kidney) of  $^{64}\text{Cu}$ -DOTA-Aoc-BN(7–14) ranged from 0.8 to 13.3% ID/g at 2 h compared to 0.1 to 4.5% ID/g at 1.5 h for the  $^{99\text{m}}\text{Tc}$ -labeled BN analogues and 0.1 to 0.4% ID/g at 1 h for the  $^{177}\text{Lu}$ -labeled BN analogues (18, 27, 28). Differences in the chelates and linkers could account for the lower tissue uptake of the  $^{99\text{m}}\text{Tc}$ -labeled BN analogues compared to  $^{64}\text{Cu}$ -DOTA-Aoc-BN(7–14). With regard to the lower uptake of  $^{177}\text{Lu}$ -DOTA-Aoc-BN(7–14) compared to  $^{64}\text{Cu}$ -DOTA-Aoc-BN(7–14) the difference may be due to the charge difference between Cu(II) and Lu(III). Alternatively, it has been demonstrated that Cu(II) can transchelate to albumin and superoxide dismutase, leading to higher blood and liver uptake (42, 43). It will be necessary to reduce this normal tissue uptake (particularly in the liver and kidney) for the clinical application of  $^{64}\text{Cu}$ -DOTA-Aoc-BN(7–14) as an imaging or therapeutic agent. The use of less lipophilic linkers should reduce the liver uptake and making the overall charge of the peptide either neutral or negative should reduce the kidney accumulation.



As discussed previously, several BN analogues have been evaluated for imaging GRPR-positive tumors using gamma ray scintigraphy. Here we show the first PET images of GRPR-positive tumors in mice using microPET (Figure 4). MicroPET has been used extensively in recent years for evaluating reporter gene expression in small animal models (44, 45), while microPET imaging of tumor antigens/receptors using radiolabeled peptides has been limited to the somatostatin receptor subtype 2 (46, 47). Transaxial images show good localization of  $^{64}\text{Cu}$ -DOTA-Aoc-BN(7–14) in PC-3 tumors in mice that did not receive a co-injection of competitor. In contrast, the tumor localization was reduced in mice that received the competitor, demonstrating GRPR-specific localization. The tumor for the mouse in Figure 4D was twice the size of the other tumors, which may account for the lack of complete inhibition as was observed in Figure 4B. In addition to the tumor, the bladder is observed due to the clearance of  $^{64}\text{Cu}$ -DOTA-Aoc-BN(7–14) through the kidney and urinary excretion. These studies demonstrate the feasibility of using positron-labeled BN analogues for PET detection of GRPR-positive neoplasms.

Although good tumor localization was observed for  $^{64}\text{Cu}$ -DOTA-Aoc-BN(7–14) in biodistribution and microPET imaging studies, we anticipated even greater localization based upon the *in vitro* results for the number of receptors per PC-3 cell. To determine if GRPR had been down regulated on PC-3 cells *in vivo*, we harvested PC-3 tumors and pancreata from mice and performed a competitive binding assay on tissue membrane preparations (Figure 5). This study showed that there were approximately 15-fold less GRPRs on PC-3 cells *in vivo* than *in vitro*, but 14-fold greater expression of GRPR per mg of PC-3 tumor than per mg of pancreas. Similar to our results (27 fmol/mg), Fanger et al. reported a level of GRPR on mouse pancreas to be 75 fmol/mg and 31 fmol/mg was reported by Hajri et al. for GRPR in rat pancreas (48, 49). Thus, greater tumor localization of  $^{64}\text{Cu}$ -DOTA-Aoc-BN(7–14) would be expected based upon the GRPR expression on tumor vs pancreas.

A preliminary biodistribution study using high specific activity  $^{64}\text{Cu}$ -DOTA-Aoc-BN(7–14) (2000 mCi/mg) did not show a difference in localization in tumor or normal tissues at 2 h postinjection when compared to the biodistribution in Figure 3, except for an increase in the pancreas to 24.1% ID/g (data not shown). This implies that GRPRs were saturated in the pancreas using the lower specific activity  $^{64}\text{Cu}$ -DOTA-Aoc-BN(7–14), thus reducing the % ID/g. We hypothesize that  $^{64}\text{Cu}$ -DOTA-Aoc-BN(7–14) did not saturate GRPRs on the PC-3 tumors, and the low uptake may be due to low blood flow. In this regard, Krohn describes a kinetic model relating blood flow to cell-bound ligand complexes (50). Krohn suggests that if ligand diffusion to the receptor is rate limiting, then the receptor number cannot be quantitated. Table 1 shows that the blood flow to the PC-3 tumor is 2.6-fold lower than the blood flow to the pancreas, which may limit diffusion of  $^{64}\text{Cu}$ -DOTA-Aoc-BN(7–14) to the tumor and underestimate the number of receptors. These results will need to be investigated further to determine if the limited tumor localization is due to low blood flow or other biochemical factors associated with PC-3 tumors. Utilization of another tumor model with similar GRPR expression and increased blood flow may help answer this question.

In conclusion, this study demonstrates that a BN analogue can be radiolabeled with the positron-emitter  $^{64}\text{Cu}$  and maintain high affinity and internalize into GRPR-positive cells. Specific tumor localization of  $^{64}\text{Cu}$ -

DOTA-Aoc-BN(7–14) in mice was visualized by microPET imaging and was confirmed by biodistribution studies. Reduction of the uptake of  $^{64}\text{Cu}$ -labeled BN analogues in normal tissues by modifying the charge of the peptide and the peptide linker group will be the focus of future studies. In addition, the relationship between blood flow and tumor localization of these analogues will be evaluated in different tumor models. This study demonstrates the potential of BN analogues for detecting GRPR-positive tumors in the clinical setting by PET imaging and possibly for radiotherapy.

#### ACKNOWLEDGMENT

We gratefully acknowledge the expert technical assistance of Sheila Bright, Synethia Kidd, and Richard Kirkman. This work was supported by a grant from the American Cancer Society RPG-00-067-01-CCE (B.E.R.) thanks to a gift from the F.M. Kirby Foundation. MicroPET imaging was supported by an NIH/NCI SAIRP grant 1 R24 CA83060 (M.J.W.). We would also like to thank the Small Animal Imaging Core of the Alvin J. Siteman Cancer Center at Washington University and Barnes-Jewish Hospital in St. Louis, Missouri for additional support of the microPET imaging. The Core is supported by an NCI Cancer Center Support Grant # 1 P30 CA91842.

#### LITERATURE CITED

- (1) Sunday, M. E., Kaplan, L. M., Motoyama, E., Chin, W. W., and Spindel, E. R. (1988) Gastrin-releasing peptide (mammalian bombesin) gene expression in health and disease. *Lab. Invest.* 59, 5–24.
- (2) Spindel, E. R., Giladi, E., Segerson, T. P., and Nagalla, S. (1993) Bombesin-like peptides: of ligands and receptors. *Recent Prog. Horm. Res.* 48, 365–391.
- (3) Moody, T. W., Carney, D. N., Cuttitta, F., Quattrocchi, K., and Minna, J. D. (1985) High affinity receptors for bombesin/GRP-like peptides on human small cell lung cancer. *Life Sci.* 37, 105–113.
- (4) Radulovic, S., Miller, G., and Schally, A. V. (1991) Inhibition of growth of HT-29 human colon cancer xenografts in nude mice by treatment with bombesin/gastrin releasing peptide antagonist (RC-3095). *Cancer Res.* 51, 6006–6009.
- (5) Pinski, J., Schally, A. V., Halmos, G., Szepeshazi, K., and Groot, K. (1994) Somatostatin analogues and bombesin/gastrin-releasing peptide antagonist RC-3095 inhibit the growth of human glioblastomas *in vitro* and *in vivo*. *Cancer Res.* 54, 5895–5901.
- (6) Qin, Y., Ertl, T., Cai, R. Z., Halmos, G., and Schally, A. V. (1994) Inhibitory effect of bombesin receptor antagonist RC-3095 on the growth of human pancreatic cancer cells *in vivo* and *in vitro*. *Cancer Res.* 54, 1035–1041.
- (7) Reubi, J. C., Wenger, S., Schumckli-Maurer, J., Schaer, J. C., and Gugger, M. (2002) Bombesin receptor subtypes in human cancers: Detection with the universal radioligand  $^{125}\text{I}$ -[D-TYR<sup>6</sup>,  $\beta$ -ALA<sup>11</sup>, PHE<sup>13</sup>, NLE<sup>14</sup>] Bombesin(6–14). *Clin. Cancer Res.* 8, 1139–1146.
- (8) Von Schrenck, T., Heinz-Erian, P., Moran, T., Mantey, S. A., Gardner, J. D., and Jensen, R. T. (1989) Neuromedin B receptor in esophagus: Evidence for subtypes of bombesin receptors. *Am. J. Physiol.* 256, 747–758.
- (9) Fathi, Z., Corjay, M. H., Shapira, H., Wada, E., Benya, R., Jensen, R., Viallet, J., Sausville, E. A., and Battey, J. F. (1993) BRS-3: a novel bombesin receptor subtype selectively expressed in testis and lung carcinoma cells. *J. Biol. Chem.* 268, 5979–5984.
- (10) Nagalla, S. R., Barry, B. J., Creswick, K. C., Eden, P., Taylor, J. T., and Spindel, E. R. (1995) Cloning of a receptor for amphibian [Phe<sup>13</sup>]bombesin distinct from the receptor for

- gastrin-releasing peptide: Identification of a fourth bombesin receptor subtype (BB4). *Proc. Natl. Acad. Sci. U.S.A.* 92, 6205–6209.
- (11) Cuttitta, F., Carney, D. N., Mulshine, J., Moody, T. W., Fedorko, J., Fischler, A., and Minna, J. D. (1985) Bombesin-like peptides can function as autocrine growth factors in human small-cell lung cancer. *Nature* 316, 823–826.
  - (12) Kiaris, H., Schally, A. V., Nagy, A., Sun, B., Armatas, P., and Szepeshazi, K. (1999) Targeted cytotoxic analogue of bombesin/gastrin-releasing peptide inhibits the growth of H-69 human small-cell lung carcinoma in nude mice. *Br. J. Cancer* 81, 966–971.
  - (13) Schally, A. V., Comaru-Schally, A. M., Nagy, A., Kovacs, M., Szepeshazi, K., Plonowski, A., Varga, J. L., and Halmos, G. (2001) Hypothalamic hormones and cancer. *Front. Neuroendocrinol.* 22, 248–291.
  - (14) Bajo, A. M., Schally, A. V., Krupa, M., Hebert, F., Groot, K., and Szepeshazi, K. (2002) Bombesin antagonists inhibit growth of MDA-MB-435 estrogen-independent breast cancers and decrease the expression of the ErbB-2/HER-2 oncoprotein and c-jun and c-fos oncogenes. *Proc. Natl. Acad. Sci. U.S.A.* 99, 3836–3841.
  - (15) Nagy, A., Armatas, P., Cai, R. Z., Szepeshazi, K., Halmos, G., and Schally, A. V. (1997) Design, synthesis, and in vitro evaluation of cytotoxic analogues of bombesin-like peptides containing doxorubicin or its intensely potent derivative, 2-pyrrolinodoxorubicin. *Proc. Natl. Acad. Sci. U.S.A.* 94, 652–656.
  - (16) Safavy, A., Khazaali, M. B., Qin, H., and Buchsbaum, D. J. (1997) Synthesis of bombesin analogues for radiolabeling with Rhenium-188. *Cancer (Suppl)* 80, 2354–2359.
  - (17) Rogers, B. E., Curiel, D. T., Mayo, M. S., Laffoon, K. K., Bright, S. J., and Buchsbaum, D. J. (1997) Tumor localization of a radiolabeled bombesin analogue in mice bearing human ovarian tumors induced to express the gastrin releasing peptide receptor by an adenoviral vector. *Cancer* 80, 2419–2424.
  - (18) Smith, C. J., Hoffman, T. J., Hayes, D. L., Owen, N. K., Sieckman, G. L., and Volkert, W. A. (2001) Radiochemical investigations of  $^{177}\text{Lu}$ -DOTA-8-Aoc-BBN[7–14] $\text{NH}_2$ : A new gastrin releasing peptide receptor (GRPr) targeting radiopharmaceutical. *J. Labelled Compd. Radiopharm.* 44, S706–S708.
  - (19) Hu, F., Cutler, C. S., Hoffman, T., Sieckman, G., Volkert, W. A., and Jurisson, S. S. (2002) Pm-149 DOTA bombesin analogues for potential radiotherapy In vivo comparison with Sm-153 and Lu-177 labeled DO3A-amide- $\beta\text{Ala}$ -BBN(7–14)- $\text{NH}_2$ . *Nucl. Med. Biol.* 29, 423–430.
  - (20) Baidoo, K. E., Lin, K. S., Zhan, Y., Finley, P., Scheffel, U., and Wagner, H. N., Jr. (1998) Design, synthesis, and initial evaluation of high-affinity technetium bombesin analogues. *Bioconjugate Chem.* 9, 218–225.
  - (21) Karra, S., Schibli, R., Gali, H., Katti, K., Hoffman, T., Higginbotham, C., Sieckman, G., and Volkert, W. (1999)  $^{99m}\text{Tc}$ -labeling and in vivo studies of a bombesin analogue with a novel water-soluble dithiadiphosphine-based bifunctional chelating agent. *Bioconjugate Chem.* 10, 254–260.
  - (22) Breeman, W. A. P., Hofland, L. J., de Jong, M., Bernard, B. F., Srinivasan, A., Kwekkeboom, D. J., Visser, T. J., and Krenning, E. P. (1999) Evaluation of radiolabeled bombesin analogues for receptor-targeted scintigraphy and radiotherapy. *Int. J. Cancer* 81, 658–665.
  - (23) Breeman, W. A. P., de Jong, M., Bernard, B. F., Kwekkeboom, D. J., Srinivasan, A., van der Pluijm, M. E., Hofland, L. J., Visser, T. J., and Krenning, E. P. (1999) Pre-clinical evaluation of [ $^{111}\text{In}$ -DTPA-Pro<sup>1</sup>, Tyr<sup>4</sup>]bombesin, a new radioligand for bombesin-receptor scintigraphy. *Int. J. Cancer* 83, 657–663.
  - (24) Van de Wiele, C., Dumont, F., Broecke, R. V., Oosterlinck, W., Cocquyt, V., Serreyn, R., Peers, S., Thornback, J., Slegers, G., and Dierckx, R. A. (2000) Technetium-99m RP527, a GRP analogue for visualization of GRP receptor-expressing malignancies: a feasibility study. *Eur. J. Nucl. Med.* 27, 1694–1699.
  - (25) Van de Wiele, C., Dumont, F., Van Belle, S., Slegers, G., Peers, S. H., and Dierckx, R. A. (2001) Is there a role for agonist gastrin-releasing peptide receptor radioligands in tumour imaging? *Nucl. Med. Commun.* 22, 5–15.
  - (26) Van de Wiele, C., Dumont, F., Dierckx, R. A., Peers, S. H., Thornback, J. R., Slegers, G., and Thierens, H. (2001) Biodistribution and dosimetry of  $^{99m}\text{Tc}$ -RP527, a gastrin-releasing peptide (GRP) agonist for the visualization of GRP receptor-expressing malignancies. *J. Nucl. Med.* 42, 1722–1727.
  - (27) La Bella, R., Garcia-Garayoa, E., Langer, M., Blauenstein, P., Beck-Sickinger, A. G., and Schubiger, P. A. (2002) In vitro and in vivo evaluation of a  $^{99m}\text{Tc}$ (I)-labeled bombesin analogue for imaging of gastrin releasing peptide receptor-positive tumors. *Nucl. Med. Biol.* 29, 553–560.
  - (28) La Bella, R., Garcia-Garayoa, E., Bahler, M., Blauenstein, P., Schibli, R., Conrath, P., Tourwe, D., and Schubiger, P. A. (2002) A  $^{99m}\text{Tc}$ -postlabeled high affinity bombesin analogue as a potential tumor imaging agent. *Bioconjugate Chem.* 13, 599–604.
  - (29) Connett, J. M., Anderson, C. J., Guo, L. W., Schwarz, S. W., Zinn, K. R., Rogers, B. E., Siegel, B. A., Philpott, G. W., and Welch, M. J. (1996) Radioimmunotherapy with a  $^{64}\text{Cu}$ -labeled monoclonal antibody: A comparison with  $^{67}\text{Cu}$ . *Proc. Natl. Acad. Sci. U.S.A.* 93, 6814–6818.
  - (30) Anderson, C. J., Jones, L. A., Bass, L. A., Sherman, E. L. C., McCarthy, D. W., Cutler, P. D., Lanahan, M. V., Cristel, M. E., Lewis, J. S., and Schwarz, S. W. (1998) Radiotherapy, toxicity and dosimetry of copper-64-TETA-octreotide in tumor-bearing rats. *J. Nucl. Med.* 39, 1944–1951.
  - (31) McCarthy, D. W., Shefer, R. E., Klinkowstein, R. E., Bass, L. A., Margeneau, W. H., Cutler, C. S., Anderson, C. J., and Welch, M. J. (1997) Efficient production of high specific activity  $^{64}\text{Cu}$  using a biomedical cyclotron. *Nucl. Med. Biol.* 24, 35–43.
  - (32) Cherry, S., Shao, Y., Silverman, R., Meadors, K., Siegel, S., Chatzizoiannou, A., Young, J., Jones, W., Moyers, J., Newport, D., Boutenouchet, A., Farquhar, T., Andreaco, M., Paulus, M., Binkley, D., Nutt, R., and Phelps, M. (1997) MicroPET: A high-resolution PET scanner for imaging small animals. *IEEE Trans. Nucl. Sci.* 44, 1161–1166.
  - (33) Defrise, M. P., Kinahan, D., Townsend, C., Michel, M., and Newport, D. (1997) Exact and approximate rebinning algorithms for 3-D PET data. *IEEE Trans. Med. Imaging* 16, 145–158.
  - (34) Rogers, B. E., McLean, S. F., Kirkman, R. L., Della Manna, D., Bright, S. J., Olsen, C. C., Myracle, A. D., Mayo, M. S., Curiel, D. T., and Buchsbaum, D. J. (1999) In vivo localization of [ $^{111}\text{In}$ ]-DTPA-D-Phe<sup>1</sup>-octreotide to human ovarian tumor xenografts induced to express the somatostatin receptor subtype 2 using an adenoviral vector. *Clin. Cancer Res.* 5, 383–393.
  - (35) Mathias, C. J., Welch, M. J., Perry, D. J., McGuire, A. H., Zhu, X., Connett, J. M., and Green, M. A. (1991) Investigation of copper-PTSM as a PET tracer for tumor blood flow. *Int. J. Rad. Appl. Instrum. B* 18, 807–811.
  - (36) Raderer, M., Kurtaran, A., Leimer, M., Angelberger, P., Niederle, B., Vierhapper, H., Vorbeck, F., Hejna, M. H., Scheithauer, W., Pidlich, J., and Virgolini, I. (2000) Value of peptide receptor scintigraphy using  $^{123}\text{I}$ -vasoactive intestinal peptide and  $^{111}\text{In}$ -DTPA-D-Phe<sup>1</sup>-octreotide in 194 carcinoid patients: Vienna University Experience, 1993 to 1998. *J. Clin. Oncol.* 18, 1331–1336.
  - (37) Cheng, Z., Chen, J., Miao, Y., Owen, N. K., Quinn, T. P., and Jurisson, S. S. (2002) Modification of the structure of a metalloprotein: synthesis and biological evaluation of  $^{111}\text{In}$ -labeled DOTA-conjugated rhenium-cyclized alpha-MSH analogues. *J. Med. Chem.* 45, 3048–3056.
  - (38) Kwekkeboom, D. J., and Krenning, E. P. (2002) Somatostatin receptor imaging. *Semin. Nucl. Med.* 32, 84–91.
  - (39) Reile, H., Armatas, P. E., and Schally, A. V. (1994) Characterization of high-affinity receptors for bombesin/gastrin releasing peptide on the human prostate cancer cell lines PC-3 and DU-145: Internalization of receptor bound  $^{125}\text{I}$ -(Tyr<sup>4</sup>) bombesin by tumor cells. *Prostate* 25, 29–38.
  - (40) Mantey, S., Frucht, H., Coy, D. H., and Jensen, R. T. (1993) Characterization of bombesin receptors using a novel, potent,

- radiolabeled antagonist that distinguishes bombesin receptor subtypes. *Mol. Pharmacol.* 43, 762–774.
- (41) Reilly, R. M., Kiarash, R., Cameron, R. G., Porlier, N., Sandhu, J., Hill, R. P., Vallis, K., Hendler, A., and Gariepy, J. (2000)  $^{111}\text{In}$ -labeled EGF is selectively radiotoxic to human breast cancer cells overexpressing EGFR. *J. Nucl. Med.* 41, 429–438.
- (42) Rogers, B. E., Anderson, C. J., Connett, J. M., Guo, L. W., Edwards, W. B., Sherman, E. L. C., Zinn, K. R., and Welch, M. J. (1996) Comparison of four bifunctional chelates for radiolabeling monoclonal antibodies with copper radioisotopes: Biodistribution and metabolism. *Bioconjugate Chem.* 7, 511–522.
- (43) Bass, L. A., Wang, M., Welch, M. J., and Anderson, C. J. (2000) In vivo transchelation of copper-64 from TETA-octreotide to superoxide dismutase in rat liver. *Bioconjugate Chem.* 11, 527–532.
- (44) Luker, G. D., Sharma, V., Pica, C. M., Dahlheimer, J. L., Li, W., Ochesky, J., Ryan, C. E., Piwnica-Worms, H., and Piwnica-Worms, D. (2002) Noninvasive imaging of protein–protein interactions in living animals. *Proc. Natl. Acad. Sci. U.S.A.* 99, 6961–6966.
- (45) Liang, Q., Gotts, J., Satyamurthy, N., Barrio, J., Phelps, M. E., Gambhir, S. S., and Herschman, H. (2002) Noninvasive, repetitive, quantitative measurement of gene expression from a bicistronic message by positron emission tomography, following gene transfer with adenovirus. *Mol. Ther.* 6, 73–82.
- (46) Li, W. P., Lewis, J. S., Kim, J., Bugaj, J. E., Johnson, M. A., Erion, J. L., and Anderson, C. J. (2002) DOTA-D-Tyr<sup>1</sup>-octreotate: A somatostatin analogue for labeling with metal and halogen radionuclides for cancer imaging and therapy. *Bioconjugate Chem.* 13, 721–728.
- (47) Uger, O., Kothari, P. J., Finn, R. D., Zanzonico, P., Ruan, S., Guenther, I., Maecke, H. R., and Larson, S. M. (2002) Ga-66 labeled somatostatin analogue DOTA-DPhe<sup>1</sup>-Tyr<sup>3</sup>-octreotide as a potential agent for positron emission tomography imaging and receptor mediated internal radiotherapy of somatostatin receptor positive tumors. *Nucl. Med. Biol.* 29, 147–157.
- (48) Fanger, B. O., Wade, A. C., and Cardin, A. D. (1991) Characterization of the murine pancreatic receptor for gastrin releasing peptide and bombesin. *Reg. Pept.* 32, 241–251.
- (49) Hajri, A., Koenig, M., Balboni, G., and Damge, C. (1996) Expression and characterization of gastrin-releasing peptide receptor in normal and cancerous pancreas. *Pancreas* 12, 25–35.
- (50) Krohn, K. A. (2001) The physical chemistry of ligand–receptor binding identifies some limitations to the analysis of receptor images. *Nucl. Med. Biol.* 28, 477–483.

BC034018L



# Synthesis of Novel Cationic Lipids Having Polyamidoamine Dendrons and Their Transfection Activity

Toshinari Takahashi,<sup>†</sup> Kenji Kono,<sup>\*,†</sup> Toshihide Itoh,<sup>‡</sup> Nobuhiko Emi,<sup>‡</sup> and Toru Takagishi<sup>†</sup>

Department of Applied Materials Science, Graduate School of Engineering, Osaka Prefecture University, 1–1 Gakuen-cho, Sakai, Osaka 599-8531, Japan, and First Department of Internal Medicine, Nagoya University School of Medicine, Nagoya 466–8550, Aichi, Japan. Received December 28, 2002; Revised Manuscript Received March 27, 2003

We designed a novel type of cationic lipid, lipids with a cationic polar group in the polyamidoamine dendron, because these dendron-bearing lipids are expected to form complexes with plasmid DNA and achieve efficient transfection of cells by synergy of endosome buffering and membrane fusion with the endosome, both of which are useful for the promotion of the transfer of plasmid DNA from endosome to cytosol. Four kinds of lipids with polyamidoamine dendrons of first to fourth generations, DL-G1, DL-G2, DL-G3, and DL-G4, were synthesized. The lipid with a dendron of a higher generation exhibited greater ability to form lipoplexes with plasmid DNA, as estimated by agarose gel electrophoresis. While the DL-G1 lipoplex did not transfect CV1 cells, the lipoplexes containing the DL-G2, DL-G3, or DL-G4 could induce transfection of the cells, and their activity was elevated with increasing generation of the dendron. Addition of dioleoylphosphatidylethanolamine (DOPE), which is known to increase fusion ability of a lipid membrane, into the lipoplexes greatly enhanced their transfection activity. In addition, the comparison with DC-Chol-containing lipoplex, which is widely used as a nonviral vector, showed that the DL-G3–DOPE lipoplex exhibits more efficient transfections. These findings imply that these dendron-bearing lipids may form the basis for a novel family of cationic lipids for efficient gene delivery.

## INTRODUCTION

Although many efforts have been made to develop nonviral vectors for gene therapy, their transfection activity is still to be improved (1, 2). While a number of systems have been reported, cationic liposomes and cationic polymers have been shown to exhibit relatively high ability to transfect various cells (3–10). These systems can associate with plasmid DNA and form complexes, which are termed lipoplexes for the complexes with cationic liposomes and polyplexes for the complexes with cationic polymers. The complexes with a positively charged surface strongly bind to cell membranes through electrostatic interaction (11).

It is currently considered that an endocytic pathway is a major pathway for DNA entry mediated by lipoplexes and polyplexes (12–15). After internalization, they are trapped in endosome, from which some fractions of DNA either included in or liberated from the complexes transfer into cytosol and subsequently enter into the nucleus (16–18). However, a large fraction of the complexes taken up in endosome is delivered to lysosome and eventually degraded (12–15). Thus, many efforts have been made to establish strategies for the efficient escape of DNA from endosome into cytosol to improve their transfection efficiency. While various approaches have been attempted for this purpose, one of the most efficient methods to elevate the transfection activity of lipoplexes is to increase their fusion ability. It is well-known that inclusion of fusogenic lipids, such as dioleoylphosphati-

dylethanolamine (DOPE) greatly improve the transfection ability of lipoplexes (19–23). It is considered that lipoplexes with high fusion ability transfer the entrapped DNA from endosome into cytosol efficiently by destabilizing and fusing with endosomal membrane (16, 23). In addition, modification of lipoplexes with various fusogenic molecules have been shown to improve the transfection activity of lipoplexes (24–27).

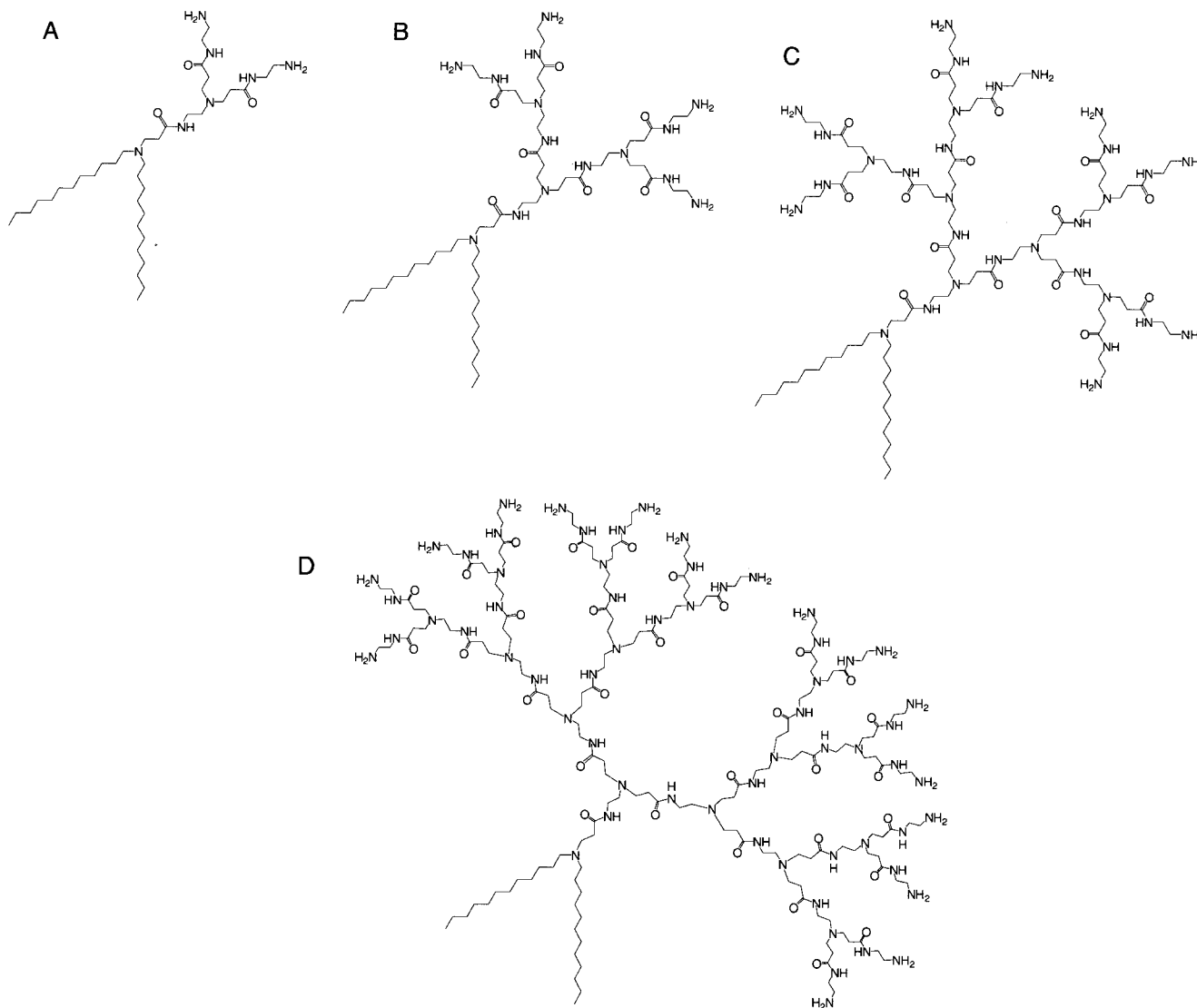
On the other hand, some cationic polymers, such as poly(ethylenimine) and polyamidoamine dendrimers, have been shown to achieve efficient transfection for various animal and human cells (6, 11, 28–30). Because these polymers possess secondary and tertiary amino groups, which become protonated under weakly acidic conditions, it is believed that these amino groups suppress the lowering of pH in endosome/lysosome by adsorbing proton and prohibit degradation of DNA in lysosome. In addition, the endosome buffering by these polymers is thought to induce osmotic swelling of the endosome interior and result in rupture of the endosome and subsequent release of DNA into cytoplasm (28, 31).

Because both the endosome buffering by secondary and tertiary amino groups and endosome fusion by fusogenic lipids are currently considered to be efficient means of enhancing transfer of DNA from endosome to cytoplasm, their combination is expected to give a highly efficient gene delivery system. Thus, we designed a new type of cationic lipids, amphiphiles composed of two long alkyl groups and a polyamidoamine dendron as headgroup. Since polyamidoamine dendrimers/dendrons have many tertiary amino groups in their interior, they would show a high buffering ability. In addition, for this type of cationic lipid, the molecular shape and the balance between the polar headgroup and the hydrophobic tails

\* Corresponding author. E-mail: kono@ams.osakafu-u.ac.jp.  
Tel: +81-722549330. Fax: +81-722549913.

<sup>†</sup> Osaka Prefecture University.

<sup>‡</sup> Nagoya University School of Medicine.



**Figure 1.** Structures of DL-G1 (A), DL-G2 (B), DL-G3 (C), and DL-G4 (D).

can be readily and precisely adjusted by controlling generation of the dendron moiety of the lipid. This is particularly important to optimize the chemical structure of the lipid molecule, because these factors affect its ability to complex with DNA and transfection (8, 32, 33). In this study, four kinds of lipid molecules having the polyamidoamine dendron of first, second, third, and fourth generations, which are termed DL-G1, DL-G2, DL-G3, and DL-G4, respectively, were synthesized (Figure 1). Their abilities to form a lipoplex with plasmid DNA and to induce transfection of CV1 cells, an African green monkey kidney cell line, were investigated. Correlation between the generation of the dendron-bearing lipids and their transfection activity, and the effect of addition of a fusogenic lipid, dioleoylphosphatidylethanolamine (DOPE), on their transfection activity, were described.

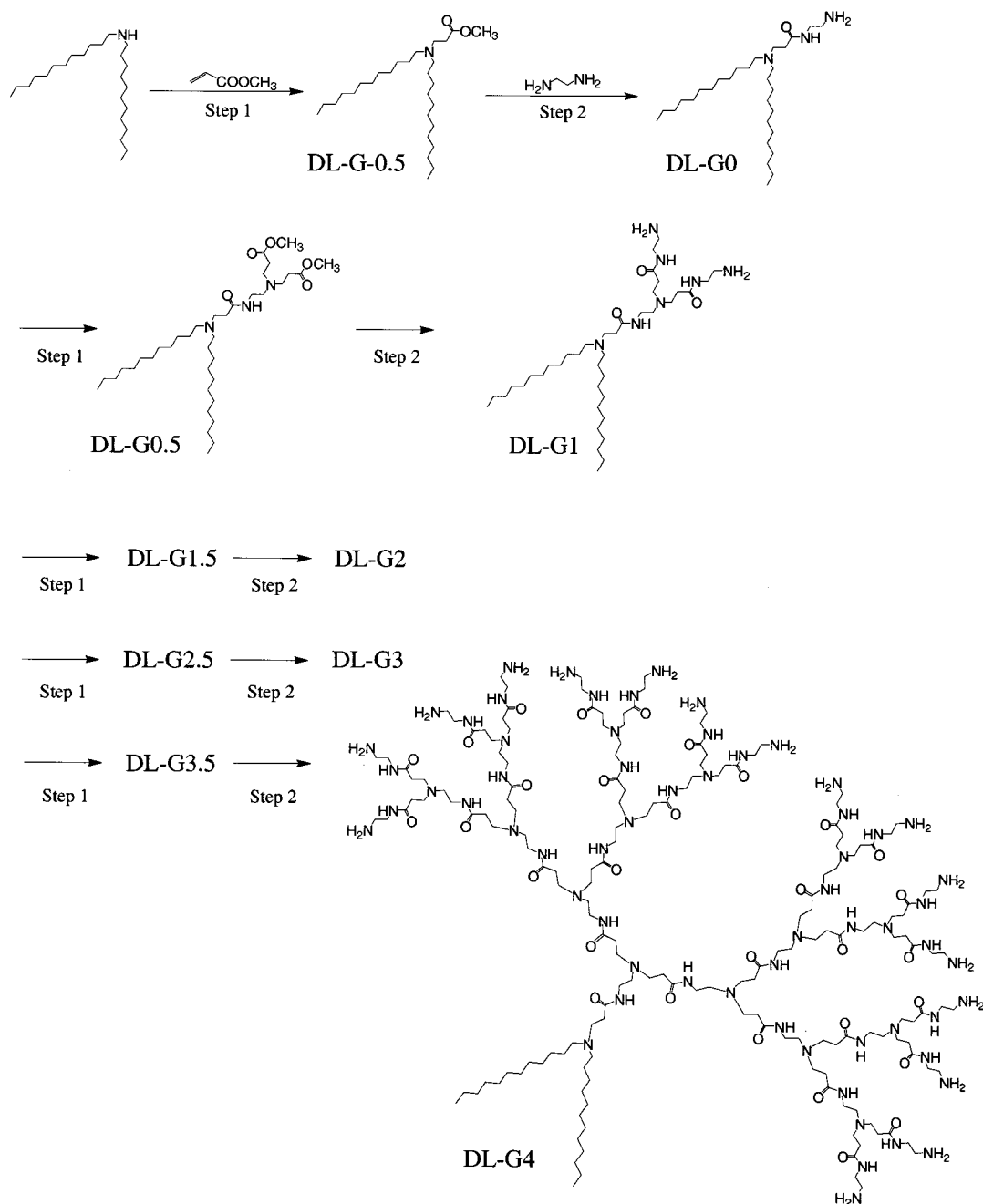
#### EXPERIMENTAL PROCEDURES

**General Methods.** DOPE was kindly donated by Nippon Oil and Fats Co. (Tokyo, Japan). Di-*n*-dodecylamine was purchased from Tokyo Kasei Kogyo (Tokyo, Japan). Methyl acrylate, ethylenediamine, and tris-(hydroxymethyl)aminomethane (Tris) were obtained from Kishida Chemical (Osaka, Japan). Sodium cyanide and ethidium bromide were supplied from Wako Pure Chemi-

cal Industries (Osaka, Japan). Fetal calf serum (FCS) was obtained from JRH Biosciences (Tokyo, Japan). Merck Kieselgel 60 (230–400 mesh) was used for silica gel chromatography. Agarose was from Sigma (St. Louis, MO). Dulbecco's modified Eagle's medium (DMEM) was from Nissui Pharmaceutical (Tokyo, Japan). 3-(4,5-Dimethyl-2-thiazolyl)-2,5-diphenyl-2*H*-tetrazolium bromide (MTT) was obtained from Dojin Laboratories (Kumamoto, Japan). Methyl acrylate and ethylenediamine were purified by distillation under reduced pressure.

3 $\beta$ -(*N,N,N*-Dimethylaminoethane)carbamoyl)cholesterol (DC-Chol) was synthesized according to the method of Gao and Huang (34). PAMAM G4 dendrimer was prepared according to the method of Tomalia et al. using ethylenediamine as the core (35, 36). <sup>1</sup>H and <sup>13</sup>C NMR spectra were recorded on a JEOL JNM-LA 400 instrument. MALDI-TOF spectra were recorded using a KOMPACT PROBE/MALDI 2 (Shimadzu, Japan).

**Synthesis of Dendron-Bearing Lipids.** A series of polyamidoamine dendron-bearing lipids were synthesized by repetition of exhaustive Michael addition with methyl acrylate using di-*n*-dodecylamine as the core material and subsequent exhaustive amidation with ethylenediamine, as reported by Tomalia et al. (35, 36). The synthetic route

**Scheme 1. Synthetic Route for Dendron-Bearing Lipids**

for the polyamidoamine dendron-bearing lipids is shown in Scheme 1.

**DL-G-0.5.** Di-*n*-dodecylamine (2.0 g, 5.7 mmol) was dissolved in purified methyl acrylate (14 mL, 0.16 mol) and the resultant solution was refluxed under nitrogen. After 18 h, unreacted methyl acrylate was removed under vacuum, and the residue was chromatographed on silica gel using petroleum ether–diethyl ether (2:1, v/v) as eluent. Yield, 96.1%;  $^1\text{H}$  NMR ( $\text{CDCl}_3$ ):  $\delta$  0.85 (m,  $\text{CH}_3$ -( $\text{CH}_2$ )<sub>9</sub>), 1.23 (s,  $\text{CH}_3$ ( $\text{CH}_2$ )<sub>9</sub>), 1.38 (m,  $\text{CH}_2\text{CH}_2\text{N}$ ), 2.35 (t,  $\text{CH}_2\text{COOCH}_3$ ), 2.40 (t,  $\text{CH}_2\text{N}$ ), 2.74 (t,  $\text{CH}_2\text{CH}_2\text{COOCH}_3$ ), 3.63 (s,  $\text{OCH}_3$ );  $^{13}\text{C}$  NMR ( $\text{CDCl}_3$ ):  $\delta$  14.1 ( $\text{CH}_3$ ( $\text{CH}_2$ )<sub>10</sub>), 22.7, 27.1, 27.5, 29.3, 29.6 and 31.9 ( $\text{CH}_3$ ( $\text{CH}_2$ )<sub>10</sub>), 32.2 ( $\text{CH}_2\text{COOCH}_3$ ), 49.3 ( $\text{CH}_2\text{CH}_2\text{COOCH}_3$ ), 51.4 ( $\text{OCH}_3$ ), 53.9 ( $\text{CH}_2\text{N}$ ), 173.3 ( $\text{COOCH}_3$ ); MALDI-TOF-MS  $m/z$  440.7 ( $[\text{M} + \text{H}]^+$ ).

**DL-G0.** DL-G-0.5 (2.2 g, 4.9 mmol) was dissolved in methanol (50 mL). The resultant solution was added

dropwise to distilled ethylenediamine (100 mL, 1.5 mol) containing sodium cyanide (48 mg, 0.98 mmol) and stirred at 45 °C under nitrogen. After 50 h, methanol and unreacted ethylenediamine were removed from the reaction mixture under vacuum. The obtained DL-G0 was purified with a Sephadex LH-20 column using methanol as eluent. Yield, 84.6%;  $^1\text{H}$  NMR ( $\text{CDCl}_3$ ):  $\delta$  0.85 (m,  $\text{CH}_3$ -( $\text{CH}_2$ )<sub>9</sub>), 1.23 (s,  $\text{CH}_3$ ( $\text{CH}_2$ )<sub>9</sub>), 1.41 (m,  $\text{CH}_2\text{CH}_2\text{N}$ ), 2.33 (t,  $\text{CH}_2\text{CONH}$ ), 2.39 (t,  $\text{CH}_2\text{N}$ ), 2.62 (t,  $\text{CH}_2\text{CH}_2\text{CONH}$ ), 2.76 (t,  $\text{CH}_2\text{NH}_2$ ), 3.25 (m,  $\text{CH}_2\text{CH}_2\text{NH}_2$ ), 8.65 (m,  $\text{CONH}$ );  $^{13}\text{C}$  NMR ( $\text{CDCl}_3$ ):  $\delta$  14.1 ( $\text{CH}_3$ ( $\text{CH}_2$ )<sub>10</sub>), 22.6, 26.6, 27.6, 29.3, 29.6, and 31.9 ( $\text{CH}_3$ ( $\text{CH}_2$ )<sub>10</sub>), 32.7 ( $\text{CH}_2\text{CONH}$ ), 41.9 ( $\text{CH}_2\text{-NH}_2$ ), 42.2 ( $\text{CH}_2\text{CH}_2\text{NH}_2$ ), 50.3 ( $\text{CH}_2\text{CH}_2\text{CONH}$ ), 53.3 ( $\text{CH}_2\text{N}$ ), 173.3 ( $\text{CONH}$ ); MALDI-TOF-MS  $m/z$  468.2 ( $[\text{M} + \text{H}]^+$ ).

**DL-G0.5.** This was prepared from DL-G0. DL-G0 (2.3 g, 4.8 mmol) dissolved in methanol (18 mL) was added to purified methyl acrylate (43.5 mL, 0.49 mol) and the



mixed solution was stirred at 35 °C for 50 h under nitrogen. The obtained material was chromatographed on silica gel using petroleum ether-diethyl ether (2:1, v/v) and then dichloromethane-methanol (9:1, v/v) as eluent. Yield, 85.4%;  $^1\text{H}$  NMR ( $\text{CDCl}_3$ ):  $\delta$  0.84 (m,  $\text{CH}_3(\text{CH}_2)_9$ ), 1.21 (s,  $\text{CH}_3(\text{CH}_2)_9$ ), 1.39 (m,  $\text{CH}_2\text{CH}_2\text{N}$ ), 2.30 (t,  $\text{CH}_2\text{-CONH}$ ), 2.38 (m,  $\text{CH}_2\text{COOCH}_3$ ), 2.39 (m,  $\text{CH}_2\text{N}$ ), 2.49 (t,  $\text{CONHCH}_2\text{CH}_2$ ), 2.67 (t,  $\text{CH}_2\text{CH}_2\text{CONH}$ ), 2.73 (t,  $\text{CH}_2\text{-CH}_2\text{COOCH}_3$ ), 3.25 (m,  $\text{CONHCH}_2$ ), 3.63 (s,  $\text{OCH}_3$ ), 7.76 (m,  $\text{CONH}$ );  $^{13}\text{C}$  NMR ( $\text{CDCl}_3$ ):  $\delta$  14.1 ( $\text{CH}_3(\text{CH}_2)_{10}$ ), 22.6, 26.7, 27.6, 29.3, 29.6, 31.9, and 32.5 ( $\text{CH}_3(\text{CH}_2)_{10}$ ), 33.1 ( $\text{CH}_2\text{COOCH}_3$ ), 36.9 ( $\text{CH}_2\text{CONH}$ ), 49.1 ( $\text{CH}_2\text{CH}_2\text{COOCH}_3$ ), 50.1 ( $\text{CH}_2\text{CH}_2\text{CONH}$ ), 51.5 ( $\text{OCH}_3$ ), 53.0 ( $\text{CH}_2\text{N}$ ), 53.5 ( $\text{CONHCH}_2\text{CH}_2$ ), 172.7 ( $\text{COOCH}_3$ ), 172.8 ( $\text{CONH}$ ); MALDI-TOF-MS  $m/z$  640.8 ( $[\text{M} + \text{H}]^+$ ).

**DL-G1.** This was prepared from DL-G0.5. DL-G0.5 (0.71 g, 1.1 mmol) dissolved in methanol (21 mL) was added to ethylenediamine (37.5 mL, 0.56 mol) containing sodium cyanide (11 mg, 0.22 mmol), and the mixed solution was stirred at 45 °C for 50 h under nitrogen. The obtained DL-G1 was purified with a Sephadex LH-20 column using methanol as eluent. Yield, 86.4%;  $^1\text{H}$  NMR ( $\text{CDCl}_3$ ):  $\delta$  0.84 (m,  $\text{CH}_3(\text{CH}_2)_9$ ), 1.22 (s,  $\text{CH}_3(\text{CH}_2)_9$ ), 1.38 (m,  $\text{CH}_2\text{CH}_2\text{N}$ ), 2.12 (m,  $\text{NH}_2$ ), 2.28 (m,  $\text{CH}_2\text{-CONHCH}_2\text{CH}_2\text{NH}_2$ ), 2.31 (m,  $\text{CH}_2\text{CONH}$ ), 2.36 (m,  $\text{CH}_2\text{N}$ ), 2.46 (t,  $\text{CONHCH}_2\text{CH}_2$ ), 2.63 (t,  $\text{CH}_2\text{CH}_2\text{CONH}$ ), 2.70 (t,  $\text{CH}_2\text{CH}_2\text{CONHCH}_2\text{CH}_2\text{NH}_2$ ), 2.79 (t,  $\text{CH}_2\text{NH}_2$ ), 3.17 (m,  $\text{CONHCH}_2$ ), 3.25 (m,  $\text{CH}_2\text{CH}_2\text{NH}_2$ ), 7.45 and 8.63 (m,  $\text{CONH}$ );  $^{13}\text{C}$  NMR ( $\text{CDCl}_3$ ):  $\delta$  14.0 ( $\text{CH}_3(\text{CH}_2)_{10}$ ), 22.6, 26.5, 27.6, 29.2, 29.6, and 31.8 ( $\text{CH}_3(\text{CH}_2)_{10}$ ), 32.9 and 34.3 ( $\text{CH}_2\text{CONH}$ ), 37.8 ( $\text{CONHCH}_2$ ), 41.3 and 41.9 ( $\text{CH}_2\text{CH}_2\text{-NH}_2$ ), 50.0 ( $\text{CH}_2\text{CH}_2\text{CONHCH}_2\text{CH}_2\text{NH}_2$ ), 50.8 ( $\text{CH}_2\text{CH}_2\text{-CONH}$ ), 52.9 ( $\text{CH}_2\text{N}$ ), 53.3 ( $\text{CONHCH}_2\text{CH}_2$ ), 173.4 and 172.9 ( $\text{CONH}$ ); MALDI-TOF-MS  $m/z$  697.4 ( $[\text{M} + \text{H}]^+$ ).

**DL-G1.5.** This was prepared from DL-G1. DL-G1 (1.5 g, 2.2 mmol) dissolved in methanol (87 mL) was added to methyl acrylate (152 mL, 1.7 mol), and the mixed solution was stirred at 35 °C for 50 h under nitrogen. The obtained material was chromatographed on silica gel using dichloromethane-methanol (9:1, v/v) as eluent. Yield, 74%;  $^1\text{H}$  NMR ( $\text{CDCl}_3$ ):  $\delta$  0.88 (m,  $\text{CH}_3(\text{CH}_2)_9$ ), 1.26 (s,  $\text{CH}_3(\text{CH}_2)_9$ ), 1.45 (m,  $\text{CH}_2\text{CH}_2\text{N}$ ), 2.37 (m,  $\text{CH}_2\text{-COOCH}_3$ ), 2.44 (m,  $\text{CH}_2\text{N}$ ), 2.56 (m,  $\text{CONHCH}_2\text{CH}_2$ ), 2.77 (m,  $\text{CH}_2\text{CH}_2\text{COOCH}_3$ ), 3.29 (m,  $\text{CONHCH}_2$ ), 3.68 (s,  $\text{OCH}_3$ ), 7.04 and 8.08 (m,  $\text{CONH}$ );  $^{13}\text{C}$  NMR ( $\text{CDCl}_3$ ):  $\delta$  14.1 ( $\text{CH}_3(\text{CH}_2)_{10}$ ), 22.7, 26.5, 27.6, 29.4, 29.6, and 31.9 ( $\text{CH}_3(\text{CH}_2)_{10}$ ), 32.7, 33.0, and 33.9 ( $\text{CH}_2\text{COOCH}_3$ ), 37.2 and 37.5 ( $\text{CONHCH}_2$ ), 49.3 and 50.0 ( $\text{CH}_2\text{CH}_2\text{COOCH}_3$ ), 50.2 ( $\text{CH}_2\text{CH}_2\text{CONH}$ ), 51.7 ( $\text{OCH}_3$ ), 52.8 ( $\text{CH}_2\text{N}$ ), 53.0 and 53.4 ( $\text{CONHCH}_2\text{CH}_2$ ), 172.3 ( $\text{COOCH}_3$ ), 172.7 and 173.1 ( $\text{CONH}$ ); MALDI-TOF-MS  $m/z$  1041.5 ( $[\text{M} + \text{H}]^+$ ).

**DL-G2.** This was prepared from DL-G1.5. DL-G1.5 (1.7 g, 1.6 mmol) dissolved in methanol (46 mL) was added to ethylenediamine (134 mL, 2.0 mol) containing sodium cyanide (32 mg, 0.66 mmol), and the mixed solution was stirred for 50 at 45 °C under nitrogen. The obtained DL-G2 was purified with a Sephadex LH-20 column using methanol as eluent. Yield, 90.8%;  $^1\text{H}$  NMR ( $\text{CDCl}_3$ ):  $\delta$  0.87 (m,  $\text{CH}_3(\text{CH}_2)_9$ ), 1.25 (s,  $\text{CH}_3(\text{CH}_2)_9$ ), 1.42 (m,  $\text{CH}_2\text{-CH}_2\text{N}$ ), 2.13 (m,  $\text{NH}_2$ ), 2.33 (m,  $\text{CH}_2\text{CONHCH}_2\text{CH}_2\text{NH}_2$ ), 2.36 (m,  $\text{CH}_2\text{N}$ ), 2.52 (m,  $\text{CONHCH}_2\text{CH}_2$ ), 2.73 (m,  $\text{CH}_2\text{-CH}_2\text{CONHCH}_2\text{CH}_2\text{NH}_2$ ), 2.82 (m,  $\text{CH}_2\text{NH}_2$ ), 3.24 (m,  $\text{CONHCH}_2$ ), 3.27 (m,  $\text{CH}_2\text{CH}_2\text{NH}_2$ ), 7.74, 7.79, and 8.58 (m,  $\text{CONH}$ );  $^{13}\text{C}$  NMR ( $\text{CDCl}_3$ ):  $\delta$  14.2 ( $\text{CH}_3(\text{CH}_2)_{10}$ ), 22.7, 26.6, 27.7, 29.4, 29.7, and 31.9 ( $\text{CH}_3(\text{CH}_2)_{10}$ ), 33.0, 34.0, and 34.3 ( $\text{CH}_2\text{CONH}$ ), 37.8 ( $\text{CONHCH}_2$ ), 41.5 and 42.2 ( $\text{CH}_2\text{CH}_2\text{NH}_2$ ), 50.2 ( $\text{CH}_2\text{CH}_2\text{CONHCH}_2\text{CH}_2\text{NH}_2$ ), 50.5 ( $\text{CH}_2\text{CH}_2\text{CONH}$ ), 53.0 ( $\text{CH}_2\text{N}$ ), 53.3 ( $\text{CONHCH}_2\text{CH}_2$ ),

172.6, 173.0, and 173.4 ( $\text{CONH}$ ); MALDI-TOF-MS  $m/z$  1153.0 ( $[\text{M}]^+$ ).

**DL-G2.5.** This was prepared from DL-G2. DL-G2 (1.7 g, 1.5 mmol) dissolved in methanol (120 mL) was added to methyl acrylate (100 mL, 1.1 mol), and the mixed solution was stirred at 30 °C for 25 h under nitrogen. The obtained material was chromatographed on silica gel using dichloromethane-methanol (85:15 and then 8:2, v/v) as eluent. Yield, 69.4%;  $^1\text{H}$  NMR ( $\text{CDCl}_3$ ):  $\delta$  0.88 (m,  $\text{CH}_3(\text{CH}_2)_9$ ), 1.26 (s,  $\text{CH}_3(\text{CH}_2)_9$ ), 1.45 (m,  $\text{CH}_2\text{CH}_2\text{N}$ ), 2.37 (m,  $\text{CH}_2\text{COOCH}_3$ ), 2.44 (m,  $\text{CH}_2\text{N}$ ), 2.56 (m,  $\text{CONHCH}_2\text{-CH}_2$ ), 2.76 (m,  $\text{CH}_2\text{CH}_2\text{COOCH}_3$ ), 3.28 (m,  $\text{CONHCH}_2$ ), 3.68 (s,  $\text{OCH}_3$ ), 7.13, 7.67 and 8.12 (m,  $\text{CONH}$ );  $^{13}\text{C}$  NMR ( $\text{CDCl}_3$ ):  $\delta$  14.1 ( $\text{CH}_3(\text{CH}_2)_{10}$ ), 22.7, 26.5, 27.6, 29.4, 29.6, 29.7, and 31.9 ( $\text{CH}_3(\text{CH}_2)_{10}$ ), 32.7 ( $\text{CH}_2\text{CONH}$ ), 33.9 ( $\text{CH}_2\text{-COOCH}_3$ ), 37.2 and 37.5 ( $\text{CONHCH}_2$ ), 49.3 and 49.9 ( $\text{CH}_2\text{-CH}_2\text{COOCH}_3$ ), 50.2 ( $\text{CH}_2\text{CH}_2\text{CONH}$ ), 51.7 ( $\text{OCH}_3$ ), 52.6 ( $\text{CH}_2\text{N}$ ), 53.0 and 53.4 ( $\text{CONHCH}_2\text{CH}_2$ ), 172.4 ( $\text{COOCH}_3$ ), 173.0 ( $\text{CONH}$ ); MALDI-TOF-MS  $m/z$  1840.7 ( $[\text{M}]^+$ ).

**DL-G3.** This was prepared from DL-G2.5. DL-G2.5 (0.12 g, 0.063 mmol) dissolved in methanol (2.5 mL) was added to ethylenediamine (5 mL, 0.075 mol) containing sodium cyanide (1.2 mg, 0.025 mmol), and the mixed solution was stirred at 45 °C for 55 h under nitrogen. The obtained DL-G3 was purified with a Sephadex LH-20 column using methanol as eluent. Yield, 88.4%;  $^1\text{H}$  NMR ( $\text{CDCl}_3$ ):  $\delta$  0.88 (m,  $\text{CH}_3(\text{CH}_2)_9$ ), 1.26 (s,  $\text{CH}_3(\text{CH}_2)_9$ ), 1.42 (m,  $\text{CH}_2\text{CH}_2\text{N}$ ), 2.37 (br,  $\text{CH}_2\text{CONHCH}_2\text{CH}_2\text{NH}_2$ ), 2.54 (br,  $\text{CONHCH}_2\text{CH}_2$ ), 2.75 (br,  $\text{CH}_2\text{CH}_2\text{CONHCH}_2\text{-CH}_2\text{NH}_2$ ), 2.83 (br,  $\text{CH}_2\text{NH}_2$ ), 3.24 (br,  $\text{CONHCH}_2$ ), 3.29 (br,  $\text{CH}_2\text{CH}_2\text{NH}_2$ ), 7.94, 8.07 and 8.57 (br,  $\text{CONH}$ );  $^{13}\text{C}$  NMR ( $\text{CDCl}_3$ ):  $\delta$  14.2 ( $\text{CH}_3(\text{CH}_2)_{10}$ ), 22.7, 26.5, 27.7, 29.4, 29.7, and 31.9 ( $\text{CH}_3(\text{CH}_2)_{10}$ ), 34.0 and 34.3 ( $\text{CH}_2\text{CONH}$ ), 37.8 ( $\text{CONHCH}_2$ ), 41.4 and 41.9 ( $\text{CH}_2\text{CH}_2\text{NH}_2$ ), 50.1 ( $\text{CH}_2\text{-CH}_2\text{CONHCH}_2\text{CH}_2\text{NH}_2$ ), 50.5 ( $\text{CH}_2\text{CH}_2\text{CONH}$ ), 52.9 ( $\text{CH}_2\text{N}$ ), 53.3 ( $\text{CONHCH}_2\text{CH}_2$ ), 172.8 and 173.1 ( $\text{CONH}$ ); MALDI-TOF-MS  $m/z$  2066.0 ( $[\text{M}]^+$ ).

**DL-G3.5.** This was prepared from DL-G3. DL-G3 (1 g, 0.49 mmol) dissolved in methanol (40 mL) was added to methyl acrylate (35 mL, 0.39 mol), and the mixed solution was stirred at 25 °C for 50 h under nitrogen. The obtained material was purified with a Sephadex LH-20 column using methanol as eluent and column chromatography on silica gel using dichloromethane-methanol (8:2, v/v) as eluent. Yield, 68.2%;  $^1\text{H}$  NMR ( $\text{CDCl}_3$ ):  $\delta$  0.88 (m,  $\text{CH}_3(\text{CH}_2)_9$ ), 1.23 (s,  $\text{CH}_3(\text{CH}_2)_9$ ), 2.37 (br,  $\text{CH}_2\text{-COOCH}_3$ ), 2.44 (br,  $\text{CH}_2\text{N}$ ), 2.54 (br,  $\text{CONHCH}_2\text{CH}_2$ ), 2.76 (br,  $\text{CH}_2\text{CH}_2\text{COOCH}_3$ ), 3.27 (br,  $\text{CONHCH}_2$ ), 3.67 (s,  $\text{OCH}_3$ ), 7.13, 7.71, and 8.10 (br,  $\text{CONH}$ );  $^{13}\text{C}$  NMR ( $\text{CDCl}_3$ ):  $\delta$  14.1 ( $\text{CH}_3(\text{CH}_2)_{10}$ ), 22.7, 29.4, 29.7, and 31.9 ( $\text{CH}_3(\text{CH}_2)_{10}$ ), 32.7 ( $\text{CH}_2\text{CONH}$ ), 33.8 ( $\text{CH}_2\text{COOCH}_3$ ), 37.2 and 37.5 ( $\text{CONHCH}_2$ ), 49.3 and 49.9 ( $\text{CH}_2\text{CH}_2\text{COOCH}_3$ ), 50.6 ( $\text{CH}_2\text{CH}_2\text{CONH}$ ), 51.7 ( $\text{OCH}_3$ ), 52.5 ( $\text{CH}_2\text{N}$ ), 53.0 ( $\text{CONHCH}_2\text{CH}_2$ ), 172.4 ( $\text{COOCH}_3$ ), 172.6 and 173.1 ( $\text{CONH}$ ).

**DL-G4.** This was prepared from DL-G3.5. DL-G3.5 (1.14 g, 0.33 mmol) dissolved in methanol (19 mL) was added to ethylenediamine (37 mL, 0.55 mol) containing sodium cyanide (6.5 mg, 0.13 mmol), and the mixed solution was stirred at 45 °C for 55 h under nitrogen. The obtained DL-G4 was purified with a Sephadex LH-20 column using methanol as eluent. Yield, 54.2%;  $^1\text{H}$  NMR ( $\text{DMSO}-d_6$ ):  $\delta$  0.85 (m,  $\text{CH}_3(\text{CH}_2)_9$ ), 1.26 (s,  $\text{CH}_3(\text{CH}_2)_9$ ), 1.37 (m,  $\text{CH}_2\text{CH}_2\text{N}$ ), 2.20 (br,  $\text{CH}_2\text{CONHCH}_2\text{CH}_2\text{-NH}_2$ ), 2.30 (br,  $\text{CH}_2\text{N}$ ), 2.57 (br,  $\text{CONHCH}_2\text{CH}_2$ ), 2.65 (br,  $\text{CH}_2\text{CH}_2\text{CONHCH}_2\text{CH}_2\text{NH}_2$ ), 3.07 (br,  $\text{CH}_2\text{CH}_2\text{NH}_2$ ), 7.91, 7.98, and 8.16 (br,  $\text{CONH}$ );  $^{13}\text{C}$  NMR ( $\text{DMSO}-d_6$ ):  $\delta$  14.0 ( $\text{CH}_3(\text{CH}_2)_{10}$ ), 22.2, 27.0, 29.1, and 31.4 ( $\text{CH}_3(\text{CH}_2)_{10}$ ), 33.3

(CH<sub>2</sub>CONH), 37.0 (CONHCH<sub>2</sub>), 41.7 (CH<sub>2</sub>CH<sub>2</sub>NH<sub>2</sub>), 49.7 (CH<sub>2</sub>CH<sub>2</sub>CONHCH<sub>2</sub>CH<sub>2</sub>NH<sub>2</sub>), 52.2 (CONHCH<sub>2</sub>CH<sub>2</sub>), 171.6 (CONH).

**Preparation of Lipoplexes.** To a dry thin membrane of the dendron-bearing lipid, phosphate-buffered saline (PBS) was added and sonicated for 2 min using a bath-type sonicator to give a suspension of the cationic lipid (DL-G1, 0.32 mM; DL-G2, 0.16 mM; DL-G3, 0.08 mM; DL-G4, 0.08 mM). Plasmid DNA p10, which contains a firefly luciferase coding sequence derived from pGL3-basic (Promega, Madison, WI) between Rous sarcoma virus LTR and polyadenylation signal (24), (1  $\mu$ g), was dissolved in 20 mM Tris-HCl buffer (pH 7.4, 50  $\mu$ L), added to a given volume (0–50  $\mu$ L) of the cationic lipid suspension, and incubated for 10 min at room temperature to afford a lipoplex with varying ratios of primary amino group of cationic lipid to DNA phosphate (N/P ratios). For the preparation of lipoplexes containing DOPE, PBS (0.5 mL) was added to a thin dry membrane of a mixture of the dendron-bearing lipid (41.7  $\mu$ g) and a given amount of DOPE and sonicated for 2 min using a bath-type sonicator. Plasmid DNA (1  $\mu$ g) dissolved in 20 mM Tris-HCl buffer (pH 7.4, 50  $\mu$ L) was added to varying volumes of the lipid suspension and incubated for 10 min at room temperature to afford lipoplexes with varying N/P ratios. For the preparation of DC-Chol-DOPE-plasmid DNA lipoplexes, PBS (2.5 mL) was added to a thin membrane of a mixture of DC-Chol (161.3  $\mu$ g) and DOPE (240  $\mu$ g) and sonicated for 2 min using a bath-type sonicator. Plasmid DNA (25  $\mu$ g) was dissolved in 20 mM Tris-HCl solution (1.25 mL). The resultant solution was added to the lipid suspension (1.25 mL) and incubated for 10 min at room temperature to afford a lipoplex with the DC-Chol/DNA phosphate ratio of 2.

**Agarose Gel Electrophoresis.** The dendron-bearing lipid-DNA complexes with varying N/P ratios (1  $\mu$ g/sample) were prepared by mixing plasmid DNA (1  $\mu$ g) dissolved in 20 mM Tris-HCl buffer (5  $\mu$ L) and cationic lipid suspension (5  $\mu$ L). Polyplexes of the polyamidoamine G4 dendrimer and plasmid DNA were prepared by the same procedure. After 10 min-incubation at room temperature, the samples (10  $\mu$ L) were electrophoresed on 0.6 wt % agarose gel in 40 mM Tris, 20 mM sodium acetate, and 2 mM EDTA buffer (pH 8.0) containing 1  $\mu$ g/mL ethidium bromide at 100 V for 30 min. The ethidium bromide-stained bands were visualized and photographed using an Eagle Eye II Still Video System (Stratagene, IN).

**Transfection.** Transfection of CV1 cells was done according to the following procedures unless otherwise noted in the text. The cells were seeded in 0.5 mL of DMEM supplemented with 10% FCS in 24-well culture plates at  $5.0 \times 10^4$  cells per well the day before transfection. The cells were washed with PBS containing 0.36 mM CaCl<sub>2</sub> and 0.42 mM MgCl<sub>2</sub> [PBS(+)] and then covered with DMEM (1 mL). The lipoplex or the polyplex containing plasmid DNA (1  $\mu$ g) was added gently to the cells and incubated at 37 °C for 4 h. Then, the cells were rinsed with PBS(+), covered with DMEM containing 10% FCS, and incubated at 37 °C. After 40 h, the cells were lysed by adding 50  $\mu$ L of Luc-PGC-50 detergent (Toyo Ink, Tokyo, Japan). A 20  $\mu$ L aliquot from each dish was used for one luciferase assay using a kit (Toyo Ink) and a Lumat LB9507 luminometer (Berthold, Bad Wildbad, Germany). The protein content of the lysate was measured by Coomassie Protein Assay Reagent (Pierce, IL) using bovine serum albumin as the standard.

**Cytotoxicity.** The cytotoxicity of the lipoplexes was assessed by MTT assay (37). The cells were treated with

the lipoplexes for 4 h and incubated for 40 h according to the above procedure. Then, the culture medium was carefully replaced with 0.2 mL of fresh DMEM containing 10% FCS and 20  $\mu$ L of MTT dissolved in PBS (5 mg/mL) was added to each well. After 2 h-incubation at 37 °C, the medium was removed, and the cells were solubilized in 500  $\mu$ L of 2-propanol containing 0.1 M HCl. The number of viable cells was determined by absorbance at 570 nm.

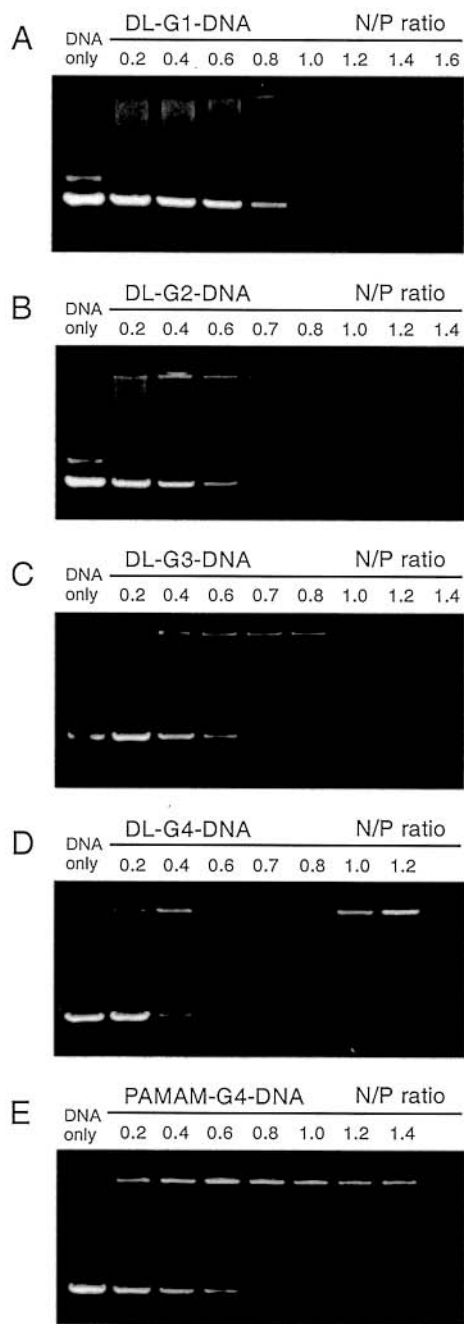
## RESULTS AND DISCUSSION

**Design, Synthesis, and Characterization of Dendron-Bearing Lipids.** It is generally considered that enhancement of escape of the introduced DNA from endosome to cytoplasm is one of the most efficient strategy for the achievement of an efficient transfection. In this study, we designed polyamidoamine dendron-bearing lipids, because we expected that with DNA and fusogenic lipids, this new type of cationic lipids could form complexes which achieve efficient gene transfection by synergy of endosome buffering induced by their tertiary amino groups (28, 31) and endosome fusion caused by fusogenic lipids (19–23). In addition, application of methodology of polyamidoamine dendrimer synthesis gives lipids with a headgroup of a desired size. This is of great importance because the dynamic shape and hydrophobic-hydrophilic balance of a lipid molecule should affect the structure of its assembly and its transfection activity.

The dendron-bearing lipids, DL-G1, DL-G2, DL-G3, and DL-G4, were synthesized according to the method of Tomalia et al. (35, 36) using di-*n*-dodecylamine as the core material. Characterization using <sup>1</sup>H NMR, <sup>13</sup>C NMR, and MALDI-TOF showed a good correspondence between the theoretically expected and experimentally obtained values for the products synthesized, as shown in the Experimental Section.

**Evaluation of Complex Formation with Plasmid DNA.** We examined the ability of the dendron-bearing lipids to form a lipoplex with plasmid DNA using agarose gel electrophoresis (Figure 2). In this experiment, the plasmid DNA was incubated with the dendron-bearing lipids for 10 min and electrophoresed on an agarose gel. As is seen in Figure 2, for all cases, the amount of free DNA decreased with increasing amount of the lipid added, indicating that these lipids have an ability to form a lipoplex with plasmid DNA. It is already known that polyamidoamine dendrimers form a complex with DNA through electrostatic interaction (38, 39). Thus, it is likely that these dendron-bearing lipids formed the complex via electrostatic interaction between plasmid DNA and their polyamidoamine dendron moiety. In the case of DL-G1, free DNA disappeared above the N/P ratio of 1.0, whereas in the case of DL-G2, the free DNA band was not observed above the N/P ratio of 0.8. Similarly, for DL-G3 and DL-G4, the free DNA band disappeared above 0.7 and 0.6, respectively. These results indicate that the lipid with a larger size of the polyamidoamine dendron has higher ability to form the lipoplex with plasmid DNA. It is likely that the dendron lipids with a larger number of amino groups bind more tightly to DNA by multivalent ionic bonds, resulting in the more efficient lipoplex formation.

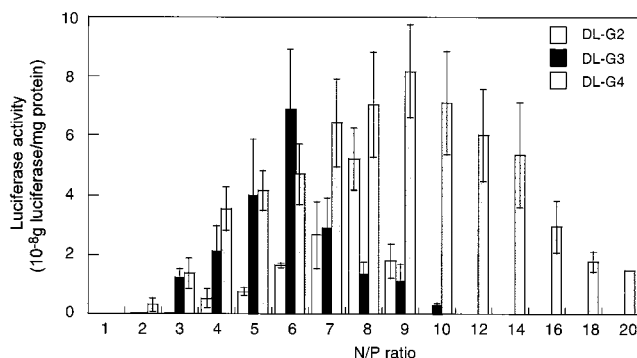
By comparison with the polyamidoamine dendrimer of the fourth generation (Figure 2), it is apparent that the DL-G4 forms a complex with DNA more efficiently than the polyamidoamine dendrimer with the same genera-



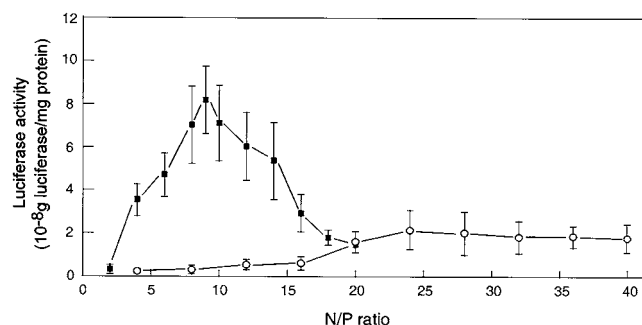
**Figure 2.** Agarose gel electrophoretic analysis of complexes of DL-G1 (A), DL-G2 (B), DL-G3 (C), DL-G4 (D), and polyamidoamine G4 dendrimer (E) with plasmid DNA. Each dendron-bearing lipid and plasmid DNA were mixed at varying charge ratios and incubated for 10 min at room temperature. Then, the mixed solution was applied to the agarose gel and electrophoresed at 100 V for 30 min.

tion. Probably, hydrophobic moiety of the lipid also contributes their complexation through hydrophobic interaction.

**Transfection Activity of Dendron-Bearing Lipid-DNA Lipoplexes.** It is well-known that transfection activity of lipoplexes varies, depending on their cationic lipid/DNA composition. Thus, we prepared the lipoplexes consisting of the dendron-bearing lipid and plasmid DNA at various N/P ratios and examined transfection of CV1 cells using these lipoplexes (Figure 3). While DL-G1 formed lipoplexes with the plasmid DNA (Figure 2), the lipoplexes with the N/P ratios between 1 and 10 did not induce expression of luciferase in CV1 cells. However, the



**Figure 3.** Luciferase activities of CV1 cells treated with DL-G2, DL-G3, and DL-G4 lipoplexes with varying N/P ratios. The cells ( $5 \times 10^4$ ) were treated with the lipoplexes containing  $1 \mu\text{g}$  of DNA. Each point represents the mean  $\pm$  SD ( $n = 6$ ).



**Figure 4.** Luciferase activities of CV1 cells treated with DL-G4 lipoplexes (■) and polyamidoamine G4 dendrimer polyplexes (○) with varying N/P ratios. The cells ( $5 \times 10^4$ ) were treated with the lipoplexes or the polyplexes containing  $1 \mu\text{g}$  of DNA. Each point represents the mean  $\pm$  SD ( $n = 6$ ).

lipoplexes containing the dendron-bearing lipids of higher generations caused transfection of CV1 cells. As shown in Figure 3, transfection activity of these lipoplexes depended on their N/P ratio. The DL-G2, the DL-G3, and the DL-G4 lipoplexes induced the highest luciferase expression in the cell at the N/P ratios of 8, 6, and 9, respectively. In comparison of these lipoplexes with the optimal N/P ratio, it is apparent that the lipoplexes with the lipid bearing the dendron of higher generation exhibited greater transfection activity and hence the DL-G4 formed the lipoplex with the highest activity among the dendron-bearing lipids. It is noteworthy that the lipoplexes of DL-G4 showed the high activity in the broad range of the N/P ratio, compared with the lipoplexes of the lipids with the lower generation dendrons.

As shown above, the DL-G4 exhibited more efficient complex formation with plasmid DNA than the polyamidoamine dendrimer of the same generation. Thus, we examined difference in transfection activity between these molecules. As is seen in Figure 4, the DL-G4 lipoplex with the N/P ratio of 9 exhibited more than 20-fold higher activity than the G4 dendrimer polyplex with the same N/P ratio. Although some elevation of transfection activity was seen at the N/P ratio above 20 for the dendrimer polyplexes, their activity is still much lower than the activity of the DL-G4 lipoplex with the optimal composition.

The G4 dendrimer did not form a complex with plasmid DNA as efficiently as the DL-G4 did. This suggests that the G4 dendrimer polyplexes are less stable. Indeed, the predominant interaction between the dendrimer/dendron-bearing lipids and DNA is electrostatic in nature. However, hydrophobic interaction by the long alkyl chains of the dendron-bearing lipids may improve stabil-



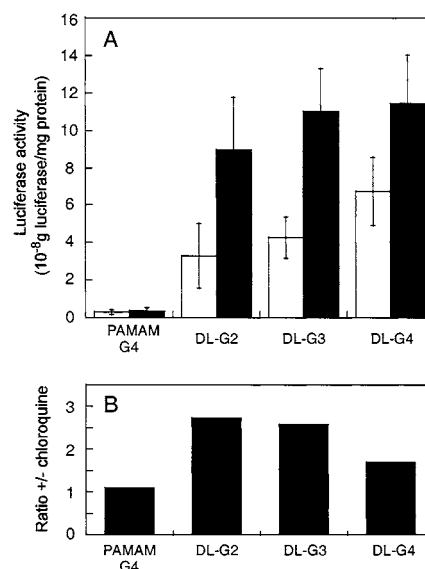
ity of their complexes formed with DNA. In fact, when varying amounts of heparin were added to suspensions of the DL-G4 lipoplex and the G4 dendrimer polyplex, both of which have the same N/P ratio of 9, less heparin was required to induce liberation of DNA from the G4 dendrimer polyplex than from the DL-G4 lipoplex, indicating that the DL-G4 lipoplex is more stable than the G4 dendrimer polyplex (result not shown).

Although DL-G2, DL-G3, and G4 dendrimer formed complexes with DNA with similar efficiency (Figure 2), these dendron-bearing lipids achieved more efficient transfection than the G4 dendrimer. Thus, it seems that the hydrophobic character of the dendron-bearing lipid lipoplexes plays an important role in their efficient transfection. In fact, many studies have revealed that introduction of hydrophobic moieties to various polycations improve their transfection activity (40–43). Because the lipoplexes of dendron-bearing lipids have hydrophobic nature due to their long alkyl groups, they could interact strongly with cellular membranes through both hydrophobic and electrostatic interactions, resulting in the high transfection activity (44).

We expected that lipoplexes containing the dendron-bearing lipids will enhance the endosome escape of DNA by the endosome buffering of the dendron tertiary amino groups. Because the numbers of tertiary amino groups of the dendron moieties of DL-G1, DL-G2, DL-G3, and DL-G4 are 1, 3, 7, and 15, respectively, it is likely that the buffering capacity of these lipids increases in this order. In fact, the transfection activity of the lipoplexes increased as the generation of the dendron of their lipid component increases, implying that there may be some relationship between the buffering ability of the dendron-bearing lipids and their transfection activity.

It is known that polyplexes formed by cationic polymers without the buffering ability, such as poly(L-lysine), do not transfect cells efficiently in the absence of an endosomotropic agent, chloroquine, whereas polyplexes made using polycations with the buffering ability, such as poly(ethylenimine), could achieve efficient transfection even in the absence of chloroquine (45). Comparison of transfection by polyplexes between in the presence and in the absence of chloroquine can be used to estimate contribution of their buffering capacity to the transfection (46). Thus, we examined influence of chloroquine on transfection of CV1 cells mediated by the dendron-bearing lipids and the polyamidoamine G4 dendrimer. As can be seen in Figure 5 A, the lipoplexes made using any dendron-bearing lipid exhibited an enhancement of transfection in the presence of chloroquine, in contrast to the G4 dendrimer polyplex, whose activity was hardly affected by chloroquine. To evaluate the effect of chloroquine on their transfection, the ratio of luciferase activity of the cells treated in the presence of chloroquine to that in the absence of chloroquine was calculated (Figure 5B). The ratio decreases in the order of DL-G2 > DL-G3 > DL-G4 > G4 dendrimer, and this is consistent with the order of the number of tertiary amino groups in these molecules (DL-G2 < DL-G3 < DL-G4), implying that their buffering ability increases in this order. Since the transfection activity of the lipoplexes of the dendron-bearing lipids also increased in the same order, it is implied that the buffering capacity of the dendron-bearing lipids might be related to their transfection activity.

**Influence of DOPE Addition on Transfection Activity of Lipoplexes.** It is generally considered that membrane fusion plays an important role in the endosome escape of DNA delivered by lipid-based systems, such as lipoplexes (13, 20, 23). A number of studies have

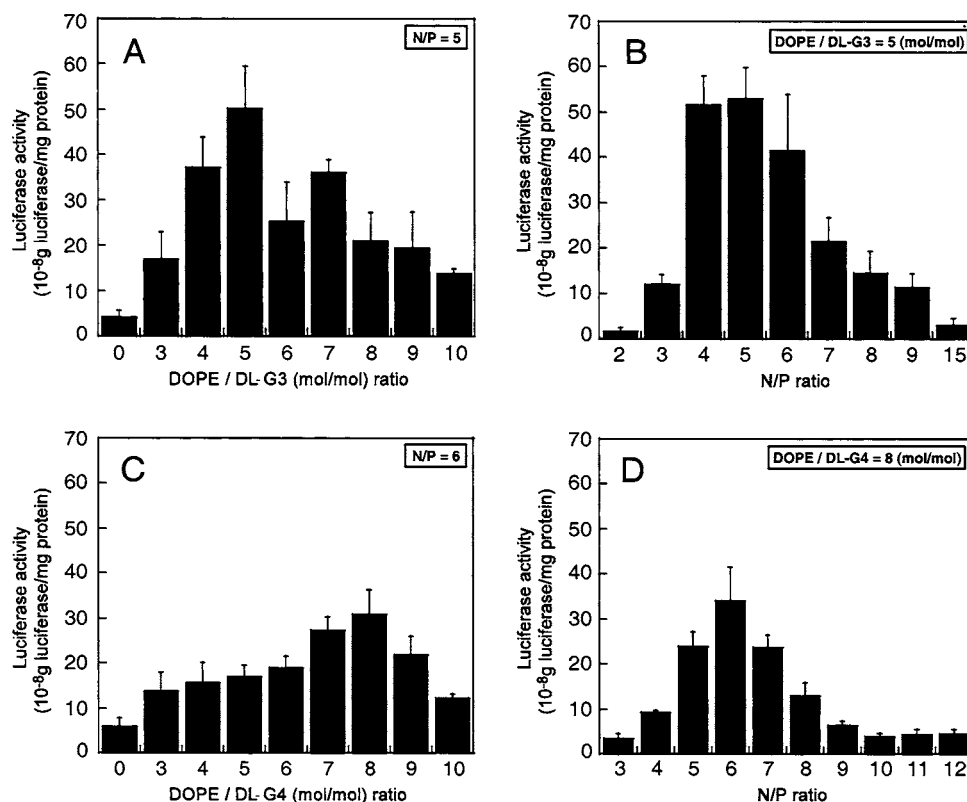


**Figure 5.** Influence of chloroquine on transfection of CV1 cells mediated by DL-G2, DL-G3, and DL-G4 lipoplexes and polyamidoamine G4 dendrimer polyplex. (A) Luciferase activity of the cells treated with the lipoplexes containing 1 μg of DNA in the absence (open bars) or presence (closed bars) of 100 μM chloroquine. The N/P ratios of lipoplexes and polyplex were 7. Each point represents the mean ± SD ( $n = 6$ ). (B) The ratio of cellular luciferase activities in the presence of chloroquine to those in the absence of chloroquine.

shown that inclusion of DOPE in cationic liposomes improves their transfection activity (21, 22, 46, 47). DOPE has a high tendency to take on a hexagonal II phase and facilitates the fusion of liposomes (22, 48–50). Thus, we examined the effect of inclusion of DOPE on the transfection activities of the DL-G3 and DL-G4 lipoplexes, both of which exhibited high transfection activity among the lipoplexes of dendron-bearing lipids.

Figure 6A depicts luciferase activity of CV1 cells treated with the DL-G3 lipoplexes containing varying amounts of DOPE. The cellular luciferase activity increased significantly, as the DOPE/DL-G3 ratio of the lipoplex increased to 5, where the activity was 12-fold higher than that of the lipoplex without DOPE. However, further increase in DOPE content of the lipoplexes abolished their activity. Because DOPE is an electronically neutral lipid, charge density of the lipoplexes should decrease with increasing DOPE content. In such lipoplexes, efficient complexation between the cationic lipid and the plasmid DNA might not occur. In addition, because their interaction with the cell membrane is based on electrostatic force, the lipoplexes with low charge density would exhibit a weak interaction with the cell. As a result, the lipoplexes with too much DOPE showed a reduced transfection activity. A similar effect of DOPE has been reported for the transfection mediated by DC-Chol-DOPE lipoplexes (21).

The influence of charge ratio of the DL-G3-DOPE lipoplexes was shown in Figure 6B. Indeed, the lipoplexes with low N/P ratios showed only limited transfection activities. This is because their positive charge is not high enough to induce strong interaction with the negatively charged cell membrane. The lipoplexes with the N/P ratios of 4–5 achieved an efficient transfection of the cells. However, further increase in the N/P ratio diminished their transfection activity. We observed that the treatment with the lipoplexes of the N/P ratio below 6 hardly affected the cell viability, but the treatment with the lipoplexes of the N/P ratio above 7 decreased the cell



**Figure 6.** The effects of DOPE content and charge ratio of DL-G3 (A, B) and DL-G4 (C, D) lipoplexes on their transfection activity. Luciferase activities of CV1 cells treated with the DL-G3–DOPE lipoplexes with varying DOPE/DL-G3 ratios (A) and varying N/P ratios (B), and the DL-G4–DOPE lipoplexes with varying DOPE/DL-G4 ratios (C) and varying N/P ratios (D). The cells ( $5 \times 10^4$ ) were treated with the lipoplexes containing  $1 \mu\text{g}$  of DNA. Each point represents the mean  $\pm$  SD ( $n = 4$ ). The N/P ratio or the DOPE/cationic lipid ratio of lipoplexes used for each experiment is shown in the figure.

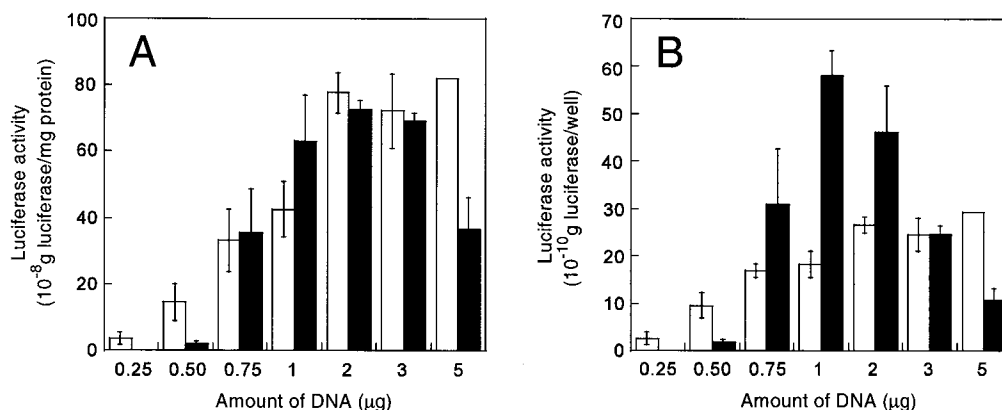
viability to some extent, indicating that the lipoplexes with higher N/P ratio are more toxic. The high toxicity may cause suppression of the gene expression in the cell. In addition, the high charge ratio will induce tight binding between the lipid and the plasmid DNA, which should inhibit liberation of the DNA from the lipoplex, which is necessary for the gene expression. As a result, the DL-G3–DOPE lipoplexes with the N/P ratio of 4–5 might have an appropriate charge density and showed high transfection activity.

A similar enhancement of transfection activity by the inclusion of DOPE was seen for the DL-G4 lipoplexes (Figures 6C and 6D). Their transfection activity became highest at the DOPE/DL-G4 ratio of 8. Also, their activity depended on the N/P ratio and showed the highest activity at the N/P ratio of 6. Indeed, the DL-G4–DOPE lipoplex with the optimal composition could transfect the cells much more efficiently than the DOPE-free lipoplex with the optimal composition. Because the DL-G4 could form a more potent lipoplex than the DL-G3, we expected that with the help of DOPE, the lipoplex with the highest activity can be obtained using this dendron-bearing lipid. However, it appears that the activity of the DL-G4–DOPE lipoplexes was somewhat lower than that of the DL-G3–DOPE lipoplexes. In addition, the DL-G4–DOPE lipoplexes required more DOPE content to gain the maximum activity than the DL-G3–DOPE lipoplex. It is well-known that the dynamic shape of a lipid molecule determines its phase preference (51, 52). Because the DL-G4 has a larger headgroup and hence might have a stronger tendency to form micellar structure than the DL-G3, the DL-G4 should stabilize more strongly a lamellar structure of DOPE, which preferentially takes on a hexagonal II phase. Thus, the lipoplex containing

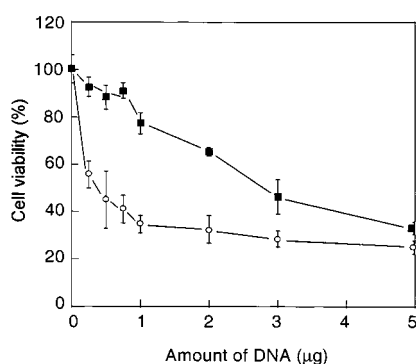
the DL-G4 required more DOPE to generate the nonbilayer structure, which plays an important role in membrane fusion and induces efficient escape of the plasmid DNA from endosome.

**Comparison of Transfection Activity between DL-G3–DOPE Lipoplex and DC–Chol–DOPE Lipoplex.** The DC–Chol–DOPE lipoplex is one of the most widely used and most intensively studied nonviral vectors (12, 33, 34). Thus, we used this lipoplex as a control to estimate the performance of the DL-G3–DOPE lipoplex, which achieved the highest transfection activity among the dendron-bearing lipid lipoplexes prepared in this study. Figure 7 shows luciferase activity of the cells treated with varying amounts of DL-G3–DOPE and DC–Chol–DOPE lipoplexes, both of which have the optimal compositions for the transfection activity. On the basis of the luciferase activity per cell, it seems that both systems possess approximately the same transfection activity under the experimental condition (Figure 7 A). However, by the comparison, based on the luciferase activity per well, which initially contained the same number of the cells, the DL-G3–DOPE lipoplex caused 2–3 times higher luciferase activity than the DC–Chol–DOPE lipoplex, indicating that the DL-G3–DOPE lipoplex possesses high transfection activity and low cytotoxicity (Figure 7 B).

The low cytotoxicity of the DL-G3–DOPE lipoplex was further confirmed by evaluating the cell viability after the treatment with the lipoplexes of the optimal compositions. As is apparent in Figure 8, the cell viability decreased significantly by the treatment with the DC–Chol–DOPE lipoplex even below  $1 \mu\text{g}$  DNA per  $5 \times 10^4$  cells, suggesting that this lipoplex is quite toxic to the cells. In contrast, the DL-G3–DOPE lipoplex showed



**Figure 7.** Luciferase activities of CV1 cells treated with varying amounts of DL-G3-DOPE (closed bars) and DC-Chol-DOPE (open bars) lipoplexes. The amounts of luciferase (g) per mg cellular protein (A) and per well (B) were shown. The DOPE/cationic lipid and N/P ratios of the DL-G3-DOPE lipoplex were 5 and 5, respectively. The DOPE/cationic lipid and N/P ratios of the DC-Chol-DOPE lipoplex were 1 and 2, respectively. Each point represents the mean  $\pm$  SD ( $n = 3$ ).



**Figure 8.** Viability of CV1 cells treated with varying amounts of DL-G3-DOPE (■) and DC-Chol-DOPE (○) lipoplexes. Viability was expressed as the percentage of the untreated control cells. Each point represents the mean  $\pm$  SD ( $n = 6$ ).

much higher cell viability especially under the treatment below 1  $\mu$ g DNA per  $5 \times 10^4$  cells, at which the lipoplex exhibited the maximum transfection activity. Therefore, these results mean that the DL-G3-DOPE lipoplex can transfect a larger number of the cells than the DC-Chol-DOPE lipoplex with the same efficiency.

In conclusion, we designed a new type of cationic lipid, which consists of the polyamidoamine dendron and two dodecyl chains, to obtain a novel gene carrier, which can transfect cells efficiently by synergy of the endosome buffering and membrane fusion with endosome. It was found that the ability of dendron-bearing lipids to form a lipoplex with plasmid DNA was elevated with increasing dendron generation. The transfection activity of their lipoplexes was shown to increase with the generation of the lipid headgroup. In addition, inclusion of DOPE, which is known to increase the fusion ability of a lipid membrane, greatly enhanced the transfection activity of the dendron-bearing lipid lipoplexes. The highest activity was achieved by the DL-G3-DOPE lipoplex, which transfected the cells more efficiently than the DC-Chol-DOPE lipoplex. In this preliminary study, we examined the dendron-bearing lipids only with the two dodecyl chains as the hydrophobic moiety. However, it can be easily imagined that the chemical structure of this moiety will affect the transfection activity of the dendron-bearing lipids. In addition, from the viewpoint of the polyamidoamine dendrimer-based transfection, the attachment of hydrophobic groups was shown to increase the transfection activity of the dendrimer. This finding may be important for the design of dendrimer-based gene carriers

with high transfection activity. We are currently investigating the correlation between the chemical structure of the polyamidoamine dendron-bearing lipids and their transfection activity as well as structures and properties of their assemblies and lipoplexes.

#### ACKNOWLEDGMENT

This work was partly supported by the Grant-in-Aid from Japanese Ministry of Education, Culture, Sports, Science, and Technology (12680839 and 13558115).

#### LITERATURE CITED

- (1) Mountain, A. (2000) Gene therapy: the first decade. *Trends Biotechnol.* 18, 119–128.
- (2) Crystal, R. G. (1995) Transfer of Genes to Humans: early lessons and obstacles to success. *Science* 270, 404–410.
- (3) Lasic, D. D., and Templeton, N. S. (2000) Bioorganic colloids: macromolecules, DNA, self-assembled particles, and their complexes. In *Gene Therapy* (Templeton, N. S., Lasic, D. D., Eds.) pp 241–266, Marcel Dekker, New York.
- (4) Lasic, D. D. (1997) *Liposomes in gene delivery*, CRC Press, Boca Raton.
- (5) Miller, A. D. (1998) Cationic liposomes for gene therapy. *Angew. Chem., Int. Ed.* 37, 1768–1785.
- (6) Brown, M. D., Schätzlein, A. G., and Uchegbu, I. F. (2001) Gene delivery with synthetic (non viral) carriers. *Int. J. Pharm.* 229, 1–21.
- (7) Felgner, P. L., Gadek, T. R., Holm, M., Roman, R., Chan, H. W., Wenz, M., Northrop, J. P., Ringold, G. M., and Danielsen, M. (1987) Lipofection: a highly efficient, lipid-mediated DNA-transfection procedure. *Proc. Natl. Acad. Sci. U.S.A.* 84, 7413–7417.
- (8) Cooper, R. G., Etheridge, C. J., Stewart, L., Marshall, J., Rudginsky, S., Cheng, S. H., and Miller, A. D. (1998) Polyamine analogues of 3 $\beta$ -[N-(N',N'-dimethylaminoethane)-carbamoyl]-cholesterol (DC-Chol) as agents for gene delivery. *Chem. Eur. J.* 4, 137–151.
- (9) Remy, J.-S., Sirlin, C., Vierling, P., and Behr, J.-P. (1994) Gene transfer with a series of lipophilic DNA-binding molecules. *Bioconjugate Chem.* 5, 647–654.
- (10) Felgner, J. H., Kumar, R., Sridhar, C. N., Wheeler, C. J., Tsai, Y. J., Border, R., Ramsey, P., Martin, M., and Felgner, P. L. (1994) Enhanced gene delivery and mechanism studies with a novel series of cationic lipid formulations. *J. Biol. Chem.* 269, 2550–2561.
- (11) Behr, J. P. (1993) Synthetic gene-transfer vectors. *Acc. Chem. Res.* 26, 274–278.
- (12) Singhal, A., and Huang, L. (1993) Gene transfer in mammalian cells using liposomes as carriers. In: *Gene Therapeutics* (Wolf, J. A., Ed.) pp 118–142, Birkhäuser, Boston.



- (13) Mönkkönen, J., and Urtti, A. (1998) Lipid fusion in oligonucleotide and gene delivery with cationic lipids. *Adv. Drug Delivery Rev.* 34, 37–49.
- (14) Friend, D. S., Papahadjopoulos, D., and Debs, R. J. (1996) Endocytosis and intracellular processing accompanying transfection. *Biochim. Biophys. Acta* 1278, 41–50.
- (15) Zabner, J., Fasbender, A. J., Moninger, T., Poellinger, K. A., and Welsh, M. J. (1995) Cellular and molecular barriers to gene transfer by a cationic lipid. *J. Biol. Chem.* 270, 18997–19007.
- (16) Xu, Y., and Szoka, F. C., Jr. (1996) Mechanism of DNA release from cationic liposome/DNA complexes used in cell transfection. *Biochemistry* 35, 5616–5623.
- (17) Pollard, H., Remy, J.-S., Loussouarn, G., Demolombe, S., and Behr, J.-P. (1996) Polyethylenimine but not cationic lipids promotes transgene delivery to the nucleus in mammalian cells. *J. Biol. Chem.* 273, 7507–7511.
- (18) Godbey, W. T., Wu, K. K., and Mikos, A. G. (1999) Tracking the intracellular path of poly(ethylenimine)/DNA complexes for gene delivery. *Proc. Natl. Acad. Sci. U.S.A.* 96, 5177–5181.
- (19) Mok, K. W. C., and Cullis, P. R. (1997) Structural and fusogenic properties of cationic liposomes in the presence of plasmid DNA. *Biophys. J.* 73, 2534–2545.
- (20) Wrobel, I., and Collins, D. (1995) Fusion of cationic liposomes with mammalian cells occurs after endocytosis. *Biochim. Biophys. Acta* 1235, 296–304.
- (21) Farhood, H., Serbina, N., and Huang, L. (1995) The role of dioleoyl phosphatidylethanolamine in cationic liposome mediated gene transfer. *Biochim. Biophys. Acta* 1235, 289–295.
- (22) Hui, S. W., Langner, M., Zhao, Y. L., Ross, P., Hurley, E., and Chan, K. (1996) The role of helper lipids in cationic liposome-mediated gene transfer. *Biophys. J.* 71, 590–599.
- (23) Noguchi, A., Furuno, T., Kawaura, C., and Nakanishi, M. (1998) Membrane fusion plays an important role in gene transfection mediated by cationic liposomes. *FEBS Lett.* 433, 169–173.
- (24) Kono, K., Torikoshi, Y., Mitsutomi, M., Itoh, T., Emi, N., Yanagie, H., and Takagishi, T. (2001) Novel gene delivery systems: complexes of fusogenic polymer-modified liposomes and lipoplexes. *Gene Ther.* 8, 5–12.
- (25) Plank, C., Zauner, W., and Wagner, E. (1998) Application of membrane-active peptides for drug and gene delivery across cellular membranes. *Adv. Drug Delivery Rev.* 34, 21–35.
- (26) Cheung, C. Y., Murthy, N., Stayton, P. S., and Hoffman, A. S. (2001) A pH-sensitive polymer that enhances cationic lipid-mediated gene transfer. *Bioconjugate Chem.* 12, 906–910.
- (27) Simões, S., Slepishkin, V., Gaspar, R., Pedrosa de Lima, M. C., and Düzgüneş, N. (1998) Gene delivery by negatively charged ternary complexes of DNA, cationic liposomes and transferrin or fusogenic peptides. *Gene Ther.* 5, 955–964.
- (28) Boussif, O., Lezoualc'h, F., Zanta, M. A., Mergny, M. D., Scherman, D., Demeneix, B., and Behr, J. P. (1995) A versatile vector for gene and oligonucleotide transfer into cells in culture and in vivo: Polyethylenimine. *Proc. Natl. Acad. Sci. U.S.A.* 92, 7297–7301.
- (29) Haensler, J., and Szoka, F. C., Jr. (1993) Polyamidoamine cascade polymers mediate efficient transfection of cells in culture. *Bioconjugate Chem.* 4, 372–379.
- (30) Tang, M., Redemann, C. T., and Szoka, F. C., Jr. (1996) In vitro gene delivery by degraded polyamidoamine dendrimers. *Bioconjugate Chem.* 7, 703–714.
- (31) Zou, S. M., Behr, J. P., Goula, D., and Demeneix, B. (2000) Gene delivery with polyethylenimine, in *Gene Therapy: Therapeutic mechanisms and strategies* (Templeton, N. S., Lasic, D. D., Eds.) pp 131–139, Marcel Dekker, NY.
- (32) Regelin, A. E., Fankhaenel, S., Gürtesch, L., Prinz, C.; von Kiedrowski, G., and Massig, U. (2000) Biophysical and lipofection studies of DOTAP analogues. *Biochim. Biophys. Acta* 1464, 151–164.
- (33) Li, S., Gao, X., Son, K., Sorgi, F., Hofland, H., and Huang, L. (1996) DC-Chol lipid system in gene transfer. *J. Controlled Release* 39, 373–381.
- (34) Gao, X., and Huang, L. (1991) A novel cationic liposome reagent for efficient transfection of mammalian cells. *Biochem. Biophys. Res. Commun.* 179, 280–285.
- (35) Tomalia, D. A., Baker, H., Dewald, J., Hall, M., Kallos, G., Martin, S., Roeck, J., Ryder, J., and Smith, P. (1985) A new class of polymers: starburst-dendritic macromolecules. *Polym. J.* 17, 117–132.
- (36) Fréchet, J. M. J., Tomalia, D. A., Eds. (2001) *Dendrimers and other dendritic polymers*, J. Wiley & Sons, West Sussex.
- (37) Mosmann, T. (1983) Rapid colorimetric assay for cellular growth and survival: application to proliferation and cytotoxicity assays. *J. Immunol. Methods* 65, 55–63.
- (38) Kukowska-Latallo, J. F., Bielinska, A. U., Johnson, J., Spindler, R., Tomalia, D. A., and Baker, J. R., Jr. (1996) Efficient transfer of genetic material into mammalian cells using Starburst polyamidoamine dendrimers. *Proc. Natl. Acad. Sci. U.S.A.* 93, 4897–4902.
- (39) Tang, M. X., and Szoka, F. C. (1997) The influence of polymer structure on the interactions of cationic polymers with DNA and morphology of the resulting complexes. *Gene Ther.* 4, 823–832.
- (40) Zhou, X., Klivanov, A. L., and Huang, L. (1991) Lipophilic polylysines mediate efficient DNA transfection in mammalian cells. *Biochim. Biophys. Acta* 1065, 8–14.
- (41) Behr, J. P., Demeneix, B., Loeffler, J. P., and Perez-Mutul, J. (1989) Efficient gene transfer into mammalian primary endocrine cells with lipopolyamine-coated DNA. *Proc. Natl. Acad. Sci.* 86, 6982–6989.
- (42) Han, S., Mahato, R. I., and Kim, S. W. (2001) Water-soluble lipopolyamine for gene delivery. *Bioconjugate Chem.* 12, 337–345.
- (43) Wang, D., Narang, A. S., Kotb, M., Gaber, A. O., Miller, D. D., Kim, S. W., and Mahato, R. I. (2002) Novel branched poly(ethylenimine)-cholesterol water-soluble lipopolymers for gene delivery. *Biomacromolecules* 3, 1197–2007.
- (44) Zhou, X., and Huang, L. (1994) DNA transfection mediated by cationic liposomes containing lipopolylysine: characterization and mechanism of action. *Biochim. Biophys. Acta* 1189, 195–203.
- (45) Brown, M. D., Schätzlein, A. G., and Uchegbu, I. F. (2001) Gene delivery with synthetic (non viral) carriers. *Int. J. Pharmaceut.* 229, 1–21.
- (46) Lim, Y., Kim, S., Suh, H., and Park, J. (2002) Biodegradable, endosome disruptive, and cationic network-type polymer as a highly efficient and nontoxic gene delivery carrier. *Bioconjugate Chem.* 13, 952–957.
- (47) Mok, K. W. C., and Cullis, P. R. (1997) Structural and Fusogenic properties of cationic liposomes in the presence of plasmid DNA. *Biophys. J.* 73, 2534–2545.
- (48) Sundler, R., Düzgüneş, N., and Papahadjopoulos, D. (1981) Control of membrane fusion by phospholipid headgroups II: the role of phosphatidylethanolamine in mixtures with phosphatidate and phosphatidylinositol. *Biochim. Biophys. Acta* 649, 751–758.
- (49) Hope, M. J., and Cullis, P. R. (1981) The role of nonbilayer lipid structures in the fusion of human erythrocytes induced by lipid fusogens. *Biochim. Biophys. Acta* 640, 82–90.
- (50) Kono, K., Iwamoto, M., Nishikawa, R., Yanagie, H., and Takagishi, T. (2000) Design of fusogenic liposomes using a poly(ethylene glycol) derivative having amino groups. *J. Controlled Release* 68, 225–235.
- (51) Cullis, P. R., and De Kruijff, B. (1979) Lipid polymorphism and the functional roles of lipids in biological membranes. *Biochim. Biophys. Acta* 559, 399–420.
- (52) Israelachvili, J. N., Marcelja, S., and Horn, R. G. (1980) Physical principles of membrane organization. *Q. Rev. Biophys.* 13, 121–200.

# pH-Sensitive Unimolecular Polymeric Micelles: Synthesis of a Novel Drug Carrier

Marie-Christine Jones,<sup>†</sup> Maxime Ranger,<sup>‡</sup> and Jean-Christophe Leroux<sup>†,\*</sup>

Canada Research Chair in Drug Delivery, Faculty of Pharmacy, University of Montreal, Montréal, Québec, Canada, H3C 3J7 and Technology Innovation, Labopharm Inc., 1208 Bergar, Laval, Québec, Canada. Received June 25, 2002; Revised Manuscript Received March 17, 2003

Novel amphiphilic star-shaped polymers showing pH-sensitivity were synthesized by atom transfer radical polymerization. These new polymers present a core-shell structure similar to polymeric micelles, but are inherently stable to dilution and are referred to as unimolecular polymeric micelles. A four-armed multifunctional initiator was used for the sequential polymerization of hydrophobic ethyl methacrylate and *tert*-butyl methacrylate and hydrophilic poly(ethylene glycol)methacrylate. Polymers of molecular weight ranging from 9000 to 20 000 were obtained. Results of dynamic light scattering showed micelle size ranging from 11 to 40 nm. Unimolecular micelles were also analyzed by static light scattering in aqueous environment. Star-shaped polymers which presented the highest molar ratio of hydrophobic monomers tended to form high molecular weight aggregates in water. Hydrolysis of the *tert*-butyl methacrylate units permitted the introduction of ionizable methacrylic acid functions. Size distributions were bimodal at both acidic and basic pH. Since, the polymers were designed as potential delivery systems for the oral administration of hydrophobic drugs, they were titrated to evaluate the degree of ionization as a function of pH. In the stomach, the carboxylic functions are expected to be fully protonated. However, in the intestine, the micelles will be more than 40% ionized. Fluorescence studies were conducted in order to evaluate the polarity of the micellar core. Results showed an increase in polarity with pH due to the ionization of the acid functions present along the polymer chains. The pH rise was associated with an increase in the *in vitro* release rate of progesterone, which was used as hydrophobic drug model.

## INTRODUCTION

Polymeric micelles (PM)<sup>1</sup> have been extensively studied as carriers for water-insoluble drugs (1). However, because micelle formation is a thermodynamic phenomenon, micelles are relatively unstable to infinitely dilute environments such as those encountered after oral or parenteral administration. To improve micelle stability, the synthesis of polymeric structures that mimic PM regarding their morphological properties has been proposed. Such polymers are referred to as unimolecular polymeric micelles (UPM) (2) and consist of covalently bound amphiphilic polymer chains. These colloids are intrinsically stable upon dilution since their formation is independent of polymer concentration. UPM have been obtained from both dendrimers (3, 4) and star polymers

(5–7). The latter form presents the advantage of being simpler to prepare since fewer synthetic steps are involved. Star polymers can be produced by the arm or core-first methods. The arm-first method involves the use of a multifunctional termination agent or the cross-linking of linear polymer chains prepared by “living”/controlled polymerization with a difunctional vinylic compound (8). In the core-first method, polymer chains are grown from a multifunctional initiator. In the present work, the latter method has been applied to the synthesis of UPM by atom transfer radical polymerization (ATRP). ATRP is a controlled radical polymerization procedure that allows control over both molecular weight and architecture. It has been previously employed to prepare polymers of varying morphologies, including linear (9, 10) and star polymers (11–13). In this study, novel nonbiodegradable water-soluble UPM with an ionizable core were developed as potential carriers for the oral delivery of hydrophobic drugs. To our knowledge, this is the first report on the use of ATRP to produce water-soluble UPM with an ionizable core. Heise et al. (5) have reported the synthesis of amphiphilic star polymers bearing an ionizable core and a hydrophobic shell. However, in that case, the micelle insolubility in water limits its application in drug delivery.

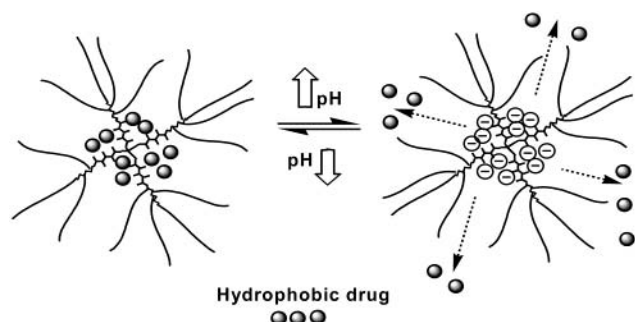
While diffusion is the sole mechanism by which drugs are released from nonbiodegradable UPM, the introduction of ionizable functions within the core is expected to modify the partition coefficient of the drug between the hydrophobic core and the surrounding aqueous milieu upon a change in pH. In the stomach, the drug would remain inside the core, protected from interactions with

\* Corresponding author: University of Montreal, Faculty of Pharmacy, 2900 Edouard-Montpetit, C.P. 6128, Succursale Centre-Ville, Montreal, Quebec, Canada H3C 3J7. Tel: (514) 343-6455. Fax: (514) 343-7738. E-mail: jean-christophe.leroux@umontreal.ca.

<sup>†</sup> University of Montreal.

<sup>‡</sup> Labopharm Inc.

<sup>1</sup> Abbreviations: ATRP, atom transfer radical polymerization; CDCl<sub>3</sub>, deuterated chloroform; CuBr, copper bromide; D<sub>2</sub>O, deuterated water; DLS, dynamic light scattering; DP, degree of polymerization; EMA, ethyl methacrylate; LALLS, low-angle laser light scattering; MAA, methacrylic acid; MALLS, multi-angle laser light scattering; MMA, methyl methacrylate; MeOD, deuterated methanol; PEGMA, poly(ethylene glycol) methacrylate; PM, polymeric micelle; PMDETA, *N,N,N',N',N'*-pentamethyldiethylenetriamine; SEC, size-exclusion chromatography; tBMA, *tert*-butyl methacrylate; THF, tetrahydrofuran; UPM, unimolecular polymeric micelles.



**Figure 1.** Theoretical drug release from a pH-sensitive UPM. It is expected that the ionization of the carboxylic functions within the micellar core will provoke an increase in polarity which in turn will aid the release of the hydrophobic drug solubilized in the core.

stomach contents by the hydrophilic shell (Figure 1). As the carrier moves toward the jejunum, the increase in polarity resulting from the ionization of acidic units would promote the release of the drug. Poorly water-soluble drugs with low or variable oral bioavailability, such as HIV-1 protease inhibitors, may mostly benefit from incorporation in the proposed UPM formulations. Although this work focuses mainly on the preparation of novel ionizable anionic UPM for the oral delivery of drugs, other types of UPM (nonionic and cationic) could be prepared by the proposed synthetic procedure (14).

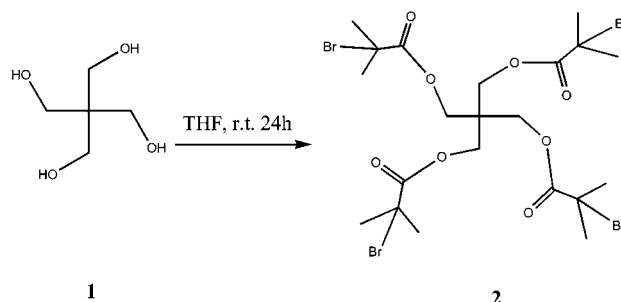
#### EXPERIMENTAL PROCEDURES

**Materials.** All chemicals were obtained from Sigma-Aldrich (Milwaukee, WI) except where otherwise stated. Tetrahydrofuran (THF) was dried over sodium using benzophenone as a dryness indicator and distilled under nitrogen prior to use. Ethyl methacrylate (EMA) and *tert*-butyl methacrylate (tBMA) were distilled under vacuum prior to use. Poly(ethylene glycol) methacrylate (PEGMA) (475 g/mol) was passed through a hydroquinone–monomethylhydroquinone inhibitor remover column and then washed with a 5% sodium hydroxide solution. PEGMA of lower molecular weight (MW) (200 and 400 g/mol) were purchased from Polysciences (Warrington, PA) and used without further purification. All other reagents were used as received. Deuterated chloroform ( $\text{CDCl}_3$ ), water ( $\text{D}_2\text{O}$ ), and methanol (MeOD) were purchased from CDN Isotopes (Pointe-Claire, QC, Canada). Radiolabeled  $^3\text{H}$ -progesterone (53.0 Ci/mmol) was obtained from Amersham Biosciences (Piscataway, NJ).

**Synthesis of ATRP Initiator: Tetrakis(2-bromo-isobutyryl) Pentaerythritol.** 2-Bromoisobutyryl bromide (0.200 mol) was slowly added to a slightly cooled solution of pentaerythritol (0.025 mol) and triethylamine (0.15 mol) in THF (Scheme 1). The solution was allowed to reach room temperature and stirred for 24 h. The mixture was then transferred to a separation funnel with 300 mL of dichloromethane and extracted successively with 10% HCl, 10% NaOH, and brine. The organic extracts were dried over  $\text{MgSO}_4$ , and the solvent was removed by rotary evaporation. The crude extract was dissolved in a small amount of dichloromethane and recrystallized in methanol. MS (positive FAB) 733.5 ( $\text{MH}^+$ ).  $^1\text{H}$  NMR ( $\delta$ , ppm,  $\text{CDCl}_3$ ): 4.33 (s, 8H); 1.94 (s, 24H).  $^{13}\text{C}$  NMR ( $\delta$ , ppm,  $\text{CDCl}_3$ ): 171.3; 77.4; 63.2; 55.6; 44.0; 31.0. Anal. C (34.60  $\pm$  0.07%), H (4.44  $\pm$  0.01%).

**Synthesis of Star-P(EMA-co-tBMA)-b-P(PEGMA).** ATRP was carried out in THF using copper bromide ( $\text{CuBr(I)}$ ) as a catalyst and *N,N,N,N,N'*-pentamethyldiethylenetriamine (PMDETA) as a ligand (Scheme 2).

**Scheme 1.** Synthesis of ATRP Multifunctional Initiator Tetrakis(2-bromoisobutyryl) Pentaerythritol (2)<sup>a</sup>



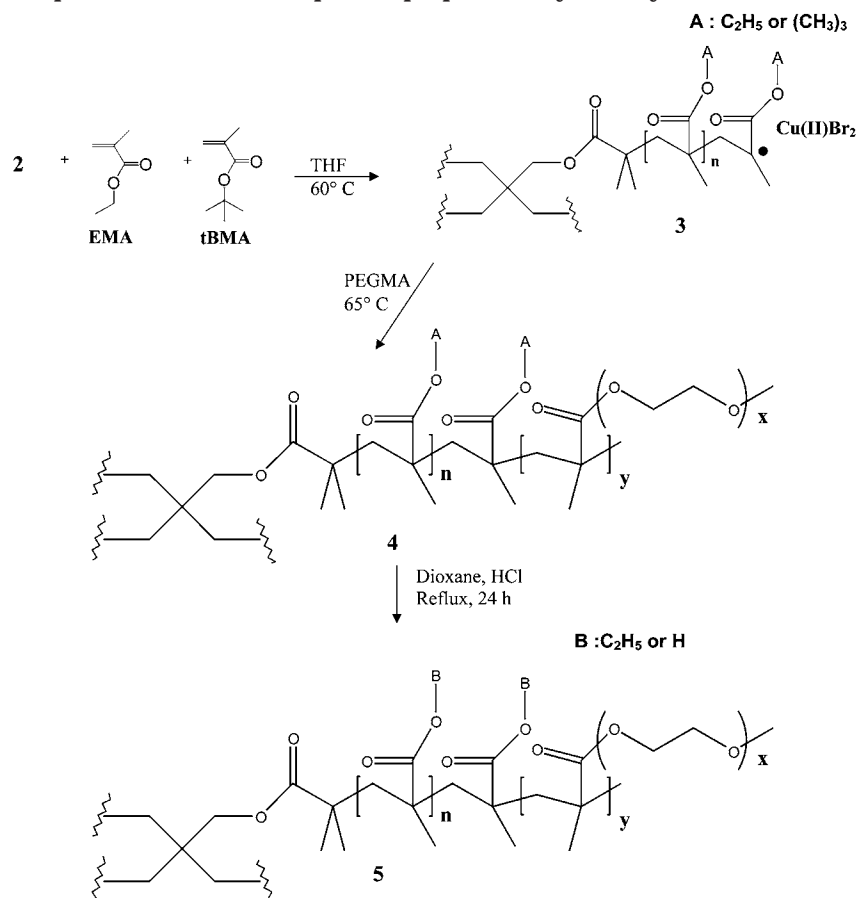
<sup>a</sup> Pentaerythritol (1) (25 mmol) is esterified by 2-bromoisobutyryl bromide (200 mmol) in the presence of triethylamine (150 mmol) in THF at room temperature.

ATRP tetrainitiator (1 mol) was added to  $\text{CuBr}$  (1.8 mol), PMDETA (3 mol), EMA (16 or 40 mol), and tBMA (16 or 40 mol) in THF (0.4 M). The mixture was degassed under argon for 15 min at room temperature and then heated to 65 °C. The hydrophobic core was reacted for 1 h at which point PEGMA (200, 400, or 475 g/mol) was added to the reaction pot. The mixture was left to further react and then poured in THF containing ethanol. The polymer was passed through a silica gel column to remove  $\text{CuBr}$ , using THF as the eluent. The solvent was evaporated under reduced pressure, and the crude polymer extract was dialyzed against water for 36 h (Spectra/Por no. 1, MW cutoff 6000–8000). The polymer was recovered by freeze-drying. All polymers are referred to by  $\text{S}_{\text{E}_x\text{T}_y\text{P}_z}\text{PY}_x$  where X is the DP of EMA (E), tBMA (T) or PEGMA (P) and Y is the MW of the PEGMA monomer divided by 100.  $\text{S}_{\text{E}_{16}\text{T}_{16}\text{P}_{25}}$ ,  $^1\text{H}$  NMR ( $\delta$ , ppm,  $\text{CDCl}_3$ ): 4.08 (m, 82H); 3.65 (m, 760H); 3.39 (s, 77H); 1.82 (m, 118H); 1.42 (s, 144H); 1.26 (m, 65H); 0.87 (m, 174H).  $\text{S}_{\text{E}_{13}\text{T}_{11}\text{P}_{34}}$ ,  $^1\text{H}$  NMR ( $\delta$ , ppm,  $\text{CDCl}_3$ ): 4.08 (m, 95H); 3.65 (m, 1258H); 3.38 (s, 116H); 1.79 (m, 117H); 1.42 (s, 105H); 1.26 (m, 47H); 0.86 (m, 177H).  $\text{S}_{\text{E}_{18}\text{T}_{17}\text{P}_{42}}$ ,  $^1\text{H}$  NMR ( $\delta$ , ppm,  $\text{CDCl}_3$ ): 4.08 (m, 124H); 3.65 (m, 1265H); 3.39 (s, 126H); 1.82 (m, 244H); 1.42 (s, 153H); 1.26 (m, 53H); 0.87 (m, 219H).  $\text{S}_{\text{E}_{24}\text{T}_{23}\text{P}_{29}}$ ,  $^1\text{H}$  NMR ( $\delta$ , ppm,  $\text{CDCl}_3$ ): 4.08 (m, 98H); 3.65 (m, 411H); 3.38 (s, 84H); 1.79 (m, 177H); 1.42 (m, 208H); 1.26 (m, 47H); 0.86 (m, 218H).

**Preparation of Star-P(EMA-co-MAA)-b-P(PEGMA).** pH-responsiveness was introduced by the hydrolysis of tBMA units into methacrylic acid (MAA). Concentrated HCl was added to a solution of the polymer bearing tBMA groups in refluxing dioxane (2.6 M). The reaction was stirred overnight. The solvent was removed by rotary evaporation, and the hydrolyzed polymer was dialyzed against water for 48 h. The polymers were recovered by freeze-drying. All hydrolyzed polymers are identified by as  $\text{S}_{\text{E}_x\text{M}_y\text{PY}_x}$ , where  $\text{M}_x$  is the DP of MAA.  $\text{S}_{\text{E}_{16}\text{M}_{16}\text{P}_{25}}$ ,  $^1\text{H}$  NMR ( $\delta$ , ppm, MeOD): 4.13 (m, 92H); 3.68 (m, 760H); 3.39 (s, 61H); 1.94 (m, 117H); 0.9–1.29 (m, 379H).  $\text{S}_{\text{E}_{13}\text{M}_{11}\text{P}_{34}}$ ,  $^1\text{H}$  NMR ( $\delta$ , ppm, MeOD): 4.13 (m, 139); 3.68 (m, 1258H); 3.39 (s, 91H); 1.94 (m, 176H); 0.9–1.29 (m, 573H).  $\text{S}_{\text{E}_{18}\text{M}_{17}\text{P}_{42}}$ ,  $^1\text{H}$  NMR ( $\delta$ , ppm, MeOD): 4.13 (m, 140H); 3.68 (m, 1265H); 3.39 (s, 92H); 1.94 (m, 177H); 0.9–1.29 (m, 576H).  $\text{S}_{\text{E}_{24}\text{M}_{23}\text{P}_{29}}$ ,  $^1\text{H}$  NMR ( $\delta$ , ppm, MeOD): 4.13 (m, 50H); 3.68 (m, 416H); 3.39 (s, 34H); 1.94 (m, 64H); 0.9–1.29 (m, 204H).

**MW Determination by Size Exclusion Chromatography.** Number ( $M_n$ ) and weight ( $M_w$ ) average molecular weights were determined using a Waters 1525 size exclusion chromatography (SEC) system equipped with a 2410 refractometer (Waters, Milford, MA) and low-



**Scheme 2. Synthesis of pH-Sensitive Star-Shaped Amphiphilic Polymers by ATRP<sup>a</sup>**

<sup>a</sup> The initiator (**2**) is first reacted with hydrophobic EMA and tBMA to yield the micellar core star-p(EMA-*co*-tBMA) (**3**). The hydrophilic shell is formed by the polymerization of PEGMA which is added to the reaction pot to obtain the star-shaped amphiphilic polymer (**4**). Hydrolysis of tBMA units of compound **4** yields the pH-sensitive UPM (**5**).

angle laser light scattering (PD2000DLS, Precision Detectors, Bellingham, MA) detector. Analyses were performed in DMF with 10 mM LiBr, at a flow rate of 1 mL/min using a set of 3 Styragel HT2, HT3, and HT4 columns (Waters, Milford, MA), maintained at 45 °C.

**Multiangle Static Light Scattering Experiments (MALLS).** Star-P(EMA-*co*-tBMA)-*b*-P(PEGMA) were analyzed by MALLS on a Malvern Autosizer 4800 equipped with a uniphase argon ion laser (488 nm) (Malvern Instruments, Worcestershire, U.K.).  $M_w$  were calculated from eq 1:

$$\frac{Kc_p}{R\theta} = \frac{1}{M_w} \left( 1 + \frac{1}{3} \langle R_g^2 \rangle q^2 \right) + 2A_2c_p \quad (1)$$

where  $c_p$  is the polymer concentration,  $A_2$  the second virial coefficient,  $R_g$  the gyration radius,  $R_\theta$  the rayleigh ratio,  $q = (4\pi n/\lambda) \sin(\theta/2)$  (where  $\theta$  is the scattering angle) and  $K = 4\pi^2 n^2 (dn/dc_p)^2 / \lambda^4 N$ , where  $n$  is the refractive index of the solvent,  $(dn/dc_p)$  the refractive index increment, and  $N$ , Avogadro's number. Values of  $dn/dc_p$  were obtained using a Fisherbrand Abbe Benchtop refractometer (Fisher Scientific Ltd., ON, Canada). The calculated  $dn/dc_p$  values were of 0.1469 mL/g and 0.1552 mL/g for S\_E18T17P442 and S\_E24T23P229, respectively. Zimm plots were obtained by measuring the intensity of the scattered light at varying angle and concentrations to obtain  $M_w$ .

**Size Analysis by Dynamic Light Scattering (DLS).** The hydrodynamic diameters were determined by DLS on a Malvern Autosizer 4800. Aqueous polymer solutions

of varying concentrations were prepared and passed through a 0.22- $\mu$ m filter prior to size determination. Size measurements were performed at a 90° angle in triplicate at 25 °C. In some experiments, pH was adjusted using small amounts of NaOH 0.5 N or HCl 0.5 N

**Potentiometric Titrations.** Aqueous solutions of the polymer were prepared (1 mg/mL) and titrated with NaOH 0.05 N. pH values were plotted as a function of the degree of ionization  $\alpha$ , where  $\alpha = C_b/C_{MAA}$  and  $C_b$  is the concentration of NaOH added to the solution,  $C_{MAA}$  is the concentration of MAA in solution. The apparent  $pK_a$  values were calculated from eq 2 (15):

$$pK_a = \text{pH} + \log \frac{1 - \alpha}{\alpha} \quad (2)$$

**Fluorescence Studies.** The local environment inside the hydrolyzed UPM was characterized by spectrofluorimetry. Pyrene was chosen as the fluorescent probe because its fluorescence is polarity-dependent. Hydrolyzed UPM solutions were prepared in water. Pyrene was added to the solution ( $2 \times 10^{-7}$  M final concentration), and pH was adjusted to 3 or 11 with small amounts of NaOH or HCl 1 M. The solutions were stirred overnight in the dark at room temperature. Excitation spectra ( $\lambda_{em} = 393$  nm) were obtained at 25 °C on a Series 2 Aminco Bowman fluorimeter (Spectronic Instruments Inc., Rochester, NY).

**In Vitro Drug Release Studies.** Drug release experiments were carried out using progesterone as a hydrophobic model drug. A solution of UPM (S\_E24M23P229, 1%

**Table 1. Characteristics of the Star-Shaped Polymers**

polymer	DP EMA	DP tBMA	DP PEGMA	PEGMA unit (g/mol)	MW of (g/mol)	NMR $M_n$	LALLS <sup>b</sup>			MALLS <sup>c</sup> $M_w$	DLS size <sup>d</sup> (nm)
							$M_n$	$M_w$	PI		
S_E16T16P225	16	16	25	200	200	9100	N/A <sup>a</sup>	N/A	N/A	N/A	15.4
S_E13T11P434	13	11	34	475	475	19670	N/A	N/A	N/A	N/A	14.3
S_E18T17P442	18	17	42	400	400	21200	32000	38700	1.20	48500	11.0
S_E24T23P229	24	23	29	200	200	11950	20850	26500	1.27	$1.4 \times 10^6$	37.3 (56%) 140.6 (44%)

<sup>a</sup> N/A: not available. <sup>b</sup> Determined in DMF with 10 mM LiBr. <sup>c</sup> Determined in H<sub>2</sub>O at 25 °C. <sup>d</sup> Polymer concentration: 0.5 mg/mL

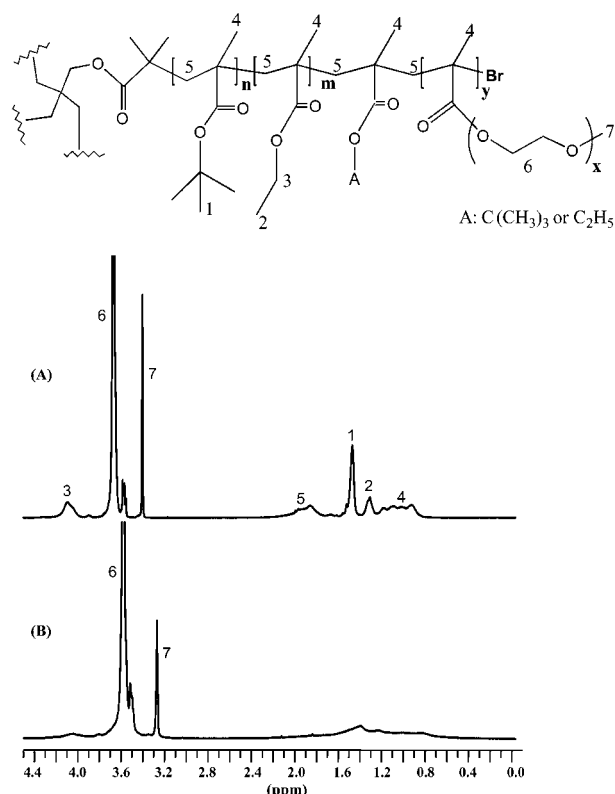
w/v), <sup>3</sup>H-progesterone (0.5  $\mu$ Ci/mL), and cold progesterone (0.05% w/v) was prepared in acetone. The solvent was removed under reduced pressure, and the resulting film was hydrated in 2 mL of simulated gastric buffer (HCl 0.06 M/NaCl 0.021 M; pH 1.2). The micelle–drug complex (5% w/w drug loading, 1  $\mu$ Ci) was transferred into a dialysis bag (MW cutoff 6000–8000) and dialyzed against simulated gastric buffer at 37 °C. When needed, the pH was adjusted to 7 or 11 after 2 h by adding NaOH (0.25% w/v)/NaH<sub>2</sub>PO<sub>4</sub> (0.12% w/v), or NaOH (0.25% w/v) to the acidic milieu. Aliquots of the dialysis milieu were taken at predetermined time intervals, and the radioactivity was measured on a LKB–Wallac 1217 Rackbeta liquid scintillation counter (Perkin-Elmer, Boston, MA). Release of free progesterone was also performed as a control. A similar procedure was used, except for the concentration of unlabeled progesterone, which was decreased by 250-fold to avoid drug precipitation in the dialysis bag.

## RESULTS AND DISCUSSION

**Star-P(EMA-co-tBMA)-b-P(PEGMA). Polymer Characterization.** Star-shaped polymers were synthesized by the core-first method. The first step consisted in the synthesis of a multifunctional initiator, tetrakis(2-bromoisobutryl) pentaerythritol, which was obtained by the esterification of pentaerythritol in the presence 2-bromoisobutryl bromide (Scheme 1). This initiator was used for the polymerization of tBMA and EMA (the core forming units) and of PEGMA (the shell forming unit) (Scheme 2). The characteristics of the polymers are presented in Table 1. The degrees of polymerization (DP) of S\_E18T17P442 as calculated by NMR spectroscopy were slightly higher than the feed ratio, but remained within the experimental error. S\_E18T17P442 and S\_E24T23P229 were analyzed by SEC equipped with a LALLS detector. Absolute  $M_n$  determined by LALLS for these two polymers were similar to those calculated by NMR spectroscopy. Relatively low polydispersity indices (<1.3) were obtained for both polymers, which is consistent with controlled radical polymerization.

**MALLS.** MALLS analysis was carried out for S\_E18T17P442 and S\_E24T23P229 (Table 1) to determine whether the amphiphilic polymer would behave as unimolecular micelles in water or self-assemble to form multimolecular structures. The absolute  $M_w$  obtained for S\_E18T17P442 was close to that observed in organic solvent suggesting the existence of true UPM. However, for S\_E24T23P229, which is more hydrophobic,  $M_w$  over a million was observed (Table 1), indicating that polymer chains tend to aggregate in water. Indeed, this polymer presents a higher proportion of hydrophobic monomers. Also, in this case the MW of the PEGMA chain used to form the micelle shell is half that of S\_E18T17P442 and may not completely shield the core from hydrophobic intermolecular interactions.

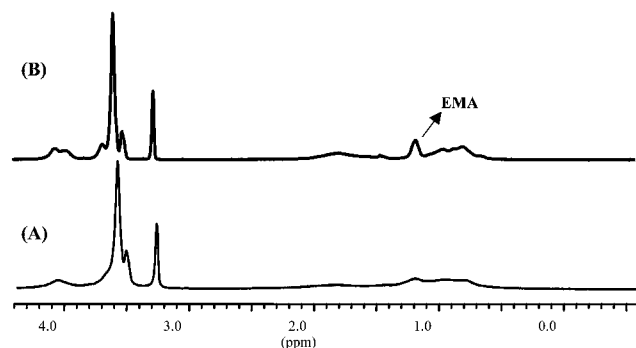
**<sup>1</sup>H NMR Spectroscopy Analysis.** Amphiphilic star polymers, just as PM, have been shown to adjust to



**Figure 2.** Study of the influence of solvent polarity on UPM conformation. <sup>1</sup>H NMR spectra (300 MHz) of UPM S\_E18T17P442 in CDCl<sub>3</sub> (A) and D<sub>2</sub>O (B). Signals 1–5 can be attributed to hydrophobic EMA and tBMA monomers while signals 6 and 7 are those of hydrophilic PEGMA. The signals for both the core and the shell were visible in apolar chloroform while only the signals of PEGMA can be seen in water.

changes in their environment by changing their conformation. To get an insight on the interactions of the micelle core with the external environment, NMR spectra were recorded in D<sub>2</sub>O and CDCl<sub>3</sub> (Figure 2). In CDCl<sub>3</sub>, the <sup>1</sup>H NMR spectrum of the UPM showed signals from both the PEGMA shell (signal 6,  $\delta$  = 3.65 ppm) and the *tert*-butyl signal from tBMA (signal 1,  $\delta$  = 1.9 ppm, tBMA was used as a reference signal for the core) since chloroform is a good solvent for both PEGMA and the two hydrophobic monomers (Figure 2A). In D<sub>2</sub>O, the signals observed were those of PEGMA whereas the signal corresponding to tBMA was not visible (Figure 2B). This indicates reduced proton mobility of the core-forming units and thus high core viscosity in aqueous media.

**Size Measurements.** DLS experiments were performed on aqueous solutions (0.5 mg/mL) of the polymers to evaluate their hydrodynamic diameter (Table 1). Small sizes (ca. 11–16 nm) were obtained for all formulations except S\_E24T23P229. Indeed, particle sizes exceeding 30 nm were observed for the latter, corroborating the results obtained by MALLS. Star polymer with the same amount of hydrophobic monomers but with differing PEGMA



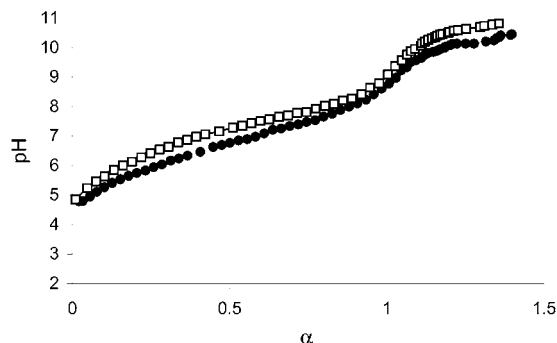
**Figure 3.** Study of the influence of pH on hydrolyzed UPM conformation.  $^1\text{H}$  NMR spectrum (300 MHz) of  $\text{S}_{\text{E}18\text{M}17\text{P}442}$  in  $\text{D}_2\text{O}$  at pH 2 (A) and pH 12 (B). Polymers were dissolved in  $\text{D}_2\text{O}$ , and the pH was adjusted using small amounts of NaOH or HCl 0.01 N. The signal of EMA (0.9 ppm, as indicated by the arrow) was used as a reporter signal for the hydrophobic core.

showed similar sizes (Table 1). Since the shell is composed of pendant PEG chains, their length may not significantly affect the hydrodynamic radius of the carrier. Hydrophobicity of the carrier seemed to be the most influential factor.  $\text{S}_{\text{E}24\text{T}23\text{P}229}$  presented the highest molar ratio of hydrophobic monomers compared to hydrophilic PEGMA and may be more prone to aggregation. Indeed, although size distribution remained unimodal and independent of concentration for all other star polymers, size increased with concentration for  $\text{S}_{\text{E}24\text{T}23\text{P}229}$  (data not shown), which is consistent with the presence of secondary aggregates, a phenomenon commonly observed with PM (16) and lipidic dendrimers (17).

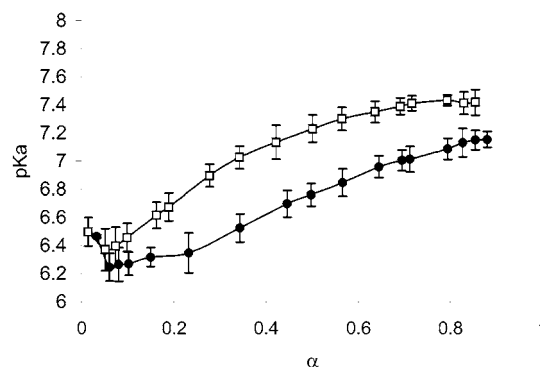
The small size of these UPM present several advantages for drug delivery applications. Small-sized carriers (<100 nm) have the advantage of longer circulation time in blood, after intravenous administration, due to decreased interactions with the mononuclear phagocyte system. This has long been recognized as one of the most attractive characteristics of PM (1). Oral absorption of polymeric carriers is also affected by size. Indeed, the size limit for particle uptake by transcytosis was evaluated at 100 nm (18). Smaller particles (50 nm) were also shown to be better absorbed than larger particles (3  $\mu\text{m}$ ) (19). Also, the high specific surface area of small drug carriers facilitates the dissolution of hydrophobic drugs in gastrointestinal fluids and increases their bioavailability (20).

**Star-P(EMA-co-MAA)-b-(PEGMA).** *Hydrolysis of tBMA Units.* pH-responsiveness was introduced by the hydrolysis of tBMA units in dioxane (2.6 M) with concentrated HCl (Scheme 2). The reaction proceeded easily and was monitored by the disappearance of the tBMA peak in the  $^1\text{H}$  NMR spectrum (data not shown). tBMA units were selectively hydrolyzed under these conditions since NMR did not show any signs of polymer degradation, and the polymer maintained its water solubility.

**$^1\text{H}$  NMR Spectroscopy Analysis.**  $^1\text{H}$  NMR spectra were recorded for hydrolyzed polymers as a function of pH. At acidic pH, only the PEGMA signals were observed (Figure 3A). As the pH is increased, electrostatic repulsion between negatively charged MAA is thought to force the polymeric chains to adopt a more extended conformation, thus allowing both the core and the shell signals to be seen (Figure 3B). Comparatively, the intensity of the signals associated to the protons of PEGMA was lower at acidic pH, than at pH 12, suggesting possible hydrogen bonding between the carboxylic functions of MAA and the oxygen atom of PEGMA (21), and reduction of the



**Figure 4.** Plot of the pH as a function of the  $\alpha$  for  $\text{S}_{\text{E}18\text{M}17\text{P}442}$  (closed circles) and  $\text{S}_{\text{E}24\text{T}23\text{P}229}$  (open squares).  $\alpha$  was calculated as  $\alpha = C_b/C_{\text{MAA}}$ . Solutions of the polymers were prepared in water (1 mg/mL) and titrated using NaOH 0.05 N. Results are a average of three measurements.

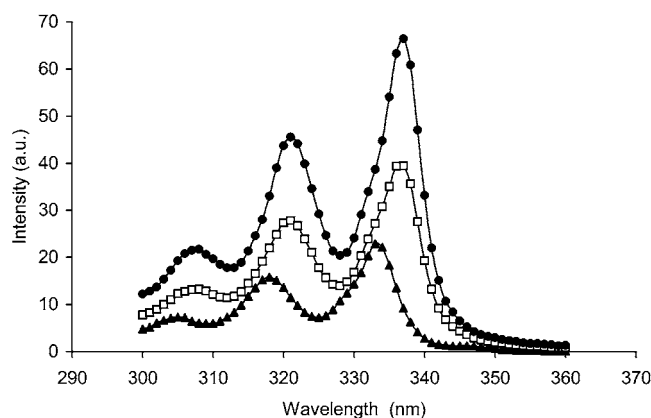


**Figure 5.** Plot of the apparent  $\text{pK}_a$  as a function of the degree of ionization ( $\alpha$ ) for  $\text{S}_{\text{E}18\text{M}17\text{P}442}$  (closed circles) and  $\text{S}_{\text{E}24\text{T}23\text{P}229}$  (open squares).  $\text{pK}_a$  values were obtained from  $\text{pK}_a = \text{pH} + \log[(1 - \alpha)/\alpha]$ . Results are presented as the average of three independent experiments  $\pm$  SD.

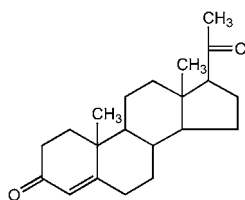
mobility of the protons implicated in the interaction. The presence of hydrogen bonding was also suspected for  $\text{S}_{\text{E}24\text{M}23\text{P}229}$  in MeOD and thought to account for the observed discrepancies in signal intensity between the NMR spectrum of  $\text{S}_{\text{E}24\text{M}23\text{P}229}$  and its nonhydrolyzed precursor (Table 1).

**Potentiometric Titrations.** Hydrolyzed UPM were titrated in order to evaluate their MAA content. The latter was approximated from the volume of NaOH corresponding to the maximum of the first derivative of pH vs NaOH volume plot (data not shown). For both  $\text{S}_{\text{E}18\text{M}17\text{P}442}$  and  $\text{S}_{\text{E}24\text{M}23\text{P}229}$ , the DP of MAA was 82–88% that of the value estimated from tBMA DP (Table 1). This slight discrepancy may be explained by the presence of MAA units located deeper in the core that may not be readily accessible by NaOH. Also, MAA protons implicated in hydrogen bonding with PEG do not readily dissociate even in the presence of NaOH and are thus not accounted for (22). Titration curves were also used to evaluate the degree of ionization ( $\alpha$ ) as a function of pH (Figure 4). The resulting curve presented a single equivalent point at  $\alpha = 1$ , which corresponds to the complete neutralization of the MAA units (15, 23) and occurred around pH 9 for both polymers studied (Figure 4). Similar results were obtained for different MAA random copolymers (24). Apparent  $\text{pK}_a$  values were extrapolated from the curves and are presented in Figure 5. Contrary to monomeric MAA, for which a single  $\text{pK}_a$  value of 4.5 (25) can be calculated, polymerized MAA shows a dependence of the  $\text{pK}_a$  value over  $\alpha$ , and higher  $\text{pK}_a$  values are generally observed (23). Neutralization of MAA has been shown to be influenced by conforma-





**Figure 6.** Fluorescence study of the effect of pH on the local environment inside UPM core. Excitation spectra of pyrene ( $2 \times 10^{-7}$  M) were obtained in water (closed triangles) and in the presence of  $S_{E24M23P229}$  (2 mg/mL) at pH 3 (closed circles) and pH 11 (open squares).  $\lambda_{em} = 393$  nm.



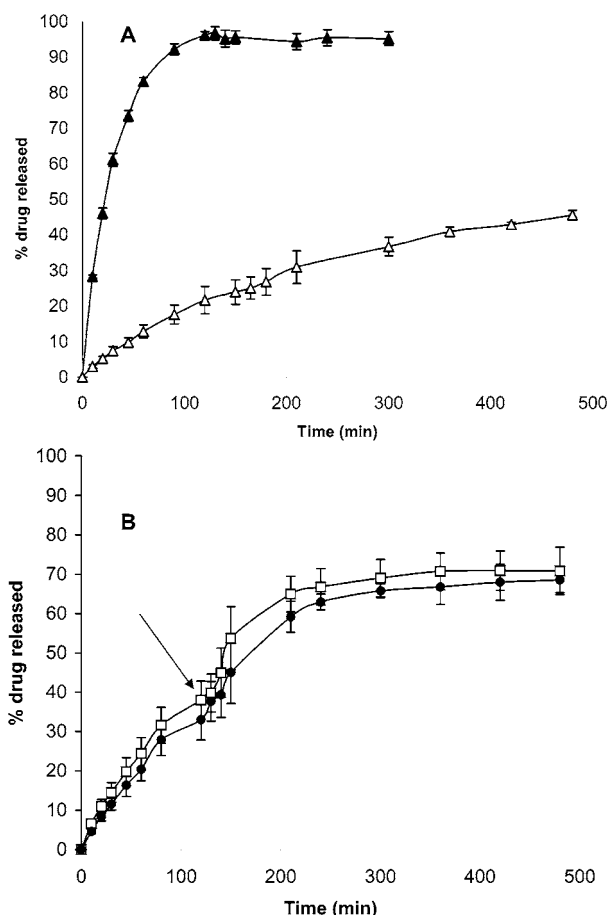
**Figure 7.** Chemical structure of progesterone.

**Table 2. Size Determination of pH-Sensitive UPM (10 mg/mL) by DLS**

pH	$S_{E18M17P442}$		$S_{E24M23P229}$	
	peak area (%)	hydrodynamic diameter (nm)	peak area (%)	hydrodynamic diameter (nm)
2	60	11	precipitate	precipitate
	40	180		
4	45	9.0	100	136
	55	158		
12	35	11.4	37	9.0
	65	170	63	178

tional changes of the polymer chain (15), usually evidenced by the presence of two inflection points in the plot of  $pK_a$  vs  $\alpha$ . However, in the present case, except for a small plateau at low  $\alpha$  values,  $pK_a$  increased steadily with  $\alpha$ . The electrostatic repulsion initially rising from the ionization of MAA units caused polymer chains to expend and translated into the plateau observed between  $\alpha = 0.05$  to 0.10 for  $S_{E24M23P229}$ , and between  $\alpha = 0.08$  to 0.23 for  $S_{E18M17P442}$  (15). Although polymer chains may experience some conformational changes due to the ionization of MAA units, the fact that chains are covalently bonded to one another prevents the occurrence of marked transitions such as the coil-to-globule transition that has been observed in other studies (15, 24). It is predicted from the titration curves that changes in the ionization of the carrier will occur as it travels through the gastrointestinal tract. Indeed, it can be hypothesized that the UPM will be fully protonated in the stomach (pH 1 to 2). As the drug carrier travels through the small intestine, the degree of ionization (20% at pH 6 in the jejunum) will reach more than 40% in the ileum (pH 7).

**Size Measurements.** The size of hydrolyzed UPM was determined in water as a function of pH (Table 2). The polymers generally presented a bimodal size distribution with a small population size around 9–11 nm and large secondary aggregates (>150 nm). The presence of large aggregates may either be attributed to hydrophobic



**Figure 8.** (A) In vitro release profiles of free (closed triangles) and  $S_{E24M23P229}$ -entrapped (5% w/w) (open triangles) progesterone against simulated gastric fluid pH 1.2 (HCl 0.06 M/NaCl 0.021 M). (B) Release profiles of  $S_{E24M23P229}$ -entrapped progesterone (5% w/w) at pH 1.2 and 7 or 11. UPM formulations were dialyzed against simulated gastric fluid pH 1.2 for 2 h at which point the pH was adjusted to either pH 11 (open squares) or pH 7 (closed circles) using NaOH (0.25% w/v) or NaOH (0.25% w/v)/ $NaH_2PO_4$  (0.12% w/v), respectively. Results are presented as the average of three independent experiments  $\pm$  SEM. The arrow indicates the time point where the pH was adjusted.

interactions or to hydrogen bonding between MAA and PEGMA units, due to the relatively high concentration of polymer (10 mg/mL), which was required to obtain an adequate signal intensity. Compared to the nonionizable polymer precursor, star-P(EMA-co-MAA)-*b*-P(PEGMA) scattered light less efficiently, and thus higher concentrations were used. In the case of  $S_{E24M23P229}$ , the polymer precipitated at pH 2, indicating insufficient steric stabilization and important hydrogen bonding between UPM. The presence of aggregates is a problem often associated with micelles leading to bimodal size distribution. Although size may influence the properties of the carrier in vivo, it will do so only if the aggregates are stable to the dilution encountered after oral or intravenous administration (26). Following oral administration, the micelles will find themselves diluted in the contents of the stomach and the small intestine. It is likely that this dilution will cause the breakdown of the secondary aggregates into single micellar entities, thus minimizing the possible effects of a bimodal size distribution on biodistribution or drug release.

**Fluorescence Studies.** Fluorescence studies were performed in order to evaluate the effect of pH variations on the local environment of the UPM core. Pyrene was chosen to conduct those assays because its fluorescence

is polarity-sensitive (27). In the case of ionizable polymers containing MAA units, it is expected that the fluorescence of pyrene will vary as the pH inside the core changes from acidic to basic. At lower pH values, the presence of unionized MAA, along with EMA, units affords a nonpolar environment. This results in increased fluorescence emission intensity, compared to the value in pure water, and a red shift of the (0,0) band from 333 to 337 nm (Figure 6). At higher pH values, the ionization of carboxylic groups renders the environment more polar, resulting in a 40% reduction of fluorescence intensity. These data confirm that pH does influence the local environment inside the core. However, even at higher pH values, the spectrum obtained is still that of pyrene in a hydrophobic environment, albeit less than at acidic pH. At least two hypotheses could be proposed to rationalize this observation. First, although polarity is effectively increased by the ionization of MAA units, the presence of hydrophobic EMA may compensate by providing hydrophobic clusters in which pyrene might be trapped. Indeed, the EMA units are randomly distributed along the hydrophobic chains. They serve to increase the hydrophobicity of the core and afford a more favorable environment for a water-insoluble compound than MAA units alone. Second, the increased polarity may promote the partial pyrene release into the aqueous milieu, which might account for the decreased emission intensity.

**In Vitro Drug Release.** Drug release from polymeric micelles will depend mainly on drug diffusion, on the stability of the carrier, and on polymer degradation (26). As the present UPM are stable to dilution and composed of nonbiodegradable polymers, diffusion will be the sole mechanism for drug release. Diffusion of the drug from the micelle may be influenced by several factors, such as core hydrophobicity. The introduction of pH-sensitive acidic functions in the core is expected to influence its polarity upon pH variations. Indeed, the increased polarity ensuing from the ionization of carboxylic functions may promote the diffusion of the drug from the core. Thus, in vitro kinetics studies were performed to evaluate the effect of pH on the release of a hydrophobic model drug. Progesterone is a hormone synthesized naturally from cholesterol with which it shares structural similarities (Figure 7). It was selected as model drug mainly because of its low solubility in water and because it does not bear any pH-sensitive functional groups, which would otherwise complicate the interpretation of the release kinetics. Figure 8A shows the release kinetics of free and entrapped progesterone at pH 1.2 and 37 °C. Under acidic conditions and at high polymer concentration, the S<sub>E24</sub>M<sub>23</sub>P<sub>29</sub> UPM solution was opalescent, probably because of hydrogen bonding between the MAA and PEGMA. From Figure 8A, it can be seen that incorporation of the drug in UPM slowed its diffusion from the dialysis bag. Indeed, in absence of polymer, 83 ± 3% of the drug was released after 60 min, and mostly all the progesterone diffused out of the bag after 2 h. Comparatively, the amount of drug released from UPM hardly reached 30% after 1 h, with a maximum of 45% after 8 h. The pH-dependence of drug release from UPM was demonstrated by alkalinizing the release medium to pH 7 or 11, after 2 h (Figure 8B). This increase in pH led to the disappearance of the opalescence observed under acidic conditions and to a relatively sharp increase in drug release. Approximately 70% progesterone was released after 5 h vs. 45% when the pH was maintained at 1.2 (Figure 8A). Release were similar at pH 11 and at pH 7 although at this pH  $\alpha$  stands at 42%. Composition seemed to influence the release of progesterone from the

UPM. The effect of pH was less evident when similar experiments were carried out using S<sub>E18</sub>M<sub>17</sub>P<sub>42</sub> instead of S<sub>E24</sub>M<sub>23</sub>P<sub>29</sub> (data not shown). Although these preliminary in vitro release kinetics are promising, improvements are still needed in order to slow the rate of release at acidic pH and to increase the total amount of drug discharged from the micelles at higher pH.

The above results show that pH-responsive UPM were produced from star polymers. These systems present structural properties similar to PM and are also of small size. Drug incorporation studies are presently being carried out to evaluate the loading capacity of these novel UPM and optimize the pH-triggered drug release. Given a reasonable incorporation capacity, such carriers may circumvent the instability problems associated with conventional micelles.

#### ACKNOWLEDGMENT

Financial support from the Natural Sciences and Engineering Research Council of Canada and the Canada Research Chair Program is acknowledged. M.C.J. and J.C.L. acknowledge scholarships from Fonds pour la Formation de Chercheurs et l'Aide à la Recherche and Fonds de Recherche en Santé du Québec.

#### LITERATURE CITED

- (1) Jones, M.-C., and Leroux, J.-C. (1999) Polymeric micelles – a new generation of colloidal drug carriers. *Eur. J. Pharm. Biopharm.* 48, 101–111.
- (2) Newkome, G. R., Moorefield, C. N., Baker, G. R., Saunders, M. J., and Grossman, S. H. (1991) Unimolecular micelle. *Angew. Chem., Int. Ed. Engl.* 30, 1178–1179.
- (3) Liu, M., Kono, K., and Fréchet, J. M. J. (2000) Water-soluble dendritic unimolecular micelles: their potential as drug delivery agents. *J. Controlled Release* 65, 121–131.
- (4) Hawker, C. J., Wooley, K. I., and Fréchet, J. M. J. (1993) Unimolecular micelles and globular amphiphiles dendritic macromolecules as novel recyclable solution agents. *J. Chem. Soc., Perkin. Trans. 1* 1287–1297.
- (5) Heise, A., Hedrick, J. L., Frank, C. W., and Miller, R. D. (1999) Starlike block copolymers with amphiphilic arms as models for unimolecular micelles. *J. Am. Chem. Soc.* 121, 8647–8648.
- (6) Liu, H., Jiang, A., Guo, J., and Uhrich, K. E. (1999) Unimolecular micelles: synthesis and characterization of amphiphilic polymer systems. *J. Polym. Sci. Part A: Polym. Chem.* 37, 703–711.
- (7) Liu, H., Farrell, S., and Uhrich, K. (2000) Drug release characteristics of unimolecular polymeric micelles. *J. Controlled Release* 68, 167–174.
- (8) Antoun, S., Gohy, J. F., and Jérôme, R. (2001) Micellization of quaternized poly(2-dimethylamino)ethyl methacrylate)-block-poly(methyl methacrylate) copolymers in water. *Polymer* 42, 3641–3648.
- (9) Ranger, M., Jones, M.-C., Yessine, M.-A., and Leroux, J.-C. (2001) From well-defined diblock copolymers prepared by a versatile atom transfer radical polymerization method to supramolecular assemblies. *J. Polym. Sci. Part A: Polym. Chem.* 39, 3861–3874.
- (10) Davis, K. A., and Matyjaszewski, K. (2000) Atom transfer radical polymerization of *tert*-butyl acrylate and preparation of block copolymers. *Macromolecules* 33, 4039–4047.
- (11) Matyjaszewski, K., Miller, P. J., Pyun, J., Kickelbick, G., and Diamanti, S. (1999) Synthesis and characterization of star polymers with varying arm number, length and composition from organic and hybrid inorganic/organic multifunctional initiators. *Macromolecules* 32, 6526–6535.
- (12) Hedrick, J. L., Trollsas, M., Hawker, C. J., Atthoff, B., Claesson, H., Heise, A., Miller, R. D., Mecerreyes, D., Jérôme, R., and Dubois, P. (1998) Dendrimer-like star block and amphiphilic copolymers by combination of ring opening and atom transfer radical polymerization. *Macromolecules* 31, 8691–8705.

- (13) Angot, S., Taton, D., and Gnanou, Y. (2000) Amphiphilic stars and dendrimer-like architectures based on poly(ethylene oxide) and polystyrene. *Macromolecules* 33, 5418–5426.
- (14) Coessens, V., Pintauer, T., and Matyjaszewski, K. (2001) Functional polymers by atom transfer radical polymerization. *Prog. Polym. Sci.* 26, 337–377.
- (15) Ravi, P., Wang, C., Tam, K. C., and Gan, L. H. (2003) Association behavior of poly(methacrylic acid)-*block*-poly(methyl methacrylate) in aqueous medium: potentiometric and laser light scattering studies. *Macromolecules* 36, 173–179.
- (16) Benahmed, A., Ranger, M., and Leroux, J.-C. (2001) Novel polymeric micelles based on the amphiphilic diblock copolymer poly(*N*-vinyl-2-pyrrolidone)-*block*-poly(D, L-lactide). *Pharm. Res.* 18, 323–328.
- (17) Sakthivel, T., Toth, I., and Florence, A. T. (1999) Distribution of a lipidic 2.5 nm diameter dendrimer carrier after oral administration. *Int. J. Pharm.* 183, 51–55.
- (18) Jani, P. U., Florence, A. T., and McCarthy, D. E. (1992) Further histological evidence of the gastrointestinal absorption of polystyrene nanospheres in rat. *Int. J. Pharm.* 84, 245–252.
- (19) Florence, A. T., Hillery, A. M., Hussain, N. and Jani, P. U. (1995) Factors affecting the oral uptake and translocation of polystyrene nanoparticles: histological and analytical evidence. *J. Drug target.* 3, 65–70.
- (20) Leroux, J.-C., Cozens, R., Roesel, J. L., Galli, B., Kubel, F., Doelker, E., and Gurny, R. (1995) Pharmacokinetics of a novel HIV-1 protease inhibitor incorporated into biodegradable or enteric nanoparticles following intravenous and oral administration. *J. Pharm. Sci.* 84, 1387–1391.
- (21) Mathur, A. M., Drescher, B., Scranton, A. B., and Klier, J. (1998) Polymeric emulsifiers based on reversible formation of hydrophobic units. *Nature* 392, 367–370.
- (22) Podhájecká, K., Stepánek, M., Procházka, K., and Brown, W. (2001) Hybrid polymeric micelles with hydrophobic cores and mixed polyelectrolyte/nonelectrolyte shells in aqueous media. 2. Studies of the shell behavior. *Langmuir* 17, 4245–4250.
- (23) Wang, C., Tam, K. C., and Jenkins, R. D. (2002) Dissolution behavior of HASE polymers in the presence of salt: potentiometric titration, isothermal titration calorimetry, and light scattering studies. *J. Phys. Chem. B* 106, 1195–1204.
- (24) Wang, C., Tam, K. C., Jenkins, R. D., and Bassett, D. R. (2000) Potentiometric titration and dynamic light scattering of hydrophobically modified alkali soluble emulsion (HASE) polymer solutions. *Phys. Chem. Chem. Phys.* 2, 1967–1972.
- (25) Borukhov, I., Andelman, D., Borrega, R., Cloitre, M., Leibler, L. and Orland, H. (2000) Polyelectrolyte titration: theory and experiment. *J. Phys. Chem. B* 104, 11027–11034.
- (26) Allen, C., Maysinger, D. and Eisenberg, A. (1999) Nano-engineering block copolymer aggregates for drug delivery. *Colloids and Surfaces B: Biointerfaces* 16, 3–27.
- (27) Astafieva, I., Zhong, X. and Eisenberg, A. (1993) Critical micellization phenomena in block polyelectrolyte solutions. *Macromolecules* 26, 7339–7352.

BC020041F



# N-Alkylated Chitosan as a Potential Nonviral Vector for Gene Transfection

Wen Guang Liu, Xin Zhang, Shu Jun Sun, Guang Jie Sun, and Kang De Yao\*

Research Institute of Polymeric Materials, Tianjin University, Tianjin 300072

Dong Chun Liang, Gang Guo, and Jing Yu Zhang

Tianjin Medical University, Tianjin 300070. Received September 15, 2002;

Revised Manuscript Received February 10, 2003

Alkylated chitosans (ACSs) were prepared by modifying chitosan (CS) with alkyl bromide. The self-aggregation of ACSs in acetic acid solution was characterized by fluorescence spectroscopy and dynamic light scattering method. The results indicate that introducing alkyl side chains leads to the self-aggregation of ACSs, and CS with a 99% deacetylation degree shows no aggregation due to the electrostatic repulsion. The electrophoresis experiment demonstrates that the complex between CS and DNA was formed at a charge ratio ( $\pm$ ) of 1/1; ACS/DNA complexes were formed at a lower charge ratio ( $\pm$ ) of 1/4. A small amount of alkylated chitosans play the same shielding role as chitosan in protecting DNA from DNase hydrolysis. Differential scanning calorimetry (DSC) and atomic force microscopy (AFM) were employed separately to investigate the thermodynamic behavior of dipalmitoyl-*sn*-glycero-3-phosphocholine (DPPC)/CS and DPPC/ACS mixtures and the variation in topological structure of DPPC membrane induced by CS and ACS. It is shown that CS and ACS can cause the fusion of DPPC multilamellar vesicles as well as membrane destabilization. In contrast, the perturbation effect induced by ACS is more evident due to the hydrophobic interaction. CS and ACS were used to transfer plasmid-encoding CAT into C<sub>2</sub>C<sub>12</sub> cell lines. Upon elongating the alkyl side chain, the transfection efficiency is increased and levels off after the number of carbons in the side chain exceeds 8. It is proposed that the higher transfection efficiency of ACS is attributed to the increasing entry into cells facilitated by hydrophobic interactions and easier unpacking of DNA from ACS carriers due to the weakening of electrostatic attractions between DNA and ACS.

## INTRODUCTION

In the past decades, chitosan (CS), a naturally occurring linear cationic polysaccharide, has been widely employed as a drug delivery system, wound dressing, anticoagulants, and scaffolds for tissue engineering owing to its biocompatibility, biodegradability, and low toxicity (1–4). Recently, increasing attention has been paid to using chitosan and its derivatives as nonviral vectors for gene transfection (5–9). For example, Mumper (10) was the first to propose to deliver a gene into a cell using chitosan as a vector. The particle sizes of chitosan/DNA complexes ranging from 150 nm to 600 nm were found to depend on the molecular weight of the chitosan (108–540 kDa) used, but not on buffer composition. The small plasmid/chitosan nanoparticles (200–300 nm) were prepared by Roy et al. (11) and were shown to transfect HEK 293 cells (human embryonic kidney cells) in vitro at a lower level than with a Lipofectamine formulation. Borchard et al. (12) synthesized trimethylated chitosan (TMO) from oligomeric chitosan, and the obtained TMOs were used to condense RSV- $\alpha$ 3 luciferase plasmid to form complexes (chitoplexes), which were investigated for their ability to transfect COS-1 and Caco-2 cell lines in the presence and absence of fetal calf serum (FCS). It was demonstrated that the transfection efficiency of the chitoplexes was not affected by FCS, whereas the trans-

fection efficiency of DOTAP (*N*-[1-(2,3-dioleoyloxy)propyl]-*N,N,N*-trimethylammonium sulfate) lipoplexes was decreased. Moreover, cells remained 100% viable in the presence of chitosan oligomers and TMOs; while the viability of DOTAP-treated cells decreased to ~50% in both cell lines. Sato et al. found that chitosan of 15 and 52 kDa obviously enhanced the transfection efficiency of luciferase plasmid (pGL3) into tumor cells. Furthermore, the transfection efficiency of chitosan/pGL3 complexes at pH 6.9 was higher than that at pH 7.6, suggesting chitosan might selectively transfect tumor in the low pH environment, but not be uptaken into normal cells. It was also observed that chitosan was resistant to serum, and while cationic liposome-associated gene expression was inhibited by serum. This resistance to serum implied that chitosan might be an efficient gene vector in vivo. Although in some cases, the uptake of chitosan/DNA nanoparticles appears to occur even in the absence of any ligand–receptor interaction, to allow for the targeted gene trafficking into specific cells, chitosan needs to be modified with various biospecific ligands. Cho's group (13, 14) developed galactosylated chitosan-*graft*-dextran and galactosylated chitosan-*graft*-PEG vectors. Galactose groups were chemically bound to chitosan for liver-targeted delivery and dextran or PEG was grafted for enhancing the complex stability in water. These systems could efficiently transfect HepG2 cells expressing asialoglycoprotein receptor (ASGR) which specifically recognizes the galactose ligands on chitosan. Leong's group

\* To whom correspondence should be addressed. E-mail address: wgliu@tju.edu.cn.

reported that binding transferrin or KNOB (C-terminal globular domain of the fiber protein) onto the surface of chitosan/DNA complex could improve gene expression level in HEK293 and HeLa cells to a different degree (15).

The advantage of chitosan-based vectors lies in not only getting away from the cytotoxicity problems that are inherent in most synthetic polymeric vehicles but also in its unique capability of transcellular transport (16, 17). However, as shown with other polycations/DNA complexes, chitosan/DNA complexes are formed by electrostatic interaction between primary amino groups and phosphate groups, which is strong enough to resist DNA unpacking within cell to a certain degree. Okano (18), Sato (19), and Kabanov (20) all reported that the incorporation of hydrophobic moieties could considerably increase the transfection efficiency. In addition, by theoretical calculations Kuhn and Levin found that for sufficiently hydrophobic amphiphilies, a charge neutralization, or even a charge inversion of the DNA–amphiphile complexes could be achieved with rather low concentration of cationic amphiphile (21).

To the best of our knowledge, to date, research work on the influence of hydrophobicity of chitosan on the properties of chitosan/DNA complexes and on the transfection efficiency of chitosan-based vectors is unavailable in the literature. In this work, we synthesized a series of alkylated chitosan (ACS) derivatives from alkyl bromide and investigated the stability of ACS/DNA complexes; an attempt was made to elucidate the mechanism of the interaction between ACS and mimic cell membrane, dipalmitoyl-*sn*-glycero-3-phosphocholine (DPPC). The CS and ACSs were used as vectors for gene transfection, and the effects of hydrophobicity of the side alkyl chain on the transfection activity were explored.

## EXPERIMENTAL SECTION

**Materials.** Chitosan (CS) ( $M_n = 50\,000$ , degree of deacetylation = 99%), DNase I was supplied by Sigma Chemical Company (St. Louis, MO). Pyrene obtained from Aldrich was purified by repeated recrystallizations from absolute ethanol. Alkyl bromides were analytically pure. pcDNA 3.1/CAT plasmid encoding chloramphenicol acetyltransferase (CAT) was purchased from Invitrogen Co. Dipalmitoyl-*sn*-glycero-3-phosphocholine (DPPC) in powder form was obtained from Fluka Co. and was used as received. Ethidium bromide and HEPES were purchased from Sigma. DMEM (Dulbecco's Modified Eagle Medium) powder was purchased from Gibco Co. Fetal bovine serum (FBS) was provided by Hyclone Co.

**Synthesis of N-Alkylated CS.** The synthetic method of N-alkylated chitosan has been reported in our previous paper (22). Briefly, 2 g of CS was added into 40 mL of 2-propanol/4 N sodium hydroxide solution and stirred at 70 °C for 30 min. The alkyl bromide was added dropwise to the mixture and allowed to react for 4 h, and then the reaction mixture was centrifuged. The obtained precipitate was washed with ethanol and then dried at vacuum to obtain the alkylated chitosan derivatives. The resultant CS derivatives from butyl bromide, octyl bromide, dodecyl bromide, and hexadecyl bromide were denoted as 4-, 8-, 12-, and 16-CS, respectively. The resultant alkylated chitosan derivatives were dialyzed for 3 days using Cellu SepH1 membrane (MWCO = 12 000) against water. The degree of substitution was determined by traditional potentiometric titration.

**Fluorescence Measurement.** Chitosan and alkylated chitosans were dissolved in 0.1 M of acetic acid, and the concentrations of sample solutions were varied from

$1.0 \times 10^{-4}$  to 5 mg/mL. Steady-state fluorescence measurement was performed on a SPEX FL212 Spectrofluorometer. For the determination of intensity ratio of the first to the third highest energy bands in the emission spectra of pyrene, the sample solution containing pyrene ( $8.0 \times 10^{-7}$  mol/L) was excited at 338 nm, and the emission spectra were recorded in the range of 350–420 nm at the scan rate of 15 nm/min. The slit openings for excitation and emission were set at 2.0 and 0.5 nm, respectively. The spectra were accumulated with an integration time of 5 s/nm.

**Dynamic Light Scattering Determination (DLS).** Dynamic light scattering measurement was carried out with an argon ion laser system tuned at 514 nm. The solutions of chitosan derivatives were filtered through a 0.5- $\mu$ m filter (Millipore) directly into a freshly cleaned 10 mm-diameter cylindrical cell. The intensity of autocorrelation was measured at a scattering angle ( $\theta$ ) of 90° with a Brookhaven BI-9000AT digital autocorrelator at room temperature. When the difference between the measured and the calculated baselines was less than 0.1%, the correlation function was accepted. The mean diameter was evaluated by the Stokes–Einstein relationship.

**CS/DNA and ACS/DNA Complex Formation.** CS was dissolved in 0.1 M sodium acetate buffer to form a solution of 1 mg/mL, and a DNA solution of 0.1 mg/mL was formed in the same way. Chitosan/DNA complexes at various charge ratios were prepared by mixing chitosan solution with DNA solution, vortexing for 15 s and incubated for 30 min at room temperature. Likewise, ACS/DNA complexes were formed. The complex formation was confirmed by electrophoresis on an 1.0% agarose gel with Tris-acetate (TAE) running buffer at 100 V for 30 min. DNA was visualized with ethidium bromide.

**DNase Resistivity.** CS/DNA or ACS/DNA complexes were placed into 2 mL of 10 mM PBS buffer containing 5 mM  $MgCl_2$  at 25 °C. To this solution was added 10 units of DNase I, and the optical density of the solution at 260 nm was recorded for 1 h.

**Differential Scanning Calorimetry Determination.** The interactions between DPPC and chitosan or its derivatives were determined with thermal analysis method reported by Fang et al. (17). Differential scanning calorimetry (DSC) scans were carried out on a Perkin-Elmer DSC-7 calorimeter. A certain amount of DPPC and chitosan mixed in 25  $\mu$ L of PBS buffer was hermetically sealed in an aluminum pan. For each DSC run, 25  $\mu$ L of plain PBS buffer was loaded in the hermetic pan and used as a blank reference. Prior to scanning, the aluminum pan loaded with sample was equilibrated at 60 °C with constant vortexing for at least 2 h in order to disperse DPPC and DPPC/CS mixtures in aqueous solution. Heating or cooling scans were recorded in the range of 25–50 °C at a scan rate of 5 °C/min. In the same manner the thermograms of ACS/DNA mixtures were recorded.

**AFM Imaging.** Two micrograms of DPPC and 0.5 mol % of chitosan were mixed together in PBS buffer and equilibrated at 60 °C with vortexing for 3 h, and then 20  $\mu$ L of mixture was deposited onto a freshly cleaved mica disk. Likewise, DPPC and DPPC/ACS mixture samples were prepared.

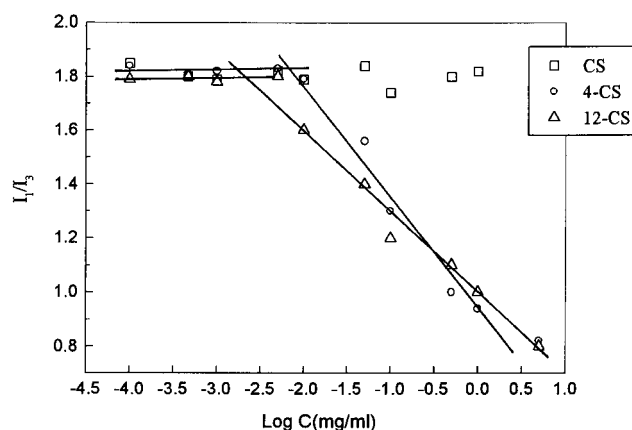
To visualize the morphological variation of DPPC membrane induced by CS/DNA or ACS/DNA complexes, 1% of DPPC was dissolved in chloroform, 20  $\mu$ L of diluted solution was deposited onto a freshly cleaved mica to form a homogeneous membrane, and then 15  $\mu$ L of CS/DNA ( $\pm = 1/1$ ) or ACS/DNA ( $\pm = 1/4$ ) complex solution was

deposited onto the DPPC-precoated mica. All the deposited solutions were dried at room temperature. The imaging was conducted on an Atomic Force Microscopy (Nanoscope a system, Digital Instruments, Inc. Santa Barbara, CA) in tapping mode, with 512 512 data acquisition at a scan speed of 1 Hz at ambient conditions.

**Cell Culture and Transfection.** C<sub>2</sub>C<sub>12</sub> cells, a mouse skeletal muscle cell line, which have been shown to be a suitable host for stable transfection experiments of exogenous DNA (23), were seeded at a density of  $5 \times 10^5$ /mL on 24-well microplates in DMEM (Dulbecco's modified Eagle's medium) containing 10% fetal bovine serum at 37 °C under a 5% CO<sub>2</sub> atmosphere. When the cells were grown to half confluency, the culture media were extracted, and rinsed with serum-free DMEM. The prepared chitosan/DNA complexes were diluted with serum-free DMEM and added into the corresponding wells (5  $\mu$ g DNA/well). After 1 h incubation, the complexes were removed, and the culture media were replaced by fresh serum-containing media and incubated for additional 48 h at 37 °C under a 5% CO<sub>2</sub> atmosphere. Then the cells were lysed with PBS solution containing 1 NP40 and 1 mmol/L PMSF and subjected to three cycles of deep freezing and thawing. The CAT concentration was determined with enzyme-linked immunosorbent assay (ELISA) method. The OD<sub>280</sub> and OD<sub>260</sub> of cell lysis solutions were measured and diluted with PBS to ensure that each sample contains the same protein concentration. The samples were added into 96-well microplates and left at 4 °C overnight. Then the solution was decanted, and 150  $\mu$ L of 4% of degreased milk powder was added, which was allowed to react at 37 °C for 2 h. After the degreased milk powder was removed, the wells were washed with PBS three times, and 100  $\mu$ L of rabbit-anti CAT IgG was added into each well, which was left at 37 °C for 1 h and followed by rinsing with 0.2% Tween-PBS. Then 100  $\mu$ L of goat-anti rabbit IgG-HRP was added into each well. After incubation at 37 °C for 1 h, 100  $\mu$ L of TMB was added, and the plate was kept in dark for 10 min. Finally 100  $\mu$ L of 2 M sulfuric acid was added to terminate the reaction, and the OD values were measured at wavelength 450 nm by plate-reader of Lab-system. The naked DNA was used as a control. Each transfection experiment was carried out in triplicate.

## RESULTS AND DISCUSSION

**Characteristics of N-Alkylated Chitosans.** The characterization of N-alkylated chitosan has been discussed in reference (22). The substitution degrees (SD) of alkylated chitosan determined by potentiometer titration are ca. 22.1%; thus, the influence of SD is negligible. In studying the formation of aggregates from hydrophobically modified polyelectrolyte in aqueous solution, pyrene is generally used as a molecular probe, and the variation in the ratio of intensity of first (373 nm) to third (383 nm) vibronic peaks  $I_1/I_3$ , the so-called polarity parameter, is quite sensitive to the polarity of microenvironment where pyrene is located (24). Thus, the change of  $I_1/I_3$  can characterize the formation of self-aggregation. Figure 1 exhibits the change of  $I_1/I_3$  value as a function of concentration of chitosan or alkylated chitosans. For 4-CS and 12-CS, at lower concentrations,  $I_1/I_3$  values remain nearly unchanged. Further increasing concentration, the intensity ratios start to decrease, implying the onset of self-association from alkylated chitosans. The critical aggregation concentration (cac) is determined by the interception of two straight lines. The cac values of alkylated chitosans are listed in Table 1. From the table, it can be seen that the cac of 12-CS is lower than that of



**Figure 1.** Variation of intensity ratio ( $I_1/I_3$ ) versus the concentration of chitosan or its derivatives.

**Table 1.** Characteristics of Alkylated Derivatives

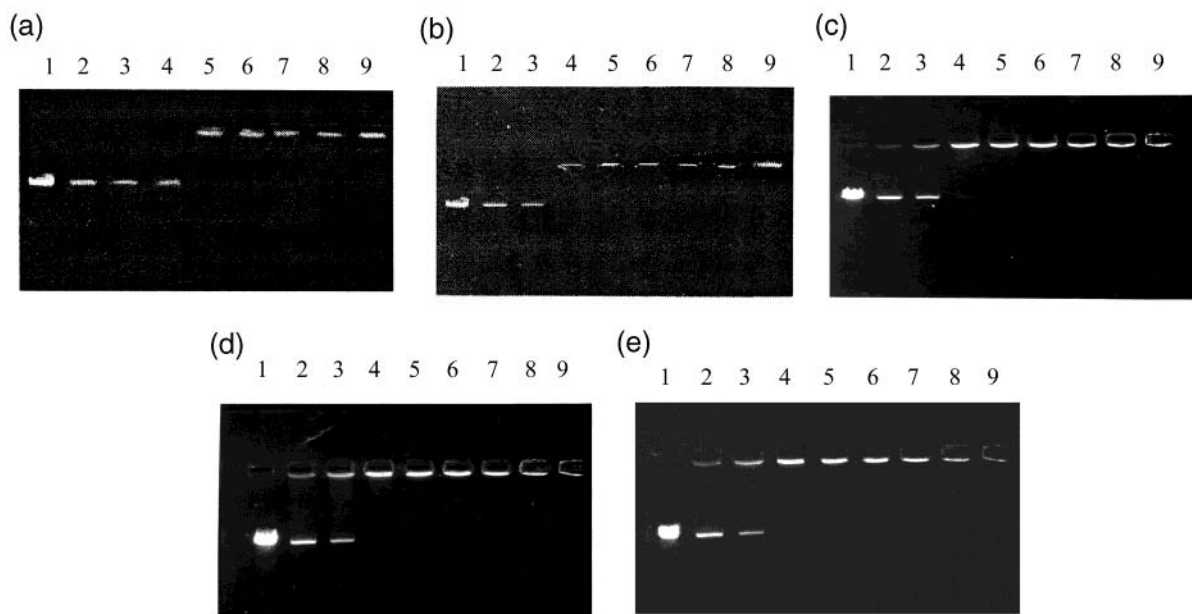
sample	critical aggregation concentration, $cac \times 10^3$ , mg/mL	mean diameter (nm)
4-CS	7.24	$261.7 \pm 30.1$
12-CS	2.33	$346.3 \pm 51.8$

4-CS. A most probable reason is that the elongation of alkyl side chains increases the hydrophobicity, rendering the self-aggregation more prone to occur. It is noted that no aggregation occurs for chitosan in the whole range of concentrations. Whereas Philippova (24) argues that there exist hydrophobic domains inherent to chitosan. In acetic acid solution, chitosan and its derivatives are positively charged, and thus electrostatic repulsion weakens the hydrophobic attraction to a certain degree. The substitution degree of chitosan used by Philippova is 88%, i.e., there still exist parts of acetyl groups which are hydrophobic in nature. These hydrophobic moieties can compete with electrostatic repulsion and lead to the hydrophobic aggregates. In contrast, the chitosan used by us is almost completely deacetylated. Therefore, the hydrophobicity of acetyl can be neglected.

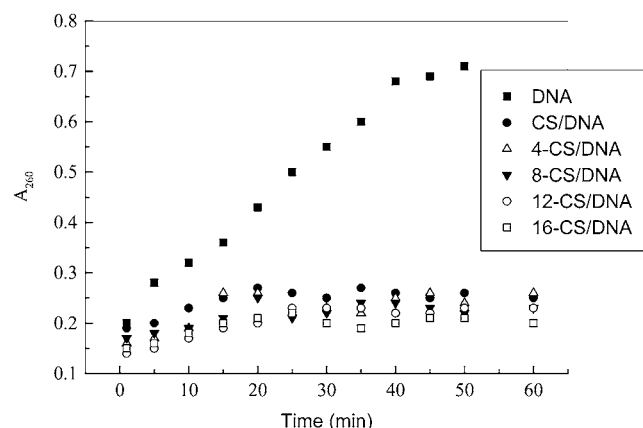
DLS data demonstrate that the mean size of self-aggregates from 12-CS is larger than that of 4-CS (Table 1), suggesting the elongation of hydrophobic side-chain facilitates the growth of the hydrophobic core of polymeric aggregates.

**Formation of CS/DNA and ACS/DNA Complexes.** The electrophoretic retardation bands on agarose gels can characterize the formation of the two oppositely charged polyelectrolyte partners since the neutralization and/or increase in molecular size of complex results in the complete retardation of DNA migration toward the anode in the electric field (25). Figure 2 shows the agarose gel electrophoresis results for CS/DNA and ACS/DNA complexes. One can see that a complete retardation occurs at charge ratio( $\pm$ ) of 1/1 for CS/DNA complex, indicating the formation of complex. While for 4-CS, 8-CS, 12-CS, and 16-CS, complexes are formed at a relative lower charge ratio of chitosan to DNA, 1/4. It is obvious that not only electrostatic interaction but also hydrophobic interaction contributes to the complex formation between DNA and chitosan derivatives. The incorporation of hydrophobic moieties might cause a cooperative binding transition of alkyl chitosan. Along with the binding of ACS onto the phosphate groups of DNA, polyanion charge neutralization occurs, and the bound ACSs facilitate the binding of subsequent ones via favorable hydrophobic interactions of alkyl side chains. At low concentration of ACS, there might be a discontinuous rising in the binding





**Figure 2.** Electrophoresis of CS/DNA (a), 4-CS/DNA (b), 8-CS/DNA (c), 12-CS/DNA (d), and 16-CS/DNA (e) complexes on an agarose gel. Lane 1: plasmid DNA; lane 2:  $\pm = 1/10$ ; lane 3: 1/1; lane 4: 1/4; lane 5: 1/1; lane 6: 2/1; lane 7: 4/1; lane 8: 8/1; lane 9: 10/1.



**Figure 3.** Variation in the optical density of DNA at 260 nm in PBS buffer containing DNase I.

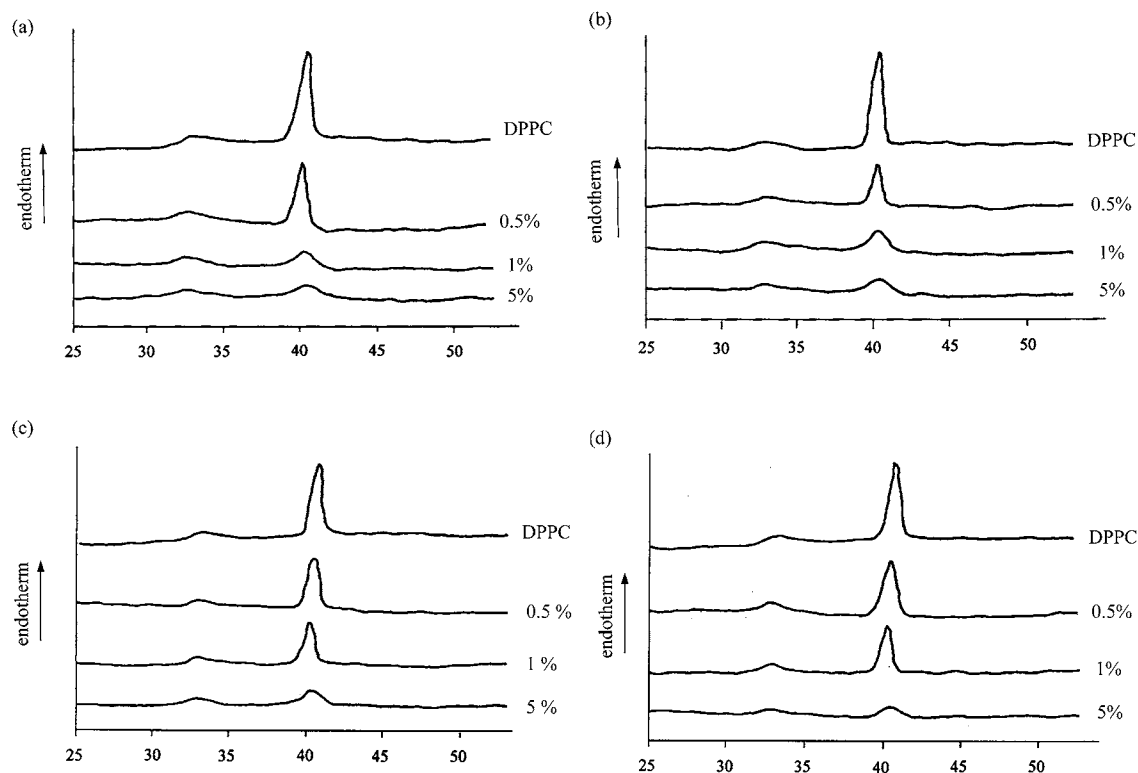
of ACS, i.e., a cooperative binding (26). Thus, even below the stoichiometric point of neutralization, the charges on the backbones of DNA are shielded by the bound hydrophobic alkyl chains. For ACS/DNA complexes, at charge ratio ( $\pm = 1/4$ ), the migration of DNA has been completely hindered. Therefore, a small amount of alkylated chitosan derivatives can condense DNA. Kuhn et al. (27) argued that lowering the amount of cationic amphiphiles could reduce the risk of unnecessary medical complications. But as a vector, the amphiphile must protect DNA from nuclease degradation.

To examine whether chitosan itself or the incorporated alkyl side chain can protect DNA from the attack of nuclease, we recorded the variation in optical density of the CS/DNA ( $\pm = 1/1$ ) and ACS/DNA ( $\pm = 1/4$ ) complexes in PBS buffer containing DNase I at 260 nm (Figure 3). The charge ratio of components is selected as 1/1 and 1/4 for CS/DNA and ACS/DNA complexes, respectively, taking account of that at these two ratios, the complexes between DNA and CS or ACS are just formed. As shown in the figure, the  $OD_{260}$  values of naked DNA increase sharply with time increasing, suggesting DNA has been degraded. In contrast, the  $OD_{260}$  values of DNA entrapped in the complexes remain lower values, and is nearly unchanged after 10 min. As expected, the complex

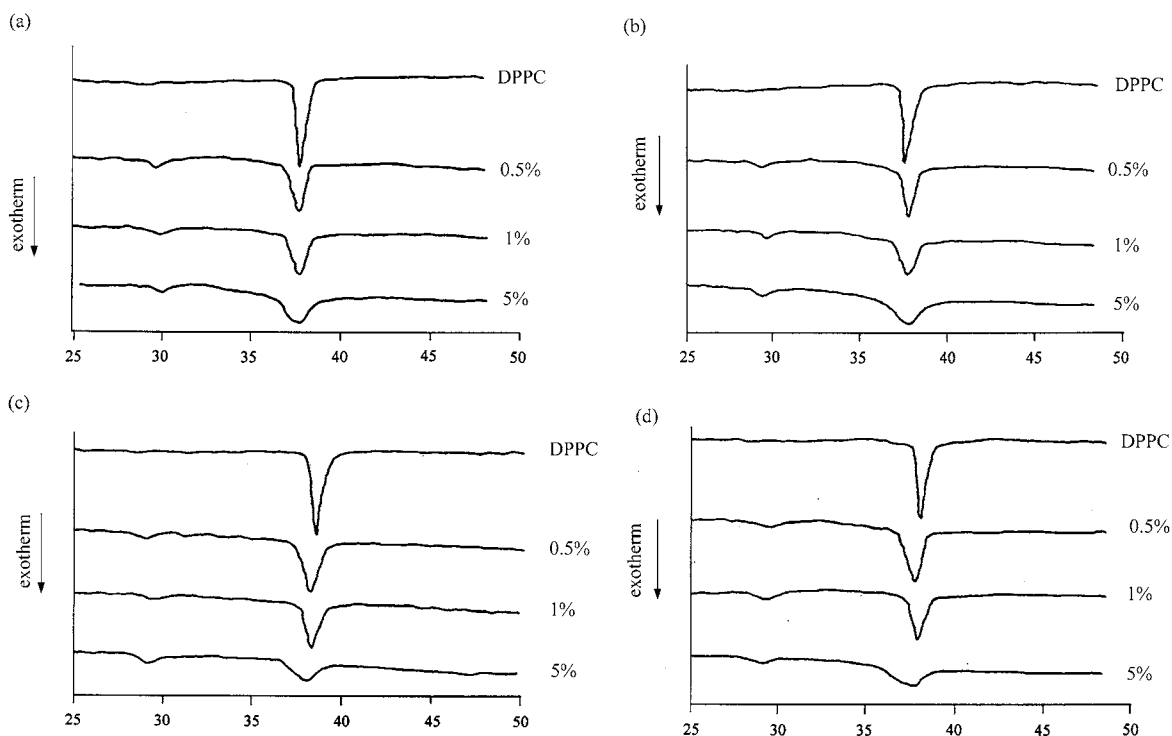
formation between DNA and chitosan can reduce the activity of DNase. It is noted that although the selected charge ratio of ACSs to DNA is lower relative to that of CS/DNA complex, an equal inhibition effect was observed for ACSs. Thus it is reasonable to consider that a small amount of alkylated chitosan can play the same shielding role as chitosan. In our previous work (27, 28), we have employed AFM to observe that the dodecylated chitosan offers a good protection for DNA, which is surmised that the hydrophobic alkyl chains incorporated lowers the permeability of DNase.

**Interactions of CS or ACS with DPPC.** Figure 4 displays the DSC heating thermograms of DPPC/CS and DPPC/ACS mixtures at different mole fractions of chitosan or its derivatives in PBS buffer. It is clearly seen that two endothermic transition peaks appear around 33 and 41.5 °C, revealing a typical gel-liquid crystalline transition occurs in DPPC multilamellar vesicles (MLV) (16). Along with the increase in the contents of CS or ACS, the peak height of main transition at 41.5 °C is considerably decreased, and the peaks are slightly broadened, an indication that the heterogeneity of membrane is enhanced. Figure 5 exhibits the DSC cooling thermograms of DPPC/CS and DPPC/ACS mixtures. Pure DPPC and all the mixtures have a major exothermic peak around 37.5 °C. For DPPC/CS and DPPC/ACS mixtures, a new exothermic transition at 30.5 °C is split from the thermograms, which implies that the incorporation of chitosan or its hydrophobic derivative results in the phase separation of DPPC.

Table 2 lists the calorimetric enthalpy of DPPC bilayer determined at different mole fractions of chitosan or its derivatives. From the table, one can see that increasing the contents of CS or ACS leads to the decrease in enthalpy of DPPC, demonstrating the addition of CS or ACS suppresses the cohesive interactions between adjacent DPPC molecules. Furthermore, with the elongation of alkyl side chain, the reduction of enthalpy is more evident. Fang et al. (17) argues that not only long-range repulsion between choline and cationic amines, but also hydrophobic interaction between chitosan and DPPC, induces bilayer destabilization. It is necessary to emphasize that the chitosan used in our experiment is fully



**Figure 4.** DSC thermograms of DPPC/CS mixtures at different mole fractions of CS or ACS in PBS during heating. (a): DPPC/CS; (b): DPPC/4-CS; (c): DPPC/12-CS; (d): DPPC/16-CS.



**Figure 5.** DSC thermograms of DPPC/CS mixtures at different mole fractions of CS or ACS in PBS during cooling. (a): DPPC/CS; (b): DPPC/4-CS; (c): DPPC/12-CS; (d): DPPC/16-CS.

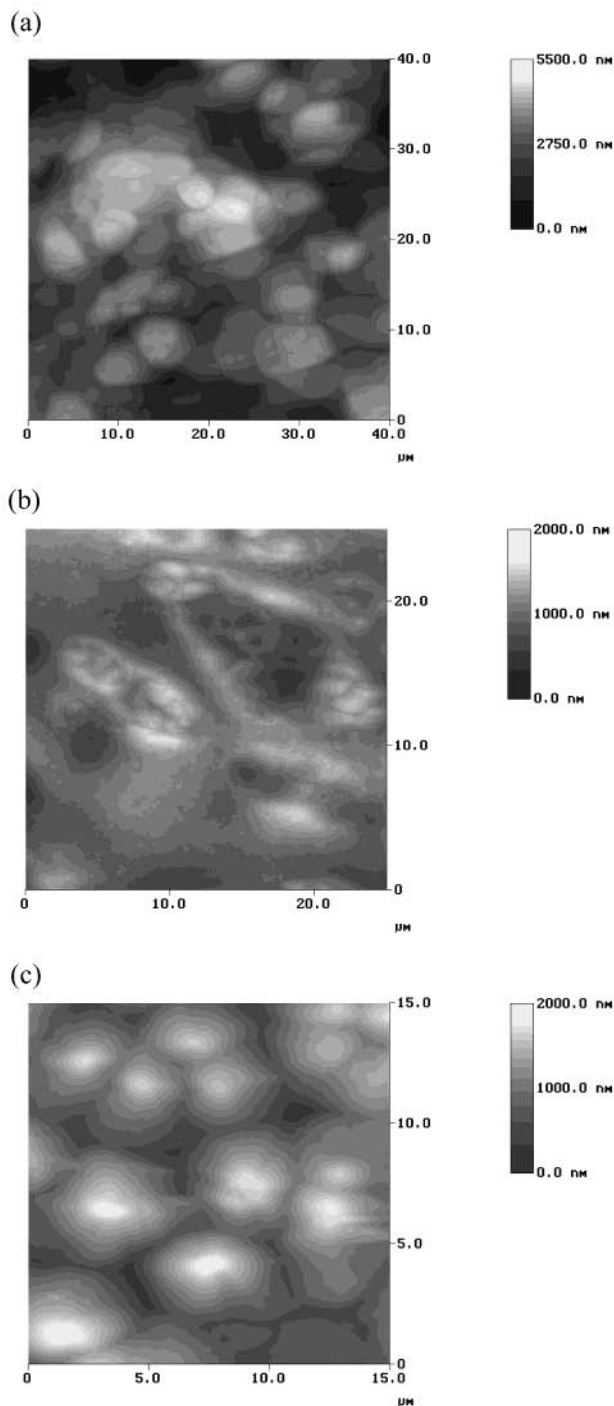
deacetylated; so the hydrophobicity from acetyl moieties can be neglected. It is obvious that the strong hydrophobic interactions are originated from alkyl side chain introduced. The longer side chains might penetrate the hydrophobic core of DPPC bilayer, and consequently enhance the disruptions of DPPC. In addition, we find no irreversible transition of DPPC during its heating and cooling as shown in the table.

Figure 6 exhibits AFM images of DPPC MLV, DPPC/CS and DPPC/12-CS mixtures. For pure DPPC, the lamellar structure of stacked bilayer with a mean diameter of 4  $\mu\text{m}$  is formed. Upon associating with chitosan, the fusion of bilayer is observed, and the surface of DPPC is indented to some extent. Similarly, the incorporation of 12-CS leads to the fusion of vesicles, and the mean size increases slightly compared to that of pure DPPC.

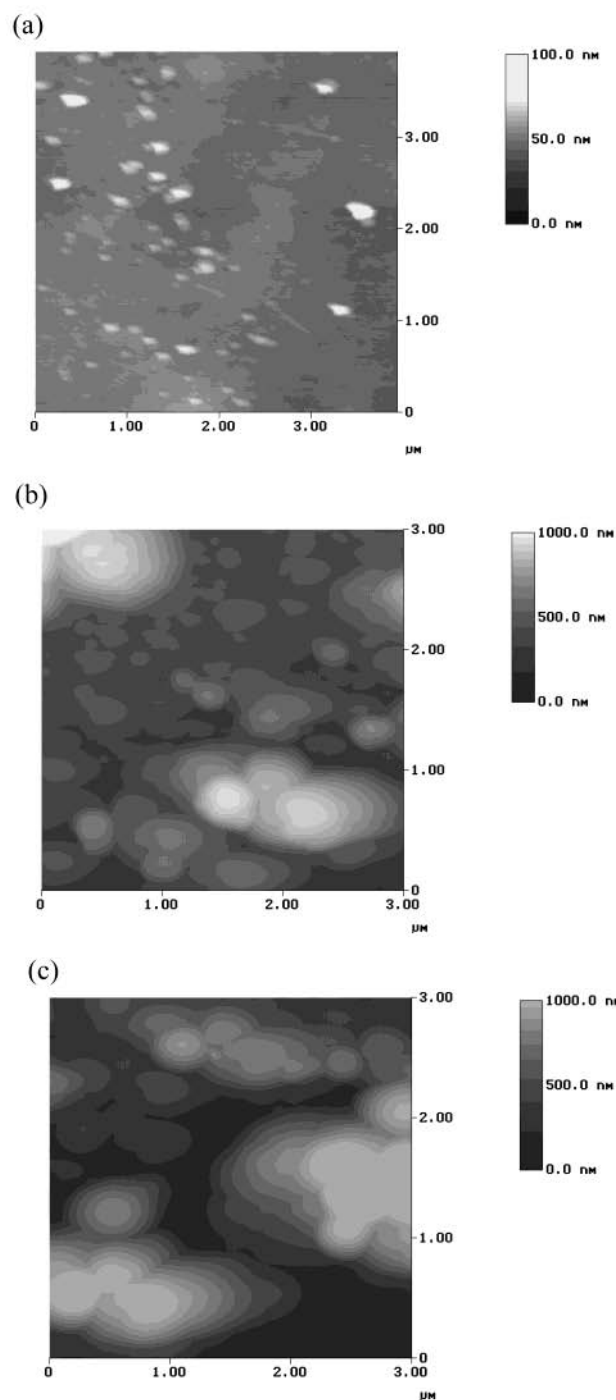
**Table 2. Calorimetric Enthalpy of DPPC Bilayer Determined at Different Mole Fractions of Chitosan or Its Derivatives<sup>a</sup>**

mole fraction (%)	CS		4-CS		12-CS		16-CS	
	$\Delta H_{\text{en}}$	$\Delta H_{\text{ex}}$	$\Delta H_{\text{en}}$	$\Delta H_{\text{ex}}$	$\Delta H_{\text{en}}$	$\Delta H_{\text{ex}}$	$\Delta H_{\text{en}}$	$\Delta H_{\text{ex}}$
0.5	6.38	6.41	5.64	5.53	5.79	5.18	4.67	4.71
1.0	4.61	4.58	3.56	3.47	3.58	3.58	3.01	3.14
5.0	1.78	1.65	1.55	1.76	1.02	1.48	1.27	1.20
DPPC	11.87	12.21						

<sup>a</sup>  $\Delta H_{\text{en}}$  is the endothermic enthalpy and  $\Delta H_{\text{ex}}$  is the exothermic enthalpy. The unit of calorimetric enthalpy is J/g.

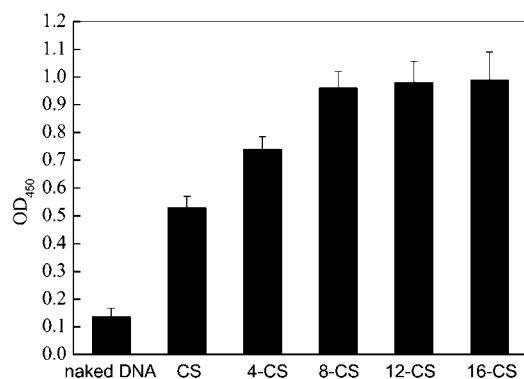
**Figure 6.** AFM images of DPPC MLV (a), DPPC/CS (b), and DPPS/12-CS (c) mixtures.

The AFM images obtained reveal that chitosan or its alkyl derivative can strongly induce the disruption of the integrity of DPPC membrane.

**Figure 7.** AFM images of naked DNA (a), the complexes of CS/DNA (b), and 12-CS/DNA (c) deposited on DPPC membranes.

To mimic the interactions between vectors with cell membrane, the DPPC membrane was first formed on mica substrates, onto which naked DNA, CS/DNA, and ACS/DNA complexes were deposited. AFM was used to examine the variation in the topological structure of DPPC (Figure 7). As shown in Figure 7a, the naked DNA molecules occur to aggregate on the surface of DPPC. The size of DNA varies from 100 to 150 nm, and the average height is about 13 nm. The aggregates of DNA are merely absorbed onto the surface of DPPC, and no perturbation of DPPC membrane was observed. In contrast, CS/DNA (Figure 7b) and 12-CS/DNA (Figure 7c) complexes lead to the strong perturbations of DPPC membrane. CS/DNA complex evolves into circular features with size ranging from 250 to 330 nm. It can be also observed that part of





**Figure 8.** Transfection efficiency of pc DNA 3.1 plasmid encoding CAT mediated by CS and ACS.

the complex particles are aggregated and form larger domains. Comparatively, 12-CS/DNA complex forms an irregular lump with larger size, and the aggregation becomes more evident.

A closer inspection of the pictures reveals that it is hard for naked DNA to enter the cell membrane due to electrostatic shielding, whereas chitosan or chitosan derivatives facilitate DNA entry into cell membrane due to the perturbation caused by electrostatic and hydrophobic interactions.

**Cell Transfection.** The transfection efficiency was evaluated in C<sub>2</sub>C<sub>12</sub> cell lines using pc DNA 3.1 plasmid encoding chloramphenicol acetyltransferase (CAT). Figure 8 shows the transfection efficiency of C<sub>2</sub>C<sub>12</sub> cells obtained with CS and ACSs. The OD<sub>450</sub> of the control group (naked DNA) is merely 0.136; in contrast, chitosan increases the transfection efficiency 4-fold. The transfection level is further increased upon elongating the alkyl side chain. For 4-CS, the transfection efficiency is increased about 5-fold. 8-CS, 12-CS, and 16-CS yields even higher transfection efficiencies with 7-fold increase compared to that of DNA alone. Nonetheless, the transfection efficiency levels off after the number of carbons in the side chain exceeds eight.

Objectively speaking, the experimental results available in the present literature on the effects of complex size upon the transfection efficiency are inconsistent. Several reports support the use of ~100 nm diameter of complex particles (24, 29), and several studies demonstrate that submicrometer or micrometer of complex particle yields higher transfection efficiency (30, 31). In studying the effects of the aggregation states on the intracellular uptake of Pluronic copolymer, Muniruzzaman et al. (32) proposed that Pluronic unimers enter into cells via a simple diffusion, whereas the Pluronic micelles are internalized through endocytosis. As shown in the aforementioned AFM images, the size of CS/DNA complex is in the range of several hundreds of nanometers and the ACS/DNA complexes form a larger size. Before complexing with DNA, the alkylated chitosans self-aggregate, and when the self-aggregates of ACS complex with DNA, a larger size of complexes tend to be generated. AFM images also imply that the complexes re-aggregate onto the cell surface before they enter into cell membrane. From the analysis above, the complexes of CS/DNA and ACS/DNA are ferried into the cell mainly via endocytosis. Moreover, the increase in hydrophobicity of chitosan derivatives raises its ability to destabilize the membrane, which facilitates DNA entry into cell. However, neither high cellular uptake, membrane destabilizing activity, endosomal escape, nor nuclear localization alone is adequate for a high transfection efficacy, which

results from complex interplay of various factors, one of which, the unpacking of complex from carrier, is the final limiting step of gene delivery (33). Chitosan has been demonstrated to possess a substantial buffering capability so that it can escape from endosome, avoiding the hydrolysis of lysosomal nuclease (34). In preparing the alkyl chitosan derivatives, only small fractions of primary amino groups were substituted, so most of amino moieties still play a role in absorbing protons of endosomal vesicles. What is more important is that aside from the ionic interactions, there are hydrophobic interactions between alkyl chitosans and DNA, and moreover a small amount of alkyl chitosans can condense DNA, which weakens the strong ionic interaction, promoting the unpacking of DNA from its cargo. Therefore, the incorporation of alkyl side chain enhances the transfection efficiency by comprehensive factors.

## CONCLUSION

Alkylated chitosans (ACSs) self-aggregate in acetic acid solution, and chitosan (CS) with 99% deacetylation degree does not aggregate due to the strong electrostatic repulsion. The complex formation between ACS and DNA requires a relatively smaller amount of ACS compared to CS due to hydrophobic interactions. CS and ACS can cause the fusion of DPPC multilamellar vesicles and the membrane destabilization. Furthermore, introducing alkyl side chains results in a more evident alteration in the topological structure of DPPC. The transfection efficiency of plasmid-encoding CAT mediated by CS and ACS into C<sub>2</sub>C<sub>12</sub> cell lines is dependent on the hydrophobicity of chitosan. Upon lengthening the alkyl side chain, the transfection efficiency is raised and levels off after the number of carbons in side chain exceeds 8. The higher transfection efficiency of ACS is presumably due to the increasing entry into cells facilitated by hydrophobic interactions and easier unpacking of DNA from ACS carriers, which is from the hydrophobicity-induced weakening of electrostatic attractions between cargo and carriers.

## ACKNOWLEDGMENT

The authors are indebted to the financial support from National Natural Science Foundation of China (Grant 50233020), Postdoctoral Foundation (Grant 2002031165), and Joint Research Project of Tianjin-Nankai Universities from the Ministry of Education, China.

## LITERATURE CITED

- (1) Thanou, M., Verhoef, J. C., and Junginger, H. E. (2001) Oral drug absorption enhancement by chitosan and its derivatives. *Adv. Drug Delivery Rev.* 52, 117–126.
- (2) Mi, F. L., Shyu, S. S., Wu, Y. B., Lee, S. T., Shyong, J. Y., and Huang, R. N. (2001) Fabrication and characterization of a spongelike asymmetric chitosan membrane as a wound dressing. *Biomaterials* 22, 165–173.
- (3) Vongchan, P., Sajomsang, W., Subyen, D., and Kongtawert, P. (2002) Anticoagulant activity of a sulfated chitosan. *Carbohydr. Res.* 337, 1233–1236.
- (4) Madhally, S. V., and Matthew, H. W. T. (1999) Porous chitosan scaffolds for tissue engineering. *Biomaterials* 20, 1133–1142.
- (5) MacLaughlin, F. C., Mumper, R. J., Wang, J., Tagliaferri, J. M., Gill, I., Hinchcliffe, M., and Rolland, A. P. (1998) Chitosan and depolymerized chitosan oligomers as condensing carriers for in vivo plasmid delivery. *J. Controlled Release* 56, 259–272.
- (6) Sato, T., Ishii, T., and Okahata, Y. (1999) In vitro gene delivery mediated by chitosan. *Proc. Int. Symp. Controlled Release Bioact. Mater.* 26, 803–804.

- (7) Janes, K. A., Calvo, P., and Alonso, M. J. (2001) Polysaccharide colloidal particles as delivery systems for macromolecules. *Adv. Drug Delivery Rev.* 47, 83–97.
- (8) Leong, K. W., Mao, H. Q., Truong-Le, V. L., Roy, K., Walsh, S. M., and August, J. T. (1998) DNA-polycation nanospheres as nonviral gene delivery vehicles. *J. Controlled Release* 53, 183–193.
- (9) Illum, L., Jabbar-Gill, I., Hinchcliffe, M., Fisher, A. N., and Davis, S. S. (2001) Chitosan as a novel nasal delivery system for vaccines. *Adv. Drug Delivery Rev.* 51, 81–96.
- (10) Mumper, R. J., Wang, J., Claspell, J. M., and Rolland, A. P. (1995) Novel polymeric condensing carriers for gene delivery. *Proc. Int. Symp. Controlled Release Bioact. Mater.* 22, 178–179.
- (11) Roy, K., Mao, H.-Q., and Leong, K. W. (1997) DNA-chitosan nanospheres: transfection efficiency and cellular uptake. *Proc. Int. Symp. Controlled Release Bioact. Mater.* 24, 673–674.
- (12) Borchard, G. (2001) Chitosans for gene delivery. *Adv. Drug Delivery Rev.* 52, 145–150.
- (13) Park, Y. K., Park, Y. H., Shin, B. A., Choi, E. S., Park, Y. R., Akaike, T., and Cho, C. S. (2000) Galactosylated chitosan-graft-dextran as hepatocyte-targeting DNA carrier. *J. Controlled Release* 9, 97–108.
- (14) Park, I. K., Kim, T. H., Park, Y. H., Shin, B. A., Choi, E. S., Chowdhury, E. H., Akaike, T., and Cho, C. S. (2001) Galactosylated chitosan-graft-poly(ethylene glycol) as hepatocyte-targeting DNA carrier. *J. Controlled Release* 76, 349–362.
- (15) Mao, H. Q., Roy, K., Truong-Le, V. L., Janes, K. A., Lin, K. Y., Wang, Y., August, J. T., Leong, K. W. (2001) Chitosan-DNA nanoparticles as gene carriers: synthesis, characterization and transfection efficiency. *J. Controlled Release* 70, 399–421.
- (16) Chan, V., Mao, H. Q., and Leong, K. W. (2001) Chitosan-induced perturbation of dipalmitoyl-sn-glycero-3-phosphocholine membrane bilayer. *Langmuir* 17, 3749–3756.
- (17) Fang, N., Chan, V., Mao, H. Q., and Leong, K. W. (2001) Interactions of phospholipid bilayer with chitosan: effect of molecular weight and pH. *Biomacromolecules* 2, 1161–1168.
- (18) Kurisawa, M., Yokoyama, M., and Okano T. (2000) Transfection efficiency increases by incorporating hydrophobic monomer units into polymeric gene carriers. *J. Controlled Release* 68, 1–8.
- (19) Sato, T., Kawakami, T., Shirakawa, N., and Okahata, Y. (1995) Preparation and characterization of DNA-lipoglutamate complexes. *Bull. Chem. Soc. Jpn.* 68, 2709–2715.
- (20) Kabavov, A. V., and Kavanov, V. A. (1995) DNA complexes with polycations for the delivery of genetic materials into cells. *Bioconjugate Chem.* 6, 7–20.
- (21) Kuhn, P. S., Levin, Y., and Barbosa, M. C. (1999) Charge inversion in DNA-amphiphile complexes: possible application to gene therapy. *Physica A* 274, 8–18.
- (22) Li, F., Liu, W. G., and Yao, K. D. (2002) Preparation of oxidized glucose-cross-linked N-alkylated chitosan membrane and in vitro studies of pH-sensitive drug delivery behavior. *Biomaterials* 23, 343–347.
- (23) McMahon, D. K., Anderson, P. A., Nassar, R., Bunting, J. B., Saba, Z. A., Oakeley, E., and Malouf, N. N. (1994) C2C12 cells: biophysical, biochemical, and immunocytochemical properties. *Am. J. Physiol. Cell Physiol.* 266, C1795–C1802.
- (24) Philippova, O. E., Volkov, E. V., Sitnikova N. L., and Khokhlov, A. R. (2001) Two types of hydrophobic aggregates in aqueous solutions of chitosan and its hydrophobic derivative. *Biomacromolecules* 2, 483–490.
- (25) Zelikin, A. N., Putnam, D., Shastri, P., Langer, R. and Izumrudov, V. A. (2002) Aliphatic Ionenenes as Gene Delivery Agents: Elucidation of Structure–Function Relationship through Modification of Charge Density and Polymer Length. *Bioconjugate Chem.* 13, 548–553.
- (26) Bae, H. S., and Hudson, S. M. (1997) The cooperative binding behavior of sodium dodecyl sulfate to cross-linked chitosan films. *J. Polym. Sci.: Part A: Polym. Chem.* 35, 3755–3765.
- (27) Liu, W. G., Yao, K. D., and Liu, Q. G. (2001) Formation of a DNA/N-dodecylated chitosan complex and salt-induced gene delivery. *J. Appl. Polym. Sci.* 82, 3391–3395.
- (28) Liu, W. G., and Yao, K. D. (2002) Chitosan and its derivatives — a promising nonviral vector for gene transfection. *J. Controlled Release*, 83, 1–11.
- (29) McGraw, T. E., and Maxfield, F. R. (1991) *Targeted Drug Delivery* (R. L. Juliano, Ed.) pp 11–41, Springer, New York.
- (30) Erbacher, P., Zou, S., Bettinger, T., Steffan, A. M., and Remy, J. S. (1998) Chitosan-based vector/DNA complexes for gene delivery: biophysical characteristics and transfection ability. *Pharm. Res.* 15, 1332–1339.
- (31) Nakanishi, M., and Noguchi, A. (2001) Confocal and probe microscopy to study gene transfection mediated by cationic liposomes with a cationic cholesterol derivative. *Adv. Drug Delivery Rev.* 52, 197–207.
- (32) Muniruzzaman, Md., Marin, A., Luo, Y., Prestwich, G. D., Pitt, W. G., Hussein, G., and Rapoport N. Y. (2002) Intracellular uptake of Pluronic copolymer: effects of the aggregation state. *Colloids Surfaces B: Biointerfaces* 25, 233–241.
- (33) Schaffer, D. V., Fidelman, N. A., Dan, N., and Lauffenburger D. A. (2000) Vector unpacking as a potential barrier for receptor-mediated polyplex gene delivery. *Biotech. Bioeng.* 67, 599–606.
- (34) Ishii, T., Okahata Y., and Sato T. (2001) Mechanism of cell transfection with plasmid/chitosan complexes. *Biochim. Biophys. Acta* 1514, 51–64.

BC020051G

## Polycation Liposome Enhances the Endocytic Uptake of Photosensitizer into Cells in the Presence of Serum

Yoshito Takeuchi,<sup>†</sup> Kohta Kurohane,<sup>‡</sup> Kanae Ichikawa,<sup>†</sup> Sei Yonezawa,<sup>†</sup> Hidetsugu Ori,<sup>§</sup> Takayuki Koishi,<sup>§</sup> Mamoru Nango,<sup>§</sup> and Naoto Oku<sup>†,\*</sup>

Department of Medical Biochemistry, School of Pharmaceutical Sciences, University of Shizuoka, 52-1 Yada, Shizuoka 422-8526, Japan, Department of Microbiology, School of Pharmaceutical Sciences, University of Shizuoka, 52-1 Yada, Shizuoka 422-8526, Japan, and Department of Applied Chemistry, Faculty of Engineering, Nagoya Institute of Technology, Gokiso-cho, Nagoya 466-8555 Japan. Received December 10, 2002; Revised Manuscript Received April 10, 2003

To construct a novel drug delivery carrier that possesses high therapeutic efficacy with low dosage, we designed polyethylenimine-modified liposome (polycation liposome, PCL) and examined the entrapment of photosensitizer, benzoporphyrin derivative monoacid ring A (BPD-MA), for antiangiogenic photodynamic therapy (PDT). Photosensitizer entrapped in PCLs showed enhanced phototoxicity for a human vascular endothelial cell line, ECV304, in comparison with that for nonmodified control liposome. Interestingly, phototoxicity of control liposomal BPD-MA was suppressed in the presence of serum, but PCL maintained the phototoxicity in the presence of serum following PCL-mediated PDT treatment due to the stability of PCL and the reduced detachment of encapsulated photosensitizer from liposome to serum. In fact, PCL enhanced the uptake level of BPD-MA to ECV304 cells despite the presence or absence of serum. Since polycation modification enhances bioavailability of the liposomal photosensitizer and this property is maintained in the presence of serum, PCL would be useful for antiangiogenic PDT.

### INTRODUCTION

Cancer chemotherapy is generally accompanied by severe side effects such as bone marrow suppression. On the contrary, photodynamic therapy (PDT)<sup>1</sup> is a modality of cancer treatments without such side effects, since a photosensitizer (such as a porphyrin, chlorin, or phthalocyanine derivatives) induces cytotoxicity only after exposure to laser light with a specific wavelength (1–4). Laser irradiation results in an induction of singlet oxygen to afford tumor destruction. In the case of hydrophobic macrocycles, it would be expected that biodistribution of administered photosensitizers in malignant tissues would be mediated by LDL in blood, selectively taken up in the tumor cells through the highly expressed LDL receptor (5–9). However, administered photosensitizer is bound by LDL and rapidly cleared by the reticuloendothelial system (RES), namely, liver and spleen, affording a reduction of the photosensitization level in the tumor. Therefore, in pursuit of a drug delivery system for such photosensitizers, lipid formulation of photosensitizers has been attempted (10–13).

In the present study, we used BPD-MA (Chart 1) as a photosensitizer. The compound is also known as Verteporfin and Visudyne and is commercialized for the treatment of choroidal neovascularization of age-related macular degeneration. Photoactivation of BPD-MA induces local damage to neovascular endothelium, resulting in vessel occlusion (14). We previously observed that antiangiogenic PDT using BPD-MA caused blood flow stasis and significant regression of tumor in comparison with conventional PDT scheduling (laser irradiation at 3 or 4 h post BPD-MA administration) (15–19). Antiangiogenic PDT was achieved by laser irradiation at 5–15 min post BPD-MA administration, and the PDT treatment damaged angiogenic vascular endothelial cells rather than tumor cells (16). Our interest in antiangiogenic PDT treatment is further motivated by development of a novel liposomal formulation targeted to vascular endothelial cells. For this purpose, we selected PCL as a carrier for a photosensitizer.

Polyethylenimine (PEI) is frequently utilized as an effective nonviral DNA vector, both in vitro (20) and in vivo (21, 22), where compacted DNA is delivered to the cytoplasm via endosome by the proton-sponge effect (23). It would be expected that PEI would adhere to the anionic plasma membrane by electrostatic interaction, even in small doses, due to the concentrated positive charges afforded by the polymerization of amino groups. Furthermore, the polycation can give high tissue selectivity and low toxicity by chemical conjugation to biofunctionalized molecules such as oligopeptides and poly(ethylene glycol).

PCL is a cationic polymer-coated liposome; specifically, cetylated PEI (cetyl-PEI, Chart 1) is located on the liposomal surface. Alkyl chains in cetyl-PEI contribute to the stability of the polycation because of the induction

\* To whom correspondence should be addressed. Tel: +81-54-264-5701. Fax: +81-54-264-5705. E-mail: oku@u-shizuoka-ken.ac.jp.

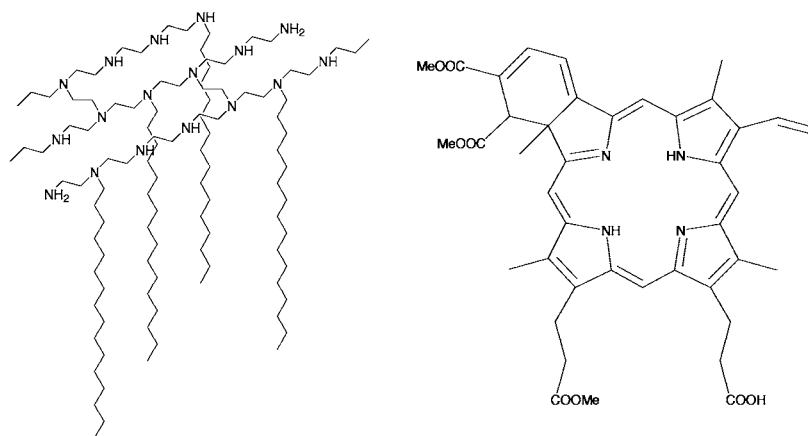
<sup>†</sup> Department of Medical Biochemistry, University of Shizuoka.

<sup>‡</sup> Department of Microbiology, University of Shizuoka.

<sup>§</sup> Nagoya Institute of Technology.

<sup>1</sup> Abbreviations: BPD-MA, benzoporphyrin derivative monoacid ring A; cetyl-PEI, cetylated polyethylenimine; DPPC, dipalmitoylphosphatidylcholine; DPPG, dipalmitoylphosphatidylglycerol; ELS, electrophoretic light scattering; FBS, fetal bovine serum; LDL, low-density lipoprotein; PCL, polycation liposome; PDT, photodynamic therapy; PEI polyethylenimine; RES, reticuloendothelial system.



**Chart 1. Chemical Structures of Cetyl-PEI (left) and BPD-MA (right)**

of hydrophobic and van der Waals interactions between the cetyl group and aliphatic hydrocarbons of lipids. We consider that PCL combines not only the above-mentioned advantages of both liposome and polycation but also enhanced endocytic uptake efficiency in the presence of serum (24, 25). In our recent study, we reported the high efficacy of BPD-MA-entrapped PCL (BPD-MA PCL) as a novel antiangiogenic liposomal drug for PDT-mediated *in vivo* cancer treatment (26). The results indicated that strong suppression of tumor growth was observed by PCL-mediated PDT treatment, and the antitumor activity was induced by destruction of tumor-derived neovasculature and subsequent apoptotic doom of tumor cells in comparison with those by BPD-MA-entrapped nonmodified control liposomes (BPD-MA liposome).

The the present study, we demonstrated the phototoxicity for the vascular endothelial cell line with BPD-MA PCLs and subsequent laser exposure. Furthermore, we described the uptake manner and the stability of liposomal structure against FBS using BPD-MA PCLs in comparison with that using BPD-MA liposomes.

## EXPERIMENTAL SECTION

**Materials.** PEI, consisting of 25%, 50%, and 25% for primary, secondary, and tertiary amino groups, respectively, with an average MW of 1800, was kindly provided by Nippon Shokubai Co., Ltd., Osaka, Japan. Polymer purification was performed by an ultrafiltration technique with an ultrafiltration apparatus equipped with a YM-1 ultrafiltration membrane (Amicon Inc., Beverly MA).  $^1\text{H}$  NMR spectra were recorded in  $\text{CDCl}_3$  with a Valian Gemini-300 instrument with tetramethylsilane as an internal standard. The visible absorption spectra were recorded on a Beckman DU-70 spectrophotometer. The purified polycation was lyophilized and stored in EtOH before the preparation of cetyl-PEI. DC-Plastikfolein Kieselgel 60 F<sub>254</sub> (Merck, Darmstadt, Germany) was used for analytical TLC. Dipalmitoylphosphatidylcholine (DPPC) and dipalmitoylphosphatidylglycerol (DPPG) were kindly provided by Nippon Fine Chemical Co., Ltd., Takasago, Hyogo, Japan, and cholesterol was purchased from Sigma Chemical Co., St. Louis, MO. BPD-MA and [ $^{14}\text{C}$ ]BPD-MA were generous gifts from QLT PhotoTherapeutics, Inc., Vancouver, British Columbia, Canada.

**Preparation of Cetylated Polyethylenimine (cetyl-PEI).** Cetyl-PEI was prepared by a similar procedure as described previously (24, 25). In brief, PEI (2.40 g,  $1.33 \times 10^{-3}$  mol) was stirred at 65 °C in EtOH (10.0 mL) for 30 min under reflux conditions and  $\text{N}_2$  bubbling, and to

the solution were added 1-bromohexadecane (3.87 mL,  $1.33 \times 10^{-2}$  mol) and triethylamine (223  $\mu\text{L}$ ,  $1.60 \times 10^{-3}$  mol). After a 7-h reaction, the solution was evaporated. The resulting solid was dissolved in 20% EtOH aqueous solution (100 mL), and the solution was ultrafiltered for 2 days, using more 20% EtOH aqueous solution (over 1000 mL). Finally, the solution was lyophilized. The stoichiometric conjugation percentage of the cetyl group, determined by  $^1\text{H}$  NMR spectra, was 24.1% per total PEI amino groups.  $^1\text{H}$  NMR ( $\text{CDCl}_3$ ):  $\delta$  0.82–0.95 (10H, t, cetyl  $\text{CH}_3$ ), 1.13–1.44 (101H, br, cetyl  $\text{CH}_2$ ), 2.36–3.19 (167H, br,  $\text{CH}_2$ ), 4.84–5.26 (32H, br, PEI amine H).

**Preparation of BPD-MA Liposome and BPD-MA PCL.** BPD-MA liposomes that were not modified cetyl-PEI were prepared as described previously (26). BPD-MA liposome consists of DPPC, cholesterol, DPPG, and BPD-MA (20/10/5/0.3 as molar ratio, respectively); on the contrary, BPD-MA PCL additionally contains cetyl-PEI at a molar ratio of 0.175, 0.875, 1.75, and 3.5 (total lipids/cetyl-PEI molar ratio: 20/0.1, 20/0.5, 20/1, 20/2, respectively). Lipids, BPD-MA, and cetyl-PEI that were dissolved in  $\text{CHCl}_3$  were evaporated to construct the thin lipid film and hydrated with PBS (300 mM as the final concentration of BPD-MA). The liposomal solution was freeze-thawed by using liquid  $\text{N}_2$  and sonicated for 15 min at 60 °C. Finally, these liposomes were sized at 100-nm diameter by extrusion through a polycarbonate membrane filter under 15 kgf/cm<sup>2</sup> of  $\text{N}_2$  pressure. The BPD-MA and phospholipid concentrations were determined before and after the extrusion step. The result supports the successful encapsulation of BPD-MA (over 98%). BPD-MA concentration was determined following extrusion by measuring the absorbance at 688 nm.

**Cell Culture.** The human vascular endothelial cell line ECV304 was used for *in vitro* investigations (27, 28). ECV304 cells ( $1 \times 10^5$  cells) were seeded in 35-mm cell culture dishes in 199 medium (Nissui Pharmaceutical Co., Ltd., Tokyo, Japan) supplemented with 10% heat-inactivated FBS (Sigma Chemical Co., St. Louis, MO) and incubated in a 5%  $\text{CO}_2$  incubator for 48 h at 37 °C.

**PDT Treatment *in Vitro*.** The medium in the cell culture dish was removed, and 199 medium supplemented with 10% heat-inactivated FBS (990  $\mu\text{L}$ ) was added. BPD-MA liposomes or BPD-MA PCLs (10  $\mu\text{L}$ ) were added (final 30–500 ng/mL in terms of BPD-MA) and incubated for 60 min. PDT treatment was performed with irradiation from the top-side of the cell culture dish using a diode-laser system, SP689 (Suzuki Motor Co., Ltd., Yokohama, Japan). The cells that were incubated with photosensitizer-entrapped liposomes were exposed

to the laser light with 2.0 J/cm<sup>2</sup> of fluence (0.25 W, 76.9 s) at 689 nm.

At 24 h after PDT treatment, the cells were washed with PBS for the removal of destroyed cells. Viable cells were determined by crystal violet dye assay. The cells were soaked in 0.5% crystal violet solution (dissolved in MeOH/H<sub>2</sub>O = 1/4 (v/v)) for 10 min following the removal of the redundant dying solution by washing in PBS attentively. The dishes were completely dried, and 33% aqueous AcOH solution (1 mL) was added to elute dye from the stained cells. Survival percentage of the cells was spectroscopically quantified by the absorbance at 630 nm, and the parameters were normalized to a control set of cells without liposomal photosensitizer treatment and laser exposure.

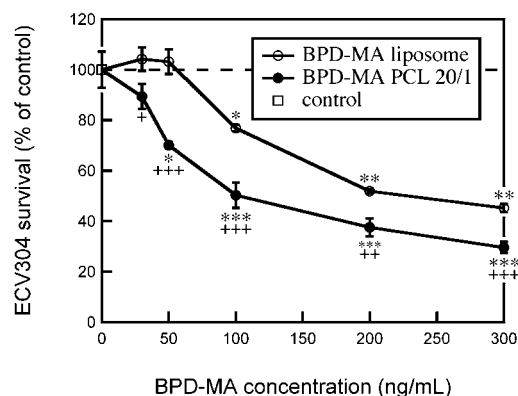
**ELS Measurement.** Preparation of BPD-MA liposomes and BPD-MA PCLs 20/1 were followed as described above. After being sized at 100-nm in diameter, the liposomal solutions were incubated in the presence and absence of an equal volume of FBS at 37 °C for 3 h. Particle sizes and  $\zeta$ -potentials of BPD-MA liposomes and BPD-MA PCLs 20/1 were recorded on a ELS-800 electrophoretic light scattering spectrophotometer (Otsuka Electronics Co., Ltd., Osaka, Japan). The results supported the assigned liposomal sizes in saline-hydrated liposomes, and the  $\zeta$ -potentials were +5.06 mV for BPD-MA liposome and +32.53 mV for BPD-MA PCL 20/1.

**Spin Column Assay.** The assay was followed Chonn's method (29). [<sup>14</sup>C]BPD-MA liposomes and [<sup>14</sup>C]BPD-MA PCLs that were hydrated with 0.3 M glucose were incubated in the presence of an equal volumes of FBS or HEPES at 37 °C for 30 min. Bio-Gel A-15 m, agarose beads 200–400 mesh (Bio-Rad Laboratories, CA), was eluted with saline three times and filled into a 1-mL cylinder with cotton cap. A spin column was prepared by centrifugation of the cylinder at 800 rpm for 30 s. The incubated liposomal samples (100  $\mu$ L) were applied to the spin column, and the first fraction was collected by centrifugation at 500 rpm for 30 s ( $n = 3$ ). After collection of the first fraction, saline (100  $\mu$ L) was applied to the spin column, and it was centrifuged at 500 rpm for 30 s. The procedure was repeated until the 12th fraction eluted. Several fractions (50  $\mu$ L) were mixed with 10 mL of Ultima-Fluor (Packard Japan, Tokyo, Japan), and the radioactivity of the <sup>14</sup>C-labeled macrocycles was determined with an Aloka LSC-3500 liquid scintillation counter.

**Cellular Uptake of BPD-MA.** ECV304 cells ( $3 \times 10^5$  cells) were seeded in 60-mm cell culture dishes and incubated in a 5% CO<sub>2</sub> incubator for 48 h at 37 °C. The medium in the cell culture dish was changed to fresh 199 medium supplemented with 10% heat-inactivated FBS (2.97 mL). BPD-MA liposomes or BPD-MA PCLs (30  $\mu$ L) were added (100 ng/mL as final concentration of BPD-MA) and incubated for 60 min. After the cells were washed with ice-cold PBS, they were dissolved in 0.1% SDS-containing 5 mM Tris buffer (1.2 mL), and the amount of BPD-MA was fluorometrically determined with an excitation wavelength of 450 nm and emission at 619.4 nm by a Hitachi F-4010 fluorescence spectrophotometer. Quantification of cell protein concentration was determined by BCA protein assay (Pierce Chemical Company, IL). Thus, BPD-MA uptake was quantitatively evaluated and represented as the amount of BPD-MA per cell protein.

## RESULTS

Cetyl-PEI was prepared using PEI and 1-bromohexadecane in EtOH at 65 °C for 6–9 h in the presence of



**Figure 1.** Phototoxicity of BPD-MA against ECV304 cells following PDT treatment in the presence of BPD-MA liposomes or BPD-MA PCLs. ECV304 cells were incubated in the presence of BPD-MA liposomes or BPD-MA PCLs 20/1 at selected BPD-MA concentrations for 60 min, and irradiated with 689-nm laser light (2.0 J/cm<sup>2</sup>). Viable cells were determined by crystal violet dye assay at 24 h after laser exposure. Data points represent the mean  $\pm$  SD of the relative absorbance at 630 nm in comparison with that of PDT-nontreated control in the absence of BPD-MA liposomes or BPD-MA PCLs ( $n = 3$ ). Asterisks and crosses indicate  $P$  vs control and an equal concentration of BPD-MA liposomes, respectively: \* and +,  $P < 0.05$ ; \*\* and ++,  $P < 0.01$ ; \*\*\* and +++,  $P < 0.001$ .

triethylamine. The grafting reaction was performed under N<sub>2</sub> atmosphere. After the reaction, the solvent was removed by evaporation and dissolved in 20% EtOH aqueous solution. Ungrafted compounds were removed by ultrafiltration technique for 2 days by filtering with 10 volumes of 20% EtOH aqueous solution. Finally, the unfiltered solution was lyophilized, resulting in a white powder. The resulting solid was soluble in CHCl<sub>3</sub> and partly soluble in H<sub>2</sub>O, so that preparation of PCL is enabled. The grafted percentage of cetyl group was determined by measuring the <sup>1</sup>H NMR spectra in CDCl<sub>3</sub>. The spectra supported the assigned structure, and the stoichiometric grafting of cetyl groups was achieved. Seven kinds of cetyl-PEIs were synthesized with varying MW of PEI (600, 1800, and 25000) and grafted percentage of cetyl group (5 to 24% per ethylenimine unit).

To optimize the MW and the grafted percentage of cetyl-PEI, PCLs were prepared using the seven types of cetyl-PEI, and the availability was determined by gene transfer assay to various cells in the presence of serum. In particular, the most effective transfection was shown by using cetyl-PEI with MW 1800 of PEI and 24% grafted percentage of cetyl group (data not shown), so that this cetyl-PEI was used for preparing PCL (24, 25).

**BPD-MA PCL Enhanced the Phototoxicity against Human Endothelium Cell Line.** Initially, the phototoxic action of BPD-MA against a human endothelial cell line, ECV304 cells, was examined by use of BPD-MA liposomes or BPD-MA PCLs 20/1. Figure 1 shows the survival for ECV304 cells in the presence of BPD-MA liposomes or BPD-MA PCLs 20/1 after laser exposure. In the range of 30–300 ng/mL in terms of BPD-MA concentration, the cells that were treated using BPD-MA PCLs 20/1 were efficiently destroyed following PDT treatment in comparison with those using an equal concentration of BPD-MA liposomes: The phototoxicity in the presence of BPD-MA PCLs 20/1 corresponded to approximately twice the dose of BPD-MA liposomes (LD<sub>50</sub>: 247.7 ng/mL for BPD-MA liposomes and 146.1 ng/mL for BPD-MA PCLs 20/1).

To verify the direct cytotoxic action of BPD-MA liposomes and BPD-MA PCLs, a large amount of photosen-

**Table 1. Stability of BPD-MA Liposome and BPD-MA PCL 20/1 in the Presence of Serum**

BPD-MA condition	serum	ELS measurement <sup>a</sup> particle size (nm)	recovery % by spin column assay <sup>b</sup>	
			liposomal fraction	serum-bound fraction
liposome	none	113.7 ± 17	100	—
liposome	50% FBS	228.3 ± 35	010	89
PCL 20/1	none	103.3 ± 17	0091 <sup>c</sup>	—
PCL 20/1	50% FBS	189.9 ± 30	0074 <sup>c</sup>	21

<sup>a</sup> All liposomes were sized at 100-nm diameter by extrusion and subsequent incubation in saline with or without an equal volume of FBS for 3 h at 37 °C. <sup>b</sup> All liposomes were sized at 100-nm diameter by extrusion and subsequent incubation in 0.15 M glucose with an equal volume of 5 mM HEPES buffer or FBS for 30 min at 37 °C. To gain the accurate recovery of liposomal and serum-bound photosensitizers, percentage of the fractions were determined by calculating the *Gaussian* distribution on the basis of the elution profile. <sup>c</sup> Accurate quantification was not possible due to the strong adsorption of PCLs to agarose beads.

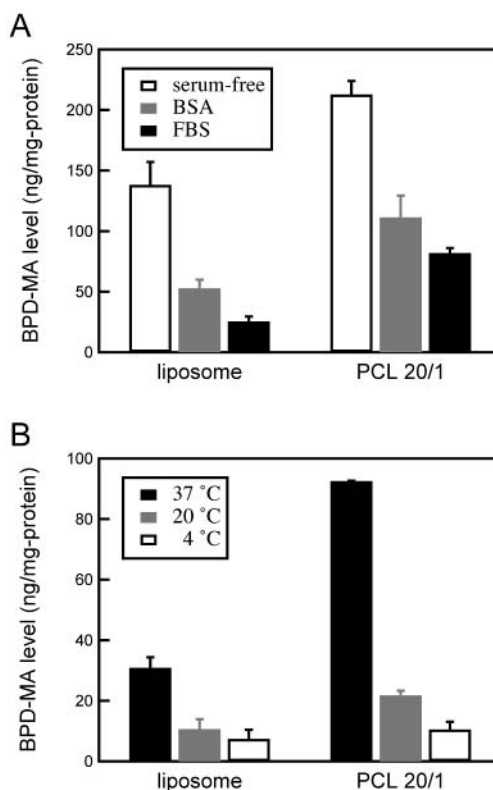
sitizers entrapped in PEI-nonmodified liposomes or PCLs (500 ng/mL in terms of BPD-MA) were applied to ECV304 cells without subsequent laser exposure. The result showed that survival for ECV304 cells was not affected, indicating no cytotoxicity of BPD-MA and PCL (data not shown). Furthermore, cytotoxicity was also not observed by laser exposure alone (2 J/cm<sup>2</sup>).

**Stability of Liposomal Photosensitizers in the Presence of Serum.** We considered that serum protein binding to liposomes resulting in aggregation of liposomes and detachment of entrapped hydrophobic drugs may occur in the presence of serum. To ascertain the stability of BPD-MA liposomes or BPD-MA PCLs in the presence of serum, electrophoretic light scattering (ELS) measurement and a spin column assay<sup>29</sup> were performed.

Initially, particle size changes of BPD-MA liposomes or BPD-MA PCLs 20/1 were evaluated after presizing at 100-nm diameter and subsequent incubation with or without 50% FBS at 37 °C for 3 h. As shown in Table 1, the ELS result indicated that the sizes of BPD-MA liposomes were determined as 228.3 ± 35 and 113.7 ± 17 nm in the presence and absence of FBS, respectively. Similarly, those of BPD-MA PCLs 20/1 were 103.3 ± 17 nm in the absence and 189.9 ± 30 nm in the presence of FBS. The aggregation of PCLs in the presence of serum was only control level.

The transfer of BPD-MA from liposome or PCL was examined by a spin column assay (Table 1). The spin column chromatogram of two types of liposomal photosensitizers preincubated in HEPES-buffered glucose solution indicated that the liposomal [<sup>14</sup>C]BPD-MA was eluted only in the void volume (data not shown). Recovery of [<sup>14</sup>C]BPD-MA was 99% for [<sup>14</sup>C]BPD-MA liposomes, although that was only 21% for [<sup>14</sup>C]BPD-MA PCLs 20/1. The latter evidence indicates that PCLs absorbed strongly to agarose gel, and [<sup>14</sup>C]BPD-MA entrapped in PCLs was strongly associated to PCL, association of which might be mediated by PEI in PCLs; on the contrary, after incubation of [<sup>14</sup>C]BPD-MA liposomes or [<sup>14</sup>C]BPD-MA PCLs with 50% FBS for 30 min, 80% or 19% of [<sup>14</sup>C]BPD-MA was eluted at the lipoprotein fractions, respectively.

**Cellular Uptake of BPD-MA.** Since the cellular uptake of liposomal BPD-MA is a potent factor for susceptibility to PDT, BPD-MA uptake level was determined by fluorescence emission spectroscopy. Fluorescence intensity of BPD-MA in the cellular fraction was proportionally increased with increasing BPD-MA concentration in the presence of either BPD-MA liposomes



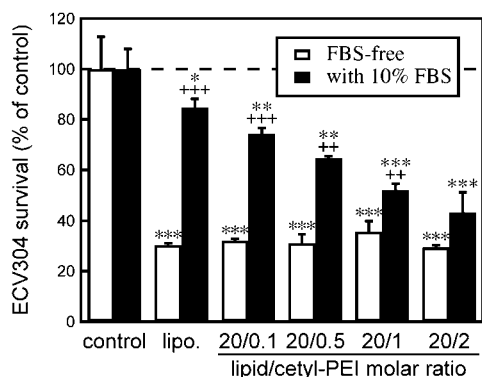
**Figure 2.** BPD-MA uptake level against ECV304 cells following addition of BPD-MA. ECV304 cells ( $3 \times 10^5$  cells) were incubated with BPD-MA liposomes or BPD-MA PCLs 20/1 (100 ng/mL in terms of BPD-MA) for 60 min at 37 °C in serum-free, 10% heat-inactivated FBS-containing, and 1.92 mg/mL of BSA-containing 199 media (A). BPD-MA uptake was also determined after addition of BPD-MA liposomes or BPD-MA PCLs in the presence of 10% heat-inactivated FBS at different incubation temperature (B). BPD-MA fluorescence levels in cell lysate (mean ± SD) were monitored by the fluorescence intensity at 691.4 nm with 450-nm excitation and normalized by the cell protein concentration determined by BCA assay.

or BPD-MA PCLs 20/1 (data not shown). Quantitative data of the incorporated photosensitizer in the presence or absence of 10% FBS is shown in Figure 2. As is apparent from Figure 2A, PCLs enhanced the BPD-MA uptake in comparison with PEI-nonmodified liposome regardless of the presence of FBS. The uptake level was increased approximately 1.5-fold in the absence of serum and 3.1-fold in the presence of 10% FBS. Furthermore, inhibition of BPD-MA uptake by FBS was reduced by using PCLs: 81.5% inhibition for BPD-MA liposomes and 61.5% inhibition for BPD-MA PCLs 20/1 in comparison with the level in the absence of serum. It is also clarified that BSA, the most abundant protein in FBS, suppressed the photosensitizer uptake to some extent.

We next examined the mechanism of BPD-MA uptake by the cells. The percentage of incorporated BPD-MA per initial amount of BPD-MA was 10.9% for PCLs 20/1 and 3.4% for PEI-unmodified liposomes after incubation at 37 °C in the presence of 10% FBS, indicating that BPD-MA uptake was improved about 3-fold by PCL formulation (Figure 2B); on the contrary, a remarkable reduction of uptake was observed in both BPD-MA liposomes or BPD-MA PCLs at the incubation temperature of 20 and 4 °C.

**Influence of Serum on the Phototoxicity by BPD-MA PCLs.** Finally we examined the phototoxicity of BPD-MA in the formulations of liposomes or PCLs in the presence of serum while changing the modified cetyl-PEI molar ratio. As shown in Figure 3, the assay revealed





**Figure 3.** Persistence of phototoxic efficiency using BPD-MA liposomes or BPD-MA PCLs in the presence of serum. ECV304 cells were incubated in the presence of BPD-MA liposomes or BPD-MA PCLs 20/1 for 60 min in the presence and absence of 10% heat-inactivated FBS, and irradiated with 689-nm laser light ( $2.0 \text{ J/cm}^2$ ). Viable cells were determined by crystal violet dye assay following 24 h after laser exposure. Data points represent the mean  $\pm$  SD of the relative absorbance at 630 nm in comparison with that of PDT-nontreated control in the absence of BPD-MA liposomes or BPD-MA PCLs 20/1 ( $n = 3$ ). Asterisks and crosses indicate  $P$  vs control and BPD-MA liposomes, respectively: \*,  $P < 0.05$ ; \*\* and ++,  $P < 0.01$ ; \*\*\* and +++,  $P < 0.001$ .

that approximately 70% phototoxicity was observed following PDT treatment in the absence of serum regardless of the cetyl-PEI molar ratio in PCLs. However strong suppression of phototoxicity was observed in the presence of 10% FBS when liposomal formulation was used. Interestingly, the suppression of phototoxicity was gradually canceled with increasing cetyl-PEI molar ratio.

## DISCUSSION

We developed BPD-MA PCL as an angiogenic vasculature-targeted drug carrier for PDT usage. Our previous *in vivo* study indicated that PCL enhances strong suppression of tumor growth following PDT treatment (26). In this paper, we described the effect of serum on the phototoxicity of liposomal photosensitizer-mediated PDT treatment to vascular endothelial cells.

We designed PCL to be taken up by the target cells efficiently: The cationic liposomal surface of PCL enhances the adherence to plasma membrane of vascular endothelial cells and accelerates the entry of PCL into cytosol via endocytic pathway (24, 25). In fact, BPD-MA PCL-mediated PDT caused strong cytotoxicity against a vascular endothelial cell line, ECV304 cells, in comparison with the nonmodified liposomes-mediated one (Figure 1). Since BPD-MA PCLs without laser exposure did not affect the cell viability, the cytotoxic action is not due to the toxicity of BPD-MA or PCL but due to the photoreaction of BPD-MA.

Uptake of liposomal drugs is frequently inhibited in the presence of serum. It is possible that administered liposomes encountered serum protein binding (30), resulting in aggregation of liposomes and detachment of entrapped hydrophobic drugs. Therefore, the aggregation of liposomes or PCLs in the presence of serum was determined by ELS measurement, and detachment level of entrapped photosensitizers was examined by a spin column assay (24). Generally, serum-mediated aggregation of liposomes induces an enormous size of concretions. As is apparent from Table 1, no significant change of liposomal size was observed, regardless of polycation modification and presence of serum. When the aggregation manner is taken into account, undesirable aggrega-

tion of liposomes does not occur in the presence of serum. The spin column assay revealed that PCLs decreased the detachment level of entrapped [ $^{14}\text{C}$ ]BPD-MA and almost all photosensitizers entrapped in PCLs retained on the agarose beads; on the contrary, photosensitizer clearance occurred primarily with nonmodified liposomes (Table 1). This result suggests that entrapped macrocycles are easily transferred from liposome to lipoproteins and that polycation modification of liposome suppresses the transfer. It is possible that PEI in PCL directly interacted with BPD-MA and suppressed the dissociation. Alternatively, polycation coating of the liposomal surface may increase the stability of liposomes, which caused stable entrapment of the photosensitizer in PCL. It is considered that adsorption of BPD-MA on the agarose beads results in the strong interaction between photosensitizer and polycation.

From the results of the BPD-MA uptake assay, the uptake level was enhanced by using BPD-MA PCLs. The uptake efficiency decreased in the presence of serum regardless of the type of liposomes. To elucidate the serum factors that suppress the uptake of BPD-MA, we examined the effect of albumin, a major serum protein, and observed that albumin also suppressed the uptake (Figure 2A). Therefore, albumin is one of the possible factors affecting the uptake. Interestingly, the suppression level of photosensitizer uptake by both BSA and FBS was reduced in BPD-MA PCLs in comparison with BPD-MA entrapped in nonmodified liposomes. The strong electrostatic interaction of polycation with the plasma membrane of vascular endothelial cells might overcome the suppression of the uptake by the serum factor(s). Besides the albumin, serum lipoprotein would affect the uptake of BPD-MA in liposomes, since a part of BPD-MA was transferred to lipoproteins especially in the presence of serum. However, the spin column data suggested that the transfer of BPD-MA to lipoprotein is suppressed by PCL formulation.

To examine the mechanism of incorporation of BPD-MA entrapped in nonmodified liposomes or PCLs into the cells, BPD-MA uptake was monitored at various temperatures. Figure 2B shows that enhanced photosensitizer uptake was observed at  $37^\circ\text{C}$ ; on the contrary, those at  $20$  and  $4^\circ\text{C}$  were significantly suppressed. The results suggested that the BPD-MA was mainly taken up in the cells via the endocytic pathway. The amount of BPD-MA in the cellular fraction after incubation at  $4^\circ\text{C}$  might reflect the bound BPD-MA on the cellular surface. From the quantitative results of Figure 2B, the endocytic BPD-MA uptake was 2.6% for BPD-MA liposomes and 9.6% for BPD-MA PCLs, and the adhered BPD-MA on the plasma membrane was calculated as 0.8% for BPD-MA liposomes and 1.2% for BPD-MA PCLs per injected BPD-MA concentration. The result also supported the enhancement of BPD-MA uptake by use of PCL. The phototoxicity following BPD-MA PCL-mediated PDT treatment was on the level of that using polycation-nonmodified control liposomes until 30 min, but significant enhancement of phototoxicity by using BPD-MA PCLs was observed after over a 30-min incubation (data not shown). The results indicated that the enhanced phototoxicity by using BPD-MA PCLs contributes to the adherence of BPD-MA PCLs to plasma membrane by electrostatic interaction and subsequent effective uptake of photosensitizer (31).

The reduced phototoxicity for ECV304 cells in the presence of serum was canceled with increasing amount of cetyl-PEI modified on the liposomal surface (Figure 3). The result indicates that stability of BPD-MA en-

trapped in PCLs against serum is dependent on the modification of polycation, and that is strongly reflected in the phototoxicity following laser exposure.

Taken together, BPD-MA PCL enhances the phototoxicity for ECV304 cells. We considered that the efficacy is induced by not only the facilitation of endocytic BPD-MA uptake by the strong electrophoretic interaction with the plasma membrane but also the persistence of the liposomal structure against serum factor(s) in comparison with nonmodified control liposome: PCL inhibits the detachment of encapsulated photosensitizer in the presence of serum. From the results of cellular uptake of BPD-MA, PCL may maintain the BPD-MA entrapment and the strong interaction with the cellular membrane. Since the cellular uptake of BPD-MA is strongly related to the phototoxicity, the phototoxicity of BPD-MA in the PCL formulation is not abolished in the presence of serum. Leunig et al. (32) have reported that the high uptake of Photofrin by endothelial cells compared with several different tumor cell lines may indicate that the vascular endothelium is a major target for PDT. Therefore, PCL may be a useful formulation of photosensitizers for practical PDT.

#### ACKNOWLEDGMENT

The authors thank Prof. Takashi Sonobe, Dr. Yasuyuki Sadzuka, and Ms. Akiko Nakade at University of Shizuoka for electrophoretic light scattering measurements. Thanks are also given to Dr. Yukihiro Namba at Nippon Fine Chemical Co., Ltd., and Mr. Katsuhiko Sato at Suzuki Motor Co., Ltd., for generous gifts of phospholipids and for providing the diode-laser apparatus, respectively.

#### LITERATURE CITED

- Gomer, C. J. (1991) Preclinical Examination of First and Second Generation Photosensitizers Used in Photodynamic Therapy. *Photochem. Photobiol.* 54, 1093–1107.
- Henderson, B. W., and Dougherty, T. J. (1992) How Does Photodynamic Therapy Work? *Photochem. Photobiol.* 55, 145–157.
- Bonnett, R. (1995) Photosensitisers of the Porphyrin and Phthalocyanine Series for Photodynamic Therapy. *Chem. Soc. Rev.* 24, 19–33.
- Dougherty, T. J., Gomer, C. J., Henderson, B. W., Jori, G., Kessel, D., Korbek, M., Moan, J., and Peng, Q. (1998) Photodynamic Therapy. *J. Natl. Cancer Inst.* 90, 889–905.
- Candide, C., Morliere, P., Maziere, J. C., Goldstein, S., Santus, R., Dubertret, L., Reyftmann, J. P., and Polonovski, J. (1986) In Vitro Interaction of the Photoactive Anticancer Porphyrin Derivative Photofrin II with Low-Density Lipoprotein, and its Delivery to Cultured Human Fibroblasts. *FEBS Lett.* 207, 133–138.
- Maziere, J. C., Santus, R., Morliere, P., Reyftmann, J. P., Candide, C., Mora, L., Salmon, S., Maziere, C., Gatt, S., and Dubertret, L. (1990) Cellular Uptake and Photosensitizing Properties of Anticancer Porphyrins in Cell Membranes and Low and High-Density Lipoproteins. *J. Photochem. Photobiol. B: Biol.* 6, 61–68.
- de Smidt, P. C., Versluis, A. J., and van Berkel, T. J. (1993) Properties of Incorporation, Redistribution, and Integrity of Porphyrin-Low-Density Lipoprotein Complexes. *Biochemistry* 32, 2916–2922.
- Nakajima, S., Takemura, T., and Sakata, I. (1995) Tumor-Localizing Activity of Porphyrin and Its Affinity to LDL, Transferrin. *Cancer Lett.* 92, 113–118.
- Shibata, Y., Matsumura, A., Yoshida, F., Yamamoto, T., Nakai, K., Nose, T., Sakata, I., and Nakajima, S. (2001) Competitive Uptake of Porphyrin and LDL via the LDL Receptor in Glioma Cell Lines: Flow Cytometric Analysis. *Cancer Lett.* 166, 79–87.
- Mayhew, E., Vaughan, L., Panus, A., Murray, M., and Henderson, B. W. (1993) Lipid-associated Methylphosphor-bide-a (Hexyl-Ether) as a Photodynamic Agent in Tumor-bearing Mice. *Photochem. Photobiol.* 58, 845–851.
- Oku, N., Doi, K., Namba, Y., and Okada, S. (1994) Therapeutic Effect of Adriamycin Encapsulated in Long-circulating Liposomes on Meth-A-Sarcoma-bearing Mice. *Int. J. Cancer* 58, 415–419.
- Polo, L., Segalla, A., Jori, G., Bocchiotti, G., Verna, G., Franceschini, R., Mosca, R., and De Filippi, P. G. (1996) Liposome-delivered 131I-labeled Zn(II)-Phthalocyanine as a Radiodiagnostic Agent for Tumours. *Cancer Lett.* 109, 57–61.
- Oku, N., Saito, N., Namba, Y., Tsukada, H., Dolphin, D., and Okada, S. (1997) Application of Long-circulating Liposomes to Cancer Photodynamic Therapy. *Biol. Pharm. Bull.* 20, 670–673.
- Ciulla, T. A., Danis, R. P., Criswell, M., and Pratt, L. M. (1999) Changing Therapeutic Paradigms for Exudative Age-related Macular Degeneration: Antiangiogenic Agents and Photodynamic Therapy. *Expert Opin. Investig. Drugs* 8, 2173–2182.
- Fingar, V. H., Kik, P. K., Haydon, P. S., Cerrito, P. B., Tseng, M., Abang, E., and Wieman, T. J. (1999) Analysis of Acute Vascular Damage after Photodynamic Therapy Using Benzoporphyrin Derivative (BPD). *Br. J. Cancer* 79, 1702–1708.
- Kurohane, K., Tominaga, A., Sato, K., North, J. R., Namba, Y., and Oku, N. (2001) Photodynamic Therapy Targeted to Tumor-induced Angiogenic Vessels. *Cancer Lett.* 167, 49–56.
- Yang, Z., Lu, X., Frazier, D. L., Panjehpour, M., and Breider, M. A. (1994) Tumor Cell-enhanced Sensitivity of Vascular Endothelial Cells to Photodynamic Therapy. *Lasers Surg. Med.* 15, 342–350.
- Dolmans, D. E., Kadambi, A., Hill, J. S., Waters, C. A., Robinson, B. C., Walker, J. P., Fukumura, D., and Jain, R. K. (2002) Vascular Accumulation of a Novel Photosensitizer, MV6401, Causes Selective Thrombosis in Tumor Vessels after Photodynamic Therapy. *Cancer Res.* 62, 2151–2156.
- Dolmans, D. E., Kadambi, A., Hill, J. S., Flores, K. R., Gerber, J. N., Walker, J. P., Rinkes, I. H., Jain, R. K., and Fukumura, D. (2002) Targeting Tumor Vasculature and Cancer Cells in Orthotopic Breast Tumor by Fractionated Photosensitizer Dosing Photodynamic Therapy. *Cancer Res.* 62, 4289–4294.
- Boussif, O., Zanta, M. A., and Behr, J. P. (1996) Optimized Galenics Improve *in Vitro* Gene Transfer with Cationic Molecules up to 1000-fold. *Gene Ther.* 3, 1074–1080.
- Abdallah, B., Hassan, A., Benoist, C., Goula, D., Behr, J. P., and Demeneix, B. A. (1996) A Powerful Nonviral Vector for *in Vivo* Gene Transfer into the Adult Mammalian Brain: Polyethylenimine. *Hum. Gene Ther.* 7, 1947–1954.
- Goula, D., Remy, J. S., Erbacher, P., Wasowicz, M., Levi, G., Abdallah, B., and Demeneix, B. A. (1998) Size, Diffusibility and Transfection Performance of Linear PEI/DNA Complexes in the Mouse Central Nervous System. *Gene Ther.* 5, 712–717.
- Behr, J.-P. (1996) The Proton Sponge: a Means to Enter Cells Viruses Never Thought of. *Med. Sci.* 12, 56–58.
- Yamazaki, Y., Nango, M., Matsuura, M., Hasegawa, Y., Hasegawa, M., and Oku, N. (2000) Polycation Liposomes, a Novel Nonviral Gene Transfer System, Constructed from Cetylated Polyethylenimine. *Gene Ther.* 7, 1148–1155.
- Oku, N., Yamazaki, Y., Matsuura, M., Sugiyama, M., Hasegawa, M., and Nango, M. (2001) A Novel Nonviral Gene Transfer System, Polycation Liposomes. *Adv. Drug Deliv. Rev.* 52, 209–218.
- Takeuchi, Y., Kurohane, K., Ichikawa, K., Yonezawa, S., Nango, M., and Oku, N. (2002) Induction of Intensive Tumor Suppression by Anti-Angiogenic Photodynamic Therapy Using Polycation-modified Liposomal Photosensitizer. *Cancer* 97, 2027–2034.
- Lucas, M., Rose, P. E., and Morris, A. G. (2000) Contrasting Effects of HSP72 Expression on Apoptosis in Human Umbilical Vein Endothelial Cells and an Angiogenic Cell Line, ECV304. *Br. J. Haematol.* 110, 957–964.

- (28) Takahashi, K., Sawasaki, Y., Hata, J., Mukai, K., and Goto, T. (1990) Spontaneous Transformation and Immortalization of Human Endothelial Cells. *In Vitro Cell Dev. Biol.* 26, 265–274.
- (29) Chonn, A., Semple, S. C., and Cullis, P. R. (1991) Separation of Large Unilamellar Liposomes from Blood Components by a Spin Column Procedure: towards Identifying Plasma Proteins which Mediate Liposome Clearance *in Vivo*. *Biochim. Biophys. Acta* 1070, 215–222.
- (30) Richter, A. M., Waterfield, E., Jain, A. K., Canaan, A. J., Allison, B. A., and Levy, J. G. (1993) Liposomal delivery of a photosensitizer, benzoporphyrin derivative monoacid ring A (BPD), to tumor tissue in a mouse tumor model. *Photochem. Photobiol.* 57, 1000–1006.
- (31) Glazunova, O. O., Korepanova, E. A., Efimov, V. S., Smirnov, A. I., and Vladimirov Yu, A. (1998) A synthetic polycation, a copolymer of 1-vinyl-3-methylimidazole iodide with maleic acid diethyl ester, increases passive ionic permeability in erythrocyte membranes modified by fatty acids. *Membr. Cell Biol.* 12, 401–409.
- (32) Leunig, A., Staub, F., Peters, J., Heimann, A., Csapo, C., Kempfski, O., and Goetz, A. E. (1994) Relation of early Photofrin uptake to photodynamically induced phototoxicity and changes of cell volume in different cell lines. *Eur. J. Cancer* 30A, 78–83.

BC025648A



## PDEPT: Polymer-Directed Enzyme Prodrug Therapy. 2. HPMA Copolymer- $\beta$ -lactamase and HPMA Copolymer-C-Dox as a Model Combination

Ronit Satchi-Fainaro,<sup>\*,†,‡</sup> Hanna Hailu,<sup>§</sup> John W. Davies,<sup>||</sup> Clive Summerford,<sup>||</sup> and Ruth Duncan<sup>\*,§</sup>

Department of Cell Research and Immunology, Faculty of Life Sciences, Tel Aviv University, Tel Aviv 69978 Israel, Centre for Polymer Therapeutics, Welsh School of Pharmacy, Cardiff University, UK, and Polymer Laboratories Ltd, Essex Road, Church Stretton, Shropshire, SY6 6EA UK. Received December 29, 2002; Revised Manuscript Received April 11, 2003

Polymer-directed enzyme prodrug therapy (PDEPT) is a novel two-step antitumor approach that uses a combination of a polymeric prodrug and polymer–enzyme conjugate to generate a cytotoxic drug rapidly and selectively at the tumor site. Previously we have shown that *N*-(2-hydroxypropyl)-methacrylamide (HPMA) copolymer-bound cathepsin B can release doxorubicin intratumorally from an HPMA copolymer conjugate PK1. Here we describe for the first time the synthesis and biological characterization of a PDEPT model combination that uses an HPMA-copolymer-methacryloyl-glycine-glycine–cephalosporin–doxorubicin (HPMA-*co*-MA-GG-C-Dox) as the macromolecular prodrug and an HPMA copolymer conjugate containing the nonmammalian enzyme  $\beta$ -lactamase (HPMA-*co*-MA-GG- $\beta$ -L) as the activating component. HPMA-*co*-MA-GG-C-Dox had a molecular weight of  $\sim 31\,600$  Da and a C-Dox content of 5.85 wt %. Whereas free  $\beta$ -L has a molecular weight of 45 kDa, the HPMA-*co*-MA-GG- $\beta$ -L conjugate had a molecular weight in the range of 75–150 kDa, and following purification no free enzyme was detectable. Against the cephalosporin C or HPMA-*co*-MA-GG-C-Dox substrates, the HPMA-*co*-MA-GG- $\beta$ -L conjugate retained 70% and 80% of its activity, respectively. In vivo  $^{125}\text{I}$ -labeled HPMA-*co*-MA-GG- $\beta$ -L showed prolonged plasma concentration and greater tumor targeting than  $^{125}\text{I}$ -labeled  $\beta$ -L due to the enhanced permeability and retention (EPR) effect. Moreover, administration of HPMA-*co*-MA-GG-C-Dox iv to mice bearing sc B16F10 melanoma followed after 5 h by HPMA-*co*-MA-GG- $\beta$ -L led to release of free Dox. The PDEPT combination caused a significant decrease in tumor growth ( $TC = 132\%$ ) whereas neither free Dox nor HPMA-*co*-MA-GG-C-Dox alone displayed activity. The PDEPT combination displayed no toxicity at the doses used, so further evaluation of this approach to establish the maximum tolerated dose (MTD) is recommended.

### INTRODUCTION

Polymer therapeutics, including polymer–protein conjugates (e.g., PEG-L-asparaginase) and polymer–drug conjugates are emerging as a new class of anticancer agents (reviewed in 1, 2). PEGylated proteins display prolonged plasma circulation times and reduced immunogenicity (3, 4), and the *N*-(2-hydroxypropyl)methacrylamide (HPMA) copolymer conjugates (5, 6) and polyglutamate–paclitaxel (7) display significant passive tumor targeting ( $>70$ -fold) due to the enhanced permeability and retention (EPR) effect (8). Once within the tumor interstitium such polymeric conjugates must usually be internalized by endocytosis to allow lysosomotropic delivery and cathepsin B-mediated liberation of active drug. Polymer-directed enzyme prodrug therapy (PDEPT) is a new two-step antitumor approach which uses a combination of a polymeric prodrug and polymer–enzyme conjugate to generate cytotoxic drug rapidly outside the tumor cells, i.e., within the tumor interstitium (9).

PDEPT offers the advantage that drug liberation can be externally triggered, and thus release of active drug is not reliant on the rate of conjugate internalization or the intracellular level of activating enzyme.

The first PDEPT combination described used HPMA-*co*-MA-GFLG-doxorubicin (PK1), a conjugate currently in Phase II clinical development (10), and HPMA-*co*-MA-GG-cathepsin B (9) to obtain in vivo proof of concept. Following endocytosis within tumor tissue, PK1 is normally degraded intracellularly by the lysosomal thiol-dependent protease cathepsin B to liberate doxorubicin (Dox) slowly. However, using the PDEPT approach it was clearly shown that subsequent (5 h) administration of HPMA-*co*-MA-GG-cathepsin B led to a dramatic and rapid (within 1 h) additional Dox release (9) consistent with interstitial liberation. We now describe the first PDEPT combination that uses a PDEPT combination that uses a nonmammalian enzyme. An HPMA copolymer-methacryloyl-Gly-Gly-cephalosporin–doxorubicin (HPMA-*co*-MA-GG-C-Dox) conjugate was synthesized as a substrate and HPMA copolymer-methacryloyl-Gly-Gly- $\beta$ -lactamase (HPMA-*co*-MA-GG- $\beta$ -L) synthesized as the activating enzyme conjugate (Figure 1).

The  $\beta$ -lactamases are small (30–45 kDa), soluble monomeric enzymes that have varying specificity. All are capable of hydrolyzing  $\beta$ -lactams to substituted  $\beta$ -amino acids (11). Some act more readily on penicillins, while others have greater activity against cephalosporins, and

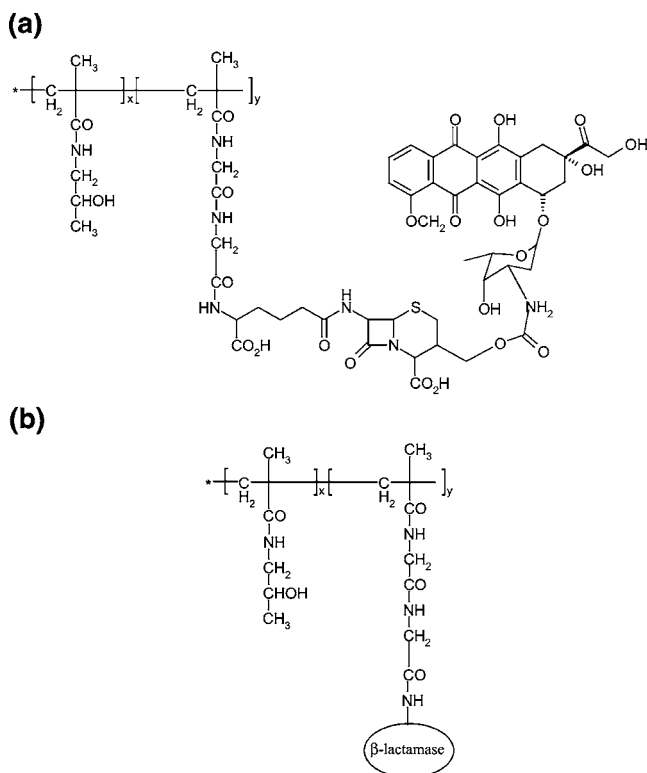
\* Corresponding authors. R.D.: Tel: +44 (0) 292 087 4180; fax: +44 (0) 292 087 4536; e-mail: duncanr@cf.ac.uk.

<sup>†</sup> Tel Aviv University.

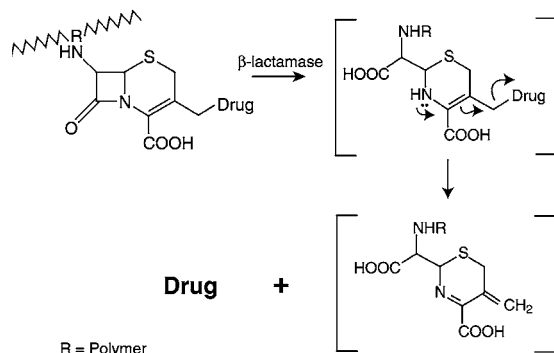
<sup>‡</sup> Present address: Dr. Ronit Satchi-Fainaro, Harvard Medical School, Children's Hospital, Surgical Research Laboratory, 320 Longwood Ave., Enders 1025, Boston, MA 02115.

<sup>§</sup> Cardiff University.

<sup>||</sup> Polymer Laboratories Ltd.



**Figure 1.** Structure of (a) HPMA-*co*-MA-GG-C-Dox and (b) HPMA-*co*-MA-GG- $\beta$ -L.



**Figure 2.** Mechanism of Dox release from HPMA-*co*-MA-GG-C-Dox by  $\beta$ -L.

the mechanism of hydrolysis involves expulsion of a 3' leaving group.  $\beta$ -Lactamases are particularly tolerant to a wide variety of substituents at this position. Cleavage of the  $\beta$ -lactam ring leads to chemical rearrangement (Figure 2) and the terminal residue, i.e., the anticancer drug, is liberated. A wide variety of cytotoxic agents bearing  $\text{NH}_2$  or OH groups can be used to create prodrugs. Cephalosporin derivatives of various mustards (12), taxol (13), and doxorubicin (14, 15) have already been described as low molecular weight prodrugs for the antibody-directed enzyme prodrug (ADEPT) approach (16). As  $\beta$ -L is not a mammalian enzyme, it should display minimal interference from mammalian inhibitors, physiological enzyme substrates, and competing endogenous enzyme systems. However, it does have the potential disadvantage of immunogenicity. Use of an HPMA copolymer conjugate is particularly attractive, as conjugation of poly(ethylene glycol) (PEG) and HPMA copolymers is well-known to reduce immunogenicity of bound proteins (4, 17, 18).

Here we describe the synthesis and characterization of the HPMA-*co*-MA-GG-C-Dox and HPMA-*co*-MA-GG-

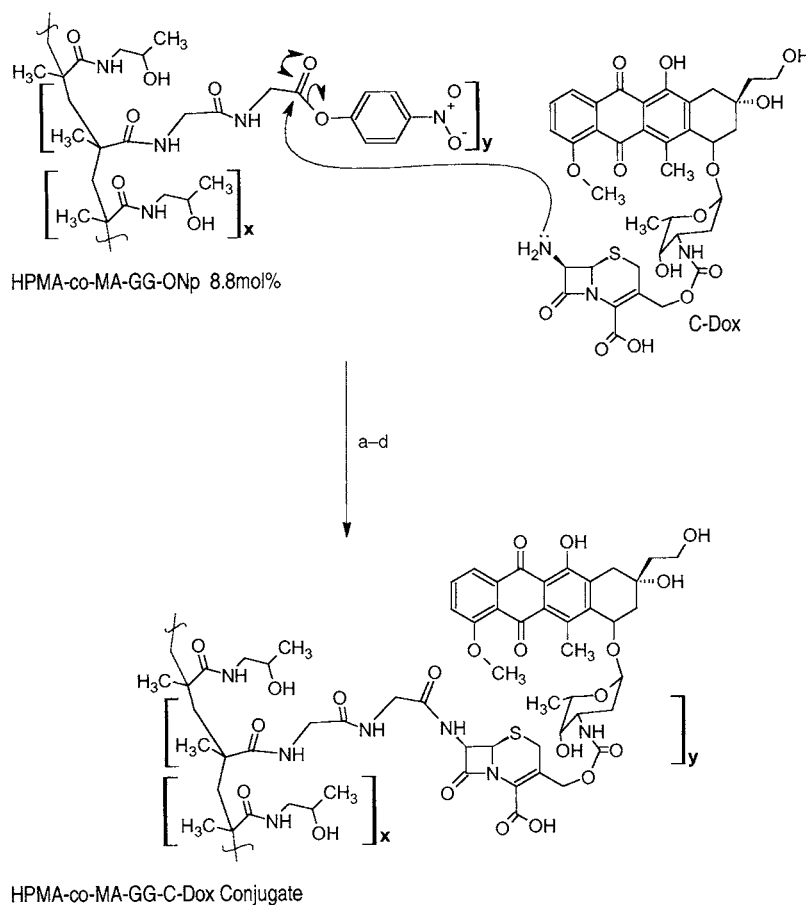
$\beta$ -L conjugates. The biological properties, including retained enzyme activity against low and high molecular weight substrates and cytotoxicity of the PDEPT combination, were studied in vitro. Finally, the pharmacokinetics of  $^{125}\text{I}$ -labeled HPMA-*co*-MA-GG- $\beta$ -L and  $^{125}\text{I}$ -labeled  $\beta$ -L and the antitumor activity of this PDEPT combination were determined in vivo using a sc B16F10 model.

## EXPERIMENTAL PROCEDURES

**Materials.** A random copolymer of HPMA copolymerized with methacryloyl-Gly-Gly-*p*-nitrophenyl ester (HPMA-*co*-MA-GG-ONp) containing 4.4 mol % of the MA-GG-ONp monomer units and with a  $M_w$  34 700 and  $M_n$  21 100 g/mol as a polymeric precursor was used for enzyme conjugation. The HPMA-*co*-MA-GG-ONp precursor used for cephalosporin-doxorubicin (C-Dox) conjugation containing 8.8 mol % of the MA-GG-ONp monomer units and had a  $M_w$  of 31 600 and  $M_n$  of 19 000 g/mol. Both were from Polymer Laboratories (UK).  $\beta$ -L from *Enterobacter cloacae* P99 was purchased from CAMR (UK). Cephalosporin C, ammonium formate, and bovine serum albumin (BSA) were from Sigma. 2-Propanol, methanol, orthophosphoric acid, and chloroform were from J. T. Baker (Israel) (all HPLC grade). Ammonia solution (32%) was from Merck (Germany). A cell proliferation assay kit with XTT reagent was from Biological Industries (Israel). C-Dox was from Ultrafine (UK). Dimethylformamide (DMF) and dimethyl sulfoxide (DMSO) were from Aldrich (UK). All other chemicals were of analytical grade from Aldrich (UK), Fisher Chemicals (UK), or BDH Ltd. (UK) unless otherwise stated.

M109 murine lung carcinoma cells were kindly donated by Professor A. Gabizon (Hadassah Medical Center, Israel). DA3 murine mammary carcinoma cells were donated by I. Witz (Tel Aviv University, Israel) and B16f10.9 murine melanoma cells were from Y. Keisari (Tel Aviv University, Israel). All cells were maintained in DMEM media supplemented with 10% fetal bovine serum (FBS, Life Technologies, Israel), 2 mM L-glutamine, and penicillin/streptomycin antibiotics at 37 °C, 5%  $\text{CO}_2$ .

**Synthesis of HPMA-*co*-MA-GG-C-Dox.** C-Dox (200 mg, 0.25 mmol) was dissolved in dry DMF (7 mL) and added to a stirred solution of the HPMA-*co*-MA-GG-ONp (662 mg) in dry DMF (5 mL) in the dark, under an argon atmosphere and at ambient temperature (25 °C). Dry triethylamine (139  $\mu\text{L}$ , 1 mmol) was then added, and the reaction was followed by TLC and HPLC. After 21 h, HPLC indicated that the quantity of free C-Dox remaining in the reaction mixture had fallen to 43%. TLC at this time also showed a faint trace of Dox aglycone. The reaction was terminated after 22 h by addition of DL-1-amino-2-propanol (40  $\mu\text{L}$ , 0.5 mmol) with stirring for a further 1 h. The reaction mixture was then added dropwise (under argon) to stirred dry diethyl ether (130 mL) which had been precooled to ca. 10 °C. The crude product precipitated as a fine reddish solid, and it was collected by filtration using a Grade 3 sintered-funnel. The crude product was then washed on the filter with small aliquots of dry diethyl ether, dry acetone, and again with dry diethyl ether. The final product was dried overnight in a vacuum oven at ambient temperature. The crude product was dissolved in dry DMF (12 mL) in the dark under an argon atmosphere. TLC at this stage showed the presence of substantial free C-Dox and a very small quantity of free Dox. PL-FDMP (150–300  $\mu\text{m}$ , 1.5 mmol/g aldehyde-functionalized) resin (811 mg) in the

Scheme 1 <sup>a</sup>

<sup>a</sup> (a) 4 equiv of Et<sub>3</sub>N/DMF/25 °C/21 h; (b) 2 equiv DL-1-amino-2-propanol, 1 h (quench remaining activated ester); (c) precip into cold Et<sub>2</sub>O, filter, wash, dry; (d) dissol DMF/PL-FDMP resin/trace AcOH/3 h (scavenge resid C-Dox), filter resin, reprecip filtrate into cold Et<sub>2</sub>O, filter product, wash, dry.

presence of a trace of acetic acid was used to scavenge this remaining free C-Dox and free Dox from solution. Within 3 h TLC showed negligible free C-Dox or Dox remained. The resin beads were removed by filtration through a sintered-funnel and quickly washed on the funnel with dry DMF (6 mL). The combined filtrates were added dropwise, under argon, to stirred dry diethyl ether (180 mL) precooled to 10 °C. After the precipitate was stirred for a further 30 min, the purified product was isolated by filtration on a Grade 3 sintered-funnel. The filter-cake was washed on the funnel successively with small aliquots of dry diethyl ether until the washings were colorless (ca. 100 mL of diethyl ether in total). The final product was collected from the sintered funnel and dried overnight in a vacuum oven at ambient temperature until constant weight. The synthesis is summarized in Scheme 1. A sample of the final HPMA-co-MA-GG-C-Dox was taken and its C-Dox content determined spectrophotometrically (UV).

**Characterization of HPMA-co-MA-GG-C-Dox during the Reaction.** *HPLC.* The HPMA-co-MA-GG-C-Dox conjugation reaction was monitored at 254 nm at ambient temperature by HPLC using a Techsphere 5 ODS column (250 × 4.6 mm) with gradient elution using eluent (A) 0.05 M triethylammonium formate, adjusted to pH 2.8 with HCl and eluent (B) acetonitrile. The flow rate used was 1 mL/min, and the gradient used was 0–8 min 30% B, 8–15 min 30% to 80% B, 15–20 min 80% to 30% B, 20–25 min 30% B. Samples applied to the column were made up using 10 µL of the reaction mixture added to

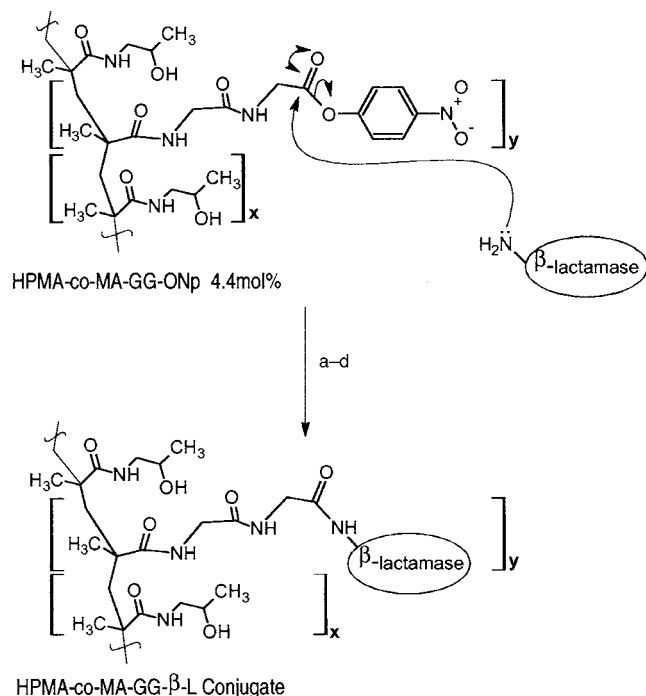
495 µL of eluent A and 495 µL of eluent B. The injection loop volume was 20 µL.

*TLC.* TLC plates (Merck, aluminum sheets, 5 × 10 cm on Silica gel 60 F<sub>254</sub>) were spotted with reaction mixture and prerun with diethyl ether (to shift the DMF reaction solvent away from sample spot). After being allowed to air-dry in fume-hood, the plates were then rerun using a dichloromethane/methanol/glacial acetic acid/water (80:20:7:3) mixture as eluent.

**Synthesis of the HPMA-co-MA-GG-β-L Conjugate.** HPMA-co-MA-GG-ONp (containing 4.4 mol % MA-GG-ONp) was dissolved in DMSO (5 mg/mL), and a solution of β-L in DMSO (5 mg/mL) was added dropwise under stirring. The reaction mixture was stirred in dark for 20 min and then terminated by adding DL-1-amino-2-propanol (20 µL) to quench any remaining unreacted ONp groups remaining on the copolymer. The final yellow solution was transferred to a VivaSpin (10 kDa MW cutoff) column and centrifuged at 4 °C at 3000g for 30 min to remove the low MW contaminants present and replace the solvent with aqueous solution. This centrifugation was repeated, with addition of phosphate buffer each time, until no visible ONp (yellow) remained. The mixture was concentrated to a final volume of 500 µL. The synthesis of HPMA-co-MA-GG-β-L is summarized in Scheme 2.

**Purification and Characterization of HPMA-co-MA-GG-β-L by FPLC.** The final HPMA-co-MA-GG-β-L conjugate was purified and characterized by FPLC and SDS-PAGE electrophoresis (gradient gels 5–15%



Scheme 2<sup>a</sup>

<sup>a</sup> (a) DMSO/25 °C/20 min; (b) DL-1-amino-2-propanol, 1 h (quench remaining activated ester); (c) ultrafiltration 10 kDa MWCO/30 min/4 °C, then aq buffer washes (repeat until visible NpOH removed); (d) concentrate and purify by FPLC.

acrylamide), and the protein content in the conjugate was determined by the Bradford assay. FPLC using a Superdex 200 HR 10/30 column (Amersham Pharmacia Biotech) with a UV (280 nm) detector and FPLC director version 1.10 software was used to analyze the final HPMA-co-MA-GG-β-L and purify it. Samples recovered from the VivaSpin (200 μL) were injected onto the FPLC column and were eluted using 0.01 M phosphate buffer containing 0.15 M NaCl, pH 7.4, at a flow rate of 0.5 mL/min. The column was calibrated using free β-L (1 mg/mL). Fractions (1 mL) were also collected and analyzed for β-L activity. The final conjugate was lyophilized and stored at -20 °C.

**Measurement of β-L Activity Using Cephalosporin C as Substrate.** All reagents were prepared in PBS, pH 7.4, containing 12.5 μg/mL BSA. Cephalosporin C was dissolved in the PBS/BSA buffer at a concentration of 300 μM. β-L was dissolved in the PBS/BSA at a concentration of 30 μg/mL. The cephalosporin solution (335 μL) and the PBS/BSA buffer (635 μL) were added to a 1.0 mL cuvette and placed in a spectrophotometer. Baseline absorbance was monitored at 260 nm for 5 min at 25 °C. Then the free or conjugated β-L (enzyme or FPLC fraction) solution (40 μL) was added to the cuvette, and activity (initial rate) was measured by monitoring the fall in absorbance at 260 nm. The specific activity was calculated as μmol/s/mg.

**Measurement of β-L Activity Using HPMA-co-MA-GG-C-Dox as Substrate.** HPMA-co-MA-GG-C-Dox was dissolved in the PBS/BSA buffer at a concentration of 300 μM cephalosporin C-equivalent. Either free or conjugated β-L was dissolved in the PBS/BSA buffer at 30 μg/mL β-L-equivalent. To a polypropylene tube were added the PBS/BSA buffer (665 μL) and the HPMA-co-MA-GG-C-Dox solution (335 μL); or 630 μL of PBS/BSA and 335 μL of HPMA-co-MA-GG-C-Dox solution together with free or conjugated β-L solution (35 μL) were added. All tubes were incubated at 37 °C. Samples (100 μL) were

taken regularly over a 5 h period. They were snap frozen in liquid nitrogen and stored at -20 °C in the dark until analyzed by HPLC.

To measure Dox release, free Dox was first extracted from each sample and then analyzed by HPLC using methods previously described (9). Briefly, daunomycin (100 ng) was added to each sample as an internal standard followed by ammonium formate buffer 1 M, pH 8.5 (100 μL), and the extraction mixture (chloroform: propan-2-ol 4:1) (5 mL). The tubes were then vortex-mixed (three times) for 20 s and centrifuged (1000g) for 30 min at 10 °C. The aqueous layer was carefully removed and the organic layer evaporated to dryness using the Techne nitrogen sample concentration at room temperature under N<sub>2(g)</sub>. The residue was then dissolved in methanol (100 μL) before analysis by HPLC.

All samples from the degradation studies and Dox calibration standards were analyzed by HPLC using a Waters μBondapak C18 125 Å 10 μm reverse phase HPLC column (3.9 × 150 mm) with a Waters Sentry Guard Column (μBondapak C18 125 Å, 10 μm, 3.9 × 20 mm) with eluent at a flow rate of 1 mL/min. Results were analyzed using a Millennium<sup>32</sup> Login Version 3.05.01 Chromatography Manager.

**Evaluation of in Vitro Cytotoxicity.** *Colony Formation Assay.* B16F10.9 melanoma cells (100) were seeded into a 24-well plate containing DMEM medium with 10% fetal calf serum (FCS) and Pen/Strep antibiotics. HPMA-co-MA-GG-C-Dox (50 μg/well Dox-equiv) alone, or the combination of HPMA-co-MA-GG-C-Dox (50 μg Dox-equiv) plus HPMA-co-MA-GG-β-L (20 μL at a 1 mg/mL concentration) were added to the cells. Treatment with free Dox (50 μg/well) or PBS were added to wells as positive and negative controls. The cells were then incubated for 8 days, fixed to the plate with 100% methanol for 20 min, and then washed with running water. The plate wells were then filled with 10% aqueous Giemsa solution. The plates were left at room temperature for 20 min and then washed again with running water and dried, and the number of colonies were counted. The average number of colonies seen following each treatment was expressed as a percentage of the untreated control.

*Cell Proliferation Assay with XTT Reagent.* The tetrazolium dye XTT (19) was used to assess cell viability. B16F10.9 cells (10<sup>3</sup> per well in 100 μL) were seeded in a flat-bottomed 96-well plate and incubated at 37 °C for 24 h. Then various concentrations of HPMA-co-MA-GG-C-Dox or HPMA-co-MA-GG-β-L or saline or Dox were added (*n* = 8). The cells were then incubated for 72 h, XTT reagent (50 μL) was added to each well, and the plate was incubated for 2 h. Spectrophotometric absorbance of the formazan product was measured at a wavelength of 450 nm using 690 nm as reference wavelength.

**Evaluation of the Body Distribution of <sup>125</sup>I-Labeled HPMA-co-GG-β-L and Free β-L in Mice Bearing B16 Melanoma sc.** All animal experiments were conducted according to the United Kingdom Coordinating Committee on Cancer Research (UKCCCR) Guidelines. Male C57BL/6J mice were inoculated with 10<sup>5</sup> viable B16F10 cells sc, and the tumor was allowed to establish until the area was approximately 50–70 mm<sup>2</sup> as measured by the product of two orthogonal diameters. Animals were injected iv with free or conjugated <sup>125</sup>I-labeled β-L (5 × 10<sup>5</sup> CPM/mouse) and animals euthanized at times up to 72 h. The main organs were dissected, and the blood was collected. The tumor, organs, and blood

samples were homogenized and read in a  $\gamma$ -counter. Results were calculated as % of administered dose/g.

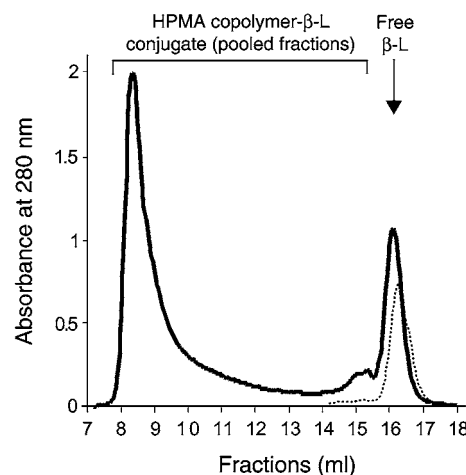
**Evaluation of Antitumor Activity of the PDEPT Combination: HPMA-co-MA-GG-C-Dox and HPMA-co-MA-GG- $\beta$ -L.** Male C57BL/6J mice ( $\sim 9$  weeks,  $\sim 20$  g) were inoculated with  $10^5$  viable B16F10 melanoma cells sc. The tumor was allowed to establish until the area was approximately 50–70 mm<sup>2</sup> as measured by the product of two orthogonal diameters. Animals (five per group) were injected iv with HPMA-co-MA-GG-C-Dox (10 mg/Kg Dox-equiv.) or HPMA-co-MA-GG-C-Dox (10 mg/kg Dox-equiv) followed after 5 h by HPMA-co-MA-GG- $\beta$ -L. As a comparison mice (five per group) were injected with either saline (100  $\mu$ L iv) or free Dox (10 mg/kg). Animals were weighed and the tumors measured daily. Mice were euthanized when the tumor reached or surpassed the size of 300 mm<sup>2</sup>. Animals were weighed daily and observed twice a day for signs of tumor progression. They were euthanized if their body weight decreased below 80% of the starting weight. Animals were monitored for general health, weight loss, and tumor progression and at termination were examined by post-mortem; tumors were dissected and weighed. Experimental data were expressed as the mean survival time, *TIC* defined as the ratio of the mean survival time of the treated animals (*T*) divided by the mean survival of the untreated control group (*C*) expressed as a percentage.

**Statistical Methods.** All the *in vitro* data are expressed as the mean  $\pm$  standard deviation of the mean (SD). All the *in vivo* data are expressed as the mean  $\pm$  standard error of the mean (SE). Statistical significance was assessed using the Student's *t*-test. *P* values of 0.05 or less were considered statistically significant.

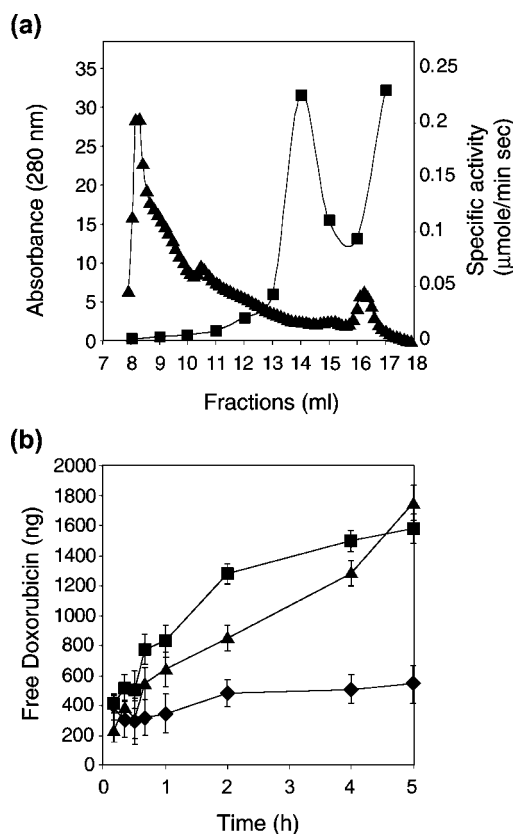
## RESULTS AND DISCUSSION

Novel treatment strategies are badly needed if cancer chemotherapy is to be significantly improved. Polymer-drug conjugates are emerging as one promising option (21). They display passive tumor targeting by the EPR effect, and lysosomotropic delivery results in marked reduction in toxicity of the bound drug. For example HPMA-co-MA-GFLG-doxorubicin (PK1) was  $\sim 5$ -fold less toxic than Dox in a Phase I study (10). Eleven such conjugates have now progressed into clinical development, and activity has been repeatedly seen in chemotherapy refractory patients (reviewed in 21). Clinically, combination chemotherapy is routinely used in an attempt to increase efficacy, bypass resistance, and minimize the peripheral toxicity that is often dose-limiting. The PDEPT concept was developed with the aim of further improving the tumor selectivity of polymer-drug conjugates (9) and also to circumvent some of the disadvantages of ADEPT (discussed in 9, 16). A model combination of HPMA-co-MA-GG-cathepsin B and HPMA-co-MA-GFLG-Dox demonstrated the practicality of the approach (9).

PDEPT involves two steps. First, systemic administration of a polymeric prodrug containing a linker designed for cleavage by the activating enzyme. This conjugate typically has a molecular weight of  $\sim 30\,000$  g/mol. Once the circulating polymer-drug conjugate has cleared (after 1–2 h due to renal elimination), a polymer-enzyme conjugate can then be administered as a second step. This conjugate has a higher molecular weight ( $\sim 50\,000$ – $100\,000$  g/mol), and thus it circulates for longer. Both conjugates display tumor targeting by the EPR effect and when they meet, activation of the prodrug leads to



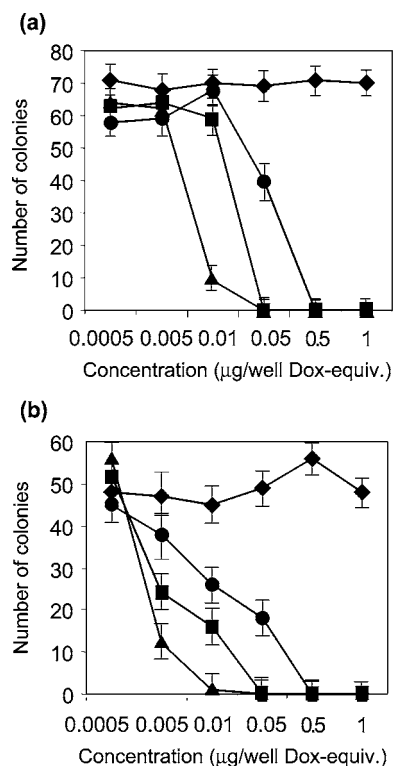
**Figure 3.** FPLC traces of free  $\beta$ -L (---) and HPMA-co-MA-GG- $\beta$ -L (—) showing the fractions pooled to give the final product.



**Figure 4.** Comparison of enzymatic activity of free  $\beta$ -L and HPMA copolymer- $\beta$ -L *in vitro*. Panel a shows the activity of  $\beta$ -L (■) in HPMA copolymer- $\beta$ -L fractions (▲) seen using cephalosporin C as a substrate. Panel b shows the release of Dox from HPMA copolymer-C-Dox when incubated with  $\beta$ -L (■) or HPMA copolymer- $\beta$ -L (▲). Release of Dox from HPMA copolymer-C-Dox in the absence of enzyme is included as a control (●). Data represent mean  $\pm$  SD.

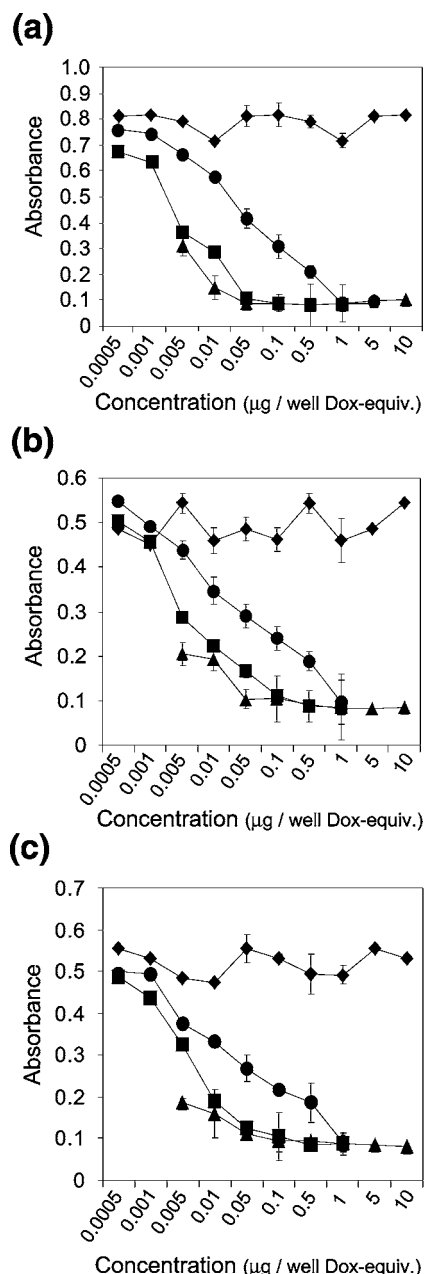
localized drug release in the tumor interstitium and therefore minimal nonspecific toxicity. The model combination of HPMA-co-MA-GG-cathepsin B and PK1 showed that a polymer-enzyme would indeed gain access to the drug conjugate in the tumor interstitium (9) and promote drug release.

The full potential of PDEPT will, however, only be fully realized if a nonmammalian enzyme is used in combination with a polymer prodrug incorporating the appropriate matching linker. The combination described here was



**Figure 5.** In vitro antitumor activity. Inhibition of colony formation after 24 h using (a) B16F10 cells and (b) DA3 cells. The data show the effect of Dox (▲), HPMA copolymer-C-Dox (●); HPMAcopolymer-C-Dox + HPMA copolymer-β-L (■) and the untreated control cells (◆). Data represent mean  $\pm$  SD.

the first attempt to achieve this goal. First the polymer prodrug, HPMA-*co*-MA-GG-C-Dox conjugate (Figure 1) was synthesized having a C-Dox content of 5.85 wt % (as determined by UV) and a  $M_w$  of  $\sim 31\,600$  g/mol. The conjugate contained neither contaminating free C-Dox nor Dox according to TLC. Synthesis of antibody- and polymer-enzyme conjugates is often problematic. Conjugation typically has a low yield (10–15%) (22, 23) and results in reduced enzyme activity. The semirandom aminolysis method used to bind the HPMA copolymer precursor to cathepsin B gave conjugates with a relatively high yield (30–35%) and also with retained enzyme activity in vitro against both a low molecular weight and macromolecular substrate (20–25%) (9). Interestingly, the HPMA-*co*-MA-GG-β-L described here had a much higher yield in respect of the bound protein (80–90%). This could be due to carrying out the aminolysis reaction in DMSO and not PBS, thus minimizing nonspecific hydrolysis. Whereas free β-L had a band at 45 kDa on SDS PAGE, the HPMA-*co*-MA-GG-β-L conjugate had a molecular weight in the range of 75–150 kDa. Following purification by FPLC (Figure 3) and pooling of conjugate fractions, no free enzyme was detectable in the final product by SDS PAGE (results not shown). During purification, all FPLC fractions were assayed for activity using cephalosporin C as substrate (Figure 4a). The recovered conjugate retained 70% of enzyme specific activity (mean:  $\sim 15$  μmol/sec/mg) against cephalosporin C. Incubation of HPMA-*co*-MA-GG-C-Dox with HPMA-*co*-MA-GG-β-L led to release of Dox, and the conjugate retained 80% of the activity of free enzyme against the macromolecular substrate (Figure 4b). No nonspecific cleavage of the β-lactamic linker occurred in buffer solutions lacking β-L over 5 h. However, slow hydrolytic release of free Dox was seen on storage of HPMA-*co*-MA-GG-C-Dox in buffer over several days. The high reten-

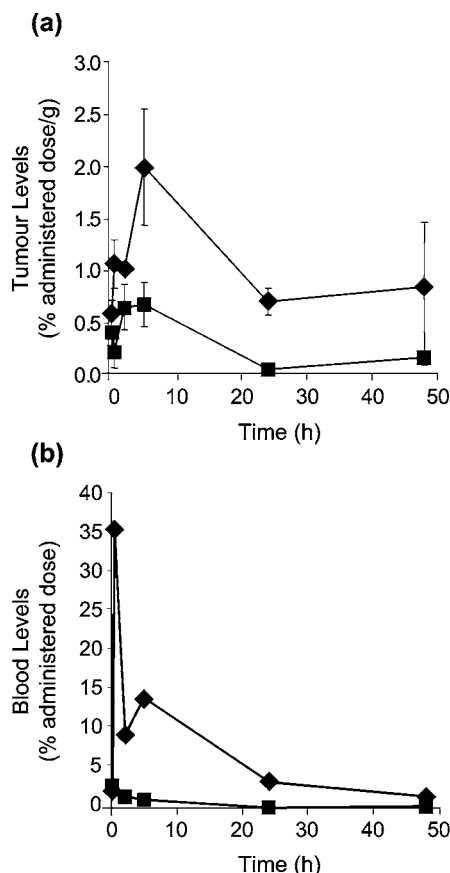


**Figure 6.** In vitro antitumor activity measured using the XTT cytotoxicity assay: (a) DA3 murine mammary carcinoma; (b) M109 murine lung carcinoma; (c) B16F10 murine melanoma. The data show the effect of Dox (▲), HPMA-*co*-MA-GG-C-Dox (●); HPMA-*co*-MA-GG-C-Dox + HPMA-*co*-MA-GG-β-L (■); and untreated control cells (◆). Data represent mean  $\pm$  SD.

tion of enzymatic activity following the relatively harsh conjugation conditions is a puzzle. It might be due to very high stability of β-L. Furthermore, it is known that this enzyme is able to undergo renaturation following denaturation (11).

Ability of HPMA-*co*-MA-GG-β-L to liberate pharmacologically active Dox from the HPMA-*co*-MA-GG-C-Dox conjugate is essential for antitumor activity. Experiments were first performed in vitro using B16F10 and DA3 cells. The plating efficiency assay revealed inhibition of colony formation when cells were treated with either the PDEPT combination or free Dox (Figure 5). Activation of HPMA-*co*-GG-C-Dox by HPMA-*co*-MA-GG-β-L resulted in a cytotoxicity profile that was similar to that seen for free Dox. In contrast, in the absence of activating enzyme, HPMA-*co*-MA-GG-C-Dox was 10-fold less cytotoxic than





**Figure 7.** Body distribution of  $^{125}\text{I}$ -labeled  $\beta\text{-L}$  and  $^{125}\text{I}$ -labeled HPMA copolymer- $\beta\text{-L}$  in mice bearing sc B16F10 tumors. Panel a shows the tumor levels of radioactivity and panel b the blood clearance. Symbols represent  $^{125}\text{I}$ -labeled  $\beta\text{-L}$  (■) and  $^{125}\text{I}$ -labeled HPMA-coMA-GG- $\beta\text{-L}$  (◆), and data are mean  $\pm$  SE.

the PDEPT combination. To further investigate this phenomenon, XTT cytotoxicity assay was conducted using three cell lines. In these experiments the PDEPT combination was also  $\sim 10$ -fold more active than HPMA-coMA-GG-C-Dox alone; 13.3-fold in DA3 cells, 7.5-fold in M109 cells, and 10-fold in B16F10.9 (Figure 6). These assays involve a 3 day incubation; thus, the cytotoxicity of HPMA-coMA-GG-C-Dox alone can be explained by the hydrolytic Dox release occurring in the meantime. Since HPMA-coMA-GG-C-Dox is only present in the circulation for a short time ( $< 5$  h), the importance of this nonspecific release in vivo would be minimal.

The above-mentioned in vitro observations justified evaluation of this PDEPT combination in vivo. It was considered important first to determine the blood clearance and tumor accumulation of the novel enzyme conjugate. It is likely that the pharmacokinetics of HPMA-coMA-GG-C-Dox will be similar to PK1 as reported previously in preclinical (24) and clinical studies (10). Free and bound  $\beta\text{-L}$  were radiolabeled with [ $^{125}\text{I}$ ]iodide using the Bolton and Hunter reagent (20). The products had a specific activity of 37  $\mu\text{Ci}/\text{mg}$  and 99.4  $\mu\text{Ci}/\text{mg}$  for  $\beta\text{-L}$  and HPMA copolymer-GG- $\beta\text{-L}$ , respectively, and their free [ $^{125}\text{I}$ ]iodide content was  $< 1\%$ , making them suitable for in vivo use.  $^{125}\text{I}$ -Labeled  $\beta\text{-L}$  had a  $t_{1/2\alpha} = 1.9$  h; the conjugate had a longer blood residence time ( $t_{1/2\alpha} = 4.7$  h) consistent with the reduced cellular clearance and/or increased resistance to proteolysis (4, 25). The plasma AUC of the conjugate was 8.2-fold greater than seen for free enzyme. The increased circulation time led to a higher conjugate tumor ac-

**Table 1.** Antitumor Activity of HPMA-coMA-GG-C-Dox and the PDEPT Combination Administered iv to C57 Black Male Mice Bearing sc B16F10

treatment	Dox dose (mg/kg)	time to progression (days $\pm$ SE)	T/C (%)	no. of toxic deaths
saline		$8.6 \pm 2$		0/5
doxorubicin	10	$10 \pm 4$	116	0/5
HPMA-coMA-GG-C-Dox	10	$9 \pm 1$	110	0/5
HPMA-coMA-GG-C-Dox + HPMA-coMA-GG- $\beta\text{-L}$	10	$12 \pm 2$	133 <sup>a</sup>	0/5

<sup>a</sup>  $p \leq 0.03$ .

cumulation (2.9-fold increase in AUC, Figure 7) attributable to passive targeting by the EPR effect.

Preliminary antitumor studies were conducted using a sc B16F10 model, which has been widely used to evaluate other polymer-drug conjugates (26). Mice showed a significantly increased survival when treated with the PDEPT combination (Table 1) and did elicit significant decrease in tumor growth rate compared with that seen in the control mice group. The PDEPT combination caused neither toxic deaths nor animal weight loss. Previous studies investigating ADEPT and using PEGylated enzymes clearly showed that antitumor activity improves dramatically following dose optimization of both the enzyme conjugate and the polymeric prodrug (27). Future studies with this new PDEPT combination will optimize these parameters and also evaluate the effect of repeated cycles of administration.

In summary, the feasibility of PDEPT strategy using a nonmammalian enzyme and the corresponding polymer prodrug has been demonstrated. The use of nonhuman proteins for parenteral therapy raises the issue of the immunogenicity. Indeed, this has been seen in clinical studies involving ADEPT (28). Cyclosporin can be used to combat the problem (29), but immunosuppression in cancer patients is not desirable. Polymer conjugation of an enzyme, for example PEGylation (30, 31), does bring the advantage of reduced protein immunogenicity. The HPMA-coMA-GG-cathepsin B and HPMA-coMA-GG- $\beta\text{-L}$  conjugates do show a significant reduction or even abrogation of the immunogenicity of the conjugated parent enzymes (32). Thus, with optimization, this PDEPT combination may provide a new and potentially immunosilent EPR-targeted approach for improved cancer chemotherapy.

#### ACKNOWLEDGMENT

This study was supported by Vectura Ltd. We thank Professor Helmut Ringsdorf and Professor Tom Connors for helpful discussions and Dr. Steve Stribbling for technical assistance.

#### LITERATURE CITED

- (1) Veronese, F. M. (2001) Peptide and protein PEGylation: a review of problems and solutions. *Biomaterials* 22, 405–417.
- (2) Duncan, R. (2003) Polymer-Anticancer Drug Conjugates. *Biomedical Aspects of Drug Targeting* (V. Muzykntov and V. Torchilin, Eds.) pp 193–210, Kluwer Academic Publishers, Boston, in press.
- (3) Francis, G. E., Delgado, C., and Fisher, D. (1992) PEG-modified proteins. *Stability of proteins pharmaceuticals (Part B)* (M. M. Ahem, Ed.) pp 235–263, Plenum Press, New York.
- (4) Francis, G. E., Fisher, D., Delgado, C., Malik, F., Gardiner, A., and Neale, D. (1998) PEGylation of cytokines and other therapeutic proteins and peptides: the importance of biological optimisation of coupling techniques. *Int. J. Hematol.* 68, 1–18.

- (5) Gianasi, E., Wasil, M., Evagorou, E. G., Keddlle, A., Wilson, G., and Duncan, R. (1999) HPMa copolymer platinates as novel antitumor agents: in vitro properties, pharmacokinetics and antitumor activity in vivo. *Eur. J. Cancer* 35, 994–1002.
- (6) Seymour, L. W., Ulbrich, K., Strohalm, J., Kopecek, J., and Duncan, R. (1990) The pharmacokinetics of polymer-bound adriamycin. *Biochem. Pharmacol.* 39, 1125–1131.
- (7) Li, C., Ke, S., Wu, Q. P., Tansey, W., Hunter, N., Buchmiller, L. M., Milas, L., Charnsangavej, C., and Wallace, S. (2000) Tumor irradiation enhances the tumor-specific distribution of poly(L- glutamic acid)-conjugated paclitaxel and its anti-tumor efficacy. *Clin. Cancer Res.* 6, 2829–2834.
- (8) Maeda, H., Wu, J., Sawa, T., Matsumura, Y., and Hori, K. (2000) Tumor vascular permeability and the EPR effect in macromolecular therapeutics: a review. *J. Controlled Release* 65, 271–284.
- (9) Satchi, R., Connors, T. A., and Duncan, R. (2001) PDEPT: polymer-directed enzyme prodrug therapy. I. HPMa copolymer-cathepsin B and PK1 as a model combination. *Br. J. Cancer* 85, 1070–1076.
- (10) Vasey, P. A., Kaye, S. B., Morrison, R., Twelves, C., Wilson, P., Duncan, R., Thomson, A. H., Murray, L. S., Hilditch, T. E., Murray, T., Burtles, S., Fraier, D., Frigerio, E., and Cassidy, J. (1999) Phase I clinical and pharmacokinetic study of PK1 [N-(2-hydroxypropyl)methacrylamide copolymer doxorubicin]: first member of a new class of chemotherapeutic agents-drug-polymer conjugates. Cancer Research Campaign Phase I/II Committee. *Clin. Cancer Res.* 5, 83–94.
- (11) Mascaretti, O. A., Danelon, G. O., Laborde, M., Mata, E. G., and Setti, E. L. (1999) Recent advances in the chemistry of beta-lactam compounds as selected active-site serine beta-lactamase inhibitors. *Curr. Pharm. Des.* 5, 939–953.
- (12) Svensson, H. P., Kadow, J. F., Vruthula, V. M., Wallace, P. M., and Senter, P. D. (1992) Monoclonal antibody-beta-lactamase conjugates for the activation of a cephalosporin mustard prodrug. *Bioconjugate Chem.* 3, 176–181.
- (13) Rodrigues, M. L., Carter, P., Wirth, C., Mullins, S., Lee, A., and Blackburn, B. K. (1995) Synthesis and beta-lactamase-mediated activation of a cephalosporin-taxol prodrug. *Chem. Biol.* 2, 223–227.
- (14) Senter, P. D., Svensson, H. P., Schreiber, G. J., Rodriguez, J. L., and Vruthula, V. M. (1995) Poly(ethylene glycol)-doxorubicin conjugates containing beta-lactamase-sensitive linkers. *Bioconjugate Chem.* 6, 389–394.
- (15) Vruthula, V. M., Svensson, H. P., and Senter, P. D. (1995) Cephalosporin derivatives of doxorubicin as prodrugs for activation by monoclonal antibody-beta-lactamase conjugates. *J. Med. Chem.* 38, 1380–1385.
- (16) Knox, R. J., Melton, R. G., and Satchi, R. (2002) Enzyme-prodrug therapies of cancer. *Polymeric Biomaterials* (S. Dumitriu, Ed.) 2nd ed., pp 895–927, Marcel Dekker, New York.
- (17) Rihova, B., Bilej, M., Vetvicka, V., Ulbrich, K., Strohalm, J., Kopecek, J., and Duncan, R. (1989) Biocompatibility of N-(2-hydroxypropyl) methacrylamide copolymers containing adriamycin. Immunogenicity, and effect on haematopoietic stem cells in bone marrow in vivo and mouse splenocytes and human peripheral blood lymphocytes in vitro. *Biomaterials* 10, 335–342.
- (18) Chapman, A. P. (2002) PEGylated antibodies and antibody fragments for improved therapy: a review. *Adv. Drug Deliv. Rev.* 54, 531–545.
- (19) Scudiero, D. A., Shoemaker, R. H., Paull, K. D., Monks, A., Tierney, S., Nofziger, T. H., Currens, M. J., Seniff, D., and Boyd, M. R. (1988) Evaluation of a soluble tetrazolium/formazan assay for cell growth and drug sensitivity in culture using human and other tumor cell lines. *Cancer Res.* 48, 4827–4833.
- (20) Bolton, A. E. and Hunter, W. M. (1973) The labeling of proteins to high specific radioactivities by conjugation to a <sup>125</sup>I-containing acylating agent. *Biochem. J.* 133, 529–539.
- (21) Duncan, R. (2002) Polymer-Drug Conjugates. *Handbook of Anticancer Drug Development* (Budman, Calvert, and Rowinsky, Eds.) Lippincott Williams & Wilkins (in press).
- (22) Svensson, H. P., Wallace, P. M., and Senter, P. D. (1994) Synthesis and characterization of monoclonal antibody-beta-lactamase conjugates. *Bioconjugate Chem.* 5, 262–267.
- (23) Niculescu-Duvaz, I., Friedlos, F., Niculescu-Duvaz, D., Davies, L., and Springer, C. J. (1999) Prodrugs for antibody- and gene-directed enzyme prodrug therapies (ADEPT and GDEPT). *Anticancer Drug Des.* 14, 517–538.
- (24) Seymour, L. W., Ulbrich, K., Styger, P. S., Brereton, M., Subr, V., Strohalm, J., Duncan, R. (1994) Tumor tropism and anticancer efficacy of polymer-based doxorubicin prodrugs in the treatment of subcutaneous murine B16F10 melanoma. *Br. J. Cancer* 70, 636–641.
- (25) Delgado, C., Francis, G. E., and Fisher, D. (1992) The uses and properties of PEG-linked proteins. *Crit. Rev. Ther. Drug Carrier Syst.* 9, 249–304.
- (26) Duncan, R., Seymour, L. W., O'Hare, K. B., Flanagan, P. A., Wedge, S., Hume, I. C., Ulbrich, K., Strohalm, J., Subr, V., Spreafico, F., Grandi, M., Ripamonti, M., Farao, M., Suarato, A. (1992) Preclinical evaluation of polymer-bound doxorubicin. *J. Controlled Release* 19, 331–346.
- (27) Springer, C. J., Bagshawe, K. D., Sharma, S. K., Searle, F., Boden, J. A., Antoniwi, P., Burke, P. J., Rogers, G. T., Sherwood, R. F., and Melton, R. G. (1991) Ablation of human choriocarcinoma xenografts in nude mice by antibody-directed enzyme prodrug therapy (ADEPT) with three novel compounds. *Eur. J. Cancer* 27, 1361–1366.
- (28) Martin, J., Stribbling, S. M., Poon, G. K., Begent, R. H., Napier, M., Sharma, S. K., and Springer, C. J. (1997) Antibody-directed enzyme prodrug therapy: pharmacokinetics and plasma levels of prodrug and drug in a phase I clinical trial. *Cancer Chemother. Pharmacol.* 40, 189–201.
- (29) Bagshawe, K. D., and Sharma, S. K. (1996) Cyclosporine delays host immune response to antibody enzyme conjugate in ADEPT. *Transplant Proc.* 28, 3156–3158.
- (30) Rihova, B., Kopecek, J., Ulbrich, K., Pospisil, M., and Mancal, P. (1984) Effect of the chemical structure of N-(2-hydroxypropyl)methacrylamide copolymers on their ability to induce antibody formation in inbred strains of mice. *Biomaterials* 5, 143–148.
- (31) Abuchowski, A., Davis, F. F., and Davis, S. (1981) Immunosuppressive properties and circulating life of Achromobacter glutaminase-asparaginase covalently attached to poly(ethylene glycol) in man. *Cancer Treat Rep.* 65, 1077–1081.
- (32) Satchi, R. (1999) *PDEPT: Polymer directed enzyme prodrug therapy*. Ph.D. Thesis, pp 193–207, London: University of London.

BC020091K

# Biodistribution of the Chimeric Monoclonal Antibody U36 Radioiodinated with a *closo*-Dodecaborate-Containing Linker. Comparison with Other Radioiodination Methods

Marika Nestor,<sup>\*,†</sup> Mikael Persson,<sup>‡</sup> Junping Cheng,<sup>†</sup> Vladimir Tolmachev,<sup>‡</sup> Guus van Dongen,<sup>||</sup> Matti Anniko,<sup>†</sup> and Kalevi Kairemo<sup>§</sup>

Division of Otolaryngology and Head & Neck Surgery, Department of Surgical Sciences, Uppsala University, Uppsala, Sweden, Division of Biomedical Radiation Sciences, and Division of Experimental Nuclear Medicine, Department of Oncology, Radiology, and Clinical Immunology, Uppsala University, Uppsala, Sweden, and Department of Otolaryngology/Head and Neck Surgery, Vrije Universiteit Medical Center, Amsterdam, The Netherlands. Received January 7, 2003; Revised Manuscript Received March 21, 2003

We have evaluated the applicability of the [(4-isothiocyanatobenzylammonio)undecahydro-*closo*-dodecaborate (1-)] (DABI) linker molecule for antibody radiohalogenation and compared it to radiohalogenation using the linker *N*-succinimidyl 4-iodobenzoate (PIB) and to direct radiohalogenation using Chloramine T. These studies were performed to assess the potential of DABI conjugates and to optimize the biological properties of halogen-labeled cMab U36. The three conjugates were evaluated in vitro for their specificity and affinity and in vivo for their biodistribution patterns in normal mice at 1.5, 6, 24, and 96 h pi. Labeling efficiencies of direct CAT labeling, indirect PIB labeling, and indirect DABI labeling were 90–95%, 60%, and 68%, respectively. This resulted in a PIB:cMab U36 molar ratio of 1.8–2.5 and a DABI:cMab U36 molar ratio of 4.1. The in vitro data demonstrated specific binding for all conjugates and similar affinities with values around  $1 \times 10^8 \text{ M}^{-1}$ . However, the in vivo data revealed accumulation of the radioiodine uptake in thyroid for the directly labeled conjugate, with a value 10 times higher than the indirectly labeled conjugates 96 h pi. Both the  $^{125}\text{I}$ -PIB-cMab U36 and  $^{125}\text{I}$ -DABI-cMab U36 conjugates yielded a low thyroid uptake with no accumulation, indicating different catabolites for these conjugates. This may favor the use of the indirectly labeled conjugates for future studies. Apart from the specific results obtained, these findings also demonstrate how the right linker molecule will provide additional opportunities to further improve the properties of an antibody–radionuclide conjugate.

## INTRODUCTION

Radioimmunotherapy (RIT) and radioimmunodiagnosis (RID) using monoclonal antibodies (MAbs) carrying cytotoxic substances (toxin, drug, or radionuclide) is a promising and realistic approach toward improving treatment and diagnosis of cancer (1). By using radioactive nuclides as the cytotoxic substance, the problem of multidrug resistance can be avoided. Also, the crossfire effect reduces the need for every cancer cell to express the antigen, since the radiation emitted by some radionuclides can kill neighboring cancer cells.

Radiohalogens are attractive candidates as radionuclides in RIT and RID since they share many chemical properties but possess a variety of half-lives and decay-modes (2). The same targeting molecule can be labeled by the same or a similar method, with a different halogen,

depending on the biomedical problem to be solved. A  $\gamma$ -emitting halogen can be used for initial detection of a tumor, whereas quantification of pharmacokinetics and dosimetry can be performed using a positron-emitter such as  $^{124}\text{I}$ .  $\beta$ - or  $\alpha$ -emitting halogens such as  $^{131}\text{I}$  and  $^{211}\text{At}$  can be applied in therapy.

A tumor-seeking protein or peptide that binds to a cellular structure will most likely be internalized, either rapidly through a clathrin-dependent pathway (3) or at a slower rate through clathrin-independent endocytosis (3, 4). After internalization, the antibody–antigen complex is degraded in the lysosome through enzymatic proteolysis. If the radiocatabolite is lipophilic, it will quickly diffuse through the lipid membranes out of the cell, causing “halogen leakage” (5–7). If the labeled degradation product instead is a bulky hydrophilic or ionic compound, it cannot penetrate the cellular membrane and remains inside the cell for a longer time (2, 5–7).

Consequently, attaching the nuclide to the antibody via an appropriate linker molecule will provide opportunities to optimize the in vivo properties of the targeting agent toward a high tumor uptake and retention of the label and a rapid whole-body clearance of labeled catabolites. In this aspect, indirect labeling methods through linker molecules that use hydrophilic anchor molecules may provide an advantage in comparison with direct labeling with tyrosine (using Chloramine T (CAT) or Iodogen)-labeled compounds. Also, the com-

\* Correspondence should be addressed to this author at Biomedical Radiation Sciences, The Rudbeck Laboratory, S-75185 Uppsala, Sweden. E-mail: marika.nestor@bms.uu.se; telephone +46 18 4713868; fax +46 18 4713432.

<sup>†</sup> Division of Otolaryngology and Head & Neck Surgery, Uppsala University.

<sup>‡</sup> Division of Biomedical Radiation Sciences, Uppsala University.

<sup>§</sup> Division of Experimental Nuclear Medicine, Uppsala University.

<sup>||</sup> Department of Otolaryngology/Head and Neck Surgery, Vrije Universiteit Medical Center.



plementarity-determining regions (CDRs) of antibodies are at risk of being damaged through direct (CAT or Iodogen) labeling, since CDRs often are tyrosine-rich regions (8). Indirect labeling is usually performed under milder conditions but often generates lower yields and is generally a more time-consuming and complicated process.

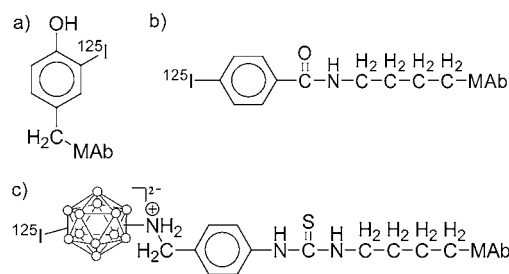
Differences between directly and indirectly radioiodinated MAbs have been observed in a number of biodistribution studies, where direct radioiodination (using CAT) have demonstrated higher accumulation of radioactivity in thyroid and stomach than indirect labeling using derivatives of benzoic acid (9–14). Studies have also shown that indirect radiohalogenation of MAbs using different linker molecules leads to differences in tissue distribution, and analysis of urine has revealed different catabolic products depending on the linker molecule used (9–14).

Recently, *N*-succinimidyl 4-(guanidinomethyl)-3-iodobenzoate has been proposed for use in labeling antibodies with radioiodine and astatine. Studies demonstrated a 3- to 4-fold improvement of radioactivity retention in comparison to the Iodogen and  $^{125}\text{I}$ -SIPC (*N*-succinimidyl 5-iodopyridine-3-carboxylate)-labeling methods (15). However, this linker has a positive charge, which might be a disadvantage since it has been demonstrated that positively charged molecules are taken up preferentially in the kidneys, (2, 16, 17), increasing the dose burden for this radiosensitive organ.

As an alternative, we propose to use polyhedral boron clusters (PBCs) as the prosthetic group. This could solve not only the problem of improving cellular retention but also that of radiocatabolite excretion. Among PBCs, boron-containing compounds such as *closo*-dodecaborate(2-),  $\text{B}_{12}\text{H}_{12}^{2-}$ , seem to be suitable for radiolabeling with halogens (18, 19). Peptides and proteins can be conjugated with various *closo*-dodecaborate(2-) containing ligands (20–22) showing that *closo*-dodecaborate can be radioiodinated in a high yield (ca. 90%) using either CAT or Iodogen. Recently, the radioiodination chemistry of  $\text{B}_{12}\text{H}_{12}^{2-}$  in aqueous solutions using CAT has been optimized (18), generating a rapid (>90% yield in 30 s) as well as efficient reaction in a wide range of pH (4–7.4). As little as 1 nmol of *closo*-dodecaborate can be iodinated with a high yield, forming highly stable boron–halogen bonds. These aspects, together with the negative charge on the dodecaborate cluster and the rapid excretion via the kidneys (19), make the  $\text{B}_{12}\text{H}_{12}^{2-}$  compounds promising as pendant groups for radiohalogenation of tumor-targeting substances for radionuclide diagnostics and therapy of cancer.

DABI, a derivative of *closo*-dodecaborate, [(4-isothiocyanatobenzylammonio)undecahydro-*closo*-dodecaborate(1-)], has recently been successfully radioiodinated at our laboratory with a high yield (93–95%) and coupled to a herceptin antibody (23, 24). This prompted us to further investigate this compound as a pendant group for radiohalogen labeling of antibodies and to compare its biodistribution with other direct and indirect labeling methods.

The chimeric monoclonal antibody (cMAb) used in these studies was cMAb U36, appearing to have much potential in RIT toward head and neck squamous cell carcinomas (HNSCCs) (25–27). The cMAb U36 recognizes the CD44 splice variant CD44v6, located on the outer cell surface (28). Clinical biodistribution studies evaluated by radioimmunoscinigraphy and by biopsy measurements in head and neck cancer patients have shown high and selective accumulation of cMAb U36 in



**Figure 1.** Structures of the three different  $^{125}\text{I}$ -antibody conjugates used. In the directly (CAT) labeled antibody (a), the  $^{125}\text{I}$  is directly attached to the tyrosine residues of the antibody. In the indirectly PIB-labeled conjugate (b), the  $^{125}\text{I}$  is connected to the antibody via the PIB linker molecule to the lysine residues of the antibody. In the case of the indirectly DABI-labeled conjugate (c), the  $^{125}\text{I}$  is attached via the DABI linker molecule to the lysine residues of the antibody.

primary tumors and lymph node metastases (29). Selective tumor accumulation to nude mice bearing human HNSCC xenografts has been demonstrated for the  $^{125}\text{I}$ -labeled cMAb U36 (using Iodogen), as well as for  $^{131}\text{I}$ - and  $^{186}\text{Re}$ -labeled MAb U36 (30–34), and recently the chimeric MAb U36 was evaluated in two clinical RIT trials using  $^{186}\text{Re}$  as a therapeutic radionuclide (25, 27).

In the present study, the cMAb U36 has been labeled with  $^{125}\text{I}$  using three different labeling techniques, i.e., direct labeling using CAT, and indirect labeling using either DABI or PIB (*N*-succinimidyl 4-iodobenzoate) linker molecules. The goal of the study was to investigate how indirect iodination of cMAb U36 using DABI affects the specificity, affinity, and biodistribution of the antibody compared to the same antibody labeled using CAT and PIB. These data were sought to investigate the feasibility of DABI as a linker molecule, as well as to optimize the biological properties of halogen-labeled cMAb U36 for possible future use in RIT and RID.

## EXPERIMENTAL PROCEDURES

**Cell Lines.** The HNSCC cell lines SCC-9 and SCC-25 (obtained from American Type Culture Collection) were cultured in a 1:1 mixture of Ham's F12 and Dulbecco's Modified Eagle Medium (DMEM), supplemented with 10% foetal calf serum, 0.4 mM hydrocortisone, 2 mM L-glutamine and antibiotics (100 IU penicillin and 100  $\mu\text{g}/\text{mL}$  streptomycin). Cells were incubated at 37 °C in an atmosphere containing humidified air with 5%  $\text{CO}_2$ . Cells were trypsinized and grown in separate dishes used for experiments 3–4 days prior to the studies.

**Antibody.** The chimeric monoclonal antibody used in these studies was cMAb U36. The selection and production of the antibody has been described previously (32, 35). The antibody was first stored in citrate buffer and then separated by size-exclusion chromatography on a NAP-5 column preequilibrated with purified (ELGA) water. It was then freeze-dried overnight and stored in  $-20$  °C.

**Direct Labeling.** Freshly prepared solution of cMAb U36 in PBS (60  $\mu\text{L}$ , 5 mg/mL) was mixed with  $^{125}\text{I}$  iodine solution (5 MBq). Reaction was initiated by adding CAT in PBS (10  $\mu\text{L}$ , 2 mg/mL) and was quenched after rigorous vortexing during 5 min by adding sodium metabisulfite (20  $\mu\text{L}$ , 2 mg/mL). Labeled antibody ( $^{125}\text{I}$ -cMAb U36) was separated from nonreacted  $^{125}\text{I}$  and low-molecular-weight reaction components by size-exclusion chromatography on a NAP-5 column preequilibrated with PBS. See Figure 1a) for the structure of the directly radioiodinated antibody.

**PIB Labeling.** Stock solution of  $^{125}\text{I}$  (45 MBq in 15  $\mu\text{L}$ ) was mixed with 10  $\mu\text{L}$  of 0.1% acetic acid, and a solution of *N*-succinimidyl 4-(trimethylstannyl)benzoate in 5% acetic acid in methanol (5  $\mu\text{L}$ , 1 mg/mL) prepared as described in (36) was then added. Labeling was started by adding CAT in water (10  $\mu\text{L}$ , 2 mg/mL) and was quenched after 5 min of vortexing by adding sodium metabisulfite (10  $\mu\text{L}$ , 4 mg/mL water). Freshly prepared solution of cMAb U36 in borate buffer, pH 9.1 (30  $\mu\text{L}$ , 10 mg/mL) was added. The solution was stirred carefully, and the coupling reaction proceeded during 30 min at 37 °C. Separation of labeled cMAb U36 ( $^{125}\text{I}$ -PIB-cMAb U36) was performed by size-exclusion chromatography on a NAP-5 column preequilibrated with PBS. See Figure 1b) for the structure of the indirectly PIB-radioiodinated antibody.

**DABI Labeling.** A solution of potassium salt of DABI in water (3  $\mu\text{L}$ , 1 mg/mL), prepared as described in (37), was mixed with stock solution of  $^{125}\text{I}$  (60 MBq in 20  $\mu\text{L}$ ). Labeling was started by adding CAT in water (10  $\mu\text{L}$ , 2 mg/mL) and was quenched after 5 min of vortexing by adding sodium metabisulfite (10  $\mu\text{L}$ , 4 mg/mL water). Freshly prepared solution of cMAb U36 in borate buffer, pH 9.1 (30  $\mu\text{L}$ , 10 mg/mL) was then added. The solution was carefully stirred, and the coupling reaction proceeded during 30 min at 37 °C. Separation of labeled cMAb U36 ( $^{125}\text{I}$ -DABI-cMAb U36) was performed by size-exclusion chromatography on a NAP-5 column preequilibrated with PBS. See Figure 1c) for the structure of the indirectly DABI-radioiodinated antibody.

**Affinity Measurements.** Kinetic affinity constants were measured using saturation curves with a fixed amount of cells and different concentrations of labeled antibody. Six dishes per data point containing approximately 50 000 cells of SCC9 or SCC25 HNSCC cells were prepared. An excess of unlabeled antibody was added to three of the dishes per data point for unspecific binding correction. These dishes also functioned as specificity controls of the antibody, since the binding of a labeled antibody conjugate that has preserved its antigen specific binding will be blocked in the dishes containing an excess of unlabeled antibody. Concentrations varying between 0.01 and 7  $\mu\text{g}$  of  $^{125}\text{I}$  labeled cMAb U36 ( $^{125}\text{I}$ -cMAb U36,  $^{125}\text{I}$ -PIB-cMAb U36, or  $^{125}\text{I}$ -DABI-cMAb U36) was then added to all dishes. Cells were incubated on ice (in order to prevent endocytosis) for 15 h. The incubation medium was then collected, and the dishes were washed six times with HAM's F12/DMEM medium. The cells were detached with 0.5 mL of trypsin-EDTA solution for 10 min in 37 °C and resuspended in 1 mL complete culture medium. Cell counting was performed on 0.5 mL of the suspension, and radioactivity measurements were performed on the remaining 1 mL in a gamma well-counter. The values were analyzed using GraphPad Prism in order to construct saturation curves and to calculate the affinity.

**Antibody Biodistribution.** All three in vivo studies were carried out in normal mice (adult female NMRI mice, BK Universal AB, Stockholm) with appropriate licenses from The Local Ethics Committee for Animal Research. Animals were housed at the Rudbeck animal facility and were allowed to acclimatize to the facility for at least a week before the start of experiments. Groups of four mice per time point were injected intravenously via tail vein with 15  $\mu\text{g}$  of 100–120 kBq  $^{125}\text{I}$ -labeled cMAb U36 diluted in PBS. Animals were sacrificed at 1.5, 6, 24, and 96 h after injection. At indicated time points, mice were anaesthetized, heart punctured, killed, and dissected. Urine and blood were collected, as well as the

**Table 1. cMAb U36 Affinity as a Function of Radioiodination Method in Two HNSCC Cell Lines**

radioiodination technique	affinity, cell line SCC9 ( $\text{M}^{-1}$ ) <sup>a</sup>	affinity, cell line SCC25 ( $\text{M}^{-1}$ ) <sup>a</sup>
direct (CAT) labeling	$0.6 \pm 0.3 \times 10^8$	$0.4 \pm 0.3 \times 10^8$
indirect PIB <sup>b</sup> labeling	$1.0 \pm 0.2 \times 10^8$	$1.5 \pm 0.6 \times 10^8$
indirect DABI <sup>c</sup> labeling	$0.8 \pm 0.3 \times 10^8$	$1.2 \pm 0.1 \times 10^8$

<sup>a</sup> Mean  $\pm$  SD ( $n = 3$ ). <sup>b</sup> *N*-Succinimidyl 4-iodobenzoate. <sup>c</sup> (4-Isothiocyanatobenzylammonio)undecahydro-*closo*-dodecaborate (1-).

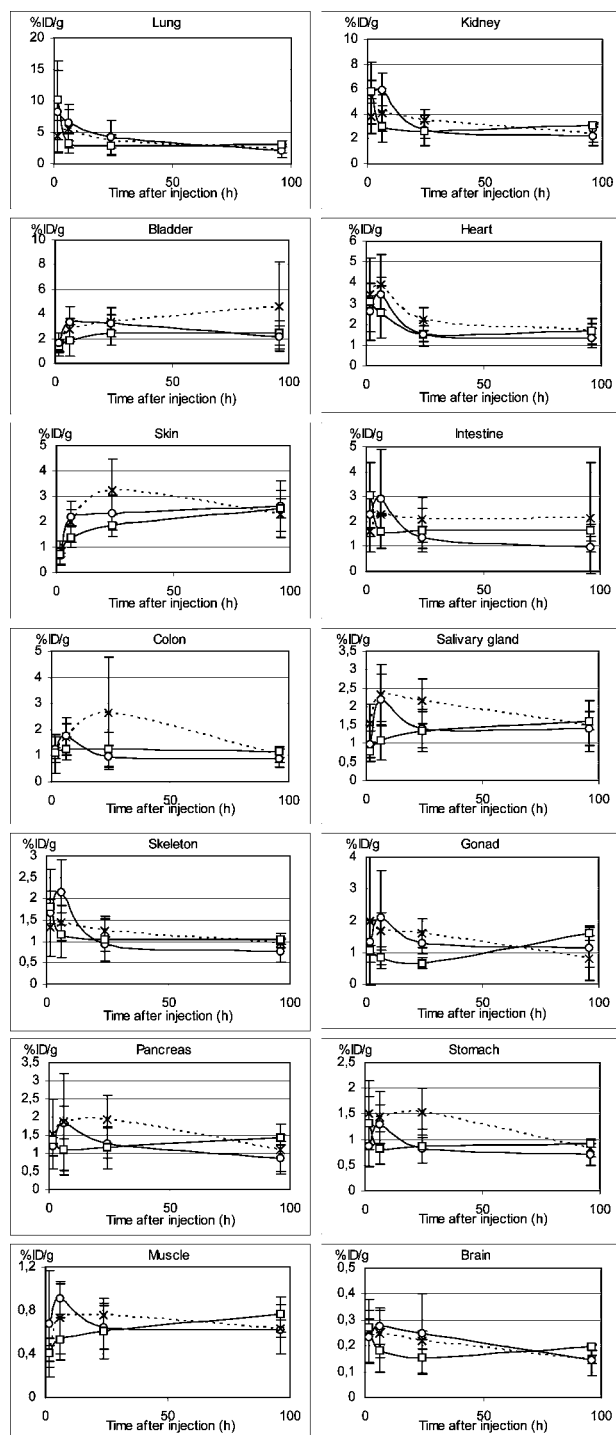
major organs and samples of brain, muscle, skeleton, and skin. The samples were then weighed, and the activity was measured. To obtain a quantitative measure of the injected radioactivity, the radioactivity of each syringe was measured before and after injection, and the radioactivity in the tails was measured after dissection. The activity expressed in percentage injected dose per gram of tissue was then calculated, and the average values were used to construct biodistribution curves. The Kruskal-Wallis test was performed in MINITAB to determine the significance of deviating values (significant if  $P < 0.05$ ).

## RESULTS

**Labeling.** Direct CAT labeling of cMAb U36 was performed with a labeling efficiency of 90–95%. PIB labeling was performed with a labeling efficiency of 60%, resulting in a PIB:cMAb U36 molar ratio of 1.8–2.5. DABI labeling was performed with a labeling efficiency of 68% and resulted in a DABI:cMAb U36 molar ratio of 4.1.

**Affinity Measurements.** The affinities of the three antibody conjugates are shown in Table 1. The differences in affinity for the three conjugates were small, with values around  $1 \times 10^8 \text{ M}^{-1}$ . Antigen specific binding of all three conjugates were clearly demonstrated in both HNSCC cell lines, as the binding of conjugates was prevented by an excess of unlabeled antibody (data not shown).

**Biodistribution.** The biodistribution of  $^{125}\text{I}$ -cMAb U36,  $^{125}\text{I}$ -DABI-cMAb U36, and  $^{125}\text{I}$ -PIB-cMAb U36 in various organs are shown in Figures 2 and 3. Figure 2 shows the organs in which no significant biodistribution difference ( $P \geq 0.05$ ) between the conjugates could be seen, and Figure 3 shows the organs in which a significant difference ( $P < 0.05$ ) could be seen for at least one of the conjugates in at least one time point. Generally, amounts in blood and organs decreased with time, with the exception for thyroid and skin. The lowest uptake was seen in brain for all three compounds. The indirectly labeled conjugates showed minor differences in tissue distribution, except in the reticuloendothelial system (i.e., liver and spleen), where the  $^{125}\text{I}$ -DABI-cMAb U36 conjugate demonstrated a higher uptake in the 1.5 and 96 h time points (see Table 2). At the 96 h time point, the  $^{125}\text{I}$ -DABI-cMAb U36 conjugate displayed a 2.2 and 2.9 times higher uptake than the other conjugates in liver and spleen, respectively. The  $^{125}\text{I}$ -DABI-cMAb U36 conjugate also displayed a higher amount of radioactivity in blood than the other conjugates at the 96 h time point. However, the most pronounced difference in uptake can be seen in thyroid starting from the 24 h time point and increasing even more at the 96 h time point. With the direct labeling technique, a radioactivity uptake corresponding to 10 times the value of the indirectly labeled compounds can be observed at the 96 h time point (see Figure 3). The thyroid uptake is clearly increasing with

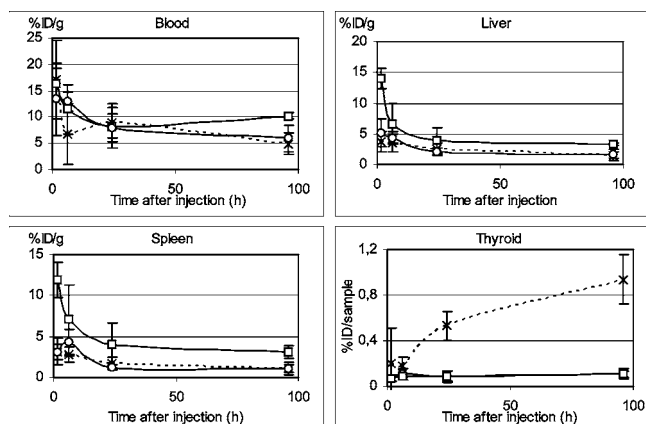


**Figure 2.** Comparison of the biodistribution of  $^{125}\text{I}$ -cMAb U36 ( $\times$ ),  $^{125}\text{I}$ -DABI-cMAb U36 ( $\square$ ), and  $^{125}\text{I}$ -PIB-cMAb U36 ( $\circ$ ) in various organs. Animals were sacrificed at 1.5, 6, 24, and 96 h after injection. The unit % ID/g refers to the activity expressed in percentage injected dose per gram of tissue. In these organs, no significant difference ( $P \geq 0.05$ ) between the conjugates could be observed. No accumulation could be seen in any organs except in skin, where some accumulation could be observed from the 24 h time point. Error bars represent standard deviations ( $N = 4$ ).

time for this conjugate, whereas the indirectly labeled conjugates show low and constant thyroid values.

## DISCUSSION

In this study we have conducted a comparative investigation of three radiohalogenation methods on the cMAb



**Figure 3.** Comparison of the biodistribution of  $^{125}\text{I}$ -cMAb U36 ( $\times$ ),  $^{125}\text{I}$ -DABI-cMAb U36 ( $\square$ ), and  $^{125}\text{I}$ -PIB-cMAb U36 ( $\circ$ ) in blood, liver, spleen, and thyroid. Animals were sacrificed at 1.5, 6, 24, and 96 h after injection. The unit % ID/g refers to the activity expressed in percentage injected dose per gram of tissue. Significant differences ( $P < 0.05$ ) could be observed at the 1.5 and 96 h time points in liver and spleen and the 96 h time point in blood, where the DABI conjugate displayed higher values. In thyroid, the directly labeled conjugate displayed significantly higher values than the indirectly labeled conjugates at the 24 and 96 h time points. Error bars represent standard deviations ( $N = 4$ ).

**Table 2.** Comparison of the % ID/g Tissue<sup>a</sup> of  $^{125}\text{I}$ -cMAb U36,  $^{125}\text{I}$ -DABI-cMAb U36, and  $^{125}\text{I}$ -PIB-cMAb U36 in Liver and Spleen

organ	time point (h)	direct (CAT) labeling	indirect PIB <sup>b</sup> labeling	indirect DABI <sup>c</sup> labeling
liver	1.5 <sup>d</sup>	$3.6 \pm 1.6$	$5.2 \pm 2.3$	$14.1 \pm 1.7$
	6	$3.5 \pm 1.4$	$4.4 \pm 1.0$	$4.8 \pm 4.5$
	24	$2.6 \pm 0.9$	$2.1 \pm 0.6$	$4.0 \pm 2.0$
	96 <sup>d</sup>	$1.5 \pm 0.9$	$1.6 \pm 0.6$	$3.4 \pm 0.2$
spleen	1.5 <sup>d</sup>	$3.1 \pm 1.0$	$3.2 \pm 1.6$	$11.9 \pm 2.2$
	6	$2.7 \pm 0.9$	$4.3 \pm 1.6$	$7.1 \pm 4.2$
	24	$1.7 \pm 0.8$	$1.3 \pm 0.3$	$4.1 \pm 2.5$
	96 <sup>d</sup>	$1.1 \pm 0.8$	$1.1 \pm 0.4$	$3.1 \pm 0.8$

<sup>a</sup> The unit % ID/g refers to the activity expressed in percentage injected dose per gram of tissue. Errors represent standard deviations ( $N = 4$ ). <sup>b</sup> *N*-Succinimidyl 4-iodobenzoate. <sup>c</sup> (4-isothiocyanatobenzylammonio)undecahydro-*closa*-dodecaborate (1-). <sup>d</sup> The DABI conjugate displayed significantly ( $P < 0.05$ ) higher values than the other conjugates at these time points.

U36. By studying the labeling effect on specificity, affinity, and biodistribution, the biological suitability of the cMAb U36 conjugates could be evaluated. Moreover, this paper describes the very first in vivo evaluation of DABI in order to assess its applicability for continued studies.

The data obtained in vitro showed antigen specific binding and minor differences in affinity for all conjugates with values around  $1 \times 10^8 \text{ M}^{-1}$ . The in vivo data pointed out a 10 times higher accumulation in thyroid for the directly labeled conjugate 96 h pi. This is consistent with a number of studies where direct radioiodination (using CAT) exhibits higher accumulation of radioactivity in thyroid than indirect labeling using derivatives of benzoic acid (9–13). Since the thyroid is known to accumulate free radioiodide, this could indicate a different catabolic pathway for the directly labeled conjugate. It has also been hypothesized that the lesser uptake of radiolabel in thyroid for the indirectly labeled compounds via benzoic derivatives is due to rapid urinary excretion of the intracellular catabolic products. This quick excretion may prevent further in vivo transforma-



tion of the catabolites and the release of free halide, resulting in a lower thyroid uptake (13, 14).

The *in vivo* data also demonstrated a higher level of  $^{125}\text{I}$ -DABI-cMAb U36 in liver and spleen compared to the other conjugates. This increase might raise some concerns about its use, even though 3.4 and 3.1% ID/g tissues in liver and spleen at the last time point is not alarmingly high. However, this higher level could indicate residualization of the DABI linker, and future xenograft studies will have to assess if the amount of residualization obtained in tumors outweigh any disadvantage of increased uptake in liver and spleen.

The increasing uptake in skin seen in this study for all three conjugates (see Figure 2) is intriguing, since the CD44v6 epitope recognized by cMAb U36 is a human epitope and should not be reactive with CD44v6 splice variants in mice. However, it has been shown for mice that skin is an important site for catabolism for the IgG<sub>1</sub> subclass (38, 39), and the epithelial uptake seen in skin in our study could be caused by this. Also, the possibility that the high skin levels were caused by urine or blood contamination cannot be ruled out, although all samples were washed before measurements.

In conclusion, among three differently radioiodinated cMAb U36 conjugates, all three conjugates showed high specific binding and similar affinities but displayed different biodistribution patterns. The directly labeled conjugate showed clear and high accumulation in thyroid, in contrast to the indirectly labeled conjugates. Both  $^{125}\text{I}$ -PIB-cMAb U36 and  $^{125}\text{I}$ -DABI-cMAb U36 showed a consistently low thyroid uptake, indicating high stability of the radiolabels and different radiocatabolites from the directly labeled conjugate. This may favor the use of these conjugates for future studies. For studies where thyroid uptake can be neglected, the direct CAT labeling method might be acceptable with unaffected affinity, offering a fast and simple labeling method with high yield. However, when the tumor target is in the throat area, the uptake in thyroid will complicate diagnosis if the tumor uptake cannot be distinguished from the thyroid uptake, and dose planning for RIT may be impossible. If instead the uptake in thyroid is low, medication to block radionuclide uptake can be avoided and the RIT process simplified. Also, the risk of causing hypothyroidism in the patient can be reduced.

Since the cMAb U36 previously has been shown to specifically target HNSCC xenograft models, the fact that the linker molecules did not considerably alter the specific binding or the affinity of the antibody is promising. This study also indicates that radioiodinated DABI conjugated to an appropriate tumor-seeking molecule can provide a stable residualizing iodine label which, if applied to a relevant targeting agent, will be of interest for imaging and therapy. Apart from the specific results obtained, these findings also demonstrate how the proper linker molecule will provide additional opportunities to further improve the properties of an antibody-radionuclide conjugate.

#### ACKNOWLEDGMENT

The authors wish to thank Dr. Igor Sivaev who prepared the potassium salt of DABI, and Dr. Anna Orlova who prepared *N*-succinimidyl 4-(trimethylstannyl)benzoate. We also wish to thank Dr. Lars Gedda for supervising the affinity experiments and Qichun Wei for help with the data collection in the DABI biodistribution experiment. This work was partly supported by grants

from Cancerfonden, Sweden (Project numbers 4462-B01-02PAA and 3980-B00-04XBB).

#### LITERATURE CITED

- (1) Potamianos, S., Varvarigou, A. D., and Archimandritis, S. C. (2000) Radioimmunosintigraphy and radioimmunotherapy in cancer: principles and application. *Anticancer Res.* 20, 925–948.
- (2) Tolmachev, V., and Sjöberg, S. (2002) Polyhedral boron compounds as potential linkers for attachment of radiohalogens to targeting proteins and peptides. A review. *Collect. Czech. Chem. Commun.* 67, 913–935.
- (3) van Deurs, B., Petersen, O. W., Olsnes, S., and Sandvig, K. (1989) The ways of endocytosis. *Int. Rev. Cytol.* 117, 131–177.
- (4) Kyriakos, R. J., Shih, L. B., Ong, G. L., Patel, K., Goldenberg, D. M., and Mattes, M. J. (1992) The fate of antibodies bound to the surface of tumor cells *in vitro*. *Cancer Res.* 52, 835–842.
- (5) Geissler, F., Anderson, S. K., Venkatesan, P., and Press, O. (1992) Intracellular catabolism of radiolabeled anti-mu antibodies by malignant B-cells. *Cancer Res.* 52, 2907–2915.
- (6) Press, O. W., Shan, D., Howell-Clark, J., Eary, J., Appelbaum, F. R., Matthews, D., King, D. J., Haines, A. M., Hamann, P., Hinman, L., Shochat, D., and Bernstein, I. D. (1996) Comparative metabolism and retention of iodine-125, yttrium-90, and indium-111 radioimmunoconjugates by cancer cells. *Cancer Res.* 56, 2123–2129.
- (7) Stein, R., Goldenberg, D. M., Thorpe, S. R., and Mattes, M. J. (1997) Advantage of a residualizing iodine radiolabel for radioimmunotherapy of xenografts of human nonsmall-cell carcinoma of the lung. *J. Nucl. Med.* 38, 391–395.
- (8) Nikula, T. K., Bocchia, M., Curcio, M. J., Sgouros, G., Ma, Y., Finn, R. D., and Scheinberg, D. A. (1995) Impact of the high tyrosine fraction in complementarity determining regions: measured and predicted effects of radioiodination on IgG immunoreactivity. *Mol. Immunol.* 32, 865–872.
- (9) Wilbur, D. S., Hadley, S. W., Hylarides, M. D., Abrams, P. G., Beaumier, P. A., Morgan, A. C., Reno, J. M., and Fritzberg, A. R. (1989) Development of a stable radioiodinating reagent to label monoclonal antibodies for radiotherapy of cancer. *J. Nucl. Med.* 30, 216–226.
- (10) Zalutsky, M. R., and Narula, A. S. (1987) A method for the radiohalogenation of proteins resulting in decreased thyroid uptake of radioiodine. *Int. J. Radiat. Appl. Instrum. [A]* 38, 1051–1055.
- (11) Zalutsky, M. R., and Narula, A. S. (1988) Radiohalogenation of a monoclonal antibody using an *N*-succinimidyl 3-(tri-*n*-butylstannyl)benzoate intermediate. *Cancer Res.* 48, 1446–1450.
- (12) Zalutsky, M. R., Noska, M. A., Colapinto, E. V., Garg, P. K., and Bigner, D. D. (1989) Enhanced tumor localization and *in vivo* stability of a monoclonal antibody radioiodinated using *N*-succinimidyl 3-(tri-*n*-butylstannyl)benzoate. *Cancer Res.* 49, 5543–5549.
- (13) Hoglund, J. (2002) On the use of  $^{76}\text{Br}$ -labelled Monoclonal Antibodies for PET. Preclinical Evaluation of Halogenated Antibodies for Diagnosis and Treatment of Cancer. *Acta Univ. Ups., Uppsala Diss. Fac. Med.*
- (14) Wilbur, D. S., Hadley, S. W., Grant, L. M., and Hylarides, M. D. (1991) Radioiodinated iodobenzoyl conjugates of a monoclonal antibody Fab fragment. *In vivo* comparisons with chloramine-T-labeled Fab. *Bioconjugate Chem.* 2, 111–116.
- (15) Vaidyanathan, G., Affleck, D. J., Li, J., Welsh, P., and Zalutsky, M. R. (2001) A polar substituent-containing acylation agent for the radioiodination of internalizing monoclonal antibodies: *N*-succinimidyl 4-guanidinomethyl-3-[ $^{131}\text{I}$ ]iodobenzoate ([ $^{131}\text{I}$ ]SGMIB). *Bioconjugate Chem.* 12, 428–438.
- (16) Behr, T. M., Becker, W. S., Sharkey, R. M., Juweid, M. E., Dunn, R. M., Bair, H. J., Wolf, F. G., and Goldenberg, D. M. (1996) Reduction of renal uptake of monoclonal antibody fragments by amino acid infusion. *J. Nucl. Med.* 37, 829–833.
- (17) Behr, T. M., Sharkey, R. M., Juweid, M. E., Blumenthal, R. D., Dunn, R. M., Griffiths, G. L., Bair, H. J., Wolf, F. G.,

- Becker, W. S., and Goldenberg, D. M. (1995) Reduction of the renal uptake of radiolabeled monoclonal antibody fragments by cationic amino acids and their derivatives. *Cancer Res.* **55**, 3825–3834.
- (18) Tolmachev, V., Lundqvist, H., Carlsson, J., Sivaev, I., Orlova, A., and Sundin, A. (1997) Labeling and in vivo evaluation of closo-dodecaborate as a linker for attachment of iodine to radiopharmaceuticals. *J. Labelled Compd. Radiopharm.* **40**, 125.
- (19) Orlova, A., Sivaev, I., Sjöberg, S., and Tolmachev, V. (2001) Radioiodination of monocarboranes. *2nd Eur. Symp. Boron Chem. (EUROBORON 2)*, (Book of Abstracts) 33.
- (20) Tolmachev, V., Koziorowski, J., Sivaev, I., Lundqvist, H., Carlsson, J., Orlova, A., Gedda, L., Olsson, P., Sjöberg, S., and Sundin, A. (1999) Closo-dodecaborate(2<sup>-</sup>) as a linker for iodination of macromolecules. Aspects on conjugation chemistry and biodistribution. *Bioconjugate Chem.* **10**, 338–345.
- (21) Orlova, A., Tolmachev, V., and Lundqvist, H. (2000) Closo-dodecaborate (2<sup>-</sup>) anion as a potential prosthetic group for attachment of radioiodine to proteins. Aspects of labeling chemistry in aqueous solutions. *Eur. J. Nucl. Med.* **27**, 1210.
- (22) Tolmachev, V., Bruskin, A., Sivaev, I., Lundqvist, H., and Sjöberg, S. (2001) Oxidative radiobromination of the dodecahydro-closo-dodecaborate (2<sup>-</sup>) anion. *2nd Eur. Symp. Boron Chem. (EUROBORON 2)*, (Book of Abstracts) 55.
- (23) Tolmachev, V., Bruskin, A., Winberg, K. J., Sivaev, I., Persson, M., Lundqvist, H., Sjöberg, S., and Carlsson, J. (2002) The use of derivatives of polyhedral boron anions (PHA), closo-dodecaborate and nido-carborate, for radiobromination of anti-HER-2 antibody Herceptin for immunoPET. (Abstracts of the 15th meeting of the International Research Group in Immunoscintigraphy and Immunotherapy (IRIST), Rotterdam, The Netherlands, May 24–25 May, 2002) *Cancer Biother. Radiopharm.* **17**, 353–354.
- (24) Tolmachev, V., Orlova, A., Bruskin, A., Sivaev, I., Persson, M., Sjöberg, S., Carlsson, J., and Lundqvist, H. (2002) The use of benzyl isothiocyanate derivative of closo-dodecaborate dianion for indirect radioiodination and radiobromination of monoclonal antibodies. *Eur. J. Nucl. Med.* **29**, Supplement 1: S76.
- (25) Colnot, D. R., Ossenkoppele, J. C., Quak, J. J., de Bree, R., Börjesson, P. C., Snow, G. B., and van Dongen, G. A. (2002) Re-infusion of Unprocessed, G.-CSF–Stimulated Whole Blood Allows Dose Escalation of 186-Re-cMab U36 Radioimmunotherapy in a Phase I Dose Escalation Study. *Clin. Cancer Res.* **8**, 3401–3406.
- (26) Colnot, D. R., Quak, J. J., Roos, J. C., de Bree, R., Wilhelm, A. J., Snow, G. B., and van Dongen, G. A. (2001) Radioimmunotherapy in patients with head and neck squamous cell carcinoma: initial experience. *Head Neck* **23**, 559–565.
- (27) Colnot, D. R., Quak, J. J., Roos, J. C., van Ling, A., Wilhelm, A. J., van Kamp, G. J., Huijgens, P. C., Snow, G. B., and van Dongen, G. A. (2000) Phase I therapy study of 186Re-labeled chimeric monoclonal antibody U36 in patients with squamous cell carcinoma of the head and neck. *J. Nucl. Med.* **41**, 1999–2010.
- (28) Van Hal, N. L., Van Dongen, G. A., Rood-Knippels, E. M., Van Der Valk, P., Snow, G. B., and Brakenhoff, R. H. (1996) Monoclonal antibody U36, a suitable candidate for clinical immunotherapy of squamous-cell carcinoma, recognizes a CD44 isoform. *Int. J. Cancer* **68**, 520–527.
- (29) de Bree, R., Roos, J. C., Quak, J. J., den Hollander, W., Snow, G. B., and van Dongen, G. A. (1995) Radioimmunoscinigraphy and biodistribution of technetium-99m-labeled monoclonal antibody U36 in patients with head and neck cancer. *Clin. Cancer Res.* **1**, 591–598.
- (30) Vrouenraets, M. B., Visser, G. W. M., Stigter, M., Oppelaar, H., Snow, G. B., and van Dongen, G. A. M. S. (2001) Targeting of Aluminum (III) Phthalocyanine Tetrasulfonate by Use of Internalizing Monoclonal Antibodies: Improved Efficacy in Photodynamic Therapy. *Cancer Res.* **61**, 1970–1975.
- (31) Vrouenraets, M. B., Visser, G. W., Loup, C., Meunier, B., Stigter, M., Oppelaar, H., Stewart, F. A., Snow, G. B., and van Dongen, G. A. (2000) Targeting of a hydrophilic photosensitizer by use of internalizing monoclonal antibodies: A new possibility for use in photodynamic therapy. *Int. J. Cancer* **88**, 108–114.
- (32) Schrijvers, A. H., Quak, J. J., Uytendinck, A. M., van Walsum, M., Meijer, C. J., Snow, G. B., and van Dongen, G. A. (1993) MAb U36, a novel monoclonal antibody successful in immunotargeting of squamous cell carcinoma of the head and neck. *Cancer Res.* **53**, 4383–4390.
- (33) van Gog, F. B., Brakenhoff, R. H., Stigter-van Walsum, M., Snow, G. B., and van Dongen, G. A. (1998) Perspectives of combined radioimmunotherapy and anti-EGFR antibody therapy for the treatment of residual head and neck cancer. *Int. J. Cancer* **77**, 13–18.
- (34) van Gog, F. B., Visser, G. W., Stroomer, J. W., Roos, J. C., Snow, G. B., and van Dongen, G. A. (1997) High dose rhenium-186-labeling of monoclonal antibodies for clinical application: pitfalls and solutions. *Cancer* **80**, 2360–2370.
- (35) Brakenhoff, R. H., van Gog, F. B., Looney, J. E., van Walsum, M., Snow, G. B., and van Dongen, G. A. (1995) Construction and characterization of the chimeric monoclonal antibody E48 for therapy of head and neck cancer. *Cancer Immunol. Immunother.* **40**, 191–200.
- (36) Koziorowski, J., Henssen, C., and Weinreich, R. (1998) A new convenient route to radioiodinated N-succinimidyl 3- and 4-iodobenzoate, two reagents for radioiodination of proteins. *Appl. Radiat. Isot.* **49**, 955–959.
- (37) Sivaev, I., Bruskin, A., Nesterov, V. V., Antipin, M. Y., Bregadze, V. I., and Sjöberg, S. (1999) Synthesis of Schiff Bases Derived from the Ammoniaundecahydro-closo-dodecaborate(1<sup>-</sup>) Anion, [B<sub>12</sub>H<sub>11</sub>NH=CHR]<sup>-</sup>, and Their Reduction into Monosubstituted Amines [B<sub>12</sub>H<sub>11</sub>(NH<sub>2</sub>CH<sub>2</sub>R)]<sup>-</sup>: A New Route to Water Soluble Agents for BNCT. *Inorg. Chem.* **38**, 5887–5893.
- (38) Henderson, L. A., Baynes, J. W., and Thorpe, S. R. (1982) Identification of the sites of IgG catabolism in the rat. *Arch. Biochem. Biophys.* **215**, 1–11.
- (39) Moldoveanu, Z., Epps, J. M., Thorpe, S. R., and Mestecky, J. (1988) The sites of catabolism of murine monomeric IgA. *J. Immunol.* **141**, 208–213.

BC034003N

# Hybridization Properties of Support-Bound Oligonucleotides: The Effect of the Site of Immobilization on the Stability and Selectivity of Duplex Formation

Kaisa Ketomäki,<sup>\*,†</sup> Harri Hakala,<sup>‡</sup> Outi Kuronen,<sup>†</sup> and Harri Lönnberg<sup>†</sup>

Department of Chemistry, University of Turku, FIN-20014 Turku, Finland, and PerkinElmer Life and Analytical Sciences, Wallac Oy, P.O. Box 10, FIN-20101 Turku, Finland. Received January 15, 2003; Revised Manuscript Received June 10, 2003

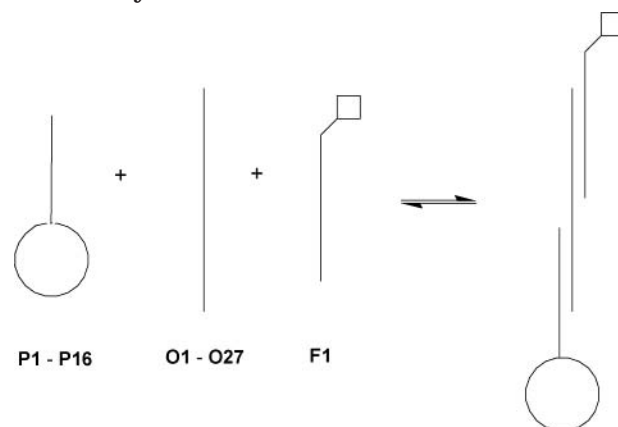
Four 12-mer oligodeoxyribonucleotide sequences were immobilized to uniformly sized (50  $\mu\text{m}$ ) polymer particles through C5-tethered thymine and N<sup>4</sup>-tethered cytosine bases at four different sites in each sequence. The effect of the site of immobilization on the efficiency and selectivity of hybridization of the particle-bound probes was quantified by a sandwich-type assay based on a time-resolved fluorometric measurement of an oligonucleotide probe labeled with a photoluminescent europium(III) chelate directly from the surface of a single particle. Immobilization through a base in the central part of the sequence was observed to destabilize the duplex more markedly than tethering through a terminal base. The effect of a one-base mismatch on the duplex stability increased with the increasing distance from the site of immobilization.

## INTRODUCTION

The so-called DNA-chip technology based on solid-supported high density oligonucleotide arrays is one of the most rapidly developing experimental techniques in molecular biology and biotechnology (1–3). An increasing number of applications dealing with analysis of gene expression (4–6), DNA polymorphism (7–10), RNA folding (11–13), and various enzyme-mediated detection methods (14–20) have gained interest. The key step in the construction of oligonucleotide arrays is immobilization of the oligonucleotide probes to a planar support. Short probes may be assembled from monomeric phosphoramidite building blocks in situ on the support (21–26). On using longer probes, the arrays are usually obtained by postsynthetic covalent immobilization of prefabricated oligonucleotides to an appropriately derivatized support. Either an oligonucleotide bearing a functionalized sidearm (27–38) or a nucleophilic phosphorothioate linkage (39, 40) is reacted with an appropriate support-bound functional group, or an underivatized oligonucleotide is cross-linked to the support through its natural functionalities either photochemically (41) or by chemical reaction with a highly reactive activated surface (42, 43). Alternatively, noncovalent immobilization based on multiple electrostatic interactions of the polyanionic oligonucleotide with a polycationic support may be applied (44).

Despite the continuously increasing number of applications of the array technique, the details of the molecular interactions occurring at the interface of the solution and solid phase are still rather poorly known (45–47). In particular, it is not clear how the site of attachment within an immobilized probe, and hence the orientation with respect to the support, affects the efficiency and selectivity of hybridization. Knowledge on such factors

**Scheme 1. Principle of the Sandwich Type Hybridization Assay**



is, however, relevant, since covalent immobilization of prefabricated underivatized oligonucleotides evidently yields arrays where several different bonding modes are present, and even on using functionalized oligonucleotides, aimed at reacting through a single functional group, interference of other functional groups may lead to nonhomogeneous arrays.

We have previously elucidated the factors affecting the efficiency of mixed-phase hybridization by using oligonucleotide-coated microscopic polymer particles (50  $\mu\text{m}$ ) as the solid phase and probes labeled with a fluorescent europium(III) chelate for quantification of the hybridization efficiency by a sandwich type assay (48–53). Accordingly, the PCR-amplified oligonucleotide forms first in solution a duplex with the fluorescently tagged probe and hybridizes then with the particle-bound probe (Scheme 1). The lanthanide ion emission is measured directly from a single particle. Special attention has been paid to the detection of point mutations (53), which plays an important role in population genetics (54) and in diagnostics of cancer (55) and viral diseases (26). It has been shown that oligonucleotide probes tethered to the support

\* To whom correspondence should be addressed. Phone +358-2-333 7639. Fax: +358-2-333 6731. E-mail: kaisa.ketomaki@utu.fi.

<sup>†</sup> University of Turku.

<sup>‡</sup> PerkinElmer Life and Analytical Sciences.



through their 3'-terminus quite well recognize a one-base mismatch present in the central or 5'-terminal region of a 10- to 12-mer support-bound probe. The hybridization efficiency is reduced by 1–2 orders of magnitude. By contrast, a mismatch at the penultimate site at the 3'-end of the immobilized probe does not appreciably destabilize the duplex, and in some cases even a stabilization takes place. Studies on microarrays have also suggested that position of the mismatch near the terminus of the probe affects the duplex stability more than the identity of the mismatch (56). To learn how susceptible the hybridization actually is to conformational constraints that result from tethering to a solid support through various sites, four 12-mer oligodeoxyribonucleotides were coupled through four different sites to 50  $\mu\text{m}$  polymer particles, and their hybridization with fully complementary 10- to 12-mer sequences, as well as with several 12-mer sequences containing a single-base mismatch at various sites, was quantified by a sandwich type assay (Scheme 1). A 35 atom long linker was used to tether the oligonucleotide from C5 of a thymidine residue to the support. It has been reported previously that on a polypropylene support the optimal spacer length is 40 atoms (57).

## EXPERIMENTAL PROCEDURES

**Preparation of Oligonucleotide-Coated Micro-particles.** The particles used for the immobilization of the oligonucleotide probes were porous uniformly sized (50  $\mu\text{m}$ ) polymer particles made of a copolymer of glycidyl methacrylate (40%) and ethylene dimethylacrylate (60%) and functionalized with primary amino groups (1 mmol  $\text{g}^{-1}$ ) by reacting the particle-bound epoxy groups with diethylenetriamine (SINTEF). The surface area of the particles was 137  $\text{m}^2 \text{g}^{-1}$ . These particles were coated with mercaptoalkyl tails by acylating the amino groups with 15-(4,4'-dimethoxytrityloxy)-12,13-dithiapentadecanoic acid in dry pyridine, using *N*-hydroxysuccinimide, *N,N*-diisopropylcarbodiimide, and 4-(dimethylamino)-pyridine as activators, and capping the rest of the amino groups with acetic anhydride in pyridine (58). The (4,4'-dimethoxytrityl) loading obtained was 6–9  $\mu\text{mol g}^{-1}$ . The disulfide bond was then reductively cleaved with DTT (0.1 mol  $\text{L}^{-1}$  in MeOH, mildly basic conditions with  $\text{Et}_3\text{N}$ ), and the mercapto-group-coated particles were treated with 2-pyridyl disulfide-activated oligonucleotides overnight in water (200–400  $\mu\text{L}$ ). The UV-spectrophotometrically determined oligonucleotide loading was 1–2  $\mu\text{mol g}^{-1}$ . The unreacted mercapto functions were capped with maleimide in a 1:1 mixture of pyridine and ethanol (1 mL of 0.5 mol  $\text{L}^{-1}$  solution), washed, and dried (49). The 2-pyridyl disulfide-activated oligonucleotides were prepared as described below.

**Preparation of Oligonucleotides.** The 2-pyridyl disulfide-activated oligonucleotides used in the preparation of oligonucleotide-coated particles were obtained as follows. Oligonucleotides bearing an aminoalkyl sidearm at desired sites were first assembled by the normal phosphoramidite strategy, using in appropriate places 5-[3-oxo-3-(*N*-trifluoroacetyl-6-aminoethyl)amino-1-propenyl]-2'-deoxyuridine or *N}^6*-(*N*-trifluoroacetyl-6-aminoethyl)-2'-deoxycytidine 3'-(2-cyanoethyl-*N,N*-diisopropylphosphoramidite) as building blocks. The former building block was a product of Glenn Research, and the latter was prepared as described previously (59). The aminoalkyl-functionalized oligonucleotides were purified by ion-exchange HPLC on a SynChropak AX-300 column (4.6 mm  $\times$  250 mm, 6.5  $\mu\text{m}$ ; buffer A, 0.05 M  $\text{KH}_2\text{PO}_4$  in 50% aqueous formamide, pH 5.6; buffer B, buffer A +

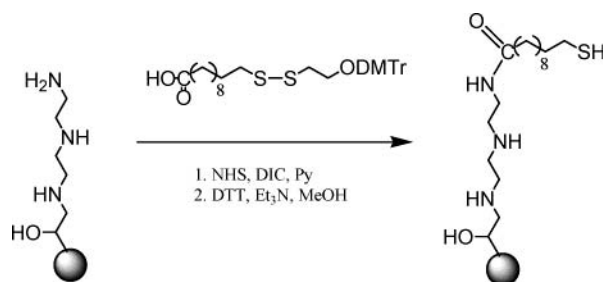
0.6 M  $(\text{NH}_4)_2\text{SO}_4$ ; flow rate 1 mL  $\text{min}^{-1}$ ; a linear gradient from 0 to 50% buffer B in 40 min) and desalted. The functionalized oligonucleotides were converted to 2-pyridyl disulfide derivatives by acylating the side chain amino function with *N*-succinimidyl 3-(2-pyridyldithio)propionate (SPDP; product of PIERCE) in 70% aq MeCN in the presence of  $\text{Et}_3\text{N}$  (100–200  $\mu\text{L}$ ). SPDP was used in 100-fold excess, and the stirring was continued overnight. The 2-pyridyl disulfide-activated oligonucleotides obtained were purified by RP-HPLC and desalted.

The target oligodeoxyribonucleotides (**O1–O27**) were assembled by normal phosphoramidite strategy and purified by ion-exchange HPLC on a SynChropak AX-300 column (4.6 mm  $\times$  250 mm, 6.5  $\mu\text{m}$ ; buffer A, 0.05 M  $\text{KH}_2\text{PO}_4$  in 50% aqueous formamide, pH 5.6; buffer B, buffer A + 0.6 M  $(\text{NH}_4)_2\text{SO}_4$ ; flow rate 1 mL  $\text{min}^{-1}$ ; linear gradient from 0 to 60% buffer B in 30 min) and desalted. The preparation of the fluorescently tagged oligodeoxyribonucleotide probe 5'-d(CX<sub>5</sub>ATATCATCTTTGGTGT)-3' (**F1**), where X stands for *N}^6*-(6-aminoethyl) 2'-deoxycytidine bearing an amino-tethered photoluminescent lanthanide chelate, {2,2',2'',2'''-[(4'-{4'''-[(4,6-dichloro-1,3,5-triazin-2-yl)amino]phenyl}-2,2':6',2''-terpyridine-6,6''-diyl)bis(methylenenitrilo)]}tetrakis(acetato)europium(III), has been described earlier (49, 51).

**Hybridization Assays.** Hybridization assays were carried out in a Tris buffer (50 mmol  $\text{L}^{-1}$ , pH = 7.5, containing 0.5 mol  $\text{L}^{-1}$  NaCl and 0.01% Tween 20). Typically 50 oligonucleotide coated particles (**P1–P16** in Table) were shaken in 10  $\mu\text{L}$  of buffer containing the target oligonucleotide (**O1–O27**) and the fluorescently tagged probe at a concentration of 17 nmol  $\text{L}^{-1}$ . The mixtures were shaken in sealed tubes with rotamix (15 rpm) at 25  $^{\circ}\text{C}$  overnight. The particles were then rapidly washed with buffer, and 10 of the particles were subjected one after another to a time-resolved measurement of the fluorescence emission directly from the particle (48). The standard deviation ranged from 5 to 20%. As shown previously (49–53), the unspecific binding was always less than 1%. The emission signal was converted to the number of the fluorescently tagged probes attached to the particle with the aid of a calibration line obtained by determining the amount of europium(III) ions released from the particle by the DELFIA protocol (60), as described previously in more detail (51, 53).

## RESULTS AND DISCUSSION

**Preparation of the Oligonucleotide-Coated Particles.** The particles used as the solid support in the mixed-phase sandwich-type hybridization assays (Scheme 1) were uniformly sized (50  $\mu\text{m}$ ) porous particles of SINTEF that were made of a copolymer of glycidyl methacrylate (40%) and ethylene dimethylacrylate (60%) and functionalized with primary amino groups (1 mmol  $\text{g}^{-1}$ ) by reacting the particle-bound epoxy groups with diethylenetriamine. The resin-bound aminoalkyl sidearms were elongated by acylating the amino groups with 15-[(4,4'-dimethoxytrityl)oxy]-12,13-dithiapentadecanoic acid (58), and the terminal mercapto function was exposed by reductive cleavage of the disulfide bond (Scheme 2). 2-Pyridyl disulfide activated oligonucleotides, bearing the activated sidearm at various sites of the 12-mer sequence, were then prepared as depicted in Scheme 3 and attached to the mercapto-derivatized particles via spontaneous disulfide bond formation in aqueous solution. Accordingly, the linker between the resin and the nucleic acid base is 36 and 32 atoms long on using immobilization through uracil and cytosine bases, re-

**Scheme 2. Preparation of Mercapto-Functionalized Particles****Table 1. Oligodeoxyribonucleotide Sequences Attached to the Particles<sup>a</sup>**

sequence on the particle <sup>b,c</sup>	sequence on the particle
<b>P1</b> S-T*GA TTC ATC GCT-5'	<b>P9</b> S-T*GA CGA TCT CAT-5'
<b>P2</b> S-TGA T*TC ATC GCT-5'	<b>P10</b> S-TGA C*GA TCT CAT-5'
<b>P3</b> S-TGA TTC ATC GCT*-5'	<b>P11</b> S-TGA CGA TC*T CAT-5'
<b>P4</b> S-TGA TTC ATC GCT*-5'	<b>P12</b> S-TGA CGA TCT CAT*-5'
<b>P5</b> S-T*AG TCA GTC GTT-5'	<b>P13</b> S-T*GA TCT ACT GAT-5'
<b>P6</b> S-TAG T*CA GTC GTT-5'	<b>P14</b> S-TGA T*CT ACT GAT-5'
<b>P7</b> S-TAG TCA GT*C GTT-5'	<b>P15</b> S-TGA TCT AC*T GAT-5'
<b>P8</b> S-TAG TCA GTC CTT*-5'	<b>P16</b> S-TGA TCT ACT GAT*-5'

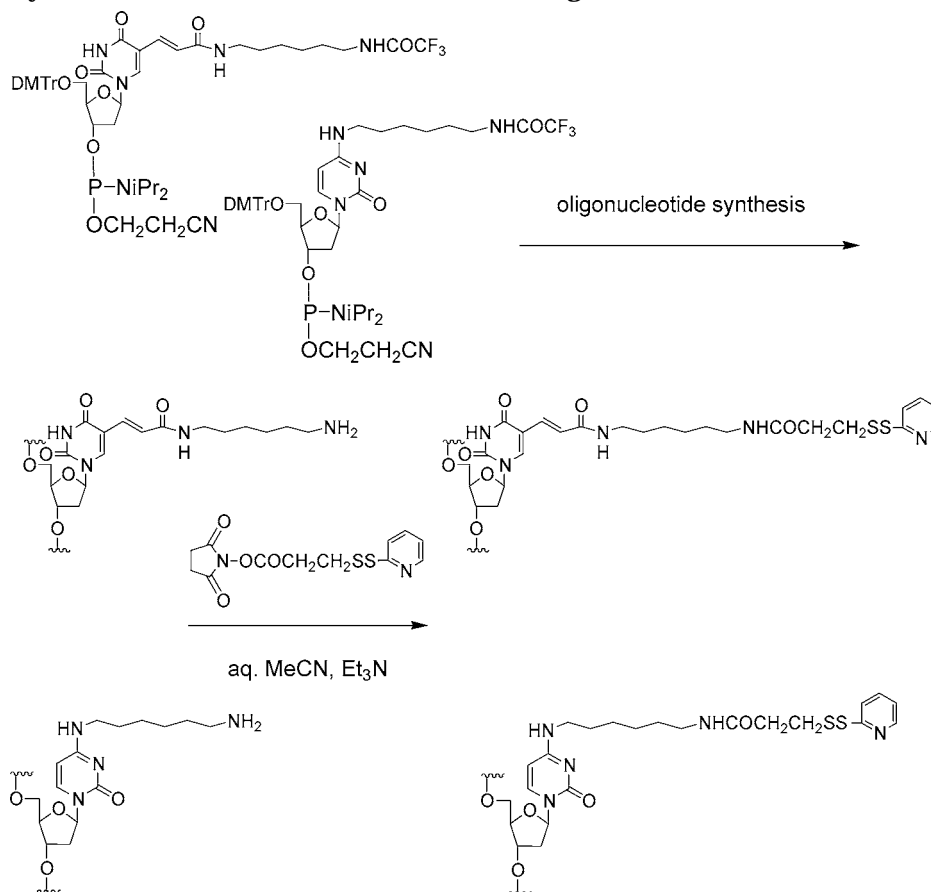
<sup>a</sup> For the structure of the linkers employed, see Chart 1. <sup>b</sup> S stands for the polymer particle. <sup>c</sup> The nucleosidic unit used for tethering is indicated by an asterisk (N\*).

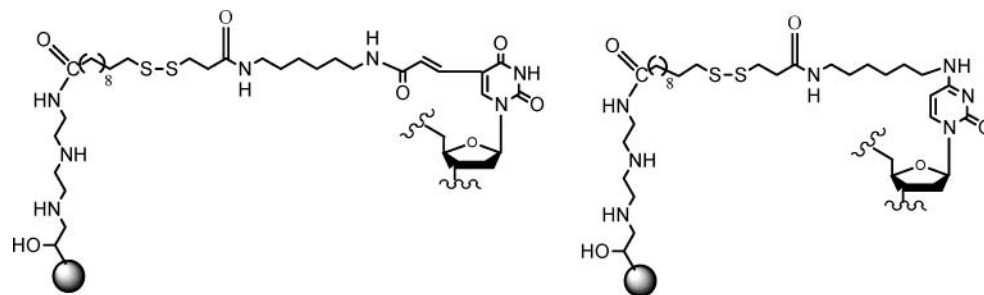
spectively. Such linkers may be expected to allow rather unhindered hybridization, since the optimal length has been previously reported to be 40 atoms (57). Table 1 lists the oligonucleotide-coated particles (**P1–P16**) prepared.

**Relationship between the Site of the Immobilization Site and Duplex Stability.** The binding efficiency of 27 oligodeoxyribonucleotides (**O1–O27**) to particles

bearing a complementary sequence (**P1–P16**) was determined by a sandwich-type setup (Scheme 1). The 5'-terminal region of these oligonucleotides was over 12 nucleotides fully or partly complementary to the support-bound probe, while a common 16 nucleotide long sequence at the 3'-terminus served to bind the fluorescently tagged probe, 5'-d(CX<sub>5</sub>ATATCATCTTTGGTGT)-3' (**F1**), where X stands for a N<sup>6</sup>-(6-aminohexyl)-2'-deoxycytidine unit labeled at the amino group with a photoluminescent lanthanide chelate. The complementarity over 16 nucleotides is sufficient to warrant virtually quantitative duplex formation between **F1** and the target oligonucleotide (**O1–O27**) (51). The intensity of the emission signal measured directly from a single particle is over a wide range proportional to the amount of the fluorescently tagged probe bound to the particle, since the quenching is negligible with photoluminescent lanthanide chelates (49–51).

Table 2 records the affinity of 14 different target sequences (**O1–O14**) to the sequence 3'-TGA TTC ATC GCT-5' immobilized to the polymer particles in four different manners (**P1–P4**). The affinity is given as the amount of the target oligonucleotide hybridized to the support-bound probes divided by the total amount of the target oligonucleotide in the assay [ $n(\text{bounds})/n(\text{total})$ ]. Among the target oligonucleotides studied, **O1** and **O2** are fully complementary with the particle-bound probe (**P1–P4**) over 12 and 11 adjacent bases, respectively, while **O3–O5** all are complementary to **P1–P4** over a sequence of 10 bases. All these oligonucleotides behave similarly: the affinity is markedly reduced when the probe is tethered to the particle through an internal (**P2**, **P3**) or 5'-terminal (**P4**) thymine base instead of the 3'-terminal base (**P1**). The markedly lower hybridization

**Scheme 3. 2-Pyridyl Disulfide Activation of Amino-Tethered Oligonucleotides**

**Chart 1. Linker Structures of the Oligonucleotide-Coated Particles****Table 2. Effect of the Site of Immobilization on the Hybridization Efficiency of Support-Bound Probes, P1–P4, at pH 7.5 and 25 °C<sup>a</sup>**

	target oligonucleotide <sup>b</sup>	P1	P2	P3	P4
<b>O1</b>	5'-ACTAAGTAGCGA-[oligo]-3'	0.28	0.08	0.05	0.15
<b>O2</b>	5'-ACTAAGTAGCGT-[oligo]-3'	0.27	0.08	0.03	0.08
<b>O3</b>	5'-ACTAAGTAGCTT-[oligo]-3'	0.19	0.07	0.02	0.03
<b>O4</b>	5'-CTAAGTAGCGT-[oligo]-3'	0.24	0.07	0.03	0.12
<b>O5</b>	5'-TAAGTAGCGA-[oligo]-3'	0.23	0.03	0.02	0.14
<b>O6</b>	5'-AGTAAGTAGCGA-[oligo]-3'	0.33	0.06	0.02	0.09
<b>O7</b>	5'-ACTAATTAGCGA-[oligo]-3'	0.07	0.03	0.01	0.03
<b>O8</b>	5'-ACTAAGTATCGA-[oligo]-3'	0.06	0.03	0.01	0.03
<b>O9</b>	5'-AGTAAGTAGCGT-[oligo]-3'	0.17	0.07	0.01	0.04
<b>O10</b>	5'-ACTAATTAGCGT-[oligo]-3'	0.07	0.03	0.00	0.02
<b>O11</b>	5'-ACTAAGTATCGT-[oligo]-3'	0.06	0.02	0.00	0.01
<b>O12</b>	5'-AGTAAGTAGCTT-[oligo]-3'	0.07	0.02	0.00	0.01
<b>O13</b>	5'-ACTAATTAGCTT-[oligo]-3'	0.03	0.00	0.00	0.00
<b>O14</b>	5'-ACTAAGTATCTT-[oligo]-3'	0.03	0.00	0.00	0.00

<sup>a</sup> The hybridization efficiency is given as  $n(\text{bound})/n(\text{total})$  for the target oligonucleotide (**O1–O8**). <sup>b</sup> The abbreviation [oligo] stands for the sequence 5'-ACACCAAGATGATATT-3', in which the nucleotides given in *italics* were used to bind the fluorescently tagged oligonucleotide **F1**. The sequence engaged in duplex formation is indicated in bold. The mismatched base is underlined.

**Table 3. Effect of the Site of Immobilization on the Hybridization Efficiency of Support-Bound Probes, P5–P8, at pH 7.5 and 25 °C<sup>a</sup>**

	target oligonucleotide <sup>b</sup>	P5	P6	P7	P8
<b>O15</b>	5'-ATCAGTCAGCAA-[oligo]-3'	0.28	0.34	0.12	0.26
<b>O16</b>	5'-ATCAGTCAGCAT-[oligo]-3'	0.24	0.22	0.14	0.33
<b>O17</b>	5'-ATCAGTCAGCTT-[oligo]-3'	0.31	0.19	0.10	0.25

<sup>a</sup> The hybridization efficiency is given as  $n(\text{bound})/n(\text{total})$  for the target oligonucleotide (**O9–O22**). <sup>b</sup> See footnote *b* in Table 2.

efficiency of the 5'-immobilized probes compared to their 3'-bound counterparts could possibly be attributed to steric hindrances resulting from interaction of the dangling end of **O1–O5** and, hence, also the fluorescently tagged probe **F1**, containing five bulky chelates, with the support. The fact that tethering through an internal base moiety (**P2**, **P3**) retards the hybridization even more markedly than immobilization through the 5'-terminal base does not, however, lend support to this interpretation, but suggests that intrachain and to a lesser extent 5'-immobilization restrict the conformational flexibility of the probe more severely than the 3'-tethering, and hence the hybridization is retarded.

Tables 3–5 summarize the corresponding data on the hybridization fully complementary oligonucleotides of three other probes, all immobilized in four different manners: hybridization of **O15–O17** to **P5–P8** (Table 3), **O18–O22** to **P9–P12** (Table 4), and **O23–O27** to **P13–P16** (Table 5). The results are very similar to those discussed above. The data in Tables 4 and 5 is consistent with the conclusions drawn above: the hybridization

**Table 4. Effect of the Site of Immobilization on the Hybridization Efficiency of Support-Bound Probes, P9–P12, at pH 7.5 and 25 °C<sup>a</sup>**

	target oligonucleotide <sup>b</sup>	P9	P10	P11	P12
<b>O18</b>	5'-ACTGCTAGAGTA-[oligo]-3'	0.28	0.05	0.02	0.06
<b>O19</b>	5'-ACTGCTAGAGTT-[oligo]-3'	0.36	0.05	0.03	0.09
<b>O20</b>	5'-ACTGCTAGAGAT-[oligo]-3'	0.43	0.04	0.02	0.13
<b>O21</b>	5'-TGCTAGAGTA-[oligo]-3'	0.33	0.07	0.02	0.07
<b>O22</b>	5'-CTGCTAGAGTT-[oligo]-3'	0.41	0.06	0.02	0.10

<sup>a</sup> The hybridization efficiency is given as  $n(\text{bound})/n(\text{total})$  for the target oligonucleotide (**O23–O27**). <sup>b</sup> See footnote *b* in Table 2.

**Table 5. Effect of the Site of Immobilization on the Hybridization Efficiency of Support-Bound Probes, P13–P16, at pH 7.5 and 25 °C<sup>a</sup>**

	target oligonucleotide <sup>b</sup>	P13	P14	P15	P16
<b>O23</b>	5'-ACTAGTACTA-[oligo]-3'	0.18	0.11	0.01	0.05
<b>O24</b>	5'-ACTAGTACTT-[oligo]-3'	0.23	0.09	0.02	0.08
<b>O25</b>	5'-ACTAGTACAT-[oligo]-3'	0.31	0.05	0.01	0.08
<b>O26</b>	5'-TAGTACTA-[oligo]-3'	0.22	0.06	0.00	0.03
<b>O27</b>	5'-CTAGTACTT-[oligo]-3'	0.27	0.07	0.01	0.07

<sup>a</sup> The hybridization efficiency is given as  $n(\text{bound})/n(\text{total})$  for the target oligonucleotide (**O28–O32**). <sup>b</sup> See footnote *b* in Table 2.

efficiency is decreased in the order **P1** > **P4** > **P2**, **P3**. Nevertheless, exceptions from this general trend appear to occur. Targets **O15–O17** do not exhibit a higher affinity to the 3'-tethered probes (**P5**) than to the intrachain (**P6**, **P7**) or 5'-immobilized (**P8**) oligonucleotides.

Another interesting question is how does the site of immobilization influence on the detection of a one-base mismatch at different parts of the probe. We have shown previously (53) that a one-base mismatch close to the 3'-end of a 3'-immobilized probe does not noticeably destabilize the duplex, while a similar mismatch in the central or 5'-terminal part of the probe reduces the hybridization efficiency by 1–2 orders of magnitude. The results of the present study are consistent fairly well with those observations. For example, a point mismatch at the penultimate position of the 5'-end of target **O6**, i.e., a site that becomes close to the 3'-end of the support-bound probe upon hybridization, does not reduce the hybridization to a 3'-immobilized probe (**P1**), but increasingly does so on shifting the site of immobilization toward the 5'-terminus (**P2** → **P3** → **P4**). When the mismatch is situated in the central part of the particle-bound probe, as on using **O7** or **O8** as a target, it becomes recognized by all the probes (**P1–P4**). Accordingly, while an intrachain tethering markedly reduces the efficiency of hybridization, it simultaneously allows rather reliable detection of a single base polymorphism at any site of the target. The affinities of the targets having a shorter complementary region (**O9–O14**) are too low to allow firm conclusions, but the behavior seems to be similar to that discussed above.



In summary, the results of the present study indicate that the selectivity of hybridization that may be achieved with a probe of a given length are markedly dependent on the site of immobilization within the probe. The 3'-immobilization generally allows more efficient hybridization than 5'- or intrachain-tethering. Reliable detection of a one-base mismatch close to the terminus used for the immobilization is, however, difficult. In fact, intrachain tethering appears to allow a rather reliable detection of a point mutation at any site within the target. Random immobilization through various sites will probably make detection of point mutation impossible.

#### ACKNOWLEDGMENT

Financial aid from the Technology Development Agency of Finland is gratefully acknowledged. PerkinElmer Life and Analytical Sciences kindly made available microfluorometer for measurements.

#### LITERATURE CITED

- (1) Ramsay, G. (1998) DNA chips: state-of-the-art. *Nature Biotechnol.* **16**, 40–44.
- (2) Niemeyer, C. M., and Blohm, D. (1999) DNA microarrays. *Angew. Chem., Int. Ed.* **38**, 2865–2869.
- (3) Aharoni, A., and Vorst, O. (2002) DNA microarrays for functional plant genomics. *Plant Mol. Biol.* **48**, 99–118.
- (4) Hoheisel, J. D. (1997) Oligomer-chip technology. *Trends Biotechnol.* **15**, 465–469.
- (5) Duggan, D. J., Bittner, M., Chen, Y., Meltzer, P., and Trent, J. M. (1999) Expression profiling using cDNA microarrays. *Nature Gen.* **21** (suppl.), 10–14.
- (6) Bowtell, D. D. L. (1999) Options available -from start to finish- for obtaining expression data by microarray. *Nature Gen.* **21** (suppl.), 25–32.
- (7) Chee, M., Yang, R., Hubbell, E., Berno, A., Huang, X. C., Stern, D., Winkler, J., Lockhart, D. J., Morris, M. S., and Fodor, S. P. A. (1996) Accessing genetic information with high-density DNA arrays. *Science* **274**, 610–614.
- (8) Hacia, J. G. (1999) Resequencing and mutational analysis using oligonucleotide microarrays. *Nature Gen.* **21** (suppl.), 42–47.
- (9) Hacia, J. G., and Collins, F. S. (1999) Mutational analysis using oligonucleotide microarrays. *J. Med. Gen.* **36**, 730–736.
- (10) Cronin, M. T. (2000) DNA oligonucleotide microarrays: application to genetic polymorphism analysis, in *Genetic polymorphisms and susceptibility to disease* (Miller, M. S., and Cronin, M. T., Eds.) pp 41–66, Taylor & Francis, London.
- (11) Milner, N., Mir, K. U., and Southern, E. M. (1997) Selecting effective antisense reagents on combinatorial oligonucleotide arrays. *Nature Biotechnol.* **15**, 537–541.
- (12) Sohail, M., Akhtar, S., and Southern, E. M. (1999) The folding of large RNAs studied by hybridization to arrays of complementary oligonucleotides. *RNA* **5**, 646–655.
- (13) Mir, K. U., and Southern, E. M. (1999) Determining the influence of structure on hybridization using oligonucleotide arrays. *Nature Biotechnol.* **17**, 788–792.
- (14) Hirschhorn, J. N., Sklar, P., Lindblad-Toh, K., Lim, Y. M., Ruiz-Gutierrez, M., Bolk, S., Langhorst, B., Schaffner, S., Winchester, E., and Lander, E. S. (2000) SBE-TAGS: an array-based method for efficient single-nucleotide polymorphism genotyping. *Proc. Natl. Acad. Sci. U.S.A.* **97**, 12164–12169.
- (15) Fan, J. B., Chen, X., Halushka, M. K., Berno, A., Huang, X., Ryder, T., Lipshutz, R. J., Lockhart, D. J., and Chakravarti, A. (2000) Parallel genotyping of human SNPs using generic high-density oligonucleotide tag arrays. *Genome Res.* **10**, 853–860.
- (16) Pastinen, T., Raitio, M., Lindroos, K., Tainola, P., Peltonen, L., and Syvänen, A.-C. (2000) A system for specific, high throughput genotyping by allele-specific primer extension on microarrays. *Genome Res.* **10**, 1031–1042.
- (17) Raitio, M., Lindroos, K., Laukkanen, M., Pastinen, T., Sistonen, P., and Syvänen, A.-C. (2001) Y-chromosomal snps in fenno-ugric-speaking populations analyzed by minisequencing on microarrays. *Genome Res.* **11**, 471–482.
- (18) Huber, M., Losert, D., Hiller, R., Harwanegg, C., Müller, M. W., and Schmidt, W. M. (2001) Detection of single base alterations in genomic DNA by solid-phase polymerase chain reaction on oligonucleotide microarrays. *Anal. Biochem.* **299**, 24–30.
- (19) Erdogan, F., Kirchner, R., Mann, W., Ropers, H.-H., and Nuber, U. A. (2001) Detection of mitochondrial single nucleotide polymorphisms using a primer elongation reaction on oligonucleotide microarrays. *Nucleic Acids Res.* **29**, e36.
- (20) Huber, M., Mündlein, A., Dornstauder, E., Schneeberger, C., Tempfer, C. B., Müller, M. W., and Schmidt, W. M. (2002) Accessing single nucleotide polymorphisms in genomic DNA by direct multiplex polymerase chain reaction amplification on oligonucleotide microarrays. *Anal. Biochem.* **303**, 25–33.
- (21) Fodor, S. P. A., Read, J. L., Pirrung, M. C., Stryer, L., Lu, A. T., and Solas, D. (1991) Light-directed, spatially addressable parallel chemical synthesis. *Science* **251**, 767–773.
- (22) Maskos, U., and Southern, E. M. (1992) Parallel analysis of oligodeoxyribonucleotide (oligonucleotide) interactions. I. Analysis of factors influencing oligonucleotide duplex formation. *Nucleic Acids Res.* **20**, 1675–1678.
- (23) Pease, A. C., Solas, D., Sullivan, E. J., Cronin, M. T., Holmes, C. P., and Fodor, S. P. A. (1994) Light-generated oligonucleotide arrays for rapid DNA-sequence analysis. *Proc. Natl. Acad. Sci. U.S.A.* **91**, 5022–5026.
- (24) McGall, G. H., Barone, A. D., Diggelmann, M., Fodor, S. P. A., Gentalen, E., and Ngo, N. (1997) The efficiency of light-directed synthesis of DNA arrays on glass substrates. *J. Am. Chem. Soc.* **119**, 5081–5090.
- (25) Pirrung, M. C., Fallon, L., and McGall, G. (1998) Proofing of photolithographic DNA synthesis with 3',5'-dimethoxybenzoinyloxycarbonyl-protected deoxynucleoside phosphoramidites. *J. Org. Chem.* **63**, 241–246.
- (26) Lipshutz, R. J., Fodor, S. P. A., Gingeras, T. R., and Lockhart, D. J. (1999) High-density synthetic oligonucleotide arrays. *Nature Gen.* **21** (suppl.), 20–24.
- (27) Stimpson, D. I., Hoijer, J. V., Hsieh, W. T., Jou, C., Gordon, J., Theriault, T., Gamble, R., and Baldeschwieler, J. D. (1995) Real-time detection of DNA hybridization and melting on oligonucleotide arrays by using optical waveguides. *Proc. Natl. Acad. Sci. U.S.A.* **92**, 6379–6383.
- (28) Timofeev, E. N., Kochetkova, S. V., Mirzabekov, A. D., and Florentiev, V. L. (1996) Regioselective immobilization of short oligonucleotides to acrylic copolymer gels. *Nucleic Acids Res.* **24**, 3142–3148.
- (29) Chrisey, L. A., Lee, G. U., and O'Farrell, C. E. (1996) Covalent attachment of synthetic DNA to self-assembled monolayer films. *Nucleic Acids Res.* **24**, 3031–3039.
- (30) Joos, B., Kuster, H., and Cone, R. (1997) Covalent attachment of hybridizable oligonucleotides to glass support. *Anal. Biochem.* **247**, 96–101.
- (31) McGovern, M. E., and Thompson, M. (1999) Thiol functionalization of surfaces for biosensor development. *Can. J. Chem.* **77**, 1678–1689.
- (32) Gerry, N. P., Witowski, N. E., Day, J., Hammer, R. P., Barany, G., and Barany, F. (1999) Universal DNA microarray method for multiplex detection of low abundance point mutations. *J. Mol. Biol.* **292**, 251–262.
- (33) Budach, W., Abel, A. P., Bruno, A. E., and Neuschafer, D. (1999) Planar waveguides as high-performance sensing platforms for fluorescence-based multiplexed oligonucleotide hybridization assays. *Anal. Chem.* **71**, 3347–3355.
- (34) Rogers, Y. H., Jiang-Baucom, P., Huang, Z. J., Bogdanov, V., Anderson, S., and Boyce-Jacino, M. T. (1999) Immobilization of oligonucleotides onto a glass support via disulfide bonds: a method for preparation of DNA microarrays. *Anal. Biochem.* **266**, 23–30.
- (35) Beier, M., and Hoheisel, J. D. (1999) Versatile derivatization of solid support media for covalent bonding on DNA-microchips. *Nucleic Acids Res.* **27**, 1970–1977.
- (36) Pirrung, M. C., Davis, J. D., and Odenbaugh, A. L. (2000) Novel reagents and procedures for immobilization of DNA on glass microchips for primer extension. *Langmuir* **16**, 2185–2191.

- (37) Kumar, A., Larsson, O., Parodi, D., and Liang, Z. (2000) Silanized nucleic acids: a general platform for DNA immobilizations. *Nucleic Acids Res.* **28**, e71.
- (38) Lenigk, R., Carles, M., Ip, N. Y., and Sucher, N. J. (2001) Surface characterization of a silicon-chip-based DNA microarray. *Langmuir* **17**, 2497–2501.
- (39) Zhao, X., Nampalli, S., Serino, A. J., and Kumar, S. (2001) Immobilization of oligodeoxyribonucleotides with multiple anchors to microchips. *Nucleic Acids Res.* **29**, 955–959.
- (40) Bordini, R., Consolandi, C., Castiglioni, B., Busti, E., Bernardi, L. R., Battaglia, C., and De Bellis, G. (2002) Investigation of the multiple anchors approach in oligonucleotide microarray preparation using linear and stem-loop structural probes. *Nucleic Acids Res.* **30**, e34.
- (41) Cheung, V. G., Morley, M., Aguilar, F., Massimi, A., Kuchlerlapati, R., and Childs, G. (1999) Making and reading microarrays. *Nature Gen.* **21** (suppl.), 15–19.
- (42) Edman, C., Raymond, D., Wu, D., Tu, E., Sosnowski, R., Butler, W., Nerenberg, M., and Heller, M. (1998) Electric field directed nucleic acid hybridization on microchips. *Nucleic Acids Res.* **25**, 4907–14.
- (43) Dolan, P. L., Wu, Y., Ista, L. K., Metzenberg, R. L., Nelson, M. A., and Lopez, G. P. (2001) Robust and efficient synthetic method for forming DNA microarrays. *Nucleic Acids Res.* **29**, e107.
- (44) Belosludtsev, Y., Iverson, B., Lemeshko, S., Eggers, R., Wiese, R., Lee, S., Powdrill, T., and Hogan, M. (2001) DNA microarrays based on noncovalent oligonucleotide attachment and hybridization in two dimensions. *Anal. Biochem.* **292**, 250–256.
- (45) Fotin, A. V., Drobyshev, A. L., Proudnikov, D. Y., Perov, A. N., and Mirzabekov, A. D. (1998) Parallel thermodynamic analysis of duplexes on oligodeoxyribonucleotide microchips. *Nucleic Acids Res.* **26**, 1515–1521.
- (46) Southern, E., Mir, K., and Shchepinov (1999) Molecular interactions on microarrays. *Nature Gen.* **21** (suppl.), 5–9.
- (47) Peterson, A. W., Heaton, R. J., and Georgiadis, R. M. (2001) The effect of surface probe density on DNA hybridization. *Nucleic Acids Res.* **29**, 5163–5168.
- (48) Lövgren, T., Heinonen, P., Hakala, H., Heinola, J., Harju, R., Takalo, H., Mikkala, V.-M., Schmid, R., Lönnberg, H., Pettersson, K., and Iitiä, A. (1997) Sensitive bioaffinity assays on individual microparticles using time-resolved fluorometry. *Clin. Chem.* **43**, 1937–1943.
- (49) Hakala, H., and Lönnberg, H. (1997) Time-resolved fluorescence detection of oligonucleotide hybridization on a single microparticle: covalent immobilization of oligonucleotides and quantitation of a model system. *Bioconjugate Chem.* **8**, 232–237.
- (50) Hakala, H., Heinonen, P., Iitiä, A., and Lönnberg, H. (1997) Detection of oligonucleotide hybridization on a single microparticle by time-resolved fluorometry: hybridization assays on polymer particles obtained by direct solid phase assembly of oligonucleotide probes. *Bioconjugate Chem.* **8**, 232–237.
- (51) Hakala, H., Mäki, E., and Lönnberg, H. (1998) Detection of oligonucleotide hybridization on a single microparticle by time-resolved fluorometry: quantitation and optimization of a sandwich type assay. *Bioconjugate Chem.* **9**, 316–321.
- (52) Hakala, H., Virta, P., Salo, H., and Lönnberg, H. (1998) Simultaneous detection of several oligonucleotides by time-resolved fluorometry: the use of a mixture of categorized microparticles in a sandwich type mixed-phase hybridization assay. *Nucleic Acids Res.* **26**, 5581–5588.
- (53) Ketomäki, K., Hakala, H., and Lönnberg, H. (2002) Mixed-phase hybridization of short oligodeoxyribonucleotides on microscopic polymer particles: effect of one-base mismatches on duplex stability. *Bioconjugate Chem.* **13**, 542–547.
- (54) Chakravarti, A. (1999) Population genetics -making sense out of sequence. *Nature Gen.* **21** (suppl.), 56–60.
- (55) Cole, K. A., Krizman, D. B., and Emmert-Buck, M. R. (1999) The genetics of cancer -a 3D model. *Nature Gen.* **21** (suppl.), 38–41.
- (56) Urakawa, H., Noble, P. A., El Fantroussi, S., Kelly, J. J., and Stahl, D. A. (2002) Single-base-pair discrimination of terminal mismatches by using oligonucleotide microarrays and neural network analyses. *Appl. Environ. Microbiol.* **68**, 235–244.
- (57) Shchepinov, M. S., Case-Green, S. C., and Southern, E. M. (1997) Steric factors influencing hybridization of nucleic acids to oligonucleotide arrays. *Nucleic Acids Res.* **25**, 1155–1161.
- (58) Salo, H., Guzaev, A., and Lönnberg, H. (1998) Disulfide-tethered solid supports for synthesis of photoluminescent oligonucleotide conjugates: hydrolytic stability and labeling on the support. *Bioconjugate Chem.* **9**, 365–371.
- (59) Hovinen, J. (1998) A simple synthesis of N<sup>6</sup>-(6-aminohexyl)-2'-deoxy-5'-O-(4,4'-dimethoxytrityl)cytidine. *Nucleosides Nucleotides* **17**, 1209–1213.
- (60) Hemmilä, I., Dakabu, S., Mikkala, V.-M., Siitari, H., and Lövgren, T. (1984) Europium as a label in time-resolved immunofluorometric assays. *Anal. Biochem.* **137**, 335–343.

BC0340058

# Glycodendritic Structures Based on Boltorn Hyperbranched Polymers and Their Interactions with *Lens culinaris* Lectin

Eva Arce,<sup>†</sup> Pedro M. Nieto,<sup>†</sup> Vicente Díaz,<sup>‡</sup> Rossana García Castro,<sup>§</sup> Antonio Bernad,<sup>§,‡</sup> and Javier Rojo<sup>\*,†</sup>

Grupo de Carbohidratos, Instituto de Investigaciones Químicas, CSIC, Isla de la Cartuja, Américo Vespucio s/n, E-41092 Sevilla, Spain, and Departamento de Inmunología y Oncología and Genetrix S.L., Centro Nacional de Biotecnología, CSIC, Cantoblanco, E- 28049 Madrid, Spain. Received January 20, 2003; Revised Manuscript Received March 4, 2003

Multivalent scaffolds bearing carbohydrates have been prepared to mediate biological processes where carbohydrates are involved. These systems consist of dendritic structures based on Boltorn H20 and H30 hyperbranched polymers to which carbohydrates are linked through a convenient spacer. Mannose has been chosen as a sugar unit to test the viability of this strategy. These glycodendritic compounds have been prepared in a few steps with good yields, showing a high solubility in physiological media and low toxicity. The binding of these dendritic polymers to the mannose-binding lectin *Lens culinaris* (LCA) was studied using STD-NMR experiments and quantitative precipitation assays. The results demonstrate the existence of a clear interaction between the mannose derivative systems and the *Lens* lectin where the dendritic scaffold does not have an important role in mannose binding but supplies the necessary multivalence for lectin cluster formation. These glycodendritic structures are able to interact with a receptor, and therefore they can be considered as promising tools for biological studies.

## INTRODUCTION

Carbohydrates play important roles in many biological processes as embryogenesis, differentiation, morula compaction, metastasis, etc. They are involved in cell–cell and cell–extracellular matrix adhesion and recognition processes through the interaction with their receptors (proteins and carbohydrates). These interactions show strong divalent cation dependence and low affinity, which is compensated in Nature by multivalent presentation of carbohydrates (1). During the past decade, chemists have focused their efforts on preparing multivalent carbohydrate model systems to study and interfere with biological processes in which carbohydrates are involved. Among the multivalent systems used, the most common are liposomes (2, 3), dendrimers (4), calixarenes (5), cyclodextrins (6), oligomers and polymers (7), and nanoparticles (8).

Dendrimers with a high degree of versatility are probably the most developed and popular multivalent systems. Unfortunately, they suffer from disadvantages, namely their tedious and expensive synthesis with several steps of separation and purification. Dendritic hyperbranched polymers, in contrast to linear polymers, present many features in common with dendrimers with the advantage of an easier synthesis with low cost (9). However, unlike dendrimers, hyperbranched polymers have to be considered only as a dendritic scaffolds presenting a polydispersity > 1 while dendrimers are monodisperse (10).

An example using successfully dendritic polymers as scaffolds for multivalent presentation of carbohydrates is PAMAM (polyamidoamine) (11); although commercially available, PAMAM is relatively expensive. In contrast, Boltorn polymers are inexpensive, commercially available hyperbranched polymers based on 2,2-bis(hydroxymethyl)propionic acid as a AB<sub>2</sub> monomer and 2,2-bis(hydroxymethyl)-1,3-propanediol as central core (12). They are supplied with different degrees of branching (generation) having a different number of primary hydroxyl groups on their surface to be functionalized: Boltorn H20 (16 OH), Boltorn H30 (32 OH), and Boltorn H40 (64 OH). Applications of Boltorn polymers have been mainly focused on their use as coatings and additives for plastics with the only exception of its use as a soluble solid support for oligosaccharides synthesis (13). To our best knowledge, these dendritic polymers have never been considered as scaffolds for multivalent presentation of biologically important ligands and for their potential application to study and intervene in biological processes (14).

Here, we present a direct strategy for the preparation of glycodendritic structures based on Boltorn polymers BH20 and BH30 (Figure 1) as a dendritic support functionalized with  $\alpha$ -D-mannose (1 and 2, respectively). Mannose oligosaccharide structures are found coating the surface of numerous infection agents such as viruses, bacteria, and fungi. Specific receptors for mannose are expressed on the surface of cells as dendritic cells and macrophages, involved on the immune system and responsible of antigen presentation (15). A natural ligand for these receptors is mannan, a highly branched mannose-containing polysaccharide isolated mainly from *Saccharomyces cerevisiae*. It consists of a  $\alpha$ (1–6) linked mannose backbone with branches of  $\alpha$ (1–2) and  $\alpha$ (1–3) linked mannose (16, 17). This mannosylated compound

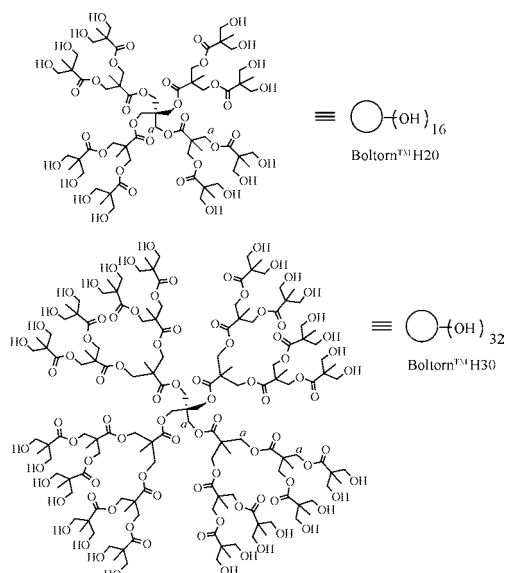
\* To whom correspondence should be addressed. E-mail: javier.rojo@iiq.cartuja.csic.es. Tel.: + 34 95 448 95 68; Fax: + 34 95 446 0565.

<sup>†</sup> Grupo de Carbohidratos.

<sup>‡</sup> Departamento de Inmunología y Oncología. Fax: + 34 91 372 0493.

<sup>§</sup> Genetrix S.L.





**Figure 1.** BoltornH20 (BH20) and BoltornH30 (BH30).

presents a high affinity for mannose receptors as legume lectins (18, 19). However, mannan cannot be used as therapeutics *in vivo* due to its toxicity and its mitogenic effect (20, 21). The design and preparation of highly mannosylated systems as potential tools for blocking the entry of these types of pathogens are of great interest (22–24). Also, the fact that mannose receptors are found in dendritic cells and macrophages can be used to stimulate the immune system through their interactions with compounds presenting antigens (25). To test the binding capabilities of our glycodendritic structures, we have selected the *Lens culinaris* lectin (LCA) which specifically recognizes glucose and mannose (26).

Lectins are a large and diverse family of proteins (many of them are commercially available) presenting carbohydrate recognition domains capable to recognize carbohydrates specifically. For this reason, they are considered as ideal models to study carbohydrate–protein interactions with new neoglycosystems. We have performed two different binding experiments with LCA and glycodendritic structures **1** and **2**: a quantitative precipitation assay and an NMR study based on saturation transfer difference (STD) experiments. These experiments have allowed demonstration of the existence of the interaction and determination of the part of the molecule involved in binding process.

Finally, cytotoxicity studies were carried out to determine the scope and the future applications of these glycodendritic systems *in vitro* and *in vivo* experiments.

#### EXPERIMENTAL PROCEDURES

**Materials.** All chemicals were obtained from Aldrich and used without further purification, unless otherwise noted. *Lens culinaris* lectin (LCA) was purchased from Sigma. Boltorn H20 and Boltorn H30 were supplied by Perstorp Specialty Chemicals. Dendritic structures were purified by dialysis against water, using water/benzoylated cellulose dialysis tubing, flat width 32 mm, MW cutoff 1 kDa obtained from Sigma.  $^1\text{H}$  and  $^{13}\text{C}$  NMR were recorded on Bruker Avance DPX 300, DRX 400, and DRX 500 MHz spectrometers. Chemical shift are in ppm with respect to TMS (Tetramethylsilane) using manufacturer indirect referencing method. 2D experiments (COSY, TOCSY, ROESY, and HMQC) were performed when necessary to assign the dendritic structures spectra. IR

spectra were recorded on a Bruker Vector 22. Optical rotations were measured with a Perkin-Elmer 341 polarimeter.

**Preparation of BH20sucOH 5.** To a solution of Boltorn H20 (5.0 g, 2.86 mmol) in pyridine (30 mL) were added succinic anhydride (5.44 g, 54.3 mmol, 1.2 equiv per OH) and a catalytic amount of DMAP (ca. 100 mg), and the mixture was stirred overnight at room temperature and concentrated. The residue was dissolved in water and concentrated again. Lyophilization afforded BH20sucOH (10.2 g, quant.) as a white solid.  $^1\text{H}$  NMR (DMSO- $d_6$ , 500 MHz):  $\delta$  4.08 (m, 56H, 28  $\text{CH}_2\text{OCO}$ ), 2.48 (m,  $2 \times 32\text{H}$ , 16  $\text{OCOCH}_2\text{CH}_2\text{COOH}$ ), 1.14 (m, 36H, 12  $\text{CH}_3$ );  $^1\text{H}$  NMR ( $\text{CD}_3\text{CN}$ , 500 MHz):  $\delta$  9.3 (broad s, 16H, 16 COOH), 4.23 (m, 56H, 28  $\text{CH}_2\text{OCO}$ ), 2.58 (m,  $2 \times 32\text{H}$ , 16  $\text{OCOCH}_2\text{CH}_2\text{COOH}$ ), 1.25 (m, 36H, 12  $\text{CH}_3$ );  $^{13}\text{C}$  NMR (DMSO- $d_6$ , 100 MHz):  $\delta$  176.3 (COOH), 176.0 (COO), 174.4 (COO), 67.7 ( $\text{CH}_2\text{O}$ ), 48.8 (C), 31.5 and 31.3 ( $\text{OCOCH}_2\text{CH}_2\text{COOH}$ ), 19.7 ( $\text{CH}_3$ );  $^{13}\text{C}$  NMR ( $\text{CD}_3\text{CN}$ , 125 MHz):  $\delta$  174.1 (COOH), 172.9 (COO), 172.8 (COO), 66.3 ( $\text{CH}_2\text{O}$ ), 47.3 (C), 29.6 and 29.2 ( $\text{OCOCH}_2\text{CH}_2\text{COOH}$ ), 17.9 ( $\text{CH}_3$ ); IR (KBr):  $\nu$  3415, 1731, 1695, 1470  $\text{cm}^{-1}$ .

**Preparation of BH30sucOH 6.** To a solution of Boltorn H30 (3.0 g, 0.88 mmol) in pyridine (30 mL) were added succinic anhydride (3.40 g, 34.0 mmol, 1.2 equiv per OH) and a catalytic amount of DMAP (ca. 100 mg), and the mixture was stirred overnight at room temperature and concentrated. The residue was dissolved in water and concentrated again. Lyophilization afforded BH30sucOH (5.83 g, quant.) as a white solid.  $^1\text{H}$  NMR (DMSO- $d_6$ , 500 MHz):  $\delta$  4.12 (m, 120H, 60  $\text{CH}_2\text{O}$ ), 2.48 and 2.42 (2m,  $2 \times 64\text{H}$ , 32  $\text{OCOCH}_2\text{CH}_2\text{COOH}$ ), 1.14 (m, 84H, 28  $\text{CH}_3$ );  $^1\text{H}$  NMR ( $\text{CD}_3\text{CN}$ , 500 MHz):  $\delta$  4.18 (m, 120H, 60  $\text{CH}_2\text{OCO}$ ), 2.54 (m,  $2 \times 64\text{H}$ , 32  $\text{OCOCH}_2\text{CH}_2\text{COOH}$ ), 1.20 (m, 84H, 28  $\text{CH}_3$ );  $^{13}\text{C}$  NMR ( $\text{CD}_3\text{CN}$ , 125 MHz):  $\delta$  174.2 (COOH), 173.0 (COO), 172.9 (COO), 66.3 ( $\text{CH}_2\text{O}$ ), 47.4 (C), 29.1 ( $\text{OCOCH}_2\text{CH}_2\text{COOH}$ ), 17.9 ( $\text{CH}_3$ ); IR (KBr):  $\nu$  3415, 1735, 1695, 1475  $\text{cm}^{-1}$ .

**Preparation of BH20sucMan 1.** To a solution of 2-aminoethyl- $\alpha$ -D-mannopyranoside (**10**) (27 mg, 0.123 mmol, 1.2 equiv per OH) and BH20sucOH **5** (20 mg, 6.39  $\mu\text{mol}$ ) in DMF: $\text{CH}_2\text{Cl}_2$  1:1 (5 mL) were added DIC (48  $\mu\text{L}$ , 0.307 mmol, 3 equiv per OH) and HOBT (41 mg, 0.307 mmol, 3 equiv per OH). The reaction mixture was stirred at room temperature for 24 h and then evaporated. The residue was washed with  $\text{Et}_2\text{O}$  and purified by dialysis to obtain compound **1** (22 mg, 60%) as a white lyophilizate.  $[\alpha]_D = +17$  ( $c = 0.9$ ,  $\text{H}_2\text{O}$ );  $^1\text{H}$  NMR ( $\text{D}_2\text{O}$ , 300 MHz):  $\delta$  4.85 (s, 16H,  $\text{H}_1$ ), 4.36–4.19 (m, 56H,  $\text{H}_a$ ), 3.92 (m, 16H,  $\text{H}_2$ ), 3.86 (m, 16H,  $\text{H}_6$ ), 3.76 (m, 16H,  $\text{H}_b$ ), 3.74 (m, 16H,  $\text{H}_6$ ), 3.69 (m, 16H,  $\text{H}_3$  or  $\text{H}_4$ ), 3.62 (m, 16H,  $\text{H}_3$  or  $\text{H}_4$ ), 3.61 (m, 16H,  $\text{H}_5$ ), 3.55 (m, 16H,  $\text{H}_c$ ), 3.40 (m, 32H,  $\text{H}_d$ ), 2.67 (m, 32H,  $\text{H}_e$ ), 2.56 (m, 32H,  $\text{H}_b$ ), 1.27 (m, 36H,  $\text{CH}_3$ );  $^{13}\text{C}$  NMR ( $\text{D}_2\text{O}$ , 75 MHz):  $\delta$  182.3 (CO), 181.6 (CO), 175.6 (CO), 100.9 ( $\text{C}_1$ ), 74.0 ( $\text{C}_5$ ), 71.2 ( $\text{C}_3$  or  $\text{C}_4$ ), 71.0 ( $\text{C}_2$ ), 68.0 ( $\text{C}_3$  or  $\text{C}_4$ ), 66.9 ( $\text{C}_a$ ), 66.8 ( $\text{C}_e$ ), 62.1 ( $\text{C}_6$ ), 47.8 (C), 40.3 ( $\text{C}_d$ ), 31.5 ( $\text{C}_c$ ), 30.9 ( $\text{C}_b$ ), 18.1 ( $\text{CH}_3$ ); IR (KBr):  $\nu$  3415, 1635, 1615, 1570  $\text{cm}^{-1}$ .

**Preparation of BH30sucMan 2.** To a solution of 2-aminoethyl- $\alpha$ -D-mannopyranoside (**10**) (26 mg, 0.116 mmol, 1.2 equiv per OH) and BH30sucOH **6** (20 mg, 3.03  $\mu\text{mol}$ ) in DMF: $\text{CH}_2\text{Cl}_2$  1:1 (5 mL) were added DIC (46  $\mu\text{L}$ , 0.291 mmol, 3 equiv per OH) and HOBT (40 mg, 0.291 mmol, 3 equiv per OH). The reaction mixture was stirred at room temperature for 24 h, then evaporated. The residue was washed with  $\text{Et}_2\text{O}$  and purified by dialysis to obtain compound **2** (27 mg, 68%) as a white lyophilizate.  $[\alpha]_D = +35$  ( $c = 0.9$ ,  $\text{H}_2\text{O}$ );  $^1\text{H}$  NMR ( $\text{D}_2\text{O}$ , 300 MHz):  $\delta$  4.84 (s, 32H,  $\text{H}_1$ ), 4.32–4.21 (m, 120H,  $\text{H}_a$ ), 3.92

(m, 32H, H<sub>2</sub>), 3.86 (m, 32H, H<sub>6</sub>), 3.76–3.57 (m, 192H, H<sub>c</sub> + H<sub>6'</sub> + H<sub>3</sub> + H<sub>4</sub> + H<sub>5</sub>), 3.40 (m, 64H, H<sub>d</sub>), 2.67 (m, 64H, H<sub>b</sub>), 2.56 (m, 64H, H<sub>c</sub>), 1.27 (m, 84H, CH<sub>3</sub>); <sup>13</sup>C NMR (D<sub>2</sub>O, 75 MHz):  $\delta$  176.2 (CO), 175.4 (CO), 175.3 (CO), 101.0 (C<sub>1</sub>), 74.2 (C<sub>5</sub>), 71.9 (C<sub>3</sub> or C<sub>4</sub>), 71.4 (C<sub>2</sub>), 68.0 (C<sub>3</sub> or C<sub>4</sub>), 67.3 (C<sub>a</sub>), 67.2 (C<sub>e</sub>), 62.2 (C<sub>6</sub>), 47.9 (C), 40.3 (C<sub>d</sub>), 31.4 (C<sub>c</sub>), 30.5 (C<sub>b</sub>), 18.4 (CH<sub>3</sub>); IR (KBr):  $\nu$  3415, 1735, 1635, 1615, 1570 cm<sup>-1</sup>.

**Preparation of BH20suclinker 3.** To a solution of 2-aminoethanol (19  $\mu$ L, 0.307 mmol, 3 equiv per OH) and BH20sucOH **5** (20 mg, 6.39  $\mu$ mol) in DMF:CH<sub>2</sub>Cl<sub>2</sub> 1:1 (5 mL) were added DIC (48  $\mu$ L, 0.307 mmol, 3 equiv per OH) and HOBT (41 mg, 0.307 mmol, 3 equiv per OH). The reaction mixture was stirred at room temperature for 24 h, then evaporated. The residue was washed with Et<sub>2</sub>O and purified by dialysis to obtain compound **3** (17 mg, 71%) as a colorless syrup. <sup>1</sup>H NMR (D<sub>2</sub>O, 400 MHz):  $\delta$  4.36–4.22 (m, 56H, H<sub>a</sub>), 3.63 (t, 32H,  $J$  = 5.7 Hz, H<sub>c</sub>), 3.31 (t, 32H,  $J$  = 5.7 Hz, H<sub>d</sub>), 2.67 (m, 32H, H<sub>b</sub>), 2.56 (m, 32H, H<sub>c</sub>), 1.27 (m, 36H, CH<sub>3</sub>); <sup>13</sup>C NMR (D<sub>2</sub>O, 100 MHz):  $\delta$  182.1 (CO), 181.3 (CO), 176.2 (CO), 66.9 (C<sub>a</sub>), 61.1 (C<sub>e</sub>), 42.5 (C<sub>d</sub>), 31.1 (C<sub>c</sub>), 30.2 (C<sub>b</sub>), 18.0 (CH<sub>3</sub>); IR (KBr):  $\nu$  3415, 1735, 1655, 1560 cm<sup>-1</sup>.

**Preparation of BH30suclinker 4.** To a solution of 2-aminoethanol (44  $\mu$ L, 0.728 mmol, 3 equiv per OH) and BH30sucOH **6** (50 mg, 7.59  $\mu$ mol) in DMF:CH<sub>2</sub>Cl<sub>2</sub> 1:1 (15 mL) were added DIC (115  $\mu$ L, 0.728 mmol, 3 equiv per OH) and HOBT (100 mg, 0.728 mmol, 3 equiv per OH). The reaction mixture was stirred at room temperature for 24 h, and then evaporated. The residue was washed with Et<sub>2</sub>O and purified by dialysis to obtain compound **4** (53 mg, 88%). <sup>1</sup>H NMR (D<sub>2</sub>O, 300 MHz):  $\delta$  4.37–4.22 (m, 120H, H<sub>a</sub>), 3.63 (t, 64H,  $J$  = 5.1 Hz, H<sub>c</sub>), 3.31 (t, 64H,  $J$  = 5.1 Hz, H<sub>d</sub>), 2.68 (m, 64H, H<sub>b</sub>), 2.57 (m, 64H, H<sub>c</sub>), 1.28 (m, 84H, CH<sub>3</sub>); <sup>13</sup>C NMR (D<sub>2</sub>O, 100 MHz):  $\delta$  182.1 (CO), 181.3 (CO), 175.6 (CO), 67.7 and 67.1 (C<sub>a</sub>), 61.4 (C<sub>e</sub>), 47.9 (C), 42.8 (C<sub>d</sub>), 31.4 (C<sub>c</sub>), 30.5 (C<sub>b</sub>), 18.3 (CH<sub>3</sub>); IR (KBr):  $\nu$  3415, 1740, 1655, 1560 cm<sup>-1</sup>.

**Quantitative Precipitation Assays.** Quantitative precipitation assays were carried out by a modification of a previously described method (27). LCA was dissolved in PBS (1 mL, 20  $\mu$ M) at pH = 7.4 containing 0.1 mM CaCl<sub>2</sub> and 0.5 mM MgCl<sub>2</sub> (PBST buffer) to make a final concentration of LCA 25  $\mu$ M (assuming MW = 49 kD). The solution was incubated for 5 h at room temperature with different concentrations of the corresponding dendritic structures and controls. After centrifugation at 10000g for 10 min, the supernatant solution was removed and the precipitated was washed two times with cold buffer. This precipitate was dissolved using a 1 M solution of methyl- $\alpha$ -D-mannopyranoside (0.8 mL) in PBST buffer. The final solution was vortexed briefly and after 10 min protein concentration was analyzed measured absorbance at 280 nm using a Perkin-Elmer Lambda 12 UV/vis spectrometer. Measurements are the average of two independent experiments. Data represented in Figure 2 are concentration of precipitation agent against concentration of LCA calculated from the experimental absorbance.

**STD NMR Experiments.** All NMR experiments were performed on a Bruker Avance DRX 500 spectrometer at 273 K. The NMR samples were prepared by dissolving the lectin in D<sub>2</sub>O solutions of dendritic compounds (1 mM and 0.5 mM for **1** and **2**, respectively) yielding a ratio of ligand molecules to lectin binding sites of 50:1. The saturation transfer difference (STD) experiments were recorded using essentially the sequence proposed by Meyer (28). A cascade of soft Gaussian-shaped pulses of 50 ms (with a power level of 80–40 Hz for the corre-

sponding square shape) was used for the saturation. The saturation times were varied from 0.25 to 2.5 s. On-resonance irradiation was done at 7 or 0 ppm while off-resonance at +30 ppm. A short spin-lock period (10–15 ms) was used prior to the acquisition in order to eliminate the remaining protein signals.

**Cell Lines and Culture Conditions.** COS-7 and 293-T cell lines were obtained from the American Type Culture Collection (Manassas, VA) and were maintained in Dulbecco's modified Eagle's medium (DMEM, Life Technologies, Inc), supplemented with 10% fetal calf serum (FCS; Gibco-BRL), 2 mM L-glutamine (Merck), streptomycin (0.1 mg/mL, Sigma), penicillin (100 U/mL, Sigma), sodium pyruvate (0.1%, Sigma), and  $\beta$ -mercaptoethanol (50  $\mu$ M, Sigma). All cell cultures were grown in a humidified 37 °C incubator with 5% CO<sub>2</sub> and periodically tested for being mycoplasma-free using a specific commercial kit (Gen-Probe, San Diego, CA).

**Cytotoxicity Studies.** Cell cultures were routinely monitored by cell scoring using a haemocytometer chamber after careful trypsinization of the adherent cell monolayer, using the trypan-blue vital dye. Cellular proliferation was determined using the MTT colorimetric assay, essentially as described by Mosmann (29), and by direct cell counting. Briefly, 10<sup>5</sup> cells/well were seeded into 96-well plates in 100  $\mu$ L of complete medium and incubated for the indicated time periods, in the presence or absence of the tested glycodendritic structures. After the cell monolayer was washed, a solution (10  $\mu$ L) of tetrazolium salt (MTT, 25 mg/mL in PBS) was then added to each well and incubated at 37 °C for 4 h. Under these conditions, MTT is reduced by living cells into an insoluble blue formazan product that is collected by centrifugation and dissolved by the addition of DMSO (100  $\mu$ L) with vigorous shaking. Plates are then read with a multiwell scanning spectrometer at 540 nm.

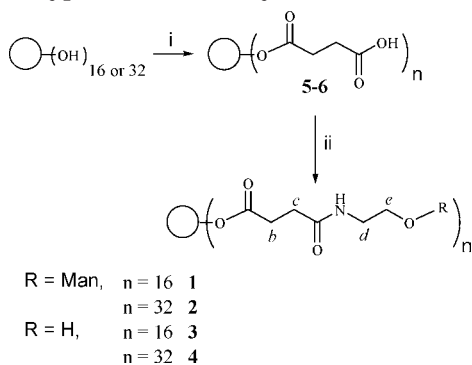
## RESULTS AND DISCUSSION

Glycodendritic polymers have been prepared linking the carbohydrate moiety to the polymer core through a spacer, giving flexibility and accessibility to the sugar for future biological applications. We have selected commercially available Boltorn H20 and H30 hyperbranched polymers as candidates to prove the viability of this strategy (Figure 1). These polymers present 16 and 32 hydroxy groups, respectively, on their surfaces, providing a multivalency comparable to other systems with biological activity described in the literature (30, 31).

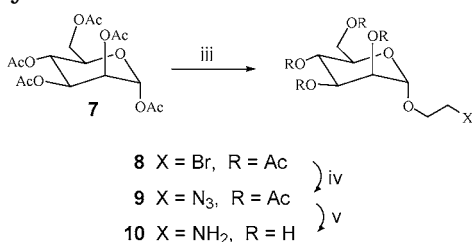
The first step of the preparation was the introduction of carboxylic groups on the dendritic core surface. This step gives a dendritic scaffold with carboxylic acid ending groups to be easily functionalized with glycoconjugates via an amide bond. This was achieved by mixing Boltorn H20 or H30 polymers and succinic anhydride in the presence of DMAP and pyridine (Scheme 1). After the mixture was stirred overnight at room temperature, the functionalized polymers were obtained (compounds **5** and **6**), as demonstrated by spectroscopic techniques.

Signals for carboxylic groups can be observed by IR spectroscopy, and the relationship between signals corresponding to the succinate methylene protons and the methyl groups of the polymer in the <sup>1</sup>H NMR spectrum confirmed the number of carboxylic groups introduced.

A simple monosaccharide ( $\alpha$ -D-mannose) has been selected as carbohydrate unit to test this methodology. More complicated oligosaccharidic structures can be envisaged for future applications. Mannose derivative **10** was prepared in four steps with good yields from the

**Scheme 1. Preparation of Dendritic Compounds 1–4 from the Hyperbranched Polymer BH20 and BH30<sup>a</sup>**

<sup>a</sup> (i) Succinic anhydride, DMAP cat., Py, 50 °C, 15 h, 100%; (ii) HOBT, DIC, DMF:CH<sub>2</sub>Cl<sub>2</sub> 1:1, **10** or HOCH<sub>2</sub>CH<sub>2</sub>NH<sub>2</sub> (1.2 equiv per OH), 24 h, 60% (**1**), 70% (**2**), 68% (**3**), or 88% (**4**).

**Scheme 2. Synthesis of Glycoconjugate 10 from Peracetylated Mannose 7<sup>a</sup>**

<sup>a</sup> (iii) HOCH<sub>2</sub>CH<sub>2</sub>Br, BF<sub>3</sub>·Et<sub>2</sub>O (5 equiv), CH<sub>2</sub>Cl<sub>2</sub>, 0 °C to room temperature, 24 h, 73%; (iv) NaN<sub>3</sub> (8 equiv), DMF, 50 °C, 15 h, 98%; (v) a) NaOMe, MeOH, rt, 15 min; (b) H<sub>2</sub> (1 atm), Pd(C), AcOEt:EtOH 1:1, rt, 20 h, 88%, two steps.

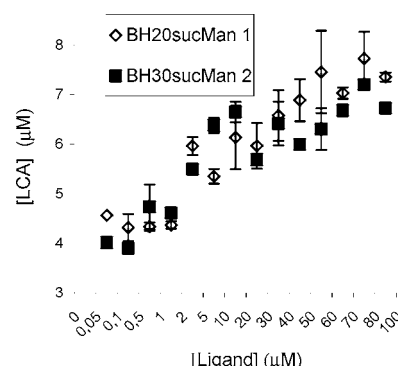
corresponding peracetylated mannose **7** following the synthetic pathway represented in Scheme 2 (32).

The spacer was introduced directly in the anomeric position by reaction with 2-bromoethanol in the presence of a large excess of BF<sub>3</sub>·Et<sub>2</sub>O (derivative **8**). Further manipulation of this chain was necessary to obtain an adequate functionalization. Substitution of bromine by azide with sodium azide in DMF gave compound **9**; deacylation under Zemplén conditions (NaOMe/MeOH) (33) and catalytic hydrogenation of the azide group rendered compound **10** ready to be attached to the dendritic cores **5** and **6**.

The final step consisted of the introduction of 16 or 32 units of **10** on the functionalized Boltorn H20 or H30 polymers **5** and **6**, respectively. This was achieved by reaction of **10** with the carboxylic acid residues of the dendritic structures **5** and **6** in the presence of 1-hydroxybenzotriazole (HOBT) and diisopropylcarbodiimide (DIC) (Scheme 1) giving glycodendritic compounds **1** and **2**. Dialysis purification afforded **1** and **2** as white solids after lyophilization. For future biological essays dendritic polymers **3** and **4**, presenting 16 and 32 linkers respectively, were prepared as control. Reaction of aminoethanol with activated Boltorn polymers **5** and **6** in the presence of HOBT and DIC gave compounds **3** and **4** which were purified by dialysis. (Scheme 1) All dendritic compounds prepared were characterized spectroscopically.

**Quantitative Precipitation Assays.** Glycodendritic structures **1** and **2** presenting several copies of mannose could form, a priori, clusters of mannose-binding lectins (as LCA) that precipitate. Quantification of the protein on this precipitate may give an idea of the efficiency of these systems based on valence (34). The formation of this precipitate clearly indicates that the ligand used is

acting as a multivalent system of the corresponding antigen. Compounds **1–4** and **10** were incubated with LCA in PBST buffer, and the amount of protein in the precipitate was measured. The absorbance observed when glycoconjugate **10** was used at concentrations up to 0.1 mM was almost zero (data not shown). This monovalent system is not capable to form a cluster with the *Lens culinaris* lectin even a high concentrations, and therefore no precipitation was detected. For compounds **3** and **4**, which present dendritic structures but without saccharidic units, a small absorbance was observed (data not shown) at the higher concentration used (0.1 mM). This could be interpreted on the base of nonspecific interactions between dendritic structures and lectin. Different behavior was observed for dendritic structures **1** and **2** which present 16 and 32 copies of mannose on their surface, respectively. Both of them present a similar profile concentration-dependent lectin precipitation. (Figure 2).

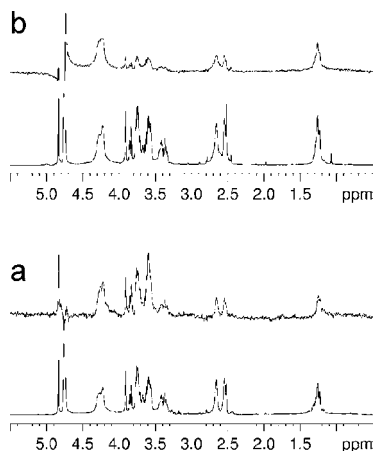


**Figure 2.** Quantitative precipitation assay. Final concentration of LCA precipitated plotted against concentration of glycodendritic compounds **1** and **2**.

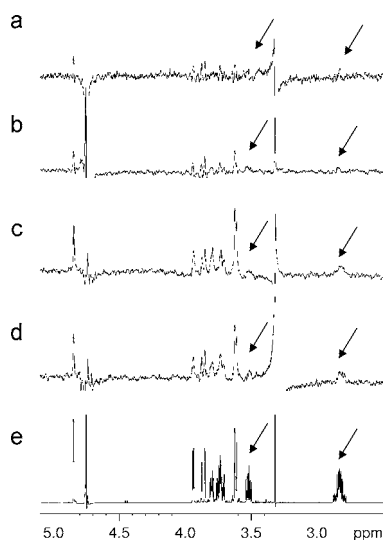
Starting at a ligand concentration of about 2 μM, there is a remarkable increase in the amount of precipitated protein which continues growing slowly with increasing ligand concentration. The maximum amount of protein precipitate during the experiment corresponds to approximately 30% of the initial amount. No significant differences were found between compounds **1** and **2**, indicating that, with these specific model systems, an increase in the number of mannose units from 16 to 32 has no influence on the binding in this particular case. These results show the importance of multivalency for cluster formation and precipitation but may also indicate that a crowded presentation of ligands on the dendritic surface might not have a positive effect on the interaction with LCA. This situation could impede the access of ligands to the protein recognition site, and therefore longer and more flexible linkers can be considered to have an important effect on ligand presentation and to promote better interaction with the protein.

**STD NMR Experiments.** STD experiments have been extensively used for ligand screening (see ref 28) and epitope mapping of molecular interactions at atomic level (35). These experiments are based on the transference of NMR saturation, through spin diffusion, from a large receptor into a small ligand due to transient binding. Thus NMR signals for those ligands interacting with a given receptor are detected. The experiment could be used also for epitope mapping. In this case, the signals corresponding to those protons closer to the receptor are detected. The method is rather robust and less sensitive to binding constant requirements than other NMR experiments as transfer NOE. We have used this methodol-





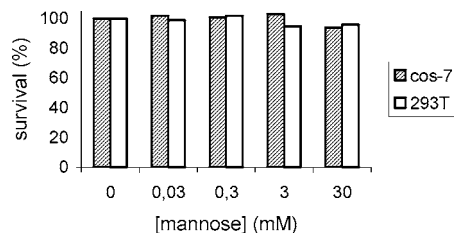
**Figure 3.** NMR Saturation transfer experiments recorded with 2.5 s of protein saturation time (top) and reference  $^1\text{H}$  NMR spectra (bottom) for (a) BH20sucMan **1** and (b) BH30sucMan **2**.



**Figure 4.** NMR Saturation transfer experiments for **10** at (a) 250, (b) 357, (c) 510, (d) 1020 ms of saturation time, and (e) reference  $^1\text{H}$  NMR spectra indicating the absence of interaction between the ethylene linker and the lectin. Arrows indicate linker ethylene moiety signals.

ogy to study the interaction of **1**, **2**, and **10** with *Lens culinaris* lectin. Similar qualitative results were found for both hyperbranched polymers and the mannose glycoconjugate **10**, indicating that the interaction of these three compounds with LCA takes place in a similar way (Figures 3 and 4). Thus, it can be concluded that attaching the carbohydrate moiety to the three-dimensional scaffold does not alter significantly its protein binding properties and only provides polyvalence.

STD technique can also yield valuable structural information identifying the regions of the ligand involved in the interaction with the receptor. We have also tried to map the epitope of the interaction of **1**, **2**, and **10** with LCA in different experimental conditions. In our case, **1** and **2**, as a consequence of their size, are in the NOE spin diffusion limit. Therefore, they should have internal saturation transfer rates comparable with the lectin-ligand ones. These features do not prevent the STD experiments although could make the observation of selectivity within the ligand difficult. This would explain the detection in the STD experiments of all the protons of the dendrimers including the internal  $\text{CH}_2$  and  $\text{CH}_3$  groups of the Boltorn polymer, even at relatively short



**Figure 5.** Percentage of survival for COS-7 and 293T cell lines in the presence of different concentrations of glycodendritic compounds **1** and **2** up to 30 mM based on number of mannose units.

saturation times of 1–0.5 s. The selectivity was improved using even shorter saturation times. In these cases, the relative intensity of the linker and polymer signals, compared with the carbohydrate ones, decreased. This result suggests that the interaction occurs mainly through the mannose residue. However, under those conditions, such short saturation times cause very low overall signal intensity. Also the spin-lock period used can induce transference of magnetization among the mannose-coupled protons, obscuring the results. Both effects prevent a deeper analysis of the specific zone of the carbohydrate involved in binding. As expected, better selectivity was observed for the case of glycoconjugate **10**, which has a more adequate size. All the mannose protons were clearly detected (Figure 4), indicating that this is the part of the molecule in contact with the lectin. The intensity of the signals from the ethylene moiety (see arrows in Figure 4) of the linker clearly decreased, which means a looser interaction of this part of the molecule with the lectin. This result confirms that the linker moiety does not interact with the protein, and therefore the sugar moiety is responsible for the interaction with LCA.

The results from these interaction experiments indicate that the lectin binding properties of the mannose are conserved in the larger glycodendritic structure. Finally, from the STD-NMR experiments it can be concluded that the linker moiety does not interact with the protein.

**Cytotoxicity Studies.** Biological application of these glycodendritic compounds relies first on good solubility in physiological conditions. Compounds **1–4** were completely soluble in aqueous buffers commonly used to perform in vitro studies. Another important issue is the compatibility of these systems with biological targets. We tested their potential toxicity against different cell lines (COS-7 and 293T). For that purpose, after exposure of cell cultures during 24 h to increasing amounts of the above-described systems, an MTT colorimetric assay was performed following the procedure described (ref 29, see Materials and Methods for more details). The results (Figure 5) indicated that compounds **1** and **2** were nontoxic in the whole concentration range tested (up to 3 mM, based on number of mannose units) and for the two cell lines included in the study. Higher concentrations (up to 30 mM) induce a moderate decrease in the cell viability (Figure 5).

Similar results were obtained for control compounds **3** and **4** (data not shown). Also, human peripheral blood mononuclear cells (PBMCs) were incubated with the glycodendritic structures and, again, cytotoxicity was not found (data not shown). Therefore, these results strongly suggest that the described glycodendritic compounds can be considered as promising candidates to carry on biological studies.

## CONCLUSIONS

In summary, we have prepared two glycodendritic structures **1** and **2** presenting 16 and 32 units of mannose, respectively, and two controls **3** and **4** without carbohydrate units based on Boltorn H20 (second generation) and H30 (third generation) hyperbranched polymers. Their solubility and their low toxicity are compatible with their use as potential tools to study biological processes. Results obtained from the interaction studies of these glycodendritic structures and a mannose-binding lectin, *Lens culinaris* lectin, using STD NMR experiments and quantitative precipitation assays demonstrate that the dendritic scaffold has no influence on the binding capabilities of mannose glycoconjugates, that being an adequate platform. On the other hand, the multivalent presentation of the sugar units is essential for lectin cluster formation, although in this particular case, no differences have been found increasing the number of sugar units from 16 to 32. In other words, the capability of these compounds to interact with biological receptors as lectins has been demonstrated.

These results open new possibilities for the design and preparation of new glycodendritic structures based on Boltorn hyperbranched polymers with different spacers and degrees of branching, including biologically important carbohydrates.

## ACKNOWLEDGMENT

This research was supported by the DGES (grants no. PB 960820 to J.R. and SAF 2001-2262 to A.B.). The authors want to thank Perstorp Specialty Chemicals for the generous gift of Boltorn polymers. We thank also Prof. M. Martín-Lomas and Dr. S. Penadés for scientific and financial support.

**Supporting Information Available:**  $^1\text{H}$  NMR (300 MHz) spectra in  $\text{D}_2\text{O}$  of glycodendritic structures **1** and **2**. This material is available free of charge via Internet at <http://pubs.acs.org>

## LITERATURE CITED

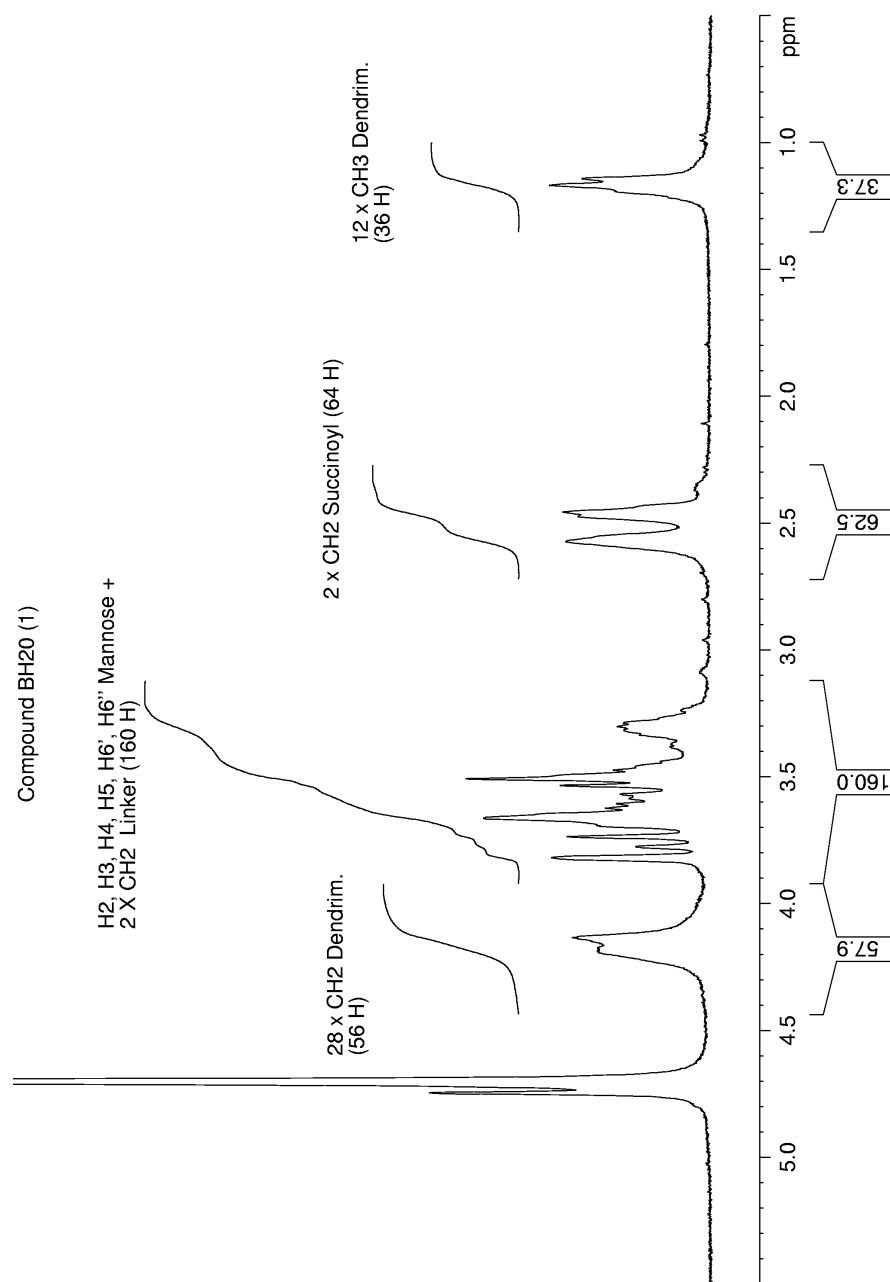
- Mammen, M., Choi, S. K., and Whitesides, G. M. (1998) Polyvalent Interactions in Biological Systems: Implications for Design and Use of Multivalent Ligands and Inhibitors. *Angew. Chem., Int. Ed.* 37, 2754–2794.
- Brewer, G. J., and Matinyan, N. (1992) Congregation of Gangliosides at the Junction between Two Model Membranes. *Biochemistry* 31, 1816–1820.
- Stewart, R. J., and Boggs, J. M. (1993) Carbohydrate-carbohydrate Interaction between Galactosylceramide-containing Liposomes and Cerebroside Sulfate-Containing Liposomes: Dependence on the Glycolipid Ceramide Composition. *Biochemistry* 32, 10666–10674.
- Röckendorf, N., and Lindhorst, T. K. (2001) Glycodendrimers. *Top. Curr. Chem.* 217, 201–238.
- Dondoni, A., Marra, A., Scherrmann, M. C., Casnati, A., Sansone, F., and Ungaro, R. (1997) Synthesis and Properties of *O*-Glycosyl Calix[4]arenes (Calixsugars). *Chem. Eur. J.* 3, 1774–1782.
- Roy, R., Hernández-Mateo, F., Santoyo-González, F. (2000) Synthesis of Persialylated beta-Cyclodextrins. *J. Org. Chem.* 65, 8743–8746.
- Roy, R. (1996) Syntheses and Some Applications of Chemically Defined Multivalent Glycoconjugates. *Curr. Opin. Struct. Biol.* 6, 692–702.
- de la Fuente, J. M., Barrientos, A. G., Rojas, T. C., Rojo, J., Cañada, J., Fernández, A., and Penadés, S. (2001) Gold Glyconanoparticles as Water-soluble Polyvalent Models to Study Carbohydrate Interactions. *Angew. Chem., Int. Ed.* 40, 2258–2261.
- Malmström, E., Johansson, M., and Hult, A. (1995) Hyperbranched Aliphatic Polyesters. *Macromolecules* 28, 1698–1703.
- Matthews, O. A., Shipway, A. N., and Stoddart, J. F. (1998) Dendrimers-branching out from Curiosities into New Technologies. *Prog. Polym. Sci.* 23, 1–56.
- Pagé, D., and Roy, R. (1997) Synthesis and Biological Properties of Mannosylated Starburst Poly(amidoamine) Dendrimers. *Bioconjugate Chem.* 8, 714–723.
- Wan, Q., Schrick, S. R., and Culbertson, B. M. (2000) Methacryloyl Derivatized Hyperbranched Polyester. 1. Synthesis, Characterization, and Copolymerization. *Pure Appl. Chem.* 11, 1301–1315.
- Kantchev, A. S., and Parquette, J. R. (1999) Disaccharide Synthesis on a Soluble Hyperbranched Polymer. *Tetrahedron Lett.* 40, 8049–8053.
- Matthews, O. A., Shipway, A. N., and Stoddart, J. F. (1998) Dendrimers-branching out from Curiosities into New Technologies. *Prog. Polym. Sci.* 23, 1–56.
- Fukasawa, M., Shimizu, Y., Shikata, K., Nakata, M., Sakakibara, R., Yamamoto, N., Hatanaka, M., and Mizuochi, T. (1998) Liposome Oligomannose-coated with Neoglycolipid, a New Candidate for a Safe Adjuvant for Induction of CD8<sup>+</sup> Cytotoxic T Lymphocytes. *FEBS Lett.* 441, 353–356 and references cited.
- Chiba, Y., Suzuki, M., Yoshida, S., Yoshida, A., Ikenaga, H., Takeuchi, M., Jigami, Y., and Ichishima, E. (1998) Production of Human Compatible High Mannose-type (Man<sub>5</sub>-GlcNAc<sub>2</sub>) Sugar Chains in *Saccharomyces Cerevisiae*. *J. Biol. Chem.* 273, 26298–26304.
- Jungmann, J., Rayner, J. C., and Munro, S. (1999) The *Saccharomyces Cerevisiae* Protein Mnn10p/Bed1p is a Subunit of a Golgi Mannosyltransferase Complex. *J. Biol. Chem.* 274, 6579–6585.
- Mislovičová, D., Gemeiner, P., Šandula, J., Masárová, J., Vikartovská, A., and Dočolomanský, P. (2000) Examination of Bioaffinity Immobilization by Precipitation of Mannan and Mannan-containing Enzymes with Legume Lectins. *Biotechnol. Appl. Biochem.* 31, 153–159.
- Mislovičová, D., Masárová, J., Švitel, J., Mendichi, R., Šoltes, L., Gemeiner, P., and Danielsson, B. (2002) Neoglycoconjugates of Mannan with Bovine Serum Albumin and their Interaction with Lectin Concanavalin A. *Bioconjugate Chem.* 13, 136–142.
- Mikami, T., Nagase, T., Matsumoto, T., Suzuki, M., Suzuki, S., and Kumano, N. (1982) Mitogenic Effect of the Mannans from *Saccharomyces Cerevisiae* on Mouse Spleen Lymphocytes. *Microbiol. Immunol.* 26, 913–922.
- Nagase, T., Mikami, T., Suzuki, S., Schuerch, C., and Suzuki, M. (1984) Lethal Effect of Neutral Mannan Fraction of Bakers' Yeast in Mice. *Microbiol. Immunol.* 28, 997–1007.
- Biessen, E. A. L., Noorman, F., van Teijlingen, M. E., Kuiper, J., Barret-Bergshoeff, M., Bijsterbosch, M. K., Rijken, D. C., and van Berkel, T. J. C. (1996) Lysine-based Cluster Mannosides that Inhibit Ligand Binding to the Human Mannose Receptor at Nanomolar Concentration. *J. Biol. Chem.* 271, 28024–28030.
- König, B., Fricke, T., Wassmann, A., Krallmann-Wenzel, U., and Lindhorst, T. K. (1998)  $\alpha$ -Mannosyl Clusters Scaffolded on Azamacrocycles: Synthesis and Inhibitory Properties in the Adhesion of Type 1 Fimbriated *Escherichia Coli* to Guinea Pig Erythrocytes. *Tetrahedron Lett.* 39, 2307–2310.
- Nagahori, N., Lee, R. L., Nishimura, S.-i., Pagé, D., Roy, R., and Lee, Y. C. (2002) Inhibition of Adhesion of Type 1 Fimbriated *Escherichia Coli* to Highly Mannosylated Ligands. *ChemBioChem* 3, 836–844.
- Grandjean, C., Rommens, C., Gras-Masse H., and Melnyk, O. (2000) One-pot Synthesis of Antigen-bearing, Lysine-based Cluster Mannosides Using Two Orthogonal Chemoselective Ligation Reactions. *Angew. Chem., Int. Ed.* 39, 1068–1072.
- Loris, R., Casset, F., Bouckaert, J., Pletincx, J., Dao-Thi, M.-h., Poortmans, F., Imbert, A., Perez, S., and Wyns, L. (1994) The Monosaccharide Binding Site of Lentil Lectin: an

- X-ray and Molecular Modelling Study. *Glycoconj. J.* 11, 507–517.
- (27) Kahn, M. I., Mandal, D. K., and Brewer, C. F. (1991) Interactions of Concanavalin A with Glycoproteins. A Quantitative Precipitation Study of Concanavalin A with the Soybean Agglutinin. *Carbohydr. Res.* 213, 69–77.
- (28) Mayer, M., and Meyer, B. (1999) Characterization of Ligand Binding by Saturation Transfer Difference NMR Spectroscopy. *Angew. Chem., Int. Ed.* 38, 1784–1788.
- (29) Mosmann, T. (1983) Rapid Colorimetric Assay for Cellular Growth and Survival: Application to Proliferation and Cytotoxicity Assays. *J. Immunol. Methods* 65, 55–63.
- (30) Baek, M. G., Rittenhouse-Olson, K., and Roy, R. (2001) Synthesis and Antibody Binding Properties of Glycodendrimers Bearing the Tumor Related T-Antigen. *J. Chem. Soc., Chem. Commun.* 257–258.
- (31) André, S., Ortega, P. J. C., Pérez, M. A., Roy, R., and Gabius, H. J. (1999) Lactose-containing Starburst Dendrimers: Influence of Dendrimer Generation and Binding-site Orientation of Receptors (Plant/Animal Lectins and Immunoglobulins) on Binding Properties. *Glycobiology* 9 1253–1261.
- (32) Lindhorst, T. K., Kötter, S., Krallmann-Wenzel, U., and Ehlers, S. (2001) Trivalent  $\alpha$ -D-Mannoside Clusters as Inhibitors of Type-1 *Fimbriae*-mediated Adhesion of *Escherichia Coli*. Structural Variations and Biotinylation. *J. Chem. Soc., Perkin Trans. 1* 823–831.
- (33) Zemplén, G. (1927) Abbau der Reduzierenden Biosen. *Ber. Dtsch. Chem. Ges.* 60, 1555–1564.
- (34) Gestwicki, J. E., Strong, L. E., Cairo, C. W., Boehm, F. J., and Kiessling, L. L. (2002) Cell Aggregation by Scaffolded Receptor Clusters. *Chem. Biol.* 9, 163–169.
- (35) Mayer, M., and Meyer, B. (2001) Group Epitope Mapping by Saturation Transfer Difference NMR to Identify Segments of a Ligand in Direct Contact with a Protein Receptor. *J. Am. Chem. Soc.* 123, 6108–6117.

BC034008K

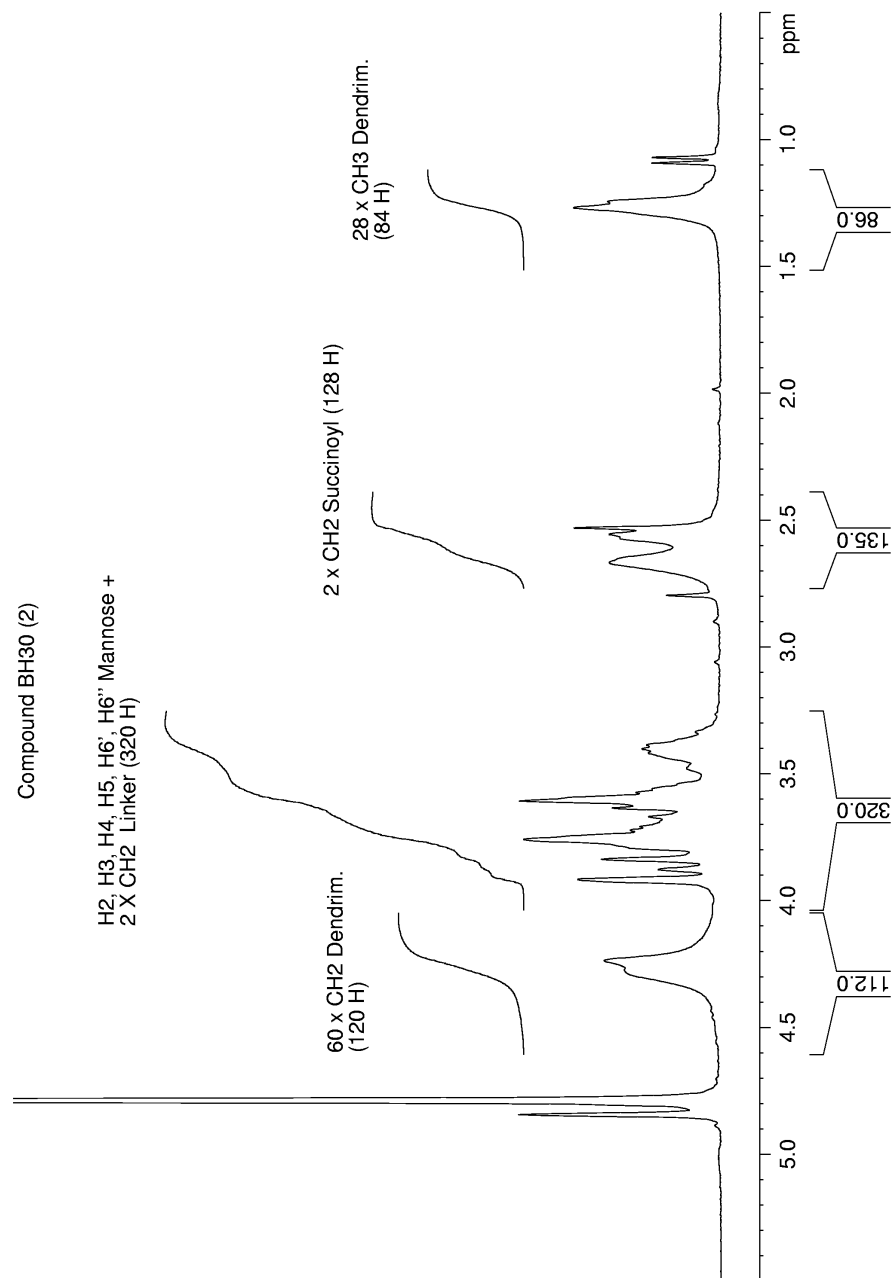


$^1\text{H}$ -NMR (300 MHz) in  $\text{D}_2\text{O}$  of Glycodendritic structure **1**



Glycodendritic structures base don Boltorn<sup>TM</sup> hyperbranched polymers and their interactions with Lens *Culinaris* lectin  
Eva Arce, Pedro M. Nieto, Vicente Díaz, Rossana García Castro, Antonio Bernad and Javier Rojo

$^1\text{H}$ -NMR (300 MHz) in  $\text{D}_2\text{O}$  of Glycodendritic structure **2**



Glycodendritic structures base don Boltorn<sup>TM</sup> hyperbranched polymers and their interactions with *Lens Culinaris* lectin  
Eva Arce, Pedro M. Nieto, Vicente Díaz, Rossana García Castro, Antonio Bernad and Javier Rojo





# A Water-Soluble Azobenzene Cross-Linker for Photocontrol of Peptide Conformation

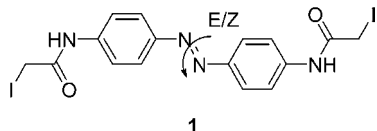
Zhihua Zhang,<sup>†</sup> Darcy C. Burns,<sup>†</sup> Janet R. Kumita,<sup>†</sup> Oliver S. Smart,<sup>‡</sup> and G. Andrew Woolley<sup>\*,†</sup>

Department of Chemistry, University of Toronto, 80 St. George St., Toronto M5S 3H6, Canada, and School of Biosciences, University of Birmingham, Edgbaston, Birmingham B15 2TT, United Kingdom. Received February 7, 2003; Revised Manuscript Received May 12, 2003

We have designed and synthesized a water-soluble, sulfonated version of an azobenzene-based thiol-reactive cross-linker that can be introduced into peptides and proteins and act as a conformational photoswitch. The sulfonated compound is shown to effect a similar degree of conformational control on a model peptide helix system, as its nonsulfonated counterpart but can be introduced without the need for any organic cosolvent. The sulfonated azobenzene cross-linker thus expands the range of proteins to which photocontrol can be applied.

## INTRODUCTION

Photocontrol of peptide/protein conformation can be a powerful tool for probing protein function in a range of biochemical systems (1–5). Chromophores, such as azobenzene, that undergo reversible *cis*–*trans* photoisomerization, can in principle be used for reversible conformational control of proteins and other biomolecules (6–14). Previously, we reported a reversible means of controlling helix stability that involved the incorporation of a photoisomerizable azobenzene cross-linking reagent (1) into an engineered peptide system (9, 15, 16).



The thiol-reactive azobenzene cross-linker was combined with peptides containing Cys residues spaced at positions *i,i*+4, *i,i*+7, and *i,i*+11 in the sequence. Photoisomerization of the cross-linker from *trans* to *cis* resulted in an increase in  $\alpha$ -helix content for the *i,i*+4 and *i,i*+7 cases and a decrease in helix content for the *i,i*+11 case as predicted based on molecular modeling studies (9, 16). Since Cys residues can be introduced via site-directed mutagenesis into proteins, this azobenzene-based cross-linker strategy offers a general way of photocontrolling protein conformation (and thereby activity). A potential drawback is the poor water solubility of the reagent. This leads to a requirement for a dimethylsulfoxide/water cosolvent during the cross-linking reaction. While many proteins will tolerate such conditions, many will not (17–19). We report here the design and synthesis of a water-soluble variant of the original cross-linking reagent. Sulfonate groups were added to the azobenzene ring system to achieve water solubility while maintaining the

symmetry and compact size of the reagent. A test of the behavior of the water soluble version with the *i,i*+11 Cys peptide indicates that it behaves similarly to the original cross-linker with a somewhat longer half-life for thermal *cis*-to-*trans* reversion.

## EXPERIMENTAL SECTION

**Synthesis of 2-Acetylamino-5-aminobenzenesulfonic Acid (3).** In a 10 mL round-bottom flask was suspended 1.294 g (6.88 mmol) of 2,5-diaminobenzenesulfonic acid (2) (Aldrich) in 10 mL of glacial acetic acid and heated to 94 °C. A volume of 0.8 mL (1.23-fold molar excess) of acetic anhydride was then added dropwise over a few minutes, and the mixture was refluxed for 2 h. Upon cooling, the product was filtered off, washed with hot acetic acid and then ether, and dried under high vacuum. The solid was resuspended in hot ethanol and the undissolved material collected by filtration to give 580 mg of a light purple solid (3). <sup>1</sup>H NMR (500 MHz, DMSO-*d*<sub>6</sub>): CH<sub>3</sub> (2.08 ppm, s, 1H), H<sub>c</sub> (7.30 ppm, dd, *J* = 2.7, 8.7 Hz, 1H), H<sub>a</sub> (7.70 ppm, d, *J* = 2.7 Hz, 1H), H<sub>b</sub> (8.39 ppm, d, *J* = 8.7 Hz, 1H) and NH (10.35 ppm, s, 1H). <sup>13</sup>C NMR (125 MHz, DMSO-*d*<sub>6</sub>): CH<sub>3</sub> (26.1 ppm), CH<sub>b</sub> (121.8 ppm), CH<sub>a</sub> (122.9 ppm), CH<sub>c</sub> (125.4 ppm), C<sub>NH2</sub> (126.5 ppm), C<sub>SO3</sub> (136.0 ppm), C<sub>acetamido</sub> (137.2 ppm), C(O) (169.0 ppm); Purity by <sup>1</sup>H NMR >97.5%; HRMS-ESI (C<sub>8</sub>H<sub>10</sub>N<sub>2</sub>O<sub>4</sub>S) calcd 230.0361 obsd 230.0365; mp >300 °C.

**Synthesis of Sodium 3,3'-Bis(sulfonato)-4,4'-bis(acetamido)azobenzene (4).** In a 50 mL round-bottom flask, 1.725 g (7 mmol) of 3 was suspended in 18 mL of distilled water, and the pH was adjusted to 8–9 by the addition of sodium carbonate (the solution turned dark brown). The solution was cooled in an ice–salt bath to –5 °C whereupon 19 mL of a sodium hypochlorite solution (available chlorine ≥4% (Aldrich)) was added dropwise over 6 min. The reaction mixture was stirred at 0 °C for 2 h and then left to stand at 4 °C for 2–3 days. The orange-yellow precipitate was collected and washed with hot ethanol to yield 130 mg of 4 as an orange solid. <sup>1</sup>H NMR (500 MHz, D<sub>2</sub>O): CH<sub>3</sub> (2.27 ppm, s, 6H), H<sub>c</sub> (7.94 ppm, dd, *J* = 2.2, 8.4 Hz, 2H), H<sub>b</sub> (8.10 ppm, d, *J* = 8.4 Hz, 2H), H<sub>a</sub> (8.28 ppm, d, *J* = 2.2 Hz, 2H); <sup>13</sup>C NMR (125 MHz, D<sub>2</sub>O): CH<sub>3</sub> (2.2 ppm), CH<sub>b</sub> (124.2 ppm), CH<sub>a</sub> (121.9 ppm), CH<sub>c</sub> (125.9 ppm), C<sub>azo</sub> (147.8 ppm), C<sub>SO3</sub>

\* Corresponding author: awoolley@chem.utoronto.ca. Telephone/fax: (416) 978-0675.

<sup>†</sup> University of Toronto.

<sup>‡</sup> University of Birmingham.

<sup>1</sup> Abbreviations: CD, circular dichroism; DMF, dimethylformamide; DMSO, dimethyl sulfoxide; TCEP, tris(carboxyethyl)phosphine; THF, tetrahydrofuran.

(136.3 ppm),  $C_{\text{acetamido}}$  (133.8 ppm),  $C(O)$  (172.4 ppm); Purity by  $^1H$  NMR >96.8%; HRMS-ESI ( $C_{16}H_{15}N_4O_8S_2^-$ ) calcd 455.0336 obsd 455.0318, 477 ( $Na^+$  adduct); mp >300 °C.

**Synthesis of Sodium 3,3'-Bis(sulfonato)-4,4'-bis(amino)azobenzene (5).** In a 25 mL round-bottom flask were added 0.55 mL of concentrated HCl and 2.75 mL of water to 15 mg (0.033 mmol) of **4**. The mixture was heated under reflux for 2.5 h and then cooled and concentrated to give a pink solid. The solid was resuspended in 8 mL of water, and the pH was adjusted to 8.5 with dilute NaOH. The solvent was evaporated under high vacuum to give 16.2 mg of a red-brown solid, compound **5**.  $^1H$  NMR (500 MHz, DMSO- $d_6$ ):  $H_c$  (7.34 ppm, dd,  $J = 2.4, 8.6$  Hz, 2H),  $H_b$  (6.70 ppm, d,  $J = 8.6$  Hz, 2H),  $H_a$  (7.94 ppm, d,  $J = 2.4$  Hz, 2H),  $NH_2$  (6.20 ppm, 4H);  $^{13}C$  NMR (125 MHz, DMSO- $d_6$ ):  $CH_b$  (115.1 ppm),  $CH_a$  (121.4 ppm),  $CH_c$  (124.6 ppm),  $C_{\text{azo}}$  (141.6 ppm),  $C_{SO_3}$  (147 ppm),  $C_{NH_2}$  (129.6 ppm); Purity by  $^1H$  NMR >98%; HRMS-ESI ( $C_{12}H_{11}N_4O_6S_2^-$ ) calcd 371.0125 obs. 371.0129, 393 ( $Na^+$  adduct); mp >300 °C.

**Synthesis of 3,3'-Bis(sulfo)-4,4'-bis(chloroacetamido)azobenzene (6).** Compound **5** (82.3 mg), chloroacetic acid (528 mg, 24 equiv), and chloroacetic anhydride (946 mg, 24 equiv) were mixed in a 5 mL round-bottom flask. The solid reaction mixture was heated to 87 °C (i.e., above its melting temperature) and stirred at this temperature for 7.5 h. The reaction mixture was cooled to room temperature, whereupon it solidified. It was washed with dichloromethane and dried under high vacuum to give 110 mg of **6**.  $^1H$  NMR (500 MHz, DMSO- $d_6$ ):  $CH_2$  (4.42 ppm, s, 4H),  $H_c$  (7.98 ppm, dd,  $J = 2.4, 8.8$  Hz, 2H),  $H_b$  (8.53 ppm, d,  $J = 8.8$  Hz, 2H),  $H_a$  (8.2 ppm, d,  $J = 2.4$  Hz, 2H),  $NH$  (11.23 ppm, s, 2H);  $^{13}C$  NMR (125 MHz, DMSO- $d_6$ ):  $CH_2$  (44.2 ppm),  $CH_b$  (121.1 ppm),  $CH_a$  (120.2 ppm),  $CH_c$  (126.8 ppm),  $C_{\text{azo}}$  (147.7 ppm),  $C_{SO_3}$  (137.4 ppm),  $C_{\text{acetamido}}$  (137.6 ppm),  $C(O)$  (165.7 ppm); Purity by  $^1H$  NMR >97%; HRMS-ESI ( $C_{16}H_{13}N_4O_8S_2Cl_2^-$ ) calcd 522.9557 obsd 522.9578; mp >300 °C.

**NMR Analysis.** Each synthetic intermediate was analyzed using 1D  $^1H$  NMR,  $^{13}C$ - $^1H$  HSQC and  $^{13}C$ - $^1H$  HMBC (CIGAR) (20) spectroscopy. All NMR experiments were performed on a 500 MHz Varian Unity spectrometer equipped with a VarianPFG2 5-mm indirect broadband probe. Data were processed using the Felix 2000 software package (Accelrys Inc.). The HSQC experiments were run in the phase sensitive mode using either 128, 256, or 512 increments in f1 and linear predicting to 2048 increments. The spectral window in f1 was 4950 Hz and in f2, 21367 Hz. Either 4 or 16 scans per increment with a relaxation delay of 1 s was used, depending on sample concentration. Acquisition time was 0.209 s with a proton pulse of 5.3  $\mu s$  and a carbon pulse of 11.5  $\mu s$ . Gaussian apodization was used in the processing. Decoupling of  $^{13}C$  was done using the WURST sequence.

The  $^{13}C$ - $^1H$  CIGAR-MBC experiments were run in the absolute value mode using 512 increments in F1 and linear predicting to 2048 increments. The spectral window in f1 was 4950 Hz and in f2, 30165 Hz. Thirty-two scans per increment and a relaxation delay of 1.0 s was used. The acquisition time was 0.207 s with a proton pulse of 5.3  $\mu s$  and a carbon pulse of 11.5  $\mu s$ . One bond filtering was done on a range of coupling constants from 130 to 165 Hz. Long-range multiple bond correlations were observed in the range 5 to 10 Hz. Sine bell apodization was used in the processing. No decoupling of  $^{13}C$  was used.

A solution of compound **4** in  $D_2O$  was analyzed by ROESY NMR spectroscopy using an 800 ms spin lock

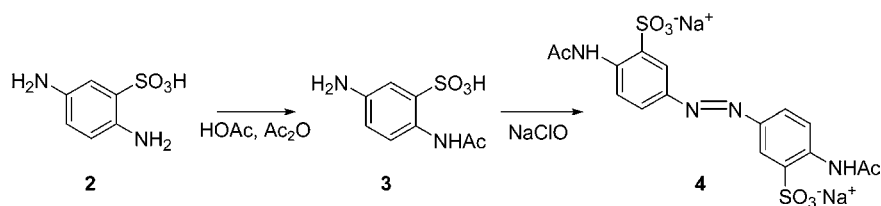
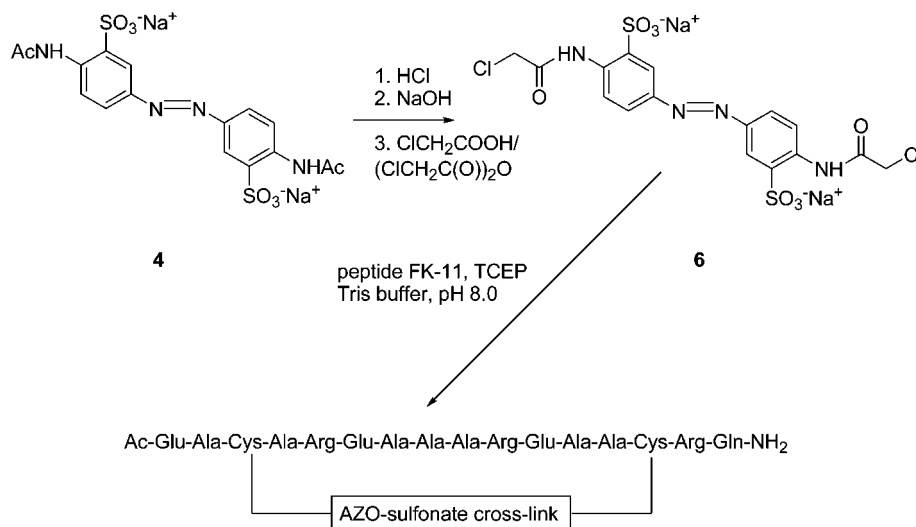
pulse train. The ROESY spectrum was acquired with 48 transients, 256 t1 increments, and 1024 complex data points over a sweep width of 5354.7 Hz in f1 and in f2. In addition, a homospoil pulse was applied at the beginning of the sequence (followed by a 1 s d1 delay period). During processing, f2 was zero-filled to 2K points, and the f1 dimension was linear predicted 2K points. The first points in f1 and f2 were corrected by multiplying the data by 0.5. A 90° sine bell squared window function was applied in both dimensions and a solvent subtraction algorithm (cnv) was employed to reduce the water signal in the two-dimensional spectrum.

**Synthesis of Glutathione-Sulfazo.** Compound **6** (2.4  $\mu\text{mol}$ ) was mixed with reduced glutathione (3.2  $\mu\text{mol}$ ) in a total volume of 600  $\mu\text{L}$  of Tris buffer, pH 8.0. The solution was stirred for 2 h under nitrogen protected from light. The desired product was isolated by HPLC (Zorbax SB-C18 column) using a linear gradient from 0 to 80% acetonitrile/ $H_2O$  (+0.1% trifluoroacetic acid) over the course of 45 min (eluted at 34% acetonitrile). MS-MALDI: (M - H)  $C_{36}H_{45}N_{10}O_{20}S_4^-$ : 1066.0 Da obsd 1065.5 Da. Purity by HPLC was >93%.

**Synthesis of FK-11 Sulfazo.** The peptide FK-11 (Ac-EACAREAAAREAAACRQ-NH $_2$ ) was prepared using standard fluorenylmethoxycarbonyl-based solid-phase peptide synthesis methods as described previously (9). To ensure the Cys residues were in the reduced form before reaction with the cross-linker, 1 mg (0.6  $\mu\text{mol}$ ) of FK-11 was dissolved in 350  $\mu\text{L}$  of a 2 mM solution of TCEP in 50 mM Tris, pH 8.0, and incubated at room-temperature overnight. The pH was checked and, if necessary, 100  $\mu\text{L}$  more 100 mM Tris buffer, pH 8.0, was added. Excess TCEP was not removed. Compound **6** (1.33  $\mu\text{mol}$  in a volume of 35  $\mu\text{L}$  of water) was added to the FK-11 peptide solution and stirred at room temperature for 20 min protected from light. Then another aliquot of the cross-linker solution (1.33  $\mu\text{mol}$  in a volume of 35  $\mu\text{L}$ ) was added, and stirring was continued for another 20 min. Finally, a third aliquot (1.33  $\mu\text{mol}$  in a volume of 35  $\mu\text{L}$ ) of cross-linker solution was added, and the solution was stirred for 40 min at room-temperature exposed to ambient light. The cross-linked peptide was then purified using HPLC (Zorbax SB-C18 column) using a linear gradient from 0 to 80% acetonitrile/ $H_2O$  (+0.1% trifluoroacetic acid) over the course of 45 min for (eluted at 37% acetonitrile). MS-MALDI: ( $C_{83}H_{126}N_{31}O_{32}S_4^-$ ): 2198.2 Da obsd 2199 Da. Purity by HPLC was >95%. Total amino acid analysis confirmed reaction of the cross-linker with Cys residues.

**UV/vis Analysis and Photoisomerization.** UV spectra were obtained with a Perkin-Elmer Lambda 2 spectrophotometer using the same thermostated quartz cell (0.1 cm path length) in which CD analysis was performed. Peptide concentrations of cross-linked species were calculated using a molar extinction coefficient of 29 000 (370 nm) for the dark-adapted azo group determined via quantitative analysis of the NMR spectrum of compound **4**.

Photoisomerization was accomplished by irradiating thermostated peptide solutions with a 70W Metal Halide Tri-Lite Lamp (World Precision Instruments) coupled to a 370  $\pm$  10 nm band-pass filter (Harvard Apparatus). Photoisomerization was complete (as judged by the lack of any further changes in UV spectra) in  $\leq 15$  min. Thermal relaxation rates were measured using a diode array spectrometer (Ocean Optics) coupled to a thermostated cuvette holder (Quantum Northwest). Spectra for pure trans and cis forms of the peptide were obtained using a Waters 996 photodiode array (PDA) detector

**Scheme 1****Scheme 2**

coupled to an HPLC system composed of a Waters 600 series controller and pump (Waters Corporation, MA). Trans and cis isomers were separated on a Zorbax SB-C18 column using a linear gradient from 0 to 80% acetonitrile/H<sub>2</sub>O (+0.1% trifluoroacetic acid) over the course of 45 min. The total concentration of the sample was calculated based on the molar extinction coefficient for the dark-adapted (trans) form. By comparing the peak areas at 315 nm (an isosbestic point), the percent of each isomer present in the sample could be determined.

**Circular Dichroism Measurements.** Circular dichroism measurements were performed with a Jasco Model J-710 spectropolarimeter. All measurements were made in a thermostated quartz cuvette (0.1 cm path length). Temperatures were measured using a microprobe directly in the sample cell. All samples were dissolved in 5 mM phosphate buffer (pH 7.0). Spectra reported are averages of three individual experiments of five scans each, with the appropriate background spectrum subtracted. A scan speed of 10 nm/min, with a 0.5 nm bandwidth, and a 4-s response time were used. The mean residue weight used for FK-11 cross-linked with the sulfonated compound was 109.1 (mass of un-cross-linked peptide divided by the number of residues). Helix content was calculated by using the simple assumption that 100% helix gives a  $\theta_{222}$  value of  $40\,000 \times [(n-4)/n]$ , where  $n$  is the number of residues (21). Using the percent cis observed by UV/vis, theoretical 100% cis CD spectra were calculated using the following equation:  $\theta(100\% \text{ cis}) = [\theta(\text{observed after irradiation}) - (\text{fraction trans} \times \theta(\text{dark-adapted}))] / \text{fraction cis}$ .

## RESULTS AND DISCUSSION

**Linker Design.** It was important that, in creating a water soluble version of the cross-linker, the photochemical properties of the cross-linker would be maintained

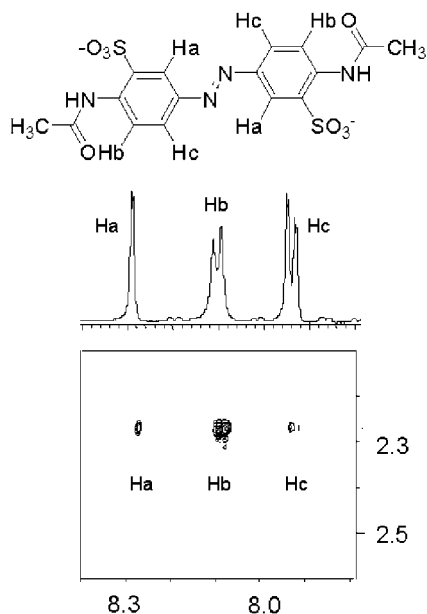
as well as the chemical reactivity, overall length, and symmetry. An asymmetric cross-linker could react in two different orientations with a peptide or protein, which would complicate analysis of conformational changes. Our strategy for producing a water soluble version of the azobenzene cross-linker was to install sulfonate groups on the rings of azobenzene (Scheme 1). Treatment of compound **2** with acetic anhydride resulted in acetylation at either amino group as well as some diacetylated compound. Isomer **3** was readily separated from the other acetylated species owing to its insolubility in hot ethanol. Oxidation of **3** led to the azobenzenesulfonate derivative **4**.

A ROESY spectrum (Figure 1) of **4** was used to determine the position of the sulfonate group on the azobenzene ring system. NOEs were observed between the methyl group and each of the three ring protons. One strong NOE (between H<sub>b</sub> and the methyl group) and two weaker NOEs (between H<sub>a</sub> and CH<sub>3</sub>, and between H<sub>c</sub> and CH<sub>3</sub>) were observed. This result is consistent with the structure shown in Scheme 1 with the sulfonate moiety meta to the azo moiety and ortho to the acetamide group.

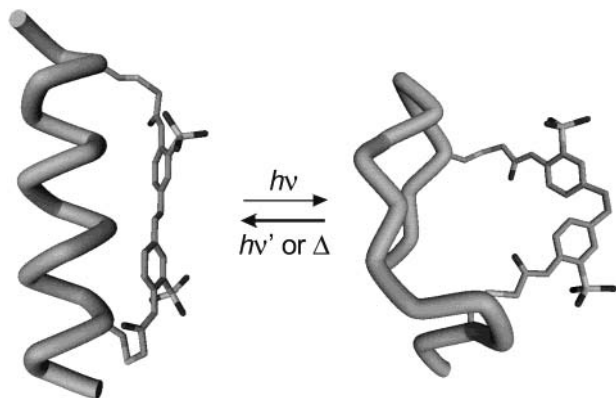
The UV/vis spectrum of this compound was similar to bis-acetamidoazobenzene (data not shown), and the compound was highly water soluble. We therefore decided to convert it into a chloroacetamido derivative (Scheme 2) and examine its ability to act as a photoswitch. The amide linkages were hydrolyzed to yield the bis-amino compound which was subsequently reacted with chloroacetic anhydride in chloroacetic acid. This compound (**6**) was reacted directly with the Cys-containing peptide FK-11 without the need for any organic cosolvent. We note that attempts to directly chloroacetylate compound **2** and then oxidize it to the azo compound proved unsuccessful.

**Photocontrol of Peptide Conformation with the Sulfo-Azobenzene Cross-Linker.** Molecular models of peptides with the sulfo-azobenzene cross-linker attached to Cys residues are shown in Figure 2. The Cys residues





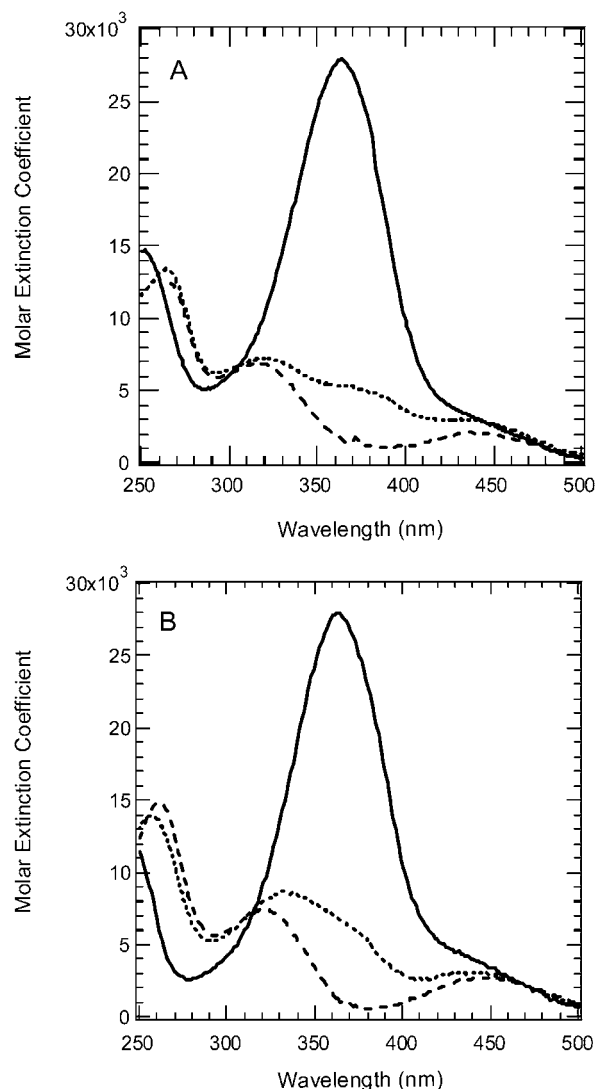
**Figure 1.** Structural analysis of compound **4**. A region of the 2D-ROESY spectrum of compound **4** is shown with its 1D spectrum overlaid above. The 1D spectrum in the aromatic region shows a doublet at 8.28 ppm ( $J = 2.2$  Hz) (labeled H<sub>a</sub>), a doublet at 8.10 ppm ( $J = 8.4$  Hz) (labeled H<sub>b</sub>), and a doublet of doublets at 7.94 ppm ( $J_1 = 8.4$  Hz,  $J_2 = 2.2$  Hz) (labeled H<sub>c</sub>). The NOE cross-peak between the methyl group and H<sub>b</sub> is substantially stronger than the NOE between the methyl group and H<sub>a</sub> or H<sub>c</sub>. This confirms the location of the sulfonate groups shown.



**Figure 2.** Schematic models of trans and cis isomers of the cross-linked peptide. The peptide backbones are represented by a ribbon. The cysteine side-chains and cross-linker are shown as sticks. Hydrogens are omitted for clarity. The trans cross-linker stabilizes a helical backbone structure of the peptide. Photoisomerization to the cis form is expected to destabilize the helix and promote unfolding. The helical model is the final frame of a 500 ps MD run after starting from a helical conformation.

have an *i,i*+11 spacing so that the trans form of the cross-linker is predicted to be compatible with an  $\alpha$ -helical conformation of the peptide whereas the cis form of the cross-linker is too short to fit such a spacing. The cis-form of the cross-linked FK-11 peptide is thus expected to partially unfold in solution.

UV/vis absorption spectra of the dark-adapted (trans form) and irradiated form of the cross-linked FK-11 peptide in aqueous solution are shown in Figure 3A. For comparison, spectra obtained with the nonsulfonated cross-linker attached to the same peptide are shown in Figure 3B. The sulfonate groups have only a minor effect on the trans spectrum. The maximum wavelength of absorbance is close to 364 nm in both cases, and the



**Figure 3.** UV-vis spectra of the cross-linked FK-11 peptide. (A) UV/vis spectrum of FK-11 cross-linked with the sulfonated azobenzene linker (40  $\mu$ M, 5 mM phosphate buffer, pH 7.0) in the dark-adapted state (solid line) and after irradiation at 370 nm (dotted line). The spectrum of the pure cis form of the peptide, measured as described in the Experimental Section is shown as a dashed line. (B) UV/vis spectra of FK-11 cross-linked with the nonsulfonated version of the cross-linker (44  $\mu$ M, 5 mM phosphate buffer, pH 7.0) in the dark-adapted state (solid line), after irradiation at 370 nm (dotted line), and in the cis-state (dashed line).

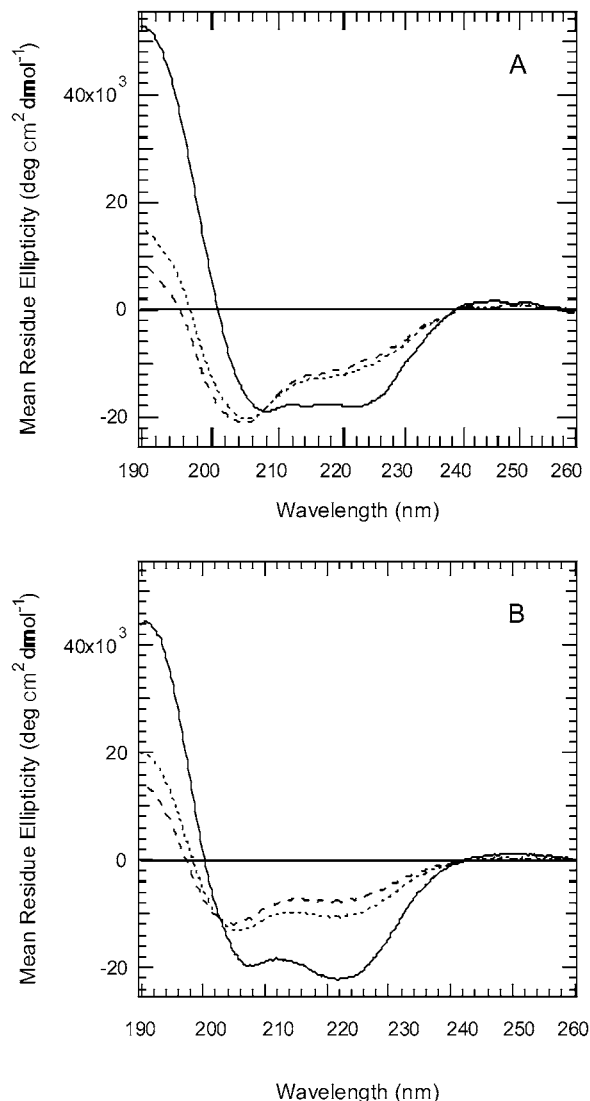
molar extinction coefficients of the two compounds are comparable.

Irradiation of a dilute solution of the FK-11 peptide cross-linked with the sulfonated cross-linker at 370 nm for 5 min ( $\sim 5$  mW) led to a solution containing 85% of the cis isomer. The degree of conversion obtained depends on the particular experimental conditions: peptide concentration, temperature, lamp intensity, and the wavelength used. Although these have not been optimized, the degree of conversion is comparable to that obtained with the nonsulfonated version of the linker and with other azobenzene compounds (13, 15, 22, 23).

Thermal reversion of the cross-linked peptide from the cis form to the trans form was measured by following the absorbance at 370 nm as a function of time after irradiation. The half-lives obtained at 25  $^{\circ}$ C and 37  $^{\circ}$ C are collected in Table 1 together with data for the nonsulfonated version of the cross-linker attached to the

**Table 1. Half-Lives for Thermal Relaxation of Cross-Linked Peptides**

	25 °C $\tau_{1/2}$ (min)	37 °C $\tau_{1/2}$ (min)
FK-11-sulfazo	35 $\pm$ 2	12 $\pm$ 0.5
FK-11-azo <sup>a</sup>	12.3 $\pm$ 0.3	2.5 $\pm$ 0.2
glutathione-sulfazo	25 $\pm$ 4	12 $\pm$ 0.5
glutathione-azo <sup>a</sup>	12.8 $\pm$ 0.3	3.5 $\pm$ 0.3

<sup>a</sup> Data from ref 9.

**Figure 4.** Effects of photoirradiation on secondary structure of cross-linked FK-11. (A). CD spectrum of FK-11 cross-linked with the sulfonated cross-linker (40  $\mu$ M, 5 mM phosphate buffer, pH 7.0) in the dark-adapted state (solid line) and after irradiation at 370 nm (dotted line). The spectrum of the pure cis form of the peptide, calculated by subtracting the residual trans signal from the irradiated spectrum, is shown as a dashed line. (B) CD spectrum of FK-11 cross-linked with the nonsulfonated cross-linker (44  $\mu$ M, 5 mM phosphate buffer, pH 7.0) in the dark-adapted state (solid line), after irradiation at 370 nm (dotted line), and the calculated spectrum for the pure cis state (dashed line).

same peptide. The rate of thermal reversion is related to the energy barrier between the cis ground state and the thermal transition state for isomerization in each case. It is noteworthy that the sulfonated version has a longer half-life, indicating a larger thermal barrier. This does not appear to be a consequence of specific interactions between the linker and the peptide since the cross-linker shows similarly slowed relaxation kinetics when

reacted with two molecules of glutathione, a small unstructured peptide.

To test whether photoisomerization of the sulfonated version of the cross-linker was able to cause the same conformational changes in FK-11 as the nonsulfonated compound, CD spectra were obtained under dark-adapted and irradiated conditions. Figure 4A shows CD spectra obtained for FK-11-sulfazo in the dark-adapted (solid line) and irradiated (dashed line) states. Figure 4B shows the corresponding CD spectra obtained for FK-11-azo. For both cases, the CD spectra of the dark-adapted states indicate the cross-linked FK-11-peptide is highly helical (65%). Irradiation causes a substantial decrease in helical content (35%). The sulfonated photoswitch is thus able to control peptide conformation in the same manner and qualitatively to the same degree as the parent cross-linker.

As previously noted (9), the CD spectrum of the dark-adapted FK-11-azo peptide has a negative band at 222 nm that is more pronounced than the band at 208 nm, a small positive ellipticity at 250 nm and exciton type CD signal at longer wavelengths (not shown). These signals have been attributed to induced CD transitions in the azobenzene chromophore caused by its proximity to the peptide (9). These features are absent in the CD spectra of the FK-11-sulfazo peptide, suggesting that the sulfonate groups disrupt or desymmetrize any such interactions. In summary, it appears that this sulfonated azobenzene cross-linker can effectively substitute for the nonsulfonated version where photocontrol of conformation is desired, but the target protein must be maintained in strictly aqueous as opposed to mixed aqueous/organic solvents. In addition a sulfonated cross-linker may be preferable if slower reversion to the dark-adapted state is desired.

#### ACKNOWLEDGMENT

We would like to acknowledge NSERC (Canada) (G.A.W.), the Volkswagen Stiftung (Germany) (G.A.W.), and the U.K. Medical Research Council (grant G.4600017 (O.S.S.)) for financial support. J.R.K. was supported by an NSERC studentship.

#### LITERATURE CITED

- (1) Adams, S. R., and Tsien, R. Y. (1993) Controlling cell chemistry with caged compounds. *Annu. Rev. Physiol.* 55, 755–784.
- (2) Curley, K., and Lawrence, D. S. (1999) Light-activated proteins. *Curr Opin. Chem. Biol.* 3, 84–88.
- (3) Miller, J. C., Silverman, S. K., England, P. M., Dougherty, D. A., and Lester, H. A. (1998) Flash decaging of tyrosine side chains in an ion channel. *Neuron* 20, 619–624.
- (4) Pan, P., and Bayley, H. (1997) Caged cysteine and thiophosphoryl peptides. *FEBS Lett.* 405, 81–85.
- (5) Willner, I., and Rubin, I. (1996) Control of the structure and functions of biomaterials by light. *Angew. Chem., Int. Ed. Engl.* 35, 367–385.
- (6) Liu, D., Karanickolas, J., Yu, C., Zhang, Z., and Woolley, G. A. (1997) Site-specific incorporation of photoisomerizable azobenzene groups into ribonuclease S. *Bioorg. Med. Chem. Lett.* 7, 2677–2680.
- (7) Hamachi, I., Hiraoka, T., Yamada, Y., and Shinkai, S. (1998) Photoswitching of the enzymatic activity of semisynthetic ribonuclease S bearing phenylazophenylalanine at a specific site. *Chem. Lett.* 6, 537–538.
- (8) James, D. A., Burns, D. C., and Woolley, G. A. (2001) Kinetic characterization of ribonuclease S mutants containing photoisomerizable phenylazophenylalanine residues. *Protein Eng.* 14, 983–991.
- (9) Flint, D. G., Kumita, J. R., Smart, O. S., and Woolley, G. A. (2002) Using an azobenzene cross-linker to either increase

- or decrease peptide helix content upon trans-to-cis photoisomerization. *Chem. Biol.* 9, 391–397.
- (10) Behrendt, R., Renner, C., Schenk, M., Wang, F., Wachtveitl, J., Oesterhelt, D., and Moroder, L. (1999) Photomodulation of the conformation of cyclic peptides with azobenzene moieties in the peptide backbone. *Angew. Chem., Int. Ed.* 38, 2771–2774.
- (11) Asanuma, H., Liang, X., Yoshida, T., and Komiyama, M. (2001) Photocontrol of DNA duplex formation by using azobenzene-bearing oligonucleotides. *ChemBioChem* 2, 39–44.
- (12) Liang, X., Asanuma, H., and Komiyama, M. (2002) Photo-regulation of DNA triplex formation by azobenzene. *J. Am. Chem. Soc.* 124, 1877–1883.
- (13) Renner, C., Behrendt, R., Heim, N., and Moroder, L. (2002) Photomodulation of conformational states. III. Water-soluble bis-cysteinyl-peptides with (4-aminomethyl) phenylazobenzoic acid as backbone constituent. *Biopolymers* 63, 382–393.
- (14) Wachtveitl, J., Nagele, T., Puell, B., Zinth, W., Kruger, M., Rudolph-Bohner, S., Oesterhelt, D., and Moroder, L. (1997). Ultrafast photoisomerization of azobenzene compounds. *J. Photochem. Photobiol. A. Chem.* 105, 283–288.
- (15) Kumita, J. R., Smart, O. S. and Woolley, G. A. (2000) Photocontrol of helix content in a short peptide. *Proc. Natl. Acad. Sci. U.S.A.* 97, 3803–3808.
- (16) Kumita, J. R., Flint, D. G., Smart, O. S., and Woolley, G. A. (2002) Photocontrol of peptide helix content by an azobenzene cross-linker: steric interactions with underlying residues are not critical. *Protein Eng.* 15, 561–569.
- (17) Fahy, G. M., Lilley, T. H., Linsdell, H., Douglas, M. S., and Meryman, H. T. (1990) Cryoprotectant toxicity and cryoprotectant toxicity reduction: in search of molecular mechanisms. *Cryobiology* 27, 247–268.
- (18) Santucci, R., Laurenti, E., Sinibaldi, F., and Ferrari, R. P. (2002) Effect of dimethyl sulfoxide on the structure and the functional properties of horseradish peroxidase as observed by spectroscopy and cyclic voltammetry. *Biochim. Biophys. Acta* 1596, 225–233.
- (19) Bhattacharjya, S., and Balaram, P. (1997) Effects of organic solvents on protein structures: observation of a structured helical core in hen egg-white lysozyme in aqueous dimethyl sulfoxide. *Proteins* 29, 492–507.
- (20) Hadden, C. E., Martin, G. E., and Krishnamurthy, V. V. (2000) Constant time inverse-detection gradient accordion rescaled heteronuclear multiple bond correlation spectroscopy: CIGAR-HMBC. *Magn. Res. Chem.* 38, 143–147.
- (21) Kallenbach, N. R. and Spek, E. J. (1998). Modified amino acids as probes of helix stability. *Methods Enzymol.* 295, 26–41.
- (22) Sporlein, S., Carstens, H., Satzger, H., Renner, C., Behrendt, R., Moroder, L., Tavan, P., Zinth, W., and Wachtveitl, J. (2002). Ultrafast spectroscopy reveals subnanosecond peptide conformational dynamics and validates molecular dynamics simulation. *Proc. Natl. Acad. Sci. U.S.A.* 99, 7998–8002.
- (23) Rau, H. (1990). Photoisomerization of Azobenzenes. In *Photochemistry and Photophysics* (J. F. Rabek, Ed.), vol. II. pp 119–141, CRC Press Inc., Boca Raton, FL.

BC0340161



# Peripheral Benzodiazepine Receptor Ligand–Melphalan Conjugates for Potential Selective Drug Delivery to Brain Tumors

Giuseppe Trapani,<sup>\*,†</sup> Valentino Laquintana,<sup>†</sup> Andrea Latrofa,<sup>†</sup> Jianguo Ma,<sup>‡</sup> Karin Reed,<sup>‡</sup> Mariangela Serra,<sup>§</sup> Giovanni Biggio,<sup>§</sup> Gaetano Liso,<sup>†</sup> and James M. Gallo<sup>‡</sup>

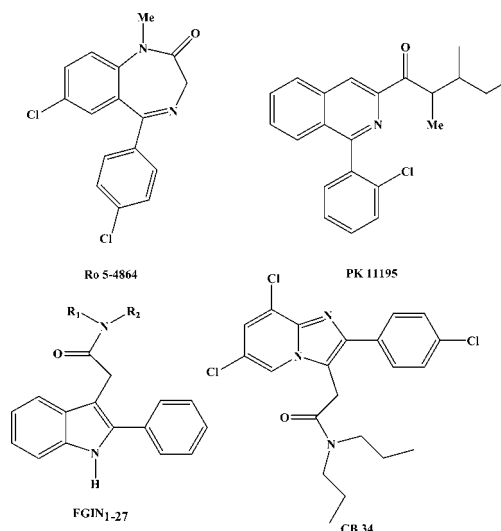
Dipartimento Farmaco-Chimico, Facoltà di Farmacia, Università degli Studi di Bari, Via Orabona 4, 70125 Bari, Italy, Dipartimento di Biologia Sperimentale, Sezione di Neuroscienze, Università di Cagliari, Cittadella Universitaria Monserrato, SS 554 Km 4.5 Monserrato (Cagliari), Italy, and Department of Pharmacology, Fox Chase Cancer Center, 7701 Burholme Avenue, Philadelphia, Pennsylvania 19111. Received February 18, 2003

To gain insight into the strategy to target PBR ligand–drug conjugates to brain tumors, novel *N*-imidazopyridinacetyl–melphalan conjugates and the corresponding ethyl esters have been prepared and evaluated for their cytotoxicity in melphalan-sensitive human (SF126, SF188) and rat (RG-2) glioma cell lines. These conjugates exhibited PBR binding affinity with IC<sub>50</sub> values ranging from 57 and 2614 nM. By a computational approach it can be predicted that these conjugates possess significant brain penetration. The stability of the conjugates in 0.05 M phosphate buffer at pH 7.4 and, in some cases, in dilute human serum solution was determined. All the ethyl ester derivatives were stable in 0.05 M phosphate buffer at pH 7.4 and their half-lives exceeded 28 h. Conversely, under the same conditions, the corresponding acids were found to undergo a fast cleavage within a few minutes. HPLC–MS analysis of the mixture from degradation in buffer and physiological medium of the representative cases allowed the identification of their main degradation products. A plausible degradation pathway accounting for the available experimental data is presented.

## INTRODUCTION

The peripheral benzodiazepine receptors (PBRs)<sup>1</sup> have been identified in various peripheral tissues as well as in glial cells in the brain (1, 2). They are pharmacologically distinct from the central benzodiazepine receptors (CBRs) which are associated with GABA<sub>A</sub> receptors and mediate classical sedative, anxiolytic, and anticonvulsant properties of benzodiazepines. From a structural point of view, PBRs are composed of at least three distinct protein subunits: an 18-kDa subunit containing binding site for isoquinolines, a 32-kDa subunit that functions as a voltage-dependent anion channel and binds benzodiazepines, and a 30-kDa subunit that functions as an adenine nucleotide carrier and also binds benzodiazepines (3). PBRs exhibit a high affinity for 4'-chlorodiazepam (Ro 5-4864), isoquinolines (PK 11195), indoleacetamides (FGIN<sub>1-27</sub>), pyrrolbenzoxazepines and phenoxyphenylacetamides (Figure 1) (4–8).

Although the functions of PBRs are still not fully clarified, growing evidence suggests that these receptors are implicated in the regulation of cell proliferation, Ca<sup>2+</sup>



**Figure 1.** Chemical structures of the most high affinity and selectivity ligands for PBRs.

\* To whom correspondence should be addressed. Phone (039) 080-5442764. Fax (039) 0805442724. E-mail: trapani@farmchim.uniba.it.

<sup>†</sup> Università degli Studi di Bari.

<sup>§</sup> Università di Cagliari.

<sup>‡</sup> Fox Chase Cancer Center.

<sup>1</sup> Abbreviations: PBRs, peripheral benzodiazepine receptors; CBRs, central benzodiazepine receptors; PK 11195, 1-(2-chlorophenyl)-*N*-methyl-*N*-(1-methylpropyl)-3-isoquinoline carboxamide; MEL, melphalan; IC<sub>50</sub>, concentration causing 50% inhibition; log BB, log C<sub>brain</sub>/C<sub>blood</sub>; NCI, National Cancer Institute; CLOG P, calculated log octanol/water partition coefficient; BBB, blood–brain barrier; SRB, sulpharodamine B; PSA, polar surface area; PBS, phosphate buffer solution.

flow, cellular respiration, and cellular immunity (9–12). Moreover, these receptors are abundant in steroidogenic tissues, in which their activation promotes cholesterol transport and neurosteroid biosynthesis (13). Besides their involvement in steroidogenesis, overwhelming experimental evidence indicates that PBR ligands are overexpressed in brain tumors compared to normal brain (14, 15). Therefore, it seems likely that these receptors could serve as a target to selectively increase anticancer drug delivery utilizing an appropriate PBR ligand–anticancer drug conjugate. This attractive strategy for PBR-mediated selective targeting of antineoplastic agents has recently been explored with a benzodiazepine–

melphalan conjugate possessing appreciable cytotoxicity in the human melphalan-resistant brain tumors cell lines (16). More recently, PBR ligand–gemcitabine conjugates, characterized by the PBR isoquinoline ligand PK 11195, have been synthesized, and a 2-fold increase in tumor target selectivity for a member of this series compared to gemcitabine alone has been demonstrated (17).

We have recently shown that some 2-phenylimidazo-[1,2-*a*]pyridine acetamides are potent and selective ligands for PBR and stimulate steroidogenesis in both the brain and periphery (18–20). Our data demonstrate that substitution at 8-position on the imidazopyridine moiety is a key factor for improving affinity and selectivity toward peripheral binding sites. In fact, members of the 8-substituted imidazopyridines show PBR selectivity  $>10^3$ – $10^5$  and are among the most selective ligands tested so far. The substitutions at 8-position and at the para-position of the phenyl ring at C(2) with a chlorine atom are crucial for high affinity and selectivity. The model compound of this new class of PBR ligands, CB 34 (Figure 1), selectively stimulated the synthesis of neuroactive steroids in rat brains with great efficacy (20) and has recently been labeled (21).

The aim of the present work was to synthesize PBR ligand–melphalan (PBR–MEL) conjugates based on the 8-substituted imidazopyridines able to bind to PBRs in vitro and to evaluate their cytotoxicity in melphalan-sensitive glioma cell lines. Thus, further insight on the feasibility of the PBR ligand–drug conjugate strategy to target brain tumor could be gained.

## EXPERIMENTAL PROCEDURES

**Apparatus.** Melting points were determined in open capillary tubes with a Büchi apparatus and are uncorrected. IR spectra were obtained on a Perkin-Elmer Spectrum one system spectrophotometer (KBr pellets for solid). Optical rotations were measured at 20 °C on a Perkin-Elmer Polarimeter 341 (10 cm cell).  $^1\text{H}$  and  $^{13}\text{C}$  NMR spectra were determined on a Varian VX Mercury instrument operating at 300 MHz. Chemical shifts are given in  $\delta$  values downfield from  $\text{Me}_4\text{Si}$  as internal standard. Mass spectra were recorded on a Hewlett-Packard 5995c GC-MS low resolution spectrometer. The mass spectra of conjugates **14**–**21** were obtained using an Agilent 1100 LC-MSD trap system VL instrument using methanol/ammonium formate 7 mM 9:1 (v/v). All compounds showed appropriate IR,  $^1\text{H}$  NMR, and mass spectra. Elemental analyses were performed on a Hewlett-Packard 185 C, H, N analyzer and agreed with theoretical values within  $\pm 0.40\%$ . High-performance liquid chromatography (HPLC) analyses were performed with a Waters Associates Model 600 pump equipped with a Waters 990 variable wavelength UV detector and a 20  $\mu\text{L}$  loop injection valve. For kinetic studies on ester PBR–MEL conjugates **14**–**17**, a reversed phase Symmetry  $\text{C}_{18}$  (25 cm  $\times$  3.9 mm; 5  $\mu\text{m}$  particles) column in conjunction with a precolumn (Sentry Guard Symmetry  $\text{C}_{18}$ , 20  $\times$  3.9 mm) was eluted with mixtures of methanol and deionized water 80/20 (v/v). The volume injected amounted was 20  $\mu\text{L}$ . The flow rate of 0.8 mL/min was maintained, and the column effluent was monitored continuously at 254 nm. Quantification of the compounds was carried out by measuring the peak areas or peak heights in relation to those of standards chromatographed under the same conditions. For kinetic studies on acid PBR–MEL conjugates **18**–**21**, a reversed phase Symmetry  $\text{C}_{18}$  (25 cm  $\times$  3.9 mm; 5  $\mu\text{m}$  particles) column in conjunction with a

precolumn (Sentry Guard Symmetry  $\text{C}_{18}$ , 20  $\times$  3.9 mm) was eluted with mixtures of methanol and acetate buffer pH 4.7 80/20 (v/v). The volume injected amounted was 20  $\mu\text{L}$ . The flow rate of 0.8 mL/min was maintained and the column effluent was monitored continuously at 254 nm. Stability studies were carried out at a controlled temperature of 37 °C ( $\pm 0.2$  °C) in a water bath. The release of melphalan from conjugate **14** was evaluated by using the reported HPLC conditions, except for the composition of elution mixture (methanol/acetate buffer, pH 4.7, 60/40 (v/v)).

The lipophilicity indexes of conjugates **14**–**21**, expressed as  $\log K' = \log(t_R - t_0)/t_0$ , were obtained eluting these compounds on a reversed phase Symmetry  $\text{C}_{18}$  (25 cm  $\times$  3.9 mm; 5  $\mu\text{m}$  particles) with mixtures of methanol and acetate buffer pH 4.7 80/20 (v/v), flux 0.8 mL/min.

TLC analyses were performed on silica gel plate 60 F254 (Merck). Silica gel 60 (Merck 70–230 mesh) was used for column chromatography. All the following reactions were performed under a nitrogen atmosphere.

**Materials.** The starting 2-aminopyridine compounds **4**, melphalan, i.e., *p*-bis(2-dichloroethyl)amino-L-phenylalanine, ethyl 1,2-dihydro-2-ethoxy-1-quinolinecarboxylate (EEDQ), *N*-hydroxysuccinimide (HO-Suc), dicyclohexylcarbodiimide (DCC), 1,1'-carbonyldiimidazole (CDI), and triethylamine (TEA) were purchased from Sigma-Aldrich (Italy). The preparation of the ethyl 3-bromo-3-benzoylpropionate compounds **3** has previously been reported (18, 19). Melphalan ethyl ester hydrochloride (**13**·HCl) was prepared as follows. A stirred solution of melphalan in ethanol (20 mL) was saturated with HCl gas and heated at 60 °C for 2 h. Excess HCl gas was removed under a stream of nitrogen, and then the solvent was evaporated under reduced pressure. The residue was washed several times with anhydrous ethyl ether and then dried under vacuum to provide **13**·HCl in quantitative yield. Treatment of **13**·HCl with  $\text{Na}_2\text{CO}_3$  solution and successive extractions with ethyl ether gave compound **13**. This compound was also obtained from Alkeran tablets (5 mg, GlaxoWellcome) according to the following procedure. Twenty five Alkeran tablets were triturated in a glass mortar, and the resulting powder was suspended in 1 L of ethanol. Hydrogen chloride gas was bubbled through the stirred ethanolic mixture and heated at 60 °C over 2 h. The resulting mixture was filtered (Whatman filter paper) and the filtrate concentrated to a small volume and then treated with water. The so obtained mixture, cooled with an ice bath, was made alkaline with dilute  $\text{Na}_2\text{CO}_3$  solution and extracted several times with ethyl ether. The organic phase, washed with water and brine, dried ( $\text{Na}_2\text{SO}_4$ ), and concentrated under reduced pressure to give a residue which was purified by silica gel column chromatography [light petroleum ether/ethyl acetate 1/1 (v/v) as eluent]. Compound **13** (90% yield) was obtained as an oil and characterized by spectral data and elemental analysis. IR(KBr) 3378, 1723, 1615  $\text{cm}^{-1}$ ;  $^1\text{H}$  NMR ( $\text{CDCl}_3$ )  $\delta$ : 1.26 (t,  $J = 6.7$  Hz, 3H,  $\text{CH}_3$ ), 1.76 (bs, 2H,  $\text{NH}_2$ ), 2.7–2.8 (m, 1H,  $\text{PhCH}$ ), 2.9–3.0 (m, 1H,  $\text{PhCH}$ ), 3.6–3.8 (m, 9H,  $\text{N}(\text{CH}_2\text{CH}_2\text{Cl})_2 + \text{CHCO}$ ), 4.18 (q,  $J = 6.7$  Hz, 2H,  $\text{CH}_2\text{OCO}$ ), 6.62 (d,  $J = 8$  Hz, 2H, Ar), 7.07 (d,  $J = 8$  Hz, 2H, Ar); MS  $m/z$  332 ( $\text{M}^+$ , 3), 230 (base). Anal. ( $\text{C}_{15}\text{H}_{22}\text{Cl}_2\text{N}_2\text{O}_2$ ) C, H, N.

Reagents used for the preparation of the buffers were of analytical grade. Fresh deionized water from all glass apparatus was used in the preparation of all the solutions. HPLC mobile phase was prepared from HPLC-grade methanol. Lyophilized human serum was obtained from Sigma-Aldrich (Italy).

**General Procedure for the Preparation of Ethyl 2-Phenylimidazo[1,2-*a*]pyridine-3-carboxylates 5–8.** To a solution of the suitably substituted 2-aminopyridine **4** (6.2 mmol) in DMF (50 mL) was added the appropriate bromoketoester **3** (6.8 mmol). The mixture was refluxed under stirring for 6–24 h. The progress of the reaction was monitored by TLC. Then the solvent was evaporated under reduced pressure, and the resulting residue was dissolved in CHCl<sub>3</sub> (20 mL), washed with 5% NaHCO<sub>3</sub>, and dried (Na<sub>2</sub>SO<sub>4</sub>). Evaporation of the solvent gave a residue which was purified by silica gel column chromatography [light petroleum ether/ethyl acetate 8/2 (v/v) as eluent].

**Ethyl 2-(4-Chlorophenyl)-6,8-dichloroimidazo[1,2-*a*]pyridine-3-acetate (5).** This compound has been previously described (21).

**Ethyl 2-Phenyl-6,8-dichloroimidazo[1,2-*a*]pyridine-3-acetate (6).** IR (KBr) 1726 cm<sup>-1</sup>; <sup>1</sup>H NMR (CDCl<sub>3</sub>) δ: 1.29 (t, *J* = 7.1 Hz, 3H, CH<sub>3</sub>), 4.01 (s, 2H, CH<sub>2</sub>CO), 4.24 (q, *J* = 7.1 Hz, 2H, CH<sub>2</sub>OCO), 7.32 (d, *J* = 1.7 Hz, 1H, Ar), 7.4–7.6 (m, 3H, Ar), 7.81 (d, *J* = 6.8 Hz, 2H, Ar), 8.14 (d, *J* = 1.7 Hz, 1H, Ar); MS *m/z* 348 (M<sup>+</sup>, 38) 275 (base); Anal. (C<sub>17</sub>H<sub>14</sub>Cl<sub>2</sub>N<sub>2</sub>O<sub>2</sub>) C, H, N.

**Ethyl 2-(4-Chlorophenyl)-8-chloroimidazo[1,2-*a*]pyridine-3-acetate (7).** IR (KBr) 1728 cm<sup>-1</sup>; <sup>1</sup>H NMR (CDCl<sub>3</sub>) δ: 1.27 (t, *J* = 7.1 Hz, 3H, CH<sub>3</sub>), 4.00 (s, 2H, CH<sub>2</sub>CO), 4.22 (q, *J* = 7.1 Hz, 2H, CH<sub>2</sub>OCO), 6.82 (t, *J* = 7 Hz, 1H, Ar), 7.32 (d, *J* = 7 Hz, 1H, Ar), 7.44 (d, *J* = 8.4 Hz, 2H, Ar), 7.79 (d, *J* = 8.4 Hz, 2H, Ar), 8.08 (d, *J* = 7 Hz, 1H, Ar); MS *m/z* 348 (M<sup>+</sup>, 29) 275 (base); Anal. (C<sub>17</sub>H<sub>14</sub>Cl<sub>2</sub>N<sub>2</sub>O<sub>2</sub>) C, H, N.

**Ethyl 2-(4-Chlorophenyl)-6-methyl-8-bromoimidazo[1,2-*a*]pyridine-3-acetate (8).** IR (KBr) 1723 cm<sup>-1</sup>; <sup>1</sup>H NMR (CDCl<sub>3</sub>) δ: 1.28 (t, *J* = 7.1 Hz, 3H, CH<sub>3</sub>), 2.36 (s, 3H, CH<sub>3</sub>-Ar), 3.96 (s, 2H, CH<sub>2</sub>CO), 4.22 (q, *J* = 7.1 Hz, 2H, CH<sub>2</sub>OCO), 7.38 (d, *J* = 1.5 Hz, 1H, Ar), 7.42 (d, *J* = 8.5 Hz, 2H, Ar), 7.78 (d, *J* = 8.5 Hz, 2H, Ar), 7.87 (d, *J* = 1.5 Hz, 1H, Ar); MS *m/z* 408 (M<sup>+</sup>, 25) 335 (base); Anal. (C<sub>18</sub>H<sub>16</sub>BrClN<sub>2</sub>O<sub>2</sub>) C, H, N.

**General Procedure for the Preparation of (Imidazo[1,2-*a*]pyridin-3-yl)acetic Acids 9–12.** To a solution of the appropriate ethyl ester **5–8** (2.3 mmol) in 95% ethanol (20 mL) was dropwise added NaOH 1 N (2 mL). The mixture was stirred at room temperature and under a nitrogen atmosphere for 4 h. Then, the solvent was evaporated under reduced pressure, and the residue was taken up with water and extracted five times with CHCl<sub>3</sub> (30 mL portions). The cooled water phase was acidified with dilute HCl. The resulting precipitate corresponded to the essentially pure carboxylic acid, which was isolated by filtration.

**[2-(4-Chlorophenyl)-6,8-dichloroimidazo[1,2-*a*]pyridin-3-yl]acetic Acid (9).** This compound has been previously described (21).

**[2-Phenyl-6,8-dichloroimidazo[1,2-*a*]pyridin-3-yl]acetic Acid (10).** IR (KBr) 3441, 1698 cm<sup>-1</sup>; <sup>1</sup>H NMR (DMSO-*d*<sub>6</sub>) δ: 4.13 (s, 2H, CH<sub>2</sub>CO), 7.3–7.5 (m, 3H, Ar), 7.64 (d, *J* = 1.6 Hz, 1H, Ar), 7.73 (d, *J* = 7.1 Hz, 2H, Ar), 8.74 (d, *J* = 1.6 Hz, 1H, Ar); MS *m/z* 276 (base); Anal. (C<sub>15</sub>H<sub>10</sub>Cl<sub>2</sub>N<sub>2</sub>O<sub>2</sub>) C, H, N.

**[2-(4-Chlorophenyl)-8-chloroimidazo[1,2-*a*]pyridin-3-yl]acetic Acid (11).** IR (KBr) 3414, 1716 cm<sup>-1</sup>; <sup>1</sup>H NMR (DMSO-*d*<sub>6</sub>) δ: 4.17 (s, 2H, CH<sub>2</sub>CO), 6.97 (t, *J* = 7 Hz, 1H, Ar), 7.50 (d, *J* = 7 Hz, 1H, Ar), 7.56 (d, *J* = 8.5 Hz, 2H, Ar), 7.78 (d, *J* = 8.5 Hz, 2H, Ar), 8.43 (d, *J* = 7 Hz, 1H, Ar); Anal. (C<sub>15</sub>H<sub>10</sub>Cl<sub>2</sub>N<sub>2</sub>O<sub>2</sub>) C, H, N.

**[2-(4-Chlorophenyl)-6-methyl-8-bromoimidazo[1,2-*a*]pyridin-3-yl]acetic Acid (12).** IR (KBr) 3422, 1734 cm<sup>-1</sup>; <sup>1</sup>H NMR (DMSO-*d*<sub>6</sub>) δ: 2.30 (s, 3H, CH<sub>3</sub>-Ar), 4.11

(s, 2H, CH<sub>2</sub>CO), 7.5–7.6 (m, 3H, Ar), 7.76 (d, *J* = 8.4 Hz, 2H, Ar), 8.29 (s, 1H, Ar); Anal. (C<sub>16</sub>H<sub>12</sub>N<sub>2</sub>BrClO<sub>2</sub>) C, H, N.

**General Procedure for Preparation of the Conjugates 14–17. Method A.** To a stirred solution of the required imidazo[1,2-*a*]pyridine-3-acetic acid **9–12** (0.93 mmol) in anhydrous THF (20 mL) was at first added EEDQ (1.2 mmol) and melphalan ethyl ester **13** (0.9 mmol) and after 15 min, TEA (1.3 mmol) dropwise. Stirring was prolonged at room temperature for 6–12 h and then the mixture poured into 20 mL of water and extracted with ethyl acetate (3 × 30 mL). The organic layer was separated, washed with water and brine, and dried over Na<sub>2</sub>SO<sub>4</sub>. Solvent was evaporated under reduced pressure, and the resulting residue was purified by silica gel column chromatography [light petroleum ether/ethyl acetate 8/2 (v/v) as eluent] to give the corresponding conjugate **14–17**.

**Method B.** To a stirred suspension of the suitably substituted 2-phenylimidazo[1,2-*a*]pyridine-3-acetic acid **10 (12)** (1.0 mmol) in anhydrous CH<sub>2</sub>Cl<sub>2</sub> (20 mL) were added HO-Suc (0.9 mmol) and DCC (0.9 mmol) at room temperature, and stirring was prolonged overnight. Then, ethyl ether was added and the resulting dicyclohexylurea precipitate removed by filtration. The filtrate was concentrated and the residue taken up with anhydrous THF (20 mL). To the resulting mixture was added melphalan ethyl ester **13** (1.0 mmol), and the stirring was prolonged overnight. Then, the reaction mixture was washed with water, made alkaline with NaHCO<sub>3</sub> solution, and extracted with ethyl acetate (3 × 30 mL). The organic phase was washed with water and brine and dried over Na<sub>2</sub>SO<sub>4</sub>. Solvent was evaporated under reduced pressure, and the residue was purified by silica gel column chromatography [light petroleum ether/ethyl acetate 8/2 (v/v) as eluent] to give the corresponding melphalan conjugate **15 (17)**.

**Method C.** A solution of the acid **9** (0.3 g, 0.85 mmol) and CDI (0.2 g, 1.3 mmol) in anhydrous THF (20 mL) was stirred at room temperature. Then, melphalan ethyl ester hydrochloride **13**·HCl (0.31 g, 0.84 mmol) was added, and the stirring was prolonged for 3 h. Then the reaction mixture was washed with water, extracted with CHCl<sub>3</sub>, and dried over Na<sub>2</sub>SO<sub>4</sub>. Solvent was evaporated under reduced pressure, and the residue was purified by silica gel column chromatography [light petroleum ether/ethyl acetate 8/2 (v/v) as eluent] to give compound **14**.

**N-(*p*-Bis(2-chloroethyl)amino-L-phenylalanine ethyl ester) [2-(4-Chlorophenyl)-6,8-dichloroimidazo[1,2-*a*]pyridin-3-yl]acetamide (14).** IR (KBr): 3340, 1727, and 1642 cm<sup>-1</sup>; <sup>1</sup>H NMR (CDCl<sub>3</sub>) δ: 1.27 (t, *J* = 7.1 Hz, 3H, CH<sub>3</sub>), 2.8–3.0 (m, 2H, CH<sub>2</sub>Ar), 3.5–3.7 (m, 8H, N(CH<sub>2</sub>CH<sub>2</sub>Cl)<sub>2</sub>), 3.84 (d, *J* = 17.8 Hz, 1H, CH<sub>2</sub>CON), 3.92 (d, *J* = 17.8 Hz, 1H, CH<sub>2</sub>CON), 4.21 (q, *J* = 7.1 Hz, 2H, CH<sub>2</sub>OCO), 4.7–4.8 (m, 1H, CHCOO), 5.98 (d, *J* = 7.3 Hz, 1H, NHCO), 6.45 (d, *J* = 8.5 Hz, 2H, Ar of melphalan moiety), 6.73 (d, *J* = 8.5 Hz, 2H, Ar of melphalan moiety), 7.3–7.4 (m, 3H, Ar), 7.57 (d, *J* = 8.4 Hz, 2H, Ar), 8.12 (s, 1H, Ar); <sup>13</sup>C NMR (CDCl<sub>3</sub>) δ: 171.3, 167.4, 145.5, 144.9, 141.1, 134.8, 131.3, 130.3, 130.1, 129.1, 125.7, 123.9, 123.6, 121.1, 120.5, 116.4, 112.1, 62.0, 53.5, 40.5, 36.3, 32.4, 14.4; MS (ESI) *m/z* 671.0 [M + H]<sup>+</sup>. Anal. (C<sub>30</sub>H<sub>29</sub>Cl<sub>5</sub>N<sub>4</sub>O<sub>3</sub>) C, H, N.

**N-(*p*-Bis(2-chloroethyl)amino-L-phenylalanine ethyl ester) (2-Phenyl-6,8-dichloroimidazo[1,2-*a*]pyridin-3-yl)acetamide (15).** IR (KBr) 3405, 1737, and 1661 cm<sup>-1</sup>; <sup>1</sup>H NMR (CDCl<sub>3</sub>) δ: 1.26 (t, *J* = 7.1 Hz, 3H, CH<sub>3</sub>), 2.9–3.0 (m, 2H, CH<sub>2</sub>Ar), 3.5–3.7 (m, 8H, N(CH<sub>2</sub>CH<sub>2</sub>Cl)<sub>2</sub>), 3.88 (d, *J* = 17.2 Hz, 1H, CH<sub>2</sub>CON), 3.96 (d, *J* = 17.2



Hz, 1H,  $\text{CH}_2\text{CON}$ ), 4.19 (q,  $J = 7.1$  Hz, 2H,  $\text{CH}_2\text{OCO}$ ), 4.7–4.8 (m, 1H,  $\text{CHCO}$ ), 5.95 (d,  $J = 7.3$  Hz, 1H,  $\text{NHCO}$ ), 6.41 (d,  $J = 8.8$  Hz, 2H, Ar of melfhalan moiety), 6.71 (d,  $J = 8.8$  Hz, 2H, Ar of melfhalan moiety), 7.36 (d,  $J = 1.8$  Hz, 1H, Ar), 7.4–7.5 (m, 3H, Ar), 7.6–7.7 (m, 2H, Ar), 8.11 (d,  $J = 1.8$  Hz, 1H, Ar). MS (ESI)  $m/z$  637.1  $[\text{M} + \text{H}]^+$ . Anal. ( $\text{C}_{30}\text{H}_{30}\text{Cl}_4\text{N}_4\text{O}_3$ ) C, H, N.

***N*-(*p*-Bis(2-chloroethyl)amino-*L*-phenylalanine ethyl ester) [2-(4-Chlorophenyl)-8-chloroimidazo[1,2-*a*]pyridin-3-yl]acetamide (16).** IR (KBr): 3410, 1737, and 1658  $\text{cm}^{-1}$ ;  $^1\text{H}$  NMR ( $\text{CDCl}_3$ )  $\delta$ : 1.25 (t,  $J = 7.1$  Hz, 3H,  $\text{CH}_3$ ), 2.8–2.3 (m, 2H,  $\text{CH}_2$ -Ar), 3.5–3.7 (m, 8H,  $\text{N}(\text{CH}_2\text{CH}_2\text{Cl})_2$ ), 3.9–4.0 (m, 2H,  $\text{CH}_2\text{CON}$ ), 4.17 (q,  $J = 7.1$  Hz, 2H,  $\text{CH}_2\text{OCO}$ ), 4.7–4.8 (m, 1H,  $\text{CHCO}$ ), 6.15 (br s, 1H,  $\text{NHCO}$ ), 6.41 (d,  $J = 8.4$  Hz, 2H, Ar of melfhalan moiety), 6.69 (d,  $J = 8.4$  Hz, 2H, Ar of melfhalan moiety), 6.87 (t,  $J = 7$  Hz, 1H, Ar); 7.3–7.4 (m, 3H, Ar), 7.58 (d,  $J = 8.4$  Hz, 2H, Ar), 8.06 (d,  $J = 7$  Hz, 1H, Ar);  $^{13}\text{C}$  NMR ( $\text{CDCl}_3$ )  $\delta$ : 171.3, 167.5, 145.4, 135.1, 130.4, 130.3, 129.1, 126.2, 124.2, 123.6, 122.6, 116.4, 113.7, 112.2, 61.8, 53.7, 53.6, 40.6, 36.3, 32.2, 29.9, 14.3; MS (ESI)  $m/z$  637.1  $[\text{M} + \text{H}]^+$ . Anal. ( $\text{C}_{30}\text{H}_{30}\text{Cl}_4\text{N}_4\text{O}_3$ ) C, H, N.

***N*-(*p*-Bis(2-chloroethyl)amino-*L*-phenylalanine ethyl ester) [2-(4-Chlorophenyl)-6-methyl-8-bromoimidazo[1,2-*a*]pyridin-3-yl]acetamide (17).** IR (KBr) 3327, 1737, and 1626  $\text{cm}^{-1}$ ;  $^1\text{H}$  NMR ( $\text{CDCl}_3$ )  $\delta$ : 1.25 (t,  $J = 7.1$  Hz, 3H,  $\text{CH}_3$ ), 2.42 (s, 3H,  $\text{CH}_3\text{Ar}$ ), 2.9–3.1 (m, 2H,  $\text{CH}_2$ -Ar), 3.5–3.7 (m, 8H,  $\text{N}(\text{CH}_2\text{CH}_2\text{Cl})_2$ ), 3.9–4.0 (m, 2H,  $\text{CH}_2\text{CON}$ ), 4.15 (q,  $J = 7.1$  Hz, 2H,  $\text{CH}_2\text{OCO}$ ), 4.7–4.8 (m, 1H,  $\text{CHCO}$ ), 6.43 (d,  $J = 8.5$  Hz, 2H, Ar of melfhalan moiety), 6.76 (d,  $J = 8.5$  Hz, 2H, Ar of melfhalan moiety), 7.29 (d,  $J = 8.1$  Hz, 2H, Ar), 7.5–7.6 (m, 3H, Ar), 8.10 (br s, 1H, Ar). MS (ESI)  $m/z$  695.0  $[\text{M} + \text{H}]^+$ . Anal. ( $\text{C}_{31}\text{H}_{32}\text{BrCl}_3\text{N}_4\text{O}_3$ ) C, H, N.

**General Procedure for Preparation of *N*-(*p*-Bis(2-chloroethyl)amino-*L*-phenylalanine) [2-Phenylimidazo[1,2-*a*]pyridin-3-yl]acetamides (18–21).** To a cooled solution of the appropriate compound **14–17** (0.2 mmol) in ethanol (10 mL) was added NaOH 1 N (0.2 mL). The reaction mixture was kept under stirring at 0 °C overnight and then concentrated. The resulting residue taken up with water was acidified with HCl 0.1 N until pH 3 and extracted several times with  $\text{CHCl}_3$  (30 mL). The organic layer was dried over  $\text{Na}_2\text{SO}_4$ , and by solvent evaporation under reduced pressure the desired compound **18–21**, respectively, was obtained.

***N*-(*p*-Bis(2-chloroethyl)amino-*L*-phenylalanine) [2-(4-Chlorophenyl)-6,8-dichloroimidazo[1,2-*a*]pyridin-3-yl]acetamide (18).** IR (KBr) 3452, 1716, 1640, 1615  $\text{cm}^{-1}$ ;  $^1\text{H}$  NMR ( $\text{DMSO}-d_6$ )  $\delta$ : 2.7–2.9 (m, 1H,  $\text{CH}_2$ -Ar), 2.9–3.1 (m, 1H,  $\text{CH}_2\text{Ar}$ ), 3.62 (s, 8H,  $\text{N}(\text{CH}_2\text{CH}_2\text{Cl})_2$ ), 4.02 (s, 2H,  $\text{CH}_2\text{CON}$ ), 4.3–4.5 (m, 1H,  $\text{CHCO}$ ), 6.56 (d,  $J = 8.4$  Hz, 2H, Ar of melfhalan moiety), 7.04 (d,  $J = 8.4$  Hz, 2H, Ar of melfhalan moiety), 7.45 (d,  $J = 8.4$  Hz, 2H, Ar), 7.65 (s, 1H, Ar), 7.82 (d,  $J = 8.4$  Hz, 2H, Ar), 8.68 (s, 1H, Ar); MS (ESI)  $m/z$  641.1  $[\text{M} - \text{H}]^-$ . Anal. ( $\text{C}_{28}\text{H}_{25}\text{Cl}_5\text{N}_4\text{O}_3$ ) C, H, N.

***N*-(*p*-Bis(2-chloroethyl)amino-*L*-phenylalanine) (2-Phenyl-6,8-dichloroimidazo[1,2-*a*]pyridin-3-yl)acetamide (19).** IR (KBr) 3298, 1716, 1638, 1615  $\text{cm}^{-1}$ ;  $^1\text{H}$  NMR ( $\text{DMSO}-d_6$ )  $\delta$ : 2.7–2.9 (m, 1H,  $\text{CH}_2$ -Ar), 2.9–3.0 (m, 1H,  $\text{CH}_2$ -Ar), 3.62 (s, 8H,  $\text{N}(\text{CH}_2\text{CH}_2\text{Cl})_2$ ), 4.03 (s, 2H,  $\text{CH}_2\text{CON}$ ), 4.3–4.4 (m, 1H,  $\text{CHCO}$ ), 6.52 (d,  $J = 8.2$  Hz, 2H, Ar of melfhalan moiety), 7.00 (d,  $J = 8.2$  Hz, 2H, Ar of melfhalan moiety), 7.3–7.5 (m, 3H, Ar), 7.62 (s, 1H, Ar), 7.80 (d,  $J = 8.0$  Hz, 2H, Ar), 8.63 (s, 1H, Ar); MS (ESI)  $m/z$  607.1  $[\text{M} - \text{H}]^-$ . Anal. ( $\text{C}_{28}\text{H}_{26}\text{Cl}_4\text{N}_4\text{O}_3$ ) C, H, N.

***N*-(*p*-Bis(2-chloroethyl)amino-*L*-phenylalanine) [2-(4-Chlorophenyl)-8-chloroimidazo[1,2-*a*]pyridin-3-yl]acetamide (20).** IR (KBr) 3296, 1711, 1644, 1615  $\text{cm}^{-1}$ ;  $^1\text{H}$  NMR ( $\text{DMSO}-d_6$ )  $\delta$ : 2.7–2.8 (m, 1H,  $\text{CH}_2\text{Ar}$ ), 2.9–3.0 (m, 1H,  $\text{CH}_2\text{Ar}$ ), 3.66 (s, 8H,  $\text{N}(\text{CH}_2\text{CH}_2\text{Cl})_2$ ), 4.00 (s, 2H,  $\text{CH}_2\text{CON}$ ), 4.3–4.4 (m, 1H,  $\text{CHCO}$ ), 6.60 (d,  $J = 8.5$  Hz, 2H, Ar of melfhalan moiety), 6.86 (t,  $J = 7$  Hz, 1H, Ar), 7.06 (d,  $J = 8.5$  Hz, 2H, Ar of melfhalan moiety), 7.46 (d,  $J = 8.5$  Hz, 2H, Ar), 7.80 (d,  $J = 8.5$  Hz, 2H, Ar), 8.23 (d,  $J = 7$  Hz, 1H, Ar), 8.72 (d,  $J = 7$  Hz, 1H, Ar);  $^{13}\text{C}$  NMR ( $\text{DMSO}-d_6$ )  $\delta$ : 173.6, 168.6, 145.5, 135.4, 130.7, 130.5, 129.1, 126.1, 124.8, 124.6, 121.8, 118.3, 112.4, 112.3, 54.4, 53.0, 41.5, 36.4, 31.2; MS (ESI)  $m/z$  607.1  $[\text{M} - \text{H}]^-$ . Anal. ( $\text{C}_{28}\text{H}_{26}\text{Cl}_4\text{N}_4\text{O}_3$ ) C, H, N.

***N*-(*p*-Bis(2-chloroethyl)amino-*L*-phenylalanine) [2-(4-Chlorophenyl)-6-methyl-8-bromoimidazo[1,2-*a*]pyridin-3-yl]acetamide (21).** IR (KBr) 3303, 1716, 1642, 1615  $\text{cm}^{-1}$ ;  $^1\text{H}$  NMR ( $\text{DMSO}-d_6$ )  $\delta$ : 2.7–2.9 (m, 1H,  $\text{CH}_2$ -Ar), 2.9–3.0 (m, 1H,  $\text{CH}_2$ -Ar), 3.65 (s, 8H,  $\text{N}(\text{CH}_2\text{CH}_2\text{Cl})_2$ ), 3.96 (s, 2H,  $\text{CH}_2\text{CON}$ ), 4.3–4.5 (m, 1H,  $\text{CHCO}$ ), 6.57 (d,  $J = 8.5$  Hz, 2H, Ar of melfhalan moiety), 7.05 (d,  $J = 8.5$  Hz, 2H, Ar of melfhalan moiety), 7.45 (d,  $J = 8.6$  Hz, 2H, Ar), 7.53 (s, 1H, Ar), 7.79 (d,  $J = 8.5$  Hz, 2H, Ar), 8.20 (s, 1H, Ar); MS (ESI)  $m/z$  665.1  $[\text{M} - \text{H}]^-$ . Anal. ( $\text{C}_{29}\text{H}_{28}\text{BrCl}_3\text{N}_4\text{O}_3$ ) C, H, N.

**Computational Calculations of Physicochemical and Penetration Characteristics of the Melfhalan Conjugates 14–21.** Lipophilicity and  $\log C_{\text{brain}}/C_{\text{blood}}$  (log BB) values were estimated by using CLOG P (v. 4, BioByte Corp) and MAREA (v. 1.4 Department of Pharmacy, Uppsala, Sweden) softwares, respectively, and are reported in Table 2.

**Stability in Buffered Solution.** The stability of the melfhalan conjugates **14–21** was studied at pH 7.4 in 0.05 M phosphate buffer at  $37 \pm 0.2$  °C in a water bath. The reaction was carried out by adding 500  $\mu\text{L}$  of a stock solution of the conjugates (5 mg in 25 mL of DMSO) to 5 mL of the buffer solution preheated at 37 °C. The final concentration of the compounds was about  $3 \times 10^{-5}$  M. The resulting solutions were vortexed and maintained in a water bath at constant temperature of  $37 \pm 0.2$  °C. Aliquots of 20  $\mu\text{L}$  were removed at appropriate intervals and either immediately analyzed or frozen at  $-20$  °C until analyzed by HPLC. Each experiment was repeated in triplicate. Pseudo-first-order rate constants for degradation of the derivatives were determined from the slopes of linear plots of the logarithms of residual melfhalan conjugate against time.

**Stability in Physiological Medium.** The stability in physiological medium of conjugates **14**, **18**, **19**, and **20** was studied at 37 °C in 0.05 M phosphate buffer and 0.14 M NaCl at pH 7.4, containing 50% v/v of human serum. The reaction was carried out by adding 100  $\mu\text{L}$  of the stock solution of compound in DMSO (7.6 mg/25 mL for **14** and 5 mg/10 mL for **18**, **19**, and **20**) to 1.6 mL of preheated serum solution, and the mixture was maintained in water bath at  $37 \pm 0.2$  °C. Aliquots of 100  $\mu\text{L}$  were withdrawn at appropriate intervals and added to 500  $\mu\text{L}$  of cold acetonitrile in order to deproteinize the serum (the final concentration of compounds being  $5.3 \times 10^{-6}$  M for **14** and  $9 \times 10^{-6}$  M for **18**, **19**, and **20**). After mixing and centrifugation for 10 min at 4000 rpm, 20  $\mu\text{L}$  of the clear supernatant was analyzed by HPLC. Each experiment was repeated in duplicate. Pseudo-first-order rate constants for degradation of the derivatives were determined from the slopes of linear plots of the logarithms of remaining melfhalan conjugate against time.

**Structural Identification of Degradation Products of 14 and 18 in Buffer and in Physiological**

**Medium.** Compound **14** was allowed to react under conditions above-reported for chemical stability except for the use of 250  $\mu\text{L}$  of stock solution of the conjugate (1 mg/5 mL of DMSO). After 24 h, to the reaction mixture was added 5 mL of  $\text{CHCl}_3$ , and it was vortexed and centrifugated. The organic phase was separated, dried over  $\text{Na}_2\text{SO}_4$ , evaporated under a stream of nitrogen, taken up with methanol (500  $\mu\text{L}$ ), purified by reversed phase HPLC, and characterized by ESI(negative mode)-MS. The same procedure was followed for compound **18** except for 2 mL of  $\text{CHCl}_3$  was added after 120 min of incubation. Compound **14** was also allowed to react under conditions above-reported for stability in physiological medium. After 120 min, an aliquot of the reaction mixture (200  $\mu\text{L}$ ) was added to 500  $\mu\text{L}$  of acetonitrile. To the resulting mixture was added water (300  $\mu\text{L}$ ), and it was vortexed and centrifugated. The supernatant (400  $\mu\text{L}$ ) was separated, treated with water (300  $\mu\text{L}$ ) and  $\text{CHCl}_3$  (500  $\mu\text{L}$ ), and then vortexed. An aliquot of 500  $\mu\text{L}$  of the chloroformic phase was dried over  $\text{Na}_2\text{SO}_4$ , evaporated under a stream of nitrogen, purified by reversed phase HPLC, and characterized by ESI (negative mode)-MS. The same procedure was followed for compound **18**. For these studies, a reversed phase Phenomenex Luna  $\text{C}_{18}$  (15 cm  $\times$  3 mm; 5  $\mu\text{m}$  particles) column in conjunction with a precolumn module was eluted in gradient HPLC conditions. The mobile phase used was the following: eluent A, methanol:deionized water:acetic acid (60:39:1, v:v:v); eluent B, methanol:deionized water:acetic acid (90:9:1, v:v:v) (injection volume 20  $\mu\text{L}$ ). Gradient 0–5 min eluent A, 5–20 min from 100% of eluent A to 100% of eluent B; 20–40 min 100% of eluent B; 40–45 min from 100% of eluent B to 100% of eluent A. Preliminary experimental work included the HPLC-ESI-MS analysis under identical experimental conditions of commercial melphalan [retention time ( $t_R$ ) 6.2 min] and the pure acids **9** ( $t_R$  5.1 min,  $m/z$  337) and **18** ( $t_R$  19 min,  $m/z$  640).

**Biological Methods. Materials.** Adult male or female Sprague–Dawley CD rats (Charles River, Como, Italy) with body masses of 200–250 g at the beginning of the experiments were maintained under an artificial 12-h-light/dark cycle (light on 08.00 to 20.00 h) at a constant temperature of  $23 \pm 2^\circ\text{C}$  and 65% humidity. Food and water were freely available, and the animals were acclimated for >7 days before use. Experiments were performed between 08.00 and 14.00 h. Animal care and handling throughout the experimental procedure were performed in accordance with the European Communities Council Directive of 24 November 1986 (86/609/EEC). The experimental protocol were approved by the Animal Ethical Committee of the University of Cagliari.

**In Vitro Receptor Binding Assays.** After sacrifice the brain was rapidly removed, the cerebral cortex was dissected, and tissues were stored at  $-80^\circ\text{C}$  until assay.

**[ $^3\text{H}$ ]Flunitrazepam Binding.** The tissues were thawed and homogenized with a Polytron PT 10 in 50 volumes of ice-cold 50 mM Tris-HCl buffer (pH 7.4) and centrifuged twice at 20 000g for 10 min. The pellet was reconstituted in 50 volumes of Tris-HCl buffer and was used for the binding assay. Aliquots of 400  $\mu\text{L}$  of tissue homogenate (0.4–0.5 mg of protein) were incubated in the presence of [ $^3\text{H}$ ]flunitrazepam at a final concentration of 0.5 nM, in a total incubation volume of 1000  $\mu\text{L}$ . The drugs were added in 100  $\mu\text{L}$  aliquots. After a 60 min incubation at  $0^\circ\text{C}$ , the assay was terminated by rapid filtration through glass-fiber filter strips (Whatman GF/B). The filters were rinsed with 2- to 4-mL portions of ice-cold Tris-HCl buffer as described above. Radioactivity bound to the filters was quantitated by liquid scintillation

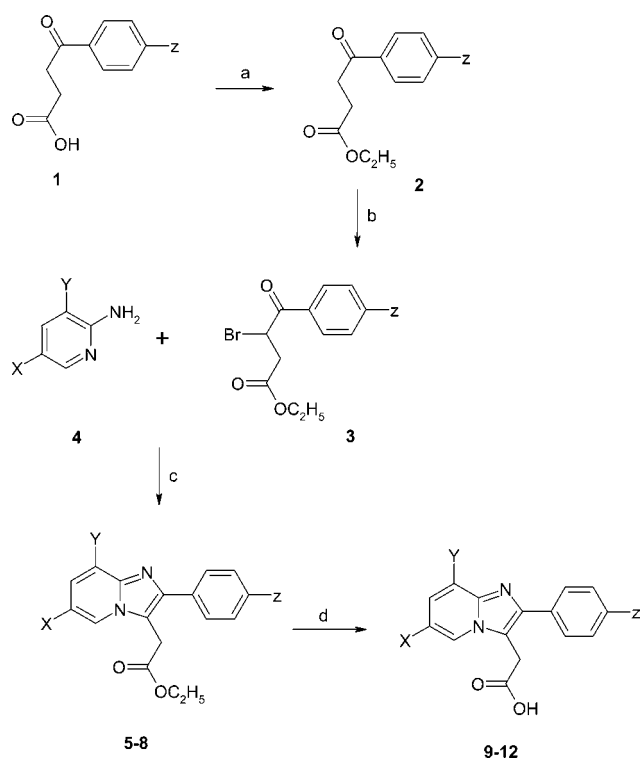
spectrometry. Nonspecific binding was determined as binding in the presence of 5  $\mu\text{M}$  diazepam and represented about 10% of total binding.

**[ $^3\text{H}$ ]PK 11195 Binding.** The tissues were thawed and homogenized in 50 volumes of Dulbecco's phosphate-buffered saline (PBS) pH 7.4 at  $4^\circ\text{C}$  with a Polytron PT 10 (setting 5, for 20 s). The homogenate was centrifuged at 40 000g for 30 min, and the pellet was resuspended in 50 volumes of PBS and recentrifuged. The new pellet was resuspended in 20 volumes of PBS and used for the assay. [ $^3\text{H}$ ]PK 11195 binding was determined in a final volume of 1000  $\mu\text{L}$  of tissue homogenate (0.15–0.20 mg protein), 100  $\mu\text{L}$  of [ $^3\text{H}$ ]PK 11195 (spec act. 85.5 Ci/mmol, New England Nuclear) at final assay concentration of 1 nM, 5  $\mu\text{L}$  of drug solution or solvent, and 795  $\mu\text{L}$  of PBS buffer (pH 7.4 at  $25^\circ\text{C}$ ). Incubations ( $25^\circ\text{C}$ ) were initiated by addition of membranes and were terminated 90 min later by rapid filtration through glass-fiber filter strips (Whatman GF/B), which were rinsed with five 4 mL volumes of ice-cold PBS buffer using a Cell Harvester filtration manifold (Brandel). Filter bound radioactivity was quantified by liquid scintillation spectrometry. Nonspecific binding was defined as binding in the presence of 10  $\mu\text{M}$  unlabeled PK 11195 (Sigma).

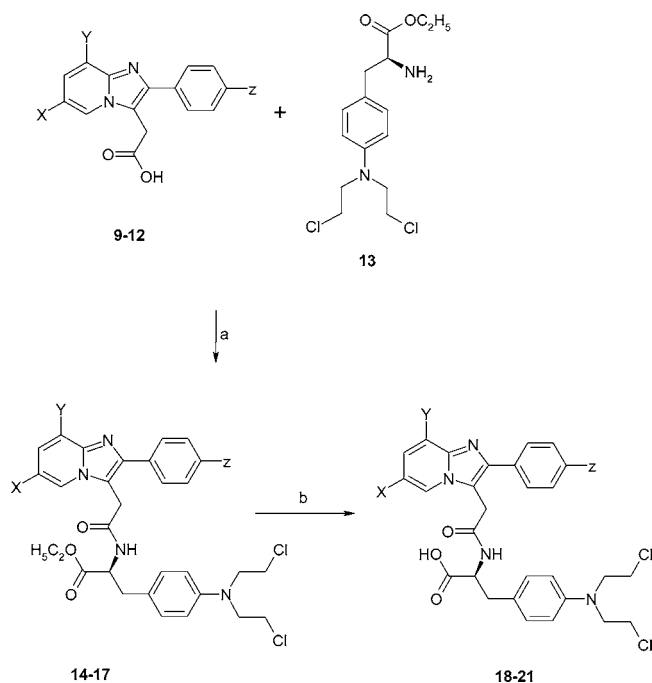
**Cytotoxicity Assays in Human SF126, SF188, and Rat RG-2 Glioma Cells.** The standard sulforhodamine B assay, used in the NCI screen (22), was used to determine cytotoxicity in the monolayer cell lines, SF126, SF188, and RG-2. All conjugates were dissolved in DMSO except for conjugate **16**, which was dissolved in ethanol at initial concentrations of 3000  $\mu\text{g/mL}$ , and except for conjugate **19**, which was prepared at 1500  $\mu\text{g/mL}$ . Drug solutions were diluted with medium to the desired concentrations, and then 100  $\mu\text{L}$  aliquots were added to the cells that were in 200  $\mu\text{L}$  of medium. Following a 3-fold serial dilution, the cells were incubated for 96 h. After the four-day incubation, the cells were fixed in 10% trichloroacetic acid (TCA) at  $4^\circ\text{C}$  for 1 h and stained with 4% SRB (dissolved in 1% of acetic acid) after  $5\times$  washing with water. Bound SRB was dissolved in 10 mM Tris-buffer after washing away the unbound SRB. The absorption at 570 nm was measured in a microplate reader, and cell survival was calculated as an absorption ratio compared to control.

## RESULTS AND DISCUSSION

**Synthetic Procedures.** As shown in Scheme 2, the new PBR ligand–melphalan conjugates **14–17** were prepared by condensation of the imidazopyridineacetic acids **9–12** with melphalan ethyl ester **13**. The condensation was successfully achieved by using ethyl 1,2-dihydro-2-ethoxy-1-quinolinecarboxylate (EEDQ) as a dehydrating agent (Method A), or DCC and HO-Suc (Method B). Method C allowed the preparation of conjugate **14** by reaction of the imidazopyridineacetic acid **9** with melphalan ethyl ester hydrochloride **13**·HCl in anhydrous THF and in the presence of CDI. The preparation of conjugate **14** was also accomplished by using Method A, but a slightly lower yield was obtained. Treatment of conjugates **14–17** with NaOH in ethanol afforded the second series of target molecules, acids **18–21**, respectively. Compounds **9–12**, in turn, were synthesized by methods previously reported by us (Scheme 1). Briefly, condensation of suitably substituted 2-aminopyridines **4** with the appropriate bromoketo esters **3** followed by alkaline hydrolysis gave the desired compounds **9–12** (Scheme 1). Compounds **3**, in turn, were prepared by reaction of esters **2** with bromine in carbon

Scheme 1<sup>a</sup>

<sup>a</sup> Reagents: (a) EtOH/HCl gas; (b) Br<sub>2</sub>/CCl<sub>4</sub>; (c) DMF, reflux; (d) NaOH/EtOH.

Scheme 2<sup>a</sup>

<sup>a</sup> Reagents: (a) Method A: EEDQ, THF; Method B: HO-Suc/DCC; Method C: CDI (b) NaOH/EtOH.

tetrachloride. Physical data for new compounds are reported in Table 1.

**Lipophilicity and Computational Approach To Estimate the Blood–Brain Barrier (BBB) Penetration of Compounds 14–21.** To be useful, a drug–conjugate targeted to the brain should have pharmacokinetic and pharmacodynamic properties that include favorable membrane permeability, intrinsic binding affinity, and conversion to a cytotoxic moiety. Membrane

Table 1. Structure and Physical Properties of Compounds 5–12, 14–21

compd	X	Y	Z	mp (°C)	yield <sup>a</sup> (%)	[α] <sub>D</sub> <sup>20</sup> <sup>b</sup>
5	Cl	Cl	Cl	<i>c</i>		
6	Cl	Cl	H	108–110	35	
7	H	Cl	Cl	156–158	30	
8	CH <sub>3</sub>	Br	Cl	173–175	33	
9	Cl	Cl	Cl	<i>c</i>		
10	Cl	Cl	H	245–247	70	
11	H	Cl	Cl	224–226	75	
12	CH <sub>3</sub>	Br	Cl	230–232	59	
14	Cl	Cl	Cl	172–174	31 (A)	+24.6
					38 (C)	
15	Cl	Cl	H	79–81	38 (A)	+14.5
					30 (B)	
16	H	Cl	Cl	70–72	55 (A)	+6.7
17	CH <sub>3</sub>	Br	Cl	69–71	41 (A)	+6.9
					32 (B)	
18	Cl	Cl	Cl	220 dec	61	
19	Cl	Cl	H	206 dec	40	
20	H	Cl	Cl	198 dec	57	
21	CH <sub>3</sub>	Br	Cl	196–198 dec	57	

<sup>a</sup> The method used is reported in parentheses. <sup>b</sup> *c* = 5 mg/mL in CHCl<sub>3</sub>. <sup>c</sup> Reference 21.

permeability is related to the drug–conjugate lipophilicity which is reflected by its partition coefficient ( $\log P$ ). The lipophilicity of compounds 14–21 was assessed, both calculating their 1-octanol/water partition coefficients, using CLOGP software, based on the fragmental method of Hansch and Leo, and measuring their retention times in RP-HPLC (Table 2). From a quantitative viewpoint, a significant linear correlation was found between the calculated  $\log P$  values and capacity factors  $\log k'$  ( $n = 8$ ,  $r^2 = 0.74$ ,  $s = 0.13$ ). This positive correlation indicates there are no significant differences in the calculated and measured lipophilicity values. Therefore, in the following calculations, we used only the lipophilicity data obtained from the CLOGP software.

$\log P$  values of 2.5 or higher were considered optimal for BBB penetration. As can be seen from Table 2, all the compounds (14–21) possessed  $\log P$  values higher than 2.5 (i.e., in the range 6.36–7.74) and appeared to be sufficiently lipophilic to cross the BBB. To gain further information on the BBB penetration properties of compounds 14–21 by passive transport, a computational study was performed. Recently, several attempts to correlate BBB penetration with physicochemical parameters have been reviewed (23). It has been clarified that the octanol–water partition coefficient ( $\log P$ ) is an important factor, although by itself correlates poorly with the  $\log C_{\text{brain}}/C_{\text{blood}}$  ( $\log BB$ ). This ratio represents a useful measure of the degree of BBB penetration. Experimental values of  $\log BB$  published to date cover the range from about –2.00 to +1.00. In particular, compounds with  $\log BB$  greater than 0.3 cross the BBB readily, while compounds with  $\log BB < -1.0$  are only poorly distributed to the brain. In addition to  $\log P$ , the importance of a molecular size descriptor has been shown (24) as well as the need to include a descriptor relating to hydrogen bond formation (23). To estimate the BBB penetration of compounds 14–21, we used the Clark model. This model relates  $\log BB$  to polar surface area (PSA, defined as the area in Å<sup>2</sup> contributed by nitrogen and oxygen atoms, plus the area of the hydrogen atoms attached to these heteroatoms) and calculated  $\log P$  (CLOG P) according to the equation:  $\log BB = -0.0148(\pm 0.001) \cdot \text{PSA} + 0.152(\pm 0.036) \cdot \text{CLOG P} + 0.139(\pm 0.073)$  (25). For compounds 14–21, we calculated a PSA in the range 62.4–72.4 Å<sup>2</sup> by using the MAREA computer program. As can be seen from the data obtained by this computa-



**Table 2. Calculated Lipophilicity, Penetration of BBB, and Chemical and Enzymatic Stability of Compounds 14–21**

compd	CLOG P <sup>a</sup>	PSA <sup>b</sup> (Å <sup>2</sup> )	log BB <sup>c</sup>	RP-HPLC log <i>K'</i> <sup>d</sup>	<i>t</i> <sub>1/2</sub> <sup>e</sup> (h) in phosphate buffer 0.05 M (pH 7.4)	<i>t</i> <sub>1/2</sub> <sup>e</sup> (min) in human serum
<b>14</b>	7.74	62.4	0.39	0.72	28	47
<b>15</b>	7.03	62.1	0.29	0.52	44	
<b>16</b>	7.03	63.9	0.26	0.48	34	
<b>17</b>	6.97	62.1	0.28	0.64	76	
<b>18</b>	7.08	71.0	0.16	0.35	0.8	120
<b>19</b>	6.36	71.7	0.04	0.08	0.67	138
<b>20</b>	6.36	72.1	0.04	0.12	0.77	55
<b>21</b>	7.01	72.5	0.13	0.28	1	
melfhalan	−0.21			−0.58		

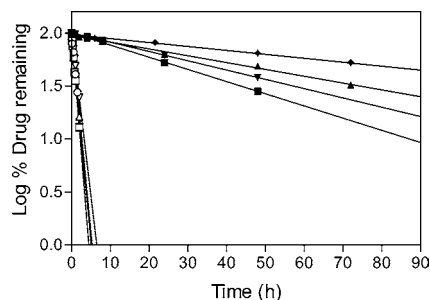
<sup>a</sup> Estimated according to CLOG P software. <sup>b</sup> Calculated according to MAREA software. <sup>c</sup> Calculated according to Clark's model (25).

<sup>d</sup> The capacity factors (*K'*) of each melfhalan conjugate has been calculated by the equation:  $K' = (t_R - t_0)/t_0$ , where *t*<sub>R</sub> is the observed retention time of the solute and *t*<sub>0</sub> is the column dead time. <sup>e</sup> Based on the loss of starting material.

**Table 3. Affinity for Rat Cerebrocortical CBR and PBR and Cytotoxicity to SF 126, SF 188, and RG-2 Glioma Cells of Compounds 14–21**

compd	IC <sub>50</sub> (nM) <sup>a</sup>		SI <sup>c</sup>	IC <sub>50</sub> (μg/mL) <sup>d</sup> SF 126 cells	IC <sub>50</sub> (μg/mL) <sup>d</sup> SF 188 cells	IC <sub>50</sub> (μg/mL) <sup>d</sup> RG-2 cells
	CBR cerebral	PBR cortex				
<b>14</b>	<i>b</i>	181 ± 8	>20 000	26.12 ± 8.95	51.43 ± 16.70	31.33 ± 1.46
<b>15</b>	<i>b</i>	521 ± 21	>9500	10.33 ± 1.35	5.01 ± 1.49	9.36 ± 1.48
<b>16</b>	<i>b</i>	1040 ± 57	>4800	6.75 ± 3.45	2.94 ± 0.23	9.75 ± 2.27
<b>17</b>	<i>b</i>	2614 ± 188	>1900	30.97 ± 14.89	7.79 ± 1.35	24.83 ± 2.10
<b>18</b>	<i>b</i>	57 ± 2	>87 000	84.32 ± 15.00	56.11 ± 4.93	27.42 ± 2.10
<b>19</b>	<i>b</i>	261 ± 15	>19 000	64.16 ± 13.52	28.37 ± 1.65	18.34 ± 2.19
<b>20</b>	<i>b</i>	1081 ± 88	>4600	82.29 ± 17.87	28.45 ± 2.03	25.03 ± 4.64
<b>21</b>	<i>b</i>	2179 ± 196	>2200	82.58 ± 14.12	39.23 ± 7.8	29.23 ± 3.65
PK 11195	24250	1.06 ± 0.06	22 877			
melfhalan	<i>e</i>	<i>e</i>	<i>e</i>	3.3	0.92 ± 0.30	6.03 ± 1.05

<sup>a</sup> Data are means ± SD of three separate experiments performed in duplicate. <sup>b</sup> No displacement up to 1 mM. <sup>c</sup> SI: selectivity index = IC<sub>50</sub>(CBR)/IC<sub>50</sub>(PBR); data are calculated considering arbitrarily the IC<sub>50</sub>(CBR) value of the conjugates as 5 mM. <sup>d</sup> Data are means ± SD (from three to five different measurements). PBR density or *B*<sub>max</sub> (pmol/mg protein) values were for each cell line; SF126: 41 ± 3.3, SF188: 22.1 ± 1.4, RG-2: 33 ± 3.1. <sup>e</sup> No receptor binding affinity.

**Figure 2.** Plots of the hydrolysis of the conjugates **14–21** at pH 7.4 in 0.05 M phosphate buffer at 37 ± 0.2 °C. **14** (■), **15** (▲), **16** (▼), **17** (◆), **18** (○), **19** (□), **20** (△), and **21** (▽).

tional approach and reported in Table 2, it can be predicted that compounds **14–21** possess significant brain penetration.

#### Stability in Buffer and Physiological Medium.

The stability of the derivatives **14–21** in buffer was determined in 0.05 M phosphate buffer at pH 7.4 as well as for selected compounds (**14**, **18**, **19**, and **20**) in dilute (50%) human serum solution at 37 °C.

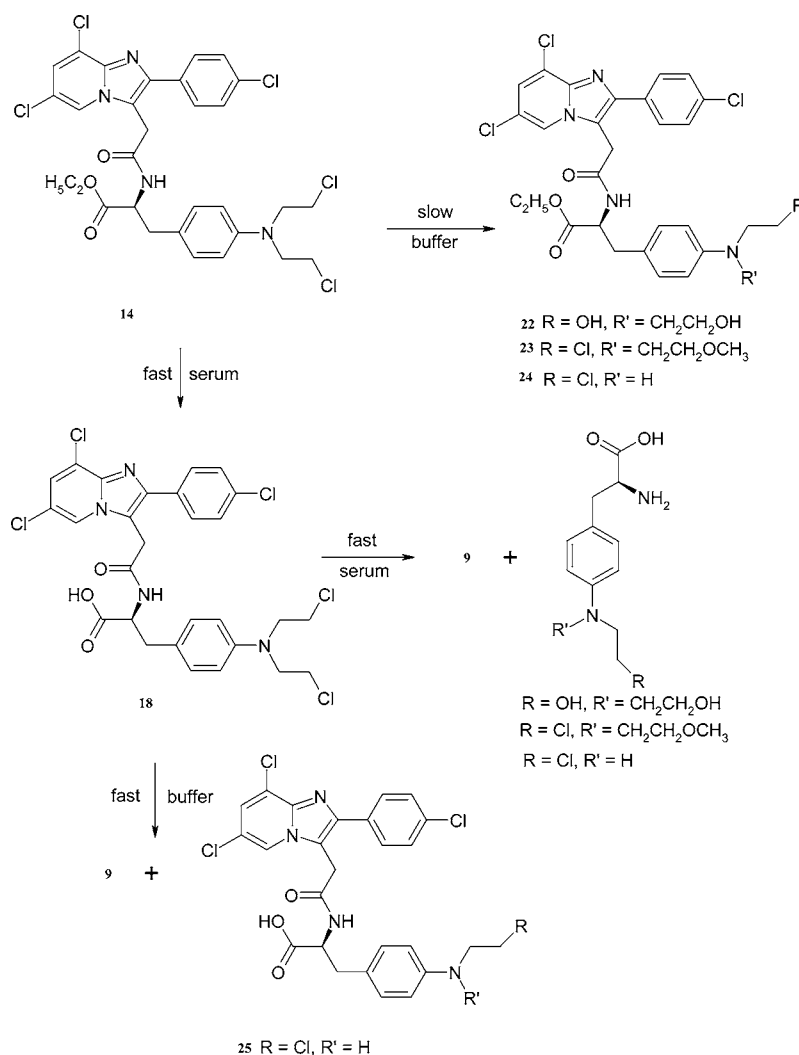
All the esters derivatives (**14–17**) were stable in 0.05 M phosphate buffer at pH 7.4, and their half-lives exceeded 28 h (Table 2). Conversely, under the same conditions, acids **18–21** were found to undergo fast cleavage within a few minutes (half-lives in the range 0.67–1 h based on the loss of starting material, Table 2 and Figure 2).

On the other hand, compounds **14**, **18**, **19**, and **20** were found unstable in serum (half-lives in the range of 47–120 min based on the disappearance of starting material, Table 2 and Figure 2). It is noteworthy that ester **14** was stable in buffered solution and unstable in human serum.

One possible explanation accounting for this finding is that ester **14** may be susceptible to enzyme (esterase)-catalyzed hydrolysis in serum, leading to compound **18** which, in turn, is rapidly cleaved in physiological medium. To gain insight into the degradation pathway of ester **14**, its main degradation products in buffer and physiological medium were characterized by LC-mass spectrometry (LC-MS). Thus, LC-MS analysis of the mixture from degradation of ester **14** in buffer after 24 h showed the presence of small amounts of degradation products of the melfhalan moiety, occurring as dihydroxymelfhalan (**22**) (*t*<sub>R</sub> 24.3 min, *m/z* 633), methoxymelfhalan (**23**) (*t*<sub>R</sub> 25.4 min, *m/z* 667), and chloroethylaminomelfhalan (**24**) (*t*<sub>R</sub> 22.5 min, *m/z* 606) derivatives, in addition to relevant quantities of the unchanged starting material **14** (*t*<sub>R</sub> 25.7 min, *m/z* 669). It is interesting to note that the formation of degradation products **22–24** can be easily rationalized taking into account the degradation of the parent nitrogen mustard (26, 27).

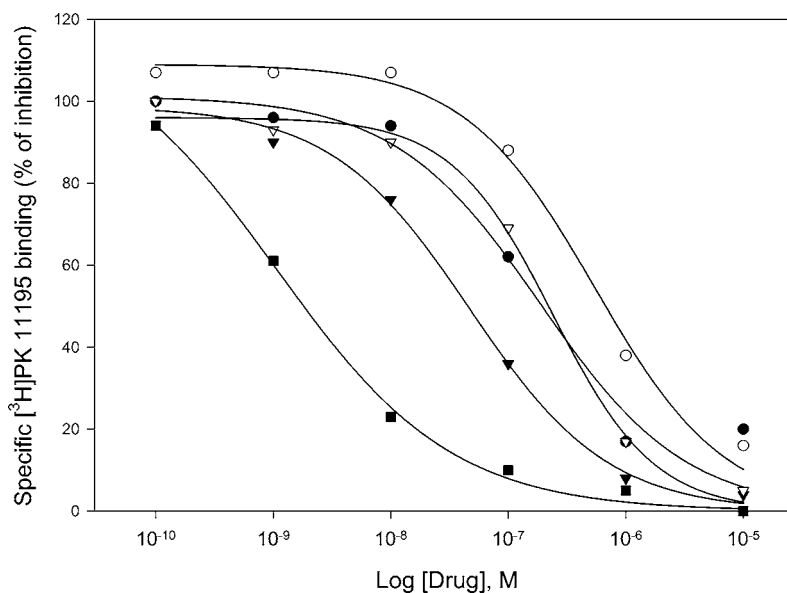
On the other hand, LC-MS analysis of the mixture from degradation of compound **14** in physiological medium after 2 h showed the presence of acids **9** (*t*<sub>R</sub> 5.1 min, *m/z* 335) and **18** (*t*<sub>R</sub> 19 min, *m/z* 639) and melfhalan degradation products together with the starting material (*t*<sub>R</sub> 25.5 min, *m/z* 669). Therefore, it can be concluded that, in physiological medium, **14** undergoes cleavage at the amide bond level. The LC-MS analysis carried out on the mixture from degradation of compound **18** in buffer showed the presence of acid **9** (*t*<sub>R</sub> 5.1 min, *m/z* 335) and a degradation product (**25**) of the melfhalan moiety of **18** (*t*<sub>R</sub> 21.6 min, *m/z* 576), aside from the starting material. The corresponding LC-MS analysis of **18** in human serum demonstrated the presence of compounds arising from the cleavage of the amide bond.

## Scheme 3



On the basis of the available experimental data, a reasonable degradation pathway may be put forward, and it is shown in Scheme 3. Compound **14** in 0.05 M phosphate buffer at pH 7.4 is stable enough, undergoing

a slow decomposition to give small amounts of degradation products involving the melphalan moiety. Under these conditions, both the ester and amide function of **14** are stable enough. Conversely, in human serum, **14**



**Figure 3.** Inhibition of [<sup>3</sup>H]PK 11195 binding to rat cerebrocortical membranes by PK 11195 (■) and by the conjugates **14** (●), **15** (○), **18** (▼), and **19** (▽). The data are means of triplicate of a representative experiment and are expressed as percentage of specific [<sup>3</sup>H]PK 11195 binding apparent in the absence of drugs.

is susceptible to esterase catalysis, yielding acid **18** which next is cleaved at the amide linkage, leading to acid **9**. The suggestion that enzymatic hydrolysis at the ester group is faster than amide cleavage is derived from the fact that the amide bond is known to be quite stable in vivo. Quite probably, the degradation of esters **15–17** and acids **19–21** proceeds through a pathway similar to that of the ester **14** and acid **18**, respectively. The fact that the acid conjugates **18–21** are less resistant than the corresponding esters **14–17** to degradation in buffer can be likely ascribed to the presence, in the former conjugates, of the carboxylic group which could promote amide cleavage.

**Affinities of Imidazopyridine Derivatives for Peripheral and Central Benzodiazepine Receptors.** The affinities of the conjugates **14–21** for CBR and PBR were evaluated by measuring their ability to compete with [<sup>3</sup>H]flunitrazepam and [<sup>3</sup>H]PK 11195 binding, respectively, to membrane preparations from rat cerebral cortex. Their affinities were compared with those of unlabeled PK 11195. The measured binding affinities for CBR and PBR expressed as IC<sub>50</sub> values as well as their ratios, as a measure of the in vitro selectivity, are shown in Table 3.

The analysis of the binding affinities of the entire set of compounds **14–21** indicated that conjugates **18**, **14**, **19**, and **15** possess, in the order given, the highest affinity for PBR (Figure 3). Moreover, the selectivity index of **18** is greater than the reference compound (PK 11195) while the selectivity indexes of conjugates **14** and **19** are comparable with that of PK 11195. The best PBR binding affinity and selectivity was observed for conjugate **18**, whereas no binding affinity for CBR and PBR was found for melphalan as such (Table 3).

The greater affinity exhibited by **18** and **14** in comparison with **19** and **15**, respectively, is consistent with previous reports where the relevant influence of the substitution at the para-position of the phenyl ring at C(2) with a chlorine atom on binding affinity and selectivity was already demonstrated (*18,19*).

**Cytotoxicity.** Cytotoxicity assays of the melphalan conjugates **14–21** were conducted in rat and human brain tumor cell lines using an SRB assay (*22*) with the results shown in Table 3. It can be seen that the ester conjugates **14–17** were more cytotoxic than the corresponding acids **18–21** but, in all cases, less toxic than melphalan alone. However, the ester conjugates **15** and **16** possessed cytotoxicity comparable to that of the parent drug.

In conclusion, synthetic routes toward imidazopyridine-PBR ligand–melphalan conjugates have been developed, and some compounds displayed suitable in vitro receptor affinity and cytotoxicity against glioma cell lines. The combined data of affinity, selectivity, and cytotoxicity support the further evaluation of conjugates **14**, **15**, **18**, and **19**. As these compounds are likely to exhibit favorable BBB penetration, their utility in a preclinical brain tumor model is warranted. Moreover, based on a comparison of affinities between these new types of PBR–MEL conjugates and a previously reported benzodiazepine–melphalan conjugate (*16*), conjugates **14**, **18**, and **19** show improved binding characteristics and warrant further evaluation.

#### ACKNOWLEDGMENT

This work was supported by a grant from Ministero dell'Università e della Ricerca Scientifica e Tecnologica (MIUR). We thank Mr Giovanni Dipinto for skillful

technical assistance in recording mass spectra and determining microanalytical data. This research was partially supported by funds provided by Regione Autonoma della Sardegna to GB.

#### LITERATURE CITED

- (1) Anholt, R. R. H., De Souza, E. B., Oster-Granite, M. L., and Snyder, S. H. (1985). Peripheral-type benzodiazepine receptors: autoradiographic localization in whole-body sections of neonatal rats. *J. Pharmacol. Exp. Ther.* **233**, 517–526.
- (2) Anholt, R. R. H., Pedersen, P. L., De Souza, E. B., and Snyder, S. H. (1986). The peripheral benzodiazepine receptor: localization to the mitochondrial outer membrane. *J. Biol. Chem.* **261**, 576–583.
- (3) McEnery, M. W., Snowman, A. M., Trifletti, R., and Snyder, S. H. (1992). Isolation of the mitochondrial benzodiazepine receptor: association with the voltage-dependent anion channel and the adenine dinucleotide carrier. *Proc. Natl. Acad. Sci. U.S.A.* **89**, 3170–3174.
- (4) Marangos, P. L., Pate, J., Boulenger, J. P., and Clark-Rosenberg, R. (1982). Characterization of peripheral-type benzodiazepine binding sites in brain using [<sup>3</sup>H]Ro 5-4864. *Mol. Pharmacol.* **22**, 26–32.
- (5) Le Fur, G., Perrier, M. L., Vaucher, N., Imbault, F., Flamier, A., Uzan, A., Renault, C., Dubroeuq, M. C., and Guerey, C. (1983). Peripheral benzodiazepine binding sites: effect of PK 11195, 1-(2-chlorophenyl)-N-(1-methylpropyl)-3-isoquinolinecarboxamide I. In vitro studies. *Life Sci.* **32**, 1839–1847.
- (6) Romeo, E., Auta, J., Kozikowski, A. P., Ma, A., Papadopoulos, V., Puia, G., Costa, E., and Guidotti, A. (1992). 2-Aryl-3-indoleacetamides (FGIN-1): a new class of potent and specific ligands for the mitochondrial DBI receptor. *J. Pharmacol. Exp. Ther.* **262**, 971–978.
- (7) Campiani, G., Nacci, V., Fiorini, I., De Filippis, M. P., Garofalo, A., Ciani, S. M., Greco, G., Novellino, E., Williams, D. C., Zisterer, D. M., Woods, M. J., Mihai, C., Manzoni, C., and Mennini, T. (1996). Synthesis, biological activity, and SARs of pyrrolobenzoxazine derivatives, a new class of specific "peripheral-type" benzodiazepine receptor ligands. *J. Med. Chem.* **39**, 3445–3450.
- (8) Okujama, S., Chaki, S., Yoshikawa, R., Ogawa, S., Suzuki, Y., Okubo, T., Nakazato, A., Nagamine, M., and Tomisawa, K. (1999). Neuropharmacological profile of peripheral benzodiazepine receptor agonists, DAA1097 and DAA1106. *Life Sci.* **16**, 1455–1464.
- (9) Cantor, E. H., Kennesey, A., Semenuk, G., and Spector, S. (1984). Interaction of calcium channel blockers with nonneural benzodiazepine binding sites. *Proc. Natl. Acad. Sci. U.S.A.* **81**, 1549–1552.
- (10) Wang, J. K. T., Morgan, J. L., and Spector, S. (1984). Benzodiazepines that bind at peripheral sites inhibit cell proliferation. *Proc. Natl. Acad. Sci. U.S.A.* **81**, 753–756.
- (11) Lenfant, M., Haumont, J., and Zavala, F. (1986). In vivo immunomodulating activity of PK 11195, a structurally unrelated ligand for "peripheral benzodiazepine-binding site: I. Potentiation in mice of the humoral response to sheep red blood cells. *Int. J. Immunopharmacol.* **8**, 825–829.
- (12) Hirsch, J. D., Beyer, C. F., Malkowitz, L., Beer, B., and Blume, A. J. (1989). Mitochondrial benzodiazepine receptors mediate inhibition of mitochondrial respiratory control. *Mol. Pharmacol.* **35**, 157–163.
- (13) Papadopoulos, V., Guarneri, P., Krueger, K. E., Guidotti, A., and Costa, E. (1992). Pregnenolone biosynthesis in C6 glioma cell mitochondria: Regulation by a mitochondrial diazepam binding inhibitor receptor. *Proc. Natl. Acad. Sci. U.S.A.* **89**, 5113–5117.
- (14) Black, K. L., Ikezaki, K., Santori, E., Becker, D. P., Vinters, H. V. (1990). Specific high-affinity binding of peripheral benzodiazepine receptor ligands to brain tumors in rat and man. *Cancer* **65**, 93–97.
- (15) Veenman, L., and Gavish, M. (2000). Peripheral-type benzodiazepine receptors: their implication in brain disease. *Drug Development Research* **50**, 355–370.
- (16) Kupczyk-Subotkowaka, L., Siahaan, T. J., Basile, A., Friedman, H. S., Higgins, P. E., Song, D., and Gallo, J. M.



- (1997). Modulation of melphalan resistance in glioma cells with a peripheral benzodiazepine receptor ligand–melphalan conjugate. *J. Med. Chem.* **40**, 1726–1730.
- (17) Guo, P., Ma, J., Li, S., Guo, Z., Adams, A. L., and Gallo J. M. (2001). Targeted delivery of a peripheral benzodiazepine receptor ligand–gemcitabine conjugate to brain tumors in a xenograft model. *Cancer Chemother. Pharmacol.* **48**, 169–176.
- (18) Trapani, G., Franco, M., Ricciardi, L., Latrofa, A., Genchi, G., Sanna, E., Tuveri, F., Cagetti, E., Biggio, G., and Liso, G. (1997). Synthesis and binding affinity of 2-phenyl-imidazo[1, 2-*a*]pyridine derivatives for both central and peripheral benzodiazepine receptors. A new series of high-affinity and selective ligands for the peripheral type. *J. Med. Chem.* **40**, 3109–3118.
- (19) Trapani, G., Franco, M., Latrofa, A., Ricciardi, L., Carotti, A., Serra, M., Sanna, E., Biggio, G., and Liso, G. (1999). Novel 2-phenyl-imidazo[1, 2-*a*]pyridine derivatives as potent and selective ligands for peripheral benzodiazepine receptors. Synthesis, binding affinity, and in vivo studies. *J. Med. Chem.* **42**, 3934–3941.
- (20) Serra, M., Madau, P., Chessa, M. F., Caddeo, M., Sanna, E., Trapani, G., Franco, M., Liso, G., Purdy, R. H., Barbaccia, M. L., and Biggio, G. (1999). 2-Phenyl-imidazo[1, 2-*a*]pyridine derivatives as ligands for peripheral benzodiazepine receptors: stimulation of neurosteroid synthesis and anticonflict action in rats. *Br. J. Pharmacol.* **127**, 177–187.
- (21) Latrofa, A., Trapani, G., Franco, M., Harris, M. J., Serra, M., Biggio, G., and Liso, G. (2001). Synthesis of the [<sup>3</sup>H]labeled potent and selective peripheral benzodiazepine receptor ligand CB 34. *J. Labelled Compd. Radiopharm.* **44**, 521–528.
- (22) Skehan, P., Storeng, R., Scudiero, D., Monks, A., McMahon, J., Vistica, D., Warren, J. T., Bokesch, H., Kenney, S., and Boyd, M. R. (1990). New colorimetric cytotoxicity assay for anticancer-drug screening. *J. Natl. Cancer Inst.* **82**, 1107–1112.
- (23) Van de Waterbeemd, H., Camenish, G., Folkers, G., Chretien, J. R., and Raevsky, O. A. (1998). Estimation of blood-brain barrier crossing of drugs using molecular size and shape, and H-bonding descriptors. *J. Drug Targeting* **6**, 151–165.
- (24) Norinder, U., and Haeberlein, M. (2002). Computational approaches to the prediction of the blood-brain distribution. *Adv. Drug Deliv. Rev.* **54**, 291–313.
- (25) Clark, D. E. (1999). Rapid calculation of polar molecular surface area and its application to the prediction of transport phenomena. 2. Prediction of blood-brain barrier penetration. *J. Pharm. Sci.* **88**, 815–821.
- (26) Brightman, K., Finlay, G., Jarvis, I., Knowlton, K., and Manktelow, C. T. (1999). A stability-indicating method for the determination of melphalan and related impurity content by gradient HPLC. *J. Pharm. Biomed. Anal.* **20**, 439–447.
- (27) Ma, D. Q., Rajewski, R. A., Velde, D. V., Stella, V. J. (2000). Comparative effects of (SBE)<sub>7m</sub>-β-CD and HP-β-CD on the stability of two anti-neoplastic agents, melphalan and carmustine. *J. Pharm. Sci.* **89**, 275–287.

BC034023P

# Modified Linear Polyethylenimine–Cholesterol Conjugates for DNA Complexation

Darin Y. Furgeson, Winter S. Chan, James W. Yockman, and Sung Wan Kim\*

Department of Pharmaceutics and Pharmaceutical Chemistry, Center for Controlled Chemical Delivery, University of Utah, Salt Lake City, Utah 84112-5820. Received April 14, 2003;  
Revised Manuscript Received May 27, 2003

Linear polyethylenimine (LPEI) is an effective nonviral gene carrier with transfection levels equal or above branched polyethylenimine (BPEI) and exhibits a lower cytotoxicity profile than BPEI. High molecular weight LPEI  $M_w$  25 k was modified with cholesterol in three different geometries: linear shaped (L), T-shaped (T), and a combined linear/T-shaped (LT) forming the LPEI–cholesterol (LPC) conjugates LPC-L, LPC-T, and LPC-LT, respectively. Physical characterization of LPC/pDNA complexes included particle size, zeta potential, *DNase* protection, mL-12 p70 expression, and cytotoxicity. The particle size was further confirmed by atomic force microscopy (AFM). The LPC-T/pDNA complexes were optimal at N/P 10/1 that resulted in a particle size of ~250 nm, which was confirmed by AFM, and a surface charge of +10 mV. These complexes also effectively protected the pDNA for up to 180 min in the presence of *DNase* I. B16-F0 cells transfected with LPC-L and LPC-T showed protein expression levels higher than LPEI alone and twice that of BPEI but without any significant loss in cell viability. These results were confirmed with EGFP flow cytometry and transfection of Renca cells. The differences in rates of transfection of the LPC/pDNA complexes is due in part to conformational changes from the point of complex formation to interaction with the plasma membrane. These conformation changes provide protection for unprotonated secondary amines in the LPEI backbone by hydrophobic protection of the cholesterol moiety that we termed “unprotonated reserves”. Finally, we show that LPC conjugates exploit receptor-mediated endocytosis via the LDL-R pathway with transgene expression levels decreasing nearly 20% after saturating the LDL-R sites on MCF-7 cells with hLDL-R-Ab.

## INTRODUCTION

Polyethylenimine (PEI) has long been used as the standard for nonviral gene delivery; however, the ideal molecular weight and geometry for PEI have not been determined (1). The molecular weights of commercial PEIs vary from 423 Da–800 kDa with linear and branched geometries. The molecular weight of BPEI has been shown to directly affect transfection efficiency while the pH of the BPEI before complexation does not (2). Recently, transfection efficiencies increased and cytotoxicity decreased with the synthesis of low molecular weight PEI ( $M_w$  11 900) with minimized branching (3), a step toward LPEI. BPEI 25 k is limited in its use primarily due to its high cytotoxicity, presumably due to the high cationic state of the numerous primary amines (4, 5); however, the best results for in vivo BPEI transfection were shown to be with  $M_w$  25 k (6). LPEI has been shown to be an effective nonviral gene carrier (7–15) with increased gene expression and decreased toxicity compared to BPEI of comparable molecular weight. The putative method of PEI gene expression is through endosomal release by osmotic swelling by the proton sponge effect; however, this endosomal release may cause local cytotoxicity due to the release of endo/lysosomal enzymes (16). LPEI  $M_w$  423 cannot efficiently buffer the low pH found in the secondary lysosome after endocyto-

sis; consequently, we have shown that a colipid is needed to facilitate gene expression (17). However, LPEI 25 k has over 520 secondary amines capable of protonation and subsequent pH buffering; therefore, this polymer does not require the use of a colipid for endosomal escape. LPEI  $M_w$  25 k should have lower cytotoxicity than BPEI  $M_w$  25 k as a higher charge density was equated with higher cytotoxicity (5).

Modifications to LPEI have been rather sparse while BPEI has been modified extensively including PEGylation (4), targeting moieties (18, 19), and lipids (20). Cholesterol conjugation to a primary amine of BPEI  $M_w$  1800 resulted in water-soluble lipopolymer (WSP) that has shown to dramatically increase transfection efficiencies and promote tumor regression when combined with a therapeutic plasmid (20–22) beyond that of the polymer itself. Conjugation of cholesterol to a secondary amine of BPEI  $M_w$  1800 has also been completed with favorable results (23). The only known LPEI carrier used in the literature is ExGen 500, an LPEI 22 k conjugate with 510 monomer units (7), that has also been modified with mannose, galactose, and RGD ligands by PolyPlustransfection (Illkirch, France). In addition, the effect of the geometry of cholesterol conjugation with cationic lipids (17) and LMW cationic polymers (20, 23) has previously been explored; however, studies with HMW cationic polymers have not been initiated. LPEI  $M_w$  25 k can adequately provide pH buffering, similar to BPEI  $M_w$  25 k, but without the deleterious effects of the high cationic charge density found with BPEI. LPEI  $M_w$  25 k should

\* To whom correspondence should be addressed: University of Utah, Center for Controlled Chemical Delivery, 30 S 2000 E Rm. 201, Salt Lake City, UT 84112-5820. Tel: (801) 581-6654. Fax: (801) 581-7848. E-mail: rburns@pharm.utah.edu.

have a lower charge density compared to BPEI  $M_w$  25 k (5) resulting in decreased cytotoxicity.

Upon the basis of the success of cholesterol conjugation with WSLP and knowing that LPEI  $M_w$  25 k should provide pH buffering similar to BPEI  $M_w$  25 k without the degree of cytotoxic side effects, we synthesized three LPEI-cholesterol (LPC) conjugates: LPC-L (linear), LPC-T (T-shaped), and LPC-LT (combined linear/T-shaped). The introduction of the cholesterol moiety should provide favorable interactions with the cell membrane as seen with WSLP in addition to sequestering regions of the LPEI backbone for future lysosomal buffering in the late endosomolytic stages.

## EXPERIMENTAL PROCEDURES

**Materials.** Linear polyethylenimine (LPEI,  $M_w$  25 000) was purchased from Polysciences, Inc. (Warrington, PA). Cholesteryl chloroformate and chlorotrimethylsilane were purchased from Aldrich Chemical Co., Inc. (Milwaukee, WI). Anhydrous methylene chloride,  $\text{CDCl}_3$ ,  $\text{D}_2\text{O}$ , acetone, ethyl acetate, triethylamine (TEA), and trifluoroacetic acid (TFA) were purchased from Sigma Chemical Company (St. Louis, MO). RQ1 RNase-free DNase and JM109 competent cells were purchased from Promega (Madison, WI). pmIL-12e was purchased from Invivogen, Inc. (San Diego, CA). pCMS-EGFP was purchased from Clontech Laboratories, Inc. (Palo Alto, CA). SeaKem GTG agarose, molecular biology grade water, Luria Broth (LB), and ethidium bromide were purchased from ISC Bio-express (Kaysville, UT). Rosewell Park Memorial Institute (RPMI 1640) medium and heat-inactivated fetal bovine serum were purchased from Hyclone (Logan, UT). Trypsin–EDTA, gentamicin reagent solution, and penicillin–streptomycin–glutamine were purchased from Gibco-BRL (Gaithersburg, MD). The Endofree Maxi Plasmid Purification Kit was purchased from QIAGEN (Valencia, CA). The PELCO mica disks, 9.9 mm diameter, were purchased from Ted Pella, Inc. (Redding, CA). BDOptEIA ELISA kits for murine interleukin-12 (mIL-12) p70 were purchased from Pharmingen (San Diego, CA). LDL-receptor antibodies were purchased from Oncogene Research Products (Boston, MA). Spectra/Por membrane tubing MWCO 6-8000 was purchased from Spectrum Laboratories, Inc. (Rancho Dominguez, CA).

**Methods.** *Synthesis of LPC-L and LPC-LT.* LPEI  $M_w$  25 000 (1.0 g, 0.04 mmol) was added to 150 mL of anhydrous methylene chloride and heated in a hot water bath for ~20 min to facilitate solubility. The sample was cooled, and additional methylene chloride was added to return the volume to 150 mL. For LPC-L, 0.018 g (0.04 mmol) of cholesteryl chloroformate was dissolved in 3 mL of anhydrous methylene chloride and added to the LPEI dropwise over 10 min; consequently, 0.036 g (0.08 mmol) of cholesteryl chloroformate was added for the synthesis of LPC-LT. These reactions were stirred overnight, and the solvent removed by rotary evaporation and purified by solvent precipitation in acetone, ethyl acetate, and excess methylene chloride. The conjugates were dried and lyophilized prior to analysis by  $^1\text{H}$  NMR (Varian Mercury 400, Inc., Palo Alto, CA) and stored at  $-20^\circ\text{C}$ . Because of the high cationic charge and multiple charge states of the LPEI, mass spectrometric analysis could not be completed.

*Synthesis of LPC-T.* LPEI  $M_w$  25 000 (1.0 g, 0.04 mmol) was added to 150 mL of anhydrous methylene chloride and heated in a hot water bath for ~20 min to break the intra- and intermolecular hydrogen bonds of the LPEI. The clear solution was removed from the hot water bath

and cooled, and additional methylene chloride was added to return the volume to 150 mL. The mixture was stirred for 15 min at room temperature after which 200  $\mu\text{L}$  of anhydrous TEA was added and stirring continued for 5 min. To protect the terminal hydroxyl group, 60  $\mu\text{L}$  (0.06 mmol) of 1 M  $\text{Si}(\text{CH}_3)_3\text{Cl}$  was added, forming an  $\text{HCl}_{(\text{g})}$  cloud over the solution. The mixture was stirred overnight. Cholesteryl chloroformate (36 mg, 0.08 mmol) was dissolved in 3 mL of anhydrous methylene chloride and added dropwise to the TMS-protected LPEI over 10 min; consequently, the cholesterol was conjugated to a secondary amine on the LPEI by a carbamate bond. The reaction was stirred overnight. Deprotection of the LPC-T-TMS was completed by adding 3 mL of TFA at which point LPC-T fell out of solution. The sample was dried on the rotavaporator, dissolved in 20 mL of ultrapure water, and purified by dialysis (MWCO 6-8000) against deionized water for 3 days. The conjugate was lyophilized and analyzed by  $^1\text{H}$  NMR (Varian Mercury 400, Inc., Palo Alto, CA) and stored at  $-20^\circ\text{C}$ . As with LPC-L and LPC-LT, the high cationic charge and multiple charge states of the LPEI prevented mass spectrometric analysis.

*Amplification and Purification of pmIL-12e.* The pmIL-12e vector was purchased from Invivogen (San Diego, CA) in which the p35 and p40 are linked by an elasti-site and driven by a human T-cell leukemia virus (HTLV) promoter. Plasmids were amplified using JM109 competent cells and purified using the QIAGEN Endofree Maxi Plasmid Purification Kit according to the protocol. UV spectrophotometry at 260/280 nm and gel electrophoresis determined the concentration, integrity, and purity of the amplified pmIL-12e. Purity was greater than 1.8, and appropriate bands were seen with restrictive enzyme digestion.

*Preparation of LPC/pmIL-12e Complexes.* LPC conjugates and BPEI were concentrated at 1.25 mg/mL in ultrapure water and stored at  $4^\circ\text{C}$  for future use. Turbidity was seen with the LPC-L and more so with the LPC-LT most likely due to intermolecular hydrogen bond formation. No visual turbidity was seen with LPC-T. The LPC solutions were heated in a warm water bath  $\sim 55^\circ\text{C}$  for 15 min to break the intra- and intermolecular hydrogen bonds of the conjugates. After being cooled to room temperature, both the LPC solutions and pmIL-12e were separately diluted to a final concentration of 5% glucose at 100  $\mu\text{L}$ , each at a pDNA concentration of 0.1 mg/mL. The LPC solution was added to the pmIL-12e solution and thoroughly mixed. Complexation was allowed for 15 min at ambient conditions. Significant aggregation of LPC-LT/pmIL-12e complexes was seen after 30 min.

*Gel Retardation Assay.* pDNA condensation by the LPC conjugates was evaluated by a gel retardation assay. The LPC/pmIL-12e complexes were electrophoresed on a 1% agarose gel pretreated with 0.5 mg/mL ethidium bromide in  $1 \times$  Tris–base–acetate–EDTA (TAE) buffer at 84 V. Naked pmIL-12e was used for the marker lane.

*DNase Protection Assay.* LPC/pmIL-12e complexes were prepared at N/P ratios 5/1, 10/1, 20/1, and 30/1 at a final pDNA concentration of 0.1 mg/mL and 500  $\mu\text{L}$  total volume. The samples were incubated at ambient conditions for 20 min. Fifty microliters of the stop solution (200 mM sodium chloride, 20 mM EDTA, and 1% SDS) was added to eight PCR tubes for each LPC/pDNA sample, representing the appropriate DNase stop times: 0, 2, 5, 15, 30, 60, and 180 min. Fifty microliters of each LPC/pDNA complex was removed and added to the 0 min incubation tube and gently mixed. To the remaining LPC/pDNA complexes, 50  $\mu\text{L}$  of RQ1 RNase-



free *DNase* (Promega, WI) was added, gently mixed, and incubated at 37 °C. At the appropriate stop times, 50  $\mu$ L of each sample was removed and added to the stop solution tube. To dissociate the pDNA from the LPCs, the samples were incubated overnight at 60 °C. The free pDNA was purified by phenol/chloroform extraction followed by ethanol precipitation. The pellets were redissolved in 10  $\mu$ L of molecular biology grade water and analyzed by 1% agarose gel electrophoresis.

**Particle Size and Zeta Potential.** LPC/pmIL-12e complexes were measured at several N/P ratios for particle size and zeta potential on a Brookhaven Instruments Corp. (Holtsville, NY) ZetaPALS. Experimental conditions were 37 °C using a 677 nm wavelength at a constant angle of 15°. Smoluchowski's formula was used to calculate the zeta potential from the electrophoretic mobility. Values for the particle size are effective mean diameters.

**Atomic Force Microscopy.** A method for determining surface morphology by AFM has been previously described (17). Briefly, 9.9 mm mica disks were soaked in 33 mM magnesium acetate for a minimum of 24 h to promote stronger pDNA binding by the divalent magnesium ions rather than the monovalent potassium ions. The mica was sonicated for 30 min in ultrapure water and subjected to glow discharge for 15 s in a vacuum between 100 and 200 mTorr. Upon exposure to air, 20  $\mu$ L of 0.1 mg/mL LPC-T/pmIL-12e complexes was placed on the mica surface for 2 min after which the mica was gently rinsed with distilled water and slowly blown dry with nitrogen. Imaging was completed at room temperature using a Digital Instruments Nanoscope II SFM (Santa Barbara, CA) in tapping mode.

**Tumor Cell Lines.** B16-F0 murine melanoma and Renca murine renal cell carcinoma cells were a gift from Dr. Wolfram Samlowski of the Huntsman Cancer Institute (Salt Lake City, UT). MCF-7 human breast carcinoma cells were donated by Dr. You Han Bae of the University of Utah (Salt Lake City, UT). The cell lines were grown and maintained in RPMI 1640 medium supplemented with 10% FBS, 100 U/mL penicillin, 100 U/mL streptomycin, and 50  $\mu$ g/mL gentamycin at 37 °C and humidified 5% CO<sub>2</sub>.

**In Vitro Transfection.** Five thousand cells (B16-F0 or Renca) were seeded on 96-well plates in RPMI 1640 containing 10% FBS and antibiotics. The plates were incubated at 37 °C and humidified 5% CO<sub>2</sub> until cell confluency reached ~70%. At this point, cells were transfected with LPC/pmIL-12e prepared at various N/P ratios ranging from 1/1–30/1. pDNA (0.1  $\mu$ g) was loaded per 100  $\mu$ L of RPMI + 10% FBS. Cells were incubated for 4 h in the presence of complexes and 10% FBS at standard incubator conditions. After 4 h, the cell media was replaced with 100  $\mu$ L of fresh RPMI + 10% FBS, and the cells were further incubated for an additional 20 h at the same conditions, resulting in a total transfection time of 24 h. The cell media was removed for ELISA as mIL-12 p70 is a secreted protein. Untreated cells in addition to cells treated with naked pDNA alone were used as controls. For the EGFP studies, 300 000 Renca or B16-F0 cells were seeded on six-well plates in RPMI 1640 supplemented with 10% FBS and antibiotics. The plates were incubated at 37 °C and humidified 5% CO<sub>2</sub> overnight. The following day the cells were transfected with 2  $\mu$ g of pCMS-EGFP in the presence of serum for 4 h after which the media was replaced with fresh RPMI 1640 + 10% FBS for an additional 44 h. Cells were trypsinized, centrifuged, and suspended in PBS prior to flow cytometry analysis.

**Cell Viability.** A Cell Counting Kit-8 (CCK-8) (Dojindo Molecular Technologies, Inc., Gaithersburg, MD) was used to evaluate the cytotoxicity of the LPC conjugates. Five thousand cells (B16-F0 or Renca) were seeded on a 96-well plate with RPMI +10% FBS and incubated at 37 °C and humidified 5% CO<sub>2</sub> until confluency reached ~70%. LPC/pmIL-12e complexes were prepared at various N/P ratios ranging from 1/1–30/1. Cells were transfected with 0.1  $\mu$ g of pmIL-12e in the presence of 10% FBS for 4 h after which the media was changed, and transfections proceeded for an additional 20 h in the presence of 10% FBS. After removal of the surrounding media containing the excreted mIL-12 p70, 10  $\mu$ L of thawed CCK-8 solution was added to each well. Plates were incubated for 1–1.5 h at the same incubator conditions after which the absorbance was read at 450 nm with a reference wavelength of 600 nm. Cell viability was calculated as

$$\text{cell viability (\%)} = (\text{OD}_{450(\text{sample})} / \text{OD}_{450(\text{control})}) \times 100$$

where OD<sub>450(sample)</sub> is the absorbance at 450 nm of the transfected cells and OD<sub>450(control)</sub> is the absorbance at 450 nm of the negative control (nontransfected cells).

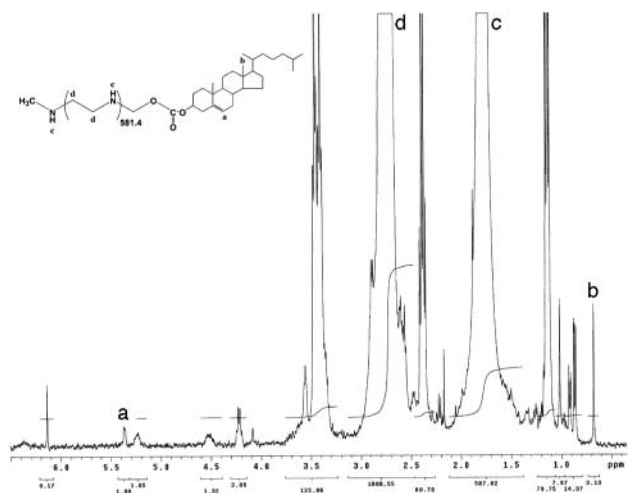
**ELISA.** mIL-12 p70 levels were measured with a BDOptEIA ELISA set for mIL-12 p70 (Pharmingen, San Diego, CA) as per the manufacturer's instructions. Cells were transfected as per the method previously described. Following the 24 h transfection time, the media was removed and assayed for secreted mIL-12 p70 by ELISA. Levels of mIL-12 p70 were reported as pg/mL.

**Flow Cytometry.** Flow cytometric analysis of EGFP-labeled Renca and B16-F0 cells was carried out using a FACScan flow cytometer and analyzed with accompanying Cell Quest software (Becton Dickinson, Franklin Lakes, NJ).

**LDL-R Ab Saturation.** MCF-7 (human breast carcinoma) cells were used in the LDL-R study to determine whether receptor-mediated endocytosis of LPC-T/pDNA complexes was also possible. To calculate the concentration of anti-LDL-R Ab needed for saturation, we assumed 10 000 LDL-R sites per cell based on a previous flow cytometry study by Li et al. (24). The concentration of anti-LDL-R Ab was determined to be approximately 0.05  $\mu$ M, assuming a fraction bound ( $f_b$ ) of 0.99 and  $K_A$  of  $2 \times 10^9$ . Five thousand MCF-7 cells were seeded onto a 96-well plate with 100  $\mu$ L of RPMI + 10% FBS. Cells were incubated at standard conditions to ~70% confluency after which a saturating concentration of the anti-LDL-R Ab was added in 100  $\mu$ L of RPMI + 10% FBS. After an incubation of 1 h, the media was removed and replaced with 100  $\mu$ L fresh RPMI + 10% FBS containing LPC-T/pmIL-12e. Cells were transfected with 0.1  $\mu$ g of pmIL-12e per 100  $\mu$ L for 4 h followed by replacing the wells with fresh media and an additional 20 h for transfection. The pmIL-12e vector was used to eliminate background levels of IL-12 p70.

## RESULTS

We synthesized three LPC conjugates in varying geometries by the addition of cholesterol to the terminal hydroxyl of LPEI (LPC-L), a secondary amine (LPC-T), or both the terminal hydroxyl and a secondary amine (LPC-LT). Following synthesis and purification, we determined the degree of cholesterol conjugation for each LPC conjugate. The target and resulting cholesterol conjugation, based upon <sup>1</sup>H NMR were LPC-L, target 1.0, actual 0.991; LPC-T, target 1.0, actual 1.401; and LPC-LT, target 2.0, actual 1.782. The <sup>1</sup>H NMR results for

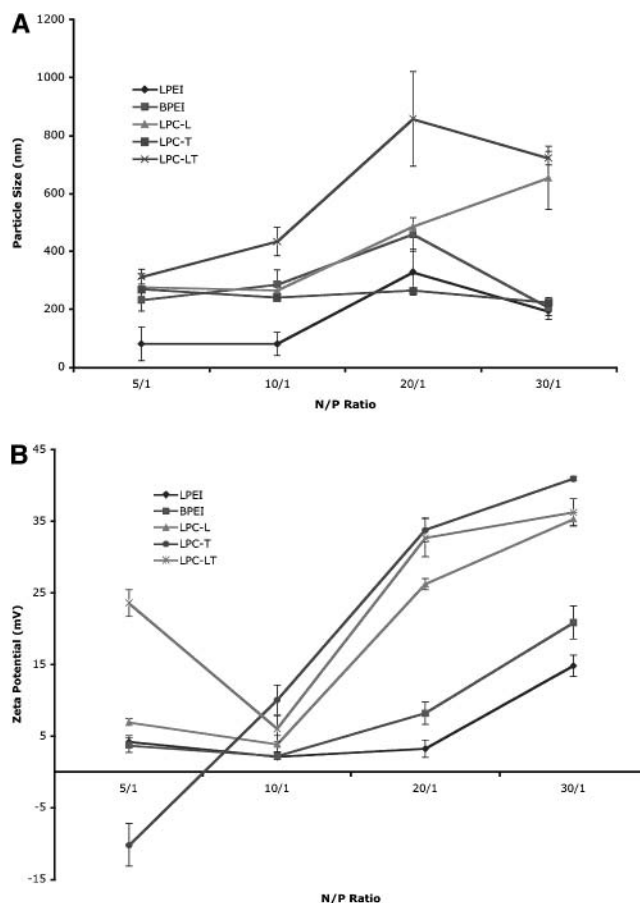


**Figure 1.**  $^1\text{H}$  NMR spectra for LPC-L ( $\text{CDCl}_3$ ).

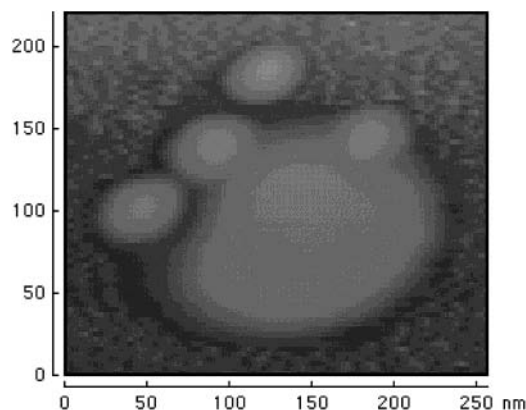
LPC-L are as follows (Figure 1):  $^1\text{H}$  NMR (400 MHz,  $\text{CDCl}_3$ )  $\delta$  0.70 [s, 3.24 H of  $\text{CH}_3$  from cholesterol (b)];  $\delta$  1.4–2.1 [587.62 H of secondary amines of LPEI backbone (c)];  $\delta$  2.5–3.15 [1808.55 H of methylene units of LPEI backbone (d)]; and  $\delta$  5.38 [s, 1.00 H of  $=\text{C}=\text{CHC}$  from cholesterol (a)]. The peak assignments were confirmed by  $\text{D}_2\text{O}$  exchange with LPC-L in which the peaks for the secondary amines disappeared. To show that the assumed geometries were correct, we first attempted to use two-dimensional NMR studies, heteronuclear multiple bond coherence (HMBC) and heteronuclear multiple quantum coherence (HMQC). Because of the HMW LPEI used in this study, the ability to identify the protons near the conjugated secondary amine was limited by the large number of methylene and secondary amine protons. Second, the terminal hydroxyl of the LPEI molecule is more reactive than any of the secondary amines. Consequently, we assumed that the reaction between LPEI and cholesterol chloroformate would result in a linear geometry (LPC-L). This assumption proved correct as our  $\text{D}_2\text{O}$  exchange studies showed (data not shown). Using the base LPEI molecule, we identified the secondary amine peaks by comparing the NMR spectra of the LPEI before and after addition of  $\text{D}_2\text{O}$ . With these studies completed, we next performed a  $\text{D}_2\text{O}$  exchange study with LPC-L. Again, comparing the spectra before and after addition of  $\text{D}_2\text{O}$ , the secondary amine peaks were no longer visible. Finally, we showed that the terminal hydroxyl peak dropped out with conjugation of cholesterol and the TMS protecting group used in the synthesis of LPC-T. Secondary amines are reactive, albeit less than primary amines; therefore, the  $^1\text{H}$  NMR spectrum of the LPC-LT conjugate showed the loss of the hydroxyl peak as well. The only other possible site for additional cholesterol conjugation is at a secondary amine.

The physicochemical properties of the LPC/pDNA complexes were further analyzed by gel retardation, particle size, zeta potential, and AFM. Gel retardation was positive for LPEI/pDNA, LPC-L/pDNA, LPC-T/pDNA, and LPC-LT/pDNA complexes at N/P 5/1 with complete DNA exclusion at  $\sim$ N/P 20/1 (data not shown).

The particle size distribution of LPC/pDNA complexes was determined by dynamic light scattering (DLS). The mean particle size for LPC-T/pDNA complexes remained relatively constant over the range of N/P 5/1–30/1 with a mean diameter of  $\sim$ 275 nm (Figure 2A). A dramatic particle size change was seen for the LPEI, LPC-L, and LPC-LT complexes from N/P 10/1 to 20/1. The LPC-LT complexes showed a particle size inappropriate for use

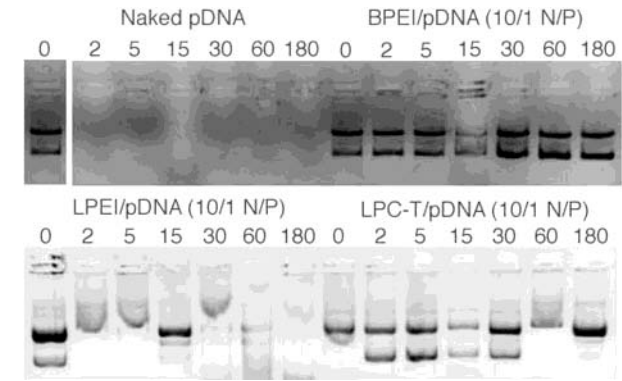


**Figure 2.** (A) Particle size data for LPC/pmIL-12e complexes. Data reported as mean  $\pm$  SD,  $n = 3$ . (B) Zeta potential data for LPC/pmIL-12e complexes. Data reported as mean  $\pm$  SD,  $n = 3$ .

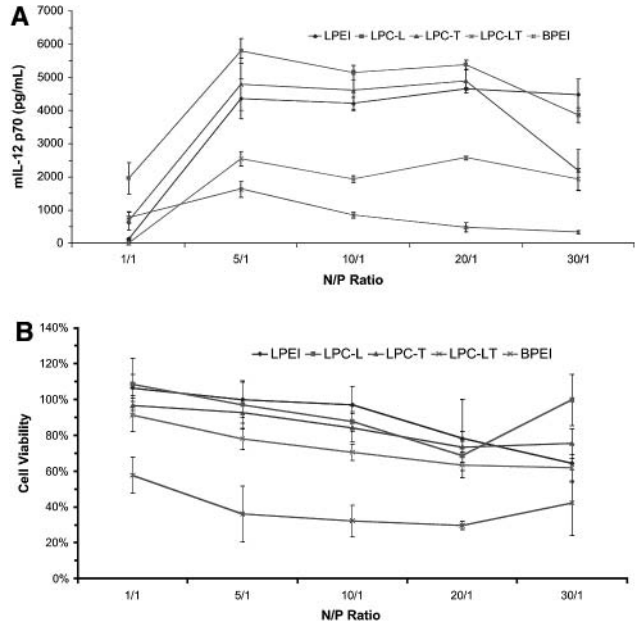


**Figure 3.** AFM image of LPC-T/pmIL-12e, N/P 10/1, 90 min after complexation.

in vivo ( $\gg$ 300 nm). The slopes of the particle size curves for LPC-LT, LPEI, and LPC-L from N/P 10/1 to 20/1 were quite similar; moreover, this trend was retained in the zeta potential measurements. LPC-T complexes were negatively charged at an N/P ratio of 5/1; however, the complexes quickly became cationic upon doubling the number of nitrogen residues to N/P 10/1 (Figure 3). Results from the AFM study show the complex morphology to be roughly spherical with a discrete particle size of  $\sim$ 250 nm at 30 and 60 min (data not shown). However, at 90 min postmixing, small satellites were seen to be merging with the  $\sim$ 250 nm LPC-T complex. We noted that the particle size for LPC-T/pmIL-12e N/P 10/1 from DLS and AFM were both  $\sim$ 250 nm. The high cationic



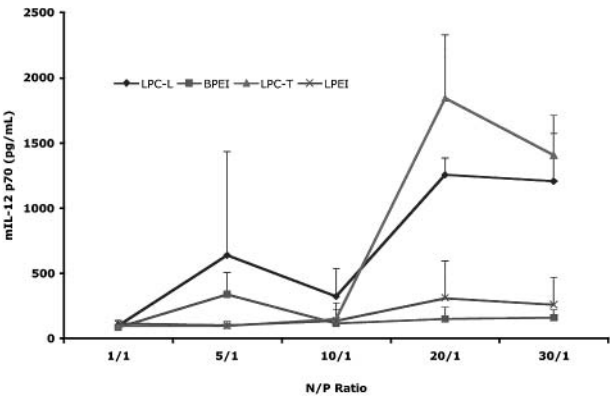
**Figure 4.** DNase protection assay for LPC-T/pmIL-12e N/P 10/1 and BPEI/pmIL-12e N/P 10/1.



**Figure 5.** (A) PEI/pmIL-12e transfection data of B16-F0 cells. mIL-12 p70 ELISA data reported as mean  $\pm$  SD,  $n = 8$ . (B) PEI/pmIL-12e cytotoxicity data for B16-F0 cells. CCK-8 data reported as mean  $\pm$  SD,  $n = 8$ .

density of BPEI, compared to LPEI, was confirmed with the DNase protection assay (Figure 4). After incubation with excess DNase, BPEI fully protected the pDNA up to 180 min while LPEI was successful up to only 60 min; however, LPC-T showed results comparable to BPEI at N/P 10/1.

In vitro transfection of B16-F0 cells (murine melanoma) showed  $\sim 2$ -fold higher mIL-12 p70 expression levels for LPEI and two of the LPC conjugates compared to BPEI over the N/P ratios that we studied (Figure 5A). All transfections were completed in the presence of 10% FBS with transgene expression levels as LPC-L > LPC-T > LPEI > BPEI > LPC-LT. The cytotoxicity profile was evaluated for the same samples used in the ELISA studies. We found a 10% difference in cytotoxicity, on average, between BPEI and the LPEI-LPC group. Renca cells (murine renal cell carcinoma) were also transfected with pmIL-12e (Figure 6), which showed the highest levels for LPC-T/pmIL-12e at N/P 20/1. There were no significant differences between the conjugates at N/P ratios below 20/1 with this cell line; moreover, the cytotoxicity profile was consistent with that previously found with B16-F0 cells (data not shown). The flow cytometry studies (Table 1) showed that LPC-L/pEGFP consistently gave the highest levels of positively trans-



**Figure 6.** PEI/pmIL-12e transfection data of Renca cells. mIL-12 p70 ELISA data reported as mean  $\pm$  SD,  $n = 8$ .

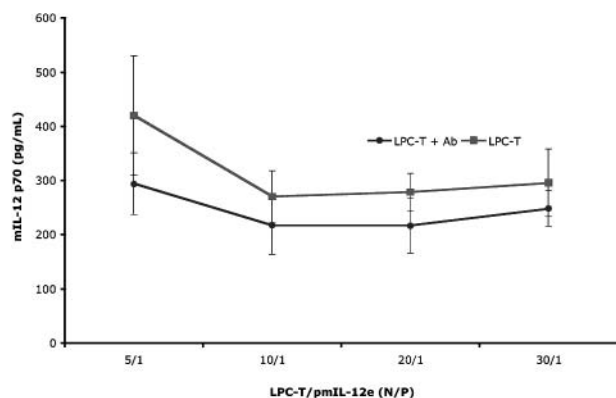
**Table 1. Flow Cytometry Data of PEGFP Expression Following Transfection of Renca and B16-F0 Cells<sup>a</sup>**

	Renca		B16-F0	
	% gated	geom mean	% gated	geom mean
C-				
average	0.38	72.73	0.43	50.74
SD	0.18	4.03	0.27	6.03
Naked pDNA				
average	0.42	69.57	0.45	48.69
SD	0.09	4.41	0.08	1.87
BPEI				
average	1.09	211.96	27.23	1552.44
SD	0.28	17.37	1.02	20.52
LPEI				
average	2.08	549.12	10.14	1416.54
SD	0.23	77.70	0.27	58.43
LPC-L				
average	32.14	2380.42	30.80	6484.99
SD	1.77	90.40	0.32	8347.57
LPC-T				
average	2.23	804.26	13.47	1269.71
SD	0.12	130.63	0.06	49.18

<sup>a</sup> The % gated indicates the percentage of cells (per 10 000) that were positive for EGFP while the geometric mean is indicative for the range of values from these gated cells. Data reported as mean  $\pm$  SD,  $n = 3$

ected cells in addition to the highest geometric mean of EGFP expression. For the Renca cells the percentage of gated cells was nearly 2-times that of BPEI for LPC-T and LPEI. LPC-L levels were nearly 32-times that of BPEI; however, there is not a direct relationship between the percentage of cells gated and geometric mean of the fluorescence detected. Both BPEI and LPEI gave significantly high percentages of B16-F0 cells that were positive for EGFP, but the geometric mean for LPC-L was more than 4-times that of BPEI. B16-F0 cells transfected with LPC-T/pEGFP showed half the percentage of positive cells, but the geometric means were quite close. The final assay was a hLDL-R saturation study showing that receptor-mediated endocytosis via the LDL-R is possible with an LPC conjugate. The LDL-R sites of human mammary carcinoma cells (MCF-7) were saturated with hLDL-R-Ab followed by transfection with LPC-T/pmIL-12e. On average mIL-12 p70 levels dropped by  $\sim 20\%$ , strongly indicating receptor-mediated endocytosis via the LDL-R pathway, in addition to the passive pathways of adsorptive endocytosis and pinocytosis (Figure 7). There was a sharp drop of mIL-12 p70 expression levels from N/P 5/1 to 10/1; however, levels remained relatively constant up to N/P 30/1 for the LPC-T and LPC-T plus LDL-R-Ab groups.





**Figure 7.** Anti-LDL-R Ab saturation study. MCF-7 cells transfected with LPC-T/pmIL-12e (N/P 10/1). mIL-12 p70 ELISA data reported as mean  $\pm$  SD,  $n = 8$ .

## DISCUSSION

Although BPEI has been used for years as the nonviral gene delivery standard of choice, LPEI is emerging as a superior alternative due to its favorable charge density and comparable pH buffering as BPEI. To better understand the structural and functional differences between BPEI and LPEI  $M_w$  25 k, we designed a number of experiments to further examine the benefits of HMW LPEI. In addition, upon the basis of the success with the LMW BPEI conjugation to cholesterol resulting in WSLP, we sought to explore whether such favorable changes could also be found with a HMW LPEI. We synthesized three new LPC conjugates in varying geometries from linear (LPC-L), to T-shaped (LPC-T), and finally to a combined conformation incorporating both the linear and T-shaped cholesterol conjugation sites (LPC-LT). The highly reactive terminal hydroxyl of LPEI provided an easy target for cholesterol conjugation, resulting in LPC-L. Protection of this reactive group was necessary to facilitate cholesterol conjugation to a secondary amine (LPC-T). Finally, saturating the reaction with excess cholesterol resulted in conjugation to both a secondary amine and the terminal hydroxyl (LPC-LT). The actual degrees of cholesterol conjugation were as expected based upon the  $^1\text{H}$  NMR studies.

The LPC conjugates were characterized by a number of methods including particle size, zeta potential, surface morphology by AFM, and gel retardation. The dramatic change in particle size for the LPEI, LPC-L, and LPC-LT complexes from N/P 10/1 to 20/1 is probably due to a conformation change of some sort resulting in a higher particle size due to intermolecular hydrogen bonding between neighboring complexes. The similar slopes within the particle size curves for LPC-LT, LPEI, and LPC-L from N/P 10/1 to 20/1 further suggest a conformation change within the LPC conjugates upon doubling the number of nitrogen residues per pDNA. Zeta potential measurements show the same trend in slope from N/P 10/1 to 20/1 for LPC-L, LPC-T, and LPC-LT (Figure 2B). LPC-T complexes exhibited a negative charge at N/P 5/1, suggesting that the total pDNA is not fully condensed. The surface charge becomes positive for LPC-T after increasing the N/P ratio to 10/1. Again, conformational changes could explain the abrupt change in surface charge for LPEI, LPC-L, and LPC-LT from N/P 5/1 to 10/1. Reorientation of the polymer complexes at this point could account for the dramatic increase in surface charge for the majority of the complexes from N/P 10/1 to 20/1. The initial negative charge of the LPC-T/pDNA complex at N/P 5/1 was interesting in that it could be accounted

for if the LPEI backbone is shielding the hydrophobic cholesterol moiety from the surrounding aqueous environment. Knowing that the charge density is less than BPEI of the same molecular weight, the number of protonated secondary amines with LPC-T available for electrostatic condensation of the pDNA is less, hence additional LPC-T conjugates are needed to effectively condense the pDNA thus producing a positive surface charge. Upon mixing 1.25 mg/mL stock solutions of the LPC conjugates, LPC-T was the only conjugate that did not require brief heating in a hot water bath to remove turbidity resulting from LPC aggregation. Aggregation effects with LPC-T/pDNA complexes were evaluated with an AFM study of the surface morphology of LPC-T/pDNA complexes at N/P 10/1. Images were taken at 30, 60, and 90 min post-mixing of LPC-T with pDNA in order to determine the potential for aggregation due to intermolecular hydrogen bonding between neighboring LPC-T complexes. The appearance of the small satellites with the AFM image suggests that LPC-T/pDNA complexes at N/P 10/1 are stable up to 90 min at ambient conditions. To evaluate the protective nature of pDNA condensation with the LPC conjugates, a *DNase* protection assay was completed. BPEI, due to its higher charge density, would condense pDNA more tightly than LPEI at the same N/P ratio. This supposition was confirmed with the *DNase* protection assay (Figure 4), which shows BPEI providing comparable pDNA protection up to 180 min in the presence of excess of *DNase*. LPEI was able to effectively protect pDNA up to 60 min while LPC-T could protect the pDNA up to 180 min, similar to BPEI. These data suggest that LPC-T forms a favorable complex conformation that shuttles the pDNA away from the deleterious *DNase* without the use of a high cationic charge density like that found with BPEI.

B16-F10 cells (murine melanoma cells) are easily transfected with polyethylenimine (PEI) (25); consequently, a close relative of this cell line, B16-F0, was specifically used to evaluate the structural differences between LPEI and BPEI. Because of the high levels of transfection, effects due to the plasmid construct were assumed to be minimal while the conformation of the PEI carriers was the dominant force in transfection levels. This finding is significant, and thus we can conclude that the different degrees of transfection are due to the PEI molecule and not from the vector (pmIL-12e). The transfections were carried out in RPMI + 10% FBS, thus the high cationic state of the BPEI/pDNA complexes may contribute to the lower transfection values due to unfavorable electrostatic interactions with serum components. Levels were expected to be low for the LPC-LT complexes due to the unfavorable complex size (Figure 2A). These data strongly suggest that LPEI and analogues may be superior to BPEI of the same molecular weight for nonviral gene delivery. The same samples used in the mIL-12 p70 study were also evaluated for cytotoxicity (Figure 5B). On average the differences in cytotoxicity were over 10%, further confirming the advantages of LPEI and its LPC analogues over BPEI. Cytotoxicity with the BPEI/pDNA complexes is due to the high cationic state of the complexes, whereas cytotoxicity with the LPEI/pDNA complexes is due to possible aggregation of the complexes by intermolecular hydrogen bonding of the LPEI backbones. This aggregation could explain the drop in cell viability at high N/P ratios. As the number of complexes increase, the ability for intermolecular hydrogen bonding also increases. Ongoing in vivo studies with the LPC conjugates are for the treatment of subcutaneous tumors and pulmonary metastases. We decided upon

Renca cells for our target cell line as they are somewhat immunogenic and are not necessarily easily transfected by PEI. Figure 6 shows the results from pmIL-12e transfections, where the highest levels were seen with LPC-T/pmIL-12e at N/P 20/1. Appreciable differences between mL-12 p70 levels were not seen below N/P 20/1; however, the trend of LPEI and LPC conjugates providing higher transfection efficiencies was retained.

The high levels of EGFP expression seen in the flow cytometry studies can be due to increased endocytosis rates, possibly due to LDL-R mediated endocytosis, increased protection of the pDNA prior to endocytosis and during lysosomal degradation, and high rates of release in the cytosolic compartment followed by nuclear translocation. We would expect a large number of cells to test positive for EGFP due to the high electrostatic binding between BPEI and pDNA; however, this tight binding of the pDNA could also prevent the pDNA from releasing quickly from this acidic environment. LPEI and the LPC conjugates possess enough cationic charge to adequately condense the pDNA, however, the release of the pDNA from the endosomal compartment should be quicker due to the less compact binding. Furthermore, cationic charge density may be even further reduced by the addition of cholesterol to the LPEI backbone (26). Upon sequestering the cholesterol from the aqueous environment, the LPC conjugate could further use the region shielding the cholesterol for endosomal buffering after endocytosis. Cleavage of the cholesterol moiety from the LPEI backbone by lipase could result in an immediate increase in proton buffering.

An additional purpose of this study was to further demonstrate mechanisms by which PEI-cholesterol conjugates could be internalized. Mechanisms by which polyplexes may be internalized into a cell include pinocytosis, adsorptive endocytosis, and receptor-mediated endocytosis. It is well-known that the human low density lipoprotein receptor (LDL-R) consists of five domains of which the outermost domain, the "ligand-binding domain", is negatively charged (27). Furthermore, Goldstein et. al confirmed that cholesteryl esters are cleaved from lipoproteins by lipase, a lysosomal acid (28). Therefore, it is plausible that LPC/pDNA complexes could exploit both of these characteristics for internalization and endosomal release of the transgenic pDNA based upon our results. Conjugation of highly hydrophobic cholesterol to a hydrophilic polymer such as PEI followed by hydration results in a complex in which the PEI reorients itself so as to shield the cholesterol from the surrounding aqueous environment. With a high molecular weight, LPEI such as that used in these studies, a number of conformations were possible dependent upon the site and degree of cholesterol conjugation. We hypothesized that the LPC-T conjugate would provide the highest transfection levels based upon a number of factors including increased water solubility by decreasing the degree of hydrogen bonding between neighboring LPEI backbones, favorable protection of the cholesterol by the hydrophilic-interactions of the two neighboring strands, and increased, late-stage pH buffering capacity after cleavage of the cholesterol from the LPEI backbone by lipase. After the late endosome fuses with the lysosome, the ethylenimine monomers used to shield the cholesterol could become available for further pH buffering, a process we termed "unprotonated reserves".

Future work will include biodistribution studies in normal and diseased mice in addition to further optimization of the LPC gene carriers by the addition of targeting ligands. PEGylation of LPC-L should provide

adequate water solubility and a resulting decrease in particle size. LPC-L showed consistently higher transgene expression; however, the particle size and degree of cytotoxicity are currently not appropriate for in vivo studies. Finally, optimization of the size and degree of conjugation of the hydrophobic moiety on the LPEI will be completed.

#### ACKNOWLEDGMENT

We thank Jay Olsen for his assistance with the NMR studies and Andras Pungor for his assistance with the AFM. This project was generously supported by Expression Genetics, Inc.

#### LITERATURE CITED

- (1) von Harpe, A., Petersen, H., Li, Y., and Kissel, T. (2000) Characterization of commercially available and synthesized polyethylenimines for gene delivery. *J. Controlled Release* 69, 309–322.
- (2) Godbey, W. T., Wu, K. K., and Mikos, A. G. (1999) Size matters: Molecular weight affects the efficiency of poly(ethylenimine) as a gene delivery vehicle. *J. Biomed. Mater. Res.* 45, 268–275.
- (3) Fischer, D., Bieber, T., Li, Y., Elsasser, H. P., and Kissel, T. (1999) A novel nonviral vector for DNA delivery based on low molecular weight, branched polyethylenimine: effect of molecular weight on transfection efficiency and cytotoxicity. *Pharm. Res.* 16, 1273–1279.
- (4) Petersen, H., Fechner, P. M., Martin, A. L., Kunath, K., Stolnik, S., Roberts, C. J., Fischer, D., Davies, M. C., and Kissel, T. (2002) Polyethylenimine-graft-poly(ethylene glycol) copolymers: influence of copolymer block structure on DNA complexation and biological activities as gene delivery system. *Bioconjugate Chem.* 13, 845–854.
- (5) Fischer, D., Li, Y., Ahlemeyer, B., Krieglstein, J., and Kissel, T. (2003) In vitro cytotoxicity testing of polycations: influence of polymer structure on cell viability and hemolysis. *Biomaterials* 24, 1121–1131.
- (6) Abdallah, B., Hassan, A., Benoist, C., Goula, D., Behr, J. P., and Demeneix, B. A. (1996) A powerful nonviral vector for in vivo gene transfer into the adult mammalian brain: polyethylenimine. *Hum. Gene Ther.* 7, 1947–1954.
- (7) Goula, D., Remy, J. S., Erbacher, P., Wasowicz, M., Levi, G., Abdallah, B., and Demeneix, B. A. (1998) Size, diffusibility and transfection performance of linear PEI/DNA complexes in the mouse central nervous system. *Gene Ther.* 5, 712–717.
- (8) Coll, J. L., Chollet, P., Brambilla, E., Desplanques, D., Behr, J. P., and Favrot, M. (1999) In vivo delivery to tumors of DNA complexed with linear polyethylenimine. *Hum. Gene Ther.* 10, 1659–1666.
- (9) Chollet, P., Favrot, M. C., Hurbin, A., and Coll, J. L. (2002) Side-effects of a systemic injection of linear polyethylenimine-DNA complexes. *J. Gene Med.* 4, 84–91.
- (10) Goula, D., Becker, N., Lemkine, G. F., Normandie, P., Rodrigues, J., Mantero, S., Levi, G., and Demeneix, B. A. (2000) Rapid crossing of the pulmonary endothelial barrier by polyethylenimine/DNA complexes. *Gene Ther.* 7, 499–504.
- (11) Zou, S. M., Erbacher, P., Remy, J. S., and Behr, J. P. (2000) Systemic linear polyethylenimine (L-PEI)-mediated gene delivery in the mouse. *J. Gene Med.* 2, 128–134.
- (12) Uduehi, A. N., Stammberger, U., Kubisa, B., Gugger, M., Buehler, T. A., and Schmid, R. A. (2001) Effects of linear polyethylenimine and polyethylenimine/DNA on lung function after airway instillation to rat lungs. *Mol. Ther.* 4, 52–57.
- (13) Wightman, L., Kircheis, R., Rossler, V., Carotta, S., Ruzicka, R., Kurs, M., and Wagner, E. (2001) Different behavior of branched and linear polyethylenimine for gene delivery in vitro and in vivo. *J. Gene Med.* 3, 362–372.
- (14) Brunner, S., Furtbauer, E., Sauer, T., Kurs, M., and Wagner, E. (2002) Overcoming the nuclear barrier: cell cycle independent nonviral gene transfer with linear polyethylenimine or electroporation. *Mol. Ther.* 5, 80–86.
- (15) Kircheis, R., Ostermann, E., Wolschek, M. F., Lichtenberger, C., Magin-Lachmann, C., Wightman, L., Kurs, M.,

- and Wagner, E. (2002) Tumor-targeted gene delivery of tumor necrosis factor- $\alpha$  induces tumor necrosis and tumor regression without systemic toxicity. *Cancer Gene Ther.* 9, 673–680.
- (16) Boussif, O., Lezoualc'h, F., Zanta, M. A., Mergny, M. D., Scherman, D., Demeneix, B., and Behr, J. P. (1995) A versatile vector for gene and oligonucleotide transfer into cells in culture and in vivo: polyethylenimine. *Proc. Natl. Acad. Sci. U.S.A.* 92, 7297–7301.
- (17) Furgeson, D. Y., Cohen, R. N., Mahato, R. I., and Kim, S. W. (2002) Novel water insoluble lipoparticulates for gene delivery. *Pharm. Res.* 19, 382–390.
- (18) Suh, W., Han, S. O., Yu, L., and Kim, S. W. (2002) An angiogenic, endothelial-cell-targeted polymeric gene carrier. *Mol. Ther.* 6, 664–672.
- (19) Benns, J. M., Maheshwari, A., Furgeson, D. Y., Mahato, R. I., and Kim, S. W. (2001) Folate-PEG-folate-graft-polyethylenimine-based gene delivery. *J. Drug Targeting* 9, 123–139.
- (20) Han, S.-O., Mahato, R. I., and Kim, S. W. (2001) Water-soluble lipopolymer for gene delivery. *Bioconjugate Chem.* 12, 337–345.
- (21) Mahato, R. I., Lee, M., Han, S., Maheshwari, A., and Kim, S. W. (2001) Intratumoral delivery of p2CMVmIL-12 using water-soluble lipopolymers. *Mol. Ther.* 4, 130–138.
- (22) Yockman, J. W., Maheshwari, A., Han, S., and Kim, S. W. (2003) Tumor regression by repeated intratumoral delivery of water soluble lipopolymers/p2CMVmIL-12 complexes. *J. Controlled Release* 87, 177–186.
- (23) Wang, D. A., Narang, A. S., Kotb, M., Gaber, A. O., Miller, D. D., Kim, S. W., and Mahato, R. I. (2002) Novel branched poly(ethylenimine)-cholesterol water-soluble lipopolymers for gene delivery. *Biomacromolecules* 3, 1197–1207.
- (24) Li, Y., Wood, N., Parsons, P. G., Yellowlees, D., and Donnelly, P. K. (1997) Expression of  $\alpha$ 2-macroglobulin receptor/low-density lipoprotein receptor-related protein on surfaces of tumour cells: a study using flow cytometry. *Cancer Lett.* 111, 199–205.
- (25) Wightman, L., Patzelt, E., Wagner, E., and Kircheis, R. (1999) Development of transferrin-polycation/DNA based vectors for gene delivery to melanoma cells. *J. Drug Targeting* 7, 292–303.
- (26) Suh, J., Paik, H.-J., and Hwang, B. K. (1994) Ionization of poly(ethylenimine) and poly(allylamine) at various pH's. *Bioorg. Chem.* 22, 318–327.
- (27) Yamamoto, T., Davis, C. G., Brown, M. S., Schneider, W. J., Casey, M. L., Goldstein, J. L., and Russell, D. W. (1984) The human LDL receptor: a cysteine-rich protein with multiple Alu sequences in its mRNA. *Cell* 39, 27–38.
- (28) Goldstein, J. L., Dana, S. E., Faust, J. R., Beaudet, A. L., and Brown, M. S. (1975) Role of lysosomal acid lipase in the metabolism of plasma low-density lipoprotein. Observations in cultured fibroblasts from a patient with cholesteryl ester storage disease. *J. Biol. Chem.* 250, 8487–8495.

BC0340565



# CORRECTIONS

---

Volume 14, Number 3, May/June 2003.

Nadia Bendifallah, Edward Kristensen, Otto Dahl,  
Uffe Koppelhus, and Peter E. Nielsen\*

## SYNTHESIS AND PROPERTIES OF ESTER- LINKED PEPTIDE NUCLEIC ACID PRODRUG CONJUGATES

Page 589. There is an error in the sequences of **PNA-10** and **PNA-11**. The second base should be a C and not a T. The corrected sequences are as follows:

**PNA-10:** Deca-eg1-CCTCTAACCTCTGTTACA-NH<sub>2</sub>

**PNA-11:** Deca-GMB2-eg1-CCTCTAACCTCTGTTACA-NH<sub>2</sub>

BC0300246

10.1021/bc0300246

Published on Web 06/21/2003

Susan K. Hobbs, Gongyi Shi, and Mark D.  
Bednarski\*

## SYNTHESIS OF POLYMERIZED THIN FILMS FOR IMMOBILIZED LIGAND DISPLAY IN PROTEOMIC ANALYSIS

Page 530. The following portion of the Acknowledgment should be removed: "We thank S. Narasimhan Danthi (National Institutes of Health) for a gift of integrin antagonist". The integrin antagonist was actually synthesized by the authors (see ref 16).

BC0300271

10.1021/bc0300271

Published on Web 06/28/2003

# CORRECTIONS

---

Volume 14, Number 3, May/June 2003.

Nadia Bendifallah, Edward Kristensen, Otto Dahl,  
Uffe Koppelhus, and Peter E. Nielsen\*

## SYNTHESIS AND PROPERTIES OF ESTER- LINKED PEPTIDE NUCLEIC ACID PRODRUG CONJUGATES

Page 589. There is an error in the sequences of **PNA-10** and **PNA-11**. The second base should be a C and not a T. The corrected sequences are as follows:

**PNA-10:** Deca-eg1-CCTCTAACCTCTGTTACA-NH<sub>2</sub>

**PNA-11:** Deca-GMB2-eg1-CCTCTAACCTCTGTTACA-NH<sub>2</sub>

BC0300246

10.1021/bc0300246

Published on Web 06/21/2003

Susan K. Hobbs, Gongyi Shi, and Mark D.  
Bednarski\*

## SYNTHESIS OF POLYMERIZED THIN FILMS FOR IMMOBILIZED LIGAND DISPLAY IN PROTEOMIC ANALYSIS

Page 530. The following portion of the Acknowledgment should be removed: "We thank S. Narasimhan Danthi (National Institutes of Health) for a gift of integrin antagonist". The integrin antagonist was actually synthesized by the authors (see ref 16).

BC0300271

10.1021/bc0300271

Published on Web 06/28/2003

## COMMUNICATIONS

---

### A Novel Approach for Affinity-Based Screening of Target Specific Ligands: Application of Photoreactive D-Glyceraldehyde-3-phosphate Dehydrogenase

Masaki Kaneda, Yutaka Sadakane, and Yasumaru Hatanaka\*

Faculty of Pharmaceutical Sciences, Toyama Medical and Pharmaceutical University,  
2630 Sugitani, Toyama 930-0194, Japan. Received April 1, 2003

---

A novel application of the photoaffinity technique has been developed for the efficient discovery of small ligand and macromolecule interaction. The approach, photoaffinity capture, uses a photoreactive protein together with immobilized ligand for the rapid screening of competitive inhibitors. The set of photoreactive glyceraldehyde-3-phosphate dehydrogenase (photo-GAPDH) and immobilized dye ligand was prepared and examined as a model system. The photo-GAPDH was shown to efficiently capture the immobilized ligand. When nonimmobilized competitive ligands were included in the system, the capture was prevented in accordance with the affinity of the ligands. The present approach would provide an efficient tool for affinity-based screening of ligand libraries.

---

Photoaffinity labeling is a useful method for the elucidation of molecular interaction processes (1). The method usually utilizes a photoreactive small ligand as a probe, which introduces cross-links on the target macromolecule (2–7). Photoreactive macromolecules such as proteins (8, 9) or oligonucleotides (10) have also been developed for probing the interactions between bio-macromolecules. However, this macromolecular probe approach has never been applied for capturing ligands that specifically enter into the internal ligand binding sphere of photoreactive macromolecules.

Here, we report a novel application of a photoreactive protein for the efficient discovery of its partner ligands. The approach uses a photoreactive protein and an im-

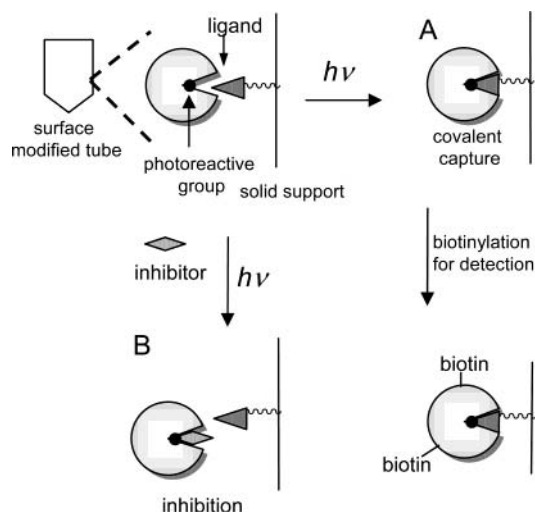
mobilized ligand for achieving efficient inhibitor screening. The protein has a photoreactive group, a diazirine, within the active site for enabling a covalent capture of a ligand (Figure 1A). The capture process can then be prevented with an inhibitor that has enough affinity for the active site (Figure 1B). Thus, the photoaffinity capture array composed of a known set of protein and ligand would provide a simple and efficient device for finding new ligands. We have examined this approach using GAPDH as a protein mold, and Cibacron Blue 3GA as an affinity ligand to be immobilized.

GAPDH is a homo-tetramer protein that catalyzes the oxidation of glyceraldehyde-3-phosphate with concomitant reduction of  $\beta$ -nicotinamide adenine dinucleotide (NAD<sup>+</sup>) (11). Each subunit of GAPDH has an active site composed with a catalytic free sulfhydryl group Cys<sup>149</sup> (12). The method for the selective modification of the active site Cys<sup>149</sup> is already established (13, 14). Thus, a

---

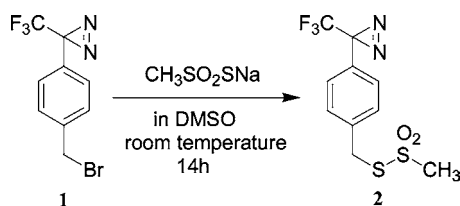
\* To whom correspondence should be addressed. Phone: +81-76-434-7515. Fax: +81-76-434-5063. E-mail: yasu@ms.toyama-mpu.ac.jp.





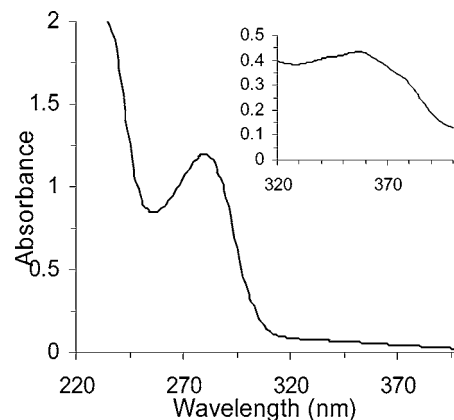
**Figure 1.** General approach of photoaffinity capture. (A) The covalent capture of target-specific ligand by photoreactive protein. (B) Application to the screening of inhibitory ligands.

sulfhydryl group selective reagent **2** was designed and synthesized for the introduction of a useful carbene precursor, a diazirine (**1**), within the active site of GAPDH. The thiosulfonate group of the reagent is known to form a disulfide linkage with the sulfhydryl group of protein (**15**).

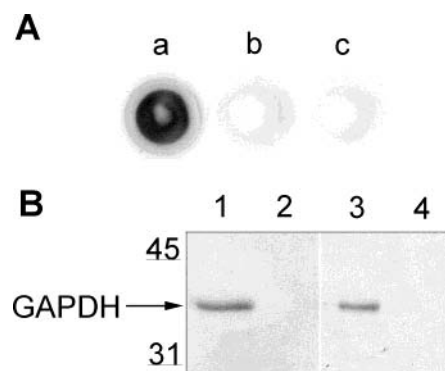


The reagent **2** was readily synthesized from a known diazirine bromide **1** (**16**) by an established derivatization method (**15**). Since the bound  $\text{NAD}^+$  of holo-GAPDH is known to inhibit the modification of the active site sulfhydryl group (**17**), the cofactor was removed before the modification reaction (**18**). The apo-GAPDH was then reacted with compound **2** for 1 h at room temperature to give photoreactive GAPDH (photo-GAPDH). After a gel filtration chromatography, the GAPDH concentration of the pooled protein fraction was determined from UV absorption at 278 nm (**19**) and also by Bradford protein assay (**20**). The diazirine concentration was independently obtained from its characteristic  $n \rightarrow \pi^*$  absorption ( $\lambda_{\text{max}}$  360,  $\epsilon = 310$ ) as shown in Figure 2 (inset). The extent of modification was calculated as 0.72 mol of diazirine per subunit of GAPDH.

For the preparation of ligand immobilized matrix, a commercially available preactivated ligand, Cibacron Blue 3GA, was used. Cibacron Blue is an affinity ligand that specifically binds to the nucleoside phosphate binding sites of dehydrogenases and kinases (**21**). Since GAPDH has a  $\text{NAD}^+$  binding site near to the  $\text{Cys}^{149}$  in active site (**17**), Cibacron Blue should locate close to the diazirine of photo-GAPDH. Cibacron Blue 3GA was immobilized on a surface aminated tube that could be easily prepared by the graft polymerization of methacrylic acid on the inner wall of polypropylene tube (**22–24**) followed by the amino scaffold coupling (Supporting Information). The Cibacron Blue immobilized tube was first used to evaluate the ligand-capturing ability of photo-GAPDH. The photo-GAPDH was incubated in the



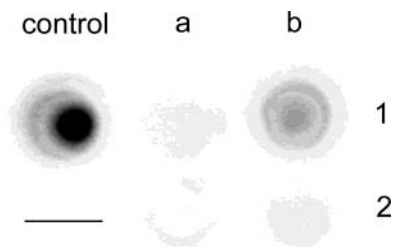
**Figure 2.** UV-vis spectra of photo-GAPDH. The UV-vis spectrum (220–400 nm) of modified GAPDH was recorded in pyrophosphate buffer pH 7.5 containing 0.1 mM EDTA. The inset shows the spectral region of 320–400 nm, which was obtained with a concentrated solution of photo-GAPDH.



**Figure 3.** Detection of cross-linked GAPDH onto immobilized Cibacron Blue ligand. (A) The photo-GAPDH was incubated in the ligand immobilized tube and examined. The GAPDH trapped on the solid matrix was visualized after biotinylation. Irradiated (spot a). Not irradiated (spot b). Irradiated then treated with 2-mercaptoethanol (spot c). (B) SDS-PAGE analysis of GAPDH without (lanes 1, 2, and 4) or with irradiation (lane 3). The affinity bound GAPDH on the immobilized Cibacron Blue 3GA was recovered with 1% SDS (lane 1). Experimental conditions were the same as the sample in lane 1 except that the Cibacron ligand was not attached on the matrix (lane 2). The photochemically cross-linked GAPDH on to the immobilized Cibacron Blue 3GA was recovered after reducing disulfide linkage with 2-mercaptoethanol (lane 3). Experimental conditions were the same as for the sample in lane 3 except that irradiation was not applied (lane 4).

Cibacron tube for 1 h at 37 °C and irradiated at 0 °C for 10 min. After the photolysis, the tube was completely washed with 1% sodium dodecyl sulfate (SDS) to remove untrapped GAPDH. The tube was then reacted with biotin *N*-hydroxysuccinimide and subjected for the chemiluminescent detection of trapped protein as shown in Figure 1. The chemiluminescence generated with a commercial kit (Wako Pure Chemical Industries, Ltd., Japan) was detected on an image analyzer (ChemiDoc, Bio-Rad Laboratories, Inc.).

The trapped GAPDH was clearly visualized as a spot when the photoaffinity capture was applied (Figure 3A, spot a). The protein was not detected when the irradiation was not applied (spot b) or the irradiated tube was treated with 2-mercaptoethanol (spot c). The latter control experiment suggests that the trapped GAPDH could be released from the matrix by cleaving the S–S linkage. To confirm the result, the GAPDH was analyzed



**Figure 4.** Photoaffinity capture in the presence of competitive small ligands. The GAPDH photoaffinity capture system was examined in the presence of Cibacron Blue 3GA (column a), ATP (column b). The concentration of additives was 100  $\mu\text{M}$  (row 1) and 600  $\mu\text{M}$  (row 2), respectively. No competitor was added to the control.

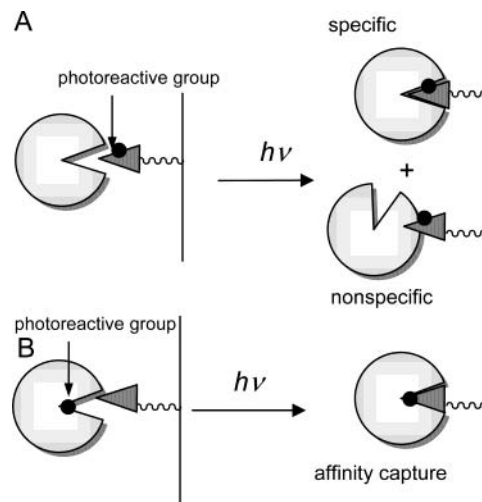
**Table 1. The Inhibition of Photoaffinity Capture in the Presence of Competitive Small Ligands.**

competitor	inhibition (% $\pm$ S. D.) <sup>a</sup>	
	100 $\mu\text{M}$	600 $\mu\text{M}$
Cibacron Blue	94.5 $\pm$ 1.5	95.9 $\pm$ 1.2
NAD <sup>+</sup>	4.5 $\pm$ 7.8	14.1 $\pm$ 5.4
ATP	51.7 $\pm$ 6.2	92.9 $\pm$ 1.9
D-glyceraldehyde-3-phosphate	13.3 $\pm$ 5.3	62.7 $\pm$ 6.8
L-tyrosine-O-phosphate	3.8 $\pm$ 5.5	6.3 $\pm$ 5.3
NADH	4.3 $\pm$ 8.2	12.8 $\pm$ 12.2
NADP <sup>+</sup>	4.1 $\pm$ 11.3	13.4 $\pm$ 5.3
NADPH	3.8 $\pm$ 2.6	12.9 $\pm$ 7.6

<sup>a</sup> The value is the average of 15 assays, and the errors are given in SD values.

with SDS-PAGE (Figure 3B). First, the photo-GAPDH was examined without the irradiation. The lane 1 demonstrate that the modification at the sulfhydryl group does not significantly reduce the recognition of Cibacron Blue. The affinity bound GAPDH was recovered from the matrix with 1% SDS and was resolved at 37 kD with the expected subunit molecular weight (lane 1), whereas no GAPDH was detected from the matrix without Cibacron Blue ligand (lane 2). The conditions for lanes 3 and 4 were the same as those for spots c and b of Figure 3A, respectively. When the irradiation was applied, the covalently trapped GAPDH on the matrix was detected only after cleaving the disulfide bond between the cross-linked moiety and Cys<sup>149</sup> (lane 3). In contrast to this, the control lane 4 showed that no GAPDH was trapped without irradiation. From the densitometric analysis, the amount of captured protein in lane 3 was determined as 36% of the bound GAPDH (lane 1). The photoaffinity capture system of photo-GAPDH and immobilized Cibacron Blue was shown to have desired nature for progression to the competitive inhibitor screening.

The GAPDH photoaffinity capture system was examined in the presence of known inhibitors, Cibacron Blue 3GA and ATP, at the concentration of 100  $\mu\text{M}$  (row 1) and 600  $\mu\text{M}$  (row 2), respectively. The addition of 100  $\mu\text{M}$  Cibacron Blue 3GA was enough for preventing the capture of GAPDH (column a row 1). ATP, a well-known inhibitor of GAPDH (25), inhibited the capture of GAPDH in a dose dependent manner as shown in the column b of Figure 4. The inhibition with various small ligands is summarized in Table 1. In the presence of NAD<sup>+</sup>, the trap of GAPDH on the matrix was moderately inhibited compared to the result of Cibacron Blue 3GA. From the study of lactate dehydrogenase and phosphoglycerate kinase, these enzymes were reported to have 10 to 100 times higher affinity for Cibacron Blue 3GA than for NAD<sup>+</sup> (26). GAPDH only uses NAD<sup>+</sup> and NADH for the enzyme reaction whereas the similar amount of the



**Figure 5.** The advantage of photoreactive protein. (A) Photoaffinity labeling of target protein with a conventional small photoreactive ligand. (B) Photoaffinity capture of small ligand by photoreactive protein.

capture inhibition was also observed with NADP<sup>+</sup> and NADPH. The similar change in the cofactor specificity was reported for an active site modified GAPDH (13). The result clearly showed that the photoaffinity capture differentiated between ligands with different affinities. The addition of substrate D-glyceraldehyde-3-phosphate inhibited the capture whereas a more bulky phosphate, L-tyrosine-O-phosphate, was ineffective. Since D-glyceraldehyde-3-phosphate binds near to the active site sulfhydryl group (27), it is interesting that the enough space for the substrate binding is still remains after the introduction of phenyl diazirine moiety. Although bulky ligands may have a conflict with the photoreactive group, the result also suggests that a small phosphate may be a candidate for a lead structure of the GAPDH inhibitor. Taken together, the results showed that the photoaffinity capture method could be a rapid and efficient approach of ligand screening.

The technique based on surface plasmon resonance spectroscopy was developed for the real-time analysis of ligand-receptor interaction (28, 29). The technique, however, requires special equipment for the analysis whereas the photoaffinity capture only uses a set of photoreactive protein and an immobilized ligand array. The advantage of the photoaffinity approach could be a simple affinity-based entry into the massive screening of ligands. Conventional methods based on the interaction between ligand and receptor usually have a problem of nonspecific binding. The advantage of current method is that the nonspecifically bound proteins can be removed from the matrix before the detection. By making the protein photoreactive, the nonspecific cross-linking is also minimized. Photoreactive small ligands often label the protein surface in a nonspecific manner (Figure 5A). The photoreactive protein limits the photochemical reaction to only the active site (Figure 5B). This directs the cross-link to the specific capture of ligands.

In summary, the application of the present method may be limited to these protein with a sulfhydryl group near the active site. The proteins have to be also stable during the modification and need to be readily available. The development of protein expression and site-specific mutagenesis, however, could provide a tailor-made (engineered) protein in which the desired sulfhydryl group is incorporated. The photoaffinity capture would be an efficient tool for affinity-based parallel screening of

ligands in the early step of the drug discovery and developments.

#### ACKNOWLEDGMENT

We are very grateful to Professor G. D. Holman (University of Bath, U. K.) for valuable advice throughout the manuscript. This work was supported by Grants-in-Aid for Scientific Research (12470504), for Encouragement of Young Scientists (13771410), and for Exploratory Research (14658185), from the Ministry of Education, Culture, Sports, Science and Technology of Japan.

**Supporting Information Available:** Synthetic procedures, NMR, MS, and elemental analysis of compound 1. Procedures for the preparation of photo-GAPDH and Cibacron immobilized tube. Conditions for photoaffinity capture experiments. These materials are available free of charge via the Internet at <http://pubs.acs.org/BC>.

#### LITERATURE CITED

- Hatanaka, Y., and Sadakane, Y. (2002) Photoaffinity Labeling in Drug Discovery and Developments: Chemical Gateway for Entering Proteomic Frontier. *Curr. Top. Med. Chem.* 2, 271–288.
- Prestwith, G. D., and Dormán G. (2000) Using Photolabile Ligands in Drug Discovery and Developments. *Trends Biotechnol.* 18, 64–77.
- Dadhish, M., Hennig, L., Findeisen, M., Sabine, G., Schumer, F., Hennig, H., Beck-Sicking, A. G., and Welzel, P. (2002) Tetrafunctional Photoaffinity Labels Based on Nakanishi's *m*-Nitroalkoxy-Substituted Phenyltrifluoromethyl-diazirine. *Angew. Chem., Int. Ed.* 41, 2293–2297.
- Strømgaard, K., Saito, D. R., Shindou, H., Ishii, S., Shimizu, T., and Nakanishi, K. (2002) Ginkgolide Derivatives for Photolabeling Studies: Preparation and Pharmacological Evaluation. *J. Med. Chem.* 45, 4038–4046.
- Mésange, F., Sebban, M., Capdevielle, J., Guillemot, J., Ferrara, P., Bayard, F., Poirot, M., and Faye, J. (2002) Identification of Two Tamoxifen Target Proteins by Photolabeling with 4-(2-Morpholinoethoxy)benzophenone. *Bioconjugate Chem.* 13, 766–772.
- Hatanaka, Y., Hashimoto, H., and Kanaoka, Y. (1998) A Rapid and Efficient Method for Identifying Photoaffinity Biotinylated Sites within Proteins. *J. Am. Chem. Soc.* 120, 453–454.
- Jahn, O., Eckart, K., Braun, O., Tezval, H., and Spiess, J. (2002) The Binding Protein of Corticotropin-Releasing Factor: Ligand-Binding Site and Subunit Structure. *Biochemistry* 99, 12055–12060.
- Wahlstrom, J. L., Randall, Jr, M. A., Lawson, J. D., Lyons, D. E., Siems, W. F., Crouch, G. J., Barr, R., and Facemyer, K. C. (2003) Structural Model of the Regulatory Domain of Smooth Muscle Heavy Meromyosin. *J. Biol. Chem.* 278, 5123–5131.
- Brown, C. E., Howe, L., Sousa, K., Alley, S. C., Carrozza, M. J., Tan, S., and Workman, J. L. (2001) Recruitment of HAT Complexes by Direct Activator Interactions with the ATM-Related Tra1 Subunit. *Science* 292, 2333–2337.
- Kovach, M. J., Tirumalai, R., and Landy, A. (2002) Site-specific Photocross-linking between  $\lambda$  Integrase and Its DNA Recombination Target. *J. Biol. Chem.* 277, 14530–14538.
- Buehner, M., Ford, G. C., Moras, D., Olsen, K. W., and Rossmann, M. G. (1974) Three-dimensional Structure of D-Glyceraldehyde-3-phosphate Dehydrogenase. *J. Mol. Biol.* 90, 25–49.
- Walker, J. E., Carne, A. F., Runswick, M. J., Bridgen, J., and Harris, J. I. (1980) D-Glyceraldehyde-3-Phosphate Dehydrogenase. *Eur. J. Biochem.* 108, 549–565.
- Hilvert, D., Hatanaka, Y., and Kaiser, E. T. (1988) A High Active Thermophilic Semisynthetic Flavoenzyme. *J. Am. Chem. Soc.* 110, 682–689.
- Hilvert, D., and Kaiser, E. T. (1985) New Semisynthetic Flavoenzymes Based on a Tetrameric Protein Template, Glyceraldehyde-3-phosphate Dehydrogenase. *J. Am. Chem. Soc.* 107, 5805–5806.
- Kenyon, G. L., and Bruice, T. W. (1977) Novel Sulfhydryl Reagents. *Methods Enzymol.* 47, 407–430.
- Nassal, M. (1984) 4'-(1-Azi-2,2,2-trifluoroethyl)phenylalanine, a Photolabile Carbene-Generating Analogue of Phenylalanine. *J. Am. Chem. Soc.* 106, 7540–7545.
- Trentham, D. R. (1968) Aspect of the Chemistry of D-Glyceraldehyde-3-phosphate Dehydrogenase. *Biochem. J.* 109, 603–612.
- Kremsky, I., and Racker, E. (1962) Separation of Oxidative from Phosphorylative Activity by Proteolysis of Glyceraldehyde-3-Phosphate Dehydrogenase. *Biochemistry* 2, 512–518.
- Murdock, A., and Koppe, O. (1964) The Content and Action of Diphosphopyridine Nucleotide in Triosephosphate Dehydrogenase. *J. Biol. Chem.* 239, 1983–1988.
- Bradford, M. M. (1976) A Rapid and Sensitive Method for the Quantitation of Microgram Quantities of Protein Utilizing the Principle of Protein-Dye Binding. *Anal. Biochem.* 72, 248–254.
- Hanggi, D. and Carr, P. (1985) Analytical Evaluation of the Purity of Commercial Preparations of Cibacron Blue F3GA and Related Dyes. *Anal. Biochem.* 149, 91–104.
- Tazuke, S., and Kimura, H. (1978) Surface Photografting. I. Graft Polymerization of Hydrophilic Monomers onto Various Polymer Films. *J. Polym. Sci.* 16, 497–500.
- Tazuke, S., and Kimura, H. (1978) Surface Photografting. 2. Modification of Polypropylene Film Surface by Graft Polymerization of Acrylamide. *Makromol. Chem.* 179, 2603–2612.
- Wenschuh, H., Volkmer-Engert, R., Schmidt, M., Schulz, M., Schneider-Mergener, J., and Reineke, U. (2000) Coherent Membrane Supports for Parallel Microsynthesis and Screening of Bioactive Peptides. *Biopolymers (Pept. Sci.)* 55, 188–206.
- Oguti, M., Gerth, E., Fitzgerald, B., and Park, J. (1973) Regulation of Glyceraldehyde-3-Phosphate Dehydrogenase by Phosphocreatine and Adenosine Triphosphate. IV. Factor affecting in vivo Control of Enzymatic Activity. *J. Biol. Chem.* 248, 5571–5576.
- Thompson, S. T., and Stellwagen, E. (1976) Binding of Cibacron Blue F3GA to Proteins Containing Dinucleotide Fold. *Proc. Natl. Acad. Sci. U.S.A.* 73, 361–365.
- Cardon, J. W., and Boyer, P. D. (1982) Subunit Interaction in Catalysis: Some Experimental and Theoretical Approaches with Glyceraldehyde-3-Phosphate Dehydrogenase. *J. Biol. Chem.* 257, 7615–7622.
- Salamon, Z., Macleod, A. H., and Tollin, G. (1997) Surface Plasmon Resonance Spectroscopy as a Tool for Investigating the Biochemical and Biophysical Properties of Membrane Protein Systems. I: Theoretical Principles. *Biochim. Biophys. Acta* 1331, 117–129.
- Salamon, Z., Macleod, A. H., and Tollin, G. (1997) Surface Plasmon Resonance Spectroscopy as a Tool for Investigating the Biochemical and Biophysical Properties of Membrane Protein Systems. II: Application to biological systems. *Biochim. Biophys. Acta* 1331, 131–152.

BC0340520



## Materials for Supporting Information

A novel approach for affinity based screening of target specific ligands: Application of photoreactive D-glyceraldehyde-3-phosphate dehydrogenase

Masaki Kaneda, Yutaka Sadakane and Yasumaru Hatanaka

## EXPERIMENTAL PROCEDURE

### Materials and Method

#### S-[4-(3-trifluoromethyl-3H-diazirin-3-yl)-benzyl]-methane thiosulfonate (**1**)

3-(4-Bromomethylphenyl)-3-trifluoromethyl-3*H*-diazirine (1.12g, 4 mmol) was dissolved in DMSO (4 ml) followed by the addition of sodium methane thiosulfonate at room temperature for 14 h. The mixture was chromatographed on silica gel (eluting with ethyl acetate/hexane = 1:3) to give *S*-[4-(3-trifluoromethyl-3*H*-diazirin-3-yl)-benzyl]-methane thiosulfonate (**1**) as a colorless solid, 1.10 g (89%). Recrystallization from ether-hexane gave colorless leaves with mp 48 – 49.5°C: <sup>1</sup>H NMR (400 MHz, CDCl<sub>3</sub>, 25°C) δ 7.45 (d, *J* = 8.0 Hz, 2H), 7.20 (d, *J* = 8.0 Hz, 2H), 4.37 (s, 2H), 2.98 (s, 3H). MS (EI) *m/z* 282 [M – N<sub>2</sub>]<sup>+</sup>; HRMS calcd for C<sub>10</sub>H<sub>8</sub>F<sub>3</sub>O<sub>2</sub>S<sub>2</sub> [M – N<sub>2</sub>]<sup>+</sup>: 281.9996, Found 281.9951. Anal. Calcd for C<sub>10</sub>H<sub>8</sub>N<sub>2</sub>F<sub>3</sub>O<sub>2</sub>S<sub>2</sub>: C, 38.70; H, 2.92; N, 9.03. Found: C, 38.51; H, 2.71; N, 9.19.

#### Preparation of photoreactive GAPDH

Prior to the modification, rabbit muscle GAPDH (SIGMA-ALDRICH CO., USA) was treated with acid washed Charcoal (SIGMA-ALDRICH CO., USA) to remove NAD<sup>+</sup>. Ten-fold excess of diazirine reagent **1** (30 mM in DMSO) was added to the resulting apo-enzyme in 0.1 M Tris-HCl buffer containing 0.1mM EDTA (pH 8.5) and the mixture was kept at room temperature. After 1 h, the reaction mixture subjected to a gel filtration on Sephadex G-25 (2 x 20 cm, pyrophosphate pH 7.5, 0.1

mM EDTA, 4 °C) for removing the excess reagent. The GAPDH fractions were pooled and used in the photoaffinity capture experiments. Separately, the amount of introduced photoreactive group was determined from the absorption maximum at 360 nm using about ten times concentrated solution of the G-25 fraction.

### Preparation of cibacron blue 3GA immobilized polypropylene tube

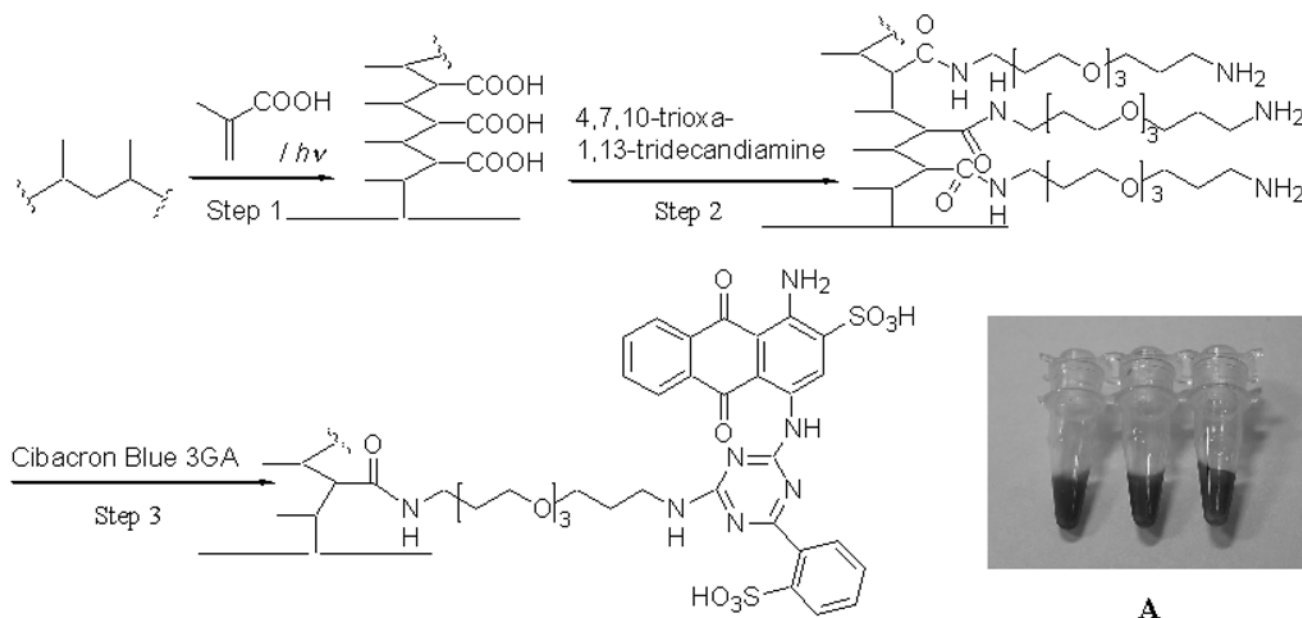


Figure SI-1. General procedure for the immobilization of Cibacron Blue 3GA on polymer tubes. A) A photograph of Cibacron Blue 3GA immobilized tubes.

Benzophenone (50 mg, 0.275 mmol) and methacrylic acid (118 mg, 1.375 mmol) were dissolved in Ar-flushed acetone (5.5 ml). 50  $\mu\text{l}$  aliquots of this solution was placed in each polypropylene tube (Nunc, IL, USA) and irradiated at 312 nm with a UV-irradiator (15 w lamp x 2) until the solution became a white solid (3 - 4 h) (Step 1). The photografted polypropylene tubes were successively washed with 1 M NaOH and 1 M HCl to result a surface carboxylated tube. For the construction of amino group, 50  $\mu\text{l}$  aliquots of 80% aqueous solution containing 4,7,10-trioxa-1,13-tridecanediamine (121 mg, 0.55 mmol), 0.3 M triethylamine, and 0.1 M 1-ethyl-3-(3-dimethylaminopropyl)-carbodiimide

hydrochloride was placed in each carboxyl tube and the tubes were allowed to react at room temperature for 5 h (Step 2). The amino modified tube were successively washed with 1 M HCl, 1 M NaOH, H<sub>2</sub>O, and methanol. 50 µl each of 0.1 M Cibacron Blue 3GA solution in 5.5 ml of coupling buffer (0.1 M sodium borate, pH 8.5, 0.15 M NaCl) was added to the amino modified tubes and were incubated at room temperature for 24 h (Step 3). The ligand immobilized tubes were successively washed with coupling buffer and water, then dried and stored at -20 °C until use. A photograph of the ligand immobilized tubes is shown in Figure SI-1 A.

### **Photoaffinity capture onto immobilized Cibacron Blue.**

The Cibacron immobilized tube was soaked with 50 mM Tris-HCl (pH 7.4) containing 0.3 M NaCl for 3 times before use. For preventing the nonspecific absorption of photoreactive GAPDH on the surface of polypropylene matrix, the tubes were preincubated for 5 h with 100 µl of blocking reagent (10% BSA in 50 mM Tris-HCl pH 7.4). Prior to the addition of photo-GAPDH, the excess BSA was removed by washing with 10 mM pyrophosphate buffer (pH 7.4) containing 0.1 mM EDTA. In the presence or absence of competitive ligands, 100 µl of photo-GAPDH solution (3 nmol) was incubated for 1 h at 37 °C. After the incubation, the tubes were irradiated at around 360 nm with a UV irradiator (15 w black-light lamp x 2) for 10 min at 0 °C. After that, the tubes were completely washed for three times with phosphate buffer saline (PBS) containing 0.1% Tween20, sonicated with 50mM Tris-HCl containing 0.15 M NaCl, 1% SDS (pH 7.4) for 20 min, and washed with 0.1% PBS containing Tween20. The tubes were kept with 100 µl of biotin *N*-hydroxysuccinimide (10 mM in 0.1M sodium carbonate containing 5% *N,N'*-dimethylformamide) for 2 h at room temperature. After that, the tubes were washed with *N,N'*-dimethylformamide and PBS. The tubes were then treated for blocking with 100 µl of 10% BSA in 50mM PBS (pH 7.4) at 37 °C for and incubated with 100 µl of streptavidin-horseradish peroxidase conjugate solution. The tubes were subjected to the conventional chemiluminescent detection using Immunostar Regents (Wako Pure Chemical Industries, Ltd. Japan).



# Synthesis and Evaluation of Water-Soluble Polymeric Bone-Targeted Drug Delivery Systems

Dong Wang,<sup>†</sup> Scott Miller,<sup>§</sup> Monika Sima,<sup>†</sup> Pavla Kopečková,<sup>†</sup> and Jindřich Kopeček<sup>\*,†,‡</sup>

Department of Pharmaceutics and Pharmaceutical Chemistry/CCCD, Department of Bioengineering, Department of Radiobiology, University of Utah, Salt Lake City, Utah 84112, USA. Received May 23, 2003

Four polymeric bone-targeting conjugates were synthesized based on poly(ethylene glycol) (PEG, two conjugates) and poly[*N*-(2-hydroxypropyl)methacrylamide] (PHPMA, two conjugates). The well-known bone-targeting compounds, alendronate and aspartic acid peptide, were used as bone-targeting moieties. Fluorescein isothiocyanate (FITC) was attached to the conjugates as a model drug for detection purposes. The bone-targeting potential of these conjugates was tested *in vitro* with hydroxyapatite (HA) and *in mice*. The data obtained indicated that these novel delivery systems could specifically accumulate in the bone tissue.

Bone is a highly specified form of connective tissue, which provides an internal support system in all vertebrates. It is also the major source of inorganic ions and actively participates in calcium homeostasis in the body (1). To maintain its normal function, bone is continuously being resorbed and rebuilt throughout the skeleton. In healthy individuals, bone resorption and formation are well balanced with the bone mass maintained in a steady state. Disturbances of this balance are characteristic of a number of bone diseases including osteoporosis, Paget's disease, osteopetrosis, bone cancer, etc. (2).

Over the past decade, our understanding of bone biology has improved dramatically (3, 4). Many molecules have been identified as new therapeutic agents for the treatment of bone diseases. Osteoprotegerin (OPG) (5), cathepsin K inhibitors (6), carbonic anhydrase II (CA2) inhibitors (7),  $\alpha\text{v}\beta 3$  integrin antagonists (8), and Src (protein tyrosine kinase pp60<sup>c-Src</sup>) homology 2 inhibitors (9) have been studied for their antiresorptive activities. Prostaglandin E series (10), prostaglandin E EP4 receptor agonists (11), statins (12), parathyroid hormone (PTH) (13), and growth factors [including transforming growth factor- $\beta$  (TGF- $\beta$ ), fibroblast growth factor (FGF), and bone morphogenetic protein (BMP)] (2) have all been considered for stimulation of bone growth. However, most of these therapeutic agents are not specific for bone, which can greatly hamper their clinical application to bone disease. The recent reports on the long-term effects of hormone replacement therapy (HRT) clearly demonstrated the adverse effects that can occur when bone therapeutic agents are not specifically targeted (14, 15).

The advantages of a bone-targeted drug delivery system for the treatment of bone diseases are obvious. Such a system could easily impart osteotropy to a

variety of bone drugs and improve their therapeutic potential. A few attempts have been made previously to target drugs to hard tissue. Tetracycline and its analogues were linked to different drugs to increase their affinity to bone (16–18). Bisphosphonates were conjugated to different macromolecules (protein, PEG<sup>1</sup>) and low molecular weight compounds to render them osteotropic (19–21). Recently, glutamic acid and aspartic acid peptides were reported being used as bone-targeting moieties to deliver drugs to the bone (22). (Scheme 1, structures of molecules with strong affinity to bone).

In the present study, we designed and synthesized water-soluble polymeric bone-targeting drug delivery systems based on PHPMA<sup>1</sup> and PEG. These systems may be used as universal vehicles for the targeted delivery of bone therapeutics. It is hypothesized that this will enable a wide variety of bone therapeutics to be covalently loaded onto these delivery systems via acid- or enzyme-cleavable spacers. Other benefits derived from these conjugates may include improved pharmacokinetic parameters, such as area under the curve (AUC), and the increased water solubility of hydrophobic drugs. In some

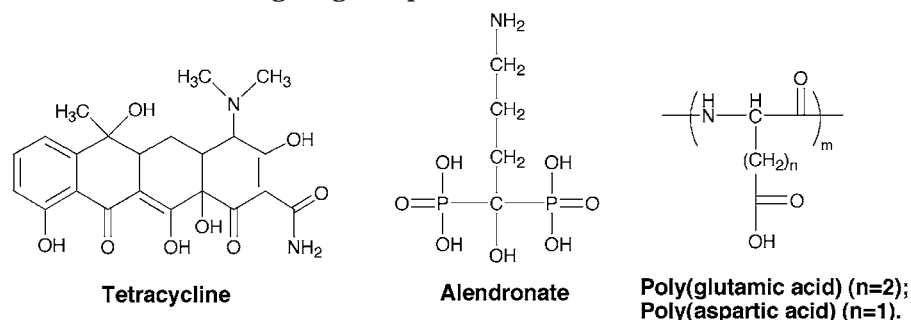
<sup>1</sup> Abbreviations: ACV, 4,4'-azobis(4-cyanopentanoic acid); D-(Asp)<sub>8</sub>, octapeptide D-aspartic acid; D-(Asp-OtBu)<sub>8</sub>, octapeptide D-aspartic acid  $\beta$ -*tert*-butyl ester; FITC-PEG-alendronate, PEG conjugate with one chain terminus linked to alendronate and the other linked to FITC; FITC-PEG-D-(Asp)<sub>8</sub>, PEG conjugate with one chain terminus linked to the N terminus of octapeptide D-aspartic acid and the other end linked to FITC; FITC-PEG-NHS, heterobifunctional PEG with FITC at one terminus and *N*-hydroxysuccinimide ester at the other; HA, hydroxyapatite; MA-FITC, *N*-methacryloylaminopropyl fluorescein thiourea; MA-GG-D-(Asp)<sub>8</sub>, *N*-methacryloylglycylglycyl-D-(aspartic acid)<sub>8</sub>; P-alendronate-FITC, conjugate of P-GG-ONp-FITC with alendronate where alendronate was linked to the polymer via Gly-Gly spacer; P-D-(Asp)<sub>8</sub>-FITC, copolymer of HPMA, MA-GG-D-(Asp)<sub>8</sub>, and MA-FITC; PEG, poly(ethylene glycol); PEG-FITC, hydrolyzed from FITC-PEG-NHS; P-GG-ONp-FITC, FITC (fluorescein isothiocyanate)-labeled HPMA [*N*-(2-hydroxypropyl)methacrylamide] copolymer containing *p*-nitrophenyl ester, where P is the HPMA copolymer backbone; P-FITC, aminolyzed from P-GG-ONp-FITC with 2-amino propanol; PHPMA, poly[*N*-(2-hydroxypropyl)methacrylamide]; TFA, trifluoroacetic acid;  $M_w$ , weight average molecular weight;

\* To whom correspondence should be addressed. University of Utah, Department of Pharmaceutics and Pharmaceutical Chemistry, 30 S 2000 E Rm. 301, Salt Lake City, UT 84112. Phone: + 801-581-4532. Fax: + 801-581-3674. E-mail: Jindrich.Kopecek@m.cc.utah.edu.

<sup>†</sup> Department of Pharmaceutics and Pharmaceutical Chemistry/CCCD.

<sup>‡</sup> Department of Bioengineering.

<sup>§</sup> Department of Radiobiology.

**Scheme 1. Structures of Some Bone-Targeting Compounds**

cases, these conjugates may also offer protection to therapeutic agents against degradation as they are transported to their target tissues (23).

Alendronate and aspartic acid peptide are well-documented bone-targeting compounds with strong bone-affinity and a primary amine useful for conjugation (19–22). These were selected as bone-targeting moieties in this study.

The conjugation of alendronate to P–GG–ONp–FITC<sup>1</sup> could only be carried out in aqueous solution due to the poor solubility of alendronate in all organic solvents. The conjugation proceeded with the gradual addition of NaOH solution to a solution of alendronate and P–GG–ONp–FITC at 25 °C. The conjugate was purified by column chromatography and dialysis, and then lyophilized.<sup>2</sup> A similar procedure was used for the synthesis of FITC–PEG–alendronate,<sup>1,3</sup> where FITC–PEG–NHS<sup>1</sup> (Nektar, formerly, Shearwater, Huntsville, AL) was used instead of P–GG–ONp–FITC. The content of alendronate in the conjugates was analyzed by HPLC, after hydrolysis with HCl (6 N) and a precolumn fluorochrome derivatization.

L-Aspartic acid hexapeptide has been used previously as a bone-targeting moiety (22). To ensure proper in vivo stability, D-aspartic acid octapeptide was used in this study.

A novel solid-phase synthesis (24) strategy was used for the synthesis of FITC–PEG–D-(Asp)<sub>8</sub>.<sup>1,4</sup> FITC–PEG–NHS was conjugated to the deprotected N-terminus of D-(Asp–OtBu)<sub>8</sub><sup>1</sup> with the C-terminus still anchored to the surface of trityl chloride resin. This was followed by TFA<sup>1</sup> cleavage to obtain the conjugate. With a similar strategy,

a polymerizable D-(Asp)<sub>8</sub><sup>1</sup> derivative, MA–GG–D-(Asp)<sub>8</sub>,<sup>1</sup> was synthesized<sup>5</sup> and copolymerized with HPMA and MA–FITC<sup>1</sup> to obtain P–D-(Asp)<sub>8</sub>–FITC.<sup>1,6</sup> These conjugates were purified by column chromatography and dialysis, and then lyophilized.

The D-(Asp)<sub>8</sub> content in these conjugates was determined by HPLC after hydrolysis with HCl (6 N) and precolumn fluorochrome derivatization. The structures of FITC–PEG–D-(Asp)<sub>8</sub> and MA–GG–D-(Asp)<sub>8</sub> were also confirmed using MALDI-TOF mass spectrometry (Supporting Information).

The characterization of all conjugates described above is summarized in Table 1. Their chemical structures are depicted in Schemes 2 and 3.

As shown in Table 1, 90% of FITC–PEG–D-(Asp)<sub>8</sub> chains have a D-(Asp)<sub>8</sub> oligopeptide attached, whereas all FITC–PEG–alendronate chains have an alendronate appended to the chain terminus. The *M<sub>w</sub>*<sup>1</sup> of HPMA copolymer conjugates was determined with size exclusion chromatography (SEC) using PBS (pH = 7.3) as eluent.

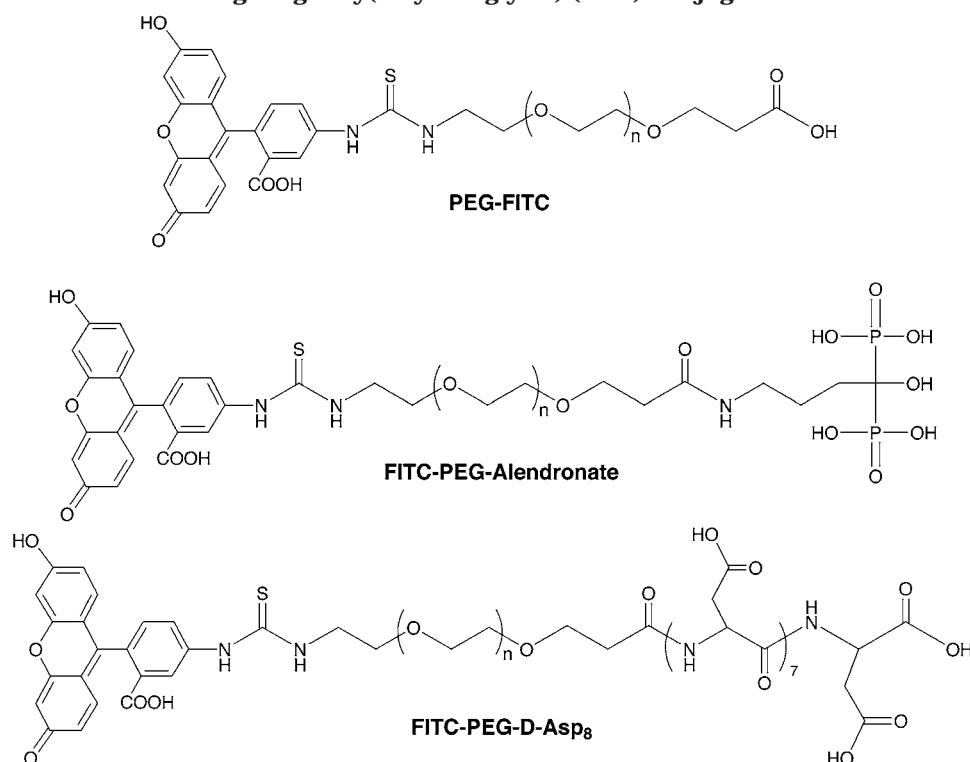
<sup>2</sup> Synthesis of P–alendronate–FITC. Alendronate (100 mg,  $3.08 \times 10^{-4}$  mol) was added in water (1 mL). With vigorous stirring of the sample, P–GG–ONp–FITC (50 mg, ONp =  $2.75 \times 10^{-5}$  mol, in 200  $\mu$ L of DMF) was dropped into the aqueous solution. NaOH (0.2 M) was then dropped into the solution. Slowly, the pH value was increased to 7. Then, in 1 h, it was further increased to 8. Afterward, the pH value was quickly raised to 9 to finish the reaction. Free ONp and alendronate were removed with PD-10 columns (Amersham Pharmacia Biotech, Piscataway, NJ). The conjugate was then dialyzed against water (MWCO 6 ~ 8 kDa). It was lyophilized to yield 36 mg of the titled product.

<sup>3</sup> Synthesis of FITC–PEG–alendronate. Alendronate (150 mg,  $4.6 \times 10^{-4}$  mol) was added in water (1 mL). With vigorous stirring of the sample, FITC–PEG–NHS (50 mg, NHS =  $2.5 \times 10^{-5}$  mol, in 200  $\mu$ L of DMF) was dropped into the aqueous solution. NaOH (0.2 M) was then dropped into the solution. Slowly, the pH value was increased to 7. Then, in 1 h, it was further increased to 8. Afterward, the pH value was quickly raised to 9 to finish the reaction. Free NHS and alendronate were removed with PD-10 columns (Amersham Pharmacia Biotech, Piscataway, NJ). The conjugate was then dialyzed against water (MWCO 2 kDa). It was lyophilized to yield 51.8 mg of the titled product, which was then analyzed with MALDI-TOF spectrometry (Supporting Information) and HPLC.

<sup>4</sup> Synthesis of FITC–PEG–D-(Asp)<sub>8</sub>. According to typical solid-phase peptide synthesis procedure (24), Fmoc–D-(Asp–OtBu) (67 mg, 0.162 mmol) was loaded onto trityl chloride resin (300 mg, 0.324 mmol of –Cl, 50% loading). Stepwise growing procedure was followed until all eight Fmoc–D-(Asp–OtBu) had been connected. As the NH<sub>2</sub> of the final Fmoc–D-(Asp–OtBu) was exposed by piperidine (20%), NHS–PEG–FITC (MW 2000, 400 mg, 0.2 mmol, in 2.5 mL DMF) and DIPEA (113  $\mu$ L, 0.648 mmol) were added. The suspension was transferred into an ampule, purge with N<sub>2</sub>, and sealed by flame. It was agitated gently for 2 days. Then the resin was dried and cleaved with TFA. The raw product was dialyzed (MWCO 2000) and further purified on FPLC with Superdex 75 column. About 90 mg of FITC–PEG–D-(Asp)<sub>8</sub> was obtained. The structure and purity of the conjugate were confirmed with MALDI-TOF mass spectrometry (Supporting Information) and amino acid analysis.

<sup>5</sup> Synthesis of MA–GG–D-(Asp)<sub>8</sub>. D-(Asp–OtBu)<sub>8</sub> protected peptide was synthesized on solid phase as described in footnote 4. After the NH<sub>2</sub> of the final Fmoc–D-(Asp–OtBu) was exposed with piperidine, MA–GG–ONp (260 mg, 0.810 mmol) and DIPEA (226  $\mu$ L, 1.296 mmol) were added (in 1.5 mL DMF). It was transferred into a vial and rotated overnight. The resin was then washed thoroughly, and the product was cleaved off with TFA. The product was then purified with a Superdex 75 column to yield about 70 mg of MA–GG–D-(Asp)<sub>8</sub>. The *m/z* (MALDI-TOF, negative ion) of the product is 1119.24 (calculated 1119.89).

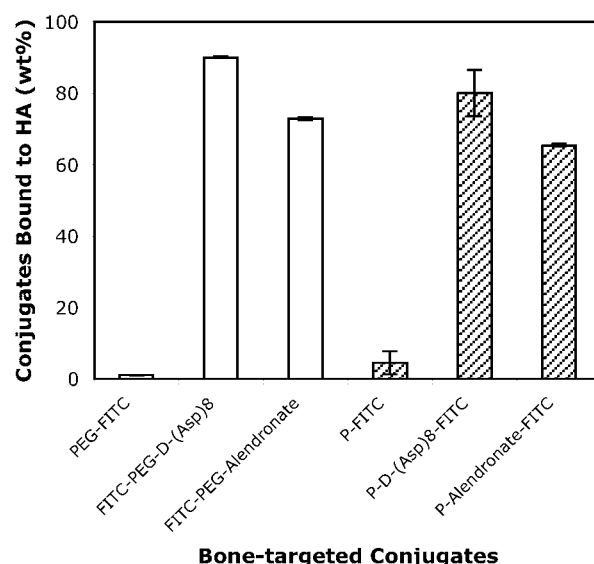
<sup>6</sup> Synthesis of P–D-(Asp)<sub>8</sub>–FITC. HPMA (50 mg,  $3.5 \times 10^{-4}$  mol) and MA–FITC (2.5 mg,  $4.6 \times 10^{-6}$  mol) were dissolved in DMSO (0.5 mL), and it was mixed with the aqueous solution (1 mL) of MA–GG–D-(Asp)<sub>8</sub> (20 mg,  $1.79 \times 10^{-5}$  mol) and ACV (5.8 mg,  $2.07 \times 10^{-5}$  mol). The solution was then purged with N<sub>2</sub> and sealed in an ampule for polymerization. It was polymerized at 50 °C for 18 h. The solution was then diluted and purified with PD-10 columns and dialyzed against water (MWCO 6~8 kDa). The polymer was then further purified with FPLC (Superdex 75). The polymer fraction was dialyzed and finally obtained 44 mg of P–D-(Asp)<sub>8</sub>–FITC.

**Scheme 2. Structures of Bone-Targeting Poly(ethylene glycol) (PEG) Conjugates****Table 1. Characterization of Polymeric Bone-Targeting Conjugates**

conjugates	MW <sup>a</sup> (kDa)	bone-targeting moiety content	
		mol/g	no./chain <sup>e</sup>
PEG-FITC <sup>b</sup>	2.4		
FITC-PEG-alendronate <sup>b</sup>	2.6	$4.3 \times 10^{-4}$	1
FITC-PEG-D-Asp <sub>8</sub> <sup>b</sup>	3.4	$2.6 \times 10^{-4}$	0.9
P-FITC <sup>c</sup>	17		
P-alendronate-FITC <sup>c</sup>	35	$6.5 \times 10^{-5}$	1.1
P-D-(Asp) <sub>8</sub> -FITC <sup>d</sup>	58	$7.6 \times 10^{-5}$	1–2

<sup>a</sup> Weight average molecular weights ( $M_w$ ) of PEG conjugates were determined with MALDI-TOF mass spectrometry (see spectra in Supporting Information);  $M_w$  of HPMA copolymer conjugates were determined with SEC using PHPMA calibrations.  $M_w$  for P-alendronate-FITC and P-D-Asp<sub>8</sub>-FITC are apparent values, which are much higher due to the increase ionic osmotic pressures by introduction of electrolytes. <sup>b</sup> Synthesized from the same precursor of NHS-PEG-FITC (MW 2.4 kDa), PEG-FITC was hydrolyzed with H<sub>2</sub>O directly from the precursor. <sup>c</sup> Synthesized from the same precursor of P-ONp-FITC, P-FITC was directly aminolyzed with 1-amino-2-propanol from the precursor. The real  $M_w$  for P-alendronate-FITC is ~17 kDa, similar to that of P-FITC. <sup>d</sup> Synthesized by copolymerization of HPMA, MA-FITC, and MA-GG-D-(Asp)<sub>8</sub>. Its estimated real  $M_w$  is 20–30 kDa. <sup>e</sup> Calculated according to the equation: no./chain = bone-targeting moiety content (mol/g)  $\times$   $M_w$  (real).

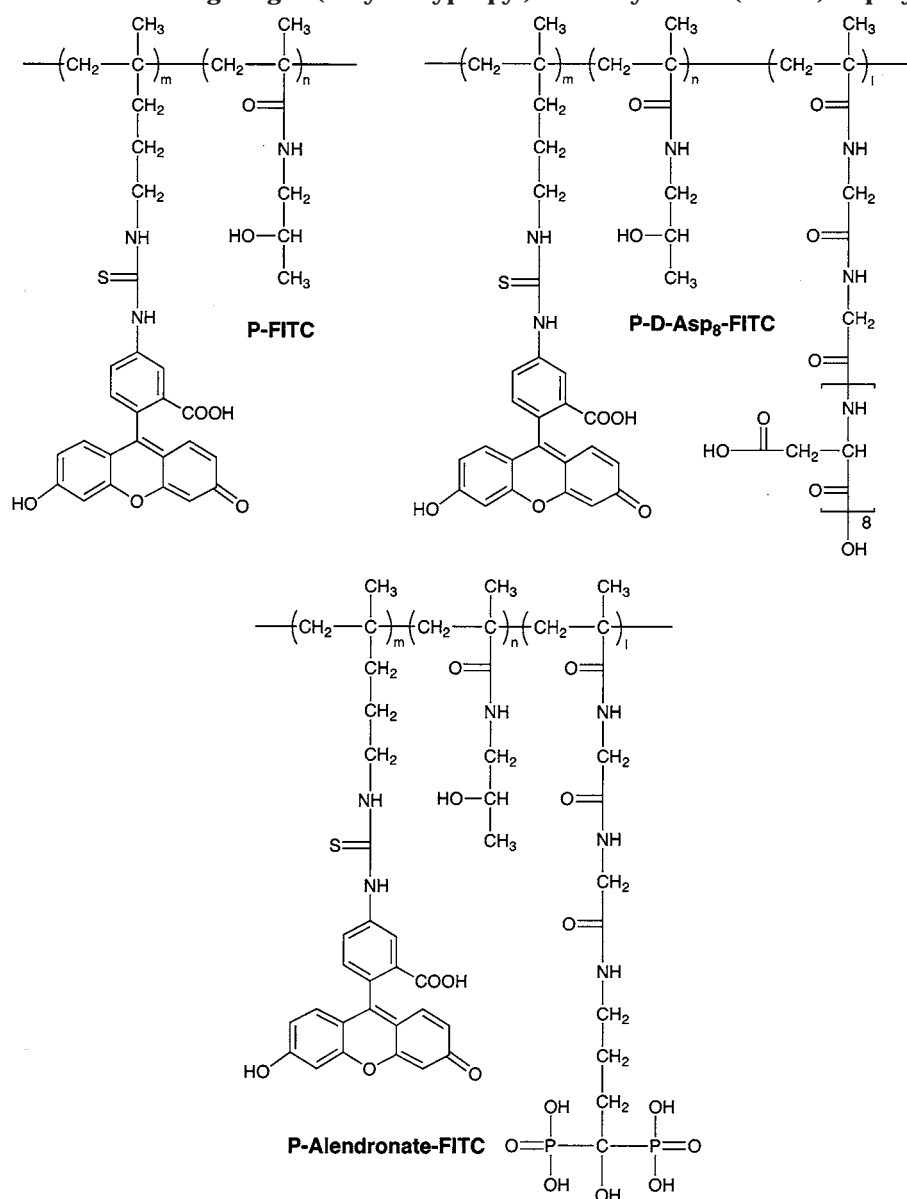
The apparent increase in molecular weight of the conjugates when compared to unmodified macromolecules is likely an artifact and the result of increased hydrodynamic volumes of the modified polymers. This may be attributed to increased ionic osmotic pressures by the introduction of electrolytes [targeting moieties, alendronate and D-(Asp)<sub>8</sub>]. P-alendronate-FITC<sup>1</sup> and P-FITC<sup>1</sup> were prepared from the same polymer precursor, P-GG-ONp-FITC ( $M_w$  = 17 kDa). Therefore, they have a similar real  $M_w$  (17 kDa). However, the apparent  $M_w$  of P-alendronate-FITC was almost doubled compared to the unmodified polymer. The HPLC analysis of the hydrolyzed P-alendronate-FITC showed that the alen-



**Figure 1.** The binding of polymeric bone-targeted conjugates to hydroxyapatite. Conjugates were dissolved in phosphate buffered saline (pH = 7.4) with a concentration of 1 mg/mL. The conjugate solution (100  $\mu$ L) and 100  $\mu$ L of the same buffer was incubated with 5 mg of hydroxyapatite powder (HA, Bio-Gel HTP, DNA grade; BIO-RAD, Hercules, CA) in an eppendorf tube for 1 h at RT. Then the HA suspension was centrifuged. The UV absorbance at 490 nm of the supernatant was monitored with a microplate reader. Background correction was applied. Data are shown as the mean standard deviation from triplicate measurements.

dronate content in the conjugate was  $4.3 \times 10^{-4}$  mol/g. Conversion to units of number of alendronate molecule per chain produced a value of 1.1 [using the equation of no./chain = bone-targeting moiety content (mol/g)  $\times$   $M_w$  (real)]. Due to the increased ionic osmotic pressure possibly caused by the introduction of D-(Asp)<sub>8</sub>, the real  $M_w$  of P-D-(Asp)<sub>8</sub>-FITC can be expected to be much lower than its apparent value of 58 kDa. Under similar



**Scheme 3. Structures of Bone-Targeting *N*-(2-Hydroxypropyl)methacrylamide (HPMA) Copolymer Conjugates**

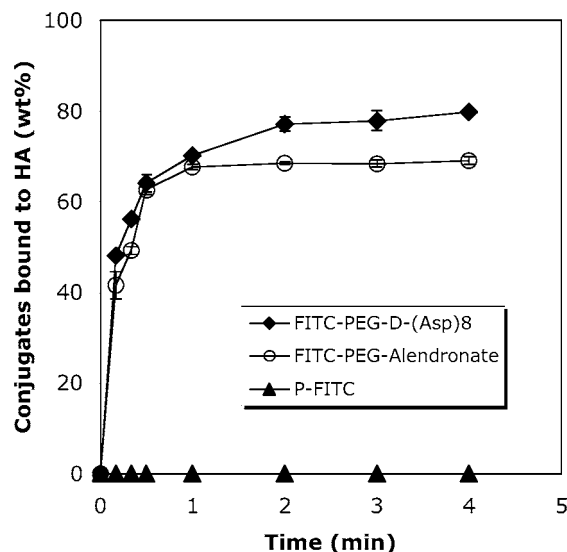
conditions, the copolymerization of HPMA and MA-FITC should yield a copolymer with an  $M_w$  of 30 kDa. Therefore, we estimate that the real  $M_w$  of P-D-(Asp)<sub>8</sub>-FITC was between 20 and 30 kDa. Since amino acid analysis of the conjugate revealed a D-(Asp)<sub>8</sub> content of  $2.6 \times 10^{-4}$ , the number of D-(Asp)<sub>8</sub> per polymer chain was estimated to be between 1 and 2 [no./chain = bone-targeting moiety content (mol/g)  $\times M_w$  (real)].

All conjugates (Table 1) were screened *in vitro* for their bone-targeting capacity using HA<sup>1</sup> powder as a model bone surface. Both bone-targeted PEG conjugates showed good binding to HA, whereas PEG-FITC<sup>1</sup> (control polymer without targeting moiety) showed no binding to HA (Figure 1). About 90% of FITC-PEG-D-(Asp)<sub>8</sub> was bound to HA, which correlated well with the fact that 90% of the FITC-PEG-D-(Asp)<sub>8</sub> chain contains D-(Asp)<sub>8</sub> (Table 1). However, only 73% of FITC-PEG-alendronate bound to HA, though each polymer chain contains an alendronate moiety (Table 1). It has been proposed (22, 25) that the domain of -COOH groups in the aspartic acid peptide and the two neighboring phosphate groups in bisphosphonate are good ligands for chelation with calcium ions. Possibly, the structure of D-(Asp)<sub>8</sub> may provide more

potential binding sites with HA surface calcium (multivalent binding) than alendronate, which contributed to its higher binding efficiency.

Analogous to the PEG conjugates, bone-targeted HPMA copolymer conjugates also showed strong binding to HA, while the control polymer (P-FITC) yielded only non-specific binding to HA (Figure 1). The higher HA binding efficiency of P-D-(Asp)<sub>8</sub>-FITC (80%) than that of P-alendronate-FITC (66%) may also be attributed to the stronger binding of D-(Asp)<sub>8</sub> compared to alendronate. However, the contribution of multiple targeting moieties per chain in the case of P-D-(Asp)<sub>8</sub>-FITC is another possibility.

The binding of the conjugates to the surface of HA was observed to occur very quickly. The result of the initial binding kinetic was shown in Figure 2. The binding of FITC-PEG-alendronate reached a plateau in 2–3 min with 69% of the conjugate bound to HA. Prolonged incubation of the conjugate with HA did not significantly improve binding efficiency (1 h, 73%, Figure 1). On the other hand, although FITC-PEG-D-(Asp)<sub>8</sub> showed a similar pattern of HA binding in the first minute, its binding continued to climb to 80% at the end of 4 min.



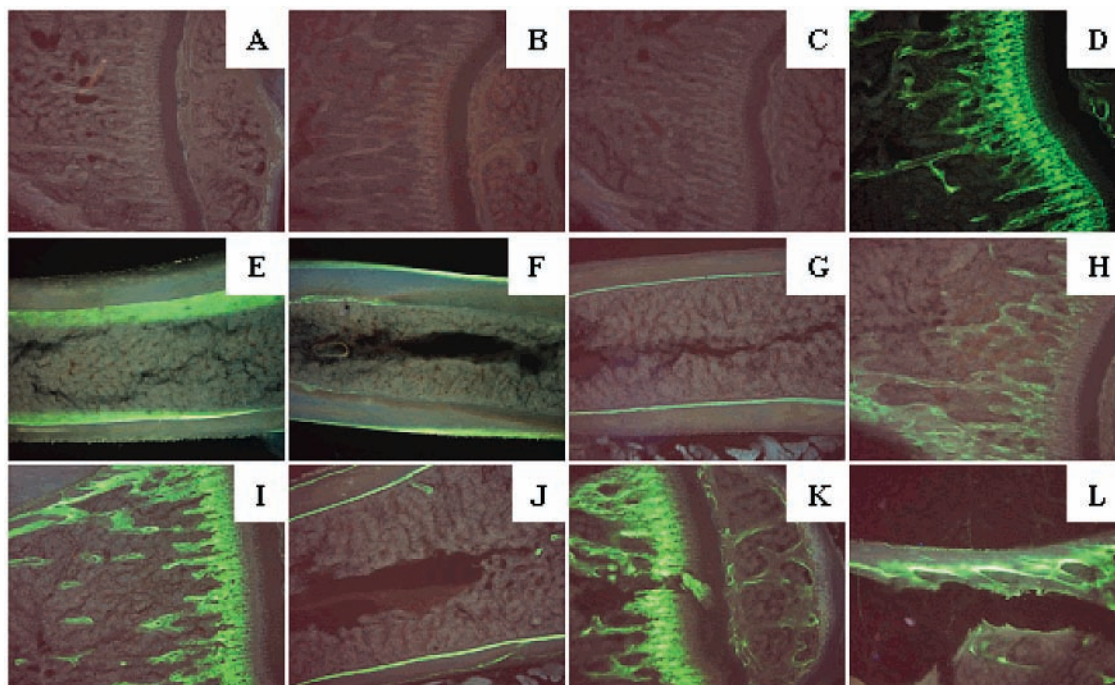
**Figure 2.** The initial binding kinetics of polymeric bone-targeted conjugates to hydroxyapatite. Conjugates were dissolved in phosphate buffered saline (pH = 7.4) with a concentration of 1 mg/mL. The conjugate solution (100  $\mu$ L) and 100  $\mu$ L of the same buffer was incubated with 5 mg of hydroxyapatite powder (HA, Bio-Gel HTP, DNA grade; BIO-RAD, Hercules, CA) at RT. At selected time intervals, the incubation was stopped by centrifugation. The UV absorbance at 490 nm of the supernatant was monitored with a microplate reader. Background correction was applied. Data are shown as the mean standard deviation from triplicate measurements.

Prolonged incubation of the FITC-PEG-D-(Asp)<sub>8</sub> with HA for 1 h led to an ultimate binding equilibrium of 90% bound. Further study is needed to understand the mechanism of these phenomena.

The bone-targeting capacity of the conjugates was evaluated *in vivo*. Balb/c mice (~20 g, male, Charles River Laboratories, Inc., Wilmington, MA) were injected i.v. (tail vein) with conjugates using an FITC dose of  $1.84 \times 10^{-5}$  mol/kg. All animals remained active with normal food and water consumption after the injection. Twenty-four hours later, the animals were sacrificed with a halothane overdose. Femurs and tibias were isolated, processed, and subjected to fluorescence microscopic analysis.

No autofluorescence was observed in the animals injected with saline (Figure 3A). In those injected with nontargeted conjugates P-FITC and PEG-FITC (Figure 3B,C), no fluorescence labeling was observed either, which indicated the absence of the FITC-labeled polymers in the bone. In contrast, all bones of animals injected with FITC-labeled bone-targeting conjugates showed bright fluorescence. Both the epiphysis and diaphysis were labeled with fluorescence. A detailed examination indicated the strongest labeling around the epiphyseal plate and the diaphyseal funnel. In addition, both the endosteum and periosteum of the diaphyseal shaft were marked with clear lines of FITC label (Figure 3D–L). It appeared that the bone-targeting delivery systems preferred to accumulate in sites associated with high rates of bone turnover, perhaps in tissues where blood supplies are abundant.

The *in vivo* binding of bone-targeting conjugates to hard tissue is much more complicated than the *in vitro* HA binding. Molecular weight and the negative charges of the conjugates have great influence on their clearance from the blood circulation via kidney glomerular filtration and liver uptake (negatively charged macromolecules can be recognized by scavenger receptor on nonparenchymal



**Figure 3.** The *in vivo* binding of polymeric bone-targeted conjugates to the bone. Bone samples were fixed with formalin, dehydrated with acetone, embedded in poly(methyl methacrylate), and sliced with a low speed diamond saw to the thickness of 100  $\mu$ m and mounted onto a plastic cover slide for observation under a fluorescence microscope (Olympus BX41, Olympus America Corp., Mellville, NY.). All images were taken under similar microscope settings. Histological nomenclature for different parts of the long bone described below can be found in ref 33. (A) Saline injection; (B) P-FITC; (C) PEG-FITC; (D) FITC-PEG-alendronate, metaphyseal primary and secondary spongiosa labeled; (E) FITC-PEG-alendronate, endosteum of diaphyseal shaft labeled; (F) FITC-PEG-alendronate, endosteum and periosteum of diaphyseal shaft labeled; (G) FITC-PEG-D-(Asp)<sub>8</sub>, endosteum of diaphyseal shaft labeled; (H) FITC-PEG-D-(Asp)<sub>8</sub>, metaphyseal spongiosa and cortex labeled; (I) P-alendronate-FITC, metaphyseal spongiosa and cortex labeled; (J) P-alendronate-FITC, endosteum and periosteum of diaphyseal shaft labeled; (K) P-D-(Asp)<sub>8</sub>-FITC, primary spongiosa and epiphysis labeled; (L) P-D-(Asp)<sub>8</sub>-FITC, endosteum of diaphyseal shaft labeled.

cells) (26, 27). The saturated calcium ions in blood could be another important factor in the bone-binding process of these conjugates. It was reported that the addition of calcium ion would enhance the adsorption of polyphosphonate onto the surface of HA. Possibly, the calcium ion binding with the polyphosphonate would enhance the collapse of the macromolecule and consequently promote HA adsorption (28). Likely, this may also apply to FITC-PEG-D-(Asp)<sub>8</sub> and P-D-(Asp)<sub>8</sub>-FITC because of their multiple charges per chain. However, both alendronate conjugates may not benefit from this due to the existence of only one alendronate on each conjugate. Apparently, conjugates binding with free calcium ions in blood may still be able to bind to the HA surface in bone. Hypothetically, it could be an energy-favorable process, in which the phosphonate or carboxylic acid groups in the conjugates would release the bound calcium ion, exchange with HA-surface phosphate, and bind to surface calcium. It is also noteworthy that the vasculature in bone is unusually porous. Because of the fenestrated capillaries or sinusoids (29) in the bone with pore size of 80–100 nm, the extravasation of the bone-targeting conjugates described here (diameter < 10 nm) (30, 31) into the bone fluid should not be hampered.

As shown in Figure 3G,H, the *in vivo* binding of FITC-PEG-D-(Asp)<sub>8</sub> to bone seems to be lower compared to the other conjugates. Most likely, this could be attributed to the high liver clearance of the conjugate from the blood circulation due to its highly negatively charged D-(Asp)<sub>8</sub> and relatively low molecular weight of PEG (2.4 kDa), which direct the conjugate to scavenger receptor. In the case of P-D-(Asp)<sub>8</sub>-FITC, 1–2 D-(Asp)<sub>8</sub> chains were introduced as side chains to the relatively high molecular weight HPMA copolymer (58 kDa). Therefore, the negative charges of D-(Asp)<sub>8</sub> may be moderately shielded and the steric hindrance of HPMA copolymer could prevent its recognition by the scavenger receptors. It is also possible that the higher molecular weight of P-D-(Asp)<sub>8</sub>-FITC could ensure a longer circulation time, which contributes to its better bone binding efficiency as well. Nevertheless, further biodistribution study is necessary to have a clear understanding of the bone-targeting efficiency of these conjugates.

In summary, bone-targeting polymeric drug delivery systems based on PEG and HPMA copolymer were successfully synthesized. Alendronate and octapeptide D-aspartic acid were introduced into the delivery system as bone-targeting moieties by either direct conjugation or copolymerization. *In vitro* and *in vivo* studies indicated that alendronate- and D-(Asp)<sub>8</sub>-based conjugates were promising candidates for bone-targeted delivery of therapeutic agents.

#### ACKNOWLEDGMENT

This work was supported in part by NIH Grant EB00251. Mass spectral data were acquired at the University of Utah Mass Spectrometry Facility, supported in part by NIH Grant P30 CA42014.

**Supporting Information Available:** MALDI-TOF mass spectra of PEG conjugates. This material is available free of charge via Internet at <http://pubs.acs.org/BC>.

#### LITERATURE CITED

- (1) Marks, S. C., Jr., and Odgren, P. R. (2002) Structure and Development of the Skeleton. *Principles of Bone Biology*, 2nd ed. (J. P. Bilezikian, L. G. Raisz, and G. A. Rodan, Eds.) pp 3–15, Academic Press, San Diego.
- (2) Odgren, P. R., and Martin, T. J. (2000) Therapeutic approaches to bone diseases. *Science* 289, 1508–1514.
- (3) Ducy, P., Zhang, R., Geoffroy, V., Ridall, A. L., and Karsenty, G. (1997) *Osf2/Cbfa1*: a transcriptional activator of osteoblast differentiation. *Cell* 89, 747–754.
- (4) (a) Takahashi, N., Udagawa, N., Takami, M. and Suda, T. (2002) Cells of Bone: Osteoclast Generation. *Principles of Bone Biology*, 2nd ed. (J. P. Bilezikian, L. G. Raisz, and G. A. Rodan, Eds.) pp 109–126, Academic Press, San Diego. (b) Väänänen, K., and Zhao, H. (2002) Osteoclast Function: Biology and Mechanism. *Principles of Bone Biology*, 2nd ed. (J. P. Bilezikian, L. G. Raisz, and G. A. Rodan, Eds.) pp 127–139, Academic Press, San Diego.
- (5) Capparelli, C., Kostenuik, P. J., Morony, S., Starnes, C., Weimann, B., Van, G., Scully, S., Qi, M., Lacey, D. L., and Dunstan, C. R. (2000) Osteoprotegerin prevents and reverses hypercalcemia in a murine model of humoral hypercalcemia of malignancy. *Cancer Res.* 60, 783–787.
- (6) Yamashita, D. S., and Dodds, R. A. (2000) Cathepsin K and the design of inhibitors of cathepsin K. *Curr. Pharm. Des.* 6, 1–24.
- (7) Minkin, C., and Jennings, J. M. (1972) Carbonic anhydrase and bone remodeling: sulfonamide inhibition of bone resorption in organ culture. *Science* 176, 1031–1033.
- (8) Engleman, V. W., Nickols, G. A., Ross, F. P., Horton, M. A., Griggs, D. W., Settle, S. L., Ruminski, P. G., and Teitelbaum, S. L. (1997) A peptidomimetic antagonist of the  $\alpha\beta 3$  integrin inhibits bone resorption *in vitro* and prevents osteoporosis *in vivo*. *J. Clin. Invest.* 99, 2284–2292.
- (9) Shakespeare, W., Yang, M., Bohacek, R., Cerasoli, F., Stebbins, K., Sundaramoorthi, R., Azimioara, M., Vu, C., Pradeepan, S., Metcalf III, C., Haraldson, C., Merry, T., Dalgarno, D., Narula, S., Hatada, M., Lu, X., van Schravendijk, M. R., Adams, S., Violette, S., Smith, J., Guan, W., Bartlett, C., Herson, J., Iuliucci, J., Weigle, M., and Sawyer, T. (2000) Structure-based design of an osteoclast-selective, nonpeptide Src homology 2 inhibitor with *in vivo* antiresorptive activity. *Proc. Natl. Acad. Sci. U.S.A.* 97, 9373–9378.
- (10) Miller, S. C., and Marks, S. C., Jr. (1994) Effects of prostaglandins on the skeleton. *Clin. Plast. Surg.* 21, 393–400.
- (11) Yoshida, K., Oida, H., Kobayashi, T., Maruyama, T., Tanaka, M., Katayama, T., Yamaguchi, K., Segi, E., Tsuboyama, T., Matsushita, M., Ito, K., Ito, Y., Sugimoto, Y., Ushikubi, F., Ohuchida, S., Kondo, K., Nakamura, T., and Narumiya, S. (2002) Stimulation of bone formation and prevention of bone loss by prostaglandin E EP4 receptor activation. *Proc. Natl. Acad. Sci. U.S.A.* 99, 4580–4585.
- (12) Mundy, G., Garrett, R., Harris, S., Chan, J., Chen, D., Rossini, G., Boyce, B., Zhao, M., and Gutierrez, G. (1999) Stimulation of bone formation *in vitro* and *in rodents* by statins. *Science* 286, 1946–1949.
- (13) Lindsay, R., and Nieves, J. (1997) Randomized controlled study of effect of parathyroid hormone on vertebral-bone mass and fracture incidence among postmenopausal women on estrogen with osteoporosis. *Lancet* 350, 550–555.
- (14) Rossouw, J. E., Anderson, G. L., Prentice R. L., LaCroix A. Z., Kooperberg C., Stefanick M. L., Jackson R. D., Beresford S. A., Howard B. V., Johnson K. C., Kotchen J. M., and Ockene J. (2002) Risks and benefits of estrogen plus progestin in healthy postmenopausal women. *J. Am. Med. Assoc.* 288, 321–333.
- (15) Lacey, J. V., Jr., Mink, P. J., Lubin, J. H., Sherman, M. E., Troisi, R., Hartge, P., Schatzkin, A., and Schairer, C. (2002) Menopausal hormone replacement therapy and risk of ovarian cancer. *J. Am. Med. Assoc.* 288, 334–341.
- (16) Pierce, W. M., Jr., and Waite, L. C. (1984) Bone-targeted carbonic anhydrase inhibitors: effect of a proinhibitor on bone resorption *in vitro*. *Proc. Soc. Exp. Bio. Med.* 186, 96–102.
- (17) Orme, M. W., and Labroo, V. M. (1994) Synthesis of  $\beta$ -estradiol-3-benzoate-17-(succinyl-12a-tetracycline): a potential bone-seeking estrogen. *Bioorg. Med. Chem. Lett.* 4, 1375–1380.
- (18) Wilson, T. M., Charifson, P. S., Baxter, A. D., and Geddie, N. G. (1996) Bone-targeted drugs. 1. Identification of het-



- erocycles with hydroxyapatite affinity. *Bioorg. Med. Chem. Lett.* **6**, 1043–1046.
- (19) Bentz, H., and Rosen, D. (1992) Targeted delivery of bone growth factors. EP 0 512 844 A1.
- (20) Uludag, H., and Yang, J. (2002) Targeting systemically administered proteins to bone by bisphosphonate conjugation. *Biotechnol. Prog.* **18**, 604–611.
- (21) Verbeke, K., Rozenski, J., Cleynhens, B., Vanbilloen, H., de Groot, T., Weyns, N., Bormans, G., and Verbruggen, A. (2002) Development of a conjugate of  $^{99m}\text{Tc}$ -EC with aminomethylenediphosphonate in the search for a bone tracer with fast clearance from soft tissue. *Bioconj. Chem.* **13**, 16–22.
- (22) Yokogawa, K., Miya, K., Sekido, T., Higashi, Y., Nomura, M., Fujisawa, R., Morito, K., Masamune, Y., Waki, Y., Kasugai, S., and Miyamoto, K. (2001) Selective delivery of estradiol to bone by aspartic acid oligopeptide and its effects on ovariectomized mice. *Endocrinology* **142**, 1228–1233.
- (23) Kozak, K. R., Crews, B. C., Ray, J. L., Tai, H. H., Morrow, J. D., and Marnett, L. J. (2001) Metabolism of prostaglandin glycerol esters and prostaglandin ethanolamides in vitro and in vivo. *J. Biol. Chem.* **276**, 36993–36998.
- (24) Chan, W. C., and White, P. D. (2000) Basic Procedures. *Fmoc Solid-Phase Peptide Synthesis, A Practical Approach*. (W. C. Chan and P. D. White, Eds.) pp 41–74, Oxford University Press Inc., New York.
- (25) Lin, J. H. (1996) Bisphosphonates: a review of their pharmacokinetic properties. *Bone* **18**, 75–85.
- (26) Yoshida, M., Mahato, R. I., Kawabata, K., Takakura, Y., and Hashida, M. (1996) Disposition characteristics of plasmid DNA in the single-pass rat liver perfusion system. *Pharm. Res.* **13**, 599–603.
- (27) Fujiwara, M., Baldeschwieler, J. D., and Grubbs, R. H. (1996) Receptor-mediated endocytosis of poly(acrylic acid)-conjugated liposomes by macrophages. *Biochim. Biophys. Acta* **1278**, 59–67.
- (28) Rawls, H. R., and Cabasso, I. (1982) Adsorption of Phosphorylated Polyelectrolytes on Hydroxyapatite. *Adsorption on and Surface Chemistry of Hydroxyapatite* (D. N. Misra, Ed.) pp 115–128, Plenum Press, New York.
- (29) Tye, C. E., Ratray, K. R., Warner, K. J., Gordon, J. A., Sodek, J., Hunter, G. K., and Goldberg, H. A. (2003) Delineation of the hydroxyapatite-nucleating domains of bone sialoprotein. *J. Biol. Chem.* **278**, 7949–7955.
- (30) Howlett, C. R., Dickson, M., and Sheridan, A. K. (1984) The fine structure of the proximal growth plate of the avian tibia: vascular supply. *J. Anat.* **139**, 115–132.
- (31) Ghandehari, H., Smith, P. L., Ellens, H., Yeh, P.-Y., and Kopeček, J. (1997) Size-dependent permeability of hydrophilic probes across rabbit colonic epithelium. *J. Pharm. Exp. Ther.*, **280**, 747–753.
- (32) Seymour, L. W., Duncan, R., Strohalm, J., and Kopeček, J. (1987) Effect of molecular weight ( $M_w$ ) of *N*-(2-hydroxypropyl)methacrylamide copolymers on body distribution and rate of excretion after subcutaneous, intraperitoneal, and intravenous administration to rats. *J. Biomed. Mater. Res.* **21**, 1341–1358.
- (33) Junqueira, L. C., Carneiro, J., and Kelley R. O. (1995) Bone. *Basic Histology*, 8th ed. (L. C. Junqueira, J. Carneiro, and R. O. Kelley, Eds.) pp 132–151, Appleton & Lange, Connecticut.

BC034090J

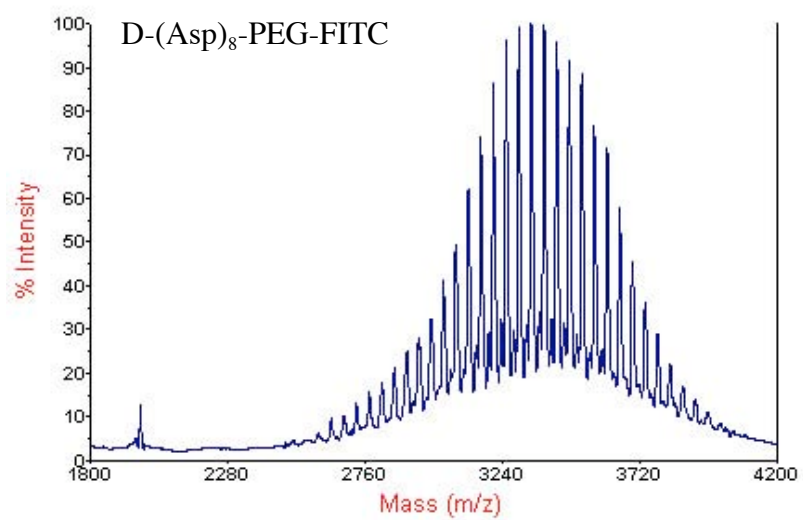
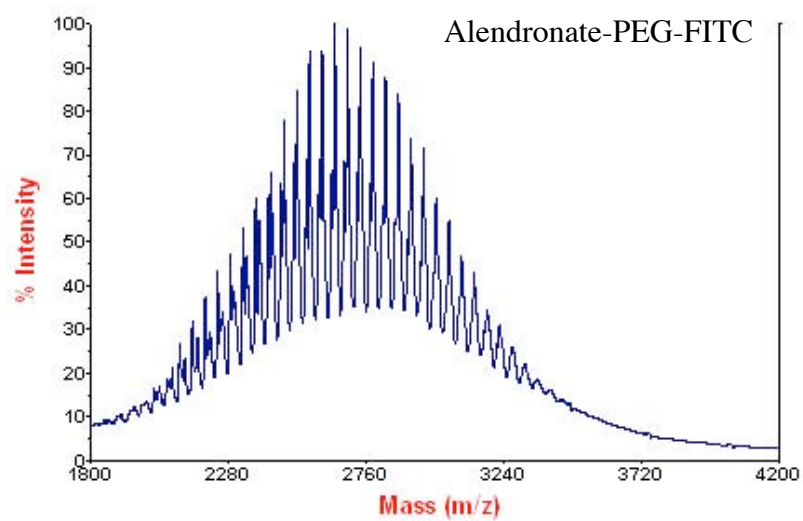
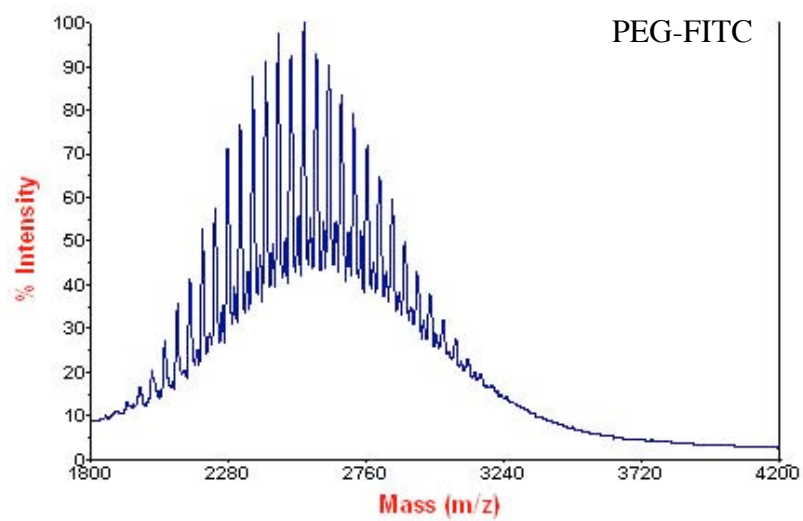
# **SUPPORTING INFORMATION**

## **SYNTHESIS AND EVALUATION OF WATER-SOLUBLE POLYMERIC BONE-TARGETED DRUG DELIVERY SYSTEM**

Dong Wang<sup>†</sup>, Scott Miller<sup>§</sup>, Monika Sima<sup>†</sup>, Pavla Kopečková<sup>†</sup>, Jindřich Kopeček<sup>†‡</sup>

<sup>†</sup>Department of Pharmaceutics and Pharmaceutical Chemistry/CCCD, <sup>‡</sup>Department of Bioengineering, <sup>§</sup>Department of Radiobiology, University of Utah, Salt Lake City, UT 84112, USA.

MALDI-TOF mass spectra of PEG conjugates





# ARTICLES

## Improved Yield and Stability of L49-sFv- $\beta$ -Lactamase, a Single-Chain Antibody Fusion Protein for Anticancer Prodrug Activation, by Protein Engineering

Charlotte F. McDonagh,\* Kevin S. Beam, Gabrielle J. S. Wu, Judy H. Chen, Dana F. Chace, Peter D. Senter, and Joseph A. Francisco

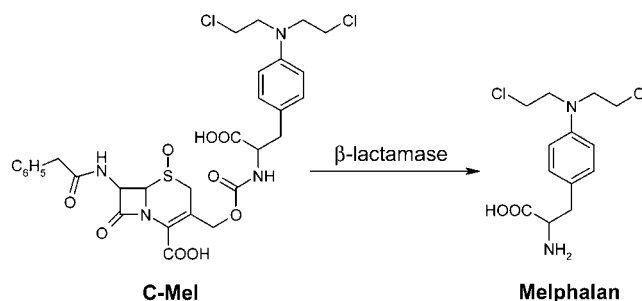
Seattle Genetics Inc., 21823 30th Drive SE, Bothell, Washington 98021. Received March 3, 2003; Revised Manuscript Received May 2, 2003

The L49 single-chain Fv fused to  $\beta$ -lactamase (L49-sFv-bL) combined with the prodrug C-Mel is an effective anticancer agent against tumor cells expressing the p97 antigen. However, large-scale production of L49-sFv-bL from refolded *E. coli* inclusion bodies has been problematic due to inefficient refolding and instability of the fusion protein. Sequence analysis of the L49-sFv framework regions revealed three residues in the framework regions at positions L2, H82B, and H91, which are not conserved for their position, occurring in <1% of sequences in Fv sequence databases. One further unusual residue, found in <3% of variable sequences, was observed at position H39. Each unusual residue was mutated to a conserved residue for its position and tested for refolding yield from inclusion bodies following expression in *E. coli*. The three V<sub>H</sub> single mutants showed improvement in the yield of active protein and were combined to form double and triple mutants resulting in a 7–8-fold increased yield compared to the parental protein. In an attempt to further improve yield, the orientation of the triple mutant was reversed to create a bL–L49-sFv fusion protein resulting in a 3-fold increase in expressed inclusion body protein and producing a 20-fold increase in the yield of purified protein compared to the parental protein. The triple mutants in both orientations displayed increased stability in murine plasma and binding affinity was not affected by the introduced mutations. Both triple mutants also displayed potent in vitro cytotoxicity and in vivo antitumor activity against p97 expressing melanoma cells and tumor xenografts, respectively. These results show that a rational protein-engineering approach improved the yield, stability, and refolding characteristics of L49-sFv-bL while maintaining binding affinity and therapeutic efficacy.

### INTRODUCTION

Antibody-directed enzyme prodrug therapy (ADEPT) is a two-step approach to cancer therapy in which monoclonal antibodies (mAbs) are used for the delivery of enzymes to tumor-cell surfaces. The localized enzymes are able to activate subsequently administered prodrugs into active anticancer agents, which can then penetrate into cells and exert cytotoxic activities (1). L49-sFv-bL is a recombinant fusion protein composed of a single-chain Fv derived from the L49 mAb and a mutated form of the *Enterobacter cloacae*  $\beta$ -lactamase (bL) (2). The L49 mAb recognizes the p97 melanotransferrin antigen expressed by human melanomas and some carcinomas (3). The  $\beta$ -lactamase enzyme rapidly catalyzes the hydrolysis of cephalosporin-containing prodrugs as melphalan (4) (Figure 1), nitrogen mustards (5), vinca derivatives (6), paclitaxel (7), doxorubicin (8), and mitomycin C (9). In vivo therapy experiments in mouse models have demonstrated the effectiveness of ADEPT for treatment of melanomas (4) and lung adenocarcinomas (10).

Previous studies utilized a fusion protein solubly expressed in *E. coli* and purified from lysed cells using



**Figure 1.**  $\beta$ -Lactamase-mediated hydrolysis of C-Mel to melphalan.

two affinity steps (3). While this allowed for the generation of modest amounts (1–4 mg/L) of purified protein from shake-flasks and small fermenters (3), it did not provide enough material for clinical development. To address this, we explored the large-scale production of L49-sFv-bL from refolded *E. coli* inclusion bodies, but encountered significant problems since the protein did not refold efficiently. Others have also reported difficulties in refolding sFv molecules (11).

Several rational engineering methods have been used to improve the refolding properties of problematic sFv fragments (11). One possibility is to graft the CDRs onto

\* Corresponding author. E-mail: cmcdonagh@seagen.com.

the framework of a more stable sFv (12, 13). However, CDR grafting has been shown to reduce the binding affinity of the sFv (14). Another method has been to compare the framework of the unstable sFv with that of a homologous stable sFv and make the appropriate changes (15). This approach is only possible if a homologous stable sFv can be identified, which was not the case for L49-sFv. Introduction of an interface disulfide bond between the  $V_H$  and  $V_L$  domain has also been used to stabilize sFv fragments (16). However, the introduction of extra cysteines into the sFv may further complicate refolding by allowing additional incorrect intramolecular disulfide bonds to form.

Sequence statistics have also been used to identify problematic amino acids in sFv frameworks. A technique, used successfully to engineer a sFv immunotoxin, has been to identify 'unusual' amino acids in the sFv frameworks by aligning the target sequence with known stable variable domains and scanning all residues for deviations from the Kabat consensus. 'Rare' residues with less than 5% frequency in the Kabat database, that were also incompatible with their solvent exposure state, were mutated to the consensus residue. Up to 18-fold increases in yield were observed although binding affinity was compromised 2–3.5-fold (17). This technique provides a straightforward initial screen to identify potential 'problem' amino acids within an sFv framework. Alignment of sFvs to their general subgroup consensus sequences has also revealed problematic framework amino acids. Stabilizing mutations have been introduced in both  $V_H$  and  $V_L$  domains using this approach (18, 19). For kappa  $V_L$  domains, this strategy was effective for approximately 60% of mutations (18).

Here, we describe a sequence alignment approach to re-engineer L49-sFv-bL. This method rapidly identified three residues in the  $V_H$  framework that, when mutated to consensus residues, improved both the yield and stability of refolded L49-sFv-bL. Binding affinity and efficacy were unaffected by the introduction of these stabilizing mutations. Further, we also investigated the effects of orientation on yield and report that positioning the  $\beta$ -lactamase protein at the amino terminus (bL-L49-sFv) increased protein yields severalfold compared to L49-sFv-bL where the  $\beta$ -lactamase fusion is positioned at the carboxyl terminus.

## EXPERIMENTAL PROCEDURES

**Mutagenesis of L49-sFv.** Mutagenesis was performed by PCR overlap extension using pfu *turbo* polymerase (Stratagene). The template used was the previously described L49-sFv-bL construct (3) cloned into pET27b (Novagen). Mutagenic primers used were sense primer 5'ACCAAGGCGAT**GTT**GTGATGACCCAA and anti-sense primer 5'TTGGGTCATCACA**AC**ATCGCCCTTGGT for F L2 V, sense primer 5'AACTGGATCCG**GCAG**TTCCAGGGAAT and anti-sense primer 5'AT-TCCCTGGGA**ACTG**CCGATCCAGTT for K H39 Q, sense primer 5'CTCCAGTTGAAT**TCT**GTGACTGCTGAG and anti-sense primer CTCAGCAGTCAC**AGA**AT-TCAACTGGAG for F H82B S, and sense primer 5'ACAGCCACATATT**ACT**GTGCAAGAAGG and anti-sense primer CCTTCTTGACAG**TA**ATATGTGGCTGT for N H91 Y (characters in bold are mutated codon). Flanking primers 5' GGATCGAGATCTCGATCCCGCGAAATT (sense) containing a *Bgl* II site (underlined) and 5'GC-CTGGCTTCTGCAGGTACCAATGTAAATA (antisense) containing a *Pst* I site (underlined) were used to amplify mutated PCR products. Products were digested with *Bgl*

II and *Pst* I (New England Biolabs) and cloned into the *Bgl* II/*Pst* I fragment of the original pET27b L49-sFv-bL construct replacing the parental sequence. Mutants were confirmed by sequencing. The reverse orientation construct FP999 was made by amplifying the  $\beta$ -lactamase cDNA from pET27b L49-sFv-bL incorporating a 5' *Nco* I site and a 3' *Hind* III site within a synthetic 6 amino acid linker (MHGTKL). The cDNA coding for L49-sFv was amplified from the expression construct incorporating a 5' *Hind* III site and a 3' *Nhe* I site. PCR products were digested with *Nco* I and *Hind* III and *Hind* III and *Nhe* I, respectively, and cloned into pET27b digested with *Nco* I and *Nhe* I.

**Protein Expression and Purification.** For small scale expression BL21(DE3) (Novagen) were transformed with parental and mutant constructs and single colonies was used to inoculate 100 mL of Terrific Broth II (TB) (QBIOSOURCE). Cells were induced at an OD of 1.0 with 1 mM IPTG (Sigma). Cells were harvested following overnight incubation and inclusion bodies were purified from the cell extracts using B-Per (Novagen) according to the manufacturers instructions. Inclusion body pellets were resuspended in 8 M urea, 2 mM DTT, 50 mM Tris-Cl pH 8.0 at a concentration of 50 mg/mL. Inclusion bodies were refolded overnight in a 50-fold dilution of 2 M urea, 0.3 M L-arginine, 50 mM Tris-Cl pH 8.0, 1 mM reduced glutathione, 0.1 mM oxidized glutathione. Protein was then dialyzed into PBS and fusion protein concentration was determined by measuring  $\beta$ -lactamase activity using the colorimetric substrate nitrocefin.

For Western analysis proteins were run on a 10% Tris/glycine gel (Novagen) and transferred to nitrocellulose. Blots were blocked with 1% BSA in PBS and then probed with a 1:5000 dilution of affinity purified rabbit polyclonal anti-serum to *E. cloacae*  $\beta$ -lactamase (3). Secondary HRP-conjugated anti-rabbit IgG was applied at 1:2000 dilution and following wash steps blots were developed using colorimetric substrate 3,3'-diaminobenzidine tetrahydrochloride (DAB) (Sigma).

For large scale expression 50 mL of TB were inoculated with transformed BL21 (DE3). After an OD<sub>600</sub> of 0.6–0.8 was reached the entire 50 mL culture was used to inoculate 500 mL of TB and grown at 37 °C with shaking in two liter flasks. At an OD<sub>600</sub> of 1, cultures were induced with 1 mM IPTG and grown overnight. Cells were harvested at 5000 rpm for 10 min, and 10 g of wet cell pellets was suspended in 500 mL of TE buffer (50 mM Tris-Cl, 1 mM EDTA, pH 8) containing 1% v/v Triton X-100 (Fisher Biotech.). The suspension was passed three times through a gaulin homogenizer at 6000–8000 psi, and inclusion bodies were collected via centrifugation. The resulting pellet was washed 2× with TE + 1% TX-100 and an additional 2× with TE alone. Washed inclusion bodies were immediately solubilized using a stator/rotor homogenizer at a concentration of 50 mg wet IB weight/mL in 10 M urea, 50 mM Tris-Cl pH 8 containing 2 mM DTT and incubated for 1 h at room temperature with gentle rotation. After reduction, solubilized inclusion bodies were filtered and concentrations of protein determined by absorbance at 280 nm using an extinction coefficient of 1.9. Solubilized inclusion bodies were immediately diluted 1:50 v/v into cold (2–8 °C) refolding buffer containing 2 M urea, 0.3 M L-arginine, 50 mM Tris-Cl, pH 8, 1 mM reduced glutathione, 0.1 mM oxidized glutathione, with stirring. Refolding was allowed to continue for 72–96 h at 2–8 °C. Five hundred milliliters of refolded fusion protein was diluted 1:3 with PBS containing additional 0.5 M NaCl and then vacuum filtered through a 0.2  $\mu$ m bottle top filter. Diluted/filtered

refold was applied to a 17 mL aminophenylboronate column (either Millipore PROSEP-PB, or Prometic Biosciences) at 1.5 mL/min previously equilibrated with five column volumes (CV) of equilibration buffer. The column was washed with 5 CV of equilibration buffer and bound protein was eluted with 50 mM diethanolamine, 0.5 M NaCl pH 11.2. The eluate was immediately neutralized with 30:1 v/v 1 M Tris-Cl pH 7.5. Neutralized PBA eluate was dialyzed against 10 mM sodium phosphate pH 7. The dialysate was filtered and bound to Macro-Prep HS (BioRad, Hercules, CA) previously equilibrated in 10 mM sodium phosphate, pH 7. The bound protein was washed with 5 CV of 10 mM sodium phosphate, pH 7, and eluted with 10 mM sodium phosphate pH 7, 250 mM NaCl. HPLC-SEC analysis was performed on an HP Agilent HPLC system. Purified L49-sFv-bL was assayed on a  $7.8 \times 300$  mm TSK G3000swxl (TosoHaas, PA) employing an isocratic gradient of PBS as the mobile phase at 1 mL/min. Recording was performed at 280 nm.

**p97 Binding Assays.** Soluble p97 (amino acids 20–710 of human p97 precursor) was cloned into pSecTag2 (Invitrogen), incorporating an Ig kappa leader sequence and a 6X his tag, and transfected into CHO cells. Stable transformants were selected and secreted protein was purified from conditioned medium on a metal chelate affinity column. Assays were performed by coating polystyrene 96-well plates with 2  $\mu$ g/mL soluble p97 in PBS overnight. The plates were blocked by adding 1% bovine serum albumin in PBS for 1 h at room temperature. Plates were emptied, and fresh blocking reagent containing serial dilutions of L49-sFv-bL samples was added. Following 1 h at room temperature, the plates were washed and developed with 0.1 mL of colorimetric  $\beta$ -lactamase substrate nitrocefin solution at 0.1 mM in PBS containing 1% DMSO. Absorbance measurements were read in an ELISA plate reader using a 490 nm filter with 610 nm as the reference wavelength.

Binding affinity was measured at 25 °C on a Biacore 2000 (Biacore analysis was performed by the Protein Interaction Facility at the University of Utah). The buffer used in the study was PBS, 0.005% P20, 0.2 mg/mL BSA. Antigen was immobilized on one flow cell surface of a CM5 sensor chip, and the others were left blank to serve as reference surfaces. For each sFv, triplicates of 0, 0.5, 2.8, 8.3, 25, 75, and 225 nM were injected across the immobilized antigen. The association and dissociation phases were monitored for 1 and 20 min, respectively. The antigen surface was regenerated with four 18-second pulses of 2.5 mM NaOH between injections.

**Stability Assays.** Stability assays were performed by incubating samples at 25  $\mu$ g/mL in mouse plasma at 37 °C. At each time point, 0, 24, 48, and 72 h, an aliquot was removed and immediately frozen at –80 °C. At the end of the experiment all aliquots were thawed and analyzed for binding to p97 using the ELISA-based assay.

**In Vitro Cytotoxicity Assay.** H3677 cells were plated into 96-well microtiter plates ( $5 \times 10^3$  cells/well in 100  $\mu$ L of RPMI 1640 media (Invitrogen) with 10% fetal bovine serum) and allowed to adhere overnight. The cells were treated with FP95, FP990, or FP999 fusion proteins at 10 nM. After 1 h at 4 °C, the plates were washed three times with medium and then concentrations of C-Mel from 0.005 nM to 100 nM were added. Melphalan was also added at the same concentrations to cells treated with medium alone. After 1 h at 37 °C, cells were washed three times with medium and incubated for 96 h at 37 °C. The cells were then incubated with 10% alamarBlue

for 3 h at 37 °C, and excitation was measured in an ELISA plate reader at 570 nm.

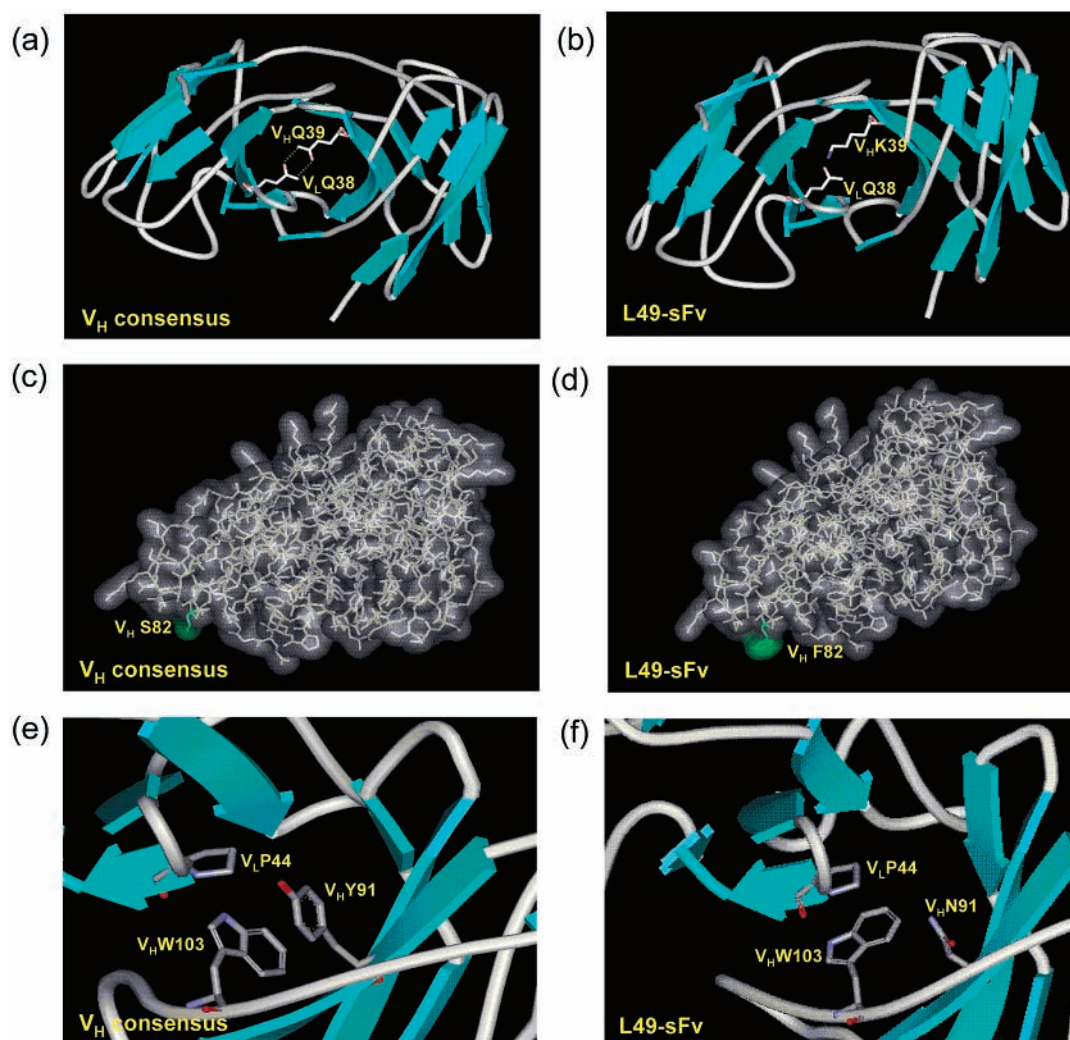
**In Vivo Therapy Experiments.** In vivo studies were performed in female BALB/c athymic mice, which were 5–6 weeks of age at the start of each study. H3677 human melanoma tumors were established as subcutaneous xenografts in donor mice and serially passaged into recipients for study. When tumors averaged approximately 100 mm<sup>3</sup>, the mice were randomized into groups of five and received either no treatment, C-Mel alone at 150 mg/kg (0.22 mmol/kg), or L49-sFv-bL (derived from either FP990 or FP999) at 1 mg/kg followed 24 h later by C-Mel at 100 mg/kg (0.14 mmol/kg) or at 150 mg/kg (0.22 mmol/kg). Tumor volume, in mm<sup>3</sup>, was defined as (length  $\times$  width<sup>2</sup>)/2. Both L49-sFv-bL and C-Mel were administered intravenously via the tail vein.

## RESULTS

**Identification of Unusual Residues in the Framework Region of L49.** To limit the effect of mutagenesis on binding affinity, CDR regions of the L49 mAb were not considered for alteration. The V<sub>H</sub> and V<sub>L</sub> chains of L49 were aligned to their consensus sequences, H-V1a and K-V2, respectively (20). Two significant differences were observed between L49 V<sub>H</sub> framework and the H-V1a consensus sequence at positions H82B (F) and H91 (N), and one significant difference was found between the L49 V<sub>L</sub> framework and its consensus at position L2 (F) (Kabat numbering). The frequency of occurrence of the three residues at these positions in the entire Kabat database (21), which currently contains greater than 14 000 V<sub>H</sub> and 6000 Kappa V<sub>L</sub> sequences, was determined as described by Chowdhury et al. (17). All three residues were found to occur in less than 1% of variable domain sequences. An additional unusual residue, occurring in less than 3% of sequences (17), was identified at position H39 (K). Further investigation of the three V<sub>H</sub> positions revealed that H39 and H91 were involved in forming the interface between the V<sub>H</sub> and V<sub>L</sub> domains (22) (Figure 2a, b, e, and f). We speculated that the presence of unusual amino acids in these two key positions disrupted the V<sub>H</sub>/V<sub>L</sub> interface resulting in an unstable molecule. The hydrophobic phenylalanine at position H82B is incompatible with its predicted exposed surface accessibility (17) (Figure 2c and 2d), which may induce instability. Literature searches did not uncover any key functions for the residue at position L2.

**Analysis of L49 sFv Framework Mutants by Measurement of p97 Binding Activity.** The four unusual residues in the L49 sFv framework were mutated to the most frequently occurring residue for that position in the Kabat database (17). The following individual mutations were introduced into L49-sFv-bL: K H39 Q, (FP930), F H82B S (FP945), N H91 Y (FP950), F L2 I (FP955) (Table 1). To efficiently assay for improved refolding characteristics, the antigen binding activities of the refolded L49-sFv-bL mutants were compared to the refolded parental molecule (FP95). The parental and four mutant fusion proteins were expressed in *E. coli* as inclusion bodies and denatured and refolded as described in Materials and Methods. The crude refolds were normalized based on  $\beta$ -lactamase activity. Binding to p97 was then determined using a solid-phase binding assay. All three V<sub>H</sub> mutants showed increases in antigen binding compared to the parental L49-sFv-bL molecule, indicating improved refolding and stability, with mutant N H91 Y having the most pronounced effect (Figure 3a). The V<sub>L</sub> single mutant, F L2 I, showed no improvement





**Figure 2.** Models showing  $V_H$  consensus sequence amino acids for H39, H82B, and H91 (panels a, c, and e, respectively) and 'rare' amino acids present in L49-sFv (panels b, d, and f). The figure was generated using crystal structure 1QOK (29), which shares 58% homology with L49-sFv. The 'rare' amino acids present in L49-sFv were introduced into the 1QOK structure using the 'mutate' function of Swiss-PdbViewer (ExPASy Molecular Biology Server). The final figure was created using WebLabViewerLite 4.0 (Molecular Simulations, Inc.).

**Table 1. Summary of Molecule Orientation and Mutations Introduced into L49-sFv**

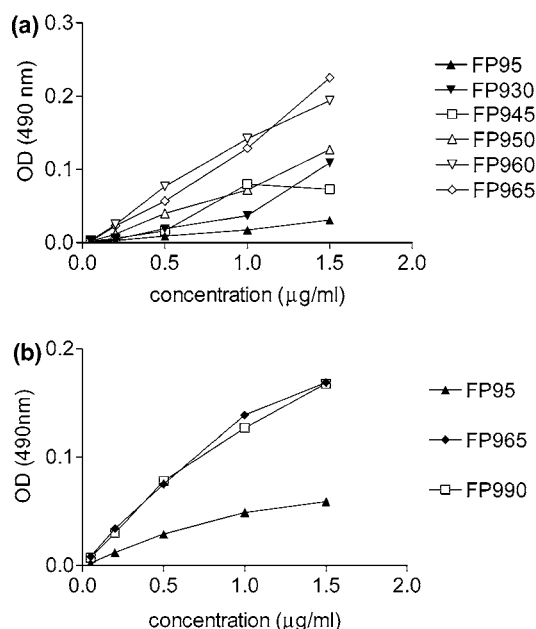
L49-sFv fusion protein	orientation	mutations
FP95	L49-sFv-bL	parental
FP930	L49-sFv-bL	K H39 Q
FP945	L49-sFv-bL	F H82B S
FP950	L49-sFv-bL	N H91 Y
FP955	L49-sFv-bL	F L2 I
FP960	L49-sFv-bL	F H82B S, N H91 Y
FP965	L49-sFv-bL	K H39 Q, N H91 Y
FP990	L49-sFv-bL	K H39 Q, F H82B S, N H91 Y
FP999	bL-L49-sFv	K H39 Q, F H82B S, N H91 Y

in antigen binding compared to the parental molecule (data not shown). As all three heavy chain mutations proved effective, the mutations were combined to create the following double and triple mutants: F H82B S/N H91 Y (FP960), K H39 Q/N H91 Y (FP965) and K H39 Q/F H82B S/N H91 Y (FP990) (Table 1). Both the double mutants and triple mutant displayed similar improvements in antigen binding activity over the single mutants (Figure 3).

**Western Analysis of L49-sFv-bL Mutants.** Western blot analysis of nonreduced crude refolds with polyclonal anti- $\beta$ -lactamase antibody showed that the parental SGN-17 molecule, FP95, exists as several different

species, indicating the presence of misfolded protein (Figure 4a). Under reducing conditions, only one band is observed (Figure 4b). Mutant FP950 and double mutants FP960 and FP965 resolve mainly to one band (Figure 4a), which suggests that the majority of protein refolds into the active conformation. The triple mutant, FP990, resolves almost completely to one band (Figure 4a) suggesting that the introduction of all three  $V_H$  mutations results in the most improved refolding characteristics.

**Expression, Purification, and Analysis of Parental and Mutated L49-sFv-bL Fusion Proteins.** Double mutants FP960 and FP965 and triple mutant FP990 all show improved refolding activity in crude lysates compared to the parental molecule and therefore all three mutant molecules were selected for further analysis. Proteins were expressed at the 1 L scale in shake flasks as described in Materials and Methods. Inclusion bodies (IBs) were obtained at a typical yield of 25% ( $\pm$  10%) wet IB mass/wet cell mass. Renatured L49-sFv-bL was purified by aminophenylboronate chromatography, dialyzed into 10 mM  $\text{Na}_2\text{PO}_4$ , and loaded onto Macro-prep HS resin. Fusion proteins were eluted in a stepwise fashion employing 250 mM NaCl. Yields of the mutated constructs showed a significant improvement compared to the parental molecule with increased yields for FP960,



**Figure 3.** Antigen binding activity of refolded L49-sFv-bL parental and mutants. (a) Binding of refolded mutants FP930 (K H39 Q), FP945 (F H82B S), FP950 (N H91 Y), FP960 (F H82B S, N H91 Y), FP965 (K H39 Q, N H91 Y), and parental protein FP95 to the p97 antigen was determined using a solid-phase binding assay. (b) Binding of refolded triple mutant FP990 (K H39 Q, F H82B S, N H91 Y) was compared to binding of double mutant FP965 (K H39 Q, N H91 Y) and wild protein FP95. All experiments were performed in duplicate.

FP965 and FP990 of 7.5-fold, 4.8-fold, and 8.2-fold, respectively (Table 2). Mutants FP965 and FP990 were greater than 95% monomeric as shown by SEC-HPLC. However, FP960 contained only 55% monomer after cation exchange purification, possibly indicating a key role for the residue at position H39 in refolding. The parental molecule, FP95, was observed as two bands by SDS-PAGE following aminophenylboronate chromatography. After ion-exchange chromatography, only the upper of these two bands was eluted. A size exclusion chromatography (SEC) binding assay was developed in which a 2:1 ratio of purified p97 antigen to purified L49-sFv-bL was

**Table 2.** Typical Expression and Purification Yields of Parental L49-sFv-bL Molecule FP95 and Mutant Molecules FP960 (F H82B S, N H91 Y), FP965 (K H39 Q, N H91 Y), FP990 (K H39 Q, F H82B S, N H91 Y), and FP999 (K H39 Q, F H82B S, N H91 Y, bL-L49-sFv orientation)<sup>a</sup>

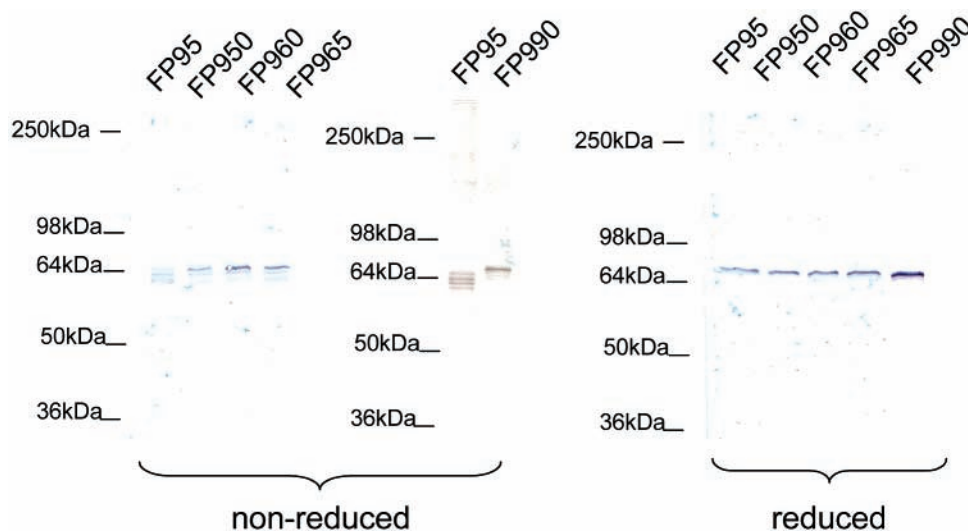
step	recovery	fusion protein				
		FP95	FP960	FP965	FP990	FP999
fermentation	g/L of culture	9.7	10.6	11.5	10.3	8.6
inclusion body prep	IB, g	3.0	2.6	2.9	3.1	3.5
	% recovery	31	24	25	30	41
solubilization	IB/g cell					
	Total mg	208	178.6	148	188	764.5
final yield	mg/L culture	4.8	36	23.1	39.2	95

<sup>a</sup> Inclusion bodies were solubilized in 10 M urea, 50 mM Tris-Cl, pH 8, containing 2 mM DTT and the concentration of protein present measured by UV spectroscopy.

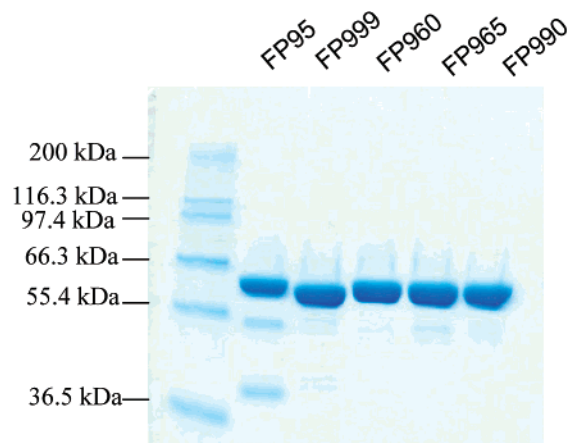
mixed and analyzed by HPLC-SEC. This assay showed that the eluted upper band bound antigen completely demonstrating that it contains the active refolded protein (data not shown). All mutants resolved as one homogeneous band during the purification process (Figure 5) and bound antigen completely in the SEC assay.

The effect of orientation on protein yield was investigated by reversing the order of the molecule so that  $\beta$ -lactamase was present at the amino terminus. As  $\beta$ -lactamase is a highly stable, well-expressed molecule positioning it at the amino terminus might drive expression of the fusion protein resulting in higher yields. The three V<sub>H</sub> mutations were introduced into this reverse orientation molecule to produce mutant FP999. This strategy was successful, resulting in almost 20-fold increased expression compared to the parental molecule. This was due to an increase in protein expression as shown by the increase in recovery of inclusion body protein (Table 2). Purified FP999 was also greater than 95% monomeric following cation exchange purification and bound completely to antigen.

**Binding Properties of Parental and Mutant L49-sFv-bL Fusion Proteins.** The binding affinities of double mutants FP960 and FP965 and triple mutants



**Figure 4.** Western analysis of refolded molecules. Ten nanomoles of FP950 (N H91 Y), FP960 (F H82B S, N H91 Y), FP965 (K H39 Q, N H91 Y), FP990 (K H39 Q, F H82B S, N H91 Y), and parental protein FP95 were separated as indicated on a 10% Tris/glycine gel under nonreducing conditions (a) or under reducing conditions (b). Proteins were transferred onto nitrocellulose and blotted with rabbit polyclonal anti- $\beta$ -lactamase antibody followed by incubation with HRP-conjugated secondary antibody. Blots were developed by addition of colorimetric substrate DAB.



**Figure 5.** Purified L49-sFv-bL parental and mutant fusion protein. Following ion exchange chromatography, FP95 (parental), FP999 (K H39 Q, F H82B S, N H91 Y, bL-L49-sFv orientation), FP960 (F H82B S, N H91 Y), FP965 (K H39 Q, N H91 Y), and FP990 (K H39 Q, F H82B S, N H91 Y) proteins were analyzed as indicated by SDS-PAGE under nonreducing conditions on a 10% Tris/glycine gel. The additional bands observed in the FP95 (parental) sample are degradation products.

**Table 3.** Binding Affinity Was Measured by Surface Plasmon Resonance Using BIAcore<sup>a</sup>

sample	$k_a$ ( $M^{-1} s^{-1}$ )	$k_d$ ( $s^{-1}$ )	$K_D$ (nM)
FP95	$3.038(2) \times 10^5$	$7.004(5) \times 10^{-4}$	2.306(1)
FP960	$3.640(4) \times 10^5$	$6.383(7) \times 10^{-4}$	1.754(1)
FP965	$4.000(6) \times 10^5$	$7.65(1) \times 10^{-4}$	1.91(1)
FP990	$4.476(1) \times 10^5$	$7.819(3) \times 10^{-4}$	1.747(1)
FP999	$3.373(3) \times 10^5$	$5.755(7) \times 10^{-4}$	1.706(1)

<sup>a</sup> Values shown are the average of triplicate readings. The data were fit to a 1:1 interaction model to obtain the shown kinetic and affinity parameter. Numbers shown in parentheses are the error in the last digit.

FP990 and FP999 were compared to the parental molecule by surface plasmon resonance. Recombinant p97 was immobilized on a BIAcore CM5 sensor chip and varying concentrations of each sFv fusion protein were injected across the chip in triplicate. The  $K_D$  values for all four mutant molecules were similar to the parental molecule, FP95, showing that introduction of the three  $V_H$  framework mutations does not adversely affect the structure of the CDR loops (Table 3). These values compared favorably with previously published data, which reported a  $K_D$  for the parental L49-sFv-bL molecule, expressed in the *E. coli* periplasm, of 1 nM using similar techniques (3).

**Stability of Parental and Mutant L49-sFv-bL in Mouse Plasma.** An effective agent for ADEPT needs to remain stable at the site of the tumor for many hours to several days to allow a high tumor-to-blood ratio to be established before application of the prodrug (1). The parental L49-sFv-bL molecule has been shown to clear rapidly from the systemic circulation with a terminal half-life  $t_{1/2\beta} = 2.5$  h. A high tumor-to-blood ratio of 141–150:1 was measured 24–48 h after the fusion protein was administered (3). To ensure that the mutated L49-sFv-bL proteins remain stable in the tumor environment for an extended time period, each mutant and the parental molecule were incubated in mouse plasma at 37 °C at a concentration of 25  $\mu$ g/mL. Aliquots were removed at 0, 24, 48, and 72 h and tested for binding to antigen using the solid-phase p97 binding assay. Mutants FP960, FP990, and FP999 were highly stable, retaining 100% antigen binding activity throughout the 72 h period. The

parental molecule, FP95, lost 84% antigen binding activity between 48 and 72 h, and mutant FP965 lost 31% activity during the same time period (Figure 6).

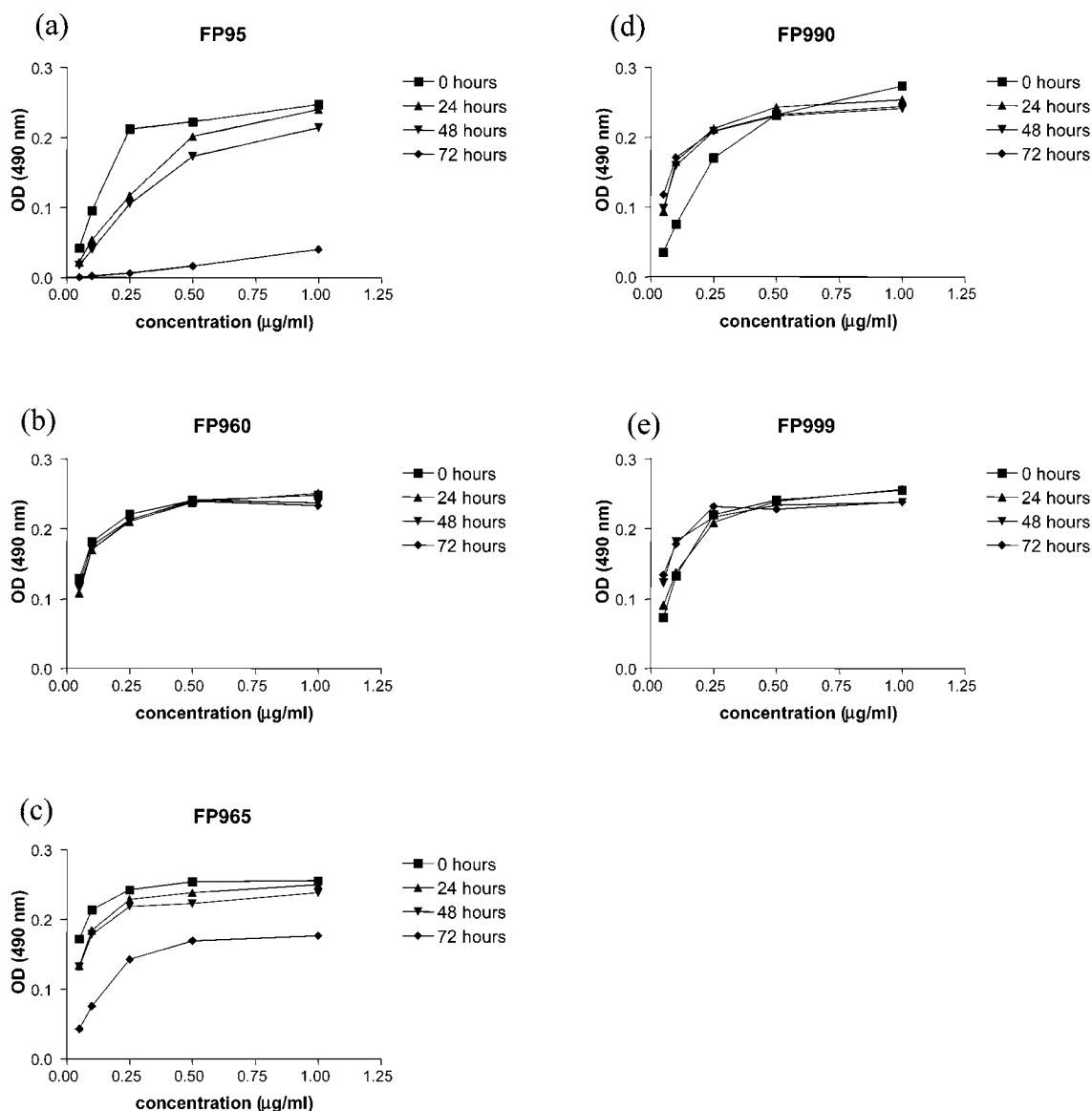
**Cytotoxicity of L49-sFv-bL Parental and Mutant Molecules.** Results from the stability studies and the properties of the mutant molecules during purification indicated that the triple mutant molecules in each orientation, FP990 and FP999, were the most suitable candidates for further study. Therefore, these two mutants and the parental molecule were tested in combination with the prodrug C-Mel, a cephalosporin-containing derivative of melphalan (4), for their effectiveness in killing cultured human melanoma H3677 cells, which express the p97 antigen. The cells were treated with 10 nM L49-sFv-bL, unbound material was washed off, and serial dilutions of C-Mel were added. C-Mel and the active drug, melphalan, were also applied to cells treated with media alone. Cell viability was measured using the redox indicator alamarBlue. The  $IC_{50}$  for C-Mel was 40  $\mu$ M while the combination of C-Mel and mutants FP990 or FP999 were equally effective in prodrug conversion resulting in an  $IC_{50}$  of 5  $\mu$ M, equivalent to the activity of melphalan (Figure 7).

**In vivo Efficacy of L49-sFv-bL Mutants.** The relative efficacy of the two triple mutants, in combination with C-Mel, was compared in H3677 human melanoma xenografts in athymic mice. This L49 antigen-positive model was previously evaluated with the parental L49-sFv-bL fusion construct and was shown to be sensitive when combined with C-Mel (4) and CCM, a prodrug of phenylenediamine mustard (3). The study was initiated with implantation, on day 0, of solid tumor obtained from donor mice, and therapy was initiated on day 7, when the tumors averaged approximately 100 mm<sup>3</sup>. Groups of mice (five/group) received either no therapy (untreated controls) or one of five therapeutic regimens: C-Mel alone at 150 mg/kg, or mutant FP990 or FP999 at 1 mg/kg followed 24 h later by C-Mel at either 100 or 150 mg/kg. Both components were administered every 7 days for a total of three injections (q7dx3) with the fusion protein administered on days 7, 14, and 21, and C-Mel administered on days 8, 15, and 22. Treatment with either mutant L49-sFv-bL molecule and C-Mel at 150 mg/kg led to complete tumor regression in all of the animals (Figure 8). Both fusion proteins also gave significant tumor regression in combination with C-Mel at 100 mg/kg. At the end of the study there were two complete regressions in the FP999 group that received 100 mg/kg C-Mel but none in the FP990 group. With the limited number of animals used in this study, the difference between these two groups is not significant. In contrast to the animals that received both L49-sFv-bL and C-Mel, C-Mel alone had no antitumor activity, indicating that the antitumor effect was specific to the combination of fusion protein and prodrug. These results show that the FP990 and FP999 constructs are highly effective when combined with C-Mel.

## DISCUSSION

The effective antitumor activity of the combination of L49-sFv-bL fusion protein with cephalosporin-containing nitrogen-mustard prodrugs C-Mel or CCM in mouse melanoma models has been previously reported (3, 4). However, development of this treatment for clinical use has been hindered by difficulties in producing sufficient quantities of L49-sFv-bL. The parental L49-sFv-bL molecule, expressed in denatured inclusion bodies, refolds inefficiently into native active protein able to bind to



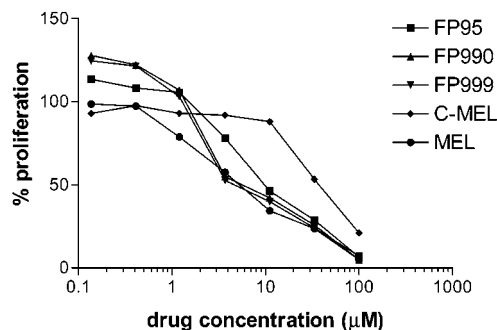


**Figure 6.** Stability of L49-sFv-bL parental and mutant molecules in mouse plasma. FP95 (a) and mutant proteins FP960 (b), FP965 (c), FP990 (d), and FP999 (e) were incubated in mouse plasma at 37 °C, and aliquots were removed at 0, 24, 48, and 72 h time points. Proteins from each time point, at indicated concentrations, were incubated in wells coated with p97, and following wash steps, protein binding was determined using  $\beta$ -lactamase substrate nitrocefin. The experiment was performed in duplicate and was repeated to confirm results.

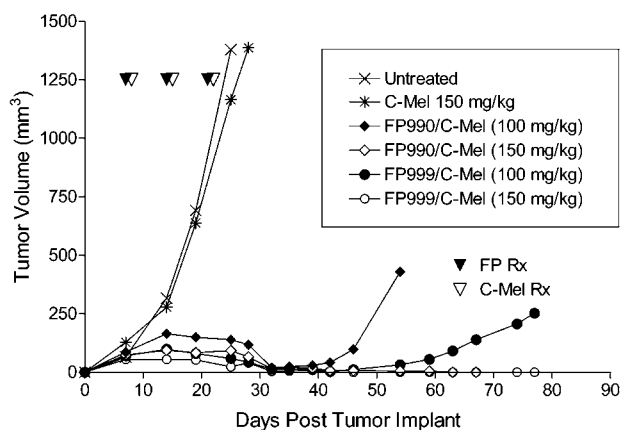
antigen, although the  $\beta$ -lactamase moiety retains activity. Therefore, it appears that the sFv portion of the molecule is responsible for the observed refolding problems. Our goal was to use a protein engineering approach to improve the refolding properties of L49-sFv-bL and increase protein yields to allow for development of this molecule into a clinical candidate.

#### Identification of Unusual Residues in L49-sFv.

Comparison of the primary framework sequences of L49 V<sub>H</sub> and V<sub>L</sub> with their subgroup consensus sequences and subsequently with the Kabat database revealed four unusual and potentially problematic residues, three in the V<sub>H</sub> and one in the V<sub>L</sub> domain. Two of the residues identified in the V<sub>H</sub> domain H39 (K) and H91 (N) are in positions involved in formation of the V<sub>H</sub>/V<sub>L</sub> interface (22). Position H39 is a glutamine in 97% of all mouse V<sub>H</sub> domains, and a lysine is present in this position in the remaining 3% of sequences (21). The glutamine side chain at position H39 forms two H bonds across the V<sub>H</sub>/V<sub>L</sub> interface with a highly conserved glutamine at position L38 (Figure 2a). In L49, the presence of a lysine at



**Figure 7.** Cytotoxic effects of mutant L49-sFv-bL molecules FP990 and FP999 in combination with C-Mel. Cytotoxic effects of parental FP95 and mutant molecules, FP990 (K H39 Q, F H82B S, N H91 Y) and FP999 (K H39 Q, F H82B S, N H91 Y, bL-L49-sFv orientation), in combination with C-Mel, were measured on H3677 melanoma cells as determined by the redox indicator alamarBlue. The effects were compared to cells treated with C-Mel or melphalan (Mel) alone. Each data point was collected in quadruplicate.



**Figure 8.** In vivo efficacy of mutant L49-sFv-bL molecules FP990 and FP999 in combination with C-Mel. Therapeutic effects of L49-sFv-bL mutants FP990 (K H39 Q, F H82B S, N H91 Y) and FP999 (K H39 Q, F H82B S, N H91 Y, bL-L49-sFv orientation) in combination with C-Mel. Athymic mice (five mice per group) were treated with L49-sFv-bL (FP990 or FP999) at 1 mg/kg followed 24 h later by C-Mel. The average tumor volumes were plotted until one or more mice were removed from the experiment due to tumor outgrowth. C-Mel was also injected without prior treatment with L49-sFv-bL.

position H39 of the  $V_H$  domain allows only one H bond to form with the glutamine at L38 instead of the two H bonds made between two glutamine side chains (Figure 2b), thus reducing the stability of the interaction. Mutation of the conserved glutamine at H39 to an alanine within Fab 57P resulted in reduced antigen binding activity despite its location at least 9 Å away from the base of the CDR loops (23). Another study, performed on a sFv, showed that increasing hydrophobic interactions at the  $V_H/V_L$  interface by mutating either H39 or L38 or both to methionine actually increases the refolding efficiency and stability while reducing antigen binding (24). Both these studies highlight the importance of the interface interaction between H39 and L38 and suggest a role for these residues in both antigen binding and folding stability.

The residue at position H91, which is a tyrosine or occasionally a phenylalanine in the majority of  $V_H$  domains, is an asparagine in L49 (Figure 2e and 2f). An asparagine occurs at position H91 in only 0.025% of heavy chains. H91 contacts position L44 across the  $V_H/V_L$  interface (22), and mutation of tyrosine at this position to alanine has been shown to eliminate antigen binding and result in reduced expression, suggesting reduced stability (23). The presence of a nonaromatic asparagine residue at position H91 in L49 may destabilize interactions with the conserved  $V_L$  domain proline at position L44, which also interacts with the highly conserved tryptophan at position H103. In the whole L49 antibody, this destabilization is probably countered by the presence of the constant domains.

The third unusual residue in the  $V_H$  domain occurs at position H82B close to the region of the variable/constant domain interface in the whole antibody (25). The L49 residue at this position is an aromatic phenylalanine, while in the majority of  $V_H$  sequences a small, relatively hydrophilic serine is present (Figure 2c and 2d). Since position H82B is generally exposed at the sFv surface (17), a phenylalanine at this position creates a hydrophobic patch, which may induce protein aggregation. Due to the close proximity of position H82B to the variable/constant interface, this phenylalanine may be buried in the L49 antibody while becoming exposed and problematic only in the sFv. Mutagenesis of hydrophobic residues

at the variable/constant interface to hydrophilic residues was shown to increase the functional expression of an anti-fluorescein sFv fragment 25-fold (25), highlighting the negative effect of hydrophobic surface residues on protein stability.

**Mutagenesis of Unusual Residues in L49-sFv-bL and Characterization of Mutants.** All three  $V_H$  mutants, FP930, FP945, and FP950 improved the refolding and antigen binding characteristics of the L49-sFv-bL molecule while the  $V_L$  mutant, for which there was no rational reason for mutagenesis, had no effect. Combinations of the three effective  $V_H$  mutants improved refolding activity further although the triple mutant FP990 showed no improvement over double mutants FP960 and FP965 when crude refolds were analyzed. Multiple disulfide-bonded species of parental L49-sFv-bL, FP95, are observed under nonreducing conditions indicating that the majority of protein is misfolded. Similar multiple bands have also been observed for another sFv fusion protein, G28-5 sFv-PE40 (26). In this case, only one of the bands could be purified by affinity chromatography over immobilized antigen, suggesting that the remaining protein was an incorrect disulfide species. The introduction of the  $V_H$  mutations into L49-sFv-bL encouraged the formation of one disulfide species, presumably active refolded protein, with the triple  $V_H$  mutant, FP990, having the most pronounced effect suggesting that all three mutations are required for optimal refolding. We found that the yields of purified double mutants, FP960 and FP965, and triple mutant, FP990, were 4.8–8.2-fold greater than for the parental, FP95, and 100% of the purified protein bound to antigen. Purified FP960, however, was found to contain high molecular weight aggregate, which may be due to the wild-type lysine residue remaining at position H39. Mutation of the conserved glutamine at position H39 of Fab 57P to alanine also resulted in formation of high molecular weight aggregates, indicating that a glutamine is preferred at this position (23). However, FP960 did remain stable during extended stability studies at 37 °C in mouse plasma while the other double mutant FP965 did not, losing activity between 48 and 72 h. When yields of purified protein, western analysis, and stability studies were compared, it was determined that all three  $V_H$  mutations are preferred for optimal refolding and stability.

Interestingly, the parental molecule, FP95, lost 84% of its activity between 48 and 72 h in mouse plasma while FP960, FP990, and FP999 remained stable. Therefore, introduction of the  $V_H$  mutations not only increases yield through more efficient refolding but also increases stability and extends the effective time period for application of prodrug. Fortunately, introduction of the  $V_H$  mutations did not decrease antigen binding affinity, as has been reported following sFv engineering (17). The three  $V_H$  mutations functioned effectively to improve the stability of the framework structure while maintaining the binding integrity of the CDR loops. We speculate that introduction of the stabilizing mutations at the  $V_H/V_L$  interface prevents disassociation of the  $V_H$  and  $V_L$  domains during refolding steps, which would expose hydrophobic residues and promote aggregation. Likewise, replacement of phenylalanine at position H82B with serine removes another hydrophobic patch from the sFv surface. As the parental molecule misfolds into several different disulfide-bonded species, the  $V_H$  mutations must also contribute to stabilization of the  $V_H$  intradomain disulfide bond.

**Effect of Reversing the Orientation of the L49-sFv-bL Fusion Protein.**  $\beta$ -Lactamases are highly

stable, well-expressed bacterial enzymes that have been fused to other proteins at both their N and C terminus without affecting enzyme activity (27, 28). Highly expressed proteins, such as glutathione-S-transferase, are commonly fused to the N terminus of less well-expressed proteins to drive expression and increase yield. Reversing the orientation of L49-sFv-bL and fusing  $\beta$ -lactamase to the N terminus of L49-sFv also had this effect with yields of FP999, containing the three V<sub>H</sub> mutations, 2.5-fold greater than its counterpart, FP990. Antigen binding affinity (Table 3) and enzyme activity (data not shown) were unaffected by the change in orientation, and stability was similar to FP990.

**Efficacy of the Re-engineered L49-sFv-bL Molecule.** As discussed, the mutations introduced into the L49-sFv-bL molecule do not adversely affect antigen-binding affinity and, as would be expected, the re-engineered molecule remains as efficacious as the original L49-sFv-bL molecule. This is also true for the reverse orientation molecule FP999. In vivo therapy studies in nude mice with subcutaneous H3677 tumors using either FP990 or FP999 in combination with C-Mel were comparable to a previous study performed with the original L49-sFv-bL molecule using an almost identical protocol (4). One therapeutic advantage of the engineered L49-sFv-bL molecule is its improved stability at 37 °C in mouse plasma. This may extend the presence of active L49-sFv-bL at the tumor and allow multiple doses of C-Mel to be applied following a single injection of L49-sFv-bL. In single dose experiments, C-Mel was most effective at 150 mg/kg concentrations, which is only half its MTD. Administering multiple lower doses of C-Mel following a single dose of L49-sFv-bL may be equally effective and, as C-Mel is likely to be rapidly cleared from circulation, improve the therapeutic window.

In conclusion, mutating only three unusual amino acids in the sFv portion of L49-sFv-bL has considerably increased the yield of active refolded protein and improved the stability of the molecule without effecting therapeutic efficacy. These improvements have allowed clinical development of the L49-sFv-bL/C-Mel combination to be considered.

#### ACKNOWLEDGMENT

We thank Jennifer Thompson and Starr Rejniak for technical assistance.

#### LITERATURE CITED

- Senter, P. D., and Springer, C. J. (2001) Selective activation of anticancer prodrugs by monoclonal antibody-enzyme conjugates. *Adv. Drug Delivery Rev.* 53, 247–264.
- Siemers, N. O., Yelton, D. E., Bajorath, J., and Senter, P. D. (1996) Modifying the specificity and activity of the *Enterobacter cloacae* P99 beta-lactamase by mutagenesis within an M13 phage vector. *Biochemistry* 35, 2104–2111.
- Siemers, N. O., Kerr, D. E., Yarnold, S., Stebbins, M. R., Vrudhula, V. M., Hellstrom, I., Hellstrom, K. E., and Senter, P. D. (1997) Construction, expression, and activities of L49-sFv-beta-lactamase, a single-chain antibody fusion protein for anticancer prodrug activation. *Bioconjugate Chem.* 8, 510–519.
- Kerr, D. E., Li, Z., Siemers, N. O., Senter, P. D., and Vrudhula, V. M. (1998) Development and activities of a new melphalan prodrug designed for tumor-selective activation. *Bioconjugate Chem.* 9, 255–259.
- Vrudhula, V. M., Svensson, H. P., Kennedy, K. A., Senter, P. D., and Wallace, P. M. (1993) Antitumor activities of a cephalosporin prodrug in combination with monoclonal antibody-beta-lactamase conjugates. *Bioconjugate Chem.* 4, 334–340.
- Meyer, D. L., Law, K. L., Payne, J. K., Mikolajczyk, S. D., Zarrinmayeh, H., Jungheim, L. N., Kling, J. K., Shepherd, T. A., and Starling, J. J. (1995) Site-specific prodrug activation by antibody-beta-lactamase conjugates: preclinical investigation of the efficacy and toxicity of doxorubicin delivered by antibody directed catalysis. *Bioconjugate Chem.* 6, 440–446.
- Rodrigues, M. L., Carter, P., Wirth, C., Mullins, S., Lee, A., and Blackburn, B. K. (1995) Synthesis and beta-lactamase-mediated activation of a cephalosporin-taxol prodrug. *Chem. Biol.* 2, 223–227.
- Vrudhula, V. M., Svensson, H. P., and Senter, P. D. (1995) Cephalosporin derivatives of doxorubicin as prodrugs for activation by monoclonal antibody-beta-lactamase conjugates. *J. Med. Chem.* 38, 1380–1385.
- Vrudhula, V. M., Svensson, H. P., and Senter, P. D. (1997) Immunologically specific activation of a cephalosporin derivative of mitomycin C by monoclonal antibody beta-lactamase conjugates. *J. Med. Chem.* 40, 2788–2792.
- Kerr, D. E., Vrudhula, V. M., Svensson, H. P., Siemers, N. O., and Senter, P. D. (1999) Comparison of recombinant and synthetically formed monoclonal antibody-beta-lactamase conjugates for anticancer prodrug activation. *Bioconjugate Chem.* 10, 1084–1089.
- Worn, A., and Pluckthun, A. (2001) Stability engineering of antibody single-chain Fv fragments. *J. Mol. Biol.* 305, 989–1010.
- Jung, S., and Pluckthun, A. (1997) Improving in vivo folding and stability of a single-chain Fv antibody fragment by loop grafting. *Protein Eng.* 10, 959–966.
- Willuda, J., Honegger, A., Waibel, R., Schubiger, P. A., Stahel, R., Zangemeister-Wittke, U., and Pluckthun, A. (1999) High thermal stability is essential for tumor targeting of antibody fragments: engineering of a humanized anti-epithelial glycoprotein-2 (epithelial cell adhesion molecule) single-chain Fv fragment. *Cancer Res.* 59, 5758–5767.
- Worn, A., and Pluckthun, A. (1999) Different equilibrium stability behavior of ScFv fragments: identification, classification, and improvement by protein engineering. *Biochemistry* 38, 8739–8750.
- Knappik, A., and Pluckthun, A. (1995) Engineered turns of a recombinant antibody improve its in vivo folding. *Protein Eng.* 8, 81–89.
- Glockshuber, R., Malia, M., Pfitzinger, I., and Pluckthun, A. (1990) A comparison of strategies to stabilize immunoglobulin Fv-fragments. *Biochemistry* 29, 1362–1367.
- Chowdhury, P. S., Vasmatzis, G., Beers, R., Lee, B., and Pastan, I. (1998) Improved stability and yield of a Fv-toxin fusion protein by computer design and protein engineering of the Fv. *J. Mol. Biol.* 281, 917–928.
- Steipe, B., Schiller, B., Pluckthun, A., and Steinbacher, S. (1994) Sequence statistics reliably predict stabilizing mutations in a protein domain. *J. Mol. Biol.* 240, 188–192.
- Wirtz, P., and Steipe, B. (1999) Intrabody construction and expression III: engineering hyperstable V(H) domains. *Protein Sci.* 8, 2245–2250.
- Kabat, E. A., Wu, T. T., Perry, H. M., Gottesman, K. S., and Foeller, C. (1991) *Sequences of Proteins of Immunological Interest*, 5th ed., Public Health Service, NIH, Washington, D.C.
- Johnson, G., and Wu, T. T. (2001) Kabat Database and its applications: future directions. *Nucleic Acids Res.* 29, 205–206.
- Chothia, C., Novotny, J., Brucoleri, R., and Karplus, M. (1985) Domain association in immunoglobulin molecules. The packing of variable domains. *J. Mol. Biol.* 186, 651–663.
- Chatellier, J., Van Regenmortel, M. H., Vernet, T., and Altschuh, D. (1996) Functional mapping of conserved residues located at the VL and VH domain interface of a Fab. *J. Mol. Biol.* 264, 1–6.
- Tan, P. H., Sandmaier, B. M., and Stayton, P. S. (1998) Contributions of a highly conserved VH/VL hydrogen bonding interaction to scFv folding stability and refolding efficiency. *Biophys. J.* 75, 1473–1482.
- Nieba, L., Honegger, A., Krebber, C., and Pluckthun, A. (1997) Disrupting the hydrophobic patches at the antibody variable/constant domain interface: improved in vivo folding



- and physical characterization of an engineered scFv fragment. *Protein Eng.* 10, 435–444.
- (26) Francisco, J. A., Gilliland, L. K., Stebbins, M. R., Norris, N. A., Ledbetter, J. A., and Siegall, C. B. (1995) Activity of a single-chain immunotoxin that selectively kills lymphoma and other B-lineage cells expressing the CD40 antigen. *Cancer Res.* 55, 3099–3104.
- (27) Francisco, J. A., Earhart, C. F., and Georgiou, G. (1992) Transport and anchoring of beta-lactamase to the external surface of *Escherichia coli*. *Proc. Natl. Acad. Sci. U.S.A.* 89, 2713–2717.
- (28) Lattemann, C. T., Maurer, J., Gerland, E., and Meyer, T. F. (2000) Autodisplay: functional display of active beta-lactamase on the surface of *Escherichia coli* by the AIDA-I autotransporter. *J. Bacteriol.* 182, 3726–3733.
- (29) Boehm, M. K., Corper, A. L., Wan, T., Sohi, M. K., Sutton, B. J., Thornton, J. D., Keep, P. A., Chester, K. A., Begent, R. H., and Perkins, S. J. (2000) Crystal structure of the anti-(carcinoembryonic antigen) single-chain Fv antibody MFE-23 and a model for antigen binding based on intermolecular contacts. *Biochem. J.* 346, 519–528.

BC0340316

## Thiol-Reactive Luminescent Lanthanide Chelates: Part 2

Pinghua Ge<sup>†</sup> and Paul R. Selvin<sup>\*,†,‡</sup>

Department of Physics and Center for Biophysics and Computational Biology, University of Illinois, Urbana, Illinois, 61801. Received February 28, 2003; Revised Manuscript Received June 20, 2003

Luminescent lanthanide complexes have unusual spectroscopic characteristics, including millisecond excited-state lifetime and sharply spiked emission spectra. These characteristics make them valuable alternatives to conventional organic fluorescent probes in detection applications and for measuring nanometer-scale conformational changes in biomolecules via resonance energy transfer. Our group has previously reported the syntheses and application of various luminescence complexes that have polyaminocarboxylate chelates coupled to a carbostyryl antenna and thiol or amine-reactive groups. Here we report the syntheses of new thiol-reactive forms of DTPA-cs124 chelates, including two iodoacetamide forms (phenylalanine-iodoacetamide and ethylenediamine iodoacetamide) and two methanethio-sulfonate forms (ethylmethanethiosulfonate and carboxyethylmethanethiosulfonate). In addition, we have developed an improved synthesis of a previously reported maleimide form.

### INTRODUCTION

Luminescent lanthanide chelate complexes are of great interest in time-resolved fluorescence assays (1–3). These complexes typically involve a chelate to bind and protect the lanthanide from solvent-quenching effects, and a covalently attached organic chromophore to act as an antenna to absorb excitation light. Their spectral characteristics include millisecond lifetime, sharply spiked emission spectra, large Stokes shifts, high quantum yield, and good solubility. These properties make them useful alternatives to radioactive probes and to organic fluorophores, particularly where there are problems of background autofluorescence (4, 5), and as donors in luminescence resonance energy transfer experiments (3, 6, 7). One group of such chelate complexes, developed in our laboratory, is the chelate diethylenetriaminepentaacetic acid covalently coupled to a chromophore, 7-amino-4-methyl-2-(1*H*)-quinolinone (carbostyryl 124, cs124). While still maintaining their high binding constants, a reactive group for attachment to biomolecules can be added to the chelate: amine reactive forms via either an anhydride or isothiocyanate (8), or thiol reactive forms via maleimide, bromoacetamide, pyridyldithio (9), or iodoacetamide (10) groups. Other thiol-reactive luminescent lanthanide chelates have been developed (11). The reactive group can be also placed on the chromophore. For example, pyridyldithio forms of DTPA and triethylenetetraamine-hexanoic acid chelates, which are luminescent with europium, have been made previously by placing the pyridyldithio group on a coumarin chromophore (12).

Our group has previously reported the syntheses of thiol-reactive maleimide, bromoacetamide, and pyridyldithio forms of DTPA-cs124 chelates (9). The maleimide form of chelate has been used in energy transfer experiments on the muscle protein myosin (13–16) and on ion channels (17). The Ebright group has made a DTPA-

cs124 iodoacetamide utilizing a diaminobenzene linker, which they have used in protein–DNA studies (10). The syntheses are two- or three-step reactions. One anhydride of DTPA dianhydride is reacted with the 7-amino group of cs124; the other anhydride is reacted with a hetero-bifunctional compound containing an amino group on one end and a thiol-reactive group on the other end. Here we present the syntheses of additional thiol-reactive DTPA-cs124 chelates, including three iodoacetamides, two methanethiosulfonates (MTS), and an improved synthesis of a maleimide form.

### EXPERIMENTAL METHODS

**Chemicals and Materials.** The following were purchased from Sigma-Aldrich: diethylenetriaminepentaacetic acid dianhydride (caDTPA), 7-amino-4-methyl-2-(1*H*)-quinolinone (carbostyryl 124, cs124), iodoacetic anhydride, anhydrous dimethyl sulfoxide (DMSO, in sure seal bottle), piperidine, ethylenediamine (redistilled), and triethylamine (for reaction). DMSO and triethylamine were dried over activated molecular sieves before use. Glacial acetic acid, methanol, acetonitrile and triethylamine (for making TEAA buffer) were purchased from Fisher Scientific.  $\beta$ -Maleimidopropionic acid hydrazide·TFA was purchased from Molecular Biosciences (Boulder, CO). 2-Aminoethyl methanethiosulfonate, hydrobromide, and (*R*)-2-amino-2-carboxyethylmethanethiosulfonate were purchased from Toronto Research Chemicals, Inc. (North York, Ontario, Canada). Fmoc-*p*-aminophenylalanine (Fmoc-*p*-amino-Phe-OH) and *p*-nitro-phenylalanine (H-*p*-nitro-phe-OH) were purchased from Bachem Bioscience Inc. (King of Prussia, PA). Maltose binding protein (MBP) was a gift from Panvera Inc. (Madison, WI). Distilled and deionized (18 M $\Omega$  cm<sup>-1</sup>) water was used throughout. All glassware was washed with a mixed acid solution and thoroughly rinsed with deionized, distilled water. All plastic labware was purchased from Bio-rad (metal-free). All chemicals were of the purest grade available.

**Purification.** Most commonly, reverse-phase high-performance liquid chromatography was performed at room temperature on a Waters model 600 system with a Dynamax 60 Å C<sub>18</sub> column (10 or 25 mm i.d.  $\times$  250 mm,

\* To whom correspondence should be addressed at Department of Physics, 1110 W. Green St., University of Illinois, Urbana, IL 61801. (217) 244–3371 (tel); (217) 244–7559 (fax); selvin@uiuc.edu.

<sup>†</sup> Department of Physics.

<sup>‡</sup> Center for Biophysics and Computational Biology.

Rainin, at 8 mL/min, respectively) using a linear gradient (solvent A = 0.1 M triethylammonium acetate, pH 6.5; solvent B = methanol, or acetonitrile). Sep-Pak C<sub>18</sub> cartridges (Waters) were used for purifying the iodoacetamide chelates. Reaction mixtures were loaded on Sep-Pak cartridges, washed with H<sub>2</sub>O, and then 1:1 MeOH/H<sub>2</sub>O. The process was monitored by shining UV light ( $\lambda$  = 365 nm) on the cartridge. The fluorescent fractions were dried under vacuum at room temperature, and the powder was stored at -80 °C.

**Spectroscopy.** NMR spectra were recorded on a Varian Unity 400 spectrometer. Time-resolved and gated luminescence measurements were made on a laboratory-built spectrometer described previously, employing a 5-ns excitation pulse at 337 nm followed by time-resolved detection of lanthanide emission (18). The number of waters in the primary coordination sphere of the lanthanide was determined via the method of Horrocks and Sudnick (19): no. of waters =  $q(\tau_{\text{H}_2\text{O}}^{-1} - \tau_{\text{D}_2\text{O}}^{-1})$ , ( $q$  = 1.05 for Eu, 4.2 for Tb). The overall quantum yield ( $Q_{\text{overall}}$ ), i.e., the probability of the lanthanide emitting given that the antenna was excited, was measured via an intensity comparison of a reactive chelate to either Tb<sup>3+</sup>- or Eu<sup>3+</sup>-DTPA-cs124, whose  $Q_{\text{overall}}$ 's have been measured to be 0.32 and 0.1, respectively (20). The efficiency of energy transfer from the antenna to the lanthanide ( $Q_{\text{transfer}}$ ) (20) was determined by comparing the number of excited lanthanides in the sample of interest to a reference sample, shortly after the excitation pulse. The reference is Tb<sup>3+</sup>- or Eu<sup>3+</sup>-DTPA-cs124, where  $Q_{\text{transfer}}$  was previously determined to be 0.67 and 0.59, respectively (20). Finally, the quantum efficiency of lanthanide emission,  $Q_{\text{Ln}}$ , i.e., the probability that the lanthanide will emit a photon given that the lanthanide was excited, was measured by comparing the lifetimes of the samples and the reference.  $Q_{\text{Ln}}$  for the reference Tb<sup>3+</sup>- and Eu<sup>3+</sup>-DTPA-cs124 was previously found to be 0.482 and 0.167, respectively (20).

**Syntheses (Figures 1 and 2). DTPA-cs124-EDA-Iodoacetamide.** DTPA-cs124-EDA (8) (5 mg, 8.5  $\mu$ mol) was dissolved in 3 mL of 10% NaHCO<sub>3</sub>. The solution was stirred in an ice bath for 15 min. Iodoacetic anhydride (14.5 mg, 42.5  $\mu$ mol) was added to the solution. The reaction mixture was stirred at 0 °C for 3 h. Cold 2.0 M H<sub>2</sub>SO<sub>4</sub> was added to the solution slowly to adjust the pH to the range of 4–5. The solution was loaded on a Sep-Pak C18 column, washed with H<sub>2</sub>O, and then 1:1 H<sub>2</sub>O/CH<sub>3</sub>OH. The elution process was monitored by shining UV 356 nm light on the cartridge. The fluorescent fraction was collected and dried under vacuum. The product was confirmed by mass spectroscopy (758, M<sup>-</sup> - 1, ESI).

**DTPA-cs124-Fmoc-*p*-NH<sub>2</sub>-Phenylalanine.** DTPA dianhydride (50 mg, 141  $\mu$ mol) was dissolved in the mixture of 0.5 mL of DMSO and 0.4 mL of triethylamine under N<sub>2</sub>. A total of 17 mg of cs124 (97.7  $\mu$ mol) in 0.5 mL of DMSO was added to the above solution dropwise via a syringe. The reaction was stirred at room temperature for 1 h. The solution was transferred to a flask containing 75 mg (187  $\mu$ mol) of Fmoc-*p*-aminophenylalanine. The reaction mixture was stirred at room temperature for 2 h. A total of 10 mL of 0.1 M TEAA was added to quench the reaction. The reaction mixture was purified by HPLC with a linear 20–40% ACN/0.1 M TEAA (pH 6.5) gradient over 40 min. The product was eluted at 33.5 min (18 mg, ~20% yield; MS: 932, M<sup>-</sup> - 1; ESI).

**DTPA-cs124- $\alpha$ -NH<sub>2</sub>-Phenylalanine.** The aqueous solution of DTPA-cs124-Fmoc-*p*-NH<sub>2</sub>-phenylalanine was concentrated, and added to 5% piperidine aqueous solu-

tion. The solution was stirred at room temperature for 2 h. Acetic acid was added to adjust the pH to ~6.5. The reaction mixture was purified by HPLC with a linear 30–50% MeOH/0.1 M TEAA (pH 6.5) gradient over 40 min. The product was eluted at 21 min (~60% yield, estimated based on its HPLC profile; MS: 710, M<sup>-</sup> - 1; ESI). <sup>1</sup>H NMR in D<sub>2</sub>O: 7.75 (1H, s), 7.06 (1H, d), 6.94 (2H, d), 6.88 (1H, d), 6.68 (2H, d), 6.00 (1H, s), 3.61–3.72 (8H, m), 3.46 (4H, s), 3.26–3.38 (3H, b), 3.22 (2H, s), 3.16 (2H, s), 2.76 (1H, dd), 2.67 (3H, s), 2.60 (1H, dd).

**DTPA-cs124- $\alpha$ -NH<sub>2</sub>-Phenylalanine-Iodoacetamide.** DTPA-cs124- $\alpha$ -NH<sub>2</sub>-phenylalanine (8 mg, 11  $\mu$ mol) was dissolved in 3 mL of 10% NaHCO<sub>3</sub>. The solution was stirred in an ice bath for 15 min. Iodoacetic anhydride (8 mg, 23  $\mu$ mol) was added to the solution. The reaction mixture was stirred at 0 °C for 3 h. Cold 2.0 M H<sub>2</sub>SO<sub>4</sub> was added to the solution slowly to adjust the pH to 2–3. A white precipitate formed. The white solid was collected and dried under vacuum (8.3 mg, 86%). The product was confirmed by its mass spectrum (878, M<sup>-</sup> - 1, ESI).

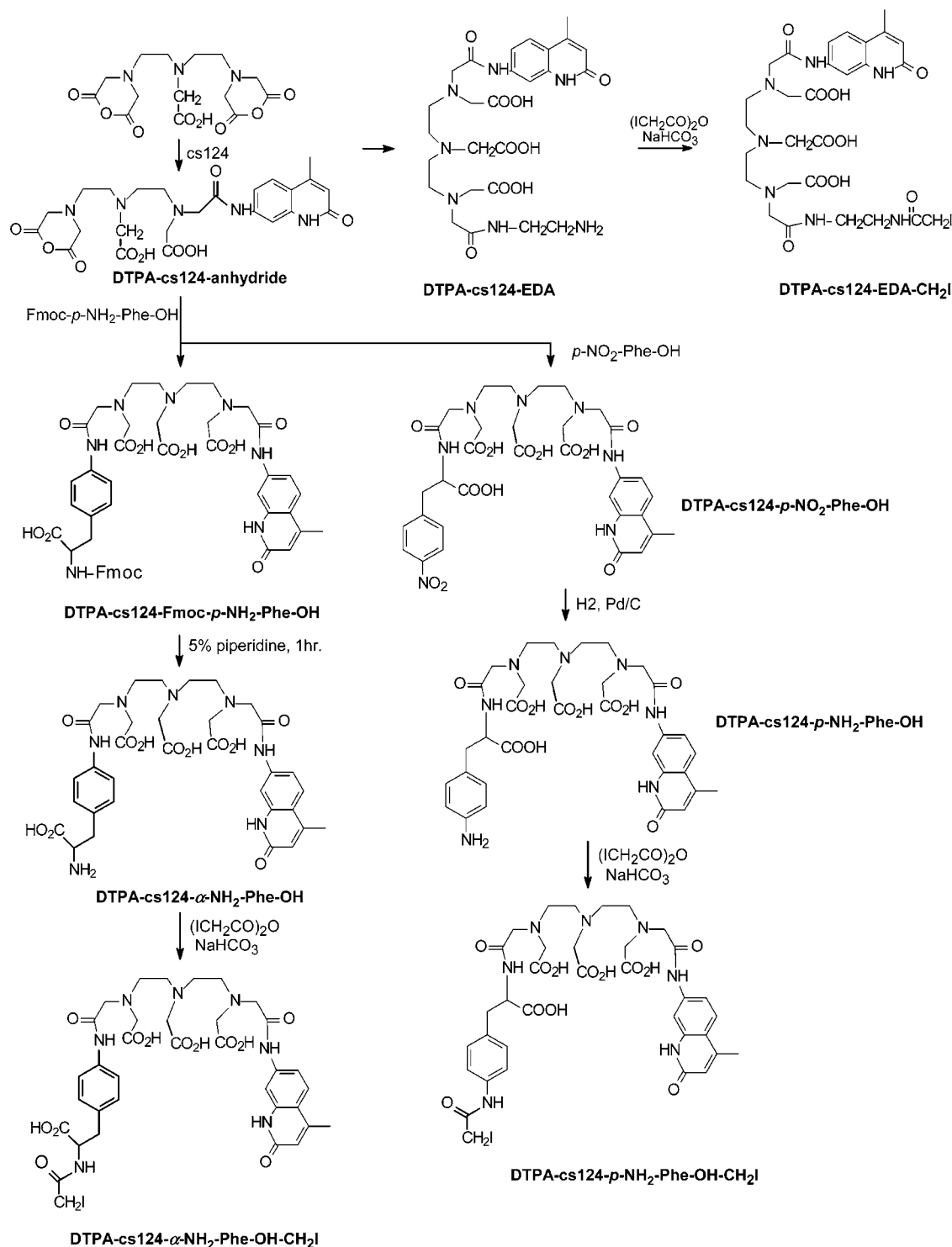
**DTPA-cs124-*p*-NO<sub>2</sub>-Phenylalanine.** DTPA dianhydride (25 mg, 70  $\mu$ mol) was dissolved in the mixture of 0.5 mL of DMSO and 0.3 mL of triethylamine under N<sub>2</sub>. A total of 10 mg of cs124 (57.5  $\mu$ mol) in 0.5 mL of DMSO was added to the above solution dropwise via a syringe. The reaction was stirred at room temperature for 1 h under N<sub>2</sub>. The solution was transferred to a flask containing 17.3 mg (82.4  $\mu$ mol) of *p*-nitrophenylalanine. The reaction mixture was stirred at room temperature for 2 h under N<sub>2</sub>. A total of 10 mL of 0.1 M TEAA was added to quench the reaction. The reaction mixture was purified by HPLC with a linear 30–50% MeOH/0.1 M TEAA (pH 6.5) gradient over 40 min. The product was eluted at 24 min. (18 mg, ~40% yield based on HPLC profile; MS: 740, M<sup>-</sup> - 1; ESI).

**DTPA-cs124-*p*-NH<sub>2</sub>-Phenylalanine.** A total of 1 mL of the concentrated HPLC elute (~5 mM) of DTPA-cs124-*p*-NO<sub>2</sub>-phenylalanine was mixed with 5 mg of 10% Pd/C, and degassed under vacuum. H<sub>2</sub> was introduced into the flask through a balloon. The reaction mixture was stirred at r.t. for 15 h. The Pd/C catalyst was filtered. The HPLC profile of the filtrate indicated the hydrogenation is 100% complete. The NMR spectrum has been previously published (8).

**DTPA-cs124-*p*-NH<sub>2</sub>-Phenylalanine-Iodoacetamide.** The HPLC-purified DTPA-cs124-*p*-NH<sub>2</sub>-phenylalanine solution was dried under vacuum. The solid residue was redissolved into 10% NaHCO<sub>3</sub>. Iodoacetic anhydride (5 mg, 14  $\mu$ mol) was added to the above solution at 0 °C, and the reaction mixture was stirred at 0 °C for 30 min. Acetic acid was added to adjust the pH to ~5. The solution was then passed through a C18 Sep-Pak cartridge. The fluorescent elutes were collected and concentrated under vacuum. Mass spectroscopy confirmed DTPA-cs124-*p*-NH<sub>2</sub>-phenylalanine-iodoacetamide (878, M<sup>-</sup> - 1, ESI), and the product was used directly in labeling experiments without further purification.

**DTPA-cs124-MTSEA.** DTPA dianhydride (30 mg, 84  $\mu$ mol) was dissolved in the mixture of 0.5 mL of DMSO and 0.2 mL of triethylamine under N<sub>2</sub>. A total of 10 mg of cs124 (57  $\mu$ mol) in 0.3 mL of DMSO was added to the solution slowly via a syringe. The reaction mixture was stirred at room temperature for 1 h. 2-Aminoethyl methanethiosulfonate-HBr (52.4 mg, 111  $\mu$ mol) in 0.5 mL of DMSO was added to the solution. The reaction mixture was stirred at room temperature for 2 h. TEAA buffer (4 mL, 0.1 M, pH 6.5) was then added to quench the reaction. The reaction mixture was purified via reverse



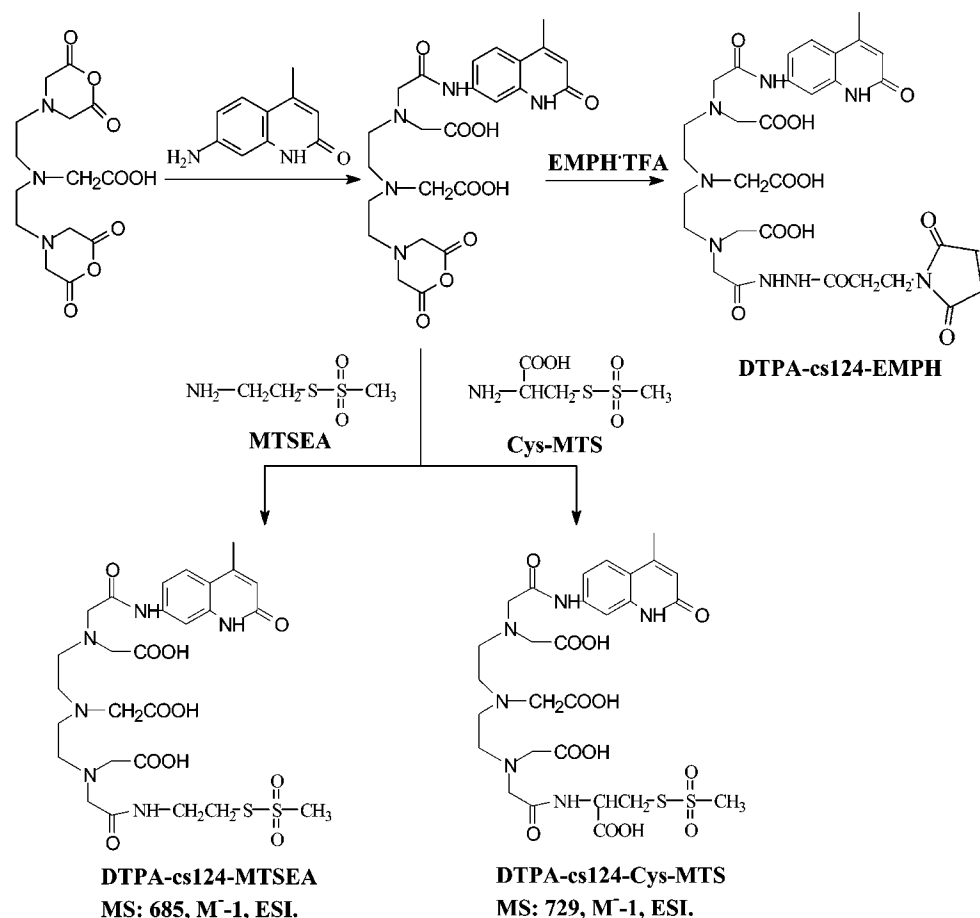


**Figure 1.** Synthetic scheme for iodoacetamide forms of DTPA-cs124.

phase HPLC with a 20–40% MeOH/TEAA (0.1 M, pH 6.5) linear gradient over 40 min. The product, DTPA-cs124-MTSEA, along with DTPA-bis-cs124, eluted at 18.5 min ( $M^-1$ : 685, DTPA-cs124-MTSEA, ESI;  $M^-1$ : 704, DTPA-bis-cs124, ESI).

**DTPA-cs124-Cys-MTS.** DTPA dianhydride (36 mg, 101  $\mu\text{mol}$ ) was dissolved in a mixture of 0.5 mL of DMSO and 0.2 mL of triethylamine under  $\text{N}_2$ . (*R*)-2-amino-2-carboxyethylmethanethiosulfonate (8.9 mg, 45  $\mu\text{mol}$ ) in 0.3 mL of DMSO was added slowly to the solution via a syringe. The reaction mixture was stirred at room temperature for 1 h. Carboxystyryl 124 (27.3 mg, 157  $\mu\text{mol}$ ) in

0.5 mL of DMSO was added to the solution and the reaction mixture stirred at room temperature for 2 h. TEAA buffer (4 mL, 0.1 M, pH 6.5) was added to quench the reaction. The reaction mixture was purified via reverse phase HPLC with a 25–40% MeOH/TEAA (0.1 M, pH 6.5) linear gradient over 40 min. The product, DTPA-cs124-Cys-MTS, was eluted at 23 min ( $M^-1$ : 729, ESI).  $^1\text{H}$  NMR in  $\text{D}_2\text{O}$ : 7.74 (1H, s), 7.23 (1H, d), 6.96 (1H, d), 6.06 (1H, s), 4.37 (1H, dd), 3.72 (2H, s), 3.67 (2H, s), 3.63 (2H, s), 3.52 (2H, s), 3.50 (2H, s), 3.42 (1H, dd), 3.33 (1H, dd), 3.15–3.3 (b) and 3.26 (s) (11H total), 2.67 (3H, s).



**Figure 2.** Synthetic scheme for maleimide and methanethiosulfonate forms of DTPA-cs124.

**DTPA-cs124-EMPH.** DTPA dianhydride (25 mg, 70.5  $\mu\text{mol}$ ) was dissolved in a mixture of 0.5 mL of DMSO and 0.2 mL of triethylamine under  $\text{N}_2$ . A total of 10 mg of cs124 (57.5  $\mu\text{mol}$ ) in 0.5 mL of DMSO was added to the above solution slowly via a syringe. The reaction was stirred at room temperature for 1 h. 3-Maleimidopropionic acid hydrazide-TFA (EMPH, 17 mg, 57.2  $\mu\text{mol}$ ) in 0.5 mL of DMSO was then added to the solution, and the mixture was stirred at room temperature for 2 h. A total of 5 mL of 0.1 M TEAA pH 6.5 was added to quench the reaction. The reaction mixture was purified via reverse phase HPLC with a 25–40% MeOH/0.1 M TEAA pH 6.5 linear gradient over 40 min. DTPA-cs124-EMPH eluted at 22 min (~30% yield, estimated by HPLC profile.  $M^-1$ : 713, ESI). The byproduct, DTPA-(cs124)<sub>2</sub>, eluted at 23.5 min.

**Addition of Metals.**  $\text{TbCl}_3$  or  $\text{EuCl}_3$  was added to the chelate in a 0.9:1 molar ratio at usually >0.5 mM concentration at pH 6–7, usually in 0.1 M TEAA, pH 6.5 buffer, and allowed to stand for 30 min at room temperature before use.

**Coupling to Biomolecules.** The labeling conditions for conjugation to muscle protein (HMM, skeletal Heavy-meromyosin, or S1 fragment of smooth muscle myosin containing a single cysteine at position 208) have been described previously (9, 13, 16). The procedure for labeling Shaker ion channels in *Xenopus* oocytes has also been published (17). The iodoacetamide and methanethiosulfonate chelates were coupled to HMM, or to maltose binding protein (MBP, a 65-kDa protein containing a single cysteine) at a typical ratio of 10:1 with the protein concentration ~15  $\mu\text{M}$ . The coupling reaction was carried out on ice overnight in 20 mM Mops, pH 7.0, 5 mM

$\text{MgCl}_2$ . The excess lanthanide chelates were removed by passing the reaction mixture through a Sephadex G-50 size exclusion column.

## RESULTS AND DISCUSSION

**Syntheses of Compounds.** Figures 1 and 2 show the synthetic pathways for the various thiol-reactive chelates. Their correct structures were judged by mass spectroscopy, UV-Vis absorption, lanthanide luminescence properties, the reactivity with thiol groups, and NMR for DTPA-cs124-Cys-MTS and DTPA-cs124- $\alpha$ - $\text{NH}_2$ -phenylalanine-iodoacetamide. Depending on the commercial availability of starting materials, the syntheses were either two-step (one-pot) reactions as for DTPA-cs124-MTSEA, DTPA-cs124-Cys-MTS, and DTPA-cs124-EMPH, or multiple-step reactions as for DTPA-cs124-EDA- $\text{CH}_2\text{I}$  and the two forms of DTPA-cs124-Phe- $\text{CH}_2\text{I}$ . The syntheses of DTPA-cs124-MTSEA and DTPA-cs124-Cys-MTS are straightforward. DTPA dianhydride was reacted with either cs124 or the corresponding amino-methanethiosulfonate reagents first, followed by the addition of the other reagents to complete the reaction. By using a combination of methanol and TEAA buffer, DTPA-cs124-Cys-MTS is well-separated from byproducts by HPLC, while DTPA-cs124-MTSEA is coincidental with the DTPA-(cs124)<sub>2</sub> byproduct.

We previously reported on the synthesis of DTPA-cs124-EMPH via a two- and three-step (one-pot) reaction, but found low yields for the two-step reaction (9). We now report conditions for the two-step (one-pot) synthesis of DTPA-cs124-EMPH that gives a satisfactory (30%) yield. In addition, by using a linear gradient of 25–40%

**Table 1. Life Times of Thiol-Reactive Tb<sup>3+</sup> Chelates Labeled to Proteins**

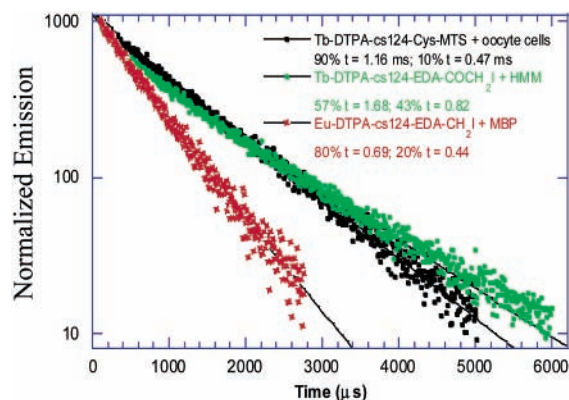
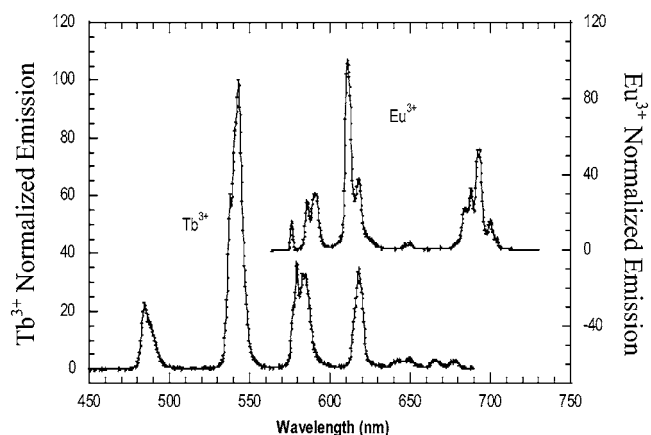
lanthanide	chelates	proteins	lifetime (ms)
Tb <sup>3+</sup>	DTPA-cs124-Phe- $\alpha$ -NH <sub>2</sub> -COCH <sub>2</sub> I	HMM <sup>a</sup>	34% 0.81
			66% 1.57
		MBP	57% 1.30
			12% 1.65
			31% 0.22
	DTPA-cs124-EDA-COCH <sub>2</sub> I	HMM	43% 0.82
			57% 1.68
		MBP	36% 1.65
			37% 0.78
			27% 0.12
	DTPA-cs124-MTSEA	myosin S1	16% 0.31
		HC208 <sup>b</sup>	84% 1.41
		MBP	56% 1.26
			44% 0.58
		Shaker K <sup>+</sup> channels in oocyte cells <sup>c</sup>	66% 1.20
			34% 0.55
	DTPA-cs124-Cys-MTS	myosin S1	90% 1.42
		HC208	10% 0.55
		MBP	79% 1.29
			21% 0.60
		Shaker K <sup>+</sup> channels in oocyte cells <sup>c</sup>	90% 1.16
			10% 0.47
		none	89% 1.53
	DTPA-cs124-Phe- $p$ -NH <sub>2</sub> -COCH <sub>2</sub> I		11% 0.44
		MBP	74% 1.46
			26% 0.37
	DTPA-cs124-EMPH	MBP	89% 1.92
			11% 0.79

<sup>a</sup> Heavy meromyosin fragment (350 kD) of skeletal myosin.<sup>b</sup> Subfragment 1 (100 kD) of smooth muscle myosin with a single cysteine at position 208 of the heavy chain. <sup>c</sup> Details of ion channel expression can be found at ref 17.

methanol/TEAA buffer, the DTPA-cs124-EMPH product is well separated from the DTPA-(cs124)<sub>2</sub> byproduct.

To synthesize an iodoacetamide chelate, one NH<sub>2</sub> group in a diamine compound was reacted with DTPA-cs124 mono anhydride to form DTPA-cs124-diamine compound in an in situ reaction. The remaining NH<sub>2</sub> group in the DTPA-cs124-diamine compound was then reacted with iodoacetic anhydride in a sodium bicarbonate solution to form the corresponding iodoacetamide chelate. All reaction mixtures were loaded onto Sep-Pak columns, and washed with H<sub>2</sub>O and 1:1 MeOH/TEAA buffer. The elution with 1:1 MeOH/TEAA buffer was dried down under vacuum and redissolved in TEAA buffer for labeling purpose without further purification. DTPA-cs124-EDA was synthesized using a published method (8). DTPA-cs124- $\alpha$ -NH<sub>2</sub>-Phe-OH was synthesized by the reaction of DTPA dianhydride with cs124 and Fmoc- $p$ -NH<sub>2</sub>-Phe-OH. The Fmoc protecting group was subsequently removed by hydrolysis with 5% piperidine to form DTPA-cs124- $\alpha$ -NH<sub>2</sub>-Phe-OH. DTPA-cs124- $p$ -NH<sub>2</sub>-Phe-OH was synthesized by the reaction of DTPA dianhydride with cs124 and  $p$ -NO<sub>2</sub>-Phe-OH. The NO<sub>2</sub> group was subsequently reduced to NH<sub>2</sub> by catalytic hydrogenation process.

**Spectroscopy of Compounds.** Tables 1 and 2 list the excited-state lifetimes of Tb<sup>3+</sup> and Eu<sup>3+</sup> measured for their complexes with the chelates labeled to proteins. Figure 3 shows three representative lifetime decays of thiol-reactive chelates labeled to HMM, MBP, and to Shaker K<sup>+</sup> expressed in an *Xenopus* oocyte. Figure 4 shows the characteristic spiked emission spectra of Tb<sup>3+</sup> and Eu<sup>3+</sup> coordinated to DTPA-cs124-Cys-MTS. All of the

**Figure 3.** Representative lifetimes of Tb<sup>3+</sup> and Eu<sup>3+</sup> complexes attached to HMM, MBP, and Shaker K<sup>+</sup> channels in oocytes.**Figure 4.** Normalized Tb<sup>3+</sup> and Eu<sup>3+</sup> emission spectra in DTPA-cs124 Cys-MTS in 0.1 M TEAA pH 6.5 at a concentration of 1  $\mu$ M. Tb<sup>3+</sup> and Eu<sup>3+</sup> display their characteristic sharply spiked spectra. Pulsed excitation was at 40 Hz, 3.5  $\mu$ J/pulse for Tb<sup>3+</sup>, 3.0  $\mu$ J/pulse for Eu<sup>3+</sup>; integration time is 1 s for Tb<sup>3+</sup> and 10 s for Eu<sup>3+</sup>.**Table 2. Life Times of Thiol-Reactive Eu<sup>3+</sup> Chelates Labeled to Proteins**

lanthanide	chelates	proteins	lifetime (ms)
Eu <sup>3+</sup>	DTPA-cs124-Phe- $\alpha$ -NH <sub>2</sub> -COCH <sub>2</sub> I	MBP	31% 0.70
			69% 0.08
	DTPA-cs124-EDA-COCH <sub>2</sub> I	MBP	80% 0.69
			20% 0.44
	DTPA-cs124-MTSEA	MBP	24% 1.05
			76% 0.62
	DTPA-cs124-Cys-MTS	MBP	77% 0.70
			23% 0.16
	unconjugated		94% 0.58
			6% 0.96
	DTPA-cs124-Phe- $p$ -NH <sub>2</sub> -COCH <sub>2</sub> I	MBP	59% 0.96
			41% 0.33
	DTPA-cs124-EMPH	MBP	14% 1.07
			37% 0.32
			49% 0.043

thiol-reactive chelates can quickly and efficiently react with thiol groups in proteins. As expected, the lifetime for both lanthanides is in the millisecond range. Although all the lifetimes are either biexponential or triexponential, the percentage of long or short lifetime components varies upon the nature of chelates and the attached proteins. In general, a high percentage of long lifetime component (0.6 ms for Eu, 1.5 ms for Tb) is advantageous. Among them, the methanethiosulfonate (MTS) chelates show biexponential fitting with a major population (typ.



**Table 3. Photophysics Data of Tb<sup>3+</sup>- and Eu<sup>3+</sup>-DTPA-cs124-Cys-MTS and Their Glutathione Adduct<sup>a</sup>**

Tb <sup>3+</sup> (Eu <sup>3+</sup> ) complexes	no. of coordinated H <sub>2</sub> O <sup>b</sup>	Q <sub>overall</sub>	Q <sub>transfer</sub>	Q <sub>Ln</sub>	τ (ms)
DTPA-cs124	1.1 (1.26)	0.324 (0.099)	66.6% (59.1%)	0.482 (0.167)	1.55 (0.62)
DTPA-cs124-Cys-MTS ( <i>n</i> = 3)	1.0 (1.0)	0.21 ± 0.003 (0.075 ± 0.004)	52% ± 1% (38% ± 3%)	0.42 ± 0.01 (0.12 ± 0.002)	1.35 ± 0.02 (0.73 ± 0.02)
DTPA-cs124-Cys-MTS-Glu ( <i>n</i> = 3)	1.02 (1.28)	0.25 ± 0.02 (0.074 ± 0.003)	54% ± 5% (44% ± 2%)	0.46 ± 0.006 (0.10 ± 0.001)	1.48 ± 0.01 (0.60 ± 0.003)

<sup>a</sup> All quantum yields (Q) and excited-state lifetimes (τ) are in H<sub>2</sub>O-based buffer. Uncertainties are reported as ± one standard deviation.

<sup>b</sup> On the basis of lifetime measurements via method of Horrocks and Sudnik (see text, (19)) in H<sub>2</sub>O and D<sub>2</sub>O. For Tb<sup>3+</sup> (Eu<sup>3+</sup>) – DTPA-cs124-Cys-MTS, the lifetimes were 1.35 ms (0.70) in H<sub>2</sub>O, and 2.3 ms (2.2 ms) in D<sub>2</sub>O. For Tb<sup>3+</sup> (Eu<sup>3+</sup>) – DTPA-cs124-Cys-MTS-Glu, the lifetimes were 1.47 ms (0.59) in H<sub>2</sub>O, and 2.29 ms (2.16) in D<sub>2</sub>O.

80–90%) having a long lifetime (ms) when unconjugated or conjugated to biomolecules.

The iodoacetamide chelates showed significantly improved labeling efficiency compared to the bromoacetamide form previously made (9). (By using higher pH, however, conjugation of a DTPA-cs124-EDA-bromoacetamide to cysteines can be improved (21)). The iodoacetamide chelates generally show a nearly equal population of the long and short lifetime components, although the ratio appears to depend on the biomolecule it is conjugated to. (DTPA-cs124-EDA-Br, which forms the same product as DTPA-cs124-EDA-I after conjugation to a thiol, showed a single-exponential signal upon conjugation to a muscle protein, the regulatory light chain (9)). In some cases when MBP was used, it became triexponential. Tb-DTPA-cs124-EMPH was also labeled to MBP. The measurement shows 89% long lifetime at 1.92 ms and 11% short lifetime at 0.79. This result is similar to when Tb-DTPA-cs124-EMPH is attached to the regulatory light chain of myosin (13).

**Photophysics of MTS Lanthanide Chelates.** We have characterized the photophysics of the Tb<sup>3+</sup>- and Eu<sup>3+</sup>- DTPA-cs124-Cys-MTS and their glutathione adducts, DTPA-cs124-Cys-MTS-Glu (Table 3). The latter was formed by reaction of the MTS-chelate with the reduced form of glutathione at pH 7.2 and purified by HPLC. The number of waters in the primary coordination sphere of Tb<sup>3+</sup>- and Eu<sup>3+</sup>-DTPA-cs124-Cys-MTS and DTPA-cs124-Cys-MTS-Glu were found to be 1.0 (1.0) and 1.02 (1.28), respectively, based on lifetime measurements of the chelates' major component in H<sub>2</sub>O and D<sub>2</sub>O. The reference complexes, Tb<sup>3+</sup>- and Eu<sup>3+</sup>-DTPA-cs124, were previously found to contain 1.1 (1.26) H<sub>2</sub>O molecules in their coordination spheres (22). These data indicate that there is no extra ligation to the lanthanides in DTPA-cs124-Cys-MTS complexes and their glutathione adducts.

We also measured the overall quantum yield (Q<sub>overall</sub>), the transfer efficiency from antenna to lanthanide (Q<sub>transfer</sub>), and the quantum yield for lanthanide emission (Q<sub>Ln</sub>) of the DTPA-cs124-Cys-MTS and its glutathione adduct (Table 3). This is accomplished by comparing the overall lanthanide intensity, the intensity of the initially excited lanthanide ions, and the average lifetimes, respectively, of the MTS-chelates to Tb<sup>3+</sup>- and Eu<sup>3+</sup>-DTPA-cs124 standards (20). We find Q<sub>overall</sub> = 0.21 (0.075) for Tb<sup>3+</sup>-(Eu<sup>3+</sup>-)DTPA-cs124-Cys-MTS and Q<sub>overall</sub> = 0.25 (0.074) for Tb<sup>3+</sup>-(Eu<sup>3+</sup>-)DTPA-cs124-Cys-MTS-Glu.

**Conclusion.** We have synthesized new thiol-reactive iodoacetamide and methanethiosulfonate forms of the luminescent lanthanide chelate, DTPA-cs124, and improved the synthesis and separation method for DTPA-cs124-EMPH. All of these chelates can easily react with thiol groups in proteins under neutral or slightly acidic condition. Generally, their lifetimes after labeling to proteins are biexponential, with a major population displaying a long lifetime. A particularly promising

chelate is DTPA-cs124-Cys-MTS, especially for ion channel studies where MTS reagents are commonly used. In addition, the ethylenediamine iodoacetamide chelate is a more reactive form of the bromoacetamide chelate which has previously been synthesized and shown to be single exponential when bound to the regulatory light chain of myosin (9). Our results demonstrate the synthetic versatility of this kind of chelate and their capability for labeling cysteines on proteins. These compounds should be useful as donors in resonance energy transfer experiments.

#### ACKNOWLEDGMENT

This work is supported by NIH Grant AR44420 and NSF Grant 9984841. We thank Baigen Mei, Marie Christenson, and Kurt Vogel from Panvera Corp. for the generous gift of MBP protein. The labeling experiments to smooth muscle myosin HC208 were done by Jeff Reifenberger. The labeling experiments to oocytes expressing *Shaker* ion channels were done by David Posson. The mass spectrometry was obtained by the Mass Spectrometry Center, University of Illinois at Urbana-Champaign.

#### LITERATURE CITED

- (1) Soini, E., and Lövgren, T. (1987) Time-resolved fluorescence of lanthanide probes and applications in biotechnology. *CRC Crit. Rev. Anal. Chem.* 18, 104–154.
- (2) Sammes, P. G., and Yahioglu, G. (1996) Modern bioassays using metal chelates as luminescent probes. *Nat. Prod. Rep.* 13, 1–28.
- (3) Selvin, P. R. (2002) Principles and biophysical applications of luminescent lanthanide probes. *Annu. Rev. Biophys. Biomol. Struct.* 31, 275–302.
- (4) Seveus, L., Vaisala, M., Hemmilla, I., Kojola, H., Roomans, G. M., and Soini, E. (1994) Use of fluorescent europium chelates as labels in microscopy allows glutaraldehyde fixation and permanent mounting and leads to reduced autofluorescence and good long-term stability. *Microsc. Res. Technol.* 28, 149–154.
- (5) Marriott, G., Heidecker, M., Diamandis, E. P., and Yan-Marriott, Y. (1994) Time-resolved delayed luminescence image microscopy using an europium ion chelate complex. *Biophys. J.* 67, 957–965.
- (6) Stryer, L., Thomas, D. D., and Meares, C. F. (1982) Diffusion-enhanced fluorescence energy transfer. In *Annu. Rev. Biophys. Bioeng.* (Mullins, L. J., Ed.) Vol. 11, pp 203–222, Annual Reviews, Inc., Palo Alto, CA.
- (7) Mathis, G. (1995) Probing molecular interactions with homogeneous techniques based on rare earth cryptates and fluorescence energy transfer. *Clin. Chem.* 41, 1391–1397.
- (8) Li, M., and Selvin, P. R. (1997) Amine-reactive forms of a luminescent DTPA chelate of terbium and europium: Attachment to DNA and energy transfer measurements. *Bioconjugate Chem.* 8, 127–132.
- (9) Chen, J., and Selvin, P. R. (1999) Thiol-reactive luminescent lanthanide chelates. *Bioconjugate Chem.* 10, 311–315.

- (10) Kapanidis, A. N., Ebright, Y. W., Ludescher, R. D., Chan, S., and Ebright, R. H. (2001) Mean DNA bend angle and distribution of DNA bend angles in the CAP-DNA complex in solution. *J. Mol. Biol.* **312**, 453–468.
- (11) Takalo, H., Mikkala, V.-M., Mikola, H., Liitti, P., and Hemmila, I. (1994). Synthesis of europium(III) chelates suitable for labeling of bioactive molecules. *Bioconjugate Chem.* **5**, 278–282.
- (12) Heyduk, E., and Heyduk, T. (1997). Thiol-reactive luminescent Europium chelates: luminescence probes for resonance energy transfer distance measurements in biomolecules. *Anal. Biochem.* **248**, 216–227.
- (13) Burmeister-Getz, E., Cooke, R., and Selvin, P. R. (1998) Luminescence resonance energy transfer measurements in myosin. *Biophys. J.* **75**, 2451–2458.
- (14) Xiao, M., Li, H., Snyder, G. E., Cooke, R., Yount, R., and Selvin, P. R. (1998) Conformational changes between the active-site and regulatory light chain of myosin as determined by luminescence resonance energy transfer: The effect of nucleotides and actin. *Proc. Natl. Acad. Sci. U.S.A.* **95**, 15309–15314.
- (15) Chakrabarty, T., Xiao, M., Cooke, R., and Selvin, P. R. (2002). Holding two heads together: stability of the myosin II rod measured by resonance energy transfer between the heads. *Proc. Natl. Acad. Sci. U.S.A.* **99**, 6011–6016.
- (16) Xiao, M., Reifengerger, J. G., Wells, A. L., Baldacchino, C., Chen, L. Q., Ge, P., Sweeney, H. L., and Selvin, P. R. (2003) An actin-dependent conformational change in myosin. *Nat. Struct. Biol.* **10**, 402–408.
- (17) Cha, A., Snyder, G. E., Selvin, P. R., and Bezanilla, F. (1999) Atomic scale movement of the voltage sensing region in a potassium channel measured via spectroscopy. *Nature* **402**, 809–813.
- (18) Xiao, M., and Selvin, P. R. (1999). An Improved instrument for measuring time-resolved lanthanide emission and resonance energy transfer. *Rev. Sci. Instrum.* **70**, 3877–3881.
- (19) Horrocks, W. D., Jr., and Sudnick, D. R. (1979). Lanthanide ion probes of structure in biology. Laser-induced luminescence decay constants provide a direct measure of the number of metal-coordinated water molecules. *J. Am. Chem. Soc.* **101**, 334–350.
- (20) Xiao, M., and Selvin, P. R. (2001). Quantum yields of luminescent lanthanide chelates and far-red dyes measured by resonance energy transfer. *J. Am. Chem. Soc.* **123**, 7067–7073.
- (21) Schelte, P., Boeckler, C., Frisch, B., and Schuber, F. (2000) Differential reactivity of maleimide and bromoacetyl functions with thiols: application to the preparation of liposomal diepitope constructs. *Bioconjugate Chem.* **11**, 118–123.
- (22) Li, M., and Selvin, P. R. (1995). Luminescent lanthanide polyaminocarboxylate chelates: the effect of chelate structure. *J. Am. Chem. Soc.* **117**, 8132–8138.

BC034029E

# Conjugates of PNA with Naphthalene Diimide Derivatives Having a Broad Range of DNA Affinities

Andriy A. Mokhir and Roland Kraemer\*

Anorganisch-Chemisches Institut, Ruprecht-Karls-Universitaet Heidelberg, Im Neuenheimer Feld 270, Heidelberg 69120, Germany. Received October 31, 2002; Revised Manuscript Received June 23, 2003

Peptide nucleic acids (PNAs) are neutral DNA analogues, which bind single-stranded DNA (ssDNA) strongly and with high sequence specificity. However, binding efficiency is dependent on the purine content of the PNA strand. This property make more difficult application of PNA as hybridization probes in, e.g., PNA chips, since at a set temperature the hybridization of a fraction of the DNA targets to the PNA probes does not obey Watson–Crick binding rules. The polypurine PNAs, for example, bind the mismatch containing DNA targets stronger, than the pyrimidine rich PNAs their fully complementary targets. Herein we show that PNA–DNA binding efficiency can be finely tuned by the conjugation of derivatives of naphthalene diimide (NADI) to the N-terminus of PNA using polyamide linkers of different lengths. This approach can potentially be used for the design of PNA probes, which bind their DNA targets with similar affinity independently of the PNA sequence.

## INTRODUCTION

Peptide nucleic acids are DNA analogues, in which the sugar–phosphate backbone has been substituted by *N*-(2-aminoethyl)-glycine units. Therefore, PNA is characterized by high chemical stability and high nucleic acid binding affinity and specificity (1). Additional desirable properties of PNA can be introduced via terminal conjugation of small molecules. The majority of such modifications reported up-to-date facilitate detection of PNA, using for example fluorescence spectroscopy (2), electrochemistry (3), and vibrational spectroscopy (4). There is just a limited number of reports on terminal modifications increasing affinity of PNA toward ssDNA significantly (5, 6). This would be important, first, because PNA–DNA duplex stability is dependent on the purine content of PNA strand, which makes applications of PNA probes more difficult (7). In particular, at a set hybridization temperature binding of mismatch polypyrimidine DNA sequences will be as efficient as binding of match polypurine DNA sequence. Second, PNA probes with high binding affinity toward ssDNA may be able to disrupt dsDNA, by forming PNA–DNA duplex and leaving one DNA strand unbound, which was reported up to now only for polypurine PNA (8). Alternative mechanism of disruption of dsDNA was reported for pseudocomplementary PNA, which bind both DNA strands (9, 10). Sequence specific dsDNA recognition, which is not restricted to polypurine/polypyrimidine DNA sequences can potentially find many applications, including, e.g., artificial restriction enzymes, gene suppression, labeling, and identification.

Although many small molecules stabilizing DNA duplexes are known and factors important for efficient ligand–dsDNA interactions are well understood (11–13), this knowledge cannot be directly applied for the design

of ligands affecting PNA–DNA duplex stability, because the PNA–DNA duplex is structurally considerably different from DNA duplex and has a lower negative charge density. Common intercalators and groove-binders are normally poor ligands for PNA–DNA duplexes (14). Therefore, further studies on new modifications stabilizing PNA–DNA duplexes are warranted. N-terminal modifications affecting PNA–DNA duplex thermal stability substantially have been reported by Okamoto et al. for 8-methoxypsoralen and Harrison et al. for polycationic peptides (for both  $\Delta T_m = + 8.0$  °C) (5). It should be noted that an alternative strategy including incorporation of nonnatural bases into the interior of PNA has proven to be successful for stabilization of PNA–DNA duplexes, but it often includes laborious synthesis (15, 16).

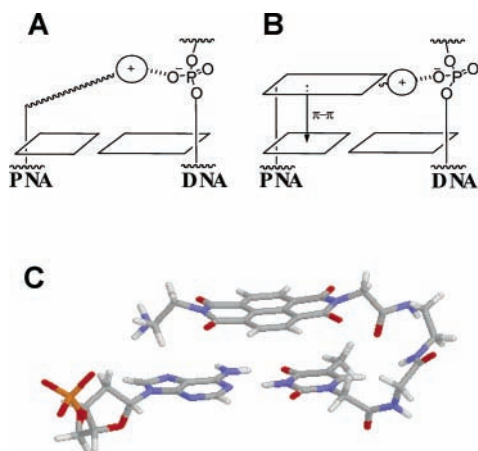
For making PNA probes having sequence independent binding affinity toward DNA, N-terminal modifiers with different stabilizing power are needed. Our strategy for generation of such a set of modifications is based, first, on modulation of  $\pi$ -stacking interactions between a planar aromatic fragment and the PNA–DNA duplex using linkers of different length. Second, the conjugate with the best linker is modified by attaching DNA binding ligands (Figure 1B), which further stabilize PNA–DNA duplex.  $\pi$ -Stacking between the planar fragment and basepairs of PNA–DNA restricts motions of the ligands to the region close to DNA, which should entropically favor ligand–DNA interactions in comparison with a fully flexible system (Figure 1A). Herein we demonstrate that this two-step approach allows generation of N-terminal PNA modifications with a broad range of effects on stability of PNA–DNA duplexes.

## EXPERIMENTAL PROCEDURES

**General.** The best commercially available chemicals from Acros (Geel, Belgium), Aldrich/Sigma/Fluka (Deisenhofen, Germany), Advanced Chemtech (Louisville, KY) and Novabiochem (Weidenmattweg, Switzerland) were obtained and used without purification. The reagents for PNA synthesis were obtained from PerSeptive

\* Corresponding author's address: Anorganisch-Chemisches Institut, Ruprecht-Karls-Universitaet Heidelberg, Im Neuenheimer Feld 270, Heidelberg 69120, Germany. Tel.: (0)6221-548438. Fax: (0)6221-548599. E-mail: roland.kraemer@urz.uni-heidelberg.de.





**Figure 1.** (A) Positively charged fragment conjugated to PNA via a flexible linker. (B) Internal motions of the modification are reduced due to  $\pi$ - $\pi$  interaction of naphthalene diimide and basepairs of PNA-DNA. This favors interaction of modification (+) with DNA (-). (C) A terminal part of **19a:26** duplex obtained from molecular modeling using Hyperchem 5.0.2.

Biosystems (Hamburg, Germany) and fluorescent metal indicators from Molecular Probes (Leiden, The Netherlands). The *N*-allyloxycarbonylthylenediamine was synthesized as described (15). MALDI-TOF mass spectra were recorded on a Bruker BIFLEX III spectrometer. The solution of 3,5-dimethoxy-4-hydroxycinnamic acid (27 mM, TFA 0.1%,  $\text{CH}_3\text{CN}$  33% in water) was used as a matrix for MALDI-TOF analysis of the PNA conjugates. Samples for mass spectrometry were prepared on a Bruker MAP II probe preparation station by dried droplet method using 1/2 probe/matrix ratio for water and water/ $\text{CH}_3\text{CN}$  solutions (HPLC fractions) and 1/20 ratio for TFA/*m*-cresol (4/1) solutions. Mass accuracy with external calibration was 0.1% of the peak mass, i.e.,  $\pm 3.0$  at  $m/z$  3000. HPLC was performed at 22 or 49 °C on a Shimadzu liquid chromatograph equipped with UV-Vis detector, column oven and Advantec SF-2100W fraction collector. Macherey-Nagel Nucleosil C4 250  $\times$  4.6 mm column with gradients of  $\text{CH}_3\text{CN}$  (0.1% TFA, solvent B) in water (0.1% TFA, solvent A) was used (gradient A: 49 °C, 0% B for 5 min, in 30 min to 35% B, in 10 min to 90% B, 90% B for 10 min; gradient B: 22 °C, 0–2% B for 5 min, in 23 min to 20% B, in 7 min to 95% B, 95% B for 10 min). NMR spectra were recorded on a Bruker Avance 200 spectrometer. UV melting experiments were performed on a Varian Cary 100 Bio UV-Vis spectrophotometer measuring absorbance at 260 nm in 1-cm black wall semimicrocuvettes with sample volume 0.7 mL, 2  $\mu\text{M}$  strand concentration in MOPS buffer (10 mM, pH 7), NaCl (50 or 150 mM), and with or without  $\text{Zn}^{2+}$  (4  $\mu\text{M}$ ). Cooling and heating rates were 0.5 °C/min. Melting points were averages of the extrema of the first derivative of the 61-point smoothed curves from at least two cooling and two heating curves. Fluorescent spectra were acquired on a Varian Cary Eclipse fluorescence spectrometer.

**Synthesis of 3.** Fmoc-Gly-OH was coupled to Wang resin (5 g, 4.5 mmol of free hydroxyl groups) using diisopropylcarbodiimide (16). Loading of Fmoc-group on the resin was found to be 0.7 mmol/g. Unreacted hydroxyl groups were capped with  $\text{Ac}_2\text{O}$ /pyridine, and Fmoc-group was deprotected with piperidine/DMF. 1,4,5,8-Naphthalene-tetracarboxylic dianhydride (3.35 g, 12.5 mmol) was suspended in pyridine (65 mL) and added to the resin. The mixture was heated to 65 °C and DIEA (4.4 mL, 25 mmol) was added. The slurry obtained was refluxed for 8 h, then filtered hot, washed thoroughly with hot (90

°C) pyridine, with DMF (2  $\times$  10 mL) and  $\text{CH}_3\text{CN}$  (2  $\times$  10 mL), and dried under vacuum ( $10^{-2}$  mbar). A solution of  $\text{Ac}_2\text{O}$  (1.9 mL, 20 mmol) in pyridine (65 mL) was added to the resin. After 30 min the resin was filtered, washed with DMF (2  $\times$  10 mL) and  $\text{CH}_3\text{CN}$  (2  $\times$  10 mL), and dried under vacuum ( $10^{-2}$  mbar). Trifluoroacetic acid in  $\text{CH}_2\text{Cl}_2$  (20%, 60 mL) was added to the resin. After the sample was shaken for 3 h, the slurry was filtered and the resin was washed with  $\text{CH}_2\text{Cl}_2$  (30 mL). The filtrates obtained were combined, volatiles were evaporated (70 mbar), and diethyl ether (200 mL) was added to the solid residue. The resulting suspension was cooled to 4 °C and kept at this temperature for 8 h. After this, the precipitate formed was filtered off, washed with diethyl ether, and dried under vacuum ( $10^{-2}$  mbar) to give yellow amorphous solid, 0.59 g, 54%. LDI-TOF MS (negative mode)  $m/z$  found 325.9, calcd. for  $\text{C}_{16}\text{H}_6\text{NO}_7$  [ $\text{M}^-$ ] 325.2.  $^1\text{H}$  NMR (200 MHz,  $\text{DMSO}-d_6$ ):  $\delta$  8.60 (s, 4H), 4.67 (s, 4H).

**Synthesis of 4.** *N*-Allyloxycarbonylthylenediamine (0.27 g, 1.8 mmol), diisopropylethylamine (0.7 mL, 4.0 mmol), and **3** (0.59 g, 1.8 mmol) were mixed together in hot pyridine (80 mL, 65 °C), and the resulting suspension was stirred at this temperature for 8 h. Then volatiles were evaporated (10 mbar, 40 °C), aqueous HCl solution (1%, 50 mL) added, and the precipitate formed was filtered, washed with water (10 mL), and dried (0.01 mbar) to give the title product 0.59 g, 70%. LDI-TOF MS (positive mode)  $m/z$  found 451.6, calcd. for  $\text{C}_{22}\text{H}_{17}\text{N}_3\text{O}_8$  [ $\text{M}^+$ ] 451.1. TLC in ethanol/ $\text{AcOH}/\text{CH}_2\text{Cl}_2$  (5/2/97):  $R_f$  0.6.  $^1\text{H}$  NMR (200 MHz,  $\text{DMSO}-d_6$ , at 60 °C):  $\delta$  8.61 (m, 4H), 6.97 (broad s, 1H), 5.66 (m, 1H), 5.08 (d,  $^3J = 17$  Hz, 1H), 4.97 (d,  $^3J = 10$  Hz, 1H), 4.68 (s, 2H), 4.27 (m, 2H), 4.11 (m, 2H), 3.28 (m, 2H).  $^{13}\text{C}$  NMR (50 MHz,  $\text{DMSO}-d_6$ ):  $\delta$  169.75, 163.50, 163.01, 156.88, 134.43, 131.66, 131.13, 127.71, 127.10, 126.79, 126.15, 117.34, 64.86, 42.26. UV-Vis:  $\lambda_{\text{max}}$  (nm) 381, 361, 344 shoulder.

**Synthesis of PNA Conjugates.** *Synthesis of PNA Part of the Conjugates.* The PNA part of the conjugates was synthesized on an Expedite 8909 PNA/DNA synthesizer according to the manufacturers' recommendations for 2  $\mu\text{molar}$  scale synthesis.

*Coupling of Monoamines and Symmetric Diamines to Polymer Bound PNA.* Bromoacetyl bromide (8.7  $\mu\text{L}$ , 100  $\mu\text{M}$ ) and DIEA (19  $\mu\text{L}$ , 110  $\mu\text{mol}$ ) in DMF (1 mL) are added to the resin bound PNA bearing free amino group. The resulting suspension is left shaking for 1 h, then filtered, the resin washed with DMF (2  $\times$  1 mL),  $\text{CH}_3\text{CN}$  (2  $\times$  1 mL), and dried under vacuum ( $10^{-2}$  mbar). Amine (100  $\mu\text{M}$ ) and DIEA (19  $\mu\text{L}$ , 110  $\mu\text{mol}$ ) in  $\text{CH}_2\text{Cl}_2$  (1 mL) are added to the resin and the resulting mixture is left on a shaker for 8 h. Then, the resin is filtered, washed with  $\text{CH}_2\text{Cl}_2$  (2  $\times$  1 mL), DMF (2  $\times$  1 mL), and  $\text{CH}_3\text{CN}$  (2  $\times$  1 mL), and dried under vacuum ( $10^{-2}$  mbar).

*Coupling of Carboxylic Acids to Polymer Bound PNA.* Carboxylic acid (100  $\mu\text{mol}$ ), HBTU (34 mg, 90  $\mu\text{mol}$ ), and HOBT (14 mg, 100  $\mu\text{mol}$ ) are dissolved in DMF (1 mL) and DIEA (38  $\mu\text{L}$ , 220  $\mu\text{mol}$ ) is added. This solution is vortexed and immediately added to  $\text{H}_2\text{N}$ -PNA<sup>PG</sup>-Rink-PS resin (2–4  $\mu\text{mol}$  of free amino-groups). The slurry obtained is left under vigorous mixing for either 0.5 h for chiral amino acids or 1 h for the others. Then, the resin is filtered, washed with DMF (2  $\times$  1 mL) and  $\text{CH}_3\text{CN}$  (2  $\times$  1 mL), and dried under vacuum ( $10^{-2}$  mbar).

*Removal of Fmoc Groups.* Piperidine/DMF (1/4) mixture (1 mL) is added to the resin bound PNA containing Fmoc protected amino group(s) (2–4  $\mu\text{mol}$ ) and the reaction is allowed to proceed for 30 min. At the end of this time the resin is filtered, washed with DMF (2  $\times$  1

**Table 1. Optimization of the Linker between Naphthalene Diimide and the N-Terminus of PNA**

no	duplex	linker <sup>a</sup>	T <sub>m</sub> (°C) <sup>b</sup>	ΔT <sub>m</sub> <sup>c</sup>
1	<b>12:26</b>	–CH <sub>2</sub> C(O)–	63.5 ± 1.1	+2.5
2	<b>19a:26</b>	–C(=O)CH <sub>2</sub> NHCH <sub>2</sub> C(O)–	68.7 ± 1.4 (57.6 ± 1.1)	+7.7 (+4.7)
3	<b>16:26</b>	–C(=O)CH(CH <sub>2</sub> NH <sub>2</sub> )NHCH <sub>2</sub> C(O)–	69.9 ± 2.3	+8.9
4	<b>14:26</b>	–C(=O)CH(NH <sub>2</sub> )(CH <sub>2</sub> ) <sub>4</sub> NHCH <sub>2</sub> C(O)–	69.2 ± 1.0	+8.2
5	<b>20:26</b>	–	61.0 ± 1.0 (52.9 ± 1.2)	0 (0)
6	<b>19a:30</b>	–C(=O)CH <sub>2</sub> NHCH <sub>2</sub> C(O)–	55.1 ± 0.3	+7.3
7	<b>20:30</b>	–	47.8 ± 0.9	0
8	<b>19f:32</b>	–C(=O)CH <sub>2</sub> NHCH <sub>2</sub> C(O)–	68.5 ± 1.4	+12.6
9	<b>25:32</b>	–	55.9 ± 0.7	0
10	<b>19e:31</b>	–C(=O)CH <sub>2</sub> NHCH <sub>2</sub> C(O)–	22.0 ± 0.7	> +7.0
11	<b>24:31</b>	–	< 15	0
12	<b>19b:27</b>	–C(=O)CH <sub>2</sub> NHCH <sub>2</sub> C(O)–	74.4 ± 2.2	+13.9
13	<b>21:27</b>	–	60.5 ± 2.1	0
14	<b>19c:28</b>	–C(=O)CH <sub>2</sub> NHCH <sub>2</sub> C(O)–	70.1 ± 1.3	+12.3
15	<b>22:28</b>	–	57.8 ± 1.1	0
16	<b>19d:29</b>	–C(=O)CH <sub>2</sub> NHCH <sub>2</sub> C(O)–	71.6 ± 1.9	+12.6
17	<b>23:29</b>	–	59.0 ± 2.0	0

<sup>a</sup> Linker connecting naphthalene diimide with N-terminus of PNA. <sup>b</sup> Melting point of PNA–DNA at 10 mM MOPS, pH 7, 50 mM NaCl, [PNA] = [DNA] = 2 μM. In brackets are melting points for 150 mM NaCl solutions. <sup>c</sup> Difference in melting points of corresponding modified and nonmodified PNA–DNA. Vertical lines in the table separate PNAs with different sequences.

mL) and CH<sub>3</sub>CN (2 × 1 mL), and dried under vacuum (10<sup>–2</sup> mbar).

**Removal of Alloc Groups.** A mixture of tetrakis(triphenylphosphine)palladium(0) complex (5 mg, 4.3 μmol) and triphenylphosphine (1 mg, 3.8 mmol) is dissolved in CH<sub>2</sub>Cl<sub>2</sub> (0.5 mL), and thoroughly purged with argon. Separately, diethylammonium hydrocarbonate (5 mg, 38 μmol) is suspended in CH<sub>2</sub>Cl<sub>2</sub>, purged with argon and added to the solution of the Pd complex. The resulting solution is added to the resin bound PNA containing Alloc protected amino group(s) (2–4 μmol) and the reaction is allowed to proceed for 2 h. At the end of this time, the resin is filtered, washed with CH<sub>2</sub>Cl<sub>2</sub> (2 × 1 mL), DMF (2 × 1 mL) and CH<sub>3</sub>CN (2 × 1 mL), and dried under vacuum (10<sup>–2</sup> mbar).

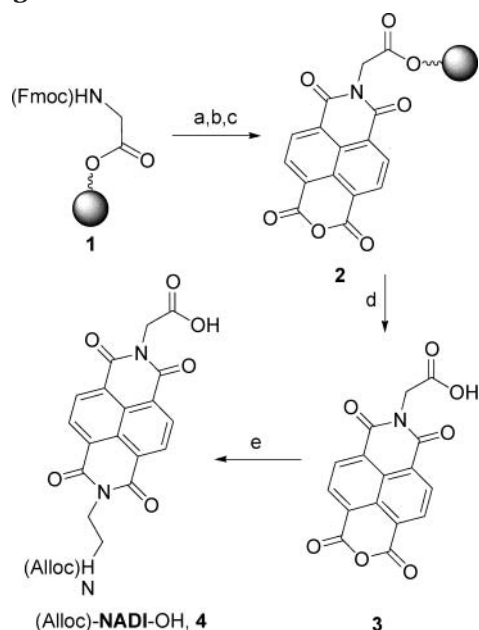
**PNA Cleavage, Deprotection, and Workup.** The resin bound PNA conjugate (0.5–4 μmol) is treated with TFA/*m*-cresol mixture (4/1 v/v, 120 μL) for 1.5 h. The resin is filtered off, the filtrate mixed with diethyl ether (2.5 mL), and the precipitate formed is filtered, washed with diethyl ether (2 × 1 mL), dried (0.01 mbar) and HPLC purified.

Compound **10**. HPLC gradient A: Rt = 25.7 min. Yield 7.0%. MALDI-TOF MS for C<sub>146</sub>H<sub>197</sub>N<sub>66</sub>O<sub>35</sub> [M+H]<sup>+</sup>: calcd 3434.6, found 3434.1. Compound **11**. HPLC gradient A: Rt = 23.6 min. Yield 8.2%. MALDI-TOF MS for C<sub>142</sub>H<sub>188</sub>N<sub>65</sub>O<sub>35</sub> [M+H]<sup>+</sup>: calcd 3363.5, found 3363.5. Compound **12**. HPLC gradient B: Rt = 43.8 min. Yield 6.1%. MALDI-TOF MS for C<sub>132</sub>H<sub>170</sub>N<sub>61</sub>O<sub>33</sub> [M+H]<sup>+</sup>: calcd 3137.3, found 3138.0. Compound **19a**. HPLC gradient A: Rt = 22.5 min. Yield 9.2%. MALDI-TOF MS for C<sub>134</sub>H<sub>173</sub>N<sub>62</sub>O<sub>34</sub> [M+H]<sup>+</sup>: calcd 3194.4, found 3194.8. Compound **19b**. HPLC gradient A: Rt = 23.0 min. Yield 10.1%. MALDI-TOF MS for C<sub>133</sub>H<sub>172</sub>N<sub>63</sub>O<sub>33</sub> [M+H]<sup>+</sup>: calcd 3179.4, found 3178.3. Compound **19c**. HPLC gradient A: Rt = 24.3 min. Yield 11.4%. MALDI-TOF MS for C<sub>134</sub>H<sub>172</sub>N<sub>65</sub>O<sub>32</sub> [M+H]<sup>+</sup>: calcd 3203.4, found 3204.7. Compound **19d**. HPLC gradient A: Rt = 24.0 min. Yield 5.2%. MALDI-TOF MS for C<sub>134</sub>H<sub>172</sub>N<sub>65</sub>O<sub>33</sub> [M+H]<sup>+</sup>: calcd 3219.4, found 3220.6. Compound **19e**. HPLC gradient A: Rt = 17.8 min. Yield 14.2%. MALDI-TOF MS for C<sub>92</sub>H<sub>120</sub>N<sub>41</sub>O<sub>22</sub> [M+H]<sup>+</sup>: calcd 2150.9, found 2149.2. Compound **19f**. HPLC gradient A: Rt = 20.0 min. Yield 11.0%. MALDI-TOF MS for C<sub>114</sub>H<sub>146</sub>N<sub>55</sub>O<sub>28</sub> [M+H]<sup>+</sup>: calcd 2733.2, found 2732.2. Compound **16**. HPLC gradient B: Rt = 43.9 min. Yield 5.1%. MALDI-TOF MS for C<sub>135</sub>H<sub>176</sub>N<sub>63</sub>O<sub>34</sub> [M+H]<sup>+</sup>: calcd 3223.4, found 3222.0. Compound **14**. HPLC

gradient B: Rt = 44.3 min. Yield 3.7%. MALDI-TOF MS for C<sub>138</sub>H<sub>182</sub>N<sub>63</sub>O<sub>34</sub> [M+H]<sup>+</sup>: calcd 3265.4, found 3265.2. Compound **18**. HPLC gradient A: Rt = 24.7 min. Yield 11.0%. MALDI-TOF MS for C<sub>128</sub>H<sub>186</sub>N<sub>63</sub>O<sub>30</sub> [M+H]<sup>+</sup>: calcd 3085.5, found 3085.9. Compound **20**. HPLC gradient A: Rt = 20.7 min. Yield 9.5%. MALDI-TOF MS for C<sub>114</sub>H<sub>159</sub>N<sub>58</sub>O<sub>28</sub> [M+H]<sup>+</sup>: calcd 2788.3, found 2786.0. Compound **21**. HPLC gradient A: Rt = 19.1 min. Yield 11.8%. MALDI-TOF MS for C<sub>113</sub>H<sub>158</sub>N<sub>59</sub>O<sub>27</sub> [M+H]<sup>+</sup>: calcd 2773.3, found 2771.8. Compound **22**. HPLC gradient A: Rt = 19.6 min. Yield 12.1%. MALDI-TOF MS for C<sub>114</sub>H<sub>158</sub>N<sub>61</sub>O<sub>26</sub> [M+H]<sup>+</sup>: calcd 2797.3, found 2796.8. Compound **23**. HPLC gradient A: Rt = 20.4 min. Yield 7.9%. MALDI-TOF MS for C<sub>114</sub>H<sub>158</sub>N<sub>61</sub>O<sub>27</sub> [M+H]<sup>+</sup>: calcd 2813.3, found 2814.1. Compound **24**. HPLC gradient A: Rt = 14.0 min. Yield 12.3%. MALDI-TOF MS for C<sub>72</sub>H<sub>106</sub>N<sub>37</sub>O<sub>16</sub> [M+H]<sup>+</sup>: calcd 1744.9, found 1743.1. Compound **25**. HPLC gradient A: Rt = 18.0 min. Yield 12.3%. MALDI-TOF MS for C<sub>94</sub>H<sub>131</sub>N<sub>51</sub>O<sub>22</sub> [M+H]<sup>+</sup>: calcd 2326.1, found 2325.0.

## RESULTS

The design of N-terminal PNA modifications utilizes a linker component, a planar aromatic fragment and a DNA binding ligand. The linker component is varied to modulate π-stacking interactions between the duplex and the planar aromatic fragment. We have chosen polyamide linkers (Table 1), since their length and flexibility can be easily controlled by a variation of amino acid fragments using commercially available derivatives. Naphthalene diimide (NADI) was selected as a planar aromatic fragment because its geometric parameters are closely related to those of natural AT and GC pairs and it efficiently interacts with DNA duplexes and to some extent with triplexes by means of π-stacking (19–21). Moreover, it offers two imide groups available for modification, positioned on opposite sides, on the line dividing this molecule into two equal parts. One imide group was used for the conjugation with PNA and the other one for the attachment of DNA binding ligands. The latter were chosen to be macrocyclic ligands: **L**<sup>1</sup> or **L**<sup>2</sup> (Scheme 2). These ligands are able to bind negatively charged DNA due to electrostatic interactions (**L**<sup>1</sup> and **L**<sup>2</sup> are positively charged at pH 7), hydrogen bonding or, when they form metal complexes with, e.g., Zn<sup>2+</sup>, due to metal coordination (e.g., LZn--OP). Moreover, they increase PNA

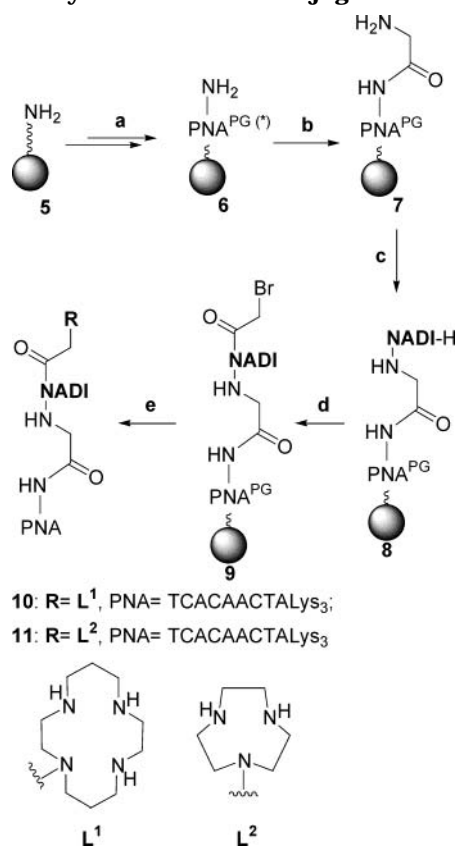
**Scheme 1. Synthesis of Naphthalene Diimide Building Block<sup>a</sup>**

<sup>a</sup>(a) Piperidine, DMF, (b) 1,4,5,8-naphthalene-tetracarboxylic dianhydride, DIEA, pyridine, (c) Ac<sub>2</sub>O, pyridine, (d) TFA, CH<sub>2</sub>Cl<sub>2</sub>, (e) *N*-(allyloxycarbonyl)ethylenediamine, DIEA, pyridine.

solubility in water in contrast to typically hydrophobic intercalators and groove binders.

**Modeling.** Molecular modeling using AMBER force field energy minimization (Hyperchem 5.0.2) was conducted to probe whether the ligands attached to the imide group of the NADI~PNA conjugate (conjugate **19a** was used as example, -NH<sub>2</sub> as the ligand) are well positioned for interaction with DNA. Geometry of the terminal basepair of the duplex was taken from a reported NMR structure (22), the NADI structure was energy-minimized using AMBER force field and initial parameters for amino acids were from Hyperchem template set. In the energy minimized structure (Figure 1C), the NADI and a basepair are positioned one over another with 3.4 Å distance between their mean planes, which indicates their  $\pi$ -stacking interaction. Distance between PNA and DNA termini in the duplex is ~18.3 Å. In the conjugate modeled the -NH<sub>2</sub> ligand is positioned on the side of the DNA strand in the PNA-DNA duplex and the distance between the point of the ligand connection and the DNA terminus is ~8.7 Å. Thus, ligands conjugated to PNA via the NADI linker are positioned 9.6 Å closer to the DNA backbone than those attached directly to the PNA terminus.

**Synthesis.** Unsymmetrically substituted intermediate **4** (Scheme 1) was required for synthesis of PNA conjugates **10–12**, **14**, **16**, and **19a–f**. This compound has a carboxylic group for coupling with the free amino group of PNA and an Alloc protected amino group, which serves for the conjugation of **L<sup>1</sup>** and **L<sup>2</sup>** (Scheme 2). Alloc group can be cleaved under mild neutral conditions, which do not affect acid (Bhoc, Boc) and base (Fmoc) sensitive groups employed in PNA protection. In known methods of synthesis of unsymmetrical naphthalene diimides (19–21), two amines are reacted with 1,4,5,8-naphthalene-tetracarboxylic dianhydride to produce a statistical product mixture, which is separated by column chromatography. Application of this methodology for synthesis of **4** has produced the desirable product with low yield, mainly because of low product solubility in organic solvents and

**Scheme 2. Synthesis of PNA Conjugates **10** and **11**<sup>a</sup>**

**10:** R = **L<sup>1</sup>**, PNA = TCACAAC<sub>2</sub>ALys<sub>3</sub>

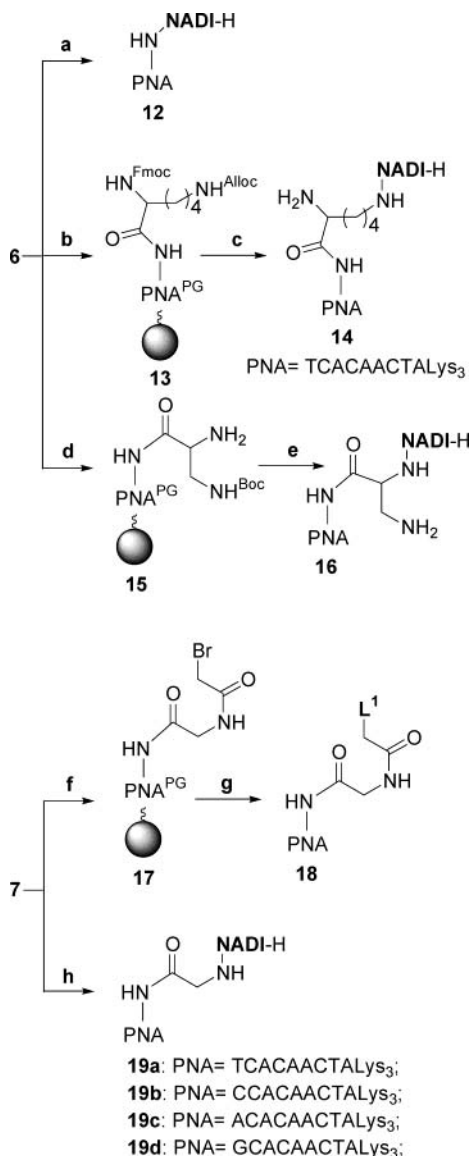
**11:** R = **L<sup>2</sup>**, PNA = TCACAAC<sub>2</sub>ALys<sub>3</sub>

<sup>a</sup>(a) PNA synthesis, (b) (1) (Fmoc)-Gly-OH, HBTU, HOBT, DIEA, DMF, (2) piperidine, DMF, (c) (1) (Alloc)-NADI-OH (**4**), HBTU, HOBT, DIEA, DMF, (2) Ac<sub>2</sub>O, pyridine, (3) Pd(PPh<sub>3</sub>)<sub>4</sub>, PPh<sub>3</sub>, (NEt<sub>2</sub>H)(HCO<sub>3</sub>), CH<sub>2</sub>Cl<sub>2</sub>, (d) bromoacetyl bromide, DIEA, DMF, (e) (1) **HL<sup>1(2)</sup>**, DIEA, CH<sub>2</sub>Cl<sub>2</sub>, (2) TFA, *m*-cresol. (\*) PG = protecting groups: Bhoc for PNA nucleobases: A, C, and G and Boc for  $\epsilon$ -NH<sub>2</sub> of PNA lysines.

similar mobility of symmetrical and unsymmetrical products in silica gel. Therefore, a new method of synthesis was developed (Scheme 1). First, compound **1** was synthesized by coupling Fmoc-Gly-OH to Wang resin under standard conditions (18), then Fmoc group was cleaved and free amino group was acylated with an excess of 1,4,5,8-naphthalene-tetracarboxylic dianhydride. After acetylation of unreacted amino groups, cleavage from the solid support and precipitation using diethyl ether compound **3** was obtained (>90% purity). Finally, the reaction of **3** with *N*-(allyloxycarbonyl)ethylenediamine gave the desired product **4** (>90% purity). In contrast to known procedures, this method can be used for combinatorial synthesis of unsymmetrical naphthalene diimides, since it does not require laborious purification and a range of suitable starting materials (monoprotected diamines and Fmoc-protected amino acids) are commercially available.

For the optimization of the interaction of naphthalene diimide with PNA-DNA basepairs product **4** was attached to the N-terminus of PNA via linkers of different length: directly (PNA **12**), via a three-atom achiral linker (PNA **19a**), three-atom chiral linker (PNA **16**) and seven-atom linker (PNA **14**). Synthesis of **19a** and **16** was performed by first coupling corresponding Fmoc protected amino acid to resin bound PNA (**6**, Scheme 2) using HBTU, HOBT, DIEA activating mixture (**7**, Scheme 2, **15**, Scheme 3) then Fmoc deprotection, acylation with **4**, Alloc cleavage using Pd<sup>0</sup> catalyst and finally cleavage from the solid support using TFA. MALDI-TOF mass spectrum of the crude product **19a** (Figure 2, **A**) il-

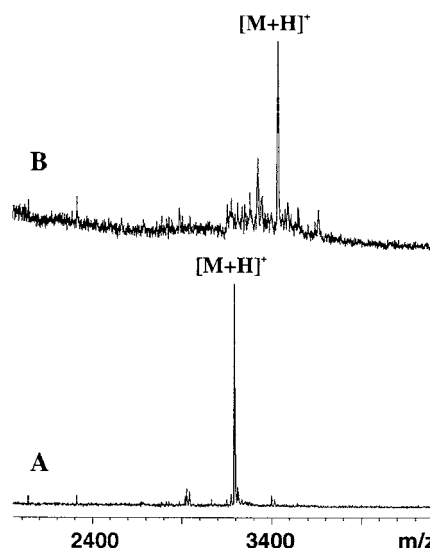


**Scheme 3. Synthesis of PNA Conjugates 12, 14, 16, 18, 19a–f<sup>a</sup>**

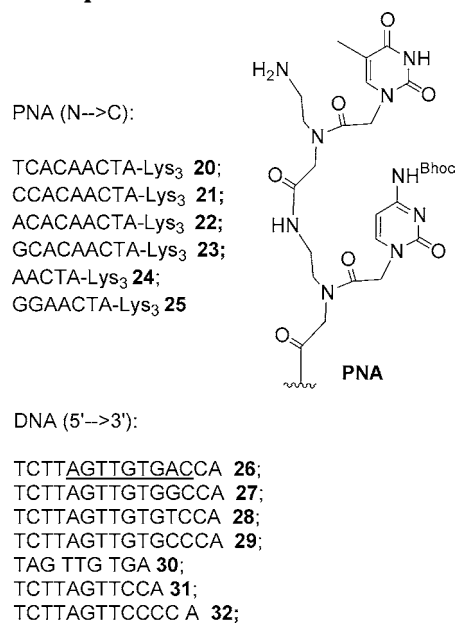
illustrates high synthesis efficiency. Compound **14** was synthesized analogously, except that after coupling Fmoc-Lys(ε-Alloc)-OH, Alloc group was cleaved first, free amino group was acylated with the **4**, and Alloc and Fmoc groups were consequently cleaved (Scheme 3).

Intermediate **8** was used for the conjugation of amines (Scheme 2). Its bromoacetylation gave intermediate **9**, which is suitable for the attachment of a variety of mono and symmetric polyamines. The desired conjugates **10**, **11** were obtained by reacting **9** with an excess of HL<sup>1</sup> or HL<sup>2</sup>. MALDI-TOF mass spectrum of crude **10** is shown in Figure 2B. Following TFA/*m*-cresol deprotection and PNA precipitation using diethyl ether the conjugates were purified in one (**12**, **14**, **16**, **18**, **19a–f**) or two (**10**, **11**) HPLC runs. Nonmodified PNA and DNA used in this study are shown in Scheme 4.

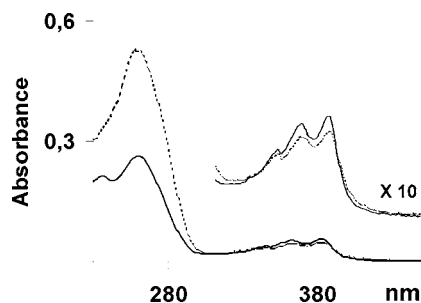
**Hybridization of PNA with ssDNA.** Naphthalene diimide stabilizes PNA–DNA duplexes best, when it is



**Figure 2.** MALDI-TOF mass spectra of crude **19a** (A) and **10** (B).

**Scheme 4 Nonmodified PNA and DNA Used for Hybridization Experiments**

attached to the N-terminus of the PNA via linkers consisting of five atoms ( $\Delta T_m = +7.7$ – $8.9$  °C, entries 2 and 3, Table 1). If the linker is longer than five atoms, its size seems to be unimportant (entry 4). However, stabilization of the duplex is much reduced when a shorter linker is used ( $\Delta T_m = 2.5$  °C, entry 1). Therefore, in all further experiments the NADI has been conjugated with the N-terminus of the PNA via the -C(O)CH<sub>2</sub>-NHCH<sub>2</sub>C(O)- linker. Analogues of **19a** with other PNA sequences (**19b–f**) were synthesized to test generality of the effect observed. In all cases, PNA–DNA duplexes were more stable than corresponding nonmodified PNA–DNA duplexes (entries 6–17, Table 1). Moreover, duplexes of PNA **19a** with long, **26** and short, **30** DNA were stabilized to the same extent ( $\Delta T_m = +7.7$  and  $+7.3$  °C respectively, entries 2 and 6). UV-spectra of the NADI~PNA show characteristic absorption bands for polynucleotides ( $\lambda_{max} = 260$  nm) and for naphthalene diimides ( $\lambda_{max} = 381$ , 361, and 344 nm) (**19–21**) (Figure 3). Upon titration of PNA solutions with complementary DNA, **26**, the intensity of the absorption bands of NADI



**Figure 3.** UV-visible spectra of **10** (solid line) and **10:26** (dotted line) recorded in MOPS buffer 10 mM pH 7, NaCl 50 mM, [PNA] = [DNA] = 2  $\mu$ M.

**Table 2.** Melting Points of PNA–DNA Duplexes

no	duplex	$T_m$ (°C) <sup>a</sup>		$\Delta T_m$ (°C) <sup>b</sup>
		[NaCl] 50 mM	[NaCl] 150 mM	
1	<b>10:26</b>	72.6 ± 0.7	61.3 ± 1.0	11.6 (8.3)
2	<b>10:26/Zn<sup>2+</sup></b>	72.0 ± 1.0	60.6 ± 1.7	11.0 (7.7)
3	<b>11:26</b>	70.3 ± 1.6	60.1 ± 1.1	9.3 (7.2)
4	<b>11:26/Zn<sup>2+</sup></b>	70.3 ± 0.7	60.2 ± 1.2	9.3 (7.3)
5	<b>18:26</b>	60.8 ± 1.8	53.1 ± 2.1	−0.2 (+0.2)
6	<b>18:26/Zn<sup>2+</sup></b>	60.5 ± 1.9	52.5 ± 1.5	−0.5 (−0.4)

<sup>a</sup> Melting point of PNA–DNA at 10 mM MOPS, pH 7, [PNA] = [DNA] = 2  $\mu$ M and with 4  $\mu$ M Zn<sup>2+</sup> or without. For melting experiments 2 equiv of Zn<sup>2+</sup> were used (4  $\mu$ M), since at lower concentrations dissociation and association curves were considerably shifted from each other (hysteresis effect). <sup>b</sup> Difference in melting points of PNA–DNA duplexes and the control **20:26** duplex at 50 mM NaCl, and in brackets at 150 mM NaCl.

decreases, which signals an intercalation of NADI in the PNA–DNA duplex (19). Moreover, melting transition of **19a:26** duplex monitored at 260 and 361 nm occurs at the same temperature, which indicates cooperative dissociation of both PNA–DNA basepairs and NADI. Importantly, the N-terminal modification of PNA with NADI does not significantly alter PNA sequence specificity toward DNA (Supporting Information).

The duplex of DNA **26** with conjugate **10**, which consists of PNA, NADI, and macrocycle **L**<sup>1</sup> melts at a temperature 3.9  $^{\circ}$ C higher than that of **19a:26** and 11.6  $^{\circ}$ C higher than nonmodified **20:26** (entries 1 and 3, Table 2). Interestingly, DNA affinity of **L**<sup>1</sup>-NH-Gly-PNA conjugate (**18**), which does not contain the NADI, is practically the same as that of the nonmodified PNA **20** (entry 5, Table 2).

Due to the high affinity of **L**<sup>1</sup> and **L**<sup>2</sup> toward Zn<sup>2+</sup>, this cation is expected to be fully bound by conjugates **10**, **11** at micromolar concentrations. In agreement with this, fluorescent Zn<sup>2+</sup> indicator Newport Green does not detect Zn<sup>2+</sup> ions in **10(11)/Zn<sup>2+</sup>** solutions (1:1, 2  $\mu$ M). However, stability of **10:26** and **11:26** duplexes is not affected by Zn<sup>2+</sup> (4  $\mu$ M).

## DISCUSSION

In the duplexes of DNA with NADI~PNA conjugates, NADI is  $\pi$ -stacking with the duplex basepairs, as it is evident from a substantial increase in thermal stability of the duplexes of PNA **19a–f** with corresponding complementary DNA ( $\Delta T_m$  = 7.7–13.9  $^{\circ}$ C, Table 1) and an apparent hypochromicity of the absorption bands of the NADI chromophore in duplexes. The absence of terminal mismatch discrimination in NADI~PNA–DNA duplexes is in agreement with intercalative binding, since alternative stacking on the terminal basepair is expected to increase terminal mismatch discrimination (23). Base-stacking interaction between the NADI and the duplex is further indicated in that melting profiles obtained at

361 nm for modified PNA–DNA duplexes exhibited cooperative increase in hyperchromicity with a midpoint in the transition that corresponded to that obtained at 260 nm (19).  $\pi$ -Stacking of naphthalene diimide with DNA duplexes and triplexes is well documented (17–19), while for PNA–DNA duplexes it is observed for the first time. This is an interesting result, because due to considerable structural differences of PNA–DNA and DNA–DNA duplexes and the lower negative charge density of the former, usual intercalators and groove-binders of double stranded DNA are often poor ligands for PNA–DNA duplexes. In contrast to naphthalene diimide, N-terminally conjugated naphthalene imide was found to stabilize the PNA–DNA duplex insignificantly ( $\Delta T_m$  = 0.5  $^{\circ}$ C) (24). Surprisingly, NADI equally stabilizes the fully matched PNA–DNA duplexes and those with a single mismatch in the terminal and penultimate positions (Supporting Information). This might indicate that the naphthalene diimide is positioned between the second and the third basepairs of the PNA–DNA duplexes. However, more detailed structural studies are required for unambiguous conclusions about the structure of these duplexes.

The five atom linker, -C(O)CH<sub>2</sub>NHCH<sub>2</sub>C(O)-, which is as well used for the attachment of nucleobases in PNA, positions NADI well for  $\pi$ -stacking in the duplex ( $\Delta T_m$  = +7.7  $^{\circ}$ C, entries 2 and 5, Table 1). The use of a shorter linker allows obtaining a PNA of lower DNA affinity ( $\Delta T_m$  = +2.5  $^{\circ}$ C, entries 1,5, Table 1), while the positively charged linker with the same number of atoms as well as the longer one give the PNAs of slightly higher DNA affinity ( $\Delta T_m$  = +8.9 and +8.2  $^{\circ}$ C, respectively, entries 3–5, Table 1). Since the stabilization trend for the five atom linker is reproduced for six PNA sequences and for two DNA targets, we believe that these effects have a general character.

The results presented in this study outline an approach for increasing efficiency of ligand–DNA interaction by a combination of proper ligand positioning and ligand motion constraining. Since the intercalator is connected with the N-terminus of PNA at one end and its orientation is fixed by  $\pi$ - $\pi$  interaction with the terminal and the penultimate basepairs of PNA–DNA, the other end is positioned at the negatively charged DNA backbone (Figure 1C). If a DNA binding ligand is attached, its orientation in relation to the DNA will be predefined by the NADI position. Such constraining of the ligand position should facilitate ligand–DNA interaction due to proximity effects, reduced possibilities for internal motions of the ligand and environment effects (duplex interior is hydrophobic, therefore polar interactions will be stronger than in water). This is illustrated by stabilization of **10:26** in comparison with **19a:26** ( $\Delta T_m$  = +3.9  $^{\circ}$ C). As expected, when **L**<sup>1</sup> is attached directly to the PNA, no stabilization is observed (entry 5, Table 2). At higher salt concentration, **10:26** melts at a temperature 3.7  $^{\circ}$ C higher than **19a:26**. This salt independent stabilization cannot be rationalized in terms of electrostatic interactions between positively charged **L**<sup>1</sup> and negatively charged DNA backbone, since it would be reduced in the presence of higher salt concentration. Hydrogen bonding (with, e.g., deprotonated phosphodiester groups of the DNA backbone) is a feasible possibility, since it is a salt independent interaction, and it is expected to be considerably stronger in the hydrophobic duplex interior than in water solution.

The method of synthesis of **10**, **11** can be easily adapted to other amine-containing ligands interacting with or modifying DNA, e.g. intercalators, groove binders, metal

binding ligands and alkylating agents. Due to the factors mentioned above for **L**<sup>1</sup>, these ligands, when positioned by the NADI in close proximity to the DNA, should have a stronger effect on the DNA than the ligands directly attached to the PNA. Finally, the N-terminal PNA modifications increasing thermal stability of PNA–DNA duplexes by 2.5, 7.7, 8.2, 8.9, 9.3, and 11.0 °C found in this study can be potentially used for the design of PNA probes, whose DNA binding affinity is sequence independent.

#### ACKNOWLEDGMENT

We thank Ruprecht-Karls-Universitaet Heidelberg, Fonds der Chemischen Industrie and Ministerium für Wissenschaft, Forschung und Kunst Baden-Württemberg for financial support. A.M. thanks Prof. C. Richert for his help on early stages of the development of this project.

**Supporting Information Available:** Melting points of duplexes of conjugate **19a** and nonmodified PNA **20** with complementary and mismatch DNAs. MALDI-TOF mass spectra of all new compounds reported in this paper. This material is available free of charge via the Internet at <http://pubs.acs.org>.

#### LITERATURE CITED

- (1) Nielsen, P. E., and Egholm, M. (1999) *An Introduction to PNA. Peptide Nucleic Acids Protocols and Applications* (Nielsen, P. E., and Egholm, M., Eds.) pp 1–19, Horizon Scientific Press, England.
- (2) Seitz, O., and Koehler, O. (2001) Convergent strategies for the attachment of fluorescing reporter groups to peptide nucleic acids in solution and on solid phase. *Chem. Eur. J.* 7, 3911–3925.
- (3) Verheijen, J. C., van der Marel, G. A., van Boom, J. H., and Metzler-Nolte, N. (2000) Transition metal derivatives of peptide nucleic acid (PNA) oligomers- synthesis, characterization, and DNA binding. *Bioconjugate Chem.* 11, 741–743.
- (4) Hess, A., and Metzler-Nolte, N. (1999) Labeling of [Leu<sup>5</sup>]-enkephalin with organometallic Mo complexes by solid-phase synthesis. *Chem. Commun.* 11, 885–886.
- (5) Okamoto, A., Tanabe, K., and Saito, I. (2001) Synthesis and properties of peptide nucleic acids containing psoralen unit. *Org. Lett.* 3, 925–927.
- (6) Uhlmann, E., Peyman, A., Breipohl, G., and Will, D. W. (1998) PNA: synthetic polyamide nucleic acids with unusual binding properties. *Angew. Chem. Int. Ed.* 37, 2796–2823.
- (7) Ratilainen, T., Holmen, A., Tuite, E., Nielsen, P. E., and Norden, B. (2000) Thermodynamics of sequence-specific binding of PNA to DNA. *Biochemistry* 39, 7781–7791.
- (8) Nielsen, P. E., and Christensen, L. (1996) Strand displacement binding of a duplex-forming homopurine PNA to a homopyrimidine duplex DNA target. *J. Am. Chem. Soc.* 118, 2287–2288.
- (9) Demidov, V. V., Protozanova, E., Izvol'sky, K. I., Price, C., Nielsen, P. E., and Frank-Kamenetskii, M. D. (2002) Kinetics and mechanism of the DNA double helix invasion by pseudocomplementary peptide nucleic acids. *Proc. Natl. Acad. Sci. U.S.A.* 99, 5953–5958.
- (10) Lohse, J., Dahl, O., and Nielsen, P. E. (1999) Double duplex invasion by peptide nucleic acid: A general principle for sequence-specific targeting of double-stranded DNA. *Proc. Natl. Acad. Sci. U.S.A.* 96, 11804–11808.
- (11) Graves, D. E., and Velea, L. M. (2000) Intercalative binding of small molecules to nucleic acids. *Curr. Org. Chem.* 4, 915–929.
- (12) Wilson, W. D. (1999) DNA intercalators. *Comprehensive Natural Products Chemistry, Vol. 7 DNA and Aspects of Molecular Biology* (Kool, E. T., Ed.) pp 427–476, Elsevier Science B. V., Amsterdam, Netherlands.
- (13) Erkkila, K. E., Odom, D. T., and Barton, J. K. (1999) Recognition and Reaction of Metallointercalators with DNA. *Chem. Rev.* 99, 2777–2795.
- (14) Wittung, P., Kim, S. K., Buchardt, O., Nielsen, P., and Norden, B. (1994) Interactions of DNA binding ligands with PNA-DNA hybrids. *Nucleic Acids Res.* 22(24), 5371–5377.
- (15) Eldrup, A. B., Christensen, C., Haaime, G., and Nielsen, P. E. (2002) Substituted 1,8-naphthyridin-2(1H)-ones are superior to thymine in the recognition of adenine in duplex as well as triplex structures. *J. Am. Chem. Soc.* 124, 3254–3262.
- (16) Armitage, B., Koch, T., Frydenlund, H., Ørum, H., and Schuster, G. B. (1998) Peptide nucleic acid (PNA)/DNA hybrid duplexes: intercalation by an internally linked anthraquinone. *Nucleic Acids Res.* 26(3), 715–720.
- (17) Cama, L. D., Ratcliffe, R. W., Wilkening, R. R., Wildonger, K. J., and Sun, W. (1999) Synthesis of naphthosultamylcarbapenems as antibacterial compounds for treatment of methicillin resistant *Staphylococcus*. *PCT Int. Appl.* AN 1999: 282219, 153 p.
- (18) Advanced ChemTech, Inc. (1998) *Advanced Chemtech Handbook of Combinatorial & Solid-Phase Organic Chemistry. A Guide to Principles, Products & Protocols* (Bennett, W. D., Christensen, J. W., Hamaker, L. K., Peterson, M. L., Rhodes, M. R., and Saneii, H. H., Eds.) Advanced ChemTech, Inc., Louisville, Kentucky.
- (19) Bevers, S., Schutte, S., and McLaughlin, L. W. (2000) Naphthalene- and perylene-based linkers for the stabilization of hairpin triplexes. *J. Am. Chem. Soc.* 122, 5905–5915.
- (20) Lokey, R. S., Kwok, Y., Guelev, V., Pursell, C. J., Hurley, L. H., and Iverson, B. L. (1997) A new class of polyintercalating molecules. *J. Am. Chem. Soc.* 119, 7202–7210.
- (21) Yen, S.-F., Gabbay, E. J., and Wilson, W. D. (1982) Interaction of aromatic imides with DNA. 1. Spectrophotometric and viscometric studies. *Biochemistry* 21, 2070–2076.
- (22) Eriksson, M., and Nielsen, P. E. (1996) Solution structure of a peptide nucleic acid–DNA duplex. *Nat. Struct. Biol.* 3, 410–413.
- (23) Blecinski, C. F., and Richert, C. (1999) Steroid-DNA interactions increasing stability, sequence-selectivity, DNA/RNA discrimination, and hypochromicity of oligonucleotide duplexes. *J. Am. Chem. Soc.* 121, 10889–10894.
- (24) Ikeda, H., Nakamura, Y., and Saito, I. (2002) Synthesis and characterization of naphthamide-containing peptide nucleic acids. *Tetrahedron Lett.* 43, 5525–5528.

BC0256345



# SUPPLEMENTARY DATA

“Conjugates of PNA with naphthalene diimide derivatives having a broad range of DNA affinities”. **Andriy A. Mokhir, Roland Kraemer**. Anorganisch-Chemisches Institut, Karl-Ruprechts University of Heidelberg, Im Neuenheimer Feld 270, Heidelberg 69120, Germany.

Table S1. Melting points of duplexes of PNA **19a** and **20** with match and mismatch DNA.

PNA	DNA target <sup>i</sup>	T <sub>m</sub> (°C) <sup>ii</sup>	T <sub>m</sub> (°C) <sup>iii</sup>
<b>19a</b>	TCT TAG TTG TGA CCA full match	68.7 ± 1.4	57.6 ± 1.0
<b>19a</b>	TCT TAG TTG TG <u>C</u> CCA	67.7 ± 1.1	57.5 ± 0.6
<b>19a</b>	TCT TAG TTG TG <u>T</u> CCA	68.5 ± 0.7	56.3 ± 0.5
<b>19a</b>	TCT TAG TTG TG <u>G</u> CCA	66.0 ± 0.9	55.8 ± 0.4
<b>19a</b>	TCT TAG TTG T <u>T</u> A CCA	56.8 ± 0.7	45.2 ± 1.1
<b>19a</b>	TCT TAG TTG <u>C</u> GA CCA	<sup>iv</sup>	-
<b>19a</b>	TCT TAG TTA <u>A</u> TGA CCA	49.8 ± 1.2	-
<b>19a</b>	TCT TAG T <u>C</u> G TGA CCA	34.1 ± 1.9	-
<b>19a</b>	TCT TAG <u>C</u> TG TGA CCA	44.2 ± 1.5	-
<b>19a</b>	TCT TAA <u>A</u> TTG TGA CCA	44.8 ± 0.9	-
<b>20</b>	TCT TAG TTG TGA CCA full match	61.0 ± 1.0	52.9 ± 1.2
<b>20</b>	TCT TAG TTG TG <u>C</u> CCA	59.2 ± 1.4	49.8 ± 1.0
<b>20</b>	TCT TAG TTG TG <u>T</u> CCA	60.2 ± 1.1	51.5 ± 2.0
<b>20</b>	TCT TAG TTG TG <u>G</u> CCA	59.5 ± 1.7	50.8 ± 1.5
<b>20</b>	TCT TAG TTG T <u>T</u> A CCA	52.9 ± 2.3	41.9 ± 1.2
<b>20</b>	TCT TAG TTG <u>C</u> GA CCA	40.8 ± 1.7	-
<b>20</b>	TCT TAG TTA <u>A</u> TGA CCA	25.9 ± 1.2	-
<b>20</b>	TCT TAG T <u>C</u> G TGA CCA	36.2 ± 0.5	-
<b>20</b>	TCT TAG <u>C</u> TG TGA CCA	31.8 ± 0.5	-
<b>20</b>	TCT TAA <u>A</u> TTG TGA CCA	30.3 ± 1.5	-

(i) Mismatched bases in DNA strands are shown using bold font and are underscored; (ii) [PNA]=[DNA]= 2 M, MOPS pH 7 10 mM, NaCl 50 mM; (iii) [PNA]=[DNA]= 2 M, MOPS pH 7 10 mM, NaCl 150 mM; (iv) irreversible transition.

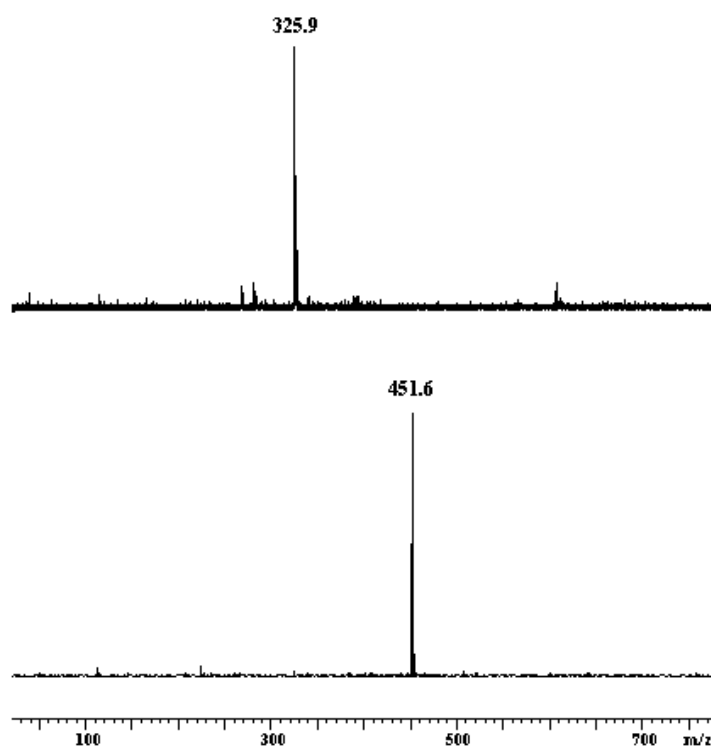


Figure S1. MALDI-TOF mass spectra of **3** (top) and **4** (bottom).

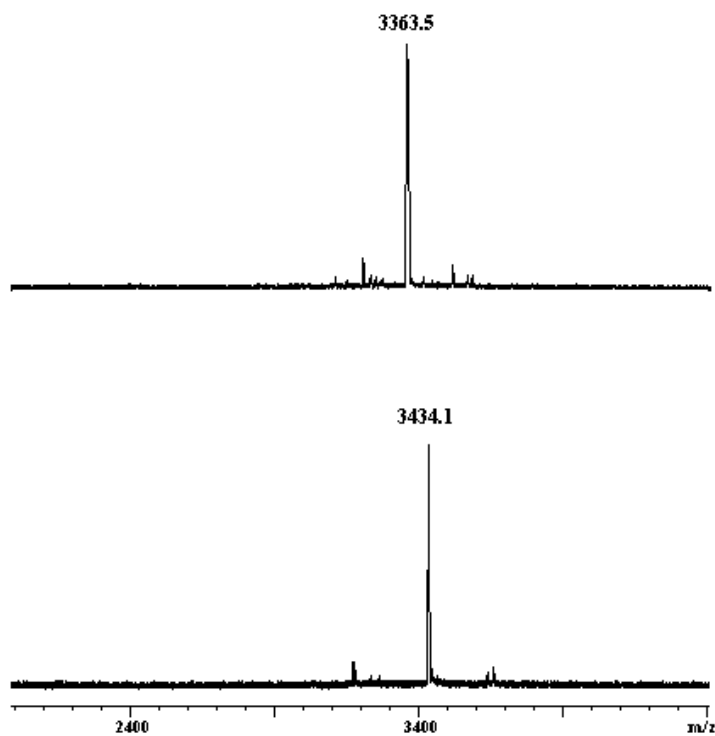


Figure S2. MALDI-TOF mass spectra of **11** (top) and **10** (bottom).

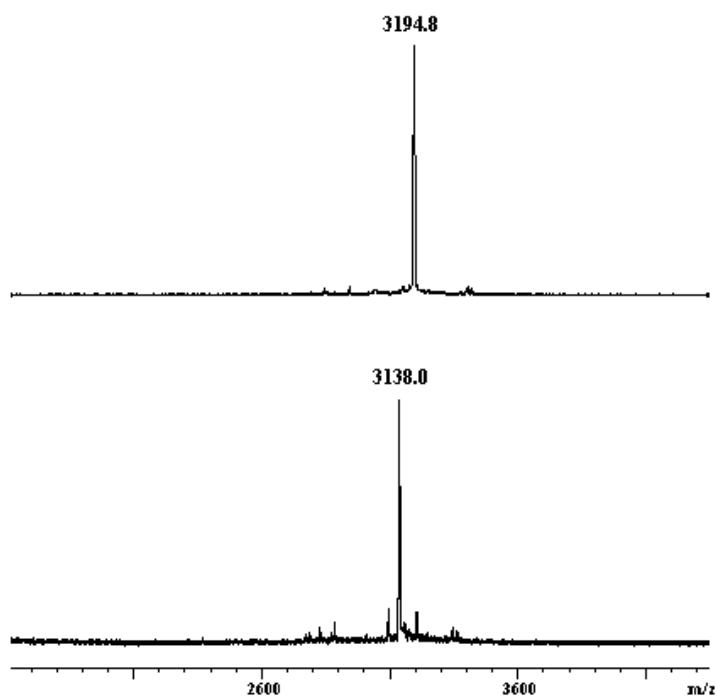


Figure S3. MALDI-TOF mass spectra of **19a** (top) and **12** (bottom).

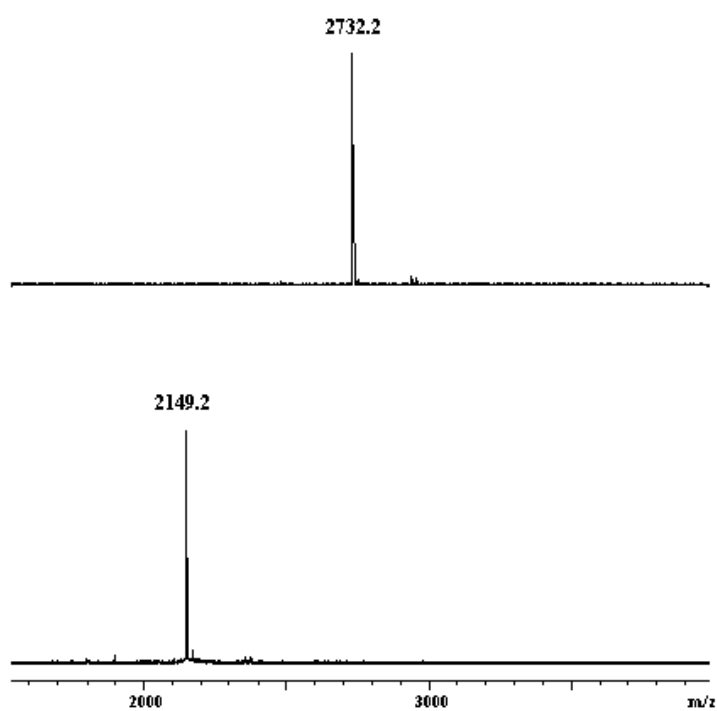


Figure S4. MALDI-TOF mass spectra of **19f** (top) and **19e** (bottom).



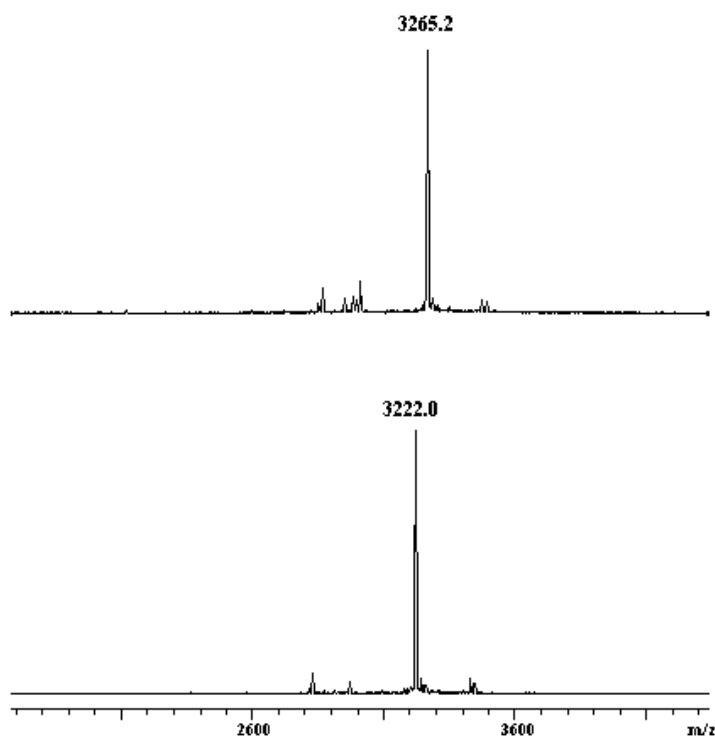


Figure S5. MALDI-TOF mass spectra of **14** (top) and **16** (bottom).

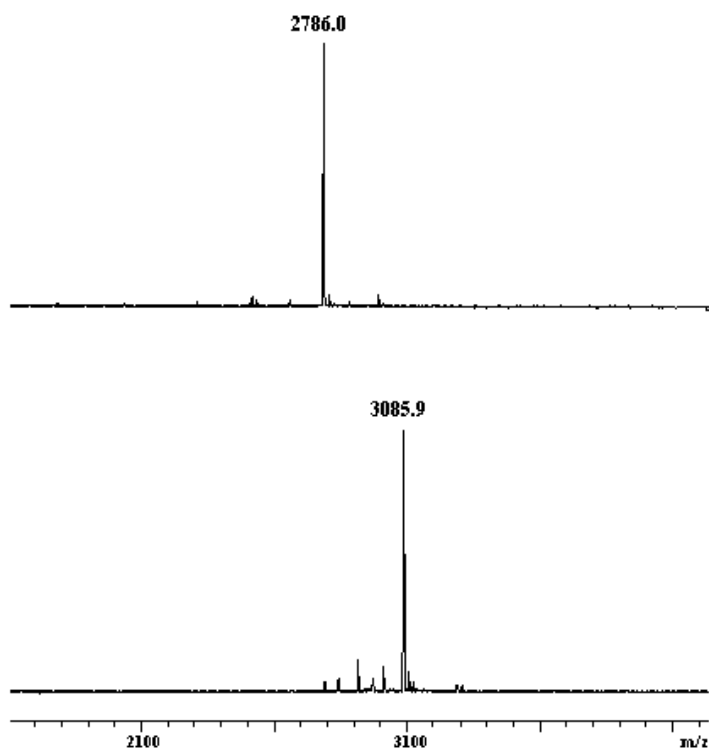


Figure S6. MALDI-TOF mass spectra of **20** (top) and **18** (bottom).

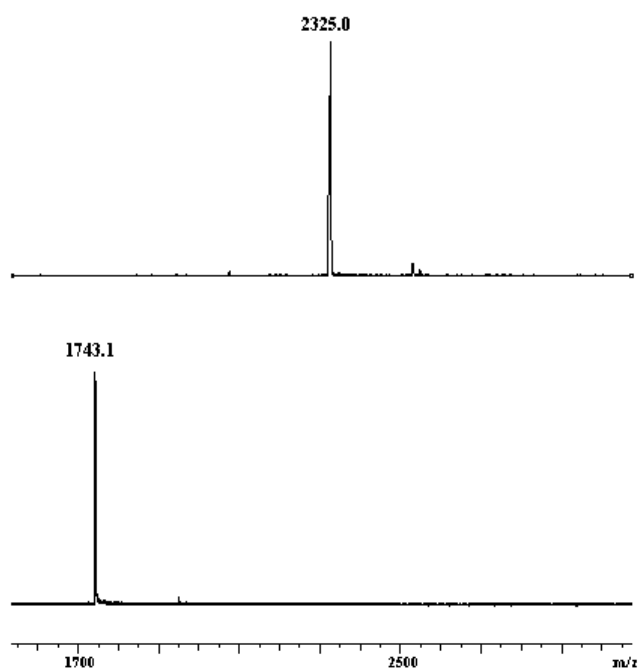


Figure S7. MALDI-TOF mass spectra of **25** (top) and **24** (bottom).

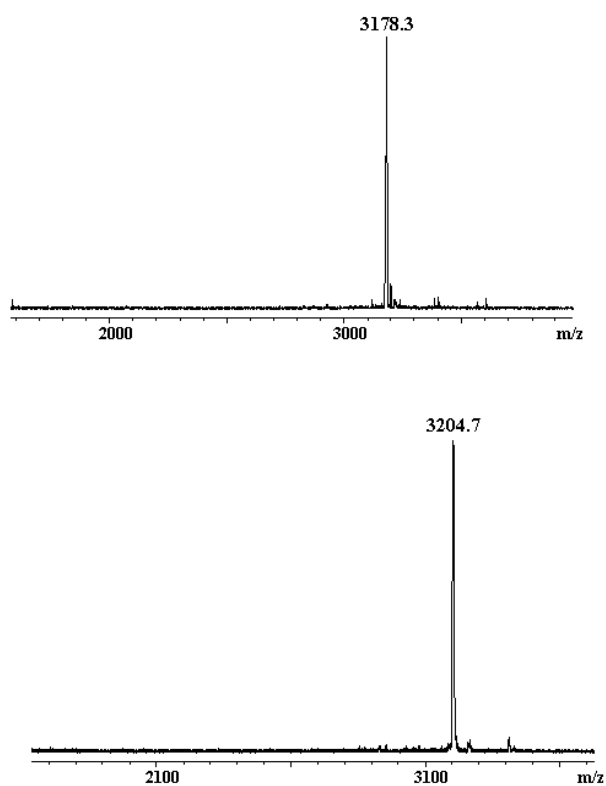


Figure S8. MALDI-TOF mass spectra of **19b** (top) and **19c** (bottom).

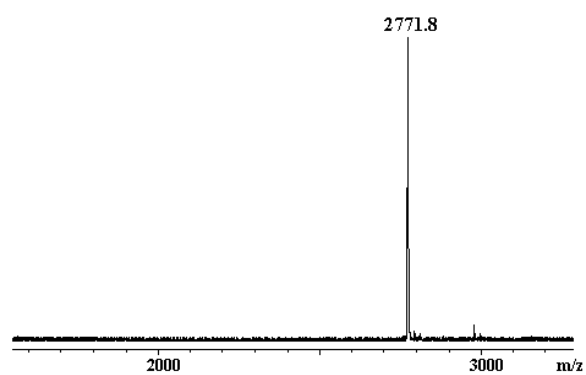
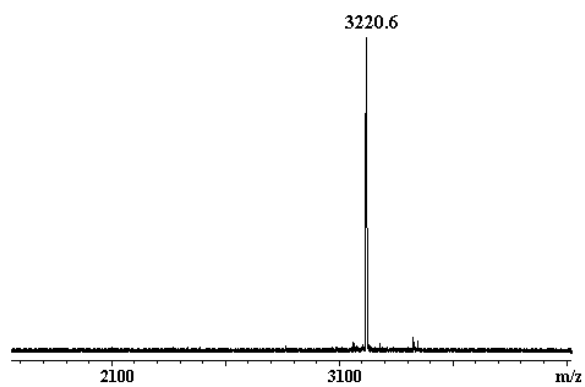


Figure S9. MALDI-TOF mass spectra of **19d** (top) and **21** (bottom).

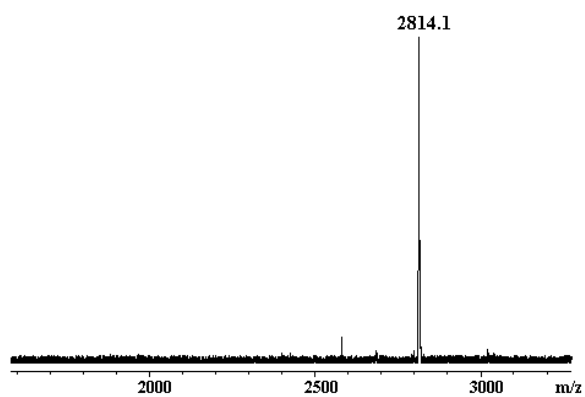
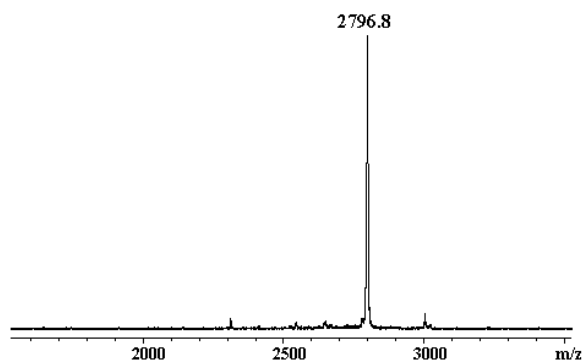


Figure S10. MALDI-TOF mass spectra of **22** (top) and **23** (bottom).



# Synthesis and Formulation of Neoglycolipids for the Functionalization of Liposomes and Lipoplexes

Eric Perouzel,<sup>†</sup> Michael R. Jorgensen,<sup>†</sup> Michael Keller,<sup>\*,†</sup> and Andrew D. Miller<sup>\*,‡</sup>

IC-Vec Ltd, Flowers Building, Armstrong Road, London SW7 2AZ, United Kingdom and Imperial College Genetic Therapies Centre, Department of Chemistry, Imperial College London, London SW7 2AZ, United Kingdom. Received May 2, 2003; Revised Manuscript Received July 10, 2003

Novel carbohydrate-based agents for the stabilization of ternary liposome:mu:DNA (LMD) nonviral vector systems are described. LMD vector systems comprise plasmid DNA (pDNA; D, 7.5 kb) expressing a reporter gene (in this instance  $\beta$ -galactosidase expressing gene) that is precondensed with the adenoviral core peptide  $\mu$  (mu, M; MRRHHRRRRASHRRMRGG) and then further packaged by means of DC-Chol:DOPE (3:2; *m/m*) cationic liposomes. Final optimized lipid:mu:pDNA ratio is typically 12:0.6:1 (w/w/w). We report the synthesis of a series of nine neoglycolipids prepared by coupling completely unprotected sugar monomers or oligomers (mannose, glucose, galactose, glucuronic acid, maltose, lactose, maltotriose, maltotetraose, and maltoheptaose) through their reducing-residue termini to an aminoxy-functionalized cholesterol-based lipid. Characterization of these novel neoglycolipids by <sup>1</sup>H NMR reveals that the coupling reaction has a major configurational preference for the  $\beta$ -anomer. Unusually, even mannose coupling results in a neoglycolipid product with a predominantly  $\beta$ -anomeric conformation (>85%). Formulation of neoglycolipids into LMD vector systems by incubation of LMD particles with neoglycolipid micelles results in the formation of a range of potential stabilized-LMD (sLMD) vector systems. Those potential sLMD systems prepared with longer chain neoglycolipids are found to have enhanced stabilities, with respect to aggregation in high ionic strength buffers, and enhanced transfection efficacies in comparison to the transfection properties of the naked first generation LMD vector system (i.e., gene delivery and expression). By contrast, when LMD vector systems are incubated with poly(ethylene glycol) DSPE-PEG micelles, resulting PEG-LMD vector systems are very stable with respect to colloidal instability and aggregation in high ionic strength buffers and in serum, but are completely refractory to transfection. These data suggest that oligosaccharides could represent an alternative to PEG as a stealth polymer able to stabilize synthetic nonviral vector systems in some fluids but without impairing transfection efficiency. Furthermore, sLMD systems prepared with longer chain neoglycolipids appear to have sufficient useful characteristics to form the basis of viable second-generation LMD vector systems after further development.

## INTRODUCTION

With the wealth of data generated by the human genome project, the use of genes for therapeutic purposes (gene therapy) is increasingly expected to revolutionize medical treatment. Well aware of the problems and high risks associated with the efficient delivery of transgenes by means of virus particles, various researchers, including chemists (1), have been searching for safer synthetic nonviral alternatives to mediate nucleic acid delivery into host cells including the use of histone proteins (2), lipids (3–5) and/or liposomes (6–8), dendrimers (9–11), or polymers (12–14). Although the transfection efficiencies of synthetic nonviral vector systems are remote from the efficiencies of viral vectors, this technology should ultimately have clinical applications given the genuine prospects that nonviral systems should have with respect to superior safety and manufacturing profiles compared

to viral systems (15–18). In the drive for clinically viable, synthetic nonviral vector systems, we recently developed a synthetic nonviral platform system known as liposome:mu:DNA (LMD) based upon cationic liposomes (L), the adenoviral core peptide  $\mu$  (mu, M) (19), and plasmid DNA (D) (20). This system showed several promising features including long-term storage characteristics, enhanced stability with respect to aggregation compared with binary cationic liposome–plasmid DNA (lipoplex, LD) systems (21).

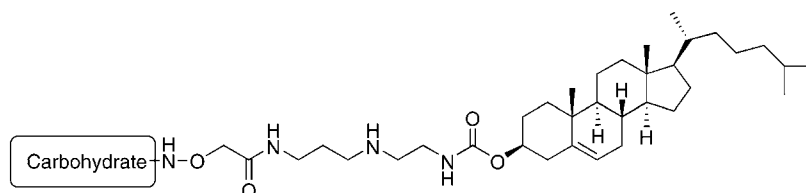
However, despite these useful characteristics, naked first generation LMD is not clinically viable owing to several clear limitations that have since come to light in more recent experiments. First, a mechanistic study comparing LD and LMD systems demonstrated that the nuclear localization sequence (NLS) of the adenoviral peptide mu is not properly exploited by the LMD system. In other words, the peptide was apparently unable to promote the active uptake of the DNA into the nucleus although mu peptide clearly harbors strong NLS characteristics (22). Second, LMD systems were found to possess inadequate stability toward aggregation in serum and other biological fluids rendering them unsuitable for routine use in vivo, even though inclusion of the mu

\* To whom correspondence should be addressed: M.K.: m.keller@icvec.com, Tel ++44 207 594 3150, Fax ++44 207 594 5803. A.D.M.: Tel ++44 207 594 5773, Fax ++44 207 594 5803.

<sup>†</sup> IC-Vec Ltd.

<sup>‡</sup> Imperial College London.

<sup>§</sup> Abbreviations: Boc, *tert*-butoxycarbonyl; br, broad; chol, cholesterol; DMF, *N,N*-dimethylformamide; DMSO, dimethyl sulfoxide; TFA, trifluoroacetic acid; THF, tetrahydrofuran.



**Figure 1.** General structure of neoglycolipids. Completely unprotected mannose, glucose, galactose, glucuronic acid, maltose, lactose, maltotriose, maltotetraose, and maltohepatose were coupled with high yields to the aminoxy functional group of aminoxy lipid **11**.

peptide had been found to confer some elements of stability over and above the stability of simple LD systems.

In the latter respect, LMD differs little from most current synthetic nonviral vector systems (23–28), with the notable exception of vector systems such as the stabilized plasmid–lipid particle (SPLP) system that takes advantage of surface-associated poly(ethylene glycol) (PEG) to provide a “stealth” barrier to serum-induced aggregation and opsonization (29–34). In general, stealth vectors are obtained by either PEGylated lipids, or surface PEGylation of existing lipo- or polyplexes. PEG is a nontoxic, neutral polyether with a large exclusion volume for most macromolecules (35). In general, PEGylation of synthetic nonviral vector systems can be carried out on condensed DNA particles using a PEG lipid insertion procedure or by means of direct surface modification. Either procedure has been shown to produce nonviral vector systems that are completely resistant to aggregation in the presence of physiological salt concentrations (150 mM NaCl) or aggregation and opsonization in the presence of serum components (25, 36–38). Unfortunately, the levels of PEG that are necessary to stabilize adequately nonviral vector system particles against aggregation in biological fluids also appear to completely inhibit the transfection process (39). This may be due to the shielding of the cationic surface of particles from interaction with the negatively charged plasma membrane of cells. However, recent evidence now suggests that PEG coats may be sufficiently interactive with plasma membranes to induce rapid PEG-particle cell entry by endocytosis, thereby implying that PEG may actually inhibit cellular transfection not by blocking cell entry but by blockading pDNA transport within the intracellular environment once cell entry has taken place (40, 41). In the first case, nontransfecting PEG particles would be cleared by macrophages postopsonization, or else in the second case by intracellular degradation post endocytosis (42).

Given the shortcomings of PEG and the lack of an obvious surrogate, we speculated that an alternative approach to escape the destructive effect of biological fluids could be to coat the surface of our lipid-based nonviral vector systems such as LMD, with oligosaccharides (43, 44). The biological functions of carbohydrates are diverse and we hoped to exploit their combined targeting potential and stabilization properties (45–47). Previous work on liposomes demonstrated the potential of neoglycolipids (48–50), and we anticipated that LMD stability in biological fluids might be enhanced by inserting such molecules into the outer cationic lipid bilayer of LMD particles. This was expected to lead to an increase in system stability under high serum and salt conditions without causing a loss in transfection efficiency (51).

Here we describe the development of a facile synthetic procedure for the preparation of a variety of diverse neoglycolipids necessary to evaluate this proposition by exploiting the high reactivity between aminoxy functional groups and a wide range of aldehydes, a reaction affinity

that is well documented in the literature (52–57) (Figure 1). In sharp contrast to other methods found in the literature describing the synthesis of neoglycolipids (58, 59), this procedure allows for the retention of the cyclic nature of the sugar unit and is far more simple and cost-effective than traditional methods applying tedious protection and deprotection steps during syntheses. Transfection and stability studies are then described in which a direct comparison is made between neoglyco-LMD vector systems and PEG-LMD vector systems prepared in a parallel fashion by inserting poly(ethylene glycol) grafted distearoylphosphatidylethanolamine (DSPE-PEG). Data suggest that oligosaccharide coats do indeed confer a combination of enhanced LMD particle stability under high salt concentrations (but not in serum) without impairing transfection efficiency.

## EXPERIMENTAL PROCEDURES

**Materials and Reagents.** All organic solvents and chemicals were purchased from Sigma-Aldrich Company LTD (Poole, Dorset, UK). Dried  $\text{CH}_2\text{Cl}_2$  was distilled with phosphorus pentoxide before use. DOPE and DSPE-PEG<sup>2000</sup> were purchased from Avanti Polar Lipid (Alabaster, AL). 3 $\beta$ -[*N,N*-dimethylaminoethane]carbamoyl]-cholesterol (DC-Chol) was synthesized in our laboratory according to published procedures (6). The adenoviral core peptide mu ( $\text{NH}_2$ -MRRHHRRRRASHRRMRGG-OH) was synthesized by the standard 9-fluorenylmethoxycarbonyl Fmoc procedure based the Wang resin and using standard Merrifield solid-phase peptide chemistry (19, 60).

Plasmid DNA pUMVC1 (pDNA; 7528bp) was obtained from the University of Michigan Vector Core (<http://www.med.umich.edu/vcore/Plasmids/>), amplified, and purified by Bayou Biolabs (LA). The concentration of pDNA was determined spectrophotometrically ( $A_{260} = 1 \approx 50 \mu\text{g/mL}$ ), and pDNA molar concentration was determined using an average nucleotide base pair molecular weight of 660 Da. OptiMEM and FCS were purchased from Gibco BRL (Lexington, KY).

**Analytical Techniques.**  $^1\text{H}$  NMR spectra were recorded at ambient temperature on either Bruker DRX400, DRX300 or JEOL GX-270Q spectrometers, with residual nonisotopically labeled solvent (e.g.,  $\text{CHCl}_3$ ,  $\delta_{\text{H}}$  7.26) as an internal reference.  $^{13}\text{C}$  NMR spectra were recorded on the same range of spectrometers at 100, 75, and 68.5 MHz, respectively, also with residual nonisotopically labeled solvent (e.g.,  $\text{CHCl}_3$ ,  $\delta_{\text{C}}$  77.2) as an internal reference. Infrared spectra were recorded on a Jasco FT/IR 620 using NaCl plates and mass spectra (positive ions electrospray) were recorded using VG-7070B or JEOL SX-102 instruments. Chromatography refers to flash column chromatography, which was performed throughout on Merck-Kieselgel 60 (230–400 mesh) with appropriate solvent. Thin-layer chromatography (TLC) was performed on precoated Merck-Kieselgel 60 F254 aluminum backed plate and visualized with ultraviolet light,

iodine, acidic ammonium molybdate(IV), acidic ethanol, vanillin, or other agents as appropriate. Neoglycolipids purity was assessed by analytical high-pressure liquid chromatography (HPLC) using a Purospher RP-18 end-capped column (5  $\mu$ m) attached to an Hitachi HPLC system. Elution was performed on RP-18 at an isocratic flow rate of 1 mL/min with CH<sub>3</sub>CN/H<sub>2</sub>O (60:40), and fractions were detected at  $A_{205}$  before collection and analysis by mass spectrometry.

**Synthesis of 2-(Cholesterylloxycarbonylamino)-ethanol (2).** A solution of cholesteryl chloroformate (99.89 g, 0.218 mol) in CH<sub>2</sub>Cl<sub>2</sub> (600 mL) was added to a stirred solution of 2-aminoethanol (29.5 mL, 0.489 mol, 2.2 equiv) in CH<sub>2</sub>Cl<sub>2</sub> (450 mL) at 0 °C over a period of 2 h. The reaction was allowed to warm to room temperature and stirring continued for a further 14 h. The reaction mixture was washed with saturated NaHCO<sub>3</sub> (2  $\times$  200 mL) and water (2  $\times$  200 mL) and dried (MgSO<sub>4</sub>), and the solvents were removed under reduced. The solid obtained was recrystallized (CH<sub>2</sub>Cl<sub>2</sub>/MeOH) to give **2** as a white solid. Yield: 99.67 g (97%); mp: 168 °C;  $R_f$  = 0.26 (acetone/ether 1:9); IR (CH<sub>2</sub>Cl<sub>2</sub>):  $\nu_{\max}$  = 3353, 2942, 2870, 1693, 1674, 1562, 1467, 1382, 1264 cm<sup>-1</sup>; <sup>1</sup>H NMR (270 MHz, CDCl<sub>3</sub>):  $\delta$  = 5.35 (d,  $J$  = 6.5 Hz, 1H, H6'), 5.25–5.29 (m, 1H, NH), 4.42–4.57 (1H, m, H3'), 3.70–3.62 (m, 2H, H1), 3.25–3.35 (m, 2H, H2), 3.12 (s, 1H, OH), 2.28–2.38 (m, 2H, H4'), 1.77–2.03 (m, 5H, H2', H7', H8'), 1.59–0.96 (m, 21H, H1', H9', H11', H12', H14'–H17', H22'–H25'), 1 (3H, s, H-19'), 0.9 (d,  $J$  = 6.5 Hz, 3H, H21'), 0.87 (d,  $J$  = 6.5 Hz, 6H, H26' and H27') and 0.67 (s, 3H, H18'); MS (FAB<sup>+</sup>):  $m/z$  = 496 [M + Na]<sup>+</sup>, 474 [M + H]<sup>+</sup>, 369 [chol]<sup>+</sup>, 255, 175, 145, 105, 95, 81, 43.

**Synthesis of 2-(Cholesterylloxycarbonylamino)-ethyl Methanesulfonate (3).** To a solution of **2** (25 g, 52.3 mmol) and triethylamine (22 mL, 0.16 mol, 3 equiv) in CH<sub>2</sub>Cl<sub>2</sub> (500 mL) at 0 °C was added dropwise a solution of methanesulfonyl chloride (10.5 mL, 0.13 mol, 2.5 equiv). The reaction mixture was allowed to warm at room temperature and stirred for 90 min. After thin-layer chromatography analysis has indicated that the reaction had gone to completion, ice was added to quench the reaction. The reaction mixture was added to saturated aqueous NH<sub>4</sub>Cl (600 mL) and extracted with ether (3  $\times$  300 mL). The combined organic layers were washed with water (2  $\times$  300 mL) and brine (250 mL) and dried (Na<sub>2</sub>SO<sub>4</sub>). Solvent was removed under reduced pressure to give a white solid, which on purification by chromatography (ether) gave **3**. Yield: 28.3 g (98%); IR (CH<sub>2</sub>Cl<sub>2</sub>):  $\nu_{\max}$  = 3453, 3342, 1716, 1531, 1377, 1137, 798 cm<sup>-1</sup>; <sup>1</sup>H NMR (270 MHz, CDCl<sub>3</sub>):  $\delta$  = 5.34 (d,  $J$  = 6.5 Hz, 1H, H6'), 5–5.1 (m, 1H, NH), 4.41–4.53 (1H, m, H3'), 4.29–4.25 (t,  $J$  = 5 Hz, 2H, H1), 3.47–3.52 (m, 2H, H2), 3.01 (s, 3H, H3), 2.24–2.36 (m, 2H, H4'), 1.74–2 (m, 5H, H2', H7', H8'), 0.9–1.6 (m, 21H, H1', H9', H11', H12', H14'–H17', H22'–H25'), 0.98 (3H, s, H-19'), 0.84 (d,  $J$  = 6.5 Hz, 3H, H21'), 0.83 (d,  $J$  = 6.5 Hz, 6H, H26' and H27') and 0.65 (s, 3H, H18'); MS (FAB<sup>+</sup>):  $m/z$  = 1104 [2M + H]<sup>+</sup>, 574 [M + Na]<sup>+</sup>, 552 [M + H]<sup>+</sup>, 369 [chol]<sup>+</sup>, 255, 175, 145, 95, 81.

**Synthesis of 4-Aza-N<sup>6</sup>-(cholesterylloxycarbonylamino)hexanol (4).** To a stirred solution of **3** (28.3 g, 51 mmol) dissolved in a minimum amount of THF was added 1-aminopropan-3-ol (160 mL, 2 mol, 39 equiv). After completion of the reaction (12 h) as monitored by thin-layer chromatography, CHCl<sub>3</sub> (350 mL) and K<sub>2</sub>CO<sub>3</sub> (20 g) were added, and the solution was vigorously stirred for 30 min. The suspension was then filtered through a short pad of Celite, washing thoroughly with CHCl<sub>3</sub>. This was washed with a saturated solution of sodium hydro-

gen carbonate and dried (Na<sub>2</sub>CO<sub>3</sub>). The solvent was removed to give **4** as a white solid. Yield: 26.1 g (96%); IR (CH<sub>2</sub>Cl<sub>2</sub>):  $\nu_{\max}$  = 3350–3210, 2937, 2850, 1531, 1460, 1380, 1220, 1120, 1040 cm<sup>-1</sup>; <sup>1</sup>H NMR (270 MHz, CDCl<sub>3</sub>):  $\delta$  = 5.33–5.35 (m, 1H, H6'), 4.92–4.96 (m, 1H, NH), 4.42–4.51 (1H, m, H3'), 3.7–3.83. (m, 2H, H5), 3.23–3.29 (m, 2H, H1), 2.73–2.57 (m, 6H, H2, H3, H4), 2.2–2.36 (m, 2H, H4'), 1.7–2 (m, 5H, H2', H7', H8'), 0.85–1.58 (m, 21H, H1', H9', H11', H12', H14'–H17', H22'–H25'), 0.98 (3H, s, H-19'), 0.84 (d,  $J$  = 6.5 Hz, 3H, H21'), 0.8 (d,  $J$  = 6.5 Hz, 6H, H26'/H27') and 0.61 (s, 3H, H18'); MS (FAB<sup>+</sup>):  $m/z$  = 543 [M + Na]<sup>+</sup>, 530 [M + H]<sup>+</sup>, 485 [M – CO<sub>2</sub>]<sup>+</sup>, 369 [chol]<sup>+</sup>, 144 [M – chol]<sup>+</sup>.

**Synthesis of 4-Aza-(Boc)-N<sup>6</sup>-(cholesterylloxycarbonylamino)hexanol (5).** To a solution of **4** (26.1 g, 49 mmol) were added Et<sub>3</sub>N (8.3 mL, 1.1 equiv) and Boc<sub>2</sub>O (10.7 g, 1 equiv) in CH<sub>2</sub>Cl<sub>2</sub> (200 mL), and the resulting solution was followed by TLC. On completion, the reaction mixture was poured into saturated aqueous NH<sub>4</sub>Cl (100 mL), washed with water, and dried (Na<sub>2</sub>SO<sub>4</sub>). The solvent was removed in vacuo to give the white solid **5**. The solvent was removed under reduced pressure to give a white solid, which on purification by chromatography (CH<sub>2</sub>Cl<sub>2</sub>/MeOH/NH<sub>3</sub> 92:7:1) gave **5**. Yield (27.9 g, 90%); IR (CH<sub>2</sub>Cl<sub>2</sub>):  $\nu_{\max}$  = 3352, 3054, 2937, 1675, 1530, 1455, 1380, 1220, 1120; <sup>1</sup>H NMR (270 MHz, CDCl<sub>3</sub>):  $\delta$  = 5.33–5.35 (m, 1H, H6'), 4.86 (m, 1H, NH), 4.42–4.5 (1H, m, H3'), 3.62–3.7 (m, 2H, H5), 3.27–3.38 (m, 6H, H1, H2, H3), 2.18–2.33 (m, 2H, H4'), 1.73–2 (m, 5H, H2', H7', H8'), 1.45 (s, 9H, Boc), 1–1.65 (m, 23H, H4, H1', H9', H11', H12', H14'–H17', H22'–H25'), 0.97 (3H, s, H-19'), 0.93 (d,  $J$  = 6.5 Hz, 3H, H21'), 0.8 (d,  $J$  = 6.5 Hz, 6H, H26' and H27') and 0.65 (s, 3H, H18'); MS (FAB<sup>+</sup>):  $m/z$  = 654 [M + Na]<sup>+</sup>, 543 [M – Boc]<sup>+</sup>, 369 [chol]<sup>+</sup>, 145, 121, 95, 69, 57.

**Synthesis of 4-Aza-(Boc)-N<sup>6</sup>-(cholesterylloxycarbonylamino)hexyl Methanesulfonate (6).** This experiment was carried out in a manner similar to the preparation of 2-(cholesterylloxycarbonylamino)ethyl methanesulfonate **3** on 44 mmol scale giving **6**. Yield (28 g, 90%); IR (CH<sub>2</sub>Cl<sub>2</sub>):  $\nu_{\max}$  = 3305, 2980, 2900, 2865, 1675, 1530, 1455, 1350, 1150; <sup>1</sup>H NMR (270 MHz, CDCl<sub>3</sub>):  $\delta$  = 5.33–5.35 (m, 1H, H6'), 4.86 (m, 1H, NH), 4.35–4.55 (m, 1H, H3'), 4.22 (t, 2H,  $J$  = 6.5 Hz, H5), 3.2–3.4 (m, 6H, H1, H2, H3), 3.01 (s, 3H, H6), 2.15–2.33 (m, 2H, H4'), 1.73–2 (m, 5H, H2', H7', H8'), 1.44 (s, 9H, Boc), 1–1.67 (m, 23H, H4, H1', H9', H11', H12', H14'–H17', H22'–H25'), 0.97 (3H, s, H-19'), 0.94 (d,  $J$  = 6.5 Hz, 3H, H21'), 0.8 (d,  $J$  = 6.5 Hz, 6H, H26' and H27') and 0.65 (s, 3H, H18'); MS (FAB<sup>+</sup>):  $m/z$  = 722 [M + Na]<sup>+</sup>, 609 [M – Boc]<sup>+</sup>, 369 [chol]<sup>+</sup>, 145, 121, 95, 69, 55.

**Synthesis of 4-Aza-(Boc)-N<sup>6</sup>-(cholesterylloxycarbonylamino)hexanamine (7).** Anhydrous DMF (200 mL) was added to **6** (25 g, 35 mmol), sodium azide (11.49, 175.7 mmol, 5 equiv), and sodium iodide (5 g, 35 mmol, 1 equiv) under nitrogen while stirring. Heating at 80 °C for 2 h resulted in completion of the reaction. The reaction mixture was allowed to cool to room temperature, the DMF removed under reduced pressure, and the residue dissolved in ethyl acetate. This was washed with water (2  $\times$  100 mL) and brine (100 mL) and dried (Na<sub>2</sub>SO<sub>4</sub>) to give after purification by chromatography (hexane/ether 1:1) **7** as a white solid. Yield (22 g, 95%); <sup>1</sup>H NMR (270 MHz, CDCl<sub>3</sub>):  $\delta$  = 5.34–5.36 (m, 1H, H6'), 4.35–4.55 (m, 1H, H3'), 4.25 (t, 2H,  $J$  = 6.5 Hz, H5), 3.2–3.5 (m, 6H, H1, H2, H3), 2.25–2.33 (m, 2H, H4'), 1.7–2.05 (m, 5H, H2', H7', H8'), 1.45 (s, 9H, Boc), 1–1.72 (m, 23H, H4, H1', H9', H11', H12', H14'–H17', H22'–H25'), 0.98 (3H, s, H-19'), 0.94 (d,  $J$  = 6.5 Hz, 3H, H21'), 0.83 (d,  $J$  = 6.5



H<sub>z</sub>, 6H, H26' and H27') and 0.64 (s, 3H, H18'); MS (FAB<sup>+</sup>):  $m/z$  = 568 [M + Na - Boc]<sup>+</sup>, 556 [M - Boc]<sup>+</sup>, 369 [chol]<sup>+</sup>, 145, 121, 95, 69, 57.

**Synthesis of 4-Aza-(Boc)-N<sup>6</sup>-(cholesteryloxycarbonylamino)hexylamine (8).** To a round-bottomed flask charged with **7** (22.75 g, 34.6 mmol) in THF (230 mL) was added trimethylphosphine in THF (1 M, 40 mL, 1.15 equiv), and the reaction was monitored by TLC. On completion the reaction was stirred with water (3 mL) and aqueous ammonia (3 mL) for 1 h, and the solvent was removed under reduced pressure affording a white crystalline powder. Yield (19.1 g, 88%); IR (CH<sub>2</sub>Cl<sub>2</sub>):  $\nu_{\max}$  = 3689, 3456, 3155, 2948, 2907, 2869, 2253, 1793, 1709, 1512, 1468, 1381, 1168; <sup>1</sup>H NMR (270 MHz, CDCl<sub>3</sub>):  $\delta$  = 5.32–5.35 (m, 1H, H6'), 4.35–4.51 (m, 1H, H3'), 3.45–3.05 (m, 8H, H1, H2, H3, H5), 2.18–2.4 (m, 2H, H4'), 1.8–2.1 (m, 5H, H2', H7', H8'), 1.46 (s, 9H, Boc), 1.01–1.72 (m, 23H, H4, H1', H9', H11', H12', H14'–H17', H22'–H25'), 0.97 (3H, s, H-19'), 0.85 (d,  $J$  = 6.5 Hz, 3H, H21'), 0.82 (d,  $J$  = 6.5 Hz, 6H, H26' and H27'), 0.64 (s, 3H, H18'); MS (FAB<sup>+</sup>):  $m/z$  = 630 [M + H]<sup>+</sup>, 530 [M - Boc]<sup>+</sup>, 369 [chol]<sup>+</sup>, 145, 121, 95, 69, 57.

**Synthesis of (Boc)aminoxycetic Acid (9).** *O*-(Carboxymethyl)hydroxylamine hemihydrochloride (1.16 g, 5.3 mmol) was dissolved in CH<sub>2</sub>Cl<sub>2</sub> (40 mL), and the pH was adjusted to 9 by addition of triethylamine (3 mL). Then, di-*tert*-butyl dicarbonate (2.36 g, 10.6 mmol, 2.0 equiv) was added, and the mixture was stirred at room temperature until TLC indicated completion of reaction. The pH was lowered to 3 by addition of diluted HCl. The reaction mixture was partitioned between saturated aqueous NH<sub>4</sub>Cl (20 mL) and CH<sub>2</sub>Cl<sub>2</sub> (30 mL). The aqueous phase was extracted with CH<sub>2</sub>Cl<sub>2</sub> (3 × 100 mL). The combined organic extracts were washed with H<sub>2</sub>O (2 × 100 mL) and dried (Na<sub>2</sub>SO<sub>4</sub>). The solvent was removed in vacuo to afford **9** as a white solid. Yield (1.86 g, 97%); IR (CH<sub>2</sub>Cl<sub>2</sub>):  $\nu_{\max}$  = 3373, 2983, 2574, 2461, 1724, 1413, 1369, 1235; <sup>1</sup>H NMR (270 MHz, CDCl<sub>3</sub>):  $\delta$  = 4.48 (s, 2H, CH<sub>2</sub>), 1.48 (s, 9H, Boc); MS (FAB<sup>+</sup>):  $m/z$  = 214 [M + Na]<sup>+</sup>, 192 [M + H]<sup>+</sup>, 135, 123, 109, 69.

**Synthesis of (Boc)aminoxylipid (10).** *N*-Hydroxysuccinimide (0.36 g, 3.13 mmol, 1 equiv), **9** (0.6 g, 3.13 mmol, 1 equiv), and *N,N*-dicyclohexylcarbodiimide (0.68 g, 3.13 mmol, 1 equiv) were dissolved in EtOAc (90 mL), and the heterogeneous mixture was allowed to stir at room-temperature overnight. The mixture was then filtered through a pad of Celite to remove the dicyclohexyl urea, which was formed as a white precipitate (rinsed with 60 mL ethyl acetate), and added to a solution of **8** (1.97 g, 3.13 mmol, 1 equiv) in THF (10 mL). A pH of 8 was maintained for this heterogeneous reaction by addition of triethylamine (6 mL). The resulting mixture was allowed to stir at room-temperature overnight. On completion the mixture was filtered, and the solvent was removed under reduced pressure to give after purification by flash-chromatography (CH<sub>2</sub>Cl<sub>2</sub>/MeOH/NH<sub>3</sub> 92:7:1) **10** as a white solid. Yield (2.3 g, 90%); <sup>1</sup>H NMR (270 MHz, CDCl<sub>3</sub>):  $\delta$  = 5.33–5.35 (m, 1H, H6'), 4.4–4.52 (m, 1H, H3'), 4.3 (s, 2H, H9), 3.2–3.42 (m, 8H, H1, H2, H4, H6), 2.23–2.35 (m, 2H, H4'), 1.7–2.1 (m, 7H, H2', H7', H8', H5), 1.44–1.46 (m, 18H, 2 Boc), 1–1.73 (m, 21H, H1', H9', H11', H12', H14'–H17', H22'–H25'), 0.98 (3H, s, H-19'), 0.85 (d,  $J$  = 6.5 Hz, 3H, H21'), 0.83 (d,  $J$  = 6.5 Hz, 6H, H26'/H27'), 0.65 (s, 3H, H18'); MS (FAB<sup>+</sup>):  $m/z$  = 803 [M + H]<sup>+</sup>, 703 [M - Boc]<sup>+</sup>, 647, 603 [M - 2Boc]<sup>+</sup>, 369, 279, 255, 235, 204, 145, 95, 69.

**Synthesis of Aminoxylipid (11).** To a solution **10** (1.1 g, 1.36 mmol, 1 equiv) in CH<sub>2</sub>Cl<sub>2</sub> (10 mL) was added

TFA (2 mL, 20.4 mmol, 15 equiv) at 0 °C. The solution was allowed to stir at room temperature for 5 h. On completion toluene was added to azeotrope TFA from the reaction mixture. The solvents were removed in vacuo to afford after purification by chromatography (CH<sub>2</sub>Cl<sub>2</sub>/MeOH/NH<sub>3</sub> 92:7:1 to 75:22:3) **11** as a white solid (709 mg, Yield: 86%); IR (CHCl<sub>3</sub>):  $\nu_{\max}$  = 3306, 2948, 2850, 2246, 1698, 1647, 1541, 1467, 1253, 1133; <sup>1</sup>H NMR (270 MHz, CDCl<sub>3</sub>):  $\delta$  = 5.26–5.4 (m, 1H, H6'), 4.4–4.52 (m, 1H, H3'), 4.12 (s, 2H, H9), 3.34–3.41 (m, 2H, H2), 3.15–3.3 (m, 2H, H4), 2.6–2.74 (m, 4H, H1/H6), 2.14–2.39 (m, 2H, H4'), 1.62–2.1 (m, 7H, H2', H7', H8', H5), 1.02–1.6 (m, 21H, H1', H9', H11', H12', H14'–H17', H22'–H25'), 0.96 (3H, s, H-19'), 0.86 (d,  $J$  = 6.5 Hz, 3H, H21'), 0.83 (d,  $J$  = 6.5 Hz, 6H, H26' and H27'), 0.66 (s, 3H, H18'); MS (FAB<sup>+</sup>):  $m/z$  = 603 [M + H]<sup>+</sup>, 369 [chol]<sup>+</sup>, 160, 137, 109, 95, 81, 69, 55.

**Synthesis of Aminoxy-mannopyranose Compound (12a).** A solution of D-mannose (266 mg, 4.8 mmol) in acetic aqueous buffer (sodium acetate/acetic acid 0.1 M, pH 4, 7 mL) and a solution of **11** (290 mg, 0.48 mmol, 10 equiv) in DMF (7 mL) was mixed and stirred for 3 days at room temperature. The solvent was removed in vacuo by freeze-drying and chromatography (CH<sub>2</sub>Cl<sub>2</sub>/MeOH/NH<sub>3</sub> 75:22:3) afforded the product **21** a white solid (233 mg, yield: 65%). The purity was further confirmed by HPLC. The final product contained of the  $\beta$ -pyranose (82%) form and  $\alpha$ -pyranose (18%) form that were not separated but characterized in the mixture. MS (FAB<sup>+</sup>):  $m/z$  = 765 [M + H]<sup>+</sup>, 787 [M + Na]<sup>+</sup>, 397, 369 [chol]<sup>+</sup>, 322, 240, 121, 109, 95, 81, 69, 57;  $\beta$ -pyranose form: <sup>1</sup>H NMR (400 MHz, CD<sub>3</sub>OD/CDCl<sub>3</sub> [75/25]):  $\delta$  = 7.64–7.62 (d,  $^3J_{1a-2a}$  = 7 Hz, 1H, H1a), 5.35–5.36 (m, 1H, H6'), 4.45–4.5 (s, 2H, H9), 4.35–4.5 (m, 1H, H3'), 4.19–4.24 (dd, 1H, H2a,  $^3J_{1a-2a}$  = 7.4 Hz,  $^3J_{2a-3a}$  = 7.7 Hz), 3.81–3.9 (m, 1H, H3'), 3.73–3.8 (m, 2H, H4a, H6a), 3.63–3.71 (m, 2H, H5a, H6a), 3.34–3.42 (m, 2H, H2), 3.27–3.30 (m, 2H, H4), 3–3.08 (m, 2H, H1), 2.9–2.98 (m, 2H, H6), 2.25–2.35 (m, 2H, H4'), 1.78–2.07 (m, 7H, H2', H7', H8', H5), 1.03–1.65 (m, 21H, H1', H9', H11', H12', H14'–H17', H22'–H25'), 1.01 (3H, s, H-19'), 0.91 (d,  $J$  = 6.5 Hz, 3H, H21'), 0.85 (d,  $J$  = 6.5 Hz, 6H, H26'/H27'), 0.69 (s, 3H, H18'); <sup>13</sup>C NMR (400 MHz, CDCl<sub>3</sub>/CD<sub>3</sub>OD [25/75]): 12.33 (C18'), 19.20 (C21'), 19.74 (C19'), 21.91 (C11'), 22.91 (C27'), 23.17 (C26'), 24.67 (C23'), 25.07 (C15'), 27.37 (C5), 28.85 (C25'), 28.96 (C2'), 29.07 (C12'), 32.76 (C7'), 32.87 (C8'), 36.38 (C2), 36.78 (C20'), 37.09 (C1) 37.76 (C22'), 37.95 (C1'), 38.4 (C4), 39.36 (C4'), 40.41 (C24'), 40.76 (C16'), 46.16 (C6), 51.19 (C9'), 57.19 (C17'), 57.75 (C14'), 64.62 (C6a), 70.19 (C2a), 70.58 (C4a), 72.12 (C3a), 72.37 (C5a), 73.11 (C9), 75.91 (C3'), 123.39 (C6'), 140.72 (C5'), 155.02 (C1a), 158.69 (NHCOOChol), 173.1 (C8);  $\alpha$ -pyranose form: identical data except, <sup>1</sup>H NMR (400 MHz, CD<sub>3</sub>OD/CDCl<sub>3</sub> [75/25]):  $\delta$  = 6.90–6.88 (d,  $^3J_{1a-2a}$  = 7 Hz, 1H, H1a), 5–5.05 (d×d, 1H, H2a,  $^3J_{1a-2a}$  = 7.3 Hz,  $^3J_{2a-3a}$  = 7.6 Hz); <sup>13</sup>C NMR (400 MHz, CDCl<sub>3</sub>/CD<sub>3</sub>OD [25/75]): 65.33 (C2a), 155.79 (C1a). <sup>1</sup>H NMR (400 MHz, CD<sub>3</sub>OD/CDCl<sub>3</sub> [75/25]): (m, 1H, H3') missing, underneath solvent peak; confirmed by <sup>1</sup>H NMR (300 MHz, DMSO):  $\delta$  = 4.67–4.82 (m, 1H, H3'). <sup>13</sup>C NMR (400 MHz, CDCl<sub>3</sub>/CD<sub>3</sub>OD [25/75]): C1 missing, underneath MeOH peak confirmed by <sup>1</sup>H/<sup>13</sup>C correlation at 400 MHz, around 49. Proton resonance assignments were confirmed using <sup>1</sup>H gradient type DQF-COSY and TOCSY; <sup>1</sup>H/<sup>13</sup>C correlation and DEPT 135 were used to assign unambiguously the carbon resonances.  $\alpha$ -pyranose form gave  $^1J^{13}\text{C1a-H1a}$  = 177 Hz and  $\beta$ -pyranose form gave  $^1J^{13}\text{C1a-H1a}$  = 167 Hz. <sup>1</sup>H phase-sensitive NOESY confirmed the observed conformation.

**Synthesis of Aminoxy-glucopyranose Compound (12b).** This was prepared with a solution of D-glucose (150 mg, 0.82 mmol) and **11** (100 mg, 0.16 mmol) in a similar way to the preparation of **12a**, stirred for 1 day, and purified by chromatography ( $\text{CH}_2\text{Cl}_2/\text{MeOH}/\text{NH}_3$  75:22:3) to afford the product **12b** as a white solid (103 mg, yield: 82%). The purity was further confirmed by HPLC. The final product contained the  $\alpha$ -pyranose (11%) anomer and the  $\beta$ -pyranose (89%) anomer that were not isolated but characterized in the mixture. (FAB<sup>+</sup>):  $m/z = 765$  [ $\text{M} + \text{H}$ ]<sup>+</sup>, 787 [ $\text{M} + \text{Na}$ ]<sup>+</sup>, 391, 369 [chol]<sup>+</sup>, 309, 290, 171, 152, 135, 123, 109, 95, 81, 69;  $\beta$ -pyranose form: (300 MHz,  $\text{CDCl}_3/\text{CD}_3\text{OD}$  [90/10]):  $\delta = 7.53\text{--}7.56$  (d,  $J = 5.6$  Hz, 1H, H1a), 5.26–5.36 (m, 1H, H6'), 4.2–4.45 (m, 3H, H9, H3'), 4.05–4.15 (m, 1H, H2a), 3.45–3.85 (m, 5H, H6a, H3a, H5a, H4a), 2.9–3.4 (m, H2, H4, MeOH), 2.9–3.15 (m, 4H, H1, H6), 2.15–2.3 (m, 2H, H4'), 1.65–2 (m, 5H, H2', H7', H8'), 0.95–1.55 (m, 23H, H5, H1', H9', H11', H12', H14'–H17', H22'–H25'), 0.93 (3H, s, H-19'), 0.84 (d,  $J = 6.5$  Hz, 3H, H21'), 0.78 (d,  $J = 6.5$  Hz, 6H, H26' and H27'), 0.62 (s, 3H, H18');  $\alpha$ -pyranose form: identical data except, <sup>1</sup>H NMR (300 MHz,  $\text{CDCl}_3/\text{CD}_3\text{OD}$  [90/10]):  $\delta = 7.22\text{--}7.24$  (d,  $J = 6.61$  Hz, 1H, H1a), 4.95–5.07 (m, 1H, H2a); <sup>1</sup>H NMR (300 MHz,  $\text{CD}_3\text{OD}$ ): (m, 1H, H3') missing, presumably underneath solvent peak; confirmed by <sup>1</sup>H NMR (300 MHz, DMSO):  $\delta = 4.7\text{--}4.86$  (m, 1H, H3').

**Synthesis of Aminoxy-galactopyranose Compound (12c).** This was prepared with a solution of D-galactose (50 mg, 0.27 mmol) and **11** (40 mg, 0.066 mmol) in a similar way to the preparation of **12a**, stirred for 1 day, and purified by chromatography ( $\text{CH}_2\text{Cl}_2/\text{MeOH}/\text{NH}_3$  75:22:3) to afford the product **12c** as a white solid (35 mg, yield: 70%). The purity was further confirmed by HPLC. The final product contained of the  $\alpha$ -pyranose (15%) form and  $\beta$ -pyranose (85%) form that were not isolated but characterized in the mixture. MS (FAB<sup>+</sup>):  $m/z = 765$  [ $\text{M} + \text{H}$ ]<sup>+</sup>, 588, 391, 369 [chol]<sup>+</sup>, 322, 290, 165, 152, 135, 121, 109, 95, 81, 69;  $\beta$ -pyranose form: <sup>1</sup>H NMR (270 MHz, DMSO):  $\delta = 7.78\text{--}7.82$  (m, 1H, NHCO of C8), 7.55–7.58 (d,  $J = 7.2$  Hz, 1H, H1a), 6.95–7.1 (m, 1H, NHCOOChol), 5.25–5.37 (m, 1H, H6'), 4.2–4.43 (m, 3H, H9, H3'), 3.2–3.9 (m, H2a, H6a, H3a, H5a, H4a, OH), 2.9–3.18 (m, 4H, H2, H4), 2.4–2.65 (m, 4H, H1, H6), 2.15–2.3 (m, 2H, H4'), 1.67–2 (m, 5H, H2', H7', H8'), 0.92–1.6 (m, 23H, H5, H1', H9', H11', H12', H14'–H17', H22'–H25'), 0.96 (3H, s, H-19'), 0.89 (d,  $J = 6.5$  Hz, 3H, H21'), 0.84 (d,  $J = 6.5$  Hz, 6H, H26'/H27'), 0.65 (s, 3H, H18');  $\alpha$ -pyranose form: identical data except, <sup>1</sup>H NMR (270 MHz, DMSO): 6.86–6.88 (d,  $J = 6$  Hz, 1H, H1a).

**Synthesis of Aminoxy-glucopyranuronic Acid Compound (12d).** This was prepared with a solution of D-glucuronic acid, sodium salt monohydrate (30 mg, 0.128 mmol, 1.5 equiv), and **11** (50 mg, 0.08 mmol) in a similar way to the preparation of **12a**, stirred for 1 day, purified by chromatography ( $\text{CH}_2\text{Cl}_2/\text{MeOH}/\text{NH}_3$  75:22:3) to afford the sodium salt of **12d** as a white solid (41 mg, Yield: 60%). The purity was further confirmed by HPLC. The final product contained of the  $\alpha$ -pyranose (85%) form and  $\beta$ -pyranose (15%) form that were not isolated but characterized in the mixture. MS (FAB<sup>+</sup>):  $m/z = 779$  [ $\text{M} + \text{H}$ ]<sup>+</sup>, 733, 588, 411, 369 [chol]<sup>+</sup>, 336, 290, 240, 214, 159, 145, 135, 121, 109, 95, 81, 69, 55;  $\beta$ -pyranose form: <sup>1</sup>H NMR (300 MHz,  $\text{CDCl}_3/\text{CD}_3\text{OD}$  [75/25]):  $\delta = 7.51\text{--}7.53$  (d,  $J = 5.9$  Hz, 1H, H1a), 5.25–5.33 (m, 1H, H6'), 4.2–4.45 (m, 3H, H9, H3'), 3.8–4.1 (m, 3H, H2a, H3a, H4a), 3.6–3.75 (m, 1H, H5a), 3.2–3.55 (m, H2, H4, MeOH), 2.7–3.15 (m, 4H, H1, H6), 2.18–2.32 (m, 2H, H4'), 1.62–2

(m, 5H, H2', H7', H8'), 0.9–1.6 (m, 23H, H5, H1', H9', H11', H12', H14'–H17', H22'–H25'), 0.93 (3H, s, H-19'), 0.83 (d,  $J = 6.5$  Hz, 3H, H21'), 0.77 (d,  $J = 6.5$  Hz, 6H, H26'/H27'), 0.6 (s, 3H, H18');  $\alpha$ -pyranose form: identical data except, <sup>1</sup>H NMR (300 MHz,  $\text{CD}_3\text{OD}$ ):  $\delta = 7.22\text{--}7.24$  (d,  $J = 6.3$  Hz, 1H, H1a), 5–5.1 (m, 1H, H2a).

**Synthesis of  $\beta$ -D-Lactose Compound (12e).** A solution of  $\beta$ -D-lactose, containing 25–30% of  $\alpha$  (1.13 g, 3.3 mmol) and **11** (200 mg, 0.33 mmol) in 14 mL of DMF/acetic aqueous buffer was stirred for 4 days at room temperature. The solvent was removed in vacuo by freeze-drying, and chromatography ( $\text{CH}_2\text{Cl}_2/\text{MeOH}/\text{NH}_3$  75:22:3) afforded the product **12e** as a white solid (145 mg, yield: 47%). The purity was further confirmed by HPLC. The final product contained of the  $\alpha$ -pyranose (15%) form and  $\beta$ -pyranose (85%) form (containing itself around 25% of  $\alpha$ -lactose) that were not isolated but characterized in the mixture. MS (FAB<sup>+</sup>):  $m/z = 927$  [ $\text{M} + \text{H}$ ]<sup>+</sup>, 588, 482, 369 [chol]<sup>+</sup>, 290, 243, 216, 178, 152, 135, 121, 109, 95, 81, 69, 55;  $\beta$ -pyranose form: <sup>1</sup>H NMR (400 MHz,  $\text{CDCl}_3/\text{CD}_3\text{OD}$  [20/80]):  $\delta_{\text{H}} = 7.69\text{--}7.71$  (d,  $^3J_{1a-2a} = 5.8$  Hz, 1H, H1a of  $\beta$  lactose), 7.66–7.68 (d,  $^3J_{1a-2a} = 6.2$  Hz, 1H, H1a of  $\alpha$  lactose), 5.35–5.37 (m, 1H, H6'), 4.37–4.6 (m, 4H, H9, H3', H2a), 4.2–4.37 (m, 1H, H1a), 3.65–4.05 (m, 7 H, H3a, H4a, H5a, H4b, H5b, H6b), 3.25–3.6 (m, 8H, H2, H4, H6a, H2b, H3b, MeOH), 3–3.2 (m, 4H, H1, H6), 2.25–2.42 (m, 2H, H4'), 1.8–2.15 (m, 5H, H2', H7', H8'), 1–1.65 (m, 23H, H5, H1', H9', H11', H12', H14'–H17', H22'–H25'), 1.01 (3H, s, H-19'), 0.91 (d,  $J = 6.5$  Hz, 3H, H21'), 0.85 (d,  $J = 6.5$  Hz, 6H, H26'/H27'), 0.69 (s, 3H, H18'); <sup>13</sup>C NMR (400 MHz,  $\text{CDCl}_3/\text{CD}_3\text{OD}$  [20/80]): 12.32 (C18'), 19.2 (C21'), 19.76 (C19'), 21.94 (C11'), 22.91 (C27'), 23.17 (C26'), 24.7 (C23'), 25.1 (C15'), 27.22 (C5), 28.89 (C25'), 29 (C2'), 29.1 (C12'), 32.8 (C7'), 32.92 (C8'), 36.29 (C22'), 36.81 (C10'), 37.12 (C1'), 37.99 (C6), 38.11 (C1), 39.48 (C2), 40.45 (C24'), 40.80 (C16'), 46.13 (C4'), 51.23 (C9'), 57.22 (C17'), 57.80 (C14'), 62.41 (C6a), 63.4 (C6a), 70.02 (C5b), 70.63 (C2a), 72.8 (C3a), 73 (C3'), 73.18 (C9), 74.75 (C2b), 76.8 (C3a), 81 (C4b), 92.39 (C1a), 105.2 (C3'), 123.42 (C6'), 140.72 (C5'), 154.8 (C1a), 156.2 (NHCOOChol), 173.17 (C8);  $\alpha$ -pyranose form: identical data except, <sup>1</sup>H NMR (400 MHz,  $\text{CD}_3\text{OD}/\text{CDCl}_3$  [80/20]):  $\delta_{\text{H}} = 7.04\text{--}7.05$  (d,  $^3J_{1a-2a} = 5.6$  Hz, 1H, H1 $\alpha$ ), 5.05–5.07 (m, 1H, H2a), 4.09–4.11 (m, 1H, H3a); <sup>1</sup>H NMR (270 MHz,  $\text{CD}_3\text{OD}$ ): (m, 1H, H3') missing, presumably underneath solvent peak; confirmed by <sup>1</sup>H NMR (300 MHz, DMSO):  $\delta = 4.7\text{--}4.85$  (m, 1H, H3'). Proton resonance assignments were confirmed using <sup>1</sup>H gradient type DQF-COSY and TOCSY; <sup>1</sup>H/<sup>13</sup>C correlation and DEPT 135 were used to assign unambiguously the carbon resonances. <sup>1</sup>H phase-sensitive NOESY confirmed conformation.

**Synthesis of Maltose Compound (12f).** This compound was prepared with a solution of D-maltose monohydrate (30 mg, 1.8 mmol, 5 equiv) and **11** (100 mg, 0.16 mmol) in a similar way to the preparation of **12e**, stirred for 1 day, and purified by chromatography ( $\text{CH}_2\text{Cl}_2/\text{MeOH}/\text{NH}_3$  75:22:3) to afford **12f** as a white solid (100 mg, yield: 65%). The purity was further confirmed by HPLC. The final product contained of the  $\alpha$ -pyranose (87%) form and  $\beta$ -pyranose (13%) form that were not isolated but characterized in the mixture. MS (FAB<sup>+</sup>):  $m/z = 927$  [ $\text{M} + \text{H}$ ]<sup>+</sup>, 765, 588, 559, 484, 369 [chol]<sup>+</sup>, 322, 290, 213, 167, 161, 143, 135, 121, 109, 95, 81, 69, 55;  $\beta$ -pyranose form: <sup>1</sup>H NMR (300 MHz,  $\text{CDCl}_3/\text{CD}_3\text{OD}$  [80/20]):  $\delta = 7.55\text{--}7.57$  (d,  $^3J_{1a-2a} = 5.3$  Hz, 1H, H1a), 5.3 (s, 1H, H6'), 4.85–5.02 (m, 1H, H3'), 4.09–4.22 (m, 1H, H1b, H36'–4 (m, 7 H, H3a, H4a, H5a, H4b, H5b, H6b), 3.2–3.6 (m, 8H, H2, H4, H6a, H2b, H3b, MeOH), 2.8–



3.1 (m, 4H, H1, H6), 2.1–2.36 (m, 2H, H4'), 1.6–2.05 (m, 5H, H2', H7', H8'), 1–1.6 (m, 23H, H5, H1', H9', H11', H12', H14'–H17', H22'–H25'), 0.93 (3H, s, H-19'), 0.83 (d,  $J = 6.5$  Hz, 3H, H21'), 0.78 (d,  $J = 6.5$  Hz, 6H, H26'/H27'), 0.6 (s, 3H, H18');  $\alpha$ -pyranose form: identical data except,  $^1\text{H}$  NMR (300 MHz,  $\text{CD}_3\text{OD}/\text{CDCl}_3$  [80/20]):  $\delta = 6.92$ – $6.94$  (d,  $J = 4.62$  Hz, 1H, H1a), 5.02–5.15 (m, 1H, H2a), 4.04–4.08 (m, 1H, H3a)

**Synthesis of Maltotriose Compound (12g).** This was prepared with a solution of maltotriose (246.4 mg, 0.46 mmol, 7 equiv) and **11** (40 mg, 0.066 mmol) in a similar way to the preparation of **12e**, stirred for 5 days, and purified by chromatography ( $\text{CH}_2\text{Cl}_2/\text{MeOH}/\text{NH}_3$  75:22:3) to afford **12f** as a white solid (61 mg, yield: 85%). The purity was further confirmed by HPLC. The final product contained of the  $\alpha$ -pyranose (15%) form and  $\beta$ -pyranose (85%) form that were not isolated but characterized in the mixture. MS (FAB<sup>+</sup>):  $m/z = 1111$  [ $\text{M} + \text{Na}$ ]<sup>+</sup>, 1089 [ $\text{M} + \text{H}$ ]<sup>+</sup>, 588, 423, 391, 369 [ $\text{chol}$ ]<sup>+</sup>, 240, 171, 159, 145, 121, 105, 95, 81, 69;  $\beta$ -pyranose form:  $^1\text{H}$  NMR (300 MHz,  $\text{CDCl}_3/\text{MeOH}$ [20/80]):  $\delta = 7.56$ – $7.58$  (d,  $J = 6$  Hz, 1H, H1a), 5.2–5.27 (m, 1H, H6'), 4.9–4.95 (m, 1H, H3'), 4.2–4.45 (m, 4H, H9, H3', H2a), 4.05–4.2 (m, 2H, H1b, H1c), 2.95–4 (m, 21H, H2, H4, H6a, H3a, H5a, H4a, H2b-6b, H2g-6 g, MeOH), 2.85–2.95 (m, 4H, H1, H6), 2.2–2.3 (m, 2H, H4'), 1.8–2.1 (m, 5H, H2', H7', H8'), 0.98–1.6 (m, 23H, H5, H1', H9', H11', H12', H14'–H17', H22'–H25'), 0.94 (3H, s, H-19'), 0.84 (d,  $J = 6.5$  Hz, 3H, H21'), 0.78 (d,  $J = 6.5$  Hz, 6H, H26'/H27'), 0.61 (s, 3H, H18');  $\alpha$ -pyranose form: identical data except,  $^1\text{H}$  NMR (300 MHz,  $\text{CDCl}_3/\text{MeOH}$ [20/80]):  $\delta = 6.85$  (d,  $J = 5.6$  Hz, 1H, H1a).

**Synthesis of Maltotetraose Compound (12h).** This was prepared with a solution of D-maltotetraose (200 mg, 0.3030 mmol) and **11** (80 mg, 0.133 mmol, stirred for 5 days and purified by chromatography ( $\text{CH}_2\text{Cl}_2/\text{MeOH}/\text{NH}_3$  75:22:3) to afford **12h** as a white solid (67.5 mg, yield: 41%). The purity was further confirmed by HPLC. The final product contained of the  $\alpha$ -pyranose (15%) form and  $\beta$ -pyranose (85%) form that were not isolated but characterized in the mixture. MS (FAB<sup>+</sup>):  $m/z = 1273$  [ $\text{M} + \text{Na}$ ]<sup>+</sup>, 1251 [ $\text{M} + \text{H}$ ]<sup>+</sup>, 588, 369 [ $\text{chol}$ ]<sup>+</sup>, 159, 145, 121, 109, 95, 81, 69; HRMS (FAB<sup>+</sup>)  $\text{C}_{59}\text{H}_{102}\text{N}_4\text{O}_{24}\text{Na}$ : [ $\text{M} + \text{Na}$ ]<sup>+</sup> calcd 1273.6782, found 1273.6821.  $\beta$ -pyranose form:  $^1\text{H}$  NMR (300 MHz,  $\text{CDCl}_3/\text{MeOH}$ [20/80]):  $\delta = 7.56$ – $7.58$  (d, 1H, H1a), 5.15–5.25 (m, 1H, H6'), 4.95–5.1 (m, 1H, H3'), 4.38–4.5 (m, 4H, H9, H3', H2a), 4.04–4.22 (m, 3H, H1b, H1g, H1d), 3.1–3.95 (m, 27H, H2, H4, H6a, H3a, H5a, H4a, H2b-6b, H2g-6g, H2d-6d, MeOH), 2.85–3.1 (m, 4H, H1, H6), 2.2–2.33 (m, 2H, H4'), 1.75–2.1 (m, 5H, H2', H7', H8'), 1–1.6 (m, 23H, H5, H1', H9', H11', H12', H14'–H17', H22'–H25'), 0.92 (3H, s, H-19'), 0.82 (d,  $J = 6.5$  Hz, 3H, H21'), 0.78 (d,  $J = 6.5$  Hz, 6H, H26'/H27'), 0.68 (s, 3H, H18');  $\alpha$ -pyranose form: identical data except,  $^1\text{H}$  NMR (300 MHz,  $\text{CDCl}_3/\text{MeOH}$ [20/80]):  $\delta = 7$  (d, 1H, H1a).

**Synthesis of Maltoheptaose Compound (12i).** This was prepared with a solution of D-maltoheptaose (100 mg, 0.08673 mmol) and **11** (30 mg, 0.0497 mmol) stirred for 7 days and purified by chromatography ( $\text{CH}_2\text{Cl}_2/\text{MeOH}/\text{NH}_3$  75:22:3) to afford **12i** as a white solid (46 mg, yield: 53%). The purity was further confirmed by HPLC. The final product contained of the  $\alpha$ -pyranose (15%) form and  $\beta$ -pyranose (85%) form that were not isolated but characterized in the mixture. MS (FAB<sup>+</sup>):  $m/z = 1759$  [ $\text{M} + \text{Na}$ ]<sup>+</sup>, 1737 [ $\text{M} + \text{H}$ ]<sup>+</sup>, 369 [ $\text{chol}$ ]<sup>+</sup>, 145, 121, 109, 95, 81;  $\beta$ -pyranose form:  $^1\text{H}$  NMR (300 MHz,  $\text{CDCl}_3/\text{MeOH}$ [20/80]):  $\delta = 7.53$ – $7.58$  (d, 1H, H1a), 5.35–5.37 (m, 1H, H6'), 4.97–5.12 (m, 1H, H3'), 4.45–4.6 (m, 4H, H9, H3', H2a),

4–4.5 (m, 6H, H1b, H1c–g), 3.1–3.9 (m, 45H, H2, H4, H6a, H3a, H5a, H4a, H2b-6b, H2c-6c, H2d-6d, H2e-6e, H2f-6f, H2g-6 g, MeOH), 2.7–3 (m, 4H, H1, H6), 2.15–2.35 (m, 2H, H4'), 1.7–2.1 (m, 5H, H2', H7', H8'), 1–1.6 (m, 23H, H5, H1', H9', H11', H12', H14'–H17', H22'–H25'), 0.94 (3H, s, H-19'), 0.84 (d,  $J = 6.5$  Hz, 3H, H21'), 0.77 (d,  $J = 6.5$  Hz, 6H, H26'/H27'), 0.63 (s, 3H, H18');  $\alpha$ -pyranose form: identical data except in  $^1\text{H}$  NMR (300 MHz,  $\text{CDCl}_3/\text{MeOH}$ [20/80]):  $\delta = 6.9$  (d, 1H, H1a).

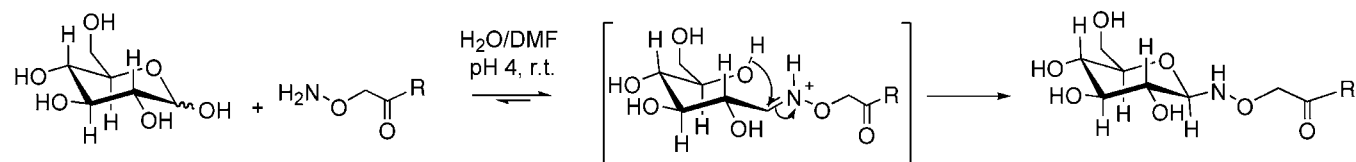
**Preparation of Liposomes DC-Chol (7.5 mg, 15  $\mu\text{mol}$ ) and DOPE (7.5 mg, 10  $\mu\text{mol}$ )** were combined in dichloromethane. The solution was transferred to a round-bottomed flask (typically 50 mL) and organic solvent removed under reduced pressure (rotary evaporator) giving a thin-lipid film that was dried for in vacuo. Following this, 4 mM HEPES buffer, pH 7.2 (3 mL) was added to the round-bottomed flask so as to hydrate the thin-lipid film. After brief sonication (2–3 min) under argon, the resulting cationic liposome suspension (lipid concentration of 5 mg/mL) was extruded 10 times through two stacked 100 nm polycarbonate filters (Millipore, Ireland) to form small unilamellar cationic liposomes (average diameter 105 nm according to PCS analysis). Lipid concentrations (approximately 4–4.8 mg/mL) were determined by inorganic phosphorus assay (61).

**Preparation of LMD and LD Systems.** First, mu:DNA (MD) particles were prepared by mixing as follows: plasmid DNA stock solutions (typically 1.2 mg/mL) were added to a vortex-mixed, dilute solution of mu peptide (1 mg/mL) in 4 mM HEPES buffer, pH 7.2. The final mu:DNA ratio was 0.6:1 (w/w), unless otherwise stated, and final plasmid DNA concentration was 0.27 mg/mL. MD containing solutions were then added slowly under vortex conditions to suspensions of extruded cationic liposomes (typically approximately 4.5 mg/mL), prepared as described above, resulting in the formation of small LMD particles with narrow size distribution ( $120 \pm 30$  nm) as measured by PCS. Final lipid:mu:DNA ratio 12:0.6:1 w/w/w. A solution of sucrose (100%, w/v) in 4 mM HEPES buffer, pH 7.2, was then added to obtain LMD particle suspensions in 4 mM HEPES buffer, pH 7.2, containing 10% w/v sucrose at the desired DNA concentration (final DNA concentration typically 0.14 mg/mL) and the whole stored at  $-80^\circ\text{C}$ . LD systems were prepared for experiments with a lipid:DNA ratio of 12:1 (w/w) following the same vortex protocol without the addition of mu peptide.

**Preparation of Stabilized LMD Systems.** Premodified, stabilized LMD were prepared by adding the defined molar percent of the stealth molecule with DC-Chol and DOPE in dichloromethane/methanol (3:1) followed by the described preparation of liposome and LMD. Postmodified stabilized LMD were prepared by incubating unmodified LMD with the required volume of an aqueous solution (1 mM) of stealth molecule (DSPE-PEG or neoglycolipid) for 2 h at room temperature.

**Particle Size Measurement.** The sizes of all LMD and potential sLMD particles were evaluated after 30 min exposure at  $37^\circ\text{C}$  to biological media by photon correlation spectroscopy (N4 plus, Coulter). The particular chosen pDNA concentration was selected for compatibility with in vitro conditions (1  $\mu\text{g}/\text{mL}$  of DNA). The parameters used were:  $20^\circ\text{C}$ , 0.089 cP, reflexive index of 1.33, angle of  $90^\circ$ ,  $\lambda = 632.8$  nm. Unimodal analysis was used to evaluate the mean particle size in OptiMEM. The size distribution program using the CONTIN algorithm was utilized to separate the subpopulation of small serum particles of less than 50 nm and to extracted the





**Figure 2.** Suggested mechanism of the reaction of glucose (and other carbohydrates with reducing termini) with aminoxy lipid **11** ( $R = 4\text{-aza-}N^6\text{-(cholesteryloxycarbonylamino)hexylamine}$ ). After the formation of an oxime bond, intramolecular acetalization affords the cyclic carbohydrate to generate closed-ring glycolipids.

calculated size of lipoplexes in OptiMEM in the presence of 10% FCS.

**Critical Micelle Concentration.** Micellar forms of the neoglycolipids or PEG-lipids were prepared by sonication of a solution of neoglycolipids (5 mM) or DSPE-PEG (1 mM) in HEPES (4 mM, pH 7) containing  $10^{-7}$  M pyrene. These stock solutions were used to generate different concentrations by serial dilutions with the same buffer. Each sample was incubated with pyrene for 24 h in darkness at 4 °C prior to measurement of fluorescence intensity on a Shimadzu RF-5301PC (Milton Keynes, UK) spectrofluorophotometer, excitation wavelength was 332 nm and emission wavelength was 392 nm.

**Turbidity Measurement.** Sixty microliters of LMD of different compositions at 100  $\mu\text{g/mL}$  were mixed with 240  $\mu\text{L}$  of serum, and the mixtures were incubated at 37 °C with gentle shaking. The absorbance at 600 nm was then recorded at different times with serum alone as blank reference.

**EtBr Exclusion Assay.** EtBr solution (2  $\mu\text{L}$ , 0.1 mg/mL) was added to a sample of 1.5  $\mu\text{g}$  ( $\approx 1.5 \mu\text{L}$ ) of DNA and 60  $\mu\text{L}$  of FCS, incubated for different lengths of time before complemented with HEPES 4 mM pH 7.2 to a final volume of 300  $\mu\text{L}$ . Samples were excited at 310 nm (slit widths of 5 nm for both the excitation and emission) and emission intensity measured at 590 nm in order to determine the effect of serum upon pDNA-intercalation by EtBr. The fluorescence emission intensity,  $I_{590}$ , usually stabilized in less than 3 min and was reported as a fraction of the maximum fluorescence obtained when EtBr was added to free plasmid DNA alone.

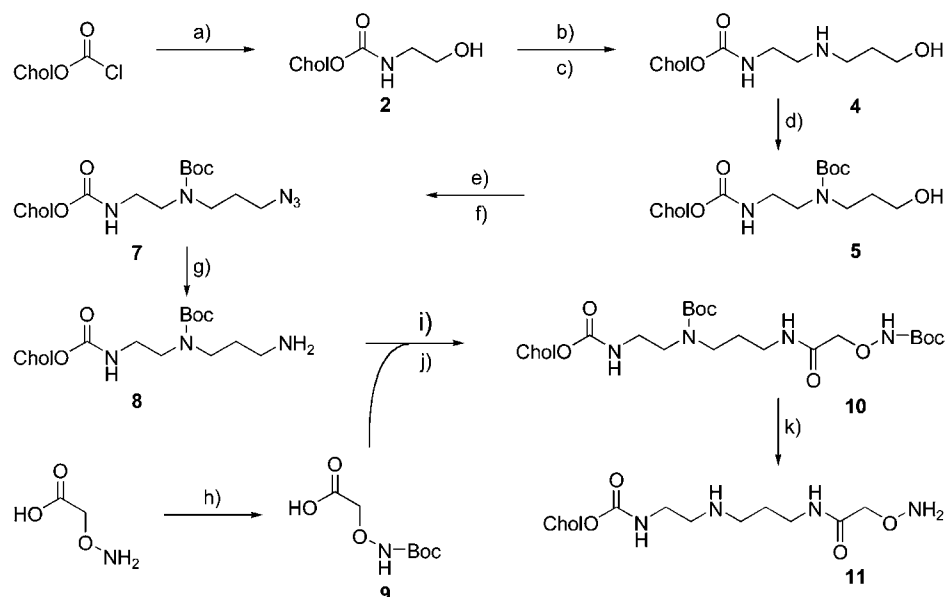
**Transfection of HeLa Cells.** Cells ( $\approx 50\,000$ ) were seeded in a 24-well culture plate in DMEM supplemented with 10% FCS and grown to approximately 70% confluence for 24 h at 37 °C in the presence of 5%  $\text{CO}_2$ . The cells were washed with PBS before the transfection media was added to each well (0.5 mL of solution with 0, 50, or 100% FCS in OptiMEM). LMD or potential sLMD systems as appropriate (5  $\mu\text{L}$ , 100  $\mu\text{g/mL}$  pDNA) were added to each well containing the HeLa cells and incubated for a transfection time of 1 h. Cells were then rinsed three times with PBS and incubated for a further 24 h in DMEM supplemented with 10% FCS prior to final determination of  $\beta$ -galactosidase ( $\beta$ -Gal) enzyme activity in cells post transfection by means of a chemiluminescent reporter gene assay kit (Roche).

## RESULTS AND DISCUSSION

**Synthesis of Neoglycolipids.** Highly convergent syntheses were devised involving first the preparation of a cholesterol-based cationic lipid containing an aminoxy functional group, followed by the chemoselective coupling of this lipid to commercially available, completely unprotected monosaccharides or oligosaccharides. Chemoselective coupling of the lipid to such unprotected sugars was enabled by the preference of the aminoxy functional group to react only with the aldehyde functional group revealed in the open-chain form of aldose monosaccharides or in the open chain form of terminal

glucose residues (reducing termini) of oligosaccharides (Figure 2). The synthesis of Boc-protected amino-lipid **8** was based upon our published methodologies for the syntheses of other cationic cholesterol-based lipids from readily available amino-alcohols as starting materials employing complementary blocking group strategies to protect secondary amino functional groups originated during syntheses (6, 22). Hence the synthesis of Boc-protected amino-lipid **8** was accomplished without major difficulty although requiring a few simple modifications to existing protocols. Compound **8** was then converted into Boc-protected aminoxy lipid **10** by means of carboxylic acid **9** (Scheme 1). Acid **9** was prepared by Boc-protection of commercially available *O*-(carboxymethyl)-hydroxylamine hydrochloride and then activated by means of *N*-hydroxysuccinimide (NHS) and *N,N*-dicyclohexylcarbodiimide (DCC) in order to promote clean acylation of aminolipid **8** in THF in situ affording **10** in good yield. Thereafter, synthesis of aminoxy lipid **11** was accomplished by Boc-deprotection of **10** with aqueous trifluoroacetic acid. Finally, the combination of aminoxy lipid **11** with a variety of aldose monosaccharides and the glucose (reducing) terminal residue of oligosaccharides was performed in order to realize a corresponding variety of neoglycolipids with a similar general formula (Figure 1). Coupling reactions were conducted under mild conditions making use of a solvent buffer system comprising DMF and aqueous acetic acid (1:1, v/v), pH 4, selected to optimize simultaneously both the combined solubilities of sugars and aminoxy lipid **11**, together with aminoxy functional group reactivity. At pH 4, the proton concentration is approximately optimal for the addition–elimination mechanism that leads to alkoxime functional group formation (Figure 2). Acid-catalyzed ring closure (acetalization) then completes the process leading to the generation of mono- and oligosaccharidoneoglycolipid products with an aminoxy-glycopyranose residue attached to the lipid moiety. Reaction times and yields of all coupling reactions carried out are given (Table 1). Further optimization could reduce the reaction times required. Analytical HPLC and NMR studies of all isolated aminoxyglycopyranose products were carried out revealing that each product was comprised of two isomers (major and minor) after workup and purification. In the case of each product, these two isomers were presumed to result from the formation of both  $\alpha$  and  $\beta$  anomers of the aminoxy glycopyranose residue during the ring closure.

**Neoglycolipid Conformations.** Conformational analysis of the neoglycolipids was performed by  $^1\text{H}$  NMR (62), with a particular emphasis upon the anomeric conformations of the aminoxy glycopyranose residue in each neoglycolipid product using heteronuclear  $^1J_{13\text{C}1\text{a}-\text{H}1\text{a}}$  coupling constants to diagnose both presence and relative proportions of  $\alpha$  and  $\beta$  anomers associated with the aminoxy anomeric carbon center (C1a) (63). The absolute value of  $^1J_{13\text{C}1-\text{H}1}$  coupling constants in typical glycopyranose ring systems depends on a number of factors including the orientation of the C1–H1 bond relative to

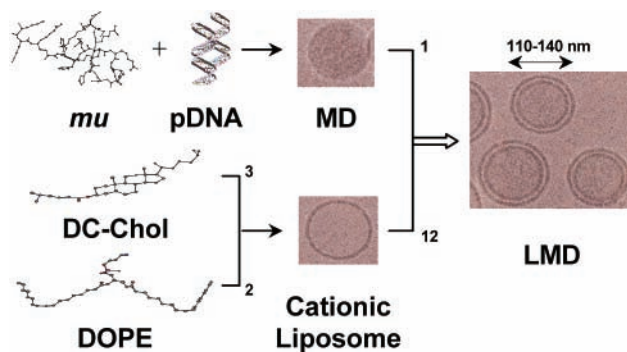
**Scheme 1. Synthesis of the Lipid Moiety<sup>a</sup>**

<sup>a</sup> Reagents: (a)  $\text{CH}_2\text{Cl}_2$ ,  $\text{HO}(\text{CH}_2)_2\text{NH}_2$  (2.2 equiv), 10 h, 97%; (b)  $\text{CH}_2\text{Cl}_2$ , 0 °C,  $\text{Et}_3\text{N}$  (3 equiv),  $\text{MsCl}$  (2.5 equiv), 10 min; then 1 h at rt, 98%; (c) THF,  $\text{HO}(\text{CH}_2)_3\text{NH}_2$  (10 equiv), 6 h, 96%; (d)  $\text{CH}_2\text{Cl}_2$ ,  $\text{Et}_3\text{N}$ ,  $\text{Boc}_2\text{O}$ , rt, 5 h, 90%; (e)  $\text{CH}_2\text{Cl}_2$ , 0 °C,  $\text{Et}_3\text{N}$  (3 equiv),  $\text{MsCl}$  (2.5 equiv), 10 min; then 2 h at rt, 90%; (f) DMF, 80 °C,  $\text{NaN}_3$  (5 equiv),  $\text{NaI}$  (1 equiv), 3 h, 95%; (g) (i) THF,  $\text{PMe}_3$  (1.15 equiv), rt, 3 h, (ii)  $\text{H}_2\text{O}/\text{NH}_3$ , 88%; (h)  $\text{CH}_2\text{Cl}_2$ ,  $\text{Et}_3\text{N}$ ,  $\text{Boc}_2\text{O}$ , rt, 5 h, 98%; (i),  $\text{EtOAc}$ ,  $N$ -hydroxysuccinimide (1 equiv),  $\text{DCC}$  (1 equiv), 10 h., rt; (j),  $\text{EtOAc}/\text{THF}$  [95/5],  $\text{Et}_3\text{N}$  (pH 8), 2 h, rt, 90%; (k)  $\text{CH}_2\text{Cl}_2$ ,  $\text{TFA}$  (15 equiv), 0 °C,  $\text{N}_2$ , 5 h, 86%.

**Table 1. Yields, Reaction Times, and Diastereoselectivity of the Formation of Neoglycolipids 12a–i**

product	carbohydrate	reaction time (days)	yield (%)	$\beta/\alpha$
<b>12a</b>	mannose	3	65	82/18
<b>12b</b>	glucose	1	80	89/11
<b>12c</b>	galactose	1	70	85/15
<b>12d</b>	glucuronic acid	1	60	85/15
<b>12e</b>	lactose	4	50	85/15
<b>12f</b>	maltose	1	65	87/13
<b>12g</b>	maltotriose	5	85	85/15
<b>12h</b>	maltotetraose	5	40	85/15
<b>12i</b>	maltoheptaose	7	55	85/15

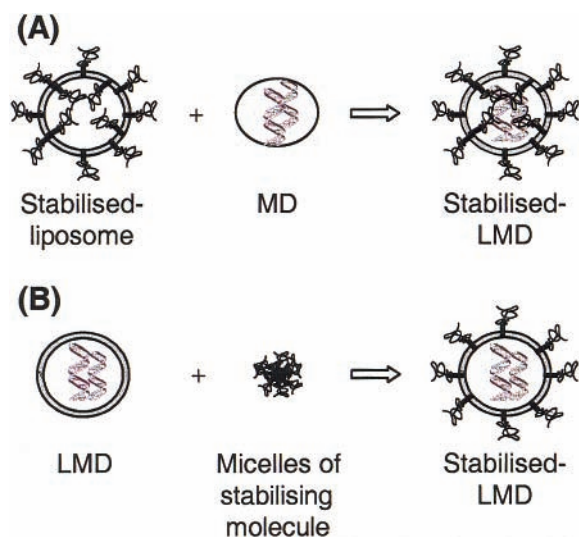
adjacent lone pairs of the glycopyranose ring oxygen atom and the electronegativity of the other substituent attached to the glycopyranose ring system. Differences between the  $^1J_{13\text{C1-H1}}$  coupling constants of  $\alpha$ - and  $\beta$ -glycopyranose ring systems have been used previously to determine relative ratios of the two anomeric conformations. Typically, the difference of  $^1J_{13\text{C1-H1eq}}(\alpha\text{-anomer})$  minus  $^1J_{13\text{C1-H1ax}}(\beta\text{-anomer})$  is  $\approx +10$  Hz. In our case, taking the aminoxy mannopyranose neoglycolipid **12a** as an example, the major isomer exhibited a  $^1J_{13\text{C1a-H1a}} = 167$  Hz and the minor isomer a value of  $^1J_{13\text{C1a-H1a}} = 177$  Hz, thereby identifying the major isomer as the  $\beta$ -anomer (approximately 80%) and the minor isomer as the  $\alpha$ -anomer (approximately 20%).  $^1\text{H}$ -phase sensitive NOESY confirmed the identification of the major and minor isomers. HPLC analysis further detailed the  $\beta:\alpha$  ratio more precisely as 82:18. Similar anomeric ratios were observed consistently throughout all the neoglycolipid series prepared as part of the studies described here (Table 1). The high  $\beta:\alpha$  ratio of 82:18 determined for the aminoxy mannopyranose neoglycolipid **12a** is unusual. Mannopyranose rings exhibit an axial hydroxyl functional group at C2 that frequently helps to promote  $\alpha$ -anomer formation. A possible explanation is that this reaction could be controlled kinetically by a pattern of hydrogen bonding between the sugar and the aminoxy linker, stabilizing the  $\beta$  anomer. For the purposes of the studies described below, we elected to proceed without



**Figure 3.** Formulation of LMD systems. Plasmid DNA (pDNA, D) is precondensed with cationic adenoviral peptide  $\mu$  (mu, M) (mu:pDNA 0.6:1, w/w) to generate MD particles ( $\text{N/P} = 0.7$ ) that are further complexed with extruded cationic liposomes prepared from cytofectin DC-Chol and neutral lipid DOPE to generate LMD vectors. Picture of LMD, MD and liposomes were obtained by cryoelectron microscopy as described previously (21).

attempting to resolve and purify each isomer separately by HPLC particularly given that we suspected isomeric mixtures may offer more benefit in terms of stabilizing synthetic nonviral vector systems in biological fluids than not. Obviously, were any of our neoglycolipids required for receptor targeting purposes then the reverse would certainly be true and additional HPLC resolution and purification would be required.

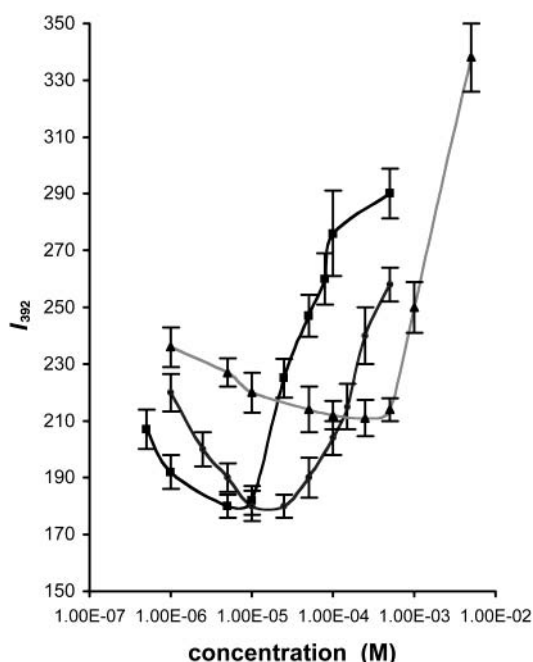
**Formulation of Stabilized LMD Systems (sLMD).** First generation LMD systems are prepared as illustrated (Figure 3) (21). To generate potential stabilized-LMD (sLMD) systems equipped with a "stealth" barrier sufficient to stabilize these systems against aggregation and inactivation in biological fluids, two alternate formulation procedures were considered as a means of introducing putative stealth molecules such as DSPE-PEG or a neoglycolipid into LMD particles. In the premodification formulation process, putative stealth molecules can be introduced into cationic liposomes prior to potential sLMD particle formation; in postmodifica-



**Figure 4.** Principles of (A) pre- and (B) postmodification of LMD particles to generate potential stabilized-LMD (sLMD) system particles.

tion, LMD particles can be prepared first and then combined with putative stealth molecules at the end of the process in order to create potential sLMD particles (Figure 4). Premodification requires that putative stealth molecules are included with the lipid mixture prior to cationic liposome formulation by either dehydration–rehydration (DRV) or reverse-phase evaporation (REV) procedures. Formulation of such a ternary mixture into cationic liposomes then results in “stabilized” cationic liposome (sL) systems wherein putative stealth molecules become distributed on both sides of the cationic liposome bilayer as part of both inner and outer leaflets. Such a distribution was thought to impede the formulation of sLMD particles as illustrated (Figure 4) by creating a steric barrier to plasmid DNA (pDNA) interactions with the cationic liposome bilayer. This is a potentially serious drawback. Hence cationic liposome-forming lipids such as the cationic lipid (cytofectin) 3 $\beta$ -[N(N,N-dimethylaminoethane)carbamoyl]cholesterol (DC-Chol) and the neutral lipid dioleoyl L- $\alpha$ -phosphatidylethanolamine (DOPE) used in our studies here, needed to be combined in a suitable solvent able to cosolubilize the putative stealth molecule as well.

The postmodification process requires that LMD particles are prepared first and stealth molecules may be surface absorbed into the outer leaflet of LMD particles to generate potential sLMD particles. The practical realization of this process was thought possible by combining LMD particles with solutions comprising putative stealth molecules at concentrations in excess of their critical micelle concentration (cmc) (64). Amphiphilic monomers such as lipids are known to transfer from one lipid phase to another via the aqueous phase (65). Hence, monomers with a relatively low cmc can therefore be expected to adopt a liposome-inserted over a solution-free state if mixed in the presence of liposome systems (66, 67). Such solution-to-liposome transfer processes have been used to generate stabilized liposome systems for drug delivery applications from liposomes and stealth molecule mixtures (68, 69). However, the main drawback of this form of postmodification process is the possibility that the transfer process may be inefficient depending upon the nature of the liposome system involved or the putative stealth molecule under investigation. The incorporation kinetics and equilibrium states of this solution-to-liposome transfer phenomenon



**Figure 5.** Determination of the cmc for DSPE-PEG (■), 12c (○), and 12g (▲). Pyrene ( $10^{-7}$  M) fluorescence intensity,  $I_{392}$ , in 4 mM HEPES, pH 7, was plotted as a function of concentration with measurements made after samples had been incubated together for 24 h in darkness at 4 °C. Means  $\pm$  SD,  $n = 3$ . The cmc was determined from the crossover point of the two straight-lines corresponding to the two domains of each curve.

**Table 2. Critical Micelle Concentrations (cmc) of Neoglycolipids Investigated in This Study**

product	carbohydrate	cmc
12a	mannose	$2 \times 10^{-5}$ M
12b	glucose	$3 \times 10^{-5}$ M
12c	galactose	$2 \times 10^{-5}$ M
12e	lactose	$7 \times 10^{-5}$ M
12f	maltose	$7 \times 10^{-5}$ M
12g	maltotriose	$4 \times 10^{-4}$ M
12h	maltotetraose	$8 \times 10^{-4}$ M

are not very well understood (68); accordingly, applications of this insertion technique in the field of nonviral gene therapy do not appear to be very numerous (70).

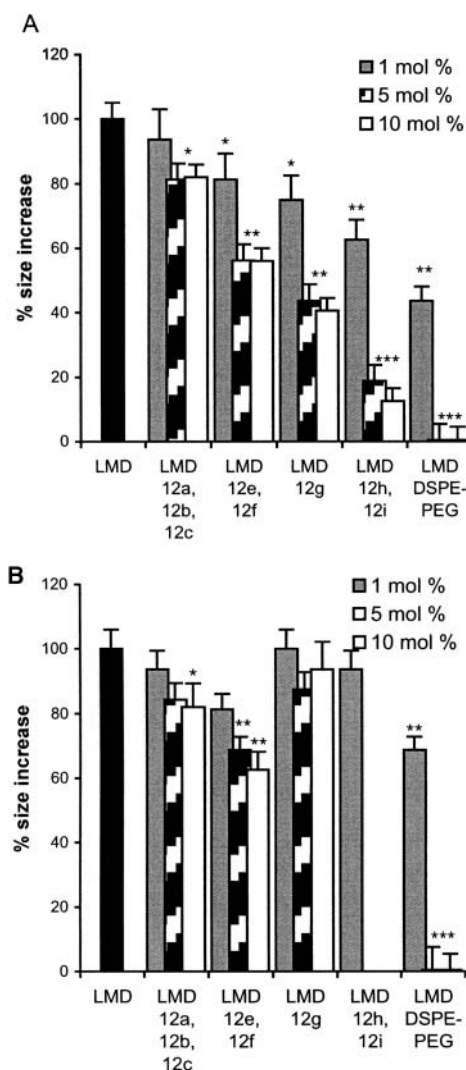
**Cmc Measurements.** Prior to the insertion of neoglycolipids or DSPE-PEG into LMD particles, the critical micellar concentrations of all these putative stealth molecules was determined as described previously by means of a fluorescence-based assay (64, 71). Pyrene fluorescence intensity,  $I_{392}$ , was measured in HEPES 4 mM, pH 7 at 20 °C and plotted as a function of stealth molecule concentration. A typical data set obtained with DSPE-PEG, 12c, and 12g is shown (Figure 5). The cmc was identified by the straight-lines crossover point corresponding to the two domains of each curve and was found to be  $8.5 \mu\text{M}$  for DSPE-PEG. This value agrees well with a DSPE-PEG cmc of  $9 \mu\text{M}$  measured by others at 37 °C in Tris-HCl buffer (72). The cmc of DSPE-PEG is significantly higher than for DSPE (more than  $10^6$  times), consistent with an increase in hydrophilicity by virtue of PEG-conjugation. Cmc values were determined for all the neoglycolipids (Table 2) as well with the exception of the glucuronic acid based compound 12d and the maltoheptaose-based compound 12i that were both poorly soluble under the assay conditions used. Compound 12i in particular was thought to be poorly soluble above millimolar concentrations owing to the peculiar properties of long chain carbohydrates. Inter-oligosaccharide



interactions in water are often cooperative, leading to higher order supramolecular structures. As an example, it is interesting to note the crystallization behavior of maltooligosaccharides; on crystallization from water, maltooligosaccharides ( $N > 5$ ) chains can adopt left-handed parallel stranded double helical conformations, which pack into monoclinic and hexagonal arrays (73, 74). The formation of such supramolecular structures by the carbohydrate headgroups is a possible explanation for the insolubility of these glycolipids. This phenomenon has been observed in different conditions with maltopentaose-based glycolipids (75–77).

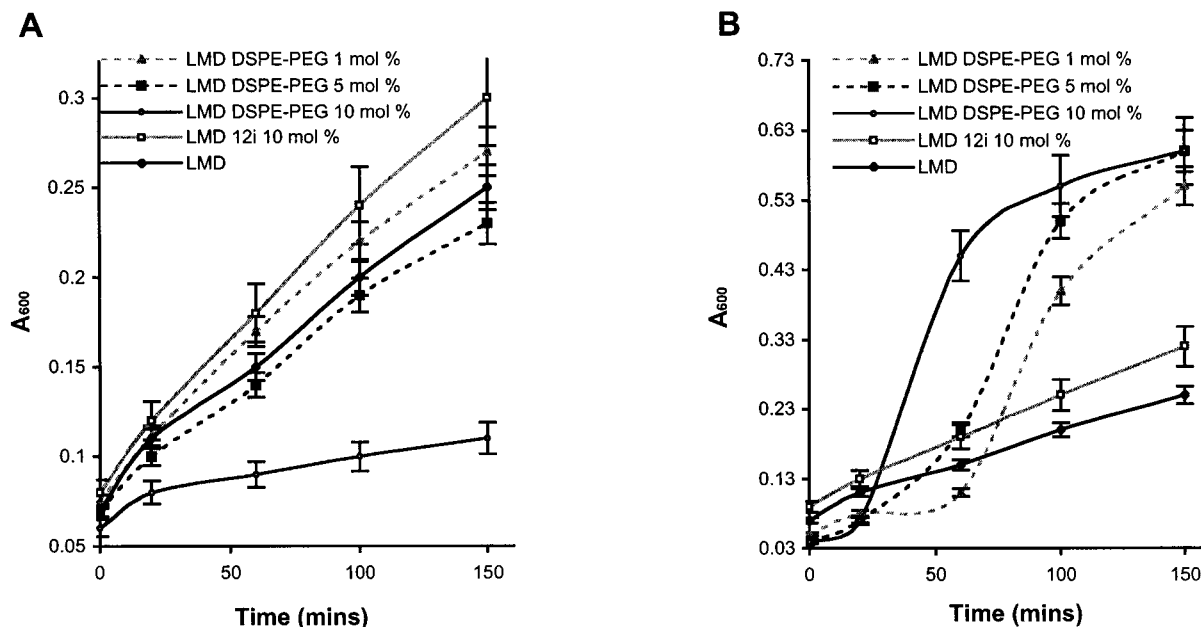
**Aggregation of Potential sLMD Systems in Salt Medium.** A variety of sLMD systems were prepared by pre- and postmodification procedures as described in the Experimental Section and then studied for stability toward salt-induced aggregation in OptiMEM. OptiMEM is the classical medium of choice for in vitro cell transfection. This serum-free tissue culture medium contains the main salts required for cell functions. It also contains the minimum amino acids and vitamins to guarantee cell survival during the transfection process. Aggregation of potential sLMD systems was followed by photon correlation spectroscopy (PCS). The colloidal instability of first generation LMD particles induced by salt results in aggregates of different sizes depending upon the incubation conditions. The higher the salt concentration, the temperature, and the time of incubation, the larger appear to be the resulting aggregates measured by PCS. Under such conditions, particles depending upon their surface properties are able to interact substantially at short range via attractive van der Waals forces, owing to the shielding of long-range electrostatic forces (78). In the case of LMD vectors, the lipids used have a strong tendency to generate hydrophobic interactions and therefore promote the formation of such aggregates. Aggregation propensities of first generation LMD particles and potential sLMD system particles were judged as a function of particle size increases after 30 min incubation at 37 °C in OptiMEM. The quality of the stealth barrier properties of either DSPE-PEG or a given neoglycolipid inserted into the surface cationic liposome bilayer were then assumed to be inversely related to the percentage particle size increase. Data are shown generated with potential sLMD systems prepared by both postmodification (Figure 6A) and premodification procedures (Figure 6B). When premodified, the best stabilization was achieved with formulations using glycolipids containing two glycosidic units. However, we were unable to formulate LMDs with glycolipids containing the longest carbohydrate units (4 or 7 units) at 5 or 10 molar %. Postmodified neoglyco-LMD systems tended to be smaller with increasing chain length of the carbohydrate unit of the glycolipid (Figure 6A). This result is consistent with increased hydrophilicity and steric repulsion (67, 79) expected if these molecules were exposed on the outer layer (molecular brushes). Particle stability induced by the largest maltoheptaose-based neoglycolipid **12i** at 10 mol % was substantial, suggesting that **12i** possessed significant stealth molecule properties in high salt conditions.

As expected, PEG-LMD systems were the most stable above 2–5 mol % PEG included by pre- or postmodification. This result reflects the widespread use of PEG as a stabilization agent in drug delivery. It is interesting to note that PEG does not interfere with the formulation when premodification technique is used even at the highest molar ratio used.



**Figure 6.** (A, B) Aggregation profile of neoglycolipid formulated stabilized LMD (sLMD) vector systems in OptiMEM. LMD formulations were incubated for 30 min at 37 °C OptiMEM at a DNA concentration of 1 mg/mL. The size increase due to salt-induced aggregation was characterized by photon correlation spectroscopy (PCS), and size increases were normalized with respect to unmodified LMD particle size increases (100%). A; postmodification: sLMD systems were prepared by incubation of LMD particles with a micellar solution of putative stealth molecules at the indicated molar ratios relative to total lipid concentration. B; premodification: sLMD systems were prepared directly from cationic liposomes formulated with the indicated molar ratios of putative stealth molecules relative to total lipid concentration. Means  $\pm$  SD,  $n = 3$ . \* $P < 0.05$ ; \*\* $P < 0.005$ ; \*\*\* $P < 0.0005$  (statistical analysis was calculated by Student's  $t$ -test when stabilized LMD were compared to unmodified LMD).

**Aggregation of Potential sLMD Systems in Serum.** Serum used in laboratories is usually derived from bovine (BS) or fetal calf (FCS). Media of cell cultures are usually supplemented with 5 to 10% serum to ensure proper cell growth. For in vitro experiments, blood is usually too difficult to handle (mainly due to clotting); therefore, experiments designed to mimic the blood and other biological fluids are frequently performed with serum alone. Serum is a complex mixture of components including serum albumin, lipoproteins, macroglobulins, fibrinogen, heparin, and fatty acids (such as oleic acid). All these components interact with LD or LMD particles rendering them ineffective for transfection either by promoting particle aggregation or disintegration (80).



**Figure 7.** (A, B) Turbidity of sLMD vector systems in FCS. LMD formulations were incubated at 37 °C in FCS at a DNA concentration of 20 mg/mL. The increase in turbidity with time was measured as a function of  $A_{600}$ . A; postmodification: sLMD vectors were prepared by incubation of LMD particles with a micellar solution of putative stealth molecules at the indicated molar ratios relative to total lipid concentration. B; premodification: sLMD systems were prepared directly from cationic liposomes formulated with the indicated molar ratios of putative stealth molecules relative to total lipid concentration. Means  $\pm$  SD,  $n = 3$ .

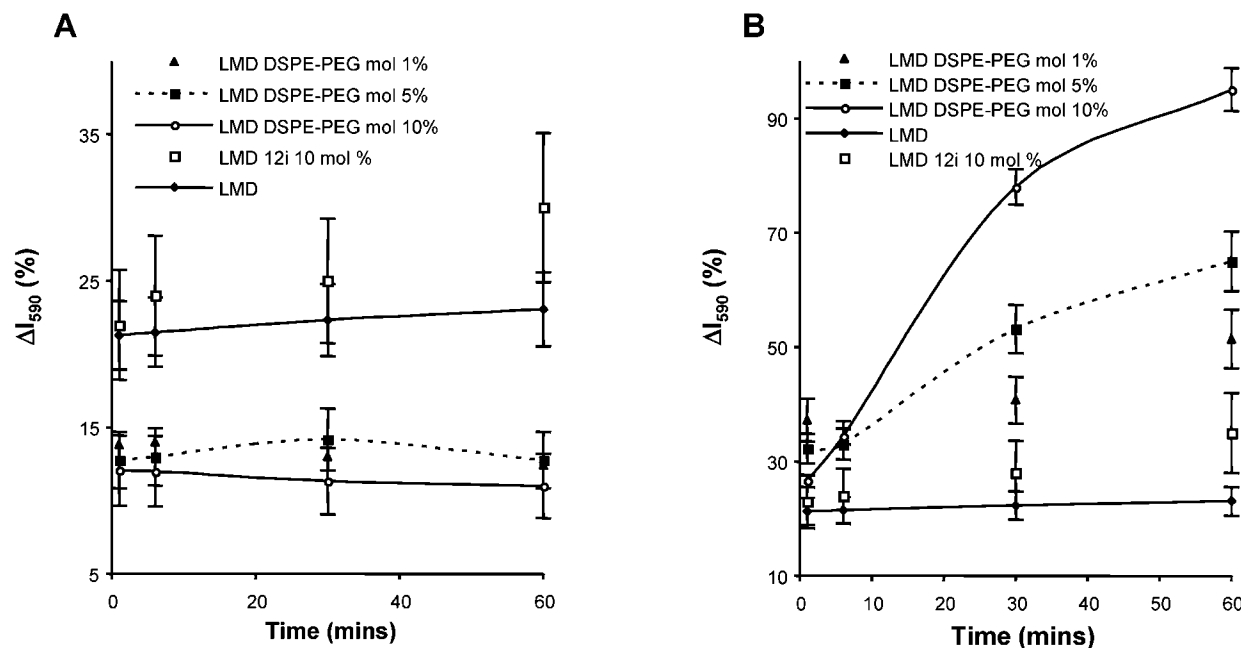
Stealth molecules such as DSPE-PEG were originated primarily for the purpose of stabilizing drug delivery liposomes against serum-induced effects. Given the fact that multicomponent serum renders PCS assays unusable owing to random scattering effects, two alternative assays were used to follow potential sLMD system stabilities in the presence of serum, namely turbidity and ethidium bromide (EtBr) exclusion assays.

Turbidity measurements are commonly used to diagnose the appearance of particle aggregation or fibrilization in solution over time. Particle aggregation causes enhanced light scattering particularly at long visible-light wavelengths  $> 600$  nm, and this is detected either by an increase in absorbance,  $A_{600}$ , above background as a function of time. Data generated does not extrapolate easily to particle size measurements, but aggregation can at least be observed qualitatively. Hence, experiments were conducted in which LMD systems were combined with FCS and changes in  $A_{600}$  monitored with time. As above, the quality of the stealth barrier properties conferred by either DSPE-PEG or neoglycolipid inserted into the cationic liposome bilayer of LMD systems were then presumed to correlate inversely with detectable increases in  $A_{600}$  over time. Data are shown for LMD systems prepared by both postmodification (Figure 7A) and premodification procedures (Figure 7B). Regrettably, all neoglycolipids, including **12i**, introduced by the postmodification procedure, proved unable to arrest particle aggregation in FCS at all in complete contrast to the effect of DSPE-PEG at 10 mol %. Therefore of the putative stealth molecules used in studies described here, only DSPE-PEG exhibited the full characteristics of a stealth molecule able to generate stable systems with respect to aggregation in both in salt medium and in serum conditions.

sLMD systems prepared from DSPE-PEG by the premodification procedure revealed an inversion of the DSPE-PEG stabilization effect (Figure 7B). While DSPE-PEG inclusion by premodification appeared sufficient to suppress aggregation initially, substantial aggregation

effects were observed to take place between 20 and 60 min after mixing with FCS suggesting that potential sLMD particles prepared from DSPE-PEG by this method were substantially metastable with respect to serum effects. It is likely that such sLMD vectors, which are stable under high salt conditions (Figure 6), are destabilized in serum by internally disruptive steric effects deriving from inner particle distributions of DSPE-PEG molecules. This behavior is a direct consequence of the premodification procedure (Figure 4). Hence this data set (Figure 7) suggests that the postmodification procedure is the preferred *modus operandi* above the premodification procedure for the preparation of future effective sLMD systems.

The ethidium bromide exclusion assay is frequently used to study the extent of pDNA charge neutralization, condensation, and encapsulation in response to cationic agents such as cationic liposomes or peptides. Ethidium bromide (EtBr), an otherwise weak fluorophore, exhibits strong fluorescence,  $I_{590}$ , following pDNA intercalation. When a saturating amount of EtBr (approximately 6:1 [nucleotide]/[EtBr]) is combined with pDNA in the presence of a cationic pDNA condensing agent, pDNA condensation, and encapsulation results in EtBr displacement (exclusion) from pDNA intercalation sites leading to a substantial fall in  $I_{590}$ . Conversely, if a condensed system such as LD, LMD, or a potential sLMD becomes destabilized for whatever reason such as by general interactions with heparin and/or dextran sulfate leading to pDNA displacement, renewed EtBr intercalation may become possible as pDNA becomes reexposed with time leading to an increase in  $I_{590}$  from a basal level (81). Experiments were conducted once again in which potential sLMD systems were combined with FCS and changes in  $I_{590}$  monitored with time. The capacities of cationic bilayer-inserted DSPE-PEG or neoglycolipid to resist particle disintegration mediated by serum components should be inversely correlated with increases in  $I_{590}$  over time in a similar way to the turbidity measurements described above. Data are shown for potential sLMD



**Figure 8.** (A and B) EtBr exclusion assay of potential stabilized-LMD (sLMD) in FCS. LMD formulations were incubated at 37 °C in FCS at DNA concentration of 25 mg/mL. Increase in EtBr fluorescence,  $I_{590}$ , was monitored as a function of time. Observed intensities,  $I_{590}$ , were normalized by dividing through the emission intensity of equivalent levels of EtBr in the presence of equivalent levels of naked pDNA alone under analogous conditions. A; postmodification: sLMD systems were prepared by incubation of LMD particles with a micellar solution of putative stealth molecules at the indicated molar ratios relative to total lipid concentration. B; premodification: sLMD systems were prepared directly from cationic liposomes formulated with the indicated molar ratios of putative stealth molecules relative to total lipid concentration. Means  $\pm$  SD,  $n = 3$ .

systems prepared by both postmodification (Figure 8A) and premodification procedures (Figure 8B). Data show that first generation LMD particles were remarkably robust with respect to disintegration, there being no apparent increase in  $I_{590}$  over time.

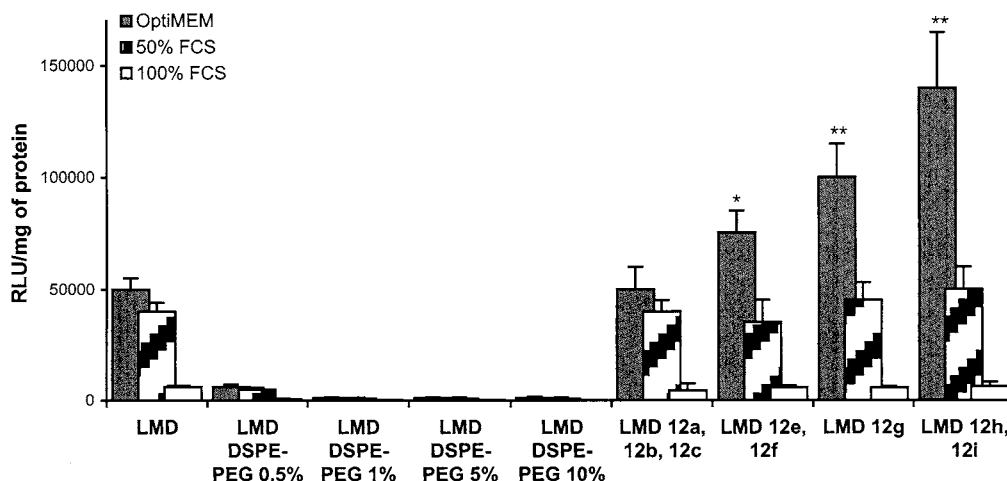
Other aspects of the exclusion assay data set indicated that neoglycolipid **12i** at 10 mol %, introduced by either the postmodification or premodification procedure, marginally impaired particle resistance to disintegration relative to first generation LMD, while DSPE-PEG at 1, 5, and 10 mol % was able to prevent particle disintegration convincingly provided that this stealth molecule was introduced by the postmodification procedure (Figure 8A). By complete contrast, when DSPE-PEG was introduced by the premodification procedure, immediate particle disintegration was observed as demonstrated by the rapid increase in  $I_{590}$  over the time period of the assay, most especially when DSPE-PEG at 10 mol % was employed (Figure 8B). This complete inversion of the DSPE-PEG stabilization effect as a direct consequence of the premodification procedure is completely in line with turbidity assay results above (Figure 7B). Furthermore, putting both data sets together suggests a degeneration process in which potential sLMD particles prepared from DSPE-PEG by the premodification procedure are first destabilized with respect to serum-induced particle disintegration by internally disruptive steric effects that derive from inner particle DSPE-PEG molecules (as mentioned above) and then subsequently become prone to aggregation. Both first generation LMD particles and neoglyco-LMD appear only to be very mildly disintegration prone in serum but substantially aggregation prone (Figures 7 and 8), characteristics that would impair their circulation profiles in vivo and result in their rapid clearance by the reticuloendothelial system.

The ability of maltoheptaose chains of **12i** to protect LMD particles from salt-induced destabilization could not be properly exploited to reduce serum protein induced

aggregation. One explanation could be that the method of postadsorption does not allow sufficient micellar insertion into the bilayer due to the peculiar cmc of **12i**. Another possibility is that the sugar chains added onto LMD are still too small to actively screen the strongly cationic LMD surface. Further increase of the carbohydrate length may induce better protection but will require the synthesis of more expensive and complex molecules. Moreover, inclusion of such long chain sugar is likely to increase recognition of the carbohydrate motifs by serum amylases, lipopolysaccharide-binding proteins, or cells with specific lectin receptors. This could result in an increased clearance rate of the lipoplexes by complement activation. We believe, therefore, that future research must primarily focus on reducing the excess of cationic charges to generate better stability. Such modification should allow in our view a more favorable harvesting of neoglycolipid properties.

**In Vitro Transfection Efficiency.** Transfection data gathered with sLMD systems demonstrate the inhibiting effects of PEG-based compounds upon transfection efficiency in marked contrast to the beneficial effects of neoglycolipids (Figure 9). The inclusion of DSPE-PEG was found to abolish transfection irrespective of the transfection conditions, in line with previously published data demonstrating the inhibitory effects of PEG upon the transfection process (40, 41). By contrast, where potential sLMD systems were prepared with neoglycolipids (postmodification), HeLa cell transfection in vitro was found to increase above first generation LMD transfection levels in proportion to the number of glycopyranose residues involved. There is an interesting correlation between increasing transfection efficiency and increasing particle stability with respect to salt-induced aggregation in OptiMEM (Figures 6 and 9). However, in serum, the transfection efficiencies of all potential sLMD systems prepared with neoglycolipids were reduced to the same levels of transfection efficiency as first generation LMD.





**Figure 9.** Transfections profile of LMD and potential stabilized LMD systems (sLMD). HeLa cells were transfected in OptiMEM, 50% FCS and 100% FCS for 1 h (48-well plate, 0.25  $\mu$ g of DNA). Unmodified reference LMD transfection is compared with transfections by potential sLMD systems prepared (postmodification procedure) with either the indicated levels of DSPE-PEG or else 7.5 mol % of each indicated neoglycolipid. Means  $\pm$  SD,  $n = 4$ . One representative of three experiments is shown. \* $P < 0.05$ ; \*\* $P < 0.005$  (statistical analysis was calculated by Student's  $t$ -test when stabilized LMD were compared to unmodified LMD).

This result is consistent with the failure of inserted neoglycolipids to make any controlling impact upon serum-induced particle aggregation (Figure 7A). Hence combining both main observations together there appears to be the suggestion of a possibility that if neoglycolipid modifications to LMD systems can be found that adequately prevent serum-induced particle aggregation, as well as salt-induced aggregation, then the result would be the development of a highly effective sLMD system, with adequate transfection competency and hence with real potential for in vivo applications.

## CONCLUSION

We have developed a simple methodology to generate neoglycolipids that we believe could be valuable for drug or gene delivery purposes and may even find more general application in carbohydrate biology. The results of our studies here also suggest that provided neoglycolipids can be identified as able to prevent serum-induced particle aggregation, as well as salt-induced aggregation, then such stealth molecules could be highly beneficial in the quest for clinically viable synthetic nonviral vector systems in view of the positive effects of neoglycolipids upon transfection efficiency. Data presented here show that none of the current neoglycolipids meet this criterion with the partial exception of maltoheptaose-based neoglycolipid **12i**. However, the possibility that alternative neoglycolipids could be developed that do meet this criterion is credible in our view. The negative impact of PEG upon transfection cannot be overstated and makes DSPE-PEG and other PEGylated stealth molecules doubtful components of a clinically viable synthetic nonviral vector system. It is interesting to note in our data reported here that the stabilizing effect of incorporating DSPE-PEG with LMD to prevent salt or serum-induced particle aggregation was only realized with 5–10 mol % of DSPE-PEG (Figures 6 and 7), while transfection was virtually abolished completely with as little as 0.5 mol % of DSPE-PEG (Figure 9). This suggests that the inhibitory effect of PEG is substantially in excess of its stabilizing stealth potential. Recent evidence suggests that PEGylated nonviral vector systems are internalized easily by cells but intracellular PEG then prevents the intramolecular trafficking of both plasmid DNA (22) and even small ODNs (40).

One alternative way to overcome the clear limitations of these neoglycolipids to confer serum stability to LMD is the postcoupling of sugars onto aminoxylipid containing LMD systems. Postcoupling allows for the stoichiometric control of surface modification without impairing particle integrity, i.e., membrane destabilization. Preliminary results along these lines obtained in our laboratories demonstrated that this novel way of covalently conjugating sugar units onto lipoplex surfaces is successful. Investigations into the serum resistance and potential targeting properties of such postcoupled systems are currently progressing and will be reported in due course.

## ACKNOWLEDGMENT

We would like to thank the Mitsubishi Chemical Corporation for supporting the Imperial College Genetic Therapies Centre. We are especially grateful to Dr. T. Tagawa for useful discussions.

## LITERATURE CITED

- (1) Marshall, E. (1999) *Science* 286, 2244–2245.
- (2) Boulikas, T., and Martin, F. (1997) *Int. J. Oncol.* 10, 317–322.
- (3) Felgner, P. L., Gadek, T. R., Holm, M., Roman, M., Chan, H. W., Wenz, M., Northrop, J. P., Ringold, G. M., and Danielsen, M. (1987) *Proc. Natl. Acad. Sci. U.S.A.* 84, 7413–7417.
- (4) Wheeler, C. J., Felgner, P. L., Tsai, Y. J., Marshall, J., Sukhu, L., Doh, S. G., Hartikka, J., Nietupski, J., Manthorpe, M., Nichols, M., Plewe, M., Liang, X. W., Norman, J., Smith, A., and Cheng, S. H. (1996) *Proc. Natl. Acad. Sci. U.S.A.* 93, 11454–11459.
- (5) Wolff, J. A., Malone, R. W., Williams, P., Chong, W., Acsadi, G., Jani, A., and Felgner, P. L. (1990) *Science* 247, 1465–1468.
- (6) Cooper, R. G., Etheridge, C. J., Stewart, L., Marshall, J., Rudginsky, S., Cheng, S. H., and Miller, A. D. (1998) *Chem.-Eur. J.* 4, 137–151.
- (7) Keller, M., Jorgensen, M. R., Perouzel, E., and Miller, A. D. (2003) *Biochemistry* 42, 6067–6077.
- (8) Miller, A. D. (1998) *Angew. Chem., Int. Ed.* 37, 1769–1785.
- (9) Bielinska, A. U., Chen, C. L., Johnson, J., and Baker, J. R. (1999) *Bioconjugate Chem.* 10, 843–850.
- (10) Sheiko, S. S., and Moller, M. (2001) *Hyperbranched macromolecules. Soft particles with adjustable shape and persistent motion capability*, Vol. 212.

- (11) Ihre, H. R., De Jesus, O. L. P., Szoka, F. C., and Frechet, J. M. J. (2002) *Bioconjugate Chem.* 13, 443–452.
- (12) Kichler, A., Leborgne, C., Coeytaux, E., and Danos, O. (2001) *J. Gene Med.* 3, 135–144.
- (13) Gao, Z. S., and Eisenberg, A. (1993) *Macromolecules* 26, 7353–7360.
- (14) Bragonzi, A., Boletta, A., Biffi, A., Muggia, A., Sersale, G., Cheng, S. H., Bordignon, C., Assael, B. M., and Conese, M. (1999) *Gene Ther.* 6, 1995–2004.
- (15) Nishikawa, M., and Huang, L. (2001) *Hum. Gene Ther.* 12, 861–870.
- (16) Anderson, W. F. (2000) *Nat. Med.* 6, 862–863.
- (17) Wasil, T., and Buchbinder, A. (2000) *Cancer Invest.* 18, 740–746.
- (18) Statham, V. S., and Morgan, R. A. (1999) *Curr. Opin. Mol. Ther.* 1, 430–436.
- (19) Keller, M., Tagawa, T., Preuss, M., and Miller, A. D. (2002) *Biochemistry* 41, 652–659.
- (20) Murray, K. D., Etheridge, C. J., Shah, S. I., Matthews, D. A., Russell, W., Gurling, H. M. D., and Miller, A. D. (2001) *Gene Ther.* 8, 453–460.
- (21) Tagawa, T., Manvell, M., Brown, N., Keller, M., Perouzel, E., Murray, K. D., Harbottle, R. P., Tecle, M., Booy, F., Brahimi-Horn, M. C., Coutelle, C., Lemoine, N. R., Alton, E. W. F. W., and Miller, A. D. (2002) *Gene Ther.* 9, 564–576.
- (22) Keller, M., Harbottle, R. P., Perouzel, E., Colin, M., Shah, I., Rahim, A., Vaysse, L., Bergau, A., Moritz, S., Brahimi-Horn, C., Coutelle, C., and Miller, A. D. (2003) *Chembiochem* 4, 286–298.
- (23) Ogris, M., Brunner, S., Schuller, S., Kircheis, R., and Wagner, E. (1999) *Gene Ther.* 6, 595–605.
- (24) McLean, J. W., Fox, E. A., Baluk, P., Bolton, P. B., Haskell, A., Pearlman, R., Thurston, G., Umemoto, E. Y., and McDonald, D. M. (1997) *Am. J. Physiol.-Heart Circul. Physiol.* 42, H387–H404.
- (25) Li, S., Tseng, W. C., Stolz, D. B., Wu, S. P., Watkins, S. C., and Huang, L. (1999) *Gene Ther.* 6, 585–594.
- (26) Sternberg, B., Hong, K., Zheng, W., and Papahadjopoulos, D. (1998) *Biochim. Biophys. Acta* 1375, 23–35.
- (27) Zou, S. M., Erbacher, P., Remy, J. S., and Behr, J. P. (2000) *J. Gene Med.* 2, 128–34.
- (28) Bragonzi, A., Dina, G., Villa, A., Calori, G., Biffi, A., Bordignon, C., Assael, B. M., and Conese, M. (2000) *Gene Ther.* 7, 1753–1760.
- (29) Fenske, D. B., MacLachlan, I., and Cullis, P. R. (2001) *Curr. Opin. Mol. Ther.* 3, 153–158.
- (30) Mok, K. W. C., Lam, A. M. I., and Cullis, P. R. (1999) *Biochim. Biophys. Acta-Biomembr.* 1419, 137–150.
- (31) Monck, M. A., Mori, A., Lee, D., Tam, P., Wheeler, J. J., Cullis, P. R., and Scherrer, P. (2000) *J. Drug Target.* 7, 439–452.
- (32) Saravolac, E. G., Ludkovski, O., Skirrow, R., Ossanlou, M., Zhang, Y. P., Giesbrecht, C., Thompson, J., Thomas, S., Stark, H., Cullis, P. R., and Scherrer, P. (2000) *J. Drug Target.* 7, 423–437.
- (33) Tam, P., Monck, M., Lee, D., Ludkovski, O., Leng, E. C., Clow, K., Stark, H., Scherrer, P., Graham, R. W., and Cullis, P. R. (2000) *Gene Ther.* 7, 1867–1874.
- (34) Zhang, Y. P., Sekirov, L., Saravolac, E. G., Wheeler, J. J., Tardi, P., Clow, K., Leng, E., Sun, R., Cullis, P. R., and Scherrer, P. (1999) *Gene Ther.* 6, 1438–1447.
- (35) Needham, D., and Kim, D. H. (2000) *Colloid Surf. B-Bio-interfaces* 18, 183–195.
- (36) Scherphof, G. L., and Kamps, J. (1998) *Adv. Drug Deliv. Rev.* 32, 81–97.
- (37) Kitson, C., Angel, B., Judd, D., Rothery, S., Severs, N. J., Dewar, A., Huang, L., Wadsworth, S. C., Cheng, S. H., Geddes, D. M., and Alton, E. (1999) *Gene Ther.* 6, 534–546.
- (38) Rosenecker, J., Naundorf, S., Gersting, S. W., Hauck, R. W., Gessner, A., Nicklaus, P., Muller, R. H., and Rudolph, C. (2003) *J. Gene Med.* 5, 49–60.
- (39) Harvie, P., Wong, F. M., and Bally, M. B. (2000) *J. Pharm. Sci.* 89, 652–663.
- (40) Song, L. Y., Ahkong, Q. F., Rong, Q., Wang, Z., Ansell, S., Hope, M. J., and Mui, B. (2002) *Biochim. Biophys. Acta-Biomembr.* 1558, 1–13.
- (41) Shi, F., Wasungu, L., Nomden, A., Stuart, M. C., Polushkin, E., Engberts, J. B., and Hoekstra, D. (2002) *Biochem. J.* 366, 333–41.
- (42) Devine, D. V., and Bradley, A. J. (1998) *Adv. Drug Deliv. Rev.* 32, 19–29.
- (43) Mori, A., Klivanov, A. L., Torchilin, V. P., and Huang, L. (1991) *FEBS Lett.* 284, 263–266.
- (44) Murahashi, N., Ishihara, H., Sakagami, M., and Sasaki, A. (1997) *Biol. Pharmacol. Bull.* 20, 704–707.
- (45) Jones, M. N. (1994) *Adv. Drug Deliv. Rev.* 13, 215–249.
- (46) Kawakami, S., Wong, J., Sato, A., Hattori, Y., Yamashita, F., and Hashida, M. (2000) *Biochim. Biophys. Acta-Gen. Subj.* 1524, 258–265.
- (47) Gabius, S., Kayser, K., Bovin, N. V., Yamazaki, N., Kojima, S., Kaltner, H., and Gabius, H. J. (1996) *Eur. J. Pharm. Biopharm.* 42, 250–261.
- (48) Xu, Z., Jayaseharan, J., and Marchant, R. E. (2002) *J. Colloid Interface Sci.* 252, 57–65.
- (49) Takeoka, S., Sakai, H., Takisada, M., and Tsuchida, E. (1992) *Chem. Lett.* 1877–1880.
- (50) Takeoka, S., Sakai, H., Ohno, H., Yoshimura, K., and Tsuchida, E. (1992) *J. Colloid Interface Sci.* 152, 351–358.
- (51) Kitamoto, D., Isoda, H., and Nakahara, T. (2002) *J. Biosci. Bioeng.* 94, 187–201.
- (52) Canne, L. E., Ferredamare, A. R., Burley, S. K., and Kent, S. B. H. (1995) *J. Am. Chem. Soc.* 117, 2998–3007.
- (53) Liu, C. F., Rao, C., and Tam, J. P. (1996) *J. Am. Chem. Soc.* 118, 307–312.
- (54) Rose, K. (1994) *J. Am. Chem. Soc.* 116, 30–33.
- (55) Peri, F., Dumy, P., and Mutter, M. (1998) *Tetrahedron* 54, 12269–12278.
- (56) Peri, F., Cipolla, L., La Ferla, B., Dumy, P., and Nicotra, F. (1999) *Glycoconjugate J.* 16, 399–404.
- (57) Cervigni, S. E., Dumy, P., and Mutter, M. (1996) *Angew. Chem., Int. Ed. Engl.* 35, 1230–1232.
- (58) Duffels, A., Green, L. G., Ley, S. V., and Miller, A. D. (2000) *Chem.-Eur. J.* 6, 1416–1430.
- (59) Dullenkopf, W., Ritter, G., Fortunato, S. R., Old, L. J., and Schmidt, R. R. (1999) *Chem.-Eur. J.* 5, 2432–2438.
- (60) Merrifield, R. B. (1986) *Science* 232, 341–347.
- (61) Fiske, C., and Subbarow, Y. (1925) *J. Biol. Chem.* 66, 375–379.
- (62) Vanhalbeek, H. (1994) *Curr. Opin. Struct. Biol.* 4, 697–709.
- (63) Bock, K., Lundt, I., and Pedersen, C. (1974) *Tetrahedron Lett.*, 1037–1040.
- (64) Astafieva, I., Zhong, X. F., and Eisenberg, A. (1993) *Macromolecules* 26, 7339–7352.
- (65) Nichols, J. (1993) in *Phospholipids Handbook*, pp 663–685, Marcel Dekker, New York.
- (66) Kanda, S., Inoue, K., Nojima, S., Utsumi, H., and Wiegandt, H. (1982) *J. Biochem. (Tokyo)* 91, 2095–2098.
- (67) Uster, P. S., Allen, T. M., Daniel, B. E., Mendez, C. J., Newman, M. S., and Zhu, G. Z. (1996) *FEBS Lett.* 386, 243–246.
- (68) Sou, K., Endo, T., Takeoka, S., and Tsuchida, E. (2000) *Bioconjugate Chem.* 11, 372–379.
- (69) Ishida, T., Iden, D. L., and Allen, T. M. (1999) *FEBS Lett.* 460, 129–133.
- (70) Fenske, D. B., Palmer, L. R., Chen, T., Wong, K. F., and Cullis, P. R. (2001) *Biochim. Biophys. Acta-Biomembr.* 1512, 259–272.
- (71) Wilhelm, M., Zhao, C. L., Wang, Y. C., Xu, R. L., Winnik, M. A., Mura, J. L., Riess, G., and Croucher, M. D. (1991) *Macromolecules* 24, 1033–1040.
- (72) Takeoka, S., Mori, K., Ohkawa, H., Sou, K., and Tsuchida, E. (2000) *J. Am. Chem. Soc.* 122, 7927–7935.
- (73) Moates, G. K., Noel, T. R., Parker, R., Ring, S. G., Cairns, P., and Morris, V. J. (1997) *Carbohydr. Res.* 299, 91–94.
- (74) Imberty, A., Chanzy, H., Perez, S., Buleon, A., and Tran, V. (1988) *J. Mol. Biol.* 201, 365–378.
- (75) Takeoka, S., Sou, K., Boettcher, C., Fuhrhop, J. H., and Tsuchida, E. (1998) *J. Chem. Soc., Faraday Trans.* 94, 2151–2158.
- (76) Hato, M., and Minamikawa, H. (1996) *Langmuir* 12, 1658–1665.

- (77) Hato, M., Minamikawa, H., and Seguer, J. B. (1998) *J. Phys. Chem. B* 102, 11035–11042.
- (78) Chiruvolu, S., Israelachvili, J. N., Naranjo, E., Xu, Z., Zasadzinski, J. A., Kaler, E. W., and Herrington, K. L. (1995) *Langmuir* 11, 4256–4266.
- (79) Klein, J., Kumacheva, E., Mahalu, D., Perahia, D., and Fetters, L. J. (1994) *Nature* 370, 634–636.
- (80) Zelphati, O., Uyechi, L. S., Barron, L. G., and Szoka, F. C. (1998) *Biochim. Biophys. Acta-Lipid Metab.* 1390, 119–133.
- (81) Xu, Y. H., and Szoka, F. C. (1996) *Biochemistry* 35, 5616–5623.

BC034068Q



# Synthesis and Physicochemical Characterization of Folate–Cyclodextrin Bioconjugate for Active Drug Delivery

Paolo Caliceti,<sup>\*,†</sup> Stefano Salmaso,<sup>†</sup> Alessandra Semenzato,<sup>†</sup> Tommaso Carofiglio,<sup>‡</sup> Roberto Fornasier,<sup>‡</sup> Maurizio Fermeleglia,<sup>§</sup> Marco Ferrone,<sup>§</sup> and Sabrina Pricl<sup>§</sup>

Department of Pharmaceutical Sciences, University of Padua, Via F. Marzolo 5, 35131 Padua, Italy, Department of Organic Chemistry, University of Padua, Via F. Marzolo 3, 35131 Padua, Italy, and Computer-aided Systems Laboratory, Department of Chemical Engineering, University of Trieste, Piazzale Europa 1, 34127 Trieste, Italy. Received May 14, 2003; Revised Manuscript Received June 18, 2003

$\beta$ -Cyclodextrin–poly(ethylene glycol)–folic acid conjugate (CD-PEG-FA) was synthesized according to a two-step procedure: (1) synthesis of CD-PEG-NH<sub>2</sub> by reaction of monotosyl-activated  $\beta$ -cyclodextrin with excess of 700 Da diamino-PEG; (2) synthesis of CD-PEG-FA by reaction of CD-PEG-NH<sub>2</sub> with succinimidyl ester-activated folic acid. The CD-PEG-NH<sub>2</sub> intermediate was purified by precipitation in acetone, and the CD-PEG-FA by gel permeation and C-18 reversed-phase chromatography. Both CD-PEG-NH<sub>2</sub> and CD-PEG-FA were analyzed by mass spectrometry, <sup>1</sup>H NMR, and UV–vis spectroscopy. All analytical methods confirmed the theoretical composition of the conjugates: the CD-PEG-NH<sub>2</sub> intermediate was composed of CD and PEG in the molar ratio of 1:1, and the CD-PEG-FA was composed of  $\beta$ -cyclodextrin, PEG, and folic acid in the molar ratio of 1:1:1. The CD-PEG-FA conjugate was highly soluble in buffer (>42 mM) as compared to the unmodified  $\beta$ -cyclodextrin (16.3 mM). Phase solubility diagrams of  $\beta$ -estradiol revealed that drug solubility increases from 11  $\mu$ M in buffer to 600  $\mu$ M in the presence of  $\beta$ -cyclodextrins and 5900  $\mu$ M with CD-PEG-FA. However, the affinity of  $\beta$ -estradiol for  $\beta$ -cyclodextrins decreased about 4 times with PEG and folic acid conjugation. Stability studies carried out using chlorambucil confirmed that the conjugate partially prevents drug degradation in buffer, although this effect was considerably lower than that obtained with  $\beta$ -cyclodextrin. Computer modeling studies showed that the folic acid linked to the  $\beta$ -cyclodextrins through a PEG spacer could partially interact with the cyclodextrin cavity. Finally, CD-PEG-FA displayed reduced hemolytic effect as compared to unmodified  $\beta$ -cyclodextrin.

## INTRODUCTION

Recent advances in tumor therapy demonstrate that successful anticancer strategies can be developed by employing proper carrier systems able to deliver probes, drugs, or genes to tumor targets. Many efforts are in progress to develop active drug targeting systems, which on one hand allow for specific drug delivery into the disease site and, on the other, limit the toxicological drawbacks due to the broad and nonspecific disposition of the therapeutic agents.

Folic acid is a small vitamin, which interacts specifically with the folate binding protein (FBP)<sup>1</sup> located in the caveole-like invaginations on the cell surface receptor (1, 2). Upon receptor interaction, the folate acid–FBP complex is taken up by cells and moves through the many organelles involved in endocytotic trafficking, providing for cytosolic deposition (2). The folic acid receptor is

overexpressed by many types of tumor cells, including ovarian, endometrial, colorectal, breast, lung, renal, neuroendocrine carcinomas, and brain metastases (3).

In virtue of its ability to be taken up by folate receptor overexpressing tumor cells, folic acid has been widely investigated as targeting molecule for active anticancer drug delivery. Proper synthesis procedures have been pointed out to link folic acid to drug carriers to produce targeting drug delivery systems. In particular, it was demonstrated that the glutamate  $\gamma$ -carboxyl group activation does not provoke significant loss of folic acid affinity for the receptor. Among the folate-based carriers described in the literature are radionuclide deferoxamine–folate complexes for radiopharmaceutical imaging, liposome–folate-encapsulated drugs; liposome–folate-encapsulated polylysine–DNA, and cytotoxin–folate conjugates (4–7).

Although successful results have been published, the therapeutic application of the folate conjugates is often limited by their large size. Indeed, it was established that, even though large molecules undergo passive accumulation into solid tumors by enhanced permeation and retention effect (EPR), the intratumor overpressure limits their penetration into the neoplastic mass (8, 9). Therefore, it seems rational to produce low molecular weight conjugates, which can easily reach the tumor site and be taken up actively by the tumor cells where the drug can be released.

Cyclodextrins are carbohydrate macrocycles which, by virtue of their ability to form molecular inclusion com-

\* To whom correspondence should be addressed. E-mail: paolo.caliceti@unipd.it. Phone: +39 049 8275695. Fax: +39 049 8275366.

<sup>†</sup> Department of Pharmaceutical Sciences, University of Padua.

<sup>‡</sup> Department of Organic Chemistry, University of Padua.

<sup>§</sup> University of Trieste.

<sup>1</sup> Abbreviations: CD, cyclodextrins; PEG, poly(ethylene glycol); FA, folic acid; CD-PEG-NH<sub>2</sub>,  $\beta$ -cyclodextrin–poly(ethylene glycol)–NH<sub>2</sub> bioconjugate; CD-PEG-FA,  $\beta$ -cyclodextrin–poly(ethylene glycol)–folic acid bioconjugate; FBP, folate binding protein; DCC, dicyclohexylcarbodiimide; NHS, *N*-hydroxysuccinimide; DMSO, dimethyl sulfoxide; TEA, triethylamine.

plexes with a wide range of hydrophobic molecules, are interesting for exploitation as a new class of conjugates for drug delivery (10, 11). Actually, cyclodextrins have been investigated to optimize the solubility, stability, and bioavailability of many drugs (12–17). Nevertheless, the parenteral administration of natural cyclodextrins, namely  $\beta$ -cyclodextrins, causes undesirable toxic effects such as hemolysis (18). To overcome these problems, semisynthetic cyclodextrins obtained by hydroxyl substitution with hydroxy-alkyl or sulfo-alkyl functions have been prepared and investigated for systemic administration (11).

Recently, cyclodextrins have been modified by conjugation of water-soluble polymers to obtain derivatives with peculiar biopharmaceutical properties (11, 19).

Aimed at exploiting cyclodextrin bioconjugates for active drug targeting, a synthetic strategy has been investigated to produce a derivative where  $\beta$ -cyclodextrins are linked to folic acid through a poly(ethylene glycol) spacer arm. The goal of this paper is to report a methodology for synthesis of cyclodextrin-PEG-folate derivatives, which possess inclusion capacity of cyclodextrin, high solubility and biocompatibility of PEG, and targetable properties of folic acid for site-directed anticancer therapy.

## MATERIALS AND METHODS

Folic acid, dicyclohexylcarbodiimide (DCC), *N*-hydroxysuccinimide (NHS), Jeffamine ED-600 (700 Da diamino-PEG), and  $\beta$ -cyclodextrin were purchased from Fluka Chemika (Buchs, Switzerland). Sephadex G25 superfine resin was obtained from Pharmacia Biotech AB (Uppsala, Sweden). Chlorambucil,  $\beta$ -estradiol, and all other reagents were supplied by Sigma (St. Louis, MO).

Analytical thin-layer chromatography (TLC) was carried out on glass sheets coated with silica gel (Merck F-254, Merck, Darmstadt, Germany). The TLC spots were visualized with the following indicators or methods: (1) tosylated-cyclodextrin and tosyl groups, UV (254 nm); (2) carbohydrates, 9.2 mL of *p*-anisaldehyde in 338 mL of 95% ethanol, 3.75 mL of glacial acetic acid, and 12.5 mL of concentrated sulfuric acid (10–20 min at 100–150 °C becomes blue to black in the presence of cyclodextrins); (3) primary aliphatic amines, a 0.3% ninhydrin in 1-butanol containing 3% acetic acid (10 min at 125–150 °C).

**Preparation of 6-Mono[*O,O*-bis(2-aminopropyl)-polypropylene glycol-*block*-poly(ethylene glycol)-*block*-polypropylene glycol]- $\beta$ -cyclodextrin.** 6-Mono-(*p*-toluenesulfonyl)- $\beta$ -cyclodextrin (0.995 g, 0.772 mmol), synthesized according to the procedure reported in the literature (20), was suspended in 35 mL of *O,O*-bis(2-aminopropyl)polypropylene glycol-*block*-poly(ethylene glycol)-*block*-polypropylene glycol (53.34 mmol) (diamino-PEG, Jeffamine ED-600), and a minimum amount of DMF was added to the suspension to obtain a clear solution. The mixture was stirred at 80 °C in a three-necked flask equipped with reflux condenser under argon atmosphere for 8–9 h. The reaction progress was checked by analytical thin-layer chromatography (TLC): 50  $\mu$ L of mixture was added to 1 mL of acetone, and the precipitate was collected by centrifugation and washed five times with 1 mL of acetone. The precipitate was dissolved in 100  $\mu$ L of methanol and analyzed by TLC plate eluted with ethyl acetate/2-propanol/water/30% ammonia (13:10:5:1.4, volume ratios). Disappearance of

the UV positive spot relative to mono(*p*-toluenesulfonyl)- $\beta$ -cyclodextrin ( $R_f = 0.05$ ) gave evidence of reaction endpoint, while the spots positive to *p*-anisaldehyde,  $I_2$ , and ninhydrin corresponded to the final product 6-mono[*O,O*-bis(2-aminopropyl)polypropylene glycol-*block*-poly(ethylene glycol)-*block*-polypropylene glycol]- $\beta$ -cyclodextrin ( $R_f = 0.006$ ). The reaction mixture was precipitated in 250 mL of acetone, and the crude product was washed five times with 20 mL of the same solvent, collected by centrifugation, and desiccated under vacuum in the presence of phosphorus pentoxide.

One milligram of CD-PEG-NH<sub>2</sub> in 1 mL of acetonitrile/water/acetic acid (50/50/1, v/v/v) was analyzed by ESI-TOF.

CD-PEG-NH<sub>2</sub> in DMSO-*d*<sub>6</sub> was analyzed by <sup>1</sup>H NMR using a Bruker Spectrospin 300 (300 MHz):  $\delta$  5.69–5.58 (br s, OH-2, of  $\beta$ -cyclodextrin, 7H), 5.66 (br s, OH-3 of  $\beta$ -cyclodextrin, 7H), 4.81 (br d, H-1 of  $\beta$ -cyclodextrin, 7H), 4.42 (br s, OH-6 of  $\beta$ -cyclodextrin, 6H), 3.78–3.42 (m, H-6–3–5 of  $\beta$ -cyclodextrin and CH<sub>2</sub>CH<sub>2</sub> of PEG, ~72H), 3.40–3.20 (m, H-4 and H-2 of  $\beta$ -cyclodextrin overlapping HOD), 1.08–0.86 (m, propyl CH<sub>3</sub> of Jeffamine ED-600, ~12H).

**Synthesis of 6-Mono{folic acid- $\gamma$ -[*O,O*-bis(2-aminopropyl)polypropylene glycol-*block*-poly(ethylene glycol)-*block*-polypropylene glycol]- $\beta$ -cyclodextrin.** 6-Mono[*O,O*-bis(2-aminopropyl)polypropylene glycol-*block*-poly(ethylene glycol)-*block*-polypropylene glycol]- $\beta$ -cyclodextrin (0.791 g, 0.438 mol) was added to 50 mL of anhydrous DMSO containing 2.884 g (5.356 mmol) of *N*-hydroxysuccinimide ester of folic acid prepared according to the procedure reported in the literature (5). TEA (320  $\mu$ L, 0.2295 mmol) was added to the reaction mixture, and pH 9.0 was maintained by addition of the same base. The reaction was stirred under dark and anhydrous conditions. After 40 h of reaction, the solution was poured dropwise into 500 mL of cold acetone, and the yellow precipitate was washed 10 times with 50 mL of acetone. The crude product was dried under vacuum in the presence of phosphorus pentoxide. The dry product was dissolved in 100 mL of 0.1 M borate buffer, pH 8.3. The solution was fractionated by gel permeation chromatography using Sephadex G25 superfine column eluted with 10 mM ammonium carbonate buffer, pH 8.0. One milliliter fractions were collected and analyzed by UV at 363 nm, iodine test, and *p*-anisaldehyde for folic acid, PEG, and cyclodextrin determination, respectively (18–20). Fractions positive to all tests were pooled and concentrated by ultrafiltration using a 500 Da cut-off membrane. Further purification was carried out using a preparative RP-C18 column (2.5 cm  $\times$  22 cm) operated on a Shimadzu SP-10 HPLC system and eluted in a gradient mode, using 10 mM ammonium acetate pH 6.5 (eluent A) and acetonitrile (eluent B), from 10% to 40% eluent B in 40 min. The UV detector was set at 363 nm. The peak corresponding to the conjugate was collected, concentrated, and desalted by ultrafiltration. The solution was lyophilized and analyzed by RP-C18 chromatography.

**UV Analysis.** Ten milligrams of  $\beta$ -cyclodextrin-PEG-folic acid, dissolved in 10 mL of 10 mM phosphate buffer, 0.15 M NaCl, pH 7.0, was analyzed by UV. The folate content in the final product was determined on the basis of the folic acid extinction coefficient value reported in the literature ( $\epsilon_M$  6.197 M<sup>-1</sup> cm<sup>-1</sup> at 363 nm and 25820 M<sup>-1</sup> cm<sup>-1</sup> at 280 nm) (21). The carrier concentrations in stock solutions were determined by UV using the same molar extinction coefficients.

<sup>1</sup>H NMR: (300 MHz, DMSO-*d*<sub>6</sub>) δ 8.63 (s, C7-H of FA, 1H), 7.64 (d, 2',6'-H of FA, 2H), 6.64 (d, 3',5'-H of FA, 2H), 5.76–5.60 (m, OH-2, OH-3 of β-cyclodextrin, 14H), 4.87–4.76 (br d, H1 of β-cyclodextrin, 7H), 4.52–4.36 (br, OH-6 of β-cyclodextrin, 6H), 4.28–4.16 (m, α-CH<sub>2</sub> of Glu of FA, 1H), 3.78–3.42 (m, H6-3-5 of β-cyclodextrin and CH<sub>2</sub>CH<sub>2</sub> of PEG, ~72H), 3.40–3.14 (m, H-4 and H-2 of β-cyclodextrin overlapping HOD), 1.08–0.86 (m, propyl CH<sub>3</sub>, Jeffamine ED-600, ~12H).

**Solubility Studies.** Five milligrams of  $\beta$ -estradiol was added to 0.1 mL of 10 mM phosphate buffer, 0.15 M NaCl, pH 7.2, containing increasing concentrations of  $\beta$ -cyclodextrin (0–16.3 mM) or equimolar amounts of  $\beta$ -cyclodextrin/PEG/folic acid (1:1:1) mixture or CD-PEG-FA (0–42 mM). The suspensions were tumbled gently for 90 h at room temperature and then centrifuged at 10000 rpm for 5 min. The  $\beta$ -cyclodextrin and  $\beta$ -cyclodextrin/PEG/folic acid mixture solutions were diluted 10 times with the same buffer, and  $\beta$ -estradiol was assessed by RP-C18 chromatography isocratically eluted with methanol/water (67:33, v/v), 0.05% trifluoroacetic acid. The UV detector was set to 280 nm. The drug content in the solutions was determined according to the peak area, which was referred to the corresponding calibration plots obtained by analysis of solutions containing different  $\beta$ -estradiol concentrations. The CD-PEG-FA solutions were added to 2 mL of acetone and centrifuged at 10000 rpm for 5 min. The supernatant was desiccated, lyophilized, redissolved in a 67% methanol/water solution, and analyzed by HPLC as reported above.

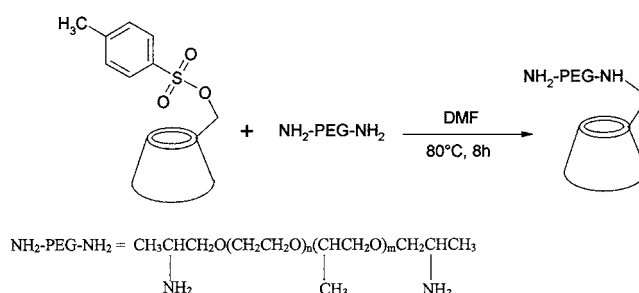
**Degradation Studies.** Five hundred microliters of 10 mM phosphate buffer, 0.15 M NaCl, pH 7.2, containing 4 mM of  $\beta$ -cyclodextrins or equimolar concentrations of CD-PEG-FA or  $\beta$ -cyclodextrin/PEG/folic acid (1:1:1 molar ratio), was added to 100  $\mu$ L of chlorambucil solution in methanol (1.2 mM). The solutions were maintained at 22  $^{\circ}$ C, and chlorambucil was estimated at scheduled times by RP-C18 column isocratically eluted with acetonitrile/water (60:40, v/v), 0.05% TFA, and detected by UV at 302 nm according to the procedure reported in the literature (22).

**Hemolysis Assay.** One milliliter of heparinized mouse blood was centrifuged at 2000 rpm for 10 min, and the precipitated erythrocytes were washed three times with 10 mM phosphate buffer, 0.15 M NaCl, pH 7.4. The erythrocytes were resuspended in the buffer to give 5% (w/v) hematocrit concentration. Hematocrit samples (30  $\mu$ L) were added to 570  $\mu$ L of buffer solutions containing  $\beta$ -cyclodextrin (0–16.3 mM) or equimolar amounts of CD-PEG-FA or  $\beta$ -cyclodextrin/PEG/folic acid 1:1:1 mixture. The samples were incubated at 37 °C for 30 min and then centrifuged at 2000 rpm for 4 min. The released hemoglobin was determined by optical density (OD) at 543 nm and expressed as (sample OD/control OD)  $\times$  100. The control corresponded to the samples containing 0 mM product (18).

**Molecular Modeling.** All simulations were performed by using AMBER 6.0 (23, 24), Cerius<sup>2</sup> (v.4.2, Accelrys, San Diego, CA), Materials Studio (v. 2.2, Accelrys), Discover (v. 2000, Accelrys), and in-house developed codes (stand-alone and add-on to the commercial software). The all-atom force field (FF) parameters set by Cornell et al. (25) (in *parm94.dat* file of the AMBER 6.0 code) was applied in all calculations.

The procedure for the generation of accurate model structures for  $\beta$ -cyclodextrin and the drugs is reported in details elsewhere (26). Accordingly, only a brief account

### Scheme 1



will be given here. The accurate model structures for the CD-PEG-FA and the drug compounds were generated and subjected to an initial energy minimization using Discover, applying a convergence criterion of  $10^{-4}$  kcal/(mol Å). The conformational search was carried out using a combined molecular mechanics/molecular dynamics simulated annealing (MDSA) protocol (27, 28). Accordingly, the relaxed structures were subjected to five repeated temperature cycles (from 310 to 1000 K and back) using constant volume/constant temperature (NVT) MD conditions. At the end of each annealing cycle, the structures were again energy minimized to converge below  $10^{-4}$  kcal/(mol Å), and only the structures corresponding to the minimum energy were used for further modeling. The electrostatic charges for the geometrically optimized drug molecules were obtained by restrained electrostatic potential fitting (29), and the electrostatic potentials were produced by single-point quantum mechanical calculations at the Hartree–Fock level with a 6-31G\* basis set. All ab initio calculations were carried out with DMol<sup>3</sup> (30), as implemented in the Cerius<sup>2</sup> modeling suite.

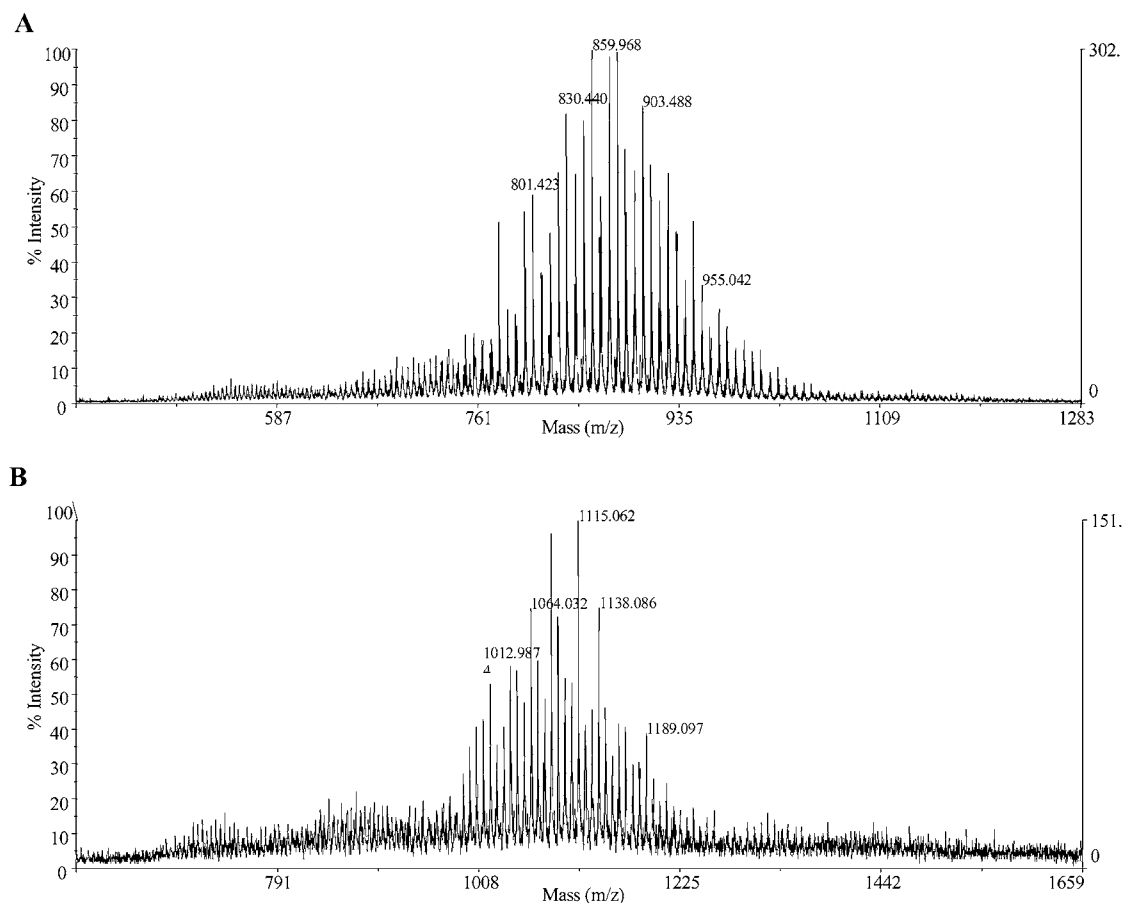
For the MD simulations, each given system was solvated by a cubic box of TIP3P water molecules (31), extended at least 10 Å in each direction from the solute. All water molecules of which the oxygen atom lied within 2.3 Å of a non-hydrogen  $\beta$ -cyclodextrin atom were removed. The periodic boundary conditions with constant pressure of 1 atm were applied, and long-range non-bonded van der Waals interactions were truncated by using a 8 Å residue-based cutoff. The particle mesh Ewald (PME) method (32) was used to treat the long-range electrostatics. Each system was gradually heated to 310 K in three intervals, allowing a 5 ps interval per each 100 K and then equilibrated for 25 ps at 310 K, followed by 2.0 ns of data collection runs. An integration time step of 2 fs has been used with constant temperature, being the temperature maintained at a constant value by the Berendsen coupling algorithm (33), with separate solute-solvent and solvent-solvent coupling.

## RESULTS

**Preparation and Characterization of Folic Acid Conjugates.** The preparation of the monosubstituted

**Conjugates.** The preparation of the monosubstituted cyclodextrin-PEG-folate conjugate (CD-PEG-FA) was carried out by a two-step procedure: (1) synthesis of CD-PEG-NH<sub>2</sub>; (2) synthesis of CD-PEG-FA. To obtain a derivative constituted by  $\beta$ -cyclodextrin, poly(ethylene glycol), and folic acid in the molar ratio of 1:1:1, monotosylated- $\beta$ -cyclodextrin was used as starting product. The reaction of monotosylated- $\beta$ -cyclodextrin, Scheme 1, with a 60-fold excess of 700 Da diamino-PEG allowed for  $\beta$ -cyclodextrin monosubstitution (CD-PEG-NH<sub>2</sub>) without formation of heterogeneous cross-linking products which could be formed because of the bifunctional nature of the diamino-PEG. The chemical structure of Jeffamine ED-





**Figure 1.** ESI-TOF mass spectra: (A)  $\beta$ -cyclodextrin-PEG; (B)  $\beta$ -cyclodextrin-PEG-folic acid.

600 (diamino-PEG) reported in Scheme 1 shows that this oligomer is composed of  $(\text{OCH}_2\text{CH}_2)$  units with 44 Da molecular weight and two terminal polypropylene glycol-aminopropyl groups. A preliminary mass spectrometry analysis showed that this oligomer has a molecular weight of about 700 Da.

The TLC analysis showed that under the selected coupling conditions the reaction was complete in 8 h as neither UV- nor *p*-anisaldehyde-positive spots relative to unreacted 6-mono(*p*-toluenesulfonyl- $\beta$ -cyclodextrin) and  $\beta$ -cyclodextrin, respectively, were detected. The ninhydrin-, iodine-, and *p*-anisaldehyde-positive spot corresponded to the final CD-PEG- $\text{NH}_2$  product. After acetone precipitation, the product recovery yield was of 72% (obtained weight/expected weight, %).

Figure 1A shows that the mass spectrum obtained with the CD-PEG- $\text{NH}_2$  conjugate exhibits a bell shaped distribution characterized by 22  $m/z$ -spaced lines centered at 900  $m/z$ . The 900  $m/z$  signal has been assigned to  $[\text{CD-PEG-NH}_2 + 2\text{H}]^{2+}$  (CD-PEG- $\text{NH}_2$  calculated molecular mass 1805 Da). The 22  $m/z$  (44 Da) mass difference between the signals corresponds to the oxyethylene unit ( $\text{CH}_2\text{CH}_2\text{O}$ ), indicating that the cluster was due to the PEG heterogeneity.

The  $^1\text{H}$  NMR analysis of the derivative showed the signals typical of  $\beta$ -cyclodextrins [ $\delta$  5.69–5.58 (br s, OH-2, of  $\beta$ -cyclodextrins, 7H), 5.66 (br s, OH-3 of  $\beta$ -cyclodextrins, 7H), 4.81 (br d, H-1 of  $\beta$ -cyclodextrins, 7H)] and polypropylene glycol-*block*-poly(ethylene glycol)-*block*-polypropylene glycol [ $\delta$  3.78–3.42 (m, H-6-3-5 of  $\beta$ -cyclodextrins and  $\text{CH}_2\text{CH}_2$  of PEG,  $\sim$ 72H), 1.08–0.86 (m, propyl  $\text{CH}_3$  of Jeffamine ED-600,  $\sim$ 12H)] which corresponded to the values reported in the literature (34). The monosubstitution of  $\beta$ -cyclodextrin with PEG was

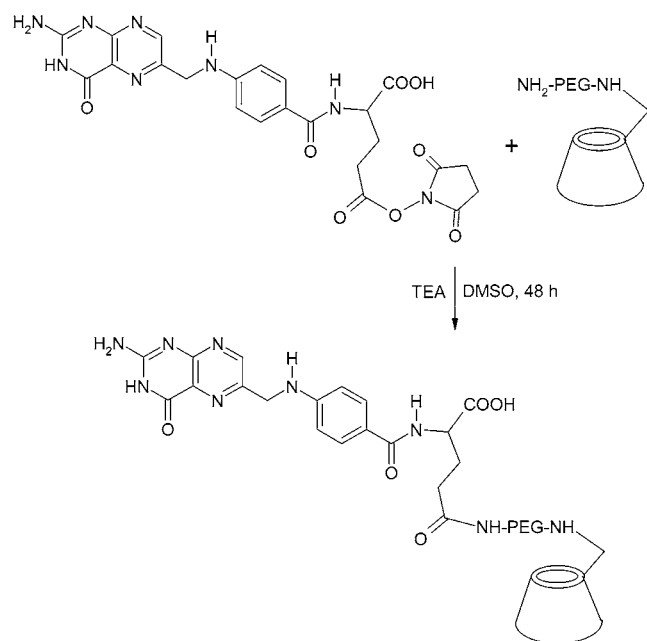
demonstrated by the H integration values of the  $\beta$ -cyclodextrin primary hydroxyl group [ $\delta$  4.48–4.32 (d, OH-6 of  $\beta$ -cyclodextrin, 6H)] and by the integration value ratios between the signal corresponding to the  $\beta$ -cyclodextrin and Jeffamine ED-600.

CD-PEG-FA was prepared by reaction of CD-PEG- $\text{NH}_2$  with excess of folic acid, which was activated as the succinimidyl ester in the presence of dicyclohexylcarbodiimide according to the procedure reported in the literature (5). The activation procedure yields 80%  $\gamma$ -carboxyl group and 20%  $\alpha$ -carboxyl group of the glutamate residue activation. The CD-PEG- $\text{NH}_2$  reaction with excess of activated folic acid (12:1 activated folic acid/CD-PEG- $\text{NH}_2$  molar ratio) yielded extensive CD-PEG- $\text{NH}_2$  derivatization in 40 h as determined by ninhydrin assay. The reaction procedure to obtain CD-PEG-FA is represented in Scheme 2.

The extensive CD-PEG- $\text{NH}_2$  derivatization avoided purification problems due to the separation of unreacted CD-PEG- $\text{NH}_2$  from CD-PEG-FA, which present similar physicochemical properties. The final product was purified from the residual folic acid and hydroxysuccinimide by gel permeation. Small amounts of free folic acid were found in the fractions containing CD-PEG-FA (positive to iodine test, *p*-anisaldehyde test and UV) probably because of the formation of folic acid/ $\beta$ -cyclodextrin inclusion complex or macromolecular aggregates. Complete elimination of free folic acid was achieved by reversed-phase chromatography, though CD-PEG-FA was eluted with a broad peak due to the PEG polydispersity. At the end of the two-step purification, the product yield was 38.6% (w/w).

Figure 1B shows the mass pattern of the conjugate, which exhibits a bell-shaped distribution of 22  $m/z$ -spaced

Scheme 2



signals centered at 1100  $m/z$  (calculated molecular mass 2229 Da). The signal  $m/z$  has been assigned to  $[\text{CD-PEG-FA} + 2\text{H}^+]^{2+}$ .

The  $^1\text{H}$  NMR showed the signals corresponding to CD [ $\delta$  5.76–5.60 (m, OH-2, OH-3 of  $\beta$ -cyclodextrins, 14H), 4.87–4.76 (br d, H-1 of  $\beta$ -cyclodextrins, 7H), 4.52–4.36 (d, OH-6 of cyclodextrins, 6H)], PEG [ $\delta$  3.78–3.42 (m, H-6-3-5 of  $\beta$ -cyclodextrins and  $\text{CH}_2\text{CH}_2$  PEG,  $\sim 72\text{H}$ ), 1.08–0.86 (m, propyl  $\text{CH}_3$  of Jeffamine ED-600,  $\sim 12\text{H}$ )], and folic acid [ $\delta$  8.63 (s, C7-H of FA, 1H), 7.64 (d, 2',6' H of FA, 2H), 6.64 (d, 3',5' H of FA, 2H), 4.28–4.16 (m,  $\alpha$ - $\text{CH}_2$  of Glu of FA, 1H)]. The results confirmed the chemical CD-PEG-FA conjugate identity and composition (1:1:1  $\beta$ -cyclodextrin/poly(ethylene glycol)/folic acid molar ratio).

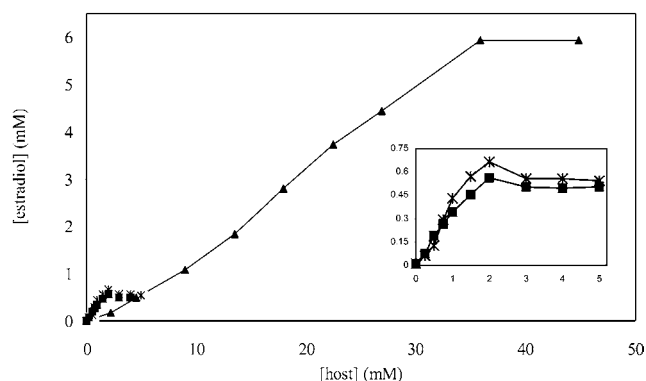
**Solubility Studies.** The ability of the CD-PEG-FA conjugate to form inclusion complexes with drugs was investigated according to the method reported by Higuchi and Connors (35).  $\beta$ -Estradiol was selected as model drug since its solubility was demonstrated to increase significantly by interaction with  $\beta$ -cyclodextrin. For comparison,  $\beta$ -estradiol phase solubility diagrams were obtained also in the presence of unmodified  $\beta$ -cyclodextrins, and  $\beta$ -cyclodextrin/diaminoPEG/folic acid 1:1:1 mixture.

The results depicted in Figure 2 show that the  $\beta$ -estradiol solubility in the presence of CD-PEG-FA conjugate is 540 and 8 times higher as compared to the solubility in physiologic buffer (3  $\mu\text{g/mL}$ ) and in  $\beta$ -cyclodextrins solution, respectively.

The apparent stability constant ( $K_c$ ) for  $\beta$ -estradiol complex was calculated by the slope of the phase-solubility diagram according to the equation:

$$K_c = \frac{\text{slope}}{S_0(1 - \text{slope})}$$

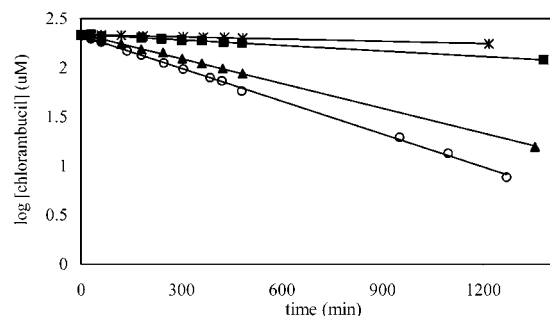
where  $S_0$  is the saturation concentration of  $\beta$ -estradiol in buffer without cyclodextrin (3  $\mu\text{g/mL}$ ) (36). The stability constants of  $\beta$ -estradiol for CD-PEG-FA,  $\beta$ -cyclodextrins, and  $\beta$ -cyclodextrin/PEG/folic acid mixture reported in Table 1 indicate that the presence of PEG/folic acid decreases the drug affinity for the  $\beta$ -cyclodextrins about



**Figure 2.** Phase-solubility diagram of estradiol in PBS, pH 7.2 at increasing concentration of  $\beta$ -cyclodextrin (\*),  $\beta$ -cyclodextrin/PEG/folic acid 1:1:1 molar ratio mixture (■), and CD-PEG-FA (▲). The inset contains a magnified phase-solubility diagram of  $\beta$ -estradiol in the presence of  $\beta$ -cyclodextrins and  $\beta$ -cyclodextrin/PEG/folic acid mixture.

**Table 1.**  $\beta$ -Estradiol Inclusion Parameters and Chlorambucil Degradation Kinetic Constants in  $\beta$ -Cyclodextrin,  $\beta$ -Cyclodextrin/PEG/Folic Acid Mixture, and CD-PEG-FA

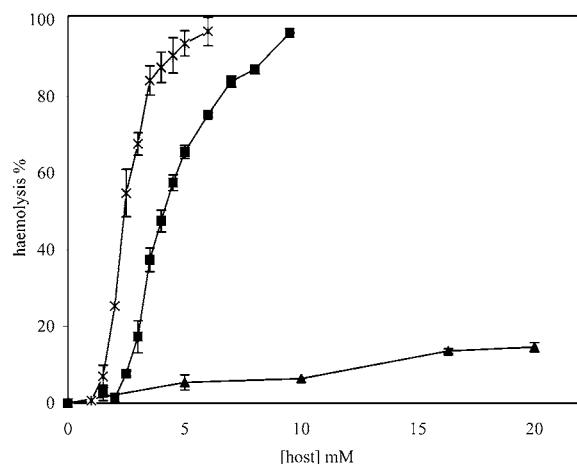
$\beta$ -Estradiol Inclusion Constants	
	$K_c$ ( $\text{M}^{-1}$ )
$\beta$ -cyclodextrin	77947
$\beta$ -cyclodextrin/PEG/folic acid 1:1:1 mol ratio mixture	54221
CD-PEG-FA	15343
Chlorambucil Degradation Kinetic Constants	
	$K_{\text{obsd}} \times 10^{-4}$ ( $\text{min}^{-1}$ )
chlorambucil	11.01
chlorambucil/ $\beta$ -cyclodextrin mixture	0.85
chlorambucil/ $\beta$ -cyclodextrin/PEG/folic acid mixture	1.88
chlorambucil/CD-PEG-FA mixture	8.38



**Figure 3.** Degradation profile of chlorambucil (200  $\mu\text{M}$ ) in PBS, pH 7.2: chlorambucil (○); chlorambucil in the presence of  $\beta$ -cyclodextrin (\*); chlorambucil in the presence of  $\beta$ -cyclodextrin/PEG/folic acid 1:1:1 molar ratio mixture (■); chlorambucil in the presence of CD-PEG-FA (▲).

30% while the conjugation of PEG and folic acid reduces the  $\beta$ -estradiol affinity about 75%.

**Stability Properties.** The degradation profiles of chlorambucil in the presence of CD-PEG-FA, unmodified  $\beta$ -cyclodextrins, and  $\beta$ -cyclodextrin/PEG/folic acid mixture 1:1:1 reported in Figure 3 show that in any case chlorambucil undergoes first-order degradation kinetics. In physiologic buffer, the free drug undergoes rapid degradation while in the presence of unmodified  $\beta$ -cyclodextrins, the drug displays high stability. In the last cases, 20% of the drug amount was degraded in 24 h. CD-PEG-FA was found to partially prevent drug degradation, although the protective effect was significantly lower than that dis-



**Figure 4.** Hemolytic effects of  $\beta$ -cyclodextrins on mouse erythrocytes in phosphate-buffered saline (pH 7.4) at 37 °C:  $\beta$ -cyclodextrin (\*);  $\beta$ -cyclodextrin/PEG/folic acid 1:1:1 molar ratio mixture (■); CD-PEG-FA (▲). Each point represents the mean of four experiments.

played by native  $\beta$ -cyclodextrins. The degradation rate constants of chlorambucil reported in Table 1 indicate that the protective effect of the CD-PEG-FA derivative is about 10 times lower than in the case of  $\beta$ -cyclodextrins.

**Hemolysis Activity.** The hemolytic properties of CD-PEG-FA were investigated by spectrophotometric evaluation of the hemoglobin released from erythrocytes incubated with increasing amounts of conjugate. For comparison, the test was carried out using equimolar amounts of  $\beta$ -cyclodextrins and  $\beta$ -cyclodextrin/PEG/folic acid 1:1:1 molar ratio mixtures.

According to the literature data, Figure 4 shows that  $\beta$ -cyclodextrins possess strong hemolytic activity, which decreases of about 50% by folic acid addition to the  $\beta$ -cyclodextrin/PEG mixture. The conjugate displayed negligible hemolytic character as compared to the native  $\beta$ -cyclodextrins or to the  $\beta$ -cyclodextrin/PEG/folic acid mixture also when high bioconjugated  $\beta$ -cyclodextrin concentrations were used.

## DISCUSSION

The synthetic procedure adopted in the present research allowed for obtaining a new  $\beta$ -cyclodextrin–poly(ethylene glycol)–folic acid bioconjugate, which can behave as a Trojan horse for active drug delivery. The hydrophobic pocket of cyclodextrins, which allows for inclusion of many lipophilic molecules, can allocate molecules to be released into specific tissues. The availability of a wide array of natural and semisynthetic cyclodextrins with different physicochemical properties represents a further advantage in the use of these polysaccharides for preparation of tailor-made drug delivery systems. Nevertheless, cyclodextrins do not have per se targeting properties; therefore, the conjugation of a targeting moiety is an essential requisite to develop systems for active delivery. For such a reason, folic acid conjugation was addressed to endow a  $\beta$ -cyclodextrin derivative which can be actively recognized by folic acid receptor overexpressing tumor cells. PEG was used as spacer arm because it confers flexibility to folic acid, allowing for its receptor interaction, and avoids problems related to the cyclodextrin steric hindrance. Actually, many studies demonstrated that PEG with a molecular weight higher than 2000 Da is required to achieve targetable colloidal systems (nanoparticles, liposomes)

(37). However, in the case of  $\beta$ -cyclodextrin we selected a shorter spacer in consideration of the lower hindrance of this small carrier.

The solubility studies carried out with  $\beta$ -estradiol demonstrated that the conjugate maintains the  $\beta$ -cyclodextrin ability to form inclusion complexes with hydrophobic drugs, although the solubilization properties of the  $\beta$ -cyclodextrin were strongly altered by PEG–folic acid conjugation. In particular, the higher solubility of  $\beta$ -estradiol in the presence of the conjugate with respect to the  $\beta$ -cyclodextrins could be attributable to the high solubility of carrier (CD-PEG-FA), which increases the complex solubility. CD-PEG-FA was in fact about three times more soluble than the unmodified  $\beta$ -cyclodextrins probably because of the presence of the freely soluble PEG and the epita-glucopyranose ring modification, which avoids the  $\beta$ -cyclodextrin precipitation. However, the affinity of  $\beta$ -estradiol for the conjugated  $\beta$ -cyclodextrins was lower than for the unmodified cyclo-polysaccharides.

The phase solubility diagram of  $\beta$ -estradiol with  $\beta$ -cyclodextrin or  $\beta$ -cyclodextrin/PEG/folic acid mixture resulted in a B-type Higuchi phase solubility diagram, both showing a good linear regression ( $R^2$  of 0.96 and 0.98 for  $\beta$ -cyclodextrin and  $\beta$ -cyclodextrin/PEG/folic acid mixture, respectively). In both cases, further addition of cyclodextrins over 2 mM did not modify the final  $\beta$ -estradiol solubility since the  $\beta$ -cyclodextrin/ $\beta$ -estradiol complex solubility end point is reached. On the other hand, the phase solubility diagram of  $\beta$ -estradiol with  $\beta$ -cyclodextrin-PEG-folic acid resulted in an  $A_p$ -type Higuchi phase solubility diagram (35, 38). Therefore, the  $\beta$ -cyclodextrin/ $\beta$ -estradiol complex is characterized by a [carrier]<sub>1</sub>: [drug]<sub>1</sub> complexation order while the CD-PEG-FA/ $\beta$ -estradiol complex is characterized by [carrier]<sub>x</sub>: [drug]<sub>1</sub> complexation order. These findings are supported by a molecular dynamics study performed on the CD-PEG-FA/ $\beta$ -estradiol complex, for which a 2:1 stoichiometry was assumed, reveals that the drug is not fully included in the cyclodextrin cavities, but gives rise to a sandwichlike molecular assembly, leading to drug dissolution (see Figure 5).

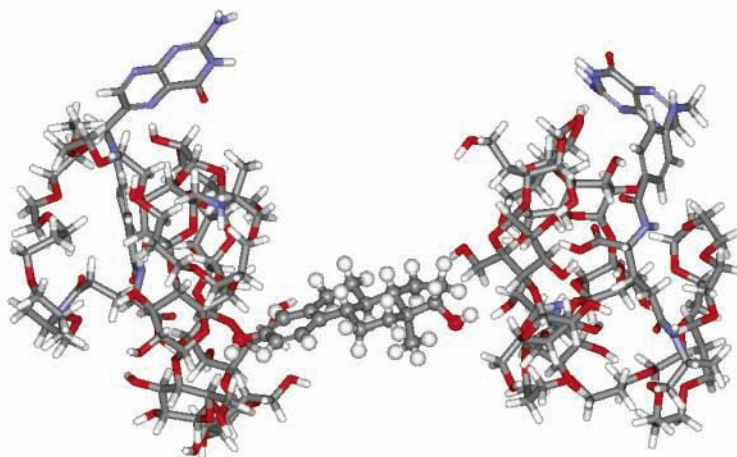
Although the phase solubility results and molecular dynamics study indicate that the  $\beta$ -cyclodextrin–PEG–folic acid/ $\beta$ -estradiol complexation takes place with [carrier]<sub>x</sub>: [drug]<sub>1</sub> stoichiometric order, the complex model was simplified to a 1:1 stoichiometric ratio to calculate the complex constant stability (35). Similar elaborations were also reported in the literature for solubility phase diagrams obtained with cholesterol and hydroxypropyl- $\beta$ -cyclodextrin (38).

The decrease in affinity constant of  $\beta$ -estradiol may be sensibly ascribed to a combination of events, such as folic acid competition for the  $\beta$ -cyclodextrins cavity and structural modification of the cyclo-glucopyranose unit. Interestingly it was demonstrated that the reduction in affinity was not due to the PEG inclusion into the cyclo-polysaccharide cavity, although the literature reports that pluronic can be included into  $\beta$ -cyclodextrins forming macromolecular structure named polyrotaxanes (39). Nevertheless, Jeffamine has only a short chain portion (end-chain propyl group) similar to the pluronic structure. On the contrary, the in vitro studies demonstrated that the addition of free folic acid significantly decreases the drug complexation, indicating that  $\beta$ -estradiol competes with folic acid in forming inclusion complexes.

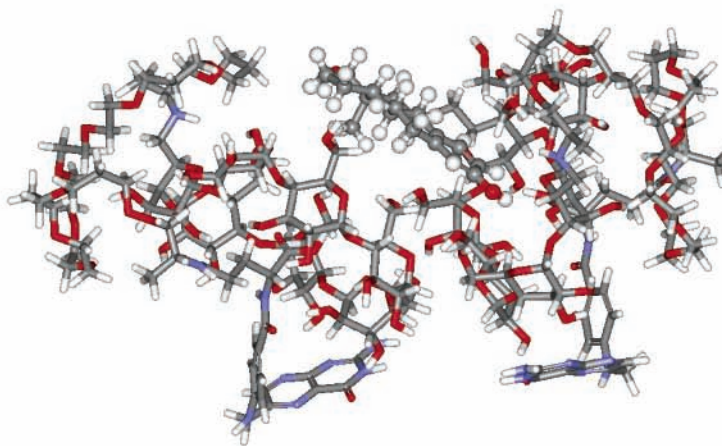
This observation is supported by the MD simulations performed on the CD-PEG-FA molecule in water, of which Figure 6 reports three snapshots. The analysis of the MD trajectories reveals that the PEG chain, by virtue



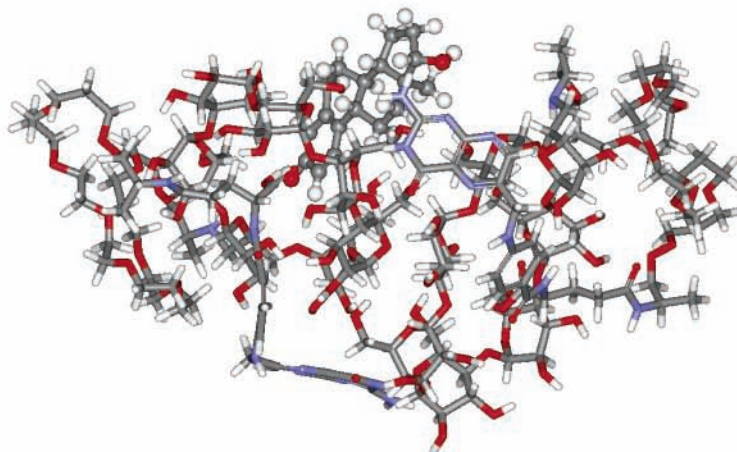
A



B



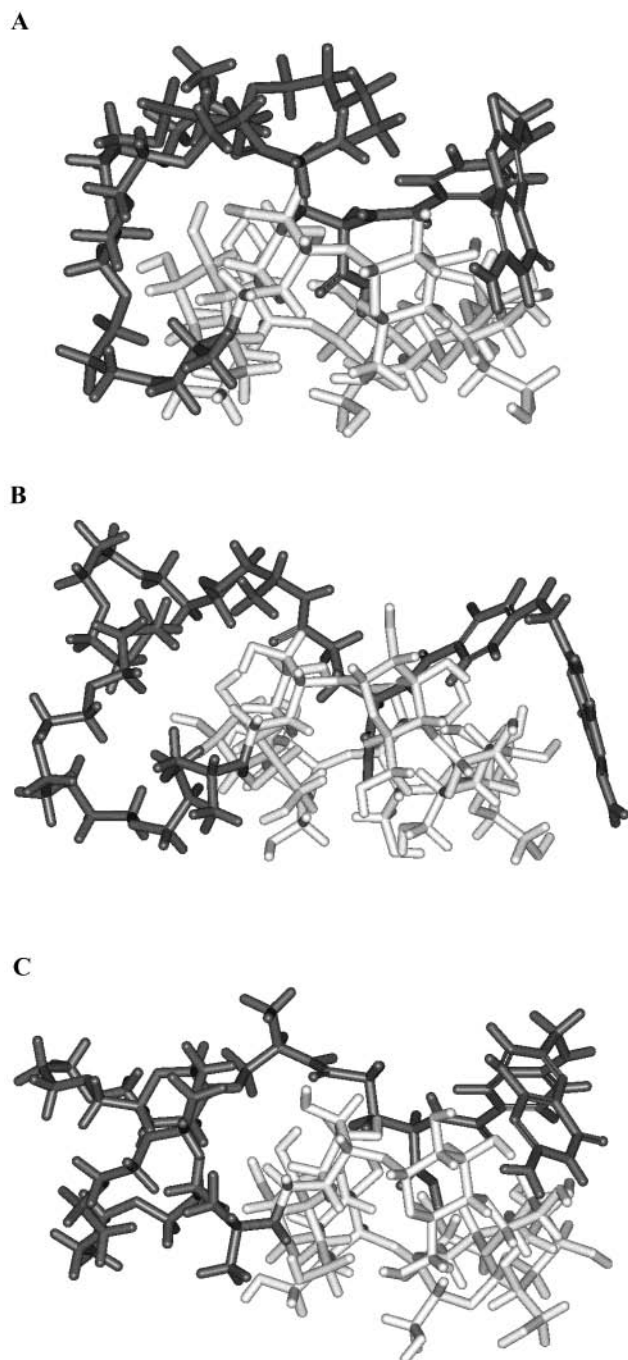
C



**Figure 5.** Three snapshots of the MD simulation performed for 2 ns at 310 K on the 1:2  $\beta$ -estradiol/CD-PEG-FA assembly in water. (A)  $t = 0$ ; (B):  $t = 1$  ns; (C):  $t = 2$  ns. For clarity,  $\beta$ -estradiol is shown in ball-and-stick representation, CD-PEG-FA is shown in stick representation, and water molecules have been omitted.

of its intrinsic flexibility, partially folds up and allows the carboxylic group of the folic acid moiety to enter the cyclodextrin cavity, thereby remaining for the entire course of the simulation. This notable affinity for the self-inclusion of the folic acid undoubtedly constitutes a hindrance for the “canonical” inclusion mechanism of drugs into this cyclodextrin bioconjugate and can be taken as one of the partial factors responsible for the

lower affinity of  $\beta$ -estradiol toward CD-PEG-FA with respect to the parent cyclodextrin. Moreover, the simulation conditions employed here mimic an infinite dilution condition; accordingly, phenomena such as cyclodextrin–cyclodextrin intermolecular interactions taking place, resulting in the inclusion of one folic acid moiety into the cyclodextrin cavity of another carrier molecule, have not been considered. This could also account for the relevant



**Figure 6.** Three snapshots taken from the MD trajectory of CD-PEG-FA in water. (A):  $t = 0.5$  ns; (B),  $t = 1$  ns; (C):  $t = 2$  ns. For clarity, the carbohydrate macrocycle is colored light gray, the PEG-FA substituents chain is colored dark gray, and water molecules have been omitted.

decrease of  $\beta$ -estradiol affinity constant, as high conjugated cyclodextrin concentrations were used in the corresponding experiments. On the other hand, this last event should be limited in the body, where very low concentration of conjugate is obtained and intermolecular displacement phenomena should be quite limited.

The lower affinity constant of  $\beta$ -estradiol for the conjugate with respect to the  $\beta$ -cyclodextrin/PEG/folic acid mixture indicates that the partial inclusion of folic acid is not the only reason of the decrease in drug complexation. Also the considerable modification of the epta-glucopyranose ring induced by the presence of the mobile PEG chain, as can be envisaged from Figure 6, plays a relevant role in preventing the inclusion of this

drug, characterized by a flat but sterically large molecular shape.

Chlorambucil is a labile drug, which undergoes first-order kinetic hydrolysis (22). Degradation kinetic order was neither affected by the presence of  $\beta$ -cyclodextrin or CD-PEG-FA. However, PEG-folic acid conjugation was found to decrease significantly the ability of  $\beta$ -cyclodextrins to prevent the chlorambucil degradation. The similar chlorambucil degradation profiles obtained by drug incubation in buffer or in the presence of the  $\beta$ -cyclodextrin conjugate indicate that the modified carbohydrate macrocycle is not effective in preventing the degradation of this labile drug.

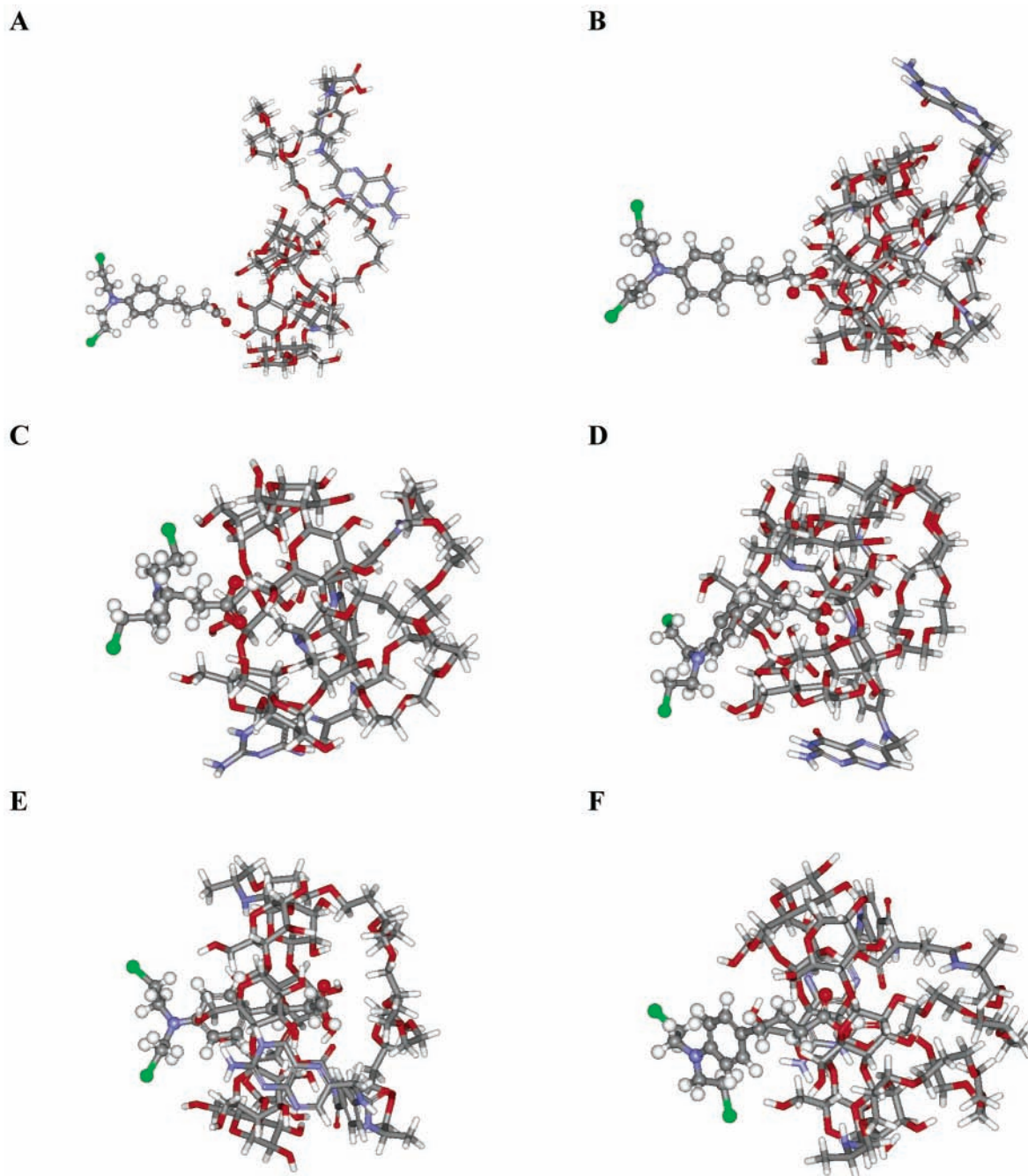
From the standpoint of molecular modeling, the possibility for chlorambucil to form stable inclusion complexes with CD-PEG-FA is suggested by several factors, such as limited drug molecular dimensions and presence of a central, disubstituted phenyl ring. Further, experimental evidence of 1:1 inclusion complexes between chlorambucil and native  $\beta$ -cyclodextrin have appeared in the literature (17). In this case, the aim of our MD simulations was to follow the dynamics of the inclusion complex formation and the behavior of the resulting supramolecular assembly during a 2 ns time period. Figure 7 shows the minimized, starting structure of the molecular assembly plus five snapshots taken from the corresponding molecular system trajectory. During the equilibration phase, the drug moves toward the cavity of CD-PEG-FA. Figure 7B shows the drug closer to the cavity with respect to the energy minimized, initial situation (Figure 7A). During the first half of dynamic simulation, the drug tends to position parallel to the cavity of the macrocycle, with the acetyl group within the cavity (0.5–1 ns, Figures 7C and 7D). Around 1.5 ns of simulation, the drug is aligned with the cavity axis and with the phenyl ring well inserted in the host (Figure 7E). The last part of the simulated period shows the slow drug release from the cavity, mainly due to the partial insertion of the folic acid into the cavity itself (Figure 7F). Since the same simulation performed on a chlorambucil/unmodified  $\beta$ -cyclodextrin system (not shown) leads to a stable complex, in which the guest is well inserted within the carbohydrate host, the observed behavior in the case of the bioconjugate carrier may partly account for a higher degree of drug degradation.

Typically,  $\beta$ -cyclodextrins display a dramatic hemolytic effects due to membrane cholesterol extraction and inclusion into the  $\beta$ -cyclodextrin cavity (14). The reduction in hemolytic effect observed with  $\beta$ -cyclodextrin/PEG/folic acid and CD-PEG-FA can be explained on the basis of the decreased affinity of  $\beta$ -cyclodextrin for cholesterol. Similarly to what was reported for  $\beta$ -estradiol, the folic acid competition with cholesterol in forming inclusion complexes can be reflected in reduced cell membrane destabilizations and hemoglobin release. The modification of the cyclo-epta-glucopyranose ring further decreases the affinity of cholesterol for the  $\beta$ -cyclodextrin cavity, dramatically reducing the hemolytic properties of this molecule. Therefore, PEG-folic acid conjugation has a significant effect in preventing nonspecific cell damage.

## CONCLUSIONS

Recent advances in modern medicinal chemistry and pharmacology point out the need for development of new carriers for active drug delivery, which enhance their therapeutic value. Actually, a number of new drugs are characterized by high pharmacological activity but relevant systemic toxicity, which limits their therapeutic application.





**Figure 7.** Energy minimized structure and five snapshots extracted from the molecular dynamics trajectory of the chlorambucil/CD-PEG-FA assembly in water at 310K. (A): energy minimized structure; (B):  $t = 0$ ; (C):  $t = 0.5$  ns; (D):  $t = 1$  ns; (E)  $t = 1.5$  ns; (F):  $t = 2$  ns. For clarity, chlorambucil is shown in ball-and-stick representation, CD-PEG-FA is shown in stick representation, and water molecules have been omitted.

A suitable strategy to prepare tailor-made targetable drug carriers is the assembly of molecules with peculiar physicochemical and biological properties. In the present study a useful synthetic strategy to obtain a new class of targetable drug carriers has been reported. Cyclodextrins, PEG, and folic acid were assembled to produce a derivative characterized by low molecular weight, high solubility, drug complexation properties, and specific recognition. The results demonstrated that the bioconjugate can form inclusion complexes with hydrophobic drugs allowing for their active delivery to the disease sites.

Finally, it is important to note that the synthetic procedure proposed in the present study can be exploited to prepare a wide array of conjugates. Indeed, bioconju-

gates with different physicochemical, biological, and biopharmaceutical properties can be obtained by proper selection of the cyclo-polysaccharide unit, PEG molecular weight, and targeting moiety.

#### ACKNOWLEDGMENT

This research was partially supported by MIUR (fondi ex-40%) and CNR.

#### LITERATURE CITED

- (1) Sudimack, J., and Lee, R. J. (2000) Targeted drug delivery via the folate receptor. *Adv. Drug Del. Rev.* 41, 147–162.
- (2) Turek, J. J., Leamon, C. P., and Low, P. S. (1993) Endocytosis of folate-protein conjugates: ultrastructural localization in KB cells. *J. Cell. Sci.* 106, 423–430.



- (3) Garin-Chesa, P., Campbell, I., Saigo, P. E., Lewis, J. L., Jr., Old, L. J., and Rettig, W. J. (1993) Trophoblast and ovarian cancer antigen LK26. Sensitivity and specificity in immunopathology and molecular identification as a folate-binding protein. *Am. J. Pathol.* **142**, 557–567.
- (4) Wang, S., Lee, R. J., Mathias, C. J., Green, M. A., and Low, P. S. (1996) Synthesis, purification, and tumor cell uptake of <sup>67</sup>Ga-deferoxamine-folate, a potential radiopharmaceutical for tumor imaging. *Bioconjugate Chem.* **7**, 56–62.
- (5) Lee, R. J., and Low, P. S. (1994) Delivery of liposomes into cultured KB cells via folate receptor-mediated endocytosis. *J. Biol. Chem.* **269**, 3198–3204.
- (6) Gottschalk, S., Cristiano, R. J., Smith, L. C., and Woo, S. L. (1994) Folate receptor mediated DNA delivery into tumor cells: potosomal disruption results in enhanced gene expression. *Gene Ther.* **1**, 185–191.
- (7) Leamon, C. P., and Low, P. S. (1994) Selective targeting of malignant cells with cytotoxin-folate conjugates. *J. Drug Target.* **2**, 101–112.
- (8) Kataoka, K. (1997) Targetable polymeric drugs. *Controlled drug delivery challenges and strategies*. (K. Park, Ed.) p 49, American Chemical Society, Washington, D.C.
- (9) Jain, R. K. (1990) Physiological barriers to delivery monoclonal antibodies and other macromolecules to tumors. *Cancer Res.* **50**, 814s–819s.
- (10) Castillo, J. A., Palomo-Canales, J., Garcia, J. J., Lastres, J. L., Bolas, F., and Torrado, J. J. (1999) Preparation and characterization of albendazole beta-cyclodextrin complexes. *Drug Dev. Ind. Pharm.* **25**, 1241–1248.
- (11) Hirayama, F., and Uekama, K. (1999) Cyclodextrin-based controlled drug release system, *Adv Drug Del. Rev.* **36**, 125–141.
- (12) Szejtli, J. (1994) Medicinal applications of cyclodextrins. *Med. Res. Rev.* **14**, 353–386.
- (13) Cho, M. J., Chen, F. J., and Huczek, D. L. (1995) Effects of inclusion complexation on the transepithelial transport of a lipophilic substance in vitro. *Pharm. Res.* **12**, 560–564.
- (14) Szente, L., and Szejtli, J. (1999) Highly soluble cyclodextrin derivatives: chemistry, properties, and trends in development. *Adv. Drug Del. Rev.* **36**, 17–28.
- (15) Bekers, O., Beijnen, J. H., Groot Bramel, E. H., Otagiri, M., Bult, A., and Underberg, W. J. M. (1989) Stabilization of mitomycins on complexation with cyclodextrins in aqueous acidic media. *Int. J. Pharm.* **52**, 239–248.
- (16) Måsson, M., Pitha, J., and Loftsson, T. (1999) Synthesis of cyclic glycerol ether cyclodextrin derivatives and investigation of their binding properties with drugs. *J. Incl. Phenom. Macrocycl. Chem.* **33**, 459–467.
- (17) Måsson, M., Loftsson, T., Jónsdóttir, S., Fridriksdóttir, H., and Petersen, D. S. (1998) Stabilisation of ionic drugs through complexation with nonionic and ionic cyclodextrins. *Int. J. Pharm.* **164**, 45–55.
- (18) Ohtani, Y., Irie, T., Uekama, K., Fukunaga, K., and Pitha, J. (1989) Differential effects of alpha-, beta- and gamma-cyclodextrins on human erythrocytes. *Eur. J. Biochem.* **186**, 17–22.
- (19) Topchieva, I. N., Elezkaya, S. V., Polyakov, V. A., and Karezin, K. I. (1996) Cyclodextrins modified with poly(ethylene oxide) as complexation and transport agents. *Abstracts of the 8th International Symposium on Cyclodextrins*, Budapest, Hungary, pp 2–20.
- (20) Petter, R. C., Salek, J. S., Sikorski, C. T., Kumaravel, G., and Fu-Tyan, L. (1990) Cooperative binding by aggregated Mono-6-(alkylamino)- $\beta$ -cyclodextrins. *J. Am. Chem. Soc.* **112**, 3860–3868.
- (21) Kranz, D. M., Patrick, T. A., Brigle, K. E., Spinella, M. J., and Roy, J. (1995) Conjugates of folate and anti-T-receptor antibodies specifically target folate-receptor-positive tumor cells for lysis. *Proc. Natl. Acad. Sci.* **92**, 9057–9061.
- (22) Klaus, F., Ed. (1987) *Analytical profiles of Drug Substances*, Vol. 16, pp 85–118, Academic Press Inc., New York.
- (23) Pearlman, D. A., Case, D. A., Caldwell, J. W., Ross, W. S., Cheatham, T. E., III, DeBolt, S., Ferguson, D., Seibel, G. L., and Kollman, P. A. (1995) AMBER, a package of computer programs for applying molecular mechanics, normal-mode analysis, molecular dynamics and free energy calculations to simulate the structural and energetic properties of molecules. *Comput. Phys. Commun.* **91**, 1–41.
- (24) Case, D. A., Pearlman, D. A., Caldwell, J. W., Cheatham, T. E., III, Ross, W. S., Simmerling, C. L., Darden, T. A., Merz, K. M., Stanton, R. V., Cheng, A. L., Vincent, J. J., Crowley, M., Tsui, V., Radmer, R. J., Duan, Y., Pitera, J., Massova, I., Seibel, G. L., Singh, U. C., Weiner, P. K., and Kollman, P. A. (1999). AMBER 6, University of California, San Francisco, CA.
- (25) Cornell, W. D., Cieplak, P., Bayly, C. I., Gould, I. R., Merz, K. M., Jr., Ferguson, D. M., Spellmeyer, D. C., Fox, T., Caldwell, J. W., and Kollman, P. A. (1995) A second generation force field for the simulation of proteins, nucleic acids and organic molecules. *J. Am. Chem. Soc.* **117**, 5179–5197.
- (26) Fermeglia, M., Ferrone, M., Lodi, A., and Prici, S. (2003) Host-guest inclusion complexes between anticancer drugs and  $\beta$ -cyclodextrin: computational studies. *Carbohydr Polym.* **53**, 15–44.
- (27) Fermeglia, M., Ferrone, M., and Prici, S. (2002) Computer-aided simulation of a dendrimer with a protoporphyrin core as potential, novel hemoprotein mimic. *Biorg. Med. Chem.* **10**, 2471–2478.
- (28) Felluga, F., Fermeglia, M., Ferrone, M., Pitacco, G., Prici, S., and Valentin, E. (2002) Computational studies on the enantioselectivity of  $\alpha$ -chymotrypsin towards  $\alpha$ -carbomethoxy- $\beta$ -lactams. *Tetrahedron: Asymmetry*. **13**, 475–489.
- (29) Bayly, C. I., Cieplak, P., Cornell, W. D., and Kollman, P. A. (1993) A well-behaved electrostatic potential based method using charge restraints for determining atom-centered charges: the RESP model. *J. Phys. Chem.* **97**, 10269–10280.
- (30) Delley, B. (1990) An all-electron numerical method for solving the local density functional for polyatomic molecules. *J. Chem. Phys.* **92**, 508–517.
- (31) Jorgensen, W. L., Chandrasekhar, J., Madura, J. D., Impey, R. W., and Klein, M. L. (1983) Comparison of simple potential functions for simulating liquid water. *J. Chem. Phys.* **7**, 926–935.
- (32) Darden, T., York, D., and Pedersen, L. (1993) Particle mesh Ewald: an  $N^2 \log(N)$  method for computing Ewald sums. *J. Chem. Phys.* **98**, 10089–10092.
- (33) Berendsen, H. J. C., Postma, J. P. M., van Gunsteren, W. F., DiNola, A., and Haak, J. R. (1984) Molecular dynamics with coupling to an external bath. *J. Chem. Phys.* **81**, 3684–3690.
- (34) Caldwell, G., Neuse, E. W., and Perlwitz, A. G. (1997) Water soluble Polyamides as potential drug carriers. IX. Polyaspartamides grafted with amine-terminated Poly(ethylene oxide) chains. *J. Appl. Pol. Sci.* **66**, 911–919.
- (35) Higuchi, T., and Connors, K. A. (1965) Phase-solubility techniques. *Adv. Anal. Chem. Instrum.* **4**, 117–212.
- (36) Slikker, W., Jr., Lipe, G. W., and Newport, G. D. (1981). High-performance liquid chromatographic analysis of estradiol-17 $\beta$  and metabolites in biological media. *J. Chromatogr. B: Biomed. Sci. Appl.* **224**, 205–219.
- (37) Gabizon, A., Horowitz, A. T., Goren, D., Tzemach, D., Mandelbaum-Shavit, F., Qazen, M. M., and Zalipsky, S. (1999) Targeting folate receptor with folate linked to extremities of poly(ethylene glycol)-grafted liposomes: in vitro studies. *Bioconjugate Chem.* **10**, 289–298.
- (38) Williams, R. O., III, Mahaguna, V., and Sriwongjanya, M. (1998) Characterization of an inclusion complex of cholesterol and hydroxypropyl- $\beta$ -cyclodextrin. *Eur. J. Pharm. Biopharm.* **46**, 355–360.
- (39) Ooya, T., and Yui, N. (1999) Polyrotaxane: synthesis, structure, and potential in drug delivery. *Crit. Rev. Ther. Drug Carrier Syst.* **16**, 289–328.

BC034080I

# A Fluorescence Resonance Energy Transfer Sensor Based on Maltose Binding Protein

Igor L. Medintz,\* Ellen R. Goldman, Michael E. Lassman, and J. Matthew Mauro\*,†

Center for Bio/Molecular Science and Engineering, Code 6900, U.S. Naval Research Laboratory, Washington D.C. 20375. Received December 3, 2002; Revised Manuscript Received April 2, 2003

A fluorescence resonance energy-transfer (FRET) sensing system for maltose based on *E. coli* maltose binding protein (MBP) is demonstrated. The FRET donor portion of the sensing system consists of MBP modified with long wavelength-excitable cyanine dyes (Cy3 or Cy3.5). The novel acceptor portion of the sensor consists of  $\beta$ -cyclodextrin ( $\beta$ -CD) modified with either the cyanine dye Cy5 or the dark quencher QSY9. Binding of the modified  $\beta$ -CD to dye-conjugated MBP results in assembly of the FRET complex. Added maltose displaces the  $\beta$ -CD–dye adduct and disrupts the FRET complex, resulting in a direct change in fluorescence of the donor moiety. In the use of these FRET pairs, MBP dissociation values for maltose were estimated (0.14–2.90  $\mu$ M). Maltose limits of detection were in the 50–100 nm range.

## INTRODUCTION

Although a variety of sensing approaches are available for sensitive real-time chemical detection, receptor-based or binding-protein-based biosensor development is a promising area (1–3). Incorporating a fluorescence resonance energy-transfer (FRET) reporter into a biosensor is especially appealing because of the potential sensitivity and specificity that can be achieved (4–7). Since FRET is intrinsically dependent upon and highly sensitive to proximity changes, it is an appealing monitoring/reporting mechanism for protein and molecular binding events and has been used extensively as a molecular or nano-scale spectroscopic ruler (4–7).

FRET is defined as the nonradiative transfer of the excited-state energy from an initially excited donor to an acceptor (5, 6). Donor molecules emit at a shorter wavelength that corresponds to or overlaps a significant portion of the acceptor molecules absorption spectrum. The energy transfer efficiency,  $E$ , is defined as the number of quanta transferred to the acceptor divided by the number of quanta absorbed by the donor and is expressed as:

$$E = \frac{1}{1 + (R/R_0)^6} \quad (1)$$

where  $R$  is the distance between the donor–acceptor pair and  $R_0$  is the donor–acceptor separation at 50% transfer efficiency (5, 6). Since there is a  $R^{-6}$  dependence, any change in distance between the donor–acceptor pair should translate to a dramatic change in energy transfer and hence fluorescence (5, 6).

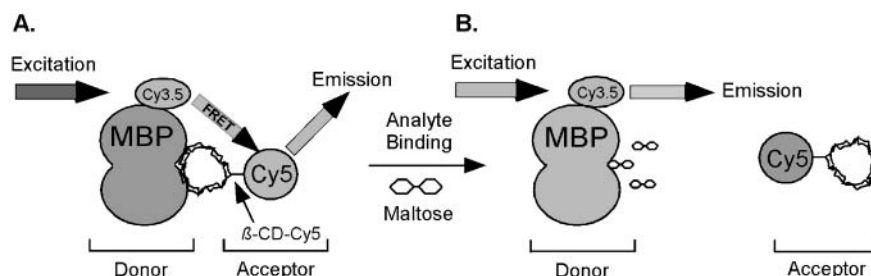
FRET has been the basis for many bioanalytical assays. For example, a Cy5-labeled antibody that bound to Cy5.5-labeled bovine serum albumin was used as a model for characterizing this particular FRET pair. This

Cy5–Cy5.5 FRET pair was subsequently applied to a homogeneous competitive immunoassay for the pesticide simazine and was shown to have a 0.3  $\mu$ g/L lower limit of detection (7). FRET has also been widely used to study many protein–protein, protein–DNA, molecular structure, and other interactions (8, 9). The use of FRET in carbohydrate analysis has not been fully exploited and remains an exciting area of research (4, 10). An energy transfer sensor complex for glucose has been described (8). The donor consisted of concanavalin A labeled with a ruthenium metal–ligand complex bound, via maltose, to insulin labeled with malachite green. The assay functioned by glucose displacement of the maltose–insulin which increased the emission intensity and lifetime of the excited ruthenium–concanavalin A complex (8).

*Escherichia coli* maltose binding protein (MBP) has proven to be an excellent model for prototyping and characterizing biosensing (3, 11–13). This periplasmic protein is involved in transcellular membrane transport of maltose and has been used in reagentless sensing of sugars. In early experiments, MBP methionine side chains were derivatized with the fluorescent reporter *N*-iodoacetyl-*N*-(5-sulfo-1-naphthyl)ethylenediamine, IAEDANS (12). A systematic increase in FRET between a tryptophan residue of MBP and IAEDANS was detected upon addition of increasing concentrations of maltose, indicating that the MBP–IAEDANS construct functioned as a quantitative FRET biosensor (12). Other MBP-based sensors exploit the effects of allosteric changes in dye-labeled MBP structure upon maltose binding, which directly affects the intrinsic fluorescence intensity, allowing this sensor to function in a reagentless manner (3, 11). Allosterically based MBP sensor variants include fluorescently labeled mutants (11, 13), an electrochemically sensitive redox MBP conjugate (14), and an amperometric trinitrotoluene (TNT) sensing nitroreductase–MBP fusion protein (15). In fact, MBP has been proposed as a model for designing and prototyping allosterically active biosensor proteins (11). An interesting FRET-based MBP sensor has recently been described in which a MBP mutant was constructed with an enhanced cyan fluorescent protein (ECFP) at the N-terminus and an enhanced

\* Corresponding authors. M. Mauro: E-mail: matt.mauro@probes.com. Tel: 591-465-8300. I. Medintz: E-mail: imedintz@cbmse.nrl.navy.mil. Tel: 202-404-6046.

† Current address: Molecular Probes, Inc., 29851 Willow Creek Rd., Eugene, OR 97602.



**Figure 1.** Schematic representation of the FRET-based sensing scheme. The FRET complex (A) consists of Cy3.5-labeled MBP (donor) with bound  $\beta$ -CD-Cy5 (acceptor), resulting in FRET. Upon addition of maltose (B), the  $\beta$ -CD-Cy5 is displaced, resulting in increased MBP-Cy3.5 donor emission. If MBP-Cy3 and  $\beta$ -CD-QSY9 (a dark quencher) are substituted, the assembled complex results in quenching of the MBP-Cy3 donor emission.

yellow fluorescent protein (EYFP) at its C-terminus (16). Upon maltose binding, the dye moieties are brought into closer proximity which alters the FRET properties. This system functioned both in single yeast cells and in vitro (16).

MBP binds a variety of sugars, with varying affinities including,  $\beta$ -cyclodextrin ( $\beta$ -CD).  $\beta$ -CD has been modified and incorporated in a variety of fluorescent sensing assays. These include a complexed boronic acid fluorophore- $\beta$ -CD probe that selectively recognized sugars and transduced signal based on changes in fluorescence (17). Dansylglycine-modified  $\beta$ -CD immobilized on a cellulose membrane decreases its fluorescent intensity upon binding guest molecules (18). Dye-modified  $\beta$ -CD complexed to copper(II) was fluorescently quenched but 'switched on' fluorescence upon binding with amino acids (19).  $\beta$ -CD has also been conjugated to a peptide in close proximity to a pyrene moiety with guest interactions monitored fluorescently (20). Dextran labeled with malachite green has also been used in a FRET sensor for serum glucose (21). However, dye-modified  $\beta$ -CD has not been used directly in a FRET-based assay.

In the work described in this report, we conjugated MBP with either of the long wavelength-excitable cyanine dyes Cy3 or Cy3.5. We also modified  $\beta$ -CD with the cyanine dye Cy5 or the dark quencher QSY9 and used the dye-modified protein and  $\beta$ -CD adduct as a FRET-based homogeneous biosensor. In this novel sensor, FRET is used to measure the concentration of maltose in solution by monitoring changes in fluorescence intensity of the donor moiety (see Figure 1 for a schematic). MBP-Cy3.5 was prepared at two different dye-to-protein ratios, 1 and 1.7, and then complexed with the  $\beta$ -CD-Cy5. MBP-Cy3 was also complexed with  $\beta$ -CD-QSY9 to enable formation of other homogeneous maltose sensor variants. One MBP-Cy3 variant was based upon MBP lysine residues modified by a Cy3-amine-active donor dye and another variant employed an engineered cysteine residue specifically labeled with Cy3-thiol-reactive energy donor dye.

## MATERIALS AND METHODS

**Maltose Binding Protein.** The DNA coding sequence for the MBP protein was contained on a standard multicopy plasmid vector containing the ampicillin resistance gene as described (11, 22). The MBP gene sequence was engineered to express a C-terminal five-histidine sequence using standard gene assembly and cloning techniques (11, 22). A mutant MBP protein with aspartate-95 changed to a cysteine (MBP D95C) was also engineered (11). These MBP derivatives were expressed in *E. coli* TOP10 cells (Stratagene La Jolla, CA) by inducing with isopropyl  $\beta$ -D-1-thiogalactopyranoside (IPTG). Induction and expression was monitored by SDS

PAGE gel electrophoresis using 8/25% Phast gels stained with Coomassie Brilliant R Blue (Amersham Pharmacia, Piscataway NJ). Expressed protein was isolated using Ni-NTA agarose (Qiagen Valencia, CA) and dialyzed against phosphate-buffered saline (PBS) at pH 7.4 to remove excess imidazole. Protein concentration was determined from the absorbance at 280 nm using an Agilent 8453 UV-vis spectrophotometer (Walbronn, Germany). Purified dialyzed protein solution was sterile filtered with a 0.2  $\mu$ M syringe filter and stored at 4 °C. MBP purified and stored in this manner remained functionally unchanged for at least 1 year (22).

**Protein Labeling.** Maleimide and NHS (*N*-hydroxy-succinimide) ester mono- or bifunctionalized Cy3, Cy3.5, and Cy5 dyes were obtained from Amersham Pharmacia and the NHS ester of QSY9 from Molecular Probes (Eugene, OR). See Figure 2 for reactive dye structures and Table 1 for their photophysical properties. Approximately 1 mg of protein was reacted with NHS-bifunctionalized Cy3 or Cy3.5 dye for 2.5 h at ~pH 9.4 in the presence of 10 mM maltose. The MBP D95C mutant was labeled with monofunctional Cy3 maleimide after disulfide reduction by Cleland's Reductacryl Reagent (Calbiochem). Labeled proteins were purified by gel filtration using PD-6 or PD-10 column chromatography (Amersham Pharmacia) to remove maltose and excess dye and then quantitated by spectrophotometry. The concentration of dye-labeled MBP was estimated using the formula:

$$[\text{MBP-dye}] = (\text{abs}_{280} - (\text{CF} \times \text{abs}_{\text{max(dye)}})) / \epsilon \quad (2)$$

where CF is the correction factor for the absorbance of the dye at 280 nm (CF for Cy3 = 0.08; CF for Cy3.5 = 0.24) and  $\text{abs}_{\text{max(dye)}}$  is the absorption measured at the dye absorbance maximum. The molar extinction coefficient ( $\epsilon$ ) value used for MBP was 69 000  $\text{M}^{-1} \text{cm}^{-1}$ . The concentration of bound dye present was estimated using:

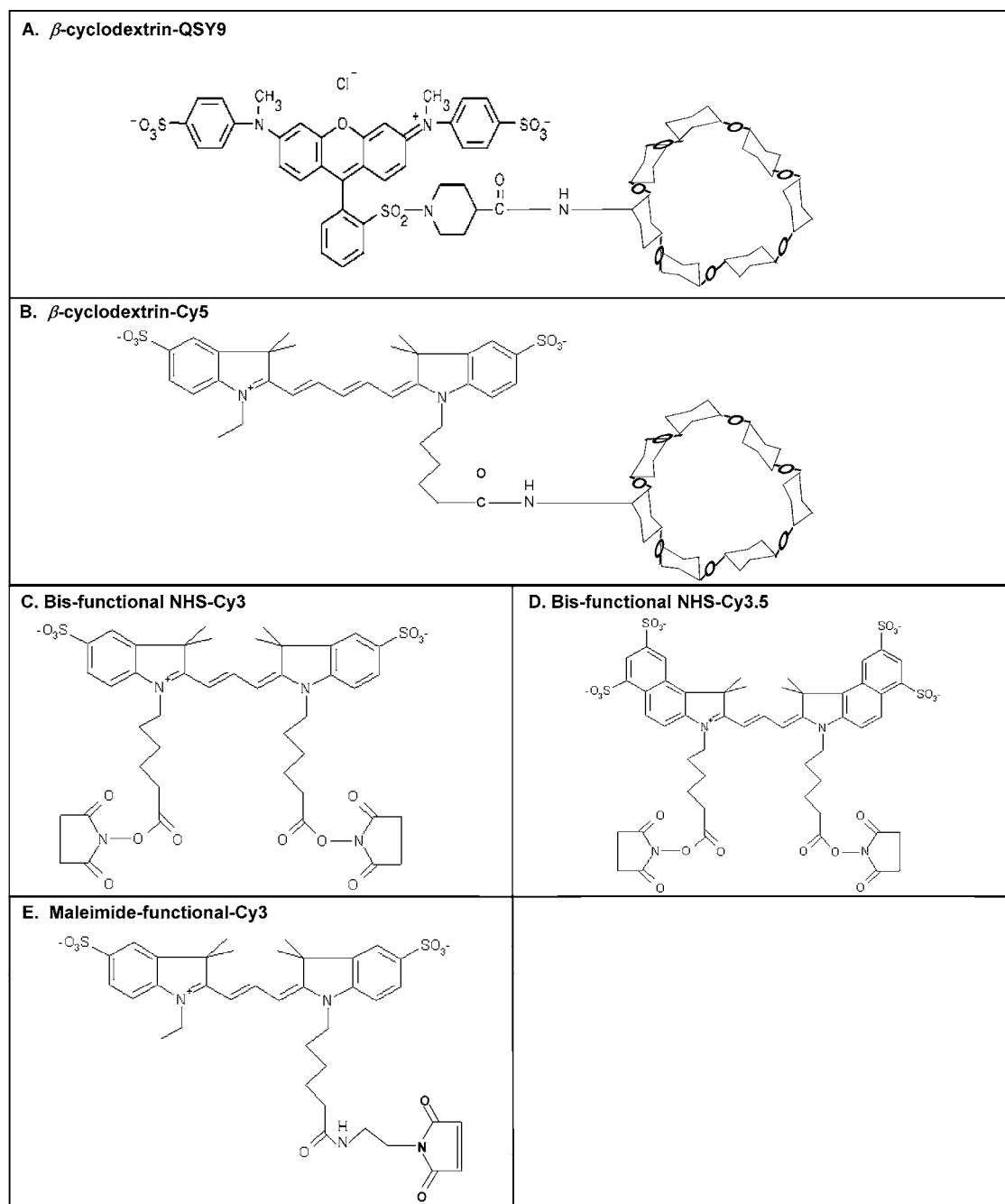
$$[\text{dye}] = \text{abs}_{\text{max(dye)}} / \epsilon_{(\text{dye})} \quad (3)$$

The molar extinction coefficients of the dyes are presented in Table 1. Estimation of final dye/protein ( $D/P$ ) ratios was made using the formula:

$$(D/P)_{\text{final}} = [\text{dye}] / [\text{MBP-dye}] \quad (4)$$

**$\beta$ -Cyclodextrin Adduct Synthesis and Purification.** An 8–10-fold molar excess of 6-monodeoxy-6-monoamino- $\beta$ -cyclodextrin,  $\beta$ -CD (Sigma, St. Louis, MO), was reacted with either monofunctional NHS-Cy5 or NHS-QSY9 for 2.5 h in 0.136 M sodium borate buffer (pH 8.5). The  $\beta$ -CD-dye adduct and excess monoamino  $\beta$ -CD were then precipitated by adding three volumes of





**Figure 2.** Chemical structure of  $\beta$ -CD-dye adducts and reactive dye intermediates. (A)  $\beta$ -CD-QSY9, (B)  $\beta$ -CD-Cy5, (C) bis-functional NHS-Cy3, (D) bis-functional NHS-Cy3.5, and (E) Cy3-maleimide.

**Table 1. Photophysical Properties of the Dyes Used**

dye	$\lambda_{\text{max}}$ abs (nm)	$\lambda_{\text{max}}$ abs bound <sup>a</sup> (nm)	$\lambda_{\text{max}}$ em (nm)	$\lambda_{\text{max}}$ em bound <sup>a</sup> (nm)	extinction coefficient (M <sup>-1</sup> cm <sup>-1</sup> )	quantum yield
Cy3	550	556	570	567	150,000	>0.15 <sup>b</sup>
Cy3.5	581	575	596	596	150,000	>0.15 <sup>b</sup>
Cy5	649	645	670	669	250,000	>0.28 <sup>b</sup>
QSY9	562	565	NA	NA	86,000	NA <sup>c</sup>

<sup>a</sup> Cy3-MBP, Cy3.5-MBP, B-CD-Cy5, B-CD-QS9. <sup>b</sup> For labeled proteins where the dye-to-protein ratio = 2. <sup>c</sup> NA = not applicable.

ethanol followed by holding the preparation at  $-20^{\circ}\text{C}$  for 1 h. The precipitate collected by centrifugation was washed four times with absolute ethanol, collected again by centrifugation ( $4^{\circ}\text{C}$ ), and dried in a vacuum centri-

fuge. Dried pellets were solubilized in HE buffer (10 mM HEPES, 1 mM EDTA buffer, pH 7.0) and product separated from unreacted  $\beta$ -CD and underivatized dye on 12% acrylamide 1 x TBE gels. The product band was excised and the  $\beta$ -CD-dye adduct eluted by passive diffusion into HE buffer. The  $\beta$ -CD-dye adduct was then concentrated and desalted using an oligonucleotide purification cartridge (OPC, Applied Biosystems, Foster City, CA). Briefly, the dilute  $\beta$ -CD-dye adduct in HEPES buffer was passed over the OPC several times to promote full binding to the resin. The bound  $\beta$ -CD-dye adduct was washed with  $\sim 35$  mL of 25 mM triethylamine ammonium acetate (TEAA) buffer (pH 7) and then eluted from the OPC with 1 mL 50% acetonitrile. The eluted product solution was aliquoted into 1.5 mL microfuge tubes, dried under vacuum, and stored at  $-20^{\circ}\text{C}$ . The

pure adducts were dissolved in PBS for quantitation and usage.

**Fluorimetry.** Fluorescence measurements were made using a SPEX Fluorolog-2 Fluorimeter (Jobin Yvon/SPEX, Edison, NJ) with excitation at 520 nm and emission monitored at right angles with slit widths set at 2–5 nm. All measurements were made at 22 °C. Titrations of dye-labeled MBP and  $\beta$ -CD–dye adducts were carried out in 3 mL of PBS. Samples were allowed to equilibrate under constant stirring at least 5 min between each reagent/sample addition. Reagent/sample addition altered the final volume by less than 5%. Where indicated, fluorescence data was corrected for inner filter effects using the formula (5):

$$F_{\text{corr}} = F_{\text{obsd}} \times \text{antilog}(\text{OD}_{\text{ex}} + \text{OD}_{\text{em}}/2) \quad (5)$$

where  $F$  is fluorescence and  $\text{OD}_{\text{ex}}$  and  $\text{OD}_{\text{em}}$  are the optical density at the wavelength of excitation and emission, respectively. Apparent dissociation values ( $K_{\text{app}}$ ) were approximated from the corrected untransformed data using the methodology of Bagshaw and Harris (23). Values correspond to the approximate dissociation constants of maltose from dye-labeled MBP under the conditions of multiple equilibria that exist in these experiments.

**Mass Spectral Analysis.** Mass spectral characterization of the  $\beta$ -cyclodextrin–dye adducts was performed using an Applied Biosystems API QSTAR Pulsar Mass Spectrometer by positive electrospray ionization (ESI). Samples were diluted in a solution of water:acetonitrile:glacial acetic acid (50:50:1) and infused into the spectrometer at a rate of 5  $\mu\text{L}/\text{min}$ . The final concentrations of the  $\beta$ -cyclodextrin–QSY9 and  $\beta$ -cyclodextrin–Cy3 adducts used for ESI infusion were 2.5 and 10  $\mu\text{M}$ , respectively.

Intact MBP and MBP–Cy3.5 were initially analyzed using sinapinic acid as the ionization matrix. For mapping the location of dye-derivatized lysine residues in MBP, tryptic digests of MBP–Cy3.5 ( $D/P$  of 1.7) were subjected to MALDI-TOF/MS peptide analyses by Commonwealth Biotechnologies, Inc. (Richmond, VA). Peptide maps from MBP–Cy3.5 were compared to those from unmodified MBP, and a unique singly labeled peptide was identified based on theoretical vs actual mass for derivitized peptides. For the peptide mapping,  $\sim 1.25$  nmol of each protein was digested with trypsin. Digested samples were analyzed using cyano-4-hydroxycinnamic acid as the ionization matrix. Spectra were acquired in both reflector and linear modes.

## RESULTS

**Mass Spectral Characterization of the  $\beta$ -Cyclodextrin–Dye Adducts and Mapping of Dye-Labeled MBP Lysine Residues.** The results of mass spectral characterization of pure  $\beta$ -cyclodextrin–dye adducts:  $\beta$ -cyclodextrin–QSY9 ( $\text{C}_{81}\text{H}_{104}\text{N}_4\text{O}_{44}\text{S}_3$ ) predicted molecular mass:1932.2, observed:1932.5;  $\beta$ -cyclodextrin–Cy5 ( $\text{C}_{75}\text{H}_{109}\text{N}_3\text{O}_{14}\text{S}_2$ ) predicted molecular mass:1771.6, observed:1771.4.

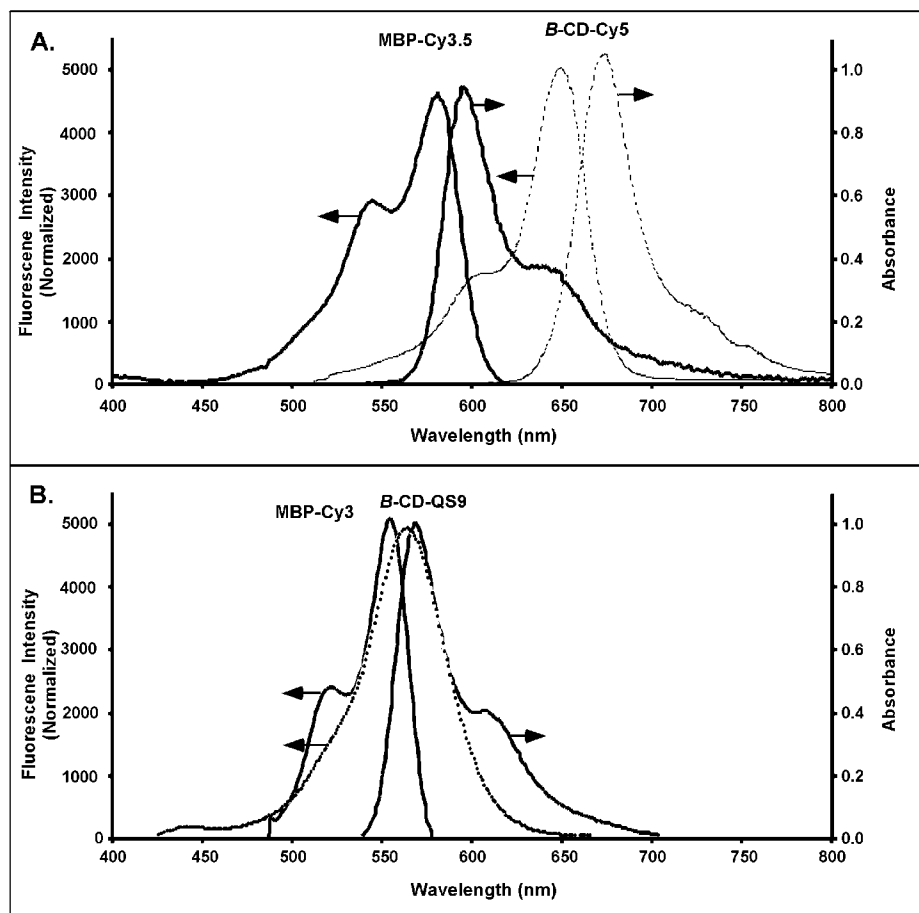
The mass spectrum of the unmodified undigested MBP corresponded to both a single charged ( $m/z$  41684) and doubly charged species ( $m/z$  20828). The mass spectrum of the undigested MBP–Cy3.5 corresponded to the presence of the Cy3.5-labeled form ( $m/z$  42694). Comparison of the mass spectra of tryptic digests for the unmodified and Cy3.5-modified MBPs identified a fragment ( $m/z$  4660.92) in the modified MBP with three missed lysine cleavage sites. This mass corresponds to a singly-Cy3.5-

labeled peptide fragment (residues 139–171) with three missed lysine cleavage sites (residues 141, 143, 145). This strongly suggests that, for any derivitized MBP molecule, one of these lysines was labeled, although from the MS data we cannot unambiguously determine which one. Each of these lysines is located at the protein surface within one turn at the end of the same helix, and since the  $D/P$  ratio for the labeled protein is relatively low, it appears that for any single protein molecule one of these lysines undergoes strong preferential labeling, as opposed to the labeling occurring randomly, by reaction with the NHS ester of the dye. As an alternative, and to contrast a sensor assembly with completely unambiguous labeling at a unique site in MBP, we also utilized a maleimide labeling strategy to target the MBP 95 cysteine residue for Cy3 conjugation ( $D/P$  for D95C–Cy3 labeled protein was 1). This labeled protein was also investigated in a sensing role, as discussed below.

The absorption and emission spectra of MBP Cy3 and MBP–Cy3.5 (both proteins labeled with amine reactive NHS esters of the dyes) are shown in Figure 3. Conjugating these dyes to MBP only slightly altered their absorbance ( $\lambda_{\text{max}}$  abs) and emission ( $\lambda_{\text{max}}$  em) maxima (Table 1). The largest spectral shift for protein bound vs free dye observed was for MBP–Cy3 and MBP–Cy3.5, both of which had their absorption maxima shifted  $\sim 6$  nm, with the MBP–Cy3 shifting to higher wavelength, and that of the MBP–Cy3.5 shifting to shorter wavelength. The identical shift in  $\lambda_{\text{max}}$  emission was noted when MBP was labeled at 95C with Cy3-maleimide or on a lysine with amino-reactive Cy3.

**Assembly of the FRET Complex.** As illustrated by the schematic in Figure 1, when a Cy3.5 dye-labeled MBP energy donor moiety binds a Cy5-labeled  $\beta$ -CD energy acceptor moiety, FRET should result, assuming the appropriate spectral overlaps and acceptable spacing between the dye centers (The same applies to the Cy3/QSY9 pair). Figure 4 presents fluorescence emission spectra of a titration of 0.1  $\mu\text{M}$  MBP–Cy3.5 FRET donor (1  $D/P$  ratio) with increasing amounts of  $\beta$ -CD–Cy5 (FRET acceptor). Comparison of the fluorescence emission of each component measured separately and when both components were mixed shows the expected FRET effect. This effect is more apparent at the higher  $\beta$ -CD–Cy5 concentrations of 0.5  $\mu\text{M}$  and 1  $\mu\text{M}$  as demonstrated by the loss in donor intensity and the corresponding gain in acceptor fluorescence intensity. This intensity gain is much greater than the directly excited signal elicited from the identical concentration of uncomplexed  $\beta$ -CD–Cy5, shown for comparison in the same plots. Incubating 0.1  $\mu\text{M}$  MBP–Cy3.5 with 1  $\mu\text{M}$  of free Cy5 dye as a control resulted in an emission spectrum essentially identical to that of the independent MBP–Cy3.5 overlaid upon 1  $\mu\text{M}$  independent  $\beta$ -CD–Cy5 shown in Figure 4, Panel C (Data not shown).

Figure 5A shows the titration of 0.1  $\mu\text{M}$  MBP–Cy3.5 (1.7  $D/P$ ) titrated with increasing amounts of  $\beta$ -CD–Cy5. This MBP–Cy3.5 preparation had a somewhat greater  $D/P$  ratio than the labeled protein used to derive the data shown in Figure 4. Stepwise addition of the acceptor portion caused a significant loss in donor fluorescence intensity almost identical to the pattern observed for MBP–Cy3.5 with the lower  $D/P$  ratio of 1 (Figure 4). This loss in donor fluorescent intensity is demonstrated by the plot in Figure 5B; an 81% drop in fluorescence intensity occurred at the wavelength corresponding to the donor's emission maximum (596 nm) as a function of  $\beta$ -CD–Cy5 concentration. The observed shift to longer wavelength of  $\beta$ -CD–Cy5 emission,  $\sim 6$ –8 nm, shown in Figure 5A,



**Figure 3.** Absorption and emission spectra of conjugated MBP-Cy3.5 (1 dye/protein ratio), solid line, and  $\beta$ -CD-Cy5, dotted line (A). MBP-Cy3 (1.7 dye/protein ratio), solid line, and  $\beta$ -CD-QSY9, dotted line (B). For emission spectra, samples were excited at 520 nm. Data are normalized for presentation. Arrows indicate the axis of reference.

is indicative of inner filter effects at higher reagent concentrations (25). Control experiments where 0.1  $\mu$ M MBP-Cy3.5 (1 *D/P*) was titrated with unlabeled  $\beta$ -CD (Figure 5C) resulted in no change in donor fluorescence. The converse control experiment where 500 nM of  $\beta$ -CD-Cy5 was titrated with increasing amounts of unlabeled MBP also showed no change in acceptor emission (Figure 5D). Additionally, in a control experiment in which dye-labeled MBP was titrated with maltose there was no effect on fluorescence (data not shown). Taken together, these results demonstrate that a FRET process is indeed taking place between the donor and acceptor components of the homogeneous sensing complex.

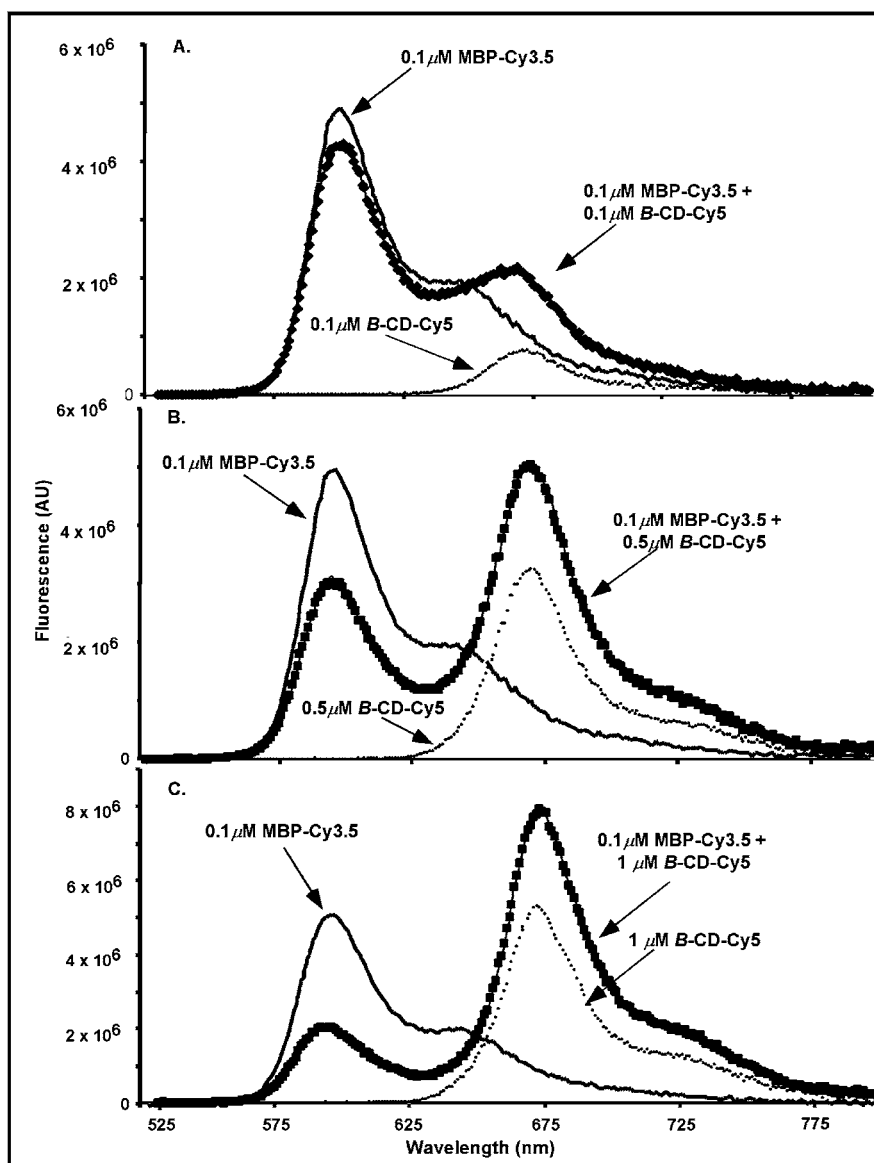
**Maltose Analysis.** Figure 5E presents plotted data from the titration of the assembled FRET complex (0.1  $\mu$ M MBP-Cy3.5 (1.7 *D/P*) – 2.5  $\mu$ M  $\beta$ -CD-Cy5) with increasing concentrations of maltose. Increasing the maltose concentration causes a systematic increase in MBP-Cy3.5 donor fluorescence intensity. The corrected fluorescence intensities as a function of added maltose are plotted in Figure 5F. An increase of 76% in Cy3.5 donor fluorescence intensity is observed for the completed titration. A similar increase in donor intensity was seen for the 0.1  $\mu$ M MBP-Cy3.5 (1 *D/P*) – 2.5  $\mu$ M  $\beta$ -CD-Cy5 FRET complex when it was titrated with increasing amounts of unlabeled  $\beta$ -CD (data not shown). From these data,  $K_{app}$  values of 0.14 and 0.15  $\mu$ M were estimated for titrations using MBP-Cy3.5 protein with 1.0 and 1.7 *D/P* ratios, respectively, see Table 2 (23).

**MBP-Cy3- $\beta$ -CD-QSY9 FRET Ensemble.** An alternate FRET complex consisting of Cy3 as the donor and

a dark quencher as energy acceptor was investigated. The dark quencher, QSY9, was conjugated to the  $\beta$ -CD and purified as described. MBP was labeled with Cy3, chosen as the energy donor in order to optimize donor-acceptor spectral overlap (see Figure 3, Panel B). This FRET pair functions in an analogous manner to the MBP-Cy3.5- $\beta$ -CD-Cy5 pair, but the dark quencher has no fluorescence emission. Figure 6A shows the titration of a 0.1  $\mu$ M MBP-Cy3-5  $\mu$ M  $\beta$ -CD-QSY9 FRET complex with increasing concentrations of maltose (MBP was labeled on lysine residues). The presence of the  $\beta$ -CD-QSY9 adduct at 5  $\mu$ M alters the shape of the Cy3 emission spectra, in comparison to uncomplexed MBP-Cy3 (Figure 3B), due to inner filter effects (25). Nonetheless, the assembly functions well in sensing maltose. Data were corrected for inner filtering at 567 nm and plotted to demonstrate the net change in fluorescence intensity as a function of maltose concentration (Figure 6B), and a  $K_{app}$  value of 0.82  $\mu$ M was estimated for maltose for this sensor complex under these conditions (Figure 6C).

**MBP-D95C-Cy3- $\beta$ -CD-QSY9 FRET Ensemble (1 *D/P*).** To evaluate a sensor assembly where the site of donor labeling was more completely controlled, a FRET ensemble was prepared that included a variant of MBP engineered with a single cysteine for unique thiol-directed labeling with a Cy3 maleimide derivative. In this case, when a 0.1  $\mu$ M MBP-D95C-Cy3 to 1  $\mu$ M  $\beta$ -CD-QSY9 sensor assembly was titrated against increasing amounts of maltose (Figure 6C), a  $K_{app}$  value of 2.90  $\mu$ M was estimated for maltose binding. The maltose sensing behavior for this assembly was found to be comparable





**Figure 4.** Titration of 0.1  $\mu\text{M}$  MBP-Cy3.5 (1 dye/protein ratio) with increasing amounts of  $\beta\text{-CD-Cy5}$ ; 0.1  $\mu\text{M}$  in A, 0.5  $\mu\text{M}$  in B, and 1  $\mu\text{M}$  in C. In each panel the fluorescence of the 0.1  $\mu\text{M}$  MBP-Cy3.5 uncomplexed (solid line), the  $\beta\text{-CD-Cy5}$  uncomplexed (dotted line), and the assembled FRET complex (solid squares) are shown. Samples were excited at 520 nm.

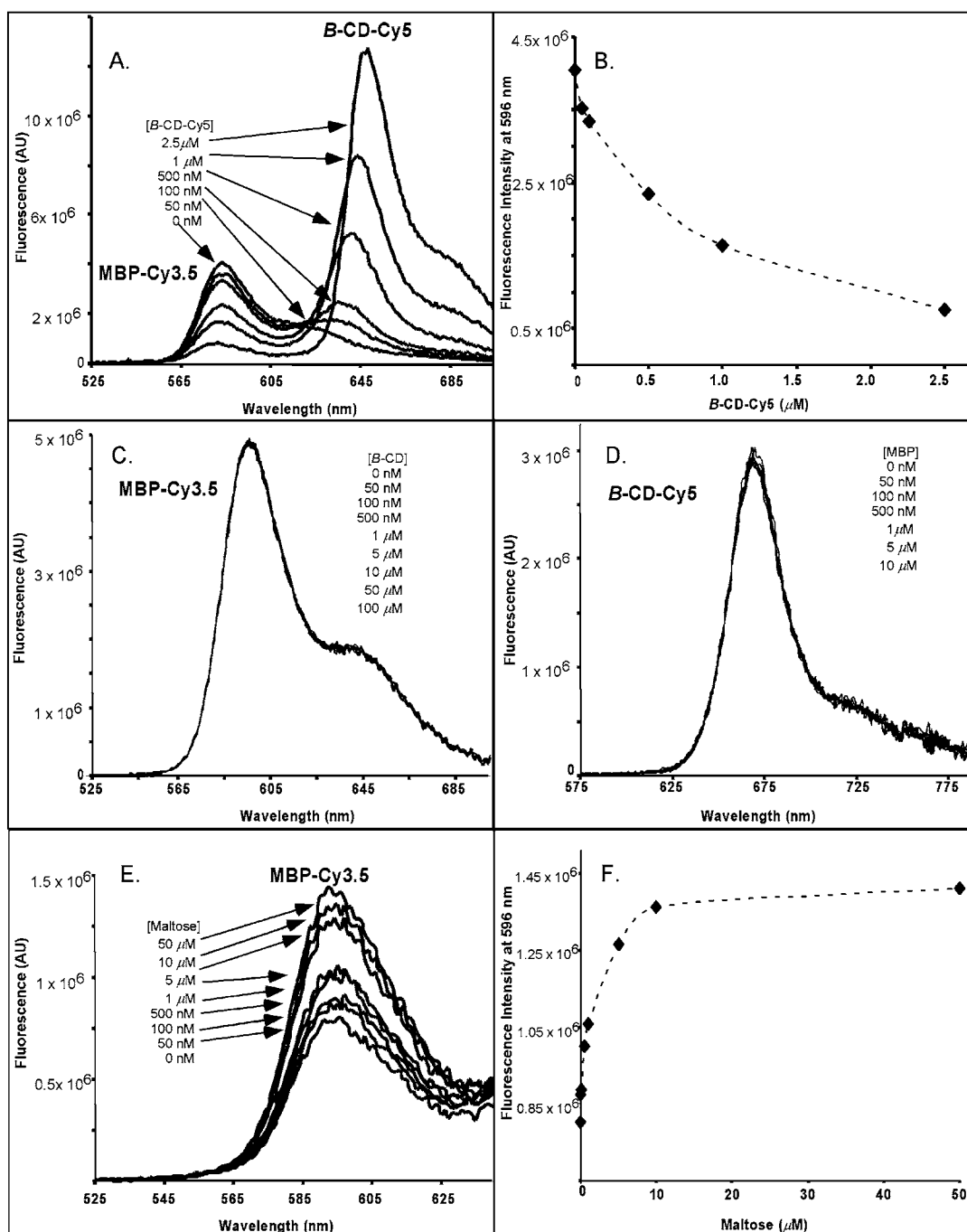
to the above examples in which the protein was modified with the Cy3 energy donor by attachment to the  $\epsilon$  amino group of lysine residues that occurred in a fortuitously selective manner in the area of residues 141–145 of MBP.

#### DISCUSSION

Wild-type, unlabeled MBP has a reported  $K_D$  of 1.8  $\mu\text{M}$  for  $\beta\text{-CD}$  and 0.9  $\mu\text{M}$  for maltose (11, 24). Since these values are similar, the appropriate concentration of maltose could compete with dye-labeled  $\beta\text{-CD}$  for binding to the protein in the present sensor assemblies. In these sensors, displacement of the labeled  $\beta\text{-CD}$  translates to loss of FRET and to an increase in donor emission. This allows measurement of maltose concentrations through the gain in donor fluorescence intensity and demonstrates that the FRET complexes can function as quantitative homogeneous biosensors. The FRET complexes are quite sensitive, with lower detection limits of 50–100 nM maltose and upper limits approaching 50  $\mu\text{M}$  (Figure 5E and Figure 6A). These assemblies are more sensitive than the previously described FRET MBP sensor that detected maltose in only the micromolar

range (3). This is likely due to the Cy3 and Cy3.5 dyes being better energy transfer donors than endogenous tryptophan residues, as well as the large extinction coefficients and high quantum yields of cyanine dyes.

Structural modeling of the present sensor assemblies indicates that the distance between the bound  $\beta\text{-CD-dyes}$  and any of the labeled donor dyes covalently attached to the protein surface will be in the 29–45 Å range. From the MBP crystal structure, the distance for each of the mapped Cy3.5 derivitized lysines to the  $\beta\text{-CD-dye}$  located in the binding pocket is as follows: lysine 141,  $\sim 40$  Å; lysine 143,  $\sim 46$  Å; lysine 145,  $\sim 45$  Å. The Förster distance corresponding to 50% energy transfer efficiency ( $R_0$ ) for the Cy3.5–Cy5 FRET pair based on spectral overlap is 66.2 Å. In the 29–45 Å range, the energy transfer efficiency increases to 91 to 98%, respectively. From the close proximity of each of these lysines, and their very similar distances from the sugar binding pocket (well under  $R_0$ ), it is clear that labeling at any one of these residues will result in effective FRET-based sensing. The  $R_0$  for the Cy3–QSY9 FRET donor–acceptor pair is 54.8 Å, and the predicted FRET efficiencies for this



**Figure 5.** (A) Fluorescence emission spectra of 0.1  $\mu\text{M}$  MBP-Cy3.5 (1.7 dye/protein ratio) titrated against increasing amounts of  $\beta\text{-CD-Cy5}$ . (B) Reduction in fluorescence intensity (uncorrected) at 596 nm for the titration shown in A. (C) Fluorescence emission spectra of 0.1  $\mu\text{M}$  MBP-Cy3.5 (1 dye/protein ratio) titrated with increasing amounts of unlabeled  $\beta\text{-CD}$ . (D) 0.5  $\mu\text{M}$   $\beta\text{-CD-Cy5}$  titrated with increasing amounts of unlabeled MBP. (E) FRET donor's emission spectra during a titration of 0.1  $\mu\text{M}$  MBP-Cy3.5 (1.7 dye/protein ratio) mixed with 2.5  $\mu\text{M}$   $\beta\text{-CD-Cy5}$  against increasing amounts of maltose. (F) Gain in fluorescence intensity (corrected) for the titration shown in E. Samples were excited at 520 nm.

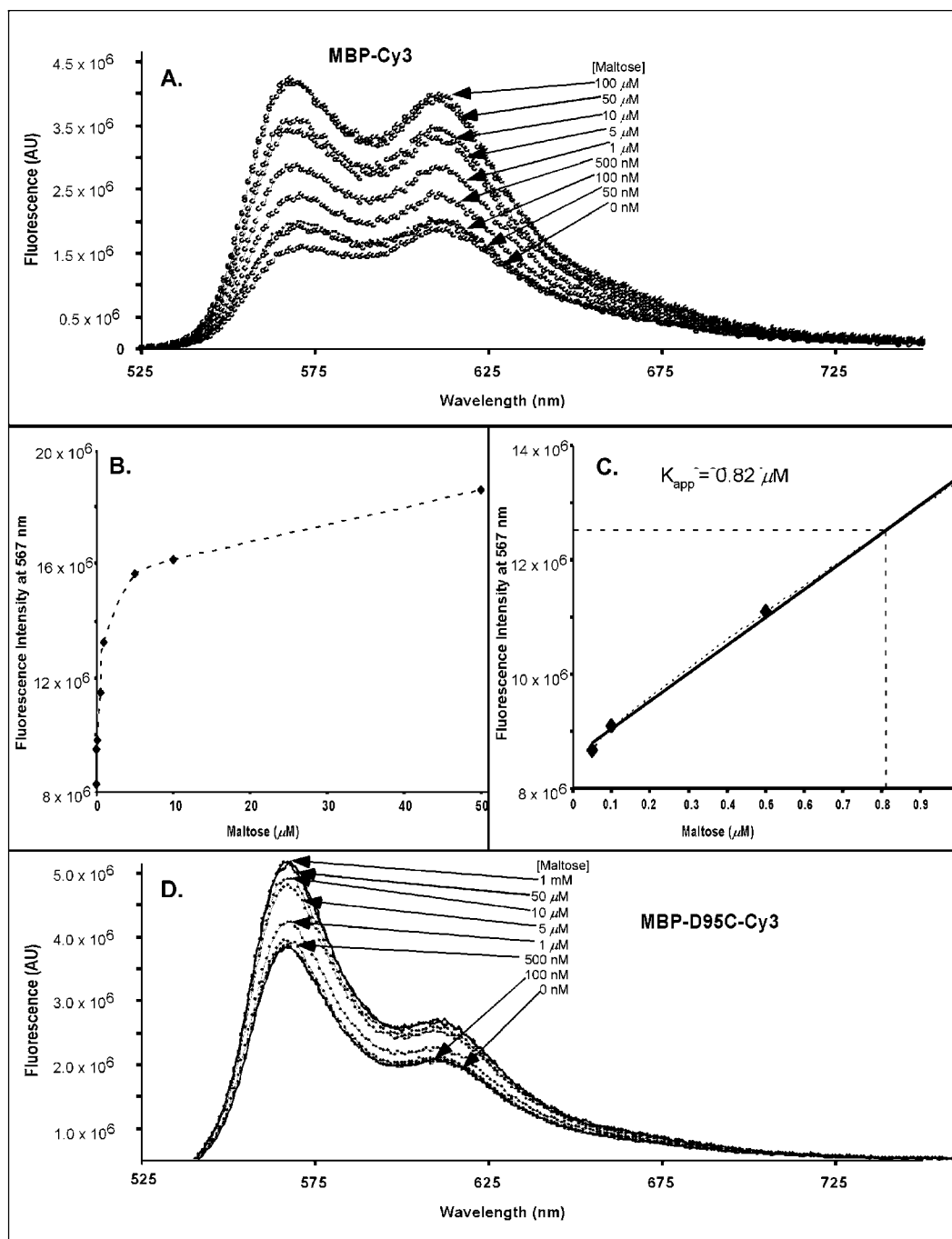
**Table 2. Properties of MBP-Dye Conjugates Used**

MBP-dye conjugate	MBP protein-dye ratio	apparent maltose dissociation values $K_{\text{app}}$ ( $\mu\text{M}$ )
MBP-D95C-Cy3	1.0	2.90
MBP-Cy3	1.7	0.82
MBP-Cy3.5	1.0	0.14
MBP-Cy3.5	1.7	0.15

pair at the 29–45 Å distance range are 98% and 77%, respectively (24, 26). The ~25 Å distance between Cy3 located at 95C and  $\beta\text{-CD-dye}$  bound in the MBP sugar

binding pocket corresponds to a predicted FRET efficiency approaching 100%. Clearly, the donor-acceptor distances in each of these complexes are ideal for sensing by the FRET mechanism to occur.

X-ray crystal structure studies and structural modeling demonstrate that while MBP binds  $\beta\text{-CD}$  and remains in an open conformation, it closes by an intramolecular conformational change so as to engulf maltose (11, 24). Previously described MBP-based sensors have exploited the conformational changes that MBP undergoes when binding maltose by measuring the effects of this allosteric



**Figure 6.** (A) Fluorescence emission spectra of 0.1  $\mu\text{M}$  MBP-Cy3 (1.65  $D/P$ ) complexed with 5  $\mu\text{M}$   $\beta\text{-CD-QSY9}$  and titrated against increasing amounts of maltose. (B) Corrected fluorescence intensity at 567 nm plotted against maltose concentration. (C) Plot of the corrected fluorescence intensity at  $1/2$  fluorescence max that was used to estimate the apparent dissociation value,  $K_{\text{app}}$  (23). (D) Titration of 0.1  $\mu\text{M}$  MBP95C-Cy3 complexed to 1  $\mu\text{M}$   $\beta\text{-CD-QSY9}$  against increasing amounts of maltose.

change upon intrinsic tryptophan fluorescence or on the fluorescence emanating from dye-labeled MBP (11). Indeed, some data suggest that fluorophore conjugation to certain MBP mutants may stabilize the maltose-bound form of the protein (11). In contrast, titrating MBP-Cy3.5 with maltose or unlabeled  $\beta\text{-CD}$  results in no fluorescence emission changes even at saturating ligand concentrations. Thus, the results presented here demonstrate that allosteric effects are silent in the present sensor complexes and that the observed sensing behavior is solely due to FRET.

These sensing assemblies make use of novel fluorescent dye-labeled  $\beta\text{-CD}$  adducts. Other activated dye labels

could undoubtedly be attached to monoamino  $\beta\text{-CD}$  to expand the potential utility of the assay. As we have shown, the basic FRET sensor system described can function in both fluorescent donor-fluorescent acceptor and fluorescent donor-dark quencher configurations. Additionally, the Cy3.5-Cy5 donor-acceptor configuration functions almost identically at two different dye/MBP ratios (1 and 1.7). This suggests that controlling the exact  $D/P$  ratio is not critical for sensor performance. The dye-labeled MBP- $\beta\text{-CD-QSY9}$  FRET pair is particularly appealing since a fluorescence increase or 'switching on' occurs in the presence of maltose, with the added benefit of no overlapping acceptor emission.



Apparent dissociation ( $K_{D,app}$ ) values were estimated from these sensor complexes for maltose and were very close to previous reported maltose  $K_d$  values. For example,  $K_{app} = 0.82 \mu\text{M}$  for a MBP-Cy3 protein versus  $0.8 \mu\text{M}$  for the acrylodan-modified C95 mutant protein (3). A  $K_{app}$  value of  $2.90 \mu\text{M}$  was determined for the MBP-D95C Cy3-labeled mutant/QSY9- $\beta$ -CD system, which correlates well with a value of  $1.5 \mu\text{M}$  for the same mutant in an unlabeled form and  $4.4 \mu\text{M}$  when the mutant is labeled with IANBD at that site (11). The 0.14 and  $0.15 \mu\text{M}$  values estimated for the MBP-Cy3.5/ $\beta$ -CD-dye systems are essentially identical to the  $K_D$  of  $0.1 \mu\text{M}$  described for the MBP Ile329Cys mutant modified with an IANBD fluorescent reporter (11).

The MBP sugar receptor used in the present MBP-based maltose sensors functioned effectively when either labeled with an energy donor in a fully directed manner (specific cysteine labeling) or when labeled with lysine-directed dye derivatives. Although labeling with the lysine-directed dye derivatives was fortuitously selective in the present case, even essentially randomly labeled protein would be highly likely to function effectively in these FRET configurations due to the moderate size of MBP, the central placement of its sugar binding site, and the favorable  $R_0$  values selected for donor-acceptor pairs. Potential applications of these sensor complexes include direct use of their maltose sensing capabilities in food production and processing (16), specifically in beer and bread production which utilize maltose as the primary sugar source and potentially other fermentative technology. Additionally, variants of this sensing scheme may be adapted for glucose monitoring of diabetic patients (8, 25) or for sensing of surface glycoproteins of potential antigens (27).

#### ACKNOWLEDGMENT

The authors thank Prof. Homme Hellinga (Duke University) for providing the plasmid with the MBP-HIS-tagged gene sequence utilized. I.L.M. was supported by a National Research Council (NRC) fellowship through the Naval Research Laboratory. M.E.L. was supported by an American Society for Engineering Education (ASEE) fellowship. The views, opinions, and/or findings described in this report are those of the authors and should not be construed as official Department of the Navy positions, policies, or decisions.

#### LITERATURE CITED

- (1) Iqbal, S. S., Mayo, M. W., Bruno, J. G., Bronk, B. V., Batt, C. A., and Chambers, J. P. (2000) A Review of Molecular Recognition Technologies for Detection of Biological Threat Agents. *Biosens. Bioelect.* 15, 549–578.
- (2) Ligler F. S., and Rowe Taitt, C. A. Eds. (2002) Optical Biosensors: Present and Future. Elsevier, The Netherlands.
- (3) Gilardi G., Zhou L. Q., Hibbert L., and Cass A. E. G. (1994) Engineering the Maltose Binding Protein for Reagentless Fluorescence Sensing. *Anal. Chem.* 66, 3840–3847.
- (4) Didenko V. V. (2001) DNA Probes Using Fluorescence Resonance Energy Transfer (FRET): Designs and Applications. *BioTechniques* 31, 1106–1121.
- (5) Lakowicz, J. R. (1999) *Principles of Fluorescence Spectroscopy*, 2nd ed., Kluwer Academic/Plenum Press, New York.
- (6) Tong, A. K., Zengmin, L., and Jingyue, J. (2002) Combinatorial Fluorescence Energy Transfer Tags: New Molecular Tools for Genomics Applications. *IEEE J. Quantum Electron.* 38, 110–121.
- (7) Schobel, U., Egelhaaf, H.-J., Brecht, A., Oelkrug, D., and G. Gauglitz. (1999) New Donor-Acceptor Pair for Fluorescent Immunoassays by Energy Transfer. *Bioconjugate Chem.* 10, 1107–1114.
- (8) Tolosa, L., Szmajcinski, H., Rao, G. and Lakowicz, J. R. (1997) Lifetime-Based Sensing of Glucose Using Energy Transfer with a Long Lifetime Donor. *Anal. Biochem.* 250, 102–108.
- (9) Chew, T. L., Wolf, W. A., Gallagher, P. J., Matsumura, F., and Chisolm, R. L. (2002) A Fluorescent Resonant Energy Transfer-based Biosensor Reveals Transient and Regional Myosin Light Chain Kinase Activation in Lamella and Cleavage Furrows. *J. Cell. Biol.* 156, 543–553.
- (10) Rice, K. G. (2001) Application of Fluorescence Resonance Energy Transfer to Analyze Carbohydrates. *Anal. Biochem.* 297, 117–122.
- (11) Marvin, J. S., Corcoran, E. E., Hattangadi, N. A., Zhang, J. V., Gere, S. A., and Hellinga, H. W. (1997) The Rational Design of Allosteric Interactions in a Monomeric Protein and its Applications to the Construction of Biosensors. *Proc. Natl. Acad. Sci. U.S.A.* 94, 4366–4371.
- (12) Zhou, L. Q., and Cass, A. E. G., (1991) Periplasmic Binding-protein Based Biosensors. 1. Preliminary-study of Maltose Binding-Protein as Sensing Element For Maltose Biosensor. *Biosens. Bioelect.* 6, 445–450.
- (13) Gilardi G., Mei G., Rosato N., Agro AF, Cass AE (1997). Spectroscopic properties of an engineered maltose binding protein. *Protein Eng.* 10, 479–86.
- (14) Benson, D. E., Conrad, D. W., de Lorimier, R. M., Trammell, S. A., and Hellinga, H. W. (2001) Design of Bioelectronic Interfaces by Exploiting Hinge-Bending Motions in Proteins. *Science* 293, 1641–1644.
- (15) Naal, Z., Park, J. H., Bernhard, S., Shapleigh, J. P., Batt, C. A., and Abruna, H. D. (2002) Amperometric TNT Biosensor Based on the Oriented Immobilization of a Nitroreductase Maltose Binding Protein Fusion. *Anal. Chem.* 74, 140–148.
- (16) Fehr, M., Frommer, W. B., and Lalonde, S. (2002) Visualization of Maltose Uptake in Living Yeast Cells by Fluorescent Nanosensors. *Proc. Natl. Acad. Sci. U.S.A.* 99, 9846–9851.
- (17) Tong, A.-J., Yamauchi, A., Hayashita, T., Zhang, Z.-Y., Smith, B. D., and Teramae, N. (2001) Boronic Acid Fluorophore/ $\beta$ -Cyclodextrin Complex Sensors for Selective Sugar Recognition in Water. *Anal. Chem.* 73, 1530–1536.
- (18) Tanabe, T., Touma, K., Hamasaki, K., and Ueno, A. (2001) Immobilized Fluorescent Cyclodextrin on a Cellulose Membrane as a Chemosensor for Molecule Detection. *Anal. Chem.* 73, 3126–3130.
- (19) Pagliari, S., Corradini, R., Galaverna, G., Sforza, S., Dossena, A., and Marchelli, R. (2000) Enantioselective Sensing of Amino Acids by Copper(II) Complexes of Phenylalanine-based Fluorescent  $\beta$ -Cyclodextrins. *Tetrahedron Lett.* 41, 3691–3695.
- (20) Hossain, M. A., Hamasaki, K., Takahashi, K., Mihara, H., and Ueno, A. (2001) Guest-Induced Diminishment in Fluorescence Quenching and Molecule Sensing Ability of a Novel Cyclodextrin-Peptide Conjugate. *J. Am. Chem. Soc.* 123, 7435–7436.
- (21) McCartney, L. J., Pickup, J. C., Rolinski, O. J., and Birch, D. J. S. (2001) Near-Infrared Fluorescence Lifetime Assay for Serum Glucose Based on Allophycocyanin-labeled Concanavalin A. *Anal. Biochem.* 292, 216–221.
- (22) Mattoussi, H., Mauro, J. M., Goldman, E. R., Anderson, G. P., Sundar, V. C., Mikolec, F. V., and Bawendi, M. G. (2000) Self-Assembly of CdSe-ZnS Quantum Dot Bioconjugates Using an Engineered Recombinant Protein. *J. Am. Chem. Soc.* 122, 12142–12450.
- (23) Bagshaw, C. R. and Harris, D. A. (1988) Measurement of Ligand Binding to Proteins. *Spectrophotometry and Spectrofluorimetry a Practical Approach* (Harris and Bashford, Eds.) pp 91–113, IRL Press, Washington, DC.
- (24) Sharff, A. J., Rodseth, L. E., and Quiocho, F. A. (1993) Refined 1.8-Å Structure Reveals the Mode of Binding of  $\beta$ -Cyclodextrin to the Maltodextrin Binding Protein. *Biochemistry* 32, 10553–10559.
- (25) Tolosa, L., Gryczynski, I., Eichhorn, L. R., Dattelbaum, J. D., Castellano, F. N., Rao, G., and Lakowicz J. R. (1999)

- Glucose Sensor for Low-cost Lifetime-based Sensing Using a Genetically Engineered Protein. *Anal. Biochem.* **267**, 114–120.
- (26) Du, H., Fuh, R. C. A., Li, J. Z., Corkan, L. A., and Lindsey, J. S. (1998) PhotochemCAD: A Computer-Aided Design and Research Tool in Photochemistry. *Photochem. Photobiol.* **68**, 141–142.
- (27) Benito, A, and Van Regenmortel, M. H. V. (1998) Biosensor Characterization of Antigenic Site A of Foot-and-Mouth Disease Virus Presented in Different Vector Systems. *FEMS Immunol. Med. Microbiol.* **21**, 101–115.

BC020062+

# Aminomodified Nucleobases: Functionalized Nucleoside Triphosphates Applicable for SELEX

Thomas Schoetzau,<sup>†</sup> Josmar Langner,<sup>†</sup> Elisabeth Moyroud, Ingo Roehl, Stefan Vonhoff, and Sven Klussmann\*

NOXXON Pharma AG, Max-Dohrn-Strasse 8-10, 10589 Berlin, Germany. Received December 13, 2002; Revised Manuscript Received March 24, 2003

5-Aminoallyl-2'-fluoro-dUTP, 5-aminoallyl-UTP, and *N*<sup>6</sup>-([6-aminoethyl]carbamoylmethyl)-ATP were systematically tested for their suitability for the systematic evolution of ligands by exponential enrichment (SELEX) process with the aim of introducing additional functionalities to RNA libraries. All three aminomodified nucleoside triphosphates proved to be compatible with the enzymatic steps required for SELEX and maintained strict Watson–Crick basepairing. Complementary RNA molecules modified with the two uridine analogues show a significantly increased melting temperature, whereas the introduction of *N*<sup>6</sup>-([6-aminoethyl]carbamoylmethyl)-ATP leads to a decreased *T*<sub>m</sub> and thus less stable basepairing. The chemical synthesis of 5-aminoallyl-2'-fluoro-dUTP is reported in detail.

## INTRODUCTION

In vitro selection of oligonucleotides, also known as systematic evolution of ligands by exponential enrichment (SELEX), was developed independently by Joyce (1), Szostak (2), and Gold (3) in the late 1980s and early 1990s. SELEX has been successfully used to obtain aptamers that bind to various molecular targets derived from many different substance classes from combinatorial nucleic acid libraries. In addition to mere binding, new ribozymes and even deoxyribozymes were selected to catalyze various reactions such as cleavage of DNA (4), ligation of RNA (5), Diels–Alder reactions (6), peptide bond formation (7), or the synthesis of pyrimidine nucleotides (8). While the sequence and structural complexity of nucleic acid libraries is high, their chemical and biophysical diversity is limited since they comprise only four different nucleotide monomers. This stands in contrast to peptides and libraries thereof, which consist of 20 different amino acids with side chains, ranging from lipophilic to hydrophilic, charged and reactive, like carboxyl, sulfhydryl, hydroxyl, guanidinium, and ammonium groups. These amino acid side chains mediate the functional variety and diversity of peptides and proteins. In analogy, modifying their constituent nucleobases is expected to enhance the binding and functional repertoire of nucleic acids.

The enzymatic generation of modified aptamers is expected to be less demanding for DNA than for RNA, where reverse transcription is required. Thus, only one enzyme, a thermostable DNA polymerase, is involved, that has to accept the modified dNTPs. In the context of DNA SELEX a series of modifications such as C5-aminomodified dUTP analogues, Lee et al. (9), 5-(1-pentynyl)-dUTP, Latham et al. (10), several highly functionalized dUTP derivatives, Sakthivel and Barbas (11), and C7-aminomodified 7-deaza-dATP, Goullain et al. (12), are closely related to our work. Perrin et al. (13) reported the simultaneous use of 5-(3-aminoallyl)-dUTP

and 8-(2-(4-imidazolyl)ethylamino)-dATP, Battersby et al. (14) employed 5-(3-aminopropynyl)-dUTP, and Santoro et al. (15) described C5-imidazole-functionalized dUTP. An overview of more modifications with expanded chemical functionalities is given by Bittker et al. (16).

For RNA SELEX modified NTPs have to be accepted and efficiently incorporated by RNA polymerases, commonly derived from phages, that seem to be more substrate-specific than thermostable DNA polymerases. In addition, RNA transcripts have to be converted to cDNA by reverse transcriptases. In both reactions, strict Watson–Crick basepairing is essential to ensure fidelity and to keep the selected information. Apart from various publications on 2'-modified NTPs, Vaish et al. (17) successfully tested 5-(3-aminopropyl)-UTP and 5-(2-mercaptoethyl)-UTP in RNA SELEX. Dewey et al. (18) used several 5-modified UTP derivatives, Ito (19) and Ito et al. (20) employed *N*<sup>6</sup>-modified ATP and *N*<sup>6</sup>-biotin-linked-CTP, and Zinnen et al. (21) introduced 2'-F-5-[(*N*-imidazole-4-acetyl) propylamine]-dUTP.

Here we report in detail about the synthesis of 5-aminoallyl-2'-fluoro-2'-deoxyuridine 5'-triphosphate **7**. We compare RNA transcription yields in the presence of **7** with 5-aminoallyl-UTP **8** and *N*<sup>6</sup>-([6-aminoethyl]carbamoylmethyl)-ATP **9**. Moreover, we show the compatibility of all three aminomodified triphosphates with the general SELEX process and discuss the thermal melting behavior of such modified RNA molecules.

## EXPERIMENTAL PROCEDURES

**General.** Aminomodified nucleoside triphosphates **8** and **9** were purchased from Sigma. Anion exchange chromatography was performed on Sephadex DEAE-A25 (400 × 26 mm), Amersham Biosciences. Analytical reversed phase HPLC was performed on Waters 2690 systems with PDA-UV detection from 200 to 300 nm and a 250 × 4 mm stainless steel column packed with Hypersil ODS (C18, 5 μm). A flow rate of 1 mL/min was used with 100 mM aq. TEAAc (pH 7) and a linear gradient of 0–25% acetonitrile.

<sup>1</sup>H-NMR spectra were obtained on a 300 MHz Varian spectrometer using the respective solvent as internal

\* To whom correspondence should be addressed: sklussmann@noxxon.net.

<sup>†</sup> Both authors contributed equally.



standard. For  $^{31}\text{P}$ - and  $^{19}\text{F}$ -NMR spectra phosphoric acid and fluorotrichloromethane were used as external standards. NMR samples of nucleotide triphosphates were dissolved in  $\text{D}_2\text{O}$  (99.9%), Aldrich. Mass spectral analysis of nucleoside triphosphates was obtained in negative mode on a Hewlett-Packard G2025A MALDI TOF with 3-hydroxy picolinic acid as matrix.

*Crotalus adamanteus* venom phosphodiesterase I and calf intestine alkaline phosphatase were purchased from USB and Roche, respectively.

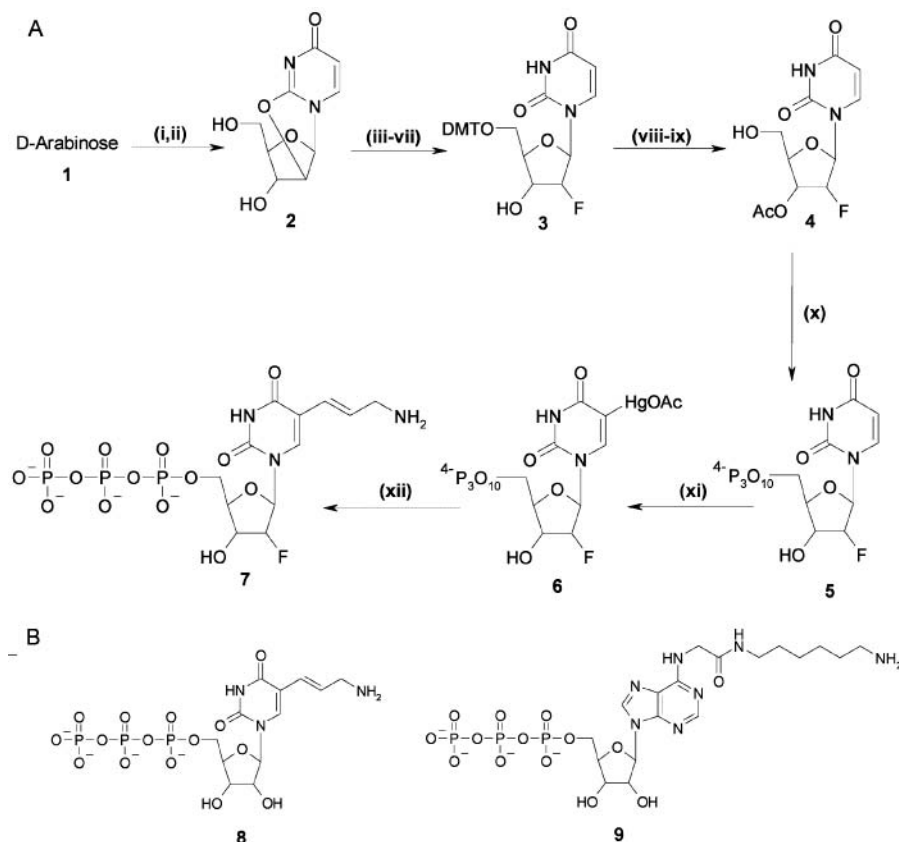
**Syntheses.** *2'-Deoxy-5'-(4,4'-dimethoxytrityl)-2'-fluoro-D-uridine 3.* 2,2'-O-Anhydro-D-uridine **2** (100 mmol) was coevaporated with anhydrous pyridine ( $2 \times 150$  mL). Pixyl chloride (220 mmol) was added to a solution of **2** (100 mmol) in anhydrous pyridine (120 mL) and the solution was stirred at room temperature overnight. The reaction was quenched with water (50 mL) and was concentrated by evaporation. The residue was dissolved in DCM (200 mL) and washed with diluted  $\text{NaHCO}_3$  solution ( $2 \times 100$  mL). The organic phase was evaporated to dryness, suspended in methanol (1200 mL) and heated to reflux for 2 h with 2 M NaOH (250 mL). After 16 h at  $4^\circ\text{C}$ , the mixture was evaporated to dryness. The residue was dissolved in DCM (300 mL) and washed with dil.  $\text{NaHCO}_3$  solution ( $2 \times 200$  mL). The organic layer was dried over  $\text{Na}_2\text{SO}_4$  and concentrated in vacuo to give 3',5'-di-*O*-pixyl-D-arabinofuranosyluridine as a yellowish foam (purity by TLC:  $>80\%$ ,  $R_f$  0.41 (DCM/MeOH 95/5)). After drying of the sample overnight, the intermediate product (40 mmol) was suspended in a mixture of DMF and  $\text{CH}_3\text{-CN}$  (1:4, v:v, 250 mL) in a Teflon bottle. The suspension was cooled to  $0^\circ\text{C}$  and (diethylamino) sulfur trifluoride (DAST) (0.2 mol) was slowly added under nitrogen. The clear brownish mixture was stirred for 10 min at  $0^\circ\text{C}$  followed by 1 h at room temperature. NaF (0.8–1.6 mol) was added and the suspension was stirred at room temperature overnight. The reaction was cooled to  $0^\circ\text{C}$  and TEA (20 mL) and methanol (60 mL) were added. After filtration and washing of the solid with methanol ( $3 \times 60$  mL), the filtrate was evaporated in vacuo, dissolved in DCM (200 mL), and extracted with water ( $2 \times 50$  mL). The organic phase was dried over  $\text{Na}_2\text{SO}_4$  and evaporated to give 3',5'-di-*O*-pixyl-2'-deoxy-2'-fluoro-D-uridine as a brownish oil ( $R_f$  0.66, DCM/MeOH 95/5). The crude compound (0.12 mol) was dissolved in a mixture of methanol and DCM (5:1, v:v, 1.2 L) and cooled to  $0^\circ\text{C}$ . 1 M HCl (150 mL) was added and the mixture was stirred for 30 min at room temperature. The solution was neutralized with aq. 1 M NaOH solution and evaporated in vacuo. The residue was dissolved in water (400 mL) and extracted with DCM ( $3 \times 200$  mL). The aqueous layer was evaporated to dryness, and coevaporated with methanol ( $2 \times 50$  mL). The residue was dissolved in methanol (150 mL), and the precipitate (NaCl) was removed by filtration and washed with methanol ( $2 \times 150$  mL). After evaporation to dryness 2'-deoxy-2'-fluoro-D-uridine ( $R_f$  0.10, DCM/MeOH 9/1) was yielded. The crude uridine analogue (60 mmol) was coevaporated with dry pyridine ( $3 \times 50$  mL) and dissolved in dry pyridine (125 mL). DMAP (30 mmol) was added and DMTCI was added in portions ( $3 \times 66$  mmol). After 2 days at room temperature, methanol (20 mL) was added and the mixture was stirred for 30 min. The solvent was evaporated and the residue was dissolved in DCM (300 mL) and washed with 5% aq.  $\text{NaHCO}_3$  solution ( $3 \times 100$  mL). The organic layer was dried over  $\text{Na}_2\text{SO}_4$  and evaporated. Silica gel chromatography using a gradient of 0 to 3% of MeOH in DCM containing 2% TEA gave **3** as a brownish foam (overall yield 20–30%,  $R_f$  0.38, DCM/MeOH 95/5).

*3'-Acetyl-2'-deoxy-2'-fluoro-D-uridine 4.* The nucleoside **4** was prepared according to a published procedure by 3'-acylation and 5'-detritylation of **3** in 81% overall yield (22).

*2'-Deoxy-2'-fluoro-D-uridine 5'-triphosphate 5.* The protected nucleoside **4** (158 mg, 550  $\mu\text{mol}$ ) was dried in vacuo overnight and dissolved in a mixture of anhydrous pyridine (550  $\mu\text{L}$ ) and dioxane (1650  $\mu\text{L}$ ) under argon. A freshly prepared 1 M solution of 2-chloro-4H-1,2,3-dioxaphosphorin-4-one (167 mg, 825  $\mu\text{mol}$ ) in anhydrous dioxane (825  $\mu\text{L}$ ) was injected into the well-stirred solution. After 20 min at room temperature, a solution of 0.5 M tri-*n*-butylammonium pyrophosphate (439 mg, 963  $\mu\text{mol}$ ) in anhydrous DMF (1926  $\mu\text{L}$ ) and tri-*n*-butylamine (550  $\mu\text{L}$ ) was added to the reaction mixture. After 20 min, a solution of 1% iodine in pyridine/water (22 mL, 98:2, v:v) was added. After stirring of the sample for 20 min, excess iodine was quenched by adding a 5% aq.  $\text{NaHSO}_3$  solution (2 mL) and the reaction solution was evaporated to dryness. After treatment with concentrated ammonia (10 mL), the product was purified using a Sephadex DEAE A-25 column with a linear gradient of 0.05 to 1 M LiCl (triphosphate eluted at  $\sim 0.7$  M LiCl). This purification was followed by reversed phase HPLC on a 15RPC column (100  $\times$  26 mm, Amersham Biosciences, buffer A: 100 mM TEAAc, pH 7; buffer B: 100 mM TEAAc, pH 7, 95% acetonitrile; gradient:  $t = 0$ –8 min 1% B,  $t = 8$ –55 min 1%  $\rightarrow$  50% B). The product containing fractions were lyophilized and transformed into lithium salt for NMR recording. Triphosphate **5** was obtained in 49% yield.  $^1\text{H}$ -NMR ( $\text{D}_2\text{O}$ , 300 MHz): 7.97 (1 H, d, H-6), 6.10 (1 H, d, H-1'), 5.96 (1 H, d, H-5), 5.20 (1 H, d, H-2'), 4.64–4.29 (4 H, m, H-3', H-4', H-5', H-5'').  $^{31}\text{P}$ -NMR ( $\text{D}_2\text{O}$ , 122 MHz):  $-4.53$  (d,  $\gamma\text{P}$ ),  $-10.27$  (d,  $\alpha\text{P}$ ),  $-19.90$  (t,  $\beta\text{P}$ ).  $^{19}\text{F}$ -NMR ( $\text{D}_2\text{O}$ , 284 MHz):  $-203.41$  (ddd). MALDI-MS: calcd for  $\text{C}_9\text{H}_{13}\text{FN}_2\text{O}_{14}\text{P}_3$  (M–H) $^-$ : 485.1, found: 483.1. RP HPLC:  $t_R = 8.6$  min.

*5-Aminoallyl-2'-deoxy-2'-fluoro-D-uridine 5'-triphosphate 7.* The nucleotide **5** (11 mg, 22  $\mu\text{mol}$ ) and mercuric acetate (38 mg, 119  $\mu\text{mol}$ ) were dissolved in 0.1 M sodium acetate buffer (2.1 mL, pH 6) and the solution was stirred for 4 h at  $50^\circ\text{C}$ . LiCl (9 mg, 220  $\mu\text{mol}$ ) was added, and the solution was extracted with EtOAc ( $7 \times 3$  mL) and DCM ( $1 \times 3$  mL). The aqueous layer was cooled to  $4^\circ\text{C}$  and ice-cold ethanol (30 mL) was added. After 30 min at  $-18^\circ\text{C}$ , the precipitate was collected by centrifugation for 30 min. The pellet was suspended in 10 mL of ethanol and the centrifugation was repeated to give nucleotide **6**, which was used without further purification in the next step.

A total of 165  $\mu\text{L}$  of allylamine solution prepared by neutralizing allylamine (1.5 mL) with ice-cold 4 M acetic acid (8.5 mL) was added to a 20 mM solution of compound **6** (22  $\mu\text{mol}$ ) in 0.1 M sodium acetate (1.1 mL, pH 5). After addition of  $\text{K}_2\text{PdCl}_4$  catalyst (7 mg, 22  $\mu\text{mol}$ ) in 220  $\mu\text{L}$  of water, the mixture was stirred at room temperature for 1 day. The precipitate was removed by filtration through a 0.8  $\mu\text{m}$  membrane filter (Nalge International). The product was purified using a Sephadex DEAE A-25 column with a linear gradient of 0.05 to 1 M LiCl (triphosphates eluted at  $\sim 0.6$  M LiCl). The purification was followed by reversed phase HPLC on a 15RPC column (100  $\times$  26 mm, Amersham Biosciences, buffer A: 100 mM TEAAc, pH 7; buffer B: 100 mM TEAAc, pH 7, 95% acetonitrile; gradient:  $t = 0$ –8 min 1% B,  $t = 8$ –55 min 1%  $\rightarrow$  50% B). The product containing fractions were lyophilized and transformed into lithium salt for NMR recording. The triphosphate **7** was obtained in 29% yield.  $^1\text{H}$ -NMR ( $\text{D}_2\text{O}$ , 300 MHz): 8.17 (1 H, s, H-6), 6.60 (1 H,



**Figure 1.** (A) Synthesis of nucleotide 7: (i) cyanamide, MeOH; (ii) methylpropiolate, EtOH aq; (iii) PxCl, Pyr; (iv) 1 M NaOH, MeOH; (v) DAST, NaF, DMF, ACN; (vi) 1 M HCl, MeOH; (vii) DMTCl, DMAP, Pyr; (viii) acetic anhydride, DMAP, Pyr; (ix) acetic acid; (x) 2-chloro-4H-1,2,3-dioxaphosphorin-4-one, dioxane, rt, 15 min, tri-*n*-butylammonium pyrophosphate, tributyl-amine, DMF, rt, 20 min; (xi) mercuric acetate, 0.1 M sodium acetate buffer (pH 6.0), 50 °C, 4 h; (xii) allylamine, K<sub>2</sub>PdCl<sub>4</sub>, 0.1 M sodium acetate buffer (pH 5), rt, 22 h; (B) Commercially available aminomodified NTPs used: 5-AA-UTP **8** and N<sup>6</sup>-[(6-aminohexyl)-carbamoylmethyl]-ATP **9**.

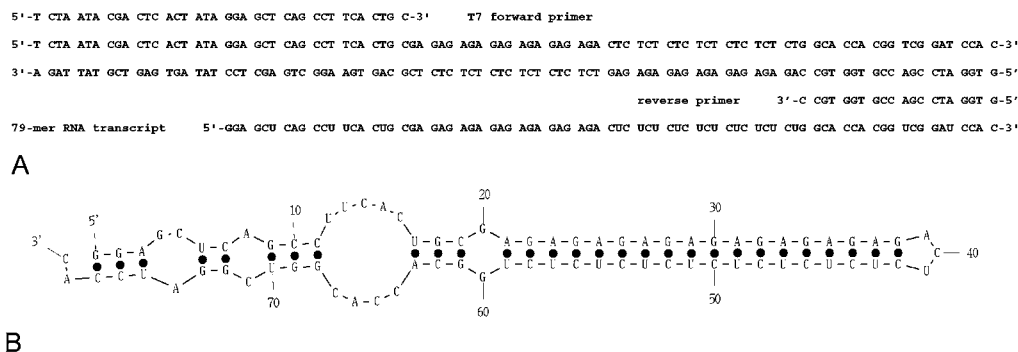
d, CH), 6.48 (1 H, dt, CH), 6.19 (1 H, d, H-1'), 5.17 (1 H, dd, H-2'), 4.75–4.33 (4 H, m, H-3', H-4', H-5', H-5''), 3.74 (2 H, d, CH<sub>2</sub>). <sup>31</sup>P-NMR (D<sub>2</sub>O, 122 MHz): −5.08 (d, γP), −10.29 (d, αP), −20.38 (t, βP). <sup>19</sup>F-NMR (D<sub>2</sub>O, 284 MHz): −203.54 (ddd). MALDI-MS: calcd for C<sub>12</sub>H<sub>18</sub>FN<sub>3</sub>O<sub>14</sub>P<sub>3</sub> [M−H]<sup>−</sup>: 540.2, found: 539.8. reversed phase HPLC: *t*<sub>R</sub> = 9.4 min.

**Base Composition of RNA Transcripts.** 0.1 OD<sub>260</sub> of RNA transcript were incubated at 37 °C in 55 μL of buffer containing 90 mM Tris-HCl (pH 7.5), 110 mM NaCl, and 15 mM MgCl<sub>2</sub> with 1.6 U alkaline phosphatase and 0.2 U snake venom phosphodiesterase for 16 h to achieve complete degradation. After precipitation with 2.5 vol of ethanol in the presence of 0.3 M sodium acetate, the pellet was discarded, the supernatant was vacuum-dried, the residue was dissolved in 120 μL of H<sub>2</sub>O and subjected to reversed phase HPLC analysis.

**In Vitro Transcription of RNA.** 17-mer/79-mer RNA transcripts were in vitro transcribed from chemically synthesized 36/98 base-pair dsDNA templates consisting of a minimal T7 promoter (positions −1 to −19) followed by the sequence of the transcript itself (positions 1–17/1–79). The 36-base-pair dsDNA T7 template for the sense 17-mer was annealed from the ssDNA molecules 5'-TCT AAT ACG ACT CAC TAT AGG ACT GAC TGA CTG ACC-3' and 5'-G<sub>OMe</sub>G<sub>OMe</sub>T CAG TCA GTC AGT CCT ATA GTG AGT CGT ATT AGA-3'. The corresponding template to generate the antisense 17-mer transcript was annealed from the ssDNA molecules 5'-TCT AAT ACG ACT CAC TAT AGG TCA GTC AGT CAG TCC-3' and 5'-G<sub>OMe</sub>G<sub>OMe</sub>A CTG ACT GAC TGA CCT ATA GTG AGT CGT ATT AGA-3'. The dsDNA template (Figure 2) to transcribe the

79-mer transcript was annealed from the ssDNA molecules 5'-TCT AAT ACG ACT CAC TAT AGG AGC TCA GCC TTC ACT GCG AGA GAG AGA GAG AGA GAG ACT CTC TCT CTC TCT CTC TCT GGC ACC ACG GTC GGA TCC AC-3' and 5'-GTG GAT CCG ACC GTG GTG CCA GAG AGA GAG AGA GAG AGA GTC TCT CTC TCT CTC TCT CTC GCA GTG AAG GCT GAG CTC CTA TAG TGA GTC GTA TTA GA-3'. All ssDNA molecules were annealed to dsDNA in 10 mM Tris-HCl, pH 8.

Typical 100 μL T7 transcription reactions with 2'-fluoro-2'-deoxypyrimidine triphosphates contained 0.5 μM template DNA, 1 mM of each NTP, 10 mM DTT, 150 U of T7 RNA/DNA polymerase (Epicentre), 10 U RNase-Out ribonuclease inhibitor (Invitrogen), 0.1 U inorganic pyrophosphatase (Sigma) in 1× Epicentre reaction buffer (40 mM Tris-HCl, pH 7.5, 6 mM MgCl<sub>2</sub>, 10 mM NaCl, 2 mM spermidine) supplemented with MgCl<sub>2</sub> to a final concentration of 12 mM. Typical 100 μL transcription reactions with all other modified NTPs contained 0.5 μM template DNA, 4 mM of each NTP, 10 mM DTT, 100 U of T7 RNA polymerase (Stratagene), 10 U RNaseOut ribonuclease inhibitor (Invitrogen), 0.1 U inorganic pyrophosphatase (Sigma) in standard T7 reaction buffer (80 mM HEPES-KOH, pH 7.5, 22 mM MgCl<sub>2</sub>, 1 mM spermidine). For radioactive body-labeling and subsequent quantification of transcript amounts on a Biorad FX Phosphorimager, 180,000–720,000 Bq [α-<sup>32</sup>P]GTP were added. Reactions were incubated for 14–16 h at 37 °C and treated with ~30 U DNaseI per 100 μL for 10 min at 37 °C to degrade dsDNA template. Full-length transcripts were purified on 7 M urea, 10–20% polyacrylamide gels. Bands were visualized by 254 nm UV-



**Figure 2.** (A) 98-mer dsDNA template for the 79-mer RNA test molecule with T7 forward and reverse primers. (B) Mfold (27) secondary structure prediction for the 79-mer RNA transcript.

shadowing on ALUGRAM SIL G/UV254 sheets (Macherey & Nagel), excised, and eluted with 30 mM sodium acetate, pH 5.5. Eluates were vacuum-concentrated to 10% of the initial volume and precipitated with 2.5 vol of an ethanol/2-propanol mixture (1:1, v:v) in the presence of 200  $\mu$ g/mL Glycogen (Roche). RNA pellets were dissolved in water and quantified UV-spectroscopically.

**Reverse Transcription and PCR.** A total of 5 pmol of 79-mer RNA was reverse transcribed at a concentration of 250 nM in the presence of 5  $\mu$ M reverse primer (5'-GTG GAT CCG ACC GTG GTG CC-3'), 500  $\mu$ M dNTPs, 10 mM DTT, 0.5 M betaine and 200 U Superscript II reverse transcriptase (Stratagene) in 1 $\times$  first strand buffer (50 mM Tris-HCl pH 8.3, 75 mM KCl, 3 mM MgCl<sub>2</sub>). Reactions were incubated for 20 min at 51 °C, diluted 1:4 (v:v) in PCR buffer (20 mM Tris-HCl pH 8.4, 50 mM KCl, 2.5 mM MgCl<sub>2</sub>) containing 1  $\mu$ M T7-forward primer 5'-TCT AAT ACG ACT CAC TAT AGG AGC TCA GCC TTC ACT GC-3', 1  $\mu$ M reverse primer (see above), 200  $\mu$ M dNTPs, 0.5 M betaine, and 5 U Taq polymerase. Ten steps of temperature cycling between 55, 72, and 94 °C were performed in a PTC-200 thermocycler (MJ research).

**DNA Sequencing.** PCR reactions were TA-cloned and sequenced by Sanger methods at GATC-Biotech, Konstanz, Germany.

**Melting Curves.** Melting curves were measured on a CARY 100 Bio instrument in 10 mM sodium phosphate buffer pH 7.0 and 100 mM NaCl. 0.7 OD<sub>260</sub> of the corresponding sense and antisense 17-mers were separately dissolved in buffer to 5  $\mu$ M concentration. Equal volumes were transferred into a new cuvette and heated to 95 °C. OD<sub>260</sub> values were recorded every 0.1 °C as the temperature was decreased to 15 °C at a rate of 0.3 °C per min, held for 5 min without recording data points, and increased again to 95 °C. This procedure was performed twice. As negative controls, melting curves for each of the 17-mers alone were recorded. Four *T<sub>m</sub>* values were calculated for each measuring cycle and averaged. Differences in the melting temperatures of modified duplex molecules compared to unmodified molecules were calculated by subtracting *T<sub>m</sub>* values of the latter from those of the former and dividing the result by the number of modified bases present in the duplex molecule.

## RESULTS AND DISCUSSION

**Design and Synthesis of Aminomodified Nucleotides.** By introducing the functional group in the nucleoside triphosphate, we expect improved affinity of such modified RNA toward certain targets. Assuming a *pK<sub>a</sub>* value between 9 and 10, the amino groups of the modified nucleoside triphosphates are expected to be protonated at neutral pH. As a consequence, the interaction between

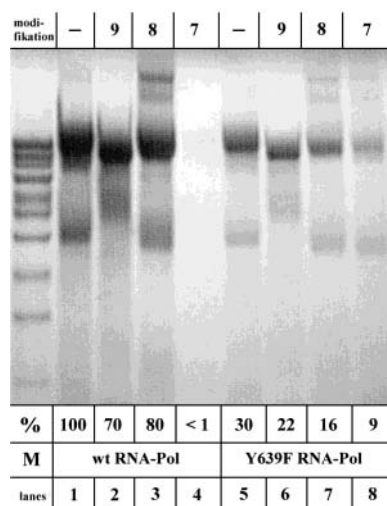
the aminomodified RNA and acidic targets should be increased. The allyl-modification at the C5-position was chosen as various modified nucleotides have proven themselves as tolerated substrates for DNA and RNA polymerases. For the synthesis of the aminomodified uridine analogue **7** the starting material D-arabinose **1** was converted to 2,2'-*O*-anhydro-D-uridine **2** according to a published procedure (23). After protection of the hydroxyl-groups with pixyl chloride and ring opening with 2 M NaOH, the crude product was fluorinated using DAST (24). To increase the concentration of fluoride, NaF was added in large excess. After treatment with 1 M HCl and neutralization, the 5'-OH group was tritylated to give nucleoside **3**. The 5'-DMT protected 2'-fluoro nucleoside **3** was obtained in five steps from 2,2'-*O*-anhydro-D-uridine **2** at 30–50 g scale without purification of the intermediates and in 20–30% overall yield.

After protection of the 3'-OH group by acetylation and subsequent detritylation under acidic conditions, nucleoside triphosphate **5** was obtained in 49% yield according to the method of Ludwig and Eckstein (25). Transformation of **5** into the mercurated uridine analogue **6** was achieved using mercury acetate. Analytical C<sub>18</sub>-HPLC showed an almost quantitative formation of **6**. Finally, 5-aminoallyl 2'-F-dUTP **7** was prepared according to the Heck reaction (26) by treating the uridine derivative **6** with allylamine in the presence of a palladium(II) catalyst. After preparative ion-exchange HPLC followed by C<sub>18</sub>-HPLC nucleotide **7** was obtained in 29% yield starting from **5**. Formation of triphosphates **5** and **7** was confirmed by <sup>1</sup>H-, <sup>19</sup>F-, <sup>31</sup>P-NMR and MALDI-MS. The UV spectrum of **7** shows a shift of  $\lambda_{\text{max}}$  from 260 nm in uridine analogue **5** to 289 nm indicating the presence of an exocyclic double bond.

**Feasibility of Modified Nucleobases for SELEX.** To be feasible for RNA SELEX, modified nucleotides have to meet certain criteria: First of all, the corresponding modified nucleoside triphosphates must be accepted as a substrate by RNA polymerases. To ensure primary sequence continuity, the modified nucleotides must form strict Watson-Crick base-pairs. In reverse transcription, modified RNA molecules must be efficient templates that do not inhibit the activity of the reverse transcriptase and finally the synthesis procedures for the corresponding triphosphates should be reasonably facile.

Feasibility tests were performed with one single transcript of a defined sequence that was originally designed to test the ability of T7 RNA polymerases to transcribe hairpin structures. This 79-mer, shown in Figure 2, is a derivative of an RNA pool frequently used at NOXXON. The original N<sub>40</sub> random region has been changed to an iteration of 10 GA purine duplets followed by 10 CU pyrimidine duplets, which presumably fold into an 18





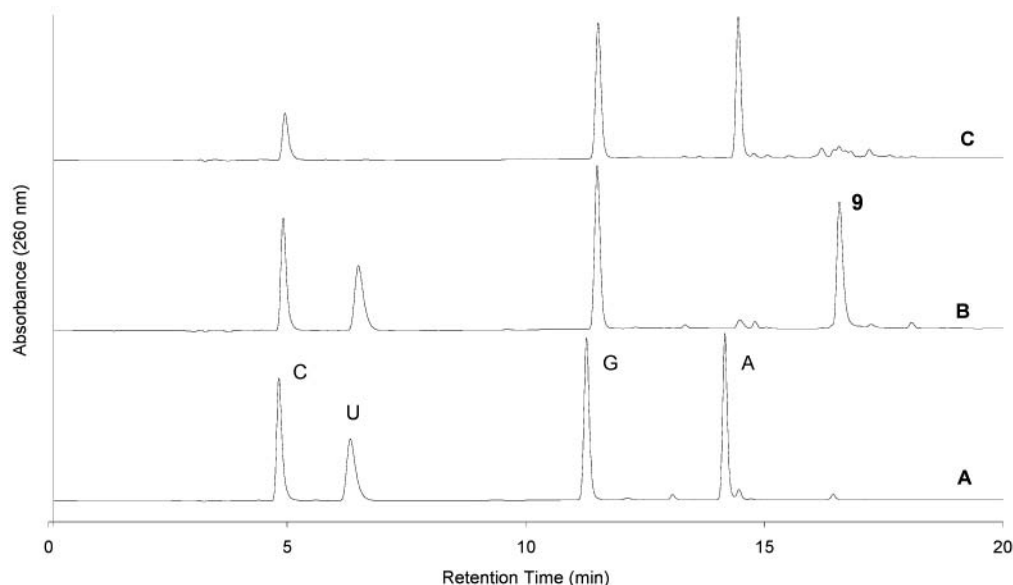
**Figure 3.** 79-mer RNA transcript modified with **7**, **8**, and **9**. Lane 1: reference transcript with unmodified nucleotides. Lane 2–4: transcripts generated with wt RNA-Pol. Lane 5–8: transcripts generated with Y639F RNA-Pol (relative yield in % to the reference). ssDNA-Marker (M) is ranging from 20 to 110 bases, 10% PAGE.

base-pair stem structure. RNA transcripts were generated from a dsDNA template, annealed from two ssDNA 98-mers, encoding the 79-mer and driven by a minimal T7 promoter. The unmodified and three differently aminomodified RNAs were transcribed using wt T7 RNA polymerase and the Y639F mutant thereof, respectively. The commercially available Y639F mutant (28) efficiently utilizes 2'-modified nucleoside triphosphates. Figure 3 shows the varying yields for the modified transcripts generated with the two different enzymes. Relative yields of radioactively body-labeled transcripts with amino-modified nucleotides compared to unmodified NTPs were visualized by 254 nm UV-shadowing and quantified on a phosphorimager. Yields obtained from wt RNA polymerase, containing **8** and **9**, are within the same range and comparable to unmodified reference transcript, whereas hardly any transcript can be detected with **7**, since the enzyme does not tolerate the 2'-F-modification. The transcription yield of mutant Y639F polymerase is

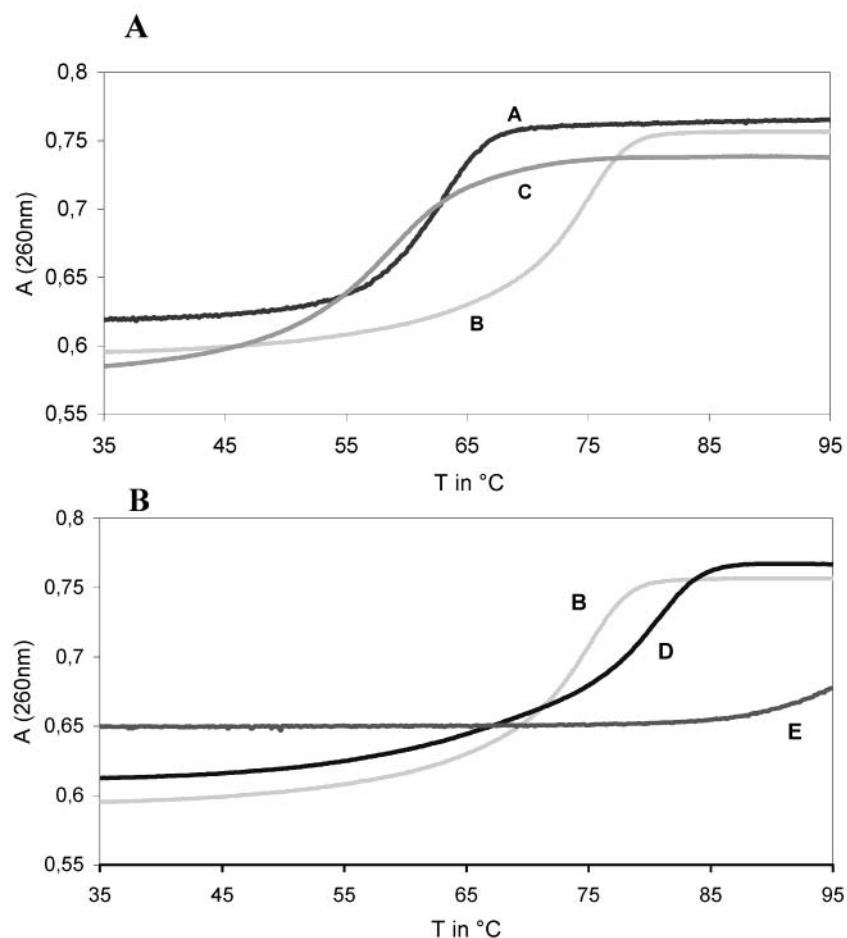
generally reduced to approximately one-third, and again the yields of transcripts containing unmodified NTPs, **8** or **9**, are within comparable ranges. With Y639F polymerase being able to tolerate 2'-modified NTPs as substrates, the transcript containing **7** is obtained at about 10% yield compared to the reference. Depending on the modification, transcripts show slightly different migration behavior in denaturing PAGE and in general appear to be larger than the corresponding band of the ssDNA marker. Byproducts that migrate above and below the intended transcript are regularly observed, but have not been investigated further.

**Base Composition.** Base composition analyses were performed to provide the first direct evidence that modified nucleotides triphosphates have been accepted and incorporated by T7 RNA polymerases. The modified 79-mer transcripts were digested with a combination of snake venom phosphodiesterase and alkaline phosphatase. The degradation products were analyzed by C18 reversed phase HPLC. Figure 4B shows the base composition of the transcript containing exocyclic-modified purine **9**. Compared to the peak of adenosine, the peak for the *N*<sup>6</sup>-derived purine nucleoside is clearly shifted to a higher retention time. Base compositions of transcripts containing the uridine analogues **7** and **8** completely lacked the peak of the corresponding uridine nucleoside (Figure 4C). These data suggest that the uridine analogues **7** and **8** were not incorporated into the transcripts. However, full-length transcripts were clearly visualized in polyacrylamide gels (Figure 3) and MALDI-TOF analyses of modified 17-mers were unambiguous (see below). The most likely explanation is that transcripts containing uridine analogues **7** or **8** cannot be completely degraded by snake venom phosphodiesterase.

Three enzymatic reactions, RNA transcription, reverse transcription, and PCR, are combined in the cyclic SELEX process. Misincorporations that occur during T7 transcription or reverse transcription cannot be monitored individually for each of the three reactions. Arising mutations cannot be observed unless the PCR product derived from the reverse transcript is sequenced. Potential mutations could arise from either T7 or reverse transcription. In both cases, the modified nucleotide may not be suitable for SELEX. To evaluate whether elevated



**Figure 4.** HPLC analysis of 79-mer RNA transcripts after nuclease digestion. (A) Unmodified RNA transcript as reference. (B) RNA transcript using modified ATP **9**. (C) RNA transcript using uridine analogue **8**.



**Figure 5.** UV melting curves of DNA (A), RNA (B), RNA containing **9** (C) in A and RNA containing 2'-F-dU (D) and **7** (E) in B.

**Table 1.** Mutational Analysis of the 79-mer Transcripts Modified with the Uridine Analogues **7**, **8** and Modified ATP **9**

79-mer RNA transcripts	unmodified	<b>7</b>	<b>8</b>	<b>9</b>	
generated with wtT7 RNA-Pol	7		3	7	sequenced molecules
	553		237	553	sequenced bases
	8		13	15	number of mutations
	1.4		5.5	2.7	percentage of mutations
generated with Y639F mutant Of T7 RNA-Pol	—	8	7	7	sequenced molecules
	—	632	553	553	sequenced bases
	—	8	15	11	number of mutations
	—	1.3	2.7	2.0	percentage of mutations

mutation rates occurred, the different transcripts were reverse transcribed, amplified by PCR, cloned, and sequenced. Furthermore, to rule out that random NTPs were utilized in place of aminommodified NTPs, T7 transcription reactions with incomplete NTP mixes, i.e., in the absence of any one of the four NTPs, were performed. The yields of these depleted transcription reactions were reduced by roughly 3 orders of magnitude and below the detection level of UV-shadowing (data not shown). As a control, the background level of sequence alterations that were observed after one mock-round of SELEX with unmodified NTPs was determined. The resultant RNA was reverse transcribed to cDNA, amplified by PCR, and sequenced in one direction. Insertions, deletions, and base exchanges were defined as phenotypic mutations. Sequence alterations could be mutations occurring during the enzymatic reactions of a SELEX round or just sequencing artifacts.

Although the number of molecules that was sequenced for each modification (see Table 1) was too low for statistics, we conclude that a maximum of a 4-fold

mutation rate in the case of **8**, a 2-fold rate for **9**, and a nearly identical rate for **7** compared to the background mutation rate observed for unmodified NTPs is tolerable, if not favorable for the SELEX procedure. In fact, modest mutation rates, achievable by error-prone PCR protocols (29, 30), are useful to extend the sequence space, that can be covered with SELEX (31).

**Melting Behavior of Nucleic Acids Containing Aminommodified Bases.** Melting temperatures were measured with two complementary single-stranded molecules, each 17 nucleotides in length, 5'-GGA CUG ACU GAC UGA CC-3' and 5'-GGU CAG UCA GUC AGU CC-3'. 17-mers were chosen, since under standard conditions at 100 mM NaCl, the complete transition would occur within a temperature range between 15 and 95 °C. Poly-GACU and poly-GUCA sequences were chosen as they do not form any stable intramolecular interactions according to the structure prediction program Mfold (27). Two additional guanines at the 5'-end of the 17-mers were introduced to initiate T7 transcription efficiently. According to the addition of two guanosine residues, two

**Table 2. Summary of the Melting Temperatures of Different 17-mer DNA and RNA Molecules Modified with Uridine Analogues 7, 8 and Modified ATP 9<sup>a</sup>**

	duplex sequence	modification	$T_m$ (°C)	$\Delta T_m$ (°C)	$\Delta T_m$ (°C) per modified base
A	5'-d(GGA CTG ACT GAC TGA CC)-3' 3'-d(CCT GAC TGA CTG ACT GG)-5'	DNA	63.0	-12.0	-
B	5'-GGA CUG ACU GAC UGA CC-3' 3'-CCU GAC UGA CUG ACU GG-5'	RNA	75.0	-	-
C	5'-GGA CUG <u>ACU</u> <u>GAC</u> UGA CC-3' 3'-CCU <u>GAC</u> <u>UGA</u> CUG <u>ACU</u> GG-5'	<b>9</b>	57.7	-17.3	-2.47
D	5'-GGA CUG ACU GAC <u>UGA</u> CC-3' 3'-CCU GAC <u>UGA</u> CUG ACU GG-5'	2'-F	80.3	+5.3	+0.76
E	5'-GGA CUG ACU GAC <u>UGA</u> CC-3' 3'-CCU GAC <u>UGA</u> CUG ACU GG-5'	<b>7</b>	> 85	n/d	n/d
F	5'-GGA CUG ACU GAC <u>UGA</u> CC-3' 3'-CCU GAC <u>UGA</u> CUG ACU GG-5'	<b>8</b>	> 85	n/d	n/d

<sup>a</sup> Modified U and A bases are underlined and boldface.  $\Delta T_m$  (°C) is the difference in  $T_m$  (°C) to the unmodified RNA (B). (n/d = could not be determined).

cytidines were added to the 3'-end to achieve perfect duplex formation. DNA, RNA, and 2'-fluoro-2'-deoxyuridine modified RNA oligonucleotides were chemically synthesized. The 17-mers containing aminomodified nucleotides **7**, **8**, and **9** were generated by in vitro transcription. T7 RNA polymerase is known to cause end heterogeneity. This arises as a result of nonspecific addition of nucleotides to the 3'-end of transcripts that are not encoded by the complementary template strand. To reduce this effect, template strands were synthesized to contain two 2'-OMe-guanidines at the 5'-ends (32). The 17-mer transcripts were analyzed by MALDI-TOF and HPLC to verify both the successful incorporation of the modified nucleobases and the correct length of the transcripts (data not shown).

All UV spectra show the typical increase of absorbance at 260 nm due to thermally induced strand separation. The thermal melting point of duplex C containing the aminomodified adenosine nucleotide **9** was significantly decreased by 17.3 °C (2.47 °C per modified base) compared to unmodified RNA and decreases by 5.3 °C compared to DNA. The steric hindrance of the bulky *N*<sup>6</sup>-linker modification is likely to cause the decreased stability of the duplex. The duplexes E and F containing the modified nucleotides **7** and **8**, respectively, were significantly more stable ( $T_m$  > 85 °C) than the control duplexes D and B. For the double substituted uridine **7**, the increase of  $T_m$  is additive for the 2'-fluoro and the 5-aminoallyl substitution. The 2'-fluoro-modification confers a RNA-like 3'-endo sugar conformation to oligonucleotides. This type of the preorganization forming an A-form duplex structure improves binding affinity toward complementary RNA (33, 34). Additionally, the aminoallyl modification of the 5-position of the nucleobase leads to an increased stability of the duplex, which can be explained by improved stacking due to the double bond (35). The positively charged amino group at neutral pH seems to have a relatively marginal effect on the  $T_m$  since incorporation of an aminopropyl-modified uridine analogue into a short DNA hairpin showed similar UV melting temperatures to the sequences bearing a uridine or thymidine residue (36).

The modified nucleotides used in this analysis met the requirements of the SELEX process. The introduction of amino functions to nucleobases increases their  $pK_a$  values and thus should result in positive charges within the

RNA molecules under neutral conditions. Positive charges and the resulting zwitterionic molecules could facilitate the identification of oligonucleotides against acidic targets. Further experiments are ongoing to support this hypothesis.

#### ACKNOWLEDGMENT

We thank Kai Gottsche for HPLC analyses and MALDI mass spectrometry analyses, Michaela Leider for transcription reactions, Bernd Eschgaeller for thoughtful comments and providing detailed information on the synthesis of 5-aminoallyl-UTP, Petra Burgstaller for helpful discussions, and Michael Courtney for critical reading of the manuscript. This work was supported by the European Union (contract no. QLG1-CT-2000-00562).

#### LITERATURE CITED

- (1) Robertson, D. L., and Joyce, G. F. (1990) Selection in vitro of an RNA enzyme that specifically cleaves single-stranded DNA. *Nature* **344**, 467–468.
- (2) Ellington, A. D., and Szostak, J. W. (1990) In vitro selection of RNA molecules that bind specific ligands. *Nature* **346**, 818–822.
- (3) Tuerk, C., and Gold, L. (1990) Systematic evolution of ligands by exponential enrichment: RNA ligands to bacteriophage T4 DNA polymerase. *Science* **249**, 505–510.
- (4) Carmi, N., Shultz, L. A., and Breaker, R. R. (1996) In vitro selection of self-cleaving DNAs. *Chem Biol.* **3**, 1039–1046.
- (5) Bartel, D. P., and Szostak, J. W. (1993) Isolation of new ribozymes from a large pool of random sequences. *Science* **261**, 1411–1418.
- (6) Tarasow, T. M., Tarasow, S. L., and Eaton, B. E. (1997) RNA-catalysed carbon–carbon bond formation. *Nature* **389**, 54–57.
- (7) Zhang, B., and Cech, T. R. (1997) Peptide bond formation by in vitro selected ribozymes. *Nature* **390**, 96–100.
- (8) Unrau, P. J., and Bartel, D. P. (1998) RNA-catalysed nucleotide synthesis. *Nature* **395**, 260–263.
- (9) Lee, S. E., Sidorov, A., Gurlain, T., Mignet, N., Thorpe, S. J., Brazier, J. A., Dickman, M. J., Hornby, D. P., Grasby, J. A., and Williams, D. M. (2001) Enhancing the catalytic repertoire of nucleic acids: a systematic study of linker length and rigidity. *Nucleic Acids Res.* **29**, 1565–1573.
- (10) Latham, J. A., Johnson, R., and Toole, J. J. (1994) The application of a modified nucleotide in aptamer selection: novel thrombin aptamers containing 5-(1-pentynyl)-2'-deoxyuridine. *Nucleic Acids Res.* **22**, 2817–2822.



- (11) Sakthivel, K., and Barbas, C. F., 3rd (1998) Expanding the potential of DNA for binding and catalysis – highly functionalized dUTP derivatives that are substrates for thermostable DNA polymerases. *Angew. Chem., Int. Ed.* **37**, 2872–2875.
- (12) Gourelain, T., Sidorov, A., Mignet, N., Thorpe, S. J., Lee, S. E., Grasby, J. A., and Williams, D. M. (2001) Enhancing the catalytic repertoire of nucleic acids. II. Simultaneous incorporation of amino and imidazolyl functionalities by two modified triphosphates during PCR. *Nucleic Acids Res.* **29**, 1898–1905.
- (13) Perrin, D. M., Garestier, T., and Helene, C. (1999) Expanding the catalytic repertoire of nucleic acid catalysts: simultaneous incorporation of two modified deoxyribonucleoside triphosphates bearing ammonium and imidazolyl functionalities. *Nucleosides Nucleotides* **18**, 377–391.
- (14) Battersby, T. R., Ang, D. N., Burgstaller, P., Jurczyk, S. C., Bowser, M. T., Buchanan, D. D., Kennedy, R. T., and Benner, S. A. (1999) Quantitative analysis of receptors for adenosine nucleotides obtained via in vitro selection from a library incorporating a cationic nucleotide analogue. *J. Am. Chem. Soc.* **121**, 9781–9789.
- (15) Santoro, S. W., Joyce, G. F., Sakthivel, K., Gramatikova, S., and Barbas, C. F., 3rd. (2000) RNA cleavage by a DNA enzyme with extended chemical functionality. *J. Am. Chem. Soc.* **122**, 2433–2439.
- (16) Bittker, J. A., Phillips, K. J., and Liu, D. R. (2002) Recent advances in the in vitro evolution of nucleic acids. *Curr. Opin. Chem. Biol.* **6**, 367–374.
- (17) Vaish, N. K., Fraley, A. W., Szostak, J. W., and McLaughlin, L. W. (2000) Expanding the structural and functional diversity of RNA: analogue uridine triphosphates as candidates for in vitro selection of nucleic acids. *Nucleic Acids Res.* **28**, 3316–3322.
- (18) Dewey, T. M., Mundt, A. A., Crouch, G. J., Zyzanski, M. C., and Eaton, B. E. (1995) New uridine derivatives for systematic evolution of RNA ligands by exponential enrichment. *J. Am. Chem. Soc.* **117**, 8474–8475.
- (19) Ito, Y. (1997) Modified nucleic acids for in vitro selection. *Nucleic Acids Symp. Ser.* **37**, 259–260.
- (20) Ito, Y., Suzuki, A., Kawazoe, N., and Imanishi, Y. (2001) In vitro selection of RNA aptamers carrying multiple biotin groups in the side chains. *Bioconj. Chem.* **12**, 850–854.
- (21) Zinnen, S. P., Domenico, K., Wilson, M., Dickinson, B. A., Beaudry, A., Mokler, V., Daniher, A. T., Burgin, A., and Beigelman, L. (2002) Selection, design, and characterization of a new potentially therapeutic ribozyme. *RNA* **8**, 214–228.
- (22) Gait, M. (1990) *Oligonucleotide Synthesis: A Practical Approach*, IRL Press, Oxford.
- (23) Codington, J. F., Doerr, I. L., and Fox, J. J. (1964) Nucleoside XVIII. Synthesis of 2'-Fluorothymidine, 2'-Fluoro-2'-deoxyuridine and other 2'-halogeno-2'-deoxynucleoside. *J. Org. Chem.* **29**, 558.
- (24) Williams, D. M., Benseler, F., and Eckstein, F. (1991) Properties of 2'-fluorothymidine-containing oligonucleotides: interaction with restriction endonuclease EcoRV. *Biochemistry* **30**, 4001–4009.
- (25) Ludwig, J., and Eckstein, F. (1989) Rapid and efficient synthesis of nucleoside 5'-O-(1-thiotriphosphates), 5'-triphosphates and 2',3'-cyclophosphorothioates using 2-chloro-4H-1,3,2-benzodioxaphosphorin-4-one. *J. Org. Chem.* **54**, 631–635.
- (26) Reck, F. (1995) Synthesis of uridine-5-propylamine derivatives and their use in affinity chromatography of *N*-acetylglucosaminyltransferases I and II. *Carbohydr. Res.* **276**, 321–335.
- (27) Mathews, D. H., Sabina, J., Zuker, M., and Turner, D. H. (1999) Expanded sequence dependence of thermodynamic parameters improves prediction of RNA secondary structure. *J. Mol. Biol.* **288**, 911–940.
- (28) Sousa, R., and Padilla, R. (1995) A mutant T7 RNA polymerase as a DNA polymerase. *EMBO J.* **14**, 4609–4621.
- (29) Fromant, M., Blanquet, S., and Plateau, P. (1995) Direct random mutagenesis of gene-sized DNA fragments using polymerase chain reaction. *Anal. Biochem.* **224**, 347–353.
- (30) Spee, J. H., de Vos, W. M., and Kuipers, O. P. (1993) Efficient random mutagenesis method with adjustable mutation frequency by use of PCR and dTTP. *Nucleic Acids Res.* **21**, 777–778.
- (31) Bittker, J. A., Le, B. V., and Liu, D. R. (2002) Nucleic acid evolution and minimization by nonhomologous random recombination. *Nat. Biotechnol.* **20**, 1024–1029.
- (32) Kao, C., Zheng, M., and Rudisser, S. (1999) A simple and efficient method to reduce nontemplated nucleotide addition at the 3'-terminus of RNAs transcribed by T7 RNA polymerase. *RNA* **5**, 1268–1272.
- (33) Cummins, L. L., Owens, S. R., Risen, L. M., Lesnik, E. A., Freier, S. M., McGee, D., Guinosso, C. J., and Cook, P. D. (1995) Characterization of fully 2'-modified oligoribonucleotide hetero- and homoduplex hybridization and nuclease sensitivity. *Nucleic Acids Res.* **23**, 2019–2024.
- (34) Sabahi, A., Guidry, J., Inamati, G. B., Manoharan, M., and Wittung-Stafshede, P. (2001) Hybridization of 2'-ribose modified mixed-sequence oligonucleotides: thermodynamic and kinetic studies. *Nucleic Acids Res.* **29**, 2163–2170.
- (35) Freier, S. M., and Altmann, K. H. (1997) The ups and downs of nucleic acid duplex stability: structure–stability studies on chemically modified DNA: RNA duplexes. *Nucleic Acids Res.* **25**, 4429–4443.
- (36) Soto, A. M., Kanika, B. I., Dande, P., Gold, B., and Marky, L. A. (2001) Incorporation of a cationic aminopropyl chain in DNA hairpins: thermodynamics and hydration. *Nucleic Acids Res.* **29**, 3638–3645.

BC0256547

# Conditionally Cleavable Radioimmunoconjugates: A Novel Approach for the Release of Radioisotopes from Radioimmunoconjugates

Craig Beeson,<sup>‡,⊥</sup> James E. Butrynski,<sup>†</sup> Michael J. Hart,<sup>‡</sup> Cynthia Nourigat,<sup>†</sup> Dana C. Matthews,<sup>†,§</sup> Oliver W. Press,<sup>†</sup> Peter D. Senter,<sup>‡</sup> and Irwin D. Bernstein<sup>\*,†,§</sup>

Clinical Research Division, Fred Hutchinson Cancer Research Center, Seattle, Washington 98109, Departments of Chemistry and Pediatrics, University of Washington, Seattle, Washington 98195, and Seattle Genetics, 21823 30th Dr. SE, Bothell, Washington 98021. Received December 14, 2002; Revised Manuscript Received July 1, 2003

One of the limitations of therapy with radiolabeled monoclonal antibodies (mAbs) is that significant toxicities can arise from circulating non-tumor-bound radiolabeled conjugate. Here, we describe a new method to reduce systemic radiation exposure from radiolabeled mAbs involving the attachment of the radioisotope through a linker that can be cleaved by an administered enzyme. To demonstrate the feasibility of this approach, we prepared a conditionally cleavable radioimmunoconjugate (RIC) composed of <sup>131</sup>I-labeled cephalosporin conjugated to Tositumomab, a mAb against the CD20 antigen. The cleavable RIC bound antigen identically to directly iodinated antibody, and in the presence of  $\beta$ -lactamase, about 80–85% of the radioisotope was released. In vivo studies in mice revealed that the cleavable RIC and the directly iodinated anti-CD20 antibody had similar biodistribution patterns. Systemically administered  $\beta$ -lactamase induced a 2–3-fold decrease in the percent injected dose (ID) of the cleavable RIC/g of blood, marrow, spleen, lung, and liver 1 h after enzyme treatment, and a 4–6-fold decrease 20 h after enzyme treatment. This was accompanied by a 20-fold increase in % ID/g in urine 1 h after enzyme treatment, indicating that the released radiolabel was rapidly excreted through the kidneys. In mice with human tumor xenografts, there was no decrease in the %ID/g in tumor 1 h after enzyme treatment, but by 4 h after enzyme injection, decreases in tumor radioactive content began to diminish the targeting advantage. These studies demonstrate that the cleavable RIC substrate is able to bind to tumor antigens and localize within human tumor xenografts and that accelerated systemic clearance can be induced with  $\beta$ -lactamase.

## INTRODUCTION

Several studies have demonstrated that radioimmunotherapy (RIT) using radiolabeled monoclonal antibodies can lead to dose-limiting toxicities through radiation exposure to normal organs. To minimize toxicity, a number of approaches have been devised to clear radiolabeled material from the systemic circulation. The most widely investigated method is commonly referred to as “pretargeting”, which involves the infusion of nonradioactive mAb conjugated with a tag that can be recognized by a radiolabeled binding partner. Biotin is the most commonly used tag, and it is recognized by radiolabeled avidin or streptavidin (1, 2). Alternatively, mAb–streptavidin conjugates can be targeted, which are then recognized by subsequently administered radiolabeled biotin-

containing compounds (3, 4). Although these approaches have yielded substantially improved tumor to normal tissue ratios of delivered radiation compared to conventional RIT, issues have arisen due to treatment complexity, endogenous biotin, immunogenicity of avidin and streptavidin, and the prolonged time that the mAb conjugate must be retained on the tumor cell surface before the radiolabel is administered.

An alternative approach for minimizing normal tissue radiation exposure involves plasmapheresis and extracorporeal immunoadsorption (ECIA). Using this method, blood is circulated ex vivo through a matrix that is capable of sequestering the radiolabeled agent and is then reinfused back into the body. Pharmacokinetic modeling studies have suggested a potential therapeutic advantage for this approach, particularly if high antibody doses and an isotope with a relatively long half-life such as <sup>131</sup>I is used (5–7). Experimentally, it has been demonstrated that the ECIA procedure removed much of the blood radioactivity due to radiolabeled mAb, and that many organs were spared from radiation exposure (8). However, ECIA is a technically difficult procedure and entails significant radiation safety risks for technicians performing the procedure. A related method for removal of circulating radiolabeled mAbs that bypasses the need for ECIA involves the formation of immune complexes with a second-step clearing mAb (5, 8–11). While some success for this approach has been reported in preclinical

\* To whom correspondence should be addressed. Fred Hutchinson Cancer Research Center, 1100 Fairview Ave. North, P.O. Box 19024, D2-373, Seattle, WA 98109. Telephone: 206-667-4886. Fax: 206-667-6084. E-mail: ibernste@fhcrc.org.

<sup>†</sup> Fred Hutchinson Cancer Research Center.

<sup>‡</sup> Department of Chemistry, University of Washington.

<sup>§</sup> Department of Pediatrics, University of Washington.

<sup>⊥</sup> Seattle Genetics.

<sup>⊥</sup> Current address: Department of Pharmaceutical Sciences, Medical University of South Carolina, Charleston, SC 29425.

<sup>1</sup> Abbreviations: ADEPT, antibody-directed enzyme prodrug therapy; ID, injected dose; ECIA, extracorporeal immunoadsorption; mAb, monoclonal antibody; RIC, radioimmunoconjugate; RIT, radioimmunotherapy; SPE, solid-phase extraction.

models, immune complexes may pose significant clinical risks including induction of nephropathies or arthropathies.

An alternative method for reducing normal organ radiation exposure from RIT has been reported, and it involves the use of linkers between the mAb carrier and the drug that can be hydrolyzed by endogenous enzymes in the liver. The rationale for this approach is that the liver, being the major organ for mAb and RIT clearance pathways, would be spared considerable radiation damage by rapid cleavage of the isotope off the mAb. This has been demonstrated using a linker that was hydrolyzed by cathepsin D, an abundant liver enzyme (12–15). The beneficial effects of this radioisotope linkage strategy were mainly restricted to the liver. We wished to extend this methodology by developing radioisotope linkers that could be cleaved in a controlled manner in the blood and in any well-perfused organs. Here, we describe the synthesis of a cephalosporin-containing linker for the attachment of radioisotopes to mAbs. The approach was designed so that the radiolabel would rapidly be released from the mAb upon the systemic administration of  $\beta$ -lactamase, where it would then be rapidly excreted through the kidneys. We also report the in vitro and in vivo properties of the first such radioimmunoconjugate.

#### MATERIALS AND METHODS

**General.** The human Ramos B lymphoma cell line (American Type Culture Collection, Bethesda, MD) was maintained in log-phase growth in RPMI media supplemented with 10% heat-inactivated bovine calf serum in a 5% CO<sub>2</sub> incubator. NOD/SCID mice were bred at the Fred Hutchinson Cancer Research Center. The anti-CD20 murine mAb Tositumomab (IgG2a) was a gift of Coulter Corporation. The G3G6 antibody, a murine IgG2a isotype control mAb, was produced by standard hybridoma techniques. All chemical reagents were obtained from Sigma/Fluka unless otherwise noted. HPLC chromatography was done with a Waters radial compression 10  $\mu$ m C18 22 mm  $\times$  30 cm column. All mass spectra were obtained on a Hewlett-Packard Quanta ion trap spectrometer using standard electrospray ionization. Synthetic procedures given below are representative of multiple preparations, and the cited yields are for the specific example.

**Synthesis: Diphenylmethyl *N*-(Boc-4-hydroxyphenylacetyl)-7-aminocephalosporanate (3).** Boc-4-hydroxyphenylacetic acid (2.83 g, 11.2 mmol), dicyclohexylcarbodiimide (2.54 g, 12.3 mmol), and triethylamine (4.69 mL, 33.6 mmol) were added to a suspension of 7-aminocephalosporanic acid **2** (3.05 g, 11.2 mmol) in 75 mL of dry dichloromethane. The resulting suspension was stirred under N<sub>2</sub> at room temperature for 18 h. The solvent was removed in vacuo, and the remaining residue was dissolved in a solution of 10 mL of dimethoxyethane and 5 mL of water at 0 °C. A solution of NaOH (4.4 mL at 19 wt %/vol, 25 mmol) was added, and the reaction was stirred at 0 °C for 20 min. A solution of diphenyldiazomethane (**16**) (10.9 g, 56 mmol) in 30 mL of ethyl acetate was added to the flask, and the solution was brought to pH 4.0 with aqueous HCl. The solution was stirred at room temperature for 1 h, brought to pH 4.0 again, and stirred for a further 18 h. After extraction with ethyl acetate and subsequent evaporation, a red oil (11.9 g) was obtained. HPLC chromatography (C18, acetonitrile:water with 0.1% TFA, ret. time = 74%) gave 1.9 g of product (25% yield) as a white fluffy powder. Analytical

HPLC (C18 Toso Haas ODS–Tm, 4.6 mm  $\times$  20 cm) using acetonitrile–water gave a single peak ( $\geq$ 95% pure) at 83% acetonitrile. Analytical HPLC (C8 Toso Haas ODS–Tm, 4.6 mm  $\times$  20 cm) using methanol–water gave a single peak ( $\geq$ 95% pure) at 47% methanol. <sup>1</sup>H NMR (CDCl<sub>3</sub>):  $\delta$  (ppm) 7.44 (m, 10H, CHPh<sub>2</sub>); 7.29 (d,  $J$  = 6 Hz, 2H, ArH); 7.13 (d,  $J$  = 6 Hz, 2H, ArH); 6.98 (s, 1H, CHPh<sub>2</sub>); 6.78 (d,  $J$  = 7 Hz, 1H, NH); 5.93 (dd,  $J_{\text{NH}}$  = 7 Hz,  $J_{7,6}$  = 5 Hz, 1H, C(7)H); 4.95 (d,  $J_{6,7}$  = 5 Hz, 1H, C(6)–H); 4.75 (br. s, 1H, OH); 4.47, 4.03 (AB dd,  $J_{\text{AB}}$  = 11 Hz, 2H, SCH<sub>2</sub>); 3.63 (dd,  $J$  = 10, 4 Hz, 2H, CH<sub>2</sub>O); 3.49 (br. s, 2H, ArCH<sub>2</sub>); 1.54 (s, 9H C(CH<sub>3</sub>)<sub>3</sub>). <sup>13</sup>C NMR (CDCl<sub>3</sub>):  $\delta$  (ppm) 174.4, 166.6, 162.2, 156.9, 141.3, 135.8, 130.4, 129.7, 129.2, 129.0, 128.6, 128.4, 127.3, 125.8, 97.5, 80.1, 61.4, 59.9, 57.6, 42.6, 27.8, 26.4. C<sub>34</sub>H<sub>34</sub>N<sub>2</sub>O<sub>8</sub>S (630.71 Da) calcd %: C 64.75, H 5.43, N 4.44, S 5.03, found %: C 64.59, H 5.21, N 4.64, S 5.02.

**3-[(1,6-Diaminohexanamidoxy)methyl]-4-hydroxyphenylacetyl-5-oxo-7-aminocephalosporanic Acid (4).** 1,1,1,2-Tetrachloroethyl orthochloroformate (32  $\mu$ mol) was added to a solution of **3** (20 mg, 32  $\mu$ mol) in dry dichloromethane at 0 °C, stirring was continued for 20 min, and then *m*-chloroperoxybenzoic acid (7.8 mg of 70 wt %/wt, 32  $\mu$ mol) was added. The reaction solution was stirred at 0 °C for 15 min under N<sub>2</sub> at which point 0.5 mL of 10% Na<sub>2</sub>S<sub>2</sub>O<sub>3</sub> was added to quench any remaining *m*-chloroperoxybenzoic acid, followed by addition of 5 mL of CH<sub>2</sub>Cl<sub>2</sub> and then washing with H<sub>2</sub>O. The solution was dried with saturated NaCl and evaporated in vacuo. The resulting oil was dissolved in THF (500  $\mu$ L at 0 °C), and to this was added 32  $\mu$ mol of mono-Boc-1,6-diaminohexane in 100  $\mu$ L of THF followed by 1 equiv of diisopropylethylamine. The crude oil obtained after evaporation was dissolved in 500  $\mu$ L of 1:1 TFA:anisole, and after 15 min this reaction mixture was evaporated to give an oily gum that was dissolved in DMSO for chromatography. After HPLC purification (C18, acetonitrile–water with 0.1% TFA, ret. time = 44% acetonitrile), **4** was obtained as a white fluffy powder (5.1 mg, 25% yield). Analytical HPLC (C18 Toso Haas ODS–Tm, 4.6 mm  $\times$  20 cm) using acetonitrile–water gave a single peak ( $\geq$ 95% pure) at 49% acetonitrile. Analytical HPLC (C8 Toso Haas ODS–Tm, 4.6 mm  $\times$  20 cm) using methanol–water gave a single peak ( $\geq$ 95% pure) at 32% methanol. <sup>1</sup>H NMR (d<sub>6</sub>-DMSO):  $\delta$  (ppm) 11.10 (br. s, 1H); 9.12 (br. s, 1H); 7.71 (br. s, 3H); 7.38 (d,  $J$  = 6 Hz, 2H, ArH); 7.24 (d,  $J$  = 6 Hz, 2H, ArH); 6.85 (t, 6 Hz, 1H, NHCH<sub>2</sub>); 6.73 (d,  $J$  = 7 Hz, 1H, NHCH); 5.78 (dd,  $J_{\text{NH}}$  = 7 Hz,  $J_{7,6}$  = 5 Hz, 1H, C(7)H); 5.13 (d,  $J_{6,7}$  = 5 Hz, 1H, C(6)H); 4.28 (dd,  $J$  = 10, 6 Hz, 2H, CH<sub>2</sub>O); 3.44 (dd,  $J$  = 14, 7 Hz, 2H, SCH<sub>2</sub>); 3.55 (br. s, 2H, ArCH<sub>2</sub>); 3.35 (m, 2H, CH<sub>2</sub>NH<sub>3</sub><sup>+</sup>); 2.97 (m, 2H, NHCH<sub>2</sub>); 2.18–2.03 (m, 4H, CH<sub>2</sub>); 1.51 (m, 2H, CH<sub>2</sub>); 1.40 (m, 2H, CH<sub>2</sub>). C<sub>23</sub>H<sub>30</sub>N<sub>4</sub>O<sub>8</sub>S (522.57 Da); MS (ES) [MH]<sup>+</sup> calc. 523.186, found 523.191.

**3-[(6-(2-Sulfo-*N*-hydroxysuccinimidobutyl)-1,6-diaminohexanamidoxy)methyl]-4-hydroxyphenylacetyl-5-oxo-7-aminocephalosporanic Acid (1).** A solution of 5.3 mg of **4** (8.4  $\mu$ mol) and 24 mg (42  $\mu$ mol) of disulfo-*N*-succinimidyl suberate (Pierce, Chicago, IL) in 1 mL of dry DMSO containing 7.3  $\mu$ L of diisopropylethylamine (42  $\mu$ mol) was stirred for 1 h at room temperature. The reaction mixture was chromatographed by HPLC (C18, acetonitrile–water with 0.1% TFA, ret. time = 48% acetonitrile) to give **1** as a white powder (6.7 mg, 92% yield). Analytical HPLC (C18 Toso Haas ODS–Tm, 4.6 mm  $\times$  20 cm) using acetonitrile–water gave a single peak ( $\geq$ 95% pure) at 43% acetonitrile. Analytical HPLC (C8 Toso Haas ODS–Tm, 4.6 mm  $\times$  20 cm) using methanol–water gave a single peak ( $\geq$ 95% pure) at 27% methanol.



$^1\text{H}$  NMR ( $d_6$ -DMSO):  $\delta$  (ppm) 11.67 (s, 1H), 11.42 (br. s, 1H); 9.43 (br. s, 1H); 7.31 (d,  $J = 6$  Hz, 2H, ArH), 7.15 (d,  $J = 6$  Hz, 2H, ArH); 6.87 (t, 7 Hz, 1H,  $\text{NHCH}_2$ ); 6.87 (t, 7 Hz, 1H,  $\text{NHCH}_2$ ); 6.65 (d,  $J = 6$  Hz, 1H,  $\text{NHCH}_2$ ); 5.76 (dd,  $J_{\text{NH}} = 6$  Hz,  $J_{7,6} = 5$  Hz, 1H, C(7)H); 5.33 (d,  $J_{6,7} = 5$  Hz, 1H, C(6)H); 4.33 (dd,  $J = 9, 6$  Hz, 2H,  $\text{CH}_2\text{O}$ ); 3.76 (dd,  $J = 9, 5$  Hz, 1H,  $\text{CH(H)CHS}$ ); 3.58 (br. s, 2H,  $\text{ArCH}_2$ ); 3.49 (dd,  $J = 12, 6$  Hz, 2H,  $\text{SCH}_2$ ); 3.34 (m, 2H,  $\text{CH}_2\text{NH}$ ); 3.31 (m, 2H,  $\text{NHCH}_2$ ); 3.12 (dd,  $J = 18, 9$  Hz, 1H,  $\text{CH(H)CHS}$ ); 2.99 (m, 2H,  $\text{CH}_2$ ); 2.70 (dd,  $J = 18, 5$  Hz, 1H,  $\text{CH(H)CHS}$ ); 2.32 (br. t,  $J \sim 7$  Hz, 2H,  $\text{COCH}_2$ ); 2.20–2.07 (m, 4H,  $\text{CH}_2$ ); 1.60–1.52 (m, 6H,  $\text{CH}_2$ ); 1.40–1.25 (m, 6H,  $\text{CH}_2$ ).  $\text{C}_{35}\text{H}_{45}\text{N}_5\text{O}_{16}\text{S}_2$  (855.89 Da) calcd %: C 49.12, H 5.30, N 8.18, S 7.49, found %: C 48.85, H 5.10, N 7.82, S 7.52.

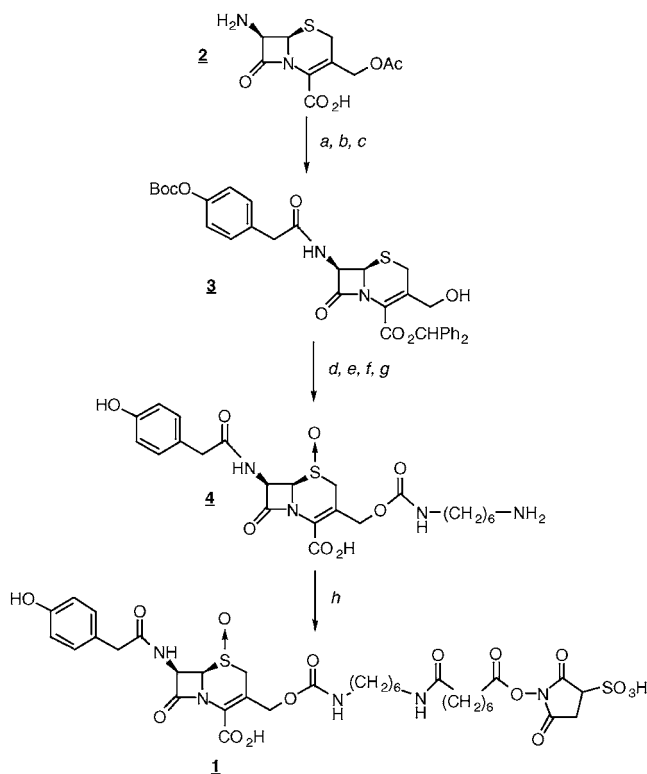
**Preparation of the Standard and Cleavable Radioimmunoconjugate.** Chloramine T was freshly prepared in deionized water to 60 mM. Carrier-free I-125 or I-131 in 0.1 M NaOH (NEN Life Sciences, Boston, MA) was neutralized with 5 volumes of 0.5 M phosphate/0.150 M NaCl buffer pH 7.4. Standard labeling of Tositumomab antibody with I-125 or I-131 was performed using the chloramine T method as previously published (3). Labeling of Tositumomab antibody with radiolabeled cleavable linker was done as follows: 8.6  $\mu\text{g}$  (10 nmol) of cleavable linker in 10  $\mu\text{L}$  of DMSO was added to 10 nmol of chloramine T and 3–5 mCi I-131, and the solution was agitated at room temperature for 5 min. The reaction was quenched with a 5 molar excess of sodium metabisulfite, and the reaction contents were added to a small reverse phase column (C18 SPE, 50 mg; Alltech, Deerfield, IL) previously equilibrated with 4% acetonitrile in water solution. Multiple aqueous washes removed unreacted iodide and aqueous soluble reagents. Acetonitrile was used to elute the radiolabeled cleavable linker. The acetonitrile solution containing radiolabeled cleavable linker was evaporated with a gentle stream of air, and B1 antibody (6 nmol in 1 mL of phosphate-buffered saline pH 7.4) was added to the dry radiolabeled cleavable linker and allowed to react for 1 h at room temperature with agitation. The cleavable radioimmunoconjugate was isolated by size exclusion chromatography (Pharmacia PD10, phosphate-buffered saline pH 7.4).

**Purification of  $\beta$ -Lactamase.**  $\beta$ -Lactamase was purified from crude penicillinase type IV, *Enterobacter cloacae*, (Sigma), according to the method of Cartwright (17). Enzymatic activities of  $\beta$ -lactamase were determined using nitrocefin as a substrate (18).

**Characterization of Cleavable Radioimmunoconjugates.** Reducing and nonreducing SDS gels of the cleavable RIC and standard size markers were run on 10–12% polyacrylamide. The gels were then dried and exposed to Kodak film for autoradiography. Immunoreactivity of the cleavable radioimmunoconjugate and standard labeled Tositumomab antibody were performed according to the method of Lindmo (19). In vitro cleaving assay were performed using 5–10  $\mu\text{L}$  (1–10  $\mu\text{g}$ ) of cleavable RIC added to an eppendorf tube with 1  $\mu\text{g}$  of  $\beta$ -lactamase enzyme. The contents were mixed and allowed to incubate for 15–60 min at 37  $^\circ\text{C}$ . Following the incubation period, 900  $\mu\text{L}$  of phosphate-buffered saline was added, the contents were mixed, the total volume was added to a PD10 (Pharmacia) size exclusion column, and 12 1 mL fractions were collected and counted on a scintillation counter.

**In Vivo Biodistribution in Murine Model.** Ten-week old NOD/SCID mice were injected in the tail vein with 25–50  $\mu\text{g}$  of standard radiolabeled antibodies or 25–50  $\mu\text{g}$  of cleavable RIC. Mice were coinjected with 400  $\mu\text{g}$

### Scheme 1. Synthesis of Cleavable Linker 1<sup>a</sup>



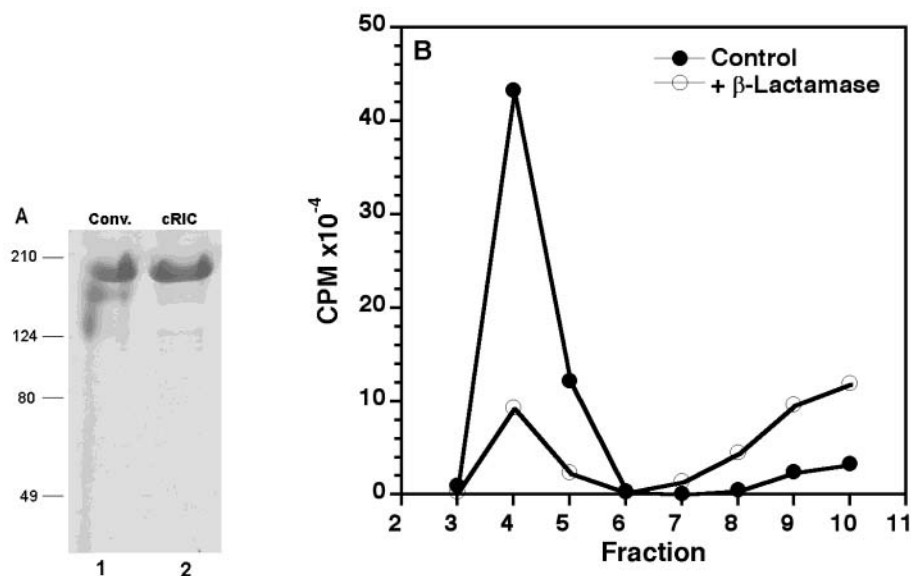
<sup>a</sup> Conditions: (a) BocOPhCH<sub>2</sub>CO<sub>2</sub>H, DCC, DIEA; (b) NaOH; (c) Ph<sub>2</sub>CN<sub>2</sub>; (d) CCl<sub>3</sub>CHClCOCl, DIEA; (e) mCPBA; (f) BocNH(CH<sub>2</sub>)<sub>6</sub>NH<sub>2</sub>; (g) TFA, anisole; (h) di-sulfoNHS suberate, DIEA.

of a nonspecific IgG2a irrelevant antibody (G3G6) to block nonspecific binding to Fc receptors in spleen, liver, and marrow, and, 5–20 h following injection of RIC, groups of mice were injected in the tail vein with 10  $\mu\text{g}$  of  $\beta$ -lactamase or buffer. Blood, urine, and tissue samples were collected immediately before and at various times after injection of enzyme or buffer. Collected body fluids and excised tissue samples were weighed, and  $^{125}\text{I}$  and  $^{131}\text{I}$  radioactivity was counted. Counts are corrected for radioactive decay using an aliquot of the injectate. The percent injected dose of radionuclide per gram (%ID/g) of fluid or tissue was calculated and is reported as the mean  $\pm$  standard deviation for  $n = 3$ –5 mice. The statistical significance between mean tissue uptake in enzyme-treated and untreated mice for a given experiment was calculated with the unpaired Student's  $t$  test for  $p < 0.05$ .

**In Vivo Biodistribution in Murine Lymphoma Xenograft Model.** NOD/SCID mice were irradiated with 375 cGy and injected with  $2 \times 10^7$  Ramos cells subcutaneously in the flank. Mice were monitored until palpable (3–10 mm) tumor nodules appeared (7–14 days) at which time mice were used for biodistribution studies as described above.

## RESULTS

**Design and Synthesis of Cleavable Linker 1.** The minimal requirements for a cleavable linker are a radio-nuclide-carrying moiety, an enzyme substrate that can be efficiently cleaved, and a protein–conjugation moiety. A cephalosporin nucleus was chosen as the cleavable enzyme substrate (compound 1, Scheme 1) since  $\beta$ -lactamase enzymes are highly specific and efficient for hydrolysis of the lactam, which then promotes spontaneous decomposition of the carbamate. In addition, there



**Figure 1.** Characterization and in vitro lactamase treatment of cleavable Tositumomab RIC. Linker **1** was iodinated with I-131 and then conjugated to Tositumomab. Shown in panel A is a nonreducing SDS-PAGE gel of the antibody labeled with linker **1** (cleavable RIC, lane 2) and antibody conventionally labeled with I-131 and chloramine T (conv., lane 1). Shown in panel B is the cpm of fractions eluted off a size exclusion column for the cleavable RIC after 1 h treatment with  $\beta$ -lactamase or buffer (control).

is no endogenous  $\beta$ -lactamase activity in mammals. The aryl group of 4-hydroxyphenylacetic acid is activated for electrophilic iodination using traditional techniques such as chloramine T, and the NHS-ester in **1** readily reacts with the  $\epsilon$ -nitrogen of lysine residues.

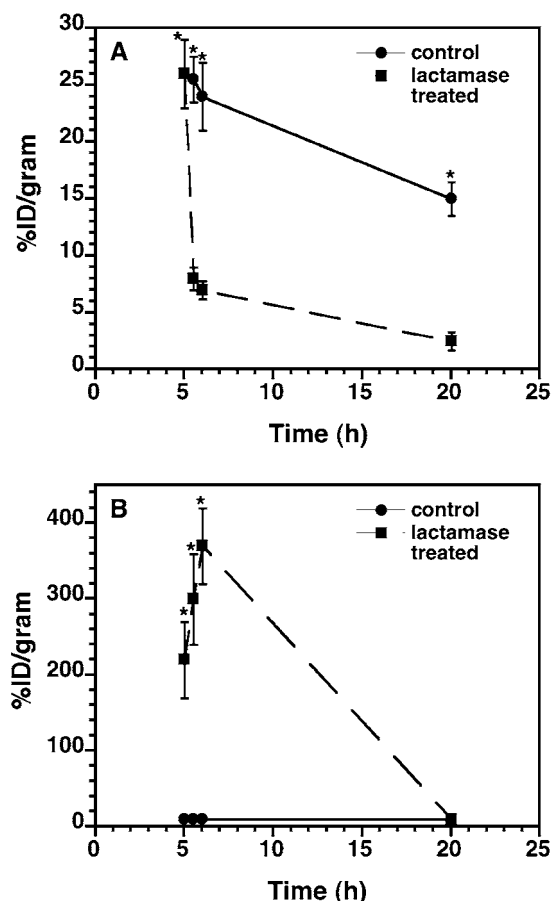
The synthesis of **1** was readily achieved using conventional side-chain protection and peptide coupling chemistries (Scheme 1). Initially 7-aminocephalosporinic acid **2** was acylated with Boc-protected 4-hydroxyphenylacetic acid. The position-3 oxymethylene acetate was hydrolyzed with base, and the carboxylic acid was protected as the diphenylmethyl ester to give the alcohol **3** with overall yields of 20–40%. The hydroxy group of **3** was activated with 1,1,1,2-tetrachloroethyl orthochloroformate, the thioether was oxidized, and the tetrachloroethyl carbonate was then coupled to mono-Boc-protected 1,6-diaminohexane to give **4** after TFA deprotection (20–30% yield from **3**). The linker **1** was then obtained from the reaction of **4** with the sulfo-NHS suberate diester (>90% yield from **4**).

**Preparation and in Vitro Characterization of Cleavable Radioimmunoconjugates.** The linker **1** was radioiodinated with chloramine T, and the iodinated linker was then incubated with Tositumomab to give the cleavable RIC. The efficiency of the cleavable RIC synthesis as assessed by percent incorporation of radioisotope into the final purified cleavable RIC was 5–10%. The cleavable RIC exhibited a molecular weight of approximately 175 kDa in nonreducing SDS PAGE analysis (Figure 1A) and comigrated with antibody radioiodinated by conventional techniques. Image analysis of gels showed about an 80% decrease of radioactivity in the region of the antibody after a 1 h treatment with  $\beta$ -lactamase (data not shown). Isolation of the cleavable radioimmunoconjugate-containing fraction by size exclusion chromatography also revealed an average 80–85% decrease in radioactive counts per minute in enzyme treated versus nontreated samples (Figure 1B). In antigen binding assays at antigen excess, the cleavable RIC, conventionally labeled RIC, and isotype control bound to 56%, 59%, and 0% of antigen-containing cells, respectively.

#### **In Vivo Cleavage and Biodistribution in Mice.**

Nonspecific uptake of IgG2a antibodies in the reticuloendothelial system in tumor and non-tumor-bearing animals was minimized by the coinjection of control IgG2a antibody against an irrelevant specificity (G3G6). We found that coinjection of 400  $\mu$ g of G3G6 was the most effective for inhibiting nonspecific uptake of radiolabeled B1 (data not shown). Various doses of radiolabeled Tositumomab were used in biodistribution experiments with the most optimal biodistributions observed after infusing 25–50  $\mu$ g of radiolabeled Tositumomab per mouse; biodistribution of the cleavable RIC in mice was identical to that of standard radioiodinated Tositumomab (data not shown). The in vivo cleavage and clearance of the  $\beta$ -lactamase-sensitive anti-CD20 cleavable RIC was demonstrated with blood clearance and urinary excretion in mice. Two hundred micrograms of cleavable Tositumomab RIC trace-labeled with I-131 was injected iv into the tail vein of NOD/SCID mice. After 5 h, 10  $\mu$ g of  $\beta$ -lactamase was administered iv to one-half of the mice, with remaining mice serving as controls. Blood clearance in enzyme-treated and control mice revealed a 3-fold decrease in %ID/g at 30 min after enzyme infusion, and a 4-fold decrease at the 20-h time point (Figure 2A). In the same mice, urine obtained 30 min following the  $\beta$ -lactamase injection showed a 300-fold increase in %ID/g compared to nontreated mice (Figure 2B).

Representative data illustrating the effects of enzymatic cleavage on radioactive uptake in normal tissues 1 and 20 h after enzyme infusion are shown in Figure 3A and 3B. At 1 h we observed a statistically significant 3-fold decrease in spleen %ID/g and a 2-fold decrease in lung and liver %ID/g in the enzyme-treated group (Figure 3A). At 20 h after enzyme infusion, we observed a statistically significant 4–6-fold decrease in marrow and spleen %ID/g, a 3–5-fold decrease in lung and liver %ID/g, and a 3-fold decrease in kidney %ID/g in the enzyme-treated group (Figure 3B). Rapid renal clearance of the low molecular weight isotope-containing moiety led to the transient 2-fold increase in the kidney %ID/g 1 h following enzyme treatment. The  $\beta$ -lactamase-mediated relative decreases in radioactive uptake shown in Figure 3

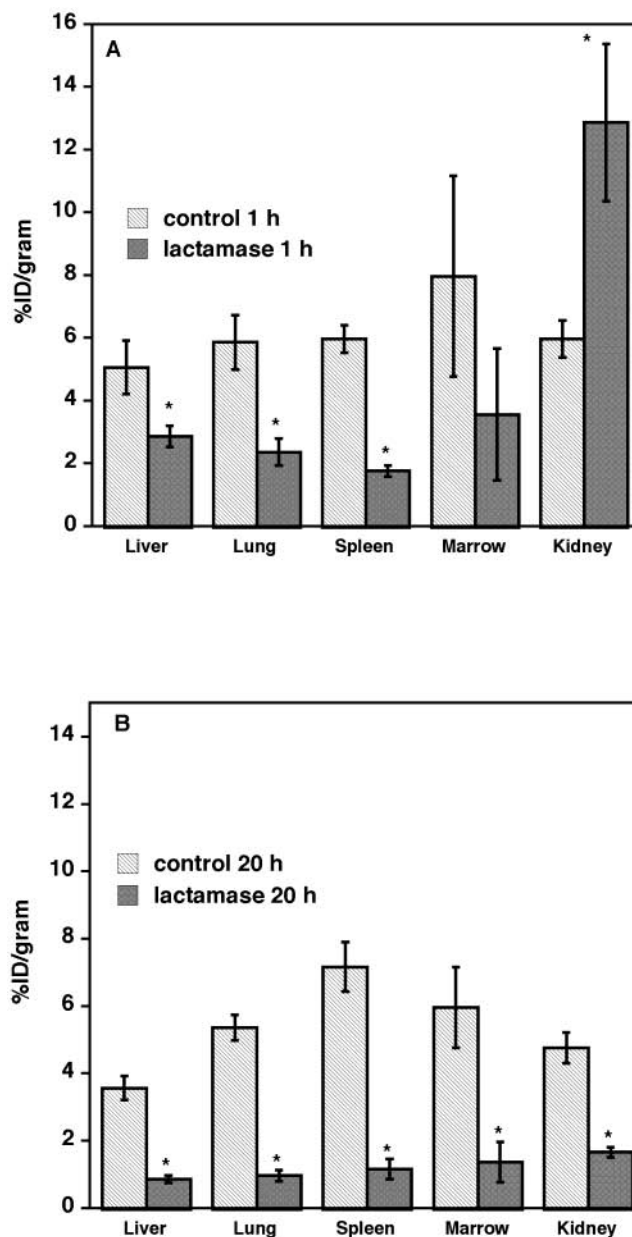


**Figure 2.** Representative clearance curves for blood (panel A) and urine (Panel B), expressed as %ID/g. Cleavable radiolabeled Tositumomab antibody was injected at time 0, and  $\beta$ -lactamase enzyme was injected 5 h later. Three mice were evaluated at each time point. Solid lines indicate enzyme-treated mice, and broken lines indicate control mice not injected with  $\beta$ -lactamase. Error bars are the standard deviation, and asterisks denote the concentrations in enzyme-treated mice that are significantly ( $p < 0.05$ ) different from the controls.

were not significantly different than those observed in other experiments where the cleavable RIC was allowed to circulate for up to 24 h before administration of  $\beta$ -lactamase (data not shown).

**In Vivo Cleavage and Biodistribution in Lymphoma Xenograft Mice.** Biodistribution studies in mice bearing lymphoma xenografts were undertaken to better determine the effects of the  $\beta$ -lactamase enzyme on the binding of radioisotope by cleavable RIC to tumor compared to normal tissues. We determined that maximum tumor localization of iodinated Tositumomab antibody occurs at 20–24 h (data not shown). Thus, the cleavable RIC was allowed to circulate for 20 h before enzyme was introduced. Immunodeficient mice with subcutaneous Ramos B lymphoma cell tumors received 25  $\mu$ g cleavable B1–RIC labeled with 18  $\mu$ Ci of I-131. Mice also received 400  $\mu$ g of irrelevant antibody to decrease nonspecific binding activity. After 20 h, one-half of the mice were treated iv into the tail vein with 6.4  $\mu$ g of  $\beta$ -lactamase, and groups of 3–4 mice each were sacrificed at later time points. Representative biodistributions for 1 and 4 h after enzyme infusion are listed in Table 1.

Evaluation of organ and tumor distribution revealed a statistically greater than 2-fold decrease in blood and marrow radioisotope concentrations 1 and 4 h after enzyme infusion. Significant decreases in radioactivity contents in lung and liver were also seen, with about a



**Figure 3.** Concentration of radioactivity in tissues expressed as %ID/g. Mice were injected with cleavable radiolabeled Tositumomab antibody at time 0, and half received  $\beta$ -lactamase enzyme at 5 h. Necropsy was performed in groups of three mice each at 1 h (panel A) and 20 h (panel B) after enzyme infusion. Error bars are the standard deviation, and asterisks denote the concentrations in enzyme-treated mice that are significantly ( $p < 0.05$ ) different from the controls.

2-fold difference 1 and 4 h after enzyme infusion. An increase in kidney radioactivity was again seen at the 1 h time point. In contrast to blood and the normal organs, tumor radioactive content was not significantly decreased 1 h after enzyme infusion. However, by 4 h, the tumor %ID/g had decreased by 40% in mice receiving enzyme. We also observed a greater than 2-fold increase in tumor/blood ratio of %ID/g at 1 h (1.3 vs 0.6) and a 50% increase at 4 h (0.9 vs 0.6) for enzyme-treated versus control. The gain in tumor/blood ratio is lost at later time points. By 20 h the biodistributions in enzyme-treated and untreated normal tissues are comparable to those illustrated in Figure 3, but the tumor radioactive content is typically reduced by about 70% compared to the control (data not shown). Thus, at these later time points there



**Table 1. I-131 RIC Biodistribution in Mice Bearing Lymphoma Xenografts at 1 h and 4 h**

tissue	%ID/g at 1 h <sup>a</sup>		%ID/g at 4 h	
	$\beta$ -lactamase	control	$\beta$ -lactamase	control
blood	5.1 <sup>d</sup> $\pm$ 0.2 <sup>b</sup> , 1.3 <sup>c,d</sup>	11.9 $\pm$ 1.0, 0.6	4.5 <sup>d</sup> $\pm$ 0.4, 0.9 <sup>d</sup>	12.1 $\pm$ 2.1, 0.6
marrow	3.6 <sup>d</sup> $\pm$ 0.2, 1.9 <sup>d</sup>	8.4 $\pm$ 0.9, 0.8	2.7 <sup>d</sup> $\pm$ 0.8, 1.5 <sup>d</sup>	6.8 $\pm$ 1.3, 3.3
lung	2.0 <sup>d</sup> $\pm$ 0.2, 3.5 <sup>d</sup>	3.7 $\pm$ 0.2, 1.9	1.6 <sup>d</sup> $\pm$ 0.2, 2.5	3.3 $\pm$ 0.9, 2.2
liver	1.4 <sup>d</sup> $\pm$ 0.1, 4.9 <sup>d</sup>	2.0 $\pm$ 0.1, 3.6	1.0 <sup>d</sup> $\pm$ 0.1, 4.0	2.0 $\pm$ 0.6, 3.6
kidney	4.0 <sup>d</sup> $\pm$ 0.2, 1.7	2.1 $\pm$ 1.22, 3.4	2.3 $\pm$ 0.2, 1.7	2.7 $\pm$ 0.4, 2.6
tumor	6.9 $\pm$ 1.0	7.1 $\pm$ 0.6	4.0 <sup>d</sup> $\pm$ 0.2	7.1 $\pm$ 1.2

<sup>a</sup> Time after iv injection of  $\beta$ -lactamase. <sup>b</sup> Standard deviation,  $n = 4$ . <sup>c</sup> Ratio of tumor/normal tissue %ID/g. <sup>d</sup> Statistically different from relevant control at  $p < 0.05$ .

is no statistically significant difference in the tumor/blood ratios for treated and untreated mice.

## DISCUSSION

This report demonstrates that a conditionally cleavable RIC that utilizes a cephalosporin-based linker can be prepared and, when exposed to  $\beta$ -lactamase, radioactivity can be released and rapidly cleared by the kidneys. In addition, in vitro antigen binding studies and in vivo studies in murine xenograft models demonstrated tumor cell localization by the conditionally cleavable RIC. The ability to target antigen was not altered by the addition of the cleavable linker to the antibody since in vitro and in vivo antigen localization of the cleavable RIC and a standard labeled RIC was nearly identical. Biodistribution experiments demonstrated in vivo cleavage of the RIC with rapid clearance of radioisotope by kidney and decreased radioactivity contents in blood and organs known to be dose limiting for RIT, namely liver, lung, and marrow. Biodistribution studies of the cleavable RIC in a tumor xenograft model demonstrated that clearance of radioactivity from the blood and dose-limiting normal organs was enhanced relative to loss at the tumor immediately following  $\beta$ -lactamase infusion. However, this advantage was transient, because  $\beta$ -lactamase treatment also caused loss of radioactive content from the tumor. Since tumor-bound conjugate is in equilibrium with nonbound cleaved and noncleaved conjugate, this decrease in tumor content could be due to exchange of bound, labeled RIC with unlabeled conjugate. Alternatively, the decrease could be due to enzyme cleavage of tumor-bound RIC. Regardless, at early time points after enzyme infusion (i.e., 1 h to 4 h), use of the cleavable RIC significantly enhanced the tumor/blood %ID/g ratio although this gain is lost at later time points (i.e., >20 h).

This study, to our knowledge, represents the initial synthesis of a conditionally cleavable radioimmunconjugates that, upon exposure to cleaving enzyme, will release the radioactive moiety in vitro or in vivo. The readily achieved release of the radioactive moiety in vivo following infusion of  $\beta$ -lactamase enzyme was successful in causing rapid clearance of radiation from blood and normal organs. However, the systemic administration of an exogenous enzyme can cause toxicity and immune responses, which are problems also encountered in antibody-directed enzyme prodrug therapies (ADEPT; 20, 21). Fortunately, the amounts of  $\beta$ -lactamase needed to clear radionuclide are considerably lower than the amounts used for ADEPT strategies, and this advantage

could be greatly increased with the use of, for example, dextran-modified  $\beta$ -lactamase, which has a very slow clearance rate and is not immunogenic (22). Although the  $\beta$ -lactamase used here also induced a loss of the radiolabel from tumor cells, the loss was delayed compared to the loss of radioactivity from normal organs. These observations suggest that effective use of a cleavable RIC for improving antibody-mediated delivery of radiolabel to tumor might be achieved if the antibodies used would not be available for cleavage following enzyme infusion. It should be possible to achieve this objective by employing antibodies that are rapidly internalized by the cell after membrane binding and subsequently retained within the cell, rather than antibodies such as Tositumomab, which are retained on the surface of cells for prolonged periods of time. In this way, enzyme-induced clearance of the radiolabel would only occur from conjugates not specifically bound to antigen and thus exposed to the enzyme. The data presented in this study also suggest that the current approach may be useful for improving tumor imaging with radiolabeled antibodies since radiolabel was cleared more rapidly from the blood than tumor or normal organs, which should allow greater discrimination between conjugate within the blood pool and at the tumor site.

## ACKNOWLEDGMENT

J.E.B. and M.J.H. contributed equally to this work. This work is supported by NIH grants CA44991 and CA86963. I.D.B. is supported by an F. M. Kirby/American Cancer Society Clinical Research Professorship.

## LITERATURE CITED

- (1) Goodwin, D. A., and Meares, C. F. (1999) Pretargeted peptide imaging and therapy. *Cancer Biother. Radiopharm.* 14, 145–152.
- (2) Goodwin, D. A., and Meares, C. F. (1997) Pretargeting: general principles. *Cancer* 80 (Suppl.), 2675–2680.
- (3) Press, O. W., Corcoran, M., Subbiah, K., Hamlin, D. K., Wilbur, D. S., Johnson, T., Theodore, L., Yau, E., Mallett, R., Meyer, D. L., and Axworthy, D. A. (2001) Comparative evaluation of conventional and pretargeted radioimmunotherapy of CD20-expressing lymphoma xenografts. *Blood* 98, 2535–2543.
- (4) Hamblett, K. J., Kegley, B., Hamlin, D., Chyan, M., Hyre, D., Press, O., Wilbur, D., and Stayton, P. (2002) A streptavidin–biotin binding system that minimizes blocking by endogenous biotin. *Bioconjugate Chem.* 13, 588–598.
- (5) DeNardo, G. L., Maddock, S. W., Sgouros, G., Scheibe, P. O., and DeNardo, S. J. (1993) Immunoadsorption: an enhancement strategy for radioimmunotherapy. *J. Nucl. Med.* 34, 1020–1027.
- (6) Sgouros, G. (1992) Plasmapheresis in radioimmunotherapy of micro-metastases: a mathematical modeling and dosimetric analysis. *J. Nucl. Med.* 33, 2167–2179.
- (7) Norrgren, K., Strand, S. E., and Ingvar, C. (1992) Contrast enhancement in RIT and modification of the therapeutic ratio in RIT: A theoretical evaluation of simulated extracorporeal immunoadsorption. *Antibody Immunoconjugate Radiopharm.* 3, 61–73.
- (8) Chen, J. Q., Strand, S. E., Tennvall, J., Lindgren, L., Hindorf, C., and Sjogren, H. O. (1997) Extracorporeal immunoadsorption compared to avidin chase: enhancement of tumor-to-normal tissue ratio for biotinylated Rhenium-188-chimeric BR96. *J. Nucl. Med.* 38, 1934–1939.
- (9) Dienhart, D. G., Kasliwal, R., and Lear, J. L. (1994) Extracorporeal immunoadsorption of radiolabeled monoclonal antibody: a method for reduction of background radioactivity and its potential role during the radioimmunotherapy of cancer. *Antibody Immunoconj. Radiopharm.* 7, 225–252.
- (10) Marshall, D., Pedley, R. B., Boden, J. A., Boden, R., and Begent, R. H. (1994) Clearance of circulating radio-antibodies

- using streptavidin or second antibodies in a xenograft model. *Br. J. Cancer* 69, 502–507.
- (11) Kobayashi, H., Sakahara, H., Hosono, M., Yao, Z. S., Toyama, S., Endo, K., and Konishi, J. (1994) Improved clearance of radiolabeled biotinylated monoclonal antibody following the infusion of avidin as a “chase” without decreased accumulation in the target tumor. *J. Nucl. Med.* 35, 1677–1684.
- (12) Studer, M., Kroger, L. A., DeNardo, S. J., Kukis, D. L., and Meares, C. F. (1992) Influence of a peptide linker on biodistribution and metabolism of antibody-conjugated benzyl-EDTA: Comparison of enzymatic digestion in vitro and in vivo. *Bioconjugate Chem.* 3, 424–429.
- (13) Stein, R., Goldenberg, D. M., Ong, G. L., Thorpe, S. R., and Mattes, M. J. (1997) Manipulation of blood clearance to optimize delivery of residualizing label-antibody conjugates to tumor cells in vivo. *J. Nucl. Med.* 38, 1392–1400.
- (14) DeNardo, G. L., Kroger, L. A., Meares, C. F., Richman, C. M., Salako, Q., Shen, S., Lamborn, K. R., Peterson, J. J., Miers, L. A., Zhong, G. R., and DeNardo, S. J. (1998) Comparison of 1,4,7,10-tetraazacyclododecane-*n,n',n'',n'''*-tetraacetic acid (DOTA)-peptide-CHL6, a novel immunoconjugate with catabolizable linker, to 2-iminothiolane-2-[*p*-(bromoacetamido)benzyl]-DOTA-CHL6 in breast cancer xenografts. *Clin. Cancer Res.* 4, 2483–2490.
- (15) Arano, Y., Wakisaka, K., Akizawa, H., Ono, M., Kawai, K., Nakayama, M., Sakahara, H., Konishi, J., and Saji, H. (1998) Assessment of the radiochemical design of antibodies with a metabolizable linkage for target-selective radioactivity delivery. *Bioconjugate Chem.* 9, 497–506.
- (16) Smith, L. I., and Howard, K. L. (1955) Preparation of diphenyldiazomethane. *Organic Syntheses*, Collect. Vol. III, p 351, Wiley, New York.
- (17) Cartwright, S. J., and Waley, S. G. (1984) Purification of beta-lactamases by affinity chromatography on phenylboronic acid-agarose. *Biochem. J.* 221, 505–512.
- (18) Shannon, K., and Phillips, I. (1980) Beta-lactamase detection by three simple methods: intralactam, nitrocefin and acidimetric. *J. Antimicrob. Chemother.* 6, 617–621.
- (19) Lindmo, T., Boven, E., Cuttitta, F., Fedorko, J., and Bunn, P. A., Jr. (1984) Determination of the immunoreactive fraction of labeled monoclonal antibodies by linear extrapolation to binding at infinite antigen excess. *J. Immunol. Methods* 72, 77–89.
- (20) Melton, R. G., and Sherwood, R. F. (1996) Antibody-enzyme conjugates for cancer therapy. *J. Natl. Cancer Inst.* 88, 153–165.
- (21) Syrigos, K. N., and Epenetos, A. A. (1999) Antibody directed enzyme prodrug therapy (ADEPT): a review of the experimental and clinical considerations. *Anticancer Res.* 19, 605–613.
- (22) Mikolajczyk, S. D., Meyer, D. L., Fagnani, R., Hagan, M. S., Law, K. L., and Starling, J. J. (1996) Dextran modification of a Fab'-β-lactamase conjugate modulated by variable pretreatment of Fab' with amine-blocking reagents. *Bioconjugate Chem.* 7, 150–158.

BC025655Z

# A Degradable Polyethylenimine Derivative with Low Toxicity for Highly Efficient Gene Delivery

M. Laird Forrest, James T. Koerber, and Daniel W. Pack\*

Department of Chemical and Biomolecular Engineering, University of Illinois at Urbana-Champaign, Urbana, Illinois 61801. Received February 5, 2003; Revised Manuscript Received May 2, 2003

Routine clinical implementation of human gene therapy awaits safe and efficient gene delivery methods. Polymeric vectors hold promise due to the availability of diverse chemistries, potentially providing targeting, low immunogenicity, nontoxicity, and robustness, but lack sufficient gene delivery efficiency. We have synthesized a versatile group of degradable polycations, through addition of 800-Da polyethylenimine (PEI) to small diacrylate cross-linkers. The degradable polymers reported here are similar in structure, size (14–30 kDa), and DNA-binding properties to commercially available 25-kDa PEI, but mediate gene expression two- to 16-fold more efficiently and are essentially nontoxic. These easily synthesized polymers are some of the most efficient polymeric vectors reported to date and provide a versatile platform for investigation of the effects of polymer structure and degradation rate on gene delivery efficiency.

## INTRODUCTION

The need for safe and efficient methods for gene delivery remains a critical stumbling block to the routine clinical implementation of human gene therapy (1). While recombinant viruses are the most efficient gene delivery vectors currently available, polymeric vectors have several advantages that make them a promising alternative. Polyplexes, comprising an electrostatic complex of cationic polymer(s) and plasmid DNA, hold potential for improved safety, easier production and purification, relatively large gene-carrying capacity, and flexibility of design. Despite their promise, none of the existing polymers is generally acceptable for human gene therapy, primarily due to lack of efficiency.

One of the most successful and widely studied gene delivery polymers reported to date is polyethylenimine (PEI), an off-the-shelf polycation containing a high density of primary, secondary, and tertiary amines, used previously as a chelator and flocculation agent (2). Due to its relatively high gene delivery efficiency and ready availability, branched, 25-kDa PEI has become a benchmark to which other polymers, especially newly designed and synthesized materials, are often compared. However, several groups have reported that PEI is cytotoxic in many cell lines; at PEI concentrations used in typical transfection protocols, cell metabolic activity may be reduced by 40–90% (3, 4). PEI toxicity appears to decrease with decreasing polymer size. For example, Gosselin et al. found transfection with 25-kDa PEI can reduce cells' adherence by 50–90% compared to a linear, low-molecular-weight, 800-Da PEI (5). However, gene transfer efficiency was reduced 30- to 50-fold with 800-Da PEI compared to the more commonly used 25-kDa PEI.

Lack of toxicity should be a major consideration in the design of any new gene delivery material. To generate

biocompatible gene delivery polymers, several degradable polycations have been reported recently. For example, several cationic polyesters have been studied (6–10) including a linear, biodegradable mimic of polylysine (6, 8) and a hyperbranched, poly(amino ester) (9), both of which exhibit negligible toxicity in comparison to the nondegradable 25-kDa PEI. A second class of degradable polycations, generated by the addition of diamines to diacrylates, has been reported by Lynn et al. (11, 12). Their strategy provides a facile route to a diversity of cationic polymer chemistries. Using a combinatorial synthesis strategy, they found polymers that exhibit 4–8-fold higher gene transfer activity than 25-kDa PEI. In addition, Pichon et al. (13) and Gosselin et al. (5) each reported gene delivery polymers comprising low-molecular-weight polycations (polylysine and PEI, respectively) cross-linked via reversible disulfide bonds. Cross-linked PEI mediated gene expression 2-fold less efficiently than the standard 25-kDa PEI, but exhibited less toxicity to cells in culture. It is expected that these polymers will decompose in the reducing environment of the cytoplasm to their low-molecular-weight constituents, which are known to exhibit reduced cytotoxicity (4). Finally, Ahn et al. (14) reported the synthesis of copolymers of low-molecular-weight PEI and difunctional poly(ethylene glycol) (PEG) succinimidyl succinate. The resulting polymers consist of short PEI and PEG ( $M_w = 2000$ ) segments cross-linked through ester linkages. These polymers showed significantly lower toxicity than 25-kDa PEI and three times more efficient transfection than the low-molecular-weight PEI starting material. However, the transfection efficiency was not compared directly to 25-kDa PEI.

Many questions remain about how to design biodegradable gene delivery polymers. Little is known about where in the cell the degradation of these polymers takes place. Further, one can only hypothesize about where degradation would be most beneficial. For example, degradation in endocytic vesicles may aid plasmid release into the cytoplasm, while keeping the plasmid in the polyplex until the vehicle reaches the nucleus may protect the DNA from enzymatic degradation. Alternatively,

\* Correspondence should be addressed to this author at Department of Chemical and Biomolecular Engineering, Box C-3, 600 S. Mathews Ave., Urbana, IL 61801. Phone: (217) 244-2816, Fax: (217) 333-5052, e-mail: dpack@uiuc.edu.



release of the plasmid from the polyplex may facilitate transport into the nucleus, for example through the nuclear pores, in which case degradation of the polymer in the cytoplasm may be desirable. Further complicating matters, little is known about how the polymer structure, including the size, cross-linking density, branching, amine density, etc., affects degradation kinetics and ultimately gene delivery efficiency.

To address these issues, we sought to develop a system that is flexible, allowing the polymer structure to be varied easily, while maintaining high gene-delivery efficiency. The polymer reported here, a biodegradable analogue of 25-kDa PEI, was produced by addition of amino groups on 800-Da PEI to diacrylates of varying spacer length following the strategy reported by Lynn et al. (11, 12). The resulting polymers are highly branched, 14–30 kDa polycations. We show that these polymers are capable of gene delivery activity two- to 16-fold greater than nondegradable, 25-kDa PEI. Importantly, these polymers show negligible toxicity in the cell lines studied to date.

## MATERIALS AND METHODS

**Cells and Plasmid DNA.** The MDA-MB-231 human breast carcinoma cell line was purchased from the American Type Culture Collection, and the C2C12 murine myoblast cell line was a gift from Prof. Stephen Kaufman (University of Illinois, Urbana, IL). All cell lines were maintained according to their respective ATCC protocols, at 37 °C and 5% CO<sub>2</sub>, but were adapted from fetal bovine serum to heat-inactivated horse serum. The 5.3-kilobase pair expression vector, pGL3 (Promega, Madison, WI), containing the luciferase gene driven by the SV40 promoter and enhancer, was grown in DH5α *E. coli* (Gibco BRL, Rockville, MD) and purified using a commercial plasmid purification kit (Bio-Rad, Hercules, CA). Plasmids were further purified by ethanol precipitation; the ratio of absorbances at 260 and 280 nm was 1.8 or greater.

**General Polymer Cross-Linking Procedure.** All reagents were purchased from Sigma-Aldrich (St. Louis, MO) and used without further purification unless noted otherwise. Cross-linking was performed following the procedure of Lynn et al. (11, 12). One gram of PEI (branched, 800 Da) was transferred to a 1-oz scintillation vial and dissolved in 3 mL of freshly distilled methylene chloride (417 mM solution). An equimolar amount of diacrylate linker (417 mM) was added dropwise, and the vial was sealed with a solvent-resistant cap. The reaction was carried out at 45 °C, with shaking, for 6 h. The polymer was then precipitated with hexanes, lyophilized (Labconco 18L Freeze-Dry System, Kansas City, MO), and stored at –80 °C.

**Synthesis of Polymer 1.** Polymer 1 was prepared according to the procedure above using 1,3-butanediol diacrylate as the cross-linker. <sup>1</sup>H NMR (400 MHz, D<sub>2</sub>O): δ = 3.95 (br m, 2 H, NHCH<sub>2</sub>CH<sub>2</sub>COOCH<sub>2</sub>, ester linker), 3.88 (br m, 2 H, NHCH<sub>2</sub>CH<sub>2</sub>COOCH(CH<sub>3</sub>), ester linker), 3.5–3.35 (br m, 2 H, OHCH<sub>2</sub>CH<sub>2</sub>, hydrolyzed ester), 3.3–2.5 (br m, 49 H, [CH<sub>2</sub>CH<sub>2</sub>N]<sub>x</sub>[CH<sub>2</sub>CH<sub>2</sub>NH]<sub>y</sub>[CH<sub>2</sub>CH<sub>2</sub>NH<sub>2</sub>]<sub>z</sub>, PEI ethylenes, 2.4 (br m, 2 H, NHCH<sub>2</sub>CH<sub>2</sub>COOCH<sub>2</sub>, ester linker), 2.33 (br m, 2 H, NHCH<sub>2</sub>CH<sub>2</sub>COOCH<sub>2</sub>, ester linker), 1.48 (br m, 2 H, COOCH<sub>2</sub>CH<sub>2</sub>, ester linker), 1.37 (t, 1 H, CH<sub>2</sub>CH<sub>2</sub>CH(CH<sub>3</sub>)OH, hydrolyzed ester), 1.2 (t, 3 H, CH<sub>2</sub>CH<sub>2</sub>CH(CH<sub>3</sub>)OCOCH<sub>2</sub>CH<sub>2</sub>NH, ester linker). Elemental anal. (mass fraction): (C: 0.409, H: 0.0853, N: 0.1784).

**Synthesis of Polymer 2.** Polymer 2 was prepared according to the procedure above using 1,6-hexanediol

diacrylate as the cross-linker. <sup>1</sup>H NMR (400 MHz, D<sub>2</sub>O): δ = 4.1–3.9 (br m, 2 H, NHCH<sub>2</sub>CH<sub>2</sub>COOCH<sub>2</sub>, ester linker), 3.55–3.35 (br m, 2 H, OHCH<sub>2</sub>CH<sub>2</sub>, hydrolyzed ester), 3.3–2.5 (br m, 90 H, [CH<sub>2</sub>CH<sub>2</sub>N]<sub>x</sub>[CH<sub>2</sub>CH<sub>2</sub>NH]<sub>y</sub>[CH<sub>2</sub>CH<sub>2</sub>NH<sub>2</sub>]<sub>z</sub>, PEI ethylenes, 2.45 (br m, 2 H, NHCH<sub>2</sub>CH<sub>2</sub>COOCH<sub>2</sub>, ester linker), 2.35 (br m, 2 H, NHCH<sub>2</sub>CH<sub>2</sub>COOCH<sub>2</sub>, ester linker), 1.2 (br m, 2 H, COOCH<sub>2</sub>CH<sub>2</sub>, ester linker), 1.1 (br m, 2 H, –COOCH<sub>2</sub>CH<sub>2</sub>– ester). Elemental anal. (mass fraction): (C: 0.412, H: 0.0986, N: 0.1754).

**Polymer Degradation Studies.** Polymers were dried in vacuo overnight. Polymer (150.0 mg) was dissolved in 1.0 mL of D<sub>2</sub>O. The solutions were then adjusted to pH 5.0 or 7.0 using deuterated buffer salts and incubated at 37 °C for specified times from 0 to 60 h. <sup>1</sup>H NMR spectra were obtained on a Varian Unity 500 MHz spectrometer with a 5-mm probe. The fraction of esters was determined by comparing δ 4.0–3.8 (ester linker [see synthesis]) and δ 3.3–2.5 ([CH<sub>2</sub>CH<sub>2</sub>N]<sub>x</sub>[CH<sub>2</sub>CH<sub>2</sub>NH]<sub>y</sub>[CH<sub>2</sub>CH<sub>2</sub>NH<sub>2</sub>]<sub>z</sub>, PEI) peaks.

**Complex Formation and Transfection.** DNA–polymer complexes (polyplexes) were prepared in 20 mM PIPES, 150 mM NaCl (pH 7.3) by addition of 150 μL of polymer to an equal volume of 3 μg of plasmid to achieve the desired polymer to DNA ratio. Polyplexes were then incubated at 4 °C for 15 min. Cells were cultured in DMEM supplemented according to ATCC protocols and plated in six-well plates at 1 × 10<sup>5</sup> cells/well 24 h prior to transfection. Immediately before transfection, the growth medium was replaced with serum-free medium, and 100 μL of polyplexes (1 μg plasmid/well) was added to each well. Transfection medium was replaced with growth medium 4 h post transfection. Luciferase expression was quantified 24 h later using a Promega luciferase assay system. Luciferase activity was measured in relative light units (RLU) using a Lumat LB 9507 luminometer (Berthold, GmbH, Germany) and converted to luciferase concentration by comparing to recombinant luciferase standards (Promega). Results were normalized to total cell protein as determined using a Bio-Rad Protein Assay Kit. All samples were run in triplicate and on two or more separate occasions.

**Cytotoxicity Determination.** Cytotoxicity was characterized as a decrease in metabolic rate measured using the XTT assay (15). Cells were plated in 96-well plates at an initial density of 50 000 cells per well in 100 μL of growth medium for 24 h. Afterward, the growth medium was replaced with fresh, serum-free medium containing the polymer of interest. Cells were incubated with polymers for 4 h, and the medium was replaced with complete growth medium for 24 h. Fresh XTT (1 mg/mL) and coenzyme Q<sub>0</sub> (80 μg/mL) stock were prepared each day in PBS and filter sterilized (0.22-μm syringe filter). Both components were diluted in PBS (0.5 μg/μL XTT and 0.04 μg/μL coenzyme Q<sub>0</sub>), and 10-μL aliquots were added to each well. The samples were incubated for 4 h at 37 °C, and the absorbance was read at 450 nm relative to blank wells prepared without cells. The cytotoxicity of polymer degradation products was measured by first incubating the degradable polymers for 60 h (PBS, 37 °C) before applying the polymers to the cells.

**Viscosity Measurements.** Polymers were dissolved in PBS to concentrations of 150 mg/mL to 20 mg/mL, and pH was adjusted to 7.3. Solution viscosity, η, was determined with an AR1000–N Rheometer with a 6-cm, 0.29° plate (TA Instruments, New Castle, DE) at 25 °C. The intrinsic viscosity, η<sub>int</sub>, was determined by η<sub>int</sub> = lim<sub>c→0</sub> [ln(η/η<sub>0</sub>)/c], where η<sub>0</sub> is solvent viscosity and c is polymer concentration. The molecular weight of cross-

linked polymers was determined using the following relationship:  $\eta_{\text{int}} = KM^a$ , where  $M$  is the molecular weight and  $K$  and  $a$  are Mark-Houwink parameters determined from PEI standards of known molecular weight.

**Gel Retardation and Dye Exclusion Assays.** Appropriate amounts of each polymer, in 10  $\mu\text{L}$  of 20 mM PIPES, 150 mM NaCl (pH 7.3), were added to an equal volume of DNA solution (500 ng/10  $\mu\text{L}$ ) to achieve the desired polymer to DNA ratio. Polyplexes were incubated at 4  $^{\circ}\text{C}$  for 15 min, after which 10  $\mu\text{L}$  was loaded and run on a 0.75% agarose gel (70 V, 1 h). Gels were visualized with Vista Green staining (Molecular Probes, Eugene, OR). For intercalating dye exclusion assays, polyplexes were prepared as above, diluted in PBS to a concentration of 1  $\mu\text{g}$  DNA/mL, and incubated at 37  $^{\circ}\text{C}$  for 24 h. Ethidium bromide (1  $\mu\text{M}$ ) was added and the fluorescence intensity measured ( $\lambda_{\text{excitation}} = 500 \text{ nm}$ ,  $\lambda_{\text{emission}} = 600 \text{ nm}$ ).

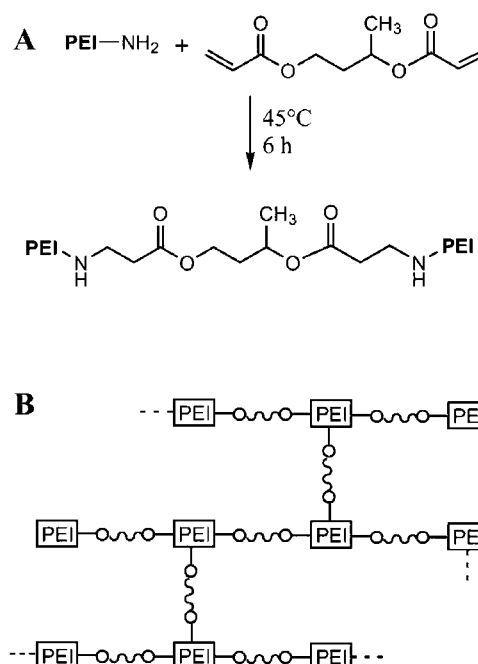
**Dynamic Light Scattering (DLS) Size Determination.** Polyplexes were prepared as in the above transfection procedure. Polyplexes were then diluted with PBS to a final concentration of 1  $\mu\text{g}$  DNA/mL. Polyplex size determination was performed on a DynaPro-MS800 (Protein Solutions, Lakewood, NJ) with Dynamics v6.3 software. The effect of polymer degradation on polyplexes was examined by incubating the complexes at 37  $^{\circ}\text{C}$  and performing light scattering analyses at specified time intervals. Samples were run in triplicate.

**Transmission Electron Microscopy.** Polyplexes were prepared as described above in the transfection procedure. Samples were placed on a carbon-coated grid and negatively stained with uranyl acetate. Micrographs were obtained using a Hitachi H600 transmission electron microscope, and 15-nm gold particles were used as size standards.

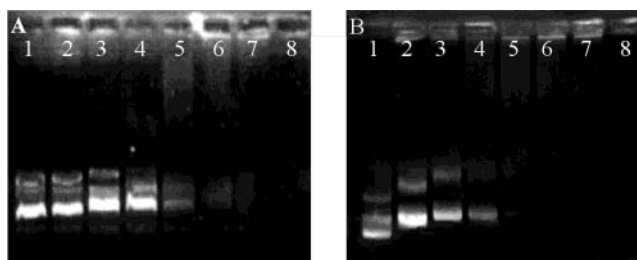
## RESULTS

**Synthesis of Degradable Polyethylenimines.** The biodegradable polyethylenimines, **1** and **2**, were synthesized by cross-linking 800-Da PEI using the diacrylate cross-linkers 1,3-butanediol diacrylate and 1,6-hexanediol diacrylate, respectively (Figure 1). The cross-linking was confirmed by observing extensive ester bond formation in the final product using  $^1\text{H}$  NMR. Although it is not possible to determine from NMR whether the observed cross-linking was inter- or intramolecular, the increased viscosity of **1** and **2**, relative to the starting material, can be directly correlated to molecular weight using Mark-Houwink theory. We determined the intrinsic viscosity of the cross-linked polymer with a cone-and-plate rheometer and, based on PEI standards, found that polymer **1** had a molecular weight of  $\sim 14 \text{ kDa}$ . Polymer **2** was found to have a molecular weight of  $\sim 30 \text{ kDa}$ . Given the starting material molecular weight of 800 Da, extensive intermolecular cross-linking apparently occurred in the formation of **1** and **2**. Previous reports have indicated that PEI with molecular weight between 10 and 70 kDa are generally efficient for gene delivery (4, 16–18).

**Characterization of Degradable Polyethylenimines.** High molecular weight PEI forms very compact particles with DNA through electrostatic attraction (19). The formation of these polyplexes can be observed as a reduction of mobility of the DNA in gel electrophoresis. We mixed DNA with increasing amounts of polymer to determine the ability of **1** and **2** to form polyplexes with DNA. Polymers **1** and **2** both completely retarded the DNA migration at a ratio of  $\sim 1:3$  (w:w) (Figure 2), indicating the formation of charge-neutral complexes.



**Figure 1.** Synthesis of degradable PEI derivatives. (A) 800-Da PEI is reacted with diacrylates (1,3-butanediol diacrylate shown) to generate the ester-cross-linked polymers. (B) The acrylate groups can react with either primary or secondary amines, resulting in a highly branched structure.

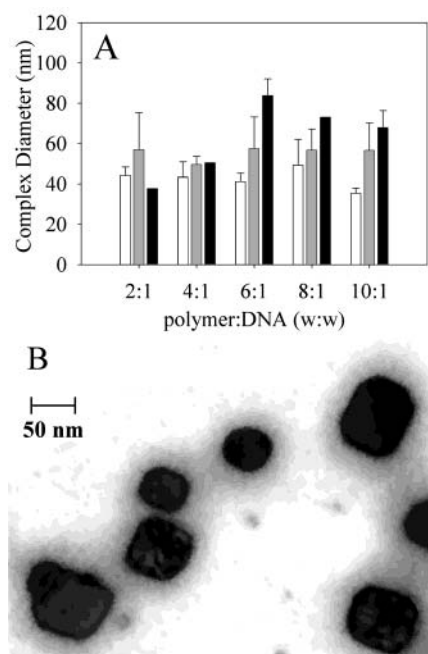


**Figure 2.** Agarose gel electrophoresis of polymer/DNA complexes. (A) Polymer **1** and (B) polymer **2** (polymer:DNA, w:w): lane 1, 0.1:1; lane 2, 0.15:1; lane 3, 0.2:1; lane 4, 0.25:1; lane 5, 0.3:1; lane 6, 0.35:1; lane 7, 0.4:1; lane 8, 0.45:1.

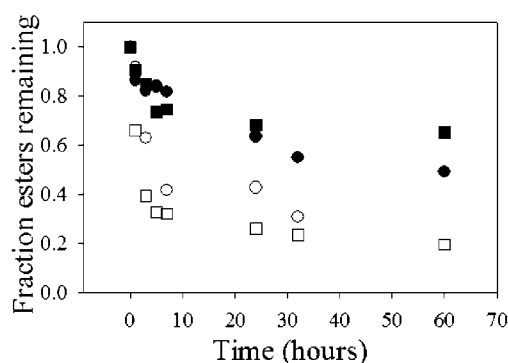
The same ratio, 1:3 w:w, of 25-kDa PEI/DNA was found to completely retard migration of plasmid (data not shown). Therefore, amidation of PEI by the cross-linker does not appear to affect its ability to condense DNA.

For efficient endocytosis and transfection to occur, the complexes must be small and compact (20). Dynamic light scattering showed that **1** and **2** formed small particles, 30 to 80 nm in diameter, over the ratio of polymer:DNA ratios examined (Figure 3A). Complexes formed in the same way using commercially available 25-kDa PEI were similar in size. The sizes of the particles were confirmed by transmission electron microscopy (TEM) using 15-nm gold particles as size standards (Figure 3B), and the complexes appeared to be compact particles. Previous reports have indicated that polyplexes in this size range are efficiently endocytosed by cells (2, 19, 21–23).

**Degradation of Polyethylenimine Derivatives.** The degradation of gene delivery polymers is an important concern for design of safe and efficient gene therapy vehicles. The commonly used 25-kDa PEI is known to be cytotoxic in many cell lines. Further, nondegradable PEI may accumulate in vivo since there is no degradation or excretion pathway, increasing its potential cytotoxicity (4). The ester bonds in **1** and **2** are susceptible to hydrolysis at physiological conditions to form the diol

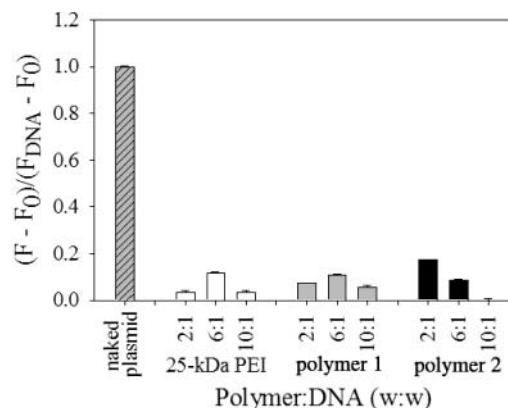


**Figure 3.** (A) Dynamic light scattering of polymer/DNA polyplexes. White bars, 25-kDa PEI; gray bars, polymer 1; black bars, polymer 2. ( $N = 3$ , error bars represent standard deviation). (B) Transmission electron microscopy of polymer/DNA complexes.

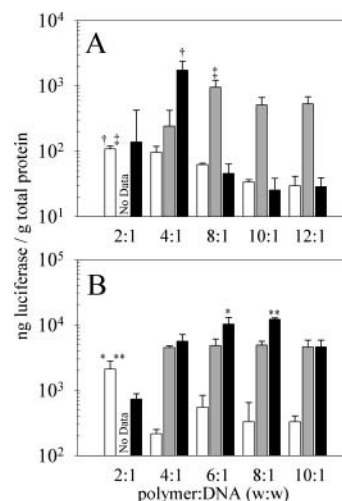


**Figure 4.** Degradation of polyethylenimine derivatives.  $\circ$ , polymer 1, pH 7.0;  $\square$ , polymer 1, pH 5.0;  $\bullet$ , polymer 2, pH 7.0;  $\blacksquare$ , polymer 2, pH 5.0. The fraction of esters remaining was determined using  $^1\text{H}$  NMR by integrating ester peaks ( $\text{COOH}$ , linker) and normalizing to the polyethylenimine backbone ( $[\text{CH}_2\text{CH}_2\text{N}]_x[\text{CH}_2\text{CH}_2\text{NH}]_y[\text{CH}_2\text{CH}_2\text{NH}_2]_z$ ).

linker and amino acid. Using NMR, we investigated the hydrolysis of the ester bond in the degradable polyethylenimines. Polymer 1 had a half-life of 4 h, and 2 had a half-life of 30 h, based on the remaining fraction of ester bonds (Figure 4). Degradation rates remained relatively constant between near-neutral, cytoplasmic conditions and endolysosomal conditions, pH 5.0. A further question was whether polymer degradation could weaken the complex, exposing the condensed DNA to cellular degradation mechanisms. Well-condensed DNA is inaccessible to intercalating dyes, such as ethidium bromide, which have a very high binding affinity for DNA (24). We found that after 24 h of incubation in PBS at 37 °C, 1 and 2 prevented ethidium bromide intercalation, suggesting that the partially degraded polymers are still capable of complexing with and protecting the plasmid (Figure 5). DLS studies also showed that degradable polyplexes remain compact for at least 6 h after formation. DNA was condensed with 1 and 2, and DLS measurements were taken at 0, 6, and 24 h postforma-



**Figure 5.** Ethidium bromide exclusion from polymer/DNA complexes. White bars, 25-kDa PEI; gray bars, polymer 1; black bars, polymer 2. Fraction DNA intercalated is calculated as  $(F - F_0)/(F_{\text{DNA}} - F_0)$ .  $F$ , fluorescence from solution containing ethidium bromide and the complexes;  $F_0$ , fluorescence from solution of ethidium bromide only; and  $F_{\text{DNA}}$ , fluorescence from solution of DNA and ethidium bromide ( $N = 3$ , error bars represent standard deviation).

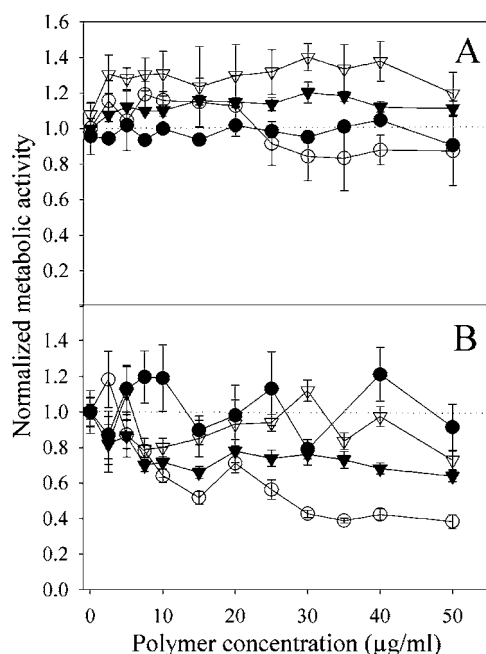


**Figure 6.** Gene delivery activity of degradable PEI derivatives. Luciferase expression in (A) MDA-MB-231 ( $\dagger$ ,  $p < 0.05$ ;  $\ddagger$ ,  $p < 0.02$ ). (B) Luciferase expression in C2C12 cells transfected with polymer/DNA polyplexes (\*,  $p < 0.005$ ; \*\*,  $p < 0.00005$ ). White bars, 25-kDa PEI; gray bars, polymer 1; black bars, polymer 2. Luciferase expression was normalized by total cellular protein ( $N = 6$ , error bars represent standard deviation).

tion. Polyplexes containing 1 and 2 increased in size by 25 and 50%, respectively, but remained smaller than 80 nm up to 6 h after being formed. This was similar to the control, 25-kDa PEI, which increased in size by 40% at 6 h. Beyond 6 h, complex aggregation and precipitation made accurate DLS measurements impossible.

**Cell Transfection Studies.** We investigated the efficacy of the cross-linked polyethylenimine polymers in gene delivery to human breast carcinoma cells, MDA-MB-231, and murine myoblasts, C2C12. Both cell lines were transfected in vitro with 1  $\mu\text{g}$  of plasmid DNA complexed with various polymers. Gene transfection efficiency was measured as luciferase enzyme activity and normalized to total cell protein (Figure 6). The starting material, 800-Da PEI, induced no measurable gene expression over the range of polymer:DNA ratios investigated (data not shown). These data are in agreement with results from other groups that have reported a lack of transfection of various cell lines using <2000-Da PEI (5, 25). In contrast, 25-kDa PEI was found to induce high levels of luciferase expression in both C2C12





**Figure 7.** Cytotoxicity of degradable PEI derivatives. Metabolic activity of (A) MDA-MB-231 and (B) C2C12 cell lines in the presence of varying amounts of 25-kDa PEI (○), 800-Da PEI (●), polymer **1** (▽), and polymer **2** (▼). Metabolic activity was normalized to controls with no polymer ( $N = 8$ , error bars represent standard deviation).

and MDA-MB-231 cell lines (Figure 6). The optimal charge ratio for 25-kDa PEI was found at a polymer:DNA ratio of 2:1 (w:w), corresponding to a nitrogen:phosphate ratio of 11:1.

DNA was condensed with **1** and **2** at various ratios and used to transfect MDA-MB-231 and C2C12 cell lines. Polymer **1** mediated luciferase expression at least 2-fold greater than 25-kDa PEI in C2C12 cells and 9-fold greater than 25-kDa PEI in MDA-MB-231 cells. Polymer **2** was even more efficient, yielding luciferase levels 6-fold greater than 25-kDa PEI in C2C12 cells and 16-fold greater than 25-kDa PEI in MDA-MB-231 cells (Figure 6).

Optimal polymer:DNA ratios were very different for the two cell lines, indicating that the polymer:DNA ratios must be optimized for each cell line of interest. Polymer **1** was most efficient at an 8:1 (w:w) ratio in MDA-MB-231 cells, while there was little change from 4:1 to 10:1 (w:w) in the C2C12 cell line. The optimal ratio for **2** was found to be 4:1 in MDA-MB-231 cells, and expression levels dropped sharply at higher and lower ratios. In C2C12 cells, the optimal ratio for polymer **2** was approximately 8:1 (w:w). Overall, much higher polymer:DNA ratios were required for optimal gene expression with **1** and **2** than with 25-kDa PEI.

**Cytotoxicity of Degradable PEI.** High molecular weight PEI has been reported to be significantly more toxic than low molecular weight PEI (3–5). To determine if the biodegradable polyethylenimine derivatives retained the low cytotoxicity of the 800-Da PEI starting material, we assayed cytotoxicity as reduced metabolic activity using the XTT assay. MDA-MB-231 cells and C2C12 cells were exposed to various concentrations of polymers for 4 h, and cytotoxicity was assayed 20 h later (Figure 7). MDA-MB-231 cells were resistant to 25-kDa PEI, and metabolic activities remained near control levels over the concentration range investigated. Metabolic activity increased slightly above baseline levels for both

**1** and **2**, indicating that the polymers were essentially nontoxic at concentrations normally used in gene therapy. The 25-kDa PEI is very cytotoxic to C2C12 cells, reducing metabolic activity by 50% at 15  $\mu\text{g/mL}$ , the concentration used in transfection studies. Polymer **1** was significantly less cytotoxic than 25-kDa PEI, reducing C2C12 metabolic activity by only 15%. Polymer **2**, which had a longer half-life than **1**, reduced metabolic activity by 30% (Figure 7). Overall, the degradable polyethylenimine derivatives were significantly less toxic than 25-kDa PEI in the C2C12 cell lines and essentially nontoxic, similar to 25-kDa PEI, in the MDA-MB-231 cells.

Since the degradable PEI's were formed using a Michael-type reaction, they may degrade via a retro-Michael reaction and form potentially harmful acrylate esters (12). Thus, we investigated the cytotoxicity of the polymer degradation products. Polymers **1** and **2** were incubated for 60 h at 37  $^{\circ}\text{C}$  in PBS and metabolic activities of MDA-MB-231 and C2C12 cells were measured after exposure to the degraded polymer mixtures. Metabolic activity of both cell types remained above the baseline level over the observed concentration range (0–50  $\mu\text{g/mL}$ ) indicating that the hydrolyzed ester linkers are essentially nontoxic, in agreement with previous reports (12).

## DISCUSSION

The primary requirements for a clinically effective vehicle for human gene therapy are efficient gene transfer and safety. Nonviral vectors, including liposomes and polymers, are typically safer but much less efficient than recombinant viruses. In addition, many polymers still exhibit significant cytotoxicity in important cell lines. As a result, less than 15% of clinical trials have employed nonviral vectors, and the majority of these used lipofection rather than polymers (26).

We hypothesize that degradable polymers will be less toxic and may also aid in other steps in the gene delivery pathway. There is a need to investigate how the polymer properties, such as molecular weight, type of degradable linkage, and structure of the monomers, impact degradability, toxicity, and gene transfer activity. Rather than synthesize entirely new polymer chemistries, we sought to design polymers around the already successful PEI building blocks that allow facile synthesis of diverse chemical structures. The amine/diacrylate addition reaction (11, 12) is a good starting point, as the chemistry is relatively simple and a wide variety of diacrylates is commercially available.

We have synthesized a set of polymers via addition of linear, low-molecular-weight PEI to two simple diacrylates with three- and six-carbon spacers, respectively. The resulting polymers are composed of several hundred PEI monomers and are highly cross-linked. The molecular weights of the polymers (14 000–30 000) are similar to the weights of other frequently used gene delivery polymers (4, 17). Ethidium bromide exclusion studies confirmed that the polymer tightly compacts plasmid DNA, and the polyplexes are small enough to be efficiently endocytosed (2, 19, 21–23, 27). In addition, complexes containing polymers **1** and **2** formed at polymer:DNA ratios similar to polyplexes containing the 800-Da PEI starting material or 25-kDa PEI. Thus, it appears that the cross-linked structures of polymers **1** and **2** have little effect on the ability of the polymers to bind and condense plasmid DNA, and polyplexes containing **1** and **2** are very similar to those of previously reported gene delivery vehicles.

Several groups have taken the approach of cross-linking low molecular weight PEI, but unfortunately the effects of the polymer degradation on gene transfer have not been directly addressed. The first report was that of Gosselin et al. (5) who cross-linked the same 800-Da PEI starting material with the amine-reactive disulfides dithiobis(succinimidylpropionate) and dimethyl-3,3'-dithiobispropionimidate. The disulfide bonds of these polymers were expected to be cleaved in the reducing environment of the cytoplasm. Cytotoxicity was significantly reduced relative to 25-kDa PEI, presumably due to degradation, but the best polymers were several times less effective than 25-kDa PEI. No data regarding the degradation kinetics of these polymers were reported. The ester-cross-linked PEI-PEG polymers of Ahn et al. (14) are also much less cytotoxic than 25-kDa PEI, but again no data regarding their degradation were given. The PEI-PEG polymers were 3-times more effective than the 1.8-kDa PEI starting material, which the authors characterize as showing almost no transfection. The transfection activities of these polymers were not compared to 25-kDa PEI, making comparison to the polymers reported here difficult.

Polymers **1** and **2** exhibit gene transfer activity 2- to 16-fold greater than 25-kDa PEI, depending on the cell line transfected, making them some of the most effective polymers reported to date. Yet it is unclear at present why these polymers are more effective than 25-kDa PEI. Potentially limiting barriers to efficient gene transfer include endocytosis, escape from endocytic vesicles into the cytoplasm, cytoplasmic motility, transport across the nuclear membrane, and unpackaging of the polyplexes (28, 29). Because of the similarity of polyplexes containing **1** or **2** as compared to 25-kDa PEI, it seems unlikely that there would be significant differences in the amounts of polyplexes endocytosed, their ability to escape from endolysosomes, their cytoplasmic motility, or their transport across the nuclear membrane. Although direct measurements must await future studies, we believe that the most advantageous properties of **1** and **2** may be their lack of toxicity and perhaps a more optimal balance between sufficiently strong binding for protection of the DNA and weaker binding of the degraded polymer possibly allowing increased efficiency of unpackaging of the polyplexes.

Reduced toxicity is undoubtedly a significant benefit of the degradable PEI as compared to 25-kDa PEI. It appears that the reduced toxicity may be correlated with polymer degradation. Polymer **2** had a significantly longer half-life than polymer **1** (>30 vs ~4 h) and was more toxic to the PEI-sensitive C2C12 cell line. And of course, nondegradable 25-kDa PEI is the most toxic. The reduced toxicity of **1** and **2** relative to 25-kDa PEI may partially explain the higher levels of gene transfer mediated with degradable PEI.

Reduced toxicity cannot be the only factor responsible for increased gene transfer, however. MDA-MB-231 cells are resistant to all three polymers, yet polymers **1** and **2** are ~10-fold better transfection agents than 25-kDa PEI in these cells. In addition, polymer **2** is more effective at gene transfer in C2C12 cells than polymer **1**, yet it is more toxic (polymer **2** reduced the metabolic activity of the cells twice as much as **1** at 15  $\mu\text{g/mL}$ ). This comparison is complicated, however, by the different molecular weights of **1** and **2**. Several studies have shown that there is a correlation between increased gene transfer activity and increased molecular weight of PEI in a similar range of polymer sizes (4, 18).

The mechanism of cytotoxicity of PEI is poorly understood. One hypothesis is that PEI aggregates on the cell surface and impairs important membrane functions (4, 30). Other possibilities are that PEI, free or in complexes with DNA, interferes with critical intracellular processes. We have shown reduced cytotoxicity even with polymers **1** and **2** that do not degrade significantly until long after most complexes have been endocytosed. Thus, our data support the importance of intra- rather than extracellular effects of PEI on the health of target cells.

Polymer degradation may also enhance transfection by facilitating the "unpackaging" of the DNA-polymer complex. Tight binding of the polymer to the plasmid is expected to hinder binding of proteins required for initiation of gene expression. In fact, several studies have found that reducing the polymer/DNA binding strength by reducing the number of positive charges (31), conjugation of PEG chains (32), or decreasing the polymer molecular weight (4, 17) leads to increased gene expression. We may expect that the degraded polymer, consisting of 800-Da PEI segments, may similarly allow more facile transcription of the plasmid.

In conclusion, we have shown that polymers comprising 800-Da PEI cross-linked with diacrylates exhibit low toxicity and can be more than 1 order of magnitude more efficient gene transfer agents than commercially available 25-kDa PEI. Low molecular weight PEI, in general, shows low cytotoxicity. In addition, the smaller polymers are hypothesized to allow easier transcription of the packaged plasmid DNA. However, small PEI polymers are known to be poor transfection agents. The degradable PEI reported here appears to provide the beneficial functions of 25-kDa PEI, but upon degradation we believe the polymer allows for more efficient transcription and interferes less with normal cell functions. Future studies will examine the effects of the polymer structure and degradation kinetics on specific barriers including cell uptake, escape from endocytic vesicles, and unpackaging.

#### ACKNOWLEDGMENT

The work was supported by awards from the American Heart Association and the National Science Foundation (BES-0120101 and BES-0134163). In addition, acknowledgment is made to the donors of the Petroleum Research Fund, administered by the ACS, for partial support of this research. We thank Amy Balija for her valuable assistance with synthesis and NMR, and also Prof. Steven C. Zimmerman (University of Illinois, Urbana, IL) and Prof. Anthony McHugh (University of Illinois) for the generous use of their equipment and facilities.

#### NOTE ADDED AFTER ASAP POSTING

In Figure 1 of the manuscript posted August 26, 2003, one of the carbonyl groups was missing in the top diacrylate. The corrected version of the manuscript was published September 8, 2003.

#### LITERATURE CITED

- (1) Verma, I. M., and Somia, N. (1997) Gene therapy – promises, problems and prospects. *Nature* 389, 239–242.
- (2) Godbey, W. T., Wu, K. K., and Mikos, A. G. (1999) Poly(ethylenimine) and its role in gene delivery. *J. Controlled Release* 60, 149–160.
- (3) Lim, Y.-B., Kim, S.-M., Suh, H., and Park, J.-S. (2002) Biodegradable, endosome disruptive, and cationic network-type polymer as a highly efficient and nontoxic gene delivery carrier. *Bioconjugate Chem.* 13, 952–957.
- (4) Fischer, D., Bieber, T., Li, Y., Elsässer, H.-P., and Kissel, T. (1999) A novel nonviral vector for DNA delivery based on

- low molecular weight, branched polyethylenimine: effect of molecular weight on transfection efficiency and cytotoxicity. *Pharm. Res.* **16**, 1273–1279.
- (5) Gosselin, M. A., Guo, W., and Lee, R. J. (2001) Efficient gene transfer using reversibly cross-linked low molecular weight polyethylenimine. *Bioconjugate Chem.* **2001**, 989–994.
- (6) Lim, Y. B., Han, S. O., Kong, H. U., Lee, Y., Park, J. S., Jeong, B., and Kim, S. W. (2000) Biodegradable polyester, poly[ $\alpha$ -(4-aminobutyl)-L-glycolic acid], as a nontoxic gene carrier. *Pharm. Res.* **17**, 811–816.
- (7) Lim, Y.-B., Choi, Y. H., and Park, J.-S. (1999) A self-destroying polycationic polymer: Biodegradable poly(4-hydroxy-L-proline ester). *J. Am. Chem. Soc.* **121**, 5633–5639.
- (8) Lim, Y.-B., Kim, C.-H., Kim, K., Kim, S. W., and Park, J.-S. (2000) Development of a safe gene delivery system using biodegradable polymer, poly[ $\alpha$ -(4-aminobutyl)-L-glycolic acid]. *J. Am. Chem. Soc.* **122**, 6524–6525.
- (9) Lim, Y.-B., Kim, S.-M., Lee, Y., Lee, W.-K., Yang, T.-G., Lee, M.-J., Suh, H., and Park, J.-S. (2001) Cationic hyperbranched poly(amino ester): A novel class of DNA condensing molecule with cationic surface, biodegradable three-dimensional structure, and tertiary amine groups in the interior. *J. Am. Chem. Soc.* **123**, 2460–2461.
- (10) Putnam, D., and Langer, R. (1999) Poly(4-hydroxy-L-proline ester): Low-temperature polycondensation and plasmid DNA complexation. *Macromolecules* **32**, 3658–3662.
- (11) Lynn, D. M., Anderson, D. G., Putnam, D., and Langer, R. (2001) Accelerated discovery of synthetic transfection vectors: Parallel synthesis and screening of a degradable polymer library. *J. Am. Chem. Soc.* **123**, 8155–8156.
- (12) Lynn, D. M., and Langer, R. (2000) Degradable poly( $\beta$ -amino esters): synthesis, characterization, and self-assembly with plasmid DNA. *J. Am. Chem. Soc.* **122**, 10761–10768.
- (13) Pichon, C., LeCam, E., Guérin, B., Coulaud, D., Delain, E., and Midoux, P. (2002) Poly[Lys-(AEDTP)]: A cationic polymer that allows dissociation of pDNA/cationic polymer complexes in a reductive medium and enhances polyfection. *Bioconjugate Chem.* **13**, 76–82.
- (14) Ahn, C.-H., Chae, S. Y., Bae, Y. H., and Kim, S. W. (2002) Biodegradable poly(ethylenimine) for plasmid DNA delivery. *J. Controlled Release* **80**, 273–282.
- (15) Stevens, M. G., and Olsen, S. (1993) Comparative analysis of using MTT and XTT in colorimetric assays for quantitating bovine neutrophil bactericidal activity. *J. Immunol. Methods* **157**, 225–231.
- (16) Remy, J.-S., Abdallah, B., Zanta, M. A., Boussif, O., Behr, J.-P., and Demeneix, B. (1998) Gene transfer with lipospermines and polyethylenimines. *Adv. Drug Deliv. Rev.* **30**, 85–95.
- (17) Bieber, T., and Elsässer, H.-P. (2001) Preparation of a low molecular weight polyethylenimine for efficient cell transfection. *Biotechniques* **30**, 74–81.
- (18) Godbey, W. T., Wu, K. K., and Mikos, A. G. (1999) Size matters: molecular weight affects the efficiency of poly(ethylenimine) as gene delivery vehicle. *J. Biomed. Mater. Res.* **45**, 268–275.
- (19) Dunlap, D. D., Maggi, A., Soria, M. R., and Monaco, L. (1997) Nanoscopic structure of DNA condensed for gene delivery. *Nucleic Acids Res.* **25**, 3095–3101.
- (20) Liu, G., Molas, M., Grossmann, G. A., Pasumarthy, M., Perales, J. C., Cooper, M. J., and Hanson, R. W. (2001) Biological properties of poly-L-lysine-DNA complexes generated by cooperative binding of the polycation. *J. Biol. Chem.* **276**, 34379–34387.
- (21) Boussif, O., Zanta, M. A., and Behr, J.-P. (1996) Optimized galenics improve in vitro gene transfer with cationic molecules up to 1000-fold. *Gene Ther.* **3**, 1074–1080.
- (22) Boussif, O., Lezoualc'h, F., Zanta, M. A., Mergny, M. D., Scherman, D., Demeneix, B., and Behr, J.-P. (1995) A versatile vector for gene and oligonucleotide transfer into cells in culture and in vivo: Polyethylenimine. *Proc. Natl. Acad. Sci. U.S.A.* **92**, 7297–7301.
- (23) Godbey, W. T., Barry, M. A., Saggau, P., Wu, K. K., and Mikos, A. G. (2000) Poly(ethylenimine)-mediated transfection: a new paradigm for gene delivery. *J. Biomed. Mater. Res.* **51**, 321–328.
- (24) Pack, D. W., Putnam, D., and Langer, R. (1999) Design of imidazole-containing endosomolytic biopolymers for gene delivery. *Biotechnol. Bioeng.* **67**, 217–223.
- (25) Godbey, W. T., Wu, K. K., and Mikos, A. G. (1997) Size matters: molecular weight affects the efficiency of poly(ethylenimine) as a gene delivery vehicle. *Proceed. Int. Symp. Control. Relat. Bioact. Mater.* **25**, 230–231.
- (26) Protocols by Vector. *J. Gene Med.* (<http://www.wiley.co.uk/genetherapy/clinical/>). Accessed Jan. 3, 2003.
- (27) Perales, J. C., Ferkol, T., Molas, M., and Hanson, R. W. (1994) An evaluation of receptor-mediated gene transfer using synthetic DNA-ligand complexes. *Eur. J. Biochem.* **226**, 255–266.
- (28) Hwang, S. J., and Davis, M. E. (2001) Cationic polymers for gene delivery: Designs for overcoming barriers to systemic administration. *Curr. Opin. Biotechnol.* **3**, 183–191.
- (29) Pack, D. W. (2001) Gene delivery polymers, in *Encyclopedia of Polymer Science and Technology* (J. I. Kroschwitz, Ed.) John Wiley & Sons, Inc., New York.
- (30) Ryser, H. J.-P. (1967) A membrane effect of basic polymers dependent on molecular size. *Nature* **215**, 934–936.
- (31) Erbacher, P., Roche, A. C., Monsigny, M., and Midoux, P. (1997) The reduction of the positive charges of polylysine by partial gluconoylation increases the transfection efficiency of polylysine/DNA complexes. *Biochim. Biophys. Acta* **1324**, 27–36.
- (32) Banaszczuk, M. G., Lollo, C. P., Kwok, D. Y., Phillips, A. T., Amini, A., Wu, D. P., Mullen, P. M., Coffin, C. C., Brostoff, S. W., and Carlo, D. J. (1999) Poly-L-lysine-graft-PEG-comb-type polycation copolymers for gene delivery. *J. Macromol. Sci., Pure Appl. Chem.* **36**, 1061–1084.

BC034014G



# Modulation of the Pharmacokinetic Properties of PNA: Preparation of Galactosyl, Mannosyl, Fucosyl, *N*-Acetylgalactosaminyl, and *N*-Acetylglucosaminyl Derivatives of Aminoethylglycine Peptide Nucleic Acid Monomers and Their Incorporation into PNA Oligomers

Ramin Hamzavi,<sup>†,‡</sup> Frédéric Dolle,<sup>§</sup> Bertrand Tavitian,<sup>||</sup> Otto Dahl,<sup>⊥</sup> and Peter E. Nielsen<sup>\*,†</sup>

Center for Biomolecular Recognition, Department of Medical Biochemistry and Genetics, University of Copenhagen, The Panum Institute, Blegdamsvej 3c, DK-2200 N Copenhagen, Denmark, Santaris Pharma A/S, Bøge Allé 3, 2970 Hørsholm, Denmark, Service Hospitalier Frédéric Joliot, Département de Recherche Médicale, CEA/DSV, 4 place du Général Leclerc, F-91401 Orsay, France, INSERM ERM 0103, Service Hospitalier Frédéric Joliot, Département de Recherche Médicale, CEA/DSV, 4 place du Général Leclerc, F-91401 Orsay, France, and Department of Chemistry, University of Copenhagen, Universitetsparken 5, DK 2100 Copenhagen Ø, Denmark. Received February 13, 2003; Revised Manuscript Received July 28, 2003

A series of *N*-(2-aminoethyl)- $\alpha$ -amino acid thymine peptide nucleic acid (PNA) monomers bearing glycosylated side chains in the  $\alpha$ -amino acid position have been synthesized. These include PNA monomers where glycine has been replaced by serine and threonine (*O*-glycosylated), derivatives of lysine and nor-alanine (*C*-glycosylated), and amide derivatives of aspartic acid (*N*-glycosylated). The Boc and Fmoc derivatives of these monomers were used for incorporation in PNA oligomers. Twelve PNA decamers containing the glycosylated units in one, two, or three positions were prepared, and the thermal stability ( $T_m$ ) of their complexes with a complementary RNA was determined. Incorporation of the glycosyl monomers reduced the duplex stability by 0–6 °C per substitution. A cysteine was attached to the amino terminus of eight of the PNA decamers (Cys-CTCATACTCT-NH<sub>2</sub>) for easy conjugation to a [<sup>18</sup>F]radiolabeled *N*-(4-fluorobenzyl)-2-bromoacetamide. The in vivo biodistribution of these PNA oligomers was determined in rat 2 h after intravenous administration. Most of the radioactivity was recovered in the kidneys and in the urine. However, *N*-acetylgalactosamine (and to a lesser extent galactose and mannose)-modified PNAs were effectively targeting the liver (40-fold over unmodified PNA). Thus, the pharmacodistribution in rats of PNA oligomers can be profoundly changed by glycosylation. These results could be of great significance for PNA drug development, as they should allow modulation and fine-tuning of the pharmacokinetic profile of a drug lead.

## INTRODUCTION

Peptide nucleic acids have shown great promise as gene targeting agents for drug discovery, especially in relation to antisense technology (1–4). Only little information is available on the pharmacokinetic behavior of PNA oligomers in animals, but the data indicate that the compounds are fairly quickly excreted in the urine (5). This is not too surprising, as these molecules are rather hydrophilic and do not bind to proteins (such as albumins in serum) in general. Therefore, it could be of significant medicinal chemical interest to develop methods that would allow (predictable) modulation or control of the pharmacokinetic profile of a given PNA oligomer. Functionalization of the PNA backbone may dramatically change the physicochemical properties of the PNA, and it is plausible that such changes would also significantly influence its biodistribution and pharmacokinetics be-

havior. Furthermore, such changes may conveniently be introduced at the  $\alpha$ -amino acid position in the PNA backbone without major influence on the DNA/RNA hybridization potency of the PNA (6, 7). As a step toward this goal we now report the synthesis of PNA Fmoc<sup>1</sup>-protected thymine monomers containing glycosyl substituents (galactosyl, mannosyl, fucosyl, *N*-acetylgalactosaminyl, and *N*-acetylglucosaminyl) in the  $\alpha$ -amino acid position, as recognition by a variety of cellular receptors relies on protein glycosylation. As the most prominent example, the asialoglycoprotein receptor of liver cells efficiently recognizes *N*-acetylgalactosamine (GalNAc), and GalNAc conjugation has been used successfully for liver (cell) targeting (8–11). We have incorporated gly-

\* Corresponding author: E-mail: pen@imbg.ku.dk; Fax: +45 35396042.

<sup>†</sup> Center for Biomolecular Recognition, University of Copenhagen.

<sup>‡</sup> Santaris Pharma A/S.

<sup>§</sup> Service Hospitalier Frédéric Joliot.

<sup>||</sup> INSERM ERM 0103.

<sup>⊥</sup> Department of Chemistry, University of Copenhagen.

<sup>1</sup> Abbreviations: BHOC, benzhydryloxycarbonyl; Boc, *tert*-butyloxycarbonyl; DBU, 1,8-diazabicyclo[5.4.0]undec-7-ene; DCC, *N,N*-dicyclohexylcarbodiimide; Dde, 1-(4,4-dimethyl-2,6-dioxocyclohexylidene)ethyl; DhbtOH, 3-hydroxy-1,2,3-benzotriazine-4(3*H*)-one; DIEA, diisopropylethylamine; EEDQ, 2-ethoxy-1-ethoxycarbonyl-1,2-dihydroquinoline; FAB, fast atomic bombardment; Fmoc, 9-fluorenylmethoxycarbonyl; HATU, *N*-[(dimethylamino)(1*H*-1,2,3-triazolo[4,5-*b*]pyridin-1-yl)methylene]-*N*-methylmethan ammonium hexafluorophosphate *N*-oxide; MALDI-TOF, matrix-assisted laser desorption/ionization time-of-flight; TFMSA, trifluoromethanesulfonic acid;  $T_m$ , melting temperature; TMG, tetramethylguanidine.

cosyl-PNA monomers into PNA decamers, and studied their relative pharmacodistribution in rats. Specifically, we observed very efficient and specific liver targeting by a PNA decamer containing three *N*-acetylgalactosaminyl substitutions.

## EXPERIMENTAL PROCEDURES

Reagents and solvents were obtained from commercial sources and used without further purification unless indicated. NMR spectra were recorded in CDCl<sub>3</sub>, CD<sub>3</sub>-OH or DMSO-*d*<sub>6</sub> on 400, 300, and 250 MHz Varian spectrometers, FAB mass spectra on a JEOL HX 110/110 mass spectrometer, and MALDI-TOF mass spectra on a Cratos Compact Maldi II spectrometer. Elemental analyses were performed by the Microanalysis Department at the Department Chemistry, University of Copenhagen. Flash chromatography was carried out using Silica Gel 60 (Merck particle size 0.040–0.063 mm). The oligomers were analyzed on a Delta Pak C<sub>18</sub> column (5 μM, 3.9 × 150 mm) and were purified on a Delta Pak C<sub>18</sub> column (15 μM, 19 × 300 mm). A linear gradient composed of A (0.1% TFA in water) and B (0.1% TFA in 10% H<sub>2</sub>O/90% acetonitrile) was used for analytical and preparative HPLC. Analytical: Time 0, 0% B. Time 35 min, 50% B (Flow, 1 mL/min). Preparative: Time 0, 15% B. Time 45 min, 40% B (Flow, 8 mL/min). The thermal stability (*T*<sub>m</sub>) measurements of PNAs were carried out with a Cary spectrophotometer 300 from Varian Optical Spectroscopy Instruments.

**Procedure a: Alkylation of Protected Amino Acids.** The *N*-protected amino acid (5 mmol) was added to a mixture of acetonitrile (10 mL) and allyl bromide (12 mL). Diisopropylethylamine (10.5 mmol) was added, and the reaction mixture was stirred for 4 h at 40 °C. Ethyl acetate was added, and the solution was extracted with aq half-saturated KHSO<sub>4</sub>, half-saturated NaHCO<sub>3</sub>, and brine. The organic phase was dried over MgSO<sub>4</sub> and evaporated under vacuum. The remaining oil (87–95%) was used for the next step without further purification.

**Procedure b: Preparation of Boc/Fmoc-Protected PNA Backbone.** The amino acid derivative (12 mmol) and Boc or Fmoc aminoacetaldehyde (10 mmol) were added to methanol (40 mL) and stirred for 10 min. Acetic acid (0.8 mL, 13 mmol) and NaBH<sub>3</sub>CN (0.6 g, 10 mmol) were added sequentially. The reaction mixture was stirred for further 1 h at room temperature. Volatiles were removed under vacuum, and the residue was dissolved in ethyl acetate and extracted with saturated aqueous NaHCO<sub>3</sub> and brine. The organic phase was dried over MgSO<sub>4</sub> and evaporated to dryness under vacuum. The residue was purified by flash chromatography, eluting with *n*-hexane/ethyl acetate (1:1 v/v) (yield 50–80%).

**Procedure c: Coupling of Thymine-1-ylacetic Acid to the PNA Backbone.** Thymine-1-ylacetic acid (17 mmol) and DhbtOH (18 mmol) were dissolved in dry DMF (50 mL). DCC (20 mmol) was added and the solution stirred for 20 min. The backbone (8.5 mmol) in dry DMF (20 mL) was added to the reaction mixture, and the mixture stirred for further 6 h at room temperature. Volatiles were removed under vacuum, and the residue was dissolved in ethyl acetate (200 mL). Insoluble DCU was filtered off and the filtrate extracted with saturated aqueous NaHCO<sub>3</sub> and brine. After being dried over MgSO<sub>4</sub>, the organic phase was evaporated to dryness. The residue was purified on a silica gel column, eluting with a gradient of 10:0 to 10:1 (v/v) ethyl acetate/methanol (yield 63–87%).

**Procedure d: Boc Deprotection and Subsequent Fmoc Protection.** The Boc-protected derivative (3 mmol) was added to a solution of triethylsilane/trifluoroacetic acid (20 mL, 5:95 v/v) at 0 °C and stirred until TLC showed absence of starting material. Toluene (50 mL) was added, and volatiles were removed under vacuum. DCM (3 × 100 mL) was added and evaporated in order to remove TFA. The residue was dissolved in diethyl ether (50 mL), and well-powdered Na<sub>2</sub>CO<sub>3</sub> (5 g) was added. The suspension was stirred for 30 min and then evaporated. The solid residue was suspended in acetonitrile (50 mL), *O*-Fmoc-*N*-hydroxysuccinimide (3.2 mmol) was added, and the mixture stirred for further 2 h. The solution was evaporated under vacuum, and the residue was purified by flash chromatography eluting with a gradient of 10:0 to 10:1 (v/v) ethyl acetate/methanol (yield 88–94%).

**Procedure e: *N*-Glycosylation.** A mixture of **20** (2 mmol), DhbtOH (2.2 mmol), and DCC (3 mmol) in DMF (10 mL) was stirred for 30 min under nitrogen. A solution of sugar-amine **S7A–E** (2 mmol) in DMF (10 mL) was added, and the reaction mixture was stirred overnight at room temperature. Volatiles were removed under vacuum, and the residue was dissolved in ethyl acetate. Insoluble DCU was filtered off and the filtrate extracted with saturated aq NaHCO<sub>3</sub> and brine. After being dried over MgSO<sub>4</sub>, the organic phase was evaporated to dryness. The residue was purified by flash chromatography eluting with a gradient of 10:0 to 10:1 (v/v) ethyl acetate/methanol (yield 60–77%).

**Procedure f: Removal of Allyl Groups.** The ester (0.1 mmol) was dissolved in THF (2 mL). (Ph<sub>3</sub>P)<sub>4</sub>Pd (0.02 mmol) and *N*-ethylaniline (1 mmol) were added and stirred at room temperature. The reaction was followed by TLC (ethyl acetate/methanol, 10:1 v/v). After complete conversion of starting material, the reaction mixture was poured dropwise into a vigorously stirred solution of diethyl ether/*n*-hexane (20 mL, 1:1 v/v). The white precipitate was collected by filtration and washed with *n*-hexane (yield 80–95%).

**Solid-Phase Synthesis.** PNA oligomers **O1**, **O2** (group **a**), and **PNA-1–8** (group **c**) were synthesized on Fmoc-Sieber-TG (Novabiochem) (50 mg) and Fmoc-PAL-PEG (Perceptive Biosystems) (50 mg) resins, respectively. A plastic syringe (2.5 mL) was used as reactor, and all reactions were carried out on a vibrator at 600 vibrations per minute. HATU (14.4 mg, 38 μmol) was dissolved in DMF (300 μL). For group **a**, HATU was first neutralized with collidine (2.2 equiv) prior to acid preactivation. For group **c**, HATU and DIPEA (2.2 equiv) were added directly into an Eppendorf tube containing the monomer (40 μmol). Acid preactivations were performed by vibration for 10 min for group **a** and 3 min for group **c**. Activated acids were transferred to the syringe containing the resin and vibrated for 30 min. The resin was washed with DMF and DCM successively. Coupling yields were determined by the Kaiser test, and capping steps were avoided. 50% Morpholine in DMF (10+5 min, group **a**) and 20% piperidine in DMF (3+2 min, group **c**) were used for deprotections. 5% water, 30% TFA in DCM (90 min) and 10% TES, 10% thioanisole in TFA (180 min) were used as cleavage condition for groups **a** and **c**, respectively. All PNAs were precipitated by draining the cleavage product into ice-cold diethyl ether and collected after centrifuging. Crude products were purified by HPLC. Acetyl groups of sugars in group **a** were removed with methanolic hydrazine (pH 9.5) solution. For group **c** acetyl removal were carried out on the resin prior to



cleavage using a mixture of TEA/water/methanol (2 mL, 5:2:3 v/v/v) vibrated overnight.

Standard PNA synthesis based on Boc chemistry (12) was used for the synthesis of **O3–O4** (group **b**). Acetyl groups were removed with methanolic hydrazine (pH 10) after cleavage and purification.

**Labeling of PNA 1–8.** All PNAs were reacted with nonlabeled *N*-(4-fluorobenzyl)-2-bromoacetamide for analytical purposes. To a solution of PNA (1.3 mg) in phosphate buffer (0.5 mL, 0.1 M, pH 8.75) was added a solution of *N*-(4-fluorobenzyl)-2-bromoacetamide in acetonitrile (0.1 M, 0.5 mL) and heated at 60 °C for 20 min. The modified PNAs were purified by semipreparative reverse-phase HPLC and were characterized by mass spectrometry analysis. Analytical data were in accordance with the expected structure.

For the fluorine-18 labeling of PNAs, we used a slight modification of the published procedure (13–16). Briefly, *N*-(4-[<sup>18</sup>F]fluorobenzyl)-2-bromoacetamide was prepared in three chemical steps from 4-cyano-*N,N,N*-trimethylanilinium trifluoromethanesulfonate. Typically, 60–90 mCi (2.2–3.3 GBq) of pure *N*-(4-[<sup>18</sup>F]fluorobenzyl)-2-bromoacetamide could be obtained in 85–95 min starting from a 550–650 mCi (20.3–24.0 GBq) aliquot of a cyclotron [<sup>18</sup>F]<sup>–</sup> production batch. The HPLC-collected fraction containing *N*-(4-[<sup>18</sup>F]fluorobenzyl)-2-bromoacetamide was concentrated to dryness at 80 °C under a nitrogen stream and redissolved in acetonitrile (0.4 mL). A solution of PNA (1.3 mg) in phosphate buffer (0.5 mL, 0.1 M, pH 8.75) and acetonitrile (0.1 mL) was rapidly added. The reactor was placed in a heating block and heated without stirring under a slight flow of nitrogen at 60 °C for 20 min. The nitrogen flow caused concentration of the reaction mixture. Distilled water (1 mL) was added, and the reaction mixture was subjected to a C-18 HPLC purification, to isolate fluorine-18-labeled PNA from unlabeled PNA and *N*-(4-[<sup>18</sup>F]fluorobenzyl)-2-bromoacetamide. The HPLC fraction containing the fluorine-18-labeled PNA was concentrated, diluted with physiological saline, and finally filtered on a 0.22 µm GS-Millipore filter (vented).

**Biodistribution Study of Radiolabeled PNAs.** Two male and two female adult Sprague–Dawley rats (200 g) were each injected with 400 µCi (14.8 MBq) of one of the [<sup>18</sup>F]-labeled PNA in the tail vein. After 2 h, the animals were sacrificed and the kidneys, liver, spleen, heart, lung, brain, flat abdominal and long leg muscle, adrenals, blood, and urine immediately collected. Aliquots of these organs were weighed, and their radioactivity was counted on a well gamma radiocounter (Packard Cobra). Radioactivity was expressed as percentage of the injected dose per gram of organ (%ID/g) and reported as the mean ± standard deviation.

**Synthesis of Glycosylated PNA Monomers and Precursors.** Note: NMR data given for all compounds in the thymine-1-ylacetylated series (**4–7**, **11–15**, **19–21**, **28**, **I–V**) correspond to their major rotamer.

***O*-(*tert*-Butyl)-L-serine Allyl Ester (**2**).** Prepared from *N*-Fmoc-*O*-(*tert*-butyl)-L-serine by the same procedure as that used for compound **2m** (83%).

***O*-(*tert*-Butyl)-L-threonine Allyl Ester (**2m**).** To *N*-Fmoc-*O*-(*tert*-butyl)-L-threonine allyl ester **1m** [prepared from *N*-Fmoc-*O*-(*tert*-butyl)-L-threonine by procedure a] (4.4 g, 10 mmol) was added 20% piperidine in DCM (50 mL). After 30 min, toluene (100 mL) was added, and volatiles were removed under vacuum. The residue was purified by flash chromatography eluting with a gradient of 10:0 to 10:1 ethyl acetate/methanol to provide **2m** (1.6 g, 75%) as a colorless oil. MS (FAB) *m/z* 216 (M

+ H); <sup>1</sup>H NMR (CDCl<sub>3</sub>): δ 5.94 (m, 1H), 5.30 (d, 1H, *J* = 17.0 Hz), 5.20 (d, 1H, *J* = 10.5 Hz), 4.55 (ABX-system, 2H, Δ = 33.8 Hz, *J*<sub>AB</sub> = 13.2 Hz, *J*<sub>AX</sub> = *J*<sub>BX</sub> = 5.8 Hz), 4.00 (dq, 1H, *J* = 6.3, 3.3 Hz), 3.26 (d, 1H, *J* = 3.3 Hz), 1.65 (s, 2H), 1.20 (d, 3H, *J* = 6.3 Hz), 1.09 (s, 9H); <sup>13</sup>C NMR (CDCl<sub>3</sub>): δ 174.51, 132.09, 118.87, 73.77, 68.63, 65.67, 60.84, 28.68, 20.94. Anal. for C<sub>11</sub>H<sub>21</sub>NO<sub>3</sub>·1/2H<sub>2</sub>O: calcd C 60.11, H 9.86, N 6.37; found C 59.87, H 9.95, N 6.34.

***N*-(2-Boc-aminoethyl)-*O*-(*tert*-butyl)-L-serine Allyl Ester (**3**).** Prepared from **2** by procedure b (68%), MS (FAB) *m/z* 345 (M + H); <sup>1</sup>H NMR (CDCl<sub>3</sub>): δ 5.96–5.89 (m, 1H), 5.26 (d, 1H, *J* = 17.2 Hz), 5.17 (d, 1H, *J* = 10.4 Hz), 5.05 (br s, 1H), 4.55 (m, 2H), 3.52 (m, 2H), 3.36 (t, 1H, *J* = 4.7 Hz), 3.20–3.10 (m, 2H), 2.80 (m, 1H), 2.60 (m, 1H), 1.37 (s, 9H), 1.08 (s, 9H); <sup>13</sup>C NMR (CDCl<sub>3</sub>): δ 172.50, 155.9, 131.74, 118.42, 118.27, 73.13, 65.263, 62.66, 61.22, 47.18, 40.03, 28.25, 27.17. Anal. for C<sub>17</sub>H<sub>32</sub>N<sub>2</sub>O<sub>5</sub>·1/2H<sub>2</sub>O: calcd C 57.77, H 9.41, N 7.93; found C 58.11, H 9.20, N 8.14.

***N*-(2-Boc-aminoethyl)-*O*-(*tert*-butyl)-L-threonine Allyl Ester (**3m**).** Prepared from **2m** by procedure b (67%), MS (FAB) *m/z* 359 (M + H); <sup>1</sup>H NMR (CDCl<sub>3</sub>): δ 5.90–5.83 (m, 1H), 5.26 (d, 1H, *J* = 17 Hz), 5.18 (d, 1H, *J*<sub>s</sub> = 10 Hz), 5.05 (br s, 1H), 4.55 (ABX-system, 2H, Δ = 30.5 Hz, *J*<sub>AB</sub> = 13.2 Hz, *J*<sub>AX</sub> = *J*<sub>BX</sub> = 5.8 Hz), 3.90 (dd, 1H, *J* = 6.3, 3.5 Hz), 3.14–3.08 (2m, 2H), 3.05 (d, 1H, *J* = 3.5 Hz), 2.80 (m, 1H), 2.70 (m, 1H), 1.37 (s, 9H), 1.18 (d, 3H, *J* = 6.2 Hz), 1.06 (s, 9H); <sup>13</sup>C NMR (CDCl<sub>3</sub>): δ 172.91, 155.88, 131.65, 118.54, 78.81, 73.66, 68.14, 66.37, 65.270, 47.51, 39.88, 28.23, 28.19, 20.49. Anal. for C<sub>18</sub>H<sub>34</sub>N<sub>2</sub>O<sub>5</sub>: calcd C 60.31, H 9.56, N 7.81; found C 60.16, H 9.98, N 7.75.

***N*-(2-Boc-aminoethyl)-*N*-(thymine-1-ylacetyl)-*O*-(*tert*-butyl)-L-serine Allyl Ester (**4**).** Prepared from **3** by procedure c (73%), mp: 70–72 °C; MS (FAB) *m/z* 511 (M + H); <sup>1</sup>H NMR (CDCl<sub>3</sub>): δ 9.08 (s, 1H), 6.83 (s, 1H), 5.87–5.77 (m, 1H), 5.6 (br s, 1H), 5.25 (d, 1H, *J* = 17.2 Hz), 5.17 (d, 1H, *J* = 10.2 Hz), 4.6–4.4 (m, 4H), 4.26 (br., 1H), 3.93 (t, 1H, *J* = 7.9 Hz), 3.77 (dd, 1H, *J* = 10.1, 3.1 Hz), 3.6–3.4 (m, 2H), 3.35 (m, 2H), 1.83 (s, 3H), 1.37 (s, 9H), 1.10 (s, 9H); <sup>13</sup>C NMR (CDCl<sub>3</sub>): δ 168.93, 167.15, 164.07, 155.85, 150.72, 140.72, 131.36, 118.84, 111.59, 110.43, 79.62, 73.84, 66.06, 60.79, 60.24, 59.50, 38.84, 33.66, 28.30, 28.10, 27.15, 12.25; HRMS (M + H)<sup>+</sup>, calcd (found) for C<sub>24</sub>H<sub>39</sub>N<sub>4</sub>O<sub>8</sub>: 511.2768 (511.2769).

***N*-(2-Boc-aminoethyl)-*N*-(thymine-1-ylacetyl)-*O*-(*tert*-butyl)-L-threonine Allyl Ester (**4m**).** Prepared from **3m** by procedure c, (76%), mp: 71–73; MS (FAB) *m/z* 525 (M + H); <sup>1</sup>H NMR (CDCl<sub>3</sub>): δ 8.60 (s, 1H), 6.90 (s, 1H), 5.95–5.85 (m, 1H), 5.50 (br s, 1H), 5.30 (d, 1H, *J* = 17.1 Hz), 5.25 (d, 1H, *J* = 10.2 Hz), 4.66 (m, 3H), 4.52–4.41 (m, 3H), 3.80 (dt, 1H, *J* = 15.3, 6.0 Hz), 3.60 (m, 1H), 3.5–3.4 (m, 2H), 1.89 (s, 3H), 1.44 (s, 9H), 1.28 (d, 3H, *J* = 6.0 Hz), 1.10 (s, 9H); <sup>13</sup>C NMR (CDCl<sub>3</sub>): δ 169.12, 167.95, 163.78, 155.78, 150.59, 140.73, 131.20, 119.41, 110.43, 79.61, 74.55, 66.14, 64.39, 39.16, 33.79, 28.69, 28.60, 28.40, 25.53, 24.87, 21.71, 12.37; HRMS (M + H)<sup>+</sup>, calcd (found) for C<sub>25</sub>H<sub>41</sub>N<sub>4</sub>O<sub>8</sub>: 525.2924 (525.2925).

***N*-(2-Fmoc-aminoethyl)-*N*-(thymine-1-ylacetyl)-L-serine Allyl Ester (**6**).** Prepared from **4** by procedure d (88%), mp: 101–103 °C; MS (FAB) *m/z* 577 (M + H); <sup>1</sup>H NMR (CDCl<sub>3</sub>): selected signals: δ 9.63 (s, 1H), 7.56–7.07 (m, 8H), 6.59 (s, 1H), 5.90 (s, 1H), 5.8–5.6 (m, 1H), 5.12 (d, 1H, *J* = 17.2 Hz), 5.05 (d, 1H, *J* = 10.4 Hz), 4.6–4.4 (overlapping s, 3H), 4.24 (s, 2H), 4–3.8 (m, 5H), 1.70 (s, 3H); <sup>13</sup>C NMR (CDCl<sub>3</sub>): δ 168.50, 168.06, 167.94, 167.07, 164.05, 162.58, 156.59, 151.33, 143.58, 143.39, 140.98, 131.14, 130.69, 127.54, 126.88, 124.82, 124.36, 119.75,



118.95, 110.90, 66.75, 66.17, 63.43, 59.47, 49.24, 48.81, 47.10, 39.45, 31.54, 12.30. Anal. for  $C_{30}H_{32}N_4O_8 \cdot \frac{1}{2}H_2O$ : calcd C 61.35, H 5.68, N 9.57; found C 61.39, H 5.53, N 9.36.

***N*-(2-Fmoc-aminoethyl)-*N*-(thymine-1-ylacetyl)-L-threonine Allyl Ester (6m).** Prepared from **4m** by procedure d (91%), mp: 99–101 °C; MS (FAB)  $m/z$  591 ( $M + H$ );  $^1H$  NMR ( $CDCl_3$ ):  $\delta$  8.90 (s, 1H), 7.6–7.1 (m, 8H), 6.60 (s, 1H), 5.8–5.6 (overlapping m, 2H), 5.12 (d, 1H,  $J = 17.2$  Hz), 5.07 (d, 1H,  $J = 10.3$  Hz), 4.50 (overlapping s, 3H), 4.42–4.26 (m, 2H), 4.20 (t, 1H,  $J = 7.4$  Hz), 4.03 (d, 2H,  $J = 6$  Hz), 3.65 (br., 1H), 3.53–3.47 (m, 1H), 3.4–3.24 (m, 3H), 2.80 (br s, 1H), 1.68 (s, 3H), 1.14 (d, 3H,  $J = 5.8$  Hz);  $^{13}C$  NMR ( $CDCl_3$ ):  $\delta$  168.67, 167.85, 163.99, 156.60, 151.10, 143.67, 143.50, 141.15, 140.98, 131.22, 127.64, 126.96, 124.88, 124.36, 119.87, 119.25, 110.75, 67.50, 66.61, 66.19, 65.16, 49.55, 48.86, 47.06, 39.41, 21.30, 12.30. Anal. for  $C_{31}H_{34}N_4O_8 \cdot \frac{1}{2}H_2O$ : calcd C 62.09, H 5.88, N 9.34; found C 62.10, H 5.86, N 9.22.

***N*-(2-Fmoc-aminoethyl)-*N*-(thymine-1-ylacetyl)-O-(2,3,4,6-tetra-O-acetyl- $\beta$ -D-galactopyranose-1-yl)-L-serine Allyl Ester (7A).** **6** (0.7 g, 1.2 mmol) and galactose trichloroacetimidate (0.75 g, 1.5 mmol) were dissolved in ethyl acetate (5 mL). Molecular sieves (0.5 g) and boron trifluoride diethyl etherate (1.2 mL, 9.5 mmol) in ethyl acetate (1 mL) were added at 0 °C. The ice bath was removed, and the reaction mixture was stirred under nitrogen overnight. Ethyl acetate (50 mL) was added, and the reaction mixture was filtered over Celite. The filtrate was extracted with ice cold half saturated aqueous  $NaHCO_3$  ( $2 \times 25$  mL) and brine, dried over  $MgSO_4$ , and evaporated to dryness. The residue was purified by flash chromatography eluting with *n*-hexanes–ethyl acetate 1:1 (v/v) to provide **7A** (0.4 g, 37%) as colorless crystals. Mp: 115–118 °C; MS (FAB)  $m/z$  907 ( $M + H$ );  $^1H$  NMR ( $CDCl_3$ ):  $\delta$  8.75 (s, 1H), 7.68–7.21 (m, 8H), 6.80 (s, 1H), 5.9–5.7 (m, 2H), 5.30 (d, 1H,  $J = 2.9$  Hz), 5.25 (d, 1H,  $J = 17.2$  Hz), 5.15 (d, 1H,  $J = 10.7$  Hz), 5.05 (d, 1H,  $J = 7.7$  Hz), 4.95 (dd, 1H,  $J = 10.4$ , 3.2 Hz), 4.7–4.3 (2m, 6H), 4.25–3.95 (m, 6H), 3.80 (t, 2H,  $J = 6.4$ ), 3.6–3.3 (m, 3H), 2.90 (br s, 1H), 2.1–1.9 (4s, 12H), 1.80 (s, 3H);  $^{13}C$  NMR ( $CDCl_3$ ):  $\delta$  169.37, 169.09, 168.96, 168.80, 166.84, 166.61, 163.09, 155.81, 149.67, 142.76, 140.27, 130.37, 126.73, 126.06, 123.91, 118.98, 118.24, 109.26, 100.03, 70.09, 69.57, 67.75, 66.38, 65.93, 65.54, 65.43, 60.22, 60.09, 47.48, 47.02, 46.29, 38.60, 19.78–19.54, 11.28. HRMS ( $M + Na$ )<sup>+</sup>, calcd (found) for  $C_{44}H_{50}N_4O_{17}Na$ : 929.3069 (929.3087).

***N*-(2-Fmoc-aminoethyl)-*N*-(thymine-1-ylacetyl)-O-(2,3,4,6-tetra-O-acetyl- $\beta$ -D-galactopyranose-1-yl)-L-threonine Allyl Ester (7mA).** The procedure is the same as that described for the synthesis of **7A** using **6m** as starting material (77%), mp: 106–108 °C; MS (FAB)  $m/z$  921 ( $M + H$ );  $^1H$  NMR ( $CDCl_3$ ) (selected signals):  $\delta$  8.54 (s, 1H), 7.78–7.76 (m, 8H), 6.95 (s, 1H), 5.92–5.82 (m, 1H), 5.81 (s, 1H), 5.38 (d, 1H,  $J = 2.5$  Hz), 5.30 (d, 1H,  $J = 17.4$  Hz), 5.20 (d, 1H,  $J = 10.4$  Hz), 5.1–4.9 (m, 3H), 4.65–4.5 (m, 4H), 4.45 (m, 2H), 4.20 (t, 2H,  $J = 7.0$  Hz), 4.07 (d, 2H,  $J = 6.4$  Hz), 3.88 (t, 1H,  $J = 6.2$  Hz), 3.60 (overlapping s, 2H), 3.43 (br s, 1H), 3.30 (br, 1H), 2.18–2.00 (3s, 12H), 1.88 (s, 3H), 1.27 (d, 3H,  $J = 5.8$  Hz);  $^{13}C$  NMR ( $CDCl_3$ ):  $\delta$  170.11, 169.89, 167.97, 163.65, 156.64, 150.35, 143.53, 141.21, 141.05, 131.31, 127.51, 126.82, 124.78, 119.80, 118.78, 110.07, 98.73, 73.34, 71.53, 70.70, 70.48, 70.01, 68.80, 66.66, 66.55, 66.17, 65.65, 64.10, 62.79, 60.84, 60.31, 48.48, 47.19, 39.70,

[21.05, 20.83, 20.67, 20.55 (sugar-acetyl groups), 17.38, 14.20, 12.29. Anal. for  $C_{45}H_{52}N_4O_{17} \cdot H_2O$ : calcd C 57.56, H 5.80, N 5.97; found C 57.51, H 5.52, N 5.82.

***N*-(Dde)-L-lysine Allyl Ester (9).** *N*<sup>2</sup>-Fmoc-*N*<sup>6</sup>-Dde-L-lysine allyl ester **8** [prepared from *N*<sup>2</sup>-Fmoc-*N*<sup>6</sup>-Dde-L-lysine by procedure a] (5.7 g, 10 mmol) was added to a solution of 20% piperidine in DCM (30 mL) and stirred for 30 min. Toluene (100 mL) was added, and volatiles were removed under vacuum. The residue was purified by flash chromatography, eluting with a gradient of 10:0 to 10:1 (v/v) ethyl acetate/methanol to provide **9** (2.5 g, 71%) as a slightly yellow oil. MS (FAB)  $m/z$  351 ( $M + H$ );  $^1H$  NMR ( $CDCl_3$ ):  $\delta$  13.34 (s, 1H), 5.9–5.8 (m, 1H), 5.27 (d, 1H,  $J = 17.3$  Hz), 5.22 (d, 1H,  $J = 10.5$  Hz), 4.56 (m, 2H), 3.40 (m, 2H), 2.49 (s, 3H), 2.30 (s, 4H), 1.77 (s, 2H), 1.74–1.38 (m, 6H), 0.97 (s, 6H);  $^{13}C$  NMR ( $CDCl_3$ ):  $\delta$  198.59, 196.83, 175.19, 173.14, 131.60, 118.51, 107.56, 65.33, 60.10, 53.92, 42.96, 33.98, 29.83, 28.59, 28.02, 22.87, 17.65; HRMS ( $M + H$ )<sup>+</sup>, calcd (found) for  $C_{19}H_{31}N_2O_4$ : 351.2284 (351.2280).

***N*-(2-Boc-aminoethyl)-*N*<sup>6</sup>-(Dde)-L-lysine Allyl Ester (10).** Prepared from **9** by procedure b (65%). MS (FAB)  $m/z$  494 ( $M + H$ );  $^1H$  NMR ( $CDCl_3$ ):  $\delta$  13.45 (s, 1H), 5.98–5.85 (m, 1H), 5.33 (d, 1H,  $J = 17.3$  Hz), 5.28 (d, 1H,  $J = 10.5$  Hz), 4.56 (m, 2H), 3.40 (m, 3H), 3.20 (m, 2H), 2.80 (m, 1H), 2.70 (m, 1H), 2.55 (s, 3H), 2.36 (s, 4H), 1.8–1.5 (m, 6H), 1.44 (s, 9H), 1.03 (s, 6H);  $^{13}C$  NMR ( $CDCl_3$ ):  $\delta$  198.79, 197.21, 174.68, 173.68, 156.37, 132.00, 119.27, 108.08, 79.47, 65.83, 60.99, 53.07, 47.83, 43.40, 40.55, 32.94, 30.35, 28.96, 28.68, 28.52, 23.35, 87, 18.18. Anal. for  $C_{26}H_{43}N_3O_6 \cdot H_2O$ : calcd C 61.03, H 8.86, N 8.21; found C 61.12, H 8.78, N 8.13.

***N*-(2-Boc-aminoethyl)-*N*<sup>2</sup>-(thymine-1-ylacetyl)-*N*<sup>6</sup>-(Dde)-L-lysine Allyl Ester (11).** Prepared from **10** by procedure c (87%), mp: 84–86 °C; MS (FAB)  $m/z$  660 ( $M + H$ );  $^1H$  NMR ( $CDCl_3$ ):  $\delta$  13.40 (s, 1H), 9.56 (s, 1H), 6.99 (s, 1H), 5.97–5.84 (m, 1H), 5.66 (s, 1H), 5.35 (d, 1H,  $J = 17.2$  Hz), 5.25 (d, 1H,  $J = 10.5$  Hz), 4.7–4.4 (m, 4H), 4.20 (m, 1H), 3.70 (m, 1H), 3.44–3.27 (m, 5H), 2.55 (s, 3H), 2.37 (s, 4H), 2.05 (m, 2H), 1.89 (s, 3H), 1.70 (m, 4H), 1.45 (s, 9H), 1.03 (s, 6H);  $^{13}C$  NMR ( $CDCl_3$ ):  $\delta$  197.81, 173.54, 170.33, 167.50, 163.94, 155.89, 150.74, 140.91, 131.26, 119.26, 110.41, 107.80, 79.85, 66.25, 60.27, 52.69, 48.30, 47.66, 42.93, 39.11, 30.01, 28.31, 28.13, 28.01, 23.36, 17.89, 12.99. Anal. for  $C_{33}H_{49}N_5O_9$ : calcd C 60.08, H 7.49, N 10.61; found C 59.70, H 7.49, N 10.50.

***N*-(2-Boc-aminoethyl)-*N*<sup>2</sup>-(thymine-1-ylacetyl)-L-lysine Allyl Ester (12).** **11** (1.4 g, 2.1 mmol) was dissolved in a mixture of allyl alcohol/hydrazine hydrate (20 mL, 10:1 v/v) and stirred for 15 min. DMF (200 mL) was added, and the reaction mixture was concentrated under high vacuum. Water was added to the remaining oil and the mixture extracted with diethyl ether. The water phase was freeze-dried to provide **12** (0.8 g, 76%) as slightly yellow crystals which were used for the next step without further purification. An aliquot was purified by HPLC and collected as a TFA salt. Mp: 81–83 °C; MS (FAB)  $m/z$  496 ( $M + H$ );  $^1H$  NMR ( $CD_3OD$ ):  $\delta$  7.34 (s, 1H), 6.03–5.94 (m, 1H), 5.37 (d, 1H,  $J = 17.2$  Hz), 5.27 (d, 1H,  $J = 10.4$  Hz), 4.8–4.6 (m, 4H), 4.37 (dd, 1H,  $J = 8.8$ , 5.0 Hz), 3.70 (m, 1H), 3.40 (overlapping s, 2H), 3.23 (m, 1H), 2.97 (t, 2H,  $J = 7.5$  Hz), 2.2–2.0 (2m, 2H), 1.90 (s, 3H), 1.70 (m, 2H), 1.49 (overlapping s, 11H);  $^{13}C$  NMR ( $CD_3OD$ ):  $\delta$  171.79, 169.81, 166.98, 158.50, 153.12, 143.74, 133.44, 119.03, 116.38, 111.11, 80.74, 67.21, 61.94, 50.21, 40.61, 29.61, 28.81, 28.37, 27.83, 24.30, 12.32. Anal. for  $C_{23}H_{37}N_5O_7 \cdot 2CF_3COOH$ : calcd C 44.82, H 5.43, N 9.68; found C 44.61, H 5.66, N 9.92.

***N*<sup>6</sup>-(2-Boc-aminoethyl)-*N*<sup>2</sup>-(thymine-1-ylacetyl)-*N*<sup>6</sup>,*N*<sup>6</sup>-bis(2,3,4,6-tetra-*O*-acetyl- $\alpha$ -D-galactopyranose-1-ylethyl)-L-lysine Allyl Ester (13A).** **12** (300 mg, 0.6 mmol) was dissolved in methanol (10 mL). **S5A** (500 mg, 2.2 equiv) was added and stirred for 10 min. Acetic acid (80  $\mu$ L, 1.3 mmol) and NaBH<sub>3</sub>CN (0.6 g, 10 mmol) were added sequentially. After 15 min the same amounts of acetic acid and NaBH<sub>3</sub>CN were added, and the reaction mixture was stirred for further 30 min at room temperature. Volatiles were removed under vacuum, and the residue was dissolved in ethyl acetate and extracted with saturated aqueous NaHCO<sub>3</sub> and brine. The organic phase was dried over MgSO<sub>4</sub> and evaporated to dryness under vacuum. The residue was purified by flash chromatography eluting with a gradient of 10:0 to 10:0.5 (v/v) ethyl acetate/methanol to provide **13A** (440 mg, 60%) as colorless crystals. Mp: 106–108 °C; MS (FAB) *m/z* 1212 (M + H); <sup>1</sup>H NMR (CDCl<sub>3</sub>): (selected signals):  $\delta$  7.00 (s, 1H), 5.90 (m, 1H), 5.50 (br s, 1H), 5.37 (d, 2H, *J* = 2.7 Hz), 5.30 (d, 1H, *J* = 17.2 Hz), 5.20 (m, 5H), 4.65–4.45 (m, 2H), 4.29 (m, 2H), 4.15 (br., 2H), 4.00 (m, 2H), 2.2–2.0 (4s, 24H), 1.80 (s, 3H), 1.40 (overlapping s, 13H); <sup>13</sup>C NMR (CDCl<sub>3</sub>):  $\delta$  170.75, 169.97, 169.65, 169.59, 167.58, 164.13, 156.00, 151.06, 141.38, 131.24, 119.06, 110.31, 79.65, 68.20, 67.44, 66.65, 66.18, 60.75, 60.18, 50.01, 39.12, 28.25, 20.66, 20.61, 20.48, 12.00; HRMS (M + H)<sup>+</sup>, calcd (found) for C<sub>55</sub>H<sub>82</sub>N<sub>5</sub>O<sub>25</sub>: 1212.5299 (1212.5360).

***N*<sup>2</sup>-(2-Boc-aminoethyl)-*N*<sup>2</sup>-(thymine-1-ylacetyl)-*N*<sup>6</sup>,*N*<sup>6</sup>-bis(2,3,4-tri-*O*-acetyl- $\alpha$ -L-fucopyranose-1-ylethyl)-L-lysine Allyl Ester (13B).** The procedure is the same as that described above for the synthesis of **13A** using **S5B**. (63%), mp: 90–92 °C; MS (FAB) *m/z* 1096 (M + H); <sup>1</sup>H NMR (CDCl<sub>3</sub>): (selected signals):  $\delta$  7.00 (s, 1H), 5.90 (m, 1H), 5.60 (br s, 1H), 5.20 (overlapping, 8H), 4.60 (overlapping, 4H), 4.20 (br s, 2H), 4.00 (m, 4H), 2.0–1.9 (3s, 18H), 1.80 (s, 3H), 1.40 (overlapping s, 13H), 1.10 (d, 6H, *J* = 3.8 Hz); <sup>13</sup>C NMR (CDCl<sub>3</sub>):  $\delta$  170.87, 170.45, 170.17, 169.95, 167.21, 164.46, 155.90, 151.11, 141.38, 131.18, 130.89, 119.34, 118.79, 110.26, 80.08, 72.51, 70.39, 69.75, 69.50, 68.07, 67.86, 66.05, 60.80, 60.08, 53.51, 50.20, 48.69, 48.01, 38.89, 36.44, 31.28, 28.09, 23.63, 21.65, 20.73, 20.60, 20.48, 20.38, 16.00, 15.47, 13.87, 11.94; HRMS (M + H)<sup>+</sup>, calcd (found) for C<sub>51</sub>H<sub>78</sub>N<sub>5</sub>O<sub>21</sub>: 1096.5189 (1096.5192).

***N*<sup>2</sup>-(2-Boc-aminoethyl)-*N*<sup>2</sup>-(thymine-1-ylacetyl)-*N*<sup>6</sup>-(2,3,4,6-tetra-*O*-acetyl- $\alpha$ -D-galactopyranose-1-ylacetyl)-L-lysine Allyl Ester (14A).** **S6A** (1.03 g, 2.64 mmol), DhbtOH (470 mg, 2.88 mmol), and DCC (740 mg, 3.6 mmol) were dissolved in DMF (20 mL) and stirred for 30 min under nitrogen. A solution of **12** (1.2 g, 2.4 mmol) in DMF (10 mL) was added, and the reaction mixture was stirred for further 3 h. Volatiles were removed under vacuum, and the residue was dissolved in ethyl acetate. Insoluble DCU was filtered off, and the filtrate was extracted with saturated aqueous NaHCO<sub>3</sub> and brine, respectively. The organic phase was dried over MgSO<sub>4</sub> and evaporated to dryness under vacuum. The residue was purified on a silica gel column eluting with ethyl acetate to provide **14A** (1.1 g, 61%) as colorless crystals, mp: 82–84 °C; MS (FAB) *m/z* 868 (M + H); <sup>1</sup>H NMR (CDCl<sub>3</sub>): (selected signals):  $\delta$  9.39 (s, 1H), 6.94 (s, 1H), 6.64 (s, 1H), 5.92–5.85 (m, 1H), 5.42 (m, 2H), 5.32 (d, 1H, *J* = 17.2 Hz), 5.25 (m, 3H), 4.75–4.45 (m, 4H), 4.3–4.1 (m, 5H), 3.60 (m, 1H), 2.60 (m, 1H), 2.45 (m, 1H), 2.15–2.00 (3s, 12H), 1.90 (s, 3H), 1.60 (br., 2H), 1.40 (overlapping s, 11H); <sup>13</sup>C NMR (CDCl<sub>3</sub>):  $\delta$  170.56, 169.85, 169.77, 169.44, 167.47, 163.93, 155.82, 151.40, 140.89, 131.23, 119.09, 110.93, 79.86, 69.23, 68.87, 68.23, 67.60, 66.82, 66.12, 60.85, 59.64, 48.88, 47.13, 38.99, 38.59,

34.74, 28.28, 28.04, 27.58, 22.79, 20.61, 20.51, 12.20.. Anal. for C<sub>39</sub>H<sub>57</sub>N<sub>5</sub>O<sub>17</sub>·1/2H<sub>2</sub>O: calcd C 53.42, H 6.67, N 7.99; found C 53.25, H 6.71, N 7.44

***N*<sup>2</sup>-(2-Boc-aminoethyl)-*N*<sup>2</sup>-(thymine-1-ylacetyl)-*N*<sup>6</sup>-(2,3,4-tri-*O*-acetyl- $\alpha$ -L-fucopyranose-1-ylacetyl)-L-lysine Allyl Ester (14B).** The procedure is the same as that described for the synthesis of **14A** using **S6B** (65%), mp: 82–84 °C; MS (FAB) *m/z* 810 (M + H); <sup>1</sup>H NMR (CDCl<sub>3</sub>) (selected signals):  $\delta$  9.64 (s, 1H), 6.94 (s, 1H), 6.88 (s, 1H), 6.0–5.8 (m, 1H), 5.50 (s, 1H), 5.37 (s, 1H), 5.30 (m, 3H), 5.16 (m, 1H), 4.8–4.6 (m, 4H), 2.15–2.00 (3s, 9H), 1.90 (s, 3H), 1.60 (m, 2H), 1.40 (overlapping s, 11H), 1.20 (d, 3H, *J* = 6.4 Hz); <sup>13</sup>C NMR (CDCl<sub>3</sub>):  $\delta$  170.42, 169.95, 169.74, 169.68, 169.55, 167.13, 163.86, 162.37, 155.81, 151.53, 140.81, 131.25, 119.08, 111.01, 79.83, 69.36, 68.43, 68.23, 67.95, 66.16, 61.64, 60.24, 48.95, 38.83, 37.41, 36.34, 35.68, 33.78, 28.72, 28.34, 27.33, 27.46, 24.80, 22.67, 20.91, 20.69, 20.62, 14.63, 14.05, 12.30; HRMS (M + H)<sup>+</sup>, calcd (found) for C<sub>37</sub>H<sub>55</sub>N<sub>5</sub>O<sub>15</sub>Na: 832.3592 (832.3594).

***N*<sup>2</sup>-(2-Boc-aminoethyl)-*N*<sup>2</sup>-(thymine-1-ylacetyl)-*N*<sup>6</sup>-(2,3,4,6-tetra-*O*-acetyl- $\alpha$ -D-mannopyranose-1-ylacetyl)-L-lysine Allyl Ester (14C).** The procedure is the same as that described for the synthesis of **14A** using **S6C** (58%), mp: 80–82 °C; MS (FAB) *m/z* 868 (M + H); <sup>1</sup>H NMR (CDCl<sub>3</sub>): (selected signals):  $\delta$  9.35 (s, 1H), 6.94 (s, 1H), 6.78 (s, 1H), 5.80 (m, 1H), 5.45 (s, 1H), 5.35 (d, 1H, *J* = 17.0 Hz), 5.25 (m, 2H), 5.13 (m, 2H), 4.6–4.5 (m, 4H), 4.30 (m, 1H), 4.20 (m, 1H), 4.10 (m, 1H), 3.60 (m, 1H), 2.15–2.00 (4s, 12H), 1.90 (s, 3H), 1.60 (br., 2H), 1.40 (overlapping s, 11H); <sup>13</sup>C NMR (CDCl<sub>3</sub>):  $\delta$  171.01, 170.47, 169.87, 169.39, 167.60, 164.35, 156.26, 151.73, 141.31, 131.64, 119.47, 111.23, 80.24, 79.01, 72.44, 71.70, 71.22, 69.85, 68.62, 67.58, 66.53, 62.23, 60.50, 50.68, 49.37, 47.90, 39.35, 39.06, 37.20, 33.09, 28.51, 27.88, 25.42, 24.76, 24.33, 21.11, 12.62; HRMS (M + H)<sup>+</sup>, calcd (found) for C<sub>39</sub>H<sub>58</sub>N<sub>5</sub>O<sub>17</sub>: 890.3647 (890.3621).

***N*<sup>2</sup>-(2-Fmoc-aminoethyl)-*N*<sup>2</sup>-(thymine-1-ylacetyl)-*N*<sup>6</sup>-(2,3,4,6-tetra-*O*-acetyl- $\alpha$ -D-galactopyranose-1-ylacetyl)-L-lysine Allyl Ester (15A)** was prepared from **14A** by procedure d (91%), mp: 93–95 °C; MS (FAB) *m/z* 990 (M + H); <sup>1</sup>H NMR (CDCl<sub>3</sub>):  $\delta$  9.33 (s, 1H), 7.6–7.1 (m, 8H), 6.64 (s, 1H), 6.51 (s, 1H), 5.8–5.6 (m, 2H), 5.27 (s, 1H), 5.15 (d, 1H, *J* = 17.0 Hz), 5.07 (m, 3H), 4.6–4.4 (m, 4H), 4.28 (overlapping s, 3H), 4.20 (m, 1H), 4.1–4.0 (m, 5H), 3.42 (m, 1H), 3.29–3.26 (overlapping s, 3H), 3.04 (br s, 2H), 2.46–2.26 (m, 2H), 2.0–1.8 (4s, 12H), 1.68 (s, 3H), 1.40 (m, 1H), 1.20 (m, 3H); <sup>13</sup>C NMR (CDCl<sub>3</sub>):  $\delta$  170.56, 170.46, 169.80, 169.72, 169.41, 169.36, 167.51, 163.98, 156.48, 151.29, 143.47, 143.44, 141.07, 131.18, 127.60, 127.49, 126.89, 124.71, 119.83, 119.03, 110.59, 77.41, 76.90, 76.39, 69.21, 68.75, 68.17, 67.64, 67.52, 66.73, 66.48, 66.06, 60.77, 59.54, 48.68, 46.97, 39.52, 38.62, 34.66, 28.16, 27.69, 22.87, 20.52, 20.43, 12.08; HRMS (M + H)<sup>+</sup>, calcd (found) for C<sub>49</sub>H<sub>60</sub>N<sub>5</sub>O<sub>17</sub>: 990.3984 (990.3940).

***N*<sup>2</sup>-(2-Fmoc-aminoethyl)-*N*<sup>2</sup>-(thymine-1-ylacetyl)-*N*<sup>6</sup>-(2,3,4-tri-*O*-acetyl- $\alpha$ -L-fucopyranose-1-ylacetyl)-L-lysine Allyl Ester (15B).** Prepared from **14B** by procedure d (89%), mp: 113–115 °C; MS (FAB) *m/z* 932 (M + H); <sup>1</sup>H NMR (CDCl<sub>3</sub>): (selected signals):  $\delta$  9.85 (s, 1H), 7.7–7.2 (m, 8H), 7.00 (s, 1H), 6.80 (s, 1H), 6.00 (s, 1H), 5.90 (m, 1H), 5.28 (s, 1H), 5.20 (m, 4H), 4.60 (overlapping s, 4H), 4.40 (m, 2H), 4.25 (br s, 1H), 4.20 (m, 2H), 2.00 (s, 9H), 1.80 (s, 3H), 1.5–1.2 (m, 4H), 1.20 (d, 3H, *J* = 6.4 Hz); <sup>13</sup>C NMR (CDCl<sub>3</sub>):  $\delta$  170.99, 170.46, 170.16, 169.98, 169.79, 169.62, 167.11, 163.90, 156.50, 151.60, 143.65, 143.31, 141.11, 131.22, 130.90, 127.65, 127.02, 126.96, 124.87, 119.88, 119.13, 110.87, 69.05,



68.19, 67.70, 66.60, 66.20, 61.55, 60.23, 48.77, 46.99, 39.32, 37.69, 35.20, 28.77, 27.46, 22.74, 20.89, 20.61, 20.56, 20.47, 14.72, 14.02, 12.15; HRMS ( $M + H$ )<sup>+</sup>, calcd (found) for  $C_{47}H_{58}N_5O_{15}$ : 932.3929 (932.3945).

***N*<sup>2</sup>-(2-Fmoc-aminoethyl)-*N*<sup>2</sup>-(thymine-1-ylacetyl)-*N*<sup>6</sup>-(2,3,4,6-tetra-*O*-acetyl- $\alpha$ -D-mannopyranose-1-ylacetyl)-L-lysine Allyl Ester (15C).** Prepared from **14C** by procedure d (88%), mp: 110–112 °C; MS (FAB)  $m/z$  990 ( $M + H$ ); <sup>1</sup>H NMR (CDCl<sub>3</sub>) (selected signals):  $\delta$  9.24 (s, 1H), 7.7–7.2 (m, 8H), 6.71 (overlapping s, 2H), 5.80 (m, 2H), 5.25 (m, 3H), 5.06 (m, 2H), 4.50 (overlapping s, 2H), 4.40 (overlapping s, 2H), 4.30 (m, 1H), 4.20 (m, 1H), 4.10 (m, 1H), 2.50 (m, 2H), 2.00 (s, 12H), 1.78 (s, 3H), 1.5–1.2 (2m, 4H); <sup>13</sup>C NMR (CDCl<sub>3</sub>):  $\delta$  170.72, 169.54, 165.72, 163.81, 151.40, 143.57, 141.17, 136.86, 131.22, 127.70, 127.01, 124.89, 119.93, 119.22, 110.10, 81.47, 67.27, 66.65, 66.24, 61.74, 47.07, 20.65, 20.43, 12.18; HRMS ( $M + H$ )<sup>+</sup>, calcd (found) for  $C_{49}H_{60}N_5O_{17}$ : 990.3984 (990.3987).

***N*-(2-Fmoc-aminoethyl)-*O*-(*t*-butyl)-L-aspartic Acid Allyl Ester (18).** To **16** [prepared from *N*-(Fmoc)-*O*-(*tert*-butyl)aspartic acid by procedure a] (4.5 g, 10 mmol) was added 20% piperidine in DCM (50 mL). After 30 min toluene (100 mL) was added, and volatiles were removed under vacuum. The residue was purified by flash chromatography, eluting with a gradient of 10:0 to 10:1 (v/v) ethyl acetate/methanol to afford **17** (1.8 g, 7.9 mmol) as a slightly yellow oil. This oil was used for procedure b, and **18** (1.7 g, 34%) was obtained as a colorless oil. MS (FAB)  $m/z$  495 ( $M + H$ ); <sup>1</sup>H NMR (CDCl<sub>3</sub>):  $\delta$  7.7–7.2 (m, 8H), 5.96–5.84 (m, 1H), 5.56 (br s, 1H), 5.35 (d, 1H,  $J = 17.3$  Hz), 5.25 (d, 1H,  $J = 10.5$  Hz), 4.60 (d, 2H,  $J = 5.9$  Hz), 4.40 (d, 2H,  $J = 7.0$  Hz), 4.20 (t, 1H,  $J = 7.0$  Hz), 3.60 (t, 1H,  $J = 7.3$  Hz), 3.30 (m, 2H), 2.90 (m, 1H), 2.7–2.5 (m, 3H), 2.30 (br s, 1H), 1.40 (s, 9H); <sup>13</sup>C NMR (CDCl<sub>3</sub>):  $\delta$  173.02, 169.89, 156.37, 143.84, 141.06, 131.47, 127.41, 126.81, 124.95, 119.71, 118.68, 81.17, 66.5, 65.62, 57.12, 47.05, 40.34, 38.97, 27.85; HRMS ( $M + H$ )<sup>+</sup>, calcd (found) for  $C_{28}H_{35}N_2O_6$ : 495.2495 (495.2480).

***N*-(2-Fmoc-aminoethyl)-*N*-(thymine-1-ylacetyl)-*O*-(*t*-butyl)-L-aspartic Acid Allyl Ester (19).** Prepared from **18** by procedure c (81%), mp: 76–77 °C; MS (FAB)  $m/z$  661 ( $M + H$ ); <sup>1</sup>H NMR (CDCl<sub>3</sub>) (selected signals):  $\delta$  9.15 (s, 1H), 7.75–7.26 (m, 8H), 6.75 (s, 1H), 5.90 (s, 1H), 5.80 (m, 1H), 5.30 (d, 1H,  $J = 17.3$  Hz), 5.20 (d, 1H,  $J = 10.5$  Hz), 4.7–4.4 (m, 5H), 4.2–4.1 (m, 3H), 1.80 (s, 3H), 1.40 (s, 9H); <sup>13</sup>C NMR (CDCl<sub>3</sub>):  $\delta$  170.49, 169.36, 167.05, 164.06, 156.52, 150.62, 143.63, 143.52, 141.09, 140.85, 131.10, 130.71, 127.57, 126.92, 124.83, 119.79, 119.24, 110.32, 82.27, 81.41, 66.84, 66.51, 60.24, 58.08, 48.85, 47.82, 47.10, 39.15, 35.41, 27.85, 14.04, 12.19; HRMS ( $M + H$ )<sup>+</sup>, calcd (found) for  $C_{35}H_{41}N_4O_9$ : 661.2874 (661.2881).

***N*-(2-Fmoc-aminoethyl)-*N*-(thymine-1-ylacetyl)-L-aspartic Acid Allyl Ester (20).** To **19** (3.3 g, 5 mmol) was added a mixture of TFA/TES (95:5 v/v, 20 mL). The reaction mixture was stirred until total conversion of starting material according to TLC. The mixture was coevaporated with DCM under vacuum, and **20** (1.87 g, 62%) was obtained as slightly yellow crystals, mp: 112–114 °C; MS (FAB) 605  $m/z$  ( $M + H$ ); <sup>1</sup>H NMR (DMSO-*d*<sub>6</sub>):  $\delta$  11.30 (s, 1H), 7.91–7.22 (m, 9H), 5.80 (m, 1H), 5.30 (d, 1H,  $J = 17.3$  Hz), 5.10 (d, 1H,  $J = 10.5$  Hz), 4.60–4.45 (m, 4H), 4.40 (t, 1H,  $J = 6.4$  Hz), 4.3–4.2 (m, 4H), 3.5–3.4 (m, 3H), 3.20 (dd, 2H,  $J = 17.0, 7.3$  Hz), 1.70 (s, 3H); <sup>13</sup>C NMR (CD<sub>3</sub>OD):  $\delta$  174.50, 170.90, 169.54, 166.94, 158.90, 152.80, 145.30, 143.64, 142.57, 142.16, 133.25, 131.09, 130.44, 128.83, 128.21, 127.13, 126.20, 121.00, 118.96, 110.89, 67.80, 67.38, 61.59, 59.96, 40.47, 35.32,

14.53, 12.34; HRMS ( $M + H$ )<sup>+</sup>, calcd (found) for  $C_{31}H_{33}N_4O_9$ : 605.2224 (605.2248).

***N*<sup>2</sup>-(2-Fmoc-aminoethyl)-*N*<sup>2</sup>-(thymine-1-ylacetyl)-*N*<sup>1</sup>-(2,3,4,6-tetra-*O*-acetyl- $\beta$ -D-galactopyranose-1-yl)-L-asparagine Allyl Ester (21A).** Prepared from **20** by procedure e using **S7A** (64%), mp: 83–85 °C; MS (FAB)  $m/z$  934 ( $M + H$ ); <sup>1</sup>H NMR (CDCl<sub>3</sub>) (selected signals):  $\delta$  9.50 (s, 1H), 7.7–7.2 (m, 8H), 6.60 (s, 1H), 5.90 (overlapping m, 2H), 5.30 (d, 1H,  $J = 1.6$  Hz), 5.25–5.15 (m, 3H), 5.05 (m, 2H), 4.6–4.4 (m, 4H), 2.1–1.9 (4s, 12H), 1.80 (s, 3H); <sup>13</sup>C NMR (CDCl<sub>3</sub>):  $\delta$  171.21, 170.22, 169.84, 169.76, 169.58, 166.56, 164.17, 156.81, 156.57, 151.39, 143.68, 143.45, 141.17, 140.94, 131.20, 127.71, 127.04, 124.89, 119.92, 119.16, 110.60, 80.39, 78.26, 72.13, 71.36, 67.86, 67.19, 66.81, 66.55, 61.44, 61.06, 57.81, 49.22, 48.92, 48.77, 47.16, 39.19, 36.00, 33.69, 25.47, 24.79, 20.71, 20.61, 20.57, 20.46 (sugar-acetyl groups), 12.26. Anal. for  $C_{45}H_{51}N_5O_{17}$ , H<sub>2</sub>O: calcd C 56.78, H 5.61, N 7.36; found C 56.87, H 5.94, N 7.57.

***N*<sup>2</sup>-(2-Fmoc-aminoethyl)-*N*<sup>2</sup>-(thymine-1-ylacetyl)-*N*<sup>1</sup>-(2,3,4-tri-*O*-acetyl- $\beta$ -L-fucopyranose-1-yl)-L-asparagine Allyl Ester (21B).** Prepared from **20** by procedure e using **S7B**, (77%), mp: 88–90 °C; MS (FAB)  $m/z$  876 ( $M + H$ ); <sup>1</sup>H NMR (CDCl<sub>3</sub>):  $\delta$  9.10 (s, 1H), 7.7–7.2 (m, 8H), 6.70 (s, 1H), 5.90 (br s, 1H), 5.80 (m, 1H), 5.30 (d, 1H,  $J = 7.6$  Hz), 5.20 (m, 2H), 5.00 (m, 2H), 4.6–4.4 (m, 4H), 4.2–4.0 (m, 4H), 3.90 (m, 1H), 3.70 (q, 1H,  $J = 6.4$  Hz), 2.2–2.0 (3s, 9H), 1.90 (s, 3H), 1.10 (d, 3H,  $J = 6.4$  Hz); <sup>13</sup>C NMR (CDCl<sub>3</sub>):  $\delta$  171.22, 170.70, 170.45, 169.91, 169.83, 167.34, 156.66, 150.75, 143.61, 141.14, 140.79, 131.13, 127.69, 127.02, 124.91, 119.91, 119.41, 110.58, 79.12, 78.30, 77.32, 76.89, 76.47, 71.39, 71.18, 70.78, 70.07, 68.63, 67.61, 66.80, 66.55, 49.27, 49.08, 47.04, 39.19, 36.06, 33.75, 25.45, 24.79, 21.17, 20.55, 20.49, 19.32, 16.00, 12.62; HRMS ( $M + H$ )<sup>+</sup>, calcd (found) for  $C_{44}H_{50}N_5O_{15}$ : 876.3303 (876.3304).

***N*<sup>2</sup>-(2-Fmoc-aminoethyl)-*N*<sup>2</sup>-(thymine-1-ylacetyl)-*N*<sup>1</sup>-(2,3,4,6-tetra-*O*-acetyl- $\beta$ -D-mannopyranose-1-yl)-L-asparagine Allyl Ester (21C).** Prepared from **20** by procedure e using **S7C** (60%), mp: 83–85 °C; MS (FAB)  $m/z$  934 ( $M + H$ ); <sup>1</sup>H NMR (CDCl<sub>3</sub>) (selected signals):  $\delta$  9.50 (s, 1H), 7.7–7.2 (m, 8H), 6.70 (s, 1H), 6.00 (br s, 1H), 5.90 (m, 1H), 5.50 (d, 1H,  $J = 8.8$  Hz), 5.45 (d, 1H,  $J = 3.2$  Hz), 5.3–5.0 (m, 4H), 4.60 (overlapping s, 2H), 4.40 (m, 2H), 4.20 (m, 3H), 4.10 (m, 2H), 2.90 (m, 1H), 2.2–1.9 (4s, 12Hs), 1.80 (s, 3H); <sup>13</sup>C NMR (CDCl<sub>3</sub>):  $\delta$  171.13, 170.95, 170.49, 170.30, 169.93, 169.85, 164.62, 157.14, 156.95, 151.54, 144.08, 141.49, 131.57, 128.04, 127.35, 125.24, 120.27, 119.56, 110.77, 74.43, 71.83, 69.87, 67.00, 66.87, 66.05, 65.62, 62.61, 58.53, 49.56, 49.34, 47.44, 39.47, 34.13, 25.83, 25.16, 21.21, 21.01, 20.95, 20.84, 12.05; HRMS ( $M + H$ )<sup>+</sup>, calcd (found) for  $C_{45}H_{52}N_5O_{17}$ : 934.3358 (934.3342).

***N*<sup>2</sup>-(2-Fmoc-aminoethyl)-*N*<sup>2</sup>-(thymine-1-ylacetyl)-*N*<sup>1</sup>-(2-acetamido-3,4,6-tri-*O*-acetyl-2-deoxy- $\beta$ -D-glucopyranose-1-yl)-L-asparagine Allyl Ester (21D).** Prepared from **20** by procedure e using **S7D** (73%), mp: 98–100 °C; MS (FAB)  $m/z$  933 ( $M + H$ ); <sup>1</sup>H NMR (CDCl<sub>3</sub>) (selected signals):  $\delta$  10.00 (s, 1H), 7.7–7.2 (m, 8H), 6.80 (s, 1H), 6.00 (br s, 1H), 5.80 (m, 1H), 5.25 (d, 1H,  $J = 17.2$  Hz), 5.18 (d, 1H,  $J = 10.2$  Hz), 5.14–5.03 (m, 2H), 4.60 (d, 2H,  $J = 5.7$  Hz), 4.40 (br s, 2H), 4.20 (m, 3H), 4.10 (m, 2H), 2.1–2.0 (4s, 12H), 1.90 (s, 3H); <sup>13</sup>C NMR (CDCl<sub>3</sub>):  $\delta$  171.78, 171.08, 170.97, 170.71, 170.51, 169.42, 169.23, 166.94, 164.52, 156.47, 151.12, 143.58, 141.06, 131.05, 130.79, 127.60, 126.92, 124.82, 119.84, 119.51, 119.17, 110.40, 79.39, 73.07, 67.89, 66.48, 61.68, 57.94, 52.75, 48.96, 48.28, 47.00, 39.14, 35.51, 33.67, 24.73, 22.74, 20.54, 20.43, 12.11. Anal. for



$C_{45}H_{52}N_6O_{16} \cdot \frac{3}{2}H_2O$ : calcd C 56.30, H 5.78, N 8.75; found C 56.43, H 5.70, N 8.72.

***N*<sup>2</sup>-(2-Fmoc-aminoethyl)-*N*<sup>2</sup>-(thymine-1-ylacetyl)-*N*<sup>1</sup>-(2-acetamido-3,4,6-tri-*O*-acetyl-2-deoxy- $\beta$ -D-galactopyranose-1-yl)-L-asparagine Allyl Ester (21E).** Prepared from **20** by procedure e using **M7E** (60%), mp: 100–102 °C; MS (FAB)  $m/z$  933 ( $M + H$ );  $^1H$  NMR ( $CDCl_3$ ) (selected signals):  $\delta$  10.20 (s, 1H), 7.9–7.0 (m, 8H), 6.80 (s, 1H), 6.30 (m, 1H), 6.10 (br s, 1H), 5.80 (m, 1H), 5.4–5.1 (m, 5H), 4.70 (m, 2H), 4.40 (s, 2H), 2.1–2.0 (m, 12H), 1.80 (s, 3H);  $^{13}C$  NMR ( $CDCl_3$ ):  $\delta$  171.78, 171.08, 170.97, 170.71, 170.51, 169.42, 169.23,  $^{13}C$  NMR ( $CDCl_3$ ):  $\delta$  172.32, 170.82, 170.54, 170.33, 170.04, 169.55, 169.37, 167.03, 164.53, 156.62, 151.35, 143.55, 141.04, 131.09, 127.59, 126.91, 124.80, 119.82, 119.07, 110.41, 79.57, 71.83, 70.46, 67.91, 67.37, 66.86, 66.70, 66.45, 61.77, 61.31, 58.59, 49.20, 48.98, 47.96, 47.01, 39.18, 23.04, 22.95, 22.77, 20.52, 12.04; HRMS ( $M + H$ )<sup>+</sup>, calcd (found) for  $C_{45}H_{53}N_6O_{16}$ : 933.3518 (933.3549).

**(Z)-*N*-(Benzyloxycarbonyl)-4-(2,3,4,6-tetra-*O*-acetyl-galactopyranose-1-yl)-2-amino-2-butenic Acid *tert*-Butyl Ester (25).** *N*-(Benzyloxycarbonyl)- $\alpha$ -(dimethoxyphosphinyl)glycine methyl ester **22** (3.5 g, 10.17 mmol) was hydrolyzed for 15 min in 1 N KOH (11.2 mL, 11.19 mmol). The reaction mixture was acidified to pH 3 by dropwise addition of 6 N HCl, resulting in the precipitation of the acid **23** as a white solid (yield 83%). **23** (4.75 g, 14 mmol) was dissolved in *tert*-butyl alcohol (150 mL) and chloroform (50 mL). EEDQ (4.4 g, 1.2 equiv) was added in one portion. After being stirred for 24 h, all volatiles were removed by rotary evaporator. The residue was dissolved in ethyl acetate (300 mL) and extracted with HCl (5%, 2  $\times$  50 mL) and brine (50 mL). The organic phase was dried over  $Na_2SO_4$  and evaporated to dryness. The residue was purified by flash chromatography eluting with ethyl acetate–toluene (2:1 v/v) to give **24** as colorless needles (5.9 g, 95%). **24** (2.2 g, 5.8 mmol) was dissolved in dry THF (20 mL). Tetramethylguanidine (0.8 mL, 10 mmol) was added at –78 °C and stirred for 5 min. **S5A** (1.9 g, 5.27 mmol) in dry THF (10 mL) was added, and the reaction mixture was allowed to reach room temperature. Volatiles were removed, and the residue was purified by flash chromatography eluting with *n*-hexane/ethyl acetate (1:1 v/v) to provide **25** (2.2 g, 66%) as a colorless oil. MS (FAB)  $m/z$  622 ( $M + H$ );  $^1H$  NMR ( $CDCl_3$ ):  $\delta$  7.40 (m, 5H), 6.50 (m, 2H), 5.40 (t, 1H,  $J = 3.0$  Hz), 5.20 (ABX-system, 2H,  $\Delta = 26.9$  Hz,  $J_{AB} = 9.1$  Hz,  $J_{AX} = 4.8$  Hz,  $J_{BX} = 3.3$  Hz), 5.15 (d, 2H,  $J = 1.3$  Hz), 4.35 (m, 1H), 4.25 (m, 1H), 4.1–4.0 (m, 2H), 2.60 (m, 1H), 2.40 (m, 1H), 2.15–2.00 (4s, 12H), 1.40 (s, 9H);  $^{13}C$  NMR ( $CDCl_3$ ):  $\delta$  170.42, 169.86, 169.68, 163.08, 153.86, 135.81, 129.60, 128.43, 128.16, 128.06, 82.06, 74.04, 71.02, 68.91, 68.51, 67.72, 67.55, 67.32, 67.25, 61.18, 27.87, 25.82, 20.62, 20.54; HRMS ( $M + H$ )<sup>+</sup>, calcd (found) for  $C_{30}H_{40}NO_{13}$ : 622.2500 (622.2495).

***N*-(2-Fmoc-aminoethyl)-4-(2,3,4,6-tetra-*O*-acetyl-galactopyranose-1-yl)-2-aminobutyric Acid *tert*-Butyl Ester (27).** **25** (2.2 g, 3.5 mmol) was dissolved in methanol (10 mL). Pd/C (50 mg) was added and the solution hydrogenated at 1 atm for 3 h. The catalyst was filtered off over Celite, and methanol was removed under vacuum. The remaining oil **26** was directly used in procedure b to afford **27** (2.1 g, 82%) as a colorless foam. MS (FAB)  $m/z$  755 ( $M + H$ );  $^1H$  NMR ( $CDCl_3$ ):  $\delta$  7.7–7.2 (m, 8H), 5.50 (overlapping s, 2H), 5.20 (m, 2H), 4.40 (d, 2H,  $J = 7$  Hz), 4.20 (overlapping s, 2H), 4.1–4.0 (m, 3H), 3.3–3.0 (m, 4H), 2.80 (m, 1H), 2.60 (m, 1H), 2.2–2.0 (4s, 12H), 1.40 (s, 9H);  $^{13}C$  NMR ( $CDCl_3$ ):  $\delta$  174.13, 170.53, 170.47, 170.40, 170.01, 169.93, 169.86, 169.76, 169.71,

169.63, 156.37, 143.79, 143.69, 141.07, 127.45, 126.82, 124.90, 119.75, 81.43, 71.60, 68.26, 68.20, 68.00, 67.80, 67.71, 67.58, 67.44, 67.35, 66.51, 61.42, 61.24, 61.07, 61.00, 60.19, 47.33, 47.05, 28.79, 27.89, 27.47, 21.75, 20.86, 20.59, 20.53, 20.46, 14.01; HRMS ( $M + H$ )<sup>+</sup>, calcd (found) for  $C_{39}H_{51}N_2O_{13}$ : 755.3391 (755.3371).

***N*-(2-Fmoc-aminoethyl)-*N*-(thymine-1-ylacetyl)-4-(2,3,4,6-tetra-*O*-acetyl-galactopyranose-1-yl)-2-aminobutyric Acid *tert*-Butyl Ester (28A).** Prepared from **27** by procedure c (66%), mp: 93–95 °C; MS (FAB)  $m/z$  951 ( $M + H$ );  $^1H$  NMR ( $CDCl_3$ ): (selected signals):  $\delta$  9.20 (s, 1H), 7.8–7.3 (m, 8H), 6.90 (s, 1H), 5.80 (s, 1H), 5.40 (d, 1H,  $J = 3.0$  Hz), 5.35–5.25 (m, 2H), 5.20 (d, 1H,  $J = 3.0$  Hz), 4.40 (m, 3H), 4.2–4.0 (m, 5H), 2.2–2.0 (4s, 12H), 1.80 (s, 3H), 1.40 (s, 9H);  $^{13}C$  NMR ( $CDCl_3$ ):  $\delta$  170.46, 169.94, 169.84, 169.07, 168.19, 166.85, 163.99, 156.44, 150.82, 143.54, 141.08, 127.59, 126.89, 124.78, 119.83, 110.23, 82.49, 72.31, 71.83, 67.49, 66.93, 66.61, 61.81, 61.29, 60.20, 59.30, 48.87, 48.40, 47.89, 46.96, 46.10, 39.98, 39.38, 33.72, 27.75, 25.41, 24.88, 22.60, 21.16, 20.86, 20.68, 20.55, 14.01, 12.16; HRMS ( $M + H$ )<sup>+</sup>, calcd (found) for  $C_{46}H_{57}N_4O_{16}$ : 921.3770 (921.3782).

***N*-(2-Fmoc-aminoethyl)-*N*-(thymine-1-ylacetyl)-*O*-(2,3,4,6-tetra-*O*-acetyl- $\beta$ -D-galactopyranose-1-yl)-L-serine (I-A).** Prepared from **7A** by procedure f (86%), mp: 124–127 °C; MS (FAB)  $m/z$  867 ( $M + H$ );  $^1H$  NMR ( $CD_3OD$ ) (selected signals):  $\delta$  7.8–7.3 (m, 9H), 5.40 (overlapping, 2H), 5.15 (m, 2H), 4.65 (overlapping s, 3H), 2.2–2.0 (4s, 12H), 1.80 (s, 3H);  $^{13}C$  NMR ( $CD_3OD$ ):  $\delta$  170.20, 170.13, 170.05, 169.75, 165.15, 143.56, 143.46, 141.98, 140.73, 133.95, 128.16, 127.99, 126.92, 126.36, 126.30, 124.40, 124.30, 119.06, 108.83, 100.26, 70.33, 70.13, 68.53, 68.44, 66.90, 65.86, 60.58, 47.95, 38.61, 18.88, 18.68, 18.59, 10.36; HRMS ( $M + H$ )<sup>+</sup>, calcd (found) for  $C_{41}H_{47}N_4O_{17}$ : 867.2936 (867.2924).

***N*-(2-Fmoc-aminoethyl)-*N*-(thymine-1-ylacetyl)-*O*-(2,3,4,6-tetra-*O*-acetyl- $\beta$ -D-galactopyranose-1-yl)-L-threonine (Im-A).** Prepared from **7mA** by procedure f (90%), mp: 128–131 °C; MS (FAB)  $m/z$  881 ( $M + H$ );  $^1H$  NMR ( $CD_3OD$ ): (selected signals):  $\delta$  7.84–7.32 (m, 9H), 5.41 (m, 1H), 5.2–5.1 (m, 2H), 2.18–2.00 (4s, 12H), 1.90 (s, 3H), 1.36 (d, 3H,  $J = 5.8$  Hz);  $^{13}C$  NMR ( $CD_3OD$ ):  $\delta$  172.06, 171.51, 167.09, 145.38, 143.86, 142.61, 128.87, 128.26, 126.26, 121.03, 116.69, 110.78, 100.40, 74.76, 72.31, 71.97, 70.66, 68.80, 67.78, 62.69, 62.49, 20.93, 20.73, 20.62, 12.41; HRMS ( $M + H$ )<sup>+</sup>, calcd (found) for  $C_{42}H_{49}N_4O_{17}$ : 881.3043 (881.3073).

***N*<sup>2</sup>-(2-Boc-aminoethyl)-*N*<sup>2</sup>-(thymine-1-ylacetyl)-*N*<sup>6</sup>,*N*<sup>6</sup>-bis(2,3,4,6-tetra-*O*-acetyl- $\alpha$ -D-galactopyranose-1-ylethyl)-L-lysine (II-A).** Prepared from **13A** by procedure f (80%), mp: 118–120 °C; MS (FAB)  $m/z$  1172 ( $M + H$ );  $^1H$  NMR ( $CD_3OH$ ): (selected signals):  $\delta$  7.40 (s, 1H), 5.45 (d, 2H,  $J = 2.7$  Hz), 5.4–5.2 (m, 4H), 4.38 (m, 4H), 3.95 (dd, 1H,  $J = 12.8, 3.6$  Hz), 2.90 (br, 2H), 2.80 (m, 2H), 2.2–2.0 (4s, 24H), 1.90 (s, 3H), 1.8–1.6 (br, 4H), 1.47 (overlapping m, 11H);  $^{13}C$  NMR ( $CD_3OH$ ):  $\delta$  172.41, 172.23, 171.91, 171.72, 171.69, 171.50, 170.39, 169.75, 167.08, 158.28, 153.16, 144.45, 144.16, 110.77, 110.57, 80.42, 71.31, 71.24, 70.29, 69.86, 69.78, 69.37, 69.20, 69.07, 66.30, 65.76, 62.88, 62.70, 54.96, 51.67, 50.87, 45.10, 40.60, 39.83, 32.81, 31.39, 30.56, 28.95, 28.88, 26.81, 26.26, 25.95, 25.66, 23.46, 23.01, 20.99, 20.79, 20.68, 12.43; HRMS ( $M + H$ )<sup>+</sup>, calcd (found) for  $C_{52}H_{78}N_5O_{25}$ : 1172.4986 (1172.5027).

***N*<sup>2</sup>-(2-Boc-aminoethyl)-*N*<sup>2</sup>-(thymine-1-ylacetyl)-*N*<sup>6</sup>,*N*<sup>6</sup>-bis(2,3,4-tri-*O*-acetyl- $\alpha$ -L-fucopyranose-1-ylethyl)-L-lysine (II-B).** Prepared from **13B** by procedure f (88%), mp: 117–120 °C; MS (FAB)  $m/z$  1056 ( $M + H$ );  $^1H$  NMR ( $CD_3OH$ ): (selected signals):  $\delta$  7.40 (s, 1H), 6.70

(m, 1H), 5.30 (overlapping, 6H), 4.30 (br. s, 2H), 4.20 (d, 2H,  $J = 6.4$  Hz), 2.2–2.0 (3s, 18H), 1.90 (s, 3H), 1.50 (overlapping s, 13H), 1.20 (m, 6H);  $^{13}\text{C}$  NMR ( $\text{CD}_3\text{OH}$ ):  $\delta$  172.19, 171.65, 166.98, 162.58, 158.30, 153.14, 144.9, 133.86, 133.18, 133.05, 130.66, 130.13, 128.83, 128.35, 123.36, 114.36, 110.83, 108.98, 80.44, 80.08, 71.82, 71.51, 69.82, 69.34, 67.49, 62.40, 54.33, 51.85, 51.32, 50.66, 45.12, 40.60, 39.81, 30.22, 28.97, 28.90, 25.24, 22.13, 21.02, 20.83, 20.67, 16.43, 12.49, 11.99; HRMS ( $\text{M} + \text{H}^+$ ), calcd (found) for  $\text{C}_{48}\text{H}_{74}\text{N}_5\text{O}_{21}$ : 1056.4876 (1056.4886).

***N*<sup>6</sup>-(2-Fmoc-aminoethyl)-*N*<sup>2</sup>-(thymine-1-ylacetyl)-*N*<sup>5</sup>-(2,3,4,6-tetra-*O*-acetyl- $\alpha$ -D-galactopyranose-1-ylacetyl)-L-lysine (IIIb-A).** Prepared from **14A** by procedure f (95%), mp: 115–118 °C; MS (FAB)  $m/z$  828 ( $\text{M} + \text{H}$ );  $^1\text{H}$  NMR ( $\text{CD}_3\text{OD}$ ): (selected signals):  $\delta$  7.37 (s, 1H), 5.44 (d, 1H,  $J = 2.6$  Hz), 5.30 (overlapping, 2H), 4.70 (m, 2H), 4.30 (m, 1H), 4.20 (m, 3H), 2.70 (m, 1H), 2.2–2.0 (4s, 12H), 1.90 (s, 3H), 1.40 (overlapping m, 11H);  $^{13}\text{C}$  NMR ( $\text{CD}_3\text{OD}$ ):  $\delta$  173.13, 172.16, 170.41–169.52, 167.69, 164.97, 156.48, 151.46, 141.90, 109.37, 78.68, 74.39, 69.32, 66.93, 60.52, 48.68, 40.93, 38.31, 37.08, 33.06, 29.22–25.82, 22.94–18.65, 10.34; HRMS ( $\text{M} + \text{H}^+$ ), calcd (found) for  $\text{C}_{36}\text{H}_{54}\text{N}_5\text{O}_{17}$ : 828.3515 (828.3515).

***N*<sup>6</sup>-(2-Fmoc-aminoethyl)-*N*<sup>2</sup>-(thymine-1-ylacetyl)-*N*<sup>5</sup>-(2,3,4,6-tetra-*O*-acetyl- $\alpha$ -D-galactopyranose-1-ylacetyl)-L-lysine (III-A).** Prepared from **15A** by procedure f (83%), mp: 130–132 °C; MS (FAB)  $m/z$  950 ( $\text{M} + \text{H}$ );  $^1\text{H}$  NMR ( $\text{CD}_3\text{OH}$ ) (selected signals):  $\delta$  7.8–7.3 (m, 9H), 5.43 (d, 1H,  $J = 2.4$  Hz), 5.30 (overlapping s, 2H), 4.70 (m, 3H), 4.40 (m, 3H), 4.3–4.1 (m, 5H), 2.7–2.5 (m, 2H), 2.2–2.0 (3s, 12H), 1.90 (s, 3H), 1.60 (br. 3H), 1.20 (m, 1H);  $^{13}\text{C}$  NMR ( $\text{CD}_3\text{OH}$ ):  $\delta$  174.33, 172.23, 172.20, 171.89, 171.56, 171.41, 170.43, 169.78, 166.98, 158.89, 153.02, 145.02, 143.91, 142.67, 128.88, 128.23, 126.22, 121.04, 110.92, 71.28, 70.14, 69.41, 69.15, 69.00, 67.81, 62.52, 61.65, 50.20, 40.80, 40.30, 35.08, 30.12, 29.78, 24.96, 20.83, 20.76, 20.72, 20.62, 12.37; HRMS ( $\text{M} + \text{H}^+$ ), calcd (found) for  $\text{C}_{46}\text{H}_{56}\text{N}_5\text{O}_{17}$ : 950.3671 (950.3666).

***N*<sup>6</sup>-(2-Fmoc-aminoethyl)-*N*<sup>2</sup>-(thymine-1-ylacetyl)-*N*<sup>5</sup>-(2,3,4-tri-*O*-acetyl- $\alpha$ -L-fucopyranose-1-ylacetyl)-L-lysine (III-B).** Prepared from **15B** by procedure f (86%), mp: 108–110 °C; MS (FAB)  $m/z$  892 ( $\text{M} + \text{H}$ );  $^1\text{H}$  NMR ( $\text{CD}_3\text{OD}$ ): (selected signals):  $\delta$  7.8–7.2 (m, 8H), 6.90 (s, 1H), 5.30 (overlapping s, 3H), 4.70 (s, 2H), 4.44 (d, 1H,  $J = 6.6$  Hz), 4.38 (m, 2H), 4.25 (m, 1H), 4.15 (d, 1H,  $J = 6.4$  Hz), 2.70 (m, 1H), 2.50 (m, 1H), 2.2–2.0 (3s, 9H), 1.85 (s, 3H), 1.6–1.3 (m, 4H), 1.20 (d, 3H,  $J = 4.4$  Hz);  $^{13}\text{C}$  NMR ( $\text{CD}_3\text{OD}$ ):  $\delta$  174.67, 172.51, 172.24, 171.51, 170.32, 169.68, 166.93, 158.86, 152.99, 145.29, 143.93, 142.62, 133.19, 131.77, 130.48, 129.92, 128.89, 128.24, 126.22, 121.83, 121.05, 117.01, 110.89, 72.044, 71.53, 69.88, 69.00, 67.81, 61.93, 42.08, 40.75, 40.12, 34.79, 30.15, 29.75, 26.77, 26.09, 24.91, 20.80, 20.59, 16.50, 12.38; HRMS ( $\text{M} + \text{H}^+$ ), calcd (found) for  $\text{C}_{44}\text{H}_{54}\text{N}_5\text{O}_{15}$ : 892.3616 (892.3635).

***N*<sup>6</sup>-(2-Fmoc-aminoethyl)-*N*<sup>2</sup>-(thymine-1-ylacetyl)-*N*<sup>5</sup>-(2,3,4,6-tetra-*O*-acetyl- $\alpha$ -D-mannopyranose-1-ylacetyl)-L-lysine (III-C).** Prepared from **15C** by procedure f (92%), mp: 115–117 °C; MS (FAB)  $m/z$  950 ( $\text{M} + \text{H}$ );  $^1\text{H}$  NMR ( $\text{CD}_3\text{OD}$ ): (selected signals):  $\delta$  8.00 (s, 1H), 7.7–7.2 (m, 8H), 6.80 (s, 1H), 5.26 (dd, 1H,  $J = 8.5$ , 3.2 Hz), 5.06 (dd, 1H,  $J = 6.7$ , 3.2 Hz), 5.13 (d, 1H,  $J = 8.5$  Hz), 4.60 (m, 2H), 4.4–4.0 (m, 8H), 2.00 (4s, 12H), 1.80 (s, 3H), 1.5–1.3 (2m, 4H);  $^{13}\text{C}$  NMR ( $\text{CDCl}_3$ ):  $\delta$  193.55, 178.08, 172.71, 172.46, 171.75, 171.56, 171.44, 166.88, 153.09, 145.27, 144.01, 142.58, 130.33, 128.89, 128.24, 126.23, 121.04, 116.26, 110.95, 73.18, 72.40, 72.30, 71.40, 70.19, 68.28, 67.88, 63.44, 62.41, 40.15,

37.31, 30.17, 25.05, 20.87, 20.71, 12.40; HRMS ( $\text{M} + \text{H}^+$ ), calcd (found) for  $\text{C}_{46}\text{H}_{55}\text{N}_5\text{O}_{17}\text{Na}$ : 972.3491 (972.3485).

***N*<sup>6</sup>-(2-Fmoc-aminoethyl)-*N*<sup>2</sup>-(thymine-1-ylacetyl)-*N*<sup>5</sup>-(2,3,4,6-tetra-*O*-acetyl- $\beta$ -D-galactopyranose-1-yl)-L-asparagine (IV-A).** Prepared from **21A** by procedure f (94%), mp: 136–138 °C; MS (FAB)  $m/z$  894 ( $\text{M} + \text{H}$ );  $^1\text{H}$  NMR ( $\text{CD}_3\text{OD}$ ) (selected signals):  $\delta$  7.8–7.3 (m, 8H), 7.20 (s, 1H), 5.45 (s, 1H), 5.37 (d, 1H,  $J = 8.5$  Hz), 5.23 (m, 2H), 4.48 (t, 1H,  $J = 6.0$  Hz), 4.42 (m, 2H), 2.2–2.0 (4s, 12H), 1.80 (s, 3H);  $^{13}\text{C}$  NMR ( $\text{CD}_3\text{OD}$ ):  $\delta$  173.62, 172.93, 172.00, 171.79, 171.53, 169.34, 166.98, 158.89, 152.90, 145.33, 143.68, 142.64, 133.85, 133.21, 130.14, 128.89, 128.27, 126.29, 121.06, 110.93, 79.30, 73.41, 73.09, 69.81, 69.03, 68.36, 62.72, 59.72, 40.46, 37.15, 34.80, 32.77, 30.19, 26.79, 26.10, 24.91, 23.73, 20.94, 20.70, 20.64, 14.51, 12.38; HRMS ( $\text{M} + \text{H}^+$ ), calcd (found) for  $\text{C}_{42}\text{H}_{48}\text{N}_5\text{O}_{17}$ : 894.3045 (894.3072).

***N*<sup>6</sup>-(2-Fmoc-aminoethyl)-*N*<sup>2</sup>-(thymine-1-ylacetyl)-*N*<sup>5</sup>-(2,3,4-tri-*O*-acetyl- $\beta$ -L-fucopyranose-1-yl)-L-asparagine (IV-B).** Prepared from **21B** by procedure f (88%), mp: 136–138 °C; MS (FAB) 836  $m/z$  ( $\text{M} + \text{H}$ );  $^1\text{H}$  NMR ( $\text{CD}_3\text{OD}$ ) (selected signals):  $\delta$  7.8–7.3 (m, 8H), 7.20 (s, 1H), 5.30 (overlapping, 2H), 5.20 (d, 1H,  $J = 5.6$  Hz), 4.66 (s, 2H), 4.4 (m, 2H), 4.25 (m, 1H), 4.00 (m, 1H), 2.2–2.0 (4s, 9H), 1.80 (s, 3H), 1.14 (d, 3H,  $J = 6.5$  Hz);  $^{13}\text{C}$  NMR ( $\text{CD}_3\text{OD}$ ):  $\delta$  172.30, 171.81, 170.68, 170.30, 169.96, 167.74, 165.39, 157.35, 151.41, 143.84, 143.74, 142.15, 141.04, 134.35, 132.27, 131.60, 131.49, 128.52, 128.40, 127.30, 126.68, 124.77, 124.07, 119.44, 109.36, 86.67, 77.61, 71.92, 71.46, 71.33, 70.51, 68.57, 68.26, 68.12, 67.93, 66.40, 58.96, 39.00, 35.92, 33.26, 25.26, 24.57, 19.27, 19.11, 19.05, 15.05, 10.90; HRMS ( $\text{M} + \text{H}^+$ ), calcd (found) for  $\text{C}_{40}\text{H}_{46}\text{N}_5\text{O}_{15}$ : 836.2990 (836.2980).

***N*<sup>6</sup>-(2-Fmoc-aminoethyl)-*N*<sup>2</sup>-(thymine-1-ylacetyl)-*N*<sup>5</sup>-(2,3,4,6-tetra-*O*-acetyl- $\beta$ -D-mannopyranose-1-yl)-L-asparagine (IV-C).** Prepared from **21C** by procedure f (95%), mp: 120–122 °C; MS (FAB)  $m/z$  894 ( $\text{M} + \text{H}$ );  $^1\text{H}$  NMR ( $\text{DMSO}-d_6$ ) (selected signals):  $\delta$  11.20 (s, 1H), 7.8–7.3 (m, 8H), 5.60 (d, 1H,  $J = 8.8$  Hz), 5.37 (dd, 1H,  $J = 10.0$ , 3.3 Hz), 5.15 (d, 1H,  $J = 3.3$  Hz), 5.00 (d, 1H,  $J = 10$ , 10 Hz), 4.60 (m, 2H), 4.30 (d, 1H,  $J = 6.0$  Hz), 2.2–2.0 (4s, 12H), 1.80 (s, 3H);  $^{13}\text{C}$  NMR ( $\text{CDCl}_3$ ):  $\delta$  170.13, 169.62, 143.91, 140.76, 127.67, 127.13, 125.17, 120.15, 108.05, 72.60, 70.88, 65.58, 47.84, 46.75, 33.39, 24.53, 21.03, 20.61, 11.99; HRMS ( $\text{M} + \text{H}^+$ ), calcd (found) for  $\text{C}_{42}\text{H}_{48}\text{N}_5\text{O}_{17}$ : 894.3045 (893.3065).

***N*<sup>6</sup>-(2-Fmoc-aminoethyl)-*N*<sup>2</sup>-(thymine-1-ylacetyl)-*N*<sup>5</sup>-(2-acetamido-3,4,6-tri-*O*-acetyl-2-deoxy- $\beta$ -D-glucopyranose-1-yl)-L-asparagine (IV-D).** Prepared from **21D** by procedure f (90%), mp: 107–110 °C; MS (FAB)  $m/z$  893 ( $\text{M} + \text{H}$ );  $^1\text{H}$  NMR ( $\text{CD}_3\text{OD}$ ): (selected signals):  $\delta$  7.8–7.3 (m, 9H), 5.34 (m, 2H), 5.04 (d, 1H,  $J = 9.7$  Hz), 4.6–3.8 (5 sets of multiplets, 10H), 2.1–1.9 (4s, 12H), 1.80 (s, 3H);  $^{13}\text{C}$  NMR ( $\text{CD}_3\text{OD}$ ):  $\delta$  173.76, 172.94, 172.43, 172.05, 171.40, 170.14, 169.26, 166.94, 158.85, 153.13, 152.87, 145.32, 143.72, 142.59, 130.13, 129.93, 128.88, 128.26, 126.24, 121.05, 111.17, 110.92, 79.53, 74.85, 74.62, 69.97, 69.82, 67.86, 63.34, 59.82, 54.28, 40.46, 37.16, 23.09, 23.01, 22.87, 22.74, 20.72, 12.39; HRMS ( $\text{M} + \text{H}^+$ ), calcd (found) for  $\text{C}_{42}\text{H}_{49}\text{N}_5\text{O}_{16}$ : 893.3205 (893.3232).

***N*<sup>6</sup>-(2-Fmoc-aminoethyl)-*N*<sup>2</sup>-(thymine-1-ylacetyl)-*N*<sup>5</sup>-(2-acetamido-3,4,6-tri-*O*-acetyl-2-deoxy- $\beta$ -D-galactopyranose-1-yl)-L-asparagine (IV-E).** Prepared from **21E** by procedure f (91%), mp: 135–137 °C; MS (FAB)  $m/z$  893 ( $\text{M} + \text{H}$ );  $^1\text{H}$  NMR ( $\text{CD}_3\text{OD}$ ): (selected signals):  $\delta$  7.8–7.3 (m, 8H), 7.20 (s, 1H), 5.40 (d, 1H,  $J = 3.1$  Hz), 5.30 (d, 1H,  $J = 9.5$  Hz), 5.20 (dd, 1H,  $J = 11.0$ , 3.3 Hz), 4.70 (s, 1H), 4.40 (m, 3H), 4.3–4.1 (m, 4H), 3.60 (m, 1H), 2.2–1.9 (4s, 12H), 1.85 (s, 3H);  $^{13}\text{C}$  NMR



(CD<sub>3</sub>OD):  $\delta$  174.06, 173.57, 172.94, 172.18, 172.05, 171.81, 171.74, 169.28, 166.98, 158.88, 153.14, 152.9, 145.34, 143.75, 142.62, 135.10, 134.97, 133.05, 131.43, 130.22, 129.95, 128.87, 128.24, 126.24, 121.03, 110.89, 80.06, 73.36, 72.71, 68.91, 68.23, 67.89, 62.86, 59.86, 40.46, 37.19, 26.55, 23.12, 20.70, 12.39; HRMS ( $M + H$ )<sup>+</sup>, calcd (found) for C<sub>42</sub>H<sub>49</sub>N<sub>6</sub>O<sub>16</sub>: 893.3205 (893.3245).

***N*-(2-Fmoc-aminoethyl)-*N*-(thymine-1-ylacetyl)-4-(2,3,4,6-tetra-*O*-acetyl-galactopyranose-1-yl)-2-aminobutyric Acid (V-A). 28A (920 mg, 1 mmol) was added to a solution of TES/TFA (10 mL, 5:95) at 0 °C and stirred until TLC showed no more starting material. DCM was added, and volatiles were removed under vacuum. The residue was crystallized by addition of diethyl ether to afford VA (830 mg, 94%) as a colorless powder, mp: 138–140 °C; MS (FAB)  $m/z$  865 ( $M + H$ ); <sup>1</sup>H NMR (CD<sub>3</sub>OH) (selected signals):  $\delta$  7.8–7.3 (m, 8H), 7.20 (s, 1H), 5.40 (overlapping, 2H), 5.30 (m, 2H), 4.70 (s, 1H), 4.60 (m, 1H), 4.50 (d, 2H,  $J = 6.6$  Hz), 4.20 (overlapping s, 3H), 4.10 (overlapping s, 2H), 3.50 (overlapping s, 3H), 3.30 (s, 1H), 2.2–2.0 (4s, 12H), 1.85 (s, 3H); <sup>13</sup>C NMR (CD<sub>3</sub>OD):  $\delta$  172.75, 171.22, 170.86, 170.75, 170.63, 170.52, 168.56, 165.80, 157.63, 151.63, 144.09, 142.89, 142.70, 141.43, 127.66, 127.01, 125.00, 119.82, 109.43, 72.16, 68.62, 68.45, 68.26, 68.08, 39.52, 33.60, 31.59, 25.58, 24.91, 24.76, 22.55, 21.73, 19.60, 19.43, 13.31, 11.16; HRMS ( $M + H$ )<sup>+</sup>, calcd (found) for C<sub>42</sub>H<sub>49</sub>N<sub>4</sub>O<sub>16</sub>: 865.3140 (865.3144).**

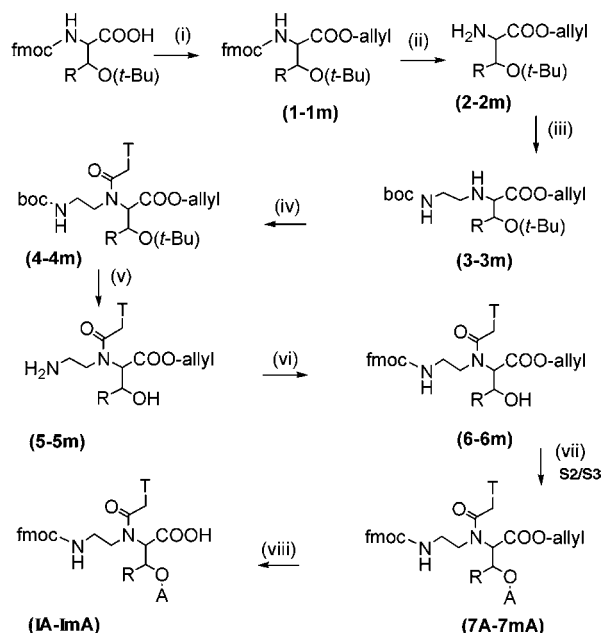
## RESULTS AND DISCUSSION

It has previously been shown that a large variety of substituents in the  $\alpha$ -position of the glycine part of the PNA backbone are tolerated without major penalties on DNA and RNA hybridization ability of the resulting PNA oligomers (3, 4). Furthermore modifications are conveniently introduced into this position by using natural  $\alpha$ -amino acids. We therefore decided to explore the possibilities of introducing glycosyl moieties in this position in the PNA backbone.

Protein glycosylation most commonly occurs via *O*-glycosylation of threonine or *N*-glycosylation of asparagine. As the *O*-glycosidic (and *N*-glycosidic) bond is both chemically and biologically fragile, besides *O*-glycosyl PNA monomers, we also synthesized *C*-glycosyl PNA monomers in which the sugar moieties are attached via amide bonds (1-methylenecarboxy sugars attached to lysine) or C–C bonds. Finally amino-sugars were amide coupled to aspartic acid. Among the sugars we chose those (e.g., mannose, galactose, and *N*-acetylgalactosamine) for which cellular receptors and/or transporters have been identified.

**Preparation of *O*-Glycosylated Serine/Threonine PNA Monomers I-A and Im-A.** The employed strategy is outlined in Scheme 1 using galactose as an example: Orthogonal protection groups for the synthesis of *O*-glycosylated PNAs were Fmoc, *tert*-butyl, and allyl for amine, hydroxyl, and carboxylic acid protection, respectively. Initially the carboxyl groups of *N*-Fmoc-*O*-(*tert*-butyl)-L-serine and *N*-Fmoc-*O*-(*tert*-butyl)-L-threonine were allylated using allyl bromide in the presence of DIPEA (17) and **1**, **1m** were obtained in high yields. Fmoc removal was achieved by piperidinolysis and gave the free amines **2**, **2m**. PNA backbones **3**, **3m** were prepared using Boc-aminoacetaldehyde (18) by reductive amination in the presence of sodium cyanoborohydride. Thymine-1-ylacetic acid (19) was attached to the backbone via an amide bond to give **4**, **4m**. Boc and *tert*-butyl group removal by TFA/scavenger gave intermediates **5**, **5m**, which were not isolated. The ethereal solution of inter-

### Scheme 1<sup>a</sup>



T = Thymine

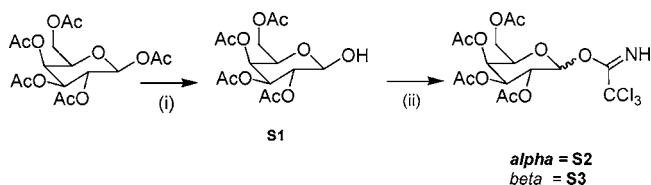
A = tetra-*O*-acetyl-galactose-1-yl

**1,2,3,4,5,6,7A,IA** R = H

**1m,2m,3m,4m,5m,6m,7mA,ImA** R = methyl

<sup>a</sup> (i) Allyl bromide, DIPEA, (ii) 20% piperidine in DMF, (iii) Boc-aminoacetaldehyde, NaBH<sub>3</sub>CN, acetic acid, (iv) thymine-1-ylacetic acid, DhbtOH, DCC, (v) 5% TES in TFA, (vi) Na<sub>2</sub>CO<sub>3</sub>, *O*-Fmoc-*N*-hydroxysuccinimide, (vii) boron trifluoride diethyl etherate, (viii) tetrakis(triphenylphosphine)palladium, *N*-ethylaniline.

### Scheme 2<sup>a</sup>



<sup>a</sup> (i) Ammonia in THF–methanol (7:3 v/v), 1.5 h, rt ( $\approx 100\%$ ), (ii) K<sub>2</sub>CO<sub>3</sub>, CCl<sub>3</sub>CN, mol sieves. 4 Å, DCM, overnight, rt, purification by silica gel chromatography (hexanes–EtOAc 2:1 v/v)  $\rightarrow$   $\alpha$ : 36%,  $\beta$ : 48%.

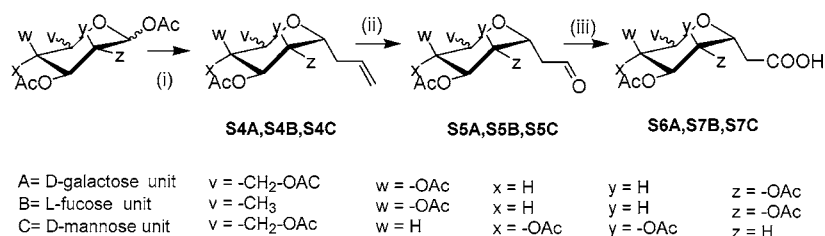
mediates were neutralized with an excess of solid sodium carbonate, and the free amine was reprotected with Fmoc using *O*-Fmoc-*N*-hydroxy succinimide to obtain **6**, **6m**.

Galactose donors were prepared by known methods as shown in Scheme 2. Commercially available  $\beta$ -D-galactose pentaacetate was converted regioselectively to the 1-*O*-deacetylated form **S1** by treatment with ammonia in THF–methanol solution (20). The galactosyl trichloroacetimidate derivatives **S2**, **S3** were prepared by the method of Schmidt et al. (21). The reaction of either  $\alpha$ - or  $\beta$ -galactosyl trichloroacetimidates with **6** and **6m** gave **7A** and **7mA** as  $\beta$  anomers. The  $\beta$ -glycosidic linkages in **7A** and **7mA** were verified by <sup>1</sup>H NMR (doublets at  $\delta$  5.05 and 5.08 ppm, respectively ( $J_{1,2} = 7.7$  Hz)). Finally the allyl groups were removed with *N*-ethylaniline in the presence of catalytic amount of (Ph<sub>3</sub>P)<sub>4</sub>Pd to give (**I-A**, **Im-A**).

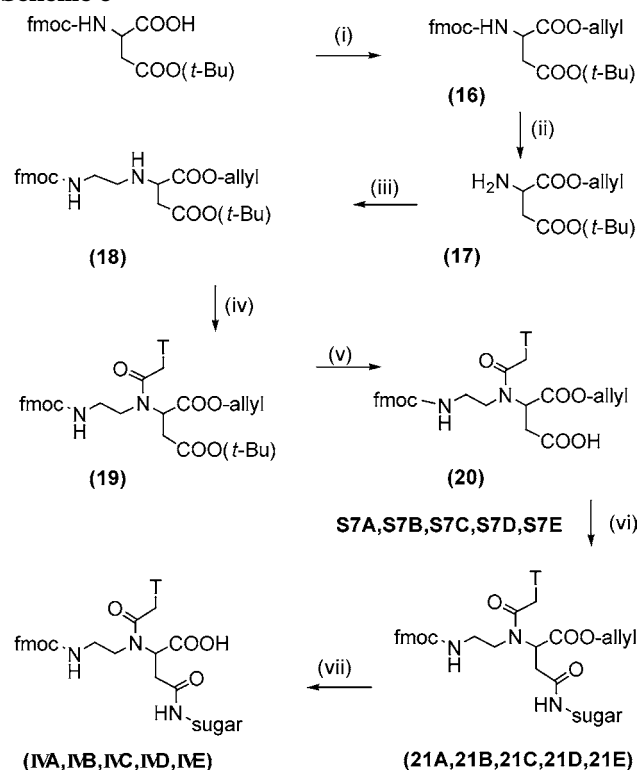
**Preparation of Lysine-Based *C*-Glycosylated PNA Monomers II-A–B, IIb-A, III-A–C.** These monomers were synthesized with galactose, mannose, or fucose and were prepared in two version with either Boc or Fmoc





Scheme 4<sup>a</sup>

<sup>a</sup> (i) Allyltrimethylsilane, (ii) OsO<sub>4</sub>, KIO<sub>4</sub>, dioxane–water (8:2 v/v), 12 h, rt (80%), (iii) 5% aqueous NaHPO<sub>4</sub>, 1 M aqueous KMnO<sub>4</sub>, *t*-BuOH, 15 min, rt (85%).

Scheme 5<sup>a</sup>

T = Thymine

sugar A = 2, 3, 4, tetra-*O*-acetyl-β-D-galactopyranose-1-yl

sugar B = 2, 3, 4, tri-*O*-acetyl-β-L-fucopyranose-1-yl

sugar C = 2,3,4,6, tetra-*O*-acetyl-β-D-mannopyranose-1-yl

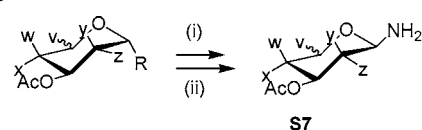
sugar D = 2-acetamido- 3, 4, 6, tri-*O*-acetyl-β-D-glucopyranose-1-yl

sugar E = 2-acetamido- 3, 4, 6, tri-*O*-acetyl-β-D-galactopyranose-1-yl

<sup>a</sup> (i) Allyl bromide, DIPEA, (ii) 20% piperidine in DMF, (iii) Fmoc-aminoacetaldehyde, NaBH<sub>3</sub>CN, acetic acid, (iv) thymine-1-ylacetic acid, DhbtOH, DCC, (v) 5% TES in TFA, (vi) DhbtOH, DCC, (vii) tetrakis(triphenylphosphine)palladium, *N*-ethyl-aniline.

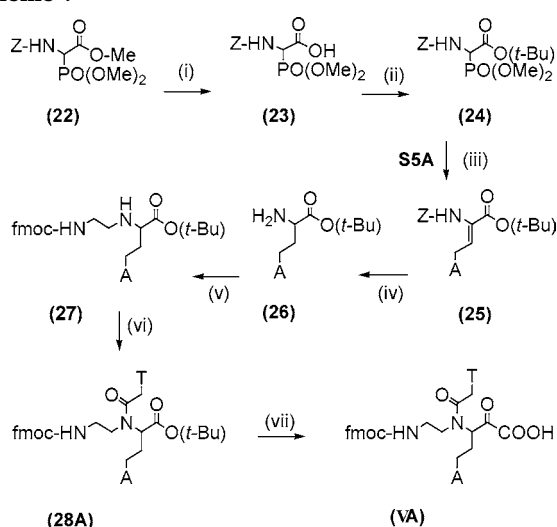
the sugar in the synthesis and deprotection steps. We found HATU–collidine as the most suitable coupling reagent. We used 50% morpholine in DMF for deprotections and 5% water, 30% TFA in DCM to cleave the BHOC groups. Finally we used methanolic hydrazine (pH 9.5) for the postcleavage deacetylation of the sugar. **O1**, **O2** were obtained in average yield (30–33%). At the present stage we do not know the optical purity of the new PNA monomers, and it is also well described that some (limited) racemization at the α-carbon does take place during solid-phase synthesis (36, 37). Thus, further studies will address this issue.

**Group b. Lysine-Based C-Glycosylated PNAs.** We initially used the Boc-strategy for the solid-phase synthesis of PNA oligomers containing lysine based C-glycosylated-

Scheme 6<sup>a</sup>

**S7A** R=Br, v=-CH<sub>2</sub>OAc, w=OAc, x=H, y=H, z=OAc, D-galactose unit  
**S7B** R=Br, v=-CH<sub>3</sub>, w=OAc, x=H, y=H, z=OAc, L-fucose unit  
**S7C** R=Br, v=-CH<sub>2</sub>OAc, w=H, x=OAc, y=H, z=H, D-mannose unit  
**S7D** R=Cl, v=-CH<sub>2</sub>OAc, w=H, x=OAc, y=H, z=NH-Ac, glucosamine unit  
**S7E** R=Cl, v=-CH<sub>2</sub>OAc, w=OAc, x=H, y=H, z=NH-Ac, galactosamine unit

<sup>a</sup> (i) NaN<sub>3</sub>, acetonitrile, (ii), PtO<sub>2</sub>, H<sub>2</sub>, methanol, 1 atm.

Scheme 7<sup>a</sup>

T = Thymine

A = 2,3,4,6-tetra-*O*-acetyl-α-D-galactopyranose-1-yl

<sup>a</sup> (i) 1 N KOH, (ii) *tert*-butyl alcohol, EEDQ, (iii) tetramethylguanidine, -78 °C, THF, (iv) Pd/C, 1 atm, (v): Fmoc-aminoacetaldehyde, NaBH<sub>3</sub>CN, acetic acid, (vi): thymine-1-ylacetic acid, DhbtOH, DCC, (vii) 5% TES in TFA.

Table 1

PNA	monomer	location of residue <sup>a</sup>	T <sub>m</sub> (°C)	RNA (M + 1)	MALDI-TOF MS found (calcd)
control			55.5	2782	(2782)
<b>O1</b>	I-A	T <sup>1</sup>	53	2986.9	(2984)
<b>O2</b>	Im-A	T <sup>1</sup>	51.5	2996.5	(2998)
<b>O3</b>	II-A	T <sup>2</sup>	55.5	3357.9	(3360)
<b>O4</b>	IIIb-A	T <sup>2</sup>	54.5	3184.7	(3184)

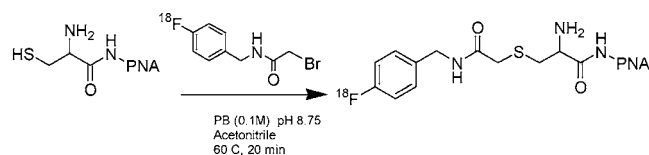
<sup>a</sup> PNA sequence: Gly-GT<sup>1</sup>AGAT<sup>2</sup>CACT-NH<sub>2</sub>.

PNA monomers **II-A** and **IIIb-A**. PNA-**O3** and PNA-**O4** were synthesized according to standard PNA solid-phase synthesis based on Boc strategy (5) (Table 1). After cleavage with TFMSA, a major side product consisting of oligomer minus one or two acetyl groups was detected

**Table 2**

PNA	monomer	location of residue <sup>a</sup>	T <sub>m</sub> (°C) RNA	MALDI-TOF MS (M + 1) found (calcd)
<b>PNA-c</b>			53.0	2738.4 (2740)
<b>PNA-1</b>	<b>III-C</b>	T <sup>2</sup> , T <sup>3</sup>	47.0	3289.2 (3290)
<b>PNA-2</b>	<b>III-B</b>	T <sup>2</sup> , T <sup>3</sup>	47.0	3262.1 (3256)
<b>PNA-3</b>	<b>IV-A</b>	T <sup>2</sup> , T <sup>3</sup>	47.0	3179.2 (3178)
<b>PNA-4</b>	<b>IV-C</b>	T <sup>2</sup> , T <sup>3</sup>	44.0	3176.5 (3178)
<b>PNA-5</b>	<b>IV-B</b>	T <sup>2</sup> , T <sup>3</sup>	41.1	3140.7 (3143)
<b>PNA-6</b>	<b>IV-D</b>	T <sup>1</sup> , T <sup>2</sup> , T <sup>3</sup>	41.1	3519.0 (3519)
<b>PNA-7</b>	<b>IV-E</b>	T <sup>1</sup> , T <sup>2</sup> , T <sup>3</sup>	40.0	3518.2 (3519)
<b>PNA-8</b>	<b>V-A</b>	T <sup>1</sup> , T <sup>2</sup> , T <sup>3</sup>	48.0	3312.0 (3309)

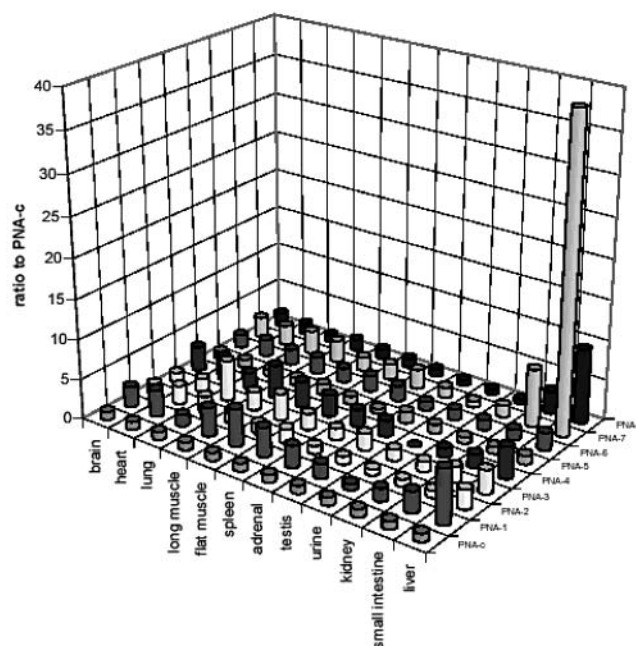
<sup>a</sup> The T<sub>m</sub> measurements were carried out in a phosphate buffer (10 mM, pH 7.0, containing 100 mM NaCl and 0.1 mM EDTA). The temperature profiles were recorded at 260 nm, and all profiles showed monophasic transitions from which the T<sub>m</sub> was determined. PNA sequence: Cys-C-T<sup>1</sup>-C-A-T<sup>2</sup>-A-C-T<sup>3</sup>-C-T-NH<sub>2</sub>.

**Scheme 8**

by MALDI and HPLC. Although the final deacetylation of both the product and the side product gave the target oligomer (yield: 25–28%), we decided to switch to the Fmoc strategy in order to avoid the use of strong acidic cleavage conditions and to obtain higher yields.

**Group c. Lysine-Based C, N and C-Glycosylated PNA's with Cysteine at the N-Terminus.** To prepare conjugates of glycosylated PNAs, we introduced cysteine as the S-trityl-protected derivative at the N-terminus of the glycosylated PNA. Deprotection of sugar hydroxyl groups were performed on the resin. Eight decamers (Cys-CTCATACTCT-NH<sub>2</sub>) were prepared containing the various glycosylated PNA monomers. These monomers were introduced at two or three positions shown as T<sup>1</sup>, T<sup>2</sup>, T<sup>3</sup> (Table 2). **PNA-1 to PNA-8** were obtained in moderate yields (40–48%). The glycosylated PNAs showed reasonable binding to complementary RNAs, with moderate reductions in thermal stability of the resulting duplexes (0–6 °C per modification) (Tables 1 and 2).

**Radiochemistry.** N-(4-[<sup>18</sup>F]fluorobenzyl)-2-bromoacetamide has been designed as a radiochemically convenient reagent (14–16), offering use of fluorine-18, the most widely used positron emitter (t<sub>1/2</sub>: 109.8 min). This labeled reagent has been used with success for the labeling of natural phosphodiester oligodeoxyribonucleotides (14, 15), as well as for the labeling of modified oligonucleotides (full phosphorothioates, hybrid meth-



**Figure 1.** Comparative biodistribution of [<sup>18</sup>F]-PNA. The figure shows the changes in organ biodistribution as a consequence of PNA conjugation relative to the unconjugated PNA-c (see Table 3 for absolute data). Radioactivity concentrations in the organs of animals 2 h after injection of a tracer dose of [<sup>18</sup>F]-PNA in anaesthetized rats are plotted as the ratio of the value for the indicated PNA to that in the corresponding organ for unconjugated PNA-c in order to reflect the increase (values > 1) or decrease (values < 1) consecutive to glycosylation of the PNA. Note the dramatic increase of hepatic uptake as a consequence of N-acetylgalactosamine (PNA-7) conjugation.

ylphosphonates/phosphodiester, or 2'-O-methyl modified oligoribonucleotides) (16). Recently, N-(4-[<sup>18</sup>F]fluorobenzyl)-2-bromoacetamide has also for the first time been successfully used in the labeling of PNAs (13). We used eight glycosylated PNA 10mers (shown in Table 2) for the preparation of labeled PNAs (Scheme 8).

**In Vivo Study of Biodistribution.** Biodistribution of the labeled PNAs were studied in rats. As shown in the results of the quantitative biodistribution studies reported in Table 3 and Figure 1, major differences were found in the organ biodistribution of the different PNAs. HPLC analysis of the urine samples showed that at least 58% of the radioactivity was recovered as intact nondegraded PNA for oligomers (**PNA-c**, **-1**, **-2**, **-4**, **-5**, **-7**, **-8**). In agreement with previous results (5) the unmodified PNA (**PNA-c**) is predominantly found in the kidneys and is rapidly excreted in the urine. In view of the reports

**Table 3. Biodistribution of [<sup>18</sup>F]-PNA<sup>a</sup>**

	PNA-c N = 5		PNA-1 N = 4		PNA-2 N = 3		PNA-3 N = 4		PNA-4 N = 4		PNA-5 N = 4		PNA-6 N = 3		PNA-7 N = 4		PNA-8 N = 4	
	mean	SD	mean	SD	mean	SD	mean	SD	mean	SD	mean	SD	mean	SD	mean	SD	mean	SD
brain	0.027	0.015	0.069	0.006	0.036	0.010	0.033	0.005	0.082	0.008	0.026	0.003	0.046	0.004	0.069	0.022	0.046	0.006
heart	0.050	0.015	0.168	0.030	0.114	0.012	0.081	0.014	0.146	0.013	0.051	0.006	0.109	0.011	0.128	0.052	0.068	0.014
lung	0.089	0.025	0.131	0.019	0.192	0.118	0.457	0.294	0.179	0.019	0.080	0.010	0.173	0.017	0.262	0.181	0.084	0.016
liver	0.096	0.030	0.651	0.227	0.234	0.061	0.282	0.127	0.380	0.046	0.108	0.023	0.214	0.033	3.755	0.583	0.901	0.242
kidney	1.136	0.445	1.838	0.800	0.998	0.313	1.451	0.693	1.290	0.321	0.911	0.215	1.459	0.198	1.679	0.281	0.673	0.350
small intestine	0.126	0.056	0.335	0.087	0.115	0.038	0.253	0.094	0.218	0.097	0.114	0.012	0.173	0.021	0.913	0.659	0.361	0.187
long muscle	0.040	0.017	0.145	0.096	0.049	0.004	0.093	0.053	0.165	0.090	0.040	0.006	0.084	0.026	0.111	0.039	0.058	0.007
flat muscle	0.052	0.026	0.247	0.139	0.063	0.008	0.174	0.129	0.169	0.066	0.070	0.042	0.095	0.041	0.091	0.033	0.067	0.003
spleen	0.055	0.025	0.204	0.041	0.099	0.013	0.112	0.085	0.154	0.011	0.053	0.008	0.113	0.007	0.111	0.038	0.063	0.010
adrenal	0.077	0.049	0.213	0.068	0.076	0.018	0.115	0.024	0.165	0.029	0.047	0.009	0.150	0.006	0.190	0.131	0.073	0.025
testis	0.076	0.050	0.142	0.050	0.076	0.014	0.160	0.133	0.155	0.021	0.112	0.080	0.084	0.009	0.101	0.026	0.056	0.006
urine	75.66	8.10	56.70	28.32	58.99	32.55	109.07	17.76	ND	ND	84.19	33.45	104.39	9.16	59.02	30.48	51.89	18.36

<sup>a</sup> Mean value and standard deviation (SD) of the radioactivity recovered from the organs of the indicated n number of animals, expressed in percent of injected dose recovered per gram of tissue, 2 h after injection of a tracer dose of [<sup>18</sup>F]-PNA in anaesthetized rats.



that naked PNAs upon systemic delivery can elicit antisense or even antigene effects in the brain in rats (38), it is also noteworthy that the lowest PNA concentration (if present at all) (for the unmodified PNA) in our study is found in the brain (Table 3).

However, the most striking effect was the 40-fold increase of the liver uptake of **PNA-7**. The *N*-acetylgalactosamine glycosylation introduced on this PNA is known to interact with the hepatic asialoglycoprotein receptor (ASGP-R) (8–11, 39). The interpretation that the carbohydrate moieties are responsible for the modification of the biodistribution by targeting to specific membrane receptors is confirmed by the observation that the other carbohydrates on the PNA known to induce interaction with the asialoglycoprotein receptor, namely mannose (**PNA-1**) and galactose (**PNA-8**) increased hepatic uptake by 6.8- and 9.4-fold relative to the unchanged **PNA-c**. Indeed it has been demonstrated that glycoproteins exposing mannose and galactose residues interact, albeit with less affinity, with the mammalian ASGP-R (39). Polydentate binding is usually advantageous when targeting asialoglycoprotein receptors, and we therefore chose to study PNA oligomers with multiple modifications. However, further systematic studies are required to reveal the optimal PNA modification in terms of number and type of glycosylation as well as spatial arrangement on the PNA oligomer. The present type of modification naturally can also be combined with terminal conjugation of sugar ligands (9).

## CONCLUSION

In the present work we have devised protocols for the synthesis of a variety of thymine PNA monomers bearing a glycosylated side chain in the backbone. Furthermore, we have incorporated these monomers into PNA oligomers and shown that the RNA hybridization potency of the latter are only slightly reduced. Finally, we have found that the pharmacokinetic behavior in rats of PNA oligomers can be profoundly changed by glycosylation. Specifically, *N*-acetylgalactosamine (and to a lesser extent galactose and mannose)-modified PNAs are effectively targeting the liver.

These results could be of great significance for PNA drug development, as they should allow modulation and fine-tuning of the pharmacokinetic profile of a drug lead, allowing cellular receptors of organs other than the liver to be targeted. Obviously, analogous receptor targeting is possible using conventional conjugation of sugar domains at either terminus of the PNA oligomer (9), but the present approach offers opportunities not available by such conjugation. Furthermore, the chemistry described may also be exploited to develop lectin binding ligands (40) based on PNA scaffolds.

## ACKNOWLEDGMENT

We are indebted to Dr. Raphaël Boisgard and Françoise Hinnen for excellent technical assistance. The financial support of the Danish Cancer Society, the Association for International Cancer Research (AICR), the French embassy in Denmark, and of EU contract QLGI-CT-2000-00562 is gratefully acknowledged.

## LITERATURE CITED

- (1) Nielsen, P. E. (2000) Antisense peptide nucleic acids. *Curr. Opin. Mol. Ther.* 2, 282–287.
- (2) Braasch, D. A., and Corey, D. R. (2002) Novel Antisense and Peptide Nucleic Acid Strategies for Controlling Gene Expression. *Biochemistry* 41, 4503–4510.
- (3) Koppelhus, U., and Nielsen, P. E. (2003) Cellular delivery of peptide nucleic acid (PNA). *Adv. Drug Delivery Rev.* 55, 267–280.
- (4) Nielsen, P. E. (2001) Peptide nucleic acids as antibacterial agents via the antisense principle. *Expert Opin. Invest. Drugs* 10, 331–341.
- (5) McMahon, B. M., Mays, D., Lipsky, J., Stewart, J. A., Fauq, A., and Richelson, E. (2002) Pharmacokinetics and tissue distribution of a peptide nucleic acid after intravenous administration. *Antisense Nucleic Acid Drug Dev.* 12, 65–70.
- (6) Haaime, G., Lohse, A., Buchardt, O., and Nielsen, P. E. (1996) Peptide nucleic acids (PNAs) containing thymine monomers derived from chiral amino acids: hybridization and solubility properties of D-lysine PNA. *Angew. Chem., Int. Ed. Engl.* 35, 1939–1941.
- (7) Puschi, A., Sforza, S., Haaime, G., Dahl, O., and Nielsen, P. E. (1998) Peptide Nucleic Acids (PNAs) with a functional backbone. *Tetrahedron Lett.* 39, 4707–4710.
- (8) Sato, H., Kato, Y., Hayasi, E., Tabata, T., Suzuki, M., Takahara, Y., and Sugiyama, Y. (2002) A novel hepatic-targeting system for therapeutic cytokines that delivers to the hepatic asialoglycoprotein receptor, but avoids receptor-mediated endocytosis. *Pharm. Res.* 19, 1736–44.
- (9) Biessen, E. A., Slidregt-Bol, K. T., Hoen, P. A., Prince, P., Van der Bilt, E., Valentijn, A. R., Meeuwenoord, N. J., Princen, H., Bijsterbosch, M. K., Van der Marel, G. A., Van Boom, J. H., and Van Berkel, T. J. (2002) Design of a targeted peptide nucleic acid prodrug to inhibit hepatic human microsomal triglyceride transfer protein expression in hepatocytes. *Bioconjugate Chem.* 13, 295–302.
- (10) Andre, S., Frisch, B., Kaltner, H., Desouza, D. L., Schuber, F., and Gabius, H. J. (2000) Lectin-mediated drug targeting: selection of valency, sugar type (Gal/Lac), and spacer length for cluster glycosides as parameters to distinguish ligand binding to C-type asialoglycoprotein receptors and galectins. *Pharm. Res.* 17, 985–90.
- (11) Lee, R. T., and Lee, Y. C. (1997) Facile synthesis of a high-affinity ligand for mammalian hepatic lectin containing three terminal *N*-acetylgalactosamine residues. *Bioconjugate Chem.* 8, 762–5.
- (12) Nielsen, P. E., and Egholm, M., Eds. (1999) *Peptide nucleic acids protocols and applications*, pp 20–39, Horizon Press, Wymondham, U.K.
- (13) Kühnast, B., Dollé, F., and Tavitian, B. (2002) Fluorine-18 Labeling of Peptide Nucleic Acids. *J. Labelled Compds. Radiopharm.* 45, 1–11.
- (14) Tavitian, B., Terrazzino, S., Kuhnast, B., Marzabal, S., Stettler, O., Dollé, F., Deverre, J.-R., Jobert, A., Hinnen, F., Bendriem, B., Crouzel, C., and DiGiamberardino, L. (1998) *In Vivo* Imaging of Oligonucleotides with Positron Emission Tomography. *Nat. Med.* 4, 467–471.
- (15) Kühnast, B., Dollé, F., Terrazzino, S., Rousseau, B., Loc'h, C., Vaufray, F., Hinnen, F., Doignon, I., Pillon, F., David, C., Crouzel, C., and B. Tavitian, (2000) A General Method to Label Antisense Oligonucleotides with Radioactive Halogens for Pharmacological and Imaging Studies. *Bioconjugate Chem.* 11, 627–636.
- (16) Kühnast, B., Dollé, F., Vaufray, F., Hinnen, F., Crouzel, C., and Tavitian, B. (2000) Fluorine-18 Labeling of Oligonucleotides Bearing Chemically-Modified Ribose-Phosphate Backbones. *J. Labelled Compds. Radiopharm.* 43, 837–848.
- (17) Egner, B. J., and Bradley, M. (1997) Monitoring the solid-phase synthesis of analogues of lysobactin and the katanosins using in situ MALDI-TOF MS. *Tetrahedron* 53, 14021–14030.
- (18) Dueholm, K. L., Egholm, M., and Buchardt, O. (1993) An efficient synthesis of Boc-aminoacetaldehyde and its application to the synthesis of N-(2-Boc-aminoethyl)glycine esters. *Org. Prep. Proced. Int.* 25, 457–461.
- (19) Nielsen, P. E., Egholm, M., Berg, R. H., and Buchardt, O. (1991) Sequence-selective recognition of DNA by strand displacement with a thymine-substituted polyamide. *Science* 254, 1497–1500.

- (20) Fiandor, J., Garcia-Lopez, M. T., De Las Heras, F. G., and Mendez-Castrillon, P. P. (1985) A facile regioselective 1-O-deacylation of peracylated glycopyranoses. *Synthesis* 1121–1123.
- (21) Schmidt, R. R., and Michel, J. (1980) Facile synthesis of Alpha-O-glycosyl and Beta-O-glycosyl imidates – Preparation of glycosides and disaccharides. *Angew. Chem., Int. Ed.* 19, 731–732.
- (22) Augustyns, K., Kraas, W., and Jung, G. (1998) Investigation on the stability of the Dde protecting group used in peptide synthesis: migration to an unprotected lysine. *J. Pept. Res.* 51, 127–133.
- (23) Rohwedder, B., Mutti, Y., Dumy, P., and Mutter, M. (1998) Hydrazinolysis of Dde: complete orthogonality with Alloc protecting groups. *Tetrahedron Lett.* 39, 1175–1178.
- (24) Giannis, A., and Sandhoff, K. (1985) Stereoselective synthesis of  $\alpha$ -C-allylglycopyranosides. *Tetrahedron Lett.* 26, 1479–1482.
- (25) Nicolaou, K. C., Hwang, C. K., and Duggan, M. E. (1989) Synthesis of the brevetoxin B IJK ring system. *J. Am. Chem. Soc.* 111, 6682–6690.
- (26) Uchiyama, T., Vassilev, V. P., Kajimoto, T., Wong, W., Lin, C. C., Huang, H., and Wong, C. (1995) Design and Synthesis of Sialyl Lewis X Mimetics. *J. Am. Chem. Soc.* 117, 5395–5396.
- (27) Broxterman, H. J. G., Van der Marel, G. A., and Van Boom, J. H. (1988) Analogues of uridine 5'-diphosphate glucose. Inhibition of glycolipid biosynthesis. *Tetrahedron Lett.* 29, 4893–4896.
- (28) Sutherland, D. P., Stark, T. M., Hughes, R., and Armstrong, R. W. (1996) Generation of C-Glycoside Peptide Ligands for Cell Surface Carbohydrate Receptors Using a Four-Component Condensation on Solid Support. *J. Org. Chem.* 61, 8350–8354.
- (29) Yusuke, S., and Junko, A., (1997) Protection of  $\Psi$  ( $\text{CH}_2\text{-NH}$ ) peptide bond with 2,4-dimethoxybenzyl group in solid-phase peptide synthesis. *Chem. Pharm. Bull.* 45, 13–17.
- (30) Antopolsky, M., and Azhayev, A. (1999) Stepwise solid-phase synthesis of peptide–oligonucleotide conjugates on new solid supports. *Helv. Chim. Acta* 82 (12), 2130–2140.
- (31) Tanaka, M., and Yamashina, I. (1973) The syntheses of various 1-N-(L-aspart-4-oyl)-glycosylamines and their analogues. *Carbohydr. Res.* 27, 175–183.
- (32) Abbot, S. D., Gagnon, L., Lagraoui, M., Kadhim, S., Attardo, G., Zacharie B., and Penney, C. L. (1998) Synthesis and Activity of Dipeptides, Linked to Targeting Ligands, as Specific NK Cell Enhancers. *J. Med. Chem.* 41, 1909–1926.
- (33) Micheel, F., and Klemer, A. (1961) Glycosyl fluorides and azides. *Adv. Carbohydr. Chem.* 16, 85–103.
- (34) Schmidt, U., Lieberknecht, A., Schanbacher, U., Beuttler, T., and Wild, J. (1982) Amino acids and peptides. Part 36. Dehydroamino acids. Part 16. Simple preparation of N-acyl-2-(diethoxyphosphoryl)glycine esters and their application in the synthesis of dehydroamino acid esters. *Angew. Chem.* 94, 797–798.
- (35) Good, L., Awasthi, S. K., Dryselius, R., Larsson, O., and Nielsen, P. E. (2001) Bactericidal antisense effects of peptide-PNA conjugates. *Nat. Biotechnol.* 19, 360–364.
- (36) Tedeschi, T., Corradini, R., Marchelli, R., Pushl, A., and Nielsen, P. E. (2002) Racemization of chiral PNAs during solid-phase synthesis: effect of the coupling conditions on enantiomeric purity. *Tetrahedron: Asymmetry* 13, 1629–1636.
- (37) Corradini, R., Di Silvestro, G., Sforza, S., Palla, G., Dossena, A., and Nielsen, P. E., et al. (1999) Direct enantiomeric separation of N-aminoethylamino acids: determination of the enantiomeric excess of chiral peptide nucleic acids (PNAs) by GC. *Tetrahedron: Asymmetry* 10, 2063–2066.
- (38) Tyler, B. M., Jansen, K., McCormick, D. J., Douglas, C. L., Boules, M., Stewart, J. A., et al. (1999) Peptide nucleic acids targeted to the neurotensin receptor and administered i.p. cross the blood-brain barrier and specifically reduce gene expression. *Proc. Natl. Acad. Sci. U.S.A.* 96, 7053–7058.
- (39) Weigel, P., and Yik, J. (2002) Glycans as endocytosis signals: the cases of the asialoglycoprotein and hyaluronan/chondroitin sulfate receptors. *Biochim. Biophys. Acta* 1572, 341–363.
- (40) Kolatkar, A. R., Leung, A. K., Isecke, R., Brossmer, R., Drickamer, K., and Weis, W. I. (1998) Mechanism of N-acetylgalactosamine binding to a C-type animal lectin carbohydrate-recognition domain. *J. Biol. Chem.* 273, 19502–19508.

BC034022X

# Residualizing Indium-111-Radiolabel for Plasmid DNA and Its Application to Tissue Distribution Study

Makiya Nishikawa,<sup>\*,†</sup> Takayuki Nakano,<sup>†</sup> Takayuki Okabe,<sup>†</sup> Nobuko Hamaguchi,<sup>†</sup> Yasuomi Yamasaki,<sup>‡</sup> Yoshinobu Takakura,<sup>‡</sup> Fumiyoshi Yamashita,<sup>†</sup> and Mitsuru Hashida<sup>†</sup>

Departments of Drug Delivery Research and Biopharmaceutics and Drug Metabolism, Graduate School of Pharmaceutical Sciences, Kyoto University, Kyoto 606-8501, Japan. Received March 6, 2003; Revised Manuscript Received July 18, 2003

To develop a suitable vector and an administration technique for in vivo gene transfer, the tissue distribution of plasmid DNA (pDNA) needs to be understood. In this study, a novel residualizing radiolabel for pDNA was developed. 4-[p-Azidosalicylamido]butylamine (ASBA) was coupled with diethylenetriaminepentaacetic acid (DTPA) anhydride, then the conjugate was reacted with pDNA by photoactivation, followed by labeling with [<sup>111</sup>In]InCl<sub>3</sub> to obtain <sup>111</sup>In-pDNA. The overall structure of pDNA was well preserved, and the retention of its transcriptional activity was 40–98%. After intravenous injection of <sup>111</sup>In-pDNA into mice, about 50% of the radioactivity was recovered in the liver within 3 min. The level remained stable for at least 2 h, followed by a very slow decrease to 45% at 24 h. This contrasted with the results obtained with <sup>32</sup>P-pDNA by nick translation, in which a rapid decrease in hepatic radioactivity was observed. The amount of radioactivity in the lung following the administration of polyethyleneimine/<sup>111</sup>In-pDNA complexes correlates well with the transgene expression. These results indicate that the novel residualizing radiolabel clearly demonstrates the cells that have taken up pDNA and, therefore, gives us useful information about how to design a better approach for nonviral in vivo gene delivery.

## INTRODUCTION

The in vivo gene transfer profile required for effective gene therapy, such as target cell-specificity of gene transfer, efficiency and duration of transgene expression, and number of transfected cells, depends on the target disease. These features are determined not only by the properties of the vector used, but also by the nature of the target cells, the route and method of administration, and the tissue distribution of the vector.

On many occasions using nonviral vectors, plasmid DNA (pDNA) encoding a target gene is used to deliver the gene to the target cell. Transgene expression by using pDNA occurs only in cells that have taken up the DNA following its administration. Therefore, the development of a vector and/or an administration technique that achieves the delivery of pDNA to the target cell in an efficient and specific manner is absolutely essential for successful in vivo gene therapy. Various approaches have been reported to improve the efficiency of in vivo gene transfer, such as complex formation with cationic vectors, electroporation, gene gun, and large-volume injection (1). These approaches improve the transgene expression by increasing the amount of pDNA delivered to the target cell.

Optimizing in vivo gene transfer by these approaches requires a detailed understanding of the tissue distribution of pDNA. To this end, several tracing methods have been used such as <sup>32</sup>P-label by nick translation (2, 3). However, radioactive metabolites, which are generated

before and after the cellular uptake of radiolabeled pDNA, often make it extremely difficult to quantitatively analyze the tissue distribution and pharmacokinetics of pDNA. Therefore, pharmacokinetic analyses of tissue distribution of pDNA complex are only possible for very short periods after in vivo administration (4, 5). For studies involving macromolecules such as antibodies, biologically active proteins, polymers, and their drug conjugates, residualizing radiolabels have been developed to trace their tissue distribution. So far, hydrophilic bi-functional chelate-radioactive metal complexes or radioiodination using sugar-containing spacers has been used as residualizing radiolabels for such compounds (6–10). In these approaches, relatively large, hydrophilic molecules are incorporated into the structure of the radiolabeled adducts. After catabolism, radioactive metabolites that are hydrophilic with a high molecular weight are hardly able to pass through biological barriers such as the plasma and lysosomal membranes (11), promising the retention of radioactivity within the cells that have taken up the radiolabeled compound.

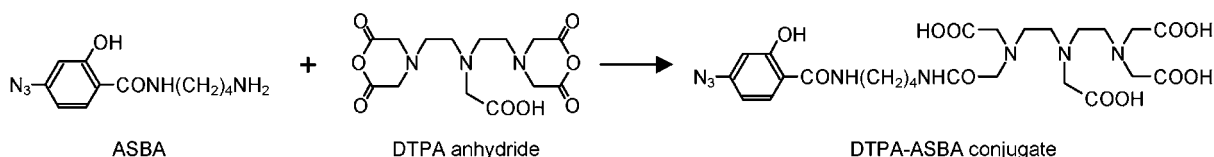
In an attempt to study the tissue distribution of pDNA, Bogdanov et al. (12) recently reported a <sup>99m</sup>Tc-label for pDNA by which the tissue distribution of pDNA can be monitored noninvasively and continuously. However, the linker for the label was cationic and interacted with pDNA in an electrostatic manner. Such an interaction altered the physicochemical properties of pDNA, as shown by agarose gel electrophoresis, which would alter the tissue distribution characteristics of pDNA. In addition to radiolabels, biotin (13) or a fluorescent dye (14) has been covalently introduced into pDNA by photoactivation. Neves et al. (14) found that fluorescently labeled pDNA retains 40% of its transcriptional activity as unlabeled pDNA. Compared with the nick translation

\* To whom correspondence should be addressed. M. Nishikawa: Phone 81-75-753-4616; Fax 81-75-753-4614; E-mail makiya@pharm.kyoto-u.ac.jp.

<sup>†</sup> Department of Drug Delivery Research.

<sup>‡</sup> Department of Biopharmaceutics and Drug Metabolism.



**Scheme 1. Synthesis of DTPA–ASBA Conjugate**

method, the supercoiled structure of pDNA was retained by this technique. In a separate experiment, a peptide nucleic acid clamp was developed as a noncovalent, but highly stable, adduct for pDNA to label it with a fluorescent dye (15). These fluorescent labels, however, will be less efficient for tissue distribution studies because they require laborious processing for quantification. The release of metabolites containing the label is another problem as far as the quantitative analysis of the tissue distribution of a labeled pDNA is concerned.

The aim of this study is to develop a residualizing radiolabel for pDNA by which we can quantitatively analyze the tissue distribution of pDNA without needing to consider the efflux of radioactive metabolites from cells. To this end, we have applied a residualizing radiolabel method for pDNA similar to that widely used for radiolabeling proteins:  $^{111}\text{In}$  label using a bifunctional chelating agent, diethylenetriaminepentaacetic acid (DTPA). Due to the low degree of reactivity of DTPA anhydride with the primary amino groups in pDNA, we newly designed a chelating agent for pDNA by conjugating DTPA anhydride to 4-[p-azidosalicylamido]butylamine (ASBA) and successfully synthesized DTPA–ASBA conjugate. Then, it was covalently coupled to pDNA by photoreaction followed by  $^{111}\text{In}$  radiolabeling. The characteristics of the  $^{111}\text{In}$ -pDNA were examined, and then the tissue distribution of radioactivity was investigated in mice after intravenous injection, and compared with data obtained with  $^{32}\text{P}$ -labeled pDNA using the nick translation method. Finally, we used  $^{111}\text{In}$ -pDNA for analyzing the tissue distribution of pDNA/nonviral vector complex and found the new residualizing radiolabel useful for designing effective gene delivery approaches.

**EXPERIMENTAL PROCEDURES**

**Chemicals.** [ $\alpha$ - $^{32}\text{P}$ ]dCTP was obtained from Amersham (Tokyo, Japan).  $^{111}\text{In}$ indium chloride ( $^{111}\text{In}$ ]InCl<sub>3</sub>) was supplied by Nihon Medi-Physics (Takarazuka, Japan). DTPA anhydride and ASBA were purchased from Dojindo (Kumamoto, Japan) and Pierce, respectively. Fetal bovine serum (FBS) was obtained from Biowhitaker (Walkersville, MD). Opti-MEM I was obtained from Gibco BRL (Grand Island, NY). Dulbecco's modified Eagle's minimum essential medium (DMEM) and other reagents for cell culture were purchased from Nissui Pharmaceutical Co., LTD (Tokyo, Japan). pDNA encoding firefly luciferase cDNA was prepared as previously reported (16). Polyethyleneimine (PEI) with an average molecular mass of 10 000 was purchased from Polysciences, Inc. (Warrington, PA). All other chemicals were of the highest grade available.

**Radiolabeling of pDNA.** To a 27.5  $\mu\text{L}$  of dimethyl sulfoxide solution of ASBA (1 mg) was added DTPA anhydride (2 mg) under dark-room conditions, and the mixture was incubated at room temperature for 1 h to obtain DTPA–ASBA conjugate (Scheme 1). Then, 25  $\mu\text{L}$  of pDNA solution (4 mg/mL) was added to the mixture and the volume was adjusted to 500  $\mu\text{L}$  with phosphate buffered saline (PBS) of pH 7.4. The mixture was immediately irradiated under a UV lamp (365 nm, Ultra-Violet Products, CA) at room temperature for 15 min to

obtain DTPA–ASBA coupled pDNA (DTPA–ASBA–pDNA). The product was purified by ethanol precipitation twice, and was dissolved in 20  $\mu\text{L}$  of acetate buffer (0.1 M, pH 6). To 10  $\mu\text{L}$  of sodium acetate solution (1 M) was added 10  $\mu\text{L}$  of [ $^{111}\text{In}$ ]InCl<sub>3</sub>, then 20  $\mu\text{L}$  of DTPA–ASBA–pDNA. The mixture was incubated at room temperature for 1 h, and unreacted [ $^{111}\text{In}$ ]InCl<sub>3</sub> was removed by ultrafiltration. The purity was checked by Sephadex G-25 column (1  $\times$  40 cm) chromatography and 1% agarose gel electrophoresis. The reaction was performed using different amounts of the starting materials, ASBA, DTPA, and pDNA. To determine the number of DTPA bound to pDNA, small amounts of free DTPA were added before radiolabeling with [ $^{111}\text{In}$ ]InCl<sub>3</sub>, followed by the separation of  $^{111}\text{In}$ -pDNA and  $^{111}\text{In}$ -DTPA by gel filtration.  $^{32}\text{P}$ -labeling of the pDNA was performed as reported previously (4).

**Animals.** All animal procedures were examined by the Ethics Committee for Animal Experiments at the Kyoto University. Female ICR mice (20–25 g) were obtained from the Shizuoka Agricultural Co-operative Association for Laboratory Animals (Shizuoka, Japan).

**Transfection to Cultured Cells.** HepG2 cells and COS7 cells were obtained from American Type Culture Collection (Manassas, VA) and maintained in DMEM supplemented with 10% FBS at 37 °C under an atmosphere of 5% CO<sub>2</sub> in air. Cells were plated on a 6-well plate at a density of about  $2 \times 10^5$  cells/well (10.5 cm<sup>2</sup>) and cultivated in 2 mL of DMEM supplemented with 10% FBS. After 24 h, the culture medium was replaced with medium containing pDNA (2  $\mu\text{g}$ ) complexed with 5  $\mu\text{L}$  of Lipofectamine 2000 (Invitrogen). Six hours later, the pDNA complex was removed and the cells were incubated for an additional 18 h. Then, the cells were scraped off and suspended in 200  $\mu\text{L}$  of PBS. The cell suspension was subjected to three cycles of freezing and thawing, followed by centrifugation at 10000g for 3 min. Ten microliters of the supernatant was mixed with 100  $\mu\text{L}$  of luciferase assay buffer (Picagene, Toyo Ink, Tokyo, Japan), and the light produced was immediately measured using a luminometer (Lumat LB 9507, EG & G Berthold, Bad Wildbad, Germany). The activity was indicated as the relative light units (RLU) per milligram of cell protein. The protein content of the cell suspension was measured using a protein assay kit (Dojindo, Kumamoto, Japan) and determined with reference to a standard curve for bovine serum albumin.

**Transgene Expression in Muscle In Vivo.** Control (unmodified) pDNA or DTPA–ASBA–pDNA was injected into the gastrocnemius muscle of anesthetized mice at a dose of 1  $\mu\text{g}$  of pDNA/50  $\mu\text{L}$  of saline. Immediately after injection, electric pulses were applied using a forceps-type electrode. Square-wave electric pulses were generated by a CUY21 electroporator (Nepa Gene, Tokyo, Japan). The parameters of the pulse were fixed at 200 V/cm for the electrical field strength, 20 ms duration, and six pulses. At 2 days after injection, the injected muscle was dissected and subjected to assays for luciferase activity and protein content.

**Tissue Distribution of Radiolabeled pDNA after Intravenous Injection.** For the tissue distribution

studies, the concentration of  $^{32}\text{P}$ - and  $^{111}\text{In}$ -pDNA was adjusted by the addition of nonradiolabeled pDNA. Each mouse was injected with  $^{111}\text{In}$ -pDNA or  $^{32}\text{P}$ -pDNA in saline ( $10\text{ }\mu\text{g}/100\text{ }\mu\text{L}$ ). At predetermined periods after injection, groups of three mice each were anesthetized with ether and blood was collected from the vena cava to obtain plasma by centrifugation at  $2000g$  for 2 min. The liver, kidney, spleen, lung, and heart were excised, rinsed with saline, and weighed.  $^{111}\text{In}$ -radioactivity of tissue samples was counted in a well-type NaI scintillation counter (ARC-500, Aloka, Tokyo, Japan).  $^{32}\text{P}$ -radioactivity was measured in a scintillation counter (LSA-500, Beckman, Tokyo, Japan) after addition of Clear-Sol I (Nacalai tesque, Kyoto, Japan) to tissue sample.

**Pharmacokinetic Analysis.** Tissue distribution of  $^{32}\text{P}$ -pDNA after intravenous injection was pharmacokinetically evaluated based on the clearance concept (17). In brief, the change in the amount of a test compound (pDNA) in a tissue with time can be described as follows:

$$\frac{dX_i}{dt} = \text{CL}_i C_p - k_{\text{efflux},i} X_i \quad (1)$$

where  $X_i$  represents an amount of pDNA in tissue  $i$  after administration,  $C_p$  is its concentration in plasma,  $\text{CL}_i$  expresses an apparent tissue uptake clearance from the plasma to tissue  $i$ , and  $k_{\text{efflux},i}$  represents an efflux rate from tissue  $i$ . When the efflux from tissues can be ignored, eq 1 is simplified to

$$\frac{dX_i}{dt} = \text{CL}_i C_p \quad (2)$$

Integration of eq 2 from time 0 to  $t_1$  gives

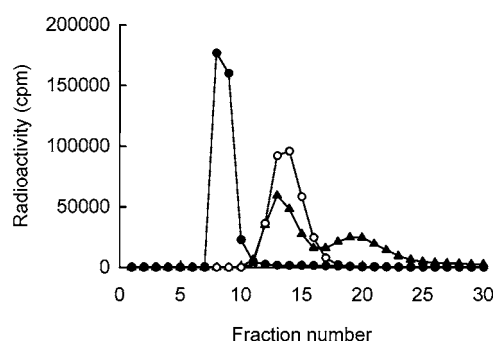
$$\text{CL}_i = \frac{X_{i,t_1}}{\text{AUC}_{0-t_1}} \quad (3)$$

where AUC is an area under the plasma concentration–time curve of pDNA. According to eq 3,  $\text{CL}_i$  is obtained by dividing the amount in a tissue by AUC. The total body clearance ( $\text{CL}_{\text{total}}$ ) was calculated by fitting an equation to the plasma concentration data of the radioactivity-time profile using the nonlinear least-squares program MULTI (18).

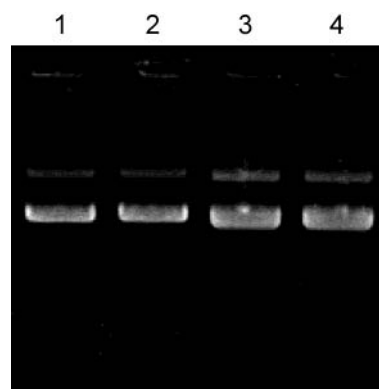
**Tissue Distribution and Transgene Expression Following Intravenous Injection of PEI/pDNA Complex.** pDNA was mixed with PEI at varying ratios and left at room temperature for 30 min. The mixture obtained was subjected to 1% agarose gel electrophoresis to check the complex formation. The N/P ratio, the ratio of the concentration of total nitrogen (N) in PEI to the phosphate groups (P) in pDNA, was used as an index of complex preparation.  $^{111}\text{In}$ -pDNA in a free or complexed form with PEI was injected into a mouse tail vein, and the tissue distribution of radioactivity was evaluated 6 h later. In separate experiments, transgene expression in the lung was measured following the injection of naked pDNA or PEI/pDNA complex. In both experiments, the dose of pDNA was fixed at  $30\text{ }\mu\text{g}/\text{mouse}$ .

## RESULTS

**Characteristics of  $^{111}\text{In}$ -pDNA.** Scheme 1 illustrates the chemistry used to prepare DTPA–ASBA conjugate. The product was analyzed by mass spectroscopy, which revealed that DTPA–ASBA was successfully obtained. Then, DTPA–ASBA conjugate was reacted with pDNA, and the final product was labeled with  $^{111}\text{In}$ . Table 1



**Figure 1.** Sephadex G-25 gel filtration profiles of  $^{111}\text{In}$ -pDNA,  $^{111}\text{In}$ -DTPA, and  $^{111}\text{In}$ -DTPA–ASBA. Each sample was applied to a Sephadex G-25 column ( $1 \times 40\text{ cm}$ ) and filtrates (40 drops/tube) were collected and radioactivity measured. Keys: (●),  $^{111}\text{In}$ -pDNA; (○),  $^{111}\text{In}$ -DTPA; (▲),  $^{111}\text{In}$ -DTPA–ASBA.



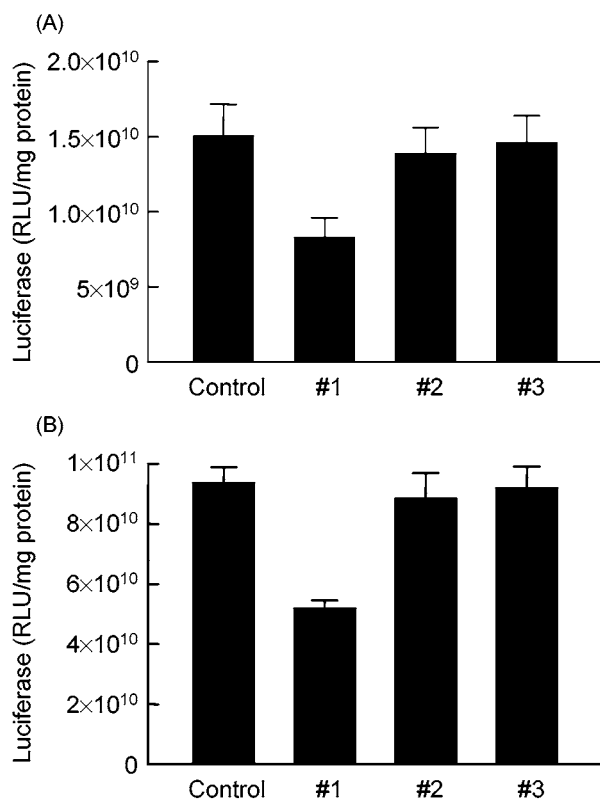
**Figure 2.** Agarose gel electrophoresis of  $^{111}\text{In}$ -pDNA. Ten micrograms of pDNA or  $^{111}\text{In}$ -pDNA was applied to 1% agarose gel and run at a constant voltage. pDNA was detected with an UV lamp. For the detection of radioactivity, the gel was cut into pieces and the radioactivity was measured in a  $\gamma$ -counter. Lanes: (1) control pDNA; (2–4)  $^{111}\text{In}$ -pDNA (lane 2, condition 3; lane 3, condition 2; lane 4, condition 1).

**Table 1. Properties of  $^{111}\text{In}$ -pDNA**

	reaction conditions				
	pDNA ( $\mu\text{g}$ )	ASBA ( $\mu\text{g}$ )	DTPA ( $\mu\text{g}$ )	no. of DTPA molecules/pDNA	specific activity (cpm/ $\mu\text{g}$ of pDNA)
1	100	1000	2000	15.8	2 000 000
2	100	500	1000	4.1	400 000
3	100	250	500	2.3	200 000

summarizes the reaction conditions and the properties of  $^{111}\text{In}$ -pDNA obtained. The number of DTPA–ASBA molecules bound to pDNA was a function of the amounts of ASBA and DTPA in the reaction mixture, and pDNA derivatives with various numbers of DTPA–ASBA molecules could be obtained. The numbers of DTPA–ASBA molecules in pDNA were calculated to be 15.8, 4.1, and 2.3, based on the amounts of radioactivity eluted in pDNA and DTPA fractions (data not shown). The specific activity of  $^{111}\text{In}$ -pDNA was as high as about  $2 \times 10^6\text{ cpm}/\mu\text{g}$  of pDNA with the largest number of DTPA–ASBA molecules (condition 1).

$^{111}\text{In}$ -pDNA showed only one peak on Sephadex G-25 column chromatography at the void volume, which could be easily distinguished from the peaks of  $^{111}\text{In}$ -DTPA and  $^{111}\text{In}$ -DTPA–ASBA (Figure 1). On agarose gel electrophoresis,  $^{111}\text{In}$ -pDNA showed almost a pattern similar to that of control pDNA (Figure 2). However, the percentages of the open circular and linear forms slightly increased with the increasing number of DTPA–ASBA molecules. The measurement of  $^{111}\text{In}$ -radioactivity of the gel indicated that more than 95% of radioactivity were



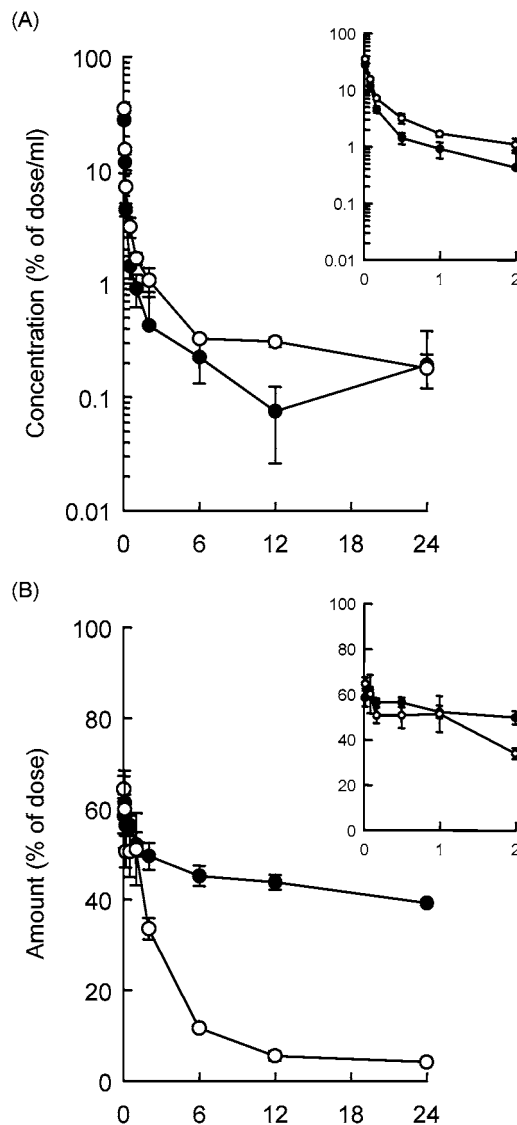
**Figure 3.** Transgene expression in (A) HepG2 and (B) COS7 cells after transfection of pDNA and DTPA-ASBA-pDNA. Cells ( $2 \times 10^5$  cells) cultured on a 12-well plate were combined with  $2 \mu\text{g}$  of pDNA complexed with Lipofectamine 2000. Results are expressed as the mean  $\pm$  SD of three wells.

detected at the positions where pDNA was visualized, suggesting that  $^{111}\text{In}$  is associated with pDNA. These distribution characteristics of  $^{111}\text{In}$ -radioactivity on the gel were confirmed by autoradiography (data not shown).

**Transgene Expression.** Gene transfection to HepG2 cells and COS7 cells with the control pDNA complex resulted in luciferase activities of  $1.5 \times 10^{10}$  and  $9.3 \times 10^{10}$  RLU/mg of protein, respectively (Figure 3). The transfection activity of the modified pDNA decreased on increasing the number of DTPA-ASBA molecules: about 97–98, 92–94, and 55% of the activity was retained after the modification of 2.3 (condition 3), 4.1 (condition 2), and 15.8 (condition 1) DTPA-ASBA molecules, respectively.

The transfection activity of the pDNA derivatives modified with DTPA-ASBA was also examined *in vivo* after intramuscular injection followed by electroporation. Again, there was successful transgene expression in mouse muscle with activity 93, 82, and 40% that of the control pDNA, respectively (data not shown). In the following tissue distribution experiments,  $^{111}\text{In}$ -pDNA with the highest specific activity (condition 1) was used.

**Tissue Distribution and Pharmacokinetic Analysis after Intravenous Injection.** Figure 4 shows the plasma concentration (A) and liver accumulation (B) time courses of radioactivity after intravenous injection of  $^{111}\text{In}$ - and  $^{32}\text{P}$ -pDNA into mice at a dose of 0.5 mg/kg. When  $^{111}\text{In}$ -pDNA was injected, radioactivity in plasma rapidly decreased with time, and a large amount of  $^{111}\text{In}$ -radioactivity was recovered in the liver (up to 50–60% of the dose), which almost leveled off for 2 h. At 24 h after injection, the radioactivity in the liver remained at about 45% of the injected dose. In a similar fashion,  $^{32}\text{P}$ -radioactivity following the injection of  $^{32}\text{P}$ -pDNA decreased in plasma with time, and there was



**Figure 4.** Plasma concentration (A) and liver accumulation (B) time courses of radioactivity in mice after intravenous injection of  $^{111}\text{In}$ -pDNA or  $^{32}\text{P}$ -pDNA at a dose of 0.5 mg/kg ( $10 \mu\text{g}/\text{mouse}$ ). Keys: (●),  $^{111}\text{In}$ -pDNA; (○),  $^{32}\text{P}$ -pDNA. Results are expressed as the mean  $\pm$  SD of three mice.

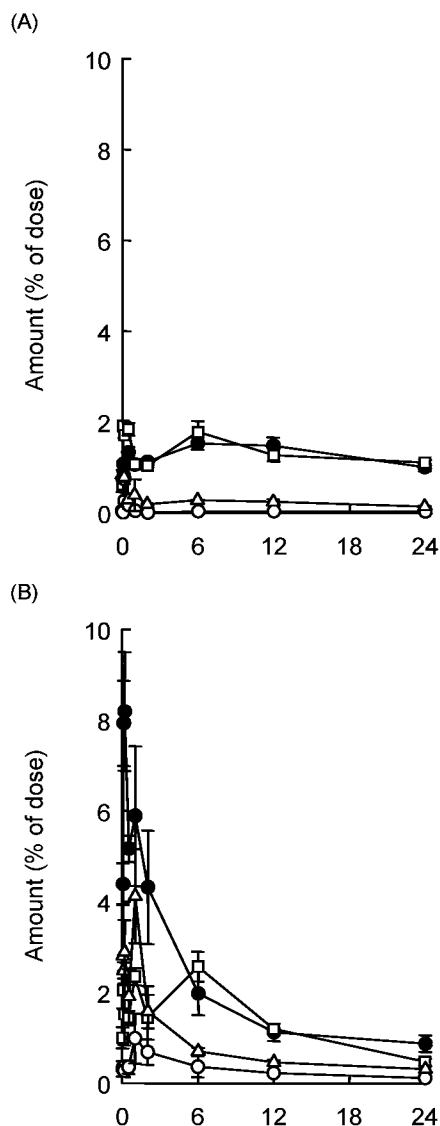
accumulation in the liver (up to 50–60% of the dose) within 3 min. However, the radioactivity in the liver fell continuously with time down to about 5% of the dose at 12 h. These results obtained with  $^{32}\text{P}$ -pDNA were basically similar to previously reported results (4, 5).

The injection of  $^{32}\text{P}$ -pDNA resulted in a relatively high, but transient, accumulation of radioactivity in organs such as the kidney, spleen, and lung, whereas  $^{111}\text{In}$ -pDNA showed less accumulation of radioactivity in these organs (Figure 5). The urinary excretion of  $^{111}\text{In}$ -radioactivity was greater than that of  $^{32}\text{P}$ -radioactivity, and about 20% of the injected dose was excreted 30 min postinjection (data not shown).

Table 2 summarizes the AUC and clearances calculated based on the radioactivity at 2 h after intravenous injection of  $^{111}\text{In}$ - and  $^{32}\text{P}$ -pDNA in mice.  $^{111}\text{In}$ -pDNA showed a greater hepatic clearance than  $^{32}\text{P}$ -pDNA, reflecting the prolonged retention of radioactivity within the liver. On the other hand, the uptake clearances for the lung, kidney, and heart were greater with  $^{32}\text{P}$ -pDNA than with  $^{111}\text{In}$ -pDNA.

**Distribution and Transgene Expression by PEI/pDNA.** Finally, we examined the correlation between the



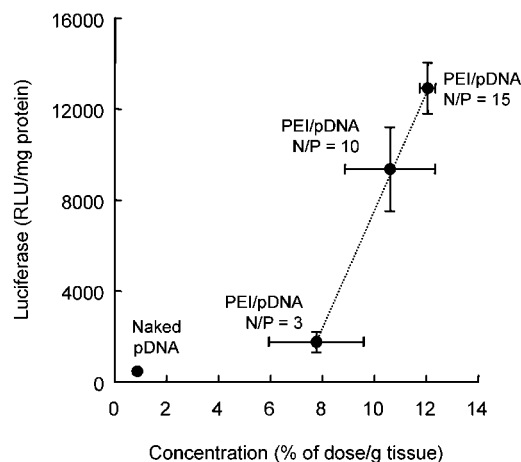


**Figure 5.** Tissue distribution-time courses of radioactivity in mice after intravenous injection of  $^{111}\text{In}$ -pDNA (A) and  $^{32}\text{P}$ -pDNA (B) at a dose of 0.5 mg/kg (10  $\mu\text{g}$ /mouse). Keys: (●), kidney; (□), spleen; (△), lung; (○), heart. Results are expressed as the mean  $\pm$  SD of three mice.

tissue distribution of  $^{111}\text{In}$ -radioactivity and transgene expression in the lung after intravenous injection of PEI/ ( $^{111}\text{In}$ )-pDNA complex into mice. It is well-known that intravenous PEI/pDNA can result in transgene expression in organs with the greatest degree in the lung, and the expression efficiency is at least partially determined by the N/P ratio of the complex (19, 20). In the present experiment, the transgene expression in the lung increased with an increase in the N/P ratio from 0 (naked) to 15. Separately, the delivery of  $^{111}\text{In}$ -pDNA to the lung was examined by determining the radioactivity in the lung at 6 h after intravenous injection of PEI/ $^{111}\text{In}$ -pDNA complex. Then, the expression was plotted against the amount of radioactivity in the organ (Figure 6). As shown in this figure, the expression in the lung correlated well with the amount of  $^{111}\text{In}$ -radioactivity in the organ, except for the case of naked  $^{111}\text{In}$ -pDNA that showed no significant luciferase activity.

#### DISCUSSION

Although pDNA amplified in, and extracted from, bacteria is one of the most promising vectors for gene



**Figure 6.** Relation between the concentration of  $^{111}\text{In}$ -radioactivity and transgene expression in the lung at 6 h after intravenous injection of ( $^{111}\text{In}$ )-pDNA at a dose of 30  $\mu\text{g}$ /mouse. Results are expressed as the mean  $\pm$  SD of three mice.

transfer both in vivo and in vitro, its transcriptional activity depends on the functional form of the plasmid: supercoiled (SC), open circular (OC), and linear (L) forms. For example, the OC and L forms of a plasmid were 90 and 10% as efficient as the SC form as far as cell transfection was concerned (21). In addition, the chemical and biological properties such as the charge density and the susceptibility to nuclease digestion depend on the structure of pDNA (22). Recently, Houk et al. (23) reported topoform-dependent pharmacokinetic characteristics of pDNA. Therefore, it is very important to investigate the tissue distribution properties of the pDNA with a structure similar to that used in gene transfer studies, namely, the SC form. To this end, various approaches have been developed to label pDNA with fluorescent probes or radioisotopes under conditions where the SC form of pDNA is hardly altered. These include covalent coupling of a fluorescent dye by photoactivation (14), radioiodination of cytidine (24), application of a fluorescent peptide nucleic acid clamp (15), and metabolic labeling using [ $^3\text{H}$ ]thymidine 5'-triphosphate (25). Other methods for labeling of pDNA could induce significant changes in the structure. In the present study, although a portion of the chemically modified pDNA showed structural alterations, most of the pDNA retained its SC form. In addition, the modified pDNA retained its transcriptional activity (40–98% as control pDNA), indicating that  $^{111}\text{In}$ -pDNA reflects the pharmacokinetic features of the unlabeled pDNA.

Various techniques have been reported to trace externally administered pDNA in vivo. Zelphati et al. (15) reported a peptide nucleic acid (PNA)-based fluorescent label for pDNA which was fully transcriptionally active. This approach would be also useful in determining the tissue distribution of pDNA, although one first needs to modify the pDNA of interest to add the PNA binding sites. In addition, the radiolabel makes it much easier to trace the in vivo distribution of labeled pDNA than any fluorescent label. PCR amplification of pDNA with an internal standard can also quantitatively determine the plasma concentration of pDNA after in vivo administration (26). An analysis based on agarose gel electrophoresis of samples containing pDNA has been used to monitor the pharmacokinetics of pDNA in rats (23). These techniques estimating the amount of pDNA by gel electrophoresis are too laborious, especially when information on the tissue distribution of pDNA is required.

**Table 2. AUC and Clearances of Radiolabeled pDNA in Mice**

compound	AUC (% of dose h/mL)	clearance ( $\mu\text{L/h}$ )					
		total	liver	lung	spleen	kidney	heart
$^{111}\text{In}$ -pDNA	2.8	36000	17800	69	374	407	3
$^{32}\text{P}$ -pDNA	3.9	25800	8670	408	372	1120	181

$^{111}\text{In}$ -labeling has been widely used in tissue distribution studies of proteins, polymers, and particulates. A chelating agent is required for labeling with  $^{111}\text{In}$ . DTPA anhydride has long been used as a bifunctional chelating agent for  $^{111}\text{In}$  labeling of many different molecules, especially monoclonal antibodies (27). Although several studies have demonstrated that other chelating agents such as 1-(4-isothiocyanatobenzyl)ethylenediaminetetraacetic acid (28) and a *N*-hydroxysulfosuccinimide ester of 1,4,7,10-tetraazacyclododecane *N,N,N',N''*-tetraacetic acid (29) can form more stable chelates with  $^{111}\text{In}$ , DTPA- $^{111}\text{In}$  chelate has sufficient chelating stability in vivo (30). After cellular uptake of  $^{111}\text{In}$ -labeled proteins followed by intracellular catabolism,  $^{111}\text{In}$  is present as  $^{111}\text{In}$ -DTPA-lysine and  $^{111}\text{In}$ -DTPA in vivo (31). These radioactive metabolites are relatively large in size and highly hydrophilic, both characteristics making them largely unable to cross biological membranes. Therefore, after cellular uptake, the  $^{111}\text{In}$ -radioactivity remains within the cells. These characteristics of  $^{111}\text{In}$ -labeling are beneficial for evaluating the pharmacokinetic characteristics of various compounds (17). This concept has been applied to the radiolabeling of pDNA for the tissue distribution study. The conjugation of DTPA-ASBA to pDNA, which would be governed by the photoreactivity of ASBA to pDNA (32), resulted in pDNA derivatives that can be efficiently radiolabeled with  $^{111}\text{In}$ . Although the exact structure needs to be elucidated,  $^{111}\text{In}$ -radioactivity remained for a significantly long period after systemic administration of  $^{111}\text{In}$ -pDNA, indicating that  $^{111}\text{In}$ -pDNA has advantages on its tissue distribution studies similar to those of  $^{111}\text{In}$ -labeled other macromolecules. As listed in Table 2,  $^{111}\text{In}$ -pDNA gave a greater hepatic clearance than  $^{32}\text{P}$ -pDNA, although  $^{32}\text{P}$ -pDNA was taken up by the liver as fast as  $^{111}\text{In}$ -pDNA. Rapid efflux of radioactive metabolites of  $^{32}\text{P}$ -pDNA will explain the difference in the hepatic clearance of these two derivatives. The released radioactive metabolites are delivered to other organs such as the lung, kidney, and heart, which increased the clearance values of  $^{32}\text{P}$ -pDNA for these organs (Table 2). Tissue uptake clearance is a useful parameter, which can be directly compared with those of others and physiological parameters such as blood flow and the rate of fluid-phase endocytosis (17). Therefore, a theoretical design of any delivery approach for pDNA can be achieved by considering the relationships between the characteristics on structures and the pharmacokinetic parameters. The present study clearly indicates that the hepatic clearance of pDNA is 20–25% of the hepatic plasma flow rate, and the clearances for other organs are about 2% or smaller than that for the liver.

As shown in Figure 6, this novel pDNA radiolabeling is very useful for developing better approaches to in vivo gene transfer because the amount of  $^{111}\text{In}$ -radioactivity in the lung correlated well with the transgene expression level. These results indicate that the organ level of pDNA delivery is important for the final output. Under the experimental settings used in the present study, about 8% of dose/g of tissue, i.e., 0.8  $\mu\text{g}$  of pDNA/lung, are needed for a detectable expression in this organ. The amount of naked pDNA delivered to the lung was too low for a significant gene expression. In a strict sense,

however, the amount of pDNA targeted to the nucleus could be a better index of transgene expression.

In conclusion, a new residualizing radiolabel for pDNA has been successfully developed. The radiolabeled pDNA can nicely designate the tissues and cells that take up the DNA after administration. Because gene transfer only occurs in the cells taking up pDNA, the tissue distribution data of pDNA can be used to evaluate the targeting ability of the vector and administration technique used. Then, a better approach can be developed based on the tissue distribution data of a vector system. Thus,  $^{111}\text{In}$ -pDNA is useful not only for evaluating the tissue distribution of pDNA and its complex with a vector system, but also for designing an effective vector for targeted delivery of pDNA.

#### ACKNOWLEDGMENT

This work was supported in part by a Grant-In-Aid for Scientific Research from the Ministry of Education, Culture, Sports, Science and Technology, Japan, and by a grant from the Ministry of Health, Labour and Welfare, Japan.

#### LITERATURE CITED

- (1) Nishikawa, M., and Huang, L. (2001) Nonviral vectors in the new millennium: delivery barriers in gene transfer. *Hum. Gene Ther.* 12, 861–870.
- (2) Rigby, P. W., Dieckmann, M., Rhodes, C., and Berg, P. (1977) Labeling deoxyribonucleic acid to high specific activity in vitro by nick translation with DNA polymerase I. *J. Mol. Biol.* 113, 237–251.
- (3) Piatyszek, M. A., Jarmolowski, A., and Augustyniak, J. (1988) Iodo-Gen-mediated radioiodination of nucleic acids. *Anal. Biochem.* 172, 356–359.
- (4) Kawabata, K., Takakura, Y., and Hashida, M. (1995) The fate of plasmid DNA after intravenous injection in mice: involvement of scavenger receptors in its hepatic uptake. *Pharm. Res.* 12, 825–830.
- (5) Kobayashi, N., Kuramoto, T., Yamaoka, K., Hashida, M., and Takakura, Y. (2001) Hepatic uptake and gene expression mechanisms following intravenous administration of plasmid DNA by conventional and hydrodynamics-based procedures. *J. Pharmacol. Exp. Ther.* 297, 853–860.
- (6) Ali, S. A., Eary, J. F., Warren, S. D., Badger, C. C., and Krohn, K. A. (1988) Synthesis and radioiodination of tyramine cellobiose for labeling monoclonal antibodies. *Int. J. Rad. Appl. Instrum. B.* 15, 557–561.
- (7) Brandt, K. D., and Johnson, D. K. (1992) Structure–function relationships in indium-111 radioimmunoconjugates. *Bioconjugate Chem.* 3, 118–125.
- (8) Demignot, S., Pimm, M. V., Thorpe, S. R., and Baldwin, R. W. (1991) Differences between the catabolism and tumour distribution of intact monoclonal antibody (791T/36) and its Fab/c fragment in mice with tumour xenografts revealed by the use of a residualizing radiolabel (dilactitol-125I-tyramine) and autoradiography. *Cancer Immunol. Immunother.* 33, 359–366.
- (9) Deshpande, S. V., Subramanian, R., McCall, M. J., DeNardo, S. J., DeNardo, G. L., and Meares, C. F. (1990) Metabolism of indium chelates attached to monoclonal antibody: minimal transchelation of indium from benzyl-EDTA chelate in vivo. *J. Nucl. Med.* 31, 218–224.
- (10) Thorpe, S. R., Baynes, J. W., and Chroneos, Z. C. (1993) The design and application of residualizing labels for studies of protein catabolism. *FASEB J.* 7, 399–405.

- (11) Duncan, J. R., and Welch, M. J. (1993) Intracellular metabolism of indium-111-DTPA-labeled receptor targeted proteins. *J. Nucl. Med.* **34**, 1728–1738.
- (12) Bogdanov, A., Jr., Tung, C. H., Bredow, S., and Weissleder, R. (2001) DNA binding chelates for nonviral gene delivery imaging. *Gene Ther.* **8**, 515–522.
- (13) Dowty, M. E., Gurevich, V., Berg, R. K., Repetto, G., and Wolff, J. A. (1992) Characterization of biotinylated and gold-labeled plasmid DNA. *Methods Mol. Cell. Biol.* **3**, 167–174.
- (14) Neves, C., Byk, G., Escriou, V., Bussone, F., Scherman, D., and Wils, P. (2000) Novel method for covalent fluorescent labeling of plasmid DNA that maintains structural integrity of the plasmid. *Bioconjugate Chem.* **11**, 51–55.
- (15) Zelphati, O., Liang, X., Hobart, P., and Felgner, P. L. (1999) Gene chemistry: functionally and conformationally intact fluorescent plasmid DNA. *Hum. Gene Ther.* **10**, 15–24.
- (16) Nishikawa, M., Yamauchi, M., Morimoto, K., Ishida, E., Takakura, Y., and Hashida, M. (2000) Hepatocyte-targeted in vivo gene expression by intravenous injection of plasmid DNA complexed with synthetic multi-functional gene delivery system. *Gene Ther.* **7**, 548–555.
- (17) Nishikawa, M., Takakura, Y., and Hashida, M. (1996) Pharmacokinetic evaluation of polymeric carriers. *Adv. Drug Delivery Rev.* **21**, 135–155.
- (18) Yamaoka, K., Tanigawara, Y., Nakagawa, T., and Uno, T. (1981) A pharmacokinetic analysis program (multi) for micro-computer. *J. Pharmacobio.-Dyn.* **4**, 879–885.
- (19) Goula, D., Benoist, C., Mantero, S., Merlo, G., Levi, G., and Demeneix, B. A. (1998) Polyethylenimine-based intravenous delivery of transgenes to mouse lung. *Gene Ther.* **5**, 1291–1295.
- (20) Morimoto, K., Nishikawa, M., Kawakami, S., Nakano, T., Hattori, Y., Fumoto, S., Yamashita, F., and Hashida, M. (2003) Molecular weight-dependent gene transfection activity of unmodified and galactosylated polyethyleneimine on hepatoma cells and mouse liver. *Mol. Ther.* **7**, 254–261.
- (21) Adami, R. C., Collard, W. T., Gupta, S. A., Kwok, K. Y., Bonadio, J., and Rice, K. G. (1998) Stability of peptide-condensed plasmid DNA formulations. *J. Pharm. Sci.* **87**, 678–683.
- (22) Poly, F., Chenu, C., Simonet, P., Rouiller, J., and Monrozier, L. J. (2000) Differences between linear chromosomal and supercoiled plasmid DNA in their mechanisms and extent of adsorption on clay minerals. *Langmuir* **16**, 1233–1238.
- (23) Houk, B. E., Martin, R., Hochhaus, G., and Hughes, J. A. (2001) Pharmacokinetics of plasmid DNA in the rat. *Pharm. Res.* **18**, 67–74.
- (24) Terebesi, J., Kwok, K. Y., and Rice, K. G. (1998) Iodinated plasmid DNA as a tool for studying gene delivery. *Anal. Biochem.* **263**, 120–123.
- (25) Wasan, E. K., Reimer, D. L., and Bally, M. B. (1996) Plasmid DNA is protected against ultrasonic cavitation-induced damage when complexed to cationic liposomes. *J. Pharm. Sci.* **85**, 427–433.
- (26) Oh, Y. K., Kim, J. P., Yoon, H., Kim, J. M., Yang, J. S., and Kim, C. K. (2001) Prolonged organ retention and safety of plasmid DNA administered in polyethylenimine complexes. *Gene Ther.* **8**, 1587–1592.
- (27) Hnatowich, D. J., Layne, W. W., Childs, R. L., Lanteigne, D., Davis, M. A., Griffin, T. W., and Doherty, P. W. (1983) Radioactive labeling of antibody: a simple and efficient method. *Science* **220**, 613–615.
- (28) Meares, C. F., McCall, M. J., Reardan, D. T., Goodwin, D. A., Diamanti, C. I., McTigue, M. (1984) Conjugation of antibodies with bifunctional chelating agents: isothiocyanate and bromoacetamide reagents, methods of analysis, and subsequent addition of metal ions. *Anal. Biochem.* **142**, 68–78.
- (29) Lewis, M. R., Raubitschek, A., and Shively, J. E. (1994) A facile, water-soluble method for modification of proteins with DOTA. Use of elevated temperature and optimized pH to achieve high specific activity and high chelate stability in radiolabeled immunoconjugates. *Bioconjugate Chem.* **5**, 565–76.
- (30) Nishikawa, M., Staud, F., Takemura, S., Takakura, Y., and Hashida, M. (1999) Pharmacokinetic evaluation of biodistribution data obtained with radiolabeled proteins in mice. *Biol. Pharm. Bull.* **22**, 214–218.
- (31) Franano, F. N., Edwards, W. B., Welch, M. J., and Duncan, J. R. (1994) Metabolism of receptor targeted <sup>111</sup>In-DTPA-glycoproteins: identification of <sup>111</sup>In-DTPA-epsilon-lysine as the primary metabolic and excretory product. *Nucleic Med. Biol.* **21**, 1023–1034.
- (32) Hermanson, G. T. (1996) Heterobifunctional Cross-linkers. *Bioconjugate Techniques* (Hermanson, G. T., Ed.) pp 228–286, Academic Press, London.

BC034032Y



# Synthesis of Trifunctional PNA–Benzophenone Derivatives for Mitochondrial Targeting, Selective DNA Binding, and Photo-Cross-Linking

Günther F. Ross,<sup>†</sup> Paul M. Smith,<sup>†</sup> Alistair McGregor, Douglass M. Turnbull, and Robert N. Lightowlers\*

School of Neurology, Neurobiology and Psychiatry, The Medical School, University of Newcastle upon Tyne, Framlington Place, Newcastle upon Tyne, NE2 4HH, UK. Received March 31, 2003; Revised Manuscript Received July 22, 2003

Mutations in mitochondrial DNA (mtDNA) cause a variety of human pathologies. In many patients, mutated and wild-type mtDNAs coexist in the same cell, a situation termed mtDNA heteroplasmy. In the absence of standard therapies for these disorders, a genetic strategy for treatment has been proposed whereby replication of mutated mtDNA is inhibited by the selective hybridization of a nucleic acid derivative, allowing propagation of the wild-type genome and correction of the associated defects. To allow for selective binding under physiological conditions, peptide nucleic acids (PNA) are being used. Two other problems, however, have to be resolved: mitochondrial import and attachment of the PNA to the target DNA to inhibit replication. Mitochondrial localization can be achieved by the addition of a caged lipophilic cation and addition of a photo-cross-linking reagent should facilitate covalent attachment. We therefore report the synthesis of benzophenone–PNA derivatives carrying a triphenylphosphonium moiety and demonstrate irreversible binding selectivity between two DNA molecules that differ by a single nucleotide.

## INTRODUCTION

Human mtDNA, a 16 569 bp circular genome, encodes 13 polypeptides and 24 RNA molecules. All 13 proteins are believed to be essential components of the enzyme complexes that couple respiration to the generation of ATP. Although clinical syndromes with an underlying mtDNA mutation such as MERRF (*myoclonus epilepsy with ragged red fibres*) and MELAS (*mitochondrial encephalopathy, lactic acidosis and stroke-like episodes*) are rare, when considered as a group, mtDNA mutations are increasingly being recognized as important genetic defects (1, 2). Epidemiological studies in the North East of England showed that as many as 1:8000 individuals carry a pathogenic mtDNA mutation and 1:17 000 have an associated clinical defect (3). There are many copies of mtDNA in each nucleated cell of the body. In the diseased state, the pathogenic allele is often represented by a major subgroup of molecules, a situation termed heteroplasmy. Dependent on the particular mutation, it is normally recessive, with ratios reported as high as 95% before a biochemical deficiency is apparent (4, 5). Mutations may take the form of rearrangements (deletions or duplications), but often the wild-type and mutated mtDNA differ by only a single base pair substitution.

In the absence of standard treatments for these disorders, we have suggested that antigenomic molecules could be made to selectively target the replicating mutated mtDNA, preventing normal replication and

allowing propagation of the wild-type molecule with time (6, 7). This antigenomic hypothesis assumes that the resultant alteration in the balance of wild-type to mutated molecule could be sufficient to reverse the biochemical and potentially the clinical defect in patients. Advances in targeting molecules to mixed-sequence duplex DNA are beginning to be made, as illustrated by recent work with pseudocomplementary peptide nucleic acid molecules (8). However, as mtDNA replicative intermediates will be single-stranded for a period during replication, it may not be necessary to target duplex mtDNA. Selective hybridization of antigenomic agents to single-stranded DNA could be effective in inhibiting mtDNA replication, particularly if this binding was irreversible. Our search for an ideal antigenomic agent has focused on peptide nucleic acids (PNAs) and derivatives. These molecules comprise a backbone of repeating *N*-(2-aminoethyl)-glycine units connected to standard purine or pyrimidine bases which are able to base pair in both Watson–Crick or Hoogsteen forms (9). As PNAs are uncharged, they show increased binding affinity when pairing with complementary oligonucleotides. DNA/PNA complexes are more sensitive to single base mismatches than the DNA duplex counterpart, and their unusual chemistry makes them resistant to degradation under physiological conditions (10, 11). Initial experiments in vitro, exploring the potential of PNAs as antigenomic agents, were promising. PNAs were able to bind to single-stranded DNA templates and inhibit polymerization by mitochondrial DNA polymerase  $\gamma$  in a sequence-selective manner, even when using an 11-mer PNA (PNA-MERRF) to target templates mimicking heteroplasmy of the common A8344G MERRF point mutation (12). By derivatizing the PNAs with the lipophilic

\* Address for correspondence: R. N. Lightowlers, School of Neurology, Neurobiology and Psychiatry, The Medical School, Framlington Place, University of Newcastle upon Tyne, Newcastle upon Tyne, United Kingdom, NE2 4HH. Telephone: (+44)-191-222-8028. Fax: (+44)-191-222-8553. E-mail: r.n.lightowlers@ncl.ac.uk.

<sup>†</sup> Both authors contributed equally to this paper.

cation, triphenylphosphonium (TPP),<sup>1</sup> the resultant molecules appeared to be imported into the mitochondrial matrix in intact cells (13). Disappointingly, however, no alteration in the levels of heteroplasmy was noted when using cells heteroplasmic for the A8344G MERRF mutation and the TPP-PNA-MERRF.

As the reported data were consistent with the TPP-PNA being imported, the lack of effect was due either to the PNA not being able to access mtDNA, or that after binding it was removed. To dissect these possibilities, we set out to synthesize a molecule that could be covalently attached to mtDNA in a sequence-selective manner. Principally, a suitable construct has to be optimized for a three-step process. First, the molecule has to be imported solely into the mitochondrial matrix. Interactions with other organelles and especially with nuclear DNA would cause severe side effects. Second, inside the matrix the agent has to bind to the mutated mtDNA and spare the wild type. Here a single mismatch has to be recognized. In the third step, a covalent cross-link to the mutated mtDNA would be ideal, inhibiting replication of the target. An alternative would be to use bis-PNAs for their extremely tight binding and ability to strand displace DNA duplexes (14). However, it has not been demonstrated that such molecules can be imported into mitochondria, and preliminary data suggest the increased size of these molecules may adversely affect their import (PMS unpublished observation). Further, the elevated pH in the mitochondrial matrix ( $\approx$  pH 7.8) would be likely to prove detrimental to the strand invasion potential.

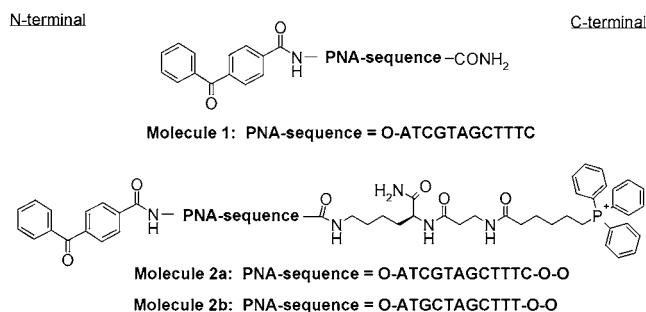
To satisfy these three requirements, we report the synthesis of a peptide nucleic acid derivative carrying a TPP moiety for mitochondrial targeting and a benzophenone system as a photoreactive cross-linker. Although unlikely to be of use for treating patients in vivo, the constructs will be essential for experiments with cells in culture to determine whether PNA derivatives do indeed bind to mtDNA in intact organelles. This information will be crucial for the design of novel targeted PNA derivatives that can be used to treat patients with mtDNA disease.

## EXPERIMENTAL PROCEDURES

**Automated Synthesis of PNA Oligomers.** PNA oligomers were synthesized on an Expedite 8909 Nucleic Acid Synthesis system (Applied Biosystems) using Fmoc/Bhoc monomers (Expedite PNA and linker AEEA-OH monomers, Applied Biosystems) and HATU activation (15). Syntheses were carried out using the standard 2  $\mu$ mol PNA protocol provided by the supplier. Reaction columns packed with Fmoc-PAL-PEG-PS resin as well as all reagents, solvents, and solutions used during the syntheses were also purchased from Applied Biosystems unless stated.

**Synthesis of PNA-BZP and PNA-BZP-TPP Conjugates.** To form 4-benzoylbenzoic acid conjugates (1,

<sup>1</sup> Abbreviations: TPP, triphenylphosphonium; Bhoc benzhydryloxycarbonyl; Fmoc, 9-fluorenylmethoxycarbonyl; Bhoc, benzhydryloxycarbonyl; AEEA, 8-amino-3,6-dioxoactanoic acid; HATU, (*O*-(7-azabenzotriazol-1-yl)-1,1,3,3-tetramethyluronium hexafluorophosphate; BZBA, 4-benzoylbenzoic acid; NHS, *N*-hydroxy succinimide; DIEA, diisopropylethylamine; DMF, *N,N*-dimethylformamide; DCM, dichloromethane; NMP, *N*-methylpyrrolidone; CPTPP, carboxypentyl triphenylphosphonium bromide; MMT, monomethoxytrityl; PFP, pentafluorophenyl; TFA, trifluoroacetic acid; IBTP, iodobutyltriphenylphosphonium iodide; ODN, oligodeoxynucleotide.



**Figure 1.** Diagrammatic representation of the PNA derivatives used in this study. Protocols for the synthesis and purification of these molecules are described in Experimental Procedures. Benzophenone-PNA **1** and the mitochondrially targeted derivatives benzophenone-triphenylphosphonium-PNAs **2a,b**. O specifies the 8-amino-3,6-dioxoactanoic acid spacer monomer. The PNA sequences of these molecules are identical except that **2b** has a single base truncation at the C-terminus.

**2a,b** Figure 1), the PNA oligomer was synthesized on solid support as described. When the automated synthesis was complete, the N-terminal Fmoc-group was removed by a final deblock step. A solution of 15 mg (46.4  $\mu$ mol, 23.2 equiv) of 4-benzoylbenzoic acid *N*-hydroxysuccinimido ester (BZBA-NHS, Molecular Probes) and 11  $\mu$ L (64.6  $\mu$ mol, 32.3 equiv) of DIEA in 300  $\mu$ L of DMF was prepared and passed back and forth through the column, 2 h at room temperature, using two 1-mL Luer slip-tip syringes attached to the ends of the column. The resin was then washed with 3  $\times$  1 mL of DMF and 3  $\times$  1 mL of DCM.

For the synthesis of PNA-conjugates **2a,b** carrying BZBA on the N-terminal and TPP on the C-terminal, two NMP-solutions were prepared and loaded onto free monomer ports of the Expedite 8909: A 0.2 M solution of carboxypentyltriphenylphosphonium bromide (CPTPP, Fluka) and a 0.2 M solution of *N*- $\alpha$ -Fmoc-*N*- $\epsilon$ -MMT-L-lysine (Bachem) (16). First, the protected amino acid was attached to the resin on the synthesizer using the standard PNA protocol and the *N*- $\alpha$ -Fmoc group was removed by a final deblock step. Then the column was removed from the synthesizer. A solution of 25 mg (52.4  $\mu$ mol, 26.2 equiv) of F-moc- $\beta$ -Ala-OPFP (Bachem) in 300  $\mu$ L of DMF was prepared and reacted manually using the two-syringe procedure described above. Subsequently, the column was replaced on the synthesizer and CPTPP was attached. The acid-labile *N*- $\epsilon$ -MMT group was removed manually by treatment with 30 mg of chloroacetic acid in 800  $\mu$ L of 4:1 (v:v) DCM/*m*-cresol for 5 h at room temperature. The resin was washed thoroughly with DCM and dried. The column was then replaced, the desired PNA-sequence was synthesized, and the N-terminal BZBA conjugation was performed as described above.

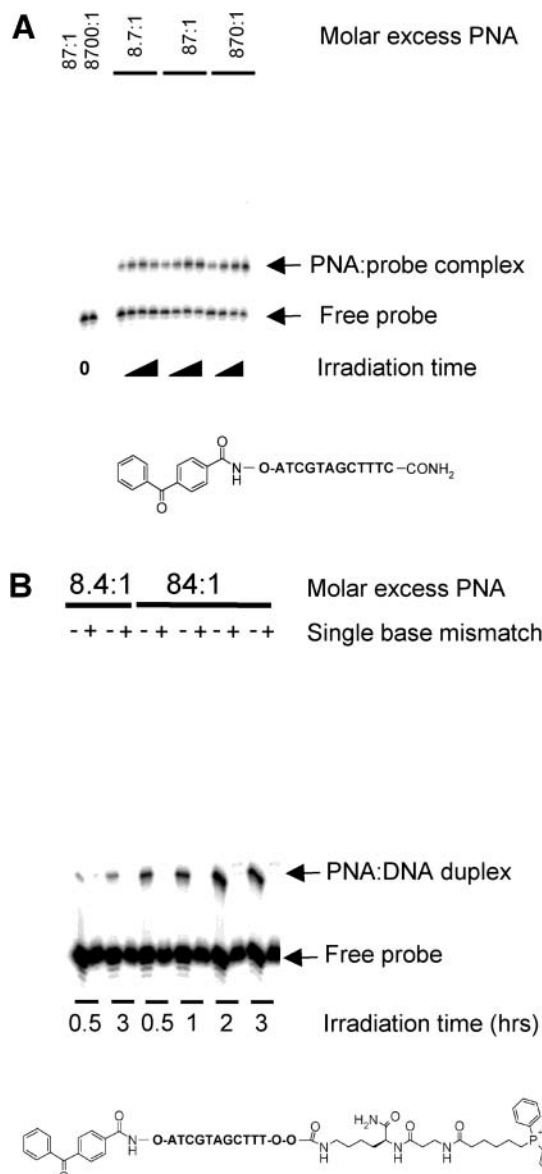
For deprotection and cleavage, dried resin carrying the PNA conjugates was transferred to a 0.2  $\mu$ m PTFE filtered microcentrifuge tube (Millipore Ultrafree-MC), TFA/*m*-cresol (200  $\mu$ L 4:1) added for 90 min and deprotected product released by centrifugation at 1200g for 5 min. Conjugates were precipitated by addition of diethyl ether and resuspended in 0.1% (v:v) TFA water prior to storage at  $-80^\circ\text{C}$ .

**Analysis and Purification of PNA Conjugates.** PNA conjugates were subjected to reverse phase HPLC on a  $C_4$  analytical column (Jones Chromatography) at a column temperature of  $55^\circ\text{C}$ . A linear gradient water/0.1% (v:v) TFA - 80% (v:v) acetonitrile/0.1% (v:v) TFA was used at a flow rate of 1 mL/min. After preparative runs,

the collected fractions were dried down in a vacuum desiccator or by blowing nitrogen over the solvent surface in a heat block at 55 °C. MALDI-TOF MS analysis of the PNA conjugates was carried out by N. Harris (Moredun Research Institute, Edinburgh) from a 4-hydroxy-3,5-dimethoxycinnamic (sinapinic) acid matrix. The correct product was considered to be confirmed if the difference between the measured and the calculated mass did not exceed 0.1%. Concentrations of PNA derivatives were calculated from measuring the optical absorbance at 260 nm (1-cm light path, 55 °C). For the PNA monomers, the established extinction coefficients given in the Expedite 8909 PNA manual were used. For the CPTTP monomer, an extinction coefficient of 3 mM<sup>-1</sup> cm<sup>-1</sup> was assumed (IBTP: 3 mM<sup>-1</sup> cm<sup>-1</sup>, 268 nm, ethanol (17)), for the BZBA unit 17 mM<sup>-1</sup> cm<sup>-1</sup> (benzophenone: 17.6 mM<sup>-1</sup> cm<sup>-1</sup>, 252 nm, ethanol (18)).

**Photo-Cross-Linking Experiments.** A 32-mer oligodeoxynucleotide (ODN) 5'-T<sub>10</sub>GAAAGCTACGAT<sub>10</sub>-3' carrying the internal sequence complementary to the PNA, was end-labeled by T4 polynucleotide kinase (Promega) and [<sup>32</sup>P]-ATP (3000 Ci mmol<sup>-1</sup> Amersham Pharmacia) following standard protocols, with unincorporated nucleotide removed using a YM3 spin column (Millipore). For part of the experiment described in Figure 2b, a similar protocol was used with a mismatched ODN containing a T-C substitution at position 17. Varying amounts of PNA were added to 0.1 pmol of ODN (of which 15 fmol was radiolabeled) in PBS, total volume 5 μL. Samples were heated to 37 °C for 5 min and then irradiated at 20 °C with a UV light source (Hybec H600 PUVA phototherapy unit) to deliver 5.1 mW cm<sup>-2</sup> for the indicated times. The light source was filtered by window glass to give a wavelength range of 330–400 nm, removing 99.984% of the total irradiance below 320 nm and 99.9985% below 315 nm. For the specificity experiments using matched and mismatched probes, samples were overlaid with mineral oil and irradiated at 37 °C in a heated water bath. Samples were denatured in 95% formamide and resolved on 16% (w:v) 19:1 polyacrylamide 8 M urea denaturing gel. Dried gels were exposed to a PhosphorImager cassette (Molecular Dynamics) and analyzed using ImageQuant software (Molecular Dynamics). Efficiency of the production of the ODN/PNA monomer following cross-linking was calculated by measuring the counts of the slower migrating species, C (PNA covalently attached to complementary oligomer), and of the faster migrating species, F (free oligo), and expressing C as a percentage of total counts, C + F. Where irradiation caused the production of large complexes, all multimers were counted together, and the counts were expressed as a percentage of the total. Table 1 records single calculations, but a sample of repeat experiments gave results entirely consistent with the reported percentages.

**Thermal Melt Analysis.** Thermal melt profiles were obtained using 1 μM of the ODN and PNA derivatives in 20 mM Tris-HCl, pH 7.5, 10 mM MgCl<sub>2</sub>, 14 mM β-mercaptoethanol, and 150 mM KCl. Mixtures were heated to 90 °C and allowed to anneal by slow cooling to room temperature. The mixture was split into two cuvettes (sample and reference). Melt profiles were measured at 260 nm using a Lambda Bio 20 UV/Visible spectrophotometer (Applied Biosystems, Cheshire UK); the temperature of the sample cuvette was modulated by a PTP-1 Peltier System (Applied Biosystems, Cheshire UK). Data were collected and analyzed using TempLab software (PE-Biosystems, Cheshire UK). Samples were heated at a rate of 0.5 °C min<sup>-1</sup>, and the sigmoidal melt curve was



**Figure 2.** Trifunctional PNA derivatives can be designed to bind irreversibly to DNA templates and to retain sequence selectivity. (A) Photo-cross-linking of a PNA/DNA complex can be induced by irradiation of a PNA conjugated to benzophenone. Molecule **1** was incubated with the ODN probe at the indicated molar excesses and irradiated as detailed in Experimental Procedures. In all cases, a single photo-cross-linked product is generated. Irradiation dosage increases from 18 to 72 J cm<sup>-2</sup>. Molecule **1** is represented under the gel. (B) Specificity of binding can still be retained by a trifunctional PNA derivative. Molecule **2b** carrying a mitochondrial targeting moiety and benzophenone was incubated with one of two ODN probes differing by a single base, as indicated. Specificity is retained at substantial molar excess, although nonspecific multimeric reaction products are noted at the higher molar concentrations. Molecule **2b** is represented under the gel.

expressed as the first derivative ( $\Delta A_{260}/\text{time}$  against unit time) to provide an accurate measurement of the melting temperature.

## RESULTS AND DISCUSSION

PNA-conjugates synthesized (Figure 1) had the sequence (N-terminal, 5')ATCGTAGCTTTC(C-terminal, 3') (molecules **1**, **2a**, and 12-mer in Table 1) or the same sequence lacking the C-terminal base (**2b** or 11-mer in Table 1). They are identical to nt12621–12632 of the rat mitochondrial genome L-strand (19). Once made, the



**Table 1. Efficiency of Cross-linking between PNA Derivative and Complementary DNA**

PNA	mass	$T_m$ (°C)	% DNA cross-linked monomer (multimer) <sup>a</sup>											
			X <sup>b</sup> : 1 PNA/DNA irradiation time (h)				10X: 1 PNA/DNA irradiation time (h)				100X: 1 PNA/DNA irradiation time (h)			
			1	2	3	4	1	2	3	4	1	2	3	4
12-mer	2923.81	54.0 ± 0.1												
1	3588.23	54.8 ± 0.1	14	31	38	45	20	41	57	61	20	42	60	64
2a	4436.96	56.9 ± 0.1	23	35	41	47	21	35	48	45	20(42)	12(49)	8(73)	8(74)
11-mer	3235.05	51.4 ± 0.3												
2b	2923.81	54.6 ± 0.4	29	34	49	37	22	34	50	55	23(9)	32(14)	36(34)	37(32)

<sup>a</sup> Samples of end-labeled oligodeoxynucleotide were mixed with the indicated molar excess of PNA derivative and irradiated at room temp for 1–4 h as shown. The percentage of single PNA/DNA complex or multimers were calculated as described in the Experimental Procedures. <sup>b</sup> X is defined as 8.7 for PNA **1**, 8.5 for **2a**, and 8.4 for **2b**.

constructs were assessed to determine whether conjugation had affected the physical characteristics of the PNA moiety and to determine the efficiency of UV-induced photo-cross-linking (gel retardation assays).

**A Benzoylbenzoic Acid PNA Conjugate Cross-Links to Single-Stranded DNA following UV Irradiation.** In this study, we decided to use the benzophenone system as a photoreactive cross-linker for several reasons. Benzophenone derivatives have extensively been used in protein, nucleic acid, and lipid biochemistry for functionalization, labeling, and cross-linking purposes (20). Upon irradiation with UV light, the benzophenone system reaches an  $n,\pi^*$  diradicaloid triplet state. Thymidine nucleosides are excellent reaction partners for this highly reactive intermediate, as two different sites are available for cross-linking reactions. The 5,6 C=C bond can be attacked in a [2+2] cycloaddition (Paterno-Buchi reaction) leading to the formation of oxetanes (21, and refs therein). Aliphatic C–H bonds of the DNA backbone are available for C–H insertion reactions; however, we found very low level photo-cross-linking efficiencies were observed using ODN partners flanked with polyguanosine residues, confirming the importance of the cycloaddition (data not shown). For the cross-linking experiments, we have therefore used ODNs complementary in sequence to the PNA and flanked by polythymidine stretches, which is also similar to the natural mtDNA sequence that flanks the PNA target site. The excited triplet state of benzophenone has an estimated lifetime of 80–120  $\mu$ s; if no suitably orientated reaction partner is found during this time, relaxation to the ground state occurs (22). The cycle of excitation–relaxation can be repeated many times until a reaction takes place. Thus, benzophenone compounds generally allow much higher yields in cross-link reactions than compounds that are only monoexcitable in a photodissociative way, such as aryl azides or diazo compounds (23). The wavelength required for the excitation of the benzophenone is about 350–360 nm. Thus, photochemical damage to DNA and proteins, which mostly occurs at shorter wavelengths, is limited.

Initially, the benzophenone–PNA conjugate **1** was synthesized. Benzophenone was linked to the N-terminal of the PNA as a benzoylbenzoic acid amide that can be assembled easily using the amine-reactive BZBA–NHS ester. One 8-amino-3,6-dioxaoctanoic acid (AEEA) linker molecule (**O**, Figure 1) was inserted between the PNA and the benzophenone to provide maximum access of the photo-cross-linker to reactive sites and avoid interference with PNA/DNA hybridization.

To assess the potential problems associated with the generation of nonspecific photo-cross-linking, studies were performed with varying molar excesses of the PNA

derivative as shown in Figure 2a. Irradiation of the ODN probe in the presence of the PNA species results in the production of a PNA/DNA duplex that is retarded in the denaturing gel (Figure 2a). Under all conditions, molecule **1** exclusively created a single cross-linked product. With an 87-fold molar excess of the PNA and an increasing dose of UVA irradiation from 18 to 72 J cm<sup>−2</sup>, the percentage of cross-linked ODN probe increased from 20 to 61% without the generation of nonspecific multiple adducts (Table 1).

**Conjugation of PNA with Benzophenone and TPP Moieties in Maximum Spatial Distance Promotes High Efficiency of Photo-Cross-Linking and Binding Specificity.** Building on the positive results with molecule **1**, the N-terminal benzoylbenzoic acid amide was chosen as the cross-linker for the generation of trifunctional PNAs. Synthesis of a variety of PNA derivatives carrying both the TPP and benzophenone moieties at the N-terminus produced molecules that showed nonspecific binding to ODNs and a UV-induced production of DNA/PNA multimers (data not shown).

To prevent the abundant formation of multiple adducts, a maximum distance between benzophenone and TPP was necessary. Thus, TPP was conjugated to the C-terminal of the PNAs **2a,b**. *N*- $\alpha$ -Fmoc-*N*- $\epsilon$ -MMT-L-lysine provides two orthogonally protected amino functions that can be manipulated independently. After the attachment of the amino acid to the resin, the  $\alpha$ -nitrogen was deprotected, followed by the addition of  $\beta$ -alanine and CPTPP. The  $\beta$ -alanine facilitates the automated assembly of CPTPP because its  $\beta$ -amino function is more reactive than the  $\alpha$ -amino function of lysine. After the assembly of the TPP-carrying moiety, the  $\epsilon$ -amino function of the lysine was liberated by mild acidolytic removal of the MMT-group using the medium-strength chloroacetic acid. Subsequently, the PNA sequence was synthesized and the N-terminal BZBA was added. The molecules **2a,b** differ only in the length of their PNA sequence. The TPP is therefore positioned distal to an  $\epsilon$ -amino and two added spacers at the C-terminal of the molecule, with benzophenone on the N-terminal.

Following confirmation of synthesis by MALDI-TOF analysis, thermal melt assays were conducted to assess the effect on the binding affinity of the molecules. Both molecules formed a PNA/DNA complex with a slightly elevated  $T_m$  than the underivatized PNA of similar length (Table 1), possibly due to the addition of the caged positive charge from the TPP. To determine their cross-linking capabilities, assays were performed as previously described. **2a** showed increased cross-linking efficiency at both 8.5:1 and 85:1 molar ratios when irradiation doses were increased (18–72 J cm<sup>−2</sup>, Table 1). Molecule **2b** also showed similar increases under identical conditions, but

the percentage of monospecific cross-link remained the major product, even in the presence of large (840-fold) molar excess of PNA.

To evaluate mismatch discrimination, molecule **2b** was tested with matched ODN probe as well as ODN carrying a single mismatch in the middle of the target sequence and was performed under physiological temperatures. As shown in Figure 2b, molecule **2b** retains an impressive selectivity even when measured with high (84-fold) molar ratios of PNA derivative, although longer irradiation times and greater PNA molar excess do begin to induce multicomplexes (data not shown). As the long term aim of this project is only to modulate the levels of heteroplasmy, this marked selectivity would appear to be ideal for such purposes.

In summary, we have been able to design and synthesize a trifunctional molecule that retains specificity of binding and efficient cross-linking after irradiation. We now intend to assess this molecule in isolated organelles and cultured cells to determine whether covalent attachment is sufficient to inhibit the de novo synthesis of mtDNA and to investigate the potential of other PNA derivatives as efficient antigenomic molecules.

#### ACKNOWLEDGMENT

R.N.L. and D.M.T. wish to thank the Wellcome Trust for funding this project (Programme Grant 056605).

#### LITERATURE CITED

- (1) Chinnery, P. F., and Turnbull, D. M. (1999) Mitochondrial DNA and disease. *Lancet* 354 (Suppl. 1), 117–121.
- (2) DiMauro, S., Bonilla, E., Davidson, M., Hirano, M., and Schon, E. (1998) Mitochondria in neuromuscular disorders. *Biochim. Biophys. Acta* 1366, 199–210.
- (3) Chinnery, P. F., Johnson, M. A., Wardell, T. M., Singh-Kler, R., and Hayes, C., et al. (2000) The epidemiology of pathogenic mitochondrial DNA mutations. *Ann. Neurol.* 48, 188–193.
- (4) Chomyn A., Martinuzzi A., Yoneda M., Daga A., Hurko O., et al. (1992) MELAS mutation in mtDNA binding site for transcription termination factor causes defects in protein synthesis and in respiration but no change in levels of upstream and downstream mature transcripts. *Proc. Natl. Acad. Sci. U.S.A.* 89, 4221–4225.
- (5) Boulet, L., Karpatis, G., and Shoubridge, E. A. (1992) Distribution and Threshold Expression of the tRNA<sup>lys</sup> Mutation in Skeletal Muscle of Patients with Myoclonic Epilepsy and Ragged Red Fibres (MERRF). *Am. J. Hum. Genet.* 51, 1187–1200.
- (6) Chrzanowska-Lightowlers, Z. M., Lightowlers, R. N., and Turnbull D. M. (1995) Gene therapy for mitochondrial DNA defects: Is it possible? *Gene Ther.* 2, 311–316.
- (7) Taylor, R. W., Chinnery, P. F., Clark, K. M., Lightowlers, R. N., and Turnbull, D. M. (1997) Treatment of mitochondrial disease. *J. Biomembr. Bioenerg.* 29, 195–205.
- (8) Demidov, V. V., Protozanova, E., Izvol'sky, K. I., Price, C., Nielsen, P. E., and Frank-Kamenetski, M. D. (2002) Kinetics and mechanism of the DNA double helix invasion by pseudocomplementary peptide nucleic acids. *Proc. Natl. Acad. Sci. U.S.A.* 99, 5953–5958.
- (9) Egholm, M., Buchart, O., Christensen, L., Behrens, C., and Freier, S. M., et al. (1993) PNA hybridizes to complementary oligonucleotides obeying the Watson–Crick hydrogen-bonding rules. *Nature* 365, 566–568.
- (10) Orum, H., Nielsen, P. E., Egholm, M., Berg, R. H., Buchardt, O., and Stanley, C. (1993) Single base pair mutation analysis by PNA directed PCR clamping. *Nucleic Acids Res.* 21, 5332–5336.
- (11) Demidov, V. V., Potaman, V. N., Frank-Kamenetskii, M. D., Egholm, M., Buchardt, O., et al. (1994) Stability of peptide nucleic acids in human serum and cellular extracts. *Biochem. Pharmacol.* 48, 1310–1313.
- (12) Taylor, R. W., Chinnery, P. F., Turnbull, D. M., and Lightowlers, R. N. (1997) Selective inhibition of mutant human mitochondrial DNA replication in vitro by peptide nucleic acids. *Nat. Genet.* 15, 212–215.
- (13) Muratovska, A., Lightowlers, R. N., Taylor, R. W., Turnbull, D. M., Smith, R. A. J., et al. (2001) Targeting of peptide nucleic acid (PNA) oligomers to mitochondria within cells by conjugation to lipophilic cations: implications for mitochondrial DNA replication, expression and disease. *Nucleic Acids Res.* 29, 1852–1863.
- (14) Kosaganov, Y., Stetsenko, D., Lubyako, E., Kvitko, N., Lazurkin, Y., and Nielsen, P. E. (2000) Effect of temperature and ionic strength on the dissociation kinetics and lifetime of PNA-DNA triplexes. *Biochemistry* 39, 11742–11747.
- (15) Casale, R., Jensen, I., and Egholm, M. 1999. Synthesis of PNA oligomers by Fmoc chemistry. In *Peptide Nucleic Acids: Protocols and Applications* (P. E. Nielsen, M. Egholm, Eds.) pp 39–50, Horizon Scientific Press, Wymondham, UK.
- (16) Dubowchik, G., and Radia, S. (1997) Monomethoxytrityl (MMT) as a versatile amino protecting group for complex prodrugs of anticancer compounds sensitive to strong acids, bases and nucleophiles. *Tetrahedron Lett.* 38, 5257–5260.
- (17) Coulter, C. V., Kelso, G. F., Lin, T.-K., Smith, R. A. J., and Murphy, M. P. (2000) Mitochondrially targeted antioxidants and thiol reagents. *Free Rad. Med. Biol.* 28, 1547–1554.
- (18) Perkampus H.-H. (1992) *UV-Vis Atlas of Organic Compounds*, VCH, Weinheim, Germany.
- (19) Gadaleta, G., Pepe, G., De Candia, G., Quagliariello, C., Sbisà, E., and Saccone, C. (1989) The Complete Nucleotide Sequence of the *Rattus norvegicus* Mitochondrial Genome: Cryptic Signals Revealed by Comparative Analysis between Vertebrates. *J. Mol. Evol.* 28, 497–516.
- (20) Dorman, G., and Prestwich, G. (1994) Benzophenone photophores in biochemistry. *Biochemistry* 33, 5661–5673.
- (21) Nakatani, K., Yoshida, T., and Saito, I. (2002) Photochemistry of benzophenone immobilised in a major groove of DNA: formation of thermally reversible interstrand cross-link. *J. Am. Chem. Soc.* 124, 2118–2119.
- (22) Prestwich, G., Dorman, G., Elliott, J., Marecak, D., and Chaudhary, A. (1997) Benzophenone photoprobes for phosphoinositides, peptides and drugs. *Photochem. Photobiol.* 65, 222–234.
- (23) Brunner, J. (1993) New photolabeling and cross-linking methods. *Annu. Rev. Biochem.* 62, 483–514.

BC034050F

# Michael-Type Addition as a Tool for Surface Functionalization

Martin Heggli,<sup>§</sup> Nicola Tirelli,<sup>\*,†,‡</sup> Andreas Zisch,<sup>†</sup> and Jeffrey A. Hubbell<sup>†</sup>

Institute for Biomedical Engineering and Department of Materials, Swiss Federal Institute of Technology (ETH) and University of Zurich, Moussonstrasse 18, CH-8044 Zurich, Switzerland, School of Pharmacy and Pharmaceutical Sciences, University of Manchester, Coupland III, Coupland Street/Oxford Road, M13 9PL Manchester, United Kingdom, and Institute for Polymers and Department of Materials, Swiss Federal Institute of Technology (ETH), Universitätstrasse 6, CH-8092 Zurich, Switzerland Received April 23, 2003; Revised Manuscript Received July 23, 2003

Michael-type addition (conjugate addition reaction between electron-poor olefins and nucleophiles, such as thiols) has been successfully used as a convenient tool for surface functionalization. Due to its mild character, this method is potentially useful for the introduction of sensitive groups, which can provide bioactivity and targeting possibilities to surfaces of, for example, colloidal carriers. As reaction partners, in our study we have used thiols, possibly present in peptidic structures, and acrylates, at the end of protein-repellant PEG chains. Satisfactory results were obtained with thiols in solution and acrylic groups bound to the surface. Alternatively, the use of thiols on the particles, even if generated in situ, did not provide useful results.

## INTRODUCTION

The surface modification of organic or inorganic materials can drastically change their interactions with an external biological environment; for example, with the introduction of appropriate chemical functionalities it is indeed possible to render them virtually invisible to biological agents ("stealth" objects) or to characterize them with a specific biological function (recognition, adhesion, release). These possibilities have been extensively used in a variety of applications ranging from the biocompatibilization of implants (1–3), to the preparation of tailor-made scaffolds for cells (4, 5), or of high signal-to-noise biosensors (6, 7).

A number of techniques has been employed for the purpose of the modification of the surface chemical composition: chemical reactions (8–12), often photoactivated (13, 14) or with a preliminary surface priming stage (e.g. silanization of an inorganic support (15)), surface phase segregation (16), chemisorption (17), or physisorption methods (10, 18), such as polyelectrolyte complexation onto charged surfaces and amphiphilic polymers absorption on hydrophobic ones (19, 20).

We have recently focused our attention onto Michael-type addition, a reaction traditionally used for the chemical modification of bioactive substances, e.g. conjugation of peptides with polymeric substrates, such as PEG (21, 22); more recently, it has also been exploited for the preparation of biofunctional hydrogels (23). The strong points of this reaction are numerous: first, its mild character and high yield in physiological conditions; second, by the use of thiols there is little competition with

naturally occurring nucleophiles: free (reduced) thiols are present in negligible concentration in a biological, extracellular environment and react faster than the most common groups (amines, alcohols, phenols) (23); at the same time, side reactions are virtually absent. Last, Michael-type addition is pH-sensitive, because deprotonated thiols are the active species (22); this allows a fine control of the reaction kinetics either with the environmental pH or with the  $pK_a$  of the nucleophile.

Despite the appealing features of this chemistry, to our knowledge yet no report exists about the use of Michael-type addition for surface functionalization. On the contrary, we believe this reaction to be of considerable interest for the surface modification of both macroscopic objects (implants, surgical instruments) and colloidal ones (drug carriers); this would complement a recent study by us (24), where surface-initiated polymerization has been developed for similar scopes, and at the same time will provide tools for the functionalization of new stimuli-responsive vesicles (25) and nanoparticles (26).

In this study we have used macroscopic beads ( $\varnothing = 10\text{--}200\ \mu\text{m}$ , see Table 1) as a model system for later application to virtually any kind of surfaces. The advantages offered by macroparticles are that they are better amenable to spectroscopical analysis than most surfaces of macroscopic objects and can be isolated, manipulated, and purified easier (e.g., by simple filtration) than any colloidal objects.

We have selected macroparticles of hydrophobic nature (cross-linked poly(styrene) (PS)), in some cases containing poly(ethylene glycol) (PEG), too. In this way they offer an acceptable model also for the surface composition and reactivity of many polymeric biomaterials: most polymers used in biomaterials applications are indeed hydrophobic, but often display a hydrophilic surface (see, for example, segmented polyurethanes, Tissue Culture PolyStyrene, gas plasma-treated polymers, such as Dacron and Teflon (27, 28), and others).

These macroparticles display nucleophilic groups such as alcohols or amines, which, differently from the systems that they should mimic, are homogeneously dispersed

\* To whom correspondence should be addressed, tel. +41 1 632 63 48, fax +41 1 632 12 14, e-mail tirelli@biomed.mat.ethz.ch or nicola.tirelli@man.ac.uk.

<sup>†</sup> Institute for Biomedical Engineering and Department of Materials, Swiss Federal Institute of Technology (ETH) and University of Zurich.

<sup>‡</sup> University of Manchester.

<sup>§</sup> Institute for Polymers and Department of Materials, Swiss Federal Institute of Technology (ETH) and University of Zurich.



**Table 1. Macroparticles Characterization Data**

particle (composition, supplier)	size <sup>a</sup> [ $\mu$ m]	modification	concentration of reactive groups <sup>b</sup> [mmol/g]	concentration of reactive groups <sup>c</sup> [mmol/g]
A (PS AM-NH <sub>2</sub> , Fluka)	160–200	amine	0.8–1.2	1.26
B (PS AM-NH <sub>2</sub> , Rapp)	2.8 (noncommercial) or 10 <sup>d</sup>	amine	0.84	0.93
C (PS AM-S-Trityl, Fluka)	65–130	S-Trityl	0.6–0.8	— <sup>e</sup>
D (PS-PEG, Fluka)	200	grafted PEG 600 OH	0.35	0.48
E (PS-PEG, Rapp)	10	grafted PEG 3000 OH	0.25	0.26

<sup>a</sup> Supplier data. <sup>b</sup> Supplier data. <sup>c</sup> Calculated from nitrogen elemental analysis for particles A, B, and C, or from TGA for particles D and E (first weight loss associated to PEG degradation). <sup>d</sup> The functionalization has been attempted on particles with two different diameter ranges, with similar results; in the paper we report the data for 2.8  $\mu$ m particles. <sup>e</sup> Not measured.

throughout the material. However, they still offer a valid model: the key step of the functionalization is performed in water, where the particles are not swollen; the reactive groups are therefore at an interface between hydrophobe and water solution, that is in the same conditions as in a water-exposed polymeric surface.

In the present study, we have compared two strategies for the use Michael-type addition, both aiming to generate a PEGylated surface (as a base for antifouling substrates) decorated with peptidic groups: (1) generation of thiols on the poly(styrene) surface of non-PEGylated particles; reaction of thiols with an excess PEG diacrylate (first Michael-type addition) and use of the excess acrylates for conjugation of a thiol-containing peptide (second Michael-type addition). (2) acrylation of a PEGylated particle and conjugation with a thiol-containing peptide.

#### EXPERIMENTAL SECTION

**Materials.** Solvents and reagents were purchased from Fluka (Buchs, Switzerland) and used without further purification unless otherwise specified. The particles were purchased from Fluka or kindly donated by Rapp Polymere (Tübingen, Germany).

**Acronyms:** SPDP (*N*-succinimidyl 3-(2-pyridyldithio)propionate), DTT (dithiotreitol), TCEP-HCl (tris-carboxyethylphosphine hydrochloride), PBS (phosphate buffer saline, 10 mM, pH = 7.4), MVPI (*N*-methyl-4-vinylpyridinium iodide), NMP (*N*-methylpyrrolidone), PEGDA (poly(ethylene glycol) diacrylate).

**Physicochemical Methods.** <sup>1</sup>H and <sup>13</sup>C NMR spectroscopy, already used for the characterization of PS-PEG particles (29), did not provide satisfactory results (too broad lines for the first technique, too poor sensitivity for the second one); infrared spectroscopy demonstrated enough sensitivity to be chosen as analytical tool. FT-IR spectra were recorded in ATR mode on a Spectrum One Perkin-Elmer spectrometer. ATR spectroscopy has a penetration depth of the order of magnitude of a micron; the results of quantitative IR analysis refer therefore only to an external shell of the particles. However, we assume these data to be representative of the overall (and bulk) composition of the particles, when dealing with reactions involving the diffusion of low molecular weight components.

Thermogravimetric analysis was performed on a Perkin-Elmer TGA 7 at a heating speed of 10 °C/min under nitrogen atmosphere (in order to reduce polystyrene oxidative degradation).

**Peptide Synthesis.** The 13 amino acids peptide was derived from the C-terminus fragment of Platelet Factor 4 (PF4) with the addition of a cysteine (*N*-acetyl-G-C-P-L-Y-K-K-I-I-K-K-L-L-E-S); the synthesis was performed by solid-state chemistry on resin using an automated peptide synthesizer (Perceptive Biosystems, Farmington, MA), with standard 9-fluorenylmethoxycarbonyl chem-

istry (30) and purified by C18 chromatography (Perceptive Biosystems Biocad 700E).

**Particle Characterization.** *Nitrogen elemental analysis* showed a 1.76 wt % or a 1.3 wt % nitrogen content of amine-functionalized Fluka particles (particles A, see Table 1) or Rapp particles (particles B), respectively, corresponding to 1.26 mmol/g or 0.93 mmol/g of amine groups, respectively.

The functionalization degree of S-trityl functionalized particles (particles C, see Table 1) was not investigated.

*Thermogravimetric analysis* on the PEG-containing particles showed a 29 wt % PEG content in the Fluka particles (particles D, see Table 1) and 62 wt % in the Rapp ones (particles E). Assuming PEG molecular weight to be 600 and 2500, respectively, according to the supplier indications, we have calculated functionalization degrees of 0.48 mmol/g and 0.26 mmol/g. The suppliers provided values of 0.35 mmol/g and 0.25 mmol/g, respectively.

*FT-IR.* Bead A: 3058 and 3025 ( $\nu$  aromatic C–H), 2920 and 2846 ( $\nu$  CH<sub>2</sub> and CH polystyrene), 1601, 1492, and 1452 ( $\nu$  aromatic ring), 1245, 1028, 742, 695 cm<sup>−1</sup>.

Bead B: 3058 and 3025 ( $\nu$  aromatic C–H), 2920 and 2847 ( $\nu$  CH<sub>2</sub> and CH polystyrene), 1601, 1492, and 1452 ( $\nu$  aromatic ring), 1028, 756, 697 cm<sup>−1</sup>.

Bead C: 3058 and 3025 ( $\nu$  aromatic C–H), 2920 and 2846 ( $\nu$  CH<sub>2</sub> and CH polystyrene), 1676 ( $\nu$  amidic C=O), 1601, 1492, and 1452 ( $\nu$  aromatic ring), 1245, 1028, 742, 695 cm<sup>−1</sup>.

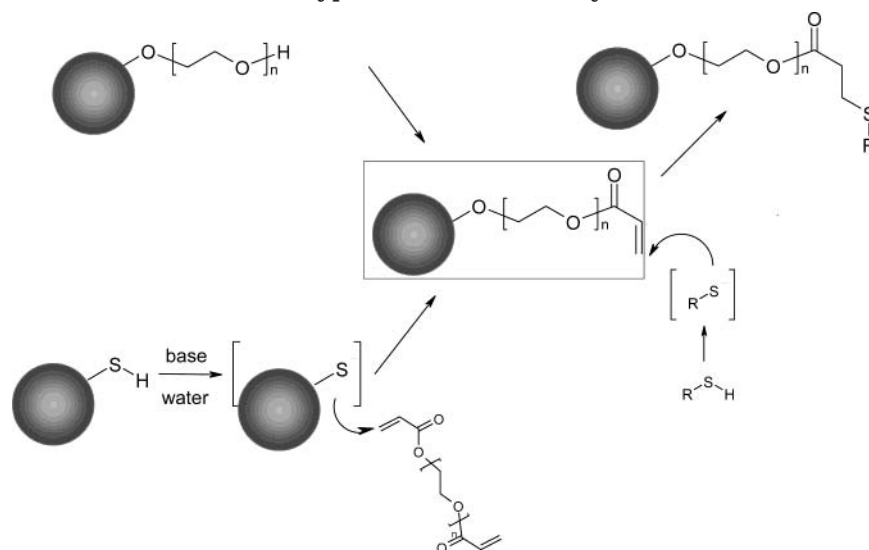
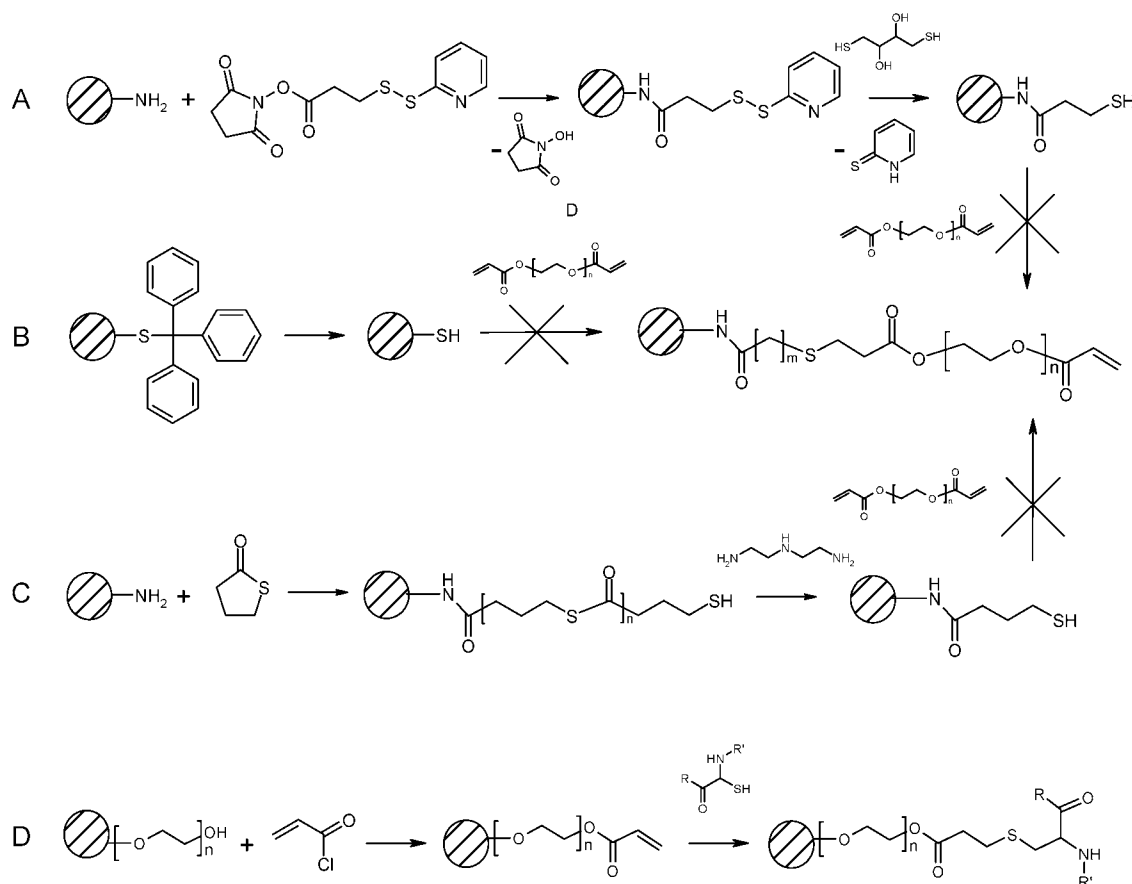
Bead D: 3500 ( $\nu$  N–H), 3058 and 3025 ( $\nu$  aromatic C–H), 2917 ( $\nu$  CH<sub>3</sub> polystyrene), 2863 ( $\nu$  CH<sub>2</sub> PEG), 1601, 1492 and 1452 ( $\nu$  aromatic ring), 1246, 1098 ( $\nu$  C–O), 845, 820, 760, 695 cm<sup>−1</sup>.

Bead E: 3500 ( $\nu$  O–H), 3058 and 3025 ( $\nu$  aromatic C–H), 2880 ( $\nu$  CH<sub>2</sub> PEG), 1601, 1492, and 1453 ( $\nu$  aromatic ring), 1466, 1342, 1280, 1246, 1100 ( $\nu$  C–O), 962, 842, 760, 699 cm<sup>−1</sup>. The absence of some polystyrene bands is coherent with a high PEG content measured in thermogravimetric analysis.

**Particle Derivatization.** The description of the reactions is followed by a list of IR peaks for a generic characterization of the product and then by a description of the analytical method for the quantification of the reaction products.

The isolation was generally performed centrifugating the particles at 14 krpm, removing the supernatant and adding another portion of solvent, vortexing with a final filtration of the solid material.

**Preparation and Use of Thiol-Displaying Particles. Thiol Generation. Beads A/B, Scheme 2A.** 20 mg particles were dispersed in 0.5 mL of solvent (THF and NMP gave equivalent results) and mixed by sonication with a solution of 2 equiv of SPDP (15 mg in 1 mL of solvent). The suspensions were stirred at room temperature for 1 h, and the particles were then filtered and washed twice in the solvent used for the reaction. In the second step pyridine-2-thione was released by treatment

**Scheme 1. Strategies for the Use of Michael-type Addition onto PEGylated Surfaces****Scheme 2. Different Approaches Used for Generation of Thiols on the Macroparticles and Successive PEGylation**

with a solution of DTT in PBS (equimolar to the amount of amine groups on the particles and hence to the maximum possible amount of SPDP present). After 15 min the particles were filtered and washed three times with PBS and immediately used for the coupling of PEGDA.

FT-IR: 3290 ( $\nu$  amidic N-H), 3058 and 3025 ( $\nu$  aromatic C-H), 2920 and 2846 ( $\nu$  CH<sub>2</sub> and CH polystyrene), 1673 ( $\nu$  amidic C=O), 1601, 1492, and 1452 ( $\nu$  aromatic ring), 1245, 1028, 742, 695 cm<sup>-1</sup>.

**Quantitative Analysis Tool.** The absorption of the solution at 342 nm (pyridine-2-thione;  $\epsilon_{342} = 8.08 \times 10^3$

M<sup>-1</sup>cm<sup>-1</sup>) is related to the deprotection yield; it reached a maximum after 15 min, corresponding for both particles A and B to a 95% conversion of amines into deprotected thiols.

**Thiol Generation. Beads A/B, Scheme 2C.** Ten milligrams of particles was dispersed in 0.5 mL of THF. A solution of 15 equiv of  $\gamma$ -thiobutyrolactone (18 mg in 0.5 mL THF) was added, and the mixture was sonicated for 10 min. The reaction was then left at room-temperature overnight. After being filtered, the particles were washed three times with THF and then treated with diethylene triamine in an amount equimolar to the

$\gamma$ -thiobutylolactone used in the first step (20  $\mu$ L of diethylene triamine) for 1 h. The particles were then washed three times with THF and immediately used for the coupling of PEGDA or of MVPI.

FT-IR (bead B): 3058 and 3025 ( $\nu$  aromatic C–H), 2920 and 2847 ( $\nu$  CH<sub>2</sub> and CH polystyrene), 1686 ( $\nu$  amidic C=O), 1601, 1492 and 1452 ( $\nu$  aromatic ring), 1028, 756, 697 cm<sup>-1</sup>.

**Quantitative analysis tool:** The concentration of thiol groups was estimated from the elemental analysis of iodine after coupling the thiols with a strong Michael-type acceptor, MVPI. Ten milligrams of particles was dispersed in 0.5 mL of NMP, and a solution of 40 mg of MVPI in NMP was prepared (0.16 mol/l); 76  $\mu$ L and 369  $\mu$ L of this solution were added to the suspensions of particles B and A, respectively (1.5 equiv). The mixture was sonicated and then stirred overnight, and then the particles were washed with NMP and twice with THF and then dried in a vacuum oven. The concentration of N and I was determined by the elemental analysis service of the Department of Chemistry, ETH Zürich. A 15% or 10% conversion of amines into deprotected thiols was recorded for particles A and B, respectively.

**Thiol Generation. Beads C, Scheme 2B.** Twenty milligrams of polystyrene AM-S-trityl microspheres was deprotected with a mixture of 950  $\mu$ L of trifluoroacetic acid (95%), 25  $\mu$ L of tris-isopropyl silane (2.5%), and 25  $\mu$ L of water (2.5%). After 2 h the deprotecting solution was removed, and the particles were washed twice with 1 mL of a solution of TCEP-HCl in PBS (pH = 8) at a concentration of 1 equiv of TCEP per thiol group. The particles were then redispersed in 0.5 mL of PBS-TCEP solution and directly used for the PEGylation reaction. No analytical tool for thiol determination was used in this case.

FT-IR: 3291 (3058 and 3025 ( $\nu$  aromatic C–H), 2920 and 2846 ( $\nu$  CH<sub>2</sub> and CH polystyrene), 1654 ( $\nu$  amidic C=O?), 1600, 1492, and 1452 ( $\nu$  aromatic ring), 1164, 1028, 742, 695 cm<sup>-1</sup>. Absence of the typical 2880 and 1100 cm<sup>-1</sup> PEG bands.

**PEGylation.** An excess of about 5 equiv PEGDA was dissolved in 0.5 mL of PBS or NMP and mixed with a suspension of 20 mg of thiol-functionalized particles in 0.5 mL of PBS or NMP. After 5 min, sonication the reaction was left at room temperature for 1 h. Then the particles were washed with PBS and three times with water.

FT-IR: absence or negligible presence of the typical Peg adsorptions at 2880 and 1100 cm<sup>-1</sup>.

**Reactions with Acrylate-Displaying Particles. Beads D/E, Scheme 2D. Acrylation.** Twelve milligrams of 2,6-di-*tert*-butyl-*p*-cresol was dissolved under dry argon in 15 mL of THF. Two hundred milligram particles were dispersed in the solvent and cooled in an ice–water bath. A 3-fold excess (compared to the hydroxy groups) of triethylamine (1.5 mL) was added. Acryloyl chloride (0.55 mL) (2 equiv) was finally added, and the suspension was stirred at 0 °C overnight.

After addition of 10 mL of water, the particles were sedimented by centrifugation. After filtration, the particles were washed three times with water and finally with ethanol to facilitate their drying.

FT-IR: 3500 ( $\nu$  O–H), 3058 and 3025 ( $\nu$  aromatic C–H), 2880 ( $\nu$  CH<sub>2</sub> PEG), 1723 ( $\nu$  ester C=O), 1601, 1492, and 1453 ( $\nu$  aromatic ring), 1466, 1342, 1280, 1246, 1100 ( $\nu$  C–O), 962, 842, 760, 699 cm<sup>-1</sup>.

**Quantitative Analysis Tool.** The  $\nu_{\text{O-H}}$  band (3500 cm<sup>-1</sup>) was normalized against the bands corresponding to  $\nu_{\text{C-H}}$  (2880 cm<sup>-1</sup>),  $\nu_{\text{C-O}}$  (1100 cm<sup>-1</sup>), and  $\delta_{\text{C-H}}$  (699

cm<sup>-1</sup>), which should be unchanged during the acrylation. The results were compared before and after the reaction:  $[\nu_{\text{O-H}}(\text{after})/\nu_{\text{O-H}}(\text{before})]_{\nu_{\text{C-H}}} = 54\%, 51\%$  and  $[\nu_{\text{O-H}}(\text{after})/\nu_{\text{O-H}}(\text{before})]_{\nu_{\text{C-O}}} = 47\%, 57\%$  for particles D and E, respectively. Averaging these values led to a  $51 \pm 2.3\%$  and  $55 \pm 2.5\%$  conversion of OH groups to acrylates, respectively, for particles D and E.

**Michael-Type Addition.** Ten milligrams of particles was dispersed in 0.5 mL of PBS. Twenty equivalents of cysteine (compared to the acrylic groups) was dissolved in 0.5 mL of PBS and added to the particle suspension. The addition of 1 equiv of TCEP-HCl (to keep cysteine in a reduced state) did not affect the yield of the reaction, as estimated from FT-IR.

After sonication, the suspension was shuttled overnight. The particles were then washed three times with water and finally with ethanol to facilitate their drying.

FT-IR: 3500 ( $\nu$  O–H), 3058 and 3025 ( $\nu$  aromatic C–H), 2880 ( $\nu$  CH<sub>2</sub> PEG), 1740–25 ( $\nu$  ester C=O), 1656 ( $\nu$  amide C=O, for peptide), 1621 and 1583 (cysteine adsorptions) 1601, 1492, and 1453 ( $\nu$  aromatic ring), 1466, 1342, 1280, 1246, 1100 ( $\nu$  C–O), 1029 (peptide adsorption), 962, 842, 760, 699 cm<sup>-1</sup>.

**Quantitative Analysis Tool.** The  $\nu_{\text{C=O}}$  band (1724 cm<sup>-1</sup>) of the acrylic ester showed a broadening after the reaction, due to the absorption of the saturated ester at 1735 cm<sup>-1</sup>. After deconvolution of the two peaks, the  $\nu_{\text{C=O}}$  absorption of the unsaturated esters was normalized against the band corresponding to  $\nu_{\text{C-H}}$  (2880 cm<sup>-1</sup>),  $\nu_{\text{C-O}}$  (1100 cm<sup>-1</sup>), and  $\delta_{\text{C-H}}$  (699 cm<sup>-1</sup>), and the obtained values were compared before and after the reaction. Values of  $65 \pm 2.8\%$  and  $9 \pm 2\%$  were obtained for the reaction of particles D or E with cysteine and the PF4-derived peptide, respectively.

## RESULTS AND DISCUSSION

Due to the ubiquitous use of PEGylated surfaces for ensuring long circulation times to colloidal carriers (31–33) and conferring antifouling properties to solid surfaces (34), we have chosen to work with PEG-displaying substrates.

More specifically, we have used PEG residues end-functionalized with acrylic groups, which were then reacted with thiols in a water environment; this reaction has been previously studied in detail, highlighting the role of thiolates as active species (23).

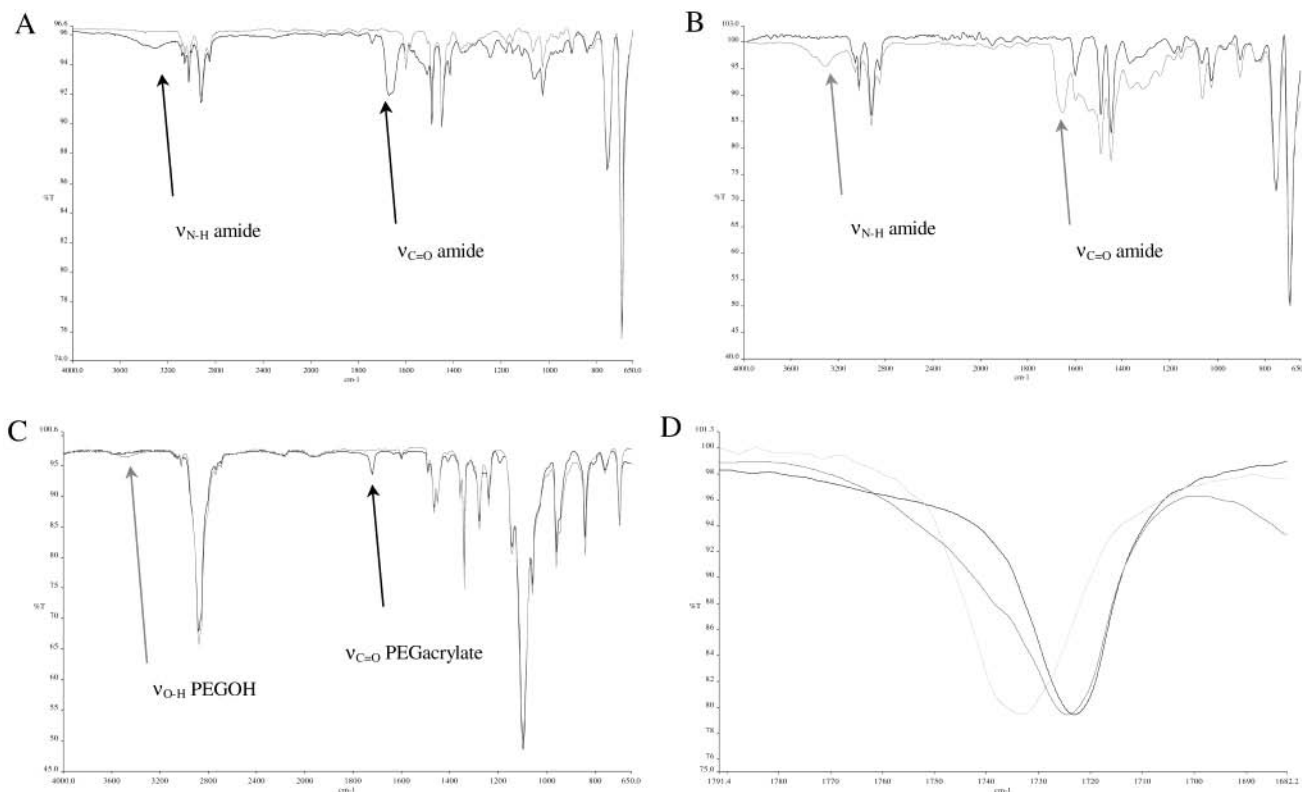
In a first approach, we have used non-PEGylated macroparticles and Michael-type addition was first exploited as a PEGylation reaction: thiols were generated on the substrate and reacted with a big excess of PEG diacrylate; in this way the polymer should mostly tethered only at one end and displays a reactive acrylate for the further functionalization step through a second Michael-type addition.

Within an alternative scheme, we have also used commercial PEG-containing particles; the PEG terminal OH groups were converted into acrylic esters and then coupled with a thiol-containing compound present in solution.

**Thiols on the Surface.** Qualitative results are reported hereafter for three synthetic strategies (Scheme 2A–C). In a first attempt, amine groups into thiols by the means of the reaction with an active ester containing a protected thiol (Scheme 2A,C).

*N*-Succinimidyl 3-(2-pyridylthio)propionate (SPDP) was reacted with both beads A and B to provide the corresponding amide (Scheme 2A; see IR spectra in Figure 1A), and then the thiol was reductively depro-





**Figure 1.** IR spectra of A: particles A before (grey) and after (black) SPDP functionalization. B: particles B before (black) and after (grey) thiobutylolactone functionalization. C: particles E before (grey) and after (black) acrylation. D: region of the ester peak for particles E after acrylation (right peak) and after Michael-type addition of cysteine (left peak) and PF4-derived peptide (broader peak), after normalization; the ester peak shifts or broadens depending on the functionalization degree.

ected by reaction with dithiothreitol (DTT). From the UV absorption of the released pyridine-2-thione, the deprotection reaction resulted almost quantitative for both particles A and B (95%). However, subsequent reaction of these thiol groups with PEG diacrylate did not lead to any detectable PEG incorporation into these particles, as revealed by the absence of  $\nu_{C-O-C}$  and  $\nu_{C=O}$  bands in IR analysis. Other methods, with potentially lower yields in thiol generation, were therefore used.

In another attempt, thiols were introduced by reacting  $\gamma$ -thiobutylolactone with the surface amine groups (Scheme 2C; see IR spectra in Figure 1B). The product of the thiolactone ring-opening polymerization was then cleaved by the reaction of a primary amine with the thioester chain, generating surface-bound thiols. The presence of amides and the absence of thioester bands in the IR spectrum after the reaction was interpreted as a sign of the quantitative thiol generation. For their analytical determination, the thiols were reacted with a powerful thiol scavenger, *N*-methyl-4-vinylpyridinium iodide; after Michael-type addition onto this compound the thiol groups were determined through the elemental analysis of iodine: they corresponded to 15% or 10% of the initial amine groups for particles A and B, respectively. After the reaction with PEG diacrylate, only traces of PEG incorporation were detected in IR spectra (weak absorption at  $1100\text{ cm}^{-1}$  ( $\nu_{C-O-C}$ ),  $\nu_{C=O}$  not detected).

A third approach, based on the use of commercial particles containing trityl-protected thiols (particles C), showed also no PEGylation (Scheme 2B).

**Thiols in Solution.** An alternative strategy for the use of Michael-type addition made use of PEGylated particles (beads D and E: cross-linked poly(styrene)-*gr*-PEG) on which acrylic groups were introduced by reaction with acryloyl chloride. The knowledge of PEG molecular

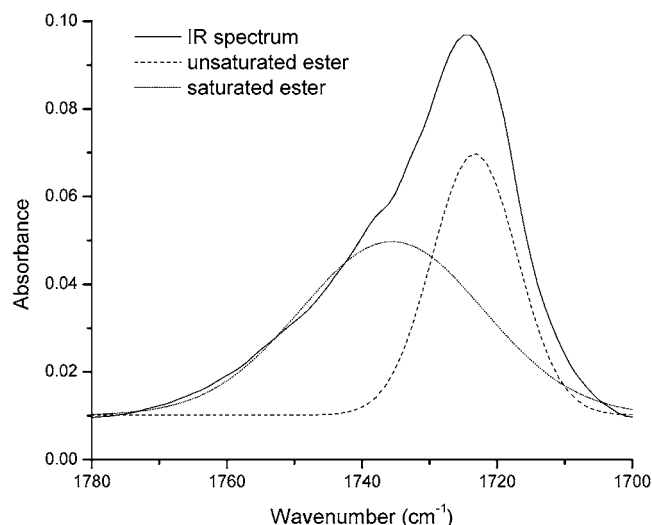
weight allowed the calculation of the degree of OH-functionalization: from thermogravimetric analysis, the weight loss due to PEG degradation (at lower temperature than poly(styrene)) provided values in accord with or higher than supplier's data for the particles E and D, respectively.

The yield of the reaction with acryloyl chloride was estimated from the signal reduction of the OH stretching vibration (see IR spectra in Figure 1C). This absorption was normalized against  $\nu_{C-H}$  ( $2880\text{ cm}^{-1}$ ),  $\nu_{C-O}$  ( $1100\text{ cm}^{-1}$ ), and  $\delta_{C-H}$  ( $699\text{ cm}^{-1}$ ), and the three results were averaged to provide a  $55 \pm 2.5\%$  or  $51 \pm 2.3\%$  conversion of OH groups to acrylates, for particles E and D, respectively.

The successive Michael-type addition was monitored using the reduction in absorption of the  $\nu_{C=O}$  vibration of the unsaturated acrylic ester, which was studied after deconvolution of the spectra and separation from the absorption of the saturated ester (Figure 2).

Two thiol-containing reagents were used as models for peptidic materials: cysteine (see IR spectra in Figure 1D) and a peptide containing 13 amino acidic residues and derived from the C-terminus of Platelet Factor 4 (PF4), with molar mass of 1774; this peptide represents an heparin-binding domain in the PF4 structure. PF4 selectively binds to regions of active angiogenesis (35), and it has been shown that this C-terminus-derived peptide retains the angiostatic effect of the whole protein (36). In a surface-supported form this peptide is potentially useful for heparin-mediated growth-factor controlled release, but also for studying the presence of PF4 receptors on the surface of cells.

The yield of the reaction was dramatically lowered by the increase in molecular mass: the peptide functional-



**Figure 2.** Deconvolution of  $\nu_{C=O}$  peak after Michael-type addition of cysteine onto acrylated polystyrene-PEG particles (particles E). The two components refer to the saturated (reacted with the PF4-derived peptide,  $1735\text{ cm}^{-1}$ ) and the unsaturated (unreacted,  $1724\text{ cm}^{-1}$ ) esters.

ized only 9% of the available acrylic groups, compared to 65% in case of cysteine.

We assume the difference to arise mostly from the more difficult diffusion of the big peptide into the polymer bead and therefore the PF4-derived peptides to be present mostly on the surface of the macroparticle. However, this does not hinder the applicability of the reaction onto carriers, where the important (and only) reactive groups are necessarily located on the surface.

## CONCLUSIONS

The present study reports on methodologies for the functionalization of surfaces with potentially bioactive components. We have used macroparticles, which facilitated the study of the functionalization techniques (easier isolation and handling of the particles), but our results are perspective useful to colloidal particles or macroscopic objects too.

Using Michael-type addition in heterogeneous conditions, we have showed that the localization of the reaction partners matters: the combination thiol on the surface/acrylate in solution, used for providing PEGylated and further reactive surfaces, showed that surface thiols lack reactivity. Disulfide formation can likely be excluded, due to the reducing reaction environment; thus, the poor reactivity is likely to ascribe to the hydrophobicity of both thiols and surface, which does not kinetically favor the reactions with products dissolved in water or in the very polar solvents (NMP).

Discarding therefore Michael-type addition as a PEGylation reaction, we have employed it for the introduction of model bioactive compounds onto previously PEGylated materials. For this purpose the reaction between supported acrylic groups and soluble thiols showed good practicality and is promising for further applications.

## ACKNOWLEDGMENT

The authors are indebted to Dr. Wolfgang Rapp (Rapp Polymere) for the free supply of particles B and E.

## LITERATURE CITED

- (1) Kasemo, B., and Gold, J. (1999) Implant surfaces and interface processes. *Adv. Dent. Res.* 13, 8.

- (2) Jones, F. H. (2001) Teeth and bones: applications of surface science to dental materials and related biomaterials. *Surf. Sci. Rep.* 42, 79.
- (3) Klee, D., and Hocker, H. (1999) Polymers for biomedical applications: Improvement of the interface compatibility. Biomedical Applications: Polymer Blends. *Adv. Polym. Sci.* 149, 1.
- (4) Cai, K. Y., Lin, S. B., and Yao, K. D. (2001) Advances in research on surface engineering of biomaterials for tissue engineering. *Prog. Chem.* 13, 56.
- (5) Folch, A., and Toner, M. (2000) Microengineering of cellular interactions. *Annu. Rev. Biomed. Eng.* 2, 227.
- (6) Heibel, C., Maus, S., Knoll, W., and Ruhe, J. (1998) Polymer-supported biomembrane models. *Organic Thin Films* (ACS Symposium Series 695) p 104, American Chemical Society, Washington.
- (7) Kasemo, B. (1998) Biological surface science. *Curr. Opin. Solid State Mater. Sci.* 3, 451.
- (8) Massia, S. P., and Hubbell, J. A. (1990) Covalently attached GRGD on polymer surfaces promotes biospecific adhesion of mammalian cells. *Ann. N.Y. Acad. Sci.* 589, 261.
- (9) Marchand-Brynaert, J., Detrait, E., Noiset, O., Boxus, T., Schneider, Y. J., and Remacle, C. (1999) Biological evaluation of RGD peptidomimetics, designed for the covalent derivatization of cell culture substrata, as potential promoters of cellular adhesion. *Biomaterials* 20, 1773.
- (10) Noiset, O., Schneider, Y. J., and Marchand-Brynaert, J. (1999) Fibronectin adsorption or and covalent grafting on chemically modified PEEK film surfaces. *J. Biomat. Sci.-Polym. E.* 10, 657.
- (11) Liu, J., Zhang, Q., Remsen, E. E., and Wooley, K. L. (2001) Nanostructured materials designed for cell binding and transduction. *Biomacromolecules* 2, 362.
- (12) Merrett, K., Griffith, C. M., Deslandes, Y., Pleizier, G., and Sheardown, H. (2001) Adhesion of corneal epithelial cells to cell adhesion peptide modified pHEMA surfaces. *J. Biomater. Sci. Polym. Ed.* 12, 647.
- (13) Chevotot, Y., Bucher, O., Leonard, D., Mathieu, H. J., and Sigrist, H. (1999) Synthesis and characterization of a photo-activatable glycoaryldiazirine for surface glycoengineering. *Bioconjugate Chem.* 10, 169.
- (14) Gao, H., Sanger, M., Luginbuhl, R., and Sigrist, H. (1995) Immunosensing with photoimmobilized immunoreagents on planar optical wave guides. *Biosens. Bioelectron.* 10, 317.
- (15) Mann, B. K., Tsai, A. T., Scott-Burden, T., and West, J. L. (1999) Modification of surfaces with cell adhesion peptides alters extracellular matrix deposition. *Biomaterials* 20, 2281.
- (16) Irvine, D. J., Ruzette, A. V., Mayes, A. M., and Griffith, L. G. (2001) Nanoscale Clustering of RGD Peptides at Surfaces Using Comb Polymers. 2. Surface Segregation of Comb Polymers in Polylactide. *Biomacromolecules* 2, 545.
- (17) McMillan, R., Meeks, B., Bensebaa, F., Deslandes, Y., and Sheardown, H. (2001) Cell adhesion peptide modification of gold-coated polyurethanes for vascular endothelial cell adhesion. *J. Biomed. Mater. Res.* 54, 272.
- (18) Quirk, R. A., Chan, W. C., Davies, M. C., Tendler, S. J., and Shakesheff, K. M. (2001) Poly(L-lysine)-GRGDS as a biomimetic surface modifier for poly(lactic acid). *Biomaterials* 22, 865.
- (19) Neff, J. A., Caldwell, K. D., and Tresco, P. A. (1998) A novel method for surface modification to promote cell attachment to hydrophobic substrates. *J. Biomed. Mater. Res.* 40, 511.
- (20) Neff, J. A., Tresco, P. A., and Caldwell, K. D. (1999) Surface modification for controlled studies of cell-ligand interactions. *Biomaterials* 20, 2377.
- (21) Romanowska, A., Meunier, S. J., Tropper, F. D., Laferrière, C. A., and Roy, R. (1994) Michael Additions for Syntheses of Neoglycoproteins. *Methods Enzymol.* 242, 90.
- (22) Lutolf, M. P., Tirelli, N., Cerritelli, S., Cavalli, L., and Hubbell, J. A. (2001) Systematic Modulation of Michael-Type Reactivity of Thiols through the Use of Charged Amino Acids. *Bioconjugate Chem.* 12, 1051.
- (23) Elbert, D. L., Pratt, A. B., Lutolf, M. P., Halstenberg, S., and Hubbell, J. A. (2001) Protein delivery from materials formed by self-selective conjugate addition reactions. *J. Controlled Release* 76, 11.

- (24) Bontempo, D., Tirelli, N., Masci, G., Crescenzi, V., and Hubbell, J. A. (2002) Thick coating and functionalization of organic surfaces via ATRP in water. *Macromol. Rapid Commun.* 23, 418.
- (25) Napoli, A., Tirelli, N., Wehrli, E., and Hubbell, J. A. (2002) Lyotropic behavior in water of amphiphilic ABA triblock copolymers based on poly(propylene sulfide) and poly(ethylene glycol). *Langmuir* 18, 8324.
- (26) Rehor, A., Tirelli, N., and Hubbell, J. A. (2002) A new living emulsion polymerization mechanism: Episulfide anionic polymerization. *Macromolecules* 35, 8688.
- (27) Ramires, P. A., Mirengi, L., Romano, A. R., Palumbo, F., and Nicolardi, G. (2000) Plasma-treated PET surfaces improve the biocompatibility of human endothelial cells. *J. Biomed. Mater. Res.* 51, 535.
- (28) Griesser, H. J., Chatelier, R. C., Gengenbach, T. R., Johnson, G., and Steele, J. G. (1994) Growth of Human-Cells on Plasma Polymers – Putative Role of Amine and Amide Groups. *J. Biomater. Sci.-Polym. Ed.* 5, 531.
- (29) Look, G. C., Holmes, C. P., Chinn, J. P., and Gallop, M. A. (1994) Methods for Combinatorial Synthesis: The Use of Fast  $^{13}\text{C}$  NMR Analysis for Gel Phase Reaction Monitoring. *J. Org. Chem.* 59, 7588.
- (30) Takahashi, N., and Creighton, T. E. (1996) On the reactivity and ionization of the active site cysteine residues of escherichia coli thioredoxin. *Biochemistry* 35, 8342.
- (31) Stolnik, S., Illum, L., and DAVIS, S. S. (1995) Long Circulating Microparticulate Drug Carriers. *Adv. Drug Delivery Rev.* 16, 215.
- (32) Peracchia, M. T., Fattal, E., Desmaele, D., Besnard, M., Noel, J. P., Gomis, J. M., M., A., D'Angelo, J., and Couvreur, P. (1999) Stealth (R) PEGylated polycyanoacrylate nanoparticles for intravenous administration and splenic targeting. *J. Controlled Release* 60, 121.
- (33) Gref, R., Luck, M., Quellec, P., Marchand, M., Dellacherie, E., Harnisch, S., Blunk, T., and Muller, R. H. (2000) 'Stealth' corona-core nanoparticles surface modified by poly(ethylene glycol) (PEG): influences of the corona (PEG chain length and surface density) and of the core composition on phagocytic uptake and plasma protein adsorption. *Colloids Surf. B* 18, 301.
- (34) Kingshott, P., and Griesser, H. J. (1999) Surfaces that resist bioadhesion. *Curr. Opin. Solid State Mater. Sci.* 4, 403.
- (35) Hansell, P., Maione, T. E., and Borgstrom, P. (1995) Selective binding of platelet factor 4 to regions of active angiogenesis in vivo. *Am. J. Physiol.* 269, H829.
- (36) Maione, T. E., Gray, G. S., Petro, J., Hunt, A. J., Donner, A. L., Bauer, S. I., Carson, H. F., and Sharpe, R. J. (1990) Inhibition of angiogenesis by recombinant human platelet factor-4 and related peptides. *Science* 247, 77.

BC0340621



# Engineered Protein A for the Orientational Control of Immobilized Proteins

Colin P. Johnson,<sup>†</sup> Irene E. Jensen,<sup>‡</sup> Anil Prakasam,<sup>‡</sup> Ravi Vijayendran,<sup>‡,||</sup> and Deborah Leckband<sup>\*,†,‡,§</sup>

Department of Chemistry, Department of Chemical and Biomolecular Engineering, and Center for Biophysics and Computational Biology, University of Illinois at Urbana–Champaign, 600 South Mathews Avenue, Urbana Illinois 61802. Received April 24, 2003; Revised Manuscript Received August 4, 2003

This work describes the genetic engineering and characterization of a histidine-tagged fragment of protein A. The histidine tag results in the site-selective immobilization of the protein A receptor and the preservation of its high ligand affinity when immobilized on solid supports. The fragment was expressed at high yield in *E. coli* and purified to homogeneity. When selectively immobilized to histidine binding matrices, the protein A fragment exhibits high affinity for soluble IgG. We further demonstrate from adsorption isotherms that the receptor exhibits a homogeneous, high affinity population at densities where steric crowding between large ligands does not affect the apparent receptor affinity. This engineered receptor is appropriate for a range of applications including sensor design or those using immobilized Fc-tagged proteins.

## INTRODUCTION

Immobilized proteins are used in an extensive array of applications, ranging from affinity chromatography to biosensors. Generally, the covalent attachment of proteins results in a substantial loss of protein activity. This loss of function has many origins, including the chemical modification of critical residues, environment-induced denaturation, and random protein orientations, some of which block the active site (1). The latter is particularly prevalent with relatively nonspecific immobilization chemistries such as amine coupling. Although they effectively anchor proteins at high density, the resulting randomly oriented protein populations exhibit broad distributions in both kinetic and thermodynamic parameters (2). These nonuniform characteristics have detrimental effects on the sensitivity, reproducibility, and predictability of devices based on surface-bound proteins, e.g., biosensors. Recent attempts to control the protein orientation in order to increase active site accessibility and reduce heterogeneity primarily focused on improving the biological activity of the proteins (3, 4), rather than on reducing the heterogeneity of the immobilized protein population (5).

Protein A binds the Fc region of the G class of immunoglobulins (IgG). It is widely used to purify antibodies and engineered proteins with Fc domain tags, and to immobilize antibodies for affinity chromatography and biosensing (6, 7). Wild type protein A comprises five highly homologous extracellular domains (8), each of which can individually bind IgG and is composed of approximately 58 amino acids. The structure of the second, B, domain in a complex with the Fc fragment of IgG was determined, and a number of studies identified

the essential residues in the Fc binding site (9, 10). It is therefore also an attractive model system for exploring the impact of site selective immobilization on the physical properties of immobilized receptors.

In this work, we describe the engineering and characterization of a truncated version of Protein A to facilitate its site selective immobilization and its binding to soluble ligands. In particular, we engineered a hexahistidine tag at the C-terminus of the excised B-domain of protein A. This construct contains a single B domain of protein A, to ensure a 1:1 stoichiometry between Fc immunoglobulin domains and the receptor. Based on the structure of the B-domain, the C-terminal location of the histidine tag is distal to the binding site, so that the active site of the immobilized protein should be fully accessible to soluble ligands. The latter should also orient Fc-tagged proteins bound to the immobilized B-domain and would therefore be useful in a wide variety of applications.

We further characterized the immobilized protein affinity and the uniformity of the immobilized protein (2) from surface plasmon resonance (SPR) measurements of IgG binding affinities. These results demonstrated that the engineered protein is functional and exhibits high affinity when site selectively immobilized on different substrates. Furthermore, the location of the histidine tag facilitates the site selective immobilization of this protein A fragment, and this further yields a homogeneous receptor population.

## MATERIALS AND METHODS

**Chemical Reagents.** 1,2-Ditridecanoyl-*sn*-glycero-3-phosphocholine (DTPC) and 1,2-dipalmitoyl-*sn*-glycero-3-phosphoethanolamine (DPPE) were purchased from Avanti Polar Lipids. 6-[9-[2,3-Bis(dodecyloxy)propyl]-3,6,9-trioxanonyl-1-oxycarboxylamino]-2-[bis(carboxymethyl)amino]hexanoic acid (NTA-TRIG-DLGE) was custom synthesized by Northern Lipids Inc. (Vancouver, BC). 1-Octadecanethiol was obtained from Aldrich. *N*-(5-Amino-1-carboxypentyl) disodium salt (AB-NTA) was purchased from Dojindo Laboratories (Japan). 1-Ethyl-3-(3-dimethylaminopropyl)carbodiimide (EDC) and *N*-

\* Corresponding author. Telephone: 217-244-0793. Fax: 217-333-5052. e-mail: leckband@scs.uiuc.edu.

<sup>†</sup> Department of Chemistry.

<sup>‡</sup> Department of Chemical and Biomolecular Engineering.

<sup>§</sup> Center for Biophysics and Computational Biology.

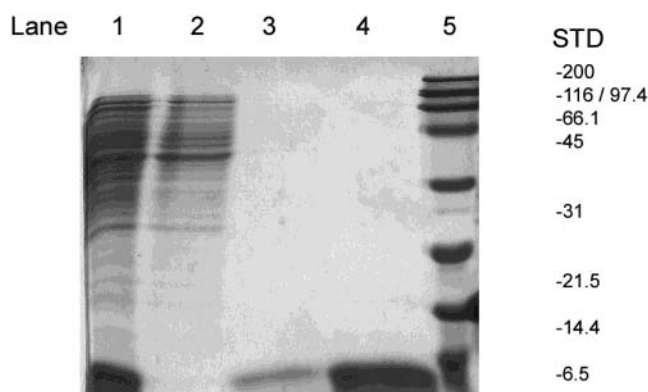
<sup>||</sup> Current address: Caliper Technologies Corp., 605 Fairchild Dr., Mountain View, CA 94043.

hydroxysulfosuccinimide (NHS) were from Pierce (Rockford, IL). Both rabbit and goat IgG were obtained from Sigma (St. Louis, MO). *N*-(Hydroxyethyl)piperazine-*N*-(2-ethanesulfonic acid) (HEPES) was purchased from Fischer Scientific (Pittsburgh, PA).

The vector pET-21b(+) and BugBuster Protein Extraction Reagent were purchased from Novagen (Madison, WI). Restriction endonucleases *Taq* DNA polymerase, T4 DNA ligase, and isopropyl  $\beta$ -D-thiogalactoside (IPTG) were all purchased from Gibco BRL (Gaithersburg, MD). Pwo polymerase was purchased from Roche (Indianapolis, IN). Oligonucleotide primers for PCR were from Integrated DNA Technologies (Indianapolis, IN). 15% SDS PAGE gels and broad range protein molecular weight standards were obtained from BioRad (Hercules, CA). Sequencing was carried out at the W. M. Keck Center for Comparative and Functional Genomics (University of Illinois Biotechnology Center, Urbana IL). GENECLEANIII was purchased from BIO101. Qiaprep Spin Miniprep kit and Ni-NTA Agarose were obtained from Qiagen (Valencia, CA). Centriprep YM-3 and PD-10 columns were purchased from, respectively, Millipore (Bedford, MA) and Amersham Pharmacia Biotech (Piscataway, NJ). Ampicillin and all other reagents were obtained from Sigma (St. Louis, MO). The plasmid pSPA-2, which contains two tandem repeats of Domain B of Protein A was a gift from Dr. M. Benedik (U. Houston, Texas).

**Protein Expression and Isolation.** Bacteria were transformed by electroporation using a Gene Pulser (BioRad). Plasmid DNA stocks were purified using Qiagen columns (Qiagen Inc., Valencia, CA) in accordance with the manufacturer's instructions. The propagation and selection of plasmids, growth of bacterial strains, and routine recombinant DNA manipulations were all performed according to the protocols described by Sambrook et al. (11).

The tandem repeat of Domain B was excised from plasmid pSPA-2 by restricting the DNA with *EcoRI* and *BamHI* (12). The resulting 375 bp fragment was excised from the agarose gel and purified using the GENECLEAN kit. This fragment was then used as a template in subsequent PCR procedures. All PCR amplifications were performed in thin-walled tubes using a Perkin-Elmer GeneAmp PCR System 2400 (Norwalk, CT). Domain B of protein A was amplified by PCR using the following synthetic oligonucleotides: (1) SPAFBhis5' (5' GAA TTC AAC ATA TGG CTG ACA ACA 3') and (2) SPAFBhis3' (5' GAT CCT CGA GAC CTT TCG GAG C 3'). *NdeI* and *XhoI* sites were engineered into the 5' ends of the SPAFBhis5' and SPAFBhis3' primers, respectively. The PCR reaction conditions were as follows: an initial hot start of 95 °C for 5 min; 80 °C for 1 min at which time 1  $\mu$ L of the polymerase Pwo was added; 94 °C 45 s, 56.5 °C 45 s, and 72 °C for 1 min, repeated 20 times; a final elongation step at 72 °C for 7 min. The reaction mixtures contained 1  $\mu$ M of each primer and 200  $\mu$ M of each dNTP in the supplied Pwo buffer, in a total volume of 50  $\mu$ L. Because the template DNA was a tandem repeat of Domain B, the PCR reaction gave two major products: namely, the original tandem repeat and a single copy of Domain B. The amplified DNA fragments generated in several reaction tubes were pooled, extracted with phenol/chloroform, precipitated with ethanol, and then cloned into the *NdeI* and *XhoI* sites of pET-21b(+) to create the plasmid pBHis12 (containing a single Domain B). Following the verification of the correct fragment insertion by restriction mapping and sequencing, the plasmid



**Figure 1.** SDS-PAGE of purified recombinant pBHis12. Protein standards (BioRad Broad Range standards, MW 6.5–200 kDa) are in lane 5. Lanes 1–4 pertain to pBHis12. Lane 1 contains total lysate of pBHis12. Lane 2 is the effluent recovered during the column loading. Lane 3 contains the flow through after the initial wash. Nearly all of the recombinant protein binds the Ni-NTA column. Lane 4 shows the pooled, concentrated recombinant protein fractions eluted with 250 mM imidazole. The protein is >97% pure (lane 4).

containing the correct insert was transformed into the *E. coli* expression host strain BL21(DE3) by electroporation.

Cells expressing a single Domain B (His<sub>6</sub>SpA<sub>B</sub>) were cultured with shaking at 37 °C in 3 mL of Luria Broth (LB) medium containing ampicillin (100  $\mu$ g mL<sup>-1</sup>) until an OD<sub>600 nm</sub> of 0.5 was reached. The cultures were then stored overnight at 4 °C. The preculture was used to inoculate 100–250 mL of LB ampicillin (100  $\mu$ g mL<sup>-1</sup>) medium, which was then incubated with shaking at 37 °C until an OD<sub>600 nm</sub> of 1 was reached. Production of the fusion protein was induced with 1 mM isopropyl  $\beta$ -thiogalactopyranoside. Bacterial cells were harvested by centrifugation 3–4 h postinduction, and the cell pellets were stored frozen at -20 °C. The soluble cell extracts from 100 to 250 mL of culture medium were prepared with BugBuster Protein Extraction Reagent.

The His<sub>6</sub>SpA<sub>B</sub> was purified on a Ni-NTA Agarose (Qiagen) column. The protein was eluted with an imidazole solution containing sodium phosphate buffer (pH 8.0) and 300 mM NaCl, according to the manufacturer's guidelines, with slight modifications, as follows. The Ni-NTA resin was first equilibrated with phosphate buffer (pH 7.2) containing 5 mM imidazole. Following protein binding to the Ni-NTA agarose, the column was washed three times with eight column volumes of phosphate buffer containing increasing imidazole concentrations (5 mM, 10 mM, and 20 mM imidazole). The protein was eluted with eight column volumes of buffer containing 250 mM imidazole. Aliquots of each fraction were submitted to 18% SDS PAGE analysis (Figure 1) according to the method of Laemmli (13). Fractions containing protein were pooled and concentrated using centrifugation filters (Centriprep YM-3) and then desalted and exchanged into phosphate buffer using a PD-10 column. Optical densities at 280 nm were determined, and protein concentration was calculated using a theoretical extinction coefficient of 1280 M<sup>-1</sup> cm<sup>-1</sup> for His<sub>6</sub>SpA<sub>B</sub>.

**Protein Immobilization.** The His<sub>6</sub>SpA<sub>B</sub> construct was site-selectively and randomly immobilized to, respectively, Ni-NTA- and *N*-hydroxysuccinimide-derivatized surfaces. The adsorption of His<sub>6</sub>SpA<sub>B</sub> was quantified by surface plasmon resonance (SPR). These measurements were carried out with a home-built instrument based on the Kretschman configuration (14). The surface

**Table 1. Density of His<sub>6</sub>SpA-B Bound to Lipid Monolayers**

immobilization chemistry	receptors/ $\mu\text{m}^2$	IgG/His <sub>6</sub> SpA-B (per unit area)
1:99 DLGE-NTA:DTPC	$3.1 \times 10^3$	0.35
1:1 DLGE-NTA:DTPC	$2.5 \times 10^4$	2.83
3:1 DLGE-NTA:DTPC	$4.6 \times 10^4$	5.20
NHS-SAM	$6.8 \times 10^4$	7.61
NTA-SAM	$1.7 \times 10^4$	1.90

density of immobilized His<sub>6</sub>SpA<sub>B</sub> was determined from the measured refractive index relative to that of a densely packed protein monolayer (14, 15). For these analyses, we used a refractive index of 1.46 for the pure protein monolayer and a monolayer thickness of 4.5 nm. The results are summarized in Table 1. From the fractional protein coverage and the known dimensions, we determined the number of proteins per square micron.

In one immobilization scheme, His<sub>6</sub>SpA<sub>B</sub> was specifically adsorbed to supported, lipid monolayers that contained a mixture of the NTA-TRIG-DLGE lipid and DTPC at a specified ratio. The mixed lipid layers were prepared by Langmuir-Blodgett deposition of the lipid film onto a hydrophobic, self-assembled alkanethiol monolayer on a thin (36 nm) gold film. The 36 nm gold film was thermally evaporated onto glass slides that were first coated with a 1 nm chromium adhesion layer. Immediately after the gold deposition, the hexadecane thiol monolayer was self-assembled onto the freshly evaporated gold from an ethanol solution containing 1 mM hexadecane thiol (14, 15).

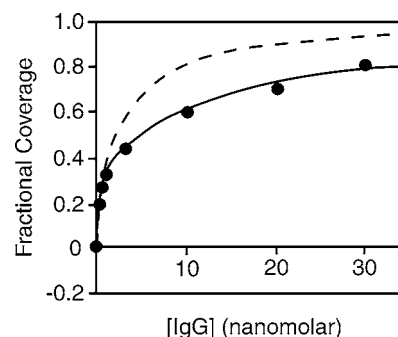
The superficial, mixed lipid monolayer was formed by spreading a 9:1 chloroform:methanol solution containing a mixture of the two lipids on the air/water surface of a Langmuir trough (NIMA 611, England). The subphase was pure water at room temperature. The NTA-DLGE:DTPC ratios used were 1:99, 1:1, and 3:1. The lipid layers were compressed to a surface pressure of 36 mN/m ( $\sim 65 \text{ \AA}^2/\text{lipid}$ ) and then deposited onto the alkanethiol monolayer at constant pressure by dipping the latter into the subphase through the air-water interface.

The His<sub>6</sub>SpA<sub>B</sub> immobilization was carried out by incubating 5  $\mu\text{M}$  His<sub>6</sub>SpA<sub>B</sub> with the lipid films for 1 h at room temperature. The incubation buffer consisted of 20 mM HEPES (pH 7.7), 100 mM NaCl, and 20  $\mu\text{M}$  NiSO<sub>4</sub>. The substrate was then washed thoroughly with buffer to remove nonspecifically bound protein.

Alternatively, the His<sub>6</sub>SpA<sub>B</sub> was immobilized to a self-assembled alkanethiol monolayer  $\omega$ -functionalized with NTA groups. Here, the carboxylic acid-terminated organothiol, 11-mercaptoundecanoic acid (MUD), was first self-assembled on a 50 nm gold film coated on a glass slide. The carboxy-terminated monolayer was then treated with a solution of 3.8 mg/mL EDC and 6.7 mg/mL NHS. A 10 mg/mL solution of AB-NTA in HEPES buffer was then reacted with the NHS ester groups on the monolayer for 1 h. The resulting surface was then treated with His<sub>6</sub>SpA<sub>B</sub> as described above for the lipid films.

The protein A fragment was also immobilized randomly on self-assembled alkanethiol monolayers using the amine-reactive moiety *N*-hydroxysuccinimide. This was done by first reacting a carboxy-terminated alkanethiol monolayer, prepared as described above, with a solution containing 3.8 mg/mL EDC and 6.7 mg/mL NHS. A 10  $\mu\text{M}$  solution of His<sub>6</sub>SpA<sub>B</sub> in 10 mM HEPES buffer at pH 7.8 was next reacted with the NHS surface functionalities. The protein bound covalently to the NHS moieties via the protein's primary amine groups.

**IgG Binding Isotherms.** The affinity of His<sub>6</sub>SpA<sub>B</sub> for soluble IgG was determined by SPR, following the



**Figure 2.** Adsorption profile for IgG binding to His<sub>6</sub>SpA<sub>B</sub> immobilized on a 1:1 NTA-DLGE:DTPC lipid monolayer. The dashed line is the nonlinear least-squares fit to the Langmuir isotherm, and the solid line through the data shows the fit to the two-site binding isotherm. The best-fit parameters are in Table 2.

injection of rabbit IgG into the flow cell above the gold-coated film. The equilibrium amounts of IgG absorbed on the monolayers were then measured at sequentially increasing bulk IgG concentrations. The IgG concentrations used were sufficiently high that the solution was not depleted during the measurement. The extent of nonspecific absorption was determined with goat IgG, which does not bind to protein A.

The binding characteristics of the systems under study were evaluated using two different thermodynamic equations: the Langmuir isotherm, a two-site Langmuir equation. Data were fit to each of these isotherms by standard nonlinear least-squares analysis. The Langmuir isotherm relates the fractional coverage of bound receptor  $f$  to the bulk analyte concentration  $c$ , according to:  $f = Kc / (1 + Kc)$ . This isotherm assumes a single population of receptors with a unique binding energy or affinity constant  $K$ .

To analyze the adsorption data, we also used the two-site Langmuir isotherm:  $f = (X_1 K_1 c / (1 + X_1 K_1 c)) + (X_2 K_2 c / (1 + X_2 K_2 c))$  where  $f$  represents the fraction of receptors bound,  $X_i$  represents the fraction of the receptors in subpopulation  $i$ ;  $K_i$  represents the affinity of subpopulation  $i$ ; and  $c$  is the solution concentration of analyte. This model assumes two independent populations of binding sites with two, distinct affinities.

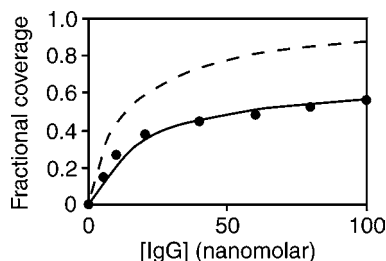
## RESULTS AND DISCUSSION

**His<sub>6</sub>SpA<sub>B</sub> Surface Densities.** The densities of protein A fragments bound to the different substrates, as quantified by SPR, are summarized in Table 1. On lipid membranes, the receptor density increases with the NTA-DLGE mole fraction in the lipid monolayer, as expected. At the highest NTA-DLGE fraction used (0.75), the His<sub>6</sub>SpA<sub>B</sub> density approaches that achieved with the random, NHS coupling chemistry, which yielded the highest protein coverage at  $6.8 \times 10^4$  receptors/ $\mu\text{m}^2$ . Site selective immobilization onto the NTA-derivatized self-assembled monolayers yielded a 3-fold lower protein density.

**IgG Adsorption Isotherms.** The results from the IgG equilibrium adsorption assays were analyzed with different adsorption isotherms, to quantify the affinity of the engineered protein and to assess the immobilized receptor heterogeneity. Both parameters were obtained from fits of the adsorption data to the isotherms described above.

Figure 2 shows adsorption isotherm for IgG binding to His<sub>6</sub>SpA<sub>B</sub>, which was bound site-selectively to a 1:1 NTA-DLGE:DTPC monolayer. Figure 3 shows the IgG adsorption onto the B-domain bound to an NHS-modified





**Figure 3.** Adsorption profile for IgG binding to His<sub>6</sub>SpA<sub>B</sub> immobilized on an NHS-functionalized self-assembled alkanethiol monolayer. The dashed line is the nonlinear least-squares fit to the Langmuir isotherm, and the solid line is the fit to the two-site isotherm. The best-fit parameters are given in Table 2.

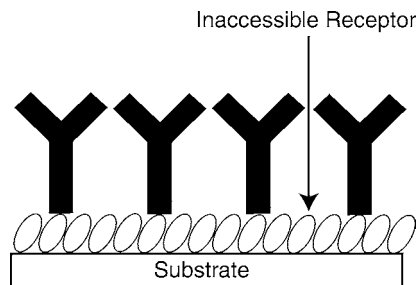
**Table 2. Fitted Parameters from IgG Adsorption Data**

immobilization chemistry	binding isotherm	affinity ( $\times 10^8 \text{ M}^{-1}$ )	population fraction	$R^2$
NHS-SAM	Langmuir	$1 \pm 1$		0.83
	two-site	$5 \pm 1$	$0.100 \pm 0.02$	0.99
		$0.020 \pm 0.008$	$0.900 \pm 0.02$	
NTA-SAM	Langmuir	$0.63 \pm 0.1$		0.80
	two-site	$2.0 \pm 0.7$	$0.39 \pm 0.07$	0.98
		$0.35 \pm 0.16$	$0.61 \pm 0.07$	
NTA-DLGE: DTPC 3:1	Langmuir	$0.2 \pm 0.1$		0.83
	two-site	$1.00 \pm 0.01$	$0.230 \pm 0.006$	0.98
		$0.02 \pm 0.01$	$0.770 \pm 0.006$	0.82
1:1	Langmuir	$0.4 \pm 0.1$		0.82
	two-site	$5.0 \pm 0.2$	$0.330 \pm 0.007$	0.99
		$0.070 \pm 0.003$	$0.670 \pm 0.007$	0.99
1:99	Langmuir	$0.9 \pm 0.1$		0.99
	two-site	$0.8 \pm 0.1$	$0.96 \pm 0.02$	0.99
		$0.031 \pm 0.01$	$0.04 \pm 0.02$	

self-assembled monolayer. The data in both cases were fit to the Langmuir isotherm. The poor fit obtained with the amine-coupled protein (Figure 3, dashed line) was expected since this immobilization method leads to a high degree of heterogeneity (2). However, we expected the His<sub>6</sub>SpA<sub>B</sub> bound to NTA-terminated substrates to form a homogeneous, oriented receptor population characterized by a unique affinity. Nevertheless, the Langmuir isotherm describes neither of these systems adequately. This was also the case with B-domain bound to an NTA-terminated SAM (data not shown). The best-fit parameters for these cases are summarized in Table 2.

One possible explanation for the finding that His<sub>6</sub>SpA<sub>B</sub> bound site-selectively to NTA-functionalized surfaces failed to exhibit Langmuir adsorption characteristics is that the receptor population is not homogeneous. This could be due to steric crowding by the relatively large, bound IgG ligands (Figure 4). Several studies have shown that, at high receptor densities, the larger, analyte molecules can crowd the surface and hinder further analyte binding (16, 17). The cross-sectional area of an IgG molecule anchored via the Fc domain is  $\sim 11,500 \text{ \AA}^2/\text{IgG}$ , and the maximum coverage would be  $\sim 8.8 \times 10^3 \text{ IgG}/\mu\text{m}^2$ . Given that the B-domain density on 50 mol % lipid monolayers is  $2.5 \times 10^4 \text{ receptors}/\mu\text{m}^2$ , about 65% of the B-domains would be unoccupied, based on steric arguments alone.

To test this hypothesis, we analyzed the results using a two-site Langmuir isotherm (Figure 2, solid line). The goodness-of-fit suggests that the His<sub>6</sub>SpA<sub>B</sub> monolayer does comprise two apparent receptor populations: namely, a smaller, high affinity population, and a larger, low affinity population. The two affinities differ by nearly 2 orders of magnitude (Table 2). Nevertheless, the high affinity population exhibits a binding constant within a



**Figure 4.** Cartoon depicting the steric interference between large IgG ligands binding to a densely packed receptor monolayer. Adjacent IgG molecules block the accessibility of IgG to some receptors on the surface. This leads to two apparent receptor subpopulations with different affinities.

factor of 10 of the IgG affinity determined from solution studies with the single B domain (18).

If the apparent population heterogeneity were indeed due to steric interference, then an increase in the B-domain density would increase the fraction of low affinity sites. Conversely, decreasing the receptor density would increase the fraction of high affinity sites. To test this, we conducted measurements with His<sub>6</sub>SpA<sub>B</sub> bound to 3:1 NTA-DLGE:DTPC monolayers. This increased the receptor surface density from  $2.5 \times 10^4$  to  $4.6 \times 10^4 \text{ receptors}/\mu\text{m}^2$  (Table 1). The results of the data fits are shown in Table 2. Although the increased receptor surface density did not significantly affect the magnitudes of the IgG affinities of the two subpopulations, the fractional amounts did change. At the higher surface density, the fraction of the low affinity receptors was greater, as expected.

We similarly investigated IgG adsorption to His<sub>6</sub>SpA<sub>B</sub> at the much lower surface density of  $3.1 \times 10^3 \text{ receptors}/\mu\text{m}^2$ . In this case, the adsorption data were well described by the Langmuir isotherm. The surface binding sites displayed a single affinity of  $1.9 \pm 0.1 \times 10^8 \text{ M}^{-1}$ , which is within a factor of 5 of the high affinity population identified at the higher protein densities. The adsorption data obtained at both high and low receptor coverage thus support the hypothesis that steric crowding by the large ligands at high densities of protein A is responsible for the two apparent His<sub>6</sub>SpA<sub>B</sub> affinities.

Although the trends described above can be explained by steric crowding, the two protein subpopulations could result from both specific IgG binding to His<sub>6</sub>SpA<sub>B</sub> and to nonspecific adsorption to the substrate. To test this possibility, we measured the nonspecific adsorption of goat IgG to both bare substrates lacking His<sub>6</sub>SpA<sub>B</sub> and to oriented immobilized His<sub>6</sub>SpA<sub>B</sub>. Protein A does not bind goat immunoglobulins so that any antibody adsorption in these control experiments should only reflect nonspecific binding. For the His<sub>6</sub>SpA<sub>B</sub> immobilization chemistries used, the adsorbed amount of goat IgG was less than 5% of the corresponding adsorption measured with rabbit IgG. Therefore, nonspecific adsorption cannot account for the observed trends.

The IgG binding to the "randomly" oriented B-domain also follows the two-site Langmuir isotherm (Figure 3, Table 2). However, in this preparation the specific activity of the bound protein is much lower. Namely, the protein surface density achieved was higher than any of the other preparations at the same time that the high affinity fraction was lower than all other systems studied. Comparing the density of "high affinity" receptors, the density was  $6.8 \times 10^3/\mu\text{m}^2$  on NHS-derivatized surfaces whereas that on the 75 mol % NTA-DLGE membrane was still higher at  $1.0 \times 10^4/\mu\text{m}^2$ , despite the lower overall

protein coverage. So another advantage of the site-selective immobilization of the protein A fragment is the higher specific activity achieved.

That randomly immobilized protein also followed the two-site model was at first surprising since a prior study showed that similarly immobilized wild type protein G and monoclonal antibody generated a heterogeneous protein population (2). The antibody thus immobilized exhibited heterogeneous ligand binding rates and binding affinities. In this case, the B-domain only has six lysines, and three are near the C-terminal histidine tag. The remaining three are outside of the binding interface. We would therefore expect the Fc binding site to be ligand accessible when the protein is linked through any of these six lysines. If this were the case, then we would not expect to see much heterogeneity in the receptor affinity, and steric occlusion in the ligand layer would have the greatest impact on the receptor efficacy, as observed here.

Binding isotherms cannot determine the ability of this engineered receptor to also orient proteins with Fc domains. However, molecular force measurements performed with an Fc-fusion protein bound to a similarly engineered histidine-tagged protein B dimer provided evidence of this orientational control. The directly measured steric thickness of the Fc-fusion protein monolayer, as well as the measured force profiles, demonstrated that the Fc-tagged protein was oriented roughly normal to the surface (19). We expect that the single B domain would similarly orient proteins on solid surfaces.

In conclusion, we describe the engineering of a fragment of protein A with a site selective immobilization anchor to control the protein orientation on solid supports. The IgG (ligand) binding isotherms show that the engineered, immobilized protein A fragment binds ligand with an affinity comparable to that of the wild type protein measured in solution. This demonstrates that site-selective immobilization and orientational control effectively preserves the potency of this receptor.

Additional studies carried out at different surface densities of the protein A fragment showed that the design parameters for producing high affinity, homogeneous, immobilized receptors include both site-selective immobilization and control of the receptor surface density. At low surface densities, the engineered receptor population exhibits a unique, high affinity, attesting to the homogeneity of the immobilized protein preparation. By contrast, at high protein densities, where the ligand footprint exceeds that of the bound protein A fragment, steric crowding between the bulky IgG ligands generates a binary receptor population, comprising both low affinity and high affinity sites. Such crowding effects have been documented previously (17). Identifying the origin of the apparent heterogeneity in this system, however, enabled us to define the conditions for achieving a uniform population of high affinity receptors.

#### ACKNOWLEDGMENT

This work was supported by the National Institutes of Health grant RO1 GM51338.

#### LITERATURE CITED

- (1) Lu, B., Smyth, M. R., and O'Kennedy, R. (1996). Oriented Immobilization of Antibodies and its Applications in Immunoassays and Immunosensors. *Analyst* 121, 29R–32R.
- (2) Vijayendran, R., Leckband, D. E. (2001) A Quantitative Assessment of Heterogeneity for Surface-Immobilized Proteins. *Anal. Chem.* 73, 471–480.
- (3) Edmiston, P. L., Saavedra, S. S. (1998) Molecular Orientation Distributions in Protein Films. 4. A Multilayer Composed of Yeast Cytochrome *c* Bound through an Intermediate Streptavidin Layer to a Planar Supported Phospholipid Bilayer. *J. Am. Chem. Soc.* 120, 1665–1671.
- (4) Edmiston P. L., Saavedra, S. S. (1998) Molecular Orientation Distributions in Protein Films: III. Yeast Cytochrome *c* Immobilized on Pyridyl Disulfide-Capped Phospholipid Bilayers *Biophys. J.* 74, 999–1006.
- (5) Lu, B., Smyth, M. R., O'Kennedy, R. (1996) Immunological activities of IgG antibody on precoated Fc receptor surfaces *Anal. Chim. Acta.* 331, 97–102.
- (6) Lu, H. C., Chen H., Lin Y. S., and Lin, J. W. (2000) A reusable and specific protein A-coated piezoelectric biosensor for flow injection immunoassay. *Biotechnol. Prog.* 16, 116–124.
- (7) Anderson, G. P., Jacoby M. A., Ligler F. S., and King, K. D. (1997) Effectiveness of Protein A For Antibody Immobilization For a Fiber Optic Biosensor. *Biosens. Bioelectron.* 12, 329–336.
- (8) Moks, T., Abrahmsen, L., Nilsson, B., Hellman, U., Sjoquist, J., Uhlen, M., (1986) Staphylococcal protein A consists of five IgG-binding domains. *Eur. J. Biochem.* 156, 637–643.
- (9) Takahashi, H., Nakanishi, T., Kami, K., Arata, Y., Shimada, I. (2000) A novel NMR method for determining the interfaces of large protein–protein complexes. *Nature Struct. Biol.* 7, 220–223.
- (10) Jendenburg, L., Tashiro, M., Tejero, R., Lyons, B., Uhlen, A. M., Montelione, G. T., Nilsson, B. (1996) The mechanism of binding staphylococcal protein A to immunoglobulin G does not involve helix unwinding. *Biochemistry* 35, 22–31.
- (11) Sambrook, J., Fritsch, E. F., Maniatis, T. (1989) *Molecular Cloning: A Laboratory Manual*, 2nd ed., Cold Spring Harbor Laboratory Press, Cold Spring Harbor, New York.
- (12) Djojonegoro, B. M., Benedik, M. J., Willson, R. C. (1994) Bacteriophage surface display of an immunoglobulin-binding domain of Staphylococcus aureus protein A. *Bio/Technology* 12, 169–72.
- (13) Laemmli, U. K. (1970) Cleavage of structural proteins during the assembly of the head of bacteriophage T4. *Nature*, 227, 680–685.
- (14) Yeung, C., Purves, T., Kloss, A. A., Kuhl, T. L., Sligar, S., Leckband, D. (1999) Cytochrome *c* Recognition of Immobilized, Orientational Variants of Cytochrome *b<sub>5</sub>*: Direct Force and Equilibrium Binding Measurements. *Langmuir* 16, 3414–3421.
- (15) Efremova, N., Bondurant, B., O'Brien, D., Leckband, D. (2000) Interaction Forces and Protein Resistance of Neutral Membranes with End-Grafted Poly(ethylene glycol). *Biochemistry* 39, 3441–3451.
- (16) Vikholm, I., Albers, W. M. (1998). Oriented Immobilization of Antibodies for Immunosensing. *Langmuir* 14, 3865–3872.
- (17) Spitznagel, T. M., Clark, D. S. (1993) Surface-Density and Orientation Effects on Immobilized Antibodies and Antibody Fragments. *Bio/Technology* 11, 825–829.
- (18) Jendeberg, L., Persson, B., Andersson, R., Karlsson, R., Uhlen, M., Nilsson, B. (1995) Kinetic Analysis of the Interaction Between Protein A Domain Variants and Human Fc Using Plasmon Resonance Detection. *J. Mol. Recognit.* 8, 270–278.
- (19) Zhu, B., Chappuis-Flament, S., Wong, E., Jensen, I. E., Gumbiner, B. M., Leckband, D. E. (2003) Functional Analysis of the Structural Basis of Homophilic Cadherin Adhesion *Biophys. J.* 84, 4033–4042.

BC034063T

# Synthesis of Poly( $\beta$ -amino ester)s Optimized for Highly Effective Gene Delivery

Akin Akinc,<sup>†,§</sup> Daniel G. Anderson,<sup>†</sup> David M. Lynn,<sup>‡</sup> and Robert Langer<sup>\*,†</sup>

Department of Chemical Engineering, Massachusetts Institute of Technology, Cambridge, Massachusetts 02139, and <sup>†</sup>Department of Chemical Engineering, University of Wisconsin, Madison, Wisconsin 53706. Received May 1, 2003; Revised Manuscript Received June 24, 2003

Several families of synthetic polymers, including degradable poly( $\beta$ -amino ester)s, have been previously shown to effectively mediate gene transfer. However, the combined impact of potentially significant factors—such as polymer molecular weight, polymer chain end-group, and polymer/DNA ratio—on different gene transfer properties has yet to be systematically investigated. The elucidation of these relationships may aid in the design of nonviral vectors with greatly enhanced transfection properties. To examine these factors, two distinct poly( $\beta$ -amino ester) structures, Poly-1 and Poly-2, were generated by adding 1,4-butanediol diacrylate and 1,6-hexanediol diacrylate, respectively, to 1-aminobutanol. Twelve unique versions of each structure were synthesized by varying amine/diacrylate stoichiometric ratios, resulting in polymers with either amine or acrylate end-groups and with molecular weights ranging from 3350 to 18 000. Using high throughput methods, all polymers were tested in quadruplicate at nine different polymer/DNA ratios ranging from 10:1 w/w to 150:1 w/w. Through the optimization of molecular weight, polymer chain end-group, and polymer/DNA ratio, these polymers successfully mediated gene transfer at levels that surpassed both PEI and Lipofectamine 2000 *in vitro*.

## INTRODUCTION

The safe and effective delivery of therapeutic genes remains a central challenge in the field of gene therapy. While the majority of current gene therapy protocols employ viral delivery systems (1), concerns regarding the safety of viral vectors have prompted many to look for synthetic alternatives (2–4). Nonviral vectors offer the promise of improved safety but have yet to match the clinical efficacy of viral systems. As a class of materials, cationic polymers have been investigated broadly in the context of nonviral gene delivery (5). These polymers not only condense DNA into structures small enough to enter cells via endocytosis, but also afford protection from nuclease degradation. To further enhance the efficacy of these systems, various groups have incorporated functional elements into polymers to improve their capacity to overcome specific barriers to gene delivery (6, 7). For example, the relatively high transfection efficiency of polyethylenimine (PEI) (8–11)—a polymer generally considered to be the standard for polymer-based gene delivery—is attributed to its “proton sponge” functionality, which allows it to overcome the lysosomal barrier to efficient gene delivery. The elucidation of additional structure–functional relationships can be accelerated by generating and screening large, structurally diverse polymer libraries. Our group has previously reported the discovery of structural elements correlating with specific gene transfer functions through the parallel synthesis and biophysical characterization of a 140-member library of unique, biodegradable poly( $\beta$ -amino ester)s (12, 13). We have recently extended this approach to the synthesis

and screening of a library containing thousands of such polymers (14).

While considerable emphasis has been placed on the use of repeat unit structure to enhance gene transfer properties, significantly less attention has been given to the investigation of nonstructural factors and their effects on gene transfer. Some of these factors, such as polymer molecular weight and polymer/DNA ratio, have been shown to impact transfection efficiency (5, 15–17). The number of polymer cation–DNA anion interactions, and thus polymer molecular weight, affects the affinity between the polymer chain and the DNA strand (17). Polymer chains that are too short do not effectively and stably condense DNA, while polymer chains that are too long retard the “unpacking” of DNA required for transcription and translation (17). Tuning polymer chain length to produce an optimal polymer–DNA affinity is likely to improve the efficacy of a given polymer-based delivery system. Polymer/DNA ratio controls the ratio of charges, affecting the complexation of polymer with DNA. This in turn impacts a number of important properties relating to gene transfer, such as the stability, cellular uptake, and cytotoxicity of the resulting complex. Although the importance of polymer molecular weight and polymer/DNA ratio have been demonstrated, to the best of our knowledge, the role of polymer chain end-groups has not yet been explored. For example, poly( $\beta$ -amino ester)s can have either amine- or acrylate-terminated chains. These polymers may have different transfection or toxicity characteristics, and therefore, controlling end-groups may be important for improving the performance of these polymer-based vectors.

Here we examine the combined effect of molecular weight, polymer/DNA ratio, and chain end-group on the transfection properties of two unique poly( $\beta$ -amino ester) structures. We demonstrate that these factors can have a dramatic effect on gene delivery function, and by

\* To whom correspondence should be addressed. E-mail: rlander@mit.edu.

<sup>†</sup> Massachusetts Institute of Technology.

<sup>‡</sup> University of Wisconsin.

<sup>§</sup> Present address: Alnylam Pharmaceuticals, Cambridge, MA 02139.



controlling these factors, we have developed poly( $\beta$ -amino ester)s that transfect better than PEI and Lipofectamine 2000, two of the best commercially available transfection reagents.

#### EXPERIMENTAL PROCEDURES

**Polymer Synthesis.** Poly-1 and Poly-2 polymers were synthesized by adding 1,4-butanediol diacrylate (99+%) and 1,6-hexanediol diacrylate (99%), respectively, to 1-aminobutanol (98%). These monomers were purchased from Alfa Aesar (Ward Hill, MA). Twelve versions each of Poly-1 and Poly-2 were generated by varying the amine/diacrylate stoichiometric ratio. To synthesize each of the 24 unique polymers, 400 mg of 1-aminobutanol was weighed into an 8 mL sample vial with Teflon-lined screw cap. Next, the appropriate amount of diacrylate was added to the vial to yield a stoichiometric ratio between 1.4 and 0.6. A small Teflon-coated stir bar was then put in each vial. The vials were capped tightly and placed on a multiposition magnetic stir-plate residing in an oven maintained at 100 °C. After a reaction time of 5 h, the vials were removed from the oven and stored at 4 °C. All polymers were analyzed by GPC. In addition, Poly-1 (amine/diacrylate = 1.025 mol/mol) and Poly-2 (amine/diacrylate = 1.025 mol/mol) were characterized by  $^1\text{H}$  NMR (300 MHz, DMSO- $d_6$ ). Poly-1: 1.25–1.45 (br  $\text{NCH}_2\text{CH}_2\text{CH}_2\text{CH}_2\text{OH}$  and  $\text{NCH}_2\text{CH}_2\text{CH}_2\text{CH}_2\text{OH}$ ), 1.50–1.65 (br  $\text{NCH}_2\text{CH}_2(\text{COO})\text{CH}_2\text{CH}_2$ ), 2.25–2.45 (br m  $\text{NCH}_2\text{CH}_2(\text{COO})\text{CH}_2\text{CH}_2$  and  $\text{NCH}_2\text{CH}_2\text{CH}_2\text{CH}_2\text{OH}$ ), 2.55–2.75 (br m  $\text{NCH}_2\text{CH}_2(\text{COO})\text{CH}_2\text{CH}_2$ ), 3.20–3.40 (br  $\text{NCH}_2\text{CH}_2\text{CH}_2\text{CH}_2\text{OH}$ ), 3.90–4.05 (br  $\text{NCH}_2\text{CH}_2(\text{COO})\text{CH}_2\text{CH}_2$ ), 4.25–4.45 (br  $\text{NCH}_2\text{CH}_2\text{CH}_2\text{CH}_2\text{OH}$ ). Poly-2: 1.20–1.45 (br  $\text{NCH}_2\text{CH}_2\text{CH}_2\text{CH}_2\text{OH}$  and  $\text{NCH}_2\text{CH}_2\text{CH}_2\text{CH}_2\text{OH}$  and  $\text{NCH}_2\text{CH}_2(\text{COO})\text{CH}_2\text{CH}_2\text{CH}_2$ ), 1.45–1.65 (br  $\text{NCH}_2\text{CH}_2(\text{COO})\text{CH}_2\text{CH}_2\text{CH}_2$ ), 2.25–2.40 (br m  $\text{NCH}_2\text{CH}_2(\text{COO})\text{CH}_2\text{CH}_2\text{CH}_2$  and  $\text{NCH}_2\text{CH}_2\text{CH}_2\text{CH}_2\text{CH}_2\text{OH}$ ), 2.55–2.70 (br m  $\text{NCH}_2\text{CH}_2(\text{COO})\text{CH}_2\text{CH}_2\text{CH}_2$ ), 3.20–3.40 (br  $\text{NCH}_2\text{CH}_2\text{CH}_2\text{CH}_2\text{OH}$ ), 3.90–4.00 (br m  $\text{NCH}_2\text{CH}_2(\text{COO})\text{CH}_2\text{CH}_2\text{CH}_2$ ), 4.25–4.45 (br  $\text{NCH}_2\text{CH}_2\text{CH}_2\text{CH}_2\text{OH}$ ).

**Gel Permeation Chromatography (GPC).** GPC was performed using a Hewlett-Packard 1100 Series isocratic pump, a Rheodyne Model 7125 injector with a 100- $\mu\text{L}$  injection loop, and a Phenogel MXL column (5  $\mu\text{m}$  mixed, 300  $\times$  7.5 mm, Phenomenex, Torrance, CA). 70% THF/30% DMSO (v/v) + 0.1 M piperidine was used as the eluent at a flow rate of 1.0 mL/min. Data were collected using an Optilab DSP interferometric refractometer (Wyatt Technology, Santa Barbara, CA) and processed using the TriSEC GPC software package (Viscotek Corporation, Houston, TX). The molecular weights and polydispersities of the polymers were determined relative to monodisperse polystyrene standards.

**Luciferase Transfection Assays.** COS-7 cells (ATCC, Manassas, VA) were seeded (14 000 cells/well) into each well of an opaque white 96-well plate (Corning-Costar, Kennebunk, ME) and allowed to attach overnight in growth medium. Growth medium was composed of 90% phenol red-free DMEM, 10% fetal bovine serum, 100 units/mL penicillin, 100  $\mu\text{g}/\text{mL}$  streptomycin (Invitrogen, Carlsbad, CA). To facilitate handling, polymer stock solutions (100 mg/mL) were prepared in DMSO solvent. Note: we have demonstrated that the small residual amount of DMSO in the transfection mixture does not affect transfection efficiency and does not result in any observable cytotoxicity. Working dilutions of each polymer were prepared (at concentrations necessary to yield the different polymer/DNA weight ratios) in 25 mM sodium acetate buffer (pH 5). Twenty five microliters of

the diluted polymer was added to 25  $\mu\text{L}$  of 60  $\mu\text{g}/\text{mL}$  pCMV–Luc DNA (Elim Biopharmaceuticals, South San Francisco, CA) in a well of a 96-well plate. The mixtures were incubated for 10 min to allow for complex formation, and then 30  $\mu\text{L}$  of the each of the polymer–DNA solutions was added to 200  $\mu\text{L}$  of Opti-MEM with sodium bicarbonate (Invitrogen) in 96-well polystyrene plates. The growth medium was removed from the cells using a 12-channel aspirating wand (V&P Scientific, San Diego, CA) after which 150  $\mu\text{L}$  of the Opti-MEM-polymer-DNA solution was immediately added. Complexes were incubated with the cells for 1 h and then removed using the 12-channel wand and replaced with 105  $\mu\text{L}$  of growth medium. Cells were allowed to grow for 3 days at 37 °C, 5%  $\text{CO}_2$ , and were then analyzed for luciferase expression. Control experiments were also performed with PEI (MW = 25 000, Sigma-Aldrich) and Lipofectamine 2000 (Invitrogen). PEI transfections were performed as described above, but using polymer:DNA weight ratios of 1:1. Lipofectamine 2000 transfections were performed as described by the vendor, except that complexes were removed after 1 h.

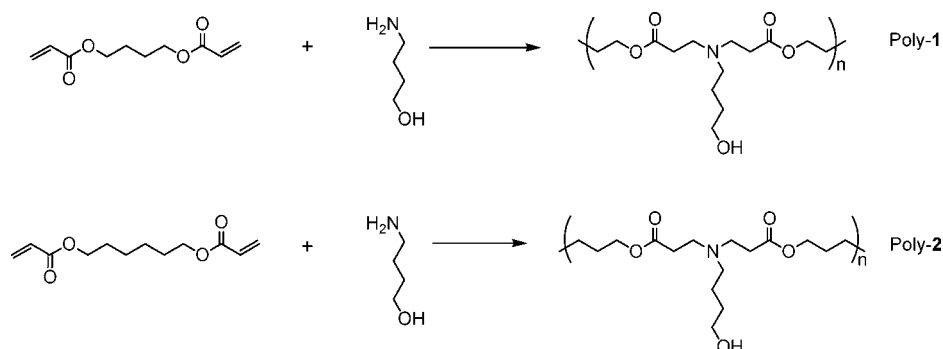
Luciferase expression was analyzed using Bright-Glo assay kits (Promega, Madison, WI). Briefly, 100  $\mu\text{L}$  of Bright-Glo solution was added to each well of the 96-well plate containing media and cells. Luminescence was measured using a Mithras Luminometer (Berthold, Oak Ridge, TN). A 1% neutral density filter (Chroma, Brattleboro, VT) was used to prevent saturation of the luminometer. A standard curve for Luciferase was generated by titration of Luciferase enzyme (Promega) into growth media in an opaque white 96-well plate.

**Measurement of Cytotoxicity.** Cytotoxicity assays were performed in the same manner as the luciferase transfection experiments with the following exception. Instead of assaying for luciferase expression after 3 days, cells were assayed for metabolic activity using the MTT Cell Proliferation Assay kit (ATCC) after 1 day. Ten microliters of MTT Reagent was added to each well. After 2 h incubation at 37 °C, 100  $\mu\text{L}$  of Detergent Reagent was added to each well. The plate was then left in the dark at room temperature for 4 h. Optical absorbance was measured at 570 nm using a SpectraMax 190 microplate reader (Molecular Devices, Sunnyvale, CA) and converted to % viability relative to control (untreated) cells.

**Cellular Uptake Experiments.** Uptake experiments were done as previously described (13), with the exception that a 12-well plate format was used instead of a 6-well plate format. COS-7 cells were seeded at a concentration of  $1.5 \times 10^5$  cells/well and grown for 24 h prior to performing the uptake experiments. Preparation of polymer/DNA complexes was done in the same manner as in the luciferase transfection experiments, the only differences being an increase in scale (2.5  $\mu\text{g}$  DNA per well of 12-well plate as opposed to 600 ng of DNA per well of 96-well plate) and the use of Cy5-labeled plasmid (18) instead of pCMV–Luc. As in the transfection experiments, complexes were incubated with cells for 1 h to allow for cellular uptake by endocytosis. The relative level of cellular uptake was quantified using a flow cytometer to measure the fluorescence of cells loaded with Cy5-labeled plasmid.

**Agarose Gel Electrophoresis Retardation Assays.** Polymer–DNA complexes were prepared as described above and run on a 1% agarose gel (TAE buffer, 90 V, 1 h). Complexes were loaded at a concentration of 200 ng DNA per well in 20  $\mu\text{L}$  volume. The loading buffer used was 10% Ficoll 400 (Amersham Pharmacia Biotech,

Scheme 1



Uppsala, Sweden) in 25 mM HEPES buffer. DNA bands were visualized by ethidium bromide staining.

**Polymer–DNA Binding Titrations.** Polymer–DNA complexes were prepared as described above and diluted in water to yield a concentration of 300 ng DNA/100  $\mu\text{L}$  solution. One hundred microliters of the aqueous solution containing the complexes was arrayed into each well of an opaque black 96-well plate. PicoGreen (Molecular Probes, Eugene, OR) solutions were prepared by diluting the supplied PicoGreen stock solution 200-fold in water containing various concentrations of NaCl. The PicoGreen solutions were prepared such that the desired salt concentration was achieved upon addition of 100  $\mu\text{L}$  of PicoGreen solution to each well containing 100  $\mu\text{L}$  of sample. After 10–15 min, the plate was analyzed using a Mithras fluorescent plate reader (Berthold, Oak Ridge, TN). Data were collected using the FITC filter set (excitation 485 nm, emission 535 nm). Fractional dye exclusion was determined by the following relationship:

$$\text{dye exclusion} = 1 - (F_{\text{sample}} - F_{\text{blank}})/(F_{\text{DNA only}} - F_{\text{blank}})$$

**GFP Transfections.** GFP transfections were carried in COS-7 (green monkey kidney), NIH 3T3 (murine fibroblast), HepG2 (human hepatocarcinoma), and CHO (Chinese Hamster Ovary) cell lines. All cell lines were obtained from ATCC (Manassas, VA) and maintained in DMEM containing 10% fetal bovine serum, 100 units/mL penicillin, 100  $\mu\text{g}/\text{mL}$  streptomycin at 37  $^{\circ}\text{C}$  in 5%  $\text{CO}_2$  atmosphere. Cells were seeded on six-well plates and grown to roughly 80–90% confluence prior to performing the transfection experiments. Polymer/DNA complexes were prepared as described above using the pEGFP–N1 plasmid (Clontech, Palo Alto, CA) (5  $\mu\text{g}/\text{well}$ ). Complexes were diluted in 1 mL Opti-MEM and added to the wells for 1 h. The complexes were then removed and fresh growth media was added to the wells. After 2 days, cells were harvested and analyzed for GFP expression by flow cytometry. Propidium iodide staining was used to exclude dead cells from the analysis.

**Flow Cytometry.** Flow cytometry was performed with a FACSCalibur (Becton Dickinson) equipped with an argon ion laser capable of exciting GFP (488 nm excitation) and a red diode laser capable of exciting Cy5 (635 nm excitation). The emission of GFP was filtered using a 530 nm band-pass filter, and the emission of Cy5 was filtered using a 650 nm long pass filter. The cells were appropriately gated by forward and side scatter and 30 000 events per sample were collected.

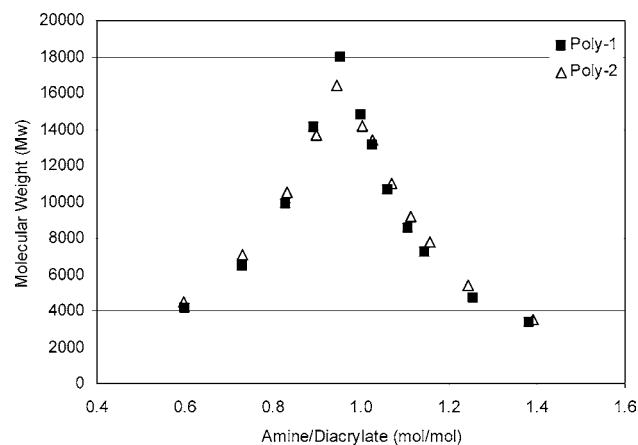
## RESULTS AND DISCUSSION

**Polymer Synthesis.** As previously described (19), the synthesis of poly( $\beta$ -amino ester)s proceeds via the con-

jugate addition of amines to acrylate groups. Because the reaction is a step polymerization, a broad, statistical distribution of chain lengths is obtained, with average molecular weight and chain end-groups controlled by monomer stoichiometry (20, 21). Molecular weight increases as the ratio of monomers nears stoichiometric equivalence, and an excess of amine or diacrylate monomer results in amine- or acrylate-terminated chains, respectively. For this class of polymers, precise control of stoichiometry is essential for controlling polymer molecular weight. While monomer stoichiometry is the most important factor affecting chain length, consideration should also be given to competing side reactions that can impact the molecular weight and structure of polymer products. In particular, intramolecular cyclization reactions, where an amine on one end of the growing polymer chain reacts with an acrylate on the other end, can limit obtained molecular weights (21). These cyclic chains may also have properties that differ from those of their linear counterparts. Also, over time, hydrolytic degradation of the polymer will result in the generation of alcohol and acid chain end-groups, potentially altering polymer properties.

In this work, we have modified the previously reported polymerization procedure (12) in order to better control monomer stoichiometry and to minimize cyclization reactions. First, the scale of synthesis was increased from roughly 0.5 g to 1 g to allow for greater control of stoichiometry. Second, all monomers were weighed into vials instead of being dispensed volumetrically. Discrepancies between actual and reported monomer densities were found to be nonnegligible in some cases, leading to inaccuracies in dispensed mass. Third, polymerizations were performed in the absence of solvent to maximize monomer concentration, thus favoring the intermolecular addition reaction over the intramolecular cyclization reaction. Eliminating the solvent also provides the added benefits of increasing the reaction rate and obviating the solvent removal step. Finally, since the previously employed methylene chloride solvent was not used, the reaction temperature could be increased from 45  $^{\circ}\text{C}$  to 100  $^{\circ}\text{C}$ . Increasing temperature resulted in an increased reaction rate and a decrease in the viscosity of the reacting mixture, helping to offset the higher viscosity of the solvent-free system. The combined effect of increased monomer concentration and reaction temperature resulted in a decrease in reaction time from roughly 5 days to 5 h. Because GPC traces of the neat polymerization products were monomodal with no monomer peaks and because NMR spectra were consistent with the hypothesized structures, polymers were used as prepared with no further purification.

We synthesized polymers Poly-1 and Poly-2 (Scheme 1) by adding 1,4-butanediol diacrylate and 1,6-hexanediol



**Figure 1.** Control of polymer molecular weight and chain end-group by varying amine/diacrylate ratio. Molecular weights ( $M_w$ ) (relative to polystyrene standards) were determined by organic phase GPC. Polymers synthesized with amine/diacrylate  $> 1$  have amine end-groups, while polymers synthesized with amine/diacrylate  $< 1$  have acrylate end-groups.

diacrylate, respectively, to 1-aminobutanol. Twelve unique versions of each polymer were synthesized by varying amine/diacrylate mole ratios between 0.6 and 1.4.

For both sets of polymers (Poly-1 and Poly-2), 7 of the 12 had amine/diacrylate ratios  $> 1$ , resulting in amine-terminated polymers, and 5 of the 12 had amine/diacrylate ratios  $< 1$ , resulting in acrylate-terminated polymers. After 5 h reaction at 100 °C, polymers were obtained as clear, slightly yellowish, viscous liquids. The polymers had observable differences in viscosity, corresponding to differences in molecular weight. Polymers were analyzed by organic phase gel permeation chromatography (GPC), employing 70% THF/30% DMSO (v/v) + 0.1 M piperidine eluent. Polymer molecular weights ( $M_w$ ) ranged from 3350 (Poly-1, amine/diacrylate = 1.38) to 18 000 (Poly-1, amine/diacrylate = 0.95), relative to polystyrene standards (Figure 1). Molecular weight distributions were monomodal with polydispersity indices (PDIs) ranging from 1.55 to 2.20 (see Supporting Information for complete PDI data). Theoretically, the maximum in molecular weight should occur at stoichiometric equivalence (amine/diacrylate = 1 mol/mol). The actual maximum in molecular weight is shifted slightly to an excess of diacrylate (Figure 1) and may be due to slight impurities in the monomers. However, consistent with theory, monomer stoichiometry was able to be utilized to control molecular weight and chain end-groups.

**Luciferase Transfection Results.** Transfection experiments were performed with all 24 synthesized polymers (12 each of Poly-1 and Poly-2) at nine different polymer/DNA ratios to determine the impact of molecular weight, polymer/DNA ratio,<sup>1</sup> and chain end-group on transfection efficiency (Figure 2). As a model system, we used the COS-7 cell line and a plasmid coding for the firefly luciferase reporter gene (pCMV-Luc) (600 ng/well). To facilitate performance of the nearly 1000 transfections (data obtained in quadruplicate), experiments

were done in 96-well plate format. Reporter protein expression levels were determined using a commercially available luciferase assay kit and a 96-well luminescence plate reader.

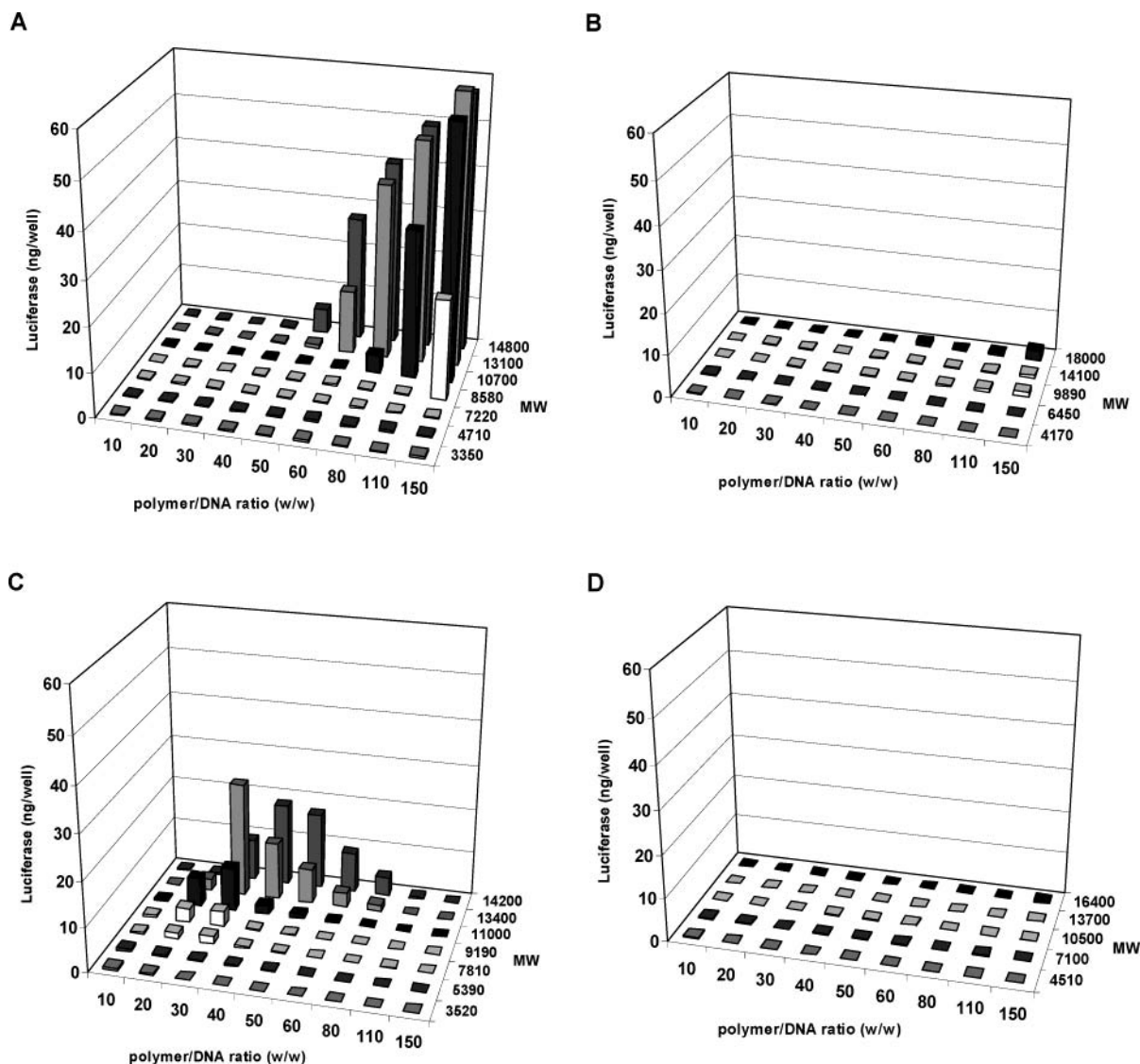
The data displayed in Figure 2 demonstrate that polymer molecular weight, polymer/DNA ratio, and chain end-group impact the transfection properties of both Poly-1 and Poly-2 polymers. One striking, and somewhat unexpected, result was that none of the acrylate-terminated polymers mediated appreciable levels of transfection under any of the evaluated conditions. This result may be more broadly applicable for poly( $\beta$ -amino ester)s, as we have yet to synthesize a polymer, using an excess of diacrylate monomer, that mediates appreciable reporter gene expression at any of the polymer/DNA ratios we have employed. These findings suggest that perhaps only amine-terminated poly( $\beta$ -amino ester)s are suitable for use as gene delivery vehicles. In contrast, there were distinct regions of transfection activity in the MW-polymer/DNA space for amine-terminated versions of both Poly-1 and Poly-2 (Figures 2A and 2C). Maximal reporter gene expression levels of 60 ng luc/well and 26 ng luc/well were achieved using Poly-1 ( $M_w = 13\ 100$ ) and Poly-2 ( $M_w = 13\ 400$ ), respectively. These results compare quite favorably with PEI (polymer/DNA = 1:1 w/w) and Lipofectamine 2000, which mediated expression levels of 6 ng luc/well and 21 ng luc/well (data not shown), respectively, under the same conditions. When an incubation time of 4 h, instead of 1 h, is employed for PEI and Lipofectamine 2000 complexes, expression levels are slightly higher, 12 ng luc/well and 27 ng luc/well (data not shown), respectively.

While the highest levels of transfection occurred using the higher molecular weight versions of both polymer structures, the optimal polymer/DNA ratios for these polymers were markedly different (polymer/DNA = 150 for Poly-1, polymer/DNA = 30 for Poly-2). The transfection results we have obtained for Poly-1 and Poly-2 highlight the importance of optimizing polymer molecular weight and polymer/DNA ratio, and the importance of controlling chain end-groups. Further, the fact that two such similar polymer structures, differing by only two carbons in the repeat unit, have such different optimal transfection parameters emphasizes the need to perform these optimizations for each unique polymer structure. To improve our understanding of the obtained transfection results, we chose to study two important delivery characteristics that directly impact transgene expression, cytotoxicity, and the ability to enter cells via endocytosis (7).

**Cytotoxicity.** As a class of materials, poly( $\beta$ -amino ester)s have been shown to be significantly less toxic than other polycations such as PEI (19). Here, we evaluated the cytotoxicities of the resultant poly( $\beta$ -amino ester)/DNA complexes using a standard MTT/thiazolyl blue dye reduction assay. The experiments were performed exactly as the transfection experiments described above, except that instead of assaying for reporter gene expression on day 3, the MTT assay was performed after day 1 (see Experimental Section). We initially hypothesized that the lack of transfection activity observed for acrylate-terminated polymers may have been due to the cytotoxicity of the acrylate end-groups. Figures 3B and 3D do indicate that high concentrations of acrylate are cytotoxic, as viability is seen to decrease with increasing polymer/DNA ratio and decreasing polymer  $M_w$  (lower  $M_w$  corresponds to a higher concentration of end-groups). However, cytotoxicity of acrylates does not sufficiently explain the lack of transfection activity at lower polymer/DNA

<sup>1</sup> We chose to use polymer/DNA weight ratios to specify the composition of complexes in order to remain consistent with our earlier publications and also because we find weight ratios to be more practical, since the overall charge on a polyamine is subject to environmental variations in pH and temperature. While DNA/polymer charge ratios are descriptive for polymers such as polylysine, they are somewhat less meaningful for polymers such as poly( $\beta$ -amino ester)s which incorporate less basic amines.



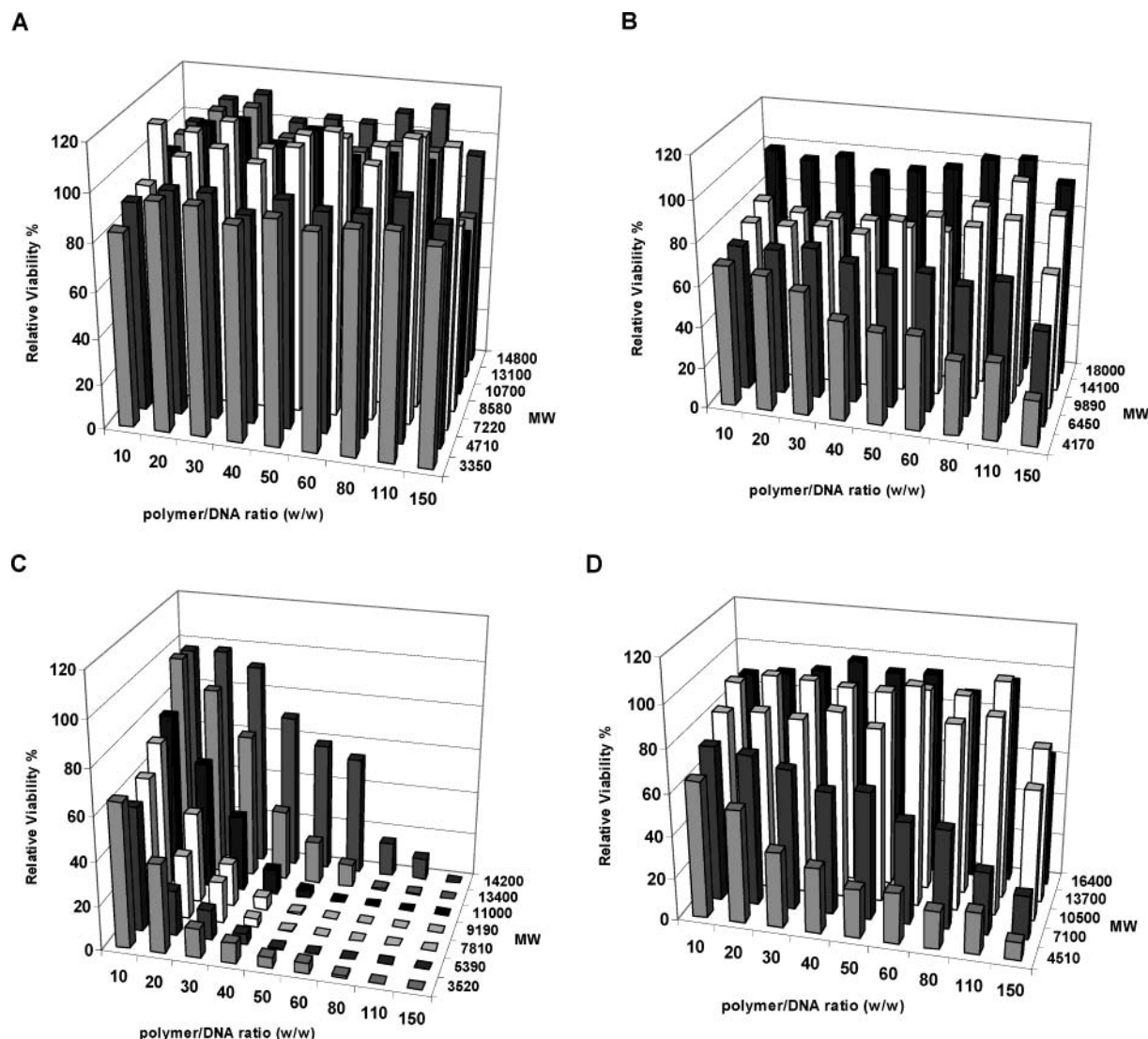


**Figure 2.** Luciferase transfection results for Poly-1 and Poly-2 as a function of polymer molecular weight, polymer/DNA ratio (w/w), and polymer end-group. (A) Poly-1, amine-terminated chains; (B) Poly-1, acrylate-terminated chains; (C) Poly-2, amine-terminated chains; (D) Poly-2, acrylate-terminated chains. Data obtained in quadruplicate (error bars not shown). Typical standard deviation = 20%.

ratios or higher molecular weights. Data shown in Figure 3A demonstrate that cytotoxicity is not a limiting factor for Poly-1 vectors, since cells remain viable even at the highest polymer/DNA ratios. On the other hand, the data displayed in Figure 3C suggest that cytotoxicity is a major factor limiting the transfection efficiency of Poly-2 vectors, especially for the lower molecular weight polymers. This result may explain why transfection activity is nonexistent or decreasing for Poly-2 vectors at polymer/DNA > 30 (see Figure 2C).

**Cellular Uptake.** The ability of polymer/DNA complexes to be taken up by cells was evaluated using a previously described flow cytometry-based technique (13) to measure the fluorescence of vector-delivered DNA. Briefly, polymer/DNA complexes were prepared using plasmid DNA covalently labeled with the fluorescent dye Cy5. To allow for comparison of the cellular uptake data with the gene expression data outlined above, complexes were formed at the same polymer/DNA ratios and in the same manner as in the transfection experiments. Labeled complexes were incubated with COS-7 cells for 1 h at 37 °C to allow for uptake. The relative level of particle uptake was then quantified by measuring the fluores-

cence of cells loaded with Cy5-labeled DNA. The results of these uptake experiments are summarized in Figure 4. Data shown in Figures 4B and 4D suggest that the lack of transfection activity for the acrylate-terminated polymers is not due to cytotoxicity, as initially thought, but rather to an inability to enter the cell. Similarly, Poly-1 complexes are severely uptake-limited at all but the highest polymer/DNA ratios (Figure 4A). These data are consistent with the fact that high levels of transfection activity using Poly-1 are not observed until very high polymer/DNA ratios are employed. The fact that transfection activity is observed at conditions where significant levels of cellular uptake is not detected may be due to the lower sensitivity of the uptake assay as compared to the luciferase gene expression assay. Poly-2 complexes show no appreciable cellular uptake at polymer/DNA ratios < 30 and increasing levels of uptake as polymer/DNA ratios increase beyond 30 (Figure 4C). This result, combined with the above cytotoxicity results, helps to explain the transfection activity of Poly-2 complexes. At polymer/DNA ratios less than 30, complexes do not effectively enter the cell, but as polymer/DNA ratios increase much beyond 30, cytotoxicity begins to limit



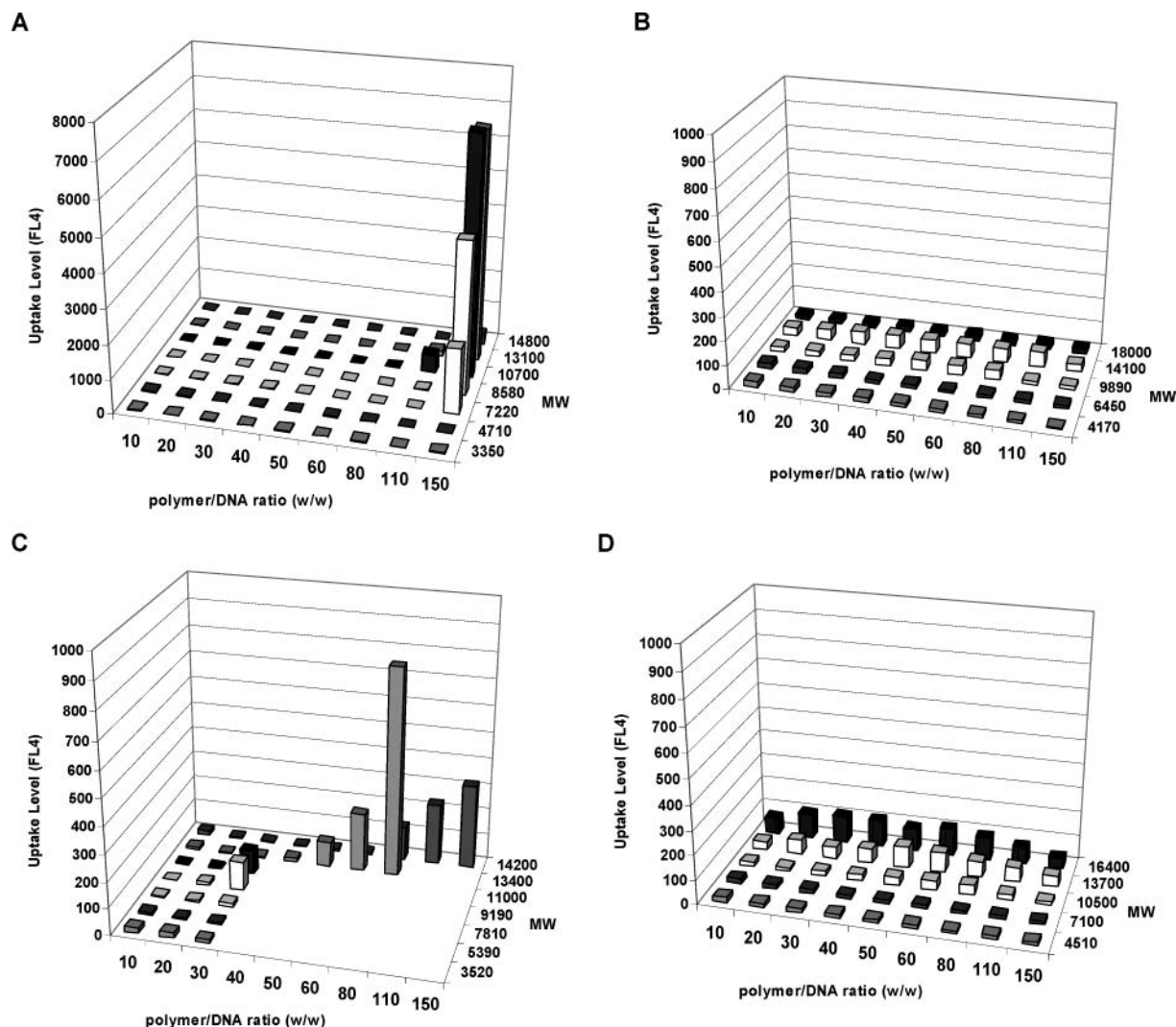
**Figure 3.** Cytotoxicity of polymer/DNA complexes prepared using Poly-1 and Poly-2 as a function of polymer molecular weight, polymer/DNA ratio (w/w), and polymer end-group. (A) Poly-1, amine-terminated chains; (B) Poly-1, acrylate-terminated chains; (C) Poly-2, amine-terminated chains; (D) Poly-2, acrylate-terminated chains. Data obtained in triplicate (error bars not shown). Typical standard deviation = 10%.

transfection efficiency, resulting in optimal transfection activity near polymer/DNA = 30.

Where endocytosis is the main route of cellular entry, the effective formation of nanometer-scale polymer/DNA complexes is one requirement for achieving high levels of cellular uptake (5, 22). We hypothesized that the poor uptake levels observed for many of the polymer/DNA complexes may have been attributable to the unsuccessful formation of stable, nanoscale complexes. Polymer/DNA complexation was investigated by agarose gel electrophoresis (Figure 5). The data indicate that the lower molecular weight amine-terminated versions of Poly-1 ( $M_w \leq 10\,700$ ) and Poly-2 ( $M_w \leq 11\,000$ ) were unable to retard the migration of DNA through an agarose gel, even at polymer/DNA ratios as high as 150:1 w/w, suggesting that these polymers may not be forming stable complexes with DNA. This is consistent with the fact that, in general, the higher molecular weight amine-terminated polymers mediated higher levels of transfection. Interestingly, significant levels of transfection were also obtained in some cases with polymers having molecular weights as low as  $\sim 8000$ . This is perhaps due to the fact that the gel electrophoresis assay does not exactly reproduce the polymer/DNA binding environment of the

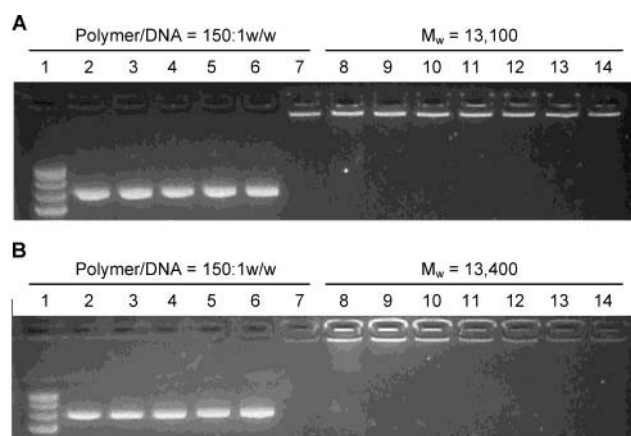
actual transfection experiment. In contrast, amine-terminated Poly-1 and Poly-2 polymers—with molecular weights of 13 100 and 13 400, respectively—were able to retard the migration of DNA at even the lowest polymer/DNA ratios investigated (10:1 w/w). The DNA binding affinity of acrylate-terminated polymers was not able to be studied using gel electrophoresis due to the poor aqueous solubility of these polymers. Furthermore, the low solubility of the acrylate-terminated polymers may be responsible for their poor uptake levels. Low solubility may limit the interaction of the polymer with the DNA residing in the aqueous phase or may result in the formation of large insoluble polymer/DNA aggregates which are unable to be efficiently internalized by cells.

**Transfection Using a Cocomplexing Agent.** Both Poly-1 and Poly-2 require relatively high polymer/DNA weight ratios to achieve high levels of gene transfer. One explanation may be that, compared to other polymers often used to compact DNA (eg. polylysine (PLL) and PEI), these polymers have relatively low amine densities. Poly-1 has a molecular weight per amine group (MW/N) of 287, and Poly-2 has a MW/N of 315. By comparison, for PLL and PEI, these figures are roughly 65 and 43, respectively. We reasoned that it might be possible to



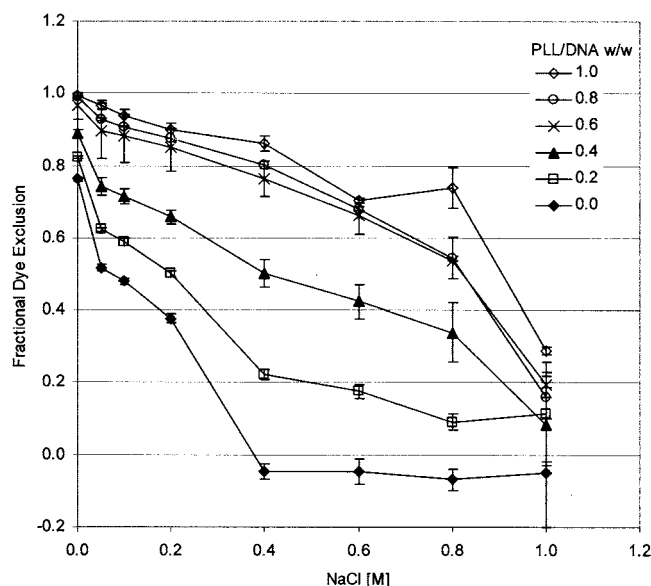
**Figure 4.** Relative cellular uptake level of polymer/DNA complexes prepared using Poly-1 and Poly-2 as a function of polymer molecular weight, polymer/DNA ratio (w/w), and polymer end-group. (A) Poly-1, amine-terminated chains; (B) Poly-1, acrylate-terminated chains; (C) Poly-2, amine-terminated chains. Note: blank squares represent conditions where cytotoxicity of the complexes prevented a reliable measurement of cellular uptake; (D) Poly-2, acrylate-terminated chains.

reduce the amount of Poly-1 or Poly-2 necessary to achieve high levels of transfection by incorporating a small amount of cocomplexing agent. We felt this approach could be especially beneficial for Poly-2 vectors, since cytotoxicity appears to be an important limitation for these vectors. To test this hypothesis, PLL was used as a model cocomplexing agent. PLL was chosen because it is a relatively poor transfection agent on its own, yet can effectively complex DNA. We focused our attention on the most promising member in each of the Poly-1 (amine-terminated,  $M_w = 13\ 100$ ) and Poly-2 (amine-terminated,  $M_w = 13\ 400$ ) sets of polymers. To first verify whether the addition of PLL could improve DNA complexation, we performed salt titrations in the presence of PicoGreen, a DNA intercalating dye. Exclusion of the intercalating dye from the DNA can be used to assess the integrity of the polymer/DNA complex (23–26). Ternary complexes were prepared with a fixed amount of Poly-1 (amine-terminated,  $M_w = 13\ 100$ ) (Poly-1/DNA = 40/1 w/w) and varying amounts of PLL (PLL/DNA = 0/1 to 1/1 w/w). The results shown in Figure 6 clearly demonstrate that the addition of PLL does improve the ability of the complex to exclude the dye from the DNA. With no PLL added, only 50 mM NaCl is required to reduce the fractional dye exclusion to one-half. However,



**Figure 5.** Polymer/DNA binding interaction determined by agarose gel electrophoresis. (A) Poly-1, amine-terminated chains, lane (1) DNA ladder control; lanes (2–7) polymer/DNA = 150:1 w/w, (2)  $M_w = 3350$ , (3) 4710, (4) 7220, (5) 8580, (6) 10700, (7) 13100; lanes (8–14)  $M_w = 13\ 100$ , (8) polymer/DNA = 10:1 w/w, (9) 20:1, (10) 40:1, (11) 60:1, (12) 80:1, (13) 110:1, (14) 150:1. (B) Poly-2, amine-terminated chains, lane (1) DNA ladder control; lanes (2–7) polymer/DNA = 150:1 w/w, (2)  $M_w = 3520$ , (3) 5390, (4) 7810, (5) 9190, (6) 11000, (7) 13400; lanes (8–14)  $M_w = 13400$ , (8) polymer/DNA = 10:1 w/w, (9) 20:1, (10) 40:1, (11) 60:1, (12) 80:1, (13) 110:1, (14) 150:1.



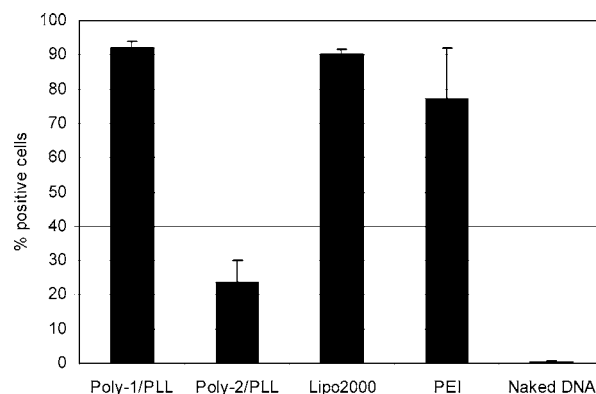


**Figure 6.** Enhancement of complex stability through the addition of PLL as a cocomplexing agent while maintaining Poly-1/DNA constant at 40:1 w/w. Complex stability determined by the exclusion of the dsDNA intercalating dye PicoGreen in the presence of varying concentrations of salt.

with the addition of PLL at PLL/DNA = 0.6:1 w/w, over 0.8 M NaCl is necessary to achieve the same reduction in dye exclusion.

The data displayed in Figures 7 indicates that, through the use of PLL as a cocomplexing agent, a significant reduction in polymer could be achieved while maintaining high levels of transfection activity. In some cases, appreciable enhancement of transfection activity was realized. As expected, this cocomplexation approach was particularly beneficial for Poly-2 vectors. It should be noted that the use of PLL on its own did not result in significant levels of transfection (Figure 7). This work, and prior work (27–30), demonstrates that the blending of polymers with complementary gene transfer characteristics can in some cases produce more effective gene delivery reagents.

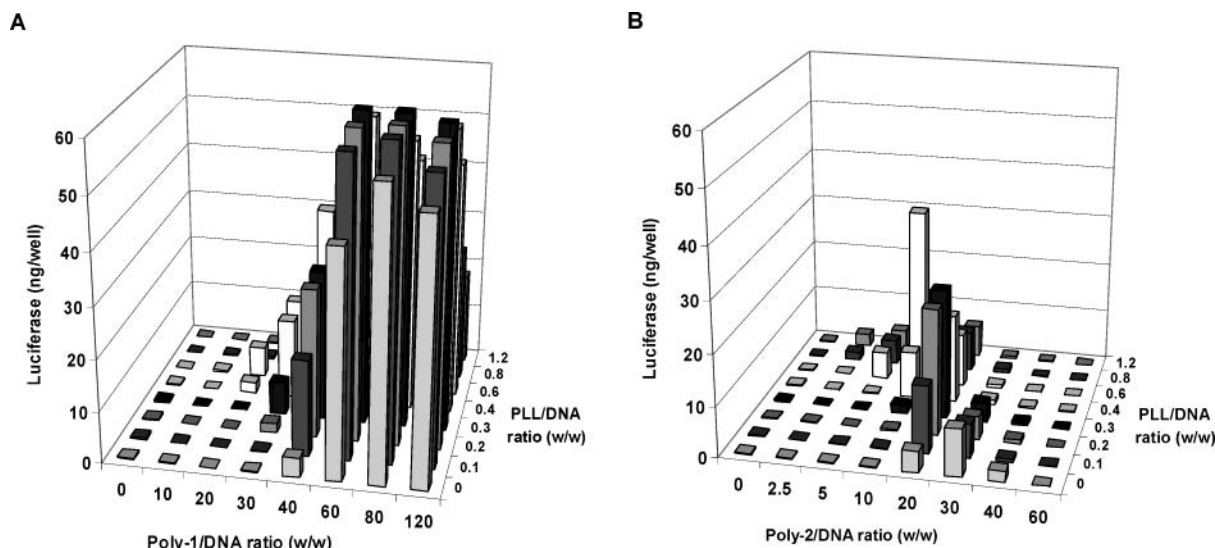
**GFP Transfections.** To further evaluate the transfection properties of the Poly-1/PLL and Poly-2/PLL



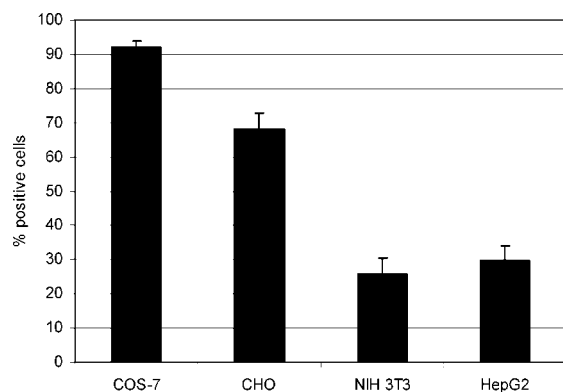
**Figure 8.** GFP gene transfer into COS-7 cells using Poly-1/PLL (Poly-1:PLL:DNA = 60:0.1:1 w/w/w), Poly-2/PLL (Poly-2:PLL:DNA = 15:0.4:1 w/w/w), Lipofectamine 2000 ( $\mu\text{L}$  reagent:  $\mu\text{g}$  DNA = 1:1), PEI (PEI:DNA = 1:1 w/w, N/P  $\sim$  8), and naked DNA. Cells were seeded on 6-well plates and grown to near confluence. Cells were incubated with complexes (5  $\mu\text{g}$  DNA/well) for 1 h, after which time complexes were removed and fresh growth media was added. Two days later GFP expression was assayed by flow cytometry. ( $n = 3$ , error bars indicate standard deviation).

blended reagents, we performed transfection experiments using a reporter plasmid coding for green fluorescent protein (pCMV-EGFP). Though the luciferase and GFP transfection assay systems both measure transfection activity, they provide different types of information. The luciferase system quantifies the total amount of exogenous luciferase protein produced by all the cells in a given well, providing a measure of cumulative transfection activity. In contrast, the GFP system can be used to quantify the percentage of cells that have been transfected, providing a cell-by-cell measure of transfection activity. Both systems are useful and offer complementary information regarding the transfection properties of a given gene delivery system.

GFP transfections were performed in a similar manner as the luciferase experiments, but were scaled up to six-well plate format (5  $\mu\text{g}$  plasmid/well). COS-7 cells were transfected using Poly-1/PLL (Poly-1:PLL:DNA = 60:0.1:1 w/w/w) and Poly-2/PLL (Poly-2:PLL:DNA = 15:0.4:1 w/w/w). Lipofectamine 2000 ( $\mu\text{L}$  reagent:  $\mu\text{g}$  DNA



**Figure 7.** Enhancement of transfection activity of Poly-1 and Poly-2 based delivery vectors through the use of PLL as a co-complexing agent. (A) Poly-1, amine-terminated chains,  $M_w = 13\,100$  blended with different amounts of PLL; (B) Poly-2, amine-terminated chains,  $M_w = 13\,400$  blended with different amounts of PLL. Data obtained in quadruplicate (error bars not shown). Typical standard deviation = 20%.



**Figure 9.** GFP gene transfer into different cell lines using Poly-1/PLL (Poly-1:PLL:DNA = 60:0.1:1 w/w/w) ( $n = 5$ , error bars indicate standard deviation). Cells were seeded on six-well plates and grown to near confluence. Cells were incubated with complexes (5  $\mu$ g DNA/well) for 1 h, after which time complexes were removed and fresh growth media was added. Two days later GFP expression was assayed by flow cytometry.

= 1:1), PEI (PEI:DNA = 1:1 w/w, N/P  $\sim$  8), and naked DNA were used as controls in the experiment. After 1 h incubation with cells, vectors were removed, and fresh growth media was added. Two days later GFP expression was assayed using a flow cytometer. Nearly all cells transfected with Poly-1/PLL were positive for GFP expression (Figure 8). Experiments indicated that Poly-2/PLL vectors were less effective, resulting in roughly 25% positive cells. Positive controls Lipofectamine 2000 and PEI were also able to mediate effective transfection of COS-7 cells under the conditions employed. Although Lipofectamine 2000 and PEI transfections resulted in nearly the same percentage of GFP-positive cells as Poly-1/PLL, the fluorescence level of GFP-positive cells was higher for Poly-1/PLL (mean fluorescence = 6033) than that of both Lipofectamine 2000 (mean fluorescence = 5453) and PEI (mean fluorescence = 2882). Multiplying the percentage of positive cells by the mean fluorescence level of positive cells provides a measure of aggregate expression for the sample and should, in theory, better correlate with the results of luciferase gene expression experiments. Quantifying total GFP expression in this manner indicates that the highest expression level is achieved by Poly-1/PLL, followed by Lipofectamine 2000 and PEI. This result is in general agreement with the luciferase expression results.

Experiments have shown that the Poly-1/PLL blend is a highly effective vector for transfecting COS-7 cells. The ability of this vector to mediate transfection in three other commonly used cell lines (CHO, NIH 3T3, and HepG2) was also investigated. It is very likely that each of these cell lines have optimal transfection conditions that differ from those used to transfect COS-7 cells; however, as a preliminary evaluation of the ability to transfect multiple cell lines, transfections were performed in the same manner and under the same conditions as the COS-7 transfections. Results indicate that Poly-1/PLL (Poly-1:PLL:DNA = 60:0.1:1 w/w/w) is able to successfully transfect CHO, NIH 3T3, and HepG2 cells, though not as effectively as COS-7 cells (Figure 9). This is not too surprising since the vector used was optimized by screening for gene transfer in COS-7 cells. We expect that the optimization of vector composition and transfection conditions specific for each cell type will result in even higher transfection levels.

## SUMMARY

In this work, we have systematically investigated the role of polymer molecular weight, polymer chain end-group, and polymer/DNA ratio on a number of important gene transfer properties. All three factors were found to have a significant impact on gene transfer, highlighting the benefit of carefully controlling and optimizing these parameters. In addition, we found that the incorporation of a small amount of PLL, used to aid complexation, could reduce the total amount of polymer required to achieve high levels of gene transfer. Through these approaches we have generated degradable polymer-based vectors that rival some of the best available nonviral vectors for in vitro gene transfer. We are currently optimizing polymer structure and formulation in the presence of serum in preparation for in vivo testing.

## ACKNOWLEDGMENT

We thank Dr. Xinqiao Jia for assistance with  $^1\text{H}$  NMR analysis of synthesized polymers. This work was supported by the NSF (through the MIT Biotechnology Process and Engineering Center) and NIH Grant EB 00244. A.A. thanks the NSF for a graduate fellowship. D.G.A. also thanks the NIH for a postdoctoral fellowship.

**Supporting Information Available:** A table showing GPC characterization of polymers used in study. This material is available free of charge via the Internet at <http://pubs.acs.org>.

## LITERATURE CITED

- <http://www.wiley.co.uk/genetherapy/clinical/> (2002).
- Felgner, P. L. (1997) Nonviral strategies for gene therapy. *Sci. Am.* 276, 102–106.
- Luo, D., and Saltzman, W. M. (2000) Synthetic DNA delivery systems. *Nat. Biotechnol.* 18, 33–37.
- Somia, N., and Verma, I. M. (2000) Gene therapy: Trials and tribulations. *Nat. Rev. Genet.* 1, 91–99.
- De Smedt, S. C., Demeester, J., and Hennink, W. E. (2000) Cationic polymer based gene delivery systems. *Pharm. Res.* 17, 113–126.
- Hwang, S. J., and Davis, M. E. (2001) Cationic polymers for gene delivery: Designs for overcoming barriers to systemic administration. *Curr. Opin. Mol. Ther.* 3, 183–191.
- Wiethoff, C. M., and Middaugh, C. R. (2003) Barriers to nonviral gene delivery. *J. Pharm. Sci.* 92, 203–217.
- Boussif, O., Lezoualc'h, F., Zanta, M. A., Mergny, M. D., Scherman, D., Demeneix, B., and Behr, J. P. (1995) A versatile vector for gene and oligonucleotide transfer into cells in culture and in vivo: polyethylenimine. *Proc. Natl. Acad. Sci. U.S.A.* 92, 7297–7301.
- Abdallah, B., Hassan, A., Benoist, C., Goula, D., Behr, J. P., and Demeneix, B. A. (1996) A powerful nonviral vector for in vivo gene transfer into the adult mammalian brain: polyethylenimine. *Hum. Gene Ther.* 7, 1947–1954.
- Behr, J. P. (1997) The Proton Sponge: A Trick to Enter Cells the Viruses Did Not Exploit. *Chimia* 51, 34–36.
- Pollard, H., Remy, J. S., Loussouarn, G., Demolombe, S., Behr, J. P., and Escande, D. (1998) Polyethylenimine but not cationic lipids promotes transgene delivery to the nucleus in mammalian cells. *J. Biol. Chem.* 273, 7507–11.
- Lynn, D. M., Anderson, D. G., Putnam, D., and Langer, R. (2001) Accelerated discovery of synthetic transfection vectors: parallel synthesis and screening of a degradable polymer library. *J. Am. Chem. Soc.* 123, 8155–8156.
- Akinc, A., Lynn, D. M., Anderson, D. G., and Langer, R. (2003) Parallel synthesis and biophysical characterization of a degradable polymer library of gene delivery. *J. Am. Chem. Soc.* 125, 5316–5323.
- Anderson, D. G., Lynn, D. M., and Langer, R. (2003) Semi-automated synthesis and screening of a large library of

- degradable cationic polymers for gene delivery. *Angew. Chem.* 42, 3153–3158.
- (15) Kabanov, A. V., and Kabanov, V. A. (1995) DNA complexes with polycations for the delivery of genetic material into cells. *Bioconjugate Chem.* 6, 7–20.
- (16) Godbey, W. T., Wu, K. K., and Mikos, A. G. (1999) Size matters: molecular weight affects the efficiency of poly-(ethylenimine) as a gene delivery vehicle. *J. Biomed. Mater. Res.* 45, 268–275.
- (17) Schaffer, D. V., Fidelman, N. A., Dan, N., and Lauffenburger, D. A. (2000) Vector unpacking as a potential barrier for receptor-mediated polyplex gene delivery. *Biotechnol. Bioeng.* 67, 598–606.
- (18) Akinc, A., and Langer, R. (2002) Measuring the pH environment of DNA delivered using nonviral vectors: Implications for lysosomal trafficking. *Biotechnol. Bioeng.* 78, 503–508.
- (19) Lynn, D. M., and Langer, R. (2000) Degradable poly( $\beta$ -amino esters): synthesis, characterization, and self-assembly with plasmid DNA. *J. Am. Chem. Soc.* 122, 10761–10768.
- (20) Flory, P. (1953) *Principles of Polymer Chemistry*, pp 40–46, 318–323, Cornell University Press, Ithaca, NY.
- (21) Odian, G. (1991) Step Polymerization *Principles of Polymerization*, pp 73–89, John Wiley & Sons, Inc., New York.
- (22) Prabha, S., Zhou, W. Z., Panyam, J., and Labhasetwar, V. (2002) Size-dependency of nanoparticle-mediated gene transfection: studies with fractionated nanoparticles. *Int. J. Pharm.* 244, 105–115.
- (23) Tsai, J. T., Furstoss, K. J., Michnick, T., Sloane, D. L., and Paul, R. W. (2002) Quantitative physical characterization of lipid-polycation–DNA lipopolyplexes. *Biotechnol. Appl. Biochem.* 36, 13–20.
- (24) Banerjee, R., Mahidhar, Y. V., Chaudhuri, A., Gopal, V., and Rao, N. M. (2001) Design, synthesis, and transfection biology of novel cationic glycolipids for use in liposomal gene delivery. *J. Med. Chem.* 44, 4176–85.
- (25) Lucas, P., Milroy, D. A., Thomas, B. J., Moss, S. H., and Pouton, C. W. (1999) Pharmaceutical and biological properties of poly(amino acid)/DNA polyplexes. *J. Drug Target.* 7, 143–56.
- (26) Ramsay, E., Hadgraft, J., Birchall, J., and Gumbleton, M. (2000) Examination of the biophysical interaction between plasmid DNA and the polycations, polylysine and poly-ornithine, as a basis for their differential gene transfection in-vitro. *Int. J. Pharm.* 210, 97–107.
- (27) Wagner, E., Plank, C., Zatloukal, K., Cotten, M., and Birnstiel, M. L. (1992) Influenza virus hemagglutinin HA-2 N-terminal fusogenic peptides augment gene transfer by transferrin-polylysine-DNA complexes: toward a synthetic virus-like gene-transfer vehicle. *Proc. Natl. Acad. Sci. U.S.A.* 89, 7934–8.
- (28) Fritz, J. D., Herweijer, H., Zhang, G., and Wolff, J. A. (1996) Gene transfer into mammalian cells using histone-condensed plasmid DNA. *Hum. Gene Ther.* 7, 1395–1404.
- (29) Pack, D. W., Putnam, D., and Langer, R. (2000) Design of imidazole-containing endosomolytic biopolymers for gene delivery. *Biotechnol. Bioeng.* 67, 217–23.
- (30) Lim, Y. B., Kim, T., Lee, J. W., Kim, S. M., Kim, H. J., Kim, K., and Park, J. S. (2002) Self-Assembled Ternary Complex of Cationic Dendrimer, Cucurbituril, and DNA: Noncovalent Strategy in Developing a Gene Delivery Carrier. *Bioconjugate Chem.* 13, 1181–1185.

BC034067Y



## SUPPLEMENTARY MATERIAL

**Table S1.** GPC characterization of polymers used in study

Structure	Amine/Diacrylate (mol/mol)	M <sub>n</sub>	M <sub>w</sub>	PDI
Poly-1	1.382	2150	3350	1.56
Poly-1	1.255	2770	4710	1.70
Poly-1	1.145	4090	7220	1.77
Poly-1	1.106	4640	8580	1.85
Poly-1	1.062	5590	10700	1.91
Poly-1	1.025	7110	13100	1.84
Poly-1	1.001	6770	14800	2.19
Poly-1	0.953	9530	18000	1.89
Poly-1	0.891	7630	14100	1.85
Poly-1	0.829	5260	9890	1.88
Poly-1	0.731	3770	6450	1.71
Poly-1	0.600	2700	4170	1.54
Poly-2	1.392	2260	3520	1.56
Poly-2	1.242	3170	5390	1.70
Poly-2	1.155	4250	7810	1.84
Poly-2	1.113	4880	9190	1.88
Poly-2	1.070	5630	11000	1.95
Poly-2	1.025	7060	13400	1.90
Poly-2	1.003	7230	14200	1.96
Poly-2	0.944	8340	16400	1.97
Poly-2	0.898	7040	13700	1.95
Poly-2	0.832	5380	10500	1.95
Poly-2	0.731	3970	7100	1.79
Poly-2	0.598	2780	4510	1.62

# Pegylated Polyethylenimine–Fab' Antibody Fragment Conjugates for Targeted Gene Delivery to Human Ovarian Carcinoma Cells

Thomas Merdan,<sup>†,‡</sup> Jon Callahan,<sup>†</sup> Holger Petersen,<sup>‡</sup> Klaus Kunath,<sup>‡</sup> Udo Bakowsky,<sup>#</sup>  
Pavla Kopečková,<sup>†</sup> Thomas Kissel,<sup>‡</sup> and Jindřich Kopeček<sup>\*,†</sup>

Department of Pharmaceutics and Pharmaceutical Chemistry, The University of Utah, 30 South, 2000 East, Salt Lake City, Utah, USA, Department of Pharmaceutics and Biopharmacy, Philipps University, Ketzerbach 63, 35032 Marburg, Germany, and Department of Pharmaceutics and Biopharmacy, Saarland University, Am Stadtwald, 66041 Saarbrücken, Germany. Received May 9, 2003; Revised Manuscript Received June 25, 2003

Specific targeting of ovarian carcinoma cells using pegylated polyethylenimine (PEG–PEI) conjugated to the antigen binding fragment (Fab') of the OV-TL16 antibody, which is directed to the OA3 surface antigen, was the objective of this study. OA3 is expressed by a majority of human ovarian carcinoma cell lines. To demonstrate the ability of the PEG–PEI–Fab' to efficiently complex DNA, an ethidium bromide exclusion assay was performed. Comparison with PEG–PEI or PEI 25 kDa showed only minor differences in the ability to condense DNA. Since conjugation of Fab' to PEG–PEI might influence complex stability, this issue was addressed by incubating the complexes with increasing amounts of heparin. This assay revealed stability similar to that of unmodified PEG–PEI/DNA or PEI 25 kDa/DNA complexes. Complexes displayed a size of approximately 150 nm with a zeta potential close to neutral. The latter property is of particular interest for potential *in vivo* use, since a neutral surface charge reduces nonspecific interactions. Binding studies using flow cytometry and fluorescently labeled DNA revealed a more than 6-fold higher degree of binding of PEG–PEI–Fab'/DNA complexes to epitope-expressing cell lines compared to unmodified PEG–PEI/DNA complexes. In OA3-expressing OVCAR-3 cells, luciferase reporter gene expression was elevated up to 80-fold compared to PEG–PEI and was even higher than that of PEI 25 kDa. The advantage of this system is its specificity, which was demonstrated by competition experiments with free Fab' in the cell culture media during transfection experiments and by using OA3-negative cells. In the latter case, only a low level of reporter gene expression could be achieved with PEG–PEI–Fab'.

## INTRODUCTION

The general feasibility of gene delivery using synthetic polymers has been demonstrated in numerous studies (1–5). Cationic polymers, such as linear or branched polyethylenimine (PEI) (2, 3), starburst dendrimers (4), or imidazole containing polymers (5), were found to be suitable for *in vitro* applications. Unmodified cationic polymers lead to complexes with DNA displaying a relatively high cationic surface charge. Therefore, nonspecific binding, as well as a fairly high toxicity due to electrostatic interactions with the negatively charged components of cellular membranes, e.g., sialic acid, remain a serious limitation for *in vivo* gene delivery (3, 6). After intravenous injection of these polyplexes, serious damage of body tissues (7) and a rather high rate of mortality (8) was observed in laboratory animals.

To progress from *in vitro* gene delivery toward *in vivo* gene therapy, vectors are needed that exhibit high stability in body fluids, minimal nonspecific interactions, low toxicity, and a targeting moiety that provides selec-

tive uptake into target cells. Since an excess of cationic polymer is necessary for complexation of DNA, the cationic surface charge needs to be shielded to reduce nonspecific interactions with blood components in nontarget tissues.

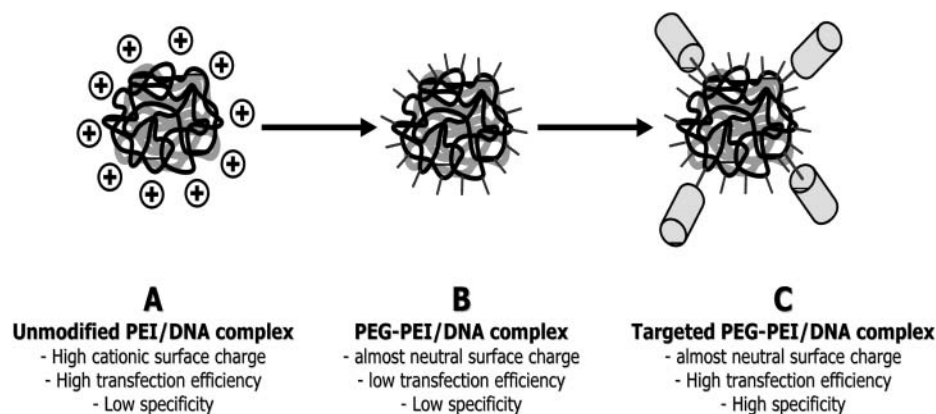
A possible strategy toward achieving an optimized polymeric gene delivery system is shown schematically in Figure 1. Polyplexes prepared with unmodified cationic polymer yield a rather high level of reporter gene expression under *in vitro* cell culture conditions (Figure 1a). Yet, due to the high cationic surface charge of these vectors, this effect is nonspecific. Pegylation (8–10) or attachment of other hydrophilic polymers, such as PHPMA (11), to cationic polymers leads to vectors with a surface charge close to neutrality (Figure 1b). Lower levels of nonspecific interactions have been demonstrated for these systems, and some have been used successfully *in vivo*. These studies have shown that such shielded gene delivery systems offer the advantage of lower toxicities and prolonged circulation times *in vivo* (8, 10). However, the resulting complexes with DNA display rather low levels of reporter gene expression. Although this property might be less favorable *in vitro*, it would be valuable for *in vivo* application because it may minimize gene expression in nontarget cells. If a targeting ligand, for example Fab', is conjugated to these polymers, the resulting complexes could then be capable of targeting specific cell types with only low levels of reporter gene expression in nontarget cells (Figure 1c).

\* Address for correspondence: Jindřich Kopeček, Department of Pharmaceutics and Pharmaceutical Chemistry, The University of Utah, 30 S 2000 E, Salt Lake City, UT 84112. Tel.: (001)–801–581–6835. Fax: (0049)–6421–282–7016. E-mail: Jindrich.Kopecek@m.cc.utah.edu.

<sup>†</sup> University of Utah.

<sup>‡</sup> Philipps University.

<sup>#</sup> Saarland University.



**Figure 1.** Rationale behind polymer modifications described in this paper. Unmodified complexes (A) displayed high levels of transfection efficiency, due solely to unspecific electrostatic interactions with cellular membranes. Pegylation of PEI (B) led to complexes with an almost neutral zeta potential; however, reporter gene expression remained at a low level. Yet, when targeting moiety was conjugated to PEG-PEI (C), the resulting PEG-PEI-Fab' complexes showed lower levels of unspecific interactions, combined with a highly specific uptake and transfection of target cells.

A variety of targeting moieties, such as transferrin (12), folate (13, 14), RGD-peptides (15, 16), different types of saccharides (17, 18), antibodies, or antibody fragments (19, 20) have been described for active gene delivery. Most studies used ligands conjugated directly to unmodified cationic polymers, such as PEI or poly(L-lysine), resulting in polymer/DNA complexes with a high cationic surface charge. Of the various targeting moieties already under investigation, antibodies and their fragments are of particular interest, due to their high specificity for their target epitopes, as well as the wide variety of possible target structures.

In this paper, we describe the use of a pegylated PEI to generate polymer/DNA complexes with a nearly neutral surface charge. We then synthesized a conjugate consisting of pegylated PEI and an antigen binding antibody fragment (Fab') that provided specific binding and efficient reporter gene expression coupled with a high specificity for target cells. Fab' was used instead of the whole monoclonal antibody due to its lower molecular weight and therefore a lower level of steric hindrance during complex formation with DNA. As a model, we used OVCAR-3 human ovarian carcinoma cells that express high levels of the OA3 surface antigen, a structure that is expressed on most human ovarian carcinomas (21, 22). The OV-TL16 antibody specifically binds to the OA3 antigen triggering subsequent internalization (22). Conjugation of OV-TL16 Fab' to PEG-PEI produced conjugates that efficiently complexed DNA. These complexes were stable and showed a very high specificity for OVCAR-3 cells as demonstrated by their enhanced binding capabilities and strongly elevated levels of reporter gene expression in vitro. Furthermore, only a low level of gene expression occurred in OA3-negative cells.

#### EXPERIMENTAL SECTION

**Chemicals and Plasmid.** PEI 25 kDa, hexamethylene diisocyanate (HMDI), PEG monomethyl ether (2 kDa), salmon testes DNA, and *N*-succinimidyl 3-(2-pyridyldithio)propionate (SPDP) were purchased from Sigma-Aldrich, Taufkirchen, Germany. Luciferase plasmid (pCMV-Luc) was produced by Plasmid Factory, Bielefeld, Germany.

**Antibody and (Fab')<sub>2</sub> Production.** OV-TL16 IgG directed against the surface antigen OA3 (21) was produced by in vitro cartridge bioreactor culture of the OV-TL16 hybridoma cell line (Cellco, Spectrum Labs, Pancho Dominguez, CA). IgG purification and pepsin

digestion to produce (Fab')<sub>2</sub> antibody fragments were performed as previously described (23).

**Cell Culture.** NIH/3T3 (Swiss mouse embryo) cell line was purchased from the German Collection of Microorganisms and Cell Cultures (DSMZ, Braunschweig, Germany). NIH:OVCAR-3 cells were purchased from the American Type Culture Collection (ATCC), Teddington, UK. Cells were cultured according to the protocols suggested by the supplier.

**Synthesis of PEG-PEI.** PEI(25k)-*g*-PEG(2k)<sub>10</sub> was synthesized via a strategy which was described previously (24). Briefly, PEG monomethyl ether (2 kDa) was dissolved in anhydrous chloroform (200 g/L) and activated with a 10-fold excess of hexamethylene diisocyanate, HMDI (60 °C, 24 h). Unreacted HMDI was carefully removed by repetitive extraction with light petrol. The reaction of activated PEG with the amino groups of PEI was carried out in anhydrous chloroform at 60 °C for 24 h. The reaction solution was precipitated in diethyl ether and the product was dried in vacuo.

**Synthesis of PEG-PEI-Fab' Conjugate.** PEG-PEI (5 mg of total polymer corresponding to 2.8 mg of PEI) was dissolved in 1 mL of reaction buffer containing 150 mM sodium chloride and 20 mM 4-(2-hydroxyethyl)-1-piperazine ethane sulfonic acid (HEPES) pH 7.5. SPDP (80 µg) was added to this solution in 80 µL of 100% ethanol while stirring and the reaction was allowed to continue for 90 min. SPDP-activated PEG-PEI was then purified by gel filtration on a PD-10 column. The amount of SPDP coupled to PEI was determined by pyridine-2-thione release upon addition of a 20-fold excess of dithiothreitol (DTT) and by measuring the absorption at 343 nm against a standard curve of pyridine-2-thione. PEG-PEI content was measured by a copper complexation assay (25).

In the second step, a 1.4-fold molar excess of freshly reduced Fab' was added in the same buffer. The reaction proceeded for 12 h at room temperature and purification was performed by ion exchange chromatography as described earlier using 0.9% NaCl, 10 mM HEPES pH 7.4 as buffer A and 3 M NaCl, 10 mM HEPES pH 7.4 as buffer B (12). The solvent was exchanged with 150 mM NaCl solution pH 7.4 via a further gel filtration step and the PEI concentration was determined by a copper complexation assay (25). The amount of Fab' per PEG-PEI was determined by UV-absorption at 280 nm with background correction using a solution of PEG-PEI with the same concentration.



**Complex Formation.** Luciferase plasmid (pCMV-Luc) and the appropriate amount of polymer were dissolved separately in a 0.9% sodium chloride solution, pH 7. The two solutions were mixed by vigorous pipetting and complexes were allowed to interact for 10 min before use. Complexes were prepared for transfection experiments with either 0.5 or 4  $\mu$ g of plasmid in 45 or 300  $\mu$ L of 0.9% NaCl and the appropriate amount of polymer or PEG–PEI–Fab' in 45 or 300  $\mu$ L of 0.9% sodium chloride solution pH 7. Flow cytometry experiments required 10  $\mu$ g of plasmid dissolved in 300  $\mu$ L of sodium chloride solution, into which the appropriate amount of polymer in 300  $\mu$ L of 0.9% NaCl was added. Complexes for the complex stability assay were formed with 1  $\mu$ g of plasmid in 50  $\mu$ L of sodium chloride solution and the appropriate amount of polymer in the same volume.

**Ethidium Bromide Exclusion Assay.** DNA condensation was measured by the decrease in ethidium bromide fluorescence, as described earlier (26). The assay was performed in 96-well plates in triplicate. Eight micrograms of salmon testes DNA was dissolved in 79  $\mu$ L of water, and 50  $\mu$ L of 60 mM Tris buffer pH 7.4 were added to each well. Volumes were equalized to 300  $\mu$ L with water. Subsequently, appropriate volumes of 0.05 mg/mL polymer solutions were added to produce N/P ratios between 0.2 and 4. These were incubated for 10 min and then 20  $\mu$ L of a 0.1 mg/mL ethidium bromide solution were added. Wells were mixed thoroughly and the fluorescence was measured using a fluorescence plate reader with excitation wavelength at 518 nm and an emission wavelength of 605 nm.

**Photon Correlation Spectroscopy.** Hydrodynamic diameters of the polymer/DNA complexes were determined by photon correlation spectroscopy. Plasmid (0.5  $\mu$ g of pCMV–Luc) in 25  $\mu$ L of 0.9% NaCl were complexed with the appropriate amount of polymer in 25  $\mu$ L of NaCl each, as described above. Measurements were performed on a Zetasizer 3000 HS from Malvern Instruments, Herrenberg, Germany (10 mW HeNe laser, 633 nm). Scattering light was detected at 90° angle through a 400  $\mu$ m pinhole. For data analysis, the viscosity (0.88 mPa s) and the refractive index (1.33) of distilled water at 25 °C were used. The instrument was routinely calibrated using Standard Reference latex particles (AZ 55 Electrophoresis Standard Kit, Malvern Instruments). Values given are the mean of five measurements.

**Measurement of Zeta Potential.** Zeta potential measurements were carried out in the standard capillary electrophoresis cell of the Zetasizer 3000 HS from Malvern Instruments at position 17.0. Measurements were performed in 0.9% NaCl, and average values were calculated with the data obtained from five runs.

**Complex Stability against Heparin.** Complexes were formed in septuplet, as described above, in a total volume of 100  $\mu$ L of sodium chloride solution at an N/P ratio of 7. To these solutions, 0.01, 0.03, 0.05, 0.1, 0.2, 0.5, and 1 IU heparin were added in 10  $\mu$ L of 0.9% sodium chloride. These solutions were mixed well and incubated for 10 min before they were applied to a 1% agarose gel containing ethidium bromide. In the eighth lane of each gel, plasmid was applied as a reference. Gels were run for 50 min at 100 V, and then scanned using a Biometra gel analyzing system.

**Atomic Force Microscopy (AFM).** The polymer–DNA complexes were prepared as described above and diluted in milliQ water (pH 5.5, 18.2 M $\Omega$ ). The formulations were directly transferred onto a silicon chip by dipping into the polyplex solution for 10 min. Atomic force microscopy was performed on a Digital Nanoscope IV

bioscope (Veeco Instruments, Santa Barbara, CA), as described elsewhere (27). The microscope was vibration-damped. Commercial pyramidal Si<sub>3</sub>N<sub>4</sub> tips (NCH–W, Veeco Instruments, Santa Barbara, CA) on a I-type cantilever with a length of 125  $\mu$ m, a resonance frequency of about 220 kHz and a nominal force constant of 36 N/m were used. All measurements were performed in tapping mode to avoid damage to the sample surface. The scan speed was proportional to the scan size. The scan frequency was between 0.5 and 1.5 Hz. Images were obtained by displaying the amplitude signal of the cantilever in the trace direction, and the height signal in the retrace direction, and both signals were simultaneously recorded. The results were visualized in amplitude mode.

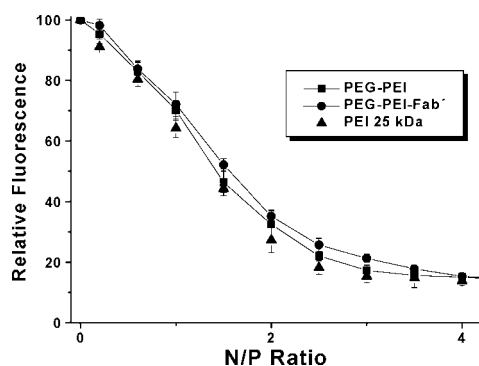
**Flow Cytometry.** Flow cytometry was performed with plasmid DNA labeled with the intercalating dye YOYO-1 (Molecular Probes, Leiden, The Netherlands), as described by Ogris et al. (28). Briefly, cells were grown for 24 h in six-well plates at a density of 400 000 cells per well. Complexes were prepared as described above and applied in fresh media with a total volume of 3 mL. After 10 min, media was aspirated and the cells were washed two times with cold (4 °C) PBS pH 7.3. Cells were suspended in PBS after detachment via trypsin incubation for 1 min. Cell suspensions were kept on ice until analysis. Flow cytometry was performed using a Becton Dickinson FACS Scan equipped with an argon laser with an excitation wavelength of 488 nm. The filter settings for emission was 530/30 nm band-pass.

**Transfection Experiments.** Transfection experiments with pCMV–Luc luciferase plasmid were performed with PEI 25 kDa, PEG–PEI, and PEG–PEI–Fab' at N/P ratios of 2.5, 3.5, 7, and 10 using 0.5 and 4  $\mu$ g of plasmid. OVCAR-3 or NIH/3T3 (negative control) cells were seeded in 12-well plates at a density of 50 000 cells per well. After 24 h, the media was removed and the complexes were added in 1.5 mL of fresh media containing different amounts of free Fab' (where applicable). Media was exchanged again after 4 h and the cells were incubated for an additional 44 h. Luciferase gene expression was quantified using a commercial kit (Promega) and photon counting on a luminometer (Sirius, Berthold). Results were measured in relative light units per second (RLU/s), which were then converted into nanograms of luciferase by creating a calibration curve with recombinant luciferase (Promega). Protein concentration in each sample was determined using a BCA assay (29). All experiments were performed in triplicate, and data were expressed in nanograms of luciferase per milligram of protein.

## RESULTS AND DISCUSSION

**Synthesis of PEG–PEI and PEG–PEI–Fab' Conjugates.** Polymer synthesis resulted in a pegylated polyethylenimine consisting of 10 PEG chains (2 kDa) grafted to one PEI 25 kDa molecule as determined by <sup>1</sup>H NMR and FT-IR spectroscopy (24). Previous investigations suggest that this degree of pegylation is suitable for obtaining vectors with a suitable size and neutral surface charge (10).

Using SPDP as a linker for coupling OV-TL16 Fab' to PEG–PEI led to efficient conjugation. SPDP modification of PEG–PEI produced a polymer containing approximately 0.5 PDP linkers per polymer. In the second step, OV-TL16 Fab' was coupled to SPDP-modified PEG–PEI. The progress and the end point of the reaction were followed by measuring pyridine-2-thione release using



**Figure 2.** Ethidium bromide exclusion assay using PEI 25 kDa, PEG-PEI, and PEG-PEI-Fab'. The ability to complex DNA was only marginally hindered by pegylation and Fab' conjugation to PEI 25 kDa.

absorption at 343 nm (data not shown). Purification of PEG-PEI-Fab' conjugate via ion exchange chromatography displayed one peak containing free Fab' shortly after application to the column in buffer A and one peak containing PEG-PEI-Fab' after changing to buffer B. UV measurement at 280 nm revealed that approximately every other polymer molecule carried one OV-TL16 Fab'. The overall polymer yield after purification was about 70%, as determined by the copper complexation assay (25).

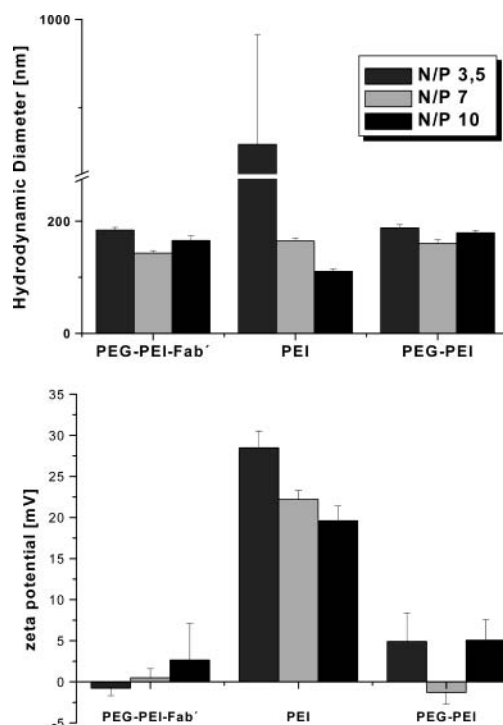
**Ethidium Bromide Exclusion Assay.** Since ethidium bromide shows fluorescence only when intercalated with DNA, the reduction of fluorescence after the addition of polymer to DNA/ethidium bromide complexes can be regarded as a measurement for the efficiency of complex formation of the polymer.

Monitoring complex formation via decrease of ethidium bromide fluorescence revealed efficient DNA complexation using the PEG-PEI-Fab' conjugate (Figure 2). The shape and position of the curve were only slightly different when compared to that of PEG-PEI or PEI 25 kDa, suggesting a similar DNA condensing ability.

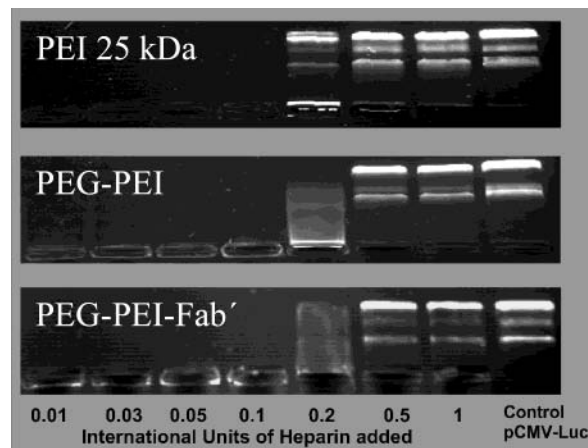
**Photon Correlation Spectroscopy.** The sizes of complexes with PEI, PEG-PEI, and PEG-PEI-Fab' at different N/P ratios are shown in Figure 3a. Complexes containing PEG displayed a similar size over N/P ratios of 3.5 to 10. Unmodified PEI 25 kDa/DNA complexes were significantly smaller at higher N/P ratios. It is very important to note that complexes of PEI 25 kDa tend to aggregate especially at low N/P ratios, with sizes increasing from about 300 to 900 nm in the first 10 min after formation (large error bar). However, those containing PEG exhibit an increase of size of less than 20 nm, probably due to efficient shielding of the cationic surface charge, thereby abolishing aggregation (data not shown). This effect has been demonstrated for pegylated PEIs in several studies (8, 24).

Furthermore, it can be summarized that all complex sizes except that of PEI 25 kDa at N/P = 3.5 are in a range that is suitable for endocytic uptake into cells (30). Remarkably, sizes of DNA complexes with PEG-PEI-Fab' are only marginally different than those of PEG-PEI/DNA complexes. Obviously, the inclusion of Fab' only slightly influences complex properties.

**Measurement of Zeta Potential.** Zeta potentials of complexes with PEI, PEG-PEI, and PEG-PEI-Fab' are shown in Figure 3b. Zeta potentials of PEG-PEI/DNA complexes are close to neutral throughout the whole N/P range tested and differences are rather small. These data suggest that the shielding effect of PEG is rather efficient, an observation that is in good agreement with



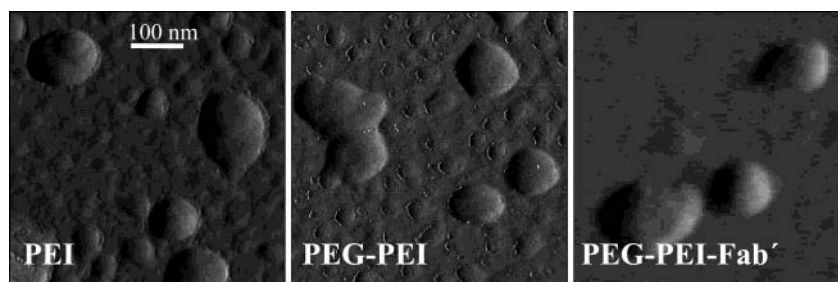
**Figure 3.** Comparison of hydrodynamic diameters and zeta potentials of complexes at three different N/P ratios.



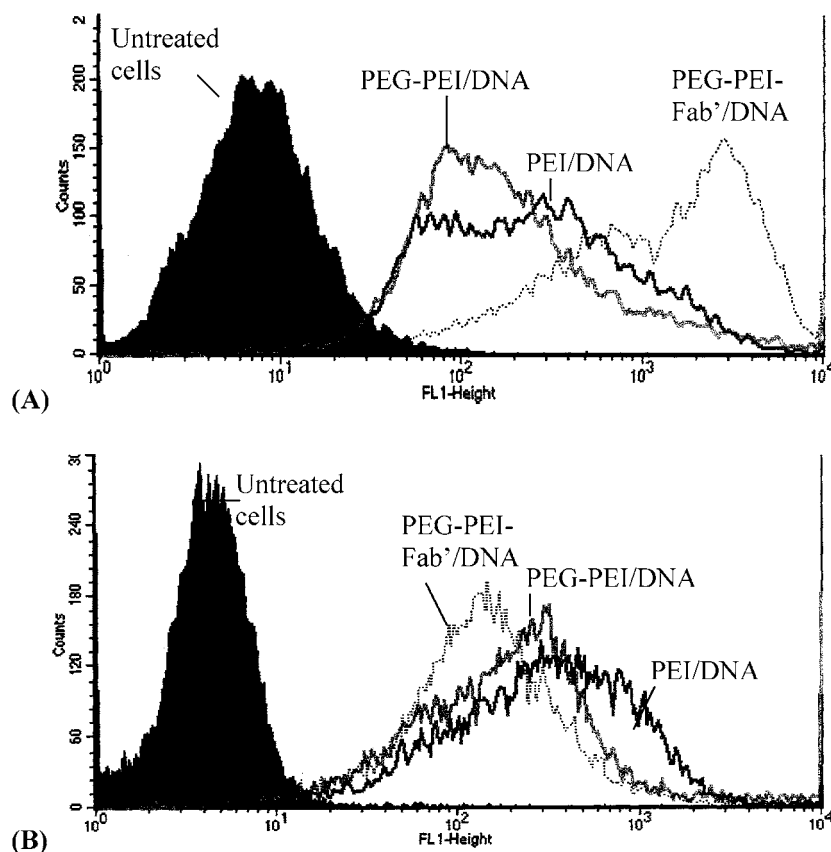
**Figure 4.** Determination of complex stability using increasing amounts of heparin. In the first seven lanes of each gel, increasing amounts of heparin were added to determine the threshold where DNA release occurs. This concentration was similar in all gels.

previous studies (9, 24, 31). Conjugation of Fab' to PEG-PEI did not lead to significant changes in surface charge of complexes at N/P ratios from 2.5 to 10. As expected, the zeta potentials of complexes with unmodified PEI were rather high. Interestingly, surface charge of these complexes decreased for N/P ratios from 3.5 and 10, although the amount of cationic polymer increased. A possible explanation for this property could be differences in complex shape and size and therefore a different exposure of cationic polymer to the surrounding media.

A neutral zeta potential is of major importance since it has been demonstrated that surface charge plays an important role for the *in vivo* fate of complexes. For example, Plank et al. found a direct relationship between opsonization of complexes via attachment of complement factors and accessible cationic surface charge (32). Furthermore, interactions of cationic polyplexes with albumin may result in the formation of large aggregates with



**Figure 5.** Atomic force microscopy images from PEI 25 kDa/plasmid, PEG–PEI/plasmid, and PEG–PEI–Fab'/plasmid complexes.



**Figure 6.** Investigation of cell binding using flow cytometry. In (A), a strongly enhanced binding of PEG–PEI–Fab'/DNA complexes to OA3-expressing OVCAR-3 cells can be observed when compared to PEG–PEI/DNA and PEI/DNA complexes at an N/P ratio 3.5. (B) Binding to NIH/3T3 cells, which do not express OA3 antigen. PEI/DNA display the strongest binding compared to PEG–PEI/DNA and PEG–PEI–Fab'/DNA complexes. The latter exhibit the least efficient binding to this non-OA3-expressing cell line at an N/P ratio of 3.5.

a reversed surface charge leading to rapid clearance by the reticuloendothelial system (33). For complexes with a neutral surface charge reduced interactions with plasma proteins, vessel endothelia or cellular blood components have been demonstrated (8, 11).

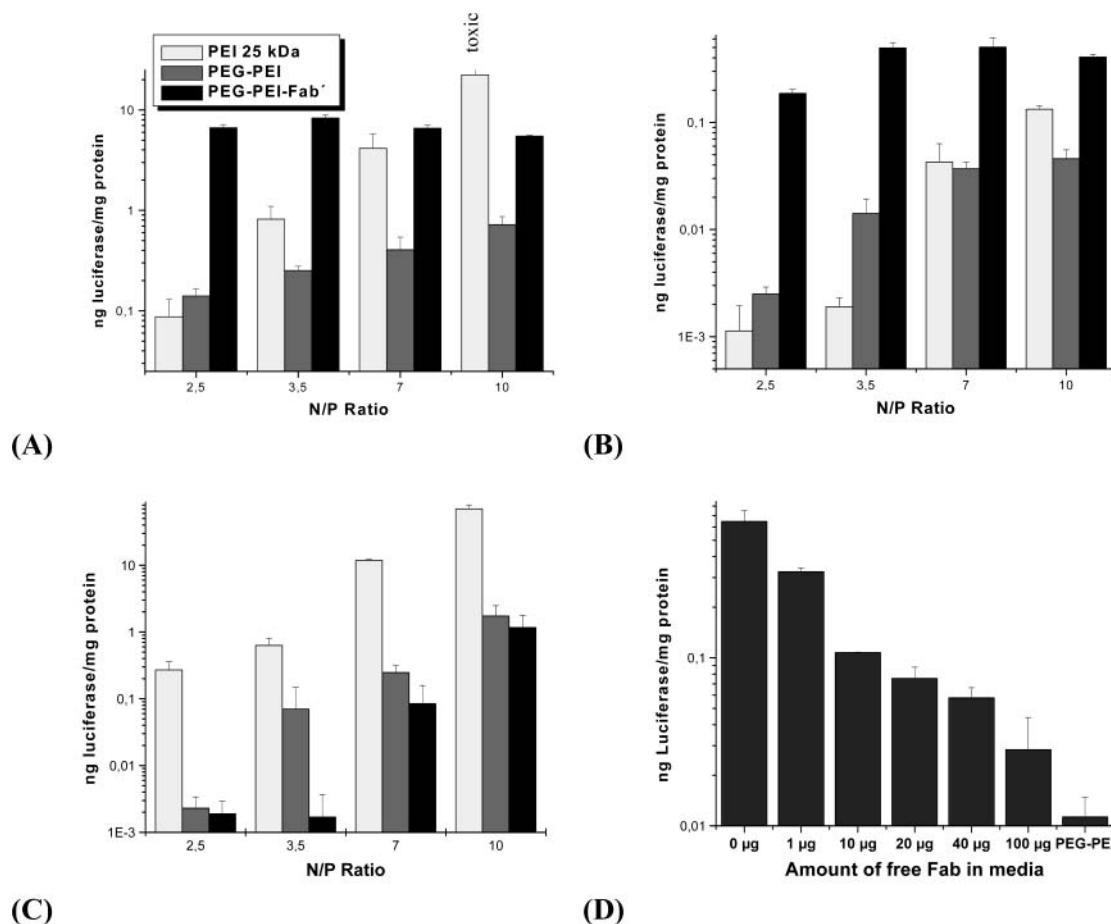
**Complex Stability against Heparin.** To evaluate complex stability, we compared levels of DNA release after incubation of PEI 25 kDa/DNA, PEG–PEI/DNA, and PEG–PEI–Fab'/DNA complexes with increasing amounts of heparin (Figure 4). Heparin, a polyanion capable of displacing DNA from polycation/DNA complexes, was chosen as a model substance for this assay. The lowest concentration of heparin where displacement occurs provides an estimation of the complex stability against polyanions. In this case, no striking differences could be detected when PEG–PEI–Fab'/DNA complexes were compared to native PEG–PEI/DNA or PEI 25 kDa/DNA complexes. In all three gels shown in Figure 4, DNA release started at the same concentration, suggesting no major influence of Fab' conjugation on complex stability.

These data are in good agreement with the DNA complexing profiles obtained in the ethidium bromide exclusion assay.

**Atomic Force Microscopy.** Images of complexes recorded under the conditions described above are shown in Figure 5. The polymers and PEG–PEI–Fab' have been shown to form defined, spherical complexes with plasmid DNA. The shape and size of complexes prepared with PEI, PEG–PEI, and PEG–PEI–Fab' were only slightly different. Size measurements from the AFM images were in good agreement with those obtained by photon correlation spectroscopy. The data indicated complex diameters around 140 nm.

**Flow Cytometry.** Flow cytometry data revealed a moderate degree of cell binding of the unmodified PEI 25 kDa/DNA complexes (Figure 6). The binding efficiency of complexes prepared with PEG–PEI is only slightly less for both cell types investigated in this study. This is somewhat surprising since surface charges of PEI/DNA complexes are about 20 mV higher than that prepared





**Figure 7.** (A) and (B) display levels of reporter gene expression in OA3-positive OVCAR-3 cells using either 4  $\mu$ g (A) or 0.5  $\mu$ g (B) of luciferase plasmid per well. Strongly enhanced levels of reporter gene expression can be observed compared to PEG-PEI, which is especially distinct at low N/P ratios. In (C), luciferase expression in OA3-negative NIH/3T3 cells using 4  $\mu$ g of pCMV-Luc per well is depicted. Here PEG-PEI-Fab'/plasmid complexes led to only low levels of reporter gene expression, stressing the high specificity of this system. (D) Levels of reporter gene expression in OVCAR-3 cells in the presence of different amounts of free Fab' in the incubation media. The higher the Fab' concentration, the lower the gene expression.

with PEG-PEI. Obviously charge is only one factor that influences cell binding. As expected, PEG-PEI-Fab'/DNA complexes show about a 6-fold higher degree of binding to OVCAR-3 cells compared to those prepared with PEI 25 kDa and PEG-PEI. However, using OA3-negative NIH/3T3 cells, PEG-PEI-Fab'/DNA complexes displayed least efficient cell binding of all three polymers. The data strongly suggest a specific binding of PEG-PEI-Fab'/DNA complexes to OA3 antigen expressing cell lines. This property is of great importance for the transfection of particular cell types *in vivo*.

**Transfection Experiments.** Data from transfection experiments using luciferase as a reporter gene are shown in Figure 7. When experiments were performed using OA3 antigen expressing OVCAR-3 cells PEG-PEI-Fab'/plasmid complexes yielded fairly high levels of reporter gene expression between N/P 2.5 and 10 using either 0.5 or 4  $\mu$ g of plasmid per well (Figure 7a,b). Expression levels were 10–80-fold higher than those of complexes prepared with PEG-PEI or unmodified PEI. In OA3-negative NIH/3T3 cells, however, reporter gene expression remained at a rather low level (Figure 7c), probably due to a lower level of cellular association as determined by flow cytometry.

In both cell lines, PEG-PEI/DNA complexes showed rather low levels of luciferase expression and only a moderate increase from N/P 2.5 to 10, probably due to the low surface charge of complexes and, therefore, a reduced uptake. Unmodified PEI, however, displayed

rather high levels of reporter gene expression at all N/P ratios with an increase of more than 2 orders of magnitude. This effect cannot be attributed to the zeta potential of complexes since it decreases with increasing N/P ratio. Increase in reporter gene expression occurs probably due to a more efficient complexation of DNA and a reduced size of complexes. This may lead to a more efficient endocytic cellular uptake.

Competition experiments with increasing amounts of Fab' in the cell culture media showed a constant decrease in reporter gene expression in the case of PEG-PEI-Fab'/DNA complexes (Figure 7d). This together with the low transfection efficiency in OA3-negative cell lines (Figure 7c) demonstrated a high degree of specificity for this gene delivery system.

Cytotoxicity of either PEG-PEI/DNA or PEG-PEI-Fab'/DNA complexes remained on a low level. At N/P = 10 using 4  $\mu$ g of DNA per well, protein content was as high as that of an untreated control containing the same amount of cells. The reason for this reduced *in vitro* toxicity is probably a reduced surface charge and therefore a reduced membrane disruptive potential of complexes as described earlier in the literature (24, 34). Unmodified PEI, however, caused a rather high cytotoxicity, leading to a protein content of as low as ~50% at this N/P ratio.

In summary, it can be stated that complexes formed with plasmid DNA and PEG-PEI-Fab' display only minor differences concerning physicochemical complex

properties compared to PEG–PEI/DNA and PEI/DNA complexes. A possible disadvantage of the method we described here may be a reduced ability of PEG–PEI–Fab' or PEG–PEI to complex DNA, or a reduced complex stability due to steric hindrance by PEG chains or the targeting moiety. However, for our system, we have been able to demonstrate that neither the grafting of ten 2 kDa PEG chains nor the conjugation of Fab' leads to significant changes in complex properties. An explanation could be that in the complex cationic PEI moiety is oriented toward the core where it efficiently interacts with DNA, leading to similar curves in the ethidium bromide exclusion assay. Hydrophilic PEG chains, as well as Fab', most likely form a shell around this core, which accounts for the efficient shielding properties and proper presentation of the targeting ligand. Consequently, complexes show a neutral zeta potential and a high level of reporter gene expression on cells expressing the OA3 antigen. The attachment of the targeting ligand to the end of a PEG spacer as described by Woodle et al. for RGD peptides (35) and Blessing et al. for EGF (epidermal growth factor) (36) could lead to further improvements of vector efficiency. This work is currently in progress.

Interestingly, the differences of reporter gene expression obtained with PEG–PEI–Fab'/DNA complexes were minor in the N/P range from 2.5 to 10. This strongly suggests an internalization or cell binding mechanism that is not related to charge. Flow cytometry data suggest that the increase in reporter gene expression with PEG–PEI–Fab'/DNA complexes when compared to PEG–PEI/DNA complexes is at least partially due to enhanced binding to OA3-positive cells. These results are in good agreement with previous studies where a variety of PEG–PEI copolymers and PEIs containing a targeting moiety have been investigated (16, 24). Advantages of the strategy described here are the possibility to produce conjugates in larger quantities and an easy one-step complex formation. Several steps are required in other strategies (8).

Due to their high specificity and low toxicity targeted vectors with PEG-shielding are attractive constructs for in vivo use. Three general approaches have been described in the literature. The first approach is the one we described here using conjugates of block polymers and a targeting moiety. In the second strategy pegylation and conjugation of a targeting moiety were performed after complex formation with unmodified PEI (36). This method was developed using EGF as a targeting moiety. Complexes prepared via this strategy showed significantly enhanced levels of reporter gene expression in target cells and almost neutral surface charges. The major disadvantage of this method compared to our procedure is that the reaction products or the reaction solvent (e.g., DMSO) may remain in the complex solution and, therefore, influence complex properties. In addition, methods for characterization the true composition of the resulting complexes with regard to the degree of pegylation, for example, are limited. Furthermore, the preparation of targeted vectors via this strategy is much more complicated than in the case of simple electrostatic vectors since several sequential steps are required.

The third approach used to obtain a targeted and pegylated vector starts with the conjugation of a targeting moiety followed by complexation with DNA. Pegylation is carried out as the last step. This strategy has been performed using EGF (36) and transferrin (8), and showed rather high levels of reporter gene expression in target cells. The advantage of this approach is the possibility of purification and characterization of the

intermediate PEI conjugate and targeting moiety. The disadvantage is the difficulty in characterizing the PEG content of the complex, the high operating expense of the pegylation process, and the possibility that reaction products may remain in the complex solution.

In conclusion, the strategy described in this paper represents a straightforward and efficient method to achieve active targeting using nonviral gene delivery systems with high specificity and low cytotoxicity. These investigations suggest that the PEG–PEI–Fab' conjugates might be promising candidates for in vivo applications.

#### ACKNOWLEDGMENT

The research was supported in part by NIH Grant CA 51578 from the National Cancer Institute. We would like to thank Eva Mohr from Philipps University, Marburg, for excellent technical support.

#### LITERATURE CITED

- (1) Boussif, O., Lezoualc'h, F., Zanta, M. A., Mergny, M. D., Scherman, D., Demeneix, B., and Behr, J. P. (1995) A versatile vector for gene and oligonucleotide transfer into cells in culture and in vivo: polyethylenimine. *Proc. Natl. Acad. Sci. U.S.A.* 92, 7297–7301.
- (2) Ferrari, S., Moro, E., Pettenazzo, A., Behr, J. P., Zacchello, F., and Scarpa, M. (1997) ExGen 500 is an efficient vector for gene delivery to lung epithelial cells in vitro and in vivo. *Gene Ther.* 4, 1100–1106.
- (3) Fischer, D., Bieber, T., Li, Y., Elsasser, H. P., and Kissel, T. (1999) A novel nonviral vector for DNA delivery based on low molecular weight, branched polyethylenimine: effect of molecular weight on transfection efficiency and cytotoxicity. *Pharm. Res.* 16, 1273–1279.
- (4) Tang, M. X., Redemann, C. T., and Szoka, F. C., Jr. (1996) In vitro gene delivery by degraded polyamidoamine dendrimers. *Bioconjugate Chem.* 7, 703–714.
- (5) Putnam, D., Gentry, C. A., Pack, D. W., and Langer, R. (2001) Polymer-based gene delivery with low cytotoxicity by a unique balance of side-chain termini. *Proc. Natl. Acad. Sci. U.S.A.* 98, 1200–1205.
- (6) Mislick, K. A., and Baldeschwieler, J. D. (1996) Evidence for the role of proteoglycans in cation-mediated gene transfer. *Proc. Natl. Acad. Sci. U.S.A.* 93, 12349–12354.
- (7) Chollet, P., Favrot, M. C., Hurbin, A., and Coll, J. L. (2002) Side-effects of a systemic injection of linear polyethylenimine-DNA complexes. *J. Gene Med.* 4, 84–91.
- (8) Ogris, M., Brunner, S., Schuller, S., Kircheis, R., and Wagner, E. (1999) PEGylated DNA/transferrin-PEI complexes: reduced interaction with blood components, extended circulation in blood and potential for systemic gene delivery. *Gene Ther.* 6, 595–605.
- (9) Wolfert, M. A., Schacht, E. H., Toncheva, V., Ulbrich, K., Nazarova, O., and Seymour, L. W. (1996) Characterization of vectors for gene therapy formed by self-assembly of DNA with synthetic block copolymers. *Hum. Gene Ther.* 7, 2123–2133.
- (10) Kunath, K., von Harpe, A., Petersen, H., Fischer, D., Voigt, K., Kissel, T., and Bickel, U. (2002) The structure of PEG-modified poly(ethylene imines) influences biodistribution and pharmacokinetics of their complexes with NF-kappaB decoy in mice. *Pharm. Res.* 19, 810–817.
- (11) Oupický, D., Howard, K. A., Koňák, Č., Dash, P. R., Ulbrich, K., and Seymour, L. W. (2000) Steric stabilization of poly-L-lysine/DNA complexes by the covalent attachment of semitelechelic poly[N-(2-hydroxypropyl)methacrylamide]. *Bioconjugate Chem.* 11, 492–501.
- (12) Kircheis, R., Kichler, A., Wallner, G., Kurs, M., Ogris, M., Felzmann, T., Buchberger, M., and Wagner, E. (1997) Coupling of cell-binding ligands to polyethylenimine for targeted gene delivery. *Gene Ther.* 4, 409–418.
- (13) Mislick, K. A., Baldeschwieler, J. D., Kayyem, J. F., and Meade, T. J. (1995) Transfection of folate-polylysine DNA

- complexes: evidence for lysosomal delivery. *Bioconjugate Chem.* 6, 512–515.
- (14) Leamon, C. P., Weigl, D., and Hendren, R. W. (1999) Folate copolymer-mediated transfection of cultured cells. *Bioconjugate Chem.* 10, 947–957.
  - (15) Erbacher, P., Remy, J. S., and Behr, J. P. (1999) Gene transfer with synthetic virus-like particles via the integrin-mediated endocytosis pathway. *Gene Ther.* 6, 138–145.
  - (16) Kunath, K., Merdan, T., Hegener, O., Häberlein, H. and Kissel, T. Integrin targeting using RGD-PEI conjugates for in vitro gene transfer. *J. Gene Med.* 5, 588–599.
  - (17) Choi, Y. H., Liu, F., Choi, J. S., Kim, S. W., and Park, J. S. (1999) Characterization of a targeted gene carrier, lactose-poly(ethylene glycol)-grafted poly-L-lysine and its complex with plasmid DNA. *Hum. Gene Ther.* 10, 2657–2665.
  - (18) Mahato, R. I., Takemura, S., Akamatsu, K., Nishikawa, M., Takakura, Y., and Hashida, M. (1997) Physicochemical and disposition characteristics of antisense oligonucleotides complexed with glycosylated poly(L-lysine). *Biochem. Pharmacol.* 53, 887–895.
  - (19) Ferkol, T., Kaetzel, C. S., and Davis, P. B. (1993) Gene transfer into respiratory epithelial cells by targeting the polymeric immunoglobulin receptor. *J. Clin. Invest.* 92, 2394–2400.
  - (20) Buschle, M., Cotten, M., Kirlappos, H., Mechtler, K., Schaffner, G., Zauner, W., Birnstiel, M. L., and Wagner, E. (1995) Receptor-mediated gene transfer into human T lymphocytes via binding of DNA/CD3 antibody particles to the CD3 T cell receptor complex. *Hum. Gene Ther.* 6, 753–761.
  - (21) Slobbe, R., Poels, L., ten Dam, G., Boerman, O., Nieland, L., Leunissen, J., Ramaekers, F., and van Eys, G. (1994) Analysis of idiotope structure of ovarian cancer antibodies: recognition of the same epitope by two monoclonal antibodies differing mainly in their heavy chain variable sequences. *Clin. Exp. Immunol.* 98, 95–103.
  - (22) Omelyanenko, V., Gentry, C., Kopecková, P., and Kopecek, J. (1998) HPMa copolymer-anticancer drug-OV-TL16 antibody conjugates. II. Processing in epithelial ovarian carcinoma cells in vitro. *Int. J. Cancer* 75, 600–608.
  - (23) Lu, Z. R., Kopecková, P., and Kopecek, J. (1999) Polymerizable Fab' antibody fragments for targeting of anticancer drugs. *Nat. Biotechnol.* 17, 1101–1104.
  - (24) Petersen, H., Fechner, P. M., Martin, A. L., Kunath, K., Stolnik, S., Roberts, C. J., Fischer, D., Davies, M. C., and Kissel, T. (2002) Polyethylenimine-graft-poly(ethylene glycol) copolymers: influence of copolymer block structure on DNA complexation and biological activities as gene delivery system. *Bioconjugate Chem.* 13, 845–854.
  - (25) von Harpe, A., Ph.D. Thesis (2000) Philipps University, Marburg, Germany.
  - (26) Petersen, H., Kunath, K., Martin, A. L., Stolnik, S., Roberts, C. J., Davies, M. C., and Kissel, T. (2002) Star-shaped poly(ethylene glycol)-*block*-polyethylenimine copolymers enhance DNA condensation of low molecular weight polyethylenimines. *Biomacromolecules* 3, 926–936.
  - (27) Oberle, V., Bakowsky, U., Zuhorn, I. S., and Hoekstra, D. (2000) Lipoplex formation under equilibrium conditions reveals a three-step mechanism. *Biophys. J.* 79, 1447–1454.
  - (28) Ogris, M., Steinlein, P., Carotta, S., Brunner, S., and Wagner, E. (2001) DNA/polyethylenimine transfection particles: influence of ligands, polymer size, and PEGylation on internalization and gene expression. *AAPS PharmSci.* 3, E21.
  - (29) Hill, H. D., Straka, J. G. (1988) Protein determination using bicinchoninic acid in the presence of sulfhydryl reagents. *Anal. Biochem.* 170, 203–208.
  - (30) Mellman, I. (1996) Endocytosis and molecular sorting. *Annu. Rev. Cell. Dev. Biol.* 12, 575–625.
  - (31) Toncheva, V., Wolfert, M. A., Dash, P. R., Oupický, D., Ulbrich, K., Seymour, L. W., and Schacht, E. H. (1998) Novel vectors for gene delivery formed by self-assembly of DNA with poly(L-lysine) grafted with hydrophilic polymers. *Biochim. Biophys. Acta* 1380, 354–368.
  - (32) Plank, C., Mechtler, K., Szoka, F. C., Jr., and Wagner, E. (1996) Activation of the complement system by synthetic DNA complexes: a potential barrier for intravenous gene delivery. *Hum. Gene Ther.* 7, 1437–1446.
  - (33) Dash, P. R., Read, M. L., Barrett, L. B., Wolfert, M. A., and Seymour, L. W. (1999) Factors affecting blood clearance and in vivo distribution of polyelectrolyte complexes for gene delivery. *Gene Ther.* 6, 643–650.
  - (34) Klemm, A. R., Young, D., and Lloyd, J. B. (1998) Effects of polyethylenimine on endocytosis and lysosome stability. *Biochem. Pharmacol.* 56, 41–46.
  - (35) Woodle, M. C., Scaria, P., Ganesh, S., Subramanian, K., Titmas, R., Cheng, C., Yang, J., Pan, Y., Weng, K., Gu, C., and Torkelson, S. (2001) Sterically stabilized polyplex: ligand-mediated activity. *J. Controlled Release* 74, 309–311.
  - (36) Blessing, T., Kurs, M., Holzhauser, R., Kircheis, R., and Wagner, E. (2001) Different strategies for formation of pegylated EGF-conjugated PEI/DNA complexes for targeted gene delivery. *Bioconjugate Chem.* 12, 529–537.

BC0340767



# Radiolabeled Constructs for Evaluation of the Asialoglycoprotein Receptor Status and Hepatic Functional Reserves

Michio Abe,<sup>†</sup> Jing Lai,<sup>†</sup> Zbigniew P. Kortylewicz,<sup>†</sup> Hideo Nagata,<sup>‡</sup> Ira J. Fox,<sup>‡</sup> Charles A. Enke,<sup>†</sup> and Janina Baranowska-Kortylewicz<sup>\*,†</sup>

University of Nebraska Medical Center, Departments of Radiation Oncology and Surgery, J. Bruce Henriksen Laboratories for Cancer Research, Omaha, Nebraska 68198. Received May 14, 2003; Revised Manuscript Received August 13, 2003

Transplantation of isolated hepatocytes may eventually replace a whole liver transplantation for the treatment of selected liver metabolic disorders and acute hepatic failure. To understand the behavior of transplanted hepatocytes, methods for longitudinal assessment of functional activity and survival of hepatocyte transplants must be developed. Targeting of asialoglycoprotein receptor (ASGPr) with various radiolabeled or Gd-labeled constructs of asialofetuin (AF) is expected to allow noninvasive and quantitative assessments of the ASGPr status in functioning hepatocytes before and after the transplant. Six new constructs of <sup>125</sup>I-, <sup>99m</sup>Tc-, <sup>153</sup>Gd-, and <sup>111</sup>In-radiolabeled AF with distinct stabilities and clearance rates were prepared and evaluated in vitro in mice, rat, porcine, and human hepatocytes, and in vivo in mice and rats. The blood and organ clearance rates, as well as liver and spleen uptake, were measured. Even extensive chemical modifications of AF with poly-L-lysine and various chelating agents do not appear to diminish AF's binding to ASGPr. Binding to isolated hepatocytes and the in vivo liver uptake studies indicate unimpaired functional activity of AF as evidenced by the rapid (<10 min) and nearly complete hepatic extraction of AF constructs from the systemic circulation. The catabolic processing and elimination of AF constructs from liver depend on the chemical modification used in the preparation of a given reagent. Radioiodinated AF has by far the shortest postabsorption (5.1 min ± 0.05 min) and elimination half-lives (2.8 ± 0.06 h) in liver. In comparison, the AF construct prepared by conjugation of DTPA- and 2-iminothiolane-substituted p-Lys with *N*-sulfosuccinimidyl 4-(*p*-maleimidophenyl)butyrate (SMPB)-modified AF (AF-SMPB-Traut-p-Lys-(<sup>111</sup>In-DTPA)<sub>20–30</sub>) has a hepatic postabsorption time of 9.1 ± 0.1 min and an elimination half-life of 44.3 ± 3.08 h, whereas [<sup>99m</sup>Tc]technetium-labeled AF appears to be permanently retained in liver. These differences in rates of liver uptake and clearance of catabolized radiolabeled AF can be used to determine functional activity of liver and transplanted hepatocytes.

## INTRODUCTION

Among the alternatives to orthotopic liver transplantation, intrasplenic transplantation of isolated hepatocytes is considered as one of the potentially most promising treatment strategies for patients with acute and chronic liver failure. Intrasplenic hepatocyte transplants are also regarded as means to achieve a temporary support of metabolic liver functions in inherited liver diseases. One of the major difficulties in this methodology is the inadequate knowledge of functional reserves and survival of transplanted hepatocytes. Development of noninvasive methods for temporal evaluation of the functional activity of hepatocytes is essential to the success of this approach. Scintigraphic studies using [<sup>111</sup>In]indium oxyquinolone-labeled hepatocytes have been used, but benefits of this method are only in a short-term assessment of the biodistribution of such a transplant (1–3). The hepatobiliary imaging with [<sup>99m</sup>Tc]-technetium iminodiacetic acid (IDA) used for the evaluation of liver transplants (4) is well suited to monitor both structural and func-

tional changes of the orthotopic grafts but is far less useful for assessment of hepatic functional reserve of the intrasplenic transplants. The primary difficulty is related to the method of <sup>99m</sup>Tc-IDA preparation. The kit consists of the chelating agent, stannous chloride, and [<sup>99m</sup>Tc]-pertechnetate and does not involve any purification steps. The whole reaction mixture is then administered as is, with some unreacted residual Sn<sup>2+</sup> and [<sup>99m</sup>Tc]pertechnetate still present. These two reagents are commonly used in nuclear medicine for in vivo and in vitro labeling of red blood cells. A proportion of circulating <sup>99m</sup>Tc-labeled red blood cells accumulates in spleen and thereby reduces contrast between transplanted hepatocytes and the spleen. An asialoglycoprotein receptor (ASGPr) scintigraphy proved to be useful in monitoring the graft and native liver functions in patients who had undergone orthotopic liver transplantation (5). ASGPr receptors on hepatocytes operate as mediators of metabolic processing for various serum glycoproteins. After binding to ASGPr, desilylated plasma proteins are transported from hepatic blood to hepatocellular lysosomes. Measurements of functioning hepatocyte mass using <sup>99m</sup>Tc-labeled diethylenetriamine-pentaacetic acid-galactosyl human serum albumin indicate that clear differences in ASGPr expression exist between normal liver and chronic liver disease. ASGPr concentrations decrease, and the degree of this change correlates with the severity of liver disease. For example,

\* Corresponding author. Janina Baranowska-Kortylewicz, Ph.D., 986850 Nebraska Medical Center, Department of Radiation Oncology, Omaha, NE 68198-6850. Telephone 402-559-8906. Fax 402-559-9127. Jbaranow@unmc.edu.

<sup>†</sup> Department of Radiation Oncology.

<sup>‡</sup> Department of Surgery.

using radiolabeled galactosylated human serum albumin, concentration of ASGPr in healthy subjects was measured at  $0.792 \pm 0.080 \mu\text{M}$ , whereas patients with chronic liver disease, such as cirrhosis, had significantly lower values ranging from  $0.0584 \pm 0.150 \mu\text{M}$ ,  $0.241 \pm 0.094 \mu\text{M}$ , and  $0.510 \pm 0.139 \mu\text{M}$ , for severe, moderate, and mild damage, respectively (6–8). However, this reagent is suitable only for short term studies. The uptake of this reagent by spleen can potentially interfere with the evaluation of intrasplenic transplants.

This study aims to establish ASGPr-based methods to monitor functional activity of hepatocytes *in vitro* before the transplant and *in vivo* when transplanted into the spleen. Several factors were considered in the design of new agents. Because the expression of ASGPr appears to correlate with the success of the hepatocyte transplant, this can be estimated beforehand through the measurement of the functional activity of this receptor in hepatocytes prepared for transplant. *In vivo*, in addition to the typically employed dynamic (morphologic) measurements of the uptake of ASGPr-targeted radiopharmaceuticals by hepatocytes, the time-course and late phase (functional) metabolic fate of the ASGPr-targeting moieties were also considered in the design of new agents and the choice of radiolabeling methods. The natural ASGPr ligand, asialofetuin, was used as a liver-specific carrier of radioisotopes. AF is a desialylated form of the native protein, a low molecular weight globulin that constitutes nearly total globulin in the blood of the fetus of ungulates. It possesses all of physical, chemical, and immunochemical characteristics of the native protein to which it can be converted by resialylation (9). Earlier studies by Morrel et al. (10, 11) and Rogers and Korfeld (9) have shown an extensive uptake of AF by the liver (over 85% of the injected dose). Most of the protein is cleared from the systemic circulation in 25 min and retained in the liver for at least 2 h. Heat denatured albumin, in amounts sufficient to significantly block phagocytic activity of the Kupffer cells, had no inhibitory effect on the liver uptake, indicating that only liver parenchymal cells are removing AF from the circulation. The uptake of AF is selective and limited to normal functioning hepatocytes through the receptor-mediated transport process. Autoradiographic studies also confirmed that this protein localizes in hepatocytes (9, 12). Because the metabolic disposition of radiolabeled AF depends on the chemical modifications necessary in the preparation of the targeting agent and the choice of the radioisotope, a comparison of the rate of uptake and clearance of metabolized/catabolized radiolabeled AF constructs is expected to provide a new insight into the functional activity of transplanted hepatocytes.

#### EXPERIMENTAL PROCEDURES

**Materials.** Diethylenetriaminepentaacetic dianhydride (DTPA-A), dithiothreitol (DTT), *N*-succinimidyl 3-(2-pyridyldithio)propionate (SPDP), *N*-sulfo-succinimidyl 4-(*p*-maleimidophenyl)butyrate (sulfo-SMPB), and 2-iminothiolane (Traut's Reagent) were from Pierce Chemical Company (Rockford, IL). All solvents, iodogen, poly-L-lysines (p-Lys), asialofetuin (AF), and gel filtration media were from Sigma-Aldrich (St. Louis, MO). Centricon filters were from Millipore Co. (Bedford, MA). Iodine-125 and indium-111 were purchased from PerkinElmer Life Sciences (Boston, MA). Technetium-99m was from Great Plains Syncor Radiopharmacy (Omaha, NE). *N*-Succinimidyl 6-hydrazinonicotinate hydrochloride (SHNH) was prepared as described by Abrams et al. (13). The method of Corson and Mears (14) was used to synthesize

(*S*)-1-*p*-isothiocyanatobenzyl-diethylenetriaminepentaacetic acid (SCN-DTPA).

**Isolation of Hepatocytes.** Mice, rat, and porcine hepatocytes were prepared using a perfusion technique of Barry and Friend (15) as modified by Seglen (16). Porcine hepatocytes were provided by Dr. Jeffrey Platt (Mayo Clinic, Rochester, MN). Male Yorkshire outbred pigs (Tufts Veterinary Facility, Garfton, MA) were used as donors. Livers were surgically removed and perfused with 1 L of cold phosphate-buffered saline (PBS) followed by 500 mL of ViaSpan (Belzer UW, Dupont) and isolated by the collagenase perfusion. The viability was assessed by trypan blue staining and was routinely >88%. The purity of the hepatocyte preparation was judged to be over 98% by immunofluorescence for class II bearing nonparenchymal cells. Isolated hepatocytes were suspended in ViaSpan and shipped to the University of Nebraska Medical Center by overnight delivery.

**Conjugation of DTPA with p-Lys [p-Lys-(DTPA)<sub>20–30</sub>] and Asialofetuin [AF-(DTPA)<sub>7</sub>].** All conjugates were prepared using methods described previously for modification of antibodies (17). Briefly, when SCN-DTPA was used, 0.1 mM solution of p-Lys hydrobromide (MW 53 900) in 0.05 M sodium carbonate buffer, pH 8.3, was reacted with 5 mM aqueous solution of SCN-DTPA at 1:300 molar ratio. The mixture was allowed to react for 2 h at room temperature. An aliquot (0.01 mL) of a crude reaction mixture was reserved for determination of the substitution ratio. The remaining mixture was transferred into an ultrafiltration device (Centricon-30) and unreacted SCN-DTPA is removed during four buffer exchanges with 1 mL of 0.05 M phosphate buffered saline, pH 7.2 (PBS). During the final buffer exchange with 0.1 M PBS, pH 7.5, the volume of the sample was reduced to achieve a concentration of p-Lys of approximately 0.2 mM. The p-Lys-DTPA conjugate was transferred into metal-free vials and stored frozen at  $-20^{\circ}\text{C}$  until ready to use. Typically 20–30 DTPA residues were associated with each molecule of p-Lys as determined using the instant thin-layer chromatography (ITLC) method (17). Reactions with DTPA dianhydride were conducted as described above with the following modification: dianhydride was dissolved in anhydrous dimethyl sulfoxide (DMSO) and used immediately. Unbound DTPA was then removed by gel filtration on Sephadex G-50 column using 0.1 M sodium phosphate buffer containing 0.1 M sodium chloride, pH 7.5. Fractions containing p-Lys-DTPA conjugate were combined and concentrated using Centricon-30. Identical methods were employed in the preparation of AF-(DTPA)<sub>7</sub>. Typically seven DTPA residues were incorporated into each molecule of AF when the reaction was conducted at 20:1 molar ratio.

**Determination of the DTPA-Protein Substitution Ratio (17).** To an aliquot of the reaction mixture containing protein, its SCN-DTPA conjugate, and unreacted (*S*)-1-*p*-isothiocyanatobenzyl-DTPA, 1 mol equiv of carrier-added  $^{111}\text{InCl}_3$  in 0.15 M acetate buffer, pH 5.3, is added. The mixture is allowed to react for 45–60 min, and a sample is withdrawn for ITLC analysis as described below. The substitution ratio is calculated using the following formula: number of DTPA molecules conjugated to one molecule asialofetuin = fraction indium bound (radioactivity associated with the origin) multiplied by the total molar equivalents of DTPA used in the conjugation reaction. The remaining reaction mixture is treated with 1000 mol equiv of diethylenetriaminepentaacetic acid, incubated for additional 5 min and analyzed

on ITLC plates to determine any nonspecific retention of indium at the plate's origin.

**Modification of Asialofetuin and p-Lys-(DTPA)<sub>20-30</sub> with 3-(2-Pyridyldithio)propionate.** AF and p-Lys are referred below as proteins. Methods used for their modification were identical. *N*-Succinimidyl 3-(2-pyridyldithio)propionate was dissolved in 95% ethanol and slowly added to proteins in 0.1 M PBS, pH 7.5, at molar ratios of 4:1 for AF and 10:1 for p-Lys-(DTPA)<sub>20-30</sub>. Reaction mixtures were left for approximately 30 min at room temperature. Unbound SPDP was removed by gel filtration on Sephadex G-50 column. Fractions containing protein were combined, and 0.1 mL aliquot was used to determine the number of 2-pyridyl disulfide residues. One milliliter of PBS was added to the SPDP-protein conjugate, and absorbance at 343 nm was recorded ( $A_1$ ). Dithiothreitol was added directly into the cuvette containing SPDP conjugates to give a final concentration of 25 mM. The reduction was allowed to proceed for 15 min, and the absorbance at 343 nm was recorded ( $A_2$ ). The molar extinction coefficient of  $8080 \text{ M}^{-1} \text{ cm}^{-1}$  was used to calculate the SPDP substitution ratio as follows: substitution ratio = concentration of 2-thiopyridone released on reduction [ $(A_2 - A_1)/8080$ ] divided by the concentration of protein.

**Modification of Asialofetuin with *N*-Sulfosuccinimidyl 4-(*p*-Maleimidophenyl)butyrate.** AF was reacted with *N*-sulfosuccinimidyl 4-(*p*-maleimidophenyl)butyrate in 20 mM sodium phosphate buffer containing 0.15 M sodium chloride, pH 7.0, at a molar ratio of 1:10 AF to SMPB. The mixture was allowed to react for 30 min at room temperature. Unbound SMPB was removed on a Sephadex G-50 column.

**Modification of p-Lys-(DTPA)<sub>20-30</sub> with the Traut's Reagent.** Traut's reagent (2-iminothiolane) in 0.16 M borate buffer, pH 8.0, was added to p-Lys-(DTPA)<sub>20-30</sub> also in 0.16 M borate buffer, pH 8.0, at a molar ratio of 20:1. The mixture was reacted for 45 min at room temperature under nitrogen. Iminothiolated protein was separated from the excess 2-iminothiolane on a Sephadex G-50 column equilibrated and eluted with PBS-EDTA.

**Preparation of 3-Mercatopropionate-Modified Asialofetuin and p-Lys-(DTPA)<sub>20-30</sub>.** SPDP conjugates prepared above were transferred into Centricon-30, and the buffer was exchanged for 0.1 M sodium acetate buffer containing 0.1 M sodium chloride, pH 4.5. DTT dissolved in water was added to a final concentration of 25 mM to liberate free thiol groups. After 30-min reduction, thiolated proteins were purified on a Sephadex G-50 column eluted with 0.1 M PBS, pH 7.5, and used immediately in the preparation of AF-p-Lys conjugates as described below.

**Conjugation of 3-Mercatopropionate-Modified Asialofetuin with 3-(2-Pyridyldithio)propionate-Modified p-Lys-(DTPA)<sub>20-30</sub> [AF-SPDP-SPDP-p-Lys-(DTPA)<sub>20-30</sub>].** 3-Mercatopropionate-modified AF in 0.1 M PBS, pH 7.5, was added to 3-(2-pyridyldithio)propionate-modified p-Lys-(DTPA)<sub>20-30</sub> in the same buffer at a molar ratio of 1:1. The reaction progress was followed by measuring 2-thiopyridone released in a thiol-disulfide exchange reaction. After approximately 18 h at 4 °C, the absorbance at 343 nm reached a plateau indicating that the conjugation was complete. AF-SPDP-SPDP-p-Lys-(DTPA)<sub>20-30</sub> conjugate was purified using a Centricon-100 at 1000g with three changes of PBS.

**Conjugation of Maleimide-Activated Asialofetuin with 3-Mercatopropionate-Modified p-Lys-(DTPA)<sub>20-30</sub> [AF-SMPB-SPDP-p-Lys-(DTPA)<sub>20-30</sub>].** Maleimide-activated asialofetuin in 20 mM sodium phos-

phate buffer containing 0.15 M sodium chloride, pH 7.0, was added to freshly prepared 3-mercaptopropionate-modified p-Lys-(DTPA)<sub>20-30</sub> in 0.1 M PBS, pH 7.5 at a molar ratio of 1:1. The reaction mixture was kept for 18 h at 4 °C. AF-SMPB-SPDP-p-Lys-(DTPA)<sub>20-30</sub> conjugate was separated from the unconjugated modified proteins using a Centricon-100 at 1000g with three buffer exchanges with 0.1 M sodium acetate, 0.1 M sodium chloride, pH 4.5. An additional purification step included the removal of potential disulfide-linked p-Lys aggregates (usually <5% total protein). To accomplish this, DTT dissolved in water was added to the conjugate to produce a final concentration of 25 mM. After 30-min reduction, DTT and liberated 3-mercaptopropionate-modified p-Lys-(DTPA)<sub>20-30</sub> were removed using a Centricon-100 at 1000g with three PBS exchanges.

**Conjugation of Maleimide-Activated Asialofetuin with Iminothiolated p-Lys-(DTPA)<sub>20-30</sub> [AF-SMPB-Traut-p-Lys-(DTPA)<sub>20-30</sub>].** Maleimide-activated AF in 20 mM sodium phosphate buffer containing 0.15 M sodium chloride, pH 7.0, was added to iminothiolated p-Lys-(DTPA)<sub>20-30</sub> at a molar ratio of 1:1. The reaction mixture was incubated for 3.5 h at room temperature. AF-SMPB-Traut-p-Lys-(DTPA)<sub>20-30</sub> conjugate was separated from unconjugated proteins using a Centricon-100 at 1000g with three changes of buffer (0.1 M sodium acetate, 0.1 M sodium chloride, pH 4.5). An additional purification step included the removal of potential disulfide linked p-Lys aggregates. To accomplish this, DTT dissolved in water was added to the conjugate to produce a final concentration of 25mM. After 30-min reduction, DTT and liberated 3-iminothiol-modified p-Lys-(DTPA)<sub>20-30</sub> were removed using a Centricon-100 at 1000g with three PBS exchanges.

**Conjugation of Asialofetuin with *N*-Succinimidyl 6-Hydrazinonicotinate Hydrochloride [AF-(SHNH)<sub>6</sub>].** To the ice-cold solution of 1 mg of AF (5 mg/mL) in 0.2 mL of 0.1 M sodium phosphate buffer, pH 7.8, in a glass tube was added 20-fold excess *N*-succinimidyl 6-hydrazinonicotinate hydrochloride. The reaction tube was wrapped in an aluminum foil to protect from light, and the mixture was reacted for a minimum of 4 h or overnight at 0–4 °C. An aliquot of the crude reaction mixture was set aside for determination of SHNH substitution ratio (18). The unreacted SHNH was removed on a BioRad de-salting column (10 cm × 1 cm) equilibrated and eluted with 0.02 M sodium citrate buffered 0.1 M saline, pH 5.2. Fractions containing AF-(SHNH)<sub>6</sub> were combined. The AF concentration was determined using the micro-BCA protein determination assay (Pierce Chemical Company). The volume of combined AF-(SHNH)<sub>6</sub> fractions was reduced using a Centricon-10 ultrafiltration device to give approximately 10 mg/mL as a final concentration of AF-(SHNH)<sub>6</sub>. The conjugate was stored at –80 °C until ready to use.

**Radiolabeling with [<sup>111</sup>In]Indium.** Aliquots of <sup>111</sup>InCl<sub>3</sub> (10 mCi/mL) in 0.05 M HCl were equilibrated with an equivalent volume of a 1:1 mixture of 0.5 M acetate buffer, pH 5.5, and 0.05 M citrate buffer, pH 5.5. AF-p-Lys-(DTPA)<sub>20-30</sub> conjugates (0.5 mg conjugate/1 mCi <sup>111</sup>In) in PBS were added to buffered [<sup>111</sup>In]indium solution, mixed, and incubated at room temperature for 40 min. The reaction progress was monitored using ITLC. The radiolabeling was stopped with 100-fold excess of DTPA just before loading onto a column. The purification of radiolabeled conjugates was accomplished on a size-exclusion Sephadex G-50 column using 0.05 M PBS as the eluant. Protein-containing radioactive fractions were combined and assayed in a dose calibrator. The labeling



efficiency and radiochemical purity were determined by ITLC and HPLC. Typically specific activities of 1.2–1.8  $\mu\text{Ci}/\mu\text{g}$  construct were obtained. This protocol was also used for radiolabeling with [ $^{153}\text{Gd}$ ]Gadolinium.

**Radiolabeling with [ $^{99\text{m}}\text{Tc}$ ]Technetium.** [ $^{99\text{m}}\text{Tc}$ ]-Pertechnetate (1 mCi) was placed in a glass test tube, and 0.005 mL of a fresh solution of Tricine in water (20 mg/mL) and 0.005 mL of a fresh solution of stannous sulfate (5 mg/mL) were added. After 15 min reduction of [ $^{99\text{m}}\text{Tc}$ ]pertechnetate, 0.4 mg of AF-(SHNH)<sub>6</sub> was added, and the mixture was allowed to react for 45 min. The reaction progress was monitored using ITLC. When protein-bound  $^{99\text{m}}\text{Tc}$  reached approximately 95% of the total radioactivity loaded on the ITLC strip, the reaction mixture was diluted with PBS, pH 7.2, to a final AF-( $^{99\text{m}}\text{Tc}$ -SHNH)<sub>6</sub> concentration of 0.5 mg/mL. Typically the radiochemical yield was >95% after a 45-min reaction. The radiolabeled product was isolated on a BioRad desalting column using PBS, pH 7.2, as the eluant with an average yield of recovery >70%. This radiolabeling protocol produces AF-( $^{99\text{m}}\text{Tc}$ -SHNH)<sub>6</sub> with a specific activity of about 2–2.5  $\mu\text{Ci } ^{99\text{m}}\text{Tc}/\mu\text{g}$  construct.

**Radioiodination of Asialofetuin.** The iodogen method (19) was used to prepare  $^{125}\text{I}$ -AF. AF in PBS, pH 7.2 was transferred into a glass tube coated with 0.1 mg iodogen. Sodium [ $^{125}\text{I}$ ]iodide was added (1 mCi/0.1 mg AF), and the mixture was reacted for 15 min. The progress of radioiodination was monitored using ITLC. The purification was accomplished on a Bio-Rad desalting column (Hercules, CA).

**Quality Controls.** *HPLC Analysis of Radiolabeled Conjugates.* Size-exclusion HPLC analysis with a Bio-sil SEC-250 column (300  $\times$  7.8 mm) with a Bio-sil SEC guard column (10  $\times$  7.8 mm) was used to determine the molecular weight and purity of the radiolabeled conjugates. A 0.05-mL sample of radiolabeled conjugate was injected into the column. The column was eluted with a buffer containing 50 mM  $\text{NaH}_2\text{PO}_4$ , 50 mM  $\text{Na}_2\text{HPO}_4$ , 100 mM NaCl, and 0.05%  $\text{NaN}_3$ , pH 6.7, at a flow rate of 0.5 mL/min. The conjugates were detected using a dual detection: the absorbance at 280 nm and the radioactivity. *Instant Thin Layer Chromatography (ITLC).* Radiolabeled conjugates were also analyzed on ITLC plates using 0.9% saline or methanol/water (1:4; v/v) as developing solvents for  $^{125}\text{I}$ -labeled constructs, or 0.15 M sodium acetate, pH 5.3, for  $^{99\text{m}}\text{Tc}$ - and  $^{111}\text{In}$ -labeled constructs. In all solvent systems, the radiolabeled protein construct remains at the origin while free radioisotopes move with the solvent front. The distribution of radioactivity on ITLC strips was monitored using a radiochromatography scanner (Vista-100, Packard Instruments).

**Stability of Constructs in Liver Homogenates.** Swiss Webster mice were anesthetized with  $\text{CO}_2$  and sacrificed by cervical dislocation. Liver (1.2 g) was homogenized in either 4.0 mL of 0.2 M acetate buffer, pH 5.0, or 4.0 mL of PBS, pH 7.2. Crude homogenates were sonicated on ice at 400 W for 1 min. The radiolabeled conjugate (0.025 mCi) was added to 1 mL of liver homogenate, and 0.1-mL portions were transferred into microcentrifuge tubes and incubated in a tissue culture incubator (5%  $\text{CO}_2$ ) at 37  $^\circ\text{C}$  for 5, 15, 30 min, and 1, 2, and 24 h. At designated time points, liver homogenates were centrifuged at 1000g for 10 min, and the supernatant was analyzed for the presence of a low and high molecular weight soluble degradation products using ITLC. Total radioactivity associated with the pellet and the supernatant was determined in a gamma counter. The supernatants collected after 2 h incubation were also analyzed on size the exclusion HPLC columns.

**In Vitro Binding and Degradation of  $^{125}\text{I}$ -AF.** Isolated hepatocytes ( $5 \times 10^5$ ) were suspended in 1 mL of Delbecco's Minimum Essential Medium (DMEM) supplemented with 10% heat inactivated fetal bovine serum (FBS). Twenty nanograms of  $^{125}\text{I}$ -AF was added to each tube and cells were incubated at 37  $^\circ\text{C}$  on a multipurpose shaker rotating at 6 rpm. At designated time points, hepatocytes were centrifuged at 3000 rpm for 5 min, and supernatants were aspirated. Cell pellets were washed twice with 1 mL of ice-cold PBS. The cell-associated radioactivity was measured in a gamma counter. The nonspecific binding was determined in the presence of a 20 000-fold (0.4 mg) excess of native, unlabeled AF. For metabolic studies, the rate of degradation was measured as the increase in the acid-soluble radioactivity accumulating in the culture medium in the presence of hepatocytes.  $^{125}\text{I}$ -AF-containing cells, washed with ice-cold PBS, were resuspended in a prewarmed to 37  $^\circ\text{C}$  DMEM supplemented with 10% heat inactivated FBS. To the cell suspension sampled immediately after mixing (time 0) and at designated time points, an equal volume of ice-cold 20% trichloroacetic acid was added. After 30 min on ice, the precipitated proteins were separated from the acid-soluble fraction by centrifugation at 4000 rpm for 10 min. The supernatant- and pellet-associated radioactivity was measured in a gamma counter.

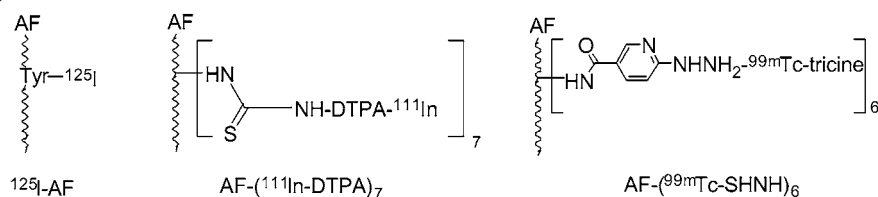
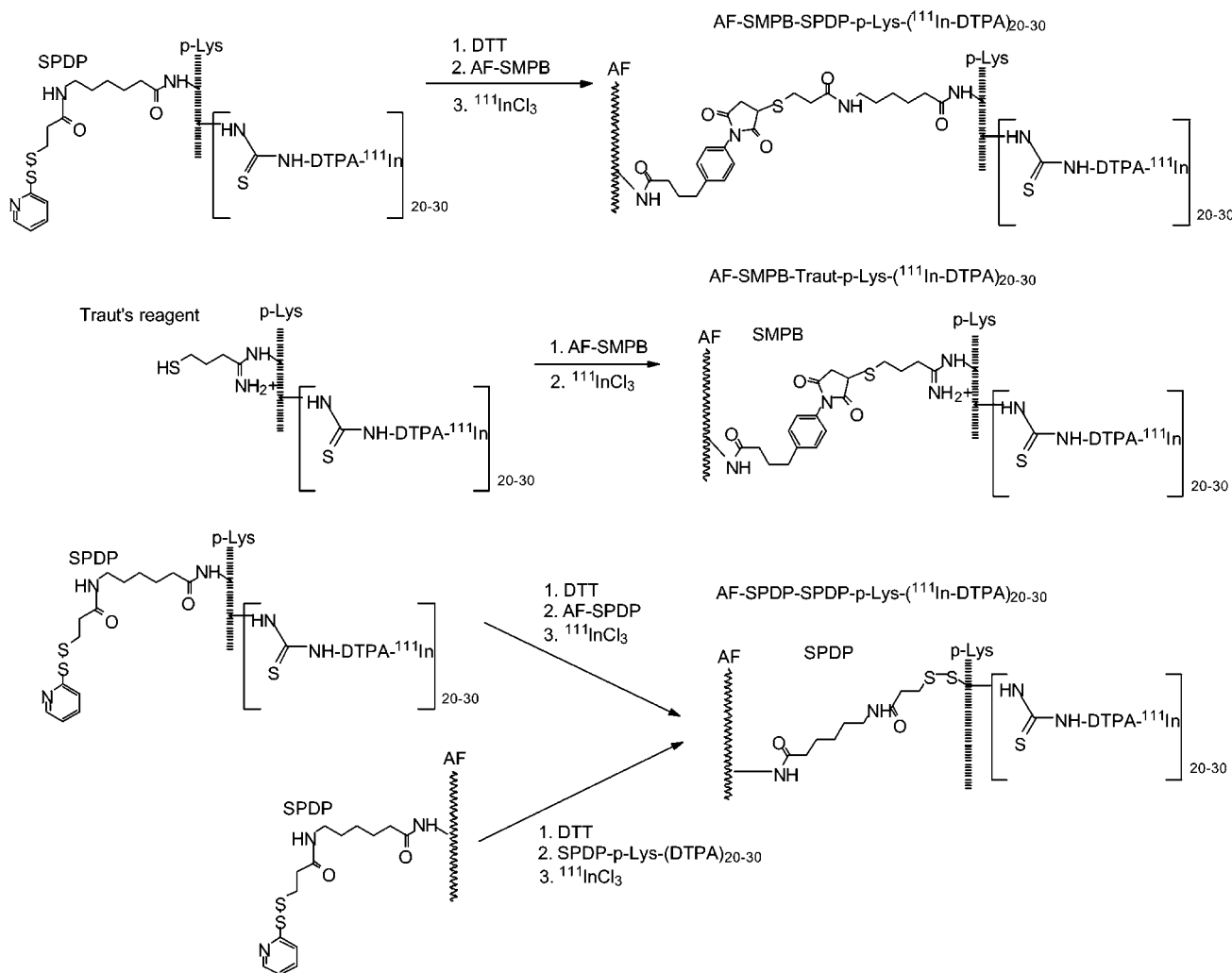
**Biodistribution.** Female, six-week-old Swiss Webster mice (Charles River Laboratories, Wilmington, MA) were used after one-week acclimation in the UNMC facilities. Radiolabeled conjugates with the specific activities  $\geq 1$  mCi/mg AF were administered via the tail vein at a dose of 2  $\mu\text{Ci}/\text{mouse}$  ( $^{111}\text{In}$ -labeled agents) or 5  $\mu\text{Ci}/\text{mouse}$  ( $^{125}\text{I}$ -AF). Mice were randomized into groups of four per time point. At 5, 15, 30, 60, 120, 180, and 1440 min after injection, mice were killed and the necropsy was performed. Tissues and blood were weighed, and their radioactive content was determined in a gamma counter. Tissue- and blood-associated radioactivity was normalized to the injected dose and the weight of the sample and expressed as percent of the injected dose per gram of tissue (%ID/g). Localization indices were calculated as tissue-to-blood ratios. Tissue and blood clearance curves were analyzed using a numerical module of a SAMM II program (SAMM Institute, University of Washington).

**Gamma Camera Imaging.** Scintigraphic images were acquired using a Technicare pinhole gamma camera in a 128  $\times$  128 matrix using a 10-min scan for each time point. The dose of 0.04 mCi of  $^{111}\text{In}$ -labeled agents was administered iv via a tail vein. Mice were kept under a light ketamine/xylazine anesthesia during the image acquisition.

## RESULTS

**Chemistry.** Two types of AF constructs were prepared: derivatives that incorporate radiolabel directly into the AF molecule and derivatives that carry additional substituents for indirect radiolabeling (Schemes 1 and 2). In directly modified AF derivatives the radiolabeling was accomplished by either radioiodination of AF with radioiodine or through an appropriate chelating group reacted with lysine residues of AF for radiometal labeling, DTPA for  $^{111}\text{In}$  and  $^{153}\text{Gd}$ , and SNHN for  $^{99\text{m}}\text{Tc}$ . The indirectly modified AF derivatives were radiolabeled with  $^{111}\text{In}$  and  $^{153}\text{Gd}$  through the p-Lys-(DTPA)<sub>20–30</sub> portion of the AF constructs.

Chemical structures of all tested AF constructs are shown in Schemes 1 and 2. For the purpose of indirect radiolabeling with  $^{111}\text{In}$  in several methods of the conjugate

**Scheme 1. Directly Radiolabeled Asialofetuin Derivatives****Scheme 2. Indirectly Radiolabeled Constructs of Asialofetuin with p-Lys**

preparation were explored. The formation of disulfide linkages was accomplished via AF-conjugated 3-mercaptopropionate displacement of 2-thiopyridine from the 3-(2-pyridyldithio)propionate portion of p-Lys conjugate. This approach was also reversed, i.e., 3-mercaptopropionate generated from SPDP on p-Lys was used to displace 2-thiopyridine on SPDP-modified AF. The use of *N*-succinimidyl 4-(4'-maleimidophenyl)butyrate (SMPB)-modified AF allowed preparation of two constructs using the reaction of the maleimide double bond with the thiol group either generated from SPDP on p-Lys or introduced as 2-iminothiolane (Traut's reagent) on p-Lys.

The synthesis of (*S*)-1-*p*-isothiocyanatobenzyl-diethylenetriaminepentaacetic acid (SCN-DTPA) was accomplished according to the method of Corson and Mears (14). The chemical modification of AF was done using either SCN-DTPA or DTPA cyclic anhydride at the protein-to-ligand ratio of 1:20. The typical degree of substitution, as determined through the carrier-added labeling of the crude reaction mixture, was found to be seven DTPA residues per one molecule of AF. The

radiochemical yield of labeling with  $^{111}\text{InCl}_3$  and  $^{153}\text{GdCl}_3$  was routinely >90%. The radioiodinated AF was prepared using the iodogen method (19) in nearly 100% radiochemical yield. For labeling with  $^{99\text{m}}\text{Tc}$ , AF was modified with *N*-succinimidyl 6-hydrazinonicotinate hydrochloride (13). On average a 6:1 molar ratio of SHNH to AF was obtained. Radiochemical yield of AF-( $^{99\text{m}}\text{Tc-SHNH}$ )<sub>6</sub> constructs was routinely >70% (corrected for decay). All constructs were purified on a size exclusion column.

AF constructs with p-Lys (MW 53 900) were modified with SCN-DTPA at a substitution ratio as high as 70 DTPA residues per p-Lys molecular without any deleterious effects on the biological activity of AF. However, for studies described here, all AF constructs were prepared to contain on an average 20–30 DTPA groups to facilitate comparison of their biological properties. Radiochemical yields for  $^{111}\text{In}$  labeling of p-Lys-(DTPA)<sub>20–30</sub> constructs with AF were typically >90%. All purifications were done on a size exclusion column much like directly radiolabeled AF. Additionally, p-Lys-AF conjugates were subjected

**Table 1. Expression of Asialoglycoprotein Receptors in Hepatocytes from Various Species Measured at 37 °C Using  $^{125}\text{I}$ -AF**

species	no. of ASGPr per cell average (standard deviation)
mouse	$2.44 \times 10^5$ ( $0.22 \times 10^5$ )
rat	$4.08 \times 10^5$ ( $0.14 \times 10^5$ )
pig	$4.00 \times 10^5$ ( $0.10 \times 10^5$ )
rat <sup>a</sup>	$2.1 \times 10^5$ ( $0.5 \times 10^5$ ) <sup>b</sup>
	$7 \times 10^4$ <sup>c</sup>

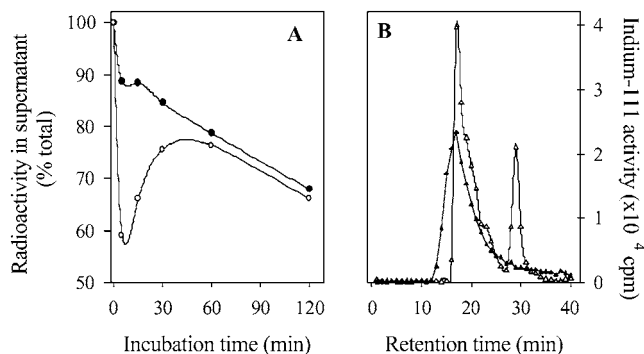
<sup>a</sup> Reference 20. <sup>b</sup> Fresh hepatocytes. <sup>c</sup> Incubated hepatocytes.

to an ultrafiltration step to remove any residual unreacted p-Lys that may have been collected with AF constructs from the size-exclusion column. In the synthesis of maleimide-based AF constructs, which requires generation of free thiols and a prolonged conjugation step, protein-containing fractions collected from the size-exclusion column went through an additional purification step after treatment with 25 mM DTT to reduce any disulfide bonds that may have contributed to the formation of p-Lys dimers and other aggregates.

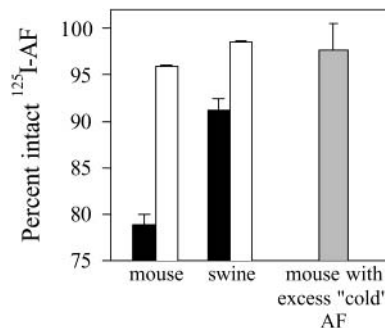
**In Vitro Studies.** Metabolic processing and binding studies in vitro were conducted to assess biological behavior of chemically modified AF and to determine differences, if any, in the recognition of the ASGP receptor. The rate of metabolic processing of each AF construct was evaluated. The stability of radiolabeled AF constructs was tested in mouse liver homogenates and in the presence of intact hepatocytes derived from mice, rat, and swine livers. Isolated fresh hepatocytes were also used to determine binding properties of AF constructs, the expression of ASGPr and the intracellular uptake of AF constructs. Hepatocytes were isolated using a perfusion technique of Barry and Friend (15) as modified by Seglen (16). Mice and rat hepatocytes were prepared on site (UNMC) and used within a couple of hours of preparation. The viability of mice hepatocytes was routinely >95%. Porcine hepatocytes were isolated and suspended in ViaSpan for shipment to UNMC by the overnight delivery. Viability as assessed by trypan blue staining was routinely >88%. Table 1 summarizes ASGP receptor recognition by AF-( $^{99\text{m}}\text{Tc}$ -SHNH)<sub>6</sub> in cells derived from mouse, rat, and pig livers. The measured number of ASGPr per cells is in good agreement with the published data (20;  $2.10 \times 10^5 \pm 0.50 \times 10^5$  for incubated hepatocytes and  $7 \times 10^4$  for fresh hepatocytes).

The stability and binding of AF constructs in liver homogenates proved to be a good predictor of the in vivo properties. This point is illustrated for AF-SPDP-SPDP-p-Lys-( $^{111}\text{In}$ -DTPA)<sub>20-30</sub> and AF-SMPB-SPDP-p-Lys-( $^{111}\text{In}$ -DTPA)<sub>20-30</sub> in Figures 1A and 1B and later in Figure 7.

Fresh liver homogenates diluted with PBS at 1-to-4 ratio (v/v) were incubated with radiolabeled  $^{111}\text{In}$  constructs. At designated time points, distribution of radioactivity associated with pellets and supernatants was determined (Figure 1A). In both cases there is a binding of AF constructs to ASGPr in liver homogenate as indicated by disappearance of  $^{111}\text{In}$  from the soluble fraction. In the case of AF-SPDP-SPDP-p-Lys-( $^{111}\text{In}$ -DTPA)<sub>20-30</sub>, a large fraction of bound radioactivity returns into the supernatant within 30 min. Further analyses of supernatants using ITLC indicated that the majority of  $^{111}\text{In}$  was still associated with larger molecular weight species that were not eluted from the origin. Size-exclusion HPLC revealed that  $^{111}\text{In}$  recovered in supernatants from liver homogenates incubated with AF-SMPB-SPDP-p-Lys-( $^{111}\text{In}$ -DTPA)<sub>20-30</sub> for 120 min was in the form of the intact construct whereas incubation of



**Figure 1.** (A) Stability of AF-SPDP-SPDP-p-Lys-( $^{111}\text{In}$ -DTPA)<sub>20-30</sub> (○) and AF-SMPB-SPDP-p-Lys-( $^{111}\text{In}$ -DTPA)<sub>20-30</sub> (●) in mouse liver homogenates diluted with PBS. (B) Radioactive HPLC profile of mouse liver homogenate supernatants collected after 120 min incubation with AF-SMPB-SPDP-p-Lys-( $^{111}\text{In}$ -DTPA)<sub>20-30</sub> (▲) and AF-SPDP-SPDP-p-Lys-( $^{111}\text{In}$ -DTPA)<sub>20-30</sub> (△). Peaks with the retention time ( $t_R$ ) of 17 min correspond to the intact construct (MW approximately 110 000); a peak at  $t_R$  of 30 min corresponds to low molecular weight (1000 < MW < 2500 Da) degradation products.



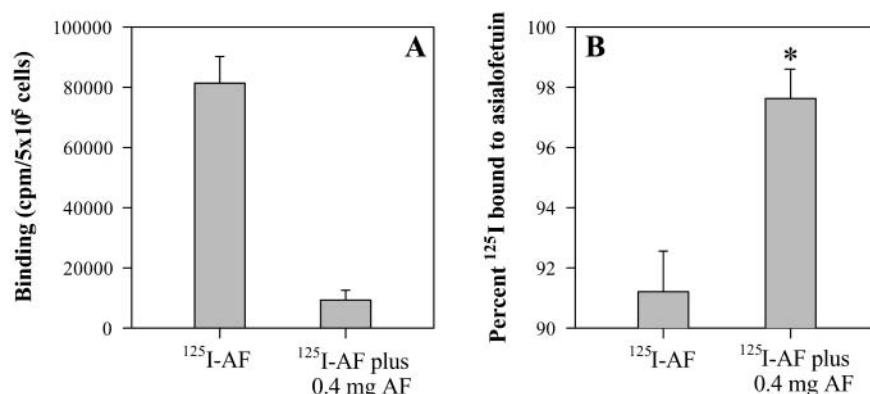
**Figure 2.** Stability of  $^{125}\text{I}$ -AF (20 ng/ $5 \times 10^5$  cells) incubated for 60 min in the presence of freshly prepared hepatocytes from mice and pigs (black bars); general stability of  $^{125}\text{I}$ -AF was evaluated under identical set of conditions in the absence of hepatocytes (white bars). The gray bar represents  $^{125}\text{I}$ -AF incubated with mice hepatocytes in the presence of 20 000-fold excess unlabeled AF sufficient to block all AF binding sites.

AF-SPDP-SPDP-p-Lys-( $^{111}\text{In}$ -DTPA)<sub>20-30</sub> for 120 min resulted in substantial degradation of the construct (Figure 1B). The in vivo fate of these constructs parallels in vitro findings (see below).

Processing of  $^{125}\text{I}$ -AF in mice and porcine hepatocytes was rapid (Figures 2 and 3).  $^{125}\text{I}$ -AF purified on a size-exclusion column was incubated in the presence of freshly prepared hepatocytes from mice and 24-h-old porcine hepatocytes. Control samples consisted of  $^{125}\text{I}$ -AF incubated under identical set of conditions in the absence of hepatocytes. A second control consisted of hepatocytes treated with the 20 000-fold excess of nonradioactive AF (0.4 mg/ $5 \times 10^5$  cells). This amount is sufficient to block AF binding sites. It is apparent that isolated hepatocytes are able to process  $^{125}\text{I}$ -AF in a receptor-dependent manner. The lesser metabolic activity observed with porcine hepatocytes is probably related to the age of these cells (prepared 24–36 h prior to use). The excess native AF inhibited binding of  $^{125}\text{I}$ -AF to porcine hepatocytes in the same way as in the case of mice hepatocytes (Figure 3). A similar result was obtained with freshly isolated rat hepatocytes, but immortalized rat hepatocytes and immortalized human hepatocytes bound neither  $^{125}\text{I}$ -AF nor ( $^{99\text{m}}\text{Tc}$ -SHNH)-AF indicating the loss of ASGPr in these cells (data not shown).

The average number of AF binding sites is similar in hepatocytes from all analyzed species (Table 1). Competition binding studies conducted with  $^{111}\text{In}$ - and





**Figure 3.** Binding and metabolic processing of  $^{125}\text{I}$ -AF in porcine hepatocytes. (A) Fresh hepatocytes were incubated with  $^{125}\text{I}$ -AF ( $20 \text{ ng}/5 \times 10^5 \text{ cells}$ ). (B) The degree of protein degradation was determined in medium collected from hepatocytes incubated with  $^{125}\text{I}$ -AF at  $37^\circ\text{C}$  for 60 min (\*  $P < 0.001$ ). Proteins were precipitated with ice-cold 10% TCA.

**Table 2. Pharmacokinetics of Hepatic Uptake and Elimination of Radiolabeled Asialofetuin and Its Constructs in Mice**

construct	absorption $t_{1/2}$ (min)	postabsorption average $t_{1/2}$ (std dev) (min)	elimination average $t_{1/2}$ (std dev) (h)
$^{125}\text{I}$ -AF	nd	5.1 (0.05)	2.8 (0.06)
AF-( $^{99\text{m}}\text{Tc}$ -SHNH) <sub>6</sub>	nd	nd	14.7 (14.7) <sup>a</sup>
AF-( $^{111}\text{In}$ -DTPA) <sub>7</sub>	6.3	29.1 (5.1)	41.0 (0.43)
AF-SPDP-SPDP-Lys-( $^{111}\text{In}$ -DTPA) <sub>20-30</sub>	nd	14.4 (7.1)	19.0 (3.52)
AF-SMPB-Traut-Lys-( $^{111}\text{In}$ -DTPA) <sub>20-30</sub>	3.8	9.1 (0.1)	44.3 (3.08)
AF-SMPB-SPDP-Lys-( $^{111}\text{In}$ -DTPA) <sub>20-30</sub>	3.3	7.9 (1.8)	36.0 (9.12)

<sup>a</sup> Corrected for decay.

**Table 3. Tissue-to-Blood Ratios Derived from Biodistribution Data of Radiolabeled Asialofetuin and Its Constructs in Mice**

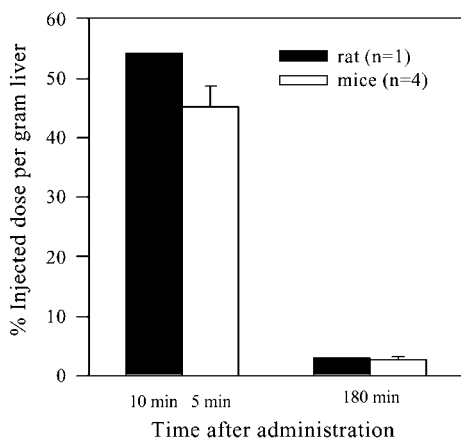
construct	time after administration (min)					
	5	15	30	60	120	1440
<b>A. Liver-to-Blood Ratios</b>						
p-Lys-( $^{111}\text{In}$ -DTPA) <sub>20-30</sub> control	0.4	0.5	0.8	1.0	1.2	5.6
AF-( $^{111}\text{In}$ -DTPA) <sub>7</sub>	58.0	130.5	257.3	323.4	718.7	830.4
AF-SMPB-SPDP-p-Lys-( $^{111}\text{In}$ -DTPA) <sub>20-30</sub>	19.6	30.6	40.3	50.2	68.3	194.3
AF-SMPB-Traut-p-Lys-( $^{111}\text{In}$ -DTPA) <sub>20-30</sub>	38.5	94.3	134.5	116.5	147.0	353.8
AF-SPDP-SPDP-p-Lys-( $^{111}\text{In}$ -DTPA) <sub>20-30</sub>	1.19	1.87	2.09	2.52	5.63	nd
$^{125}\text{I}$ -AF	75	nd	3.2	3.1	2.4 <sup>a</sup>	nd
( $^{99\text{m}}\text{Tc}$ -SHNH) <sub>6</sub> -AF	71.6	nd	63.0	69.4	54.3	nd
<b>B. Kidney-to-Blood Ratios</b>						
p-Lys-( $^{111}\text{In}$ -DTPA) <sub>20-30</sub> control	2.5	6.5	9.4	19.9	26.3	203.6
AF-( $^{111}\text{In}$ -DTPA) <sub>7</sub>	24.5	69.7	142.9	175.8	416.4	673.9
AF-SMPB-SPDP-p-Lys-( $^{111}\text{In}$ -DTPA) <sub>20-30</sub>	2.3	5.2	8.22	12.2	17.8	69.4
AF-SMPB-Traut-p-Lys-( $^{111}\text{In}$ -DTPA) <sub>20-30</sub>	3.1	8.0	13.6	14.7	17.6	54.6
AF-SPDP-SPDP-p-Lys-( $^{111}\text{In}$ -DTPA) <sub>20-30</sub>	0.7	2.5	4.4	4.7	13.3	nd
$^{125}\text{I}$ -AF	0.54	nd	0.15	0.14	0.13 <sup>a</sup>	nd
( $^{99\text{m}}\text{Tc}$ -SHNH) <sub>6</sub> -AF	1.12	nd	2.6	4.2	4.4	nd
<b>C. Spleen-to-Blood Ratios</b>						
p-Lys-( $^{111}\text{In}$ -DTPA) <sub>20-30</sub> control	0.1	0.15	0.2	0.3	0.3	2.9
AF-( $^{111}\text{In}$ -DTPA) <sub>7</sub>	5.4	13.2	20.4	28.9	61.4	74.0
AF-SMPB-SPDP-p-Lys-( $^{111}\text{In}$ -DTPA) <sub>20-30</sub>	4.4	4.6	5.7	6.8	8.3	40.1
AF-SMPB-Traut-p-Lys-( $^{111}\text{In}$ -DTPA) <sub>20-30</sub>	9.2	19.5	22.4	20.1	19.4	46.0
AF-SPDP-SPDP-p-Lys-( $^{111}\text{In}$ -DTPA) <sub>20-30</sub>	0.21	0.29	0.37	0.36	0.57	nd
$^{125}\text{I}$ -AF	1.9	nd	0.56	0.56	0.48 <sup>a</sup>	nd
( $^{99\text{m}}\text{Tc}$ -SHNH) <sub>6</sub> -AF	4.4	nd	7.0	27.5	25.2	nd

<sup>a</sup> 180 min.

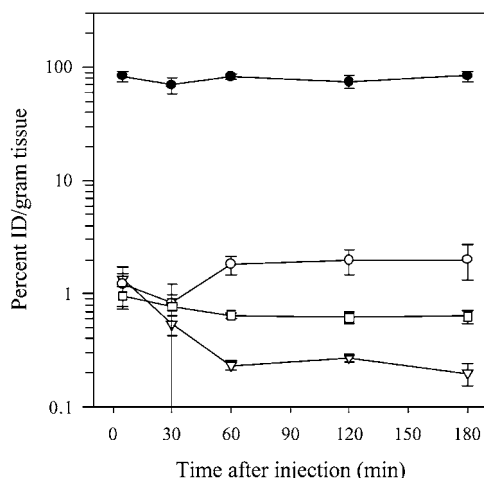
$^{99\text{m}}\text{Tc}$ -labeled constructs of AF indicated that binding and cell uptake of these agents are similar to  $^{125}\text{I}$ -AF data shown in Figure 3. Modification of AF with p-Lys did not impair binding of  $^{111}\text{In}$ -labeled constructs to hepatocytes. However, the catabolic processing of radiometal-labeled constructs in the presence of viable hepatocytes is considerably slower than degradation of  $^{125}\text{I}$ -AF. A 60-min incubation time sufficient to degrade approximately 20% of  $^{125}\text{I}$ -AF results in less than 1% degradation of  $^{111}\text{In}$ - or  $^{153}\text{Gd}$ -labeled directly labeled AF constructs under identical conditions.

In addition to controls containing only buffer and radiolabeled AF constructs, fixed hepatocytes were also used as a control to verify that binding of radiolabeled

AF to its receptor does not contribute to the degradation of this protein. Stability of radiolabeled AF in the presence of fixed hepatocytes was similar to that measured in incubation medium in the absence of cells. While binding of  $^{125}\text{I}$ -AF to fresh porcine hepatocytes and to fixed cells was very similar,  $95.14 \pm 4.47\%$  versus  $82.90 \pm 4.94$ , respectively, within the scope and timeline of the experiments the degradation of  $^{125}\text{I}$ -AF in the presence of fixed porcine cells was not facilitated by the presence of fixed hepatocytes. The very slow loss of radiolabel was related only to the radiolysis or chemical degradation. Likewise, fresh murine hepatocytes metabolized on average  $21.05 \pm 0.02\%$   $^{125}\text{I}$ -AF per hour, but the loss of



**Figure 4.** Liver uptake of  $^{125}\text{I}$ -AF in rats and mice at various times after administration. Rats received 0.05-mCi dose of  $^{125}\text{I}$ -AF; mice received 0.005-mCi dose. At designated times animals were killed and necropsy performed.



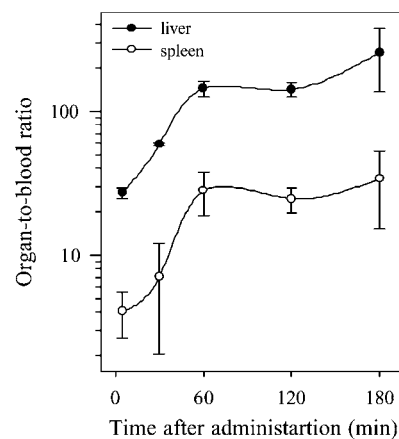
**Figure 5.** Biodistribution of  $(^{99\text{m}}\text{Tc-SHNH})_6\text{-AF}$  in mice: ● liver; ○ spleen; □ kidney; ▽ blood. Mice ( $n = 5$ ) received 0.05 mCi dose iv via a tail vein in normal saline (data is corrected for decay).

radioactivity from  $^{125}\text{I}$ -AF in the presence of fixed mouse hepatocytes was less than 0.5% during the same time.

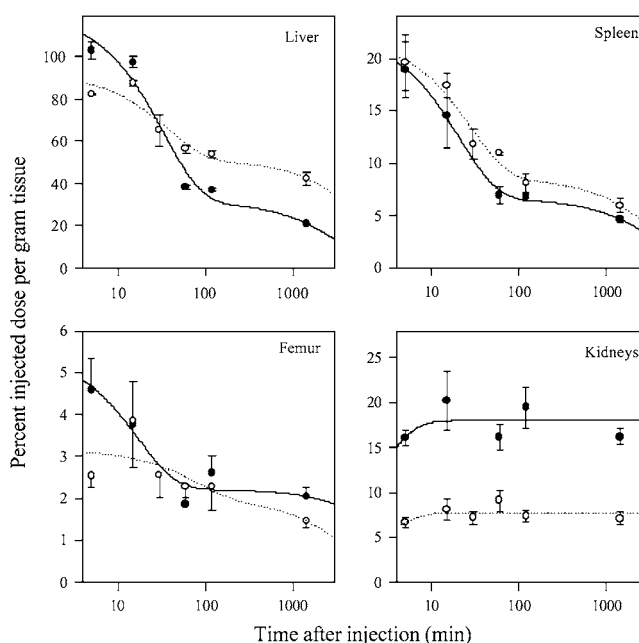
**In Vivo Studies.** Radioiodinated  $^{125}\text{I}$ -AF rapidly localizes in liver wherein it is promptly deiodinated (Figure 4). Analyses of serum samples from mice and rats treated with  $^{125}\text{I}$ -AF revealed that at 5 and 10 min postinjection, 46% ( $n = 1$  rat) and  $54.8\% \pm 3.5\%$  ( $n = 4$  mice) of the total circulating radioactivity is already in the form of free [ $^{125}\text{I}$ ]-iodide. A similar analysis of the 180-min serum sample, indicated that only 2.95% ( $n = 1$  rat) and  $2.74 \pm 0.47\%$  ( $n = 4$  mice) of circulating  $^{125}\text{I}$  was still in the form of intact  $^{125}\text{I}$ -AF. The hepatic postabsorption half-life was  $5.1 \pm 0.05$  min (Table 2).

Hepatic uptake of  $^{99\text{m}}\text{Tc-SHNH})_6\text{-AF}$  in mice is rapid and highly selective (Figure 5). Five minutes after injection nearly 85% of the injected dose is localized in liver, and this level is maintained up to 3 h after injection. Some uptake of  $\text{AF-(}^{99\text{m}}\text{Tc-SHNH})_6$  is also observed in spleen, with  $0.83 \pm 0.40\%$  injected dose at 30 min and  $2.00 \pm 0.98\%$  at 180 min after injection. The liver-to-blood ratio and spleen-to-blood ratios are  $144.3 \pm 18.4$  and  $28.0 \pm 9.3$ , respectively, 1 h after injection (Figure 6, Tables 3A, 3C).

The liver uptake of  $^{111}\text{In}$ -labeled AF constructs indicated that all tested reagents specifically targeted hepatocytes and recognized AFGPr irrespective of the chemical modification of AF. However, systemic and liver

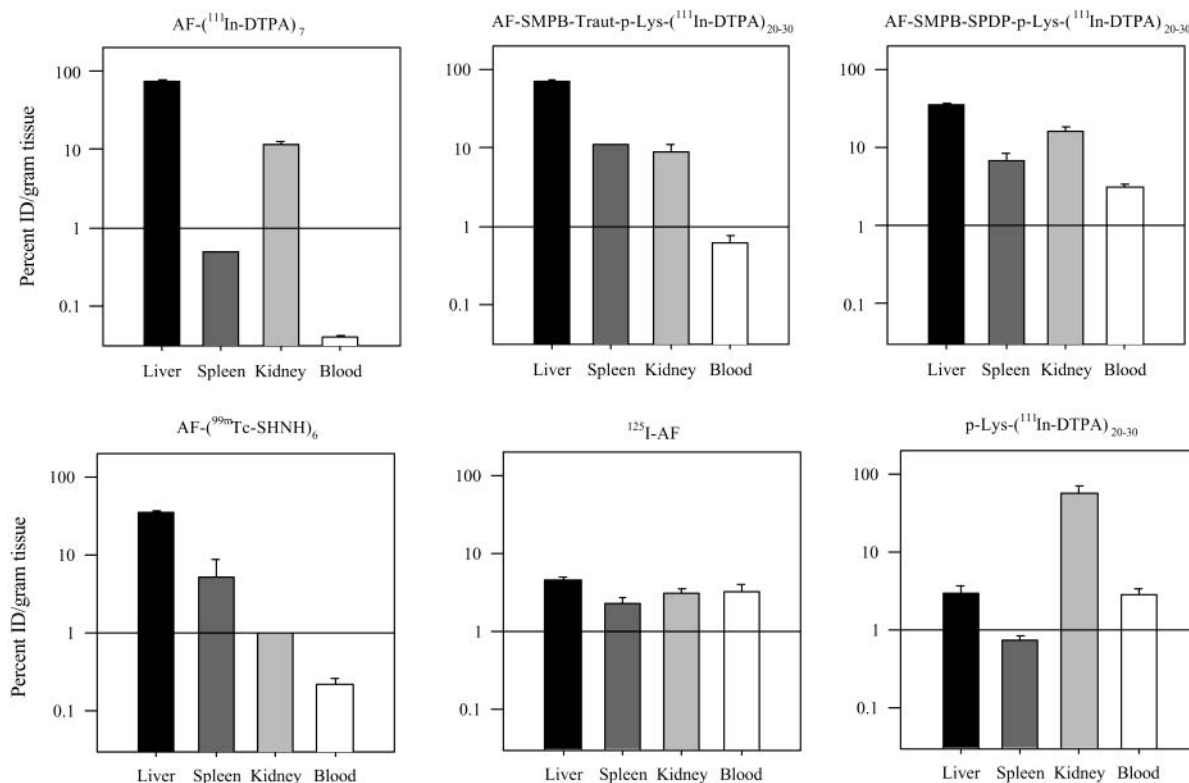


**Figure 6.** Organ-to-blood ratio in normal mice treated with 0.05 mCi  $^{99\text{m}}\text{Tc-SHNH})_6\text{-AF}$  administered IV in 0.2 mL of normal saline. At indicated time points mice ( $n = 5$ ) were killed, and necropsy was performed.

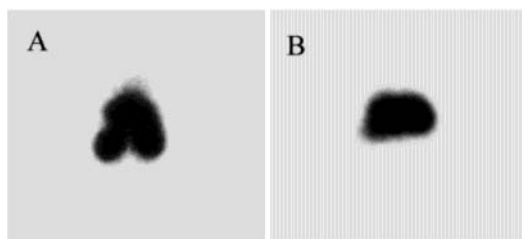


**Figure 7.** Tissue clearance curves for  $\text{AF-SMPB-SPDP-p-Lys-(}^{111}\text{In-DTPA)}_{20-30}$  (black symbols, solid lines) and  $\text{AF-SMPB-Traut-p-Lys-(}^{111}\text{In-DTPA)}_{20-30}$  (white symbols, dotted lines) in selected tissues. Data for liver, spleen, and femur were fitted into a biexponential model and are indicated with solid and dotted lines.

clearance rates were strongly influenced by the chemical structure of the conjugates.  $\text{p-Lys-(DTPA)}_{20-30}$  constructs labeled with  $^{111}\text{In}$  were used as a nonspecific control for all  $^{111}\text{In}$ -labeled AF-p-Lys conjugates. Tables 3A, 3B, and 3C show tissue-to-blood ratios for studied constructs. The uptake and in vivo processing of two AF constructs radiolabeled with  $^{111}\text{In}$  is shown in Figures 7. There is a favorable clearance from systemic circulation and normal spleen accompanied by a considerable retention of the released radioisotope in liver and kidneys (up to 24 h). Constructs containing SPDP linkages appear to be less stable, and 60 min after administration the radioactivity associated with kidneys is clearly visible in planar images (Figure 9A). The degradation of maleimide-based constructs is slower (Figures 8, 9B, 10). The Traut's reagent- and SPDP-based maleimide constructs have similar degradation rates and pharmacokinetics, but the liver uptake of  $\text{AF-SMPB-SPDP-p-Lys-(}^{111}\text{In-DTPA)}_{20-30}$  is lower and  $^{111}\text{In}$  released from this construct appears in



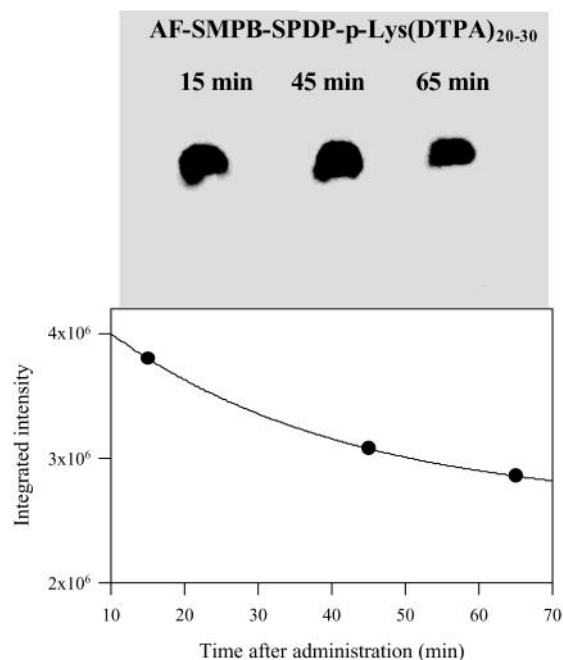
**Figure 8.** Comparison of distribution of various AF constructs in mice 60 min after intravenous administration.



**Figure 9.** Planar images in mice acquired 60 min after iv injection (tail) of 40  $\mu$ Ci <sup>111</sup>In-labeled (A) AF-SPDP-SPDP-p-Lys-(<sup>111</sup>In-DTPA)<sub>20-30</sub> and (B) AF-SMPB-SPDP-p-Lys-(<sup>111</sup>In-DTPA)<sub>20-30</sub>. Images were acquired using a Technicare pinhole gamma camera; acquisition matrix 128  $\times$  128; time of acquisition 600 s.

systemic circulation faster. Liver-to-blood ratios at 30 min after injection are 40 and 135 for AF-SMPB-SPDP-p-Lys-(<sup>111</sup>In-DTPA)<sub>20-30</sub> and AF-SMPB-Traut-p-Lys-(<sup>111</sup>In-DTPA)<sub>20-30</sub>, respectively.

The kidney-to-blood ratio for AF-SMPB-SPDP-p-Lys-(<sup>111</sup>In-DTPA)<sub>20-30</sub> is measured at 30 min after administration at 8 and for AF-SMPB-Traut-p-Lys-(<sup>111</sup>In-DTPA)<sub>20-30</sub> at nearly 14. The lack of the uptake of the radiometal released from AF constructs in the bone and/or bone marrow indicates that the metabolites released from the liver do not contain free metal (Figure 7; femur). In vitro stability studies in liver homogenates and human serum confirmed the absence of free metal in incubated reaction mixtures (Figures 1A, 1B). Hepatic half-lives for all constructs in mice are summarized in Table 2. Three reagents had a measurable absorption phase with a half-life < 6 min. The postabsorption and elimination half-lives appeared to be related to the rate of hepatic degradation of a given construct. The shortest half-life was measured for <sup>125</sup>I-AF at 5 min. Of the DTPA-modified AF, AF-SPDP-SPDP-p-Lys-(<sup>111</sup>In-DTPA)<sub>20-30</sub> construct was eliminated from liver approximately twice as fast as the other three reagents.



**Figure 10.** Liver images acquired after iv administration of 40  $\mu$ Ci AF-SMPB-SPDP-p-Lys-(<sup>111</sup>In-DTPA)<sub>20-30</sub>. Data were analyzed using a Scion Image software.

## DISCUSSION

The ability of asialofetuin to target asialoglycoprotein receptor has long been recognized as a convenient tool for the delivery of various vectors such as liposomes, recombinant lipoproteins, and polymers for drug or gene delivery to the liver, especially to hepatocytes (21, 22). The results of our studies indicate that appropriately radiolabeled AF can also be used to monitor the metabolic and functional activity of hepatocytes before and after transplant. The rapid metabolic removal of radioiodine



from AF and its rapid clearance should allow for a simple and noninvasive evaluation of metabolic activity of hepatocytes pre- and posttransplant. Kinetic measurements of  $^{125}\text{I}$  plasma levels can be supplemented with a more traditional evaluation of the ASGPr status with either  $^{99\text{m}}\text{Tc}$ - or  $^{111}\text{In}$ -AF constructs. It is expected that because of such rapid kinetics of  $^{125}\text{I}$ -AF its concentrations in liver and spleen as a function of time postadministration will provide good estimates of activities and function of the spleen-transplanted hepatocytes. The evaluation of tissue-to-blood ratios supports this conclusion. Using the more stable AF constructs labeled with indium-111, the in vivo quantification of ASGPr, the total receptor concentrations per liter of hepatic plasma or per volume of transplanted hepatocytes in the spleen, can be measured. One  $^{111}\text{In}$ -labeled AF construct, AF-SMPB-SPDP-p-Lys-( $^{111}\text{In}$ -DTPA) $_{20-30}$  appears to have a superior liver targeting and metabolic stability. Images acquired 60 min postinjection indicate that the majority of the radiotracer is localized in liver. This may be a reagent of choice for determination of ASGPr concentration in transplanted hepatocytes. As shown in the images in Figure 10 the hepatocyte uptake of AF-SMPB-SPDP-p-Lys-( $^{111}\text{In}$ -DTPA) $_{20-30}$  is virtually 100% with undetectable redistribution into systemic circulation and other organs. Normal spleen is not apparent in the images, and the uptake measured during the necropsy is also insignificant (see spleen-to-blood ratio in Table 2C), indicating that a presence of a viable population of transplanted hepatocytes in the spleen should be detectable in planar images particularly in larger animals with impaired liver function. These data appear to indicate that several of the proposed constructs can also be utilized for functional MR imaging. In preliminary experiments, conjugation ratios of up to 60–70 DTPA residues per one poly-L-lysine molecule were achieved. This number of paramagnetic chelates should be sufficient to bring about measurable  $T_1$  relaxation time changes. The in vivo studies of carrier-added  $^{153}\text{Gd}$ -DTPA-AF constructs (20 DTPA residues/p-Lys) in mice indicate that nearly 100% of the injected radioactivity localizes in the liver at 5 min after the intravenous administration (data not shown). Studies to correlate the in vitro ASGPr status and function with the survival of intrasplenic hepatocyte transplants are in progress.

#### ACKNOWLEDGMENT

This research was supported in part by the LB595 grant from the Nebraska Department of Health.

#### LITERATURE CITED

- (1) Bohnen, N. I., Charron, M., Reyes, J., Rubinstein, W., Strom, S. C., Swanson, D., and Towbin, R. (2000) Use of indium-111-labeled hepatocytes to determine the biodistribution of transplanted hepatocytes through portal vein infusion. *Clin. Nucl. Med.* 25, 447–450.
- (2) Gupta, S., Lee, C. D., Vemuru, R. P., and Bhargava, K. K. (1994)  $^{111}\text{In}$  labeling of hepatocytes for analysis of short-term biodistribution of transplanted cells. *Hepatology* 19, 750–757.
- (3) Gupta, S., Yerneni, P. R., Vemuru, R. P., Lee, C. D., Yellin, E. L., and Bhargava, K. K. (1993) Studies on the safety of intrasplenic hepatocyte transplantation: relevance to ex vivo gene therapy and liver repopulation in acute hepatic failure. *Hum. Gene Ther.* 4, 249–257.
- (4) Hawkins, R. A., Hall, T., Gambhir, S. S., Busuttil, R. W., Huang, S. C., Glickman, S., Marciano, D., Brown, R. K., and Phelps, M. E. (1988) Radionuclide evaluation of liver transplants. *Semin. Nucl. Med.* 18, 199–212.
- (5) Sakahara, H., Kiuchi, T., Nishizawa, S., Saga, T., Nakamoto, Y., Sato, N., Higashi, T., Tanaka, K., and Konishi, J. (1999) Asialoglycoprotein receptor scintigraphy in evaluation of auxiliary partial orthotopic liver transplantation. *J. Nucl. Med.* 40, 1463–1467.
- (6) Kudo, M., Todo, A., Ikekubo, K., Yamamoto, K., Vera, D. R., and Stadalnik, R. C. (1993) Quantitative assessment of hepatocellular function through in vivo radioreceptor imaging with technetium 99m galactosyl human serum albumin. *Hepatology* 17, 814–819.
- (7) Miki, K., Kubota, K., Inoue, Y., Vera, D. R., and Makuuchi, M. (2001) Receptor measurements via Tc-GSA kinetic modeling are proportional to functional hepatocellular mass. *J. Nucl. Med.* 42, 733–737.
- (8) Pimstone, N. R., Stadalnik, R. C., Vera, D. R., Hutak, D. P., and Trudeau, W. L. (1994) Evaluation of hepatocellular function by way of receptor-mediated uptake of a technetium-99m-labeled asialoglycoprotein analog. *Hepatology* 20, 917–923.
- (9) Rogers, J. C., and Kornfeld, S. (1971) Hepatic uptake of proteins coupled to fetuin glycopeptide. *Biochem. Biophys. Res. Commun.* 45, 622–629.
- (10) Morell, A. G., Irvine, R. A., Sternlieb, I., and Schneiberg, I. H. (1968) Physical and chemical studies on ceruloplasmin: V. Metabolic studies on sialic acid-free ceruloplasmin in vivo. *J. Biol. Chem.* 243, 155–159.
- (11) Morell, A. G., Gregoriadis, G., and Scheinberg, I. H. (1971) The role of sialic acid in determining the survival of glycoprotein in the circulation. *J. Biol. Chem.* 246, 1461–1467.
- (12) Roseng, L., Tolleshaug, H., and Berg, T. (1992) Uptake, intracellular transport, and degradation of poly(ethylene glycol)-modified asialofetuin in hepatocytes. *J. Biol. Chem.* 267, 22987–22993.
- (13) Abrams, M. J., Juweid, M., Tenkate, C. I., Schwartz, D. A., Hauser, M. M., Gaul, F. E., Fuccello, A. J., Rubin, R. H., Strauss, H. W., and Fischman, A. J. (1990) Technetium-99m-human polyclonal IgG radiolabeled via the hydrazino nicotinamide derivative for imaging focal sites of infection in rats. *J. Nucl. Med.* 31, 2022–2028.
- (14) Corson, D. T., and Meares, C. F. (2000) Efficient multigram synthesis of the bifunctional chelating agent (*S*)-1-*p*-isothiocyanatobenzyl-diethylenetriaminepentaacetic acid. *Bioconjugate Chem.* 11, 292–299.
- (15) Berry, M. N., and Friend, D. S. (1969) High yield preparation of isolate rat liver parenchymal cells: A biochemical and fine structural study. *J. Cell Biol.* 43, 506–520.
- (16) Seglen, P. O. (1976) Preparation of isolated rat liver cells. *Methods Cell. Biol.* 13, 29–83.
- (17) Baranowska-Kortylewicz, J., Dalrymple, G. V., Quadri, S. M., and Harrison, K. A. (1995) Radiolabeling of antibodies for therapy and diagnosis. *Methods Mol. Biol.* 51, 423–439.
- (18) Claessens, R. A., Boerman, O. C., Koenders, E. B., Oyen, W. J., van der Meer, J. W., and Corstens, F. H. (1996) Technetium-99m labeled hydrazinonicotinamido human non-specific polyclonal immunoglobulin G for detection of infectious foci: a comparison with two other technetium-labeled immunoglobulin preparations. *Eur. J. Nucl. Med.* 23, 414–421.
- (19) Fraker, P. J., and Speck, J. C., Jr. (1978) Protein and cell membrane iodinations with a sparingly soluble chloroamide, 1,3,4,6-tetrachloro-3a,6a-diphenylglycoluril. *Biochem. Biophys. Res. Commun.* 80, 849–857.
- (20) Weigel, P. H., and Oka, J. A. (1983) The surface content of asialoglycoprotein receptors on isolated hepatocytes is reversibly modulated by changes in temperature. *J. Biol. Chem.* 258, 5089–5102.
- (21) Wu, J., Nantz, M. H., and Zern, M. A. (2002) Targeting hepatocytes for drug and gene delivery: emerging novel approaches and applications. *Front. Biosci.* 7d, 717–725.
- (22) Fiume, L., Di Stefano, G., Busi, C., Mattioli, A., Bonino, F., Torrani-Cerenzia, M., Verme, G., Rapisetta, M., Bertini, M., and Gervasi, G. B. (1997) Liver targeting of antiviral nucleoside analogues through the asialoglycoprotein receptor. *J. Viral. Hepat.* 4, 363–370.

# Synthesis of Linear, $\beta$ -Cyclodextrin-Based Polymers and Their Camptothecin Conjugates

Jianjun Cheng,<sup>†</sup> Kay T. Khin,<sup>†</sup> Gregory S. Jensen,<sup>†</sup> Aijie Liu,<sup>†</sup> and Mark E. Davis<sup>\*,‡</sup>

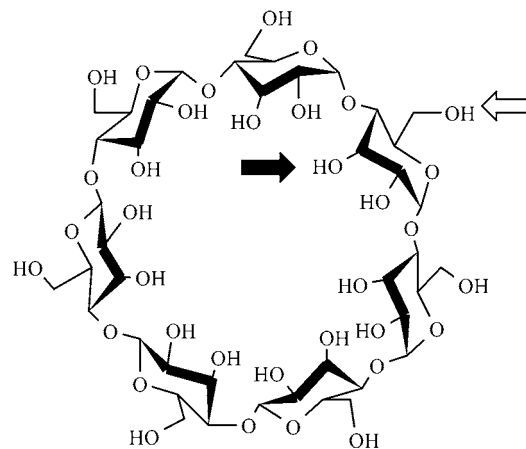
Insert Therapeutics, Inc., 2585 Nina Street, Pasadena, California 91107, and Division of Chemical Engineering, California Institute of Technology, Pasadena, California 91125. Received May 29, 2003; Revised Manuscript Received July 22, 2003

6<sup>A</sup>,6<sup>D</sup>-Bis-(2-amino-2-carboxylethylthio)-6<sup>A</sup>,6<sup>D</sup>-dideoxy- $\beta$ -cyclodextrin **1**, a diamino acid derivative of  $\beta$ -cyclodextrin, is synthesized and condensed with difunctionalized PEG comonomers to give linear, high molecular weight ( $M_w$  over 50 kDa)  $\beta$ -cyclodextrin-based polymers (**2–4**) with pendant functionality (carboxylate). **2–4** are all highly soluble in aqueous solutions (over 200 mg/mL). 20-*O*-trifluoroglycinylcampthecin, **5a**, and 20-*O*-trifluoroglycinylglycinylglycinylcampthecin, **5b**, are synthesized and conjugated to **2** to give polymer–campthecin (CPT) prodrugs. The solubility of CPT is increased by more than three orders of magnitude when it is conjugated to **2**. The rates of CPT release from the conjugates **HGGG6** (high molecular weight polymer ( $M_w$  97 kDa), glyglygly linker and 6 wt % CPT loading) and **HG6** (high MW polymer ( $M_w$  97 kDa), gly linker and 6 wt % CPT loading) in either mouse or human plasma are dramatically accelerated over the rates of pure hydrolysis at pH = 7.4, indicating the presence of enzymatic cleavage as a rate-determining step at this pH in the release of the CPT. The pH of aqueous solution has a large effect on hydrolysis rate of CPT from **HGGG6** and **HG6**; the lower the pH, the slower the rate in the range at  $4.1 \leq \text{pH} \leq 13.1$ . The  $\text{IC}_{50}$ 's of polymer **2e**, CPT, and the CPT conjugates **HG6** and **HGGG6** are found to be cell-line dependent with LS174T, HT29, A2780, and PC3 cells using in vitro MTT assays. The parent polymer **2e** has very low toxicity to all cultured cells tested.

## INTRODUCTION

Numerous small molecules have been investigated for use as antitumor agents. Many of these compounds have been found to have limited clinical effectiveness due in part to their high toxicity, low solubility, and/or other poor pharmaceutical parameters. It has been demonstrated that conjugation of an anticancer molecule to a water-soluble polymer can greatly enhance its aqueous solubility and reduce its cytotoxicity in vitro and in vivo (1–3). High molecular weight (MW) polymers can increase the accumulation of drug in tumor tissue through the so-called enhanced permeability and retention (EPR) effects (4). Therefore, development of polymeric drug delivery vehicles has attracted much attention because of these enhancing features of the polymer–drug conjugates over the parent drug molecules. Polymers that can be used for the conjugation of antitumor agents should have low-toxicity, low-immunogenicity, and high water solubility.

Cyclodextrins (CDs) are cyclic oligosaccharides consisting of ( $\alpha$ -1,4)-linked- $\alpha$ -D-glucopyranose units, and several of their derivatives are known to have low toxicity and lack immunogenicity in humans (5). CDs contain lipophilic cone-shaped cavities that are surrounded by hydrophilic shells that possess a large number of primary and secondary hydroxyls (Figure 1). These hydroxyl groups render many of the CD derivatives highly water-soluble. Therefore, CDs may be excellent building blocks



**Figure 1.** Hydroxyl groups located on the edged of the  $\beta$ -cyclodextrin ring. Primary hydroxyl groups are denoted by an open arrow. Secondary hydroxyl groups are denoted by a solid arrow.

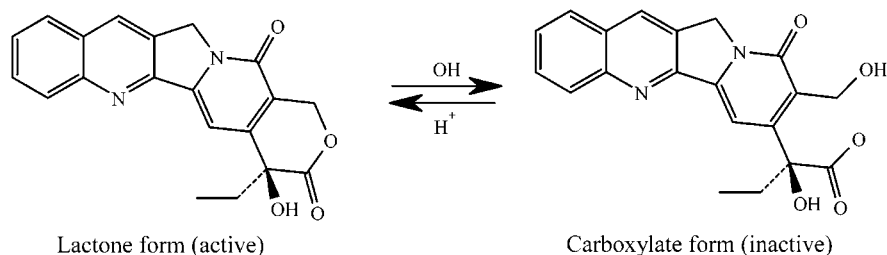
for the synthesis of safe and water-soluble polymers for drug delivery. However, due to the multi-functionality of CD molecules (Figure 1), most CD-containing polymers that have been extensively studied are heavily cross-linked (6). The structures of these polymers are complex and make their characterization difficult.

It is possible to selectively convert only two of the many hydroxyls (e.g., 21 hydroxyls for  $\beta$ -CD) of CDs to other functionalities to give disubstituted CD derivatives (7). If properly functionalized, these CD derivatives can be used for the synthesis of linear polymers where the CD moiety is incorporated to the polymer backbone. We have described the synthesis of  $\beta$ -CD-based, linear polycations

\* To whom correspondence should be addressed. E-mail: mdavis@cheme.caltech.edu. Tel: (626) 395–4251; Fax: (626) 568–8743.

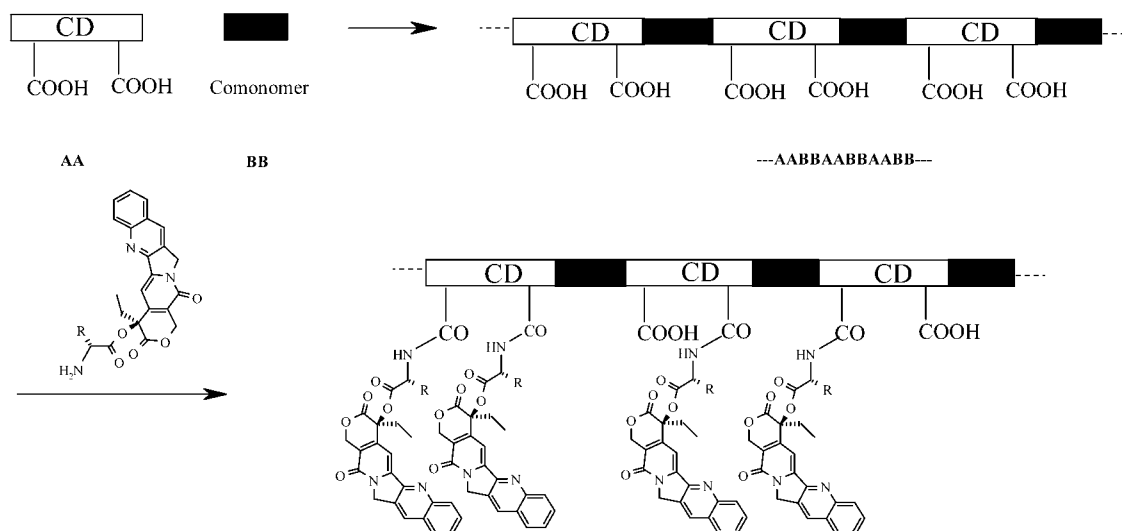
<sup>†</sup> Insert Therapeutics, Inc.

<sup>‡</sup> California Institute of Technology.



**Figure 2.** CPT structure and pH-dependent equilibrium between the lactone and carboxylate form. Lactone form is favored at acidic pH.

**Scheme 1**



(around 6 kDa) as nonviral vectors for systemic gene delivery (8–12).

20(S)-camptothecin (CPT) was first isolated from the Chinese tree, *Camptotheca acuminata*, in the 1960s (13), and has shown a broad range of anticancer activity in animal models (14, 15). CPT has low aqueous solubility in the lactone form and can be highly toxic in its carboxylate form (16). The lactone is essential for anti-cancer activity, while the carboxylate is inactive and favored at physiological pH (see Figure 2) (17, 18). Serum albumin preferentially binds the carboxylate form of CPT and forces the distribution of CPT to further disfavor the lactone form (16–18). These features of CPT result in rapid lactone-ring opening and a loss of antitumor function. Despite these difficulties, CPT-based drugs, e.g., topotecan and irinotecan, are currently approved for use in humans (19, 20).

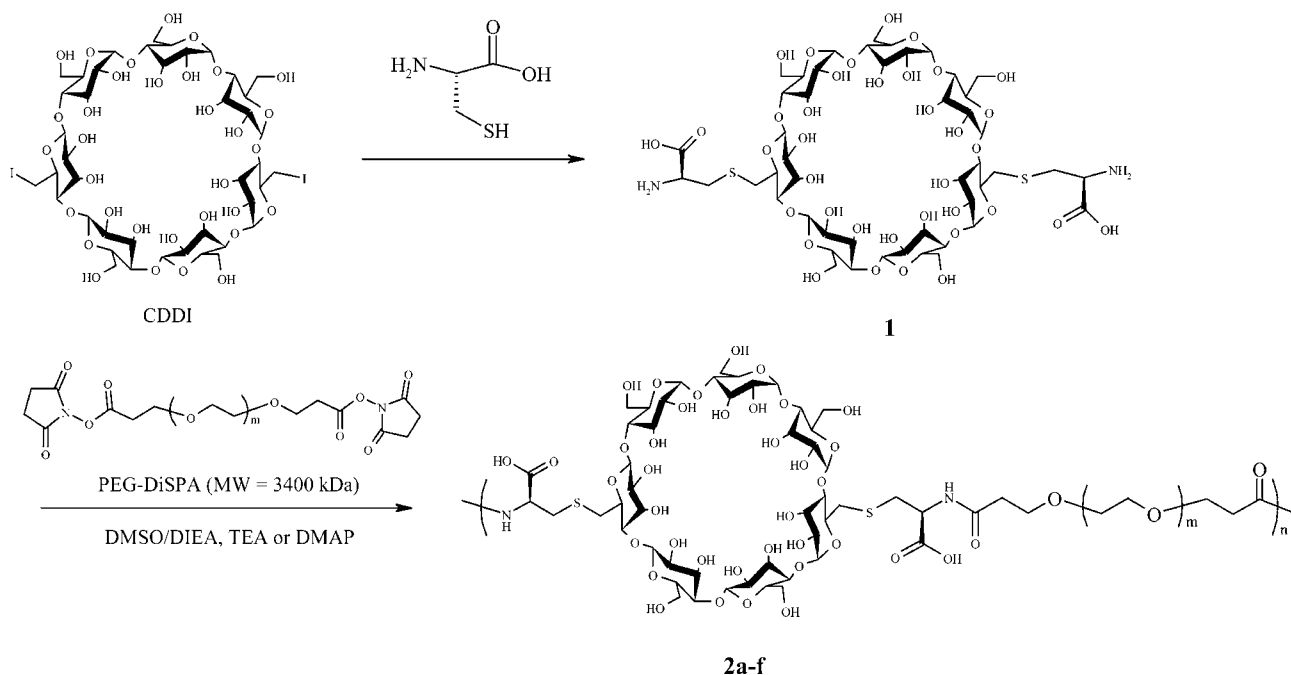
It has been reported that substitution on 20-OH of CPT can substantially reduce the tendency for lactone ring opening (21). Covalent attachment of CPT via this site (20-OH) to water-soluble polymers such as poly(ethylene glycol) (PEG) (22–24), poly-*N*-(2-hydroxypropyl)methacrylamide (HPMA) (25, 26) and poly-*L*-glutamic acid (PG) (27–29) have been reported. In this study, we show the first syntheses of linear, water-soluble, high molecular weight ( $M_w$  over 50 kDa), CD-based polymers (CDPs) that contain pendant carboxylate groups, and conjugate CPT to them for use as antitumor therapeutics. CPT functionalized at the 20-OH position was covalently coupled to the polymer to give the conjugate as illustrated in Scheme 1. The synthesis and properties of these types of conjugates are presented here.

## EXPERIMENTAL PROCEDURES

**General.** All the anhydrous solvents, HPLC grade solvents, and other common organic solvents were purchased from commercial suppliers and used without further purification. Poly(ethylene glycol) dipropionic-succinimide (PEG-DiSPA, MW 3400), poly(ethylene glycol) dibutanoylsuccinimide (PEG-DiSBA, MW 3400), and poly(ethylene glycol) dibenzotriazolecarbonate (PEG-DiBTC, MW 3400) were purchased from Nektar (Huntsville, AL). Poly(ethylene glycol) di-*p*-nitrophenolcarbonate (PEG-DiNPC, MW 3400) was acquired from Sigma (St. Louis, MO). CPT was purchased from Boehringer Ingelheim (Ingelheim, Germany). Human plasma was purchased from Sigma and reconstituted with DI water. Mouse plasma was prepared by centrifuge removal of blood cells of fresh blood samples collected from BALB/C female mice (Charles River). 6<sup>A</sup>,6<sup>D</sup>-Diiodo-6<sup>A</sup>,6<sup>D</sup>-dideoxy- $\beta$ -cyclodextrin (CDDI, Scheme 2) was synthesized according to previous reported procedure (8). Deionized water (18-M $\Omega$ -cm) was obtained by passing in-house deionized water through a Barnstead E-pure purification system. NMR spectra were recorded on a Bruker AMX 500 MHz or a Varian 300 MHz spectrometer. Mass spectral (MS) analysis was performed using either an electrospray mass spectrometer equipped with LCQ ion trap (Thermo Finnigan) and fitted with an electrospray ionization source or a MALDI-TOF mass spectrometer (Voyager DE-PRO, Applied Biosystems). MWs of the polymer samples were analyzed on a GPC system equipped with a Hitachi L-6200 Intelligent Pump, an Anspec RI detector (ERC-7512, Erma, Inc.), a Precision Detectors DLS detector (PD 2020), and double gel permeation columns (PL-aquagel-OH-40 8  $\mu$ m 300  $\times$  7.5 mm, Polymer Laboratory) calibrated using poly(ethylene gly-



Scheme 2



Poly(CDDCys-PA-PEG)

Abbr: PA = propanoicamide bond between PEG and CD

col) standard and eluted using PBS (1×) at a concentration of 20–50 mg/mL and at a 0.7 mL/min flow rate at ambient temperature. CD derivatives were analyzed with a C-18 reverse phase column on a HPLC system equipped with an UV detector (System Gold 168 Detector, Beckman Coulter) and an evaporative light scattering (ELS) detector (Sedex 75, Sedere, France). CPT, CPT derivatives, and polymer–CPT conjugates were analyzed on HPLC systems with a C-18 reverse phase column (HIRPB-4438, 4.6 × 150 mm, Richard Scientific) equipped with a fluorescence detector (FD-500, GTI/Spectro Vision, Grotton Technology, Inc.) using a gradient of potassium phosphate buffer (pH 4.1) and acetonitrile. Excitation and emission wavelengths of the fluorescence detector were set at 370 and 440 nm, respectively.

**6<sup>A</sup>,6<sup>D</sup>-Bis-(2-amino-2-carboxylethylthio)-6<sup>A</sup>,6<sup>D</sup>-dideoxy-β-cyclodextrin, 1 (Scheme 2).** A total of 167 mL of 0.1 M sodium carbonate buffer were degassed for 45 min in a 500-mL two-neck round-bottom flask equipped with a magnetic stir bar, a condenser, and septum. To this solution were added 1.96 g (16.2 mmol) of L-cysteine and 10.0 g (73.8 mmol) of 6<sup>A</sup>,6<sup>D</sup>-diiodo-6<sup>A</sup>,6<sup>D</sup>-dideoxy-β-cyclodextrin (CDDI, Scheme 2). The resulting suspension was heated at a reflux temperature for 4.5 h until the solution turned clear (colorless). The solution was then cooled to room temperature and acidified to pH 3 using 1 N HCl. The product was precipitated by slow addition of acetone (3 times weight ratio of the solution). This afforded 9.0 g of crude material containing CD-biscysteine (90.0%), unreacted cyclodextrin, CD-monocysteine, and cystine. The resulting solid was subjected to anionic exchange column chromatography (SuperQ650M, Tosoh Bioscience) using a gradient elution of 0–0.4M ammonium bicarbonate. All fractions were analyzed by HPLC. The desired fractions were combined, and the solvent was reduced to 100 mL under vacuum. The final product was either precipitated by adding acetone or by adding methanol (3 times weight ratio of the solution). **1** was obtained in 60–80% yield. <sup>1</sup>H NMR (D<sub>2</sub>O) δ 5.08 (m,

Table 1. Polymerization of **1** with Difunctionalized PEG

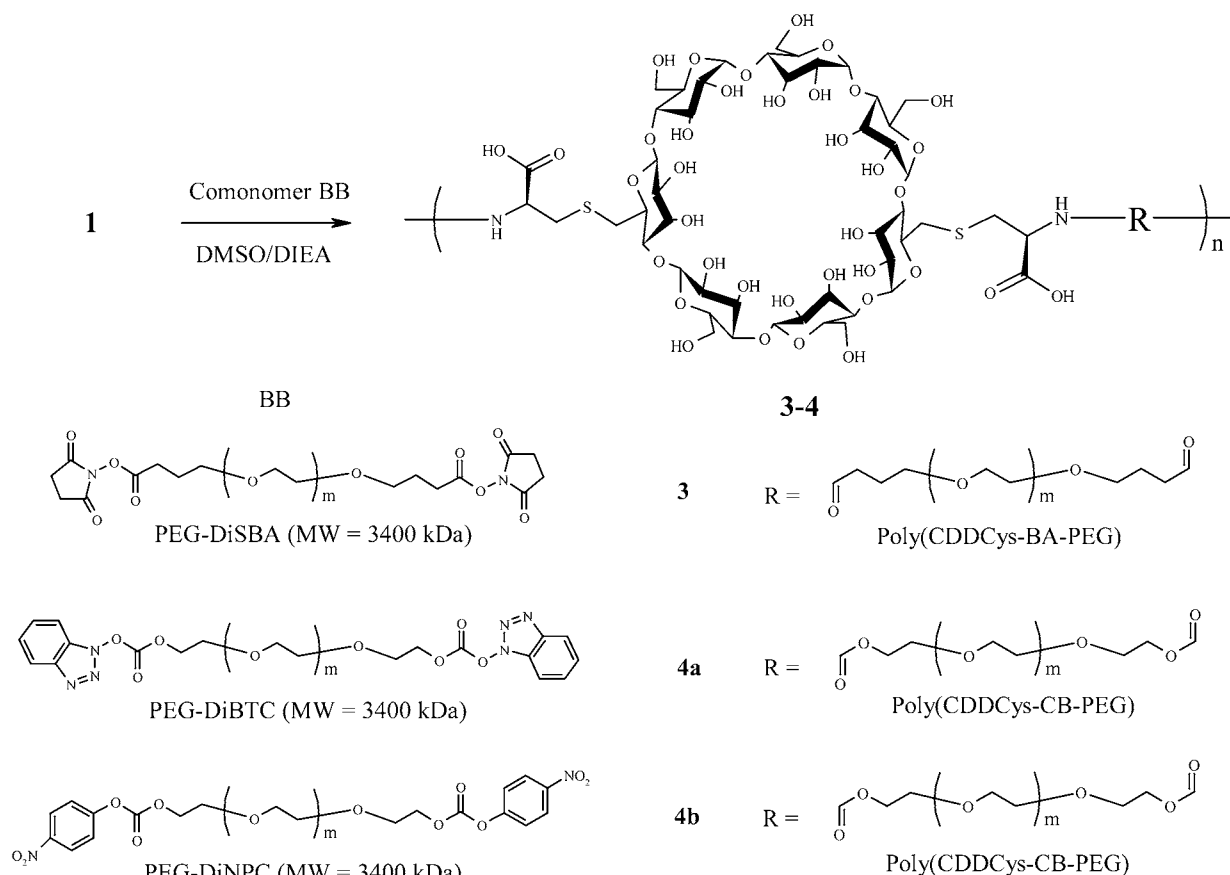
CDP	PEG comonomer	base	polymer- ization time (h)	<i>M<sub>w</sub></i> (kDa)	<i>M<sub>n</sub></i> (kDa)	<i>M<sub>w</sub></i> / <i>M<sub>n</sub></i>	yield (%)
<b>2a<sup>a</sup></b>	PEG-DiSPA	DIEA	120	57.4	41.7	1.38	90
<b>2b<sup>a</sup></b>	PEG-DiSPA	DMAP	120	54.2	38.1	1.42	91
<b>2c<sup>a</sup></b>	PEG-DiSPA	TEA	120	57.4	42.6	1.35	91
<b>2d<sup>b</sup></b>	PEG-DiSPA	DIEA	120	93.6	58.0	1.48	96
<b>2e<sup>b</sup></b>	PEG-DiSPA	DIEA	144	97.3	58.0	1.67	94
<b>2f<sup>b</sup></b>	PEG-DiSPA	DIEA	2	35.3	25.6	1.38	95
<b>3</b>	PEG-DiSBA	DIEA	120	114.7	77.9	1.47	96
<b>4a</b>	PEG-DiBTC	DIEA	120	67.6	39.4	1.47	95
<b>4b</b>	PEG-DiNPC	DIEA	120	86.5	57.2	1.51	96

<sup>a</sup> **1** was washed with acetone before polymerization. <sup>b</sup> **1** was washed with methanol before polymerization.

7H, CD-2-CH), 3.79–3.94 (m, 30H, CD-3,4-CH, CD-CH<sub>2</sub>, Cys-CH), 3.49–3.62 (m, 14H, CD-5, 6-CH), 2.92–3.30 (m, 4H, Cys-CH<sub>2</sub>). <sup>13</sup>C NMR (D<sub>2</sub>O) δ 172.3, 101.9, 83.9, 81.6, 81.5, 73.3, 72.2, 72.0, 60.7, 54.0, 34.0, 30.6. ESI/MS (*m/z*): 1342 [M]<sup>+</sup>, 1364 [M + Na]<sup>+</sup>.

**Synthesis of Poly(CDDCys-PA-PEG), 2a (Scheme 2).** **1** (after precipitation with acetone, 63 mg, 0.047 mmol) and PEG-DiSPA (MW 3400, 160 mg, 0.047 mmol) were dried under vacuum for 8 h. Anhydrous DMSO (1.26 mL) was added to the mixture under argon. After 10 min of stirring, anhydrous diisopropylethylamine (DIEA, 19 μL, 2.3 equiv) was added under argon. The reaction mixture was stirred under argon for 120 h. The polymer containing solution was dialyzed using a 10 000 MWCO membrane (Spectra/Por 7) against water for 48 h and lyophilized to yield 196 mg of **2a** (92%, Table 1). *M<sub>w</sub>* = 57.4 kDa, *M<sub>n</sub>* = 41.7 kDa, *M<sub>w</sub>*/*M<sub>n</sub>* = 1.38. <sup>1</sup>H NMR (D<sub>2</sub>O) δ 5.08 (m, CD-2-H), 4.27 (m, Cys-CH), 2.72–3.76 (m, CD-3,4,5,6-CH, CD-CH<sub>2</sub>, PEG-CH<sub>2</sub>), 2.44 (m, Cys-CH<sub>2</sub>).

Synthesis of other poly(CDDCys-PA-PEG) (**2b–f**), poly(CDDCys-BA-PEG) (**3**), and poly(CDDCys-CB-PEG) (**4a**) (Schemes 2 and 3) were achieved under polymerization condition similar to that of **2a**. Details for the polymer-

**Scheme 3**

Abbr: BA = butanoicamide bond; CB = carbamate bond

ization conditions, monomer selection, polymer molecular weight, polydispersity, and yields are listed in Table 1. **3**:  $^1\text{H}$  NMR ( $\text{D}_2\text{O}$ )  $\delta$  5.10 (m, CD-2-H), 4.25–4.37 (m, Cys-CH), 2.72–3.86 (m, CD-3,4,5,6-CH, CD- $\text{CH}_2$ , PEG- $\text{CH}_2$ ), 2.21 (m, Cys- $\text{CH}_2$ ). **4a–b**:  $^1\text{H}$  NMR ( $\text{D}_2\text{O}$ )  $\delta$  5.05 (m, CD-2-H), 4.56 (m, Cys-CH), 2.70–3.93 (m, CD-3,4,5,6-CH, CD- $\text{CH}_2$ , PEG- $\text{CH}_2$ ), 2.38 (m,  $-\text{OCH}_2\text{CH}_2\text{CH}_2\text{C}(\text{O})-\text{NH}-$ ), 2.34 (m, Cys- $\text{CH}_2$ ), 1.90 (m,  $-\text{OCH}_2\text{CH}_2\text{CH}_2\text{C}(\text{O})-\text{NH}-$ ).

**Molecular Weight Control of CD Polymers.** **1** (after precipitation with methanol) (56.2 mg, 0.0419 mmol) and PEG-DiSPA (147 mg, 0.0419 mmol) were dried under vacuum for 4–8 h. To the mixture was added dry DMSO (1.1 mL) under argon. After 10 min stirring of the sample, DIEA (16  $\mu\text{L}$ , 2.2 equiv) was added under argon. A portion of polymerization solution (150  $\mu\text{L}$ ) was removed and precipitated with ether at selected times (2, 18, 43, 70, 168, and 288 h). MWs of the precipitated polymers were determined as described above.

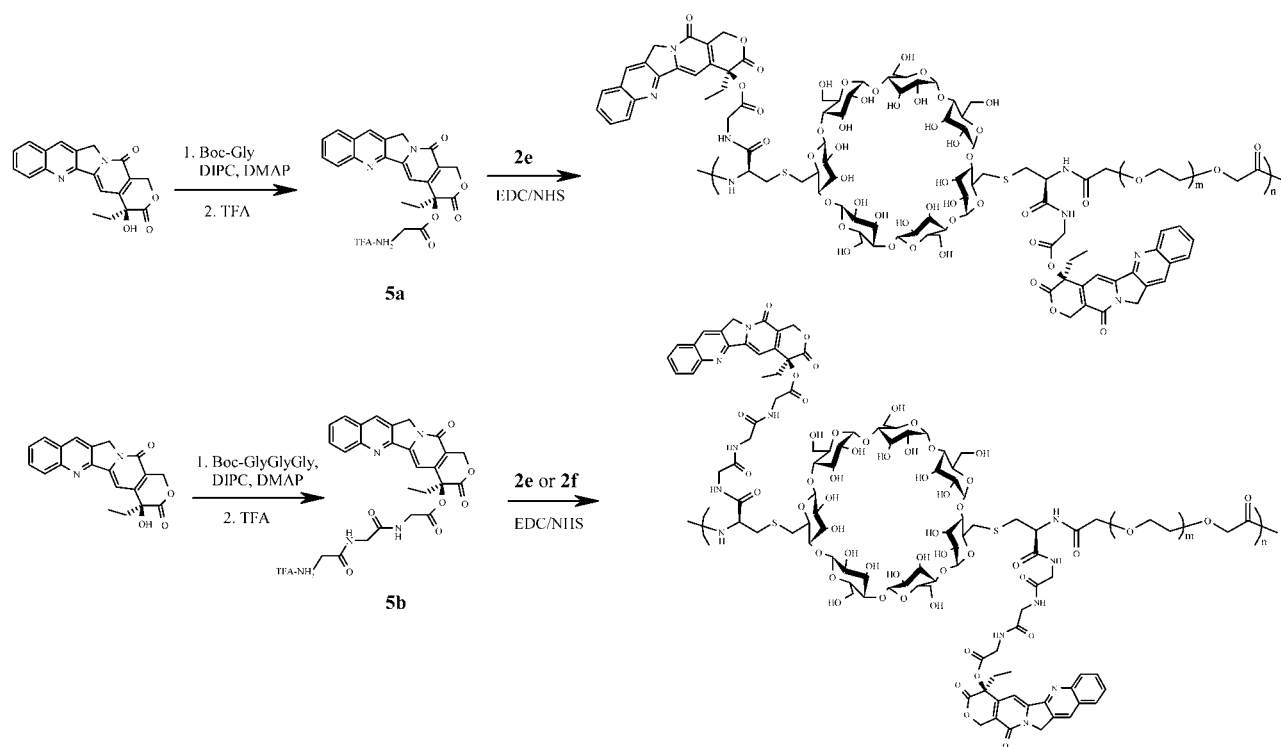
**20-Hydroxyl-Modified Camptothecin.** Synthesis of 20-*O*-trifluoroglycinyllcamptothecin (**5a**) and 20-*O*-trifluoroglycinyllglycinyllcamptothecin (**5b**) were synthesized according to previous reported procedures (23) with slight modification.

**Synthesis of 5a (Scheme 4).** *t*-Boc-glycine (0.9 g, 4.7 mmol) was dissolved in 350 mL of anhydrous methylene chloride at room temperature, and to this solution were added DIPC (0.75 mL, 4.7 mmol), DMAP (382 mg, 3.13 mmol), and CPT (0.55 g, 1.57 mmol) at 0  $^\circ\text{C}$ . The reaction mixture was allowed to warm to room temperature and remain stirring for 16 h. The organic solution was extracted with cold pH 2 aqueous solution, dried with

$\text{MgSO}_4$ , and evaporated under reduced pressure to yield a light yellow solid, that was recrystallized from methanol to give camptothecin-20-ester of *t*-Boc-glycine 0.45 g (57%):  $^1\text{H}$  NMR( $\text{DMSO}-d_6$ )  $\delta$  7.5–8.8 (m), 7.3 (s), 5.5 (s), 5.3 (s), 4 (m), 2.1 (m), 1.6 (s), 1.3 (d), 0.9 (t). Camptothecin-20-ester of *t*-Boc-glycine (0.608 g, 1.2 mmol) was dissolved in a mixture of methylene chloride (10 mL) and TFA (10 mL) and stirred at room temperature for 1 h. Solvent was removed and the residue was recrystallized from methylene chloride and ether to give 0.55 g of **5a** (87%).  $^1\text{H}$  NMR ( $\text{DMSO}-d_6$ )  $\delta$  7.7–8.5 (m); 7.2 (s), 5.6 (s), 5.4 (s), 4.4 (m), 2.2 (m), 1.6 (d), 1.0 (t),  $^{13}\text{C}$  NMR ( $\text{DMSO}-d_6$ )  $\delta$  168.6, 166.6, 156.5, 152.2, 147.9, 146.2, 144.3, 131.9, 130.6, 129.7, 128.8, 128.6, 128.0, 127.8, 119.0, 95.0, 77.6, 66.6, 50.5, 47.9, 30.2, 15.9, 7.9. ESI/MS ( $m/z$ ) expected 405; Found 406 ( $\text{M}+\text{H}$ ).

**Synthesis of 5b (Scheme 4).** *t*-Boc-GlyGlyGly (1.359 g, 4.7 mmol) was dissolved in 350 mL of anhydrous methylene chloride at room temperature and to this solution were added DIPC (0.75 mL, 4.7 mmol), DMAP (382 mg, 3.13 mmol), and CPT (0.55 g, 1.57 mmol) at 0  $^\circ\text{C}$ . The reaction mixture was allowed to warm to room temperature and remain stirring for 16 h. The organic solution was extracted with cold pH 2 aqueous solution, dried with  $\text{MgSO}_4$ , and evaporated under reduced pressure to yield a light yellow solid, which was recrystallized from methanol to give camptothecin-20-ester of *t*-Boc-GlyGlyGly 0.47 g (65%):  $^1\text{H}$  NMR( $\text{DMSO}-d_6$ )  $\delta$  8.40 (s), 8.25 (d), 7.91 (d), 7.78 (m), 7.65 (t), 7.26 (s), 7.05 (br, s), 5.65 (d), 5.40 (d), 5.25 (s), 5.10 (br, s), 3.75–4.42 (m), 2.15–2.35 (m), 1.45 (s), 0.95 (t) Camptothecin-20-ester of *t*-Boc-GlyGlyGly (1.5 g, 2.08 mmol) was dissolved in a mixture

Scheme 4



of methylene chloride (20 mL) and TFA (20 mL) and stirred at room temperature for 1 h. Solvent was removed under vacuum, and the residue was redissolved in methylene chloride. The solution was poured into ether to give an instant yellow precipitate. The precipitate was filtered and washed with cold ether to give 1.31 g of **5b** (86%).  $^1\text{H}$  NMR ( $\text{DMSO}-d_6$ )  $\delta$  8.79 (s), 7.75–8.61 (m), 7.10 (s), 5.55 (s), 3.90–4.37 (m), 3.86 (s), 3.54 (s), 2.11–2.23 (m), 0.95 (t). ESI/MS ( $m/z$ ) expected 519; Found 520 ( $M+H$ ).

**Synthesis of Poly(CDDCys-PA-PEG)-CPT Conjugates.** *Synthesis of Poly(CDDCys-PA-PEG)-GlyGlyGly-CPT (HGGG6).* **2e** (1.37 g, 0.30 mmol of repeat unit) was dissolved in dry DMSO (136 mL). The mixture was stirred for 10 min. **5b** (419 mg, 0.712 mmol, 2.36 equiv), DIEA (0.092 mL, 0.712 mmol, 2.36 equiv), EDC (172 mg, 0.903 mmol, 3 equiv), and NHS (76 mg, 0.662 mmol, 2.2 equiv) were added to the polymer solution and stirred for ca. 15 h. The polymer was precipitated with ethyl ether (1 L). The ether was poured out and the precipitate was washed with  $\text{CH}_3\text{CN}$  ( $3 \times 100$  mL). The precipitate was dissolved in water (600 mL). Some insoluble solid was filtered through 0.2  $\mu\text{m}$  filters. The solution was dialyzed using 25 000 MWCO membrane (Spectra/Por 7) for 10 h at 10–15  $^\circ\text{C}$  in DI water. Dialysis water was changed every 60 min. The polymer–drug conjugate solution was sterilized by passing it through 0.2  $\mu\text{m}$  filters. The solution was lyophilized to yield a yellow solid (1.42 g, 85%).

*Synthesis of Poly(CDDCys-PA-PEG)-GlyGlyGly-CPT (LGGG10).* Conjugation of **5b** to **2f** was performed in a manner similar to that used to produce **HGGG6** except that this conjugate was dialyzed with 10 000 MWCO membrane (Spectra/Por 7) instead of with 25 000 MWCO membrane. The yield of **LGGG10** was 83%.

*Synthesis of Poly(CDDCys-PA-PEG)-Gly-CPT (HG6).* Conjugation of **5a** to **2e** was performed in a manner similar to that used to produce **HGGG6**. The yield of **HG6** was 83%.

*Synthesis of Poly(CDDCys-PA-PEG)-GlyGlyGly-CPT (HGGG10).* **2e** (1.5 g, 0.33 mmol of repeat unit) was dissolved in dry DMSO (150 mL). The mixture was stirred for 10 min. **5b** (941 mg, 1.49 mmol, 4.5 equiv), DIEA (0.258 mL, 1.49 mmol, 4.5 equiv), EDC (283 mg, 1.49 mmol, 4.5 equiv), and NHS (113 mg, 0.99 mmol, 3 equiv) was added to the polymer solution and stirred for ca. 24 h. Another portion of EDC (142 mg, 0.75 mmol, 2.3 equiv) and NHS (56 mg, 0.5 mmol, 1.5 equiv) were added to the conjugation solution. The polymer was stirred for an additional 22 h. The workup procedure was same as that for the synthesis of **HGGG6**. The yield of **HG6** was 77%.

**Determination of wt % CPT on the Conjugates.** Stock solutions of **HGGG6**, **LGGG10**, **HG6**, and **HGGG10** were prepared at a concentration of 10 mg/mL in DMSO. An aliquot of corresponding stock solution was diluted to 100  $\mu\text{g/mL}$  using 1 N NaOH. CPT was completely hydrolyzed in this basic solution and transformed to its carboxylate form within 2 h at room temperature. An aliquot of this solution was diluted to 10  $\mu\text{g/mL}$  using 8.5%  $\text{H}_3\text{PO}_4$ , and the CPT carboxylate form was transformed to its lactone form. 30  $\mu\text{L}$  of this solution was injected into the HPLC. The peak area from the CPT lactone form was integrated and compared to a standard curve.

**Comparison of Lactone Stability of CPT and 5 in Phosphate Buffered Saline (PBS).** CPT or **5** (**5a** and **5b**) was dissolved in DMSO at 1 mg/mL and then diluted to 1  $\mu\text{g/mL}$  with PBS ( $1\times$ , pH 7.4). 30  $\mu\text{L}$  of solution were injected into the HPLC at room temperature at selected time intervals. The peak area from the CPT lactone form of CPT or **5** (**5a** and **5b**) were integrated.

**Release of CPT from HGGG6 and HG6.** *Release of CPT in PBS.* **HGGG6** and **HG6** were prepared at 1 mg/mL in PBS ( $1\times$ , pH 7.4). A 100  $\mu\text{L}$  aliquot of the solution was transferred to a 1.5 mL Eppendorf tube and incubated at 37  $^\circ\text{C}$ . The incubated samples were quenched at selected time intervals and stored at  $-80$   $^\circ\text{C}$  until the



analysis. Each solution was diluted with 8.5%  $\text{H}_3\text{PO}_4$  to a 5 mL total volume in a volumetric flask. 30  $\mu\text{L}$  of such solution was injected into the HPLC. The peak area from the CPT lactone form was integrated and compared to a standard curve.

Analysis for the release of CPT from **HGGG6** and **HG6** in PBS containing acetyl cholinesterase (an esterase, 100 units/mL), in  $\text{KH}_2\text{PO}_4$  buffer (pH 6.1, 0.1 M) and in the  $\text{KH}_2\text{PO}_4$  buffer (pH 6.1, 0.1 M) containing cathepsin B (a cysteine proteinase, 200  $\mu\text{M}$ , preactivated on ice for 30 min in this buffer containing 2 mM DTT and 1 mM EDTA) were performed in a manner similar to that described above for PBS alone.

**Release of CPT in Human Plasma.** An aliquot of **HGGG6** and **HG6** stock solution were diluted to give final concentration of 0.5 mg/mL in PBS (1 $\times$ , pH 7.4). This solution was added to a lyophilized powder of human plasma to reconstitute 100% human plasma by the recommended amount. The solution was divided into equal volume (250  $\mu\text{L}$ ) to 1.5 mL Eppendorf tubes, incubated at 37  $^\circ\text{C}$ , and stopped at selected time point. Samples were stored at  $-80^\circ\text{C}$  until the analysis. Samples were separated from plasma by solid-phase extraction columns. The solid-phase extraction cartridge (Oasis HLB 1  $\text{cm}^3$  cartridge from Waters) was preconditioned with 1 mL of acetonitrile and then with 1 mL of 8.5%  $\text{H}_3\text{PO}_4$  before loading. Samples were acidified with equal volume of 8.5%  $\text{H}_3\text{PO}_4$  prior to loading. After the acidified solution was loaded on the cartridge, the bed was washed with  $3 \times 1$  mL of water. Released CPT and polymer conjugate were eluted with  $3 \times 1$  mL of a solution mixture of acetonitrile and potassium phosphate buffer (pH 4.1) (60/40 v/v). The eluted solution was diluted to 5 mL total volume in a 5 mL volumetric flask. 30  $\mu\text{L}$  of such solution was injected into the HPLC. The peak area from the CPT lactone form was integrated and compared to a standard curve.

Release of CPT from **HGGG6** and **HG6** in PBS containing 4% human plasma (PBS/reconstituted human plasma solution = 96/4 (v/v)), in mouse plasma and in reconstituted human albumin (PBS solution) were performed in a manner similar to that described above for pure human plasma.

**Release of CPT in Solution at Variable Different pH.** **HGGG6** and **HG6** were prepared at 1 mg/mL in buffer solution with pH values ranging from acidic (pH = 1.2) to basic (pH = 13.1) and incubated at 37  $^\circ\text{C}$  for 24 h. An aliquot of each solution was diluted with 8.5%  $\text{H}_3\text{PO}_4$  to about 100  $\mu\text{g}/\text{mL}$ . 30  $\mu\text{L}$  of such solution was injected into HPLC. The peak area from the CPT lactone form was integrated and compared to a standard curve.

**$\text{IC}_{50}$  via MTT Assay.** The human ovarian carcinoma A2780 cell line was obtained from the European Collection of Cell Cultures (Salisbury, Wiltshire, UK). The human colorectal adenocarcinoma HT29, human prostate carcinoma PC-3, and human colonic adenocarcinoma LS174T cell lines were obtained from the American Type Culture Collection (Rockville, MD). Cells were seeded in 96-well plates at 5000 cells/well and grown in medium containing 10% fetal bovine serum at 37  $^\circ\text{C}$  for 24 h in a humidified 5%  $\text{CO}_2$  atmosphere. The medium was replaced with fresh medium containing CPT, **2e**, **HGGG6** or **HG6** in concentrations ranging from 1 nM to 10  $\mu\text{M}$  of CPT and **2e** (CPT equivalent for **HGGG6** and **HG6**). At each concentration, three wells per plate were treated. The effect of the compounds on cell growth was measured by the MTT assay after 72 h. The medium was removed, the cells were rinsed with PBS, MTT solution was added at a concentration of 0.5 mg/mL, and the plates were

incubated for 4 h at 37  $^\circ\text{C}$ . The medium was removed and the formazan crystals were solubilized in DMSO. Absorbance was measured at 560 nm using a SPEC-TRAFluor Plus plate reader (Tecan, Durham, NC). The percentage of cell survival was calculated relative to untreated cells, and  $\text{IC}_{50}$ 's were determined from plots of dose versus cell survival.

## RESULTS

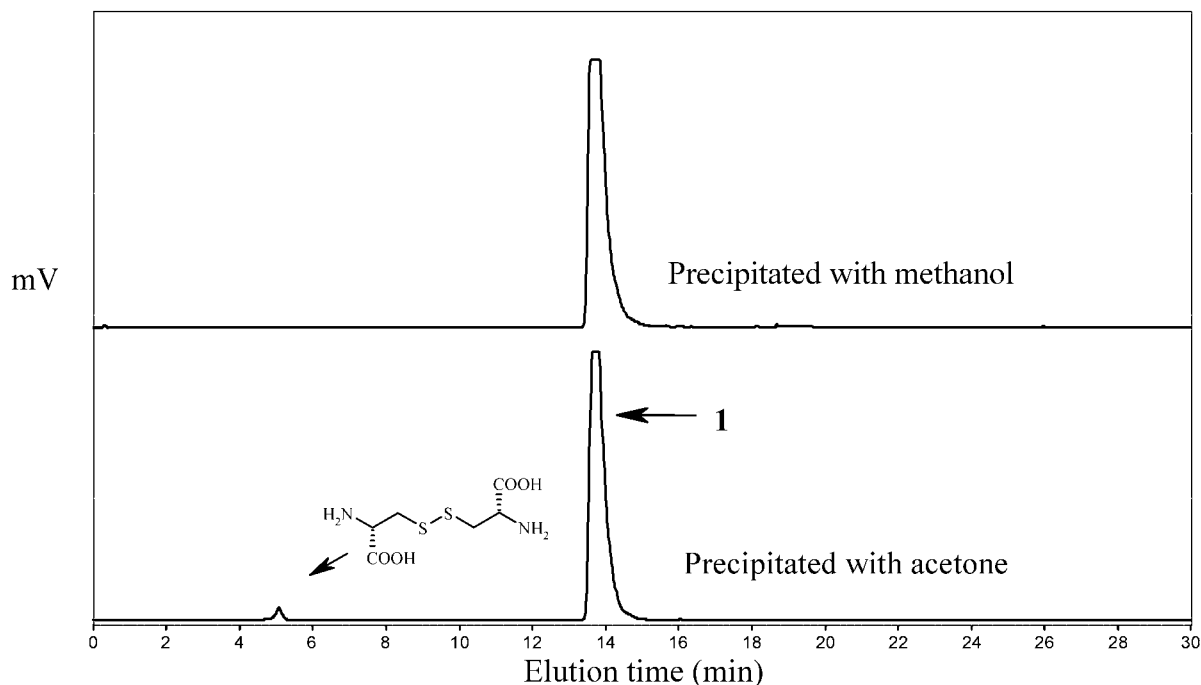
**Synthesis of Difunctionalized Cyclodextrin Monomer, 1.** 6<sup>A</sup>, 6<sup>D</sup>-bis-(2-amino-2-carbonylthio)-6<sup>A</sup>,6<sup>D</sup>-dideoxy- $\beta$ -cyclodextrin, **1**, was synthesized from 6<sup>A</sup>,6<sup>D</sup>-diiodo-6<sup>A</sup>,6<sup>D</sup>-dideoxy- $\beta$ -cyclodextrin (CDDI, Scheme 2) in a basic buffer solution (pH 11.6, sodium bicarbonate buffer) at 100  $^\circ\text{C}$  (Scheme 2). High pH buffer was essential to increase the nucleophilicity of the thiol group on the L-cysteine. This reaction was complete within 5 h. **1** was isolated from other impurities in yields between 60 and 80% using a final anion exchange. After the purification, **1** usually still contained small amounts of free cystine, a side product from the oxidation of cysteine. To achieve higher purity product, **1** was dissolved in water and precipitated with either acetone or methanol. Cystine cannot be completely removed by the acetone-precipitation method as detectable amounts of cystine (0.5–1 wt %) still remains in **1** (Figure 3). Precipitation of **1** with methanol completely removes cystine (Figure 3), most likely due to the higher solubility of cystine in methanol as compared to acetone.

**Polymerization of 1 with PEG Comonomers.** Polymerization of **1** with PEG-DiSPA was carried out in anhydrous DMSO solution under argon (Scheme 2). Addition of a nonnucleophilic organic base (such as DIEA) was essential for this polymerization as no viscosity changes of the polymerization solutions were observed after 48 h if no base was added. When 2.3 equiv of DIEA was added, the viscosity of polymerization solution increased dramatically after 4–6 h of reaction. DIEA deprotonates the amino groups of **1** to render them more nucleophilic for coupling with PEG-DiSPA. There were essentially no differences in the polymerizations if other bases, such as TEA or DMAP, were used (**2b–c**, Table 1). Polymerization using **1** recovered by the two different precipitation methods (acetone and methanol) produced polymers with different MWs. **1** that was purified by the methanol precipitation method (contains no free cystine) gave higher MW polymer (**2d–e**) as compared to the less pure **1** that was obtained from the acetone precipitation method (**2a**). Polymerization of **1** with PEG-DiSPA typically produced polymer in yields greater than 90%.

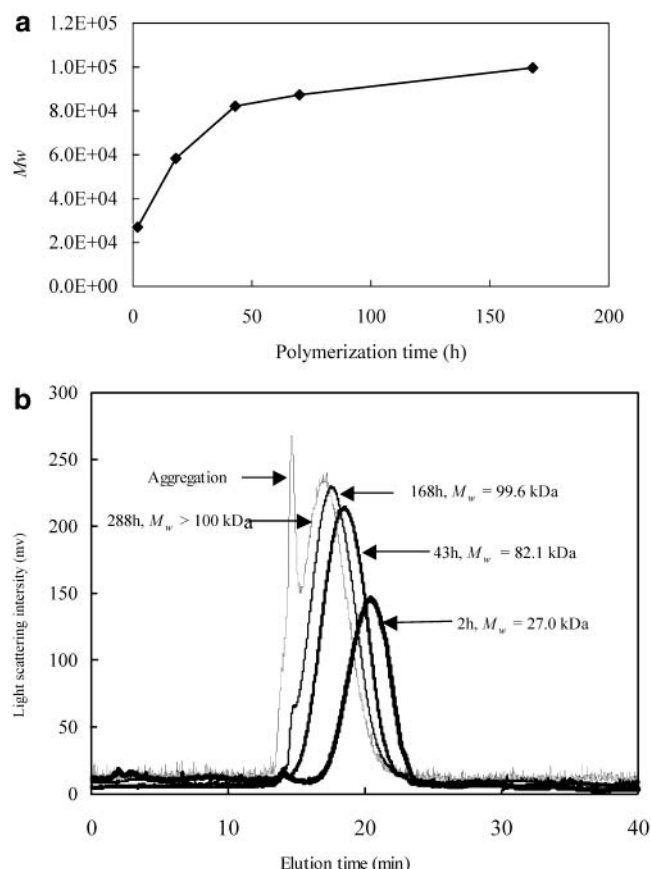
As shown in Figure 4a, the polymer MW increased to around 80 kDa over the course of 48 h of reaction, then gradually increased to around 100 kDa after the polymerization was carried out for another 4–5 days. Prolonged polymerization (> 1 week) generally produced aggregation that rendered the MW measurements inaccurate (Figure 4b).

**1** was polymerized with other activated monomers such as PEG-DiSBA, PEG-DiBTC, and PEG-DiNPC (Scheme 3). Reaction of **1** with PEG-DiSBA gave a polymer **3** with similar linkages as **2** (amide bond, but one more  $-\text{CH}_2$  group than **2** at the linker) with  $M_w$  over 100 kDa, while reaction of **1** with PEG-DiBTC and PEG-DiNPC generated polymers (**4a** and **4b**, respectively) with connecting carbamate moiety and  $M_w$ 's over 50 kDa (Table 1).

Polymers **2–4** are highly soluble in aqueous solution. They can be easily dissolved in water or phosphate buffered saline (PBS) solution at concentrations of at



**Figure 3.** Purification of **1** by precipitation with acetone or methanol.



**Figure 4.** (a) Molecular weights of poly(CDDCys-PA-PEG) as a function of polymerization times. (b) GPC curves of poly(CDDCys-PA-PEG) as a function of polymerization times.

least 200 mg/mL. Solubility of these polymers in aqueous solution at concentrations higher than 200 mg/mL was not attempted due to the high viscosity. These polymers were also soluble in DMF, DMSO, and methanol, slightly soluble in  $\text{CH}_3\text{CN}$  and  $\text{CHCl}_3$ , but insoluble in THF and ethyl ether.

**Table 2.** Properties of Polymer–CPT Conjugates

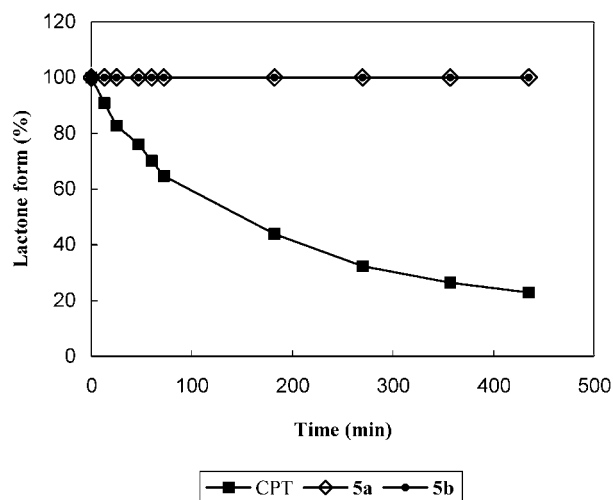
polymer	CPT-linker	CPT (wt %)	conjugate <sup>a</sup>	yield (%)
<b>2e</b>	<b>5b</b>	6.1	<b>HGGG6</b>	85
<b>2f</b>	<b>5b</b>	10.2	<b>LGGG10</b>	83
<b>2e</b>	<b>5a</b>	6.8	<b>HG6</b>	87
<b>2e</b>	<b>5b</b>	9.6	<b>HGGG10</b>	77

<sup>a</sup> Abbreviations: **H** = high  $M_w$  polymer (97 kDa), **L** = low  $M_w$  polymer (35 kDa), **GGG** = triglycine linker, **G** = glycine linker, **6** = drug loading around 6 wt %, **10** = drug loading around 10 wt %.

**Synthesis of Poly(CDDCys-PA-PEG)–CPT Conjugates.** CPT was reacted with *N*-*tert*-butoxycarbonyl (Boc) glycine or triglycine to form an ester bond between the 20-hydroxyl group of CPT and the carboxylate of the amino acid in the presence of diisopropylcarbodiimide and DMAP. **5a** and **5b** were obtained after removing the BOC groups of the corresponding ester intermediate with trifluoroacetic acid (TFA) (Scheme 4). **5a** and **5b** were isolated with yields over 50%.

**5a** and **5b** were conjugated to **2e** or **2f** (Scheme 4 and Table 2) using conventional coupling methods. Due to the instability of the ester linker of **5a** and **5b** in aqueous solution, the conjugation was conducted in anhydrous DMSO under argon. An organic base was required to deprotonate the TFA salts of **5a** and **5b** to facilitate the coupling. For polymer conjugation with **5b**, the weight percent (wt %) drug loading was around 6–10% (a prolonged reaction time did not lead to higher loadings). The theoretical maximum drug loading is around 13% using PEG with MW of 3400 Da; maximum values can be increased by decreasing the MW of the PEG segments. Solubilities of all conjugates in water or PBS were more than 200 mg/mL (equivalent to a 12–20 mg of CPT/mL for 6–10 wt % drug loading, respectively).

**CPT Lactone Ring Stability by 20-Substitution.** The rate of lactone ring opening for **5a**, **5b**, and CPT were studied in PBS buffer (pH 7.4). Both **5a** and **5b** were very stable against ring-opening, and no carboxylate forms of **5a** and **5b** were detected throughout the study (7 h). On



**Figure 5.** Lactone stability of CPT, **5a** and **5b** in PBS (pH 7.4).

**Table 3.** Half-life ( $t_{1/2}$ , in h) of the Release of CPT from **HG6** and **HGGG6**<sup>a</sup>

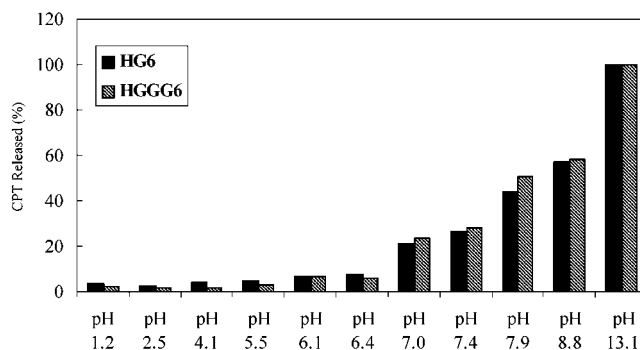
conjugate	PBS <sup>b</sup>	4% HP <sup>c</sup>	HP <sup>d</sup>	MP <sup>e</sup>	Alb <sup>f</sup>	Ac Cho <sup>g</sup>	pH 6.1 buffer <sup>h</sup>	Cath B (pH 6.1) <sup>i</sup>
<b>HG6</b>	59	25	1.7	2.6	62	33	>144	>144
<b>HGGG6</b>	32	22	1.6	2.2	73	43	>144	>144

<sup>a</sup>  $t_{1/2}$  is defined as time (h) for the release of half of the total conjugated CPT. Abbreviations: HP means human plasma, MP means mouse plasma. <sup>b</sup> pH 7.4 PBS 1× buffer. <sup>c</sup> Reconstituted human plasma mixed with PBS (v/v = 4/96). <sup>d</sup> Reconstituted human plasma. <sup>e</sup> Fresh mouse plasma. <sup>f</sup> In reconstituted human albumin PBS buffer. <sup>g</sup> In the presence of acetyl cholinesterase PBS solution (100 units/mL). <sup>h</sup> pH 6.1 phosphate buffer (0.1M). <sup>i</sup> pH 6.1 phosphate buffer in the presence of cathepsin B.

the other hand, more than 60% of the CPT lactone form was transformed to its carboxylate form in the same period of time (Figure 5).

**Release of CPT from Conjugates.** The release of CPT from two polymer-CPT conjugates (**HG6** and **HGGG6**) with identical MW ( $M_w$  97 kDa) and very similar drug loading (ca. 6 wt %) was investigated. The release kinetics for CPT from **HG6** and **HGGG6** was measured at 37 °C in different aqueous solutions (Table 3). In PBS (1×, pH 7.4), the half-lives ( $t_{1/2}$ ) for releasing CPT from **HG6** and **HGGG6** were 59 and 32 h, respectively. The half-lives decreased to 25 and 22 h, respectively, in the presence of 4% human plasma, and to 1.7 and 1.6 h, respectively, in 100% human plasma and 2.6 and 2.2 h, respectively, in 100% mouse plasma. CPT release rates for both **HG6** and **HGGG6** in the presence of albumin or acetyl cholinesterase were on the same order of magnitude as in PBS. In a buffer solution at a pH lower than PBS (pH 6.1) with or without the enzyme cathepsin B (active at pH 6.1 (30)), less than 50% of total conjugated CPT was released from both **HG6** and **HGGG6** for times up to 144 h (Table 3).

The pH of aqueous solution has great effect on the CPT release rates from both **HG6** and **HGGG6**. The amounts of CPT released from **HG6** and **HGGG6** at 37 °C after 24 h in buffer solutions with pHs ranging from 1.1 to 13.1 are illustrated in Figure 6. The glycyl-CPT ester bonds of both **HG6** and **HGGG6** were very stable in acidic pH (1.1–6.4) as less than 7% of CPT were released in 24 h. The CPT hydrolysis rate was drastically increased with an increase of pH to pH 7 or above. CPT was completely hydrolyzed at pH 13 in 24 h. The polymer backbone of **2e** was stable against degradation at pH 5 or above, and



**Figure 6.** Release of CPT from **HG6** and **HGGG6** at various pH (37 °C, 24 h).

**Table 4.** IC<sub>50</sub> of CPT, Unconjugated Polymer **2e** and CPT Conjugates **HG6** and **HGGG6** in Various Cell Lines

cell line	<b>2e</b> (μM)	CPT (μM)	<b>HG6</b> (μM)	<b>HGGG6</b> (μM)
LS174T	>300	0.005	0.050	0.010
HT29	300	0.020	0.050	0.030
A2780	100	0.007	0.025	0.020
PC3	>300	0.075	0.25	0.15

slowly degrades to low MW species over a period of several months at pH 4 or below (data not shown).

The **HG6** hydrolysis solution (PBS) was analyzed by HPLC and the fraction containing the released CPT molecule (same retention time as authentic CPT) was investigated by mass spectroscopy. The molecular weight of this molecule is identical to that of authentic CPT demonstrating that the component released is pure CPT.

**IC<sub>50</sub> Measurement by MTT Assay.** The toxicities of **2e**, CPT, and the conjugates (**HG6** and **HGGG6**) were tested in various cell lines (Table 4) using the MTT assay. The IC<sub>50</sub>'s of **2e** were in a range of 100 to 450 μM, indicating that this polymer was very nontoxic to all cell lines tested. The IC<sub>50</sub> of CPT was around 5 nM in LS174T cells, and ca. 75 nM in PC3 cells. The IC<sub>50</sub> of **2e** was thus at least 3 orders of magnitude higher than that of CPT. In all cell lines tested, the IC<sub>50</sub> values decreased in the order **HG6**, **HGGG6**, and CPT.

## DISCUSSION

The general strategy for the design of the linear, CD-containing polymers with pendant functionalities via the condensation of a difunctionalized CD monomer (AA) with a comonomer (BB) for the conjugation of CPT is illustrated in Scheme 1. Due to the existence of numerous hydroxyl groups on cyclodextrins, syntheses involving CD molecules typically require protection and deprotection of these hydroxyls to avoid side reactions such as cross-linking. Here, the design of a difunctionalized CD molecule allows straightforward use as a monomer for the construction of linear polymers without the need of tedious protection/deprotection chemistry during the polymerization. CD-diamino acids are used as monomers since amino groups are much more reactive for certain types of condensation reactions (e.g., coupling to succinimide) when compared to hydroxyl groups, and the carboxylates remain intact during polycondensation for use in the conjugation of CPT.

Synthesis of the CD diamino acid monomer was first attempted by reacting  $N_\alpha$ -CBZ-lysine with CDDI. However, no product was isolated. The result is likely due to the low reactivity of the amino groups of lysine for substitution of the iodo group of CDDI that is adjacent to the bulky CD moiety. It has been reported that thiol group, as compared with amino group, has a much higher



reactivity for this substitution reaction (8, 9). For example, reaction between CDDI and dicysteamine gives predominantly CD-dicysteamine with amino terminal groups. Therefore, L-cysteine, an amino acid containing a thiol group, was chosen to react amino acid moieties onto the CD (Scheme 2). **1** was successfully synthesized using this strategy and was purified with good yield (60–80%).

Due to the bulky size of the CD, a disuccinimide compound with relatively long distance between these reactive groups is used to minimize the steric hindrance between CD molecules in the construction of polymer chains. PEG-DiSPA (MW 3400) is a good comonomer for such polymerization. **1** is a multifunctionalized  $\beta$ -CD derivative containing two amino, two carboxylates, and 19 hydroxyl groups. The amino groups of **1** ( $pK_a = 10.8$  (31)) are protonated after purification by ion exchange and are not reactive toward PEG-DiSPA. Nonnucleophilic organic bases, such as DIEA, DMAP, or TEA, whose  $pK_a$ 's are in a range of 11–12, can deprotonate the amino groups of **1** to render them very nucleophilic and facilitate coupling with the succinimides of PEG-DiSPA (the hydroxyls of the CD are not reactive to succinimide comonomers). Linear, CD-based polymers with  $M_w$ 's greater than 50 kDa can be easily synthesized using this method. To the best of our knowledge, this is the first synthesis of water-soluble, linear,  $\beta$ -CD polymers with high MW ( $M_w > 50$  kDa) and with pendant functional groups. No cross-linking was observed in these polymers.

As shown in Table 1, the purity of **1** plays an important role in the achievement of high MW polymers. Although there is only ca. 0.5–1 wt % free cystine in acetone-precipitated **1** (Figure 3), the mole percentage is around 3–6% due to its small molecular weight (240 g/mol) compared to **1** (1341 g/mol). Chain termination due to the presence of the impurity is likely one of the reasons lower MW polymers are obtained (Table 1).

As shown in Figure 4a for the polymerization of **1** (methanol-precipitated) with PEG-DiSPA, the  $M_w$  of poly(CDDCys-PA-PEG) (**2**) increases to around 80 kDa during the first 2 days of reaction and then slowly increases to ca. 100 kDa after another 3–5 days of reaction. Although the polymer MW should continue to increase with prolonged reaction time in this step-growth polymerization (as long as polymerization is not terminated), polymer aggregation normally occurs in this polymerization system when reaction is carried out for more than one week that can be easily identified since it gives a sharp peak in the gel permeation chromatography (GPC) with a retention time earlier than that of nonaggregated polymer peak (Figure 4b).

In addition to PEG-DiSPA, **1** was polymerized with comonomers that contain different functional groups such as benzotriazolecarbonate (PEG-DiBTC) or nitrophenolcarbonate (PEG-NPC). **1** condenses with these difunctionalized molecules to create linear, CD polymers with the desired connecting bonds (Table 1).

Direct conjugation of CPT to the CDPs **2–4** is problematic due to the existence of the hydroxyl groups on the CD rings. Therefore, conjugation of CPT to this type of polymer is performed by converting the 20-OH moiety of CPT into an ester via coupling to an amino acid or peptide linkers (transforms CPT hydroxyl group to a more reactive amino end group), and subsequently grafting the functionalized CPT intermediates onto the polymer backbone at the pendant carboxylate sites. It was also found that CPT lactone form (the antitumor active form) was greatly stabilized when CPT was transformed to its amino acid or oligopeptide derivatives via the ester

linkage at the 20-OH site (Figure 5). Therefore, CPT should be maintained in its lactone form after conjugation to the CDP via the amino acid or oligopeptide linkers.

Insertion of linkers between CPT and polymer backbone has the advantage that CPT hydrolysis rates can be adjusted by altering the size and/or nature of the linkers. Although study of CPT conjugates with PEG showed that the introduction of amino acids with bulky side chains such as the leucine or proline can substantially lower hydrolysis rates of CPT in PBS and in plasma (32), excellent antitumor efficacy was found in PEG–CPT conjugates with linkers such as glycine or alanine that are known to release CPT with higher hydrolysis rates (32). Several recent *in vivo* studies of polymer–CPT conjugates have used glycine or similar linkers (27, 29, 32). Therefore, glycine and triglycine were chosen in this study to conjugate CPT to poly(CDDCys-PA-PEG).

To confirm that there was no interchain cross-linking reactions between the hydroxyls of the cyclodextrin and the pendent carboxylate groups under such coupling conditions, **2e** was treated with same coupling reagents and the molecular weight of this polymer was analyzed before and after such treatment. No increase in molecular weight was observed for this polymer after treatment. Solubilities of the polymer–CPT conjugates with the two different linkers have values greater than 200 mg/mL (equivalent to a 12–20 mg of CPT/mL) in aqueous solution. For comparison, the solubility of CPT (lactone form) is 4  $\mu$ g/mL at the same condition as those for testing the polymer–CPT conjugates. Therefore, the solubilities of the CPT lactone form are increased for more than three orders of magnitude when conjugated to **2e**.

Dramatic, accelerated release of CPT from both **HG6** and **HGGG6** in the presence of plasma was observed (Table 3), and indicates that the release of CPT is enhanced by mechanism other than pure hydrolysis. Similar release rates in the presence of human or rat plasma have been reported by others using PEG–CPT conjugates with a glycine linker (32). Although the conjugate with the triglycine linker (**HGGG6**) releases CPT faster than the one with the glycine linker (**HG6**) in PBS (pure hydrolysis), the difference is less in plasma (enzyme-induced release dominates). Release rates of **HG6** and **HGGG6** in mouse or human plasma are essentially the same (Table 3). The release of CPT from both **HG6** and **HGGG6** was also analyzed in the presence of cathepsin B, acetyl cholinesterase and albumin, and none show any dramatic effects on the release rate of CPT.

The CPT hydrolysis from both **HG6** and **HGGG6** decrease substantially in acidic pH (Table 3 and Figure 6). A possible mechanism for uptake of polymer–drug conjugates into tumor cells is via an endocytotic pathway. Conjugates internalized in this manner can be contained in intracellular compartments such as endosomes and lysosomes that have low pH (pH 4–6.5) (33). Therefore, the dramatic decrease in CPT release in acidic pH may play a role in the therapeutic efficacy of these conjugates.

CDPs **2–4** have backbones that are repeating units of two species (PEG and CD) that are known for their low toxicities and low immunogenicities. Other linear, CD-based polymers have also been reported to have low toxicity and lack an immune response in animals (8). Therefore, it is not surprising to observe high  $IC_{50}$  values for **2e** in various cultured cells (Table 4).

In summary,  $\beta$ -cyclodextrin-based, linear polymers were synthesized and used for the conjugation of camptothecin. These polymers are extremely soluble in aqueous solution and show low toxicity to cultured cells. When

conjugated to the CD polymers **2e** and **2f**, the solubility of CPT is increased by more than 3 orders of magnitudes. These polymer–CPT conjugates have been tested in a xenograft mouse model and the results will be reported elsewhere (34). Initial tumor reduction studies reveal that these conjugates have enhanced efficacy over CPT alone and one of the commercial analogues of CPT (irinotecan). Comparisons to the other polymer conjugates of CPT are difficult since dosing schedules and amounts are not the same. However, Conover et al. dosed mice containing LS174t colon tumors with PEG–CPT conjugates on days 1, 5, and 9 and repeated the dosing schedule every 21 days (32). In our study, we dosed mice containing LS174t colon tumors on days 1, 5, and 9 (no repeat dosing) (34). The median tumor sizes for the PEG–CPT treated animals were 20–29% of the median size of the tumors in the placebo treated animals when these tumors reached 1000 mg (32). By comparison, the cyclodextrin-containing polymer conjugates of CPT gave median tumor sizes that ranged from 10 to 12% of the median size of the tumors in the control group when they reached 1000 mg (34). Thus, the conjugates presented here reveal properties that are different from other polymer–CPT conjugates that have been reported previously.

#### ACKNOWLEDGMENT

We thank Drs. Nathalie Bellocq, Leonard Borrmann, Christopher Dardt, and Suzie Hwang Pun of Insert Therapeutics, Inc., for their helpful discussions. M. E. Davis is a consultant to and has financial interest in Insert Therapeutics, Inc.

#### LITERATURE CITED

- (1) Duncan, R., Dimitrijevic, S., and Evagorou, E. (1996) The role of polymer conjugates in the diagnosis and treatment of cancer. *S. T. P. Pharma. Sci.* **6**, 237–263.
- (2) Duncan, R., Gac-Breton, S., Keane, R., Musila, R., Sat, Y. N., Satchi, R., and Searle, F. (2001) Polymer-drug conjugates, PDEPT and PELT: basic principles for design and transfer from the laboratory to clinic. *J. Controlled Release* **74**, 135–146.
- (3) Duncan, R., and Kopecek, J. (1984) Soluble synthetic polymers as potential drug carriers. *Adv. Polym. Sci.* **57**, 51–101.
- (4) Matsumura, Y., and Maeda, H. (1986) A new concept for macromolecular therapeutics in cancer-chemotherapy: mechanism of tumoritropic accumulation of proteins and the antitumor agent SMANCS. *Cancer Res.* **6**, 6387–6392.
- (5) Uekama, K., Hrayama, F., and Irie, T. (1998) Cyclodextrin drug carrier systems. *Chem. Rev.* **98**, 2045–2076.
- (6) Fenyvesi, E. (1988) Cyclodextrin polymers in the pharmaceutical industry. *J. Inclusion Phenom. Macrocyclic Chem.* **6**, 537–545.
- (7) Tabushi, I., Shimokawa, K., and Fujita, K. (1977) Specific bifunctionalization on cyclodextrin. *Tetrahedron Lett.* **18**, 1527–1530.
- (8) Hwang, S. J., Bellocq, N. C., and Davis, M. E. (2001) Effects of structure of  $\beta$ -cyclodextrin-containing polymers on gene delivery. *Bioconjugate Chem.* **12**, 280–290.
- (9) Gonzalez, H., Hwang, S. J., and Davis, M. E. (1999) New class of polymers for the delivery of macromolecular therapeutics. *Bioconjugate Chem.* **10**, 1068–1074.
- (10) Reineke, T. M., and Davis, M. E. (2003) Structural effects of carbohydrate-containing polycations on gene delivery. 1. Carbohydrate size and its distance from charge centers. *Bioconjugate Chem.* **14**, 247–254.
- (11) Reineke, T. M., and Davis, M. E. (2003) Structural effects of carbohydrate-containing polycations on gene delivery. 2. Charge center type. *Bioconjugate Chem.* **14**, 255–261.
- (12) Popielarski, S. R., Mishra, S., and Davis, M. E. (2003) Structural effects of carbohydrate-containing polycations on gene delivery. 3. Cyclodextrin type and functionalization. *Bioconjugate Chem.* **14**, 672–678.
- (13) Wall, M. E., Wani, M. C., Cook, C. E., Palmer, K. H., McPhail, A. T., and Sim, G. A. (1966) Plant antitumor agents. I. Isolation and structure of camptothecin, a novel alkaloidal leukemia and tumor inhibitor from *camptotheca acuminata*. *J. Am. Chem. Soc.* **88**, 3888–3890.
- (14) Muggia, F. M., Dimery, I., and Arbus, S. G. (1996) Camptothecin and its analogs. *Ann. NY Acad. Sci.* **803**, 213–223.
- (15) Rothenberg, M. L. (1997) Topoisomerase I inhibitors: review and update. *Ann. Oncol.* **9**, 837–855.
- (16) Hertzberg, R. P., Caranfa, M. J., and Hecht, S. M. (1989) On the mechanism of topoisomerase-I inhibition by camptothecin-evidence for binding to an enzyme DNA complex. *Biochemistry* **28**, 4629–4638.
- (17) Mi, Z., and Burke, T. G. (1994) Marked interspecies variations concerning the interactions of camptothecin with serum albumins: a frequency-domain fluorescence spectroscopic study. *Biochemistry* **33**, 12540–12545.
- (18) Mi, Z., and Burke, T. G. (1994) Differential interactions of camptothecin lactone and carboxylate forms with human blood components. *Biochemistry* **33**, 10325–10336.
- (19) ten Bokkel Huinink, W. W., Gore, M., and Carmichael, J. (1997) Topotecan versus paclitaxel for the treatment of recurrent epithelial ovarian cancer. *J. Clin. Oncol.* **15**, 2183–2193.
- (20) Van Cutsem, M., Cunningham, D., and ten Bokkel Huinink, W. W. (1999) Clinical activity and benefit of irinotecan (CPT-11) in patients with colorectal cancer truly resistant to 5-fluorouracil (5-FU). *Eur. J. Cancer* **35**, 54–59.
- (21) Zhao, H., Lee, C., Sai, P., Choe, Y., Boro, M., Pentri, A., Guan, S., and Greenwald, R. B. (2000) 20-O-Acylcamptothecin derivatives: evidence for lactone stabilization. *J. Org. Chem.* **65**, 4601–4606.
- (22) Greenwald, R. B., Pendri, A., Conover, C. D., Gilbert, C. W., Yang, R., and Xia, J. (1996) Drug delivery systems. 2. Camptothecin 20-O-poly(ethylene glycol) ester transport forms. *J. Med. Chem.* **39**, 1938–1940.
- (23) Greenwald, R. B., Pendri, A., Conover, C. D., Lee, C., Choe, Y. H., Gilbert, C., Martinez, A., Xia, J., Wu, D. C., and Hsue, M. (1998) Camptothecin-20-PEG ester transport forms: the effect of spacer groups on antitumor activity. *Bioorg. Med. Chem.* **6**, 551–562.
- (24) Rowinsky, E. K., Rizzo, J., Ochoa, L., Takimoto, C. H., Forouzes, B., Schwartz, G., Hammond, L. A., Patnaik, A., Kwiatek, J., Goetz, A., Denis, L., McGuire, J., and Tolcher, A. W. (2003) A phase I and pharmacokinetic study of pegylated camptothecin as a 1-hour infusion every 3 weeks in patients with advanced solid malignancies. *J. Clin. Oncol.* **21**, 148–157.
- (25) Zama, M., vandeVen, M., Farao, M., Gratton, E., Ghiglieri, A., Castelli, M. G., Fontana, E., d'Argy, R., Fiorino, A., Pesenti, E., Suarato, A., and Caiolfa, V. R. (2003) Camptothecin poly[N-(2-hydroxypropyl) methacrylamide] copolymers in antitopoisomerase-I tumor therapy: intratumor release and antitumor efficacy. *Mol. Cancer Ther.* **2**, 29–40.
- (26) Caiolfa, V. R., Zama, M., Fiorino, A., Frigerio, E., Pellizzoni, C., d'Argy, R., Ghiglieri, A., Castelli, M. G., Farao, M., Pesenti, E., Gogli, M., Angelucci, F., and Suarato, A. (2000) Polymer-bound camptothecin: initial biodistribution and antitumor activity studies. *J. Controlled Release* **65**, 105–119.
- (27) Bhatt, R., Vries, P. D., Tulinsky, J., Bellamy, G., Baker, B., Singer, J. W., and Klein, P. (2003) Synthesis and in vivo antitumor activity of poly(L-glutamic acid) conjugates of 20-(S)-camptothecin. *J. Med. Chem.* **46**, 190–193.
- (28) Zou, Y., Wu, Q., Tansey, W., Chow, D., Hung, M., Charnsangavej, C., Wallace, S., and Li, C. (2001) Effectiveness of water soluble poly(L-glutamic acid)-camptothecin conjugate against resistant human lung cancer xenografted in nude mice. *Int. J. Oncol.* **18**, 331–336.
- (29) Singer, J. W., Bhatt, R., Tulinsky, J., Buhler, K. R., Heasley, E., Klein, P., and Vries, P. D. (2001) Water-soluble poly(L-glutamic acid)-gly camptothecin conjugates enhance

- camptothecin stability and efficacy in vivo. *J. Controlled Release* 74, 243–247.
- (30) Mach, L., Mort, J. S., and Glossl, J. (1994) Maturation of human procathepsin B. Proenzyme activation and proteolytic processing of the precursor to the mature proteinase, in vitro, are primarily unimolecular processes. *J. Biol. Chem.* 269, 13030–13035.
- (31) Stryer, L. (1998) *Biochemistry* (Fourth ed.), p 43, W. H. Freeman and Company, New York.
- (32) Conover, C. D., Greenwald, R. B., Pendri, A., and Shum, K. L. (1999) Camptothecin delivery systems: the utility of amino acid spacers for the conjugation of camptothecin with poly(ethylene glycol) to create prodrugs. *Anti-Cancer Drug Des.* 14, 499–506.
- (33) Duncan, R. (2003) The dawning era of polymer therapeutics. *Nature Rev. Drug Discov.* 2, 347–360.
- (34) Cheng, J., Khin, K. T., and Davis, M. E. Antitumor activity of  $\beta$ -cyclodextrin polymer-camptothecin conjugates. *Cancer Res.*, submitted.

BC0340924



## A Comparison of in Vitro and in Vivo Stability in Mice of Two Morpholino Duplexes Differing in Chain Length

Jiang He, Guozheng Liu, Surong Zhang, Jean-Luc Vanderheyden, Ning Liu, Changbin Liu, Yumin Zhang, Suresh Gupta, Mary Rusckowski, and Donald J. Hnatowich\*

Division of Nuclear Medicine, Department of Radiology, University of Massachusetts Medical School, 55 Lake Avenue North, Worcester, Massachusetts 01655. Received June 19, 2003

The stability of hybridized duplexes is an important criterion for any radiopharmaceutical application of DNAs or their analogues such as phosphorodiamidate morpholinos (MORFs). Objective: The stabilities in vitro and in mice of the duplex between MORF and its complement (cMORF) were investigated for two different chain lengths, a 15-mer MORF compared to the identical MORF but elongated to a 25-mer. Methods: The hybridization characteristics of the 15-mer MORF with its complementary 15-mer and that of the 25-mer with its complementary 25-mer MORF were measured using surface plasmon resonance (SPR) analysis. For radiolabeling with  $^{99m}\text{Tc}$ , the 15- and 25-mer MORF, both with a primary amine via a 10-member linker on the 3' equivalent end, were conjugated with NHS-MAG<sub>3</sub>. The 15- and 25-mer cMORFs were conjugated via their amines to carbodiimidazole treated poly(methyl vinyl ether-*alt*-maleic acid) (PA) such that about 50 cMORFs were attached to each polymer molecule in both cases (estimated MWs about 300 and 450 kDa, respectively). After hybridization in vitro, both the PA-cMORF15- $^{99m}\text{Tc}$ -MORF15 and PA-cMORF25- $^{99m}\text{Tc}$ -MORF25 homoduplexes were evaluated by size exclusion HPLC in saline, after incubation in 37 °C serum and in urine obtained 30 min post IV administration to normal mice. Biodistributions were obtained up to 18 h post administration. Results: By SPR, the affinity constants for the homoduplexes were both about  $10^9 \text{ M}^{-1}$  with the 25/25 only about 25% higher than the 15/15. However, the affinity constants for the 15/25 and 25/15 heteroduplexes showed a surprisingly 13-fold difference. By HPLC analysis, all duplexes were stable in saline; however, analysis of serum incubates and urine containing PA-cMORF15- $^{99m}\text{Tc}$ -MORF15 showed an immediate and pronounced low molecular weight peak that was identified by a shift assay to be  $^{99m}\text{Tc}$ -MORF15. The comparable peak in both fluids was much less pronounced in the case of PA-cMORF25- $^{99m}\text{Tc}$ -MORF25. Whole body radioactivity levels also fell much more rapidly in mice receiving the 15-mer conjugate (65 vs 30% eliminated at 18 h) and biodistribution results showed higher kidney levels for the 15-mer conjugate. Results with the PA-cMORF25- $^{99m}\text{Tc}$ -MORF15 heteroduplex were more similar to that obtained with the 15-mer homoduplex than the 25-mer homoduplex. Conclusion: Despite what is reported to be high hybridization affinities, both the homoduplex and heteroduplexes prepared with  $^{99m}\text{Tc}$ -MORF15 were found to be unstable in serum and in vivo toward dissociation to free  $^{99m}\text{Tc}$ -MORF15. By contrast, homoduplex prepared with  $^{99m}\text{Tc}$ -MORF25 showed higher stability. These differences in hybridization stability may be important considerations in radiopharmaceutical design.

### INTRODUCTION

This laboratory has been investigating the potential of DNA and DNA-like oligomers for radiopharmaceutical use. We earlier examined both the phosphodiester and phosphorothioate DNAs (1, 2). Subsequently, we examined peptide nucleic acids (PNAs)<sup>1</sup> as the first commercially available DNA analogue (3). Recently, we have begun examining phosphorodiamidate morpholinos (MORFs), another commercially available DNA analogue (4). Apart from pharmacokinetic behavior, one important criteria of DNA and other oligomers for radiopharmaceutical use is hybridization stability. Although melting temperatures and affinity constants provide a measure of stability (5–7), oligomers under consideration for in vivo use should be studied in 37 °C serum and, preferably, in animals.

One unique feature of oligomers for radiopharmaceutical design is the ability to alter base sequence and chain length. In preliminary studies from this laboratory, MORFs labeled with  $^{99m}\text{Tc}$  showed significant differences in biodistribution depending upon chain length (and therefore base sequence) from 15- to 25-mer (8). This present investigation was conducted to further establish the influence of base sequence and chain length, now on hybridization stability. A 15-mer MORF (MORF15) and a 25-mer MORF (MORF25) were separately conjugated to a polymer (PA) and hybridized in vitro with complementary MORF15 (cMORF15) and complementary

\* To whom correspondence should be addressed: Prof. Donald J. Hnatowich, Division of Nuclear Medicine, Department of Radiology, University of Massachusetts Medical School, 55 Lake Avenue North, Worcester, MA 01655. Phone: 1-508-856-4256. Fax: 1-508-856-4572. E-mail: donald.hnatowich@umassmed.edu.

<sup>1</sup> Abbreviations: MORF, phosphorodiamidate morpholino; SPR, surface plasmon resonance; PA, poly(methyl vinyl ether-*alt*-maleic acid); PNA, peptide nucleic acid; NHS-MAG<sub>3</sub>, *N*-hydroxysuccinimidyl *S*-acetylmercaptoacetyltriglycine; DMF, dimethylformamide; NMP, *N*-methyl-2-pyrrolidinone; DIEA, diisopropylethylamine; RUs, resonance units; EDTA, ethylenediaminetetraacetic acid; HEPES, *N*-[2-hydroxyethyl]piperazine-*N'*-[2-ethanesulfonic acid];  $k_a$ , association rate constant;  $k_d$ , dissociation rate constant;  $K_A$ , affinity constant;  $^{99m}\text{Tc}$ , 99m-technetium.

MORF25 (cMORF25) respectively, each radiolabeled with  $^{99m}\text{Tc}$  via  $\text{MAG}_3$ . The stability of each duplex was then investigated in vitro and in vivo in mice.

## MATERIALS AND METHODS

All MORFs and cMORFs whether biotinylated or amine modified on the 3' equivalent end were purchased purified (Gene-Tools, Corvallis, OR) and were used as received. The MORF15 base sequence was 5'-equivalent-TGT-ACG-TCA-CAA-CTA-linker-primary amine (or biotin) and that of MORF25 was T-GGT-GGT-GGG-MORF15. The base sequences of the cMORFs were complementary with the linker and primary amine also on the 3'-equivalent end. The molecular masses ranged from 5000 to 9000 Da. The MORFs were therefore identical to those used by us previously (4, 8). *N*-Hydroxysuccinimidyl *S*-acetylmercaptoacetyltriglycine (NHS- $\text{MAG}_3$ ) was synthesized in house according to published procedures, and the structure was confirmed by elemental analysis, proton NMR, and mass spectroscopy (9). Normal male CD-1 mice were purchased with a mean body weight of 20–30 g (Charles River laboratories, Wilmington, MA). The serum was from normal male CD-1 mice. Poly(methyl vinyl ether-*alt*-maleic acid) (PA, average MW ca. 45 000), anhydrous dimethylformamide (DMF), *N*-methyl-2-pyrrolidinone (NMP), diisopropylethylamine (DIEA), and 1,1'-carbonyldiimidazole were purchased (Sigma-Aldrich, St. Louis, MO). All other chemicals were reagent grade and were used without purification. A radionuclide generator (Bristol-Myers Squibb Medical Imaging, Inc., North Billerica, MA) provided the  $^{99m}\text{Tc}$ -pertechnetate.

**Synthesis and Radiolabeling of  $\text{MAG}_3$ -Conjugated MORF.** A solution of MORF15 or MORF25 was prepared at a concentration of 2 mg/mL in 0.1 M HEPES buffer pH 8.0. A 50 mg/mL solution of NHS- $\text{MAG}_3$  in anhydrous DMF was then added dropwise to the stirred MORF solution until a  $\text{MAG}_3$  to MORF molar ratio of 20:1 was reached. After incubation at room temperature overnight, the conjugated oligomer was purified on a  $0.7 \times 20$  cm P4 (Bio-Gel, Bio-Rad, Melville, NY) gel filtration column eluted with 0.25 M ammonium acetate buffer, pH 5.2. The UV absorbency at 265 nm of fractions off the column was measured (U-2000, Hitachi Instruments, Danbury, CT). Concentration of conjugated oligomer was estimated with respect to MORF at this frequency using a molar absorbency value of 158 000 for MORF15 and 258 350 for MORF25 reported by the manufacturer. Samples were stored as such at  $-20^\circ\text{C}$  for further use.

Generally, 7  $\mu\text{g}$  of the  $\text{MAG}_3$ -conjugated MORF was labeled on each occasion. To 25  $\mu\text{L}$  of the  $\text{MAG}_3$ -MORF solution in acetate buffer was added 0.5 mg of sodium tartrate from a fresh 50 mg/mL solution in pH 9.3 buffer (0.5 M ammonium bicarbonate, 0.25 M ammonium acetate, 0.18 M ammonium hydroxide), followed by 0.5–3 mCi of  $^{99m}\text{Tc}$ -pertechnetate. Finally, 4  $\mu\text{g}$  of stannous chloride dihydrate from a fresh 1 mg/mL solution in 10 mM HCl was quickly added with agitation. The final pH was about 7.6. After heating at  $100^\circ\text{C}$  for 20 min, the entire labeled  $\text{MAG}_3$ -MORF15/25 preparation was purified on a  $0.7 \times 20$  cm P4 column using 50 mM phosphate buffered-saline pH 7.2 as eluant. Labeling efficiency was calculated as the percentage of radioactivity eluting as  $^{99m}\text{Tc}$ -MORF compared to the total radioactivity applied to the column.

Each P4-purified preparation of radiolabeled  $\text{MAG}_3$ -MORF was analyzed by size exclusion HPLC using a single  $1 \times 30$  cm Superose 12 column (Amersham

Pharmacia Biotech, Piscataway, NJ) with 50 mM phosphate buffer pH 7.2 as eluant. In-line UV absorbency at 265 nm and radioactivity were used to identify and quantitate peak fractions. Recovery of radioactivity was routinely determined.

**Synthesis of PA-cMORF.** The polymer PA was previously used in this laboratory as a platform for the construction of PNA polymers (10) and MORF polymers (4). The polymer (10 mg) was dissolved in 1.0 mL of the aprotic solvent *N*-methyl pyrrolidinone (NMP) and to this was added 20.4 mg of 1,1'-carbonyldiimidazole and 3.0  $\mu\text{L}$  of diisopropylethylamine (DIEA). The mixture was incubated at room temperature for 2 h. To 500  $\mu\text{L}$  of a 2.0 mg/mL solution of cMORF15 or cMORF25 in NMP, a designated amount of the activated PA mixture and the equivalent moles of DIEA were added to reach a 100:1 molar ratio of cMORF to PA. The mixture was incubated overnight at room temperature.

An aliquot of the solution prior to purification was used to estimate the average number of cMORF groups bonded to each PA molecule by SE HPLC with UV detection at 265 nm. Since PA does not absorb appreciably at 265 nm, the peak areas of free, nonconjugated cMORF and of PA-coupled cMORF15/25 were compared. As an alternative method of estimating the average number of groups per molecule, radiolabeled MORF15 and MORF25 were used to measure the groups per molecule of PA-cMORF15 and PA-cMORF25, respectively. Each was added at tracer concentrations to an aliquot of its polymer and the radioactivity on free, nonconjugated cMORF compared to that on PA-coupled cMORF was determined. The PA-cMORF conjugates were purified by open column gel filtration chromatography on  $1 \times 30$  cm Sephadex G100 column (Amersham Pharmacia Biotech, Piscataway, NJ) using water as eluant. The concentration of PA-cMORFs in the recovered fractions with respect to cMORFs was estimated by UV absorbency using the above molar absorbency values.

**Surface Plasmon Resonance Measurements.** Recent improvements in instrumentation for biomolecular interaction analysis by surface plasmon resonance (SPR) has made it easier to measure rates of association and dissociation directly. Thus, SPR may be used to measure the rate of binding of an analyte on a surface to which its partner has been immobilized (11). SPR is an optical phenomenon that arises when light illuminates thin conducting films under specific conditions. SPR permits the generation of sensorgrams in which the refractive index changes due to this binding are measured in resonance units (RUs) (12). In this investigation, surface plasmon resonance was used to estimate the association rate constants for duplex formation between immobilized cMORFs and MORFs. The analysis was performed on a BIAcore-2000 (BIAcore, Piscataway, NJ) instrument operating at room temperature. Biotinylated cMORF15 and biotinylated cMORF25 were each added to a streptavidin-dextran-coated sensor chip only until a response of about 200 RUs was reached. The absence of mass transfer effects was confirmed by running separately one concentration of free MORF at three different flow rates (10, 30, and 75  $\mu\text{L}/\text{min}$ ) and demonstrating identical RU responses in all cases. Solutions of free MORF were prepared at six concentrations (0.0–5.0  $\mu\text{M}$ ) in the same running buffer (10 mM HEPES, 150 mM sodium chloride, 3.4 mM  $\text{Na}_2\text{-EDTA}$ , 0.005% P20, pH 7.4). Dissociation was followed for 25 min and the chip surface was regenerated by injection of 100 mM HCl. In-line reference subtraction was performed at each concentration to correct for bulk refractive index changes. The resulting

sensorgrams were analyzed using instrument software (BIAevaluation 3.0, BIAcore) by assuming 1:1 Langmuir interactions.

**Stability of Radiolabeled Polymer in Mouse Serum.** The polymer conjugates of PA-cMORF15 and PA-cMORF25 were usually radiolabeled by adding trace amount of  $^{99m}\text{Tc}$ -MORF15 or  $^{99m}\text{Tc}$ -MORF25 respectively to prepare the homoduplexes followed by incubation at room temperature for 30 min. Occasionally, PA-cMORF25 was radiolabeled in this manner with  $^{99m}\text{Tc}$ -MORF15 to form the heteroduplex. When necessary to provide a radiolabeled polymer of at least 95% radiochemical purity, the preparation was purified by ultrafiltration (Microcon 100 kDa MWCO, Millipore Corporation, Bedford, MA). Quality control by size exclusion HPLC was routinely performed. Repeat measurements by HPLC were then used to assess the stability of the radiolabeled polymer conjugate following incubation in mouse serum at 37 °C for 1 h. Serum aliquots were removed and analyzed by HPLC using 50 mM sodium phosphate buffer pH 7.2 as eluant. Recoveries with respect to radioactivity were routinely measured.

**Urine Analysis.** Normal CD-1 male mice received by tail vein 0.1 mL of saline containing about 20–100  $\mu\text{Ci}$  of both radiolabeled homoduplex polymers carrying 2–4  $\mu\text{g}$  of cMORF. The mice were then sedated by halothane inhalation and urine was collected at 0.5 h postinjection. Urine radioactivity and whole body radioactivity after urine removal were both measured in a dose calibrator. A shift assay was performed on the urine samples by HPLC analysis before and after the addition of PA-cMORF to establish whether the  $^{99m}\text{Tc}$  in urine was still bound to MORF. Recoveries were routinely measured.

**Biodistribution of Radiolabeled Polymer in Normal Mice.** In groups of four, normal CD-1 male mice each received by tail vein 0.1 mL of saline containing about 20–100  $\mu\text{Ci}$  of each of the four PA-cMORF- $^{99m}\text{Tc}$ -MORF in each case carrying 2–4  $\mu\text{g}$  of cMORF. Use of a large polymer such as PA was important to this measurement because its slow clearance provided sufficient time for dissociation of the duplex to become evident. Whole body radioactivity was monitored over 18 h by repeatedly placing individual mice in a dose calibrator. Thereafter, the mice were sedated by halothane inhalation and sacrificed by cervical dislocation. Blood was removed by cardiac puncture, the mice were then dissected, and selected organs were removed and rinsed in saline and weighed before counting in a NaI (TI) well counter along with blood samples and an aliquot of the injectate. The biodistributions are reported as the percentage of the injected dose per gram (%ID/g) of tissue corrected for background radioactivity, physical decay during counting, and retention of radioactivity in the tail.

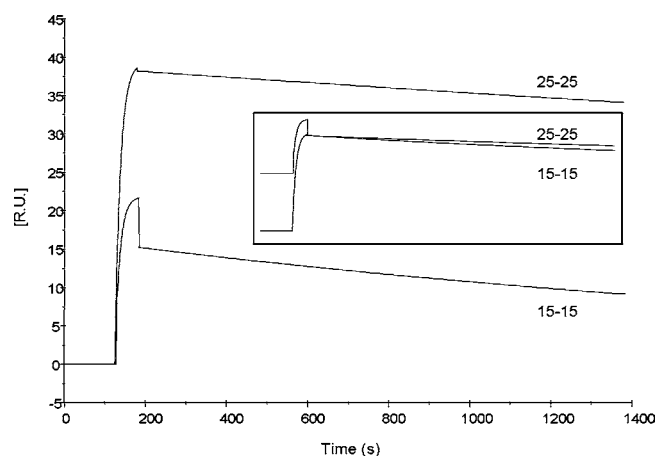
## RESULTS

**PA-cMORF15/25 Conjugates.** The HPLC chromatographic profiles of both PA-cMORF15 and PA-cMORF25 after conjugation but before purification all showed by both radioactivity and 265 nm UV detection two roughly equal peaks, one at 14 min due to PA-cMORF and a second at 26 or 28 min due to free cMORF15 or cMORF25, respectively. In both cases, an average of 40–50 groups of cMORF per PA molecule was calculated from the ratio of UV peak areas (at this frequency, the absorbency of PA is negligible). The HPLC profiles of radioactivity were used to determine the number of cMORF on PA molecule in solution that are accessible to radiolabeled MORF. The  $^{99m}\text{Tc}$ -MORF15 or  $^{99m}\text{Tc}$ -MORF25 added at tracer con-

**Table 1. Kinetics Constants of Single-Stranded MORFs Hybridization Obtained from BIAcore<sup>a</sup>**

MORFs	$k_a$ (1/Ms)	$k_d$ (1/s)	$K_A$ (1/M)
25–25	$1.01(0.02) \times 10^5$	$9.25(0.29) \times 10^{-5}$	$1.10(0.05) \times 10^9$
15–15	$3.80(0.23) \times 10^5$	$4.30(0.20) \times 10^{-4}$	$8.87(0.81) \times 10^8$
15–25	$2.08(0.07) \times 10^5$	$2.19(0.14) \times 10^{-4}$	$9.50(0.92) \times 10^8$
25–15	$1.73(0.06) \times 10^4$	$2.52(0.26) \times 10^{-4}$	$6.92(1.00) \times 10^7$

<sup>a</sup> 25–25: MORF25 binding to immobilized biotinylated cMORF25. 15–15: MORF15 binding to immobilized biotinylated cMORF15. 15–25: MORF15 binding to immobilized biotinylated cMORF25. 25–15: MORF25 binding to immobilized biotinylated cMORF15. (standard deviation in parentheses).  $N = 4$ .

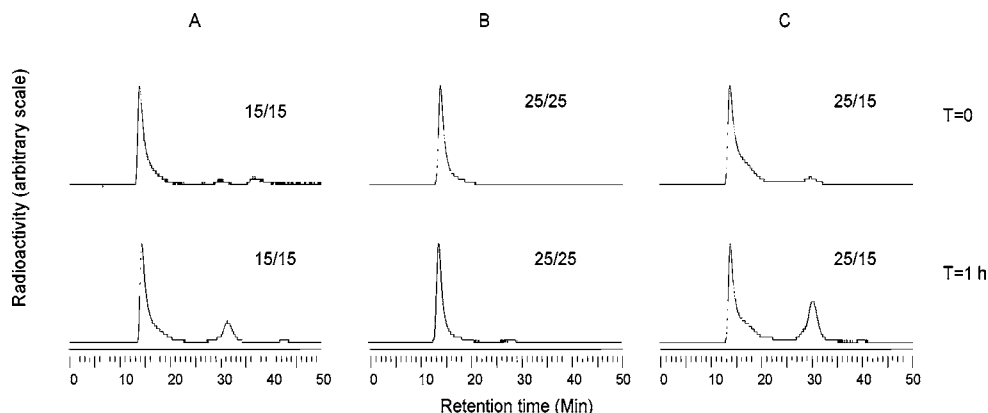


**Figure 1.** Representative sensorgrams obtained from BIAcore for MORF25 binding to immobilized biotinylated cMORF25 (25–25) and MORF15 binding to immobilized biotinylated cMORF15 (15–15). The decreased  $k_d$  of MORF25 is clearly visible in a normalized overlay sensorgrams obtained for dissociation phase(boxed inlay).

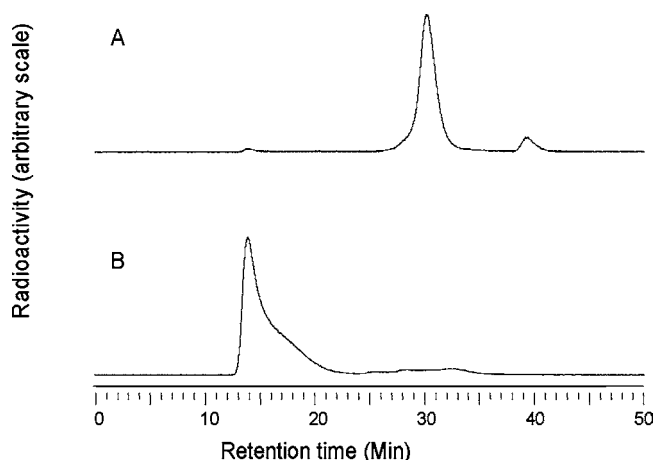
centrations to unpurified PA-cMORF15 or PA-cMORF25 respectively distributes between free cMORFs and cMORF accessible on PA polymer according to their relative concentration. In this way, the average number of cMORFs accessible to hybridization in solution was estimated in both cases to be about  $40 \pm 5$  in good agreement with the UV results to suggest that all cMORFs on both PAs are accessible to free MORF in solution. The final molecular masses were calculated to be 300 and 450 kDa, respectively.

**Surface Plasmon Resonance.** The association rate constants ( $k_a$ ), the dissociation rate constants ( $k_d$ ), and the affinity constants ( $K_A = k_a/k_d$ ) determined using SPR analysis are summarized in Table 1. Between the two homoduplexes, the 25-mer MORF showed about a 4-fold lower association rate, but a dissociation rate about a 5-fold lower such that its affinity constant was about 25% higher than that of the 15-mer MORF. A surprising result of these measurements on the heteroduplexes was the large difference in association rate constants depending upon which MORF was immobilized and which was free. Thus, while the dissociation rate constants were about the same, the association rate constant for MORF15 binding to immobilized MORF25 was about 12-fold higher than the reverse. For this reason, the affinity constants between the heteroduplexes showed a large difference with hybridization of MORF25 to immobilized MORF15 showing the lowest value among all four combinations. Figure 1 presents typical sensorgrams for the hybridization of MORF25 to immobilized cMORF25 and MORF15 to immobilized cMORF15 obtained at room temperature showing association during injection followed by dissociation. The lower dissociation constant for the MORF15 homoduplex relative to the MORF25 het-





**Figure 2.** Size exclusion HPLC radiochromatograms of PA-cMORF15- $^{99m}\text{Tc}$ MORF15 (A), PA-cMORF25- $^{99m}\text{Tc}$ MORF25 (B), and PA-cMORF25- $^{99m}\text{Tc}$ MORF15 (C) in saline (top row) and after 1 h incubation in 37 °C serum (bottom row).

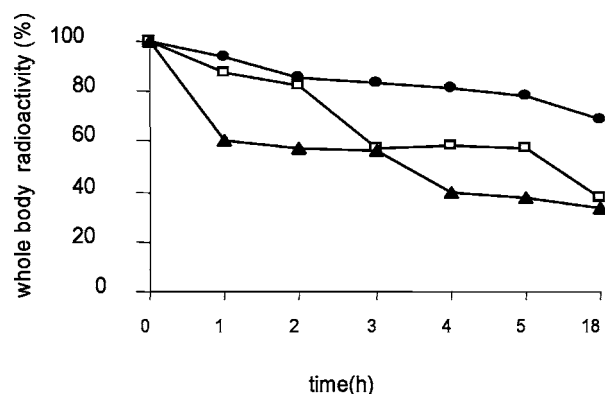


**Figure 3.** Size exclusion HPLC radiochromatograms of urine obtained 30 min post administration to mice of PA-cMORF15- $^{99m}\text{Tc}$ MORF15 before (A) and after (B) the addition of PA-cMORF15.

eroduplex is clearly visible over the 25 min dissociation period.

**Stability of Radiolabeled Polymer Conjugate in Mouse Serum.** Figure 2 presents HPLC radiochromatograms of radiolabeled PA-cMORF15 (panel A) and PA-cMORF25 (panel B) homoduplexes and radiolabeled PA-cMORF25- $^{99m}\text{Tc}$ -MORF15 heteroduplex (panel C) in saline (top row) and after 1 h in 37 °C serum incubation (bottom row). Before incubation, all three samples show only the polymer peak at 14 min, but only the PA-cMORF25 homoduplex continues to show only this peak after incubation. By contrast, both the PA-cMORF15 homoduplex and PA-cMORF25 heteroduplexes in serum show a prominent second peak at 26–28 min. In both cases, this latter peak has been shown to be due to free labeled MORF15 by a shift assay in which this peak disappears following addition of PA-cMORF15. The figure therefore presents evidence for rapid hybridization instability only in 37 °C serum and only in the case of MORF15, either as the homoduplex or the heteroduplex.

**Analysis of Urine from Mice Administered Radiolabeled Polymer.** Figure 3 (panel A) presents a HPLC radiochromatogram of urine pooled from three mice at 0.5 h post administration of PA-cMORF15- $^{99m}\text{Tc}$ -MORF15. The radiochromatogram shows one prominent peak at 28 min suggestive of free  $^{99m}\text{Tc}$ -MORF15. That this peak is indeed due to free MORF15 is shown by the shift in the radiochromatographic profile (panel B) after the addition of PA-cMORF15. The addition has resulted in a complete shift in the radioactivity profile



**Figure 4.** Whole body radioactivity levels vs time in normal mice receiving PA-cMORF15- $^{99m}\text{Tc}$ MORF15 (□, 15/15), PA-cMORF25- $^{99m}\text{Tc}$ -MORF25 (●, 25/25) or PA-cMORF25- $^{99m}\text{Tc}$ -MORF15 (▲, 25/15).

to higher molecular weight (earlier retention time) due to polymer hybridization. That the urine from mice receiving PA-cMORF25- $^{99m}\text{Tc}$ -MORF25 contained much less radioactivity (<2%ID) compared to mice receiving PA-cMORF15- $^{99m}\text{Tc}$ -MORF15 (>15%ID) is further evidence for increased instability of the latter complex. A shift assay was not attempted on urine from mice receiving PA-cMORF25- $^{99m}\text{Tc}$ -MORF25 because of the lower radioactivity level.

**Whole Body Radioactivity Retention.** The whole body radioactivity over 18 h post administration of the three radiolabeled polymers is shown in Figure 4. The average whole body radioactivity fell much more rapidly (only 35 vs 70% remaining at 18 h) following administration of  $^{99m}\text{Tc}$ -MORF15 whether on a homoduplex or heteroduplex. Since all three polymers have molecular masses beyond the 60 kDa cutoff for glomerular filtration, the rapid clearance must be the result of in vivo instability. Furthermore, urine radioactivity obtained from mice receiving PA-cMORF25- $^{99m}\text{Tc}$ -MORF15 and PA-cMORF15- $^{99m}\text{Tc}$ -MORF15 was essentially identical and much higher than that from animals receiving PA-cMORF25- $^{99m}\text{Tc}$ -MORF25 (20–30 vs 2–5% ID). This evidence shows that an important fraction of  $^{99m}\text{Tc}$ -MORF15, whether hybridized in a homoduplex or heteroduplex, rapidly dissociated in vivo.

**Biodistribution in Normal Mice.** Table 2 presents the biodistribution at 18 h in percent injected dosage per gram for the three radiolabeled polymers. Both polymers radiolabeled with  $^{99m}\text{Tc}$ -MORF15 exhibited significantly lower liver and spleen level but higher kidney level than that of the PA-cMORF25 homoduplex. Despite being

**Table 2. Biodistribution in Normal Mice at 18 h Post Administration of Polymer<sup>a</sup>**

organ	25/25	25/15	15/15
liver	20.5(4.24)	12.3(2.13)	17.9(5.33)
heart	0.53(0.18)	0.15(0.02)	0.44(0.20)
kidney	1.47(0.39)	2.62(1.51)	3.67(1.17)
lung	0.44(0.10)	0.19(0.05)	0.71(0.13)
spleen	16.5(6.83)	5.61(0.71)	7.26(1.81)
muscle	0.08(0.07)	0.03(0.01)	0.07(0.01)
blood	0.15(0.12)	0.02(0.0)	0.05(0.02)
whole body	69.0(0.82)	29.7(2.06)	34.0(6.53)

<sup>a</sup> PA-cMORF15-<sup>99m</sup>Tc-MORF15 (15/15), PA-cMORF25-<sup>99m</sup>Tc-MORF25 (25/25) and PA-cMORF25-<sup>99m</sup>Tc-MORF15 (25/15). %ID/g (standard deviation in parenthesis). *N* = 5.

hybridized to the same polymer, the biodistribution of PA-cMORF25-<sup>99m</sup>Tc-MORF15 is obviously more similar to that of PA-cMORF15-<sup>99m</sup>Tc-MORF15 than PA-cMORF25-<sup>99m</sup>Tc-MORF25.

## DISCUSSION

The use of oligomers such as DNAs, PNAs, and MORFs in the design of radiopharmaceuticals would benefit from an improved understanding of their in vitro properties and their behavior in vivo. That oligomers may exist in a large number of distinct chemical forms without apparent impairment of their hybridization properties is an advantage not enjoyed by many biologicals and will explain the large variety of available oligomers. Just as phosphorothioate DNAs display properties unique from that of the phosphodiester DNAs, PNAs, and MORFs display their own unique properties. It may therefore be possible eventually to select among different oligomers for those with particular properties suited to a particular application. This may be especially true for oligomers because of the ability to vary not only the backbone supporting the nitrogenous bases but also both the chain length and base sequence (13, 14). We have recently noted that the pharmacokinetics of MORFs when radiolabeled with <sup>99m</sup>Tc show important differences depending upon chain sequences and base lengths (8). The objective of this present investigation was to extend these observations by examining the influence of chain length on the hybridization stabilities in vivo of two MORFs.

Using surface plasmon resonance, both the association and dissociation rate constant, and therefore the affinity constants for all four combinations of MORFs were measured. The affinity constants for both homoduplexes averaged about 10<sup>9</sup> M<sup>-1</sup> and therefore are respectable for PNA duplexes (15) or DNA duplexes (5) of comparable lengths. As shown in Table 1, the 25-mer homoduplex displayed the highest affinity of the four combinations while one of the heteroduplexes, 25-mer MORF on immobilized 15-mer cMORF showed the lowest affinity by about a factor of 13. Surprisingly, the other heteroduplex, 15-mer MORF on immobilized 25-mer cMORF showed affinities comparable to that of the homoduplexes. Possibly the difference may be due to steric hindrance exhibited when hybridizing the 25-mer MORF to the small 15-mer, that may be less severe when the 15-mer is hybridized to the immobilized 25-mer.

While affinity constants may reflect in vivo stabilities, they do not necessarily predict the kinetics of dissociation. The evidence of this investigation is definitive in showing instabilities toward hybridization dissociation in the case of the 15-mer MORF in 37 °C serum and in vivo. Incubations in saline at room temperature for the homoduplexes and the heteroduplex of this investigation showed by HPLC no evidence of dissociation over at least

24 h. However, after only 1 h in 37 °C serum, the homoduplexes and the heteroduplex prepared with <sup>99m</sup>Tc-cMORF15 showed by HPLC evidence for free <sup>99m</sup>Tc-cMORF15. The <sup>99m</sup>Tc-cMORF15 was also shown to be the most prominent radiolabeled species present in urine of mice receiving the radiolabeled polymers. Furthermore, whole body retention of radioactivity was much lower in animals administered polymers labeled with <sup>99m</sup>Tc-MORF15. Evidence for free <sup>99m</sup>Tc-MORF25 was in all cases much less prominent. In conclusion, hybridization stability in the case of morpholinos was shown to be dependent upon chain length when subjected to 37 °C serum environments both in vitro and in vivo. If this phenomenon can be shown to be general and not restricted to the particular base sequence selected for this investigation, then hybridization stability may be an important criterion in the selection of oligomers as potential radiopharmaceuticals.

## ACKNOWLEDGMENT

Financial support for this investigation was provided in part by the National Institutes of Health (CA 79507). The authors are grateful to Dr. Kara Herlihy (BIAcore, Inc., Piscataway, NJ) for helpful suggestions and Mr. Bhavesh Patel (Theseus Imaging, Boston, MA) for valuable assistance with the BIAcore measurements.

## NOTE ADDED AFTER ASAP POSTING

Changes to the captions of Figures 3 and 4 were made to the version posted August 27, 2003. The corrected version was reposted August 29, 2003.

## LITERATURE CITED

- (1) Hnatowich, D. J., Winnard, P., Jr., Virzi, F., Fogarasi, M., Sano, T., Smith, C. L., Cantor, C. R., and Rusckowski, M. (1995) Labeling deoxyribonucleic acid oligonucleotides with <sup>99m</sup>Tc. *J. Nucl. Med.* 36, 2306–2314.
- (2) Hnatowich, D. J., Mardirossian, G., Fogarasi, M., Sano, T., Smith, C. L., Cantor, C. R., Rusckowski, M., and Winnard, P., Jr. (1996) Comparative properties of a technetium-99m-labeled single-stranded natural DNA and a phosphorothioate derivative in vitro and in vivo in mice. *Pharm. Exp. Ther.* 276, 326–334.
- (3) Mardirossian, G., Lei, K., Rusckowski, M., Chang, F., Qu, T., Egholm, M., and Hnatowich, D. J. (1997) In vivo hybridization of technetium-99m-labeled peptide nucleic acid (PNA). *J. Nucl. Med.* 38, 907–913.
- (4) Mang'era, K., Liu, G., Wang, Y., Zhang, Y., Liu, N., Gupta, S., Rusckowski, M., Hnatowich D. J. (2001) Initial investigations of <sup>99m</sup>Tc-labeled morpholinos for radiopharmaceutical applications. *Eur. J. Nucl. Med.* 28, 1682–1689.
- (5) Niemeyer, C. M., Burger, W., and Hoedemakers, R. M. (1998) Hybridization characteristics of biomolecular adaptors, covalent DNA-streptavidin conjugates. *Bioconj. Chem.* 9, 168–175.
- (6) Hashem, G. M., Pham, L., Vaughan, M. R., and Gray, D. M. (1998) Hybrid oligomer duplexes formed with phosphorothioate DNAs: CD spectra and melting temperatures of S-DNA. RNA hybrids are sequence-dependent but consistent with similar heteronomous conformations. *Biochemistry* 37, 61–72.
- (7) Jaroszewski, J. W., Clausen, V., Cohen, J. S., and Dahl, O. (1996) NMR investigations of duplex stability of phosphorothioate and phosphorodithioate DNA analogues modified in both strands. *Nucleic Acids Res.* 24, 829–834.
- (8) Liu, G., Zhang, S., He, J., Liu, N., Gupta, S., Rusckowski, M., and Hnatowich, D. J. (2002). The influence of chain length and base sequence on the pharmacokinetic behavior of <sup>99m</sup>Tc-morpholinos in mice. *Quart. J. Nucl. Med.* 46, 233–243.
- (9) Winnard, P., Jr., Chang, F., Rusckowski, M., Mardirossian, G., and Hnatowich, D. J. (1997) Preparation and use of NHS-

- MAG<sub>3</sub> for technetium-99m labeling of DNA. *Nuclear Med. Biol.* 24, 425–432.
- (10) Wang, Y., Chang, F., Zhang, Y., Liu, N., Liu, G., Gupta, S., Rusckowski, M., and Hnatowich, D. J. (2001) Pretargeting with amplification using polymeric peptide nucleic acid (PNA). *Bioconj. Chem.* 12, 807–816.
- (11) Jonsson, U., Fagerstam, L., Ivarsson, B., Johnsson, B., Karlsson, R., Lundh, K., Lofas, S., Persson, B., Roos, H., Ronnberg, I., Sjolander, S., Stenberg, E., Stahlberg, R., Urbaniczky, C., Ostlin, H., and Malmqvist, M. (1991) Real-time biospecific interaction analysis using surface plasmon resonance and a sensor chip technology. *Biotechniques* 11, 620–627.
- (12) Malmqvist, M. (1993) Biospecific interaction analysis using biosensor technology. *Nature* 36, 186–187.
- (13) Braasch, D. A., and Corey, D. R. (2002) Novel antisense and peptide nucleic acid strategies for controlling gene expression. *Biochemistry* 41, 4503–4510.
- (14) Hnatowich, D. J. (2000) Antisense and Nuclear Medicine. Where are we now? *Cancer Biother. Radiopharm.* 15, 447–457.
- (15) Jensen, K. K., Orum, H., Nielsen, P. E., and Norden, B. (1997) Kinetics for hybridization of peptide nucleic acids (PNA) with DNA and RNA studied with the BIAcore technique. *Biochemistry* 36, 5072–5077.

BC0341019



# Affinity Capture-Facilitated Preparation of Aequorin–Oligonucleotide Conjugates for Rapid Hybridization Assays

Kyriaki Glynou,<sup>†</sup> Penelope C. Ioannou,<sup>\*,†</sup> and Theodore K. Christopoulos<sup>\*,‡,§</sup>

Department of Chemistry, University of Athens, Athens, Greece 15771, and Department of Chemistry, University of Patras, Patras, Greece 26500, and Institute of Chemical Engineering and High-Temperature Chemical Processes, P.O. Box 1414, Patras, Greece 26500. Received June 19, 2003

We report a general procedure for the preparation of biomolecular conjugates that combine the molecular recognition properties of oligonucleotides with the high detectability of the photoprotein aequorin. Central to the conjugation protocols is the use of recombinant aequorin fused to a hexahistidine tag. In one protocol, an amino-modified oligonucleotide was treated with a homobifunctional cross-linker carrying two *N*-hydroxysuccinimide ester groups, and the derivative was allowed to react with (His)<sub>6</sub>-aequorin. A second strategy involved the introduction of protected sulfhydryl groups into (His)<sub>6</sub>-aequorin and subsequent reaction with a heterobifunctional linker containing a *N*-hydroxysuccinimide and a maleimide group. The strong, but reversible, binding of (His)<sub>6</sub>-aequorin to Ni<sup>2+</sup>-nitrilotriacetic acid agarose enabled the rapid and effective removal of the unreacted oligonucleotide, which otherwise diminishes the performance of the hybridization assay by competing with the conjugate for the complementary target sequence. Aequorin–oligo conjugates prepared by affinity capture showed similar performance with those purified by anion-exchange HPLC. The conjugates were applied to the development of rapid bioluminometric hybridization assays. The analytical range extended from 2 to 2000 pmol/L of target DNA. The reproducibility was less than 10%. The conjugate obtained from a reaction of 10 nmol of (His)<sub>6</sub>-aequorin is sufficient for about 5000 hybridization assays. The proposed conjugation strategy is general because a variety of reporter proteins can be fused to hexahistidine tag by using suitable vectors that are commercially available.

## INTRODUCTION

In recent years, nucleic acid analysis by hybridization has undergone a transition from radioactive labels to nonradioactive alternatives which was driven by the need to improve the detectability and facilitate automation while avoiding problems associated with the use and disposal of radioisotopes (1). (Chemi)bioluminometric hybridization assays are used widely because they are amenable to automation and offer superior detectability over conventional spectrophotometric and fluorometric ones (2).

Aequorin is a photoprotein composed of a 189-amino acid polypeptide chain (apoequorin), the imidazopyrazine chromophore coelenterazine, and oxygen that is attached to coelenterazine as a peroxide (3–5). When Ca<sup>2+</sup> binds to aequorin, it induces a conformational change that triggers the oxidation of coelenterazine by the bound oxygen to produce coelenteramide, CO<sub>2</sub>, and light at 470 nm. Aequorin is an excellent reporter molecule since it can be detected at the attomole level in the presence of excess Ca<sup>2+</sup> (6). The cloning of apoequorin cDNA (7, 8) has enabled the expression of recombinant aequorin in bacteria and its subsequent use as a reporter in immunoassays (9, 10) and hybridization

assays (9, 11–14). In these studies it was observed that although the aequorin reaction does not entail a substrate turnover, it provides a high detectability that is comparable to enzyme reporters (e.g., alkaline phosphatase) with chemiluminogenic substrates. Moreover, the detection of aequorin is complete within 3 s following the addition of Ca<sup>2+</sup>, which is a significant advantage over enzyme reactions that require much longer incubation times.

Aequorin-based bioluminometric hybridization assays may be performed by two strategies. In the 'indirect labeling' approach, a ligand (such as biotin or the hapten digoxigenin) is attached to the DNA probe, and the hybrids are detected by using a specific binding protein conjugated or complexed to the photoprotein. Thus, the hapten digoxigenin has been attached to the probe and an aequorin–antidigoxigenin was used for detection (12). Alternatively, biotin was used as a ligand, and the hybrids were detected by an aequorin–streptavidin conjugate or a streptavidin–biotinylated aequorin complex (11, 15). The 'direct labeling approach' employs aequorin conjugated to the DNA probe (16). The advantage of the latter arises from the elimination of an incubation step and a washing step, thus reducing significantly the time required for assay completion. However, the preparation of aequorin–DNA conjugates requires laborious chromatographic procedures followed by concentration steps, to remove the unreacted DNA probe which otherwise competes with the conjugate for hybridization to the target sequence.

Recently, we reported a simple method for expression and purification of aequorin in one step, based on

\* Corresponding authors: P.C.I.; T.K.C.: Tel. (+30)2107274574; (+30)2610997130. FAX: (+30)2107274750; (+30)2610997118. E-mail: ioannou@chem.uoa.gr; tkc@chemistry.upatras.gr.

<sup>†</sup> University of Athens.

<sup>‡</sup> University of Patras.

<sup>§</sup> Institute of Chemical Engineering and High-Temperature Chemical Processes.

immobilized metal-ion affinity chromatography (17). A hexahistidine-coding sequence was fused upstream of aequorin cDNA. The (His)<sub>6</sub>-apoequorin fusion protein was purified from crude cellular extracts by using a Ni<sup>2+</sup>-nitrilotriacetic acid agarose column. This procedure lasted only a few hours and gave aequorin of high purity and activity whereas previous methods required precipitation of aequorin from the culture medium at pH 4.2, resuspension, overnight dialysis, and purification by DEAE-cellulose chromatography followed by aequorin regeneration.

In the present work we demonstrate that besides enabling one-step purification of the photoprotein from bacterial cultures, the hexahistidine tag greatly facilitates the preparation of conjugates of aequorin to DNA probes for the development of high-throughput hybridization assays. Conjugates are prepared by using either homobifunctional or heterobifunctional cross-linking reagents.

## EXPERIMENTAL SECTION

**Instrumentation.** Ion-exchange chromatography was performed using an HPLC system from GBC Scientific Equipment Pty (Dandenong, Victoria, Australia) consisting of the LC1150 quaternary gradient pump, the LC1205 UV/Vis Detector, and the WinChrom management System. A strong anion-exchange column Hypersil SAX (150 × 4.6 mm) was employed (GBC Scientific Equipment). Bioluminescence was measured by using the PhL microplate Luminometer/Photometer manufactured by Mediators (Vienna, Austria). Polymerase chain reaction (PCR) was carried out in a Hybaid Omn-E thermal cycler (Middlesex, UK). A digital camera, Kodak DC 120, and the Gel Analyzer software for DNA and protein documentation were purchased from Kodak (New York, NY). Microcentrifuge Mikro 20 was from Hettich GmbH (Tutlingen, Germany).

**Materials.** Sulfo-succinimidyl 4-[*N*-maleimidomethyl]-cyclohexane-1-carboxylate (Sulfo-SMCC), *N*-succinimidyl *S*-acetylthioacetate (SATA), and bis(sulfosuccinimidyl) suberate (BS<sup>3</sup>) were obtained from Pierce Chemical Co (Rockford, IL). Bovine serum albumin (BSA) was from Serva (Heidelberg, Germany), blocking reagent was from Roche (Mannheim, Germany). Sephadex G-25 Spin Pure columns were purchased from CPG (Lincoln Park, NJ). Ni<sup>2+</sup>-Nitrilotriacetic acid (Ni-NTA) agarose was obtained from Qiagen (Hilden, Germany). Microcon YM-10 centrifugal filter devices were from Millipore (Bedford, MA). All oligonucleotides were synthesized by MWG Biotech (Ebersberg, Germany). The 20mer 5'-biotin-GTC CTT CCC CAG AGT TCA GT-3' and the 31mer 5'-TTT TTC TAG AAA CAC CAT CCC TCC TCG AAC C-3' were used as the upstream (UP) and downstream primer (DP), respectively, for the PCR of the cDNA of prostate-specific membrane antigen (PSMA). The 24mer 5'-NH<sub>2</sub>-TTT GTT TGT TTC CCA ATT TTT AGT was used as the target specific probe (p). Ultrapure 2'-deoxyribonucleoside 5'-triphosphates (dNTPs) were purchased from HT Biotechnology (Cambridge, UK). *Tth* DNA polymerase was from Biotools (Madrid, Spain). (His)<sub>6</sub>-tagged recombinant apoequorin was expressed in *E. coli* JM109 cells and purified as described previously (17).

**Conjugation of (His)<sub>6</sub>-aequorin to Oligonucleotides Using a Homobifunctional Cross-Linking Reagent.** The 5'-amino-modified oligonucleotide probe, p, was dissolved in distilled water to a final concentration of 0.4 mmol/L. An 8.5-μL aliquot (3.4 nmol of probe) was then mixed with 4.5 μL of 0.5 mol/L sodium bicarbonate,

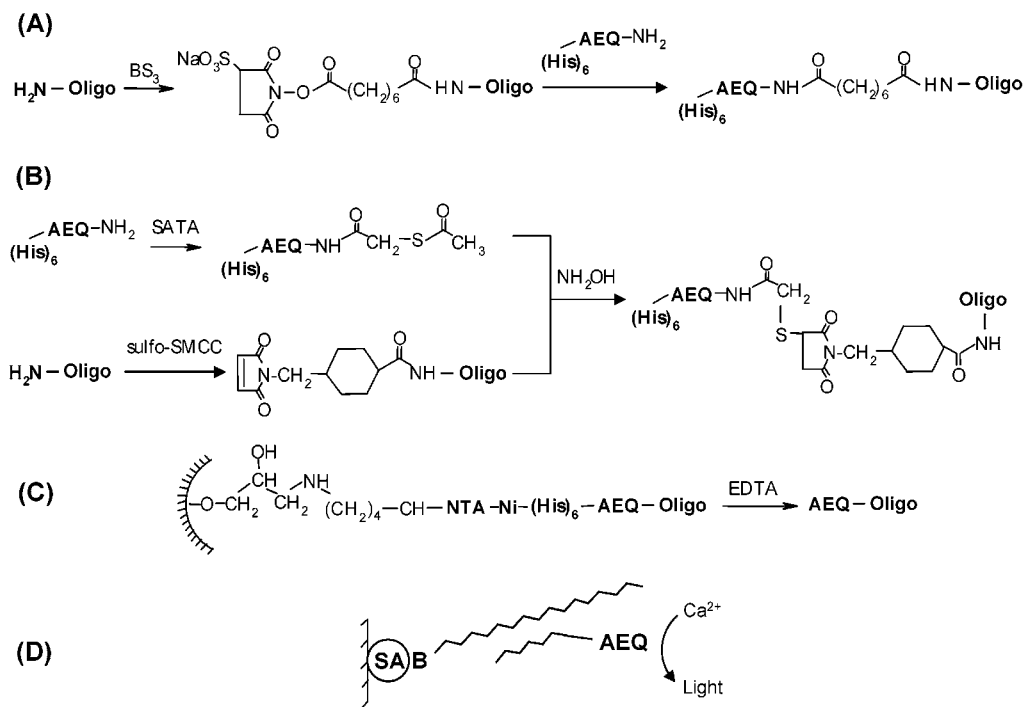
pH 8, and 9.7 μL of 20 g/L BS<sup>3</sup> (dissolved in DMSO). The mixture was incubated for 15 min at ambient temperature in the dark, and the unreacted BS<sup>3</sup> was removed by gel filtration using spin-pure G-25 column prehydrated with distilled water. The derivatized oligonucleotide (~32 μL) was mixed with 9.3 μL of 0.2 mol/L sodium phosphate buffer, pH 8.6, containing 5 mmol/L EDTA and 61 μL of 165 μmol/L aequorin solution (10 nmol) in 50 mmol/L *N*-(3-sulfopropyl)morpholine (MOPS), pH 7.2, 1 mol/L KCl, 5 mmol/L EGTA and 0.3 mol/L glucose. KCl was added to give a final concentration of 2 mol/L, and the mixture was incubated for 12–16 h at 4 °C in the dark.

**Conjugation of (His)<sub>6</sub>-aequorin to Oligonucleotides Using a Heterobifunctional Cross-Linking Reagent.** Sulfhydryl groups were first introduced into aequorin by using SATA. A 61-μL aliquot of 165 μmol/L aequorin (10 nmol), in 50 mmol/L MOPS, pH 7.2, 1 mol/L KCl, 5 mmol/L EGTA and 0.3 mol/L glucose, was mixed with 1.8 μL 1.25 g/L SATA solution (10 nmol) in DMSO and 6.9 μL of 0.2 mol/L sodium phosphate buffer, pH 8.0, 5 mmol/L EDTA and 2 mol/L KCl. The reaction mixture was incubated for 90 min at ambient temperature in the dark. Excess SATA was removed by ultrafiltration using the Microcon YM-10 centrifugal filter device. Prior to ultrafiltration, the reaction mixture was diluted with 0.4 mL of a buffer solution (20 mmol/L phosphate buffer, pH 7.5, containing EDTA 0.5 mmol/L and KCl 0.2 mol/L) and it was centrifuged at 10000 rpm, in the microcentrifuge, for 50 min at 4 °C. This step was repeated, and then the retentate was collected by centrifugation at 3000 rpm for 3 min (retentate volume about 8 μL).

The 5'-amino-modified oligonucleotide probe was activated by reacting with the heterobifunctional cross-linking reagent sulfo-SMCC. An 8.5-μL aliquot of oligonucleotide, p, solution (3.4 nmol) was mixed with 3.9 μL of 0.5 mol/L sodium bicarbonate, pH 8, and 7.4 μL of 20 g/L sulfo-SMCC (340 nmol) solution in DMSO. Following 30 min incubation at ambient temperature in the dark, the excess of sulfo-SMCC was removed by gel filtration using a G-25 Spin Pure column prehydrated with water.

The reaction between SATA-derivatized aequorin and maleimide-activated oligonucleotide was initiated by the addition of hydroxylamine. A 30-μL aliquot of maleimide-activated oligo was mixed with 8 μL of SATA-aequorin, 10.5 μL of 0.5 mol/L NH<sub>2</sub>OH, and 5.2 μL of 0.2 mol/L phosphate buffer, pH 7.5, containing 5 mmol/L EDTA. Then, KCl was added to a final concentration of 2 mol/L, and the mixture was incubated for 12–16 h at 4 °C.

**Purification of Oligonucleotide-Conjugated (His)<sub>6</sub>-aequorin Using Ni-NTA Agarose.** A 35-μL aliquot of Ni-NTA agarose slurry was placed to a disposable spin column and centrifuged at 3000 rpm (in the microcentrifuge) for 3 min at ambient temperature, and the flow-through was discarded. Ni-NTA agarose was shaken gently in the column for 25 min with 0.2 mL of blocking solution (20 mmol/L NaH<sub>2</sub>PO<sub>4</sub>, 0.5 mmol/L EDTA, 0.2 mol/L KCl, pH 7.5, 10 g/L BSA, and 1.5 mL/L Tween-20). The mixture was then centrifuged at 3000 rpm for 3 min, and the flow-through was discarded. The conjugation reaction mixture was diluted about 10 times with water so that the final concentration of EDTA did not exceed 0.5 mmol/L, and then it was loaded onto the spin column. Following a 20 min incubation period, under gentle agitation, the mixture was centrifuged, and the flow-through was discarded. Ni-NTA agarose was washed with 0.1 mL of 20 mmol/L NaH<sub>2</sub>PO<sub>4</sub>, 0.5 mmol/L EDTA, 0.2 mol/L KCl, pH 7.5. The bound conjugate was eluted by applying 3 × 0.1 mL of a solution containing 20 mmol/L NaH<sub>2</sub>PO<sub>4</sub>, 0.1 mol/L EDTA, 0.2 mol/L KCl, pH



**Figure 1.** Outline of the strategies used for preparation and purification of conjugates of hexahistidine-tagged photoprotein aequorin to oligonucleotide probes. (A) Conjugation through a homobifunctional cross-linking reagent. (B) Conjugation through a heterobifunctional cross-linker. (C) Affinity capture-facilitated purification of the conjugates. (D) Hybridization assay configuration. SA = Streptavidin; B = Biotin.

7.5. The eluate was concentrated to a volume of 20 to 40  $\mu\text{L}$  using a Microcon filter device.

**Purification of Oligonucleotide-Conjugated  $(\text{His})_6$ -aequorin by HPLC.** A 20- $\mu\text{L}$  aliquot of the concentrated eluate from the previous step was injected onto a Hypersil SAX anion-exchange column. Initially the mobile phase contained 55% buffer A (10 mmol/L Tris-HCl, 2 mmol/L EDTA pH 7.5) and 45% buffer B (10 mmol/L Tris-HCl, 2 mmol/L EDTA and 1 mol/L NaCl pH 7.5). After 10 min, a linear gradient of 3.25% buffer B/min was applied until buffer B reached to 58%. The composition of the mobile phase was kept constant for 10 min, and then a linear gradient of 3.8% buffer B/min was applied until buffer B reached 100%. The flow rate was 1 mL/min. During separation, 1-mL fractions were collected, and the activity of aequorin was measured.

**Polymerase Chain Reaction.** The target DNA was a 263-bp fragment synthesized by amplifying the prostate-specific membrane antigen (PSMA) cDNA. PCR was performed in a total volume of 50  $\mu\text{L}$  consisting of 75 mmol/L Tris-HCl (pH 9.0), 20 mmol/L  $(\text{NH}_4)_2\text{SO}_4$ , 50 mmol/L KCl, 2 mmol/L  $\text{MgCl}_2$ , 0.2 mmol/L dNTPs, 25 pmol each of the upstream (biotinylated) and downstream primer, and 1.5 units of *Tth* DNA polymerase. Amplification was carried out for 35 cycles using the following program: 95  $^\circ\text{C}$ , 15 s (1 min for the first cycle), 60  $^\circ\text{C}$ , 15 s, 72  $^\circ\text{C}$ , 30 s (10 min for the last cycle). The PCR products were stored at 4  $^\circ\text{C}$  until hybridization. The concentration of the stock solutions of target DNA was determined by densitometry from pictures of ethidium bromide-stained agarose gels using the  $\phi\text{X174}$  DNA fragments as calibrators.

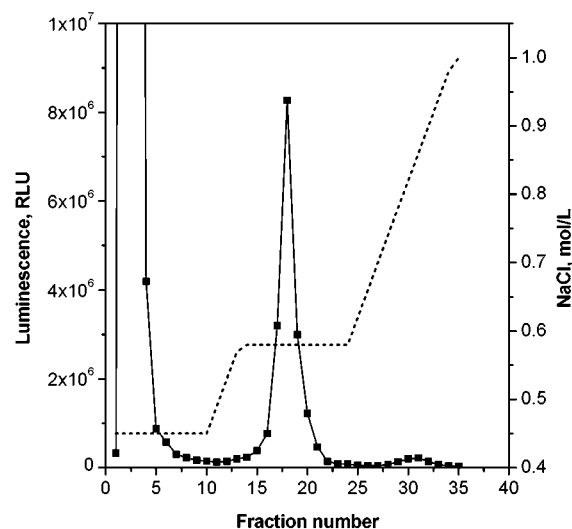
**Hybridization Assays Using Oligonucleotide Probe-Conjugated Aequorin.** Opaque polystyrene wells were coated overnight at ambient temperature with 50  $\mu\text{L}$  of 1.4 mg/L streptavidin diluted in phosphate-buffered saline (PBS). Prior to use, the wells were washed three times with wash solution (50 mmol/L Tris-HCl, 0.15

mol/L NaCl, 2 mmol/L EGTA, pH 7.5, and 1 mL/L Tween-20). Biotinylated PCR products were diluted in blocking solution (10 g/L blocking reagent in 0.1 mol/L maleic acid, 0.15 mol/L NaCl, 2 mmol/L EGTA, and 1.5 mL/L Tween-20), and then 50  $\mu\text{L}$  was pipetted into the wells. The DNA fragments were allowed to bind to streptavidin for 30 min with shaking. The wells were washed three times, and then the nonbiotinylated strand was dissociated by incubating for 20 min with 50  $\mu\text{L}$  of 0.2 mol/L NaOH. The wells were washed three times, and 50  $\mu\text{L}$  of oligonucleotide probe-conjugated aequorin (22 nmol/L with respect to aequorin), diluted in blocking solution containing 10% DMSO, was added. Following 30 min incubation at 37  $^\circ\text{C}$ , the wells were washed three times and placed in the luminometer. The activity of aequorin was measured by injecting 50  $\mu\text{L}$  of triggering solution (20 mmol/L Tris-HCl, 25 mmol/L  $\text{CaCl}_2$ , pH 7.5) into each well and integrating the signal for 3 s.

## RESULTS AND DISCUSSION

The principle of affinity capture-facilitated preparation of aequorin-oligonucleotide conjugates is illustrated diagrammatically in Figure 1. The vector pHISAEQ (17) was used for expression of recombinant  $(\text{His})_6$ -aequorin in *E. coli* and subsequent purification of the photoprotein. Two conjugation strategies were studied in the course of the present work using an oligonucleotide probe modified with a primary amino group at the 5' end. The first approach involves reaction of the probe with an excess (100-fold) of the homobifunctional cross-linking reagent  $\text{BS}^3$  that contains two *N*-hydroxysuccinimide groups. By adding an excess of  $\text{BS}^3$ , the bridging of two oligonucleotides by the cross-linker was avoided and one succinimide group remained free on the derivatized oligo for subsequent reaction with primary amino groups of aequorin ( $\epsilon$ -amino groups of lysine residues). Following synthesis of the conjugate, the effective removal of the unreacted oligonucleotide is crucial because it competes



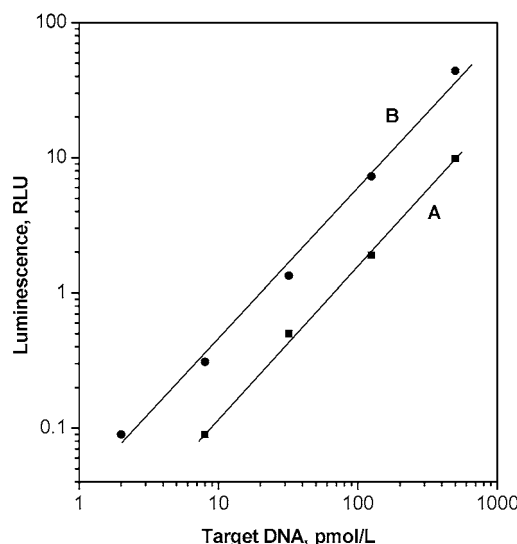


**Figure 2.** Chromatogram of aequorin-conjugated oligonucleotide synthesized using homobifunctional linker (BS<sup>3</sup>). The conjugation reaction was performed with 5 nmol of (His)<sub>6</sub>-aequorin and 5 nmol of oligonucleotide modified with BS<sup>3</sup> (1:100 molar ratio). The luminescence of the eluted fractions are plotted versus the fraction number.

with the aequorin-oligo conjugate for hybridization to the target DNA sequence. The hexahistidine tag of aequorin enables the affinity capture of the conjugate to Ni-NTA agarose and removal of the free oligo by washing. The conjugate is then eluted with EDTA and used directly in hybridization assays.

The second approach involves chemical modification of (His)<sub>6</sub>-aequorin with SATA to introduce protected thiol groups. The amino group of the probe was converted to a maleimide group by reacting with the heterobifunctional cross-linker sulfo-SMCC. The SATA-modified aequorin was then mixed with the SMCC-oligo, and the reaction was initiated by deprotecting the sulfhydryl group with hydroxylamine. Again, the conjugate was captured on Ni-NTA agarose for effective removal of the free probe.

**Conjugation of (His)<sub>6</sub>-aequorin to DNA Using a Homobifunctional Cross-Linker.** The conjugation reaction products were first separated by HPLC using an anion-exchange column. Elution was accomplished by applying a NaCl gradient. Five nanomoles of (His)<sub>6</sub>-aequorin were conjugated to BS<sup>3</sup>-derivatized oligo at a 1:1 molar ratio. Fractions (1 mL) were collected, and the luminescence of aequorin was measured by pipetting 50  $\mu$ L from a 100-fold dilution of each fraction into a microtiter well, adding 50  $\mu$ L of triggering solution and integrating the light emission for 3 s. The chromatographic profile of the conjugation reaction mixture, presented as luminescence versus the fraction number, is shown in Figure 2. Unreacted (His)<sub>6</sub>-aequorin is eluted first followed by the aequorin-DNA conjugate (fractions 15–23). A small peak also appears at fractions 28–33 that corresponds to higher oligo-aequorin molar ratios. According to absorbance data (260 nm), the free oligonucleotide was eluted at fractions 25 to 31. Fractions from the first conjugate peak were pooled, supplemented with 1 g/L BSA and 200 g/L glycerol, and stored at –20 °C. Pooled fractions from the first conjugate peak were tested further as a detection reagent in hybridization assays. Biotinylated (through PCR) target DNA (263 bp) was captured on the surface of polystyrene microtiter wells coated with streptavidin. One strand was removed by NaOH treatment followed by hybridization with the

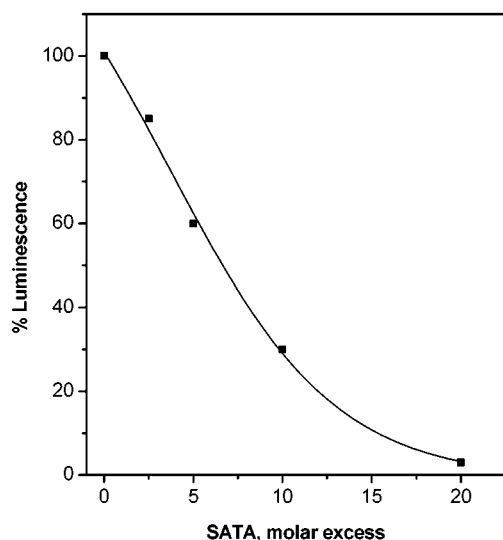


**Figure 3.** Luminescence as a function of the target DNA concentration. The hybridization assay was performed as described under Materials and Methods using aequorin-oligonucleotide conjugates prepared with a homobifunctional linker and purified: (A) by anion-exchange HPLC and (B) by affinity capture on Ni-NTA agarose and anion-exchange chromatography.

aequorin-oligonucleotide conjugate. The excess of conjugate was removed by washing and the bioluminescent reaction of bound aequorin was triggered by the addition of Ca<sup>2+</sup>. The effect of the conjugate concentration on the signal of the assay was studied in the range of 0.08 to 0.64 nmol/L at 0.2 nmol/L target DNA. The optimized conjugate concentration was found to be 0.45 nmol/L (calculated on the basis of aequorin activity). Subsequently, the luminescence was studied as a function of the concentration of target DNA, and the results are presented in Figure 3. Signal-to-background (S/B) ratios of 1.2 and 2.8 were obtained for 8 and 32 pmol/L of target DNA, respectively. The background is defined as the luminescence signal in the absence of target DNA, and it is due to the nonspecific binding of the detection reagent to the surface of the microtiter well.

Subsequently, we investigated whether affinity capture of the aequorin-DNA conjugate on Ni-NTA agarose, through the hexahistidine tag, could facilitate its purification by replacing the anion-exchange HPLC step. Initial affinity capture experiments were carried out by using (His)<sub>6</sub>-aequorin. A solution containing 10 nmol of (His)<sub>6</sub>-aequorin (the amount typically used in conjugation reactions) was incubated, under gentle agitation, with 10–50  $\mu$ L of Ni-NTA agarose slurry for various time intervals between 20 and 75 min. The aequorin was eluted with EDTA. These experiments showed that the capture of aequorin to agarose matrix was efficient, but the yield of the elution of bound aequorin was relatively low (40–60%). This was attributed to the nonspecific binding (adsorption) of the photoprotein directly to agarose. To decrease the adsorption of aequorin, blocking of Ni-NTA agarose (prior to the affinity capture) was investigated by applying various concentrations of bovine serum albumin. The most efficient blocking of agarose was achieved by using a 10 g/L BSA solution containing 1.5 mL/L Tween-20. Under these conditions, the recovery of bound (His)<sub>6</sub>-aequorin was about 90%. The optimized affinity capture protocol was applied to the purification of aequorin-oligo conjugates from the free oligo.

The performance of aequorin-oligo conjugates purified both by affinity capture and anion-exchange HPLC, was



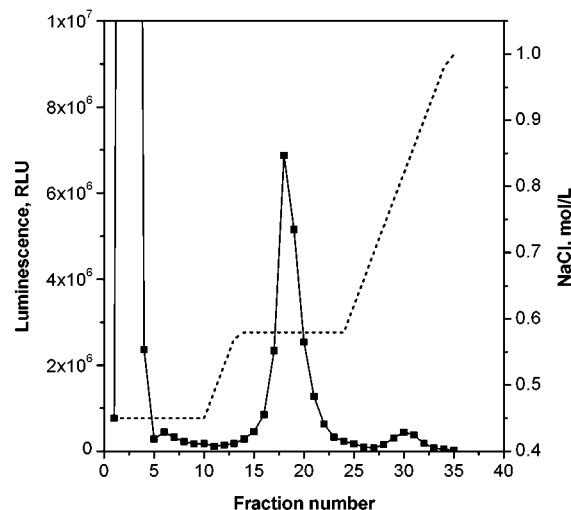
**Figure 4.** Effect of SATA on the activity of aequorin. A constant amount of (His)<sub>6</sub>-aequorin (0.5 nmol) was treated with various amounts of SATA for 90 min, and the luminescence was measured as described in the Experimental Section. The percent luminescence is plotted versus the molar ratio SATA:aequorin. The value 100% is defined as the signal obtained from non-derivatized (with SATA) aequorin.

tested in hybridization assays. The results are also presented in Figure 3. It is observed that the signals were four times higher with the affinity-purified conjugate compared to the one purified only by HPLC. This was attributed to the more effective removal of unreacted probe by affinity capture. As low as 2 pmol/L target DNA was detected using this conjugate with a signal-to-background ratio of 1.8. Moreover, we found that conjugates purified by a single rapid affinity capture step offer the same detectability and analytical range as those purified both by affinity capture and HPLC.

The reproducibility of the hybridization assay was tested by analyzing samples containing 3.2, 12.4, 50, and 400 pmol/L of target DNA. The CVs were 2, 9, 2, and 2%, respectively ( $n = 3$ ).

**Conjugation of (His)<sub>6</sub>-aequorin to DNA Using a Heterobifunctional Cross-Linker.** It is known that treatment of aequorin with cross-linkers containing a maleimide group results in a rapid inactivation of the photoprotein due to derivatization of cysteine groups that appear to play an important role in the Ca<sup>2+</sup>-dependent bioluminescent reaction (16, 18). This problem was circumvented either by introducing extra thiol groups to aequorin (16) or by substituting the cysteines with serines (through site-directed mutagenesis) and simultaneous introduction of a single cysteine at a position that has no effect on the activity (19, 20). The latter approach has only been applied to immunoassay development.

We have converted the amino group of the probe to a maleimide group by treating with sulfo-SMCC. Protected thiol groups were introduced to (His)<sub>6</sub>-aequorin by reacting with SATA. The effect of SATA on the activity of (His)<sub>6</sub>-aequorin was studied at molar ratios (Aeq:SATA) ranging from 1:1 to 1:20, and the results are presented in Figure 4. It is observed that at 1:1 and 1:5 Aeq:SATA ratios 100% and 85% of the activity of aequorin was preserved after derivatization. At a higher excess of SATA, aequorin is inactivated as it is concluded by the rapid drop of luminescence. The SATA-derivatized aequorin was mixed with SMCC-modified oligo and hydroxylamine was added to expose the thiol groups. Figure 5 presents the chromatographic analysis of the conjugation

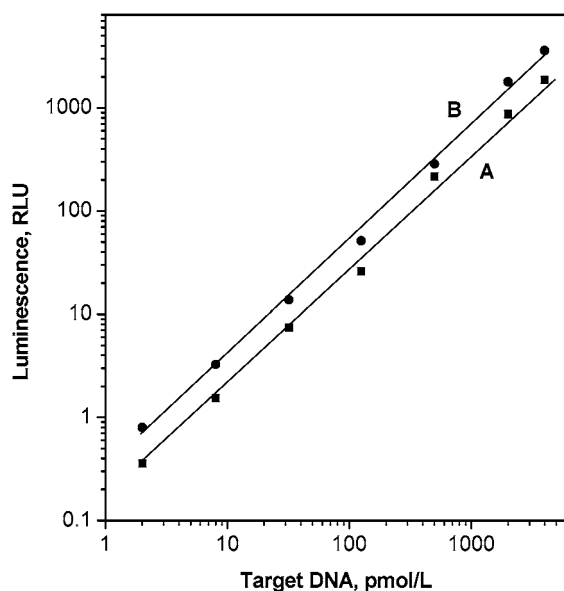


**Figure 5.** Chromatogram of aequorin-conjugated oligonucleotide synthesized using a heterobifunctional linker. The conjugation reaction was performed with 5 nmol of (His)<sub>6</sub>-aequorin modified with SATA (1:1 molar ratio) and 1.7 nmol of oligonucleotide modified with sulfo-SMCC (1:100 molar ratio). The reaction product was purified from unreacted oligonucleotide by Ni-NTA agarose and by anion-exchange HPLC. The luminescence of the eluted fractions are plotted versus the fraction number.

reaction mixture by anion-exchange HPLC. Fractions 15–23 contain the conjugate. The small conjugate peak collected in fractions 26–31 corresponds to higher oligo:aequorin molar ratios. By comparing the chromatographic data from Figures 2 and 5, it is deduced that the elution volumes of aequorin-oligo conjugates prepared by using either homobifunctional or heterobifunctional cross-linkers were identical.

We assessed the performance of conjugates purified (a) by affinity capture and anion-exchange HPLC and (b) by a single affinity capture step. The effect of the concentration of the affinity purified conjugate was studied in the range of 4.4–35 nmol/L and the optimum concentration was 11 nmol/L. Then, a series of hybridization assays was performed at various concentrations of target DNA and aequorin-oligo conjugates (a and b) were employed as detection reagents. In Figure 6, the luminescence is plotted as a function of target DNA concentration. A linear response was obtained for both conjugates in the range of 2 to 2000 pmol/L target DNA. The conjugate that was purified only by affinity capture gave higher signals. However, the S/B ratios at 2 pmol/L target DNA were 3.9, for the conjugate that was purified by affinity capture and HPLC, and 2.9 for the conjugate that was only subjected to affinity capture. The slight decrease in the S/B ratio is due to the higher background signal caused by the presence of unreacted aequorin. We have also tested conjugates prepared with (His)<sub>6</sub>-aequorin derivatized with 1-, 2.5-, and 5-fold molar excess of SATA. It was found that the 1:1 molar ratio gave the highest signal and lowest background.

To summarize, (His)<sub>6</sub>-aequorin-oligo conjugates prepared by affinity capture followed by HPLC and conjugates purified simply by affinity capture on the Ni-NTA agarose slurry showed similar performance. This fact greatly simplifies the preparation of oligonucleotide conjugated aequorin because it eliminates the necessity for HPLC purification. HPLC requires costly instrumentation and long time to setup, to carry out the separation and to concentrate the pooled fractions. By comparing the two conjugation chemistries studied, we found that



**Figure 6.** Calibration graph for the hybridization assay of amplification product from the PSMA cDNA, using aequorin–oligonucleotide conjugate prepared with SATA-sulfo-SMCC chemistry and purified: (A) by Ni–NTA agarose and anion-exchange chromatography and (B) by Ni–NTA agarose.

conjugates prepared with the heterobifunctional reagent protocol showed about 2 times higher S/B ratios than those prepared using the homobifunctional cross-linker. However, conjugation using the homobifunctional linker is simpler because it requires fewer reaction steps. Assessment of the performance of the conjugates showed that the detectability and analytical range are similar to those obtained previously (12) by using the ‘indirect labeling’ approach in which a digoxigenin-labeled probe hybridized to the target and the hybrids were reacted with antidigoxigenin–aequorin conjugate. The hybridization assay, however, is much faster and less costly when using the aequorin–DNA conjugate because the antibody incubation and washing steps are eliminated. The conjugate obtained from a reaction that uses 10 nmol of (His)<sub>6</sub>-aequorin is sufficient for about 5000 hybridization assays.

The proposed method for preparing conjugates is general because a variety of reporter proteins can be fused to a hexahistidine tag at their N- or C-terminus without significant loss of activity, by using suitable vectors that are available commercially.

#### ACKNOWLEDGMENT

This work was supported by a research grant from the General Secretariat of Research and Technology (GSRT) of Greece and Medicon Hellas, SA. We also acknowledge the financial support from the Secretariat of the Research Committee of the University of Athens and a Karatheodory research grant from the University of Patras.

#### LITERATURE CITED

- (1) Christopoulos, T. K. (1999) Nucleic acid analysis. *Anal. Chem.* 71, 425R.
- (2) Lewis, L. C., and Daunert, S. (2000) Photoproteins as luminescent labels in binding assays. *Fresenius J. Anal. Chem.* 366, 760.
- (3) Jones, K., Keenan, M., and Keenan, M. (1999) Glowing jellyfish, luminescence and a molecule called coelenterazine. *Trends Biotechnol.* 17, 477.
- (4) Shimomura, O., and Johnson, F. H. (1978) Peroxidized coelenterazine, the active group in the photoprotein aequorin. *Proc. Natl. Acad. Sci. U.S.A.* 75, 2611.
- (5) Head, J. F., Inouye, S., Teranishi, K., and Shimomura, O. (2000) The crystal structure of the photoprotein aequorin at 2.3 Å resolution. *Nature* 405, 372.
- (6) Kendall, J. M., and Badminton, M. N. (1998) Aequorea Victoria bioluminescence moves into an exciting new era. *Trends Biotechnol.* 16, 216.
- (7) Inouye, S., Noguchi, M., Sakaki, Y., Takagi, Y., Miyata, T., Iwanaga, S., Miyata, T., and Tsuji, F. I. (1985) Cloning and sequencing analysis of cDNA for the luminescent protein aequorin. *Proc. Natl. Acad. Sci. U.S.A.* 82, 3154.
- (8) Prasher, D., McCann, R. O., and Cormier, M. J. (1985) Cloning and expression of the cDNA coding for aequorin, a bioluminescent calcium-binding protein. *Biochem. Biophys. Res. Commun.* 126, 1259.
- (9) Stults, N. L., Stocks, N. F., Rivera, H., Gray, J., McCann, R. O., O’Kane, D., Cummings, R. D., Cormier, M. J., and Smith, D. F. (1992) Use of recombinant biotinylated aequorin in microtiter and membrane-based assays: purification of recombinant apoaequorin from *Escherichia coli*. *Biochemistry* 31, 1433.
- (10) Sgoutas, D. S., Tuten, T. E., Verras, A. A., Love, A., and Barton, E. G. (1995) AquaLite bioluminescence assay of thyrotropin in serum evaluated. *Clin. Chem.* 41, 1637.
- (11) Galvan, B., and Christopoulos, T. K. (1996) Bioluminescence hybridization assays using recombinant aequorin. Application to the detection of prostate-specific antigen mRNA. *Anal. Chem.* 68, 3545.
- (12) Verhaegen, M., and Christopoulos, T. K. (1998) Quantitative polymerase chain reaction based on a dual-analyte chemiluminescence hybridization assay for target DNA and internal standard. *Anal. Chem.* 70, 4120.
- (13) Laios, E., Ioannou, P. C., and Christopoulos, T. K. (2001) Enzyme-amplified aequorin-based bioluminescent hybridization assays. *Anal. Chem.* 73, 689.
- (14) Actor, J. K. (2000) Bioluminescent quantitation and detection of gene expression during infectious disease. *Comb. Chem. High Throughput Screen.* 3, 273.
- (15) Verhaegen, M., and Christopoulos, T. K. (2002) Bacterial expression of in vivo-biotinylated aequorin for direct application to bioluminescent hybridization assays. *Anal. Biochem.* 306, 314.
- (16) Stults, N. L., Rivera, H. N., Burke-Payne, J., Ball, R. T., and Smith, D. F. (1997) Preparation of stable conjugates of recombinant aequorin with proteins and nucleic acids, in *Bioluminescence and Chemiluminescence: Molecular reporting with photons* (Hastings, J. W., Kricka, L. J., Stanley, P. E., Eds), p 423, John Wiley and Sons, Chichester, UK.
- (17) Glynnou, K., Ioannou, P. C., and Christopoulos, T. K. (2003) One-step purification and refolding of recombinant photoprotein aequorin by immobilized metal-ion affinity chromatography. *Protein Expr. Purif.* 27, 384.
- (18) Erikaku, T., Zenno, S., and Inouye, S. (1991) Bioluminescent immunoassay using a monomeric Fab’-photoprotein aequorin conjugate. *Biochem. Biophys. Res. Commun.* 174, 1331.
- (19) Lewis, J. C., Cullen, L. C., and Daunert, S. (2000) Site-specifically labeled photoprotein-thyroxine conjugates using aequorin mutants containing unique cysteine residues: applications for binding assays. *Bioconjugate Chem.* 11, 140.
- (20) Shrestha, S., Paeng, I. R., and Daunert, S. (2002) Cysteine-free mutant of aequorin as a photolabel in immunoassay development. *Bioconjugate Chem.* 13, 269.



# TECHNICAL NOTES

## Anaerobic $^{90}\text{Y}$ - and $^{177}\text{Lu}$ -Labeling of a DOTA-Conjugated Nonpeptide Vitronectin Receptor Antagonist

Shuang Liu,\* Thomas D. Harris, Charles E. Ellars, and D. Scott Edwards

Bristol-Myers Squibb Medical Imaging, 331 Treble Cove Road, North Billerica, Massachusetts 01862.

Received September 23, 2002; Revised Manuscript Received April 7, 2003

This study describes the discovery and development of an anaerobic formulation for the routine preparation of  $^{90}\text{Y}$  and  $^{177}\text{Lu}$  complexes ( $^{90}\text{Y}$ -TA138 and  $^{177}\text{Lu}$ -TA138) of a DOTA-conjugated nonpeptide vitronectin receptor antagonist (TA138: 3-sulfon-*N*-[[4,7,10-tris(carboxymethyl)1,4,7,10-tetraazacyclododec-1-yl]acetyl]-L-alanyl-*N*-[2-[4-[[[(1*S*)-1-carboxy-2[[[1,4-dihydro-7-[(1*H*-imidazol-2-ylamino)methyl]-1-methyl-4-oxo-3-quinolinyl]carbonyl]amino]ethyl]amino]-sulfonyl]-3,5-dimethylphenoxy]-1-oxobutyl]-amino]ethyl]-3-sulfo-L-alaninamide). Since  $^{90}\text{Y}$ -TA138 and  $^{177}\text{Lu}$ -TA138 are very sensitive to radiolytic degradation, exclusion of oxygen is necessary during the radiolabeling. Using the anaerobic formulation,  $^{90}\text{Y}$ -TA138 and  $^{177}\text{Lu}$ -TA138 can be prepared in high yield and high specific activity. The anaerobic formulation described in this study is particularly useful for  $^{90}\text{Y}$ - and  $^{177}\text{Lu}$ -labeling of DOTA-conjugated small biomolecules, which are sensitive to the radiolytic degradation during radiolabeling.

### INTRODUCTION

We have been interested in the development of diagnostic and therapeutic radiopharmaceuticals based on small biomolecules (1–17). Recently, we reported the  $^{90}\text{Y}$ - and  $^{177}\text{Lu}$ -labeling of a DOTA-conjugated cyclic peptide vitronectin receptor antagonist (Figure 1: SU015). Through a series of radiolabeling experiments, we found that there are many factors influencing the  $^{90}\text{Y}$ -chelation rate of the DOTA conjugate (16). These include the purity of the DOTA conjugate (SU015), the pH, reaction temperature, and heating time, as well as the presence of trace metal contaminants. The  $^{90}\text{Y}$ -chelation rate of SU015 is slow room temperature and can be accelerated by raising the pH of the reaction mixture or/and elevating the heating temperature. Under optimized conditions (pH 7.2–7.8 and heating at 50–100 °C for 5–10 min), the minimal amount of SU015 required to achieve RCP of 95% for the complex  $^{90}\text{Y}$ -SU015 is  $\sim 25\ \mu\text{g}$  for 20 mCi of  $^{90}\text{YCl}_3$  corresponding to a SU015: $^{90}\text{Y}$  ratio of  $\sim 30:1$  (16).

As a continuation of our interest in the development of new diagnostic and therapeutic radiopharmaceuticals, we now present the synthesis of  $^{90}\text{Y}$  and  $^{177}\text{Lu}$  complexes of a DOTA-conjugated nonpeptide vitronectin receptor antagonist (Figure 1: TA138). It was found that complexes  $^{90}\text{Y}$ -TA138 and  $^{177}\text{Lu}$ -TA138 are extremely prone to radiolytic degradation. Exclusion of oxygen is required for the successful  $^{90}\text{Y}$ - and  $^{177}\text{Lu}$ -labeling of TA138. Through a series of experiments, we have developed an anaerobic formulation for routine preparation of  $^{90}\text{Y}$ -TA138 and  $^{177}\text{Lu}$ -TA138. This formulation is particularly

useful for radiolabeling of small biomolecules, which are sensitive to the radiolytic degradation during radiolabeling.

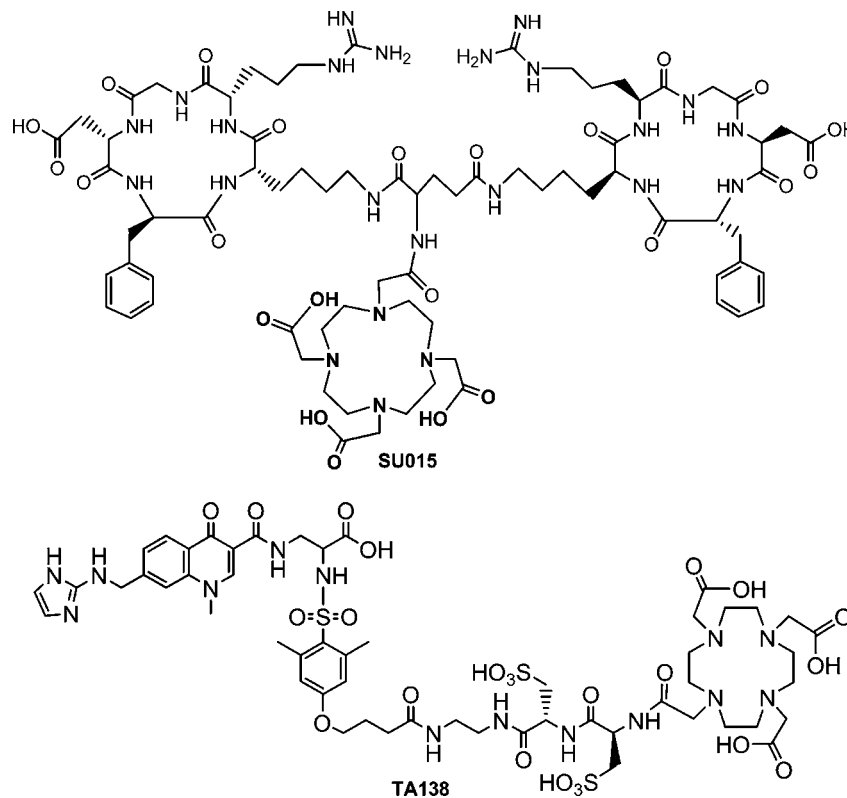
### EXPERIMENTAL SECTION

**Materials.** Acetic acid (ultrapure), ammonium hydroxide (ultrapure), diethylenetriaminepentaacetic acid (DTPA), sodium ascorbate (AA), and sodium gentisate (GA) were purchased from either Aldrich or Sigma Chemical Co. and were used as received.  $^{90}\text{YCl}_3$  (in 0.05 N HCl) was purchased from NEN Life Sciences, N. Billerica, MA. High specific activity  $^{177}\text{LuCl}_3$  was obtained from University of Missouri Research Reactor, Columbia, MO. DOTA tris(*tert*-butyl) ester was obtained from Macrocyclics, Richardson, TX. The synthesis of 2-([4-(3-*N*-[2-((2*R*)-2-((2*R*)-2-[(*tert*-butoxy)carbonylamino]-3-sulfopropyl]-3-sulfopropyl)ethyl]carbamoyl]propoxy)-2,6-dimethylphenyl]sulfonyl)amino)(2*S*)-3-([1-methyl-4-oxo-7-([1-(triphenylmethyl)imidazol-2-yl]amino)methyl](3-hydroquinolyl)]carbonylamino)propanoic acid (DPC-AG-1522) will be reported elsewhere (18).

**Analytical Methods.** The LC-MS data were collected using a HP1100 LC/MSD system with an API-electrospray interface. The LC-MS method used a Zorbax SB-C<sub>18</sub> column (4.6 mm  $\times$  150 mm, 3.5  $\mu\text{m}$  particle size). The flow rate was 1 mL/min with mobile phase gradient starting from 95% solvent A (25 mM ammonium acetate buffer, pH = 6.8) and 5% solvent B (acetonitrile) to 85% A and 15% B at 40 min.

The HPLC method 1 used a HP-1100 HPLC system with a UV/visible detector ( $\lambda = 230\ \text{nm}$ ), an IN-US radiodetector, and a Zorbax C<sub>18</sub> column (4.6 mm  $\times$  250 mm, 80 Å pore size). The flow rate was 1 mL/min with a gradient mobile phase starting from 92% solvent A (0.025 M ammonium acetate buffer, pH 6.8) and 8% solvent B (acetonitrile) to 90% solvent A and 13% solvent B at 18

\* To whom correspondence should be addressed. Current address: Department of Industrial and Physical Pharmacy, Division of Nuclear Pharmacy, School of Pharmacy, Purdue University, 575 Stadium Dr., West Lafayette, IN 47907-2051. Tel: 765-494-0236 (S.L.); Fax: 765-496-3367; E-mail: shuang.liu@pharmacy.purdue.edu.



**Figure 1.** Structures of DOTA-conjugated vitronectin receptor antagonists (SU015 and TA138).

min. The mobile phase was isocratic using 40% of solvent A and 60% solvent B from 19 to 25 min.

The HPLC method 2 used a HP-1050 HPLC system with a Rainin Dynamax UV/visible detector (model UV-C,  $\lambda = 230$  nm) and a Zorbax C<sub>18</sub> column (4.6 mm  $\times$  250 mm, 80 Å pore size). The flow rate was 1 mL/min with the mobile phase starting 10% of solvent A (0.1% TFA in water) and 90% solvent B (0.1% TFA in acetonitrile) to 20% solvent A and 80% of solvent B at 20 min, followed by an isocratic wash using 40% of solvent A and 60% solvent B from 21 to 26 min.

The TLC method used the C<sub>18</sub> reverse phase glass plates and a mobile phase containing methanol, acetone, and saline (2:1:1 = v:v:v). By this method, <sup>90</sup>Y-TA138 and <sup>177</sup>Lu-TA138 migrate to the solvent front while [<sup>90</sup>Y/<sup>177</sup>Lu]colloid and [<sup>90</sup>Y/<sup>177</sup>Lu]acetate remain at the origin. The corrected RCP was calculated by subtracting the percentage of [<sup>90</sup>Y/<sup>177</sup>Lu]colloid and [<sup>90</sup>Y/<sup>177</sup>Lu]acetate obtained by TLC from that obtained by radio-HPLC.

**Synthesis of 2-[(4-{3-[N-(2-[(2R)-2-[(2R)-3-Sulfo-2-(2-{1,4,7,10-tetraaza-4,7,10-tris[(*tert*-butoxycarbonyl)methyl]cyclododecyl}acetyl)amino)propyl]-3-sulfopropyl}ethyl)carbamoyl]propoxy}-2,6-dimethylphenyl)sulfonyl]amino)-(2S)-3-[1-methyl-4-oxo-7-([1-(triphenylmethyl)imidazol-2-yl]amino)methyl](3-hydroquinolyl)]carbonylamino}propanoic Acid (DPC-AG1613).** DPC-AG1522 (2.95 g, 2.20 mmol) was dissolved in 25/75 TFA/DCM (40 mL). The solution was stirred at room temperature for 60 min and was then concentrated under vacuum to give the free amine as an amber oil. Trituration with anhydrous diethyl ether (6  $\times$  50 mL) gave a colorless solid. The solid was dried under vacuum for 60 min to give 3.07 g of the title compound. LC-MS:  $m/z = 1241.3$  for  $[M + H]^+$  (25%) and 999.3 for  $[M + H - \text{Trt}]^+$  (42%). The free amine was dissolved in anhydrous DMF (30 mL) and DIEA (0.128 mL). In a separate flask, DOTA tris(*tert*-butyl) ester (2.10 g, 3.67 mmol) was dissolved in anhydrous DMF (21 mL)

and DIEA (0.85 mL). The solution was treated with HBTU (1.16 g, 3.06 mmol) and stirred under nitrogen at room temperature for 15 min. The activated DOTA tris(*tert*-butyl) ester was added to the solution of the free amine prepared above. The reaction mixture was stirred at room temperature for 1.5 h. DMF was removed under vacuum. The oily residue was triturated with EtOAc (5  $\times$  50 mL) to afford a pale yellow solid (4.54 g). This solid was purified in four separate runs by HPLC on a Vydac C<sub>18</sub> Pharmaceutical column (50  $\times$  250 mm) using a gradient mobile phase from 65% A (0.1 M NaOAc, pH 5.0) and 35% B (ACN) to 53% A and 47% B at 60 min and a flow rate of 80 mL/min. The collected fractions were diluted with two volumes of water and desalted by HPLC using the same Vydac C<sub>18</sub> column. The column was equilibrated with 13.5% ACN containing 0.1% TFA, and the diluted product fractions were pumped onto the column. The column was desalted by eluting isocratically using 22.5% ACN containing 0.1% TFA for 10 min at 88 mL/min. Product was eluted using a 1.8%/min gradient of 22.5 to 31.5% ACN containing 0.1% TFA followed by a 0.45%/min gradient mobile phase of 31.5 to 49.5% ACN containing 0.1% TFA. The collected fractions were combined and lyophilized to give the title compound as a colorless solid (2.58 g, 65.3%). LC-MS:  $m/z = 1795.6$  for  $[M + H]^+$  (60%) and 1553.5  $[M + H - \text{Trt}]^+$  (50%). High-resolution MS:  $m/z = 1795.744$  for C<sub>85</sub>H<sub>115</sub>N<sub>14</sub>O<sub>23</sub>S<sub>3</sub>,  $[M + H]^+$  (calcd 1795.7422).

**Synthesis of 3-Sulfon-N-[4,7,10-tris(carboxymethyl)1,4,7,10-tetraaza-cyclododec-1-yl]acetyl]-L-alanyl-N-[2-[4-[[[(1S)-1-carboxy-2[[[1,4-dihydro-7-[(1*H*-imidazol-2-ylamino)methyl]-1-methyl-4-oxo-3-quinolyl]carbonyl]amino]ethyl]amino]sulfonyl]-3,5-dimethylphenoxy]-1-oxobutyl]amino]ethyl]-3-sulfo-L-alaninamide (TA138).** A solution of DPC-AG1613 (2.50 g, 1.39 mmol) in 94/6 TFA/Et<sub>3</sub>SiH (75 mL) was heated at 70 °C under nitrogen for 60 min and concentrated under vacuum. The resulting oily solid was

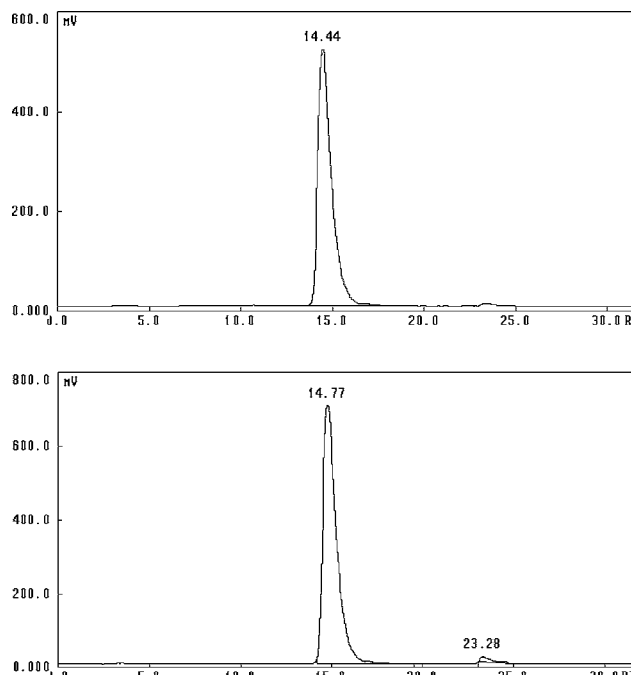
partitioned between diethyl ether (40 mL) and 5% aqueous ACN. The ether layer was extracted with 5% aqueous ACN (2 × 30 mL). The combined aqueous extracts were lyophilized to give crude TA138 (1.99 g) as a pale yellow solid. TA138 was purified in seven separate runs by HPLC on a Vydac C<sub>18</sub> Pharmaceutical column (50 × 250 mm) using a 0.45%/min gradient of 4.5 to 22.5% ACN containing 0.1% TFA at a flow rate of 80 mL/min. The collected product fractions from the seven runs were combined and lyophilized to give the title compound as its TFA salt. A second lyophilization from neutral ACN/water gave TA138 (1.55 g, 80.5%) as a fluffy solid. MS:  $m/z$  = 1385.4 for  $[M + H]^+$  (29%) and 693.3 for  $[M + 2H]^{2+}$  (100%). High-resolution MS:  $m/z$  = 1385.442 for C<sub>54</sub>H<sub>77</sub>N<sub>14</sub>O<sub>23</sub>S<sub>3</sub>,  $[M + H]^+$  (calcd 1385.4448).

**A General Procedure for Synthesis of <sup>90</sup>Y-TA138 and <sup>177</sup>Lu-TA138.** To a shielded, clean 5 mL vial were added 10–100 μg of TA138, 2–10 mg of sodium gentisate (GA), and 0–20 mg of sodium ascorbate (AA) dissolved in 1.0 mL of 0.5 M ammonium acetate buffer (pH = 6.0–8.0). The mixture was degassed under vacuum (<0.5 mmHg) for ~2 min. Upon addition of 10–40 μL of <sup>90</sup>YCl<sub>3</sub> or <sup>177</sup>LuCl<sub>3</sub> stock solution (20 ± 2 mCi) in 0.05 N HCl, the reaction mixture was heated at 95 °C for 5–30 min. For <sup>90</sup>Y-TA138, a sample of the resulting solution was diluted 50-fold with 2 mM DTPA solution (pH = 5) and analyzed by radio-HPLC (Method 1). For <sup>177</sup>Lu-TA138, samples of the resulting solution were diluted 2-fold with 2 mM DTPA solution (pH = 5) and then analyzed by HPLC (injection volume = ~5 μL). Each condition was run twice, and the radiochemical purity (RCP) data are presented as an average of two independent measurements.

**Synthesis of <sup>89</sup>Y-TA138.** To a clean 5 mL vial containing 70 mg of TA138, 10 mg of GA, and 50 mg of Y(NO<sub>3</sub>)<sub>3</sub>·4H<sub>2</sub>O was added 1.0 mL of 0.5 M ammonium acetate buffer (pH = 7.5). The reaction mixture was heated at 100 °C for 20 min. After being cooled to room temperature, a sample of the resulting solution was filtered. The product was separated from the filtrate by HPLC (Method 2) purification. The collected mobile phases were combined and then lyophilized to give a white powder (45 mg). The retention time was 14.5 min with the purity > 98% by HPLC (Method 1). LC-MS:  $m/z$  = 1472.1 for C<sub>54</sub>H<sub>73</sub>N<sub>14</sub>O<sub>23</sub>S<sub>3</sub>Y, (M + H)<sup>+</sup>, 736.2 for C<sub>54</sub>H<sub>74</sub>N<sub>14</sub>O<sub>23</sub>S<sub>3</sub>Y, (M + 2H)<sup>2+</sup>.

## RESULTS

**Discovery of the Anaerobic Formulation.** We first tried to prepare <sup>90</sup>Y-TA138 using the procedure described in our previous communication (16). TA138 was allowed to react with <sup>90</sup>YCl<sub>3</sub> in the ammonium acetate buffer (0.5 M, pH = 7.5) at 100 °C for 5 min. GA (10 mg for 20 mCi of <sup>90</sup>YCl<sub>3</sub>) was used as the stabilizer to prevent radiolytic degradation of <sup>90</sup>Y-TA138 during radiolabeling. The total volume was 0.5 mL, and the <sup>90</sup>YCl<sub>3</sub> concentration was 40 mCi/mL. We used 100 μg of TA138 for 20 mCi of <sup>90</sup>YCl<sub>3</sub>. The yield for <sup>90</sup>Y-TA138 prepared in the presence of oxygen was only 85–90% with a large wash peak (5–8%) at ~23 min. We also found that <sup>90</sup>Y-TA138 was not stable in the HPLC autosampler vial in the presence of air unless GA or AA (10 mg/mL) is added. If the autosampler vial is sealed, <sup>90</sup>Y-TA138 remains relatively stable for 2 h. These observations suggest that the instability and low yield of <sup>90</sup>Y-TA138 might be caused by the presence of oxygen dissolved in solution. That led to the discovery of an anaerobic formulation for routine preparations of <sup>90</sup>Y-TA138 and <sup>177</sup>Lu-TA138.



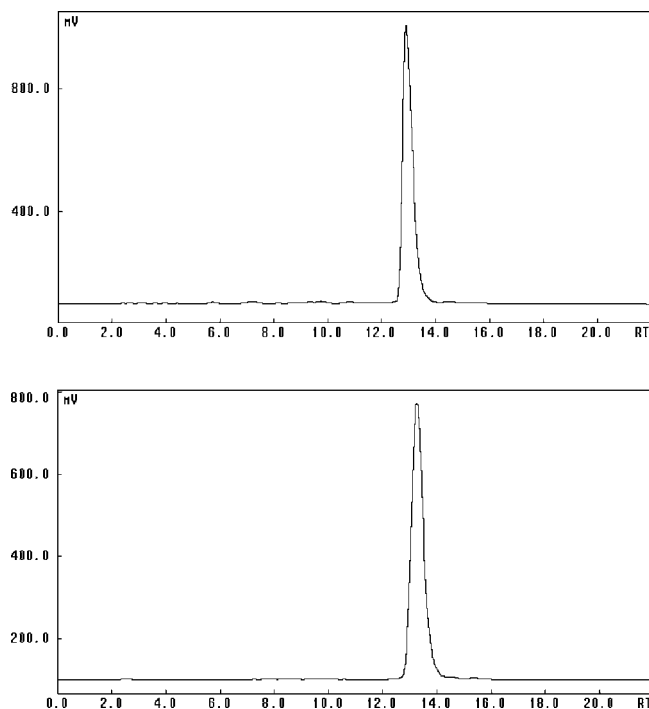
**Figure 2.** Radio-HPLC chromatograms (method 1) of <sup>90</sup>Y-TA138 (top) and <sup>177</sup>Lu-TA138 (bottom).

**Synthesis of <sup>90</sup>Y-TA138 and <sup>177</sup>Lu-TA138.** <sup>90</sup>Y-TA138 can be readily prepared in high yield (RCP > 95%) using the anaerobic formulation, in which TA138 is allowed to react with <sup>90</sup>YCl<sub>3</sub> in the degassed buffer solution (pH = 6.0–7.5) at 100 °C for 5–30 min. Exclusion of oxygen is required for successful radiolabeling, and can be achieved either by degassing under vacuum or by bubbling nitrogen through the reaction mixture before the addition of <sup>90</sup>YCl<sub>3</sub>. GA (2 mg/20 mCi) and AA (20 mg/20 mCi) are used as stabilizers to prevent radiolytic degradation of <sup>90</sup>Y-TA138 during radiolabeling. Both 0.5 M ammonium acetate and 0.1 M TRIS (tris(hydroxymethyl)amino-methane) can be used as buffers for the radiolabeling. The heating time depends on the pH of the buffer solution. Heating at 100 °C for 30 min is needed for successful radiolabeling if the pH is at 6.0. Heating at 100 °C for 5 min is usually sufficient to achieve RCP > 95% if the pH is > 7.5. We typically use 100 μg of TA138 for 20 mCi of <sup>90</sup>YCl<sub>3</sub> (TA138:<sup>90</sup>Y ~170:1) for most of the radiolabeling experiments. However, under optimized conditions <sup>90</sup>Y-TA138 can be prepared in high yield (RCP > 95%) using 20 μg of TA138 for 20 mCi of <sup>90</sup>YCl<sub>3</sub> corresponding to a TA138:<sup>90</sup>Y ratio of ~32:1. <sup>177</sup>Lu-TA138 can also be prepared in high yield using the same anaerobic formulation.

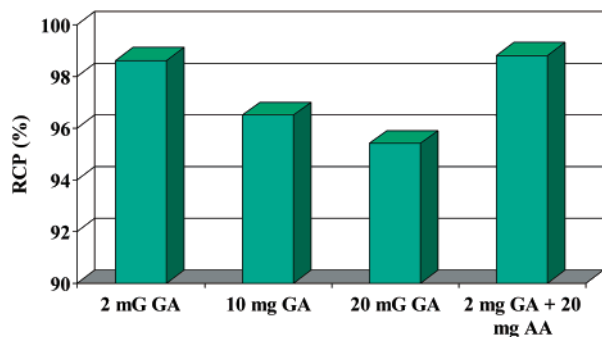
**HPLC Analysis of <sup>90</sup>Y-TA138 and <sup>177</sup>Lu-TA138.** <sup>90</sup>Y-TA138 and <sup>177</sup>Lu-TA138 were analyzed by a reversed phase HPLC method using a gradient mobile phase. Figures 2 show typical radio-HPLC chromatograms of <sup>90</sup>Y-TA138 and <sup>177</sup>Lu-TA138. There are some small peaks (the void-volume peak at ~2.5 min and the wash-peak at ~23 min) due to radioimpurities in <sup>90</sup>Y-TA138 and <sup>177</sup>Lu-TA138 preparations. Since these radioimpurities are less than 1.0%, no further characterization was performed. The HPLC retention time of <sup>177</sup>Lu-TA138 is almost identical to that of <sup>90</sup>Y-TA138.

**Synthesis of <sup>89</sup>Y-TA138.** <sup>89</sup>Y-TA138 was prepared by reaction TA138 with excess of yttrium(III) nitrate tetrahydrate and was separated from the reaction mixture by HPLC purification. <sup>89</sup>Y-TA138 has been characterized by HPLC and LC-MS methods. The HPLC concordance





**Figure 3.** HPLC concordance of  $^{90}\text{Y}$ -TA138 (bottom,  $\beta$ -detector) and  $^{89}\text{Y}$ -TA138 (top, UV detector).

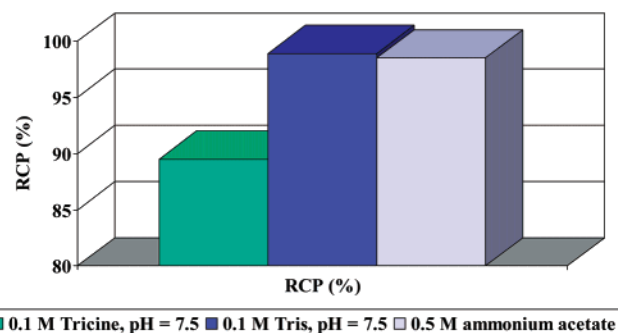


**Figure 4.** Effect of sodium gentisate (GA) concentration on RCP of  $^{90}\text{Y}$ -TA138.

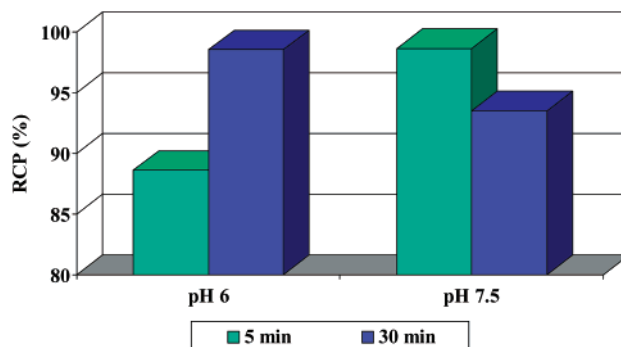
experiment (Figure 3) showed that  $^{90}\text{Y}$ -TA138 and  $^{89}\text{Y}$ -TA138 have the same HPLC elution profiles under identical chromatographic conditions. The LC-MS shows the monoprotonated molecular ion,  $(\text{M} + \text{H})^+$ , peak at  $m/z = 1472.1$  for  $[\text{C}_{54}\text{H}_{73}\text{N}_{14}\text{O}_{23}\text{S}_3\text{Y}]^+$  and diprotonated molecular ion,  $(\text{M} + 2\text{H})^{2+}$ , peak at  $m/z = 736.2$  for  $[\text{C}_{54}\text{H}_{74}\text{N}_{14}\text{O}_{23}\text{S}_3\text{Y}]^{2+}$ .

**Stabilizer Concentration.** In this experiment, we prepared  $^{90}\text{Y}$ -TA138 using 100  $\mu\text{g}$  of TA138, 2–20 mg of GA, 20 mCi of  $^{90}\text{YCl}_3$ , and 0.5 M ammonium acetate buffer (pH = 7.5). The reaction mixture was heated at 100  $^\circ\text{C}$  for 5 min. Figure 4 shows the effect of GA concentration on RCP of  $^{90}\text{Y}$ -TA138. Lower GA concentration gives better RCP for  $^{90}\text{Y}$ -TA138. However, 2 mg of GA is not sufficient to maintain the solution stability of  $^{90}\text{Y}$ -TA138. We have to use AA (20 mg for 20 mCi of  $^{90}\text{YCl}_3$ ) as the second stabilizer. AA can be added to the reaction mixture before addition of  $^{90}\text{YCl}_3$  or after radiolabeling.

**Buffer Agent.** The purpose of this experiment is to see if other buffer agents can be used to replace ammonium acetate for  $^{90}\text{Y}$ -labeling of DOTA–biomolecule conjugates at pH 6.0–8.5. The buffer agents tested include tricine [ $N$ -[tris(hydroxymethyl)methyl]glycine] ( $\text{pK}_a = 8.15$  at 20  $^\circ\text{C}$ ) and TRIS ( $\text{pK}_a = 8.3$  at 20  $^\circ\text{C}$ ). We



**Figure 5.** Effect of the buffering agent on RCP of  $^{90}\text{Y}$ -TA138.

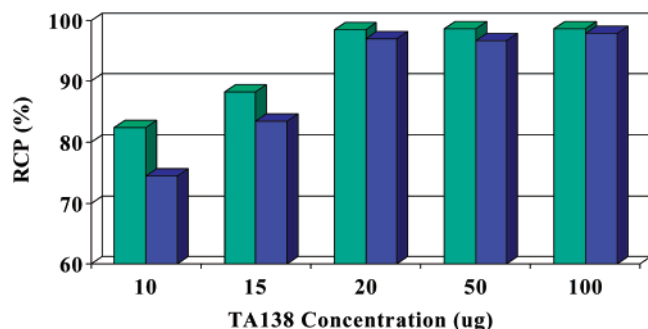


**Figure 6.** Effect of the pH and heating time on RCP of  $^{90}\text{Y}$ -TA138.

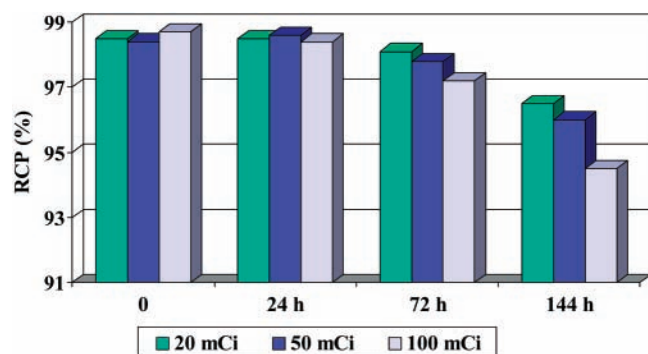
prepared  $^{90}\text{Y}$ -TA138 using 100  $\mu\text{g}$  of TA138, 2 mg of GA, 20 mg of AA, and 20 mCi of  $^{90}\text{YCl}_3$  for the radiolabeling. The buffer concentration was 0.5 M for ammonium acetate and 0.1 M for tricine and TRIS. The pH in the mixture was 7.5 before addition of  $^{90}\text{YCl}_3$ . The reaction mixture was heated at 100  $^\circ\text{C}$  for 5 min. Figure 5 shows that TRIS and ammonium acetate are comparable as buffer agents for the preparation of  $^{90}\text{Y}$ -TA138. Tricine is not a good buffer agent because it is a stronger chelator and may interfere with the  $^{90}\text{Y}$ -chelation of the DOTA conjugate. Since it has been used for the radiolabeling of various biomolecules, we chose 0.5 M ammonium acetate as the buffer agent for most radiolabeling experiments in this study.

**Buffer pH and Heating Time.** We prepared  $^{90}\text{Y}$ -TA138 using 100  $\mu\text{g}$  of TA138, 2 mg of GA, 20 mg of AA, and 20 mCi of  $^{90}\text{YCl}_3$  in 1.0 mL of 0.5 M ammonium acetate buffer. The pH in the reaction mixture was 6.0 or 7.5 before addition of  $^{90}\text{YCl}_3$ . The reaction mixture was heated at 100  $^\circ\text{C}$  for 5 or 30 min. Figure 6 shows the effect of pH and heating time on RCP of  $^{90}\text{Y}$ -TA138. Obviously, 30 min heating at 100  $^\circ\text{C}$  is needed for successful radiolabeling (RCP > 95%) if the pH is 6.0. Heating at 100  $^\circ\text{C}$  for 5 min is sufficient to achieve 95% RCP if the pH is 7.5. At pH > 7.5, longer heating time often results in more degradation of  $^{90}\text{Y}$ -TA138. We also found that  $^{90}\text{Y}$ -TA138 has less degradation at pH 6.0 during storage postlabeling.

**$^{90}\text{Y}$ - and  $^{177}\text{Lu}$ -Labeling Efficiency of TA138.** We studied the  $^{90}\text{Y}$ - and  $^{177}\text{Lu}$ -labeling efficiency of TA138 by determining the minimal amount of TA138 required to achieve 95% RCP for  $^{90}\text{Y}$ -TA138 and  $^{177}\text{Lu}$ -TA138. We prepared  $^{90}\text{Y}$ -TA138/ $^{177}\text{Lu}$ -TA138 using 10, 20, 50, or 100  $\mu\text{g}$  of TA138, 2 mg of GA, 20 mg of AA for 20 mCi of  $^{90}\text{YCl}_3$ / $^{177}\text{LuCl}_3$  in 1.0 mL of 0.5 M ammonium acetate buffer (pH = 6.0). The heating temperature was 100  $^\circ\text{C}$ , and the heating time was 30 min. Figure 7 shows the effect of TA138 concentration on RCP for  $^{90}\text{Y}$ -TA138. At pH 6.0, the minimal amount of TA138 required to achieve



**Figure 7.** Effect of the TA138 level ( $\mu\text{g}/20 \text{ mCi } ^{90}\text{Y}$ ) on RCP of  $^{90}\text{Y}$ -TA138 (left) and  $^{177}\text{Lu}$ -TA138 (right).



**Figure 8.** Solution stability of  $^{90}\text{Y}$ -TA138 at different activity levels.

95% RCP for  $^{90}\text{Y}$ -TA138 is about 20  $\mu\text{g}$  for 20 mCi of  $^{90}\text{YCl}_3$  corresponding to a TA138: $^{90}\text{Y}$  ratio of  $\sim 32:1$ . The same labeling efficiency can also be achieved at pH 7.5 except that the reaction mixture is heated at 100  $^\circ\text{C}$  for only 5 min.  $^{177}\text{Lu}$ -TA138 can also be prepared in high yield (RCP > 95%) under the same anaerobic conditions.

**Solution Stability of  $^{90}\text{Y}$ -TA138 at  $-78^\circ\text{C}$ .** We prepared  $^{90}\text{Y}$ -TA138 using 100  $\mu\text{g}$  of TA138, 2 mg of GA, 20 mg of AA, and 20 mCi of  $^{90}\text{YCl}_3$  in the 1.0 mL of 0.5 M ammonium acetate buffer (pH = 6.0). For the vials containing 100 mCi and 200 mCi of activity, all the component levels were increased proportionally so that the concentration of each component in the reaction mixture is constant. The reaction mixture was heated at 100  $^\circ\text{C}$  for 30 min. After radiolabeling, all the vials containing  $^{90}\text{Y}$ -TA138 were kept in a dry ice box ( $-78^\circ\text{C}$ ). Samples of the reaction mixture were analyzed by radio-HPLC at 0, 24, 56, and 144 h. Figure 8 shows the RCP change over 6 days for  $^{90}\text{Y}$ -TA138. Apparently,  $^{90}\text{Y}$ -TA138 remains stable in the kit matrix when stored at  $-78^\circ\text{C}$ .

## DISCUSSION

**DOTA Conjugate Design.** Angiogenesis is a requirement for tumor growth and metastasis (19–21). The angiogenic process depends on vascular endothelial cell migration and invasion and is regulated by cell adhesion receptors (22–31). The integrin  $\alpha_v\beta_3$  (vitronectin receptor) is such a cell adhesion receptor and interacts with proteins and peptides containing the RGD tripeptide sequence. A number of peptide and nonpeptide vitronectin receptor antagonists have been synthesized and studied for their antitumor activity (25–35). Radiolabeled vitronectin receptor antagonists (peptides and peptidomimetics) have been studied as new radiotracers for noninvasive tumor imaging and monitoring  $\alpha_v\beta_3$  expression (36–42).

We are interested in the quinolone-based nonpeptide vitronectin receptor antagonist (Figure 1: TA138) due to its high binding affinity and specificity for the integrin  $\alpha_v\beta_3$  receptor (18). DOTA is chosen for  $^{177}\text{Lu}$ - and  $^{90}\text{Y}$ -chelation due to its ability to form lutetium and yttrium complexes with high thermodynamic stability and kinetic inertness (42–46). The dicyclic acid linker (Figure 1) is used as a pharmacokinetic modifier to increase the hydrophilicity and to improve the renal clearance of the  $^{177}\text{Lu}$ - and  $^{90}\text{Y}$ -labeled DOTA conjugates (46).

**Anaerobic Synthesis of  $^{90}\text{Y}$ -TA138.** Radiopharmaceuticals comprising  $\beta$ -emitting radionuclides may undergo autoradiolysis during preparation and storage. Radiolysis is caused by the formation of free radicals such as hydroxyl and superoxide radicals (47) and is dependent on the concentration of the radionuclide and oxygen dissolved in the reaction mixture (48). To prevent radiolysis, a radiolytic stabilizer is often used during or/and after the radiolabeling (17, 49, 50). However, the use of the stabilizer cannot totally eliminate the oxygen dissolved in the reaction mixture. The combination of oxygen and the high-energy  $\beta$ -particles will result in formation of a large number of superoxide radicals, which are very reactive toward organic molecules.

It should be noted that different biomolecules have different sensitivity toward radiolysis. For the  $^{90}\text{Y}$ -labeled cyclic peptide ( $^{90}\text{Y}$ -SU015), it can be prepared in high yield in the presence of oxygen (16). The HPLC-purified  $^{90}\text{Y}$ -SU015 remains stable for several hours in saline. For  $^{90}\text{Y}$ -TA138, however, exclusion of oxygen is necessary during the radiolabeling. Addition of a stabilizer (GA or AA) in the HPLC autosampler vial is also needed to maintain the solution stability of the  $^{90}\text{Y}$ -TA138 sample.

**$^{90}\text{Y}$ - and  $^{177}\text{Lu}$ -Labeling Kinetics.** The  $^{90}\text{Y}$ -chelation kinetics of DOTA conjugates is largely dependent on the radiolabeling conditions, such as the pH in the reaction mixture, reaction time, and heating temperature (46, 51–56). Meares and co-workers (53) recently reported optimized conditions for  $^{90}\text{Y}$ -chelation of DOTA immunoconjugates. It was found that the time required to chelate 94% of  $^{90}\text{Y}$  was 17–148 min at pH 6.5, but it was only 1–10 min at pH 7.5 when the concentration of DOTA conjugate was 97–870  $\mu\text{M}$  and  $^{90}\text{Y}$  concentration was in the range of 0.83–6.1  $\mu\text{M}$  (53). In this study, we found that heating the reaction mixture at 100  $^\circ\text{C}$  for 30 min is needed to achieve 95% RCP for  $^{90}\text{Y}$ -TA138 if the pH is 6.0 while 5 min heating at 100  $^\circ\text{C}$  is sufficient if the pH is 7.5. In addition, the choice of radiolabeling conditions also depends on the chemical and radiolytic stability of the specific DOTA conjugate.

A major advantage in using DOTA for  $^{90}\text{Y}$ - and  $^{177}\text{Lu}$ -chelation is its capability to form yttrium and lutetium chelates with extremely high solution stability (43–46). However, studies have shown that the  $^{90}\text{Y}$ -chelation efficiency of DOTA derivatives is much lower than that of acyclic chelators such as DTPA (51, 54). The trace metal ( $\text{Ca}^{2+}$ ,  $\text{Fe}^{2+}$ , and  $\text{Zn}^{2+}$ ) contamination also has the more significant effect on the radiolabeling efficiency of the DOTA conjugate (51, 52, 55). Therefore, excess DOTA conjugate is often used to compensate for the presence of the trace metals and to achieve a high yield radiolabeling (RCP > 95%). As demonstrated in this study,  $^{90}\text{Y}$ -TA138 can be prepared in high yield under optimized conditions using 20  $\mu\text{g}$  of TA138 for 20 mCi of  $^{90}\text{YCl}_3$ . Although the specific activity of  $^{177}\text{Lu}$  ( $\sim 20 \text{ Ci/mg}$ ) is much lower than that of  $^{90}\text{Y}$  ( $\sim 500 \text{ Ci/mg}$ , carrier free),  $^{177}\text{Lu}$ -TA138 can be prepared in high yield (RCP > 95%) using the same anaerobic formulation.

In addition to the anaerobic condition, a stabilizer is needed during the radiolabeling. In our previous communication (16), we found that the GA level has minimal effect on the RCP of  $^{90}\text{Y}$ -SU015. In this study, however, we found that a high level of GA (20 mg/20 mCi) gives lower RCP for  $^{90}\text{Y}$ -TA138. Therefore, we have to use a combination of 2 mg of GA and 20 mg of AA for 20 mCi of  $^{90}\text{Y}$ . We also noticed that GA and ammonium acetate buffer can be totally replaced with AA (20–100 mg/mL or 100–500 mM) due to the fact that AA is not only a radiolytic stabilizer but also a buffer agent at pH 4–6. That led to the discovery of the anaerobic AA formulation, details of which will be reported as a separate communication (57).

Controlling pH is very important in the manufacturing process in order to have consistency and reproducibility. Although ammonium acetate has been used as a buffer agent for radiolabeling of biomolecules, including antibodies (44, 50, 51) and small peptides (14–17, 56), its buffer capacity is low if the pH is  $> 6.0$ . Therefore, a better buffer agent is needed for the  $^{90}\text{Y}$ -labeling of a DOTA conjugate at pH 6.0–8.0. In this study, we tested tricine ( $\text{p}K_a = 8.15$  at 20 °C) and TRIS ( $\text{p}K_a = 8.3$  at 20 °C), both of which have been used in various pharmaceutical compositions (58). Results from radiolabeling experiments show that TRIS is comparable to ammonium acetate as a buffer agent for the  $^{90}\text{Y}$ -labeling of the DOTA conjugate while tricine is not a good buffer agent due to its stronger chelating capability. Ammonium citrate has also been reported to interfere with the  $^{90}\text{Y}$ -labeling of DOTA immunoconjugates (53).

**Solution Stability of  $^{90}\text{Y}$ -TA138.** Unlike diagnostic radiopharmaceuticals, therapeutic radiopharmaceuticals have to be manufactured and released under GMP (good manufacturing practice) conditions and delivered for clinic applications. Therefore, the new therapeutic radiopharmaceutical must retain its chemical and biological integrity during release and transportation. In this study, we used GA and AA as radiolytic stabilizers in the anaerobic formulation and stored  $^{90}\text{Y}$ -TA138 at low temperature ( $-78$  °C/dry ice). Under these conditions,  $^{90}\text{Y}$ -TA138 remains stable for at least two half-lives of  $^{90}\text{Y}$ .

## CONCLUSIONS

In this study, we describe the discovery and development of an anaerobic formulation for the  $^{90}\text{Y}$ - and  $^{177}\text{Lu}$ -labeling of a DOTA-conjugated nonpeptide vitronectin receptor antagonist (TA138). It was found that difference biomolecules have different sensitivity toward radiolytic degradation and require different radiolabeling conditions. Using the anaerobic formulation,  $^{90}\text{Y}$ -TA138 can be prepared in high yield and high specific activity (20  $\mu\text{g}$  of TA138 for 20 mCi of  $^{90}\text{Y}$  corresponding to a TA138: $^{90}\text{Y}$  ratio of  $\sim 30:1$ ).  $^{177}\text{Lu}$ -TA138 can be prepared in high yield using the same anaerobic formulation.  $^{90}\text{Y}$ -TA138 remains stable in the formulation matrix when stored at  $-78$  °C. The amount of radiolytic stabilizer used in the formulation and storage temperature should be adjusted according to the sensitivity of a specific radiolabeled DOTA conjugate toward radiolytic decomposition. The anaerobic formulation described in this study is extremely useful for  $^{90}\text{Y}$ - and  $^{177}\text{Lu}$ -labeling of DOTA-conjugated small biomolecules, which are sensitive to the radiolytic degradation during radiolabeling.

## LITERATURE CITED

- (1) Liu, S., Edwards, D. S., Looby, R. J., Harris, A. R., Poirier, M. J., Barrett, J. A., Heminway, S. J., and Carroll, T. R. (1996)

- Labeling a hydrazinonicotinamide-modified cyclic IIB/IIIA receptor antagonist with  $^{99\text{m}}\text{Tc}$  using aminocarboxylates as co-ligands. *Bioconjugate Chem.* 7, 63–70.
- (2) Liu, S., Edwards, D. S., Looby, R. J., Harris, A. R., Poirier, M. J., Rajopadhye, M., Bourque, J. P., and Carroll, T. R. (1996) Labeling cyclic GPIIB/IIIA receptor antagonists with  $^{99\text{m}}\text{Tc}$  by the preformed chelate approach: Effects of chelators on properties of  $^{99\text{m}}\text{Tc}$ -chelator-peptide conjugates. *Bioconjugate Chem.* 7, 196–202.
- (3) Barrett, J. A., Damphousse, D. J., Heminway, S. J., Liu, S., Edwards, D. S., and Carroll, T. R. (1996) Biological evaluation of  $^{99\text{m}}\text{Tc}$ -labeled cyclic GPIIB/IIIA receptor antagonists in canine arteriovenous shunt and deep vein thrombosis models: effects of chelators on biological properties of  $^{99\text{m}}\text{Tc}$ -chelator-peptide conjugates. *Bioconjugate Chem.* 7, 203–208.
- (4) Liu, S., Edwards, D. S., and Barrett, J. A. (1997)  $^{99\text{m}}\text{Tc}$ -labeling of highly potent small peptides. *Bioconjugate Chem.* 8, 621–636.
- (5) Edwards, D. S., Liu, S., Barrett, J. A., Harris, A. R., Looby, R. J., Ziegler, M. C., Heminway, S. J., and Carroll, T. R. (1997) A new and versatile ternary ligand system for technetium radiopharmaceuticals: water soluble phosphines and tricine as coligands in labeling a hydrazino nicotinamide-modified cyclic glycoprotein IIB/IIIA receptor antagonist with  $^{99\text{m}}\text{Tc}$ . *Bioconjugate Chem.* 8, 146–154.
- (6) Barrett, J. A., Crocker, A. C., Damphousse, D. J., Heminway, S. J., Liu, S., Edwards, D. S., Lazewatsky, J. L., Kagan, M., Mazaika, T. J., and Carroll, T. R. (1997) Biological evaluation of thrombus imaging agents utilizing water soluble phosphines and tricine as coligands to label a hydrazinonicotinamide-modified cyclic glycoprotein IIB/IIIA receptor antagonist with  $^{99\text{m}}\text{Tc}$ . *Bioconjugate Chem.* 8, 155–160.
- (7) Liu, S., Edwards, D. S., and Harris, A. R. (1998) A novel ternary ligand system for technetium radiopharmaceuticals: imine-N containing heterocycles as coligands in labeling a hydrazinonicotinamide-modified cyclic platelet glycoprotein IIB/IIIA receptor antagonist with  $^{99\text{m}}\text{Tc}$ . *Bioconjugate Chem.* 9, 583–595.
- (8) Edwards, D. S., Liu, S., Harris, A. R., and Ewels, B. A. (1999)  $^{99\text{m}}\text{Tc}$ -labeling hydrazones of a hydrazinonicotinamide conjugated cyclic peptide. *Bioconjugate Chem.* 10, 803–807.
- (9) Edwards, D. S., Liu, S., Ziegler, M. C., Harris, A. R., Crocker, A. C., Heminway, S. J., Barrett, J. A., Bridger, G. J., Abrams, M. J., and Higgins, J. D. (1999) RP463: A stabilized technetium-99m complex of a hydrazino nicotinamide conjugated chemotactic peptide for infection imaging. *Bioconjugate Chem.* 10, 884–891.
- (10) Liu, S., and Edwards, D. S. (1999)  $^{99\text{m}}\text{Tc}$ -labeled small peptides as diagnostic radiopharmaceuticals. *Chem. Rev.* 99, 2235–2268.
- (11) Liu, S., Edwards, D. S., Harris, A. R., Heminway, S. J., and Barrett, J. A. (1999) Technetium complexes of a hydrazinonicotinamide-conjugated cyclic peptide and 2-hydrazinopyridine: Synthesis and characterization. *Inorg. Chem.* 38, 1326–1335.
- (12) Liu, S., Edwards, D. S., Ziegler, M. C., and Harris, A. R. (2002)  $^{99\text{m}}\text{Tc}$ -Labeling of a hydrazinonicotinamide-conjugated LTB4 receptor antagonist useful for imaging infection. *Bioconjugate Chem.* 13, 881–886.
- (13) Liu, S., Edwards, D. S., Ziegler, M. C., Harris, A. R., Heminway, S. J., and Barrett, J. A. (2001)  $^{99\text{m}}\text{Tc}$ -Labeling of a hydrazinonicotinamide-conjugated vitronectin receptor antagonist. *Bioconjugate Chem.* 12, 624–629.
- (14) Liu, S., Cheung, E., Rajopadyhe, M., Williams, N. E., Overoye, K. L., and Edwards, D. S. (2001) Isomerism and solution dynamics of  $^{90}\text{Y}$ -labeled DTPA- biomolecule conjugates. *Bioconjugate Chem.* 12, 84–91.
- (15) Liu, S., and Edwards, D. S. (2001) Synthesis and characterization of two  $^{111}\text{In}$ -labeled DTPA-peptide conjugates. *Bioconjugate Chem.* 12, 630–634.
- (16) Liu, S., Cheung, E., Rajopadyhe, M., Ziegler, M. C., and Edwards, D. S. (2001)  $^{90}\text{Y}$ - and  $^{177}\text{Lu}$ -labeling of a DOTA-conjugated vitronectin receptor antagonist for tumor therapy. *Bioconjugate Chem.* 12, 559–568.



- (17) Liu, S., and Edwards, D. S. (2001) Stabilization of  $^{90}\text{Y}$ -labeled DOTA-biomolecule conjugates using gentisic and ascorbic acid. *Bioconjugate Chem.* **12**, 554–558.
- (18) Harris, T. D., Kalogeropoulos, S., Nguyen, T., Liu, S., Bartis, J., Ellars, C. E., Edwards, D. S., Onthinks, D., Yalamanchili, P., Robinson, S. P., Lazewatsky, J., and Barrett, J. A. (2003) Design, synthesis and evaluation of radiolabeled integrin  $\alpha_v\beta_3$  antagonists for tumor imaging and radiotherapy. *Cancer Biother. Radiopharm.*, in press.
- (19) Folkman, J. (1995) Angiogenesis in cancer, vascular, rheumatoid and other disease. *Nature Med.* **1**, 27–31.
- (20) Mousa, S. A. (1998) Mechanism of angiogenesis in vascular disorders: potential therapeutic targets. *Drugs Future* **23**, 51–60.
- (21) Matter, A. (2001) Tumor angiogenesis as a therapeutic target. *Drug Discovery Today* **6**, 1005–1024.
- (22) Weinstat-Saslow, D., and Steeg, P. S. (1994) Angiogenesis and colonization in tumor metastatic process: basis and applied advances. *FASEB* **8**, 401–407.
- (23) Blood, C. H., and Zetter, B. R. (1990) Tumor interactions with the vasculature: angiogenesis and tumor metastasis. *Biochim. Biophys. Acta* **1032**, 410.
- (24) Gasparini, G., Brooks, P. C., Biganzoli, E., Vermeulen, P. B., Bonoldi, E., Dirix, L. Y., Ranieri, G., Miceli, R., and Cheresch, D. A. (1998) Vascular integrin  $\alpha_v\beta_3$ : a new prognostic indicator in breast cancer. *Clin. Can. Res.* **4**, 2625–2634.
- (25) Ferrara, N., and Alitalo, K. (1999) Clinical applications of angiogenic growth factors and their inhibitors. *Nature Med.* **5**, 1359–1364.
- (26) Brower, V. (1999) Tumor angiogenesis-new drug on the block. *Nature Biol.* **17**, 963–968.
- (27) Brooks, P. C., Montgomery, A. M. P., Rosenfeld, M., Reisenfeld, R., Hu, T., Klier, G., and Cheresch, D. A. (1994) Integrin  $\alpha_v\beta_3$  antagonists promote tumor regression by inducing apoptosis of angiogenic blood vessels. *Cell* **79**, 1157–1164.
- (28) Giannis, A., and Rübsam, F. (1997) Integrin antagonists and other low molecular weight compounds as inhibitors of angiogenesis: new drugs in cancer therapy. *Angew. Chem., Int. Ed. Engl.* **36**, 588–590.
- (29) Haubner, R., Gratias, R., Diefenbach, B., Goodman, S. L., Jonczyk, A., and Kessler, H. (1996) Structural and functional aspect of RGD-containing cyclic pentapeptides as highly potent and selective integrin  $\alpha_v\beta_3$  antagonists. *J. Am. Chem. Soc.* **118**, 7461–7472.
- (30) Haubner, R., Finsinger, D., and Kessler, H. (1997) Stereoisomeric peptide libraries and peptidomimetics for designing selective inhibitors of the  $\alpha_v\beta_3$  integrin for a new cancer therapy. *Angew. Chem., Int. Ed. Engl.* **36**, 1374–1389.
- (31) Drake, C. J., Cheresch, D. A., and Little, C. D. (1995) An antagonist of integrin  $\alpha_v\beta_3$  prevents maturation of blood vessels during embryonic neovascularization. *J. Cell Sci.* **108**, 2655–2661.
- (32) Allman, R., Cowburn, P., and Manson, M. (2000) In vitro and in vivo effects of a cyclic peptide with affinity for the  $\alpha_v\beta_3$  integrin in human melanoma cells. *Eur. J. Cancer* **36**, 410–422.
- (33) Miller, W. H., Alberts, D. P., Bhatnager, P. K., Bondinell, W. E., Callahan, J. F., Calvo, R. R., Cousins, R. D., Erhard, K. F., Heerding, D. A., Keenan, R. M., Kwon, C., Manley, P. J., Newlander, K. A., Ross, S. T., Samanen, J. M., Yuan, C. C. K., Haltiwanger, R. C., Gowen, M., Hwang, S. M., James, I. E., Lark, M. W., Rieman, D. J., Stroup, G. B., Azzarano, L. M., Slayers, K. L., Smith, B. R., Ward, K. W., Johanson, K. O., and Huffman, W. F. (2000) Discovery of orally active nonpeptide vitronectin receptor antagonists based on a 2-benzazepine Gly-Asp mimetic. *J. Med. Chem.* **43**, 22–26.
- (34) Keenan, R. M., Miller, W. H., Barton, L. S., Bondinell, W. E., Cousins, R. D., Eppley, D. F., Hwang, S. M., Kwon, C., Lago, M. A., Nguyen, T. T., Smith, B. R., Uzinskas, I. N., and Yuan, C. C. K. (1999) Orally bioavailable nonpeptide vitronectin receptor antagonists containing 2-aminopyridine arginine mimetics. *Bioorg. Med. Chem. Lett.* **9**, 1801–1806.
- (35) Batt, D. G., Petraitis, J. J., Houghton, G. C., Modi, D. P., Gain, G. A., Corjay, M. H., Mousa, S. A., Bouchard, P. J., Forsythe, M. S., Harlow, P. P., Barbera, F. A., Spitz, S. M., Wexler, R. R., and Jadhav, P. K. (2000) Disubstituted indazoles as potent antagonists for the integrin  $\alpha_v\beta_3$ . *J. Med. Chem.* **43**, 41–58.
- (36) Haubner, R., Wester, H.-J., Reuning, U., Senekowisch-Schmidtke, R., Diefenbach, B., Kessler, H., Stöcklin, G., and Schwaiger, M. (1999) Radiolabeled  $\alpha_v\beta_3$  integrin antagonists: a new class of tracers for tumor imaging. *J. Nucl. Med.* **40**, 1061–1071.
- (37) Van Hagen, P. M., Breeman, W. A. P., Bernard, H. F., Schaar, M., Mooij, C. M., Srinivasan, A., Schmidt, M. A., Krenning, E. P., and de Jong, M. (2000) Evaluation of a radiolabeled cyclic DTPA-RGD analogue for tumor imaging and radionuclide therapy. *Int. J. Cancer (Radiat. Oncol. Invest.)*, **8**, 186–198.
- (38) Haubner, R., Wester, H. J., Weber, W. A., Mang, C., Ziegler, S. I., Goodman, S. L., Senekowisch-Schmidtke, R., Kessler, H., and Schwaiger, M. (2001) Noninvasive imaging of  $\alpha_v\beta_3$  integrin expression using  $^{18}\text{F}$ -labeled RGD-containing glycopeptide and positron emission tomography. *Cancer Res.* **61**, 1781–1785.
- (39) Haubner, R., Wester, H. J., Burkhart, F., Senekowisch-Schmidtke, R., Weber, W., Goodman, S. L., Kessler, H., and Schwaiger, M. (2001) Glycolated RGD-containing peptides: tracer for tumor targeting and angiogenesis imaging with improved biokinetics. *J. Nucl. Med.* **42**, 326–336.
- (40) Weber, W. A., Haubner, R., Vabulienė, E., Kuhnast, B., Webster, H. J., and Schwaiger, M. (2001) Tumor angiogenesis targeting using imaging agents. *Quart. J. Nucl. Med.* **45**, 179–182.
- (41) Cheesman, E. H., Sworin, M. J., Liu, S., Onthank, D. C., Barrett, J. A., and Edwards, D. S. (2001) Nonpeptide vitronectin antagonists labeled with Tc-99m for imaging tumors, 222nd American Chemical Society National Meeting, Chicago, Aug 26–30, 2001, MEDI-077.
- (42) Harris, T. D., Kalogeropoulos, S., Bartis, J., Edwards, D. S., Liu, S., Onthank, D. C., and Barrett, J. A. (2001) Radiolabeled indazole-based  $\alpha_v\beta_3$  antagonists as potential tumor imaging agents. *J. Labelled Compd. Radiopharm.* **44** (Suppl. 1), S60–S62.
- (43) Moi, M. K., and Meares, C. F. (1988) The peptide way to macrocyclic bifunctional chelating agents: synthesis of 2-(p-nitrobenzyl)-1,4,7,10-tetraazacyclododecane-N,N',N'',N'''-tetraacetic acid and study of its yttrium(III) complex. *J. Am. Chem. Soc.* **110**, 6266–6267.
- (44) Li, M., and Meares, C. F. (1993) Synthesis, metal chelate stability studies, and enzyme digestion of a peptide-linked DOTA derivative and its corresponding radiolabeled immunoconjugates. *Bioconjugate Chem.* **4**, 275–283.
- (45) Caravan, P., Ellison, J. J., McMurry, T. J., and Lauffer, R. B. (1999) Gadolinium(III) chelates as MRI contrast agents: structure, dynamics, and applications. *Chem. Rev.* **99**, 2293–2352, and references therein.
- (46) Liu, S., and Edwards, D. S. (2001) Bifunctional chelators for target specific therapeutic lanthanide radiopharmaceuticals. *Bioconjugate Chem.* **12**, 7–34, and references therein.
- (47) Garrison, W. M. (1987) Reaction mechanisms in radiolysis of peptides, polypeptides, and proteins. *Chem. Rev.* **87**, 381–398.
- (48) Berger, R. (1982) Radical scavengers and the stability of  $^{99\text{m}}\text{Tc}$ -radiopharmaceuticals. *Int. J. Appl. Radiat. Isot.* **33**, 1341–1344.
- (49) Chakrabarti, M. C., Le, N., Paik, C. H., De Graff, W. G., and Carrasquillo, J. A. (1996) Prevention of radiolysis of monoclonal antibody during labeling. *J. Nucl. Med.* **37**, 1384–1388.
- (50) Salako, Q. A., O'Donnell, R. T., and DeNardo, S. J. (1998) Effects of radiolysis on yttrium-90-labeled lym-1 antibody preparations. *J. Nucl. Med.* **39**, 667–670.
- (51) Lewis, M. R., Raubitschek, A., and Shively, J. E. (1994) A facile, water-soluble method for modification of proteins with DOTA. Use of elevated temperature and optimized pH to

- achieve high specific activity and high chelate stability in radiolabeled immunoconjugates. *Bioconjugate Chem.* 5, 565–576.
- (52) Stimmel, J. B., Stockstill, M. E., and Kull, F. C., Jr. (1995) Yttrium-90 chelation properties of tetraazatetraacetic acid macrocycles, diethylenetriaminepentaacetic acid analogues, and a novel terpyridine acyclic chelator. *Bioconjugate Chem.* 6, 219–225.
- (53) Kulis, D. L., DeNardo, S. J., DeNardo, G. L., O'Donnell, R. T., and Meares, C. F. (1998) Optimized conditions for chelation of yttrium-90-DOTA immunoconjugates. *J. Nucl. Med.* 39, 2105–2110.
- (54) Lewis, M. R., and Shively, J. E. (1998) Maleimidocysteineamido-DOTA derivatives: New reagents for radiometal chelate conjugation to antibody sulfhydryl groups undergo pH-dependent cleavage reactions. *Bioconjugate Chem.* 9, 72–86.
- (55) Stimmel, J. B., and Kull, F. C., Jr. (1998) Samarium-153 and lutetium-177 chelation properties of selected macrocyclic and cyclic ligands. *Nucl. Med. Biol.* 25, 117–125.
- (56) Heppler, A., Froidevaux, S., Mäcke, H. R., Jermann, E., Béhé, M., Powell, P., and Hennig, M. (1999) Radiometal-labeled macrocyclic chelator-derived somatostatin analogue with superb tumor-targeting properties and potential for receptor-mediated internal therapy. *Chem. Eur. J.* 5, 1974–1981.
- (57) Liu, S. Unpublished data.
- (58) Nema, S., Washkuhn, R. J., and Brendel, R. J. (1997) Excipients and their use in injectable products. *J. Pharm. Sci., Technol.* 51, 166–171.

BC020061H

# Postsynthetic Conjugation of Biopolymers with High Molecular Mass Poly(ethylene glycol): Optimization of a Solution Process Tested on Synthetic Oligonucleotides

Maurizio Ballico,<sup>§</sup> Susanna Cogoi,<sup>#</sup> Sara Drioli,<sup>§</sup> and Gian M. Bonora<sup>\*,§</sup>

Department of Chemical Science, University of Trieste, Via Giorgieri, 1 - 34127 Trieste, Italy, and  
Department of Biological Science and Technologies, University of Udine, P.le Kolbe, 4-33100 Udine, Italy.  
Received February 13, 2003; Revised Manuscript Received May 22, 2003

The reaction of oligonucleotides with high molecular weight monomethoxy poly(ethylene glycol)s (MPEGs) has been tested to set up a convenient procedure for the postsynthetic conjugation in solution of biopolymers. A first oligonucleotide was previously modified in 5', using a liquid-phase procedure, with a linker carrying a terminal primary amino group to enhance its nucleophilic reactivity. Two procedures commonly utilized for the activation of the terminal OH groups of the MPEG were evaluated, that is, the reaction with pNO<sub>2</sub>-phenyl chloroformate and with *N,N*-disuccinimidyl carbonate. Both water as well as organic solution conditions were employed and compared. In a second test, a 3'-amino modified, commercial 20-mer was also conjugated in a microscale condition to verify the effect of size and concentration of MPEG on the postsynthetic conjugation of these biopolymers under troublesome synthetic conditions.

## INTRODUCTION

The pharmacological properties of synthetic oligonucleotides can be modulated by their conjugation with proper molecules (1). The rationale of these modifications is dictated by the necessity to get better cellular uptake, biostability, and pharmacokinetic properties. Among the molecules described in the literature, it is possible to distinguish between low and high molecular mass units. Within the first group, lipophilic conjugates, as cholesterol and other steroids, vitamins, and folic acid have been widely employed (2). Oligosaccharides and peptides have been considered for their ability to deliver oligonucleotides specifically to the targeted cells (3). Cleaving and cross-linking agents have been also proposed to improve the overall biological performances (4). Furthermore, large conjugating molecules as proteins and antibodies have been linked, and great attention turned to polyamines as polycationic carriers (5).

Among the different biocompatible polymers, poly(ethylene glycol) (PEG) was extensively investigated on the basis of previous success achieved with the PEGylation of protein (6). In fact, this procedure is well on its way to becoming a standard component of the pharmaceutical tool box, since PEG possesses a unique set of properties, including analytical methods for conjugate characterization, absence of toxicity, immunogenicity, and antigenicity, low mass-dependent elimination via the kidney, and high solubility in water and other organic media. At the oligonucleotide level, the presence of high molecular weight PEGs has showed a minimal effect on the hybridization behavior, while a clear enhancement of in vivo stability and cellular permeation has been observed, without any adverse toxic effect (7).

Additionally, taking advantage from the recent procedure capable of producing pure, selectively and reversibly protected bifunctional PEGs (8), it is easy to imagine the production of PEG conjugates carrying on the same chain an oligonucleotide and an additional molecule as a peptide, a steroid, an intercalator, or whatever can be devised to further improve their pharmacological properties.

The coupling of PEG to a bioactive molecule is achieved by a polymeric derivative having an activated functional group at one or both termini (9), chosen on the basis of the reactive groups of the molecule to be PEG-conjugated. In case of oligonucleotides, since they offer only low nucleophilic functions as primary OH groups, is quite difficult to attain an extensive modification through a direct reaction with PEGs. Moreover, the introduction of a large PEG chain by classical solid-phase procedures, commonly used for much postsynthetic oligonucleotide modification, suffers from the phase heterogeneity of the process that implies poor reactivity and unpredictable kinetic effects. An acceptable yield of these reactions has been described in the literature only using PEGs of lower molecular weight following the standard phosphoramidite conditions (10). However, the adverse effects are enhanced with the increasing of the mass of the conjugating polymer (11), as demanded due to its better biological performances observed with sizes up to 20–40 kDa. An oligonucleotide conjugation using a larger PEG molecule in a classical solution reaction has been reported; a very large excess of the ester-activated form of polymer was employed, but the yield of condensation was not discussed (12).

For all these reasons, we decided to investigate the postsynthetic PEG conjugation in solution of synthetic oligonucleotides to ascertain the optimum level of modification achievable through this procedure. To avoid the low reactivity of the terminal hydroxyl group, and to likely extend this procedure even at the peptide level, a

\* To whom correspondence should be addressed. Tel: +390405583927; fax: +390405583903; e-mail: bonora@units.it.

<sup>§</sup> University of Trieste.

<sup>#</sup> University of Udine.



terminal amino function was introduced on the oligonucleotides. The two most used chemical activations of the OH functions of PEG, namely, the *N,N*-disuccinimidyl and the *p*NO<sub>2</sub>-phenyl carbonate derivatives, were used both in water as well as in organic solution, and compared. The effects of concentration and molecular size of PEG were also investigated.

## MATERIALS AND METHODS

**Oligonucleotide Synthesis.** The oligonucleotides were a fully thioate 15-mer synthesized in our laboratory and a commercial, partially thioate 20-mer, modified with the 3'-amino-modifier C7 CPG linker (MWG-Biotech AG, Ebersberg (D)). Both were used without any further purification. The monomethoxy PEGs (MPEG)s of 5 and 10 kDa were obtained from Fluka, Bucks (Switzerland).

**Introduction of the Amino-Linker.** A 5'-terminal primary amino group was introduced, following the described procedure, on the fully thioate 15-mer obtained by liquid-phase synthesis on PEG (HELP technique) (13) after standard detritylation of the crude product.

**Conjugation with the 5'-Amino-Modifier Phosphoramidite, MMt-Protected.** A total of 1.00 g of MPEG<sub>10000</sub>-(3')-15-mer-(5')-OH (15.6  $\mu$ mol of 5'-OH groups) was dehydrated by coevaporation with 3  $\times$  5 mL of anhydrous AcCN in a three-neck vessel. Through the rubber septa, the MPEG-supported oligonucleotides were dissolved by injecting with a syringe 5.0 mL of anhydrous AcCN; successively, 100  $\mu$ mol of the 2-[2-(4-monomethoxytrityl)-aminoethoxy]ethyl-(2-cyanoethyl)-(N,N-diisopropyl)-phosphoroamidite (Glen Research) as 5'-amino-modifier phosphoroamidite (6 times excess) and 400  $\mu$ mol of 1H-tetrazole (24 times excess) were injected simultaneously through the septa. The mixture was kept under stirring, at room temperature and under argon atmosphere, for 5 min. The MPEG-bound product was precipitated from the solution, kept in an ice bath, by the addition of 100 mL of TBME under vigorous stirring. A white solid was filtered, washed with ether, and collected. To remove the residual excess of reagents, the product was recrystallized from EtOH. A total of 0.98 g of product were collected and dried under vacuum. On the basis of the monomethoxytrityl (MMt) absorbance at 472 nm ( $\epsilon$  = 51 900 in 70% HClO<sub>4</sub>/EtOH = 3/2 (v/v)) a functionalization degree of 67% was measured. The product was reacted again using the reported conditions, but with a prolonged reaction time (15 min). A final 86.5% degree of functionalization was achieved.

**Oxidation of the Phosphate Bond.** A total of 0.98 g of MPEG-(3')-15-mer-(5')-NH-MMt were dissolved in 7 mL of anhydrous AcCN. In an ice bath, and under stirring, 0.6 mL of *tert*-butyl hydroperoxide (80% in di-*tert*-butyl-hydroperoxide/water 3:2, Fluka, Bucks (Switzerland)) were added and the reaction was left under stirring at 0 °C for 15 min. The product was precipitated with 100 mL of TBME. A total of 0.97 g of a white powder were collected, washed with ether, and dried under vacuum over KOH pellets.

**Deprotection and Detachment of the Oligonucleotides.** A total of 0.80 g of MPEG-(3')-15-mer-(5')-NH-MMt were dissolved in 200 mL of concentrated NH<sub>4</sub>OH and stored, in a tightly closed vessel, in an oven at 50 °C for 18 h. The solution was coevaporated to dryness from distilled water until the ammonia was completely eliminated. The residual was dissolved in distilled water (100 mL) and extracted with ether (4  $\times$  100 mL). After lyophilization, 0.79 g of a white solid was collected. The MPEG was removed by dissolving the product in 8 mL of a 0.5%

solution of NH<sub>4</sub>OH and precipitating the oligonucleotides in an ice bath, under vigorous stirring, with 150 mL of acetone. After centrifugation of the sample (0 °C, 20 min, 4000 rpm), 0.30 g of 3'-OH-15-mer-(5')-NH-MMt, as ammonium salt, was quantitatively recovered and lyophilized. The supporting MPEG was eventually recovered from the acetone solution.

**Deprotection of the Terminal Amino Group.** A total of 0.30 g of the (3')-OH-15-mer-(5')-NHMMt were dissolved in 75 mL of a 4:1 (v/v) solution of glacial AcOH in water. The solution was left under stirring for 4 h at room temperature. A pale yellow color was developed. After addition of 8 mL of distilled water, the solution was extracted with ether (5  $\times$  75 mL). The residual was dissolved in water and lyophilized. A total of 0.29 g of a white product was collected. Less than 0.05% of MMt was still present.

### Activation of Terminal OH Groups of MPEG.

**Reaction with *p*NO<sub>2</sub>-Phenyl Chloroformate (MPEG-*p*NO<sub>2</sub>-Phenyl Carbonate).** A total of 5.0 g of MPEG<sub>5000</sub> (MW = 5 kDa), equivalent to 1.0 mmol of terminal OH groups, were coevaporated from anhydrous toluene and connected to a rotatory pump for 30 min for a complete dehydration. The solid residual was dissolved in 20 mL of anhydrous CH<sub>2</sub>Cl<sub>2</sub> and cooled in an ice-bath. Under stirring, 0.4 g of *p*NO<sub>2</sub>-phenyl chloroformate (2 times excess) was added, together with 1 equiv of TEA (0.28 mL). The reaction was left under stirring at room temperature; the pH was maintained around 8 with TEA. After 24 h, the product was precipitated from an ice-bath solution, under stirring, with TBME (200 mL), filtered, washed with <sup>1</sup>PrOH and ether, and dried under vacuum over KOH pellets. The collected product was recrystallized from EtOH. A total of 5.12 g was collected.

**Reaction with *N,N*-Disuccinimidyl Carbonate (MPEG-OSu Carbonate).** A total of 5.0 g of MPEG<sub>5000</sub>, equivalent to 1.0 mmol of terminal OH groups, was coevaporated from anhydrous toluene and connected to a rotatory pump for 30 min for a complete dehydration. The residue was added with 1.0 mL of anhydrous pyridine, and the slurry suspension was dissolved with 5 mL of anhydrous CH<sub>2</sub>Cl<sub>2</sub> and 2 mL of anhydrous AcCN. Under stirring, at room temperature, 0.64 g of *N,N*-disuccinimidyl carbonate were added (2.5 times excess). The reaction was left to react overnight. The product was precipitated from an ice-bath solution, under stirring, with TBME (200 mL), filtered, washed with <sup>1</sup>PrOH and ether, and dried under vacuum over KOH pellets. The product was recrystallized from AcOEt. A total of 5.15 g was collected.

**Conjugation of the 5'-Amino-Oligonucleotide with MPEG.** These experiments were performed with the HELP-synthesized 15-mer to set up the best conjugating conditions.

**Synthesis in Organic Media (Heterogeneous).** A total of 0.1 g of MPEG<sub>5000</sub>-(5') OH-activated (20  $\mu$ mol) was dissolved in 1.0 mL of CHCl<sub>3</sub>. A total of 0.05 g of the OH-(3')-15-mer-(5')-NH<sub>2</sub> (10  $\mu$ mol) and 0.8  $\mu$ L of TEA was added. The suspension was kept under vigorous stirring at room temperature. The insoluble solid was a white powder collected by addition, in an ice-bath and under stirring, of 100 mL of TBME. The product was washed with <sup>1</sup>PrOH and ether, and dried under vacuum.

**Synthesis in Aqueous Media (Homogeneous).** A total of 0.05 g of the OH-(3')-15-mer-(5')-NH<sub>2</sub> (10  $\mu$ mol) were dissolved in 1.0 mL of a buffer solution of Na<sub>2</sub>CO<sub>3</sub>/NaHCO<sub>3</sub> at pH = 9.0. 0.1 g of MPEG<sub>5000</sub>-(5') OH-activated (20  $\mu$ mol) were added and left under stirring at room temperature. After 72 h, the solution was evaporated to dryness in a rotavapor. The residue was suspended in

20 mL of  $\text{CHCl}_3$  and left under stirring for 10 min. The insoluble material was filtered, and the  $\text{CHCl}_3$  solution was dried with anhydrous  $\text{Na}_2\text{SO}_4$ . A white solid was collected by addition, in an ice-bath and under vigorous stirring, of 100 mL of TBME. The product was washed with  $\text{PrOH}$  and ether, and dried under vacuum.

**Analytical Methods.** The NMR spectra were collected in  $\text{DMSO}-d_6$  on a JEOL EX 400 spectrometer using TMS as internal standard.

The RP chromatography was performed on a Progel-TSK OligoDNA (column  $15 \times 0.46$  cm) with the following gradient: eluent A: TEAAc 0.05 M, pH = 7.0; eluent B: TEAAc 0.05 M, pH = 7.0/AcCN 20:80 (for 2 min: 10%B; from 2 to 40 min: 40% B). The GPC was performed on a PL aquagel-OH 30- $8\mu\text{m}$  (column  $30 \times 0.75$  cm) eluted with water milliQ.

A HPLC Hewlett-Packard series 1100 system equipped with a Lambda-Max model 481 UV/Vis detector was used.

The gel-electrophoresis was performed in a Mighty Small II cell (Amersham Pharmacia Biotech) equipped with a Power Pac 3000 power supply (Bio-Rad), in denaturing conditions (urea 7 M) on 20% polyacrylamide. Conditions: 2 h of prerunning at 55 °C, 600 V, 30 W, 50 mA; 45 min of running at 55 °C, 600 V, 30 W, 50 mA. After running, the gel was incubated overnight in a Stains All solution (0.01% Stains All in 50% formamide), washed with water, and then analyzed on a Phosphor-imager (Bio-Rad).

The amount of  $\text{NH}_2$  was calculated using the colorimetric TNBS test as follows: 250  $\mu\text{L}$  of TNBS 0.03 M in borate buffer at pH = 9.3 was added to 1 mg of sample. The solution was diluted to 10 mL with borate buffer at pH = 9.3, stirred, and allowed to stand for 30 min at room temperature. Absorbance at 421 nm ( $\epsilon = 12\,860$ ) was measured.

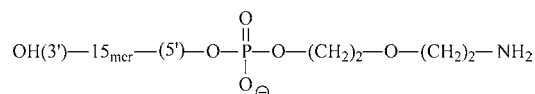
## RESULTS AND DISCUSSION

**Introduction of the 5'- $\text{NH}_2$  Terminal Linker.** To overcome the low nucleophilicity of the terminal OH group of the oligonucleotides, and consequently to increase the expected yield of the postsynthetic conjugation of these molecules, a linker carrying a primary amino group is required. This was introduced on the HELP-synthesized thioate 15-mer using a reagent that allows the standard amidite procedure and ensures high condensation yields and fast reaction times. It is important to observe that, in principle, the same conjugation reaction between a high molecular mass polymer, as PEG, and a biomolecule will likely be extended, on similar reaction conditions, on peptides or other biologically active molecules provided with a proper amino function. This reaction was performed on the oligonucleotides supported on a MPEG polymer using a liquid-phase procedure to take advantage of the presence of the soluble supporting polymer. In fact, it is possible to drive the reaction to high yield values using an excess of reagents, but saving advantageous homogeneous conditions; any unreacted material is easily removed by the usual precipitation and filtration procedure at the end of the reaction. Successively, the hydrolysis of the MPEG-supporting bond will permit the recovery of free  $\text{NH}_2$ -terminal modified oligonucleotides.

In Scheme 1, the structure of the  $\text{NH}_2$ -terminal modified oligonucleotides is reported.

Up to near 90% of modification was achieved on the MPEG-(3')-15-mer-(5')-OH. The removal of the terminal MMT amino-protecting group did not offer any drawback, while the final hydrolytic cleavage of the MPEG-

**Scheme 1. Free 15-mer Thioate Carrying the Amino Linker at the 5'-Position**



**Table 1. Yields and Reaction Solvent of the MPEG-Conjugation Reactions**

activated MPEG <sub>5000</sub>	reaction solvent	conjugation yield (%)
MPEG-pNO <sub>2</sub> phenyl carbonate	$\text{CHCl}_3$	10
	$\text{H}_2\text{O}$	10
MPEG-Osu carbonate	$\text{CHCl}_3$	15
	$\text{H}_2\text{O}$	65

supporting ester bond was obtained, as usually, during the terminal deprotection procedure of the oligonucleotides chain. From the starting MPEG-supported oligonucleotides, the expected amount of free 5'- $\text{NH}_2$ -oligonucleotide was eventually collected. Only the final, full-sequence oligonucleotides carried the reacting amino group, since the reaction was performed on a crude product subjected, at the end of the chain assembly, to a capping procedure that irreversibly modified any still unreacted groups. Hence, only the terminal DMT-protected nucleotide will be able to further react with the linker, once deprotected. The hydrolyzed, supporting MPEG was almost completely removed from the reaction mixture by dissolving in acetone that solubilizes only the polymer, while the insoluble oligonucleotide was filtered out and collected. An UV analysis of the aqueous and organic solutions confirmed these results, since less than 0.05% of the calculated total absorbance at 260 nm due to the oligonucleotide was measured in acetone solution, while the starting MPEG-OH was recovered after precipitation with ether.

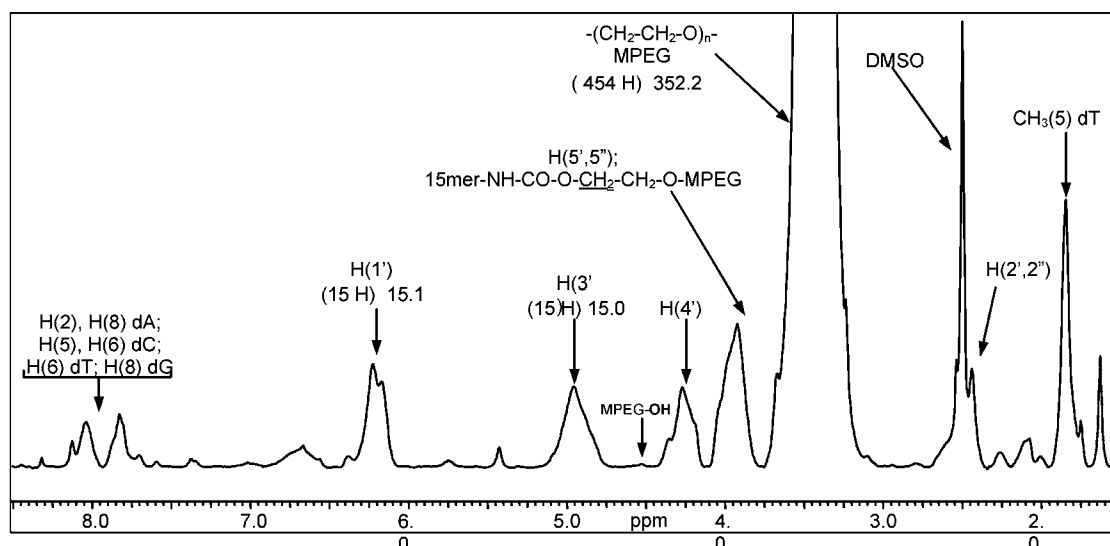
### Conjugation with High Molecular Weight MPEGs.

To obtain a stable linkage between MPEG and the conjugating molecule, the OH-terminal groups of polymer must be activated. Two quite common conditions were chosen, that is the reaction with the pNO<sub>2</sub>-phenyl chloroformate and that with the *N,N*-disuccinimidyl carbonate. Both will give a reactive intermediate that will form a stable urethane linkage with the  $\text{NH}_2$  group of the biomolecule. The two reactions, very popular as MPEG-modifying procedures, were compared for their behavior toward the same oligonucleotides. In addition, the reactivity of the two activated MPEGs was verified both in organic as well as in aqueous conditions to investigate if it was possible to avoid the time-consuming dehydration of the final product obtained from water solution.

All these experiments were performed using a 15-mer synthesized by a large scale, liquid-phase procedure using the PEG-supported procedure (13).

The sequence of the fully phosphorothioated oligonucleotide was (5')- $\text{NH}_2$ linker-d(TCTCAGT<sub>3</sub>G<sub>4</sub>T<sub>2</sub>)-OH-(3')

In  $\text{CHCl}_3$ , the conjugation was obviously achieved in heterogeneous conditions, but a likely solubilization of the product due to the presence of the amphipilic, large molecular weight MPEG was expected. However, with the proceeding of the reaction, only a very low solubilization of the reaction mixture was observed. On the other hand, the reaction performed in aqueous solution, characterized by the homogeneity of the reaction mixture, will reasonably offer a better reactivity, even if some adjunctive workup will be demanded. In any case, the presence of MPEG on the final product granted the usual advantages given by the soluble polymer-supported reactions, as the easy purification procedures. The overall results

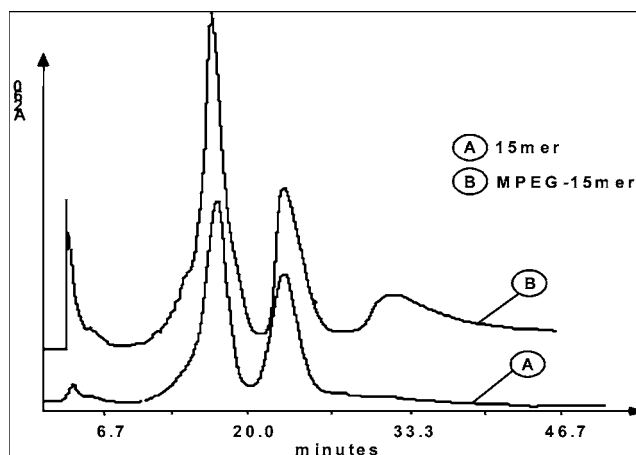


**Figure 1.**  $^1\text{H}$  NMR in  $\text{DMSO}-d_6$  of the crude MPEG-(5')-NH-15-mer-(3')-OH obtained from the water solution of the OSu-activated polymer.

as a function of the reaction conditions are summarized in Table 1 where yields were calculated from  $^1\text{H}$  NMR spectra in  $\text{DMSO}-d_6$ .

By comparing the results it is easy to observe that the best reaction conditions are achieved from the conjugation with the MPEG OSu-activated in water solution, where less than 30% of the unreacted, starting amino groups were still present, as measured by the TNBS test. In case of the  $\text{pNO}_2$ -phenyl carbonate, almost the same result was observed for both the organic and the aqueous reaction, that is, near 10% of conjugation yield; a similar value was achieved from the reaction of MPEG-OSu in  $\text{CHCl}_3$ . A 2:1 ratio between MPEG and oligonucleotides was used in all these experiments, but a high conjugation yield can be predicted increasing the excess of activated polymer. In Figure 1 a representative  $^1\text{H}$  NMR spectra is reported, where the ratio between  $\text{H}(1')$  and  $\text{H}(3')$  protons of the oligonucleotides and the internal  $\text{CH}_2$  of the MPEG's chain can be used to evaluate the reaction. The yields have been calculated taking into account that some free MPEG resulting from the oligonucleotide synthesis was still present in about 20% of the overall amount, as calculated from the chromatographic analyses of the crude, deblocked material. The final value was in line with the amount of unreacted, free  $\text{NH}_2$  of the starting oligonucleotide as evaluated from the TNBS colorimetric test. In addition, the intensity of residual signals due to the terminal OH group of MPEG, as well as those of the OH-activating moieties, confirms that the MPEG signals are almost due to the stable conjugate.

In Figure 2 the RP-HPLC chromatograms of the starting, free oligonucleotide and of its MPEG-conjugated, obtained by a water-based, OSu-activated procedure, are reported. It is possible to recognize a broad, late-running peak due to the MPEG-oligonucleotide. The two first peaks can be originated by the intermolecular associations of the starting oligonucleotide, as confirmed by its analysis under more diluted conditions (data not shown), in which the decrease of intensity of the second peak is paralleled by an increase of the first one. However, some nonconjugated, shorter oligonucleotides were still present in the sample. In fact, a crude synthetic mixture was used in which all the wrong sequences were previously capped and, consequently, made unable to be modified by the introduction of the  $\text{NH}_2$  linker and, successively, of the MPEG moiety. Furthermore, the intensity of the MPEG-



**Figure 2.** RP HPLC of the starting 15-mer (A) and of its MPEG-conjugated form (B).

conjugated peak is lower than expected from  $^1\text{H}$  NMR results, likely due to the presence of the conjugated polymer that decreases the UV absorbance of the conjugated sample compared with the free oligonucleotide. The  $\text{CHCl}_3$  fraction of the same reaction, once chromatographed, showed only traces of the same materials, as expected.

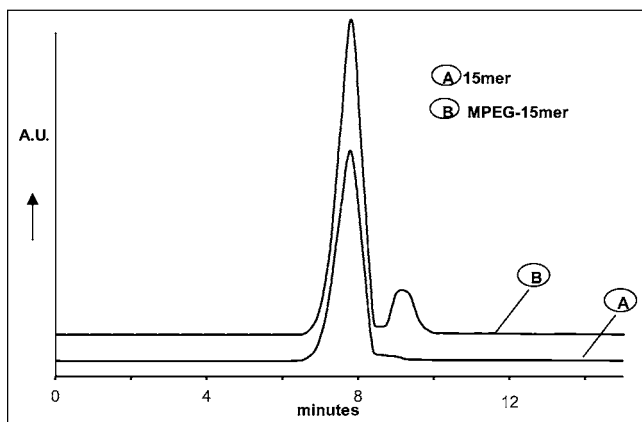
These results are supported by a GPC investigation, where the peaks were monitored using the UV absorbance and the refractive index. As reported in Figure 3, in this case it is possible to observe a new peak assignable to the PEG-conjugated oligonucleotide. Its low intensity is, as said, very likely due to the presence of the conjugating polymer, while only a single peak due to unreacted oligonucleotides is observed with this chromatographic support.

As a conclusion, we can reasonably assume that the best reaction condition demands the use of MPEG-OSu carbonate in a basic, buffered aqueous solution.

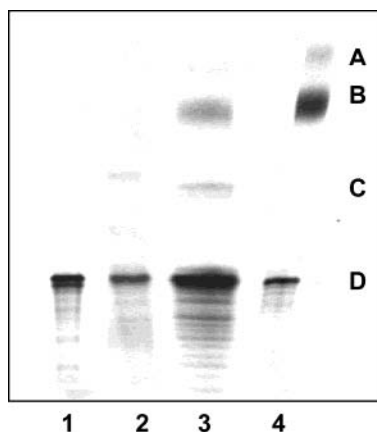
A further study investigated the effect of the molecular size of the conjugating MPEG on the condensation yield, as well as the excess of the reacting polymer.

As a sample oligonucleotide a commercial 20-mer, partially thioated, was in this case employed to additionally evaluate the efficiency of this PEG-conjugating procedure in a very low-scale condition. The new sequence,





**Figure 3.** GPC of the starting 15-mer (A) and of its MPEG-conjugated form (B). The arrow indicates the elution time of a standard sample of the starting MPEG<sub>5000</sub>.



**Figure 4.** Gel-electrophoresis of the commercial 20-mer and of its crude MPEG-conjugated derivatives (Lane 1, starting 20-mer; lane 2, 20-mer + MPEG<sub>10000</sub> = 1:2; lane 3, 20-mer + MPEG<sub>5000</sub> = 1:2; lane 4, 20-mer + MPEG<sub>5000</sub> = 1:10).

(5′)-OH-d(GpsA<sub>2</sub>GapsAGapsAGAGpsA<sub>2</sub>GA<sub>2</sub>GpsAG)-NH<sub>2</sub>-(3′), where ps = phosphorothioate bond, was used as control in a recent anti-gene activity study (14). The NH<sub>2</sub>-terminal group was present on the 3′-terminal position, as given by the standard synthetic procedure used for this commercial product that adopts a 2-DMT-6-Fmoc-amino-hexane-1-succinoyl linker supported on a long chain alkylamino-CPG solid-phase support. Due to the low abundance of the starting material, the conjugation procedure was performed on a microscale, using 1/100 of the sample employed in the previous experiment. Less than 1.0 mg of oligonucleotide was utilized. The main problem arose from the manipulation of the reaction mixture since a minimum volume reaction was demanded to maintain the reagent concentration as high as possible. A MPEG<sub>10000</sub> (10 kDa) OSu-activated was initially employed consequently to the increased size of the oligonucleotide, with a twice-excess with respect to the oligonucleotide. Successively, the same reactions were performed using a MPEG<sub>5000</sub> with a 2:1 and with a 10:1 excess of polymer. The final purification was performed by a molecular sieves chromatography, using a Bio-Rad P-4 column, eluted with water milliQ. The MPEG-oligonucleotide was collected with the void volume of the column. The small fragments of the oligonucleotide were mostly present in the late-running peak. The crude products were analyzed by a gel-electrophoresis on polyacrylamide. The results are reported in Figure 4.

It can be observed that only a larger excess of the activated MPEG guarantees in this case an efficient

modification of the terminal NH<sub>2</sub> moiety of the oligonucleotides, while an increased size of the polymer makes almost inefficient the conjugation reaction, at least on these conditions. As observed in lanes 3 and 4, the amount of the MPEG-conjugates is enhanced using an higher excess of polymer, as seen at the level B. The level A shows a larger derivative likely arising from the impurity of PEG<sub>10000</sub> present in the starting MPEG<sub>5000</sub>, as observed from its GPC analysis (not shown); alternatively some aggregation of the MPEG-conjugate cannot be excluded. Some aggregation due to the oligonucleotide sequence can be also envisaged from the spots at level C; their disappearance in lane 4 is very likely due to the reaction with the polymer that reduced the amount of free 20-mer still present. At the level D are clearly recognizable the spots due to free oligonucleotides in the starting crude, commercial sample.

These results are complementary to those obtained with the shorter oligonucleotide and are here included as an example of a postsynthetic PEG conjugation performed on a quite low scale using a commercial product. A similar downscaling was not performed on the fully thioated 15-mer, but a comparable result can be reasonably expected.

## CONCLUSIONS

In conclusion, an efficient procedure for the conjugation in solution of oligonucleotides, and very likely of other biomolecules carrying a reactive NH<sub>2</sub> function, can be set up using properly activated, high molecular weight PEGs in water solution.

A main problem could arise from the low abundance of rare products that hampers an efficient procedure, owing to a difficult manipulation of samples. However, a technical solution to these drawbacks can be reasonably devised.

From the chemical point of view, the reactivity of the OSu-activated MPEGs behaves efficiently in buffered, basic water solution. The same reaction in organic solution suffers for the phase heterogeneity that reduces dramatically the conjugation yield. A clear advantage derives from the amphiphilic properties of the polymer that allow for a convenient purification procedure and recovery of products.

## ACKNOWLEDGMENT

This work was supported by grants from Regione Friuli-Venezia Giulia (Italy), L.R. 3/98, and from MIUR-Italy (Cofin 2001). The authors thanks Prof. Luig Xodo (University of Udine-Italy) for the helpful discussions.

## LITERATURE CITED

- (1) Manoharan, M. (2001) Oligonucleotide conjugates in anti-sense technology. In *Antisense Drug Technology* (Crooke, S., Ed.) pp 391–469, Marcel Dekker, Inc.
- (2) MacKellar, C., Grahham, D., Will, D. W., Burgess, S., and Brown, T. (1992) Synthesis and physical properties of anti-HIV antisense oligonucleotides bearing terminal lipophilic groups. *Nucleic Acids Res.* 20, 3411–3417.
- (3) Garcia de la Torre, B., Albericio, F., Saison-Behmoaras, E., Bachi, A., and Eritja, R. (1999) Synthesis and binding properties of oligonucleotides carrying nuclear localization sequences. *Bioconj. Chem.* 10, 1005–1012.
- (4) Magda, D., Wright, M., Crofts, S., Lin, A., and Sessler, J. L. (1997) Metal complex conjugate of antisense DNA which displays ribozyme-like activity. *J. Am. Chem. Soc.* 119, 6947–6948.

- (5) Markiewicz, W. T., Godzina, P., Markiewicz, M., and Astriab, A. (1998) Synthesis of a polyamino-oligodeoxyribonucleotide combinatorial library, *Nucleosides Nucleotides* 17, 1871–1880.
- (6) Kodera, Y., Matsushima, A., Hiroto, M., Nishimura, H., Ishii, A., Ueno, T., and Inada, Y. (1998) PEGylation of proteins and bioactive substances for medical and technical applications. *Prog. Polym. Sci.* 23, 1233–1271.
- (7) Pang, S. N. J. (1993) Final report on the safety assessment of poly(ethylene glycol)s. *J. Am. Coll. Toxicol.* 12, 429–456.
- (8) Drioli, S., Benedetti, F., and Bonora, G. M. (2001) Pure, homobifunctional poly(ethylene glycol) orthogonally protected: synthesis and characterization. *React. Funct. Polym.* 48, 119–128.
- (9) Zalipsky, S. (1995) Chemistry of poly(ethylene glycol) conjugates with biologically active molecules. *Adv. Drug Delivery Rev.* 16, 157–182.
- (10) Tarasow, T. M., Tinnermeier, D., and Zyzniewski, C. (1997) Characterization of oligodeoxyribonucleotide-poly(ethylene glycol) conjugates by electrospray mass spectrometry. *Bioconj. Chem.* 8, 89–93.
- (11) Jäschke, A., Fürste, J. P., Nordhoff, E., Hillenkamp, F., Cech, D., and Erdmann, V. A. (1994) Synthesis and properties of oligodeoxyribonucleotide-poly(ethylene glycol) conjugates. *Nucleic Acids Res.* 22, 4810–4017.
- (12) Wlotzka, B., Leva, S., Eschgfäller, B., Burmeister, J., Kleinjung, F., Kaduk, C., Muhn, P., Hess-Stumpp, H., and Klusmann, S. (2002) In vivo properties of an anti\_GnRG Spiegelmer: an example of an oligonucleotide-based therapeutic substance class. *Proc. Natl. Acad. Sci. U.S.A.* 99, 8899–8902.
- (13) Bonora, G. M., Rossin, R., Zaramella, S., Cole, D. L., and Ravikumar, V. T. (2000) A liquid-phase process suitable for large-scale synthesis of phosphorothioate oligonucleotides. *Org. Process Res. Dev.* 4, 225–231.
- (14) Cogoi, S., Ballico, M., Bonora, G. M., Quadrifoglio, F., and Xodo, L. E. (2003) Inhibition of Ki-ras gene by a triple helix-forming oligonucleotide conjugated to high-molecular weight poly(ethylene glycol) in carcinoma pancreatic cells, submitted for publication.

BC034020C

# Activated Clearance of a Biotinylated Macromolecular MRI Contrast Agent from the Blood Pool Using an Avidin Chase

Hisataka Kobayashi,<sup>†,\*</sup> Satomi Kawamoto,<sup>‡</sup> Robert A. Star,<sup>||</sup> Thomas A. Waldmann,<sup>†</sup> Martin W. Brechbiel,<sup>§</sup> and Peter L. Choyke<sup>⊥</sup>

Metabolism Branch, Center for Cancer Research, National Cancer Institute, National Institutes of Health, Bethesda, Maryland 20892, Department of Radiology, School of Medicine, Johns Hopkins University, Baltimore, Maryland 21287, Radioimmune & Inorganic Chemistry Section, Radiation Oncology Branch, National Cancer Institute, National Institutes of Health, Bethesda, Maryland 20892, Renal Diagnostics and Therapeutics Unit, National Institutes of Diabetes and Digestive and Kidney Diseases, National Institutes of Health, Bethesda, Maryland 20892, and Diagnostic Radiology Department, Clinical Center, National Institutes of Health, Bethesda, Maryland 20892. Received April 28, 2003; Revised Manuscript Received June 18, 2003

The enhancement characteristics of a contrast agent are dependent on its pharmacokinetics within the body. In the case of macromolecular contrast agents, prolonged enhancement of the blood pool is seen after the first dose, limiting opportunities for repeated injection in the same session. If the enhancement within the blood pool could be intentionally switched off, the macromolecular contrast agents could be used both to define blood volume and vessel permeability, properties that could be useful in studying angiogenesis. In the current study, the avidin–biotin system was coupled to a dendrimer-based macromolecular MRI contrast agent to switch enhancement from the blood pool to the liver. Because avidin causes rapid trapping of the contrast agent in the liver, the blood pool cleared within 2 min of the injection of avidin. This system can be applied to all dendrimer-based macromolecular MRI contrast agents to investigate blood volume and vascular permeability. Moreover, it permits the repeated injection of the contrast agent and the “avidin switch” during a single MR experiment.

## INTRODUCTION

The enhancement characteristics of a contrast agent are dependent on its pharmacokinetics. The blood pool macromolecular contrast agents remain within the circulation during the acquisition of vascular MR images (1, 2). Macromolecular MRI contrast agents can be used to analyze blood volume, vascular permeability, and other characteristics of tumor angiogenesis. However, it can be difficult to differentiate the contribution of each parameter to the signal intensity within a tumor (3–5). A significant limitation of macromolecular agents is that their clearance is slow, preventing repeated measurements within the same MRI session (6). This is especially limiting when performing MRI before and soon after angiogenic inhibitor therapy to detect early changes in tumor vessels. Therefore, if the enhancement in the vascular structures could be intentionally “switched off” or cleared from the blood pool, the macromolecular contrast agents could be applied more widely to the investigation of tumor angiogenesis.

Avidin “chase”, which was developed by us to improve the pharmacokinetics of monoclonal antibody cancer

therapy, is a method that can be used to clear macromolecules quickly from the circulation by increasing their uptake in the liver (7, 8). Avidin “chase” was also used as an essential step of the three-step method for cancer radioimmunotherapy (9–11). Dafni et al. has recently reported the application of an avidin “chase” to a macromolecular albumin-based MRI contrast agent to analyze the extravascular leakage from the tumor vessels (5). In the current study, we synthesized a dendrimer-based blood pool macromolecular MRI contrast agent, which contains 5 biotins and 210 gadolinium ions. We then used an avidin “chase” to clear the blood pool of the agent. We evaluated its pharmacokinetics and the effects of the avidin “chase” by dynamic MRI.

## EXPERIMENTAL PROCEDURES

**PAMAM Dendrimer.** A generation-6 PAMAM dendrimer (G6) (Dendritech, Inc., Midland, MI) with an ethylenediamine core, 256 primary terminal amino groups, and a molecular weight of 58 048 Da was used in the current study (12).

**Preparation of the Biotinylated Contrast Agent.** Four mg/mL of G6 (170 nmol) was dissolved in PBS, pH 7.4, and mixed with 10 mg/mL solution of 1.7 mmol of sulfosuccinimidyl-6-(biotinamide) hexanoate (Bt) (NHS-LC-biotin, MW = 340 Da; Pierce Chemical Co., Rockford, IL) in DMSO at a molar ratio of 1:10, at room temperature for 30 min. The mixture was applied to a diafiltration membrane (Centricon 30, Amicon, Inc., Beverly, MA) to remove unbound Bt as well as to change the buffer to 0.1 M phosphate buffer, pH 9. After purification, a small aliquot of biotinylated G6 (Bt-G6) was examined using a

\* To whom correspondence should be addressed. Tel.: 1–301-435-8344. Fax: 301-496-9956. E-mail: kobayash@mail.nih.gov.

<sup>†</sup> Metabolism Branch, National Cancer Institute.

<sup>‡</sup> Johns Hopkins University.

<sup>§</sup> Radiation Oncology Branch, National Cancer Institute.

<sup>||</sup> National Institutes of Diabetes and Digestive and Kidney Diseases.

<sup>⊥</sup> Diagnostic Radiology Department, National Institutes of Health.



modified HABA assay, which was previously described in detail elsewhere (13, 14). In brief, the 2-(4'-hydroxy-azobenzene)benzoic acid (HABA; Pierce Chemical Co., Rockford, IL) reagent was prepared according to the manufacturer's instructions by adding 10 mg of avidin and 600  $\mu$ L of 10 mM HABA to 19.4 mL of PBS. One hundred microliters of serially diluted Bt-G6 solutions was added to 900  $\mu$ L of the avidin-HABA solutions. Then, the absorbance was measured at 500 nm. Approximately 4.8 biotin molecules were determined to be conjugated to each G6 molecule on the average.

The biotinylated G6 was concentrated to  $\sim$ 5 mg/mL and reacted with a 256-fold molar excess of 2-(*p*-isothiocyanatobenzyl)-6-methyl-diethylenetriaminepentaacetic acid (1B4M, MW = 555 Da) (44  $\mu$ mol) at 40  $^{\circ}$ C. The reaction was maintained at pH 9 with 1 M NaOH for 24 h. An additional equal amount of 1B4M was added to the mixture after 24 h as a solid, and the pH was maintained as before for another 24 h. The resulting preparation was purified by diafiltration using a Centricon 30 (Amicon Co., Beverly, MA). Approximately  $97 \pm 2\%$  of the amine groups on the surface of the G6 dendrimer reacted with the 1B4M, as determined by  $^{153}\text{Gd}$  (NEN DuPont, Boston, MA) labeling of the reacted samples (2,15). In brief,  $\sim$ 500 000 cpm ( $\sim$ 0.4 pmol) of  $^{153}\text{Gd}$  citrate were added to  $\sim$ 40  $\mu$ g/10  $\mu$ L ( $\sim$ 160 pmol) of the reaction mixture before diafiltration and incubated in 0.2 M acetate buffer for 15 min at room temperature. Then, the fractions bound to the conjugates and free 1B4M were separated using a PD-10 column (Pharmacia) and counted, after which the numbers of 1B4M chelates bound to the conjugate were calculated by the quantification of the radioactivity in the fraction bound relative to that of the conjugates.

Approximately 3 mg of biotinylated G6 dendrimer-1B4M conjugate [ $\text{Bt}_5\text{-G6-(1B4M-Gd)}_{251}$ ] (containing 4  $\mu$ mol 1B4M) were mixed with 8  $\mu$ mol of nonradioactive Gd(III) citrate in 0.3 M citrate buffer for 2 h at 40  $^{\circ}$ C. The excess Gd in each preparation was removed by diafiltration using a Centricon 30 (Amicon Co.) while simultaneously changing the buffer to 0.05 M PBS. The purified samples were diluted to 0.5 mL with 0.05 M PBS and passed through a 0.22  $\mu$ m filter (Amicon Co.), and 100  $\mu$ L of this solution was used as the MRI contrast agent for each mouse. Using a replacement assay involving  $^{153}\text{Gd}$ , we determined that 85% of the 1B4M (209.5 ions/molecule) on the dendrimer-1B4M conjugates were indeed chelating Gd(III) atoms (2). In brief, approximately 300 000 cpm of  $^{153}\text{Gd}$  was added with 0.1  $\mu$ mol of nonradioactive Gd(III) to 5  $\mu$ L of the injected samples and incubated in 0.5 M citrate buffer for 2 h at 40  $^{\circ}$ C, after which the bound and unbound fractions were separated using a PD-10 column (Pharmacia).

**Quality Control Studies. Molecular Purity.** The purity of the contrast agent was analyzed by a size-exclusion HPLC equipped with a TSK G2000 SW column (TosoHaas, Philadelphia, PA; 0.066 M PBS; pH 7.2; 1 mL/min) using a UV detector at 280 nm absorbance.

**Binding Ability to Avidin.** The binding ability to avidin-sephalose gel (Pierce Chemical Co.) of  $^{153}\text{Gd}$ -labeled  $\text{Bt}_5\text{-G6-(1B4M-Gd)}_{251}$  (MW = 240 kDa) was examined (8, 16). In brief, 3 ng/0.1  $\mu$ Ci of  $\text{Bt}_5\text{-G6-(1B4M-Gd)}_{251}$  was incubated with 0.5 mL of avidin-sephalose gel for 15 min at room temperature. Then the gel fraction was washed and separated from the supernatant by a paper filter. The radioactivity of both fractions was counted with a  $\gamma$ -counter (Perkin-Elmer, Boston, MA).

**$R_1$  Relaxivity.** The  $R_1$  relaxivity of the  $\text{Bt}_5\text{-G6-(1B4M-Gd)}_{251}$  contrast agent was calculated from the T1 data

obtained from all samples of 5, 10, and 20  $\mu$ molGd/mL and PBS and then compared with that of the nonbiotinylated  $\text{G6-(1B4M-Gd)}_{256}$  contrast agent. We used an inversion recovery spin-echo imaging sequence with various TI 50, 100, 200, and 400 ms and TR/TE: 6000/15 ms, using a 1.5-Tesla superconductive magnet unit (Signa LX, General Electric Medical System, Milwaukee, WI) with a high-resolution wrist coil (General Electric Medical System). All images were obtained in three slices with an 8 cm field of view and a 2 mm slice thickness,  $256 \times 256$  matrix, and two excitations were averaged. The best slice was selected, and the data obtained from 12 mm<sup>2</sup> areas at the center of the tubes were averaged and used to calculate  $R_1$  values.

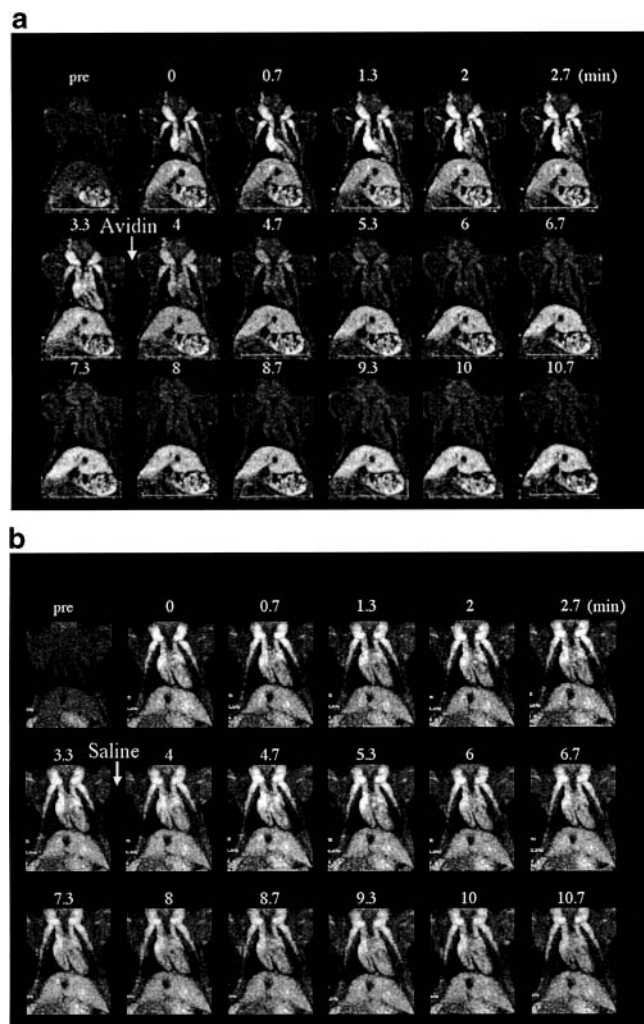
**Dynamic MRI Study.** To evaluate the pharmacokinetics and effects of the avidin "chase", serial dynamic MR images of normal mice ( $n = 9$ ) were obtained before and after injection of 0.03 mmolGd/kg (30% of clinical dose) of  $\text{Bt}_5\text{-G6-(1B4M-Gd)}_{251}$  followed by injection with 100  $\mu$ L of either saline containing 400  $\mu$ g of avidin ( $n = 5$ ) or PBS ( $n = 4$ ) at 4 min (six frames) postinjection of the contrast agent. A 1.5-Tesla superconductive magnet unit (Signa LX, Milwaukee, WI) and a commercially available high-resolution wrist coil with a custom mouse holder were employed for image acquisition. The mice were anesthetized with 1.15 mg of sodium pentobarbital (Dainabot, Osaka, Japan) and placed in the center of the coils. The 3D-fast-spoiled gradient echo technique (TR/TE 10/4.1 ms; TI 29 ms; flip angle 30 $^{\circ}$ ; scan time 35 s; frequency encoding  $\times$  phase encoding steps  $256 \times 192$ ; two excitations; slice encoding steps 14; with fat-suppression technique and serial 3D data acquisition) was used to acquire 20 images every 40 s from 0 (immediately after injection) to 12.3 min after injection of the contrast agents for all mice studied. The coronal images were reconstructed with 2-mm thick sections with 1-mm overlap. The field of view was  $8 \times 4$  cm, and the size of each voxel was  $0.32 \times 0.42 \times 2$  mm<sup>3</sup>. The serial dynamic data were analyzed using an Advantage Windows version 3 (GE). In addition, to evaluate the whole body pharmacokinetics, whole body 3D-MR angiograms were reconstructed with the maximum intensity projection (MIP) method.

## RESULTS

**Quality Control Studies.** The elution time of the  $\text{Bt}_5\text{-G6-(1B4M-Gd)}_{251}$  contrast agent (17.2 min) was similar to that of nonbiotinylated  $\text{G6-(1B4M-Gd)}_{256}$  contrast agent (17.1 min). The chemical purity of  $\text{Bt}_5\text{-G6-(1B4M-Gd)}_{251}$  was 99%. Ninety one percent of the radioactivity of  $^{153}\text{Gd}$ -labeled  $\text{Bt}_5\text{-G6-(1B4M-Gd)}_{251}$  sample was bound to the avidin-sephalose gel. The  $R_1$  relaxivity of  $\text{Bt}_5\text{-G6-(1B4M-Gd)}_{251}$  ( $33 \text{ mM}^{-1} \text{ s}^{-1}$ ) was the same as that of  $\text{G6-(1B4M-Gd)}_{256}$  contrast agent ( $33 \text{ mM}^{-1} \text{ s}^{-1}$ ).

**Dynamic MRI Study.** The time intensity curves in the inferior vena cava and the liver obtained by dynamic MRI of mice injected with  $\text{Bt}_5\text{-G6-(1B4M-Gd)}_{251}$  contrast agent followed by the injection of PBS without avidin demonstrate slow clearance from the blood pool and rapid enhancement followed by a steady state in the liver (Figure 1b and 2). This pattern is similar to that previously reported with  $\text{G6-(1B4M-Gd)}_{256}$  agent (17). The only difference between these molecules is the presence of an additional five biotin molecules that did not appear to affect the pharmacokinetic properties of the agent.

The time intensity curves of the inferior vena cava and the liver of mice injected with  $\text{Bt}_5\text{-G6-(1B4M-Gd)}_{251}$  contrast agent followed by an avidin "chase" are shown

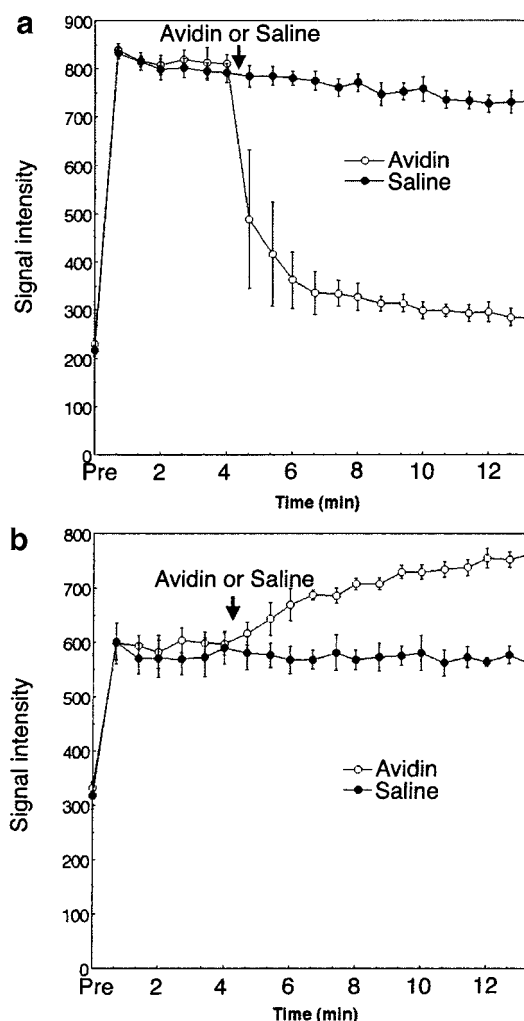


**Figure 1.** 2D-dynamic chest and abdominal MRIs of mice with avidin (a) and saline (b) injection at 4 min postinjection with  $\text{Bt}_5\text{-G6-(1B4M-Gd)}_{251}$  contrast agent.

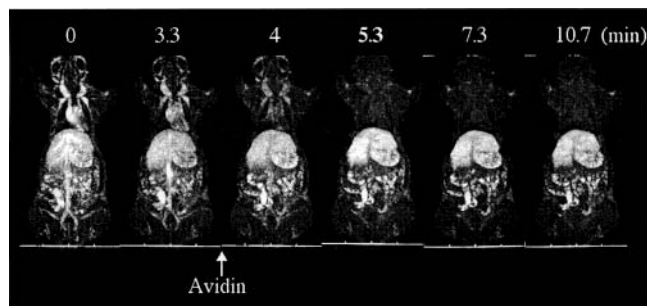
in Figure 2; the signal intensity in the vessels quickly decreased within 2 min of the avidin “chase” to nearly the preinjection level (Figure 1a and 2a). The signal intensity in the liver gradually increased after injection with avidin (Figure 1a and 2b). Therefore, the vascular enhancement faded out within 2 min after injection with avidin while the signal intensity of the liver increased after injection of avidin as shown on serial whole-body MRIs (Figure 3).

#### DISCUSSION

The avidin “chase” system is a simple but efficient system to quickly clear biotinylated macromolecule from the circulation to the liver (8). The avidin “chase” system has been reported to improve the pharmacokinetics of radiolabeled monoclonal antibodies for the radioimmunotherapy for cancer (8, 18, 19). Briefly, circulating biotinylated macromolecules such as antibodies are quickly cleared from the blood pool within 20 min after injection of avidin and accumulate in the liver internalizing into either hepatocytes or the reticuloendothelial system (8, 20). Although the intravascular component and avidin itself were cleared quickly, the extravascular component was cleared much more slowly, that is, over a period of 4–6 h (20–22). Therefore, this method potentially differentiates the vascular component (blood volume) from the extravascular component (permeability)



**Figure 2.** Time intensity curves of the inferior vena cava (a) and the liver (b) in mice with avidin ( $n = 5$ ) or saline ( $n = 4$ ) injections at 4 min postinjection with  $\text{Bt}_5\text{-G6-(1B4M-Gd)}_{251}$  contrast agent.



**Figure 3.** Serial whole body 3D-MRIs (maximum intensity projection) of mice with avidin injection at 4 min postinjection with  $\text{Bt}_5\text{-G6-(1B4M-Gd)}_{251}$  contrast agent showed that the enhancement disappeared not only from the central circulation but also from the peripheral blood vessels within 2 min postinjection of an avidin chase.

if the total time to clear the blood pool could be kept to a minimum.

In the current study, the avidin “chase” system was successfully applied to a dendrimer-based macromolecular MRI contrast agent. The pharmacokinetics of this agent were evaluated specifically in regards to the rate of disappearance of the agent from the circulation by dynamic MRI. This clearing process of the contrast agent was revealed to be much quicker than we expected from the results of the conventional pharmacokinetic studies



(8) because the conventional methods including scintigraphy had technical difficulties to serially monitor the drug kinetics at every single minute.

The advantage of dendrimer-based macromolecular MRI contrast agents over an albumin-based agent is that molecules of a specific size could be made with chemical conformity. That enables us to use a molecule of an appropriate size for a specific purpose (22). The rapid clearance of the contrast agent from the blood pool may permit the nearly simultaneous assessment of both the blood volume and vessel permeability and allow repeated injections during a single MR session in animal models.

In conclusion, the successful synthesis and application of an avidin chase system to dendrimer-based macromolecular MRI contrast agents enabled us to rapidly clear blood pool contrast agents from the circulation. This system might be a good method to analyze the characteristics of angiogenic vessels especially before and after therapy. In addition to evaluating tumor angiogenesis and response to therapy this contrast agent system may be useful for monitoring the stimulation of angiogenesis in ischemic disease and demonstrating the effects of vascular disease in organs such as the kidney.

#### LITERATURE CITED

- Ogan, M. D., Schmiedl, U., Moseley, M. E., Grodd, W., Paajanen, H., and Brasch, R. C. (1987) Albumin labeled with Gd-DTPA. An intravascular contrast-enhancing agent for magnetic resonance blood pool imaging: preparation and characterization. *Invest. Radiol.* **22**, 665–671.
- Kobayashi, H., Sato, N., Hiraga, A., Saga, T., Nakamoto, Y., Ueda, H., Konishi, J., Togashi, K., and Brechbiel, M. W. (2001) 3D-micro-MR angiography of mice using macromolecular MR contrast agents with polyamidoamine dendrimer core with references to their pharmacokinetic properties. *Magn. Reson. Med.* **45**, 454–460.
- Kobayashi, H., Sato, N., Kawamoto, S., Saga, T., Hiraga, A., Ishimori, T., Konishi, J., Togashi, K., and Brechbiel, M. W. (2001) 3D MR angiography of intratumoral vasculature using a novel macromolecular MR contrast agent. *Magn. Reson. Med.* **46**, 579–585.
- Shirakawa, K., Kobayashi, H., Heike, Y., Kawamoto, S., Brechbiel, M. W., Kasumi, F., Iwanaga, T., Konishi, F., Terada, M., and Wakasugi, H. (2002) Hemodynamics in vasculogenic mimicry and angiogenesis of inflammatory breast cancer xenograft. *Cancer Res.* **62**, 560–566.
- Dafni, H., Israely, T., Bhujwalla, Z. M., Benjamin, L. E., and Neeman, M. (2002) Overexpression of vascular endothelial growth factor 165 drives peritumor interstitial convection and induces lymphatic drain: magnetic resonance imaging, confocal microscopy, and histological tracking of triple-labeled albumin. *Cancer Res.* **62**, 6731–6739.
- Kobayashi, H., Kawamoto, S., Saga, T., Sato, N., Hiraga, A., Konishi, J., Togashi, K., and Brechbiel, M. W. (2001) Micro-MR angiography of normal and intratumoral vessels in mice using dedicated intravascular MR contrast agents with high generation of polyamidoamine dendrimer core: reference to pharmacokinetic properties of dendrimer-based MR contrast agents. *J. Magn. Reson. Imaging* **14**, 705–713.
- Sinitsyn, V. V., Mamontova, A. G., Checkneva, Y. Y., Shnyra, A. A., and Domogatsky, S. P. (1989) Rapid blood clearance of biotinylated IgG after infusion of avidin. *J. Nucl. Med.* **30**, 66–69.
- Kobayashi, H., Sakahara, H., Hosono, M., Yao, Z. S., Toyama, S., Endo, K., and Konishi, J. (1994) Improved clearance of radiolabeled biotinylated monoclonal antibody following the infusion of avidin as a chase without decreased accumulation in the target tumor. *J. Nucl. Med.* **35**, 1677–1684.
- Paganelli, G., Magnani, P., Zito, F., Villa, E., Sudati, F., Lopalco, L., Rossetti, C., Malcovati, M., Chiolerio, F., Seccamani, E., Siccardi, A. G., and Fazio, F. (1991) Three-step monoclonal antibody tumor targeting in carcinoembryonic antigen-positive patients. *Cancer Res.* **51**, 5960–5966.
- Paganelli, G., Magnani, P., and Fazio, F. (1993) Pretargeting of carcinomas with the avidin–biotin system. *Int. J. Biol. Markers* **8**, 155–159.
- Chinol, M., Casalini, P., Maggiolo, M., Canevari, S., Omodeo, E. S., Caliceti, P., Veronese, F. M., Cremonesi, M., Chiolerio, F., Nardone, E., Siccardi, A. G., and Paganelli, G. (1998) Biochemical modifications of avidin improve pharmacokinetics and biodistribution, and reduce immunogenicity. *Br. J. Cancer* **78**, 189–197.
- Tomalia, D. A., Naylor, A. M., and Goddard, W. A., III (1990) Starburst dendrimers: Molecular-level control of size, shape, surface chemistry, topology, and flexibility from atoms to macroscopic matter. *Angew. Chem., Int. Ed. Engl.* **29**, 138–175.
- Green, N. M. (1975) Avidin. *Adv. Protein Chem.* **29**, 85–133.
- Kobayashi, H., Sun, B. F., Yoo, T. M., Le, N., Kim, M. K., Paik, C. H., Pastan, I., Waldmann, T. A., and Carrasquillo, J. A. (1999) Methods to avoid adverse effect of circulating antigen on biodistribution of  $^{125}\text{I}$ -labeled antiTac dsFv: pre-injection of intact antibody versus clearance of antigen with avidin-biotin system. *J. Nucl. Med.* **40**, 1381–1391.
- Kobayashi, H., Sakahara, H., Hosono, M., Shirato, M., Kondo, S., Miyatake, S., Kikuchi, H., Namba, Y., Endo, K., and Konishi, J. (1994) Scintigraphic detection of neural-cell-derived small-cell lung cancer using glioma-specific antibody. *J. Cancer Res. Clin. Oncol.* **120**, 259–262.
- Kobayashi, H., Kawamoto, S., Saga, T., Sato, N., Ishimori, T., Konishi, J., Ono, K., Togashi, K., and Brechbiel, M. W. (2001) Avidin–dendrimer–(1B4M-Gd)(254): a tumor-targeting therapeutic agent for gadolinium neutron capture therapy of intraperitoneal disseminated tumor which can be monitored by MRI. *Bioconjugate Chem.* **12**, 587–593.
- Kobayashi, H., Sato, N., Kawamoto, S., Saga, T., Hiraga, A., Haque, T. L., Ishimori, T., Konishi, J., Togashi, K., and Brechbiel, M. W. (2001) Comparison of the macromolecular MR contrast agents with ethylenediamine-core versus ammonia-core generation-6 polyamidoamine dendrimer. *Bioconjugate Chem.* **12**, 100–107.
- Paganelli, G., Stella, M., Zito, F., Magnani, P., De Nardi, P., Mangili, F., Baratti, D., Veglia, F., Di Carlo, V., Siccardi, A. G., and Fazio, F. (1994) Radioimmunoguided surgery using iodine-125-labeled biotinylated monoclonal antibodies and cold avidin. *J. Nucl. Med.* **35**, 1970–1975.
- Paganelli, G., Magnani, P., Zito, F., Lucignani, G., Sudati, F., Truci, G., Motti, E., Terreni, M., Pollo, B., Giovanelli, M., Canal, N., Scotti, G., Comi, G., Koch, P., Maecke, H. R., and Fazio, F. (1994) Pre-targeted immunodetection in glioma patients: tumour localization and single-photon emission tomography imaging of  $[^{99\text{m}}\text{Tc}]\text{PnAO}$ -biotin. *Eur. J. Nucl. Med.* **21**, 314–321.
- Kobayashi, H., Sakahara, H., Endo, K., Hosono, M., Yao, Z. S., Toyama, S., and Konishi, J. (1995) Comparison of the chase effects of avidin, streptavidin, neutravidin, and avidin-ferritin on a radiolabeled biotinylated antitumour monoclonal antibody. *Jpn. J. Cancer Res.* **86**, 310–314.
- Kobayashi, H., Sakahara, H., Endo, K., Yao, Z. S., Toyama, S., and Konishi, J. (1995) Repeating the avidin chase markedly improved the biodistribution of radiolabelled biotinylated antibodies and promoted the excretion of additional background radioactivity. *Eur. J. Cancer* **31A**, 1689–1696.
- Kobayashi, H., Sakahara, H., Endo, K., Yao, Z. S., and Konishi, J. (1996) Inflammation-seeking scintigraphy with radiolabeled biotinylated polyclonal IgG followed by the injection of avidin chase. *Nucl. Med. Biol.* **23**, 29–32.
- Kobayashi, H., and Brechbiel, M. W. (2003) Gadolinium-based macromolecular MRI contrast agents. *Mol. Imaging* **2**, 1–10.



# High Efficiency Synthesis of a Bioconjugatable Near-Infrared Fluorochrome

Wellington Pham, Wen-Fu Lai, Ralph Weissleder, and Ching-Hsuan Tung\*

Center for Molecular Imaging Research, Massachusetts General Hospital, Harvard Medical School, Charlestown, Massachusetts 02129. Received May 5, 2003; Revised Manuscript Received August 1, 2003

Near-infrared (NIR) fluorochromes have become important reporter molecules for many biomedical applications, including FACS sorting, confocal microscopy, and more recently in vivo imaging. While the structures of several stable 800 nm fluorochromes have been published, their synthesis is often complex and there are difficulties in rapidly purifying these compounds in large quantities. Here we report on the synthesis of NIR820,  $\text{ex/em} = 790/820$ , with excellent physicochemical properties. Importantly, NIR820 is conveniently synthesized in a three-step reaction and can be purified by flash column chromatography rather than by HPLC. NIR820 is chemically stable and can be directly coupled to peptides during the solid-phase synthesis. In addition, NIR820 is also suitable for conjugation to proteins and other affinity molecules in aqueous buffer.

## INTRODUCTION

Fluorescence imaging is widely used in microscopy, and recently the technology has been extended to in vivo imaging of biological targets and disease (1). Unlike microscopy, in vivo imaging is preferably performed in the NIR region (700–900 nm) because of more efficient tissue penetration of photons (2) and minimal autofluorescence (3) in this region. A number of different NIR fluorochromes have been described with variable stabilities, quantum efficiencies, and ease of synthesis. Typically, cyanine dyes contain two heterocyclic rings linked by a polymethine bridge which extends the unsaturated system from one end of an aromatic ring to the other. (4–6). NIR fluorescence properties depend on the structure of the terminal aromatic rings (7) but also on the length of the polymethine bridge. Each introduction of an additional  $\text{CH}=\text{CH}$  bond in the latter can cause red shifts by about 100 nm, however, at the expense of chemical stability.

Ideal NIR fluorochromes for in vivo imaging will ultimately have to be produced in large batches because of the large amounts necessary for in vivo imaging (about 50 nmol/kg bodyweight). Preferred compounds have to be exceedingly stable for regulatory purposes and/or to directly use NIRF in solid-phase peptide synthesis under harsh conditions. Furthermore, ideal compounds should have high quantum yields, narrow excitation and emission peaks, aqueous solubility, low albumin binding, and a functional group for bioconjugation (8). Here we describe an efficient, optimized synthesis of a cyclohepta methine fluorochrome, NIR820. The fluorochrome was conveniently prepared using a three-step reaction and purified by a flash column chromatography at gram quantities rather than requiring HPLC. Due to its excellent chemical stability, NIR820 was suitable for solid-phase chemistry in DMF, and protein-labeling in aqueous phase.

## EXPERIMENTAL PROCEDURES

**Apparatus and Reagents.** Unless otherwise stated, reagents and solvents were obtained from commercial sources without further purification. Thin layer chromatography (TLC) was obtained from Polygram SIL G/UV<sub>254</sub> plates (Bodman, Aston, PA) using reagent-graded solvents. Flash column chromatography was performed on silica gel 60, (230–400 mesh, Bodman). All moisture or air-sensitive reactions were carried out under a static argon atmosphere. Nuclear magnetic resonance (NMR) spectra were obtained with a Varian 400 MHz in  $\text{CD}_3\text{OD}$  with TMS as a standard. Chemical shifts are reported in parts per million downfield from tetramethylsilane, and coupling constants are reported in hertz. High performance liquid chromatography (HPLC) was performed on the Hitachi D-7000 incorporated with Diode Array Detector L-7455. ES and MALDI-TOF mass spectra were determined by Harvard Mass Spectrometry Facility (Cambridge, MA) and Tufts Core Mass Spectrometry Facility (Boston, MA), respectively. Absorption and emission spectra were determined using Hitachi U-3000 Spectrophotometer and F-4500 Fluorescence Spectrophotometer, respectively. The relative fluorescence quantum yield was determined using the model:

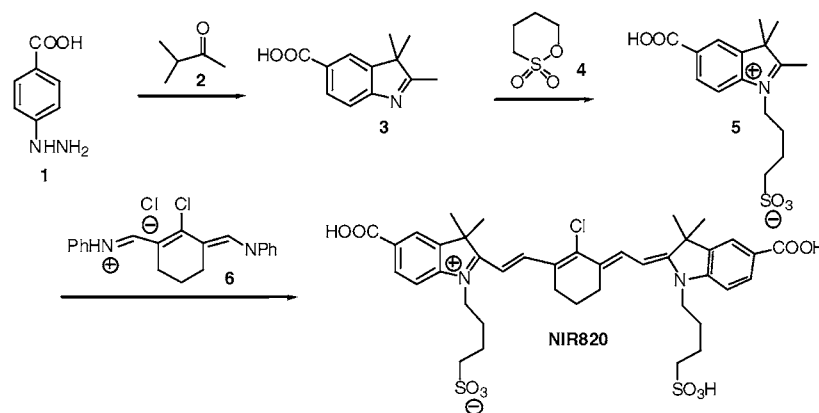
$$\phi_{\text{F}(x)} = (A_{\text{s}}/A_{\text{x}})(F_{\text{x}}/F_{\text{s}})(n_{\text{x}}/n_{\text{s}})^2 \phi_{\text{F}(s)}$$

where  $\phi_{\text{F}}$  is the fluorescence quantum yield,  $A$  is the absorbance,  $F$  is the area under the emission curve, and  $n$  is the refractive index of the solvents using in measurement (9). The subscript s and x represent for standard and to the unknown, respectively.

**2,3,3-Trimethyl-3*H*-indole-5-carboxylic Acid (3)** (10). Glacial acetic acid (15 mL) was added to a mixture of 4-hydrazinobenzoic acid **1** (1.0 g, 6.6 mmol, Aldrich, Milwaukee, WI), methyl isopropyl ketone **2** (1.1 mL, 9.9 mmol, Aldrich), and sodium acetate (1.1 g, 13.2 mmol) in a round-bottomed flask fitted with a condenser. The brown suspension was refluxed for 8 h, and the solvent was removed under reduced pressure with a rotavapor. The residue was redissolved into a clear solution using water and methanol (9:1). Undissolved material was

\* To whom correspondence should be addressed: Ching H. Tung, Ph.D., Center for Molecular Imaging Research, Massachusetts General Hospital, 149 13th St., Rm. 5406, Charlestown, MA 02129, (Tel): (617) 726–5779, (Fax): (617) 726–5708, e-mail: tung@helix.mgh.harvard.edu.

Scheme 1. Synthesis of NIR820



filtered off, the filtrate was allowed to stand at room temperature, and the crystal **3** (0.94 g, 70%) was collected by filtration.  $^1\text{H}$  NMR (400 MHz,  $\text{CD}_3\text{OD}$ )  $\delta$  8.0 (m, 2H, Ar H), 7.50 (d,  $J$  = 8.8 Hz, 1H, Ar H), 2.35 (s, 3H,  $\text{CH}_3$ ), 1.37 (s, 6H,  $2\text{CH}_3$ ).

**NIR820 Synthesis.** 1,4-Butane sultone **4** (3.8 mmol, 383.7  $\mu\text{L}$ , Aldrich) followed by anhydrous toluene (15 mL) were added to a flamed-dried flask containing indole **3** (500 mg, 2.5 mmol), and the suspension was refluxed for 18 h. The precipitate intermediate **5** was collected by filtration and recrystallized with methanol and ether to provide a pink powder (647 mg, 76%).

A suspension of pink powder intermediate **5** (100 mg, 0.29 mmol), *N*-[(3-(anilino-methylene)-2-chloro-1-cyclohexen-1-yl)methylene]aniline monohydrochloride **6** (58 mg, 0.16 mmol, Aldrich), and sodium acetate (55.1 mg, 0.67 mmol) in absolute ethanol (20 mL) was refluxed for 2 h. The mixture was cooled to room temperature, and the solvent was removed using a rotavapor. Chromatography from 8:2 to 1:9 of methylene chloride:methanol afforded 87.2 mg (67%) of green solid material of NIR820:  $R_f$  = 0.7 (1:9  $\text{CH}_2\text{Cl}_2/\text{MeOH}$ );  $^1\text{H}$  NMR (400 MHz,  $\text{CD}_3\text{OD}$ )  $\delta$  8.47 (d,  $J$  = 14.0 Hz, 2H,  $\text{CH}=\text{N}$ ), 8.08 (m, 4H, Ar H), 7.36 (d,  $J$  = 8.8 Hz, 2H, Ar H), 6.39 (d,  $J$  = 14.0 Hz, 2H,  $\text{CH}=\text{N}$ ), 4.23 (br t, 4H,  $\text{CH}_2-\text{N}=\text{N}$ ), 2.91 (t,  $J$  = 6.8 Hz, 4H,  $\text{CH}_2-\text{SO}_3$ ), 2.78 (br, t, 4H, cyclohexene- $\text{CH}_2$ ), 2.02 (br, m, 10H,  $\text{CH}_2-\text{CH}_2$ , cyclohexene- $\text{CH}_2$ ), 1.80 (s, 12H,  $\text{CH}_3$ ). MS (ES) calcd ( $\text{M}^+$ ) ( $\text{C}_{40}\text{H}_{47}\text{ClN}_2\text{O}_{10}\text{S}_2$ ) 815.39, found 815.30.

**NIR820-NHS.** Diisopropyl carbodiimide (37.6  $\mu\text{L}$ , 0.24 mmol) was added dropwise to a green solution containing NIR820 (62.5 mg, 0.08 mmol) and *N*-hydroxysuccinimide (NHS, 36.8 mg, 0.32 mmol) in 0.1 M  $\text{NaH}_2\text{PO}_4$  (1.0 mL). The reaction mixture was stirred in the dark for 5 h, and the mixture was filtered and purified by HPLC to afford the green solid NIR820-NHS (19.7 mg, 27%). MS (ES) calcd. ( $\text{M}^+$ ) ( $\text{C}_{44}\text{H}_{50}\text{ClN}_3\text{O}_{12}\text{S}_2$ ) 912.46, found 912.20.

**NIR-820 Labeled Peptides Synthesis.** A model NIR capped peptide was synthesized directly using an automatic synthesizer (PS3, Rainin, Woburn, MA) and Fmoc chemistry using Rink amide MBHA resin (0.72 mmol/g) and 2-(1*H*-benzotriazole-1-yl)-1,1,3,3-tetramethyluronium hexafluorophosphate (HBTU)/*N*-hydroxybenzotriazole (HOBt) as the activating reagents. The excess of Fmoc-amino acids were incorporated onto resin in a 4:1 ratio. NIR820 (121.5 mg, 0.15 mmol) was first activated with HBTU (57 mg, 0.15 mmol) and HOBt (20.3 mg, 0.15 mmol) in DMF (5 mL) under argon for 2 h and then reacted with the peptide resin overnight. The green resin was filtered and washed with DMF ( $3 \times 10$  mL) and MeOH ( $3 \times 10$  mL) following by treatment with deprotection solution (90:5:3:2 TFA/thioanisole/ethanedithiol/

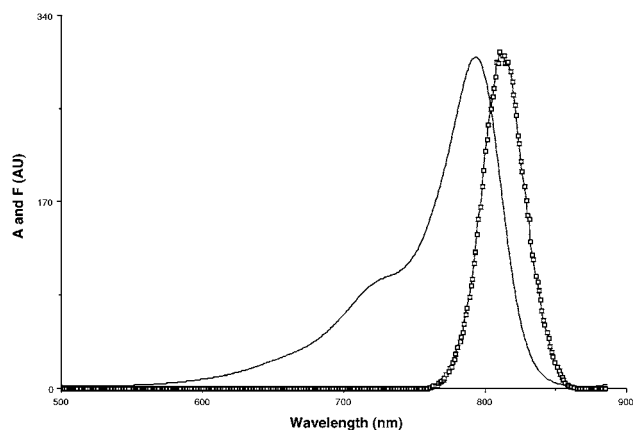
anisole) and purified by C18 reversed-phase HPLC using 0.1% TFA and acetonitrile as elution buffers to afford a fluorescence peptide. MS (MALDI-TOF) calcd ( $\text{M} - \text{H}^+$ ) 1772.57 found 1772.41, UV-vis (PBS)  $\lambda_{\text{ex}}$  = 793 nm,  $\lambda_{\text{em}}$  = 826 nm. The model peptide was NIR820-GVPLSLTMGC, a nonsense motif with no known biological binding partner.

**Protein Conjugation.** The activated NHS ester of NIR820 in DMSO was reacted with human transferrin (Tf, 200  $\mu\text{M}$ ) in PBS buffer (pH = 7.4) for 2 h. The product was purified by sephadex G25 column (18 cm) with PBS as the eluent. The loading efficiency was determined by absorption measurement at 790 nm (extinction coefficient 184 000  $\text{M}^{-1} \text{cm}^{-1}$ ) for the dye and 280 nm for the Tf (extinction coefficient 93 600  $\text{M}^{-1} \text{cm}^{-1}$ ). On average each Tf contains 1.3 NIR820.

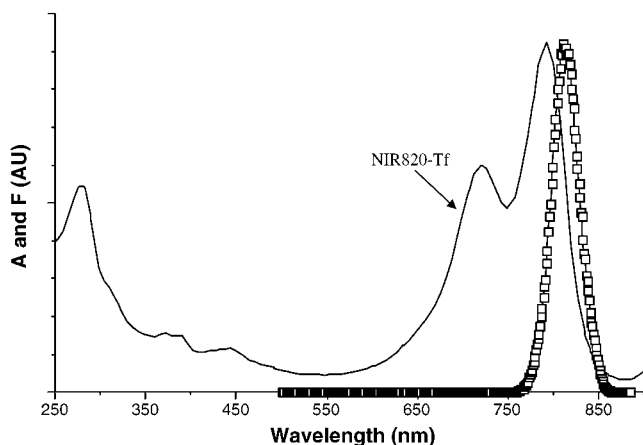
**Cell Lines and Cell Cultures.** Rat 9L gliosarcoma cells (Brain Tumor Research Center, San Francisco, CA) or rat gliosarcoma cells (9L-3.9) stably overexpressing an altered form of the human transferrin receptor (TfR) (11) were grown in Dulbecco's modified Eagle's medium (DMEM, Cellgro, Mediatech, Washington, DC) containing 10% fetal bovine serum (FBS, Cellgro) at 37  $^\circ\text{C}$  in humidified 6% carbon dioxide atmosphere. The cells were grown to 70% confluence on glass cover slips for the uptake experiments. After incubating with NIR820 labeled transferrin (1.0  $\mu\text{M}$ ) for 1 h at 37  $^\circ\text{C}$ , cells were washed three times with PBS and then subjected to fluorescence microscopy (Zeiss, Axiovert). The band-pass excitation filter is 730–750 nm, and the long-pass emission filter is 780 nm. (Omega Optical, Brattleboro, VT). The fluorescent images were digitally captured using a CCD-SPOT RT digital camera and compiled using Adobe Photoshop software (v7.0).

## RESULTS AND DISCUSSION

NIR820 (Scheme 1) was designed to allow simple synthesis and efficient purification avoiding HPLC. We furthermore designed the molecule to fluoresce above 800 nm and be compatible with solid-phase peptide synthesis under harsh conditions. As described previously (4–7), cyanine dyes with four conjugated double bond polymethine bridges fluoresce above 800 nm. However, the chemical stability decreases as the unsaturated bridge chain increases. To improve the chemical stability, a cyclic halogenated polymethine bridge was introduced to replace the less stable linear version (10, 12, 13). Terminal sulfonate moieties were introduced to improve water solubility and enable flash column chromatography. Carboxyl groups were used for subsequent NHS activation.



**Figure 1.** Excitation (790 nm) and emission (820 nm) spectra of NIR820 in methanol.

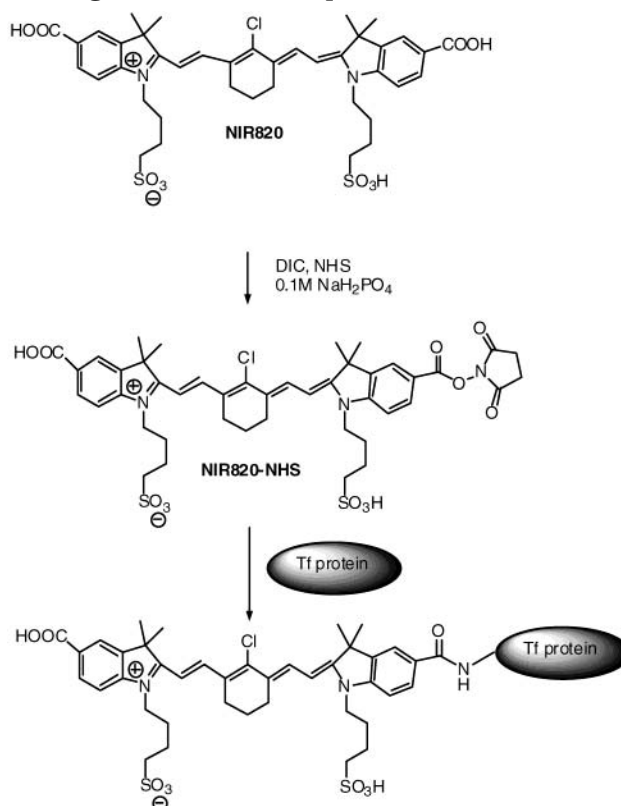


**Figure 2.** The absorption of NIR820-Tf and its emission spectra. All the measurement were performed in PBS, pH = 7.4.

The synthesis of NIR820 was started by reacting commercially available 4-hydrazinobenzoic acid **1** with methyl isopropyl ketone **2** to result in 2,3,3-trimethyl-3*H*-indole-5-carboxylic acid **3** following a published protocol (Scheme 1) (10). The collected compound **3** was then reacted with 1,4-butane sultone **4** in anhydrous toluene, forming a precipitated intermediate **5** which was collected by filtration and recrystallized to provide a pink powder. Refluxing the intermediate **5** with compound **6** in absolute ethanol for 2 h formed the desired product NIR820. The final product was purified using conventional column chromatography at 1-g scale, sufficient material for over 100 patient doses. NIR820 absorbs maximally at 790 nm and emits maximally at 820 nm in methanol (Figure 1) with a molar extinction coefficient of 184000, and a quantum yield of 0.08.

Direct labeling of peptides with NIR fluorochromes during solid-phase synthesis is a favorable approach for synthesizing targeted fluorescent imaging agents. To facilitate direct synthesis, the fluorochrome must be chemically stable under all synthesis and cleavage conditions and be available in sufficiently large quantities. To demonstrate the utility of NIR820 in solid-phase chemistry, we synthesized a model molecule, NIR820-GVPLSLTMGC. The NIR820 fluorochrome was coupled to peptide as an amino acid residue using standard HOBt/HBTU coupling reagent but with extended coupling time. The peptide was then cleaved and deported using 95% TFA. After the purification, the structure of the terminally NIR labeled peptide was confirmed by mass spectrum analysis. NIR820 was compatible with

## Scheme 2. Selective Activation of NIR820 and Labeling of Tf Protein in Aqueous Conditions



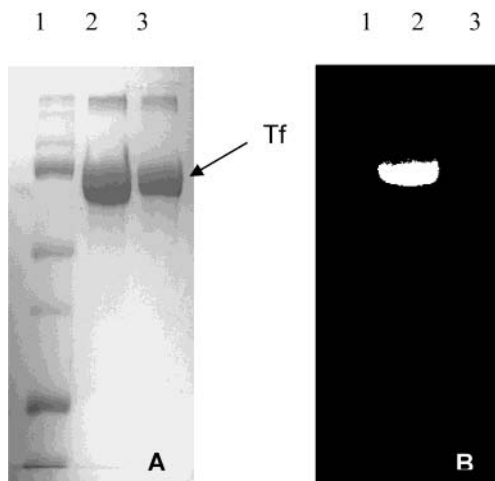
all reaction conditions and retained its excitation and emission with a minor red shift to 793 and 826 nm.

The ability of NIR820 to serve as a generic label was furthermore tested by using proteins. We chose human transferrin (Tf) as a model protein because of the abundance of its known receptors and our prior work in targeting transferrin receptor (11). The human transferrin receptor (TfR) is a transmembrane glycoprotein and is ubiquitously present on most mammalian cells being responsible for cellular acquisition of iron. TfR overexpression is found in many malignant tumors (14, 15), and hence the Tf/TfR system has been proposed for therapeutic and diagnostic targeting. For example, Tf was used to conjugate a diphtheria toxin, CRM107, as a chemotherapeutic reagent to treat brain tumors (16), or with monocrySTALLINE iron oxide MION nanoparticles to detect gene expression using MRI (11, 17).

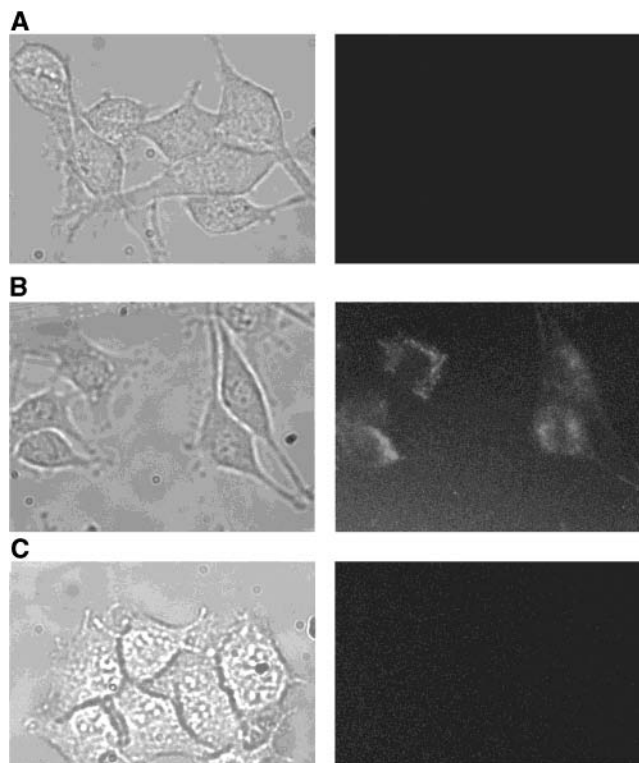
For protein labeling under aqueous conditions, NIR820 was first converted to the NHS activated ester. To avoid inter- or intramolecular cross-linking of the proteins, only one carboxyl group on NIR820 was activated (Scheme 2) by optimizing reaction conditions. The prepared NIR820-NHS was stable in the dark at  $-20^{\circ}\text{C}$  at least for 6 months without any deterioration. The labeling of Tf with NIR820 was carried out in PBS (pH = 8), and the labeled product was isolated using Sephadex size-exclusion column. On average, 1.3 NIR820 molecules were attached to each Tf under the chosen labeling conditions. The absorbance and emission spectra of the labeled protein indicated that NIR820 retained its optical property after the coupling reaction (Figure 2). The labeling of NIR820-Tf was further characterized by SDS-PAGE (Figure 3). NIR imaging of the gel showed a brightly fluorescent band of NIR820-Tf but not of unlabeled Tf.

A cell culture experiment was subsequently conducted to verify that NIR labeled Tf is taken up by cells lines overexpressing the receptor. For these experiments we





**Figure 3.** Tf labeled with NIR820 was analyzed by SDS-PAGE and visualized by light imaging (A) and NIRF imaging at 800 nm excitation (B). Lane 1, molecular marker; lane 2, NIR820-Tf; lane 3, Tf.



**Figure 4.** Light and NIRF imaging of wild-type 9L compared to engineered 9L3.9 cells. Images were acquired 1 h after incubation with the NIR820-TfR. (A) 9L with probe, (B) 9L3.9 with probe, and (C) 9L3.9 without probe.

used 9L3.9 gliosarcoma cells engineered to overexpress TfR and 9L gliosarcomas with baseline TfR levels (11). Previously, it has been shown that the 9L3.9 has 5-fold increase in TfR expression (18). Following incubation of cells with NIR820-Tf for 1 h, fluorescence was primarily found inside of 9L3.9 cells (Figure 4). The result indicates that NIR labeled Tf is taken up efficiently by the overexpressed receptor and that NIR820-Tf labeling does not block the internalization of Tf. Without conjugating to Tf, the NIR820 cannot penetrate the cell membrane by itself (data not shown).

In conclusion, we reported an efficient approach for the synthesis of a scalable water-soluble NIR dye with 820 nm emission in a time and cost-efficient manner. NIR820

is chemically stable and suitable for solid-phase peptide synthesis as well as for protein labeling. We anticipate that this and related molecules as well as their synthesis procedure should be widely applicable for NIR detection of biological affinity molecules.

#### ACKNOWLEDGMENT

We would like to thank Dr. Gail Newton and Dr. Umar Mahmood for technical support. This research was supported by NIH P50-CA86355, BAA NO1-CO17016, and RO1-CA99385.

#### LITERATURE CITED

- Weissleder, R.; V. Ntziachristos (2003) Shedding light onto live molecular targets. *Nat. Med.* 9, 123–8.
- Ntziachristos, V., j. Ripoll, and R. Weissleder (2002) Can near-infrared fluorescence propagate through human organs for noninvasive clinical examinations? *Optics Lett.* 27, 333–335.
- Georgakoudi, I., Mueller, M. G., and Feld, M. S. (2002) *Intrinsic Fluorescence Spectroscopy of Biological Tissue in Fluorescence in Biomedicine*, New York, Marcel Dekker.
- Licha, K. (2002) Contrast agents for optical imaging. *Top Curr. Chem.* 222, 1–29.
- Sekar, N. (2000) Reactive cationic dyes – an update. *Colourage Annu.* 27–28.
- Mujumdar, S. R., Mujumdar, R. B., Grant, C. M., and Waggoner, A. S. (1996) Cyanine-labeling reagents: sulfo benzindocyanine succinimidyl esters. *Bioconjugate Chem.* 7, 356–62.
- Lin, Y., Weissleder, R., and Tung, C. H. (2002) Novel near-infrared cyanine fluorochromes: synthesis, properties, and bioconjugation. *Bioconjugate Chem.* 13, 605–10.
- Flanagan, J. H., Jr., Khan, S. H., Menchen, S., Soper, S. A., and Hammer, R. P. (1997) Functionalized tricarbo-cyanine dyes as near-infrared fluorescent probes for biomolecules. *Bioconjugate Chem.* 8, 751–6.
- Fery-Forgues, S., and D. Lavabre (1999) Are fluorescence quantum yields so tricky to measure? a demonstration using familiar stationery products. *J. Chem. Edu.* 76, 1260–1264.
- Terpetschnig, E., Szmazinski, H., Ozinskas, A., and J. R. Lakowicz (1994) Synthesis of squaraine-N-hydroxysuccinimide esters and their biological application as long-wavelength fluorescent labels. *Anal. Biochem.* 217, 197–204.
- Weissleder, R., Moore, A., Mahmood, U., Bhorade, R., Benveniste, H., Chiocca, E. A., et al. (2000) In vivo magnetic resonance imaging of transgene expression. *Nat. Med.* 6, 351–5.
- Reynolds, G. A., Drexhage, K. H. (1977) Stable heptamethine pyrylium dyes that absorb in the infrared. *J. Org. Chem.* 42, 885–8.
- Slominskii, Y. L., Radchenko, I. D. and Tolmachev, A. I. (1979) Polymethine dyes with hydrocarbon bridges. Effect of substituents in the chromophore on the color of tricarbo-cyanines. *Zhurnal Organicheskoi Khimii* 15, 400–407.
- Faulk, W. P., Hsi, B. L., and Stevens, P. J. (1980) Transferrin and transferrin receptors in carcinoma of the breast. *Lancet* 2, 390–2.
- Gatter, K. C., Brown, G., Trowbridge, I. S., Woolston, R. E., and Mason, D. Y. (1983) Transferrin receptors in human tissues: their distribution and possible clinical relevance. *J. Clin. Pathol.* 36, 539–45.
- Hagihara, N., Walbridge, S., Olson, A. W., Oldfield, E. H., and Youle, R. J. (2000) Vascular protection by chloroquine during brain tumor therapy with Tf-CRM107. *Cancer Res.* 60, 230–4.
- Hogemann, D., Josephson, L., Weissleder, R., and Basilion, J. P. (2000) Improvement of MRI probes to allow efficient detection of gene expression. *Bioconjugate Chem.* 11, 941–6.
- Moore, A., Basilion, J. P., Chiocca, E. A., and Weissleder, R. (1998) Measuring transferrin receptor gene expression by NMR imaging. *Biochim. Biophys. Acta* 1402, 239–49.

BC034070H

# Ascorbic Acid: Useful as a Buffer Agent and Radiolytic Stabilizer for Metalloradiopharmaceuticals

Shuang Liu,<sup>\*,†</sup> Charlie E. Ellars,<sup>‡</sup> and D. Scott Edwards<sup>‡</sup>

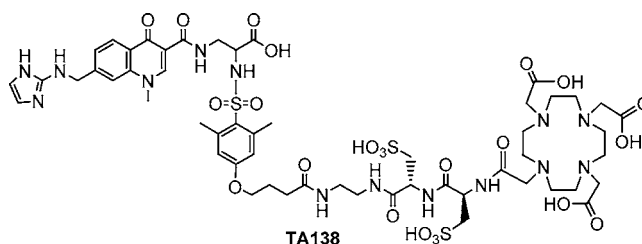
Department of Industrial and Physical Pharmacy, School of Pharmacy, Purdue University, 575 Stadium Mall Drive, West Lafayette, Indiana 47907-2051 and Discovery R & D, Bristol-Myers Squibb Medical Imaging, 331 Treble Cove Road, North Billerica, Massachusetts 01862. Received June 26, 2003; Revised Manuscript Received August 1, 2003

The goal of this study is to explore the use of ascorbic acid (AA) as a buffer agent and a radiolytic stabilizer for preparation and stabilization of radiolabeled DOTA–biomolecule conjugates. Results from a titration experiment show that 0.1 M AA solution has sufficient buffer capacity at pH 5.0 while 0.5 M AA solution is useful even at pH 6.0. The radiolabeling experiment using TA138, a DOTA-conjugated nonpeptide integrin  $\alpha_v\beta_3$  receptor antagonist, clearly demonstrates that AA is a good buffer agent for pH control and an excellent antioxidant for stabilization of metal-labeled diagnostic ( $^{111}\text{In}$ ) and therapeutic ( $^{90}\text{Y}$  and  $^{177}\text{Lu}$ ) radiopharmaceuticals if the radiolabeling is performed at pH 5–6. There is no need for the additional stabilizer (e.g., gentisic acid) and buffer agent such as ammonium acetate. The anaerobic AA formulation described in this study is particularly useful for radiolabeling of small biomolecules, which are sensitive to the radiolytic degradation during radiolabeling.

## INTRODUCTION

There has been a great current interest in radiolabeled small biomolecules (peptides and nonpeptides) as diagnostic and therapeutic radiopharmaceuticals (1–15). Radiopharmaceuticals comprising  $\alpha$ - or  $\beta$ -emitting radionuclides often undergo radiolysis during preparation and storage (11). During radiolysis, emissions from the radionuclide attack the metal chelate, targeting biomolecule, and other compounds in proximity, which results in decomposition or destruction of the metal chelate or/and the biomolecule. Since the tumor uptake is largely dependent on the receptor binding of the radiolabeled biomolecule, radiolytic degradation may lead to the decreased therapeutic efficacy and unwanted radiation toxicity to normal organs. Thus, it is important that the radionuclide remains linked to the targeting moiety, and specificity of the targeting biomolecule is preserved.

A radiopharmaceutical composition usually contains a bifunctional chelator-conjugated biomolecule (BFC–BM), a buffer agent for pH control, a weak chelator to prevent metal–colloid formation, and a stabilizer to prevent radiolytic degradation of the radiolabeled BFC–BM conjugate. The pH is critical for the success and reproducibility of the  $^{90}\text{Y}$ - or  $^{111}\text{In}$ -labeling. When it is used at high concentrations, ammonium acetate can serve as a buffer agent and weak chelator. As a matter of fact, ammonium acetate has been widely used as the buffer agent for the radiolabeling of various DOTA–BM and DTPA–BM conjugates (16–25). The stabilizer can be added into the reaction mixture before or after radiolabeling. However, the combination of ammonium acetate and stabilizer often results in high osmolarity of the radiopharmaceutical composition. Therefore, there is a



**Figure 1.** TA138: a DOTA-conjugated vitronectin receptor antagonist.

need for a new agent, which can serve both as a buffer agent for pH control and as a stabilizer to stabilize the radiolabeled BFC–BM conjugate.

TA138 (Figure 1) is a DOTA-conjugated nonpeptide integrin  $\alpha_v\beta_3$  receptor antagonist that binds with high affinity and specificity to integrin  $\alpha_v\beta_3$  receptors overexpressed on endothelial cells of tumor neovasculature and tumor cells (26–30).  $^{90}\text{Y}$ -TA138 has demonstrated significant therapeutic effects in several preclinical tumor models, including c-neu Oncomouse, HCT116, and HT460 xenografts (31). Since  $^{90}\text{Y}$  is a pure  $\beta$ -emitter,  $^{111}\text{In}$ -TA138 was chosen as the imaging surrogate for biodistribution and dosimetry determination. To support the clinical studies, it is necessary to develop a robust formulation for routine preparation of  $^{90}\text{Y}$ -TA138 and  $^{111}\text{In}$ -TA138.

In our previous contribution (38), we reported synthesis of complexes  $^{90}\text{Y}$ -TA138 and  $^{177}\text{Lu}$ -TA138. Through a series of radiolabeling experiments, we developed an anaerobic formulation for routine preparation of  $^{90}\text{Y}$ -TA138 and  $^{177}\text{Lu}$ -TA138. It was found that  $^{90}\text{Y}$ -TA138 and  $^{177}\text{Lu}$ -TA138 are very sensitive to radiolytic degradation, and exclusion of oxygen is necessary during the radiolabeling. Using the anaerobic formulation,  $^{90}\text{Y}$ -TA138 and  $^{177}\text{Lu}$ -TA138 can be prepared in high yield and high specific activity. We also found that Tris ( $\sim 0.1$  M, pH = 6.0–8.0) and ascorbic acid (AA:  $\sim 0.1$  M, pH = 5.0–7.0) can also be used as buffer agents to replace ammonium acetate in the anaerobic formulation. Since AA is a known

\* To whom correspondence should be addressed. Phone: 765-494-0236 (S.L.); fax 765-496-3367; e-mail: lius@pharmacy.purdue.edu.

<sup>†</sup> Purdue University.

<sup>‡</sup> Bristol-Myers Squibb Medical Imaging.

radiolytic stabilizer and has the buffer capacity at pH 4–6, there is no need for gentisic acid and ammonium acetate in the formulation matrix if the radiolabeling is performed at pH 5–6. That led us to explore the possibility of using AA as a buffer agent for pH control and a radiolytic stabilizer for stabilization of the radiopharmaceutical during or/and after radiolabeling. In this report, we present an anaerobic formulation for routine preparation of radiometal-labeled small biomolecule radiopharmaceuticals. This formulation is particularly useful for small biomolecules sensitive to radiolytic degradation during radiolabeling.

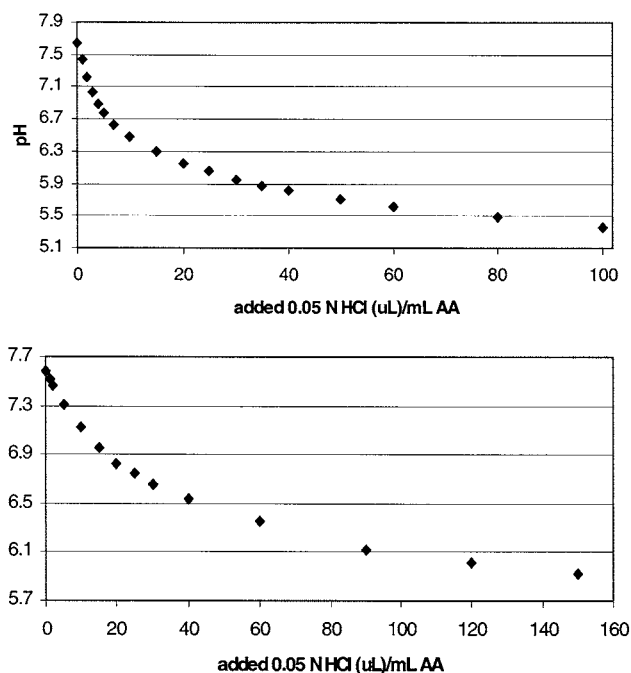
## EXPERIMENTAL SECTION

**Materials.** Ammonium acetate, ascorbic acid (sodium salt), and diethylene-triaminepentaacetic acid (DTPA) were purchased from Sigma/Aldrich Chemical Co. and were used as received.  $^{90}\text{YCl}_3$  and  $^{111}\text{InCl}_3$  (in 0.05 N HCl) were purchased from PerkinElmer Life Sciences, N. Billerica, MA. High specific activity  $^{177}\text{LuCl}_3$  was obtained from University of Missouri Research Reactor, Columbia, MO. Synthesis of TA138, 3-sulfon-*N*-[[4,7,10-tris(carboxymethyl)1,4,7,10-tetraaza-cyclododec-1-yl]acetyl]-L-alanyl-*N*-[2-[4-[[[(1*S*)-1-carboxy-2[[[1,4-dihydro-7-[(1*H*-imidazol-2-ylamino)methyl]-1-methyl-4-oxo-3-quinolinyl]carbonyl]amino]ethyl]amino]sulfonyl]-3,5-dimethylphenoxy]-1-oxobutyl]amino]ethyl]-3-sulfo-L-alaninamide, has been reported in our previous communication (25).

**Analytical Methods.** The radio-HPLC method used a HP-1100 HPLC system with a UV/visible detector ( $\lambda = 230$  nm), an IN-US radio-detector, and a Zorbax C<sub>18</sub> column (4.6 mm  $\times$  250 mm, 80 Å pore size). The flow rate was 1 mL/min with a gradient mobile phase starting from 92% solvent A (0.025 M ammonium acetate buffer, pH 6.8) and 8% solvent B (acetonitrile) to 90% solvent A and 10% solvent B at 18 min. The mobile phase was isocratic using 40% of solvent A and 60% solvent B from 19 to 25 min. The isocratic condition was used to make sure that more lipophilic radioimpurities were washed out from the column. The TLC method used the C<sub>18</sub> reverse phase glass plates and a mobile phase containing methanol, acetone, and saline (2:1:1 = v:v:v). By this method, the radiolabeled DOTA-conjugate migrates to solvent front while unchelated radiometal (metal-colloid and metal-acetate complex) remain at the origin. The corrected radiochemical purity (RCP) was calculated by subtracting the percentage of unchelated radiometal obtained by TLC from that obtained by radio-HPLC.

**General Procedure for the Synthesis of  $^{90}\text{Y}$ -TA138.** To a 5 mL vial containing 50  $\mu\text{g}$  of TA138 was added 0.5 mL of the AA buffer (0.1 or 0.5 M; pH = 5.0–7.0). The solution was degassed under vacuum (<1 mmHg) for ~2 min. Upon addition of 10–15  $\mu\text{L}$  of  $^{90}\text{YCl}_3$  (~10 mCi) in 0.05 N HCl, the reaction mixture was heated at 50 °C or 95 °C for 5 or 35 min. After radiolabeling, a sample of the resulting solution was added to a 2 mL HPLC autosampler vial containing a mixture of 0.5 mL of AA and 0.5 mL of 2 mM DTPA solution and was then analyzed by radio-HPLC and TLC. Each sample was run twice, and the RCP data are presented as an average of two independent measurements.

**Synthesis of  $^{177}\text{Lu}$ -TA138.** To a clean sealed 5 mL vial was added 1.0 mL of 0.1 M AA buffer (pH = 5.0) containing 100  $\mu\text{g}$  of TA138. The solution was degassed under vacuum (<1 mmHg) for ~2 min. Upon addition of 25  $\mu\text{L}$  of  $^{177}\text{LuCl}_3$  solution (~20 mCi) in 0.05 N HCl,



**Figure 2.** The pH titration curves for 0.1 M (top) and 0.5 M (bottom) AA solutions.

the reaction mixture was heated at 95 °C for 30 min. After being cooled to room temperature, a sample of the resulting solution was diluted 2-fold with 2 mM DTPA solution, analyzed by HPLC and TLC. The mixture was kept at –78 °C for 5 days, and then reanalyzed using the same HPLC and TLC methods.

**Synthesis of  $^{111}\text{In}$ -TA138.** TA138 (40–100  $\mu\text{g}$ ) was dissolved in 1.5 mL of AA buffer (0.1 M at pH 5.0 or 0.5 M at pH = 6.0). The solution was immediately degassed under vacuum (<1 mmHg) for ~2 min. Upon addition of  $^{111}\text{InCl}_3$  solution (2–2.5 mCi) in 0.05 N HCl, the reaction mixture was heated at 95 °C for 30 min. After being cooled to room temperature, a sample of the resulting solution was analyzed by radio-HPLC and TLC. The resulting mixture was kept at room temperature for 24 h and was then reanalyzed using the same HPLC and TLC methods.

## RESULTS

**The pH Titration Experiment.** In this experiment, sodium ascorbate was used as the starting material to prepare 0.1 M (20 mg/mL) and 0.5 M (100 mg/L) AA solutions. The original pH in both solutions was ~7.6. Since  $^{90}\text{YCl}_3$ ,  $^{111}\text{InCl}_3$  and  $^{177}\text{LuCl}_3$  are all dissolved in 0.05 N HCl solution, we used 0.05 N HCl to titrate both AA solutions. Figure 2 shows the titration curves (pH versus added 0.05 M HCl/mL AA) for 0.1 M (top) and 0.5 M (bottom) AA solutions.

**Radiolabeling Experiment.** This experiment was designed to explore the possibility of using AA as a buffer agent for pH control and as a radiolytic stabilizer for stabilization of  $^{90}\text{Y}$ -TA138. We used 100  $\mu\text{g}$  of TA138 for 20 mCi of  $^{90}\text{Y}$  to make sure that TA138 was in large excess. We also fixed the  $^{90}\text{Y}$ :TA138 ratio (10 mCi/50  $\mu\text{g}$ /mL) to explore other factors influencing the radiolabeling yield of  $^{90}\text{Y}$ -TA138. Four factors were considered in the experimental design. These include pH value (5, 6, and 7), heating time (5 and 35 min), AA level (20 and 100 mg/mL), and temperature (50 °C and 95 °C). There were 20 conditions (Table 1) for the radiolabeling experiment. Each condition contains 2–3 vials unless specified. The



**Table 1. Radiolabeling Results (at ~10 mCi Level)**

pH	heating time (min)	temp (°C)	AA level (mg/mL)	average RCP (%) for $^{90}\text{Y}$ -TA138
5.0	35	95	100	$96.2 \pm 0.8$ ( $n = 2$ )
5.0	35	95	20	$98.5 \pm 0.3$ ( $n = 6$ )
5.0	5	95	100	$95.3 \pm 1.3$ ( $n = 3$ )
5.0	5	95	20	$98.1 \pm 0.4$ ( $n = 6$ )
6.0	35	95	100	$97.8 \pm 0.8$ ( $n = 6$ )
6.0	35	95	20	$98.5 \pm 0.5$ ( $n = 3$ )
6.0	5	95	100	$97.5 \pm 0.7$ ( $n = 2$ )
6.0	5	95	20	$98.7 \pm 0.3$ ( $n = 3$ )
7.0	35	95	100	$97.3 \pm 0.6$ ( $n = 2$ )
7.0	35	95	20	$98.4 \pm 0.3$ ( $n = 3$ )
7.0	5	95	100	$98.0 \pm 0.5$ ( $n = 3$ )
7.0	5	95	20	$98.5 \pm 0.4$ ( $n = 2$ )
5.0	5	50	20	$17.5 \pm 15.3$ ( $n = 3$ )
5.0	35	50	100	$74.4 \pm 7.5$ ( $n = 3$ )
5.0	35	50	20	$36.2 \pm 9.4$ ( $n = 2$ )
6.0	5	50	100	$38.4 \pm 8.6$ ( $n = 3$ )
7.0	5	50	100	$78.5 \pm 2.3$ ( $n = 2$ )
7.0	5	50	20	$80.6 \pm 3.5$ ( $n = 2$ )
7.0	35	50	100	$91.2 \pm 1.5$ ( $n = 3$ )
7.0	35	50	20	$87.1 \pm 2.7$ ( $n = 2$ )

**Table 2. RCP Performance of the AA Formulation for  $^{90}\text{Y}$ -TA138 (at 100 mCi level)**

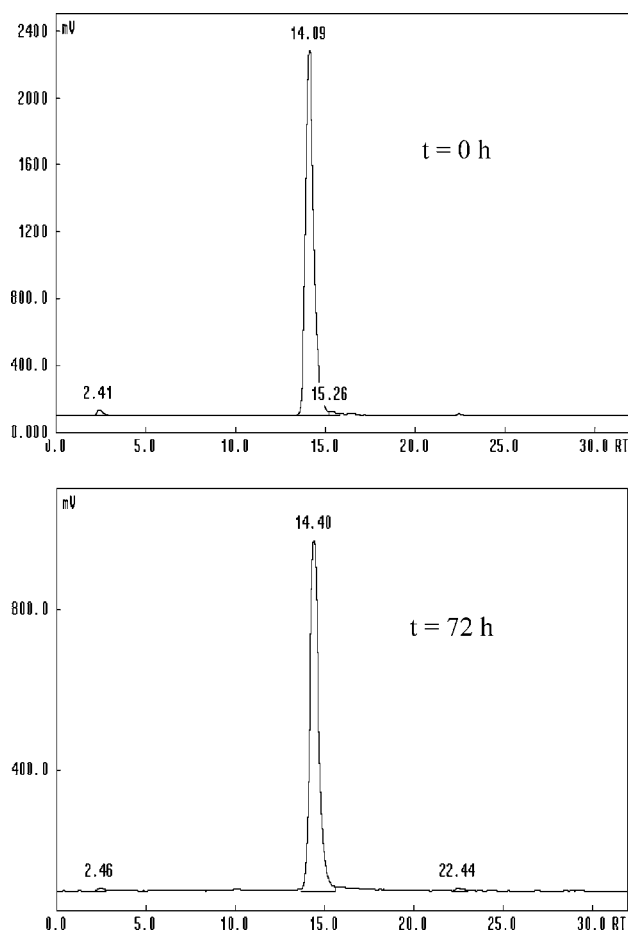
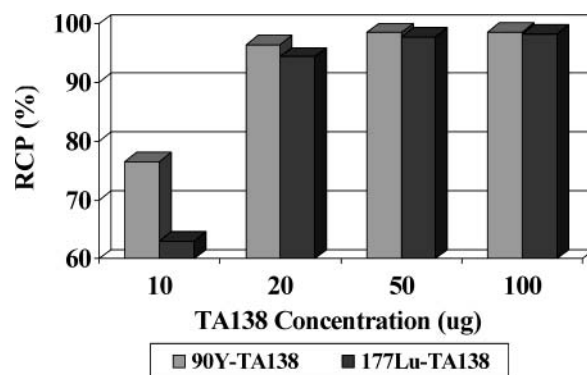
buffer concn	buffer pH	HPLC RCP (%)	TLC RCP (%)
0.1 M (20 mg/mL)	6.0 ( $n = 3$ )	$98.4 \pm 0.6/T = 0$	$99.7 \pm 0.2/T = 0$
0.1 M (20 mg/mL)	6.0 ( $n = 3$ )	$97.8 \pm 0.2/T = 3 \text{ d}$	$99.5 \pm 0.4/T = 3 \text{ d}$
0.5 M (100 mg/mL)	5.0 ( $n = 3$ )	$98.9 \pm 0.5/T = 0$	$99.2 \pm 0.1/T = 0$
0.5 M (100 mg/mL)	5.0 ( $n = 3$ )	$98.3 \pm 0.6/T = 3 \text{ d}$	$99.4 \pm 0.2/T = 3 \text{ d}$

activity level in each vial was ~10 mCi. The RCP data for the radiolabeled vials are summarized in Table 1.

**Solution Stability of  $^{90}\text{Y}$ -TA138.** In this experiment, we prepared six  $^{90}\text{Y}$ -TA138 vials at a 100 mCi level using 0.1 M AA (pH = 5.0;  $n = 3$ ) or 0.5 M AA (pH = 6.0;  $n = 3$ ), and studied the solution stability of  $^{90}\text{Y}$ -TA138 at  $-78^\circ\text{C}$  over 3 days. The TA138 concentration was 100  $\mu\text{g}/\text{mL}$ , and the activity concentration was 20 mCi/mL. Radiolabeling was readily accomplished by adding 100 mCi of  $^{90}\text{YCl}_3$  (in 0.05 N HCl) into the degassed AA solution containing TA138 and heating the reaction mixture at  $95^\circ\text{C}$  for 30 min. After the radiolabeling, a sample of the resulting solution was analyzed by radio-HPLC and TLC. Vials containing  $^{90}\text{Y}$ -TA138 were then placed in a lead pig and stored at  $-78^\circ\text{C}$  for 3 days. Frozen vials were allowed to thaw for 30–40 min at room temperature. Samples were analyzed by radio-HPLC and TLC. The RCP data at  $t = 0$  and  $t = 3$  days postlabeling are listed in Table 2. As an example, Figure 3 shows the typical radio-HPLC chromatograms of  $^{90}\text{Y}$ -TA138 at 0 and 72 h post-labeling.

**$^{90}\text{Y}$ -Labeling Efficiency of TA138 Using the AA Formulation.** We studied the  $^{90}\text{Y}$ -labeling efficiency of TA138 by determining the minimal amount of TA138 required to achieve 95% RCP for  $^{90}\text{Y}$ -TA138. We prepared  $^{90}\text{Y}$ -TA138 using 10, 20, 50, and 100  $\mu\text{g}$  of TA138 for 20 mCi of  $^{90}\text{YCl}_3$  in 1.0 mL of 0.5 M AA buffer (pH = 6.0). The heating temperature was  $95^\circ\text{C}$ , and the heating time was 30 min. Figure 4 shows the effect of TA138 concentration on the RCP for  $^{90}\text{Y}$ -TA138. At pH 6.0, the minimal amount of TA138 required to achieve 95% RCP for  $^{90}\text{Y}$ -TA138 is about 20  $\mu\text{g}$  for 20 mCi of  $^{90}\text{YCl}_3$  corresponding to a TA138: $^{90}\text{Y}$  ratio of ~30:1. In all cases, the formation of [ $^{90}\text{Y}$ ]colloid was minimal.

**AA Formulation for  $^{177}\text{Lu}$ -TA138.** We also used the AA formulation to prepare  $^{177}\text{Lu}$ -TA138. Radiolabeling was easily accomplished by adding  $^{177}\text{LuCl}_3$  solution (~20 mCi) into 1.0 mL of the degassed AA solution (0.5 M at pH = 6) containing 100  $\mu\text{g}$  of TA138 and heating the

**Figure 3.** Radio-HPLC chromatograms of  $^{90}\text{Y}$ -TA138 at  $-78^\circ\text{C}$ .**Figure 4.** The effect of TA138 concentration on RCP of  $^{90}\text{Y}$ -TA138 and  $^{177}\text{Lu}$ -TA138.

reaction mixture at  $95^\circ\text{C}$  for 30 min. The RCP for  $^{177}\text{Lu}$ -TA138 was >95%.  $^{177}\text{Lu}$ -TA138 remains stable at  $-78^\circ\text{C}$  for at least 5 days. Under optimized conditions (0.1–0.5 M, pH = 5.0–6.0), the minimal amount of TA138 required to achieve 95% RCP for  $^{177}\text{Lu}$ -TA138 is ~20  $\mu\text{g}$  for 20 mCi of  $^{177}\text{LuCl}_3$  (Figure 4) even though the specific activity of  $^{177}\text{Lu}$  is much higher than that of  $^{90}\text{Y}$ .

**AA Formulation for  $^{111}\text{In}$ -TA138.** We also carried out a radiolabeling study using the AA formulation for preparation of  $^{111}\text{In}$ -TA138. Radiolabeling was accomplished by simply adding  $^{111}\text{InCl}_3$  (~2.0 mCi) into 1.5 mL of the degassed AA solution (0.5 M at pH = 6.0 or 0.1 M at pH = 5.0) containing TA138 (67  $\mu\text{g}/\text{mL}$ ) and heating the mixture at  $95$ – $100^\circ\text{C}$  for 30 min. The RCP data for  $^{111}\text{In}$ -TA138 are summarized in Table 3. The TA138 concentration can be varied from 40  $\mu\text{g}$  to 100  $\mu\text{g}$  for 2.0–

**Table 3. RCP Performance of the AA Formulation for RP748 (at ~ 2.5 MCi Level)**

<sup>111</sup> In source	buffer pH	RCP (%) HPLC	TLC RCP(%)
NEN ( <i>n</i> = 4)	6.0	97.5 ± 0.4	99.6 ± 0.3
Indiclor ( <i>n</i> = 3)	6.0	97.2 ± 0.6	99.5 ± 0.3
NEN ( <i>n</i> = 3)	5.0	98.5 ± 0.2	99.6 ± 0.2
Indiclor ( <i>n</i> = 3)	5.0	97.2 ± 0.5	99.7 ± 0.2

2.5 mCi of <sup>111</sup>InCl<sub>3</sub>. Apparently, the <sup>111</sup>In-labeling efficiency was not as high as that for <sup>90</sup>Y and <sup>177</sup>Lu, probably due to the presence of trace metal contaminants from the <sup>111</sup>InCl<sub>3</sub> source (11).

## DISCUSSION

A radiolytic stabilizer is a radical scavenging antioxidant, which reacts readily with hydroxyl and superoxide radicals (32). In general, the ideal stabilizer possesses the following characteristics: low or no toxicity, no interference with the receptor binding of the radiolabeled compound, and the ability to stabilize the radiopharmaceutical composition for a reasonable period of time during preparation, release, storage, and transportation. AA is a known antioxidant and has been used for stabilization of both diagnostic and therapeutic radiopharmaceuticals (23, 24, 33–37). It has a *pK<sub>a</sub>* of 4.2 with high buffer capacity at pH 3.5–5.5. At higher concentrations (>50 mg/mL or 0.25 M), it may also have sufficient buffer capacity at the pH range 5.5–6.0. Since AA contains two hydroxyl groups, one of which is deprotonable at pH > 4.2, it can also be used as a weak chelator to prevent the formation of radiometal colloid. If AA is used at pH 4.0–6.0, there is no need for extra buffer agent in the formulation matrix. In doing so, it will eliminate the use of ammonium acetate and reduce the osmolarity of the radiopharmaceutical composition.

To demonstrate the utility of AA as a buffer agent, we performed a titration experiment, in which 0.1 M (20 mg/mL) and 0.5 M (100 mg/L) AA solutions were titrated with the 0.05 N HCl. Figure 2 shows the titration curves for 0.1 and 0.5 M AA solutions. For an ideal buffer agent, the pH change should not exceed 0.2 units after addition of 20 μL of 0.05 N HCl solution and during radiolabeling. If one assumes that the activity concentration for <sup>90</sup>YCl<sub>3</sub> and <sup>177</sup>LuCl<sub>3</sub> is about 1.0 mCi/μL, the volume of the <sup>90</sup>YCl<sub>3</sub> or <sup>177</sup>LuCl<sub>3</sub> stock solution for a 20 mCi activity in 1.0 mL of the AA buffer solution is about 20 μL. Obviously, 0.1 M AA solution has sufficient buffer capacity at pH 5.0 while 0.5 M AA solution has the buffer capacity even at pH 6.0.

The radiolabeling experiment was designed to explore the optimal conditions for routine preparation of <sup>90</sup>Y-TA138. Since <sup>90</sup>Y-TA138 is sensitive to radiolytic degradation, exclusion of oxygen is required during radiolabeling. Results from the radiolabeling experiments show that heating temperature is the most dominant factor. Heating the reaction mixture at 95 °C for 5–35 min is required to achieve high yield radiolabeling (RCP > 95%). It is interesting to note that the pH shows little effect on the RCP at pH = 5.0–7.0 if the heating temperature is 95 °C. At pH < 6.0, lower AA level seems to give a slightly better RCP for <sup>90</sup>Y-TA138 while it does not have a significant effect on the RCP of <sup>90</sup>Y-TA138 at pH = 7.0. Longer heating time gives slightly better RCP at 95 °C, particularly at pH = 5.0.

It should be noted that the radiolabeling experiment was performed at ~10 mCi level of <sup>90</sup>Y. There is often a relatively large variability (5–15%) between vials heated at 50 °C. There is also a large variability between different batches of <sup>90</sup>YCl<sub>3</sub>. Similar results have been

reported for the <sup>90</sup>Y-labeling of DOTA-conjugated antibodies (16–20). Thus, the RCP difference of ~2.0% between different vials may not be significant within the experimental error. Results from the radiolabeling experiment suggest that <sup>90</sup>Y-TA138 can be prepared in high yield (RCP > 95%) under the following conditions: 100 μg TA138 for 20 mCi of <sup>90</sup>Y in 1 mL of degassed AA buffer solution (0.1–0.5 M at pH 5.0; 0.5 M at pH 6.0), and heating the reaction mixture at 95 °C for 30–35 min.

To further validate the anaerobic AA formulation, we prepared six <sup>90</sup>Y-TA138 vials at 100 mCi level using 0.1 M AA (pH = 5.0; *n* = 3) or 0.5 M AA (pH = 6.0; *n* = 3). We studied the solution stability of <sup>90</sup>Y-TA138 at –78 °C over 72 h. The radio-HPLC and TLC data clearly demonstrated that <sup>90</sup>Y-TA138 can be prepared in high yield (RCP > 95%) using the anaerobic AA formulation (0.1–0.5 M, pH = 5–6), and it remains stable at –78 °C for at least 72 h. Very high specific activity can be achieved for <sup>90</sup>Y-TA138. At pH 6.0, the minimal amount of TA138 required to achieve 95% RCP for <sup>90</sup>Y-TA138 is ~20 μg for 20 mCi of <sup>90</sup>YCl<sub>3</sub> (Figure 4) corresponding to a TA138:<sup>90</sup>Y ratio of ~30:1. The anaerobic AA formulation is also good for routine preparation of <sup>177</sup>Lu-TA138 and <sup>111</sup>In-TA138. Very high <sup>177</sup>Lu-labeling efficiency has been achieved even though the specific activity of <sup>177</sup>Lu is much higher than that of <sup>90</sup>YCl<sub>3</sub>. The source of <sup>111</sup>InCl<sub>3</sub> has no significant effect on the RCP of <sup>111</sup>In-TA138 (Table 3).

## CONCLUSION

This study clearly shows that ascorbic acid is a good buffer agent for pH control and an excellent antioxidant for stabilization of metal-labeled diagnostic (<sup>111</sup>In) and therapeutic (<sup>90</sup>Y and <sup>177</sup>Lu) radiopharmaceuticals. If the radiolabeling is performed at pH 5–6, there is no need for an additional stabilizer or buffer agent in the formulation matrix. The anaerobic AA formulation described in this study is simple and is particularly useful for radiolabeling of small biomolecules sensitive to the radiolytic degradation during radiolabeling.

**Acknowledgment** is made to Dr. Thomas D. Harris for the synthesis of TA138 (3-sulfon-*N*-[[4,7,10-tris(carboxymethyl)-1,4,7,10-tetraaza-cyclododec-1-yl]acetyl]-*L*-alanyl-*N*-[2-[4-[[[(1*S*)-1-carboxy-2-[[[1,4-dihydro-7-[(1*H*-imidazol-2-ylamino)methyl]-1-methyl-4-oxo-3-quinolinyl]carbonyl]amino]ethyl]amino]sulfonyl]-3,5-dimethylphenoxy]-1-oxobutyl]amino]ethyl]-3-sulfo-*L*-alaninamide).

## LITERATURE CITED

- (1) Anderson, C. J., and Welch, M. J. (1999) Radiolabeled agents (non-technetium) for diagnostic imaging. *Chem. Rev.* 99, 2219–2234.
- (2) Liu, S., and Edwards, D. S. (1999) <sup>99m</sup>Tc-labeled small peptides as diagnostic radiopharmaceuticals. *Chem. Rev.* 99, 2235–2268.
- (3) Jurisson, S., and Lydon, J. D. (1999) Potential technetium small molecule radiopharmaceuticals. *Chem. Rev.* 99, 2205–2218.
- (4) Volkert, W. A., and Hoffman, T. J. (1999) Therapeutic radiopharmaceuticals. *Chem. Rev.* 99, 2269–2292.
- (5) Heppeler, H., Froidevaux, S., Eberle, A. N., and Maecke, H. R. (2000) Receptor targeting for tumor localization and therapy with radiopeptides. *Current Pharmaceutical Design* 6, 971–994.
- (6) Boerman, O. C., Oyen, W. J. G., and Corstens, F. H. M. (2000) Radio-labeled receptor-binding peptides: a new class of radiopharmaceuticals. *Semin. Nucl. Med.* 30, 195–208.
- (7) Heppeler, H., Froidevaux, S., Eberle, A. N., and Maecke, H. R. (2000) Receptor targeting for tumor localization and therapy with radiopeptides. *Curr. Pharm. Des.* 6, 971–994.

- (8) Kwekkeboom, D., Krenning, E. P., and de Jong, M. (2000) Peptide receptor imaging and therapy. *J. Nucl. Med.* **41**, 1704–1713.
- (9) Signore, A., Annovazzi, A., Chianelli, M., Coretti, F., Van de Wiele, C., Watherhouse, R. N., and Scopinaro, F. (2001) Peptide radiopharmaceuticals for diagnosis and therapy. *Eur. J. Nucl. Med.* **28**, 1555–1565.
- (10) Hoffman, T. J., Quinn, T. P., and Volkert, W. A. (2001) Radiometalated receptor-avid peptide conjugates for specific in vivo targeting of cancer cells. *Nucl. Med. Biol.* **28**, 527–539.
- (11) Liu, S., and Edwards, D. S. (2001) Bifunctional chelators for target specific therapeutic lanthanide radiopharmaceuticals. *Bioconjugate Chem.* **12**, 7–34.
- (12) Breeman, W. A. P., de Jong, M., Kwekkeboom, D. J., Valkema, R., Bakker, W. H., Kooij, P. P. M., Visser, T. J., and Krenning, E. P. (2001) Somatostatin receptor imaging and therapy of pancreatic endocrine tumors. *Eur. J. Nucl. Med.* **28**, 1421–1429.
- (13) Liu, S., and Edwards, D. S. (2002) Fundamentals of receptor-based diagnostic metalloradiopharmaceuticals. *Topics in Current Chem.* **222**, 259–278.
- (14) Jong, M., Kwekkeboom, D., Valkema, R., and Krenning, E. P. (2003) Radiolabeled Peptides for tumor therapy: current status and future directions. *Eur. J. Nucl. Med.* **30**, 463–469.
- (15) Fichna, J., and Janecka, A. (2003) Synthesis of target-specific radiolabeled peptides for diagnostic imaging. *Bioconjugate Chem.* **14**, 3–17.
- (16) Lewis, M. R., Raubitschek, A., and Shively, J. E. (1994) A facile, water soluble method for modification of proteins with DOTA. Use of elevated temperature and optimized pH to achieve high specific activity and high chelate stability in radiolabeled immunoconjugates. *Bioconjugate Chem.* **5**, 565–576.
- (17) Stimmel, J. B., Stockstill, M. E., and Kull, F. C., Jr. (1995) Yttrium-90 chelation properties of tetraazatetraacetic acid macrocycles, diethylenetriaminepentaacetic acid analogues, and a novel terpyridine acyclic chelator. *Bioconjugate Chem.* **6**, 219–225.
- (18) Kulis, D. L., DeNardo, S. J., DeNardo, G. L., O'Donnell, R. T., and Meares, C. F. (1998) Optimized conditions for chelation of yttrium-90-DOTA immunoconjugates. *J. Nucl. Med.* **39**, 2105–2110.
- (19) Lewis, M. R., and Shively, J. E. (1998) Maleimidocysteine-amido-DOTA derivatives: New reagents for radiometal chelate conjugation to antibody sulfhydryl groups undergo pH-dependent cleavage reactions. *Bioconjugate Chem.* **9**, 72–86.
- (20) Stimmel, J. B., and Kull, F. C., Jr. (1998) Samarium-153 and lutetium-177 chelation properties of selected macrocyclic and cyclic ligands. *Nucl. Med. Biol.* **25**, 117–125.
- (21) Liu, S., Cheung, E., Rajopadyhe, M., Williams, N. E., Overoye, K. L., and Edwards, D. S. (2001) Isomerism and solution dynamics of  $^{90}\text{Y}$ -labeled DTPA-biomolecule conjugates. *Bioconjugate Chem.* **12**, 84–91.
- (22) Liu, S., and Edwards, D. S. (2001) Synthesis and characterization of two  $^{111}\text{In}$  labeled DTPA-peptide conjugates. *Bioconjugate Chem.* **12**, 630–634.
- (23) Liu, S., Cheung, E., Rajopadyhe, M., Ziegler, M. C., and Edwards, D. S. (2001)  $^{90}\text{Y}$ - and  $^{177}\text{Lu}$ -labeling of a DOTA-conjugated vitronectin receptor antagonist for tumor therapy. *Bioconjugate Chem.* **12**, 559–568.
- (24) Liu, S., and Edwards, D. S. (2001) Stabilization of  $^{90}\text{Y}$ -labeled DOTA-biomolecule conjugates using gentisic and ascorbic acid. *Bioconjugate Chem.* **12**, 554–558.
- (25) Liu, S., Ellars, C., and Edwards, D. S. (2003) Anaerobic  $^{90}\text{Y}$ - and  $^{177}\text{Lu}$ -labeling of a DOTA-conjugated nonpeptide vitronectin receptor antagonist. *Bioconjugate Chem.*, in press.
- (26) Folkman, J. (1995) Angiogenesis in cancer, vascular, rheumatoid and other disease. *Nat Med* **1**, 27–31.
- (27) Mousa, S. A. (1998) Mechanism of angiogenesis in vascular disorders: potential therapeutic targets. *Drugs Future* **23**, 51–60.
- (28) Mousa, S. A. (2000) Integrins as novel drug discovery targets: potential therapeutic and diagnostic implications. *Emerg. Ther. Targets* **4**, 143–153.
- (29) Carmeliet, P. (2000) Mechanism of angiogenesis and atherogenesis. *Nat. Med.* **6**, 389–395.
- (30) Zitzmann, S., Ethemann, V., and Schwab, M. (2000) Arginine-Glycine-Aspartic acid (RGD)-peptide binds to both tumor and tumor endothelial cells in vivo. *Cancer Res.* **62**, 5139–5143.
- (31) Harris, T. D., Kalogeropoulos, S., Nguyen, T., Liu, S., Bartis, J., Ellars, C. E., Edwards, D. S., Onthank, D., Yalamanchili, P., Robinson, S. P., Lazewatsky, J., and Barrett, J. A. (2003) Design, synthesis and evaluation of radiolabeled integrin  $\alpha_v\beta_3$  antagonists for tumor imaging and radiotherapy. *Cancer Biother. Radiopharm.* **18**, 631–645.
- (32) Garrison, W. M. (1987) Reaction mechanisms in radiolysis of peptides, polypeptides, and proteins. *Chem. Rev.* **87**, 381–398.
- (33) Berger, R. (1982) Radical scavengers and the stability of  $^{99\text{m}}\text{Tc}$ -radiopharmaceuticals. *Int. J. Appl. Radiat. Isot.* **33**, 1341–1344.
- (34) Chakrabarti, M. C., Le, N., Paik, C. H., De Graff, W. G., and Carrasquillo, J. A. (1996) Prevention of radiolysis of monoclonal antibody during labeling. *J. Nucl. Med.* **37**, 1384–1388.
- (35) Salako, Q. A., O'Donnell, R. T., and DeNardo, S. J. (1998) Effects of radiolysis on yttrium-90-labeled lym-1 antibody preparations. *J. Nucl. Med.* **39**, 667–670.
- (36) Kulis, D. L., DeNardo, S. J., DeNardo, G. L., O'Donnell, R. T., and Meares, C. F. (1998) Optimized conditions for chelation of yttrium-90-DOTA immunoconjugates. *J. Nucl. Med.* **39**, 2105–2110.
- (37) Knapp, F. F., Jr. (Russ), Beets, A. L., Gohlke, S., Zamora, P. O., Bender, H., Palmedo, H., and Biersack, H.-J. (1997) Availability of rhenium-188 from the alumina-based tungsten-188/rhenium-188 generator for preparation of rhenium-188-labeled radiopharmaceuticals for cancer treatment. *Anticancer Res.* **17**, 1783–1796.

BC034109I



## ARTICLES

---

### Multistep Fluorescence Resonance Energy Transfer in Sequential Chromophore Array Constructed on Oligo-DNA Assemblies

Yuichi Ohya,\* Kentaro Yabuki, Masafumi Hashimoto, Atsushi Nakajima, and Tatsuro Ouchi

Department of Applied Chemistry, Faculty of Engineering & High Technology Research Center, Kansai University, Suita, Osaka 564-8680, Japan. Received February 28, 2003; Revised Manuscript Received July 24, 2003

---

Sequential arrays of chromophores at regulated distances were constructed on a noncovalent DNA molecular assembly system in aqueous media. Photoinduced fluorescence resonance energy transfer (FRET) behaviors were then observed. We designed a number of chromophore/oligo-DNA conjugates with varying sequences. The chromophores eosin (Eo), TexasRed (TR), and tetramethylrhodamine (Rho) were employed as the energy donor, acceptor, and mediator, respectively, based on overlapping excitation and emission spectra. The chromophores were attached via aminolinkers to the 5'-terminals of 10mer oligo-DNAs consisting of AT rich sequences. The arrangement of Eo-Rho or Rho-TR with 10-residue (1 pitch of duplex) distances was ensured by duplex formation of the conjugates with a 20mer matrix oligo-DNA composed of complementary sequences to the conjugates. Single-step FRET from Eo to Rho and from Rho to TR was confirmed on the duplex. The three chromophore conjugates were then mixed with longer matrix oligo-DNAs (30 or 40mer) consisting of complementary sequences to the conjugates, producing Eo-(Rho)<sub>*n*</sub>-TR (*n* = 1 or 2) arrays with 10-residue distances. Multistep FRET from Eo to TR through the Rho mediator(s) was observed on the molecular assemblies. This photoenergy transmission system offers a good model for a photoenergy transmission system mimicking photosynthetic systems.

---

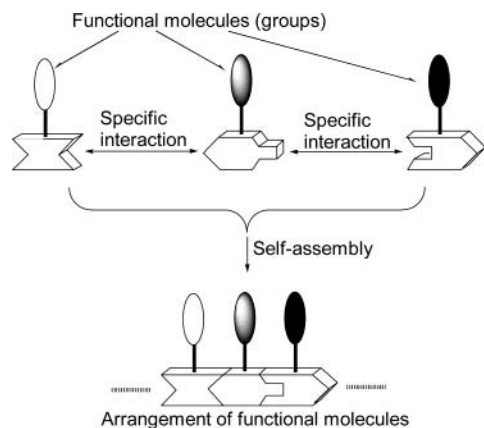
#### INTRODUCTION

In natural systems, the arrangement of functional molecules and groups with regulated distances, orders, and orientations provide highly efficient functionality. For example, in natural photosynthetic systems, the arrangement of porphyrin derivatives with regulated distance and geometry through noncovalent interaction provide highly efficient photoinduced energy transfer (1–3). To achieve noncovalent “homo” arrangement of one

kind of molecule or functional group, solid crystal, liquid crystalline systems or Langmuir–Blodgett film techniques may be useful. However, to achieve “hetero” and sequential arrangement of different kinds of molecules or functional groups, such systems are not effective. When constructing this type of system, numerous sets of specific noncovalent interactions should be provided (Figure 1). In natural and artificial systems, several types of noncovalent specific interactions, such as host–guest molecule, antigen–antibody, avidin–biotin, and saccharide–lectin, are known. However, it is difficult to include a wide variety of these specific interactions, and most of them require relatively large spaces.

---

\* Corresponding author. Phone +81-6-6368-0818, fax +81-6-6339-4026, e-mail yohya@ipcku.kansai-u.ac.jp.

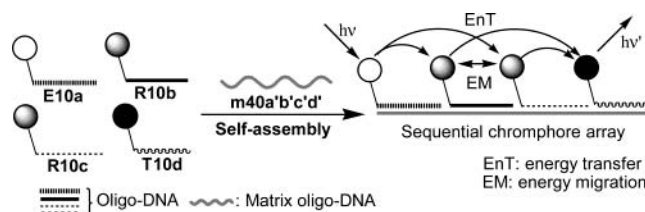


**Figure 1.** Arrangement of functional molecules or groups by self-assembly through specific interactions.

The biological tasks of nucleic acids (DNA and RNA) are genetic information storage and propagation. A single chain of poly- or oligo-nucleotide is able to interact specifically with its complementary counterpart chain through sequence-specific hydrogen bonding. By focusing on this property of nucleic acids, a wide variety of noncovalent binding pairs, binding donors, and binding acceptors, with high specificity and stability, can easily be provided simply by varying the oligo-DNA sequences. Oligo-DNA is therefore useful molecular glue for constructing molecular assembly systems. In fact, high-molecular-weight supramolecular polyassembly systems using complementary oligo-DNAs as binding groups have been reported both by our group (4) and Takenaka et al. (5). Seeman reported topological DNA assembly systems of various shapes and sizes (6–10). These characteristics of oligo-DNA facilitate the sequential arrangement of functional molecules.

As described above, in natural photosynthetic systems, arrangement of porphyrin derivatives with regulated distances and geometry through noncovalent interaction provide highly efficient photoinduced energy transfer. Arrangement of chromophores (multichromophore array) would therefore provide a good model for artificial photosynthetic systems. Chromophore arrangements using noncovalent interactions have been studied as models for artificial photosynthetic systems (11–17). Arrangements of chromophores in polymeric systems and the energy or electron transfer have also been investigated as models for photon-harvesting systems (18–20); however, the flexibility of the polymer chains interfered with the distance-controlled spatial arrangement of the chromophores. Sisido et al. attempted to arrange chromophores along a relatively rigid polypeptide  $\alpha$ -helix and reported energy or electron transfer in such systems (21–23). The high rigidity and regularity of DNA duplex may prove to be more practical and applicable for ensuring distance-controlled spatial arrangement of chromophores.

The DNA duplex contains a rich  $\pi$ -electron system comprising four bases stacked upon one another. A number of researchers have investigated the kinetics of electron transfer (ET) (24–29) and hole transport (30–32) through the DNA duplex as well as conductivity of the DNA duplex (33–35). Labeling of oligo- and polynucleotides with fluorescent probes is a classical but still very important technique for analysis of DNAs and RNAs. Spectral changes of the probes and fluorescent resonance energy transfer (FRET) or ET between probes covalently attached to DNAs and RNAs have been investigated for detection of duplex or triplex DNA formations (36, 37), for structural analyses of DNA and



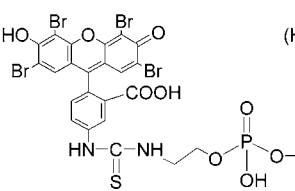
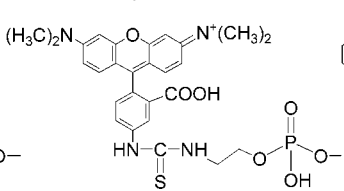
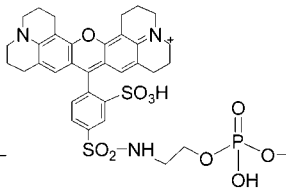
**Figure 2.** Schematic representation array constructed by mixing with complementary matrix oligo-DNA.

RNA (38–40), and for diagnostic detection of specific genes (41–43).

Specific chromophores with overlapping excitation and emission spectra that are arranged in order of excitation energy level should form a “photoenergy transmission pathway”. Such systems would provide a good model for artificial photosynthetic systems and assist our understanding of the natural photosynthetic system. We previously utilized DNA duplex formation to construct sequential arrangements of the three chromophores fluorescamine, rhodamine B, and fluorescein to act as the photoenergy donor, acceptor and mediator, respectively. We then reported the FRET behavior in aqueous media (44). Multistep photoinduced energy transfer from fluorescamine to rhodamine B through one or more fluorescein mediators was actually observed. However, the thermodynamic stability of the system was less than ideal, as only five residues were used for complementarity-determining regions. FRET systems involving three chromophores on DNAs have also reported by other groups (45–48).

In the present study, we designed a new series of chromophore/oligo-DNA conjugates with 10mer oligo-DNA as complementarity-determining regions. Using these, we constructed a relatively stable sequential arrangement of chromophores separated by a regulated distance and produced a multistep FRET in a noncovalent molecular assembly system in aqueous media. Three different chromophores with overlapping excitation and emission spectra were utilized: eosin (Eo), TexasRed (TR), and tetramethylrhodamine (Rho), as the photoenergy donor, acceptor, and mediator, respectively. These were attached to the 5'-terminals of 10mer oligo-DNAs displaying differing sequences. The sequences and the structure of the conjugates synthesized and matrix oligo-DNAs were shown in Table 1. The sequences of these oligo-DNAs were carefully chosen after considering several factors. We previously reported primitive study on energy transfer behavior in a similar system consisting of GC rich oligo-DNAs; however, the energy transfer efficiencies were not so high (49). Then we revealed that guanine residue(s) possessed a fluorescent quenching effect on chromophores attached to oligo-DNA when guanine was located near the chromophore (50). Guanine residues have also been reported to exhibit charge transport ability through a hole transport mechanism (30, 31). To avoid such unexpected quenching phenomena, we ensured that only A–T pairs were located near the chromophores (terminal regions of oligo-DNAs) in the chromophore/oligo-DNA conjugate. Moreover, the sequences were chosen to avoid formation of unexpected three-dimensional structures by intramolecular hydrogen bonding. The resulting conjugates were mixed with matrix oligo-DNA (30 or 40mer) consisting of complementary sequences for the conjugates in order to construct a sequential Eo-(Rho)<sub>n</sub>-TR array (where  $n = 1$  or 2) in a DNA duplex with 10 residues separating each chromophore component (Figure 2). The most common

**Table 1. Sequences and Abbreviations of the Compounds Used**

<div style="display: flex; justify-content: space-around; align-items: flex-start;"> <div style="text-align: center;"> <p>Eo = Eosin =</p>  </div> <div style="text-align: center;"> <p>Rho = Tetramethylrhodamine =</p>  </div> <div style="text-align: center;"> <p>TR = Texas Red® =</p>  </div> </div>		
abbreviation	structure(sequenced)	
<b>E10a</b>	Eo-5'-TTTTCTGATA3'	[Eo/oligo-DNA]
<b>R10b</b>	Rho-5'-ATTAGCTATT3'	[Rho/oligo-DNA(1)]
<b>R10c</b>	Rho-5'-ATTTCGAATT3'	[Rho/oligo-DNA(2)]
<b>T10d</b>	TR-5'-TATGTTCTAT3'	[TR/oligo-DNA]
<b>10a</b>	5'-TTTTCTGATA3'	
<b>10b</b>	5'-ATTAGCTATT3'	
<b>10c</b>	5'-ATTTCGAATT3'	
<b>10d</b>	5'-TATGTTCTAT3'	
<b>m20a'b'</b>	5'-AATAGCTAAT-TATCAGAAA3'	
<b>m20b'd'</b>	5'-ATAGAACATA-AATAGCTAAT3'	
<b>m30a'b'd'</b>	5'-ATAGAACATA-AATAGCTAAT-TATCAGAAA3'	
<b>m40a'b'c'd'</b>	5'-ATAGAACATA-AATTTCGAAAT-AATAGCTAAT-TATCAGAAA3'	

conformation for natural DNA duplex is B-form, where 10 residues form one turn. Chromophores on the DNA duplex were thus assumed to be arranged on the same side of the DNA duplex separated by one helical pitch (34 Å). The FRET behavior between the three chromophores was then investigated by monitoring fluorescence spectra in buffer solution.

#### EXPERIMENTAL PROCEDURES

**General Methods.** The UV-vis absorption and fluorescence spectra were recorded on UV-2500PC (Shimadzu, Japan) and F4010 (Hitachi, Japan) spectrophotometers, respectively. CD spectra were measured using a J-600 (JASCO, Japan). MALDI-TOF-MS experiments were performed on an AXIMA CFR (Shimadzu, Japan) [negative mode, matrix: 3-hydroxyphenylacetic acid ( $H_2O$ /acetonitrile = 7/3)] after samples were treated with 0.1 M diammonium hydrogen citrate solution. Reverse-phase HPLC was carried out using a Tosco-8020 system with a TSKgel OligoDNA RP column.

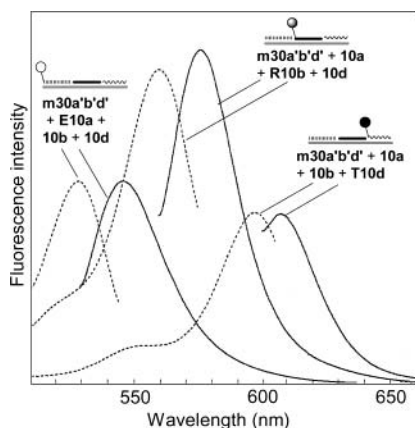
**Materials.** Eosin isothiocyanate (EITC), tetramethylrhodamine isothiocyanate (TRITC), and Texas Red sulfonyl chloride (TRS-Cl) were purchased from Molecular Probes, Inc. (USA). 5'-End-free fully protected oligo-DNAs on solid support (control pore glass, CPG), biotinyl-oligo-DNA, and nonmodified oligo-DNAs were obtained from Hokkaido System Science Co Ltd. (Japan). Aminoethanol, ethyl trifluoroacetate, 1*H*-tetrazole/acetonitrile solution and anhydrous acetonitrile were purchased from Wako Pure Chemical Ind. (Japan). 2-Cyanoethyl-*N,N,N,N*-tetraisopropylphosphorodiamidite was purchased from Aldrich Chemical Co. Inc. (Milwaukee, WI). Water was purified using a reverse-osmotic membrane. DMF and other organic solvents were purified by usual distillation methods. Other materials were of reagent grade and used without further purification. Synthesis of chromophore/oligo-DNA conjugates was performed according to the methods reported previously (49). Structures and sequences of the oligo-DNAs and chromophore/oligo-DNA conjugates synthesized are shown in Table 1. Synthetic procedures and spectral data of the conjugates are available in the Supporting Information.

**Spectroscopic Studies.** Concentration of unmodified oligo-DNA was calculated from the UV absorbance at 260 nm ( $A_{260}$ ), and extinction coefficients were determined using the nearest-neighbor approximation. Concentration

of each chromophore/oligo-DNA conjugate was determined using UV-vis absorbance at 525, 554, and 597 nm for Eo/oligo-DNA **E10a**, Rho/oligo-DNA **R10b** and **R10c**, and TR/oligo-DNA **T10d**, respectively. Conjugate concentration in solution was confirmed by the fact that their hypochromicity with complementary unmodified oligo-DNAs was maximal at 1/1 molar ratio. Hypochromicity measurement was performed by monitoring  $A_{260}$  of the solution containing the conjugate and complementary oligo-DNA in various ratios. Melting curves were recorded by starting at 60 °C sufficiently above  $T_m$  and reducing temperature at a rate of 10 °C/h to 10 °C sufficiently below  $T_m$ . Absorbance values were continuously recorded at intervals of 5 °C. CD spectra were measured on a JASCO J-600 using quartz cells of 0.5-cm path length at 15 °C. Concentrations of each conjugate and matrix oligo-DNA were  $1.0 \times 10^{-5}$  M. Fluorescence measurements were performed on a Hitachi F4010, using a  $1 \times 1$  cm quartz cell. Excitation wavelengths used were 525, 554, and 597 nm for Eo, Rho, and TR, respectively. Fluorescence spectra for the mixture of several chromophore/oligo-DNA conjugates and complementary matrix oligo-DNA were obtained by varying the mixing ratios. The following procedure is an example of the titration of **E10a** and **m20a'b'** with **R10b**. "Solution A", containing **E10a** ( $5.0 \times 10^{-7}$  M) and **m20a'b'** ( $5.0 \times 10^{-7}$  M), and "Solution B" containing **E10a** ( $5.0 \times 10^{-7}$  M), **m20a'b'** ( $5.0 \times 10^{-7}$  M), and **R10b** ( $40.0 \times 10^{-7}$  M) were prepared. The fluorescence spectra of "Solution A" were measured under titration with "Solution B". The final ratio of **R10b** to **E10a** was 4.0. All fluorescence experiments were performed at 5 °C in 0.05 M Tris-HCl buffer (pH 7.5) containing 0.5 M NaCl. The fluorescence intensity of each chromophore in mixed systems containing two or more chromophores was calculated by decomposition of the obtained spectra to the emission spectra of each chromophore. Excitation spectra were measured on the equipment described above at an emission wavelength of 609 nm.

**QCM Measurement.** Sequential duplex formation of chromophore/oligo-DNA conjugates with matrix oligo-DNA was investigated by 27-MHz quartz crystal microbalance (QCM) analysis at 15 °C. Experiments were carried out using the same equipment and methods as previously reported (51). In this experiment, 30mer matrix oligo-DNA-3'-biotinylated through a tetraethylene



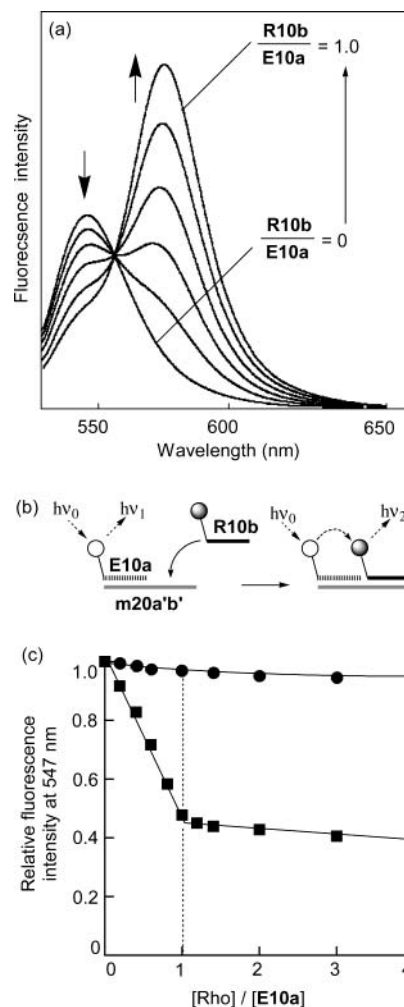


**Figure 3.** Excitation and emission spectra of Eo, Rho and TR in duplex form. Excitation spectra shown dotted lines and emission spectra shown solid lines. The excitation wavelengths for emission spectra of Eo, Rho and TR were 525 nm, 554 nm and 597 nm, respectively. Emission wavelengths for excitation spectra of Eo, Rho and TR were 574 nm, 578 nm and 609 nm, respectively.

glycol spacer (bio-**m30a'b'd'**) was used as a matrix oligo-DNA. Bio-**m30a'b'd'** (400 pmol) was added to an avidin-immobilized QCM sensor tip immersed in 8 mL of 10 mM Tris·HCl–1 mM EDTA–200 mM NaCl buffer (pH 7.8). After frequency decreased to  $-150$  Hz, the sensor tip was washed with water and 50 mM Tris·HCl–500 mM NaCl buffer (pH 7.5) and dipped into 8 mL of 50 mM Tris·HCl–500 mM NaCl buffer (pH 7.5). A frequency decrease of 1 Hz corresponded to a mass increase of  $0.61 \pm 0.1$  ng  $\text{cm}^{-2}$  on the QCM electrode (51–53). The frequency decrease of 150 Hz corresponded  $91.5$  ng  $\text{cm}^{-2}$  (1 pmol on  $4.9$  mm $^2$ ) binding of bio-**m30a'b'd'** to avidin immobilized on the sensor tip. Chromophore/oligo-DNA conjugates (**E10a**, **R10b**, **T10d**) were then sequentially added to the solution, and frequency changes were observed.

## RESULTS AND DISCUSSION

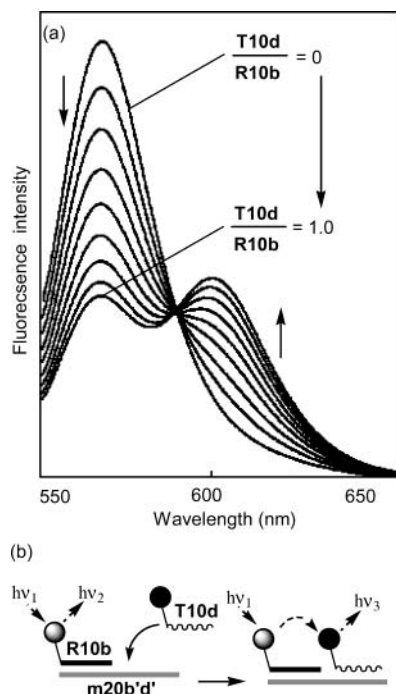
We selected Eo, TR, and Rho as the photoenergy donor, acceptor, and mediator, respectively, because of their overlapping excitation and emission wavelength ranges. The excitation and emission spectra of the chromophore/oligo-DNA conjugates in duplex form are shown in Figure 3. The  $\lambda_{\text{max}}$  values of excitation/emission spectra for Eo/oligo-DNA, Rho/oligo-DNA, and TR/oligo-DNA were 525/547 nm, 554/578 nm, and 597/609 nm, respectively. The  $T_m$  value of the stoichiometric mixture of **E10a**, **R10b**, **T10d**, and **m30a'b'd'** was determined to be ca.  $37^\circ\text{C}$  in 0.05 M Tris·HCl–0.5 M NaCl buffer (pH 7.5). The 30mer matrix oligo-DNA **m30a'b'd'** was composed of 3 units of 10mer oligo-DNA, each one of which was complementary with **E10a**, **R10b**, or **T10d**. The melting curve seemed to display a single transition point and no obvious double or triple transition points. This indicates that each of the 10mer units had similar  $T_m$  values. The  $T_m$  value of the stoichiometric mixture of matrix oligo-DNA **m30a'b'd'** and the three types of oligo-DNA **10a**, **10b**, and **10d**, having the same sequences as **E10a**, **R10b**, and **T10d**, was ca.  $37^\circ\text{C}$ . The mixture of conjugates and matrix oligo-DNA revealed that the chromophores attached to the 5'-terminals of oligo-DNA exerted almost no effect on formation of the duplex (thermal dissociation curves are available in the Supporting Information). On the basis of the results, further fluorescence measurements were performed at  $5^\circ\text{C}$ , which is sufficiently lower than the  $T_m$ . Specific and nonspecific interactions of chromophores with single- and double-stranded DNA, such as intercalation,



**Figure 4.** (a) Fluorescence spectra for titration of **E10a** and **m20a'b'** complex with **R10b** in 0.05 M Tris·HCl–0.5 M NaCl buffer (pH 7.5) at  $5^\circ\text{C}$ .  $[\text{m20a'b}'] = [\text{E10a}] = 5.0 \times 10^{-7}$  M,  $[\text{R10b}]/[\text{E10a}] = 0\text{--}1.0$ . Excitation wavelength: 525 nm. (b) Schematic representation of procedure. (c) Plots of relative fluorescence intensity at 547 nm vs ratio of  $[\text{Rho}]/[\text{E10a}]$ . Square **R10b**; circle 1:1 mixture of **10b** and free Rho.  $[\text{m20a'b}'] = [\text{E10a}] = 5.0 \times 10^{-7}$  M. Excitation wavelength: 525 nm.

were not observed in either UV or fluorescence spectra measurements.

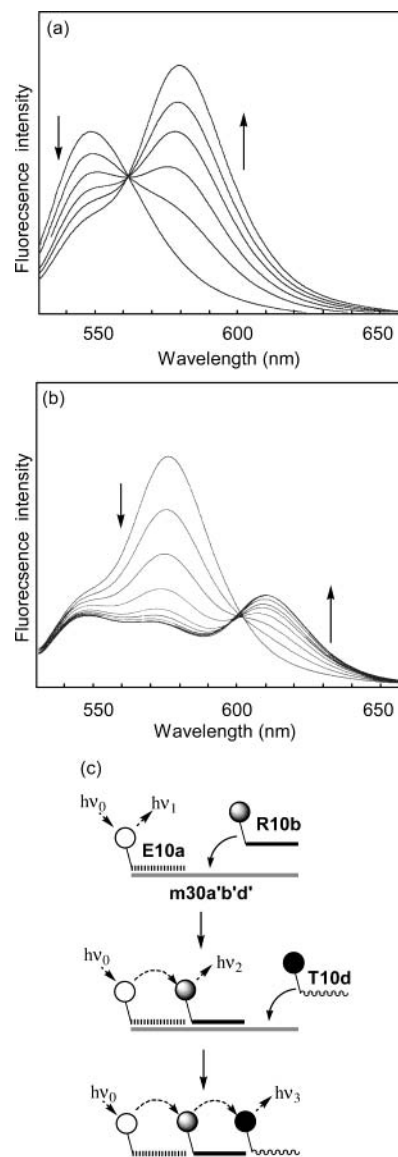
Before studying multistep FRET, we investigated single-step FRET behaviors between two chromophores. Experiments were performed using 20mer matrix oligo-DNA, donor/oligo-DNA displaying complementarity with the 10 3'-terminal residues of the matrix oligo-DNA and acceptor/oligo-DNA displaying complementarity with the 10 5'-terminal residues of the matrix oligo-DNA. Figure 4a shows the fluorescence spectra for titration of **E10a** (donor) and the 20mer matrix oligo-DNA **m20a'b'** with **R10b** (acceptor). Fluorescence spectra were measured at an excitation wavelength of 525 nm ( $\lambda_{\text{max}}$  of Eo) in 0.05 M Tris·HCl–0.5 M NaCl buffer (pH 7.5) at  $5^\circ\text{C}$ . A schematic illustration of the experimental procedure is shown in Figure 4b. Quenching of fluorescence from donor chromophores (Eo) and increased fluorescence from acceptor chromophores (Rho) were observed on addition of **R10b**. Effective quenching and increased fluorescence of Rho were not observed when a mixture of free Rho and oligo-DNA **10b** was added instead of **R10b**. Figure 4c shows relative fluorescence intensity of Eo at 547 nm vs the molar ratio of **R10b** to **E10a**. The donor (Eo) quenching was almost saturated when the molar ratio



**Figure 5.** (a) Fluorescence spectra for titration of **R10b** and **m20b'd'** complex with **T10d** in 0.05 M Tris·HCl–0.5 M NaCl buffer (pH 7.5) at 5 °C.  $[\text{m20b'd}'] = [\text{R10b}] = 5.0 \times 10^{-7}$  M,  $[\text{T10d}]/[\text{R10b}] = 0\text{--}1.0$ . Excitation wavelength: 554 nm. (b) Schematic representation of the procedure.

of **R10b** to **E10a** was 1. The same experiment was performed for the combination of **R10b** and **T10d**. Figure 5a shows the fluorescence spectra for titration of **R10b** (donor) and a 20mer matrix oligo-DNA **m20b'd'** with **T10d** (acceptor). Fluorescence spectra were measured at an excitation wavelength of 554 nm ( $\lambda_{\text{max}}$  of Rho) in 0.05 M Tris·HCl–0.5 M NaCl buffer (pH 7.5) at 5 °C. A schematic illustration of the experimental procedure is shown in Figure 5b. Quenching of fluorescence from donor chromophores (Rho) and increased fluorescence from acceptor chromophores (TR) was observed on the addition of **T10d**. Effective quenching and increased fluorescence of TR were not observed when a mixture of free TR and oligo-DNA **10d** was added instead of **T10d**. These results suggest that single-step FRET from Eo to Rho and from Rho to TR occurred along the 20bp DNA duplex.

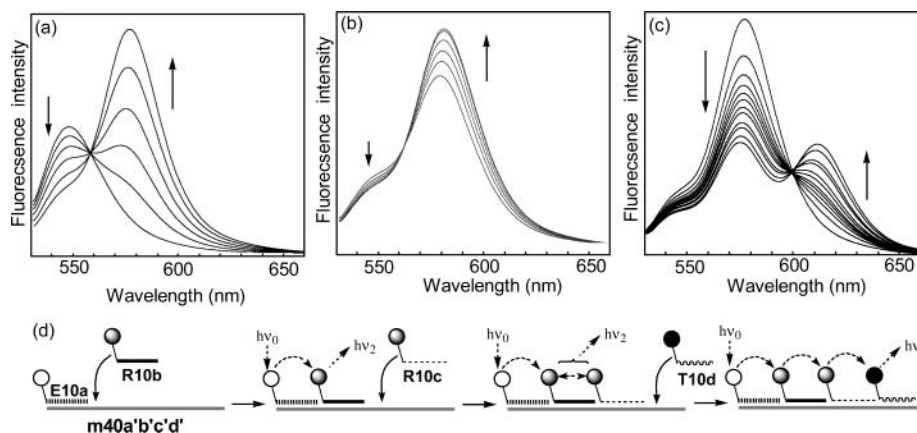
Single-step FRET was successfully observed between two chromophores, and we therefore investigated two-step energy transfer from Eo (donor) through Rho (mediator) to TR (acceptor) on a duplex with a 30mer matrix oligo-DNA **m30a'b'd'**. As an initial step, **E10a** displaying complementarity with the 10 3'-terminal residues of the matrix oligo-DNA was mixed with matrix oligo-DNA **m30a'b'd'** in a 1:1 ratio. The complex formed was then titrated with an equivalent amount **R10b** displaying complementarity with the 10 central residues of the **m30a'b'd'**. The obtained solution of **E10a**, **R10b** and **m30a'b'd'** (1:1:1 ratio) was then titrated with **T10d** displaying complementarity with the 10 5'-terminal residues of **m30a'b'd'**. Figures 6a and 6b show the fluorescence spectra of the two-step titration for the complex of **m30a'b'd'** and **E10a** with **R10b**, and subsequent titration with **T10d**. Fluorescence spectra were measured at an excitation wavelength of 525 nm ( $\lambda_{\text{max}}$  of Eo) in 0.05 M Tris·HCl–0.5 M NaCl buffer (pH 7.5) at 5 °C. A schematic illustration of the experimental procedure is shown in Figure 6c. Initially, quenching of Eo and



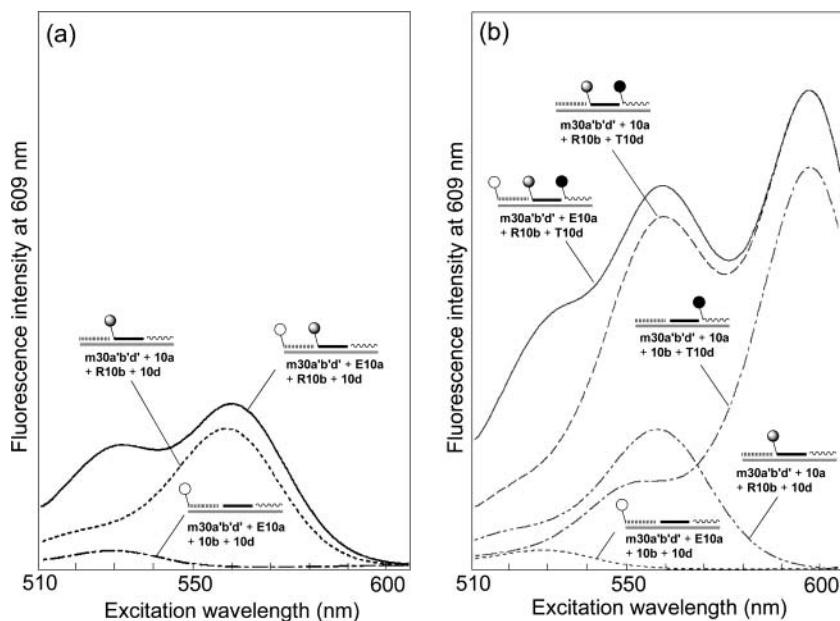
**Figure 6.** Fluorescence spectra for titration of **E10a** and **m30a'b'd'** complex with **R10b** (a) and **T10d** (b) in 0.05M Tris·HCl–0.5M NaCl buffer (pH 7.5) at 5 °C.  $[\text{m30a'b'd}'] = [\text{E10a}] = 5.0 \times 10^{-7}$  M.  $[\text{R10b}]/[\text{E10a}] = 0\text{--}1.0$ .  $[\text{T10d}]/[\text{E10a}] = 0\text{--}2.0$ . Excitation wavelength: 525 nm. (c) Schematic representation of the procedure.

increased fluorescence from Rho were observed on addition of **R10b**, as shown in Figure 4. Quenching of Rho and increased fluorescence from TR were then observed on addition of **T10d**, as shown in Figure 5. The fact that obvious fluorescence from TR was observed at an excitation wavelength of 525 nm indicates that the photoenergy transferred from Eo to Rho was further transferred to TR by two-step FRET.

We then investigated multistep FRET from Eo (donor) through two Rhos (mediators) to TR (acceptor) on a duplex with a 40mer matrix oligo-DNA **m40a'b'c'd'** containing 20 complementary residues with **R10b** and **R10c** in the central region. Initially, **R10b** (complementary with residues 21–30 of **m40a'b'c'd'**) was added to the 1:1 ratio mixture of **m40a'b'c'd'** with **E10a** (complementary with the residues 31–40 of **m40a'b'c'd'**) to a final ratio of 1:1:1. The complex formed was then titrated with an equivalent amount **R10c** (complementary with residues 11–20 of **m40a'b'c'd'**). This complex, **E10a**, **R10b**, **R10c** and **m40a'b'c'd'** (1:1:1:1 ratio), was titrated



**Figure 7.** Fluorescence spectra for titration of **E10a** and **m40a'b'c'd'** complex with **R10b** (a), **R10c**, (b), and **T10d** (c) in 0.05M Tris·HCl-0.5M NaCl buffer (pH 7.5) at 5 °C.  $[\mathbf{m40a'b'c'd'}] = [\mathbf{E10a}] = 5.0 \times 10^{-7}$  M.  $[\mathbf{R10b}]/[\mathbf{E10a}] = 0-1.0$ ,  $[\mathbf{R10c}]/[\mathbf{E10a}] = 0-1.0$ ,  $[\mathbf{T10d}]/[\mathbf{E10a}] = 0-4.0$ . Excitation wavelength: 525 nm. (d) Schematic representation of the procedure.



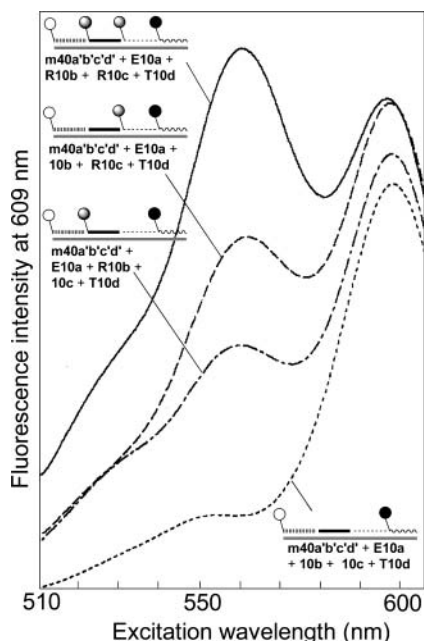
**Figure 8.** Excitation spectra for complexes (a) (**m30a'b'd' + E10a + 10b + 10d**), (**m30a'b'd' + 10a + R10b + 10d**), (**m30a'b'd' + E10a + R10b + 10d**), and (b) (**m30a'b'd' + E10a + 10b + T10d**), (**m30a'b'd' + 10a + R10b + T10d**), (**m30a'b'd' + 10a + 10b + T10d**), (**m30a'b'd' + E10a + R10b + T10d**), (**m30a'b'd' + 10a + R10b + T10d**), and (**m30a'b'd' + 10a + 10b + T10d**) in 0.05 M Tris·HCl-0.5 M NaCl buffer (pH 7.5) at 5 °C. Emission wavelength: 609 nm.  $[\mathbf{E10a}] = [\mathbf{R10b}] = [\mathbf{T10d}] = [\mathbf{10a}] = [\mathbf{10b}] = [\mathbf{m30a'b'd'}] = 5.0 \times 10^{-7}$  M.

with **T10d** displaying complementarity with the residues 1–10 of **m40a'b'c'd'**. Figures 7a–c show changes in fluorescence spectra for the three-step titration of complex of **m40a'b'c'd'** and **E10a** with **R10b**, **R10c** and the subsequent titration with **T10d**. Fluorescence spectra were measured at an excitation wavelength of 525 nm ( $\lambda_{\max}$  of Eo) in 0.05 M Tris·HCl-0.5 M NaCl buffer (pH 7.5) at 5 °C. A schematic illustration of the experimental procedure is shown in Figure 7d. Quenching of Eo and increased fluorescence from Rho were observed on addition of **R10b**, as shown in Figures 4 and 6. Slightly quenching of Eo and somewhat increased fluorescence from Rho were observed on addition of **R10c**. Furthermore, quenching of Rho and increased fluorescence from TR were observed on addition of **T10d**, as shown in Figures 5 and 6. The fact that obvious fluorescence from TR was observed at excitation of 525 nm indicates that the photoenergy transferred from Eo through the two Rhos was further transferred to TR. These results suggest that energy migration between the two Rhos occurred.

To determine the energy transfer efficiency, excitation spectra were measured for the chromophore/oligo-DNA

assembly systems in 0.05 M Tris·HCl-0.5 M NaCl buffer (pH 7.5) at 5 °C. The emission wavelength was 609 nm ( $\lambda_{\max}$  of emission of TR) for all excitation spectra. Figures 8 and 9 show typical excitation spectra for the 30mer and 40mer assembly systems, respectively. Combinations of the conjugates, control oligo-DNAs and matrix oligo-DNA are illustrated in the figures. Figure 8a suggests FRET from Eo to Rho occurred. Eo (**E10a + 10b + 10d + m30a'b'd'**) showed very little excitation, because Eo does not show effective emission at 609 nm. Rho (**10a + R10b + 10d + m30a'b'd'**) showed some excitation around 560 nm, corresponding with absorbance by Rho. However, the Eo–Rho system (**E10a + R10b + 10d + m30a'b'd'**) showed double the maximum excitation as each of Rho and Eo showed. The difference between (**E10a + R10b + 10d + m30a'b'd'**) and (**10a + R10b + 10d + m30a'b'd'**) was larger than that for (**E10a + 10b + 10d + m30a'b'd'**). This suggests that effective energy transfer from Eo to Rho in (**E10a + R10b + 10d + m30a'b'd'**) occurred. In Figure 8b, FRETs from Rho to TR and from Eo to TR were shown. TR (**10a + 10b + T10d + m30a'b'd'**) showed substantial excitation around 600 nm corresponding with absorbance by TR. The Rho-TR





**Figure 9.** Excitation spectra for complex (**m40a'b'c'd' + E10a + 10b + 10c + T10d**), (**m40a'b'c'd' + E10a + R10b + 10c + T10d**), (**m40a'b'c'd' + E10a + 10b + R10c + T10d**) and (**m40a'b'c'd' + E10a + R10b + R10c + T10d**) in 0.05 M Tris-HCl-0.5 M NaCl buffer (pH 7.5) at 5 °C. Emission wavelength: 609 nm.  $[E10a] = [R10b] = [R10c] = [T10d] = [10a] = [10b] = [10c] = [10d] = [m40a'b'c'd'] = 5.0 \times 10^{-7}$  M.

system (**10a + R10b + T10d + m30a'b'd'**) showed double the maximum excitation as each of Rho and TR showed. The difference between (**10a + R10b + T10d + m30a'b'd'**) and (**10a + 10b + T10d + m30a'b'd'**) was larger than that for (**10a + R10b + 10d + m30a'b'd'**). This indicates that effective energy transfer from Rho to TR in (**10a + R10b + T10d + m30a'b'd'**) occurred. Furthermore, for the Eo-Rho-TR system (**E10a + R10b + T10d + m30a'b'd'**), a peak at around 520 nm, corresponding with Eo, was observed in addition to the spectra seen with (**10a + R10b + T10d + m30a'b'd'**). The difference between these systems was larger than that for (**E10a + 10b + 10d + m30a'b'd'**). This suggests that absorption of Eo contributed to fluorescence at 609 nm: photon-energy absorbed by Eo was effectively transferred to TR.

In Figure 9, FRETs in the quadruplex system on 40mer matrix oligo-DNA. The Y-axis of Figure 9 is the same as Figures 8a and 8b. Eo-(blank)-(blank)-TR system (**E10a + 10b + 10c + T10d + m30a'b'c'd'**) showed almost same excitation spectra as TR (**10a + 10b + 10c + T10d + m30a'b'c'd'**). No effective energy transfer from Eo to TR separated 30 residues. Eo-Rho-(blank)-TR system (**E10a + R10b + 10c + T10d + m30a'b'c'd'**) and Eo-(blank)-Rho-TR system (**E10a + 10b + R10c + T10d + m30a'b'c'd'**) showed excitation peak around 560 nm. The intensity was larger in the latter, which had shorter distance (10 residues) between Rho and TR. In Eo-Rho-Rho-TR system, larger excitation peak for Rho was observed because this system two Rhos. In addition to the Rho excitation peak, small peak corresponding with Eo was observed around 520 nm. This suggest some energy transfer from Eo to TR separated 30 residues. Quantitative for all excitation spectra below.

On the basis of the titration fluorescence spectra and excitation spectra, we were able to estimate quenching efficiency ( $Q(\%)$ ) and energy transfer efficiency ( $T(\%)$ ). Quenching efficiency ( $Q(\%)$ ) based on fluorescence quench-

ing of the donor chromophore was calculated using the following equation:

$$Q(\%) = (q - q_0)/(1 - q_0) \times 100$$

where  $q = 1 - I/I_0$ , and represents the quenching with acceptor/oligo-DNA conjugate,  $q_0$  is the quenching with free chromophore and oligo-DNA without chromophore,  $I$  is the fluorescence intensity, and  $I_0$  is the fluorescence intensity of donor/oligo-DNA conjugate.

Energy transfer ( $T(\%)$ ) based on excitation spectra was calculated using the following equation (54):

$$T_{app}(\%) = \frac{A_{(x)}}{A_{(100)}} \times 100 = \left\{ \frac{\phi_D F_D}{\phi_A F_A} (1 - T) + T \right\} \times 100$$

$T_{app}$  is the apparent energy transfer,  $A_{(100)}$  is the emission spectrum,  $A_{(x)}$  is the excitation spectrum of measurement system,  $\phi_D$  and  $\phi_A$  are the quantum yields of donor and acceptor chromophore, and  $F_D$  and  $F_A$  are the fluorescence of donor and acceptor chromophore/area of the emission spectrum.

The  $Q(\%)$ ,  $T_{app}(\%)$ , and  $T(\%)$  obtained for the molecular assemblies of chromophore/oligo-DNA conjugates with matrix oligo-DNAs summarized in Table 2. The efficiencies for one-step FRET from Eo to Rho and from Rho to TR were 32.3% and 36.3%, respectively. Direct energy transfer from Eo to TR in Eo-(blank)-TR system was 0%, because the 20 residue distance and small overlap of absorbance and emission spectra. In contrast, the Eo-Rho-TR system showed effective energy transfer (23.7% efficiency). The effect of Rho as a mediator was clear. The two-step energy transfer efficiency from Eo to TR though Rho was smaller than that of the one-step FRETs, but larger than their product. When comparing the Eo-Rho system and the Eo-(blank)-Rho system, energy transfer efficiency decreased depending the distance. This is not exactly in line with the Förster equation, probably due to the flexibility of the spacer groups and friction of the chromophores. Single Rho mediator systems, Eo-Rho-(blank)-TR system and Eo-(blank)-Rho-TR system, showed 13.8% and 8.5% of energy transfer efficiencies, respectively. On the other hand, the Eo-Rho-Rho-TR system having two Rho mediators showed larger energy transfer efficiency (21.6%), which was similar to that of the Eo-Rho-TR system (23.7%). These results indicate energy migration between two Rho mediators.






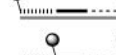



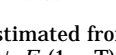
Sequential and quantitative duplex formation of chromophore/oligo-DNA conjugates with matrix oligo-DNA was investigated by QCM analysis. The following Sauerbrey equation was for the AT-cut shear mode QCM (55),

$$\Delta F = - \frac{2F_0^2}{A\sqrt{\rho_q \mu_q}} \Delta m$$

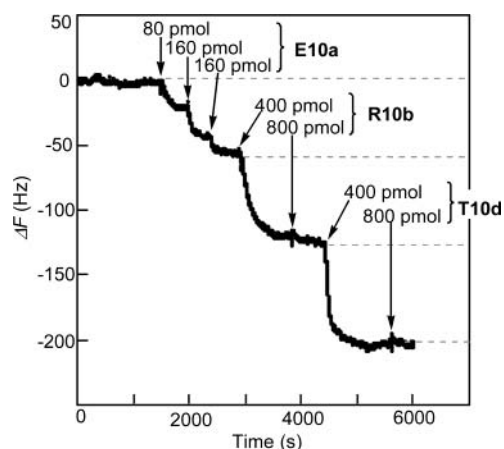
where,  $\Delta F$  is the measured frequency change (Hz),  $F_0$  the fundamental frequency of the QCM ( $27 \times 10^6$  Hz),  $\Delta m$  is the mass change (g),  $A$  is the electrode area ( $4.9 \text{ mm}^2$ ),  $\rho_q$  is the density of quartz ( $2.65 \text{ g cm}^{-3}$ ), and  $\mu_q$  is the shear modulus of quartz ( $2.95 \times 10^{11} \text{ dyn cm}^{-2}$ ). Previous calibration for the 27 MHz QCM showed that a frequency decrease of 1 Hz corresponded to a  $0.61 \text{ ng cm}^{-2}$  mass increase (53).

Typical results for the assembly of **E10a**, **R10b**, and **T10d** with **m30a'b'd'** are shown in Figure 10. First, 80 pmol of **m30a'b'd'** was added to **m30a'b'd'** bound to avidin-immobilized QCM sensor tip (total concentration of **E10a**

**Table 2. Quenching and Energy Transfer Efficiencies**

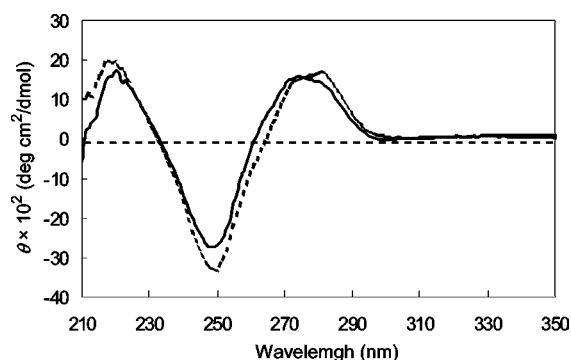
		$Q(\%)^a$	$T_{app}(\%)^b$	$T(\%)^c$
$E0 \rightarrow Rho$		50.2	45.8	32.3
$E0 \rightarrow (blank) \rightarrow TR$		5.4	2.4	0
$Rho \rightarrow TR$		62.5 <sup>d</sup>	46.8	36.3
$E0 \rightarrow Rho \rightarrow TR$		53.1	26.2	23.7
$E0 \rightarrow (blank) \rightarrow Rho$		13.6	27.8	9.7
$E0 \rightarrow (blank) \rightarrow (blank) \rightarrow TR$		0	0	0
$Rho \rightarrow (blank) \rightarrow TR$		9.9 <sup>d</sup>	34.1	21.1
$E0 \rightarrow Rho \rightarrow (blank) \rightarrow TR$		49.5	16.6	13.8
$E0 \rightarrow (blank) \rightarrow Rho \rightarrow TR$		11.7	11.5	8.5
$E0 \rightarrow Rho \rightarrow Rho \rightarrow TR$		57.5	24.2	21.6

<sup>a</sup> Quenching efficiency of donor. <sup>b</sup> Apparent energy transfer estimated from excitation spectra. <sup>c</sup> Energy transfer efficiency calculated from the following equation:  $T_{app}(\%) = A_{(X)}/A_{(100)} \times 100 = \{\phi_D F_D / \phi_A F_A (1 - T) + T\} \times 100$  where  $A_{(100)}$ , emission spectrum;  $A_{(X)}$ , excitation spectrum of measurement system;  $\phi_{D(A)}$ , quantum yield of donor (acceptor) chromophore;  $F_{D(A)}$ , fluorescence of donor (acceptor) chromophore/area of emission spectrum. <sup>d</sup> Calculated from quenching of Rho.



**Figure 10.** Typical time dependencies of QCM frequency for immobilized **m30a'b'd'** responding to addition of **E10a**, **R10b**, and **T10d** in 0.05 M Tris·HCl–0.5 M NaCl buffer (pH 7.5) at 15 °C.

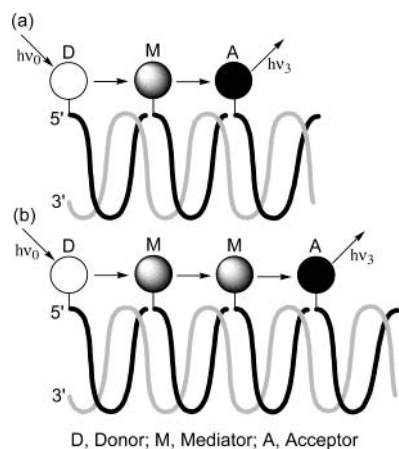
= 10 nM). A decrease in frequency was observed and a further 160 pmol of **E10a** was added. After this second addition of **E10a**, a larger decrease in frequency was observed (twice the decrease observed with the first addition). Following this, a further 160 pmol of **E10a** was added, and slight decreases in frequency and saturation of frequency change were observed. These results indicate that 400 pmol of **E10a** was an excess for immobilized **m30a'b'd'** and that the **m30a'b'd'** on QCM sensor tip quantitatively bound to **E10a**. The decrease in frequency was 59.5 Hz after total **E10a** addition (400 pmol). Second, 400 pmol of **R10b** was added to the solution, and a similar decrease in frequency (62.2 Hz) as seen with **E10a** (400 pmol) was observed. After confirmation of no further **R10b** binding by addition of excess **R10b** (800 pmol), 400 pmol of **T10d** was added to the solution. A slightly higher but similar decrease in frequency (75.0 Hz) as observed with **E10a** (400 pmol) was observed. No further **T10d** binding was confirmed by addition of excess **T10d** (800 pmol). These results indicate that almost the same amounts of **E10a**, **R10b**, and **T10d** bound to **m30a'b'd'**, and each 10-residue region of **m30a'b'd'** was quantitatively by **E10a**, **R10b** and **T10d**. From these



**Figure 11.** CD Spectrum for equivalent mixture of **m40a'b'c'd'**, **E10a**, **R10b**, **R10c**, and **T10d** (solid line), and equivalent mixture of **m40a'b'c'd'**, **10a**, **10b**, **10c**, and **10d** (dashed line) in 0.05 M Tris·HCl–0.5 M NaCl buffer (pH 7.5) at 15 °C. Concentration of each conjugate and oligo-DNA =  $1.0 \times 10^{-5}$  M.

results, formation of the expected assembly of chromophore/oligo-DNA conjugates with matrix oligo-DNA, as shown in Figure 2, was strongly suggested.

In order to obtain information about the conformation of the assembly, CD spectra were measured for equivalent mixtures of chromophore/oligo-DNA conjugates and matrix oligo-DNA at 15 °C. Figure 11 shows a typical example for equivalent mixtures of **E10a**, **R10b**, **R10c**, **T10d**, and **m40a'b'c'd'**, which were used in the experiment shown in Figure 7. Strong negative and positive cotton effects were observed around 250 and 280 nm, respectively. This pattern displays the typical characteristics of a B-form DNA duplex and is almost the same as that seen for the equivalent mixture of **10a**, **10b**, **10c**, **10d**, and **m40a'b'c'd'**. The assembly system of the four kinds of chromophore/oligo-DNA conjugates with the 40mer matrix oligo-DNA therefore displayed a B-form double helical conformation. Other systems, such as **E10a**, **R10b**, **T10d**, and **m30a'b'd'**, showed similar results. Figure 12 shows geometrical illustrations for assemblies of the three types of chromophore/oligo-DNAs and matrix oligo-DNA (30 or 40mer) assuming B-form double helical conformation. As the B-form DNA duplex has 10 residues per turn (34 Å), the system was believed



**Figure 12.** Schematic illustration geometry of chromophore arrays constructed on oligo-DNA assemblies. (a) 1:1:1 mixture of **E10a**, **R10b**, **T10d**, and **m30a'b'd'**, (b) 1:1:1:1 mixture of **E10a**, **R10b**, **R10c**, **T10d**, and **m40a'b'c'd'**.

to have all chromophores on the same side of the duplex at one-pitch distance (34 Å), as shown in Figure 12.

## CONCLUSIONS

Three chromophores (Eo, Rho, and TR) were attached to the 5'-terminal ends of 10mer oligo-DNAs in order to produce chromophore/oligo-DNA conjugates. Programmed sequential arrangements of chromophores separated by regulated distances of about one pitch of DNA duplex (34 Å) on noncovalent molecular assembly systems in aqueous media were then constructed by mixing conjugates with longer matrix oligo-DNAs. Multistep FRET from Eo to TR through one or two Rho mediators was observed on the molecular assemblies. The results suggested that photon-energy transfer occurred from Eo to TR separated by a long distance (three helical pitches, 104 Å) through Rho mediators via a multistep FRET on the molecular assemblies. The information obtained from these systems will be useful in constructing a photon-collecting antenna for an artificial photosynthetic system, as well as in enhancing our understanding of the mechanisms of energy transfer behavior in noncovalent molecular assembly system, such as natural photosynthetic systems. In subsequent research, details of the FRET behaviors of chromophores on oligo-DNA assemblies should be investigated using measurements of fluorescence lifetime and transition state absorption spectra of the chromophores.

## ACKNOWLEDGMENT

A part of this study was financially supported by a Grant-in-Aid for Scientific Research on Priority Areas from The Ministry of Education, Science, Sports and Culture, Japan. The authors express their thanks to Prof. Yoshio Okahata, Department of Biomolecular Engineering Tokyo Institute of Technology, for his assistance in QCM analysis.

**Supporting Information Available:** Experimental procedures for synthesis of chromophore/oligo-DNA conjugates, spectral data for conjugates, melting curves of assemblies, and illustration of QCM analysis. This material is available free of charge via the Internet at <http://pubs.acs.org/BC>.

## LITERATURE CITED

(1) McDermott, G., Prince, S. M., Freer, A. A., Hawthornthwaite-Lawless, A. M., Papiz, M. Z., Cogdell, R. J., and Isaacs,

N. W. (1995) Crystal-Structure of an Integral Membrane Light-Harvesting Complex from Photosynthetic Bacteria. *Nature* 374, 517–521.

(2) Van Grondelle, R., Dekker, J. P., Gillbro, T., and Sundstrom, V. (1994) Energy-Transfer and Trapping in Photosynthesis. *Biochim. Biophys. Acta* 1187, 1–65.

(3) Moser, C. C., and Dutton, P. L. (1992) Engineering Protein-Structure for Electron-Transfer Function in Photosynthetic Reaction Centers. *Biochim. Biophys. Acta* 1101, 171–176.

(4) Ohya, Y., Noro, H., Komatsu, M., Ouchi, T. (1996) Synthesis of Symmetric Oligo-DNA Dimers and Their Formation of Polymeric Supramolecular Assembly. *Chem. Lett.* 447–448.

(5) Takenaka, S., Funatsu, Y., and Kondo, H. (1996) Spontaneous Formation of a Molecular Net Assembly by Using Nucleotide Complementarity. *Chem. Lett.* 891–892.

(6) Zhang, Y., and Seeman, N. C. (1994) Construction of a DNA-Truncated Octahedron. *J. Am. Chem. Soc.* 116, 1661–1669.

(7) Chen, J., and Seeman, N. C. (1991) Synthesis from DNA of Molecule with the Connectivity of a Cube. *Nature* 350, 631–633.

(8) Seeman, N. C. (1991) Construction of 3-Dimensional Stick Figures from Branched DNA. *DNA Cell Biol.* 10, 475–486.

(9) Winfree, E., Liu, F., Wenzler, L. A., and Seeman, N. C. (1998) Design and Self-Assembly of Two-Dimensional DNA Crystals. *Nature* 394, 539–544.

(10) Mao, C., Sun, W., and Seeman, N. C. (1999) Designed Two-Dimensional DNA Holliday Junction Arrays Visualized by Atomic Force Microscopy. *J. Am. Chem. Soc.* 121, 5437–5443.

(11) Sessler, J. L., Wang, B., and Harriman, A. (1993) Long-Range Photoinduced Electron-Transfer in an Associated but Noncovalently Linked Photosynthetic Model System. *J. Am. Chem. Soc.* 115, 10418–10419.

(12) Sessler, J. L., Wang, B., and Harriman, A. (1995) Photoinduced Energy-Transfer in Associated but Noncovalently Linked Photosynthetic Model Systems. *J. Am. Chem. Soc.* 117, 704–714.

(13) Berman, A., Izraeli, E. S., Levanon, H., Wang, B., and Sessler, J. L. (1995) Photoinduced Intraensemble Electron-Transfer in a Base-Paired Porphyrin-Quinone System – Time-Resolved EPR Spectroscopy. *J. Am. Chem. Soc.* 117, 8252–8257.

(14) Osuka, A., Yoneshima, R., Shiratori, H., Okada, T., Taniguchi, S., and Mataga, N. (1998) Electron Transfer in a Hydrogen-Bonded Assembly Consisting of Porphyrin-Diimide. *Chem. Commun.* 1567–1568.

(15) Tecilla, P., Dixon, R. P., Slobodkin, G., Alavi, D. S., Waldeck, D. H., and Hamilton, A. D. (1990) Hydrogen-Bonding Self-Assembly of Multichromophore Structures. *J. Am. Chem. Soc.* 112, 9408–9410.

(16) Tamiaki, H., Miyatake, T., Tanikaga, R., Holzwarth, A. R., and Schaffner, K. (1996) Self-Assembly of an Artificial Light-Harvesting Antenna: Energy Transfer from a Zinc Chlorin to a Bacteriochlorin in a Supramolecular Aggregate. *Angew. Chem., Int. Ed. Engl.* 35, 772–774.

(17) Hunter, C. A., and Hyde, R. K. (1996) Photoinduced Energy and Electron Transfer in Supramolecular Porphyrin Assemblies. *Angew. Chem., Int. Ed. Engl.* 35, 1936–1939.

(18) Webber, S. E. (1985) Intramolecular Energy Transfer in Polymers. *New Trends in The Photochemistry of Polymers* (N. S. Allen and J. F. Rabek, Eds.) pp 19–41, Elsevier, London.

(19) Ren, X.-X., and Guillet, J. E. (1985) Studies of the Antenna Effect in Polymer-Molecules. 9. Energy-Transfer, Migration, and Photoreactivity of Copolymers of 1-Naphthylmethyl Methacrylate and [2-(9,10-Anthraquinonyl)]Methyl Methacrylate. *Macromolecules* 18, 2012–2019.

(20) Bai, F., Chang, C.-H., and Webber, S. E. (1986) Photon-Harvesting Polymers – Singlet Energy-Transfer in Anthracene-Loaded Alternating and Random Copolymers of 2-Vinylnaphthalene and Methacrylic-Acid. *Macromolecules* 19, 2484–2494.

(21) Sisido, M. (1989) Photoinduced Electron-Transfer on a Single Alpha-Helical Polypeptide-Chain. *J. Am. Chem. Soc.* 111, 6790–6796.

(22) Inai, Y., Sisido, M., and Imanishi, Y. (1991) Photoinduced Electron-Transfer on a Single Alpha-Helical Polypeptide-



- Chain-Evidence of a Through-Space Mechanism. *J. Phys. Chem.* 95, 3847–3851.
- (23) Sisido, M. (1989) One-Dimensional Aromatic Crystals in Solution. 9. Synthesis, Conformation, and Chiroptical Spectroscopy of Poly[LYS(Z)2-PYRALA] in Solution. *Macromolecules* 22, 3280–3285.
- (24) Brum, A. M., and Harriman, A. (1992) Dynamics of Electron-Transfer Between Intercalated Polycyclic Molecules – Effect of Interspersed Bases. *J. Am. Chem. Soc.* 114, 3656–3660.
- (25) Murphy, C. J., Arkin, M. R., Jenkins, Y., Ghatilia, N. D., Bossmann, S. H., Turro, N. J., and Barton, J. K. (1993) Long-Range Photoinduced Electron-Transfer Through a DNA Helix. *Science* 262, 1025–1029.
- (26) Meade, T. J., and Kayyem, J. F. (1995) Electron-Transfer Through DNA – Site-Specific Modification of Duplex DNA with Ruthenium Donors and Acceptors. *Angew. Chem., Int. Engl. Ed.* 34, 352–354.
- (27) Kelley, S. O., and Barton, J. K. (1999) Electron-Transfer Between Bases in Double Helical DNA. *Science* 283, 375–381.
- (28) Lewis, F. D., Wu, T., Zhang, Y., Letsinger, R. L., Greenfield, S. R., and Wasielewski, M. R. (1997) Distance-Dependent Electron Transfer in DNA Hairpins. *Science* 277, 673–676.
- (29) Barnett, R. N., Cleveland, C. L. Joy, A., Landman, U., and Schuster, G. B. (2001) Charge Migration in DNA: Ion-Gated Transport. *Science* 294, 567–571.
- (30) Meggers, E., Micheal-Beyerle, M. E., and Giese, B. (1998) Sequence Dependent Long-Range Hole Transport in DNA. *J. Am. Chem. Soc.* 120, 12950–12955.
- (31) Giese, B., Amaudrut, J., Kohler, A. K., Spormann, M., and Wessely, S. (2001) Direct Observation of Hole Transfer Through DNA by Hopping Between Adenine Bases and by Tunneling. *Nature* 412, 318–320.
- (32) Lewis, F. D., Liu, X., Liu, J., Miller, S. E., Hayes, R. T., and Wasielewski, M. R. (2000) Direct Measurement of Hole Transport Dynamics in DNA. *Nature* 406, 51–53.
- (33) Fink, H.-W., Schonenberger, C. (1999) Electrical Conduction Through DNA Molecules. *Nature* 398, 407–410.
- (34) Porath, D., Bezryadin, A., de Vries, S., and Dekker, C. (2000) Direct Measurement of Electrical Transport Through DNA Molecules. *Nature* 403, 635–638.
- (35) Nakayama, H., Ohno, H., and Okahata, Y. (2001) Intramolecular Electron Conduction Along DNA Strands and Their Temperature Dependency in a DNA-Aligned Cast Film. *Chem. Commun.* 2300–2301.
- (36) Cardullo, R. A., Agrawal, S., Flores, C., Zamecnik, P. C., and Wolf, D. E. (1988) Detection of Nucleic-Acid Hybridization by Nonradiative Fluorescence Resonance Energy-Transfer. *Proc. Natl. Acad. Soc. U.S.A.* 85, 8790–8794.
- (37) Mergny, J. L., Garestier, T., Rougee, M., Lebedev, A. V., Chassignol, M., Thung, N. T., and Helene, C. (1994) Fluorescence Energy-Transfer Between 2 Triple Helix-Forming Oligonucleotides Bound to Duplex DNA. *Biochemistry* 33, 15321–15328.
- (38) Murchie, A. I. H., Clegg, R. M., von Kitzing, E., Duckett, D. R., Diekmann, S., and Lilley, D. M. J. (1989) Fluorescence Energy-Transfer Shows That the 4-Way DNA Junction is a Right-Handed Cross of Antiparallel Molecules. *Nature* 341, 763–766.
- (39) Mergny, J. L., Botorine, A. S., Garestier, T., Belloc, F., Rougee, M., Bulychec, N. V., Koshkin, A. A., Bourson, J., Levedev, A. V., Valeur, B., Thuong, N. T., and Helene, C. (1994) Fluorescence Energy-Transfer as a Probe for Nucleic-Acid Structures and Sequences. *Nucleic Acids Res.* 22, 920–928.
- (40) Morrison, L. E., Hadler, T. C., and Stols, L. M. (1989) Solution-Phase Detection of Polynucleotides Using Interacting Fluorescent Labels and Competitive Hybridization. *Anal. Biochem.* 183, 231–244.
- (41) Tyagi, S., and Kramer, F. R. (1996) Molecular Beacons: Probes that Fluoresce Upon Hybridization. *Nat. Biotech.* 14, 303–308.
- (42) Clegg, R. M., Murchie, A. I. H., Zechel, A., and Lilley, D. M. J. (1993) Observing the Helical Geometry of Double-Stranded DNA in Solution by Fluorescence Resonance Energy-Transfer. *Proc. Natl. Acad. Soc. U.S.A.* 90, 2994–2998.
- (43) Morrison, L. E., and Stols, L. M. (1993) Sensitive Fluorescence-Based Thermodynamic and Kinetic Measurements of DNA Hybridization in Solution. *Biochemistry* 32, 3095–3104.
- (44) Ohya, Y., Yabuki, K., Komatsu, M., and Ouchi, T. (2000) Sequential Arrangement of Chromophores and Energy Transfer Behavior on Oligonucleotides Assemblies. *Polym. Adv. Technol.* 11, 845–855.
- (45) Kawahara, S., Uchimar, T., and Murata, S. (1999) Sequential Multistep Energy Transfer: Enhancement of Efficiency of Long-Range Fluorescence Resonance Energy Transfer. *Chem. Commun.* 563–564.
- (46) Horsey, I., Furey, W. S., Harrison, J. G., Osborne, M. A., and Balasubramanian, S. (2000) Double Fluorescence Resonance Energy Transfer to Explore Multicomponent Binding Interactions: a Case Study of DNA Mismatches. *Chem. Commun.* 1043–1044.
- (47) Tong, A. K., Jackusch, S., Li, Z., Zhu H.-R., Akins, D. L., Turro, N. J., and Ju, J. (2001) Triple Fluorescence Energy Transfer in Covalently Trichromophore-Labeled DNA. *J. Am. Chem. Soc.* 123, 12923–12924.
- (48) Liu, J., Lu, Y. (2002) FRET Study of a Trifluorophore-Labeled DNase. *J. Am. Chem. Soc.* 124, 15208–15216.
- (49) Ohya, Y., Yabuki, K., Tokuyama, M., and Ouchi, T. (2003) Construction of Sequential Chromophore Arrays on Oligo-DNA Assembly and Their Energy Transfer Behavior. *Supramol. Chem.* 15, 45–54.
- (50) Ohya, Y., Yabuki, K., and Ouchi, T. (2003) Sequence Dependence of Fluorescent Quenching of Chromophores Covalently Bonded to Oligo-DNA before and after Duplex Formation. *Supramol. Chem.* 15, 149–154.
- (51) Caruso, F., Furlong, D. N., Niikura, K., and Okahata, Y. (1998) In Situ Measurement of DNA Immobilization and Hybridization Using a 27 MHz Quartz Crystal Microbalance. *Colloids and Surfaces, B: Biointerfaces* 10, 199–204.
- (52) Okahata, Y., Kawase, M., Niikura, K., Ohtake, F., Furusawa, H., and Ebara, Y. (1998) Kinetic Measurements of DNA Hybridization an Oligonucleotide-Immobilized 27-MHz Quartz Crystal Microbalance. *Anal. Chem.* 70, 1288–1296.
- (53) Ebara, Y., Itakura, K., and Okahata, Y. (1996) Kinetic Studies of Molecular Recognition Based on Hydrogen Bonding at the Air–Water Interface by Using a Highly Sensitive Quartz-Crystal Microbalance. *Langmuir* 12, 5165–5170.
- (54) Uemura, A., Kimura, S., and Imanishi, Y. (1983) Investigation on the Interactions of Peptides in the Assembly of Liposome and Peptide by Fluorescence. *Biochim. Biophys. Acta* 729, 28–34.
- (55) Sauerbrey, G. (1959) The use of quartz oscillators for weighing thin layers and for microweighing. *Z. Physik* 155, 206.

BC034028M

# Multivalent Poly(ethylene glycol)-Containing Conjugates for In Vivo Antibody Suppression

David S. Jones,\* Michael J. Branks, Mary-Ann Campbell, Keith A. Cockerill, Jeffrey R. Hammaker, Christina A. Kessler, Eric M. Smith, Anping Tao, Huong-Thu Ton-Nu, and Tong Xu

La Jolla Pharmaceutical Company, 6455 Nancy Ridge Drive,

San Diego, California 92121 Received June 19, 2003; Revised Manuscript Received August 19, 2003

Poly(ethylene glycol) (PEG) was incorporated into multivalent conjugates of the N-terminal domain of  $\beta_2$ GPI (domain 1). PEG was incorporated to reduce the rate of elimination of the conjugates from plasma and to putatively improve their efficacy as toleragens for the suppression of anti- $\beta_2$ GPI antibodies and the treatment of antiphospholipid syndrome (APS). Three structurally distinct types of multivalent platforms were constructed by incorporating PEG into the platform structures in different ways. The amount of PEG incorporated ranged from about 5000 g per mole to about 30000 g per mole. The platforms were functionalized with either four or eight aminooxy groups. The conjugates were prepared by forming oxime linkages between the aminooxy groups and N-terminally glyoxylated domain 1 polypeptide. The plasma half-life of each conjugate, labeled with  $^{125}\text{I}$ , was measured in both mice and rats. The half-lives of the conjugates ranged from less than 10 min to about 1 h in mice, and from less than 3 h to about 19 h in rats. The ability of five tetravalent conjugates to suppress anti-domain 1 antibodies in immunized rats was also measured. Incorporation of PEG in the conjugates significantly reduced the doses required for suppression, and the amount of reduction correlated with the amount of PEG incorporated.

## INTRODUCTION

B cell tolerance is a new approach to the treatment of B cell-mediated autoimmune diseases in which autoantibodies are pathogenic. The approach relies on multivalent presentation of B cell epitopes that are devoid of T cell epitopes to suppress the formation of antibody-producing cells immunospecifically and, therefore, selectively suppress pathogenic antibody formation. More information on the underlying principles of B cell tolerance can be found in recent review articles (1–3). Molecules designed to selectively suppress a pathogenic antibody response are called B cell toleragens. They are composed of multiple B cell receptor epitopes or mimetic epitopes connected to nonimmunogenic multivalent platforms. B cell toleragens have been successfully used to reduce antibody levels in animal models and in humans suffering from autoimmune diseases. Toleragens composed of double-stranded oligonucleotides (dsON) were developed for treating systemic lupus erythematosus (SLE). Those toleragens suppressed anti-dsON antibodies in mice immunized with dsON (4, 5). Human clinical trials have demonstrated suppression of anti-double-stranded DNA antibodies in patients suffering from SLE (6).

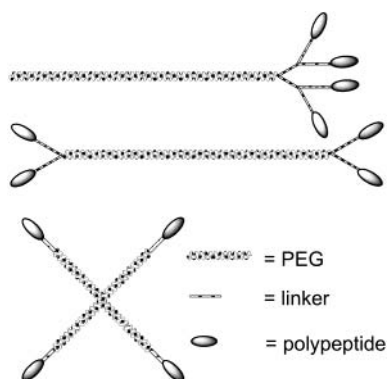
Toleragens composed of mimetic epitopes of  $\beta_2$ GPI are under development for treating antiphospholipid syndrome (APS), a condition in which anti- $\beta_2$ GPI antibodies (also referred to as anti-phospholipid antibodies) are believed to cause thrombotic events. Toleragens prepared using peptide mimics of  $\beta_2$ GPI were effective in suppressing anti-peptide antibody formation in an animal model; however, the peptides themselves bound the anti- $\beta_2$ GPI antibodies of only a small subset of patients (7). The

N-terminal domain of  $\beta_2$ GPI (domain 1) was recently discovered to recognize a high percentage of (APS) patient antisera (8). A toleragen composed of domain 1 was effective in suppressing anti-domain 1 antibodies in mice immunized with domain 1 (9). Antibody suppression in mice, using both the peptide toleragens and the domain 1 toleragen, required in vitro treatment of primed spleen cells followed by transfer into immune-ablated hosts. The domain 1 toleragen was, however, effective in vivo in rats immunized with domain 1. The difference in in vivo effectiveness of the toleragens in mice and rats was attributed to differential rates of clearance for the two species, and it became apparent that the effectiveness of toleragens could be improved by decreasing their rate of clearance from circulation.

Rapid clearance is a problem that is often encountered in the development of polypeptide-based therapeutic drugs that are generally administered parenterally. Frequent dosing of such drugs is not desirable, because it increases the cost of drug and is inconvenient for the patient. Continuous infusion is often necessary to maintain an effective drug concentration. In general, proteins of less than approximately 70 kDa, the size of albumin, will clear from blood by passing through the glomerular membrane in a size dependent manner (10).

A solution to rapid kidney clearance of drugs is to increase their physical size. That can be accomplished by attaching the drug to a macromolecule of sufficient size to prevent it from passing through the glomerular membrane (11). There are numerous examples of conjugates of polypeptides and macromolecules that have been prepared to enhance efficacy. Adriamycin and mitomycin C have been attached to 70 kDa dextran to prepare forms of those drugs that are more persistent in the circulation (12, 13). Attachment of poly(ethylene glycol) (PEG) to polypeptides has been widely used to improve their clinical effectiveness (11, 14, 15). In addition to reducing

\* To whom correspondence should be addressed. Tel.: (858) 646-6628. Fax: (858) 626 2845. E-mail: dave.jones@ljpc.com.



**Figure 1.** Three distinct types of PEG-containing conjugate structures.

kidney clearance and providing prolonged in vivo circulation half-lives, "PEGylated" proteins may be less susceptible to proteolysis or clearance by receptor-mediated mechanisms, and they may be less immunogenic and antigenic (16). Other advantageous properties of PEG are its water solubility, its amenability to chemical modification at one or both termini, and its availability in a variety of molecular weight ranges with low polydispersity. Some examples of polypeptides that have been attached to PEG to prolong their circulation half-lives include antibody fragments (17), granulocyte colony stimulating factor (18), bovine hemoglobin (19), growth hormones (20), insulin (21), and interferon  $\alpha$ -2a (22). Several PEGylated polypeptides have been approved for treating human diseases. Further examples, of which there are many, may be found in recent review articles (14, 15).

This report describes new anti- $\beta_2$ GPI specific toleragens that were constructed from novel PEG-containing platforms designed to provide longer circulatory half-lives and therefore greater efficacy. Our aim was to incorporate PEG into the platforms before attachment of domain 1 in order to avoid nonselective modification of the polypeptide and to provide a well-defined conjugate. The syntheses of three novel structurally distinct types of PEG-containing platforms are described, as is the use of these platforms to prepare multivalent conjugates of domain 1. The structural varieties of conjugates are shown graphically in Figure 1. Summaries of pharmacokinetic data and in vivo tolerance data are also presented for the new conjugates.

#### EXPERIMENTAL PROCEDURES

**Abbreviations.** DIPEA, diisopropylethylamine; NHS, *N*-hydroxysuccinimide; DCC, 1,3-dicylohexylcarbodiimide; CDI, 1,1'-carbonyldiimidazole; HOBt, 1-hydroxybenzotriazole hydrate; Et<sub>3</sub>N, triethylamine; Boc, *tert*-butoxycarbonyl; TFA, trifluoroacetic acid; PBS, phosphate buffered saline; TA/D1, transaminated domain 1.

**General.** Monomethoxypoly(ethylene glycol) benzo-triazolyl carbonates of molecular weight 11690 g/mol (mPEG<sub>12K</sub>-BTC), 5215 g/mol (mPEG<sub>5K</sub>-BTC), 22334 g/mol (mPEG<sub>20K</sub>-BTC), 32120 g/mol (mPEG<sub>30K</sub>-BTC), poly(ethylene glycol) bis(benzotriazolyl) carbonate of molecular weight 21529 g/mol (PEG<sub>20K</sub>-bis-BTC), and mono-Boc-diaminopoly(ethylene glycol) of molecular weight 5094 g/mol (BocNH-PEG<sub>(5K)</sub>-NH<sub>2</sub>) were obtained from Shearwater Polymers, Huntsville, AL (now Nektar Therapeutics). *N*-(Benzyloxycarbonyloxy)succinimide was obtained from Aldrich Chemical Co., Milwaukee, WI.

Silica gel chromatography was performed on silica gel (230–400 Mesh ASTM) purchased from Baxter. TLC was

performed on silica gel plates (EM Separations cat. no. 5554). PBS was prepared by dissolving 175 g of NaCl, 6.5 g of NaH<sub>2</sub>PO<sub>4</sub>·H<sub>2</sub>O, and 40.9 g of Na<sub>2</sub>HPO<sub>4</sub>·7H<sub>2</sub>O in H<sub>2</sub>O and diluting to a final volume of 20 L. Sodium acetate 100 mM pH 4.6 buffer was prepared by dissolving 0.820 g (10 mmol) of sodium acetate in 95 mL of water, adding acetic acid to obtain a pH of 4.6, and adding water to obtain a volume of 100 mL. Tris acetate 100 mM pH 8.0 buffer was prepared by dissolving 1.21 g of tris-(hydroxymethyl)aminomethane in 95 mL of water, adding acetic acid to obtain a pH of 8.0, and adding water to obtain a volume of 100 mL. NMR spectra were recorded on a Bruker AC-300 spectrometer with a broad band probe. Low resolution mass spectra were recorded on a Finnigan LCQ electrospray mass spectrometer or obtained from the Mass Spectroscopy Lab at the Scripps Research Institute, San Diego, CA. High-resolution MALDI mass spectra were obtained from the Mass Spectroscopy Lab at the Scripps Research Institute, San Diego, CA. High-resolution FAB mass spectra were obtained from the Mass Spectrometry Laboratory at the University of California at Berkeley, Berkeley, CA. Optical densities of plate wells were obtained with a Power Wave 340 Microplate Spectrophotometer from Bio-Tek Instruments, Winooski, VT. Gamma counts were measured with a Cobra gamma counter from Packard Instruments, Downers Grove, IL. Protein concentrations were determined by UV absorbance at 280 nm using a molar extinction coefficient of 9531 L mol<sup>-1</sup> cm<sup>-1</sup> (1.35 mL mg<sup>-1</sup> cm<sup>-1</sup>) for the domain 1 polypeptide. Nunc Maxisorp Immunoplates were obtained from Nalge Nunc International, Rochester, NY. Recombinant human  $\beta_2$ GPI was obtained from Sigma, St. Louis, MO. Nonfat dry milk was produced by Carnation, Solon, OH. Alkaline phosphatase-conjugated goat anti-rat IgG was obtained from Jackson ImmunoResearch, West Grove, PA. Female CD-1 mice were obtained from The Jackson Laboratories, Bar Harbor, ME. Male Sprague–Dawley rats were obtained from Charles River, Hingham, MA.

**S-Acetyl-6-(*N*-*tert*-butyloxycarbonyl)aminoxyhexane-1-thiol, Compound 2.** To a solution of 77 mg (0.67 mmol) of potassium thioacetate in 15 mL of acetone was added 209 mg (0.61 mmol) of 6-(*N*-*tert*-butyloxycarbonyl)aminoxy-1-iodohexane (23), and the mixture was stirred at room temperature for 18 h. The acetone was removed under vacuum, and the residue was partitioned between 50 mL of CH<sub>2</sub>Cl<sub>2</sub> and 3 × 25 mL of 1 N NaOH. The CH<sub>2</sub>Cl<sub>2</sub> layer was dried (Na<sub>2</sub>SO<sub>4</sub>), filtered, and concentrated to a brown oil. Purification by silica gel chromatography (15/85 EtOAc/hexanes) provided 166 mg (94%) of compound 2 as a colorless oil: <sup>1</sup>H NMR (CDCl<sub>3</sub>)  $\delta$  1.39 (m, 4H), 1.48 (s, 9H), 1.59 (m, 4H), 2.32 (s, 3H), 2.86 (t, 2H), 3.82 (t, 2H), 7.10 (s, 1H); <sup>13</sup>C NMR (CDCl<sub>3</sub>)  $\delta$  25.5, 28.0, 28.4, 28.6, 29.1, 29.5, 30.8, 76.7, 81.6, 157.1, 196.0; HRMS (MALDI) calculated for (M + Na): C<sub>13</sub>H<sub>25</sub>NaO<sub>4</sub>S: 314.1396. Found: 314.1402.

**6-(*N*-*tert*-butyloxycarbonyl)aminoxyhexane-1-thiol, Compound 3.** Compound 2 (50 mg, 172  $\mu$ mol) and 22  $\mu$ L (17.4 mg, 85.8  $\mu$ mol) of tri-*n*-butylphosphine was placed under nitrogen, and 2 mL of a nitrogen sparged 1 M solution of NaOH in MeOH was added to the mixture. The mixture was stirred for 18 h at room temperature, and 172  $\mu$ L (180 mg, 3 mmol) of TFA was added. The mixture was partitioned between 25 mL of EtOAc and 3 × 25 mL of 1 N HCl, and the combined aqueous layers were extracted with 25 mL of EtOAc. The combined EtOAc extracts were dried (Na<sub>2</sub>SO<sub>4</sub>), filtered, and concentrated. The resulting oil was purified by silica gel chromatography (15/85/0.1 EtOAc/hexanes/MeOH) to



provide 28 mg (65%) of **3** as a colorless oil:  $^1\text{H}$  NMR ( $\text{CDCl}_3$ )  $\delta$  1.32 (t, 1H), 1.40 (m, 4H), 1.49 (s, 9H), 1.62 (m, 4H), 2.53 (d of t, 2H), 3.84 (t, 2H), 7.09 (s, 1H);  $^{13}\text{C}$  NMR ( $\text{CDCl}_3$ )  $\delta$  24.4, 25.3, 27.8, 28.0, 28.2, 33.7, 76.6, 81.5, 156.8; HRMS (MALDI) calculated for ( $\text{M} + \text{Na}$ ):  $\text{C}_{11}\text{H}_{23}\text{NaNO}_3\text{S}$ : 272.1291. Found: 272.1294.

**Preparation of Compound 5 from Compound 2 without Isolation of Compound 3.** Compound **2** (13 mg, 45  $\mu\text{mol}$ ) and 6  $\mu\text{L}$  (4.5 mg, 22.3  $\mu\text{mol}$ ) of tri-*n*-butylphosphine was placed under nitrogen, and 3 mL of a nitrogen sparged solution of 4/1 6 N  $\text{NH}_4\text{OH}/\text{CH}_3\text{CN}$  was added to the mixture. The mixture was stirred for 1 h at room temperature and concentrated under vacuum. The residue was dissolved in 3 mL of a nitrogen-sparged solution of 10/90 water/ $\text{CH}_3\text{CN}$ . The resulting solution of **3** was kept under nitrogen atmosphere, and 10 mg (7.44  $\mu\text{mol}$ ) of compound **4** (prepared as described in ref 5) was added, followed by 8  $\mu\text{L}$  (5.77 mg, 44.6  $\mu\text{mol}$ ) of DIPEA. The mixture was stirred for 18 h and concentrated under vacuum. The residue was purified by silica gel chromatography (multiple step gradient, 1/99 to 5/95 to 7.5/92.5 to 10/90 to 15/85  $\text{MeOH}/\text{CH}_2\text{Cl}_2$ ) to provide 14 mg (93%) of **5** as a colorless oil: TLC (10/90  $\text{MeOH}/\text{CH}_2\text{Cl}_2$ ),  $R_f$  = 0.3;  $^1\text{H}$  NMR ( $\text{CDCl}_3$ )  $\delta$  1.51 (m, 92H), 2.22 (t, 8H), 2.54 (t, 8H), 3.19 (m, 24H), 3.38 (brd s, 8H), 3.75 (m, 12H), 3.82 (t, 4H), 4.19 (t, 4H), 7.38 (brd s, 8H), 7.94 (s, 4H);  $^{13}\text{C}$  NMR ( $\text{CDCl}_3$ )  $\delta$  12.2, 17.2, 18.3, 25.0, 25.2, 26.2, 27.6, 28.0, 28.2, 28.8, 28.9, 32.6, 35.8, 39.3, 42.5, 54.2, 64.3, 69.0, 70.1, 76.2, 81.0, 156.6, 156.7, 169.2, 173.5; mass spectrum (ES)  $m/z$  calculated for  $\text{C}_{92}\text{H}_{173}\text{N}_{14}\text{O}_{26}\text{S}_4$  ( $\text{M} + \text{H}$ ): 2018. Found: 2018; HRMS (ESI) ( $\text{M} + 2\text{Na}$ ) $^{+2}$  calculated for  $\text{C}_{92}\text{H}_{172}\text{Na}_2\text{N}_{14}\text{O}_{26}\text{S}_4$ : 1031.5617. Found: 1031.5633.

**6-(*N*-*tert*-Butyloxycarbonyl)aminooxyhexanoic Acid, Compound 7.** To a magnetically stirred solution of 7.2 g (26 mmol) of compound **6** (**23**) in 10 mL of EtOH was added 5 mL of 50% w/w NaOH solution in water. The reaction was done in 5 min, as determined by TLC (1/5 EtOAc/hexanes). The reaction mixture was concentrated, and the residue was partitioned between 20 mL of  $\text{CH}_2\text{Cl}_2$  and 20 mL of 1 N HCl solution. The layers were separated, and the aqueous layer was extracted with 6  $\times$  10 mL portions of  $\text{CH}_2\text{Cl}_2$ . The combined  $\text{CH}_2\text{Cl}_2$  layers were dried ( $\text{MgSO}_4$ ), filtered, and concentrated to give 6.5 g (99%) of compound **7** as a colorless oil.  $^1\text{H}$  NMR ( $\text{CDCl}_3$ )  $\delta$  1.44 (m, 2H), 1.48 (s, 9H), 1.66 (m, 4H), 2.37 (t, 2H), 3.85 (t, 2H), 7.20 (s, 1H);  $^{13}\text{C}$  NMR ( $\text{CDCl}_3$ )  $\delta$  24.6, 25.5, 27.8, 28.4, 34.0, 76.6, 82.0, 157.5, 179.3; HRMS (MALDI) calculated for ( $\text{M} + \text{Na}$ ):  $\text{C}_{11}\text{H}_{21}\text{NaNO}_5$ : 270.1312. Found: 270.1309.

**Synthesis of Compound 8.** To a magnetically stirred solution of 1.00 g (4.04 mmol) of compound **7** in 10 mL of  $\text{CH}_2\text{Cl}_2$  at 0  $^\circ\text{C}$  was added 511 mg (4.44 mmol) of NHS followed by 1.25 g (6.06 mmol) of DCC. The mixture was brought to room temperature within 1 h. The mixture was stirred for 16 h, 750  $\mu\text{L}$  of acetic acid was added, and the mixture was placed in the freezer for 30 min. The solids were removed by filtration, and the filtrate was concentrated to a viscous oil. Purification by silica gel chromatography (15/85 acetone/toluene) provided 1.13 g (81%) of compound **8** as a white amorphous solid:  $^1\text{H}$  NMR ( $\text{CDCl}_3$ )  $\delta$  1.48 (s, 9H), 1.51 (m, 2H), 1.68 (m, 2H), 1.79 (m, 2H), 2.63 (t, 2H), 2.84 (br. s, 4H), 3.87 (t, 2H), 7.18 (br. s, 1H);  $^{13}\text{C}$  NMR ( $\text{CDCl}_3$ )  $\delta$  24.32, 25.07, 25.53, 27.42, 28.16, 30.77, 76.13, 81.51, 156.89, 168.45, 169.15; HRMS (MALDI) calculated for ( $\text{M} + \text{Na}$ ):  $\text{C}_{15}\text{H}_{24}\text{NaN}_2\text{O}_7$ : 367.1476. Found: 367.1474.

**Synthesis of Compound 9.** A magnetically stirred solution of 1.49 g (11.4 mmol) of 6-aminocaproic acid and

958 mg (11.4 mmol) of  $\text{NaHCO}_3$  in 144 mL of water was cooled to 0  $^\circ\text{C}$ . To the solution was added 27.8 mL of  $\text{CH}_3\text{CN}$  followed by a solution of 1.31 g (3.80 mmol) of compound **8** in 30 mL of  $\text{CH}_3\text{CN}$ . The mixture was brought to room temperature within an hour and stirred for 18 h. The mixture was concentrated, and the residue was partitioned between 70 mL of 1 N HCl and 2  $\times$  70 mL of  $\text{CH}_2\text{Cl}_2$ . The combined  $\text{CH}_2\text{Cl}_2$  layers were washed with brine, dried ( $\text{MgSO}_4$ ), filtered, and concentrated. Purification by silica gel chromatography 45/55/0.5 acetone/toluene/acetic acid provided 1.18 g (86%) of compound **9** as a viscous oil.  $^1\text{H}$  NMR ( $\text{CDCl}_3$ )  $\delta$  1.42 (m, 4H), 1.49 (s, 9H), 1.53 (m, 2H), 1.65 (m, 6H), 2.20 (t, 2H), 3.38 (t, 2H), 2.88 (q, 2H), 3.86 (t, 2H), 5.84 (br t, 1H), 7.67 (br s, 1H);  $^{13}\text{C}$  NMR ( $\text{CDCl}_3$ )  $\delta$  24.1, 25.3, 25.4, 26.1, 27.5, 28.2, 29.0, 33.7, 36.4, 76.4, 81.7, 157.2, 173.4, 177.6; HRMS (MALDI) calculated for ( $\text{M} + \text{Na}$ ):  $\text{C}_{17}\text{H}_{32}\text{NaN}_2\text{O}_6$ : 383.2152. Found: 383.2141.

**Synthesis of Dimer Cassette, Compound 10.** To a magnetically stirred solution of 1.09 g (3.04 mmol) of compound **9** in 11 mL of EtOAc was added 493 mg (3.04 mmol) of CDI. The reaction was stirred under  $\text{N}_2$  for 1 h, and 160  $\mu\text{L}$  (152 mg, 1.48 mmol) of diethylenetriamine was added followed by 423  $\mu\text{L}$  (307 mg, 3.03 mmol) of  $\text{Et}_3\text{N}$  at which time a precipitate formed. The mixture was stirred for 3 h and partitioned between 25 mL of  $\text{H}_2\text{O}$  and 200 mL of  $\text{CH}_2\text{Cl}_2$ . The  $\text{CH}_2\text{Cl}_2$  layer was washed with 25 mL of  $\text{H}_2\text{O}$  and 25 mL of brine, dried ( $\text{MgSO}_4$ ), filtered, and concentrated. Purification by silica gel chromatography (step gradient 17/83/0.5  $\text{MeOH}/\text{CH}_2\text{Cl}_2$ /concd  $\text{NH}_4\text{OH}$  to 20/80/0.5  $\text{MeOH}/\text{CH}_2\text{Cl}_2$ /concd  $\text{NH}_4\text{OH}$ ) provided 851 mg (73%) of compound **10** as a light yellow, glassy solid.  $^1\text{H}$  NMR ( $\text{CD}_3\text{OD}$ )  $\delta$  1.38 (m, 8H), 1.46 (s, 9H), 1.49 (m, 4H), 1.62 (m, 12 H), 2.18 (t, 4H), 2.20 (t, 4H), 2.75 (t, 4H), 3.16 (t, 4H), 3.30 (t, 4H), 3.77 (t, 4H);  $^{13}\text{C}$  NMR ( $\text{CD}_3\text{OD}$ )  $\delta$  26.5, 26.6, 26.8, 27.6, 28.6, 28.8, 30.2, 37.0 (36.98), 37.0 (37.02), 39.7, 40.2, 49.4, 77.2, 81.9, 159.1, 176.0, 176.5; HRMS (MALDI) calculated for ( $\text{M} + \text{H}$ ):  $\text{C}_{38}\text{H}_{74}\text{N}_7\text{O}_{10}$ : 788.5491. Found: 788.5488.

**Compound 12.** To a solution of 1.50 g (7.76 mmol) of compound **11** (prepared as described in ref 24) and 1.30 g (15.52 mmol) of  $\text{NaHCO}_3$  in 20 mL of  $\text{H}_2\text{O}$  at 0  $^\circ\text{C}$  was added a solution of 2.32 g (9.31 mmol) of *N*-(benzyloxycarbonyloxy)succinimide dissolved in 20 mL of dioxane. Cooling was discontinued, and the mixture was stirred for 4 h at room temperature. The mixture was acidified to approximately pH 1 with 1 N HCl and partitioned between 20 mL of 1 N HCl and 100 mL of  $\text{CH}_2\text{Cl}_2$ . The aqueous layer was extracted with four additional 50 mL portions of  $\text{CH}_2\text{Cl}_2$ . All of the  $\text{CH}_2\text{Cl}_2$  extracts were combined, dried ( $\text{MgSO}_4$ ), filtered, and concentrated. The residue was dissolved in 30 mL of  $\text{CH}_2\text{Cl}_2$  and cooled to 0  $^\circ\text{C}$ . To the solution was added 6.26 g (31.0 mmol) of 4-nitrophenylchloroformate followed by addition of 5 mL (4.91 g, 62.1 mmol) of pyridine dropwise over approximately 2 min during which time a precipitate formed. Cooling was discontinued, and the mixture was allowed to stir for 3 h at room temperature. The precipitate was removed by filtration and washed with approximately 20 mL of  $\text{CH}_2\text{Cl}_2$ . Approximately 1 mL of water was added to the filtrate, and the mixture was stirred for 5 min and shaken with 50 mL of 1 N HCl. The organic layer was collected, and the aqueous layer was extracted with 50 mL of  $\text{CH}_2\text{Cl}_2$ . The combined organic layers were washed successively with four 25 mL portions of saturated  $\text{NaHCO}_3$  solution, 25 mL of 1 N HCl, and 25 mL of brine, dried ( $\text{MgSO}_4$ ), filtered, and concentrated. Purification by silica gel chromatography (loaded in  $\text{CH}_2\text{Cl}_2$  and eluted with 50/50 EtOAc/hexanes) provided 3.81 g (75%) of

compound **12** as a viscous oil:  $^1\text{H}$  NMR ( $\text{CDCl}_3$ )  $\delta$  3.48–3.82 (m, 12H), 4.39 (m, 4H), 5.12 (s, 2H), 7.34 (m, 7H), 8.23 (d, 2H);  $^{13}\text{C}$  NMR ( $\text{CDCl}_3$ )  $\delta$  47.8, 48.2, 67.2, 68.0, 68.1, 68.2, 68.3, 69.6, 69.9, 121.7, 125.2, 127.8, 128.0, 128.5, 136.6, 145.4, 152.4, 155.4, 156.1; HRMS mass spectrum (MALDI) ( $\text{M} + \text{Na}$ ) calculated for  $\text{C}_{30}\text{H}_{31}\text{N}_3\text{O}_{14}$ : 680.1698. Found 680.1697.

**Compound 13.** A solution of 294 mg (0.45 mmol) of compound **12** in 30 mL of pyridine was added to a flask containing 775 mg (0.98 mmol) of compound **10**. Triethylamine (249  $\mu\text{L}$ , 1.81 mmol, 1.79 mmol) was added, and the mixture was stirred at room temperature under nitrogen atmosphere for 18 h. Most of the pyridine was removed under reduced pressure, and the residue was partitioned between 100 mL of  $\text{CH}_2\text{Cl}_2$  and  $3 \times 20$  mL of 1 N HCl. The  $\text{CH}_2\text{Cl}_2$  extract was washed with 20 mL of brine, dried ( $\text{MgSO}_4$ ), filtered, and concentrated to a yellow oil. Purification by silica gel chromatography (step gradient: 5/95/0.1 to 10/90/0.1 to 15/85/0.1 MeOH/ $\text{CH}_2\text{Cl}_2$ /HOAc) provided 633 mg (72%) of compound **13** as a viscous oil:  $^1\text{H}$  NMR ( $\text{CD}_3\text{OD}$ )  $\delta$  1.20–1.52 (m, 24H), 1.43 (s, 36H), 1.60 (m, 24H), 2.16 (m, 16H), 3.12 (m, 8H), 3.33 (m, 20H), 3.50–3.70 (m, 16H), 3.76 (t, 8H), 4.16 (m, 4H), 5.12 (s, 2H), 7.36 (brd s, 5H), 7.93 (m, 4H);  $^{13}\text{C}$  NMR ( $\text{CD}_3\text{OD}$ )  $\delta$  26.6, 26.8, 27.6, 28.7, 28.8, 30.2, 37.0, 38.7, 39.0, 40.2, 40.3, 65.8, 68.3, 70.1, 70.3, 70.5, 77.2, 81.9, 128.8, 129.2, 129.7, 138.1, 158.0, 158.1, 159.1, 176.0, 176.2; HRMS mass spectrum (MALDI) ( $\text{M} + \text{Na}$ ) calculated for  $\text{C}_{94}\text{H}_{167}\text{N}_3\text{O}_{28}$ : 1977.1997. Found 1977.1899.

**Compound 14.** A solution of 300 mg (0.15 mmol) of compound **13** and 8.8  $\mu\text{L}$  (9.2 mg, 0.13 mmol) of acetic acid in 20 mL of MeOH was purged with  $\text{H}_2$ . To the solution was added 75 mg of 10% palladium on carbon. A hydrogen-filled balloon was attached, and the mixture was stirred for 2 h. The flask was purged with nitrogen, the catalyst was removed by filtration, and the mixture was concentrated to provide 282 mg (quantitative yield) of compound **14** as a gummy solid:  $^1\text{H}$  NMR ( $\text{CD}_3\text{OD}$ )  $\delta$  1.38 (m, 16H), 1.48 (m, 44H), 1.65 (m, 24H), 2.20 (t, 16H), 2.83 (t, 4H), 3.17 (t, 8H), 3.38 (m, 16H), 3.63 (t, 4H), 3.69 (t, 4H), 3.78 (t, 4H), 4.21 (m, 4H);  $^{13}\text{C}$  NMR ( $\text{CD}_3\text{OD}$ )  $\delta$  26.7, 27.0, 27.8, 28.8, 28.9, 30.3, 37.1, 38.8, 39.1, 40.3, 49.9, 66.0, 70.4, 70.9, 77.3, 82.0, 158.2, 159.2, 176.1, 176.3; mass spectrum (ESI) ( $\text{M} + \text{H}$ ) $^+$  calculated for  $\text{C}_{86}\text{H}_{162}\text{N}_{15}\text{O}_{26}$ : 1821. Found 1821; HRMS (MALDI) ( $\text{M} + \text{Na}$ ) calculated for  $\text{C}_{86}\text{H}_{162}\text{N}_{15}\text{O}_{26}$ : 1821.1809. Found 1821.1803.

**Compound 16b.** To a solution of 20 mg (11.0  $\mu\text{mol}$ ) of compound **14** in 5 mL of DMF was added 103 mg (8.8  $\mu\text{mol}$ ) of compound **15b** (mPEG<sub>12K</sub>-BTC) followed by 5  $\mu\text{L}$  (3.6 mg, 35.9  $\mu\text{mol}$ ) of  $\text{Et}_3\text{N}$ . The mixture was stirred at room temperature for 18 h and concentrated. The residue was purified by silica gel chromatography (multistep gradient: 5/95 to 15/85 to 20/80 MeOH/ $\text{CH}_2\text{Cl}_2$ ) to provide 109 mg (92%) of compound **16b** as a waxy solid:  $^1\text{H}$  NMR ( $\text{CDCl}_3$ )  $\delta$  1.37 (m, 16H), 1.49 (m, 44H), 1.65 (m, 24H), 2.20 (t, 16H), 3.20 (q, 8H), 3.36 (m, 16H), 3.61 (m, 4H), 3.68 (m, approximately 1056H), 3.84 (t, 8H), 3.91 (m, 4H), 4.23 (m, 4H); mass spectrum (MALDI) average  $m/z$  calculated for  $\text{C}_{610}\text{H}_{1208}\text{N}_{15}\text{O}_{289}$ : 13370. Found: 13711.

**Compound 16a.** This compound was prepared in 69% yield using essentially the same procedure used for the preparation of compound **16b**; however, compound **15a** (mPEG<sub>5K</sub>-BTC) was used:  $^1\text{H}$  NMR (4:1  $\text{CDCl}_3/\text{CD}_3\text{OD}$ )  $\delta$  1.37 (m, 16H), 1.49 (m, 44H), 1.65 (m, 24H), 2.20 (t, 16H), 3.20 (q, 8H), 3.36 (m, 16H), 3.61 (m, 4H), 3.68 (m, approximately 468H), 3.84 (t, 8H), 3.91 (m, 4H), 4.23 (m, 4H); mass spectrum (MALDI) average  $m/z$  calculated for  $\text{C}_{316}\text{H}_{619}\text{N}_{15}\text{O}_{142}$ : 6898. Found: 6800.

**Compound 16c.** This compound was prepared in 92% yield using essentially the same procedure used for the preparation of compound **16b**; however, compound **15c** (mPEG<sub>20K</sub>-BTC) was used:  $^1\text{H}$  NMR (5:1  $\text{CDCl}_3/\text{CD}_3\text{OD}$ )  $\delta$  1.37 (m, 16H), 1.49 (m, 44H), 1.65 (m, 24H), 2.20 (t, 16H), 3.20 (q, 8H), 3.36 (m, 16H), 3.61 (m, 4H), 3.68 (m, approximately 2024H), 3.84 (t, 8H), 3.91 (m, 4H), 4.23 (m, 4H); mass spectrum (MALDI) average  $m/z$  calculated for  $\text{C}_{1094}\text{H}_{2175}\text{N}_{15}\text{O}_{531}$ : 24023. Found: 23400.

**Compound 16d.** This compound was prepared in 54% yield using essentially the same procedure used for the preparation of compound **16b**; however, compound **15d** (mPEG<sub>30K</sub>-BTC) was used:  $^1\text{H}$  NMR (5:1  $\text{CDCl}_3/\text{CD}_3\text{OD}$ )  $\delta$  1.37 (m, 16H), 1.49 (m, 44H), 1.65 (m, 24H), 2.20 (t, 16H), 3.20 (q, 8H), 3.36 (m, 16H), 3.61 (m, 4H), 3.68 (m, approximately 2,900H), 3.84 (t, 8H), 3.91 (m, 4H), 4.23 (m, 4H); mass spectrum (MALDI) average  $m/z$  calculated for  $\text{C}_{1538}\text{H}_{3663}\text{N}_{15}\text{O}_{753}$ : 33818. Found: 33775.

**Compound 17.** To a solution of 54 mg (29.6  $\mu\text{mol}$ ) of compound **14**, 9 mg (13.5  $\mu\text{mol}$ ) of compound **12**, and 8 mg (53.9  $\mu\text{mol}$ ) of HOBT in 5 mL of anhydrous pyridine was added 15  $\mu\text{L}$  (10.9 mg, 107.8  $\mu\text{mol}$ ) of  $\text{Et}_3\text{N}$ . The mixture was stirred for 18 h and concentrated to a viscous oil. The residue was purified by HPLC using a 24 mm  $\times$  30 cm  $\text{C}_{18}$  column (gradient 30% to 60% B over 60 min; A =  $\text{H}_2\text{O}/0.1\%$  TFA, B =  $\text{CH}_3\text{CN}/0.1\%$  TFA) to provide 17 mg (31%) of compound **17** as a waxy white solid:  $^1\text{H}$  NMR ( $\text{CD}_3\text{OD}$ )  $\delta$  1.20–1.51 (m, 48H), 1.43 (s, 72H), 1.60 (m, 48H), 2.19 (t, 32H), 3.14 (t, 16H), 3.32 (m, 32H), 3.50 (m, 12H), 3.59 (m, 12H), 3.64 (m, 12H), 3.78 (t, 16H), 4.18 (m, 12H), 5.12 (s, 2H), 7.32 (m, 5H);  $^{13}\text{C}$  NMR ( $\text{CD}_3\text{OD}$ )  $\delta$  26.6, 26.8, 27.6, 28.6, 28.8, 30.2, 37.0, 38.7, 39.0, 40.2, 65.8, 68.3, 70.2, 70.6, 77.2, 81.9, 128.8, 129.2, 129.3, 129.7, 129.9, 138.2, 157.8, 157.9, 158.0, 159.1, 176.0, 176.2; HRMS (ESI) ( $\text{M} + 3\text{Na}$ ) $^{+3}$  calculated for  $\text{C}_{190}\text{H}_{343}\text{N}_3\text{O}_{60}$ : 1362.8134. Found: 1362.8224.

**Compound 18.** A solution of 9 mg (2.24  $\mu\text{mol}$ ) of compound **17** in 10 mL of MeOH was placed under an  $\text{H}_2$  atmosphere by applying partial vacuum and filling with  $\text{H}_2$ . To the solution was added 10 mg of 10% palladium on carbon, a  $\text{H}_2$ -filled balloon was attached, and the mixture was stirred at room temperature for 2 h. The flask was purged with  $\text{N}_2$ , the catalyst was removed by filtration, and the filtrate was concentrated to provide 6 mg (69%) of compound **18** as a colorless gum:  $^1\text{H}$  NMR ( $\text{CD}_3\text{OD}$ )  $\delta$  1.23–1.50 (m, 48H), 1.48 (s, 72H), 1.61 (m, 48H), 2.19 (t, 32H), 3.08 (brd t, 4H), 3.17 (t, 16H), 3.38 (m, 36H), 3.52 (m, 8H), 3.63 (t, 8H), 3.70 (m, 12H), 3.78 (t, 16H), 4.21 (m, 12H);  $^{13}\text{C}$  NMR ( $\text{CD}_3\text{OD}$ )  $\delta$  26.7, 26.9, 27.7, 28.7, 28.9, 30.2, 37.1, 38.8, 39.1, 40.3, 65.9, 70.3, 77.2, 81.9, 158.0, 158.1, 159.1, 176.0, 176.2; mass spectrum (ESI) ( $\text{M} + \text{H}$ ) $^+$  calculated for  $\text{C}_{182}\text{H}_{338}\text{N}_{31}\text{O}_{58}$ : 3887. Found 3887. HRMS (ESI) ( $\text{M} + 3\text{Na}$ ) $^{+3}$  calculated for  $\text{C}_{182}\text{H}_{337}\text{N}_{31}\text{O}_{58}$ : 1318.1350. Found: 1318.1419.

**Compound 19.** To a solution of 13 mg (3.34  $\mu\text{mol}$ ) of compound **18** in 5 mL of pyridine was added 60 mg (2.68  $\mu\text{mol}$ ) of compound **15c** (mPEG<sub>20K</sub>-BTC) followed by 5  $\mu\text{L}$  (3.6 mg, 35.9  $\mu\text{mol}$ ) of  $\text{Et}_3\text{N}$ . The mixture was stirred at room temperature for 18 h and concentrated. The residue was purified by silica gel chromatography (multistep gradient: 10/90 to 15/85 to 20/80 MeOH/ $\text{CH}_2\text{Cl}_2$ ) to provide 45 mg (68%) of compound **19** as a waxy solid:  $^1\text{H}$  NMR ( $\text{CDCl}_3$ )  $\delta$  1.30 (m, 32H), 1.50 (m overlapping s at 1.48, 88H), 1.67 (m, 48H), 2.24 (t, 32H), 3.23 (m, 16H), 3.41 (m, 32H), 3.65 (m, approximately 2024H), 3.70 (t, 24H), 3.89 (m, 16H), 4.21 (m, 12H); mass spectrum (MALDI) average  $m/z$  calculated for  $\text{C}_{1127}\text{H}_{2227}\text{N}_{31}\text{O}_{531}$ : 24696. Found: 23270.



**Compound 21.** To a solution of 22 mg (27.3  $\mu\text{mol}$ ) of compound **10** in 5 mL of pyridine was added 236 mg (10.9  $\mu\text{mol}$ ) of compound **20** (PEG<sub>20K</sub>-bis-BTC) followed by 8  $\mu\text{L}$  (5.8 mg, 57.4  $\mu\text{mol}$ ) of Et<sub>3</sub>N. The mixture was stirred at room temperature for 18 h and concentrated. The residue was purified by silica gel chromatography (multistep gradient; 5/95 to 10/90 to 15/85 to 20/80 MeOH/CH<sub>2</sub>Cl<sub>2</sub>) to provide 242 mg (96%) of compound **21** as a white solid: <sup>1</sup>H NMR (CDCl<sub>3</sub>)  $\delta$  1.35 (m, 16H), 1.48 (m, 44H), 1.61 (m, 24H), 2.20 (m, 16H), 3.22 (m, 8H), 3.52–3.96 (m, approximately 2000H), 4.23 (m, 4H); mass spectrum (MALDI) average  $m/z$  calculated for C<sub>1040</sub>H<sub>2068</sub>N<sub>14</sub>O<sub>504</sub>: 22836. Found: 23246.

**Compound 24.** To a solution of 3.87 mg (4.85  $\mu\text{mol}$ ) of compound **22** (25) in 5 mL of pyridine was added 124 mg (24.2  $\mu\text{mol}$ ) of compound **23** (BocNH-PEG<sub>(5K)</sub>-NH<sub>2</sub>) and 5  $\mu\text{L}$  (3.63 mg, 35.9  $\mu\text{mol}$ ) of Et<sub>3</sub>N, and the mixture was stirred for 18 h and concentrated under vacuum. The residue was purified by silica gel chromatography (step gradient; 5/95 to 15/85 MeOH/CH<sub>2</sub>Cl<sub>2</sub>) to provide 77 mg (77%) of compound **24** as a white solid: <sup>1</sup>H NMR (CDCl<sub>3</sub>)  $\delta$  1.48 (s, 36H), 3.32 (m, 16H), 3.52–3.96 (m, approximately 1818H), 4.10 (m, 8H); mass spectrum (MALDI) average  $m/z$  calculated for C<sub>933</sub>H<sub>1860</sub>N<sub>8</sub>O<sub>464</sub>: 20604. Found: 21340.

**Compound 25.** Compound **24** (77 mg, 3.73  $\mu\text{mol}$ ) was dissolved in 5 mL of TFA, and the mixture was allowed to stand for 3 h. The TFA was removed under a stream of N<sub>2</sub>, and the residue was dissolved in 5 mL of CH<sub>2</sub>Cl<sub>2</sub>. To the resulting solution was added a solution of 7.72 mg (22.4  $\mu\text{mol}$ ) of compound **8** in 5 mL of CH<sub>2</sub>Cl<sub>2</sub> followed by 35  $\mu\text{L}$  (25.4 mg, 251  $\mu\text{mol}$ ) of Et<sub>3</sub>N. (Note: The pH of the mixture should be checked and adjusted accordingly with Et<sub>3</sub>N to make sure it is basic.) The mixture was stirred under nitrogen for 18 h and partitioned between 50 mL of CH<sub>2</sub>Cl<sub>2</sub> and three 25 mL portions of 1 N HCl. The CH<sub>2</sub>Cl<sub>2</sub> layer was washed with brine, dried (MgSO<sub>4</sub>), filtered, and concentrated. Purification by silica gel chromatography (step gradient; 5/95 to 10/90 MeOH/CH<sub>2</sub>Cl<sub>2</sub>) provided 42 mg (53%) of compound **25** as waxy solid: <sup>1</sup>H NMR (CDCl<sub>3</sub>)  $\delta$  1.40 (m, 8H), 1.48 (s, 36H), 1.66 (m, 16H), 2.18 (t, 8H), 3.32 (m, 16H), 3.38–3.89 (m, approximately 1818H), 4.10 (m, 8H), 4.97 (t, 4H), 6.43 (t, 4H), 7.47 (s, 4H); mass spectrum (MALDI) average  $m/z$  calculated for C<sub>957</sub>H<sub>1904</sub>N<sub>12</sub>O<sub>472</sub>: 21122. Found: 21796.

**Synthesis of Compound 1a (LJP 1027).** Compound **5** (4.1 mg,  $2.05 \times 10^{-6}$  mol) was treated with 3 mL of a solution of 1/9 TFA/CH<sub>2</sub>Cl<sub>2</sub> for 2 h at room temperature. The mixture was concentrated to an oil under vacuum, and immediately 200  $\mu\text{L}$  of 0.1 M pH 8.0 tris acetate buffer was added followed by 200  $\mu\text{L}$  of CH<sub>3</sub>CN. The resulting solution was added to a helium sparged solution of 87 mg ( $12.1 \times 10^{-6}$  mol) of TA/D1 in 10.9 mL of 0.1 M pH 4.6 sodium acetate buffer using approximately 0.5 mL of CH<sub>3</sub>CN to rinse residual material into the reaction mixture. The mixture was allowed to stand for 16 h at room temperature, and the resulting mixture was purified by preparative HPLC (1 in.  $\times$  30 cm diphenyl column (Vydak), 12 mL/min, gradient 27% to 45% B over 40 min; A = H<sub>2</sub>O/0.1% TFA, B = CH<sub>3</sub>CN/0.1% TFA). The fractions containing product were lyophilized to provide 34 mg (55%) of compound **1a** as a white powder: mass spectrum (ESI)  $m/z$  calculated for C<sub>1352</sub>H<sub>2104</sub>N<sub>338</sub>O<sub>370</sub>S<sub>24</sub>: 29783. Found: 29783.

**Synthesis of Compound 1g (LJP 1082).** Compound **21** (318 mg,  $13.9 \times 10^{-6}$  mol) was treated with 16 mL of a solution of 1/1 TFA/CH<sub>2</sub>Cl<sub>2</sub> for 30 min at room temperature. The mixture was concentrated to an oil under vacuum, and immediately 3 mL of 0.1 M pH 8.5 Tris

acetate buffer was added followed by 3 mL of CH<sub>3</sub>CN. The resulting solution was added to a helium-sparged solution of 532 mg ( $7.53 \times 10^{-5}$  mol) of TA/D1 in 35 mL of 0.1 M pH 4.6 sodium acetate buffer using 2 mL of CH<sub>3</sub>CN to rinse residual material into the reaction mixture. The pH was adjusted to between 4.4 and 4.6 by addition of approximately 2.4 mL of 5 N NaOH solution, and the mixture was allowed to stand for 16 h. The pH was adjusted to 7 by addition of 5 N NaOH solution, and the mixture was dialyzed against water followed by 10 mM pH 7 sodium phosphate solution for approximately 16 h until a conductivity of 1.0 mmho was obtained. The resulting solution was purified in three portions by cation exchange chromatography (2 cm  $\times$  17 cm column packed with Toyopearl CM650M (TosoHass); flow rate 8 mL/minute; gradient 2–13% B 0–120 min; A = 9/1 10 mM pH 7 sodium phosphate/CH<sub>3</sub>CN, B = A + 1 M NaCl). The fractions containing product were partially lyophilized to reduce the volume and dialyzed against water. The desalted solution was lyophilized to provide 413 mg (59%) of compound **1g** as a white powdery solid: mass spectrum (MALDI) average  $m/z$  calculated for C<sub>2300</sub>H<sub>4000</sub>N<sub>338</sub>O<sub>848</sub>S<sub>20</sub>: 50600. Found: 51620.

**Compound 1b (LJP 1078).** Compound **1b** was prepared in a manner essentially similar to that described for compound **1g**. A mole ratio of 6.0/1.0 of TA/D1/compound **16a** was used resulting in an overall yield of 55% of compound **1b**: mass spectrum (MALDI) average  $m/z$  calculated for C<sub>1576</sub>H<sub>2551</sub>N<sub>339</sub>O<sub>486</sub>S<sub>20</sub>: 34666. Found: 35025.

**Compound 1c (LJP 1081).** Compound **1c** was prepared in a manner essentially similar to that described for compound **1g**. A mole ratio of 8.0/1.0 of TA/D1/compound **16b** was used resulting in an overall yield of 35% of compound **1c**: mass spectrum (MALDI) average  $m/z$  calculated for C<sub>1870</sub>H<sub>3140</sub>N<sub>339</sub>O<sub>633</sub>S<sub>20</sub>: 41143. Found: 41922.

**Compound 1d (LJP 1077).** Compound **1d** was prepared in a manner essentially similar to that described for compound **1g**. A mole ratio of 6.0/1.0 of TA/D1/compound **16c** was used resulting in an overall yield of 59% of compound **1d**: mass spectrum (MALDI) average  $m/z$  calculated for C<sub>2354</sub>H<sub>4107</sub>N<sub>339</sub>O<sub>875</sub>S<sub>20</sub>: 51802. Found: 51636.

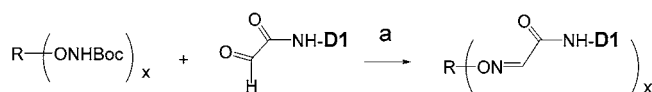
**Compound 1e (LJP 1086).** Compound **1e** was prepared in a manner essentially similar to that described for compound **1g**. A mole ratio of 6.6/1.0 of TA/D1/compound **16d** was used resulting in an overall yield of 31% of compound **1e**: mass spectrum (MALDI) average  $m/z$  calculated for C<sub>2808</sub>H<sub>5015</sub>N<sub>339</sub>O<sub>1102</sub>S<sub>20</sub>: 61803. Found: 61739.

**Compound 1f (LJP 1084).** Compound **1f** was prepared in a manner essentially similar to that described for compound **1g**. A mole ratio of 12.0/1.0 of TA/D1/compound **19** was used resulting in an overall yield of 11% of compound **1f**: mass spectrum (MALDI) average  $m/z$  calculated for C<sub>3710</sub>H<sub>6219</sub>N<sub>579</sub>O<sub>1251</sub>S<sub>40</sub>: 81638. Found: 81893.

**Compound 1h (LJP 1083).** Compound **1h** was prepared in a manner essentially similar to that described for compound **1g**. A mole ratio of 5.4/1.0 of TA/D1/compound **25** was used resulting in an overall yield of 61% of compound **1h**: mass spectrum (MALDI) average  $m/z$  calculated for C<sub>2217</sub>H<sub>3836</sub>N<sub>336</sub>O<sub>816</sub>S<sub>20</sub>: 48898. Found: 49390.

**Measurement of Anti-domain 1 Antibodies in Rats.** Nunc Maxisorp Immunoplates were coated overnight with 50  $\mu\text{L}$  of 5  $\mu\text{g/mL}$  of recombinant human  $\beta$ -2-GPI in pH 9.6 carbonate buffer at 4 °C. Subsequent steps were carried out at room temperature. Plates were washed 3 $\times$  with PBS and then blocked by treating with 250  $\mu\text{L}$  of a 2% solution of nonfat dry milk for 1 h in PBS. Plates were washed 3 $\times$  with PBS, and then wells were treated for 1 h with 50  $\mu\text{L}$  of serial dilutions of each serum sample in PBS in triplicate. Plates were washed 3 $\times$  with



**Scheme 1<sup>a</sup>**

<sup>a</sup> Reagents and conditions: (a) pH 4.6 sodium acetate buffer;  $R$  = multivalent platform,  $x = 4$  or  $8$ ,  $D1$  = domain 1 polypeptide of  $\beta_2$ GPI (amino acid sequence RTCPK PDDL P FSTV V PLKTF YEPGE EITYS CKPGY VSRGG MRKFI CPLTG LWPIN TLKCT PR).

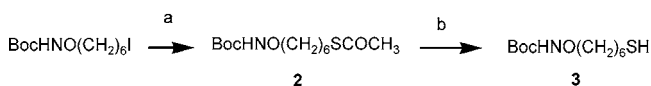
PBS, and then the wells were treated for 1 h with 50  $\mu$ L of alkaline phosphatase-conjugated goat anti-rat IgG diluted 1:2000 in PBS/0.1% BSA. Plates were washed 3 $\times$  with H<sub>2</sub>O and developed for 20 min with chromogenic substrate solution consisting of 10 gm of phenolphthalein monophosphate, 97.4 mL of 2-amino-2-methyl-1-propanol, 9.62 mL of H<sub>2</sub>O, and 21 mL HCl of concd HCl solution. Color development was stopped by adding 50  $\mu$ L of 0.2 M Na<sub>2</sub>HPO<sub>4</sub> to each well, and optical absorbance at 550 nm was measured. Nominal antibody units were assigned to the standard pool, and the concentrations of anti-domain 1 antibody (units/mL) in test sera were derived from the standard curve. Serum from nonimmunized animals was used as a control, and a pool of sera from immunized animals was used to generate a standard curve of antibody levels at various dilutions. Percent suppression of anti-domain 1 antibody by the various multivalent domain 1 conjugates was calculated by comparison to PBS-treated controls.

**Measurement of Plasma Half-Life of Conjugates in Rats and Mice.** The compounds were radiolabeled with <sup>125</sup>I by the iodine monochloride method (26) and injected iv into female CD-1 mice or male Sprague-Dawley rats. Mouse plasma samples were collected periodically for 1 h, and rat plasma samples were collected for 24 h. The amount of radiolabeled drug was detected using a gamma counter. Pharmacokinetic parameters were calculated using WinNonLin software (Pharsight, Mountain View, CA). Plasma half-lives were calculated from the areas under the time-concentration curves using the formula  $t_{1/2} = \ln 2(AUC/C_0)$  assuming a single component first-order elimination at  $t = t_{1/2}$ .

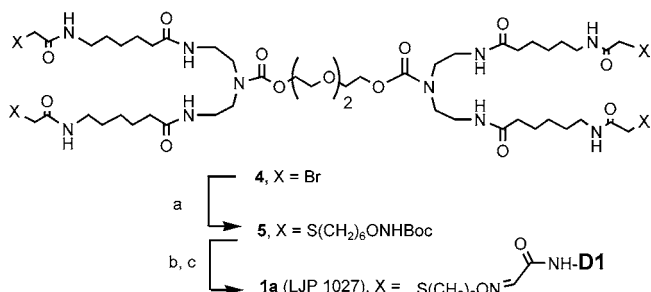
**RESULTS AND DISCUSSION**

Three types of novel PEG-containing platforms were designed and synthesized, and they were used to prepare multivalent conjugates of domain 1. The types of platform differ in the way PEG was incorporated. In one type of platform monomethoxy PEG, which has only one end available for attachment chemistry, was attached to a platform intermediate with a free secondary amine. A second type of platform was prepared in which bivalent PEG is incorporated as an integral part of the platform by branching at each end of the PEG chain. The third type of platform was prepared with PEG incorporated into each of four branching arms of the platform. A non-PEG-containing platform was also prepared. All of the platforms contained either four or eight Boc-protected aminoxy groups. Each of the platforms was converted to a multivalent domain 1 conjugate by a two step process involving removal of the Boc-protecting groups and subsequent reaction of the free aminoxy groups with transaminated domain 1 (TA/D1) as described in Scheme 1. TA/D1 is a derivative of domain 1 that has been N-terminally glyoxylated by a transamination reaction as previously described (9).

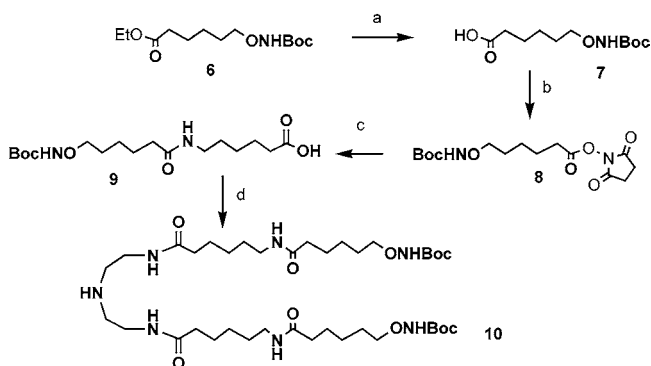
The non-PEG containing conjugate, compound **1a**, was prepared to serve as a non-PEG control. The synthesis began with the preparation of a thiol-containing Boc-

**Scheme 2<sup>a</sup>**

<sup>a</sup> Reagents and conditions: (a) KSCoCH<sub>3</sub>, acetone; (b) tri-*n*-butylphosphine, aqueous NaOH, MeOH.

**Scheme 3<sup>a</sup>**

<sup>a</sup> Reagents and conditions: (a) Compound **3**, DIPEA, 9/1 H<sub>2</sub>O/CH<sub>3</sub>CN; (b) 1/9 TFA/CH<sub>2</sub>Cl<sub>2</sub>; (c) transaminated domain 1, pH 4.6 aqueous NaOAc, CH<sub>3</sub>CN.

**Scheme 4<sup>a</sup>**

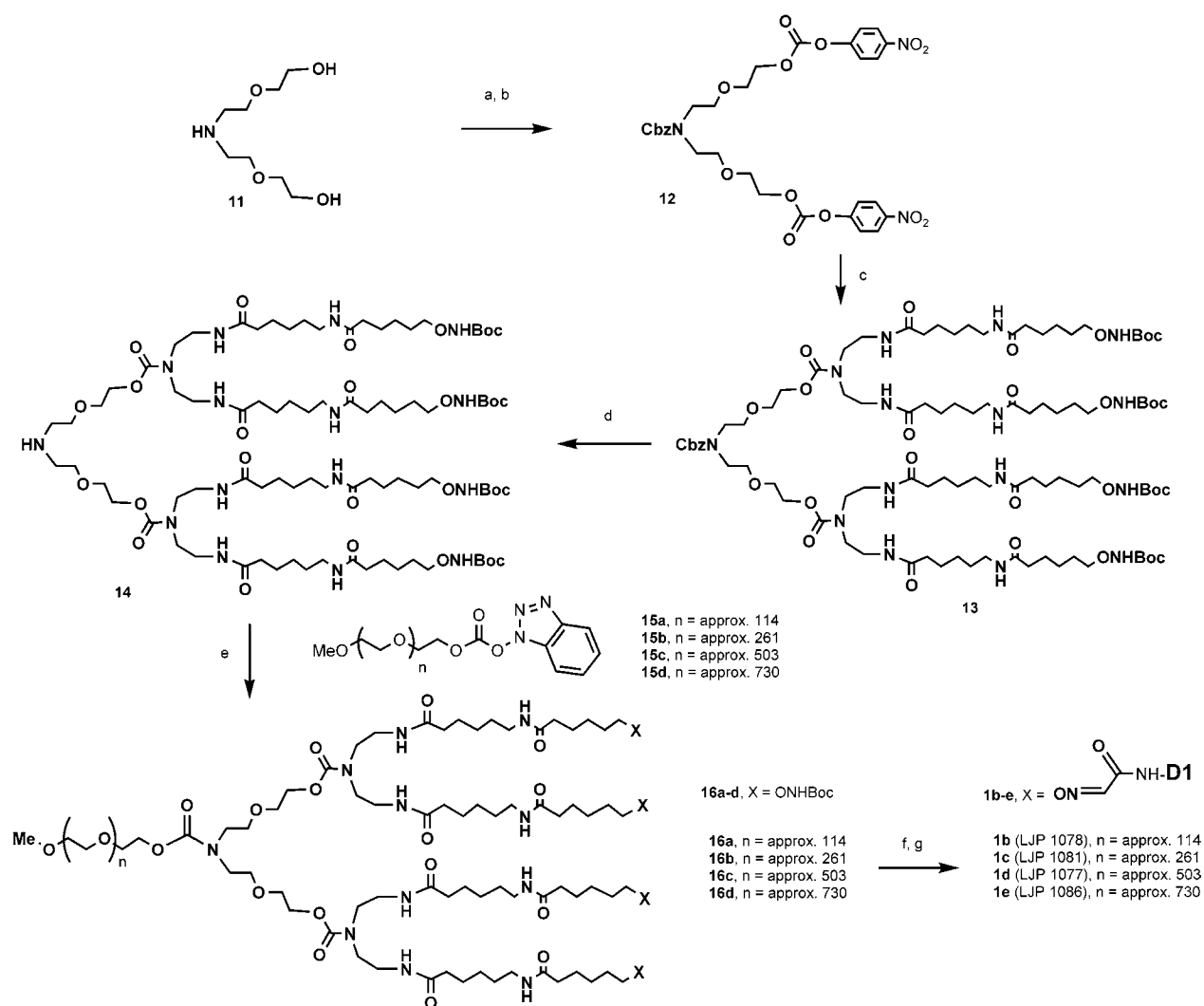
<sup>a</sup> Reagents and conditions: (a) NaOH, H<sub>2</sub>O/EtOH; (b) NHS, DCC, CH<sub>2</sub>Cl<sub>2</sub>; (c) 6-aminocaproic acid, NaHCO<sub>3</sub>, H<sub>2</sub>O, CH<sub>3</sub>CN; (d) CDI, EtOAc, diethylenetriamine, Et<sub>3</sub>N.

protected aminoxy linker, compound **3**, as described in Scheme 2. The linker was prepared from 6-iodo-*N*-Boc-1-aminoxyhexane (**2**) by reaction with potassium thioacetate to provide compound **2**. Hydrolysis of **2** with ammonium hydroxide provided compound **3**. The ammonium hydroxide and solvent were removed, and the crude thiol was used directly in the next step.

Reaction of **3** with compound **4** provided the tetravalent Boc-protected aminoxy platform, compound **5**, as described in Scheme 3. The Boc protecting groups were removed by treating with trifluoroacetic acid, and TA/D1 was attached to the resulting free aminoxy groups to provide conjugate **1a** (LJP 1027).

A series of domain 1 toleragens were prepared with attached monomethoxy PEG of different molecular weights. The synthesis of these molecules began by preparing a bivalent Boc-protected aminoxy linker, compound **10**, with a free secondary amine as diagrammed in Scheme 4. Compound **6** was prepared as described previously (23), and it was saponified to provide compound **7**. Compound **7** was converted to the *N*-hydroxy-succinimidyl ester, compound **8**, which was used to acylate 6-aminocaproic acid to provide compound **9**. Treatment of compound **9** with carbonyldiimidazole followed by diethylenetriamine provided the key intermediate, compound **10**, also referred to as the dimer cassette.

A tetravalent Boc-protected aminoxy scaffold with a free secondary amine attachment site was prepared as

Scheme 5<sup>a</sup>

<sup>a</sup> Reagents and conditions: (a) *N*-(benzyloxycarbonyloxy)succinimide, NaHCO<sub>3</sub>, H<sub>2</sub>O, dioxane; (b) 4-nitrophenylchloroformate, pyridine; (c) compound **10**, pyridine, Et<sub>3</sub>N; (d) H<sub>2</sub>, Pd/C, acetic acid, MeOH; (e) Et<sub>3</sub>N, DMF; (f) TFA/CH<sub>2</sub>Cl<sub>2</sub>; (g) transaminated domain 1 polypeptide, 100 mM pH 4.6 sodium acetate, CH<sub>3</sub>CN.

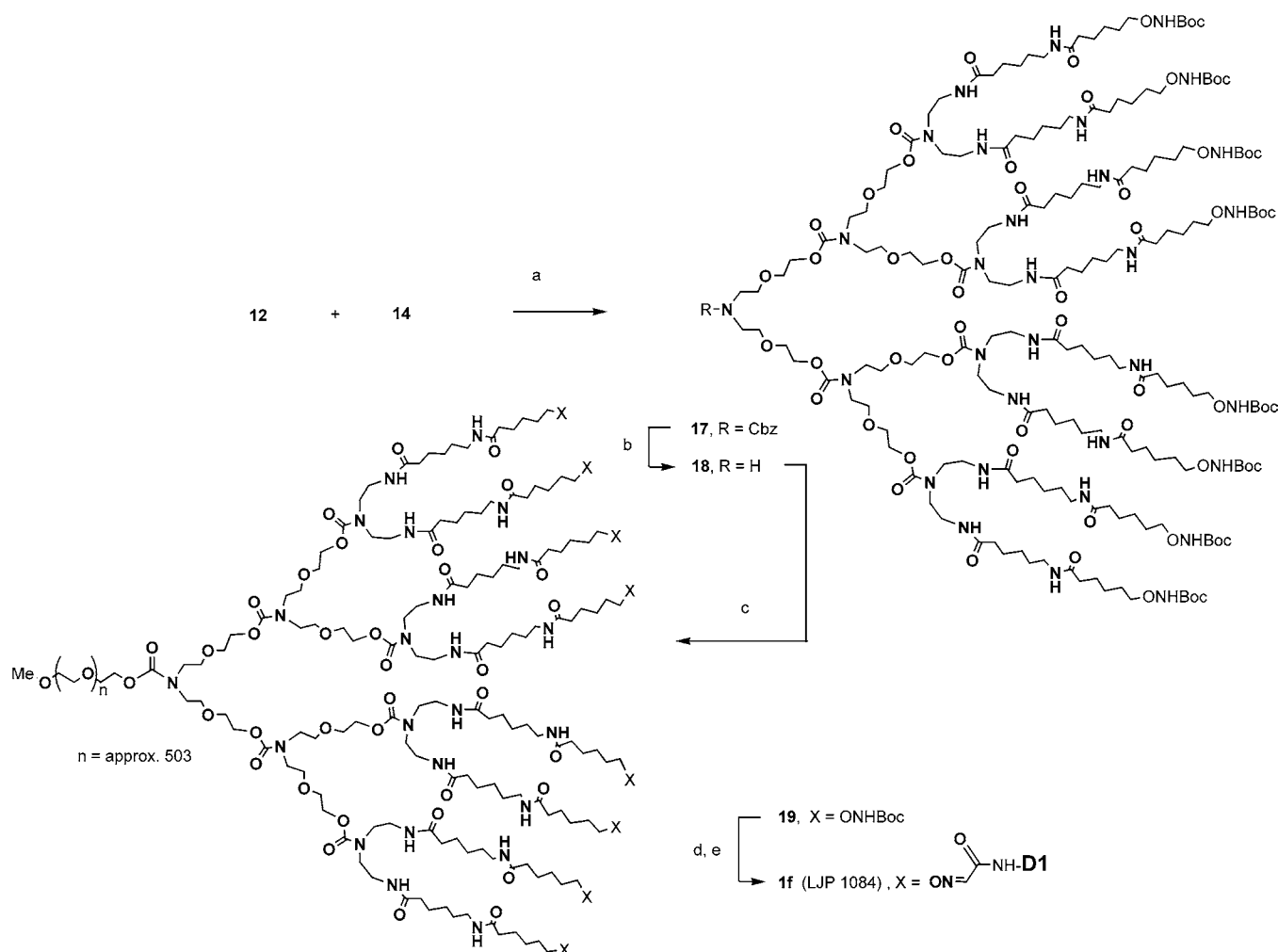
described in Scheme 5. Compound **12** was prepared in two steps from bis(2-(2-hydroxyethoxy)ethyl)amine, compound **11**, which was prepared as previously described (24). Compound **11** was first treated with *N*-(benzyloxycarbonyloxy)succinimide to place a Cbz protecting group on the secondary nitrogen atom. The hydroxyl groups were subsequently converted to 4-nitrophenyl carbonate esters using 4-nitrophenyl chloroformate. Compound **12** was reacted with compound **10** to provide compound **13**, and the Cbz protecting group was removed by hydrogenolysis to provide compound **14**. Compound **14**, also referred to as a tetramer cassette, was connected to monomethoxy-PEG of various average molecular weights. Thus reaction of compound **14** with hydroxybenzotriazole esters of methoxy-PEG with average molecular weights of approximately 5000 g/mol, 12000 g/mol, 20000 g/mol, and 30000 g/mol, compounds **15a–d**, gave rise to PEG-containing Boc-protected tetraivalent platforms **16a–d**. The Boc protecting groups were removed by treating with trifluoroacetic acid, and TA/D1 was attached to the free aminoxy groups to provide conjugates **1b–e**.

An octavalent analogue was prepared as described in Scheme 6. Condensation of the tetramer cassette, compound **14**, with compound **12** provided the Cbz-protected octamer cassette, compound **17**. The Cbz protecting group was removed by hydrogenolysis to provide the octamer

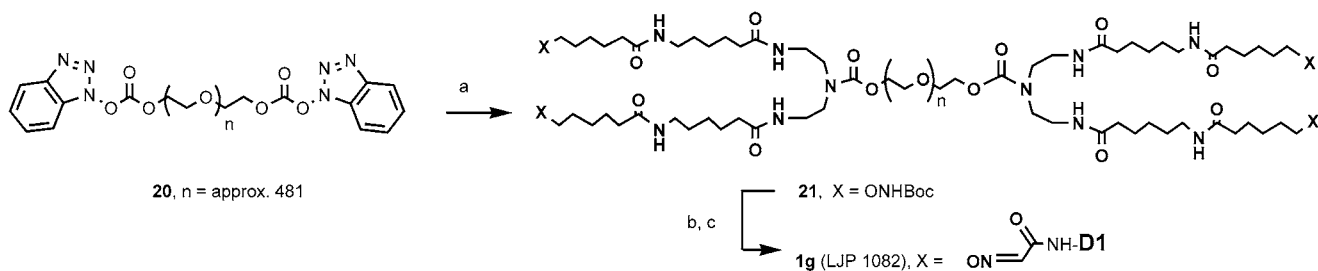
cassette, compound **18**. The octamer cassette was connected to methoxy-PEG with an average molecular weight of approximately 20000 g/mol using essentially the same chemistry described above for the tetraivalent analogues, and the resulting platform was similarly deprotected and conjugated with TA/D1 to provide compound **1f**.

The second type of PEG containing domain 1 conjugate was prepared as described in Scheme 7. The synthesis began by attaching a dimer cassette to each end of PEG. Thus, the bis(hydroxybenzotriazolyl) carbonate ester of PEG with a molecular weight of approximately 20000 g/mol, compound **20**, was treated with 2 equiv of compound **10** to provide compound **21**. Compound **21** was deprotected and treated with TA/D1 under standard conditions to provide compound **1g**.

The third class of PEG-containing conjugates was prepared by incorporation of PEG into each of the linking arms of the platform as described in Scheme 8. This example incorporates a total of approximately 20000 g/mol of PEG with 5000 g/mol of PEG in each arm. Thus, tetraivalent 4-nitrophenyl carbonate ester **22** was reacted with mono-Boc-diamino-PEG of approximately 5000 g/mol, compound **23**, to provide the branched Boc-protected tetraamine **24**. The protecting groups were removed, and the resulting tetraamine was condensed with compound

**Scheme 6<sup>a</sup>**

<sup>a</sup> Reagents and conditions: (a) HOBT, Et<sub>3</sub>N, pyridine; (b) H<sub>2</sub>, Pd/C, MeOH; (c) **15c**, Et<sub>3</sub>N, pyridine; (d) TFA/CH<sub>2</sub>Cl<sub>2</sub>; (e) transaminated domain 1 polypeptide, 100 mM pH 4.6 sodium acetate, CH<sub>3</sub>CN.

**Scheme 7<sup>a</sup>**

<sup>a</sup> Reagents and conditions: (a) compound **10**, Et<sub>3</sub>N, pyridine; (b) TFA/CH<sub>2</sub>Cl<sub>2</sub>; (c) transaminated domain 1 polypeptide, 100 mM pH 4.6 sodium acetate, CH<sub>3</sub>CN.

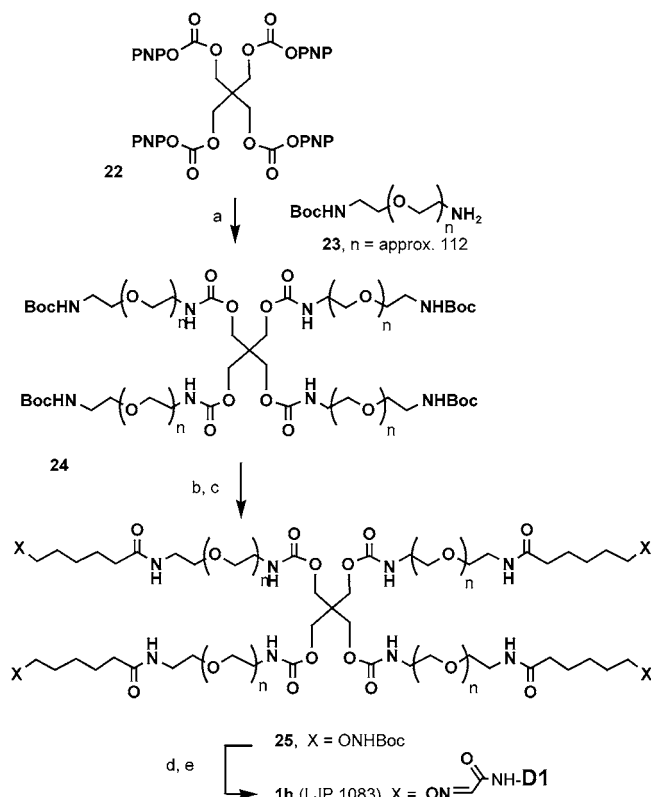
**8** to give the tetravalent aminoxy platform, compound **25**. The platform was deprotected and treated with TA/D1 under standard conditions to provide compound **1h**.

The pharmacokinetics of several radiolabeled domain 1 conjugates was studied, as was their ability to suppress anti-domain 1 antibodies and the relevant antibody producing cells in vivo. Pharmacokinetics and antibody suppression data is summarized for the tetravalent conjugates presented in this report. The potency of five tetravalent conjugates as toleragens was evaluated for their ability to suppress antibody levels in rats immunized with domain 1. Rats were primed with a conjugate of domain 1 and KLH (**9**) and adjuvant, treated with toleragen, and boosted.<sup>1</sup> Serum samples were col-

lected, and anti-domain 1 antibody levels were measured using an ELISA. Table 1 summarizes the results of the antibody suppression experiments. It is clear that the three 20 kDa PEG conjugates (**1d**, **1g**, and **1h**) are required in lower doses to achieve significant antibody

<sup>1</sup> Lewis rats (Harlan, Indianapolis, IN) weighing approximately 200 g were immunized ip with 10  $\mu$ g of domain 1-KLH conjugate in alum with pertussis as adjuvant. Three weeks after the primary immunization, groups of four animals were treated iv with toleragen (0.88, 8.8, or 88 nmol/kg; 2.5, 0.25, and 0.025 mg of polypeptide per kilogram of body weight) or PBS control. Five days after treatment, animals were boosted ip with 10  $\mu$ g of domain 1-KLH conjugate, and sera samples were collected 7 days after boost.)



Scheme 8<sup>a</sup>

<sup>a</sup> Reagents and conditions: (a)  $\text{Et}_3\text{N}$ , pyridine; (b) TFA; (c) compound **8**,  $\text{Et}_3\text{N}$ ,  $\text{CH}_2\text{Cl}_2$ ; (d) TFA/ $\text{CH}_2\text{Cl}_2$ ; (e) transaminated domain 1 polypeptide, 100 mM pH 4.6 sodium acetate,  $\text{CH}_3\text{CN}$ .

Table 1. Percent Reduction of Anti-domain 1 Antibodies in Immunized Rats<sup>a</sup>

compound	dose per kg body weight		
	0.88 nmol	8.8 nmol	88 nmol
<b>1a</b> (no PEG)	32	36	76 <sup>b</sup>
<b>1b</b> (5K PEG)	34	73	86 <sup>b</sup>
<b>1d</b> (20 K PEG)	61 <sup>b</sup>	82 <sup>b</sup>	89 <sup>b</sup>
<b>1g</b> (20 K PEG)	72 <sup>b</sup>	89 <sup>b</sup>	96 <sup>b</sup>
<b>1h</b> (20 K PEG)	73 <sup>b</sup>	93 <sup>b</sup>	94 <sup>b</sup>

<sup>a</sup> Lewis rats; percent reduction compared with PBS treated controls. <sup>b</sup>  $p \leq 0.05$ . For a brief description of the protocol see footnote 1.

suppression. The 5 kDa PEG conjugate **1b** appears to be marginally more effective than **1a**, which contains no PEG.

The rates of elimination of all of the conjugates were measured in mice and in rats. The conjugates were radiolabeled with  $^{125}\text{I}$  using the iodine monochloride method (26), and the plasma concentrations of the compounds were measured in female CD-1 mice and in male Sprague–Dawley rats dosed at 1 mg/kg.<sup>2</sup> The shapes of the time vs concentration curves were quite different in mice than in rats. In mice most of the conjugate cleared from plasma during the initial phase, whereas in rats most of the clearance took place during the second phase. The half-lives of the conjugates in both species are reported in Table 2. It is evident that, among the tetravalent conjugates, increases in the amount of PEG correlate with reduction in clearance rates. Increasing the molecular weight by increasing the number of

Table 2. Plasma  $t_{1/2}$  of Conjugates in Mice<sup>a</sup> and Rats<sup>b</sup>

compound	mice (h)	rats (h)
<b>1a</b> (no PEG)	$0.11 \pm .01$	$1.5 \pm .3$
<b>1b</b> (5K PEG)	$0.12 \pm .04$	$6.7 \pm .6$
<b>1c</b> (12K PEG)	$0.20 \pm .04$	$7.7 \pm .4$
<b>1d</b> (20K PEG)	$0.37 \pm .03$	$8.5 \pm .6$
<b>1e</b> (30K PEG)	$1.03 \pm .37$	$18.9 \pm .6$
<b>1f</b> (20K PEG)	$0.13 \pm .01$	$7.4 \pm .8$
<b>1g</b> (20K PEG)	$0.37 \pm .38$	$9.5 \pm .5$
<b>1h</b> (20K PEG)	$0.44 \pm .02$	$8.7 \pm .2$

<sup>a</sup> Female CD-1; <sup>b</sup> Male Sprague–Dawley.

copies of domain 1 polypeptide from four to eight, however, resulted in a possible increase in clearance. Compound **1f**, having 20 kDa PEG, has eight polypeptide domains and appears to clear marginally faster than the other conjugates with 20 kDa PEG.

## CONCLUSION

We have described the preparation of three novel types of multivalent PEG-containing platforms. The platforms were used to prepare well-defined conjugates of the first domain of  $\beta_2\text{GPI}$ , and the conjugates were studied for efficacy as B cell toleragens. It is clear that incorporation of PEG into the conjugates improved their effectiveness in suppressing the formation of anti-domain 1 antibodies in rats that were immunized with domain 1. In general as the molecular weight contribution from PEG increased, lower doses of toleragen were required. As the amount of PEG incorporated into the molecules was increased, the amount of suppression at all doses increased. The trend is most noticeable at the medium and low doses (8.8 and 0.88 nmol/kg). The improved efficacy of these conjugates is most likely a result of their persistence in circulation.

It is likely that in addition to size-dependent kidney filtration, clearance of the conjugates can take place by other mechanisms such as uptake by various tissues, and incorporation of PEG may also affect the rates of clearance by those mechanisms. Conversely, glomerular filtration rates can depend on properties other than size. Comparison of the clearance rate of compound **1d** with that of compound **1f** shows that increasing the number of polypeptide epitopes actually appears to result in faster clearance; whereas, one might expect the opposite if size were the only factor affecting clearance. The domain 1 polypeptide is positively charged due to an excess of positively charged amino acids, and it is well-known that charge can affect clearance from circulation. The glomerular filtration rate of anionic IgG has been shown to be slower than that of cationic IgG (28). Similarly, it has been demonstrated that the kidney filtration rate of dextran depends on charge, with positively charged molecules clearing faster than negatively charged molecules (29).

It is noteworthy that the spacing of the epitopes does not seem to significantly affect the ability of the conjugates to suppress antibody formation in the immunized rat model in which they were tested. The results with the three tetravalent conjugates (**1d**, **1g**, and **1h**), which contain 20000 MW PEG and are quite different in structure, show that they are remarkably similar in both their pharmacokinetic profiles and their ability to suppress antibody formation. Information on the relative abilities of the three structurally distinct tetravalent conjugates (**1d**, **1g**, and **1h**) to cluster B cell surface receptors would provide additional insight into the mechanism of B cell tolerance. Future studies will be aimed at further probing the structure activity relationships of

<sup>2</sup> Equivalent pharmacokinetics was demonstrated between the Lewis rats used in the present efficacy studies and the Sprague–Dawley rats.)

B cell toleragens with the goal of developing improved therapies for autoimmune diseases.

#### ACKNOWLEDGMENT

We thank La Jolla Pharmaceutical Company for supporting this work.

**Supporting Information Available:** Mass spectral data for conjugates, HPLC methods for conjugates, and estimates of purity. This material is available free of charge via the Internet at <http://pubs.acs.org>.

#### LITERATURE CITED

- (1) Goodnow, C. C. (2001) Pathways for Self-Tolerance and the Treatment of Autoimmune Diseases. *Lancet* 357, 2115–2121.
- (2) Healy, J. I., and Goodnow, C. C. (1998) Positive Versus Negative Signaling by Lymphocyte Antigen Receptors. *Annu. Rev. Immunol.* 16, 645–670.
- (3) Coggeshall, K. M. (2000) Positive and Negative Signaling in B Lymphocytes. *Curr. Top. Microbiol. Immunol.* 245, 213–260.
- (4) Jones, D. S., Hachmann, J. P., Osgood, S. A., Hayag, M. S., Barstad, P. A., Iverson, G. M., and Coutts, S. M. (1994) Conjugates of Double-Stranded Oligonucleotides With Poly-(Ethylene Glycol) and Keyhole Limpet Hemocyanin: a Model for Treating Systemic Lupus Erythematosus. *Bioconjugate Chem.* 5, 390–399.
- (5) Jones, D. S., Barstad, P. A., Feild, M. J., Hachmann, J. P., Hayag, M. S., Hill, K. W., Iverson, G. M., Livingston, D. A., Palanki, M. S., Tibbetts, A. R., and et al. (1995) Immunospecific Reduction of Antioligonucleotide Antibody-Forming Cells With a Tetrakis-Oligonucleotide Conjugate (LJP 394), a Therapeutic Candidate for the Treatment of Lupus Nephritis. *J. Med. Chem.* 38, 2138–2144.
- (6) Furie, R. A., Cash, J. M., Cronin, M. E., Katz, R. S., Weisman, M. H., Aranow, C., Liebling, M. R., Hudson, N. P., Berner, C. M., Coutts, S., and de Haan, H. A. (2001) Treatment of Systemic Lupus Erythematosus With LJP 394. *J. Rheumatol.* 28, 257–265.
- (7) Jones, D. S., Coutts, S. M., Gamino, C. A., Iverson, G. M., Linnik, M. D., Randow, M. E., Ton-Nu, H. T., and Victoria, E. J. (1999) Multivalent Thioether-Peptide Conjugates: B Cell Tolerance of an Anti- Peptide Immune Response. *Bioconjugate Chem.* 10, 480–488.
- (8) Iverson, G. M., Victoria, E. J., and Marquis, D. M. (1998) Anti-Beta2 Glycoprotein I ( $\beta_2$ GPI) Autoantibodies Recognize an Epitope on the First Domain of  $\beta_2$ GPI. *Proc. Natl. Acad. Sci. U. S. A.* 95, 15542–15546.
- (9) Jones, D. S., Cockerill, K. A., Gamino, C. A., Hammaker, J. R., Hayag, M. S., Iverson, G. M., Linnik, M. D., McNeeley, P. A., Tedder, M. E., Ton-Nu, H. T., and Victoria, E. J. (2001) Synthesis of LJP 993, a Multivalent Conjugate of the N-Terminal Domain of  $\beta_2$ GPI and Suppression of an Anti- $\beta_2$ GPI Immune Response. *Bioconjugate Chem.* 12, 1012–1020.
- (10) Knauf, M. J., Bell, D. P., Hirtzer, P., Luo, Z. P., Young, J. D., and Katre, N. V. (1988) Relationship of Effective Molecular Size to Systemic Clearance in Rats of Recombinant Interleukin-2 Chemically Modified With Water-Soluble Polymers. *J. Biol. Chem.* 263, 15064–15070.
- (11) Katre, N. V. (1993) The Conjugation of Proteins With Poly-(Ethylene Glycol) and Other Polymers; Altering Properties of Proteins to Enhance Their Therapeutic Potential. *Adv. Drug Delivery Rev.* 10, 91–114.
- (12) Ueda, Y., Munechika, K., Kikukawa, A., Kanoh, Y., Yamanouchi, K., and Yokoyama, K. (1989) Comparison of Efficacy, Toxicity and Pharmacokinetics of Free Adriamycin and Adriamycin Linked to Oxidized Dextran in Rats. *Chem. Pharm. Bull. (Tokyo)* 37, 1639–1641.
- (13) Hashida, M., Kato, A., Takakura, Y., and Sezaki, H. (1984) Disposition and Pharmacokinetics of a Polymeric Prodrug of Mitomycin C, Mitomycin C-Dextran Conjugate, in the Rat. *Drug Metab. Dispos.* 12, 492–499.
- (14) Fuertges, F., and Abuchowski, A. (1993) The Clinical Efficacy of Poly(Ethylene Glycol)-Modified Proteins. *J. Controlled Release* 11, 139–148.
- (15) Bailon, P., and Berthold, W. (1998) Poly(Ethylene Glycol)-Conjugated Pharmaceutical Proteins. *Pharm. Sci. Technol. Today* 1, 352–356.
- (16) Mehvar, R. (2000) Modulation of the Pharmacokinetics and Pharmacodynamics of Proteins by Polyethylene Glycol Conjugation. *J. Pharm. Pharm. Sci.* 3, 125–136.
- (17) Chapman, A. P., Antoniwi, P., Spitali, M., West, S., Stephens, S., and King, D. J. (1999) Therapeutic Antibody Fragments With Prolonged in Vivo Half-Lives. *Nat. Biotechnol.* 17, 780–783.
- (18) Bowen, S., Tare, N., Inoue, T., Yamasaki, M., Okabe, M., Horii, I., and Eliason, J. F. (1999) Relationship Between Molecular Mass and Duration of Activity of Polyethylene Glycol Conjugated Granulocyte Colony-Stimulating Factor Mutein. *Exp. Hematol.* 27, 425–432.
- (19) Conover, C. D., Gilbert, C. W., Shum, K. L., and Shorr, R. G. (1997) The Impact of Polyethylene Glycol Conjugation on Bovine Hemoglobin's Circulatory Half-Life and Renal Effects in a Rabbit Top-Loaded Transfusion Model. *Artif. Organs* 21, 907–915.
- (20) Clark, R., Olson, K., Fuh, G., Marian, M., Mortensen, D., Teshima, G., Chang, S., Chu, H., Mukku, V., Canova-Davis, E., Somers, T., Cronin, M., Winkler, M., and Wells, J. A. (1996) Long-Acting Growth Hormones Produced by Conjugation With Polyethylene Glycol. *J. Biol. Chem.* 271, 21969–21977.
- (21) Hinds, K. D. and Kim, S. W. (2002) Effects of PEG Conjugation on Insulin Properties. *Adv. Drug Deliv. Rev.* 54, 505–530.
- (22) Bailon, P., Palleroni, A., Schaffer, C. A., Spence, C. L., Fung, W. J., Porter, J. E., Ehrlich, G. K., Pan, W., Xu, Z. X., Modi, M. W., Farid, A., Berthold, W., and Graves, M. (2001) Rational Design of a Potent, Long-Lasting Form of Interferon: a 40 KDa Branched Polyethylene Glycol-Conjugated Interferon Alpha-2a for the Treatment of Hepatitis C. *Bioconjugate Chem.* 12, 195–202.
- (23) Jones, D. S., Hammaker, J. R., and Tedder, M. E. (2000) A Convenient Synthesis of N-(tert-Butyloxycarbonyl) Aminoxy Ethers. *Tetrahedron Lett.* 41, 1531–1533.
- (24) Bordunov, A. V., Hellier, P. C., Bradshaw, J. S., Dalley, N. K., Kou, X., Zhang, X. X., and Izatt, R. M. (1995) Synthesis of New Pyridinoazacrown Ethers Containing Aromatic and Heteroaromatic Proton Ionizable Substituents. *J. Org. Chem.* 60, 6097–6102.
- (25) Jones, D. S., Tedder, M. E., Gamino, C. A., Hammaker, J. R., and Ton-Nu, H.-T. (2001) Synthesis of Multivalent Carbonate Esters by Divergent Growth of Branched Carbamates. *Tetrahedron Lett.* 42, 2069–2072.
- (26) Contreras, M. A., Bale, W. F., and Spar, I. L. (1983) Iodine Monochloride (ICl) Iodination Techniques. *Methods Enzymol.* 92, 277–292.
- (27) Cockerill, K. A., Smith, E., Jones, D. S., Branks, M. J., Hayag, M., Victoria, E. J., Linnik, M. D., and Campbell, M.-A. (2003) In Vivo Characterization of Bioconjugate B Cell Toleragens with Specificity for Autoantibodies in Antiphospholipid Syndrome. *Int. Immunopharmacol.* 3, 1667–1675.
- (28) Di Mario, U., Cancelli, A., Pietravalle, P., Altamore, G., Mariani, G., De Rossi, M. G., Bernardini, G., Pasquale, A., Borgia, M. C., Frontoni, S., et al. (1990) Anionic Versus Cationic Immunoglobulin Clearance in Normal Subjects: a Novel Approach to the Evaluation of Charge Permselectivity. *Nephron* 55, 400–407.
- (29) Brenner, B. M., Hostetter, T. H., and Humes, H. D. (1978) Glomerular Permselectivity: Barrier Function Based on Discrimination of Molecular Size and Charge. *Am. J. Physiol.* 234, F455–460.

BC034103T

# A Targeted Peptide Nucleic Acid To Down-Regulate Mouse Microsomal Triglyceride Transfer Protein Expression in Hepatocytes

Sabine M. W. van Rossenberg,<sup>†</sup> Karen M. Sliedregt-Bol,<sup>‡</sup> Perry Prince,<sup>†</sup> Theo J. C. van Berkel,<sup>†</sup> Jacques H. van Boom,<sup>‡</sup> Gijs A. van der Marel,<sup>‡</sup> and Erik A. L. Biessen<sup>\*,†</sup>

Leiden/Amsterdam Center for Drug Research, Division of Biopharmaceutics, and Leiden Institute of Chemistry, Gorlaeus Laboratories, Leiden University, P.O. Box 9502, 2300 RA Leiden, The Netherlands  
Received March 19, 2003; Revised Manuscript Received August 26, 2003

Peptide nucleic acids (PNA's) have shown to hold potential as antisense drugs. In this study we have designed PNA drugs for the microsomal triglyceride transfer protein (MTP), which is known to play a critical role in the assembly of atherogenic lipoproteins, and have converted the most potent drug into a liver-targeted prodrug. First, we have synthesized three PNA sequences targeting domains on the mouse MTP mRNA, which were not involved in intrastrand base-pairing interactions as judged from its secondary structure. Only one of the PNA's, PNA569, showed dose-dependent inhibition of MTP expression in a cell-free system for coupled transcription/translation of MTP. Second, to improve the cellular uptake of this PNA drug, we have conjugated PNA569 to a high affinity ligand for the asialoglycoprotein receptor, K(GalNAc)<sub>2</sub>. As compared to the parent PNA, the prodrug PNA-K(GalNAc)<sub>2</sub> was found to display to a markedly improved capacity to inhibit MTP mRNA expression in parenchymal liver cells. A glycoconjugated nonsense control appeared to be ineffective. In conclusion, the design of a targeted PNA is described to reduce MTP expression in parenchymal liver cells by 70%. The presented approach for targeted tissue-specific down-regulation of genes by PNA's may be valid for other genes as well.

## INTRODUCTION

Peptide nucleic acids (PNA's) are DNA analogues, in which the phosphate backbone has been replaced by an *N*-(2-aminoethyl)glycine pseudopeptide backbone. The achiral, uncharged, and rather flexible peptide backbone permits a more stable hybridization to DNA and RNA oligomers and thus a higher sequence specificity (1, 2). PNA's have been used to block protein expression both at a transcriptional and at a translational level (3). As compared to other more commonly used nucleotide analogues, cellular uptake of PNA's tends to be even lower, which has hampered the application of PNA oligomers in an in vivo setting (4, 5). Accordingly, therapeutic PNA activity has been demonstrated in cell-free translation/transcription systems (6) and after microinjection in individual cells (7). Cutrona et al. (8) have recently described that PNA uptake by Burkitt's lymphoma cells was considerably enhanced after conjugation to a so-called nuclear location signal (NLS), leading to a significant down-regulation of the target gene, *c-myc*. Likewise, several other groups have reported an improved PNA uptake after conjugation to an NLS (9, 10) and to intracellular translocation peptides (11). Another strategy was pursued by Chiarantini et al. (12) who successfully applied opsonized erythrocytes to selectively deliver entrapped PNA to monocytes/macrophages. Although

these approaches appear to be effective in vitro, reports showing effective transfection in vivo are scarce (13, 14).

In this study we have explored to the potential of targeted PNA delivery. PNA drugs have been designed against the murine microsomal triglyceride protein (MTP), which is a rate-limiting key enzyme in the assembly of atherogenic apoB100-containing lipoproteins by parenchymal liver cells (15, 16). MTP activity was found to correlate with the blood levels of these lipoproteins (17), making MTP an excellent target for therapeutic intervention in hyperlipidemia. From the secondary structure of murine MTP mRNA, we selected three regions that were not involved in base-pairing reactions and synthesized PNA sequences targeting these domains. The most potent PNA drug was subsequently conjugated to a high affinity tag for the asialoglycoprotein receptor (ASGPr), K(GalNAc)<sub>2</sub>, which was previously shown effective in redirecting (oligo)nucleotides and peptides to this receptor (18, 19). We demonstrate that the activity of antisense PNA's can be considerably improved through K(GalNAc)<sub>2</sub>-aided targeting to the asialoglycoprotein receptor.

## EXPERIMENTAL PROCEDURES

**Materials.** Tris-saturated biophenol, pH 8, was purchased from Biosolve Ltd. (Valkenswaard, The Netherlands). Ribogreen was from Molecular Probes (Eugene, OR). Superscript II reverse transcriptase and RNaseH were obtained from Life Technologies (Frederick, MD). Oligonucleotides and Goldstar DNA polymerase were from Eurogentec (Seraing, Belgium). The TnT in vitro transcription/translation assay was from Promega (Leiden, The Netherlands). All other chemicals were of analytical grade.

\* To whom correspondence should be addressed. Tel: +31-(0)71-5276040. Fax: +31-(0)71-5276032. E-mail: biessen@lacdr.leidenuniv.nl.

<sup>†</sup> Leiden/Amsterdam Center for Drug Research, Division of Biopharmaceutics.

<sup>‡</sup> Leiden Institute of Chemistry.



**Synthesis.** Synthesis of the PNA025, PNA341, PNA569, control PNA, and the PNA glycoconjugates were performed as previously described (20). PNA's were routinely checked for purity (RP-HPLC, high-resolution mass spectroscopy) and chemical identity (mass spectroscopy) as described (20).

**Cell-Free Assay for Coupled Transcription/Translation (TnT).** MuMTP cDNA was cloned in an T7 polymerase promote driven transcription vector for use in the transcription/translation assay (TnT). The TnT assay was performed as follows. TnT mixtures were prepared containing 5  $\mu$ L of rabbit reticulocyte lysate (RRL), 0.4  $\mu$ L of reaction buffer, 0.2  $\mu$ L of T7-polymerase, 0.2  $\mu$ L of amino acid mixture (1 mM) without methionine, 0.4  $\mu$ L of  $^{35}$ S-methionine (2  $\mu$ Ci), and 0.4  $\mu$ L of muMTP plasmid (0.5  $\mu$ g/ $\mu$ L) with or without PNA025, PNA341, PNA569, or nonsense PNA (500 nM; total volume 10  $\mu$ L) and subsequently incubated for 60 min at 30 °C. Next, 25  $\mu$ L of protein sample buffer (62 mM Tris, 12.5% glycerol (v/v), 1.25% SDS (w/v), 2.5% (v/v)  $\beta$ -mercaptoethanol, and 0.25% (w/v) bromophenol blue pH 6.8) were added, and the mixture was denatured for 3 min at 95 °C. Samples were applied to a 15% denaturing SDS-polyacrylamide gel, and the gel was run for 30 min at 100 V and subsequently for 1 h at 200 V in 0.02 M Tris, 0.16 M glycine, and 0.1% SDS (w/v). Gels were fixed in a solution of 45% methanol (v/v) and 0.5 M acetic acid and autoradiographed by exposure to a phosphor-imager screen for 2 days. As a measure of muMTP synthesis, we have quantified the amount of incorporated  $^{35}$ S-methionine using ImageQuant software (Molecular Dynamics, Sunnyvale, CA).

**Isolation of Mouse Parenchymal Liver Cells.** Parenchymal liver cells were isolated from anaesthetized mice (10–12 weeks old male C57bl/6KH mice; 22–27 g; Broekman Institute BV, Someren, The Netherlands) by perfusion of the liver for 10 min at 37 °C with collagenase (type IV, 0.05%, w/v) according to the method of Seglen (21). Cells were >99% pure as judged by light microscopy. Nonviable cells were removed by density gradient centrifugation (10 min; 100g) after diluting the cell suspension 1:1 with Percoll, and the viable cells (>98%) were subsequently washed and dissolved in the incubation medium.

**Down-Regulation of MTP mRNA in Mouse PC Cells.** Mouse parenchymal liver cells were incubated 3 h after seeding ( $2 \times 10^5$  cells/well) with PNA's. Cells were incubated for 4 h at 37 °C in the absence or the presence of PNA569, PNA569-K(GalNAc)<sub>2</sub>, or nonsense PNA-K(GalNAc)<sub>2</sub> (200nM). After incubation, medium was removed, 1 mL medium was added, and cells were incubated for 24 h at 37 °C. Cells were lysed, total RNA was isolated, and the muMTP-to-muGAPDH amplicon ratio was determined by quantitative radioactive RT-PCR as described below.

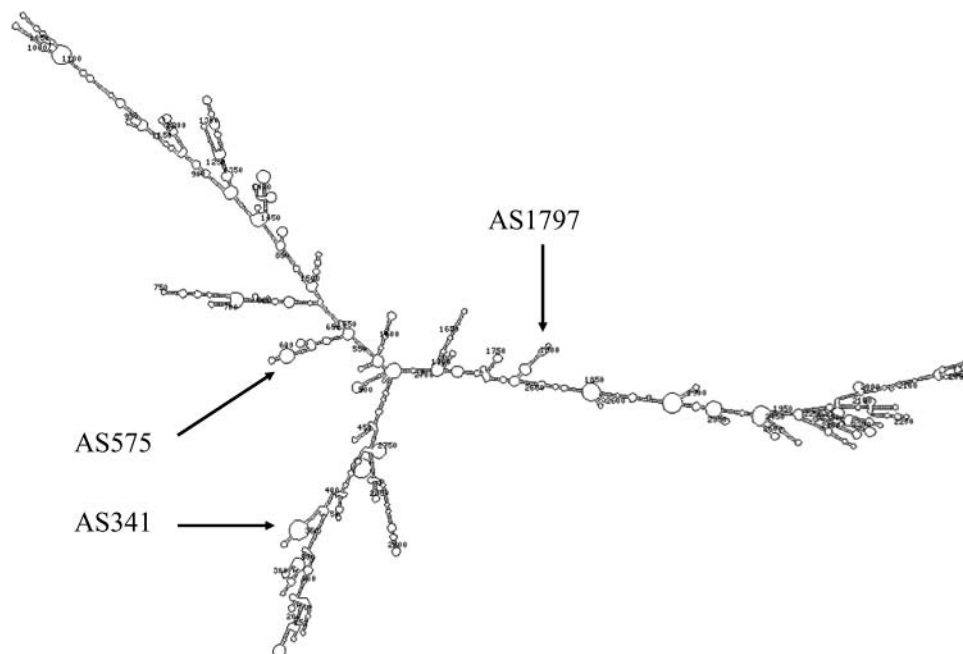
**Quantitative Radioactive RT-PCR of Murine MTP.** The relative abundance of murine MTP mRNA was monitored through quantitative RT-PCR with glyceraldehyde-3-phosphate dehydrogenase (GAPDH) as an internal standard. Total RNA was isolated from mA3/F2 or parenchymal liver cells by lysis in GTC solution (4 M guanidinium isothiocyanate; 25 mM sodium citrate buffer, pH 7.0; 0.5% *N*-lauroyl sarcosine; and 0.1 M  $\beta$ -mercaptoethanol) according to Chomczynski and Sacchi (22). After phenol–chloroform extraction, the total RNA was precipitated by adding 2.5 volumes of ice-cold ethanol. The mixture was placed at –20 °C for at least 1 h and centrifuged for 45 min at 10000g. Pellets were washed twice with 70% ethanol in DEPC-treated water and were

dissolved in 20  $\mu$ L of DEPC-treated Tris/EDTA buffer (10 mM Tris-HCl, 1 mM EDTA, pH 8.0). The RNA concentration in the samples was determined with the RNA-specific fluorescent dye Ribogreen according to the procedure of Jones et al. and using yeast tRNA as calibration standard (yield: 6–18  $\mu$ g/ $6 \times 10^5$  cells) (23). Total RNA (2  $\mu$ g) was reverse transcribed using 100 Units Superscript II reverse transcriptase (Life Technologies, Gaithersburg, MD) and subsequently amplified in the presence of [ $^{32}$ P]- $\alpha$ -dCTP (0.8  $\mu$ Ci) and Taq polymerase (0.4 Units, Eurogentec, Brussels, Belgium) using muMTP primers (forward: 5'-gga.aaa.ccg.caa.gac.agc; reversed: 5'-ctt.gt-t.ggg.ctc.ggt.agg; 100 ng). cDNA was amplified for 22 rounds using the following cycling parameters: denaturing step 30 min at 95 °C, annealing step: 60 min at 54 °C; elongation step 2 min at 72 °C. Unless otherwise stated, muGAPDH primers (forward: 5'-gag.cga.gac-.ccc.act.aac; reversed: 5'-atg.agc.cct.tcc.aca.atg; 100 ng) were added after four cycles, and the mixture was amplified according to the above protocol for another 18 cycles. Aliquots of 20  $\mu$ L were mixed with 2.5  $\mu$ L of loading buffer (40% (w/v) sucrose, 0.25% (w/v) bromophenol blue, 0.25% (w/v) xylene cyanol) and subjected to electrophoresis on 10% polyacrylamide gel (1.5 mm thickness) under nondenaturing conditions in 1  $\times$  TBE buffer (0.1 M Tris, 0.1 M boric acid, 2.5 mM EDTA, pH 8.0). The gels were fixed with 7% acetic acid, washed five times with water, and exposed overnight to a phosphor-imager screen. The intensity of the muMTP and muGAPDH amplicons was quantified using ImageQuant software (Molecular Dynamics, Sunnyvale, CA). To minimize RT reaction variability, all RNA samples were reverse transcribed simultaneously by using a RT "master mix". Formation of muMTP amplicons in the presence or the absence of muGAPDH primers was identical. Intraexperimental variation in the muMTP-to-muGAPDH amplicon ratio amounted to 13% and 18% starting from a single batch of cDNA and mRNA, respectively ( $n = 5$ ). The RT-PCR signal was completely linear under the conditions used in this study, and the PCR efficiency per cycle was close to the theoretical maximum.

**Data Processing.** Saturation binding data and substrate curves of initial uptake were analyzed according to a single site binding model using nonlinear regression (Prism, GraphPAD Software, Inc., San Diego, CA). Values are expressed as means  $\pm$  SEM. Data variance was analyzed statistically by means of one-way ANOVA with Dunnet's Post testing.

## RESULTS

**Antisense Sequences.** In search of effective antisense drugs for muMTP, we have selected a set of potentially active sequences targeting different regions on the muMTP. On the basis of secondary structure analysis (Mfold vs 3.1; 24), we have identified sites which are not likely involved in base pairing reactions (i.e. hairpins and pseudoknots) and might thus be accessible to antisense drug hybridization (Figure 1). Three sequences were selected from the single strand frequency plot (plotting the chance that a single nucleotide is involved in base-pairing; obtained from the 25 energetically most favorable secondary RNA structures). Two domains (341 and 569), corresponding with the highest peaks from the plot, were selected as PNA target, while PNA025 was designed as it appeared to be the most accessible site near the translation initiation codon. These PNA sequences were synthesized, purified, and subsequently tested for their ability to inhibit muMTP synthesis (Table 1).



**Figure 1.** Identification of potential antisense sites. Mapping of the secondary structure of muMTP mRNA using the Mfold algorithm (24). Arrows indicate the specific mRNA regions targeted by the PNA antisense drugs.

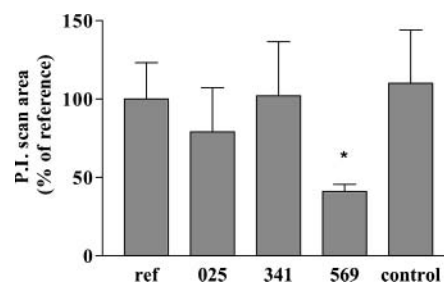
**Table 1.** Sequences of PNA Drugs Used in This Study

PNA	sequences
025	GGA TCA TGC TGG CTC CCT
341	TCC CTA TGA TCT TAG GTG
569	TTT TGA CCA CTT TGT
569-cluster	TTT TGA CCA CTT TGT-K(GalNAc) <sub>2</sub>
nonsense	TTT CCA TGA CTT CTT TGT
nonsense cluster	CAT ATA CAT TGA TC-K(GalNAc) <sub>2</sub>

**Effect of PNA on muMTP Synthesis in a Cell-Free System.** To evaluate the antisense activity of the selected sequences, a cell-free assay for coupled transcription/translation (TnT) was developed. Basically, muMTP mRNA was transcribed from a T7 polymerase promoter-flanked muMTP cDNA construct and translated in situ under the agency of rabbit reticulocyte lysate (RLL) and <sup>35</sup>S-methionine. Synthesis of full length <sup>35</sup>S-labeled muMTP (96 kD) was established by PAGE electrophoresis and subsequent autoradiography.

The selected PNA sequences were first tested for their capacity to inhibit muMTP transcription or translation in the TnT assay at a concentration of 500 nM. From Figure 2 only PNA569 appeared to be capable of inhibiting muMTP synthesis. PNA025, PNA341, and the nonsense PNA control did not show any inhibition of muMTP. Since PNA569 seemed to display antisense activity, we investigated the concentration dependency of its effect. PNA569 appeared to inhibit muMTP expression in a concentration-dependent fashion (Figure 3a). Maximal inhibition of <sup>35</sup>S-muMTP synthesis was attained at 500 nM, while the EC<sub>50</sub> was calculated to be 357 nM. PNA569 also affected luciferase synthesis from a T7 polymerase promoter driven luciferase vector, albeit at a much lower potency (EC<sub>50</sub> = 15 μM) (Figure 3b). Apparently, a rather narrow concentration window exists, in which PNA569 is able to specifically down-regulate muMTP synthesis.

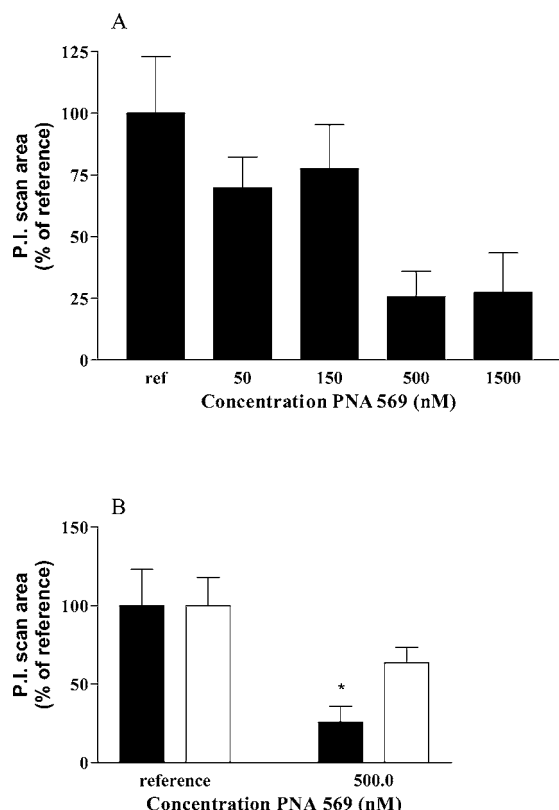
**In Vitro Binding Studies.** We and others have previously shown that conjugation of drugs oligonucleotides and proteins to a cell-specific ligand is a powerful strategy to improve their uptake by the target tissue (25, 20). In analogy this strategy may also prove effective for PNA's and will result in higher antisense activity. Hence



**Figure 2.** Potency of PNA's to inhibit muMTP expression in a cell-free system for coupled transcription/translation. The expression of <sup>35</sup>S-met muMTP was measured by a rabbit reticulocyte lysate-containing in vitro assay for coupled transcription/translation in the presence of PNA025, PNA341, PNA569, or nonsense PNA (500 nM). The results are expressed as percentage of the amount of full length <sup>35</sup>S-met muMTP synthesized in the absence of PNA's. Statistical significant difference relative to control is indicated by \* ( $P < 0.05$ ). Data are means  $\pm$  SEM of three determinations in triplicate.

we have prepared a glycoconjugated PNA prodrug to target parenchymal liver cells, by coupling PNA to K(GalNAc)<sub>2</sub>, a high affinity ligand for the asialoglycoprotein receptor on this cell type (20). The affinity of PNA-K(GalNAc)<sub>2</sub> for the asialoglycoprotein receptor (ASGPr) was monitored in an in vitro competition assay of <sup>125</sup>I-ASOR binding to mouse parenchymal liver cells. PNA-K(GalNAc)<sub>2</sub> gave complete and monophasic inhibition of <sup>125</sup>I-ASOR binding with an affinity that was similar to that of the glycoside ligand itself ( $K_d$  = 77 nM; data not shown) (19, 20). This indicates that attachment of the PNA to the K(GalNAc)<sub>2</sub> did not dramatically affect the affinity for the ASGPr.

**Antisense Effect of PNA and PNA-K(GalNAc)<sub>2</sub> in Vitro.** A quantitative radioactive RT-PCR-based assay was set up to measure muMTP mRNA levels in parenchymal liver cells. We have evaluated the effect of the most potent PNA and its glycoconjugate on muMTP expression in freshly isolated parenchymal liver cells. Cells were incubated for 4 h with 200 nM of PNA569, PNA569-K(GalNAc)<sub>2</sub>, or nonsense PNA-K(GalNAc)<sub>2</sub>. After 24 h, cells were harvested, and their muMTP content was measured relative to that of the GAPDH

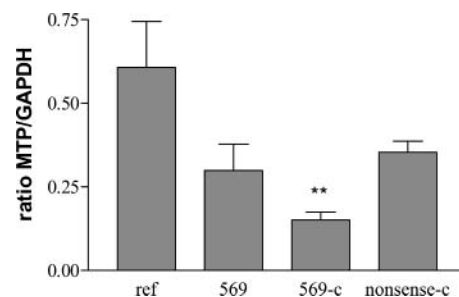


**Figure 3.** (A) Dose dependency of inhibitory effect of PNA569 on muMTP expression in the TnT assay. (B) Inhibitory effect of PNA569 (500 nM) on muMTP expression and luciferase in the TnT assay. The expression of  $^{35}\text{S}$ -Met muMTP and  $^{35}\text{S}$ -Met luciferase was measured in the TnT assay in the presence of 50–1500 nM of PNA569. The results are expressed as percentage of the amount of  $^{35}\text{S}$ -Met muMTP formed in the absence of PNA. Statistical significant difference relative to luciferase down-regulation is indicated by \* ( $P < 0.05$ ). Data are means  $\pm$  SEM of three determinations in triplicate.

housekeeping gene. Figure 4 shows that the muMTP-to-GAPDH ratio was significantly reduced after incubation with PNA569-K(GalNAc)<sub>2</sub> ( $p < 0.05$ ), while the parent PNA569 and a nonsense glycoconjugate (nonsense PNA-K(GalNAc)<sub>2</sub>) gave only a minor nonsignificant reduction of mRNA MTP levels.

## DISCUSSION

Over the past few years, PNA have emerged as one of the most promising antisense or anti-gene drugs (26, 27). In this study we selected a set of potentially active PNA sequences against muMTP. MTP is essential for the assembly and secretion of apoB-containing lipoproteins and as such an interesting target for the therapeutic intervention in hyperlipidemia. Potential PNA target sequences were identified by secondary structure analysis of muMTP mRNA using a computerized Mfold algorithm, which was previously shown to generate accurate predictions of the RNA folding pattern (24). Three sequences were subsequently synthesized and tested for their activity in a cell-free assay for coupled transcription/translation (TnT). This assay has already been successfully used for the initial validation of phosphodiester and phosphorothioate nucleotides targeting the glutathione S-transferase Mu1/2 gene (28). As shown in this study, the TnT assay is also appropriate for testing PNA drugs. Our results show that, of the antisense drugs tested, only PNA569 was able to induce a specific inhibition of muMTP synthesis. The activity of PNA569 was less than



**Figure 4.** Down-regulation of MTP mRNA in mouse parenchymal liver cells by PNA and PNA-K(GalNAc)<sub>2</sub>. The expression of muMTP mRNA was measured after incubation of parenchymal liver cells with PNA569, PNA-K(GalNAc)<sub>2</sub>, or nonsense PNA-K(GalNAc)<sub>2</sub> (200 nM). The results are expressed as the ratio between MTP and GAPDH. Statistical significant difference relative to control is indicated by \*\* ( $P < 0.01$ ). Data are means  $\pm$  SEM of three determinations in triplicate.

that of a phosphodiester analogue targeting the same site ( $\text{EC}_{50} = 18$  nM). PNA025 and PNA341 appeared to be ineffective, which concurs with the poor activity of phosphodiester drugs targeting the same sites (ODN025 and ODN341 gave only 29% and 81% inhibition at 150 nM, respectively) [Vrins et al., manuscript in preparation]. Nevertheless this apparent similarity may not necessarily reflect a corresponding mode of action, as the phosphodiester probably act inhibitory via RNaseH-mediated target strand degradation, whereas the antisense activity of PNA's was reported not to involve RNaseH-mediated degradation (29–31). From the in vitro assay it can also be concluded that at higher concentrations (>500 nM), PNA569 inhibits luciferase synthesis as well. This inhibition may be attributed to a nonspecific aptameric effect rather than by specific hybridization of the PNA to the luciferase cDNA, since no homology was observed between the MTP and luciferase cDNA.

Second, we have demonstrated in this study the inhibition of muMTP mRNA levels by mouse parenchymal liver cells after conjugation of the PNA569 with a high affinity ligand for the asialoglycoprotein receptor. Although recently a number of potent MTP inhibitors have been developed (32), this PNA569 conjugate offers the advantage of only inhibiting liver MTP, leaving MTP expression in the intestine unaffected. Previous studies in our lab confirmed that, upon injection into mice, K(GalNAc)<sub>2</sub>-derivatized PNA mainly accumulated in the liver, while intestinal uptake was only marginal (20). This PNA was directed against human MTP and did not cross-hybridize to murine MTP cDNA, thus hampering in vivo evaluation in a mouse model for hyperlipidemia. Here we present a targeted PNA prodrug that upon incubation with parenchymal liver cells effected a significant reduction of mouse MTP expression by 70%. This reduction was neither observed for a glycoconjugated control PNA, establishing that the PNA inhibited muMTP expression in a sequence dependent fashion, nor for the parental PNA569 drug. The actual mode of action of the glycoconjugated PNA remains to be solved. It has been reported that PNA-RNA heteroduplexes are not degraded by RNase H (33), suggesting that the antisense effect of PNA569 is attributable to steric interference with translation or to RNA destabilization. PNA was reported to promote a sequence-specific lowering of mRNA levels (34). Aldrian-Herrada et al. (35) proposed that hybridization of antisense PNA to the target may interdict mRNA translation by shuttling the PNA/RNA hybrids into the proteasome compartment leading to its



degradation. Theoretically mRNA down-regulation might reflect an RT-PCR artifact. PNA-RNA hybrids are known to be resistant to phenol extraction and urea treatment (36). Reverse transcription of the PNA/MTP might be less efficient, which will translate in a seemingly reduced mRNA level. Unpublished studies within our lab showed that RT-PCR interference may occur at PNA concentrations > 100–500 nM. However, as PNA569 was also a potent inhibitor in the TnT assay, the latter is not a very plausible explanation. In either case, the observed PNA-induced reduction in muMTP mRNA levels clearly demonstrates that the antisense PNA was able to enter parenchymal liver cells and to hybridize to the corresponding intracellular target. The fact that PNA-RNA heteroduplexes do not induce cleavage of the mRNA target by Rnase H can be considered an advantage as nonspecific effects due to the interaction of the antisense or nonsense PNA with other mRNA molecules are less likely to result in a temporary arrest of translation (9).

In conclusion, we demonstrate a marked inhibition of muMTP expression in freshly isolated parenchymal liver cells by a glycoconjugated PNA drug. This glycoconjugated PNA will provide an excellent tool for therapeutic evaluation of MTP down-regulation in a mouse model for hyperlipidemia.

#### ACKNOWLEDGMENT

This work was supported by CW/STW project 349-4779 and The Netherlands Heart Foundation project M93.001

#### LITERATURE CITED

- (1) Good, L., and Nielsen, P. E. (1997) Progress in developing PNA as a gene-targeted drug. *Antisense And Nucleic Acid Drug Development*. Aug 7, 431–437.
- (2) Nielsen, P. E. (1999) Peptide nucleic acids as therapeutic agents. *Curr. Opin. Struct. Biol.* 9, 353–7.
- (3) Mologni, L., Nielsen, P. E., and Gambacorti-Passerini, C. (1999) In vitro transcriptional and translational block of the bcl-2 gene operated by peptide nucleic acid. *Biochem. Biophys. Res. Commun.* 264, 537–43.
- (4) Gray, G. D., Basu, S., and Wickstrom, E. (1997) Transformed and immortalized cellular uptake of oligodeoxynucleoside phosphorothioates, 3'-alkylamino oligodeoxynucleotides, 2'-O-methyl oligoribonucleotides, oligodeoxynucleoside methylphosphonates, and peptide nucleic acids. *Biochem. Pharmacol.* 53, 1465–76.
- (5) Bonham, M. A., Brown, S., Boyd, A. L., Brown, P. H., Bruckenstein, D. A., Hanvey, J. C., Thomson, S. A., Pipe, A., Hassman, F., Bisi, J. E., and et al. (1995) An assessment of the antisense properties of RNase H-competent and steric-blocking oligomers. *Nucleic Acids Res.* 23, 1197–203.
- (6) Good, L., and Nielsen, P. E. (1998) Inhibition of translation and bacterial growth by peptide nucleic acid targeted to ribosomal RNA. *Proc. Natl. Acad. Sci. U. S. A.* 95, 2073–6.
- (7) Hanvey, J. C., Pepper, N. J., Bisi, J. E., Thomson, S. A., Cadilla, R., Josey, J. A., Ricca, D. J., Hassman, C. F., Bonham, M. A., Au, K. G., and et al. (1992) Antisense and antigenic properties of peptide nucleic acids. *Science* 258, 1481–5.
- (8) Cutrona, G., Carpaneto, E. M., Ulivi, M., Roncella, S., Landt, O., Ferrarini, M., and Boffa, L. C. (2000) Effects in live cells of a c-myc anti-gene PNA linked to a nuclear localization signal. *Nat. Biotechnol.* Mar. 18, 300–303.
- (9) Rapozzi, V., Burm, B. E., Cogoi, S., Van Der Marel, G. A., Van Boom, J. H., Quadrifoglio, F., and Xodo, L. E. (2002) Antiproliferative effect in chronic myeloid leukaemia cells by antisense peptide nucleic acids. *Nucleic Acids Res.* 30, 3712–21.
- (10) Branden, L. J., Mohamed, A. J., and Smith, C. I. (1999) A peptide nucleic acid-nuclear localization signal fusion that mediates nuclear transport of DNA. *Nat. Biotechnol.* 17, 784–7.
- (11) Pooga, M., Soomets, U., Hallbrink, M., Valkna, A., Saar, K., Rezaei, K., Kahl, U., Hao, J. X., Xu, X. J., Wiesenfeld-Hallin, Z., Hokfelt, T., Bartfai, A., and Langel, U. (1998) Cell penetrating PNA constructs regulate galanin receptor levels and modify pain transmission in vivo. *Nat. Biotechnol. Sep.* 16, 857–861.
- (12) Chiarantini, L., Cerasi, A., Fraternali, A., Andreoni, F., Scari, S., Giovine, M., Clavarino, E., and Magnani, M. (2002) Inhibition of macrophage iNOS by selective targeting of antisense PNA. *Biochemistry* 41, 8471–7.
- (13) Penichet, M. L., Kang, Y. S., Pardridge, W. M., Morrison, S. L., and Shin, S. U. (1999) An antibody-avidin fusion protein specific for the transferrin receptor serves as a delivery vehicle for effective brain targeting: initial applications in anti-HIV antisense drug delivery to the brain. *J. Immunol.* 163, 4421–6.
- (14) Braun, K., Peschke, P., Pipkorn, R., Lampel, S., Wachsmuth, M., Waldeck, W., Friedrich, E., and Debus, J. (2002) A biological transporter for the delivery of peptide nucleic acids (PNA's) to the nuclear compartment of living cells. *J. Mol. Biol.* 318, 237–43.
- (15) Tietge, U. J., Bakillah, A., Maugeais, C., Tsukamoto, K., Hussain, M., and Rader, D. J. (1999) Hepatic overexpression of microsomal triglyceride transfer protein (MTP) results in increased in vivo secretion of VLDL triglycerides and apolipoprotein B. *J. Lipid Res.* 40, 2134–9.
- (16) Hui, T. Y., Olivier, L. M., Kang, S., and Davis, R. A. (2002) Microsomal triglyceride transfer protein is essential for hepatic secretion of apoB-100 and apoB-48 but not triglyceride. *J. Lipid Res.* 43, 785–93.
- (17) Raabe, M., Kim, E., Veniant, M., Nielsen, L. B., and Young, S. G. (1998) Using genetically engineered mice to understand apolipoprotein-B deficiency syndromes in humans. *Proc. Assoc. Am. Physicians* 110, 521–30.
- (18) Zhang, X., Simmons, C. G., and Corey, D. R. (2001) Liver cell specific targeting of peptide nucleic acid oligomers. *Bioorg. Med. Chem. Lett.* 11, 1269–1272.
- (19) Van Rossenberg, S. M., Slidregt-Bol, K. M., Meeuwenoord, N. J., Van Berkel, T. J., Van Boom, J. H., Van Der Marel, G. A., and Biessen, E. A. (2002) Targeted lysosome disruptive elements for improvement of parenchymal liver cell specific gene delivery. *J. Biol. Chem.* 16, 16.
- (20) Biessen, E. A., Slidregt-Bol, K., PA, T. H., Prince, P., Van der Bilt, E., Valentijn, A. R., Meeuwenoord, N. J., Princen, H., Bijsterbosch, M. K., Van der Marel, G. A., Van Boom, J. H., and Van Berkel, T. J. (2002) Design of a targeted peptide nucleic acid prodrug to inhibit hepatic human microsomal triglyceride transfer protein expression in hepatocytes. *Bioconjugate Chem.* 13, 295–302.
- (21) Seglen, P. O. (1976) *Methods Cell. Biol.* 13, 29–83.
- (22) Chomczynski, P., and Sacchi, N. (1987) Single-step method of RNA isolation by acid guanidinium thiocyanate-phenol-chloroform extraction. *Anal. Biochem.* 162, 156–9.
- (23) Jones, L. J., Yue, S. T., Cheung, C. Y., and Singer, V. L. (1998) RNA quantitation by fluorescence-based solution assay: RiboGreen reagent characterization. *Anal. Biochem.* 265, 368–74.
- (24) Zuker, M., and Jacobson, A. B. (1998) Using reliability information to annotate RNA secondary structures. *RNA* 4, 669–79.
- (25) Liang, K. W., Hoffman, E. P., and Huang, L. (2000) Targeted delivery of plasmid DNA to myogenic cells via transferrin-conjugated peptide nucleic acid. *Mol. Ther.* 1, 236–43.
- (26) Kaushik, N., Basu, A., Palumbo, P., Myers, R. L., and Pandey, V. N. (2002) Anti-TAR polyamide nucleotide analog conjugated with a membrane-permeating peptide inhibits human immunodeficiency virus type 1 production. *J. Virol.* 76, 3881–91.
- (27) Mologni, L., Marchesi, E., Nielsen, P. E., and Gambacorti-Passerini, C. (2001) Inhibition of promyelocytic leukemia (PML)/retinoic acid receptor-alpha and PML expression in acute promyelocytic leukemia cells by anti-PML peptide nucleic acid. *Cancer Res.* 61, 5468–73.
- (28) 't Hoen, P. A., Out, R., Commandeur, J. N., Vermeulen, N. P., van Batenburg, F. H., Manoharan, M., van Berkel, T.

- J., Biessen, E. A., and Bijsterbosch, M. K. (2002) Selection of antisense oligodeoxynucleotides against glutathione S-transferase Mu. *RNA* 8, 1572–83.
- (29) Gee, J. E., Robbins, I., van der Laan, A. C., van Boom, J. H., Colombier, C., Leng, M., Raible, A. M., Nelson, J. S., and Lebleu, B. (1998) Assessment of high-affinity hybridization, RNase H cleavage, and covalent linkage in translation arrest by antisense oligonucleotides. *Antisense Nucleic Acid Drug Dev.* 8, 103–11.
- (30) Uhlmann, E. (1998) Peptide nucleic acids (PNA) and PNA–DNA chimeras: from high binding affinity towards biological function. *Biol. Chem.* 379, 1045–52.
- (31) Larsen, H. J., Bentin, T., and Nielsen, P. E. (1999) Antisense properties of peptide nucleic acid. *Biochim. Biophys. Acta* 1489, 159–66.
- (32) Chang, G., Ruggeri, R. B., and Harwood, H. J., Jr. (2002) Microsomal triglyceride transfer protein (MTP) inhibitors: discovery of clinically active inhibitors using high-throughput screening and parallel synthesis paradigms. *Curr. Opin. Drug Discovery Dev.* 5, 562–70.
- (33) Knudsen, H., and Nielsen, P. E. (1996) Antisense properties of duplex- and triplex-forming PNA's. *Nucleic Acids Res.* 24, 494–500.
- (34) Tyler, B. M., Jansen, K., McCormick, D. J., Douglas, C. L., Boules, M., Stewart, J. A., Zhao, L., Lacy, B., Cusack, B., Fauq, A., and Richelson, E. (1999) Peptide nucleic acids targeted to the neurotensin receptor and administered i.p. cross the blood-brain barrier and specifically reduce gene expression. *Proc. Natl. Acad. Sci. U. S. A.* 96, 7053–8.
- (35) Aldrian-Herrada, G., Desarmenien, M. G., Orcel, H., Boissin-Agasse, L., Mery, J., Brugidou, J., and Rabie, A. (1998) A peptide nucleic acid (PNA) is more rapidly internalized in cultured neurons when coupled to a retro-inverso delivery peptide. The antisense activity depresses the target mRNA and protein in magnocellular oxytocin neurons. *Nucleic Acids Res.* 26, 4910–6.
- (36) Rowley, P. T., Kosciulek, B. A., and Kool, E. T. (1999) Circular antisense oligonucleotides inhibit growth of chronic myeloid leukemia cells. *Mol. Med.* 5, 693–700.

BC0340417

# Synthesis of Radiometal-Labeled and Fluorescent Cell-Permeating Peptide–PNA Conjugates for Targeting the *bcl-2* Proto-oncogene

Fabio Gallazzi,<sup>†</sup> Yi Wang,<sup>‡</sup> Fang Jia,<sup>‡</sup> Nalini Shenoy,<sup>§</sup> Linda A. Landon,<sup>||</sup> Mark Hannink,<sup>||</sup> Susan Z. Lever,<sup>§,⊥</sup> and Michael R. Lewis<sup>\*,†,⊗</sup>

Molecular Biology Program, Department of Veterinary Medicine and Surgery, Department of Chemistry, Department of Biochemistry, University of Missouri Research Reactor, and Department of Radiology, University of Missouri–Columbia, Columbia, Missouri 65211. Received May 16, 2003; Revised Manuscript Received September 18, 2003

The B-cell lymphoma/leukemia-2 (*bcl-2*) proto-oncogene has been associated with the transformation of benign lesions to malignancy, disease progression, poor prognosis, reduced survival, and development of resistance to radiation and chemotherapy in many types of cancer. The objective of this work was to synthesize an antisense peptide nucleic acid (PNA) complementary to the first six codons of the *bcl-2* open reading frame, conjugated to a membrane-permeating peptide for intracellular delivery, and modified with a bifunctional chelating agent for targeting imaging and therapeutic radiometals to tumors overexpressing *bcl-2*. Four peptide–PNA constructs were synthesized by a combination of manual and automated stepwise elongation techniques, including *bcl-2* antisense conjugates and nonsense conjugates with no complementarity to any known mammalian gene or DNA sequence. The PNA sequences were synthesized manually by solid-phase 9-fluorenylmethoxycarbonyl (Fmoc) techniques. Then a fully protected lysine monomer, modified with 1,4,7,10-tetraazacyclododecane-*N,N,N',N''*-tetraacetic acid (DOTA) for radiometal chelation, was coupled manually to each PNA sequence. Synthesis of the DOTA–PNA conjugates was followed by automated elongation with a peptide sequence (PTD-4-glycine, PTD-4-G), known to mediate cellular internalization of impermeable effector molecules, or its retro-inverso analogue (*ri*-PTD-4-G). Preparation of the four conjugates required an innovative synthetic strategy, using mild acid conditions to generate hydrophobic, partially deprotected intermediates. These intermediates were purified by semipreparative reversed-phase HPLC and completely deprotected to yield pure peptide–PNA conjugates in 6% to 9% overall yield. Using modifications of this synthetic strategy, the *ri*-PTD-4-G conjugate of *bcl-2* antisense PNA was prepared using a lysine derivative of tetramethylrhodamine (TMR) for fluorescence microscopy. Plasma stability studies showed that <sup>111</sup>In-DOTA-labeled *ri*-PTD-4-G–anti-*bcl-2* PNA was stable for 168 h at 37 °C, unlike the conjugate containing the parent peptide sequence. Scanning confocal fluorescence microscopy of TMR-labeled *ri*-PTD-4-G–anti-*bcl-2* PNA in Raji lymphoma cells demonstrated that the retro-inverso peptide was active in membrane permeation and mediated cellular internalization of the antisense PNA into the cytoplasm, where high concentrations of *bcl-2* mRNA are expected to be present.

## INTRODUCTION

Apoptosis, or programmed cell death, is a major pathway by which both chemotherapeutic drugs and ionizing radiation kill tumor cells (1). The B-cell lymphoma/leukemia-2 (*bcl-2*)<sup>1</sup> gene is a member of a relatively new category of proto-oncogenes involved in cell survival, by blocking apoptosis (2). The *bcl-2* gene product is an inner mitochondrial membrane protein that heterodimerizes with and inhibits a conserved homolog, bax, which accelerates cell death in response to apoptotic

stimuli (3). Overexpression of *bcl-2* in stably transfected cell lines has been implicated in the development of both drug (4–6) and radiation (7–9) resistance.

The *bcl-2* cellular oncogene was discovered by Croce and co-workers, after cloning the chromosome 18 breakpoint region in non-Hodgkin's lymphoma (NHL) (10). Over 85% of follicular lymphomas and approximately 20% of large cell lymphomas carry a t(14;18) translocation (11–13), juxtaposing the *bcl-2* gene with the IgH promoter and deregulating *bcl-2* expression. However, mechanisms other than translocation may deregulate *bcl-2* expression (14, 15) in lymphoma. In addition, 84% of acute myeloid leukemias (16), 80–100% of malignant cells in multiple myeloma (17), and 60–90% of many nonlymphoid malignancies, including breast (18), lung (19, 20), colon (21, 22), prostate (23, 24), neuroendocrine cancers (25), and malignant melanomas (26) overexpress *bcl-2*. In these cancers *bcl-2* expression is often associated with transformation of benign lesions to malignancy, disease progression, and poor prognosis.

Clinical understanding of the role of *bcl-2* in disease progression and treatment response or failure will be-

\* To whom correspondence should be addressed: Michael R. Lewis, Ph.D., Department of Veterinary Medicine and Surgery, College of Veterinary Medicine, 379 E. Campus Drive, University of Missouri–Columbia, Columbia, MO 65211. Phone: (573) 814-6000, ext. 3703. Fax: (573) 814-6551. E-mail: LewisMic@missouri.edu.

<sup>†</sup> Molecular Biology Program.

<sup>‡</sup> Department of Veterinary Medicine and Surgery.

<sup>§</sup> Department of Chemistry.

<sup>||</sup> Department of Biochemistry.

<sup>⊥</sup> University of Missouri Research Reactor.

<sup>⊗</sup> Department of Radiology.



come increasingly important as drugs that act to down-regulate *bcl-2* mRNA and protein are developed. While the majority of NHL patients respond well initially to conventional chemotherapy, *bcl-2* overexpression has been identified as an independent predictor of increased relapse, shorter disease-free intervals, and poor cause-specific survival (27, 28). The most important recent advances in the treatment of NHL have been the development of targeted immunotherapy and radioimmunotherapy (RIT). The pan-B cell, anti-CD20 monoclonal antibody rituximab down-regulates *bcl-2* through a STAT3- and IL-10-mediated pathway (29, 30), sensitizing lymphoma cells in vitro to apoptotic killing by cytotoxic drugs (31). Data emerging from ongoing Phase III clinical trials suggest that addition of rituximab to combination chemotherapy may improve survival in patients with aggressive lymphoma. Yttrium-90-ibritumomab (Zevalin), the radiolabeled analogue of rituximab, has shown considerable efficacy for RIT of relapsed NHL (32). Zevalin RIT showed a significantly greater response rate than rituximab in a randomized Phase III trial and has effected responses in rituximab-refractory patients. Recent findings that tumor *bcl-2* mRNA and protein levels decrease in response to RIT (33) suggest that down-regulation of *bcl-2* may play a significant role in response to low dose-rate radiation.

Another alternative therapy involves the use of an antisense oligonucleotide, which is complementary to the first six codons of *bcl-2* mRNA and is able to reduce *bcl-2* gene expression. G3139, a DNA phosphorothioate oligonucleotide, has shown efficacy against B-cell lymphoma in tumor-bearing SCID mice (34) and is currently in clinical trials for antisense therapy of *bcl-2*-positive NHL (35). Preliminary results indicated that two of nine patients experienced a reduction in tumor burden. However, more encouraging was the fact that six of eight patients who went on to receive further chemotherapy achieved responses. Similarly, six of 14 patients with *bcl-2*-positive metastatic melanoma in a Phase I/II trial of G3139 and dacarbazine achieved objective responses (36). Thus, *bcl-2* antisense treatment may overcome drug resistance.

Peptide nucleic acid (PNA) (37) is a DNA-like molecule in which the deoxyribose phosphodiester backbone of DNA has been replaced by (2-aminoethyl)glycine units, to which the nucleobases are attached by methylenecar-

bonyl linkers. Compared to DNA oligonucleotides, the superior biological stability and greater affinity and specificity of PNA for complementary mRNA sequences (38) make it extremely attractive for antisense applications. However, poor cellular uptake of unmodified PNAs has limited their utility in vitro and in vivo. Several groups have demonstrated that PNA uptake in target cells can be increased substantially by conjugation to cell membrane-permeating peptides (39–43), such as *Drosophila* Antennapedia (43–58) (pAntp) (44) or an uncleaved peptide from the HIV Tat protein transduction domain (45). Using alanine residue substitution to identify the basic residues critical for cell membrane transduction, Dowdy and co-workers prepared a synthetic protein transduction domain, YARAAARQARA (PTD-4) (46), that was 33-fold more active than the Tat sequence.

The results of these studies suggest that tumor proto-oncogenes such as *bcl-2* might be targeted by radiolabeled, cell-permeating peptide–PNA constructs for in vivo imaging and targeted radiotherapy of cancer. Previously we demonstrated that a radiometal-labeled PTD-4–anti-*bcl-2* PNA conjugate bound to *bcl-2* mRNA with high specificity and thermodynamic stability in cell-free systems (47). We report here the solid-phase synthesis of antisense peptide–PNA conjugates for targeting imaging and therapeutic radiometals to tumor cells expressing high levels of *bcl-2* mRNA. The antisense PNA was based on the 18-residue sequence of G3139, while an 18-mer nonsense PNA did not correspond to any known mammalian gene or DNA sequence in a BLAST database search. The *bcl-2* antisense and nonsense PNAs were conjugated with a new derivative of 1,4,7,10-tetraazacyclododecane-*N,N,N',N''*-tetraacetic acid (DOTA), designed for chelation of radiometals and fully protected for solid-phase peptide and PNA synthesis. The DOTA–PNA conjugates were then coupled by solid-phase techniques to glycine, a small amino acid spacer, followed by PTD-4 or its retro-inverso analogue (*ri*-PTD-4).

Preparation of these DOTA conjugates required the development of an innovative solid-phase synthetic strategy, involving cleavage from the resin and partial deprotection of the peptide–PNA conjugates under mildly acidic conditions. This strategy allowed hydrophobic intermediates to be separated from unreacted PNA by semipreparative reversed-phase HPLC (RP-HPLC). In contrast, tetramethylrhodamine (TMR)-labeled PNA conjugates could be prepared in a straightforward manner by standard solid-phase synthesis, cleavage, deprotection, and purification techniques. Plasma stability studies demonstrated that *ri*-PTD-4 was much more stable to proteolytic degradation than the parent sequence, and scanning confocal fluorescence microscopy studies of the TMR conjugates showed that *ri*-PTD-4-mediated cellular internalization of the antisense PNA in NHL cells known to express high levels of *bcl-2* mRNA.

## EXPERIMENTAL PROCEDURES

**General.** All reagents were HPLC or peptide synthesis grade.  $\text{CDCl}_3$ , phenol, and EDT were obtained from Aldrich Chemical Co. (Milwaukee, WI). Anhydrous *N*-methylpyrrolidinone (NMP), *N,N*-dimethylformamide (DMF), dichloromethane (DCM), acetonitrile, and methanol were obtained from Fisher Scientific, Inc. (Pittsburgh, PA). Trifluoroacetic acid (TFA) was obtained from VWR Scientific Products (St. Louis, MO). All standard, protected Fmoc amino acid derivatives, 2-(1*H*-benzotriazol-1-yl)-1,1,3,3-tetramethyluronium hexafluorophosphate (HBTU), and 1-hydroxybenzotriazole (HOBt) were ob-

<sup>1</sup> Abbreviations: *bcl-2*, B-cell lymphoma/leukemia-2 gene; Bhoc, benzhydryloxycarbonyl; BLAST, Basic Local Alignment Search Tool; DCM, dichloromethane; DIEA, *N,N*-diisopropylethylamine; DMF, *N,N*-dimethylformamide; DOTA, 1,4,7,10-tetraazacyclododecane-*N,N,N',N''*-tetraacetic acid; DOTA(OtBu)<sub>3</sub>, DOTA tris(*tert*-butyl) ester; EDT, ethanedithiol; EDTA, ethylenediaminetetraacetic acid; ESI-MS, electrospray ionization mass spectrometry; FKD, *N*-α-(9-fluorenylmethoxycarbonyl)-*N*-ε-[tris(*tert*-butyl)DOTA]-L-lysine; FKT, *N*-α-(9-fluorenylmethoxycarbonyl)-*N*-ε-[tetramethylrhodamine-(5-carbonyl)]-L-lysine; Fmoc, 9-fluorenylmethoxycarbonyl; HATU, 2-(1*H*-7-azabenzotriazol-1-yl)-1,1,3,3-tetramethyluronium hexafluorophosphate; HBTU, 2-(1*H*-benzotriazol-1-yl)-1,1,3,3-tetramethyluronium hexafluorophosphate; HOAt, 1-hydroxy-7-azabenzotriazole; HOBt, 1-hydroxybenzotriazole; KD, *N*-ε-(DOTA)-L-lysine; KT, *N*-ε-[tetramethylrhodamine-(5-carbonyl)]-L-lysine; LC-MS, liquid chromatography–mass spectrometry; NHL, non-Hodgkin's lymphoma; NMP, *N*-methylpyrrolidinone; OtBu, *tert*-butoxy; PNA, peptide nucleic acid; PTD-4, synthetic protein transduction domain-4; *ri*-PTD-4, retro-inverso PTD-4; RP, reversed-phase; TA, thioanisole; TFA, trifluoroacetic acid; TIS, triisopropylsilane; TMR, tetramethylrhodamine; TNBS, 2,4,6-trinitrobenzenesulfonic acid; XAL PEG PS resin, xanthenylamide-poly(ethylene glycol)polystyrene.

tained from Novabiochem (San Diego, CA). *N*- $\alpha$ -(9-Fluorenylmethoxycarbonyl)-*N*- $\epsilon$ -[tetramethylrhodamine-(5-carbonyl)]-L-lysine (FKT) was purchased from Molecular Probes, Inc. (Eugene, OR). 2-(1*H*-7-Azabenzotriazol-1-yl)-1,1,3,3-tetramethyluronium hexafluorophosphate (HATU), 1-hydroxy-7-azabenzotriazole (HOAt), all Fmoc/Bhoc protected monomers for PNA synthesis, and Fmoc-XAL PEG PS resin were obtained from PerSeptive Biosystems (Framingham, MA). DOTA tris(*tert*-butyl) ester (DOTA-(OtBu)<sub>3</sub>) was procured from Macrocyclics (Dallas, TX), and *N*- $\alpha$ -Fmoc-L-lysine was purchased from Advanced ChemTech (Louisville, KY). Piperidine, *m*-cresol, *N,N*-diisopropylethylamine (DIEA), thioanisole (TA), triisopropylsilane (TIS), and 2,4,6-trinitrobenzenesulfonic acid (TNBS) were purchased from Fluka (Milwaukee, WI). <sup>111</sup>InCl<sub>3</sub> was obtained from Mallinckrodt, Inc. (St. Louis, MO). Ultrapure water (18 M $\Omega$ -cm resistivity) was used for all procedures. All laboratory glassware was washed with a mixed acid solution (48) and thoroughly rinsed with ultrapure water. Manual reaction vessels were obtained from Chemglass, Inc. (Vineland, NJ). Normal phase TLC plates (Silica Gel 60 F254, plastic-backed) were purchased from EM Science (Gibbstown, NJ).

An Advanced ChemTech ACT Model 396 Omega Multiple Biomolecular Synthesizer was used for automated solid-phase synthesis. <sup>1</sup>H NMR analysis of purified *N*- $\alpha$ -(9-fluorenylmethoxycarbonyl)-*N*- $\epsilon$ -[tris(*tert*-butyl)DOTA]-L-lysine was performed using a Bruker DRX 300 MHz spectrometer (Bruker BioSpin, Westmont, IL), and elemental analysis of the compound was performed by Atlantic Microlab (Norcross, GA). ESI-MS analyses were performed on a Finnigan TSQ7000 mass spectrometer (Thermo Finnigan, San Jose, CA). A Waters (Milford, MA) NovaPak C18 column (3.9  $\times$  300 mm) was used for the LC-MS analysis.

Analytical and semipreparative RP-HPLC were performed on a Beckman Coulter System Gold chromatograph equipped with a 168 diode array detector, a 507e auto-injector, and the 32 KARAT software package (Beckman Coulter, Fullerton, CA). A Keystone Scientific, Inc. (San Jose, CA) C-18 Kromosil column (4.6  $\times$  150 mm, 5  $\mu$ m, 100 Å) was used for analytical HPLC. For semipreparative HPLC, a Waters Prep NovaPak, HR-C18 column (7.8  $\times$  300 mm, 6  $\mu$ m, 60 Å) was used. The flow rate was maintained at 1.0 mL/min for analytical runs and at 4.0 mL/min for semipreparative purification. The wavelengths used for UV detection were 214 and 260 nm for analytical RP-HPLC and 235 and 245 nm for semipreparative RP-HPLC, respectively. Eluents used in all runs consisted of solvent A (0.1% TFA/H<sub>2</sub>O) and solvent B (0.1% TFA/CH<sub>3</sub>CN). Three different gradients were used: (1) "Full Gradient": linear from 5% to 95% solvent B in 45 min, (2) "FKD Gradient" (optimized for semipreparative purification of *N*- $\alpha$ -(9-fluorenylmethoxycarbonyl)-*N*- $\epsilon$ -[tris(*tert*-butyl)DOTA]-L-lysine): linear from 45% to 50% solvent B in 20 min, and (3) "Semiprep Gradient" (optimized for semipreparative purification of hydrophobic, partially deprotected peptide-PNA conjugate precursors): sequential linear from 10% to 20% solvent B in 20 min (step 1), 20% to 30% solvent B in 10 min (step 2), 30% to 50% solvent B in 5 min (step 3), and 50% to 60% solvent B in 20 min (step 4). Isocratic conditions were applied after steps 1 and 2 to permit all hydrophilic species and *m*-cresol to elute, prior to application of steps 3 and 4.

Size exclusion HPLC was performed on a Waters Delta 600 chromatograph equipped with a manual Rheodyne injector, a 2487 dual wavelength UV detector, a Packard (Downers Grove, IL) 500TR Flow Scintillation Analyzer

with a GAMMA-C flow cell for <sup>111</sup>In, a Waters busSAT/IN analog-digital interface, and the Millennium 32 software package. A Phenomenex (Torrance, CA) BioSep-SEC-S 3000 column (7.8  $\times$  300 mm, 5  $\mu$ m, 290 Å), an isocratic mobile phase of 100 mM NaH<sub>2</sub>PO<sub>4</sub>/0.05% NaN<sub>3</sub>, pH 6.8, and a flow rate of 1.0 mL/min were used. Molecular weights estimated by size exclusion HPLC were calculated from a calibration curve generated using a Bio-Rad (Hercules, CA) molecular weight standard.

Raji Burkitt's lymphoma cells were obtained from the American Type Culture Collection (Manassas, VA). Suspension cultures of cells were maintained in exponential growth phase in RPMI 1640 medium (Mediatech, Inc., Herndon, VA), supplemented with 10% fetal bovine serum, 2 mM L-glutamine, and 48  $\mu$ g/mL gentamycin, at 37 °C and 5% CO<sub>2</sub>. Cell viability was determined to be >98% by trypan blue exclusion and hemacytometry.

**PNA Synthesis.** Syntheses of anti-*bcl-2* PNA (tctc-cagcgtgcgcat) and nonsense PNA (tgtgtgtgcacaccttg) were performed in a manual reaction vessel. Fmoc/Bhoc chemistry was used with the following PNA monomers: Fmoc-A(Bhoc)-OH, Fmoc-C(Bhoc)-OH, Fmoc-G(Bhoc)-OH, and Fmoc-T-OH. Fmoc-XAL PEG PS resin was used as a solid support at a substitution level of 0.18 mmol/g. Each cycle of elongation consisted of (1) Fmoc deprotection with 25% piperidine in DMF for 2 cycles of 1 min at room temperature, (2) washing with DMF, DCM, and twice with NMP for 1 min each at room temperature, (3) coupling using a molar ratio of resin:monomer:HATU:DIEA:2,6-lutidine = 1.0:3.0:2.7:3.0:4.5; 5 min of preactivation followed by a 25-min coupling at room temperature, after which the process was repeated, (4) capping with 2 mL of 5% acetic anhydride/6% 2,6-lutidine in DMF for 5 min at room temperature, and (5) washing with NMP, DCM, and twice with DMF for 1 min each at room temperature. All chemical steps were followed by a TNBS test on the resin, and the resulting colorimetric reaction indicated the presence of free primary amines after Fmoc deprotection and the absence of primary amino groups after the coupling and capping steps. After 6, 12, and 18 cycles, aliquots of the resin-bound PNAs were cleaved and Bhoc-deprotected with *m*-cresol:TFA (1:19) for 30 min, and LC-MS analysis was performed to confirm that the observed masses were consistent with the calculated molecular weights of the Fmoc-protected intermediates.

***N*- $\alpha$ -(9-Fluorenylmethoxycarbonyl)-*N*- $\epsilon$ -[tris(*tert*-butyl)DOTA]-L-lysine (FKD, 1).** To 1 mL of anhydrous NMP was added sequentially 218 mg (0.381 mmol) of DOTA(OtBu)<sub>3</sub>, 134 mg (0.352 mmol) of HATU, and 5.1 mg (0.038 mmol) of HOAt with continuous stirring. The reaction mixture was stirred at room temperature for 1.5 h, after which normal phase TLC, using acetone as the mobile phase, showed that formation of the DOTA-(OtBu)<sub>3</sub>-OAt active ester was complete (*R*<sub>f</sub> = 0.66). Then 133 mg (0.360 mmol) of *N*- $\alpha$ -Fmoc-L-lysine was added, and the reaction mixture was stirred at room temperature for 10 min. After quenching the reaction with H<sub>2</sub>O, the reaction mixture was taken into ethyl acetate and extracted with H<sub>2</sub>O, while maintaining the pH at 6.0 with 5% NaHCO<sub>3</sub>. The organic phase was acidified with TFA and washed with water, after which the solvent was removed in vacuo. The residue was dissolved in 1 mL of ethyl acetate and added to 25 mL of diethyl ether with vigorous stirring and cooling to -20 °C. The thick oily precipitate was washed with cold diethyl ether and dried in vacuo, after which it was dissolved in acetonitrile. Unreacted *N*- $\alpha$ -Fmoc-L-lysine was precipitated by dropwise addition of 0.2% TFA, and this process was repeated four to five times. The supernatant was concentrated to



a minimum volume, and the pH of the remaining aqueous solution was adjusted to 6.0 with 5%  $\text{NaHCO}_3$ . The desired product was extracted into ethyl acetate, which was washed with  $\text{H}_2\text{O}$  and evaporated to dryness in vacuo. The resulting oil was dissolved in 1 mL of ethyl acetate, to which was added 15 mL of diethyl ether with vigorous stirring to precipitate the product. After discarding the supernatant, the product was dried in vacuo to yield 308 mg (92.7%) of **1** as a white, microcrystalline solid. Normal phase TLC ( $\text{CHCl}_3:\text{CH}_3\text{OH}:\text{conc'd NH}_4\text{OH}$ , 13:3:1)  $R_f = 0.45$ ; RP-HPLC, Full Gradient,  $t_R = 31.2$  min (98.6% purity); ESI-MS  $m/z$  calcd for  $\text{C}_{49}\text{H}_{74}\text{N}_6\text{O}_{11}$  ( $\text{M} + \text{H}^+$ ) = 924.2, found 923.9 ( $\text{M} + \text{H}^+$ ), 462.5 ( $\text{M} + 2\text{H}^{2+}$ ).

Alternatively, DOTA(OtBu)<sub>3</sub> (658 mg, 1.15 mmol), HATU (427 mg, 1.12 mmol), and HOAt (67.0 mg, 0.492 mmol) were dissolved in 2 mL of NMP at room temperature. The resulting pale yellow solution was stirred for 1.5 h. To this solution of the active ester was added 410 mg (1.11 mmol) of *N*- $\alpha$ -Fmoc-L-lysine. After dissolution, stirring was continued for an additional 2 h. The reaction was quenched by the addition of 1 mL of  $\text{H}_2\text{O}$  and diluted with 40 mL of ethyl acetate. The organic phase was washed with  $3 \times 20$  mL of  $\text{H}_2\text{O}$ . The organic phase was then acidified with the addition of 100  $\mu\text{L}$  of TFA. The organic layer was washed again with  $2 \times 20$  mL of  $\text{H}_2\text{O}$  and concentrated in vacuo, leaving a pale yellow, viscous oil (820 mg, 80.0%). Analytical RP-HPLC under Full Gradient conditions indicated the purity of the crude product to be >89%. The crude product was dissolved in 10 mL of  $\text{CH}_3\text{CN}:\text{H}_2\text{O}$  (1:1). The product was purified by semipreparative RP-HPLC, using the optimized FGD Gradient. The collected fractions, eluting at  $t_R = 26.5$  min, were pooled and lyophilized, yielding 416 mg (40.6%) of **1** as a white solid.  $^1\text{H}$  NMR (300 MHz,  $\text{CDCl}_3$ )  $\delta$  1.4 (s, 27 H), 1.5 (s, 6 H), 2.7 (s, 2 H), 2.7–3.8 (br complex m, 28 H), 4.0 (br s, 1H), 4.2 (t, 2H), 7.3 (dt, 4H), 7.5 (d, 2H), 7.6 (d, 2H); ESI-MS  $m/z$  calcd for  $\text{C}_{49}\text{H}_{74}\text{N}_6\text{O}_{11}$  ( $\text{M} + \text{H}^+$ ) = 924.2, found 923.7 ( $\text{M} + \text{H}^+$ ), 462.4 ( $\text{M} + 2\text{H}^{2+}$ ). Anal. ( $\text{C}_{49}\text{H}_{74}\text{N}_6\text{O}_{11} \cdot 4\text{TFA} \cdot 2\text{H}_2\text{O}$ ): C, H, N: calcd 5.94; found 6.52.<sup>2</sup>

**PTD-4-G-KD-anti-*bcl-2* PNA (2).** Fmoc-anti-*bcl-2* PNA on XAL PEG PS resin was deprotected at the *N*-terminus with 25% piperidine in DMF for two cycles of 1 min at room temperature, followed by washing with DMF, DCM, and twice with NMP for 1 min each at room temperature. A solution containing 40  $\mu\text{mol}$  of **1**, 40  $\mu\text{mol}$  of HOAt, 32  $\mu\text{mol}$  of HATU, and 100  $\mu\text{mol}$  of DIPEA in NMP was stirred for 15 min at room temperature. The resulting mixture was added to 9  $\mu\text{mol}$  of anti-*bcl-2* PNA on 100 mg of XAL PEG PS resin and mixed by nitrogen bubbling for 45 min in a reaction vessel for manual peptide synthesis. This process was repeated twice, after which the resin was reacted for 5 min with 5% acetic anhydride and 6% 2,6-lutidine in DMF at room temperature.

After removal of the *N*-terminal Fmoc group with 25% piperidine in DMF for two cycles of 25 min at room temperature, KD-anti-*bcl-2* PNA resin was then sequentially elongated with PTD-4-G, using the multiple automated synthesizer and standard Fmoc coupling chemistry. The peptide chain was assembled by sequential acylation with protected amino acids, which were activated in situ with HBTU/HOBt. Recoupling at each cycle with a minimal 15-fold molar excess of activated amino

acid derivative was performed, to minimize the production of truncated species. Each cycle of elongation involved the following steps: (1) Fmoc deprotection with 25% piperidine in DMF/NMP for one cycle of 1 min and three cycles of 10 min at room temperature, (2) washing with NMP for four cycles of 1 min at room temperature, (3) coupling with in situ activated amino acid (amino acid: HBTU:HOBt:DIEA molar ratio = 1:0.9:1:2) in NMP for two cycles of 25 min at room temperature, and (4) washing with NMP for two cycles of 1 min at room temperature.

To detach hydrophobic, partially deprotected intermediate products from the resin, two sequential procedures were evaluated in a reaction vessel: (1) reaction with 1% TFA/5% *m*-cresol in DCM for eight cycles of 15 min at room temperature, followed by filtration; and (2) reaction with 50% TFA/5% *m*-cresol in DCM for one cycle of 30 min at room temperature, followed by filtration. The partially deprotected intermediates were isolated by precipitation with cold diethyl ether and evaporation to dryness under a stream of nitrogen. Crude intermediates from both procedures were analyzed by RP-HPLC, using Full Gradient conditions, and then purified by semipreparative RP-HPLC, using Semiprep Gradient conditions. The purified intermediates, eluting from 37 to 41 min retention time for procedure 1 and from 33 to 38 min for procedure 2, were pooled, lyophilized, and then fully deprotected with 87.5% TFA containing 2.5% each of  $\text{H}_2\text{O}$ , phenol, TA, EDT, and TIS for 4 h at room temperature. After this treatment, 4.5 mg (7.7%) of **2** was isolated by precipitation with cold diethyl ether and lyophilized to a white solid. ESI-MS:  $m/z$  2190.0 ( $\text{M} + 3\text{H}^{3+}$ ), 1642.5 ( $\text{M} + 4\text{H}^{4+}$ ), 1314.2 ( $\text{M} + 5\text{H}^{5+}$ ), 1095.1 ( $\text{M} + 6\text{H}^{6+}$ ), 938.9 ( $\text{M} + 7\text{H}^{7+}$ ). The observed molecular ions were consistent with the theoretical molecular weight of **2**, calcd ( $\text{M} + \text{H}^+$ ) = 6569.1.

**PTD-4-G-KD-nonsense PNA (3).** Fmoc-nonsense PNA on XAL PEG PS resin was deprotected at the *N*-terminus with 25% piperidine in DMF for two cycles of 1 min at room temperature, followed by washing with DMF, DCM, and twice with NMP for 1 min each at room temperature. A solution containing 20  $\mu\text{mol}$  of **1**, 20  $\mu\text{mol}$  of HOAt, 18  $\mu\text{mol}$  of HATU, and 60  $\mu\text{mol}$  of DIPEA in NMP was stirred for 15 min at room temperature. The resulting mixture was added to 5  $\mu\text{mol}$  of nonsense PNA on 45 mg of XAL PEG PS resin and mixed by nitrogen bubbling for 45 min in a reaction vessel for manual peptide synthesis. This process was repeated twice, after which the resin was reacted for 5 min with a large excess of acetic anhydride (5% v/v) and 2,6-lutidine (6% v/v) in DMF at room temperature. After Fmoc removal with 25% piperidine in DMF for two cycles of 25 min, KD-nonsense-PNA resin was then sequentially elongated with PTD-4-G on the multiple automated synthesizer, as described for **2**.

To cleave hydrophobic, partially deprotected intermediates from the resin, the following three procedures were performed in sequence of increasing acidity: (1) reaction with 5% TFA, containing 5% each of  $\text{H}_2\text{O}$ , *m*-cresol, and TIS in DCM, for four cycles of 15 min at room temperature, followed by filtration; (2) reaction with 25% TFA, containing 5% each of  $\text{H}_2\text{O}$ , *m*-cresol, and TIS in DCM, for two cycles of 15 min at room temperature, followed by filtration; and (3) reaction with 50% TFA, containing 5% *m*-cresol and 2.5% each of  $\text{H}_2\text{O}$ , TIS, TA, and phenol in DCM, for one cycle of 40 min at room temperature, followed by filtration. The partially deprotected intermediates were isolated by precipitation with cold diethyl ether and evaporation to dryness under nitrogen. These

<sup>2</sup> Elemental analysis for *N*- $\alpha$ -(9-fluorenylmethoxycarbonyl)-*N*- $\epsilon$ -[tris(*tert*-butyl)DOTA]-L-lysine (FKD): Theoretical ( $\text{C}_{49}\text{H}_{74}\text{N}_6\text{O}_{11} \cdot 4\text{TFA} \cdot 2\text{H}_2\text{O}$ ): calcd C, 48.37%; H, 5.84%; N, 5.94%; found C, 48.52%; H, 6.14%; N, 6.52%.



intermediates were analyzed by RP-HPLC, using Full Gradient conditions, and intermediates from procedures 1 and 2 were purified by semipreparative RP-HPLC, using the Semiprep Gradient. The purified intermediates, eluting from 43 to 49 min retention time, were pooled and lyophilized, after which the resulting mixture was treated for 4 h at room temperature with 87.5% TFA containing 2.5% of each of H<sub>2</sub>O, phenol, TA, EDT, and TIS, to afford the completely deprotected product. After precipitation with cold diethyl ether and lyophilization, 3.0 mg (9.1%) of **3** was isolated as a white solid. ESI-MS: *m/z* 2211.1 (M + 3H)<sup>3+</sup>, 1658.0 (M + 4H)<sup>4+</sup>, 1326.9 (M + 5H)<sup>5+</sup>, 1106.1 (M + 6H)<sup>6+</sup>, 948.1 (M + 7H)<sup>7+</sup>. The observed molecular ions were consistent with the theoretical molecular weight of **3**, calcd (M + H)<sup>+</sup> = 6629.2.

***ri*-PTD-4-G-KD-anti-*bcl-2* PNA (4).** *ri*-PTD-4-G-KD-anti-*bcl-2* PNA was prepared from 4  $\mu$ mol of anti-*bcl-2* PNA on 45 mg of XAL PEG PS resin. The synthetic procedure was identical to that employed for **2**, except that after coupling of glycine, all D-amino acid analogues of the PTD-4 residues were added in the reverse sequence. Hydrophobic, partially deprotected crude intermediates were obtained from the three sequential cleavage procedures with increasing TFA concentrations, identical to those utilized for **3**. The partially deprotected intermediates were isolated by precipitation with cold diethyl ether and evaporation to dryness under nitrogen. Crude intermediate products from procedures 1 and 2 were analyzed and purified by RP-HPLC, as described for **2**, and the fraction eluting at 45 to 52 min retention time was collected. After full deprotection and isolation of the final product, using the procedures employed for **2**, 1.7 mg (6.5%) of **4** was obtained as a white solid. ESI-MS: *m/z* 2188.5 (M + 3H)<sup>3+</sup>, 1642.1 (M + 4H)<sup>4+</sup>, 1313.6 (M + 5H)<sup>5+</sup>, 1094.8 (M + 6H)<sup>6+</sup>, 938.7 (M + 7H)<sup>7+</sup>, 821.3 (M + 8H)<sup>8+</sup>, 730.4 (M + 9H)<sup>9+</sup>. The observed molecular ions were consistent with the theoretical molecular weight of **4**, calcd (M + H)<sup>+</sup> = 6569.1.

***ri*-PTD-4-G-KD-nonsense PNA (5).** *ri*-PTD-4-G-KD-nonsense-PNA was synthesized from 9  $\mu$ mol of nonsense PNA on 104 mg of XAL PEG PS resin, using a procedure identical to that employed for **3**, except that the *ri*-PTD-4 sequence was elongated after coupling of glycine. Hydrophobic, partially deprotected crude intermediates were obtained from the three sequential cleavage procedures using increasing TFA concentrations, identical to those employed for **3**. The partially deprotected intermediates were isolated by precipitation with cold diethyl ether and evaporation to dryness under nitrogen. Crude intermediate products from procedures 1 and 2 were analyzed and purified by RP-HPLC, as described for **3**, and the fraction eluting at 42 to 52 min retention time was collected. After full deprotection and isolation of the final product, using the procedures employed for **3**, 3.6 mg (6.1%) of **5** was obtained as a white solid. ESI-MS: *m/z* 2209.8 (M + 3H)<sup>3+</sup>, 1657.9 (M + 4H)<sup>4+</sup>, 1326.4 (M + 5H)<sup>5+</sup>, 1104.8 (M + 6H)<sup>6+</sup>, and 947.6 (M + 7H)<sup>7+</sup>. The observed molecular ions were consistent with the theoretical molecular weight of **5**, calcd (M + H)<sup>+</sup> = 6629.2.

**KT-anti-*bcl-2* PNA (6).** Fmoc-anti-*bcl-2* PNA on XAL PEG PS resin was deprotected at the N-terminus using a procedure identical to that employed for **2**. A solution containing 20  $\mu$ mol of FKT, 20  $\mu$ mol of HOAt, 18  $\mu$ mol of HATU, and 60  $\mu$ mol of DIPEA in NMP was stirred for 15 min at room temperature. The resulting mixture was added to 8  $\mu$ mol of anti-*bcl-2* PNA on 90 mg of XAL PEG PS resin and mixed by nitrogen bubbling for 45 min in a reaction vessel for manual peptide synthesis. This process

was repeated twice, after which the resin was reacted for 5 min with 5% acetic anhydride and 6% 2,6-lutidine in DMF at room temperature. The crude product was cleaved from 45 mg (4  $\mu$ mol) of the resin and deprotected with 87.5% TFA containing 2.5% H<sub>2</sub>O, phenol, TA, EDT, and TIS each for 2 h at room temperature, after which it was purified by semipreparative RP-HPLC, using Semiprep Gradient conditions. The peak eluting at *t<sub>R</sub>* = 34.0 min was collected, and 1.3 mg (6.1%) of **6** was isolated as a magenta solid, after precipitation with cold diethyl ether and lyophilization. RP-HPLC, Full Gradient, *t<sub>R</sub>* = 16.5 min (>99.5% purity); ESI-MS *m/z* 1784.0 (M + 3H)<sup>3+</sup>, 1338.2 (M + 4H)<sup>4+</sup>, 1070.8 (M + 5H)<sup>5+</sup>. The observed molecular ions were consistent with the theoretical molecular weight of **6**, calcd (M + H)<sup>+</sup> = 5333.1.

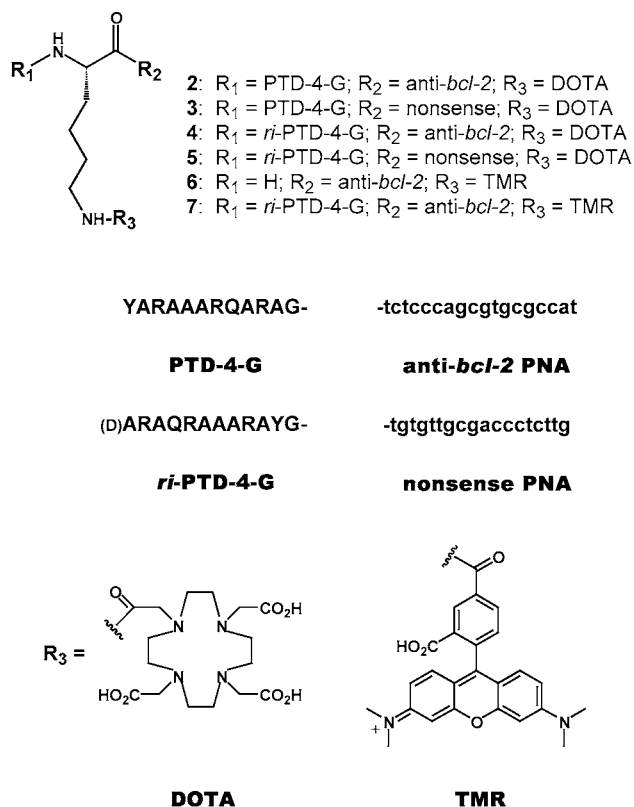
***ri*-PTD-4-G-KT-anti-*bcl-2* PNA (7).** *ri*-PTD-4-G-KT-anti-*bcl-2* PNA was synthesized from 4  $\mu$ mol of Fmoc-deprotected KT-anti-*bcl-2* PNA on 45 mg of XAL PEG PS resin, using a procedure for elongation of the *ri*-PTD-4-G sequence identical to that employed for **4**. The crude product was cleaved from the resin, deprotected, and purified by semipreparative RP-HPLC using the procedures employed for **6**. The peak eluting at *t<sub>R</sub>* = 35.5 min was collected, and 1.8 mg (6.8%) of **7** was obtained as a magenta solid, after precipitation with cold diethyl ether and lyophilization. RP-HPLC, Full Gradient, *t<sub>R</sub>* = 16.1 min (>99.5% purity); ESI-MS *m/z* 2197.3 (M + 3H)<sup>3+</sup>, 1648.4 (M + 4H)<sup>4+</sup>, 1319.4 (M + 5H)<sup>5+</sup>, 1099.1 (M + 6H)<sup>6+</sup>, 942.2 (M + 7H)<sup>7+</sup>, 824.6 (M + 8H)<sup>8+</sup>, 733.3 (M + 9H)<sup>9+</sup>. The observed molecular ions were consistent with the molecular weight of **7**, calcd (M + H)<sup>+</sup> = 6593.5.

**Plasma Stability Studies.** Compounds **2** and **4** were labeled with <sup>111</sup>In as described previously (47). An aliquot of 948  $\mu$ Ci of <sup>111</sup>In-labeled **2** (4.89  $\mu$ g) or 915  $\mu$ Ci of <sup>111</sup>In-labeled **4** (4.47  $\mu$ g) was added to 1 mL of mouse plasma. The resulting mixtures were incubated at 37 °C for 168 h. Aliquots of 100  $\mu$ L of the mixtures were analyzed by size exclusion HPLC at 0, 0.25, 1, 4, 24, 48, 96, and 168 h of incubation, to determine conjugate and chelate stability.

**Scanning Confocal Fluorescence Microscopy Studies.** An aliquot of **6** (0.18 mg/mL, 34  $\mu$ M) or **7** (0.72 mg/mL, 109  $\mu$ M) in 0.2 M ammonium acetate, pH 5.0, was added to a final concentration of 2.5  $\mu$ M in a suspension of Raji cells (1  $\times$  10<sup>7</sup> cells/mL) in 2.0 mL of RPMI 1640 medium at 37 °C and 5% CO<sub>2</sub>. Cells and supernatants from 100  $\mu$ L of the suspension were separated by centrifugation at 1, 5, and 30 min and at 2 h of incubation. After removal of the supernatant, the cells were fixed by addition of 100  $\mu$ L of 4% formaldehyde and washed with 1% formaldehyde to remove any fluorescent probe in solution. Formaldehyde was not added for fluorescence microscopy of live Raji cells. Live Raji cells were incubated with **6** or **7** as described above and immediately analyzed by fluorescence microscopy. Digital microscopy was performed with an Olympus IX70 microscope/Bio-Rad Radiance 2000 scanning confocal fluorescence system, interfaced to a photomultiplier tube array and computer workstation. Excitation of TMR was accomplished at 568 nm, followed by image acquisition using a 580 nm long path emission filter. All fluorescence microscopy studies were performed using identical microscope settings, and all images were acquired in the medial plane.

## RESULTS AND DISCUSSION

The optimized procedure for the preparation of cell-permeating peptide-PNA conjugates (Figure 1) for

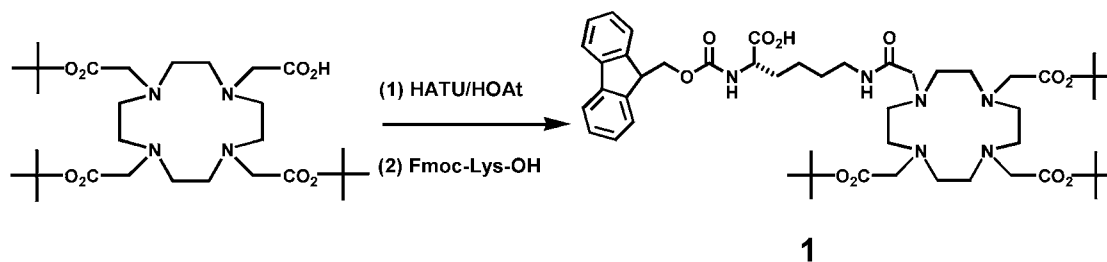


**Figure 1.** Structures of DOTA- and TMR-conjugated PTD-4-G and *ri*-PTD-4-G *bcl-2* antisense and nonsense PNA conjugates. PNA residues are indicated in lower case letters, and peptide residues are indicated in upper case letters.

radiometal targeting of the *bcl-2* proto-oncogene consisted of a combination of manual solid-phase synthesis of PNA sequences and automated solid-phase synthesis of peptide sequences, using standard Fmoc chemistry. Manual syntheses of PNAs were undertaken in order to perform sequential Fmoc deprotection of the growing PNA oligomers under carefully controlled conditions. Unlike peptides, upon Fmoc deprotection, PNA can undergo an alkaline pH-dependent *N*-acyl transfer rearrangement that converts the primary *N*-terminus into an unreactive amide (49). When the automated multiple biomolecular synthesizer was used for PNA synthesis, truncated PNA species or degraded products were often obtained. This problem was likely mechanical in nature and probably resulted from exposure of the PNA to piperidine for periods longer than 1 min during Fmoc deprotection. When PNAs were synthesized manually, piperidine reactions were carried out in precise 1-min cycles, and no evidence of *N*-acyl transfer rearrangement was observed. Using manual solid-phase synthesis techniques, the desired sequences could be prepared in their entirety.

To incorporate a macrocyclic chelating agent into any sequence position of a peptide-PNA conjugate, a new

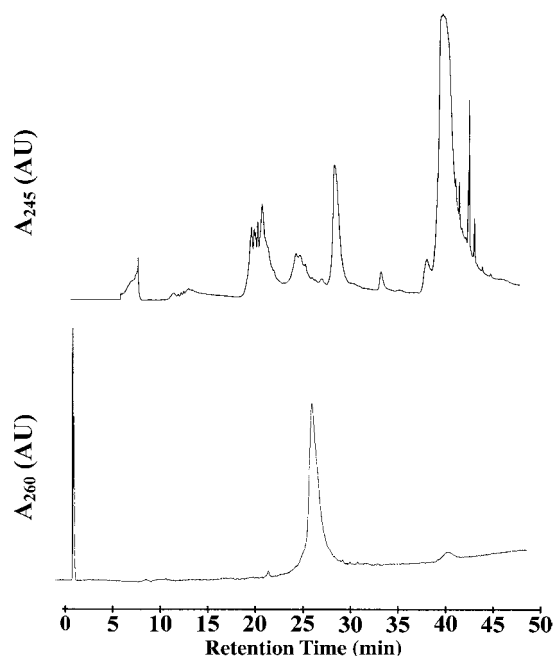
#### Scheme 1



derivative of DOTA, *N*- $\alpha$ -(9-fluorenylmethoxycarbonyl)-*N*- $\epsilon$ -[tris(*tert*-butyl)DOTA]-L-lysine (FKD, **1**), was prepared as a fully protected building block for solid-phase Fmoc chemistry. DOTA chelates a wide variety of radiometals for diagnostic imaging and targeted radiotherapy, including  $^{111}\text{In}$  ( $T_{1/2}$  = 67.4 h; EC 849 keV (100%);  $\gamma$  173 keV (89%), 247 keV (94%)) and  $^{90}\text{Y}$  ( $T_{1/2}$  = 64.0 h;  $\beta^-$  2.27 MeV (100%)), respectively, with extremely high in vivo stability (50). The synthesis of **1** is shown in Scheme 1. Compound **1** was prepared in a one-pot, two-step process, by activating commercially available DOTA tris(*tert*-butyl) ester with HATU and HOAt and reacting the resulting active ester with commercially available *N*- $\alpha$ -Fmoc-L-lysine. An extensive solvent extraction workup under carefully controlled pH conditions afforded **1** in high yield and 98.6% purity. The only impurity detected by analytical RP-HPLC was the dilysine adduct of DOTA tris(*tert*-butyl) ester (1.4%). Alternatively, compound **1** was obtained in somewhat lower yield using a simplified solvent extraction procedure, followed by semipreparative RP-HPLC. Using a mobile phase gradient optimized for purification of **1**, the bifunctional DOTA derivative was obtained in analytically pure form. Furthermore, this procedure greatly simplified scale-up of the reaction and purification of the desired product. To date, over 1.7 g of **1** have been prepared using these two procedures.

Coupling of **1** to *bcl-2* antisense and nonsense PNAs was followed by sequential automated elongation of the PNA conjugate with the cell-permeating PTD-4-G peptide sequence. Cleavage of the constructs from the resin, with concomitant deprotection, was followed by attempts to purify the crude products by semipreparative RP-HPLC and characterize them by LC-MS. It was discovered that neither the final products nor the unmodified PNA oligomers were retained on RP-HPLC, and both unmodified PNA and DOTA-derivatized PTD-4-G-PNA conjugates coeluted at the solvent front. Therefore, direct separation of the fully deprotected peptide-PNA conjugates from unmodified PNA byproducts was not possible.

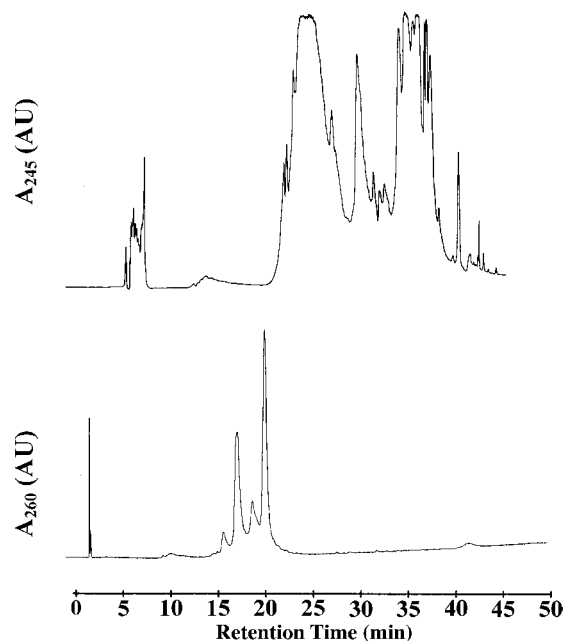
To solve this problem, an innovative strategy was devised to detach each conjugate from the resin under mildly acidic conditions, using dilute TFA and a partial cocktail of radical scavengers, to leave most of the protecting groups on the peptide residues. While it was predicted that the crude intermediates obtained by this process would consist of a mixture of different compounds, corresponding to various protecting groups remaining on the peptide, it was hypothesized that these partially protected conjugates would be very hydrophobic and retained on RP-HPLC. This strategy offered the possibility of separating the hydrophobic, partially deprotected intermediates from the very hydrophilic unreacted PNA. By collecting the hydrophobic components and subsequently treating them with a high concentration of TFA in full radical scavenger cocktail, the fully deprotected final products could be obtained.



**Figure 2.** (Top) Semipreparative RP-HPLC chromatogram, using Semiprep Gradient conditions, of intermediate products obtained after cleavage of **2** with 1% TFA containing 5% *m*-cresol. (Bottom) Analytical RP-HPLC chromatogram, using Full Gradient conditions, of hydrophobic, partially deprotected species purified after cleavage of **2** with 1% TFA containing 5% *m*-cresol.

This strategy was ultimately successful for the preparation of PTD-4-G-KD-anti-*bcl-2* PNA (**2**), after developing procedures for cleavage and partial deprotection. Initially two sets of conditions were evaluated, where the concentration of TFA was varied. It was surmised that 1% TFA would be sufficiently acidic to detach the conjugate from the resin without any risk of removing protecting groups, as is the case for the similarly labile 2-chlorotrityl chloride resin. However, after eight cycles of reaction with 1% TFA containing 5% *m*-cresol, only a small amount of crude intermediate product was obtained. After diethyl ether precipitation, the partially deprotected peptide-PNA was purified by semipreparative RP-HPLC, eluting at 37 to 41 min retention time (Figure 2, top). Analytical RP-HPLC (Figure 2, bottom) of the main fraction collected showed that it consisted of a relatively pure hydrophobic species.

The resin was then treated with 50% TFA containing 5% *m*-cresol to ensure full detachment of the conjugate from the resin. Under these conditions, it was anticipated that most of the protecting groups would probably be removed, possibly complicating the subsequent HPLC purification. A much larger quantity of crude intermediate product was obtained and purified by semipreparative RP-HPLC (Figure 3, top). The chromatogram showed that this mixture contained a large amount of hydrophilic species, which had to be discarded because this fraction, eluting at 21 to 29 min retention time, was contaminated with unmodified PNA. The major hydrophobic fraction, eluting at 33 to 38 min retention time, was collected, subjected to analytical RP-HPLC (Figure 3, bottom), and lyophilized. To remove the protecting groups still present, the lyophilized samples obtained by cleavage with 1% and 50% TFA were treated with concentrated TFA and a full cocktail of radical scavengers, in each case yielding a single product, for which ESI-MS analysis showed a pattern of multiply charged molecular ions consistent with the calculated molecular weight of **2**.

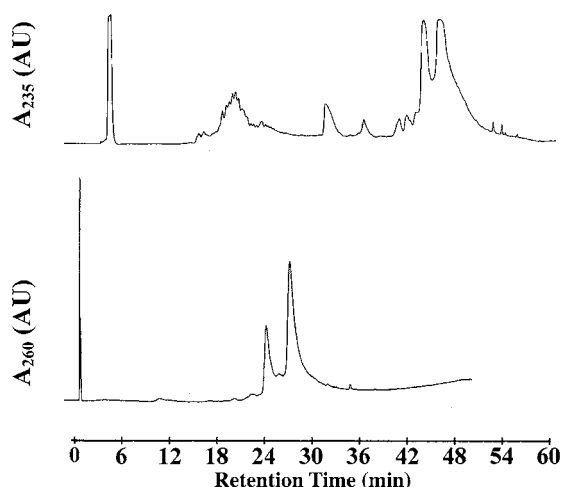


**Figure 3.** (Top) Semipreparative RP-HPLC chromatogram, using Semiprep Gradient conditions, of intermediate products obtained after cleavage of **2** with 50% TFA containing 5% *m*-cresol. (Bottom) Analytical RP-HPLC chromatogram, using Full Gradient conditions, of hydrophobic, partially deprotected species purified after cleavage of **2** with 50% TFA containing 5% *m*-cresol.

As observed previously during the synthesis of **2**, the final deprotected *bcl-2* antisense peptide-PNA conjugate was not retained upon subsequent RP-HPLC analysis and eluted with the solvent front. This result confirmed that the procedure for purification of the partially protected precursor was necessary to separate the PTD-4 conjugate from unreacted PNA and obtain the desired product in pure form. In addition, it was concluded that neither 1% TFA nor 50% TFA was an optimal treatment for generating a relatively small number of hydrophobic, partially deprotected precursors in the highest possible yield. Cleavage with 1% TFA gave a relatively pure hydrophobic product, but in low yield, while cleavage with 50% TFA afforded an excessive amount of fully deprotected conjugate, which could not be isolated in pure form by semipreparative RP-HPLC. Therefore, intermediate acid concentrations were then evaluated to optimize the cleavage, deprotection, and purification conditions.

In the synthesis of PTD-4-G-KD-nonsense PNA (**3**), once the protected conjugate had been assembled, the resin was reacted with increasing concentrations of TFA in partial radical scavenger cocktail, until detachment of the partially deprotected intermediates occurred. First, cleavage with four cycles of 5% TFA containing 5% H<sub>2</sub>O, *m*-cresol, and TIS each was attempted, followed by reaction with two cycles of 25% TFA containing 5% H<sub>2</sub>O, *m*-cresol, and TIS each, and finally reaction with one cycle of 50% TFA containing 5% *m*-cresol and 2.5% H<sub>2</sub>O, TIS, TA, and phenol each. Using 5% TFA, a modest amount of product was obtained, but the conjugate was not completely cleaved from the resin. When 25% TFA was employed, a substantially larger quantity of crude intermediate was obtained. Semipreparative RP-HPLC purification (Figure 4, top) afforded mainly very hydrophobic species, eluting at 43 to 49 min retention time, and a relatively small hydrophilic fraction, eluting at 17 to 24 min retention time. Analytical RP-HPLC of the hydrophobic fraction collected revealed that it was com-





**Figure 4.** (Top) Semipreparative RP-HPLC chromatogram, using Semiprep Gradient conditions, of intermediate products obtained after cleavage of **3** with 25% TFA containing 5% H<sub>2</sub>O, *m*-cresol, and TIS each. (Bottom) Analytical RP-HPLC chromatogram, using Full Gradient conditions, of hydrophobic, partially deprotected species purified after cleavage of **3** with 25% TFA containing 5% H<sub>2</sub>O, *m*-cresol, and TIS each.

posed of two major intermediates (Figure 4, bottom). No additional product was recovered from reaction with 50% TFA. The purified hydrophobic species generated by cleavage and slight deprotection with 5% and 25% TFA were pooled and lyophilized, after which they were completely deprotected with concentrated TFA and full radical scavenger cocktail. A single product was isolated, and ESI-MS analysis revealed a pattern of multiply charged molecular ions consistent with the calculated molecular weight of **3**.

Conjugates **2** and **3** were previously labeled to high specific activities with <sup>111</sup>In and <sup>90</sup>Y, and the specificity and stability of hybridization of <sup>90</sup>Y-labeled **2** with *bcl-2* mRNA in cell-free systems was compared to that of the corresponding <sup>32</sup>P-labeled anti-*bcl-2*-DNA (47). While <sup>90</sup>Y-labeled **2** showed equivalent specificity and superior thermodynamic stability in *bcl-2* mRNA binding, the plasma stability of <sup>111</sup>In-labeled **2** was suboptimal, as proteolytic degradation of the PTD-4 sequence was evident after 24 h at 37 °C. Therefore, the *ri*-PTD-4 analogues of **2** and **3** were synthesized in order to improve plasma stability. The retro-inverso peptide, which consists of all D-amino acids in the reverse sequence, places the basic residues of PTD-4 critical for cell permeation in approximately the same three-dimensional spatial configuration as the parent peptide. Thus, *ri*-PTD-4 should retain biological activity mediating cellular internalization of the PNA conjugates and show greater proteolytic stability than the parent peptide. Aldrian-Herrada et al. (39) demonstrated that the retro-inverso counterpart of pAntp was active in causing PNA conjugates to permeate target cells and presumed that it was much more stable to proteolysis. However, before now *ri*-PTD-4 had not been synthesized and evaluated for biological activity and stability.

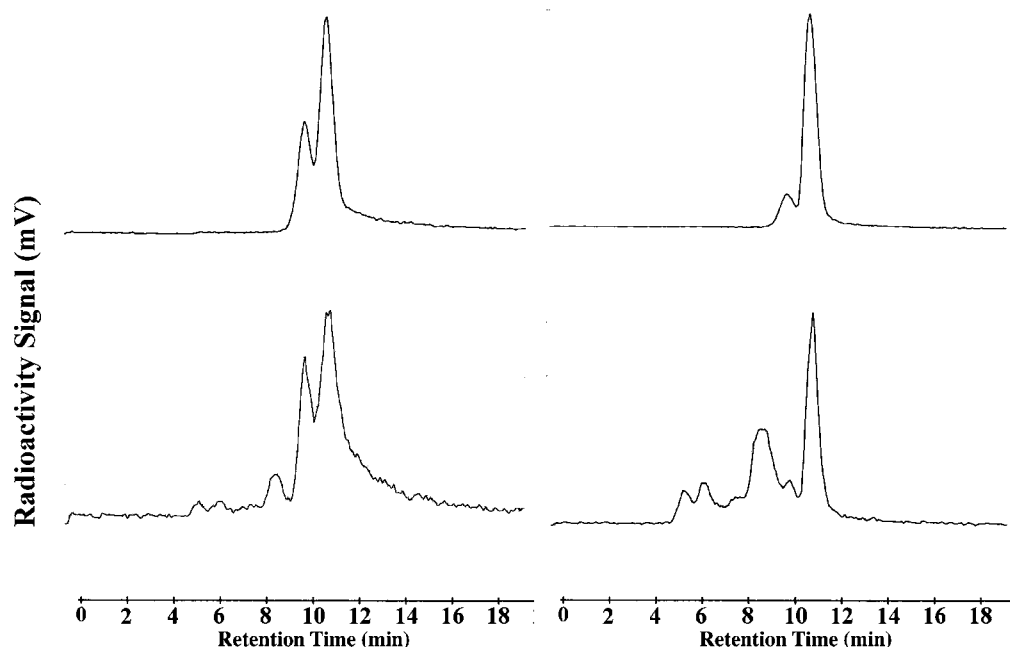
DOTA-conjugated *ri*-PTD-4 constructs of *bcl-2* antisense (**4**) and nonsense (**5**) PNAs were prepared based on the methods developed for the syntheses of the parent PTD-4 conjugates **2** and **3**. As in the case of conjugate **3**, optimized sequential cleavage and slight deprotection using 5% TFA, followed by 25% TFA, in partial radical scavenger cocktail, was employed. These reaction conditions readily afforded hydrophobic precursors. These precursors were purified by semipreparative RP-HPLC,

completely deprotected in concentrated TFA and full radical scavenger cocktail, precipitated with diethyl ether, and lyophilized to yield **4** and **5**. ESI-MS analysis of **4** and **5** were consistent with the calculated molecular weights of the desired products.

Conjugates **2** and **4** were labeled with <sup>111</sup>In at specific activities of 1298 Ci/mmol and 1370 Ci/mmol, respectively, using a previously published procedure (47). The radiolabeled conjugates were incubated in mouse plasma for 168 h at 37 °C (Figure 5). The retention time of <sup>111</sup>In-labeled **2** shifted reproducibly from 11.4 min immediately upon mixing to 11.5 min at 168 h. In addition, the radiolabeled conjugate peak, initially sharp, showed considerable tailing by 168 h of incubation in plasma. After 168 h at 37 °C, an aliquot of the plasma mixture was spiked with pure <sup>111</sup>In-KD-anti-*bcl-2* PNA and analyzed by size exclusion HPLC. The species corresponding to 11.5 min retention time coeluted with the radiolabeled PNA lacking the PTD-4 sequence, with no observed changes in the chromatographic profile. These results suggested that considerable degradation of PTD-4 by plasma proteases and peptidases had occurred. In contrast, the peak corresponding to <sup>111</sup>In-labeled **4** remained sharp during the 168-h incubation in plasma at 37 °C, its retention time changed by less than 0.02 min, and the lack of lower molecular weight species indicated that *ri*-PTD-4 was stable to plasma proteases and peptidases. During the course of these experiments, the protein-bound fraction of <sup>111</sup>In-labeled **2** changed relatively little, from 28.8% at 0 h to 34.5% at 168 h. By comparison, the protein-bound fraction of <sup>111</sup>In-labeled **4** increased over 4-fold, from 13.7% to 60.2%, during the 168-h incubation in plasma. In the case of conjugate **4**, the major component of protein-associated <sup>111</sup>In (41.7%) eluted at 9.24 min, consistent with the molecular weight of immunoglobulin G (158 kDa). Since transferrin (80 kDa) is the main indium-binding protein in plasma, this result suggested that little, if any, dissociation of <sup>111</sup>In from the DOTA chelate occurred. Instead the protein-associated fractions of <sup>111</sup>In likely resulted from non-specific binding of the radiolabeled peptide-PNA conjugate. Under the size exclusion HPLC conditions employed, transferrin could not be separated from albumin (69 kDa). However, the peak eluting in this molecular weight range, at 10.5 min retention time, corresponded to approximately 6% of the total radioactivity. In addition, no low molecular species corresponding to <sup>111</sup>In transchelated by EDTA in the plasma was observed, a further indication of the kinetic stability of the DOTA chelate.

The superior proteolytic stability of <sup>111</sup>In-labeled **4** rendered it the more suitable peptide-antisense-PNA conjugate to evaluate for tumor *bcl-2* targeting in NHL cells in culture and lymphoma-bearing SCID-hu mouse models. However, prior to initiating these studies, the ability of *ri*-PTD-4 to mediate cellular internalization of anti-*bcl-2* PNA required validation. Therefore, anti-*bcl-2* PNA was conjugated to a lysine derivative of the red fluorescent dye tetramethylrhodamine (TMR) in the same sequence position as DOTA, after which the *ri*-PTD-4-G sequence was added.

KT-anti-*bcl-2* PNA (**6**) was synthesized manually using modifications of the procedures for synthesizing the DOTA-conjugated PNAs. Unlike the DOTA conjugates, the hydrophobic nature of the tetramethylrhodamine residue allowed for isolation of **6** by standard peptide and PNA cleavage, deprotection, and purification conditions. Following assembly, the crude product was cleaved from the resin and completely deprotected, using concentrated



**Figure 5.** (Left) Size exclusion HPLC chromatograms of  $^{111}\text{In}$ -labeled **2** after 0 h (top) and 168 h (bottom) of incubation in mouse plasma at 37 °C. (Right) Size exclusion HPLC chromatograms of  $^{111}\text{In}$ -labeled **4** after 0 h (top) and 168 h (bottom) of incubation in mouse plasma at 37 °C.

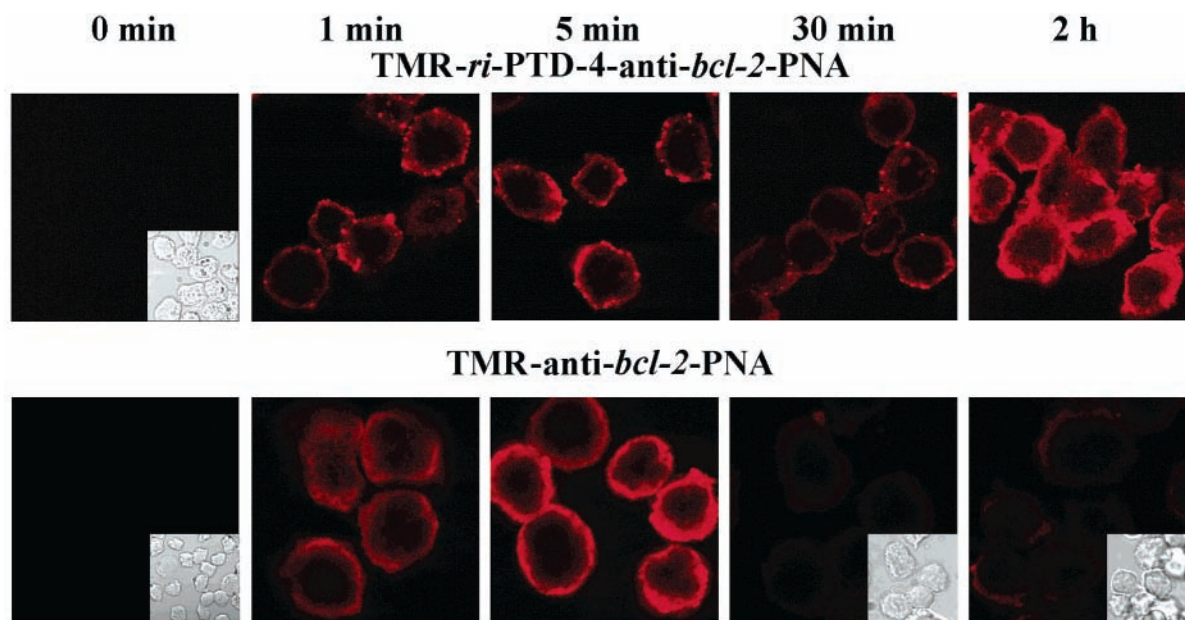
TFA and full radical scavenger cocktail, and then purified by semipreparative RP-HPLC. The 33.5 min retention time of **6** allowed for easy separation from the unreacted PNA byproduct. Compound **6** was also conjugated to *ri*-PTD-4-G by automated, stepwise elongation with the peptide sequence using standard Fmoc chemistry. The *ri*-PTD-4-G-KT-anti-*bcl-2* PNA conjugate (**7**) had a retention time of 35.5 min on semipreparative RP-HPLC, also affording easy separation from unmodified PNA. Following RP-HPLC purification, conjugates **6** and **7** were isolated by diethyl ether precipitation and lyophilization. ESI-MS analyses showed patterns of molecular ions that were consistent with the calculated molecular weights of the conjugates. Analytical RP-HPLC analysis of **6** and **7** indicated that the purity of both TMR conjugates was >99.5%.

To determine whether *ri*-PTD-4 was active in cell permeation and mediated cellular internalization of anti-*bcl-2* PNA, scanning confocal microscopy studies were performed with conjugates **6** and **7** in Raji Burkitt's lymphoma cells, after fixation with 4% formaldehyde at various incubation times. Raji cells express high levels of homogeneous 6.5-kb *bcl-2* mRNA (51). During the course of these studies, fluorescence in Raji cells was much more intense with **7** than with **6** at all time points from 0 to 2 h of incubation, but the fluorescence intensity from each conjugate was normalized to the value at 5 min, to show qualitative differences between the two compounds. As shown in Figure 6, at 1 to 5 min, fluorescence from both conjugates was confined largely to the plasma membrane, and a small amount of cytoplasmic staining observed with **7**. By 30 min, cell-associated fluorescence from **7** had decreased considerably, and that from **6** had nearly disappeared. However, after 2 h of incubation, widespread, intense fluorescence was seen in the cytoplasm of essentially all cells exposed to **7**, while little to no fluorescence was observed from **6** at the same time point. The fluorescence microscopy studies demonstrated that *ri*-PTD-4 was active in permeation of the plasma membrane and mediated cellular internalization of the *bcl-2* antisense PNA. Furthermore,

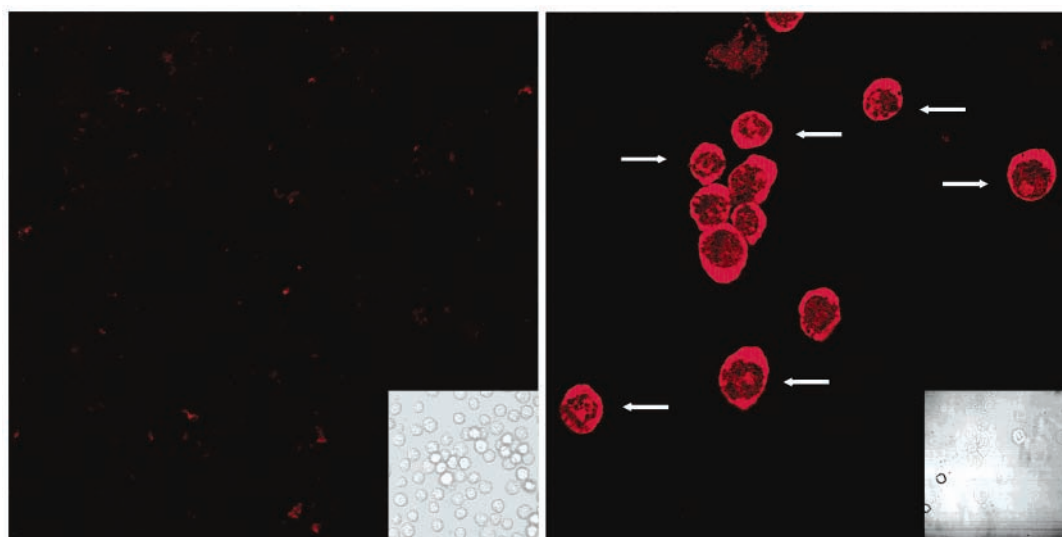
internalization of the *ri*-PTD-4 conjugate **7** in Raji cells delivered the antisense PNA predominantly into the cytoplasm, where concentrations of mRNA, including *bcl-2*, are highest.

Recently, Richard et al. (52) demonstrated that cell fixation with 3.7% formaldehyde caused subcellular redistribution artifacts during fluorescence microscopy studies of cell-penetrating peptides. In that report, fixation of HeLa and CHO cells led to redistribution of fluorescein- and Alexa 488-conjugated Tat peptide into the nucleus, whereas no nuclear uptake was observed in live cells. When Dowdy and co-workers (46) examined the uptake of fluorescein-conjugated PTD-4 in fixed Jurkat cells, both nuclear and cytoplasmic localization were visualized by fluorescence microscopy. To test whether cell fixation led to redistribution artifacts in the present studies, scanning confocal fluorescence microscopy of conjugates **6** and **7** in live Raji cells was performed. Association of **6** and **7** with live cells from 0 to 2 h of incubation was qualitatively similar to the results obtained with fixed cells (data not shown). At 2 h, very little membrane-bound fluorescence from **6** was observed in live Raji cells (Figure 7, left), and essentially all cells incubated with **7** showed internalization of the compound and widespread, intense cytoplasmic staining (Figure 7, right). Surprisingly, though, approximately 50% of live Raji cells incubated with the *ri*-PTD-4 conjugate **7** exhibited nuclear uptake after 2 h of incubation. This result was contrary to the findings of Richard et al. (52), but they studied different cell-permeating peptides in cells of epithelial origin.

The nuclear localization of **7** in live lymphoma cells, but not in fixed cells, suggests that the uptake mechanisms of cell-permeating peptide conjugates are complex and remain poorly understood. As reviewed by Moulton and Moulton (53) and Vives et al. (54), most publications on cell-permeating peptides highlighted energy-independent processes that occurred at low temperatures and in the presence of drugs that inhibit active transport. However, these reviews pointed to recent reports strongly suggesting that arginine-rich peptide



**Figure 6.** Scanning confocal fluorescence microscopy images of Raji cells incubated with **7** (top) or **6** (bottom) at 37 °C and 5% CO<sub>2</sub>, then fixed with 4% formaldehyde. Transmission images of cells with little or no fluorescence are shown in the lower right corner of some panels.



**Figure 7.** Scanning confocal fluorescence microscopy images of live Raji cells incubated with **6** (left) or **7** (right) at 37 °C and 5% CO<sub>2</sub> for 2 h. Arrows indicate cells with nuclear accumulation of **7**. Transmission images of the cells are shown in the lower right corner insets.

conjugates are internalized by an energy-dependent endocytotic pathway. Furthermore, early assay techniques produced artifacts leading to widespread acceptance of the nonendocytotic, membrane-permeating model as the mechanism of uptake.

Using fluorescein conjugates and live COS7 cells, Dom et al. (55) demonstrated that cellular uptake of pAntp is a two-step process. The first step is phase transfer from a hydrophilic to a hydrophobic environment, which is probably mediated by charge neutralization in the presence of negatively charged lipids. Phase transfer of pAntp is then followed by further translocation across the membrane bilayer, a process dependent on a critical tryptophan residue at position 6.

Thorén and colleagues (56) showed that pAntp was internalized by PC-12 and V79 cells via an endocytotic mechanism that could be abrogated at 4 °C or by depleting ATP. In contrast, they observed only an energy-independent, nonendocytotic pathway for R<sub>7</sub>W in the

same cell lines. Behavior of the Tat peptide in those studies was more complex. It showed substantial endocytosis in PC-12 cells, as well as energy-independent uptake. However, in V79 cells, Tat peptide internalization was exclusively energy-independent and led to uniform uptake in the cytoplasm and nuclear accumulation, similar to the subcellular distribution of conjugate **7** in the present studies.

Piwnicka-Worms and co-workers (57) found evidence for a membrane permeability barrier to Tat uptake in well-differentiated epithelial cells that form tight junctions in monolayer culture. They observed a complete lack of internalization of fluorescein-conjugated Tat peptide in monolayers of MDCK and CaCo-2 cells, but treatment with membrane permeabilizing agents resulted in immediate translocation. In contrast, epithelial cells that do not form tight junctions in monolayer culture, such as HeLa and KB 3-1, showed facile cytoplasmic and nucleolar accumulation of the fluorescent Tat conjugate.



However, it should be noted that these fluorescence microscopy studies were performed on paraformaldehyde-fixed cells. Piwnicka-Worms's group have also examined the effects of sequence and chirality on cell permeation activity (58). Screening a library of 42 <sup>99m</sup>Tc-labeled basic domain peptides in live Jurkat cells, Piwnicka-Worms and colleagues found that D-peptides were more active in cell permeation, a result not attributable to decreased proteolytic stability of the corresponding L-sequences. Furthermore, peptide uptake was dependent on length, sequence, and the type of radiometal chelate, with D-Tat-Orn<sup>6</sup> and (D-Arg)<sub>9</sub> having the greatest activity. Taken together, the results of these and the present studies indicate that further investigation of the uptake mechanisms of cell-permeating peptides is clearly warranted.

## CONCLUSION

In the present work, an innovative solid-phase synthesis strategy was developed to prepare, purify, and characterize a variety of cell-permeating peptide-PNA conjugates for targeting imaging and therapeutic radiometals to the *bcl-2* cellular oncogene. The strategy was based on cleavage and partial deprotection of resin-bound DOTA-conjugated peptide-PNA constructs, followed by RP-HPLC separation of the hydrophobic precursors from the hydrophilic unreacted PNA. Using this approach, *bcl-2* antisense and nonsense PNA sequences were conjugated to a new bifunctional derivative of DOTA, which can be incorporated into any position of a peptide-PNA conjugate, and to peptides that mediate cell permeation and internalization of the PNA. Peptide-PNA conjugates for both radiometal and fluorophore labeling were obtained in high purity and 6% to 9% overall yield by this synthetic strategy and modifications of the procedure. The <sup>111</sup>In-labeled retro-inverso PTD-4-G-KD-anti-*bcl-2* PNA conjugate showed superior plasma stability to the parent PTD-4-G construct. Moreover, scanning confocal fluorescence microscopy studies with the analogous tetramethylrhodamine conjugate demonstrated that retro-inverso PTD-4 was active in mediating internalization of anti-*bcl-2* PNA in Raji NHL cells, which are known to express high basal levels of *bcl-2* mRNA. Retro-inverso PTD-4-G-KT-anti-*bcl-2* PNA showed nuclear accumulation in approximately 50% of live cells, but formaldehyde fixation resulted in artifactual redistribution into the cytoplasm only. Further optimization of the design and synthesis of internalizing peptide-PNA conjugates for in vivo tumor uptake could generate powerful oncogene-targeting tools for both diagnostic imaging and targeted radiotherapy of cancer.

## ACKNOWLEDGMENT

This work was supported by NIH Grant CA86290 (W.A. Volkert, PI) and a grant from the University of Missouri Research Reactor Research Partnerships Initiative (to M.R.L.). The authors would like to thank Dr. Mayandi Sivaguru of the University of Missouri-Columbia Molecular Cytology Core, for valuable assistance in performing the fluorescence microscopy studies. We also acknowledge the Department of Veterans Affairs, for providing resources and the use of facilities at the Harry S Truman Memorial Veterans' Hospital in Columbia, MO, and the University of Missouri Research Reactor, for purchasing the Advanced ChemTech ACT Model 396 Omega Multiple Biomolecular Synthesizer used in this research.

**Supporting Information Available:** ESI mass spectra of all peptide-PNA conjugates. This material is available free of charge via the Internet at <http://pubs.acs.org>.

## LITERATURE CITED

- (1) Milas, L., Stephens, L. C., and Meyn, R. E. (1994) Relation of Apoptosis to Cancer Therapy. *In Vivo* 8, 665–674.
- (2) Hockenbery, D., Nuñez, G., Millman, C., Schreiber, R. D., and Korsmeyer, S. J. (1990) Bcl-2 is an inner mitochondrial membrane protein that blocks programmed cell death. *Nature* 348, 334–336.
- (3) Oltvai, Z. N., Millman, C. L., and Korsmeyer, S. J. (1993) Bcl-2 Heterodimerizes In Vivo with a Conserved Homolog, Bax, That Accelerates Programmed Cell Death. *Cell* 74, 609–619.
- (4) Miyashita, T., and Reed, J. C. (1992) *bcl-2* Gene Transfer Increases Relative Resistance of S49.1 and WEHI7.2 Lymphoid Cells to Cell Death and DNA Fragmentation Induced by Glucocorticoids and Multiple Chemotherapeutic Drugs. *Cancer Res.* 52, 5407–5411.
- (5) Miyashita, T., and Reed, J. C. (1993) Bcl-2 Oncoprotein Blocks Chemotherapy-Induced Apoptosis in a Human Leukemia Cell Line. *Blood* 81, 151–157.
- (6) Reed, J. C., Kitada, S., Takayama, S., and Miyashita, T. (1994) Regulation of chemoresistance by the *bcl-2* oncoprotein in non-Hodgkin's lymphoma and lymphocytic leukemia cell lines. *Ann. Oncol.* 5, S61–S65.
- (7) Sentman, C. L., Shutter, J. R., Hockenbery, D., Kanagawa, O., and Korsmeyer, S. J. (1991) *bcl-2* Inhibits Multiple Forms of Apoptosis but Not Negative Selection in Thymocytes. *Cell* 67, 879–888.
- (8) Strasser, A., Harris, A. W., and Cory, S. (1991) *bcl-2* Transgene Inhibits T Cell Death and Perturbs Thymic Self-Censorship. *Cell* 67, 889–899.
- (9) Mirkovic, N., Voehringer, D. W., Story, M. D., McConkey, D. J., McDonnell, T. J., and Meyn, R. E. (1997) Resistance to radiation-induced apoptosis in Bcl-2-expressing cells is reversed by depleting cellular thiols. *Oncogene* 15, 1461–1470.
- (10) Tsujimoto, Y., Cossman, J., Jaffe, E., and Croce, C. M. (1985) Involvement of the *bcl-2* Gene in Human Follicular Lymphoma. *Science* 228, 1440–1443.
- (11) Yunis, J. J., Oken, M. M., Kaplan, M. E., Ensrud, K. M., Howe, R. R., and Theologides, A. (1982) Distinctive Chromosomal Abnormalities in Histologic Subtypes of Non-Hodgkin's Lymphoma. *N. Engl. J. Med.* 307, 1231–1236.
- (12) Tsujimoto, Y., Finger, L. R., Yunis, J., Nowell, P. C., and Croce, C. M. (1984) Cloning of the Chromosome Breakpoint of Neoplastic B Cells with the t(14;18) Chromosome Translocation. *Science* 226, 1097–1099.
- (13) Levine, E. G., Arthur, D. C., Frizzera, G., Peterson, B. A., Hurd, D. D., and Bloomfield, C. D. (1985) There Are Differences in Cytogenetic Abnormalities Among Histologic Subtypes of the Non-Hodgkin's Lymphomas. *Blood* 66, 1414–1422.
- (14) Pezzella, F., Tse, A. G. D., Cordell, J. L., Pulford, K. A. F., Gatter, K. C., and Mason, D. Y. (1990) Expression of the *bcl-2* Oncogene Protein Is Not Specific for the 14; 18 Chromosomal Translocation. *Am. J. Pathol.* 137, 225–232.
- (15) Zutter, M., Hockenbery, D., Silverman, G. A., and Korsmeyer, S. J. (1991) Immunolocalization of the Bcl-2 Protein Within Hematopoietic Neoplasms. *Blood* 78, 1062–1068.
- (16) Karakas, T., Maurer, U., Weidmann, E., Miething, C. C., Hoelzer, D., and Bergmann, L. (1998) High expression of *bcl-2* mRNA as a determinant of poor prognosis in acute myeloid leukemia. *Ann. Oncol.* 9, 159–165.
- (17) Puthier, D., Pellat-Deceunynck, C., Barillé, S., Robillard, N., Rapp, M.-J., Juge-Morineau, N., Harousseau, J.-L., Bataille, R., and Amiot, M. (1999) Differential expression of Bcl-2 in human plasma cell disorders according to proliferation status and malignancy. *Leukemia* 13, 289–294.
- (18) Lanzafame, S., Emmanuele, C., Torrisi, A., and Magro, G. (1998) Correlated Expression of BCL-2 Protein, Estrogen Receptor, Cathepsin D and Low Growth Fraction (PCNA) in Intracystic Papillary Breast Carcinoma. *Pathol. Res. Pract.* 194, 541–547.

- (19) Pezzella, F., Turley, H., Kuzu, I., Tungekar, M. F., Dunnill, M. S., Pierce, C. B., Harris, A., Gatter, K. C., and Mason, D. Y. (1993) *bcl-2* Protein in Non-Small-Cell Lung Carcinoma. *N. Engl. J. Med.* **329**, 690–694.
- (20) Jiang, S.-X., Sato, Y., Kuwao, S., and Kameya, T. (1995) Expression of *bcl-2* Oncogene Protein is Prevalent in Small Cell Lung Carcinomas. *J. Pathol.* **177**, 135–138.
- (21) Sinicrope, F. A., Ruan, S. B., Cleary, K. R., Stephens, L. C., Lee, J. J., and Levin, B. (1995) *bcl-2* and p53 Oncoprotein Expression during Colorectal Tumorigenesis. *Cancer Res.* **55**, 237–241.
- (22) Yang, H.-B., Chow, N.-H., Sheu, B.-S., Chan, S.-H., Chien, C.-H., and Su, I.-J. (1999) The Role of *bcl-2* in the Progression of the Colorectal Adenoma-Carcinoma Sequence. *Anticancer Res.* **19**, 727–730.
- (23) Colombel, M., Symmans, F., Gil, S., O'Toole, K. M., Chopin, D., Benson, M., Olsson, C. A., Korsmeyer, S., and Buttyan, R. (1993) Detection of the Apoptosis-Suppressing Oncoprotein *bcl-2* in Hormone-Refractory Human Prostate Cancers. *Am. J. Pathol.* **143**, 390–400.
- (24) Sullivan, G. F., Amenta, P. S., Villanueva, J. D., Alvarez, C. J., Yang, J.-M., and Hait, W. N. (1998) The Expression of Drug Resistance Gene Products during the Progression of Human Prostate Cancer. *Clin. Cancer Res.* **4**, 1393–1403.
- (25) Wang, D.-G., Johnston, C. F., and Buchanan, K. D. (1997) Oncogene Expression in Gastroenteropancreatic Neuroendocrine Tumors. Implications for Pathogenesis. *Cancer* **80**, 668–675.
- (26) Cerroni, L., Soyer, H. P., and Kerl, H. (1995) *bcl-2* Protein Expression in Cutaneous Malignant Melanoma and Benign Melanocytic Nevi. *Am. J. Dermatopathol.* **17**, 7–11.
- (27) Hermine, O., Haïoun, C., Lepage, E., d'Agay, M.-F., Briere, J., Lavignac, C., Fillet, G., Salles, G., Marolleau, J.-P., Diebold, J., Reyes, F., and Gaulard, P. (1996) Prognostic Significance of *bcl-2* Protein Expression in Aggressive Non-Hodgkin's Lymphoma. *Blood* **87**, 265–272.
- (28) Hill, M. E., MacLennan, K. A., Cunningham, D. C., Vaughan Hudson, B., Burke, M., Clarke, P., Di Stefano, F., Anderson, L., Vaughan Hudson, G., Mason, D., Selby, P., and Linch, D. C. (1996) Prognostic Significance of BCL-2 Expression and *bcl-2* Major Breakpoint Region Rearrangement in Diffuse Large Cell Non-Hodgkin's Lymphoma: A British National Lymphoma Investigation Study. *Blood* **88**, 1046–1051.
- (29) Alas, S., Emmanouilides, C., and Bonavida, B. (2001) Inhibition of Interleukin 10 by Rituximab Results in Down-Regulation of Bcl-2 and Sensitization of B-Cell Non-Hodgkin's Lymphoma to Apoptosis. *Clin. Cancer Res.* **7**, 709–723.
- (30) Alas, S., and Bonavida, B. (2001) Rituximab Inactivates Signal Transducer and Activation of Transcription 3 (STAT3) Activity in B-Non-Hodgkin's Lymphoma through Inhibition of the Interleukin 10 Autocrine/Paracrine Loop and Results in Down-Regulation of Bcl-2 and Sensitization to Cytotoxic Drugs. *Cancer Res.* **61**, 5137–5144.
- (31) Demidem, A., Lam, T., Alas, S., Hariharan, K., Hanna, N., and Bonavida, B. (1997) Chimeric Anti-CD20 (IDEC-C2B8) Monoclonal Antibody Sensitizes a B Cell Lymphoma Cell Line to Cell Killing by Cytotoxic Drugs. *Cancer Biother. Radiopharm.* **12**, 177–186.
- (32) Witzig, T. E. (2001) Radioimmunotherapy for patients with relapsed B-cell non-Hodgkin's lymphoma. *Cancer Chemother. Pharmacol.* **48** (Suppl 1), S91–S95.
- (33) Kroger, L. A., DeNardo, S. J., DeNardo, G. L., Xiong, C. Y., Winthrop, M. D., and Gumerlock, P. H. (1999) Effect of <sup>67</sup>Cu-2IT-BAT-Lym-1 Therapy on *BCL-2* Gene and Protein Expression in a Lymphoma Mouse Model. *Clin. Cancer Res.* (Suppl.) **5**, 3010s–3014s.
- (34) Cotter, F. E., Johnson, P., Hall, P., Pocock, C., Al Mahdi, N., Cowell, J. K., and Morgan, G. (1994) Antisense oligonucleotides suppress B-cell lymphoma growth in a SCID-hu mouse model. *Oncogene* **9**, 3049–3055.
- (35) Webb, A., Cunningham, D., Cotter, F., Clarke, P. A., di Stefano, F., Ross, P., Corbo, M., and Dziekanowska, Z. (1997) *BCL-2* antisense therapy in patients with non-Hodgkin lymphoma. *Lancet* **349**, 1137–1141.
- (36) Jansen, B., Wacheck, V., Heere-Ress, E., Schlagbauer-Wadl, H., Hoeller, C., Lucas, T., Hoermann, M., Hollenstein, U., Wolff, K., and Pehamberger, H. (2000) Chemosensitization of malignant melanoma by BCL2 antisense therapy. *Lancet* **356**, 1728–1733.
- (37) Nielsen, P. E., Egholm, M., Berg, R. H., and Buchardt, O. (1991) Sequence Selective Recognition of DNA by Strand Displacement with a Thymine-substituted Polyamide. *Science* **254**, 1497–1500.
- (38) Larsen, H. J., Bentin, T., and Nielsen, P. E. (1999) Antisense properties of peptide nucleic acid. *Biochim. Biophys. Acta* **1489**, 159–166.
- (39) Aldrian-Herrada, G., Desarménien, M. G., Orcel, H., Boissin-Agasse, L., Méry, J., Brugidou, J., and Rabié, A. (1998) A peptide nucleic acid (PNA) is more rapidly internalized in cultured neurons when coupled to a retro-inverso delivery peptide. The antisense activity depresses the target mRNA and protein in magnocellular oxytocin neurons. *Nucleic Acids Res.* **26**, 4910–4916.
- (40) Pooga, M., Soomets, U., Hällbrink, M., Valkna, A., Saar, K., Rezaei, K., Kahl, U., Hao, J.-X., Xu, X.-J., Wiesenfeld-Hallin, Z., Hökfelt, T., Bartfai, T., and Langel, U. (1998) Cell penetrating PNA constructs regulate galanin receptor levels and modify pain transmission in vivo. *Nat. Biotechnol.* **16**, 857–861.
- (41) Koppelhus, U., Awasthi, S. K., Zachar, V., Holst, H. U., Ebbesen, P., and Nielsen, P. E. (2002) Cell-Dependent Differential Cellular Uptake of PNA, Peptides, and PNA-Peptide Conjugates. *Antisense Nucleic Acid Drug Dev.* **12**, 51–63.
- (42) Braun, K., Peschke, P., Pipkorn, R., Lampel, S., Wachsmuth, M., Waldeck, W., Friedrich, E., and Debus, J. (2002) A Biological Transporter for the Delivery of Peptide Nucleic Acids (PNAs) to the Nuclear Compartment of Living Cells. *J. Mol. Biol.* **318**, 237–243.
- (43) Kaushik, N., Basu, A., Palumbo, P., Myers, R. L., and Pandey, V. N. (2002) Anti-TAR Polyamide Nucleotide Analogue Conjugated with a Membrane-Permeating Peptide Inhibits Human Immunodeficiency Virus Type 1 Production. *J. Virol.* **76**, 3881–3891.
- (44) Derossi, D., Joliot, A. H., Chassaing, G., and Prochiantz, A. (1994) The Third Helix of the Antennapedia Homeodomain Translocates through Biological Membranes. *J. Biol. Chem.* **269**, 10444–10450.
- (45) Fawell, S., Seery, J., Daikh, Y., Moore, C., Chen, L. L., Pepinsky, B., and Barsom, J. (1994) Tat-mediated delivery of heterologous proteins into cells. *Proc. Natl. Acad. Sci. U.S.A.* **91**, 664–668.
- (46) Ho, A., Schwarze, S. R., Mermelstein, S. J., Waksman, G., and Dowdy, S. F. (2001) Synthetic Protein Transduction Domains: Enhanced Transduction Potential in Vitro and in Vivo. *Cancer Res.* **61**, 474–477.
- (47) Lewis, M. R., Jia, F., Gallazzi, F., Wang, Y., Zhang, J., Shenoy, N., Lever, S. Z., and Hannink, M. (2002) Radiometal-Labeled Peptide-PNA Conjugates for Targeting *bcl-2* Expression: Preparation, Characterization, and in Vitro mRNA Binding. *Bioconjugate Chem.* **13**, 1176–1180.
- (48) Thiers, R. E. (1957) Contamination in Trace Element Analysis and Its Control. *Methods Biochem. Anal.* **5**, 273–335.
- (49) Eriksson, M., Christensen, L., Schmidt, J., Haaima, G., Orgel, L., and Nielsen, P. E. (1998) Sequence dependent N-terminal rearrangement and degradation of peptide nucleic acid (PNA) in aqueous solution. *New J. Chem.* **22**, 1055–1059.
- (50) Volkert, W. A., and Hoffman, T. J. (1999) Therapeutic Radiopharmaceuticals. *Chem. Rev.* **99**, 2269–2292.
- (51) Graninger, W. B., Seto, M., Boutain, B., Goldman, P., and Korsmeyer, S. J. (1987) Expression of Bcl-2 and Bcl-2-Ig Fusion Transcripts in Normal and Neoplastic Cells. *J. Clin. Invest.* **80**, 1512–1515.
- (52) Richard, J. P., Melikov, K., Vives, E., Ramos, C., Verbeure, B., Gait, M. J., Chernomordik, L. V., and Lebleu, B. (2003) Cell-penetrating Peptides. A Reevaluation of the Mechanism of Cellular Uptake. *J. Biol. Chem.* **278**, 585–590.
- (53) Moulton, H. M., and Moulton, J. D. (2003) Peptide-assisted delivery of steric-blocking antisense oligomers. *Curr. Opin. Mol. Ther.* **5**, 123–132.

- (54) Vives, E., Richard, J. P., Rispal, C., and Lebleu, B. (2003) TAT Peptide Internalization: Seeking the Mechanism of Entry. *Curr. Protein Pept. Sci.* 4, 125–132.
- (55) Dom, G., Shaw-Jackson, C., Matis, C., Bouffieux, O., Picard, J. J., Prochiantz, A., Mingeot-Leclercq, M.-P., Brasseur, R., and Rezsöházy, R. (2003) Cellular uptake of Antennapedia Penetratin peptides is a two-step process in which phase transfer precedes a tryptophan-dependent translocation. *Nucleic Acids Res.* 31, 556–561.
- (56) Thorén, P. E. G., Persson, D., Isakson, P., Goksör, M., Önfelt, A., and Nordén, B. (2003) Uptake of analogues of penetratin, Tat(48–60), and oligoarginine in live cells. *Biochem. Biophys. Res. Commun.* 307, 100–107.
- (57) Violini, S., Sharma, V., Prior, J. L., Dyszlewski, M., and Piwnicka-Worms, D. (2002) Evidence for a Plasma Membrane-Mediated Permeability Barrier to Tat Basic Domain in Well-Differentiated Epithelial Cells: Lack of Correlation with Heparan Sulfate. *Biochemistry* 41, 12652–12661.
- (58) Gammon, S. T., Villalobos, V. M., Prior, J. L., Sharma, V., and Piwnicka-Worms, D. (2003) Quantitative Analysis of Permeation Peptide Complexes Labeled with Technetium-99m: Chiral and Sequence-Specific Effects on Net Cell Uptake. *Bioconjugate Chem.* 14, 368–376.

BC034084N



# Polyacetal–Doxorubicin Conjugates Designed for pH-Dependent Degradation

Ryan Tomlinson,<sup>†,‡</sup> Jorge Heller,<sup>§</sup> Steve Brocchini,<sup>\*,‡</sup> and Ruth Duncan<sup>\*,†</sup>

Centre for Polymer Therapeutics, Welsh School of Pharmacy, Cardiff University, King Edward VII Avenue, Cardiff, CF10 3XF, UK, Biomedical Polymers Group, Department of Pharmaceutics, The School of Pharmacy, University of London, 29–39 Brunswick Square, London, WC1N 1AX, UK, and A. P. Pharma, 123 Saginaw Drive, Redwood City, California, California 94063. Received May 22, 2003; Revised Manuscript Received August 1, 2003

Terpolymerization of poly(ethylene glycol) (PEG), divinyl ethers, and serinol can be used to synthesize water soluble, hydrolytically labile, amino-pendent polyacetals (APEGs) suitable for drug conjugation. As these polyacetals display pH-dependent degradation (with faster rates of hydrolysis at acidic pH) and they are not inherently hepatotropic after intravenous (iv) injection, they have potential for development as biodegradable carriers to facilitate improved tumor targeting of anticancer agents. The aim of this study was to synthesize a polyacetal–doxorubicin (APEG–DOX) conjugate, determine its cytotoxicity in vitro and evaluate its potential for improved tumor targeting in vivo compared to an HPMA copolymer–DOX conjugate in clinical development. Amino-pendent polyacetals were prepared, and following succinylation (APEG–succ), the polymeric intermediate conjugated to DOX via one of three methods using carbodiimide mediated coupling (1-ethyl-3-(3-dimethylaminopropyl)-carbodiimide (EDC) in aqueous solution was the most successful). The resultant APEG–DOX conjugates had a DOX content of 3.0–8.5 wt %, contained <1.2% free DOX (relative to total DOX content) and had a  $M_w = 60000$ – $100000$  g/mol and  $M_w/M_n = 1.7$ – $2.6$ . In vitro cytotoxicity studies showed APEG–DOX to be 10-fold less toxic toward B16F10 cells than free DOX ( $IC_{50} = 6$   $\mu$ g/mL and 0.6  $\mu$ g/mL respectively), but confirmed the serinol-succinoyl-DOX liberated during main-chain degradation to be biologically active. When administered iv to C57 black mice bearing subcutaneous (sc) B16F10 melanoma, APEG–DOX of  $M_w = 86000$  g/mol, and 5.0 wt % DOX content exhibited significantly ( $p < 0.05$ ) prolonged blood half-life and enhanced tumor accumulation compared to an HPMA copolymer–GFLG–DOX conjugate of  $M_w = 30000$  g/mol and 6.2 wt % DOX content. Moreover, APEG–DOX exhibited lower uptake by liver and spleen. These observations suggest that APEG anticancer conjugates warrant further development as novel polymer therapeutics for improved tumor targeting.

## INTRODUCTION

Of the many polymer–anticancer drug conjugates that have been proposed (1), 11 have now entered Phase I/II clinical trials (2). These first polymer therapeutics have predominantly used *N*-(2-hydroxypropyl)methacrylamide (HPMA) copolymers (3–8), poly(ethylene glycol) (PEG) (9, 10), or polyglutamate (PGA) (11, 12) as the carrier combined with established drugs such as doxorubicin, paclitaxel, camptothecin, and platinates (2). Clinical studies confirmed the safety of HPMA copolymers, PEG and PGA, and they are now being used as a platform to generate second generation polymer therapeutics containing experimental drugs, that have new therapeutic targets or that are delivered as drug combinations. For example, the antiangiogenic conjugate HPMA copolymer–TNP470 (13), HPMA copolymer conjugates containing natural products (14–17), and the HPMA copolymer-based drug combinations PDEPT (18), PELT (19), and those using catalytic antibodies (20).

Tumor targeting of long circulating polymer conjugates occurs as a result of the enhanced permeability and retention (EPR) effect (21, 22). This passive phenomenon arises because of tumor vasculature hyperpermeability (allowing polymer extravasation) and the lack of tumor tissue lymphatic drainage which subsequently promotes polymer retention. The magnitude of EPR-mediated targeting is directly proportional to the plasma concentration of circulating conjugate (23, 24). So far those conjugates tested clinically all have a  $M_w$  of  $\leq 40000$  g/mol. In the case of HPMA copolymer and PEG conjugates, which are non-biodegradable in the polymer main chain, this ensures polymer is not retained in the body therefore minimizing the danger of cumulative storage. However, this relatively low molecular weight brings the disadvantage of less than optimal EPR-mediated tumor targeting.

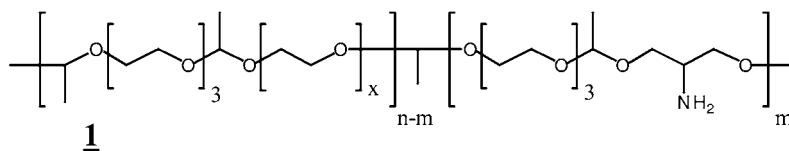
To improve further tumor targeting, we have been searching for novel water-soluble biodegradable polymeric carriers that are 'biocompatible', contain a pendent functionality for drug attachment, and have plasma pharmacokinetics that will maximize tumor targeting while minimizing normal tissue exposure. Several degradable polymer families have been investigated including PEG–polyester carbonates (25), dextrans (26), *cis*-aconityl polymers (27), and amino-PEG (APEG) polyacetals

\* Corresponding authors. duncanr@cf.ac.uk. Tel: +44 (0) 292 087 4180; Fax: +44 (0) 292 087 4536 or steve.brocchini@ulsop.ac.uk. Tel +44 (0) 207 753 5802; Fax +44 (0) 207 753 5942.

<sup>†</sup> University of London.

<sup>‡</sup> Cardiff University.

<sup>§</sup> A. P. Pharma.



**1** (28). The amino-pendent polyacetals **1** are particularly attractive as novel water-soluble carriers as they are designed to display pH-dependent hydrolytic degradation to liberate monomeric components once internalized into endosomal and lysosomal compartments of the cell. At pH 7.4 they lose 10% of their molecular weight over 72 h, whereas 40% of the molecular weight is lost over 24 h at pH 5.5 (28). Additionally these polyacetals are not inherently hepatotropic following intravenous (iv) injection, and no toxicity in vitro has yet been observed for either the intact polymer or its degradation products (28).

The aims of this study were to further optimize the synthesis of polyacetals **1** (structure **1**) to produce a weight average molecular weight ( $M_w$ ) greater than the renal threshold and to prepare the first APEG antitumor conjugates **2** using doxorubicin (DOX) as a model. The in vitro cytotoxicity of the conjugate **2** and its degradation products were studied. Finally, the pharmacokinetics of APEG–DOX **2** were determined after iv injection and compared with HPMa copolymer–GFLG–DOX to assess whether the polyacetal conjugate **2** has potential for improved tumor targeting.

## MATERIALS AND METHODS

**Materials.** Tri(ethylene glycol) divinyl ether, PEG and *p*-toluenesulfonic acid monohydrate (*p*-TSA) were from Aldrich (Dorset, UK). Fisher supplied the succinic anhydride, 1-ethyl-3-(3-dimethylaminopropyl)carbodiimide (EDC) *N*-hydroxysuccinimide (NHS), and *N,N*-dicyclohexylcarbodiimide (DCC). Dichloromethane (DCM), tetrahydrofuran (THF), and toluene were from BDH (Dorset, UK). Before use, THF was distilled from sodium–benzophenone, and DCM was distilled from CaH. Medical grade O<sub>2</sub>, N<sub>2</sub> and CO<sub>2</sub> (all 95% v/v) and liquid nitrogen were supplied by BOC (Surrey, UK). All other reagents were of general laboratory grade and were from Aldrich. Sephadex LH20 was from Pharmacia LKB Biotechnology.

Murine melanoma cells (B16F10) were kindly donated by Prof. I. Hart (St. Thomas's Hospital, London, UK). Tissue culture grade dimethyl sulfoxide (DMSO), 3-(4,5-dimethylthiazol-2-yl)-2,5-diphenyltetrazolium bromide (MTT), trypan blue, and optical grade DMSO were from Sigma (Dorset, UK). Trypsin, foetal calf serum (FCS), and RPMI 1640 were from Gibco BRL Life Technologies (Paisley, UK).

**Synthesis of Amino-Pendent Polyacetals 1.** Amino-pendent polyacetals **1** were prepared essentially as previously described (28) but with an additional drying step involving Fmoc-serinol. Two molecular weights of PEG were used in this study, 3400 and 2900 g/mol. Briefly, PEG<sub>3400</sub> (5.0052 g, 1.5 mmol) and *p*-TSA (12 mg, 0.05 mmol) were weighed into a 100 mL double-necked round-bottomed flask equipped with a magnetic stirrer bar. The compounds were dried in this flask at 80 °C in a vacuum (0.1 mmHg) for 3 h to remove water. After cooling, the vacuum pump was turned off as the reaction vessel was purged with nitrogen. A solution of the Fmoc serinol diol **4** (0.4616 g, 1.5 mmol) in freshly distilled THF (10 mL) was added by syringe. The THF was evaporated in a vacuum at 80 °C, for 30 min with continuous stirring. After cooling, the reaction vessel was purged with

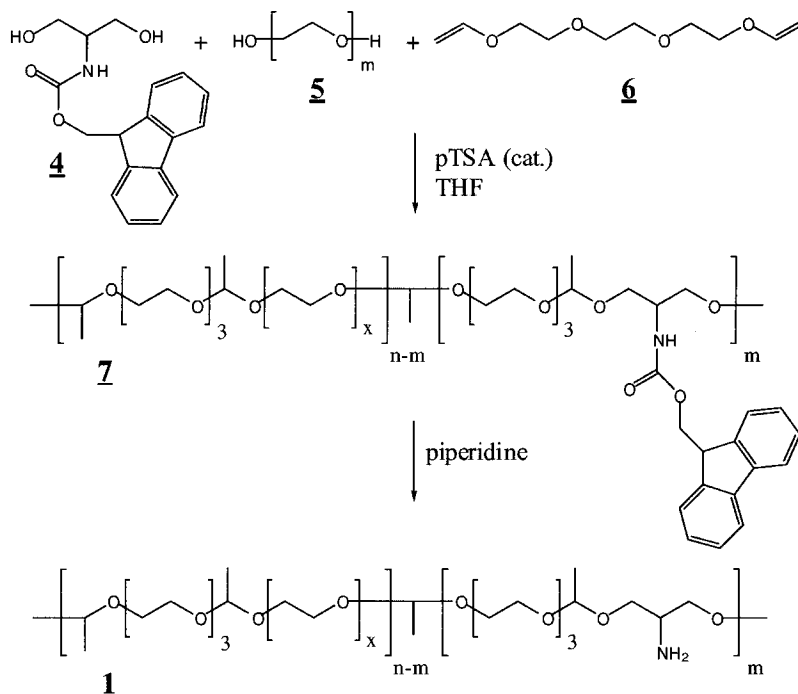
nitrogen, and freshly distilled THF (20 mL) was added by syringe. A solution of tri(ethylene glycol) divinyl ether **6** (0.601 mL, 3 mmol) in freshly distilled THF (10 mL) was then added by syringe, and the reaction mixture was stirred for 3 h at ambient temperature (Scheme 1). Additional THF was added if the reaction mixture became too viscous to stir. Triethylamine (0.3 mL) was added to complex *p*-TSA and the mixture poured into a stirred solution of hexane (100 mL) to precipitate a white solid. After 10 min, the precipitate was filtered, stirred again in hexane, and isolated. Residual solvent was removed in a vacuum to give the polymer as a white solid. A typical Fmoc-protected amino-polyacetal **7** had a  $M_w$  of 65000 g/mol ( $M_w/M_n = 2.0$ ) as determined by aqueous GPC calibrated with PEG standards. NMR (<sup>1</sup>H, 500 MHz, CDCl<sub>3</sub>):  $\delta = 1.23$ – $1.30$  (3H, m, acetal CH<sub>3</sub>),  $4.75$ – $4.78$  (1H, m, acetal CH),  $7.27$ – $7.73$  (8H, m, Ar).

The Fmoc group was removed by adding (2.0509 g) of the protected polymer **7** to a stirred solution of 20% piperidine in acetonitrile (10 mL) at ambient temperature. TLC (ethyl acetate, UV detection) was used to monitor the reaction which was complete after 0.5 h. The mixture was washed with hexane (30 mL) and the CH<sub>3</sub>CN evaporated in vacuo. The resulting oil was poured into stirred hexane (30 mL) to yield the desired amino-pendent polyacetal **1** as a white solid in quantitative yield. NMR (1H, 500 MHz, CDCl<sub>3</sub>) indicated complete removal of the Fmoc-protection by the absence of characteristic peaks at 7.3–7.8, 4.6, and 4.3. The molecular weight characteristics of the final amino-pendent polyacetal **1** was  $M_w$  65100 g/mol ( $M_w/M_n$  1.89) as determined by aqueous GPC (PEG calibrants) was the same as seen for the Fmoc-protected polyacetal **7**.

**Polyacetal Succinylation. Preparation of Succinoylated APEG 9.** Succinic anhydride (0.0853 g,  $8.5 \times 10^{-4}$  mol) and (dimethylamino)pyridine (DMAP) (0.1014 g,  $8.3 \times 10^{-4}$  mol) were added to a solution of APEG **1** (0.716 g,  $2.1 \times 10^{-4}$  mol NH<sub>2</sub> equiv) and triethylamine (100  $\mu$ L) in anhydrous THF (13 mL) with stirring at ambient temperature under a nitrogen atmosphere. The reaction mixture was stirred for 24 h, and the solution was poured into a solution of diethyl ether (50 mL) to precipitate the succinoylated APEG **9** as a white solid. After filtration, the polymer was dissolved in distilled H<sub>2</sub>O (~15 mL), dialyzed (Spectra Por membrane,  $M_w$  cutoff 2000 g/mol) at 4 °C against distilled H<sub>2</sub>O (2  $\times$  5 l) for 24 h, and lyophilized to yield succinoylated APEG **9** (0.693 g, yield > 95%). GPC (PBS, 1.0 mL/min, PEG calibrants) indicated no change in molecular weight characteristics (64800 g/mol,  $M_w/M_n = 2.0$ ). NMR (<sup>1</sup>H, 500 MHz, CD<sub>3</sub>OD):  $\delta = 2.4$ – $2.5$  (4H, s, NHCOCH<sub>2</sub>CH<sub>2</sub>COOH).

**Conjugation of Doxorubicin To Give APEG–DOX 2.** Three methods were examined for the conjugation of DOX to APEG **1** (Scheme 2).

(A) *Conjugation Mediated by N,N*-Dicyclohexylcarbodiimide (DCC). To a 25 mL flask equipped with a magnetic stirrer bar were added the HCl salt of DOX (9.8 mg,  $1.7 \times 10^{-5}$  mol) and triethylamine (7.1  $\mu$ L,  $5.1 \times 10^{-5}$  mol) in anhydrous methanol (3 mL) to a solution of succinoylated APEG **9** (57.7 mg,  $1.7 \times 10^{-5}$  mol COOH equiv) and DCC (7.0 mg,  $3.4 \times 10^{-5}$  mol) in anhydrous

**Scheme 1. Terpolymerization Gave the Fmoc-Protected Amino-Pendent Polyacetal 7 That Was Deprotected To Give APEG 1**

THF (10 mL). The reaction was stirred under  $N_2$  at ambient temperature for 72 h. Monitoring the disappearance of the free DOX ( $R_f = 0.33$ ) by TLC (butan-1-ol:acetic acid:water, 4:1:5 (29)) indicated that the reaction proceeded slowly and not to completion. Evaporation of the reaction mixture gave a residue that was dissolved in methanol (2–3 mL), and the APEG–DOX **2** was purified twice by LH20 Sephadex column separation ( $2.5 \times 40$  cm). The conjugate fractions were pooled, methanol was evaporated, and the residue was dissolved in water and lyophilized to yield the red conjugate **2** (54.0 mg, yield > 85%).

(B) *Conjugation Mediated by N-Hydroxysuccinimide (NHS) and DCC.* To a stirred solution of succinylated APEG **9** (47.0 mg,  $1.4 \times 10^{-5}$  mol) in anhydrous THF (10 mL) under  $N_2$  were added NHS (5.0 mg,  $4.2 \times 10^{-5}$  mol) and DCC (5.8 mg,  $2.8 \times 10^{-5}$  mol). The reaction mixture was stirred for 2 h at ambient temperature. A solution of DOX·HCl (8.0 mg,  $1.4 \times 10^{-5}$  mol) and triethylamine (5.8  $\mu$ L,  $4.2 \times 10^{-5}$  mol) in anhydrous methanol (3 mL) was then added and the reaction continued for a further 48 h. TLC (butan-1-ol:acetic acid:water, 4:1:5) was used to monitor the reaction. The conjugate was isolated and purified as described in (A) above to yield APEG–DOX **2** (42.3 mg; yield 85%).

(C) *Conjugation Mediated by NHS and 1-Ethyl-3-(3-dimethylaminopropyl)carbodiimide (EDC).* To an aqueous solution (distilled  $H_2O$ , 5 mL) of succinylated APEG **9** (52.2 mg,  $1.5 \times 10^{-5}$  mol COOH equiv) was added EDC (12.2 mg,  $6 \times 10^{-5}$  mol) followed by NHS (4.2 mg,  $3 \times 10^{-5}$  mol). The reaction mixture was stirred for 30 min and then DOX·HCl (8.8 mg,  $1.5 \times 10^{-5}$  mol) in distilled  $H_2O$  (4 mL) was added followed by the dropwise addition of triethylamine (4.3  $\mu$ L,  $3 \times 10^{-5}$  mol) over 2 min with rapid stirring. The reaction was stirred a further 24 h. Progress was monitored by TLC (butan-1-ol:acetic acid:water, 4:1:5) for the disappearance of free DOX. The crude reaction mixture was lyophilized and redissolved in methanol and purified using LH20 Sephadex column chromatography ( $2.5 \times 40$  cm) as described in method A above. APEG–DOX **2** was isolated as a red solid following

evaporation of methanol, dissolution in distilled  $H_2O$  and subsequent lyophilization (52.2 mg; yield 90.5%).

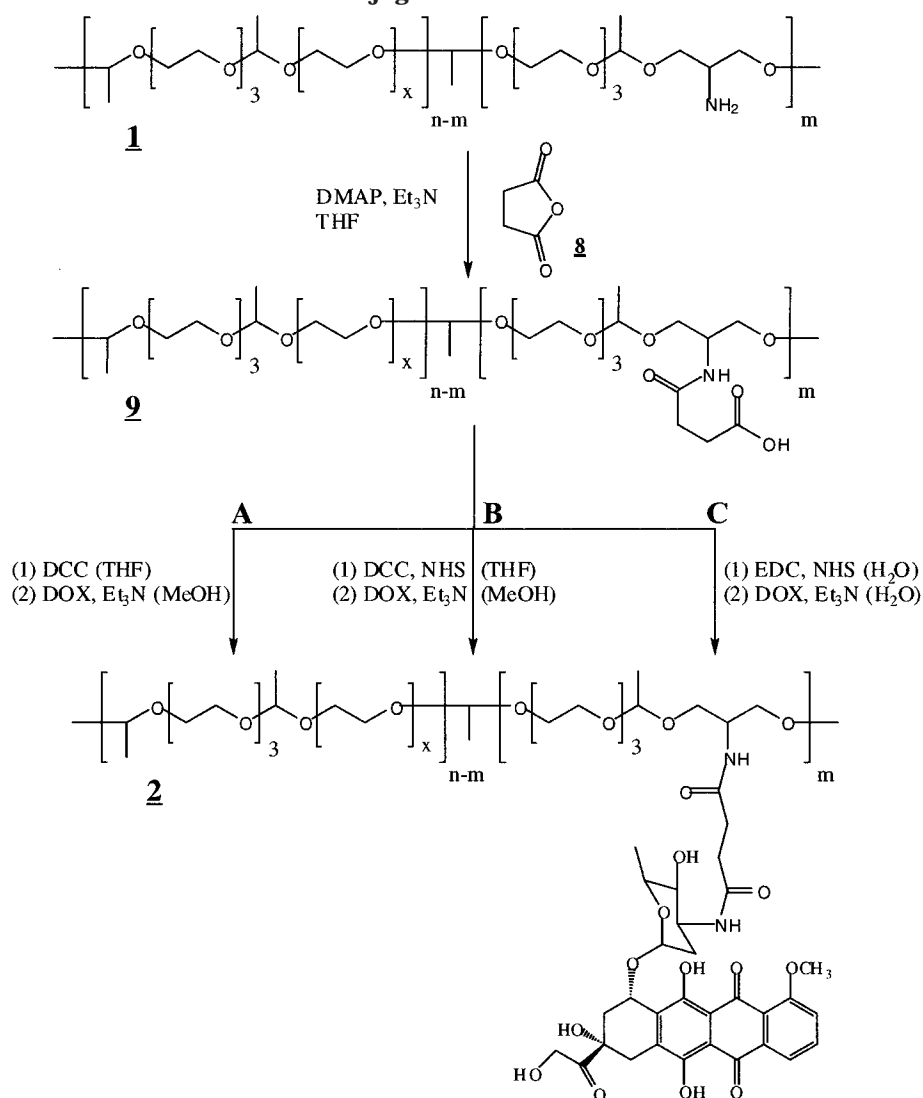
**Characterization of Polyacetals and Polyacetal–DOX Conjugates.** *Molecular Weight Determination.* Aqueous gel permeation chromatography (GPC). Method 1: Waters Ultrahydrogel 1000 and 250 columns (7.8 mm ID  $\times$  30 cm) eluted using phosphate-buffered saline (0.7–1.0 mL/min) and UV and RI detectors in series were used with PEG calibrants. Method 2: Triple detection GPC (triSEC–Viscotek) using RI, viscosimetry, and light scattering (90°) detectors. Waters Ultrahydrogel 1000 and 250 columns (7.8 mm ID  $\times$  30 cm) and eluted using 0.2 M  $NaNO_3$  diluted with  $CH_3CN$  (10 v/v%) (0.7 mL/min); the narrow calibrant was PEG and broad calibrant was dextran.

*Determination of Free Doxorubicin in the APEG–DOX Conjugate.* APEG–DOX (1 mg) was dissolved in methanol (900  $\mu$ L). HCl (0.1 M; 100  $\mu$ L) was added and the solution left for 30 min. Aliquots (100  $\mu$ L) were then subjected to HPLC (C-18 reverse phase  $\mu$ Bondapak column eluted at 0.4 mL/min with 29% propan-2-ol in distilled water adjusted to pH 3.2 using *o*-phosphoric acid as mobile phase; detection by UV at 485 nm; data analysis using a PowerChrom system). Free DOX (500 ng/100  $\mu$ L) was used as standard, both with and without the addition of HCl, to confirm that under these conditions that no degradation of DOX or formation of the aglycone had taken place.

*Determination of Total Doxorubicin Content.* APEG–DOX (1 mg) was dissolved in methanol (1 mL), HCl (2 M; 1 mL) was added, and the solution was heated at 50  $^{\circ}C$  for 1.5 h to generate the aglycone (30). A standard curve was generated using free DOX aglycone (1 mg/mL methanol) exposed to the same conditions followed by serial dilutions to the range of 20–400 ng/100  $\mu$ L. Aliquots (100  $\mu$ L) of the degraded samples were then subjected to HPLC analysis as described above. All samples were kept in the dark and stored in polypropylene tubes at 4  $^{\circ}C$ .

*Determination of APEG–DOX and HPMA Copolymer DOX in Tissue Samples.* This method was adopted from



**Scheme 2. Reaction Routes Utilized for the Conjugation of Doxorubicin to APEG 1**

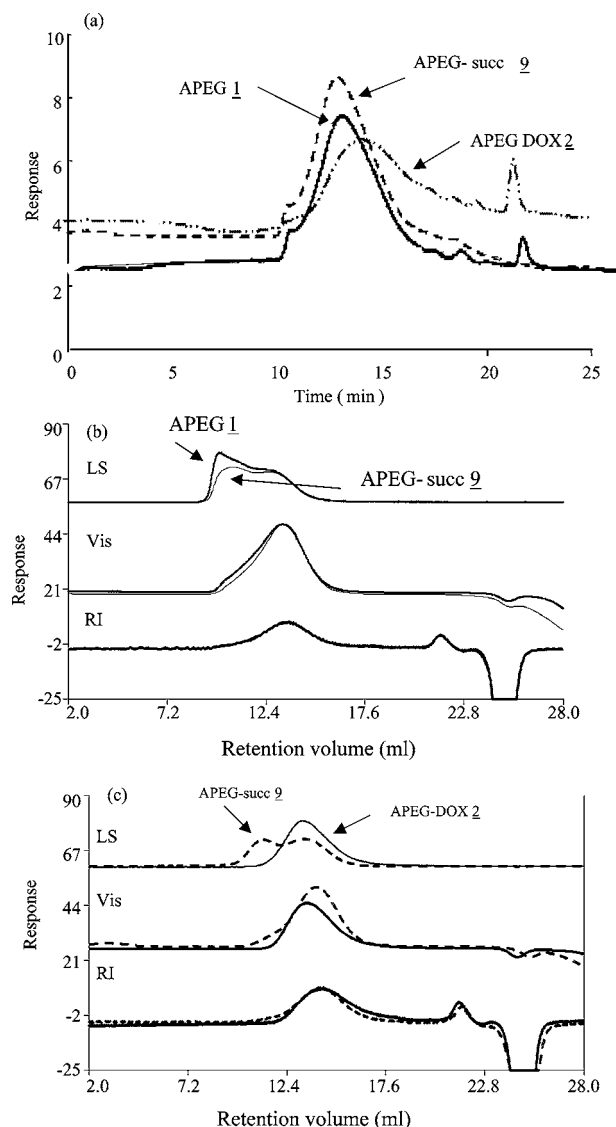
Wedge (*31*) and used to examine the total DOX content of tumor, plasma, and major organs in the body distribution studies. Organs were homogenized in water to a known volume (2–4 mL). Homogenate (975  $\mu$ L;  $n = 2$ ) was pipetted into a 15 mL polypropylene tube, and for plasma, 50  $\mu$ L was diluted with 925  $\mu$ L of distilled water. To each tube was added 25  $\mu$ L of a daunomycin solution (10  $\mu$ g/mL dissolved in distilled water). The tubes were vortexed, and HCl (2 M; 1 mL) was added. Samples were then heated to 50  $^{\circ}$ C for 25 min. Ammonium formate (1 M; approximately 1.5 mL) was added to adjust the pH to 8.5. The samples were revortexed, and NaOH (2 M; 1.0 mL) was added to neutralize the acid. Next chloroform:propan-2-ol (4:1; 5.0 mL) was added and the thoroughly mixed before centrifugation at 1000*g* for 30 min at 4  $^{\circ}$ C. The organic layer was carefully removed and evaporated under flowing N<sub>2</sub> to leave a residue that was redissolved in methanol (100  $\mu$ L) that was then analyzed by HPLC (as described but using fluorescence for detection; excitation at 480 nm and emission at 560 nm). Calibration curves were generated by extraction of DOX, APEG–DOX, or HPMA copolymer DOX from rat liver homogenate or distilled water for plasma samples.

#### Cytotoxicity of APEG–DOX Conjugates in Vitro.

In vitro cytotoxicity was determined using the MTT assay (*32*). B16F10 cells were seeded into 96-well microtiter plates at a density of  $1 \times 10^4$  cells/well. After 24 h, when

the cells had adhered, media was removed, the sample polymers (0.0–1.0 mg/mL media) were added, and free DOX was used as a reference standard. The cells were returned to the incubator for a further 67 h. After this time, MTT solution (20  $\mu$ L; 5 mg/mL in sterile-filtered PBS) was added to each well, and the plates were reincubated for a further 5 h. The formazan crystals were dissolved in DMSO, and the concentration was read at 550 nm using a microtiter plate reader. Cells grown in media alone were used as a reference for 100% viability. The results were expressed as viability (%) relative to a control containing no polymer.

**Body Distribution of APEG–DOX in Mice Bearing a Subcutaneous B16F10 Tumor.** All experiments were conducted according to UKCCCR Guidelines governing experiments with neoplasia (*33*). B16F10 cells ( $1 \times 10^5$ ) were injected sc into C57/B black mice and the tumor allowed to establish to a palpable size (25–50 mm<sup>2</sup>). Polymer conjugates, APEG–DOX or HPMA copolymer DOX, were then injected iv (5 mg/kg DOX-equiv) via the tail vein and the animals killed at the specified time points ( $n = 3$ ). A blood sample was taken and immediately centrifuged (1000*g* at 4  $^{\circ}$ C) to isolate the plasma. The tumor, liver, heart, spleen, kidneys, and lungs were removed, washed in PBS, and stored at –20  $^{\circ}$ C. Total blood volume of the mouse was calculated assuming 5.77 mL per 100 g body weight (*34*). The



**Figure 1.** Comparison of the GPC profiles of APEG, APEG-succ, and APEG-DOX. (a) Traces for APEG 1, APEG-succ 9, and APEG-DOX 2 obtained using aqueous GPC with RI detection only (method 1). (b) Traces obtained using a triple detection aqueous GPC (method 2) of APEG 1 and APEG-Succ 9. (c) Traces obtained using the triple detection system for APEG-DOX 2 (5 wt % loading) and APEG-Succ 9 from which the DOX conjugate was derived.

concentration of DOX in each organ was determined by HPLC as described above and was expressed as a percentage of the injected dose per gram of organ.

**Statistics.** Statistical significance was calculated using the students' *t*-test (two tailed). Statistical significance was defined as  $p < 0.05$ .

## RESULTS AND DISCUSSION

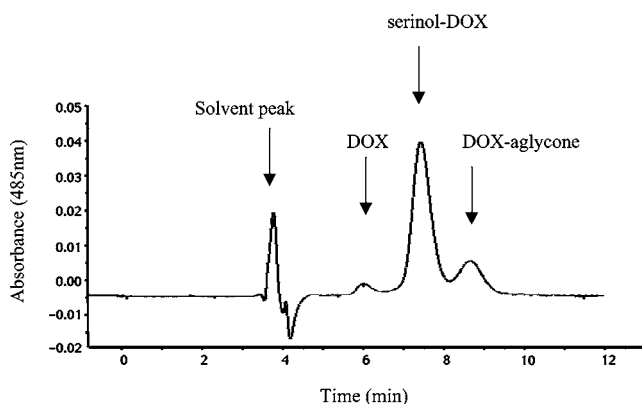
Polymer therapeutics have already demonstrated their ability to provide new, improved medicines, particularly in the treatment of cancer and infectious diseases (35). Design of biocompatible, biodegradable polymers does, however, remain a significant challenge if this concept is to be more widely applied. This was our motivation for preparation of amine-pendent polyacetals **1** (28). It was considered particularly important to design a polymeric carrier that would be stable in the circulation, but show triggered pH-dependent degradation after cellular internalization into the acidic vesicles (endosomes and lysosomes) of the endocytic pathway.

**Table 1.** Characteristics of Different Batches of APEG-DOX 2

polymer conjugate	total DOX (wt %) UV <sup>a</sup>	total DOX (wt %) HPLC <sup>b</sup>	free DOX (% total DOX) <sup>c</sup>	$M_w$ (g/mol) <sup>d</sup>	$M_w/M_n$ <sup>d</sup>
APEG <sub>3400</sub> DOX	3.8	5.0	0.9	99500	1.7
APEG <sub>3400</sub> DOX <sup>e</sup>	NA	5.0	0.85	86000	2.6
APEG <sub>2900</sub> DOX	4.2	5.3	1.2	77600	1.9
APEG <sub>2900</sub> DOX	3.9	5.4	0.77	57000	2.6
APEG <sub>2900</sub> DOX	6.3	8.5	0.79	92000	2.5

<sup>a</sup> The total DOX loading was determined by UV spectroscopy.

<sup>b</sup> The total DOX loading determined HPLC analysis. <sup>c</sup> Free DOX determined by HPLC. <sup>d</sup> Molecular weight determined by triple detection GPC, Method 2. <sup>e</sup> The batch used for in vivo studies.

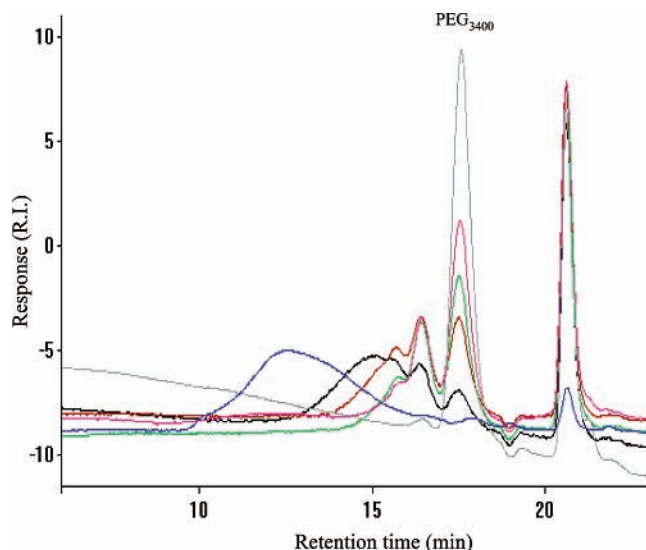


**Figure 2.** A typical HPLC chromatogram APEG-DOX 2 after acid hydrolysis (0.1 N HCl, 30 min at room temperature). The elution of free DOX, serinol-succ-DOX, and DOX aglycone is shown.

The terpolymerization process utilized to make the first amine-pendent polyacetals **1** (APEG) (Scheme 1) (28) has been improved here to ensure that polymers of molecular weight greater than the renal threshold ( $M_w > 40000$  g/mol) could be reproducibly prepared. Adventitious water in the starting reagents, especially PEG, gives polyacetals of variable and sometimes moderate molecular weight ( $M_w$  25000–78000 g/mol;  $M_w/M_n = 1.8$ –2.0). Here considerable care was taken to ensure that glassware, reagents and solvents were dry. The resultant Fmoc-polyacetals **7** were readily deprotected to give the desired APEG **1** that later gave APEG-DOX conjugates of  $M_w$  60000–100000 g/mol and  $M_w/M_n = 1.7$ –2.6. No evidence of degradation in the polymer main-chain was observed during the deprotection step. For the polymerization two molecular weights of PEG were used (2900 and 3400 g/mol). The proportion of Fmoc-serinol **4** to PEG **5** dictated the relative amount of amino pendent functionality in APEG **1**. A 1:1 ratio of these diol monomers was used throughout this study, and incorporation of this ratio of monomers in the polymer main-chain was confirmed by <sup>1</sup>H NMR. There was little difference in the characteristics of polymers (and their conjugates) synthesized using different molecular weight PEGs so PEG<sub>3400</sub> was used to prepare all APEG-DOX batches used for biological evaluation.

### Synthesis and Characterization of APEG-Succ 9.

To synthesize APEG-succ **9** as a precursor polymer for DOX conjugation, APEG **1** was succinoylated with an excess of succinic anhydride (Scheme 2). Complete succinoylation is essential to avoid polymer cross-linking during DOX conjugation. <sup>1</sup>H NMR analysis of APEG-Succ **9** indicated the succinoyl methylene (CH<sub>2</sub>) protons were at 2.4–2.5 ppm. The relative integrals of these protons



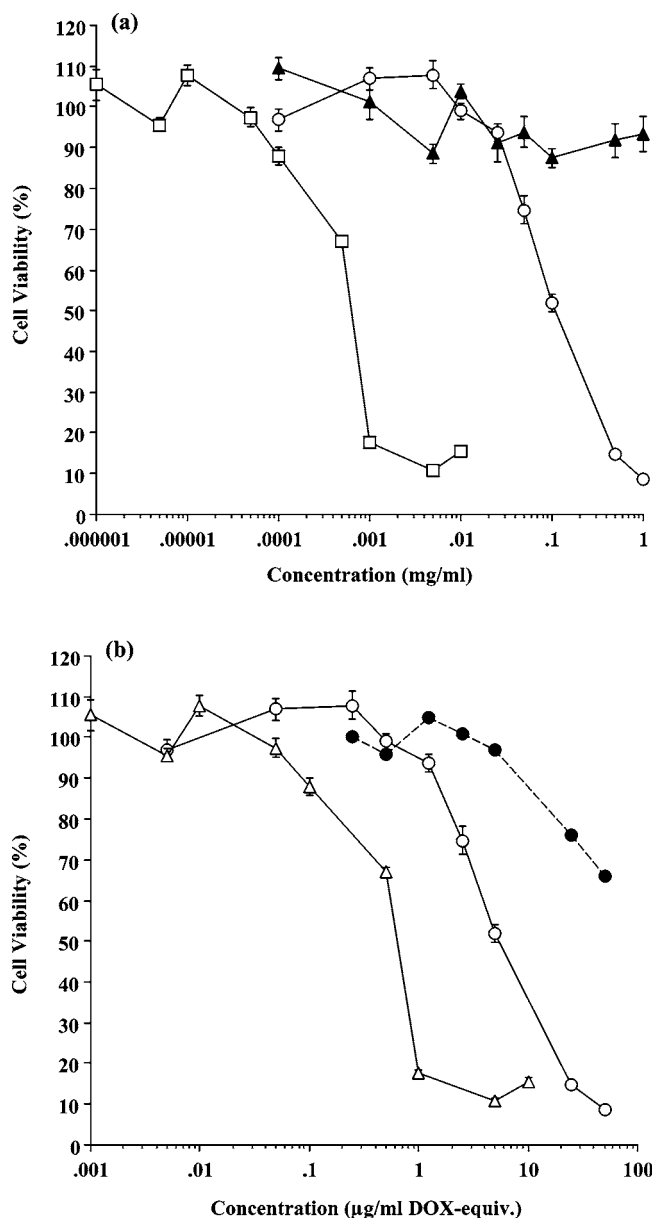
**Figure 3.** Degradation of APEG-DOX at acid pH followed by GPC. APEG-DOX was incubated at pH 3.2 for 22 h at room temperature. The data show superimposed GPC traces (obtained using method 1) indicating main-chain polyacetal hydrolysis with time leading to decreasing molecular weight of the polymer and generation of PEG<sub>3400</sub>.

and the acetal methyl proton at 1.2 ppm could be used to estimate the degree of succinylation. This was always in the range 85–100%. Since the ratio of Fmoc serinol **4** to PEG **5** was 1:1, the number of pendent chains equaled the degree of polymerization. Also, since the molecular weight of the PEG monomer was either 2900 or 3400 g/mol, the degree of polymerization was always ~14–20.

Polymers susceptible to main-chain degradation must be evaluated carefully after each reaction and purification step to determine whether there has been any inadvertent loss in molecular mass. Analysis of APEG-Succ **9** by aqueous GPC (method 1; Figure 1a) showed no significant change in molecular weight during succinylation (Scheme 2; **1**→**9**). To gain further insight into the molecular weight characteristics of these polymers in solution, APEG **1** and the succinylated APEG **9** derivative were also analyzed by triple detection aqueous GPC (RI, viscosimetry and 90° light scattering detectors) (Figure 1b). Light scattering indicated the presence of some higher molecular weight species, but their concentration was low since these species were not detectable by RI. They probably represent polymer aggregates, a phenomena that might be expected due to the high PEG content of the precursors **1** and **9**. Polymer aggregation in aqueous solution has been frequently reported and related to polymer-drug loading, polymer hydrophobicity, temperature, and/or the concentration of the polymer in the eluant (36–38).

#### Synthesis and Characterization of APEG-DOX.

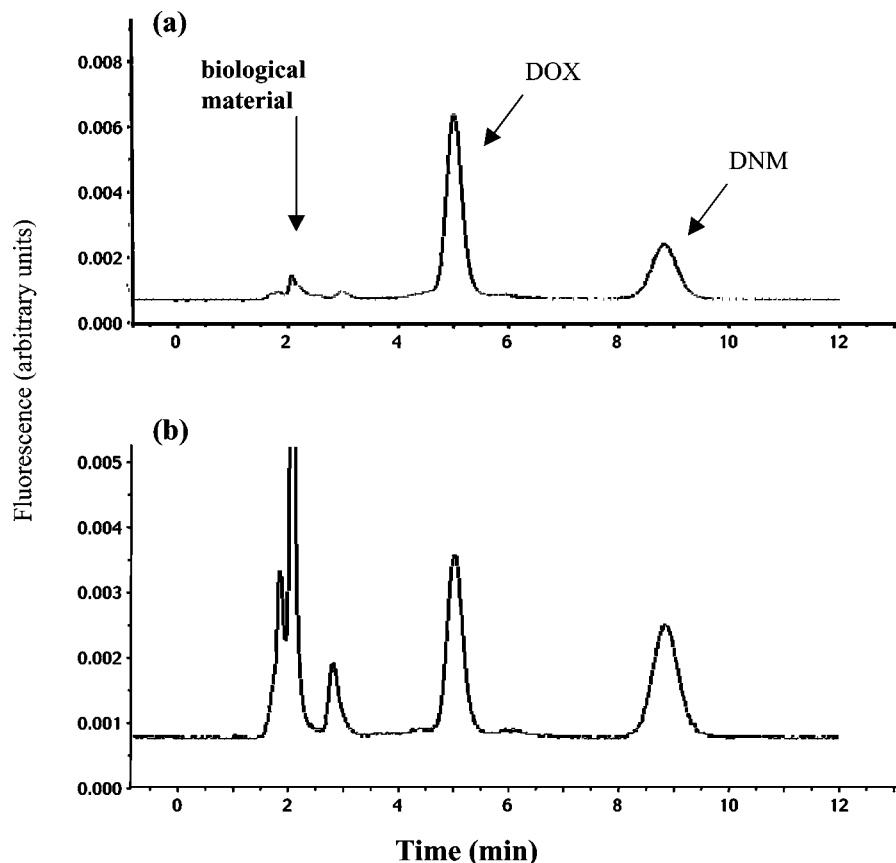
Three synthetic approaches were explored as a means of DOX conjugation to APEG-succ **9** (Scheme 2, reactions A, B, and C). DCC-mediated conjugation (reaction A) produced APEG-DOX conjugates with a DOX content of 3.0–5.0 wt %. This is a low yield since the theoretical maximum for DOX loading is 11.1 wt %, and it is probably due to competitive esterification with methanol. Formation of the NHS ester by DCC in THF prior to the addition of DOX (reaction B) gave no better yield (DOX content 5.4 wt %). These two approaches were therefore abandoned in favor of DOX conjugation using EDC in aqueous solution (reaction C), as this route gave conjugates with a much better yield (8.5 wt % DOX content).



**Figure 4.** In vitro cytotoxicity of APEG-DOX assessed using B16F10 cells. (a) Cytotoxicity of free DOX (□), APEG-DOX **2** (○) and APEG-succ **9** (▲) expressed as compound concentration. (b) Data for free DOX (△) and APEG-DOX **2** (○) in this case expressed as relative DOX concentration. Knowing that this APEG-DOX conjugate contains 1% free DOX the cytotoxicity attributable to this contamination is also shown (●). Data represent mean ± SE ( $n = 6$ ).

The DOX content of all APEG-DOX batches synthesized are given in Table 1. Total DOX content was determined either by UV spectroscopy or HPLC analysis after acidic hydrolysis of the conjugate at 50 °C to liberate DOX aglycone **10**. Use of the UV extinction coefficient to estimate total drug content is easy and routinely used by many. However, reliance on these values is not advisable, as the extinction coefficient often changes after drug conjugation, and any resultant inaccuracy would give a dangerous measure of clinical dose (2). For this reason, validated techniques had to be developed to determine the total and free DOX content of HPMA copolymer-DOX conjugates (39). In this case it is noteworthy that the DOX content of APEG-DOX measured by HPLC was consistently 20–40% higher than that measured by UV (Table 1). Also important to note is the DOX loading capacity (8.5 wt %) of APEG **1** conjugates



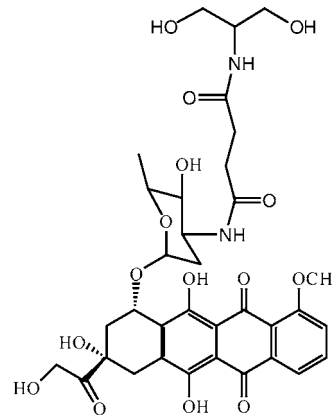


**Figure 5.** Typical HPLC traces used to determine total DOX content of biological samples in the biodistribution studies. (a) Plasma; (b) tumor. Elution of DOX-aglycone and DNM-aglycone is shown. In both cases a small amount of sample residue is present, but this elutes close to the solvent peak and is well resolved from the peaks of interest.

compares favorably with other polymer–DOX conjugates tested clinically (HPMA copolymer-gly phe-leu-gly–DOX 8.5 wt % (4), or proposed as potential clinical candidates (PEG–DOX, 2.5–5 wt % (40) and poly(glutamic acid)–DOX, 5–16 wt % (41).

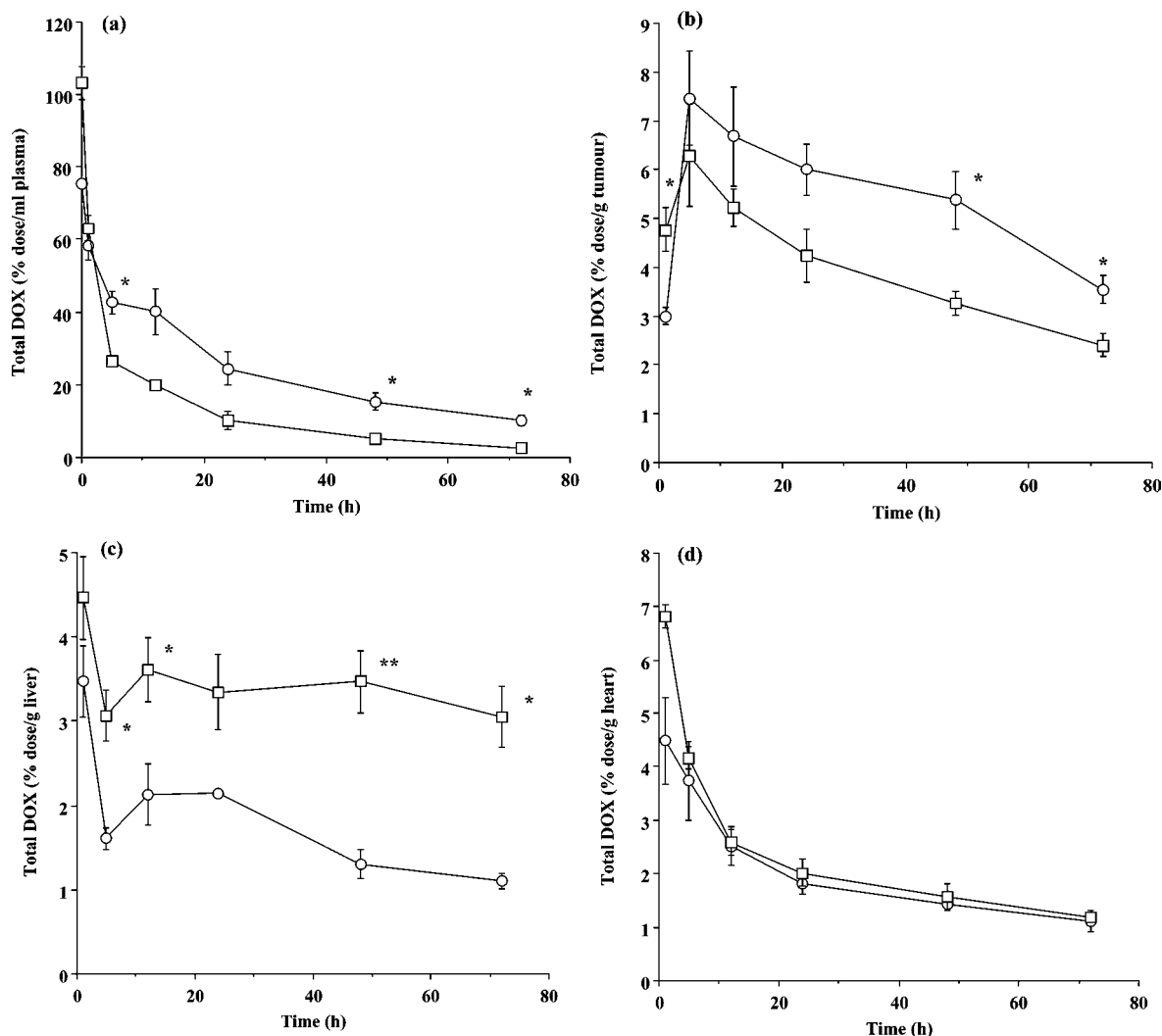
In all cases the free DOX content of APEG–DOX conjugates was  $\leq 1.2\%$  of the total DOX content (Table 1). Determination of free DOX levels required development of a new analytical method, as the extraction techniques previously employed for isolation of DOX from HPMA copolymer–DOX conjugates (30, 31, 40) led to partitioning of APEG–DOX into both organic and aqueous phases (chloroform:propan-2-ol (4:1)/water). Gradient HPLC (40) was also impossible due to retention of the APEG–DOX conjugates on the C-18  $\mu$ bondapak columns used. The method developed used mild degradation of the polyacetal polymer backbone using 0.1 M HCl at room temperature for 30 min to generate serinol-succ–DOX **11** (structure 2) without causing generation of DOX-aglycone **10** from free DOX in the sample. This allowed HPLC separation and quantitation of both serinol-succ–DOX **11** and free DOX. A typical HPLC chromatogram of the hydrolyzed APEG–DOX **2** is shown in Figure 2. DOX is known to be stable in the pH range 3.0–6.5 (29), and indeed free DOX exposed to the conditions used here for 4 h did not produce any DOX-aglycone **10**. Therefore it was concluded that the DOX aglycone present in these samples arose from subsequent degradation of the isolated serinol-succ–DOX **10**. The standard curve was generated for free DOX exposed to these analytical conditions was used to calculate the free drug content in each APEG–DOX sample (Table 1).

APEG–DOX **2** conjugates showed a decrease in the polymer aggregation behavior compared to that of the



### 10

APEG-succ **9** precursor on GPC (Figure 1c). There was no evidence of polymer cross-linking during DOX conjugation, and in fact some batches of APEG–DOX **2** had an apparently lower molecular weight than the precursor from which they were generated (Figure 1a). This was likely due to DOX conjugation causing a diminution of polymer hydrodynamic radius (14). Degradation of the polymer did not occur during DOX conjugation, as the viscosimetry and RI signals showed neither an increase in heterodispersity nor appearance of lower molecular weight degradation products (e.g. PEG). Importantly, dual channel GPC using RI and UV detectors in series also indicated that the DOX had bound homogeneously across the polymer molecular weight range (results not shown).



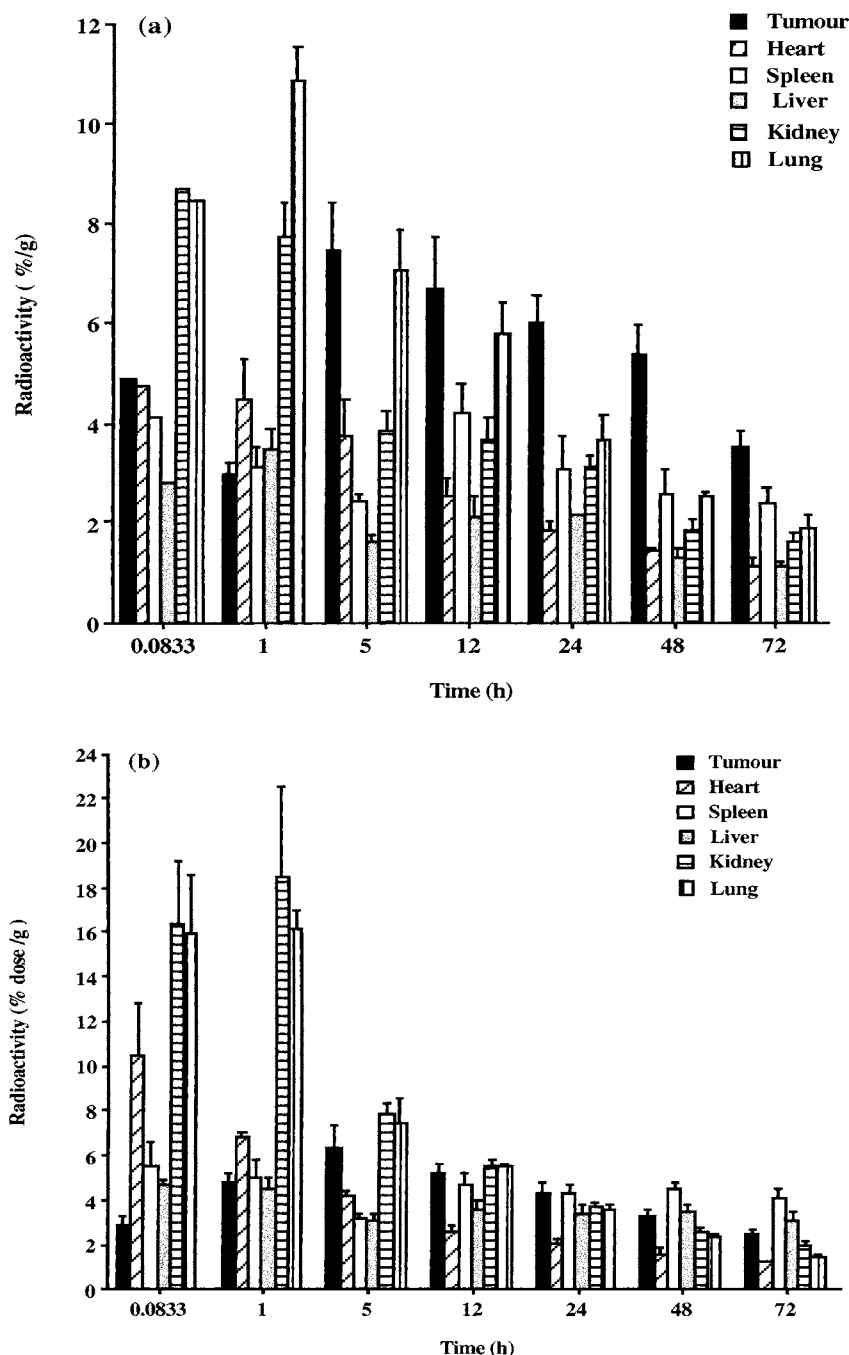
**Figure 6.** The biodistribution of APEG-DOX and for comparison HPMA copolymer-DOX administered iv (5 mg/kg DOX-equivalent) to mice bearing sc B16F10 melanoma tumors. In all cases total DOX content is shown after injection of APEG-DOX (○) or HPMA copolymer-DOX (□). (a) Plasma (expressed as percent dose per mL of plasma); (b) tumor; (c) liver; (d) heart. Organ data are expressed as % dose/g tissue. In all cases the data represent mean values  $\pm$  SEM ( $n = 3$ ) and statistical significance is indicated by \*  $p < 0.05$  and \*\*  $p \leq 0.01$ .

**pH-Dependent Degradation of APEG-DOX.** Incubation of APEG-DOX conjugates at pH 3.2 (Figure 3) led to a reduction in polymer molecular weight and appearance of degradation products with time. Complete degradation of the polymer backbone occurred over 24–48 h. This observation was consistent with the earlier studies which showed that APEG 1 and APEG-succ 9 rapidly degraded at pH 6.5 and 5.5, but not at pH 7.4 (28), and confirmed that DOX conjugation to the APEG main-chain did not impair backbone degradation. Moreover, these observations suggested that serinol-succ-DOX would be efficiently liberated intracellularly following conjugate internalization.

**In Vitro Cytotoxicity of APEG-DOX.** Before in vivo valuation, it was important to verify the potential antitumor activity of the APEG-DOX conjugate. Whereas APEG-succ was not cytotoxic against B16F10 cells up to concentrations of 1 mg/mL, the APEG-DOX 2 conjugate had an  $IC_{50}$  value of 6  $\mu$ g/mL (DOX-equivalent) (Figure 4). This was 10-fold lower than observed for free DOX ( $IC_{50} = 0.6 \mu$ g/mL). Activity of APEG-DOX is not simply attributable to the small amount of free DOX in the sample (~1% of total DOX) (Figure 4b). It is well-known that polymer conjugates display lower  $IC_{50}$  values in vitro than those for the parent compound due to their changed

cellular pharmacokinetics (slower endocytic captured compared with rapid transmembrane passage of free drug) (3). The relatively 'high'  $IC_{50}$  value observed for APEG-DOX compared with HPMA copolymer-DOX conjugates suggests that serinol-succinoyl-DOX 10 is, like other anthracycline prodrugs (42), a potent antitumor agent.

**In Vivo Pharmacokinetics of APEG-DOX.** The rationale for development of an APEG-DOX conjugate was the desire to produce improved EPR-mediated tumor targeting. Thus it was essential to establish that APEG-DOX would be long circulating (and not hepatotropic) and demonstrate improved tumor targeting compared to the HPMA copolymer-DOX, a conjugate currently undergoing clinical development (4). The biodistribution of APEG-DOX 2 ( $M_w = 86000$  g/mol,  $M_w/M_n = 2.6$ ; DOX content 5.0 wt %) and HPMA copolymer-gly phe-leu-gly-DOX ( $M_w = 30000$  g/mol,  $M_w/M_n = 1.3$ –1.5; 6.2 wt % DOX) in C57 mice bearing a sc B16F10 tumor was investigated after iv administration of both conjugates at a dose of 5 mg/kg DOX-equivalent. An HPLC assay was used to quantitate the total DOX content of plasma and tissues, and in this case daunomycin was used as an internal reference standard (Figure 5). The results obtained are summarized in Figures 6 and 7.



**Figure 7.** Comparison of the body distribution of APEG-DOX (panel a) and HPMA copolymer-gly phe-leu-gly-DOX (panel b) in all tissues after iv administration to C57 mice bearing sc B16F10 melanoma. The results are expressed as % dose/g for all tissues. (mean  $\pm$  SE and  $n = 3$ ).

Both APEG-DOX and HPMA copolymer-DOX displayed a biphasic pattern of plasma clearance with a  $t_{1/2\alpha}$  of  $\sim 1$  h (Figure 6a). The similarity in this early phase clearance can be attributed to the polydispersity of APEG-DOX which contained a significant proportion of the injected sample of  $M_w$  lower than the renal threshold ( $< 40000$  g/mol), i.e., of similar  $M_w$  to HPMA copolymer-DOX. Plasma levels of APEG-DOX were, however, significantly higher ( $p < 0.05$ ) than seen for HPMA copolymer-DOX after 5, 48, and 72 h (Figure 6a). The  $t_{1/2\beta}$  for HPMA copolymer-DOX and APEG-DOX were 3.5 and 19 h, respectively, and after 24 and 72 h, the administered dose remaining in the circulation was 20% and 8% for APEG-DOX compared with 8% and 2% for HPMA copolymer-DOX. During the second phase of elimination the higher molecular weight polyacetal-DOX

fraction circulated longer leading to a 2-fold increase in the plasma area under the curve ( $AUC_{1-72h}$ ).

Although tumor accumulation of HPMA copolymer-DOX was significantly higher at 1 h ( $p < 0.05$ ) (Figures 6b and 7b), APEG-DOX displayed elevated tumor levels at 48 and 72 h ( $p < 0.05$ ). The peak tumor levels attained by both polymers was seen after 5 h and were 7.5 and 6.3% dose/g for APEG-DOX and HPMA copolymer-DOX, respectively. The tumor  $AUC_{1-72h}$  of APEG-DOX was 1.4-fold higher than observed for the HPMA copolymer conjugate.

Prolonged plasma circulation is the driving force for increased tumor targeting (23, 24); however, this phenomenon can potentially also lead to increased normal tissue exposure to the anthracycline. This would obviously be disadvantageous as it might lead to nonspecific



toxicity. Interestingly, liver accumulation ( $AUC_{1-72h}$ ) for HPMA copolymer-DOX was 2-fold higher than APEG-DOX (Figures 6c and 7). Similarly, HPMA copolymer-DOX showed a spleen  $AUC_{1-72h}$  that was 1.5-fold higher than that of APEG-DOX (Figure 7). PEG is an extremely hydrophilic polymer, and it has been widely used to prolong the plasma circulation of proteins and liposomal drug carriers (43, 44). It is probable that the high PEG content within the APEG backbone is responsible for this lower APEG-DOX uptake by the reticuloendothelial system.

The two conjugates showed similar (no significant difference) uptake by heart and lung (Figures 6d and 7). DOX conjugation to HPMA copolymers was shown to abrogate cardiotoxicity commonly associated with DOX therapy during Phase I trials (4). Thus the low heart levels of DOX seen here after administration of APEG-DOX bodes well for reduced cardiotoxicity of this conjugate. The relatively high kidney levels seen at 1 h after administration of both polymers results from their ongoing renal elimination (Figure 7). Significantly higher kidney levels of HPMA copolymer-DOX were seen after 5 and 12 h ( $p < 0.05$ ) probably due to its continued excretion over this time. No progressive accumulation was seen for either HPMA copolymer-DOX or the longer circulating APEG-DOX in any organ (Figure 7).

## CONCLUSIONS

High molecular weight APEGs were used to synthesize APEG-DOX conjugates ( $M_w = 60000-100000$  g/mol;  $M_w/M_n = 1.7-2.6$ ) via a succinoylated intermediate. Conjugates had a DOX content of up to 8.5 wt % and a free DOX of <1.2% total DOX. APEG-DOX maintains the ability to display pH-dependent polymer main-chain degradation, and the serinol-succ-DOX liberated displays antitumor activity in vitro. In vivo biodistribution studies in animals bearing a sc B16F10 tumor confirmed that APEG-DOX had prolonged plasma circulation (2-fold) compared to HPMA copolymer-DOX. This led to a 1.4-fold increase in DOX tumor targeting, but moreover, administration of APEG-DOX led to significantly less deposition of DOX in liver and the spleen. This is the first conjugate designed for pH-triggered intracellular main-chain degradation. The data presented here suggest that further in vivo studies are warranted to define the therapeutic index of APEG-DOX, and synthesis APEG-DOX conjugates with narrower polydispersity, moreover with all polymer chains of  $M_w$  > than the renal threshold, would maximize the tumor targeting potential of this novel polymeric carrier.

## ACKNOWLEDGMENT

R.T. is grateful to A.P. Pharma for supporting his Ph.D. studentship.

**Supporting Information Available:** Tables of biodistribution data. This material is available free of charge via the Internet at <http://pubs.acs.org>.

## LITERATURE CITED

- Brocchini, S., and Duncan, R. (1999) Pendant drugs, release from polymers. In *Encyclopaedia of Controlled Drug Delivery* (Mathiowitz, E., Ed.) pp 786-816, John Wiley & Sons, New York.
- Duncan, R. (2003) Polymer-drug conjugates. In *Handbook of Anticancer Drug Development*. (Budman, H., Calvert, H., and Rowinsky, E., Eds.) pp 239-260, Lippincott Williams and Wilkins, Baltimore.
- Duncan, R. (1992) Drug-polymer conjugates: potential for improved chemotherapy. *Anti-Cancer Drugs* 3, 175-210.
- Vasey, P., Kaye, S. B., Morrison, R., Twelves, C., Wilson, P., Duncan, R., Thomson, A. H., Murray, L. S., Hilditch, T. E., Murray, T., Burtles, S., Fraier, D., Frigerio, E., and Cassidy, J. (1999) Phase I clinical and pharmacokinetic study of PK1 (*N*-(2-hydroxypropyl)methacrylamide copolymer doxorubicin): first member of a new class of chemotherapeutic agents - drug-polymer conjugates. *Clin. Cancer Res.* 5, 83-94.
- Gianasi, E., Buckley, R. G., Latigo, J., Wasil, M., and Duncan, R. (2002) HPMA copolymers platins containing dicarboxylate ligands. Preparation, characterisation and in vitro and in vivo evaluation. *J. Drug Targeting* 10, 549-556.
- Seymour, L. W., Ferry, D. R., Anderson, D., Hesslewood, S., Julyan, P. J., Poyner, R., Doran, J., Young, A. M., Burtles, S., and Kerr, D. J. (2002) Hepatic drug targeting: Phase I evaluation of polymer bound doxorubicin. *J. Clin. Oncol.* 20, 1668-1676.
- Meerum Terwogt, J. M., ten Bokkel Huinink, W. W., Schellens, J. H., Schot, M., Mandjes, I. A., Zurlo, M. G., Rocchetti, M., Rosing, H., Koopman, F. J., and Beijnen, J. H. (2001) Phase I clinical and pharmacokinetic study of PNU166945, a novel water soluble polymer-conjugated pro-drug of paclitaxel. *Anti-Cancer Drugs* 12, 315-323.
- Schoemaker, N. E., van Kesteren, C., Rosing, H., Janesen, S., Swart, M., Lieverst, J., Frasier, D., Breda, M., Pellizzoni, C., Spinelli, R., Porro, M. G., Beijnen, J. H., Schellens, J. H., and Ten Bokkel Huinink, W. W. (2002) A phase I and pharmacokinetic study of MAG-CPT, a water soluble polymer conjugate of camptothecin. *Br. J. Cancer* 87, 608-614.
- Greenwald, R. B., Choe, Y. H., McGuire, J., and Conover, C. D. (2003) Effective drug delivery by PEGylated drug conjugates. *Adv. Drug Delivery Rev.* 55, 217-250.
- Ochoa, L., Tolcher, A., Rizzo, J., Schwartz, G., Patnaik, A., Hammond, L., McCreery, H., Denis, L., Hidalgo, M., Kwiatek, J., McGuire, J., and Rowinsky, E. (2000) A Phase I study of PEG-camptothecin (PEGCPT) in patients with advanced solid tumours: A Novel formulation for an insoluble but active agent. *Proc. Am. Soc. Clin. Oncol.* 19, 19.
- Li, C., Price, J. E., Milas, L., Hunter, N. R., Ke, S., Yu, D. F., Chamsangavej, C., and Wallace, S. (1999) Antitumour activity of poly(L-glutamic acid)-paclitaxel on syngeneic and xenografted tumours. *Clin. Cancer Res.* 5, 891-897.
- Todd, R., Sludden, J., Boddy, A. V., Griffin, M. J., Robson, L., Cassidy, J., Bissett, D., Main, M., Brannan, M. D., Elliott, S., Fishwick, K., Verrill, M., and Calvert, H. (2001) Phase I and pharmacological study of CT-2103, a poly(L-glutamic acid)-paclitaxel conjugate. *Proc. Am. Assoc. Cancer Res.* 42, 2883.
- Satchi-Fainaro, R., Mamluk, R., Puder, M., Greene, A. K., Soker, S., and Folkman, J. (2002) Polymer therapeutics of angiogenesis inhibitors: HPMA copolymer-TNP-470 conjugate. *Proc. Int. Symp. Controlled Release Bioact. Mater.* 29, 209-210.
- Searle, F., Gac-Breton, S., Keane, R., Dimitrijevic, S., Brocchini, S., and Duncan, R. (2001) *N*-(2-hydroxypropyl)-methacrylamide copolymer-6-(3-aminopropyl)-ellipticine conjugates, synthesis, characterisation and preliminary in vitro and in vivo studies. *Bioconjugate Chem.* 12, 711-718.
- Kasuya, Y., Lu, Z.-R., Kopeckova, P., Tabibi, S. E., and Kopecek, J. (2002) Influence of the structure of drug moieties on the in vitro efficacy of HPMA copolymer-geldanamycin derivative conjugates. *Pharm. Res.* 19, 115-123.
- Varticovski, L., Lu, Z. R., Mitchell, K., De Aas, I., and Kopecek, J. (2001) Water-soluble HPMA copolymer-wortmannin conjugate retains phosphoinositide 3-kinase inhibitory activity in vitro and in vivo. *J. Controlled Release* 74, 275-281.
- Vicent, M. J., Manzanaro, S., De la Fuente, J. A., and Duncan, R. (2003) HPMA copolymer-1,5-diazaanthraquinone conjugates as novel anticancer agents. *Proc. Int. Symp. Controlled Release Bioact. Mater.* 30, 486.
- Satchi-Fainaro, R., Connors, T. A., and Duncan, R. (2001) PDEPT: Polymer directed enzyme prodrug therapy I. HPMA

- copolymer-cathepsin B and PK1 as a model combination. *Br. J. Cancer* 85, 1070–1076.
- (19) Duncan, R., Gac-Breton, S., Keane, R., Musila, R., Sat, Y. N., Satchi-Fainaro, R., and Searle, F. (2001) Polymer-drug conjugates, PDEPT and PELT: Basic principles for design and transfer from the laboratory to the clinic. *J. Controlled Release* 74, 135–146.
  - (20) Gopin, A., Pessah, N. M., Shanks, M., Rader, C., and Shabat, D. (2003) A chemical adapter system designed to link a tumour-targeting device with a prodrug and an enzymatic trigger. *Angew. Chem., Int. Ed.* 42, 327–332.
  - (21) Matsumura, Y., and Maeda, H. (1986) A new concept for macromolecular therapies in cancer chemotherapy: mechanism of tumouritropic accumulation of proteins and the antitumour agent SMANCS. *Cancer Res.* 6, 6387–6392.
  - (22) Seymour, L. W., Ulbrich, K., Styger, P. S., Brereton, M., Subr, V., Strohalm, J., and Duncan, R. (1994) Tumouritropism and anticancer efficacy of polymer-based doxorubicin prodrugs in the treatment of subcutaneous murine B16F10 melanoma. *Br. J. Cancer* 70, 636–641.
  - (23) Seymour, L. W., Miyamoto, Y., Maeda, H., Brereton, M., Strohalm, J., Ulbrich, K., and Duncan, R. (1995) Influence of molecular weight on passive tumour accumulation of a soluble macromolecular drug carrier. *Eur. J. Cancer* 31, 766–770.
  - (24) Noguchi, Y., Wu, J., Duncan, R., Strohalm, J., Ulbrich, K., Akaike, T., and Maeda, H. (1998) Early phase tumour accumulation of macromolecules: A great difference in clearance rate between tumour and normal tissues. *Jpn. J. Cancer Res.* 89, 307–314.
  - (25) Vincenzi, V., Ferruti, P., Ford, J., and Duncan, R. (2002) Synthesis and preliminary biological evaluation of novel functionalised poly(ethyleneglycol)-poly(ester-carbonate) block copolymers as novel biodegradable polymeric carriers. *Macromol. Biosci.* 1, 164–169.
  - (26) Hreczuk-Hirst, D., Chicco, D., German, L., and Duncan, R. (2001) Dextrins as potential carriers for drug targeting: Tailored rates of dextrin degradation by introduction of pendant groups. *Int. J. Pharm.* 230, 57–66.
  - (27) Clochard, M., Rankin, S., and Brocchini, S. (2000) Synthesis of soluble polymers for medicine that degrade by intramolecular acid catalysis. *Macromol. Rapid Commun.* 21, 853–859.
  - (28) Tomlinson, R., Klee, M., Garrett, S., Heller, J., Duncan, R., and Brocchini, S. (2002) Pendant chain functionalised polyacetals that display pH-dependent degradation: A platform for the development of novel polymer therapeutics. *Macromolecules* 35, 473–480.
  - (29) Vigevari, A., and Williamson, M. J. (1980) Doxorubicin. In *Analytical profiles of drug substances* (Florey, K., Ed.) Vol 9, pp 245–274, Academic Press, New York.
  - (30) Fraier, D., Frigerio, E., Pianezzola, E., Strolin Benedetti, M., Cassidy, J., and Vasey, P. (1995) A sensitive procedure for the quantitation of free and *N*-(2-hydroxypropyl)methacrylamide polymer-bound doxorubicin (PK1) and some of its metabolites, 13-dihydrodoxorubicin, 13-dihydrodoxorubicinone and doxorubicinone in human plasma and urine by reverse phase HPLC with fluorometric detection. *J. Pharm. Biomed. Anal.* 13, 625–631.
  - (31) Wedge, S. R. (1991) Mechanism of action of polymer anthracyclines: potential to overcome multidrug resistance. Ph.D. Thesis, Keele University, UK.
  - (32) Sgouras, D., and Duncan, R. (1990) Methods for the evaluation of biocompatibility of soluble synthetic polymers which have potential for biomedical use: 1-Use of the tetrazolium-based colorimetric assay (MTT) as a preliminary screen for evaluation of *In vitro* cytotoxicity. *J. Mater. Sci. Mater. Med.* 1, 61–68.
  - (33) United Kingdom Coordinating Committee on Cancer Research (UKCCCR) (1998) Guidelines for the welfare of animals in experimental neoplasia (2nd ed.) *Br. J. Cancer* 77, 1–10.
  - (34) Dreyer, G., and Ray, W. (1910) The blood volume of mammals as determined by experiments upon rabbits, Guinea-pigs and mice and its relationship to body weight and surface area expressed in a formula. *Philos. Trans. R. Soc. Sci. London* 201, 133–160.
  - (35) Duncan, R. (2003) The dawning era of polymer therapeutics. *Nat. Rev. Drug Discovery* 2, 347–360.
  - (36) Konak, C., Helmstedt, M., and Bansil, R. (2000) temperature-dependence of dynamics of solutions of triblock copolymer in a selective solvent. *Polymer* 41, 9311–9315.
  - (37) Konak, C., Rath, R. C., Kopeckova, P., and Kopecek, J. (1998) Photoassociation of watersoluble copolymers containing photochromic spirobenzopyran moieties. *Polym. Adv. Technol.* 9, 641–648.
  - (38) Konak, C., Oupicky, D., Chytrý, V., and Ulbrich, K. (2000) Thermally controlled association in aqueous solutions of diblock copolymers of poly[*N*-(2-hydroxypropyl)methacrylamide] and poly(*N*-isopropylacrylamide). *Macromolecules* 33, 5318–5320.
  - (39) Configliacchi, E., Razzano, G., Rizzo, V., and Vigevari, A. (1996) HPLC methods for the determination of bound and free doxorubicin and of bound and free galactosamine in methacrylamide polymer-drug conjugates. *J. Pharm. Biomed. Anal.* 15, 123–129.
  - (40) Rodrigues, P. C. A., Beyer, U., Schumacher, P., Roth, T., Fiebig, H. H., Unger, C., Messori, L., Orioli, P., Paper, D. H., Mulhaupt, R., and Kratz, F. (1999) Acid-sensitive poly(ethylene glycol) conjugates of doxorubicin: Preparation, *in vitro* efficacy and intracellular distribution. *Bioorg. Med. Chem.* 7, 2517–2524.
  - (41) Hoes, C. J. T., Grooten, J., Feijen, J., Duncan, R., Hume, I. C., Bhakoo, M., and Bouma, J. M. W. (1993) Biological properties of adriamycin bound to biodegradable polymeric carriers. *J. Controlled Release* 23, 37–54.
  - (42) Huang, P. S., and Ollif, A. (2001) Drug targeting strategies in cancer therapy. *Curr. Opin. Genetics Dev.* 11, 104–110.
  - (43) Harris, J. M., and Chess, R. B. (2003) Effect of pegylation on pharmaceuticals. *Nat. Rev. Drug Discovery* 2, 214–221.
  - (44) Allen, T. M. (2002) Ligand-targeted therapeutics in anti-cancer therapy. *Nature Rev. Drug Discovery* 2, 750–763.

BC030028A

# Diphtheria Toxin–Epidermal Growth Factor Fusion Protein and Pseudomonas Exotoxin–Interleukin 13 Fusion Protein Exert Synergistic Toxicity against Human Glioblastoma Multiforme Cells

Tie Fu Liu, Mark C. Willingham, Stephen B. Tatter, Kimberley A. Cohen, A. Corinne Lowe, Andrew Thorburn, and Arthur E. Frankel\*

Departments of Cancer Biology, Surgery, Pathology and Comparative Medicine, Wake Forest University School of Medicine, Winston-Salem, North Carolina 27157. Received July 1, 2003; Revised Manuscript Received October 7, 2003

The cytotoxicity of combinations of a diphtheria toxin–human epidermal growth factor fusion protein (DAB<sub>389</sub>EGF) and a Pseudomonas exotoxin–human interleukin 13 fusion protein (IL13PE38QQR) was tested against 14 human glioma cell lines. After cells were cultured for 48 h with various concentrations of the fusion proteins, the percentage reductions in thymidine incorporation were determined. Seven of fourteen cell lines were highly sensitive to DAB<sub>389</sub>EGF alone, and six cell lines were highly sensitive to IL13PE38QQR alone with IC<sub>90</sub>'s < 100 pM. When combined, synergistic cell killing was observed for seven of the cell lines based upon concave isobolograms and combination indices (CI's) of 0.2 to 0.7. Supraadditive cytotoxicity was confirmed by measurements of induction of apoptosis. Receptor expression was assessed by flow cytometry and confocal microscopy. Marked heterogeneity of expression of EGFR and IL13R $\alpha$ 2 was seen on all the glioma cell lines. This heterogeneity may contribute to incomplete cell killing with the individual fusion proteins and synergistic cell kill with the combination. These results suggest that both fusion proteins may yield antitumor effects in patients with recurrent gliomas and that combination fusion protein intracranial therapy of malignant gliomas may yield an improved therapeutic index.

## INTRODUCTION

There are 17 000 cases of primary brain tumors per year in the United States (1). Over 80% of these tumors are infiltrative astrocytomas/GBM<sup>1</sup> which arises from malignant transformation of astrocytes (2). In most cases, treatment is unsatisfactory with a median survival of one year for newly diagnosed patients and six months for patients with recurrent disease (3). The two-year survival rate for GBM patients is less than 20%. Both local spread of tumor cells beyond sites of surgery and radiation and chemotherapy- and radiation-resistant tumor cells contribute to the development of refractory disease (4, 5). Novel agents with different mechanisms of action are needed.

One such class of therapeutics is fusion proteins consisting of protein synthesis-inactivating peptide toxins fused to brain tumor-selective ligands. The ligand directs the molecule to the glioma cell surface; after internalization and translocation to the cytosol, the peptide toxin moiety catalytically inactivates protein synthesis leading to cell death. Fusion proteins targeting brain tumor Tf receptors, IL13 receptors, IL4 receptors, and EGFR have been prepared and administered by CED directly into the brain tumor interstitium of patients with refractory GBM (6–9). CED creates a bulk flow that supplements diffusion and leads to achievement of drug concentrations

hundreds-fold greater than by systemic infusion for large areas of the brain parenchyma (10). Fusion protein CED therapy has yielded remissions lasting years in a significant fraction of patients. However, not every patient responds and toxicities to normal brain have occurred. Thus, there is a need to improve the technology.

Since most brain tumors are heterogeneous in their expression of receptors and even glioma cell lines display cell-to-cell variations in receptor density, we reasoned that combinations of fusion proteins targeting different receptors would enhance glioma cell kill and permit lower doses of each fusion protein to be used—reducing normal brain toxicity. In this paper, we tested the cytotoxicity of combinations of DAB<sub>389</sub>EGF and IL13PE38QQR fusion proteins targeting the EGFR and IL13R. Fourteen human glioma cell lines were evaluated. Combination indices and isobolograms were used to assess the presence and degree of synergy (11). In addition, we measured the expression of each of the receptors and estimated the level of receptor heterogeneity.

## MATERIALS AND METHODS

**Fusion Proteins and Antibodies.** DAB<sub>389</sub>EGF was a gift of Ligand Pharmaceuticals (San Diego, CA). The fusion protein was synthesized and partially purified as previously described (12). Vials contained sterile filtered and lyophilized 500  $\mu$ g of DAB<sub>389</sub>EGF, phosphate-buffered saline pH 7.2, 1% mannitol, and 50  $\mu$ M EDTA. Vials were stored at –80 °C. Fusion protein was prepared for experiments by adding 2 mL of sterile water and gently agitating. Dissolved fusion protein was stored at 4 °C. Lot number was 3E13EB2.

IL13PE38QQR was a gift of NeoPharm (Lake Forest, IL). The fusion protein was synthesized and partially

\* To whom correspondence should be addressed. Phone: (336) 716–3313; fax: (336) 716–0255; e-mail: afrankel@wfubmc.edu.

<sup>1</sup> Abbreviations: GBM, glioblastoma multiforme; IL, interleukin; Tf, transferring; CED, convection-enhanced delivery; EGFR, epidermal growth factor receptor; PE, Pseudomonas exotoxin; DT, diphtheria toxin; MTD, maximum tolerated dose; DLT, dose-limiting toxicity.



purified as described (13). Vials contained sterile filtered IL13PE38QQR at 200  $\mu\text{g/mL}$  in normal saline with 0.2% human serum albumin. Material was stored in aliquots at  $-80^\circ\text{C}$  until used.

Murine monoclonal antibody anti-IL13R $\alpha$ 2 and R-phycoerythrin (PE)-conjugated murine monoclonal antibody anti-IL13R $\alpha$ 2 was purchased from Diaclone SAS (Besancon, France). Mouse anti-EGFR antibody conjugated to fluorescein isothiocyanate (FITC), mouse isotype control antibody IgG2b $\kappa$  conjugated to FITC, and PE-conjugated mouse isotype control antibody IgG1 were obtained from BD Biosciences (Mountain View, CA). Mouse IgG and rhodamine-conjugated goat anti-mouse IgG were purchased from Jackson ImmunoResearch (West Grove, PA).

**Cell Lines.** Cell lines U373MG and U138MG were obtained from the Wake Forest University Tissue Culture Core Laboratory. Cell lines A172, DBTRG05MG, T98G, U87MG, and U118MG were purchased from the American Type Culture Collection (Rockville, MD). Cell lines LN405, GAMG, DKMG, GMS10, 42MGBA, SNB19, and 8MGBA were purchased from the Deutsche Sammlung von Mikroorganismen und Zellkulturen GmbH (braunschweig, Germany). Cells were cultured at  $37^\circ\text{C}$  in a humidified atmosphere containing 5%  $\text{CO}_2$  in air and maintained as described previously (14).

**Cell Cytotoxicity Assays.** Aliquots of 5000 cells were incubated in triplicate in 100  $\mu\text{L}$  of medium (same as that used to grow the cells) in Costar 96-well flat-bottomed plates. After 24 h, DAB<sub>389</sub>EGF, IL13PEQQR, or both in medium were added to each well to yield concentrations ranging from 0 to 1000 pM, and the cells were incubated at  $37^\circ\text{C}$  in 5%  $\text{CO}_2$  for another 48 h. After the incubation, 0.5  $\mu\text{Ci}$  of [ $^3\text{H}$ ]thymidine (NEN DuPont, Boston, MA) in 50  $\mu\text{L}$  of medium was added to each well, and incubation was continued for an additional 16 h at  $37^\circ\text{C}$  in 5%  $\text{CO}_2$ . Plates were frozen at  $-80^\circ\text{C}$  and thawed; cell lysates were harvested using a Skatron Cell Harvester (Skatron Instruments, Lier, Norway) on to glass fiber mats; and the cpm of incorporated radiolabel were counted using an LKB liquid scintillation counter gated for  $^3\text{H}$ . The  $\text{IC}_{90}$  was defined as the concentration of toxin that inhibited thymidine incorporation by 90% compared to control wells. The percentage of maximum [ $^3\text{H}$ ]thymidine incorporation was plotted versus the log of the toxin concentration, and nonlinear regression with a variable-slope sigmoidal dose-response curve was generated along with  $\text{IC}_{90}$  with use of GraphPad Prism software (GraphPad Software, San Diego, CA). All assays were performed in triplicate. Multiple drug-effect analysis was done using CalcuSyn software (BioSoft, Ferguson, MO). Both the  $\text{IC}_{90}$  isobologram and the  $\text{IC}_{90}$  combination index (CI) were derived using the software and the equation of T. C. Chou (11). The  $\text{CI} = A/A_0 + B/B_0$ .  $A_0$  and  $B_0$  are individual drug concentrations producing the effect;  $A$  and  $B$  are the drug concentrations in the combination yielding the same effect. Isobolograms are graphs of  $A$  versus  $B$  with individual points ( $A$ ,  $B$ ) noted yielding the desired effect. The graphs of ( $A$ ,  $B$ ) points for a given effect yield concave, straight lines or convex curves for synergistic, additive or antagonistic interactions, respectively.

For analysis of nuclear morphology, cells were treated with the drugs for 48 h then stained with Hoescht 3258 as previously described (15). Cells were deposited onto slides using a cytospinner and scored for apoptotic nuclei by fluorescence microscopy.

**Flow Cytometry.** Aliquots of 1 000 000 cells were pelleted at 600g and resuspended in 80  $\mu\text{L}$  of phosphate

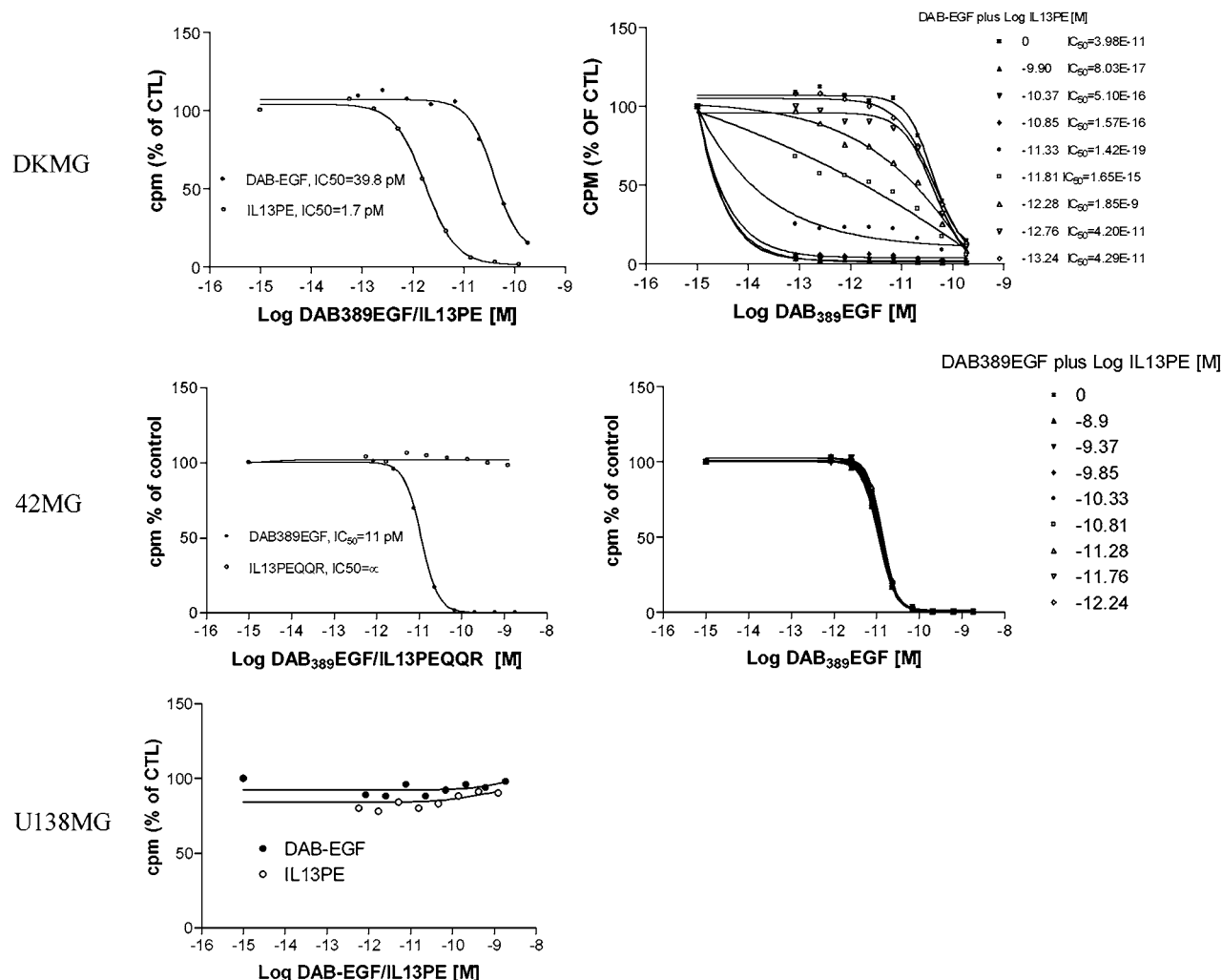
buffered saline (PBS) with 1% bovine serum albumin (BSA). Different aliquots were incubated with 10  $\mu\text{L}$  of PE-conjugated mouse IgG1 anti-IL13R $\alpha$ 2 antibody or PE-conjugated mouse IgG1 isotype control antibody. After 45 min on ice, cells were washed with PBS/BSA and incubated with 10  $\mu\text{L}$  of FITC conjugated mouse anti-EGFR antibody or FITC conjugated mouse IgG2b $\kappa$  isotype control antibody. After 30 min on ice, cells were washed with PBS/BSA and resuspended in 1 mL of PBS/BSA. A volume of 250  $\mu\text{L}$  of 3.7% formaldehyde was added to each tube, and the cells were assayed on an EPICS-XL flow cytometer (Coulter, Hialeah, FL) with filters set for simultaneous PE and FITC fluorescence detection. Gates were based on isotype control antibody staining such that there were  $<2\%$  positive cells with isotype control PE- and FITC-conjugated antibodies. Ten thousand cells were evaluated for PE and/or FITC positivity. Receptor heterogeneity was estimated by the ratio of the sum of single (PE or FITC) stained cells to doubly PE- and FITC-stained cells. Flow cytometric analysis was performed on cells on two separate occasions.

**Confocal Microscopy.** Number 1 coverslips were precoated with 0.1 mg/mL poly-L-lysine (Sigma) for 5 min at room temperature and rinsed three times with PBS. Ten thousand cells were grown on the precoated coverslips in six-well culture plates overnight at  $37^\circ\text{C}/5\% \text{CO}_2$ . The coverslips were then rinsed with cold PBS/0.1% sodium azide and blocked with 10% normal goat serum in PBS/0.1% sodium azide (blocking buffer) for 30 min. Cells were then incubated with 10  $\mu\text{g/mL}$  mouse anti-human IL13R $\alpha$ 2 monoclonal antibody or IgG1 mouse control antibody for 1 h in blocking buffer followed by incubation for another 1 h with 15  $\mu\text{g/mL}$  goat anti-mouse IgG conjugated to rhodamine at  $4^\circ\text{C}$  in blocking buffer. Cells were then incubated with 10  $\mu\text{g/mL}$  mouse IgG in PBS/0.1% sodium azide (second blocking buffer) for 30 min and 1 h with a 1:10 dilution of FITC-conjugated anti-EGFR or FITC-mouse IgG2b $\kappa$  control antibody at  $4^\circ\text{C}$  also in second blocking buffer. After all incubations with antibodies, slides were washed three times with cold PBS/0.1% sodium azide. Slides were postfixed with 3.7% formaldehyde in PBS and mounted in mounting medium (Victor Labs, Burlingame, CA). The staining was analyzed in a LSM 510 microscope (Zeiss) with the LSM 510 image browser software.

**Statistical Analysis.** Linear regression analysis was used to correlate  $\text{IC}_{90}$ 's and CI's with mean fluorescence intensity and percent single positive and doubly positive cells using GraphPad software.

## RESULTS

**Glioma Cell Lines Are Sensitive to Fusion Proteins.** Thirteen of fourteen glioma cell lines were killed by DAB<sub>389</sub>EGF alone, and seven cell lines were highly sensitive with mean  $\text{IC}_{90}$ s of 4 to 58 pM (Table 1). Similarly, seven of the glioma cell lines were killed by IL13PE38QQR and six were highly sensitive with  $\text{IC}_{90}$ 's of 6 to 85 pM (Table 1). Interestingly, the cell lines most sensitive to DAB<sub>389</sub>EGF were not the same as those most sensitive to IL13PE38QQR. Only three cell lines (U373MG, SNB19, and GMS10) were highly sensitive ( $\text{IC}_{90} < 100 \text{ pM}$ ) to both fusion proteins. When cells were exposed to a mixture of both fusion proteins, synergistic cell killing was observed for seven of the cell lines with combination indices (CI's) of 0.3 to 0.7 (Figure 1 and Table 1). Isobolographic analyses confirmed concave isoboles for these cell lines (Figure 2). For analysis of



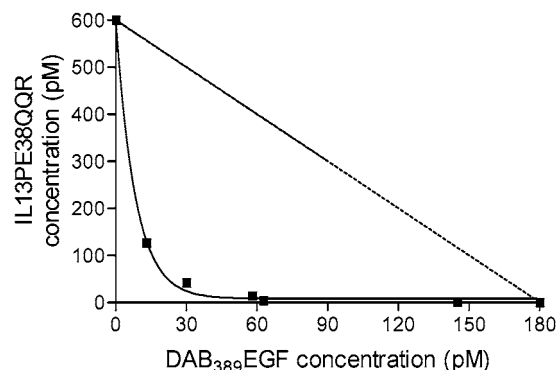
**Figure 1.** Glioma cell cytotoxicity by DAB<sub>389</sub>EGF and IL13PE38QQR. Ten thousand cells were incubated 48 h with the indicated concentrations of fusion proteins and then pulsed with 1  $\mu$ Ci of <sup>3</sup>H-thymidine and harvested onto glass fiber mats using a cell harvester and counted on a Betaplate scintillation counter. Cell lines noted in the left margin. The left panels show single agent treatments; the right panels show the effect of the combinations. Among the three displayed cell lines, only DKMG shows synergistic drug interaction. The other two cell lines lack sensitivity to IL13PE38QQR or both DAB<sub>389</sub>EGF and IL13PE38QQR.

**Table 1. Fusion Protein Cytotoxicity to Human Glioma Cell Lines<sup>a</sup>**

cell line	IC <sub>90</sub> (pM)		ratio IC <sub>90</sub> 's	CI (90% cell kill)
	DAB <sub>389</sub> EGF	IL13PE38QQR		
U87MG	10	>6000	<0.01	—
GAMA	15	>6000	<0.02	—
8MGBA	18	>6000	<0.02	—
U373MG	33	13	2.5	0.18
SNB19	34	8	4.3	0.66
GMS10	48	56	0.9	0.99
42MGBA	67	>6000	<0.07	—
LN405	103	85	1.2	0.29
DKMG	142	15	9.3	0.57
T98G	178	>6000	<0.14	—
DBTRG05MG	198	1899	0.10	0.46
A172	270	6.2	44	0.36
U118MG	402	6824	0.06	0.47
U138MG	>6000	>6000	—	—

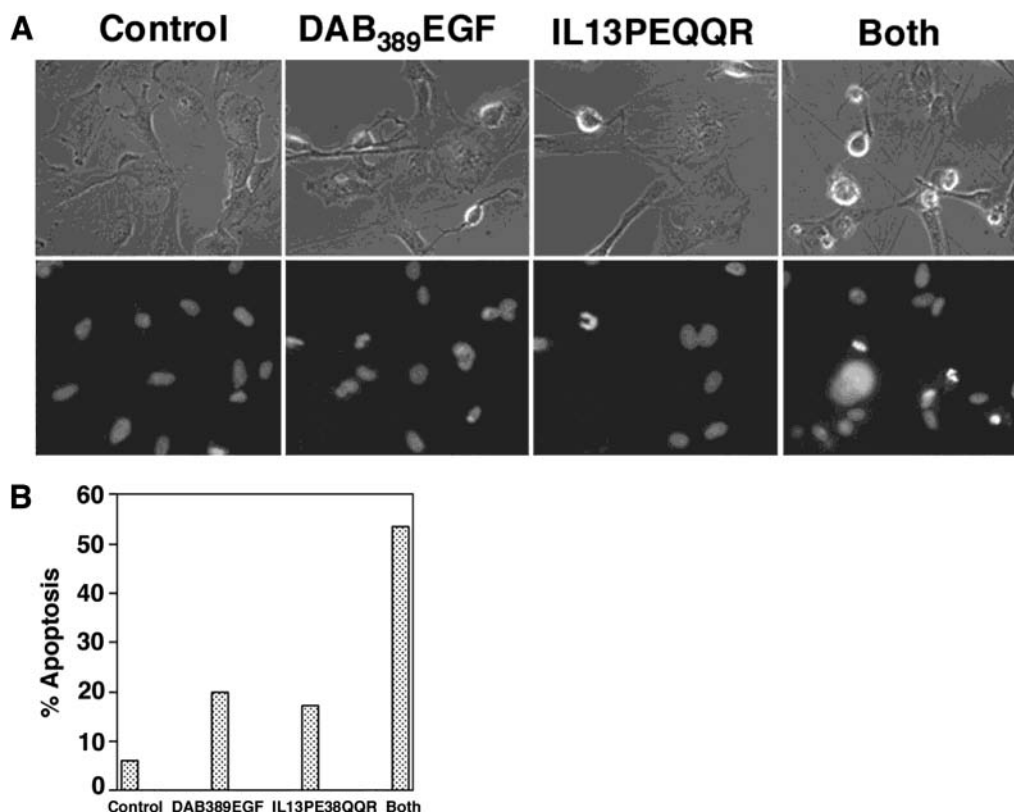
<sup>a</sup> Cytotoxicity assays performed in triplicate as described in text.

supraadditivesensitivity of the fusion protein mixture, the cells had to show at least partial sensitivity to each fusion protein alone (IC<sub>90</sub> ≤ 1000 pM). U373MG cell apoptosis was greater with combination of DAB<sub>389</sub>EGF and IL13PE38QQR than with either agent alone at the same protein concentrations (Figure 3).



**Figure 2.** Isobologram showing 90% inhibition of thymidine incorporation of LN405 cells with exposure to combinations of DAB<sub>389</sub>EGF and IL13PEQQR. The mean combination index was 0.29 determined by CalcuSyn software. CI values of 0.1–0.4 demonstrate strong synergism. The points were fitted by nonlinear regression using GraphPad software (solid line;  $R^2 = 0.99$ ). The dotted line exhibits the theoretical combinations with additive effect; points below the dotted line are associated with a synergistic effect; points above the dotted line are associated with an antagonistic effect. The DAB<sub>389</sub>EGF/IL13PEQQR shows synergism at different concentrations.

**Glioma Cell Lines Show Heterogeneous Expression of EGFR and IL13R $\alpha$ 2.** By two color immuno-



**Figure 3.** Supraadditive fusion protein-induced U373MG cell nuclear fragmentation. A. Phase and fluorescence micrograph at  $32\times$  of DAB<sub>389</sub>EGF, IL13PE38QQR, or combination DAB<sub>389</sub>EGF plus IL13PE38QQR-treated U373MG Hoechst 33258-stained cells. B. Histogram with percent apoptosis (fragmented nuclei) versus drug. DAB<sub>389</sub>EGF yielded 20% apoptosis at 21 pM for 48 h; IL13PE38QQR yielded 17% apoptosis at 14 pM for 48 h; the combination of the two fusion proteins at the same concentrations yielded 54% apoptosis at 48 h.

fluorescence and flow cytometry, all of the glioma cell lines displayed cell-to-cell variations in expression of both EGFR and IL13R $\alpha$ 2 (Figure 4 and Table 2). EGFR was expressed on a greater percentage of cells and at higher density than IL13R $\alpha$ 2 on each of the cell lines. The cell line U138MG was the only cell line with very low levels of both individual receptors. The fraction of cells expressing both receptors varied from 1% to 40% among the cell lines. The DAB<sub>389</sub>EGF fusion protein potency (IC<sub>90</sub>) correlated with the percent total EGFR positive cells ( $p < 0.0001$ ) but not the mean EGFR density measured by flow cytometry ( $p = 0.11$ ). Most of the correlation between percent positive cells and potency was secondary to the influence of two low potency cell lines (A172 and U138MG) which each had low percent EGFR positive cells. There was no correlation between IL13PE38QQR potency (IC<sub>90</sub>) and either IL13R $\alpha$ 2 density ( $p = 0.33$ ) or percent IL13R $\alpha$ 2-positive cells ( $p = 0.33$ ). Synergy (CI) did not correlate with either the percent receptor doubly positive cells ( $p = 0.70$ ) or the ratio of single positive to doubly positive cells ( $p = 0.95$ ). Immunofluorescence confocal microscopy confirmed the results from flow cytometry (Figure 5).

## DISCUSSION

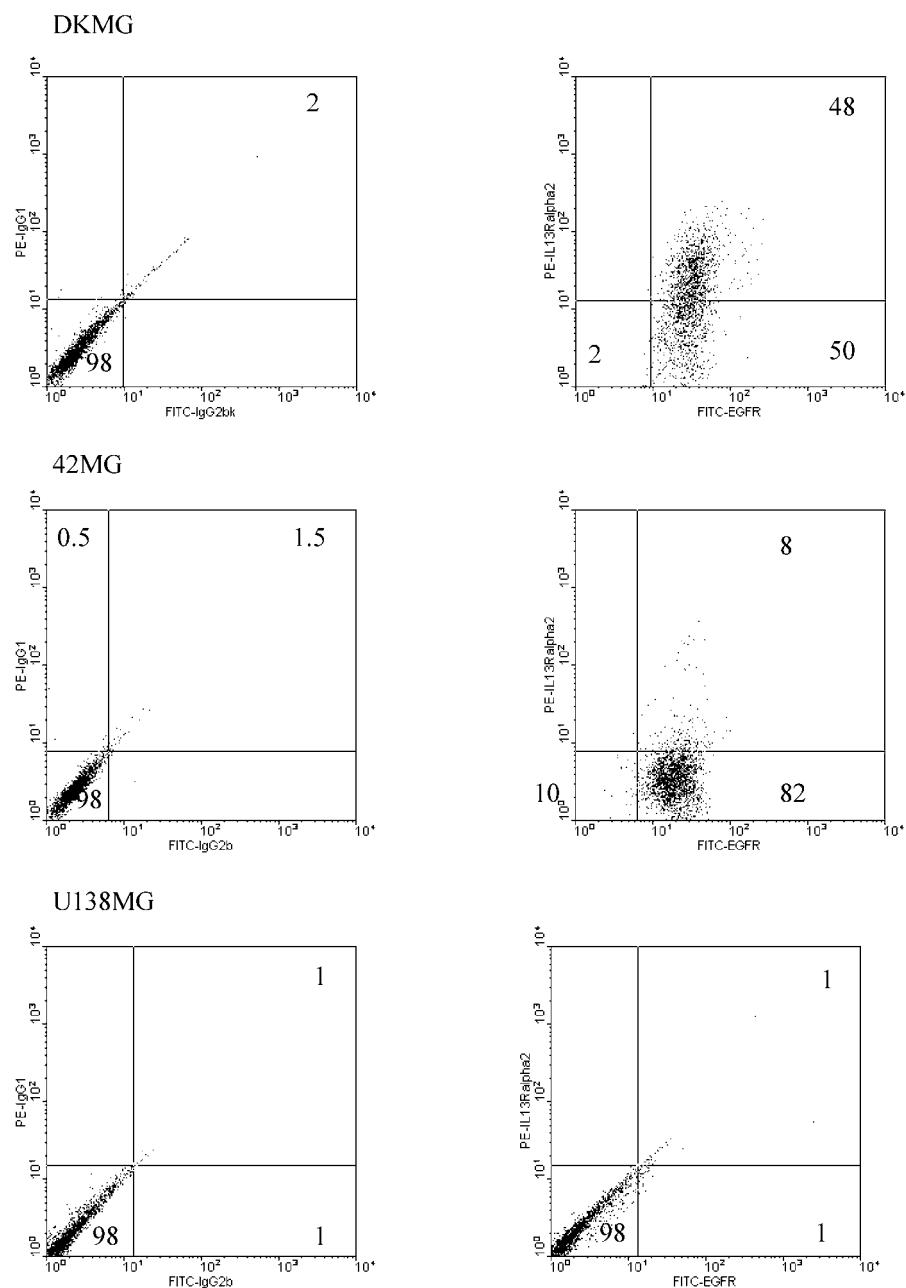
Both DAB<sub>389</sub>EGF and IL13PE38QQR were potently cytotoxic to a number of human glioma cell lines. This confirms and extends previous observations with DAB<sub>389</sub>EGF and IL13PE38QQR (13, 16, 17). Since both these fusion proteins require receptor expression on the tumor cells for binding and intoxication and there is minimal or absent expression of the receptors in normal brain, they should be excellent single agents for CED therapy

of brain tumors. In preliminary phase I/II studies, fusion proteins targeted to each of these receptors showed antitumor efficacy (8, 9).

Our study is the first demonstration that some gliomas may not respond equally to EGFR and IL13R $\alpha$ 2-directed fusion proteins. We found six out of fourteen glioma cell lines that displayed marked differences in sensitivity to DAB<sub>389</sub>EGF and IL13PE38QQR with IC<sub>90</sub> ratios of approximately 10-fold or more. This suggests that although responses may be seen in refractory glioma patients to each fusion protein, they may be different for different fusion proteins in different patients. We recently completed an immunohistochemical survey of 39 patients with high-grade gliomas and found markedly different receptor expression for EGFR and IL13R $\alpha$ 2 for nine of the patients (18). In contrast, only two of the patient samples lacked both EGFR and IL13R $\alpha$ 2. Thus, inclusion of immunohistochemical reactivity in fusion protein CED clinical trials may improve remission rates. Alternatively, combinations of EGFR- and IL13R $\alpha$ 2-directed fusion proteins may also yield improved response rates. This is consistent with the clinical results to date (8, 9). Not every patient responded to individual EGFR- or IL13R $\alpha$ 2-directed fusion proteins, and many of the responses were transient. Neurotoxicities were observed at higher doses. In an effort to widen the therapeutic index with these agents, we examined the anti-glioma activity in vitro of a combination of fusion proteins targeting the two receptors.

Combinations of agents for treatment of cancer patients have been sought for a long time. The hypothesis has been that individual agents could be used at lower doses to achieve the same antitumor effect and that the



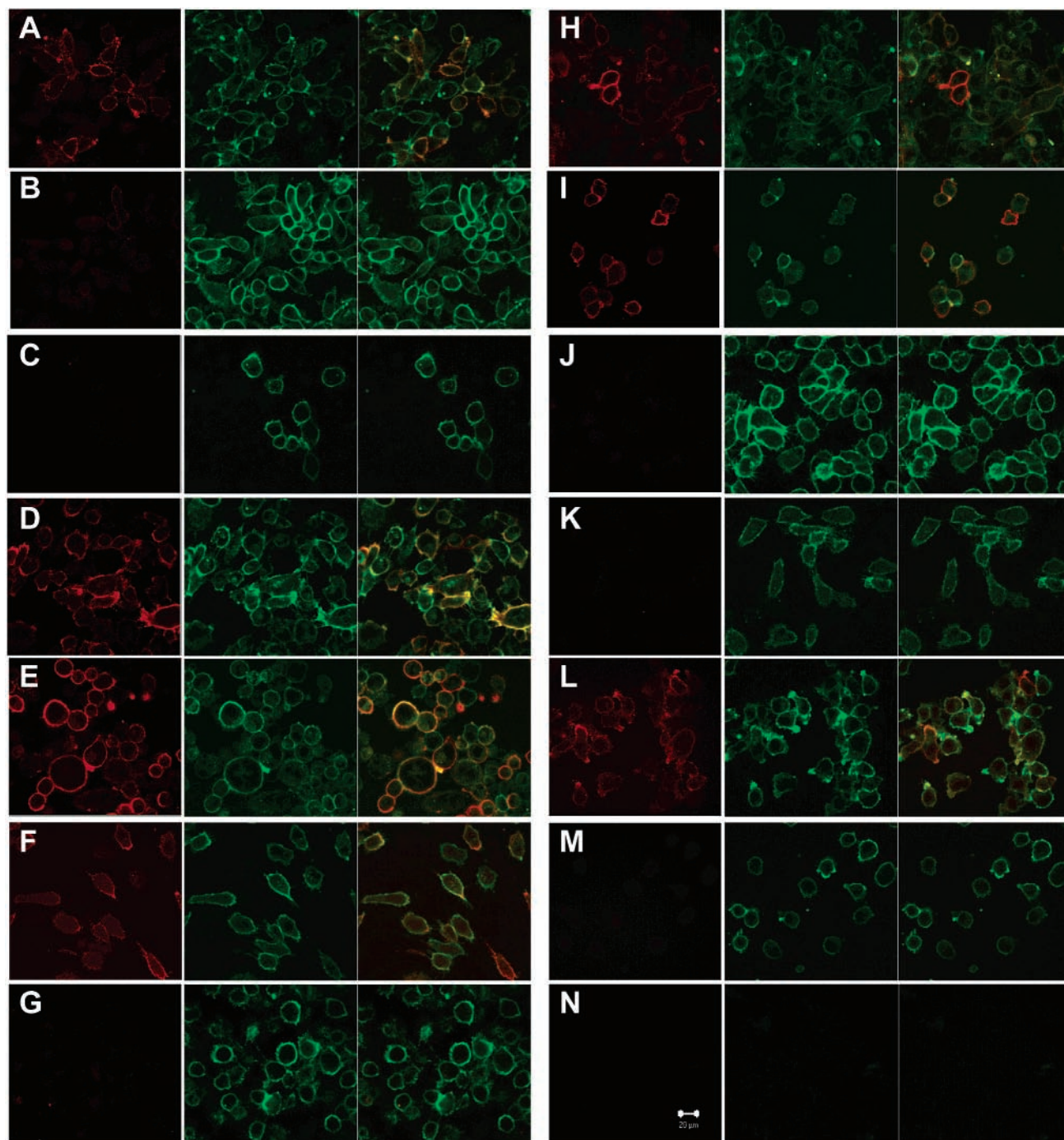


**Figure 4.** Flow cytometry of glioma cell lines stained with FITC- and PE-labeled antibodies. Dot-plots showing glioma cells as individual points. The left panels show the isotype control IgG2b–FITC fluorescence on the *x*-axis and isotype control IgG1–PE fluorescence on the *y*-axis. The right panels show the anti-EGFR–FITC fluorescence on the *x*-axis and anti-IL13Rα2–PE fluorescence on the *y*-axis. Note DKMG has doubly stained cells whereas 42MG has only EGFR and U138MG lacks EGFR and IL13Rα2.

**Table 2. Receptor Expression on Human Glioma Cell Lines<sup>a</sup>**

cell line	EGFR alone		IL13Rα2 alone		EGFR + IL13Rα2
	density (mean)	positive (%)	density (mean)	positive (%)	positive (%)
U87MG	22.72	92	1.01	0	5
GAMA	21.09	64	1.45	0	20
8MGBA	12.09	53	4.21	0	40
U373MG	2.79	73	0.48	0	15
SNB19	11.39	53	5.18	0	35
GMS10	42.24	76	3.19	0	24
42MGBA	12.68	82	0.56	0	8
LN405	24.92	75	1.95	0	17
DKMG	26.73	50	6.27	0	48
T98G	19.85	57	4.08	0	36
DBTRG05MG	17.46	71	0.63	0	12
A172	29.43	95	0.08	0	4
U118MG	25.7	91	1.18	0	8
U138MG	1.88	1	0.12	0	1

<sup>a</sup> Flow cytometry performed as described in the text.



**Figure 5.** Confocal immunofluorescence microscopy. EGFR and IL13R $\alpha$ 2 were detected as described in text. Left hand photomicrographs are IL13R $\alpha$ 2 staining (red); middle photomicrographs shows EGFR staining (green); and right-hand photomicrographs show combined EGFR and IL13R $\alpha$ 2 staining (yellow). Bar equals 20  $\mu$ m. Cell lines are listed as follows: A: U87MG, B: GAMG, C: 8MGBA, D: U373MG, E: SNB-19, F: GMS10, G: 42MGBA, H: LN405, I: DKMG, J: T98G, K: DBTRG05MG, L: A172, M: U118MG, and N: U138MG.

individual agent toxicities would be consequently reduced. Efficacy would be maintained. Recent dramatic successes with combinations of rituximab, cyclophosphamide, vincristine, doxorubicin, and prednisone for lymphomas and trastuzumab with taxanes for breast cancer support the hypothesis. However, clinical evidence of additive or supraadditive efficacy of combinations for brain tumors is not available. Since protein synthesis inactivating toxins kill cells by a different mechanism than DNA or proliferation damaging drugs and have nonoverlapping side effects (minimal myelosuppression or mucositis), immunotoxin/cytotoxic drug combinations have been tested for a number of malignancies. Fewer

studies have been done with immunotoxin combinations since rarely have there been two agents available for a given cancer. Again, the hypothesis is that differentially targeted toxins will yield less damage to normal tissues when used in combination. Lower doses of each may be used, and fewer normal tissues should have both receptors. The combination of DAB<sub>389</sub>EGF and IL13PE38QQR yielded synergistic toxicity to seven of the fourteen cell lines. The combination indices of 0.2 to 0.7 suggested excellent supraadditive toxicity. The results confirm and extend our previous observation of synergistic cell kill on a single glioma cell line (16). While no similar studies have been done in brain tumors, there are two studies

in breast carcinoma (19, 20), two studies in lymphoma (21, 22), and three studies in leukemias (23–25) demonstrating supraadditive toxicity with mixtures of antibody–toxin conjugates. Quantitative isobolographic analyses were only performed in the breast cancer studies where combination indices of 0.1 to 0.4 were observed. Single mixture studies suggested synergistic toxicities in the lymphoma and leukemia studies. These findings in different tumor types lead to the hypothesis that, when several different cell surface receptors are present on a tumor, mixtures of fusion proteins targeting the different receptors may yield an improved therapeutic index.

The molecular mechanism for the synergistic toxicity is undefined. We examined the possible role of receptor heterogeneity. EGFR and IL13R $\alpha$ 2 were measured on individual cells by flow cytometry and epifluorescence microscopy. Populations of cells with only EGFR or IL13R $\alpha$ 2 were found in all seven cell lines. We hypothesize that only mixtures of fusion proteins can efficiently kill such mixed populations. We were not able to correlate CI with the degree of heterogeneity because of the narrow range in CIs. Comparisons using transfected cells with defined numbers of each receptor will help confirm or negate this hypothesis. Other groups have correlated immunotoxin synergy with receptor heterogeneity (19, 20, 26). Other factors may also play a role in the observed synergy such as total cell surface-bound fusion protein or modulation of internalization. Increased antibody binding to EGFR and IL13R $\alpha$ 2 was observed over the amount for each receptor alone for all seven glioma cell lines showing synergistic cell kill. Increased cell surface-bound toxin conjugate was reported with mixtures of the different conjugates in one of the leukemia studies (24). While we did not study rates of receptor internalization, such increased internalization was reported with cocktails of immunotoxins in a breast carcinoma and a lymphoma study (20, 22).

IL13R $\alpha$ 2 expression was lower than EGFR expression. The different physiology of the two receptors likely accounts for the difference. Cell line culture conditions and the choice of monoclonal antibodies may have also influenced the difference in measured cell surface receptor densities.

Regardless of mechanism, the synergistic toxicity of DAB<sub>389</sub>EGF and IL13PE38QQR will permit use of lower doses of each fusion protein in brain tumor CED therapy to achieve the same degree of cell kill. This should reduce toxicities to normal brain tissues which may express low levels of individual receptors. Testing of the combinations in animal models should help test whether the mixture provides a wider therapeutic index. Both these agents show promise for efficacy in clinical trials of patients with radiotherapy and chemotherapy refractory recurrent high-grade gliomas and should undergo further development both as single and combination agents.

#### ACKNOWLEDGMENT

The work was supported in part by the National Institutes of Health grants R01CA76178 (A.F.), R21CA090550 (A.F.), and R01CA090263 (A.F.). We thank Ligand Pharmaceuticals and NeoPharm for gifts of fusion proteins, and the WFU Tissue Culture Core Laboratory for storage and maintenance of the glioma cell lines. We thank Raj K. Puri for guidance and critical review of the manuscript.

#### LITERATURE CITED

- (1) Greenlee, R. T., Hill-Harmon, M. B., Murray, T., and Thun, M. (2001) Cancer statistics, 2001. *CA Cancer J. Clin.* 51, 15–36.
- (2) Polednak, A. P. and Flannery, J. T. (1995) Brain, other central nervous system, and eye cancer. *Cancer (Phila.)*, 75 (Suppl. 1), 330–337.
- (3) Glioma Meta-analysis Trialists (GMT) Group. (2002) Chemotherapy in adult high-grade glioma: a systemic review and meta-analysis of individual patient data from 12 randomised trials. *Lancet* 359, 1011–1018.
- (4) Esteller, M., Garcia-Foncillas, J., Andion, E., Goodman, S. N., Hidalgo, O. F., Vanaclocha, V., Baylin, S. B., and Herman, J. G. (2000) Inactivation of the DNA-repair gene MGMT and the clinical response of gliomas to alkylating agents. *N. Engl. J. Med.* 343, 1350–1354.
- (5) Gaspar, L. E., Fisher, B. J., Macdonald, D. R., LeBer, D. V., Halperin, E. C., Schold, S. C., and Cairncross, J. G. (1992) Supratentorial malignant glioma: patterns of recurrence and implications for external beam local treatment. *Int. J. Radiat. Oncol. Biol. Phys.* 24, 55–57.
- (6) Oldfield, E. H., Broaddus, W. C., Bruce, J., Task, T., Laske, D. W., McDonald, J., Patel, S. J., Weingart, J. D., Wharen, R. E., and Youle, R. J. (2000) Phase II trial of convection-enhanced distribution of recombinant immunotoxin in patients with recurrent malignant gliomas. *Proc. Am. Assoc. Neurol. Surgeons* 18, 94–95.
- (7) Rand, R. W., Kreitman, R. J., Patronas, N., Varricchio, F., Pastan, I., and Puri, R. K. (2000) Intratumoral administration of recombinant circularly permuted interleukin-4-Pseudomonas exotoxin in patients with high-grade glioma. *Clin. Cancer Res.* 6, 2157–2165.
- (8) Prados, M. D., Lang, F. F., Strauss, L. C., Fleming, C. K., Aldape, K., Kunwar, S., Yung, W. A., Chang, S. M., Husain, S. R., Gutin, P. H., Raizer, J. J., Piepmeyer, J. M., Berger, M., McDermott, M., and Puri, R. K. (2002) Intratumoral and intracerebral microinfusion of IL13-PE38QQR cytotoxin: phase I/II study of pre- and post-resection infusions in recurrent resectable malignant glioma. *Proc. ASCO* 21, 69b.
- (9) Sampson, J. R., Reardon, D., Akabani, G., Archer, G., Friedman, A., Friedman, H., Herndon, J., McLendon, R., Penne, K., Paolino, A., Tourt-Uhlig, S., Quinn, J., Rich, J., Williams, R., Marcus, S., Pastan, I., and Bigner, D. D. (2002) A phase I study of intratumoral infusion of a recombinant chimeric protein composed of transforming growth factor (TGF)- $\alpha$  and a mutated form of the Pseudomonas exotoxin (TP-38) for the treatment of malignant brain tumors. *Proc. ASCO* 21, 13b.
- (10) Laske, D. W., Morrison, P. F., Lieberman, D. M., Cortes, M. E., Reynolds, J. C., Stewart-Henney, P. A., Koong, S. S., Cummins, A., Paik, C. H., and Oldfield, E. H. (1997) Chronic interstitial infusion of protein to primate brain: determination of drug distribution and clearance with single-photon emission computerized tomography imaging. *J. Neurosurg.* 87, 586–594.
- (11) Chou, T. C. and Talalay, P. (1983) Analysis of combined drug effects: a new look at a very old problem. *Trends Pharmacol. Sci.* 4, 450–454.
- (12) Cohen, K. A., Liu, T. F., Bissonette, R., Puri, R. K., and Frankel, A. E. (2003) DAB<sub>389</sub>EGF fusion protein therapy of refractory glioblastoma multiforme. *Curr. Pharm. Biotech.* 4, 39–49.
- (13) Barth, S. (2001) hIL13-PE38QQR. *NeoPharm. Curr. Opin. Invest. Drugs* 2, 1309–1313.
- (14) Liu, T. F., Cohen, K. A., Willingham, M. C., Ramage, J. G., Thorburn, A. M., and Frankel, A. E. (2003) A diphtheria toxin-epidermal growth factor fusion protein is cytotoxic to human glioblastoma multiforme cells. *Cancer Res.* 63, 1834–1837.
- (15) Morgan, M. J., Thorburn, J., Thomas, L., Maxwell, T., Brothman, A. R., and Thorburn, A. (2001) An apoptosis signaling pathway induced by the death domain of FADD selectively kills normal but not cancerous prostate epithelial cells. *Cell Death Differ.* 8, 696–705.
- (16) Liu, T. F., Cohen, K. A., Willingham, M. C., Tatter, S. B., Puri, R. K., and Frankel, A. E. (2003) Combination fusion protein therapy of refractory brain tumors: demonstration of efficacy in cell culture. *J. Neuro-Oncol.*, in press.
- (17) Debinski, W., Obiri, N. I., Powers, S. K., Pastan, I., and Puri, R. K. (1995) Human glioma cells overexpress receptors



- for interleukin 13 and are extremely sensitive to a novel chimeric protein composed of interleukin 13 and *Pseudomonas* exotoxin. *Clin. Cancer Res.* 1, 1253–1258.
- (18) Liu, T. F., Tatter, S. B., Willingham, M. C., Yang, M., Hu, J. J., and Frankel, A. E. (2003) Growth factor receptor expression varies among high grade gliomas and normal brain: epidermal growth factor receptor has excellent properties for interstitial fusion protein therapy. *Mol Cancer Ther.* 2, 783–787.
- (19) Yu, Y. H., Crews, J. R., Cooper, K., Ramakrishnan, S., Houston, L. L., Leslie, D. S., George, S. L., Lidor, Y., Boyer, C. M., Ring, D. B., and Bast, R. C. (1990) Use of immunotoxins in combination to inhibit clonogenic growth of human breast carcinoma cells. *Cancer Res.* 50, 3231–3238.
- (20) Crews, J. R., Maier, L. A., Yu, Y. H., Hester, S., O'Briant, K., Leslie, D. S., DeSombre, K., George, S. L., Boyer, C. M., Argon, Y., and Bast, R. C. (1992) A combination of two immunotoxins exerts synergistic cytotoxic activity against human breast cancer cell lines. *Int. J. Cancer* 51, 772–779.
- (21) Flavell, D. J., Noss, A., Pulford, K. A., Ling, N., and Flavell, S. U. (1997) Systemic therapy with 3BIT, a triple combination cocktail of anti-CD19, –CD22, and –CD38-SAPORIN immunotoxins, is curative of human B-cell lymphoma in severe combined immunodeficient mice. *Cancer Res.* 57, 4824–4829.
- (22) Ghetie, M. A., Tucker, K., Richardson, J., Uhr, J. W., and Vitetta, E. S. (1994) Eradication of minimal disease in severe combined immunodeficient mice with disseminated Daudi lymphoma using chemotherapy and an immunotoxin cocktail. *Blood* 84, 702–707.
- (23) Flavell, D. J., Boehm, D. A., Noss, A., Warnes, S. L., and Flavell, S. U. (2001) Therapy of human T-cell acute lymphoblastic leukaemia with a combination of anti-CD7 and anti-CD38-SAPORIN immunotoxins is significantly better than therapy with each individual immunotoxin. *Br. J. Cancer* 84, 571–578.
- (24) Herrera, L., Farah, R. A., Pellegrini, V. A., Aquino, D. B., Sandler, E. S., Buchanan, G. R., and Vitetta, E. S. (2000) Immunotoxins against CD19 and CD22 are effective in killing precursor B acute lymphoblastic leukemia cells in vitro. *Leukemia* 14, 853–858.
- (25) Vallera, D. A., Ash, R. C., Zanjani, E. D., Kersey, J. H., LeBien, T. W., Beverley, P. C. L., Neville, D. M., and Youle, R. J. (1983) Anti-T cell reagents for human bone marrow transplantation: ricin linked to three monoclonal antibodies. *Science* 222, 512–515.
- (26) Katz, F. E., Janossy, G., Cumber, A., Ross, W., Blacklock, H. A., Tax, W. and Thorpe, P. E. (1987) Elimination of T cells from human peripheral blood and bone marrow using a cocktail of three anti-T cell immunotoxins. *Br. J. Haematol.* 67, 407–411.

BC034111+

# Uptake and Metabolism of a Dual Fluorochrome Tat-nanoparticle in HeLa Cells

A. M. Koch,<sup>†</sup> F. Reynolds,<sup>‡</sup> M. F. Kircher,<sup>‡</sup> H. P. Merkle,<sup>†</sup> R. Weissleder,<sup>‡</sup> and L. Josephson<sup>\*‡</sup>

Department of Chemistry and Applied BioSciences, Drug Formulation & Delivery, Swiss Federal Institute of Technology Zurich (ETHZ), Winterthurerstrasse 190 8057 Zurich, Switzerland, and Center for Molecular Imaging Research, Massachusetts General Hospital/Harvard Medical School, Building 149, 13th Street, Charlestown, Massachusetts 02129. Received July 16, 2003

The ability to use magnetic nanoparticles for cell tracking, or for the delivery of nanoparticle-based therapeutic agents, requires a detailed understanding of probe metabolism and transport. Here we report on the development and metabolism of a dual fluorochrome version of our tat-CLIO nanoparticle termed Tat(FITC)-Cy3.5-CLIO. The nanoparticle features an FITC label on the tat peptide and a Cy3.5 dye directly attached to the cross-linked coating of dextran. This nanoparticle was rapidly internalized by HeLa cells, labeling 100% of cells in 45 min, with the amount of label per cell increasing linearly with time up to 3 h. Cells loaded with nanoparticles for 1 h retained 40–60% of their FITC and Cy3.5 labels over a period of 72 h in label-free media. Over a period of 144 h, or approximately 3.5 cell divisions, the T2 spin-spin relaxation time of cells was not significantly changed, indicating retention of the iron oxide among the dividing cell population. Using confocal microscopy and unfixed cells, both dyes were nuclear and perinuclear (broadly cytoplasmic) after Tat(FITC)-Cy3.5-CLIO labeling. Implications of the rapid labeling and slow excretion of the Tat(FITC)-Cy3.5-CLIO nanoparticle are discussed for cell tracking and drug delivery applications.

## INTRODUCTION

The ability of membrane-translocating peptides to move materials through the plasma membrane or even cell layers and tissues has the potential to lead to the development of new types of pharmaceuticals, which can overcome cellular barriers for the delivery of current compounds. The membrane-translocating sequence of the tat protein of HIV (tat-peptide) has been used to ferry diagnostic and therapeutic agents across membranes and has led to new forms of cyclosporine (1), improved radiotherapies (2), and new methods for intracellular delivery of DNA and enzymes (3–5). However, the development of tat peptide-based pharmaceuticals would be furthered, not merely by studies on the efficacy of such compounds, but by a thorough understanding of the transport and degradation of tat-like probes.

The relationship between probe utility on one hand and probe metabolism and transport on the other can be illustrated with tat-CLIO (tat-cross-linked iron oxide), a magnetic nanoparticle to which tat peptides have been attached (6, 7). Tat-CLIO-loaded cells have been used to study cell movement in vivo in a variety of medically important applications including stem cell engraftment (7) and T cell infiltration in adoptive immunotherapy (8). In magnetic resonance (MR) cell tracking applications, excretion of the nanoparticle after internalization, if it occurs, limits the observation time of labeled cells. On the other hand, for the tat-mediated delivery of therapeutic agents, particularly for delivery of agents across epithelial or endothelial barriers, internalization without externalization would not permit tat-drug conjugates to

pass through cell layers and achieve tissue penetration. In the liver tat-CLIO crosses endothelial barriers in the vasculature and is found in the parenchyma (9). The tat-mediated delivery of a diverse type of molecules including fluorochromes, peptides, and enzymes through tissues in vivo has been reported (10, 11).

With the interrelated, long-term objectives of understanding the fate of Tat-CLIO-loaded cells followed by magnetic resonance (MR) tracking in vivo, and determining the ability of Tat-CLIO to undergo transepithelial or transendothelial transport, we examined the uptake and excretion of dual fluorochrome, multimodal (fluorescent and magnetic) tat-nanoparticles. Here we describe a Tat-CLIO that is detectable by its effects on MR with one fluorochrome, fluorescein isothiocyanate (FITC), attached to each tat peptide, Tat(FITC), and a second fluorochrome, Cy3.5, is attached to the coating of nanoparticle (cross-linked iron oxide, CLIO). We term this form of tat-CLIO Tat(FITC)-Cy3.5-CLIO, to denote its dual fluorochrome labels. On the basis of fluorescent activated cell sorter (FACS) analysis, Tat(FITC)-Cy3.5-CLIO was rapidly internalized and slowly excreted by HeLa cells. On the basis of effects on the cellular T2 (spin-spin relaxation time), the superparamagnetic iron oxide nanoparticle cores were not eliminated during the 7-day observation period. Implications of this pharmacokinetic pattern are described for cell tracking and pharmaceutical targeting applications.

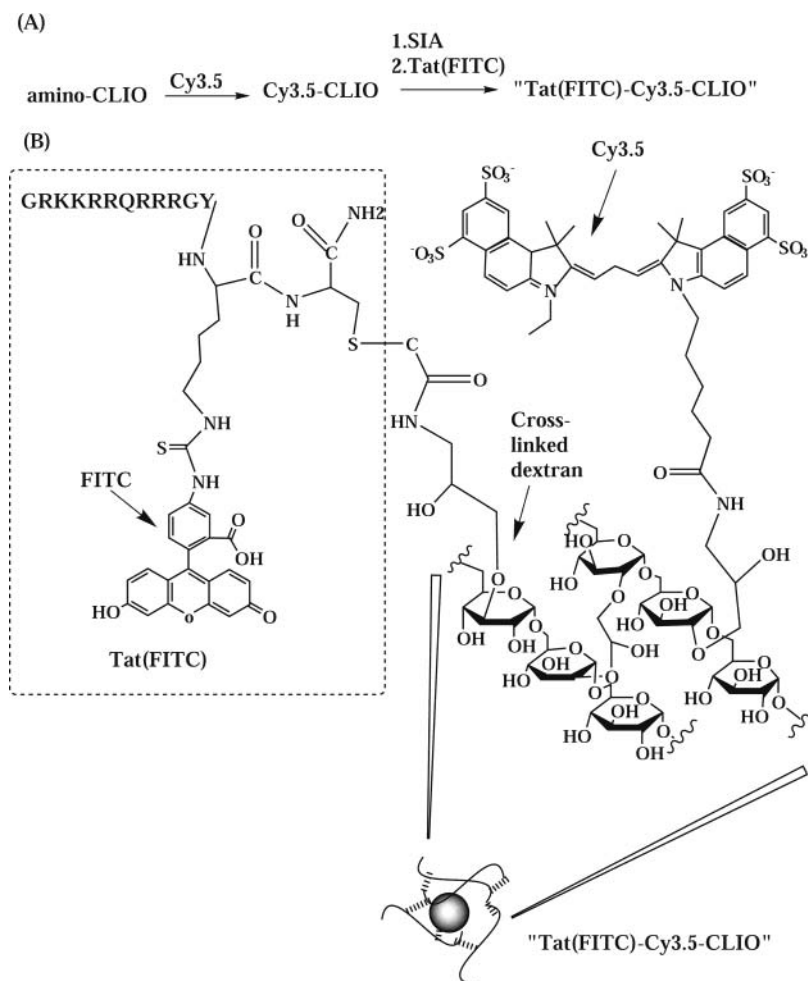
## MATERIALS AND METHODS

**Nanoparticle Synthesis.** To synthesize dual fluorochrome-labeled magnetic nanoparticles, the dye Cy3.5 was first attached to the amines of a cross-linked dextran-coated nanoparticle termed amino-CLIO, to yield Cy3.5-CLIO. The tat peptide, denoted Tat(FITC), was attached to the nanoparticle using the bifunctional reagent, suc-

\* Corresponding author. Phone: 617-726-6478, Fax: 617-726-5788, e-mail: ljosephson@partners.org.

<sup>†</sup> Swiss Federal Institute of Technology Zurich.

<sup>‡</sup> Massachusetts General Hospital/Harvard Medical School.



**Figure 1.** Synthesis and features of Tat(FITC)-3.5-CLIO. (A) Synthetic scheme. (B) Schematic diagram showing features of Tat(FITC)-3.5-CLIO. Tat(FITC) is the peptide GRKKRRQRRRGYK(FITC)C-NH<sub>2</sub>. Succinimidyl iodoacetate (SIA) gives a thioether (S-C) linkage between the peptide and the nanoparticle.

**Table 1.** Physical Properties of Tat(FITC)-Cy3.5-CLIO

nanoparticle	Cy3.5/nanoparticle	Tat(FITC)/nanoparticle	size (nm)
Tat(FITC)-Cy3.5-CLIO	1.4	24	49.1

cinimidyl iodoacetate (SIA), as shown in Figure 1A. A schematic representation of the structure of Tat(FITC)-Cy3.5-CLIO is shown in Figure 1B.

A tat peptide, termed Tat(FITC), with the sequence GRKKRRQRRRGYK(FITC)C-NH<sub>2</sub> was synthesized and purified as described (9). The amino-CLIO nanoparticle was prepared as described (6, 12).

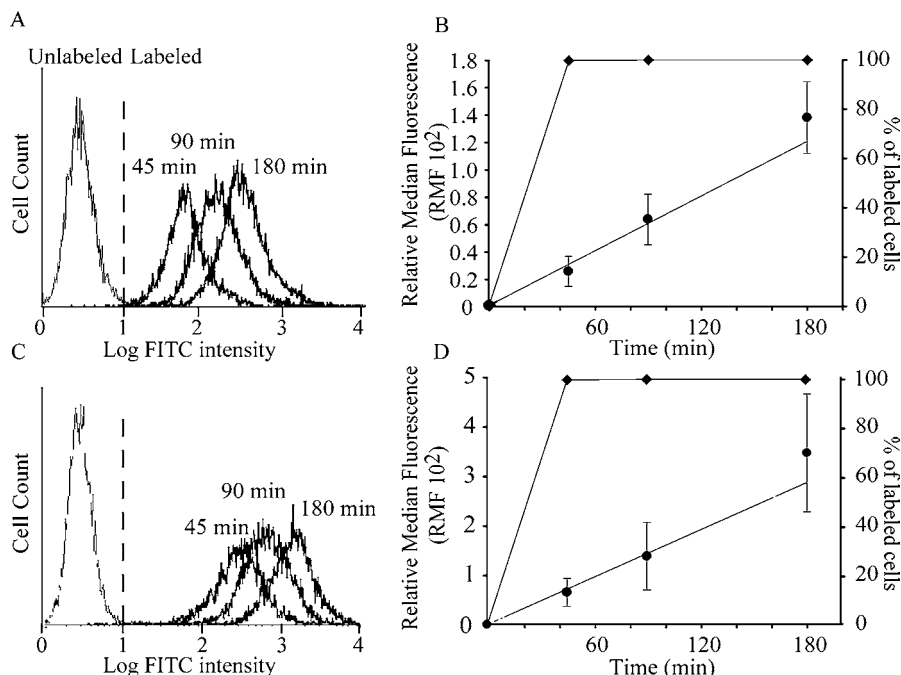
Cy 3.5-CLIO was prepared by adding 175  $\mu$ L of amino-CLIO (2 mg Fe) to one tube of monofunctional Cy3.5 dye as supplied by the manufacturer (Amersham Biosciences, Little Chalfont, UK). The mixture was vortexed and allowed to sit for a minimum of 2 h. Reaction with Cy3.5 consumes 1.4 amino groups per nanoparticle, out of a total of 40–60 amino groups per nanoparticle. Cy 3.5-CLIO was added to *N*-succinimidyl iodoacetate (SIA, 4 mg, 14  $\mu$ mol, Molecular Bioscience, Boulder, CO) in 100  $\mu$ L of DMSO. The mixture was vortexed, allowed to sit for 1 h, and purified with a PD-10 desalting column (Sigma) in 0.02 M citrate, 0.15 M NaCl, pH 8. A single separation step was used to remove unreacted Cy3.5 and SIA.

Tat(FITC)-Cy3.5-CLIO was prepared by adding Tat(FITC) (60  $\mu$ L, 5 mM) in 0.1% v/v trifluoroacetic acid to SIA activated Cy3.5-CLIO (2 mg Fe). The mixture was vortexed and allowed to react for 1–2 h, and unreacted

peptide was removed by ultrafiltration (Minicon YM-30, Millipore, Bedford, MA). The number of attached Cy3.5 and FITC dyes was determined spectrophotometrically, for fluorescein ( $\epsilon_{494} = 73000$ ) and for Cy3.5 ( $\epsilon_{581} = 150000$ ). Iron was determined spectrophotometrically (8), and the ratios of Cy3.5 or Tat(FITC) per nanoparticle were calculated assuming 2064 iron atoms per CLIO particle (13). Properties of the nanoparticle are summarized in Table 1. We previously demonstrated that the ability of cells to internalize tat peptide magnetic nanoparticles increases with increasing numbers of peptides per nanoparticle (14). The Tat(FITC)-Cy3.5-CLIO nanoparticle we employed is similar to that of Zhao et al. but differs in the use of two chemically distinct fluorochromes and in the use of a thioether rather than a disulfide linkage. The thioether-linked Tat(FITC)-Cy3.5-CLIO had improved stability between the peptide and nanoparticle when incubated in cell culture media compared to the disulfide-linked nanoparticle (Koch and Josephson, unpublished observations).

**Cell Culture.** HeLa cells were cultured in MEM (minimum essential medium) containing 10% FBS, supplemented with penicillin (100 units/mL)/streptomycin (100  $\mu$ g/mL), sodium pyruvate (1 mM), and nonessential amino acids (0.1 mM) at 37  $^{\circ}$ C in a humidified atmosphere





**Figure 2.** Uptake of Tat(FITC)-Cy3.5-CLIO nanoparticle or Tat(FITC) peptide. (A) Progressive increase in cell associated fluorescence with Tat(FITC)-Cy3.5-CLIO as shown in the FACS profile (frequency distribution of labeled cells). Dotted line is the demarcation between labeled and unlabeled cells. (B) Data from A are plotted as the median fluorescence of labeled cells divided by median unlabeled cells (relative median fluorescence, RMF). (C and D) Increase in cell fluorescence with Tat(FITC) peptide obtained as in A and B, respectively.

containing 5% CO<sub>2</sub>. Media, balanced salt solutions, and supplements were from Cellgro (Mediatech Inc, Herndon, VA). HeLa cells were cultured as exponentially growing subconfluent monolayers, except when used in experiments lasting 72 h and more, where cells were allowed to reach confluency.

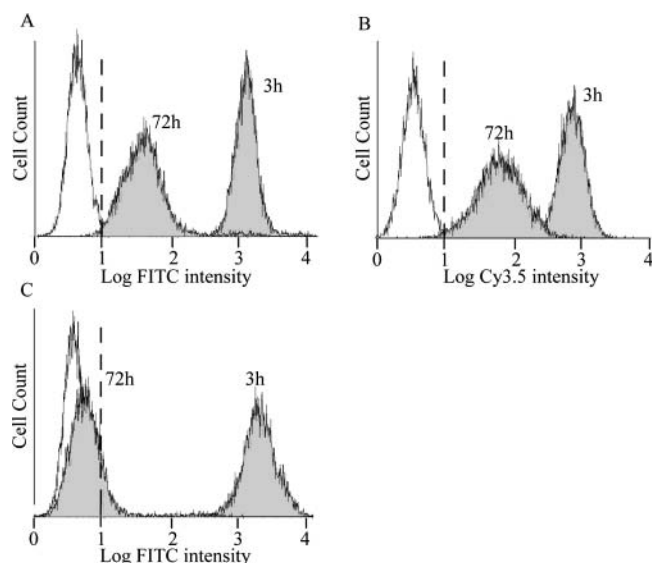
**FACS Analysis. Uptake Studies.** Exponentially growing HeLa cells were trypsinized and seeded at a density of  $10^5$  cells/well in 12 well plates (Becton Dickinson, Bedford, MA). About 18 h later, cells were labeled for 1 h with Tat(FITC)-Cy3.5-CLIO (50  $\mu$ g Fe/mL), or Tat(FITC) peptide (5  $\mu$ M) added in complete cell culture medium. Medium was sterile-filtered (0.2  $\mu$ m, low protein binding, Gelman, Ann Arbor, MI) before addition to cells. After 45, 90, or 180 min, cells were washed 4 $\times$  with HBSS, trypsinized for 7 min, counted, fixed in 2% paraformaldehyde (Fisher Scientific, reagent grade), and analyzed by flow cytometry on a FACS Calibur (Becton Dickinson, Franklin Lakes, NJ) within 2 h after trypsinization. A total of 10 000 cells per sample was analyzed. The numbers of cells with a fluorescence intensity higher than unlabeled cells was used to calculate percent of labeled cells. The baseline was determined by analyzing unlabeled control cells. RMF (relative median fluorescence) was calculated by dividing the median of the labeled cells by the median of an unlabeled cell population.

**Retention in Cells.** HeLa cells were labeled with Tat(FITC)-Cy3.5-CLIO (50  $\mu$ g Fe/mL which corresponds to 7.5  $\mu$ M Tat(FITC) peptide), or Tat(FITC) peptide (5  $\mu$ M) as described for the uptake studies. After 1 h of labeling, cells were washed 4 $\times$  with HBSS, and then not immediately trypsinized and analyzed, but incubated in fresh cell culture medium for 3, 24, 48, or 72 h. At respective time points, cells were trypsinized and analyzed as described for uptake studies.

**Confocal Fluorescence Microscopy.** HeLa cells were cultured on Lab-Tek Chambered Coverglass (Nalge Nunc, Naperville, IL) with a density of  $3 \times 10^4$  cells/cm<sup>2</sup>. Cells were labeled as described for FACS analysis with

either Tat(FITC)-Cy3.5-CLIO (50  $\mu$ g/mL Fe) or free Tat(FITC) peptide (5  $\mu$ M). Cells were observed immediately after labeling, after 24 h and after 72 h. Brightfield and fluorescence images were obtained with a Zeiss Plan-Neofluar 40 $\times$  objective using a Zeiss Axiovert 200 confocal microscope (Zeiss, Jena, Germany) equipped with Argon (488 nm) and HeNe (543 nm) lasers for fluorescence. Exposure time for fluorescence was adjusted at each time point to localize fluorochromes. Background fluorescence was determined by analyzing unlabeled cells. Image acquisition and analysis was done using LSM 5 PASCAL Software.

**MR Imaging.** HeLa cells were seeded in cell culture flasks (175 cm<sup>2</sup>) at a density of  $5 \times 10^4$  cells/cm<sup>2</sup> and allowed to adhere overnight. Cells were washed with fresh cell culture medium and then incubated for 4 h with sterile filtered Tat(FITC)-Cy3.5-CLIO (200  $\mu$ g Fe/mL). Cells were trypsinized (5 min) and divided into new cell culture flasks (175 cm<sup>2</sup>), with each flask containing  $2 \times 10^6$  cells. Two flasks were harvested immediately, cells of another eight flasks were allowed to adhere and kept in culture for different time points up to 96 h. At each time point, adherent cells were washed 4 $\times$  with HBSS, trypsinized, transferred to a conical cell culture tube, centrifuged down, and washed three times with HBSS. Finally, cells were resuspended in warm 0.5% agarose to yield a volume of 100  $\mu$ L and put on ice. The number of cells ranged from  $2.5 \times 10^6$  cells at start of the experiment to  $31 \times 10^6$  cells after 7 days, with a doubling time of 24 h at the beginning and then decreasing to 48 h at the end of the experiment. Immobilized cells were then imaged with a 7T MR Scanner (Siemens, Massachusetts General Hospital, Boston, MA). T2 values were from signal intensity data obtained at six echo times (20, 40, 60, 80, 120 ms), with a repetition time of 2 s. Data were fit to the standard exponential transverse relaxation model used previously (15).

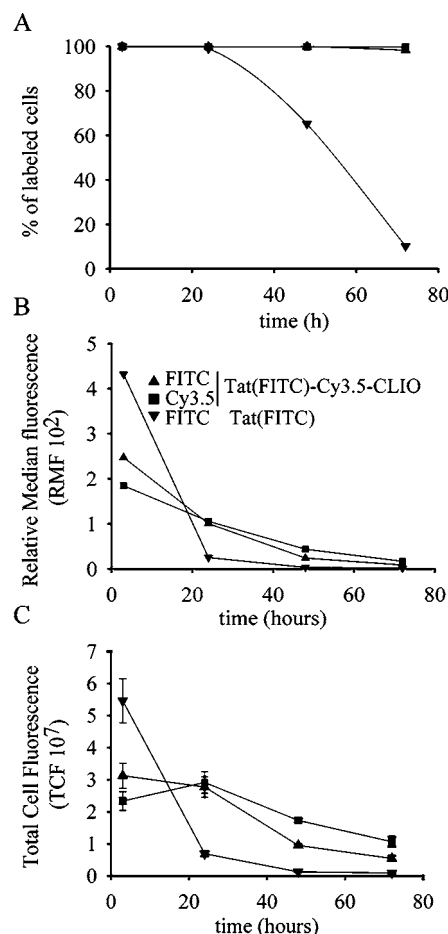


**Figure 3.** Retention of the Tat(FITC)-Cy3.5-CLIO nanoparticle and Tat(FITC) peptide in HeLa cells. HeLa cells were labeled for 1 h with Tat(FITC)-Cy3.5-CLIO (A and B) or Tat(FITC) peptide (C) and washed. Cells were incubated in fresh cell culture medium for 3, 24, 48, or 72 h, trypsinized, and analyzed by flow cytometry. A relative median fluorescence (RMF) is calculated (median labeled/median unlabeled) and, together with additional time points, shown in Figure 4.

## RESULTS

**Uptake of Tat(FITC)-Cy3.5-CLIO.** The uptake of Tat(FITC)-Cy3.5-CLIO was monitored by FACS analysis based on FITC as shown in Figure 2. Figure 2A demonstrates that exposing cells to Tat(FITC)-Cy3.5-CLIO results in a uniform labeling of cells and that the amount of cell-associated nanoparticle increases with the time of incubation. Cell labeling was expressed using two parameters, the percent labeled cells and the relative median fluorescence or RMF, obtained by dividing the median fluorescence of labeled cells by the median fluorescence of unlabeled cells. The dotted line indicates a clear division between labeled and unlabeled cells that occurred at the short incubation time of 45 min. RMF and percent of labeled cells are plotted in Figure 2B, which demonstrates that nanoparticle accumulation (RMF) increased at a constant rate over the 180 min incubation period. Also shown are comparable data for the uptake of the tat(FITC), the peptide of the Tat(FITC)-Cy3.5-CLIO nanoparticle, see Figures 2C and 2D. Again labeling was rapid and highly uniform, and cell-associated fluorescence increased over the 180 min incubation period.

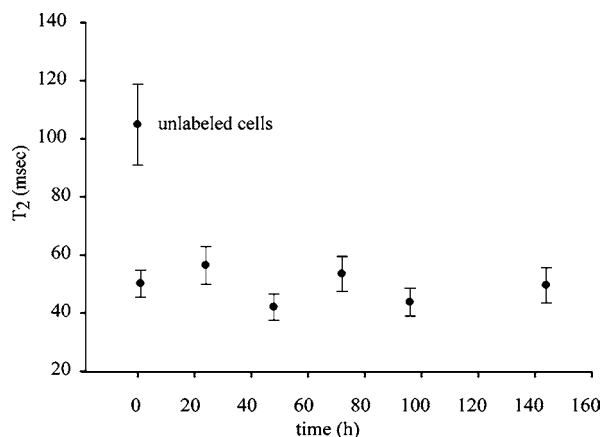
**The Retention of Tat(FITC)-Cy3.5-CLIO in Cells by Fluorescence.** We next examined the retention of both FITC fluorescence and Cy3.5 fluorescence of Tat(FITC)-Cy3.5-CLIO in cells, when cells were loaded for 1 h with Tat(FITC)-Cy3.5-CLIO nanoparticle or Tat(FITC) peptide and were then incubated in media for up to 72 h. Representative FACS histograms after cells have been in media for 3 and 72 h are shown in Figures 3A–C. Data from the 3 and 72 h time points, together with additional time points, are presented in Figure 4. As shown in Figure 4A, after 72 h cells loaded with Tat(FITC)-Cy3.5-CLIO were still labeled, that is had higher fluorescence than a population of unlabeled cells, by either FITC or Cy3.5 fluorescence. On the other hand, after 72 h, more than 80% of cells labeled with Tat(FITC) peptide at the beginning of the experiment were unlabeled. Figures 4B and 4C show the fluorescence of Tat-



**Figure 4.** Retention of fluorescence of cells loaded with the Tat(FITC)-Cy3.5-CLIO nanoparticle or the Tat(FITC) peptide. Cells were loaded for 1 h and analyzed by flow cytometry. For all graphs, (▼) is the FITC fluorescence from the Tat(FITC) peptide, (▲) is the FITC fluorescence from Tat(FITC)-Cy3.5 CLIO, and (■) is the Cy3.5 fluorescence from Tat(FITC)-Cy3.5 CLIO. (A) Percent of labeled cells versus time. (B) Fluorescence per cell as RMF versus time. (C) Total cellular fluorescence (TCF) versus time, where TCF equals RMF times cell number. Experiment is representative for two similar experiments: each data point (A, B) is the median fluorescence intensity of 10 000 cells per sample. Errors bars in (C) represent variations in cell number.

(FITC)-Cy3.5-CLIO or Tat(FITC) peptide loaded cells uncorrected for cell division (B) or corrected for cell division (C). As shown in Figure 4B, the RMF of peptide-loaded cells decreased rapidly, while the FITC and Cy3.5 fluorescence from Tat(FITC)-Cy3.5-CLIO-loaded cells decreased similarly and more slowly than peptide-loaded cells. For Figure 4C, total cell fluorescence (TCF) was obtained by multiplying cell number times the RMF. For Tat(FITC)-Cy3.5-CLIO-loaded cells, the loss of TCF was less than the loss of fluorescence per cell (RMF), indicating that a major source of fluorescence loss was the distribution of the labels to daughter cells.

A second way of ascertaining the retention of the Tat(FITC)-Cy3.5-CLIO is by determining the T2 spin-spin relaxation times of cells. Cells were loaded with nanoparticle and allowed to proliferate in nanoparticle-free media for up to 144 h, and T2 was determined periodically. With this method, nanoparticles can be distributed between dividing cells, but the entire population of cells is retained and analyzed. As shown in Figure 5, the T2 of cells decreases from  $105 \pm 10$  ms to  $50 \pm 5$  ms, indicating the internalization of superparamagnetic iron oxide, and did not increase during the 144 h incubation



**Figure 5.** T<sub>2</sub> relaxation times of cells labeled with the Tat(FITC)-Cy3.5-CLIO. Cells were labeled (4 h), washed, and incubated in fresh cell culture medium for up to 7 days.

period, indicating retention of the superparamagnetic iron oxide core of the Tat(FITC)-Cy3.5-CLIO nanoparticle.

We next examined the intracellular distribution of Tat(FITC)-Cy3.5-CLIO and Tat(FITC) by confocal microscopy as a function of time after loading (Figure 6). Cells were unfixed, to prevent shifts in distribution due to fixation (16), and exposure time was adjusted to correct for the loss of fluorescence (Figure 4B). Nanoparticle-loaded cells showed fluorescence in the nucleus and cytoplasm with either FITC or Cy3.5 immediately after labeling or 24 h after labeling. By 72 h after loading, nuclear fluorescence was not observed. Tat(FITC) also showed a broad intracellular distribution after labeling and after 24 h, whereas after 72 h, fluorescence was similar to unlabeled cells. Overlays of FITC and Cy3.5 fluorescence (yellow in Figures 6C, F, and I) showed a similar distribution of FITC and Cy3.5 fluorescence.

## DISCUSSION

The general design we employed for dual fluorochrome labeled nanoparticles features one fluorochrome directly attached to the cross-linked dextran, Cy3.5, with a second supplied by a FITC-labeled peptide (Figure 1). This allows different peptides to be attached to the same parent nanoparticle with different linkages and valences, and the fate of peptide and nanoparticle can be tracked by fluorescence. Here we use a dual fluorochrome-labeled nanoparticle, Tat(FITC)-Cy3.5-CLIO, with 24 copies of Tat(FITC) attached through a thioether linkage per nanoparticle, and used this nanoparticle to monitor the fate of the Tat(FITC) peptide and nanoparticle (Cy3.5-CLIO) after administration to cells. Tat(FITC)-Cy3.5-CLIO-loaded cells lost fluorescence from FITC and Cy3.5 with a similar time course (Figure 4), and patterns of intracellular distribution of both fluorochromes (Figure 6) were similar. This suggests that Cy3.5 and FITC remain attached to the nanoparticle coating of cross-linked, polymeric dextran and that this coating was poorly excreted over the time course of our experiments. This result was in contrast to a disulfide-linked Tat(FITC)-Cy3.5-CLIO, made as described (14), where FITC fluorescence was far more rapidly lost than Cy3.5 fluorescence (data not shown). Nanoparticles with disulfide linkage between Tat(FITC) and the Cy3.5-CLIO undergo an intracellular separation of Tat(FITC) and Cy3.5-CLIO, with rapid elimination of the Tat(FITC) peptide and retention of Cy3.5-CLIO. High concentrations of glutathione are believed to create a reducing

environment in cells, which can break disulfide bonds (17). Similar results with disulfide-linked conjugates have been obtained by others; see for example, ref 18.

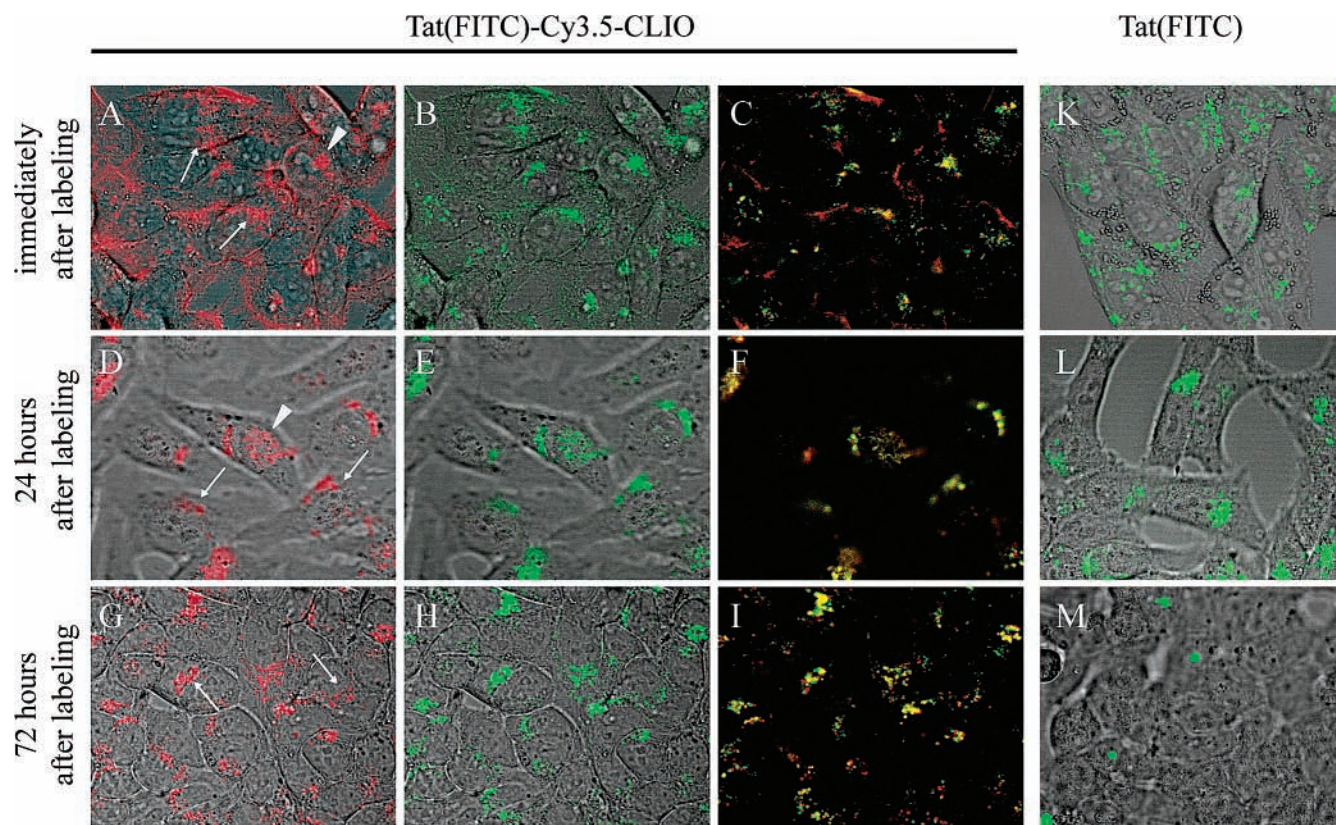
**Tat(FITC) Peptide versus Tat(FITC)-Cy3.5-CLIO Nanoparticle Metabolism.** Both Tat(FITC) and Tat(FITC)-CLIO were rapidly internalized, labeling the population of HeLa cells uniformly, with increasing levels of intracellular fluorescence per cell over the 180 min incubation period (Figure 2). While the internalization of the Tat(FITC) and Tat(FITC)-Cy3.5-CLIO were similar, the fates of the peptide and nanoparticle after internalization were quite different. Tat(FITC)-loaded cells showed a sharp decrease in RMF and TCF after 24 h in peptide-free media (Figures 4B and 4C), and by 72 h more than 80% of cells were unlabeled (Figure 4A). With Tat(FITC)-Cy3.5 CLIO, when a correction was made for cell division, cells retained their fluorescence after 24 h in media and lost only about 50% of their FITC or Cy3.5 over the next 48 h. When cells were loaded with Tat(FITC)-Cy3.5-CLIO and incubated in nanoparticle-free media, T<sub>2</sub> dropped and did not change over a 144 h incubation period, indicating a general lack of excretion of the superparamagnetic iron oxide core of the nanoparticle. Hence the Tat(FITC) peptide rapidly labeled cells, but fluorescence was rapidly lost, presumably due to the excretion of the peptide or a fragment. The Tat(FITC)-Cy3.5-CLIO also rapidly labeled cells, but the excretion was either slow, based on the retention of fluorescence, or not detectable based on relaxation time measurements. The dominant pathway for nanoparticle elimination was distribution to daughter cells after cell division.

The Tat(FITC)-Cy3.5-CLIO nanoparticle is a highly stable nanoparticle because dextran is tightly bound to the surface of the iron oxide by cross-linking, and a reduction-insensitive thioether bond is used to attach the peptide to the nanoparticle. Separation of Cy3.5 and FITC is unlikely, based on the nanoparticle design (Figure 1) that requires a proteolytic cleavage between two highly modified amino acids, the C-terminal cysteine attached to the CLIO nanoparticle, and the penultimate lysine, attached to FITC. Degradation of a major part of the tat peptide may occur without severing the bonds between FITC or Cy3.5 and the coating of cross-linked dextran. The similar retention of the Cy3.5 and FITC fluorescence by cells (Figures 3 and 4) is consistent with this high chemical stability and suggests that both fluorochromes remain attached to the cross-linked coating of dextran after internalization by cells.

HeLa cells loaded with Tat(FITC)-Cy3.5-CLIO were unable to digest the superparamagnetic iron oxide sufficiently to cause T<sub>2</sub> to increase during our 144 h observation period. When injected intravenously, superparamagnetic iron oxides are phagocytosed, with a drop in the T<sub>2</sub> of the liver and spleen (19, 20). Over a period of days, T<sub>2</sub> increases back to normal values, due to dissolution of the iron oxide crystal, with the iron joining normal body pools. Our studies suggest that lifetime of superparamagnetic iron oxide in HeLa cells is considerably longer than in phagocytic cells. The retention of T<sub>2</sub> depression is a desirable feature that can allow cells to be tracked by MRI in vivo for long periods of time.

The ability of tat peptide to deliver a variety of agents of varying sizes and chemical compositions into cells in vitro and in vivo has been explored (1, 21). Particularly intriguing is the potential of the tat peptide to deliver macromolecules such as proteins or enzymes (10, 22, 23) and nanoparticles (9) both into cells and across endo-





**Figure 6.** Localization of Tat(FITC)-Cy3.5-CLIO or Tat(FITC) peptide as a function of time by confocal microscopy of unfixed cells. Cells were labeled with Tat(FITC)-Cy3.5-CLIO (A–I) or Tat(FITC) peptide (K–M). FITC fluorescence is shown in green and Cy3.5 fluorescence in red. The two are superimposed in yellow (C, F, I). Cells were labeled (1 h) analyzed immediately (A–C, K), after 24 h (D–F, L) or after 72 h (G–I, M). Exposure time was adjusted to give similar overall fluorescence intensities at all time points. Arrows indicate perinuclear distribution. Arrowheads indicate nuclear distribution.

thelial and epithelial barriers in vivo. However, a recent study examining radiolabeled tat peptide transport across bladder as an epithelial layer did not find evidence of such transport (24). The loss of cellular fluorescence of Tat(FITC)-Cy3.5-CLIO suggests that the transcellular passage of the nanoparticle, if it occurs, will be a slow and inefficient process compared to internalization. Attempts to study tat-mediated transcellular nanoparticle transport should use analytical methods of very high sensitivity that can detect very stable features of the tat macromolecule or nanoparticle. In the current study we followed the fate of cellular fluorescence for 72 h and internalized superparamagnetic iron oxide over 144 h, a time period during which the fate of a technetium 99m-labeled tat peptide-magnetic nanoparticle would be difficult to observe due to radiochemical decay ( $t_{1/2} = 6$  h) (24). On the other hand, a recently developed enzyme immunoassay method for detecting immunoreactive fluorescein, a method that is nonisotopic and which measures difficult to metabolize fluorescein, might provide an accurate view of the magnitude of the transcellular passage of tat-nanoparticles (25). Using the FITC immunoassay the transcellular transport of Tat(FITC)-Cy3.5-CLIO using CaCo-2 cell monolayers has been observed to have a lag period time course (Koch et al., manuscript in preparation). Studies of metabolism of Tat(FITC) peptide and Tat(FITC)-Cy3.5-CLIO, such as the current one, can lead to insights regarding the likely rates of tat-mediated, transcellular transport in and through cell layers, and guide the selection of analytical tools to measure such transport.

#### ACKNOWLEDGMENT

This work was supported in part by NIH Grants R01 CA86782.

#### LITERATURE CITED

- (1) Rothbard, J. B., Garlington, S., Lin, Q., Kirschberg, T., Kreider, E., and McGrane, P. L. et al. (2000) Conjugation of arginine oligomers to cyclosporin A facilitates topical delivery and inhibition of inflammation. *Nat. Med.* 6, 1253–1257.
- (2) Polyakov, V., Sharma, V., Dahlheimer, J. L., Pica, C. M., Luker, G. D., and Piwnica-Worms, D. (2000) Novel Tat-peptide chelates for direct transduction of technetium-99m and rhenium into human cells for imaging and radiotherapy. *Bioconjugate Chem.* 11, 762–771.
- (3) Eguchi, A., Akuta, T., Okuyama, H., Senda, T., Yokoi, H., Inokuchi, H. et al. (2001) Protein transduction domain of HIV-1 Tat protein promotes efficient delivery of DNA into mammalian cells. *J. Biol. Chem.* 276, 26204–10.
- (4) Ford, K. G., Souberbielle, B. E., Darling, D., and Farzaneh, F. (2001) Protein transduction: an alternative to genetic intervention? *Gene Ther.* 8, 1–4.
- (5) Snyder, E. L., and Dowdy, S. F. (2001) Protein/peptide transduction domains: potential to deliver large DNA molecules into cells. *Curr. Opin. Mol. Ther.* 3, 147–152.
- (6) Josephson, L., Tung, C. H., Moore, A., and Weissleder, R. (1999) High-efficiency intracellular magnetic labeling with novel superparamagnetic-Tat peptide conjugates. *Bioconjugate Chem.* 10, 186–191.
- (7) Lewin, M., Carlesso, N., Tung, C. H., Tang, X. W., Cory, D., Scadden, D. T. et al. (2000) Tat peptide-derivatized magnetic nanoparticles allow in vivo tracking and recovery of progenitor cells. *Nat. Biotechnol.* 18, 410–414.
- (8) Kircher, M. F., Allport, J. R., Graves, E. E., Love, V., Josephson, L., Lichtman, A. H. et al. (2003) In vivo high

- resolution 3D imaging of antigen-specific cytotoxic T-lymphocyte trafficking to tumors. *Cancer Res.*, in press.
- (9) Wunderbaldinger, P., Josephson, L., and Weissleder, R. (2002) Tat peptide directs enhanced clearance and hepatic permeability of magnetic nanoparticles. *Bioconjugate Chem.* **13**, 264–8.
- (10) Schwarze, S. R., Ho, A., Vocero-Akbani, A., and Dowdy, S. F. (1999) In vivo protein transduction: delivery of a biologically active protein into the mouse. *Science* **285**, 1569–1572.
- (11) Schwarze, S. R., and Dowdy, S. F. (2000) In vivo protein transduction: intracellular delivery of biologically active proteins, compounds and DNA. *Trends Pharmacol Sci.* **21**, 45–48.
- (12) Josephson, L., Perez, J. M., and Weissleder, R. (2001) Magnetic nanosensors for the detection of oligonucleotide sequences. *Angewandte Chemie, International Edition*, **40**, 3204–3206.
- (13) Shen, T., Weissleder, R., Papisov, M., Bogdanov, A., Jr., and Brady, T. J. (1993) Monocrystalline iron oxide nanocompounds (MION): physicochemical properties. *Magn Reson Med*, **29**, 599–604.
- (14) Zhao, M., Kircher, M. F., Josephson, L., and Weissleder, R. (2002) Differential conjugation of tat Peptide to superparamagnetic nanoparticles and its effect on cellular uptake. *Bioconjugate Chem.* **13**, 840–844.
- (15) Hogemann, D., Ntziachristos, V., Josephson, L., and Weissleder, R. (2002) High throughput magnetic resonance imaging for evaluating targeted nanoparticle probes. *Bioconjugate Chem.* **13**, 116–121.
- (16) Richard, J. P., Melikov, K., Vives, E., Ramos, C., Verbeure, B., Gait, M. J. et al. (2003) Cell-penetrating peptides. A reevaluation of the mechanism of cellular uptake. *J. Biol. Chem.* **278**, 585–590.
- (17) Meister, A. (1995) Glutathione metabolism. *Methods Enzymol.* **251**, 3–7.
- (18) Trail, P. A., Willner, D., Knipe, J., Henderson, A. J., Lasch, S. J., Zoeckler, M. E. et al. (1997) Effect of linker variation on the stability, potency, and efficacy of carcinoma-reactive BR64-doxorubicin immunoconjugates. *Cancer Res.* **57**, 100–105.
- (19) Weissleder, R., Stark, D. D., Engelstad, B. L., Bacon, B. R., Compton, C. C., White, D. L. et al. (1989) Superparamagnetic iron oxide: pharmacokinetics and toxicity. *AJR Am. J. Roentgenol.* **152**, 167–173.
- (20) Ferrucci, J. T., and Stark, D. D. (1990) Iron oxide-enhanced MR imaging of the liver and spleen: review of the first 5 years. *AJR Am J Roentgenol.* **155**, 943–950.
- (21) Vives, E., Brodin, P., Lebleu, B. (1997) A truncated HIV-1 Tat protein basic domain rapidly translocates through the plasma membrane and accumulates in the cell nucleus. *J. Biol. Chem.* **272**, 16010–16017.
- (22) Schwarze, S. R., Hruska, K. A., and Dowdy, S. F. (2000) Protein transduction: unrestricted delivery into all cells? *Trends Cell Biol.* **10**, 290–295.
- (23) Fawell, S., Seery, J., Daikh, Y., Moore, C., Chen, L. L., Pepinsky, B. et al. (1994) Tat-mediated delivery of heterologous proteins into cells. *Proc. Natl. Acad. Sci. U. S. A.* **91**, 664–668.
- (24) Violini, S., Sharma, V., Prior, J. L., Dyszlewski, M., and Piwnicka-Worms, D. (2002) Evidence for a plasma membrane-mediated permeability barrier to Tat basic domain in well-differentiated epithelial cells: lack of correlation with heparan sulfate. *Biochemistry* **41**, 12652–12661.
- (25) Kelly, K. A., Reynolds, F., Weissleder, R., and Josephson, L. (2003) FITC-hapten immunoassay for determination of peptide–cell interactions. *Anal. Chem.*, submitted.

BC034123V



# Transferrin-Containing, Cyclodextrin Polymer-Based Particles for Tumor-Targeted Gene Delivery

Nathalie C. Bellocq,<sup>†</sup> Suzie H. Pun,<sup>†,§</sup> Gregory S. Jensen,<sup>†</sup> and Mark E. Davis<sup>\*,‡</sup>

Insert Therapeutics, Inc., Pasadena, California and California Institute of Technology, Pasadena, California  
Received July 17, 2003

Transferrin is a well-studied ligand for tumor targeting due to upregulation of transferrin receptors in numerous cancer cell types. Here, we report the development of a transferrin-modified, cyclodextrin polymer-based gene delivery system. The delivery system is comprised of a nanoparticle (formed by condensation of a cyclodextrin polycation with nucleic acid) that is surface-modified to display poly(ethylene glycol) (PEG) for increasing stability in biological fluids and transferrin for targeting of cancer cells that express transferrin receptor. A transferrin-PEG-adamantane conjugate is synthesized for nanoparticle modification. The transferrin conjugate retains high receptor binding and self-assembles with the nanoparticles by adamantane (host) and particle surface cyclodextrin (guest) inclusion complex formation. At low transferrin modification, the particles remain stable in physiologic salt concentrations and transfect K562 leukemia cells with increased efficiency over untargeted particles. The increase in transfection is eliminated when transfections are conducted in the presence of excess free transferrin. The transferrin-modified nanoparticles are appropriate for use in the systemic delivery of nucleic acid therapeutics for metastatic cancer applications.

## INTRODUCTION

One of the most challenging applications of gene therapy is its use against metastatic cancer. The delivery of nucleic acid therapeutics to disseminated tumor sites demands a vehicle capable of systemic administration that will be able to localize in tumor areas. While viral vectors containing therapeutic genes have shown anti-tumor responses via direct tumoral injections, these vectors generally suffer from immunogenicity issues that make repeat systemic administrations problematic (1, 2). Nonviral vectors, whose assets include low T-cell and humoral immunogenicity, offer a viable alternative approach. In addition, nonviral vectors can be readily modified with ligands for cell targeting.

Transferrin (Tf), an iron-binding glycoprotein, is a well-studied ligand for tumor targeting (3, 4). Iron-loaded (holo-) transferrin is recognized by and binds to transferrin receptors on cell surfaces. Transferrin is then endocytosed into acidic compartments. The drop in pH triggers the iron dissociation, and the iron-poor (apo-) transferrin is recycled to the cell surface and released (4). Expression of transferrin receptor (Tf-R) is elevated in rapidly dividing cells due to a need for iron; therefore, Tf-R is often upregulated on surfaces of malignant cells and has been used as a tumor-targeting ligand for several drug delivery systems (5).

Anticancer agents such as doxorubicin have been conjugated to transferrin for tumor targeting (6–8). Transferrin has also been used for targeting nonviral gene delivery vehicles to cancerous cells (9–19). However, the synthesis and characterization of these multicomponent materials is often not completely defined or con-

trolled. For example, doxorubicin–transferrin conjugates were initially prepared by glutaraldehyde cross-linking between the amines on the transferrin (lysine) and the doxorubicin. These conjugates exhibited cytotoxic activity to tumor cell lines (20, 21). However, polymeric products are likely to be formed using this cross-linking method, and the resulting conjugates are poorly defined from a chemical point of view (4). In addition, the binding affinities of the conjugates are significantly reduced from the affinity of the natural protein (21). The “second generation” doxorubicin–transferrin synthesis was improved by Kratz and colleagues by thiolating transferrin with Traut's reagent and then reacting it with maleimide derivatives of doxorubicin (7). Advantages of this approach include less random cross-linking and also the incorporation of a potentially reversible hydrazone linkage. However, the resulting conjugates still contained ~10% transferrin dimers that were not separated from the monomeric conjugates (7). Numerous other transferrin–doxorubicin conjugates have been prepared and one has even been explored for human use in a phase I clinical trial (22).

For targeted gene delivery, approaches include direct transferrin conjugation onto activated surfaces of polycation/nucleic acid complexes (17) or linkage via biotin/streptavidin interactions to plasmid DNA (19). One method of transferrin conjugation to poly(ethylenimine) that has yielded promising *in vivo* targeting of tumors involves oxidation of carbohydrate groups associated with the transferrin followed by reductive amination with the primary amines of poly(ethylenimine) (23). These literature examples show the potential of tumor-targeting via transferrin–Tf-R interactions.

We have developed a cyclodextrin-based polymer delivery system that has the potential of being used for systemic nucleic acid delivery (24). The delivery system consists of two components. The first component is a cyclodextrin-containing polycation that is used for nucleic acid condensation into nanoparticles (25, 26), and the

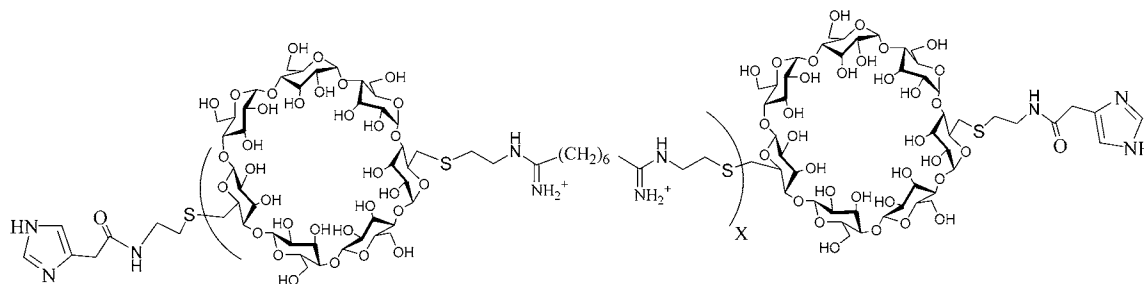
\* To whom correspondence should be addressed. E-mail: mdavis@cheme.caltech.edu.

<sup>†</sup> Insert Therapeutics, Inc.

<sup>‡</sup> California Institute of Technology.

<sup>§</sup> Current address: Department of Bioengineering, University of Washington, Seattle, WA 98195.





## CDP-Imid

second component is an adamantane-terminated modifier for stabilizing the particles in order to (i) minimize interactions with plasma and (ii) target cell surface receptors (27). The specific ligands contained in the second component mediate cell targeting specificity, e.g., Tf ligands for cells with Tf-R. The two components self-assemble with nucleic acids to form stable and uniform sub-100 nm particles. The modular design of this delivery system allows each component to be synthesized and characterized separately.

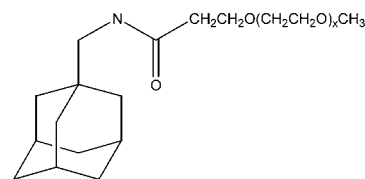
Here, we investigate the synthesis of transferrin-poly(ethylene glycol)-adamantane (Tf-PEG-AD) conjugates (second component of the delivery system) and their use in formulating a complete delivery system for systemic application. In subsequent reports, we will show that these delivery vehicles can successfully target and deliver either oligonucleotides (28, 29) or plasmids (30, 31) to subcutaneous tumors in nude mice. These constructs can be used as targeting ligands as described above. The process of attaching PEG to a protein is typically achieved by reacting an activated PEG reagent through either the carbohydrate moiety or through the lysine residues (32). Since a typical protein possesses a number of such groups, each having different reactivities and degrees of accessibility, the resulting product contains a family of species that is characterized by a distribution in both the number and position of attachment of the PEG group. Below, we describe an example of a fairly well-defined and characterized preparation of transferrin-PEG conjugates. We report on (i) the effect of the site of modification (lysine residue versus carbohydrate moiety), and (ii) the effect of the degree of modification (number of PEG chains per protein) on the binding affinity toward transferrin receptors. These transferrin-PEG conjugates are used to formulate transferrin-modified particles and some of their properties are presented. The particles are demonstrated to mediate transferrin-mediated delivery of nucleic acids to cultured cells.

## EXPERIMENTAL PROCEDURES

**Material Synthesis.**  *$\beta$ -Cyclodextrin Polymers (CDP-Imid).*  $\beta$ CDP was synthesized according to previously described procedures (25, 26). The number of methylene groups separating the charges in the polycation backbone was chosen to be six to maximize transfection efficiency (26). Imidazole was conjugated to the  $\beta$ CDP polymer by amidation of the primary amines at the end of the polymer with 4-imidazoleacetic acid (Aldrich, St. Louis, MO) (33). In a typical experiment, 200 mg (33.3  $\mu$ mol) of  $\beta$ CDP was dissolved in 800  $\mu$ L of 25 mM MES (pH 6.5) buffer to which was added 4-imidazoleacetic acid, sodium salt hydrate (49.3 mg, 0.333 mmol). This solution was used to dissolve 1-ethyl-3-(3-dimethylaminopropyl)car-

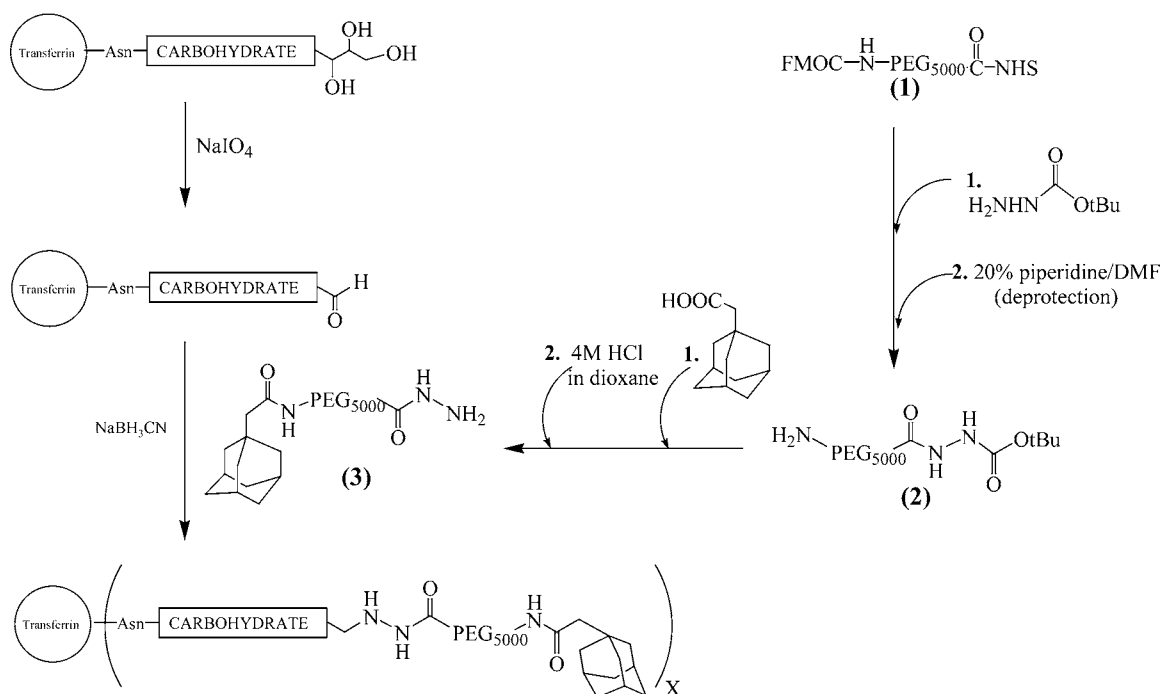
bodiimide (EDC) (0.128 g, 0.666 mmol). Then, *N*-hydroxy-succinimide (NHS) (3.83 mg, 33.3  $\mu$ mol) dissolved in 200  $\mu$ L of 25 mM MES (pH 6.5) buffer was added immediately to the polymer solution. The resulting solution was stirred for 24 h at room temperature and then dialyzed against water using a Spectra Por membrane 1000 MWCO. The solution was lyophilized to dryness. The imidazole content was determined by the TNBS assay (34), followed by UV measurements to quantify the amount of unreacted polymer end groups. The imidazole conjugation was 73%.

*Adamantane-PEG<sub>5000</sub> (AD-PEG).* AD-PEG was synthesized according to published procedures (27). In brief, PEG<sub>5000</sub>-SPA (Nektar AL, Huntsville, AL) was reacted with 5 equiv of 1-adamantane-methylamine (Aldrich) dissolved in dichloromethane. The resulting solution was stirred at room temperature for 4 h. The solvent was removed in vacuo, and water was added to the remaining solution. The solution was centrifuged at 15K rcf for 15 min in order to remove unreacted 1-adamantane-methylamine. The aqueous portion was collected and dialyzed (Slide-A-Lyzer 3500 MWCO, Pierce, Rockford, IL) for 24 h against water. The dialyzed solution was then lyophilized to yield a white, fluffy powder. The product was analyzed on a Beckman Coulter Gold HPLC system equipped with a Richards Scientific Sedere Evaporative Light Scattering detector using a C18 reversed phase column. The product was found to be pure (retention time of PEG<sub>5000</sub>-SPA: 10.7 min; retention time of product: 12.1 min). The product was also confirmed by mass spectroscopy Maldi-ToF analysis.



## AD-PEG

*Transferrin Conjugation via Carbohydrate Groups (Figure 1).* The synthesis involves three steps. First, Fmoc-NH-PEG<sub>5000</sub>-NHS (1) (Nektar AL, 0.2 mmol, 1 g) was added to a round-bottom flask equipped with a stir bar. To this was added *tert*-butyl carbazate (Aldrich, 1.6 mmol, 0.2112 g) dissolved in 7 mL of dichloromethane/ethyl acetate (1:1). The resulting solution was stirred overnight at room temperature. The next day, the solvents were removed in vacuo. The Fmoc group was removed by dissolving the resulting solid in 10 mL of 20% piperidine in dimethylformamide and stirring at room



**Figure 1.** Synthesis of Tf-PEG-AD by carbohydrate conjugation.

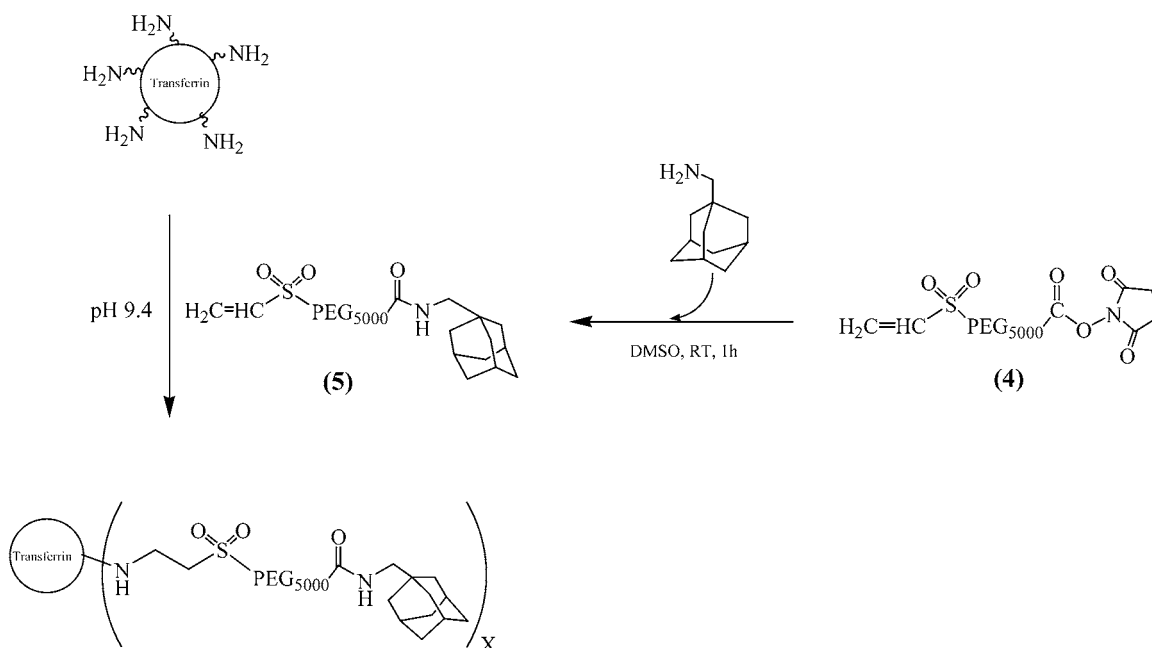
temperature for 5 h. The solvent was removed in vacuo, and the residue was redissolved in water. The solution was centrifuged to remove the undissolved Fmoc group and then dialyzed overnight in Pierce's Slide-A-Lyser, 3500 MWCO. The solution was then lyophilized to afford 790 mg of  $\text{H}_2\text{N}-\text{PEG}_{5000}-\text{NHNHCOOtBu}$  (**2**).

In the second step, *N*-hydroxysuccinimide (Aldrich, 0.24 mmol, 27.3 mg) and adamantanecarboxylic acid (Aldrich, 0.39 mmol, 71.2 mg) were dissolved in 7 mL of dichloromethane and added to **2** (0.16 mmol, 790 mg). To this resulting solution was added 1,3-dicyclohexylcarbodiimide (Aldrich, 1.6 mmol, 0.326 g) dissolved in 3 mL of dichloromethane. The resulting solution was stirred overnight at room temperature. The next day, the solid formed was filtered on a fine glass frit, and the filtrate was concentrated on a rotary evaporator under vacuum. The residue was dissolved in 10 mL of water and centrifuged to remove the unreacted adamantanecarboxylic acid. The solvent was removed in vacuo, and the residue was redissolved in 6 mL of 4 M HCl in dioxane in order to deprotect the *tert*-butoxycarbonyl group and stirred at room temperature for 4 h. The solvent was then removed in vacuo, and the residue was redissolved in water. The resulting solution was dialyzed overnight in Pierce's Slide-A-Lyser (Rockford, IL), 3500 MWCO, and lyophilized to afford 635 mg of  $\text{AD}-\text{PEG}_{5000}-\text{NHNH}_2$  (**3**). This product was analyzed on a Beckman Coulter Gold HPLC system equipped with a Richards Scientific Sedere Evaporative Light Scattering detector using a C18 reversed phase column. The product was also confirmed by mass spectroscopy Maldi-ToF analysis.

In the third step, **3** was conjugated to transferrin according to the protocol described previously by Wagner et al. (23). A solution of 100 mg (1.28  $\mu\text{mol}$ ) of human transferrin (iron poor) (Sigma-Aldrich) in 1 mL of a 30 mM sodium acetate buffer (pH 5) was subjected to gel filtration on a Sephadex G-25 (Supelco) column. The resulting 4 mL of solution containing transferrin (monitoring: UV absorption at 280 nm) was cooled to 0 °C and 80  $\mu\text{L}$  of a 30 mM sodium acetate buffer (pH 5) containing

4 mg (19  $\mu\text{mol}$ ) of sodium periodate was added. The mixture was kept in an ice bath and in the dark for 2 h. For removal of the low molecular weight products, an additional gel filtration (Sephadex G-25, 30 mM sodium acetate buffer (pH 5)) was performed. This yielded a solution containing about 85 mg (1.09  $\mu\text{mol}$ ) of oxidized transferrin. The modified transferrin solution was promptly added to a solution containing 10.9 mg (2.2  $\mu\text{mol}$ ) of  $\text{AD}-\text{PEG}_{5000}-\text{NHNH}_2$  (**3**) in 1 mL of 100 mM sodium acetate (pH 5). The resulting solution was stirred overnight at room temperature. The pH was then brought to 7.5 by addition of 1 M sodium bicarbonate, and four portions of 9.5 mg (150  $\mu\text{mol}$ ) of sodium cyanoborohydride each were added at 1 h intervals. After 4 h, the PEGylated transferrin was purified and concentrated using a Centricon YM-50,000 NMWI device (Millipore). This concentrated solution was subjected to hydrophobic interaction chromatography media (Tosoh Bioscience Butyl-650S) packed into a 10 cm bed height  $\times$  1 cm I.D. column. The products were eluted using a gradient mobile phase from 1.7 M to no ammonium sulfate in 0.1 M potassium phosphate buffered at pH 7.0. The column was run at room temperature, and the elution profile was monitored by UV absorbance at 280 nm. The UV-active fractions were then analyzed on a Beckman Coulter HPLC system equipped with a system gold 168 detector and a Butyl-NPR (Tosoh Bioscience) hydrophobic interaction column using a linear gradient from 1.7 to 0 M ammonium sulfate in 0.1 M potassium phosphate buffered at pH 7.0 at a 1 mL/min flow rate.

**Transferrin Conjugation via Lysine Groups (Figure 2).** Vinyl sulfone- $\text{PEG}_{5000}$ -NHS (**4**) (Nektar AL, 0.147 mmol, 0.5 g) was added to a round-bottom flask equipped with a stir bar and dissolved in 5 mL of DMSO. To this was added adamantanemethylamine (Aldrich, 0.147 mmol, 0.0243 g). The resulting solution was stirred 1 h at room temperature. The solvent was removed in vacuo, and the residue was redissolved in water. The resulting mixture was dialyzed overnight against a 3500 MWCO membrane



**Figure 2.** Synthesis of Tf-PEG-AD by lysine conjugation.

(Spectra Por). The solution was then lyophilized to afford 0.49 g of vinyl sulfone-PEG<sub>5000</sub>-AD (5).

In the second step, 0.49 g (0.1 mmol) of vinyl sulfone-PEG<sub>5000</sub>-AD (5) were added to a solution of 1 g (12.5  $\mu$ mol) of human transferrin (iron poor) (Sigma-Aldrich) in 30 mL of a 0.1 M sodium tetraborate buffer (pH 9.4) and stirred at room temperature for 2 h. The PEGylated transferrin was purified from the unreacted vinyl sulfone-PEG<sub>5000</sub>-AD (5) and concentrated using a Centricon plus YM-50,000 NMWI device (Millipore). This concentrated solution was subjected to hydrophobic interaction chromatography media (Tosoh Bioscience Butyl-650S) packed into a 30 cm bed height  $\times$  4 cm I.D. column. The products were eluted using a gradient mobile phase from 1.7 M to no ammonium sulfate in 0.1 M potassium phosphate buffered at pH 7.0. The column was run at room temperature, and the elution profile was monitored by UV absorbance at 280 nm. The UV active fractions were then analyzed on a Beckman Coulter HPLC system equipped with a system gold 168 detector and a Butyl-NPR (Tosoh Bioscience) hydrophobic interaction column using a linear gradient from 1.7 M to no ammonium sulfate in 0.1 M potassium phosphate buffered at pH 7.0 at a 1 mL/min flow rate (Figure 3A). The product was also confirmed by mass spectroscopy MALDI-ToF analysis (Figure 3B).

**Synthesis of Transferrin-Fluorescein.** Fluorescein-5-thiosemicarbazide, the hydrazide derivative of fluorescein (35) was conjugated to the transferrin via carbohydrate groups (23). A solution of 50 mg (0.64  $\mu$ mol) of human transferrin (iron poor) (Sigma-Aldrich) in 1 mL of ice cold 30 mM sodium acetate buffer (pH 5) was subjected to gel filtration on a Sephadex G-25 (Supelco) column. The resulting 2 mL of solution containing transferrin (monitoring: UV absorption at 280 nm) was cooled to 0  $^{\circ}$ C, and 40  $\mu$ L of a 30 mM sodium acetate buffer (pH 5) containing 2 mg (9.5  $\mu$ mol) of sodium periodate was added. The mixture was kept in an ice bath and in the dark for 2 h. For removal of the low molecular weight products an additional gel filtration (Sephadex G-25, 30 mM sodium acetate buffer, pH 5) was performed. This yielded a solution containing about 43 mg (0.55  $\mu$ mol) of oxidized transferrin. The modified transferrin solution was promptly added to 0.5 mg/mL fluorescein-5-thio-

semicarbazide. The resulting solution was stirred 30 min in the dark at room temperature. The resulting transferrin-fluorescein was then subjected to gel filtration on a Sephadex G-25 (Supelco) column.

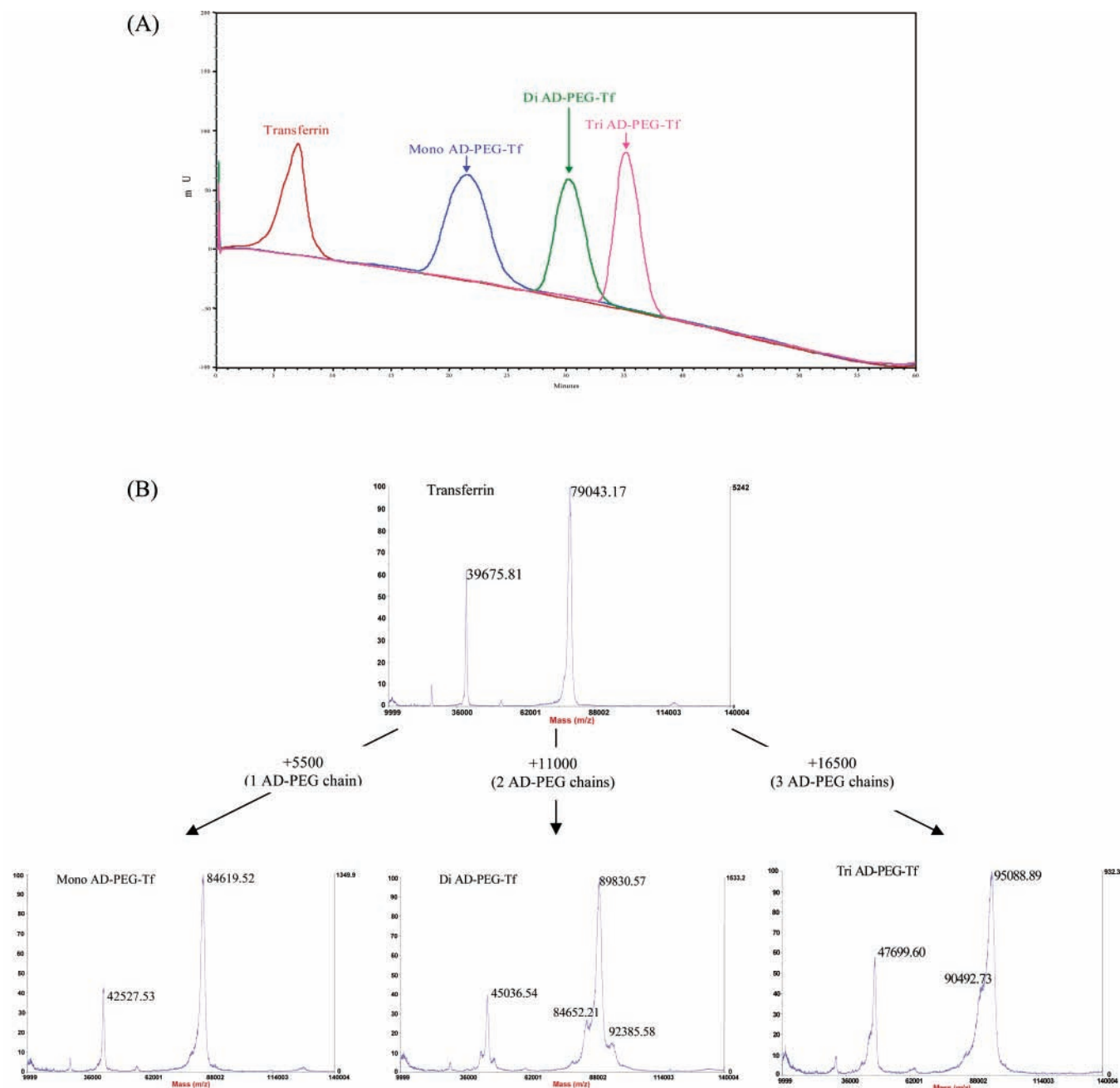
**Iron-Loading of Transferrin Conjugates.** A 40 mg amount of apo-transferrin-based compound (apo-transferrin or apo-transferrin-PEG-AD) was dissolved in 700  $\mu$ L of dH<sub>2</sub>O. To this solution was added 200  $\mu$ L of 5 mM iron citrate and 100  $\mu$ L of 84 mg/mL NaHCO<sub>3</sub>. This solution was allowed to stand for 2–3 h and then dialyzed against dH<sub>2</sub>O overnight. The iron-loading efficiency was calculated by determining the ratio of absorbance at 465 nm (from the oxidized iron) to absorbance at 280 nm (from the tryptophan residues in the protein) and normalizing to the  $A_{465}/A_{280}$  ratio of commercially available holo-transferrin (ratio is denoted as iron-loading in the figures).

**Cell Culture and Cellular Studies.** *Cells and Plasmids.* PC-3 (human prostate carcinoma) and K562 (chronic myelogenous leukemia) cells were purchased from the ATCC. Cells were cultured according to recommended procedures. Media and supplements were purchased from Gibco BRL (Gaithersburg, MD). Plasmid pGL3-CV (Promega, Madison, WI) containing the luciferase gene under the control of the SV40 promoter was amplified and purified by Elim Biopharmaceuticals (Hayward, CA).

**Competitive Binding Studies.** PC-3 cells or K562 cells were plated at 300,000 cells/well in six-well plates. After 24 h, cells were exposed to 250 nM of Tf-fluor (fluorescein-labeled transferrin) with various amounts of unlabeled transferrin or Tf-PEG-AD in MEM media containing 1% BSA. 15 min after exposure, media was removed and cells washed with PBS and prepared for analysis by flow cytometry. For competitive binding studies using particle formulations, the same procedure was followed except Tf or Tf-PEG-AD was first formulated with particles (as described in the following paragraph) and then added to the media at a final concentration of 75 nM.

**Tf-Particle Formulations.** Transferrin-modified particles were prepared at a final DNA concentration of 1 mg/mL. Equal volumes of the four components (plasmid pGL3-CV, CDP-Imid, AD-PEG, and Tf-(PEG-AD))





**Figure 3.** (A) Purification and isolation of transferrin conjugates by hydrophobic interaction chromatography and (B) confirmation of desired products Maldi-ToF mass spectroscopy.

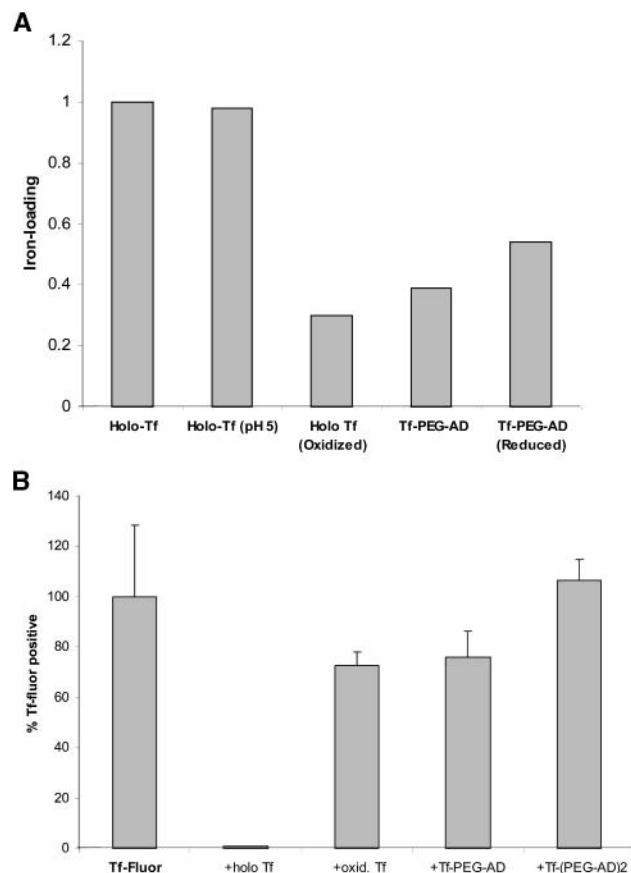
were mixed by adding the three polymer solutions (premixed) to the DNA solution and pipeting gently to mix. CDP-Imid was added at a 3  $\pm$  to DNA. AD-PEG and Tf-(PEG-AD)<sub>x</sub> were included such that the total moles of AD-PEG and Tf-(PEG-AD)<sub>x</sub> is equal to the total moles of cyclodextrin. For particle size and zeta potential determination, particles were prepared, diluted to 5  $\mu$ g/mL in dH<sub>2</sub>O, and analyzed using a ZetaPals dynamic light scattering detector (DLS, Brookhaven Instruments Corporation, Holtsville, NY).

**Tf-Particle Transfection Studies.** K562 cells were plated in 24-well plates at 40,000 cells/well in 0.2 mL Opti-MEM (Invitrogen). Particle-containing solutions (with or without holo-transferrin as a competitive inhibitor) were then added to each well. Five hours after transfection, 0.8 mL of complete media was added to each well. Cells were collected by centrifugation 48 h post-transfection, washed with PBS, lysed and analyzed for luciferase activity by addition of Promega's luciferase assay reagent and light

measurements integrated over 10 s with a Monolight 3010C luminometer (Pharmingen, San Diego, CA).

## RESULTS

**Tf-PEG-AD Synthesized by Carbohydrate Conjugation.** Transferrin-poly(ethyleneglycol)-adamantane (Tf-PEG-AD) was synthesized by carbohydrate conjugation according to literature procedures (Figure 1) (12, 23). In brief, the vicinal diols in the apo-transferrin glycan chains were oxidized to aldehydes with sodium periodate and reacted by reductive amination with adamantane-PEG-hydrazide. The Tf-PEG-AD conjugates were purified by hydrophobic interaction chromatography and iron-loaded with iron citrate in sodium bicarbonate. The iron-loading efficiency of the conjugates was measured by the ratio of the UV absorption at 465 nm (iron-loaded transferrin) to the absorption at 280 nm (total protein)



**Figure 4.** (A). Comparison of iron-loading efficiency of transferrin, oxidized transferrin, and Tf-PEG-AD (synthesized by carbohydrate conjugation). Proteins were purified at each step of the reaction by gel filtration and iron-loaded with iron citrate in sodium bicarbonate. Iron-loading efficiency was measured by the ratio of UV absorption at 465 nm to 280 nm and normalized by the  $A_{465}/A_{280}$  ratio for holo-transferrin. (B) Relative binding of Tf-PEG-AD conjugates (synthesized by carbohydrate conjugation) to Tf-R. PC-3 cells were exposed to 250 nM of Tf-fluor in the presence of transferrin or various transferrin-based conjugates for 15 min. Cells were collected, washed, and analyzed by FACS for cellular association of Tf-fluor.

and normalized by the  $A_{465}/A_{280}$  ratio for holo-transferrin (Figure 4A). The Tf-PEG-AD conjugate had only 40% iron-loading efficiency. The transferrin iron-loading efficiency was then determined at each step in the synthesis process: in the pH 5 reaction buffer, after oxidation, after reaction with AD-PEG-hydrazide, and after hydrazone reduction with sodium cyanoborohydride. Each product was isolated by gel filtration before iron-loading. Efficient iron-loading was obtained at pH 5 (98%), but was substantially reduced after oxidation with sodium periodate (30%). The loss in iron-loading efficiency of the oxidized Tf was maintained upon conjugation to the AD-PEG and was not reversible; the addition of a reducing agent only slightly increased iron-loading efficiency of the conjugated Tf (54%).

The Tf-PEG-AD conjugates were tested for transferrin receptor-binding affinity. PC-3, a human prostate carcinoma cell line that expresses elevated levels of transferrin receptor (Tf-R) (36), were exposed to 250 nM of fluorescein-labeled transferrin (Tf-fluor) and 100 nM of hTf (holo-transferrin), Tf-PEG-AD, or Tf-(PEG-AD)<sub>2</sub>, and analyzed for Tf-fluor cellular association (Figure 4B). Transferrin conjugates with high receptor binding affinities should compete efficiently against Tf-fluor for receptor binding sites, thus reducing average

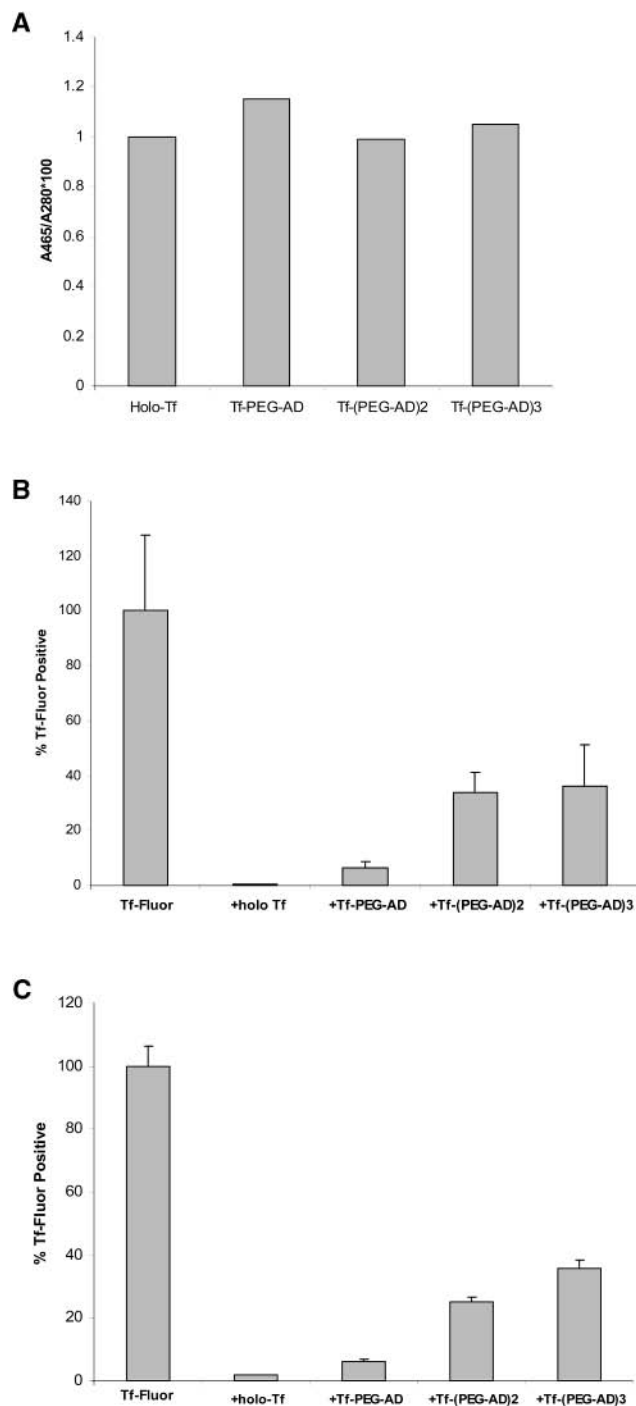
cell fluorescence. The fraction of cells in each sample with Tf-fluor/Tf-R binding above a threshold value was determined by flow cytometry and normalized by the fraction of fluorescein positive cells in samples exposed to 250 nM Tf-fluor alone. The native holo-Tf ligand has the highest binding affinity for the Tf-R and prevents Tf-fluor/Tf-R association (0.6% fluorescein positive cells), even at 40% the concentration of Tf-fluor. Oxidized transferrin has significantly reduced Tf-R binding affinity (72%), as do the purified Tf-PEG-AD (76%) and Tf-(PEG-AD)<sub>2</sub> (107%) conjugates. Because the synthesis of Tf-PEG-AD via the reductive amination scheme causes a significant reduction in the Tf/Tf-R binding, another conjugation method was pursued.

#### Tf-PEG-AD Synthesized by Lysine Conjugation.

A second approach was used to prepare Tf-PEG-AD conjugates (Figure 2). Tf was modified at surface-available lysines via reaction with adamantane-PEG-vinyl sulfone. The Tf-PEG-AD conjugates were separated and purified by hydrophobic interaction column (Figure 3A). Each conjugate (Tf-PEG-AD, Tf-(PEG-AD)<sub>2</sub>, and Tf-(PEG-AD)<sub>3</sub>), could therefore be isolated. Clean separation of the mono-, di-, and trisubstituted transferrins was demonstrated by HPLC analysis with products confirmed by MALDI-ToF mass spectroscopy (Figure 3B). Transferrin is an 80 kDa protein, and the molecular weight of PEG-AD is approximately 5300. As expected, mass spectroscopy of the transferrin yields a sharp signal at 79 kDa. The isolated fractions for Tf-PEG-AD, Tf-(PEG-AD)<sub>2</sub>, and Tf-(PEG-AD)<sub>3</sub> reveal peaks at 84.6 kDa, 89.8 kDa, and 95.1 kDa, respectively. The purified transferrin conjugates were then iron-loaded as described above. Unlike the conjugates synthesized by transferrin oxidation and Schiff base formation, Tf-PEG-AD's prepared by reaction with surface lysines retain high iron-loading efficiencies (all around 100% iron loading, Figure 5A).

The Tf-(PEG-AD), Tf-(PEG-AD)<sub>2</sub>, and Tf-(PEG-AD)<sub>3</sub> compounds were analyzed for receptor-binding to transferrin receptors on both PC-3 and K562 cells as described above (Figure 5B and 5C). The monosubstituted Tf-PEG-AD showed the highest binding affinity to Tf-R of the three conjugates and was only slightly reduced from the native holo-transferrin protein (for PC-3, 6% cells with Tf-fluor association compared with 0.6% in the presence of holo-transferrin and for K562, 6% cells with Tf-fluor association compared with 2% in the presence of holo-transferrin). The ability of Tf-(PEG-AD)<sub>2</sub> to bind to Tf-R was affected by PEG-AD conjugation (34% of PC-3 and 25% of K562 cells fluorescein positive), and Tf-(PEG-AD)<sub>3</sub> revealed the lowest receptor-binding of the three conjugates (36% cells fluorescein positive for both PC-3 and K562 cells). Therefore, the monosubstituted Tf-PEG-AD synthesized by lysine conjugation was used for all further experiments described.

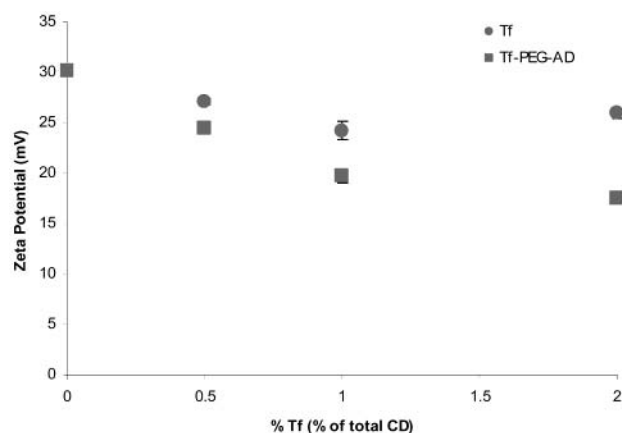
**Formulation of Tf-Modified Particles.** Transferrin-modified particles were prepared by mixing the following components (prepared in water solutions) in equal volumes: (1) CDP-Imid, a linear, cyclodextrin-based polycation that condenses and protects plasmid DNA, (2) adamantane-PEG (AD-PEG), a particle modifier that provides for PEGylation to give stabilization against nonspecific interactions including self-aggregation, (3) AD-PEG-Tf (synthesized by lysine conjugation), another modifier that introduces transferrin for targeting to Tf-R-expressing cells (for controls, holo-transferrin was used instead of AD-PEG-Tf), and (4) plasmid DNA. The first three components are premixed and added to the fourth solution. Particles were prepared with various



**Figure 5.** (A) Comparison of iron-loading efficiency of transferrin and Tf-PEG-AD conjugates synthesized by lysine reaction. Iron-loading efficiency was measured by the ratio of UV absorption at 465 nm to 280 nm and normalized by the  $A_{465}/A_{280}$  ratio for holo-transferrin. Relative binding of Tf-PEG-AD conjugates (synthesized by lysine conjugation) to Tf-R to PC3 (5B) and K562 (5C) cells. Cells were exposed to 250 nM of Tf-fluor in the presence of transferrin or various transferrin-based conjugates for 15 min. Cells were collected, washed, and analyzed by FACS for cellular association of Tf-fluor.

amounts of Tf or Tf-PEG-AD (0%, 0.5%, 1%, and 2% of total cyclodextrins by mole).

The particle size and surface charge were measured by dynamic light scattering and zeta potential, respectively. Average particle diameter of all formulations was ~100 to 150 nm. Transferrin modification was verified by monitoring the average zeta potential of the particles



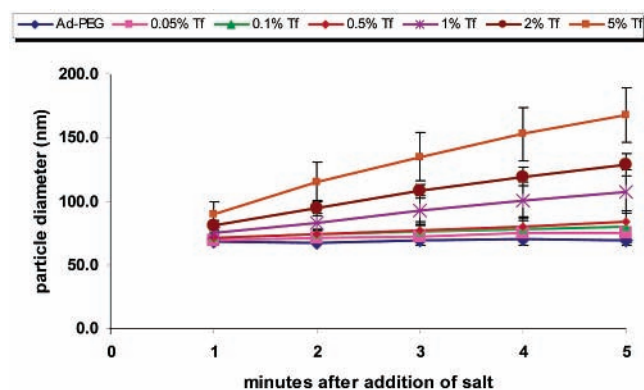
**Figure 6.** Zeta potential of transferrin modified particles. Transferrin-modified particles were prepared at 3 +/- (CDP-Imid to pGL3-CV) with 100% adamantane modification (total of AD-PEG and Tf-PEG-AD). Particles were analyzed using a ZetaPals dynamic light scattering detector.

(Figure 6). Transferrin is an anionic protein; therefore, transferrin association with the positively charged particles should decrease the surface charge. Addition of free transferrin decreases average particle zeta potential from +30 mV to +25 mV (at 1% and 2% transferrin to CD). The effect of transferrin on surface charge levels off at 1% (~+25 mV for both 1% and 2% transferrin). The zeta potential of particle formulations with Tf-PEG-AD also decreased with higher concentration of Tf-PEG-AD, and indicated successful modification of particles with Tf-PEG-AD. At 1% and 2% Tf-PEG-AD, average particle zeta potentials are +20 mV and +17 mV, respectively.

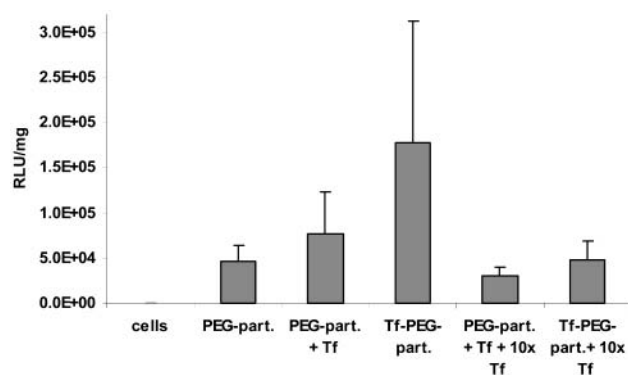
Transferrin-modified particles (Tf-PEG-particle) should also have higher association to transferrin receptors on cell surfaces than Tf-PEG-AD because the Tf-PEG-particle has the ability to bind to several Tf-R while Tf-PEG-AD/Tf-R binding is a single interaction event. PC-3 cells were exposed for 15 min to 250 nM of Tf-fluor and 75 nM of Tf or Tf-PEG-AD in the presence and absence of CDP-Imid-based particles (at a 2 Tf per 100 cyclodextrin mole ratio). The cells were prepared and analyzed by flow cytometry as described previously for the receptor binding assay. Particle addition alone did not affect Tf-fluor association to PC-3 cells. However, formulation of Tf-PEG-AD with particles reduces the percentage of fluorescein positive cells by 15% from the percentage when exposed directly to Tf-PEG-AD and Tf-fluor. Similarly, exposure of cells to Tf in the presence of particles only reduces the percentage by 6%.

The salt stability of various Tf-PEG-particle formulations was determined by monitoring particle size in physiological salt solutions by dynamic light scattering. Tf-PEG-particles were formulated with 0%, 0.05%, 0.1%, 0.5%, 1.0%, 2%, and 5% Tf-PEG-AD (of total cyclodextrins by mole with the remaining balance to 100% comprised of AD-PEG) in a small volume (40  $\mu$ L) of water. PBS, pH 7.2, was then added (1.2 mL) and average particle diameter recorded every minute for 5 min (Figure 7). Unmodified particles aggregated rapidly in salt (final diameter of 300 nm), but PEGylated particles remained stable with diameters of ~70 nm. The stability of Tf-modified particles depended on the amount of Tf-PEG-AD present during formulation. Formulations with 0.05%, 0.1%, and 0.5% Tf-PEG-AD were stable in salt (respective diameters of 75, 80, and 83 nm after 5 min in salt solutions) while formulations with 1%, 2%, and 5% Tf-PEG-AD aggregated slowly upon salt addition (107, 129, and 168 nm after 5 min, respectively).





**Figure 7.** Salt stability of transferrin-modified particles. Transferrin-modified particles were prepared at 3  $\pm$  (CDP-Imid to pGL3-CV) with 100% adamantane modification (total of AD-PEG and Tf-PEG-AD). PBS (1.2 mL) was added to the particle solution and average particle diameter every minute for 5 min by dynamic light scattering.



**Figure 8.** Luciferase transfection of transferrin-particles to K562 cells. K562 cells were plated in 24-well plates and exposed to 1  $\mu$ g of pGL3-CV in four formulations: particles modified with 100% AD-PEG, particles modified with 100% AD-PEG, and mixed with 0.05% holo-Tf (by mole to cyclodextrins), particles modified with 100% AD-PEG and 0.05% Tf-PEG-AD (Tf-PEG-part.), and Tf-PEG-part. mixed with 10 equiv of holo-Tf (with respect to Tf-PEG-AD). Experiments were conducted with five replicates with average values shown.

**In Vitro Transfection of Tf-Modified Particles to K562 Cells.** Tf-PEG-particles containing pGL3-CV were formulated at 0.05% Tf-PEG-AD (and 99% AD-PEG) and 3  $\pm$  charge ratio (ratio of polymer to plasmid charge by mole) and used to transfect K562 cells. Control samples included PEGylated particles (PEG-particles, 1 AD-PEG to 1 cyclodextrin by mole), PEG-particles formulated with holo-Tf (at 0.05% Tf by mole cyclodextrin), PEG-particles formulated with holo-Tf (at 0.05% Tf by mole cyclodextrin) mixed with 10 equiv of free holo-Tf, and Tf-PEG-particles mixed with 10 equiv of free holo-Tf. Transfections were carried out in serum-free media, and cells were lysed and analyzed for luciferase activity 48 h after transfection with results reported in relative light units per mg of protein (RLU/mg protein, protein levels determined by Lowry protein assay, Figure 8). The positively charged, PEGylated particles transfected K562 cells ( $4.6 \times 10^4$  RLU/mg). Formulation of these particles with holo-Tf increased delivery efficiency by 1.7-fold ( $7.7 \times 10^4$  RLU/mg). The Tf-PEG-particles, with Tf attachment to the particles via inclusion complex formation, demonstrated the highest luciferase expression ( $1.8 \times 10^5$  RLU/mg) with a 4-fold enhancement over the PEG-particles. To confirm specific transfection enhancement by Tf-mediated delivery, Tf-PEG-particle transfections were also conducted in the presence of 10

equiv of holo-Tf. These samples did not reveal much increase in luciferase gene delivery ( $4.7 \times 10^4$  RLU/mg) over the PEGylated particle. The transfection by particles formulated with holo-Tf was likewise reduced in the presence of free transferrin ( $3 \times 10^4$  RLU/mg). In addition, no toxicity was observed in any of the samples.

## DISCUSSION

The goal of this work is to develop a transferrin-mediated, tumor-targeting gene delivery system that is chemically well-defined. Although targeting to tumors via mixtures of transferrin and liposomal or polymeric delivery systems has been reported (15, 16, 18, 37), the characteristics and efficacy of these constructs are highly dependent on formulation methods. We strived to prepare stable formulations without significantly diminished interaction affinity between the transferrin targeting ligand and Tf-R on the surfaces of carcinoma cells. Here, Tf-PEG-AD conjugates were synthesized for assembly with cyclodextrin-containing particles by inclusion complex formation between the adamantanes and particle surface displayed cyclodextrins. The Tf-PEG-AD interacts with the particles through charge (anionic Tf-cationic particles) and inclusion complexation formation (AD-CD).

A Tf-PEG-AD ligand was first synthesized by sodium periodate oxidation of the apo-transferrin carbohydrate moieties followed by a reductive amination reaction with AD-PEG-hydrazide (Figure 1). The synthesis protocol was adapted from published procedures for preparing Tf-poly(L)lysine and Tf-poly(ethylenimine) conjugates (12, 13, 23). The various transferrin products were purified by hydrophobic interaction chromatography, an established method for isolation of PEGylated proteins (38, 39). The mono-, di-, and tri-PEGylated transferrins were successfully isolated and converted to the iron-loaded form by iron citrate treatment in bicarbonate. A distinct difference in color was noted between holo-Tf and holo-Tf-PEG-AD solutions at the same concentrations. This discrepancy was quantified by measuring the UV absorbance at 465 nm (for the oxidized iron) and 280 nm (for total protein concentration). The results confirmed that the Tf-PEG-AD conjugates suffered from low iron-loading efficiency. The amount of iron-loading into transferrin was therefore measured at each reaction step, and the cause of reduced iron-loading was determined to be the oxidation of transferrin with sodium periodate (Figure 4A). The oxidized transferrin was separated from excess sodium periodate by chromatography before iron citrate treatment. Iron-loading of oxidized transferrin was only 30%, and efficiency was not recovered by reaction with AD-PEG-hydrazide or by subsequent reduction with sodium cyanoborohydride. The iron-loading protocol conditions (concentration of iron citrate and iron-loading time) were also varied in an attempt to increase efficiencies, but did not result in any substantial improvements.

The binding affinity of the transferrin conjugates for Tf-R on surfaces of cultured cells was assessed by monitoring the competitive binding against fluorescently labeled transferrin (Figure 4B). Holo-transferrin completely displaces the fluorescently labeled transferrin, even at a reduced concentration (the Tf-fluor was also synthesized by reductive amination with fluorescein hydrazide and has lower receptor binding affinity than the natural ligand). The transferrin iron-loading efficiency was found to be a good indicator of receptor binding. Transferrin with low iron-loading efficiencies

(oxidized transferrin and Tf-PEG-AD conjugates) also had low receptor binding. Indeed, apo-transferrin is reported to have lower binding affinity for the transferrin receptor at physiologic pH to unloading after recycling to cell surfaces (40).

After finding that the affinity for the Tf-R was greatly reduced when conjugating AD-PEG to Tf via carbohydrate oxidation, an alternative synthetic approach was pursued. Tf-PEG-AD was synthesized by reaction of lysine amines with a vinyl sulfone that was prepared as AD-PEG-vinyl sulfone (Figure 2). The vinyl sulfone group is known to be highly selective at pH 7 for reaction with sulfhydryl groups (relative to reaction with amino groups). However, it has been shown that the reaction with lysine sites occurs slowly at pH 9.4 and is essentially complete (41). A reaction conducted at pH 7 revealed that the vinyl sulfone did not react with cysteine thiols groups of transferrin because no free thiols are available on the protein surface (as confirmed by Ellman's titration (34)). The Tf-PEG-AD conjugates were thus synthesized at pH 9.4 by reaction between the vinyl sulfone and the lysine groups. The resulting product was a physical mixture of conjugates with variable number of attachments of AD-PEG chains. These conjugates were purified and Tf-PEG-AD, Tf-(PEG-AD)<sub>2</sub>, and Tf-(PEG-AD)<sub>3</sub> were isolated by hydrophobic interaction chromatography (Figure 3A) with product confirmation by Maldi-ToF mass spectroscopy (Figure 3B). Iron-loading was efficient for all transferrin conjugates synthesized by lysine conjugation (Figure 5A). During this process, it was found that it was important to freeze the protein conjugates slowly in dry ice before lyophilization. Rapid freezing in liquid nitrogen impaired the iron-loading efficiency.

The transferrin conjugates were tested for transferrin receptor binding to both PC-3 and K562 cell lines. PC-3, an adherent cell line, and K-562, a suspension cell line, have upregulated transferrin receptors on their surfaces; K-562 cells are reported to have  $1.5 \times 10^5$  Tf-R per cell (40, 42). Unlike transferrin conjugates synthesized by carbohydrate reaction, all lysine-reacted Tf-PEG-AD were able to compete effectively with fluorescein-labeled transferrin for receptor binding in both cell lines (6–36% fluorescein positive cells for lysine-reacted conjugates compared with 76–100% fluorescein positive cells for carbohydrate-reacted conjugates, Figure 5B and 5C). The transferrin receptor binding affinity was decreased by modification with multiple PEGs. While Tf-PEG-AD demonstrated slightly lower binding constants from the natural ligand, the difference was larger for the di- and tri-PEGylated conjugates. With higher PEGylation events, it becomes more likely for the reaction site to interfere with the ligand/receptor binding site. In addition, a multi-PEGylated protein may be sterically inhibited from receptor interactions. On the basis of these receptor binding studies, the mono-Tf-PEG-AD conjugate was used for all subsequent experiments.

Transferrin-modified particles were formulated using the Tf-PEG-AD conjugate. The Tf-modified particles are composed of four components: the nucleic acid of interest, a polycation for condensation of nucleic acid, AD-PEG for particle stabilization, and AD-PEG-Tf for tumor targeting. CDP-Imid, a linear, cyclodextrin-based polycation end-modified with imidazoles, was used as the nucleic acid condensing agent. The parent cyclodextrin-based polymer has been optimized structurally for in vitro transfection and the imidazoles further boost transfection efficiency and act as buffers in endosomes (24). The increased gene expression may be occurring by

mechanisms similar to those proposed for histidylated polymers and poly(ethylenimine) (43, 44). AD-PEG<sub>5000</sub> was used because previous experiments demonstrated that a molecular weight of 5000 was necessary for stabilizing cyclodextrin-based particles in salt-containing media (27).

The particles were formulated by mixing the three polymer solutions together and then adding the polymer solution to the nucleic acid solution. The polymers and DNA self-assembled quickly (in seconds) to form particles with diameters ~100–150 nm (as measured by dynamic light scattering). The amount of Tf-PEG-AD (by mole % to cyclodextrin) included in the formulations ranged from 0% to 2% with the balance (to 100% CD) consisting of AD-PEG. This range was chosen by estimating the amount of Tf that can pack around a 100 nm sphere, subject to space constraints.

The zeta potential for each of the formulations was also measured (Figure 6). As expected, the zeta potentials decrease with increasing concentration of Tf or Tf-PEG-AD in the formulations. Transferrin, an anionic protein, decreases zeta potential as it associates with the positively charged particle surface via electrostatic interactions. Formulations with Tf-PEG-AD have a larger impact on zeta potential, likely due to the higher surface affinity resulting from both inclusion complex formation and electrostatic interactions. With both ligands, the decrease in zeta potential levels off in the formulations with 1–2% transferrin and likely indicates surface saturation.

Incorporation of the Tf-PEG-AD ligand in the particle was further confirmed by competitive receptor-binding studies. Fluorescein-labeled transferrin and either transferrin or Tf-PEG-AD were incubated with PC-3 cells, both as free ligands in solution and as a component in a particle formulation. The percentage of fluorescein-positive cells, indicating Tf-fluor binding to receptors, was determined by flow cytometry. The fluorescence profile of the cells was the same for cells exposed to 250 nM Tf-fluor alone and to 250 nM Tf-fluor/PEGylated particles (no Tf on the particles); therefore, the presence of particles alone does not affect Tf-fluor association with PC-3 cells. Formulation of 250 nM Tf-fluor/75 nM Tf-PEG-AD with the particles reduced the number of fluorescein positive cells by 15% as compared with 250 nM Tf-fluor/75 nM Tf-PEG-AD alone, while formulation of 250 nM Tf-fluor/75 nM Tf with the particles reduced the number by 6% as compared with 250 nM Tf-fluor/75 nM Tf alone. The difference in receptor binding between free ligand and ligand formulated with particles (keeping the concentration of transferrin constant) can therefore be attributed to an increase in binding affinity resulting from multidentate interactions between the ligand-modified particles and cell surface receptors. The stronger interaction between Tf-PEG-AD and the CDP-Imid particles (as opposed to Tf and particle) is reflected in the larger difference in receptor binding affinity between free ligand and ligand/particle formulations.

It has been demonstrated previously that AD-PEG imparts salt stability to cyclodextrin-based particles by forming a hydrophilic layer on the particle surface (27). It is expected that, above certain proportions, incorporation of the large and bulky Tf-PEG-AD ligand will interfere with the PEG layer and eliminate its stabilization effect. The particle sizes of several Tf-particle formulations were monitored by dynamic light scattering to determine their salt stability in 150 mM PBS (Figure 7). Formulations with 0%, 0.05%, 0.1%, and 0.5% Tf-PEG-AD were stable, whereas average particle diam-



eters of formulations with 1%, 2%, and 5% Tf-PEG-AD increased steadily after salt addition (although not to the extent of the unmodified particles).

The Tf-particle formulation was then tested for gene delivery efficiency to K562 cells (Figure 8). K562 cells are suspension cells that are notoriously difficult to transfect. The PEGylated particles are positively charged and can bind via electrostatic interaction with proteoglycans on the cell surface with eventual uptake by endocytosis (45). Formulations with 0.05% transferrin result in a 1.7-fold increase in delivery efficiency. The transferrin associates with the particles by electrostatic interactions and may facilitate cell association and uptake. The Tf-PEG-AD particle preparations (with 0.05% Tf-PEG-AD) demonstrate the highest transfection, a 4-fold increase over AD-PEG-particles. The enhanced transfection is due to transferrin-mediated uptake; the addition of excess transferrin (10 equiv) as a competitor for the Tf-R eliminates the transfection enhancement.

In summary, we describe the synthesis, purification, and in vitro use of a transferrin conjugate for targeting to tumor cells that are known to have upregulated transferrin receptors. While the potential of transferrin-mediated targeting has been clearly demonstrated by others in the field (4, 7, 8, 14, 23, 46–49), we focused on preparing delivery systems with high receptor binding affinities. To this end, monofunctionalized Tf-PEG-AD conjugates were synthesized and purified by hydrophobic interaction chromatography. Isolation of the monofunctionalized transferrin is important for maintaining high receptor binding affinity. Sato et al. also isolated Tf-DNA conjugates by selecting conjugates that bind strongly to Tf-R affinity columns (19). However, most other conjugation chemistries for transferrin impair receptor binding or result in polymeric products. Glutaraldehyde cross-linking of transferrin with drug molecules forms polymeric products (4) with receptor binding affinities half that of transferrin (21), SPDP cross-linking of Tf with polycations yields multiple populations (including polymeric products) (50), and reaction by carbohydrate oxidation adversely affects receptor binding (as described previously). The transferrin conjugates described here are monofunctionalized and retain high receptor binding affinity. Physicochemical characterization and in vitro studies demonstrate that these conjugates should be useful in providing transferrin receptor-targeted drug delivery systems. The synthesis and purification protocols discussed here can also be extended to prepare transferrin conjugates for small molecule delivery. Applications of the transferrin-modified nucleic acid delivery system described herein are currently being investigated for the in vivo delivery of both oligonucleotide and plasmids in mouse xenograph models (29, 31).

#### ACKNOWLEDGMENT

We thank Prof. Ernest Beutler (Scripps Institute) for his scientific advice and Mona Shahgholi (California Institute of Technology) for her assistance with MALDI-ToF analysis. Mark E. Davis is a consultant to and has financial interest in Insert Therapeutics, Inc.

#### LITERATURE CITED

- (1) Green, N., and Seymour, L. (2002) Adenoviral vectors: systemic delivery and tumor targeting. *Cancer Gene Ther.* 9, 1036–42.
- (2) Nielsen, L., and Maneval, D. (1998) P53 tumor suppressor gene therapy for cancer. *Cancer Gene Ther.* 5, 52–63.
- (3) Singh, M. (1999) Transferrin as a targeting ligand for liposomes and anti-cancer drugs. *Curr. Pharm. Des.* 5, 443–51.
- (4) Qian, Z. M., Li, H., Sun, H., and Ho, K. (2002) Targeted drug delivery via the transferrin receptor-mediated endocytosis pathway. *Pharm. Rev.* 54, 561–587.
- (5) Thorstensen, K., and Romslo, I. (1993) The transferrin receptor: its diagnostic value and its potential as therapeutic target. *Scand. J. Clin. Lab Invest.* 53, 113–120.
- (6) Li, H., Sun, H., and Qian, Z. M. (2002) The role of the transferrin-transferrin-receptor system in drug delivery and targeting. *Trends in Pharm. Sci.* 23, 206–209.
- (7) Kratz, F., Beyer, U., Roth, T., Tarasova, N., Collery, P., Lechenault, F., Cazabat, A., Schumacher, P., Unger, C., and Falken, U. (1998) Transferrin conjugates of doxorubicin: synthesis, characterization, cellular uptake, and in vitro efficacy. *J. Pharm. Sci.* 87, 338–346.
- (8) Kratz, F., Beyer, U., Schumacher, P., Kruger, M., Zahn, H., Roth, T., Fiebig, H., and Unger, C. (1997) Synthesis of new maleimide derivatives of daunorubicin and biological activity of acid labile transferrin conjugates. *Bioorg. Med. Chem. Lett.* 7, 617–622.
- (9) Cotten, M., Längle-Rouault, F., Kirlappos, H., Wagner, E., Mechtler, K., Zenke, M., Beug, H., and Birnstiel, M. (1990) Transferrin-polycation-mediated introduction of DNA into human leukemic cells: Stimulation by agents that affect the survival of transfected DNA or modulate transferrin receptor levels. *Proc. Natl. Acad. Sci. U.S.A.* 87, 4033–4037.
- (10) Kircheis, R., Blessing, T., Brunner, S., Wightman, L., and Wagner, E. (2001) Tumor targeting with surface-shielded ligand-polycation DNA complexes. *J. Controlled Release* 72, 165–170.
- (11) Kircheis, R., Wightman, L., Schreiber, A., Robitza, B., Rossler, V., Kurs, M., and Wagner, E. (2001) Polyethylenimine/DNA complexes shielded by transferrin target gene expression to tumors after systemic application. *Gene Ther.* 8, 28–40.
- (12) Kircheis, R., Kichler, A., Wallner, G., Kurs, M., Ogris, M., Felzmann, T., Buchberger, M., and Wagner, E. (1997) Coupling of cell-binding ligands to polyethylenimine for targeted gene delivery. *Gene Ther.* 4, 409–418.
- (13) Ogris, M., Steinlein, P., Kurs, M., Mechtler, K., Kircheis, R., and Wagner, E. (1998) The size of DNA/transferrin-PEI complexes is an important factor for gene expression in cultured cells. *Gene Ther.* 5, 1425–1433.
- (14) Ogris, M., Brunner, S., Schüller, S., Kircheis, R., and Wagner, E. (1999) PEGylated DNA/transferrin-PEI complexes: reduced interaction with blood components, extended circulation in blood and potential for systemic gene delivery. *Gene Ther.* 6, 595–605.
- (15) Simoes, S., Slepishkin, V., Gaspar, R., Pedrosa de Lima, M., and Düzgünes, N. (1998) Gene delivery by negatively charged ternary complexes of DNA, cationic liposomes and transferrin or fusogenic peptides. *Gene Ther.* 5, 955–964.
- (16) Xu, L., Frederik, P., Pirollo, K. F., Tang, W.-H., Rait, A., Xiang, L.-M., Huang, W., Cruz, I., Yin, Y., and Chang, E. (2002) Self-assembly of a virus-mimicking nanostructure system for efficient tumor-targeted gene delivery. *Hum. Gene Ther.* 13, 469–481.
- (17) Fisher, K., Ulbrich, K., Subr, V., Ward, C., Mautner, V., Blakey, D., and Seymour, L. (2000) A versatile system for receptor-mediated gene delivery permits increased entry of DNA into target cells, enhanced delivery to the nucleus and elevated rates of transgene expression. *Gene Ther.* 7, 1337–1343.
- (18) Seki, M., Iwakawa, J., Cheng, H., and Cheng, P.-W. (2002) p53 and PTEN/MMAC1/TEP1 gene therapy of human prostate PC-3 carcinoma xenograft, using transferrin-facilitated lipofection gene delivery strategy. *Human Gene Therapy* 13, 761–773.
- (19) Sato, Y., Yamauchi, N., Takahashi, M., Sasaki, K., Fukaura, J., Neda, H., Fujii, S., Hirayama, M., Itoh, Y., Koshita, Y., Kogawa, K., Kato, J., Sakamaki, S., and Niitsu, Y. (2000) In vivo gene delivery to tumor cells by transferrin-streptavidin-DNA conjugate. *FASEB J.* 14, 2108–2118.



- (20) Yeh, C., Taylor, C., and Faulk, W. (1984) Transferrin binding by peripheral blood mononuclear cells in human lymphomas, myelomas and leukemias. *Vox Sang.* 46, 217–223.
- (21) Berczi, A., Ruthner, M., Szuts, V., Fritzer, M., Schweinzer, E., and Goldenberg, H. (1993) Influence of conjugation of doxorubicin to transferrin on the iron uptake by K562 cells via receptor-mediated endocytosis. *Eur. J. Biochem.* 213, 427–436.
- (22) Faulk, W., Taylor, C., Yeh, C., and McIntyre, J. (1990) Preliminary clinical study of transferrin-adriamycin conjugate for drug delivery to acute leukemia patients. *Mol. Biother.* 2, 57–60.
- (23) Wagner, E., Cotten, M., Mechtler, K., Kirlappos, H., and Birnstiel, M. L. (1991) DNA-binding transferrin conjugates as functional gene-delivery agents: synthesis by linkage of polylysine or ethidium homodimer to the transferrin carbohydrate moiety. *Bioconjugate Chem.* 2, 226–231.
- (24) Davis, M., Pun, S., Bellocq, N., Reineke, T., Popielarski, S., Mishra, S., and Heidel, J. (2003) Self-assembling nucleic acid delivery vehicles via linear, water-soluble, CD-containing polymers. *Curr. Med. Chem.*, in press.
- (25) Gonzalez, H., Hwang, S., and Davis, M. (1999) New class of polymers for the delivery of macromolecular therapeutics. *Bioconjugate Chem.* 10, 1068–74.
- (26) Hwang, S., Bellocq, N., and Davis, M. (2001) Effects of Structure of Beta-Cyclodextrin-Containing Polymers on Gene Delivery. *Bioconjugate Chem.* 12, 280–290.
- (27) Pun, S. H., and Davis, M. (2002) Development of a Non-Viral Gene Delivery Vehicle for Systemic Application. *Bioconjugate Chem.* 13, 630–639.
- (28) Bellocq, N., Pun, S., Grubbs, B., Jensen, G., Liu, A., Cheng, J., Mavis, M., Bakker, A., Janssens, B., Floren, W., Janicot, M., Peeters, J., and Brewster, M. (2002). Development of transferrin-modified, cyclodextrin-based particles for the delivery of RNA-cleaving DNA enzyme (DNAzyme) molecules. Paper presented at the 2nd International Symposium on Tumor Targeted Delivery Systems, Rockville, MD.
- (29) Pun, S., Bakker, A., Bellocq, N., Grubbs, B., Jensen, G., Liu, A., Cheng, J., Janssens, B., Floren, W., Peeters, J., Janicot, M., Mavis, M., and Brewster, M. Transferrin-targeted, cyclodextrin polymer-based gene delivery systems. II. Applications in the delivery of RNA-cleaving DNA enzyme (DNAzyme) molecules. Manuscript in preparation.
- (30) Bellocq, N. C., Davis, M. E., Engler, H., Jensen, G. S., Liu, A., Machemer, T., Maneval, D. C., Quijano, E., Pun, S. H., Schleup, T., and Wen, S. (2003). Transferrin-targeted, cyclodextrin polycation-based gene vector for systemic delivery. Presented at the American Society of Gene Therapy Annual Conference, Washington, D. C.
- (31) Schleup, T., Bellocq, N., Davis, M., Engler, H., Liu, A., Machemer, T., Maneval, D., Philopena, J., Quijano, E., Pun, S. H., and Wen, S. Tumor-targeted nonviral gene delivery vehicle for systemic delivery. Manuscript in preparation.
- (32) Larson, R., Menard, V., Jasobs, H., and Kim, S. (2001) Physicochemical characterization of poly(ethylene glycol)-modified anti-GAD antibodies. *Bioconjugate Chem.* 12, 861–9.
- (33) Sehgal, D., and Vijay, I. (1994) A method for the high efficiency of water-soluble carbodiimide-mediated amidation. *Anal. Biochem.* 218, 87–91.
- (34) Hermanson, G. T. (1996) *Bioconjugate Techniques*, p 132, Academic Press, Rockford, IL.
- (35) Hermanson, G. T. (1996) *Bioconjugate Techniques*, pp 313–315, Academic Press, Rockford, IL.
- (36) Keer, H., Kozlowski, J., Tsai, Y., Lee, C., McEwan, R., and Grayhack, J. (1990) Elevated transferrin receptor content in human prostate cancer cell lines assessed in vitro and in vivo. *J. Urol.* 143, 381–385.
- (37) Xu, L., Pirollo, K. F., Tang, W.-H., Rait, A., and Chang, E. (1999) Transferrin-liposome-mediated systemic p53 gene therapy in combination with radiation results in regression of human head and neck cancer xenografts. *Hum. Gene Ther.* 10, 2941–2952.
- (38) Snider, J., Neville, C., Yuan, L.-C., and Bullock, J. (1992) Characterization of the heterogeneity of poly(ethylene glycol)-modified superoxide dismutase by chromatographic and electrophoretic techniques. *J. Chromatogr.* 599, 141–155.
- (39) Seely, J. E., and Richey, C. W. (2001) Use of ion-exchange chromatography and hydrophobic interaction chromatography in the preparation and recovery of poly(ethylene glycol)-linked proteins. *J. Chromatogr. A* 908, 235–241.
- (40) Klausner, R., VanRenswoude, J., Ashwell, G., Kempf, C., Schechter, A., Dean, A., and Bridges, K. (1983) Receptor-mediated Endocytosis of Transferrin in K562 Cells. *J. Biol. Chem.* 258, 4715–4724.
- (41) Morpurgo, M., Veronese, F., Kachensky, D., and Harris, J. (1996) Preparation and characterization of poly(ethylene glycol) vinyl sulfone. *Bioconjugate Chem.* 7, 363–8.
- (42) Barabas, K., and Faulk, W. (1993) Transferrin Receptors Associate with Drug Resistance in Cancer Cells. *Biochem. Biophys. Res. Commun.* 197, 702–708.
- (43) Pack, D., Putnam, D., and Langer, R. (2000) Design of imidazole-containing endosomolytic biopolymers for gene delivery. *Biotechnol. Bioeng.* 67, 217–23.
- (44) Boussif, O., Lezoualc'h, F., Zanta, M., Mergny, M., Scherman, D., Demeneix, B., and Behr, J.-P. (1995) A versatile vector for gene and oligonucleotide transfer into cells in culture and in vivo: Polyethylenimine. *Proc. Natl. Acad. Sci. U.S.A.* 92, 7297–7301.
- (45) Mislick, K., and Baldeschwieler, J. (1996) Evidence for the role of proteoglycans in cation-mediated gene transfer. *Proc. Natl. Acad. Sci. U.S.A.* 93, 12349–12354.
- (46) Dash, P., Read, M., Fisher, K., Howard, K., Wolfert, M., Oupicky, D., Subr, V., Strohalm, J., Ulbrich, K., and Seymour, L. (2000) Decreased Binding to Proteins and Cells of Polymeric Gene Delivery Vectors Surface Modified with a Multivalent Hydrophilic Polymer and Retargeting through Attachment of Transferrin. *J. Biol. Chem.* 275, 3793–3802.
- (47) Fritzer, M., Szekeres, T., Szuts, V., Jarayam, H., and Goldenberg, H. (1996) Cytotoxic Effects of a Doxorubicin-Transferrin Conjugate in Multidrug-Resistant KB Cells. *Biochem. Pharm.* 51, 489–493.
- (48) Wagner, E., Zenke, M., Cotten, M., Beug, H., and Birnstiel, M. L. (1990) Transferrin-polycation conjugates as carriers for DNA uptake into cells. *Proc. Natl. Acad. Sci. U.S.A.* 87, 3410–3414.
- (49) Liang, K. W., Hoffman, E. P., and Huang, L. (2000) Targeted delivery of plasmid DNA to myogenic cells via transferrin-conjugated peptide nucleic acid. *Mol. Ther.* 1, 236–243.
- (50) Wagner, E., Cotten, M., Foisner, R., and Birnstiel, M. (1991) Transferrin-polycation–DNA complexes: The effect of polycations on the structure of the complex and DNA delivery to cells. *Proc. Natl. Acad. Sci. U.S.A.* 88, 4255–4259.

BC034125F

# Inter- and Intramolecular Fluorescence Quenching of Organic Dyes by Tryptophan

Nicole Marmé,<sup>†</sup> Jens-Peter Knemeyer,<sup>†</sup> Markus Sauer,<sup>\*,‡</sup> and Jürgen Wolfrum<sup>†</sup>

Physikalisch-Chemisches Institut, Universität Heidelberg, Im Neuenheimer Feld 253, 69120 Heidelberg, Germany and Fakultät für Physik, Angewandte Laserphysik und -spektroskopie, Universität Bielefeld, Universitätsstrasse 25, 33615 Bielefeld, Germany. Received July 23, 2003; Revised Manuscript Received September 23, 2003

Steady-state and time-resolved fluorescence measurements were performed to elucidate the fluorescence quenching of oxazine, rhodamine, carbocyanine, and bora-diaza-indacene dyes by amino acids. Among the natural amino acids, tryptophan exhibits the most pronounced quenching efficiency. Especially, the red-absorbing dyes ATTO 655, ATTO 680, and the oxazine derivative MR 121 are strongly quenched almost exclusively by tryptophan due to the formation of weak or nonfluorescent ground-state complexes with association constants,  $K_{\text{ass}}$ , ranging from 96 to 206 M<sup>-1</sup>. Rhodamine, fluorescein, and bora-diaza-indacene derivatives that absorb at shorter wavelengths are also quenched substantially by tyrosine residues. The quenching of carbocyanine dyes, such as Cy5, and Alexa 647 by amino acids can be almost neglected. While quenching of ATTO 655, ATTO 680, and the oxazine derivative MR121 by tryptophan is dominated by static quenching, dynamic quenching is more efficient for the two bora-diaza-indacene dyes Bodipy-FL and Bodipy630/650. Labeling of the dyes to tryptophan, tryptophan-containing peptides, and proteins (streptavidin) demonstrates that knowledge of these fluorescence quenching processes is crucial for the development of fluorescence-based diagnostic assays. Changes in the fluorescence quantum yield of dye-labeled peptides and proteins might be used advantageously for the quantification of proteases and specific binding partners.

## INTRODUCTION

To date, the use of fluorescently labeled proteins and nucleic acids in various biological and medical relevant assays represents standard technology. Usually, the presence or absence of target molecules is monitored by an increase or decrease in fluorescence intensity of one dye interacting via short-range electronic or long-range dipole–dipole interactions with a second dye (1–5). Deteriorations of the interaction geometry or efficiency are caused, for example, by specific binding or cleavage events. Especially, the use of fluorescence resonance energy transfer (FRET) between a donor, D, and an acceptor dye, A, has increased considerably in the field of biondiagnostics during the past decade (6–8). Other important methods rely on two-color cross-correlation to monitor specific binding events at the single molecule level (9–11). That is, probe and target molecule are labeled with two spectrally distinguishable fluorescent dyes. The two dyes are excited using two different lasers or two-photon excitation with a single laser line and their fluorescence is recorded on two spectrally separated detectors. Colocalization of the two dyes in the observation volume is reflected by a higher cross correlation amplitude.

On the other hand, the absorption and emission spectra, fluorescence quantum yield, and fluorescence lifetime of dyes often vary with environmental conditions. Hence, instead of using interactions between two extrinsic probes, many fluorescent dyes can be used as sensors

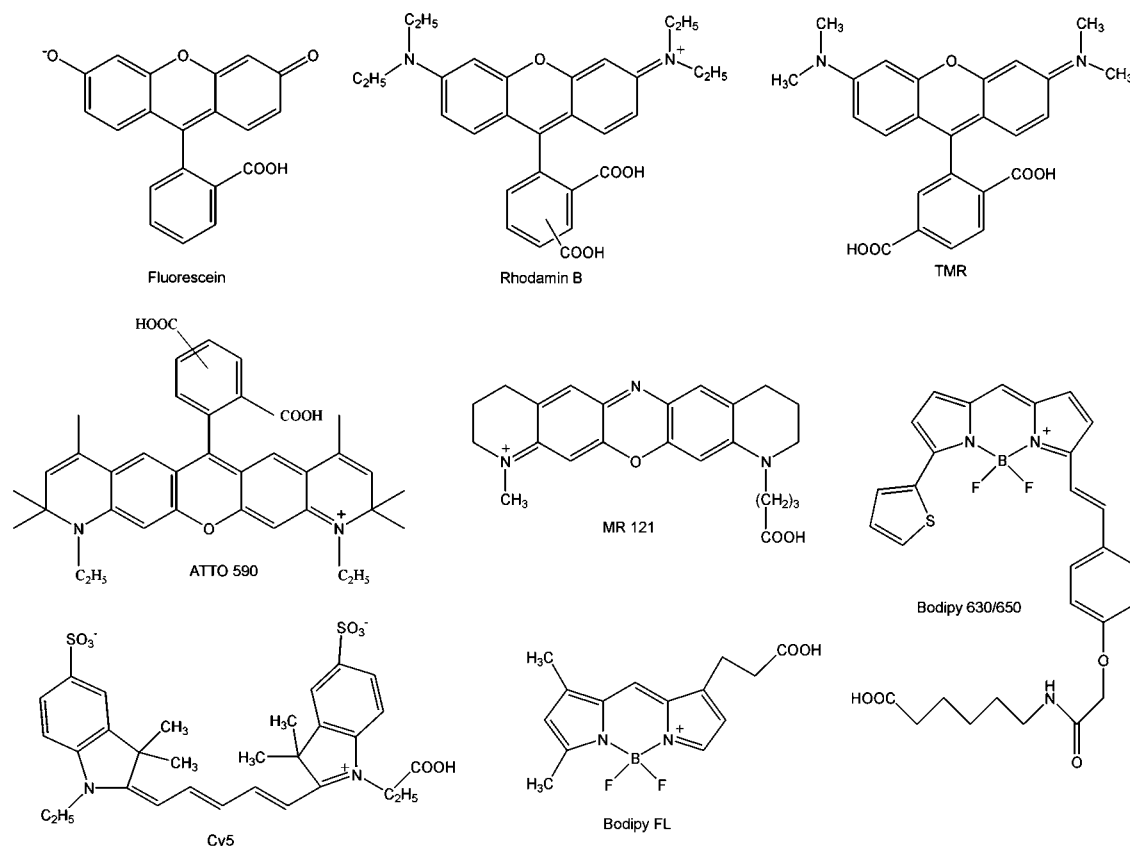
to probe their local environments in biological and analytical applications. For example, interactions of fluorophores with DNA bases can be used for the specific detection of DNA or RNA sequences at the single molecule level (12, 13). Nucleobase-specific interactions have been reported for coumarin (14), rhodamine (15–17), oxazine (12, 13, 18), and bora-diaza-indacene (19) dyes. Nucleobase-specific quenching relies on the differences in specific properties of naturally occurring nucleotides, in particular, the low oxidation potential of the DNA base guanosine (14, 20) and the tendency of many fluorophores to aggregate in aqueous environment to decrease their water accessible area. Thus, dependent on the reduction potential of the fluorophore used, efficient photoinduced electron transfer (PET) can occur between the first excited singlet-state of the dye and the ground-state guanosine (18, 21). With careful design of conformationally flexible probes, e.g. DNA-hairpins that carry several guanosine residues in the complementary stem sequence and the use of appropriate fluorophores (rhodamine and oxazine dyes are well suited candidates), efficient single molecule sensitive DNA-hairpins can be produced (12). If quenching interactions between the fluorophore and the guanosine residue are deteriorated upon specific binding to the target, for example, due to binding of a complementary DNA sequence, or due to cleavage by an endonuclease enzyme, fluorescence of the DNA-hairpin is restored. Although this quenching effect is not always desirable, it can be used to develop new, highly sensitive probes for the detection of specific DNA sequences or proteins (12, 13, 18).

Intra- and intermolecular fluorescence quenching experiments with different dyes and amino acids in water have revealed that a similar mechanism holds true for

\* Corresponding author. Phone: +49-521-106-5450. Fax: +49-521-106-2958. E-mail: sauer@physik.uni-bielefeld.de.

<sup>†</sup> Universität Heidelberg.

<sup>‡</sup> Universität Bielefeld.



**Figure 1.** Molecular structures of fluorescein, rhodamine B, tetramethylrhodamine (TMR), Bodipy-FL, MR 121, ATTO 590, and Bodipy 630/650 investigated in inter-, and intramolecular quenching experiments. The molecular structures of some of the investigated dyes are available, while for other dyes the structures are proprietary (Alexa 647, ATTO 655, ATTO 680).

some amino acids. It has been shown that the fluorescence quantum yield of some fluorescein and bora-diazaindacene derivatives is quenched substantially by tryptophan, and to a smaller degree partly by tyrosine and methionine residues (22–24). The oxidation potential,  $E_{ox}$ , of tryptophan is  $\sim 1V$  (25, 26) even lower than that of dG, so the resulting quenching efficiency can be expected to be relatively strong. The strong fluorescence quenching efficiency of oxazine derivatives by tryptophan residues has been used in oxazine-labeled peptide epitopes to detect the presence of p53-autoantibodies in serum samples of patients (27). The underlying method involves the detection of reversible fluorescence quenching of dyes by tryptophan residues in labeled short peptides derived from the antibody recognition sequence of p53. In the free peptide in aqueous solution fluorescence is reduced, due to the formation of ground-state complexes between the dye and the tryptophan residue and subsequent efficient fluorescence quenching. Binding to the antibody via the tryptophan-containing recognition sequence initiates a spontaneous conformational change in the peptide accompanied by a strong increase in fluorescence intensity. Similar quenching interactions between an oxazine derivative and a tryptophan residue have been used to study intramolecular contact formation in peptides at the single molecule level (28). In contrast to electronic energy transfer-based systems where long-range dipole–dipole interactions occur, efficient electron transfer-based fluorescence quenching within these peptides requires close contact between the fluorophore and the tryptophan.

Consideration of these quenching effects of fluorescent dyes in peptides or proteins by neighboring amino acids is crucial for the development of new fluorescence-based assays. Motivated by these considerations, we measured steady-state and time-resolved intermolecular fluores-

cence quenching of different fluorophores (MR121, ATTO 655, ATTO 680, Cy5, ATTO 590, Alexa 647, tetramethylrhodamine, rhodamine B, Bodipy-FL, Bodipy 630/650, and fluorescein) by several amino acids. Among the fluorophores investigated, the red-absorbing oxazine derivative MR121 and the dyes ATTO 655 and ATTO 680 show the most pronounced quenching efficiency by tryptophan. Other amino acids (tyrosine, phenylalanine, methionine, and histidine) showed only minor quenching efficiencies. The fluorescence intensity and lifetime of the carbocyanine dyes Cy5 and Alexa 647 are only slightly influenced by the presence of amino acids. To investigate intramolecular fluorescence quenching, the fluorophores were covalently attached to amino acids, a tryptophan-containing peptide, and streptavidin. Each hydrophobic binding pocket of streptavidin contains four tryptophan residues that are involved in strong biotin binding (23, 29). We demonstrate that knowledge of the fluorescence quenching behavior of fluorophores by amino acids has to be considered for the design of biological or medical assays.

## EXPERIMENTAL PROCEDURES

**Fluorescent Dyes and Conjugates.** The dyes used in this study were obtained as free carboxy acids, or *N*-hydroxysuccinimidyl esters. ATTO 590, ATTO 655, and ATTO 680 were purchased from ATTO-TEC (Siegen, Germany), Cy5 from Amersham Pharmacia Biotech (Freiburg, Germany), fluorescein, rhodamine B (RB) and tetramethylrhodamine (TMR), Bodipy 630/650, and Bodipy-FL from Molecular Probes (Göttingen, Germany). The oxazine derivative MR121 was kindly provided by K. H. Drexhage (Universität-Gesamthochschule, Siegen). Molecular structures of the fluorophores investigated are shown in Figure 1. When dissolved in water, *N*-hydroxy-



succinimidyl esters are believed to be deactivated within minutes to hours. MR121 and RB were converted into their *N*-hydroxysuccinimyl esters using an equimolar amount of *N*-(3-dimethylaminopropyl)-*N*-ethylcarbodiimide hydrochloride (EDC) and *N*-hydroxysuccinimide (NHS) in acetonitrile. For coupling to the amino groups of amino acids or peptides, 20  $\mu$ L of the activated dyes (0.1 mM in acetonitrile) was mixed with an excess of amino acids or peptides in 50  $\mu$ L of carbonate buffer (0.1 M, pH 8.3). Fluorescent dyes were coupled to the amino group of the lysine residue of the *N*-terminal protected peptide lysine-glycine-glycine-glycine-tryptophan (KGGGW). The reaction solution was incubated for 6 h at room temperature, and the product was purified by HPLC (Hewlett-Packard, Böblingen, Germany) using a reversed-phase column (Knauer, Berlin, Germany) with octadecylsilane-hypersil C18. Separation was performed in 0.1 M triethylammonium acetate, using a linear gradient from 0% to 75% acetonitrile in 20 min. Yields >90% were obtained. To ensure low labeling degrees, the coupling to streptavidin was carried out in 50  $\mu$ L carbonate buffer (0.1 M, pH 8.3) using 20  $\mu$ L of the activated dye solution (0.1 mM in acetonitrile) and a 100-fold excess of streptavidin. Purification of the product was performed with NAP-columns (Sephadex G-25). Absorption measurements revealed an average label degree of <1.

**Spectroscopy.** Absorption spectra were taken on a Cary 500 UV-vis-NIR spectrometer (Varian, Darmstadt, Germany). Corrected fluorescence spectra were performed using a Cary Eclipse fluorescence spectrometer (Varian, Darmstadt, Germany). To avoid reabsorption and reemission effects, concentrations were kept strictly below 1  $\mu$ M (typically 0.1  $\mu$ M) in all measurements. Relative fluorescence quantum yields,  $\Phi_{f,rel}$ , of the fluorescently labeled constructs were measured with respect to the fluorescence intensity of the free dyes under otherwise similar conditions.

Ensemble fluorescence lifetime measurements were performed on a 5000MC spectrometer (IBH, Glasgow, U.K.) using the time-correlated single-photon counting (TCSPC) technique. As excitation sources served a pulsed laser diode emitting at 635 nm with a pulse length of  $\sim$ 200 ps (fwhm), or LEDs emitting at 495 or 590 nm with pulse lengths of  $\sim$ 1 ns (fwhm) at repetition rates of 1 MHz. With this setup, instrument response functions (IRFs) of 220 ps (fwhm) for the laser diode and  $\sim$ 1 ns for the LEDs (fwhm) were measured. The apparatus enables the measurement of fluorescence lifetimes down to 40 ps (for the pulsed laser diode), and  $\sim$ 200 ps (for the pulsed LED). Typically, 3000–5000 photon counts were collected in the maximum channel using 4096 channels. The decay parameters were determined by least-squares deconvolution, and their quality was judged by the reduced  $\chi^2$  values and the randomness of the weighted residuals. In the case that a monoexponential model was not adequate to describe the measured decay, a multiexponential model was used to fit the decay (eq 1),

$$I(t) = I(0) \sum a_i \tau_i \quad (1)$$

where  $a_i$  are the preexponential factors that describe the ratio of the excited species and  $\tau_i$  denote their lifetimes.

## RESULTS AND DISCUSSION

**Intermolecular Fluorescence Quenching of Dyes by Tryptophan.** To investigate intermolecular fluorescence quenching efficiencies, steady-state fluorescence experiments with tetramethylrhodamine (TMR), ATTO

**Table 1. Relative Fluorescence Quantum Yields,  $\Phi_{f,rel}$ , of Fluorescein, Bodipy-FL, TMR, ATTO 590, MR121, ATTO 655, ATTO 680, and Cy5 in Unbuffered Water in the Presence of 30 mM L-Tryptophan (Trp), L-Tyrosine (Tyr), L-Phenylalanine (Phe), L-Methionine (Met), and L-Histidine (His)<sup>a</sup>**

$\Phi_{f,rel}$	Trp	Tyr	Phe	Met	His
fluorescein	0.57 (0.89)	0.83 (0.96)	0.98	0.86	0.94
Bodipy-FL	0.48 (0.85)	0.70 (0.92)	0.95	0.81	0.93
TMR	0.43 (0.77)	0.66 (0.91)	0.89	0.92	0.88
ATTO 590	0.42 (0.80)	0.60 (0.88)	0.96	0.98	1.00
MR 121	0.17 (0.63)	0.82 (0.96)	0.95	0.98	0.98
ATTO 655	0.13 (0.54)	0.83 (0.97)	1.00	1.00	0.99
ATTO 680	0.16 (0.64)	0.91 (0.98)	1.00	1.00	1.00
Cy5	0.91 (0.97)	1.00	1.00	1.00	1.00

<sup>a</sup> Due to lower solubility of Tyr, measurements were performed with 6 mM. The values given (30 mM Tyr) were calculated assuming a linear dependence of fluorescence intensity from quencher concentration. Measured values for 6 mM Tyr are given in brackets. For better comparison, the values in brackets given for Trp quenching are measured from solutions containing 6 mM Trp.

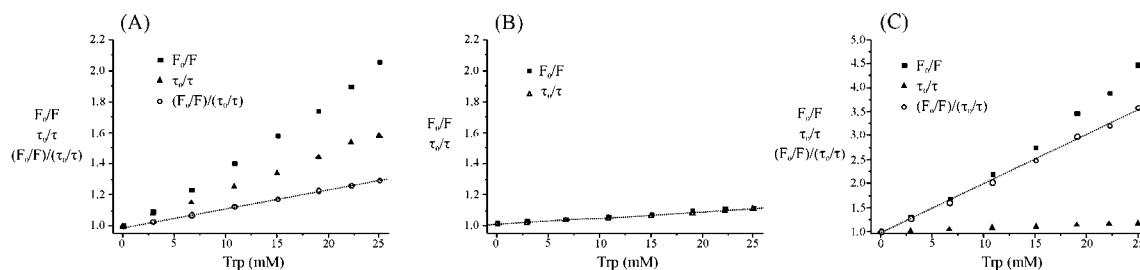
590, Bodipy-FL, fluorescein, MR121, ATTO 655, ATTO 680, and Cy5 were performed with the most potent fluorescence quenchers among the natural amino acids, i.e., the amino acids methionine (Met) and histidine (His), as well as the aromatic amino acids tryptophan (Trp), tyrosine (Tyr), and phenylalanine (Phe). The results are summarized in Table 1. As expected (22–24), among the amino acids investigated, tryptophan exhibits the most pronounced fluorescence quenching. In addition, for the green/yellow-absorbing fluorophores Bodipy-FL, TMR, and ATTO 590, substantial quenching by tyrosine is observed. On the other hand, the quenching efficiency of tyrosine is much less pronounced for most of the red-absorbing fluorophores (MR 121, ATTO 655, and ATTO 680). All other amino acids show only small quenching efficiencies. To summarize, the red-absorbing oxazine derivative MR121 as well as the two ATTO dyes ATTO 655 and ATTO 680 are almost exclusively quenched by tryptophan. On the other hand, rhodamine, and boradiaz-indacene derivatives that absorb at shorter wavelengths, are also quenched substantially by tyrosine residues. The quenching of the carbocyanine dye Cy5 by amino acids is generally very low.

In the following intermolecular studies we restricted our investigations to fluorescence experiments with the most efficient quencher tryptophan. To interpret intermolecular quenching efficiencies of tryptophan, bimolecular quenching experiments with the fluorophores were performed in aqueous solution. Bimolecular static and dynamic quenching constants,  $k_{q,s}$ , and  $k_{q,dyn}$ , were determined from steady-state and time-resolved fluorescence quenching experiments using Stern–Volmer analysis (eqs 2 and 3),

$$F_0/F = 1 + K_s[Q] = 1 + k_{q,s}\tau_0[Q] \quad (2)$$

$$\tau_0/\tau = 1 + K_{dyn}[Q] = 1 + k_{q,dyn}\tau_0[Q] \quad (3)$$

where  $\tau_0$  and  $F_0$  are the fluorescence lifetime and intensity in the absence of a quencher,  $\tau$  and  $F$  are the fluorescence lifetime and intensity in the presence of the quencher  $Q$  with the concentration  $[Q]$ , and  $K_s$  and  $K_{dyn}$  denote the static and dynamic Stern–Volmer constant, respectively. All quenching experiments yielded identical results, within error, in phosphate-buffered saline (PBS) pH 7.4 and unbuffered H<sub>2</sub>O. The fluorescence decays of all fluorophores investigated remain almost monoexpo-



**Figure 2.** Static and dynamic bimolecular Stern–Volmer plots of the bora-diaza-indacene dye Bodipy-FL (A), the carbocyanine dye Cy5 (B), and the oxazine derivative MR121 (C) with Trp in PBS buffer, pH 7.4.

**Table 2.** Fluorescence Lifetimes,  $\tau_0$ , of  $10^{-7}$  M Solutions of Fluorescent Dyes in the Absence of Trp in PBS Buffer, pH 7.4<sup>a</sup>

	$\tau_0$ (ns)	$k_{q,dyn}$ ( $\times 10^9$ M <sup>-1</sup> s <sup>-1</sup> )	$K_{dyn}$ (M <sup>-1</sup> )	$K_{ass.}$ (M <sup>-1</sup> )
fluorescein	3.98	2.4	9.6	16.0
Bodipy-FL	5.80	4.0	23.0	12.0
RB	1.52	4.3	6.5	9.3
TMR	2.25	4.3	9.7	14.0
ATTO 590	3.96	4.0	16.0	15.0
Bodipy 630/650	4.23	3.3	14.0	7.7
MR121	1.81	4.0	7.3	96.0
ATTO 655	1.79	5.1	9.1	206.0
ATTO 680	1.71	4.5	7.7	144.0
Alexa 647	1.0	2.3	2.3	
Cy5	1.0	3.9	3.9	

<sup>a</sup> Fluorescence lifetimes were measured at the emission maxima ( $\chi^2 = 0.90$ –1.15). In addition, the dynamic Stern–Volmer and bimolecular dynamic quenching constants  $K_{dyn}$  and  $k_{q,dyn}$ , respectively, and the association constants,  $K_{ass.}$ , are given (3 $\sigma$ -error estimation: 10% for  $k_{q,s.}$  and  $k_{q,dyn}$ ).  $K_{ass.}$  was determined at Trp concentrations 0–10 mM.  $K_{q,dyn}$  was determined from the longer, quencher-dependent fluorescence lifetime.

nential independent of the Trp concentration. In some cases an additional shorter or longer fluorescence decay component appeared with an amplitude smaller than 0.05. Therefore, bimolecular dynamic quenching constants,  $k_{q,dyn}$ , were calculated from the quencher dependent fluorescence lifetime with an amplitude > 0.95 (Table 2). Figure 2a–c show three typical static and dynamic Stern–Volmer plots. Bodipy-FL (Figure 2a) shows a combination of dynamic and static quenching while Cy5 exhibits only weak dynamic quenching (Figure 2b). In the case of the oxazine derivative MR121, and the two dyes ATTO 655 and ATTO 680, the Stern–Volmer plots are dominated by strong static quenching (Figure 2c). In addition, Stern–Volmer plots obtained from steady-state measurements display upward curvatures for almost all dyes investigated. These deviations from linearity with increasing quencher concentration indicate the presence of at least two populations of fluorophores. The fact that (i) static quenching is much higher than expected for a diffusion-controlled bimolecular reaction and (ii) all dyes investigated show almost monoexponential fluorescence decays independent of the quencher concentration, strongly support the idea of the formation of weak or nonfluorescent ground-state complexes between the fluorophores and Trp in aqueous solutions. Dependent on the relative conformations and resulting interaction geometries, the complexes can be considered as essentially nonfluorescent. Then, the association constant,  $K_{ass.}$ , can be calculated via eq 4 by plotting  $(F_0/F)/(\tau_0/\tau)$  versus the quencher concentration (Figure 2a and 2c).

$$\frac{F_0}{F} = (1 + K_{dyn}[Q])(1 + K_{ass.}[Q]) \quad (4)$$

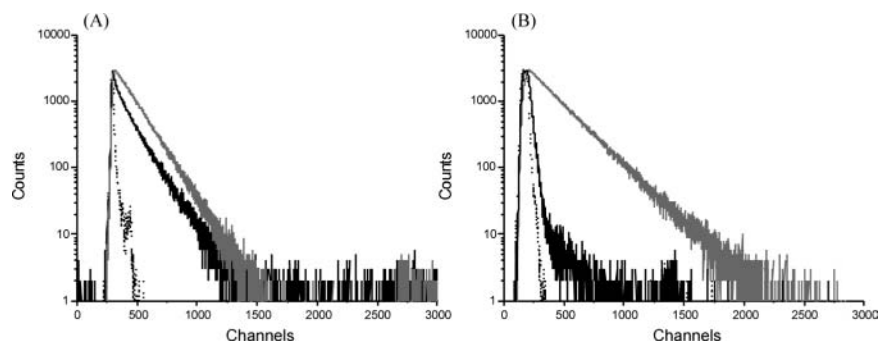
**Table 3.** Relative Fluorescence Quantum Yields,  $\Phi_{f,rel}$ , of Fluorescein, Bodipy-FL, and ATTO 655 Amino Acid Conjugates

$\Phi_{f,rel}$	Trp-dye	Tyr-dye	Phe-dye	Met-dye	His-dye
fluorescein	0.25	0.55	0.95	0.77	0.79
Bodipy-FL	0.02	0.15	0.91	0.30	0.70
ATTO 655	0.03	0.63	1.00	0.99	1.00

As can be seen in Table 2, bimolecular dynamic quenching constants,  $k_{q,dyn}$ , vary between  $2.0$  and  $5.0 \times 10^9$  M<sup>-1</sup> s<sup>-1</sup> for all dyes investigated. On the other hand, the bimolecular static quenching efficiencies calculated at low quencher concentrations (0–10 mM) differ significantly. Here, the red-absorbing dyes MR121, ATTO 655, and ATTO 680 exhibit the highest association constants,  $K_{ass.}$ , of 96–206 M<sup>-1</sup> with Trp. Fluorescence quenching is dominated by the formation of nonfluorescent ground-state complexes, i.e., static quenching. Quenching of ATTO 590, fluorescein, TMR, and RB by Trp comprises static and dynamic quenching with comparable efficiency while for the two bora-diaza-indacene dyes Bodipy-FL and Bodipy630/650, dynamic quenching is more efficient than static quenching (compare  $K_{dyn}$  and  $K_{ass.}$  in Table 2). Carbocyanine derivatives, such as Cy5 and Alexa 647, show solely dynamic quenching (Table 2).

**Intramolecular Fluorescence Quenching of Dyes by Tryptophan in Peptides and Proteins.** Table 3 shows the relative fluorescence quantum yields,  $\Phi_{f,rel}$ , measured for fluorescein, Bodipy-FL, and ATTO 655 coupled to the aliphatic amino group of the amino acids Trp, Tyr, Phe, Met, and His. As expected from intermolecular quenching experiments (Table 1), ATTO 655 is almost exclusively quenched when directly coupled to Trp. Besides the Trp-conjugate, only the Tyr-conjugate exhibits measurable fluorescence quenching. Comparison of the fluorescence quantum yield and fluorescence decay of the ATTO 655-labeled Trp conjugate (Figure 3a) demonstrates mainly static quenching. This supports the idea that fluorescence quenching is dominated by the formation of weak or nonfluorescent ground-state complexes that exhibit fluorescence lifetimes shorter than the time-resolution of our apparatus used to measure the time-resolved fluorescence decays (~40 ps). The short fluorescence lifetime of 230 ps with an amplitude of 0.16 measured for the ATTO 655-Trp conjugate (Table 4) cannot account for a relative fluorescence quantum yield,  $\Phi_{f,rel}$  of 0.03. The main part of the fluorescence decay is dominated by the nearly unquenched fluorescence lifetime of the free dye of ~1.8 ns with an amplitude of 0.84. Similar fluorescence characteristics were measured for the MR121 and ATTO 680 Trp-conjugate (Table 4).

The fluorescence quantum yields of the Bodipy-FL amino acid conjugates show the following sequence: Trp < Tyr < Met < His < Phe (Table 3).  $\Phi_{f,rel}$  for the Trp-conjugate is similar to the value measured for the ATTO 655 Trp-conjugate indicating strong quenching interactions. Furthermore, both Bodipy-FL and ATTO 655



**Figure 3.** Fluorescence decays of the free dyes (gray) and Trp conjugates (black) (A) ATTO 655, and (B) Bodipy-FL in PBS buffer, pH 7.4. In addition, the instrument response functions (IRFs) are given. Excitation was performed using a pulsed LED (490 nm) or a laser diode emitting (635 nm). Fluorescence was detected at the emission maxima (12.5 ps/channel).

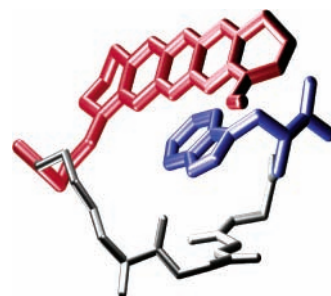
**Table 4. Relative Fluorescence Quantum Yields,  $\Phi_{f,rel}$ , Fluorescence Lifetimes,  $\tau_i$ , and Corresponding Amplitudes,  $a_i$ , of Trp, Peptide, and Streptavidin Conjugates of Different Dyes in the Absence and Presence of an Excess of Biotin**

	$\Phi_{f,rel}$	$\tau_1$ (ns)/ $a_1$	$\tau_2$ (ns)/ $a_2$
MR121–Trp	0.03	0.47/0.37	1.81/0.63
MR121–Lys-(Gly) <sub>3</sub> -Trp	0.10	0.50/0.07	1.60/0.93
MR121–streptavidin/+biotin	0.11/0.72	0.28/0.31	1.99/0.69
ATTO 655–Trp	0.03	0.23/0.16	1.77/0.84
ATTO 655–Lys-(Gly) <sub>3</sub> -Trp	0.08	1.45/1.00	
ATTO 655–streptavidin/+biotin	0.05/0.58	0.28/0.34	1.49/0.66
ATTO 680–Trp	0.01	0.21/0.30	1.30/0.70
ATTO 680–Lys-(Gly) <sub>3</sub> -Trp	0.09	1.35/1.00	
ATTO 680–streptavidin/+biotin	0.11/0.82	0.21/0.39	1.78/0.61
Bodipy-FL–Trp	0.02	0.44/0.95	4.95/0.05
Bodipy-FL–Lys-(Gly) <sub>3</sub> -Trp	0.27	2.52/1.00	
Bodipy-FL–streptavidin/+biotin	0.09/0.65	1.41/0.22	5.43/0.78
fluorescein–Trp	0.25	1.10/0.20	1.85/0.80
fluorescein–Lys-(Gly) <sub>3</sub> -Trp	0.57	2.87/1.00	
fluorescein–streptavidin/+biotin	0.06/0.17	0.75/0.64	2.85/0.36
Cy5–Trp	0.59	0.79/1.00	
Cy5–Lys-(Gly) <sub>3</sub> -Trp	0.80	0.41/0.15	0.97/0.85
Cy5–streptavidin/+biotin	0.90/0.90	0.71/0.20	1.71/0.80

exhibit similar bimolecular dynamic quenching constants,  $k_{q,dyn}$ , of  $\sim 4 \times 10^9 \text{ M}^{-1} \text{ s}^{-1}$  (Table 2). However, as ATTO 655 shows a high association constant ( $206 \text{ M}^{-1}$ ) promoting the formation of weak or nonfluorescent ground-state complexes, the tendency of Bodipy-FL to associate with Trp is less pronounced. That is, most of the ATTO 655 molecules are associated with the Trp residue in ground-state complexes whereas Bodipy-FL molecules are either still accessible for dynamic quenching or Bodipy-FL/Trp complexes exhibit a less optimal interaction geometry for efficient quenching. This is reflected in the fluorescence decay of the Bodipy-FL conjugate (Figure 3). The fluorescence decay can be fitted almost monoexponentially revealing a short fluorescence lifetime of 440 ps with an amplitude of 0.95 (Table 4).

As can be seen in Table 2, static and dynamic quenching efficiencies measured from intermolecular fluorescence quenching experiments with fluorescein and amino acids are similar. The corresponding fluorescein conjugates show only moderate fluorescence quenching with relative fluorescence quantum yields,  $\Phi_{f,rel}$ , ranging from 0.25 for the Trp-conjugate to 0.95 for the Phe-conjugate (Table 3). In the case of the Trp-conjugate, the measured fluorescence lifetimes of 1.10 ns and 1.85 ns with amplitudes of 0.20 and 0.80, respectively (Table 4), account almost for the observed decrease in fluorescence intensity.

To further evaluate the quenching interactions between organic dyes and Trp residues and, in particular, the distance dependence of quenching, the dyes were



**Figure 4.** Model for the formation of weak or nonfluorescent ground-state complexes between the oxazine derivative MR121 and the Trp residue in the peptide MR121-Lys-(Gly)<sub>3</sub>-Trp. Due to the flexibility of the glycine residues, the oxazine derivative MR121 (red) can adopt a nearly coplanar stacking conformation with respect to the Trp residue (blue).

coupled to the terminal lysine residue of the peptide: Lys-Gly-Gly-Gly-Trp. Because of the relatively flexible glycine residues intramolecular contact and complex formation between the dyes and the Trp residue is possible. Table 4 shows the relative fluorescence quantum yields and fluorescence lifetimes of the Trp and peptide conjugates of MR121, ATTO 655, ATTO 680, Bodipy-FL, fluorescein, and Cy5. For all dyes investigated, fluorescence quenching is diminished in the peptide conjugates. The low fluorescence quantum yields measured for MR121, ATTO 655, and ATTO 680 demonstrate again the formation of weak or nonfluorescent ground-state complexes between the dyes and the terminal Trp residue (Figure 4). The fluorescence lifetimes are slightly reduced and can be fitted satisfactorily using a monoexponential model. Only in the case of the MR 121 conjugate does a second shorter decay component of 500 ps with an amplitude of 0.07 appear. For the Bodipy-FL conjugate the quantum yield increases substantially from 0.02 for the Trp conjugate to 0.27 for the peptide conjugate (Table 4). In addition, the fluorescence lifetime increases from 440 ps to 2.52 ns. This indicates that static quenching within ground-state complexes plays only a minor role in these peptides. For fluorescein, the fluorescence quantum yield and lifetime increase while Cy5 is only slightly quenched in all conjugates investigated.

Assuming quenching electron transfer from the Trp residue to the dye, at least two mechanisms have to be considered (30): through-space and through-bond. Due to the flexibility of the peptide used in our studies, a clear answer cannot be given. However, our data indicate that contact formation between the Trp residue and the chromophore is required for efficient quenching. This implies that electron transfer through-bond is only of minor importance. Hence, the distinct dynamic quenching measured for dyes such as Bodipy-FL might reflect



collisions between the terminal Trp residue and the dye due to the flexibility of the peptide. That is, the fluorescence lifetime of Bodipy-FL-labeled peptides that contain a Trp residue might eventually be used to reveal contact formation rates in peptides (28, 31).

The results demonstrate that knowledge of the spectroscopic behavior of the dyes used to label peptides or proteins is crucial for the design of biological relevant applications. Because of the importance of the biotin-streptavidin techniques, dyes were covalently attached to streptavidin and the effect of biotin binding was investigated (Table 4). The strong binding of biotin to the 60 kDa protein streptavidin ( $K_D = 10^{-15}$  M) has become a standard tool in molecular biology (32, 33). Each hydrophobic binding pocket of streptavidin contains four tryptophan residues that are involved in strong biotin binding (22). With the exception of Cy5, the fluorescence of all streptavidin conjugates is substantially quenched (Table 4). While the increase in fluorescence quantum yield is less pronounced in the case of the fluorescein conjugate,  $\Phi_{f,rel}$  of the MR 121, ATTO 655, ATTO 680, and Bodipy-FL conjugate shows a dramatic increase upon addition of an excess biotin (Table 4). As in the case of the peptide and Trp conjugates, it is likely that the strong reduction in fluorescence intensity is caused by reversible quenching of the dye with tryptophan residues of streptavidin. The strong increase in fluorescence intensity of the MR121, ATTO 655, ATTO 680, and Bodipy-FL streptavidin conjugate upon binding to biotin is advantageous for biological applications where washing steps have to be avoided.

## CONCLUSIONS

The fluorescence quenching of various fluorescent dyes by amino acids, and in particular by tryptophan, is studied and compared using steady-state and time-resolved fluorescence spectroscopy. The red-absorbing oxazine derivative MR121 and the two ATTO dyes ATTO 655 and ATTO 680 are almost exclusively quenched by tryptophan while rhodamine and bora-diaza-indacene derivatives that absorb at shorter wavelengths are also quenched substantially by tyrosine residues. The quenching of the carbocyanine dye Cy5 by amino acids is generally very low. Fluorescence quenching of the red-absorbing dyes MR 121, ATTO 655, and ATTO 680 by tryptophan is dominated by the formation of nonfluorescent ground-state complexes, i.e., static quenching, with association constants,  $K_{ass.}$ , ranging from of 96–206 M<sup>-1</sup>. On the other hand, quenching of various rhodamine derivatives and fluorescein comprises static and dynamic quenching with comparable efficiency. For the two bora-diaza-indacene dyes Bodipy-FL and Bodipy630/650, dynamic quenching is more efficient than static quenching. Selective fluorescence quenching of dyes by tryptophan residues in proteins has great potential for the development of diagnostic applications (21, 27), and new methods for the direct measurement of submicrosecond intramolecular contact formation in biopolymers at the single molecule level (28). Furthermore, the data show that changes in the fluorescence quantum yield of dye-labeled peptides might be used in developing fluorescence-based assays, e.g., protease assays.

## ACKNOWLEDGMENT

The authors wish to thank Prof. K. H. Drexhage (Universität-Gesamthochschule Siegen) for providing the oxazine derivative MR121. This work was supported

by the Bundesministerium für Bildung, Wissenschaft, Forschung und Technologie (Grants 311864 and 13N8349).

## LITERATURE CITED

- (1) Haugland, R. P. (1996) *Handbook of fluorescent probes and research chemicals*, 6th ed., Molecular Probes, Eugene, OR.
- (2) Cardullo, R. A., Agrawal, S., Flores, C., Zamecnik, P. C., and Wolf, D. E. (1988) Detection of nucleic acid hybridization by nonradiative fluorescence resonance energy transfer. *Proc. Natl. Acad. Sci. U.S.A.* 85, 8790–8794.
- (3) Tyagi, S., and Kramer, F. R. (1996) Molecular beacons: probes that fluoresce upon hybridization. *Nat. Biotechnol.* 14, 303–308.
- (4) Tyagi, S., Marras, S. A. E., and Kramer, F. R. (2000) Wavelength-shifting molecular beacons. *Nat. Biotechnol.* 18, 1191–1196.
- (5) Marras, S. A. E., Kramer, F. R., and Tyagi, S. (2002) Efficiencies of fluorescence resonance energy transfer and contact-mediated quenching in oligonucleotide probes. *Nucleic Acid Res.* 30, e122.
- (6) Förster, T. (1949) Experimentelle und theoretische Untersuchung des zwischenmolekularen Übergangs von Elektronenanregungsenergie. *Zeitschrift für Naturforschung* 4a, 321–327.
- (7) Weiss, S. (1998) Fluorescence spectroscopy of single biomolecules. *Science* 283, 1676–1683.
- (8) Gordon, G. W., Berry, G., Liang, X. H., Levine, B., and Herman, B. (1998) Quantitative fluorescence resonance energy transfer measurements using fluorescence microscopy. *Biophys. J.* 74, 2702–2713.
- (9) Schuille, P., Meyer-Almes, F. J., and Rigler, R. (1997) Dual-color fluorescence cross-correlation spectroscopy for multi-component diffusional analysis in solution. *Biophys. J.* 72, 1878–1886.
- (10) Heinze, K. G., Rarbach, M., Jahnz, M., and Schuille, P. (2002) Two-photon fluorescence coincidence analysis: Rapid measurements of enzyme kinetics. *Biophys. J.* 83, 1671–1681.
- (11) Hom, E. F. Y., and Verkman, A. S. (2002) Analysis of coupled bimolecular reaction kinetics and diffusion by two-color fluorescence correlation spectroscopy: Enhanced resolution of kinetics by resonance energy transfer. *Biophys. J.* 83, 533–546.
- (12) Knemeyer, J. P., Marmé, N., and Sauer, M. (2000) Probes for detection of specific DNA sequences at the single molecule level. *Anal. Chem.* 72, 3717–3724.
- (13) Piester, O., Barsch, H., Buschmann, V., Heinlein, T., Knemeyer, J. P., Weston, K. D., and Sauer, M. (2003) A single molecule sensitive DNA-hairpin system based on intramolecular electron transfer. *Nano Lett.* 3, 979–982.
- (14) Seidel, C. A. M., Schulz, A., and Sauer, M. (1996) Nucleobase-specific quenching of fluorescent dyes. 1. Nucleobase one-electron redox potentials and their correlation with static and dynamic quenching efficiencies. *J. Phys. Chem.* 100, 5541–5553.
- (15) Sauer, M., Han, K. T., Ebert, V., Müller, R., Schulz, A., Seeger, S., Wolfrum, J., Arden-Jacob, J., Deltau, G., Marx, N. J., Zander, C., and Drexhage, K. H. (1995) New fluorescent dyes in the red region for biodiagnostics. *J. Fluoresc.* 5, 247–261.
- (16) Edman, L., Mets, Ü., and Rigler, R. (1996) Conformational transitions monitored for single molecules in solution. *Proc. Natl. Acad. Sci. U.S.A.* 93, 6710–6715.
- (17) Eggeling, C., Fries, J. R., Brand, L., Günther, R., and Seidel, C. A. M. (1998) Monitoring conformational dynamics of a single molecule by selective fluorescence spectroscopy. *Proc. Natl. Acad. Sci. U.S.A.* 95, 1556–1561.
- (18) Heinlein, T., Knemeyer, J. P., Piester, O., and Sauer, M. (2003) Nucleobase-specific quenching of fluorescent dyes in DNA-hairpins. *J. Phys. Chem. B* 107, 7957–7964.
- (19) Kurata, S., Kanagawa, T., Yamada, K., Torimura, M., Yokomaku, T., Kamagata, Y., and Kurane, R. (2001) Fluorescent quenching-based quantitative detection of specific DNA/RNA using BODIPY FL-labeled probe or primer. *Nucleic Acids Res.* 29, e34.

- (20) Lewis, F. D., Letsinger, R. L., and Wasielewski, M. R. (2001) Dynamics of photoinduced charge transfer and hole transport in synthetic DNA hairpins. *Acc. Chem. Res.* **34**, 159–170.
- (21) Sauer, M. (2003) Single molecule sensitive fluorescence sensors based on intramolecular photoinduced electron transfer. *Angew. Chem., Int. Ed.* **115**, 1790–1793.
- (22) Watt, R. M., and Voss, E. W. (1977) Mechanism of quenching of fluorescein by anti-fluorescein IgG antibodies. *Immunochemistry* **14**, 533–541.
- (23) Emans, N., Biwersi, J., and Verkman, A. S. (1995) Imaging of endosome fusion in BHK fibroblasts based on a novel fluorimetric avidin–biotin assay. *Biophys. J.* **69**, 716–728.
- (24) Karolin, J., Johansson, L. B.-A., Strandberg, L., and Ny, T. (1994) Fluorescence and absorption spectroscopic properties of dipyrrometheneboron difluoride (BODIPY) derivatives in liquids, lipid membranes, and proteins. *J. Am. Chem. Soc.* **116**, 7801–7806.
- (25) Wagenknecht, H. A., Stemp, E. D. A., and Barton, J. K. (2000) Evidence of electron transfer from peptides to DNA: Oxidation of DNA-bound tryptophan using the flash-quench technique. *J. Am. Chem. Soc.* **122**, 1–7.
- (26) DeFelippis, M. R., Murthy, C. P., Broitman, F., Weinraub, D., Faraggi, M., and Klapper, M. H. (1991) Electrochemical properties of tyrosine phenoxyl and tryptophan indolyl radicals in peptides and amino acid analogues. *J. Phys. Chem.* **95**, 3416–3419.
- (27) Neuweiler, H., Schulz, A., Vaiana, A., Smith, J., Kaul, S., Wolfrum, J., and Sauer, M. (2002) Peptide-based molecular beacons for the detection of p53-autoantibodies in human sera. *Angew. Chem., Int. Ed.* **114**, 4769–4773.
- (28) Neuweiler, H., Schulz, A., Böhmer, A., Enderlein, J., and Sauer, M. (2003) Measurement of submicrosecond intramolecular contact formation in peptides at the single molecule level. *J. Am. Chem. Soc.* **125**, 5324–5330.
- (29) Gruber, J. H., Kahn, C. D., Kada, G., Riener, C. K., Harms, G. S., Ahler, W., Dax, T. G., and Knaus, H. (2000) Anomalous fluorescence enhancement of Cy3 and Cy3.5 versus anomalous fluorescence loss of Cy5 and Cy7 upon covalent linking to IgG and noncovalent binding to avidin. *Bioconjugate Chem.* **11**, 696–704.
- (30) Adams, D. M., Brus, L., Chidsey, C. E. D., Creager, S., Creutz, C., Kagan, C. R., Kamat, P. V., Lieberman, M., Lindsay, S., Marcus, R. A., Metzger, R. M., Michel-Beyerle, M. E., Miller, J. R., Newton, M. D., Rolison, D. R., Sankey, O., Schanze, K. S., Yardley, J., and Zhu, X. (2003) Charge transfer on the nanoscale: Current status. *J. Phys. Chem. B* **107**, 6668–6697.
- (31) Hudgins, R. R., Huang, F., Gramlich, G., and Nau, W. M. (2002) A fluorescence-based method for direct measurement of submicrosecond intramolecular contact formation in biopolymers: An exploratory study with polypeptides. *J. Am. Chem. Soc.* **124**, 556–564.
- (32) Weber, P. C., Ohlendorf, D. H., Wendolowski, J. J., and Salemme, F. R. (1989) Structural origins of high-affinity biotin binding to streptavidin. *Science* **243**, 85–88.
- (33) Chevalier, J., Yi, J., Michel, O., and Ming, T. X. (1997) Biotin and digoxigenin as labels for light and electron microscopy in situ hybridization probes: Where do we stand? *J. Histochem. Cytochem.* **45**, 481–91.

BC0341324

# DNA Electrochemistry as a Probe of Base Pair Stacking in A-, B-, and Z-Form DNA

Elizabeth M. Boon and Jacqueline K. Barton\*

Division of Chemistry and Chemical Engineering, California Institute of Technology,  
Pasadena, California 91125. Received August 5, 2003; Revised Manuscript Received September 11, 2003

DNA-mediated charge transport (CT) chemistry is sensitive to DNA structure and base pair stacking. In an electrochemical assay based upon DNA CT, DNA-modified electrode surfaces are used to examine the electrochemical reduction of methylene blue (MB), a small molecule that binds to the DNA film by intercalation. Here electrochemically we probe CT in the three primary conformations of double-stranded nucleic acids, A-, B-, and Z-form DNA. The A-form is examined in the context of a DNA/RNA hybrid duplex and Z-DNA, in duplexes containing d(mCG)<sub>8</sub> sequences at high Mg<sup>2+</sup> concentrations. We find that both A- and B-DNA support efficient DNA CT as measured by MB reduction in the DNA film; a lower level of reduction is evident with the Z-form film. Furthermore, mismatches incorporated into A-form duplexes, as in B-form duplexes, disrupt MB reduction, thus providing a strategy for mutation detection through testing of RNA transcripts at DNA electrodes.

## INTRODUCTION

Charge transport (CT) through double helical DNA has been shown to be exquisitely sensitive to coupling within the base pair stack (1–11). Sequence-dependent DNA structure, including the presence of mismatches or base lesions, as well as conformational dynamics and local flexibility, all contribute to this coupling and thus to the efficiency of DNA CT chemistry. This sensitivity to base stacking provides the foundation for applications of DNA CT to probe nucleic acid structure, particularly those utilizing electrochemistry experiments on DNA films (12–20).

In DNA CT measurements by electrochemistry at DNA films, DNA oligonucleotide duplexes modified with a thiol linker are self-assembled on gold electrode surfaces (12–20). A redox-active intercalator, such as methylene blue (MB), is bound noncovalently to the close-packed DNA films. We have shown that noncovalent intercalators bind near the solution-accessible interface of these densely packed DNA-modified surfaces and that the ratio of intercalator to DNA oligonucleotide duplex is approximately 1:1, eliminating the need for covalent labeling (12, 16–20). The reduction of the intercalator at the top of the film through a DNA-mediated reaction serves as the probe for DNA base pair stacking within the film: if the stacking is intact, MB is efficiently reduced at the DNA-modified film; however, the presence of an intervening mismatch or other stacking perturbation results in an attenuation of MB reduction (15–19). The signal from MB can be amplified in an electrocatalytic cycle in which reduced MB is used as a catalyst for the reduction of a species diffusing in solution outside of the DNA film (usually ferricyanide) (16, 17, 19). Importantly, whether the direct or catalytic reduction of MB is monitored, reduction of MB has been shown to take place via CT through the DNA base stack (12, 20).

DNA-mediated CT electrochemistry therefore provides an exquisitely sensitive means to monitor nucleic acid

structure and stacking. Even small perturbations in base pair stacking, as is associated with some base lesions, diminish the efficiency of MB reduction (15–19). Using this technique, all single base mismatches within a DNA duplex have been detected as well as several common DNA base damage products (17). Furthermore, the electrochemical reduction of DNA intercalators bound to DNA-modified electrodes has been used to monitor DNA–protein interactions (18) as well as the hybridization of antisense oligonucleotides (19). Due to this sensitivity to very small changes in DNA base pair stacking, this electrochemical assay may be generally exploited in probing nucleic acid structure and stacking.

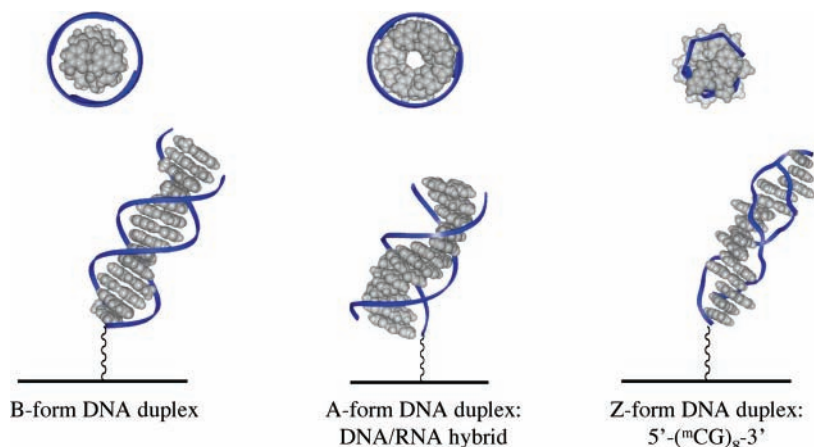
In that context, we examine here three primary conformations of double-stranded nucleic acids, A-, B-, and Z-form DNA (21, 22). RNA duplexes as well as dehydrated DNA duplexes adopt A-form helical structure. In addition, DNA/RNA hybrids adopt a helical structure that is very similar to A-form DNA (23–26). Within these hybrid duplexes in solution, the RNA strand generally maintains A-form characteristics, while the DNA strand adopts a sequence dependent structure intermediate between A- and B-form DNA. DNA/RNA hybrid duplexes are common *in vivo* as a product of reverse transcriptase activity (e.g. HIV reverse transcriptase), normal transcription of DNA into mRNA, as well as during DNA replication as an intermediate in lagging strand synthesis, and antisense therapy (27–30).

The third major nucleic acid duplex structure is Z-form DNA (21, 22, 31). Z-DNA is a left-handed helix, in contrast to right-handed A- and B-form helices. This structure is generally adopted by oligonucleotides that have sequences of alternating pyrimidines and purines (usually alternating dGdC) in the presence of high salt concentrations. Physiologically, Z-form DNA is thought to form *in vivo* during transcription as a result of torsional strain generated by a moving polymerase and it is suspected to play a role in gene regulation (32–38).

To demonstrate the utility of our DNA CT-based electrochemical assay in reporting on changes in DNA structure and  $\pi$ -stacking, here we demonstrate the

\* To whom correspondence should be addressed at jkbarton@caltech.edu.





**Figure 1.** Schematic illustration of the electrochemical reduction of MB bound to thiol-terminated A-, B-, and Z-form DNA duplexes on gold electrode surfaces. Also shown are views of A-, B-, and Z-form DNA down the helical axis.

application of electrochemistry at DNA-modified electrode surfaces to probe stacking in DNA/RNA hybrids as well as Z-form DNA duplexes (Figure 1).

#### EXPERIMENTAL PROCEDURES

**Materials.** DNA oligonucleotides were synthesized on an ABI DNA Synthesizer using standard solid-phase techniques. Incorporation of 5-methyl-cytidine (5-Me-C) was accomplished using the respective phosphoramidite. All DNA synthesis reagents were obtained from Glen Research. Purified RNA single strands were purchased from Dharmacon Research, Inc., in the 2'-bis(acetoxy-ethoxy)methyl ether form and deprotected and desalted immediately prior to hybridization. Unless otherwise indicated, all reagents and solvents were purchased in their highest available purity and used without further purification.

**Preparation of DNA-Modified Surfaces.** Thiol-modified oligonucleotides were prepared as previously described (12–20). After stringent purification by HPLC (Hewlett-Packard HPLC using a reverse-phase C18 column and an acetonitrile/ 50 mM ammonium acetate gradient), the single strands were quantitated by UV–visible spectroscopy (Beckman) using the standard extinction coefficients for the nucleotides. For DNA and DNA/RNA hybrids of mixed sequence, these thiol-modified single strands were hybridized in a 1:1 molar ratio to purified unmodified complements. The 5'-(CG)<sub>8</sub>-3' duplexes were made by mixing the thiol strand in a 1:5 ratio with the unmodified strand so that statistically each duplex would have only one or no thiols to avoid dithiol duplexes in the self-assembly mixture. Duplex structure was characterized by CD spectroscopy (Aviv CD spectrometer).

The resultant duplexes were deposited on polycrystalline gold electrodes for 12–24 h (100  $\mu$ M duplex in 5 mM phosphate, 50 mM NaCl buffer, pH 7; 100 mM MgCl<sub>2</sub> is added to the duplexes after hybridization just prior to self-assembly). Unless otherwise noted, before electrochemical measurements, the electrodes were rinsed thoroughly with 5 mM phosphate, 50 mM NaCl buffer, pH 7. As electrodes containing a high surface coverage of DNA are most useful for our experiments, surfaces were routinely assayed for coverage by monitoring the attenuation of the oxidation of ferrocyanide (12).

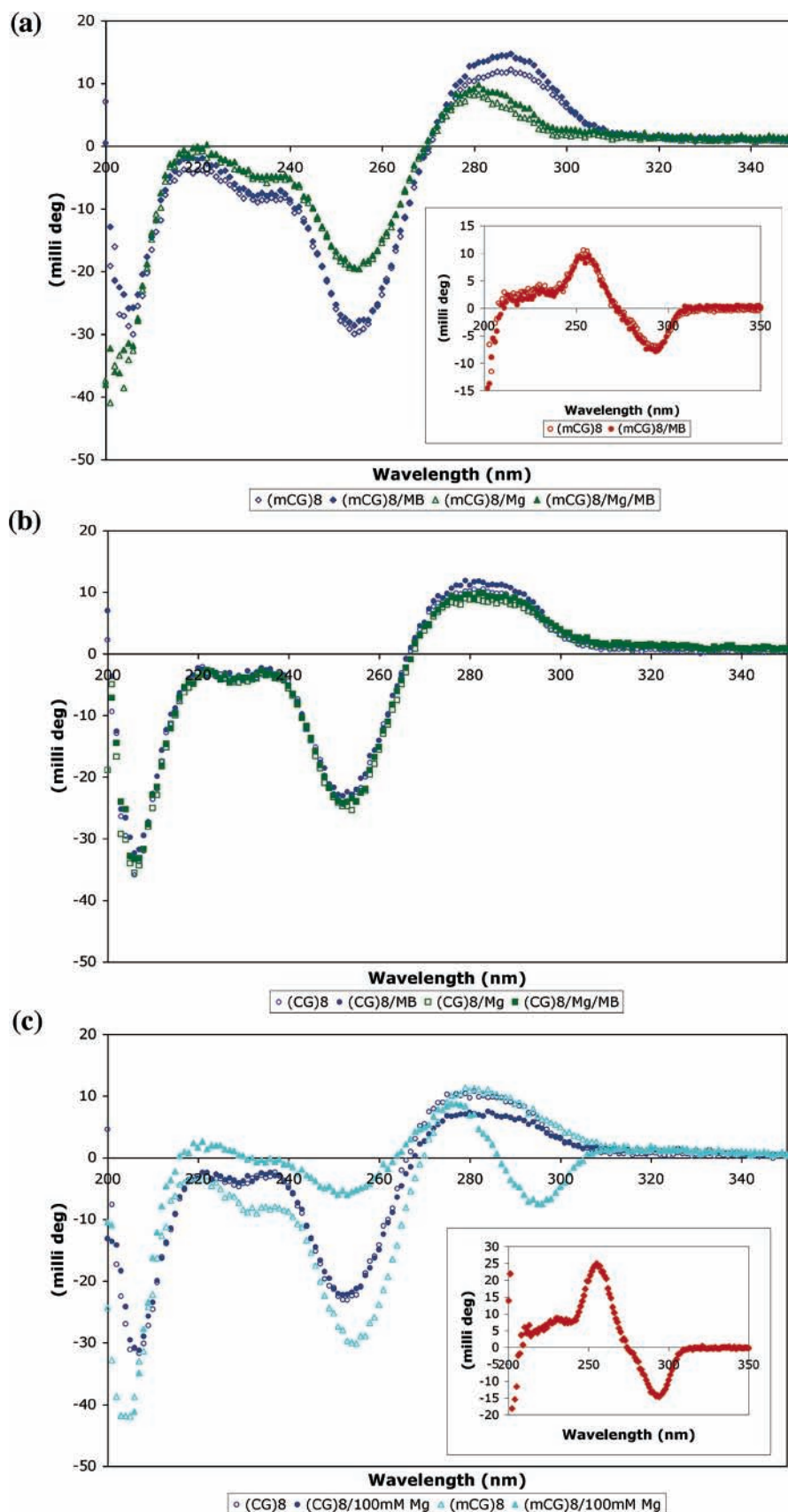
**Electrochemical Measurements.** Cyclic voltammetry and chronocoulometry was carried out on 0.02 cm<sup>2</sup> gold electrodes using a Bioanalytical Systems (BAS) Model CV-50W electrochemical analyzer. A normal three-

electrode configuration consisting of a modified gold-disk working electrode, a saturated calomel reference electrode (SCE, Fisher Scientific), and a platinum wire auxiliary electrode was used. A modified Luggin capillary separated the working compartment of the electrochemical cell from the reference compartment. Potentials are reported versus SCE. Volumes of 3 mL were typically employed. Unless specifically noted, all measurements were recorded at  $20 \pm 2$  °C in 5 mM sodium phosphate containing 50 mM NaCl, pH 7, that had been thoroughly degassed with Ar.

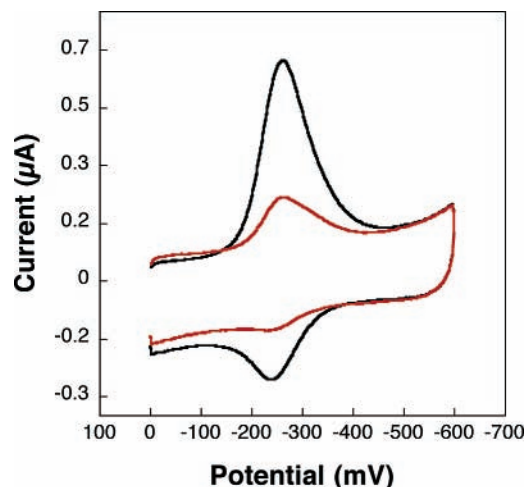
#### RESULTS

**Electrochemical Probe of Base Pair Stacking in Z-Form DNA Duplexes.** Duplexes with uninterrupted sequences of (CG)<sub>n</sub> usually form Z-DNA at very high ionic strength. MB binding to DNA is inhibited at high ionic strength; however, binding to DNA films is reduced by about 50% at 50 mM MgCl<sub>2</sub> (20, 40). Thus, to examine stacking in Z-form DNA, the duplexes 5'-(mCG)<sub>8</sub>-3' and 5'-(CG)<sub>8</sub>-3' were synthesized. Methylation of cytosine has been shown to stabilize Z-form structure at lower ionic strength than normally required to form Z-DNA within an alternating GC duplex (39). We hypothesized we could promote Z-form DNA in the methylated (5'-(mCG)<sub>8</sub>-3') but not wildtype (5'-(CG)<sub>8</sub>-3') duplex at low ionic strength (10 mM Mg<sup>2+</sup>), giving B- and Z-form DNA to compare by electrochemistry at DNA-modified surfaces.

CD and UV–vis experiments were thus carried out to monitor the conformations of 5'-(mCG)<sub>8</sub>-3' and 5'-(CG)<sub>8</sub>-3' at various ionic strengths. Each duplex (3  $\mu$ M) was incubated with either 10 or 100 mM Mg<sup>2+</sup> overnight in 5 mM Pi, pH 7. B- to Z-form structural transitions in the methylated duplex, but not the wildtype duplex, are very clearly seen in Z–B difference spectra using both 10 and 100 mM Mg<sup>2+</sup> (Figure 2). A maximum peak of about 25 millidegrees at 254 nm, a minimum of 15 millidegrees at 293 nm, and isochromism at 277 nm were observed in the difference spectra and are indicative of B- to Z-transition. Importantly, CD spectra taken after the addition of 3  $\mu$ M MB do not disrupt this structure. UV–visible spectroscopy was especially useful in examining MB binding to both 5'-(mCG)<sub>8</sub>-3' and 5'-(CG)<sub>8</sub>-3'. Hypochromism of the MB absorption band at 668 nm shows that MB stacks with the B- and Z-form duplexes in the presence of 10 mM Mg<sup>2+</sup> to similar extents, 6% for the methylated duplex, 10% for the un-methylated duplex. At 100 mM Mg<sup>2+</sup> there is very little MB binding to either duplex, as expected for such a high ionic strength (20, 40).



**Figure 2.** Circular dichromism of 5'-(CG)<sub>8</sub>-3' and 5'-(mCG)<sub>8</sub>-3' duplexes in the presence of MgCl<sub>2</sub> and MB. (a) CD of 5'-(mCG)<sub>8</sub>-3' (3  $\mu$ M duplex) in 5 mM phosphate, pH 7 buffer only (open blue), with 10 mM MgCl<sub>2</sub> (open green), with 3  $\mu$ M MB (closed blue), and with 10 mM MgCl<sub>2</sub> and 3  $\mu$ M MB (closed green). The inset shows the Z-B difference spectra (with MgCl<sub>2</sub> – no MgCl<sub>2</sub>) for this duplex with (closed red) and without (open red) MB. (b) CD of 5'-(CG)<sub>8</sub>-3' (3  $\mu$ M duplex) in 5 mM phosphate, pH 7 buffer only (open blue), with 10 mM MgCl<sub>2</sub> (open green), with 3  $\mu$ M MB (closed blue), and with 10 mM MgCl<sub>2</sub> and 3  $\mu$ M MB (closed green). (c) CD of 5'-(CG)<sub>8</sub>-3' (blue) and 5'-(mCG)<sub>8</sub>-3' (cyan) in 5 mM phosphate, pH 7 buffer only (open) and with 100 mM MgCl<sub>2</sub> (closed). The inset shows the Z-B difference spectrum (with MgCl<sub>2</sub> – no MgCl<sub>2</sub>) for 5'-(mCG)<sub>8</sub>-3'.

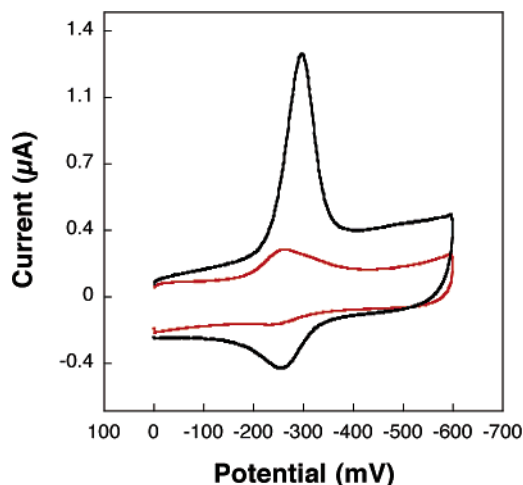


**Figure 3.** Cyclic voltammetry of  $2 \mu\text{M MB}^+$  at a gold electrodes modified with the thiol-terminated duplex  $\text{SH-5'-(CG)}_8\text{-3'}$  (black; B-form) or  $\text{SH-5'-(mCG)}_8\text{-3'}$  (red; Z-form) in 5 mM phosphate, 50 mM NaCl, 10 mM  $\text{MgCl}_2$  buffer, pH 7. Voltammograms were obtained with scan rate ( $\nu$ ) = 100 mV/s, electrode area ( $A$ ) =  $0.02 \text{ cm}^2$ .

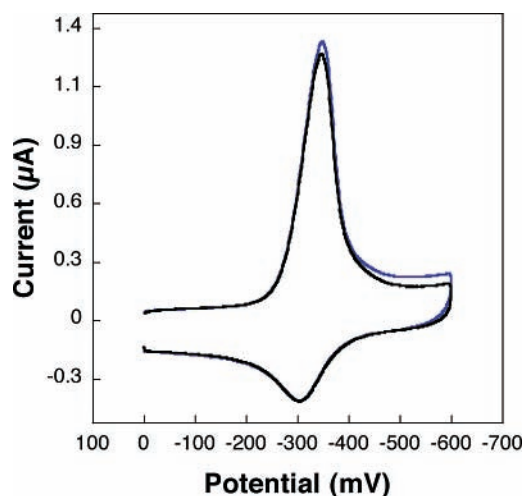
The UV-vis and CD experiments clearly indicate that at 10 mM  $\text{MgCl}_2$ , a B- to Z-form transition takes place only in the methylated duplexes and that MB binds to both B- and Z-form DNA at this ionic strength (41, 42). The structural mode of binding to the Z-form is not clear, however. Nonetheless, these experiments provide us with a system to compare the effect of differing nucleic acid structure on the efficiency of MB reduction at a DNA film, as we are able to form both B- and Z-DNA at equivalent ionic strengths within alternating CG duplexes, and MB binds to both types of DNA film.

To determine the efficiency of charge transport in Z-form DNA, the DNA duplexes  $\text{SH-5'-(mCG)}_8\text{-3'}$  and  $\text{SH-5'-(CG)}_8\text{-3'}$  were both incubated with 100 mM  $\text{Mg}^{2+}$  overnight to promote the Z-form structure in the methylated duplexes (Figure 2c) followed by self-assembly on clean gold electrode surfaces for an additional 12 h, still in the presence of 100 mM  $\text{Mg}^{2+}$ . After assembly of the DNA, the electrodes were rinsed with 5 mM Pi, 50 mM NaCl, 10 mM  $\text{Mg}^{2+}$ , pH 7, and electrochemistry experiments with  $2 \mu\text{M MB}$  in 10 mM  $\text{Mg}^{2+}$ , 5 mM Pi, 50 mM NaCl, pH 7 buffer solution were carried out. The electrochemistry was carried out at lower  $\text{Mg}^{2+}$  concentrations due to reduced MB binding at high ionic strength (20, 40). In all cases, however, the electrochemistry was accomplished within minutes of reducing the ionic strength of the DNA films, thus there was not sufficient time for a Z- to B-conversion, considering the very slow nature of this structural transition, and that at 10 mM  $\text{Mg}^{2+}$ , Z-form DNA is favorable in the methylated duplexes (Figure 2a).

Figure 3 shows the cyclic voltammograms for MB reduction on B- and Z-form DNA films. It is evident that there is less MB reduction within the Z-form duplex ( $\text{SH-5'-(mCG)}_8\text{-3'}$ ) than within the B-form duplex ( $\text{SH-5'-(CG)}_8\text{-3'}$ ), despite evidence of MB binding to both duplexes. Nonetheless, some reduction is evident with both conformations. There is a decrease in the peak current as well as a positive shift in the potential of the MB electrochemical signal in this experiment as compared to analogous experiments conducted with B-form DNA without  $\text{Mg}^{2+}$  in the electrochemistry solution (see Figure 5 for example). We have previously studied the effect of ionic strength on the electrochemistry of MB at DNA-modified electrodes (20) and this is the expected conse-



**Figure 4.** Cyclic voltammetry of  $2 \mu\text{M MB}^+$  at a gold electrodes modified with the thiol-terminated duplex  $\text{SH-5'-(mCG)}_8\text{-3'}$  in 5 mM phosphate, 50 mM NaCl, 10 mM  $\text{MgCl}_2$  buffer, pH 7 (red; Z-form) and after incubation in 5 mM phosphate, 50 mM NaCl (no  $\text{MgCl}_2$ ) buffer, pH 7 overnight (black; converted to B-form). Voltammograms were obtained with scan rate ( $\nu$ ) = 100 mV/s, electrode area ( $A$ ) =  $0.02 \text{ cm}^2$ .



**Figure 5.** Cyclic voltammetry of  $2 \mu\text{M MB}^+$  at a gold electrode modified with the thiol-terminated sequence  $\text{SH-5'-AGTA-CAGTCATCGCG}$  hybridized to a fully base paired DNA (black; B-form) and RNA (blue; A-form) complements in 5 mM phosphate, 50 mM NaCl buffer, pH 7. Voltammograms were obtained with scan rate ( $\nu$ ) = 100 mV/s, electrode area ( $A$ ) =  $0.02 \text{ cm}^2$ .

quence of 10 mM  $\text{Mg}^{2+}$ . It should be noted that the asymmetrical MB signal observed with both B- and Z-form (and A-form, see Figure 5) DNA is typical for MB electrochemistry at gold electrode surfaces. This is attributed to the lower DNA binding affinity of MB in its reduced form (20).

A critical experimental observation is that when the same Z-form DNA electrode is rinsed and incubated overnight in 5 mM Pi, 50 mM NaCl, pH 7 buffer (no  $\text{Mg}^{2+}$ ), the electrochemical behavior is similar to the B-form DNA films (Figure 4), indicating that a Z- to B-form structural transition has taken place on the electrode surface. Importantly, this experiment suggests that the initial attenuation of MB reduction is due to the Z-form helical structure.

Therefore we can conclude that at an electrode surface under conditions where Z-form DNA is formed and MB can bind, reduction of MB mediated by the Z-form structure is attenuated. Whether this occurs primarily owing to poor coupling of MB within the Z-form structure



or poor coupling within the Z-form DNA stack itself cannot be established. Intercalation into Z-form DNA has been studied with several intercalators, but not MB (41). More commonly, binding of the intercalator promotes a transition to the B-form (42). Given that an overnight incubation of the Z-form-modified electrode at low ionic strengths is required for return of the B-form signal, MB clearly does not cause this structural transition within the film; possibly this is due to the smaller size and weaker binding of MB compared, for example, to daunomycin (16), an intercalator that does promote a Z- to B-structural transition. It should be noted that intercalation into Z-form DNA has also been reported to support a polarized intercalation site (43).

**Electrochemical Probe of Base Pair Stacking In DNA/RNA Hybrid Duplexes.** To compare the stacking of DNA/RNA hybrid duplexes (A-form) to DNA duplexes (B-form), gold electrode surfaces were modified with SH-5'-AGTACAGTCATCGCG-3' hybridized to either a DNA or RNA single stranded complementary oligonucleotide. Following rinsing with 5 mM phosphate, 50 mM NaCl, pH 7 buffer, these nucleic acids films were incubated with 2  $\mu$ M MB in the same buffer and investigated by cyclic voltammetry. Intercalation of MB within A-DNA or DNA/RNA hybrids has not been systematically studied, but intercalators, such as ethidium (42, 45, 46), daunomycin (42), and anthraquinone (47), have been shown to bind to DNA/RNA hybrids. The electrochemical data presented here provide additional evidence that MB binds to the DNA/RNA hybrids used in these studies. Figure 5 illustrates that both surfaces facilitate efficient reduction of MB, comparable to that seen for the reduction of MB at DNA films (17). This result therefore suggests that the base pair stacking in the DNA/RNA hybrid A-form (44) supports DNA CT.

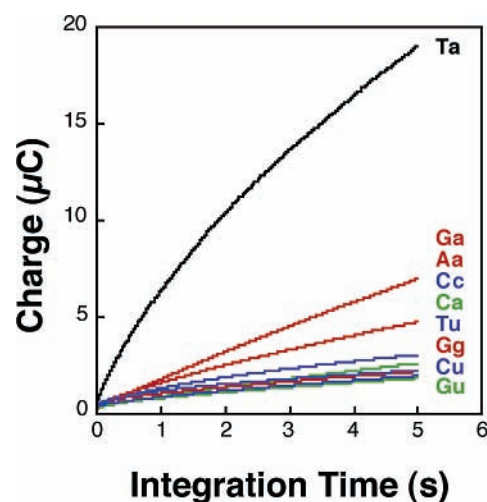
**Mutation Detection in DNA/RNA Hybrid Duplexes.** Because efficient MB reduction is observed in A-form DNA/RNA hybrids, indicating the base pair stacking supports DNA CT, the effect of base stacking perturbations on this alternate duplex structure was examined. We incorporated all possible single base mismatches into DNA/RNA hybrid duplexes formed using SH-5'-AGTACAGTCATCGCG-3' (the surface-bound strand was DNA and the complements were RNA). As electrocatalysis has been shown to increase sensitivity to minor changes in base pair stacking, particularly when followed by chronocoulometry (see especially ref 17), we used electrocatalytic reduction of ferricyanide ( $\text{Fe}(\text{CN})_6^{3-}$ ) by MB to evaluate mismatch detection in DNA/RNA hybrids (16, 17, 19). Due to poor DNA CT in Z-form DNA, we did not further investigate the effect of mismatches within this type of helix.

In separate experiments, electrode surfaces modified with DNA/RNA hybrid duplexes incorporating all possible single base mismatches (Table 1) were interrogated in electrocatalytic chronocoulometric analyses, monitoring charge accumulation at  $-350$  mV (vs SCE), the reduction potential of MB, with  $0.5$   $\mu$ M methylene blue (MB) as the intercalated catalyst and  $2.0$  mM  $\text{Fe}(\text{CN})_6^{3-}$  as the solution-borne substrate. Incorporation of a mismatch into the duplex significantly attenuates the electrocatalytic response of methylene blue at these DNA/RNA hybrid films (Figure 6); all possible mutations were easily detected. In fact, sensitivity to mutations was almost identical to our previously published DNA/DNA results (17). Mismatch detection in this system is amplified due to the catalytic nature of the detection system. In this assay, fewer MB molecules are reduced at the mismatched DNA electrode due to reduced efficiency of

**Table 1. Mismatch Detection in DNA/RNA Hybrids**

Sequence	$Q$ ( $\mu\text{C}$ ) <sup>a</sup>
SH-5' AGTACAGTCATCGCG <sup>b</sup> ucaugucaguagcgc	21.8 (1.8)
SH-5' AGTACAGTCATCGCG ucauguca <u>a</u> uagcgc	3.4 (0.7)
SH-5' AGTACAGTCATCGCG ucaugu <u>a</u> aguagcgc	6.7 (1.2)
SH-5' AGTACAGTCATCGCG ucauguc <u>u</u> guagcgc	3.5 (1.1)
SH-5' AGTACAGTCATCGCG ucaugu <u>u</u> aguagcgc	2.7 (0.9)
SH-5' AGTACAGTCATCGCG ucauguca <u>u</u> uagcgc	1.6 (0.7)
SH-5' AGTACAGTCATCGCG ucauguca <u>c</u> uagcgc	4.1 (1.1)
SH-5' AGTACAGTCATCGCG ucaugug <u>a</u> aguagcgc	2.4 (0.8)
SH-5' AGTACAGTCATCGCG ucaug <u>a</u> caguagcgc	5.5 (0.8)

<sup>a</sup> Integrated charge after 5 s of electrocatalysis at  $-350$  mV. Values are based on more than five trials each, and results are comparable for experiments run side by side or from different sample preparation. <sup>b</sup> SH-5' stands for  $\text{SH}(\text{CH}_2)_2\text{CONH}(\text{CH}_2)_6\text{NHCO}$  attached to the 5' OH of the DNA single strand.



**Figure 6.** Chronocoulometry at  $-350$  mV of  $2.0$  mM  $\text{Fe}(\text{CN})_6^{3-}$  plus  $0.5$   $\mu$ M MB<sup>+</sup> at a gold electrode modified with the thiol-terminated sequence SH-5'-AGTACAGTCATCGCG hybridized to a fully base paired RNA complement (Ta) and complements that introduce single base mismatches into the DNA/RNA hybrid. Red lines are purine-purine mismatches, blue are pyrimidine-purine mismatches, and green are pyrimidine-pyrimidine mismatches.

the DNA-mediated CT reaction: the steady-state concentration of active catalyst is lower, and a diminished overall catalytic rate results (48). Improved signal differentiation is achieved with increasing sampling time, a result that reflects the catalytic nature of this assay. The error analysis for each mismatch is presented in Table 1.

## DISCUSSION

**MB Reduction at DNA-Modified Surfaces is a Sensitive Assay of DNA Structure and Base Pair Stacking.** In the experiments reported here, efficient

DNA-mediated CT, as measured by MB reduction at DNA-modified electrodes, was observed in A- and B-form DNA, but not appreciably in Z-form DNA. These results are consistent with previous reports of CT in DNA/RNA hybrid duplexes as well as part ribose, part deoxyribose chimeric duplexes (45, 47, 49). It was determined that these mixed A-form/B-form nucleic acids do facilitate long range DNA-mediated CT chemistry as measured by guanine oxidation, fluorescence quenching, and transient absorption spectroscopy. In addition, we have previously found efficient reduction of MB bound to DNA/RNA hybrid antisense duplexes on gold electrodes (19).

In our previous experiments at DNA-modified electrodes, we have shown the reduction of bound intercalators to be a direct measurement of the integrity of DNA base pair stacking (15–19). Thus, these results suggest that DNA/RNA hybrids are well stacked. This is fully consistent with what is known about the structure and stacking of this type of nucleic acid duplex. Although the overall structure of DNA and DNA/RNA hybrids are significantly different (21–26), both types of nucleic acid duplexes appear to be well stacked as estimated by base overlap for DNA and DNA/RNA dinucleotides (45). Furthermore, experimental and theoretical determinations of stacking energies have also indicated that both types of duplexes display similar extents of stacking between adjacent base pairs (50–55). The structural dynamics of DNA/RNA hybrid duplexes has been studied by NMR (56–58) and found to be different than of DNA duplexes; for example, the base pair lifetime of an r(A–U) base pair in an RNA duplex is significantly shorter than the d(A–T) base pair lifetime in a DNA duplex, a consequence of A-form structure, not substitution of U for T (56). This suggests there is increased dynamics in A-form DNA over that in B-form DNA. In line with increased dynamics in A-form duplexes, DNA CT studies have shown that increased dynamics and flexibility aids, rather than hinders, DNA CT (7, 49, 59). Thus both A- and B-form duplexes are well stacked, but there is increased flexibility and dynamics in A-form DNA and this increased dynamical motion helps facilitate DNA CT.

Less efficient, but not completely attenuated, charge transport chemistry was observed with Z-form DNA at gold surfaces. This is understood based on the differences in base stacking in this nucleic acid structure. Z-DNA differs structurally and dynamically from B-form (21, 22, 31). Due to the alternating syn–anti sugar puckers present in Z-form DNA, there is some *inter*-strand stacking, but not *intra*-strand stacking as in A- and B-form DNA. The distance between base pairs is farther, 3.8 Å, as compared to 3.4 Å seen in A- and B-form DNA, which probably contributes reduced electronic coupling between base pairs. Significantly, the base-pair opening rate of Z-DNA, as measured by proton exchange, is much slower than it is in B-form DNA (60). Additionally, EPR and thermal measurement suggest that Z-DNA is a more rigid structure than B-DNA (61–63). Consistent with the hypothesis that some flexibility and dynamical motion helps DNA CT, it is expected that the converse would also be true, and, indeed, we do not observe efficient CT in our electrochemical system with Z-DNA.

It is additionally possible that less MB reduction is observed in the Z-form films because MB does not intercalate within Z-form DNA, and thus the signal observed in these experiments is due exclusively to intercalation into a B-form duplex. Although we cannot rigorously eliminate this possibility, the hypochromism observed in the MB absorption band upon addition of Z-form DNA in solution is consistent with some level of

DNA binding. Our data furthermore are not consistent with MB inducing a Z- to B-form structural transition (41, 42). Instead these data indicate that poor stacking within the Z-form film and/or between MB and the Z-form helix limits CT. It should be noted that long-range DNA CT as measured by guanine oxidation has been observed in a hairpin Z-form DNA structure (64). These data were explained in terms of hole hopping by the guanine radical cation to effect damage at long range. In the experiments here on DNA films, we monitor a reduction of the bound intercalator and on a much slower time scale. These differences may be important in distinguishing between these experiments.

**Mismatch Biosensors Based on Charge Transport through DNA/RNA Hybrids.** We have been interested in developing sensors based on DNA CT to efficiently detect mismatches within nucleic acid duplexes for clinical applications (15–17). As efficient reduction of MB bound to DNA/RNA hybrid duplexes was observed (Figure 5) and found to be sensitive to mismatches (Figure 6), these hybrid duplexes are candidates for DNA CT applications. Furthermore, due to the presence of DNA/RNA hybrids as a part of cellular biochemistry, as well as, in general, higher copy numbers of mRNA than genomic DNA within the cell, in assays for interrogating cellular samples, it may be preferable to test mRNA transcripts rather than genomic DNA. In this scenario, patient mRNA would be hybridized to a chip or electrode modified with single stranded DNA, resulting in DNA/RNA hybrids. With the high sensitivity of mismatch detection we have demonstrated in electrochemical detection based on DNA CT and the possibility of a high copy number of mRNA within the cell, it may be possible to screen for mutations without the use of amplifying techniques such as PCR.

Mismatches are generally stacked in a DNA duplex but undergo greater dynamical motion than well paired bases (65–67). Thus it seems that *some* added DNA dynamics and flexibility is helpful for DNA-mediated CT, but too much motion, leading to destacking, can severely hamper the charge transport reaction. Base pair lifetime measurements within B-form DNA have indicated that mismatches do significantly decrease the base pair lifetime locally at the mismatched site (8). Presumably, mismatches within A-form DNA also provide too much flexibility and motion for efficient charge transport chemistry. Within A-form RNA duplexes, mismatches, especially GA mismatches, are common, but the mismatches are not well stacked, and thus our electrochemical detection assay is well-suited to detection of mismatches in A- as well as B-form DNA.

DNA CT is now a well studied phenomenon. Many different experiments have shown that efficient CT reactions can take place in well stacked DNA duplexes, causing many researchers to search for physiological consequences of this DNA-mediated reaction. Given the presence of A-, B-, and Z-form DNA *in vivo*, and their differing abilities to sustain CT reactions, this might raise new possibilities for CT *in vivo* as well as in practical clinical applications.

#### ACKNOWLEDGMENT

We are grateful to the National Institutes of Health (GM61077) for their financial support of this research and to Melanie O'Neill for assistance with DNA figures.

#### LITERATURE CITED

- (1) Boon, E. M., and Barton, J. K. (2002) Charge Transport in DNA. *Curr. Opin. Struct. Biol.* 12, 320–329.



- (2) Nunez, M. E., and Barton, J. K. (2000) Probing DNA charge transport with metallointercalators. *Curr. Opin. Chem. Biol.* 4, 199–206.
- (3) Schuster, G. B. (2000) Long-range charge transfer in DNA: Transient structural distortions control the distance dependence. *Acc. Chem. Res.* 33, 253–260.
- (4) Giese, B. (2002) Long-distance electron transfer through DNA. *Annu. Rev. Biochem.* 71, 51–70.
- (5) Delaney, S., and Barton, J. K. (2003) Long Range DNA Charge Transport. *J. Org. Chem.* 68, 6475–6483.
- (6) Hall, D. B., Holmlin, R. E., and Barton, J. K. (1996) Oxidative DNA Damage through Long-Range Electron Transfer. *Nature* 382, 731–735.
- (7) Nunez, M. E., Hall, D. B., Barton, and J. K. (1999) Long-Range Oxidative Damage to DNA: Effects of Distance and Sequence. *Chem. Biol.* 6, 85–97.
- (8) Bhattacharya, P. K., Barton, and J. K. (2001) Influence of intervening mismatches on long-range guanine oxidation in DNA duplexes. *J. Am. Chem. Soc.* 123, 8649–8656.
- (9) Kelley, S. O., Holmlin, R. E., Stemp, E. D. A., and Barton, J. K. (1997) Photoinduced electron transfer in ethidium-modified DNA duplexes: Dependence on distance and base stacking. *J. Am. Chem. Soc.* 119, 9861–9870.
- (10) Kelley, S. O., and Barton, J. K. (1999) Electron transfer between bases in double helical DNA. *Science* 283, 375–381.
- (11) Rajski, S. R., Kumar, S., Roberts, R. J., and Barton, J. K. (1999) Protein-modulated DNA electron transfer. *J. Am. Chem. Soc.* 121, 5615–5616.
- (12) Kelley, S. O., Barton, J. K., Jackson, N. M., and Hill, M. G. (1997) Electrochemistry of methylene blue bound to a DNA-modified electrode. *Bioconjugate Chem.* 8, 31–37.
- (13) Kelley, S. O., Barton, J. K., Jackson, N. M., McPherson, L. D., Potter, A. B., Spain, E. M., Allen, M. J., and Hill, M. G. (1998) Orienting DNA helices on gold using applied electric fields. *Langmuir* 14, 6781–6784.
- (14) Boon, E. M., Barton, J. K., Sam, M., Hill, M. G., and Spain, E. M. (2001) Morphology of 15-mer duplexes tethered to Au-(111) probed using scanning probe microscopy. *Langmuir* 17, 5727–5730.
- (15) Kelley, S. O., Jackson, N. M., Hill, M. G., and Barton, J. K. (1999) Long-range electron transfer through DNA films. *Angew. Chem., Int. Ed.* 38, 941–945.
- (16) Kelley, S. O., Boon, E. M., Barton, J. K., Jackson, N. M., and Hill, M. G. (1999) Single-base mismatch detection based on charge transduction through DNA. *Nucleic Acids Res.* 27, 4830–4837.
- (17) Boon, E. M., Ceres, D. M., Drummond, T. G., Hill, M. G., and Barton, J. K. (2000) Mutation detection by electrocatalysis at DNA-modified surfaces. *Nature Biotechnol.* 18, 1096–1100.
- (18) Boon, E. M., Salas, J. E., and Barton, J. K. (2001) An electrical probe of protein-DNA interactions on DNA-modified surfaces. *Nature Biotechnol.* 20, 282–286.
- (19) Boon, E. M., Barton, J. K., Pradeepkumar, P. I., Isaksson, J., Petit, C., and Chattopadhyaya, J. (2002) An electrochemical probe of DNA stacking in an antisense oligonucleotide containing a C3'-endo-locked sugar. *Angew. Chem., Int. Ed.* 41, 3402.
- (20) Boon, E. M., Jackson, N. M., Whightman, M. D., Kelley, S. O., Hill, M. G., and Barton, J. K. (2003) Intercalative stacking: A critical feature of DNA charge transport electrochemistry. *J. Phys. Chem. B*, in press.
- (21) Saenger, W. (1984) *Principles of Nucleic Acid Structure*, Springer-Verlag, New York.
- (22) Hartmann, B., and Lavery, R. (1996) DNA structural forms. *Q. Rev. Biophys.* 29, 309–368.
- (23) Gyi, J. I., Lane, A. N., Conn, G. L., and Brown, T. (1998) Solution structures of DNA center dot RNA hybrids with purine-rich and pyrimidine-rich strands: Comparison with the homologous DNA and RNA duplexes. *Biochemistry* 37, 73–80.
- (24) Gyi, J. I., Conn, G. L., Lane, A. N., and Brown, T. (1996) Comparison of the thermodynamic stabilities and solution conformations of DNA center dot RNA hybrids containing purine-rich and pyrimidine-rich strands with DNA and RNA duplexes. *Biochemistry* 35, 12538–12548.
- (25) Fedoroff, O. Y., Salazar, M., and Reid, B. R. (1993) Structure of a DNA-RNA hybrid duplex – why RNase-H does not cleave pure RNA. *J. Mol. Biol.* 233, 509–523.
- (26) Shakked, Z., Guerin-Guzikevich, G., Eisenstein, M., Frolov, F., and Rabinovich, D. (1989) The conformation of the DNA double helix in the crystal is dependent on its environment. *Nature* 342, 456–460.
- (27) Adams, R. L. P., Knowler, J. T., and Leader, D. P. (1986) *The Biochemistry of Nucleic Acids*, 10th ed. Chapman and Hall, London.
- (28) Hansen, U. M., and McClure, W. R. (1980) Role of the sigma-subunit of Escherichia-Coli RNA-polymerase in initiation 0.2. Release of sigma from ternary complexes. *J. Biol. Chem.* 255, 9564–9570.
- (29) Varmus, H. (1988) Retroviruses. *Science* 240, 1427–1435.
- (30) Stephenson, M. L., and Zamecnik, P. C. (1978) Inhibition of rous-sarcoma viral-RNA translation by a specific oligodeoxyribonucleotide. *Proc. Natl. Acad. Sci. U.S.A.* 75, 285–288.
- (31) Wang, A. H.-J., Quigley, G. J., Kolpak, F. J., Crawford, J. L., Van Boom, J. H., Van Der Marel, G. A., and Rich, A. (1979) Molecular-structure of a left-handed double helical DNA fragment at atomic resolution. *Nature* 282, 680–686.
- (32) Gagna, C. E., and Lambert, W. C. (2003) The halting arrival of left-handed Z-DNA. *Med. Hypoth.* 60, 418–423.
- (33) Suram, A., Rao, J. K. S., Latha, K. S., and Viswamitra, M. A. (2002) First evidence to show the topological change of DNA from B-DNA to Z-DNA conformation in the hippocampus of Alzheimer's brain. *NeuroMol. Med.* 2, 289–297.
- (34) Oh, D.-B., Kim, Y.-G., and Rich, A. (2002) Z-DNA-binding proteins can act as potent effectors of gene expression in vivo. *Proc. Nat. Acad. Sci. U.S.A.* 99, 16666–16671.
- (35) Gagna, C. E., Lambert, W. C., Kuo, H. R., and Farnsworth, P. N. (1997) Localization of B-DNA and Z-DNA in terminally differentiating fiber cells in the adult lens. *J. Histochem. Cytochem.* 45, 1511–1521.
- (36) Rothenburg, S., Koch-Nolte, F., and Haag, F. (2001) DNA methylation and Z-DNA formation as mediators of quantitative differences in the expression of alleles. *Immunol. Rev.* 184, 286–298.
- (37) Herbert, A., and Rich, A. (1999) Left-handed Z-DNA: structure and function. *Genetica* 106, 37–47.
- (38) Rich, A. (1996) The biology of left-handed Z-DNA. *J. Biol. Chem.* 271, 11595–11598.
- (39) Sugiyama, H.; Kawai, K., Matsunaga, A., Fujimoto, K., Saito, I.; Robinson, H., and Wang, A. H.-J. (1996) Synthesis, structure and thermodynamic properties of 8-methylguanine-containing oligonucleotides: Z-DNA under physiological salt conditions. *Nucleic Acids Res.* 24, 1272–1278.
- (40) Hagmar, P., Pierrou, S., Nielsen P., Norden, B., and Kubista, M. (1992) Ionic-strength dependence of the binding of methylene-blue to chromatin and calf thymus DNA. *J. Biomol. Struct. Dyn.* 9, 667–679.
- (41) Qu X. G., Trent J. O., Fokt I., and Chaires, J. B. (2000) Allosteric chiral-selective drug binding to DNA. *Proc. Natl. Acad. Sci. U.S.A.* 97, 12032–12037.
- (42) Ren, J., and Chaires, J. B. (1999) Sequence and structural selectivity of nucleic acid binding ligands. *Biochemistry* 38, 16067–16075.
- (43) Taylor, E. R., and Wiechelman, K. (1998) Polarized intercalation site in Z-DNA. *Supramol. Chem.* 9, 37–46.
- (44) Wang, A. H. J., Fujii, S., van Boom, J. H., van der Marel, G. A., Boeckel, S. A. A., and Rich, A. (1982) Molecular structure of r(gcgc)d(tatagc) – a DNA RNA hybrid helix joined to double helical DNA. *Nature* 299, 601–604.
- (45) Odom, D. T., and Barton, J. K. (2001) Long-range oxidative damage in DNA/RNA duplexes. *Biochemistry* 40, 8727–8737.
- (46) Olmsted, J., and Kearns, D. R. (1977) Mechanism of ethidium-bromide fluorescence enhancement on binding to nucleic-acids. *Biochemistry* 16, 3647–3654.
- (47) Sartor, V.; Henderson, P. T., and Schuster, G. B. (1999) Radical cation transport and reaction in RNA/DNA hybrid duplexes: Effect of global structure on reactivity. *J. Am. Chem. Soc.* 121, 11027–11033.
- (48) Boon, E. M., Barton, J. K., Bhaghat, V., Nersissian, M., Wang, W., and Hill, M. G. (2003) The Reduction of Ferricya-



- nide by Methylene Blue at a DNA-modified Rotating Disc Electrode. *Langmuir*, in press.
- (49) O'Neill, M. A., and Barton, J. K. (2002) 2-aminopurine: A probe of structural dynamics and charge transfer in DNA and DNA: RNA hybrids. *J. Am. Chem. Soc.* **124**, 13053–13066.
- (50) Stivers, J. T. (1998) 2-aminopurine fluorescence studies of base stacking interactions at abasic sites in DNA: metal-ion and base sequence effects. *Nucleic Acids Res.* **26**, 3837–3844.
- (51) Xu, D. G., and Nordlund, T. M. (2000) Sequence dependence of energy transfer in DNA oligonucleotides. *Biophys. J.* **78**, 1042–1058.
- (52) Nordlund, T. M., Xu, D. G., and Evans, K. O. (1993) Excitation-energy transfer in DNA – duplex melting and transfer from normal bases to 2-aminopurine. *Biochemistry* **32**, 12090–12095.
- (53) Kool, E. T. (2001) Hydrogen bonding, base stacking, and steric effects in DNA replication. *Annu. Rev. Biophys. Biomol. Struct.* **30**, 1–22.
- (54) Guckian, K. M., Schweitzer, B. A., Ren, R. X. F., Sheils, C. J., Tahmassebi, D. C., and Kool, E. T. (2000) Factors contributing to aromatic stacking in water: Evaluation in the context of DNA. *J. Am. Chem. Soc.* **122**, 2213–2222.
- (55) Bommarito, S., Peyret, N., and SantaLucia, J. (2000) Thermodynamic parameters for DNA sequences with dangling ends. *Nucleic Acids Res.* **28**, 1929–1934.
- (56) Snoussi, K., and Leroy, J.-L. (2001) Imino proton exchange and base-pair kinetics in RNA duplexes. *Biochemistry* **40**, 8898–8904.
- (57) Maltseva, T. V., Zarytova, V. F., and Chattopadhyaya, J. (1995) Base-pair exchange kinetics of the imino and amino protons of the 3'-phenazinium tethered DNA-RNA duplex, r((5')gauugaa(3'))-d((5')tcaatc(3')-pzn), and their comparison with those of B-DNA duplex. *J. Biochem. Biophys. Methods* **30**, 163–177.
- (58) Gyi, J. I., Lane, A. N., Conn, G. L., and Brown, T. (1998) The orientation and dynamics of the C2'-OH and hydration of RNA and DNA-RNA hybrids. *Nucleic Acids Res.* **26**, 3104–3110.
- (59) O'Neill, M. A., and Barton, J. K. Unpublished data.
- (60) Kochoyan, M., Leroy, J. L., and Gueron, M. (1990) Processes of base-pair opening and proton-exchange in Z-DNA. *Biochemistry* **29**, 4799–4805.
- (61) Keyes, R. S., and Bobst, A. M. (1995) Detection of internal and overall dynamics of a 2-atom-tethered spin-labeled DNA. *Biochemistry* **34**, 9265–9275.
- (62) Otokiti, E. O., and Sheardy, R. D. (1997) Effect of base pair A/C and G/T mismatches on the thermal stabilities of DNA oligomers that form B–Z junctions. *Biochemistry* **36**, 11419–11427.
- (63) Strobel, O. K., Keyes, R. S., Sinden, R. R., and Bobst, A. M. (1995) Rigidity of a B–Z region incorporated into a plasmid as monitored by electron paramagnetic resonance. *Arch. Biochem. Biophys.* **324**, 357–366.
- (64) Abdou, I. M., Sartor, V., Cao, H., and Schuster, G. B. (2001) Long-distance radical cation migration in Z-form DNA. *J. Am. Chem. Soc.* **123**, 6696–6697.
- (65) Hunter, W. N., Leonard, G. A., Brown, T. (1998) Hydrogen-bonding patterns observed in the base pairs of duplex oligonucleotides. *ACS Symp. Ser.* **682**, 77–90.
- (66) Luxon, B. A., and Gorenstein, D. G. (1995) Comparison of X-ray and NMR-determined nucleic acid structures. *Methods Enzymol.* **261**, 45–73.
- (67) Peyret, N., Seneviratne, P. A., Allawi, H. T., and SantaLucia, J. (1999) Nearest-neighbor thermodynamics and NMR of DNA sequences with internal A center dot A, C center dot C, G center dot G, and T center dot T mismatches. *Biochemistry* **38**, 3468–3477.

BC034139L

# Multivalent Conjugates of Poly- $\gamma$ -D-glutamic Acid from *Bacillus licheniformis* with Antibody F(ab') and Glycopeptide Ligands

Emmanuel J. F. Prodhomme,<sup>†</sup> Alison L. Tutt,<sup>‡</sup> Martin J. Glennie,<sup>‡</sup> and Timothy D. H. Bugg<sup>\*,†</sup>

Department of Chemistry, University of Warwick, Coventry CV4 7AL, U.K., and Tenovus Research Laboratory, General Hospital, Tremona Road, Southampton SO16 6YD, U.K.. Received February 22, 2002;

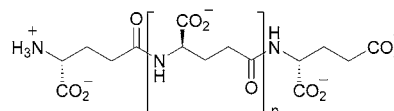
Revised Manuscript Received August 28, 2003

Poly- $\gamma$ -D-glutamic acid from *Bacillus licheniformis* is a water-soluble, nontoxic, nonimmunogenic exopolymer. Using synthetic linkers, the  $\alpha$ -carboxylate side chains of PGA were conjugated to an exposed thiol side chain of an antibody F(ab') fragment, Mc109F4. Analysis of the PGA–Mc109F4 conjugate by gel filtration HPLC revealed a mixture of multivalent conjugates. The PGA–Mc109F4 conjugate retained biological activity, but showed a lower binding affinity to target BCL3B3 cells than free Mc109F4 F(ab')<sub>2</sub> by flow cytometry, and a lower efficacy for BCL3B3 growth inhibition than free Mc109F4 F(ab')<sub>2</sub>. PGA was also conjugated with the free amino group of glycopeptide antibiotic vancomycin. The PGA–vancomycin conjugate showed slightly lower antibacterial activity than free vancomycin versus susceptible *Bacillus subtilis*, but slightly higher activity versus intrinsically resistant *Leuconostoc mesenteroides*.

## INTRODUCTION

Microorganisms which can survive in the human body commonly utilize nonimmunogenic cell surface exopolymers to evade the human immune system. These biopolymers are therefore attractive reagents for the formation of conjugates which could operate successfully in the human body. One such exopolymer is poly- $\gamma$ -D-glutamic acid (Figure 1), a  $\gamma$ -linked polypeptide of D-glutamic acid of molecular mass 100–300 kDa, found in several strains of *Bacillus* (1), including soil bacterium *Bacillus licheniformis* (1, 2), and the human pathogen *Bacillus anthracis* (1, 3). We have previously shown that  $\gamma$ -PGA from *Bacillus licheniformis* can be covalently modified in aqueous solution with amines bearing a UV chromophore (4), giving a modified polymer of reduced molecular weight (10–15 kDa). Early literature reports of PGA conjugates (5, 6) suggested that this biopolymer would be a useful template for functionalization with bioactive molecules. In this paper we describe methods for conjugation of PGA with an antibody F(ab'), and with a glycopeptide antibiotic.

Targeting of cytotoxic drugs via comodification of the drug to a water-soluble polymer with a cell-specific antibody is an attractive approach for anticancer chemotherapy (7). Tumor-specific antibody F(ab') fragments have been successfully conjugated to *N*-(2-hydroxypropyl)methacrylamide (HPMA) with cytotoxic agents adriamycin (8) or doxorubicin (9) to give cytotoxic conjugates. Methods have also been developed for the attachment of antibody F(ab') fragments, via a reactive thiol group, to poly- $\alpha$ -lysine (10, 11), poly[2-(dimethylamino)ethyl methacrylate] (12), and poly(ethylene oxide)-poly(propylene oxide) triblock copolymers (13). In this study, we used the F(ab') fragment of antibody Mc109G4, a monoclonal



**Figure 1.** Structure of poly- $\gamma$ -D-glutamic acid.

rat IgG2a antibody (mAb) with activity against idiotype determinants carried by the IgM molecule of the BCL<sub>1</sub> lymphoma (14).

The glycopeptide antibiotic vancomycin exerts its antibacterial effects via complexation of the peptidyl-D-Ala-D-Ala termini of peptidoglycan on the surface of Gram-positive bacterial cell walls (15). Recent studies by Williams et al. have demonstrated that members of the vancomycin group of glycopeptide antibiotics form dimers, and that the dimerization is cooperative with ligand binding (15, 16). Thus, multivalent derivatives of vancomycin which are able to bind the target ligands cooperatively might have enhanced affinity for bacterial peptidoglycan, particularly for vancomycin-resistant strains containing peptidyl-D-Ala-D-Lac termini, for which vancomycin shows low affinity (15). Synthetic dimers (17) and trimers (18, 19) of vancomycin have been reported to show enhanced binding of L-Lys-D-Ala-D-Ala and enhanced antibacterial activity against vancomycin-resistant strains. Polymers derived from a vancomycin-containing monomer have also been reported to show enhanced antibacterial activity (20, 21). We therefore also investigated the effects of conjugating vancomycin to  $\gamma$ -PGA.

## EXPERIMENTAL SECTION

**General.** Poly- $\gamma$ -D-glutamic acid was prepared from *Bacillus licheniformis* ATCC 9945a by the method of Troy (2) and was stored as a powder at 4 °C. *N*-butoxycarbonyl-1,2-diamine was prepared by the method of Krapcho and Kuell (22). Chemicals and biochemicals were purchased from Sigma-Aldrich.

*N*-Butoxycarbonyl-[2,2'-(ethylenedioxy)bis-ethylamine] was prepared by a modification of the method of Krapcho and Kuell (22). A solution of di-*tert*-butyl dicarbonate (2.18 g, 10 mmol) in dioxane (30 mL) was added

\* To whom correspondence should be addressed. Tel 02476-573018. Fax 02476-524112. E-mail t.d.bugg@warwick.ac.uk.

<sup>†</sup> University of Warwick.

<sup>‡</sup> Tenovus Research Laboratory.

<sup>†</sup> Abbreviations used: PGA, poly- $\gamma$ -D-glutamic acid; FITC, fluorescein isothiocyanate; EDC, *N*-ethyl-*N*-(3-dimethylaminopropyl)carbodiimide hydrochloride.

to 2,2'-(ethylenedioxy)bis-ethylamine (7.3 mL, 5 equiv) in dioxane (30 mL) over 2.5 h. The reaction mixture was stirred at room temperature for 22 h. Solvent was then removed under reduced pressure. Water (50 mL) was added to the residue, and the insoluble bis-substituted product removed by filtration. The filtrate was extracted with dichloromethane (3  $\times$  50 mL), the extracts were combined and dried (MgSO<sub>4</sub>), and the solvent was evaporated at reduced pressure to give the product as a clear oil (2.2 g, 63%).  $R_f$  0.10 (9:1 CH<sub>2</sub>Cl<sub>2</sub>/EtOH);  $\delta_H$  (300 MHz, CDCl<sub>3</sub>) 5.65 (1H, br s, NH), 3.55 (4H, s, OCH<sub>2</sub>-CH<sub>2</sub>O), 3.45 (4H, m, NHCH<sub>2</sub>CH<sub>2</sub>O), 3.25 (2H, m, BocNHCH<sub>2</sub>-CH<sub>2</sub>O), 2.80 (2H, t,  $J$  = 7 Hz, H<sub>2</sub>NCH<sub>2</sub>CH<sub>2</sub>O), 1.40 (9H, s, tBu) ppm;  $\delta_C$  (75 MHz, CDCl<sub>3</sub>) 156.0, 78.7, 73.3, 70.1, 66.9, 41.6, 40.2, 28.3 ppm.

**Preparation of *N*-Carboxyalkylmaleimides 1a,b.** A solution of maleic anhydride (2.94 g, 30 mmol) in acetic acid (100 mL) was added to a solution of 6-aminocaproic acid (3.94 g, 30 mmol) in acetic acid (100 mL). The reaction was stirred for 3 h at room temperature, yielding a white precipitate, which was filtered, yielding *N*-maleamyl-6-aminocaproic acid (4.6 g, 67%).  $R_f$  0.25 (9:1 CH<sub>2</sub>Cl<sub>2</sub>/EtOH); mp 159–161 °C;  $\delta_H$  (300 MHz, *d*<sub>6</sub>-DMSO) 9.15 (1H, br, COOH), 6.40 (1H, d,  $J$  = 11 Hz, CH=C), 6.25 (1H, d,  $J$  = 11 Hz, CH=C), 3.15 (2H, q,  $J$  = 6 Hz, NCH<sub>2</sub>), 2.20 (2H, t,  $J$  = 7 Hz, CH<sub>2</sub>COOH), 1.45 (4H, m), 1.30 (2H, m) ppm;  $\delta_C$  (75 MHz, *d*<sub>6</sub>-DMSO) 174.5, 165.5, 165.4, 133.1, 131.8, 40.4, 33.6, 28.2, 26.0, 24.2 ppm;  $m/z$  (ES<sup>+</sup>) 230.1 (MH<sup>+</sup>, 60%).

*N*-Maleamyl-6-aminocaproic acid (0.92 g, 4.0 mmol) was dissolved in dry toluene (100 mL), to which was added triethylamine (1.1 mL, 8.0 mmol). The reaction was refluxed for 1 h in a Dean–Stark apparatus, with removal of water. The toluene solution was decanted and evaporated under reduced pressure to give a solid, which was dissolved in water (20 mL), acidified (HCl) to pH 2.0. The product was extracted with ethyl acetate (2  $\times$  20 mL), washed with sat. sodium chloride solution (5 mL), dried (MgSO<sub>4</sub>), and evaporated at reduced pressure to give *N*-carboxypentylmaleimide **1b** as a white solid (0.42 g, 50%).  $R_f$  0.72 (9:1 CH<sub>2</sub>Cl<sub>2</sub>/EtOH); mp 79–80 °C; UV/vis  $\lambda_{max}$  319 nm;  $\delta_H$  (300 MHz, *d*<sub>6</sub>-acetone) 10.1 (1H, br, COOH), 6.70 (2H, s, CH=C), 3.30 (2H, t,  $J$  = 6 Hz, NCH<sub>2</sub>), 2.15 (2H, t,  $J$  = 7 Hz, CH<sub>2</sub>COOH), 1.45 (4H, qui,  $J$  = 7 Hz), 1.20 (2H, qui,  $J$  = 7 Hz) ppm;  $\delta_C$  (75 MHz, *d*<sub>6</sub>-acetone) 206.0, 174.3, 134.9, 37.7, 33.7, 28.7, 26.6, 24.9 ppm.

The same procedure was used to prepare *N*-carboxymethylmaleimide **1a** from glycine, in 46% overall yield.  $R_f$  0.35 (9:1 CH<sub>2</sub>Cl<sub>2</sub>/EtOH); mp 113–114 °C; UV/vis  $\lambda_{max}$  318 nm;  $\delta_H$  (300 MHz, *d*<sub>6</sub>-acetone) 6.35 (2H, s, CH=C), 4.15 (2H, s, CH<sub>2</sub>) ppm;  $\delta_C$  (75 MHz, *d*<sub>6</sub>-acetone) 206.0, 168.8, 135.4, 38.6 ppm.

**Preparation of *N*-Boc-ethylenediaminylcarboxyalkylmaleimides 2a,b.** Isobutyl chloroformate (129  $\mu$ L, 1.0 mmol) was added to a solution of *N*-carboxypentylmaleimide (0.21 g, 1.0 mmol) and triethylamine (0.2 mL) in THF (10 mL) at 0 °C, and the reaction was stirred for 15 min at room temperature. A solution of *N*-butoxycarbonylethylenediamine (0.16 g, 1.0 mmol) and triethylamine (0.2 mL) in THF (10 mL) was then added, and the reaction was stirred for 16 h at room temperature. The solution was filtered and solvent evaporated under reduced pressure. The resulting oil was triturated with diethyl ether to give *N*-butoxycarbonyl-*N*-6-(*N*-maleimyl)-aminoethanylethylenediamine **2b** as a pale yellow gum (0.165 g, 45%).  $R_f$  0.70 (9:1 CH<sub>2</sub>Cl<sub>2</sub>/EtOH);  $\delta_H$  (300 MHz, CDCl<sub>3</sub>) 6.60 (2H, s, CH=C), 6.15 (1H, br s, NH), 4.90 (1H, br s, NH), 3.45 (2H, t,  $J$  = 6 Hz, NCH<sub>2</sub>), 3.2–3.3

(4H, m, NHCH<sub>2</sub>CH<sub>2</sub>NH), 2.10 (2H, t,  $J$  = 7 Hz, CH<sub>2</sub>CO), 1.55 (4H, qui,  $J$  = 7 Hz), 1.35 (9H, s, tBu), 1.25 (2H, qui,  $J$  = 7 Hz) ppm;  $\delta_C$  (75 MHz, CDCl<sub>3</sub>) 174.0, 171.0, 159.7, 134.2, 80.2, 40.9, 40.4, 37.8, 36.6, 28.5, 28.4, 26.5, 25.2 ppm;  $m/z$  (ES<sup>+</sup>) 354.3 (MH<sup>+</sup>, 100%).

The same procedure was used to prepare *N*-butoxycarbonyl-*N*-6-(*N*-maleimyl)aminoethanylethylenediamine **2a** from *N*-carboxymethylmaleimide (**1a**) and *N*-butoxycarbonylethylenediamine, in 51% yield. Mp 133–135 °C;  $\delta_H$  (300 MHz, CDCl<sub>3</sub>) 7.0 (1H, br s, NH), 6.70 (2H, s, CH=C), 5.05 (1H, br s, NH), 4.10 (2H, s, NCH<sub>2</sub>), 3.2–3.3 (4H, m, NHCH<sub>2</sub>CH<sub>2</sub>NH), 1.35 (9H, s, tBu) ppm;  $\delta_C$  (75 MHz, CDCl<sub>3</sub>) 170.0, 167.0, 158.0, 134.2, 80.0, 41.7, 40.9, 40.4, 28.5 ppm;  $m/z$  (ES<sup>+</sup>) 298.2 (MH<sup>+</sup>, 100%).

**Preparation of Boc-protected Maleimides 3a,b.** Isobutyl chloroformate (129  $\mu$ L, 1.0 mmol) was added to a solution of *N*-carboxypentylmaleimide (0.21 g, 1.0 mmol) and triethylamine (0.2 mL) in THF (10 mL) at 0 °C, and the reaction was stirred for 15 min at room temperature. A solution of *N*-butoxycarbonyl-[2,2'-(ethylenedioxy)bis-ethylamine] (0.248 g, 1.0 mmol) and triethylamine (0.2 mL) in THF (10 mL) was then added, and the reaction was stirred for 16 h at room temperature. The solution was filtered and solvent evaporated under reduced pressure. The resulting oil was triturated with diethyl ether to give maleimide **3b** as a pale yellow gum (0.176 g, 40%).  $R_f$  0.75 (9:1 CH<sub>2</sub>Cl<sub>2</sub>/EtOH);  $\delta_H$  (300 MHz, CDCl<sub>3</sub>) 6.60 (2H, s, CH=C), 6.15 (1H, br s, NH), 5.65 (1H, br s, NH), 3.55 (4H, s, OCH<sub>2</sub>CH<sub>2</sub>O), 3.50 (2H, t,  $J$  = 6 Hz), 3.40 (4H, m), 3.25 (2H, m), 2.85 (2H, t,  $J$  = 7 Hz, BocNHCH<sub>2</sub>-), 2.1 (2H, t,  $J$  = 7 Hz, CH<sub>2</sub>CO), 1.55 (4H, m), 1.40 (9H, s, tBu), 1.30 (2H, m) ppm;  $\delta_C$  (75 MHz, CDCl<sub>3</sub>) 173.8, 171.2, 157.0, 134.4, 78.7, 73.1, 70.3, 67.2, 41.9, 39.9, 37.7, 36.4, 28.4, 28.2, 26.3, 24.9 ppm;  $m/z$  (ES<sup>+</sup>) 442.3 (MH<sup>+</sup>, 45%).

The same method was used to prepare *N*-Boc maleimide **3a** from maleimide acid **2a**, in 48% yield.  $R_f$  0.64 (9:1 CH<sub>2</sub>Cl<sub>2</sub>/EtOH);  $\delta_H$  (300 MHz, CDCl<sub>3</sub>) 6.70 (2H, s, CH=C), 6.40 (1H, br s, NH), 4.95 (1H, br s, NH), 4.15 (2H, s, NCH<sub>2</sub>CO), 3.60 (4H, s, OCH<sub>2</sub>CH<sub>2</sub>O), 3.50 (4H, m), 1.40 (9H, s, tBu) ppm;  $\delta_C$  (75 MHz, CDCl<sub>3</sub>) 170.3, 167.8, 158.0, 134.7, 79.8, 73.8, 70.3, 70.1, 41.9, 41.4, 39.9, 28.5 ppm;  $m/z$  (ES<sup>+</sup>) 387.2 (MH<sup>+</sup>, 40%).

**Preparation of Maleimide Linkers 4a,b and 5a,b.** Boc-protected maleimide **2b** (90 mg, 0.25 mmol) was stirred in a 1:1 mixture of trifluoroacetic acid and dichloromethane (10 mL) at room temperature for 30 min. Solvent was removed under reduced pressure, and the residue was coevaporated with toluene to remove excess trifluoroacetic acid, to give the deprotected maleimide **4b** (trifluoroacetate salt) as a brown oil (61 mg, 96%).  $\delta_H$  (300 MHz, CDCl<sub>3</sub>) 7.90 (2H, br s, NH), 6.60 (2H, s, CH=C), 6.35 (1H, br s, NH), 3.50 (2H, t,  $J$  = 6 Hz, NCH<sub>2</sub>), 3.25 (2H, q,  $J$  = 5 Hz, NHCH<sub>2</sub>), 3.05 (2H, m, NHCH<sub>2</sub>), 2.15 (2H, t,  $J$  = 7 Hz, CH<sub>2</sub>CO), 1.60 (4H, qui,  $J$  = 7 Hz), 1.25 (2H, qui,  $J$  = 7 Hz) ppm;  $\delta_C$  (75 MHz, CDCl<sub>3</sub>) 174.4, 172.1, 133.7, 40.7, 39.6, 37.5, 36.3, 28.2, 26.0, 24.7 ppm;  $m/z$  (ES<sup>+</sup>) 254.1 (MH<sup>+</sup>, 100%).

The same procedure was used to prepare maleimide **4a** from Boc-protected maleimide **2a**, in 94% yield.  $\delta_H$  (300 MHz, CDCl<sub>3</sub>) 8.05 (2H, br s, NH), 7.05 (1H, br s, NH), 6.70 (2H, s, CH=C), 4.10 (2H, s, NCH<sub>2</sub>), 3.20 (2H, t,  $J$  = 5 Hz, NHCH<sub>2</sub>), 3.05 (2H, m, NHCH<sub>2</sub>) ppm;  $\delta_C$  (75 MHz, CDCl<sub>3</sub>) 170.0, 167.0, 134.2, 41.7, 40.9, 40.4 ppm;  $m/z$  (ES<sup>+</sup>) 198.3 (MH<sup>+</sup>, 100%).

The same procedure was used to prepare maleimide **5a** from Boc-protected maleimide **3a**, in 95% yield.  $\delta_H$  (300 MHz, CDCl<sub>3</sub>) 7.80 (2H, br s, NH), 6.75 (2H, s, CH=C), 6.20 (1H, br s, NH), 4.10 (2H, s, NCH<sub>2</sub>CO), 3.65 (4H,



s, OCH<sub>2</sub>CH<sub>2</sub>O), 3.55 (4H, m), 3.35 (2H, m), 3.15 (2H, m, NCH<sub>2</sub>) ppm;  $\delta_C$  (75 MHz, CDCl<sub>3</sub>) 170.8, 168.3, 134.2, 71.5, 70.8, 70.2, 41.3, 41.1, 38.9 ppm;  $m/z$  (ES<sup>+</sup>) 287.5 (MH<sup>+</sup>, 60%).

The same procedure was used to prepare maleimide **5b** from Boc-protected maleimide **3b**, in 93% yield.  $\delta_H$  (300 MHz, CDCl<sub>3</sub>) 8.30 (2H, br s, NH), 6.60 (2H, s, CH=C), 6.10 (1H, br s, NH), 3.60 (4H, s, -OCH<sub>2</sub>CH<sub>2</sub>O-), 3.45 (2H, t,  $J$  = 6 Hz), 3.35 (2H, m), 3.25 (2H, m), 3.15 (2H, m), 2.65 (2H, t,  $J$  = 7 Hz, NHCH<sub>2</sub>), 2.10 (2H, t,  $J$  = 7 Hz, CH<sub>2</sub>CO), 1.50 (4H, m), 1.20 (2H, m) ppm;  $\delta_C$  (75 MHz, CDCl<sub>3</sub>) 173.6, 170.7, 134.1, 73.9, 70.2, 67.7, 41.7, 39.1, 37.1, 36.5, 28.9, 27.1, 25.3 ppm;  $m/z$  (ES<sup>+</sup>) 342.5 (MH<sup>+</sup>, 50%).

#### Preparation of *N*-Succinylethane 1,2-Diamine (**6**).

Succinic anhydride (0.86 g, 1.1 equiv) was added to a solution of *N*-Boc-ethylene 1,2-diamine (1.25 g, 7.85 mmol) in toluene (250 mL). The reaction was heated at 60 °C for 4 h, then cooled. The product, which crystallized upon cooling, was filtered and dried to give *N*-Boc *N*-succinylethylene 1,2-diamine as white crystals (1.826 g, 90%). Mp 124–126 °C;  $\delta_H$  (300 MHz, *d*<sub>6</sub>-DMSO) 12.05 (1H, br s, COOH), 7.85 (1H, br s, NH), 6.75 (1H, br s, NH), 3.05 (2H, t,  $J$  = 7 Hz, NCH<sub>2</sub>), 2.95 (2H, t,  $J$  = 7 Hz, NCH<sub>2</sub>), 2.40 (2H, t,  $J$  = 7 Hz, COCH<sub>2</sub>), 2.30 (2H, t,  $J$  = 7 Hz, COCH<sub>2</sub>), 1.40 (9H, tBu) ppm;  $\delta_C$  (75 MHz, CD<sub>3</sub>OD) 176.2, 174.8, 158.4, 80.0, 40.7, 40.5, 31.4, 30.2, 28.7 ppm;  $m/z$  (ES<sup>+</sup>) 261.4 (MH<sup>+</sup>, 100%).

*N*-Boc-*N*-succinylethylene 1,2-diamine (0.2 g, 0.77 mmol) was added to a 1:1 mixture (10 mL) of trifluoroacetic acid and dichloromethane at room temperature for 30 min. Solvent was removed under reduced pressure, and the residue was coevaporated with toluene to remove excess trifluoroacetic acid, to give *N*-succinylethylene 1,2-diamine **6** (trifluoroacetate salt) as a brown oil (0.117 g, 95%).  $\delta_H$  (300 MHz, *d*<sub>6</sub>-DMSO) 11.70 (1H, br s, COOH), 8.20 (1H, br s, NH), 7.85 (2H, br s, NH), 6.75 (1H, br s, NH), 3.25 (2H, t,  $J$  = 7 Hz, NCH<sub>2</sub>), 2.85 (2H, t,  $J$  = 7 Hz, NCH<sub>2</sub>), 2.40 (2H, t,  $J$  = 7 Hz, COCH<sub>2</sub>), 2.30 (2H, t,  $J$  = 7 Hz, COCH<sub>2</sub>) ppm;  $\delta_C$  (75 MHz, *d*<sub>6</sub>-DMSO) 175.0, 172.2, 39.4, 38.7, 31.2, 29.7 ppm;  $m/z$  (ES<sup>+</sup>) 161.0 (MH<sup>+</sup>, 10%).

**Toxicity of Poly- $\gamma$ -D-glutamic Acid.** PGA was incubated with the EHRB human B cell line at 20 and 100  $\mu$ g/mL concentration for 24 h, then stained with propidium iodide to detect apoptotic cells, as described by Nicoletti et al. (23). Uptake of <sup>3</sup>H-thymidine into EHRB cells was also assayed, at 100 and 10  $\mu$ g/mL concentrations of PGA, as previously described (24). Animal toxicity was assessed by injection of PGA (1 mg) intra-peritoneally into mice. No signs of toxicity (morbidity, coat appearance, diarrhea) were observed.

**Modification of Poly- $\gamma$ -D-glutamic Acid with Maleimide Linkers.** Poly- $\gamma$ -D-glutamic acid (35 mg, 0.27 mmol available sites) was dissolved in water (10 mL), to which was added the appropriate amine (0.27 mmol), triethylamine (38  $\mu$ L, 0.3 mmol), *N*-ethyl-*N*-(3-dimethylaminopropyl)carbodiimide hydrochloride (53 mg, 0.27 mmol), and hydroxybenzotriazole (37 mg, 0.27 mmol). The reaction mixture was stirred for 24 h at room temperature, then dialyzed against water (1 L), and freeze-dried, to give the PGA–maleimides as pale brown solids. Maleimide-modified polymers were characterized by UV and NMR spectroscopy. Observed  $\lambda_{\max}$  values: PGA–**4a**, 306 nm; PGA–**4b**, 317 nm; PGA–**5a**, 304 nm; PGA–**5b**, 299 nm.

**Conjugation of Poly- $\gamma$ -D-glutamic Acid with Antibody Mc109F4 F(ab').** Buffers: 1 M NTE8 buffer stock contains 25 mM Tris, 12.5 mM EDTA, and 1 M NaCl, adjusted to pH 8.0, which was diluted 5-fold for use. AE

buffer contains 50 mM sodium acetate and 0.6 mM EDTA, adjusted to pH 5.2 with acetic acid. PBS buffer contains 10 mM sodium phosphate (pH 7.4) and 150 mM NaCl.

F(ab')<sub>2</sub> fragments were obtained by proteolytic digestion of antibody Mc109F4, as previously described (25). F(ab')<sub>2</sub> fragments (5–12 mg/mL, 1.0 mL) in 0.2 M NTE8 buffer were reduced by addition of 100  $\mu$ L of 200 mM  $\beta$ -mercaptoethanol, followed by incubation at 30 °C for 30 min, then cooled to 4 °C. Reduced F(ab')SH was separated from reducing agent by passage through a Sephadex G25 column (80  $\times$  2.4 cm) in 50 mM AE buffer. Fractions from the G25 column were analyzed by HPLC gel filtration (Phenomenex BioSep-SEC–S3000 column, 1.0 mL/min flow rate, monitored at 280 nm, retention times F(ab')<sub>2</sub> 8.6 min, F(ab')SH 9.4 min,  $\beta$ -mercaptoethanol 12.5 min).

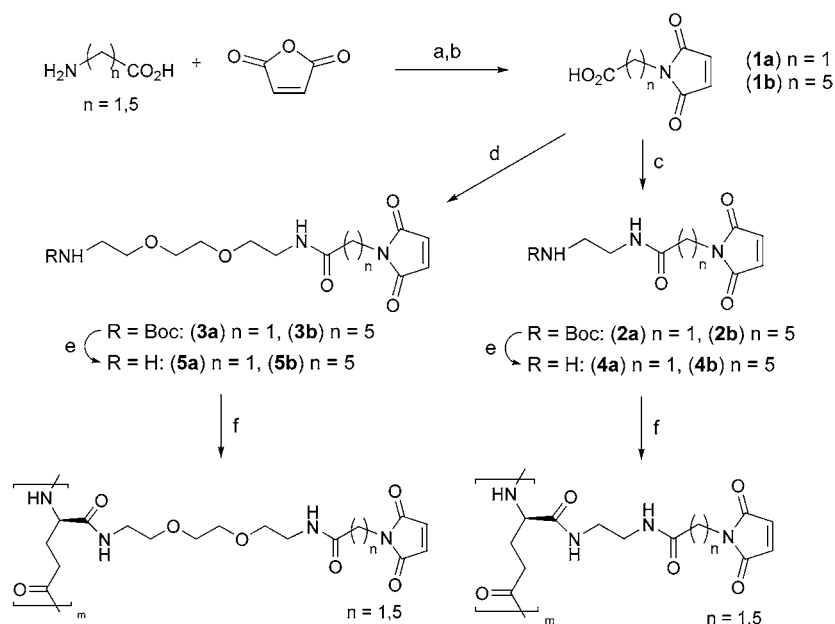
Fractions containing F(ab')SH and free of  $\beta$ -mercaptoethanol were pooled and immediately treated with a solution of maleimide-activated PGA (160 mg) in water (1 mL). The molar ratio of reagents was 5:1 PGA–maleimide (moles of glutamic acid):antibody F(ab'). The mixture was left to react at 4 °C for up to 14 days and monitored by HPLC gel filtration (retention time of conjugate 7.3 min). The conjugate was purified by passage through two AcA44 gel filtration columns (120  $\times$  2.0 cm) in series, in 0.2 M NTE8 buffer. Two main protein peaks were observed: the first being the PGA–F(ab') conjugate, and the second being unreacted F(ab')<sub>2</sub> and F(ab')SH. The PGA–F(ab') conjugate was pooled, concentrated using an Amicon device, and dialyzed into PBS.

HPLC gel filtration was carried out using a Phenomenex BioSep-SEC–S3000 column, eluting with 50 mM sodium acetate buffer pH 5.2 containing 0.5 mM EDTA at a flow rate of 1.0 mL/min. Molecular weight calibration was carried out using authentic samples of poly- $\alpha$ -D-glutamic acid (Sigma): 12000–14000 Da (9.1 min); 16000–32000 (8.2 min); 45000–65000 (6.6 min).

**Analysis of Interaction of PGA–**5b**–Mc109F4 Conjugate with BCL3B3 Cells.** BCL<sub>1</sub> 3B3 cells were analyzed by indirect immunofluorescent staining using a FACS vantage (Becton Dickinson, Mountain View, CA), as described previously (14). BCL3B3 cells were incubated for 30 min with the conjugate or control antibody, then washed and incubated with goat anti-rat IgG-FITC (Strattech Scientific Ltd, Luton UK), then washed and analyzed by flow cytometry. Protein concentration of 25  $\mu$ g/mL was used in each assay. Concentration of F(ab') in PGA–**5b**–Mc109F4 estimated by measurement of A<sub>280</sub> and comparison with standard sample of Mc109F4.

A growth assay to assess direct effects of mAb or derivatives on BCL<sub>1</sub>3B3 target tumor cells in vitro was carried out as described previously (24). The cells (5  $\times$  10<sup>4</sup>) were grown in various concentrations (1–25  $\mu$ g/mL) of antibodies for 42 h, then pulsed with <sup>3</sup>H-thymidine and harvested 6 h later, and growth was assessed by <sup>3</sup>H incorporation.

**Preparation of PGA–Vancomycin Conjugates.** Poly- $\gamma$ -D-glutamic acid (30 mg, 0.23 mmol available sites) was dissolved in water (5 mL), to which was added the *N*-succinylethane 1,2-diamine (**6**, 30 mg, 0.23 mmol), triethylamine (32  $\mu$ L, 0.25 mmol), *N*-ethyl-*N*-(3-dimethylaminopropyl)carbodiimide hydrochloride (45 mg, 0.23 mmol), and hydroxybenzotriazole (32 mg, 0.23 mmol). The reaction mixture was stirred for 15 min at room temperature. Vancomycin hydrochloride (35 mg, 0.23 mmol, Sigma) and triethylamine (32  $\mu$ L, 0.25 mmol) were then added, and the reaction mixture was stirred overnight at room temperature. The mixture was then

**Scheme 1. Synthesis of Maleimide Linkers 4, 5<sup>a</sup>**

<sup>a</sup> a, AcOH; b,  $\text{NEt}_3$ , toluene,  $\Delta$ , 46% ( $n = 1$ ) and 34% ( $n = 5$ ); c,  $\text{BocNHCH}_2\text{CH}_2\text{NH}_2$ , isobutyl chloroformate,  $\text{NEt}_3$ , THF, 51% ( $n = 1$ ) and 45% ( $n = 5$ ); d,  $\text{BocNH}(\text{CH}_2\text{CH}_2\text{O})_2\text{CH}_2\text{CH}_2\text{NH}_2$ , isobutyl chloroformate,  $\text{NEt}_3$ , THF, 48% ( $n = 1$ ), 40% ( $n = 5$ ); e,  $\text{CF}_3\text{COOH}$ ,  $\text{CH}_2\text{Cl}_2$ , 90–96%; f, PGA, EDC, HOBT,  $\text{NEt}_3$ ,  $\text{H}_2\text{O}$ .

dialyzed against water (1 l) and freeze-dried, to give the PGA–6–vancomycin conjugate (30 mg) as a fluffy off white solid. The PGA–vancomycin conjugate was prepared using the same method, omitting linker 6, and using 0.1 equiv of EDC, HOBT, vancomycin, and triethylamine. PGA–vancomycin conjugates were analyzed by BioSep S3000 HPLC gel filtration, as described above.

**Assay of Antibacterial Activity of PGA–Vancomycin Conjugates.** Overnight cultures of *Bacillus subtilis* W23 and *Lactobacillus casei* subsp. *casei* (ATCC393) were grown in Luria broth at 37 °C and then spread onto the surface of an LB plate, and excess liquid was removed. Filter disks (Whatman no.1, 20 mm) were placed onto the plate, and an aliquot (100  $\mu\text{l}$ ) of a 1 mg/mL solution of the antibiotic or conjugate was added to the disk. The plate was then grown overnight at 37 °C. A zone of growth inhibition was observed around each filter disk, whose radius from the outside of the disk was measured.

**RESULTS**

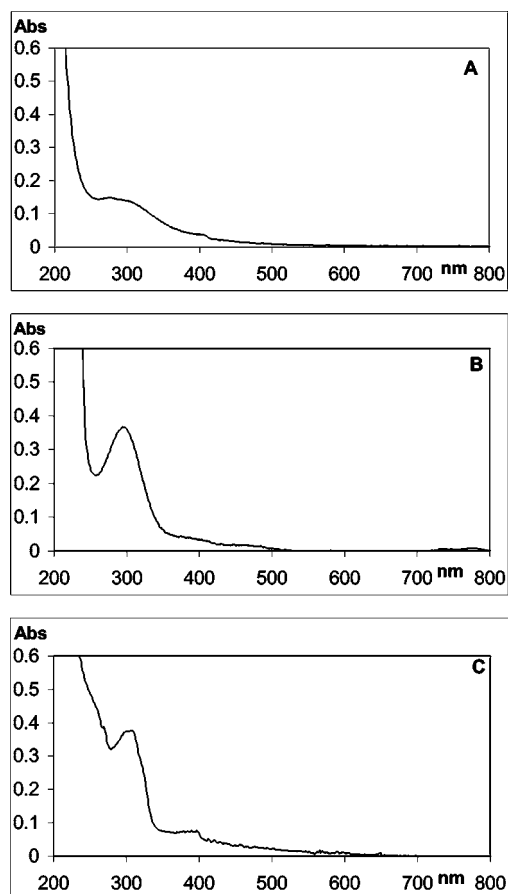
**Toxicity of Native PGA.** Poly- $\gamma$ -D-glutamic acid (PGA) was prepared from *Bacillus licheniformis* ATCC 9945a using the procedure of Troy (2), yielding approximately 120 mg of pure polymer from a 100 mL culture, as a freeze-dried powder. The toxicity of PGA was tested in cell culture, against a sensitive EHRB cell line. Using the method of Nicoletti et al. to measure % apoptotic cells (23), no toxicity was observed at 20  $\mu\text{g}/\text{mL}$  PGA (11.2%) compared to a control (11%), although slight toxicity was observed at 100  $\mu\text{g}/\text{mL}$  (18.1%). Using a  $^3\text{H}$ -thymidine uptake assay (24) on EHRB cells, 100 and 10  $\mu\text{g}/\text{mL}$  PGA showed 78% and 88% counts compared to untreated cells. Injection of a 1 mg dose of PGA into mice resulted in no observable toxicity.

**Synthesis and Attachment of Maleimide Linkers to PGA.** Proteolytic digestion of IgG immunoglobulins, followed by reduction of the  $\text{F}(\text{ab}')_2$  dimer product (100 kDa), generates an antibody  $\text{F}(\text{ab}')_1$  fragment (50 kDa) bearing a unique reactive thiol group (25). To conjugate an antibody  $\text{F}(\text{ab}')_1$  to PGA, a synthetic linker is required

which can be attached to the  $\alpha$ -carboxyl group of PGA and subsequently selectively with the thiol group. Preliminary experiments using bromoacetyl- and iodoacetyl-containing linkers revealed that thiol conjugation with these linkers required high pH conditions and proceeded in low yield; therefore, the synthesis of linkers containing reactive maleimide groups was undertaken. The maleimide functional group, known to react selectively with thiol nucleophiles (26), was attached via a variable length chain to a primary amine group, which could be attached to PGA.

The synthesis of four maleimide-containing linkers is illustrated in Scheme 1. Maleic anhydride was reacted with glycine to give the corresponding maleamic acid, which was converted to maleimide **1a** by treatment with triethylamine in refluxing toluene (27). In a similar fashion, 6-aminohexanoic acid was converted to maleimide **1b**. Each maleimide acid was coupled to mono-Boc-ethylenediamine, to give maleimides **2a,b**, and also to a longer, more polar linker containing an ethylene glycol spacer, yielding maleimides **3a,b**. Deprotection under acidic conditions gave the deprotected maleimide linkers **4a,b** and **5a,b** containing 9, 13, 15, and 19 atom spacers, respectively.

Each linker was attached to PGA using water-soluble carbodiimide EDC, and the modified polymers were dialyzed and lyophilized. The attachment of maleimide linkers to PGA was monitored by UV and NMR spectroscopy. Maleimides **4** and **5** showed characteristic UV/visible absorption peaks at  $\lambda_{\text{max}}$  300–315 nm, due to the maleimide chromophore. PGA–maleimide conjugates showed peaks at 300–315 nm by UV/visible spectroscopy, demonstrating that immobilization of the maleimide had taken place (see Figure 2). NMR signals for the maleimide group could also be observed at  $\delta_{\text{H}}$  6.75 ppm and  $\delta_{\text{C}}$  135 ppm in the  $^1\text{H}$  and  $^{13}\text{C}$  NMR spectra of the modified polymer (see Figure 3). After storage for >24 h, the UV absorption of the modified polymers gradually decreased, suggesting that intramolecular reaction was taking place between the maleimide groups and free carboxylate side chains of the polymer. Therefore, samples of activated

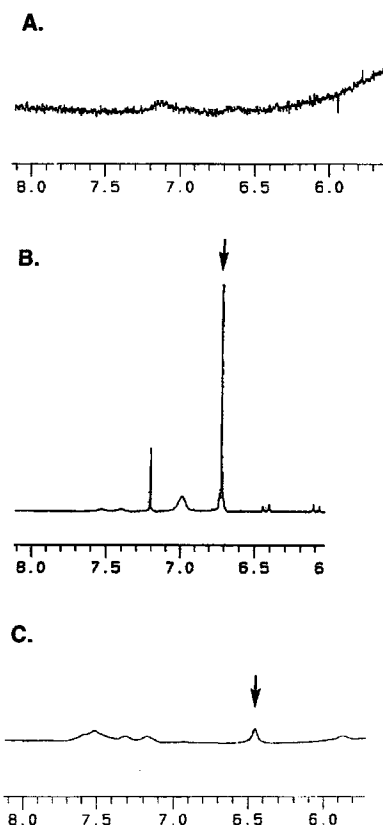


**Figure 2.** UV/visible spectra of (A)  $\gamma$ -PGA; (B) linker **4a**; (C) PGA modified by linker **4a**. The absorption of the maleimide chromophore can be seen at  $\lambda_{\max}$  300 nm.

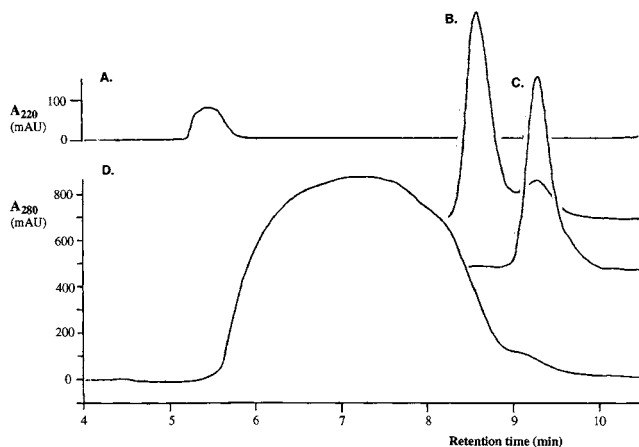
polymer for conjugation reactions were prepared immediately prior to use.

**Conjugation with Antibody Mc109F4 F(ab').** Antibody Mc109F4 IgG was subjected to proteolytic cleavage by treatment with bromelain, to give the F(ab')<sub>2</sub> dimer (100 kDa). Treatment with  $\beta$ -mercaptoethanol then gave the F(ab')-SH monomer (50 kDa), which was separated from excess reducing agent by G25 gel filtration chromatography. Preparation of F(ab')-SH could be conveniently monitored by HPLC gel filtration, using a Phenomenex BioSep-S3000 column, which could resolve F(ab')<sub>2</sub> and F(ab') with retention times 8.6 and 9.4 min, respectively (see Figure 4B,C). Freshly reduced F(ab')-SH was mixed with the maleimide-activated polymer, in a 1:1 ratio of reduced F(ab')-SH to maleimide linker, in 50 mM acetate buffer pH 5.2, and left to react at 4 °C.

Reaction of the maleimide-activated polymer with reduced F(ab')-SH was monitored by HPLC gel filtration. Analysis of native PGA gave a single peak at 5.5 min (Figure 4A), whereas the maleimide-activated polymers gave peaks at 9.0–9.2 min, implying that fragmentation of the native polymer had taken place during modification, as observed previously (4). Molecular weight calibration was attempted using samples of poly- $\alpha$ -D-glutamic acid, which gave the following retention times: 44–64 kDa, 6.6 min; 17–31 kDa, 8.2 min; 11–13 kDa, 9.1 min. Using these data, we can tentatively assign a molecular weight for the activated PGA of 11–13 kDa, which matches previous estimates (4), and a  $M_r$  for native PGA of  $110 \pm 40$  kDa. The reason for the fragmentation of PGA upon modification is not known: it may be due to EDC-mediated cleavage (4) or the existence of a depolymerase enzyme (28).



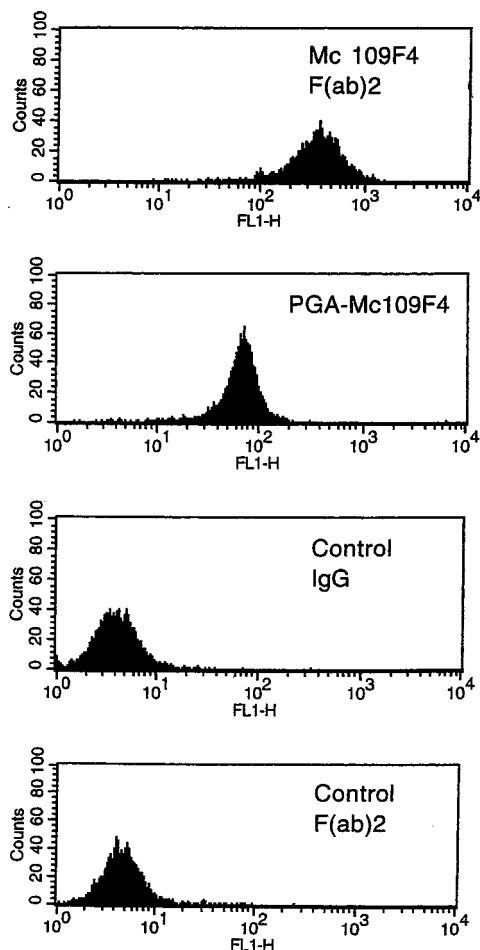
**Figure 3.** 300 MHz <sup>1</sup>H NMR spectra of (A)  $\gamma$ -PGA; (B) linker **4b**; (C) PGA modified by linker **4b**. The position of the maleimide C=CH is indicated by arrows in B and C.



**Figure 4.** HPLC gel filtration (Bio-Sep S3000) analysis of (A) native PGA, (B) Fab<sub>2</sub> (50 kDa), (C) Fab-SH (25 kDa), (D) Fab-PGA conjugate. Retention times of poly- $\alpha$ -D-glutamic acid standards: 44–64 kDa, 6.6 min; 17–31 kDa, 8.2 min; 11–13 kDa, 9.1 min.

Analysis of the PGA–Mc109F4 conjugate by HPLC gel filtration gave a large, broad peak at 5.8–8.7 min, followed by small peak at 9.1 min (see Figure 4D). The peak at 9.1 min probably corresponds to residual activated polymer. A slight shoulder is visible at 8.2 min, which (from the difference in retention times of the F(ab') and F(ab')<sub>2</sub> peaks) probably corresponds to the 1:1 PGA–F(ab') conjugate, and the remainder of the peak to higher PGA(F(ab'))<sub>n</sub> conjugates. Maximum absorbance is observed at retention time 7.3 min, suggesting that the most abundant conjugates are PGA(F(ab'))<sub>2</sub> and PGA–(F(ab'))<sub>3</sub>.



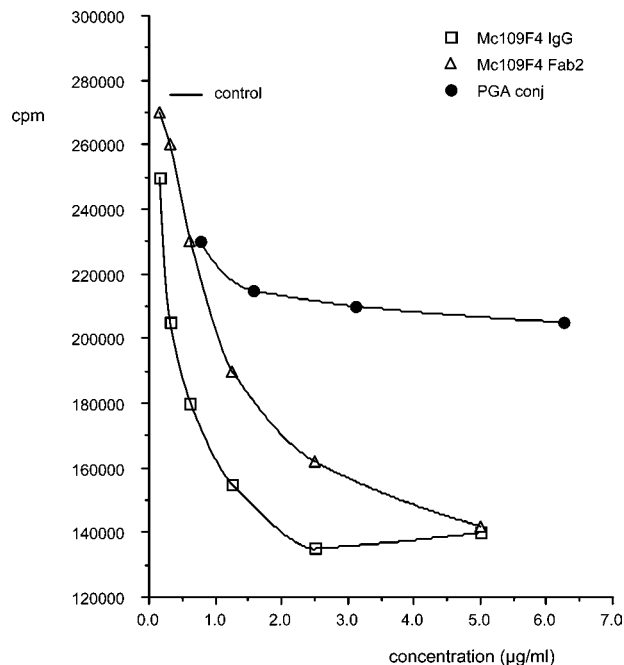


**Figure 5.** Binding of PGA-5b-Mc109F4 conjugate to BCL3B3 cells assessed by flow cytometry. Procedure described in Experimental Section. Samples of control IgG and F(ab)<sub>2</sub> antibodies were included, which have no interaction with BCL3B3 cells. Each protein sample was assayed at 25  $\mu$ g/mL concentration. Strength of binding interaction assessed by mean channel fluorescence ( $x$ -axis).

Conjugation of activated PGA to F(ab')-SH was found to take place slowly, requiring several days at 4  $^{\circ}$ C to reach completion, with most successful conjugation using PGA-5a and PGA-5b. The reactivity of samples of activated PGA was variable, low reactivity being observed for stored samples, perhaps due to intramolecular reaction of carboxylate side chains of PGA with maleimide groups, and 'burying' of maleimide groups in the hydrophobic core of PGA. However, by carrying out the functionalization of PGA with the PEG-maleimide linkers rapidly, coupling of antibody F(ab')-SH was successfully achieved. The PGA-5a-F(ab') and PGA-5b-F(ab') conjugates were purified by AcA44 gel filtration and concentrated prior to storage.

#### Biological Activity of PGA-Mc109F4 Conjugate.

The PGA-5b-Mc109F4 conjugate was tested for binding to target BCL3B3 cells (14) using flow cytometry, as shown in Figure 5. BCL3B3 cells were incubated for 30 min with the conjugate or control antibody, washed and incubated with anti-antibody conjugated to fluorescent dye FITC, and then washed and analyzed by flow cytometry. Antibody Mc109F4 IgG and F(ab)<sub>2</sub> showed a mean channel fluorescence of 600 and 400 units, respectively, at 25  $\mu$ g/mL concentration, respectively, whereas the PGA-Mc109F4 conjugate recorded only 70 units at 25  $\mu$ g/mL concentration. A control antibody F(ab)<sub>2</sub> gave a reading of only 4 units at 25  $\mu$ g/mL concentration. Thus,



**Figure 6.** Growth inhibition of BCL3B3 cells of Mc109F4 IgG (open squares), Mc109F4 F(ab)<sub>2</sub> (open circles), and PGA-5b-Mc109F4 conjugate (filled circles) assessed by <sup>3</sup>H-thymidine incorporation (in cpm), at 0.1–6  $\mu$ g/mL protein concentration. Procedure described in Experimental Section. Result of control assay (addition of medium only) is indicated.

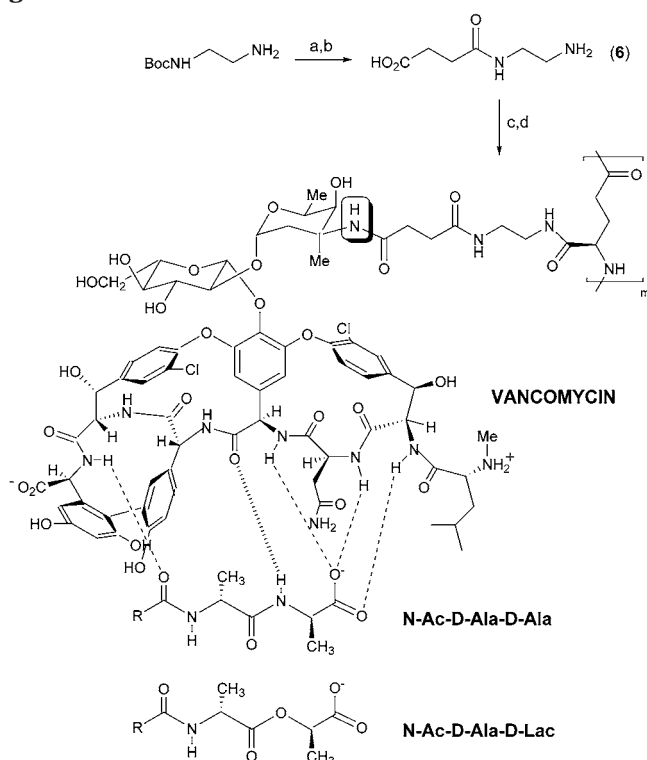
the PGA-Mc109F4 conjugate does bind to BCL3B3 cells, but less strongly than the parent antibody F(ab'), indicating that conjugation to the polymer has reduced its biological activity.

Since antibody Mc109F4 is known to inhibit the growth of BCL3B3 (14), the effect of the PGA-5b-Mc109F4 conjugate upon BCL3B3 growth was also investigated, as shown in Figure 6. The cells ( $5 \times 10^4$ ) were grown in various concentrations of antibodies for 42 h, pulsed with <sup>3</sup>H-thymidine, and harvested 6 h later, and growth was assessed by <sup>3</sup>H incorporation (24). Approximately 20% growth inhibition was observed at 1  $\mu$ g/mL PGA-Mc109F4; however, only 25% inhibition was observed at 6.25  $\mu$ g/mL conjugate (and 30% inhibition at 25  $\mu$ g/mL conjugate), whereas 5  $\mu$ g/mL Mc109F4 F(ab)<sub>2</sub> caused 50% growth inhibition. In conclusion, the conjugated antibody fragment does retain its biological activity, but has reduced efficacy compared with the free antibody.

**Conjugation of  $\gamma$ -PGA with Vancomycin.** The glycopeptide antibiotic vancomycin is a very interesting ligand for immobilization to PGA, since the dimerization of the antibiotic is believed to promote its antibacterial effects (15). The presence of a free primary amine, on the vancosamine sugar of the glycopeptide, provided a convenient point of conjugation to PGA, as shown in Scheme 2.

Two conjugates of PGA with vancomycin were prepared. Conjugation of PGA directly to vancomycin was carried out, using the water-soluble carbodiimide EDC. A second conjugate was also prepared, using an eight-atom spacer 6, prepared from Boc-ethylene 1,2-diamine and succinic anhydride, as shown in Scheme 2.

Analysis of the PGA-vancomycin and PGA-6-vancomycin conjugates by BioSep S3000 gel filtration gave new single peaks at retention times 16.7 and 16.4 min, respectively ( $\gamma$ -PGA 5.5 min, vancomycin 11.3 min), indicating that conjugates had been formed. The high retention times are indicative of an interaction between

**Scheme 2. Preparation of PGA–Vancomycin Conjugate<sup>a</sup>**

<sup>a</sup> a. Succinic anhydride, toluene, 90%; b. CF<sub>3</sub>COOH, CH<sub>2</sub>Cl<sub>2</sub>, 95%; c. γ-PGA, EDC, HOBT, Et<sub>3</sub>N, H<sub>2</sub>O; d., vancomycin, EDC, HOBT, Et<sub>3</sub>N, H<sub>2</sub>O.

**Table 1. Antibacterial Activities of PGA–Vancomycin Conjugates**

zone of inhibition vs	<i>Bacillus subtilis</i> (Vm-sensitive), mm	<i>Lactobacillus casei</i> (Vm-resistant), mm
vancomycin (1 mg/mL)	14	3
PGA–vancomycin conjugate (1 mg/mL)	8	5
PGA–6–vancomycin conjugate (1 mg/mL)	9	5

the glycoside portion of vancomycin and the column, as observed for other glycoside derivatives (data not shown); therefore, it is not possible to estimate an  $M_r$  for the conjugates.

**Antibacterial Activity of PGA–Vancomycin Conjugates.** The antibacterial activities of the two PGA–vancomycin conjugates were assessed by filter disk assays on agar plates and compared directly with free vancomycin. Measurement of the zone of growth inhibition around the filter disk containing the antibiotic provides a measure of antibacterial potency. The results are summarized in Table 1.

Against a vancomycin-susceptible strain of *Bacillus subtilis*, the PGA–vancomycin and PGA–6–vancomycin conjugates were found to show antibacterial activity (8 mm and 9 mm zones, respectively) at 1 mg/mL concentration. At the same concentration, free vancomycin showed a 14 mm zone of inhibition. Thus, it appears that the immobilized vancomycin retains its biological activity, but with somewhat reduced biological efficacy.

High-level vancomycin resistance, both plasmid-mediated resistance in *Enterococcus* strains (29) and intrinsic resistance in lactic acid bacteria (30), is known to be associated with the presence of peptidyl-D-Ala-D-Lac termini in the cell wall peptidoglycan, for which vancomycin has low affinity, since one hydrogen bond between

vancomycin and the terminal D-alanine is absent. Synthetic vancomycin dimers (17) and vancomycin-based polymers (20) have been reported to show higher activity against vancomycin-resistant strains. Therefore, the antibacterial activity of the PGA–vancomycin conjugates was also assayed against a vancomycin-resistant strain of *Lactobacillus casei*, using the filter disk assay. Both conjugates showed a 5 mm zone of inhibition, whereas free vancomycin showed a 3 mm zone of inhibition. It appears, therefore, that the PGA–vancomycin conjugates possess slightly higher antibacterial activity against vancomycin-resistant strains, although not markedly higher activity.

**DISCUSSION**

We have previously shown that small molecular weight amines can be immobilized onto PGA in aqueous solution using a water-soluble carbodiimide, EDC (4). In this paper we describe the preparation of linkers for the attachment of protein ligands to PGA via thiol side chains. The most successful linker was found to be maleimide linker 5b, containing an ethylene glycol spacer capable of hydrogen bonding with the aqueous solvent. Using this linker, we were able to conjugate the Mc109F4 F(ab'), to give a mixture of PGA(F(ab'))<sub>n</sub> conjugates. The conjugated antibody F(ab') was found to retain its biological recognition properties, but showed reduced binding efficacy and cell growth inhibition, compared with the free antibody F(ab'). We have also immobilized the glycopeptide antibiotic vancomycin to PGA and have shown that the immobilized ligand also retains its biological activity, but with slightly reduced efficacy. In this case, however, there is some indication of enhanced biological activity against vancomycin-resistant strains, against which the free ligand shows low affinity.

This work establishes the feasibility of attaching bioactive molecules and macromolecules such as cell-specific antibody F(ab') fragments to nontoxic, nonimmunogenic biopolymers such as PGA. The observation that the immobilized ligands retain their biological activity implies that antibody–polymer conjugates could in principle be used to target cytotoxic drugs in the human body (7), although the reduced biological efficacy of the immobilized F(ab') implies that there are inherent practical difficulties in this approach. Biopolymers such as PGA provide interesting alternatives to man-made polymers for antibody F(ab') immobilization (8–13), which may prove to have certain advantages for biocompatibility.

**ACKNOWLEDGMENT**

We would like to thank EPSRC for the award of a Project Studentship (GR/L60968) to E.J.P.

**LITERATURE CITED**

- (1) Thorne, C. B., Gomez, C. G., Noyes, H. E., and Housewright, R. D. (1954). Production of glutamyl polypeptide by *Bacillus subtilis*. *J. Bacteriol.* 68, 307–315.
- (2) Troy, F. A. (1973). Chemistry and biosynthesis of poly(γ-D-glutamyl) capsule in *Bacillus licheniformis*. *J. Biol. Chem.* 248, 305–315.
- (3) Uchida, I., Makino, S., Sasakawa, C., Yoshikawa, M., Sugimoto, C., and Terakado, N. (1993). Identification of a novel gene, *dep*, associated with depolymerization of the capsular polymer in *Bacillus anthracis*. *Mol. Microbiol.* 9, 487–496.
- (4) King, E. C., Watkins, W. J., Blacker, A. J., and Bugg, T. D. H. (1998). Covalent Modification in Aqueous Solution of Poly-γ-D-Glutamic Acid from *Bacillus licheniformis*. *J. Polym. Sci. Part A: Polym. Chem.* 36, 1995–1999.

- (5) Alkan, S. S., Nitecki, D. E., and Goodman, J. W. (1971). Antigen recognition and the immune response: the capacity of L-tyrosine-azobenzenearsonate to serve as a carrier for a macromolecular hapten. *J. Immunol.* 107, 353–358.
- (6) Blanchard, T. G., Thorne, C. B., and MacDonald, A. B. (1988). The use of polyglutamic acid as a delivery system for anti-idiotypic vaccines. *FASEB J.* 2, A1257.
- (7) Putnam, D., and Kopecek, J. (1995). Polymer conjugates with anticancer activity. *Adv. Polym. Sci.* 122, 55–123.
- (8) Kunath, K., Kopeckova, P., Minko, T., and Kopecek, J. (2000). HPMa copolymer-anticancer drug-OV-TL16 antibody conjugates. 3. The effect of free and polymer-bound adriamycin on the expression of some genes in the OVCAR-3 human ovarian carcinoma cell line. *Eur. J. Pharm. Biopharm.* 49, 11–15.
- (9) Jelinkova, M., Strohalm, J., Plocova, D., Subr, V., St'astny, M., Ulbrich, K., and Rihova B. (1998). Targeting of human and mouse T-lymphocytes by monoclonal antibody-HPMA copolymer-doxorubicin conjugates directed against different T-cell surface antigens. *J. Controlled Release* 52, 253–270.
- (10) Trubetskoy, V. S., Narula, J., Khaw, B. A., and Torchilin, V. P. (1993). Chemically optimized antimyosin F(ab') conjugates with chelating polymers – importance of the nature of the protein-polymer single-site covalent bond for biodistribution and infarction localization. *Bioconjugate Chem.* 4, 251–255.
- (11) Slinkin, M. A., Klivanov, A. L., and Torchilin, V. P. (1991). Terminal-modified polylysine-based chelating polymers – highly efficient coupling to antibody with minimal loss in immunoreactivity. *Bioconjugate Chem.* 2, 342–348.
- (12) van Dijk-Wolthuis, W. N. E., van de Wetering, P., Hinrichs, W. L. J., Hofmeyer, L. J. F., Liskamp, R. M. J., Crommelin, D. J. A., and Hennink, W. E. (1999). A versatile method for the conjugation of proteins and peptides to poly[2-(dimethylamino)ethyl methacrylate]. *Bioconjugate Chem.* 10, 687–692.
- (13) Li, J. T., Carlsson, J., Lin, J. N., and Caldwell, K. D. (1996). Chemical modification of surface active poly(ethylene oxide)-poly(propylene oxide) triblock copolymers. *Bioconjugate Chem.* 7, 592–599.
- (14) George, A. J. T., McBride, H. M., Glennie, M. J., Smith, L. J., and Stevenson, F. K. (1991). Monoclonal Antibodies Raised Against the Idiotypic of the Murine B Cell Lymphoma, BCL<sub>1</sub> Act Primarily with Heavy Chain Determinants. *Hybridoma* 10, 219–227.
- (15) Williams, D. H. (1996). The glycopeptide story: how to kill the deadly "superbugs". *Nat. Prod. Rep.* 13, 469–477.
- (16) Beauregard, D. A., Maguire, A. J., Williams, D. H., and Reynolds, P. E. (1997). Semiquantitation of cooperativity in binding of vancomycin group antibiotics to vancomycin-susceptible and -resistant organisms. *Antimicrob. Agents Chemother.* 41, 2418–2423.
- (17) Sundram, N., Griffin, J. H., and Nicas, T. I. (1996). Novel vancomycin dimers with activity against vancomycin-resistant enterococci. *J. Am. Chem. Soc.* 119, 10286.
- (18) Rao, J., Lahiri, J., Isaacs, L., Weis, R. M., and Whitesides, G. M. (1998). A trivalent system from vancomycin: D-Ala-D-Ala with higher affinity than avidin: biotin. *Science* 280, 708–711.
- (19) Rao, J., Lahiri, J., Weis, R. M., and Whitesides, G. M. (2000). Design, synthesis and characterisation of a high affinity trivalent system derived from vancomycin and L-Lys-D-Ala-D-Ala. *J. Am. Chem. Soc.* 122, 2698–2710.
- (20) Arimoto, H., Nishimura, K., Kinumi, T., Hayakawa, I., and Uemura, D. (1999). Multivalent polymer of vancomycin: enhanced antibacterial activity against VRE. *J. Chem. Soc. Chem. Commun.* 1361–1362.
- (21) Arimoto, H., Oishi, T., Nishijima, M., and Kinumi, T. (2001). Affinity of a vancomycin polymer with bacterial surface models. *Tetrahedron Lett.* 42, 3347–3350.
- (22) Krapcho, A. P., and Kuell, C. S. (1990). Monoprotected diamines N-tert-butoxycarbonyl- $\alpha$ ,  $\omega$ -alkanediamines from  $\alpha$ ,  $\omega$ -alkanediamines. *Synth. Commun.* 20, 2559–2564.
- (23) Nicoletti, I., Migliorati, G., Pagliacci, M. C., Grignani, F., and Riccardi, C. (1991). A rapid and simple method for measuring thymocyte apoptosis by propidium iodide staining and flow cytometry. *J. Immunol. Methods* 139, 271–279.
- (24) Tutt, A. L., French, R. R., Illidge, T. M., Honeychurch, J., McBride, H. M., Penfold, C. A., Fearon, D. T., Parkhouse, R. M. E., Klaus, G. G. B., and Glennie, M. J. (1998). Monoclonal antibody therapy of B cell lymphoma: signaling activity on tumor cells appears more important than recruitment of effectors. *J. Immunol.* 161, 3176–3185.
- (25) Glennie, M. J., Tutt, A. L., and Greenman, J. (1993). Preparation of multispecific F(ab')<sub>2</sub> and F(ab')<sub>3</sub> antibody derivatives. In *Tumour Immunobiology, a practical approach* (Gallagher, G., Rees, R. C., and Reynolds C. W., Eds.) pp 225–44, Oxford University Press, Oxford.
- (26) Wong, S. S. (1993). *Chemistry of protein conjugation and cross-linking*, CRC Press, New York.
- (27) Reddy, P. Y., Kondo, S., Toru, T., and Ueno, Y. (1997). Lewis acid and hexamethyldisilazane-promoted efficient synthesis of N-alkyl and N-arylimide derivatives. *J. Org. Chem.* 62, 2652–2654.
- (28) King, E. C., Blacker, A. J., and Bugg, T. D. H. (2000). Enzymatic Breakdown of Poly- $\gamma$ -D-glutamic Acid in *Bacillus licheniformis*: Identification of a Polyglutamyl  $\gamma$ -Hydrolase Enzyme. *Biomacromolecules* 1, 75–83.
- (29) Bugg, T. D. H., Wright, G. D., Dutka-Malen, S., Arthur, M., Courvalin, P., and Walsh, C. T. (1991). Molecular Basis for Vancomycin Resistance in *Enterococcus faecium* BM4147: Biosynthesis of a Depsipeptide Peptidoglycan Precursor by Vancomycin Resistance Proteins VanH and VanA. *Biochemistry* 30, 10408–10415.
- (30) Handwerker, S., Pucci, M. J., Volk, K. J., Liu, J., and Lee, M. S. (1994). Vancomycin-resistant *Leuconostoc mesenteroides* and *Lactobacillus casei* synthesize cytoplasmic peptidoglycan precursors that terminate in lactate. *J. Bacteriol.* 176, 260–264.

BC020019M



# A Novel Family of L-Amino Acid-Based Biodegradable Polymer–Lipid Conjugates for the Development of Long-Circulating Liposomes with Effective Drug-Targeting Capacity

Josbert M. Metselaar,<sup>†,||</sup> Peter Bruin,<sup>†</sup> Leo W. T. de Boer,<sup>‡</sup> Tom de Vringer,<sup>‡</sup> Cor Snel,<sup>†</sup> Christien Oussoren,<sup>†</sup> Marca H. M. Wauben,<sup>§,||</sup> Daan J. A. Crommelin,<sup>†,||</sup> Gert Storm,<sup>†,||</sup> and Wim E. Hennink<sup>\*,†</sup>

Department of Pharmaceutics, Utrecht Institute for Pharmaceutical Sciences, Utrecht University, The Netherlands, Department Infectious Diseases and Immunology, Division of Immunology, Faculty of Veterinary Medicine, Utrecht University, The Netherlands, Yamanouchi Europe BV, Leiderdorp, The Netherlands, and Members of UNYPHAR, a network collaboration between the universities of Groningen, Leiden, Utrecht, and the pharmaceutical company Yamanouchi. Received March 11, 2003; Revised Manuscript Received June 27, 2003

The objective of this study was to develop biodegradable polypeptide–lipid conjugates for the design of polymer-coated long-circulating liposomes (LCL). Lipid conjugates of poly(hydroxyalkyl L-asparagine/L-glutamine) were synthesized and incorporated into 0.15  $\mu\text{m}$  dipalmitoyl phosphatidylcholine (DPPC)–cholesterol liposomes. Circulation times and biodistribution were assessed in rats using a radioactive lipid marker. Evaluation of the therapeutic activity of prednisolone phosphate loaded in 0.1  $\mu\text{m}$  PHEA–DPPC–cholesterol liposomes in a rat experimental arthritis model was performed to demonstrate the drug-targeting potential of the polymer-coated liposomes. Coating of liposomes with poly(hydroxyethyl L-asparagine) (PHEA) and poly(hydroxyethyl L-glutamine) (PHEG) extended the circulation half-life to a similar extent as poly(ethylene glycol) (PEG), which is normally used for the preparation of LCL. Glutamine polymers with a hydroxypropyl or a hydroxybutyl group instead of hydroxyethyl group also yield prolonged circulation, however, not to the same extent as PHEA/G. The pharmacokinetic properties of PHEA-liposomes were independent of the lipid dose even at very low lipid doses of around 50 nmol per rat. PLP was successfully entrapped in PHEA-liposomes. These liposomes were shown to be stable in the circulation and equally effective in rat experimental arthritis as PLP encapsulated in PEG-liposomes. PHEA and PHEG are attractive alternative polymers for the design of LCL: their performance is similar to that of PEG-liposomes but they have the advantage of being biodegradable.

## INTRODUCTION

Liposomes are small spherical particles that consist of one or more lipid bilayers enclosing an aqueous interior (1). Liposomes are highly suitable as drug carriers, as they are composed of natural lipids and offer the opportunity to incorporate a wide variety of therapeutic agents for the purpose of drug-targeting (2). Biodistribution studies in laboratory animals showed that intravenously (iv) injected liposomes predominantly home to cells of the mononuclear phagocyte system (MPS) that is present in liver, spleen, and bone marrow. As a result, liposomes show generally a short circulation half-life after iv administration (3, 4).

The development of bilayer surface modifications that were able to reduce rapid uptake by the MPS represented a major step forward to the successful clinical application of liposomes (5). Incorporation of a lipid conjugate of the

water-soluble polymer poly(ethylene glycol) (PEG) results in a polymeric layer around the liposome, which reduces the adhesion of plasma proteins that would otherwise cause rapid recognition of the liposomes by MPS-phagocytes. With a PEG-coating, liposomes oppose rapid uptake by the MPS and acquire a prolonged circulation property. With these so-called 'long-circulating liposomes' (LCL) drug-targeting to tissues other than liver, spleen, and bone marrow became possible. Indeed, LCL were shown to selectively accumulate at sites of enhanced vascular permeability as found in tumors and inflamed areas in the body (6, 7). This form of targeted drug delivery resulted in increased therapeutic efficacy and/or reduced toxicity of several cytostatic, antifungal, and antibacterial drugs and led to the market approval of liposomal doxorubicin as the first commercially available liposomal cytostatic agent (8–11).

Besides PEG a few other polymers have also been shown to induce prolonged circulation behavior of liposomes upon attachment to their surface (12). Woodle and co-workers investigated oxazoline-derived polymers, Maruyama et al. designed poly(glycerol)-coated liposomes, while Torchilin and co-workers developed several water-soluble vinyl-based polymers for the creation of long-circulating liposomes. All groups reported circulation half-lives comparable to PEG-liposomes (13–18). Up to now, PEG-liposomes are the only polymer-coated lipo-

\* Address correspondence to Wim E. Hennink, Department of Pharmaceutics, Faculty of Pharmacy, Sorbonnelaan 16, 3584 CA Utrecht, The Netherlands. Tel: +31-30-2537304. Fax: +31-30-2517839. E-mail: W.E.Hennink@pharm.uu.nl.

<sup>†</sup> Department of Pharmaceutics, Utrecht University.

<sup>§</sup> Department Infectious Diseases and Immunology, Utrecht University.

<sup>‡</sup> Yamanouchi Europe BV.

<sup>||</sup> Members of UNYPHAR.

some that have been approved for clinical use. However, despite the fact that low-molecular weight PEG has been shown to be nontoxic and to be readily excreted by the kidneys, the biological fate of (liposome-associated) PEG after cellular uptake is not known (19, 20). Since PEG is expected not to be easily intracellularly degraded, it cannot be excluded that PEG may affect cell functioning at the long term (21).

It was the objective of this study to design a biodegradable and biocompatible polymer–lipid conjugate for the development of LCL. To achieve minimal toxicity of the polymer as well as the compounds that are formed upon biodegradation, we selected natural L-amino acids as starting material for the synthesis of polymer–lipid conjugates in this study. Besides the advantage of being intracellularly degradable, such poly(L-amino acid)–lipid conjugates are expected to be degraded by proteolytic enzymes that are present at pathological target tissues such as tumors and sites of inflammation. Therefore, these polymer–lipid conjugates may allow the incorporation of bilayer functionalities that have to remain shielded in the circulation until arrival at the pathological target sites where they can perform their specific function.

The present study investigates the feasibility of polymers based on hydroxyalkyl derivatives of L-glutamine and L-asparagine as monomers. Poly(hydroxyethyl L-glutamine) (PHEG) was selected as a starting polymer, as PHEG is known to be water-soluble, biocompatible, and degradable by isolated enzymes (e.g. papain, chymotrypsin, and Pronase) as well as cocktails of lysosomal extracts and kidney homogenates (22–25). Subsequently, structure–activity relationships were established by replacing the hydroxyethyl side group with other hydroxyalkyl groups and selecting L-asparagine as backbone monomer instead of glutamine. Different lipid molecules were evaluated to ensure stable anchoring of the polymer–lipid conjugates in the liposome bilayer. In addition, the effect of the polymer grafting density on the liposome surface and the effect of lipid dose on the circulation half-life were assessed. Finally, the feasibility of liposomal incorporation and targeting an antiinflammatory glucocorticoid to inflamed sites in an experimental animal model of arthritis was evaluated.

## MATERIALS AND METHODS

**Synthesis and Characterization of Different PEG–Lipid Conjugates.** PEG5000–lipid conjugates were synthesized from methoxy-PEG5000-isocyanate, commercially available from Shearwater Polymers, Huntsville, AL, and long-chain alkylamines: octadecylamine (stearylamine)  $\text{NH}_2\text{-C}_{18}\text{H}_{37}$  (ODA), having a single  $\text{C}_{18}$ -tail, and dioctadecylamine (distearylamine)  $\text{NH-(C}_{17}\text{H}_{35})_2$  (DODA) and 1-heptadecyl-octadecylamine  $\text{NH}_2\text{-CH-(C}_{17}\text{H}_{35})_2$  (HOA), both with a double alkyl tail. Isocyanate groups reacted with these primary and secondary alkylamines rapidly at room temperature to form ureas of a general formula:  $\text{mPEG-NH-CO-NH-R}$  in case of a primary amine (ODA,  $\text{R} = \text{C}_{18}\text{H}_{37}$  or HOA,  $\text{R} = \text{CH(C}_{17}\text{H}_{35})_2$ ) or  $\text{mPEG-NH-CO-N-R}_2$  in case of a secondary amine (DODA,  $\text{R}$  being a  $\text{C}_{18}$ -tail).

All three PEG5000 derivatives were synthesized in exactly the same way. For the synthesis of the PEG5000-stearyl derivative, a solution of 300 mg of methoxy-PEG-isocyanate (0.06 mmol, MW 5000, Shearwater Polymers) and 18 mg (0.07 mmol) of ODA in 1.5 mL of chloroform was stirred at room temperature for ca. 0.5–1 h. The solution was then precipitated into 20–30 mL petroleum ether. A fine white powder (220 mg, 75%) was obtained

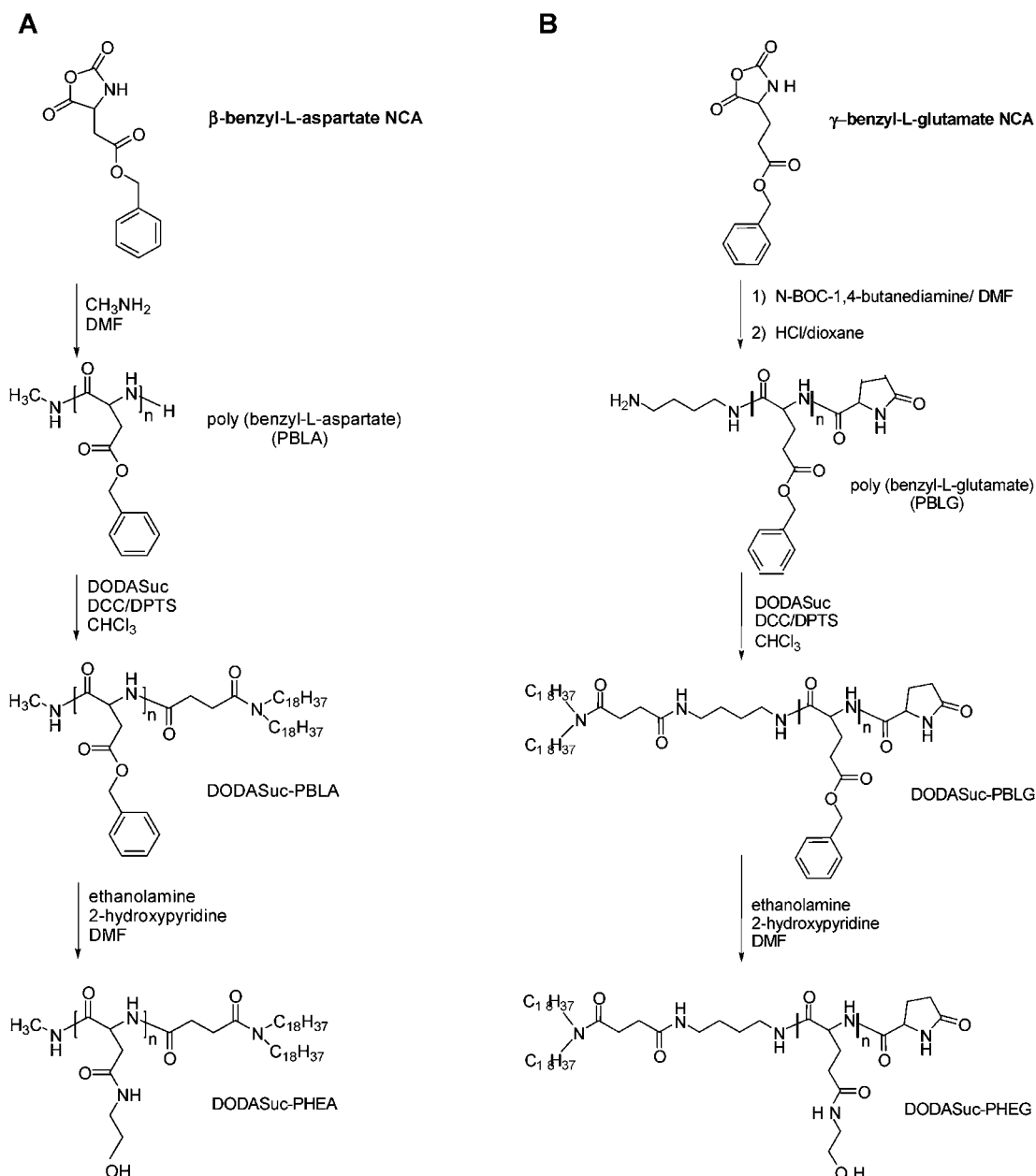
after filtration and drying.  $^1\text{H}$  NMR ( $\text{CDCl}_3$ ,  $\delta$  in ppm relative to TMS): PEG: 3.6 ( $\text{CH}_2\text{O}$ ); stearyl anchor: 1.2 ( $\text{CH}_2$ ) and 0.8 ( $\text{CH}_3$ ). The ratio of PEG and stearyl peak integrals confirms the presence of one stearyl group per PEG moiety. MALDI-TOF confirms the molecular structure of the PEG–lipid conjugates: e.g.  $\text{Na}^+$ -adduct of the most abundant peaks of the PEG–stearyl conjugate:  $m/z$  5459 ( $n = 115$ ), 5503 ( $n = 116$ ), 5547 ( $n = 117$ ), etc.

**Synthesis and Characterization of PHEA–DODASuc.** Synthesis of poly(L-hydroxyethyl asparagine)-*N*-succinyldioctadecylamine (PHEA–DODASuc) is schematically represented in Scheme 1 A. To a solution of 3 g of  $\beta$ -benzyl L-aspartate *N*-carboxy anhydride (NCA) (synthesized as described by Fuller et al. (26)) dissolved in 9 mL of dry dimethylformamide (DMF) (Aldrich-Chemie, Steinheim, Germany) was added 0.3 mL of a 2 M solution of methylamine in tetrahydrofuran (THF) (Aldrich) as initiator. The solution (initially clear, after ca. 2 h cloudy) was stirred for 1 day under a nitrogen atmosphere at room temperature and then precipitated into water (150 mL), collected by filtration, and dried. Yield: 2 g of poly(benzyl L-aspartate) (PBLA).

Polymer–lipid coupling was performed to obtain the PBLA–DODASuc conjugate. Briefly, a solution of 2 g of PBLA in 5 mL of chloroform containing ca. 150 mg of triethylamine (Merck, Darmstadt, Germany) was added to a solution of 200 mg of dicyclohexylcarbodiimide (DCC) (Acros Chimica, Geel, Belgium), 15 mg of 4-(dimethylamino)pyridinium 4-toluenesulfonate (DPTS) (Acros), and 350 mg of *N*-succinyldioctadecylamine (DODASuc; for synthesis see (27)) in 6 mL of chloroform that had been stirred for 1 h. The mixture was stirred for 1 day and then precipitated into methanol. The polymeric product was filtered off and dried in vacuo. Yield: 1.4 g of PBLA–DODASuc. Aminolysis of 1.4 g of PBLA–DODASuc was performed with ca. 4 mL of ethanolamine (Aldrich), using 0.4 g of 2-hydroxypyridine (Aldrich) as a catalyst, in 10 mL of DMF solution at 40 °C for 1 day, yielding PHEA–DODASuc. Yield: 0.8 g after dialysis (molecular weight cut off 500) and freeze-drying. Characterization:  $^1\text{H}$  NMR ( $\text{DMSO-}d_6$ ) ( $\delta$  in ppm relative to TMS): distearyl: 0.8 ( $\text{CH}_3$ ), 1.2 ( $\text{CH}_2$ ), 1.4 ( $\text{CH}_2\text{N}$ ); PHEA: 2.4–2.8 ( $\beta\text{-CH}_2$ ), 3.2 and 3.4 (hydroxyethyl), 4.6 ( $\alpha\text{-CH} + \text{OH}$ ), 7.8–8.5 (NH). From the ratio of integrals of the distearyl signals and the  $\alpha\text{-CH}$  signal, the molecular weight of the polymer part of the conjugate was calculated to be ca. 3000 g/mol.

MALDI-TOF confirms the molecular structure of the PHEA–DODASuc conjugate as depicted in Scheme 1 A.  $\text{Na}^+$ -adduct:  $m/z$  2397.5 ( $n = 11$ ), 2555.6 ( $n = 12$ ), 2713.6 ( $n = 13$ ), 2871.9 ( $n = 14$ ), etc.

**Synthesis and Characterization of Poly(L-hydroxyalkyl glutamine)–DODASuc Conjugates.** Synthesis of poly(hydroxyethyl glutamine) (PHEG)–lipid conjugates is schematically shown in Scheme 1B. To a solution of 3 g of  $\gamma$ -benzyl L-glutamate NCA (for synthesis see (26)) in 8 mL of dry DMF was added a solution of 0.1 g of *N*-BOC-1,4-diaminobutane (Fluka, Zwijndrecht, The Netherlands) in chloroform as initiator. This solution was stirred for 1 day under a nitrogen atmosphere at room temperature. After precipitation into ca. 100 mL of methanol, the polymer was filtered off and dried, yielding 2 g of PBLG with a BOC-protected amino end group. To remove BOC, a solution of 1.7 g of PBLG–diaminobutane-BOC in 12 mL of 2 M HCl/dioxane was stirred for 4 h and then added dropwise to ca. 150 mL of water in which approximately 10 g of  $\text{NaHCO}_3$  was dissolved. The product was filtered off, washed with water, and dried in vacuo. Yield: 1.4 g of PBLG–diaminobutane.

**Scheme 1. Synthesis of Poly(hydroxylalkyl L- asparagines/glutamine)–Lipid Conjugates<sup>a</sup>**

<sup>a</sup> (A) Schematic representation of PHEA–DODASuc synthesis strategy. (B) Schematic representation of the synthesis of PHEG–DODASuc. Note that DODASuc is attached to PHEA at the amino end group (on the right) of the poly(amino acid) backbone, whereas to PHEG it is attached to the carboxylic end (on the left, using diaminobutane to connect the poly(amino acid) backbone to DODASuc).

Deprotection was complete as demonstrated by NMR analysis.

To obtain the PBLG–DODASuc conjugate, 340 mg of DODASuc, 180 mg of DCC, and 15 mg of DPTS were dissolved in 5 mL of chloroform. The solution was stirred for 1 h at room temperature. Next, a solution of 1.4 g of PBLG–diaminobutane and 120 mg of triethylamine in 8 mL of chloroform was added. After stirring overnight at room temperature the obtained solution was added dropwise to an excess of methanol (ca. 150 mL). The polymeric product was filtered off, washed, and dried. Yield: 1.2 g of PBLG–DODASuc. <sup>1</sup>H NMR (CDCl<sub>3</sub>) ( $\delta$  in ppm relative to TMS): distearyl signals at 0.8–0.9 (CH<sub>3</sub>) and 1.2–1.4 (methylene protons); PBLG: 2.2 and 2.6 ( $\beta,\gamma$ -CH<sub>2</sub>), 4.0 ( $\alpha$ -CH), 5.0 (benzyl CH<sub>2</sub>), 7.3 (phenyl).

Aminolysis with ethanolamine was performed to obtain PHEG–DODASuc: 1.2 g of PBLG–DODASuc (see above) and 0.5 g of 2-hydroxypyridine were dissolved in 10 mL

of DMF. Then ca. 4 mL of ethanolamine was added dropwise. After being stirred for 24 h at 40 °C under a nitrogen atmosphere, the solution was precipitated into ca. 200 mL of diethyl ether. The precipitate was dissolved in water, dialyzed (molecular weight cut off 500), and subsequently freeze-dried yielding 0.8 g of PHEG–DODASuc conjugate. Characterization: <sup>1</sup>H NMR (DMSO-*d*<sub>6</sub>) ( $\delta$  relative to TMS): distearyl signals at 0.8–0.85 (CH<sub>3</sub>) and 1.2–1.5 (methylene protons); PHEG: 1.7–2.2 ( $\beta,\gamma$ -CH<sub>2</sub>), 3.1 and 3.3 (hydroxyethyl), 4.2 ( $\alpha$ -CH), 4.7 (OH), 7.8 and 8.2 (NH). From the ratio of integrals of the distearyl signals and the  $\alpha$ -CH signal molecular weight of PHEG was calculated to be ca. 4000. By varying the monomer/initiator ratio, similar conjugates with different PHEG molecular weights (3000 and 8000) were synthesized.

MALDI-TOF confirms the molecular structure of the PHEG–DODASuc conjugate as depicted in Scheme 1B.



Na<sup>+</sup>-adduct:  $m/z$  3064.5 ( $n = 13$ ), 3236.1 ( $n = 14$ ), 3408.7 ( $n = 15$ ), 3580.6 ( $n = 16$ ), 3752.9 ( $n = 17$ ), 3924.7 ( $n = 18$ ), 4096.7 ( $n = 19$ ), 4268.4 ( $n = 20$ ), 4441.1 ( $n = 21$ ), 4613.3 ( $n = 22$ ), 4785.1 ( $n = 23$ ), etc.

The same procedure of aminolysis but with 3-propanolamine instead of ethanolamine yielded PHPG-DODASuc. Characterization: <sup>1</sup>H NMR (DMSO-*d*<sub>6</sub>) ( $\delta$  in ppm relative to TMS): distearyl signals at 0.8–0.85 (CH<sub>3</sub>) and 1.2–1.5 (methylene protons); PHPG: 1.7–2.2 ( $\beta$ , $\gamma$ -CH<sub>2</sub>), 1.5 and 3.1 and 3.3 (hydroxypropyl), 4.2 ( $\alpha$ -CH), 4.6 (OH), 7.8 and 8.2 (NH). MALDI-TOF: Na<sup>+</sup>-adduct:  $m/z$  3623 ( $n = 15$ ), 3810 ( $n = 16$ ), 3996 ( $n = 17$ ), 4182 ( $n = 18$ ), 4368 ( $n = 19$ ), 4555 ( $n = 20$ ), etc.

To obtain PHBG-DODASuc, the same procedure of aminolysis of PBLG-DODASuc was repeated with 4-butanolamine (Merck). Stirring was performed for 48 h instead of 24 h at 40 °C. <sup>1</sup>H NMR (DMSO-*d*<sub>6</sub>) ( $\delta$  in ppm relative to TMS): distearyl signals at 0.8–0.85 (CH<sub>3</sub>) and 1.2–1.5 (methylene protons); PHBG: 1.7–2.2 ( $\beta$ , $\gamma$ -CH<sub>2</sub>), 1.4 and 3.1 and 3.3 (hydroxybutyl), 4.2 ( $\alpha$ -CH), 4.5 (OH), 7.8 and 8.2 (NH).

**Preparation of Radiolabeled Liposomes for Comparative Pharmacokinetics.** Liposomes were prepared as described previously (28). Briefly, a lipid mixture in ethanol with a molar ratio composition of 1.85:0.15:1.0 (DPPC:polymer-lipid conjugate:cholesterol) was prepared. Such molar ratio results in liposomes containing 7.5% polymer-lipid conjugate as a percentage of the total amount of phospholipid. To the mixture was added [<sup>3</sup>H]-cholesteryl oleyl ether as a nondegradable liposome lipid phase marker. A lipid film was created by rotary evaporation under reduced pressure. The lipid film was hydrated with phosphate-buffered saline (PBS) at an initial total lipid concentration of 20  $\mu$ mol/mL. The liposomes were sized by multiple extrusion using a medium-pressure extruder equipped with two stacked polycarbonate membrane filters, one with a pore size of 200 nm on top of one with 100 nm pores. Components that were not incorporated in liposomes were removed by gel filtration on a PD-10 column (Pharmacia, Uppsala, Sweden) eluted with PBS.

**Characterization of Liposome Preparations.** Radioactivity of the liposomal dispersions was assayed in an Ultima Gold liquid scintillation cocktail purchased from Hewlett Packard (Groningen, The Netherlands) and counted in a Philips PW 4700 liquid scintillation counter. Lipid content of the liposomal dispersion was determined by assessing the radioactivity of the liposomes before and after preparation. The mean particle size of the liposomes was determined by dynamic light scattering (29) with a Malvern 4700 system (Malvern, UK). The mean size ranged between 140 and 160 nm. In addition to the mean particle size, the system reports a polydispersity index (a value between 0 and 1; 0 indicating that a complete monodisperse system is obtained, whereas 1 indicates maximal variation in particle size). All liposome preparations used had a polydispersity index of below 0.15. In Table 1 the composition and characteristics of the different liposome types are summarized. Liposome preparations were stored under nitrogen at 4 °C and used within one week after preparation.

**Comparative Pharmacokinetics of Polymer-Coated <sup>3</sup>H-Labeled Liposomes in Rats.** Male Wistar rats with an approximate body weight of 200 g were used (outbred, SPF-quality, Utrecht University, The Netherlands). Besides the different poly(hydroxyalkyl L-amino acid)-coated liposomes, nonpolymer-coated ('bare') liposomes and liposomes coated with PEG2000 coupled to distearyl phosphatidylethanolamine (PEG-DSPE) were

**Table 1. Liposome Composition and Characteristics. Means of Three Measurements Are Shown**

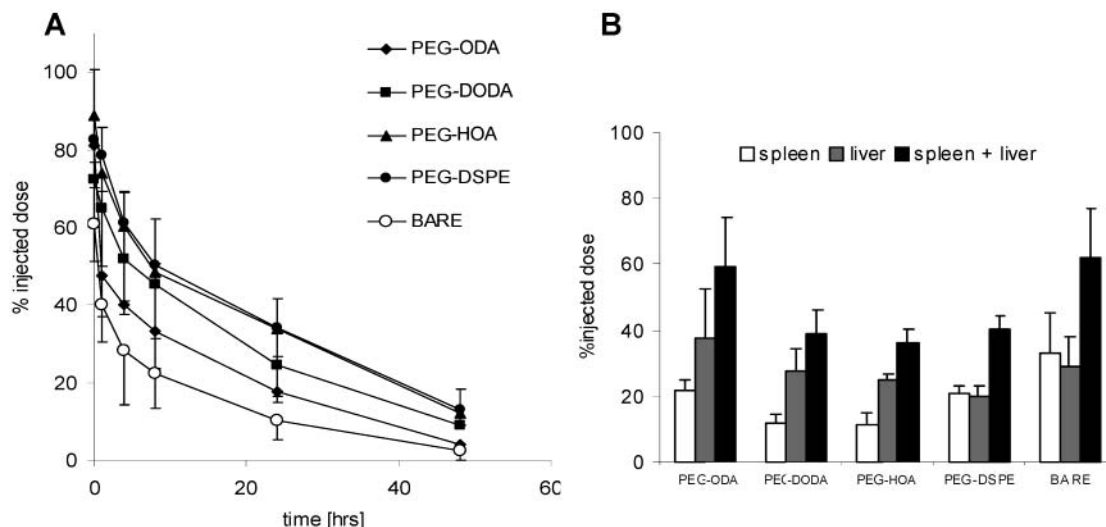
	grafting density (%)	composition DPPC:Chol:PLC <sup>a</sup>	mean diameter (nm)	polydispersity index
BARE(no polymer)	0	2:1	151 $\pm$ 2	0.13 $\pm$ 0.02
PEG-DSPE	7.5	1.85:1.0:0.15	139 $\pm$ 2	0.11 $\pm$ 0.01
PHEG-DODASuc	1	1.98:1.0:0.02	151 $\pm$ 2	0.09 $\pm$ 0.01
	2.5	1.95:1.0:0.05	156 $\pm$ 2	0.08 $\pm$ 0.01
	7.5	1.85:1.0:0.15	151 $\pm$ 2	0.07 $\pm$ 0.02
	15	1.85:1.0:0.30	160 $\pm$ 1	0.07 $\pm$ 0.01
PHEA-DODASuc	7.5	1.85:1.0:0.15	146 $\pm$ 2	0.09 $\pm$ 0.02
PHPG-DODASuc	7.5	1.85:1.0:0.15	153 $\pm$ 1	0.09 $\pm$ 0.02
PHBG-DODASuc	7.5	1.85:1.0:0.15	148 $\pm$ 2	0.07 $\pm$ 0.04

<sup>a</sup> PLC: Polymer-lipid conjugate.

prepared and evaluated as 'negative' and 'positive' controls, respectively. Single-dose intravenous injections of liposomal preparations containing 5  $\mu$ mol of total lipid and approximately 50 kBq of radioactivity were given in the tail vein. Blood samples of 100  $\mu$ g were collected from the opposite tail vein of each rat at the following time points postinjection: 5 min and 1, 4, 8, 24, and 48 h. Radioactivity in blood samples was determined by adding Solvable tissue solubilizer (NEN, Dreieich, Germany) and 35% hydrogen peroxide. After overnight incubation, the samples were assayed in Ultima Gold scintillation cocktail (Packard BioScience B. V., Groningen, The Netherlands) and counted for radioactivity with a Philips PW 4700 liquid scintillation counter. At 48 h postinjection liver and spleen were dissected, homogenized and processed according to the same method as described for the blood samples. Besides tissue and blood samples, the radioactivity of the injected dose was also counted. The % injected dose in the organs was calculated by dividing the total radioactivity of the organs by the injected dose. The total radioactivity of the blood was calculated by multiplying the radioactivity of the blood samples with the total mass of the blood of each rat, which is defined as 7% of the total body weight. The results are presented as the mean  $\pm$  standard deviation of the percentage of the injected dose of four rats.

**Liposome Preparation for Assessing Drug-Targeting Potential.** Liposomes containing the antiinflammatory glucocorticoid prednisolone phosphate (PLP) were prepared as described previously (30). In brief, a lipid film containing 7.5% PHEA-DODASuc or PEG-DSPE was created by rotary evaporation and hydrated with a solution of 100 mg/mL prednisolone phosphate (PLP) (Bufo, Uitgeest, The Netherlands) in water at a initial lipid concentration of 100  $\mu$ mol of lipid per mL dispersion. Liposomes were sized to approximately 90 nm by multiple extrusion. A smaller size than the liposomes used in the comparative pharmacokinetic studies was chosen, as this may further increase target localization of the liposomes. PLP was removed by repeated dialysis using Slide-A-Lyzer dialysis cassettes with a molecular weight cut off of 10 000 (Pierce, UK) against PBS. Phospholipid content was determined with a phosphate assay in the organic phase after extraction of the liposomal preparations with chloroform (31). The aqueous phase after extraction was used for determining the PLP content by HPLC. Each milliliter of liposomal preparation contained around 5 mg of PLP and approximately 60  $\mu$ mol of phospholipid.

**Pharmacokinetics of PLP Encapsulated in Polymer-Coated Liposomes.** For assessment of in vivo stability in the circulation and pharmacokinetic behavior of PLP in polymer-coated liposomes, the PLP plasma concentration was measured at the time of injection, at



**Figure 1.** Pharmacokinetics and distribution to the MPS of PEG5000 conjugated with different anchor molecules incorporated with a grafting density of 7.5% in 150 nm DPPC-cholesterol liposomes. (A) % Injected dose in blood-curves of PEG5000-ODA (closed diamonds), PEG5000-DODA (closed squares), PEG5000-HOA (closed triangles), PEG5000-DSPE (closed circles), and bare liposomes without polymer-lipid conjugate (open circles). (B) Distribution to spleen (open bars), liver (gray bars), and total distribution to the MPS (liver and spleen) (black bars). Results are expressed as the mean percentage of the injected dose of four rats  $\pm$  SD.

24 and 48 h postinjection. The PLP-plasma concentration was compared with PLP in PEG-liposomes, as the latter has been shown to be completely stable in the circulation by comparing the plasma concentration of a radioactive liposome marker to the plasma concentration of encapsulated PLP (30). In the same study, plasma levels of PLP could hardly be detected after iv injection of free PLP, which strongly suggests that all PLP measured in plasma after injection of liposomal PLP must be liposome-associated. To measure PLP in plasma samples, plasma was extracted according to a method reported by Derendorf et al. (32). The extracts were assayed with a reversed-phase HPLC method, using UV-absorption detection at 254 nm.

**Therapeutic Activity of PLP-Containing Polymer-Coated Liposomes in Adjuvant Arthritis.** The Dutch Committee of Animal Experiments approved the animal studies. Male inbred Lewis rats between 7 and 9 weeks of age (170–200 g) were obtained from Maastricht University, Maastricht, The Netherlands. Adjuvant arthritis was induced according to Koga and Pearson (33). Briefly, incomplete Freund's adjuvant containing heat-inactivated *Mycobacterium tuberculosis* was subcutaneously injected at the base of the tail. Paw inflammation started around day 10 after the immunization and reached maximal severity around day 20, after which the inflammation process gradually resolved. The rats were daily scored for the visual signs of inflammation. All rats were treated on day 15 postimmunization, when the average score of all rats in the experiment is about half the maximal scores reached in these experiments. The effect of treatment on clinical scores and body weight was monitored up to 4 weeks posttreatment.

**Statistical Analysis.** For statistically assessing and comparing therapeutic efficacy in different groups, the nonparametric Wilcoxon/Kruskal-Wallis test (rank sums) was used. For evaluating differences between groups regarding other parameters, one-way analysis of variance was used. *P* values of less than 0.05 were considered significant.

## RESULTS

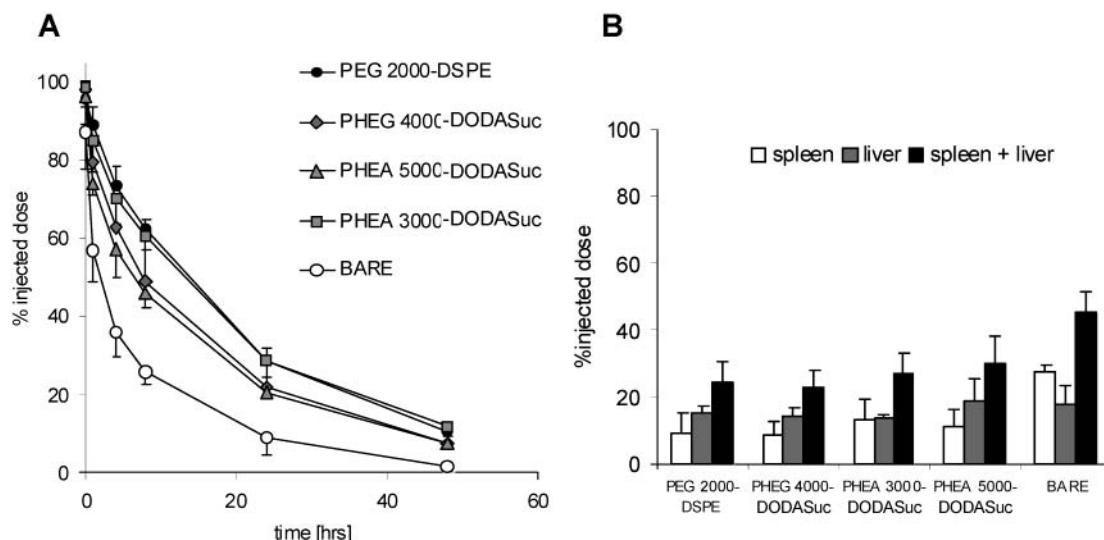
**Synthesis of PHEA- and PHEG-DODASuc Conjugates.** Poly(hydroxyethyl L-asparagine) (PHEA) and

poly(hydroxyethyl L-glutamine) (PHEG) were synthesized starting from benzyl L-aspartate NCA and benzyl L-glutamine NCA, respectively, as shown in Scheme 1. Polymerization of these L-amino acid benzyl ester NCA monomers was followed by aminolysis with alkanolamines. Molecular weights in the range of 2000–5000 were obtained via a primary amine initiated polymerization of these side group-protected amino acid NCA monomers. The molecular weight of the polymer is controlled by the molar ratio of monomer/initiator. *N*-Succinyldioctadecylamine (DODASuc) (lipid anchor) could be coupled to the polypeptide's amino end group. Polymerization of benzyl L-aspartate initiated by a primary amine (e.g., methylamine) yields a polypeptide (PBLA) with an amino end group. In contrast, polymerization of benzyl glutamate NCA initiated by a primary amine results in the formation of a polypeptide (PBLG) without an amino end group. As could be concluded from MALDI-TOF, a five-membered lactam end group is formed by an intramolecular reaction of the amino end group with the benzyl ester group. The terminal amino group is lost.

Conjugation of DODASuc to PBLG, therefore, requires a slightly modified approach: first, benzyl L-glutamate NCA is polymerized using BOC-butanediimine (one amino group is BOC (tertiary butoxycarbonyl)-protected; the other amino group is not) as an initiator. The resulting PBLG containing a protected amino group is deprotected and then coupled to DODASuc using dicyclohexylcarbodiimide (DCC). Amphiphilic conjugates resulted after the polypeptides were made water-soluble by the aminolysis reaction of the benzyl ester side groups with alkanolamines (e.g., ethanolamine).

**Preparation and Characterization of Polymer-Coated Liposomes.** In Table 1 the characteristics of the polymer-coated liposomes are presented. The resulting mean diameter and polydispersity of PHEG-, PHPG-, PHBG-, and PHEA-coated liposomes are comparable to those of PEG-liposomes. All preparations appeared to be physically stable upon storage, and no signs of aggregation were found.

**Selection of Suitable Anchor Molecules.** Figure 1A shows the plasma concentration-time profiles of liposomes coated with different PEG5000 conjugates after iv injection. For the evaluation of the anchor molecules,



**Figure 2.** Pharmacokinetics and distribution to the MPS of PHEA and PHEG versus PEG incorporated with a grafting density of 7.5% in 150 nm DPPC-cholesterol liposomes. (A) %-injected dose in blood-curves of PEG2000-DSPE (closed circles), PHEG4000-DODASuc (gray diamonds), PHEA5000-DODASuc (gray triangles), PHEA3000-DODASuc (gray squares), and bare liposomes without polymer-lipid conjugate (open circles). (B) Distribution to spleen (open bars), liver (gray bars) and total distribution to the MPS (liver and spleen) (black bars). Results are expressed as the mean percentage of the injected dose of four rats  $\pm$  SD.

PEG5000 was chosen instead of PEG2000, as a molecular mass of PEG5000 more closely resembles the molecular mass of most of the polymers tested in this study. We coupled PEG5000 to a series of lipid anchor molecules and compared liposomes coated with these conjugates to liposomes without PEG ('bare' liposomes). Clearly, octadecylamine (ODA) as a lipid anchor results in little prolongation of circulation time, suggesting that one single  $C_{18}$ -tail is not sufficient for stable grafting. Dioctadecylamine (DODA) and heptadecyl octadecylamine (HOA) yield improved prolongation of circulation behavior, similar to the phospholipid anchor distearyl phosphatidylethanolamine (DSPE), which is generally used for stable grafting of PEG on the liposome bilayer. Apparently, two alkyl tails are required for sufficient grafting stability. We selected DODA as the standard anchor molecule for synthesis of PHEA-and the different poly(hydroxyalkyl L-glutamine)-lipid conjugates.

Figure 1B shows the tissue distribution to the MPS organs. The DODA- and HOA-PEG conjugates significantly reduce the hepatosplenic uptake of liposomes. As hepatosplenic uptake is the main cause of liposome elimination from the circulation, these data are in agreement with plasma concentration-time profiles shown in Figure 1A.

**Successful Prolongation of Circulation Half-Life with PHEG- and PHEA-DODASuc.** In Figure 2A it is shown that coating liposomes with 7.5% PHEG4000 or PHEA3000 and PHEA5000 all coupled to *N*-succinyl-DODA (DODASuc) results in almost similar circulation behavior as compared to 7.5% PEG2000-DSPE, the conjugate which is most often used for the preparation of LCL. These results are in line with the tissue distribution data shown in Figure 2B, which shows that all four polymer-lipid conjugates significantly reduce MPS uptake from the circulation.

**Selection of Optimal Grafting Density with PHEG-DODASuc.** In Table 2 the effect of different grafting densities of PHEG4000 on circulation behavior and hepatosplenic uptake is shown. Although plasma concentration-time profiles show little differences at 4 and 24 h, hepatosplenic uptake at 48 h indicates that decreasing the grafting density to 2.5% and 1% or

**Table 2. Percentage of Injected Dose<sup>a</sup> of PHEG-Liposomes in the Circulation at 4 and 24 h Postinjection and Uptake by MPS Organs at 48 h**

PHEG grafting density, %	blood circulation		liver uptake	spleen uptake
	4 h	24 h	48 h	48 h
1	55 $\pm$ 2	22 $\pm$ 1	52 $\pm$ 9	11 $\pm$ 6
2.5	56 $\pm$ 8	22 $\pm$ 1	38 $\pm$ 7	15 $\pm$ 2
7.5	61 $\pm$ 6	23 $\pm$ 4	23 $\pm$ 5	7 $\pm$ 2
15	49 $\pm$ 4	17 $\pm$ 3	32 $\pm$ 5	9 $\pm$ 1

<sup>a</sup> Mean  $\pm$  SD of four rats per group.

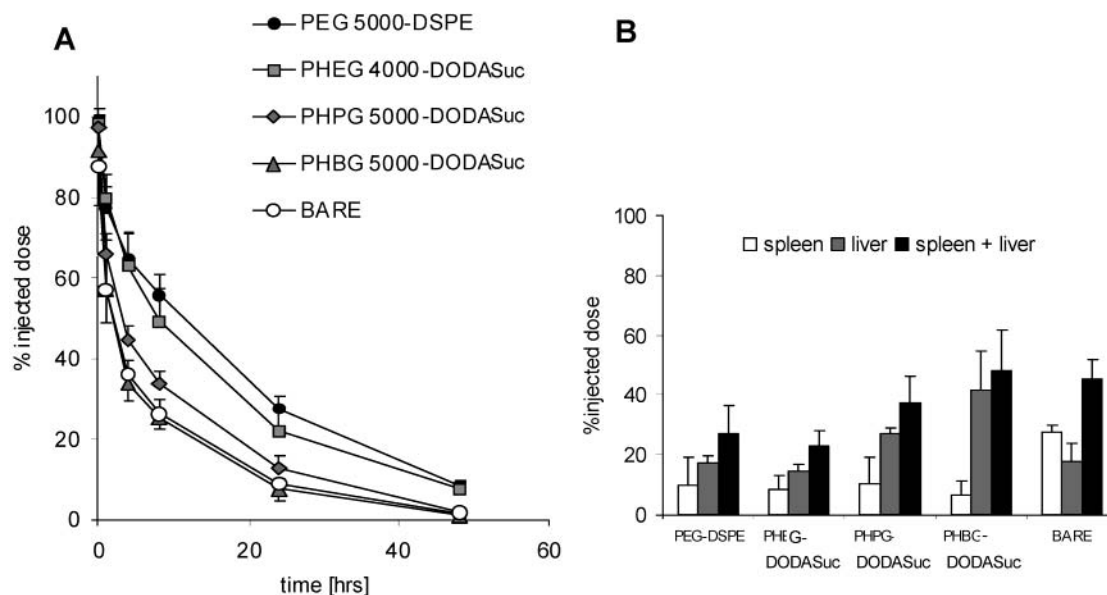
increasing the density to 15% leads to enhanced removal of liposomes by the MPS.

**Effect of the Side Group.** Introduction of longer hydroxyalkyl side groups to the poly(L-glutamine) backbone, such as hydroxypropyl and hydroxybutyl instead of hydroxyethyl, results in reduced prolongation of circulation time and enhanced MPS uptake to the level of 'bare' liposomes (Figure 3). The hydroxyethyl side group appears to be the optimal side group for the poly(hydroxyalkyl L-glutamine)-lipid conjugates.

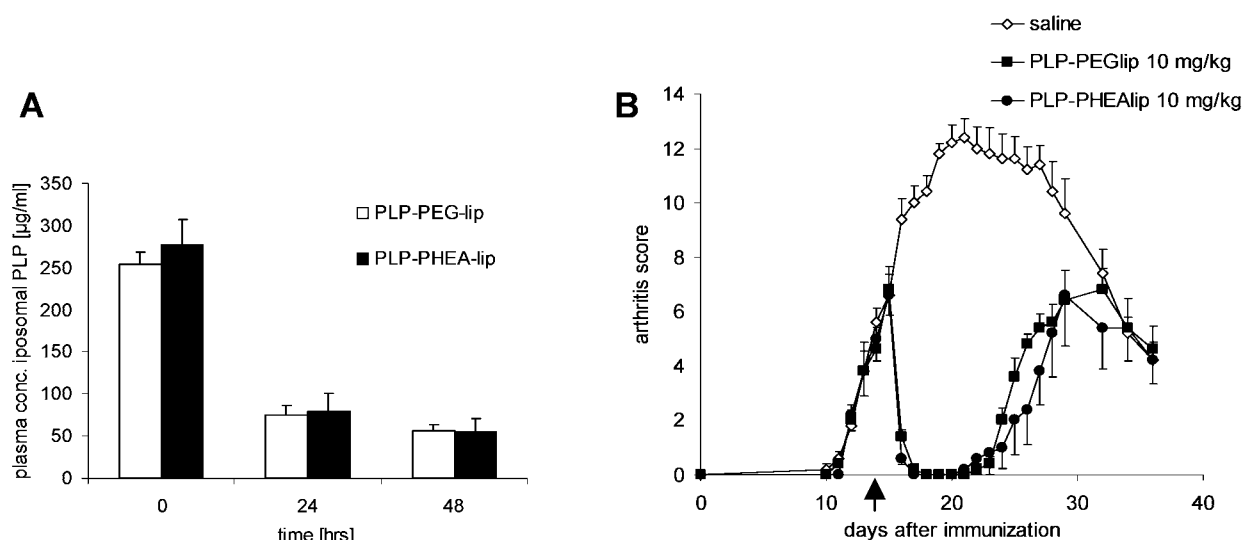
**Effect of Lipid Dose.** Table 3 shows the % injected dose of liposomes still present in the circulation at 4 and 24 h postinjection of PEG-coated liposomes and PHEA-coated liposomes, both at 4 different dose levels ranging from 0.005 to 5  $\mu$ mol lipid per rat. At a dose of 0.05  $\mu$ mol and especially at 0.005  $\mu$ mol, PHEA-liposomes show improved circulation behavior as compared to PEG-liposomes. PEG-liposomes are very rapidly eliminated at the 5 nmol dose level, and they are hardly present in the circulation at 24 h postinjection, whereas 9% of the injected PHEA-liposomes still circulates at 24 h at the same dose level.

**Drug-Targeting Potential.** Prednisolone phosphate (PLP) was encapsulated in both PEG- and PHEA-liposomes and injected in adjuvant arthritis rats. In this experimental arthritis model we previously showed that the therapeutic activity of PLP was dramatically increased by encapsulation in PEG-liposomes. Figure 4A shows the plasma concentration of liposomally encapsulated PLP. The % fractions of the injected dose of PLP in PHEA-liposomes in the circulation at 24 and 48 h equals





**Figure 3.** Pharmacokinetics and distribution to the MPS of different poly(hydroxyalkyl L-glutamine)s incorporated with a grafting density of 7.5% in 150 nm DPPC-cholesterol liposomes. (A) %-injected dose in blood-curves of PEG2000-DSPE (closed circles), PHEG4000-DODASuc (gray squares), PHPG5000-DODASuc (gray diamonds), PHBG5000-DODASuc (gray triangles), and bare liposomes without polymer-lipid conjugate (open circles). (B) Distribution to spleen (open bars), liver (gray bars) and total distribution to the MPS (liver and spleen) (black bars). Results are expressed as the mean percentage of the injected dose of four rats  $\pm$  SD.



**Figure 4.** Pharmacokinetics and therapeutic activity of PHEA- versus PEG-liposomal PLP in rat experimental arthritis. (A) Plasma concentration at 0, 24, and 48 h postinjection of 10 mg/kg PLP in PHEA-liposomes (open bars) and PEG-liposomes (closed bars). Results are expressed as the mean concentration ( $\mu$ g/mL) of five rats  $\pm$  SD. (B) Daily arthritis score after induction of adjuvant arthritis at day 0 and treatment at day 15 (arrow) with 10 mg/kg PLP (120  $\mu$ mol/kg phospholipid) in PHEA-liposomes (closed circles), 10 mg/kg in PEG-liposomes (closed squares), and saline (open diamonds). Results are expressed as the mean of five rats  $\pm$  SEM.

**Table 3.** Percentage of the Injected Dose<sup>a</sup> of Liposomes in Circulation at 4 and 24 h Postinjection

lipid dose, $\mu$ mol	PEG-liposomes		PHEA-liposomes	
	4 h	24 h	4 h	24 h
5	66 $\pm$ 7	29 $\pm$ 6	57 $\pm$ 4	27 $\pm$ 9
0.5	71 $\pm$ 10	26 $\pm$ 5	57 $\pm$ 5	18 $\pm$ 2
0.05	46 $\pm$ 7	12 $\pm$ 3	61 $\pm$ 4	20 $\pm$ 1
0.005	5 $\pm$ 3	1 $\pm$ 1	33 $\pm$ 5	9 $\pm$ 2

<sup>a</sup> Mean  $\pm$  SD of four rats per group.

PLP in PEG-liposomes. As PLP-PEG-liposomes composed of DPPC and cholesterol have been shown not to leak PLP in the circulation, such may therefore also be assumed for PLP-PHEA-liposomes. The circulation half-life of these liposomes is somewhat longer than reported with the radiolabeled liposomes in this study. However,

this is most likely a result of a relatively small diameter of approximately 90 nm as compared to the radiolabeled liposomes (between 140 and 160 nm). Figure 4B shows that 10 mg/kg PLP-PHEA-liposomes induces a similar reversal of the inflammation reaction as 10 mg/kg PLP-PEG-liposomes. Both preparations induce a strong anti-inflammatory effect lasting for two weeks.

## DISCUSSION

In this paper biodegradable polymer-lipid conjugates based on amino acids are evaluated regarding their capacity to confer a long-circulation property to liposomes upon attachment to their lipid bilayer surface. Besides the polymer itself, also the choice of the lipid bilayer anchor deserves attention, as stable grafting of a polymer to the liposome bilayer is essential for achieving long-

circulating behavior. Therefore, in this study the suitability of different lipid anchor molecules was evaluated with PEG5000 as a model polymer (Figure 1). The results show that successful prolongation of liposome circulation time can only be realized with anchor molecules with two stearyl chains. PEG coupled to DODA and HOA resulted in similar prolongation of circulation behavior as PEG-DSPE, which is at present most often used in liposome technology. In agreement with the findings of Webb et al., coupling of the polymer to a single alkyl chain yielded inferior results, most likely due to insufficient grafting stability (34). As DODA was easier to obtain from commercial sources than HOA, all polypeptides were tested in subsequent experiments with DODA as liposome anchor molecule.

The approach of L-amino acid-based polymer-lipid conjugates proved to be successful with PHEG4000 and PHEA3000 and -5000, all coupled to DODASuc. The plasma concentration-time profiles as well as uptake by liver and spleen showed that these polymer-lipid conjugates prolonged the circulation time and reduced the uptake by the MPS to the same extent as PEG2000-DSPE (Figure 2). As has been shown in the literature for PEG, lowering the grafting density of PHEG to 1 mol % resulted in increased uptake by the MPS (35). Interestingly, also a grafting density of 15 mol % PHEG increased MPS-uptake. However, the circulation times of liposomes grafted with 1, 2.5, 7.5, and 15 mol % PHEG did not differ significantly.

The results in this study show that coating the liposomes with poly(L-glutamine) with longer hydroxyalkyl side chains (PHPG and PHBG) instead of PHEG resulted in decreased circulation half-lives (Figure 3). An explanation for this observation may be found in the conformation of the polymers when dissolved in water. It has been suggested that suitable stealth polymers should be flexible and adopt a random conformation (36). For example, dextran has a lower chain flexibility than PEG due to its carbohydrate backbone. When grafted on liposomes, dextran is not able to prolong circulation times (37). Altschuler et al. showed that for poly(hydroxyalkyl-L-glutamine)s the degree of conformational freedom is optimal with hydroxyethyl as a side group and conformational freedom decreases for longer hydroxyalkyl groups. The use of hydroxypropyl and, even more so, hydroxybutyl resulted in the formation of  $\alpha$ -helices in the polymer (38). The decrease in flexibility of these polymers correlates with the observed decrease of circulation half-life.

An important advantage of polymer-coated LCL over LCL without polymer-lipid conjugates is that incorporation of PEG leads to dose-independent pharmacokinetics over a broad dose range (39). To evaluate whether this phenomenon also applies to liposomes coated with poly(hydroxyalkyl L-amino acid)-lipid conjugates, pharmacokinetics of PHEA-liposomes were compared with PEG-liposomes at four different lipid doses ranging from 0.005 to 5  $\mu$ mol total lipid per rat. The lowest dose level at which the PEG-liposomes appeared to show dose-independent kinetics was around 500 nmol/rat (Table 3) which corresponds with earlier reported data (40). Interestingly, with PHEA-liposomes dose-dependency of the pharmacokinetics was less pronounced even at a 10-fold lower dose. PHEA-liposomes may therefore offer an additional advantage over PEG-liposomes in cases when very low lipid doses are preferred, such as in scintigraphic detection of sites of pathology (7).

The final aim of this study was to show that successful drug targeting is possible, with liposomes exposing

biodegradable polypeptide-lipid conjugates. Within the scope of this thesis, a PEG-liposomal formulation of prednisolone phosphate (PLP) was developed that was shown to efficiently contain the drug in the circulation and to highly effectively deliver the encapsulated drug to inflamed joints in experimental arthritis (30). Incorporation of PEG increased the circulation half-life of the liposomal formulation from 6 h to 18 h, which was shown to be necessary to achieve sufficient local delivery for complete reversal of the development of joint inflammation. The present study shows that the use of PHEA-liposomes as PLP carrier results in a similar pharmacokinetic profile of encapsulated PLP. Also, the therapeutic activity of 10 mg/kg PLP-PHEA-liposomes in rat adjuvant arthritis was equal to that of 10 mg/kg PLP-PEG-liposomes. We reported earlier that nonencapsulated PLP was inactive at this dose level (30). The observation that a dramatic improvement of the therapeutic effect of PLP can be achieved with PHEA-liposomes clearly points to the drug targeting potential of this formulation.

In conclusion, we present a novel sterically stabilized liposome formulation performing similarly to PEG-liposomes regarding in vivo long-circulation behavior and drug-targeting potential. These novel polymer-coated liposomes are the first that are sterically stabilized with a biodegradable polymer coating.

#### LITERATURE CITED

- (1) Bangham, A. D., and Horne, R. W. (1964) Negative staining of phospholipids and their structural modification by surface-active agents as observed in the electron microscope. *J. Mol. Biol.* 8, 660-668.
- (2) (1998) *Medical applications of liposomes* (D. D. Lasic, and D. Papahadjopoulos, Eds.) Elsevier Science BV, Amsterdam.
- (3) Karlowsky, J. A., and Zhanel, G. G. (1992) Concepts on the use of liposomal antimicrobial agents: applications for aminoglycosides. *Clin. Infect. Dis.* 15, 654-667.
- (4) Bakker-Woudenberg, I. A., Storm, G., and Woodle, M. C. (1994) Liposomes in the treatment of infections. *J. Drug Target.* 2, 363-371.
- (5) Oku, N., and Namba, Y. (1994) Long-circulating liposomes. *Crit. Rev. Ther. Drug Carrier Syst.* 11, 231-270.
- (6) Gabizon, A., Catane, R., Uziely, B., B. Kaufman, B., Safra, T., Cohen, R., Martin, F., Huang, A., and Barenholz, Y. (1994) Prolonged circulation time and enhanced accumulation in malignant exudates of doxorubicin encapsulated in polyethylene-glycol coated liposomes. *Cancer Res.* 54, 987-992.
- (7) Laverman, P., Boerman, O. C., Oyen, W. J. G., Dams, E. T. M., Storm, G., and Corstens, F. H. M. (1999) Liposomes for scintigraphic detection of infection and inflammation. *Adv. Drug Del. Rev.* 37, 225-235.
- (8) Massing, U., and Fuxius, S. (2000) Liposomal formulations of anticancer drugs: selectivity and effectiveness. *Drug Resist. Update* 3, 171-177.
- (9) Muggia, F. M. (2001) Liposomal encapsulated anthracyclines: new therapeutic horizons. *Curr. Oncol. Rep.* 3, 156-162.
- (10) Tollema, J., Klingspor, L., and Ringden, O. (2001) Liposomal amphotericin B (AmBisome) for fungal infections in immunocompromised adults and children. *Clin. Microbiol. Infect.* 7 S 2, 68-79.
- (11) Schiffelers, R., Storm, G., and Bakker-Woudenberg I. (2001) Liposome-encapsulated aminoglycosides in pre-clinical and clinical studies. *J. Antimicrob. Chemother.* 48, 333-344.
- (12) Moghimi, S. M., Hunter, A. C., and Murray, J. C. (2001) Long-circulating and target-specific nanoparticles: theory to practice. *Pharmacol. Rev.* 53, 283-318.
- (13) Woodle, M. C., Engbers, C. M., and Zalipsky S. New amphipatic polymer-lipid conjugates forming long-circulating reticuloendothelial system-evading liposomes. *Bioconjugate Chem.* 5, 493-496.
- (14) Maruyama, K., Okuizumi, S., Ishida, O., Yamauchi, H., Kikuchi, H., and Iwatsuru, M. (1994) Phosphatidylpoly-

- glycerols prolong liposome circulation in vivo. *Int. J. Pharm.* 111, 103–107.
- (15) Torchilin, V. P., Shtilman, M. I., Trubetskoy, V. S., Whiteman, K., and Milstein A. M. (1994) Amphiphilic vinyl polymers effectively prolong liposome circulation time in vivo. *Biochim. Biophys. Acta* 1195, 181–184.
- (16) Torchilin, V. P., Trubetskoy, V. S., Whiteman, K., Caliceti, P., Ferruti, P., and Veronese F. M. (1995) New synthetic amphiphilic polymers for steric protection of liposomes in vivo. *J. Pharm. Sci.* 84, 1049–1053.
- (17) Torchilin, V. P., Levchenko, T. S., Whiteman, K. R., Yaroslavov, A. A., Tsatsakis, A. M., Rizos, A. K., Michailova, E. V., and Shtilman, M. I. (2001) Amphiphilic poly-N-vinylpyrrolidones: synthesis, properties and liposome surface modification. *Biomaterials* 22, 3035–3044.
- (18) Whiteman, K. R., Subr, V., Ulbrich, K., and Torchilin, V. P. (1999) Attachment of HEMA derivatives to the liposome surface makes them long-circulating. *Proc. Int. Symp. Controlled Release Bioact. Mater.* 26, 1064–1065.
- (19) Wang, Z. Y., and Stern I. J. (1975) Disposition in rats of a polyoxypropylene-polyoxyethylene copolymer used in plasma fractionation. *Drug Metab. Dispos.* 3, 536–542.
- (20) Kwon, G. S., Yokoyama, M., Okano, T., Sakurai, Y., and Kataoka K. (1993) Biodistribution of micelle-forming polymer-drug conjugates. *Pharm. Res.* 10, 970–974.
- (21) Hunter, A. C., and Moghimi, S. M. (2002) Therapeutic synthetic polymers: a game of Russian roulette? *Drug Discovery Today* 7, 998–1001.
- (22) Pytela, J., Kotva, R., Metalova, M., and Rypacek, F. (1990) Degradation of N5-(2-hydroxyethyl)-L-glutamine and L-glutamic acid homopolymers and copolymers by papain. *Int. J. Biol. Macromol.* 12, 241–246.
- (23) Rypacek, F., Pytela, J., Kotva, R., and Skarda, V. (1997) Biodegradation of poly(amino acid)s: evaluation methods and structure-to-function relationships. *Macromol. Symp.* 123, 9–24.
- (24) Pytela, J., Saudek, V., Drobnik, J., and Rypacek, F. (1989) Poly(N5-hydroxyalkylglutamines). IV. Enzymatic degradation of N5-(2-hydroxyethyl)-L-glutamine homopolymers and copolymers. *J. Controlled Release* 10, 17–25.
- (25) Chiu, H. C., Kopeckova, P., Deshame, S. S., and Kopecek, J. (1997) Lysosomal degradability of poly( $\alpha$ -amino acids). *J. Biomed. Mater. Res.* 34, 381–392.
- (26) Fuller, W. D., Verlander, M. S., and Goodman, M. (1976) A procedure for the facile synthesis of amino acid N-carboxyanhydrides. *Biopolymers* 15, 1869–1871.
- (27) Schmitt, L., Dietrich, C., and Tampé, R. (1994) Synthesis and characterization of chelator-lipids for reversible immobilization of engineered proteins at self-assembled lipid interfaces. *J. Am. Chem. Soc.* 116, 8485–8491.
- (28) Amselem, S., Gabizon, A., and Barenholz, Y. (1993) A large-scale method for the preparation of sterile and non-pyrogenic liposomal formulations of defined size distributions for clinical use. *Liposome Technology* (G. Gregoriadis, Ed.) pp 501–525, CRC Press, Boca Raton, FL.
- (29) Finsy, R. (1994) Particle sizing by quasi-elastic light scattering. *Adv. Colloid Interface Sci.* 52, 79–143.
- (30) Metselaar, J. M., Wauben, M. H. M., Wagenaar-Hilbers, J. P. A., Boerman, O. C., and Storm, G. (2003) Complete remission of experimental arthritis by joint targeting of glucocorticoids with long-circulating liposomes. *Arthritis Rheum.* 48, 2059–2066.
- (31) Rouser, G., Fkeischer, S., and Yamamoto, A. (1970) Two-dimensional thin layer chromatographic separation of polar lipids and determination of phospholipids by phosphorus analysis of spots. *Lipids* 5, 494–496.
- (32) Derendorf, H., Rohdewald, P., Hochhaus, G., and Möllmann, H. (1986) HPLC determination of glucocorticoid alcohols, their phosphates and hydrocortisone in aqueous solutions and biological fluids. *J. Pharm. Biomed. Anal.* 4, 197–206.
- (33) Koga, T., and Pearson, C. M. (1973) Immunogenicity and arthritogenicity in the rat of an antigen from *Mycobacterium tuberculosis* wax D. *J. Immunol.* 111, 599–608.
- (34) Webb, M. S., Saxon, D., Wong, F. M., Lim, H. J., Wang, Z., Bally, M. B., Choi, L. S., Cullis, P. R., and Mayer, L. D. (1998) Comparison of different hydrophobic anchors conjugated to poly(ethylene glycol): effects on the pharmacokinetics of liposomal vincristine. *Biochim. Biophys. Acta* 1372, 272–282.
- (35) Schiffelers, R. M., Bakker-Woudenberg, I. A., Snijders, S. V., Storm, G. (1999) Localization of sterically stabilized liposomes in *Klebsiella pneumoniae*-infected rat lung tissue: influence of liposome characteristics. *Biochim. Biophys. Acta* 1421, 329–339.
- (36) Torchilin, V. P., Omelyanenko, V., Papisov, M. I., Bogdanov, A. A., Jr., Trubetskoy, V. S., Herron, D. I. N., and Gentry, C. A. (1994) Poly(ethyleneglycol) on the liposome surface: On the mechanism of polymer-coated liposome longevity. *Biochim. Biophys. Acta* 1195, 11–20.
- (37) Papisov, M. I. (1998) Theoretical considerations of RES-avoiding liposomes: Molecular mechanics and chemistry of liposome interactions. *Adv. Drug Delivery Rev.* 32, 119–138.
- (38) Altschuler, E. L., Hud, N. V., Mazrimas, J. A., and Rupp, B. (2000) Structure of polyglutamine. *FEBS Lett.* 472, 166–168.
- (39) Allen, T. M., and Hansen, C. (1991) Pharmacokinetics of stealth versus conventional liposomes: effect of dose. *Biochim. Biophys. Acta* 1068, 133–141.
- (40) Laverman, P., Boerman, O. C., Oyen, W. J. G., Corstens, F. H. M., and Storm, G. (2001) In vivo applications of PEG liposomes: unexpected observations. *Crit. Rev. Ther. Drug Carrier Syst.* 18, 551–566.

BC0340363



# Dinuclear Copper(II) Complex as Nitric Oxide Scavenger in a Stimulated Murine Macrophage Model

Laura Chiarantini,<sup>\*,†</sup> Aurora Cerasi,<sup>†</sup> Luca Giorgi,<sup>‡</sup> Mauro Formica,<sup>‡</sup> Maria Francesca Ottaviani,<sup>‡</sup> Michela Cangiotti,<sup>‡</sup> and Vieri Fusi<sup>\*,‡</sup>

Institute of Biochemistry "Giorgio Fornaini" and Istituto di Scienze Chimiche, Università degli Studi di Urbino "Carlo Bo", Italy. Received April 15, 2003; Revised Manuscript Received July 20, 2003

Nitric oxide is a gaseous, short-living free radical which behaves as an important signaling molecule with pleiotropic capacities including vasodilatation, neurotransmission, and microbial and tumor cell killing, as well as in tissue damage and organ-specific autoimmune disorders. Here, a synthesized, dinuclear copper complex system in vitro obtained by the simple aza-phenolic ligand 2,6-bis{[bis-(2-aminoethyl)amino]methyl}phenol (L) and Cu(II) ion has been used. The stability constants of ligand L with Cu(II) ion were determined through potentiometric measurements in aqueous solution ( $37.1 \pm 0.1$  °C,  $I = 0.15$  M of NaCl) to mimic the biological medium. The measurements demonstrated that  $[\text{Cu}_2\text{H}_-1\text{L}(\text{OH})]^{2+}$  (DCu) is the predominant species present in solution at pH 7.4. The molecular structure of the ligand in this species permits the cooperation of the two copper ions in assembling the substrate, thus the complex can be used as a receptor for small molecules such as NO. As a biological model, we chose the production of NO catalyzed by inducible nitric oxide synthase obtained from RAW 264.7 murine macrophage cell line stimulated with LPS, which enabled us to prove that NO is coordinated by the DCu complex, modifying its EPR spectra. The coordination of NO with DCu reduces the level of nitrite in the culture medium of stimulated RAW 264.7 macrophages without any inhibition in the expression of iNOS.

## INTRODUCTION

Nitric oxide (NO) can be synthesized by several cell types in mammalian tissues and the mechanism of its synthesis and functions have been the focus of wide investigation (1). NO plays a role as an autocrine and paracrine mediator in several physiological conditions. In particular, the effect of NO in the regulation of vascular homeostasis, as well as its involvement in neurotransmission and in host defense against infectious agents, has been demonstrated (2–4).

However, it has also been reported that imbalances in intracellular NO levels may be responsible for various pathological alterations, such as septic shock, hypertension, stroke, and neurodegenerative disease (5). The production of nitric oxide is catalyzed by the enzyme nitric oxide synthase (NOS). NOS is constituted by a family of enzymes that catalyze the NADPH-dependent conversion of L-arginine to nitric oxide and L-citrulline. Three isoforms of nitric oxide synthase have been identified and cloned (6). Brain (nNOS or type I) and endothelial (eNOS or type III) enzymes are constitutively expressed, and their enzymatic activity is regulated by changes in concentration of free  $\text{Ca}^{2+}$  (7–9). The third member of the family is the inducible (type II) nitric oxide synthase (iNOS), which is expressed in many different cell types after induction and produces high levels of NO

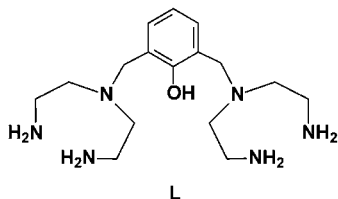
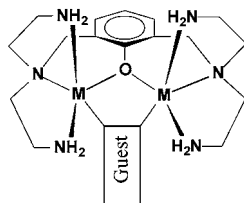
(6). In fact, iNOS is regulated at the transcriptional level by endotoxin and cytokines and is independent of calcium concentration in the physiological range. When activated by endotoxin, macrophages elicit the formation of inflammatory cytokines, which then activate macrophages and other cells to promote iNOS gene induction. Overproduction of NO, primarily by iNOS, has been implicated in a wide variety of disease states (10). Therefore, it is crucial to regulate the excess NO produced by iNOS when considering inflammatory reactions. Most of the currently used pharmacological inhibitors of iNOS may also affect the other two isoforms of NOS and interfere with unrelated metabolic cell pathways to some degree (2, 3). One strategy for the inhibition of NO is to scavenge or remove excess NO produced during pathological processes, avoiding inhibition of the NO metabolic pathway. For this purpose we have used a dinuclear copper complex  $[\text{Cu}_2\text{H}_-1\text{L}(\text{OH})]^{2+}$  (DCu) as a scavenger for NO.

Binuclear transition metal complexes play a central role in a variety of fields. In fact, binuclear metal complexes are successful devices for the recognition and assembly of external species of various nature such as inorganic and organic species (11–14). Many natural biological sites, such as the active centers of several metalloenzymes, are produced by two transition metal ions; thus synthetic binuclear receptors can be used to mimic the active centers (15–18). Recently, we reported the synthesis and the coordination properties of the noncyclic ligand L (Figure 1) containing a phenol moiety separating two triaza-polyamine fragments toward several M(II) metal cations (19–22). Solid-state and solution studies highlighted the ability of L to assemble two transition metal ions in close proximity. In this way, the two metals cooperate to bind a new species ( $\text{OH}^-$ ,  $\text{Cl}^-$ ,  $\text{R-O}^-$ ,  $\text{N}_3^-$ ,  $\text{O}_2$ , and others), which is coordinated in a

\* Corresponding authors. Prof. Laura Chiarantini, Institute of Biochemistry "Giorgio Fornaini", Università degli Studi di Urbino "Carlo Bo", Via Saffi 2, 61029 Urbino (PU), Italy. Phone: +39 0722 305260. Fax: +39 0722 320188. E-mail: l.chiarantini@uniurb.it. Prof. Vieri Fusi, Istituto di Scienze Chimiche, Università degli Studi di Urbino "Carlo Bo", Piazza Rinascimento 6, Urbino (PU), Italy.

<sup>†</sup> Institute of Biochemistry "Giorgio Fornaini".

<sup>‡</sup> Istituto di Scienze Chimiche.

**Figure 1.** Ligand L.**Figure 2.** Coordination models of the  $[M_2(H-1L)]^{2+}$  complex with a potential guest.

bridge disposition between the two metals as schematically depicted in Figure 2.

The data demonstrate that the DCu species was able to lower nitrite levels (an indicator of NO presence), in the culture supernatant produced by LPS-stimulated RAW 264.7 macrophage cell line. It is also demonstrated that, through electron paramagnetic resonance (EPR) spectra analysis, the ability of the DCu species to bind the NO produced in vitro.

Here it is shown that the DCu species decreases the free NO level but does not interfere with the expression of iNOS protein in macrophage cell line.

#### MATERIAL AND METHODS.

**Synthesis.** Ligand 2,6-bis{[bis(2-aminoethyl)amino]methyl}phenol L and its solid copper complex  $[Cu_2H-1L(OH)](ClO_4)_2$  were prepared as previously described (19). An aqueous solution at pH 7.4 of this copper complex was freshly prepared by dissolving a known amount of  $[Cu_2H-1L(OH)](ClO_4)_2$  in water and adjusting to pH 7.4 and promptly used. Solvents and starting materials were used as purchased.

**EMF Measurements.** Equilibrium constants for protonation and complexation reactions with L were determined by pH-metric measurements ( $pH = -\log [H^+]$ ) in 0.15 M NaCl at  $T = 37.1^\circ C$ , using the fully automatic equipment previously described (23); the EMF data were acquired with the PASAT computer program. The combined glass electrode was calibrated as a hydrogen concentration probe by titrating known amounts of HCl with  $CO_2$ -free NaOH solutions and determining the equivalent point by Gran's method (24, 25), which gives the standard potential  $E^\circ$  and the ionic product of water ( $pK_w = 13.40$  (1) at  $T = 37.1^\circ C$  in 0.15 M NaCl). At least three potentiometric titrations were performed for each system in the pH range 2.5–11, using different molar ratios of Cu(II)/L ranging from 1:1 to 2:1.

The HYPERQUAD computer program was used to process the potentiometric data (26, 27). All titrations were treated either as single sets or as separate entities without significant variation in the values of the determined constants.

**UV-vis Spectroscopy.** UV absorption spectra were recorded at  $T = 37.1^\circ C$  on a Varian Cary-100 spectrophotometer equipped with a temperature control unit.

**Cell Culture.** All experiments were performed on mouse macrophage cell line RAW 264.7 (kindly supplied by Prof. Umberto Benatti, Genova) cultured in DMEM

supplemented with 10% heat-inactivated foetal calf serum (FCS), 2.0 mM glutamine, and 1% antibiotics. Cultures were maintained in exponential growth at  $37^\circ C$  in a humidified atmosphere of 95% air–5%  $CO_2$ .

**Cell Activation.** RAW 264.7 cells were incubated for 24 h in FCS-free DMEM culture medium at  $37^\circ C$  at 80% of confluence. Cell stimulation to promote iNOS synthesis in intact murine macrophages was achieved by adding 1  $\mu g/mL$  lipopolysaccharide (LPS) from *Escherichia coli* (serotype 0111:B4, Sigma, St. Louis, MO) for 30 min, and then the cells were washed and maintained in the serum free (without phenol red) DMEM medium with several concentrations (0.001–10.0  $\mu M$ ) of DCu or ligand L or  $Cu(ClO_4)_2$  for 18 h to elicit the expression of iNOS and the production of NO.

**Cellular Toxicity.** RAW 264.7 cells were seeded in 96-well plates (Greiner, International PBI, Italy) at a concentration of  $1 \times 10^4$  cells/mL (100  $\mu L$ /well) and treated with several concentrations of DCu or ligand L or  $Cu(ClO_4)_2$  (0.1–10.0  $\mu M$ ) for 24 h.

The in vitro toxicity of RAW 264.7 cells in the presence of several compounds was tested by MTT assay (28, 29). Briefly, 5 mg/mL of 3-(4,5-dimethylthiazol-2-yl)-2,5-diphenyltetrazolium bromide (MTT) in PBS was sterilized by filtration. At the time indicated, 10  $\mu L$  of MTT solution was added, and plates were incubated at  $37^\circ C$  for 4 h. Then 100  $\mu L$  of 0.4% of 0.04 N HCl in 2-propanol was added and thoroughly mixed to dissolve the dark blue crystals. The plates were then read on a Microplate Reader (Benchmark, Bio-Rad), using a test wavelength of 570 nm and a reference wavelength of 630 nm. The experiments were run in quadruplicate.

**Measurement of Nitrate/Nitrite.** Total nitrate and nitrite was measured by enzymatic reduction of nitrate to nitrite analysis using the Griess assay (30) which provides a measure of total NO produced by the RAW 264.7 cells. Nitrate was converted to nitrite by the action of nitrate reductase from *Aspergillus niger* (Sigma, Milan, Italy). Briefly, after RAW 264.7 cells were treated with several concentrations of DCu, ligand L, or  $Cu(ClO_4)_2$  in the presence of LPS, the supernatants were immediately centrifuged at 750g in an Eppendorf microcentrifuge to remove cells in suspension. Then 100  $\mu L$  aliquots of culture supernatants were incubated with 50  $\mu M$  NADPH, 5  $\mu M$  FAD, and 0.01 U of nitrate reductase for 20 min at  $37^\circ C$ . After this incubation, the medium was mixed with 100  $\mu L$  of Griess reagent (1% sulfanilamide, 0.1% N-(1-naphthylethylenediamine dihydrochloride in 5%  $H_3PO_4$ ) and incubated at room temperature for 10 min. The absorbance at 540 nm was measured with a spectrophotometer. Nitrite levels were determined using  $NaNO_2$  as a standard.

**Detection of iNOS by Western Blot Analysis.** iNOS in the RAW 264.7 macrophage cell line was detected by Western blot as described previously (31). Briefly, after cells ( $1 \times 10^6$  cells/dishes) ( $\Phi$  35 mm, Sarstedt, Italy) were stimulated with LPS and treated with tested compounds, they were scraped and lysed with a lysis buffer containing 50 mM Tris-HCl, pH 7.6, 0.25 M sucrose, 2% (w/v) SDS, 2  $\mu g/mL$  leupeptin, 1  $\mu g/mL$  pepstatin, 2 mM phenylmethylsulfonyl fluoride (PMSF), 5 mM EDTA, and 5 mM N-ethylenemaleimide. Cellular extracts were immediately boiled for 5 min, sonicated to shear the DNA, and centrifuged at 10 000g in an Eppendorf microcentrifuge to remove insoluble debris. Protein content was assayed by Lowry's method (32). Equal amounts of protein extracts (20  $\mu g$ ) were resolved on 8% SDS-polyacrilamide gels, transferred to nitrocellulose membranes (Amersham Pharmacia Biotech, UK), and then detected with an

**Table 1. Protonation Constants (log *K*) of L Determined by Means of Potentiometric Measurements in 0.15 M NaCl Aqueous Solution at 37.0 °C**

reaction	log <i>K</i>
$L + H^+ = HL^+$	10.47(1) <sup>a</sup>
$HL^+ + H^+ = H_2L^{2+}$	9.40(1)
$H_2L^{2+} + H^+ = H_3L^{3+}$	9.02(1)
$H_3L^{3+} + H^+ = H_4L^{4+}$	7.52(2)
$H_4L^{4+} + H^+ = H_5L^{5+}$	2.59(4)

<sup>a</sup> Values in parentheses are the standard deviations of the last significant figure.

**Table 2. Logarithm of the Equilibrium Constants Determined in 0.15 M NaCl Aqueous Solution at 37.0 °C for the Complexation Reactions of L with Cu(II) Ion**

reaction	log <i>K</i>
$Cu^{2+} + L = CuL^{2+}$	20.90(2)
$Cu^{2+} + L + H^+ = CuLH^{3+}$	29.72(3)
$Cu^{2+} + L + 2H^+ = CuLH_2^{4+}$	33.13(4)
$Cu^{2+} + L + 3H^+ = CuLH_3^{5+}$	36.29(7)
$2Cu^{2+} + L = Cu_2L^{4+}$	29.59(2)
$2Cu^{2+} + L = Cu_2H_{-1}L^{3+} + H^+$	25.03(2)
$2Cu^{2+} + L + H_2O = Cu_2H_{-1}L(OH)^{2+} + 2H^+$	19.09(5)

<sup>a</sup> Values in parentheses are the standard deviations of the last significant figure.

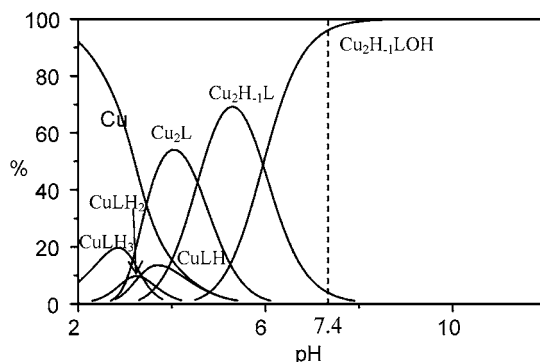
antibody specific against iNOS (M-19, Santa Cruz Biotechnology Inc., Santa Cruz, CA). The secondary antibody was horseradish peroxidase-conjugated goat anti-rabbit IgG and immune complexes were visualized with the ECL detection kit (Amersham Life Science, UK) according to the manufacturer's instructions. Membranes were stripped and reprobed with an antibody against actin (Sigma, Milan, Italy). Immunoreactive bands were quantitated by laser densitometry and iNOS levels were normalized to actin.

**EPR Analysis: Samples and Instrumentation.** For EPR analyses, the media from culture supernatant was collected in 2 mm glass tubes sealed at both sides and stored in liquid nitrogen before the measurements. EPR spectra were recorded by means of a EMX-Bruker spectrometer operating at X band (9.5 GHz) and interfaced to a IBM PC computer (Bruker software) for data acquisition and handling. The temperature was controlled with a Bruker ST3000 variable-temperature assembly.

The spectra were considered valid only on condition of reproducibility of the spectral line shape. Radical survival was nevertheless controlled by reproducibility of the EPR signal intensity. No variation of the EPR spectra was found after 1 day, after storing the samples in liquid nitrogen.

## RESULTS

**Chemical and UV Analysis.** Table 1 and Table 2 report the protonation constant and the stability constants of ligand L with Cu(II), respectively, for both equilibrium reactions determined potentiometrically in aqueous 0.15 M NaCl solution at 37.0 °C. The constants values are similar to those determined in 0.15 M N(CH<sub>3</sub>)<sub>4</sub>-Cl solution at 25.0 °C previously discussed (19). The experimental condition was chosen to mimic the same culture medium condition of the dinuclear system used in the in vitro studies. The distribution diagram of the species of the L/Cu(II) system as a function of pH is reported in Figure 3. The diagram shows that in the culture medium at pH 7.4, the species [Cu<sub>2</sub>H<sub>-1</sub>L(OH)]<sup>2+</sup> (DCu) is prevalent in solution and thus can be considered the active species for the interaction with nitric oxide.

**Figure 3.** Distribution diagrams of the species as a function of pH in 0.15 M NaCl aqueous solution at 37.0 °C for the system L/Cu(II): [Cu<sup>2+</sup>] = 2 × 10<sup>-3</sup> M; [L] = 1 × 10<sup>-3</sup> M.

The crystal structure of the DCu species was previously reported (19), and it can be depicted as in Figure 2; in this case, the guest is OH<sup>-</sup> anion.

To understand whether the environment of the two copper ions was modified in the presence of the biological medium, UV spectra were recorded in aqueous solutions containing L and Cu(II) in a 1:2 molar ratio at pH 7.4 using either NaCl ionic strength of the potentiometric measurements or culture medium at 37 °C. Dinuclear complex dissolved in the culture medium was used in the 0.5–100 mM range. The spectrum recorded at pH 7.4 in 0.15 M NaCl aqueous solution, where the DCu species is prevalent in solution, shows two bands at λ<sub>max</sub> 243 (ε = 9300 cm<sup>-1</sup> mol<sup>-1</sup> dm<sup>3</sup>) and 288 (ε = 4900 cm<sup>-1</sup> mol<sup>-1</sup> dm<sup>3</sup>) nm, due to the phenolate moiety engaged in the coordination of the metals; in the visible region, two more bands showing λ<sub>max</sub> 408 nm (ε = 450 cm<sup>-1</sup> mol<sup>-1</sup> dm<sup>3</sup>) attributed to phenolate metal charge transfer and a large band showing λ<sub>max</sub> 725 nm (ε = 420 cm<sup>-1</sup> mol<sup>-1</sup> dm<sup>3</sup>), due to the d–d electron transfer, are also observed. These four bands, having approximately the same profiles and ε, are also present in the culture medium, suggesting that the DCu species are preserved.

**Effects of DCu on Nitrite Level.** Nitrite production was measured in the culture medium of RAW 264.7 murine macrophage cell line treated with DCu species or ligand L or Cu(ClO<sub>4</sub>)<sub>2</sub> (0.001–10.0 μM) as described in Materials and Methods.

Nitrite levels in stimulated macrophages, whether treated or not with ligand L or Cu(ClO<sub>4</sub>)<sub>2</sub> at the several concentrations tested, did not show any differences (Figure 4). On the contrary, stimulated macrophages treated with DCu showed a reduced level of nitrite. The percentage of inhibition of nitrite level is shown in Figure 4.

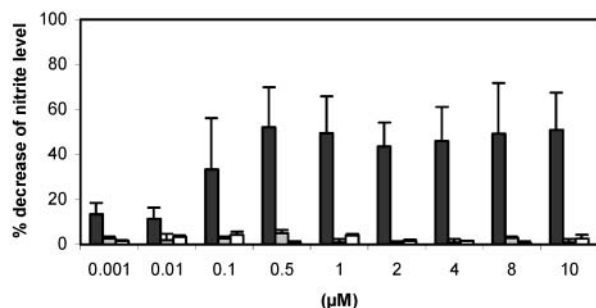
All the compounds used were tested to exclude any toxic effect on the cell line. Data are shown in Figure 5.

**Effects of DCu on iNOS Expression.** To examine the effect of DCu, ligand L, or Cu(ClO<sub>4</sub>)<sub>2</sub> on iNOS protein expression, RAW 264.7 cells were stimulated with 1 μg/mL of LPS for 30 min and subsequently treated with the above-mentioned compounds for 18 h. The cellular extracts were prepared and tested for iNOS expression by western blot analysis as described in Materials and Methods.

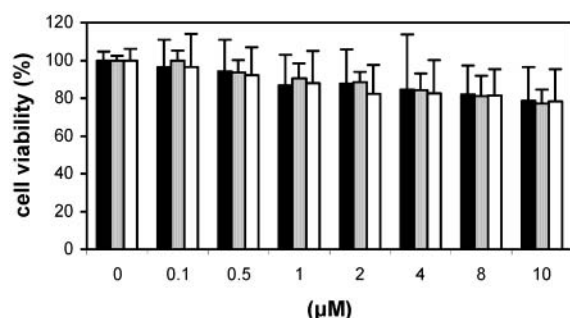
The evaluation of iNOS levels by laser densitometry of the immunoreactive band normalized to actin is reported (Figure 6).

Immunoblot analysis of unstimulated macrophage cellular extracts revealed no iNOS expression (Figure 6, lane 1). LPS-activated cells treated with DCu at several

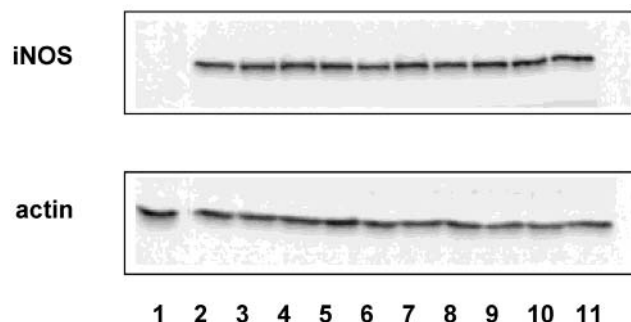




**Figure 4.** Effects of DCu on nitrite level. Cells ( $1 \times 10^6$  cells) were incubated for 30 min with LPS ( $1 \mu\text{g/mL}$ ) and further incubated for 18 h in DMEM (without phenol red) culture medium with several concentrations of DCu (column black), ligand L (column gray) or  $\text{Cu}(\text{ClO}_4)_2$  (column white). Nitrite levels in the supernatants of culture medium were measured using Griess reagent as described in Materials and Methods. The values are the mean  $\pm$  SD of three different experiments. For all samples:  $p \leq 10^{-3}$  (vs LPS stimulated).



**Figure 5.** MTT assay in RAW 264.7 cells. Murine macrophage cell line ( $10^4/\text{well}$ ) was incubated for 24 h with different concentrations (0.1–10  $\mu\text{M}$ ) of DCu (column black), ligand L (column gray), or  $\text{Cu}(\text{ClO}_4)_2$  (column white). Each data point represents the mean  $\pm$  SD of quadruplicate samples from two different experiments.

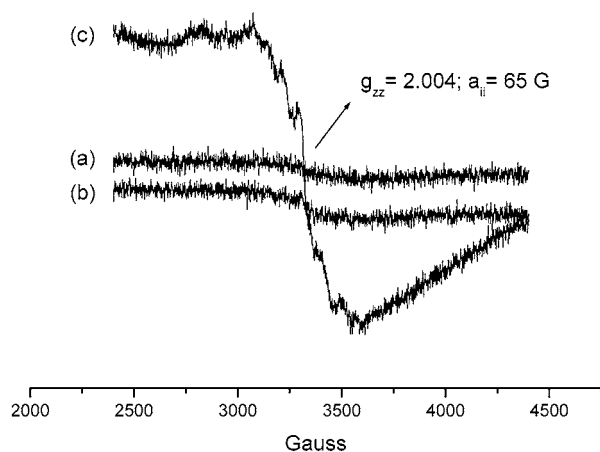


**Figure 6.** iNOS expression in stimulated RAW 264.7 cells. Immunoblot analysis of iNOS levels in murine macrophages not stimulated (lane 1) and LPS stimulated (lane 2–11). DCu was present at the concentration of 0.001  $\mu\text{M}$  (lane 3); 0.01  $\mu\text{M}$  (lane 4); 0.1  $\mu\text{M}$  (lane 5); 0.5  $\mu\text{M}$  (lane 6); 1.0  $\mu\text{M}$  (lane 7); 2.0  $\mu\text{M}$  (lane 8); 4.0  $\mu\text{M}$  (lane 9); 8.0  $\mu\text{M}$  (lane 10); and 10.0  $\mu\text{M}$  (lane 11). Blots were probed with anti iNOS and actin antibodies. More details on the stimulation protocol are described in Materials and Methods.

concentrations (0.001–10.0  $\mu\text{M}$ ) showed no significant effect on the iNOS protein level (Figure 6, lanes 2–11).

Even when ligand L or  $\text{Cu}(\text{ClO}_4)_2$  were used, the iNOS expression was not affected (data not shown).

**EPR Analysis.** EPR experiments were performed on DCu or ligand L dissolved in NaCl 0.15 M aqueous solution at pH 7.4 or in culture medium. Murine macrophages stimulated with LPS or unstimulated were grown in the presence or absence of DCu or ligand L, and on these media, EPR spectra were performed. Spectra



**Figure 7.** EPR spectra at  $-196^\circ\text{C}$  of DCu (a) and of murine macrophages stimulated with LPS, grown in the absence (b) and in the presence of DCu (c).

obtained from culture medium alone were also recorded as negative control.

All the EPR spectra were recorded at different temperatures,  $37^\circ\text{C}$ ,  $-103^\circ\text{C}$ , and at  $-196^\circ\text{C}$ . Spectra of DCu or ligand L in 0.15 M NaCl aqueous solution in the culture medium or in media obtained from unstimulated macrophages in the presence or absence of the two compounds appeared EPR silent at all temperatures. This is expected since dinuclear copper complexes in solution show a detectable signal only at temperatures low enough to provide a powder spectrum, due to spin-exchange effect, ferro- or ferri-magnetic properties correlated to fast relaxation (33–38). On the contrary, DCu in the presence of NO generated by LPS-stimulated macrophages showed a detectable EPR signal. The EPR signals, obtained at  $-196^\circ\text{C}$  for stimulated cells in the absence and in the presence of DCu, and for DCu alone, are shown in Figure 7. The broad line, centered at  $g = 2.004$  ( $g$  values were measured compared to diphenylpicryl hydrazide-DPPH ( $g = 2.0036$ ) added as an external reference) is attributed, on the basis of similar spectra reported in the literature, to the perpendicular adsorption of mononuclear copper complexes and shows a partial resolution of the hyperfine coupling between the unpaired electron and the nuclear spins of nitrogen nuclei ( $a_{\text{N}}$  = 65 G). The parallel adsorptions, centered at  $g_{\text{N}}$ , approximately 2.21, are poorly resolved and not shown. No further EPR lines were found in different field ranges. The spectrum at  $37^\circ\text{C}$  is a very noisy broad signal (not shown) centered at  $g$ , approximately 2.1. The signals shown in Figure 7 address the purpose of the present study: a significant spectral variation occurs because of the linking of NO, produced by stimulated cells, to the dinuclear  $\text{Cu}(\text{II})$  complex. The spectrum resulting from mononuclear  $\text{Cu}(\text{II})$ , in the presence of NO, indicates that the NO coordination influences the environment of copper ions in DCu. This can occur through the formation of a structure similar to that reported in the literature for an equivalent DCu complex coordinating  $\text{NO}^-$  (39), and probably an electron transfer also occurs between NO and  $\text{Cu}(\text{II})$ .

## DISCUSSION

In this *in vitro* biological model, exposure of macrophages to the proinflammatory bacteria LPS induces the expression of iNOS and the consequent production of a large amount of NO responsible for tissue damage and

autoimmune diseases. Therefore, the reduction of NO concentration without interfering with NOS enzyme is desirable.

Recent attention has been directed toward the development of synthetic metal receptors, formed by transition metal ions capable of coordinating NO molecules (40). Many of the synthetic metal receptors present copper ion as the coordinating center (41, 42).

Synthetic dinuclear complexes, in which the two metal ions are placed in close proximity, are good metal receptors for small molecules; the binding center is formed by both metal ions and they cooperate to bind the molecule in a stable, coordinated bridge disposition between the two metal ions (19, 21, 43). This knowledge prompted us to synthesize a dinuclear copper complex (DCu) having the two Cu(II) ions placed close to each other and to investigate whether DCu acts as a NO scavenger, forming a stable complex.

The selectivity of this scavenger for the nitric oxide responsible for pathological effects is not based on specificity for any particular enzyme, but rather on compartmental localization and rate of reaction with NO. To prove that DCu in a physiological environment, such as the culture medium, is the active species for NO coordination, potentiometric and UV/Vis measurements were performed; the formation constants of the complexed species for the system L/Cu(II) calculated by potentiometric measurements in 0.15 M NaCl aqueous solution at 37 °C revealed the presence of a stable dinuclear complex (DCu) in solution (Table 2 and Figure 3), representing the only species present at pH 7.4. Moreover, UV/Vis spectra on L/Cu(II) in aqueous solution or in culture medium proved that the DCu complex is preserved in the biological medium and therefore can be considered the active species interacting with NO. MTT experiments on DCu showed no toxicity on RAW 264.7 in the concentration range tested. The biological experiments show that it is the DCu complex and not the ligand L or Cu(ClO<sub>4</sub>)<sub>2</sub> that was able to reduce nitrite accumulation in the culture medium of the LPS-stimulated RAW 264.7 macrophage cell line (Figure 4) without inhibiting iNOS protein expression as shown in Figure 6.

To determine if the DCu complex is involved in NO reduction, EPR experiments were performed to exploit the magnetic properties of both DCu and NO species. As expected, the DCu complex is EPR silent in all media used in absence of NO; this property is due to the closeness of the two Cu(II) ions which, in solution, produce a spin-exchange effect correlated to fast relaxation. As well, the medium containing NO alone is also EPR silent. At the same time, the EPR spectra recorded in the presence of both NO and DCu show detectable signals below -103 °C that could be generated by the presence of a stable DCu-NO complex. These spectra are due to the mononuclear copper complex, and they can be obtained by a spatial separation of the two copper ions in DCu which can be achieved by the coordination of a molecule of NO in a bridge disposition as observed in similar studies (39). However, redox processes involving coordinated NO and Cu(II) ions cannot be excluded although they should represent a minority since the oxidation products of NO (nitrite or nitrate) decrease in the experiments. Certainly, the EPR signals are due to Cu(II) ion when NO binding occurs. This could be explained by the separation of the two Cu(II) ions in the complexed species which behave, for EPR experiments, as a mononuclear complex. In this case, it results that NO acts on DCu complex generating an EPR signal and probably facilitates the electron transfer between the

metal ions and the ligand. Currently, inorganic chemical studies on the NO-DCu system in aqueous solution are in progress to elucidate these aspects.

In fact, all the experiments performed in biological conditions are not suitable to unequivocally identify the stoichiometry of the complex DCu-NO formed, mainly due to the low concentration of the solutions used. However, previous studies (19, 21) on the coordination properties of DCu indicate that it binds external species through cooperation of both metal ions; thus it is possible to hypothesize that DCu binds only one NO molecule in a bridge disposition as shown in Figure 2, preserving the oxidation state of the two copper ions.

Our model provides unequivocal evidence that DCu reduces nitrite accumulations in RAW 264.7-stimulated cell line by scavenging NO produced while not inhibiting iNOS expression. The low toxicity of DCu, together with its activity in the cells studied, indicates a potential use in biological models where the removal of NO is advisable. Moreover, the success of DCu as a NO scavenger in vitro points out the potential of the synthesis and investigation of new dinuclear copper complexes suitable for the detection of NO produced in vitro/vivo.

#### ACKNOWLEDGMENT

This work was supported by MIUR PRIN 2002 and by CIB 2002 project.

#### LITERATURE CITED

- (1) Lamas, S., Pèrez Sala, D., and Moncada S. (1998) Nitric Oxide: From discovery to the clinic. *Trends Pharmacol. Sci.* 19, 436-438.
- (2) Nathan, C. (1992) Nitric oxide as a secretory product of mammalian cells. *FASEB J.* 6, 3051-3064.
- (3) Moncada, S., and Higgs, A. (1993) The L-arginine-nitric oxide pathway. *N. Engl. J. Med.* 329, 2002-2012.
- (4) MacMicking, J., Xie, Q., and Nathan, C. (1997) Nitric oxide and macrophage function. *Annu. Rev. Immunol.* 15, 323-350.
- (5) Miyasaka, N., and Hirata, Y. (1997) Nitric oxide and inflammatory arthritides. *Life Sci.* 61, 2073-2081.
- (6) Xie, W., Cho, H., Kashiwabara, Y., Baum, M., Weidner, J. R., Elliston, K., Mumford, R., and Nathan, C. (1994) Carboxyl terminus of inducible nitric oxide synthase. Contribution to NADPH binding and enzymic activity. *J. Biol. Chem.* 269, 28500-28505.
- (7) Sessa, W. C., Harrison, J. K., Barber, C. M., Zeng, D., Durieux, M. E., D'Angelo, D. D., Lynch, K. R., and Peach, M. J. (1992) Molecular cloning and expression of a cDNA encoding endothelial cell nitric oxide synthase. *J. Biol. Chem.* 267, 15274-15276.
- (8) Nakane, M., Schmidt, H., Pollock, J. S., Forstermann, U., and Murad, F. (1993) Cloned human brain nitric oxide synthase is highly expressed in skeletal muscle. *FEBS Lett.* 316, 175-180.
- (9) Lyons, C. R., Orloff, G. J., and Cunningham, J. M. (1992) Molecular cloning and functional expression of an inducible nitric oxide synthase from a murine macrophages cell line. *J. Biol. Chem.* 267, 6370-6374.
- (10) Szabò, C. (1995) Alteration in nitric oxide production in various forms of circulatory shock. *New Horiz. (Baltimore)* 3, 2-32.
- (11) Guerrierio, P., Tamburini, S., and Vigato, P. A. (1995) From mononuclear to polynuclear macrocyclic or macroacyclic complexes. *Coord. Chem. Rev.* 110, 17-243.
- (12) Dapporto, P., Formica, M., Fusi, V., Micheloni, M., Paoli, P., Pontellini, R., Romani, P., and Rossi, P. (2000) Polyamine macrocycles incorporating a phenolic function: their synthesis, basicity, and coordination behavior toward metal cations. Crystal structure of a binuclear nickel complex. *Inorg. Chem.* 39, 2156-2163.
- (13) Aoki, S., and Kimura, E. (2000) Highly selective recognition of thymidine mono- and diphosphate nucleotides in aqueous

- solution by ditopic receptors zinc(II)-bis(cyclen) complexes (Cyclen = 1,4,7,10-Tetraazacyclododecane). *J. Am. Chem. Soc.* **122**, 4542–4548.
- (14) Murthy, N. M., Mahroof-Tahir, M., and Karlin, K. D. (2001) Dicopper(I) complexes of unsymmetrical binucleating ligands and their dioxygen reactivities. *Inorg. Chem.* **40**, 628–635.
- (15) Lippard, S. J., and Berg, J. M. (1994) *Principles of Bioinorganic Chemistry*, University Science Books, Mill Valley, CA.
- (16) Reedijk, J., and Bouwman, E. (1993) *Bioinorganic Catalysis* (Reedijk, J., and Bouwman, E., Eds.) 2nd ed., Dekker, New York.
- (17) Karlin, K. D. (1993) Metalloenzymes, structural motifs, and inorganic models. *Science* **261**, 701–708.
- (18) Wilcox, D. E. (1996) Binuclear metallohydrolases. *Chem. Rev.* **96**, 2435–2458.
- (19) Dapporto, P., Formica, M., Fusi, V., Micheloni, M., Paoli, P., Pontellini, R., and Rossi, P. (2000) Synthesis of a flexible ligand for assembling two metal ions in close proximity. Crystal structures of binuclear nickel and copper complexes. *Inorg. Chem.* **39**, 4663–4665.
- (20) Ceccanti, N., Formica, M., Fusi, V., Micheloni, M., Pardini, R., Pontellini, R., and Tinè, M. R. (2001) Anaerobic and aerobic complexation of Co(II) by a polyamine ditopic ligand containing the phenolic moiety. *Inorg. Chim. Acta* **321**, 153–161.
- (21) Dapporto, P., Formica, M., Fusi, V., Micheloni, M., Paoli, P., Pontellini, R., and Rossi, P. (2001) Addition of small molecules by Zn(II) and Cu(II) dinuclear complexes obtained by an amino-phenolic ligand. Crystal structures of the dinuclear zinc complex assembling butanolate and azide anions. *Inorg. Chem.* **40**, 6186–6192.
- (22) Formica, M., Fusi, V., Micheloni, M., Giorgi, L., and Pontellini, R. (2001) Two triaza-polyamine units linked together by different aromatic spacers, coordination properties towards metal cations of a new compartmental ligand. *Polyhedron* **21**, 1351–1356.
- (23) Wei, C. C., Wang, Z. Q., Wang, Q., Meade, A. L., Hemann, C., Hille, R., and Stuehr, D. J. (2001) Rapid kinetic studies link tetrahydrobiopterin radical formation to heme-dioxy reduction and arginine hydroxylation in inducible nitric-oxide synthase. *J. Biol. Chem.* **276**, 315–319.
- (24) Fontanelli, M., and Micheloni, M. (1990) Presented at 1st Spanish–Italian Congress Thermodynamics of Metal Complexes, Peñíscola, June 3–6, University of Valencia, Spain, abstract 41, ED. Servicio de Publicaciones, Castellon, Spain.
- (25) Gran, G. (1952) Determination of the equivalence point in potentiometric titrations. *Analyst* **77**, 661–671.
- (26) Rossotti, F. J., and Rossotti, H. (1965) Potentiometric titrations using Gran plots—a textbook omission. *J. Chem. Educ.* **2**, 375–378.
- (27) Gans, P., Sabatini, A., and Vacca, A. (1996) Investigation of equilibria in solution. Determination of equilibrium constants with HYPERQUAD suite of programs. *Talanta* **43**, 1739–1753.
- (28) Mosmann, T. (1983) Rapid colorimetric assay for cellular growth and survival: application to proliferation and cytotoxicity assays. *J. Immunol. Methods* **65**, 55–63.
- (29) Pessina, A., Gribaldo, L., Mineo, E., and Neri, M. G. (1994) In vitro short-term and long-term cytotoxicity of fluoroquinolones on murine cell lines. *Indian J. Exp. Biol.* **32**, 113–118.
- (30) Stuehr, D. J., and Nathan, C. F. (1989) Nitric oxide. A macrophage product responsible for cytostasis and respiratory inhibition in tumor target cells. *J. Exp. Med.* **169**, 1543–1555.
- (31) Chiarantini, L., Cerasi, A., Fraternali, A., Andreoni, F., Scarfi, S., Giovine, M., Clavarino, E., and Magnani, M. (2002) Inhibition of macrophage iNOS by selective targeting of antisense PNA. *Biochemistry* **41**, 8471–8477.
- (32) Lowry, O. H., Rosebrough, N. J., Farr, A. L., and Randall, R. J. (1951) Protein measurement with the folin phenol agent. *J. Biol. Chem.* **193**, 265–275.
- (33) Richardson, H. W., Wasson, J. R., Estes, W. E., and Hatfield, W. E. (1977) Spectral and magnetic properties of linear-chain amino acid complexes of copper(II), bis(d,1- $\alpha$ -aminobutyrate)- and bis(1-asparaginato)copper(II). *Inorg. Chim. Acta* **23**, 205–209.
- (34) Richardson, H. W., Wasson, J. R., and Hatfield, W. E. (1977) Spectral and magnetic properties of copper(II) furoate and copper(II) thiophene-2-carboxylate. *J. Mol. Struct.* **36**, 83–91.
- (35) Doedens, R. J. (1976) Structure and metal–metal interactions in copper(II) carboxylate complexes. *Prog. Inorg. Chem.* **21**, 209–231.
- (36) Kato, M., and Muto, Y. (1988) Factors affecting the magnetic properties of dimeric copper(II) complexes. *Coord. Chem. Rev.* **92**, 45–83.
- (37) Kahn, O. (1985) Binuclear complexes with predictable magnetic properties. *Angew. Chem.* **97**, 837–853.
- (38) Gutierrez, L., Alzuet, G., Borrás, J., Castineiras, A., Rodriguez-Forte, A., and Ruiz, E. (2001) Inorg. Copper(II) complexes with 4-amino-N-[4,6-dimethyl-2-pyrimidinyl]benzenesulfonamide. Synthesis, crystal structure, magnetic properties, EPR, and theoretical studies of a novel mixed  $\mu$ -carboxylato, NCN-bridged dinuclear copper compound. *Inorg. Chem.* **40**, 3089–3096.
- (39) Paul, P. P., Tyeklár, Z., Farooq, A., Karlin, K. D., Liu, S., Zubieta, J. (1990) Isolation and X-ray structure of a dinuclear copper-nitrosyl complex. *J. Am. Chem. Soc.* **112**, 2430–2432.
- (40) Schnepfensieper, T., Finkler, S., Czup, A., Van Eldik, R., Heus, M., Nieuwenhuizen, P., Wreesmann, C., and Abma, W. (2001) Tuning the reversible binding of NO to iron(II) aminocarboxylate and related complexes in aqueous solution. *Eur. J. Inorg. Chem.* **491**–501.
- (41) Schnider, J. L., Carrier, S. M., Ruggiero, C. E., Young, V. G., Jr., and Tolman, W. B. (1998) Influences of ligand environment on the spectroscopy properties and disproportionation reactivity of copper-nitrosyl complexes. *J. Am. Chem. Soc.* **120**, 11408–11418.
- (42) Padden, K. M., Krebs, J. F., MacBeth, C. E., Scarrow, R. C., and Borovik, A. S. (2001) Immobilized metal complexes in porous organic host: development of a material for the selective and reversible binding of nitric oxide. *J. Am. Chem. Soc.* **123**, 1072–1079.
- (43) Dapporto, P., Formica, M., Fusi, V., Micheloni, M., Paoli, P., Pontellini, R., Romani, P., and Rossi, P. (2000) Polyamine macrocycles incorporating a phenolic function: their synthesis, basicity, and coordination behavior toward metal cations. Crystal structure of a binuclear nickel complex. *Inorg. Chem.* **39**, 2156–2163.

BC030022L



# Prolonged Oxygen-Carrying Ability of Hemoglobin Vesicles by Coencapsulation of Catalase in Vivo

Yuji Teramura, Hideo Kanazawa, Hiromi Sakai, Shinji Takeoka, and Eishun Tsuchida\*

Advanced Research Institute for Science and Engineering, Waseda University, Tokyo 169-8555, Japan  
Received April 23, 2003; Revised Manuscript Received August 21, 2003

Hemoglobin (Hb) vesicles (particle diameter, ca. 250 nm) have been developed as Hb-based oxygen carriers in which a purified Hb solution is encapsulated with a phospholipid bilayer membrane. The oxidation of Hb to nonfunctional ferric Hb (metHb) was caused by reactive oxygen species, especially hydrogen peroxide ( $\text{H}_2\text{O}_2$ ), in vivo in addition to autoxidation. We focused on the enzymatic elimination of  $\text{H}_2\text{O}_2$  to suppress the metHb formation in the Hb vesicles. In this study, we coencapsulated catalase with Hb within vesicles and studied the rate of metHb formation in vivo. The Hb vesicles containing  $5.6 \times 10^4$  unit  $\text{mL}^{-1}$  catalase decreased the rate of metHb formation by half in comparison with Hb vesicles without catalase. We succeeded in prolonging the oxygen-carrying ability of the Hb vesicle in vivo by the coencapsulation of catalase.

## INTRODUCTION

Ferrous hemoglobin (Hb) reversibly binds oxygen molecules to carry oxygen to terminal tissues and is gradually autoxidized to nonfunctional ferric Hb (metHb). In red blood cells, reduction systems such as NADH-cytochrome  $b_5$ , NADPH-flavin, glutathione, and ascorbic acid reduce metHb to ferrous Hb. Superoxide dismutase (SOD) and catalase exist in the cell to eliminate the superoxide anion ( $\text{O}_2^{\cdot-}$ ) and hydrogen peroxide ( $\text{H}_2\text{O}_2$ ), respectively, and the percentage of metHb in red blood cells is normally maintained at less than 1.0% (1, 2).

At present, several hemoglobin (Hb)-based oxygen carriers, which have been developed as red blood cell substitutes (3–5), are generally classified into two types: one is the acellular-type modified Hb molecules such as intramolecularly cross-linked Hb (6), recombinant cross-linked Hb (7), intermolecularly polymerized Hb (8), and poly(ethylene glycol) (PEG)-conjugated Hb (9). The other is a cellular-type Hb such as Hb vesicles (10) or liposome-encapsulated Hb (11), in which Hb molecules are encapsulated with a phospholipid bilayer membrane. Some of the acellular-type Hb modifications have advanced to phase III clinical trials (12, 13). Though the Hb vesicles have not yet been clinically studied, their excellent oxygen-carrying ability and high safety have been confirmed in vivo (10, 14–19).

When using Hb-based oxygen carriers, the oxidation of ferrous Hb to metHb is an important issue (20). Enzymes such as SOD and catalase, and enzymes in metHb reduction systems have been used to limit the metHb formation (21, 22). In the case of acellular Hb, the rate of metHb formation in blood circulation was suppressed compared with that in vitro, because metHb was reduced by reductants contained in the plasma such as ascorbic acid and glutathione. For example, about 40% glutaraldehyde-polymerized bovine Hb was reported to be oxidized to metHb at 72 h after a 90% exchange transfusion in ovines, and no further increase in the metHb percentage was observed (23). In the dextran-

conjugated Hb, the metHb percentage was maintained at 35%, 12 h after the 50% exchange transfusion in guinea pigs (24). On the other hand, in the Hb vesicles, the reductants in plasma are not available because of their low membrane permeability. Among the reactive oxygen species (ROS) such as nitric oxide (NO),  $\text{O}_2^{\cdot-}$ , and  $\text{H}_2\text{O}_2$ , which are known to promote metHb formation,  $\text{H}_2\text{O}_2$  can permeate through the bilayer membrane, and a relatively large amount of  $\text{H}_2\text{O}_2$  such as 4–5  $\mu\text{M}$  is constantly generated in normal human plasma (25). Therefore, we considered that such exogenous  $\text{H}_2\text{O}_2$  should be a cause of the metHb formation in addition to the autoxidation of Hb and endogenous  $\text{H}_2\text{O}_2$  generated by the autoxidation of Hb in the Hb vesicles. Therefore, the metHb formation of Hb vesicles was expected to be suppressed by  $\text{H}_2\text{O}_2$  elimination.

Although the rate of metHb formation was actually suppressed in vitro by the coencapsulation of catalase, the rate was dramatically increased in vivo. This was because catalase, which was purchased for laboratory use, was contaminated with LPS, and the resulting catalase-coencapsulated Hb vesicles were also highly contaminated with LPS ( $>10$  EU  $\text{mL}^{-1}$ ). We considered that the LPS would promote the rate of metHb formation in vivo because the inflammatory reaction would produce reactive oxygen species. In this study, we prepared the Hb vesicles coencapsulating LPS-free catalase (below 0.1 EU  $\text{mL}^{-1}$ ) and administered the Hb vesicle dispersion to Wistar rats (20  $\text{mL kg}^{-1}$ ) to study the suppression of the rate of metHb formation by the coencapsulation of catalase.

## MATERIALS AND METHODS

**1. Removal of Lipopolysaccharide (LPS) from Catalase.** A catalase solution (from bovine liver, Sigma, St Louis, MO) was mixed with a 10% Triton X-114 solution (Pierce Chemical, Rockford, IL) and incubated at 4 °C for 30 min. After the mixed solution was incubated at 37 °C for 40 min to separate into two phases, the aqueous phase containing catalase was centrifuged at 5000 rpm for 20 min, and the catalase solution was dialyzed against the water for injection at 4 °C for 24 h.

\* To whom correspondence should be addressed. E-mail: eishun@waseda.jp.

The determination of LPS was carried out with limulus assay (Limulus ES-II, Wako Pure Chemical, Osaka). The catalase solution was mixed with the LAL reagent, and the concentration of LPS was determined from the gelation time (Toxinometer ET-201, Wako Pure Chemical). The catalase activity was measured from the decreasing rate of the absorbance at 240 nm when the 0.06% (v/v)  $\text{H}_2\text{O}_2$  solution (2.9 mL) was mixed with the catalase solution (0.1 mL) at 25 °C.

**2. Preparation of Hb Vesicles Coencapsulating Catalase (26–28).** Hb was purified from outdated human red blood cells donated from Japanese Red Cross Blood Center (27). After the hemolyzed solution was separated from stromata, the ligand exchange of Hb from  $\text{O}_2$  to carbon monoxide (CO) was carried out by CO gas flowing. The proteins other than carbonylHb (HbCO) were denatured by heat treatment (60 °C for 12 h) and removed as precipitates. Pyridoxal 5'-phosphate (PLP, Sigma) as an allosteric effector was added to the HbCO solution (36 g  $\text{dL}^{-1}$ ) at a 2.5:1 molar ratio of PLP to Hb, and the catalase solution was added to it. Mixed lipid [1,2-dipalmitoyl-*sn*-glycero-3-phosphatidylcholine (DPPC, Nippon Fine Chemical, Osaka)/cholesterol (Nippon Fine Chemical)/1,5-dipalmitoyl-L-glutamate-*N*-succinic acid (DPEA, Nippon Fine Chemical)/1,2-distearoyl-*sn*-glycero-3-phosphatidylethanolamine-*N*-PEG (PEG molecular weight was 5000, Sunbright DSPE-50H, H-form, NOF Co., Tokyo), 5/5/1/0.033 by molar ratio] powder was dispersed with the HbCO solution, and the dispersion was stirred at 10 °C for 12 h. The resulting dispersion of multilamellar vesicles was extruded through the membrane filters (FM series, pore size; 3.00, 0.80, 0.65, 0.45, 0.30, 0.22  $\mu\text{m}$ , Fuji Film Co., Tokyo) with a Remolino (Millipore Co., Ltd., Bedford, MA). The Hb vesicles with an average diameter of 250 nm were prepared after extrusion through the membrane filter with 0.22  $\mu\text{m}$  pore size. After the separation of unencapsulated Hb by ultracentrifugation (10000g, 60 min), the precipitate of the Hb vesicles was redispersed into saline. Finally, the Hb concentration of the dispersion was adjusted to 10 g  $\text{dL}^{-1}$ . After Hb vesicles were solubilized with Triton X, the concentration of Hb was determined by a cyanometHb method. In this study,  $[\text{catalase}]_{\text{fed}}$  was defined as the catalase concentration at the mixed solution of Hb and catalase used in the preparation of the Hb vesicles.

The particle diameter of the Hb vesicles was measured by a dynamic light scattering method (N4 PLUS, Beckman Coulter, Fullerton, CA).

**3. Measurement of the Rate of methHb Formation of the Hb Vesicle in Vivo.** Wistar rats (195–210 g) were used in the experiments. They were anesthetized with diethyl ether, and the Hb vesicle dispersion was administered to the tail vein (20 mL  $\text{kg}^{-1}$ ). The sample was the Hb vesicles coencapsulating catalase (0–5.6  $\times 10^4$  unit  $\text{mL}^{-1}$ ). The blood withdrawn from the tail vein was centrifuged (12000g, 5 min) to collect the Hb vesicles in the upper phase of the precipitate. The methHb percentage was calculated based on the intensity ratio at 405 and 430 nm, which were identified as methHb and deoxyHb, respectively, under the nitrogen condition.

## RESULTS AND DISCUSSION

The catalase from bovine liver purchased for laboratory use was contaminated with LPS and was not acceptable for in vivo administration. We tried to remove LPS from the catalase solution using a nonionic detergent, Triton X-114. A solution of Triton X-114, which has a cloud point at 20 °C, is homogeneous below this point and is

separated into an aqueous phase and a detergent phase above that point (29). LPS is highly lipophilic and is transferred from an aqueous phase containing catalase into the organic phase of Triton X-114. We mixed a catalase solution ( $2.5 \times 10^3$  unit  $\text{mL}^{-1}$ ) with a Triton X-114 solution (10%, v/v) at 4 °C and separated the mixed solution into two phases at 37 °C to collect the aqueous phase containing catalase. The LPS concentration of the resulting catalase solution was reduced to 0.0038 EU  $\text{mL}^{-1}$  from  $>10$  EU  $\text{mL}^{-1}$  without significant dilution. We coencapsulated this purified catalase with Hb in the vesicles.

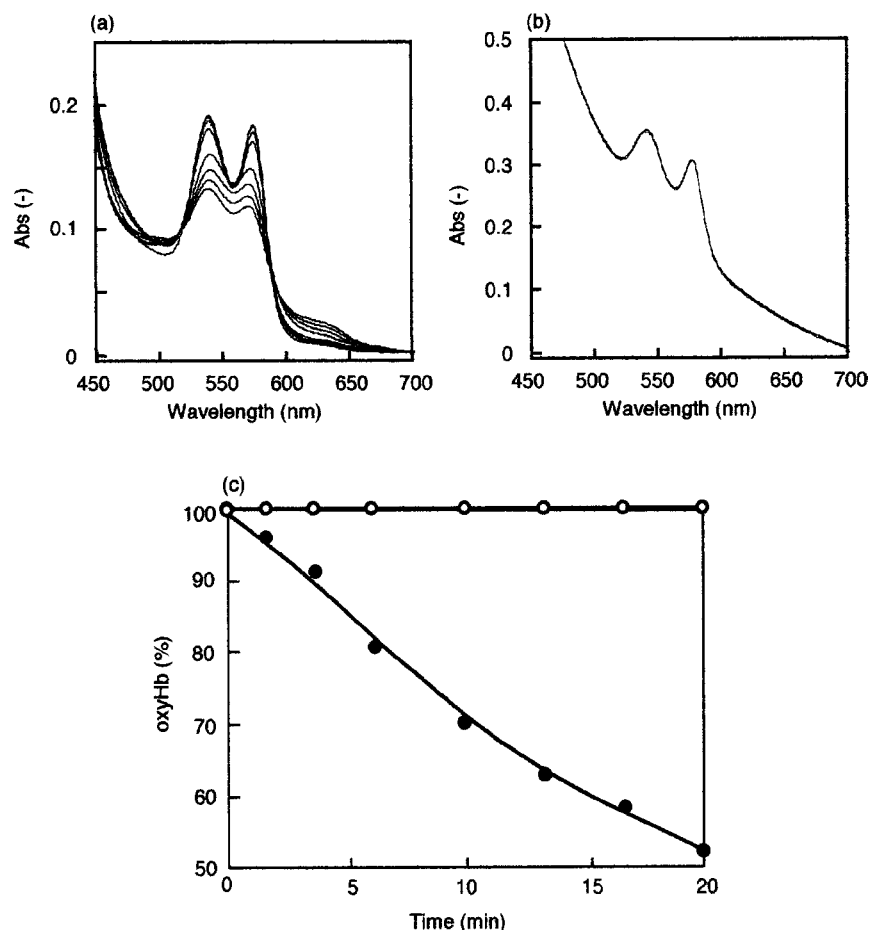
We then examined the stability of the catalase activity in a solution state at 37 °C. The catalase activities after incubation for 24, 48, and 56 h were 82, 82, and 81%, respectively. The constant activity of around 80% at 37 °C for more than 56 h indicate that the catalase should be tolerable during the in vivo study because the circulation half-life of the Hb vesicles was around 24 h in rats (20 mL  $\text{kg}^{-1}$ ).

The particle diameter of the Hb vesicles was  $251 \pm 80$  nm, and the oxygen affinity ( $P_{50}$ ) was 30 Torr. For all the Hb vesicles used in this study, oxyHb and methHb were more than 97% and less than 3%, respectively. Neither HbCO nor ferrylHb was detected. After the catalase-coencapsulated Hb vesicles were dissolved by the addition of Triton X, the resulting solution was analyzed by electrophoresis (IEF-PAGE). From the band of catalase, it was confirmed that the catalase was exactly coencapsulated in the Hb vesicles. We tried to measure the catalase activity of the Hb vesicles, however, due to the catalase-like activity of Hb, this activity could not be determined. Therefore,  $[\text{catalase}]_{\text{fed}}$  was defined as the catalase concentration at the mixed solution of Hb and catalase in the preparation process.

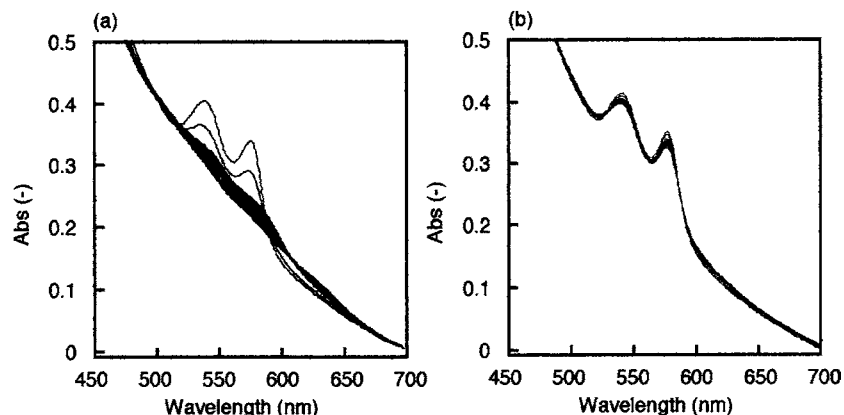
The LPS concentration in the resulting Hb vesicle dispersion ( $[\text{Hb}] = 10$  g  $\text{dL}^{-1}$ ) was below 0.1 EU  $\text{mL}^{-1}$ , which was measured by limulus assay after the solubilization of the Hb vesicles with poly(ethylene glycol) 10-lauryl ether (30).

We studied the reactivity of the Hb vesicles against ROS ( $\text{O}_2^{\cdot -}$  and  $\text{H}_2\text{O}_2$ ). The rate of  $\text{O}_2^{\cdot -}$  produced in a 106  $\mu\text{M}$  hypoxanthine/0.32 unit  $\text{mL}^{-1}$  xanthine oxidase system was 0.9  $\mu\text{M s}^{-1}$ , which was determined by cytochrome *c* (31). Catalase was also added to this system to eliminate  $\text{H}_2\text{O}_2$  from the immediate dismutation of  $\text{O}_2^{\cdot -}$  ( $k = 8.5 \times 10^5 \text{ M}^{-1} \text{ s}^{-1}$ ). As shown in Figure 1a, for the Hb solution, the peaks at 542 and 577 nm, identified as oxyHb, were gradually converted to the peak at 630 nm, identified as methHb, indicating that Hb underwent a one-electron oxidation to methHb by  $\text{O}_2^{\cdot -}$ . On the other hand, in the Hb vesicle dispersion, the UV-vis spectrum, where a large decline in the baseline from the lower wavelength typically shows the turbidity of the vesicles, did not change at all as shown in Figure 1b. This indicated that  $\text{O}_2^{\cdot -}$  could not permeate through the bilayer membrane due to the electrostatic repulsion from the negatively charged membrane (Figure 1c). Therefore, if the exogenous  $\text{O}_2^{\cdot -}$  would attack the Hb vesicles, it should have little influence on the methHb formation.

Next, we analyzed the reaction of  $\text{H}_2\text{O}_2$  with the Hb vesicles as shown in Figure 2a ( $[\text{heme}] = 12 \mu\text{M}$ ,  $[\text{H}_2\text{O}_2] = 120 \mu\text{M}$ ); oxyHb was converted to methHb via ferrylHb as an intermediate. In our previous report (19),  $\text{H}_2\text{O}_2$  permeated through the bilayer membrane, and Hb in the vesicles reacted with  $\text{H}_2\text{O}_2$  in a catalase-like reaction to produce methHb or ferrylHb ( $\text{Fe}^{\text{IV}}=\text{O}$ ) in the presence of excess  $\text{H}_2\text{O}_2$ . In the case of the Hb vesicles coencapsulating catalase ( $[\text{catalase}] = 4.2 \times 10^4$  unit  $\text{mL}^{-1}$ , Figure



**Figure 1.** Spectral changes of (a) the Hb solution and (b) the Hb vesicle dispersion ( $[\text{heme}] = 12 \mu\text{M}$ ) during the reaction with  $O_2^{\cdot-}$  at  $37^\circ\text{C}$  ( $0.9 \mu\text{M s}^{-1}$ ). The repetitive scanning was started at a 2 min interval. (c) Changes of the oxyHb in the Hb solution (●) and the Hb vesicle dispersion (○) during the reaction with  $O_2^{\cdot-}$ .



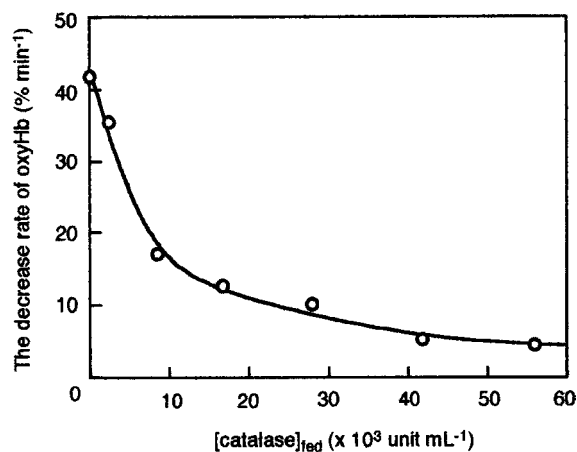
**Figure 2.** Spectral changes of (a) the Hb vesicle dispersion ( $[\text{heme}] = 12 \mu\text{M}$ ) and (b) catalase-coencapsulating Hb vesicle dispersion ( $[\text{heme}] = 12 \mu\text{M}$ ,  $[\text{catalase}]_{\text{fed}} = 4.2 \times 10^4 \text{ unit mL}^{-1}$ ) during the reaction with  $H_2O_2$  at  $37^\circ\text{C}$ . The repetitive scanning was started at a 2 min interval.

2b), a very small amount of oxyHb was converted to metHb without the formation of ferrylHb. This is because the reaction of Hb or catalase with  $H_2O_2$  should be competitive in the vesicles. Most of the  $H_2O_2$  should be eliminated by catalase, and a small amount of  $H_2O_2$  should react with Hb to form metHb (the elimination rate of catalase is about a thousand times greater than that of Hb). We measured the time course of the oxyHb percentage after the addition of 10-fold excess  $H_2O_2$  to oxyHb in the vesicles and calculated the initial decreasing rate of oxyHb (Figure 3). The Hb vesicles without catalase showed a decreasing rate of  $42\% \text{ min}^{-1}$ , whereas the Hb

vesicles with catalase showed a lower decreasing rate, depending on the concentration of catalase ( $[\text{catalase}]_{\text{fed}}$ ). The rate decreased to  $5.0\% \text{ min}^{-1}$  when more than  $5.0 \times 10^4 \text{ unit mL}^{-1}$  was coencapsulated within the vesicle. In this case, the ratio of Hb to catalase was calculated to be 35. We confirmed that the metHb formation of the Hb vesicles by exogenous  $H_2O_2$  could be effectively suppressed by catalase-coencapsulation.

We next examined the catalase encapsulation effect on the autooxidation-derived  $H_2O_2$ , namely endogenous  $H_2O_2$ . We measured the rate of metHb formation in the Hb vesicles at 40 Torr of oxygen partial pressure ( $PO_2$ ) in



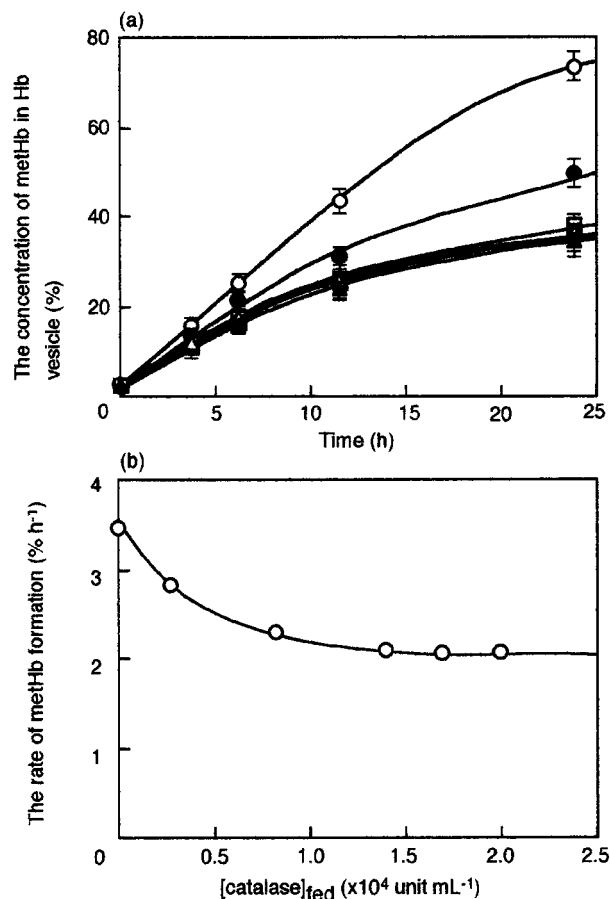


**Figure 3.** The relationship between the decrease rate of oxyHb in the vesicle ([heme] = 12  $\mu$ M) and the coencapsulated catalase during the reaction with  $\text{H}_2\text{O}_2$  ( $[\text{H}_2\text{O}_2]$  = 120  $\mu$ M).

vitro. When the  $\text{PO}_2$  is approximately the  $P_{50}$  of Hb, the rate of metHb formation tends to show a maximum (32, 33), and the average oxygen partial pressure in mixed venous blood is estimated to be 40 Torr. Therefore, we used the constant oxygen partial pressure of 40 Torr to measure the rate of metHb formation of the Hb vesicle dispersion for estimation of the *in vivo* behavior. As shown in Figure 4a, the rate of metHb formation in the Hb vesicles was 3.5%  $\text{h}^{-1}$ , and in the case of the catalase-coencapsulating Hb vesicles, the rate of metHb formation was significantly reduced from 2.8 to 2.0%  $\text{h}^{-1}$  with an increase in the encapsulated catalase concentration from  $2.8 \times 10^3$  to  $1.7 \times 10^4$  unit  $\text{mL}^{-1}$ . However, the rate of metHb formation was not reduced even when  $2.0 \times 10^4$  unit  $\text{mL}^{-1}$  catalase was coencapsulated (Figure 4b). Inside the vesicle, Hb is autoxidized to metHb with the production of  $\text{O}_2^{\cdot-}$ , and the resulting  $\text{O}_2^{\cdot-}$  immediately caused a one-electron oxidation of Hb to metHb and the  $\text{O}_2^{\cdot-}$  became  $\text{H}_2\text{O}_2$ . On the other hand, the  $\text{O}_2^{\cdot-}$  was immediately dismutated to  $\text{H}_2\text{O}_2$ . As previously reported, the resulting endogenous  $\text{H}_2\text{O}_2$  also autoxidizes Hb to metHb, or metHb via ferrylHb. Therefore, the autoxidation of Hb should trigger a further oxidation accompanied by the production of reactive oxygen species. In fact, in the group of catalase-coencapsulating Hb vesicles, the reduction of the metHb formation rate indicates that the metHb formation was suppressed by the elimination of the endogenous  $\text{H}_2\text{O}_2$ . The 2.0%  $\text{h}^{-1}$  rate of metHb formation of the Hb vesicles coencapsulating more than  $1.7 \times 10^4$  unit  $\text{mL}^{-1}$  catalase showed that the metHb formation by  $\text{H}_2\text{O}_2$ , which was produced by the autoxidation of Hb in the vesicle, could be completely suppressed by catalase.

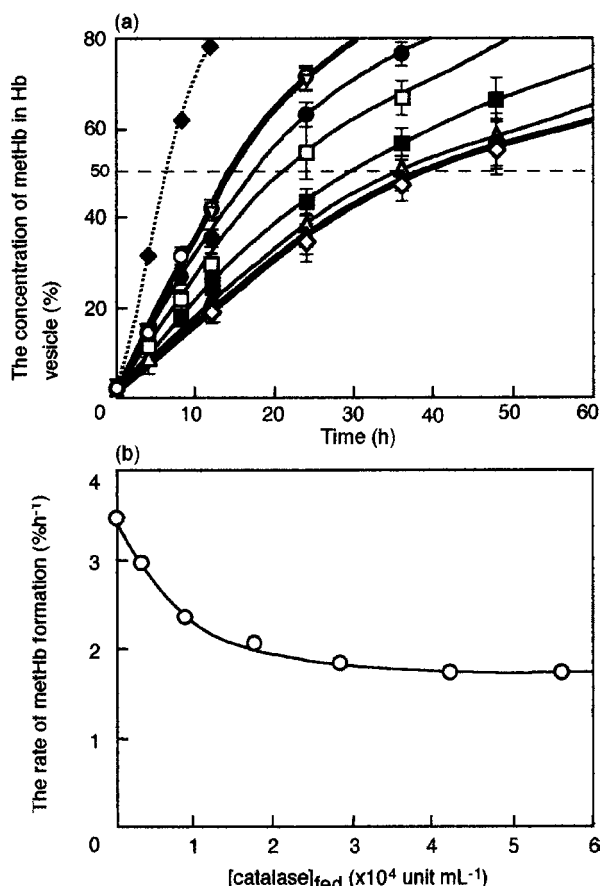
It is expected that SOD, which dismutates two  $\text{O}_2^{\cdot-}$  and two  $\text{H}^+$  to  $\text{H}_2\text{O}_2$  and  $\text{O}_2$ , should contribute to the reduction of the metHb formation rate. In the Hb solution ([Hb] = 2.0 g  $\text{dL}^{-1}$ ) containing SOD ( $2.0 \times 10^3$  unit  $\text{mL}^{-1}$ ) and catalase ( $2.0 \times 10^4$  unit  $\text{mL}^{-1}$ ), the rate of the metHb formation at 37  $^\circ\text{C}$  under atmospheric conditions was 1.3%  $\text{h}^{-1}$ , which was reduced to 74% compared with a bare Hb solution (1.8%  $\text{h}^{-1}$ ). However, the rate was almost the same as that of the Hb solution containing catalase (1.4%  $\text{h}^{-1}$ , [catalase] =  $2.0 \times 10^4$  unit  $\text{mL}^{-1}$ ). From this experiment, we used only catalase as an effective prolongation tool of the Hb function in the Hb vesicles.

To study the rate of the metHb formation *in vivo*, the Hb vesicles were injected into the rat tail vein (20 mL  $\text{kg}^{-1}$ ). It was confirmed that the LPS concentration in



**Figure 4.** (a) Changes of metHb percentage in the Hb vesicles at 40 Torr of oxygen partial pressure ([Hb] = 2.0 g  $\text{dL}^{-1}$ ). The control is catalase-free Hb vesicles ( $\circ$ ). The encapsulated catalase in the Hb vesicle was  $2.8 \times 10^3$  ( $\bullet$ ),  $8.4 \times 10^3$  ( $\square$ ),  $1.4 \times 10^4$  ( $\blacksquare$ ),  $1.7 \times 10^4$  ( $\triangle$ ), and  $2.0 \times 10^4$  unit  $\text{mL}^{-1}$  ( $\blacktriangle$ ). (b) The relationship between  $[\text{catalase}]_{\text{enc}}$  and the rate of metHb formation.

these samples was below 0.1 EU  $\text{mL}^{-1}$ , approved for *in vivo* administration. If LPS-contaminated Hb vesicles were injected, the rate of metHb formation should dramatically increase. In the catalase-coencapsulated Hb vesicles ( $[\text{catalase}] = 2.8 \times 10^4$  unit  $\text{mL}^{-1}$ ), where the LPS concentration was 10 EU  $\text{mL}^{-1}$ , the rate of metHb formation was 8.0%  $\text{h}^{-1}$  (dotted line in Figure 5a), whereas the rate was 2.9%  $\text{h}^{-1}$  in the catalase-coencapsulated sample of which the LPS concentration was 0.1 EU  $\text{mL}^{-1}$ . LPS is a major constituent of the outer envelope of Gram-negative bacteria; therefore, it is an extremely potent stimulator of the mammalian immune system and causes the activation of macrophages (34, 35), which should increase the rate of metHb formation by elevation of the reactive oxygen species concentration such as  $\text{H}_2\text{O}_2$ . In this case, there was no effect of the encapsulation with catalase in the Hb vesicles. The effect of such inflammation should exceed the effect of catalase coencapsulation. Therefore, we used the samples where the LPS concentration was below 0.1 EU  $\text{mL}^{-1}$  in order to accurately measure the rate of metHb formation. In the catalase-free Hb vesicles, the rate of the metHb formation was 3.4%  $\text{h}^{-1}$ , and the time for 50% metHb formation ( $T_{50\% \text{metHb}}$ ) was 14 h. On the other hand, in the groups of catalase-coencapsulated Hb vesicles ( $[\text{catalase}] = 2.8 \times 10^3$ ,  $8.4 \times 10^3$ ,  $1.7 \times 10^4$ ,  $2.8 \times 10^4$ ,  $4.2 \times 10^4$ , and  $5.6 \times 10^4$  unit  $\text{mL}^{-1}$ ), the rates of metHb formation were 2.9, 2.3, 2.0, 1.8, 1.7, and 1.7%  $\text{h}^{-1}$ , respectively, and the  $T_{50\% \text{metHb}}$  were 18, 22, 29, 36, 38, and 39 h, respectively. Figure 5a



**Figure 5.** (a) Changes of metHb percentage in the Hb vesicles in vivo (20 mL kg<sup>-1</sup>, Wistar rat). The control is catalase-free Hb vesicles (○) and the mixture of the Hb vesicle dispersion and the catalase solution ( $5.6 \times 10^4$  unit mL<sup>-1</sup>, ▽). The encapsulated catalase in the Hb vesicle was  $2.8 \times 10^3$  (●),  $8.4 \times 10^3$  (□),  $1.7 \times 10^4$  (■),  $2.8 \times 10^4$  (△),  $4.2 \times 10^4$  (▲), and  $5.6 \times 10^4$  unit mL<sup>-1</sup> (◇). The dotted line (◆) is the LPS-contaminated Hb vesicles ([catalase] =  $2.8 \times 10^4$  unit mL<sup>-1</sup>). (b) The relationship between [catalase]<sub>fed</sub> and the rate of metHb formation.

showed the changes in the metHb concentration, indicating that the rest of metHb in the Hb vesicles was the functional ferrous Hb (oxyHb). In the case of the administration of the mixture of the catalase-free Hb vesicle dispersion and catalase solution ( $5.6 \times 10^4$  unit mL<sup>-1</sup>), there was no significant difference from the control groups (catalase-free Hb vesicles) as shown in Figure 5a. These results showed that the administered catalase rapidly disappeared from the blood stream and could not eliminate hydrogen peroxide.

It was confirmed that, by catalase-coencapsulation, the rate of metHb formation was reduced and the  $T_{50\% \text{metHb}}$  was also prolonged. As shown in Figure 5b, the rate of metHb formation was saturated when the catalase concentration was over  $4.2 \times 10^4$  unit mL<sup>-1</sup> in comparison with  $1.7 \times 10^4$  unit mL<sup>-1</sup> in vitro as shown in Figure 4b. Such a high catalase concentration in vivo suggests that metHb formation should be caused by the exogenous H<sub>2</sub>O<sub>2</sub> from the blood circulation in addition to the endogenous H<sub>2</sub>O<sub>2</sub>. It is indicated that the saturated metHb formation rate should be due to the substantial autooxidation of Hb because of the elimination of endogenous and exogenous H<sub>2</sub>O<sub>2</sub>.

## CONCLUSION

Catalase coencapsulated in the Hb vesicle could eliminate H<sub>2</sub>O<sub>2</sub>, which was not only produced by the Hb

autooxidation in the vesicle but also generated in vivo, and the rate of metHb formation in the Hb vesicle could thus be effectively suppressed by catalase coencapsulation. We succeeded in substantially prolonging the oxygen-carrying ability of the Hb vesicles in vivo by coencapsulating catalase.

## ACKNOWLEDGMENT

This work was supported in part by Health and Labor Sciences Research Grants, Research on Pharmaceutical and Medical Safety, Ministry of Health, Labor and Welfare, Japan, Grants in Aid for Scientific Research (B) from the Ministry of Education, Science, Sports, and Culture, Japan (12558112), and 21COE "Practical Nano-Chemistry" from MEXT, Japan. One of the authors (Y.T.) thanks Research Fellowships of the Japan Society for the Promotion of Science for Young Scientists.

## LITERATURE CITED

- (1) Shikama, K. (1984) A controversy on the mechanism of autooxidation of oxyhemoglobin and oxyhemoglobin: oxidation, dissociation, or displacement? *Biochem. J.* 223, 279–280.
- (2) Tomoda, A., Yoneyama, T., and Tsuji, A. (1981) Changes in intermediate hemoglobins during autooxidation of hemoglobin. *Biochem. J.* 195, 485–492.
- (3) Tsuchida, E., Ed. (1998) *Blood substitutes: present and future perspectives*. Elsevier Science, Amsterdam.
- (4) D'Agnillo, F., and Chang, T. M. S. (1998) Polyhemoglobin-superoxide dismutase-catalase as a blood substitute with antioxidant properties. *Nat. Biotechnol.* 16, 667–671.
- (5) Riess, J. G., (2001) Oxygen carriers ("blood substitutes")—raison d'être, chemistry, and some physiology. *Chem. Rev.* 101, 2797–2920.
- (6) Przybelski, R. J., Daily, E. K., and Birnbaum, M. L. (1997) The pressor effect of hemoglobin—good or bad? In *Advances in Blood Substitutes: Industrial Opportunities and Medical Challenges* (Winslow, R. M., Vandegriff, K. D., and Intaglietta, M., Eds.) Birkhauser, Boston.
- (7) Murray, J. A., Ledlow, A., Launspach, J., Evans, D., Loveday, M., and Conklin, J. L. (1995) The effects of recombinant human hemoglobin on esophageal motor function in humans. *Gastroenterology* 109, 1241–1248.
- (8) Gould, S. A., Moore, E. E., Hoyt, D. B., Burch, J. M., Haenel, J. B., Garcia, J., DeWoskin, R., and Moss, G. S. (1998) The first randomized trial of human polymerized hemoglobin as a blood substitute in acute trauma and emergency surgery. *J. Am. Coll. Surg.* 187, 113–122.
- (9) McCarthy, M. R., Vandegriff, K. D., and Winslow, R. M. (2001) The role of facilitated diffusion in oxygen transport by cell-free hemoglobins: implications for the design of hemoglobin-based oxygen carriers. *Biophys. Chem.* 92, 103–117.
- (10) Sakai, H., Horinouchi, H., Tomiyama, K., Ikeda, E., Takeoka, S., Kobayashi, K., and Tsuchida, E. (2001) Hemoglobin-vesicles as oxygen carriers, Influence on phagocytic activity and histopathological changes in reticuloendothelial system. *Am. J. Pathol.* 159, 1079–1088.
- (11) Rudolph, A. S., Sulpizio, A., Hieble, P., MacDonald, V., Chavez, M., and Feuerstein, G. (1997) Liposome encapsulating attenuates hemoglobin-induced vasoconstriction in rabbit arterial segment. *J. Appl. Physiol.* 82, 1826–1835.
- (12) Mullon, J., Giacompe, G., Clagett, C., McCune, D., and Dillard, T. (2000) Transfusions of polymerized bovine hemoglobin in a patient with severe autoimmune hemolytic anemia. *N. Engl. J. Med.* 342, 1638–1643.
- (13) Sloan, E. P., Koenigsberg, M., Gens, D., Cipolle, M., Runge, J., Mallory, M. N., Rodman, G. Jr. (1999) Diaspirin cross-linked hemoglobin (DCLHb) in the treatment of severe traumatic hemorrhagic shock: a randomized controlled efficacy trial. *JAMA* 282, 1857–1864.

- (14) Sakai, H., Yuasa, M., Onuma, H., Takeoka, S., and Tsuchida, E. (2000) Synthesis and physicochemical characterization of a series of hemoglobin-based oxygen carriers: objective comparison between cellular and acellular types. *Bioconjugate Chem.* **11**, 56–64.
- (15) Sakai, H., Hara, H., Yuasa, M., Tsai, A. G., Takeoka, S., Tsuchida, E., and Intaglietta, M. (2000) Molecular dimensions of Hb-based O<sub>2</sub> carriers determine constriction of resistance arteries and hypertension in conscious hamster model. *Am. J. Physiol. (Heart Circ. Physiol.)* **279**, H908–H915.
- (16) Izumi, Y., Sakai, H., Hamada, K., Takeoka, S., Yamahata, T., Kato, R., Nishide, H., Tsuchida, E., and Kobayashi, K. (1996) Physiologic responses to exchange transfusion with hemoglobin vesicles as an artificial oxygen carrier in anesthetized rats: changes in mean arterial pressure and renal cortical tissue oxygen tension. *Circ. Care. Med.* **24**, 1869–1873.
- (17) Sakai, H., Takeoka, S., Park, S.-I., Kose, T., Izumi, Y., Yoshizu, A., Nishide, H., Kobayashi, K., and Tsuchida, E. (1997) Surface-modification of hemoglobin vesicles with poly(ethylene glycol) and effects on aggregation, viscosity, and blood flow during 90%-exchange transfusion in anesthetized rats. *Bioconjugate Chem.* **8**, 15–22.
- (18) Kyokane T., Norizumi, S., Taniai, H., Yamaguchi, T., Takeoka, S., Tsuchida, E., Naito, M., Ishimura, Y., and Suematsu, M. (2001) Carbon monoxide from heme catabolism protects against hepatobiliary dysfunction in endotoxin-treated rat liver. *Gastroenterology* **120**, 1227–1240.
- (19) Takeoka, S., Teramura, Y., Atoji, T., and Tsuchida, E. (2002) Effect of Hb-encapsulation with vesicles on H<sub>2</sub>O<sub>2</sub> reaction and lipid peroxidation. *Bioconjugate Chem.* **13**, 1302–1308.
- (20) Nagababu, E., Ramasamy, S., Rifkind, J. M., Jia, Y., and Alayash, A. I. (2002) Site-specific cross-linking of human and bovine hemoglobins differentially alters oxygen binding and redox side reactions producing rhombic heme and heme degradation. *Biochemistry* **41**, 7407–7415.
- (21) Chang, T. M. S. (2003) Future generations of red blood cells substitutes. *J. Intern. Med.* **253**, 527–535.
- (22) Takahashi, A. (1995) Characterization of neo red cells (NRCs), their function and safety in vivo tests. *Artif. Cells Blood Substitutes Immobilization Biotechnol.* **23**, 347–354.
- (23) Lee, R., Neya, K., Svizzero, T. A., and Vlahakes, G. J. (1995) Limitations of the efficacy of hemoglobin-based oxygen carrying solutions. *J. Appl. Physiol.* **79**, 236–242.
- (24) Faivre, B., Menu, P., Labrude, P., and Vigneron, C. (1998) Hemoglobin Autoxidation/oxidation mechanism and methemoglobin prevention or reduction processes in the bloodstream. *Artif. Cells Blood Substitutes Immobilization Biotechnol.* **26**, 17–26.
- (25) Yamamoto, Y., Brodsky, M. H., Baker, J. C., and Ames, B. N. (1987) Detection and characterization of lipid hydroperoxides at picomole levels by high-performance liquid chromatography. *Anal. Biochem.* **160**, 7–13.
- (26) Takeoka, S., Ohgushi, T., Terasa, K., Ohmori, T., and Tsuchida, E. (1996) Layer-controlled hemoglobin vesicles by interaction of hemoglobin with a phospholipid assembly. *Langmuir* **12**, 1755–1759.
- (27) Sakai, H., Takeoka, S., Yokohama, H., Seino, Y., Nishide, H., and Tsuchida, E. (1993) Purification of concentrated hemoglobin using organic solvent and heat treatment. *Protein Expr. Purif.* **4**, 563–569.
- (28) Sou, K., Naito, Y., Endo, T., Takeoka, S., and Tsuchida, E. (2003) Effective encapsulation of proteins into size-controlled phospholipid vesicles using freeze-thawing and extrusion. *Biotechnol. Prog.* **19**, 1547–1552.
- (29) Bordier, C. (1981) Phase separation of integral membrane proteins in Triton X-114 solution. *J. Biol. Chem.* **256**, 1604–1607.
- (30) Sakai, H., Hisamoto, S., Fukutomi, I., Sou, K., Takeoka, S., and Tsuchida, E. (2004) Detection of lipopolysaccharide in hemoglobin-vesicles by Limulus Amebocyte test with kinetic-turbidimetric gel clotting analysis and pretreatment of surfactant. *J. Pharm. Sci.*, in press.
- (31) McCord, J. M., and Fridovich, I. (1969). Superoxide dismutase. An enzymic function for erythrocuprein (hemocuprein). *J. Biol. Chem.* **244**, 6049–6055.
- (32) Levy, A., Zhang, L., and Rifkind, J. M. (1988) Hemoglobin: a source of superoxide radical under hypoxic conditions. *Oxy Radicals Mol. Biol. Pathol., Proc. Upjohn-UCLA Symp.*, 11–25.
- (33) Mansouri, A., and Winterhalter, H. (1973) Nonequivalence of chains in hemoglobin oxidation. *Biochemistry* **12**, 4946–4949.
- (34) Raetz, C. R. (1990) Biochemistry of endotoxins, *Annu. Rev. Biochem.* **59**, 129–170.
- (35) Wright, S. D., Ramos, R. A., Tobias, P. S., Ulevitch, R. J., and Mathison, J. C. (1990) CD14, a receptor for complexes of lipopolysaccharide (LPS) and LPS binding protein. *Science* **249**, 1431–1433.

BC0340619



# Evaluation of the Human Melanoma Targeting Properties of Radiolabeled $\alpha$ -Melanocyte Stimulating Hormone Peptide Analogues

Yubin Miao,<sup>†,‡</sup> Donna Whitener,<sup>†</sup> Weiwei Feng,<sup>†,||</sup> Nellie K. Owen,<sup>§</sup> Jianqing Chen,<sup>†,||</sup> and Thomas P. Quinn<sup>\*,†,‡</sup>

Departments of Biochemistry, Radiology, and Internal Medicine, University of Missouri—Columbia, Columbia, Missouri 65211, and Harry S. Truman Memorial Veterans Hospital, Columbia, Missouri 65201. Received May 5, 2003; Revised Manuscript Received August 20, 2003

The purpose of this study was to evaluate the human MC1 receptor-mediated melanoma targeting properties of two metal cyclized  $\alpha$ -MSH peptide analogues,  $^{188}\text{Re}-(\text{Arg}^{11})\text{CCMSH}$  and  $^{188}\text{Re}\text{-CCMSH}$ . Initially, the presence and density of the MC1 receptor were determined on a bank of human melanoma cell lines. All eight human melanoma cell lines tested in this study displayed the MC1 receptor at a density of 900 to 5700 receptors per cell. Receptor affinity and biodistribution properties of  $^{188}\text{Re}-(\text{Arg}^{11})\text{CCMSH}$  and  $^{188}\text{Re}\text{-CCMSH}$  were evaluated in a cultured TXM13 human melanoma-xenografted Scid mouse model. Biodistribution results demonstrated that  $3.06 \pm 0.68\%$  ID/g of  $^{188}\text{Re}-(\text{Arg}^{11})\text{CCMSH}$  accumulated in the tumors 1 h postinjection and greater than 65% of the activity at 1 h postinjection remained in the tumors at 4 h after dose administration. Whole body clearance of  $^{188}\text{Re}-(\text{Arg}^{11})\text{CCMSH}$  was very rapid, with approximately 82% of injected dose cleared through urinary system at 4 h postinjection. There was very little activity in blood and major organs such as liver, lung, and muscle except for the kidney.  $^{188}\text{Re}\text{-CCMSH}$  exhibited similar tumor uptake and retention in TXM13 human melanoma-xenografted Scid mice as  $^{188}\text{Re}-(\text{Arg}^{11})\text{CCMSH}$ . However, the kidney uptake value of  $^{188}\text{Re}\text{-CCMSH}$  was two times higher than that of  $^{188}\text{Re}-(\text{Arg}^{11})\text{CCMSH}$ . The results of this study indicate that the MC1 receptor is present on the surface of a large number of human melanoma cells, which makes the MC1 receptor a good imaging or therapeutic target. Moreover, the biodistribution properties of  $^{188}\text{Re}-(\text{Arg}^{11})\text{CCMSH}$  and  $^{188}\text{Re}\text{-CCMSH}$  highlight their potential as therapeutic agents for human melanoma.

## INTRODUCTION

Malignant melanoma has become a serious public health problem due to its increase in incidence (1). In 2001, it was estimated that there were 51 400 cases of malignant melanoma newly reported and 7800 fatalities in the United States (1). It is estimated that more than 1.3% of Americans will develop malignant melanoma during their lifetimes (2). Moreover, metastatic melanoma deposits are difficult to discover and are resistant to conventional chemotherapy and external beam radiation therapy (2). Therefore, there is a great need to develop novel treatment approaches for metastatic melanoma.

Radiolabeled antibodies and antibody fragments have been investigated extensively to target melanoma and its metastases (3–5). However, their success has been limited because of the intrinsic limitations of radiolabeled antibodies and antibody fragments, such as slow circulation clearance (6, 7) and reduced rates of tumor penetra-

tion (8, 9). Recently,  $^{123}\text{I}$ -labeled *N*-(2-diethylaminoethyl)-4-iodobenzamide ( $^{123}\text{I}$ ]BZA) and *N*-(2-diethylaminoethyl)-3-iodo-4-methoxybenzamide ( $^{123}\text{I}$ ]IMBA) have exhibited high tumor uptake value ranging from 5 to 20 %ID/g in B16 tumor model (10, 11). However, their clinical application may be impeded due to the disadvantages of iodine-123, such as routine availability and high cost. More promising results were obtained with  $^{131}\text{I}$ -labeled *N*-(2-diethylaminoethyl)benzamide derivatives (12). In comparison with  $^{123}\text{I}$ ]BZA and  $^{123}\text{I}$ ]IMBA, superior tumor uptake and retention of (4-acetamido-*N*-(2-diethylaminoethyl)-5- $^{131}\text{I}$ ]iodo-2-methoxybenzamide) provided considerable potential for melanoma imaging and radionuclide therapy. However, the high liver uptake (9.86 %ID/g at 6 h pi) and slow clearance (3.72 %ID/g at 24 h pi) might limit its therapeutic application.

Another class of promising agents for melanoma imaging and therapy are  $\alpha$ -melanocyte stimulating hormone ( $\alpha$ -MSH) peptide analogues. Wild-type  $\alpha$ -MSH is a small tridecapeptide (Ac-Ser<sup>1</sup>-Tyr<sup>2</sup>-Ser<sup>3</sup>-Met<sup>4</sup>-Glu<sup>5</sup>-His<sup>6</sup>-Phe<sup>7</sup>-Arg<sup>8</sup>-Trp<sup>9</sup>-Gly<sup>10</sup>-Lys<sup>11</sup>-Pro<sup>12</sup>-Val<sup>13</sup>-NH<sub>2</sub>), which is involved in the control of skin pigmentation. The biological activity of  $\alpha$ -MSH is mediated through interactions with the melanocortin 1 (MC1) receptor (13). The melanocortin receptors belong to the superfamily of G-protein-coupled receptors (GPCRs). At the present time, five melanocortin receptors, namely MC1 receptor to MC5 receptor, have been identified and cloned (37–43). The MC1 receptor is mainly expressed in melanocytes and leukocytes and involved in skin pigmentation and animal coat coloration (13, 37, 44). The MC2 receptor has been found in the

\* Corresponding author: Thomas P. Quinn, 117 Schweitzer Hall, Department of Biochemistry, University of Missouri—Columbia, Columbia, MO 65211. Phone: (573) 882-6099; Fax: (573) 884-4812; E-mail: quinnt@missouri.edu.

<sup>†</sup> Department of Biochemistry, University of Missouri—Columbia.

<sup>‡</sup> Department of Radiology, University of Missouri—Columbia.

<sup>‡</sup> Department of Internal Medicine, University of Missouri—Columbia.

<sup>§</sup> Harry S Truman Memorial Veterans Hospital.

<sup>||</sup> Current address: Bracco Research USA, Princeton, NJ 08540.

adrenal gland and regulates glucocorticoneogenesis (37). The MC3 receptor and MC4 receptor have been identified in the brain for the control of feeding behavior and energy homeostasis (45). The MC5 receptor is expressed in a variety of peripheral tissues and participated in mediating exocrine gland function (46). Among the members of melanocortin receptors, the MC1 receptor has been the most widely studied (13–16, 44). The MC1 receptor has been identified both on human and mouse melanoma cells (14, 15). More than 80% of human metastatic melanoma tumor samples have been found to bear MC1 receptor (16). Nanomolar receptor affinity of  $\alpha$ -MSH and many of its analogues for the MC1 receptor make MC1 receptor an attractive target for the development of new melanoma targeting peptide pharmaceuticals.

Recently, several  $\alpha$ -MSH analogues have been examined for their abilities to target melanoma (17–20, 52–53). In our lab, a novel class of metal-cyclized  $\alpha$ -MSH analogues has been developed for melanoma imaging and therapy (21–23). Three cysteine were introduced into the amino acid sequence of CCMSH (Ac-Cys<sup>3</sup>-Cys<sup>4</sup>-Glu<sup>5</sup>-His<sup>6</sup>-D-Phe<sup>7</sup>-Arg<sup>8</sup>-Trp<sup>9</sup>-Cys<sup>10</sup>-Lys<sup>11</sup>-Pro<sup>12</sup>-Val<sup>13</sup>-NH<sub>2</sub>) to site-specifically coordinated radiometals such as <sup>99m</sup>Tc and <sup>188</sup>Re. Peptide cyclization with <sup>99m</sup>Tc and <sup>188</sup>Re made the molecules resistant to chemical and proteolytic degradation in vivo while retaining high bioactivities (22, 23). Both <sup>99m</sup>Tc-CCMSH and <sup>188</sup>Re-CCMSH exhibited excellent tumor uptake and retention and rapid whole body clearance in B16/F1 murine melanoma bearing C57 mice (22, 23). However, the presence of nonspecific kidney activity associated with <sup>188</sup>Re-CCMSH administration indicated that nephrotoxicity might be a problem with high doses used in melanoma therapy trials. Therefore two strategies, chemical modification of the peptide and amino acid coinfusion, were investigated to reduce renal uptake of <sup>188</sup>Re-CCMSH in our previous report (23). The substitution of Lys at 11th position of <sup>188</sup>Re-CCMSH with Arg yielded <sup>188</sup>Re-(Arg<sup>11</sup>)CCMSH, which possessed superior tumor uptake and lower renal activity accumulation in B16/F1 murine melanoma bearing C57 mice. The renal uptake value of <sup>188</sup>Re-CCMSH was significantly decreased by amino acid coinfusion as well (approximately 50%); however, the tumor/kidney ratio of <sup>188</sup>Re-(Arg<sup>11</sup>)CCMSH was higher than that of <sup>188</sup>Re-CCMSH with amino acid coinfusion (23). The superior tumor uptake and lower kidney accumulation of <sup>188</sup>Re-(Arg<sup>11</sup>)CCMSH greatly enhanced its potential as a melanoma therapeutic agent.

The receptor binding characteristics and in vivo biodistribution properties of radiolabeled  $\alpha$ -MSH peptides are most often analyzed in the murine melanoma B16 series of cell lines and in the C57–B16/F1 syngenic murine melanoma mouse model (48, 57). However, if radiolabeled  $\alpha$ -MSH peptides are to be effective in melanoma imaging and therapy, they must be able to bind a wide variety of human melanoma cells and show favorable biodistribution properties in human melanoma xenografts. Differences between the human and murine MC1 receptor, tumor morphology, and physiology could have a significant impact on the imaging and therapeutic potential of radiolabeled MSH peptide analogues. In this study, the prevalence of the MC1 receptor on human melanoma was determined in a bank of human melanoma cell lines. The tumor targeting properties of two <sup>188</sup>Re cyclized  $\alpha$ -MSH peptide analogues, namely <sup>188</sup>Re-(Arg<sup>11</sup>)CCMSH and <sup>188</sup>Re-CCMSH, were determined in a TXM13 human melanoma-xenografted, severely compromised immunodeficient (Scid) mouse model. The in vitro receptor binding affinities of (Arg<sup>11</sup>)CCMSH, CC-

MSH, and nonradioactive rhenium-conjugated Re-(Arg<sup>11</sup>)-CCMSH and Re-CCMSH in TXM13 human melanoma cells were examined by a competitive displacement cell binding assay using <sup>125</sup>I-Tyr<sup>2</sup>-NDP ([Nle<sup>4</sup>, D-Phe<sup>7</sup>] $\alpha$ -MSH). Pharmacokinetic properties of <sup>188</sup>Re-(Arg<sup>11</sup>)CCMSH and <sup>188</sup>Re-CCMSH were determined in TXM13 human melanoma-xenografted Scid mice to evaluate their potential for human melanoma therapy. Results presented in this study demonstrated that both <sup>188</sup>Re-(Arg<sup>11</sup>)CCMSH and <sup>188</sup>Re-CCMSH exhibited substantial tumor uptake and good retention in TXM13 human melanoma-xenografted Scid mice, which highlighted their potential as therapeutic agents for human melanoma.

## MATERIALS AND METHODS

**Chemicals and Reagents.** Amino acids and resin were purchased from Advanced ChemTech Inc (Louisville, KY). <sup>188</sup>ReO<sub>4</sub><sup>-</sup> was obtained from a <sup>188</sup>W/<sup>188</sup>Re generator from Oak Ridge National Laboratory. All chemicals used in this study were purchased from Fischer Scientific and used without further purification. The human melanoma cell lines were obtained from National Cancer Institute except for the TXM13 cell line was supplied by Dr. Isaiah J. Fidler and Dr. Janet Price from the Cell Biology Department, University of Texas M. D. Anderson Cancer Center.

**MC1 Receptor Quantitation Assay.** The  $B_{\max}$  of the human melanoma cell lines were determined by a method previously described (23). Briefly,  $1 \times 10^6$  human melanoma cells were incubated at 37 °C for 1.5 h in the presence of an increasing concentration of <sup>125</sup>I-(Tyr<sup>2</sup>)-NDP (1.56 nCi to 200 nCi) in 0.5 mL of binding media (MEM with 25 mM HEPES, pH 7.4, 0.2% BSA, 0.3 mM 1,10-phenanthroline). The reaction media was aspirated after incubation. Cells were rinsed with 0.5 mL of ice-cold pH 7.4, 0.2% BSA/0.01 M PBS three times. The activity in cells was measured in a NaI well counter. Nonspecific binding was determined by incubating cells and <sup>125</sup>I-(Tyr<sup>2</sup>)-NDP with nonradioactive NDP at a final concentration of 10  $\mu$ M. Scatchard plots were obtained by plotting the ratio of specific binding to free <sup>125</sup>I-Tyr<sup>2</sup>-NDP vs concentration of specific binding (fmole/million cells). The  $B_{\max}$  was the X intercept of linear regression line.

**Peptide Purification.** High performance liquid chromatography (HPLC) analysis was performed on an ISCO system (Lincoln, NE) equipped with absorption detector and Packard radiometric detector (Meriden, CT). Water containing 5 mM hydrogen chloride and acetonitrile were used as HPLC solvents A and B, respectively. A C-18 reverse phase column (218TP54, Vydac, Hesperia, CA) was used to purify <sup>188</sup>Re conjugates with a flow rate of 1.0 mL/min. A 20-min gradient of 18–28% acetonitrile in H<sub>2</sub>O/5 mM HCl was used for radiolabeled peptide purification.

**Preparation of <sup>188</sup>Re-Labeled  $\alpha$ -MSH Peptides.** The  $\alpha$ -MSH peptide analogues, CCMSH and (Arg<sup>11</sup>)-CCMSH, were synthesized by using Fmoc chemistry on amide resin with a Synergy 432A desktop solid-phase peptide synthesizer (Applied Biosystems, Foster City, CA) as previously described (23). The peptides were deprotected, cleaved from the resin, and purified by RP-HPLC. The identities of peptides were confirmed by electrospray ionization mass spectrometry (Mass Consortium Corp., San Diego, CA).

Radiolabeling of <sup>188</sup>Re- $\alpha$ -MSH peptides was accomplished by a method previously described (23). Briefly, 200  $\mu$ L of 6 mg/mL SnCl<sub>2</sub> in an aqueous 0.2 M sodium glucoheptonate solution and 200  $\mu$ L of fresh <sup>188</sup>ReO<sub>4</sub><sup>-</sup>

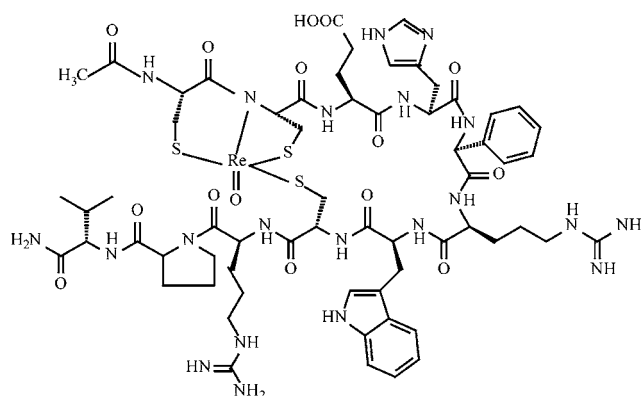
eluant (1–4 mCi) were added into a reaction vial. The mixture was incubated at 75 °C for 30 min. Ten microliters of a 1 mg/mL peptide solution were added into the mixture. After being adjusted to pH 8.5 with 1 N NaOH, the resulting solution was incubated at 75 °C for 30 min. The radiolabeled peptide was purified to single species by RP-HPLC. Purified peptide samples were purged with N<sub>2</sub> gas for 20 min to remove the acetonitrile. The pH of final solution was adjusted to 5 with 0.1 N NaOH and normal saline for animal studies. Quality controls were performed by RP-HPLC (Figure 3).

**Competitive Binding Assay.** The IC<sub>50</sub> values for the  $\alpha$ -MSH peptide analogues were determined by competitive binding assays with <sup>125</sup>I-Tyr<sup>2</sup>-NDP (Amersham Pharmacia Biotech, UK) in TXM13 human melanoma cells. Briefly, TXM13 cells were harvested from the culture flasks with a 0.02% EDTA solution, seeded into a 24-well cell culture plate (5 × 10<sup>5</sup>/well), and incubated at 37 °C overnight. After being washed once with binding media (MEM with 25 mM HEPES, pH 7.4, 0.2% BSA, 0.3 mM 1,10-phenanthroline), the cells were incubated at 37 °C for 2 h with approximately 100 000 cpm of <sup>125</sup>I-Tyr<sup>2</sup>-NDP in the presence of increasing concentrations of  $\alpha$ -MSH analogues in 0.3 mL of binding media. The reaction media was aspirated after incubation. Cells were rinsed with 0.5 mL of ice-cold pH 7.4, 0.2% BSA/0.01 M PBS twice and lysed in 0.5 mL of 1 N NaOH for 5 min. The activity in cells was measured in a NaI well counter. The competitive binding curves were obtained by plotting the percentage of <sup>125</sup>I-Tyr<sup>2</sup>-NDP bound to cells vs concentrations of displacing peptides. The IC<sub>50</sub> values for the peptides were calculated by using the Graft software (Erithacus Software Limited, UK).

**In Vivo Pharmacokinetics Studies.** The pharmacokinetics of <sup>188</sup>Re-CCMSH and <sup>188</sup>Re-(Arg<sup>11</sup>)CCMSH were performed in TXM13 human melanoma-xenografted Scid female mice (Harlan, Indianapolis, IN). The Scid mice were housed in sterile microisolator cages in a temperature and humidity-controlled room. The animals were fed with autoclaved food and water for a week prior to the tumor cell inoculation. The Scid mice were inoculated subcutaneously with 5 × 10<sup>6</sup> TXM13 human melanoma cells in the both flanks. After four weeks, when the weight of tumors reached approximately 0.3 g, 3–8  $\mu$ Ci of <sup>188</sup>Re-labeled peptide was injected into each mouse through the tail vein for in vivo pharmacokinetics studies. Groups of five mice per each time point were used for the biodistribution studies. The mice were sacrificed at 1, 4, and 24 h postinjection, and tumors and organs of interest were harvested, weighed, and counted. Blood values were taken as 6.5% of the whole body weight. The results were expressed as percent injected dose/gram (%ID/g) and as percent injected dose (%ID). All the animal studies were conducted in compliance with Institutional Animal Care and Committee Approval. Statistical analysis was performed using the Student's *t*-test for unpaired data. A 95% confidence level was chosen to determine the significance between compounds, with *p* < 0.05 being significantly different.

## RESULTS AND DISCUSSION

A bank of human melanoma cell lines were examined for presence and number of MC1 receptors. The human melanoma cell lines were derived from metastatic deposits from various organs as well as from primary tumors that were either producing melanin (melanonic) or not melanin producing (amelanonic). All of the human melanoma cell lines displayed MC1 receptors. The recep-



**Figure 1.** Structure of Re-(Arg<sup>11</sup>)CCMSH; Ac-Cys-Cys-Glu-His-D-Phe-Arg-Trp-Cys-Arg-Pro-Val-NH<sub>2</sub>.

**Table 1.** MC1 Receptor Numbers on Human Melanoma Cells

cell line	receptor number (sites/cell)
TXM13	5700
UACC62	1000
M14	1500
SKMEL5	1000
SKMEL28	900
3M	5000
UACC257	2800
LOX	1000

tor numbers ranged from 900 to 5700 receptors per cell (Table 1). There was no correlation between the experimentally determined receptor number and melanonic state of the cells or the location of the original isolate. All of the human melanoma cell lines exhibited 1.4–8 times fewer receptor numbers per cell than the murine B16/F1 cell line. These results suggest that in general human melanoma cells have fewer MC1 receptors than the B16/F1 murine melanoma cell line. Lower MC1 receptor numbers may translate into lower melanoma tumor uptake of radiolabeled  $\alpha$ -MSH peptide analogues in vivo and certainly highlight the need to produce and administer high specific activity preparations for imaging and therapy.

The biodistribution and tumor targeting properties of two <sup>188</sup>Re-cyclized  $\alpha$ -MSH peptide analogues (<sup>188</sup>Re-(Arg<sup>11</sup>)CCMSH and <sup>188</sup>Re-CCMSH) were determined in the TXM13 human melanoma-xenografted Scid mice. The TXM13 human melanoma xenograft model is robust and well characterized for tumor establishment and metastatic potential, making it attractive for biodistribution analyses as well as future therapy studies (47). Initially, the binding affinities of the Re-cyclized and apo  $\alpha$ -MSH peptide analogues were examined in cultured TXM-13 human melanoma cells. The  $\alpha$ -MSH peptide analogues, namely CCMSH, (Arg<sup>11</sup>)CCMSH, Re-CCMSH and Re-(Arg<sup>11</sup>)CCMSH were synthesized and purified by RP-HPLC, and the identities of peptides were confirmed by electrospray ionization mass spectrometry. An illustration of the Re-(Arg<sup>11</sup>)CCMSH structure is shown in Figure 1. Results from in vitro competitive binding assay of peptides performed in TXM13 human melanoma cells revealed that both the peptides with or without nonradioactive rhenium cyclization bound to the human melanoma cells with nanomolar range affinities (Figure 2). The introduction of the ReO core in the peptide sequence slightly decreased the binding affinity of the peptide (Table 2). A list of the peptide sequences, IC<sub>50</sub> values, and molecular weights of CCMSH, (Arg<sup>11</sup>)CCMSH, and their Re-cyclized derivatives is presented in Table 2. The

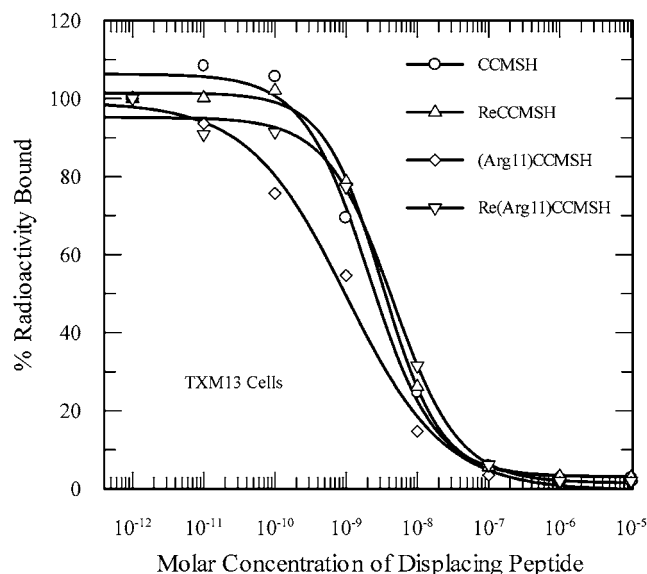


**Table 2. Molecular Weights (MW), Sequences, and IC<sub>50</sub> Values of  $\alpha$ -MSH Peptide Analogues**

peptide	sequence	IC <sub>50</sub> (nM)	calcd MW	measured MW
CCMSH	Ac-CCEHdFRWCKPV-NH <sub>2</sub>	2.1	1448.7	1448
ReCCMSH	Ac-(ReO)CCEHdFRWCKPV-NH <sub>2</sub>	3.2	1646.9	1648
(Arg <sup>11</sup> )CCMSH	Ac-CCEHdFRWCRPV-NH <sub>2</sub>	1.0	1476.7	1476
Re(Arg <sup>11</sup> )CCMSH	Ac-(ReO)CCEHdFRWCRPV-NH <sub>2</sub>	4.4	1674.9	1676
NDP	Ac-SYSNleEHdFRWGKPV-NH <sub>2</sub>	0.21 <sup>a</sup>	1647 <sup>a</sup>	1647 <sup>a</sup>
<sup>125</sup> I-Tyr <sup>2</sup> -NDP	Ac-S( <sup>125</sup> I)YSNleEHdFRWGKPV-NH <sub>2</sub>	ND <sup>b</sup>	1772 <sup>b</sup>	ND <sup>b</sup>

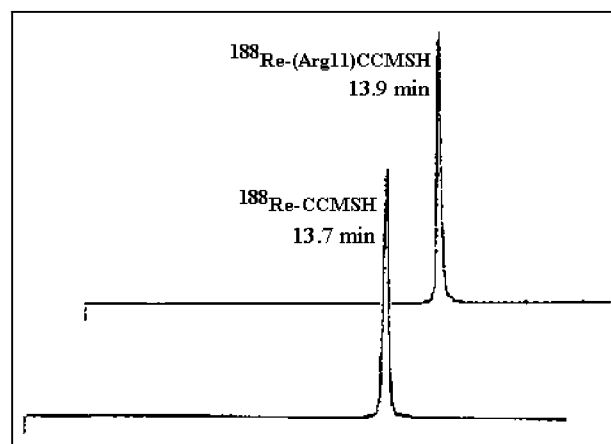
<sup>a</sup> Data cited from Chen, J. Q., et al. (2000) *Cancer Res.* 60, 5649–5658. The IC<sub>50</sub> was determined in B16/F1 murine melanoma cells.

<sup>b</sup> ND, data not determined.

**Figure 2.** Competitive binding curves of CCMSH, Re-CCMSH, (Arg<sup>11</sup>)CCMSH, and Re-(Arg<sup>11</sup>)CCMSH in TXM13 human melanoma cells.

low nanomolar binding affinities of the  $\alpha$ -MSH peptide analogues for the human MC1 receptors on the TXM-13 cells were similar to the affinity values determined for the murine MC1 receptor on B16/F1 cells. Similarity in ligand affinities between the human and mouse MC1 receptors was consistent with their shared amino acid identity of 75% (37). However, sequence alignments also revealed gaps and stretches of nonconservative amino acid substitutions that could result in ligand selectivity difference between the two receptors.

The pharmacokinetics and tumor targeting properties of <sup>188</sup>Re-(Arg<sup>11</sup>)CCMSH and <sup>188</sup>Re-CCMSH were determined in TXM13 human melanoma-xenografted Scid mice. CCMSH and (Arg<sup>11</sup>)CCMSH were labeled with <sup>188</sup>Re through a glucoheptonate transchelation reaction, using stannous chloride as a reducing agent. <sup>188</sup>Re-CCMSH and <sup>188</sup>Re-(Arg<sup>11</sup>)CCMSH were separated completely from their nonlabeled counterparts by RP-HPLC. Quality control of the purified <sup>188</sup>Re-CCMSH and <sup>188</sup>Re-(Arg<sup>11</sup>)CCMSH for animal studies was performed by RP-HPLC (Figure 3). The biodistribution of <sup>188</sup>Re-CCMSH and <sup>188</sup>Re-(Arg<sup>11</sup>)CCMSH in TXM13 tumor-bearing Scid mice at 1 h, 4 h, and 24 h postinjection is shown in Table 3. Substantial tumor uptake of <sup>188</sup>Re-(Arg<sup>11</sup>)CCMSH was exhibited in TXM13 human melanoma-xenografted Scid mice. For example, there was  $3.06 \pm 0.68\%$  ID/g of <sup>188</sup>Re-(Arg<sup>11</sup>)CCMSH accumulated in the tumors 1 h after dose administration. Greater than 65% of the activity at 1 h postinjection remained in the tumors at 4 h after dose administration. Even 24 h later, there was  $0.93 \pm 0.49\%$  ID/g of <sup>188</sup>Re-(Arg<sup>11</sup>)CCMSH remaining in the tumors. The tumor uptake of <sup>188</sup>Re-(Arg<sup>11</sup>)CCMSH was similar to the tumor uptake values of <sup>111</sup>In-labeled bombesin (53)

**Figure 3.** HPLC quality control of <sup>188</sup>Re-CCMSH and <sup>188</sup>Re-(Arg<sup>11</sup>)CCMSH.

and minigastrin (54) evaluated in human tumor xenograft models. For example, <sup>111</sup>In-labeled bombesin and minigastrin exhibited up to 3.63 %ID/g and 5 %ID/g at 1 h postinjection (53, 54) compared to <sup>188</sup>Re-(Arg<sup>11</sup>)CCMSH that displayed 3.06 %ID/g at the same time point. The corresponding <sup>90</sup>Y-labeled bombesin and minigastrin analogues displayed therapeutic efficacy in their respective human tumor xenograft models (55, 56). It is expected that the uptake of <sup>188</sup>Re-(Arg<sup>11</sup>)CCMSH will be sufficient to show therapeutic effects in human melanoma-xenografted Scid mouse model.

Whole body clearance of <sup>188</sup>Re-(Arg<sup>11</sup>)CCMSH was very rapid, with approximately 82% of injected dose cleared through urinary system at 4 h postinjection. Greater than 98% of the injected dose was washed out of body by 24 h postinjection. There was very little activity in blood and major organs such as liver, lung, and muscle except for the kidneys. High tumor/blood and tumor/normal tissue uptake ratios were demonstrated as early as 1 h postinjection (Table 4). Although the majority of <sup>188</sup>Re-(Arg<sup>11</sup>)CCMSH in the kidneys cleared rapidly, there was still  $6.24 \pm 1.14\%$  ID/g of activity present in the kidneys at 4 h after injection. Hence, nephrotoxicity would likely be a dose-limiting factor if <sup>188</sup>Re-(Arg<sup>11</sup>)CCMSH was used for melanoma therapy trials. In comparison with <sup>188</sup>Re-(Arg<sup>11</sup>)CCMSH, <sup>188</sup>Re-CCMSH exhibited similar tumor uptake and retention properties. However, the kidney uptake value of <sup>188</sup>Re-CCMSH was two times higher than that of <sup>188</sup>Re-(Arg<sup>11</sup>)CCMSH at 1 h and 4 h postinjection, which would compromise its application for melanoma therapy. The biodistribution data of <sup>188</sup>Re-CCMSH demonstrated that whole body clearance of <sup>188</sup>Re-CCMSH was rapid as well. Approximately 91% of injected dose was washed out of body through urinary system at 4 h postinjection. Greater than 99% of the injected dose was cleared out of body by 24 h postinjection. The accumulation of <sup>188</sup>Re-CCMSH activity in blood and blood rich organs such liver and lung was similar to that of <sup>188</sup>Re-(Arg<sup>11</sup>)CCMSH. In contrast to <sup>188</sup>Re-CCMSH, slightly

**Table 3. Pharmacokinetics of  $^{188}\text{Re}$ -CCMSH and  $^{188}\text{Re}$ -(Arg $^{11}$ )CCMSH in TXM13 Human Melanoma-Xenografted Scid Mice<sup>a</sup>**

tissues	1 h		4 h		24 h	
	CCMSH	Arg $^{11}$ CCMSH	CCMSH	Arg $^{11}$ CCMSH	CCMSH	Arg $^{11}$ CCMSH
Percent Injected Dose/Gram						
tumor	1.98 $\pm$ 0.26	3.06 $\pm$ 0.68 <sup>b</sup>	2.20 $\pm$ 0.24	2.02 $\pm$ 0.27	0.87 $\pm$ 0.33	0.93 $\pm$ 0.49
brain	0.02 $\pm$ 0.04	0.07 $\pm$ 0.04	0.08 $\pm$ 0.09	0.02 $\pm$ 0.05	0.01 $\pm$ 0.01	0.07 $\pm$ 0.08
blood	0.43 $\pm$ 0.05	0.84 $\pm$ 0.32 <sup>b</sup>	0.01 $\pm$ 0.00	0.04 $\pm$ 0.05	0.04 $\pm$ 0.07	0.09 $\pm$ 0.11
heart	0.35 $\pm$ 0.34	0.74 $\pm$ 0.62	0.24 $\pm$ 0.17	0.20 $\pm$ 0.28	0.06 $\pm$ 0.09	0.11 $\pm$ 0.18
lung	0.90 $\pm$ 0.08	1.57 $\pm$ 0.65	0.16 $\pm$ 0.22	0.21 $\pm$ 0.13	0.06 $\pm$ 0.04	0.03 $\pm$ 0.03
liver	0.48 $\pm$ 0.02	0.83 $\pm$ 0.44	0.11 $\pm$ 0.04	0.37 $\pm$ 0.12 <sup>c</sup>	0.03 $\pm$ 0.01	0.04 $\pm$ 0.02
spleen	0.12 $\pm$ 0.14	0.30 $\pm$ 0.34	0.06 $\pm$ 0.06	0.25 $\pm$ 0.19 <sup>b</sup>	0.07 $\pm$ 0.10	0.09 $\pm$ 0.11
kidneys	19.92 $\pm$ 5.30	9.70 $\pm$ 3.69 <sup>b</sup>	12.56 $\pm$ 0.89	6.24 $\pm$ 1.14 <sup>d</sup>	0.39 $\pm$ 0.12	0.27 $\pm$ 0.06 <sup>b</sup>
muscle	0.07 $\pm$ 0.08	0.16 $\pm$ 0.19	0.04 $\pm$ 0.04	0.27 $\pm$ 0.22	0.02 $\pm$ 0.04	0.06 $\pm$ 0.02
pancreas	0.18 $\pm$ 0.06	0.33 $\pm$ 0.24	0.13 $\pm$ 0.17	0.17 $\pm$ 0.10	0.01 $\pm$ 0.01	0.04 $\pm$ 0.03 <sup>b</sup>
Percent Injected Dose						
stomach	0.28 $\pm$ 0.05	0.46 $\pm$ 0.23	0.16 $\pm$ 0.14	0.52 $\pm$ 0.46	0.02 $\pm$ 0.01	0.04 $\pm$ 0.03
intestines	3.71 $\pm$ 0.49	7.47 $\pm$ 1.36	3.51 $\pm$ 1.52	10.98 $\pm$ 2.21	0.08 $\pm$ 0.03	0.19 $\pm$ 0.08
urine	83.24 $\pm$ 1.28	74.30 $\pm$ 5.86	91.03 $\pm$ 2.30	82.51 $\pm$ 3.02	99.51 $\pm$ 0.06	98.83 $\pm$ 0.54

<sup>a</sup> The data are presented as percent injected dose/gram or as percent injected dose (mean  $\pm$  SD,  $n = 5$ ). <sup>b</sup> 0.05 >  $P$  > 0.01. <sup>c</sup> 0.01 >  $P$  > 0.001. <sup>d</sup> 0.001 >  $P$ .

**Table 4. The Tumor/normal Tissues Uptake Ratio of  $^{188}\text{Re}$ -CCMSH and  $^{188}\text{Re}$ -(Arg $^{11}$ )CCMSH in TXM13 Human Melanoma-Xenografted Scid Mice**

ratios	1 h		4 h		24 h	
	CCMSH	Arg $^{11}$ CCMSH	CCMSH	Arg $^{11}$ CCMSH	CCMSH	Arg $^{11}$ CCMSH
tumor/blood	4.60	3.64	220.00	50.50	21.75	10.33
tumor/kidney	0.10	0.32	0.18	0.32	2.23	3.44
tumor/lung	2.20	1.95	13.75	9.62	14.50	31.00
tumor/liver	4.13	3.69	20.00	5.46	29.00	23.25
tumor/muscle	28.29	19.13	55.00	7.48	43.50	15.50

more  $^{188}\text{Re}$ -(Arg $^{11}$ )CCMSH activity was excreted through GI system, indicating that the lipophilicity of  $^{188}\text{Re}$ -(Arg $^{11}$ )CCMSH was higher than that of  $^{188}\text{Re}$ -CCMSH. This hypothesis was consistent with HPLC results, in which  $^{188}\text{Re}$ -(Arg $^{11}$ )CCMSH exhibited a greater retention time than  $^{188}\text{Re}$ -CCMSH under the same reverse-phase elution gradient (Figure 3).

The tumor uptake of  $^{188}\text{Re}$ -CCMSH and  $^{188}\text{Re}$ -(Arg $^{11}$ )CCMSH were lower 1 h and 4 h postinjection in the TXM13 human melanoma-xenografted Scid mice than in the B16/F1 murine melanoma model (23). For example, the uptake of  $^{188}\text{Re}$ -CCMSH and  $^{188}\text{Re}$ -(Arg $^{11}$ )CCMSH in the B16/F1 murine melanoma mouse model was  $9.78 \pm 2.00$  %ID/g and  $16.37 \pm 3.27$  %ID/g at 4 h postinjection and  $1.94 \pm 0.47$  %ID/g and  $3.50 \pm 2.32$  %ID/g 24 h postinjection (23) compared to  $2.02 \pm 0.24$  %ID/g and  $2.20 \pm 0.27$  %ID/g at 4 h postinjection and  $0.87 \pm 0.33$  %ID/g and  $0.93 \pm 0.49$  %ID/g 24 h postinjection in the TXM13 human melanoma xenograft model. The significant tumor uptake value difference between B16/F1 murine melanoma and TXM13 human melanoma models were attributed to MC1 receptor density and the in vivo behavior differences between two cell lines. In this report, it was shown that the MC1 receptor density on human melanoma cells, including TXM13, was lower than that of B16/F1 cells. Moreover, based on the histopathological results showed in our previous report, TXM13 cells formed amelanonic solid tumors with extensive necrotic centers as opposed to the nonnecrotic gelatinous composition of B16/F1 murine melanoma tumors (22). Differences in tumor morphology could significantly affect the tumor uptake of radioactivity on a per gram basis. Necrotic centers present in the TXM13 human melanoma tumors contribute to the total mass of the tumors but contain few viable melanoma cells capable of  $^{188}\text{Re}$ -CCMSH and  $^{188}\text{Re}$ -(Arg $^{11}$ )CCMSH uptake. Rhenium-188-CCMSH uptake is likely to be localized to rapidly proliferating melanoma cells located around the surface of the TXM13

human melanoma tumors (22). Therefore, the overall percent activity per gram of TXM13 human melanoma tumors is reduced when compared to B16/F1 murine melanoma tumors that lack significant necrotic regions and are almost entirely composed of viable melanoma cells capable of rhenium-188-CCMSH uptake.

Numerous  $\alpha$ -MSH analogues, based on the high affinity NDP sequence [Nle $^4$ ,D-Phe $^7$ ]- $\alpha$ -MSH, have been synthesized and characterized as tumor targeting agents (18–20, 50). NDP radiolabeled with  $^{125}\text{I}$  or  $^{18}\text{F}$  exhibited high receptor affinities in vitro and rapid pharmacokinetics in vivo; however, they did not display high tumor uptake and retention (20, 50). Recently, Froidevaux et al. (51, 52) described the characterization of a novel 8 amino acid DOTA-conjugated MSH analogue, DOTA-MSH $_{(\text{oct})}$ , that was based on the high affinity NDP MSH sequence. Indium-111-labeled DOTA-MSH $_{(\text{oct})}$  displayed rapid pharmacokinetics and good tumor uptake, highlighting its melanoma imaging potential. Tumor uptake values were  $4.31 \pm 0.30$  %ID/g at 4 h and  $1.17 \pm 0.13$  %ID/g 24 h postinjection in the B16/F1 murine melanoma mouse model (52). Murine melanoma uptake of  $^{111}\text{In}$ -DOTA-MSH $_{(\text{oct})}$  was 2 times and 1.2 times greater than  $^{188}\text{Re}$ -(Arg $^{11}$ )CCMSH in human melanoma at 4 and 24 h postinjection. This difference was expected since we routinely see a 5–10-fold reduction in xenografted human melanoma compared to B16/F1 murine melanoma tumors. No characterization of  $^{111}\text{In}$ -DOTA-MSH $_{(\text{oct})}$  was reported for a human melanoma-xenografted model making direct biodistribution comparisons difficult. However, a comparison of  $^{111}\text{In}$ -DOTA-MSH $_{(\text{oct})}$  with  $^{111}\text{In}$ -DOTA-ReCCMSH(Arg $^{11}$ ) in the B16/F1 murine melanoma mouse model showed that  $^{111}\text{In}$ -DOTA-ReCCMSH(Arg $^{11}$ ) displayed 4 times the tumor uptake 4 h and 7 times the uptake of  $^{111}\text{In}$ -DOTA-MSH $_{(\text{oct})}$  at 24 h postinjection (49). Moreover, the kidney uptake of  $^{111}\text{In}$ -DOTA-ReCCMSH(Arg $^{11}$ ) was 1.8 and 1.2 times less than  $^{111}\text{In}$ -DOTA-MSH $_{(\text{oct})}$  at 4 h and 24 h postinjection (49). Although  $^{111}\text{In}$ -

DOTA-MSH<sub>(oct)</sub> exhibited high affinity for the MC1 receptor, it may be cleared too rapidly from the blood stream for optimal tumor uptake.

Nonspecific kidney accumulation is a common problem associated with radiolabeled peptide and small protein administration (24–26). Cationic peptides and proteins bind to the negatively charged surface of tubule cells via electrostatic interaction when they are generally filtered in the glomerulus and reabsorbed in the cells of the proximal tubule (24). Therefore, two strategies of chemical modification of the molecule and basic amino acid coinfusion have been employed to decrease renal accumulation by masking the electrostatic interaction between molecule and the surface of tubular cells (24–31). For instance, Kim and Kobayashi et al. reported the use of 2,3,5,6-tetrafluorophenyl (TFP)-glycolate to neutralize the positive charges and lower the isoelectric point of anti-Tac disulfide-bonded variable region single-chain Fv fragments (dsFv) and humanized anti-Tac Fab fragments. Their findings indicated that neutralizing the positive charges decreased the kidney accumulation of the glycolated conjugates without impairing their tumor uptake (32–35). Recently, Akizawa et al. investigated the effect of molecular charges on renal uptake of <sup>111</sup>In-DTPA-conjugated peptide by substitution of the N-terminal D-phenylalanine of <sup>111</sup>In-DTPA-D-Phe<sup>1</sup>-Octreotide with L-aspartic acid, L-lysine, L-methionine, and L-phenylalanine. They found that the net charges of <sup>111</sup>In-DTPA-D-Phe<sup>1</sup>-Octreotide derivatives significantly affected their kidney uptake. The strategy of increasing negative charges in peptide molecules might be used to decrease the renal uptake of <sup>111</sup>In-DTPA-conjugated low molecular weight peptides (36). An analysis of biodistribution comparison of <sup>188</sup>Re-CCMSH and <sup>188</sup>Re-(Arg<sup>11</sup>)-CCMSH in this work revealed that the charge distribution of peptide molecule might be another important factor, which affected the renal uptake of peptide. Theoretically, the positive charge of Arg is same as Lys; however, the positive charge distribution is different between the Arg guanidinium group and Lys primary amine. The biodistribution data demonstrated that the kidney uptake value of <sup>188</sup>Re-(Arg<sup>11</sup>)-CCMSH was approximately 50% of that of <sup>188</sup>Re-CCMSH 1 h and 4 h postinjection. Moreover, coinfusion of positively charged amino acids reduced the kidney retention of <sup>188</sup>Re-CCMSH by more than 50% while only reducing that of <sup>188</sup>Re-(Arg<sup>11</sup>)-CCMSH by 40% in our previous report (23). This supports the assertion that difference in charge distribution on the side chain greatly influences nonspecific charge–charge interaction and could be responsible for reduced kidney retention of <sup>188</sup>Re-(Arg<sup>11</sup>)-CCMSH. Arg at 11th position of CCMSH peptide sequence played a critical role in decreasing the renal uptake value of <sup>188</sup>Re-labeled CCMSH peptide analogues. The coinfusion of basic amino acid or amino acids combination, such as L-lysine, L-arginine, D-lysine, and combination of L-lysine and L-arginine, have been proved to be effective in decreasing the renal uptake of radiolabeled peptides and antibodies (24–31). It was also clearly demonstrated by our previous report that L-lysine coinjection could significantly decrease the renal uptake of <sup>188</sup>Re-CCMSH and <sup>188</sup>Re-(Arg<sup>11</sup>)-CCMSH in B16/F1 murine melanoma bearing C57 mice (23). Hence, the strategy of L-lysine coinfusion could potentially be employed to enhance the therapeutic efficacy of <sup>188</sup>Re-(Arg<sup>11</sup>)-CCMSH by further decreasing the nephrotoxicity in human melanoma therapy trials.

In conclusion, all eight human melanoma cell lines tested in this study displayed the MC1 receptor. Bio-

distribution results demonstrated that both <sup>188</sup>Re-(Arg<sup>11</sup>)-CCMSH and <sup>188</sup>Re-CCMSH exhibited substantial tumor uptake and good retention, coupled with rapid whole body clearance in TXM13 human melanoma-xenografted Scid mice model. Human melanoma-targeting properties of <sup>188</sup>Re-(Arg<sup>11</sup>)-CCMSH and <sup>188</sup>Re-CCMSH accentuated their potential as therapeutic agents for human melanoma.

#### ACKNOWLEDGMENT

The authors would like to thank Drs. Wynn A. Volkert, Susan L. Deutscher, Silvia S. Jurisson, and Timothy J. Hoffman for their helpful discussion, and Gary L. Sieckman and Dana G. Mazuru for their technical assistance. This work was supported by a grant (ER61661) from the Department of Energy (to T.P.Q.) and a grant from the University of Missouri Life Science Mission Enhancement Postdoctoral Fellowship (to Y.M.).

#### LITERATURE CITED

- (1) Greenlee, R. T., Hill-Harmon, M. B., Murray, T., and Thun, M. (2001) Cancer statistics, 2001. *CA Cancer J. Clin.* 51, 15–36.
- (2) Marghood, A. A., Slade, J., Salopek, T. G., Kopf, A. W., Bart, R. S., and Rigel, D. S. (1995) Basal cell and squamous cell carcinomas are important risk factors for cutaneous malignant melanoma. *Cancer* 75, 707–714.
- (3) Larson, S. M., Brown, J. P., Wright, P. W., Carrasquillo, J. A., Hellstorm, I., and Hellstorm, K. E. (1983) Imaging of melanoma with I-131-labeled monoclonal antibodies. *J. Nucl. Med.* 24, 123–129.
- (4) Wahl, R. L., Swanson, N. A., Johnson, J. W., Natale, R., Petry, N. A., Mallette, S., Kasina, S., Reno, J., Sullivan, K., and Abrams, P. (1992) Clinical experience with Tc-99m labeled (N<sub>2</sub>S<sub>2</sub>) anti-melanoma antibody fragments and single photon emission computed tomography. *Am. J. Physiol. Imaging* 7, 48–58.
- (5) Loeffler, K. U., Brautigam, P., Simon, J. C., Althausen, S. R., Wuttig, C., and Witschel, H. (1996) Immunoscintigraphy for ocular melanoma: a reliable diagnostic technique? *Graefes Arch. Clin. Exp. Ophthalmol.* 234, 100–104.
- (6) Halpern, S. E., and Bartholomew, R. (1995) Pharmacokinetics of an indium-111-labeled IgG monoclonal antibody over a prolonged period. *Eur. J. Nucl. Med.* 22, 1323–1325.
- (7) Carrasquillo, J. A., Abrams, P. G., Schroff, R. W., Reynolds, J. C., Woodhouse, C. S., Morgan, A. C., Keenan, A. M., Foon, K. A., Perentesis, P., and Marshall, S. (1988) Effect of antibody dose on the imaging and biodistribution of In-111 9.2.27 anti-melanoma monoclonal antibody. *J. Nucl. Med.* 29, 39–47.
- (8) Kwok, C. S., Cole, S. E., and Liao, S. K. (1988) Uptake kinetics of monoclonal antibodies by human melanoma multicell spheroids. *Cancer Res.* 48, 1856–1863.
- (9) Ong, G. L., and Mattes, M. J. (1989) Penetration and binding of antibodies in experimental human solid tumors grown in mice. *Cancer Res.* 49, 4264–4273.
- (10) Nicholl, C., Mohammed, A., Hull, W. E., Bubeck, B., and Eisenhut, M. (1997) Pharmacokinetics of iodine-123-IMBA for melanoma imaging. *J. Nucl. Med.* 38, 127–133.
- (11) Mohammed, A., Nicholl, C., Titsch, U., and Eisenhut, M. (1997) Radioiodinated N-(alkylaminoalkyl)-substituted 4-methoxy-, 4-hydroxy-, and 4-aminobenzamide: Biological investigations for the improvement of melanoma-imaging agents. *Nucl. Med. Biol.* 24, 373–380.
- (12) Eisenhut, M., Hull, W. E., Mohammed, A., Mier, W., Lay, D., Just, W., Gorgas, K., Lehmann, W. D., and Haberkorn, U. (2000) Radioiodinated N-(2-diethylaminoethyl)benzamide derivatives with high melanoma uptake: Structure-affinity relationships, metabolic fate, and intracellular localization. *J. Med. Chem.* 43, 3913–3922.
- (13) Hruby, V. J., Sharma, S. D., Toth, K., Jaw, J. Y., Al-Obeidi, F., Sawyer, T. K., and Hadley, M. E. (1993) Design, synthesis,



- and conformation of superpotent and prolonged acting melanotropins. *Ann. N. Y. Acad. Sci.* 680, 51–63.
- (14) Tatro, J. B., and Reichlin, S. (1987) Specific receptors for alpha-melanocyte-stimulating hormone are widely distributed in tissues of rodents. *Endocrinology* 121, 1900–1907.
- (15) Siegrist, W., Solca, F., Stutz, S., Giuffrè, L., Carrel, S., Girard, J., and Eberle, A. N. (1989) Characterization of receptors for alpha-melanocyte-stimulating hormone on human melanoma cells. *Cancer Res.* 49, 6352–6358.
- (16) Tatro, J. B., Wen, Z., Entwistle, M. L., Atkins, M. B., Smith, T. J., Reichlin, S., and Murphy, J. R. (1992) Interaction on an  $\alpha$ -melanocyte stimulating hormone-diphtheria toxin fusion protein with melanotropin receptors in human metastases. *Cancer Res.* 52, 2545–2548.
- (17) Bard, D. R., Knight, C. G., and Page-Thomas, D. P. (1990) A chelating derivative of  $\alpha$ -melanocyte stimulating hormone as a potential imaging agent for malignant melanoma. *Br. J. Cancer* 62, 919–922.
- (18) Bagutti, C., Stolz, B., Albert, R., Bruns, C., Pless, J., and Eberle, A. N. (1994)  $^{111}\text{In}$ -DTPA-labeled analogues for alpha-melanocyte-stimulating hormone for melanoma targeting: receptor binding in vitro and in vivo. *Int. J. Cancer* 58, 740–755.
- (19) Wraight, E. P., Bard, D. R., Maughan, C. G., Knight, C. G., and Page-Thomas, D. P. (1992) The use of a chelating derivative of alpha-melanocyte stimulating hormone for the clinical imaging of malignant melanoma. *Br. J. Radiol.* 65, 112–118.
- (20) Vaidyanathan, G., and Zalutsky, M. R. (1997) Fluorine-18-labeled  $[\text{Nle}^4, \text{D-Phe}^7]\text{-}\alpha\text{-MSH}$ , an  $\alpha$ -melanocyte stimulating hormone analogue. *Nucl. Med. Biol.* 24, 171–178.
- (21) Giblin, M. F., Wang, N. N., Hoffman, T. J., Jurisson, S. S., and Quinn, T. P. (1998) Design and characterization of  $\alpha$ -melanotropin peptide analogues cyclized through rhenium and technetium metal coordination. *Proc. Natl. Acad. Sci. U.S.A.* 95, 12814–12818.
- (22) Chen, J. Q., Cheng, Z., Hoffman, T. J., Jurisson, S. S., and Quinn, T. P. (2000) Melanoma-targeting properties of  $^{99\text{m}}$ -Technetium-labeled cyclic  $\alpha$ -melanocyte-stimulating hormone peptide analogues. *Cancer Res.* 60, 5649–5658.
- (23) Miao, Y., Owen, N. K., Whitener, D., Gallazzi, F., Hoffman, T. J., and Quinn, T. P. (2002) In vivo evaluation of  $^{188}\text{Re}$  labeled alpha-melanocyte stimulating hormone peptide analogues for melanoma therapy. *Int. J. Cancer* 101, 480–487.
- (24) Mørgenson, C. E., and Sølling, K. (1977) Studies on renal tubular protein reabsorption: partial and near complete inhibition by certain amino acids. *Scand. J. Clin. Lab Invest.* 37, 477–486.
- (25) Silbernagl, S. (1988) The renal handling of amino acids and oligopeptides. *Physio. Rev.* 68, 912–986.
- (26) Maack, T., Johnson, V., Kan, S. T., Figueiredo, J., and Sigulem, D. (1979) Renal filtration, transport, and metabolism of low molecular weight proteins: a review. *Kidney Int.* 16, 251–270.
- (27) Behr, T. M., Sharkey, R. M., Juweid, M. E., Blumenthal, R. D., Dunn, R. M., Bair, H. J., Wolf, F. G., Becker, W. S., and Goldenberg, D. M. (1995) Reduction of the renal uptake of radiolabeled monoclonal antibody fragments by cationic amino acids and their derivatives. *Cancer Res.* 55, 3825–3834.
- (28) Behr, T. M., Becker, W. S., Sharkey, R. M., Juweid, M. E., Dunn, R. M., Bair, H. J., Wolf, F. G., and Goldenberg, D. M. (1996) Reduction of renal uptake of monoclonal antibody fragments by amino acid infusion. *J. Nucl. Med.* 37, 829–833.
- (29) Behr, T. M., Goldenberg, D. M., and Becker, W. S. (1998) Reduction the renal uptake of radiolabeled antibody fragments and peptides for diagnosis and therapy: present status, future prospects and limitations. *Eur. J. Nucl. Med.* 25, 201–212.
- (30) Bernard, B. F., Krenning, E. P., Breeman, W. A. P., Rolleman, E. J., Bakker, W. H., Visser, T. J., Macke, H., DeJong, M. (1997) D-lysine reduction of Indium-111 octreotide and Yttrium-90 octreotide renal uptake. *J. Nucl. Med.* 38, 1929–1933.
- (31) Valkema, R., DeJong, M., Kooij, P. P., Kwekkeboom, D. J., and Krenning, E. P. (2001) Effective and safe inhibition of renal uptake of radiolabeled peptides by combined lysine and arginine infusion. *J. Nucl. Med.* 42, 37P.
- (32) Kim, I. S., Yoo, T. M., Kobayashi, H., Kim, M.-K., Le, N., Han, E. S., Wang, Q.-C., Pastan, I., Carrasquillo, J. A., and Paik, C. H. (1997) Acylation with glycolate lowers pI of dsFv and reduce renal uptake of its Tc-99m label. *J. Labelled Compd. Radiopharm.* 15, 422–424 (Abstract).
- (33) Kim, I. S., Yoo, T. M., Kobayashi, H., Kim, M.-K., Le, N., Wang, Q.-C., Pastan, I., Carrasquillo, J. A., and Paik, C. H. (1999) Chemical modification to reduce renal uptake of disulfide-bonded variable region fragment of anti-Tac monoclonal antibody labeled with  $^{99\text{m}}$ Tc. *Bioconjugate Chem.* 10, 447–453.
- (34) Kobayashi, H., Le, N., Kim, I. S., Kim, M.-K., Pie, J.-E., Drumm, D., Paik, D. S., Waldmann, T. A., and Paik, C. H. (1999) The pharmacokinetic characteristics of glycolated humanized anti-Tac Fabs are determined by their isoelectric points. *Cancer Res.* 59, 422–430.
- (35) Kobayashi, H., Kim, I. S., Drumm, D., Kim, M.-K., Paik, D. S., Le, N., Waldmann, T. A., Carrasquillo, J. A., and Paik, C. H. (1999) Favorable effects of glycolate conjugation on the biodistribution of humanized anti-Tac Fab Fragment. *J. Nucl. Med.* 40, 837–845.
- (36) Akizawa, H., Arano, Y., Mifune, M., Iwado, A., Saito, Y., Mukai, T., Uehara, T., Ono, M., Fujioka, Y., Ogawa, K., Kiso, Y., and Saji, H. (2001) Effect of molecular charges on renal uptake of  $^{111}\text{In}$ -DTPA-conjugated peptides. *Nucl. Med. Biol.* 28, 761–768.
- (37) Mountjoy, K. G., Robbins, L. S., Mortrud, M. T., and Cone, R. D. (1992) The cloning of a family of genes that encode the melanocortin receptors. *Science* 257, 1248–1251.
- (38) Gantz, I., Konda, Y., Tashiro, T., Shimoto, Y., Miwa, H., Munzert, G., Watson, S. J., Del Valle, V., and Yamada, T. (1993) Molecular cloning of a novel melanocortin receptor. *J. Biol. Chem.* 268, 8246–8250.
- (39) Gantz, I., Miwa, H., Konda, Y., Shimoto, Y., Tashiro, T., Watson, S. J., Del Valle, V., and Yamada, T. (1993) Molecular cloning, expression, and gene localization of a fourth melanocortin receptor. *J. Biol. Chem.* 268, 15174–15179.
- (40) Barret, P., MacDonald, A., Helliwell, R., Davidson, G., and Morgan, P. (1994) Cloning and expression of a new member of the melanocyte-stimulating hormone receptor family. *J. Mol. Endocrinol.* 12, 203–213.
- (41) Desarnaud, F., Labbé, O., Eggerickx, D., Vassart, G., and Parmentier, M. (1994) Molecular cloning, functional expression and pharmacological characterization of a mouse melanocortin receptor gene. *Biochem. J.* 299, 366–373.
- (42) Labbé, O., Desarnaud, F., Eggerickx, D., Vassart, G., and Parmentier, M. (1994) Molecular cloning, of a mouse melanocortin 5 receptor gene widely expressed in peripheral tissues. *Biochemistry* 33, 4543–4549.
- (43) Fathi, Z., Iben, L. G., and Parker, E. M. (1995) Cloning, expression, and tissue distribution of a fifth melanocortin receptor subtype. *Neurochem. Res.* 20, 107–113.
- (44) Lu, D., Våge, D. I., and Cone, R. D. (1998) A ligand-mimetic model for constitutive activation of the melanocortin-1 receptor. *Mol. Endocrinol.* 12, 592–604.
- (45) Abbot, C. R., Rossi, M., Kim, M. S., Al Ahmed, S. H., Taylor, G. M., Ghatei, M. A., Smith, D. M., and Bloom, S. R. (2000) Investigation of the melanocytes stimulating hormones on food intake. Lack of evidence to support a role for the melanocortin-3-receptor. *Brain Res.* 869, 203–210.
- (46) Chen, W. B., Kelly, M. A., Opitz Araya, X., Thomas, R. E., Low, M. J., and Cone, R. D. (1997) Exocrine gland dysfunction in MC5-R deficient mice: Evidence for coordinated regulation of exocrine gland function by melanocortin peptides. *Cell* 91, 789–798.
- (47) Zhang, R. D., Price, J. E., Schackert, G., Itoh, K., and Fidler, I. J. (1991) Malignant potential of cells isolated from lymph node or brain metastases of melanoma patients and implications for prognosis. *Cancer Res.* 51, 2029–2035.

- (48) Fidler, I. J. (1975) Biological behavior of malignant melanoma cells correlated to their survival in vivo. *Cancer Res.* 35, 218–224.
- (49) Cheng, Z., Chen, J. Q., Miao, Y., Owen, N. K., Quinn, T. P., Jurisson, S. S. (2002) Modification of the structure of a metalloprotein: synthesis and biological evaluation of  $^{111}\text{In}$ -labeled DOTA-conjugated rhenium-cyclized  $\alpha$ -MSH analogues. *J. Med. Chem.* 45, 3048–3056.
- (50) Garg, P. K., Alston, K. L., Welsh, P. C., Zalutsky, M. R. (1996) Enhanced binding and inertness to dehalogenation of  $\alpha$ -melanotropic peptides labeled using N-succinimidyl 3-iodobenzoate. *Bioconjugate Chem.* 7, 233–239.
- (51) Froidevaux, S., Calame-Christe M., Sumanovski, L., Tanner H., and Eberle A. N. (2003) DOTA  $\alpha$ -melanocyte-stimulating hormone analogues for imaging metastatic melanoma lesions. *Ann. N. Y. Acad. Sci.* 994, 378–383.
- (52) Froidevaux, S., Calame-Christe M., Tanner H., Sumanovski, L., Eberle A. N. (2002) A novel DOTA- $\alpha$ -melanocyte-stimulating hormone analogue for metastatic melanoma diagnosis. *J. Nucl. Med.* 43, 1699–1706.
- (53) Hoffman, T. J., Gali, H., Smith, C. J., Sieckman, G. L., Hayes, D. L., Owen, N. K., and Volkert, W. A. (2003) Novel series of  $^{111}\text{In}$ -labeled bombesin analogues as potential radiopharmaceuticals for specific targeting of gastrin-releasing peptide receptors expressed on human prostate cancer cells. *J. Nucl. Med.* 44, 823–831.
- (54) Behr, T. M., and Béhé, M. P. (2002) Cholecystokinin-B/Gastrin receptor-targeting peptides for staging and therapy of medullary thyroid cancer and other Cholecystokinin-B receptor-expressing malignancies. *Semin. Nucl. Med.* 32, 97–109.
- (55) Hoffman, T. J., Smith, C. J., Gali, H., Owen, N. K., Sieckman, G. L., Hayes, D. L., Foster, B., Volkert, W. A. (2001)  $^{111}\text{In}/^{90}\text{Y}$  radiolabeled peptides for targeting prostate cancer; a matched pair gastrin releasing peptide (GRP) receptor localizing radiopharmaceutical. *J. Nucl. Med.* 42, 274P (abstract).
- (56) Behr, T. M., Béhé, M. P., Angerstein, C., Hübner, M., Becker, W. (2001) Cholecystokinin(CCK)-B/Gastrin-receptor binding peptides for diagnosis and therapy of metastatic medullary thyroid cancer. *J. Nucl. Med.* 42, 157P (abstract).
- (57) Fidler, I. J., Nicolson, G. L. (1976) Organ selectivity for implantation survival and growth of B16 melanoma variant tumor lines. *J. Natl. Cancer Institute* 57, 1199–1202.

BC034069I

# Growth of Large Polymer–Actin Complexes

Akira Kakugo,<sup>†</sup> Kazuhiro Shikinaka,<sup>†</sup> Kanae Matsumoto,<sup>†</sup> Jian Ping Gong,<sup>\*,†,‡</sup> and Yoshihito Osada<sup>†</sup>

Graduate School of Science Hokkaido University, and Presto, JST,  
Sapporo 060-0810, Japan. Received May 6, 2003; Revised Manuscript Received August 28, 2003

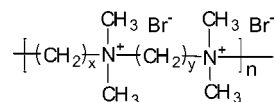
Polymer–actin complexes as large as 10–50  $\mu\text{m}$  with filamentous, branched, stranded, and ring shapes are obtained when fluorescent phalloidin-labeled F-actin is mixed with some synthetic polymers carrying positive charges such as poly-L-lysine,  $x,y$ -ionene bromide polymers. All growth of these complexes occurs cooperatively at some certain critical polymer concentrations, regardless of the chemical structure of the polymer, while the morphology of the complexes is substantially influenced by the chemical structure of the polymer. Poly-Lys–actin complex grows preferentially along the filament axis even above the critical concentration. 3,3-ionene–actin complexes show completely homogeneous filaments below the critical concentration but forms bundles at a higher concentration. Occasionally, ring shape complexes can be observed in the 6,6-ionene–actin complex.

## INTRODUCTION

Recently, we have constructed an adenosine triphosphate (ATP)-fueled soft gel machine constructed from chemically cross-linked actin gel and myosin gel (1). Actins and myosins are major components of muscle proteins and play an important role in dynamic motion of creatures that is caused by the molecular deformation using the chemical energy released by hydrolysis of ATP. We have found that chemically cross-linked giant actin gel filaments, several tens of times the length of native actin filaments, move along a chemically cross-linked myosin fibrous gel with a velocity as high as that of native actins, by coupling to ATP hydrolysis. This result indicates that muscle proteins can be tailored into desired shape and size without sacrificing their bioactivities. The above-described giant actin gel filaments were obtained by forming complexes with poly-L-Lysine (p-Lys) by subsequent chemical cross-linking (1). However, the self-organized growth process of actin-p-Lys complexes has not been clarified yet.

In this paper we systematically study the complex formation between actins and various kinds of polycations, such as p-Lys and  $x,y$ -ionene bromide polymers ( $x = 3$  or 6;  $y = 3, 4, 6, 10$ , or 12).  $x,y$ -ionene polymers are cationic polymers having positive charges on their chain backbone with periodical alkyl spacers  $x$  and  $y$  (Chart 1). Native actins (G-actin), which are globular proteins of 5 nm in diameter, form thin filaments with a diameter about 9 nm in living muscle. In physiological ionic solution (F-buffer), G-actins extracted from muscles undergo self-assembly reaction polymerization transferring to a single-stranded filament with a pitch of 5.9 nm which resembles the actin filaments within sarcomere (2). This actin filament polymerized from G-actin in physiological ionic solution is called F-actin. The F-actins of several nanometers in length can be conveniently observed under a fluorescence microscope by binding fluorescent phalloidin to the F-actins. Since the isoelectric point of actins is pH 4.7, F-actins in F-buffer of pH 7.2 are negatively

**Chart 1. Molecular Structure of  $x,y$ -ionene Bromide Polymers**



charged. Therefore, they were assumed to form complexes with cationic polymers through electrostatic interaction. When synthetic polymers carrying positive charges are mixed with fluorescent phalloidin-labeled F-actin, polymer–actin complexes grew with time. The complex growth kinetics and thermodynamics are investigated and compared with the morphological features of the complexes by using fluorescent optical images and transmission electron microscope (TEM) images.

## EXPERIMENTAL PROCEDURES

**Sample Preparations.**  $x,y$ -ionene ( $x = 3$  or 6;  $y = 3, 4, 6, 10$ , or 12) bromide polymers ( $x,y$ -ionene), which have the chemical structures as shown in Chart 1, were synthesized by the method reported previously (3). The intrinsic viscosities of 6,6- and 6,12-ionene polymers in 0.4 M LiBr aqueous solution at 25  $^\circ\text{C}$  were 0.19 and 0.22 dL/g, respectively. The viscosity value of the 6,6-ionene polymer corresponds to a weight-average molecular weight of  $1.9 \times 10^4$ . Poly-L-lysine hydrochloride (p-Lys) and poly-D-glutamic acid sodium salt (p-Glu) were purchased from Peptide Institute Inc. Deoxyribonucleic acid sodium salt (DNA) was purchased from Sigma Chemical Co. Poly(ethylene glycol) (PEG) was purchased from Aldrich Chemical Co., Inc.

G-actins (0.1 mg/mL) were obtained from scallops by the method of Spudich et al. (4). Fluorescently labeled F-actins were obtained by stoichiometrically mixing G-actins and rhodamine–phalloidin (Molecular Probes No. 4171) in F-buffer (5 mM HEPES (pH 7.2), 0.2 mM ATP, 0.2 mM  $\text{CaCl}_2$ , 100 mM KCl, 2 mM  $\text{MgCl}_2$ ) for 24 h at 4  $^\circ\text{C}$ . Phalloidin bonds to G-actin stoichiometrically and stabilizes the F-actin against depolymerization at a decreased critical concentration of actin.

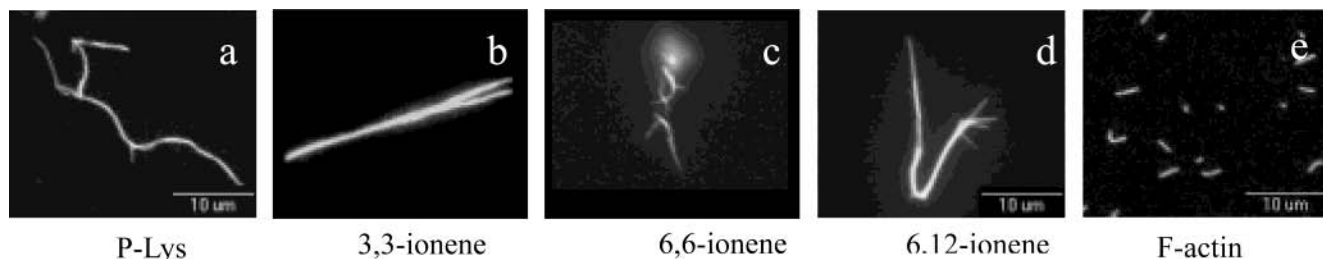
**Measurement.** The rhodamine–phalloidin-labeled F-actin (later denotes as F-actin) solution was diluted to 0.001 mg/mL with F-buffer and mixed with various kinds

\* To whom correspondence should be addressed. E-mail: gong@sci.hokudai.ac.jp.

<sup>†</sup> Graduate School of Science.

<sup>‡</sup> Presto, JST.





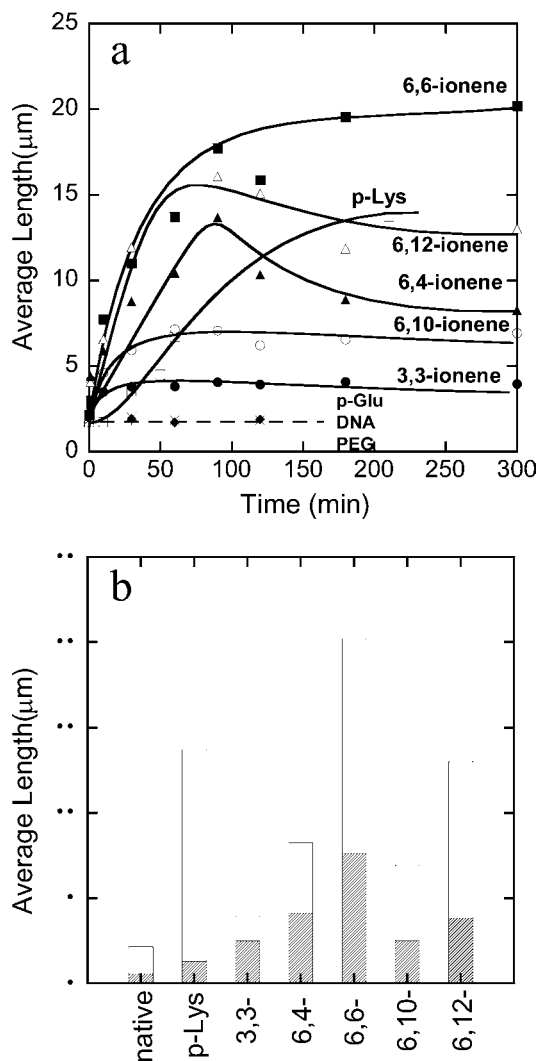
**Figure 1.** Fluorescence microscope images of polymer-actin complexes formed by mixing F-actin and various cationic polymers at room temperature. (a) p-Lys, (b) 3,3-ionene, (c) 6,6-ionene, (d) 6,12-ionene, (e) F-actin only. The molar ratio of ammonium cation of polymer to monomeric actin was kept constant at 30:1 for *x,y*-ionene polymers and 100:1 for p-Lys, which corresponding-to-weight ratios of [3,3-ionene]/[actin] = 0.41 g/g, [6,6-ionene]/[actin] = 0.61 g/g, [6,12-ionene]/[actin] = 0.81 g/g, [p-Lys]/[actin] = 0.35 g/g. Actin concentration was 0.001 mg/mL.

of polymers with a prescribed weight ratio of [polymer]/[F-actin] at room temperature. A cover glass was placed on a slide glass equipped with two spacers 1.1–1.4 mm high at both sides to form a flow-cell. Solution of F-actin and polymer mixture about 30  $\mu\text{m}$  was introduced into the flow-cell by a micropipet at a prescribed time after mixing. The flow-cell was then placed on the stage of a fluorescence microscope (Olympus BX 50) and observed under a  $\times 60$  objective. F-actins and its complexes with polymers absorbed on the slide glass surface can be clearly visualized under a microscope. The fluorescence images were recorded by a CCD-camera (Olympus CD-300T-RC), and images of filament length were analyzed by using a computer-analyzing program (MetaMorph, Nippon ROPER). The length of filaments, measured from the contour length of long axis, was the average over 50 samples. Transmission electron microscopy (TEM) was performed by using a JEOL (JEM-1200EX) at 120 kV acceleration voltage. A drop of F-actin-polymer mixture of about 10  $\mu\text{L}$  was put on carbon-coated 200-mesh grids that were rendered hydrophilically by glow discharge in a reduced pressure. After waiting for 180 s for adsorption, the grids were stained by one drop of phosphotungstic acid (pH 7.2). The length or width of filament was the average over 20 samples.

## RESULTS AND DISCUSSION

Figure 1a–d shows some examples of fluorescence microscope images of polymer-actin complexes obtained by mixing F-actins with p-Lys (Figure 1a) and *x,y*-ionene polymers (Figure 1b–d) for 120 min. One can see that large filamentous, stranded and branched complexes of 20–30  $\mu\text{m}$  in size are formed in the presence of p-Lys and 3,3-, 6,6-, 6,12- ionene polymers and their morphological nature, both of size and shape, are strongly in contrast to that of native F-actin (Figure 1e). Figure 2a shows time courses of the average length of the complexes in the presence of various kinds of polymers. Polymers have been mixed with following weight ratios keeping the actin concentration constant at 0.001 mg/mL as well as the molar ratio of ammonium cation of polymer to actin monomer of F-actin as 100:1 for p-Lys and 30:1 for ionene polymers: [p-Lys]/[actin] = 0.35 g/g, [3,3-ionene]/[actin] = 0.41 g/g, [6,4-ionene]/[actin] = 0.54 g/g, [6,6-ionene]/[actin] = 0.61 g/g, [6,10-ionene]/[actin] = 0.74 g/g, [6,12-ionene]/[actin] = 0.81 g/g.

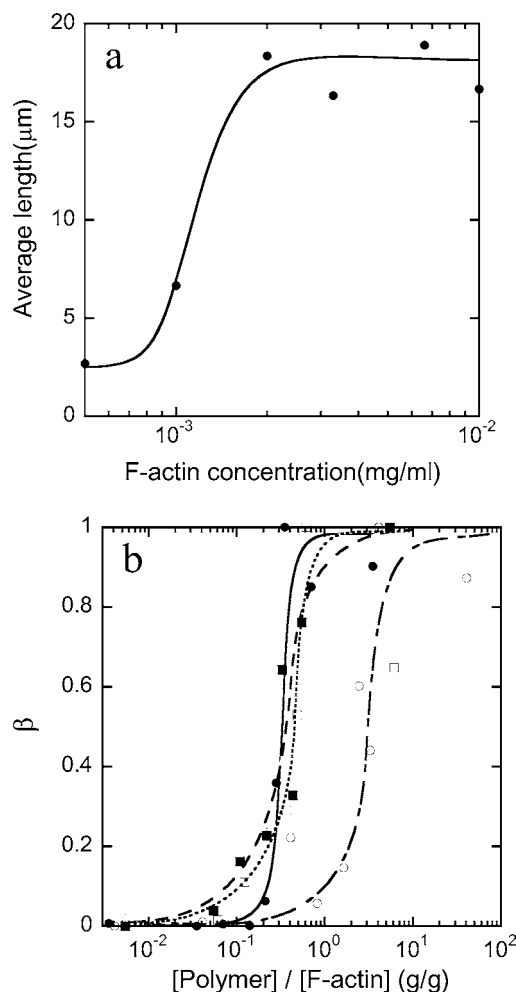
The number-average length of fluorescence image of F-actins is 2.14  $\mu\text{m}$  with a standard deviation of 0.11  $\mu\text{m}$  (average over 784 samples) in the F-buffer. However, polymer-actin complexes grow with time and reach as large as 5–20  $\mu\text{m}$  within one or 2 h, which is about 2–10 times larger than that of native F-actin. The growth profiles depend on the chemical structure of the



**Figure 2.** (a) Time courses of polymer-actin complexes growth. (●): 3,3-ionene-actin complexes, (▲): 6,4-ionene-actin complexes, (■): 6,6-ionene-actin complexes, (○): 6,10-ionene-actin complexes, (△): 6,12-ionene-actin complexes, (□): p-Lys-actin complexes, (◆): p-Glu-actin complexes, (×): [DNA-actin complexes, (+): PEG-actin complexes. (b) Average length of polymer-actin complexes observed from fluorescence microscope images (white columns) and from transmission electron microscopy (TEM) images (shade columns) at 210–300 min. The molar ratio of ammonium cation to monomeric actin was 30:1 for *x,y*-ionene polymers and 100:1 for p-Lys. The corresponding weight ratios were as follows: [3,3-ionene]/[actin] = 0.41 g/g, [6,4-ionene]/[actin] = 0.54 g/g, [6,6-ionene]/[actin] = 0.61 g/g, [6,10-ionene]/[actin] = 0.74 g/g, [6,12-ionene]/[actin] = 0.81 g/g, [p-Lys]/[actin] = 0.35 g/g, [p-Glu]/[actin] = 0.36 g/g, [DNA]/[actin] = 0.77 g/g, [PEG]/[actin] = 0.10 g/g. Actin concentration: 0.001 mg/mL.

polycations. P-Lys shows a relatively slow growth profile but gives out a large complex. On the other hand, 3,3-ionene polymer gives the smallest complexes. These results indicate that hydrophobicity and charge density of the ionene polymers are important in complex formation. The average lengths of actin-polymer complexes are shown in Figure 2b. To confirm that this kind of actin growth is due to the complex formation via electrostatic interaction between the negatively charged actins and positively charged polymers, we further studied the actin growth in the mixture solution of actins and negatively charged polymers such as p-Glu, DNA, and neutral polymer, such as PEG at a molar ratio of monomeric units of polymer to F-actin of 100:1, which corresponding-to-weight ratios of [p-Glu]/[actin] = 0.36 g/g, [DNA]/[actin] = 0.77 g/g, [PEG]/[actin] = 0.10 g/g. As shown in Figure 2a, the F-actins do not grow into large filaments with time in the presence of these anionic or neutral polymers. Therefore, the formation of polymer-actin complexes should be attributed to the electrostatic interaction between actins and cationic polymers. As shown in Figure 2a, although 3,3-ionene has a similar high charge density as that of p-Lys that has charged moiety on its side chain, it shows a much less ability of complex growth. This indicates that although the complex formation is initiated by the electrostatic interaction, the flexibility of the charged moiety is important. The complicated  $x,y$  value dependence of the complex growth observed in  $x,y$ -ionene polymers might be associated with the complementary effect between the charge density and the flexibility of the charged moiety. Both 3,3-ionene and 6,10-ionene form short complexes because the former has a high charge density but with a less flexibility, while the latter has a high flexibility but with a low charge density. 6,6-Ionene gives longest complex due to its proper charge density and flexibility. Here, we could not find a clear role related to the hydrophobicity of the  $x,y$ -ionene polymers. The decrease in the filament length after 100 min of complex formation observed for 6,4- and 6,12-ionene complexes seems to be due to the aggregation of the complex.

Since the formation of polymer-actin complexes is an equilibrium reaction, the morphological features of the product should depend not only on time and polymer structure, but also on concentrations of actins and polymers. Figure 3a shows the effect of actin concentration on the equilibrium size of the polymer-actin complexes when mixed with p-Lys of a constant concentration ( $3.5 \times 10^{-4}$  mg/mL). When the actin concentration exceeds 0.001 mg/mL, the actin complexes increase the length steeply with the increase in the concentration and then saturate to a length around 15–20  $\mu$ m. Figure 3b shows the effect of p-Lys concentration on the relative length  $\beta$  of polymer-actin complexes in the equilibrium at a constant actin concentration (0.001 mg/mL). Here  $\beta$  is defined as a ratio of average length to maximum length of actin-polymer complex. No actin growth is observed at all when the mixing ratio of p-Lys to actin is lower than 0.14 g/g, indicating that the polymer-actin complex does not form at such a low concentration. However, the length of polymer-actin complexes abruptly increases when the mixing ratio of p-Lys to F-actin exceeds 0.21 g/g. Thus, there exists a critical p-Lys concentration to form complex, indicating that the complex formation is cooperative. The similar cooperative behavior was also observed in the complex formation with ionene polymers, and the critical mixing ratios of 3,3-, 6,4-, 6,6-, 6,10-, and 6,12-ionene to F-actin were about 0.81, 0.054, 0.12, 0.024, and 0.022 g/g at a constant



**Figure 3.** Average length of polymer-actin complexes as a function of F-actin concentration (a) and dependence of  $\beta$  on the mixing ratio of polymer to actin (b). Here  $\beta$  is defined as the ratio of average length to maximum length of actin-polymer complex. (●): p-Lys; (○): 3,3-ionene; (■): 6,4-ionene; (□): 6,6-ionene. Data in part a were obtained at [p-Lys] =  $3.5 \times 10^{-4}$  mg/mL at 60 min and in part b at an actin concentration of 0.001 mg/mL at 90 min.

F-actin concentration (0.001 mg/mL), respectively (Figure 3b). These results explain why we observed a shortest complex length of 3,3-ionene in Figure 2a performed at [3,3-ionene]/[actin] = 0.41 g/g, which was less than the critical value of 0.81 g/g. Now, we can conclude that interaction between polymers and actins behave cooperatively, and polymer-actin complexes are formed only when both F-actin concentration and the mixing ratio exceed the critical values.

From Figure 3b we can obtain the binding constant ( $K$ ) as well as the other thermodynamic parameters of the actin-polymer interaction by the following equation (5–7).  $K = K_0 u = 1/(C_s)_{0.5}$ , where  $K_0$  is the binding constant of the cationic polymer bound to an isolated binding site on the actin filament (initiation process),  $(C_s)_{0.5}$  is the cationic polymer concentration at  $\beta = 0.5$  ( $\beta$  is defined as a ratio of average length to maximum length of actin-polymer complex), and  $u$  is the cooperative parameter which tells the extra interaction energy between the binding sites (propagation process). The value of  $u$  can be calculated from the slope of the growth profile at the half-length point.  $(d\beta/d \ln C_s)_{0.5} = \sqrt{u/4}$ .  $K_0$  and  $u$  as well as the total binding energy ( $\Delta F_{\text{total}} = -RT \ln K$ ) and cooperative energy change ( $\Delta F_{\text{coop.}} = -RT \ln$

**Table 1.** Thermodynamic Interaction Parameters of Complex Formation between F-Actin and Various Cationic Polymers

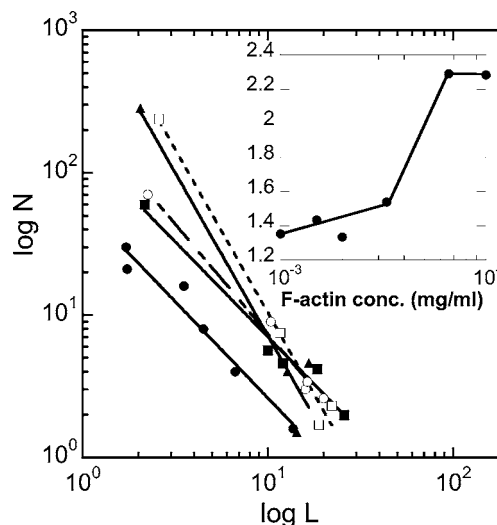
polymer	$K$ [ $10^6$ ]	$u$	$K_0$ [ $10^5$ ]	$\Delta F_{\text{total}}$ [ $\text{kJ mol}^{-1}$ ]	$\Delta F_{\text{coop.}}$ [ $\text{kJ mol}^{-1}$ ]
p-Lys	3.7	31	1.2	-37	-8.5
3,3-	0.3	32	0.1	-31	-8.6
6,4-	2.9	4.4	6.6	-37	-3.7
6,6-	2.4	20	1.2	-36	-7.4
6,10-	1.1	7.0	1.5	-34	-4.8
6,12-	1.6	2.2	7.1	-35	-1.9

$u$ ) were calculated, and the results are summarized in Table 1. One can see a large value of the cooperative parameter ( $u$ ) and therefore a large cooperative energy ( $\Delta F_{\text{coop.}}$ ) change for p-Lys and 3,3-ionene, and the smallest value of cooperative parameter is observed for 6,12-ionene, which is 1 order of magnitude smaller than the  $u$  value of the other polymers. On the contrary, 6,12-ionene shows the highest binding constant of the initiation process ( $K_0$ ).

The growth of polymer-actin complexes in size is accompanied by a substantial decrease in the number of actin filament. Figure 4 shows a logarithmic plot of the number ( $N$ ) as a function of the length ( $L$ ) of polymer-actin complexes at various actin concentrations at a constant mixing ratio of [p-Lys]/[actin] = 0.35 g/g. As shown in the figure, the number of complexes ( $N$ ) decreases with increase in the length ( $L$ ), and they follow a power law as  $N \propto L^{-\alpha}$ . The exponent  $\alpha$  that is the fractal dimension ( $\delta$ ) should characterize the growth process of the complexes. If  $\alpha$  is 1, the complexes grow one-dimensionally, i.e., the actins aggregate along the axis of filament. If  $\alpha > 1$ , lateral growth occurs simultaneously with the longitudinal growth. When the fractal dimension  $\alpha$  is plotted against the concentration of actin, we obtain Figure 4 (insert) which shows an abrupt increase in  $\alpha$  at an actin concentration of 0.0033 mg/mL. When the concentration of actin is lower than this concentration,  $\alpha$  is ca. 1.4, but abruptly increases to 2.2 when it exceeds this concentration. In other words, at low concentration the complexes grow preferentially along the filament axis extending their length, but above the critical concentration, they begin to grow in lateral direction as well.

As shown in Figure 2 that among  $x,y$ -ionenes, 6,6-ionenes form the longest polymer-actin complexes which is followed by 6,12-, 6,4-, 6,10-, and 3,3-ionene. Therefore, we further investigate the fractal dimension of the complexes with  $x,y$ -ionenes. It is found that  $\alpha$  values were 2.1, 2.9, 2.2, 3.5, and 2.3, for 3,3-, 6,4-, 6,6-, 6,10-, and 6,12-ionenes, respectively, at a constant actin concentration (0.001 mg/mL) and molar ratio of ammonium cation to actin monomer unit (30:1). These results indicate that 6,4-, 6,10-, and 6,12-ionenes grow in a three-dimensional direction, and 3,3-, 6,6-ionene promotes a preferential growth along the filament direction with a less vague growth in the lateral direction. Since the complex length of 3,3-ionene is much shorter than that of 6,6-ionene, we can expect that much thinner filaments were formed in 3,3-ionene than that in 6,6-ionene.

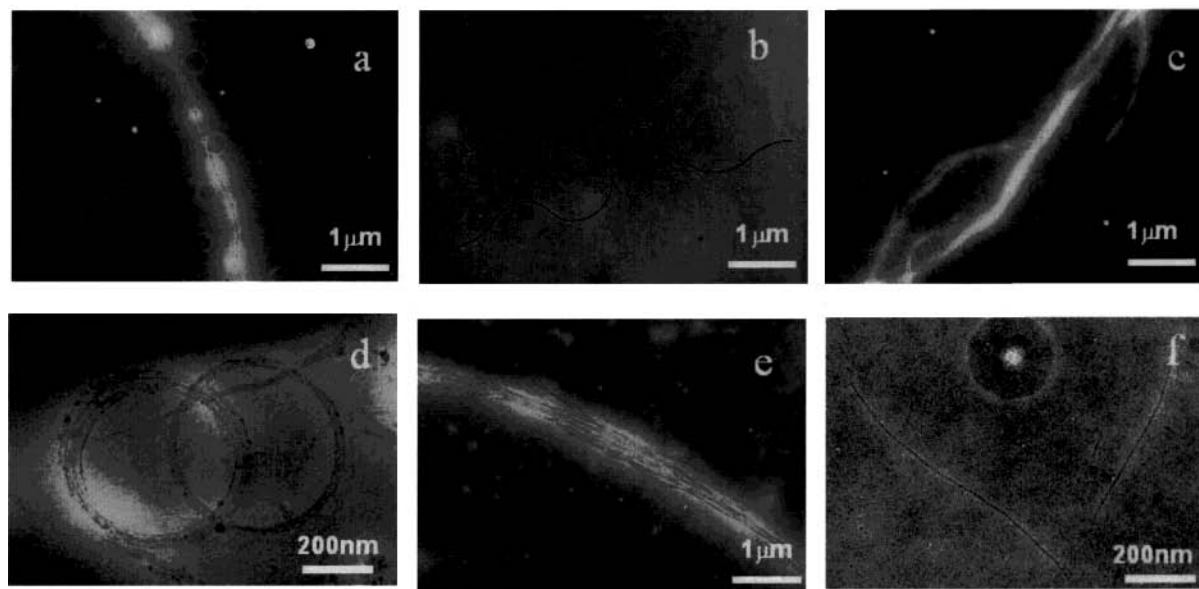
As the lateral structures of the polymer-actin complexes are too small to be clearly observed by fluorescent optical microscope, we further studied polymer-actin complexes by TEM, using the negative staining technique. Figure 5 shows the TEM images of the actin complexes prepared at a molar ratio of ammonium cation of polymer to monomeric actin as 100:1 for p-Lys and 30:1 for ionene polymers at a constant F-actin concentration

**Figure 4.** Logarithmic plot of number of p-Lys-actin complexes ( $N$ ) as a function of length ( $L$ ) for different F-actin concentration after 90 min.  $N$  and  $L$  follow a power law  $N \propto L^{-\alpha}$  where the exponent  $\alpha$  depends on actin concentration as shown in the inserted figure. Actin concentration: (closed circle): 0.001 mg/mL, (closed square): 0.002 mg/mL, (open circle): 0.0033 mg/mL, (open square): 0.0066 mg/mL, (closed triangle): 0.01 mg/mL. The molar ratio of ammonium cation to monomeric actin was 100:1.

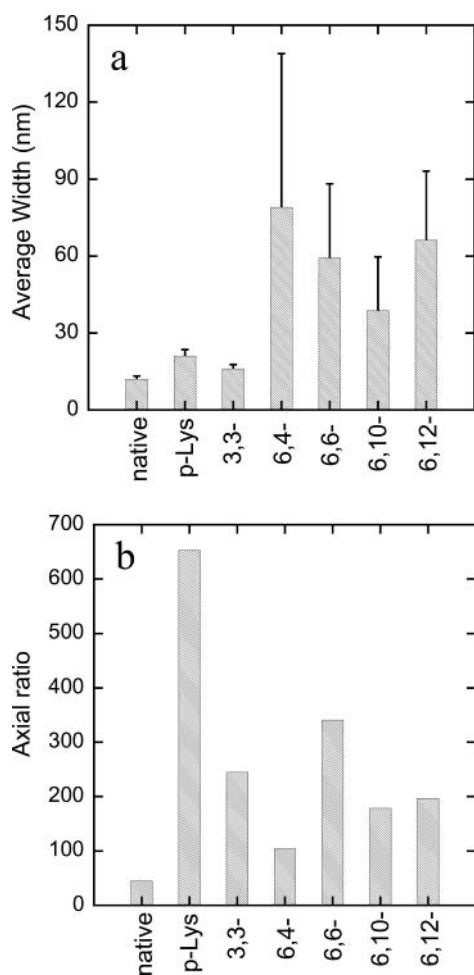
0.001 mg/mL. As shown in Figure 5a, actin forms a relatively homogeneous and thin filament in the presence of p-Lys, which agrees well with the small fractal dimension at a F-actin concentration 0.001 mg/mL in Figure 4 (insert). We also found that actin is able to form an extremely homogeneous nanoscale wire (nanowire) with 3,3-ionene (Figure 5b), and this is also in agreement with the prediction from the fractal dimension value. Filamentous complexes are observed in the presence of 6,6-ionene, (Figure 5c). Occasionally, a ring-shaped complex (nano-ring) is observed in a 6,6-ionene-actin complex (Figure 5d).

The average width of the p-Lys-actin complex is 21.0 nm with a standard deviation of 2.6 nm. Compared with the native F-actins that have an average width of 12.1 nm with a standard deviation of 1.2 nm, p-Lys-actin complexes are only slightly thicker than that of the native F-actin with almost the same width scattering. 3,3-ionene complexes also showed a very thin and homogeneous wirelike morphology showing an average width of 16.1 nm with a standard deviation of 1.7 nm. However, from Figure 3b, we know that at a molar ratio of ammonium cation to actin monomer as 30:1, the 3,3-ionene polymer concentration is still below the critical concentration. Since the complex morphology is strongly dependent on the polymer concentration, we further investigated the 3,3-ionene-actin complex at a molar ratio of ammonium cation to actin monomer of 300:1 ([3,3-ionene]/[actin] = 4.1 g/g), which is above the critical concentration of complex formation. As shown in Figure 5e, bundles of thin filaments are formed when the 3,3-ionene polymer exceeds the critical concentration. Similar morphology are observed for other  $x,y$ -ionene polymers above their critical concentration. Actin-6,4-, 6,6-, 6,10-, and 6,12-ionene complexes have an average width of 79.0 nm, 59.3, 38.7, and 66.1 nm with a standard deviation of 60, 29, 21, and 27 nm, respectively (Figure 6a). The large scattering in the width of actin-6,4-, 6,6-, 6,10-, and 6,12-ionene complexes quantitatively indicates the randomness of the morphology of the complexes.





**Figure 5.** Transmission electron microscopy (TEM) images of polymer–actin complexes formed by mixing F-actin and various polymers at room temperature for 240 min. (a) p-Lys, (b) 3,3-ionene, (c) 6,6-ionene, (d) 6,6-ionene, (e) 3,3-ionene, (f) F-actin only. Mixing molar ratios are the same as fluorescence microscope observation (Figure 1), except for part e which is carried out at 300:1 ([3,3-ionene]/[actin] = 4.1 g/g). Actin concentration: 0.001 mg/mL.



**Figure 6.** Average width of polymer–actin complexes obtained at 240 min by TEM images (a), and axial ratios of polymer–actin complexes evaluated by dividing the average length of complex obtained from fluorescence image by the average width obtained from TEM images (b). Error bar means standard deviation.

The average length of the complexes as observed by TEM showed a similar dependence on the polymers, but the absolute values of the length are about 2 times shorter than that obtained from fluorescent observations (Figure 2b). This discrepancy is due to the breakage of the long filament during the sample drying process for TEM measurements.

The axial ratio of polymer–actin complexes, which is the ratio of the average length from fluorescence image (Figure 2b) to the average width from TEM images, was estimated (Figure 6b). We find that the axial ratios are 653, 245, 104, 340, 179, and 196 for p-Lys, 3,3-, 6,4-, 6,6-, 6,10-, and 6,12-ionene, respectively. This tendency in the axis ratio values well coincides with that of the growth fractal dimension  $\alpha$  as estimated from the fluorescent images of the complex during growth process. For example, P-Lys showed a smallest fractal dimension (Figure 4) which agrees well with the highest axial ratio. Furthermore, 3,3-, and 6,6-ionene showed a relatively smaller fractal dimension, and this is in agreement with a relatively high axial ratio of the complex as shown in Figure 6b.

As a conclusion, p-Lys keeps the axial growth even above the critical concentration of cooperative growth, forming long and thin filaments, while  $\alpha,\gamma$ -ionene polymers change their growth mode from axial to lateral at the critical concentration and their average width at the concentration which gives half-length point is dominated by the cooperative energy ( $F_{\text{coop}}$ ) between actin and ionene polymers. Thus, designed micro-order polymer–actin complexes could be obtained by changing the structure of cationic polymer and other conditions. The motility of these actin–ionene complexes will be explored in future studies.

#### ACKNOWLEDGMENT

This research is financially supported by PRESTO, JST, and the Ministry of Education, Science, Sports, and Culture, Japan (Grand-in-Aid of Creative Scientific Research).

## LITERATURE CITED

- (1) Kakugo, A., Sugimoto, S., Gong, J. P., and Osada, Y. (2002) Gel machines constructed from chemically cross-linked actins and myosins. *Adv. Mater.* **14**, 1124–1126.
- (2) Oosawa, F., Asakura, S., Hotta, K., Imai, N., and Ooi, T. (1959) G–F transformation of actin as a fibrous condensation. *J. Polymer. Sci.* **37**, 323–336.
- (3) Chen, L., Yu, S. Y., Kagami, Y., Gong, J. P., and Osada, Y. (1998) Surfactant binding of polycations carrying charges on the chain backbone: Cooperativity, stoichiometry and crystallinity. *Macromolecules* **31**, 787–794.
- (4) Spudich, J. A., and Watt, S. (1971) The regulation of rabbit skeletal muscle contraction. I. Biochemical studies of the interaction of the tropomyosin-troponin complex with actin and the proteolytic fragments of myosin. *J. Biol. Chem.* **246**, 4866–4871.
- (5) Hayakawa, K., Santerre, J. P., and Kwak, J. C. (1983) Study of surfactant-polyelectrolyte interactions. Binding of dodecyl- and tetradecyltrimethylammonium bromide by some carboxylic polyelectrolytes. *Macromolecules* **16**, 1642–1645.
- (6) Gong, J. P., Mizutani, T., and Osada, Y. (1996) A comparative study on the cooperative binding of surfactants with solubilized polymers and networks. *Polym. Adv. Technol.* **7**, 797–804.
- (7) Satake, I., and Yang, J. T. (1976) Interaction of sodiumdecyl sulfate with poly (L-ornithine) and poly (L-lysine) in aqueous solution. *Biopolymers* **15**, 2263–2275.
- (8) Gong, J. P., Kagami, Y., Yamada, K., and Osada, Y. (1990) Fractal pattern formation of metal containing polymeric thin films prepared by plasma reaction. *Bull. Chem. Soc. Jpn.* **63**, 1578–1583.

BC0340722

# Fully Detachable Molecular Umbrellas as Peptide Delivery Agents

Bingwen Jing, Vaclav Janout, and Steven L. Regen\*

Department of Chemistry, Lehigh University, Bethlehem, Pennsylvania 18015. Received May 7, 2003;  
Revised Manuscript Received October 8, 2003

A persulfated molecular umbrella, derived from cholic acid and spermidine, has been covalently attached to H-Tyr-D-Ala-Gly-Phe-D-Leu-OH (DADLE) by use of an *o*-dithiobenzyl carbamate linkage. Treatment of the resulting conjugate (**1**) with glutathione in solution resulted in the liberation of the free form of the peptide. Addition of **1** to glutathione-entrapped liposomes, prepared from 1-palmitoyl-2-oleoyl-*sn*-glycero-3-phosphocholine (POPC), 1-palmitoyl-2-oleoyl-*sn*-glycero-3-phosphatidylglycerol (POPG), and cholesterol [POPC/POPG/cholesterol, 72/4/24 (mol/mol/mol)], resulted in the delivery of DADLE into their aqueous interior.

## INTRODUCTION

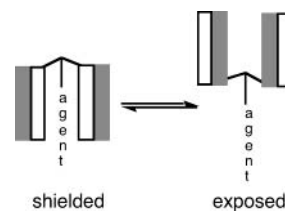
Molecular umbrellas are a unique class of amphiphiles that are capable of shielding an attached agent from an incompatible environment. Typically, such molecules are composed of a central scaffold that contains two or more facially amphiphilic units (*1*). When a hydrophilic agent is attached to an umbrella molecule, immersion in water favors an exposed conformation such that intramolecular hydrophobic interactions are maximized (*2*). Alternatively, when immersed in a hydrophobic environment, the molecular umbrella can shield the agent by providing a hydrophobic exterior (*2*). A stylized illustration of shielded and exposed conformers is shown in Scheme 1. Here, the shaded and unshaded rectangles represent hydrophobic and hydrophilic faces, respectively.

Recent mechanistic studies have provided strong evidence that facial amphiphilicity plays a major role in umbrella transport across lipid bilayers (*3*). The fact that facial amphiphilicity is more important than the hydrophobic/hydrophilic balance of such molecules, in promoting bilayer transport, lends strong support for an umbrella mechanism; that is, a permeation pathway involving monolayer insertion of a shielded conformer, transbilayer diffusion and entry to the opposite membrane/water interface.

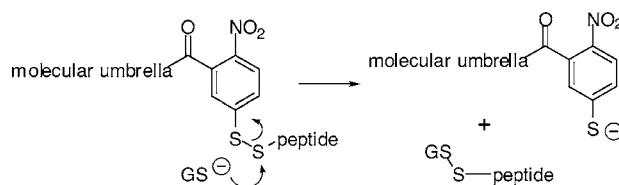
Previous molecular umbrellas that we have designed for peptide transport have employed a 2-nitrobenzoyl-5-dithio moiety as a detachable handle (*3*). When these conjugates enter the aqueous interior of a liposome that contains glutathione (GSH), the peptide is released by means of a thiolate–disulfide exchange reaction (Scheme 2) (*4*). The fact that mammalian cells contain millimolar concentrations of GSH within their cytoplasm adds relevance to such a strategy from a prodrug standpoint. Two distinct limitations associated with this approach, however, are the need of a cysteine residue for umbrella attachment/detachment, and the peptide is released in a non-native state; that is, as a glutathione conjugate.

In this paper, we introduce a new design strategy for the synthesis of molecular umbrella–peptide conjugates that (i) takes advantage of GSH-based thiolate–disulfide interchange reactions, (ii) circumvents the need for a

Scheme 1



Scheme 2



cysteine residue for attachment of the peptide to the umbrella, and (iii) allows for the release of the native form of the peptide.

## EXPERIMENTAL SECTION

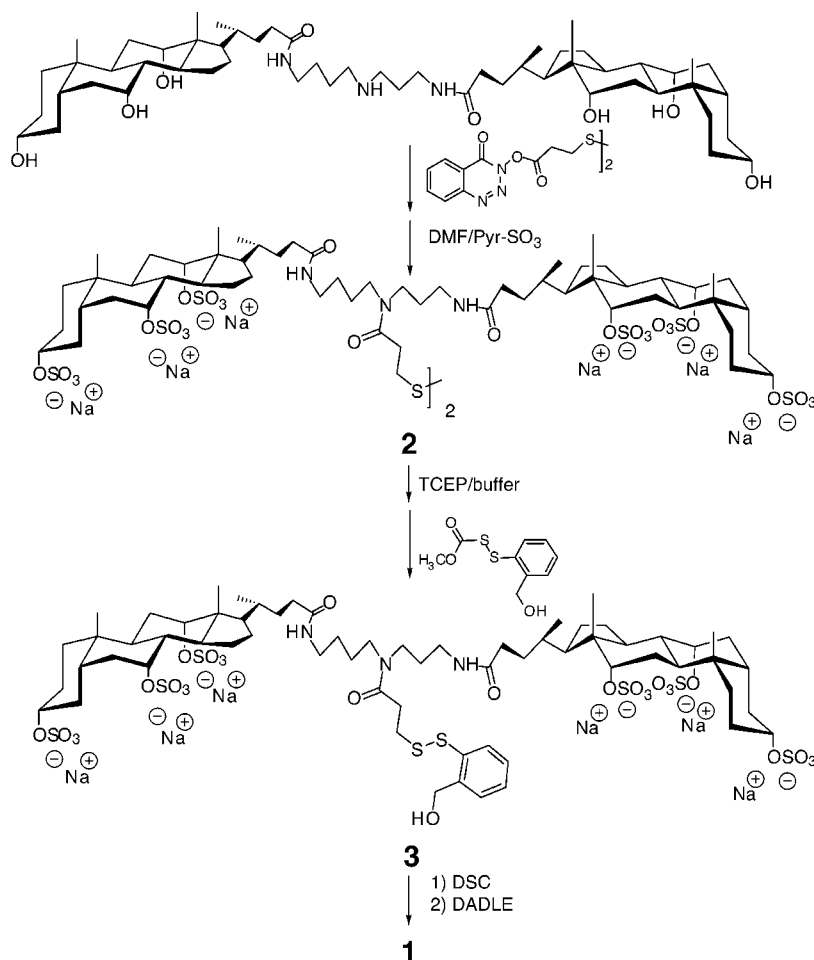
**General Methods.** Unless stated otherwise, all reagents were obtained from commercial sources and used without further purification. House-deionized water was purified using a Millipore Milli-Q-filtering system containing one carbon and two ion-exchange stages. All <sup>1</sup>H NMR spectra were recorded on a 360 MHz instrument; chemical shifts are reported in ppm relative to residual solvent. All UV spectra were recorded using a Carey 300 Bio UV–Visible spectrophotometer operating at ambient temperature. MALDI spectra were obtained using an Applied Biosystems DE-STR MALDI-TOF instrument operating in the linear, negative mode with an accuracy of ±0.2%; reflector mode analyses afforded an accuracy of ±0.02%. A standard buffer that was used in this work (referred to as “buffer”) was composed of 10 mM NaCl, 1.0 mM EDTA, and 2 mM PIPES, pH 7.2. The synthetic route that was used to prepare **1** is outlined in Scheme 3.

**2-(Methoxycarbonyldithio)benzyl Alcohol.** A solution of 1.4 g (9.99 mmol) of 2-mercaptobenzyl alcohol in 20 mL of dichloromethane was added, dropwise, to a

\* To whom correspondence should be addressed. E-mail: slr0@lehigh.edu.



Scheme 3



cooled (0 °C) solution prepared from 1 mL (10.98 mmol) of methoxycarbonylsulfonyl chloride and 60 mL of dichloromethane, under a nitrogen atmosphere. After stirring for 2 h, the mixture was washed, sequentially, with saturated sodium bicarbonate, and saturated sodium chloride, and the organic layer then dried over anhydrous MgSO<sub>4</sub>. Removal of solvent under reduced pressure, followed by column chromatographic purification [silica, chloroform/ethyl acetate (10/1, v/v)] afforded 1.20 g (52%) of 2-(methoxycarbonyldithio)benzyl alcohol having an  $R_f$  = 0.47 and <sup>1</sup>H NMR (CDCl<sub>3</sub>, 360 MHz)  $\delta$  ppm: 7.65–7.27 (m, 4 H), 4.85 (s, 2 H, CH<sub>2</sub>OH), 3.83 (s, 3 H, OCH<sub>3</sub>), 2.99 (s, 1H, OH). FAB for C<sub>9</sub>H<sub>10</sub>O<sub>3</sub>S<sub>2</sub> (M<sup>+</sup>) calcd: 230. found 230.

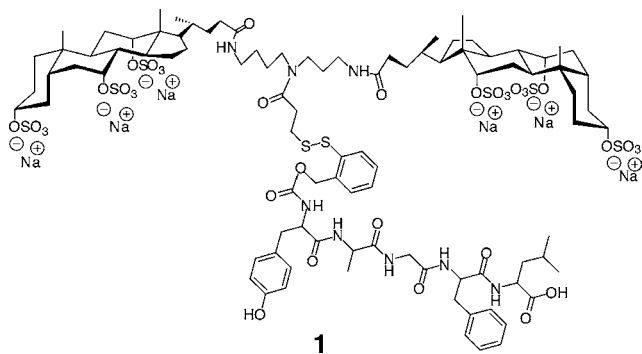
**3,3'-Dithiopropionic Acid Bis-3-hydroxyl-1,2,3-benzotriazin-4(3H)-onyl Ester.** A solution was prepared from 0.500 g (2.378 mmol) of dithiopropionic acid, 1.008 g (6.18 mmol) of 3-hydroxyl-1,2,3-benzotriazin-4(3H)-one, 1.135 g (5.5 mmol) of *N,N*-dicyclohexylcarbodiimide (DCC), and 20 mL of CH<sub>2</sub>Cl<sub>2</sub>. After stirring the mixture overnight at room temperature, the resulting insoluble urea was removed by filtration. The filtrate was then poured into 100 mL of a saturated aqueous NaHCO<sub>3</sub> solution. The organic layer was separated and concentrated under reduced pressure, and the residue was purified by recrystallization from ethanol to give 1.31 g (75%) of the desired diester having <sup>1</sup>H NMR(CD<sub>3</sub>OD):  $\delta$  ppm: 8.43 (dd, 2 H), 8.41 (dd, 2 H), 8.22 (td, 2 H), 8.07 (td, 2 H), 3.40 (t, 4 H), 3.27 (t, 4 H). FAB for C<sub>20</sub>H<sub>16</sub>N<sub>6</sub>O<sub>6</sub>S<sub>2</sub> (MH<sup>+</sup>) calcd: 501. found 501.

***N,N'*-Bis[*N,N'*-spermidinebischoleamideyl]-3,3'-dithiopropionebisamide, Persulfate (2).** To a solution

of 1.186 g (1.28 mmol) of *N,N'*-spermidinebis(choleamide) in 10 mL of DMF was added 669  $\mu$ L (3.84 mmol) of diisopropylethylamine (DIPEA) (2). After stirring for 10 min, 315 mg (0.63 mmol) of 3,3'-dithiopropionic acid bis-3-hydroxyl-1,2,3-benzotriazin-4(3H)-one ester was directly added as a powder. After stirring overnight, the mixture was concentrated under reduced pressure. Purification by column chromatography [silica, chloroform/methanol/water (30/9/1, v/v/v)] afforded 970 mg (75%) of the corresponding bis-steroid dimer having  $R_f$  = 0.57 and <sup>1</sup>H NMR (CD<sub>3</sub>OD)  $\delta$  ppm: 3.89 (s, 4 H), 3.74 (s, 4 H), 3.26 (m, 4 H), 3.14–3.11 (m, 8 H), 2.90 (brs, 4 H), 2.74 (brs, 4 H), 2.30–2.10 (m, 8 H), 2.10–2.00 (m, 8 H), 1.95–1.00 (m, 100 H), 1.04 (s, 12 H), 0.97 (s, 12 H), 0.66 (s, 12 H).

Sulfation was then carried out using standard procedures (5). Thus, 320 mg (0.148 mmol) of the bis-steroid dimer was dissolved in 10 mL of DMF at 0 °C, followed by direct addition of 848 mg (5.33 mmol) of Pyr-SO<sub>3</sub>. After the mixture was stirred for 5.5 h at room temperature, 10 mL of cold water was added, followed by addition of saturated sodium bicarbonate until the pH of the mixture was 10. The combined solvent was removed under reduced pressure, and the residue was purified by column chromatography [silica, chloroform/methanol/water (5/4/1, v/v/v)] to give 323 mg (67%) of the hexasulfated dimer (Na<sup>+</sup> salt) having  $R_f$  = 0.29 and <sup>1</sup>H NMR (CD<sub>3</sub>OD)  $\delta$  ppm: 4.67 (s, 4 H), 4.45 (s, 4 H), 4.13 (s, 4 H), 3.35–3.10 (m, 16 H), 2.99 (br, 4 H), 2.83 (br, 4 H), 2.40–0.90 (m, 120 H), 0.76 (s, 12 H). MALDI for C<sub>116</sub>H<sub>184</sub>N<sub>6</sub>O<sub>54</sub>S<sub>14</sub>Na<sub>11</sub> (M–Na) calcd: 3226. found 3231.

***N*<sup>1</sup>,*N*<sup>3</sup>-(Spermidine-bis-choleamideyl)-*N*<sup>2</sup>-(3-dithio-2-hydroxymethyl-1-phenyl)propionamide, Persulfate **3**.** The sulfated dimer conjugate **2** (1.81 g, 0.556 mmol) was dissolved in 20 mL of a 1.0 M phosphate buffer (pH 7.3) and mixed with 10 mL of a 1.0 M phosphate buffer containing 240 mg (0.835 mmol) of tris-(2-carboxyethyl)phosphine hydrochloride (TCEP), which was adjusted to pH 7.3. After stirring for 50 min at room temperature, the solution was concentrated under reduced pressure, and the residue dissolved in 100 mL of methanol (the inorganic salts were removed by filtration). The solution, which contained the corresponding thiol monomer, was concentrated to ca. 50 mL, and 140  $\mu$ L (1.0 mmol) of triethylamine then added to it. To the resulting solution was added, dropwise, a second solution, which was prepared from 307 mg (1.335 mmol) of 2-(methoxycarbonyldithio)benzyl alcohol plus 50 mL of methanol. After addition was complete, the mixture was stirred at room temperature for 5 h. Subsequent removal of solvent under reduced pressure and purification by column chromatography [silica, chloroform/methanol/water (60/40/10, v/v/v)] afforded 804 mg (41%) of **3** having  $R_f$  = 0.42 and  $^1\text{H}$  NMR ( $\text{CD}_3\text{OD}$ )  $\delta$  ppm: 7.76 (m, 1 H), 7.47 (m, 1 H), 7.30 (m, 2 H), 4.77 (s, 2 H), 4.65 (s, 2 H), 4.43 (s, 2 H), 4.12 (br, 2 H), 3.31 (m, 2 H), 3.15 (m, 6 H), 2.95 (m, 2 H), 2.73 (m, 2 H), 2.35–0.85 (m, 66 H), 0.75 (s, 6 H). MALDI (reflector mode  $\pm 0.02\%$ ) for  $\text{C}_{65}\text{H}_{99}\text{N}_3\text{O}_{28}\text{S}_8\text{Na}_5(\text{M}-\text{Na})$  calcd: 1740. found 1740.



**{3-(*N*<sup>2</sup>-Propionamideyl-*N*<sup>1</sup>,*N*<sup>3</sup>-spermidine-bis-choleamideyl)-2-dithiobenzyl-DADLE-carbamate, Persulfate **1**.** To a solution made from 35.3 mg (0.02 mmol) of **3** and 1 mL of DMF were added 51.2 mg (0.2 mmol) of *N,N*-disuccinimidyl carbonate (DSC) and 28  $\mu$ L (0.2 mmol) of triethylamine. The mixture was stirred for 15 h under a nitrogen atmosphere at room temperature, followed by removal of most of the solvent under reduced pressure; a small amount of DMF remained in order to keep the product in solution. Addition of 10 mL of acetone resulted in the precipitation of the DSC-activated ester, which was washed thoroughly with acetone, collected by filtration and freeze-dried for 2 h. This activated ester was then dissolved in 1 mL of DMF, and the resulting solution then added, dropwise, to a solution made from the sodium salt of DADLE [prepared by treating 13 mg (0.0228 mmol) of DADLE with 2 equiv of  $\text{NaHCO}_3$  in a minimum volume of water, followed by freeze-drying] plus 0.5 mL of DMF. The resulting mixture was stirred for 10 h at room temperature. The solvent was then removed under reduced pressure, and the umbrella-peptide conjugate was purified once by preparative thin-layer chromatography [silica, chloroform/methanol/water (60/40/10, v/v/v);  $R_f$  = 0.3], twice by reverse phase preparative thin-layer chromatography [C-18 silica (VWR Scientific), methanol/water (3/2, v/v)], and one final

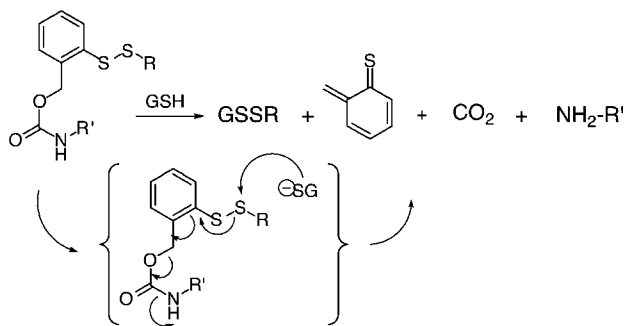
preparative thin-layer chromatography [silica, chloroform/methanol/water (60/40/10, v/v/v)] to give 10 mg of **1** having  $R_f$  = 0.51, and  $^1\text{H}$  NMR ( $\text{CD}_3\text{OD}$ , 360 MHz)  $\delta$  ppm: 7.75 (m, 1 H), 7.35–7.10 (m, 8 H), 7.08 (d, 2 H), 6.71 (d, 2 H), 5.20 (m, 2 H), 4.65 (s, 3 H), 4.45 (s, 2 H), 4.33 (m, 2 H), 4.15 (br, 3 H), 3.95 (m, 2 H), 3.30 (m, 2 H), 3.15–2.85 (m, 12 H), 2.68 (m, 2 H), 2.45–0.90 (m, 72 H), 0.73 (m, 12 H). MALDI (reflector mode  $\pm 0.02\%$ ) for  $\text{C}_{95}\text{H}_{135}\text{N}_8\text{O}_{36}\text{S}_8\text{Na}_6(\text{M}-\text{Na})$  calcd: 2358. found 2358.

**Efflux of DADLE from Cholesterol-Rich Liposomes.** A unilamellar liposomal dispersion (ca. 200 nm diameter) was prepared by standard extrusion methods using 42 mg of a mixture of POPC/POPG/cholesterol (72/4/24, mol/mol/mol) and 1.40 mL of buffer that was 1.0 mM in DADLE (**6**). The dispersion was dialyzed (three times) against 1 L of buffer for 24 h, using a dialysis tubing having a 300 kDa MW cutoff. The dispersion was then placed into a 2 mL dialysis cell, equipped with a 100 nm Nuclepore membrane. An analysis for the release of DADLE from the liposomes was made by monitoring the receiving side (23  $^\circ\text{C}$ ) by withdrawing 0.5 mL and reacting it with 0.1 mL of a 2.0 mM fluorescamine solution in acetone for 5 min. The fluorescence intensity at 480 nm was then recorded and compared with a calibration curve. Immediately after withdrawing the 0.5 mL aliquot, 0.5 mL of fresh buffer was added to the receiving side in order to maintain a constant volume of 1.0 mL.

To test for binding of DADLE to the liposomes, a related experiment was carried out in which empty liposomes were first incubated with an external solution of DADLE for 24 h, and then the resulting dispersion was dialyzed against an equal volume of buffer. In principle, if the binding of DADLE to the liposomes were negligible, then exactly 50% of the total quantity of DADLE that was added to the dispersion should be present in the receiving side of the dialysis cell, that is, the side that does not contain liposomes. Thus, 430  $\mu$ L of a liposomal dispersion that was devoid of DADLE was incubated with 430  $\mu$ L of a 50  $\mu\text{M}$  solution of DADLE in buffer for a period of 24 h. Subsequent dialysis against 860  $\mu$ L of buffer for 24 h, and analysis of the receiving side showed the presence of 50% of the total DADLE that was incubated with the liposomes. These results indicate, therefore, that there is negligible binding of DADLE to the liposomes.

**Reaction of **1** with GSH in Solution.** A solution of **1** in buffer (1.00 mM, 0.80 mL) was mixed with 0.80 mL of 3.0 mM in glutathione in buffer at room temperature. The course of the reaction was monitored by UV (264 nm) and also by thin-layer chromatography. For UV analysis, 140  $\mu$ L-aliquots were withdrawn and diluted with 240  $\mu$ L of buffer, and the UV absorption was recorded. Analysis by thin-layer chromatography (silica gel,  $\text{CHCl}_3/\text{CH}_3\text{OH}/\text{H}_2\text{O}$ , 60/40/10, v/v/v) showed the complete disappearance of **1** ( $R_f$  0.3) after 8 h. At that time, a portion of the liberated DADLE was isolated by thin-layer chromatography (silica gel,  $\text{CHCl}_3/\text{CH}_3\text{OH}/\text{H}_2\text{O}$ , 65/30/2, v/v/v) using 10  $\mu$ L aliquots of the solution. The band corresponding to the free peptide ( $R_f$  0.65) was extracted with  $2 \times 0.5$  mL of buffer and filtered using glass wool. A 0.5 mL portion was then analyzed after reaction with 100  $\mu$ L of 2 mM fluorescamine in acetone for 5 min. The fluorescence intensity at 480 nm was then compared with a calibration curve.

**Delivery of DADLE to the Aqueous Interior of Cholesterol-Rich Liposomes.** A unilamellar liposomal dispersion (200 nm diameter) was prepared by standard extrusion methods using 60 mg of a mixture of POPC/

**Scheme 4**

POPG/cholesterol (72/4/24, mol/mol/mol) plus 2.0 mL of buffer containing 3.0 mM glutathione (**6**). The dispersion was dialyzed (three times) against 1 L of buffer for 28 h using dialysis tubing with a 300 kDa MW cutoff. The absence of external glutathione was confirmed by taking an 800- $\mu$ L aliquot and subjecting it to dialysis for 35 min against 800  $\mu$ L of buffer, using a dialysis cell that was equipped with a 100 nm Nuclepore membrane. Under these conditions, the half-life for permeation of glutathione across this membrane is 33 min. Analysis of the receiving side, by use of Ellman's assay [5,5'-dithiobis-(2-nitrobenzoic acid), DTNB], indicated that  $<0.9$   $\mu$ M of external thiol was present in the dispersion. An analysis of the glutathione that was entrapped within the vesicles was then made by dissolving a 20  $\mu$ L aliquot of the dispersion in a solution that was made from 0.266 mL of ethanol plus 0.133 mL of buffer that contained 20% of sodium dodecyl sulfate (w/w). To this mixture was added 20  $\mu$ L of 2.0 mM DTNB in buffer. The glutathione concentration of the resulting solution was found to be 427  $\mu$ M.

To 0.99 mL of the glutathione-entrapped dispersion was added 0.99 mL of a 80  $\mu$ M solution of **1** in buffer at 23  $^{\circ}$ C. Aliquots (200  $\mu$ L) of the resulting dispersion were withdrawn as a function of time and were mixed with 200  $\mu$ L of a solution that was made from 0.133 mL of ethanol plus 0.066 mL of buffer containing 20% of sodium dodecyl sulfate (w/w). The absorbance at 264 nm was then measured after 1 min of mixing. It should be noted that under these dilute conditions, the rate of reaction of glutathione with **1** is negligible (i.e.,  $<0.7\%$ ).

After the transport experiment was completed, 550  $\mu$ L of the dispersion was dialyzed for 2.5 h at 23  $^{\circ}$ C against 550  $\mu$ L of buffer and analyzed, separately, for glutathione (Ellman's assay) and for amino group content (fluorescamine assay). Specifically, 300  $\mu$ L of the receiving side of the dialysis cell was reacted with 20  $\mu$ L of 2.0 mM DTNB, and the absorbance measured at 410 nm. The concentration of glutathione was found to be 0.82  $\mu$ M. In a separate experiment, 250  $\mu$ L of the receiving side was diluted with an equal volume of buffer, followed by addition of 100  $\mu$ L of a 2.0 mM solution of fluorescamine in acetone. The DADLE concentration (total amino group concentration minus the glutathione concentration) was 1.54  $\mu$ M.

## RESULTS AND DISCUSSION

**Design and Synthesis of a Fully Detachable Molecular Umbrella–Peptide Conjugate.** To create a fully detachable molecular umbrella conjugate, we have chosen to follow a prodrug strategy that has previously been introduced by Senter (7,8). Specifically, this strategy involves a thiol-induced reductive fragmentation of a benzyl carbamate disulfide (Scheme 4). In the present work, umbrella–peptide conjugate (**1**) was designed as

a synthetic target in order to test the feasibility of such an approach for the construction of a fully detachable molecular umbrella. In essence, conjugate **1** was deemed as a target worthy for three reasons. First, there has been considerable interest in finding ways to improve the transport of opioid peptides such as H-Tyr-D-Ala-Gly-Phe-D-Leu-OH (DADLE) across hydrophobic barriers (9–12). Thus, conjugates such as **1** could have direct therapeutic relevance. Second, an *o*-dithiobenzyl carbamate was selected as a linkage unit due to the ready availability of 2-mercaptobenzyl alcohol from commercial sources. Third, a persulfated form of molecular umbrella was used to ensure reasonable water solubility of the resulting conjugate. Previous studies from our laboratory have shown that such umbrella molecules can transport GSH across phospholipid bilayers (13).

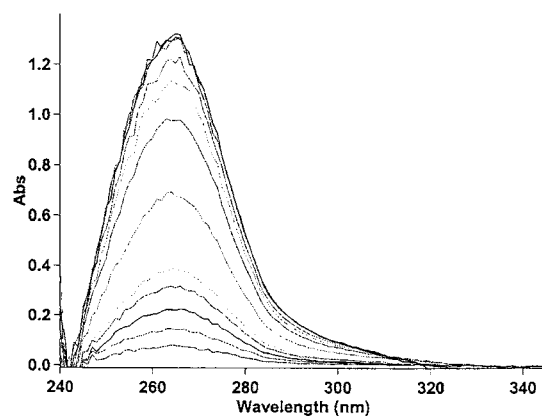
Our synthesis of **1** was accomplished via the sequence of reactions that are summarized in Scheme 3. Thus, acylation of *N,N*-spermidinebis(choleamide) with an activated form of 3,3'-dithiopropionic acid [activated with 3-hydroxy-1,2,3-benzotriazin-4*H*(3*H*)-one], followed by sulfation with Pyr-SO<sub>3</sub> yielded umbrella dimer **2**. Subsequent reduction with TCEP to give the corresponding umbrella thiol and coupling with an activated form of 2-mercaptobenzyl alcohol (prepared by reaction with methoxycarbonylsulfonyl chloride) afforded **3**. Finally, activation of the benzylic hydroxyl group with *N,N*-disuccinimidyl carbonate (DSC), followed by direct coupling with DADLE produced the desired conjugate, **1**.

**Impermeability of Cholesterol-Rich Phospholipid Membranes toward DADLE.** To confirm that DADLE, itself, does not readily cross cholesterol-rich phospholipid bilayers, this pentapeptide was entrapped within the aqueous interior of unilamellar liposomes (200 nm diameter), which were prepared using a POPC/POPG/cholesterol composition of 72/4/24 (mol/mol/mol). Upon removal of nonentrapped DADLE by gel filtration, subsequent dialysis revealed negligible release of the peptide ( $<0.3\%$ ) from the liposomes after 72 h at 23  $^{\circ}$ C. Related experiments that were carried out, in which empty liposomes were incubated with buffer solutions of DADLE, further revealed that this peptide has negligible affinity to such membranes (see Experimental Section for details).

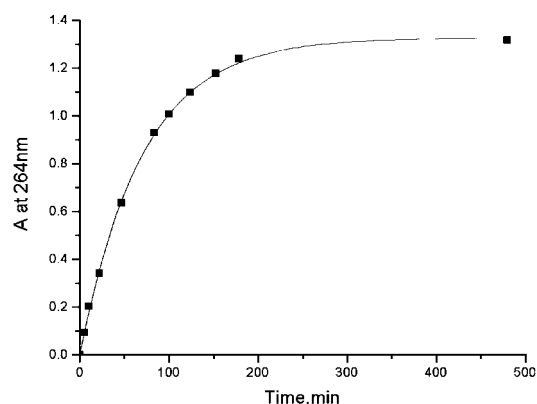
**Reaction of **1** with Glutathione in Solution.** Before attempting the delivery of DADLE to the aqueous interior of liposomes, we first confirmed the ability of GSH to release DADLE from **1** in homogeneous solution. For this purpose, an aqueous solution of **1** was treated with 1.5 mM GSH in PIPES buffer at 23  $^{\circ}$ C. During the course of the reaction, the solution became effervescent and a UV absorption emerged at 264 nm (Figure 1). The putative *o*-thiobenzoquinone methide product and/or cyclic oligomers are presumed to be responsible for this absorbance (14). A plot of the increase in the UV absorbance as a function of time obeyed simple first-order kinetics (Figure 2). When the UV absorption reached a maximum, thin-layer chromatography confirmed the complete disappearance of **1** and the appearance of the free form of DADLE. Isolation of DADLE from the product mixture by preparative thin-layer chromatography afforded a ca. 82% isolated yield of the peptide.

**Delivery of DADLE into Cholesterol-Rich Liposomes.** Peptide delivery experiments were next carried out with **1**, using liposomal targets that were made from a lipid mixture that was similar to the one used to demonstrate the impermeability of DADLE. In this case, glutathione was first entrapped within the aqueous interior of the liposomes and **1** was added, externally, to





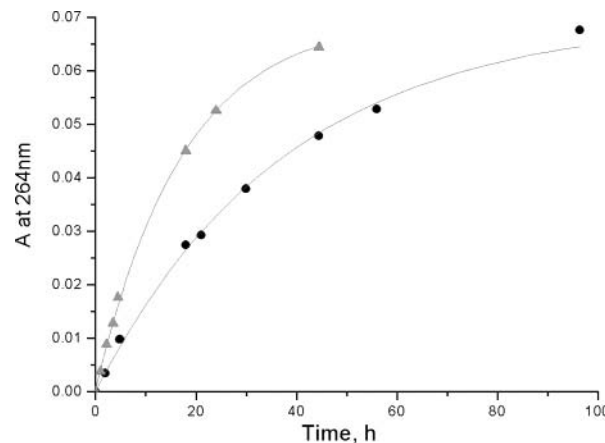
**Figure 1.** Changes in UV spectrum upon reaction of 0.50 mM of **1** with 1.5 mM GSH at 23 °C in PIPES buffer.



**Figure 2.** Increase in UV absorbance at 264 nm as a function of time (data taken from Figure 1). The solid lines represents a theoretical curve for a first-order process.

the dispersion. Using procedures that are described in the Experimental Section, the progress of the reaction could be followed by monitoring the increase in the UV absorption at 264 nm. For this analysis, aliquots of the dispersion were destroyed by addition of an ethanolic solution of sodium dodecyl sulfate (SDS) in order to avoid interference from light scattering by the liposomes. It should be noted that GSH and **1** undergo a significant dilution upon addition of the ethanolic solution. This results in a minimal extent of reaction, provided that the UV measurement is made within ca. 2 min of the addition. Similar to what was found in homogeneous solution, the increase in the absorbance at 264 nm followed first-order kinetics (Figure 3). The fact that the observed first-order rate constant was directly proportional to the concentration of entrapped GSH (i.e., the pseudo first-order rate constant increased from  $2.47 \times 10^{-2} \text{ h}^{-1}$  to  $5.87 \times 10^{-2} \text{ h}^{-1}$  on going from 1.25 to 3.00 mM entrapped GSH) indicates that the rate of peptide delivery is controlled by chemical reaction, and that permeation across the bilayer is a relatively fast process (Figure 3).

To confirm that DADLE was, in fact, released within the aqueous interior of the vesicles, we sought evidence that (i) leakage of entrapped glutathione was negligible and (ii) DADLE was fully retained by the dispersion upon dialysis. If leakage of glutathione were negligible, this would provide compelling evidence that chemical reaction has taken place within the aqueous interior of the vesicles. Since we have found that DADLE exhibits negligible binding to POPC/POPG/cholesterol-based liposomes, complete retention of DADLE by such a dispersion, after being subjected to dialysis, would provide



**Figure 3.** Increase in UV absorption at 264 nm as a function of time for reaction of 40  $\mu\text{M}$  of **1** with 200 nm diameter liposomes made from POPC/POPG/cholesterol ratio of 72/4/24 (mol/mol/mol), (19 mM in total lipid concentration present in the dispersion), which contained (●) 1.25 mM and (▲) 3.00 mM of entrapped GSH at 23 °C. The solid lines represent theoretical curves for first-order processes.

compelling evidence that this peptide is entrapped within the vesicle interior. With this rationale in mind, we carried out a delivery experiment similar to the one that is described above. Upon completion of the reaction (UV analysis), a portion of the dispersion was subjected to dialysis for 2.5 h using an equal volume of buffer. Analysis of the source and receiving side of the dialysis cell showed that more than 99.6% of the glutathione was present in the source (liposome) side. Given the fact that glutathione crosses such dialysis membranes with a half-life of ca. 33 min, we can conclude that leakage of glutathione from the vesicles is negligible. In a separate analysis, we have found that >96% of the DADLE was associated with the source (liposome) side of the dialysis cell. Since the half-life for permeation of free DADLE across this dialysis membrane is ca. 53 min, this results provides strong evidence that DADLE has become entrapped within these vesicles.

In summary, the results reported herein demonstrate the feasibility of creating a fully detachable molecular umbrella that can deliver a peptide into model cells containing physiologically relevant concentrations of entrapped glutathione. Efforts aimed at exploiting such systems, with a view toward drug delivery, are currently in progress.

#### ACKNOWLEDGMENT

We are grateful to the National Institutes of Health (PHS Grant GM51814) for support of this research.

**Supporting Information Available:**  $^1\text{H}$  NMR spectrum of **1**. This material is available free of charge via the Internet at <http://pubs.acs.org>.

#### LITERATURE CITED

- (1) Janout, V., Lanier, M., and Regen, S. L. (1996) Molecular Umbrellas. *J. Am. Chem. Soc.* 118, 1573.
- (2) Janout, V., Lanier, M., and Regen, S. L. (1997) Design and Synthesis of Molecular Umbrellas. *J. Am. Chem. Soc.* 119, 640.
- (3) Janout, V., Staina, I. V., Bandyopadhyay, P., and Regen, S. L. (2001) Evidence for and Umbrella Mechanism of Bilayer Transport. *J. Am. Chem. Soc.* 123, 9926–9927.
- (4) Abbreviations: GSH, glutathione; PIPES, piperazine-*N,N*-bis(2-ethanesulfonic acid); TCEP, tris(2-carboxyethyl)phos-

- phine hydrochloride; DADLE, H-Tyr-D-Ala-Gly-Phe-D-Leu-OH; POPC, 1-palmitoyl-2-oleoyl-*sn*-glycero-3-phosphocholine; POPG, 1-palmitoyl-2-oleoyl-*sn*-glycero-3-phosphatidylglycerol; DTNB, 5,5'-dithiobis(2-nitrobenzoic acid); Pyr-SO<sub>3</sub>, pyridine sulfur trioxide.
- (5) Kunou, M., Koizumi, M., Shimizu, K., Kawase, M., and Hatanaka, K. (2000) Synthesis of Sulfated Colominic Acids and Their Interaction with Fibroblast Growth Factors. *Biomacromolecules* 1, 451.
  - (6) Mayer, L. D., Hope, M. J., and Cullis, P. R. (1986) Vesicles of Variable Size Produced By A Rapid Extrusion Procedure. *Biochim. Biophys. Acta*, 858, 161.
  - (7) Senter, P. D., Pearce, W. E., Greenfield, R. S. (1990) Development of a Drug-Release Strategy Based on the Reductive Fragmentation of Benzyl Carbamate Disulfides. *J. Org. Chem.* 55, 2975–2978.
  - (8) Zalipsky, S., Qazen, M., Walker, J. A., Mullah, N., Quinn, Y. P., and Huang, S. K. (1999) New Detachable Poly(ethylene glycol) Conjugates: Cysteine-Cleavable Lipopolymers Regenerating Natural Phospholipid, Diacyl Phosphatidylethanolamine. *Bioconjugate Chem.* 10, 703–707.
  - (9) Bak, A., Siahaan, T. J., Gudmundsson, O. S., Friis, G. J., and Borchardt, R. T. (1999) Synthesis and Evaluation of the Physicochemical Properties of Esterase-Sensitive Cyclic Prodrugs of Opioid Peptides Using an (Acyloxy)alkoxy Linker. *J. Peptide Res.* 53, 393–402.
  - (10) Gudmundsson, O. S., Jois, S.D. S., Velde, D. G., Vander, Siahaan, T. J., Wang, B., and Borchardt, R. T. (1999) The Effect of Conformation On the Membrane Permeation of Coumarinic Acid- and Phenylpropionic acid-based Cyclic Prodrugs of Opioid Peptides. *J. Peptide Res.* 53, 383–392.
  - (11) Bak, A., Gudmundsson, O. S., Griis, G. J., Siahaan, J., and Borchardt, R. T. (1999) Acyloxyalkoxy-Based Cyclic Prodrugs of Opioid Peptides: Evaluation of the Chemical and Enzymatic Stability as Well as Their Transport Properties Across Caco-2 Cell Monolayers. *Pharm. Res.* 16, 24–29.
  - (12) Rasmuswami, V., Zhu, X., Romanowski, M., Haaseth, R. C., Misicka, A., Lipkowski, A. W., Hruby, V. J., and O'Brien, D. F. (1996) Lipid Membrane Permeability of Modified c[D-Pen<sup>2</sup>, D-Pen<sup>5</sup>] Enkephalin Pept.. *Int. J. Pept. Protein Res.* 48, 87–94.
  - (13) Janout, V., Zhang, L. H., Staina, I. V., DiGiorgio, C., and Regen, S. L. (2001) Molecular Umbrella-Assisted Transport of Glutathione Across a Phospholipid Membrane. *J. Am. Chem. Soc.* 123, 5401.
  - (14) Kanakarajan, K., and Meier, H. (1983) Cycloaddition reactions of benzothietane. *J. Org. Chem.* 48, 881.

BC034074M

# No Enhancement of Nuclear Entry by Direct Conjugation of a Nuclear Localization Signal Peptide to Linearized DNA

Mitsuhide Tanimoto,<sup>†,‡</sup> Hiroyuki Kamiya,<sup>†,‡</sup> Noriaki Minakawa,<sup>†</sup> Akira Matsuda,<sup>†</sup> and Hideyoshi Harashima<sup>\*,†,‡</sup>

Graduate School of Pharmaceutical Sciences, Hokkaido University, Kita-12, Nishi-6, Kita-ku, Sapporo 060-0812, Japan and CREST, Japan Science and Technology, Japan. Received May 8, 2003;

Revised Manuscript Received October 6, 2003

Efficient nuclear entry of exogenous DNA is one of the key factors toward gene therapy success with nonviral vectors. To re-address the effects of a nuclear localization signal (NLS) peptide attached directly to DNA, we prepared three dumbbell-shaped, green fluorescent protein (GFP)-encoding DNAs containing one or two NLS peptides. The peptide was conjugated to the loop-forming oligodeoxynucleotides by cross-linking reactions between the peptide and a modified uracil base with a dioxaoctylamino linker, and the oligonucleotides were then ligated to the DNA molecules. The NLS-conjugated DNA dumbbells were microinjected into the cytosols and nuclei of simian COS-7 cells. In addition, unconjugated DNA dumbbells, with or without a modified uracil base, were also examined for comparison. The GFP gene was expressed with efficiencies in the order of the unmodified DNA  $\geq$  the NLS-conjugated DNA  $>$  the unconjugated DNA with the base modification, with both cytosolic and intranuclear microinjections. Thus, we concluded that (i) one or two NLS peptide(s) did not dramatically improve the nuclear entry of DNA and that (ii) chemical modification of DNA reduced the transcription efficiency or stability in the nucleus.

## INTRODUCTION

Nonviral vectors are highly attractive in gene therapy due to their excellent safety profile, despite their low transgene expression efficiency in comparison to viral vectors. The intracellular disposition, especially the DNA entry into the nucleus, is a very important issue for high transgene expression (1). Intranuclear microinjections of DNA result in about 100- to 1000-fold more efficient expression than cytoplasmic microinjections (2, 3). Thus, the nuclear entry pathway(s) of exogenous DNA are of great interest. One proposed mechanism is the trafficking of DNA when the nuclear membrane disappears at the M phase of cell division (4). However, the nuclear entry occurs in nondividing cells (5) and at a very early time point during the transfection (6), suggesting that DNA could enter the nucleus in the presence of the nuclear membrane. We and others pointed out the possibility that the cationic liposomal lipid and the nuclear envelope may fuse, and thus the exogenous DNA may enter the nucleus (4, 6). An alternative explanation is the nuclear pore complex (NPC)-mediated import of DNA. Although the contribution of this putative pathway to the nuclear entry of DNA is unclear, it has been proven to be useful for the delivery of a protein conjugated with nuclear localization signal (NLS) peptides (7).

Recently, chemical conjugations of the NLS peptide to DNA molecules have been attempted to improve the nuclear entry. Sebestyén et al. used a cross-linker to conjugate the NLS peptide to the N3-position of adenine bases in double-stranded DNA (8). The introduction of 60–100 NLS peptides/kbp DNA was efficient for nuclear

uptake in digitonin-permeabilized cells. However, no increase in the nuclear uptake of the modified DNA was observed after microinjection into the cytoplasm of living cells, and the transgene expression was completely abolished due to the high modification level. In contrast, Zanta et al. synthesized a loop-forming oligodeoxynucleotide (ODN) cross-linked with the NLS peptide, and this modified loop-forming ODN was then enzymatically ligated to linearized double-stranded DNA (9). This NLS–DNA was transfected with a cationic polymer, polyethylenimine (PEI), and a single NLS peptide reportedly could enhance transgene expression from ten- to hundreds-fold, depending on the cell lines used. However, the nuclear entry effects of the NLS peptide attached to DNA are still open to dispute (10). Zanta et al. obtained their results using PEI-mediated transfection. However, PEI may enter the nucleus together with DNA (11).

In this study, we reexamined the effects of the NLS peptide conjugated to DNA by cytosolic and intranuclear microinjections. In addition, we compared the expression of the transgene on chemically modified and unmodified DNA molecules. Our results suggest that (i) one or two NLS peptide(s) did not dramatically improve the nuclear entry of DNA and that (ii) chemical modification of DNA reduced the transcription efficiency or stability in the nucleus.

## MATERIALS AND METHODS

**General.** COS-7 cells were from the RIKEN Cell Bank (Tsukuba, Japan). The plasmid pQBI 25–63, containing the cytomegalovirus promoter and the green fluorescent protein (GFP) gene (3), was purified with a Qiagen (Valencia, California) EndoFree Mega kit. The SV40 large T antigen NLS peptide (NH<sub>2</sub>-PKKKRKVEDPYC) with C-terminal amidation was obtained from Sigma Genosys Japan (Ishikari, Japan) in the purified form.

Physical data were measured as follows: The NMR spectra were recorded with a JEOL GX-270 spectrometer,

\* To whom correspondence should be addressed: Tel +81–11–706–3919. Fax +81–11–706–4879. E-mail harasima@pharm.hokudai.ac.jp.

<sup>†</sup> Hokkaido University.

<sup>‡</sup> CREST.



**Table 1. Oligodeoxynucleotides Used in This Study**

ODN	sequence (5'→3') <sup>a</sup>
ODN-1	dGATCTGGCTCGCCTGTTTTTCAGGCGAGCCA
ODN-2	dAGCTTGGCTCGCCTGTTTTTCAGGCGAGCCA
ODN-3	dGATCTGGCTCGCCTGTTXTTCAGGCGAGCCA
ODN-4	dGATCTGGCTCGCCTGTTXTTCAGGCGAGCCA
ODN-5	dAGCTTGGCTCGCCTGTTXTTCAGGCGAGCCA

<sup>a</sup>X represents the modified uracil derivative conjugated or unconjugated to the NLS peptide. The italicized and underlined sequences represent sticky ends and loop-forming sites, respectively. Annealed ODN-2 and ODN-5 have an end compatible with *Hind* III, and the others have that compatible with *Bgl* II.

with CDCl<sub>3</sub> as the solvent and tetramethylsilane as the internal standard. Chemical shifts are reported in parts per million ( $\delta$ ), and signals are expressed as s (singlet), d (doublet), t (triplet), q (quartet), or m (multiplet). Mass spectra were measured on a JEOL JMS-D300 spectrometer. Matrix-assisted laser desorption/ionization time-of-flight mass spectrometry (MALDI-TOF-MS) was conducted with Applied Biosystems Voyager System 1065 (Appera, Norwalk, CT). Edman peptide sequencing analysis was carried out with Procise 492 (Appera, Norwalk, CT). TLC was done on Merck Kieselgel F254 precoated plates. The silica gel used for column chromatography was Merck silica gel 5715.

**5-*N*-(8-Trifluoroacetylaminio-3,6-dioxaoctyl)carbamoyl-5'-*O*-dimethoxytrityl-2'-deoxyuridine (3).** To a solution of **1** (**12**) (2.1 g, 3.2 mmol) in pyridine (30 mL) was added 2,2'-(ethylenedioxy)bis(ethylamine) (1.4 mL, 9.6 mmol), and the mixture was stirred for 1 h at room temperature. The solvent was removed in vacuo, and the residue was coevaporated with toluene to give crude **2**. The resulting **2** was dissolved in MeOH (80 mL), and Et<sub>3</sub>N (2.7 mL, 19.2 mmol) and ethyl trifluoroacetate (2.3 mL, 19.2 mmol) were added to the solution. The reaction mixture was stirred at room temperature until compound **2** was consumed on TLC analysis. The solvent was removed in vacuo, and the residue was purified on a neutral silica gel column with 5–10% EtOH in CHCl<sub>3</sub> to give **3** (1.8 g, 70% as white foam): FAB-MS: *m/z* 800 (M<sup>+</sup>); FAB-HRMS: calcd for C<sub>39</sub>H<sub>43</sub>N<sub>4</sub>O<sub>11</sub>NaF<sub>3</sub> (MNa<sup>+</sup>): 823.2747. found: 823.2750; <sup>1</sup>H NMR (CDCl<sub>3</sub>)  $\delta$  9.10 (s, 1H), 8.80 (m, 1H), 8.61 (s, 1H), 7.59 (m, 1H), 7.41–6.82 (m, 13H), 6.15 (t, 1H, *J* = 6.6 Hz), 4.33 (m, 1H), 4.00 (q, 1H, *J* = 4.6 Hz), 3.78 (s, 6H), 3.62–3.52 (m, 12H), 3.47 (dd, 1H, *J* = 4.6 and 9.9 Hz), 3.37 (dd, 1H, *J* = 4.6 and 9.9 Hz), 2.45 (m, 1H), 2.45 (ddd, 1H, *J* = 6.6, 4.0, and 13.9 Hz), 2.21 (ddd, 1H, *J* = 6.6, 7.3, and 13.9 Hz).

**5-*N*-(8-Trifluoroacetylaminio-3,6-dioxaoctyl)carbamoyl-5'-*O*-dimethoxytrityl-3'-*O*-(2-cyanoethoxy-1)*N,N*-diisopropylamino)phosphoryl-2'-deoxyuridine (4).** After successive coevaporation with pyridine, **3** (80 mg, 0.1 mmol) was dissolved in CH<sub>2</sub>Cl<sub>2</sub> (5 mL) containing *N,N*-diisopropylethylamine (35  $\mu$ L, 0.2 mmol). 2-Cyanoethyl *N,N*-diisopropylphosphoramidochloride (33  $\mu$ L, 0.15 mmol) was added to the solution, and the reaction mixture was stirred for 1 h at room temperature. The mixture was diluted with CHCl<sub>3</sub> and washed with saturated aqueous NaHCO<sub>3</sub> and brine. The separated organic layer was dried (Na<sub>2</sub>SO<sub>4</sub>) and concentrated in vacuo. The residue was purified on a neutral silica gel column with 60–100% AcOEt in hexane to give **4** (61 mg, 61% as white foam): <sup>31</sup>P NMR (CDCl<sub>3</sub>)  $\delta$  149.93, 149.53.

**Oligodeoxyribonucleotides.** ODNs with the modified uracil derivative were designed to incorporate it in the loop consisting of five pyrimidine bases and to make a 5'-protruding end compatible with the *Bgl* II or *Hind* III restriction enzyme (ODN-3 to ODN-5, Table 1). These

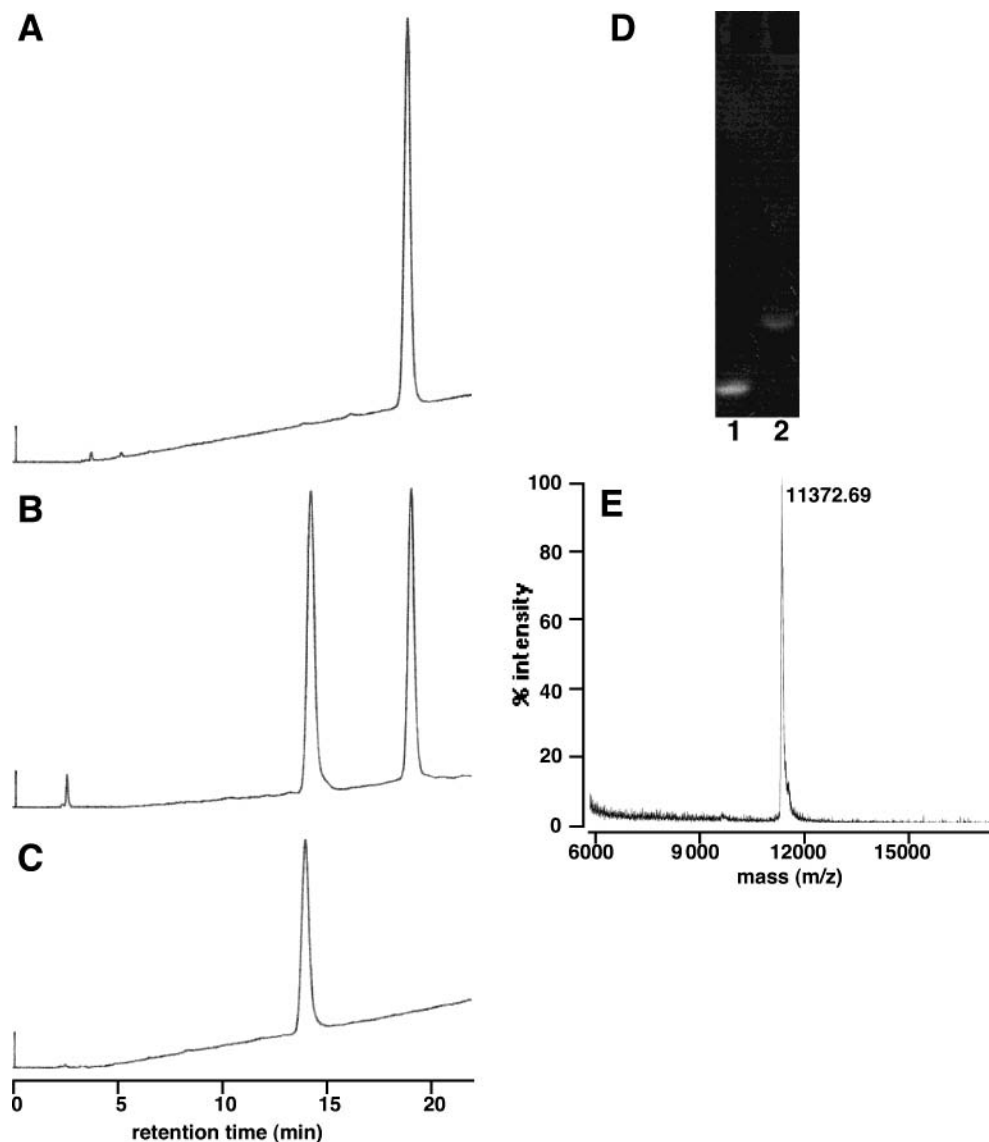
ODNs were synthesized using the phosphoramidite derivative **4** on an ABI model 381A DNA/RNA synthesizer. These ODNs were purified essentially as described (13).

The NLS peptide was conjugated to an ODN essentially as described (9), using 4-(*N*-maleimidomethyl)-cyclohexane-1-carboxylic acid *N*-hydroxysuccinimide ester (SMCC) as a bifunctional cross-linker. Namely, an ODN containing the modified uracil base(s) (16.1 nmol) was dissolved in 10 mM of sodium phosphate buffer (pH 7.5), and a 20 molar excess of SMCC (in DMF) was added. After an incubation for 1 h at room temperature, the same amount of SMCC was added, and the reaction mixture was then incubated at room temperature for another 1 h. The unreacted SMCC was removed with a NICK Column (Amersham Biosciences, Piscataway, NJ). A 20 molar excess of the NLS peptide was added, and the reaction mixture was incubated at room temperature overnight. In the case of ODN-4, containing two modified uracil bases, the amounts of SMCC and the NLS peptide were twice those described above. The conjugated ODNs were purified by anion-exchange HPLC, using a TSK-GEL DEAE-2SW column (4.6  $\times$  250 mm, Tosoh, Japan) with a linear gradient of ammonium formate (450 mM to 650 mM) in 20% aqueous acetonitrile. A new peak eluted at 15 min, faster than the unconjugated ODN (starting material, 18 min), and this peak was collected as an NLS-conjugated ODN (Figure 1). When ODN-4 containing two modified uracil bases was used, two peaks (8 and 12 min) that eluted faster than the unconjugated ODN (17 min) were observed. The 8 min peak was collected as the ODN containing two NLS peptides. The faster elution upon anion-exchange HPLC corresponded to the conjugation of the positively charged peptide. The ammonium formate was removed by gel filtration using Sephadex-G-25 (Amersham Biosciences).

The unmodified ODNs (ODN-1 and ODN-2, Table 1) were obtained from Hokkaido System Science (Sapporo, Japan) in the purified form. These ODNs were annealed and 5'-phosphorylated by T4 polynucleotide kinase and ATP.

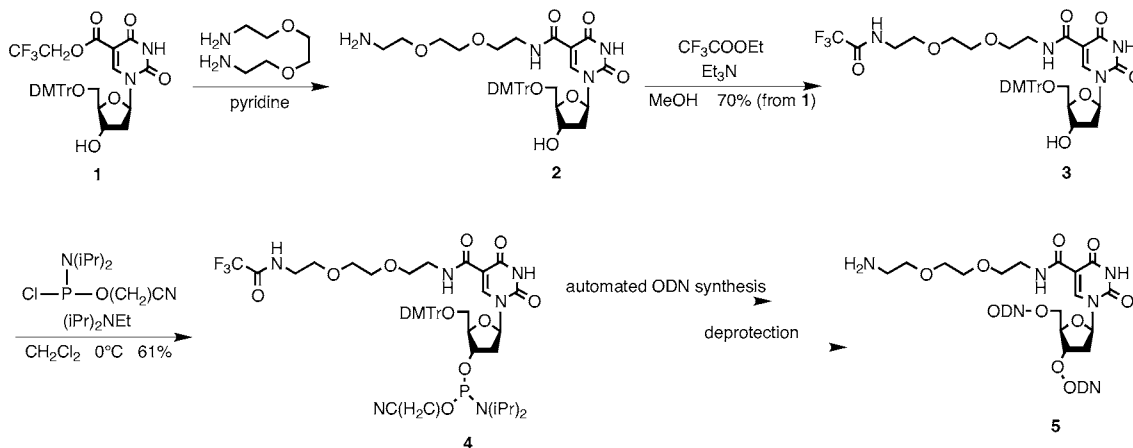
**Preparation of Linearized DNA Dumbbells.** The plasmid pQBI 25–63 was digested with *Bgl* II and *Hind* III, according to the manufacturer's instructions. The digested DNA was loaded onto a low melting point agarose gel. The linearized DNA was recovered from the gel by visualization with UV irradiation in the presence of a thin-layer chromatography plate. The DNA was then purified as described in the literature (14). The purified 2.3-kb DNA was mixed and joined with the corresponding ODNs (DNA:ODN = 1:100), as reported previously (3). After ethanol precipitation, the ligated DNA was purified by anion-exchange HPLC using a TSK-gel DNA-NPR column ( $\phi$ 4.6  $\times$  75 mm, Tosoh, Japan), essentially as described (15).

**Microinjection.** Cells were microinjected at day 1 postplating. In this procedure, we used a semiautomatic injection system (Eppendorf transjector 5246, Hamburg, Germany) attached to the Eppendorf micromanipulator 5171. Intranuclear and cytosolic microinjections were performed with the Z (depth) limit option using a 0.2-s injection time and a 10–200 hectopascal-injection pressure. The DNA was diluted with an injection buffer solution (0.5% tetramethylrhodamine-labeled dextran in phosphate-buffered saline). At 24 h postinjection, GFP expression was monitored by fluorescence microscopy, and the ratio of cells expressing GFP to tetramethylrhodamine-positive cells was calculated.



**Figure 1.** Conjugation of the NLS peptide and ODN-3. (A–C) Behavior upon anion-exchange HPLC. Unconjugated ODN-3 (A), mixture of the conjugation reaction (B), and conjugated ODN-3 after purification (C) are shown. (D) Polyacrylamide gel electrophoresis. Lane 1, unconjugated ODN-3; lane 2, conjugated ODN-3. (E) Molecular weight analysis by MALDI-TOF-MS. The calculated molecular weight of conjugated ODN-3 is 11364.

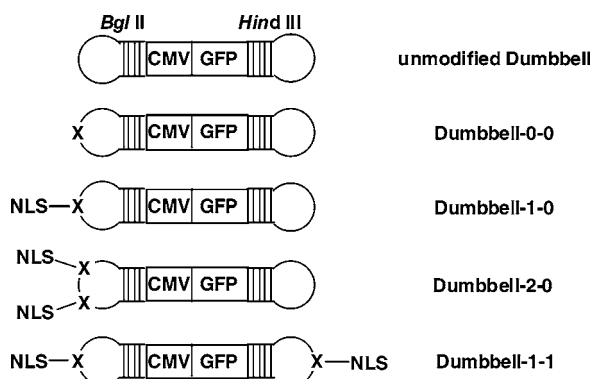
#### Scheme 1



#### RESULTS AND DISCUSSION

**Design of DNA Dumbbells.** A modified uracil base with a dioxaoctylamino linker (5), for conjugation to the NLS peptide, was incorporated into the ODNs, as shown

in Scheme 1. The conjugation of an ODN containing the modified uracil base and the NLS peptide was conducted using a bifunctional cross-linker, essentially as described (9). The conjugated ODNs were separated from the



**Figure 2.** Structures of DNA dumbbells containing the GFP gene used in this study. X, the modified uracil derivative; NLS, NLS peptide; CMV, CMV promoter. *Bgl* II and *Hind* III represent the restriction enzyme sites used for the ligation of loop-forming ODNs.

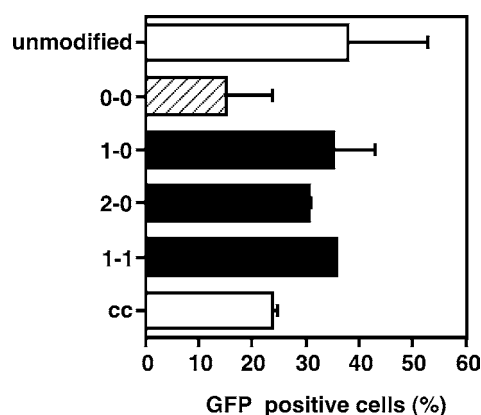
unconjugated ODNs by anion-exchange HPLC. Successful conjugation of an ODN and the positively charged peptide was indicated by chromatographic behavior upon anion-exchange HPLC (Figure 1A–C), lower mobility than the unconjugated ODN upon polyacrylamide gel electrophoresis (Figure 1D), molecular weight analysis by matrix-assisted laser desorption ionization time-of-flight mass spectrometry (MALDI-TOF-MS, Figure 1E), and sequencing of N-terminal 10 amino acids upon the Edman analysis (data not shown).

We prepared three DNA dumbbells with the NLS peptide (Figure 2). The NLS peptide-conjugated ODN-3 and ODN-4 (Table 1) were used to construct Dumbbell-1-0 and Dumbbell-2-0, respectively, which contain one and two peptide(s) in the loop near the *Bgl* II site. These DNA dumbbells contain the unmodified loop-forming ODN-2 near the *Hind* III site. Dumbbell-1-1 contains NLS peptides in both loops, using ODN-3 and ODN-5 conjugates. As controls, two DNA dumbbells were constructed: Dumbbell-0-0, which was capped with ODN-2 and unconjugated ODN-3, and the unmodified Dumbbell capped with ODN-1 and ODN-2. The unmodified Dumbbell was used to examine the effects of the base modification in comparison with Dumbbell-0-0. These DNA dumbbells were purified by anion-exchange HPLC to remove the unligated ODNs, which could possibly compete with the nuclear entry of NLS-conjugated DNA dumbbells via the NPC.

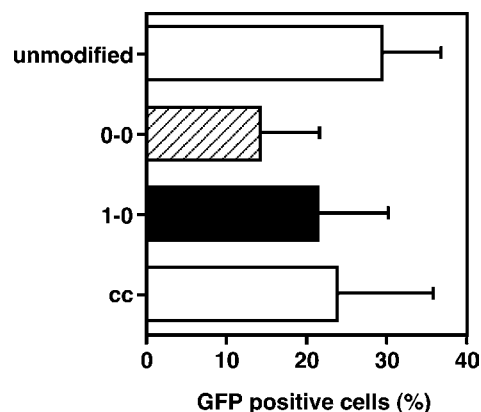
**Cytosolic Microinjection.** First, we microinjected various DNA dumbbells (10000 copies/cell) into the cytoplasm of simian COS-7 cells. GFP expression was monitored by fluorescence microscopy, and the ratio of cells expressing GFP to those containing the labeled dextran in their nuclei was calculated. Figure 3 shows the percentage of GFP-positive cells at 24 h postinjection.

When microinjected into the cytoplasm of simian COS-7 cells, approximately 40% of the cells expressed GFP, in the case of the unmodified Dumbbell. The GFP genes on the NLS-conjugated DNA dumbbells (Dumbbell-1-0, -1-1, and -2-0) were expressed with an efficiency similar to or slightly less than the unmodified Dumbbell (~35%, Figure 3). Thus, no dramatic increase in transgene expression was observed by the conjugation of the NLS peptide to DNA molecules, when we attached one or two peptide(s) per DNA.

Interestingly, Dumbbell-0-0 showed decreased GFP expression, as compared with that of the unmodified Dumbbell (~15%, Figure 3). This result suggests that the presence of the modified base suppressed transgene



**Figure 3.** Expression efficiencies of the GFP gene in COS-7 cells by cytoplasmic microinjection of DNAs. The DNA (10000 copies) was injected, and the expression was examined at 24 h postinjection. The data are expressed as means  $\pm$  standard deviation of two separate experiments. The datum of Dumbbell-1-1 is that obtained in a single injection experiment. cc represents closed circular plasmid DNA.



**Figure 4.** Expression efficiencies of the GFP gene in COS-7 cells by intranuclear microinjection of DNAs. The DNA (1000 copies) was injected, and the expression was examined at 24 h postinjection. The data are expressed as means  $\pm$  standard deviation of two separate experiments. cc represents closed circular plasmid DNA.

expression, for by one or two reasons: (i) the nuclear entry of the modified dumbbell (Dumbbell-0-0) occurred less efficiently than that of unmodified Dumbbell, and/or (ii) the expression of the gene on the modified Dumbbell-0-0 was reduced in the nucleus by the base modification. Moreover, the fact that the NLS-conjugated DNAs showed better expression than that of Dumbbell-0-0 (and similar expression to the unmodified Dumbbell) suggests the possibilities that the peptide improved the nuclear entry and/or the expression in the nucleus.

**Intranuclear Microinjection.** Next, we microinjected various DNAs (100 copies/nucleus) into the nuclei of simian COS-7 cells. We microinjected only Dumbbell-1-0 as the NLS-conjugated DNA, because very similar results were obtained with the three NLS-dumbbells in the cytosolic microinjection experiments described above.

As shown in Figure 4, results similar to those obtained with the cytosolic microinjection experiments were observed. Dumbbell-0-0 showed decreased GFP expression as compared with that of the unmodified Dumbbell. The transgene on the NLS-conjugated DNA dumbbell (Dumbbell-1-0) was expressed more efficiently than that on Dumbbell-0-0 (~20% and ~15%, respectively), and with less efficiency than that on the unmodified Dumbbell (~30%). Thus, the efficiencies of GFP expression by the



cytosolic microinjections, shown above, mainly depended on the event(s) in the nucleus.

**Effects of the Modified Base and the NLS Peptide.** On the basis of the results obtained with the cytosolic and intranuclear microinjections, we found that (i) one or two NLS peptide(s) did not dramatically improve the nuclear entry of DNA and that (ii) chemical modification of the DNA decreased the transgene expression. Although the actual reason(s) for the latter is unclear, the transcription efficiency or stability in the nucleus may be reduced by the introduction of the modified base. The uracil derivative used in this study was incorporated in the loop near the *Bgl*II site (Figure 2), and thereby near the promoter region. Thus, transcriptional factors may load less efficiently than on unmodified DNA. Alternatively, the modified base may be recognized by DNA repair enzyme(s) with endonuclease function(s). The NLS-conjugated DNA dumbbells, in contrast, showed GFP expression similar to that of the unmodified Dumbbell. The NLS-conjugation 'shielded' the effects of the base modification in the transcription and/or excision reactions. The peptide consists of positively charged amino acid residues and may interact with the DNA phosphate backbone. If this putative interaction occurs in the loop region, then the cellular protein(s) may hardly recognize the modification.

We showed that one or two NLS peptide(s) conjugated to DNA did not enhance transgene expression dramatically, at least when the naked DNA was microinjected into the cytoplasm. Thus, the nuclear entry of DNA appears to be similar with and without the peptide. The NLS peptide used in this study is positively charged and may interact with the DNA phosphate backbone. Thus, the NLS peptide might not act as a nuclear entry device. This interpretation is in contrast to the results of Zanta et al. (9), who reported ten- to hundreds-fold increased transgene expression by the conjugation of the NLS peptide to the loop region of dumbbell-shaped DNA. Improved transgene expression was also reported with a noncovalently bound NLS peptide. Brandén et al. combined a peptide nucleic acid (PNA) molecule to the NLS peptide, and this NLS-PNA was attached to plasmid DNA containing a sequence complementary to the PNA molecules (16). They reported that the addition of the NLS-PNA enhanced PEI-mediated transgene expression 3- to 5-fold. Interestingly, both Zanta et al. and Brandén et al. obtained their results using PEI-mediated transfection. Godbey et al. observed the intracellular trafficking of a PEI-DNA complex by confocal microscopy and found that both PEI and DNA entered the nucleus as a complex (11). Thus, PEI may alter the transcription efficiency of the delivered DNA. The NLS peptide may enhance the transcription, since the transcriptional factors may be loaded more efficiently if the interaction between the PEI and DNA is impaired. It should be emphasized that the combination of cytosolic and intranuclear microinjections enables separate considerations of the nuclear entry and the events inside the nucleus.

Recently, attachment of the NLS peptide to plasmid DNA using a triple helix-forming padlock ODN was reported (17). Upon transfection experiments, no enhancement of transgene expression was observed. Very recently, Nagasaki et al. reported the covalent conjugation of the NLS peptide to plasmid DNA, by diazo coupling through a PEG chain (18). They observed by fluorescence microscopy that the NLS peptide did not enhance the nuclear entry of the circular plasmid DNA upon cytosolic microinjection, although the conjugation of 5.1 NLS peptides per DNA increased the transgene expression

4-fold upon transfection. Their results agree with our present results, on the point that a small number of NLS peptides could not enhance the nuclear entry remarkably.

In this study, we observed that (i) one or two NLS peptide(s) did not dramatically improve the nuclear entry of a linearized DNA dumbbell and that (ii) chemical modification of the DNA reduced the transcription efficiency or stability in the nucleus. These results suggest that the NLS peptide should be attached to a DNA-carrying molecule, not to the DNA itself, to enhance the nuclear entry of DNA via the NPC.

#### ACKNOWLEDGMENT

This work was supported in part by Grants-in-Aid for Scientific Research on Priority Areas, from the Ministry of Education, Culture, Sports, Science and Technology of Japan, a Grant-in-Aid for Scientific Research (B) from the Japan Society for the Promotion of Science, and a Grant-in-Aid from the Uehara Memorial Foundation.

#### LITERATURE CITED

- (1) Kamiya, H., Tsuchiya, H., Yamazaki, J., and Harashima, H. (2001) Intracellular trafficking and transgene expression of viral and nonviral gene vectors. *Adv. Drug Del. Rev.* 52, 153–164.
- (2) Pollard, H., Remy, J. S., Loussouarn, G., Demolombe, S., Behr, J. P., and Escande, D. (1998) Polyethylenimine but not cationic lipids promotes transgene delivery to the nucleus in mammalian cells. *J. Biol. Chem.* 273, 7507–7511.
- (3) Kamiya, H., Yamazaki, J., and Harashima, H. (2002) Size and topology of exogenous DNA as determinant factors of transgene transcription in mammalian cells. *Gene Ther.* 9, 1500–1507.
- (4) Tseng, W. C., Haselton, F. R., and Giorgio, T. D. (1999) Mitosis enhances transgene expression of plasmid delivered by cationic liposomes. *Biochim. Biophys. Acta* 1445, 53–64.
- (5) Ludtke, J. J., Sebestyén, M. G., and Wolff, J. A. (2002) The effect of cell division on the cellular dynamics of microinjected DNA and dextran. *Mol. Ther.* 5, 579–588.
- (6) Kamiya, H., Fujimura, Y., Matsuoka, I., and Harashima, H. (2002) Visualization of intracellular trafficking of exogenous DNA delivered by cationic liposomes. *Biochem. Biophys. Res. Commun.* 298, 591–597.
- (7) Tachibana, R., Harashima, H., Shono, M., Azumano, M., Niwa, M., Futaki, S., and Kiwada, H. (1998) Intracellular regulation of macromolecules using pH-sensitive liposomes and nuclear localization signal: qualitative and quantitative evaluation of intracellular trafficking. *Biochem. Biophys. Res. Commun.* 251, 538–544.
- (8) Sebestyén, M. G., Ludtke, J. J., Bassik, M. C., Zhang, G., Budker, V., Lukhtanov, E. A., Hagstrom, J. E., and Wolff, J. A. (1998) DNA vector chemistry: the covalent attachment of signal peptides to plasmid DNA. *Nat. Biotechnol.* 16, 80–85.
- (9) Zanta, M. A., Belguise-Valladier, P., and Behr, J. P. (1999) Gene delivery: a single nuclear localization signal peptide is sufficient to carry DNA to the cell nucleus. *Proc. Natl. Acad. Sci. U.S.A.* 96, 91–96.
- (10) Cartie, R., and Reszka, R. (2002) Utilization of synthetic peptides containing nuclear localization signals for nonviral gene transfer systems. *Gene Ther.* 9, 157–167.
- (11) Godbey, W. T., Wu, K. K., and Mikos, A. G. (1999) Tracking the intracellular path of poly(ethylenimine)/DNA complexes for gene delivery. *Proc. Natl. Acad. Sci. U.S.A.* 96, 5177–5181.
- (12) Nomura, Y., Ueno, Y., and Matsuda, A. (1997) Site-specific introduction of functional groups into phosphodiester oligodeoxynucleotides and their thermal stability and nuclease-resistance properties. *Nucleic Acids Res.* 25, 2784–2791.
- (13) Kamiya, H., and Kasai, H. (1997) Substitution and deletion mutations induced by 2-hydroxyadenine in *Escherichia coli*: Effects of sequence contexts in leading and lagging strands. *Nucleic Acids Res.* 25, 304–310.

- (14) Sambrook, J., Fritsch, E. F., and Maniatis, T. (1989) *Molecular Cloning: A Laboratory Manual*, 2nd ed., pp 6.30–6.31, Cold Spring Harbor Laboratory Press, Woodbury, NY.
- (15) Kamiya, H., and Kasai, H. (2000) 2-Hydroxy-dATP is incorporated opposite G by *Escherichia coli* DNA polymerase III resulting in high mutagenicity. *Nucleic Acids Res.* **28**, 1640–1646.
- (16) Brandén, L. J., Mohamed, A. J., and Smith, C. I. (1999) A peptide nucleic acid-nuclear localization signal fusion that mediates nuclear transport of DNA. *Nat. Biotechnol.* **17**, 784–787.
- (17) Roulon, T., Hélène, C., and Escudé, C. (2002) Coupling of a targeting peptide to plasmid DNA using a new type of padlock oligonucleotide. *Bioconjugate Chem.* **13**, 1134–1139.
- (18) Nagasaki, T., Myohoji, T., Tachibana, T., Futaki, S., and Tamagaki, S. (2003) Can Nuclear Localization Signals Enhance Nuclear Localization of Plasmid DNA? *Bioconjugate Chem.* **14**, 282–286.

BC034075E

# Influence of Targeting Ligand Flexibility on Receptor Binding of Particulate Drug Delivery Systems

Verena Olivier,<sup>†,||</sup> Iris Meisen,<sup>‡</sup> Barbara Meckelein,<sup>†,||</sup> Timothy R. Hirst,<sup>§,⊥</sup> Jasna Peter-Katalinic,<sup>‡</sup> M. Alexander Schmidt,<sup>†</sup> and Andreas Frey<sup>†,||,\*</sup>

Institut für Infektiologie, Zentrum für Molekularbiologie der Entzündung, von-Esmarch-Strasse 56, Westfälische Wilhelms-Universität, D-48149 Münster, Germany, Institut für Medizinische Physik und Biophysik, Robert-Koch-Strasse 31, Westfälische Wilhelms-Universität, D-48149 Münster, Germany, and Department of Pathology & Microbiology, School of Medical Sciences, University of Bristol, Bristol BS8 1TD, United Kingdom. Received May 9, 2003; Revised Manuscript Received September 3, 2003

Receptor-mediated drug targeting via nanoengineered particulate delivery systems is an emerging field. However, little is known about how such magic bullets should be assembled to yield optimal targeting efficiency. Here we investigated the influence of targeting ligand flexibility on binding of ligand-coated microparticles to cell surface receptors. Using the ganglioside G<sub>M1</sub>-binding B subunit of cholera toxin as ligand and fluorescent microparticles as a model delivery system, conjugates with different numbers of linkages between ligand and particle were prepared and tested for their efficiency to bind to live fibroblast monolayers. Our results show that multiple bonds between ligand and particle reduce the targeting rate by up to 50% compared to constructs where ligands are attached via single aliphatic chains. Thus, for maximum performance, targeted particulate drug delivery systems should be assembled such that ligands are attached via single  $\sigma$  bonds only, allowing the ligand molecules to adopt an optimal binding conformation.

## INTRODUCTION

Functional genomics, proteomics, and glycomics along with emerging technologies such as molecular breeding are expected to yield drugs with ever increasing potency and molecular specificity. Yet, except for anti-infectiva where foreign organisms are to be attacked, molecular specificity does not necessarily translate into cell type- or organ-specificity since the molecular target of the drug may be expressed at multiple locations throughout the body, exerting different functions at different sites. The predicament can be solved only when the drug is combined with a delivery technology that directs the compound exclusively to its desired site of action. This dilemma is most apparent in gene therapy and cancer medication, but also in areas less obvious such as oral vaccination where targeted delivery may be desirable.

Orally administered proteinaceous antigens rapidly fall prey to the digestive enzymes of the gastrointestinal tract and give rise to oral immune tolerance, the default reaction of the mucosal immune system (1). To overcome this, it is believed that antigens must be delivered in intact form selectively to M cells, a special epithelial cell type overlying the organized mucosa-associated lymphoid tissue (2). To meet this requirement, we devised an M

cell targeting strategy which exploits differences in cell surface receptor accessibility (3) and requires the antigen to be 30 nm in diameter and coated with a ligand directed against plasma membrane ganglioside G<sub>M1</sub>. Since we observed considerable differences in targeting efficiency in a cell culture model system depending on how the targeting ligand was attached to a particle surface (3, 4), we have chosen in this study to investigate the influence of rigidity of ligand attachment on the efficiency of ligand-mediated particle targeting.

## EXPERIMENTAL PROCEDURES

**Production of Recombinant CTB.** Recombinant cholera toxin B-subunit (rCTB) was prepared as described previously (5). Briefly, rCTB was expressed in secreted form in *Vibrio* sp. 60 containing the inducible vector pATA13 (6). rCTB was harvested from the culture supernatant by ultrafiltration and the concentrated retentate fraction subjected to hydrophobic interaction and cation exchange chromatography (5). The purified rCTB was desalted by gel permeation chromatography, equilibrated in Dulbecco's phosphate-buffered saline (D-PBS), pH 7.4, snap-frozen in liquid N<sub>2</sub> and stored at -80 °C until required.

**Biotinylation of CTB.** Mixtures of 5  $\mu$ M rCTB and either 75, 25, or 8.35  $\mu$ M NHS-LC-biotin (water soluble biotin (long arm) NHS, sulfosuccinimidyl-6-(biotinamido)-hexanoate; Vector, Burlingame, CA) in a total volume of 200  $\mu$ L of D-PBS were allowed to react for 30 min at RT on an end-to-end-mixer at 4 rpm before the reaction was quenched by adding 400  $\mu$ L of 200  $\mu$ M lysine in D-PBS to a final concentration of 133  $\mu$ M. The solution was dialyzed extensively against D-PBS at 4 °C for 48 h using Slide-A-Lyzer Dialysis Cassettes (MWCO 10 000 Da; Pierce, Bonn, Germany), snap-frozen in liquid N<sub>2</sub> and stored at -80 °C.

\* Corresponding author. Laborgruppe Mukosaimmunologie, Abteilung Klinische Medizin, Forschungszentrum Borstel, Parkallee 22, D-23845 Borstel, Germany. Phone: +49-4537-188-562. Fax: +49-4537-188-693. E-mail: afrey@fz-borstel.de.

<sup>†</sup> Institut für Infektiologie.

<sup>‡</sup> Institut für Medizinische Physik und Biophysik.

<sup>§</sup> University of Bristol.

<sup>||</sup> Present address: Laborgruppe Mukosaimmunologie, Abteilung Klinische Medizin, Forschungszentrum Borstel, Parkallee 22, D-23845 Borstel, Germany.

<sup>⊥</sup> Present address: A14 - Main Quadrangle, The University of Sydney, NSW 2006, Australia.



**Preparation of CTB-Coated Particles.** CTB-coated microparticles (CTB-P) and biocytin-quenched control particles (Control-P) were prepared by coupling biotinylated CTB or biocytin (*N*- $\epsilon$ -biotinyl-L-lysine) (Sigma, Taufkirchen, Germany) to avidin-coated, carboxy-modified, fluorescent latex particles (Molecular Probes, Eugene, OR) of 1  $\mu$ m nominal size as described earlier (3). In 500  $\mu$ L of D-PBS,  $5 \times 10^8$  or  $1 \times 10^9$  red fluorescent particles were reacted under rocking at 1.5 rpm for 72 h at 4 °C in the dark with 21  $\mu$ g (0.361 nmol) or 43  $\mu$ g (0.738 nmol) of the differently biotinylated CTBs. Thus, regardless of its degree of biotinylation, CTB was applied in a 5.5-fold molar excess over the maximally achievable CTB particle load (approximately 80 000 CTB molecules per 1- $\mu$ m particle, as calculated according to (3)). For the control particles,  $4 \times 10^9$  green fluorescent particles in 1000  $\mu$ L of D-PBS were reacted under the same conditions with 149  $\mu$ g (400 nmol) biocytin, representing a 110-fold molar excess of biocytin over biotin binding sites. Unreacted ligand was removed by centrifugation at  $1100 \times g$  and gently resuspending the particles in 1.8 mL of distilled water. Washes were repeated 10–12 times for all preparations before the particles were stored at concentrations of  $2 \times 10^8$  to  $3 \times 10^9$  particles/mL in 0.1 M HEPES–NaOH, pH 7.4, at 4 °C in the dark.

**G<sub>M1</sub> Binding Assay.** High-bind ELISA plates (Corning, Wiesbaden, Germany) coated overnight at 4 °C with 75  $\mu$ L/well of 5 ng/mL ganglioside G<sub>M1</sub> (Alexis, Grünberg, Germany) in D-PBS were washed three times with 300  $\mu$ L/well of D-PBS and blocked with 250  $\mu$ L/well of 0.1% (w/v) ovalbumin (OVA) (Sigma) in D-PBS for 6–8 h at RT. After four washes with D-PBS, plates were incubated overnight at 4 °C with 75  $\mu$ L/well of serially diluted biotinylated CTB in 0.1% (w/v) OVA/D-PBS, washed six times with PBST (D-PBS, 0.05% (v/v) Tween 20), and incubated for 90 min at RT with 75  $\mu$ L/well of 1  $\mu$ g/mL (8 pmol streptavidin/mL) peroxidase-labeled streptavidin (Vector) in 0.1% (w/v) OVA/D-PBS. After six washes with PBST, plates were developed using the 3,3',5,5'-tetramethylbenzidine substrate system of Frey et al. (7).

**Nano-Electrospray Ionization Mass Spectrometric Determination of Biotinylation.** Biotinylated CTB (5  $\mu$ g) was dialyzed extensively against 20% (v/v) acetic acid for 48 h at 4 °C in QuixSep microdialysis chambers (Roth, Karlsruhe, Germany) using Spectra/Por7 dialysis membranes (MWCO 3500; Spectrum, Rancho Dominguez, CA), lyophilized, and redissolved in 8.6  $\mu$ L of 25% (v/v) acetic acid (final concentration 10  $\mu$ M CTB) of which 5  $\mu$ L (50 pmol) was used for mass spectrometry. Measurements were carried out on a nano-electrospray Q-TOF instrument fitted with a Z-spray nano-ESI source (Micromass, Manchester, UK) using omega nanospray glass capillaries prepared from borosilicate glass (Hilgenberg, Malsfeld, Germany) on a Kopf vertical pipet puller, model 720 (David Kopf Instruments, Tujunga, CA). Electrospray potential (900–1100 V) was applied via a stainless steel wire electrode inside the nanospray source (8).

**Biochemical Determination of Biotinylation.** The differently biotinylated CTBs were serially diluted (2-fold, 6.7  $\mu$ g/mL–3.3 ng/mL) in 0.1% (w/v) BSA/PBS and 3  $\mu$ L of each dilution was pipetted onto nitrocellulose membranes (4.5  $\times$  13 cm, 0.2  $\mu$ m pore size; Schleicher & Schuell, Dassel, Germany). After being dried and washed twice with 20 mL of D-PBS and once with PBST, membranes were blocked for 5 h in 20 mL of blocking solution (1% (w/v) casein (Hammarsten grade; BDH, Poole, UK), 0.02% (w/v) thimerosal, 0.05% (v/v) Tween 20 in D-PBS) at RT. Dotted CTB labeled with a 15-, 5-, or 1.67-fold molar excess of biotinylation reagent was

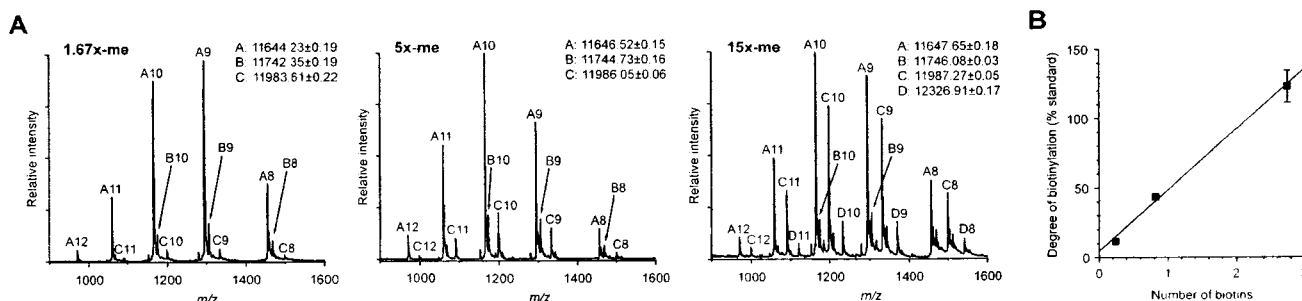
then incubated in 20 mL of blocking solution for 24 h at 4 °C with 6834 ng (54.4 pmol), 2278 ng (18.1 pmol), or 759 ng (6.0 pmol) peroxidase-labeled streptavidin, each representing a 20-fold molar excess of streptavidin over the maximum amount of biotin theoretically present on the membrane. After four washes in PBST and two in D-PBS, 800  $\mu$ L of LumiLight<sup>PLUS</sup> Western blotting substrate (Roche, Mannheim, Germany) was applied, and chemiluminescence was quantitated on a Lumi-Imager-F1 (Roche). Serially diluted OVA (2-fold, 6.7  $\mu$ g/mL–3.3 ng/mL) biotinylated with a 15-fold molar excess of NHS-LC-biotin served as standard.

**Binding of Microparticles to BALB/c 3T3 Fibroblasts.** BALB/c 3T3 fibroblasts (clone A31; ATCC, Rockville, MD) were grown in high glucose (25 mM) Dulbecco's modified Eagle's medium (DMEM) (PAA Laboratories, Linz, Austria) supplemented with 10% (v/v) newborn calf serum (defined grade; Hyclone, Bonn, Germany), 2 mM glutamine, 100 U/mL penicillin/100  $\mu$ g/mL streptomycin, and 25 mM HEPES (PAA) at 37 °C in a humidified atmosphere containing 10% (v/v) CO<sub>2</sub>. For particle binding, cells (passages 70–86) were seeded onto round (13 mm diameter) glass coverslips (Bellco, Vineland, NJ) in 24-well tissue culture plates and used at 14–17 days post confluence. Monolayers were washed gently five times with 1 mL of prewarmed (37 °C) D-PBS containing 0.9 mM CaCl<sub>2</sub> and 0.5 mM MgCl<sub>2</sub> (CM-PBS) before 500  $\mu$ L of a suspension containing  $2.5 \times 10^7$  particles/mL each of CTB-P and Control-P in DMEM, 4 mM glutamine, and 25 mM HEPES were applied. For competition assays, coverslips were preincubated for 15 min with 250  $\mu$ L of 20  $\mu$ g/mL CTB in DMEM, 4 mM glutamine, and 25 mM HEPES before 250  $\mu$ L of  $5 \times 10^7$  particles/mL each of CTB-P and Control-P in the same buffer were added. After 60 min at 37 °C, coverslips were washed gently five times with 1 mL of prewarmed CM-PBS, fixed in 1 mL of 3% (w/v) paraformaldehyde in D-PBS for 90–120 min at RT in the dark, and washed three times in D-PBS and once in distilled water and mounted on glass slides with Mowiol 4–88 (Calbiochem-Novabiochem, Bad Soden, Germany) containing 2.5% (w/v) DABCO (1,4-diazabicyclo-[2.2.2]octane; Sigma). Cells were examined en face with a Zeiss Axiophot microscope equipped for epifluorescence (Zeiss, Jena, Germany) and were either photographed or recorded with a video camera.

**Statistics.** For quantitation of microparticle binding, digital images of five randomly selected nonoverlapping regions (top, bottom, center, left, and right) of each coverslip were printed and counted manually. Statistical analysis was performed using the StatView 4.51 software (Abacus Concepts, Berkeley, CA). Mixed probes of test- and control particles were considered paired samples. Results of independent experiments were treated as unpaired samples. Statistical analyses were considered significant only if  $p < 0.05$ .

## RESULTS AND DISCUSSION

When particle surfaces are to be derivatized with biomolecules, coupling is often achieved in an ill-defined manner, either by physisorption via van der Waals and electrostatic forces or by chemisorption after preactivation of the surface or in a one-pot reaction with a condensation reagent. Although macromolecules bound this way may generally retain their biological activity, it is extremely difficult to assess the degree of their functionality once the bioconjugate is formed. To tackle this problem we devised a strategy to bind a ligand to a polyvalent microparticle via a defined number of linkers.



**Figure 1.** Analysis of CTB biotinylation. A: Representative nano-ESI MS analysis in positive ion mode of CTB biotinylated with 1.67-, 5-, and 15-fold molar excess (1.67×-me, 5×-me, 15×-me) of NHS-LC-biotin. Species A: unmodified CTB; species B: phosphoric acid adduct of the CTB monomer; species C: monobiotinylated CTB; species D: CTB carrying two biotin labels. B: Regression analysis of mass spectrometric versus biochemical analysis of CTB biotinylation. Degrees of biotinylation deduced from the nano-ESI MS data closely correlate (simple regression  $R^2$ : 0.997; one-way ANOVA,  $p < 0.05$ ) with background-corrected signal intensities (mean  $\pm$  standard error) obtained from a dot-blot biotin detection assay where biotinylated ovalbumin served as standard (100%).

This enables us to deduce the rigidity of the conjugate and investigate its influence on the functionality of the probe.

As a ligand the ganglioside  $G_{M1}$ -binding B subunit of cholera toxin (CTB) was chosen. CTB (SWISS-PROT: P01556) is a torus- or donut-shaped homopentameric protein of 58222 Da bearing five identical receptor binding sites arranged in 5-fold symmetry at the bottom of the torus (9) and 10 potentially derivatizable amino functions on each subunit. While one of them (Lys-91) tolerates derivatization (10, 11), although it is directly involved in  $G_{M1}$ -binding (9), succinylation of a second lysine (Lys-34) does not impair the biological activity of its own but that of a neighboring subunit (10). Besides that, integrity of the lone tryptophan (Trp-88) is crucial for  $G_{M1}$ -binding (10).

To link CTB to the particle surface we decided to biotinylate the ligand to various degrees at its amino functions thus creating single or multiple bonds when coupling it to avidin-coated microparticles.

**Differently Biotinylated CTBs.** Recombinant CTB was produced in functional pentameric form in a *Vibrio* species and biotinylated with NHS-LC-biotin (sulfo-succinimidyl-6-(biotinamido)hexanoate), an active ester derivative of biotin, which carries a flexible 2.2 nm spacer and reacts with  $\alpha$ - and  $\epsilon$ -amino functions of proteins. Since preservation of at least about 50% of its  $G_{M1}$ -binding activity requires that no more than 30% of the amino functions of CTB be converted into amide bonds (12), a maximum of a 15-fold molar excess of NHS-LC-biotin should be used for derivatization when assuming full conversion of the active ester. We therefore carried out three different biotinylation reactions with 1.67-, 5-, and 15-fold molar excess of NHS-LC-biotin.

The actual degree of biotinylation was determined using nano-electrospray ionization mass spectrometry (nano-ESI MS). In Figure 1A the resulting spectra are shown, depicting a representative analysis of CTB, biotinylated with 1.67-, 5-, or 15-fold molar excess of NHS-LC-biotin. Several species named A, B, C, D were detected in each spectrum. The different charge states, +8 to +12, obtained for each species allowed the determination of the average molecular masses which are given in each spectrum. Species A represents the unmodified CTB-monomer (calcd average mass 11 645.36). Species B is generated by a noncovalent phosphoric acid adduct of the unmodified CTB-monomer (calcd average mass 11 743.36). Species C is assigned to a monoderivatized monomer (calcd average mass 11 984.82) and species D corresponds to a CTB monomer derivatized with 2 biotin moieties (calcd average mass 12 324.28). On the

**Table 1.** Degree of Biotinylation of CTB Depending on the Amount of Biotinylation Reagent Used

molar excess of biotinylation reagent	derivatization as determined by	
	nano-ESI-MS: no. of biotins per pentamer <sup>a</sup>	dot-blot: biotinylation as % of standard <sup>b</sup>
15-fold	2.75 $\pm$ 0.10	122.79 $\pm$ 11.61
5-fold	0.82 $\pm$ 0.06	43.39 $\pm$ 2.20
1.67-fold	0.24 $\pm$ 0.00	11.37 $\pm$ 0.85

<sup>a</sup> Data are derived from three different  $m/z$  ratios. <sup>b</sup> Data are derived from five different dot blots of each sample. Results are given as mean  $\pm$  standard error.

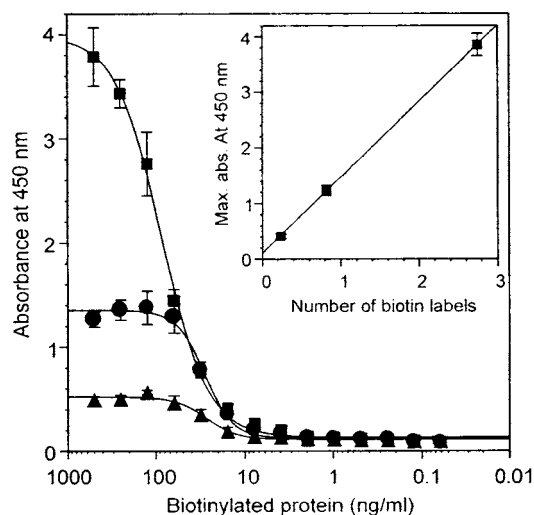
basis of these data the average degree of biotinylation of a CTB pentamer can be deduced by comparing the background-corrected relative signal intensities of the unmodified and differently biotinylated CTB monomers using eq 1,

$$\text{biotins per CTB pentamer} = \frac{c + 2d}{100 + c + d} \times 5 \quad (1)$$

where  $c$  is the relative signal intensity of CTB monomers carrying 1 biotin label,  $d$  the relative signal intensity of CTB monomers carrying two biotin labels, and the signal intensity of nonbiotinylated CTB monomer is set 100%. The respective degrees of biotinylation obtained with 1.67-, 5-, or 15-fold excess of NHS-LC-biotin are summarized in Table 1. They were confirmed in a quantitative dot-blot assay, which correlated strongly with the mass spectrometric data (Figure 1B). The relative differences in signal intensity between the differently biotinylated CTBs were normalized on a standard and are included in Table 1.

According to these data, the actual derivatization yield for CTB is directly correlated with the molar excess of NHS-LC-biotin applied (simple regression  $R^2$ : 1.0, one-way ANOVA,  $p < 0.025$ ) while the reaction yields for biotinylation reagent increased slightly from 14.3% for a 1.67-fold molar excess over 16.5% for a 5-fold excess to 18.3% for a 15-fold molar excess. Thus, no signs of saturation in the derivatization reactions are visible, which is to be expected when less than five amino functions are derivatized on a homopentameric protein molecule.

**Biological Activity of the Differently Biotinylated CTBs.** Due to the five equal receptor binding sites, CTB is markedly tolerant toward derivatization of its primary amino functions. Hybrid CTB pentamers renatured from equal amounts of monomers which were either formylated at Trp-88 or succinylated at Lys-34 have only 1.25



**Figure 2.** Biological activity of biotinylated CTB. ELISA-type assay with serial dilutions of CTBs derivatized with 1.67- ( $\Delta$ ), 5- ( $\bullet$ ), and 15- ( $\blacksquare$ ) fold molar excess of NHS-LC-biotin. Conjugates were captured on ganglioside  $G_{M1}$ -coated microtiter plates and visualized via streptavidin–horseradish peroxidase and a colorogenic substrate. Data represent mean  $\pm$  standard error of three independent experiments. Inset: Regression analysis of signal intensities of streptavidin-binding to  $G_{M1}$ -captured biotinylated CTB versus degree of biotinylation. Background-corrected absorbances extrapolated for saturated  $G_{M1}$ -binding (mean  $\pm$  standard error) closely correlate (simple regression  $R^2$ : 1.0; one-way ANOVA,  $p < 0.005$ ) with degrees of biotinylation determined by mass spectrometry.

functional receptor binding sites left but still retain 40% of the original affinity for  $G_{M1}$  (10). Consequently, CTB should tolerate the up to 2.75 biotins which we introduced even if labeling occurred exclusively at amino groups essential for receptor interaction. However, affinity may decrease with progressive labeling under these circumstances. Moreover, selective biotinylation of these sites will attach the CTB molecule to the avidin-coated microparticle the wrong way around with its receptor binding interface pointing toward the particle core. We therefore needed to know whether biotin was present at locations (top and/or side of the torus) which would allow CTB to conjugate to avidin-coated particles in the desired

way and whether this biotinylation pattern persists for the different degrees of biotinylation.

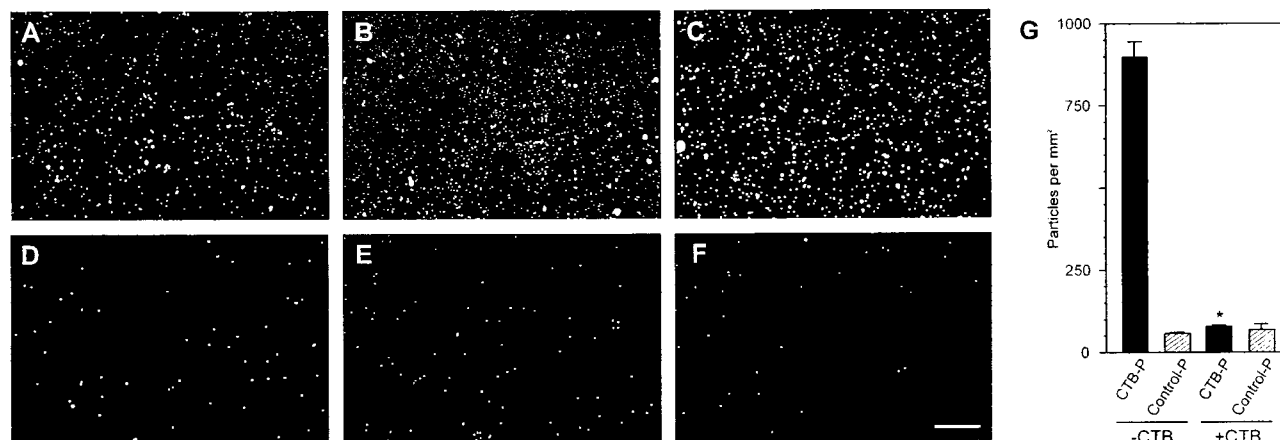
To address this question, soluble biotinylated CTB was first allowed to bind to a  $G_{M1}$ -coated microtiter plate before the biotin moieties were detected with a streptavidin–horseradish peroxidase conjugate. In this setup, biotinylation of amino functions located at the bottom of the torus, i.e., the  $G_{M1}$ -binding interface of CTB, cannot be detected because they are buried beneath the CTB molecule inaccessible for streptavidin–horseradish peroxidase.

Since signals were not only detectable but also increased linearly with the number of biotins per CTB pentamer (Figure 2), all three preparations did indeed carry labels at the desired part of the torus and exhibited a similar affinity for  $G_{M1}$ , although the result does not imply that some kind of site-selective labeling has occurred. Nevertheless, a substantial proportion of biotinylated CTB in each preparation can link to avidin-coated particles such that their  $G_{M1}$ -binding site points away from the particle core and all preparations are comparable in their biological activity.

#### Targeting Efficiency of Microparticles Conjugated with CTB in Mono- or Polyvalent Manner.

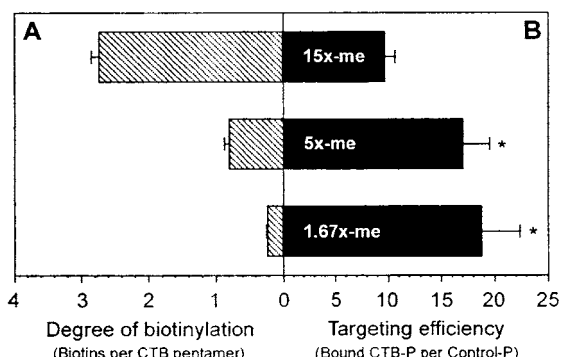
Since molecules biotinylated at an unfavorable position cannot be eliminated from a preparation we decided to circumvent this predicament by using rather large particles of 1  $\mu$ m diameter as an experimental delivery system. They offer a parking area for approximately 80 000 CTB molecules (3, 4), enough to generate a surface coat that is representative of the original distribution of top/side- and bottom-labeled CTB. Since the proportion of bottom-labeled CTB was shown to be constant in all preparations, its effect will then be canceled out when comparing the biological activity of different CTB-coated particles (CTB-P). As internal control for binding assays, inert microparticles of different color (Control-P) were prepared by quenching their biotin binding sites in a charge neutral manner using excess biocytin.

BALB/c 3T3 fibroblasts were chosen as an appropriate target cell since they express high levels of  $G_{M1}$  receptor (13) which is readily accessible to the 1  $\mu$ m particles used here (3, 4). To simulate a real targeting situation, cells were grown as confluent monolayers and then exposed



**Figure 3.** CTB-mediated binding of microparticles to BALB/c 3T3 fibroblasts. Cell monolayers (133 mm<sup>2</sup>) were exposed to  $2.5 \times 10^7$  particles each of CTB-P (A–C) and Control-P (D–F) for 1 h at 37 °C. Particles had been coated with CTB derivatized with 1.67-fold (A), 5-fold (B), or 15-fold (C) molar excess of biotinylation reagent. Particle binding was visualized by fluorescence microscopy and quantitated. Binding of CTB-P was significantly higher than binding of Control-P for all CTB-P preparations (two-tailed, paired  $t$ -tests,  $p < 0.0005$ ), scale bar, 200  $\mu$ m. G: In the presence of 10  $\mu$ g/mL free CTB binding of CTB-P prepared from CTB derivatized with 1.67-fold molar excess of biotinylation reagent was significantly lower (\*) than in the absence of free CTB (two-tailed, unpaired  $t$ -test,  $p < 0.0001$ ) and indistinguishable from control levels (Control-P) (two-tailed, paired  $t$ -test,  $p \approx 0.9$ ). Data given are means  $\pm$  standard error.



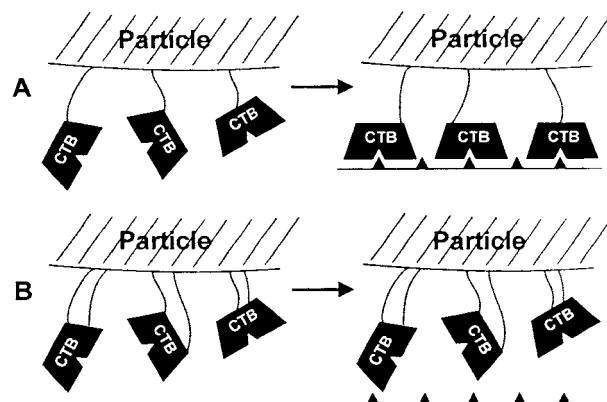


**Figure 4.** Influence of degree of biotinylation on the binding of CTB-particles to BALB/c 3T3 fibroblasts. A: Degree of biotinylation of CTB derivatized with 1.67-, 5- and 15-fold molar excess (1.67 $\times$ -me, 5 $\times$ -me, 15 $\times$ -me) of biotinylation reagent. The number of biotin labels per CTB pentamer (mean  $\pm$  standard error) represents the maximum number of ligand-particle bonds. B: Efficiency of CTB-mediated particle binding to apical surfaces of cultured BALB/c 3T3 fibroblasts. Data from seven independent experiments are displayed as  $n$ -fold better binding of CTB-P than Control-P (geometric mean  $\times/\div$  standard error). Particles coated with CTBs that can form no more than one single bond with avidin particles (1.67 $\times$ -me and 5 $\times$ -me) showed significantly higher binding (\*) to cell surfaces than particles coated with CTB that can form multiple bonds with a particle (15 $\times$ -me) (one-way ANOVA, Fisher's PLSD,  $p < 0.05$ ).

to a suspension of  $2 \times 10^5$  CTB-P per  $\text{mm}^2$  along with the same number of Control-P as internal standard in physiological buffer. All three CTB-P preparations showed binding to the apical plasma membranes of 3T3 fibroblasts (Figure 3A–C) which was significantly higher than that of Control-P (Figure 3D–F). Binding was exclusively mediated via the ligand since competition with soluble CTB reduced binding of CTB-P to control levels as exemplified in Figure 3G for CTB-P prepared with 1.67-fold molar excess of biotinylation reagent.

However, when comparing the targeting efficiency of the different CTB-P preparations significantly lower binding was observed for particles derived from CTB which was derivatized with a 15-fold than for particles coated with CTB derivatized with 1.67- or 5-fold molar excess of biotinylation reagent (Figure 4). Binding of the former CTB-P which may contain a mean of 2.75 bonds between ligand and particle (Figure 4A) was reduced significantly by up to 50% (one-way ANOVA, Fisher's PLSD,  $p < 0.05$ ) compared to preparations in which CTB is linked via no more than a single bond (calculated average values: 0.82 and 0.24 bonds, respectively) to the experimental particulate delivery system (Figure 4B). As chemical bonds occur in integers only, both a 0.82- and a 0.24-fold biotinylated CTB should of course behave the same in that only the biotinylated matter reacts with the particle while the nonbiotinylated CTB is lost during CTB-P preparation. As 0.24-fold biotinylated ligand still harbors less double-labels than 0.82-fold labeled CTB it should perform even better than the latter on particulate delivery systems which was indeed the case (Figure 4B). However, differences between these two CTB-P preparations were not statistically significant.

In conclusion, our results demonstrate that conjugating targeting ligands via multiple bonds to particulate delivery systems impairs the performance of the final conjugate to a significant extent. A possible reason for this adverse behavior is proposed in Figure 5. It shows that a monovalent aliphatic linker gives a ligand considerably more freedom to rotate and bend than bi- or polyvalent linkages which will tether it in a rotational



**Figure 5.** Proposed effect of ligand flexibility on targeting efficiency. Schematic diagram of ligand-particle conjugates binding to cell surfaces. Ligands conjugated to a particle surface via a single  $\sigma$  bond (A) are able to adopt an optimal position for receptor interaction. Ligands conjugated via multiple bonds to a particle surface (B) are sterically constrained which prevents them to adopt an optimal binding position.

axis tangential to the particle surface or even totally immobilize it in a position that is dictated by the location of the cross-linker on the ligand and therefore by the relative reactivities of its surface functional groups.

For optimal targeting efficiency drug targeting systems should therefore be designed such that the targeting ligand is attached via a single  $\sigma$  bond only. A powerful technology to achieve such tailored linkers on proteins may arise from current efforts to expand the genetic code in order to incorporate unnatural amino acids (14) which eventually will provide a solitary handle for attaching the ligand to the particulate drug delivery system. Alternatively, protein ligands may be substituted by chemically less complex molecules such as peptides where a single attachment handle can readily be introduced (15).

#### ACKNOWLEDGMENT

This work was supported by the Deutsche Forschungsgemeinschaft (grant no. FR 958/2-2&3). B.M. is a recipient of a personal stipend from the state of Nordrhein-Westfalen.

#### LITERATURE CITED

- (1) Garside, P., and Mowat, A. M. (2001) Oral tolerance. *Semin. Immunol.* 13, 177–185.
- (2) Neutra, M. R., Frey, A., and Kraehenbuhl, J. P. (1996) Epithelial M cells: gateways for mucosal infection and immunization. *Cell* 86, 345–348.
- (3) Frey, A., Giannasca, K. T., Weltzin, R., Giannasca, P. J., Reggio, H., Lencer, W. I., and Neutra, M. R. (1996) Role of the glycocalyx in regulating access of microparticles to apical plasma membranes of intestinal epithelial cells: implications for microbial attachment and oral vaccine targeting. *J. Exp. Med.* 184, 1045–1059.
- (4) Frey, A., Meckelein, B., and Schmidt, M. A. (1999) Grafting protein ligand monolayers onto the surface of microparticles for probing the accessibility of cell surface receptors. *Bioconjugate Chem.* 10, 562–571.
- (5) Richards, C. M., Aman, A. T., Hirst, T. R., Hill, T. J., and Williams, N. A. (2001) Protective mucosal immunity to ocular herpes simplex virus type 1 infection in mice by using *Escherichia coli* heat-labile enterotoxin B subunit as an adjuvant. *J. Virol.* 75, 1664–1671.
- (6) Aman, A. T., Fraser, S., Merritt, E. A., Rodighiero, C., Kenny, M., Ahn, M., Hol, W. G., Williams, N. A., Lencer, W. I., and Hirst, T. R. (2001) A mutant cholera toxin B subunit

- that binds GM1- ganglioside but lacks immunomodulatory or toxic activity. *Proc. Natl. Acad. Sci. U.S.A.* **98**, 8536–8541.
- (7) Frey, A., Meckelein, B., Externest, D., and Schmidt, M. A. (2000) A stable and highly sensitive 3,3',5,5'-tetramethylbenzidine-based substrate reagent for enzyme-linked immunosorbent assays. *J. Immunol. Methods* **233**, 47–56.
- (8) Alving, K., Paulsen, H., and Peter-Katalinic, J. (1999) Characterization of O-glycosylation sites in MUC2 glycopeptides by nanoelectrospray QTOF mass spectrometry. *J. Mass Spectrom.* **34**, 395–407.
- (9) Merritt, E. A., Sarfaty, S., van den Akker, F., L'Hoir, C., Martial, J. A., and Hol, W. G. (1994) Crystal structure of cholera toxin B-pentamer bound to receptor GM1 pentasaccharide. *Protein Sci.* **3**, 166–175.
- (10) De Wolf, M. J., and Dierick, W. S. (1994) Regeneration of active receptor recognition domains on the B subunit of cholera toxin by formation of hybrids from chemically inactivated derivatives. *Biochim. Biophys. Acta* **1223**, 285–295.
- (11) McCann, J. A., Mertz, J. A., Czworkowski, J., and Picking, W. D. (1997) Conformational changes in cholera toxin B subunit-ganglioside GM1 complexes are elicited by environmental pH and evoke changes in membrane structure. *Biochemistry* **36**, 9169–9178.
- (12) Ludwig, D. S., Holmes, R. K., and Schoolnik, G. K. (1985) Chemical and immunochemical studies on the receptor binding domain of cholera toxin B subunit. *J. Biol. Chem.* **260**, 12528–12534.
- (13) Critchley, D. R., Streuli, C. H., Kellie, S., Ansell, S., and Patel, B. (1982) Characterization of the cholera toxin receptor on Balb/c 3T3 cells as a ganglioside similar to, or identical with, ganglioside GM1. No evidence for galactoproteins with receptor activity. *Biochem. J.* **204**, 209–219.
- (14) Wang, L., and Schultz, P. G. (2002) Expanding the genetic code. *Chem. Commun. (Cambridge, U.K.)* 1–11.
- (15) Akerman, M. E., Chan, W. C., Laakkonen, P., Bhatia, S. N., and Ruoslahti, E. (2002) Nanocrystal targeting in vivo. *Proc. Natl. Acad. Sci. U.S.A.* **99**, 12617–12621.

BC034077Z

## 2,3,5,6-Tetrafluorophenyl *N*-(*S*-Benzoylthioacetyl)glycylglycyl-*p*-aminobenzoate, a Heterobifunctional $^{99m}\text{Tc}$ Ligand for Precomplexed Antibody Labeling

O. Calderon Sanchez,<sup>†,‡</sup> A. Mohammed,<sup>†</sup> W. Mier,<sup>†</sup> K. Graham,<sup>†</sup> J. Schuhmacher,<sup>§</sup> S. O. Arndt,<sup>||</sup> U. Haberkorn,<sup>†</sup> R. Mocelo,<sup>‡</sup> and M. Eisenhut<sup>\*,§</sup>

Department of Nuclear Medicine, University of Heidelberg, Heidelberg, Germany; Laboratory of Organic Synthesis, Faculty of Chemistry, Havana University, Cuba; Department of Radiopharmaceutical Chemistry, DKFZ Heidelberg, 69120 Heidelberg, Germany; and Merck KGaA, 64293 Darmstadt, Germany. Received May 28, 2003; Revised Manuscript Received July 23, 2003

Heterobifunctional  $^{99m}\text{Tc}$  ligands are useful for antibody labeling using the precomplexation route. The aim of this work was to synthesize a ligand, which has sufficient chemical stability to be complexed with  $^{99m}\text{Tc}$  without inactivating the reactive conjugation group. Using 2,3,5,6-tetrafluorophenyl *N*-(*S*-benzoylthioacetyl)glycylglycyl-*p*-aminobenzoate (OC2) >60% of the  $^{99m}\text{Tc}$  complex was obtained at 80 °C in 20 min, which was separated from the free ligand and impurities by HPLC. After solvent evaporation,  $^{99m}\text{Tc}$ -OC2 was conjugated with the monoclonal antibody mAb425 in 50% radiochemical yield. In all, the labeling method required about 1 h preparation time. The immunoreactive fraction of the  $^{99m}\text{Tc}$ -OC2 mAb425 conjugate was 81%, indicating preserved binding capability after conjugation. Compared to recently described methods, which need in situ activation of the  $^{99m}\text{Tc}$  complex, the application of OC2 saved time and reduced the number of manipulations with radioactive material.

### INTRODUCTION

In the past, several types of heterobifunctional ligands have been presented in the literature, which were mainly designed for the labeling of antibodies with  $^{99m}\text{Tc}$ . In this context, heterobifunctionality is defined by two different molecular entities: on the one side, a chelating structure element for  $^{99m}\text{Tc}$  complexation and, on the other, a reactive structure element for covalent protein linkage. Depending on the primary reaction route for one of the two functions, the ligands have been classified as pre-conjugation (postconjugation labeling) or as precomplexation agents. Both routes are associated with advantages and disadvantages: (1) Precomplexation has the unique feature of radiolabeling antibodies with  $^{99m}\text{Tc}$  in an equimolar tracer/ligand fashion. In addition, the thermal energy supply necessary for chelate formation precedes the conjugation with thermosensitive proteins; (2) Pre-conjugation has the advantage of preparing antibody chelate conjugates in advance, which may be split into sample fractions, ready to use on demand. The amount of ligands conjugated per mole of protein are in most cases  $\gg 1$  in order to secure good labeling yields. Consequently, the resulting biological function may be impaired by the amount of added ligands.

With reference to precomplexation several types of ligands have been described, which comprise an activated

ester in the side chain. In 1987 the first heterobifunctional ligand was presented by Fritzberg et al. showing that 4,5-bis(ethylcarbonylmercaptoacetamide)pentanoic acid was capable of being activated with 2,3,5,6-tetrafluorophenol (TFP) after  $^{99m}\text{Tc}$  complexation (1, 2). Later on,  $^{99m}\text{Tc}$  complexes of  $\text{MAG}_3$  (3) and partially hydrolyzed L,L-ECD (4) were activated in a similar manner.

Cyclopentadienyltricarbonyl complexes and boronic acid adducts of  $^{99m}\text{Tc}$  dioxime complexes were also used for the precomplexation route of  $^{99m}\text{Tc}$  labeling of antibodies. The former complex was synthesized in a double ligand transfer reaction using 1,1'-bis(methoxycarbonyl)-ferrocene, [ $^{99m}\text{Tc}$ ]pertechnetate,  $\text{Cr}(\text{CO})_6$ , and  $\text{CrCl}_3$ , which was then hydrolyzed and subsequently activated using TFP (5).  $^{99m}\text{Tc}$  dioxime complexes were obtained using mixtures of dimethylglyoxime (DMG) and 3-isothiocy-anatophenylboronic acid (PICT), which was heated with [ $^{99m}\text{Tc}$ ]pertechnetate in the presence of stannous chloride, forming the reactive  $^{99m}\text{TcCl}(\text{DMG})_3\text{PICT}$  complex (6).

The syntheses of chelators exhibiting an activated ester group have been described for the preconjugation route. NHS esters of *S*-Bz-MAG<sub>3</sub> and 6-(4'-(4''-carboxyphenoxy)-butyl)-2,10-dimercapto-2,10-dimethyl-4,8-diazaundecane (NHS-BAT ester) were used for that purpose but complexation with  $^{99m}\text{Tc}$  was so far not described (7) or failed.<sup>1</sup>

The aim of this work was to synthesize a heterobifunctional ligand, which offers sufficient chemical stability for long-term storage and that could be complexed with  $^{99m}\text{Tc}$  without inactivating the reactive conjugation group. One of the ligands that fulfills these requirements was 2,3,5,6-tetrafluorophenyl *N*-(*S*-benzoylthioacetyl)glycylglycyl-*p*-aminobenzoate (OC2). The synthesis of this ligand,

\* Corresponding author: Michael Eisenhut, Ph.D., Department of Radiopharmaceutical Chemistry, Deutsches Krebsforschungszentrum, Im Neuenheimer Feld 280, 69120 Heidelberg, Germany. Tel +49-6221-42-2443. Fax +49-6221-42-2430. E-mail m.eisenhut@dkfz.de.

<sup>†</sup> University of Heidelberg.

<sup>‡</sup> Havana University.

<sup>§</sup> DKFZ Heidelberg.

<sup>||</sup> Merck KGaA.

<sup>1</sup> M. Eisenhut, unpublished result.



**Table 1. Atom Numbering for the Assignments of NMR Signals**

2	
3	
4	
OC2	

the evaluation of optimal  $^{99m}\text{Tc}$  complexation conditions, and the conjugation to a monoclonal antibody are described.

#### MATERIALS AND METHODS

All commercially available chemicals were of analytical grade and used without further purification.  $^{99m}\text{Tc}$ -pertechnetate was obtained via a generator from CIS bio international (Gif/Yvette Cedex, France). HPLC was carried out on LATEK systems equipped with variable UV (Latek, Heidelberg) and  $\gamma$  radiation detectors (Berthold, Bad Wildbad, Germany). Reversed-phase HPLC columns used were Nucleosil C18 (5  $\mu\text{m}$ , 270  $\times$  4 mm or 270  $\times$  8 mm) (Macherey & Nagel, Düren, Germany). The solvents consisted of MeOH and 0.1% trifluoroacetic acid in water. Protein conjugation yields were determined by instant thin-layer chromatography using silica-coated glass fiber sheets (Pall, Ann Arbor, MI). Size exclusion chromatography (SEC) was performed with Sephadex G 25 (Pharmacia, Freiburg, Germany). The monoclonal antibody used for the conjugation experiments was the anti-EGF receptor antibody mAb425 (Merck, Darmstadt, Germany). The immunoreactive assay was performed with A431 cells, a squamous carcinoma cell line expressing the EGF receptor (Merck, Darmstadt, Germany).

Confirmation of the compounds' structure was obtained with the following analytical methods: MALDI-TOF mass spectrometry (MALDI III TOF spectrometer, Kratos/Shimadzu, Duisburg, Germany), elemental analysis (Microanalytical Laboratory, Chemistry Department, University of Heidelberg),  $^1\text{H}$  and  $^{13}\text{C}$  NMR spectroscopy (Bruker AM-300 spectrometer, Rheinstetten, Germany), where possible assignments of the  $^1\text{H}$  and  $^{13}\text{C}$  NMR resonances are according to the numbering shown in Table 1, and IR spectra (FTIR Jasco Spectrophotometer FT/IR-460).

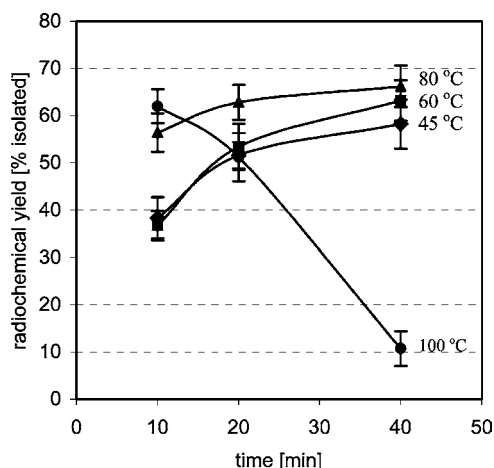
**S-Benzoylmercaptoactetyldiglycine (2).** Glycylglycine (5.94 g, 45 mmol) was dissolved in water (45 mL) by dropwise addition of 1 N NaOH and added in one portion to a solution of succinimidyl *S*-benzoylthioglycolate (17.58 g, 60 mmol) (**8**) in 360 mL of ethanol at 55 °C. The mixture was heated under reflux for 2.5 h and then stirred at room temperature for 12 h. After solvent evaporation, the colorless residue was extracted twice with boiling acetonitrile and recrystallized twice from 20% water in methanol. An additional recrystallization from 2-propanol resulted in 9.5 g (68%) of product, mp: 198–200 °C (lit.: 198–200 °C (**9**)).  $^1\text{H}$  NMR (DMSO- $d_6$ )

$\delta$  (ppm): 3.78 (d, 4H,  $\text{CH}_2$ -11  $\text{CH}_2$ -14); 3.89 (s, 2H,  $\text{CH}_2$ -8); 7.52–7.94 (m, 5H, *H*-Ar); 8.20 (t, 1H, *NH*-13); 8.49 (t, 1H, *NH*-10).  $^{13}\text{C}$  NMR (DMSO- $d_6$ )  $\delta$  (ppm): 32.55 ( $\text{CH}_2$ -8); 40.69 ( $\text{CH}_2$ -14); 42.32 ( $\text{CH}_2$ -11); 126.97 (*C*-3 *C*-5, Ar); 129.23 (*C*-2 *C*-6, Ar); 134.16 (*C*-1, Ar); 136.01 (*C*-4, Ar); 167.31, 169.07 (*CO*-9 *CO*-12); 171.17 (*CO*-15); 190.46 (*CO*-7). IR (KBr,  $\text{cm}^{-1}$ ): 3600–2600 (m, br,  $\nu\text{OH}$ ); 3267 (m,  $\nu\text{NH}$ ); 3100 (m,  $\nu\text{CH}$ , Ar); 1720 (m,  $\nu\text{C}=\text{O}$ , COOH); 1658 (s,  $\nu\text{C}=\text{O}$ , *S*-*C*=O); 1628 (s,  $\nu\text{C}=\text{O}$ , *N*-*C*=O, amide I); 1575 (m,  $\delta\text{NH}$ , amide II); 913 (m,  $\gamma\text{OH}$ ); 688 (m,  $\gamma\text{CH}$ , Ar).

**S-Benzoylmercaptoactetyldiglycine N-Hydroxysuccinimide Ester (3) (10).** Solid *N,N*-dicyclohexylcarbodiimide (5.15 g, 25 mmol) was added in portions to a refluxing solution of *S*-benzoylmercaptoactetyldiglycine (7.34 g, 23 mmol) and *N*-hydroxysuccinimide (2.65 g, 23 mmol) in 100 mL of acetonitrile. The mixture was stirred overnight at room temperature. The precipitate was collected by filtration and washed twice with hot acetonitrile and with hot tetrahydrofuran. The precipitate was collected by filtration and finally recrystallized from ethyl acetate to yield 2.54 g (27%) of a white solid; mp: 145–147 °C.  $^1\text{H}$  NMR (DMSO- $d_6$ )  $\delta$  (ppm): 2.80 (s, 4H,  $\text{CH}_2$ -17  $\text{CH}_2$ -18); 3.81 (d, 2H,  $\text{CH}_2$ -11); 3.88 (s, 2H,  $\text{CH}_2$ -8); 4.28 (d, 2H,  $\text{CH}_2$ -14), 7.53–7.94 (m, 5H, *H*-Ar); 8.50 (s br, 2H, *NH*-10 *NH*-13);  $^{13}\text{C}$  NMR (DMSO- $d_6$ )  $\delta$  (ppm): 25.34 ( $\text{CH}_2$ -17  $\text{CH}_2$ -18); 32.36 ( $\text{CH}_2$ -8); 38.14 ( $\text{CH}_2$ -14); 42.07 ( $\text{CH}_2$ -11); 126.79 (*C*-3 *C*-5, Ar); 126.79 (*C*-2 *C*-6, Ar); 133.95 (*C*-1, Ar); 135.90 (*C*-4, Ar); 166.11, 167.1 (*CO*-9 *CO*-12); 169.31 (*CO*-15); 169.79 (*CO*-16 *CO*-19); 190.19 (*CO*-7); IR (KBr,  $\text{cm}^{-1}$ ): 1817m, 1781m, 1753s ( $\nu\text{C}=\text{O}$ , active ester); 1659 (m,  $\nu\text{C}=\text{O}$ , *S*-*C*=O); 1628 (m,  $\nu\text{C}=\text{O}$ , *N*-*C*=O, amide I); 1217 (s,  $\nu\text{C}-\text{O}$ ). Mass spec (mw = 310.3) observed: 333.4 (*M* + *Na*) $^+$ .

**N-(S-Benzoylthioacetyl)glycylglycyl-4-aminobenzoic Acid (4).** *S*-Benzoylmercaptoactetyldiglycine *N*-hydroxysuccinimide ester (2.03 g, 5 mmol) and 4-aminobenzoic acid (0.68 g, 5 mmol) were dissolved in acetonitrile (35 mL), and the solution was heated under reflux for 5 h, during which a white precipitate formed. To the solution was added 100 mL of acetonitrile, and the mixture was heated under reflux for additional 30 min. The reaction mixture was filtered warm, and the product was washed with acetonitrile to obtain a white solid (1.56 g, 73%); mp: 266–268 °C (dec).  $^1\text{H}$  NMR (DMSO- $d_6$ )  $\delta$  (ppm): 3.80 (d, 2H,  $\text{CH}_2$ -11); 3.90 (s, 2H,  $\text{CH}_2$ -8); 3.93 (d, 2H,  $\text{CH}_2$ -14); 7.51–7.95 (m, 9H, *H*-Ar); 8.29 (t, 1H, *NH*-10); 8.57 (t, 1H, *NH*-13); 10.11 (s, 1H, *NH*-16).  $^{13}\text{C}$  NMR (DMSO- $d_6$ )  $\delta$  (ppm): 32.36 ( $\text{CH}_2$ -8); 42.58, 42.76 ( $\text{CH}_2$ -11  $\text{CH}_2$ -14); 118.34 (*C*-18 *C*-22, Ar); 125.67 (*C*-20, Ar); 126.77 (*C*-3 *C*-5, Ar); 129.02 (*C*-2 *C*-6, Ar); 130.18 (*C*-19 *C*-21, Ar); 133.95 (*C*-1, Ar); 135.88 (*C*-4, Ar); 142.51 (*C*-17, Ar); 167.04 (*CO*-23); 167.44, 167.97, 168.99 (*CO*-9 *CO*-12 *CO*-15); 190.23 (*CO*-7). IR (KBr,  $\text{cm}^{-1}$ ): 3600–2300 (m, br,  $\nu\text{OH}$ ); 3279 (s,  $\nu\text{NH}$ ); 1701 (s,  $\nu\text{C}=\text{O}$ , COOH); 1659 (s,  $\nu\text{C}=\text{O}$ , *S*-*C*=O); 1626, 1602 (s,  $\nu\text{C}=\text{O}$ , *N*-*C*=O, amide I); 1535 (s,  $\delta\text{NH}$ , amide II). Mass spec (mw = 429.4) observed: 452.4 (*M* + *Na*) $^+$ .

**2,3,5,6-Tetrafluorophenyl N-(S-Benzoylthioacetyl)glycylglycyl-4-aminobenzoate (OC2).** *N*-(*S*-Benzoylthioacetyl)glycylglycyl-4-aminobenzoic acid (1.07 g, 2.5 mmol) and 2,3,5,6-tetrafluorophenol (0.83 g, 5.0 mmol) were dissolved in dimethylformamide (20 mL) and cooled in an ice–water bath. *N,N*-Dicyclohexylcarbodiimide (1.03 g, 5 mmol) dissolved in dimethylformamide (5 mL) was added dropwise over 30 min. The reaction mixture was stirred at 0 °C for 2 h and then at room-temperature overnight. After removal of the insoluble *N,N*-dicyclohexylurea by filtration, the solvent was evaporated in



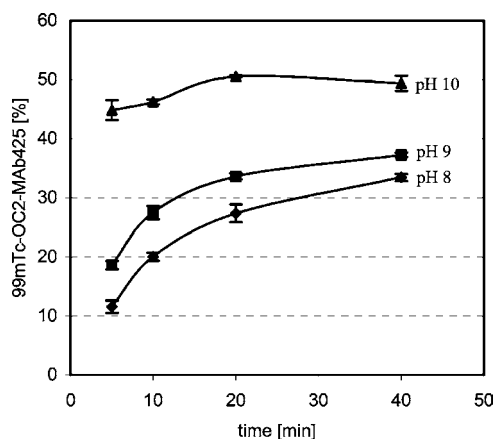
**Figure 1.** Radiochemical yields of  $^{99m}\text{Tc}$ -OC2 formation as a function of reaction temperature and time.

vacuo and the residue recrystallized twice from 2-propanol yielding 0.49 g (34%) of a colorless solid; mp: 243–245 °C (dec).  $^1\text{H}$  NMR ( $\text{DMSO}-d_6$ )  $\delta$  (ppm): 3.81 (d, 2H,  $\text{CH}_2$ -11); 3.91 (s, 2H,  $\text{CH}_2$ -8); 3.97 (d, 2H,  $\text{CH}_2$ -14); 7.51–8.11 (m, 10H,  $H$ -Ar); 8.30 (t, 1H,  $\text{NH}$ -10); 8.57 (t, 1H,  $\text{NH}$ -13); 10.28 (s, 1H,  $\text{NH}$ -16); H, 3.43; N, 7.30; S, 5.57.  $^{13}\text{C}$  NMR ( $\text{DMSO}-d_6$ )  $\delta$  (ppm): 32.31 ( $\text{CH}_2$ -8); 42.58, 42.82 ( $\text{CH}_2$ -11  $\text{CH}_2$ -14); 104.40 ( $C$ -27, Ar); 118.85 ( $C$ -18  $C$ -22, Ar); 119.97 ( $C$ -20, Ar); 126.76 ( $C$ -3  $C$ -5, Ar); 129.00 ( $C$ -2  $C$ -6, Ar); 131.66 ( $C$ -19  $C$ -21, Ar); 133.92 ( $C$ -1, Ar); 135.86 ( $C$ -4, Ar); 144.85 ( $C$ -17, Ar); 161.60 ( $\text{CO}$ -23, Ar); 167.47, 168.42, 169.05 ( $\text{CO}$ -9,  $\text{CO}$ -12,  $\text{CO}$ -15, Ar); 190.19 ( $\text{CO}$ -7). IR (KBr,  $\text{cm}^{-1}$ ): 3314 (m,  $\nu\text{NH}$ ); 1754 (m,  $\nu\text{C}=\text{O}$ ,  $\text{COOT-FP}$ ); 1650 (s, br,  $\text{N}-\text{C}=\text{O}$ ); 1601 (m,  $\text{N}-\text{C}=\text{O}$ , amide I); 1524 (s,  $\delta\text{NH}$ , amide II); 1085 (m,  $\nu\text{C}-\text{F}$ ); Mass spec ( $m/z$  = 577.5) observed: 600.3 ( $M + \text{Na}$ ) $^+$ . Anal. ( $\text{C}_{26}\text{H}_{19}\text{F}_4\text{N}_3\text{O}_6\text{S}$ ) C, H, N, S.

**$^{99m}\text{Tc}$  Complexation of OC2.**  $^{99m}\text{Tc}$  complexation was performed by mixing 100  $\mu\text{L}$  of 1 mM OC2 (dimethylformamide) with 10  $\mu\text{L}$  of 50 mM potassium gluconate ( $\text{H}_2\text{O}$ ), 1  $\mu\text{L}$  of acetic acid, and 300  $\mu\text{L}$  of [ $^{99m}\text{Tc}$ ]pertechnetate eluate (up to 1 GBq in 0.9% NaCl solution). After the addition of 1  $\mu\text{L}$  of 50 mM stannous chloride in 50 mM potassium gluconate, the mixture was heated for the indicated time periods at indicated temperatures (Figure 1). The resulting reaction mixture was loaded on a reversed-phase  $\text{C}_{18}$  column, and the  $^{99m}\text{Tc}$ -OC2 complex separated from the free ligand. The product eluted after 8.5 min using isocratic conditions at 80% MeOH/20% 0.1% TFA in water and after 18 min using a gradient of 60 to 100% MeOH in 30 min. Under these conditions, the ligand eluted after 4 and 17.6 min, respectively. For protein conjugation, the collected  $^{99m}\text{Tc}$ -OC2 eluate was evaporated to dryness.

**$^{99m}\text{Tc}$ -OC2 Antibody Conjugation.** For the measurements of the conjugation kinetics (Figure 2) freeze-dried monoclonal antibody mAb425 was dissolved and adjusted to pH 8, 9, and 10 at a concentration of 67  $\mu\text{M}$ . Samples of 1 mg (100  $\mu\text{L}$ ) were transferred to the dried  $^{99m}\text{Tc}$ -OC2 complex and reacted for 5, 10, 20, and 40 min at 30 °C. Two microliter aliquots were taken from the mixture and spotted on silica-coated glass fiber sheets. The sheets were developed with methanol. The  $^{99m}\text{Tc}$  complexes of OC2 and of compound 4 migrated to the front, while the labeled antibody remained at the start.

Preparation of high-dose labeled antibody was performed with size exclusion chromatography. The complete reaction mixture was transferred to an 8 mL Sephadex G25 column and eluted with PBS (pH 7.4). The



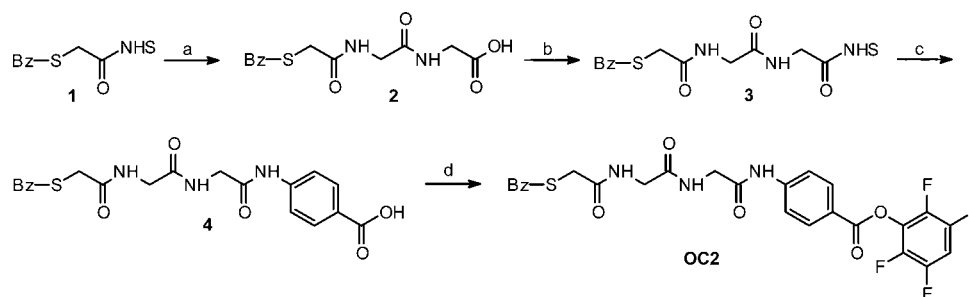
**Figure 2.** Conjugation yields of  $^{99m}\text{Tc}$ -OC2-mAb425 formation at 30 °C as a function of pH and time.

labeled antibody was recovered between 4 and 6 mL. With 67  $\mu\text{M}$  antibody concentration and at pH 10 about 50% radiochemical yield was obtained after 15 min reaction time.

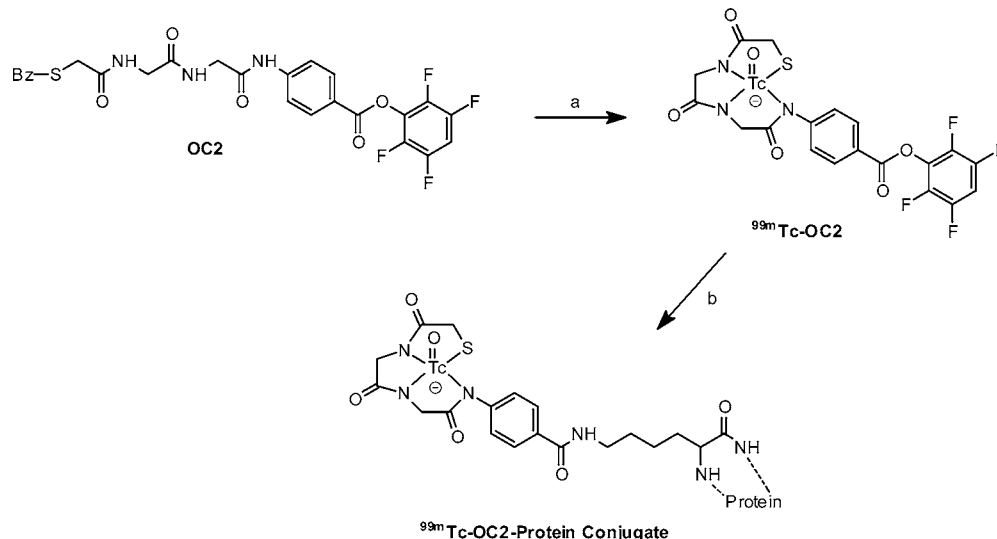
**Immunoreactivity of the  $^{99m}\text{Tc}$ -OC2 Antibody Conjugate.** The immunoreactivity of the radiolabeled mAb425 was determined by a modified cell-binding assay of Lindmo et al. (17). Aliquots of the  $^{99m}\text{Tc}$ -OC2 antibody conjugate (10 ng/50  $\mu\text{L}$ ) were incubated for 1 h at 37 °C with  $6.25 \times 10^4$  to  $1 \times 10^6$  A431 cells. Cells were washed twice, and the radioactivity of the pellet was counted. The maximum cell-bound counts, corrected for nonspecific binding and expressed as a percentage of the total counts, were taken to be the immunoreactivity.

## RESULTS AND DISCUSSION

**Synthesis of 2,3,5,6-Tetrafluorophenyl *N*-(*S*-Benzoylthioacetyl)glycylglycyl-4-aminobenzoate (OC2).** Scheme 1 illustrates the course of synthesis of the heterobifunctional ligand OC2. The preparation steps are straightforward and resemble partly those which lead to *S*-Bz-MAG<sub>3</sub> (12). Starting with succinimidyl *S*-benzoylthioglycolate 1 and the sodium salt of H-Gly-Gly-OH, *S*-benzoylmercaptoacetyldiglycine 2 was formed in high yield. An excess of the NHS ester and elevated temperature was chosen to allow complete turnover of H-Gly-Gly-OH. Coprecipitation of the latter compound during the workup of compound 2 was, therefore, diminished. Because of the limited solubility of compound 2, the formation of the NHS ester 3 had to be performed in refluxing  $\text{CH}_3\text{CN}$ . Although the reaction resulted in an almost quantitative conversion into the product, losses during workup could not be avoided. The NHS ester 3 was then reacted with 4-aminobenzoic acid in refluxing  $\text{CH}_3\text{CN}$ . The triamide 4 precipitated as a white solid from the reaction solution. The purity of the precipitate was high enough to continue with the synthesis. This compound has been described before using, however, an alternative synthesis route and investigated as a renal imaging agent (13, 14). The activation of compound 4 with 2,3,5,6-tetrafluorophenol was performed using *N,N*-dicyclohexylcarbodiimide. To obtain complete turnover of compound 4, double molar excess of the latter compounds was used. Owing to the good solubility of all components, the reaction was performed at 0 °C in dimethylformamide. Pure OC2 was obtained after recrystallization from 2-propanol. The chemical stability of OC2 was not investigated in detail. However, storage of solid OC2 at ambient temperature showed no decomposition after

**Scheme 1<sup>a</sup>**

<sup>a</sup> Reagents and conditions: (a) H-Gly-Gly-OH, NaOH, 55 °C; (b) NHS, DCC, CH<sub>3</sub>CN, reflux; (c) 4-NH<sub>2</sub>-Ph-CO<sub>2</sub>H, CH<sub>3</sub>CN, reflux; (d) TFP, DCC, DMF, 0 °C.

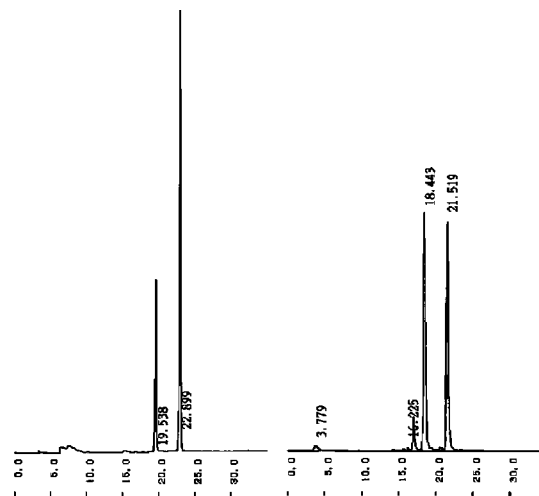
**Scheme 2 <sup>99m</sup>Tc Complexation of OC2 and Conjugation of the <sup>99m</sup>Tc-OC2 Complex with an Antibody<sup>a</sup>**

<sup>a</sup> Reagents and conditions: (a) [<sup>99m</sup>Tc]pertechnetate, potassium gluconate, AcOH, Sn<sup>2+</sup>, 80 °C/20 min; (b) mAb425, pH 9–10, 30 °C/10 min.

more than one year. On the other hand, formation of about 20% of the free acid **4** was observed after one month standing in dimethylformamide solution.

**<sup>99m</sup>Tc Complexation of OC2.** <sup>99m</sup>Tc complexation of OC2 was performed with [<sup>99m</sup>Tc]pertechnetate eluate and potassium gluconate using the stannous chloride reduction method. Heating at increasing temperatures and various time periods resulted in increased labeling yields. The results are illustrated in Figure 1. The temperature and the reaction time significantly influenced the radiochemical yield of complex formation. The optimum complexation temperature obtained from these experiments centered around 80 °C at which >60% radiochemical yield was obtained within 20 min. At higher temperatures this yield can be attained in a shorter time period, however, with the risk of hydrolysis of the TFP ester <sup>99m</sup>Tc-OC2 at later time points.

While the tracer concentration of the <sup>99m</sup>Tc complex of OC2 precludes macroscopic characterization, the structures shown in Scheme 2 are proposed to be in accordance with the <sup>99</sup>Tc-MAG<sub>3</sub> and [Ph<sub>4</sub>P][<sup>99</sup>TcO(MAG<sub>2</sub>-pABA)] complexes (12, 14). The influence of the aromatic amide nitrogen on the complex formation was, however, unknown. Therefore, competition experiments were carried out using equimolar amounts of compound **4**, the free acid of OC2, and *S*-Bz-MAG<sub>3</sub>, which were both complexed together at 80 °C for 10 and 30 min. Figure 3 presents an example of these experiments, which indicates that similar ligand reactivities lead to about the same amount of <sup>99m</sup>Tc complex formation.



**Figure 3.** HPLC of <sup>99m</sup>Tc complexes obtained with a mixture of equimolar amounts of compound **4** and *S*-Bz-MAG<sub>3</sub> after 30 min at 80 °C. Assignments of peaks: UV at 254 nm (left), 19.5 min *S*-Bz-MAG<sub>3</sub>, 22.9 min compound **4**; gamma trace (right), 16.2 min <sup>99m</sup>Tc complex of an impurity originating from compound **4**, 18.4 min <sup>99m</sup>Tc-MAG<sub>3</sub>, 21.5 min <sup>99m</sup>Tc-**4**. HPLC conditions: gradient of 0 to 100% MeOH in 30 min using 0.1% TFA in water as aqueous phase at 0.7 mL/min.

HPLC purification of the complete reaction mixture yielded <sup>99m</sup>Tc-OC2 complex in about 60% radiochemical yield and high radiochemical purity. Isocratic HPLC conditions described in the Materials and Methods section were preferred, not only because of saving time, but



**Table 2. Time Course for Precomplexation and Conjugation Using OC2**

step time	preparation step
20 min	<sup>99m</sup> Tc complexation
10 min	HPLC separation
10 min	eluate evaporation
15 min	protein conjugation
10 min	SEC and sterile filtration
65 min	total preparation time

also to ensure ligand-free <sup>99m</sup>Tc-OC2 preparations. The eluate was collected in a 10 mL glas tube and evaporated to dryness using a rotavapor run under oil pump vacuum. Both steps, HPLC and evaporation, were finished within 20 min. The <sup>99m</sup>Tc-OC2 complex was stable in solution and after evaporation for >24 h.

**<sup>99m</sup>Tc-OC2 Antibody Conjugation.** Solutions (67 μM) of monoclonal antibody mAb425 formulated at pH 8, 9, and 10 were reacted at 30 °C with the dried <sup>99m</sup>Tc-OC2 complex. The conjugation yields were monitored at the indicated reaction-time periods as shown in Figure 2. The time course of the labeling yield was clearly dominated by the pH of the reaction mixture, with the reaction time increasing for reactions performed at pH 8 and 9. The conjugation performed at pH 10 seemed to attain the endpoint just after 20 min. Raising the conjugation temperature up to 50 °C did not improve the conjugation yield at pH 10 (data not shown). Starting with 1 GBq [<sup>99m</sup>Tc]pertechnetate, specific activities of 36 ± 8 GBq/μmol (or 280 ± 53 MBq/mg) mAb425 (*n* = 3) were obtained. Owing to the high molar excess of the antibody, higher specific activities can be expected by increasing the [<sup>99m</sup>Tc]pertechnetate dose. Optimal conditions have to be evaluated for individual mAbs.

The conjugation reaction was expected to have a negligible influence on receptor binding, because <sup>99m</sup>Tc-OC2 was separated from the free ligand OC2. The immunoreactivity assay performed with A431 cells confirmed this assumption. An 81% immunoreactivity was obtained proving the binding integrity of <sup>99m</sup>Tc-OC2-mAb425.

In conclusion, OC2 represents a versatile heterobifunctional <sup>99m</sup>Tc chelating agent, which can be used as a precomplexation tool for antibody labeling. The time course of the labeling method is summarized in Table 2 indicating that about 1 h preparation time was needed for all manipulations. Compared to recently described methods, which need in situ activation of the <sup>99m</sup>Tc complex (e.g., *S*-Bz-MAG<sub>3</sub>, (3)), the application of OC2 saves time and manipulation steps with radioactive material.

#### ACKNOWLEDGMENT

We would like to thank W.E. Hull for NMR spectroscopy, W.D. Lehmann for MS measurements, and U. Bauder-Wüst as well as R. Matys (all DKFZ Heidelberg) for cell-binding experiments. Sample material of mAb425 was obtained as a gift from Merck KGaA, Darmstadt. O.C. was supported by a grant from the Deutscher Akademischer Austauschdienst (DAAD).

#### LITERATURE CITED

- (1) Fritzberg, A. R. (1987) Advances in <sup>99m</sup>Tc-labeling of antibodies. *Nuklearmedizin* 26, 7–12.
- (2) Fritzberg, A. R., Abrams, P. G., Beaumier, P. L., Kasina, S., Morgan, A. C., Rao, T. N., Reno, J. M., Sanderson, J. A., Srinivasan, A., Wilbur, D. C., Vanderheyden, J. L. (1988) Specific and stable labeling of antibodies with technetium-99m with a diamide dithiolate chelating agent. *Proc. Natl. Acad. Sci. U.S.A.* 85, 4025–4029.
- (3) Yoo, T. M., Chang, H. K., Choi, C. W., Webber, K. O., Le, N., Kim, I. S., Eckelman, W. C., Pastan, I., Carrasquillo, J. A., Paik, C. H. (1997) Technetium-99m labeling and biodistribution of anti-TAC disulfide-stabilized Fv fragment. *J. Nucl. Med.* 38, 294–300.
- (4) Verbeke, K., Verbeke, A., Vanbilloen, H., Verbruggen, A. (2002) Preparation and preliminary evaluation of <sup>99m</sup>Tc-EC-For-MLFK. *Nucl. Med. Biol.* 29, 585–592.
- (5) Spradau, T. W., Katzenellenbogen, J. A. (1998) Protein and peptide labeling with (cyclopentadienyl)tricarbonyl rhenium and technetium. *Bioconjugate Chem.* 9, 765–772.
- (6) Linder, K. E., Wen, M. D., Nowotnik, D. P., Malley, M. F., Gougoutas, J. Z., Nunn, A. D., Eckelman, W. C. (1991) Technetium labeling of monoclonal antibodies with functionalized BATOs. 1. TcCl(DMG)3PITC. *Bioconjugate Chem.* 2, 160–170.
- (7) Winnard, P., Jr., Chang, F., Rusckowski, M., Mardirossian, G., Hnatowich, D. J. (1997) Preparation and use of NHS-MAG<sub>3</sub> for technetium-99m labeling of DNA. *Nucl. Med. Biol.* 24, 425–432.
- (8) Brandau, W., Bubeck, B., Eisenhut, M., Taylor, D. M. (1988) Technetium-99m labeled renal function and imaging agents: III. Synthesis of <sup>99m</sup>Tc-MAG<sub>3</sub> and biodistribution of byproducts. *Int. J. Rad. Appl. Instrum. [A]* 39, 121–129.
- (9) Bormans, G., Cleynhens, B., Adriaens, P., Vanbilloen, H., De Roo, M., Verbruggen, A. (1995) Investigation of the labeling characteristics of <sup>99m</sup>Tc-mercaptoacetyltriglycine. *Nucl. Med. Biol.* 22, 339–349.
- (10) Hjelstuen, O. K., By, B. C., Cleynhens, B., Ormstad, H. M., Roald, T. E., Tonnesen, H. H., Bremer, P. O., Verbruggen, A. M. (1999) Comparative evaluation of <sup>99m</sup>Tc-MAG2-oligonucleotides with phosphodiester or phosphorothioate backbones: Preparation, stability and biodistribution. *J. Labelled Compd. Radiopharm.* 42, 737–760.
- (11) Lindmo, T., Boven, E., Cuttitta, F., Fedorko, J., Bunn, P. A. Jr. (1984) Determination of the immunoreactive fraction of radiolabeled monoclonal antibodies by linear extrapolation to binding at infinite antigen excess. *J. Immunol. Methods* 72, 77–89.
- (12) Fritzberg, A. R., Kasina, S., Eshima, D., Johnson, D. L. (1986) Synthesis and biological evaluation of technetium-99m MAG<sub>3</sub> as a hippuran replacement. *J. Nucl. Med.* 27, 111–116.
- (13) Hansen, L., Cini, R., Taylor, A., Jr., Marzilli, L. G. (1992) Rhenium(V) oxo complexes relevant to technetium renal imaging agents derived from mercaptoacetylglucylglycylaminobenzoic acid isomers. Structural and molecular mechanistic studies. *Inorg. Chem.* 31, 2801–2808.
- (14) Hansen, L., Marzilli, L. G., Eshima, D., Malveaux, E. J., Folks, R., Taylor, A. Jr. (1994) Evaluation of technetium-99m-triamide-mercaptide complexes designed to identify properties favoring renal tubular transport. *J. Nucl. Med.* 35, 1198–1205.

BC034091B

# Polyplexes Assembled with Internally Quaternized PAMAM-OH Dendrimer and Plasmid DNA Have a Neutral Surface and Gene Delivery Potency

Jung Hoon Lee, Yong-beom Lim, Joon Sig Choi, Yan Lee, Tae-il Kim, Hyun Jin Kim, Jae Keun Yoon, Kwan Kim, and Jong-sang Park\*

School of Chemistry & Molecular Engineering, Seoul National University, Kwanak-ku, Seoul 151-742, Korea  
Received June 5, 2003; Revised Manuscript Received September 11, 2003

Interior tertiary amine groups of PAMAM-OH dendrimers (hydroxyl-terminated polyamidoamine, PAMAM) were modified by methylation to make these polymers have a more cationic character, which enabled electrostatic interaction between PAMAM-OH and plasmid DNA. A methylation reaction was dose-dependent, producing internally quaternized PAMAM-OH (QPAMAM-OH), thereby making tertiary amine/quaternary amine ratio adjustment possible. More highly condensed particles of plasmid DNA were formed as the degree of quaternization increased, whereas unmodified polymer (PAMAM-OH) could not. The location of positive charges in the internal position of QPAMAM-OH resulted in the formation of neutral polyplexes in which  $\zeta$  potential leveled off near the zero value even at high charge ratios (+/−) of 10. A light scattering experiment showed that the polyplex formed by QPAMAM-OH was very small with the size of 53.3 nm at the optimum condition. QPAMAM-OH/DNA polyplexes were round-shaped with the more compact and small particles formed as the charge ratio increased. QPAMAM-OH showed much reduced cytotoxicity compared with starburst PAMAM and branched polyethyleneimine (PEI) in which shielding of interior positive charges by surface hydroxyls might be the reason for this favorable result. These results suggest that QPAMAM-OH could be a promising tool as a nonviral vector both by itself and in conjugated form with targeting ligands.

## INTRODUCTION

Numerous gene delivery systems based on viral (1–3) and nonviral (4, 5) vectors have been developed and tried so far. Recently, several recurring issues about safety of viral vectors have led to a careful reconsideration of the use of them in human clinical trials such as in Gelsinger's case (6, 7). Moreover, they have significant limitation in large-scale production and available DNA size they can carry. In response to these problems, nonviral gene delivery systems such as cationic polymers or cationic lipids have attracted great attention to achieve a breakthrough in the development of an "ideal" gene carrier (8).

Several polymeric materials have been investigated as candidates for gene delivery; among them, cationic polymers with hydrophilic segments are gaining attention (9–14). It is because hydrophilic segments detoxify cationic polymers (11, 12), improve solubility (12, 13, 15) and prevent polycation/DNA complexes from aggregation *in vivo*.

Starburst PAMAM dendrimers are highly branched spherical polymers characterized by primary amine groups at the surface and tertiary amine groups in the interior. The polyplexes formed by PAMAM showed efficient transfection in which the primary amine groups participate in DNA binding and the tertiary amine groups exert endosome buffering effect (14, 16, 17). Biological behavior of dendrimers depends to a large extent on their surface groups. In one example, it was

reported that amine-terminated PAMAM dendrimer interacted with bovine serum albumin more strongly than carboxyl-terminated one (18). Serum albumin has been considered to cause aggregation of nonviral carriers *in vivo* (19).

PAMAM-OH dendrimers are structurally identical to PAMAM except that surface amine functions have been replaced by hydroxyl groups. Absence of surface primary amine groups in PAMAM-OH makes this polymer nearly neutral which might be advantageous in terms of cytotoxicity and an aggregation problem. However, PAMAM-OH is nearly unable to form DNA polyplex because of the low  $pK_a$  of interior tertiary amines (20).

To overcome this hurdle, we introduced internal quaternary ammonium salt to the tertiary amine of PAMAM-OH dendrimers by methylation in order to provide binding sites for negatively charged plasmid DNA. Some polymers containing quaternary ammonium groups have been known to make polyplexes with DNA more efficiently than the polymers having primary or secondary amine groups. In addition, the polyplexes of quaternary amine-based polymers were relatively smaller compared to those prepared by cationic polymers containing primary and tertiary amine groups (21). Quaternary amine-based polymers are cationic at most pHs as a strong polyelectrolyte, while the charge density in the primary amine-based polymers depend on the pH of media (22).

From such a viewpoint, here we report the synthesis and characterization of internally quaternized PAMAM-OH. We expected that interior quaternary amine groups of QPAMAM-OH would interact negatively charged DNA while preserving a neutral polymer and/or a polyplex surface, which would act affirmatively with regard to cytotoxicity and an aggregation behavior of polyplexes.

\* To whom correspondence should be addressed. Jong-sang Park, School of Chemistry & Molecular Engineering, Seoul National University, San 56-1, Shillim-dong, Kwanak-ku, Seoul 151-742, Korea, Tel: 82-2-880-6660, Fax: 82-2-877-5110, E-mail: pfjspark@plaza.snu.ac.kr.

**Table 1. Quaternization of PAMAM-OH G4<sup>a</sup>**

PAMAM-OH	0.27 Q	0.52 Q	0.78 Q	0.97 Q
CH <sub>3</sub> I	0.5 equiv	0.75 equiv	0.9 equiv	4.16 equiv
temperature	25 °C	37.5 °C	37.5 °C	37.5 °C

<sup>a</sup> Equiv means the equivalent moles of methyl iodide relative to interior tertiary amines in PAMAM-OH G4.

## EXPERIMENTAL PROCEDURES

**Materials.** PAMAM-OH G4, PAMAM G4 (Starburst), Methyl iodide, anhydrous *N,N*-dimethylformamide (DMF), and PEI (average molecular weight 25 kDa) were purchased from Aldrich (Milwaukee, WI). PGL3-control vector (plasmid DNA) was purchased from Promega (Madison, WI). Fetal bovine serum (FBS) and Dubecco's modified Eagle's medium (DMEM) were purchased from GIBCO (Gaithersburg, MD).

**Synthesis of Quaternized PAMAM-OH (QPAMAM-OH).** The solvent (methanol) was vacuum-evaporated and dried from manufacturer's PAMAM-OH solution prior to reaction. After redissolving PAMAM-OH (0.1 g, 7  $\mu$ mol) in DMF (0.5 mL), methyl iodide of various molar ratios diluted in DMF (0.5 mL) was added. The mixture was stirred at each optimal reaction temperature (Table 1). After 24 h, the mixture was precipitated into diethyl ether and vacuum-dried and the residue obtained was redissolved in 1 mL of water. The solution was placed into a dialysis membrane (SpectraPore, MwCO 6000–8000) and dialyzed against 2 M NaCl and pure water in succession. Freeze-drying of water resulted in a white powder of QPAMAM-OH. <sup>1</sup>H NMR (300 MHz, D<sub>2</sub>O)  $\delta$  2.47 (br m, CH<sub>2</sub>CO), 2.69 (br m, NCH<sub>2</sub>CH<sub>2</sub>NHCO), 2.88 (br m, NCH<sub>2</sub>CH<sub>2</sub>), 3.15 (s, CH<sub>3</sub>), 3.34 (br m, CH<sub>2</sub>CH<sub>2</sub>OH), 3.52 (br m, CH<sub>2</sub>N<sup>+</sup>), 3.66 (br m, CH<sub>2</sub>OH).

**Ethidium Bromide Exclusion Assay.** Ethidium bromide (1.0  $\mu$ g) in 10  $\mu$ L of water and plasmid DNA (1.0  $\mu$ g) in 10  $\mu$ L of water were mixed for 10 min at room temperature. After incubation, the plasmid DNA/ethidium bromide mixture was added to quaternized PAMAM-OH dendrimers with various charge ratios, ranging from 0.25 to 10 (+/–) and incubated further for 30 min. The charge ratio was calculated by relating the number of quaternary amine groups of QPAMAM-OH derivatives and the number of phosphate groups of DNA. The complexes were diluted to a total of 2 mL of Hepes buffered saline (HBS, 25 mM Hepes, 150 mM NaCl, pH 7.4) prior to measuring fluorescence intensity with a spectrofluorometer (JASCO FP-750). Excitation ( $\lambda_{\text{ex}}$ ) and emission ( $\lambda_{\text{em}}$ ) wavelengths were 260 and 600 nm, respectively. The fluorescence of the DNA solution in HBS with ethidium bromide was calculated as 100%. The buffer containing ethidium bromide only without DNA was used as a blank control.

**Dynamic Light Scattering (DLS) Measurement.** The size of complexes was determined using a BI-200SM Goniometer (Brookhaven Instruments Corporation, Holtsville, NY) with a Lexel laser model 95 argon laser (100 mW output power at a wavelength of 514.5 nm). Correlator, PD2000 (Precision Detectors) was used and the scattering angle was 90°. Complexes were formed at a final concentration of 5  $\mu$ g/mL plasmid DNA in water. DNA stock solution was added to QPAMAM-OH derivatives or PAMAM G4 prepared at various concentrations. DLS was performed in triplicate with the sampling time set to automatic.

**$\zeta$  Potential Measurement.** The complexes of PAMAM or 0.97 QPAMAM-OH and plasmid DNA at various charge ratios were prepared in water. Surface charges were measured using a Zetasizer (Malvern Instrument

Ltd, Malvern UK) equipped with a He–Ne laser at a wavelength of 680 nm.

**Atomic Force Microscopy (AFM).** Atomic force microscopy (Nanoscope IIIa System, Digital Instruments, Inc., Santa Barbara, CA) was used for imaging the shape of complexes at 4 (N/P or  $\pm$  ratio). Complexes were formed at a total of 1  $\mu$ g/mL of plasmid DNA concentration in water. In the case of PAMAM-OH/plasmid mixture, 2.5 mM of MgCl<sub>2</sub> was applied to the solution. Complexes containing 1 ng of plasmid DNA were applied to freshly cleaved mica and incubated on the mica for 5 min. After incubation, excess fluid was wicked off using filter paper. The solution was dried at room temperature prior to imaging. The image mode was set to tapping mode and average scan speed was 2 Hz.

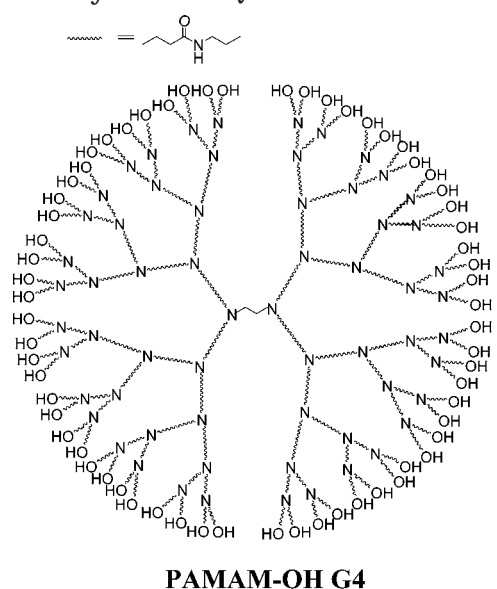
**Cytotoxicity Assay in Vitro.** For the cytotoxicity assay, an MTT assay was performed (23). 293T cells were seeded at a density of  $1 \times 10^4$  cells/well in a 96-well plate and grown in 95  $\mu$ L of DMEM containing 10% FBS for 24 h, supplying 5% CO<sub>2</sub> at 37 °C. After treating cells with PEI 25 kDa, PAMAM G4, PAMAM-OH G4, and QPAMAM-OHs for 1 day, 25  $\mu$ L of MTT stock solution (5 mg/mL) was added to each well and incubated for 2 h. Then, 100  $\mu$ L of extraction buffer (20% w/v of SDS in 50% DMF, pH 4.7) was added. Absorbance was measured at 570 nm after overnight incubation.

**Transfection.** 293T cells ( $5 \times 10^4$  cells/well) were seeded in 24-well plates and grown in 600  $\mu$ L of DMEM containing 10% FBS for 1 day. Polyplexes of plasmid DNA and dendrimers were prepared by mixing 0.5 mL of plasmid DNA (4  $\mu$ g/mL) and 0.5 mL of PAMAM or QPAMAM-OHs at various N/P or charge ratios, respectively, in FBS-free DMEM, and the mixtures were incubated for 30 min at room temperature. Following 4 h treatment of polyplexes, the medium was replaced by 1 mL of DMEM containing 10% FBS. Cells were incubated further for 2 days at 37 °C. After the growth medium was removed, cells were washed with PBS and lysed for 30 min at room temperature by 100  $\mu$ L of Reporter lysis buffer (Promega, Madison, WI). The lysate was cleared by centrifugation. Luciferase activity was measured using a LB 9507 luminometer (Berthold, Germany), and the protein content was measured by Micro BCA assay reagents (Pierce, Rockford, IL).

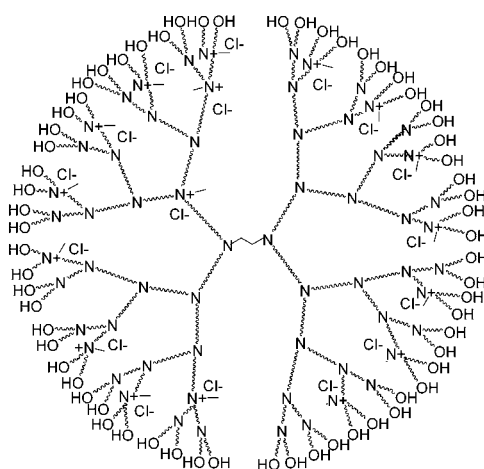
## RESULTS AND DISCUSSION

**Synthesis of QPAMAM-OHs.** QPAMAM-OHs with various degrees of internal quaternization were synthesized by partial or near complete methylation of interior tertiary amine groups (Scheme 1). The peak area of N<sup>+</sup>-methyl group was compared to the total proton numbers of unmodified PAMAM-OH, as confirmed by empirical estimation and theoretical calculation by <sup>1</sup>H NMR (Figure 1). From the <sup>1</sup>H NMR spectra, the degree of quaternization was determined by dividing the experimental proton numbers of the N-methyl groups (3.15 ppm) with the calculated total proton numbers that were obtained by assuming that all the tertiary amines were completely methylated. Careful control over the reaction conditions, e.g., the amount of methyl iodide and reaction temperature, made it possible to produce QPAMAM-OHs with various degrees of quaternization. <sup>1</sup>H NMR spectra showed that surface hydroxyl groups were not reacted with methyl iodide. The significant chemical shift changes occurred at carbons c, d due to the chemical environment of positively charged nitrogen. Chloride salt of QPAMAM-OHs with the various quaternization degree of 27% (0.27 QPAMAM-OH), 52% (0.52 QPAMAM-OH), 78% (0.78



**Scheme 1. Synthesis of QPAMAM-OH<sup>a</sup>**

1. CH<sub>3</sub>I  
2. 2M NaCl dialysis

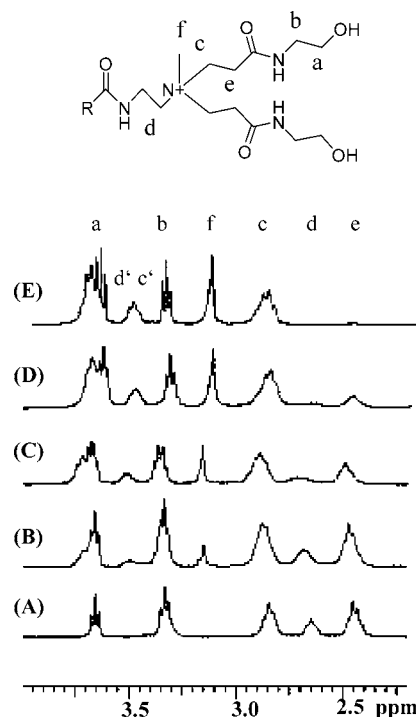


<sup>a</sup> Tertiary amine groups of PAMAM-OH were converted into quaternary amine groups at a degree of 27 % (0.27 QPAMAM-OH), 52 % (0.52 QPAMAM-OH), 78 % (0.78 QPAMAM-OH) and 97 % (0.97 QPAMAM-OH), respectively.

QPAMAM-OH), and 97% (0.97 QPAMAM-OH) were obtained after dialysis and lyophilization.

The PAMAM-OH dendrimers were transformed to be functional by equipping quaternary amine groups for DNA condensation, the hydroxyl groups of their surface for low cytotoxicity, and internal positively charged amines by modifying tertiary amines to quaternary ammonium salts, which screened their charges due to the exterior hydroxyl groups leading to neutral surface charges.

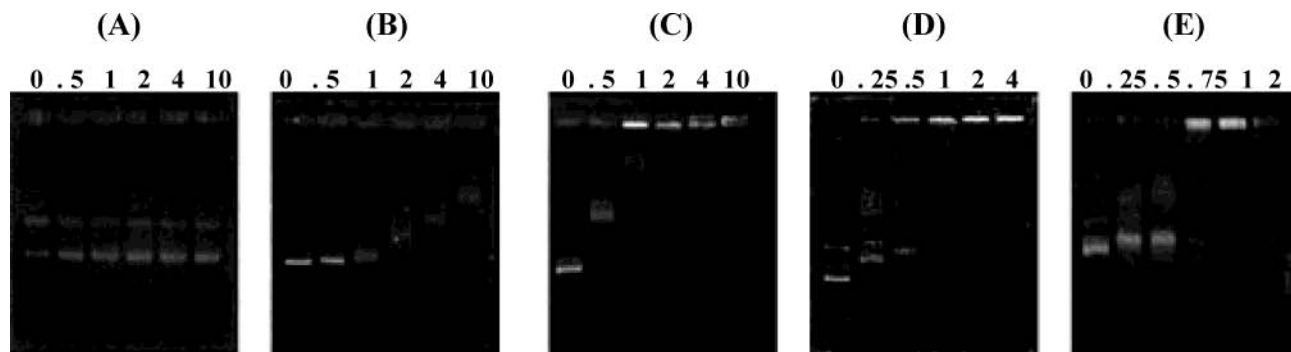
**Analysis of Complex Formation by Agarose Gel Electrophoresis and Ethidium Bromide Exclusion Assay.** The PAMAM-OHs having various degrees of quaternization and plasmid DNA were mixed, and the mixtures were electrophoresed in agarose gel to see if



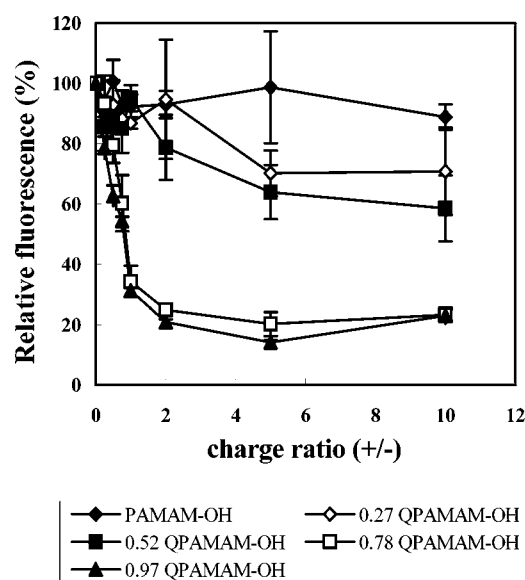
**Figure 1.** <sup>1</sup>H NMR spectra of QPAMAM-OH derivatives. (A) PAMAM-OH G4, (B) 0.27 QPAMAM-OH, (C) 0.52 QPAMAM-OH, (D) 0.78 QPAMAM-OH, and (E) 0.97 QPAMAM-OH. c' and d' are shifted peaks from c and d after quaternization.

polyplexes could be formed by interior positive charges (Figure 2). No indication of polyplex formation between PAMAM-OH and DNA was found (Figure 2A). Low pK<sub>a</sub> values of PAMAM-OH's interior tertiary amines and ensuing low charge density should be the reason for this. Slowly migrating bands in Figure 2B might be the polyplex of 0.27 QPAMAM-OH and DNA; however, no complete retardation of DNA was observed in this polymer. It was observed that the number of charges per copolymer was an important factor in condensing DNA into small particles and in determining other physicochemical characteristics of a polymer/DNA complex (24). As the degree of quaternization increased, complete retardation of DNA was observed (Figure 2C, 2D, and 2E). More highly quaternized polymers were more efficient in polyplex formation. The polyplex formation in 0.97 QPAMAM-OH was nearly stoichiometric.

As shown in Figure 3, ethidium bromide exclusion assay was performed to quantify and confirm the complex formation ability of QPAMAM-OHs. Initial fluorescence of DNA and ethidium bromide complex decreased as dendrimers bound to DNA, releasing intercalated ethidium bromide. In 0.27 QPAMAM-OH, the relative fluorescence intensity decreased to 70% at a charge ratio of 5 and plateaued after that point. A low charge density of 0.27 QPAMAM-OH might be the reason and it is in line with the electrophoresis result (vide ante). DNA was completely retarded by 0.52 QPAMAM-OH above a charge ratio of 2 in the electrophoresis experiment; however, ethidium exclusion did not go beyond around 60% even at a charge ratio of 10. The unexpected phenomenon was revealed that interaction between 0.52 QPAMAM-OH and DNA is too weak to change DNA conformation sufficiently to exclude intercalated ethidium. 0.78 QPAMAM-OH and 0.97 QPAMAM-OH expelled ethidium from DNA, completely above a charge ratio of about 2. In summary, as the degrees of quaternization



**Figure 2.** Agarose gel band shift assay. (A) PAMAM-OH/plasmid DNA polyplexes, (B) 0.27 QPAMAM-OH/plasmid DNA polyplexes, (C) 0.52 QPAMAM-OH/plasmid DNA polyplexes, (D) 0.78 QPAMAM-OH/plasmid DNA polyplexes, and (E) 0.97 QPAMAM-OH/plasmid DNA polyplexes. Charge ratios (+/-) are indicated above each lane. In the case of PAMAM-OH/DNA, numbers of each lane are represented N/P ratios. The charge ratio was calculated by relating the number of quaternary amine groups of QPAMAM-OH derivatives and the number of phosphate groups of DNA, and the N/P ratio was calculated from the number of tertiary amines of PAMAM-OH and the number of phosphate groups of DNA. Samples were electrophoresed in 0.7% agarose gel at 100 V for 40 min in Tris-borate buffer.



**Figure 3.** Ethidium bromide exclusion assay. N/P ratio of PAMAM-OH G4 and charge ratio (+/-) of QPAMAM-OH/plasmid DNA was 0.25, 0.5, 0.75, 1, 2, 5, and 10. Data are expressed as a mean relative fluorescence intensity (%),  $n = 3$  at each ratio and the mean  $\pm$  standard deviation are shown at each data point.

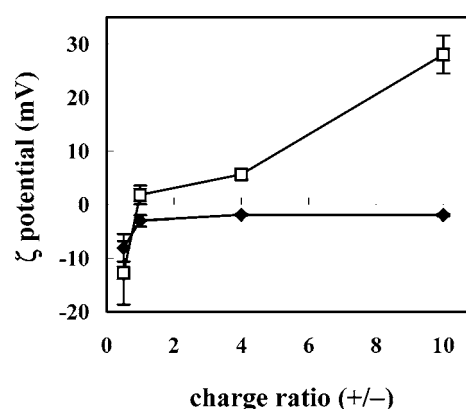
**Table 2. The Complex Size of QPAMAM-OH/DNA Polyplexes and PAMAM/DNA Polyplexes As Determined by Dynamic Light Scattering**

(+/-)	PAMAM	0.52 Q	0.78 Q	0.97 Q
1	168.0	680.2	157.0	129.3
2	126.0	122.6	108.4	111.3
4	86.4	90.9	84.8	74.0
10	78.0	66.1	51.3	53.3

<sup>a</sup> Data are the mean diameter (nm) of each polyplex observed in water at 5  $\mu$ g/mL of plasmid DNA concentration. Charge ratio in PAMAM was calculated on the assumption that only primary amines are protonated in near neutral pH

(97% > 78% > 52% > 27%) in QPAMAM-OH increased, the formation of polyplexes was more efficient.

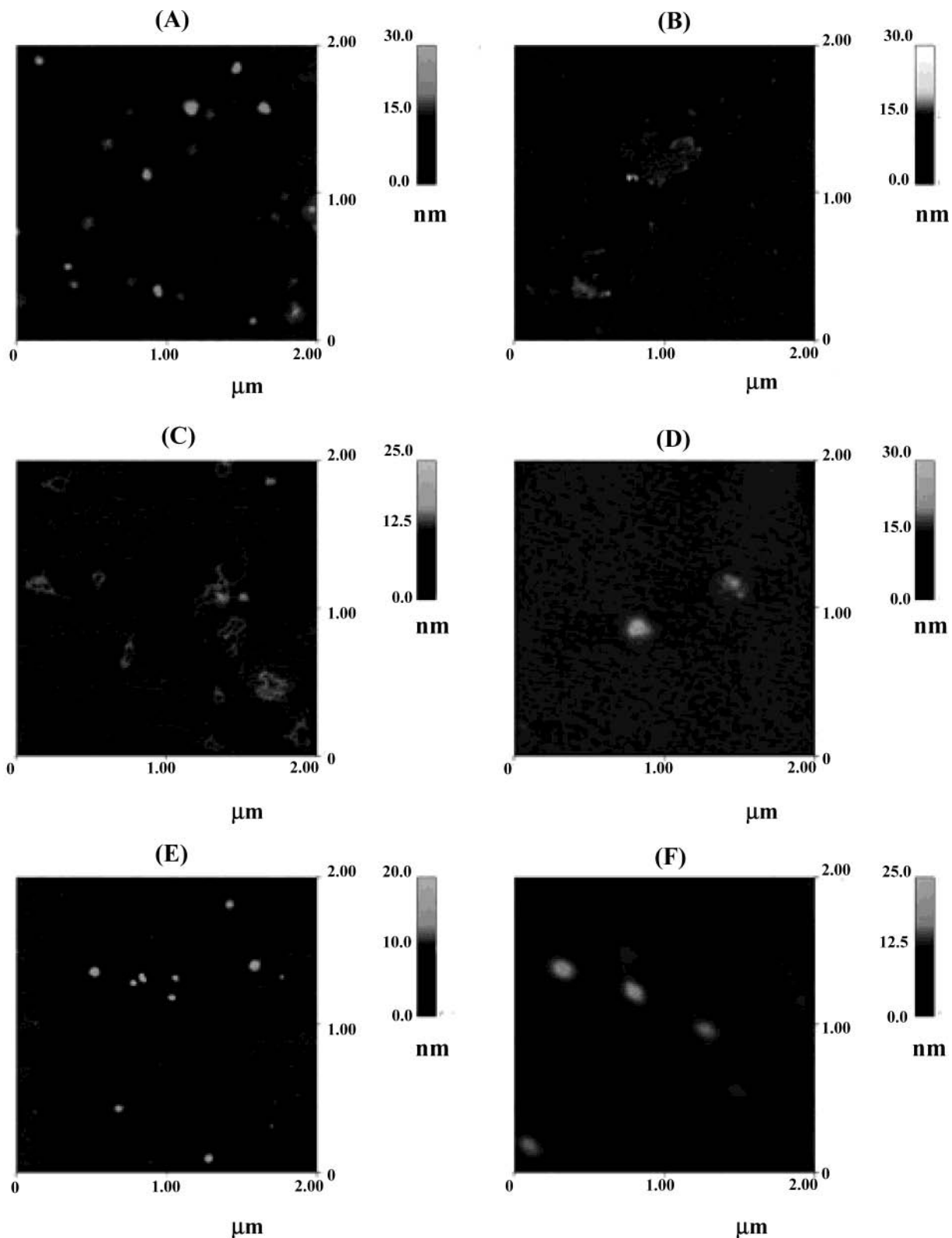
**Characterization of QPAMAM-OHs/DNA Particles.** For analysis of particle size, we performed dynamic light scattering measurements. Briefly, in the presence of quaternary amine-based PAMAM-OH, relatively smaller, compared to primary amine-based PAMAM, particles were formed (Table 2). Interestingly, in the case of 0.52 QPAMAM-OH, very large particles (680.2



**Figure 4.** Surface charge of particles measured by  $\zeta$  potential experiments. The polyplexes of 0.97 QPAMAM-OH ( $\blacklozenge$ ) or PAMAM G4 ( $\square$ ) and plasmid DNA were formed at 0.5, 1, 4, and 10 of charge ratios (+/-). Results are shown as mean  $\pm$  standard deviation ( $n = 3$ ).

nm) were detected at a charge ratio of 1 due to the poor ability of complex formation with DNA. This is also seen from the neutralization between DNA and 0.52 QPAMAM-OH, in which cancellation of net charge (25) and minimization of charge-to-charge repulsion between complex particles might cause the large particles (26). However, increasing the charge ratio up to 2, the particle size became small (122.6 nm). The size distribution of the particles of more quaternized QPAMAM-OHs with DNA was below 157 nm at all charge ratios, which means these particles were small enough to be taken up by receptor-mediated endocytosis requiring a smaller size than 150 nm (27). It can be also noted that the diameter of complex particles gradually decreased as the degree of quaternization in QPAMAM-OH increased. This result indicates that the more compact polyplexes are produced at higher degrees of QPAMAM-OHs. We believe from these results that plasmid DNA having an extended structure can contact and bind to internal positive charges.

The surface charges of particles were determined by  $\zeta$  potential measurements (Figure 4). The surface charge of PAMAM G4 particles increased as increasing charge ratios and positive  $\zeta$  potentials were observed above a charge ratio of 1. For QPAMAM-OH, although the charge ratio was increased up to 10, its surface charge never went to values beyond zero. Starburst PAMAM-OH dendrimers are highly branched macromolecules that have a specific size, spherical shape, and rigid conformation, and it seems likely that the dendrimer has enough



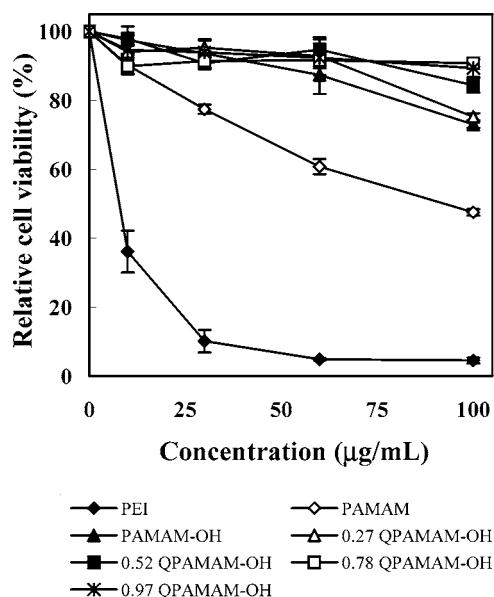
**Figure 5.** Particle morphology imaged by AFM at charge ratio (+/-) = 4. (A) PAMAM G4, (B) PAMAM-OH G4, (C) 0.27 QPAMAM-OH, (D) 0.52 QPAMAM-OH, (E) 0.78- QPAMAM-OH, and (F) 0.97 QPAMAM-OH.

inner space (28) to accommodate large plasmid DNA molecules. This should be the reason hydroxyl groups exposed at their surface are able to screen internal positive charges even increasing their charge ratios. Thus, the condensates are considered to be electrostatically neutralized at their surface.

The morphology and size of the complexes depending on the degree of quaternization was investigated by

atomic force microscopy (AFM) at a charge ratio of 4.0 (Figure 5). Only free plasmid DNA, or very large and loose condensates were observed for PAMAM-OH/DNA polyplexes and 0.27 QPAMAM-OH/DNA polyplexes. 0.52 QPAMAM-OH showed partially condensed structures of DNA. These results were reconfirmed by ethidium bromide exclusion assay results in which no sharp decrease of relative fluorescence was observed by 0.52



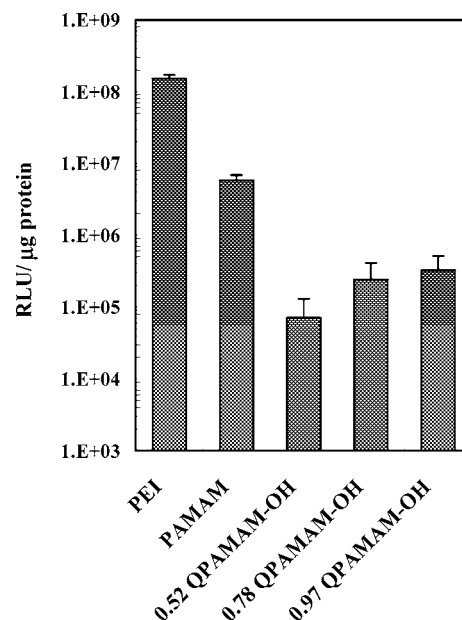


**Figure 6.** Cytotoxicity assay on 293T cell after exposing the cells with PAMAM-OH, QPAMAM-OH, PAMAM G4, and PEI 25kDa at various concentrations. Relative cell viability (RCV, %) is expressed as a percentage of viable cells divided by untreated cells.

QPAMAM-OH. The images of polyplexes composed of 0.78 QPAMAM-OH and 0.97 QPAMAM-OH were observed to be small and spherical particles.

**Cytotoxicity Issue.** Cytotoxic effects of polycations are mainly mediated by interactions of the polymers with cell membranes and/or by cellular uptake of the polymers, and subsequent activation of intracellular signal transduction pathways (29). We examined the cytotoxicity of QPAMAM-OHs with various degrees of quaternization, comparing it with PAMAM G4 and branched PEI (25 kDa) (Figure 6). The cells exposed to PAMAM G4 were more viable than that treated with PEI. In general, the relative cell viability (RCV) of both PEI and PAMAM G4 decreased significantly as the concentration increased. However, quaternized PAMAM-OHs were less toxic than PAMAM G4 and PEI 25kDa. The RCV (%) of all quaternized PAMAM-OH derivatives was over 90% throughout all the concentration levels tested.

The cytotoxicity of cationic macromolecules has been studied and reported extensively so far. One hypothesis is that their toxicity results from the interaction between positively charged polymers and negatively charged cell membranes leading to a haemolytic effect (30, 31). The presence of primary amines has a significant toxic effect on red blood cells, causing them to agglutinate (32). So, many strategies to decrease cytotoxicity of polymers were reported as follows. The cytotoxicity of polyallylamine was reported to be decreased by substituting primary amine groups with amido hydroxyl groups (11). It was also reported that the quaternization of the PEI polymer resulted in a decrease of toxicity (33). The fact that all QPAMAM-OHs were less cytotoxic than their parent dendrimer (PAMAM) should be the result of shielding interior positive charges by surface hydroxyls and of quaternization. Dendrimer-shielding of a surface charge confirmed by  $\zeta$  potential measurement might be the major reason for reduced toxicity, minimizing the direct contact of these polycations to cell membrane. In addition, an inverse correlation between cytotoxicity and degree of quaternization was observed: PAMAM-OH > 0.26 QPAMAM-OH > 0.52 QPAMAM-OH > 0.78 QPAMAM-OH  $\approx$  0.97 QPAMAM-OH with cell cytotoxicity mirroring



**Figure 7.** Transfection efficiency in 293T cell at charge ratio (+/-) = 6. Data are expressed as a RLU (Relative light unit) per  $\mu$ g protein.

the degree of quaternization. The results suggest that the cytotoxicity is a function of the nature of the polycation charged moiety (primary, secondary, tertiary, or quaternary amine group) rather than its charge density (34). The quaternary amines were always charged and strongly hydrophilic; thus, the majority of quaternary amine-containing PAMAM-OHs appeared to be less toxic than tertiary amine-containing PAMAM-OH. Moreover, the higher density of quaternary amine-containing PAMAM-OH benefited from improved hydrophilicity and showed less cytotoxicity. Therefore, the transformation of the water-soluble polymers had previously resulted in a marked reduction in toxicity (33, 35).

Introducing quaternary amines to PAMAM-OH resulted not only in less cytotoxicity, but also the ability for condensation with plasmid DNA while the parent PAMAM-OH could not. These hydroxyl group-modified dendrimer-based delivery systems are supposed to be useful for reduction of the toxicity of PAMAM dendrimers.

**Transfection Efficiency in Vitro.** The gene delivery efficiency of QPAMAM-OH/DNA polyplexes as judged by luciferase gene expression was tested on 293T cell lines. The result (Figure 7) indicated that the transfection efficiency of QPAMAM-OH was lower than that of PAMAM G4 and PEI. The neutral surface charge of QPAMAM-OH/DNA polyplexes, as shown by measurement of the  $\zeta$  potential, might decrease chances of the polyplexes to bind electrostatically to cell-matrix and cell-cell anchoring proteins, such as heparan sulfate proteoglycans (36, 37).

In principle, cellular uptake of a polycation is a nonspecific process. A positively charged complex binds to a negatively charged cell membrane with electrostatic interaction. However, anionic proteoglycans are too ubiquitous for cationic particles to reach specific targeting organs in vivo. Therefore, the introduction of a system which decreases the surface charge of particles is necessary to avoid such a nonspecific uptake into cells. QPAMAM-OHs have such a low nonspecific interaction potential due to the neutral surface of particles; however,

they should be equipped with cell-surface targeting residues that could trigger their receptor-mediated endocytosis.

Although the transfection efficiency of QPAMAM-OH derivatives was lower by 1 order of magnitude than PAMAM G4, our particles have the merit of much lower cytotoxicity and the chance to attach a ligand at the hydroxyl groups of their surface. These properties are useful for the strategy of receptor-mediated transfection by attaching a ligand as is being done in our further works.

## CONCLUSION

We introduced quaternary ammonium salts that were placed in an internal location of starburst PAMAM-OH dendrimer (generation 4) by methylation of interior tertiary amines of PAMAM-OH. Improvements were made, not only in the ability to bind to DNA, but also in the cytotoxicity. The surface hydroxyl functionalities of QPAMAM-OHs could provide low cytotoxicity, and the polyplex of the polymer exhibited a neutral surface charge. Another major advantage of QPAMAM-OH dendrimers is that unreacted hydroxyl groups can be exploited for the conjugation of targeted ligands in order to provide cell entry by receptor-mediated endocytosis, while maintaining decreased nonspecific interaction with ubiquitous cellular proteins.

## ACKNOWLEDGMENT

We acknowledge the support of this work by the Korea Research Foundation (2001-015-DP0344), the Korea Science and Engineering Foundation (R02-2002-000-00011-0), and the SRL-Molecular Therapy Research Center, in Sungkyunkwan University. We thank Prof. Doo Soo Chung for giving access to DLS.

## LITERATURE CITED

- (1) Verma, I. M., and Somia, N. (1997) Gene therapy -- promises, problems and prospects. *Nature* 389 239–242.
- (2) Lotze, M. T., and Kost, T. A. (2002) Viruses as gene delivery vectors: application to gene function, target validation, and assay development. *Cancer Gene Ther.* 9, 692–699.
- (3) Walther, W., and Stein, U. (2000) Viral vectors for gene transfer: a review of their use in the treatment of human diseases. *Drugs* 60, 249–271.
- (4) Nishikawa, M., and Huang, L. (2001) Nonviral vectors in the new millennium: delivery barriers in gene transfer. *Hum. Gene Ther.* 12, 861–870.
- (5) Li, S., and Huang, L. (2000) Nonviral gene therapy: promises and challenges. *Gene Ther.* 7, 31–34.
- (6) Ferber, D. (2001) Gene therapy. Safer and virus-free? *Science* 294, 1638–1642.
- (7) Lehrman, S. (1999) Virus treatment questioned after gene therapy death. *Nature* 401, 517–518.
- (8) Brown, M. D., Schatzlein, A. G., and Uchegbu, I. F. (2001) Gene delivery with synthetic (non viral) carriers. *Int. J. Pharm.* 229, 1–21.
- (9) Choi, J. S., Lee, E. J., Choi, Y. H., Jeong, Y. J., and Park, J. S. (1999) Poly(ethylene glycol)-*block*-poly(l-lysine) Dendrimer: Novel linear polymer/dendrimer block copolymer forming a spherical water-soluble polyionic complex with DNA. *Bioconjugate Chem.* 10, 62–65.
- (10) Kim, T. I., Jang, H. S., Joo, D. K., Choi, J. S., and Park, J. S. (2003) Synthesis of diblock copolymer, methoxypoly(ethylene glycol)-*block*-polyamidoamine dendrimer and its generation-dependent self-assembly with plasmid DNA. *Bull. Korean Chem. Soc.* 24, 123–125.
- (11) Boussif, O., Delair, T., Brua, C., Veron, L., Pavirani, A., and Kolbe, H. V. (1999) Synthesis of polyallylamine derivatives and their use as gene transfer vectors in vitro. *Bioconjugate Chem.* 10, 877–883.
- (12) Ahn, C. H., Chae, S. Y., Bae, Y. H., and Kim, S. W. (2002) Biodegradable poly(ethylenimine) for plasmid DNA delivery. *J. Controlled Release* 80, 273–282.
- (13) Ward, C. M., Pechar, M., Oupicky, D., Ulbrich, K., and Seymour, L. W. (2002) Modification of pLL/DNA complexes with a multivalent hydrophilic polymer permits folate-mediated targeting in vitro and prolonged plasma circulation in vivo. *J. Gene Med.* 4, 536–547.
- (14) Luo, D., Haverstick, B., Nadya, K., Han, E., and Saltzman, W. M. (2002) Poly(ethylene glycol)-Conjugated PAMAM Dendrimer for Biocompatible, High-Efficiency DNA Delivery. *Macromolecules* 35, 3456–3462.
- (15) Mannisto, M., Vanderkerken, S., Toncheva, V., Elomaa, M., Ruponen, M., Schacht, E., and Urtti, A. (2002) Structure–activity relationships of poly(L-lysines): effects of pegylation and molecular shape on physicochemical and biological properties in gene delivery. *J. Controlled Release* 83, 169–182.
- (16) Kukowska-Latallo, J. F., Bielinska, A. U., Johnson, J., Spindler, R., Tomalia, D. A., and Baker, J. R., Jr. (1996) Efficient transfer of genetic material into mammalian cells using Starburst polyamidoamine dendrimers. *Proc. Natl. Acad. Sci. U.S.A.* 93, 4897–4902.
- (17) Eichman, J. D., Bielinska, A. U., Kukowska-Latallo, J. F., and Baker, J. R., Jr. (2000) The use of PAMAM dendrimers in the efficient transfer of genetic material into cells. *Pharm. Sci. Technol. Today* 3, 232–245.
- (18) Klajnert, B., and Bryszewska, M. (2002) Fluorescence studies on PAMAM dendrimers interactions with bovine serum albumin. *Bioelectrochemistry* 55, 33–35.
- (19) Godbey, W. T., and Mikos, A. G. (2001) Recent progress in gene delivery using nonviral transfer complexes. *J. Controlled Release* 72, 115–125.
- (20) Tomalia, D. A., Baker, H., Dewald, J., Hall, M., Kallos, G., Martin, S., Roeck, J., Ryder, J., and Smith, P. (1985) A new class of polymers: Starburst-dendritic macromolecules. *Polym. J.* 17, 177–182.
- (21) Wolfert, M. A., Dash, P., Nazarova, R., O., Oupicky, D., Seymour, L. W., Smart, S., Strohalm, J., and Ulbrich, K. (1999) Polyelectrolyte vectors for gene delivery: influence of cationic polymer on biophysical properties of complexes formed with DNA. *Bioconjugate Chem.* 10, 993–1004.
- (22) Bronich, T. K., Nguyen, H. K., Eisenberg, A., and Kabanov, A. V. (2000) Recognition of DNA Topology in Reactions between Plasmid DNA and Cationic Copolymers. *J. Am. Chem. Soc.* 122, 8339–8343.
- (23) Hansen, M. B., Nielsen, S. E., and Berg, K. (1989) Reexamination and further development of a precise and rapid dye method for measuring cell growth/cell kill. *J. Immunol. Methods* 119, 203–210.
- (24) Choi, J. S., Joo, D. K., Kim, C. H., Kim, K., and Park, J. S. (2000) Synthesis of a Barbell-like Triblock Copolymer, Poly(l-lysine) Dendrimer-*block*-Poly(ethylene glycol)-*block*-Poly(l-lysine) Dendrimer, and Its Self-Assembly with Plasmid DNA. *J. Am. Chem. Soc.* 122, 474–480.
- (25) Yaroslavov, A. A., Sukhishvili, S. A., Obolsky, O. L., Yaroslavova, E. G., Kabanov, A. V., and Kabanov, V. A. (1996) DNA affinity to biological membranes is enhanced due to complexation with hydrophobized polycation. *FEBS Lett.* 384, 177–180.
- (26) Jeong, J. H., Song, S. H., Lim, D. W., Lee, H., and Park, T. G. (2001) DNA transfection using linear poly(ethylenimine) prepared by controlled acid hydrolysis of poly(2-ethyl-2-oxazoline). *J. Controlled Release* 73, 391–399.
- (27) Perales, J. C., Ferkol, T., Molas, M., and Hanson, R. W. (1994) An evaluation of receptor-mediated gene transfer using synthetic DNA-ligand complexes. *Eur. J. Biochem.* 226, 255–266.
- (28) Carnahan, M. A., and Grinstaff, M. W. (2001) Synthesis and characterization of polyether-ester dendrimers from glycerol and lactic acid. *J. Am. Chem. Soc.* 123, 2905–2906.
- (29) Fischer, D., Lib, Y., Ahlemeyerc, B., Krieglsteinc, J., and Kissel, T. (2003) In vitro cytotoxicity testing of polycations:

- influence of polymer structure on cell viability and hemolysis. *Biomaterials* 24, 1121–1131.
- (30) Malik, N., Wiwattanapatapee, R., Klopsch, R., Lorenz, K., Frey, H., J. Weener, W., Meijer, E. W., Paulus, W., and Duncan, R. (2000) Dendrimers: relationship between structure and biocompatibility in vitro, and preliminary studies on the biodistribution of <sup>125</sup>I-labeled polyamidoamine dendrimers in vivo. *J. Controlled Release* 65, 133–148.
- (31) Jevprasesphant, R., Penny, J., Jalal, R., Attwood, A., Mckeown, N. B., and D'Emanuele, A. (2003) The influence of surface modification on the cytotoxicity of PAMAM dendrimers. *Int. J. Pharm.* 252, 263–266.
- (32) Dekie, L., Toncheva, V., Dubruel, P., E., Schacht, H. Barrett, L., and Seymour, L. W. (2000) Poly L-glutamic acid derivatives as vectors for gene therapy. *J. Controlled Release* 65, 187–202.
- (33) Brownlie, A., Uchegbu, I. F., and Schatzlein, A. G. (2002) *Controlled Release Society 29th Annual Meeting Proceedings*, #105, Controlled Release Society, Memphis, TN.
- (34) Zelikin, A. N., Putnam, D., Shastri, P., Langer, R., and Izumrudov, V. A. (2002) Aliphatic ionenes as gene delivery agents: Elucidation of structure–function relationship through modification of charge density and polymer length. *Bioconjugate Chem.* 13, 548–553.
- (35) Brown, M. D., Schatzlein, A., Brownlie, A., Jack, V., Wang, W., Tetley, L., Gray, A. I., and Uchegbu, I. F. (2000) Preliminary characterization of novel amino acid based polymeric vesicles as gene and drug delivery agents. *Bioconjugate Chem.* 11, 880–891.
- (36) Blessing, T., Remy, J. S., and Behr, J. P. (1998) Monomolecular collapse of plasmid DNA into stable virus-like particles. *Proc. Natl. Acad. Sci. U.S.A.* 95, 1427–1431.
- (37) Zuber, G., Dauty, E., Nothisen, M., Belguise, P., and Behr, J. P. (2001) Towards synthetic viruses. *Adv. Drug Delivery Rev.* 52, 245–253.

BC034095G



# A Quantitative Analysis and Chemical Approach for the Reduction of Nonspecific Binding Proteins on Affinity Resins

Tsuruki Tamura, Tomohiro Terada, and Akito Tanaka\*

Chemistry Department, Reverse Proteomics Research Institute Co., Ltd. 2–6–7 Kazusa-Kamatari, Chiba 292-0818, Japan. Received June 18, 2003; Revised Manuscript Received September 2, 2003

Tubulin and actin often bind nonspecifically to affinity chromatography resins, complicating research toward identifying the cellular targets of small molecules. Reduction of nonspecific binding proteins is important for the success of such biochemical approaches. To develop strategies to circumvent this problem, we quantitatively investigated the binding of tubulin and actin to a series of affinity resins bearing 15 variant ligands on 3 commercially available polymer supports. Nonspecific protein binding was proportional to the hydrophobicity of the affinity resins and could be quantitatively correlated to the CLOGP values of the ligands, which are a measure of compound hydrophobicity. When compounds had CLOGP values greater than 1.5, (amount of tubulin) =  $0.73 \times \text{CLOGP} - 1.1$  ( $n = 7$ ,  $r = 0.97$ ), and (amount of actin) =  $0.42 \times \text{CLOGP} - 0.79$  ( $n = 7$ ,  $r = 0.99$ ). On the basis of these studies, we designed a novel hydrophilic poly(ethylene glycol) (PEG) spacer (**26**) for the conjugation of ligands to chromatography resins. As predicted by our binding algorithm, introduction of this spacer reduced the amount of nonspecific protein binding in proportion to the number of ethylene glycol units.

## INTRODUCTION

Affinity chromatography matrixes bearing bioactive compounds such as medicines, natural products, and toxins play an important role in the discovery of novel drug targets and the elucidation of drug mechanisms. Their effectiveness has been demonstrated by the discovery of FKBP12 (1), HDAC (2), and Ref-1 (3) as specific binding proteins of FK506 (1), Trapoxin, and E-3330, respectively. The successful isolation of target proteins by affinity chromatography depends on the synthesis of polymeric resins that can bind to the cellular target with maximum selectivity and efficiency. The nonspecific binding of cellular proteins to affinity matrixes is therefore a significant limitation to this biochemical approach. In particular, tubulin and actin often interfere with affinity chromatography studies, due to their high abundance and the similarity of their molecular weights (50 kDa and 42 kDa, respectively) to many putative target proteins.

Commercially available resins for the synthesis of affinity matrixes can be structurally classified as two types: one consisting of sugar derivatives such as agarose (4) or sepharose (5), and the other based upon methacrylate polymers (6). A wide variety of sugar-based resins are commonly used as bioseparators in molecular biology fields, but these supports are often irreversibly denatured in several synthetic conditions, such as organic solvents and strong acids and bases (7). These properties significantly restrict chemical approaches such as increasing the ligand density on the resin and synthesizing affinity resins bearing structurally complex compounds. In contrast, functional polymers such as poly(methacrylate) derivatives are stable under most synthetic conditions, which allow the synthesis of more effective affinity resins. This is attractive for organic chemists since the recent development of combinatorial chemistry allows us to synthesize a variety of compounds on functional polymers (8–10). However, methacrylate polymers bearing bioactive compounds often show high levels of nonspecific protein binding in comparison to agarose resins with the same ligands. Therefore, the reduction of nonspecific protein binding to methacrylate derivatives is now desired.

The phrase “nonspecific protein binding” is usually used to represent proteins that bind to affinity resins based on physical adsorption rather than specific binding such as “lock and key” interactions between ligands and receptors (11). They were usually thought to bind to the resin through hydrophobic interactions (11, 12), and indeed methacrylate resins are more hydrophobic than agarose-derived supports. As there are no systematic studies of the relationship between nonspecific protein binding and the physical and chemical characteristics of affinity resins, we quantitatively investigated these interactions using 3 kinds of polymeric supports and 15 arbitrarily selected ligands. These studies demonstrated that (1) the profile of nonspecific binding proteins is approximately constant throughout the series of affinity

\* To whom correspondence should be addressed. Tel: +81-438-52-3990, fax: +81-438-52-3986, tanaka-a@reprori.jp.

<sup>1</sup> The following abbreviations were used: AcOEt, ethyl acetate; BB, Bromophenol Blue; buffer A, an aqueous solution of 25mM Tris-HCl (pH 7.4), 0.25 M sucrose; CHCl<sub>3</sub>, chloroform; CH<sub>2</sub>Cl<sub>2</sub>, dichloromethane; DMAP, *N,N*-dimethylaminopyridine; DMF, dimethylformamide; DMSO, dimethyl sulfoxide; EDC, *N*-ethyl-*N*-(3-(dimethylamino)propyl)carbodiimide; EDC HCl, *N*-ethyl-*N*-(3-(dimethylamino)-propyl)carbodiimide hydrochloride; EtOH, ethanol; FK506, immunosuppressant tacrolimus; HOBt, 1-hydroxy-benzotriazole; 2-ME, 2-mercaptoethanol, MeOH, methanol; MgSO<sub>4</sub>, magnesium sulfate; NMP, *N*-methyl-2-pyrrolidone; Pd-C, palladium on activated carbon; PEG, poly(ethylene glycol); PyBOP, bromotris(pyrrolidino)phosphonium hexafluorophosphate; rt, room temperature; sat. NaHCO<sub>3</sub> aq, saturated aqueous solution of sodium bicarbonate; SDS, sodium dodecyl sulfate; TBDPS, *tert*-butyldiphenylsilyl; TBS, *tert*-butyldimethylsilyl; TBS-OTf, *tert*-butyldimethylsilyl trifluoromethanesulfonate; THF, tetrahydrofuran; TFA, trifluoroacetic acid; Tr, trityl.

resins bearing different compounds, and (2) a linear relationship exists between amount of the nonspecific protein binding and ligand hydrophobicity, as measured by CLOGP values. Moreover, we determined that introduction of a hydrophilic spacer is effective for reduction of the nonspecific binding proteins.

## EXPERIMENTAL PROCEDURES

Thin-layer chromatography (TLC) was performed on Merck silica gel 60 F-254 plates. For normal chromatography, Merck silica gel type 60 (size 70–230) was used. All evaporation was performed with a rotary evaporator under reduced atmosphere. The structures of all compounds were confirmed by a LC-MS (Agilent 1100 Series LC/MSD) and 400 MHz proton nuclear magnetic resonance spectroscopy (Bruker, Avance-series 400). The chemical shift values are reported in parts per million on the  $\delta$  scale from internal standard tetramethylsilane. No attempt was made to maximize the yields.


**Mono-TBS-Protected FK506 (2) (13).** FK506 (**1**, 1 g, 1.24 mmol) was dissolved with benzene, evaporated in vacuo, and then dried in vacuo for 1 h to remove water completely.  $\text{CH}_2\text{Cl}_2$  (20 mL) was added and cooled under ice–water conditions, lutidine (0.58 mL, 4.97 mmol) and TBS-OTf (1.15 g, 4.35 mmol) were added thereto, and the mixture was stirred for 1 h. To the reaction mixture was added MeOH (0.2 mL), and then it was poured into a mixture of  $\text{CH}_2\text{Cl}_2$  and sat.  $\text{NaHCO}_3$ . The separated organic layer was washed with water and brine and dried over  $\text{MgSO}_4$ . After filtration, the filtrate was evaporated in vacuo and then purified by chromatography on silica gel (eluted with 20% AcOEt in *n*-hexane). Fractions including the target compound were collected and evaporated in vacuo to give a 24,32-di-TBS protected FK506 derivative (0.62 g), which was used in the next reaction.

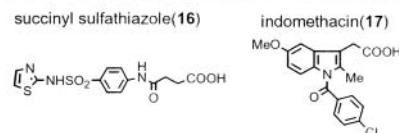
A mixture of the di-TBS protected FK506 (1.87 g, 1.81 mmol), toluenesulfonic acid monohydrate (86.1 mg, 0.453 mmol),  $\text{CH}_2\text{Cl}_2$  (20 mL), and MeOH (20 mL) was stirred at rt for 1 h. The reaction mixture was poured into a mixture of AcOEt and sat.  $\text{NaHCO}_3$ . Separated organic layer was washed with water and brine and dried over  $\text{MgSO}_4$ . After filtration, the filtrate was evaporated in vacuo and then purified by chromatography on silica gel (eluted with 15% acetone in *n*-hexane). Fractions including the target compound were collected and evaporated in vacuo to give **2** (1.33 g, 80%). MS (*m/z*): 918 ( $\text{M}^+$ ), 940 ( $\text{M} + \text{Na}$ ).

**FK506 with a Linker Moiety (3).** A mixture of **2** (138 mg, 0.15 mmol), suberic acid mono-TBDPS ester (86.7 mg, 0.218 mmol), DMAP, (16.5 mg, 0.098 mmol), EDC·HCl (69.1 mg, 0.261 mmol), and  $\text{CH}_2\text{Cl}_2$  (1 mL) was stirred at room temperature for 1.5 h. This mixture was poured into a mixture of AcOEt and an aqueous solution of ammonium chloride. The organic layer was washed with water and brine and dried over  $\text{MgSO}_4$ . After filtration, the filtrate was evaporated in vacuo and then purified by chromatography on silica gel (eluted with 20% AcOEt in *n*-hexane). Fractions including the target compound were collected and evaporated in vacuo to give a crude protected intermediate (44 mg, 24.6%).  $^1\text{H}$  NMR ( $\text{CDCl}_3$ )  $\delta$ : –0.1–0.1 (6H, m), 0.70–2.65 (71H, m), 2.69–3.96 (16H, m), 3.89–5.69 (10H, m), 7.35–7.69 (10H, m).

A mixture of the protected intermediate (44 mg, 0.037 mmol), 48% HF aqueous solution (0.12 mL), and acetonitrile was stirred at room-temperature overnight. This mixture was poured into a mixture of AcOEt and an aqueous solution of ammonium chloride. The organic layer was washed with water and brine and dried over

**Table 1. Structure of Ligands Studied in This Work and Their CLOGP Values**

	
R-COOH	CLOGP *
<i>fatty acids</i>	
<b>5</b> $\text{CH}_3\text{COOH}$	–0.07
<b>6</b> $\text{CH}_3(\text{CH}_2)_2\text{COOH}$	0.85
<b>7</b> $\text{CH}_3(\text{CH}_2)_4\text{COOH}$	1.77
<b>8</b> $\text{CH}_3(\text{CH}_2)_6\text{COOH}$	2.67
<b>9</b> $\text{CH}_3(\text{CH}_2)_8\text{COOH}$	4.04
<b>10</b> $\text{CH}_3(\text{CH}_2)_{12}\text{COOH}$	5.41
<b>11</b> $\text{CH}_3(\text{CH}_2)_{14}\text{COOH}$	6.33
<b>12</b> $\text{CH}_3(\text{CH}_2)_{16}\text{COOH}$	7.69
<i>bioactive and related compounds</i>	
<b>13</b> $\text{Ph}(\text{CH}_2)_2\text{COOH}$	1.41
<b>14</b> $\text{PheNHCO}(\text{CH}_2)_3\text{COOH}$	1.32
<b>15</b> 3-pyridylacetic acid	0.30
<b>16</b> succinyl sulfathiazole	0.74
<b>17</b> indomethacin	3.69
<b>18</b> Ac-L-Trp-OH	0.13
<b>4b</b> $_{32}\text{-FK506-COOH}$	7.48



$\text{MgSO}_4$ . After filtration, the filtrate was evaporated in vacuo and then purified by chromatography on silica gel (eluted with 5% MeOH in  $\text{CHCl}_3$ ). Fractions including the target compound were collected and evaporated in vacuo to give **3** (14.2 mg, 40%).  $^1\text{H}$  NMR ( $\text{CDCl}_3$ )  $\delta$ : 0.82 and 0.85 (3H, d,  $J = 6.5$  Hz, Me), 0.91 and 0.94 (3H, d,  $J = 6.4$  Hz, Me), 0.96 and 1.00 (3H, d,  $J = 6.5$  Hz, Me), 0.8–1.2 (3H, m) 1.3–2.4 (39H, m), 2.46 (1H, m), 2.72 and 2.79 (1H, dd,  $J = 16, 2.4$  Hz), 3.02 (1H, m), 2.95–4.0 (14 H), 3.76 and 4.42 (1H, m), 4.22 and 4.86 (1H, brs, OH), 4.69 (1H, dt,  $J_t = 9.2$  Hz,  $J_d = 4.4$  Hz,  $\text{CH-OOC-linker}$ ), 4.61 and 5.02 (1H, m), 4.95–5.10 (4H, m), 5.19 and 5.32 (1H, each s,  $\text{CH}$ ), 5.71 (1H, m,  $\text{CH=CH}_2$ ). MS (*m/z*): 960 ( $\text{M}^+$ ).

**Affinity Resin Bearing FK506 on Toyopearl (4b).** A mixture of **3** (38.4 mg, 0.04 mmol), Toyopearl (Tosho, AF-Amino-650M, cat. 08002, 100  $\mu\text{L}$ , 0.01 mmol), EDC·HCl (9.2 mg, 0.048 mmol), HOBT (6.5 mg, 0.048 mmol), and DMF (1 mL) was shaken at room temperature for 6 h. After removal of solvents by filtration, the resin was washed with DMF. The reaction ratio was determined by the ninhydrin test (82%). The resin was mixed with a 20% DMF solution of acetic anhydride at rt for 1 h and was washed with DMF and 20% aqueous solution of EtOH.

The synthesis of affinity resins bearing FK506 on AffiGel (**4a**, BIO-RAD, AffiGel 102 Gel, cat. 153–2401) and TentaGel (**4c**, Fluka, TentaGel S- $\text{NH}_2$ , cat. 86364) were carried out according to a similar manner. AffiGel was used after washed with DMF five times. Other resins (**5–18**, Table 1) were prepared according to a similar manner.

**Mono-O-Trityl-Protected Pentaethylene Glycol (20).** To a mixture of pentaethylene glycol (**19**, 10 g, 42.0 mmol), DMAP (0.9 g, 7.4 mmol), and pyridine (100 mL)

was added triphenylmethyl chloride (11.6 g, 41.6 mmol) at rt, and the mixture was stirred at 35 °C overnight. After evaporation in vacuo, the resulting mixture was poured into a mixture of  $\text{CHCl}_3$  and water. The organic layer was washed with sat.  $\text{NaHCO}_3$  aq and brine and dried over  $\text{MgSO}_4$ . After filtration, the filtrate was evaporated in vacuo and then purified by chromatography on silica gel (eluted with 1.6% MeOH in  $\text{CHCl}_3$ ). Fractions including the target compound were collected and evaporated in vacuo to give **20** (10.4 g, 51.2%).  $^1\text{H}$  NMR ( $\text{CDCl}_3$ )  $\delta$ : 3.16 (2H, t,  $J = 5.3$  Hz,  $\text{CH}_2\text{OTr}$ ), 3.49 (2H, m,  $\text{CH}_2\text{OH}$ ), 3.55–3.66 (16H, m), 7.14–7.41 (15H, m).

**2-(2-Tritylhydroxyethoxy-(2-ethoxy-(2-ethoxy-(2-ethoxy-(2-ethoxy))))acetic Acid (21).** To a mixture of **20** (10.2 g, 21.2 mmol), THF (200 mL), and DMF (50 mL) was added 60% sodium hydride (3.1 g, 77.4 mmol) under nitrogen atmosphere over 10 min at 0 °C, and the mixture was stirred at the same temperature for 30 min. After 2-bromoacetic acid (6.5 g, 46.8 mmol) was added thereto, the mixture was stirred at rt for 1 h and then cooled at 0 °C, and sodium hydride (11.6 g, 290 mmol) was added. The mixture was stirred at rt for 1 h and was poured into a mixture of AcOEt and water. This mixture was adjusted to pH 6 by addition of 2 M potassium hydrogen sulfate. The separated organic layer was washed with brine and dried over  $\text{MgSO}_4$ . After the filtration, filtrate was evaporated in vacuo and then purified by chromatography on silica gel (eluted with 15% MeOH in  $\text{CHCl}_3$ ). Fractions including the target compound were collected and evaporated in vacuo to give crude **21** (12.4 g).  $^1\text{H}$  NMR ( $\text{CDCl}_3$ )  $\delta$ : 3.34 (2H, t,  $J = 5.2$  Hz), 3.76–3.84 (18H, m), 4.13 (2H, s,  $\text{CH}_2\text{COOH}$ ), 7.30–7.83 (15H, m).

**2-(2-Tritylhydroxyethoxy-(2-ethoxy-(2-ethoxy-(2-ethoxy-(2-ethoxy))))acetic Acid Benzyl Ester (22).** A mixture of the above crude **21** (12.4 g), DMAP (0.29 g, 2.4 mmol), benzyl alcohol (3.1 mL, 30.0 mmol), EDC·HCl (4.5 g, 23.5 mmol), and  $\text{CH}_2\text{Cl}_2$  (100 mL) was stirred at rt overnight. The reaction mixture was poured into a mixture of  $\text{CHCl}_3$  and water. The separated organic layer was washed with sat.  $\text{NaHCO}_3$  aq and brine and dried over  $\text{MgSO}_4$ . After filtration, the filtrate was evaporated in vacuo and then purified by chromatography on silica gel (eluted with 50% AcOEt in *n*-hexane). Fractions including the target compound were collected and evaporated in vacuo to give crude **22** (12.0 g, 90.1%).  $^1\text{H}$  NMR ( $\text{CDCl}_3$ )  $\delta$ : 3.16 (2H, t,  $J = 5.4$  Hz), 3.55–3.65 (18H, m), 4.11 (2H, s), 5.11 (2H, s,  $\text{CH}_2\text{Ph}$ ), 7.15–7.40 (20H, m).

**2-(2-Hydroxyethoxy-(2-ethoxy-(2-ethoxy-(2-ethoxy-(2-ethoxy))))acetic Acid Benzyl Ester (23).** A mixture of **22** (12.0 g, 1.59 mmol), 5% TFA in  $\text{CH}_2\text{Cl}_2$  (150 mL), and water (150 mL) was stirred at 0 °C for 10 min. The reaction mixture was poured into sat.  $\text{NaHCO}_3$  aq. The separated organic layer was washed with brine and dried over  $\text{MgSO}_4$ . After filtration, the filtrate was evaporated in vacuo and then purified by chromatography on silica gel (eluted with 1.5% MeOH in  $\text{CHCl}_3$ ). Fractions including the target compound were collected and evaporated in vacuo to give crude **23** (7.0 g, 95.0%).  $^1\text{H}$  NMR ( $\text{CDCl}_3$ )  $\delta$ : 3.30 (2H, t,  $J = 5.2$  Hz,  $\text{CH}_2\text{OH}$ ), 3.62–3.76 (18H, m), 4.12 (2H, s), 5.20 (2H, s), 7.36–7.41 (5H, m).

**2-(2-Azidoethoxy-(2-ethoxy-(2-ethoxy-(2-ethoxy-(2-ethoxy))))acetic Acid Benzyl Ester (24).** To a mixture of **23** (7.0 g, 18.1 mmol), DMAP (0.4 g, 3.3 mmol), and pyridine (45 mL) was added *p*-toluenesulfonyl chloride (5.2 g, 27.2 mmol) at 0 °C. After the mixture was stirred at rt overnight, *p*-toluenesulfonyl chloride (5.2 g, 27.2 mmol) and DMAP (120 mg, 0.98 mol) were added

thereto at 0 °C. The reaction mixture was stirred at rt for 2 h and poured into a mixture of EA and water. The separated organic layer was washed with sat.  $\text{NaHCO}_3$  aq, water, and brine and dried over  $\text{MgSO}_4$ . After filtration, the filtrate was evaporated in vacuo to give a crude tosylate intermediate, which was used in the following reaction.

A mixture of this crude intermediate,  $\text{NaN}_3$  (11.8 g, 0.18 mol), and DMF was stirred at 60 °C for 1 h. The reaction mixture was stirred at rt for 2 h and then poured into a mixture of AcOEt and water. The separated organic layer was washed with sat.  $\text{NaHCO}_3$  aq, water, and brine and dried over  $\text{MgSO}_4$ . After filtration, the filtrate was evaporated in vacuo, and the resulting residue was purified by chromatography on silica gel (eluted with 25% AcOEt in *n*-hexane). Fractions including the target compound were collected and evaporated in vacuo to give crude **24** (3.3 g, 44.3%).  $^1\text{H}$  NMR ( $\text{CDCl}_3$ )  $\delta$ : 3.31 (2H, t,  $J = 5.2$  Hz,  $\text{CH}_2\text{N}_3$ ), 3.54–3.87 (18H, m), 4.13 (2H, s), 5.12 (2H, s), 7.20–7.30 (5H, m).

**2-(2-Aminoethoxy-(2-ethoxy-(2-ethoxy-(2-ethoxy-(2-ethoxy))))acetic Acid Benzyl Ester (25).** A mixture of **24** (1.94 g, 4.72 mmol), 10% Pd–C (0.5 g), and MeOH (50 mL) was stirred under hydrogen atmosphere at rt for 2.5 h. After filtration, the filtrate was evaporated in vacuo, to give crude **25** (1.4 g, 100%) which was used in the next reaction without further purifications. MS ( $m/z$ ): 296 ( $\text{M}^+$ ).

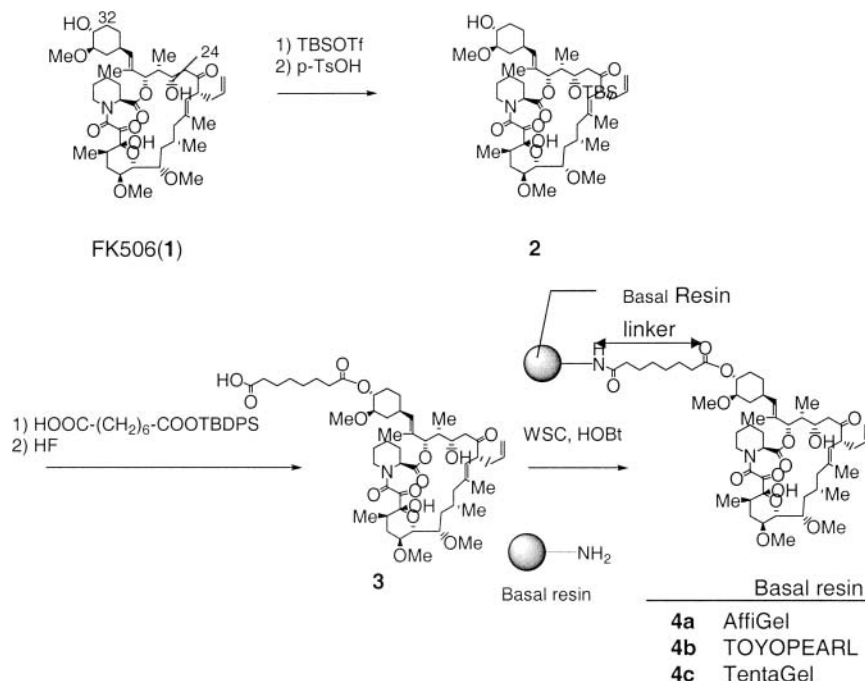
**2-(2-*N*-Fmoc-aminoethoxy-(2-ethoxy-(2-ethoxy-(2-ethoxy-(2-ethoxy))))acetic Acid Benzyl Ester (26).** To a mixture of **25** (1.25 g, 4.23 mmol) and 10% aqueous solution of  $\text{NaHCO}_3$  was added a mixture of 9-fluorenylmethoxycarbonyloxysuccinimide (2.15 g, 6.37 mmol) and dimethoxyethane (14 mL) at rt, and the mixture was stirred at rt overnight. After filtration, the filtrate was washed with 2 M  $\text{NaHSO}_4$  and brine and dried over  $\text{MgSO}_4$ . After filtration, the filtrate was evaporated in vacuo and then purified by chromatography on silica gel (eluted with 0.7% MeOH in  $\text{CHCl}_3$ ). Fractions including the target compound were collected and evaporated in vacuo to give **13** (1.38 g, 63.0%).  $^1\text{H}$  NMR ( $\text{CDCl}_3$ )  $\delta$ : 3.34 (2H, t,  $J = 5.0$  Hz,  $\text{FmocNHCH}_2$ ), 3.50–3.71 (18H, m), 4.05 (2H, s), 4.12 (1H, t,  $J = 7.0$  Hz), 4.33 (2H, d,  $J = 7.0$  Hz), 5.57 (1H, s,  $\text{FmocNH}$ ), 7.22–7.95 (8H, m). Anal. Calcd for  $\text{C}_{27}\text{H}_{37}\text{NO}_{10}$  (monohydrate): C, 60.55; H 6.96; N 2.62. Found: C, 60.72; H 6.92; N 2.42.

**Representative Procedure for Introduction of the Hydrophilic Spacer on Resins.** A mixture of **13** (21 mg, 0.04 mmol), Toyopearl (100  $\mu\text{L}$ , 0.01 mmol), PyBOP (26 mg, 0.05 mmol), *N,N*-diisopropylethylamine (17  $\mu\text{L}$ , 0.10 mmol),  $\text{CH}_2\text{Cl}_2$  (0.4 mL), and NMP (0.1 mL) was shaken at rt for 4 h. After filtration, the resin was washed with DMF five times. The reaction ratio was determined by the ninhydrin test (81%). After the resin was washed with DMF carefully, 0.5 mL of a mixture (acetic anhydride: $\text{CH}_2\text{Cl}_2$ :NMP = 1:8:2) was added for acetyl capping of remained amines. The reaction mixture was shaken at rt for 3 h and then washed with DMF more than five times. The capping reaction was confirmed by the ninhydrin test.

This Fmoc resin was mixed with 0.5 mL of a mixture (piperidine:DMF: $\text{CH}_2\text{Cl}_2$  = 1:4:4) at rt for 3 h. After filtration, the resin was five times washed with DMF to afford the objective resins bearing the hydrophilic spacer **13**. The amount of amine was estimated by the ninhydrin (79  $\mu\text{mol/mL}$ ).

**Preparation of Rat Brain Lysate.** Preparation of tissue extracts of rat brain. Fresh rat brain were homogenized (1:10, wt/vol) in buffer A. The homogenate was





**Figure 1.** Synthesis of affinity resins bearing FK506.

centrifuged at 9500 rpm for 10 min. After supernatant was separated, it was centrifuged at 50 000 rpm for 30 min again. Obtained supernatant was used for lysate and kept at  $-80^{\circ}\text{C}$  before use.

**Binding Assay on Affinity Resins.** The lysate as crude tissue extracts were diluted by buffer A and total protein concentration was prepared about 7 mg/mL. This lysate was stirred calmly with affinity resin at  $4^{\circ}\text{C}$  for about 15 h to adsorb the nonspecific binding proteins or specific binding proteins. A typical mixture has a total volume of 1.0 mL, consisting of buffer A, 10  $\mu\text{L}$  of beads that is previously equilibrated by buffer A, and 0.5 mL of tissue extract. After incubation, the resins were precipitated by centrifugation in a microcentrifuge at 12 000 rpm for 1 min. The resins were washed five times with 1.0 mL of buffer A. The washed beads were then resuspended in 20  $\mu\text{L}$  of SDS sample buffer solution (nakalai, sample buffer solution with 2-ME(2 $\times$ ) for SDS-PAGE, cat. 30566-22, including 4% (w/v) SDS, 20% (v/v) glycerol, 0.01% (w/v) BB, 10% (v/v) 2-mercaptoethanol, 0.125 M Tris pH 6.8), shaken at  $25^{\circ}\text{C}$  for 10 min, and centrifuged for 1 min. The supernatant was subjected to SDS-PAGE followed by CBB staining.

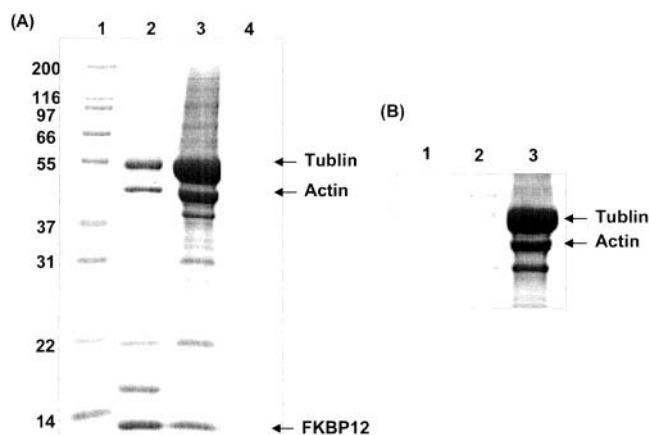
## RESULTS AND DISCUSSION

**Nonspecific Protein Binding on Commercially Available Resins Bearing FK506.** To understand the effect of polymer structure on the amount of nonspecific protein binding, we first synthesized affinity resins bearing a common ligand, FK506 (1, Figure 1), on three types of commercially available and widely used resins, AffiGel, Toyopearl, and TentaGel. AffiGel, a polymer of sugar derivatives, is thought to have hydrophilic surface properties and is now one of the most popular resins for preparation of affinity matrixes (14). AffiGel is not suitable for organic synthesis, because it is easily denatured in organic synthesis conditions and becomes denatured even in DMF (15). Thus, chemical approaches using this resin are limited. Toyopearl consists of poly-(glycidyl methacrylate) whose epoxy moieties have been chemically converted to a hydrophilic spacer after the initial polymerization reaction (its detailed structure is

not published) (16). TentaGel is a polystyrene polymer with long PEG spacers and is often used as resin for the synthesis peptide libraries (17).

FK506 (1) is an immunosuppressive drug that targets to FKBP12 (FK506 binding protein) with a  $K_d$  of 0.4 nM (18). Structure and functions of the complex of FK506 (1) and FKBP12 have been well-characterized at molecular level by S. L. Schreiber et al. (19–21). Since the molecular weight of FKBP12 (12 kDa) differs significantly from that of actin (42 kDa) and tubulin (50 kDa), it is easy to observe and compare the amounts of specific and nonspecific protein binding. Introduction of a linker moiety onto FK506 (1) to connect it to the resins was carried out on a hydroxyl group at the 32 position of FK506 (1, Figure 1) because crystal structure studies indicate that this position is not involved in the binding of FK506 with FKBP12 (21). The synthesis of affinity resins bearing FK506 (1) is shown in Figure 1. Selective protection of a hydroxyl group at the 24 position of FK506 (1) was carried out by two steps, and the linker moiety was introduced by a standard esterification protocol, followed by deprotection of TBS and TBDPS in acidic conditions, giving the FK506 derivative (3). Conjugation of 3 to the base resins, AffiGel, Toyopearl, and TentaGel, was performed by EDC and HOBt in DMF to give the affinity resins (4a–c). Although ligand immobilization onto AffiGel is usually carried out in an aqueous solution using excess amount of ligand and condensation reagents such as EDC and HOBt, or preactivated ligand, 3 was conjugated to AffiGel in DMF to conserve compound.

We mixed the FK506 bearing resins (4a–c) with lysate prepared from rat brain using a simple buffer (buffer A; 0.25 M sucrose, 25 mM Tris-HCl, pH 7.4). Rat brain lysate was thought to be suitable since it includes both the specific binding protein, FKBP12, and the nonspecific binding proteins such as tubulin and actin. The binding proteins to each affinity resin were completely eluted by a SDS sample buffer solution, after extensive washes using buffer A. Eluted proteins were resolved by SDS-polyacrylamide gel electrophoresis, and the identification of tubulin, actin, and FKBP12 were performed by MALDI-TOF mass spectrometry peptide mass fingerprinting after



**Figure 2.** Binding proteins on the resins (A) eluted by SDS sample buffer, (B) eluted proteins by three different buffers. (A) Lane 1, molecular weight ladder; lane 2, eluted proteins from AffiGel bearing FK506; lane 3, that from Toyopearl bearing FK506, lane 4, that from TentaGel bearing FK506. (B) Lane 1, eluted proteins by 1.4 M NaCl; lane 2, that by 8 M urea; lane 3, that by the SDS sample buffer.

in-gel digestion. As determined by binding competition with soluble FK506, we confirmed that only FKBP12 specifically interacts with the FK506-bearing resins and that other proteins such as tubulin and actin are non-specific binding proteins.

A comparison of the protein binding profiles using the three affinity resins is shown in Figure 2A. AffiGel resin (**4a**, lane 2) and Toyopearl resin (**4b**, lane 3) could capture the target protein, FKBP12. However, TentaGel (**4c**, lane 4) failed to sequester significant amounts of proteins including FKBP12 even though it is often used as a resin for peptide libraries. The reason for this result with TentaGel was not clear (*22*). With respect to nonspecific protein binding, Toyopearl resin (lane 3, Figure 2A) bound several proteins with high efficiency, whereas the AffiGel support exhibited much less nonspecific binding (lane 2, Figure 2A). Nonspecifically bound tubulin and actin were observed in particularly large quantities, obscuring any specific protein binding in the 40–55 kDa molecular weight range. To understand the origins of actin and tubulin binding to the Toyopearl resin, we attempted to elute the proteins by three kinds of buffers (Figure 2B); that is, we first washed the Toyopearl resin by 1.4 M NaCl and 8 M urea, which are thought to be able to disturb ionic interaction between proteins and resins, and then washed by the SDS sample buffer solution. The SDS sample buffer is thought to disturb hydrophobic interaction as well, because it includes a high concentration (4%) of the surface-active agent, SDS. As shown in Figure 2B, the nonspecific binding proteins such as actin and tubulin were eluted only by this sample buffer, which indicated that the binding to Toyopearl resins come from hydrophobic interaction not hydrogen bonding, which coincides with Hofstee's result in which several proteins nonspecifically bind to *n*-octyl-agarose through hydrophobic interaction (*11*).

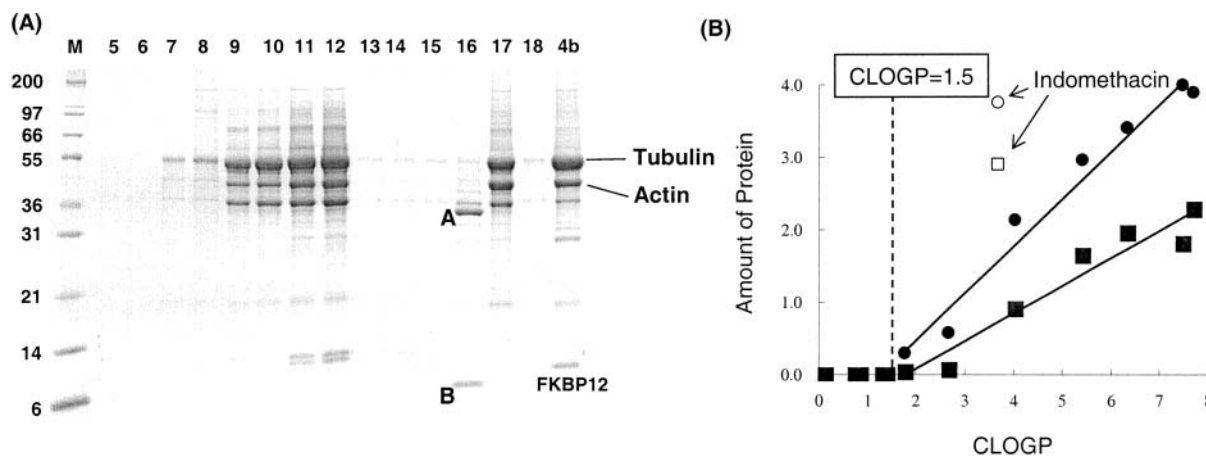
Assuming that binding of nonspecific protein binding to affinity resins is due to hydrophobic interactions, it is logical that much more nonspecific binding is observed with the Toyopearl surface than the AffiGel support, because the matrix surface of AffiGel is more hydrophilic than that of Toyopearl.

**Quantitative Study on Relationship between Nonspecific Protein Binding and Ligand Hydrophobicity.** Aiming to reduce the nonspecific binding of

proteins to the Toyopearl resins, we attempted to quantify the relationship between amount of tubulin and actin binding and hydrophobic property of affinity resins. For this purpose, we synthesized fifteen affinity resins bearing various ligands on Toyopearl and profiled the proteins bound to these resins after the supports were mixed with the rat brain lysate. These ligands were arbitrarily selected, and their structures were shown in Table 1 with their CLOGP values. CLOGP values are a representative descriptor of a compound's hydrophobicity and are often used in QSAR (quantitative structure–activity relationships) studies were calculated by CLOGP program (Version 4.72, Daylight Chemical Information Systems Inc.). All ligands have a carboxylic acid which was used to immobilize the compounds to the amino group of Toyopearl resin as shown in Table 1. Compounds **5–12**, saturated fatty acids, were selected to discuss about effect of simple hydrophobicity of ligands. We also selected some compounds to address the effects of several chemical moieties such as phenyl ring (**13**), amide bond (**14**), pyridine ring (**15**), and amino acid (**18**), which often appear in bioactive compounds and drugs. Some drugs, such as succinyl sulfathiazole (**16**) and indomethacin (**17**), were also selected with FK506 (**4b**) to investigate the effects of drug structure.

Protein binding to each affinity resin was shown in Figure 3A. Proteins binding to the resins were obtained by elution using the SDS sample buffer solution. Proteins from resins bearing hydrophilic ligands such as acetic acid (lane 5), butyric acid (lane 6), 3-phenylpropionic acid (lane 13), glutarallic acid (lane 14), 3-pyridylacetic acid (lane 15), and *N*-acetyltryptophan (lane 18) were almost undetectable. Proteins were observed from other resins while the amount was different each other. Amounts of proteins in lane 7 and 8 were very low compared with others. The large difference in amounts between lane 8 and lane 9 was particularly noteworthy because their structural difference is only three methylenes, indicating that this difference arose from nonstructural distinction. Visible protein species in Figure 3A were similar to each other and almost the same as that from the FK506 resin except for two unknown proteins (A, B) in lane 16 and FKBP12 in lane 4b, while the structures of each ligand on the resin were very diverse. Proteins at 36 kDa in lane 10, 11, 12, and 17 were identified as glyceraldehyde-3-phosphate dehydrogenase [EC 1.2.1.12] by mass spectrum analysis; however, we have not determined whether the 36 kDa bands in lane 9 and 4b are also the same enzyme or not. We also do not know the physiological relevance of the binding of this enzyme to fatty acid-containing resins. On the other hand, the total amount of nonspecific binding differed in a manner that correlated with ligand hydrophobicity. For example, resins bearing less hydrophobic ligands (CLOGP < 1.5) such as acetic acid (**5**), butyric acid (**6**), phenylpropionic acid (**13**), glutarallic acid (**14**), 3-pyridylacetic acid (**15**), and succinyl sulfathiazole (**16**) exhibited little nonspecific binding, while those bearing hydrophobic ligands (CLOGP > 1.5) sequestered much more nonspecific protein. To address this relationship quantitatively, we measured the amount of the largest proteins, tubulin and actin, and plotted them with CLOGP values of ligands (Figure 3B).

Measurement of actin and tubulin on the gel were carried out by a GS-710 Calibrated Imaging Densitometer (BIO-RAD, software; Quantity One-4.1.0). In lane 16, there were three visible and unidentified proteins (11, 34, and 36 kDa proteins); however, tubulin and actin were not detected. This plot demonstrated that the amount of nonspecific protein binding has a linear relationship with



**Figure 3.** (A) Binding proteins on resins bearing various ligands. (B) A plot of estimated amount of tubulin and actin with CLOGP values of each ligands on the resins. (A) Lanes 4b, 5–18 showed binding proteins on each resin bearing compounds **4b**, **5**–**18** (Table 1), respectively. (B) The amount of actin and tubulin was measured by a GS-710 Calibrated Imaging Densitometer (BIO-RAD, software; Quantity One-4.1.0). The linear equations were obtained by Microsoft Excel 2002. CLOGP values were calculated by CLOGP program (Version 4.72, Daylight Chemical Information Systems Inc.).

a simple descriptor for a compound's hydrophobicity, CLOGP. Indomethacin-containing resin (**17**) is the only exception for this trend, demonstrating much more nonspecific binding than would be expected for its CLOGP value. A statistical analysis of the other 14 affinity matrixes resulted in the following algorithms:

$$(\text{amount of tubulin}) = 0.73 \times \text{CLOGP} - 1.1 \quad (n = 7, r = 0.97) \quad (\text{A})$$

$$(\text{amount of actin}) = 0.42 \times \text{CLOGP} - 0.79 \quad (n = 7, r = 0.99) \quad (\text{B})$$

when CLOGP values of compounds were over 1.5, except for that bearing indomethacin (Figure 3B). The reason for the unusually high levels of nonspecific binding observed with the indomethacin-containing resin is not clear.

To our knowledge, this is the first report to quantitatively describe the relationship between nonspecific protein binding and a single descriptor of ligand character with excellent regression factors, 0.97 for tubulin (eq A) and 0.99 for actin (eq B), respectively.

Toyopearl resin bearing ligands whose CLOGP value is less than 1.5 in this work exhibit little nonspecific protein binding. In this study, we found the relationship between ligand hydrophobicity and the amount of actin and tubulin capture; however, we observed the relationship using only a series of affinity resins which consist of Toyopearl as the base resin and the 15 ligands shown in Table 1. Thus, now we actually do not have enough data to discuss whether this relationship can be generally observed in other series of affinity resins or if the 1.5 CLOGP value is universal or variable. We believe that the critical CLOGP value will be more than 1.5 when a hydrophilic basal resin such as AffiGel is used since the hydrophobicity of the resin–ligand conjugate could be a vital factor in addition to that of ligand alone.

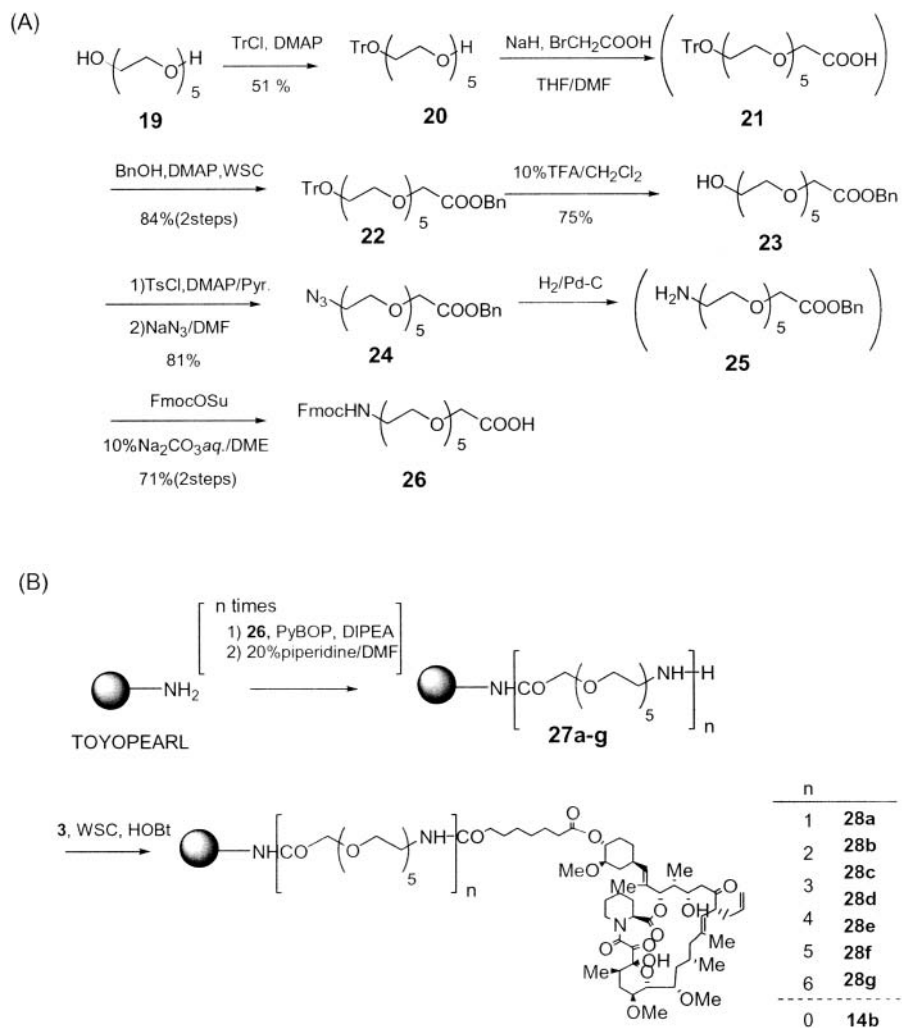
These results indicated the representative nonspecific binding proteins, actin and tubulin, bind to hydrophobic affinity resins without regard to molecular shapes of ligands. High-affinity binding to the resin was indicated because these proteins were not eluted by washing with 1.4 M NaCl and 8 M urea, as shown in Figure 2B. These results are surprising because high-affinity protein–ligand interactions are generally believed to involve a “lock and key” relationship (20). It is difficult to imagine

a common pharmacophore of stearic acid and FK506, yet their affinity resins gave very similar proteins as shown in Figure 3A. We believe that the reason for this unusual binding could be that the proteins denature to variable degrees (21) upon contact with hydrophobic ligands in an aqueous solution. Such protein denaturation would likely involve the binding of aromatic and aliphatic amino acids by the resin-bound ligands, disrupting the core hydrophobic interactions that maintain protein stability.

**Chemical Approach To Reduce Nonspecific Protein Binding.** The results in Figure 3B indicate that an increase of ligand hydrophilicity on Toyopearl resins can decrease the amount of nonspecific protein binding. Therefore, we next attempted to reduce nonspecific protein binding by introduction of a hydrophilic spacer between the base resin and ligands. We designed a hydrophilic spacer based upon poly(ethylene glycol) (PEG) (**26**, Figure 4). PEG derivatives are known to be hydrophilic and are sometimes used as hydrophilic moieties in surface-active agents (25). PEG derivatives are also known to have few unfavorable biological effects. These properties of PEG derivatives were thought to be suitable for a spacer moiety in affinity resins, as seen with TentaGel (17). The hydrophilic spacer (**26**) has an amino acid-like structure that allows study of its repetition effects while usual PEG derivatives are synthesized by the polymerization process and their exact structure is not known (26). The amino group was protected by an Fmoc (9-fluorenylmethoxycarbonyl) to facilitate the synthesis of polymer on resin by the Fmoc strategy. FK506 was also used as a ligand on the affinity resin to compare to that in Figure 1B.

The synthesis of hydrophilic spacer (**26**) is shown in Figure 4A. Single protection of a pentaethylene glycol (**19**) was carried out by using trityl chloride, followed by alkylation of the remaining hydroxyl group to introduce the acetic acid moiety, to give **21**. After introduction of a benzyl group at the carboxylic acid, the trityl group was removed under acidic conditions to afford **23**. The hydroxyl group was converted to an azide group via a *p*-toluenesulfonyl group (**24**). Both the conversion of azide group to amino group and the removal of the benzyl group were performed by hydrogenation. Finally, an Fmoc group was introduced to the amino group to give the desired Fmoc-protected hydrophilic spacer monomer (**26**). The synthesis of FK506 affinity resins bearing the





**Figure 4.** (A) Synthesis of a hydrophilic spacer (**26**). (B) Synthesis of FK506 affinity resins bearing  $n$  mers of the hydrophilic spacer between solid phase and FK506.

hydrophilic spacer between solid phase and FK506 is shown in Figure 4B. Toyopearl resin was used as basal base similar to that of Lane 3 in Figure 1B. Repetitions of the spacer monomer (**26**) on resins were carried out by the Fmoc strategy using PyBOP as a condensation reagent. Finally, introduction of FK506 derivative with the linker moiety at the end of the PEG moiety was performed by using EDC and HOBT to give the desired resin (**28a–g**).

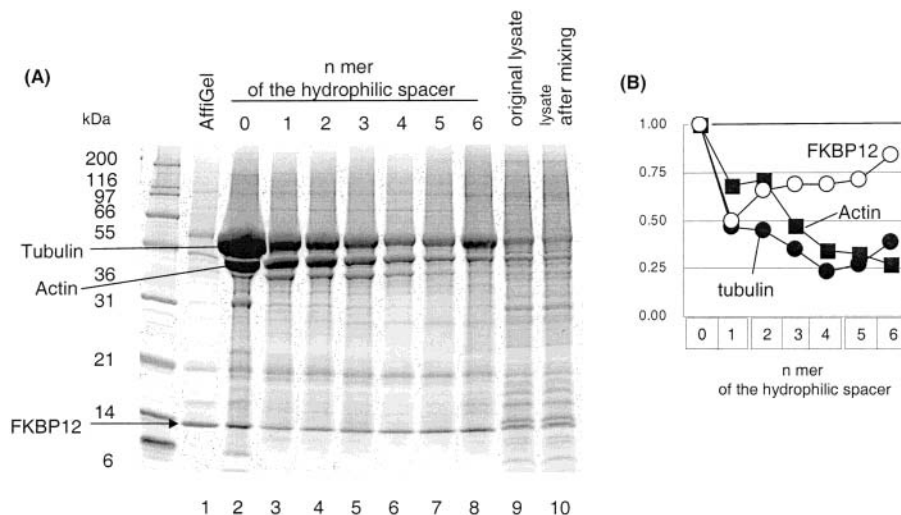
We analyzed the protein binding to each resin after mixing with rat brain lysate as shown in Figure 1B (Figure 5). As shown in Figure 5A, introduction of the hydrophilic spacer was very effective for reduction of the nonspecific protein binding, as expected, and the repetition effect is also obvious while the binding of the target protein, FKBP12, is almost constant throughout the resin series (Figure 5B). The affinity resin bearing a hexamer of the hydrophilic spacer ( $n = 6$ , lane 8 in Figure 5A) yields the same amount of FKBP12 to that without any spacer ( $n = 0$ , lane 2 in Figure 5A) while giving over four times less amount of nonspecific binding proteins. These results reinforce our observations shown in Figure 3B and demonstrate the effectiveness of the introduction of hydrophilic spacer. The effectiveness by introduction of the spacer in Figure 5A was obvious, but the estimated effect in Figure 5B did not seem to be consistent with that in Figure 5A; that is, the amount of tubulin and actin in lane 2 appear to be less. We thought the amount of protein was underestimated by the imaging densitometer

because the shape of the tubulin band was irregular due to an excessive amount on the gel.

The unfavorable proteins were still observed even in lane 8, and Figure 5B indicated that the effect appeared to reach near the maximum, but their amounts were still greater than that of the target protein, FKBP12. We thought the most important factor suggested by Figure 3A is that reduction of the hydrophobicity near the resin surface is vital to reduce the amount of proteins. Thus, the first introduction is very drastic (lane 3 compared with lane 2 in Figure 5A), because it causes introduction of hydrophilicity near the surface. However, addition of the hydrophilic spacer causes introduction of hydrophilicity at an area far from the surface because of repetition, so that the effectiveness decreased. This prompted our next project in which hydrophilicity was introduced near the surface to reduce the unfavorable proteins, which will be reported in the future.

## CONCLUSION

Tubulin and actin are often found as nonspecific binding proteins in affinity chromatography studies, interfering with research toward the identification of drug targets. Reduction of nonspecific protein binding is important for the success of such biochemical approaches. Although it is known that nonspecific binding proteins tend to stick to hydrophobic affinity resins, there is no systematic and quantitative study on the relationship



**Figure 5.** (A) Reduction effect on introduction of the hydrophilic spacer. (B) A plot of the estimated amount of nonspecific binding proteins (tubulin and actin) and the specific binding protein (FKBP12) with repetition numbers of the spacer. (A) Lane 1, molecular weight maker; lane 2, AffiGel bearing FK506 (**4a**); lane 3, Toyopearl bearing FK506 without the hydrophilic spacer ( $n = 0$ , **4b**), lane 4–9, that with  $n$  mer of the hydrophilic spacer ( $n = 1$  to 6, **28a–g**); lane 10, original lysate prepared from rat brain; lane 11, lysate after mixed with **4b**. (B) The amount of actin and tubulin was measured by a GS-710 Calibrated Imaging Densitometer (BIO-RAD, software; Quantity One-4.1.0), and all were represented as a ratio compared to the value of lane 2 ( $n = 0$ ).

between affinity resin hydrophobicity and amount of the nonspecific protein binding. We therefore first compared nonspecific binding proteins on three kinds of affinity resins, consisting of commercially available and widely used base resins AffiGel, Toyopearl, and TentaGel, with a common ligand, FK506 (Figure 2). This study showed that the hydrophilic resin, AffiGel, has low levels of nonspecific protein binding while Toyopearl exhibits much higher levels. Unfortunately, AffiGel is not chemically stable while functional polymers, Toyopearl and TentaGel, are stable in most chemical conditions, which restricts chemical modification and synthesis of desired affinity resins. Thus, the development of novel methods to reduce nonspecific protein binding to functional polymers such as Toyopearl is needed.

To reduce the unfavorable proteins, we first scrutinized the relationship between ligand hydrophobicity and the amount of the nonspecific protein binding using a series of 15 affinity resins bearing variant ligands on Toyopearl (Table 1, Figure 3A). These results showed that the amount increased in proportion to a simple descriptor of hydrophobicity of ligands, CLOGP (Figure 3B). A statistical calculation on the amount of representative nonspecific binding proteins, actin and tubulin, with CLOGP of ligands exhibited a strong correlation; that is, (amount of tubulin) =  $0.73 \times \text{CLOGP} - 1.1$  ( $n = 7$ ,  $r = 0.97$ ), (amount of actin) =  $0.42 \times \text{CLOGP} - 0.79$  ( $n = 7$ ,  $r = 0.99$ ) when CLOGP values of compounds were over 1.5, with the exception of Toyopearl conjugated to indomethacin. On the other hand, resins bearing hydrophilic ligands, whose CLOGP is less than 1.5, showed small amounts of actin and tubulin. According to our knowledge, this is the first report that shows the a quantitative relationship between the amount of nonspecific protein binding and affinity resin hydrophobicity.

Since this relationship suggested that reducing ligand hydrophobicity will be effective for the minimizing of the nonspecific protein binding to affinity matrixes, we next attempted to introduce hydrophilic spacer (**26**) between the ligand and base resin (Figure 5A and 5B). The amount of nonspecific protein binding proteins decreased in proportion to the number of spacer monomers while that of the target protein, FKBP12, is essentially constant. These results exhibited the effectiveness of the

introduction of a hydrophilic spacer to reduce the unfavorable proteins on Toyopearl resin.

It is known that the addition of surface-active agents into affinity chromatography buffers is effective for reducing nonspecific protein binding, because such reagents can noncovalently convert hydrophobic surfaces to hydrophilic ones. But the use of surface-active agents is not always useful because their addition sometimes causes the denaturation of the target proteins while the introduction of a hydrophilic spacer is not thought to affect the activities of proteins. Dextran, a sugar derivative and similar to agarose, has been used as a hydrophilic spacer to reduce nonspecific binding as well (27); however, it is chemically unstable like that of AffiGel. On the other hand, the PEG type of hydrophilic spacer (**26**) is chemically stable, making it suitable for a variety of applications. We believe that the utility of the PEG type spacer is not restricted to affinity resins but that these moieties could also have useful applications in the reduction of nonspecific protein binding on artificial materials in life science. We also apply the spacer on gold surfaces for SPR (surface plasmon resonance) chemistry to reduce noise in the BIACORE experiments and observed similar results described in this paper (data will be reported). Therefore, results described in this work could be effective for reduction of nonspecific protein binding in a wide range of experimental studies involving native proteins.

The nonspecific binding proteins were still observed even after repeated introduction of the spacer (Figure 5A), which indicated that the effect reaches a maximum and that it may be difficult to remove them completely only by introduction of the PEG spacer. We are now developing other hydrophilic and chemically stable spacers and other methods to introduce hydrophilicity on the surface of affinity resins to completely eliminate the nonspecific proteins. Their synthesis and application will be reported in the future.

#### ACKNOWLEDGMENT

We thank Dr. Isao Nakanishi (Exploratory Research Laboratories, Fujisawa Pharmaceutical Co., Ltd.) for calculation of CLOGP values. We also express our thanks

to Prof. James K. Chen (Department of Molecular Pharmacology, Stanford University School of Medicine) and Dr. Masayuki Haramura (Reverse Proteomics Research Institute Co., Ltd.) for critical reading of this manuscript.

## LITERATURE CITED

- (1) Harding, M. W., Galat, A., Uehling, D. E., and Schreiber, S. L. (1989). A receptor for the immunosuppressant FK506 is a cis-trans peptidyl-prolyl isomerase. *Nature* **341**, 758–760.
- (2) Taunton J., Hassig, C. A., and Schreiber, S. L. (1996) A mammalian histone deacetylase related to the yeast transcriptional regulator Rpd3p. *Science* **272**, 408–411.
- (3) Shimizu, N., Sugimoto, K., Tang, J., Nishi, T., Sato, I., Hiramoto, M., and Handa, H., et al. (2000). High-performance affinity beads for identifying drug receptors. *Nat. Biotechnol.* **18**, 877–881.
- (4) Information on one of agarose derivatives, "AffiGel", can be found at the web site of Bio-Rad Laboratories, Inc. (<http://www.bio-rad.com>).
- (5) Information on one of sepharose derivative can be found at the web site of Amersham Biosciences (<http://bioprocess.apbiotech.com>).
- (6) Information on one of methacrylate derivatives, "Toyopearl", can be found at the web site of TOSOH Corporation (<http://www.tosoh.com>).
- (7) The glycoside bonds are usually unstable in the presence of strong acids, etc., and the unprotected hydroxyl moieties in the agarose or sepharose sometimes react with reagents.
- (8) Borman, S. (2001) Combinatorial Chemistry. *C&E News* **79**, 49–58.
- (9) Kawaguchi, H., and Fujimoto, F. (1999). Smart latexes for bioseparation. *Bioseparation* **7**, 253–258.
- (10) Kawaguchi, H. (2000). Functional polymer microspheres. *Prog. Polym. Sci.* **25**, 1171–1210.
- (11) (a) Hofstee, B. H. J. (1974). Nonspecific binding of proteins by substituted agarose. *Adv. Exp. Med. Biol.* **42**, 43–59. (b) Hofstee, B. H. J. (1973). Immobilization of enzymes through noncovalent binding to substituted agarose. *Biochem. Biophys. Res. Commun.* **53**, 1137–1144.
- (12) Haynes, C. A., and Norde, W. (1994). Globular proteins at solid/liquid interfaces. *Colloids Surf. B Biointerfaces* **2**, 517–566.
- (13) The synthesis of mono TBS-protected FK506 was carried out by a manner similar to that of ascomycin described in the following literature: Hyun, O., Szumiloski, J. L., Beattie, T. R., Goulet, M. T., Staruch, M. J. et al. (1997). C32-Amino derivatives of the immunosuppressant ascomycin. *Bioorg. Med. Chem. Lett.* **7**, 2199–2204.
- (14) Harding, M. W., Galat, A., Uehling, D.E., and Schreiber, S. L. (1989) A receptor for the immunosuppressant FK506 is a cis-trans peptidyl-prolyl isomerase. *Nature* **341**, 758.
- (15) As described in the text, AffiGel is stable in aqueous solution and usually used in aqueous solutions. However, it is impossible to use an excess amount of ligand for immobilization since we usually synthesize the compound with linker moiety via more than several synthetic steps, and only small amounts are available. Thus, the immobilization reaction, such as amide formation, needed to be carried out in organic solvent to avoid the presence of water. But AffiGel is sometimes irreversibly denatured in organic solvent and sometimes gives false-positive targets; for example, we found a novel nonspecific binding protein when we synthesized affinity material bearing FK506 in acetonitrile while it was not detected when prepared in an aqueous solution.
- (16) Ito, K., Ma, X., Azmi, N., Huang, H. S., Fujii, M., and Yoshimoto, T. (2003) Novel aminopeptidase specific for glycine from *Actinomucor elegans*. *Biosci. Biotechnol. Biochem.* **67**, 83–8.
- (17) Hiemstra, H. S., Benckhuijsen, W. E., Amons, R., Rapp, W., and Drijfhout, J. W. (1998) A new hybrid resin for stepwise screening of peptide libraries combined with single bead Edman sequencing. *J. Pept. Sci.* **4**, 282–8.
- (18) Siekierka, J. J., Hung, S. H., Poe, M., Lin, C. S., and Sigal, N. H. (1989). A cytosolic binding protein for the immunosuppressant FK506 has peptidyl-prolyl isomerase activity but is distinct from cyclophilin. *Nature* **341**, 755–757.
- (19) Harding, M. W., Galat, A., Uehling, D. E., and Schreiber, S. L. (1989) A Receptor for the Immunosuppressant FK506 is a cis-trans Peptidyl-Prolyl Isomerase. *Nature* **341**, 758.
- (20) Liu, J., Farmer, J. D., Lane, W. S., Friedman, J., Weissman, I., and Schreiber, S. L. (1991) Calcineurin is a Common Target of Cyclophilin-Cyclosporin A and FKBP–FK506 Complexes. *Cell* **66**, 807–815.
- (21) Van Duyn, G. D., Standaert, R. F., Karplus, P. A., Schreiber, S. L., and Clardy, J. (1991) Atomic Structure of FKBP–FK506, an Immunophilin-Immunosuppressant Complex. *Science* **252**, 839–842.
- (22) TentaGel is used as basal matrix in peptide library screening. We thought that proteins only bind to the very outside surface of TentaGel, so it works well only when hydrophilic ligands such as peptides are immobilized on it, and it does not work when hydrophobic ligands such as FK506 are on it because they tend to bind to the hydrophobic basal resin, which consists of polystyrene. It is usually impossible because the length of spacer moiety of the usual affinity resins is not enough while the length of TentaGel is very long; the average number of PEG polymer is ca. 66.
- (23) Dean, P. M. (1987) Molecular foundation of drug-receptor interaction. Cambridge University Press, England.
- (24) It was known that enzyme activities were still observed after absorption on *n*-octyl-agarose (11). These results indicated that the conformation of proteins was not unique; that is, some of them were completely denatured and others were partially denatured; moreover, native proteins can also bind on the surface that are occupied by various conformational states of the enzymes.
- (25) There are many surface-active agents that include PEG in their structures as a hydrophilic moiety; for examples, polyoxyethylene(23) lauryl ether ("Brij 35") and other "Brij" series, polyoxyethylene branched monocyclohexyl ether ("Triton") and other "Triton" series, and polyoxyethylene(20) sorbitan monolaurate ("Tween20") and others in the "Tween" series.
- (26) For example, the average repetition number of oxyethylene unit of TentaGel's PEG moiety is 68, and the number is not unique.
- (27) Dextran is used as hydrophilic spacer in the Biacore chips. Dextran plays as a spacer between gold foil and ligands in the Biacore system. We have observed nonspecific binding proteins after treatment of the gold foil bearing a ligand via the Dextran spacer with acetonitrile (data not shown).

BC034099L



# The [ $^{99m}\text{Tc}(\text{N})(\text{PNP})$ ] $^{2+}$ Metal Fragment: A Technetium-Nitrido Synthron for Use with Biologically Active Molecules. The *N*-(2-Methoxyphenyl)piperazyl-cysteine Analogues as Examples

C. Bolzati,<sup>\*,†</sup> A. Mahmood,<sup>‡</sup> E. Malagò,<sup>§</sup> L. Uccelli,<sup>§</sup> A. Boschi,<sup>§</sup> A. G. Jones,<sup>‡</sup> F. Refosco,<sup>†</sup> A. Duatti,<sup>§</sup> and F. Tisato<sup>†</sup>

ICIS, CNR Corso Stati Uniti, 4, 35020 Padova, Italy, Harvard Medical School and Brigham and Woman's Hospital, Boston, Massachusetts 02115, and Laboratory of Nuclear Medicine, Department of Clinical and Experimental Medicine, University of Ferrara, Via L. Borsari, 46, 44100 Ferrara, Italy. Received June 19, 2003; Revised Manuscript Received August 27, 2003

The incorporation of a bioactive molecule into a nitrido-containing  $^{99m}\text{Tc}$ -complex has been successfully achieved by using the [ $\text{TcN}(\text{PNP})$ ] $^{2+}$  metal fragment. In this strategy, the strong electrophilic [ $\text{TcN}(\text{PNP})$ ] $^{2+}$  metal fragment efficiently reacts with bifunctional chelating ligands having a  $\pi$ -donor atom set, such as *N*-functionalized *O,S*-cysteine. The 2-methoxyphenylpiperazine (2-MPP) pharmacophore, which displays preferential affinity for 5HT<sub>1A</sub> receptors, was conjugated to the amino group of cysteine to obtain 2-MPPP-cys-OS, where 2-MPPP is 3-[4-(2-methoxyphenyl)piperazin-1-yl]propionate. The asymmetric Tc(V)-nitrido complexes, [ $^{99g/99m}\text{Tc}(\text{N})(\text{PNP})(2\text{-MPPP-cys-OS})$ ] (PNP = PNP3, PNP4), were obtained in high yield (95%), by simultaneous addition of PNP and 2-MPPP-cys-OS ligand to a solution containing a starting  $^{99g/99m}\text{Tc}$ -nitrido precursor. A mixture of syn and anti isomers was observed, the latter being the thermodynamically favored species. In vitro challenge experiments using the anti isomers with glutathione and cysteine indicated that no transchelation reaction occurs. Assessment of the in vitro 5HT<sub>1A</sub> receptor-affinity of the technetium complexes revealed that only the *anti*-PNP4 complex possesses some affinity for the receptor, but displayed negligible brain uptake in biodistribution studies in rats in vivo.

## INTRODUCTION

One aspect of radiopharmaceutical development focuses on the design and synthesis of imaging agents that target specific receptors and transporters involved in certain pathological conditions. In vivo imaging via positron emission tomography (PET) provides the means to visualize receptor and transporter densities in living subjects and to estimate the inhibition of receptor, transporter density, and binding of endogenous (neurotransmitter) or exogenous (e.g. neuroleptic drug) ligands. This methodology is of general importance in elucidating how various neuropsychiatric conditions unfold in human subjects and for establishing the mechanism and efficacy of drug-treatment strategies. In this regard, investigation of the serotonergic system, which is implicated in several neuropsychiatric disorders including anxiety, depression, schizophrenia, and Alzheimer's disease, has been a subject of particular interest. Recent reports have described [ $^{11}\text{C}$ ]WAY-100635 as a  $^{11}\text{C}$ -labeled radioligand that may provide a means to noninvasively image the 5HT<sub>1A</sub> receptors with PET (1, 2). While this agent is a potent and selective 5HT<sub>1A</sub> receptor antagonist, its initial high signal-to-noise ratio is compromised by the in vivo formation of small amounts of labeled metabolites that bind nonspecifically in various brain regions, thereby reducing image contrast. Thus the search for and devel-

opment of new 5HT<sub>1A</sub> radioligands is under active investigation (3, 4).

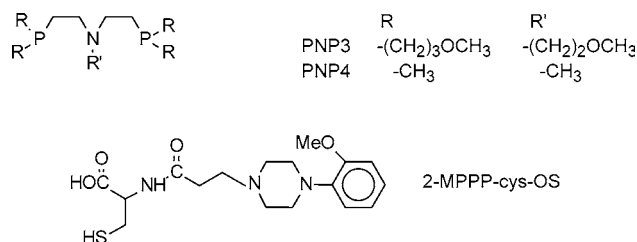
Given the general availability in most nuclear medicine facilities of single-photon-emission tomography (SPECT) instrumentation compared with that for PET, the widespread availability of  $^{99}\text{Mo}$ – $^{99m}\text{Tc}$  generators, and the near ideal imaging characteristics of  $^{99m}\text{Tc}$  via SPECT, the potential utility of a technetium-99m-labeled receptor-specific agent for 5HT<sub>1A</sub> would be of interest. Thus, over the past few years various approaches have been proposed for synthesizing  $^{99m}\text{Tc}$ -complexes capable of selectively binding central nervous system (CNS) 5HT<sub>1A</sub> receptors. Most of the reported complexes are based on the monooxo-Tc(V) core (5–11), with one utilizing the organometallic [ $^{99m}\text{Tc}(\text{CO})_3$ ] $^{+}$  metal fragment (12). Among all these strategies, however, the  $\text{Tc}\equiv\text{N}$  core has yet to be developed for synthesizing  $^{99m}\text{Tc}$ -labeled, receptor-targeting radiopharmaceuticals. To explore the utility of the  $\text{Tc}\equiv\text{N}$  core, we have developed a simplified route to incorporate biologically active molecules into stable  $^{99m}\text{Tc}$ -nitrido complexes. The strategy relies on the presence of asymmetric complexes containing two different polydentate ligands bound to the [ $\text{Tc}\equiv\text{N}$ ] $^{2+}$  core (13). The synthesis entails the initial preparation of the substitution inert [ $\text{Tc}(\text{N})(\text{PXP})$ ] $^{2+}$  moiety, a strongly electrophilic fragment, that selectively reacts with bidentate chelating ligands (YZ) possessing  $\pi$ -donors as coordinating atoms, to form heterocomplexes of the type [ $\text{Tc}(\text{N})(\text{YZ})(\text{PXP})$ ] $^{0/+}$  (14, 15); thus, for example, cysteine readily reacts as a bidentate ligand with the precursor complex [ $^{99m}\text{Tc}(\text{N})(\text{PXP})\text{Cl}_2$ ] via [O-, S-] or [NH<sub>2</sub>, S-] coordination in a nearly stoichiometric ratio, demonstrating that a terminal cys-

\* Author for correspondence. Phone +39 049 8295958. Fax +39 049 8702911. E-mail: bolzati@icis.cnr.it.

<sup>†</sup> ICIS.

<sup>‡</sup> Harvard Medical School and Brigham and Woman's Hospital.

<sup>§</sup> University of Ferrara.



**Figure 1.** Diphosphine (PNP) and bifunctional ligands utilized in this study.

teine group can act as an efficient chelating system for this metal fragment.

The general requirements for a compound to cross the blood–brain barrier (BBB) in appreciable amounts must be met when designing complexes to target CNS receptors. These include that the complex be neutral in charge, lipophilic in character, and possess a molecular weight lower than 700 Da. Considering these criteria, we focused on di-negative [O-,S-], N-functionalized, cysteine-containing ligands, with the cysteine N-terminus conjugated via a propionate link to the biological molecule of interest, the arylpiperazine [(2-methoxyphenyl)piperazine], known to be active toward the 5HT<sub>1A</sub> subclass of serotonergic receptors. The final bidentate ligand (2-MPPP-cys-OS), when reacted with the [<sup>99m</sup>Tc(N)(PXP)Cl<sub>2</sub>] fragment would thus provide Tc≡N-based neutral, lipophilic complexes and a means of assessing the feasibility of this approach.

Herein we report the application of this labeling procedure to the preparation of asymmetrical <sup>99g</sup>/<sup>99m</sup>Tc-nitrido complexes with the diphosphine ligands PNP3 and PNP4 and the bidentate chelating ligand 2-MPPP-cys-OS (Figure 1).

#### EXPERIMENTAL PROCEDURES

**Caution!** <sup>99g</sup>Tc is a weak β<sup>-</sup>-emitter ( $E_{\beta^-} = 0.292$  MeV,  $t_{1/2} = 1.12 \times 10^5$  years). All manipulations were carried out in laboratories approved for low-level radioactivity use. Handling milligram amounts of <sup>99g</sup>Tc does not present a serious health hazard since common laboratory glassware provides adequate shielding and all work is performed in approved and monitored hoods and glove-boxes. Bremsstrahlung is not a significant problem due to the low energy of the β-particles; however, proper radiation safety procedures must be followed at all times, and particular care should be taken when handling solid samples.

**General.** All chemicals and reagents were purchased from Aldrich Chemicals. All solvents were reagent grade and were used without further purification. Due to the tendency of the diphosphine ligands to oxidize, all the solvents used in reactions with PNP3 and PNP4 were previously degassed to remove dissolved trace oxygen.

Commercially available NH<sub>4</sub>[<sup>99g</sup>TcO<sub>4</sub>] (Oak Ridge National Laboratories) was purified from a black contaminant (<sup>99g</sup>TcO<sub>2</sub> × *n*H<sub>2</sub>O) by addition of H<sub>2</sub>O<sub>2</sub> and NH<sub>4</sub>OH solutions followed by recrystallization as NH<sub>4</sub>[<sup>99g</sup>TcO<sub>4</sub>] from hot water. Technetium-99m as Na[<sup>99m</sup>TcO<sub>4</sub>] was eluted from a <sup>99</sup>Mo–<sup>99m</sup>Tc generator provided by Nymed Amersham-Sorin (Saluggia, Italy). [<sup>99g</sup>Tc(N)Cl<sub>2</sub>(PPh<sub>3</sub>)<sub>2</sub>] was prepared as previously described (16). The diphosphine ligands bis(dimethoxypropylphosphinoethyl)methoxyethylamine, [PNP3 = (CH<sub>3</sub>OC<sub>3</sub>H<sub>6</sub>)<sub>2</sub>P(CH<sub>2</sub>)<sub>2</sub>N(C<sub>2</sub>H<sub>4</sub>OCH<sub>3</sub>)(CH<sub>2</sub>)<sub>2</sub>P(C<sub>3</sub>H<sub>6</sub>OCH<sub>3</sub>)<sub>2</sub>] and bis(dimethylphosphinoethyl)methylamine [PNP4 = (CH<sub>3</sub>)<sub>2</sub>P(CH<sub>2</sub>)<sub>2</sub>N(CH<sub>3</sub>)(CH<sub>2</sub>)<sub>2</sub>P(CH<sub>3</sub>)<sub>2</sub>] were purchased from Argus Chemicals (Prato, Italy). [<sup>3</sup>H]-8-Hydroxy-*N,N*-dipropyl-2-amino-

tetralin ([<sup>3</sup>H]-8-OH-DPAT, specific activity = 147.2 Ci/mmol) and Aquasure were purchased from New England Nuclear Research Products (NEN, Boston, MA). Female Sprague–Dawley rats were acquired from Morini (Reggio Emilia, Italy).

Elemental analyses (C, H, N, S) were performed on a Carlo Erba 1106 elemental analyzer. FT IR spectra were recorded on a Nicolet 510P Fourier transform spectrometer, in the range 4000–200 cm<sup>-1</sup> and in KBr mixture using a Spectra-Tec diffuse-reflectance collector accessory. <sup>1</sup>H, <sup>13</sup>C, and <sup>31</sup>P NMR spectra were collected on a Bruker 300 instrument, using SiMe<sub>4</sub> as internal reference (<sup>1</sup>H and <sup>13</sup>C) and 85% aqueous H<sub>3</sub>PO<sub>4</sub> as external reference (<sup>31</sup>P).

Chromatographic purification of the compounds was accomplished on silica gel columns: for the bifunctional ligand, 120 × 5 cm, 70–230 mesh (Aldrich) and for the asymmetrical <sup>99g</sup>Tc-complexes, 30 × 2 cm, 70–230 mesh (Merck). Thin-layer chromatography (TLC) (SiO<sub>2</sub> F<sub>254</sub>S, Merck) and high performance liquid chromatography (HPLC) analyses were used to evaluate the radiochemical purity (RCP) and stability of the compounds. Radioactivity on TLC plates was detected and measured using a Cyclone instrument equipped with a phosphorus imaging screen and OptiQuant image analysis software (Packard, Meridian, CT). HPLC was performed on a Beckman System Gold instrument equipped with a programmable solvent Model 126, a sample injection valve 210A, a scanning detector Module 166, and a radioisotope detector Model 170. HPLC analysis was carried out on a reversed-phase Hamilton PRP-1 precolumn (45 × 4.1 mm), and a reversed-phase Hamilton PRP-1 column (250 × 4.1 mm, Ø = 10 μm) using the chromatographic condition reported in Table 1; flow rate: 1 mL/min. Log *k'*<sub>0</sub> of the complexes was determined by HPLC chromatography as reported previously (17). The results are summarized in Table 1.

**3-[4-(2-Methoxyphenyl)piperazin-1-yl]propionic Acid Methyl Ester (1).** 1-(2-Methoxyphenyl)piperazine hydrochloride (2-MPP) (4 g, 0.017 mol) and *N,N*-diisopropylethylamine (4.49 g, 0.035 mol) were dissolved in CH<sub>2</sub>Cl<sub>2</sub> (150 mL). To this solution was added methyl 3-bromopropionate (1.947 g, 0.012 mol), and the reaction mixture was stirred at room-temperature overnight. The solvent was evaporated, and the residual oil was suspended in water (50 mL) and extracted with CH<sub>2</sub>Cl<sub>2</sub> (50 mL × 3). The combined CH<sub>2</sub>Cl<sub>2</sub> layers were reduced in volume, and the resulting pale yellow oil was purified by silica gel chromatography eluting with CH<sub>2</sub>Cl<sub>2</sub> followed by a 3% MeOH/CH<sub>2</sub>Cl<sub>2</sub> solution (3.51 g, 72%). <sup>1</sup>H NMR (CDCl<sub>3</sub>) δ: 6.97–6.82 (4H, Ar), 3.82 (s, 3H, OCH<sub>3</sub>), 3.66 (s, 3H, CH<sub>3</sub>), 3.06 (m, 4H, CH<sub>2</sub>), 2.76 (t, 2H, CH<sub>2</sub>CO), 2.65 (m, 4H, CH<sub>2</sub>), 2.54 (t, 2H, CH<sub>2</sub>). Anal. Calcd for C<sub>15</sub>H<sub>22</sub>N<sub>2</sub>O<sub>3</sub>: C, 64.73; H, 7.97; N 10.06; O, 17.24; found: C, 64.72; H, 7.79; N, 10.06; O, 17.02.

**3-[4-(2-Methoxyphenyl)piperazin-1-yl]propionate (2).** Compound 1 (3.42 g, 12.3 mmol) was dissolved in MeOH (30 mL), and 10 mL of an aqueous solution containing KOH (1.034 g, 18.4 mmol) was added. The reaction mixture was stirred at room temperature for 1 h. The solvent was evaporated, and the residue, dissolved in the minimum amount of CH<sub>2</sub>Cl<sub>2</sub>, was purified by chromatography using a short silica gel column eluted with 20% MeOH/CH<sub>2</sub>Cl<sub>2</sub> solution (3.01 g, 81%). <sup>1</sup>H NMR (CDCl<sub>3</sub>) δ: 7.08–6.89 (4H, Ar), 3.89 (s, 3H, OCH<sub>3</sub>), 3.24 (m, 4H, CH<sub>2</sub>), 3.02 (m, 4H, CH<sub>2</sub>), 2.96 (t, 2H, CH<sub>2</sub>CO), 2.63 (t, 2H, CH<sub>2</sub>). Anal. Calcd for C<sub>14</sub>H<sub>19</sub>KN<sub>2</sub>O<sub>3</sub>: C, 55.60; H, 6.33; N, 9.26; O, 15.87; found: C, 55.02; H, 6.55; N, 9.31; O, 15.8.

**Table 1. Chromatographic Data for <sup>99g/99m</sup>Tc Complexes**

complex	<i>M<sub>w</sub></i>	<i>R<sub>f</sub></i> (SiO <sub>2</sub> )	retention time (min)		% yields		Log <i>P</i>	Log <i>k</i> '	ref
			<sup>99g</sup> Tc	<sup>99m</sup> Tc	<sup>99g</sup> Tc	<sup>99m</sup> Tc			
[Tc(N)Cl <sub>2</sub> (PNP3)]	667.52	0.0 <sup>a</sup>	18.65 <sup>c</sup>	19.3 + mix <sup>c</sup>					
[Tc(N)Cl <sub>2</sub> (PNP4)]	391.14	0.0 <sup>b</sup>	22.01 <sup>d</sup>	22.5 + mix <sup>d</sup>					
<i>anti</i> -[Tc(N)(2-MPPP-cys-OS)(PNP3)]	962.07	0.5 <sup>a</sup>	23.58 <sup>c</sup>	23.86 <sup>c</sup>	48.5	89	2.42	4.84	
<i>syn</i> -[Tc(N)(2-MPPP-cys-OS)(PNP3)]	962.07	0.4 <sup>a</sup>	23.02 <sup>c</sup>	23.28 <sup>c</sup>	43.6	9.6		4.84	
<i>anti</i> -[Tc(N)(2-MPPP-cys-OS)(PNP4)]	685.69	0.5 <sup>b</sup>	27.48 <sup>d</sup>	27.82 <sup>d</sup>	38.6	73.6	1.88	3.28	
<i>syn</i> -[Tc(N)(2-MPPP-cys-OS)(PNP4)]	685.69	0.4 <sup>b</sup>	26.37 <sup>d</sup>	26.66 <sup>d</sup>	33.6	7.6		3.28	
[Tc(N)(2-MPPP-cys-OS) <sub>2</sub> ]	843.91	0.0 <sup>a,b</sup>	—	mix <sup>c,d</sup>	—	—			
[Tc(N)(OS-TA)(PNP4)]				21.1 <sup>d</sup>					
[Tc-HMPAO]							1.90		18
[Tc-ECD]							1.64		18

<sup>a</sup> TLC: MeOH (2% NH<sub>4</sub>OH 20%)/CHCl<sub>3</sub> (10/90). <sup>b</sup> TLC: CH<sub>2</sub>Cl<sub>2</sub>/MeOH/NH<sub>4</sub>OH 20% (89/10/1). <sup>c</sup> HPLC: Reverse-phase C<sub>18</sub> column; A = 5 mM DMGA, pH 7 (DMGA = 3,3-dimethylglutaric acid), B = CH<sub>3</sub>CN. Gradient: 0–5 min, B, 0%, 5–20 min, B, 70%, 25–30 min, B, 70%, 30–35 min, B, 0%. <sup>d</sup> Reverse-phase C<sub>18</sub> column, A = TFA 0.01 M, pH 3 (TFA = trifluoroacetic acid), B = CH<sub>3</sub>CN. Gradient 0–2 min, B, 0%; 2–23 min, B, 30%, 25–30 min, B, 70%, 30–35 min, B, 70%, 35–40 min, B, 0%.

**2-Amino-3-tritylsulfanyl-propionic Acid Ethyl Ester (3).** A suspension of (S)-trityl-L-cysteine (1.125 g, 3.1 mmol) and ethyl *p*-toluenesulfonate (2.250 g, 6.2 mmol) in dry ethanol was refluxed under an argon atmosphere for 48 h, during which time dissolution occurred. After evaporation of the solvent, the residue was dissolved in 30 mL of an aqueous solution of KHCO<sub>3</sub> (pH 8) and extracted three times with an equal volume of CH<sub>2</sub>Cl<sub>2</sub>. The combined organic phases were evaporated, and the pale yellow oil was redissolved in the minimum amount of CH<sub>2</sub>Cl<sub>2</sub>. Finally, Et<sub>2</sub>O was added to precipitate a white powder. The precipitate was separated by filtration, and the ether filtrate was evaporated to obtain the crude ester. Purification was achieved by SiO<sub>2</sub> chromatography, eluting with a 2% MeOH/CH<sub>2</sub>Cl<sub>2</sub> solution (0.97 g, 80%) <sup>1</sup>H NMR (CDCl<sub>3</sub>) δ: 7.46–7.23 (15H, Ar), 4.14 (q, 2H, CH<sub>2</sub>O), 3.22 (m, 1H, CHNH<sub>2</sub>), 2.59 (q, 1H, CH<sub>2</sub>S), 2.50 (q, 1H, CH<sub>2</sub>S), 1.25 (t, 3H, CH<sub>3</sub>). Anal. Calcd for C<sub>24</sub>H<sub>25</sub>N<sub>2</sub>O<sub>2</sub>S: C, 73.62; H, 6.44; N, 3.58; S, 8.19; found: C, 73.02; H, 6.96; N, 3.66; S, 8.06.

**2-{3-[4-(2-Methoxyphenyl)piperazin-1-yl]propionylamino}-3-trityl-sulfanylpropionic Acid Ethyl Ester (4).** Compounds **2** (0.310 g, 1.15 mmol) and **3** (0.45 g, 1.15 mmol) were dissolved in CH<sub>2</sub>Cl<sub>2</sub> (30 mL). The solution was cooled at –78 °C in a dry ice acetone bath, and 1-(3-dimethylaminopropyl)-3-ethylcarbodiimide (EDC) (0.330 g, 1.73 mmol), previously dissolved in the minimum amount of DMF, was added. The reaction mixture was stirred at –78 °C, under argon atmosphere for 1 h, allowed to reach room temperature, and stirred overnight. The solvent was removed, and the residue was subjected to H<sub>2</sub>O/CH<sub>2</sub>Cl<sub>2</sub> extraction. The combined CH<sub>2</sub>Cl<sub>2</sub> layers were dried with anhydrous Na<sub>2</sub>SO<sub>4</sub>, evaporated to minimum volume, and purified by SiO<sub>2</sub> chromatography eluting with 3% MeOH/CH<sub>2</sub>Cl<sub>2</sub> solution (0.70 g, 96%). <sup>1</sup>H NMR (CDCl<sub>3</sub>) δ: 9.53 (d, 1H, NH), 7.36–7.18 (15H, Ar), 7.03–6.80 (4H, Ar), 4.73 (m, 1H, CHNH), 4.15 (t, 2H, CH<sub>2</sub>N<sub>pip</sub>), 3.87 (s, 3H, OCH<sub>3</sub>), 3.14 (m, 4H, CH<sub>2</sub>N<sub>pip</sub>), 2.93 (m, 2H, CH<sub>2</sub>CO), 2.79 (m, 4H, CH<sub>2</sub>N<sub>pip</sub>), 2.64 (q, 1H, CH<sub>2</sub>OC(O)), 2.53 (q, 1H, CH<sub>2</sub>OC(O)), 2.45 (d, 2H, CH<sub>2</sub>S), 1.25 (t, 3H, CH<sub>3</sub>). Anal. Calcd for C<sub>38</sub>H<sub>43</sub>N<sub>3</sub>O<sub>4</sub>S: C, 71.56; H, 6.79; N, 5.58; S, 5.03; found: C, 70.18; H, 6.80; N, 6.59; S, 5.03.

**2-{3-[4-(2-Methoxyphenyl)piperazin-1-yl]propionylamino}-3-trityl-sulfanylpropionic Acid (5).** Compound **4** (2.027 g, 0.0032 mol) was dissolved in MeOH (30 mL), and 5 mL of an aqueous solution containing KOH (0.267 g, 0.005 mol) was added. The reaction mixture was stirred at room temperature for 1 h. After the solvent was evaporated, the residue was redissolved in water, the pH was adjusted to 3 with HCl (2 M), and

the ligand was extracted with CH<sub>2</sub>Cl<sub>2</sub> (30 mL × 3). The combined CH<sub>2</sub>Cl<sub>2</sub> layers were reduced to a minimum volume with the pure hydrochloride salt precipitating as a white powder with the addition of anhydrous Et<sub>2</sub>O (1.61 g, 83%). The powder was dissolved in methanol and treated with KHCO<sub>3</sub> to obtain the free base. <sup>1</sup>H NMR (CD<sub>3</sub>COOD) δ: 7.85 (s, 1H, NH), 7.42–7.21 (15H, Ar), 7.10–6.93 (4H, Ar), 4.44 (t, 1H, CHNH), 3.89 (s, 3H, OCH<sub>3</sub>), 3.37–3.26 (m, 12H, alkyl), 2.73–2.66 (m, 4H, alkyl). FT IR (cm<sup>–1</sup>): [3258 ν (NH)], [2930–2835 ν (CH<sub>2</sub>–CH<sub>2</sub>)], [1750 ν (COOH)], [1683 ν (CONH)], [1240 ν (OCH<sub>3</sub>)], [743, 701 ν (CH=CH)]. Anal. Calcd for C<sub>36</sub>H<sub>39</sub>N<sub>3</sub>O<sub>4</sub>S·2HCl: C, 63.38; H, 6.05; N, 6.15; S, 4.7; found: C, 63.46; H, 6.85; N, 6.31; S, 4.59.

**2-{3-[4-(2-Methoxyphenyl)piperazin-1-yl]propionylamino}-3-sulfhydryl-propionic Acid (2-MPPP-cys-OS) (6).** Trityl deprotection of the thiol was performed by dissolving **5** (0.2 g, 0.293 mmol) in trifluoroacetic acid (TFA) (5 mL). The resulting yellow solution was stirred for 5 min, and then triethylsilyl hydride was added by drops until the solution became colorless. The solution was evaporated to dryness to remove TFA and subsequently dried under vacuum and used without further purification.

**Synthesis of [<sup>99g</sup>Tc(N)Cl<sub>2</sub>(PNP3)] (7).** To [Tc(N)Cl<sub>2</sub>(PPh<sub>3</sub>)<sub>2</sub>] (118 mg, 0.166 mmol) suspended in CH<sub>2</sub>Cl<sub>2</sub> (10 mL) was added PNP3 (120 mg, 0.248 mmol) dissolved in CH<sub>2</sub>Cl<sub>2</sub> (5 mL). The solution was stirred at reflux for 30 min. The initial orange-pink solution changed color to yellow. After the solution was cooled, the solvent was removed by a gentle stream of nitrogen and the oily residue was washed with Et<sub>2</sub>O, dissolved in the minimum amount of EtOH, and precipitated with *n*-hexane. The yellow powder was collected by filtration, washed with Et<sub>2</sub>O and *n*-hexane again, and dried under vacuum (94.04 mg, 85%). <sup>1</sup>H NMR (CDCl<sub>3</sub>) δ: 3.44–1.63 (H, alkyl). <sup>31</sup>P NMR (CDCl<sub>3</sub>) δ: 31.0 (broad singlet). FT IR (cm<sup>–1</sup>): [1054 ν (Tc≡N)], [2979–2817 ν (C–H)]. Anal. Calcd for C<sub>23</sub>H<sub>51</sub>N<sub>2</sub>O<sub>5</sub>P<sub>2</sub>Cl<sub>2</sub>Tc: C, 41.38; H, 7.71; N, 4.21; found: C, 40.57; H, 7.87; N, 4.51.

**Synthesis of [<sup>99g</sup>Tc(N)Cl<sub>2</sub>(PNP4)] (8).** To [Tc(N)Cl<sub>2</sub>(PPh<sub>3</sub>)<sub>2</sub>] (90 mg, 0.130 mmol) suspended in CH<sub>2</sub>Cl<sub>2</sub> (10 mL) was added PNP4 (30 mg, 0.145 mmol) dissolved in EtOH (5 mL). The solution was stirred at room temperature for 30 min during which time the initial orange-pink solution changed color to yellow. The solvent was removed by a gentle stream of nitrogen, and the residue was washed with Et<sub>2</sub>O and treated with *n*-hexane. The precipitated yellow residue was redissolved in methanol, and a residual white powder was separated by filtration. The yellow filtrate was evaporated, and the residue was



treated with Et<sub>2</sub>O to provide a yellow precipitate, which was collected by filtration, washed with Et<sub>2</sub>O and *n*-hexane, and dried under vacuum (40.67 mg, 80%). <sup>1</sup>H NMR (CDCl<sub>3</sub>) δ: 2.47 (m, 4H, NCH<sub>2</sub>), 2.26 (m, 2H, PCH<sub>2endo</sub>), 2.11 (s, 3H, NCH<sub>3</sub>), 1.92 (m, 2H, PCH<sub>2exo</sub>), 2.02, 1.99, 1.78, 1.76 (4s, 12H, PCH<sub>3</sub>). <sup>13</sup>C NMR (CDCl<sub>3</sub>) δ: 51.88 (NCH<sub>2</sub>), 46.20 (NCH<sub>3</sub>), 27.65, 27.45 (PCH<sub>2</sub>), 17.96, 17.76, 14.98, 14.76 (PCH<sub>3</sub>). <sup>31</sup>P NMR (CDCl<sub>3</sub>) δ: 23.1 (bs). FT IR (cm<sup>-1</sup>): [1045 ν (Tc≡N)], [2971–2804 ν (C–H)]. Anal. Calcd for C<sub>9</sub>H<sub>23</sub>N<sub>2</sub>Cl<sub>2</sub>P<sub>2</sub>Tc: C, 27.63; H, 5.90; N, 7.16; found: C, 27.01; H, 5.79; N, 7.01.

**Synthesis of [<sup>99g</sup>Tc(N)(2-MPPP-cys-OS)(PNP3)] Anti (9a) and Syn (9b).** *Method A:* Compound **7** (57.3 mg, 0.086 mmol) was dissolved in EtOH (5 mL) along with five drops of neat Et<sub>3</sub>N. To this solution was added 2-MPPP-cys-OS ligand (41 mg, 0.108 mmol) dissolved in CH<sub>2</sub>Cl<sub>2</sub> (5 mL). The reaction mixture was stirred at reflux for 60 min. No apparent color change from yellow was observed during the reaction. After the solution was cooled, the solvent was removed, and the residue was washed with Et<sub>2</sub>O. The yellow oily residue was dissolved in the minimum amount of CHCl<sub>3</sub> and chromatographed on a silica column, preconditioned with CHCl<sub>3</sub>, and eluted with a mixture of CHCl<sub>3</sub>/MeOH/NH<sub>4</sub>OH (20%) (95/5/3). Two yellow bands were separated and collected; the first fraction was identified (vide infra) as the pure anti isomer **9a** (35%, based on Tc) and the second fraction as the pure syn isomer **9b** (29%, based on Tc).

*Method B:* To [<sup>99g</sup>Tc(N)Cl<sub>2</sub>(PPh<sub>3</sub>)<sub>2</sub>] (29.32 mg, 0.041 mmol) suspended in CH<sub>2</sub>Cl<sub>2</sub> (5 mL) were added PNP3 (20 mg, 0.043 mmol) dissolved in CH<sub>2</sub>Cl<sub>2</sub> (5 mL), 2-MPPP-cys-OS ligand (37.08 mg, 0.060 mmol) dissolved in CH<sub>2</sub>Cl<sub>2</sub> (5 mL), and neat Et<sub>3</sub>N (five drops). Within 10 min the initial orange-pink solution turned yellow. The reaction mixture was further stirred at room temperature under a nitrogen atmosphere, for 1 h. The solvent was evaporated, and the crude yellow residue was dissolved in CHCl<sub>3</sub> (1 mL) and chromatographed on silica. After the column was eluted with the mobile phase described above, two yellow bands were separated and isolated as yellow oily residues. The first fraction was identified as the anti isomer **9a** (48.5%, based on Tc) and the second fraction as the syn isomer **9b** (43.6%, based on Tc). These two isomers were identical to those prepared by method A, as confirmed by TLC, HPLC, and NMR data.

Complex **9a** was soluble in chlorinate solvents and in alcohols, and insoluble in diethyl ether and *n*-hexane. <sup>1</sup>H NMR (CDCl<sub>3</sub>) δ: 8.04 (d, 1H, NHC(O)), 7.00–6.82 (4H, C<sub>6</sub>H<sub>4</sub>OCH<sub>3</sub>), 4.83 (m, 1H, CHNHC(O)), 3.85 (s, 3H, C<sub>6</sub>H<sub>4</sub>OCH<sub>3</sub>), 3.36–3.19 (5s, 15H, aliphatic OCH<sub>3</sub>), 3.32 and 2.41 (m, 2H, S–CH<sub>2exo</sub> and S–CH<sub>2endo</sub>), 3.16 and 2.74 (bs, 4H+4H, CH<sub>2pip</sub>), 3.55–1.55 (36H+4H, CH<sub>2</sub> groups). <sup>13</sup>C NMR (CDCl<sub>3</sub>) δ: 177.65, 170.75 (C=O), 152.28, 141.42, 122.75, 120.96, 118.39, 111.21 (C<sub>6</sub>H<sub>4</sub>OCH<sub>3</sub>), 73.14, 72.93, 72.63, 72.48, 68.34 (CH<sub>2</sub>O), 58.67, 58.57 (OCH<sub>3</sub>), 56.63 (SCH<sub>2</sub>CH), 55.37 (C<sub>6</sub>H<sub>4</sub>OCH<sub>3</sub>), 54.13 (CH<sub>2</sub>N<sub>pip</sub>), 53.03 (CH<sub>2pip</sub>), 51.54 (NCH<sub>2</sub>CH<sub>2</sub>OCH<sub>3</sub>), 50.48 (CH<sub>2pip</sub>), 47.27, 46.13 (NCH<sub>2</sub>CH<sub>2</sub>P), 33.47, 29.70 (SCH<sub>2</sub>CH), 25.77, 24.77, 23.85, 22.80, 18.20, 16.27 (PCH<sub>2</sub>CH<sub>2</sub>CH<sub>2</sub>OCH<sub>3</sub>). <sup>31</sup>P NMR (CDCl<sub>3</sub>) δ: 32.8 (broad s), 25.4 (broad s). FT IR (cm<sup>-1</sup>): [1050 ν (Tc≡N)], [3300 ν (NH)], [2933–2817 ν (C–H)], [1732 ν (CO)O], [1636 ν NH(CO)], [1240 ν (OCH<sub>3</sub>)], [749 ν (b, CH=CH)]. Anal. Calcd for C<sub>40</sub>H<sub>74</sub>N<sub>5</sub>O<sub>9</sub>P<sub>2</sub>Stc: C, 49.93; H, 7.75; N, 7.27; S, 3.34; found: C, 49.85; H, 7.8; N, 7.28; S, 3.32.

Complex **9b** was soluble in chlorinate solvents and alcohols and insoluble in diethyl ether and *n*-hexane. <sup>1</sup>H NMR (CDCl<sub>3</sub>) δ: 8.26 (d, 1H, NHC(O)), 7.00–6.82 (4H, C<sub>6</sub>H<sub>4</sub>OCH<sub>3</sub>), 4.73 (m, 1H, CHNHC(O)), 3.86 (s, 3H, C<sub>6</sub>H<sub>4</sub>OCH<sub>3</sub>), 3.36–3.20 (5s, 15H, aliphatic OCH<sub>3</sub>), 3.21 (m, 2H, SCH<sub>2</sub>CH), 3.14 and 2.76 (4H+4H, CH<sub>2pip</sub>), 3.60–1.55 (36H+4H, CH<sub>2</sub> groups). <sup>13</sup>C NMR (CDCl<sub>3</sub>) δ: 176.81, 171.15 (C=O), 152.01, 141.42, 122.68, 120.89, 118.27, 111.10 (C<sub>6</sub>H<sub>4</sub>OCH<sub>3</sub>), 73.19, 73.01, 72.73, 72.33, 68.03, 58.67, 58.51, 56.56 (SCH<sub>2</sub>CH), 55.44 (C<sub>6</sub>H<sub>4</sub>OCH<sub>3</sub>), 53.99, 52.98, 51.34, 50.40, 47.24, 46.03, 33.42, 29.70 (SCH<sub>2</sub>CH), 25.60, 24.82, 23.65, 22.40, 17.97, 16.23. <sup>31</sup>P NMR (CDCl<sub>3</sub>) δ: 34.6 (broad s), 27.1 (broad s). FT IR (cm<sup>-1</sup>): [1049 ν (Tc≡N)], [3374 ν (NH)], [2949–2810 ν (CH)], [1660–1636 ν (CO)O, ν NH(CO)], [1240 ν (OCH<sub>3</sub>)], [749 ν (b, CH=CH)]. Anal. Calcd for C<sub>40</sub>H<sub>74</sub>N<sub>5</sub>O<sub>9</sub>P<sub>2</sub>Stc: C, 49.93; H, 7.75; N, 7.27; S, 3.34; found: C, 49.7; H, 7.71; N, 7.3; S, 3.35.

**Synthesis of [<sup>99g</sup>Tc(N)(2-MPPP-cys-OS)(PNP4)] Anti (10a) and Syn (10b).** *Method A:* To compound **8** (33.56 mg, 0.086 mmol) dissolved in EtOH (5 mL) were added neat Et<sub>3</sub>N (five drops) and 2-MPPP-cys-OS ligand (39 mg, 0.103 mmol) dissolved in CH<sub>2</sub>Cl<sub>2</sub> (5 mL). The mixture was stirred at reflux for 60 min. No color change from the initial yellow was observed throughout the reaction. After the solution was cooled, the solvent was removed by a gentle stream of nitrogen and the residue was washed with Et<sub>2</sub>O followed by *n*-hexane. The yellow oil was dissolved in the minimum amount of CH<sub>2</sub>Cl<sub>2</sub> and loaded onto a silica column conditioned with CH<sub>2</sub>Cl<sub>2</sub>. The column was eluted with a mixture of CH<sub>2</sub>Cl<sub>2</sub>/MeOH/NH<sub>4</sub>OH (20%) (89/10/1), and two yellow bands were separated and collected. The eluate was evaporated, and the residues were treated with Et<sub>2</sub>O to precipitate the complexes. The first pale yellow product was identified as the pure anti isomer **10a** (35%, based on Tc) and the second lemon-yellow complex as the pure syn isomer **10b** (19%, based on Tc).

*Method B:* To [<sup>99g</sup>Tc(N)Cl<sub>2</sub>(PPh<sub>3</sub>)<sub>2</sub>] (30.6 mg, 0.043 mmol) suspended in CH<sub>2</sub>Cl<sub>2</sub> (5 mL) were added PNP4 (10 mg, 0.048 mmol) dissolved in CH<sub>2</sub>Cl<sub>2</sub> (5 mL), 2-MPPP-cys-OS ligand (38 mg, 0.062 mmol) dissolved in CH<sub>2</sub>Cl<sub>2</sub> (5 mL), and an excess of Et<sub>3</sub>N (five drops). The reaction mixture was stirred at reflux for 1 h under nitrogen atmosphere. The initial orange-pink solution turned yellow. After the solution was cooled, the solvent was evaporated, and the resulting oily residue was dissolved in CH<sub>2</sub>Cl<sub>2</sub> (1 mL) and chromatographed on a silica column using the conditions described above. Two fractions were collected, **10a** (48.5%, based on Tc) and **10b** (19.5%, based on Tc). These two isomers were identical to those prepared by method A, as confirmed by TLC, HPLC, and NMR data.

Complex **10a** was soluble in chlorinate solvents and alcohols and insoluble in diethyl ether. <sup>1</sup>H NMR (CDCl<sub>3</sub>) δ: 8.33 (d, 1H, NHC(O)), 6.98–6.83 (4H, C<sub>6</sub>H<sub>4</sub>OCH<sub>3</sub>), 4.89 (m, 1H, CHNHC(O)), 3.86 (s, 3H, C<sub>6</sub>H<sub>4</sub>OCH<sub>3</sub>), 3.34 (dd, 1H, SCH<sub>2exo</sub>), 2.47 (m, 1H; SCH<sub>2endo</sub>), 3.17 (bs, 4H, CH<sub>2pip</sub>), 2.78 (m 6H; CH<sub>2pip</sub>, CH<sub>2zen</sub>), 2.47 (m, 2H, CH<sub>2zen</sub>), 2.6–1.9 (8H, PCH<sub>2</sub>CH<sub>2</sub>N), 2.0 (s, 3H, NCH<sub>3</sub>), 1.78, 1.75, 1.72, 1.69 (4s, 12H, P–CH<sub>3</sub>). <sup>13</sup>C NMR (CDCl<sub>3</sub>) δ: 177.95–170.67 (C=O), 152.19, 141.29, 122.70, 120.88, 118.39, 111.10 (C<sub>6</sub>H<sub>4</sub>OCH<sub>3</sub>), 56.92 (SCH<sub>2</sub>CH), 55.32 (OCH<sub>3</sub>), 54.13 (CH<sub>2</sub>N), 52.97, 50.36 (CH<sub>2pip</sub>); 51.80, 51.19 (PCH<sub>2</sub>CH<sub>2</sub>N), 45.05 (NCH<sub>3</sub>), 33.28 (C(O)CH<sub>2</sub>CH<sub>2</sub>N), 30.13 (SCH<sub>2</sub>CH), 28.27 (d), 26.19 (d, P–CH<sub>2</sub>), 19.13 (d), 15.46 (d), 13.55 (d), 11.75 (d, P–CH<sub>3</sub>). <sup>31</sup>P NMR (CDCl<sub>3</sub>) δ: 20.0 (broad s), 14.0 (broad s). FT IR (cm<sup>-1</sup>): [1047 ν (Tc≡N)], [3296 ν (NH)], [2936–2826 ν (–CH)], [1700–1636 ν (CO)O, ν NH(CO)], [1240 ν (OCH<sub>3</sub>)], [747, 726 ν (b, CH=CH)]. Anal. Calcd for C<sub>26</sub>H<sub>46</sub>N<sub>5</sub>O<sub>4</sub>P<sub>2</sub>Stc: C, 45.55; H, 6.76; N, 10.22; S, 4.68; found: C, 45.2; H, 6.78; N, 10.18; S, 4.71.

Complex **10b** was soluble in chlorinate solvents and alcohols and insoluble in diethyl ether. <sup>1</sup>H NMR (CDCl<sub>3</sub>) δ: 8.33 (d, 1H, NHC(O)), 6.98–6.83 (4H, C<sub>6</sub>H<sub>4</sub>OCH<sub>3</sub>), 4.89 (m, 1H, CHNHC(O)), 3.86 (s, 3H, C<sub>6</sub>H<sub>4</sub>OCH<sub>3</sub>), 3.34 (dd, 1H, SCH<sub>2exo</sub>), 2.47 (m, 1H; SCH<sub>2endo</sub>), 3.17 (bs, 4H, CH<sub>2pip</sub>), 2.78 (m 6H; CH<sub>2pip</sub>, CH<sub>2zen</sub>), 2.47 (m, 2H, CH<sub>2zen</sub>), 2.6–1.9 (8H, PCH<sub>2</sub>CH<sub>2</sub>N), 2.0 (s, 3H, NCH<sub>3</sub>), 1.78, 1.75, 1.72, 1.69 (4s, 12H, P–CH<sub>3</sub>). <sup>13</sup>C NMR (CDCl<sub>3</sub>) δ: 177.95–170.67 (C=O), 152.19, 141.29, 122.70, 120.88, 118.39, 111.10 (C<sub>6</sub>H<sub>4</sub>OCH<sub>3</sub>), 56.92 (SCH<sub>2</sub>CH), 55.32 (OCH<sub>3</sub>), 54.13 (CH<sub>2</sub>N), 52.97, 50.36 (CH<sub>2pip</sub>); 51.80, 51.19 (PCH<sub>2</sub>CH<sub>2</sub>N), 45.05 (NCH<sub>3</sub>), 33.28 (C(O)CH<sub>2</sub>CH<sub>2</sub>N), 30.13 (SCH<sub>2</sub>CH), 28.27 (d), 26.19 (d, P–CH<sub>2</sub>), 19.13 (d), 15.46 (d), 13.55 (d), 11.75 (d, P–CH<sub>3</sub>). <sup>31</sup>P NMR (CDCl<sub>3</sub>) δ: 20.0 (broad s), 14.0 (broad s). FT IR (cm<sup>-1</sup>): [1047 ν (Tc≡N)], [3296 ν (NH)], [2936–2826 ν (–CH)], [1700–1636 ν (CO)O, ν NH(CO)], [1240 ν (OCH<sub>3</sub>)], [747, 726 ν (b, CH=CH)]. Anal. Calcd for C<sub>26</sub>H<sub>46</sub>N<sub>5</sub>O<sub>4</sub>P<sub>2</sub>Stc: C, 45.55; H, 6.76; N, 10.22; S, 4.68; found: C, 45.2; H, 6.78; N, 10.18; S, 4.71.

**Table 2. pH and Temperature Dependence of Syn → Anti Isomerization for Complex *syn*-[<sup>99m</sup>Tc(N)(2-MPPP-cys-OS)(PNP4)] (10b)**

buffer	pH	T, °C	% of <i>syn</i> -[ <sup>99m</sup> Tc(N)(2-MPPP-cys-OS)(PNP4)] (10b)					
			0	12 h	24 h	3 d	5 d	7 d
Ac <sup>-</sup> /HAc	5.0	4	92.0	86.0	82.3	77.6	71.4	69.7
Ac <sup>-</sup> /HAc	5.0	25	92.1	81.1	79.6	72.2	65.8	55.5
Ac <sup>-</sup> /HAc	5.0	37	92.0	77.2	65.3	47.2.2	21.3	10.8
H <sub>2</sub> PO <sub>4</sub> <sup>-</sup> /HPO <sub>4</sub> <sup>2-</sup>	7.5	4	93.5	87.0	83.3	77.7	73.4	71.2
H <sub>2</sub> PO <sub>4</sub> <sup>-</sup> /HPO <sub>4</sub> <sup>2-</sup>	7.5	25	93.5	82.1	80.6	72.0	65.2	54.5
H <sub>2</sub> PO <sub>4</sub> <sup>-</sup> /HPO <sub>4</sub> <sup>2-</sup>	7.5	37	93.5	77.2	66.5	45.0	23.3	11.6
HCO <sub>3</sub> <sup>-</sup> /CO <sub>3</sub> <sup>2-</sup>	9.0	4	91.0	85.0	81.3	76.7	73.4	71.2
HCO <sub>3</sub> <sup>-</sup> /CO <sub>3</sub> <sup>2-</sup>	9.0	25	91.0	80.1	78.6	72.2	65.4	54.3
HCO <sub>3</sub> <sup>-</sup> /CO <sub>3</sub> <sup>2-</sup>	9.0	37	91.0	75.2	66.3	44.0	20.1	10.9
water	—	4	93.0	87.0	83.3	77.7	73.4	71.2
water	—	25	93.0	82.1	80.6	72.0	65.2	54.5
water	—	37	93.0	77.2	66.3	45.2	20.3	10.6

% of <i>syn</i> -[ <sup>99m</sup> Tc(N)(2-MPPP-cys-OS)(PNP4)] (10b)						
	0	15 min	60 min	120 min	6 h	24 h
water	90.0	87.2	83.3	71.3	39.7	10.2
water	90.0	11.5	11.6	12.0	—	—

δ: 8.31 (m, 1H, NH-C(O)), 6.99–6.84 (4H, C<sub>6</sub>H<sub>4</sub>OCH<sub>3</sub>), 4.76 (m, 1H, CHNHC(O)), 3.86 (s, 3H, C<sub>6</sub>H<sub>4</sub>OCH<sub>3</sub>), 3.24 (m, 2H, SCH<sub>2</sub>CHNH), 3.16 (bs, 4H, CH<sub>2</sub>pip), 2.81 (m, 2H, CH<sub>2</sub>en), 2.74 (bs, 4H, CH<sub>2</sub>pip), 2.46 (m, 2H, CH<sub>2</sub>en), 2.6–1.85 (8H, PCH<sub>2</sub>CH<sub>2</sub>N), 2.09 (s, 3H, NCH<sub>3</sub>), 2.00–1.70 (4s, 12H, PCH<sub>3</sub>). <sup>31</sup>P NMR (CDCl<sub>3</sub>) δ: 21.3 (broad s), 14.6 (broad s). FT IR (cm<sup>-1</sup>): [1047 ν (Tc≡N)], [3370 ν (NH)], [2971–2818 ν (CH)], [1652–1636 ν (CO)O, ν NH(CO)], [1240 ν (OCH<sub>3</sub>)], [747, 726 ν (b, CH=CH)]. Anal. Calcd for C<sub>26</sub>H<sub>46</sub>N<sub>5</sub>O<sub>4</sub>P<sub>2</sub>Stc: C, 45.55; H, 6.76; N, 10.22; S, 4.68; found: C, 45.3; H, 6.65; N, 10.20; S, 4.65.

**Syn → Anti Isomerization of [<sup>99m</sup>Tc(N)(2-MPPP-cys-OS)(PNP3/4)].** *Effect of pH:* In a propylene test tube containing EtOH (0.250 mL) and an alcoholic solution of the selected <sup>99m</sup>Tc-complex (10 mM, 0.050 mL) was added the appropriate buffer solution at pH 5–9 (0.250 mL). The mixture was vortexed and incubated at various temperatures (4 °C, 25 °C, 37 °C) for one week. A control reaction containing an equal volume of water, instead of buffer solution, was maintained in parallel. Aliquots of the reaction mixtures were withdrawn and analyzed by TLC and HPLC chromatography at appropriate time intervals (0 h, 12 h, 24 h, 3 d, 5 d, 7 d). The results are summarized in Table 2.

*Effect of Temperature:* In a propylene test tube containing EtOH (0.250 mL) and an alcoholic solution of the selected <sup>99m</sup>Tc-complex (10 mM, 0.050 mL), H<sub>2</sub>O (0.250 mL) was added. The mixture was vortexed and kept at 50 °C or 100 °C for various times (0, 15 min, 60 min, 120 min, 6 and 24 h). Aliquots of the reaction mixtures were withdrawn at the appropriate time and analyzed immediately by TLC and HPLC chromatography (Table 2).

*Challenge Reaction with Thioacetate:* In a propylene test tube containing EtOH (0.250 mL) and an alcoholic solution of **10b** (10 mM, 0.050 mL) was added an aliquot of an aqueous solution of sodium *O,S*-thioacetate (OS-TA) (20.0 mM). The volume of the resulting solutions, having final **10b**/thioacetate molar ratios of 1/1, 1/5, and 1/10, were adjusted to 0.5 mL with water. The mixtures were vortexed and heated at 50 °C or 100 °C for 24 h. A control reaction containing an equal volume of water without thioacetate was run in parallel. At 15 min, 4 h, and 24 h, aliquots of the reaction mixtures were withdrawn and analyzed by TLC and HPLC chromatography. The results are summarized in Table 3.

**Preparation of [<sup>99m</sup>Tc(N)(2-MPPP-cys-OS)(PNP3/4)] Anti (11a, 12a) and Syn (11b, 12b).** *Method A:* Na[<sup>99m</sup>TcO<sub>4</sub>] (0.250 mL, 50.0 MBq/3.0 GBq) was added to a

**Table 3. Incubation of *syn*-[<sup>99m</sup>Tc(N)(2-MPPP-cys-OS)(PNP4)] (10b) with Sodium *O,S*-Thioacetate (OS-ta)**

ratio <b>10b</b> /OS-ta	°C	time	<i>syn</i> - <b>10b</b>	<i>anti</i> - <b>10a</b>	<b>13</b> -(OS-ta)
1/1	50	15 min	93.3	6.6	0.1
1/5	50	15 min	91.4	7.3	1.3
1/5	50	4 h	51.4	31.6	17.0
1/5	50	24 h	4.9	51.8	43.3
1/5	100	15 min	23.3	68.0	8.7

vial containing succinic dihydrazide (SDH) (5.0 mg) and SnCl<sub>2</sub> (0.1 mg) suspended in saline (0.1 mL) and ethanol (1.0 mL). The vial was kept at room temperature for 15 min giving a mixture of <sup>99m</sup>Tc-nitrido precursors [<sup>99m</sup>Tc≡N]<sub>mix</sub><sup>2+</sup>. The appropriate diphosphine ligand (PNP3 or PNP4) (1.0 mg), dissolved in EtOH (0.1 mL), was then added, and the reaction mixture was left standing for 30 min at room temperature. To the resulting intermediate complex [<sup>99m</sup>Tc(N)(PNP3/4)]<sup>2+</sup> was added an ethanolic solution (0.1 mL) containing the 2-MPPP-cys-OS ligand (1 mg, 1.6 × 10<sup>-3</sup> mmol), and the solution was heated at 100 °C for 30 min. TLC and HPLC characterization showed the presence of two separate radioactive spots, which resulted from the formation of two distinct isomeric forms (**a** and **b**) of the complex [<sup>99m</sup>Tc(N)(2-MPPP-cys-OS)(PNP3/4)]. Total radiochemical purity (RCP) as determined by TLC and HPLC chromatography for the two isomers was 90.4% for [<sup>99m</sup>Tc(N)(2-MPPP-cys-OS)(PNP3)] (**11a**, 78.3%; **11b**, 12.1%) and 80.7% for [<sup>99m</sup>Tc(N)(2-MPPP-cys-OS)(PNP4)] (**12a**, 65.7%; **12b**, 15%).

*Method B:* To a mixture of [Tc≡N]<sub>mix</sub><sup>2+</sup> prepared as above, an ethanolic solution (0.1 mL) containing 2-MPPP-Cys-OS (1 mg, 1.6 × 10<sup>-3</sup> mmol) was added, and the reaction vial was left to stand at room temperature for 30 min. The reaction mixture was then treated with PNP3 or PNP4 (1.0 mg) dissolved in EtOH (0.1 mL) and heated at 100 °C for 30 min. Total RCP determined by TLC and HPLC chromatography for the two isomers was 42% for [<sup>99m</sup>Tc(N)(2-MPPP-cys-OS)(PNP3)] (**11a**, 35.9%; **11b**, 6.1%) and 45% for [<sup>99m</sup>Tc(N)(2-MPPP-cys-OS)(PNP4)] (**12a**, 40.5%; **12b**, 4.5%). These products exhibited the same chromatographic profiles as those obtained by method A.

*Method C:* To [Tc≡N]<sub>mix</sub><sup>2+</sup> prepared as above, the appropriate diphosphine (PNP3 or PNP4) (1.0 mg) dissolved in EtOH (0.1 mL) and 2-MPPP-Cys-OS (0.1 mg, 0.16 × 10<sup>-3</sup> mmol) dissolved in EtOH (0.1 mL) were added simultaneously, and the reaction mixture was



heated at 100 °C for 30 min. Total RCP determined by TLC and HPLC chromatography was 98% for [<sup>99m</sup>Tc(N)-(2-MPPP-cys-OS)(PNP3)] (**11a**, 85%; **11b**, 13%) and 85.4% for [<sup>99m</sup>Tc(N)-(2-MPPP-cys-OS)(PNP4)] (**12a**, 76.9%; **12b**, 8.5%). In both cases, the major compound, **11a** or **12a**, isolated by HPLC (*t<sub>R</sub>* **11a** = 23.4 min, *t<sub>R</sub>* **12a** = 27.8 min), was concentrated on a Sep pack C18 column rinsed with H<sub>2</sub>O and eluted using EtOH (3 × 0.5 mL). The second fraction containing all the activity was diluted with saline (1/10 EtOH/saline) and utilized for in vitro stability studies and in vivo biodistribution studies. After this purification the RCP's of both complexes, evaluated by TLC and HPLC chromatography, was >95%. In all cases the pH of the reaction mixture, measured at the end of the reaction, was 7.5.

**Preparation of [<sup>99m</sup>Tc(N)(OS-ta)(PNP4)] (OS-ta = Thioacetate) (**13**).** This complex was synthesized as reported earlier (*14*).

**Determination of Partition Coefficients (Log *P*).** After HPLC purification, Log *P* values of the thermodynamically stable *anti*-Tc-99m complexes (**11a**, **12a**) were determined by measuring the activity that partitioned between *n*-octanol (3.0 mL) and aqueous phosphate buffer (3.0 mL, 0.1 M, pH 7.4) under strict equilibrium conditions. Results are presented in Table 1. The syn to anti conversion of **11b** and **12b** complexes precluded the measurements of their Log *P*, and these were therefore not determined by this method.

**Stability Studies.** Compound **11a** or **12a** (100 μL) was added to a 5-mL propylene test tube containing rat serum (900 μL) or saline (900 μL). The resulting mixture was incubated at 37 °C for 2 h and assayed at 15, 30, 60, and 120 min by TLC for any changes in radiochemical purity. The complexes were found to be stable.

**Glutathione (GSH) and Cysteine Challenge.** To a 5-mL propylene test tube containing phosphate buffer (250.0 μL, 0.2 M, pH 7.4) were added water (100.0 μL), **11a** or **12a** (100.0 μL), and an aliquot (50.0 μL) of an aqueous stock solution of GSH (10.0 mM). The mixture was vortexed and incubated at 37 °C for 2 h. A control reaction containing an equal volume of H<sub>2</sub>O instead of GSH was studied in parallel. At 15, 30, 60, and 120 min, aliquots of the reaction mixture were withdrawn and analyzed by TLC and HPLC chromatography. The complexes were found to be inert toward substitution by GSH. A study using cysteine hydrochloride (10.0 mM and 1.0 mM) as the challenge ligand demonstrated a similar stability toward cysteine transchelation.

**Receptor-Binding Assays and Calculations.** The 5-HT<sub>1A</sub>-radioligand-binding assay was performed with rat (Sprague Dawley) cerebral cortex membrane prepared according to published procedures (*19, 20*). The net content of protein was determined via the Bradford method (Comassie Brilliant Blue, Biorad) using human serum albumin as a standard (*21*).

Competitive binding assays were performed in triplicate using [<sup>3</sup>H]-8-OH-DPAT as the radioligand, in a final volume of 0.250 mL. Briefly, aliquots (0.1 mL) corresponding to 0.15 mg of membrane protein were mixed with Tris-HCl buffer (50 mM, pH 7.7), [<sup>3</sup>H]-8-OH-DPAT (0.025 mL, 1 nM final concentration), and increasing concentrations (0.125 mL, 1 nM–10 μM) of the competing <sup>99m</sup>Tc-complex (**9a**, **9b**, **10a**, and **10b**). Incubations were carried out at 25 °C for 30 min. The reaction was terminated by the addition of ice-cold assay buffer (3 mL) followed by separation of bound from free radioligand by rapid filtration of the reaction mixture through Whatman GF/B glass-fiber filters. The filters were rinsed three times with ice-cold Tris-HCl buffer (3 × 3 mL). Filter-

**Table 4. Inhibition Constant, *K<sub>i</sub>* (nM), for the Displacement of 1.0 nM [<sup>3</sup>H]-8-OH-DPAT from Rat Cerebral Cortex Membranes 5HT<sub>1A</sub> Receptors**

compound	<i>K<sub>i</sub></i> (nM)
2-MPP	150 (± 12)
<i>anti</i> -[ <sup>99m</sup> Tc(N)(2-MPPP-cys-OS)(PNP3)] <b>9a</b>	>10000
<i>syn</i> -[ <sup>99m</sup> Tc(N)(2-MPPP-cys-OS)(PNP3)] <b>9b</b>	>10000
<i>anti</i> -[ <sup>99m</sup> Tc(N)(2-MPPP-cys-OS)(PNP4)] <b>10a</b>	800 (±17)
<i>syn</i> -[ <sup>99m</sup> Tc(N)(2-MPPP-cys-OS)(PNP4)] <b>10b</b>	>10000

bound radioactivity (<sup>99m</sup>Tc) was measured by liquid scintillation counting using a beta counter (LS 5081, Beckman) with a window set to exclude the interference from the tritium channel. IC<sub>50</sub> values were obtained graphically and the inhibition constant (*K<sub>i</sub>*) was calculated according to the Cheng and Prusoff equation (*22*) (Table 4).

**Animal Studies.** Female Sprague–Dawley rats weighing 200–250 g were anesthetized with an intramuscular injection of a mixture of ketamine (80 mg kg<sup>-1</sup>) and xylazine (19 mg kg<sup>-1</sup>). Compound **12a** (100 μL, 300–370 kBq) was injected via the jugular vein. The animals (*n* = 3) were sacrificed by cervical dislocation at 0, 2, 10, 20, and 60 min postinjection. Immediately after sacrifice of the rats, blood was withdrawn from the heart through a syringe and counted. Organs were excised, rinsed with saline, weighed, and counted in a gamma counter. The results are expressed as percentage injected dose per gram (% ID g<sup>-1</sup>) for each organ and blood (Table 5).

## RESULTS

**Preparation of the Bifunctional Ligand.** As outlined in Scheme 1, 2-{3-[4-(2-methoxyphenyl)piperazin-1-yl]propionylamino}-3-tritylsulfanypropionic acid (**5**) was obtained by coupling the amino group of the *S*-trityl-cysteine ethyl ester (**3**) to the carboxylic group of 3-[4-(2-methoxyphenyl)piperazin-1-yl]propionate (**2**) in CH<sub>2</sub>-Cl<sub>2</sub> in the presence of EDC, followed by base hydrolysis of the ester group. Compound **2** was obtained by a two-step reaction through N-alkylation of 1-(2-methoxyphenyl)piperazine hydrochloride (2-MPP) with methyl 3-bromopropionate, and subsequent hydrolysis to the corresponding acid under basic conditions. The final product 2-MPPP-cys-OS (**6**) was activated by removing the *S*-trityl protecting group from cysteine thiolate with TFA in the presence of triethylsilyl hydride to produce the free thiol ligand. The resulting bifunctional ligand is composed of a potentially bioactive moiety with affinity for 5HT<sub>1A</sub> receptors tethered to a bidentate chelating system having the thiol and carboxyl oxygen atoms of the cysteine as π-donor coordinating atoms.

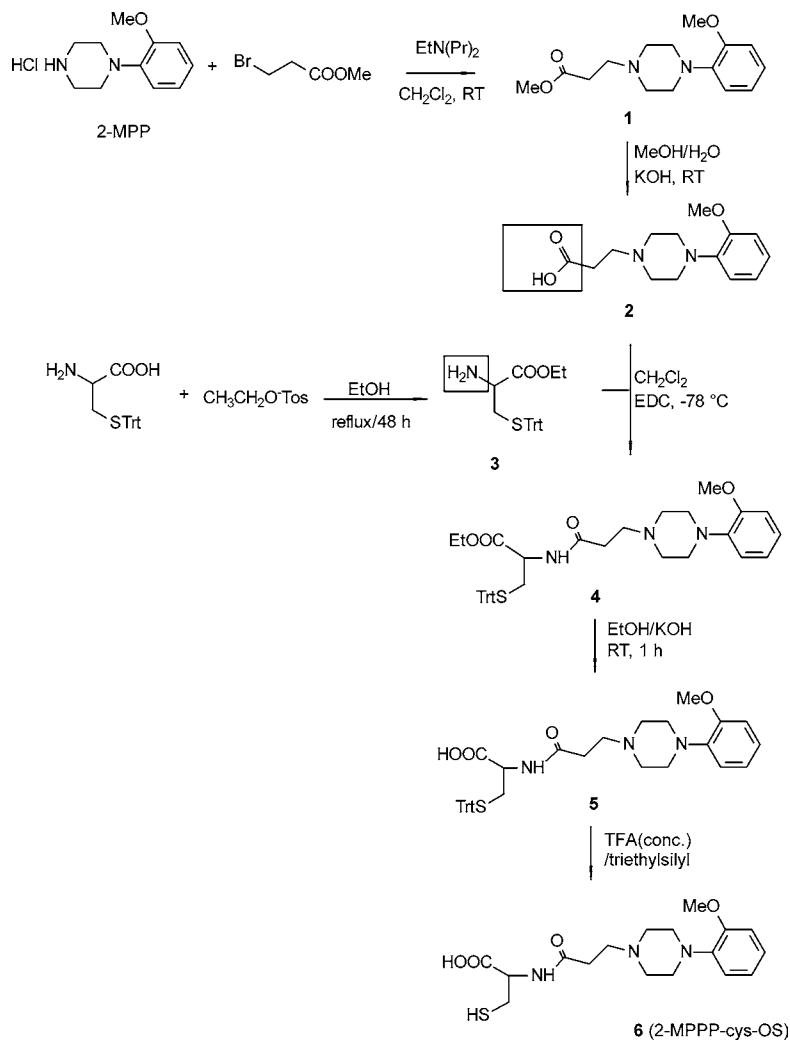
**Preparation and Characterization of <sup>99m</sup>Tc-labeled Compounds.** The intermediate compounds [<sup>99m</sup>Tc(N)Cl<sub>2</sub>(PNP3/4)] (**7**, **8**) have been prepared, in high yield, via ligand-exchange reaction of the labile precursor [<sup>99m</sup>Tc(N)Cl<sub>2</sub>(PPh<sub>3</sub>)<sub>2</sub>] with the appropriate diphosphine ligand in CH<sub>2</sub>Cl<sub>2</sub> solution (Scheme 2). IR absorption spectra exhibit typical medium intense bands at 1054 (**7**) and 1045 (**8**) cm<sup>-1</sup>, attributable to ν[Tc≡N] along with characteristic absorptions of coordinated alkylidiphosphine ligand in the 2979–2808 cm<sup>-1</sup> region. Elemental analyses, as reported in the Experimental Section, are also in good agreement with the proposed formulation.

Magnetic equivalence of the diphosphine phosphorus, results in <sup>31</sup>P NMR spectra of the intermediate complexes **7** and **8** exhibiting a broad singlet at room-temperature centered at δ = 31.0 and 23.1, respectively. Similar signal broadening is found in diamagnetic d<sup>2</sup> Tc-complexes and is attributed to the quadrupole relaxation induced by the



**Table 5. Biodistribution in Rats of 12a (% I.D. dose/g)**

organ	0 min	2 min	10 min	20 min	30 min	60 min
blood	$3.65 \pm 0.25$	$1.42 \pm 0.13$	$0.53 \pm 0.13$	$0.22 \pm 0.02$	$0.18 \pm 0.08$	$0.01 \pm 0.01$
brain	$0.29 \pm 0.03$	$0.14 \pm 0.02$	$0.04 \pm 0.01$	$0.02 \pm 0.00$	$0.02 \pm 0.00$	$0.01 \pm 0.00$
heart	$1.83 \pm 0.15$	$0.91 \pm 0.15$	$0.33 \pm 0.0$	$0.16 \pm 0.02$	$0.08 \pm 0.00$	$0.07 \pm 0.01$
lungs	$1.72 \pm 0.09$	$1.01 \pm 0.07$	$0.4 \pm 0.01$	$0.21 \pm 0.02$	$0.09 \pm 0.00$	$0.08 \pm 0.00$
liver	$2.7 \pm 0.49$	$3.22 \pm 0.01$	$2.08 \pm 0.02$	$0.79 \pm 0.17$	$0.40 \pm 0.01$	$0.38 \pm 0.03$
stomach	$0.65 \pm 0.08$	$0.50 \pm 0.04$	$1.06 \pm 0.30$	$4.25 \pm 2.16$	$2.42 \pm 1.39$	$4.75 \pm 1.41$
spleen	$0.74 \pm 0.03$	$0.64 \pm 0.05$	$0.20 \pm 0.01$	$0.12 \pm 0.00$	$0.06 \pm 0.00$	$0.06 \pm 0.01$
kidneys	$2.16 \pm 0.18$	$5.77 \pm 0.34$	$1.50 \pm 0.21$	$0.70 \pm 0.01$	$0.50 \pm 0.07$	$0.46 \pm 0.05$
intestine	$2.00 \pm 0.04$	$6.37 \pm 0.04$	$10.80 \pm 0.40$	$16.65 \pm 1.13$	$13.33 \pm 1.51$	$18.31 \pm 2.09$
muscle	$0.14 \pm 0.04$	$0.18 \pm 0.02$	$0.10 \pm 0.02$	$0.08 \pm 0.01$	$0.05 \pm 0.00$	$0.08 \pm 0.0$

**Scheme 1**

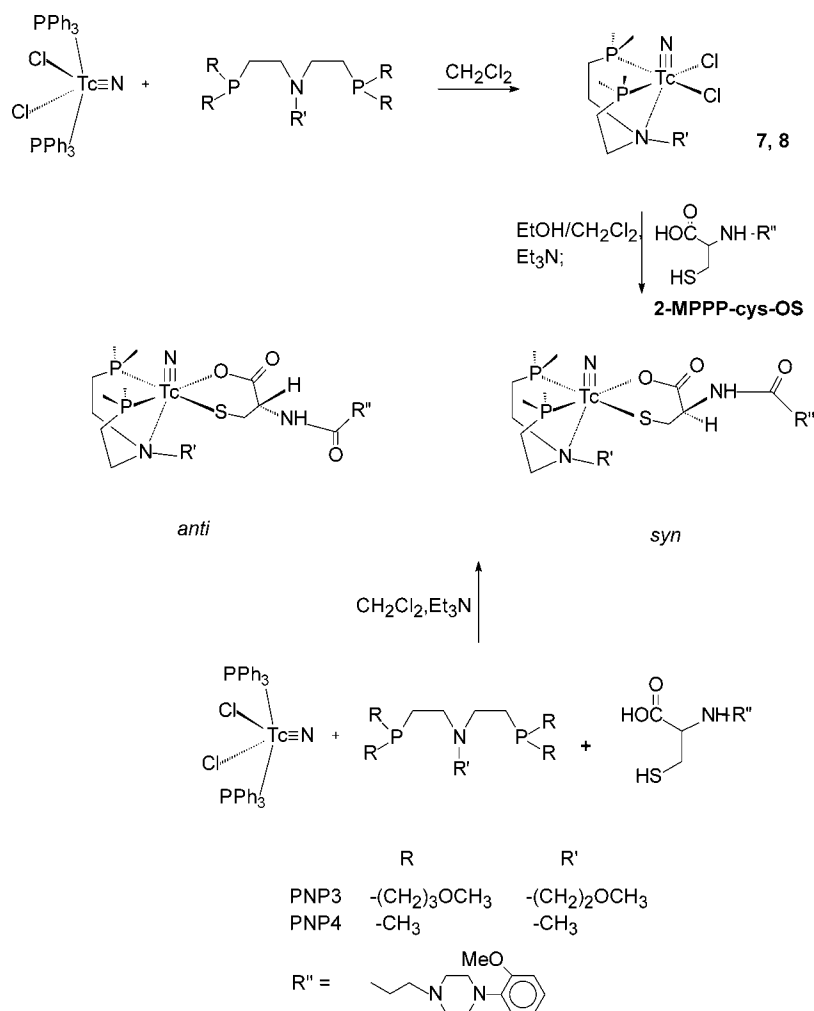
$^{99}\text{Tc}$  nucleus ( $I = 9/2$ ) on the neighboring P atoms (16).  $^1\text{H}$  and  $^{13}\text{C}$  spectra show relatively complex patterns consistent with the molecular structure depicted in Scheme 2, in which the asymmetry introduced by the terminal nitrido group removes the equivalence of the substituents on P (syn and anti oriented) and makes the methylene protons of the diphosphine chain diastereotopic. The molecular structure of an isostructural Re complex,  $[\text{Re}(\text{N})\text{Cl}_2(\text{PNP}2)]$  ( $\text{PNP}2 = \text{bis}[(2\text{-diphenylphosphino)ethyl]methoxyethylamine}$ ), has recently been solved by X-ray diffraction analysis (15), and the spectroscopic properties exhibited by this Re complex compared well with the complexes depicted in Scheme 2.

As detailed in Scheme 2, these intermediate compounds react with the bidentate dinegative ligand 2-MPPP-cys-OS resulting in stable neutral asymmetrical compounds of the type  $[\text{M}(\text{N}(\text{2-MPPP-cys-OS})(\text{PNP}3/4)]$

(9, 10). The same heterocomplexes are formed with the simultaneous addition of the two polydentate ligands ( $\text{PNP}3/4$  and 2-MPPP-cys-OS) to the labile precursor  $[\text{M}(\text{N})\text{Cl}_2(\text{PPh}_3)_2]$  in  $\text{CH}_2\text{Cl}_2$  solution in the presence of an excess of  $\text{Et}_3\text{N}$ . Under the synthetic conditions reported, no symmetric disubstituted compounds of the type  $[\text{M}(\text{N})(\text{PNP}3/4)_2]$  and  $[\text{M}(\text{N})(\text{2-MPPP-cys-OS})_2]$  have been detected.

For  $[\text{M}(\text{N})(\text{2-MPPP-cys-OS})(\text{PNP}3/4)]$ , two distinct isomeric forms have been isolated and identified as syn or anti isomers depending on the orientation of the N-substituted cysteine pendant group with respect to the central  $\text{Tc} \equiv \text{N}$  terminal core. The final isomeric ratio, evaluated by TLC and HPLC chromatography, is approximately 50/50 for 9a and 9b and 70/30 for 10a and 10b. In both cases, the two isomers were separated by silica column chromatography and were relatively stable

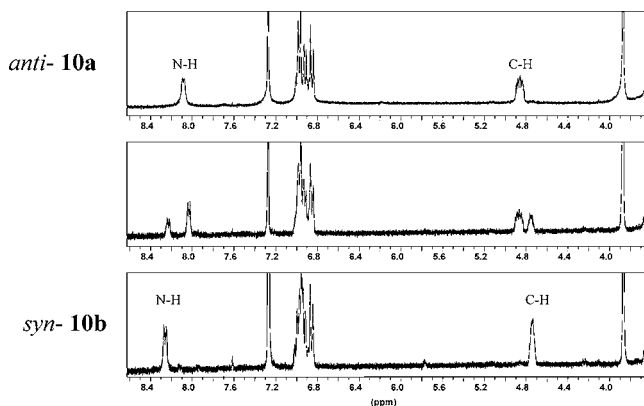
## Scheme 2



on this time scale. IR spectra of these asymmetric Tc(V)-nitrido complexes show typical absorptions of the intermediate compounds with two additional vibrations at 1732–1638 and 1240  $\text{cm}^{-1}$ , characteristic of 2-MPPP-cys-OS, indicating that the bifunctional chelating ligand is coordinated to the metal fragment  $[\text{}^{99\text{g}}\text{TcN}(\text{PNP3/4})]^{2+}$ . The expected bands of the technetium nitrogen multiple bond, appear in the region 1050–1047  $\text{cm}^{-1}$ , but no significant difference in the Tc $\equiv$ N stretch between syn and anti species has been observed.

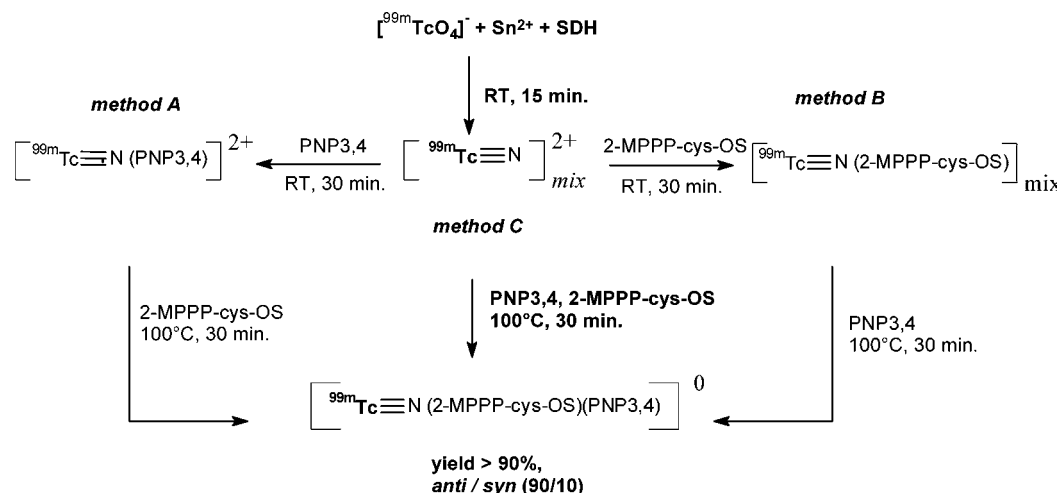
The complete characterization of two isomeric forms was obtained by multinuclear NMR spectroscopy. Coordination of the asymmetric S,O-cysteine fragment on the equatorial plane removes the magnetic equivalence of the facing diphosphine phosphorus. Consequently, the  $^{31}\text{P}$  NMR spectrum of each nitrido heterocomplex has two distinct broad signals. Syn and anti isomers are distinguished by the different proton patterns of the coordinated cysteine framework, as previously determined in similar isomeric pairs,  $[\text{}^{99\text{g}}\text{Tc}(\text{O})(\text{RP294})]$  (RP294 = dimethylglycyl-L-seryl-L-cysteinylglycinamide) (23) and  $[\text{Re}(\text{N})(\text{PNP2})(\text{N-ac-cys})]$  (PNP2 = aryldiphosphine and N-ac-cys = N-acetyl-L-cysteine) (24), containing N,S-carboxylic-substituted cysteine and O,S-amine-substituted cysteine, respectively. The assignment of the anti isomer in complexes **9** and **10** is based on the assumption that the pertinent NH and methyne protons of cysteine are shifted upfield and downfield, respectively, relative to the corresponding proton resonances in the syn isomer (Figure 2).

The syn  $\rightarrow$  anti isomerization of **9b** and **10b** was found to occur relatively slowly and to be an irreversible and temperature-dependent process. In fact, by monitoring the conversion by TLC or HPLC for **10b** (see Table 2), we observed that the isomerization reached the final 90/10 anti/syn ratio only after one week at 37  $^\circ\text{C}$ , and after only 15 min at 100  $^\circ\text{C}$ . A faster syn  $\rightarrow$  anti conversion was observed for the syn-PNP3 complex. On the other hand, no variation of the reverse anti  $\rightarrow$  syn conversion was observed by either varying the pH of the mixture from 5 to 9 or the temperature.



**Figure 2.** Proton NMR spectra in the 8.4–3.5 ppm region of *anti*- $[\text{}^{99\text{g}}\text{Tc}(\text{N})(2\text{-MPPP-cys-OS})(\text{PNP4})]$  **10a** (top), of *syn*- $[\text{}^{99\text{g}}\text{Tc}(\text{N})(2\text{-MPPP-cys-OS})(\text{PNP4})]$  **10b** (bottom), and mixture of **10a** and **10b** (middle).

## Scheme 3



To clarify the mechanism of isomer conversion, *syn*- $[^{99g}\text{TcN}(2\text{-MPPP-cys-OS})(\text{PNP4})]$  (**10b**) was incubated with an equimolar or excess amount of the less hindered cysteine-mimicking molecule *O,S*-thioacetate sodium salt at 50 °C and 100 °C. As reported in Table 3, in addition to the expected *syn* → *anti* conversion, the chromatographic profile reveals the presence of a more hydrophilic peak (see Scheme 4) identified as  $[^{99g}\text{TcN}(\text{O,S-thioacetate})(\text{PNP4})]$  (**13**) by comparison with an authentic sample prepared in earlier studies (17). The production of **13** is increased with time by using an excess of *O,S*-thioacetate or by raising the temperature.

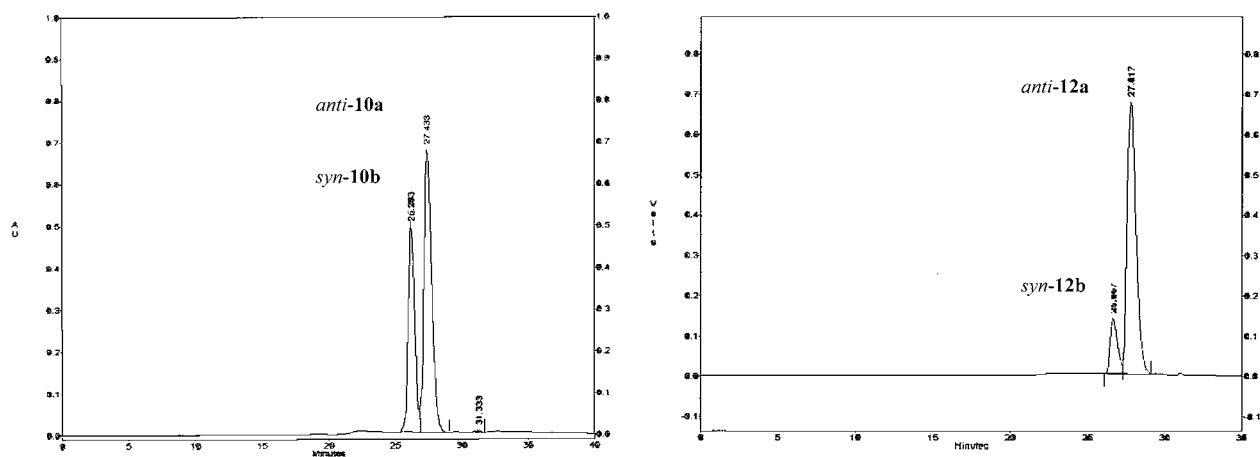
**Preparation of  $^{99m}\text{Tc}$ -Labeled Compounds.** Methods employed for preparing neutral tracer asymmetric  $^{99m}\text{Tc}$ -nitrido complexes of the type  $[^{99m}\text{Tc}(\text{N})(\text{PNP3/4})-(2\text{-MPPP-cys-OS})]$  are outlined in Scheme 3. The labeling procedures have been carried out using either a two- or a three-step approach.

In all preparations the first step is to generate a mixture of  $^{99m}\text{Tc}$ -nitrido precursors, all containing the  $[\text{Tc}\equiv\text{N}]^{2+}$  core, through the reduction of pertechnetate with tin(II) chloride in the presence of SDH as donor of the nitrido nitrogen atom. The three-step procedure (method A) entails formation of the strongly electrophilic  $[^{99m}\text{Tc}(\text{N})(\text{PNP})]^{2+}$  intermediate fragment by addition of the appropriate diphosphine ligand (PNP3/4) to the starting  $^{99m}\text{Tc}$ -nitrido mixture. The preparation is then completed by addition of 2-MPPP-cys-OS, which selectively reacts with the intermediate fragment to yield the

final asymmetric complexes. An analogous three-step procedure (method B) reverses the order of addition of the reagents. The yield, however, is somewhat reduced. The optimal labeling procedure involves only two separate steps (method C). After production of the mixture  $[^{99m}\text{Tc}\equiv\text{N}]_{\text{mix}}^{2+}$ , the appropriate diphosphine and bidentate 2-MPPP-cys-OS ligand are simultaneously added to the reaction vial to afford the final product in high yield, after 30 min at 100 °C. Chromatographic characterization indicates that the chemical nature of the final complexes is independent of the preparation method utilized.

The chemical identity of the  $^{99m}\text{Tc}$ -complexes were established by comparison of their chromatographic properties with those of the corresponding complexes obtained at the macroscopic level with the long-lived  $^{99g}\text{Tc}$  isotope (see Table 1 and Figure 3). The  $\log k'_0$  values were determined for each compound by reversed-phase HPLC using various mixtures of methanol/buffer (pH 7.4) as eluant, these served as a measure of the relative lipophilicity of the complexes particularly when traditional octanol/water ( $\log P$ ) ratios (Table 1) could not be determined due to *syn* → *anti* isomer conversion.

All  $^{99m}\text{Tc}$ -complexes exist in two distinct isomeric forms (see  $^{99g}\text{Tc}$ ) but with an *anti*/*syn* isomeric ratio of 90/10 irrespective of the diphosphine utilized. This difference in the tracer  $^{99m}\text{Tc}$  synthesis, compared with the macroscopic  $^{99g}\text{Tc}$  synthesis is attributed to the higher temperature employed in the *nca*  $^{99m}\text{Tc}$  synthesis which accel-



**Figure 3.** RP-HPLC comparison of  $[^{99m}\text{Tc}(\text{N})(2\text{-MPPP-cys-OS})(\text{PNP4})]$  (**12**) complexes with  $[^{99g}\text{Tc}(\text{N})(2\text{-MPPP-cys-OS})(\text{PNP4})]$  (**10**) analogue.



erates the syn to anti conversion observed at room temperature with the  $^{99g}\text{Tc}$ -complexes.

Consequently, only the anti  $^{99m}\text{Tc}$  isomers were isolated by HPLC (RCP > 95%) and utilized for both in vitro stability and in vivo biodistribution studies after appropriate dilution with saline.

**Stability.** Complexes **11a** and **12a** exhibit a good in vitro stability and no significant change in radiochemical purity after 2 h of incubation at 37 °C, thus indicating the high stability and substitution inertness of these compounds.

**Biological Studies.** The in vitro affinity for the 5HT<sub>1A</sub> receptors of the underivatized 2-MPP compound and of the technetium complexes (**9a**, **9b**, **10a**, **10b**) was assessed by measuring the ability of the compounds to compete with [ $^3\text{H}$ ]-8-OH-DPAT binding in isolated membranes from rat cerebral cortex. The inhibition binding-constant ( $K_i$ ) values, measured at 25 °C (Table 4), show that only complex **10a** (*anti*-PNP4) possesses some affinity compared with that observed for the free 2-MPP ligand, while a complete absence of receptor affinity is observed for the other complexes.

For biodistribution studies of the  $^{99m}\text{Tc}$ -compound **12a** in female Sprague–Dawley rats, the radiolabeled compound was purified before injection to remove excess unlabeled cold ligand. The radiochemical purity of the purified compound was verified prior to in vivo administration and the tissue distribution of the complexes is summarized as % ID/g tissue in Table 5.

The complex exhibits rapid blood clearance with the activity mainly eliminating through both the hepatobiliary system and the urinary tract. Only a small fraction of the injected activity ( $\approx 0.14\%$  ID at 2 min) crosses the BBB, followed by a rapid wash out. A very high intestinal uptake is observed at 2 min postinjection.

## DISCUSSION

In this study a new route for incorporating a bioactive molecule into stable  $^{99m}\text{Tc}$ -nitrido compounds is reported. The method is based on the chemical properties of the electrophilic nitrido metal fragment [ $^{99g/99m}\text{Tc}(\text{PNP})$ ] $^{2+}$ . The structural framework of these moieties contains a pseudo tridentate diphosphine ligand (PNP) coordinated to the technetium-nitrido group and two labile sites usually filled by halogens which complete the pseudo-octahedral environment. The [ $^{99g/99m}\text{Tc}(\text{PNP})$ ] $^{2+}$  metal fragment is an activated intermediate which selectively reacts with bidentate chelating ligands carrying  $\pi$ -donor atoms (YZ) to form the final complex [ $\text{Tc}(\text{N})(\text{YZ})(\text{PXP})$ ] $^{0/+}$  which is characterized by an asymmetric arrangement of two polydentate ligands around the metal center.

Neutral asymmetric complexes [ $^{99g}\text{Tc}(\text{N})(2\text{-MPPP-cys-OS})(\text{PNP})$ ] are prepared in high yield by ligand-exchange reactions of [ $^{99g}\text{Tc}(\text{N})\text{Cl}_2(\text{PNP})$ ] with the bifunctional ligand 2-MPP-cy-OS, or, alternatively, by direct reaction of the relevant diphosphine (PNP3 or PNP4) and 2-MPPP-cys-OS with the labile precursor [ $^{99g}\text{Tc}(\text{N})\text{Cl}_2(\text{PPh}_3)_2$ ]. As indicated in Scheme 2, the heterocomplexes display a metal fragment, composed of a terminal  $\text{Tc}\equiv\text{N}$  multiple bond with an ancillary diphosphine ligand, and are coordinated to the thiolate sulfur and carboxylate oxygen of the 2-MPPP-cys-OS ligand. Upon coordination to the metal fragment, 2-MPPP-cys-OS adopts two distinct isomeric forms depending on the relative syn or anti orientation of the *O,S*-cys-piperazinyl group with respect to the  $\text{Tc}\equiv\text{N}$  terminal group. The isolated syn isomer slowly and irreversibly converts to the anti isomer in a temperature-dependent process.

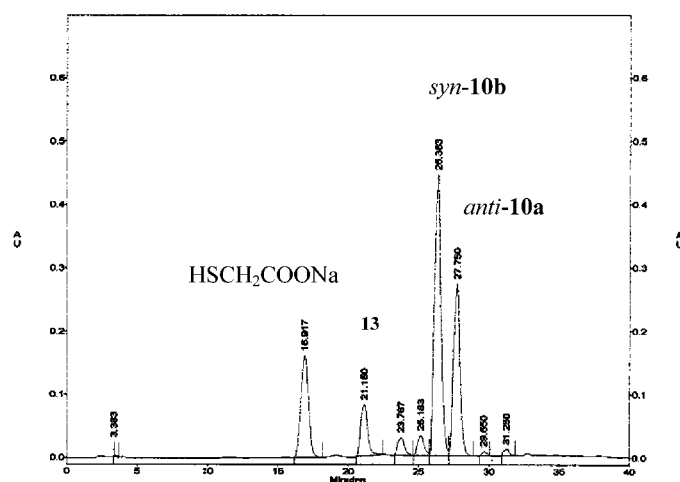
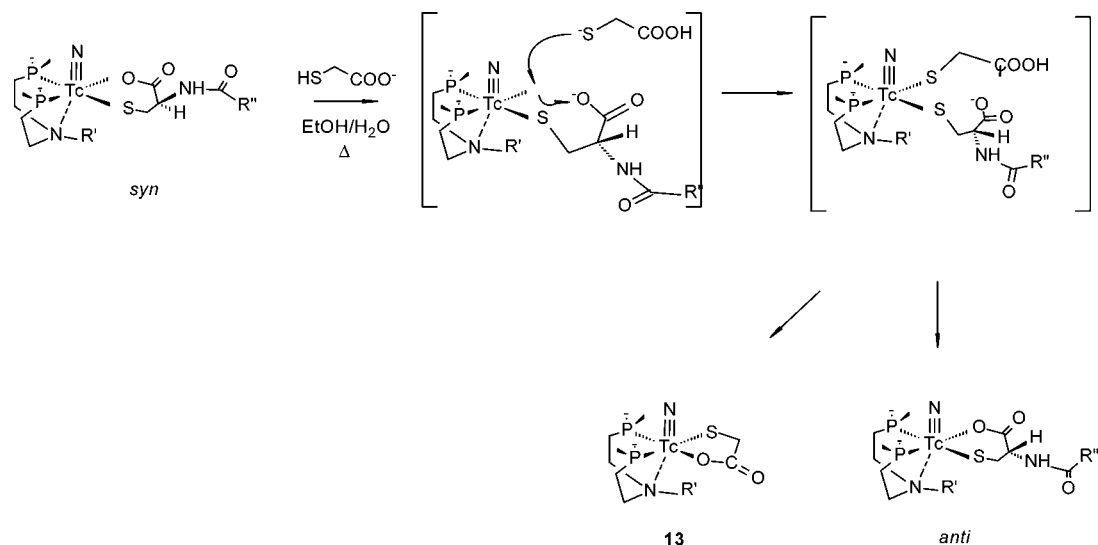
pH does not modify the course of this syn  $\rightarrow$  anti conversion (Table 2). This lack of acid–base sensitivity is likely due to the pseudo-octahedral geometry of the nitrido heterocomplex, where the position trans to the nitrido group is already occupied by the PNP tertiary amine nitrogen, thus preventing the insertion of additional molecules (e.g., water). A dissociative mechanism for this syn  $\rightarrow$  anti conversion is proposed based on the temperature dependence of the conversion process and the formation, in addition to syn  $\rightarrow$  anti transformed complex, of a more hydrophilic [ $\text{Tc}(\text{N})(\text{OS-ta})(\text{PNP})$ ] species when the syn complex is incubated with equimolar or excess amounts of a less hindered cysteine-mimicking *S,O*-thioacetate (Scheme 4). These observations support a mechanism which requires the dissociation of the carboxylate oxygen of 2-MPPP-cys-OS and the insertion of the thioacetate thiolate, resulting in production of the hydrophilic [ $\text{Tc}(\text{N})(\text{OS-ta})(\text{PNP})$ ] species together with isomerization of the syn to anti [ $\text{Tc}(\text{N})(2\text{-MPPP-cys-OS})(\text{PNP})$ ]. This behavior also suggests that the anti isomer is the sterically and thermodynamically favored conformation of these heterocomplexes.

The chromatographic profile (Figure 3) shows that the complexes synthesized at the millimolar level are identical to those prepared at n.c.a. level, the only difference being the increased anti/syn isomeric ratio, which is attributed to the higher temperature employed in the former  $^{99m}\text{Tc}$  synthesis. At the n.c.a. level asymmetric  $^{99m}\text{Tc}$ -nitrido complexes are efficiently prepared through three alternative routes as indicated in Scheme 3. The most efficient labeling procedure involves only two steps, mixing in the same reaction vial both the PNP and 2-MPPP-cys-OS ligand with the starting mixture of [ $^{99m}\text{Tc}\equiv\text{N}$ ] $^{2+}_{\text{mix}}$  nitrido precursor. Alternatively, intermediate Tc-nitrido diphosphine complex can also be formed prior to reacting with the  $\pi$ -donor 2-MPPP-cys-OS ligand present in the same reaction vial to give the desired nitrido heterocomplex in high yield. The most salient feature of these reactions is that no formation of the symmetric complexes [ $^{99m}\text{Tc}(\text{N})(\text{PNP})_2$ ] $^{2+}$  and [ $^{99m}\text{Tc}(\text{N})(2\text{-MPPP-cys-OS})_2$ ] are detected under a broad range of experimental conditions.

In vitro stability studies carried out on the anti isomers show that these compounds are stable in aqueous solutions and serum and are inert toward transchelation with free glutathione and cysteine, suggesting that the arrangement of two  $\pi$ -acceptor phosphorus and two  $\pi$ -donor atoms around the [ $\text{Tc}\equiv\text{N}$ ] $^{2+}$  core possess a high thermodynamic stability and kinetic inertness.

Despite these promising physicochemical properties, in vitro binding studies of the technetium complexes (**9a**, **9b**, **10a**, **10b**) with the 5HT<sub>1A</sub> receptors show that only complex **10a** (*anti*-PNP4) retains some affinity for the 5HT<sub>1A</sub> receptors. The complete loss of receptor affinity observed for complexes containing the PNP3 phosphine could be attributed to the larger steric hindrance imparted to the metal fragment by this phosphine. The relatively smaller complex formed with PNP4 displayed  $K_i$  values of the same order of magnitude as the underivatized 2-MPP ligand (**22**). For PNP4 complexes, the partial loss of affinity may be attributed to the interaction of the piperazinyl fragment with the aminomethyl PNP pendant group. This suggests that affinity could be improved by further manipulating the structure, e.g., by increasing the length of the spacer between the piperazine moiety and the cysteine fragment, eliminating the amide link in the linker arm, or using an alkyl link between the MPP and the bidentate coordinating groups. Studies with this focus are in progress.

## Scheme 4



Although both the molecular weight and the lipophilicity of the *anti*-PNP4 complex are in the appropriate range required for crossing the BBB, in vivo biodistribution data displayed negligible brain uptake. This low affinity toward the receptor along with the rapid blood clearance of the complex may reduce the bioavailability of the tracer thus limiting the brain uptake. In non-CNS peripheral sites, such as the intestine, in our opinion, the accumulation may reflect an excretory pathway via the hepatobiliary system for these molecule rather than binding to peripheral 5HT<sub>1A</sub> receptors, particularly since the complex displays only low affinity toward the receptor in vitro.

## CONCLUSIONS

This work describes application of a new labeling procedure for incorporating a bioactive molecule into a stable asymmetric  $^{99m}\text{Tc}$ -nitrido complex. The chemistry is based on the use of the  $[\text{Tc}(\text{N})(\text{PNP})]^{2+}$  metal fragment which, once formed, selectively reacts with bidentate ligands, such as bifunctional N-derivatized cysteine ligand carrying the bioactive 2-MPP fragment. The resulting neutral species are easily prepared both at macroscopic and n.c.a. levels and exhibit remarkable stability toward glutathione or cysteine challenge. Despite these promising properties, the lack of BBB penetration indicates that these particular complexes may not be useful for CNS-receptor mapping. However, the

experimental evidence that the incorporation of the  $[\text{Tc}(\text{N})(\text{PNP})]^{2+}$  molecular fragment with a bioactive molecule (2-MPP) maintains its affinity for 5HT<sub>1A</sub> receptors suggests that this class of complexes might be useful for peripheral applications (25) and that this strategy may be applied to other receptor-targeting molecules with appropriately modified bidentate chelates.

## ACKNOWLEDGMENT

The authors are indebted to Nihon Medi-Physic, Tokyo, Japan, for financial support of this work. The authors wish to thank Anna Rosa Moresco for her work on the elemental analysis.

## LITERATURE CITED

- (1) Pike, V. W., Hallidin, C., McCarron, J. A., Lundkvist, C., Hirani, E., Olsson, H., Hume, S. P., Karlsson, P., Osman, S., Swahn, C. G., Hall, H., Wikström, H., Mensonidas, M., Poole, K. G., and Farde, L. (1998) [carbonyl- $^{11}\text{C}$ ]Desmethyl-WAY-100635 (DWAY) is a potent and selective radioligand for central 5-HT<sub>1A</sub> receptor in vitro and in vivo. *Eur. J. Nucl. Med.* 25, 338–346.
- (2) Mensonides-Harsema, M. M., Liao, Y., Böttcher, H., Bartoszyk, G. D., Greiner, H. E., Harting, J., de Boer, P., and Wikström, H. V. (2000) Synthesis and in Vitro and in Vivo Functional Studies of *Ortho*-Substituted phenylpiperazine and *N*-Substituted 4-*N*-(*o*-Methoxyphenyl)aminopiperidine Analogues of WAY100365. *J. Med. Chem.* 43, 432–439.

- (3) Pike, V. W., Halldin, C., Wikström, H., Marchais, S., McCarron, J. A., Sandell, J., Nowicki, B., Swahn, C. G., Osman, S., Hume, S. P., Constantinos, M., André, B., and Farde, L. (2000) Radioligands for the Study of Brain 5-HT<sub>1A</sub> Receptors in *Vivo*-development of Some New Analogues of WAY. *Nucl. Med. Biol.* 27, 449–455.
- (4) Lang, L., Jagoda, E., Schmall, B., Sassaman, M., Ma, Y., and Eckelman, W. C. (2000) Floro Analogues of WAY-100365 with Varying Pharmacokinetics Properties. *Nucl. Med. Biol.* 27, 457–462.
- (5) Kung, H. F., Bradshaw, J. E., Chumpradit, S., Zhuang, M.-P., Kung, M.-P., and Mu, M. (1995) Rhenium and other Metals in Chemistry and Nuclear Medicine. New TcO(III) and ReO(III) N<sub>2</sub>S<sub>2</sub> complexes as potential CNS 5-HT<sub>1A</sub> receptor imaging agents, in *Technetium and Rhenium in Chemistry and Nuclear Medicine 4* (M. Nicolini, G. Bandoli, and U. Mazzi, Eds.) pp 293–298, SGEEditoriali, Padova, Italy.
- (6) Mahmood, A., Kronauge, J. F., Barbarics, E., Freiberg, E., Madras, B. K., Li, J., Davison, A., and Jones, A. G. (1999) *Technetium, Rhenium and other Metals in Chemistry and Nuclear Medicine 5* (M. Nicolini, and U. Mazzi, Eds.) pp 393–399, SGEEditoriali, Padova, Italy.
- (7) Johannsen, B., Berger, R., Brust, P., Pietzsch, H. J., Scheunemann, M., Seifert, S., Spies, H., and Syher, R. (1997) Structural modification of receptor-binding technetium-99m complexes in order to improve brain uptake. *Eur. J. Nucl. Med.* 24, 316–319.
- (8) Heimbold, I., Drews, A., Syhre, R., Kretzschmar, M., Pietzsch, H. J., and Johannsen, B. (2002) A novel technetium-99m radioligand for the 5-HT<sub>1A</sub> receptor derived from desmethyl-WAY100635 (DWAY). *Eur. J. Nucl. Med.* 29, 82–87.
- (9) León, A., Rey, A., Mallo, L., Pirmettis, I., Papadopoulos, M., León, E., Pagano, M., Manta, E., Incerti, M., Raptopoulou, C., Terzis, A., and Chiotellis, E. (2002) Novel mixed ligand technetium complexes as 5-HT<sub>1A</sub> receptor imaging agents. *Nucl. Med. Biol.* 29, 217–226.
- (10) Heimbold, I., Drews, A., Kretzschmar, M., Varnäs, K., Hall, H., Halldin, C., Syhre, R., Kraus, W., Pietzsch, H.-J., Seifert, S., Brust, P., and Johannsen, B. (2002) Synthesis, biological and autoradiographic evaluation of a novel Tc-99m radioligand derived from WAY 100635 with high affinity for the 5-HT<sub>1A</sub> receptor and the alpha1-adrenergic receptor. *Nucl. Med. Biol.* 29, 375–387.
- (11) Drews, A., Pietzsch, H.-J., Syhre, R., Seifert, S., Varnäs, K., Hall, H., Halldin, C., Kraus, W., Karlsson, P., Johnsson, C., Spies, H., and Johannsen, B. (2002) Synthesis and biological evaluation of technetium (III) mixed ligand complexes with high affinity for the cerebral 5-HT<sub>1A</sub> receptor and the alpha1-adrenergic receptor. *Nucl. Med. Biol.* 29, 389–398.
- (12) Alberto, R., Schibli, R., Schubiger, A. P., Abram, U., Pietzsch, H.-P., and Johannsen, B. (1999) First application of *fac*-[<sup>99m</sup>Tc(OH<sub>2</sub>)<sub>3</sub>(CO)<sub>3</sub>]<sup>+</sup> in bioorganometallic chemistry: design, structure, and in vitro affinity of a 5HT<sub>1A</sub> receptor ligand labeled with <sup>99m</sup>Tc. *J. Am. Chem. Soc.* 121, 6076–6077.
- (13) Bolzati, C., Boschi, A., Duatti, A., Prakash, S., Uccelli, L., Refosco, F., Tisato, F., and Bandoli, G. (2000) Geometrically Controlled Selective Formation of Nitrido Technetium(V) Asymmetrical Heterocomplexes with Bidentate Ligands. *J. Am. Chem. Soc.* 122, 4510–4511.
- (14) Boschi, A., Bolzati, C., Benini, E., Malagò, E., Uccelli, L., Duatti, A., Piffanelli, A., Refosco, F., and Tisato, F. (2001) A novel approach to the high-specific-activity labeling of small peptides with the technetium-99m fragment [<sup>99m</sup>Tc(N)-(PXP)]<sup>2+</sup> (PXP = Diphosphine ligand). *Bioconjugate Chem.* 12, 1035–1042.
- (15) Bolzati, C., Boschi, A., Uccelli, L., Tisato, F., Refosco, F., Cagnolini, A., Duatti, A., Prakash, S., Bandoli, G., and Vittadini, A. (2002) Chemistry of the strong electrophilic metal fragment [<sup>99</sup>Tc(N)(PXP)]<sup>2+</sup> (PXP = Diphosphine ligand). A novel tool for the selective labeling of small molecules. *J. Am. Chem. Soc.* 124, 11468–11479.
- (16) Abram, U., Lorenz, B., Kaden, L., and Scheller, D. (1988) Nitrido Complexes of Technetium with Tertiary Phosphines and Arsines *Polyhedron* 7, 285–289.
- (17) Boschi, A., Uccelli, L., Bolzati, C., Duatti, A., Sabba, N., Moretti, E., Di Domenico, G., Zavattini, G., Refosco, F., and Giganti, M. (2003) Biological Evaluation of monocationic Asymmetrical Nitride Tc-99m Heterocomplexes Showing High Heart Uptake and Improved Imaging Properties. *J. Nucl. Med.* 44, 806–814.
- (18) Moretti, J. L., Caglar, M., and Weinmann, P. (1995) Cerebral Perfusion Imaging Tracers for SPECT: Which One to Choose? *J. Nucl. Med.* 36, 359–363.
- (19) Dalpiaz, A., Gessi, S., Borea, P. A., and Gilli, G. (1995) Binding thermodynamics of serotonin to rat-brain 5-HT<sub>1A</sub>, 5-HT<sub>2A</sub>, 5-HT<sub>3</sub> receptors. *Life Sci.* 57, 141–146.
- (20) Dalpiaz, A., Borea, P. A., Gessi, S., and Gilli, G. (1996) Binding thermodynamic of 5-HT<sub>1A</sub> receptor ligands. *Eur. J. Pharmacol.* 312, 107–114.
- (21) Bradford, M. M. (1976) A rapid and sensitive method for the quantification of microgram quantities of proteins utilizing the principle of protein dye-binding. *Anal. Biochem.* 72, 248–254.
- (22) Cheng, Y. C., and Prusoff, W. H. (1973) *Biochem. Pharmacol.* 22, 3099–3108.
- (23) Wong, E., Fauconnier, T., Bennett, S., Valliant, J., Nguyen, T., Lau, F., Lu, L. F. L., Pollak, A., Bell, R. A., and Thornback, J. R. (1997) Rhenium (V) and Technetium (V) Oxo Complexes of an N<sub>2</sub>N'S Peptide Chelator: Evidence of Interconversion between the Syn and Anti Conformations. *Inorg. Chem.* 36, 5799–5808.
- (24) Tisato, F., Refosco, F., Cagnolini, A., Bandoli, G., Bolzati, C., Uccelli, L., Boschi, A., Prakash, S., and Duatti, A. (1999) Reliable synthesis of asymmetrical nitrido Tc(V) and Re(V) heterocomplexes, in *Technetium, Rhenium and other Metals in Chemistry and Nuclear Medicine 5* (M. Nicolini, and U. Mazzi, Eds.) pp 133–138, SGEEditoriali, Padova, Italy.
- (25) Nock, B. A., Maina, T., Malagò, E., Duatti, A., Porchia, M., Refosco, F., and Tisato, F. (2002) Synthesis of Asymmetrical Heterocomplexes of the [<sup>99m</sup>Tc/<sup>99g</sup>Tc(N)(PNP)]<sup>2+</sup> Fragment with Cysteine-Functionalized Biotin, in *Technetium, Rhenium and other Metals in Chemistry and Nuclear Medicine 6* (M. Nicolini, and U. Mazzi, Eds.) pp 479–481, SGEEditoriali, Padova, Italy.

BC034100G



# Oligomeric Assembly and Ligand Binding of the Members of Protein Family YER057c/YIL051c/YJGF

Edita Mistiniene,<sup>\*,†</sup> Virginijus Lukša,<sup>‡</sup> Jolanta Sereikaite,<sup>§</sup> and Vytautas Naktinis<sup>‡</sup>

Institute of Biotechnology, V. Graičiūno 8, Vilnius 2028, Lithuania, SICOR Biotech UAB, V. Graičiūno 8, Vilnius 2028, Lithuania, and Vilnius Gediminas Technical University, Sauletekio al. 11, Vilnius 2040, Lithuania. Received June 23, 2003; Revised Manuscript Received September 24, 2003

Proteins UK114 and p14.5 are both members of the putative family of small proteins YER057c/YIL051c/YjgF. The biological role of these proteins is not understood very well, and in addition, their oligomeric structure in solution remains controversial. We therefore investigated the oligomeric structure of UK114 and p14.5 using a number of methods. Both proteins have exhibited a homotrimeric structure in solution. Indeed the trimeric structure of the two proteins appeared to be so similar that when protein subunits derived from different species were mixed, stable heterotrimeric complexes (monomer ratio of 1:2 and 2:1 of UK114 and p14.5, respectively) could be formed in vitro. Furthermore, the trimeric structure of both UK114 and p14.5 proved essential for the stoichiometric hydrophobic ligand, such as fatty acid binding activity of the two proteins.

## INTRODUCTION

Perchloric acid- or trifluoroacetic acid-soluble extracts from liver or kidney of mammals have been shown to contain regularly identifiable proteins of currently unknown function. UK114 is one of the three proteins found in perchloric acid-soluble extract of goat liver (1, 2). UK114 is located in the cytoplasm of normal cells, while in a wide variety of tumors it is also expressed on the cell surface (3), to suggest that tumors, which express UK114 on the cell membrane, could be subjected to antibody-mediated cytotoxicity. Indeed, administration of the UK-specific antibodies in vivo specifically suppresses growth of human colon cancer HT29 cells xenografted into *nu/nu* mice (4, 5). Preliminary evidence on an anticancer efficacy of UK114-containing preparations in humans has also been reported (3, 6).

The mode of biological action of these proteins however remains undefined. Melloni et al. demonstrated that UK114 activated the protease  $\mu$ -calpain and showed its similarity to other activators, such as long chain acyl-coAs-binding proteins or activators from bovine brain (7, 8). PSP (perchloric acid-soluble protein), a homologue of UK114, from rat liver and kidney, on the other hand, has been shown to inhibit a cell-free protein synthesis in a rabbit reticulocyte lysate system (9, 10). PSP may also be involved in fatty acid binding and in intracellular metabolism of fatty acids (11). A 14.5 kDa trichloroacetic acid-soluble p14.5 protein from human mononuclear monocytes has also been isolated and characterized. Human recombinant p14.5 appears similar to PSP in its ability to inhibit protein synthesis in vitro (12). Hrp12, a homologue from mouse, described by Samuel et al., has specifically been assigned the function of a translation inhibitor, though it also exhibited features of a heat shock protein (13).

All these proteins were identified as constituting a new hypothetical family of small proteins, the YER057c/YIL051c/YjgF family (12). The amino acid sequences of the members of this family are highly conserved throughout the evolutionary tree, from prokaryotes to eukaryotes. Approximately 30 proteins sharing sequence similarity of 32–93% have currently been assigned to this family.

3-D structures in crystal are currently available for two bacterial member proteins of the family, a purine regulatory protein from *Bacillus subtilis* (14) and YjgF from *E. coli* (15). In both cases, data obtained was consistent with the proteins forming symmetric trimers in crystals. Recently, the crystal structure of the first mammalian protein UK114 from this family has also revealed the trimeric organization (16). Information about oligomeric structure in solution for members of the YER057c/YIL051c/YjgF family is controversial. Preliminary X-ray data on PSP was indicative of two molecules being present per asymmetric unit (17), a conclusion supported with size exclusion chromatographic data, which was consistent with the dimeric structure of the protein in solution (9). A monomeric structure of a homologue protein from human mononuclear monocytes, p14.5, has been reported (12). Recently, the first NMR study of the member of YjgF/YER057c/UK114 family HI0719 from *Haemophilus influenzae* in solution showed trimeric structure (18). There is no clear evidence of oligomeric structures for mammalian members of this family in solution.

Such controversy over the oligomeric structure of these very similar and evolutionarily well preserved proteins in solution generates a significant hurdle for efforts made to understand the biological role of these proteins. We therefore made our own routine gel filtration chromatographic measurements and then applied a carefully designed gentle chemical cross-linking method to two proteins of the YER057c/YIL051c/YjgF family, namely, UK114 and p14.5, in solution. We supported this approach by characterizing the conditions of ESI-MS<sup>1</sup> (electrospray ionization mass spectrometry) analysis required for identification of the oligomeric state of the

\* Corresponding author. Fax +37052 60 21 16, tel +37052 60 21 19, e-mail: Editami@ibt.lt.

<sup>†</sup> Institute of Biotechnology.

<sup>‡</sup> SICOR Biotech UAB.

<sup>§</sup> Vilnius Gediminas Technical University.

proteins. In the present study the first homotrimeric solution structure was confirmed for two mammalian members of the YER057c/YIL051c/YjgF family. Furthermore, the trimeric structure in solution was demonstrated to be so similar for the two proteins that stable heterotrimeric complexes could be formed in vitro. Indeed, our evidence indicates that the maintenance of the trimeric structure of these proteins in solution may be critical to their ability to bind hydrophobic ligands, such as free fatty acids, one possible mode of action of these proteins.

## EXPERIMENTAL PROCEDURES

**Materials.** Recombinant UK114 and p14.5 expressed in *Escherichia coli* were a kind gift from SICOR Biotech UAB (Lithuania). Protein molecular weight markers for SDS-PAGE were obtained from MBI Fermentas (Lithuania). Lipidex 1000 was obtained from Packard Instrument Company. <sup>3</sup>H-labeled fatty acids were obtained from Amersham Pharmacia Biotech, England. Scintillation cocktail Rotiszint Eco Plus was obtained from ROTH. 1,3,5-Triacryloyl-hexahydro-*s*-triazine (TAT) was prepared as described by T. L. Gresham and T. R. Steadman (19) and recrystallized from water. Ethylene glycol bis-(succinimidylsuccinate) (EGS) and 8-anilino-1-naphthalenesulfonic acid (ANS) were obtained from Sigma.

**Cross-Linking by TAT.** The solution containing 0.025 mM of UK114 or p14.5 in 0.05 M borate buffer pH 9.2 was incubated for 5 min at 30 °C, and then TAT was added to a concentration of 2.8 mM. The reaction mixture was incubated at 30 °C; samples were withdrawn after 5, 15, 30, 60, 120, 180, and 300 min, and the reaction was stopped by acidification to pH 5.0. The samples were analyzed by SDS-PAGE to identify cross-linked protein forms.

**SDS-PAGE.** SDS-PAGE was carried out on the Mighty Small electrophoresis unit (Hoefer Scientific Instruments, San Francisco, CA) according to the method of Laemmli (20). The acrylamide concentration used in the gel was 15%. Proteins were stained with Coomassie Brilliant Blue R-250 or silver.

**Kinetic Measurements.** Kinetics of TAT reaction with glycine amino groups were measured spectrophotometrically in a thermostated cell at 275 nm, under pseudo-first-order conditions. Five kinetic runs were carried out for each experiment. Pseudo-first-order rate constants were calculated with eq 1, using linear-regression program GraphPad:

$$k = \frac{1}{t} \ln \frac{A_0 - A_{\text{inf}}}{A_t - A_{\text{inf}}} \quad (1)$$

where  $A_0$  is the initial absorbance,  $A_t$  is the absorbance at the time  $t$ , and  $A_{\text{inf}}$  is the final absorbance, after completion of the reaction. Light absorbance of glycine at 275 nm is negligible.

**Size Exclusion Chromatography.** (a) *Nondenaturing Conditions.* Size exclusion chromatography was performed on Superdex200 HR 300×10 mm column

(Amersham Pharmacia, Sweden), equilibrated with 10mM potassium phosphate buffer, pH 7.0, 0.3 M NaCl using FPLC Akta-explorer 100 (Amersham Pharmacia, Sweden). Protein samples were applied, and isocratic elution was carried out at a flow rate of 0.5 mL/min.

(b) *Denaturing Conditions.* The column, as described above, was equilibrated with 10 mM potassium phosphate buffer, pH 7.0, 0.3 M NaCl, 7 M GdnHCl. Protein samples were incubated in 7 M GdnHCl for 24 h at ambient temperature and applied on the column, and isocratic elution was carried out at a flow rate of 0.5 mL/min.

**Separation of Heterotrimers by Anion Exchange Chromatography.** The mixture of 100 μL of UK114 solution (1 mg/mL) in 10 mM phosphate buffer pH 7.4 and 100 μL of p14.5 solution (1 mg/mL) in the same buffer and 200 μL of 3 M urea water solution was incubated for 2.5 h at 30 °C. Then the mixture was diluted to 2 mL with 10 mM glycine-NaOH buffer, pH 9.0, and chromatographed on Mono Q HR 5/5 in a gradient of 30 column volumes in the same buffer, containing 0.1 M NaCl at flow rate of 1 mL/min using FPLC Akta-explorer 100 (Amersham Pharmacia, Sweden). Collected peaks were analyzed using isoelectric focusing.

**Electrospray Ionization Mass Spectrometry.** The method was developed according to the published procedure (21).

(a) *Mild Conditions.* All samples prior to mass spectrometry were dialyzed against 0.1% acetic acid in water. The HP 1100 MSD (mass selective detector) was used for the acquisition of the electrospray ionization mass spectra. Mass spectra were in positive ion mode, over mass range 500–2900  $m/z$ . The samples (protein concentration 0.5 mg/mL) were delivered to the analyzer using a 30 mL/min flow of 1.0% acetic acid. The temperature of drying gas was 150 °C. Nitrogen was used for drying and nebulizing.

(b) *Denaturing Conditions.* All samples prior to mass spectrometry were purified by RP-HPLC using reversed phase column Hi-Pore RP-304 (250 × 4.6 mm, Bio-Rad); solvent A: 0.1% trifluoroacetic acid in water, solvent B: 0.1% trifluoroacetic acid in acetonitrile/water (90/10, v/v). The column was initially equilibrated with solvent A at flow rate of 1 mL/min. After the injection, the column was eluted with a 4 min linear gradient to 50% B followed by a 64 min linear gradient to 70% B and 65 min to 90% B. Chromatographic analysis was performed on a HP 1100 Series HPLC system. Collected peaks were lyophilized and dissolved in acetonitrile/water/acetic acid (49.5/49.5/1, v/v/v).

Mass spectra were in positive ion mode, over mass range 500–2900  $m/z$ . The samples (protein concentration 0.05 mg/mL) were delivered to the analyzer using a 50 mL/min flow of acetonitrile/water/acetic acid (49.5/49.5/1, v/v/v). The temperature of drying gas was 350 °C. Nitrogen was used for drying and nebulizing.

**Delipidation by Lipidex Chromatography.** Delipidation by Lipidex chromatography was carried out according to the method described by J. F. Glatz (22). Lipidex 1000 was washed free of methanol in a column by elution with 10 bed volumes of 10 mM potassium phosphate buffer (pH 7.4), containing 0.01% NaN<sub>3</sub>. The gel was transferred to a glass vial and stored at 4 °C as Lipidex-buffer suspension (1/1, v/v).

The lipid components in the protein samples were recovered by chromatography on a column (10'×60 mm) of Lipidex1000 equilibrated with 10 mM potassium

<sup>1</sup> Abbreviations: AEC, anion exchange chromatography; ANS, 8-anilino-1-naphthalenesulfonic acid; DMSO, dimethyl sulfoxide; ESI-MS, electrospray ionization mass spectrometry; GdnHCl, guanidine hydrochloride; I-FABP, intestinal fatty acid binding protein; RP-HPLC, reversed phase high performance liquid chromatography; SDS-PAGE, sodium dodecyl sulfate polyacrylamide gel electrophoresis; SEC, size exclusion chromatography; TAT, 1,3,5-triacryloyl-hexahydro-*s*-triazine; TNF-α, tumor necrosis factor.

phosphate buffer pH 7.4 at room temperature. All proteins were eluted in a void volume.

**Free Fatty Acid Binding Assay.** For the assay of fatty acid binding activity, protein samples (2 mM) were incubated in 1.5 mL polyethylene test tubes in 10 mM potassium phosphate buffer pH 7.4 with various concentrations of  $^3\text{H}$ -fatty acid. The final volume was 0.45 mL. After incubation for 10 min at 37 °C, the test tubes were cooled in ice water. Unbound fatty acid was removed from the solution by adding of 0.05 mL of ice cold Lipidex1000/water suspension, incubated for 10 min at 0 °C, and centrifuged for 2 min at 20000*g* and 4 °C. An aliquot of supernatant was assayed for radioactivity by liquid scintillation counting. Fatty acid binding was calculated from the amount of radioactivity present in the supernatant and was expressed as mol of fatty acid per mol of monomeric protein.

**ANS Binding Assay.** All fluorescence experiments were performed on a Perkin-Elmer Luminescence Spectrometer LS50B. For the ANS binding assay, protein samples (9.1  $\mu\text{M}$ ) in 2 mL 10 mM potassium phosphate buffer pH 7.4 were titrated with increasing ANS concentration. ANS emission spectra (excitation  $\lambda_{\text{max}}$  365 nm) were recorded in the range of 350–650 nm, slit widths 5 nm.

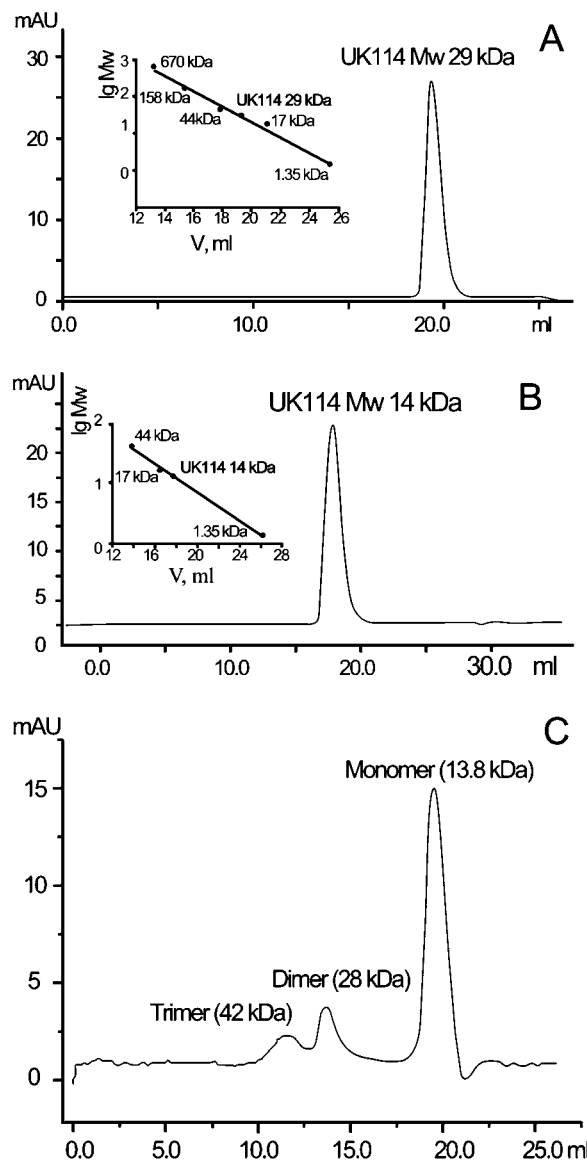
## RESULTS

**Size Exclusion Chromatography.** Size exclusion chromatography provides means by which the state of aggregation of proteins can be effectively determined, provided that the subunit–subunit interaction forces are sufficiently strong to withstand such a nonequilibrium analysis. As it is shown in Figure 1A, the UK114 protein behavior on Superdex200 was consistent with the molecular mass of 29 kDa. These experiments were performed at an initial protein concentration of  $\sim 70 \mu\text{M}$ . Reductions of protein concentration to 1.4  $\mu\text{M}$  did not affect the gel-filtration behavior of the protein, to indicate that the oligomeric state of the protein was stable through the range of the concentrations tested. The gel-filtration behavior of the p14.5 human analogue of UK114 was exactly the same as that of UK114.

The molecular mass of UK114 derived from the gene sequence has been reported to be 14166 Da (23), to suggest that UK114 may exist in a dimeric state under the experimental conditions described above. Indeed, when UK114 was subjected to gel-filtration using 6 M guanidine hydrochloride (Gdn·HCl) in a mobile phase, the elution volume was consistent with molecular weight of 14.0 kDa (Figure 1B), a number in good agreement with the expected molecular mass of monomeric subunit.

**Electrospray Ionization Mass Spectrometry.** Significant evidence has now been reported to suggest that proper adjustment of experimental conditions used in the performance of ESI-MS experiments is required to provide insight into oligomeric structure. Without such precisely defined conditions, quaternary structure can be easily disrupted by low pH, high organic solvent content, high temperature of drying gases, and high flow rate of mobile phase (24). When these disruptive forces are not controlled, only covalent protein interactions usually survive, and a precise molecular mass of the protein monomeric subunits is obtained. Quaternary structure of the protein, however, can be maintained throughout the course of analysis by careful adjustment of these disruptive factors, such that the molecular mass of the complex can be established.

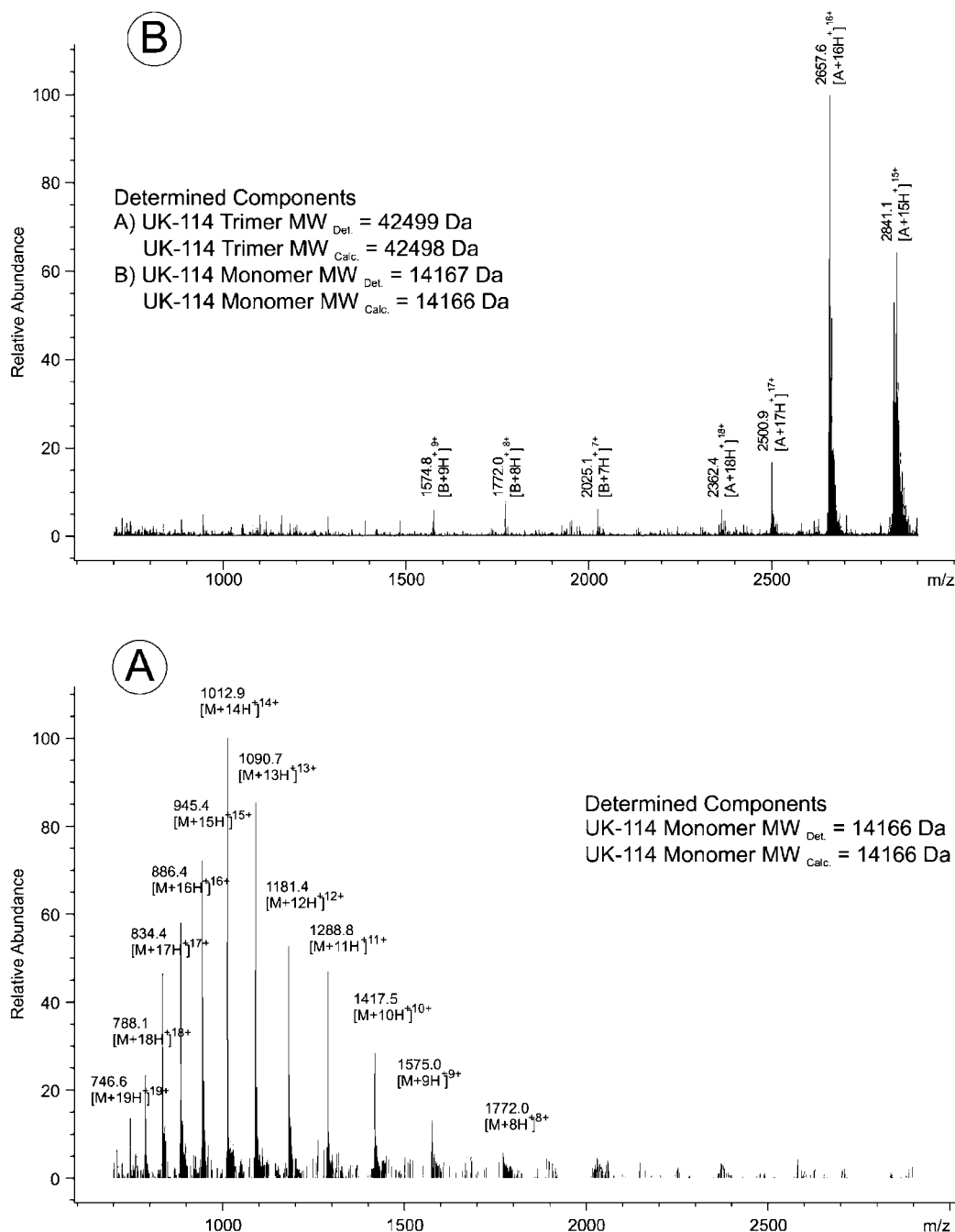
Initially, we subjected UK114 to ESI-MS analysis under denaturing conditions where disruption of oligo-



**Figure 1.** Size exclusion chromatography of UK114 on Superdex200 HR 300 $\times$ 10 mm using FPLC Akta-explorer100 (Amersham Pharmacia, Sweden). The column was equilibrated with 10 mM potassium phosphate buffer, pH 7.0, 0.3 M NaCl (A), buffer A also containing 6 M Gdn HCl (B) and buffer A with 0.1% SDS (C). UK114 samples of 200  $\mu\text{L}$  (1 mg/mL) in the A buffer (A), in the B buffer (B) and UK114 3 h cross-linked with TAT in 0.1% SDS (C) were applied and isocratic elution was carried out at flow rate of 0.5 mL/min.

meric state of the protein was expected. Denaturing ESI-MS conditions include RP-HPLC with high organic solvent concentration for sample preparation and rigorous ionization parameters (high temperature, high concentration of organic solvent in mobile phase, and high flow rate of mobile phase) for ESI-MS. The data (Figure 2A) demonstrated a typical ESI-MS spectrum of the protein, consisting of multiply charged  $[\text{M} + n\text{H}]^{n+}$  ions, with charges ranging from +8 to +19. The set of ions detected corresponded to the protein average mass of  $14166 \pm 1$  (mean  $\pm$  SD) Da. This value was in excellent agreement with the theoretically calculated mass of 14.166 kDa for the monomeric form of UK114. Using denaturing conditions, i.e., RP-HPLC for sample preparation and rigorous conditions for ESI-MS ionization, it is not clear enough which of the factors are mainly responsible for destruction of trimeric structure.





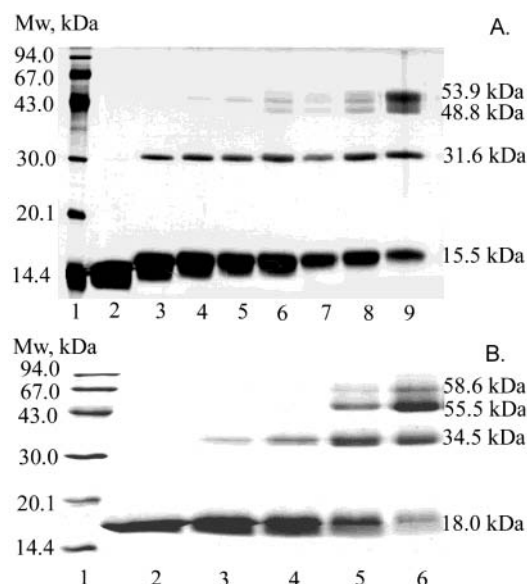
**Figure 2.** Mass spectrum of UK114 under denaturing (A) and mild conditions (B).

To preserve noncovalent protein complexes, we used mild sample preparation conditions, i.e., dialysis against 0.1% acetic acid in water, and milder ionization parameters for ESI-MS. Organic solvent was not used in the mobile phase for ESI-MS; lower temperature and lower flow rate of mobile phase were applied. After using mild sample preparation conditions together with mild ionization parameters, a significant change in the overall spectrum was observed (Figure 2B). Two protein components were detected on the spectrum, a major component of  $42499 \pm 3$  kDa which corresponded with the trimeric form of UK114, and a minor component of  $14166 \pm 1$  kDa, which was clearly reflective of monomeric form of the protein. At the same time no dimeric form was detected.

**Chemical Cross-Linking.** The formation of protein oligomers in solution is commonly investigated by cross-linking studies in which closely associated subunits are

cross-linked in such a manner that the so-formed quaternary structure can be subsequently isolated and analyzed. Two cross-linking agents, 1,3,5-triacryloyl-hexahydro-*s*-triazine (TAT) (25, 26) and ethylene glycol bis(succinimidylsuccinate) (EGS) (27), were therefore used to probe the quaternary structure of UK114.

TAT is a trifunctional chemical cross-linking agent, previously demonstrated to be extremely stable, simple and convenient to use in the generation of cross-linking patterns, which are characteristic of the native structure of the proteins (25, 26, 28). We have previously described its use in concentrations of 4.5–30-fold molar excess of TAT active groups over the concentrations of amino groups in the protein, defining the oligomeric state of such well-characterized monomeric, dimeric, or trimeric proteins, such as human growth hormone, interferon- $\gamma$ , and tumor necrosis factor alpha (TNF- $\alpha$ ), respectively (25, 28).



**Figure 3.** SDS-PAGE (15%) of UK114 (A) and TNF- $\alpha$  (B) cross-linked by TAT. A. Lane 1, protein markers; lane 2, unmodified UK114; lane 3–9, samples taken at 5, 15, 30, 60, 120, 180, and 300 min. B. Lane 1, protein markers; lane 2, unmodified TNF- $\alpha$ ; lane 3–6, samples taken at 30, 60, 120, and 300 min.

Every attempt was made to ensure that the experimental conditions, adjusted to specific characteristics of UK114, exclusively promoted the cross-linking of true molecular contacts rather than accidental protein molecular collisions. First, UK114 was incubated with TAT at a molar ratio of 30:1 of TAT acrylic groups:UK114 amino groups, at pH 9.2. Next, the aliquots of the reaction mixture were withdrawn at increasing time intervals and subjected to denaturing SDS–PAGE analysis. The profile obtained by applying this experimental approach to the well-known trimeric protein, tumor necrosis factor  $\alpha$ , is indicated in Figure 3B. Characteristically, the TAT interaction with the trimeric protein resulted in an early intermediate of dimeric form. The presence of cross-linked dimers on PAGE gels does not mean that they actually exist in the solution. Cross-linked dimers may be not yet completely cross-linked trimers. If trimer is the main form of a protein in solution, cross-linked trimers become dominant on PAGE at the completion of cross-linking process, as is shown on the Figure 3 for TNF and UK114. Then trimeric structures appeared gradually, and no higher oligomers were detected after long time incubation. A detailed explanation of the kinetics of the cross-linking profile of TNF- $\alpha$  has previously been reported (26, 28).

**Table 1.** Detected Species of TAT-Cross-Linked UK114

ESI-MS experimental data mol mass, Da <sup>a</sup>	suggested protein structure	calcd mol mass, Da	percent from the total amount of identified (UK114) <sub>T</sub> +nTAT
Monomer			
14914	+3 TAT	14914	9.4
15161	+4 TAT	15163	16.2
15410	+5 TAT	15412	16.4
15661	+6 TAT	15661	16.7
15909	+7 TAT	15910	15.9
Dimer			
30081	+7 TAT	30077	4.8
30850	+10 TAT	30850	3.9
31843	+14 TAT	31820	6.1
Trimer			
45988	+14 TAT	45987	5.6
46244	+15 TAT	46236	5.0

<sup>a</sup> UK114 cross-linked with TAT pH 9.2, 3 h at 30 °C.

As it is demonstrated in Figure 3A, the cross-linking profile obtained with UK114 was the same as that of TNF- $\alpha$ . Two predominant species with apparent molecular mass in a range of 48–54 kDa were observed as the ultimate products of cross-linking reaction. It has previously been demonstrated that these two molecular species resemble two different steric isoforms of the cross-linked trimer, the linear and ring-shape isoforms (29). Therefore, the similarity of cross-linking profiles of UK114 with those of the trimeric TNF- $\alpha$  protein was consistent with the trimeric structure of UK114 in solution.

Since the most favorable TAT cross-linking conditions included a pH of 9.2, we questioned whether the reaction kinetics and the end product profile were similar under physiological conditions. We reproduced the cross-linking reaction results using ethylene glycol bis(succinimidylsuccinate) at pH 7.2.

To further support the observation that UK114 formed trimers in solution, we subjected the products of the TAT 3 h (Figure 3A, lane 8) cross-linking reaction to more detailed characterization. Size exclusion chromatography under mild denaturing conditions (in the presence of 0.1% SDS) revealed that the 3 h reaction mixture was composed of three principal components, with their molecular masses being consistent with monomeric, dimeric, and trimeric forms of UK114 (Figure 1C). The behavior of UK114 in the presence of SDS is no more exceptional: experimental molecular mass of the cross-linked trimer is near the calculated one (42 and 43.2 kDa, respectively).

Extending this analysis of the TAT reaction products, we used ESI-MS. Main components of a complex mixture of monomeric, dimeric, and trimeric structures of UK114 3 h cross-linked with TAT (Figure 3A, lane 8) were identified. They are listed in Table 1. Up to seven TAT moieties were attached to the monomeric UK114 form, a number in good agreement with the fact that the UK114 monomer contains seven lysine residues in polypeptide chain. Two principal forms of trimeric UK114 were confirmed in the reaction mixture, with 14 and 15 covalently attached TAT moieties, respectively.

All the methods used for probing the quaternary structure led us to conclude that two mammalian proteins from the YjgF/YER057c/UK114 family UK114 and p14.5 exist as homotrimers in solution, like their bacterial homologue HI0719 (18).

**The Interaction between Subunits in the Trimeric Structure.** Having established the TAT cross-linking technique as a reliable tool for probing quaternary structure of UK114, we addressed the issue of the nature of interaction between monomeric subunits in the tri-

**Table 2. Pseudo-First-Order Rate Constants for the Reaction of TAT with Glycine Amino Group in KCl Solution<sup>a</sup>**

concentration of KCl, M	$k \times 10^4, \text{s}^{-1}$
0	$5.02 \pm 0.06^b$
1	$4.62 \pm 0.08$
2	$4.75 \pm 0.07$
3	$4.85 \pm 0.05$

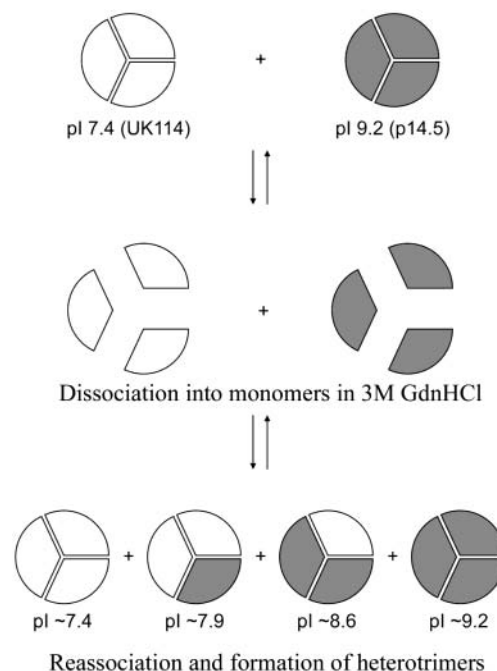
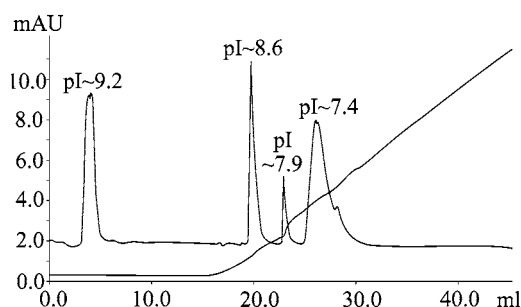
<sup>a</sup> Initial concentrations: TAT,  $6.9 \times 10^{-4}$  M; glycine, 0.07 M; 30 °C and pH 9.0. <sup>b</sup> Standard deviations are given.

meric structure. It was expected that if electrostatic interactions were predominant in forming trimers, then the disruption of such interactions by increasing ionic strength would preclude the formation of trimers in the cross-linking reaction. We added KCl to the cross-linking reaction mixture and monitored UK114 trimer formation by SDS–PAGE analysis. Our results indicated that the elevation of KCl concentration to 0.5 M considerably reduced the formation of the trimeric structure. The further elevation of salt concentration to 2.5 M completely abolishes recovery of the trimeric form.

To eliminate the possibility that the inhibitory effect of high salt concentration on the formation of the UK114 trimeric structure was due to the inhibition of the TAT reaction with amino groups, we performed a study where kinetic parameters of the TAT reaction with amino group of model compound, glycine, were measured. As shown in Table 2, pseudo-first-order rate constant of the reaction remained unchanged through the range of KCl concentrations from 0 to 3 M, to suggest that we could exclude the possibility that observed inhibiting effect of elevated salt concentrations on the formation of the trimeric structure of UK114 was due to the inability of TAT to react under these conditions.

To explore the possible contribution of hydrophobic interactions in UK114 trimer formation, we added dimethyl sulfoxide (DMSO) to the cross-linking reaction mixture and monitored trimer formation by SDS–PAGE analysis. This chaotropic reagent, when present in concentrations of up to 10%, is known to disrupt hydrophobic interactions of proteins (30). DMSO in concentrations up to 15% had no effect on trimerization, to suggest that the role of hydrophobic interactions in the association of monomeric subunits was insignificant.

**Heterotrimer Formation.** Alignment of the sequence of UK114 with that of p14.5 revealed a striking 86% similarity in primary structure. The cross-linking experiments described above, then repeated using p14.5, generated results very similar to those described for UK114. It was therefore interesting to explore the possibility of creating chimeric structures in vitro. To do so, we exploited the fact that the two proteins, despite significant overall similarity, had very different isoelectric points, pI 7.4 and pI 9.2, for UK114 and p14.5, respectively. We also exploited the fact that we could reversibly dissociate UK114 into subunits and reassociate the trimer structure afterward. If one mixed the two proteins, then subjected the mixture to mild denaturation, to cause the break down of trimers into monomers, and then removed denaturant, monomeric subunits would reassociate into the trimers. Under such conditions, four species of trimers theoretically should form (Figure 4). Two species would resemble the original UK114 and p14.5 trimers, while two would be chimeric structures with monomer ratios of 1:2 and 2:1, UK114 and p14.5, respectively. All four trimeric species would be characterized by different pI values, to allow their separation in a properly selected chromatographic system.

**Figure 4.** Hypothetical scheme for the formation of hetero-trimers of UK114 and p14.5 subunits.**Figure 5.** The chromatographic separation of the dissociated–associated mixture of UK114 and p14.5. Solution of UK114 and p14.5 (1 mg/mL of each) in 3 M Gdn–HCl was incubated for 2.5 h at 30 °C and diluted with 3 volumes of 10 mM glycine–NaOH, pH 9.0. Samples of reaction mixture (2 mL) were chromatographed on Mono Q HR5/5 in a gradient of 30 column volumes in the same buffer, containing 0.1 M NaCl at flow rate of 1 mL/min using FPLC Akta-explorer100 (Amersham Pharmacia, Sweden).

As indicated in Figure 5, heterotrimer formation was achieved using the scheme described above, and the heterotrimers formed were separable. The nature of all the species formed was confirmed by isoelectrofocusing analysis.

**Free Fatty Acid Binding.** PSP, a protein from rat liver, also a homologue of both UK114 and p14.5, is known as a fatty acid binding protein (11). Because of the significant homologies between these proteins, UK114 and p14.5 may also bind free fatty acids, the possibility we investigated. The principle of the method we exploited involved the incubation of the protein with varying amounts of <sup>3</sup>H-labeled fatty acid, removal of unbound free fatty acid on Lipidex1000, and measurement of the remaining labeled complex. Two known proteins were used for comparison: I-FABP, which has previously been demonstrated to stoichiometrically bind 1 mol of fatty acid per mol of protein (31, 32), and TNF- $\alpha$ , a cytokine, whose biological function is apparently not related to fatty acid metabolism (33, 34) and which therefore served as a negative control. The data generated for binding of oleic acid are presented in Table 3. The same results were



**Table 3. Binding Activity of  $^3\text{H}$ -Labeled Oleic Acid**

protein	$B_{\text{max}}$ , mol/mol monomeric protein
I-FABP	$1.10 \pm 0.20$
UK114	$0.90 \pm 0.15$
p14.5	$0.70 \pm 0.17$
TNF- $\alpha$	$0.09 \pm 0.04$

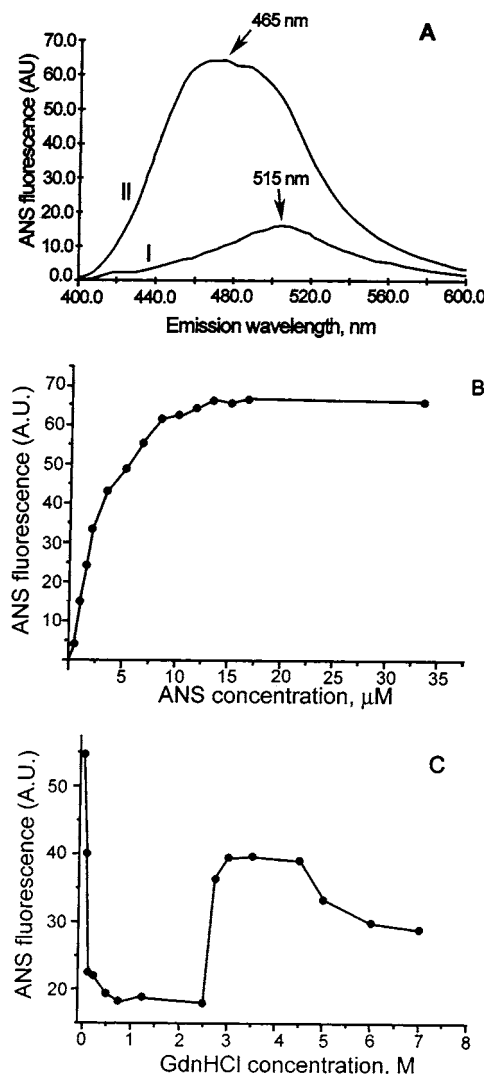
obtained in palmitic acid binding experiments. Both fatty acids bind to UK114 (or p14.5) in a saturable manner. This indicates the specific nature of the binding. The stoichiometry of both complexes was very close 1:1 (mol fatty acid per mol monomer protein). As it was expected, the protein known to bind fatty acids specifically (I-FABP) manifested 1:1 stoichiometric binding activity, while the binding activity of TNF- $\alpha$ , the negative control, barely exceeded the background level.

These results suggest that UK114 maintains three fatty acid binding sites per trimeric molecule. Further, the apparent dissociation constant of the complex UK114-fatty acid decreased while increasing the saturation of the protein with ligand, to suggest cooperative character of the fatty acid binding.

To exclude the possibility that the free fatty acid binding observed was a random event, we addressed the correlation between structural integrity of the protein and its binding ability. Specifically we evaluated binding at various stages of thermal inactivation. Samples of UK114 were incubated at 37, 60, and 80 °C for 20 min, and at 100 °C for 1 min, and their ability to bind fatty acid was measured as described above. The results of this study revealed that the UK114 gradually lost binding activity with thermal inactivation, starting from 60 °C with only minor activity remaining after heating for 1 min at 100 °C. These data confirmed the specific nature of the binding observed.

**ANS Binding.** Stoichiometric binding activity of fatty acid suggests the presence of three binding sites per trimeric protein. We found that UK114 and p14.5 are able to bind the hydrophobic fluorescent dye ANS in their native state. The fluorescent probe ANS is traditionally used to detect molten globules, i.e. partly folded proteins that accumulate under mild conditions (35). ANS fluorescence is sensitive to the polarity of its microenvironment; upon binding to the apolar surfaces, its emission maximum is shifted to shorter wavelengths and the emission intensity is enhanced. ANS is believed to bind to molten globules due to the presence of solvent-exposed hydrophobic patches, which are a particular characteristic of this protein state (36). Certain proteins also bind ANS in the native state, however, provided this conformation displays exposed hydrophobic sites (37). Fluorescence emission spectra of ANS in the presence or absence of UK114 (or p14.5) are shown in Figure 6A. In water, ANS fluoresce is negligible and exhibits a maximum emission wavelength ( $\lambda_{\text{max}}$ ) of  $\sim 515$  nm. In the presence of UK114 (or p14.5) under native conditions (pH 7.4), ANS fluorescence displays a pronounced increase in intensity with a concomitant shift of  $\lambda_{\text{max}}$  to 465 nm, both of which indicate transfer of ANS to a less polar environment. These data show that UK114 and p14.5 bind ANS in the native state.

The affinity of the interaction between ANS and UK114 (or p14.5) was examined by titration of UK114 (or p14.5) with ANS while following the ANS emission at 465 nm. The resulting binding curves, displayed in Figure 6B, show that ANS binds to UK114 (or p14.5) in a saturable manner.  $K_d$  values for UK114 and p14.5 are 2.2 and 2.4  $\mu\text{M}$ , respectively. These experiments yield a binding stoichiometry of  $1.1 \pm 0.2$  mol ANS/mol mono-



**Figure 6.** A. ANS binding to native UK114. Fluorescence of 9.1  $\mu\text{M}$  ANS in the absence and presence of 9.1  $\mu\text{M}$  UK114 at 25 °C in 10 mM potassium phosphate buffer pH 7.4. ANS fluorescence is a very weak exhibiting a  $\lambda_{\text{max}}$  of  $\sim 515$  nm (I). Upon addition of UK114 the fluorescence of ANS increase with a concomitant shift of  $\lambda_{\text{max}}$  to 465 nm (II). ANS was excited at 365 nm. B. Affinity of ANS to UK114 interaction. Titration of 9.1  $\mu\text{M}$  UK114 with ANS in 10 mM potassium phosphate buffer pH 7.4. ANS was excited at 365 nm. C. ANS binding to UK114 with increasing concentration of Gdn-HCl. 9.1  $\mu\text{M}$  UK114 was preincubated 5h at 25 °C in 10 mM potassium phosphate buffer pH 7.4 with increasing Gdn-HCl concentration. ANS binding was monitored by 365 nm excitation and 465 nm emission.

meric protein and support the presumption that proteins UK114 and p14.5 exhibit three ligand binding sites per trimeric molecule.

To prove the importance of quaternary structure for ligand binding, we investigated the ANS binding under denaturation of UK114 with GdnHCl. The profile of ANS emission intensity with increasing GdnHCl concentration shows two maxima (Figure 6C). The ANS fluorescence intensity decreases and reaches minimum at 0.25 M GdnHCl. It may be explained by disruption of trimeric structure and intersubunit binding sites. Further increase of emission intensity at GdnHCl concentration above 2.75 M is related with unfolding of UK114 to molten globule, when hydrophobic surfaces of protein are exposed to a greater extent compared with a native state.

To confirm disruption of quaternary structure we performed size-exclusion chromatography of UK114 in

the presence of GdnHCl. UK114 was incubated in various concentrations of GdnHCl and applied to a TSK G2000SW FPLC size-exclusion column equilibrated with buffer containing an identical concentration of GdnHCl. In the absence of GdnHCl UK114 eluted as a single peak, corresponding to native trimeric protein, increasing of GdnHCl concentration up to 0.25 M UK114 also eluted as a single peak, but with elution volume, corresponding with monomeric form. This transition from trimer to monomer occurred having the same GdnHCl concentration as the losing of specific binding of ANS (Figure 6C). With further increase of GdnHCl concentration, the peak, corresponding to monomeric UK114, gradually shifted to earlier elution times, suggesting that monomer of UK114 was unfolded and a molecule with increased apparent volume produced. The midpoint of the unfolding curve was 2.5 M.

## DISCUSSION

The highly conserved protein family YER057c/YIL051c/YjgF is comprised of ~30 homologues exhibiting varying degrees of sequence homology from 32 to 93%. Some of them have been identified as proteins soluble in strong acids, but most sequences from this protein's group were hypothetical and identified by genome projects. Despite the sequence conservation through evolution and the high degree of homology between members of the YER057c/YIL051c/YjgF family, no common biological function has been allocated to it yet. With the mounting evidence as to the potentially high clinical value of the biotherapeutics being developed on the basis of proteins of this family (6), the deciphering of biochemical mechanisms underlying their clinical actions becomes increasingly urgent.

In this paper we describe the oligomeric structures and ligand binding properties of two recombinant DNA-derived members of the YER057c/YIL051c/YjgF family: perchloric acid-soluble protein from goat liver, UK114, and its analogue from human monocytes, p14.5, proteins that manifest 86% sequence similarity.

Indications as to biological function of these proteins could potentially be derived from the details of their structural organization. However, in the case of the YER057c/YIL051c/YjgF family evidence on oligomeric state in solution has supported conclusions of monomeric to trimeric forms. Gel-filtration data used to demonstrate the native state of the protein yielded results interpreted to be consistent with the dimeric form (9, 12). Indeed, we also initially produced gel-filtration data indicative of the dimeric form for both UK114 and p14.5 in solution. However, we extended our study of the oligomeric state of these proteins by applying a carefully designed cross-linking technique. The formation of UK114 (and p14.5) trimers was observed under a variety of conditions in water solution. Direct evidence of trimeric structure was obtained by using nondisrupting ESI-MS analysis. In fact, our results as well as crystallographic data (16) indicate that these proteins are trimeric under physiological conditions.

The apparent conflict between cross-linking, ESI-MS and gel-filtration data may be explained by the UK114 (and p14.5) protein assuming an extremely compact structure in solution, such that effective hydrodynamic radii of the proteins were substantially smaller than the radii of reference proteins used for gel-filtration column calibration. Support of this explanation has now been provided by X-ray study data (16) of the crystal form of UK114, which revealed the dimensions of highly sym-

metric homotrimeric UK114 of  $\sim 48 \times 45 \times 43$  Å. The apparently more compact spatial organization of UK114 could provide a clue into the misleading gel-filtrational behavior of this protein, compared with conventional reference proteins.

To delineate the character of the interaction forces, which keep separate subunits in trimeric form, we exploited cross-linking methodology, where reaction conditions were altered to limit either hydrophobic or electrostatic protein interactions. The overall electrostatic interaction was demonstrated to be the major factor in the trimerization of the protein. Information on monomer: monomer surface interactions retrieved from recent crystal data (16) was consistent with our observation. The UK114 molecule possesses an extensive network of hydrogen bonds and electrostatic interactions throughout the subunits contact surface. The number of complementary interactions between oppositely charged ionizable groups on the contact surfaces between monomers was sufficient to confirm that electrostatic interaction played the major role in the stabilization of UK114 trimer. The critical putative interaction points identified from the 3-D structure now provide a basis for future site-specific mutagenesis studies directed at further biochemical confirmation of the role of these putative contacts in maintaining trimeric organization of the protein.

Further, the high degree of sequence similarity between UK114 and p14.5, together with the proven trimeric structure of the two proteins, led us to hypothesize that there could be a high similarity in tertiary structure such that the monomeric subunits from one protein could be interchangeable with the monomeric subunits from the other in their respective trimeric states. We successfully demonstrated that such a possibility could be implemented *in vitro* by exploring the finding that each of the proteins could be dissociated into monomers under mild conditions and then reassembled into functional trimers by removing the denaturing agent. By mixing the two original proteins, dissociating them into monomers, and later reassociating them, we produced chimeric trimers containing two subunits from one protein and one subunit from another. The heterotrimers formed were sufficiently stable to withstand anionic exchange chromatographic separation, and isoelectric focusing in a way analogous to that of the original homotrimers, to indicate an extremely close if not identical spatial organization of monomers in these two proteins. We plan to explore this observation further in future eukaryote genetic knock-out models (38).

Stable trimeric organization could potentially play an important role in the biological function of the protein, specifically its ability to bind hydrophobic ligands, such as free fatty acids. We confirmed that these two proteins bind fatty acid with  $K_d \sim 2.0$   $\mu$ M, forming one to one stoichiometric complex (mol of fatty acid per mol of monomeric protein), a finding similar to that of PSP from rat (11). The ability of these proteins to bind hydrophobic ligands in their native state was also demonstrated with fluorescent dye ANS. The binding isotherm is rectangular hyperbolic and reaches saturation, suggesting that binding is specific, i.e. a well-defined number of binding sites exist. Indeed, titrating of UK114 (or p14.5) with ANS at concentrations well above  $K_d$  indicates a 1:1 (mol of dye per mol of monomeric protein) binding stoichiometry. Stoichiometric ligand binding activities suggest the presence of three binding sites per trimeric protein. Indeed, trimeric UK114 in a crystalline state contains three hydrophobic solvent-exposed cavities, created between

interacting subunits (16), as it was shown previously for some members of the YER057c/YIL051c/YjgF family (14, 15, 18).

It was found that oleic acid displaces ANS bound to UK114, i.e. the two substances compete for the same binding sites. We also demonstrated that ligand binding activity exhibits only trimeric protein. UK114 lost ANS binding ability when trimer was disrupted to monomer under unfolding, induced by GdnHCl.

In conclusion, these findings may have important biological implications. Despite the mentioned above multifunctionality of the proteins from YER057c/YIL051c/YjgF family, high similarity in quaternary structures suggest that these proteins use the same biochemical way for the manifestation of their biological function. Trimeric organization of the two proteins of the YER057c/YIL051c/YjgF family has been shown to be a critical structural feature in ligand binding, one potential mode of action of these proteins. The structural elements, which direct formation of the trimeric state of the protein, are apparently preserved throughout the evolutionary tree to support a correlation between structural organization and function of these proteins. The data presented therefore could target further studies of the structure–function relationship of these proteins, to elucidate their respective mechanisms of action.

#### ACKNOWLEDGMENT

We thank prof. G. Dienys for helpful comments and discussion, Barbara Richmond-Smith for critical reading of the manuscript and L. Noreika for technical assistance. This work was supported by Lithuanian State Science and Studies Foundation, grant no. G-053.

#### LITERATURE CITED

- (1) Bartorelli, A., Biancardi, C., Cavalca, V., Ferrara, R., Botta, M., Arzani, C., Colombo, I., Berra, B., Ceciliani, F., Ronchi, S., and Bailo, M. (1996) Purification and Partial Characterization of Proteins Present in a Perchloric Acid Extract of Goat Liver. *J. Tumor Marker Oncol.* 11, 57–61.
- (2) Ceciliani, F., Biancardi, C., Cavalca, V., Ferrara, R., Botta, M., Bailo, M., Arzani, C., Berra, B., Ronchi, S., and Bartorelli, A. (1996) Structural Characterization of the Small Molecular Weight Proteins Present in UK101. *J. Tumor Marker Oncol.* 11, 63–66.
- (3) Bussolati, G., Guena, M., Bussolati, B., Millesimo, M., Botta, M., and Bartorelli, A. (1997) Cytolytic and tumor inhibitory antibodies against UK114 protein in the sera of cancer patients. *Int. J. Oncol.* 10, 779–798.
- (4) Bartorelli, A., Berra, B., Ronchi, S., Biancardi, C., Cavalca, V., Bailo, M., Mor, C., Ferrara, R., Botta, M., Arzani, C., and Clemente, C. (1994) Immunocytochemical Reactivity of Mamalian Liver Antigen (UK101) in Human Tumors and non Neoplastic Tissues. *J. Tumor Marker Oncol.* 9, 37–47.
- (5) Bartorelli, A., Bussolati, B., Millesimo, M., Gugliotta, P., and Bussolati, G. (1996) Antibody – dependent cytotoxic activity on human cancer cells expressing UK114 tumor membrane antigen. *Int. J. Oncol.* 8, 543–548.
- (6) Mor, C., Garibaldi, A., Bissi, O., Concas Benevelli, D., Di Mattia, D., Gajani, M. R., Gilardoni, E., Liverani, A., Mancini, S., Santi, C., and Bartorelli, A. (1997) On the compassionate use of UK101 in metastatic cancer. *J. Tumor Marker Oncol.* 12, 29–37.
- (7) Melloni, E., Michetti, M., Salamino, F., and Pontremoli, S. (1998) Molecular and functional properties of a calpain activator protein specific for  $\mu$  – isoforms. *J. Biol. Chem.* 273, 12827–12831.
- (8) Melloni, E., Averna, M., Salamino, F., Sparatore, B., Minafra, R., and Pontremoli, S. (2000) Acyl – CoA – binding protein is a potent m – Calpain activator. *J. Biol. Chem.* 275, 82–86.
- (9) Oka, T., Tsuji, H., Noda, C., Sakai, K., Hong, Y., Suzuki, I., Munoz, S., and Natori, Y. (1995) Isolation and Characterization of a Novel Perchloric Acid –soluble Protein Inhibiting Cell-free Protein synthesis. *J. Biol. Chem.* 270, 30060–30067.
- (10) Morishita, R., Kawagoshi, A., Sawasaki, T., Madin, K., Ogasawara, T., Oka, T., and Endo, Y. (1999) Ribonuclease Activity of Rat Liver Perchloric Acid-Soluble Protein, a Potent Inhibitor of Protein Synthesis. *J. Biol. Chem.* 274, 20688–20692.
- (11) Sasagawa, T., Oka, T., Tokumura, A., Nishimoto, Y., Munoz, S., Kuwahata, M., Okita, M., Tsuji, H., and Natori, Y. (1999) Analysis of the fatty acid components in a perchloric acid – soluble protein. *Biochim. Biophys. Acta* 1437, 317–324.
- (12) Schmiedeknecht, G., Kerkhoff, C., Orso, E., Aslanidis, C., Nagy, G. M., Knuechel, R., and Schmit, G. (1996) Isolation and characterization of 14.5 – kDa trichloroacetic – acid – soluble translational inhibitor protein from human monocytes that is upregulated upon cellular differentiation. *Eur. J. Biochem.* 242, 339–351.
- (13) Samuel, S. J., Tzung, S. P., and Cohen, S. A. (1997) Hrp12, a novel heat- responsive, tissue- specific, phosphorylated protein isolated from mouse liver. *Hepatology* 25, 1213–1222.
- (14) Sinha, S., Rappu, P., Lange, S. C., Mantsala, P., Zalkin, H., and Smith, J. L. (1999) Crystal structure of *Bacillus subtilis*, a purine regulatory protein and member of the highly conserved YjgF family. *Proc. Natl. Acad. Sci.* 96, 13074–13079.
- (15) Volz, K. (1999) A test case for structure – based functional assignment: The 1.2Å crystal structure of the yjgF gene product from *Escherichia coli*. *Protein Sci.* 8, 2428–2437.
- (16) Deriu, D., Briand, C., Mistiniene, E., Naktinis, V., and Gruetter, M. G. (2003) Crystal structure and oligomeric state of the mammalian tumor associated antigen UK114. *Acta Crystallogr. D Biol. Crystallogr.* 59 (Pt 9), 1676–8.
- (17) Carugo, K. D., Saraste, M., and Oka, T. (1999) Crystalization and preliminary X – ray diffraction studies of a perchloric acid soluble protein (PSP) from rat liver. *Acta Crystallogr. D Biol. Crystallogr.* 55, 667–668.
- (18) Parsons, L., Bonander, N., Eisenstein, E., Gilson, M., Kairys, V., and Orban, J. (2003) Solution Structure and Functional Ligand Screening of HI0719, a Highly Conserved Protein from Bacteria to Humans in the YjgF/YER057c/UK114 Family. *Biochemistry* 42, 80–89.
- (19) Gresham, T. L., and Steadman, T. R. (1949) Triazines from formaldehyde and nitriles. *J. Am. Chem. Soc.* 71, 1872–1873.
- (20) Laemmli, U. K. (1970) Laemmli cleavage of structural proteins during the assembly of the head of bacteriophage T4. *Nature* 227, 680–685.
- (21) Konerman, L., Collings, B. A., and Douglas, D. J. (1997) Cytochrome c Folding Kinetics Studied by Time-Resolved Electrospray Ionization Mass Spectrometry. *Biochemistry* 36, 5554–5559.
- (22) Glatz, J. F. C., and Veerkamp, J. H. (1983) A radiochemical procedure for the assay of fatty acid binding by proteins. *Anal. Biochem.* 1, 89–95.
- (23) Colombo, I., Ceciliani, F., Ronchi, S., Bartorelli, A., and Berra, B. (1998) cDNA cloning and *Escherichia coli* expression of UK114 tumor antigen. *Biochim. Biophys. Acta* 1442, 49–59.
- (24) Pramanik, B. N., Bartner, P. L., Mirza, U. A., Liu, Y.-H., and Ganguly, A. K. (1998) Electrospray Ionization Mass Spectrometry for the Study of Noncovalent Complexes: an Emerging Technology. *J. Mass Spectrom.* 33, 911–920.
- (25) Dienys, G., Sereikaite, J., Gavenas, G., Kvederas, R., and Bumelis, V. A. (1998) Cross-linking of protein subunits by 1,3,5-triacryloyl-hexahydro-s-triazine. *Bioconjugate Chem.* 9, 744–748.
- (26) Dienys, G., Sereikaite, J., Lukša, V., Jarutienė, O., Mištiniene, E., and Bumelis, V. A. (2000) Dimerization of human growth hormone in the presence of metal ions. *Bioconjugate Chem.* 11, 646–651.
- (27) Loster, K., and Josic, D. (1997) Analysis of protein aggregates by combination of cross-linking reactions and chromatographic separations. *J. Chromatogr. B.* 699, 439–461.



- (28) Kvederas, R., Mištinienė, E., Sereikaitė, J., Lukša, V., Dienys, G., and Bumelis, V. A. (2000) Association of tumor necrosis factor alpha in water solution. *Biologija* 2, 253–256.
- (29) Horiguchi, T., Miwa, Y., and Shigesada, K. (1997) The quaternary geometry of transcription termination factor rho: assignment by chemical cross – linking. *J. Mol. Biol.* 269, 514–528.
- (30) Fountoulakis, M., Juranville, J. F., Maris, A., Ozmen, L., and Garotta, G. (1990) One Interferon  $\gamma$  Receptor Binds One Interferon  $\gamma$  Dimer. *J. Biol. Chem.* 15, 19758–19767.
- (31) Nemezc, G., Hubbell, T., Jefferson, J. R., Lowe, J. B., and Schroeder, F. (1991) Interaction of fatty acids with recombinant rat intestinal and liver fatty acid –binding proteins. *Arch. Biochem. Biophys.* 1, 300–309.
- (32) Kirk, W. R., Kurian, E., and Prendergast, F. G. (1996) Characterization of the sources of protein–ligand affinity: 1-sulfonato-8-(1') anolinonaphthalene binding to intestinal fatty acid binding protein. *Biophys. J.* 1, 69–83.
- (33) Aggarwal, B. B., Kohr, W. J., Hass, P. E., Moffat, B., Spencer, S. A., Henzel, W. J., Bringman, T. S., Nedwin, G. E., Goeddel, D. V., and Harkins, R. N. (1985) Human Tumor Necrosis Factor. *J. Biol. Chem.* 25, 2345–2354.
- (34) Creasey, A. A., Doyle, L. V., Reynolds, T., Jung, T., Lin, L. S., and Vitt, C. R. (1987) Biological effects of Recombinant Human Tumor Necrosis factor and Its Novel Muteins on Tumor and Normal Cell Lines. *Cancer Res.* 47, 145–149.
- (35) Reddy, G. B., Srinivas, V. R., Ahmad, N., and Surolia, A. (1999) Molten globule-like state of peanut lectin monomer retains its carbohydrate specificity. Implications in protein folding and legume lectin oligomerization. *J. Biol. Chem.* 274, 4500–3.
- (36) Matulis, D., Baumann, C. G., Bloomfield, V. A., and Lovrien, R. E. (1999) 1-anilino-8-naphthalene sulfonate as a protein conformational tightening agent. *Biopolymers* 49, 451–8.
- (37) Mogensen, J. E., Wimmer, R., Larsen, J. N., Spangfort, M. D., and Otzen, D. E. (2002) The major birch allergen, Bet v 1, shows affinity for a broad spectrum of physiological ligands. *J. Biol. Chem.* 277, 23684–23692.
- (38) Gedvilaite, A., Sasnauskas, K., and Naktinis, V. (2001) Functional complementation of the yeast MMD1 gene mutation by the goat UK114 cDNA. Presented at the XXth International Conference on Yeast Genetics and Molecular Biology, Prague, Aug 26–31, 2001, abstract 07–11.

BC0341066

# Synthesis of a New Heterobifunctional Linker, *N*-[4-(Aminooxy)butyl]maleimide, for Facile Access to a Thiol-Reactive $^{18}\text{F}$ -Labeling Agent

Tatsushi Toyokuni,\* Joseph C. Walsh, Alan Dominguez, Michael E. Phelps, Jorge R. Barrio, Sanjiv S. Gambhir, and Nagichettiar Satyamurthy

Crump Institute for Molecular Imaging, Department of Molecular & Medical Pharmacology, David Geffen School of Medicine at UCLA, Los Angeles, California 90095-1770. Received June 25, 2003; Revised Manuscript Received August 25, 2003

A new heterobifunctional linker containing an aldehyde-reactive aminooxy group and a thiol-reactive maleimide group, namely *N*-[4-(aminooxy)butyl]maleimide, was synthesized as a stable HCl salt by *O*-alkylation of either *N*-hydroxyphthalimide or *N*-(4-monomethoxytrityl)hydroxylamine, followed by *N*-alkylation of maleimide, in an overall yield of 18% (seven steps) or 29% (five steps), respectively. This heterobifunctional linker allowed a simple and efficient synthesis of a maleimide-containing thiol-reactive  $^{18}\text{F}$ -labeling agent. Thus, *N*-{4-[(4- $^{18}\text{F}$ ]fluorobenzylidene)aminooxy]butyl}maleimide (specific activity:  $\sim 3000$  Ci/mmol at end of synthesis) was synthesized in two steps involving the preparation of 4- $^{18}\text{F}$ fluorobenzaldehyde, followed by its aminooxy-aldehyde coupling reaction to the heterobifunctional linker, with an overall radiochemical yield of  $\sim 35\%$  (decay corrected) within  $\sim 60$  min from end of bombardment. Initial  $^{18}\text{F}$ -labeling experiments were carried out using a thiol-containing tripeptide glutathione (GSH) and a 5'-thiol-functionalized oligodeoxynucleotide (5'-*S*-ODN) in phosphate-buffered saline (PBS, pH 7.5). After standing at room temperature for 10 min, the  $^{18}\text{F}$ -labeled GSH and 5'-*S*-ODN were obtained in  $^{18}\text{F}$ -labeling yields of  $\sim 70\%$  and  $\sim 5\%$  (decay-corrected), respectively. The heterobifunctional linker is easy to synthesize and provides a facile access to the maleimide-containing thiol-reactive  $^{18}\text{F}$ -labeling agent, which could be advantageously employed in the development of  $^{18}\text{F}$ -labeled biomolecules for use with positron emission tomography.

## INTRODUCTION

As medicine moves toward treatment at the molecular level, complementary molecular diagnostic tools will be of vital importance. In this regard, molecular imaging techniques, namely positron emission tomography (PET) (1, 2) and single photon emission computed tomography (SPECT) (3), are of particular interest due to their ability to noninvasively and repeatedly track radiolabeled probes in living subjects. Advances in basic medical sciences have led to an appreciation of biomolecules that selectively target a particular disease at the cellular level. Examples for this approach include peptide (4) and nucleic acid probes (aptamers) (5), monoclonal antibodies (6), and antisense oligodeoxynucleotides (ODNs) (7). Synthetic and engineered variants of these biomolecules are also being developed to improve their native chemical and biological characteristics. Such variants of biomolecules can be potential target-specific imaging probes for PET and SPECT when they are labeled with appropriate radioisotopes (8–11). PET in general is superior to SPECT in terms of sensitivity and spatial resolution. Among the routinely available positron-emitting isotopes,  $^{18}\text{F}$  is the most attractive isotope due to its relatively long half-life (110 min) which permits multistep radiosyntheses. Furthermore, better quality PET images can be

obtained from  $^{18}\text{F}$ -labeled radiotracers due to the short range of positrons emitted by the radioisotope. Accordingly, recent years have seen a growing interest in the development of  $^{18}\text{F}$ -labeled biomolecules for target-specific PET imaging probes (12, 13).

Radiofluorination of biomolecules generally utilizes  $^{18}\text{F}$ -labeled intermediates which are synthesized by nucleophilic [ $^{18}\text{F}$ ]fluorination of precursor compounds. These  $^{18}\text{F}$ -labeled intermediates are subsequently converted into amine-reactive (14–18) or thiol-reactive (14, 19, 20) functional groups. Such indirect approaches are required since nucleophilic radiofluorination reactions are carried out with anhydrous [ $^{18}\text{F}$ ]fluoride ion in polar aprotic solvents under strong basic conditions, which are frequently detrimental to sensitive functional groups. Nonetheless, a few direct [ $^{18}\text{F}$ ]fluorinations of preformed active esters have been reported. However, these direct methods are not selective and suffer from either the need of an extensive HPLC purification (21) or low specific activity of the final product (22). The amine-reactive  $^{18}\text{F}$ -labeling agent *N*-succinimidyl 4- $^{18}\text{F}$ fluorobenzoate has currently found considerable applications in  $^{18}\text{F}$ -labeling of peptides (23–25), proteins (16, 26), and ODNs (27). Nevertheless, the preparation of this agent requires at least three major synthetic steps: (1) [ $^{18}\text{F}$ ]fluorination of an aromatic aldehyde/ester precursor, (2) a functional group transformation to the corresponding carboxylic acid, and (3) formation of its *N*-succinimidyl ester. In order for  $^{18}\text{F}$ -labeling of biomolecules to be a routine procedure, there is a need for simpler and more efficient  $^{18}\text{F}$ -labeling methods.

\* Correspondence should be addressed to: LA Tech Center, Department of Molecular and Medical Pharmacology, David Geffen School of Medicine at UCLA, 6140 Bristol Parkway, Culver City, CA 90230. Phone: (310) 670-8695. Fax: (310) 670-8428. E-mail: ttyokuni@mednet.ucla.edu.

We herein report that a novel heterobifunctional linker containing an aldehyde-reactive aminoxy group and a thiol-reactive maleimide group facilitates a facile access to a maleimide-containing thiol-reactive  $^{18}\text{F}$ -labeling agent obtainable via readily available 4- $^{18}\text{F}$ fluorobenzaldehyde (28–32).

## EXPERIMENTAL METHODS

**General.** All reagents and solvents were purchased from commercial suppliers and used without further purification, except for THF and MeCN which were distilled under  $\text{N}_2$  from sodium benzophenone ketyl and  $\text{CaH}_2$ , respectively. The 5'-thiol functionalized 15-mer ODN,  $\text{HS}-(\text{CH}_2)_6\text{OPO}_3\text{-AACGTTGAGGGGCAT}$ , was purchased from Genset (Paris, France) as the *S*-trityl protected form, which was deprotected according to the manufacture's protocol just before use. Reactions were monitored by TLC on 0.25-mm thickness silica gel plates containing  $\text{UV}_{254}$  indicator. Flash column chromatography was performed on silica gel 60 (0.032–0.063 mm). Melting points were determined with a Fisher-Johns melting point apparatus and are uncorrected. Elemental analyses were done by Galbraith Laboratories in Knoxville, TN.

$^1\text{H}$  and  $^{13}\text{C}$  NMR spectra were recorded using either a Bruker AM360, Bruker ARX400, or Bruker Avance 500 spectrometer using TMS as the internal standard. High-resolution mass spectra were recorded on an IonSpec HiResMALDI spectrometer (MALDI) or a VG Analytical 70VSE spectrometer (FAB). MALDI-TOF MS was obtained at The Scripps Research Institute, La Jolla, CA.

No-carrier-added  $^{18}\text{F}$ fluoride ( $\sim 600$  mCi; specific activity:  $> 10\,000$  Ci/mmol) was produced by 11 MeV proton bombardment of 95%  $^{18}\text{O}$ -enriched  $\text{H}_2\text{O}$  via  $^{18}\text{O}(\text{p},\text{n})^{18}\text{F}$  nuclear reaction using a RDS-112 cyclotron. HPLC was performed with a Rainin-HP system equipped with a UV detector (250 nm) and a Bioscan  $\gamma$  detector. Semi-preparative HPLC was carried out using a C-18 column (Phenomenex Aqua, 5  $\mu\text{m}$ ,  $250 \times 10$  mm) with MeCN–water (1:1 v/v for 8 min followed by 7:3 v/v) at 5 mL/min. For analytical HPLC, a C-18 column (Phenomenex Aqua, 5  $\mu\text{m}$ ,  $250 \times 4.6$  mm) was used with a linear gradient elution of 5–80% solvent B in solvent A over 20 min at 1 mL/min, where solvent A: 0.1 M triethylammonium acetate (TEAA) (pH 7) containing 5% MeCN; solvent B: 0.1 M TEAA (pH 7) containing 70% MeCN. The specific activity was determined by on-line measurements of radioactivity and UV absorption.

***N*-[4-(*tert*-Butyldimethylsiloxy)butoxy]phthalimide (3).** DEAD (1.10 mL, 7.07 mmol) was added dropwise over a period of 1 h to a solution of 4-(*tert*-butyldimethylsiloxy)butanol (33) (2) (1.20 g, 5.87 mmol), *N*-hydroxyphthalimide (1.13 g, 6.93 mmol) and  $\text{Ph}_3\text{P}$  (1.83 g, 6.80 mmol) in THF (15 mL) at 0 °C. The mixture was then stirred at room-temperature overnight. The reaction mixture was poured into water and extracted with  $\text{Et}_2\text{O}$ . The  $\text{Et}_2\text{O}$  extract was washed with water and dried ( $\text{MgSO}_4$ ). After concentration of the ethereal solution, the residue was purified by flash column chromatography with hexanes– $\text{Et}_2\text{O}$  (3:2 v/v) to give **3** (1.74 g, 85%) as a clear colorless oil. The  $^1\text{H}$  NMR data were in agreement with the literature values (34).

***N*-(4-Hydroxybutoxy)phthalimide (4).** The reaction was carried out in a neoprene flask. A mixture of **3** (1.70 g, 4.87 mmol), 48% aqueous HF (0.79 mL, 19.5 mmol), and MeCN (20 mL) was stirred at room temperature for 30 min. The reaction mixture was poured into water and extracted with  $\text{Et}_2\text{O}$ . The  $\text{Et}_2\text{O}$  extract was dried ( $\text{MgSO}_4$ )

and concentrated. The residue was purified by flash column chromatography with  $\text{Et}_2\text{O}$  to give **4** (0.98 g, 85%) as a clear colorless oil. The  $^1\text{H}$  NMR data were in agreement with the reported values (34).

**4-(Aminoxy)butanol (5).** A solution of **4** (0.98 g, 4.16 mmol) and hydrazine (0.62 mL, 19.4 mmol) in EtOH (20 mL) was refluxed for 2.5 h. A white precipitate that formed was removed by filtration, and the filtrate was concentrated to dryness. The residue was purified by flash column chromatography with  $\text{CHCl}_3$ –MeOH (17:3 v/v) containing 1%  $\text{Et}_3\text{N}$  to give **5** (0.35 g, 80%) as a pale yellow oil. Vanillin was used to visualize spots on TLC plates. The  $^1\text{H}$  NMR data were in agreement with the literature values (35).

**4-[(4-Monomethoxytrityl)aminoxy]butanol (6).** From **5**. 4-Methoxytrityl chloride (0.96 g, 3.11 mmol) was added dropwise over a period of 15 min to a solution of **5** (0.34 g, 3.23 mmol) and  $\text{Et}_3\text{N}$  (0.45 mL, 3.23 mmol) in  $\text{CH}_2\text{Cl}_2$  (7 mL) at 0 °C. The mixture was stirred at room temperature for 90 min. After concentration of the mixture, the residue was purified by flash column chromatography with  $\text{CH}_2\text{Cl}_2$ –MeOH (95:1 v/v) to give **6** (0.85 g, 70%) as a clear colorless oil.  $^1\text{H}$  NMR (360 MHz,  $\text{CDCl}_3$ )  $\delta$  1.44 (br quint,  $J = 6$  Hz, 2H) and 1.54 (br quint,  $J = 6$  Hz, 2H) ( $\text{CCH}_2\text{CH}_2\text{C}$ ), 3.47 (t,  $J = 6.1$  Hz, 2H,  $\text{CH}_2\text{OH}$ ), 3.71 (t,  $J = 6.1$  Hz, 2H,  $\text{CH}_2\text{ON}$ ), 3.79 (s, 3H, *OMe*), 6.29 (br s, 1H, *NH*), 6.82 (br d,  $J = 9$  Hz, 2H) and 7.22–7.35 (m, 12H) (*Ar*).  $^{13}\text{C}$  NMR (90 MHz,  $\text{CDCl}_3$ )  $\delta$  24.77, 29.56, 55.08, 62.41, 73.34, 73.76, 112.86, 126.68, 127.57, 128.90, 130.16, 136.52, 144.57, 158.20. HRMS (FAB) calcd for  $\text{C}_{24}\text{H}_{28}\text{NO}_3$  [ $\text{M} + \text{H}$ ] $^+$  378.2069, found 378.2063.

From **13** (for preparation of **13**, see below). A 1 M solution of  $\text{Bu}_4\text{NF}$  in THF (17.8 mL, 17.8 mmol) was added to a solution of **13** (4.38 g, 8.92 mmol) in THF (20 mL). The mixture was stirred at room temperature for 3 h. The reaction mixture was poured into water and extracted with  $\text{Et}_2\text{O}$ . The  $\text{Et}_2\text{O}$  extract was dried ( $\text{MgSO}_4$ ) and concentrated. The residue was purified by flash column chromatography with  $\text{CH}_2\text{Cl}_2$ –MeOH (95:1 v/v) to give **6** (3.36 g, quantitative) as a clear colorless oil.

***N*-[4-[(4-Monomethoxytrityl)aminoxy]butyl]-maleimide (7).** DEAD (0.19 mL, 1.22 mmol) was added dropwise over a period of 1 h to a solution of **6** (0.38 g, 1.00 mmol),  $\text{Ph}_3\text{P}$  (0.31 g, 1.18 mmol), and maleimide (0.12 g, 1.23 mmol) in THF (15 mL) at 0 °C. The mixture was then stirred at room-temperature overnight. The reaction mixture was poured into water and extracted with  $\text{Et}_2\text{O}$ . The  $\text{Et}_2\text{O}$  extract was dried ( $\text{MgSO}_4$ ) and concentrated. The residue was purified by flash column chromatography with hexanes– $\text{Et}_2\text{O}$  (3:2 v/v) to give **7** (0.25 g, 55%) as a clear colorless oil.  $^1\text{H}$  NMR (400 MHz,  $\text{CDCl}_3$ )  $\delta$  1.44–1.48 (m, 4H,  $\text{CCH}_2\text{CH}_2\text{C}$ ), 3.41 (t,  $J = 6.7$  Hz, 2H,  $\text{CH}_2\text{N}$ ), 3.66 (t,  $J = 5.8$  Hz, 2H,  $\text{CH}_2\text{ON}$ ), 3.79 (s, 3H, *OMe*), 6.30 (br s, 1H, *NH*), 6.64 (s, 2H, maleimide), 6.82 (br d,  $J = 9$  Hz, 2H) and 7.21–7.35 (m, 12H) (*Ar*).  $^{13}\text{C}$  NMR (100 MHz,  $\text{CDCl}_3$ )  $\delta$  25.34, 25.71, 37.66, 55.20, 73.34, 73.48, 112.96, 126.76, 127.68, 129.06, 130.37, 134.02, 136.66, 144.73, 158.29, 170.84. HRMS (MALDI) calcd for  $\text{C}_{28}\text{H}_{28}\text{N}_2\text{O}_4\text{Na}$  [ $\text{M} + \text{Na}$ ] $^+$  479.1947, found 479.1937.

***N*-[4-(Aminoxy)butyl]maleimide (8).** HCl gas was bubbled into a solution of **7** (0.12 g, 0.27 mmol) in  $\text{Et}_2\text{O}$  (15 mL) at 0 °C for 1 min. The mixture was stirred at the same temperature for an additional 5 min. The resulting white precipitate was collected by filtration. Recrystallization from MeCN afforded **8** (0.058 g, quantitative) as the HCl salt: mp 131–132 °C.  $^1\text{H}$  NMR (400 MHz,  $\text{CD}_3\text{OD}$ )  $\delta$  1.60–1.70 (m, 4H,  $\text{CCH}_2\text{CH}_2\text{C}$ ), 3.53 (t,  $J = 6.2$  Hz, 2H,  $\text{CH}_2\text{N}$ ), 4.02 (t,  $J = 5.8$  Hz, 2H,  $\text{CH}_2\text{ON}$ ),



6.81 (br s, 2H, *maleimide*). Anal. Calcd for  $\text{C}_8\text{H}_{13}\text{ClN}_2\text{O}_3$ : C, 43.55; H, 5.94; Cl, 16.07; N, 12.70. Found: C, 43.45; H, 6.20; Cl, 16.14; N, 12.71.

**N-(4-Monomethoxytrityl)hydroxylamine (10).** 4-Monomethoxytrityl chloride (50.0 g, 162 mmol) was added to a solution of  $\text{NH}_2\text{OH}\cdot\text{HCl}$  (10.4 g, 162 mmol) and  $\text{Et}_3\text{N}$  (35.3 mL, 324 mmol) in DMF (450 mL). The resulting cloudy mixture was stirred at room-temperature overnight. The mixture was poured into water and extracted with  $\text{Et}_2\text{O}$ . The  $\text{Et}_2\text{O}$ -extract was washed with water and dried ( $\text{MgSO}_4$ ). After concentration, the residue was triturated with hexanes to afford a yellow solid. Recrystallization from EtOH gave **10** (35.3 g, 72%) as white crystals: mp 112–113 °C. The  $^1\text{H}$  and  $^{13}\text{C}$  NMR data were in agreement with the values reported in the literature (36).

**1-(tert-Butyldimethylsiloxy)-4-[(4-monomethoxytrityl)aminooxy]butane (13).** 1-(tert-Butyldimethylsiloxy)-4-iodobutane (**37**) (5.60 g, 17.8 mmol) was added to a solution of **10** (4.53 g, 14.9 mmol) and NaH (60% dispersion in mineral oil, 0.54 g, 17.8 mmol) in DMF (50 mL). The mixture was stirred at room-temperature overnight. The reaction mixture was poured into water and extracted with  $\text{Et}_2\text{O}$ . The  $\text{Et}_2\text{O}$  extract was washed with water and dried ( $\text{MgSO}_4$ ). After concentration, the residue was purified by flash column chromatography with hexanes– $\text{Et}_2\text{O}$  (9:1 v/v) to give **13** (4.38 g, 60%) as a clear colorless oil.  $^1\text{H}$  NMR (360 MHz,  $\text{CDCl}_3$ )  $\delta$  0.03 (s, 6H,  $\text{SiMe}_2$ ), 0.87 (s, 9H, *t*-Bu), 1.40 (br quint,  $J = 6$  Hz, 2H) and 1.52 (br quint,  $J = 6$  Hz, 2H) ( $\text{CCH}_2\text{CH}_2\text{C}$ ), 3.52 (t,  $J = 6.5$  Hz, 2H,  $\text{CH}_2\text{OTBDMS}$ ), 3.67 (t,  $J = 6.4$  Hz, 2H,  $\text{CH}_2\text{ON}$ ), 3.80 (s, 3H, *OMe*), 6.25 (s, 1H, *NH*), 6.82 (br d,  $J = 9$  Hz, 2H) and 7.21–7.31 (m, 12H) (*Ar*).  $^{13}\text{C}$  NMR (100 MHz,  $\text{CDCl}_3$ )  $\delta$  –5.40, 14.01, 25.84, 29.37, 31.47, 55.01, 62.80, 73.28, 73.75, 112.78, 126.59, 127.49, 128.94, 130.23, 136.65, 144.69, 158.15. HRMS (MALDI) calcd for  $\text{C}_{30}\text{H}_{41}\text{NO}_3\text{NaSi}$  [ $\text{M} + \text{Na}$ ] $^+$  514.2753, found 514.2747.

**N-{4-[(4-Fluorobenzylidene)aminooxy]butyl}-maleimide (16- $^{19}\text{F}$ ).** 4-Fluorobenzaldehyde (**15- $^{19}\text{F}$** ) (27.0  $\mu\text{L}$ , 0.25 mmol) was added to a solution of **8**·HCl (36.6 mg, 0.17 mmol) in DMF (2 mL). The mixture was stirred at room temperature for 30 min. The reaction mixture was poured into water and extracted with  $\text{Et}_2\text{O}$ . The  $\text{Et}_2\text{O}$  extract was washed with water and dried ( $\text{MgSO}_4$ ). After concentration, the residue was purified by flash column chromatography with hexanes– $\text{Et}_2\text{O}$  (3:2 v/v) to give **16- $^{19}\text{F}$**  (44 mg, 91%) as a white powder: mp 79–81 °C.  $^1\text{H}$  NMR (360 MHz,  $\text{CD}_3\text{OD}$ )  $\delta$  1.65–1.75 (m, 4H,  $\text{CCH}_2\text{CH}_2\text{C}$ ), 3.57 (t,  $J = 6.7$  Hz, 2H,  $\text{CH}_2\text{N}$ ), 4.15 (t,  $J = 6.0$  Hz, 2H,  $\text{CH}_2\text{ON}$ ), 6.68 (s, 2H, *maleimide*), 7.07 (br t,  $J = 9$  Hz, 2H) and 7.54 (br dd,  $J = 9, 6$  Hz, 2H) (*Ar*), 8.02 (s, 1H,  $\text{CH}=\text{NOR}$ ). HRMS (FAB) calcd for  $\text{C}_{15}\text{H}_{16}\text{FN}_2\text{O}_3$  [ $\text{M} + \text{H}$ ] $^+$  291.1145, found 291.1142. Anal. Calcd for  $\text{C}_{15}\text{H}_{15}\text{FN}_2\text{O}_3$ : C, 62.06; H, 5.21; F, 6.54; N, 9.65. Found: C, 62.37; H, 5.50; F, 6.60; N, 9.32.

**N-{4-[(4- $^{18}\text{F}$ )Fluorobenzylidene)aminooxy]butyl}-maleimide (16- $^{18}\text{F}$ ).** *Step 1: Preparation of 4- $^{18}\text{F}$ -Fluorobenzaldehyde (15- $^{18}\text{F}$ ).* Cyclotron-produced [ $^{18}\text{F}$ ]-fluoride (~600 mCi; specific activity: >10000 Ci/mmol) was transferred to a reaction vessel containing Kryptofix 222 (7 mg) and  $\text{K}_2\text{CO}_3$  (0.7 mg) in MeCN–water (25:1 v/v, 0.7 mL). After water was evaporated at 110 °C with a stream of nitrogen gas, the residue was dried further by the azeotropic distillation with MeCN (3  $\times$  0.2 mL). A solution of (4-formylphenyl)trimethylammonium triflate (**28**) (**14**) (8 mg, 0.026 mmol) in DMSO (0.7 mL) was added and the mixture was heated at 120 °C for 10 min. After dilution with water (7 mL), the mixture was passed

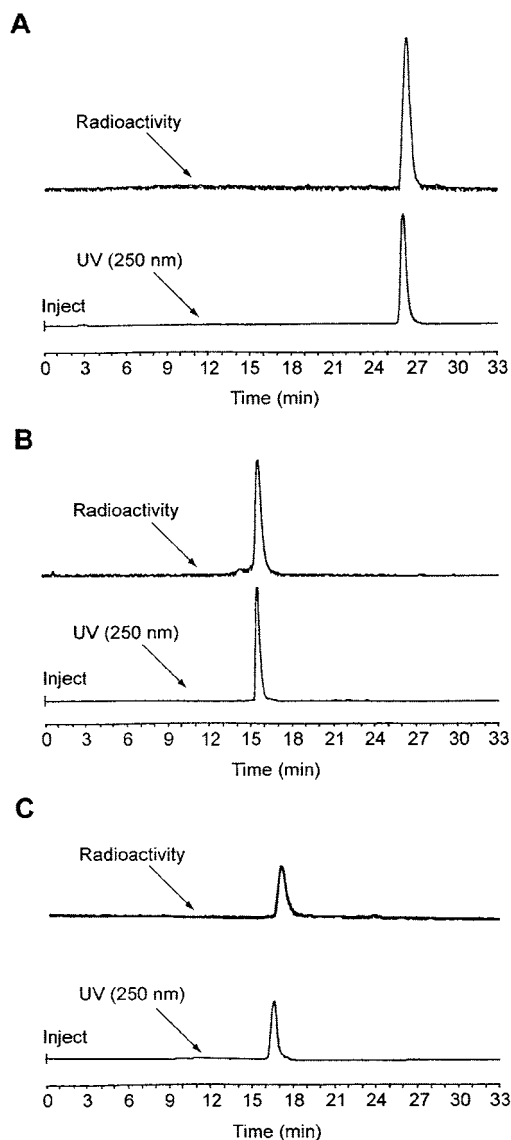
through a Waters Sep-Pak C-18 cartridge (1 mL). The cartridge was washed with water (2  $\times$  5 mL), and the product **15- $^{18}\text{F}$**  was eluted with MeOH (1.5 mL) into a vial containing **8**·HCl (8.00 mg, 0.036 mmol). The yield of **15- $^{18}\text{F}$**  was ~250 mCi (~50% decay-corrected) at ~20 min after end of bombardment (EOB).

*Step 2: Aminooxy-Aldehyde Coupling Reaction.* The mixture was gently agitated with a stream of nitrogen gas for 15 s and allowed to stand at room temperature for 15 min. The reaction mixture (~1.5 mL) was purified by semipreparative HPLC. The chemically and radiochemically pure fraction (~5 mL;  $t_R$  ~16 min) was collected, diluted with water (25 mL), and passed through a Waters Sep-Pak C-18 cartridge (1 mL). The cartridge was washed with  $\text{H}_2\text{O}$  (2  $\times$  5 mL), and the product was eluted with MeCN (1 mL) to afford **16- $^{18}\text{F}$**  (~140 mCi; ~70% decay corrected). The overall radiochemical yield was ~35% (decay corrected) at ~60 min after EOB. The chemical and radiochemical purities as well as chemical identity were confirmed by analytical HPLC by reference to **15- $^{19}\text{F}$**  ( $t_R$  ~26.5 min) (Figure 1A). The specific activity was found to be ~3000 Ci/mmol at end of synthesis (EOS).

**Coupling of 16- $^{19}\text{F}$  with Glutathione (GSH) (17).** A solution of **16- $^{19}\text{F}$**  (16 mg, 0.055 mmol) in DMF (0.5 mL) was added dropwise to a solution of GSH (**17**) (17 mg, 0.055 mmol) in phosphate-buffered saline (PBS, pH 7.5) (1 mL). The mixture was stirred at room temperature for 10 min. At this time TLC indicated the disappearance of **16- $^{19}\text{F}$**  ( $R_f$  0.3; hexanes– $\text{Et}_2\text{O}$  3:2) and the appearance of one major product ( $R_f$  0.6; *n*-BuOH–EtOH– $\text{H}_2\text{O}$ –AcOH 4:2:2:1). After dilution with water (5 mL), the mixture was passed through a Waters Sep-Pak C-18 cartridge (1 mL). The cartridge was washed with water (2  $\times$  5 mL), and the product was eluted with MeOH (5 mL). Evaporation of the MeOH eluate afforded  $^{19}\text{F}$ -GSH **19- $^{19}\text{F}$**  (26 mg, 79%) as a pale yellow solid.  $^1\text{H}$  NMR (400 MHz,  $\text{CD}_3\text{OD}$ )  $\delta$  1.50 (br s, 4H,  $\text{NOCH}_2\text{CH}_2\text{CH}_2\text{CH}_2\text{N}$ ), 1.98–2.03 (m, 2H) and 2.37–2.40 (m, 2H) (Glu  $\text{C}_\beta\text{H}_2\text{C}_\gamma\text{H}_2$ ), 2.41–3.20 (m, 4H, Cys  $\text{C}_\beta\text{H}_2$ , succinimide  $\text{CH}_2$ ), 3.38 (br s, 2H,  $\text{NOCH}_2\text{CH}_2\text{CH}_2\text{CH}_2\text{N}$ ), 3.56–3.69 (m, 3H, Glu  $\text{C}_\alpha\text{H}$ ,  $\text{NOCH}_2\text{CH}_2\text{CH}_2\text{CH}_2\text{N}$ ), 3.83–3.89 (m, 1H, succinimide  $\text{CH}$ ), 3.98 (br s, 2H, Gly  $\text{C}_\alpha\text{H}_2$ ), 4.51 (m, 1H, Cys  $\text{C}_\alpha\text{H}$ ), 6.98 (br t,  $J = 9$  Hz, 2H, *Ar*), 7.40–7.44 (m, 2H, *Ar*), 7.98 (d,  $J = 2.8$  Hz, 1H,  $\text{CH}=\text{NOR}$ ). HRMS (FAB) calcd for  $\text{C}_{25}\text{H}_{33}\text{FN}_5\text{O}_9\text{S}$  [ $\text{M} + \text{H}$ ] $^+$  597.1905, found 597.1904.

**$^{18}\text{F}$ -Labeling of GSH 17.** A portion (~20 mCi, ~140  $\mu\text{L}$ ) of the MeCN eluate containing **16- $^{18}\text{F}$**  (see above) was added to a solution of **17** (4 mg) in PBS (pH 7.5) (1 mL). The mixture was gently agitated and left at room temperature for 10 min. Analytical HPLC indicated the total consumption of **16- $^{18}\text{F}$**  ( $t_R$  ~26.5 min) and the appearance of a new radioactive peak ( $t_R$  ~15.5 min). After dilution with water (5 mL), the mixture was passed through a Waters Sep-Pak C-18 cartridge (1 mL). The cartridge was washed with water (2  $\times$  5 mL), and the activity was eluted with MeOH (1 mL) to yield  $^{18}\text{F}$ -GSH **19- $^{18}\text{F}$**  (~12 mCi, ~70% decay corrected). The labeling time was ~30 min. The chemical and radiochemical purities as well as chemical identity were confirmed by analytical HPLC by reference to **19- $^{19}\text{F}$**  ( $t_R$  ~15.5 min) (Figure 1B).

**Coupling of 16- $^{18}\text{F}$  with 5'-Thiol-Functionalized Oligodeoxynucleotide (5'-S-ODN) 18.** A solution of **16- $^{18}\text{F}$**  (150  $\mu\text{g}$ ) in MeCN (20  $\mu\text{L}$ ) was added to a solution of 5'-S-ODN **18** (~100  $\mu\text{g}$ ) in PBS (pH 7.5) (0.2 mL). After gentle agitation, the mixture was left at room temperature for 40 min. The mixture was purified by analytical HPLC and the peak at  $t_R$  ~16.5 min was collected (20



**Figure 1.** Analytical HPLC profiles of (A) the maleimide-containing  $^{18}\text{F}$ -labeling agent **16- $^{18}\text{F}$**  coinjected with the standard **16- $^{18}\text{F}$** , (B) the  $^{18}\text{F}$ -labeled glutathione **19- $^{18}\text{F}$**  coinjected with the standard **19- $^{18}\text{F}$** , and (C) the  $^{18}\text{F}$ -labeled 5'-thiol-functionalized oligodeoxynucleotide **20- $^{18}\text{F}$**  coinjected with the standard **20- $^{18}\text{F}$** . Column: Phenomenex Aqua (C-18, 5  $\mu\text{m}$ , 250  $\times$  4.6 mm); elution protocol: a linear gradient elution of 5–80% solvent B (0.1 M TEAA, pH 7, 70% MeCN) in solvent A (0.1 M TEAA, pH 7, 5% MeCN) over 20 min; flow rate: 1 mL/min.

$\mu\text{L}$  each injection). After lyophilization, the product  $^{19}\text{F}$ -5'-S-ODN **20- $^{18}\text{F}$**  was characterized by MALDI-TOF MS: calcd for  $\text{C}_{169}\text{H}_{213}\text{FN}_{64}\text{O}_{93}\text{P}_{15}\text{S}$  [ $\text{M} + \text{H}$ ] $^{+}$  5141, found 5138.

**$^{18}\text{F}$ -Labeling of 5'-S-ODN **18**.** A portion ( $\sim 30$  mCi,  $\sim 160$   $\mu\text{L}$ ) of the MeCN eluate containing **16- $^{18}\text{F}$**  (see above) was added to a solution of **18** ( $\sim 400$   $\mu\text{g}$ ) in PBS (pH 7.5) (160  $\mu\text{L}$ ). The mixture was gently agitated and left at room temperature for 10 min. After dilution with water (5 mL), the mixture was passed through a Waters Sep-Pak C-18 cartridge (1 mL). The cartridge was washed with water ( $2 \times 5$  mL), and the activity was eluted with EtOH (1 mL). The EtOH eluate was concentrated to  $\sim 200$   $\mu\text{L}$  and diluted with PBS (pH 7.5) (800  $\mu\text{L}$ ). The mixture was applied to a NAP-10 gel-filtration cartridge with PBS (pH 7.5) as an eluting solvent. The eluate was fractionated ( $\sim 1$  mL each) and analyzed by analytical HPLC. The second fraction was found to contain chemically and

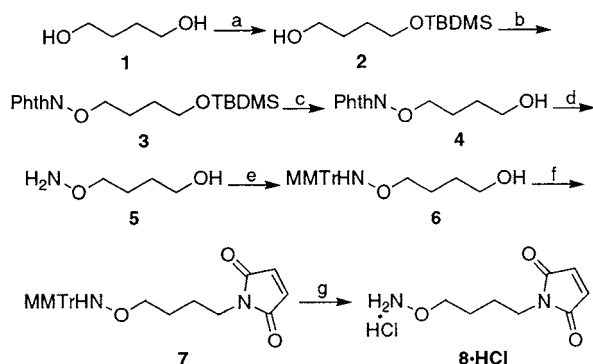
radiochemically pure  $^{18}\text{F}$ -5'-S-ODN **20- $^{18}\text{F}$**  ( $t_{\text{R}} \sim 16.5$  min) (Figure 1C). The radioactivity was  $\sim 1$  mCi ( $\sim 5\%$  decay-corrected) and the labeling time was  $\sim 60$  min.

## RESULTS AND DISCUSSION

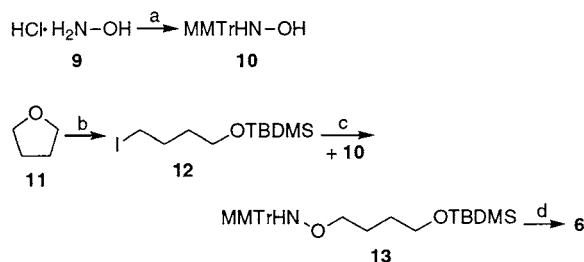
Thiol-reactive agents have been widely used to modify peptides and proteins at specific sites (38–40). This is because under physiological conditions a thiol group is more nucleophilic than amines. The thiol-reactive agents include maleimides, vinyl sulfones, haloacetyl derivatives, bromomethyl derivatives, and pyridyl disulfides, among which maleimides are the most preferable due to their highest selectivity toward the thiol group. Therefore, maleimide-containing thiol-reactive  $^{18}\text{F}$ -labeling agents are of particular interest for the selective introduction of  $^{18}\text{F}$  at a predetermined site. In 1988 Shiue et al. reported a multistep preparation of two maleimide-containing  $^{18}\text{F}$ -labeling agents starting from 1- $^{18}\text{F}$ fluoro-4-nitrobenzene or 4- $^{18}\text{F}$ fluorobenzonitrile (19). They also reported unsuccessful direct  $^{18}\text{F}$ fluorination of pre-formed maleimides. The likely reason for their failure is that the strongly basic conditions required for radiofluorination with  $^{18}\text{F}$ fluoride are not compatible with base-labile maleimides. Since then little efforts have been made on the development of maleimide-containing thiol-reactive  $^{18}\text{F}$ -labeling agents (41–43).

We therefore envisioned the thiol-reactive maleimide **16** (Scheme 3) as a potential precursor for modifying peptides and proteins. Condensation of the readily available 4- $^{18}\text{F}$ fluorobenzaldehyde (28–32) with the aminoxy maleimide **8** was a key step in the preparation of **16**. The choice of the aminoxy derivative **8** instead of the corresponding amine was based on the enhanced reactivity of the aminoxy group toward carbonyl groups and the greater stability of the oxime ethers formed (44). The hydrazide maleimide derivatives, such as BMPH, EMCH, and KMH (45), are commercially available as aldehyde- and thiol-reactive heterobifunctional linkers, in which the hydrazide group reacts with carbonyl groups forming stable hydrazones. However, the aminoxy group is more attractive for time-restricted PET radiochemistry (46) because of its greater nucleophilicity than the hydrazide group (47–49). Although a number of examples are described in bioconjugate chemistry (50–55), aminoxy chemistry has not been previously utilized in PET radiochemistry.

**Synthesis of the Heterobifunctional Linker **8** (Scheme 1).** The conventional route to aminoxy ethers involves an *O*-alkylation of *N*-hydroxyphthalimide (PhthNOH) with alkylating agents (56). The Mitsunobu reaction has also been shown effective for this transformation with alcohols (57). We employed the Mitsunobu reaction for the preparation of the *N,O*-protected aminoxy alcohol **3**. The monosilyl ether **2**, prepared from 1,4-butanediol (**1**) as reported (33), was subjected to the Mitsunobu reaction condition using PhthNOH as a nucleophile and DEAD and  $\text{PPh}_3$  as activators. The desired compound **3** was obtained in 85% yield from **2**. This product was previously prepared from the tosylate of the monosilyl ether **2** in 60% yield (2 steps) (34). Removal of the phthalimido group requires strong basic/nucleophilic conditions, under which decomposition of the maleimide group can occur. Accordingly, the phthalimide group was replaced with an acid-labile 4-monomethoxytrityl (MMTr) group before the introduction of the maleimide group. Desilylation of **3** and subsequent hydrazinolysis of **4** afforded the aminoxy alcohol **5**, which upon treatment with MMTrCl gave rise to the *N*-tritylaminoxy alcohol

Scheme 1<sup>a</sup>

<sup>a</sup> Reagents and conditions (yield): (a) ref 34 (81%); (b) PhthNOH, Ph<sub>3</sub>P, DEAD, THF, 0 °C→rt, overnight (85%); (c) 48% aq HF, MeOH, 30 min (85%); (d) NH<sub>2</sub>NH<sub>2</sub>, EtOH, reflux, 2.5 h (80%); (e) MMTTrCl, Et<sub>3</sub>N, CH<sub>2</sub>Cl<sub>2</sub>, 0 °C→rt, 90 min (70%); (f) maleimide, Ph<sub>3</sub>P, DEAD, THF, 0 °C→rt, overnight (55%); (g) HCl(g), Et<sub>2</sub>O, 0 °C, 5 min (quantitative).

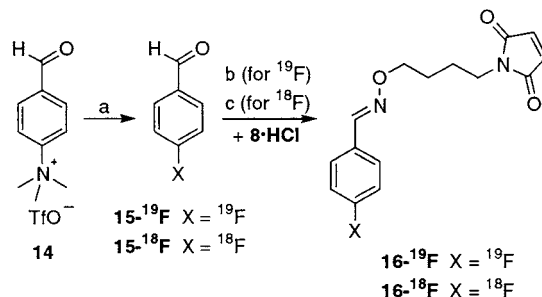
Scheme 2<sup>a</sup>

<sup>a</sup> Reagents and conditions (yield): (a) MMTTrCl, Et<sub>3</sub>N, DMF, overnight (72%); (b) ref 37 (89%); (c) NaH, DMF, overnight (60%); (d) Bu<sub>4</sub>NF, THF, 3 h (quantitative).

**6.** An alternative synthesis of **5** was reported in the literature involving *O*-alkylation of PhthNOH with 4-bromobutyl acetate (35).

*N*-Alkylmaleimides are in general prepared by reaction of alkylamines with maleic anhydride, followed by cyclization of the maleamic acid intermediates (58). Direct *N*-alkylation of maleimide with alkyl halides is reported to be unsuccessful, except for the use of the heavy metal salts of maleimide (59, 60). Once again the Mitsunobu reaction proved to be effective for the direct *N*-alkylation of maleimide (61). Thus, treatment of **6** with maleimide under the Mitsunobu condition furnished the desired *N*-tritylaminoxy maleimide **7** in good yields. Detritylation of **7** by bubbling HCl gas through the Et<sub>2</sub>O solution rapidly precipitated the heterobifunctional linker **8** as a stable HCl salt in quantitative yield. The overall yield of **8** was 18% (seven steps from **1**).

**An Improved Synthesis of the Key Intermediate 6 (Scheme 2).** To eliminate the undesirable protecting group manipulation (*N*Phth → *N*MMTr), *O*-alkylation of the *N*-tritylhydroxylamine **10** was investigated. *N*-Tritylation of hydroxylamine (**9**) with MMTTrCl in pyridine was reported to be problematic necessitating two consecutive chromatographic purifications of **10** (52% yield) (36). In our hands the reaction was straightforward in DMF containing Et<sub>3</sub>N and simple recrystallization was enough to provide pure **10** in a 72% yield without column chromatography. The siloxyiodobutane **12** was prepared from THF (**11**) using TBDMSI as reported (37). *O*-Alkylation of **10** was successful by reaction with NaH and **12** in DMF to furnish the desired protected aminoxy alcohol **13**, the desilylation of which afforded the key intermediate **6**. Thus, the overall yield of **8** was improved to 29% (five steps from **11**).

Scheme 3<sup>a</sup>

<sup>a</sup> Reagents and conditions (yield): (a) K<sup>18</sup>F, Kryptofix 222, DMSO, 120 °C, 10 min (~50% decay corrected); (b) DMF, 30 min (91%); (c) MeOH, 15 min (~70% decay corrected).

**Synthesis of the Maleimide-Containing Thiol-Reactive  $^{18}\text{F}$ -Labeling Agent **16- $^{18}\text{F}$**  (Scheme 3).** The efficiency of the aminoxy-aldehyde coupling reaction was first evaluated by reaction of **8**·HCl with commercially available 4-fluorobenzaldehyde (**15- $^{19}\text{F}$** ). The coupling reaction proceeded essentially to completion within 30 min at room temperature affording the nonradioactive standard **16- $^{19}\text{F}$**  in a 91% yield. The aminoxy group proved to be highly chemoselective toward the aldehyde group over the maleimide group. Although **16- $^{19}\text{F}$**  could exist as *E*- and *Z*-isomers, the <sup>1</sup>H NMR spectrum revealed only one isomer evidenced by a single oxime proton (*CH*=NOR) at  $\delta$  8.02. It is reported that the chemical shifts of the oxime protons are characteristic of the *E*- and *Z*-isomers, e.g.,  $\delta$  7.56 for *E* and  $\delta$  6.95 for *Z* (62). Accordingly, **16- $^{19}\text{F}$**  was tentatively assigned to possess the *E*-configuration.

Synthesis of the maleimide-containing thiol-reactive  $^{18}\text{F}$ -labeling agent **16- $^{18}\text{F}$**  began with the radiochemical synthesis of 4-[ $^{18}\text{F}$ ]fluorobenzaldehyde (**15- $^{18}\text{F}$** ) by [ $^{18}\text{F}$ ]-fluoride-for-trimethylammonium substitution on 4-(formylphenyl)trimethylammonium triflate (**14**) at 120 °C for 10 min (28). After rapid Sep-Pak (C-18) purification, **15- $^{18}\text{F}$**  was subjected to the aminoxy-aldehyde coupling reaction with the linker **8**·HCl. The coupling reaction proceeded efficiently in ~70% coupling yield (decay corrected) within 15 min at room temperature. After HPLC purification, the radioactive fraction (5 mL) was reconstituted in acetonitrile (1 mL) using the solid-phase extraction technique (63). Acetonitrile is the choice of cosolvent particularly for modification of peptides due to its preventive effect against peptide aggregation (64). The chemical and radiochemical purity of **16- $^{18}\text{F}$**  was verified by analytical HPLC (Figure 1A). Coelution of the radioactive peak with the UV peak of the **16- $^{19}\text{F}$**  confirmed the identity. The overall radiochemical yield was ~35% (decay corrected) and the total reaction time was ~60 min from EOB. The specific activity was determined to be ~3000 Ci/mmol at EOS.

**Model  $^{18}\text{F}$ -Labelings of Glutathione (GSH) (**17**) and 5'-Thiol-Functionalized ODN (5'-S-ODN) **18** (Scheme 4).** The  $^{18}\text{F}$ -labeling ability of **16- $^{18}\text{F}$**  was preliminarily assessed by using a tripeptide GSH (**17**) and a 5'-S-ODN **18** as model thiol-containing/functionalyzed biomolecules. Both  $^{18}\text{F}$ -labelings were performed in PBS (pH 7.5) at room temperature for 10 min. The  $^{18}\text{F}$ -labeled GSH **19- $^{18}\text{F}$**  (Figure 1B) and 5'-S-ODN **20- $^{18}\text{F}$**  (Figure 1C) were obtained in over 95% purities after Sep-Pak (C-18) purification and sequential Sep-Pak (C-18) and NAP-10 purification, respectively, without the use of HPLC. The  $^{18}\text{F}$ -labeling yields (unoptimized) were ~70% and ~5% (decay corrected) for **19- $^{18}\text{F}$**  and **20- $^{18}\text{F}$** , respectively. The isolated yields of **19- $^{18}\text{F}$**  (~12 mCi) and





- (28) Haka, M. S., Kilbourn, M. R., Watkins, G. L., and Toorngian, S. A. (1989) Aryltrimethylammonium trifluoromethanesulfonates as precursors to aryl [ $^{18}\text{F}$ ]fluorides: improved synthesis of [ $^{18}\text{F}$ ]GBR-13119. *J. Labelled Compd. Radiopharm.* 27, 823–833.
- (29) Wilson, A. A., Dannals, R. F., Ravert, H. T., and Wagner, H. N., Jr. (1990) Reductive amination of [ $^{18}\text{F}$ ]fluorobenzaldehydes: radiosyntheses of [2- $^{18}\text{F}$ ]- and [4- $^{18}\text{F}$ ]fluorodexetimides. *J. Labelled Compd. Radiopharm.* 28, 1189–1199.
- (30) Plenevaux, A., Fowler, J. S., Dewey, S. L., Wolf, A. P., and Guillaume, M. (1991) The synthesis of no-carrier-added DL-4-fluorine-18-labeled fluorodeprenyl via the nucleophilic aromatic substitution reaction. *Appl. Radiat. Isot.* 42, 121–127.
- (31) Stone-Elander, S., and Elander, N. (1993) Fast chemistry in microwave fields: nucleophilic  $^{18}\text{F}$ -radiofluorinations of aromatic molecules. *Appl. Radiat. Isot.* 44, 889–893.
- (32) Iwata, R., Pascali, C., Bogno, A., Horvath, G., Kovacs, Z., Yanai, K., and Ido, T. (2000) A new, convenient method for the preparation of 4-[ $^{18}\text{F}$ ]fluorobenzyl halides. *Appl. Radiat. Isot.* 52, 87–92.
- (33) Nicolaou, K. C., Prasad, C. V. C., Hwang, C.-K., Duggan, M. E., and Veale, C. A. (1989) Cyclizations of hydroxy dithioketals. New synthetic technology for the construction of oxocenes and related medium-ring systems. *J. Am. Chem. Soc.* 111, 5321–5330.
- (34) Cozzi, P., Giordani, A., Menichincheri, M., Pillan, A., Pinciroli, V., Rossi, A., Tonani, R., Volpi, D., Tamburin, M., Ferrario, R., Fusar, D., and Salvati, P. (1994) Agents combining thromboxane receptor antagonism with thromboxane synthase inhibition: [[2-(1H-imidazol-1-yl)ethylidene]amino]oxy]alkanoic acids. *J. Med. Chem.* 37, 3588–3604.
- (35) Mikola, H., and Hänninen, E. (1992) Introduction of aliphatic amino and hydroxy groups to keto steroids using *O*-substituted hydroxylamines. *Bioconjugate Chem.* 3, 182–186.
- (36) Canle, M. L., Clegg, W., Demirtas, I., Elsegood, M. R. J., Haider, J., Maskill, H., and Miatt, P. C. (2001) *N*-Trityl-hydroxylamines: preparations, structures, base strengths, and reactions with nitrous acid and perchloric acid. *J. Chem. Soc., Perkin Trans. 2* 2001, 1742–1747.
- (37) Nyström, J.-E., McCanna, T. D., Helquist, P., and Amouroux, R. (1988) Cleavage of tetrahydrofuran by *tert*-butyldimethylsilyl iodide and further transformations of the resulting 1-silyloxy-4-iodobutane. *Synthesis* 1988, 56–58.
- (38) Brinkley, M. (1992) A brief survey of methods for preparing protein conjugates with dyes, haptens, and cross-linking reagents. *Bioconjugate Chem.* 3, 2–13.
- (39) Wilbur, D. S. (1992) Radiohalogenation of proteins: an overview of radionuclides, labeling methods, and reagents for conjugate labeling. *Bioconjugate Chem.* 3, 433–470.
- (40) Hermanson, G. T. (1996) *Bioconjugate Techniques*, Academic Press, San Diego, CA.
- (41) Kuhnast, B., Dolle, F., and Tavitian, B. (2002) Fluorine-18 labeling of peptide nucleic acids. *J. Labelled Compd. Radiopharm.* 45, 1–11.
- (42) Patt, J. T., and Patt, M. (2002) Reaction of [ $^{18}\text{F}$ ]4-fluorobenzenediazonium cations with cysteine or the cysteinyl group: preparation of  $^{18}\text{F}$ -labeled S-aryl-cysteine and a radio-labeled peptide. *J. Labelled Compd. Radiopharm.* 45, 1229–1238.
- (43) Li, Z., Ding, Y.-S., Gifford, A., Fowler, J. S., and Gatley, J. S. (2003) Synthesis of structurally identical fluorine-18 and iodine isotope labeling compounds for comparative imaging. *Bioconjugate Chem.* 14, 287–294.
- (44) Abele, E., and Lukevics, E. (2000) Recent advances in the chemistry of oximes. *Org. Prep. Proced. Int.* 32, 235–264.
- (45) 2003/2004 *Pierce Applications Handbook and Catalog*, Pierce, IL.
- (46) Fowler, J. S., and Wolf, A. P. (1997) Working against time: rapid radiotracer synthesis and imaging the human brain. *Acc. Chem. Res.* 30, 181–188.
- (47) Jencks, W. P. (1959) Studies on the mechanism of oxime and semicarbazone formation. *J. Am. Chem. Soc.* 81, 475–481.
- (48) Yarema, K. J., Mahal, L. K., Bruehl, R. E., Rodriguez, E. C., and Bertozzi, C. R. (1998) Metabolic delivery of ketone groups to sialic acid residues: application to cell surface glycoform engineering. *J. Biol. Chem.* 273, 31168–31179.
- (49) Houdier, S., Legrand, M., Boturyn, D., Croze, S., Defrancq, E., and Lhomme, J. (1999) A new fluorescent probe for sensitive detection of carbonyl compounds. *Anal. Chim. Acta* 382, 253–263.
- (50) Boturyn, D., Boudali, A., Constant, J.-F., Defrancq, E., and Lhomme, J. (1997) Synthesis of fluorescent probes for the detection of abasic sites in DNA. *Tetrahedron* 53, 5485–5492.
- (51) Salo, H., Virta, P., Hakala, H., Prakash, T. P., Kawasaki, A. M., Manoharan, M., and Lönnberg, H. (1999) Aminoxy functionalized oligonucleotides: preparation, on-support derivatization, and postsynthetic attachment to polymer support. *Bioconjugate Chem.* 10, 815–823.
- (52) Bark, S. J., Schmid, S., and Hahn, K. M. (2000) A highly efficient method for site-specific modification of unprotected peptides after chemical synthesis. *J. Am. Chem. Soc.* 122, 3567–3573.
- (53) Hang, H. C., and Bertozzi, C. R. (2001) Chemoselective approaches to glycoprotein assembly. *Acc. Chem. Res.* 34, 727–736.
- (54) Neuner, P., Gallo, P., Orsatti, L., Fontana, L., and Monaci, P. (2003) An efficient and versatile synthesis of bisPNA-peptide conjugates based on chemoselective oxime formation. *Bioconjugate Chem.* 14, 276–281.
- (55) Thumshirn, G., Hersel, U., Goodman, S. L., and Kessler, H. (2003) Multimeric cyclic RGD peptides as potential tools for tumor targeting: solid-phase peptide synthesis and chemoselective oxime ligation. *Chem. Eur. J.* 9, 2717–2725.
- (56) Rougny, A., and Daudon, M. (1976) Use of *N*-hydroxyl-imides for the synthesis of primary alkoxylamines. *Bull. Soc. Chim. Fr.* 5–6, 833–838.
- (57) Mitsunobu, O. (1981) The use of diethyl azodicarboxylate and triphenylphosphine in synthesis and transformation of natural products. *Synthesis* 1981, 1–28.
- (58) Mehta, N. B., Phillips, A. P., Lui, F. F., and Brooks, R. E. (1960) Maleamic and citraconamic acids, methyl esters, and imides. *J. Org. Chem.* 25, 1012–1015.
- (59) Schwartz, A. L., and Lerner, L. M. (1974) Preparation of *N*-substituted maleimides by direct coupling of alkyl or aralkyl halides with heavy metal salts of maleimide. *J. Org. Chem.* 39, 21–23.
- (60) Yoon, U. C., Cho, S. J., Lee, Y.-J., Mancheno, M. J., and Mariano, P. S. (1995) Investigations of novel azomethine ylide-forming photoreactions of *N*-silylmethylimides. *J. Org. Chem.* 60, 2353–2360.
- (61) Walker, M. A. (1994) The Mitsunobu reaction: a novel method for the synthesis of bifunctional maleimide linkers. *Tetrahedron Lett.* 35, 665–668.
- (62) Karabatsos, G. J., and Hsi, N. (1967) Structural studies by nuclear magnetic resonance-XI: conformations and configurations of oxime *O*-methyl ethers. *Tetrahedron* 23, 1079–1095.
- (63) Lemaire, C., Plenevaux, A., Aerts, J., Fiore, G. D., Brihaye, C., Bars, D. L., Comar, D., and Luxen, A. (1999) Solid-phase extraction – an alternative to the use of rotary evaporators for solvent removal in the rapid formulation of PET radiopharmaceuticals. *J. Labelled Compd. Radiopharm.* 42, 63–75.
- (64) Ni, J., Singh, S., and Wang, L.-X. (2003) Synthesis of maleimide-activated carbohydrates as chemoselective tags for site-specific glycosylation of peptides and proteins. *Bioconjugate Chem.* 14, 232–238.

# Synthesis and Comparison of Antibody Recognition of Conjugates Containing Herpes Simplex Virus Type 1 Glycoprotein D Epitope VII<sup>1</sup>

Gábor Mezö,<sup>†</sup> Eliandre de Oliveira,<sup>‡,§</sup> Dimitrios Krikorian,<sup>||</sup> Matty Feijlbrief,<sup>⊥</sup> Annamária Jakab,<sup>†</sup> Vassilios Tsikaris,<sup>||</sup> Constantinos Sakarellos,<sup>||</sup> Sytske Welling-Wester,<sup>⊥</sup> David Andreu,<sup>§,⊗</sup> and Ferenc Hudecz<sup>\*,†</sup>

Research Group of Peptide Chemistry, Hungarian Academy of Sciences, Eötvös L. University, Budapest 112, P.O. Box 32, H-1518, Hungary, Department of Organic Chemistry, University of Barcelona, Barcelona, Spain, Department of Chemistry, University of Ioannina, Ioannina, Greece, and Department of Medicinal Microbiology, University of Groningen, Groningen, The Netherlands. Received July 2, 2003; Revised Manuscript Received September 23, 2003

Synthetic oligopeptides comprising linear or continuous topographic B-cell epitope sequences of proteins might be considered as specific and small size antigens. It has been demonstrated that the strength and specificity of antibody binding could be altered by conjugation to macromolecules or by modification in the flanking regions. However, no systematic studies have been reported to describe the effect of different carrier macromolecules in epitope conjugates. To this end, the influence of carrier structure and topology on antibody recognition of attached epitope has been studied by comparing the antibody binding properties of a new set of conjugates with tetratuftsin analogue (H-[Thr-Lys-Pro-Lys-Gly]<sub>4</sub>-NH<sub>2</sub>, T20) sequential oligopeptide carrier (SOC<sub>n</sub>), branched chain polypeptide, poly[Lys(Ser<sub>i</sub>-DL-Ala<sub>m</sub>)] (SAK), multiple antigenic peptide (MAP), and keyhole limpet hemocyanine (KLH). In these novel constructs, peptide <sup>9</sup>LKNleADPNRFRGKDL<sup>22</sup> ([Nle<sup>11</sup>]-9–22) representing an immunodominant B cell epitope of herpes simplex virus type 1 glycoprotein D (HSV-1 gD) was conjugated to polypeptides through a thioether or amide bond. Here we report on the preparation of sequential and polymeric polypeptides possessing chloroacetyl groups in multiple copies at the α- and/or ε-amino group of the polypeptides and its use for the conjugation of epitope peptides possessing Cys at C-terminal position. We have performed binding studies (direct and competitive ELISA) with monoclonal antibody (Mab) A16, recognizing the HSV gD-related epitope, [Nle<sup>11</sup>]-9–22, and conjugates containing identical and uniformly oriented epitope peptide in multiple copies attached to five different macromolecules as carrier. Data suggest that the chemical nature of the carrier and the degree of substitution have marked influence on the strength of antibody binding.

## INTRODUCTION

Synthetic oligopeptides comprising linear or continuous topographic B-cell epitope peptides corresponding to sequences of proteins might be considered as specific and small size antigens. It has been demonstrated that the strength and specificity of antibody binding could be altered by conjugation of peptide epitopes to macromolecules or by the substitution of amino acids in the flanking regions of the epitope (1). Such constructs are frequently applied to induce specific immune responses against the covalently attached peptide epitopes for antibody production to identify gene products or for

synthetic vaccine construction (2, 3). An additional application of synthetic oligopeptides and their conjugates is the use in diagnostic microbiologic assays to determine the presence of antibodies against particular microorganisms in patients' sera (4, 5). So far, branched chain polypeptide epitope conjugates have been analyzed with respect to the effect of the carrier macromolecule on immune recognition (6). Here we extend these studies to analyze the effect of the structure and topology of the carrier macromolecule on antibody recognition of epitope. For this we have included sequential oligopeptide carriers (tetratuftsin analogue (H-[Thr-Lys-Pro-Lys-Gly]<sub>4</sub>-NH<sub>2</sub>, T20) (7), and Ac-[Lys-Aib-Gly]<sub>4</sub>-NH<sub>2</sub>, SOC<sub>4</sub> (8)),<sup>2</sup> polymeric branched chain polypeptide, poly[Lys(Ser<sub>i</sub>-DL-Ala<sub>m</sub>)] (SAK) (9, 10), Lys-dendrimer construct (multiple antigenic peptide (MAP) (11) (Figure 1), and the widely used keyhole limpet hemocyanin (KLH) (12) as carrier.

In these novel constructs our model peptide <sup>9</sup>LKNleADPNRFRGKDL<sup>22</sup> ([Nle<sup>11</sup>]-9–22) representing an immunodominant B cell epitope from herpes simplex virus type 1 glycoprotein D (HSV gD-1) was conjugated to synthetic polypeptides mentioned above through a thioether or amide bond (Figure 1). HSV, with its two closely related serotypes (HSV-1 and HSV-2), is one of the most common infectious agents in man. Glycoprotein D of HSV

\* Corresponding author. Fax: 36–1–372–2620, Tel: 36–1–372 2828, e-mail: hudecz@szerves.chem.elte.hu.

<sup>†</sup> Eötvös L. University.

<sup>‡</sup> University of Barcelona.

<sup>§</sup> Present address: Barcelona Science Park-University of Barcelona, Josep Samitier, 08028 Barcelona, Spain.

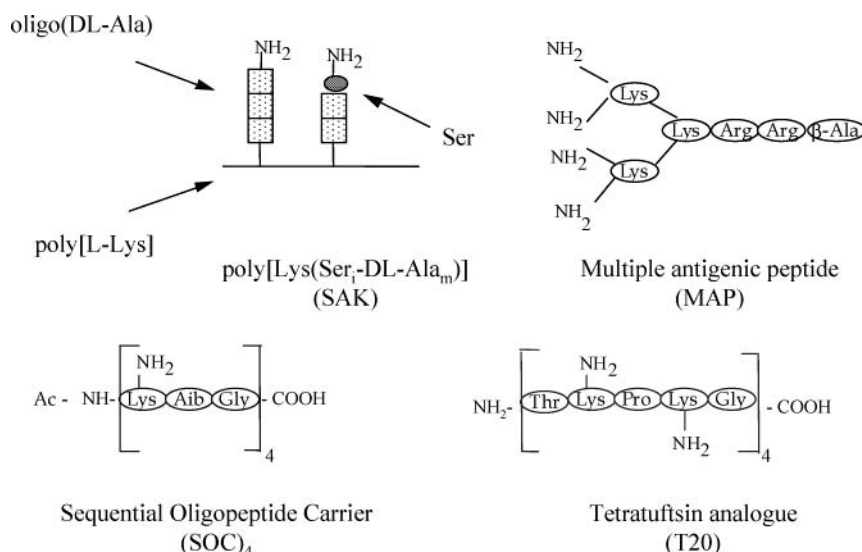
<sup>||</sup> University of Ioannina.

<sup>⊥</sup> Present address: Department of Experimental and Health Sciences, Pompeu Fabra University, 08003 Barcelona, Spain.

<sup>⊗</sup> University of Groningen.

<sup>1</sup> Part of the work has been presented at the 7th International Symposium on Solid-Phase Synthesis & Combinatorial Chemical Libraries, Sept 18–22, 2001, Southampton, England, UK.





**Figure 1.** Schematic structure of conjugates in which a peptide epitope corresponding to the 9–22 region of glycoprotein D of HSV-1 is connected with multivalent synthetic sequential (SOC<sub>4</sub>, tetratuftsin analogue), polymeric (SAK), or dendrimeric (MAP) peptide carrier.

is a highly conserved glycoprotein and is >98% similar among HSV strains. It is a major target of both humoral and cellular immune responses of the human host (13). Mature gD-1 is a glycoprotein consisting of 369 amino acids with an *N*-terminal ectodomain of 316 residues and with three *N*-linked oligosaccharide attachment sites. The X-ray crystal structure, comprising residues 1–254, of a soluble ectodomain of gD was published (14).

There are many well-defined coupling methods for the attachment of biologically active peptides to carriers through amide bonds (water-soluble carbodiimide (15), active ester (16), BOP (17)), or via disulfide bridge (heterobifunctional reagents such as SPDP (18) or Cys-(Npys) (19)). An alternative strategy for thiol-based conjugation is the introduction of a thioether bond. This can be achieved by heterobifunctional reagents with a maleimido (MBS (20), SMCC (21)), or iodoacetyl (SIAB (22)) moiety. The simplest way to incorporate an  $\alpha$ -haloacetyl group is to use a corresponding activated ester derivative such as a *p*-nitrophenyl ester of iodoacetic acid

(23). For conjugation, usually small peptides with terminal (24, 25) or internal (24)  $\alpha$ -bromo- or chloroacetyl groups are prepared, and the partner protein or polymer possesses the SH function. Peptides with a chloro- or bromoacetyl group were used for repetitive ligation of  $\alpha$ -helical peptide segments (26), assembly of peptide vaccines composed of T helper and B cell epitopes (27), or for attachment of peptides to antibodies (28). Sporadic reports are available in the literature on the reverse strategy. Jones et al. (29) reported on the synthesis and favorable tolerogenic activity of a peptide–PEG conjugate in which four copies of cyclic mimotope peptides containing an SH group were attached with iodo- or bromoacetylated PEG derivatives. During the preparation of a three-component conjugate, Grandjean et al. (30) have conjugated 2-thioethyl- $\alpha$ -D-mannopyranoside with a construct containing a single copy of a toxoid-derived epitope TT(830–846) peptide and glyoxylyl-*N*-chloroacetylated-L-lysine dendrimers. In this conjugate, four copies of the SH-carbohydrate component were attached to a tetrameric chloroacetylated Lys dendrimer.

Here we report on the preparation of sequential and polymeric polypeptides possessing chloroacetyl groups in multiple copies at the  $\alpha$ - and/or  $\epsilon$ -amino group of the polypeptides and its use for the conjugation of epitope peptides possessing a Cys at C-terminal position. With these constructs, we have performed a comparative study to understand of the effect of carrier structure on antibody recognition. Five conjugates containing different macromolecules as carrier, but identical and uniformly oriented epitope peptide from gD of herpes simplex virus (<sup>9</sup>LKNleADPNRFRGKDL<sup>22</sup>, [Nle<sup>11</sup>]-9–22), were prepared. Binding studies with monoclonal antibody (Mab) A16, recognizing the HSV gD-related epitope, [Nle<sup>11</sup>]-9–22 (31), were performed by direct and competitive ELISA. Data suggest that the chemical nature of the carrier and the degree of substitution have marked influence on the strength of antibody binding.

## EXPERIMENTAL PROCEDURES

Abbreviations used in this paper follow the rules of the IUPAC–IUB Commission of Biochemical Nomenclature (32) in accordance with the recommended nomenclature of graft polymers (32).

<sup>2</sup> Abbreviation: Ac, acetyl; Aib, aminoisobutyric acid, Boc, *tert*-butoxycarbonyl; BOP, benzotriazol-1-yloxytris(dimethylamino)phosphonium hexafluorophosphate; Bzl, benzyl; cHex, cyclohexyl; ClZ, 2-chlorobenzoyloxycarbonyl; DCC, *N,N*-dicyclohexylcarbodiimide; DCM, dichloromethane; DCU, *N,N*-dicyclohexylurea; DIEA, *N,N*-diisopropylethylamine; DMF, *N,N*-dimethylformamide; *DP<sub>n</sub>*, average ratio of polymerization; DTT, dithiothreitol; ESI, electrospray ionisation; FAB-MS, fast atom bombardment mass spectrometry; HATU, 2-(7-aza-1*H*-benzotriazol-1-yl)-1,1,3,3-tetramethyluronium hexafluorophosphate; HOBt, 1-hydroxybenzotriazole; HPLC, high performance liquid chromatography; HSV gD, Herpes simplex virus glycoprotein D; KLH, keyhole limpet hemocyanin; MALDI, matrix-assisted laser desorption; MAP, multiple antigenic peptide; MBHA, 4-methylbenzhydrylamine; MBS, *N*-(3-maleimidobenzoyloxy)succinimide; Mab, monoclonal antibody; Meb, 4-methylbenzyl; MeOH, methanol; MS, mass spectrometry; Npys, 3-nitro-2-pyridinesulfenyl; PEG, poly(ethylene glycol); SAK, poly[Lys(Ser<sub>0.9</sub>-DL-Ala<sub>3.5</sub>)]<sub>4</sub>; SIAB, *N*-succinimidyl 4-(iodoacetyl)-aminobenzoate; SMCC, succinimidyl 4-(*N*-maleimidomethyl)-cyclohexane-1-carboxylate; SOC, sequential oligopeptide carrier; SPDP, *N*-succinimidyl 3-(2-pyridyldithio)propionate; TBTU, 2-(1*H*-benzotriazol-1-yl)-1,1,3,3-tetramethyluronium tetrafluoroborate; TFA, trifluoroacetic acid; TLC, thin-layer chromatography; Tos, tosyl; UV, ultraviolet.

**Table 1. Characteristics of Polypeptide Carriers and Their [Nle<sup>11</sup>]-9–22 Conjugates**

carrier/conjugate	code	epitope/ conjugate (mol/mol) <sup>a</sup>	M + H <sup>+</sup> calcd/found
H- <sup>9</sup> Leu-Lys-Nle-Ala-Asp-Pro-Asn-Arg-Phe-Arg-Gly-Lys-Asp-Leu <sup>22</sup> -NH <sub>2</sub>	[Nle <sup>11</sup> ]-9–22	-	1641.9/1642.0 <sup>b</sup>
H- <sup>9</sup> Leu-Lys-Nle-Ala-Asp-Pro-Asn-Arg-Phe-Arg-Gly-Lys-Asp-Leu <sup>22</sup> -Cys-NH <sub>2</sub>	[Nle <sup>11</sup> ]-9–22-C	-	1744.9/1745.2 <sup>b</sup>
Ac-[Lys([Nle <sup>11</sup> ]-9–22)-Aib-Gly] <sub>4</sub> -OH	Ac-[SOC <sub>4</sub> ([Nle <sup>11</sup> ]-9–22) <sub>4</sub> ]	4.0	7641.0/7640.1 <sup>b</sup>
Ac-[Lys(ClAc)-Aib-Gly] <sub>4</sub> -OH	Ac-[SOC <sub>4</sub> (ClAc) <sub>4</sub> ]	-	1447.3/1447.2 <sup>b</sup>
Ac-[Lys([Nle <sup>11</sup> ]-9–22-Cys)-Aib-Gly] <sub>4</sub> -OH	Ac-[SOC <sub>4</sub> ([Nle <sup>11</sup> ]-9–22-C) <sub>4</sub> ]	4.0	8281.4/8281.2 <sup>b</sup>
H-[Thr-Lys-Pro-Lys(ClAc)-Gly] <sub>4</sub> -NH <sub>2</sub>	T20(ClAc) <sub>4</sub>	-	2364.5/2364.3 <sup>b</sup>
H-[Thr-Lys-Pro-Lys(Nle <sup>11</sup> )-9–22-Cys)-Gly] <sub>4</sub> -NH <sub>2</sub>	T20 ([Nle <sup>11</sup> ]-9–22-C) <sub>4</sub>	4.0	9202.5/9202.1 <sup>b</sup>
poly[Lys(ClAc)-Ser <sub>0.9</sub> -DL-Ala <sub>3.5</sub> ]	SAK(ClAc) <sub>1</sub>	-	n.t. <sup>c</sup>
poly{Lys([Nle <sup>11</sup> ]-9–22-Cys) <sub>x</sub> -Ser <sub>0.9</sub> -DL-Ala <sub>3.5</sub> }	SAK([Nle <sup>11</sup> ]-9–22-C) <sub>x</sub>	X <sup>d</sup>	n.t.
Lys(ClAc) <sub>2</sub> -Lys[Lys(ClAc) <sub>2</sub> ]-Arg-Arg-βAla-NH <sub>2</sub>	MAP(ClAc) <sub>4</sub> <sup>e</sup>	-	1089.4/1089.9 <sup>f</sup>
Lys{[Nle <sup>11</sup> ](9–22-Cys)} <sub>2</sub> -Lys[Lys{[Nle <sup>11</sup> ]-9–22-Cys}] <sub>2</sub> -Arg-Arg-βAla-NH <sub>2</sub>	MAP([Nle <sup>11</sup> ]-9–22-C) <sub>4</sub>	4.0	7919.4/7942.4 <sup>g</sup>

<sup>a</sup> Molar ratio calculated from the amino acid composition. <sup>b</sup> ESI-MS. <sup>c</sup> Not tested. <sup>d</sup> Four conjugates were X = 4.4, 5.4, 13.2, or 26.4. <sup>e</sup> Chloroacetyl groups at all four (α- and ε-) amino ends. <sup>f</sup> MALDI. <sup>g</sup> Na<sup>+</sup> adduct, MALDI.

**Synthesis of Epitope Peptides H-<sup>9</sup>LKNleADPNRFRGKDL<sup>22</sup>-NH<sub>2</sub> ([Nle<sup>11</sup>]-9–22) and H-<sup>9</sup>LKNleADPNRFRGKDL<sup>22</sup>C-NH<sub>2</sub> ([Nle<sup>11</sup>]-9–22-Cys).** The HSV gD-1 epitope peptide, H-<sup>9</sup>LKNleADPNRFRGKDL<sup>22</sup>-NH<sub>2</sub> ([Nle<sup>11</sup>]-9–22) and its elongated derivative with C-terminal Cys (H-<sup>9</sup>LKNleADPNRFRGKDL<sup>22</sup>C-NH<sub>2</sub>) ([Nle<sup>11</sup>]-9–22-Cys), were synthesized manually by solid-phase synthesis using an MBHA resin (0.5 g, 1.1 mmol/g capacity) and the Boc/Bzl strategy. The following *N*<sup>t</sup>-Boc-protected amino acids were used: Asp(OcHex), Lys(CIZ), Arg(Tos), and Cys(Meb). The protocol of the synthesis was the following: (i) deprotection with 33% TFA/DCM (2+20 min); (ii) DCM washing (5 × 0.5 min); (iii) neutralization with 10% DIEA/DCM (3 × 1 min); (iv) DCM washing (4 × 0.5 min); (v) coupling with three equivalent amino acid derivatives—DCC—HOBT in DCM—DMF 4:1 or 1:4 (v/v) mixture depending on the solubility of Boc-amino acid derivatives (60 min); (vi) DMF washing (1 × 0.5 min); (vii) DCM washing (2 × 0.5 min); (viii) ninhydrin (34) or isatin (35) assay. The peptides were cleaved from the resin by the aid of liquid HF in the presence of *p*-cresol and DTT (HF—*p*-cresol—DTT = 10 mL:1 g:0.1 g) for 1.5 h at 0 °C. The crude products were purified by RP-HPLC using a Delta Pak C<sub>18</sub> semipreparative column (300 × 19 mm, 10 μm, 300 Å). The purified peptides were analyzed by RP-HPLC (*t*<sub>R</sub> = 30.9 min for [Nle<sup>11</sup>]-9–22, and *t*<sub>R</sub> = 31.4 min for [Nle<sup>11</sup>]-9–22-Cys), amino acid analysis (data not shown) and ESI-MS (Table 1).

**Synthesis of Chloroacetylated Tetrafluorotyrosine Analogue (H-[Thr-Lys-Pro-Lys(ClAc)-Gly]<sub>4</sub>-NH<sub>2</sub>, T20-(ClAc)<sub>4</sub>).** Chloroacetylated tetrafluorotyrosine analogue (H-[Thr-Lys-Pro-Lys(ClAc)-Gly]<sub>4</sub>-NH<sub>2</sub>, T20(ClAc)<sub>4</sub>) was synthesized using MBHA resin (0.5 g, 1.1 mmol/g capacity) and the Boc/Bzl strategy. The following *N*<sup>t</sup>-Boc-protected amino acids were used: Lys(CIZ), Lys(Fmoc), and Thr(Bzl). The protocol described above for the epitope peptide was used. Chloroacetyl groups were introduced at the *N*<sup>t</sup>-amino group of Lys residues using chloroacetic acid pentachlorophenyl ester in 5 equiv excess in DMF after removal of *N*<sup>t</sup>-Fmoc groups by 20% piperidine/DMF. The chloroacetylated peptides were cleaved from the resin by the aid of anhydrous HF—*m*-cresol—*p*-thiocresol (10 mL:0.5 mL:0.5 g) for 1.5 h at 0 °C (36). The crude product was purified by RP-HPLC using a Delta Pak C<sub>18</sub> semipreparative column (300 × 19 mm, 10 μm, 300 Å). The purified peptides were analyzed by RP-HPLC (*t*<sub>R</sub> = 23.7 min), amino acid analysis and ESI-MS (Table 1). The yield was 65%.

**Synthesis of Chloroacetylated Sequential Oligopeptide (Ac-[Lys(ClAc)-Aib-Gly]<sub>4</sub>-OH, Ac-[SOC<sub>4</sub>(ClAc)<sub>4</sub>].** Chloroacetylated sequential oligopeptide carrier (Ac-[Lys(ClAc)-Aib-Gly]<sub>4</sub>-OH, Ac-[SOC<sub>4</sub>(ClAc)<sub>4</sub>]) was synthesized using a PAM resin and the Boc/Bzl strategy.

Boc-Lys(Fmoc) as side chain protected amino acid derivative was used. The protocol for the synthesis was as follows: (i) deprotection with 40% TFA/DCM (1 × 2 min, 1 × 13 min); (ii) washing DCM (3 × 1 min), MeOH (3 × 1 min), DCM (3 × 1 min); (iii) neutralization with 10% DIEA/DCM (2 × 2 min); (iv) washing DCM (3 × 1 min), MeOH (3 × 1 min), DCM (3 × 1 min); (v) coupling of three equivalent amino acid derivatives—TBTU—HOBT in DCM/DMF 1:1 (60 min); (vi) washing DCM (3 × 1 min), MeOH (3 × 1 min), DCM (3 × 1 min) vii) ninhydrin assay. Chloroacetyl groups were introduced at the *N*<sup>t</sup>-amino group of Lys residue by chloroacetic acid pentachlorophenyl ester as described above after removal of *N*<sup>t</sup>-Fmoc groups by 40% piperidine/DMF. The product was cleaved from the resin with anhydrous HF in the presence of anisole and phenol (10% v/v) as scavengers at –8 °C for 30 min and 0 °C for 1 h. The crude product was purified by RP-HPLC using a Supelco Discovery C<sub>18</sub> semipreparative column (250 mm × 10 mm, 5 μm). The purified peptides were analyzed by RP-HPLC (*t*<sub>R</sub> = 40.5 min) and ESI-MS (Table 1). The yield was 42%.

**Conjugation of Peptide H-<sup>9</sup>LKNleADPNRFRGKDL<sup>22</sup>C-NH<sub>2</sub> ([Nle<sup>11</sup>]-9–22-Cys) with Sequential Oligopeptides Using Thioether Linkage.** 40 mg of sequential glycopeptides Ac-(Lys(ClAc)-Aib-Gly)<sub>4</sub>-OH (Ac-[SOC<sub>4</sub>(ClAc)<sub>4</sub>]) or H-[Thr-Lys-Pro-Lys(ClAc)-Gly]<sub>4</sub>-NH<sub>2</sub> (T20(ClAc)<sub>4</sub>) containing four chloroacetyl groups was dissolved in 40 mL of 0.1 M Tris-HCl (pH 8.0) .1.2–1.4 equiv (calculated for the chloroacetyl content of the oligopeptides) of epitope peptide ([Nle<sup>11</sup>]-9–22-Cys) was added to the solution of chloroacetylated oligopeptides over a period of time in solid form. The mixtures were stirred at RT. The reaction was monitored by RP-HPLC and proceeded for 24–72 h. The conjugates were purified by RP-HPLC and were characterized by *t*<sub>R</sub> values (*t*<sub>R</sub> = 31.8 min for Ac-[SOC<sub>4</sub>(ClAc)<sub>4</sub>], *t*<sub>R</sub> = 31.0 min for T20-(ClAc)<sub>4</sub>), the amino acid compositions, and mass value presented in Table 1. The yields of purified conjugates were over 60% in all cases. The conjugates were designated as Ac-[SOC<sub>4</sub>([Nle<sup>11</sup>]-9–22-C)<sub>4</sub>] and T20([Nle<sup>11</sup>]-9–22-C)<sub>4</sub>, respectively.

**Synthesis of Chloroacetylated Multiple Antigenic Peptide (ClAc-Lys(ClAc)-Lys(ClAc-Lys(ClAc))-Arg-Arg-βAla-NH<sub>2</sub>, MAP(ClAc)<sub>4</sub>).** The lysine dendrimer (ClAc-Lys(ClAc)-Lys(ClAc-Lys(ClAc))-Arg-Arg-βAla-NH<sub>2</sub>, MAP(ClAc)<sub>4</sub>), was synthesized stepwise using MBHA resin (0.7 mmol/g, 145 mg) of. The side chains of Arg and Lys were protected with Tos and Boc groups, respectively, the latter to allow creation of the dendrimeric structure. The synthesis protocol was as follows: (i) deprotection with 30% TFA/DCM (2+20 min); (ii) DCM washing (6 × 1 min); (iii) neutralization with 5% DIEA/DCM (3 × 1 min); (iv) DCM washing (4 × 0.5 min); (v) DMF washing



(3 × 0.5 min); (vi) coupling with 3 equiv of Boc-amino acid, in the presence of an equimolar amount of TBTU and 2-fold molar excess DIEA in DMF for 1 h; (vii) DMF washing (3 × 0.5 min); (viii) DCM washing (3 × 0.5 min); (ix) ninhydrin test. After assembly of the peptide chain was completed, the Boc protecting groups of the two outlying Lys residues were removed as above, and the resulting  $\alpha$ - and  $\epsilon$ -amino groups were acylated with chloroacetyl chloride (3 equiv) in the presence of DIEA (3 equiv) in DCM. The peptide was deprotected and cleaved off the resin by treatment with HF/*p*-cresol (9:1; v/v) for 1 h at 0 °C. The product was purified by semipreparative RP-HPLC and resulted in homogeneous material ( $t_R$  = 22.4) characterized by amino acid analysis and MALDI-TOF mass spectrometry (Table 1). The yield was 50%.

**Conjugation of the peptide H-<sup>9</sup>LKNleADPNRFRGKDL<sup>22</sup>C-NH<sub>2</sub> ([Nle<sup>11</sup>]-9-22-Cys) with Chloroacetylated Multiple Antigenic Peptide (ClAc-Lys(ClAc)-Lys(ClAc-Lys(ClAc))-Arg-Arg- $\beta$ -Ala-NH<sub>2</sub>, MAP(ClAc)<sub>4</sub>) Using a Thioether Linkage.** Conjugation was performed by reacting 14 mg (8  $\mu$ mol) of [Nle<sup>11</sup>]-9-22-Cys peptide with 1.1 mg (1  $\mu$ mol) of MAP(ClAc)<sub>4</sub> in 0.1 M Tris-HCl buffer, pH 8, under N<sub>2</sub> atmosphere. The reaction was monitored by RP-HPLC. After 24 h the expected tetravalent MAP([Nle<sup>11</sup>]-9-22-C)<sub>4</sub> was found by MALDI-TOF mass spectrometry as a minor component of the main peak. Preparative HPLC purification resulted in a homogeneous fraction, that was characterized by RP-HPLC ( $t_R$  = 19.3 min) and MALDI-TOF MS (linear mode). The yield was 55%. The conjugate was designated as MAP-[Nle<sup>11</sup>]-9-22-C)<sub>4</sub>.

**Tandem Synthesis of Conjugate (Ac-SOC<sub>4</sub>([Nle<sup>11</sup>]-9-22)<sub>4</sub>) Composed of Sequential Oligopeptide Carrier (SOC<sub>4</sub>) and H-<sup>9</sup>LKNleADPNRFRGKDL<sup>22</sup>-NH<sub>2</sub> ([Nle<sup>11</sup>]-9-22) with an Amide Linkage.** The conjugate was prepared by tandem synthesis on a PAM resin using the Boc/Bzl strategy. The following side chain protected *N*<sup>t</sup>-Boc amino acids were used: Asp(OBzl), Lys(Fmoc) and Arg(Tos). First the carrier Ac-[Lys(Fmoc)-Aib-Gly]<sub>4</sub>-OH was synthesized. After completion and *N*<sup>t</sup>-acetylation by acetic anhydride, the *N*<sup>t</sup>-Fmoc-group was removed and the epitope peptide was built up on the  $\epsilon$ -amino groups of lysines according to the Ac-[SOC<sub>4</sub>(ClAc)]<sub>4</sub> protocol described above. The conjugate was cleaved from the resin with HF in the presence of anisole and phenol (10% v/v) as scavengers at -8 °C for 30 min and 0 °C for 1 h. The crude product was purified by RP-HPLC using a Supelco Discovery C<sub>18</sub> semipreparative column (250 mm × 10 mm, 5  $\mu$ m). The purified conjugate was analyzed by RP-HPLC and ESI-MS (Table 1). The yield was 20%. The conjugates were designated as Ac-[SOC<sub>4</sub>([Nle<sup>11</sup>]-9-22)<sub>4</sub>].

**Synthesis of Chloroacetylated Branched Polypeptide Poly[Lys(ClAc-Ser<sub>1</sub>-DL-Ala<sub>m</sub>)] (SAK(ClAc)<sub>j</sub>).** Branched chain polymer polypeptide poly[Lys(Ser<sub>0.9</sub>-DL-Ala<sub>3.5</sub>)] (SAK) with polylysine backbone was produced as described earlier (9). Briefly, poly[Lys] was synthesized by polymerization of *N*<sup>t</sup>-carboxy-*N*<sup>t</sup>-benzyloxycarbonyl-lysine anhydride (average degree of polymerization: 60). After cleavage of the protecting groups, poly[Lys(DL-Ala<sub>3.5</sub>)] (AK) was prepared by grafting of short oligomeric DL-Ala side chains using the respective *N*<sup>t</sup>-carboxy-alanine anhydride onto the  $\epsilon$ -amino groups of poly[Lys]. Benzyloxycarbonyl-protected amino acid derivative (Z-Ser-OPcp) was coupled to the end of the side chains of AK by the HOBt-catalyzed active ester method (37). Blocking groups were removed completely with HBr in

glacial acetic acid. The composition of SAK was determined by amino acid analysis. The size and molecular weight of polymer was calculated from the amino acid composition and the sedimentation analysis of polylysine (38).

Chloroacetylation of SAK was carried out as follows: 80 mg (0.145 mmol) SAK-HBr salt ( $\overline{DP}_n$  = 60,  $M_{w,monomer}$  = 550) was dissolved in 1 mL water, and the solution was diluted with 4 mL of DMF. Chloroacetyl groups were introduced at the *N*<sup>t</sup>-amino group of Ser residues by chloroacetic acid pentachlorophenyl ester. Six different SAK-ClAc-OPcp ratios were used (1:1, 1:0.8, 1:0.6, 1:0.5, 1:0.4, and 1:0.3 mol/mol; 50 mg, 40 mg, 30 mg, 25 mg, 20 mg, 15 mg of ClAc-OPcp, respectively), and the active ester was added to the polymer-containing solution dissolved in 5 mL of DMF. The reaction mixtures were stirred overnight at room temperature. The solution was dialyzed for 2 days in Visking tubes (cut-off 8000–12000) against 0.1% acetic acid and freeze-dried. According to the Cl analysis of six SAK derivatives: 46.5%, 45.9%, 48.5%, 41.3%, 30.1%, and 21.7% of the side chains were blocked by ClAc groups, respectively.

**Conjugation of the Peptide H-<sup>9</sup>LKNleADPNRFRGKDL<sup>22</sup>C-NH<sub>2</sub> ([Nle<sup>11</sup>]-9-22-Cys) with Chloroacetylated Branched Polypeptide Poly[Lys(ClAc-Ser<sub>1</sub>-DL-Ala<sub>m</sub>)] (SAK(ClAc)<sub>j</sub>) Using a Thioether Linkage.** For conjugation of epitope peptide to chloroacetylated SAK, four differently substituted carriers were applied. Fifteen milligrams of SAK(ClAc)<sub>48.5</sub>, SAK(ClAc)<sub>41.3</sub>, SAK(ClAc)<sub>30.1</sub>, or SAK(ClAc)<sub>21.7</sub> (acetate salt form) was dissolved in 100 mL of 0.1 M Tris-HCl (pH 8.2). A 1.2 equiv (calculated for the chloroacetyl content of the polymers) amount of epitope peptide (23.4 mg, 20 mg, 14.8 mg, and 10.6 mg, respectively) were added in two portions to the solution. The conjugations proceeded for 24 h, and then they were terminated by addition of an excess of Cys to block the unreacted chloroacetyl groups. The solutions were dialyzed in Visking tubes (cut-off 8000–12000) for 2 days against water. The average degree of substitution was calculated from the amino acid analysis. Depending on the input molar ratio, 44%, 22%, 9%, and 7% of the side chains were substituted by epitope peptide, respectively. The conjugates were designated as SAK([Nle<sup>11</sup>]-9-22-C)<sub>x</sub>.

**Conjugation of the Peptide H-<sup>9</sup>LKNleADPNRFRGKDL<sup>22</sup>C-NH<sub>2</sub> ([Nle<sup>11</sup>]-9-22-Cys) with Keyhole Limpet Hemocyanin (KLH) Using a Thioether Linkage.** The conjugation involved three steps: (i) KLH activation with *m*-maleimidobenzoic acid *N*-hydroxysuccinimido ester (MBS), (ii) Sephadex G25 purification, and (iii) coupling of the peptide epitope to the purified, activated protein (19). Briefly, to 3.75 mg of KLH in 0.01 M PBS was added dropwise 112  $\mu$ L of a 20 mg/mL solution of MBS in DMF. After 30 min the reaction mixture was loaded onto a Sephadex G-25 column (16 × 1 cm) eluted with 0.05 M PBS, pH 6, at a flow rate of 20 mL/h, to separate the KLH-MBS adduct from excess MBS and nonactivated KLH. One milliliter fractions were collected and monitored at  $\lambda$  = 280 nm. The KLH-MBS adduct usually was eluted in fractions 5–10. To the pooled, KLH-MBS-containing fractions was slowly added 3.75 mg of freeze-dried peptide. The pH was adjusted to 7.5 with 0.1 M NaOH, and the reaction was allowed to proceed for 3 h and then dialyzed in Visking tube (MW cut-off 8000–12000 Da) against 4 × 1 L of 10 mM PBS, pH 8. An aliquot of the peptide-KLH conjugate solution was hydrolyzed and subjected to amino acid analysis (see below) to determine the molar peptide/KLH ratio. The conjugate was designated as MAP([Nle<sup>11</sup>]-9-22-C)<sub>4</sub>.



**RP-HPLC.** RP-HPLC analysis of peptides [Nle<sup>11</sup>]-9–22, [Nle<sup>11</sup>]-9–22-C, T20(CIAC)<sub>4</sub>, and conjugates Ac-[SOC<sub>4</sub>([Nle<sup>11</sup>]-9–22-C)<sub>4</sub>], T20 ([Nle<sup>11</sup>]-9–22-C)<sub>4</sub>, was performed using a Phenomenex Jupiter C<sub>18</sub> (250 × 4.6 mm, 5 μm, 300 Å) reverse phase column with Knauer apparatus (H. Knauer, Bad Homburg, Germany). The instrument was assembled from two HPLC Pumps 64, a variable wavelength monitor, and functionalized by HPLC Software/Hardware Package Version 2.21 A. The type of columns, gradients, and solvents are summarized below. Eluent A was 0.1% TFA in water, and eluent B was 0.1% TFA in acetonitrile–water (80:20 V/V). A linear gradient (0 min 0% B; 5 min 0% B; 50 min 90% B) at a flow rate of 1 mL/min was used as mobile phase. Detection was performed at λ = 220 nm. Purification was carried out on a Phenomenex Jupiter C<sub>18</sub> (250 × 10 mm, 10 μm, 300 Å) semipreparative column using the same eluents at a flow rate of 5 mL/min. The gradient was 0 min 10% B; 5 min 10% B; 50 min: 50% B. Detection was carried out at λ = 220 nm.

HPLC analysis of Ac-[Lys([Nle<sup>11</sup>]-9–22)-Aib-Gly]<sub>4</sub>-OH was performed using a Supelco Discovery C<sub>18</sub> (250 mm × 4.6 mm, 5 μm, 300 Å) reverse phase column with a Waters instrument equipped with a Waters 616 pump and a Waters 996 photodiode array detector. Eluent A was 0.1% TFA in water, and eluent B was 0.1% TFA in acetonitrile. A linear gradient 15% to 35% acetonitrile in 0.1% TFA at a flow rate of 1 mL/min. Purification was carried out on a Waters 4000 semipreparative instrument using a Supelco Discovery C<sub>18</sub> (250 mm × 10 mm, 5 μm, 300 Å) column with the same linear gradient at a flow rate of 4.7 mL/min. Detection was carried out at λ = 214 nm.

HPLC analysis of ClAc-Lys(CIAC)-Lys(CIAC-Lys(CIAC))-Arg-Arg-β-Ala-NH<sub>2</sub> (MAP(CIAC)<sub>4</sub>) and its epitope conjugate was performed on a Shimadzu (Japan) HPLC system using a Vydac C<sub>18</sub> column, linear 10–40% gradient of acetonitrile (0.036% TFA) into water (0.045% TFA) over 30 min at 1 mL/min. Purification was carried out on a Vydac C<sub>18</sub> column (200 mm × 25 mm, 20 μm) in a Waters Delta Prep 4000 system using a linear 10 to 30% gradient of acetonitrile (0.1% TFA) into water (0.1% TFA) over 60 min at 3 mL/min flow rate. Detection was performed at λ = 214 nm.

**Amino Acid Analysis.** The amino acid composition of sequential oligopeptides (SOC<sub>n</sub>, tetratuftsin analogue), branched polypeptide (SAK), keyhole limpet hemocyanin (KLH), epitope peptide, and their conjugates was determined by amino acid analysis using a Beckman (Fullerton, CA) model 6300 amino acid analyzer. Prior to the analysis, samples were hydrolyzed in 6 M HCl in sealed and evacuated tubes at 110 °C for 24 h.

**Mass Spectrometry.** Positive ion electrospray ionization mass spectrometric (ESI-MS) analyses of peptides [Nle<sup>11</sup>]-9–22, [Nle<sup>11</sup>]-9–22-C, T20(CIAC)<sub>4</sub>, and conjugates Ac-[SOC<sub>4</sub>([Nle<sup>11</sup>]-9–22-C)<sub>4</sub>], T20 ([Nle<sup>11</sup>]-9–22-C)<sub>4</sub>, were performed on a PE API 2000 triple quadrupole mass spectrometer (Sciex, Toronto, Canada). Spray voltage was set to 4.8 kV, and 30 V orifice voltage was applied. Samples were dissolved in methanol–water (1:1 V/V) mixture containing 0.1% acetic acid, and 5 μL of sample was injected at a flow rate of 100 μL/min. The instrument was used in Q<sub>1</sub> scan mode in the range of *m/z* 400–1700, with a step size of 0.3 amu and a dwell time of 0.5 ms.

Positive and negative ion electrospray ionization mass spectrometric (ESI-MS) analyses of Ac-[Lys([Nle<sup>11</sup>]-9–22)-Aib-Gly]<sub>4</sub>-OH and Ac-[Lys(CIAC)-Aib-Gly]<sub>4</sub>-OH were performed on a Micromass Platform LC-MS. Capillary and cone voltages were set to 3 kV and 40 V, respectively.

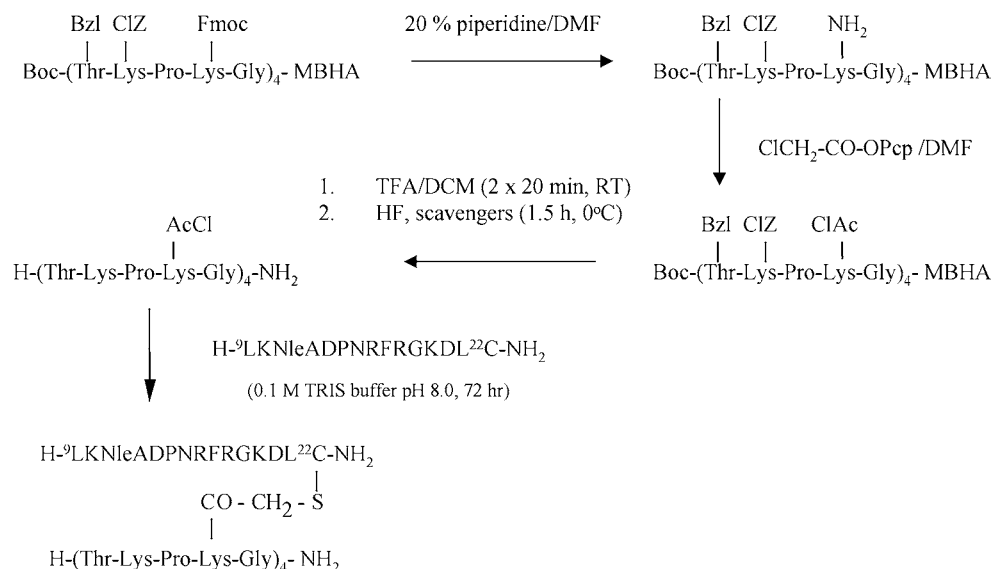
Samples were dissolved in water/acetonitrile/trifluoroacetic acid (1/1/0.05 V/V/V).

MALDI-TOF mass spectra of ClAc-Lys(CIAC)-Lys(CIAC-Lys(CIAC))-Arg-Arg-β-Ala-NH<sub>2</sub> (MAP(CIAC)<sub>4</sub>) and its epitope conjugate were recorded in a Voyager DE-STR instrument (Applied Biosystems, Foster City, CA) operating routinely in the linear mode and using α-cyano-4'-hydroxycinnamic acid as matrix.

**Enzyme-Linked Immunosorbent Assay (ELISA).** Throughout the ELISA studies culture medium of the hybridoma cell line Mab A16 was used. The preparation of Mab A16 has been described earlier (31, 39, 40). Briefly, Mab A16 was isolated after immunization of mice with extracts of HSV-1 infected cells. Hybridomas reactive with HSV were isolated. The isolated hybridomas were screened for reactivity with HSV specific proteins. Mab A16, isotype IgG2a, is reactive with HSV glycoprotein D. The Mab A16 is a conformation-independent monoclonal antibody and is classified together with Mabs LP14, ID3 as a group VII monoclonal antibody of gD (39, 41). The epitope of group VII Mabs is located within residues 9–19 of mature gD (39, 42).

In the direct ELISA, a standard dilution, containing an excess Mab A16, was used in combination with serial dilutions of the conjugates, used as coating antigen. For the direct ELISA, 96-well ELISA plates (Greiner Labortechnik, Germany) were coated with serial dilutions of peptide 9–22 and the conjugates (dilutions started at 100 ng/well). The dilutions were made in coating buffer (0.05 M sodium carbonate-bicarbonate buffer, pH 9.6). Plates were incubated overnight 4 °C or 2 h at 37 °C. After coating, the plates were washed three times with washing buffer (0.3% Tween-20, 1.0 M NaCl, in phosphate-buffered saline, pH 7.2 (PBS)). The monoclonal antibody A16 was diluted in dilution buffer (0.3% Tween-20, 0.2 M NaCl, in PBS), and 100 μL of the standard dilution Mab A16 was added to each well. Thereafter, the plates were incubated at room temperature for 1 h and subsequently washed three times with washing buffer. Then 100 μL of peroxidase-conjugated goat anti-mouse IgG (Dako, Denmark) diluted 1000 times in dilution buffer was added to each well, and the plates were incubated at 37 °C for 1 h. After incubation, the plates were washed three times with washing buffer and 100 μL of *o*-phenylenediamine dihydrochloride (0.5 mg/mL) in substrate buffer (0.05 M sodium phosphate-citrate buffer, pH 5.0) with 100 μL of 30% hydrogen peroxide per 100 mL of substrate buffer was added. After 30 min, the reaction was stopped by adding 50 μL of 2 M H<sub>2</sub>SO<sub>4</sub> and the absorbance at λ = 490 nm was measured. The concentration of the peptide/conjugate construct which gave an OD<sub>490</sub> of 1.0 by a standard dilution of Mab A16 was calculated.

The competition ELISA was performed as described earlier (31, 39). Briefly, 2-fold dilution series of peptide LKNleADPNRFRGKDL ([Nle<sup>11</sup>]-9–22) of gD and the conjugates containing peptide ([Nle<sup>11</sup>]-9–22) were preincubated for 2 h at room temperature with optimal concentrations (dilution 800×) of Mab A16 (38). After preincubation, the residual binding capacity of Mab A16 in the preincubation mixture was determined by ELISA in microtiter wells coated with peptide ([Nle<sup>11</sup>]-9–22 (0.5 μg/well)). As standard, a serial dilution of peptide ([Nle<sup>11</sup>]-9–22 with a fixed dilution of Mab A16 was always included: approximately 3 pmol of peptide ([Nle<sup>11</sup>]-9–22 present per 100 μL resulted in an OD<sub>490</sub> of 1.0. The relative amount of peptide ([Nle<sup>11</sup>]-9–22 present in the conjugates giving a residual OD<sub>490</sub> of 1.0 was estimated graphically from plots of OD vs peptide concentrations.



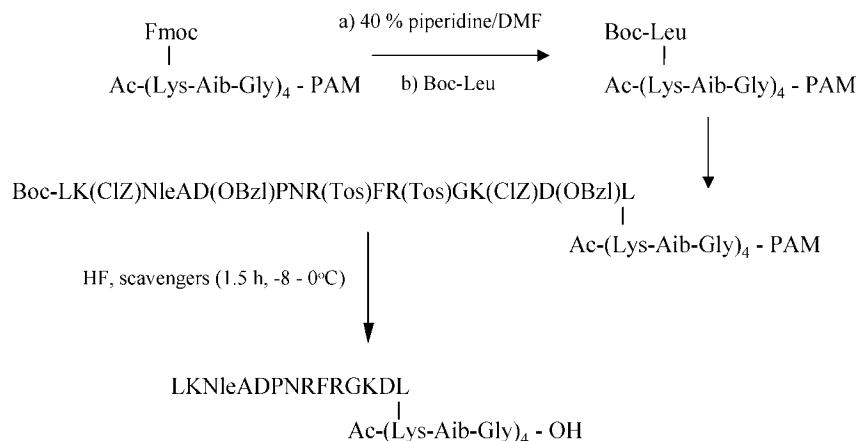
**Figure 2.** Outline of the synthesis of ([Nle<sup>11</sup>]-9-22-Cys) conjugate with chloroacetylated tetratuftsin analogue T20(ClAc)<sub>4</sub> by introduction of a thioether bond.

## RESULTS AND DISCUSSION

**Synthesis and Chemical Characterization of [Nle<sup>11</sup>]-9-22-polypeptide Conjugates.** The coupling of epitope peptide with the sequence according to herpes simplex virus type 1 glycoprotein D (HSV gD-1) was coupled to sequential polypeptide carriers (SOC<sub>4</sub> (8), tetratuftsin analogue T20 (7), to branched chain polymeric polypeptide SAK (10, 43), and to Lys-dendrimer (11) (Figure 1) by the introduction of thioether linkage. For this, thiol group was incorporated by elongation the peptide with a Cys residue at its C-terminal, H-<sup>9</sup>LKNleADPNRFRGKDL<sup>22</sup>C-NH<sub>2</sub>. Simultaneously, sequential oligopeptides and Lys-dendrimers were assembled by solid-phase synthesis using the Boc/Bzl strategy and MBHA or PAM resins. Chloroacetyl groups were introduced into the polypeptides by chloroacetic acid pentachlorophenyl ester after removal of Fmoc groups (tetratuftsin analogue, SOC<sub>n</sub>) or Boc-groups (Lys-dendrimer). It should be noted that the chloroacetylated derivative of the SOC<sub>4</sub> oligopeptide (Ac-[Lys(ClAc)-Aib-Gly]<sub>4</sub>-OH), the tetratuftsin analogue (H-[Thr-Lys-Pro-Lys(ClAc)-Gly]<sub>4</sub>-NH<sub>2</sub>), and the Lys-dendrimer (ClAc-Lys(ClAc)-Lys(ClAc-Lys(ClAc))-Arg-Arg-β-Ala-NH<sub>2</sub>) were tetravalent, e.g., contained four ClAc groups. The synthesis of the chloroacetylated tetratuftsin derivative is outlined in Figure 2. The scheme indicates that selective side chain protection strategy was used to provide access only to every second Lys residues in the sequence. After removal of Fmoc blocking groups, the chloroacetyl moiety was introduced. This strategy allowed us to design the number and position of epitopes after conjugation. In the case of SOC<sub>4</sub> oligopeptide (Ac-[Lys(ClAc)-Aib-Gly]<sub>4</sub>-OH) and Lys-dendrimer, all four ε- and α- plus ε-amino groups were chloroacetylated. The synthetic peptides containing chloroacetyl moiety at their N<sup>ε</sup>- and/or N<sup>α</sup>-Lys amino groups were cleaved from the resins by HF in the presence of appropriate scavengers by the simultaneous liberation of the peptide and cleavage of Bzl, Tos, and ClZ protections (an example of the strategy is shown in Figure 2). Compounds were purified on RP-HPLC prior to the conjugation. Conjugation reactions were carried out in solution using 0.1 M Tris-HCl (pH 8.0). To avoid dimerization, the cysteine containing epitope peptide ([Nle<sup>11</sup>]-9-22-Cys) was added in solid form to the solution of chloroacetylated polypeptides (1 mg/mL) over a period

of time. The reaction was monitored by HPLC and mass spectrometric analysis of samples and proceeded for 2–3 days. For conjugation of peptide H-<sup>9</sup>LKNleADPNRFRGKDL<sup>22</sup>C-NH<sub>2</sub> ([Nle<sup>11</sup>]-9-22-Cys) with tetratuftsin analogue (H-[Thr-Lys-Pro-Lys(ClAc)-Gly]<sub>4</sub>-NH<sub>2</sub>), the formation of thioether linkage is a stepwise and time-consuming process. First, we observed the appearance of the monosubstituted compound. After 3.5 h, two additional peaks were present: the conjugate with two copies of the epitope peptide and also the dimeric form of the peptide. At 29 h no unsubstituted chloroacetyl tuftsin analogue was present in the reaction mixture which was predominated by conjugates containing three or four copies of the epitope peptides. After reduction with DTT, at the end of the reaction (72 h) mainly the tetravalent target compound and peptide [Nle<sup>11</sup>]-9-22-Cys applied in excess were present. It should be noted that the excess of the Cys-peptide was recovered. Conjugates were purified by RP-HPLC and characterized by *t<sub>R</sub>* values, amino acid compositions from amino acid analysis, and relative molar mass. Even the Lys-dendrimer conjugation reaction resulted in a satisfactory end product. The yields of purified conjugates were over 60%.

For the preparation of multivalent epitope conjugates, branched chain polymeric polypeptide (SAK) was reacted with chloroacetic acid pentachlorophenyl ester in DMF–water (9:1, v/v) solution. The conjugation with peptide [Nle<sup>11</sup>]-9-22-Cys resulting in a thioether linkage between the carrier and epitope peptide was performed similarly to the MAP, SOC<sub>4</sub>, and tetratuftsin analogue constructs. The conjugation reaction was terminated after 24 h by addition of an excess of Cys to block the unreacted chloroacetyl groups. The crude product was dialyzed against water to remove of uncoupled peptide and Cys. By using various input peptide/polymer molar ratios, we have prepared conjugates in which 7–44% of the side chains were substituted by the epitope peptide, as determined from amino acid analysis. The KLH conjugate of peptide [Nle<sup>11</sup>]-9-22-Cys was prepared by using *N*-succinimidyl *m*-maleimidobenzoate activated protein as described in the literature (20). For comparison, we have produced a conjugate of the SOC<sub>4</sub> oligopeptide. In this tetravalent construct—instead of a thioether bond—an amide linkage connected the epitope and to the carrier (Figure 3). For this, a tandem solid-phase synthesis



**Figure 3.** Outline of the tandem synthesis of  $[(\text{Nle}^{11})\text{-9-22}]$  conjugate with sequential oligopeptide carrier (Ac-(SOC<sub>4</sub>)) using an amide bond.

**Table 2.** Binding of HSV Glycoprotein D Type 1 Specific Monoclonal Antibody A16 to  $[(\text{Nle}^{11})\text{-9-22}]$  Epitope-conjugates. The Effect of the Carrier and of the Degree of Epitope Substitution

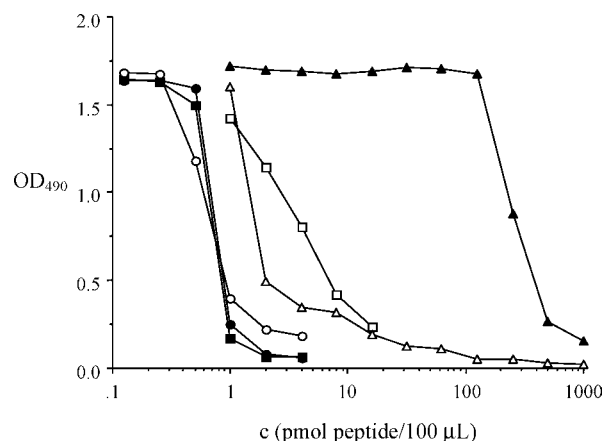
peptide/conjugate	carrier	linkage	degree of substitution epitope/conjugate (mol/mol) <sup>a</sup>	direct ELISA <sup>b</sup> (ng/100 $\mu\text{L}$ )	competition ELISA <sup>c</sup> (pmol/100 $\mu\text{L}$ )
<sup>9</sup> LKNleADPNRFRGKDL <sup>22</sup>	-	-	-	51.2	3.0
<sup>9</sup> LKRADPNRFRGKDL <sup>22</sup>	-	-	-	41.7	2.0
Ac-[SOC <sub>4</sub> [(Nle <sup>11</sup> )-9-22-C] <sub>4</sub> ]	Ac-(SOC) <sub>4</sub>	amide	4.0	9.3	0.62
Ac-[SOC <sub>4</sub> [(Nle <sup>11</sup> )-9-22-C] <sub>4</sub> ]	Ac-[SOC <sub>4</sub> (AcCl)] <sub>4</sub>	thioether	4.0	2.9	0.7
T20[(Nle <sup>11</sup> )-9-22-C] <sub>4</sub>	T20	thioether	4.0	3.4	0.72
SAK[(Nle <sup>11</sup> )-9-22-C] <sub>x</sub>	SAK	thioether	9.0	3.4	1.5
SAK[(Nle <sup>11</sup> )-9-22-C] <sub>x</sub>	SAK	thioether	22.0	0.5	0.74
SAK[(Nle <sup>11</sup> )-9-22-C] <sub>x</sub>	SAK	thioether	44.0	1.3	1.3
MAP[(Nle <sup>11</sup> )-9-22-C] <sub>4</sub>	MAP	thioether	4.0	7.5	n.i. <sup>d</sup>
KLH[(Nle <sup>11</sup> )-9-22-C] <sub>x</sub>	KLH	thioether	270	13.6	157.0

<sup>a</sup> Molar ratio calculated from the amino acid composition. <sup>b</sup> The lowest amount in ng peptide per 100  $\mu\text{L}$  to obtain an OD = 1.0. <sup>c</sup> pmol peptide per 100  $\mu\text{L}$  needed to obtain a residual OD = 1.0. Values are based on the amounts of epitope peptide present in the conjugate. <sup>d</sup> Not interpretable.

strategy was used. After completion of the assembly of the 68-mer conjugate, the compound was cleaved from the resin by HF in the presence of appropriate scavengers.

**Comparison of the Reactivity of the Peptide  $[(\text{Nle}^{11})\text{-9-22}]$  Conjugates against Mab A16.** The peptide conjugates were compared for reactivity against Mab A16 in the direct and competition ELISA. In direct ELISA, two different properties of the conjugates are measured: the reactivity of the conjugates against Mab A16, and the coating properties of the conjugates to the polystyrene of the ELISA plates. Coating of the conjugates to the polystyrene may affect the accessibility of the epitope by the Mab and makes interpretation of the results difficult. Differences in reactivity could be due either to the nature of the conjugates or to the binding properties of the conjugates to the polystyrene. Therefore, the reactivity of the conjugates and the Mab in solution were determined as well in the competition ELISA.

In the direct ELISA peptide conjugates, peptide  $[(\text{Nle}^{11})\text{-9-22}]$  and the conjugates were coated to ELISA plates. Subsequently Mab A16 and peroxidase-conjugated anti-monoclonal antibody was added. The results are summarized in Table 2. For peptide  $[(\text{Nle}^{11})\text{-9-22}]$ , 51.2 ng per 100  $\mu\text{L}$  was required for coating to obtain an OD<sub>490</sub> of 1.0. Substantially less of the conjugated peptide was needed. It should be noted that the comparison was made based on the amount of the epitope peptide present in the conjugates and not on the total amount of conjugate. For the conjugates of Ac-[SOC<sub>4</sub>[(Nle<sup>11</sup>)-9-22-C]<sub>4</sub>], T20-[(Nle<sup>11</sup>)-9-22-C]<sub>4</sub>, and SAK[(Nle<sup>11</sup>)-9-22-C]<sub>x</sub> roughly the same amount, approximately 3–4 ng of peptide, present in the conjugates was required, while for Ac-[SOC<sub>4</sub>-



**Figure 4.** Reactivity of HSV glycoprotein D type 1 specific monoclonal antibody A16 to  $[(\text{Nle}^{11})\text{-9-22}]$  epitope conjugates in competition ELISA. The effect of the carrier on the binding. Peptide 9-22 ( $\square$ ), T20  $[(\text{Nle}^{11})\text{-9-22-C}]_4$  ( $\bullet$ ), Ac-[SOC<sub>4</sub>[(Nle<sup>11</sup>)-9-22-C]<sub>4</sub>] ( $\circ$ ), Ac-[SOC<sub>4</sub>[(Nle<sup>11</sup>)-9-22-C]<sub>x</sub>] ( $\triangle$ ), KLH  $[(\text{Nle}^{11})\text{-9-22-C}]_x$  ( $\blacktriangle$ ).

$[(\text{Nle}^{11})\text{-9-22}]_4$  and KLH  $[(\text{Nle}^{11})\text{-9-22-C}]_x$  conjugates, slightly more (9.3 and 13.6 ng, respectively) conjugated peptide was needed. The carriers without peptide  $[(\text{Nle}^{11})\text{-9-22}]$  did not show any reactivity with Mab A16 (data not shown).

To compare the binding properties of the different conjugates to Mab A16, competition ELISAs were performed (Figure 4). Serial dilutions of peptide  $[(\text{Nle}^{11})\text{-9-22}]$ , the conjugates, and the carriers were preincubated with optimal concentrations of Mab A16. The residual binding capacity of Mab A16 in the mixtures was

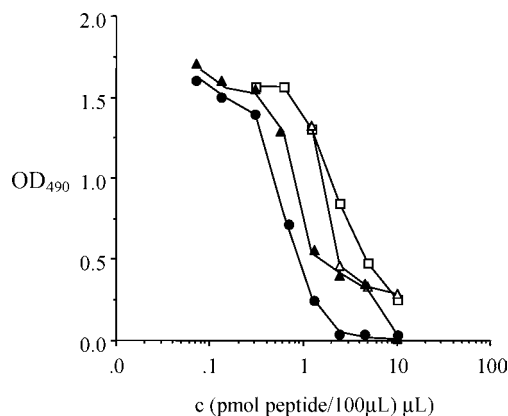


determined in microtiter wells coated with peptide [Nle<sup>11</sup>]-9-22. The relative amount of peptide in the conjugates giving an OD<sub>490</sub> of 1.0 was estimated graphically from plots of OD vs peptide concentrations. We found that the chemical nature of the carrier has marked effects on the antibody binding (Table 2).

Conjugates Ac-[SOC<sub>4</sub>([Nle<sup>11</sup>]-9-22-C)<sub>4</sub>], T20([Nle<sup>11</sup>]-9-22-C)<sub>4</sub>, and Ac-[SOC<sub>4</sub> ([Nle<sup>11</sup>]-9-22)<sub>4</sub>] all required similar amounts of peptide, which was approximately five times less than that needed of the nonconjugated peptide [Nle<sup>11</sup>]-9-22, to inhibit the binding of peptide [Nle<sup>11</sup>]-9-22 and Mab A16. Of the SAK conjugate (SAK([Nle<sup>11</sup>]-9-22-C)<sub>x</sub>), slightly more was required than of the Ac-[SOC<sub>4</sub>([Nle<sup>11</sup>]-9-22-C)<sub>4</sub>], T20([Nle<sup>11</sup>]-9-22-C)<sub>4</sub>, and Ac-[SOC<sub>4</sub> ([Nle<sup>11</sup>]-9-22)<sub>4</sub>], conjugates, but still less than the amount of the nonconjugated peptide. Of the KLH-([Nle<sup>11</sup>]-9-22-C)<sub>x</sub> conjugate, approximately 50-fold excess peptide was required than of the nonconjugated peptide [Nle<sup>11</sup>]-9-22, to obtain the same level of inhibition. None of the carriers without peptide [Nle<sup>11</sup>]-9-22 could inhibit the reactivity between peptide [Nle<sup>11</sup>]-9-22 and Mab A16. A possible explanation for the higher reactivity of the conjugates Ac-[SOC<sub>4</sub>([Nle<sup>11</sup>]-9-22-C)<sub>4</sub>], T20([Nle<sup>11</sup>]-9-22-C)<sub>4</sub>, Ac-[SOC<sub>4</sub> ([Nle<sup>11</sup>]-9-22)<sub>4</sub>], and SAK([Nle<sup>11</sup>]-9-22-C)<sub>x</sub> in comparison to KLH([Nle<sup>11</sup>]-9-22-C)<sub>x</sub> conjugate could be that in the conjugates with the higher reactivity, the distances between the [Nle<sup>11</sup>]-9-22 peptide molecules are smaller than in KLH([Nle<sup>11</sup>]-9-22-C)<sub>x</sub> conjugate. As a consequence, the [Nle<sup>11</sup>]-9-22 peptide molecules in close vicinity of each other could possibly cooperate with the IgG combining sites of the Mab in the formation of di- or multivalent immune complexes. In agreement with this explanation are earlier results, in which we found that dimers of peptide [Nle<sup>11</sup>]-9-21 of gD have approximately a 5–10-fold higher binding to Mabs than the monomer of peptide [Nle<sup>11</sup>]-9-21.

Combining the results of the direct and competition ELISA indicates that the differences in binding of Mab A16 as observed for the KLH([Nle<sup>11</sup>]-9-22-C)<sub>x</sub> versus the other conjugates in the competition ELISA is partly overridden by the coating properties of these conjugates, as shown by less pronounced differences in the direct ELISA.

Next, we studied whether the amount of peptide [Nle<sup>11</sup>]-9-22 coupled to the carrier molecule had effect on the reactivity of the conjugate and Mab A16. Therefore, three conjugates of the SAK carrier were synthesized in which 9%, 22%, and 44% of the reactive groups were replaced by peptide [Nle<sup>11</sup>]-9-22-C. These SAK conjugates with a different average degree of substitution were studied in the direct and competition ELISA, and the results are summarized in Figure 5 and Table 2. The direct ELISA results show that the different average degree of substitution of peptide [Nle<sup>11</sup>]-9-22-C in the SAK([Nle<sup>11</sup>]-9-22-C)<sub>x</sub> conjugate has only a small effect on the reactivity, when the conjugate is coated. The conjugate with 22% average degree of substitution proved to be the most efficient. The results of the competition ELISA (Figure 5) show that the SAK([Nle<sup>11</sup>]-9-22-C)<sub>x</sub> conjugate with 22% substitution rate of peptide [Nle<sup>11</sup>]-9-22 are slightly more effective in the binding of Mab A16 in solution than the SAK([Nle<sup>11</sup>]-9-22-C)<sub>x</sub> conjugates with the 9% and 44% substitution rates. The results of the direct and competition ELISA combined give the impression that the SAK([Nle<sup>11</sup>]-9-22-C)<sub>x</sub> conjugate with 9% substitution rate of peptide [Nle<sup>11</sup>]-9-22 is slightly less efficiently coated than those with substitution rates of 22% and 44%. The reactivity of the SAK([Nle<sup>11</sup>]-9-22-C)<sub>x</sub> conjugate with 22% substitution rate of peptide



**Figure 5.** Reactivity of HSV glycoprotein D type 1 specific monoclonal antibody A16 to [Nle<sup>11</sup>]-9-22 epitope-SAK conjugates in competition ELISA. The effect of the degree of epitope substitution. Peptide 9-22 (□), SAK([Nle<sup>11</sup>]-9-22-C)<sub>9</sub> (△), SAK([Nle<sup>11</sup>]-9-22-C)<sub>22</sub> (●), SAK([Nle<sup>11</sup>]-9-22-C)<sub>44</sub> (▲).

[Nle<sup>11</sup>]-9-22 was comparable to the Ac-[SOC<sub>4</sub>([Nle<sup>11</sup>]-9-22-C)<sub>4</sub>], T20([Nle<sup>11</sup>]-9-22-C)<sub>4</sub>, and Ac-[SOC<sub>4</sub> ([Nle<sup>11</sup>]-9-22)<sub>4</sub>] conjugates.

## CONCLUSION

In this paper we described a conjugation method for linking Cys-peptides with sequential, dendrimeric, or polymeric polypeptide possessing chloroacetyl groups by formation of a stable (44) thioether linkage. We found that the incorporation of ClAc moiety with a chloroacetic acid pentachlorophenyl ester or chloroacetyl chloride is simple and results in the desired product. The coupling of peptide [Nle<sup>11</sup>]-9-22-Cys to the macromolecules under mild conditions (0.1 M Tris-HCl, pH 8.0) produced tetra- and multivalent conjugates with uniformly oriented epitope peptides. The results of the monoclonal antibody binding experiments with the various conjugates clearly indicated that the carrier bound peptide epitopes are recognized more efficiently than free peptides in all multivalent peptide conjugates except in the dendrimeric and KLH conjugate. We found that the binding properties of conjugates could differ 2.5–50-fold depending on the carrier, the average degree of substitution, and the experimental system used. In conclusion, our results indicate that well-characterized synthetic carriers with well-defined substitution degree of epitopes may open new possibilities not only in their use as target antigen in diagnostic assays, but also when applied as tools in molecular biology to prepare antisera with desired specificity.

## ACKNOWLEDGMENT

These studies were supported by grants by the Hungarian Research Fund (OTKA T-14964, T-032425, T-03838, and T-043576), from the Hungarian-Spanish Intergovernmental Program (5/1998), and from the "Peptide based synthetic antigens against infectious diseases" COST Chemistry Action (D13/0007/00).

## LITERATURE CITED

- (1) Hudecz, F. (2001) Manipulation of epitope function by modification of peptide structure: a minireview. *Biologicals* 29, 197–207.
- (2) Müller, G. M., Shapira, M., and Arnon, R. (1982) Anti-influenza response achieved by immunization with a synthetic conjugates. *Proc. Natl. Acad. Sci. US* 79, 5042–5046.
- (3) Neurath, A. R., Kent, S. B. H., and Strick, N. (1982) Specificity of antibodies elicited by a synthetic peptide having

- a sequence in common with a fragment of a virus protein, the hepatitis B surface antigen. *Proc. Natl. Acad. Sci. U.S.A.* 79, 7871–7875.
- (4) Pau, C. P., Lam, L. L., Spira, T. J., Black, J. B., Stewart, J. A., Pellett, P. E., and Respass, R. A. (1998) Mapping and serodiagnostic application of a dominant epitope within the human herpesvirus 8 ORF 65-encoded protein. *J. Clin. Microbiol.* 36, 1574–1577.
  - (5) Olepado, D. K., Klapper, P. E., and Marsden, H. S. (2000) Peptide base enzyme-linked immunoassays for detection of anti-HSV-2 IgG in human sera. *J. Virol. Methods* 87, 63–70.
  - (6) Hudecz, F., and Price, M. R. (1992) Monoclonal antibody binding to peptide epitopes conjugated to synthetic branched polypeptide carriers. Influence of the carrier upon antibody recognition. *J. Immunol. Methods* 147, 201–210.
  - (7) Mezö, G., Kalászi, A., Reményi, J., Mihala, N., Majer, Zs., Hilbert, Á., Láng, O., Köhida, L., Barna, K., and Gaál, D. (2001) Synthesis of new carrier molecules based on repeated tuftsin sequences. In *Peptides 2000* (J. Martinez, J.-A., Fehrentz, Eds.) pp 253–254, EDK, Paris, France.
  - (8) Tsikaris, V., Sakarellos, C., Cung, M. T., Marraud, M., and Sakerellos-Daitsiotis, M. (1996) Concept and design of a new class of sequential oligopeptide carriers (SOC) for covalent attachment of multiple antigenic peptides. *Biopolymers* 38, 291–293.
  - (9) Hudecz, F., and Szekerke, M. (1980) Investigation of drug–protein interactions and the drug-carrier concept by the use of branched polypeptides as model systems. Synthesis and characterization of the model peptides. *Collect. Czech. Chem. Commun.* 45, 933–940.
  - (10) Mezö, G., Kajtár, J., Nagy, I., Szekerke, M., and Hudecz, F. (1997) Carrier design: Synthesis and conformational studies of poly[L-lysine] based branched polypeptides with hydroxyl groups. *Biopolymers* 42, 719–730.
  - (11) Tam, J. P., and Lu, Y. A. (1989) Vaccine engineering: enhancement of immunogenicity of synthetic peptide vaccines related to hepatitis in chemically defined models consisting of T- and B-cell epitopes. *Proc. Natl. Acad. Sci. U.S.A.* 86, 9084–9088.
  - (12) Bartel, A., and Campbell, D. (1959) Some immunochemical differences between associated and dissociated hemocyanin. *Arch. Biochem. Biophys.* 82, 2332–2336.
  - (13) Hall, M. J., and Katrak, K. (1986) The quest for a herpes simplex virus vaccine: background and recent developments. *Vaccine* 4, 138–150.
  - (14) Carfi, A., Willis, S. H., Whitbeck, J. C., Krummenacher, C., Cohen, G. H., Eisenberg, R. J., and Wiley, D. C. (2001) Herpes simplex virus glycoprotein D bound to the human receptor HveA. *Mol. Cell* 8, 169–179.
  - (15) Dean, C., Claassen, E., Gerritse, K., Zegers, N. D., and Boersma, W. J. A. (1990) A novel carbodiimide coupling method for synthetic peptides. *J. Immunol. Methods* 129, 119–125.
  - (16) Atassi, M. Z., Kazim, A. L., and Sakata, S. (1981) High yield coupling of peptides to protein carriers. *Biochim. Biophys. Acta* 670, 300–302.
  - (17) Mezö, G., Mezö, I., Pimm, M. V., Kajtár, J., Seprödi, A., Teplán, I., Kovács, M., Vincze, B., Pályi, I., Idei, M., Szekerke, M., and Hudecz, F. (1996) Synthesis, conformation, biodistribution and hormone related in vitro antitumor effect of GnRH antagonist branched polypeptide conjugate. *Bioconjugate Chem.* 7, 642–650.
  - (18) Carlsson, J., Drevin, H., and Axen, R. (1978) Protein thiolation and reversible protein–protein conjugation. N–Succinimidyl 3-(2-pyridyldithio) propionate, a new heterobifunctional reagent. *Biochem. J.* 173, 723–728.
  - (19) Mezö, G., Mihala, N., Andreu, D., and Hudecz, F. (2000) Conjugation of epitope peptides to branched chain polypeptides via Cys(Npys). *Bioconjugate Chem.* 11, 484–491.
  - (20) Kitagawa, T., and Aikawa, T. (1976) Enzyme coupled immunoassay of insulin using a novel coupling reagent. *J. Biochem.* 79, 233–236.
  - (21) Kato, K., Haruyama, Y., Hamaguchi, Y. and Ishikawa, E. (1978) Comparison of three enzyme-linked procedures for the quantitative determination of guinea pig anti-porcine insulin antibody. *J. Biochem. (Tokyo)* 84, 93–102.
  - (22) Weltman, J. K., Hohnson, S. A., Langevin, J., and Riester, E. F. (1983) N–Succinimidyl(4-iodoacetyl)aminobenzoate: A new heterobifunctional cross-linker. *BioTechniques* 1, 148–152.
  - (23) Hudson, E. N., Weber, G. (1973) Synthesis and characterization of two fluorescent sulfhydryl reagents. *Biochemistry* 12, 4154–4161.
  - (24) Inman, J. K., Highet, P. F., Kolodny, N., and Robey, F. A. (1991) Synthesis of N- $\alpha$ -(tert-butoxycarbonyl)-N- $\epsilon$ -[N-(bromoacetyl)- $\beta$ -alanyl]-L-lysine: its use in peptide synthesis for placing a bromoacetyl cross-linking function at any desired sequence position. *Bioconjugate Chem.* 2, 458–463.
  - (25) Lindner, W., and Robey, F. A. (1987) Automated synthesis and use of N-chloroacetyl-modified peptides for the preparation of synthetic peptide polymers and peptide–protein immunogens. *Int. J. Pept. Protein Res.* 30, 794–800.
  - (26) Futaki, S., Ishikawa, T., Niwa, M., Kitagawa, K., and Yagami, T. (1997) Embodying a stable alpha-helical protein structure through efficient chemical ligation via thioether formation. *Bioorg. Med. Chem.* 5, 1883–1891.
  - (27) Zeng, W., Ghosh, S., Macris, M., Pagnon, J., and Jackson, D. C. (2001) Assembly of synthetic peptide vaccines by chemoselective ligation of epitopes: influence of different chemical linkages and epitope orientations on biological activity. *Vaccine* 19, 3843–3852.
  - (28) Wilson, K. M., Catimel, B., Mitchellhill, K. I. and Kemp, B. E. (1994) Simplified conjugation chemistry for coupling peptides to F(ab') fragments: autologous red cell agglutination assay for HIV-1 antibodies. *J. Immunol. Methods* 175, 267–273.
  - (29) Jones, D. S., Coutts, S. M., Gamino, C. A., Iverson, G. M., Linnik, M. D., Randow, M. E., Ton-Nu, H. T., and Victoria, E. J. (1999) Multivalent thioether-peptide conjugates: B cell tolerance of an anti-peptide immune response. *Bioconjugate Chem.* 10, 480–488.
  - (30) Grandjean, C., Santraine, V., Fruchart, J. S., Melnyk, O., and Gras-Masse, H. (2002) Combined thioether/hydrazone chemoselective ligation reactions for the synthesis of glyco-cluster-antigen peptide conjugates. *Bioconjugate Chem.* 13, 887–892.
  - (31) Van der Ploeg, J. R., Drijfhout, J. W., Feijlbrief, M., Bloemhoff, W., Welling, G. W., and Welling-Wester, S. (1989) Immunological properties of multiple repeats of a linear epitope of herpes simplex virus type 1 glycoprotein D. *J. Immunol. Methods* 124, 211–217.
  - (32) IUPAC–IUB Commission on Biochemical Nomenclature. (1972) *Biochem. J.* 127, 753–756.
  - (33) IUPAC–IUB Commission on Biochemical Nomenclature. (1984) *Eur. J. Biochem.* 138, 9–37.
  - (34) Kaiser, E., Colescott, R. L., Bossinger, C. D., and Cook, P. I. (1970) Color test for detection of free terminal amino groups in the solid-phase synthesis of peptides. *Anal. Biochem.* 34, 595–598.
  - (35) Kaiser, E., Bossinger, C. D., Colescott, R. L., and Olsen, D. B. (1980) Color test for terminal prolyl residues in the solid-phase synthesis of peptides. *Anal. Chim. Acta.* 118, 149–151.
  - (36) Ivanov, B. B., and Robey, A. F. (1996) Effective use of free thiols as scavengers for HF cocktails to deprotect bromo- and chloroacetyl synthetic peptides. *Peptide Res.* 9, 305–307.
  - (37) Mezö, G., Votavova, H., Hudecz, F., Kajtár, J., Sponar, J., and Szekerke, M. (1988) Conformation of branched polypeptides: The influence of DL-alanine oligomer spacers in the side chains. *Collect. Czech. Chem. Commun.* 53, 2843–2853.
  - (38) Hudecz, F., Kovács, P., Kutassi-Kovács, S., and Kajtár, J. (1984) GPC, CD and sedimentation analysis of poly-Lys and branched chain poly-Lys-poly-DL-Ala polypeptides. *Colloid Polym. Sci.* 262, 208–212.
  - (39) Welling-Wester, S., Feijlbrief, M., Koedijk, D. G. A. M., Drijfhout, J. W., Weijer, A. J., Scheffer, A. J., and Welling, G. W. (1994) Analogues of peptide 9–21 of glycoprotein D of herpes simplex virus and their binding to group VII monoclonal antibodies. *Arch. Virol.* 138, 331–340.
  - (40) Scheffer, A. J., Koedijk, D. G. A. M., Abee, T., Osterhaus, A. D. M. W. (1984) Monoclonal antibodies against herpes simplex virus type 1 glycoprotein D. In *Development*

- Biological Standards* (M. Barme, W. Hennesen, Eds.) vol. 57, pp 269–274, Karger, Basel.
- (41) Eisenberg R. J., Long D., Ponce de Leon M., Matthews J. T., Spear P. G., Gibson M. G., Lasky L. A., Berman P., Golub E., Cohen G. H (1985) Localization of epitopes of herpes simplex virus type 1 glycoprotein D. *J. Virol.* 53, 634–644.
- (42) Lasonder, E., Schellekens, G. A., Koedijk, D. G., Damhof, R. A., Welling-Wester, S., Feijlbrief, M., Scheffer, A. J., Welling, G. W. (1996) Kinetic analysis of synthetic analogues of linear-epitope peptides of glycoprotein D of herpes simplex virus type 1 by surface plasmon resonance. *Eur. J. Biochem.* 240, 209–214.
- (43) Hudecz, F., Pimm, M. V., Rajnavölgyi, É., Mezö, G., Fabra, A., Gaál, D., Kovács, A. L., Horváth, A., and Szekerke, M. (1999) Carrier design: New generation of polycationic branched polypeptides containing OH groups with prolonged blood survival and diminished in vitro cytotoxicity. *Bioconjugate Chem.* 10, 781–790.
- (44) Beekman, N. J., Schaaper, W. M., Langeveld, J. P., Boshuizen, R. S., and Meloen, R. H. (2001) The nature of the bond between peptide and carrier molecule determines the immunogenicity of the construct. *J. Pept. Res.* 58, 237–245.

BC0341122



# Organomercury Bioconjugate Synthesis and Characterization by Matrix-Assisted Laser Desorption Ionization Mass Spectrometry

Caryn K. Prudenté\* and Margaret C. Hausman

Department of Chemistry, University of Southern Maine, 96 Falmouth Street, Portland, Maine 04104.  
Received July 11, 2003; Revised Manuscript Received August 21, 2003

Synthesis of an organomercury hapten and conjugation of the hapten to proteins and peptides is described. Starting with allylamine, synthesis of the organomercury hapten was completed in five steps using readily available and inexpensive reagents. The key transformation in the synthesis, intramolecular oxymercuration, was achieved in good yield and under mild conditions. Hapten conjugation was afforded via disuccinimide active ester coupling chemistry, and the resulting conjugates were analyzed by matrix-assisted laser desorption ionization mass spectrometry (MALDI-MS). To exploit the accurate mass measuring capabilities of MALDI-MS, the conjugates were digested with trypsin prior to analysis. The masses of the peptides resulting from tryptic digestion of the organomercury conjugates were accurately measured, and five hapten attachments were identified in the mass range of 1000–2200 *m/z*. The organomercury bioconjugate synthesized in this study was designed to contain a stable carbon–metal bond, constituting an underutilized approach for preparing protein–metal complexes and may result in mAbs consisting of unique recognition capabilities.

## INTRODUCTION

Mercury has played a rich role and has made diverse contributions to the field of bioconjugate chemistry. For example, mercury's unique electronic properties have proved useful in designing electrochemical-based thiol assay methods (1). Mercury metal has aided electron microscopy characterization of proteins (2) and has been incorporated into fluorescent peptide and protein tags (3). More recently, there has been interest in developing anti-mercury mAbs for their potential use as diagnostic tools capable of providing highly specific, inexpensive, easy to use mercury detection assays (4, 5). Our interest in this area prompted us to design and prepare a synthetic organomercury hapten that is amenable to protein conjugation methods. Mercury metal, mercury salts, and organomercury compounds are ubiquitous and persistent environmental toxins, and the associated health hazards to humans, mammals, and aquatic systems are of keen interest (6).

The preparation of metal containing bioconjugates for the purpose of generating mAbs capable of binding metals and metal ions has been the focus of numerous research efforts over the last 20 years (7–12). Generally, the approach taken to generate metal-based bioconjugates has been to chemically modify carriers by covalently attaching EDTA<sup>1</sup> or other structurally similar metal chelating agents (7–11). The chelating species facilitates encapsulation of a metal in a cagelike structure on the carrier's surface via formation of coordination bonds between the electron rich atoms of the chelate and the electron deficient metal atom. The earliest examples of bioconjugates prepared with the metal chelation methodology have resulted in several useful substrates. These substrates have found practical applications as metal-labeled therapeutic antibodies (8, 13), magnetic reso-

nance imaging substrates (14, 15), and radioimaging techniques (16). One recent extension of the EDTA chelation methodology has been the synthesis of a fluorescent optical sensor designed to detect Hg<sup>2+</sup> ions (17). In this work, Hg<sup>2+</sup> is trapped in a cagelike structure arising from a porphyrin dimer. Preliminary work has shown that the chemical sensor is capable of detecting Hg<sup>2+</sup> at concentrations of 10<sup>−4</sup> to 10<sup>−7</sup> M with high degrees of specificity preferentially over other divalent metal ions.

One shortcoming of the chelation methodology is that EDTA is known to form stable coordination complexes with virtually all of the transition metals (8). Because of the nonselective nature of EDTA–metal complexes, efforts to develop immunoassays based on mAbs elicited from EDTA–metal bioconjugates have been thwarted by poor sensitivity and lack of metal specificity (10). Additionally, mAbs generated via EDTA-encapsulated metal bioconjugates often display poor selectivity between the metal–chelate analyte and metal-free chelate (18).

Currently, there are only a few examples of protocols that have yielded metal binding antibodies from methodologies other than chelate complexation. Benkovic and co-workers have chemically modified the binding site of a specific antibody to accommodate complexation of Zn<sup>2+</sup> ion (19). The catalytic hydrolysis rate of the resulting Ab–Zn<sup>2+</sup> substrate was observed to increase relative to the native enzyme. In another approach, Wylie and co-workers covalently attached glutathione, a tripeptide of glutamic acid, cysteine, and glycine, to KLH via carbodiimide chemistry (20). Mercuric chloride (HgCl<sub>2</sub>) was then attached to the glutathione-modified carrier by sulfur-mediated ligand exchange. Mercury ions have a particularly high affinity for thiols; the binding constant between cysteine and mercury is on the order of 10<sup>14</sup> (21).

Our overall strategy was to synthesize a structurally simple, but chemically robust, organomercury hapten, which was obtained via an intramolecular oxymercuration reaction. The synthetic hapten was covalently bonded

\* To whom correspondence should be addressed at University of Southern Maine. Phone: (207) 780-4005. Fax: (207) 228-8288. E-mail: prudente@maine.edu.

to BSA and a model peptide through an amine positioned at a site removed from the carbon–mercury bond. MALDI/FT-ICR MS<sup>1</sup> was used to unequivocally characterize the resulting bioconjugates. The short-term goals of this project have been completed, and we are currently preparing to initiate a mAb development program with the organomercury bioconjugate resulting from this work. In this paper we describe the complete synthesis of the organomercury hapten, conjugation of the hapten, and the results obtained from MALDI-MS characterization of the bioconjugates.

## EXPERIMENTAL PROCEDURES

**Materials and Methods.** All reagents were purchased from Sigma-Aldrich at the highest purity available and used without further purification, except where noted. Allylamine, di-*tert*-butyl dicarbonate, *m*CPBA, and benzyl bromide were purchased from Acros. BS<sup>3</sup> was purchased from Pierce and C-18 Zip Tips were purchased from Millipore.

<sup>1</sup>H NMR and <sup>13</sup>C NMR were recorded on a Bruker Avance 400 Fourier transform spectrometer at 400 MHz for hydrogen and 100 MHz for carbon using tetramethylsilane (TMS) as an internal standard. HiResMALDI-FTMS (IonSpec, Irvine, CA) equipped with a 4.7 T actively shielded superconducting magnet was used to record all MALDI-MS. The MALDI source uses a 337-nm nitrogen laser and a 10-faceted sample probe. Flash chromatography was carried out on a SiO<sub>2</sub> column (32–63 μm particle size) at an elution rate of 2 in./min. GC/MS was done on a Hewlett-Packard Series 5988A equipped with an EC-1 column, 30 m, 0.25 mm i.d., 0.25 μm film thickness (Alltech, Deerfield, IL), injector 250 °C, detector 280 °C, oven 40 °C, programmed at a rate of 10 °C/min to 280 °C. EI, CI (CH<sub>4</sub>), and CI (NO/CH<sub>4</sub>) MS were collected. Infrared spectroscopy was carried out on a Nicolet 210 FTIR. Melting points were determined in open glass capillary tubes with a Mel-Temp II Melting Point Apparatus and were not corrected.

The toxicological properties of the organomercury compounds prepared in this study have not been characterized. All mercury-containing compounds were handled using standard safety guidelines, which included protective clothing, safety goggles, and doubled gloves. Whenever possible, substrates were reduced in situ with NaBH<sub>4</sub> to avoid excessive handling of mercury containing substrates.

**Organomercury Hapten Synthesis.** *tert*-Butyl Allylcarbamate. To a solution of allylamine (**1**) (4.87 mL, 65 mmol) in 80 mL of double-distilled H<sub>2</sub>O was added 40 mL of 1.5 M Na<sub>2</sub>CO<sub>3</sub>, followed by 13.9 mL of di-*tert*-butyl carbonate (63.7 mmol), and the solution was stirred overnight at room temperature. The desired product, a white precipitate, was filtered and recrystallized from water. If precipitate did not form, the reaction mixture was extracted with CH<sub>2</sub>Cl<sub>2</sub>, and the combined extracts were washed with HCl (1 M) and brine, dried over Na<sub>2</sub>SO<sub>4</sub>, and concentrated in vacuo. Regardless of purification method, the product was obtained in 85% as a white solid: mp 30–32 °C; <sup>1</sup>H NMR (CDCl<sub>3</sub>) δ 1.40 (s, 9H, CH<sub>3</sub>), 3.75 (m, 2H, CH<sub>2</sub>), 4.65 (br s, 1H, NH), 5.13 (m, 2H, =CH<sub>2</sub>), 5.85 (m, 1H, =CH); <sup>13</sup>C NMR (CDCl<sub>3</sub>) δ 28.6 (CH<sub>3</sub>), 43.3 (CH<sub>2</sub>), 79.6 (quaternary C), 115.9 (=CH<sub>2</sub>), 135.1 (CH=), 156.0 (C=O); FTIR cm<sup>-1</sup> 3450 (νNH), 3056 (ν=CH<sub>2</sub>), 2976 (νCH), 1710 (νC=O), 1502 (νC–N), 1272 (νC–O); GC/MS CI (CH<sub>4</sub>) *m/z* 142 [(M + 41) – 56]<sup>+</sup>, 130 [(M + 29) – 56]<sup>+</sup>, 102 [(M + 1) – 56]<sup>+</sup>.

*tert*-Butyl (Oxiran-2-ylmethyl)carbamate (**2**). To a solution of the protected amine (5 g, 31.9 mmol) in 60 mL of

CH<sub>2</sub>Cl<sub>2</sub> was slowly added excess dry *m*CPBA (8.77 g, 51 mmol), allowing the *m*CPBA to dissolve between additions. The reaction was stirred with a magnetic stir bar overnight at room temperature. To precipitate unreacted *m*CPBA and byproduct *m*-chlorobenzoic acid, the reaction mixture was placed in the refrigerator overnight, filtered, and washed with cold CH<sub>2</sub>Cl<sub>2</sub>. The filtrate was stirred magnetically for 1 h in 1 M Na<sub>2</sub>CO<sub>3</sub>, and the aqueous layer was extracted with CH<sub>2</sub>Cl<sub>2</sub>. The pooled CH<sub>2</sub>Cl<sub>2</sub> layers were washed with brine, dried over Na<sub>2</sub>SO<sub>4</sub>, and concentrated in vacuo, to obtain a clear, colorless slightly viscous oil (84%): <sup>1</sup>H NMR (CDCl<sub>3</sub>) δ 1.45 (s, 9H, CH<sub>3</sub>), 2.59 (dd, 1H, CH<sub>2</sub>O), 2.78 (dd, 1H, CH<sub>2</sub>O), 3.08 (m, 1H, NHCH<sub>2</sub>), 3.20 (m, 1H, ring CH), 3.51 (m, 1H, NHCH<sub>2</sub>), 4.89 (br s, 1H, NH); <sup>13</sup>C NMR (CDCl<sub>3</sub>) δ 28.7 (CH<sub>3</sub>), 42.0 (CH), 45.4 (CH<sub>2</sub>O), 51.2 (NHCH<sub>2</sub>), 80.0 (quaternary C), 156.3 (C=O); IR cm<sup>-1</sup> 3438 (νNH), 3046 (νCH<sub>2</sub> ring), 2978 (νsp<sup>3</sup>CH), 1707 (νC=O), 1509 (νC–N), 1263 and 1168 (νC–O–C); GC/MS CI (CH<sub>4</sub>) *m/z* 202 [M + 29]<sup>+</sup>, 174 [M + 1]<sup>+</sup>, 158 [(M + 41) – 56]<sup>+</sup>, 146 [(M + 29) – 56]<sup>+</sup>, 118 [(M + 1) – 56]<sup>+</sup>.

*tert*-Butyl (2-Hydroxy-5-hexen-1-yl)carbamate (**3**). Allylmagnesium bromide (1 M in ether, 57 mL, 57.8 mmol) was transferred via a cannula to a round-bottom flask equipped with reflux condenser, magnetic stir bar, and nitrogen inlet. The ether was evaporated under nitrogen flow to yield a white solid paste. Dry dioxane (100 mL) was added via cannula to the dried allylmagnesium bromide, and the mixture was stirred magnetically under nitrogen for 2.5 h to precipitate MgBr<sub>2</sub>. A solution of **2** (2 g, 11.6 mmol) in 5 mL of dioxane was added, and the reaction was refluxed for 2 h. A slight excess of 1 M NH<sub>4</sub>Cl(aq) was added, and the reaction was stirred magnetically overnight at room temperature. Dioxane and H<sub>2</sub>O were removed in vacuo to yield a yellow oil (**3**) and white solid. The product was extracted with CH<sub>2</sub>Cl<sub>2</sub> and diH<sub>2</sub>O. The combined organic layers were washed with brine, dried over Na<sub>2</sub>SO<sub>4</sub>, and concentrated in vacuo to yield a yellow viscous oil (80%). GC analysis of the crude product indicates a 20:1 ratio of regioisomers. The crude product was purified by flash chromatography (10% acetone:CH<sub>2</sub>Cl<sub>2</sub>) to yield a pale yellow viscous oil (65%): <sup>1</sup>H NMR (CDCl<sub>3</sub>) δ 1.45 (s, 9H, CH<sub>3</sub>), 1.55 (q, 2H, HOCHCH<sub>2</sub>), 2.16 (m, 2H, allylic CH<sub>2</sub>), 2.72 (br s, 1H, OH), 3.04 (m, 1H, NHCH<sub>2</sub>), 3.30 (m, 1H, NHCH<sub>2</sub>), 3.71 (br s, 1H, NH), 4.98 (m, 2H, =CH<sub>2</sub>), 5.06 (m, 1H, CHOH), 5.84 (m, 1H, CH=); <sup>13</sup>C NMR (CDCl<sub>3</sub>) δ 28.8 (CH<sub>3</sub>), 30.2 (allylic CH<sub>2</sub>), 34.2 (HOCHCH<sub>2</sub>), 47.0 (NHCH<sub>2</sub>), 71.5 (CHOH), 80.0 (quaternary C), 115.5 (=CH<sub>2</sub>), 138.6 (=CH), 157.2 (C=O); FTIR cm<sup>-1</sup> 3339 (δOH), 3069 (ν=CH), 2978 (νsp<sup>3</sup>CH), 2923 (νsp<sup>3</sup>CH), 1687 (νC=O), 1513 (νC–N), 1362 (νOH), 1255 and 1160 (νC–O); GC/MS CI *m/z* 216 [M + 1]<sup>+</sup>, 200 [(M + 41) – 56]<sup>+</sup>, 188 [(M + 29) – 56]<sup>+</sup>, 170 [(M + 29) – 56]<sup>+</sup>, 160 [(M + 1) – 56]<sup>+</sup>, 142 [(M + 1) – 56 – H<sub>2</sub>O]<sup>+</sup>, 116 [(M + 1) – 56 – CO<sub>2</sub>]<sup>+</sup>; CI(NO/CH<sub>4</sub>) *m/z* 214 [M – 1]<sup>+</sup>, 158 [(M – 1) – 56]<sup>+</sup>, 140 [(M – 1) – 56 – H<sub>2</sub>O]<sup>+</sup>.

*tert*-Butyl [(5-Methyl mercuric chloride tetrahydrofuran-2-yl)methyl]carbamate (**4**). Grignard product **3** (200 mg, 0.93 mmol) was dissolved in 5 mL of freshly distilled CH<sub>3</sub>CN in a round-bottom flask equipped with magnetic stir bar and argon gas inlet/outlet. Mercuric acetate (0.591 g, 1.9 mmol) was dissolved in 10 mL of CH<sub>3</sub>CN and added to the solution of **3**. The mixture was stirred overnight at room temperature under argon gas, after which time the reaction mixture became clear and colorless. Brine was added and the resulting mixture was stirred 3 h at room temperature. Excess NaHCO<sub>3</sub> (250 mg, 3.0 mmol) was added to the crude mixture to

neutralize the acetic acid formed. Acetonitrile was removed in vacuo, and the remaining mixture was extracted with  $\text{CH}_2\text{Cl}_2$ . The organic layers were combined, washed with brine, dried over  $\text{Na}_2\text{SO}_4$ , and concentrated in vacuo. The desired product was purified by flash chromatography (2:1 hexane:ethyl acetate) to yield a viscous, yellow oil (270 mg, 65%):  $^1\text{H}$  NMR ( $\text{CDCl}_3$ )  $\delta$  1.47 (s, 9H,  $\text{CH}_3$ ), 1.65 (m, 2H, ring  $\text{CH}_2$ ), 2.15 (m, 2H, ring  $\text{CH}_2$ ), 2.19 (m, 1H,  $\text{CH}_2\text{Hg}$ ), 2.32 (m, 1H,  $\text{CH}_2\text{Hg}$ ), 3.06 (m, 1H,  $\text{NHCH}_2$ ), 3.35 (m, 1H,  $\text{NHCH}_2$ ), 4.15 (m, 1H,  $\text{CHCH}_2\text{Hg}$ ), 4.23 (m, 1H,  $\text{OCHCH}_2$ ), 5.08 (br s, 1H, NH);  $^{13}\text{C}$  NMR ( $\text{CDCl}_3$ )  $\delta$  28.8 ( $\text{CH}_3$ ), 30.0 (ring  $\text{CH}_2$ ), 36.8 ( $\text{CH}_2\text{Hg}$ ), 38.6 (ring  $\text{CH}_2$ ), 45.0 ( $\text{NHCH}_2$ ), 77.9 ( $\text{OCHCH}_2$ ), 78.7 ( $\text{CHCH}_2\text{Hg}$ ), 78.8 (quaternary C), 156.1 ( $\text{C}=\text{O}$ ); FTIR  $\text{cm}^{-1}$  3384 (br,  $\nu\text{NH}$ ), 2975 ( $\nu\text{sp}^3\text{CH}$ ), 2928 ( $\nu\text{sp}^3\text{CH}$ ), 1752 ( $\nu\text{C}=\text{O}$ ), 1703 ( $\nu\text{C}=\text{O}$ ), 1505 ( $\nu\text{C}-\text{N}$ ), 1265 and 1170 ( $\nu\text{C}-\text{O}-\text{C}$ ); HRMS calcd for  $\text{C}_{11}\text{H}_{20}\text{NO}_3\text{HgClNa}$  474.0729, found 474.0730.

*tert*-Butyl [(5-Methyltetrahydrofuran-2-yl)methyl]carbamate (**6**). To crude **4** (60 mg, 0.113 mmol) dissolved in 2 mL of  $\text{CH}_2\text{Cl}_2$  was added 7.56 mg of  $\text{NaBH}_4$  (0.2 mmol) dissolved in 1 mL of 10 M NaOH and stirred magnetically for 2 h. The resulting mixture was filtered through Celite with  $\text{CH}_2\text{Cl}_2$  to remove the mercury metal formed. The filtrate was extracted with double-distilled  $\text{H}_2\text{O}$ , and the organic layer was washed with brine, dried over  $\text{Na}_2\text{SO}_4$ , and concentrated in vacuo to yield a viscous yellow oil:  $^1\text{H}$  NMR ( $\text{CDCl}_3$ )  $\delta$  1.19 (d, 3H,  $\text{CH}_3$ ), 1.42 (s, 9H,  $\text{CH}_3$ ), 1.52 (m, 2H, ring  $\text{CH}_2$ ), 2.01 (m, 2H, ring  $\text{CH}_2$ ), 3.12 (m, 1H,  $\text{NHCH}_2$ ), 3.36 (m, 1H,  $\text{NHCH}_2$ ), 4.05 (m, 1H,  $\text{OCHCH}_2$ ), 4.07 (m, 1H,  $\text{CHCH}_3$ ), 5.04 (br s, 1H, NH);  $^{13}\text{C}$  NMR ( $\text{CDCl}_3$ )  $\delta$  21.4 ( $\text{CH}_3$ ), 28.8 ( $\text{CH}_3$  tBOC), 29.6 (ring  $\text{CH}_2$ ), 34.2 (ring  $\text{CH}_2$ ), 45.1 ( $\text{NHCH}_2$ ), 76.2 ( $\text{CHCH}_3$ ), 77.9 ( $\text{OCHCH}_3$ ), 79.5 (quaternary C), 156.5 ( $\text{C}=\text{O}$ ); GC/MS EI (diastereomer ratio 1:1.7; identical fragmentation patterns were seen for both diastereomers)  $m/z$  159 [ $\text{M} - 56$ ] $^+$ , 142 [ $\text{M} - 56 - \text{H}_2\text{O}$ ] $^+$ , 98 [ $\text{M} - 117$ ] $^+$  (117 = tBOCOC(O)NHCH), 85 [ $\text{M} - 130$ ] $^+$  (130 = tBOCOC(O)NHCH<sub>2</sub>), 57 [*tert*-butyl fragment] $^+$ .

(5-Methylmercuric chloride tetrahydrofuran-2-yl)-methylamine (**5**). A large excess of TFA (1.0 mL, 12.9 mmol) was added to **4** (100 mg, 0.22 mmol) in 1.0 mL of  $\text{CH}_2\text{Cl}_2$ , and the mixture was stirred magnetically overnight at room temperature. TFA and  $\text{CH}_2\text{Cl}_2$  were removed in vacuo to yield a pale yellow viscous oil, which was extracted with  $\text{CH}_2\text{Cl}_2$  and double-distilled  $\text{H}_2\text{O}$ . The aqueous layer was basified with NaOH (12.9 mmol), and  $\text{CH}_2\text{Cl}_2$  was added to precipitate any remaining salts. The mixture was filtered, and the filtrate was concentrated in vacuo to yield a viscous yellow oil (65%), which was used in the conjugation protocols without further purification.

**Conjugation of Organomercury Hapten 5 and MALDI-MS Characterization.** Prior to MALDI-MS analysis samples were purified using a C-18 zip tip and were eluted with 50%  $\text{CH}_3\text{CN}$  in 0.1% TFA. The purified samples (0.5  $\mu\text{L}$ ) were added to the matrix (0.5  $\mu\text{L}$  of 40 mg DHB in 250  $\mu\text{L}$  of  $\text{CH}_3\text{CN}$  and 250  $\mu\text{L}$  of 0.1% TFA/ $\text{H}_2\text{O}$  stock solution), and the 1  $\mu\text{L}$  mixture was placed on the MALDI probe. Protein concentrations were typically 120  $\mu\text{g}/\text{mL}$ .

**BSA–Benzylamine Model Conjugates.** A 5 mg/mL stock solution of BSA was prepared in 20 mM phosphate buffer, pH 7.5. Just prior to use, 15 mg of  $\text{BS}^3$  ( $2.62 \times 10^{-2}$  mmol) was dissolved in 5 mL of 20 mM phosphate buffer, pH 7.5. To the  $\text{BS}^3$  solution, 2.28  $\mu\text{L}$  of benzylamine ( $2.08 \times 10^{-2}$  mmol) was added, and 1.7 mL aliquots of this solution were removed at time 0, 1, and 5 min and added to 200  $\mu\text{L}$  aliquots of the BSA solution.

The three reactions were stirred for 45 min at room temperature, quenched with benzylamine (1  $\mu\text{L}$ ,  $9.15 \times 10^{-3}$  mmol), and stirred for an additional 1.0 h. Each conjugate was dialyzed exhaustively (dialysis membrane tubing MWCO 10 000) against 20 mM phosphate buffer, pH 7.5.

**Tryptic Digestion of BSA–Benzylamine Model Conjugates.** Each of the above conjugates (60  $\mu\text{g}$ ) was dissolved in 100  $\mu\text{L}$  of urea (6 M in 25 mM  $\text{NH}_4\text{HCO}_3$ ). To each mixture was added 5 mL of DTT (200 mM in 25 mM  $\text{NH}_4\text{HCO}_3$ ), and the reactions were vortexed and then gently rotated for 1 h at room temperature. After adding 20  $\mu\text{L}$  of iodoacetamide (200 mM in 25 mM  $\text{NH}_4\text{HCO}_3$ ), the reactions proceeded for 1 h at room temperature in the dark. To consume unreacted iodoacetamide, 20  $\mu\text{L}$  of DTT (200 mM in 25 mM  $\text{NH}_4\text{HCO}_3$ ) was added, followed by 900  $\mu\text{L}$  of 25 mM  $\text{NH}_4\text{HCO}_3$ . The resulting mixtures were enzymatically digested with 20  $\mu\text{L}$  of trypsin (0.1  $\mu\text{g}/\mu\text{L}$  in 25 mM  $\text{NH}_4\text{HCO}_3$ ) and incubated overnight at 37  $^\circ\text{C}$ . Each sample was concentrated to approximately 0.5 mL. Identical fragmentation patterns were observed in the MALDI-MS for all three conjugates. MALDI/FT-ICR MS: Unconjugated BSA peptides were observed at  $m/z$  1283.725, 1439.835, 1479.805, and 1567.716. These unconjugated peptides were also identified in the digested sample of conjugate **9** (corresponding to residues 361–371, 360–371, 421–433, and 347–359, respectively). Peptides coupled to 1 equiv of benzylamine were observed at  $m/z$  1062.638 (452–459), 1092.654 (242–248), 1236.758 (210–218), 1246.735 (233–218), and 1886.138 (437–451). Numbers in parentheses indicate the tryptic peptide residue that is coupled to benzylamine. Residues 452–459, 242–248, and 437–451 were also observed as hapten attachment points in the MALDI-MS of digested conjugate **9**.

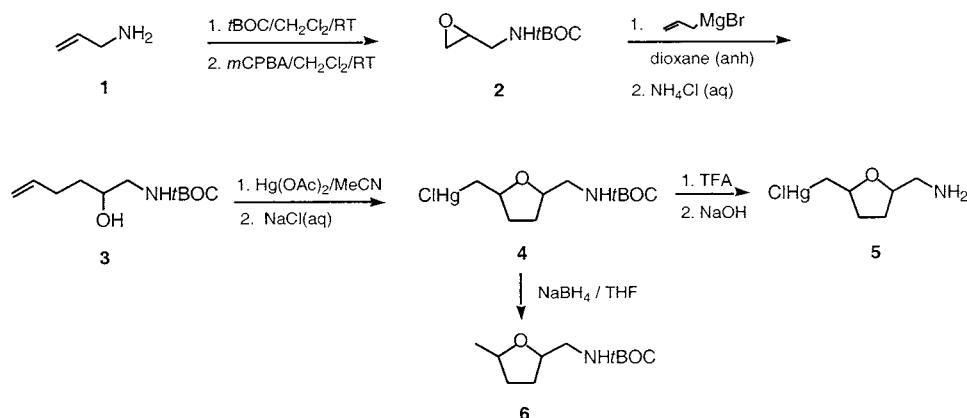
**Model Peptide and Organomercury Hapten 5 Conjugations.** A 5 mg/100  $\mu\text{L}$  stock solution of hapten **5** was prepared in 20 mM phosphate buffer at pH 7.5. Just prior to use,  $\text{BS}^3$  was dissolved in 20 mM phosphate buffer at pH 7.5 to yield a 0.3 mg/100  $\mu\text{L}$  solution. To 400  $\mu\text{L}$  of the  $\text{BS}^3$  solution ( $2.02 \times 10^{-3}$  mmol) was added 7.0  $\mu\text{L}$  of hapten stock solution (5:BS<sup>3</sup> 0.5:1 molar ratio), and the solution was mixed for 5 min. A 0.5 mg/100  $\mu\text{L}$  peptide solution was prepared in 20 mM phosphate buffer at pH 7.5, and 200  $\mu\text{L}$  was added to the 5/BS<sup>3</sup> solution. The reaction was magnetically stirred for 1 h at room temperature, quenched with a 0.5 mol equiv of the hapten **5** stock solution, and stirred another 1 h at room temperature. The sample volume was reduced to approximately 0.5 mL in vacuo. MALDI/FT-ICR MS  $m/z$ : 1440.740 [ $\text{MH} - \text{HCl}$ ] $^+$ , 987.616 (uncoupled peptide), 1143.698 (peptide and  $\text{BS}^3$  only); with CsI added to the matrix  $m/z$  1568.604 [ $\text{M} + \text{H}$ ] $^+$  of peptide–mercuric iodide conjugate, 1440.740 [ $\text{MH} - \text{HI}$ ] $^+$ .

**BSA–Organomercury Hapten Conjugation (9).** To 100  $\mu\text{L}$  ( $1.42 \times 10^{-2}$  mmol) of a 50 mg/mL hapten **5** stock solution in double-distilled water was added 400  $\mu\text{L}$  ( $2.99 \times 10^{-5}$  mmol) of a 5 mg/mL BSA solution in 20 mM phosphate buffer at pH 7.5. The pH of this solution was adjusted to 7.5. Immediately after preparation, 340  $\mu\text{L}$  ( $1.75 \times 10^{-2}$  mmol) of a 30 mg/mL  $\text{BS}^3$  stock solution in 20 mM phosphate buffer at pH 7.5 was added to the hapten **5**/BSA mixture, and the reaction was stirred magnetically for 1 h at room temperature. The reaction was quenched with 0.5 equiv of the hapten stock solution (50  $\mu\text{L}$ ,  $7.14 \times 10^{-3}$  mmol) and stirred magnetically for 30 min.

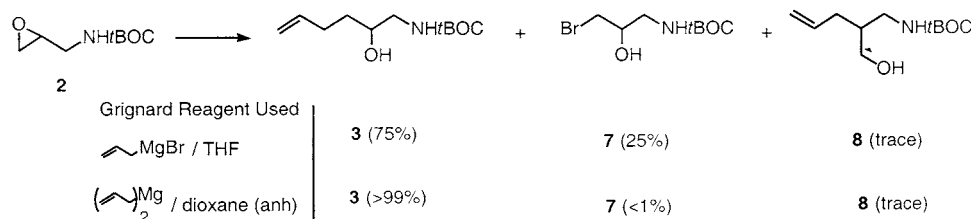
**Tryptic Digestion of Conjugate 9.** The protocol previously described for the digestion of the BSA–



## Scheme 1



## Scheme 2



benzylamine conjugate was not suitable because of potential coupling between DTT and the mercury. Consequently, the digest of the BSA-hapten conjugate **9** was done without DTT. The conjugate was purified on a Sephadex G-25 column (20 mM phosphate buffer, pH 7.2) and was concentrated in vacuo. A 0.125 mg/mL solution was prepared by adding 0.5 mL of 100 mM  $\text{NH}_4\text{HCO}_3$  to the purified conjugate. To 100  $\mu\text{L}$  of the conjugate solution was added 100  $\mu\text{L}$  of trypsin (10  $\mu\text{g}/\text{mL}$  in 25 mM  $\text{NH}_4\text{HCO}_3$ ), and the mixture was reacted overnight at 37  $^\circ\text{C}$ . The sample was concentrated to dryness in vacuo, and the resulting fragmented conjugate was taken up in 5  $\mu\text{L}$  of 0.1% TFA. MALDI-MS unconjugated BSA peptides were observed at  $m/z$  847.5 (161–167), 1283.7 (361–371), 1439.8 (360–371), 1479.8 (421–433), 1567.7 (347–359), 1639.9 (437–451), and 2045.1 (168–183). Peaks at  $m/z$  1283.7, 1439.8, 1479.8, and 1567.7 were also observed in the digested benzylamine conjugate. BSA-hapten conjugate peptides were observed at  $m/z$  1270.6 (452–459), 1300.6 (242–248), 1646.7 (25–34), 1702.7 (35–44), 1802.6 (24–34), and 2093.2 (437–451) all corresponding to  $[\text{MH} - \text{HCl}]^+$ . Loss of water  $[\text{MH} - \text{HCl} - \text{H}_2\text{O}]^+$  from peaks at  $m/z$  1646.7, 1702.7, and 2093.2 lead to peaks at  $m/z$  1628.7, 1684.7, and 2075.2, respectively.

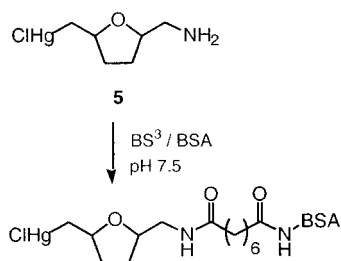
## RESULTS AND DISCUSSION

**Organomercury Hapten Synthesis.** Synthesis of the organomercury hapten **5** (Scheme 1) was initiated by protecting allylamine with *tert*-butyl carbamate (*t*-Boc). Using standard protocols, the protection proceeded cleanly at room temperature in  $\text{CH}_2\text{Cl}_2$  (22). Recrystallization of the crude reaction mixture provided *t*-Boc-allylamine, which was converted directly to epoxide **2** by reaction with *m*CPBA in  $\text{CH}_2\text{Cl}_2$  under standard conditions (23). The desired epoxide was routinely prepared in greater than 80% yield and was used without further purification. GC data of the crude reaction mixture indicated pure product, as did the sharp melting point of the crystalline solid. Both the amine protection reaction and the epoxidation reaction were readily amenable to scale-up (>5 g batch size) without further optimization.

Initially the nucleophilic ring opening reaction of epoxide **2** in the presence of allylmagnesium bromide in THF appeared to provide the desired hydroxy alkene **3**, albeit in poor yield. Upon further characterization, it was found that the desired product was contaminated by a significant amount of bromohydrin byproduct **7** (Scheme 2). Several purification methods were attempted in order to isolate the desired hydroxy alkene (**3**) from the crude reaction mixture, but under all conditions investigated, bromohydrin contamination remained unacceptable.

Etheral solutions of Grignard reagents tend to exist as equilibrium mixtures of alkylmagnesium bromide, magnesium bromide, and dialkylmagnesium (24). When magnesium bromide is present in solution, epoxide **2** is susceptible to bromide ion-mediated nucleophilic ring opening reactions, thus forming the bromohydrin as a byproduct. Hydroxy alkene **3** was prepared successfully upon addition of anhydrous dioxane to allylmagnesium bromide prior to reacting with epoxide **2**. Dioxane promotes precipitation of magnesium bromide, shifting the equilibrium toward higher concentrations of dialkylmagnesium (25, 26). When the resulting enriched solution of dialkylmagnesium was reacted with epoxide **2**, the desired hydroxy alkene (**3**) was formed without the problematic bromohydrin present. GC analysis of the crude reaction mixture indicated that the product consisted of a 20:1 mixture of regioisomeric ring-opened products (**3** and **8**).

With hydroxy alkene **3** in hand, optimization of the intramolecular oxymercuration cyclization, the key synthetic transformation in the synthesis, was explored. The organomercury precursor (**3**) was designed to readily accommodate intramolecular mercury-mediated cyclization to generate a mercurio cyclic ether. Oxymercuration reactions have been extensively studied and the intramolecular reaction of  $\gamma$ -hydroxy alkenes was well suited for preparing the target organomercury hapten (27–30) because these reactions are fast, high yielding, and occur under extremely mild conditions (28). The reaction is also highly versatile, accommodating numerous alkene structures, and tolerant of many organic functional groups (29,

**Scheme 3**

30). The resulting carbon–mercury bond is especially chemically and thermally stable (28). Additionally, organomercury compounds are air stable and therefore amenable to routine purification and characterization techniques.

The oxymercuration reaction proceeded smoothly upon addition of mercuric acetate to a solution of hydroxy alkene **3** in acetonitrile. The organomercury compounds prepared in this study were not amenable to routine GC-MS analysis, presumably due to their low volatility; therefore, the course of the cyclization reaction was followed via TLC. When starting material was no longer observed, the reaction mixture was quenched with NaCl to facilitate mercury ligand exchange, yielding cyclic mercuric chloride **4** (Scheme 1). The organomercury substrate was purified via column chromatography and was isolated in good yield. The exact mass of mercuric chloride **4** was determined by high-resolution MALDI/FT-ICR MS. The experimental exact mass found for the sodiated parent ion of **4** ( $[M + Na]^+$ ) was 474.0730 *m/z* and the calculated mass was 474.0729 *m/z*. The isotopic distribution of Hg was observed in the MS and proved to be a very useful diagnostic tool in characterizing the organomercury hapten and the bioconjugates coupled with the hapten.

A small sample of the crude oxymercuration reaction mixture was reduced with  $\text{NaBH}_4$  to generate cyclic ether **6** (Scheme 1). GC analysis of the reaction mixture after reduction revealed a 1:1.7 mixture of cyclic diastereomers. In the proton NMR of a purified sample of the reduced product, two methyl doublets were observed, providing additional evidence that the mercuric chloride (**4**) was formed as a pair of diastereomers.

The final step in the synthesis of organomercury hapten **5**, deprotection of cyclic mercuric chloride **4** was carried out in excess TFA, which was removed in vacuo prior to quenching the crude reaction mixture with 1 equiv of NaOH. The free amine organomercury hapten **5** was coupled directly to BSA without further purification (Scheme 3). In designing the organomercury hapten, we had intended to prepare a water-soluble substrate to facilitate protein conjugation protocols. Hapten **5** was moderately water soluble upon deprotection and basification to the free amine.

**Conjugation of Organomercury Hapten.** Prior to conjugating organomercury hapten **5** to BSA, hapten carrier coupling conditions were optimized with benzylamine serving as a model hapten. Benzylamine was selected as a suitable model hapten because it is an inexpensive, water-soluble aliphatic amine, and has a  $pK_a$  similar to hapten **5**. Additionally, benzylamine would be a useful analyte for testing the feasibility of MALDI/FT-ICR MS as a viable method for characterizing the resulting bioconjugates.

The bioconjugate prepared in this work constitutes a novel approach to achieving an organometallic–protein complex, in which the metal is covalently bound to the

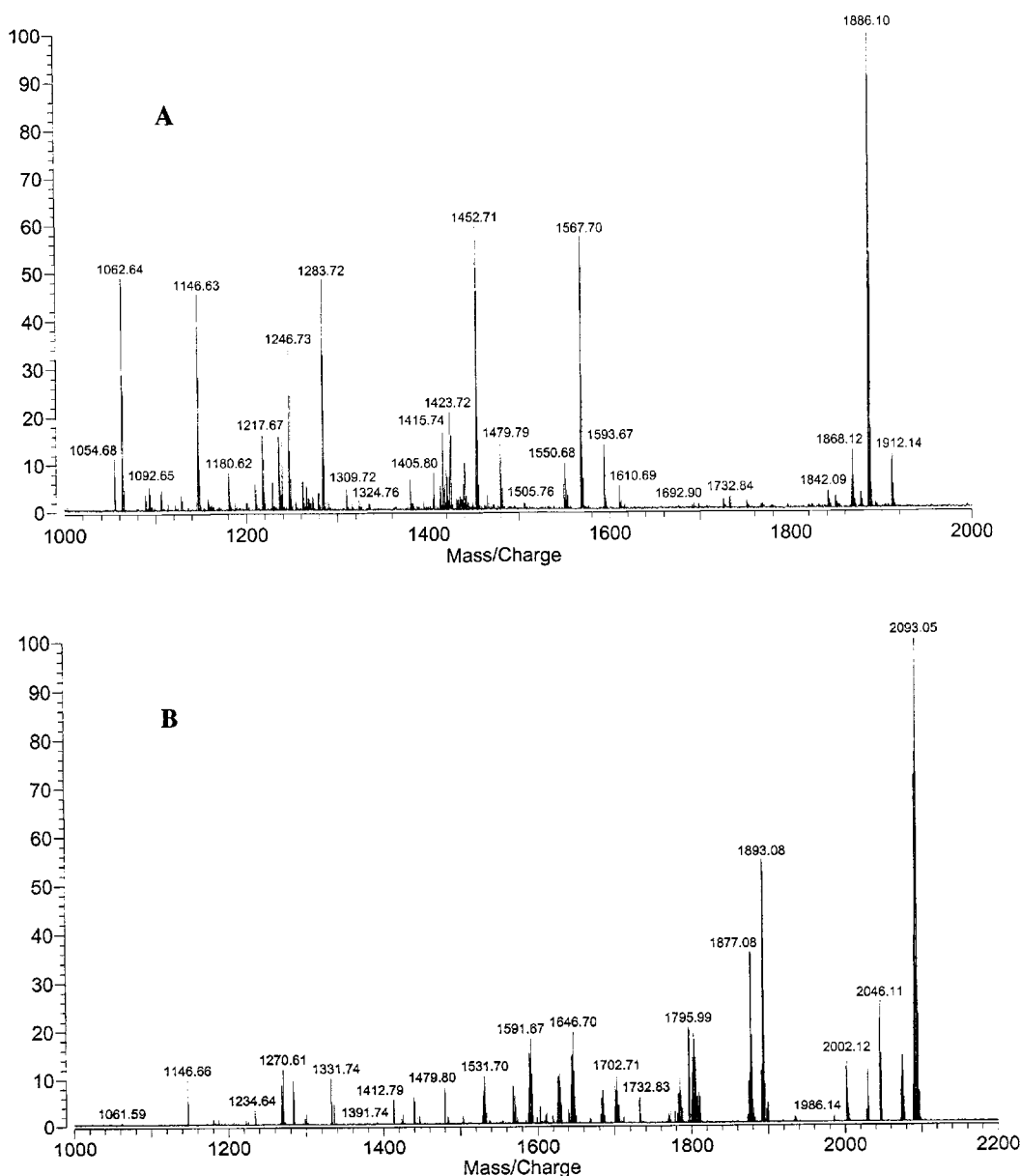
protein.  $\text{BS}^3$ , a commercially available homobifunctional (disuccinimide ester) cross-linking reagent that targets amine functional groups and forms stable amide linkages (31, 32), was utilized to covalently couple organomercury hapten **5** to BSA and in all the model conjugates prepared in this study. Upon coupling, a linker arm distance of 14 atoms separates the mercury atom from the protein in bioconjugate **9** (Scheme 3). We propose that the hydrophobic, nonpeptide character of the linker arm will provide more optimal immunological response and result in mAbs consisting of unique recognition capabilities, compared to the anti-mercury Ab previously prepared (20).

Succinimide esters are commonly used amine reactive cross-linking reagents, but can be problematic because undesirable ester hydrolysis becomes favorable at pH levels most suited for promoting nucleophilic substitution by unprotonated amines. Active ester coupling reactions are typically preformed in pH ranges of 7.0–7.5 (33). In this pH range the concentration of unprotonated amine is low, but the rate of the nucleophilic substitution reaction is sufficiently fast (10 min) relative to the succinimide ester hydrolysis rate, which is on the order of hours. The reaction conditions examined for the model coupling consisted of incubating a 1:2 molar ratio of benzylamine and  $\text{BS}^3$  for varying times (0, 1, and 5 min) in pH 7.5 phosphate buffer prior to coupling with BSA. The preincubation was intended to maximize monosubstitution of  $\text{BS}^3$  with benzylamine and limit protein cross coupling. BSA–phosphate buffer solution was added to each reaction mixture after the  $\text{BS}^3$ –benzylamine preincubation, and the solutions were allowed to react an additional 45 min at room temperature. The conjugates were dialyzed and enzymatically digested with trypsin. MALDI/FT-ICR MS analysis of the model conjugates revealed that preincubating  $\text{BS}^3$  with benzylamine at different time intervals did not significantly affect the molar ratio of benzylamine to protein in the bioconjugates.

Since the model conjugation reactions with benzylamine indicated that the extent of hapten coupling was not sensitive to incubation times, organomercury hapten **5** was covalently coupled to BSA via  $\text{BS}^3$  cross-linking reagent under slightly modified reaction conditions. BSA and hapten **5** were dissolved initially in pH 7.5 phosphate buffer. A concentrated stock solution of  $\text{BS}^3$  was prepared in pH 7.5 phosphate buffer and immediately added to the hapten–carrier solutions. After incubating for 1 h, each reaction was quenched with an additional aliquot of hapten and stirred for 30 more minutes at room temperature.

**MALDI Characterization of Conjugates.** The techniques suitable for characterizing the bioconjugates prepared in this study were limited. UV spectroscopy, a very common bioconjugate characterization method, was not possible because hapten **5** does not contain any UV detectable chromophores. Another example of a routine method for characterizing carrier:hapten ratios is TNBS colorimetric assays (34), which quantify the number of lysine residues that have been modified upon conjugation of a hapten to a protein carrier. Hampered by competitive hydrolysis of  $\text{BS}^3$ , there is the possibility that the hydrolyzed linker alone occupies some of the lysine sites. Consequently, the results of a TNBS assay would not distinguish between lysine residues that had been modified by covalent attachment of hapten- $\text{BS}^3$  linker from those that had been modified only by the addition of hydrolyzed linker.

MALDI-MS techniques have been shown to be very powerful and accurate tools for analyzing complex bio-



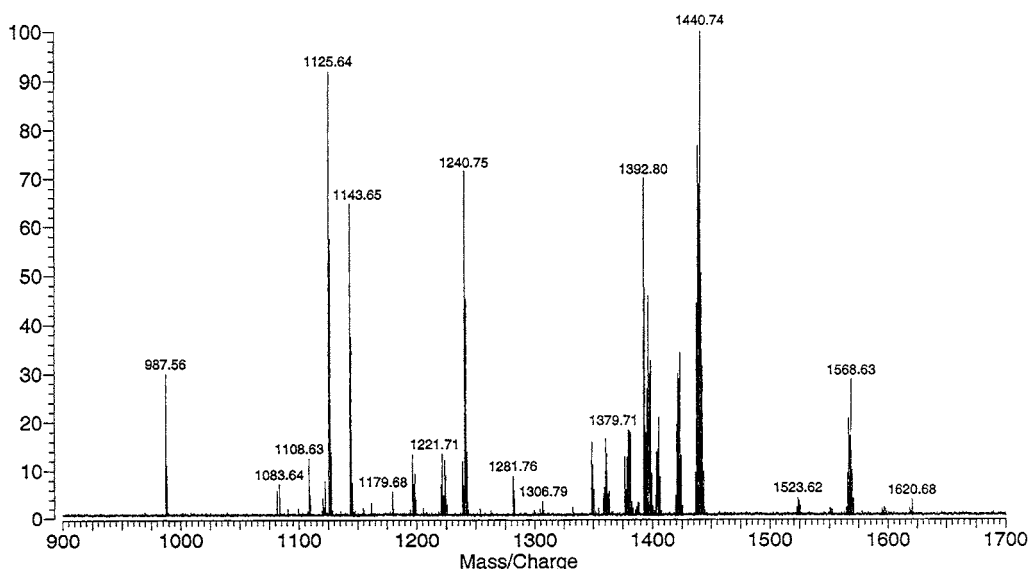
**Figure 1.** MALDI MS of trypsin digested conjugates. A. Benzylamine-BSA conjugate. B. Organomercury hapten-BSA conjugate **9**.

conjugate structures (35–40). For example, in a comparative study, Adamczyk and co-workers demonstrated that MALDI-MS is a significantly more accurate analytical tool than either UV spectroscopy or TNBS colorimetric assays for determining the extent of coupling of low molecular weight haptens to protein carriers (37). MALDI-MS is a sensitive ionization technique (detection limits in the low attomole range have been demonstrated) that generates primarily singly charged  $[M + H]^+$  ions for peptides and proteins (35, 40). These ions undergo limited subsequent fragmentation and are ideally suited for characterization of mixtures of structurally complex substrates (39). MALDI is most commonly used in combination with TOF mass analyzers; however, the MALDI/FT-MS used in this study has ultrahigh mass resolution, coupled with ppm mass accuracy. In addition, MS/MS techniques can be used for structural characterization (40, 41).

The mass range of the MALDI/FT-MS is lower than that of a MALDI/TOF and analysis of the intact BSA conjugates was not possible (41–43). Consequently, the

conjugates were digested with trypsin to produce peptides of an appropriate mass for MALDI/FT-MS analysis (39). With this approach, modifications to specific regions of BSA can be identified through the accurate measurement of the masses of the tryptic peptides. As a test of this approach, a sample of unmodified BSA and the benzylamine model bioconjugates were enzymatically digested with trypsin (39, 44). The monoisotopic masses of the peptides resulting from tryptic digestion of the benzylamine bioconjugates were compared to native BSA's tryptic peptides. A MALDI/FT-MS (mass range 1000–2000  $m/z$ ) spectrum of a digested benzylamine-BSA conjugate is shown in Figure 1A. The spectrum shows that five benzylamine-coupled peptides are detected along with four peptides without the amine attached. Unconjugated BSA peptides are observed at  $m/z$  1283.7, 1439.8, 1479.8, and 1567.7. Peptides coupled to 1 equiv of benzylamine are observed at  $m/z$  1062.6, 1092.7, 1236.8, 1246.7, and 1886.1 (Figure 1A). This experiment revealed that the BS<sup>3</sup> coupling protocol was effective in covalently attaching the aliphatic amine model hapten to BSA, and





**Figure 2.** MALDI-MS of hapten **5** coupled to model peptide (KKRAARATS-amide), base peak ( $[MH - HCl]^+$ ) observed at  $m/z$  1440.74.

**Table 1.** Mass (measured vs calculated) of BSA Peptide Fragments Observed in MALDI MS (Figure 1B) after Tryptic Digestion of Organomercury Bioconjugate **9**

measured mass ( $m/z$ )	calculated mass ( $m/z$ ) <sup>a</sup>	ppm	AA sequence in tryptic peptide	residue number
847.5141	847.5036	12.4	(R)LSQKFPK <sup>b</sup>	161–167
1283.7059* <sup>c</sup>	1283.7106	−3.7	(R)HPEYAVSVLLR	361–371
1439.8123*	1439.8117	0.4	(R)RHPEYAVSVLLR	360–371
1479.8036*	1479.7954	5.5	(K)LGEYGFQNALIVR	421–433
1567.7456*	1567.7427	1.8	(K)LGEYGFQNALIVR	347–359
1639.9261*	1639.9378	−7.1	(R)KVPQVSTPTLVEVSR	437–451
2045.1175	2045.0280	43.8	(R)RHPYFYAPELLYYANK	168–183
1270.6136	1270.6127	0.7	(R)SLGKVGTR <sup>d</sup>	452–459
1300.6356	1300.6264	7.1	(R)LSQKFPK	242–459
1646.7043	1646.7249	−12.5	(R)DTHKSEIAHR	25–34
1702.7185	1702.7439	−14.9	(R)DTHKSEIAHR	35–44
2093.0579	2093.0623	−2.1	(R)KVPQVSTPTLVEVSR	437–451

<sup>a</sup> Calculated monoisotopic masses are given. <sup>b</sup> Unmodified lysine residues shown in *italic*. <sup>c</sup> Calibration peaks are indicated by an asterisk. <sup>d</sup> Lysine residues coupled to hapten **5** shown in **bold**.

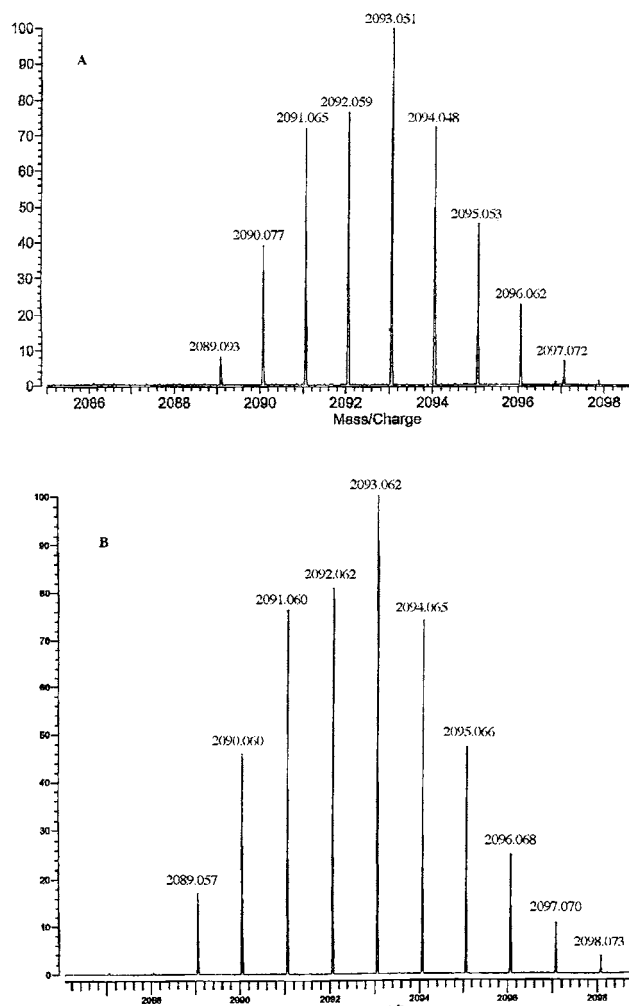
that tryptic digestion coupled with MALDI-MS would provide a convenient method for accurately measuring hapten attachment sites in the bioconjugates.

To investigate the behavior of peptides containing organomercury moieties under MALDI-MS conditions, the synthetic hapten (**5**) was coupled via BS<sup>3</sup> to a commercially available peptide, nine amino acids in length and containing a terminal lysine (KKRAARATS-amide). Upon examination of the MS data, the  $[M + H]^+$  peak ( $m/z$  1476.7) was not detected; however, several peaks containing mercury were apparent. The base peak in the spectrum, containing one mercury, corresponds to  $[MH - HCl]^+$  at  $m/z$  1440.7. The mass spectra of organomercury halides are often dominated by loss of the halide, and the facile loss of HCl in this case may prevent detection of the intact  $[M + H]^+$  peak. When cesium iodide was added to the matrix/peptide–conjugate mixture, iodine-mediated ligand exchange with the mercuric chloride hapten was favorable, and a peak at  $m/z$  1568.6 corresponding to the  $[M + H]^+$  parent ion of the peptide–mercuric iodide conjugate was observed (Figure 2). A distinct peak, clearly containing mercury, at  $m/z$  1440.7 was also observed in this spectrum. This peak arises from the parent ion minus HCl or HI ( $[MH - HCl]^+$ ,  $[MH - HI]^+$ ), respectively. MS/MS of the  $m/z$  1568.6  $[M + H]^+$  ion showed a peak at  $m/z$  1440 resulting from loss of HI, demonstrating that the  $m/z$  1440 peak results from an

ionization-induced fragmentation of the protonated parent ion. The  $[MH - HCl]^+$  ion was found to be characteristic of the other peptide–organomercury conjugates. Other peaks observed in the spectrum included the unreacted peptide ( $m/z$  987.6) and peptide coupled to hydrolyzed BS<sup>3</sup> ( $m/z$  1143.7) and a peak at  $m/z$  1240.8 arising from loss of HgCl from the  $[M + H]^+$  parent ion. (Figure 2). The MS/MS experiment indicated that  $m/z$  1240.8 is also an ionization-induced fragment.

Confident that MALDI-MS was a viable tool for analyzing peptides covalently bound to mercury, BSA–organomercury bioconjugate **9** was digested with trypsin, and the resulting peptide fragments were analyzed by MALDI-MS. Analysis of the model peptide–organomercury conjugates had revealed that the peak of key diagnostic value arises from loss of HCl from the parent ion ( $[MH - HCl]^+$ ). There are five hapten attachment sites apparent in the MS of the tryptic fragments of conjugate **9** in the range of 1000–2200  $m/z$ .

The exact mass of all the peptide fragments expected upon tryptic digestion of BSA and of each peptide coupled to the organomercury hapten through a BS<sup>3</sup> linker were calculated by the Web version of Protein Prospector (45) and compared to the experimental masses measured in the digested sample of **9**. Several tryptic peptide fragments without any hapten attachment are observed at  $m/z$  847.5, 1283.7, 1439.8, 1479.8, 1567.7, 1639.9, and



**Figure 3.** Expansion of  $m/z$  2093.0579 peak arising from hapten **5** coupled to tryptic peptide composed of amino acid sequence KVPQVSTPTLVEVSR (437–451). A. Experimentally measured peak, including isotopic distribution of mercury. B. Calculated monoisotopic mass and isotope distribution.

2045.1. Four of these peptides are consistent with the peptides identified in the MS of the digested benzylamine model conjugate. The calculated monoisotopic masses of each of these hapten free peptide fragments were compared to the experimentally measured mass values and are shown in Table 1. The peaks at  $m/z$  1270.6, 1300.6, 1646.7, 1702.7, and 2093.1 all correspond to a BSA tryptic peptide coupled to organomercury hapten **5** ( $[MH - HCl]^+$ ). The calculated monoisotopic mass of these peptides compared to the measured mass is also presented in Table 1. Fragmentation of water from peaks at  $m/z$  1646.7, 1702.7, and 2093.1 gives rise to the peaks observed at  $m/z$  1628.7, 1684.7, and 2075.2, respectively. The peak at  $m/z$  1802.6 was initially interpreted as a sixth hapten attachment site, as it clearly displays the mercury isotopic pattern evident in other peaks and matched the calculated mass (1802.8266  $m/z$ ) for hapten **5** coupled to lysine 28 in the peptide containing amino acids 24–34 (RDTHKSEIAHR). This peak, however, is a result of BSA's multiple possible tryptic cleavage points, which can generate peptide fragments containing overlapping amino acid sequences. The peak at  $m/z$  1646.7, which arises from hapten **5** coupled to the peptide composed of amino acids 25–34 (DTHKSEIAHR), already accounts for coupling between the hapten and lysine 28. The  $m/z$  1893.1 peak is consistent with the loss

of Hg from the  $m/z$  2093.5 peak, but in this case a MS/MS experiment did not identify this peak as arising from ionization-induced fragmentation. Surprisingly, there were no peaks corresponding to peptides coupled to hydrolyzed BS<sup>3</sup> in the mass range investigated.

The expanded spectrum of the peak measured at  $m/z$  2093.2 is compared to the theoretical isotopic distribution and the calculated monoisotopic mass for hapten **5** coupled to the tryptic peptide fragment containing amino acids 437–451 in Figure 3A and 3B, respectively. The experimentally measured mass, 2093.0579  $m/z$ , has a mass accuracy of  $-2.1$  ppm relative to the calculated mass value (2093.0623  $m/z$ ). The symmetrical nature observed in the peaks shown in Figure 3 was a reoccurring pattern found in all the peptide fragments containing an organomercury moiety. The peaks at  $m/z$  2089.1–2093.1 and 2095.1 arise from the mercuric isotopes of mass 198–202 and 204, respectively.

Aided by MALDI-MS, we were able to validate our conjugation protocol through the examination of model conjugates, and specifically identify sites containing covalently linked organomercury hapten **5** by accurate mass measurements. It was also demonstrated that our approach to preparing a metal–protein complex via formation of a stable organometallic bond was successful. As MALDI-MS analysis of conjugates becomes a more widely exploited technique, it may provide the opportunity to correlate epitope density, hapten conformation and linker arm length and structure to immune response.

#### ACKNOWLEDGMENT

This work was supported by CIB (Center for Innovation in Biotechnology) in Augusta, ME, and by the University of Southern Maine Faculty Senate. The MALDI instrumentation used in this study was supported by the National Science Foundation under Grant No. CHE-0116416. The NMR (400 MHz) instrumentation was supported by the National Science Foundation under Grant No. 9724321. The authors thank Professor Elizabeth Stemmler at Bowdoin College for her assistance in collecting and analyzing MALDI-MS data.

#### LITERATURE CITED

- (1) Kolthoff, I. M. et al (1954) Amperometric Mercurimetric Titration of Sulfhydryl Groups in Biologically Important Substances. *Anal. Chem.* 26, 366.
- (2) Azadova, N. B., et al (1965) Action of Proflavine on the Development of Sendai Virus in HEp 2-Cells. *Br. J. Exp. Path.* 47, 121.
- (3) Leavis, P. C., and Lehrer, S. S. (1974) A Sulfhydryl-Specific Fluorescent Label, S-Mercuric-N-Dansylcysteine. Titrations of glutathione and Muscle Proteins. *Biochemistry* 13, 3042.
- (4) Wylie, D. E., Carlson, L. D., Carlson, R., Wagner, F. W., and Schuster, S. M. (1991) Detection of Mercuric Ions in Water by ELISA with a Mercury-Specific Antibody. *Anal. Biochem.* 194, 381.
- (5) Marx, A., and Hock, B. (2000) Monoclonal Antibody-Based Enzyme Immunoassay for Mercury (II) Determination. *Methods* 22, 49.
- (6) Brummer, O., La Clair, J. J., and Janda, K. D. (2001) Practical Screening of Mercury Contamination in Fish Tissue. *Bioorg. Med. Chem.* 9, 1067.
- (7) Mears, C. F., and Wensel, T. G. (1984) Metal Chelates as Probes of Biological Systems. *Acc. Chem. Res.* 17, 202.
- (8) Reardon, D. T., Meares, C. F., Goodwin, D. A., McTigue, M., David, G. S., Stone, M. R., Leung, J. P., Bartholomew, R. M., and Frincke, J. M. (1985) Antibodies Against Metal Chelates. *Nature* 316, 265.

- (9) Sieving, P. F., Watson, A. D., and Rocklage, S. M. (1990) Preparation and Characterization of Paramagnetic Poly-chelates and Their Protein Conjugates. *Bioconjugate Chem.* 1, 65.
- (10) Blake, D. A., Chadrabarti, P., Khosraviani, M., Hatcher, F. M., Westhoff, C. M., Goebel, P., Wylie, D. E., and Blake, R. C. II. (1996) Metal Binding Properties of a Monoclonal Antibody Directed toward Metal-Chelate Complexes. *J. Biol. Chem.* 271, 27677.
- (11) Jones, R. M., Yu, H., Delehanty, J. B., and Blake, D. A. (2002) Monoclonal Antibodies That Recognize Minimal Differences in the Three-Dimensional Structures of Metal-Chelate Complexes. *Bioconjugate Chem.* 13, 408.
- (12) Civitello, E. R., Leniek, R. G., Hossler, K. A., Haebe, K., and Stearns, D. M. (2001) Synthesis of Peptide–Oligonucleotide Conjugates for Chromium Coordination. *Bioconjugate Chem.* 12, 399.
- (13) Siiman, O., Burshteyn, A., Maples, J. A., and Whitesell, J. K. (2000) Tris 93-mercaptopropyl-N-glycylaminomethane as a New Linker to Bridge Antibody with Metal Particles for Biological Cell Separations. *Bioconjugate Chem.* 11, 349.
- (14) Brasch, R. C. (1992) Contrast Enhancement in MRI: Images of the Future. *Adv. MRI Contrast* 1, 28.
- (15) Shreve, P., and Aisen, A. M. (1986) Monoclonal Antibodies Labeled with Paramagnetic Ion Chelates. *Magn. Reson. Med.* 3, 336.
- (16) Schwartz, D. A., Abrams, M. J., Hauser, M. M., Gaul, F. E., Larsen, D. R., and Zubieta, J. A. (1991) Preparation of Hydrazino-Modified Proteins and Their Use for the Synthesis of  $^{99m}\text{Tc}$ –Protein Conjugates. *Bioconjugate Chem.* 2, 333.
- (17) Zhang, X.-B., et al. (2002) An Optical Fiber Chemical Sensor for Mercury Ions Based on a Porphyrin Dimer. *Anal. Chem.* 74, 821.
- (18) Khosraviani, M., Blake, R. C., II, Pavlov, A. R., Lorbach, S. C., Yu, H., Delehanty, J. B., Brechbiel, M. W., and Blake, D. A. (2000) Binding Properties of a Monoclonal Antibody Directed Toward Lead–Chelate Complexes. *Bioconjugate Chem.* 11, 207.
- (19) Stewart, J. D., Roberts, V. A., Crowder, M. W., Getzoff, E. D., and Benkovic, S. J. (1994) Creation of a Novel Biosensor for Zn(II). *J. Am. Chem. Soc.* 116, 415.
- (20) Wylie, D. E., Lu, D., Carlson, L. D., Carlson, R., Babacan, K. F., Schuster, S. M., and Wagner, F. W. (1992) Monoclonal Antibodies Specific for Mercuric Ions. *Proc. Natl. Acad. Sci.* 89, 4104.
- (21) Martell, A. E., and Smith, R. M. (1974) *Critical Stability Constants*, Plenum Press, New York.
- (22) Greene, T. W. (1981) *Protective Groups in Organic Synthesis*, Chapter 7, Wiley, New York.
- (23) Smith, M. B., March, J. (2001) *Advanced Organic Chemistry: Reactions, Mechanism, and Structure*, Wiley, New York.
- (24) Salinger, R. M., and Mosher, H. S. (1964) Infrared Spectral Studies of Grignard Solutions. *J. Am. Chem. Soc.* 86, 1782.
- (25) Smith, M. B., and Becker, W. E. (1966) The Constitution of the Grignard Reagent II. The Reaction between  $\text{R}_2\text{Mg}$  and  $\text{MgX}_2$  in Ether. *Tetrahedron* 22, 3027.
- (26) Parris, G. E., and Ashby, E. C. (1971) The Composition of Grignard Compounds: VII. The Composition of Methyl and *tert*-Butyl Magnesium Halides and Their Dialkyl Magnesium Analogues in Diethyl Ether and THF as Inferred from Nuclear Magnetic Resonance Spectroscopy. *J. Am. Chem. Soc.* 93, 1206.
- (27) Larock, R. C. (1978) Organomercury Compounds in Organic Synthesis. *Angew. Chem., Int. Ed. Engl.* 17, 27.
- (28) LaRock, R. C. (1985) *Reactivity and Structure Concepts in Organic Chemistry, Vol 22, Organomercury Compounds in Organic Synthesis*, Chapter 7, Springer-Verlag, New York.
- (29) Imagawa, H. I., Shigarak, T., Suzuki, T., Takao, H., Yamada, H., Sugihara, T., and Nishizawa, M. (1998) Intramolecular Oxymercuration with Mercuric Triflate. *Chem. Pharm. Bull.* 46, 1341.
- (30) Nishizawa, M., Kashima, T., Sakakibara, M., Wakabayashi, A., Takahashi, K., Takao, H., Imagawa, H., and Sugihara, T. (2001) Intramolecular Oxymercuration of 4-Hexen-1-ols: Kinetic vs Thermodynamic Products Regulated by Mercuric Salts. *Heterocycles* 54, 529.
- (31) Staros, J. V. (1982) N-Hydroxy Sulfo Succinimide Active Esters: bis(N-hydroxysulfo-succinimide) Esters of Two Dicarboxylic Acids are Hydrophilic, Membrane-Impermeant Protein Cross-Linkers. *Biochemistry* 21, 3950.
- (32) Paek, S.-H., et al (1993) Defined Analyte-Enzyme Conjugates as Signal Generators in Immunoassays. *Anal. Biochem.* 210, 145.
- (33) Aslam, M., and Dent, A. (1998) *Bioconjugation: Protein Coupling Techniques for the Biomedical Sciences*, MacMillan Reference LTD, London.
- (34) Shinoda, T., and Tsuzukida, Y. (1974) Identification of Rapidly Trinitrophenylating Amino Groups of Human Bence-Jones Proteins. *J. Biochem.* 75, 23.
- (35) Karas, M., et al (1990) Principles and Applications of Matrix-Assisted UV Laser Desorption/Ionization Mass Spectrometry. *Anal. Chem. Acta* 241, 175.
- (36) Chait, B. T., and Kent, S. B. H. (1992) Weighing Naked Proteins: Practical High Accuracy Mass Measurement of Peptides and Proteins. *Science* 257, 1885.
- (37) Adamczyk, M., Buko, A., Chen, Y.-Y., Fishpaugh, J. R., Gebler, J. C., and Johnson, D. D. (1994) Characterization of Protein-Hapten Conjugates. 1. Matrix-Assisted Desorption Ionization Mass Spectrometry of Immuno BSA–Hapten Conjugates and Comparison with Other Characterization Methods. *Bioconjugate Chem.* 5, 631.
- (38) Yang, T., Horejsh, D. R., Mahan, K. J., Zaluzec, E. J., Watson, T. J., and Gage, D. A. (1996) Mapping Cross-Linking Sites in Modified Proteins with Mass Spectrometry: An Application to Cross-Linked Hemoglobins. *Anal. Biochem.* 242, 55.
- (39) Yasuzawa, T., and Tomer, K. B. (1997) Structural Determination of the Conjugate of Human Serum Albumin with Mitomycin C Derivative, KW-2149, by Matrix-Assisted Laser Desorption/Ionization Mass Spectrometry. *Bioconjugate Chem.* 8, 391.
- (40) Fenselau, C. (1997) MALDI MS and Strategies for Protein Analysis. *Anal. Chem.* 69, A661.
- (41) Buchanan, M. V., and Hettich, R. L. (1993) Fourier Transform Mass Spectrometry of High-Mass Biomolecules. *Anal. Chem.* 65, 245A.
- (42) Castoro, J. A., and Wilkins, C. L. (1993) Ultrahigh-Resolution Matrix-Assisted Laser Desorption/Ionization of Small Proteins by Fourier Transform Mass Spectrometry. *Anal. Chem.* 65, 2621.
- (43) Solouki, T., and Russell, D. H. (1992) Laser Desorption Studies of High Mass Biomolecules in Fourier Transform Ion Cyclotron Resonance Mass Spectrometry. *Proc. Natl. Acad. Sci. U.S.A.* 89, 5701.
- (44) <http://masspec.scripps.edu/information/samprep/solidigest.html>.
- (45) <http://prospector.ucsf.edu>.
- (46) Abbreviations: MALDI/FT-ICR MS, matrix-assisted laser desorption ionization Fourier transform ion cyclotron resonance mass spectroscopy; EDTA, ethylenediamine tetraacetic acid; KLH, keyhole limpet hemocyanin; *t*-Boc, *tert*-butyl carbamate; *m*CPBA, *m*-chloroperoxy benzoic acid; THF, tetrahydrofuran; DEP, direct exposure probe; TFA, trifluoroacetic acid; BSA, bovine serum albumin; BS<sup>3</sup>, bis[sulfosuccinimidyl]-suberate; DMSO, dimethyl sulfoxide; TNBS, trinitrobenzene sulfonic acid; TOF, time-of-flight DTT, dithiothreitol; DHB, 2,5-dihydroxybenzoic acid.



# Asymmetrical Nitrido Tc-99m Heterocomplexes as Potential Imaging Agents for Benzodiazepine Receptors

Alessandra Boschi,<sup>†</sup> Licia Uccelli,<sup>†</sup> Adriano Duatti,<sup>\*,†</sup> Cristina Bolzati,<sup>‡</sup> Fiorenzo Refosco,<sup>‡</sup> Francesco Tisato,<sup>‡</sup> Romeo Romagnoli,<sup>§</sup> Pier Giovanni Baraldi,<sup>§</sup> Katia Varani,<sup>§</sup> and Pier Andrea Borea<sup>§</sup>

Laboratory of Nuclear Medicine, Department of Clinical & Experimental Medicine, University of Ferrara, 44100 Ferrara, Italy, Department of Pharmaceutical Sciences, University of Ferrara, 44100 Ferrara, Italy, and Istituto di Chimica Inorganica e delle Superfici - CNR, 35127 Padua, Italy. Received July 17, 2003; Revised Manuscript Received August 21, 2003

The design, synthesis, and biological evaluation of nitrido technetium-99m complexes for imaging benzodiazepine receptors are described. The design was performed by selecting the precursor biologically active substrate desmethyldiazepam, and the reactive metal-containing fragment  $[^{99m}\text{Tc}(\text{N})(\text{PXP})]^{2+}$  (PXP = diphosphine ligand) as molecular building-blocks for assembling the structure of the final radiopharmaceuticals through the application of the so-called 'bifunctional' and 'integrated' approaches. This required the synthesis of the ligands  $\text{H}_2\text{BZ1}$ ,  $\text{H}_2\text{C1}$ , and  $\text{H}_2\text{C2}$  (Figures 1 and 2) derived from desmethyldiazepam. In turn, these ligands were reacted with  $[^{99m}\text{Tc}(\text{N})(\text{PXP})]^{2+}$  to afford the complexes  $[^{99m}\text{Tc}(\text{N})(\text{PXP})(\text{L})]$  ( $\text{L} = \text{BZ1}, \text{C1}, \text{C2}$ ). The chemical nature of the resulting Tc-99m radiopharmaceuticals was investigated using chromatographic methods, and by comparison with the analogous complexes prepared with the long-lived isotope Tc-99g and characterized by spectroscopic and analytical methods. Results showed that the complexes  $[^{99m}\text{Tc}(\text{N})(\text{PXP})(\text{L})]$  are neutral and possess an asymmetrical five-coordinated structure in which two different bidentate ligands, PXP and L, are coordinated to the same  $\text{Tc}\equiv\text{N}$  core. With the ligand  $\text{H}_2\text{BZ1}$ , two isomers were obtained depending on the syn or anti orientation of the pendant benzodiazepine group relative to the  $\text{Tc}\equiv\text{N}$  multiple bond. Biodistribution studies of Tc-99m complexes were carried out in rats, and affinity for benzodiazepine receptors was assessed through in vitro binding experiments on isolated rat's cerebral membranes using the corresponding Tc-99g complexes.

## INTRODUCTION

Benzodiazepine receptors are ubiquitously involved in the GABA postsynaptic receptor complex. In particular, the biochemical evidence indicates that benzodiazepine receptors are part of the  $\text{GABA}_A$  receptor chloride ion channel complex. Alterations of benzodiazepine receptor distribution are involved in many pathological states of the central nervous system (1–4). Positron emission tomography (PET) and single photon emission tomography (SPET) are unique technologies for the noninvasive monitoring of receptor patterns in integrated organisms without affecting their in vivo stability. Various radiopharmaceuticals have been proposed as suitable candidates for the application of these imaging procedures to the evaluation of benzodiazepine receptor distribution (5, 6). It has been showed previously that the derivative Iomazenil labeled with the  $\gamma$ -emitting radionuclide I-123 possesses useful biological characteristics, and it is currently employed as imaging agent for the diagnosis of various brain diseases related to alterations of benzodiazepine receptors (7). Nonetheless, since production of I-123 is performed through a neutron reactor, its routine clinical use is strongly limited. Analogous compounds labeled with the short-lived, positron-emitting nuclides C-11 and F-18 have been also described (8–13). However,

the main limitation with this type of radionuclides comes from the fact that their production requires the use of an on-site cyclotron, an apparatus that is not widely accessible in all nuclear medicine centers.

The  $\gamma$ -emitting nuclide technetium-99m possesses almost ideal nuclear properties for SPET imaging and is readily available in all nuclear medicine centers through the use of a transportable  $^{99}\text{Mo}/^{99m}\text{Tc}$  generator (14). These advantages account for the widespread use of Tc-99m radiopharmaceuticals in routine clinical practice. They further suggest that the search for a useful Tc-99m tracer for imaging benzodiazepine receptor distribution would be highly desirable. However, the preparation of a diagnostic agent of this type would appear immediately as a rather difficult task due to the strict, structural requirements that should be attained by such a compound in order to penetrate the intact blood–brain barrier (BBB) and localize selectively into the target receptor. For instance, a first prerequisite indicates that diffusion through BBB can be achieved only for complexes having a neutral charge and a suitable lipophilic character. Moreover, the molecular shape of the potential Tc-99m receptor imaging agent has to fit correctly the target receptor site to allow the setting up of a selective interaction (15–17).

The above considerations clearly point out the need for a preliminary design of the structure of a Tc-99m complex before coming to its actual synthesis. In the last years, two main approaches to the design of Tc-99m receptor imaging agents have been proposed. Both strategies start initially with the selection of a convenient biologically

\* Author for correspondence. Phone: 39-0532-236545. Fax: 39-0532-236589. E-mail: dta@unife.it.

<sup>†</sup> Department of Clinical & Experimental Medicine.

<sup>‡</sup> ICIS, CNR.

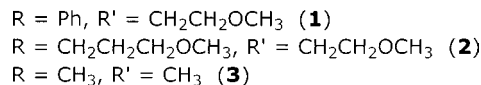
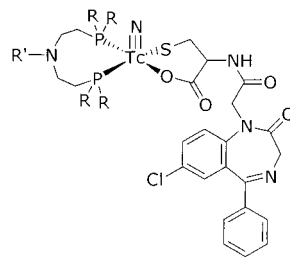
<sup>§</sup> Department of Pharmaceutical Sciences.

active molecule or drug know to have affinity for a specific receptor. After this common input, the two methods diverge. The so-called 'bifunctional' or 'pendant' approach literally suggests to append the bioactive group to a metal complex through a suitable linkage. This can be conveniently accomplished using a 'bifunctional ligand' that could be viewed as a composite molecule combining a strong chelating group for the radiometal with the biomolecule by means of a suitable linker connecting these two moieties. After the radiometal has been engaged by the chelating system, the resulting 'conjugate' complex retains the bioactive group into its structure as an appended side chain. Instead, the other procedure, called 'integrated approach', puts its focus on the selected biomolecule itself that may serve as a mold for assembling the structure of the final Tc-99m receptor radiopharmaceutical. The key step is to identify a region in its structure that is not essential for preserving its biological properties. The final radiopharmaceutical, therefore, is assembled by replacing this nonessential part with a metal-containing fragment having a molecular shape and dimension similar to the substituted portion of the original biomolecule in order to fit almost exactly into the same position. Obviously, the ultimate success of both design strategies lies in their ability to keep unaltered the intrinsic biological behavior of the starting biomolecule (17, 14, 18–20).

A key, theoretical advantage of the two approaches outlined above originates from their representation of the molecular structure of a radioactive tracer as consisting of different 'pieces' or 'fragments', which can be, at least in principle, conveniently assembled to build up the final radiopharmaceutical. However, the merging of the various fragments to yield a stable product is not always simple to accomplish and, for practical purposes, this has been obtained only through the application of the bifunctional approach.

In recent years, an alternative approach to the problem of assembling the various parts of a receptor-specific Tc-99m radiopharmaceutical has emerged. This method is based on the chemical properties of certain types of substitution-labile technetium complexes showing a marked reactivity only toward ligands having some specific set of coordinating atoms. In these complexes, a few coordination positions are occupied by a set of ligands that are tightly bound to the metal center. The resulting strong ligand field allows a significant stabilization of the metal oxidation state preventing the complex to undergo oxidation–reduction reactions. The remaining positions of the coordination arrangement are usually spanned by weakly bound ligands that could be easily replaced by some other incoming ligand carrying a specific set of donor atoms. As a consequence, the reaction between the precursor complex and the hypothetical incoming ligand is expected to be kinetically favored and should produce the final substituted complex in very high yield. Such a behavior can be efficiently exploited for assembling a 'robust' Tc-99m fragment with a biomolecule including the appropriate set of coordinating atoms. The high affinity of the precursor metal fragment for the specific donor set on the bioactive ligand would ensure the perfect fitting of these two molecular building blocks to form the final, combined complex (21).

The first example of the application of the above 'metal fragment' approach have been reported, a few years ago, by Alberto and co-workers. This is based on the chemical properties of the precursor, aquo-carbonyl, metal complex  $[^{99m}\text{Tc}(\text{CO})_3(\text{H}_2\text{O})_3]^+$ . In this species, the fragment  $[^{99m}\text{Tc}(\text{CO})_3]^+$  constitutes the chemically inert portion of



**Figure 1.** Chemical structure of complexes **1–3**.

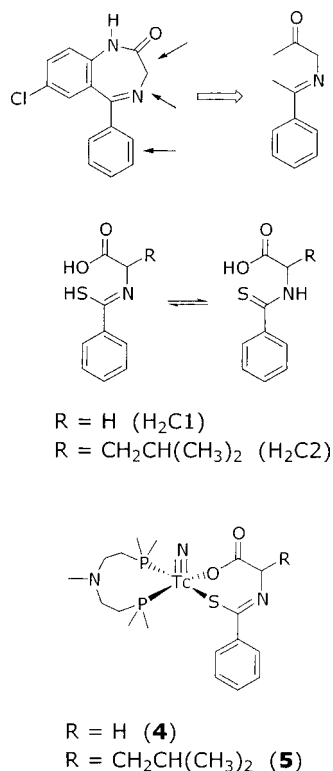
the complex. On the contrary, the three water molecules are weakly coordinated and, thus, can be easily replaced by some substituting ligand having the appropriate set of donor atoms. Under these conditions, the reaction between the metal fragment  $[^{99m}\text{Tc}(\text{CO})_3]^+$  and the incoming ligand becomes highly selective allowing the efficient assemblage of these two pieces to afford the final complex. Therefore, the precursor complex  $[^{99m}\text{Tc}(\text{CO})_3(\text{H}_2\text{O})_3]^+$  can be conveniently used as a synthon for the synthesis of a variety of Tc-99m carbonyl derivatives (22–24).

Very recently, we described the second definite example of the 'metal fragment' approach by studying the synthesis of a novel class of asymmetrical nitrido heterocomplexes characterized by the presence of two different bidentate ligands bound to the same Tc<sup>5+</sup> center. It was found that this novel type of mixed-ligand complexes was efficiently prepared by reacting the precursor complex  $[^{99m}\text{Tc}(\text{N})(\text{PXP})\text{Cl}_2]$  (PXP = diphosphine ligand) with bidentate chelating ligands carrying  $\pi$ -donors as coordinating atoms. In these reactions, the arrangement of atoms  $[^{99m}\text{Tc}(\text{N})(\text{PXP})]^{2+}$ , composed by a Tc≡N group coordinated to a chelating diphosphine ligand PXP, behaves as 'robust' metal fragment, and the two chlorine atoms can be easily displaced by the incoming  $\pi$ -donor ligand to afford the asymmetrical complex  $[^{99m}\text{Tc}(\text{N})(\text{PXP})(\text{L})]^{0/+}$ . Thus, the metal synthon  $[^{99m}\text{Tc}(\text{N})(\text{PXP})]^{2+}$  could be conveniently utilized to obtain a very broad class of asymmetrical nitrido Tc(V) complexes with a variety of bidentate ligands (25–27).

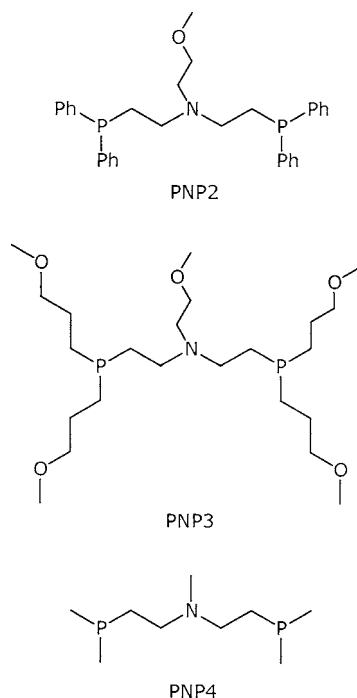
In this paper, we describe the application of the labeling method based on the metal fragment  $[^{99m}\text{Tc}(\text{N})(\text{PXP})]^{2+}$  to the preparation of a series of Tc-99m complexes with bidentate ligands derived from the benzodiazepine receptor drug desmethyldiazepam showed in Figure 1. This latter compound has been modified in two different ways to allow the application of both the bifunctional and integrated approaches as described in the following sections. The resulting ligands H<sub>2</sub>BZ1, H<sub>2</sub>-C1, and H<sub>2</sub>C2 were then reacted with  $[^{99m}\text{Tc}(\text{N})(\text{PXP})]^{2+}$  to afford asymmetrical Tc-99m complexes, which have been characterized by chromatographic methods and their biological properties evaluated both in vitro and in vivo. A drawing of the structure of the new complexes and the corresponding numbering scheme are illustrated in Figures 1 and 2 for the ligands H<sub>2</sub>BZ1, and H<sub>2</sub>C1 and H<sub>2</sub>C2, respectively.

## EXPERIMENTAL SECTION

All reactions were carried out under an inert atmosphere of dry nitrogen, unless otherwise described. Organic solutions were dried over anhydrous Na<sub>2</sub>SO<sub>4</sub>. Dry DMF was distilled from calcium chloride and stored over molecular sieves (3 Å).



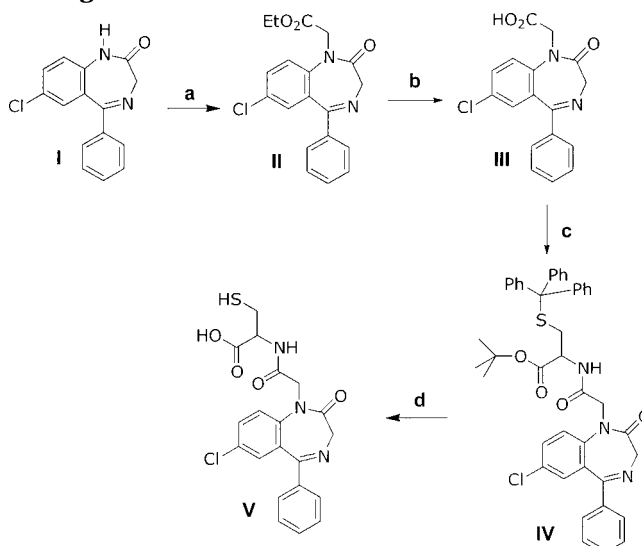
**Figure 2.** Chemical structure of the ligands **H<sub>2</sub>C1** and **H<sub>2</sub>C2**, and of complexes **3** and **5**.



**Figure 3.** The PNP-type diphosphine ligands.

The diphosphine ligands **PNP2**, **PNP3**, and **PNP4**, shown in Figure 3, were prepared as reported elsewhere or obtained from Argus Chemicals (Florence, Italy). The ligand **H<sub>2</sub>BZ1** was obtained using a procedure detailed below and illustrated in Scheme 1. The ligands (L)-*N*-thiobenzoyl glycine (**H<sub>2</sub>C1**) (**28**) and (L)-*N*-thiobenzoyl leucine (**H<sub>2</sub>C2**) (**29**) (Figure 2) have been synthesized following literature procedures. Succinic dihydrazide [SDH =  $H_2NNH(OC)CH_2CH_2(CO)NHNH_2$ ] and  $SnCl_2 \cdot 2H_2O$  were purchased from Aldrich Chimica (Milan, Italy). A generous supply of the compound 7-chloro-1,3-

**Scheme 1.** Schematic Drawing of the Preparation of the Ligand **H<sub>2</sub>BZ1**<sup>a</sup>



<sup>a</sup> Reagents and conditions: (a) NaH,  $BrCH_2CO_2Et$ ; (b) LiOH, THF/MeOH/ $H_2O$  (3:1:1); (c) EDCI, HOBT, *S*-trityl cysteine *tert*-butyl ester, DMF, rt, 18 h; (d)  $Et_3SiH$ , TFA, DCM, rt.

dihydro-5-phenyl-2*H*-1,4-benzodiazepin-2-one (desmethyldiazepam or nordazepam) was obtained as a gift from FIS S.p.A. (Vicenza, Italy). [ $^3H$ ]-Ro151788 (85.0 Ci/mmol) and [ $^3H$ ]-flunitrazepam (85.0 Ci/mmol) were provided by New England Nuclear.

Tc-99g as  $[NH_4][^{99g}TcO_4]$  was obtained from Oak Ridge National Laboratory. Samples were dissolved in water and treated with excess aqueous ammonia and 30% hydrogen peroxide at 80 °C prior to use to eliminate residual  $TcO_2$ . Solid samples of purified ammonium pertechnetate were obtained by slow evaporation of the solvent by heating at 40 °C. *Caution!* Tc-99g is a weak  $\beta$ -emitter ( $E_{\beta max} = 0.292$  MeV,  $t_{1/2} = 2.12 \times 10^5$  years). When handled in milligram amounts, it does not present a serious health hazard as normal laboratory glassware provides adequate shielding. Bremstrahlung is not a significant problem due to the low energy of the  $\beta$ -particle. However, a laboratory approved for low-level radiation equipped with gloves-boxes and monitored hoods, and normal radiation safety procedures should be used to prevent contamination and inhalation. The complex  $[^{99g}Tc(N)Cl_2(PPh_3)_2]$  was prepared as described previously (30).

TLC chromatography was performed on Merck silica gel plates. TLC chromatograms were analyzed with a Packard Cyclone instrument equipped with a phosphor imaging screen and OptiQuant image analysis software. HPLC was performed on a Beckman System Gold Instrument equipped with a programmable solvent Module 126, a scanning detector Module 166, and a radioisotope detector Module 170. Chromatographic runs were performed on a reversed-phase C18 column (Beckman Ultrasphere,  $4.6 \times 250$  mm) with a reversed-phase C18 precolumn (Beckman Ultrasphere,  $4.6 \times 45$  mm) or, alternatively, on a semipreparative reversed-phase C18 column (Beckman Ultrasphere,  $10.0 \times 250$  mm). The radiochemical purity (RCP) of Tc-99m complexes was expressed as the ratio between the activity associated with a single radiocompound, revealed as a single spot on a TLC strip, and the total activity on the strip or, alternatively, as the percent of the area under the corresponding HPLC peak.

Positive ion fast atom bombardment mass spectra (FAB+) of selected complexes in an NBA matrix were



recorded on a VG 30–250 spectrometer (VG Instrument) at the probe temperature. Xe was used as the primary beam gas and the ion gun was operated at 8 keV (ca.  $1.28 \times 10^{-15}$  J) and 100  $\mu$ A. Elemental analyses (C, H, N, S) were carried out on a Carlo Erba 1106 Elemental Analyzer. FT IR spectra were recorded on a Nicolet 510P Fourier transform spectrometer in the range 4000–200  $\text{cm}^{-1}$  in KBr mixtures using a Spectra-Tech diffuse-reflectance collector accessory. IR spectra of the ligands  $\text{H}_2\text{BZ1}$ ,  $\text{H}_2\text{C1}$ , and  $\text{H}_2\text{C2}$  were recorded on a Perkin-Elmer 781 IR spectrophotometer. Proton and  $^{31}\text{P}$  NMR spectra were collected in  $\text{CDCl}_3$  and  $d_6$ -DMSO solutions on a Bruker AC-200 instrument using  $\text{SiMe}_4$  as internal reference ( $^1\text{H}$ ) and 85% aqueous  $\text{H}_3\text{PO}_4$  as external reference ( $^{31}\text{P}$ ).

**Preparation of (7-Chloro-2-oxo-5-phenyl-2,3-dihydro-benzo[*e*][1,4]diazepin-1-yl)acetic Acid Ethyl Ester (II).** A mixture of sodium hydride (50% dispersion in mineral oil, 288 mg, 6 mmol) and desmethyldiazepam (I) (1.35 g, 5 mmol) in DMF (5 mL) was stirred at room temperature for 0.5 h. Ethyl bromoacetate (1 g., 6 mmol) in DMF (2 mL) was then added, and the reaction mixture was stirred further for 18 h at room temperature and decomposed with ice. The resulting mixture was extracted with EtOAc ( $2 \times 15$  mL) and the organic phase washed with water (10 mL), brine (5 mL) and finally dried over  $\text{Na}_2\text{SO}_4$ . After evaporation under vacuum, the residue was purified by flash-chromatography (EtOAc/petroleum ether, 7:3, v/v) to give **II** (1.48 g, yield = 81%) as a white solid.

**Preparation of (7-Chloro-2-oxo-5-phenyl-2,3-dihydro-benzo[*e*][1,4]diazepin-1-yl)acetic Acid (III).** Lithium hydroxide monohydrate (252 mg, 6 mmol) was added to a solution of **II** (732 mg, 2 mmol) in 15 mL of THF/MeOH/ $\text{H}_2\text{O}$  (3:1:1) at room temperature. The reaction mixture was stirred for 3 h, concentrated under vacuum, and then diluted with water (10 mL) and extracted with EtOAc ( $3 \times 10$  mL). The combined organic extracts were washed with brine (5 mL), dried over  $\text{Na}_2\text{SO}_4$ , and concentrated under vacuum. Flash chromatography (EtOAc) afforded **III** (494 mg, yield = 75%) as a white solid.

**Preparation of (S)-2-[2-(7-Chloro-2-oxo-5-phenyl-2,3-dihydro-benzo[*e*][1,4]diazepin-1-yl)acetylaminol]-3-tritylsulfanylpropionic Acid *tert*-Butyl Ester (IV).** EDC (960 mg, 5 mmol, 1.25 equiv), HOBt (675 mg, 5 mmol), and *S*-trityl cysteine *tert*-butyl ester (1.68 g., 4 mmol) were added to a solution of **III** (1.31 g, 4 mmol) in dry DMF (10 mL) cooled at 0 °C (29). This mixture was stirred for 24 h and then concentrated in vacuo. The residue was dissolved in EtOAc (10 mL) and washed with water (5 mL) and brine (5 mL). The organic layer was dried over  $\text{Na}_2\text{SO}_4$  and concentrated in vacuo. The resulting residue, purified by column chromatography using EtOAc/ $\text{CH}_2\text{Cl}_2$  (2:8, v/v), furnished the derivatives **IV** (1.82 g, yield = 62%) as a white solid.

**Preparation of (S)-2-[2-(7-Chloro-2-oxo-5-phenyl-2,3-dihydro-benzo[*e*][1,4]diazepin-1-yl)acetylaminol]-3-mercaptopropionic Acid (V).** The compound **IV** (730 mg, 1 mmol) was stirred for 3 h, at room temperature, in a mixture of TFA/ $\text{CH}_2\text{Cl}_2$  (1:1, 5 mL) containing  $\text{Et}_3\text{SiH}$  (0.8 mL, 582 mg, 5 equiv). The volatiles were removed in vacuo, and the residue was diluted with 5% aqueous  $\text{NaHCO}_3$  (5 mL). The aqueous mixture was extracted with  $\text{CH}_2\text{Cl}_2$  ( $3 \times 5$  mL), and the combined organic extracts were dried over  $\text{Na}_2\text{SO}_4$  and concentrated in vacuo. The resulting pale-yellow solid was used for the next reactions without any further purification.

(V)  $\text{C}_{20}\text{H}_{18}\text{N}_3\text{O}_4\text{SCL}$ . Calcd (%): C, 55.62; H, 4.20; N, 9.73; S, 7.41. Found (%): 55.68; H, 4.25; N, 9.69; S, 7.20.

**Synthesis of the Intermediate Complexes [ $^{99\text{g}}\text{Tc}(\text{N})(\text{PXP})\text{Cl}_2$ ] (PXP = PNP2, PNP3, PNP4).** The dichloride derivatives of the metal synthon [ $^{99\text{g}}\text{Tc}(\text{N})(\text{PXP})\text{Cl}_2$ ] $^{2+}$  were obtained starting from the precursor nitrido complex [ $^{99\text{g}}\text{Tc}(\text{N})\text{Cl}_2(\text{PPh}_3)_2$ ]. A representative procedure is given below for the ligand PNP3.

[ $^{99\text{g}}\text{Tc}(\text{N})\text{Cl}_2(\text{PPh}_3)_2$ ] (94 mg, 0.132 mmol) was suspended in dichloromethane (10 mL) and then reacted with PNP3 (73 mg, 0.145 mmol) at reflux temperature, for 30 min. The starting pink-orange solution turned to yellow. The solvent was removed by passing a weak stream of nitrogen, and a yellow solid was collected, which was washed with isopropyl alcohol, diethyl ether, and *n*-hexane. The yellow compound was dissolved in the minimum amount of chloroform, and the resulting solution was treated with diethyl ether. The precipitation of yellow microcrystalline powder was observed, which was then dried by overnight high-vacuum suction.

Yields expressed as (number of moles of the final complex/number of moles of the starting complex)  $\times 100$  were in the range 75–80%.

**Synthesis of the Complexes [ $^{99\text{g}}\text{Tc}(\text{N})(\text{L})(\text{PXP})$ ] ( $\text{H}_2\text{L} = \text{H}_2\text{BZ1}$ ,  $\text{H}_2\text{C1}$ ,  $\text{H}_2\text{C2}$ ; PXP = PNP2, PNP3, PNP4) (1–5).** The asymmetrical heterocomplexes [ $^{99\text{g}}\text{Tc}(\text{N})(\text{PXP})(\text{L})$ ] were prepared by reacting the ligand  $\text{H}_2\text{L}$  with the intermediate complexes [ $^{99\text{g}}\text{Tc}(\text{N})(\text{PXP})\text{Cl}_2$ ]. A representative procedure is given below for the ligands PNP3 and  $\text{H}_2\text{BZ1}$ .

[ $^{99\text{g}}\text{Tc}(\text{N})(\text{PNP3})\text{Cl}_2$ ] (51 mg, 0.077 mmol) was dissolved in 10 mL of a ethanol/dichloromethane mixture (1:1 v/v) under a nitrogen atmosphere. Triethylamine (0.2 mL) was added to the mixture followed by  $\text{H}_2\text{BZ1}$  (40 mg, 0.092 mmol). The reaction solution was refluxed for 60 min while keeping the nitrogen flux. After cooling, the solvent was removed by passing a weak nitrogen stream. A solid was collected and then washed with isopropyl alcohol, diethyl ether, and *n*-hexane. The resulting compound was dissolved in the minimum amount of acetonitrile, and the resulting solution was filtered and treated with diethyl ether. The slow precipitation of microcrystalline powder was observed, which was washed with diethyl ether and further dried by overnight high-vacuum suction.

Yields expressed as (number of moles of the final complex/number of moles of the starting complex)  $\times 100$  were in the range 70–80%.

HPLC chromatography of the yellow products isolated from reactions with the ligands  $\text{H}_2\text{BZ1}$  and PXP (PXP = PNP2, PNP3, PNP4) revealed that these species were actually composed by a mixture of two different compounds **A** and **B**, which were assigned to the syn and anti isomers of the complexes 1–3 (see Results and Discussion). However, the relative yields of the two isomers were found to be dependent on the type of diphosphine ligand utilized. Specifically, when PXP = PNP2 and PNP3, complex **A** was obtained almost quantitatively with a relative yield > 95%. On the contrary, with the ligand PNP4, the relative yields of compounds **A** and **B** were 79% and 21%, respectively.

Spectroscopic data and elemental analyses for Tc-99g complexes are reported in Table 3. Due to the low yields of isomer **B** for complexes 1–3, only isomer **A** was fully characterized.

**Preparation of the Complexes [ $^{99\text{m}}\text{Tc}(\text{N})(\text{PXP})(\text{BZ1})$ ] (PXP = PNP2, PNP3, PNP4).**  $\text{Na}^{99\text{m}}\text{TcO}_4$  (50 MBq) was added to a vial containing 5.0 mg of SDH, 0.1 mg of  $\text{SnCl}_2$  (suspended in 0.1 mL of saline) and 1.0 mL

**Table 1. IR and <sup>1</sup>H NMR Spectral Data of Compounds II–V**

compd	IR, (KBr) cm <sup>-1</sup>	<sup>1</sup> H NMR
<b>II</b>	1737, 1684, 1610, 1486, 1403, 1351, 1324, 1206, 1029, 698	1.28 (t, <i>J</i> = 7.2 Hz, 3H), 3.96 (d, <i>J</i> = 11.2 Hz, 1H), 4.24 (m, 2H), 4.53 (d, <i>J</i> = 17.2 Hz, 1H), 4.62 (d, <i>J</i> = 17.2 Hz, 1H), 4.94 (d, <i>J</i> = 11.2 Hz, 1H), 7.32 (m, 2H), 7.51 (m, 4H), 7.67 (m, 2H) <sup>a</sup>
<b>III</b>	3417, 1670, 1606, 1484, 1414, 1395, 1318, 826	3.76 (d, <i>J</i> = 10.6 Hz, 1H), 4.01 (d, <i>J</i> = 16.2 Hz, 1H), 4.22 (d, <i>J</i> = 16.2 Hz, 1H), 4.53 (d, <i>J</i> = 10.6 Hz, 1H), 7.11 (m, 1H), 7.55 (m, 7H), 13.1 (bs, 1H) <sup>b</sup>
<b>IV</b>	3400, 1680, 1485, 1325, 1153, 698	1.28 (s, 9H), 2.24 (m, 1H), 3.29 (s, 2H), 3.84 (d, <i>J</i> = 10.6 Hz, 1H), 4.01 (m, 1H), 4.48 (d, 7.8 Hz, 1H), 4.53 (d, <i>J</i> = 10.6 Hz, 1H), 7.33 (m, 23H), 8.62 (d, <i>J</i> = 7.2 Hz, 1H) <sup>b</sup>
<b>V</b>	3421, 1677, 1560, 1484, 1326, 1194, 828	2.39 (m, 1H), 2.82 (m, 2H), 3.84 (s, 2H), 4.24 (m, 1H), 4.57 (s, 2H), 7.19 (m, 1H), 7.54 (m, 7H), 8.23 (t, <i>J</i> = 5.8 Hz, 1H), 13.04 (bs, 1H) <sup>b</sup>

<sup>a</sup> CDCl<sub>3</sub> solutions. <sup>b</sup> d<sub>6</sub>-DMSO solutions.**Table 2. Chromatographic and Lipophilicity Data for the Prepared Complexes**

complex	TLC ( <i>R</i> <sub>f</sub> ) <sup>a</sup>	HPLC ( <i>t</i> <sub>R</sub> , min)	P	log <i>P</i>
<b>1A, 1B</b>	0.69, 0.57 <sup>b</sup>	43.9, 40.0 <sup>c</sup>	5758, 3167	3.76, 3.50
<b>2A, 2B</b>	0.62, 0.51 <sup>b</sup>	28.4, 25.8 <sup>f</sup>	441, 175	2.64, 2.24
<b>3A, 3B</b>	0.41, 0.30 <sup>c</sup>	30.1, 23.1 <sup>g</sup>	99, 43	1.99, 1.63
<b>4</b>	0.60 <sup>d</sup>	28.3 <sup>g</sup>		
<b>5</b>	0.50 <sup>d</sup>	33.6 <sup>g</sup>		

<sup>a</sup> SiO<sub>2</sub>. <sup>b</sup> EtOH/CHCl<sub>3</sub>/C<sub>6</sub>H<sub>6</sub> (0.7:3:1.5). <sup>c</sup> EtOH/CHCl<sub>3</sub>/C<sub>6</sub>H<sub>6</sub> (1.5:2:1.5). <sup>d</sup> EtOH/CHCl<sub>3</sub>/toluene/NH<sub>4</sub>Ac (0.5 mol dm<sup>-3</sup>) (6:3:3:1). <sup>e</sup> Et<sub>3</sub>N (0.1 mol dm<sup>-3</sup>) in aqueous H<sub>3</sub>PO<sub>4</sub> (1.0 mol dm<sup>-3</sup>) (45%)/CH<sub>3</sub>CN (55%). Flow rate, 4 mL/min. <sup>f</sup> A = Et<sub>3</sub>N (0.1 mol dm<sup>-3</sup>) in aqueous H<sub>3</sub>PO<sub>4</sub> (1.0 mol dm<sup>-3</sup>), B = CH<sub>3</sub>CN. Gradient: 0 min, B = 20%, 1–5 min, B = 45%, 5–31 min, B = 45% (isocratic), 31–32 min, B = 20%. Flow rate, 1.0 mL/min. <sup>g</sup> Et<sub>3</sub>N (0.1 mol dm<sup>-3</sup>) in aqueous H<sub>3</sub>PO<sub>4</sub> (1.0 mol dm<sup>-3</sup>) (65%)/CH<sub>3</sub>CN (35%). Flow rate, 3 mL/min.

of ethanol. The reaction mixture was kept at room temperature for 30 min. Then, 1.0 mg of the appropriate PXP ligand (dissolved in 0.25 mL of ethanol) and 2.5 mg of H<sub>2</sub>BZ1 (dissolved in 0.25 mL of ethanol) were added to the reaction vial, which was heated at 100 °C for 30 min. Chromatographic characterization of the resulting Tc-99m complexes (Table 1) showed the presence of two distinct products, **A** and **B**, with relative yields in the range 80–85% and 10–15%, respectively. Overall yields ranged between 90 and 96%.

**Preparation of the Complexes [<sup>99m</sup>Tc(N)(PNP4)-(L<sup>1</sup>)] (L<sup>1</sup> = C1, C2).** Na[<sup>99m</sup>TcO<sub>4</sub>] (50 MBq) was added to a vial containing 5.0 mg of SDH, 0.1 mg of SnCl<sub>2</sub> (suspended in 0.1 mL of saline), 0.5 mL of saline, and 0.5 mL of ethanol. The reaction mixture was kept at room temperature for 30 min. Then, 0.25 mL of a phosphate buffer (PBS, pH = 7.4), 0.1 mg of PNP4 (dissolved in 0.3 mL of ethanol), and 10.0 mg of H<sub>2</sub>L<sup>1</sup> (dissolved in 0.3 mL of ethanol) were added to the reaction vial, which was heated at 100 °C for 1 h. Yield > 90%. Chromatographic characterization is reported in Table 2.

**Determination of Partition Coefficients (Log *P*).** After HPLC purification, Log *P* values of Tc-99m complexes **1–3** were determined by measuring the activity partitioned between *n*-octanol (3.0 mL) and aqueous phosphate buffer (3.0 mL, 0.1 mol dm<sup>-3</sup>, pH = 7.4) under equilibrium conditions. Results are reported in Table 2. On the contrary, due to the impossibility to attain a true equilibrium condition with complexes **4** and **5**, their Log *P* values were not determined.

**Serum Stability.** After HPLC purification, 100 μL of the selected Tc-99m complex were added to a propylene test tube (5 mL) containing 900 μL of rat serum or, alternatively, 900 μL of saline. The resulting mixture was incubated at 37 °C for 2 h. RCP changes in time were checked at 15, 30, 60, and 120 min by TLC.

**In Vitro Reaction with Glutathione (GSH) and Cysteine.** A phosphate buffer (250 μL, 0.2 mol dm<sup>-3</sup>, pH = 7.4), water (100 μL), the appropriate HPLC-purified Tc-99m complex (100 μL), and an aliquot (50 μL) of a

stock aqueous solution of GSH (0.01 mol dm<sup>-3</sup>) were mixed in a propylene test tube (5 mL), and the mixture was incubated at 37 °C for 2 h. For the blank experiment, an equal volume of water was added in place of the GSH solution. Aliquots of the resulting solutions were withdrawn at 15, 30, 60, and 120 min after incubation and analyzed by TLC chromatography.

The same procedure applied above for GSH challenge was performed in two separate experiments using two different aqueous solutions of cysteine hydrochloride (0.01 and 0.001 M, respectively).

**Animal Studies.** All animal experiments were performed in compliance with relevant national laws and with the *Principles of Laboratory Animal Care* (NIH Publication #85-23, revised 1985). Purified fractions of the complexes were obtained by HPLC separation. Before injection, the collected activity was further diluted with PBS (0.1 M, pH, 7.4) to give a final solution that was 10% in ethanol content. Using Tc-99m complexes of **1–3**, both peaks corresponding to the two isomers **A** and **B** were recovered, and the resulting mixture was injected for biodistribution studies. Female Sprague–Dawley rats weighing 200–250 g were anesthetized with an intramuscle injection of a mixture of ketamine (80 mg kg<sup>-1</sup>) and xilazine (19 mg kg<sup>-1</sup>). A jugular vein was surgically exposed, and 100 μL (300–370 kBq) of the solution containing the radioactive complex was injected. The animals (*n* = 3) were sacrificed by cervical dislocation at different times postinjection. The blood was withdrawn from the heart through a syringe immediately after the sacrifice and counted. Harvested organs were rinsed in saline, weighed, and counted in a γ-counter. Results expressed as %ID/g tissue are reported in Tables 4–8. Brain uptake at 2 min was always corrected by subtracting blood activity measured at the same time point after injection of the radiocompound <sup>99m</sup>Tc-DTPA (diethylenetriaminepentaacetic acid = DTPA), which is unable to penetrate the intact BBB.

**In Vitro Binding Studies.** Binding affinities of [<sup>3</sup>H]-Ro151788 and [<sup>3</sup>H]-flunitrazepam were assayed as previously described with the following modifications (31, 32). Male Sprague–Dawley rats, weighing 200–250 g, were killed by decapitation and each cerebral cortex was extracted and stored at –80 °C until use. For assay, cerebral cortex was homogenized in 50 volumes (w/v) ice-cold assay buffer (0.050 M Tris-citrate buffer, pH = 7.1) with an Ultra-Turrax homogenizer (Jenkel & Kunkel) at a setting of 4 for 30 s. The resulting homogenate was centrifuged at 48000 × *g* for 10 min with a L8–50 M/E ultracentrifuge (Beckman). The isolated pellet was resuspended in 20-vol assay buffer and further homogenized at the same settings as detailed above. The resulting homogenate was, then, centrifuged once again. The described procedure was repeated four times and the final pellet was resuspended in 20-vol assay buffer.

The bindings of both [<sup>3</sup>H]-Ro151788 and [<sup>3</sup>H]-flunitrazepam were routinely assessed in triplicate (*n* = 3),

**Table 3. Spectroscopic Data and Elemental Analyses<sup>a</sup> for Tc-99g Complexes**

complex	MW (g mol <sup>-1</sup> )	FAB MS <i>m/z</i> [MH] <sup>+</sup>	<sup>1</sup> H NMR, $\delta$ (ppm)	<sup>31</sup> P NMR (ppm)	IR (cm <sup>-1</sup> ) $\nu$ (Tc=N)	elemental analysis
<b>1A</b>	1041	1042	7.79–6.85 (H <sub>arom</sub> ; 28H), 7.22 (NH <sub>cys</sub> ; 1H), 4.97 (CH <sub>cys</sub> ; 1H), 3.25, 2.33 (CH <sub>2cys</sub> ; 2H), 4.34 (CH <sub>2BZ1</sub> ; AB; 2H), 4.29 (CH <sub>2BZ1</sub> ; AB; 2H), 3.19 (OCH <sub>3PNP2</sub> ; 3H), 3.50–2.15 (various CH <sub>2PNP2</sub> ; 12H)	22.7 (bs), 33.2 (bs)	1051	C <sub>51</sub> H <sub>51</sub> N <sub>5</sub> O <sub>5</sub> P <sub>2</sub> SCITc: C, 58.71 (58.78); H, 4.85 (4.89); N, 6.67 (6.72); S, 3.00 (3.07)
<b>2A</b>	1025	1026	7.54–7.21 (H <sub>arom</sub> ; 8H), 7.16 (NH <sub>cys</sub> ; 1H), 4.93 (CH <sub>cys</sub> ; 1H), 3.30, 2.40 (CH <sub>2cys</sub> ; 2H), 4.35 (CH <sub>2BZ1</sub> ; AB; 2H), 4.30 (CH <sub>2BZ1</sub> ; AB; 2H), 3.30 (OCH <sub>3PNP3</sub> ; 12H), 3.14 (OCH <sub>3PNP3</sub> ; 3H), 3.53–1.77 (various CH <sub>2PNP3</sub> ; 36H)	22.8 (bs), 30.4 (bs)	1053	C <sub>43</sub> H <sub>67</sub> N <sub>5</sub> O <sub>9</sub> P <sub>2</sub> SCITc: C, 50.40 (50.34); H, 6.56 (6.53); N, 6.79 (6.83); S, 3.05 (3.12)
<b>3A</b>	749	750	7.57–7.22 (H <sub>arom</sub> ; 8H), 7.29 (NH <sub>cys</sub> ; 1H), 4.86 (CH <sub>cys</sub> ; 1H), 3.25, 2.38 (CH <sub>2cys</sub> ; 2H), 4.40 (CH <sub>2BZ1</sub> ; AB; 2H), 4.33 (CH <sub>2BZ1</sub> ; AB; 2H), 2.60–1.85 (various CH <sub>2PNP4</sub> ; 8H), 1.94 (NCH <sub>3PNP4</sub> ; 3H), 1.73–1.65 (PCH <sub>3PNP4</sub> ; 12H)	14.3 (bs), 20.2 (bs)	1057	C <sub>29</sub> H <sub>39</sub> N <sub>5</sub> O <sub>4</sub> P <sub>2</sub> SCITc: C, 46.50 (46.45); H, 5.23 (5.20); N, 9.29 (9.34); S, 4.18 (4.27)
<b>4</b>	513	514	7.67–7.27 (H <sub>arom</sub> ; 5H), 4.21 (CH <sub>2C1</sub> ; 2H), 2.60–1.86 (various CH <sub>2PNP4</sub> ; 8H), 2.07 (NCH <sub>3PNP4</sub> ; 3H), 1.76–1.68 (PCH <sub>3PNP4</sub> ; 12H)	14.6 (bs), 20.8 (bs)	1058	C <sub>18</sub> H <sub>30</sub> N <sub>3</sub> O <sub>2</sub> P <sub>2</sub> STc: C, 42.21 (42.13); H, 5.83 (5.85); N, 8.11 (8.19); S, 6.17 (6.23)
<b>5</b>	569	570	7.62–7.29 (H <sub>arom</sub> ; 5H), 3.98 (CH <sub>2C2</sub> ; 1H), 1.86–1.84 (CH <sub>2C2</sub> , CH <sub>2C2</sub> ; 3H), 1.17 (CH <sub>3C2</sub> ; 6H), 2.68–1.80 (various CH <sub>2PNP4</sub> ; 8H), 2.03 (NCH <sub>3PNP4</sub> ; 3H), 1.83–1.72 (PCH <sub>3PNP4</sub> ; 12H)	15.0 (bs), 19.8 (bs)	1060	C <sub>22</sub> H <sub>38</sub> N <sub>3</sub> O <sub>2</sub> P <sub>2</sub> STc: C, 46.49 (46.42); H, 6.69 (6.67); N, 7.32 (7.32); S, 5.54 (5.62)

<sup>a</sup> Theoretical values are in parentheses.**Table 4. Biodistribution of the Complex [99mTc(N)(PNP2)(BZ1)]**

organ	2 min	10 min	30 min	60 min
blood	2.85 ± 0.32	0.57 ± 0.06	0.30 ± 0.13	0.24 ± 0.04
brain	0.11 ± 0.00	0.02 ± 0.00	0.01 ± 0.00	0.01 ± 0.00
heart	0.80 ± 0.00	0.28 ± 0.02	0.20 ± 0.06	0.21 ± 0.00
lung	1.53 ± 0.40	1.01 ± 0.15	0.37 ± 0.12	0.39 ± 0.08
liver	8.19 ± 1.66	9.77 ± 0.91	7.73 ± 2.09	5.63 ± 0.45
kidney	1.37 ± 0.29	1.05 ± 0.14	0.93 ± 0.21	1.06 ± 0.05

<sup>a</sup> Values represent % ID/g wet tissue ± standard deviations (*n* = 4).**Table 5. Biodistribution of the Complex [99mTc(N)(PNP3)(BZ1)]<sup>a</sup>**

organ	2 min	10 min	30 min	60 min
blood	0.90 ± 0.20	0.28 ± 0.04	0.11 ± 0.00	0.06 ± 0.00
brain	0.05 ± 0.01	0.01 ± 0.00	0.03 ± 0.00	0.04 ± 0.00
heart	0.37 ± 0.02	0.11 ± 0.07	0.05 ± 0.01	0.03 ± 0.01
lung	0.59 ± 0.07	0.26 ± 0.02	0.09 ± 0.01	0.06 ± 0.01
liver	3.67 ± 0.97	1.12 ± 0.32	0.05 ± 0.02	0.03 ± 0.02
kidney	3.76 ± 0.07	1.49 ± 0.46	0.40 ± 0.04	0.25 ± 0.03

<sup>a</sup> Values represent % ID/g wet tissue ± standard deviations (*n* = 4).**Table 6. Biodistribution of the Complex [99mTc(N)(PNP4)(BZ1)]**

organ	2 min	10 min	30 min	60 min
blood	1.59 ± 0.09	0.58 ± 0.05	0.37 ± 0.04	0.25 ± 0.01
brain	0.09 ± 0.01	0.05 ± 0.01	0.02 ± 0.01	0.02 ± 0.01
heart	0.55 ± 0.05	0.25 ± 0.03	0.16 ± 0.02	0.10 ± 0.02
lung	1.13 ± 0.13	0.51 ± 0.04	0.32 ± 0.02	0.19 ± 0.01
liver	2.01 ± 0.18	1.09 ± 0.15	0.66 ± 0.07	0.57 ± 0.05
kidney	6.58 ± 0.64	4.71 ± 0.62	4.16 ± 0.94	4.38 ± 0.53

<sup>a</sup> Values represent % ID/g wet tissue ± standard deviations (*n* = 4).

at 0 °C, and using 100  $\mu$ L of the above membrane preparation with a concentration in the range (0.20–4.0)  $\times 10^{-9}$  M. At the end of the incubation period, 3.0 mL of ice-cold assay buffer were added to each incubation tube, and its contents were immediately filtered under reduced pressure through a Whatman GF/B glass-fiber filter. Each filter was, then, washed three times with 3.0 mL of ice-cold buffer. Filter-bound radioactivity was measured by liquid scintillation spectrometry after addition of 3.0 mL of Aquasure (Packard), using a LS 5081  $\beta$ -counter (Beckman). Nonspecific binding was defined as the binding measured in the presence of  $1.0 \times 10^{-5}$  M nitrazepam (FIS). Specific binding was calculated by

**Table 7. Biodistribution of the Complex [99mTc(N)(PNP4)(C1)]**

organ	2 min	10 min	30 min	60 min
blood	0.53 ± 0.03	0.18 ± 0.03	0.06 ± 0.00	0.04 ± 0.00
brain	0.02 ± 0.00	0.01 ± 0.00	0.00 ± 0.00	0.00 ± 0.00
heart	0.20 ± 0.01	0.08 ± 0.01	0.04 ± 0.01	0.03 ± 0.00
lung	0.35 ± 0.05	0.18 ± 0.04	0.06 ± 0.01	0.09 ± 0.03
liver	4.51 ± 0.59	1.68 ± 0.25	0.48 ± 0.10	0.35 ± 0.10
kidney	4.35 ± 0.88	0.70 ± 0.19	0.20 ± 0.01	0.15 ± 0.02

<sup>a</sup> Values represent % ID/g wet tissue ± standard deviations (*n* = 4).**Table 8. Biodistribution of the Complex [99mTc(N)(PNP4)(C2)]**

organ	2 min	10 min	30 min	60 min
blood	0.83 ± 0.11	0.18 ± 0.03	0.09 ± 0.00	0.05 ± 0.00
brain	1.03 ± 0.13	0.53 ± 0.02	0.08 ± 0.00	0.01 ± 0.00
heart	0.96 ± 0.03	0.22 ± 0.09	0.04 ± 0.01	0.02 ± 0.00
lung	0.65 ± 0.09	0.36 ± 0.03	0.06 ± 0.01	0.06 ± 0.01
liver	5.98 ± 0.65	1.92 ± 0.20	0.87 ± 0.07	0.09 ± 0.02
kidney	2.94 ± 0.07	0.68 ± 0.18	0.32 ± 0.05	0.12 ± 0.02

<sup>a</sup> Values represent % ID/g wet tissue ± standard deviations (*n* = 4).

subtracting the nonspecific binding from the total binding and expressed as fmol/mg of protein. The total protein content was determined by Bradford's method (Comassie Brilliant Blue, Biorad) using human serum albumin as a standard (Kabi-vitrum).

To study the effect of the free ligands and of the corresponding Tc-99g complexes **1–5** and on the specific binding of [<sup>3</sup>H]-Ro151788 and [<sup>3</sup>H]-flunitrazepam, binding inhibition experiments were conducted on isolated membranes obtained as described before. In particular, with complexes **1** and **2**, only the main isomeric form **A** was utilized. On the contrary, with complex **3** both isomers **A** and **B** were isolated and evaluated. In a typical experiment, 100  $\mu$ L of the membrane suspension and a final concentration of  $1.0 \times 10^{-9}$  M, the radioligand [<sup>3</sup>H]-Ro151788 (or, alternatively, of [<sup>3</sup>H]-flunitrazepam), dissolved in a Tris-citrate buffer, were used. The total volume was 0.250 mL, and the tubes were incubated for 1 h at 0 °C until incubation was stopped by rapid filtration through a glass-fiber filter as described above. Each filter was washed three times with 3.0 mL of ice-cold buffer and radioactivity measured. Interference of  $\beta$ -emission from <sup>99g</sup>Tc ( $E_{\beta\text{max}} = 0.212$  MeV,  $T_{1/2} = 2.02 \times 10^5$  y) on <sup>3</sup>H counting was significant only at the highest <sup>99g</sup>Tc concentrations as radioactivity was determined by



adjusting  $\beta$ -counter's window to exclude 85% of  $^{99g}\text{Tc}$  counts from the tritium channel. The 15%  $^{99g}\text{Tc}$  spill was subtracted from the  $^3\text{H}$  counts.

Results expressed as  $K_i$  values of the competing ligand (I) ( $K_i$  = dissociation constant at equilibrium), were determined according to the Cheng–Prusoff equation  $K_i = \text{IC}_{50}/(1 + [\text{R}]/K_R)$ , where  $\text{IC}_{50}$  is the concentration of I inhibiting 50% of radioligand's binding at the radioligand concentration  $[\text{R}]$ .

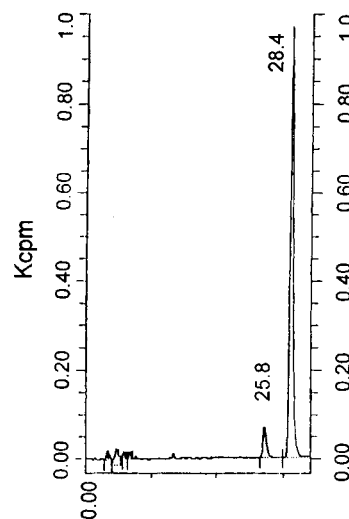
## RESULTS

**Synthesis of the Ligands.** The preparation of the ligand  $\text{H}_2\text{BZ1}$  (**V**) has been accomplished by a synthetic sequence according to the reactions showed in Scheme 1. Starting from the commercially available desmethyldiazepam (**I**), alkylation with ethyl bromoacetate in DMF in the presence of sodium hydride gave the intermediate **II** (**33**). This derivative was then transformed into the corresponding acid **III** (**34**) by basic hydrolysis with lithium hydroxide. 1-[3-(Dimethylamino)propyl]-3-ethylcarbodiimide (EDCI) promoted the coupling of **III** with S-trityl cysteine *tert*-butyl ester (**35**) to furnish compound **IV** that was finally transformed into **V** after removal of both trityl and Boc protecting groups by treatment with a mixture of triethylsilane ( $\text{Et}_3\text{SiH}$ ) and trifluoroacetic acid ( $\text{CF}_3\text{CO}_2\text{H}$ ) in DCM (**36**).

**Preparation and Characterization of Tc-99m and Tc-99g Complexes.** The Tc-99m analogues of complexes **1–5** were prepared through a simple two-step procedure involving the reaction of a nitrido Tc-99m precursor with the ligands PXP and  $\text{H}_2\text{L}$ . The preliminary step of this procedure was carried out at room temperature and led to the formation of a nitrido Tc-99m precursor through the reaction of  $[\text{}^{99m}\text{TcO}_4]^-$  with SDH in the presence of  $\text{SnCl}_2$  as reducing agent (**37**, **38**). This was then followed by the simultaneous addition of the two ligands PXP and  $\text{H}_2\text{L}$  that, after a short heating at  $100^\circ\text{C}$ , gave rise to the final asymmetrical complexes  $[\text{}^{99m}\text{Tc}(\text{N})(\text{PXP})(\text{L})]$  in high yield ( $>90\%$ ). In these reactions, no formation of the symmetrical complexes,  $[\text{}^{99m}\text{Tc}(\text{N})(\text{L})_2]$ , containing two identical bidentate ligands was detected.

Tc-99m complexes **1–5** were characterized by chromatographic methods. Results are reported in Table 2. When  $\text{L} = \text{BZ1}$ , both TLC and HPLC chromatography revealed that the resulting complexes formed as an isomeric pair, and that one isomer was predominant with a radiochemical yield in the range 60–85%. The formation of the two isomers was determined by the syn or anti orientation of the bioactive group of desmethyldiazepam relative to the terminal  $\text{Tc}\equiv\text{N}$  group. A representative HPLC chromatogram for the Tc-99m complex **2** is reported in Figure 4. The syn and anti isomers were separated by HPLC and their chemical properties measured independently. Partition coefficients of the syn and anti isomers of Tc-99m complexes **1–3** are given in Table 2.

Complexes **1–5** were prepared with the long-lived isotope Tc-99g through a simple ligand-substitution reaction of the weakly bound  $\text{Cl}^-$  groups by  $\text{L}$  onto the dichloride derivative of the metal synthon  $[\text{}^{99g}\text{Tc}(\text{N})(\text{PXP})]^{2+}$  in a dichloromethane/ethanol mixture. As observed in preparations with the  $\gamma$ -emitting nuclide Tc-99m, no formation of the symmetrical, disubstituted complexes ( $[\text{}^{99g}\text{Tc}(\text{N})(\text{L})_2]$ ) was detected also in reactions with Tc-99g. Characterization was accomplished by elemental analysis, infrared,  $^1\text{H}$  and  $^{31}\text{P}$  NMR spectra, and mass spectra (Table 3). Results supported the view that the complexes possess a five-coordinated geometry



**Figure 4.** HPLC chromatogram of the Tc-99g complex **2**.

with a  $\text{Tc}\equiv\text{N}$  group bound to the two phosphorus atoms of a neutral PXP ligand, and the negatively charged  $\text{O}^-$  and  $\text{S}^-$  atoms of one dianionic  $\text{L}$  ligand. The ligand BZ1 is coordinated through the terminal cysteine moiety (Figure 1), while the ligands C1 and C2 bind to the metal ion in the thiol form through the deprotonated SH and COOH functional groups (Figure 2). As a result, the complexes possess a vanishing charge.

The chemical identity of Tc-99m complexes was assessed by comparing their HPLC chromatograms with those of the corresponding Tc-99g analogues. A close matching of HPLC retention times of Tc-99m complexes with those of the analogous Tc-99g is usually taken as a strong indication that the two series of compounds have the same chemical structure. Indeed, HPLC chromatography of Tc-99g complexes displayed a pattern similar to that observed for the analogous Tc-99m complexes. In particular, HPLC of the complexes **1–3** showed the presence of two peaks at the same retention times of the corresponding Tc-99m complexes, thus giving further support for the existence of a syn, anti isomeric pair. The origin of syn and anti isomerism is presumably due to the chirality of the central carbon atom of the coordinated cysteine ring, allowing the pendant benzodiazepine group to assume a syn or anti position with respect to the apical  $\text{Tc}\equiv\text{N}$  group within the pseudo square pyramidal arrangement. However, a major difference between the two concentration scales was observed. Specifically, at the macroscopic level, one isomer was obtained almost quantitatively with complexes **1** and **2**, the other isomer being produced in a very small amount ( $<4\%$ ). In contrast, the two isomers of complex **3** were produced in the percentage ratio 75:20.

**Stability.** The complexes **1–3** were found to be stable both in physiological solution and in plasma. They were also inert toward transchelation by cysteine and glutathione. On the contrary, though the complexes **4** and **5** were almost stable in physiological solution, its RCP in serum decreased to 60% after 2 h. Moreover, transchelation by both cysteine and glutathione was complete in  $0.01\text{-mol dm}^{-3}$  solutions after 1 h. Despite this, the kinetics of transchelation and of decomposition in serum were considered sufficiently slow for conducting biodistribution studies in animals.

**Biological Evaluation.** The ability of the resulting Tc-99m complexes to penetrate the intact blood–brain barrier (BBB) was evaluated in rats. In particular, mixtures of syn and anti isomers were used for biodis-

tribution studies with the Tc-99m analogues of **1–3**. Biodistribution data are reported in Tables 4–8.

Affinity for benzodiazepine receptors was assessed through in vitro binding experiments on isolated membranes of rat's brain using the Tc-99g complexes **1–5**. Specifically, the mixture of syn and anti isomers of complexes **1** (isomeric ratio 96:2) and **2** (isomeric ratio 93:4) were used for in vitro measurements. In contrast, the binding affinities of both isomers of complex **3** were separately evaluated.

Results revealed that the complexes **1–4** did not show any relevant brain uptake. In contrast, a significant brain localization was observed for complex **5** at 2 min after injection, but followed by a fast washout. Competitive, in vitro binding experiments were carried out on isolated rat cerebral membranes and demonstrated that complexes **1–5** do not possess a strong affinity for benzodiazepine receptors. Specifically,  $K_i$  values for complexes **1–5** and for the free ligand H<sub>2</sub>BZ1, measured in competitive inhibition experiments with [<sup>3</sup>H]-RO151788, were >1  $\mu$ M. In contrast,  $K_i$  of the compound diazepam used as a reference was 7.5 nM.

## DISCUSSION

The chemical structure of the ligand HBZ1 was designed by considering a plain application of the 'bifunctional approach'. In fact, the bifunctional ligand HBZ1 can be viewed as composed of two different molecular pieces formed by a cysteine group and a diazepam derivative linked together. The cysteine group provides the chelating system for the metal, while the diazepam derivative plays the role of a biologically active moiety. A key advantage of this procedure is that the species H<sub>2</sub>BZ1 is capable to coordinate as a dianionic ligand, through the deprotonated thiol sulfur atom and the carboxylic oxygen atom of the cysteine group, thus ensuring that the resulting complexes possess a neutral charge. This is a necessary requirement to promote the passage of the blood–brain barrier by a Tc-99m radiopharmaceutical.

The coupling between the strong electrophilic metal fragment [Tc(N)(PXP)]<sup>2+</sup> and the nucleophilic  $\pi$ -donor bidentate ligand H<sub>2</sub>BZ1 led to the formation of the neutral asymmetrical heterocomplexes **1–3**. These preparations provide a definite example of the application of the 'metal fragment approach' based on the selective reaction of a precursor metal synthon with a ligand possessing a specific set of coordinating atoms. The strong affinity of the nucleophilic [S<sup>-</sup>,O<sup>-</sup>]-cysteine chelating system for the fragment [Tc(N)(PXP)]<sup>2+</sup> allowed us to obtain the final products in high-yield and without the concomitant formation of the corresponding symmetrical nitride complexes containing two identical BZ1 ligands.

Although complexes **1–3** were found to be stable in solution and resistant to transchelation by cysteine and GSH, complexes **4** and **5** showed a lower stability and kinetic inertness. This fact could be presumably attributed to the largest seven-membered chelating ring formed by the ligands H<sub>2</sub>C1 and H<sub>2</sub>C2 upon coordination to the metal center as compared to the shorter six-membered ring formed by the ligand H<sub>2</sub>BZ1.

Biodistribution studies in rats were carried out mostly to assess the ability of the resulting complexes to cross the BBB barrier. This requires that a suitable mechanism for trapping the activity into the cerebral tissue for a sufficient time should be operative. Biological results revealed that Tc-99m analogues of complexes **1–3** are not able to localize into the rat brain, and this behavior

was irrespective of syn and anti isomerism. Moreover, in vitro binding experiments showed that complexes **1–3** have lost almost entirely the affinity for benzodiazepine receptors. Binding affinities of both the syn and anti isomers of complex **3** were evaluated in separate experiments, but no significant difference was observed between the two isomeric forms. This fact indicates that receptor interaction does not provide a suitable brain trapping mechanism for these complexes, and therefore no clear insight into their ability to penetrate the intact BBB could be obtained. A possible explanation of this outcome could be found by considering that previous studies of NOESY NMR spectra of analogous asymmetrical heterocomplexes designed to target 5HT1A receptors revealed the existence of a weak interaction between the pendant bioactive moiety and the group attached to the nitrogen atom of the PNP ligand in both the syn and anti configurations. This interaction prevented the bioactive group to acquire the correct configuration for binding to the receptor and could be also effective in complexes discussed here (39).

The biological evaluation of complexes containing the BZ1 ligand gave support to the conclusion that the bifunctional approach might not provide an efficient route to the design of benzodiazepine receptor-specific nitrido Tc-99m radiopharmaceuticals starting from the metal fragment [<sup>99m</sup>Tc(N)(PXP)]<sup>2+</sup>. Therefore, the alternative 'integrated approach' was utilized in the attempt to lower the molecular size of the complexes while maintaining the biological activity of the starting drug. According to this method, the design of the 'integrated complex' was performed by seeking for a region of desmethyldiazepam that is considered nonessential for preserving its biological properties and could be, therefore, conveniently replaced by the metal-containing fragment. Previous studies (40) showed that binding affinity for this drug is associated with the region indicated by arrows in Figure 1. Thus, the phenyl ring fused with the seven-membered ring in the precursor biomolecule was completely removed to give an open system as illustrated in Figure 2. As a final step, thiol and carboxylic groups were placed at the two terminus of the resulting open system to provide the required  $\pi$ -donor atoms for binding to the metal fragment [<sup>99m</sup>Tc(N)(PXP)]<sup>2+</sup>. Figure 2 shows the chemical representation of the final ligands (H<sub>2</sub>C1 and H<sub>2</sub>C2) designed through the application of the integrated design. These compounds easily reacted in the thiol form with the fragment [<sup>99m</sup>Tc(N)(PNP4)]<sup>2+</sup> to afford the final Tc-99m complexes **4** and **5** pictured in Figure 2. Although the integrated concept was essential in providing the route to complexes **4** and **5**, these compounds cannot be strictly considered as true 'integrated complexes'. Indeed, the molecular size and dimension of the metal fragment [<sup>99m</sup>Tc(N)(PNP4)]<sup>2+</sup> evidently do not fit within the structure of that unessential part of the H<sub>2</sub>BZ1 ligand brought aside to give the ligands H<sub>2</sub>C1 and H<sub>2</sub>C2. A classification like that of a 'benzodiazepine mimetic' may, therefore, appear more appropriate.

Biological evaluation of complexes **4** and **5** still gave results not entirely satisfactory. Actually, though both complexes **4** and **5** possessed the correct matching of physical characteristics such as molecular weight and lipophilicity, only **5** showed a significant brain uptake at 2 min postinjection. Moreover, affinity of these complexes for benzodiazepine receptors was found to be almost negligible. These data suggest that the chemical modification brought about by the application of the integrated design has caused a strong perturbation of the starting bioactive drug. The difference in brain uptake

observed between complexes **4** and **5** is not easily interpretable considering that they differ only by a lateral isobutyl group, though the relative instability of these complexes in physiological conditions may also play a role in providing a biological trapping mechanism into the cerebral tissue. Investigation of these aspects is currently underway.

## CONCLUSIONS

The present study illustrates the application of the 'metal-fragment' approach based on the metal synthon  $[\text{Tc}(\text{N})(\text{PXP})]^{2+}$  to the design and synthesis of a new class of small-molecule Tc-99m radiopharmaceuticals for imaging benzodiazepine receptors in the central nervous system. Results indicate that the labeling method is highly efficient and sufficiently flexible to be potentially utilized in the preparation of diagnostic tracers for a wide range of biological targets. As demonstrated by the weak brain accumulation of complex **5**, there does not apparently exist any basic molecular feature of these complexes preventing their passage of the BBB barrier. However, since BBB crossing appears to be better favored for complexes having a reduced molecular size, it appears reasonable to expect that asymmetrical heterocomplexes containing the light PNP4 diphosphine ligand might find some potential application in the study of Tc-99m radiopharmaceuticals for the central nervous system. Moreover, though poor binding affinities for benzodiazepine receptors were found for the complexes described here, a careful selection of the most suitable length of the spacer connecting the metal fragment to the benzodiazepine moiety may prevent any perturbation of this latter group by the inorganic block, thus leaving the biomolecule free to interact with the receptor.

## ACKNOWLEDGMENT

This work was supported by Nihon Medi-Physics Co., Ltd., Tokyo, Japan.

## LITERATURE CITED

- Weissman, B. A., and Raveh, L. (2003) Peripheral Benzodiazepine Receptors: on Mice and Human Brain Imaging. *J. Neurochem.* **84**, 432–437.
- Johnston, G. A. (2002) Medicinal Chemistry and Molecular Pharmacology of GABA(C) Receptors. *Curr. Top. Med. Chem.* **2**, 903–913.
- Siegel, E. (2002) Mapping of the Benzodiazepine Recognition Site on GABA(A) Receptors. *Curr. Top. Med. Chem.* **2**, 833–839.
- Teuber, L., Watjens, F., and Jensen, L. H. (1999) Ligands for the Benzodiazepine Binding Site – a Survey. *Curr. Pharm. Des.* **5**, 317–343.
- Hatazawa, J., and Shimosegawa, E. (1998) Imaging Neurochemistry of Cerebrovascular Disease with PET and SPECT. *Q. J. Nucl. Med.* **42**, 193–198.
- Richardson, M. P. Functional Imaging in Epilepsy. (2002) *Seizure* **11** (Suppl. A), 139–156.
- Millet, P., Graf, C., Buck, A., Walder, B., and Ibanez, V. (2002) Evaluation of Tissue Models for PET and SPECT Benzodiazepine Binding Parameters. *Neuroimage* **17**, 928–942.
- Muller, J., Saur, D., Klutmann, S., Weiller, C., Rother, J., and Clausen, M. (2002) Experience with  $^{123}\text{I}$ -Iomazenil SPECT in Acute Cerebral Infarction. *Nucl. Med. Commun.* **23**, 1191–1196.
- Bremner, J. D., Innis, R. B., White, T., Fujita, M., Silbersweig, D., Goddard, A. W., Staib, L., Stern, E., Cappiello, A., Woods, A., Baldwin, R., and Charney, D. S. (2000) SPECT [I-123]Iomazenil Measurement of the Benzodiazepine Receptor in Panic Disorder. *Biol. Psychiatry* **47**, 96–106.
- Juhász, C., Chugani, D. C., Muzik, O., Shah, J., Watson, C., Canady, A., and Chugani, H. T. (2001) Relationship of Flumazenil and Glucose Abnormalities to Neocortical Epilepsy Surgery Outcome. *Neurology* **56**, 1650–1658.
- Ohya, M., Senda, M., Ishiwata, K., Kitamura, S., Mishina, M., Ishii, K., Toyama, H., Oda, and K., Katayama, Y. (1999) Preserved Benzodiazepine Receptors in Alzheimer's Disease Measured with C-11 Flumazenil PET and I-123 Iomazenil SPECT in Comparison with CBF. *Ann. Nucl. Med.* **13**, 309–315.
- Lingford-Hughes, A., Hume, S. P., Feeney, A., Hirani, E., Osman, S., Cunningham, V. J., Pike, V. W., Brooks, D. J., and Nutt, D. J. (2002) Imaging of GABA-Benzodiazepine Receptor Subtype Containing the Alpha5-Subunit In Vivo with  $^{11}\text{C}$ [Ro15–4513 Positron Emission Tomography. *J. Cereb. Blood Flow Metab.* **22**, 878–889.
- Levêque, P., Labar, D., and Gallez, B. (2001) Biodistribution, Binding, Specificity and Metabolism of  $^{18}\text{F}$ Fluoroethylflumazenil in Rodents. *Nucl. Med. Biol.* **28**, 809–814.
- Schwochau, K. (2000) *Technetium. Chemistry and Radiopharmaceutical Applications*, Wiley-VCH, Weinheim, Germany.
- Kung, H. F., Kung, M. P., and Choi, S. R. (2003) Radiopharmaceuticals for Single-Photon Emission Computed Tomography Brain Imaging. *Sem. Nucl. Med.* **33**, 2–13.
- Kung, H. F., Yu, C. C., Billings, J., Molnar, M., and Blau, M. (1985) Synthesis of New Bis(Aminoethanethiol) (BAT) Derivatives: Possible Ligands for  $^{99\text{m}}\text{Tc}$  Brain Imaging Agents. *J. Med. Chem.* **29**, 1280–1284.
- Hom, R. K., and Katzenellenbogen, J. A. (1997) Technetium-99m-Labeled Receptor-Specific Small-Molecule Radiopharmaceuticals: Recent Developments and Encouraging Results. *Nucl. Med. Biol.* **24**, 485–498.
- Chi, D. Y., Neil, J. P., Anderson, C. J., Welch, M. J., and Katzenellenbogen, J. A. (1994) Homodimeric and Heterodimeric Bis(aminethiol) Oxometal Complexes with Rhenium(V) and Technetium(V). Control of Heterodimeric Complex Formation and an Approach to Metal Complexes That Mimic Steroid Hormones. *J. Med. Chem.* **37**, 928–937.
- Katzenellenbogen, J. A., Minutolo, F., Spradau, T. W., and Skaddan, M. B. (1999) Preserving Bioactivity of Small Molecules Labeled with Technetium and Rhenium: an Organometallic Approach. *Technetium, Rhenium and Other Metals in Chemistry and Nuclear Medicine V* (Nicolini, M., Mazzi, U., Eds.) pp 363–372, SG Editoriali, Padova, Italy.
- Jurisson, S. S., and Lydon, J. D. (1999) Potential Technetium Small Molecule Radiopharmaceuticals. *Chem. Rev.* **99**, 2205–2215.
- Duatti, A. (1999) Advances in the Chemistry of Technetium and Rhenium. From Ligands and Cores to Biocomplexes. *Technetium, Rhenium and Other Metals in Chemistry and Nuclear Medicine V* (Nicolini, M., Mazzi, U., Eds.) pp 3–17, SG Editoriali, Padova, Italy.
- Egli, A., Alberto, R., Tannahill, L., Schibli, R., Abram, U., Schaffland, A., Waibel, R., Tourwe, D., Jeannin, L., Iterbeke, K., and Schubiger, P. A. (1999) Organometallic  $^{99\text{m}}\text{Tc}$ -aquaion Labels Peptide to an Unprecedented High Specific Activity. *J. Nucl. Med.* **40**, 1913–1917.
- Correia, J. D., Domingos, A., Santos, I., Alberto, R., Ortner, K. (2001) Re Tricarbonyl Complexes with Ligands Containing P, N, N and P, N, O Donor Atom Set: Synthesis and Structural Characterization. *Inorg. Chem.* **40**, 5147–5151.
- Alberto, R., Ortner, K., Wheatley, N., Schibli, R., and Schubiger, A. P. (2001) Synthesis and Properties of Boranocarbonate: A Convenient in Situ CO Source for the Aqueous Preparation of  $^{99\text{m}}\text{Tc}(\text{OH})_2(\text{CO})_3^+$ . *J. Am. Chem. Soc.* **123**, 3135–3136.
- Bolzati, C., Boschi, A., Uccelli, L., Tisato, F., Refosco, F., Cagnolini, A., Duatti, A., Prakash, S., Bandoli, G., Vittadini, A. (2002) Chemistry of the Strong Electrophilic Metal Fragment  $^{99\text{m}}\text{Tc}(\text{N})(\text{PXP})]^{2+}$  (PXP = Diphosphine Ligand). A Novel Tool for the Selective Labeling of Small Molecules. *J. Am. Chem. Soc.* **124**, 11468–11479.



- (26) Bolzati, C., Boschi, A., Duatti, A., Prakash, S., Uccelli, L., Refosco, F., Tisato, F., and Bandoli, (2000) G. Geometrically Controlled Selective Formation of Nitrido Technetium(V) Asymmetrical Heterocomplexes with Bidentate Ligands. *J. Am. Chem. Soc.* **122**, 4510–4511.
- (27) Boschi, A., Bolzati, C., Benini, E., Malagò, E., Uccelli, L., Duatti, A., Piffanelli, A., Refosco, F., and Tisato, F. (2001) A Novel Approach to the High-Specific Activity Labeling of Small Peptides with the Technetium-99m Fragment  $[^{99m}\text{Tc}(\text{N})(\text{PXP})]^{2+}$  (PXP = Diphosphine Ligand). *Bioconjugate Chem.* **12**, 1035–1042.
- (28) Yokoyama, M., Menjo, Y., Watanabe, M., and Togo, H. (1994) Synthesis of Oxazoles and Thiazoles Using Thioimides. *Synthesis* 1467–1470.
- (29) Gatewood, E. S., and Johnson, T. B. (1926) Thio-amides. VI. A preliminary Study of Some Amino Acid Derivatives Containing Sulfur in Thio-amide Combination. *J. Am. Chem. Soc.* **48**, 2900–2905.
- (30) Baldas, J., Bonnyman, J., and Williams, G. A. (1986) Studies of Technetium Complexes. 9. Use of the Tetrachloronitridotechnetate(VI) Anion for the Preparation of Nitrido Complexes of Technetium. Crystal Structure of Bis(8-quinolinethiolato)nitridotechnetium(V). *Inorg. Chem.* **25**, 150–153.
- (31) Gessi, S., Dalpiaz, A., Varani, K., and Borea, P. A. (1999) Temperature dependence and GABA modulation of beta-carboline binding to rat cerebellum benzodiazepine receptors. *Life Sci.* **64**, 185–192.
- (32) Bradford, M. M. (1976) A Rapid and Sensitive Method for the Quantification of Microgram Quantities of Protein Utilizing the Principle of Protein Dye-Binding. *Anal. Biochem.* **72**, 248–254.
- (33) Archer, G. A., and Sternbach, L. H. 1-Substituted benzodiazepin-2-ones. U.S. Pat. 3,236,838, 1966.
- (34) Usui, Y., Yukio, H., Mikami, I., and Masuda, T. (1970) Benzodiazepines. I. Synthesis of New 1,4-Benzodiazepine Derivatives. *Takeda Kenkyusho Ho.* **1**, 145–152.
- (35) Gibson, F. S., Bergmeier, S. C., and Rapoport, H. (1994) Selective Removal of an N-Boc Protecting Group in the Presence of a *tert*-butyl Ester and Other Acid-sensitive Groups. *J. Org. Chem.* **59**, 3216–3218.
- (36) Pearson, D. A., Blanchette, M., Baker, M. L., and Guidon, C. A. (1989) Trialkylsilanes as Scavengers for the Trifluoroacetic Acid Deblocking of Protecting Groups in Peptide Synthesis. *Tetrahedron Lett.* **30**, 27339–2742.
- (37) Pasqualini, R., Duatti, A., Bellande, E., Comazzi, V., Brucato, V., Hoffschir, D., Fagret, D., and Comet, M. (1994) Bis(dithiocarbamate) Nitrido Technetium-99m Radiopharmaceuticals: a Class of Neutral Myocardial Imaging Agents. *J. Nucl. Med.* **35**, 334–341.
- (38) Bolzati, C., Uccelli, L., Boschi, A., Malagò, E., Duatti, A., Tisato, F., Refosco, F., Pasqualini, R., Piffanelli, A. (2000) Synthesis of a Novel Class of Nitrido Tc-99m Radiopharmaceuticals with Phosphino-Thiol Ligands Showing Transient Heart Uptake. *Nucl. Med. Biol.* **24**, 369–374.
- (39) Bolzati, C., Mahmood, A., Malagò, E., Boschi, A., Uccelli, L., Friebe, M., Jones, A. G., and Duatti, A. (2002) Asymmetric Tc–Nitrido Complexes for Imaging 5HT<sub>1A</sub> Receptor. *Technetium, Rhenium and Other Metals in Chemistry and Nuclear Medicine VI* (Nicolini, M., Mazzi, U., Eds.) pp 369–374. SG Editoriali, Padova, Italy.
- (40) Borea, P. A., Gilli, G., Bertolasi, V., and Ferretti, V. (1987) Stereochemical Features Controlling Binding and Intrinsic Activity Properties of Benzodiazepine-Receptor Ligands. *Mol. Pharmacol.* **31**, 334–344.

BC034124N

# Efficient and Expedient Two-Step Pyranose-Retaining Fluorescein Conjugation of Complex Reducing Oligosaccharides: Galectin Oligosaccharide Specificity Studies in a Fluorescence Polarization Assay

Christopher T. Öberg,<sup>†,§</sup> Susanne Carlsson,<sup>‡</sup> Eric Fillion,<sup>†,\*</sup> Hakon Leffler,<sup>‡,\*</sup> and Ulf J. Nilsson<sup>§,\*</sup>

Department of Chemistry, University of Waterloo, 200 University Avenue West, Waterloo, Ontario N2L 3G1, Canada, Section MIG, Institute of Laboratory Medicine, Lund University, Sölvegatan 23, 223 62 Lund, Sweden, and Organic and Bioorganic Chemistry, Lund University, P.O. Box 124, 221 00 Lund, Sweden. Received July 21, 2003

Fluorescence labeling of naturally occurring saccharides provides a tool for studying lectins. A practical and efficient two-step protocol for fluorescence labeling of reducing sugars without disrupting their pyranose structure has been developed, consisting of generation of the amino sugar using  $\text{NH}_4\text{HCO}_3$ -(s)/ $\text{NH}_3$ (aq, concentrated) followed by BOP-mediated acylation with derivatives of 5- or 6-carboxy-fluorescein. The acylated conjugates were subsequently run against galectins-1, -3, and -8,  $\beta$ -galactoside recognizing lectins of current interest, in a fluorescence polarization binding assay. Upon analyzing a collection of isomerically pure 5- and 6-carboxyfluorescein derivatives with different tether lengths, we found that conjugates based on 5-carboxyfluorescein gave significantly better results than the ones based on 6-carboxyfluorescein and that galectins-1 and -8 favored conjugates with different tether lengths than did galectin-3. The results show that fluorescence labeling can be chemically tuned to find optimal probes for individual galectins but also probes interacting well with many galectins.

## INTRODUCTION

The galectins, a subfamily of animal lectins, are defined by shared conserved sequence elements and affinity for  $\beta$ -galactosides, with about 10 members in humans (1). Galectins are implicated in, most notably, cancer, inflammation, and immunity among many other cellular events; however, a comprehensive description of their overall biological function has so far been elusive (2, 3).

Our research groups have been particularly interested in expressing and studying galectin-1, -3, and -8. One method employed in probing their function has been to develop inhibitors with  $K_d$ <sup>1</sup> in the low micromolar range (4). With the prospect of learning more about the galectins' functions, we have also developed a simple method for the screening of naturally occurring  $\beta$ -galactosides and their fine specificity. A fluorescence polarization (FP) assay was chosen to measure the affinity between galec-

tins and naturally occurring saccharides because it is a highly sensitive and robust method (5).

For the FP assay, fluorescently labeled saccharides are needed. A library of such probes can be used to profile the specificity of a target lectin by measuring their direct binding to the lectin by FP. A selected probe can also be used to screen the potency of nonfluorescent saccharides as inhibitors of the probe–lectin interaction.

The aim of the present investigation was to develop an efficient and practical method to label natural saccharides with a fluorophore to be used as probes. The well-studied carboxyfluorescein was chosen as the fluorescent moiety due to suitable properties such as appropriate excitation lifetime, relatively high absorptivity, high quantum yield, and ready availability. It was considered desirable to keep the reducing saccharide residue in the ring (pyranose) form, as this appears to be required for efficient binding of galectins in many cases (6–8) (Figure 1). Therefore, reductive amination, commonly used to tag saccharides, could not be used (9). Instead glycosylamines were first generated using a published one-step introduction of a primary amine onto the reducing end (10) and then conjugated with a suitable carboxyfluorescein derivative selected out of a premade library with different tethers and other features. A simple, mild, one-step procedure to conserve and not to alter complex saccharides was devised for the final conjugation. This convergent strategy is similar to one reported during this research by Danishefsky et al. for glycopeptide synthesis in which the glycan was also the limiting factor (11).

## EXPERIMENTAL PROCEDURES

**General Procedures.** HPLC. Waters Instrument: The HPLC system consisted of a Waters 600 Controller,

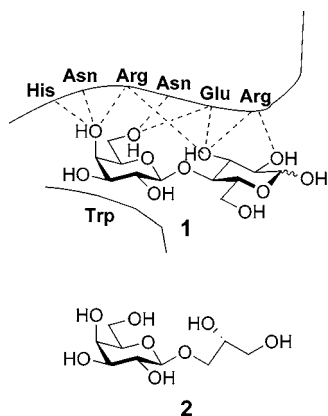
\* To whom correspondence should be addressed: E.F.: Phone +1-(519) 888-4567 ext: 2470, Fax +1-(519) 746-0435, E-mail efillion@uwaterloo.ca; H.L.: Phone +46-46-173270, Fax +46-46-137468, E-mail hakon.leffler@mig.lu.se; U.J.N.: Phone +46-46-2228218, Fax +46-46-2228209, E-mail ulf.nilsson@bioorganic.lth.se.

<sup>†</sup> University of Waterloo.

<sup>‡</sup> Institute of Laboratory Medicine, Lund University.

<sup>§</sup> Organic and Bioorganic Chemistry, Lund University.

<sup>1</sup> Abbreviations used: BOP, benzotriazol-1-yloxytris(dimethylamino)phosphonium hexafluorophosphate; DIPA, diisopropylamine; DIPEA, diisopropylethylamine; GABA,  $\gamma$ -aminobutyric acid; CRD, carbohydrate recognition domain; Gal, galactose; galectin-8N, the N-terminal CRD of galectin-8 expressed as a thioredoxin fusion protein; Glc, glucose; GlcNAc, acetyl glucosamine; HOBt 1-hydroxybenzotriazole;  $K_D$ , dissociation constant; o.n. = overnight;  $P_{\text{max}}$ , maximum polarization value; rt, room temperature.



**Figure 1.** Schematic of galectin interaction with lactose **1** and an analogue **2**. The lactose is depicted to resemble its natural conformation. Parts of the galectin are drawn around it with the conserved signature amino acids indicated interacting with the saccharide via hydrogen bonds (dotted lines) or hydrophobic interaction (the Trp residue). Based on Figure 4 in Barondes et al., 1994 (7).

a Waters 2487 Dual Wavelength Absorbance Detector, and a Waters 600 Pump equipped with No. 3 pump heads, a Rheodyne 7725i injector, and a 5 mL sample loop. A Waters Nova-Pak HR Silica column (25 × 100 mm, 6  $\mu$ m, 60 Å) with corresponding Guard-Pak (25 × 10 mm) was fitted in a radial compression module. The flow rate was 14 mL/min, and a gradient mobile phase was employed (CH<sub>3</sub>CN:H<sub>2</sub>O 10:90 up to 23:77 over 26 min and then up to 100:0 over an additional 20 min). Millenium<sup>32</sup> (v. 3.20) software was used for data acquisition and analysis.

**Beckman System Gold Instrument:** The HPLC system consisted of a Programmable Solvent Module 126 equipped with a Rheodyne 7725i injector and a 5 mL sample loop, a Programmable Detector Module 166, a Pharmacia LKB Frac-100 fraction collector, and Supelco Supelcosil column (SPLC-18-DB, 10 × 250 mm, 5  $\mu$ m). The Beckman System Gold Personal Chromatography Software (v. 7.0) was used for controlling the HPLC system and for data acquisition and analysis.

The flow rate was 5 mL/min, and a gradient mobile phase was used (CH<sub>3</sub>CN 0.1% TFA/H<sub>2</sub>O 0.1% TFA 5:95 was held for 3 min before being raised to 25:75 over 30 min and then up to 100:0 over additional 20 min).

**NMR.** <sup>1</sup>H NMR were performed on Bruker Avance 300 or Bruker Avance 500 machines. All samples were run at room temperature using a zg30 pulsprogram. Compounds **16** and **17** were run on a Bruker Avance DRX400.

**MS.** Two mass spectrometers were used. A Q-TOF Global, Micromass (UK) was used in high-resolution mode. Samples were dissolved in MeOH with clusters of CF<sub>3</sub>COONa used as internal standard and injected using direct infusion. Samples run in negative mode unless otherwise stated. An ABI-Sciex Qstar, Canada, with an ESI-TurboIon source and with the QTOF geometry. The instrument was used in positive mode.

**TLC.** Glass backed plates from Silicycle were used for TLC (60 Å, 250  $\mu$ m, F-254 indicator). Eluents were CH<sub>2</sub>-Cl<sub>2</sub>:CH<sub>3</sub>OH:H<sub>2</sub>O 100:10:1, 65:35:5, or 50:50:10.

**Chemicals and Solvents.** Chemicals were supplied by Sigma-Aldrich and used as is unless otherwise noted. Me<sub>2</sub>SO was either from SureSeal bottle or distilled under vacuum over CaH<sub>2</sub> prior to use, EtOH was of HPLC grade, and CH<sub>3</sub>NO<sub>2</sub> and DIPA were distilled from CaH<sub>2</sub> prior to use. LNT-2 and LNnT were generously donated by Dr. David Zopf at Neose Inc., Philadelphia, PA.

**Synthetic Procedures.** *General Procedure for the Coupling of Methyl Ester-Protected Amino Acids with 5- or 6-Carboxyfluorescein.* 5- or 6-Carboxyfluorescein (700 mg, 1.29 mmol), amino acid methyl ester hydrochloride (2.57 mmol), BOP (683 mg, 1.54 mmol), and HOBT (209 mg, 1.54 mmol), in dry glassware, were dissolved in Me<sub>2</sub>SO (12.9 mL) and DIPEA (1.34 mL) and stirred at room temperature for 13 h. NaOH (aq, 1 N, 12.9 mmol) was slowly added and the reaction mixture stirred for 30 min after final addition at room temperature. HCl (aq, 1 N, 22 mmol) was added causing precipitation. The reaction mixture was diluted with Me<sub>2</sub>SO, loaded onto a C18-silica column (5 g), and washed with HCOOH (aq, 1%, 300 mL). The C18-column was eluted with MeOH (100 mL), and the MeOH was removed in vacuo. The remaining solids were redissolved in CH<sub>2</sub>Cl<sub>2</sub> and minimal amount of MeOH and purified using flash chromatography (CH<sub>2</sub>-Cl<sub>2</sub>:MeOH:HCOOH 100:2:1 → 100:5:1 → 100:7.5:1 → 100:10:1) to give the product.

*General Procedure for the Coupling of Lactosylamine with 5- or 6-Carboxyfluorescein and their Carboxylic Acid Derivatives.* Carboxylic acid (0.179 mmol), crude lactosylamine **10/11** (30.5 mg, 0.089 mmol), BOP (87 mg, 0.197 mmol), and HOBT (26.6 mg, 0.197 mmol) in dry glassware, were dissolved in Me<sub>2</sub>SO (1.8 mL) and DIPEA (78  $\mu$ L, 0.45 mmol) and stirred at room temperature for 15 h. The reaction mixture was diluted with Me<sub>2</sub>SO, loaded onto a C18-silica column (5 g), and washed with a 1% HCOOH solution (aq, 150 mL). The C18-column was eluted with CH<sub>3</sub>CN:MeOH (70:30). The solvents were removed in vacuo, and the residue was redissolved in Me<sub>2</sub>SO (2 mL) followed by H<sub>2</sub>O (6 mL) and purified using HPLC divided over two runs (see procedure for Waters Instrument). The pure fractions from the two runs were pooled to give the product.

*General Procedure for the Coupling of Reducing Oligosaccharides in 1–2 mg Scale with 5- or 6-Carboxyfluorescein and Their Carboxylic Acid Derivatives.* Reducing oligosaccharide (3.66  $\mu$ mol), NH<sub>4</sub>HCO<sub>3</sub> (1.16 mg, 14.6  $\mu$ mol), and NH<sub>3</sub> (aq, 25%, 146  $\mu$ L) were stirred at 43 °C for 19 h in a sealed Eppendorf vial. A stream of air was used to remove some NH<sub>3</sub> from the stirred solution before the remainder was lyophilized over 18 h. Carboxylic acid (14.6  $\mu$ mol), BOP (7.1 mg, 16.1  $\mu$ mol), and HOBT (2.2 mg, 16.1  $\mu$ mol) were added to the crude in the vial followed by addition of Me<sub>2</sub>SO (146  $\mu$ L) and DIPEA (36.6  $\mu$ mol). The reaction was kept in the dark and stirred at room temperature for 6 h. The reaction mixture was purified without previous workup on the Beckman HPLC system to give the product.

*(2R)-2,3-Dihydroxypropyl  $\beta$ -D-Galactopyranoside.* Fully acetylated galactose (100 mg, 0.26 mmol) and (2S)-2,3-propylideneglycerol (67 mg, 0.51 mmol) were dissolved in CH<sub>2</sub>Cl<sub>2</sub> (2.56 mL). BF<sub>3</sub>·OEt<sub>2</sub> (35.4  $\mu$ L, 0.28 mmol) was added at room temperature under N<sub>2</sub> atmosphere and the reaction stirred for 3 h. The reaction mixture was diluted with CH<sub>2</sub>Cl<sub>2</sub> and washed with NaHCO<sub>3</sub> (aq, sat, 3 × 10 mL), and the organic phase was dried over MgSO<sub>4</sub> and concentrated in vacuo. The residue was purified by flash chromatography over silica gel (toluene:acetone 7:1) to give 37.5 mg of the glycosylated galactose intermediate. The intermediate was dissolved in AcOH (aq, 80%, 10 mL) and stirred at 60 °C for 3 h before solvents were removed in vacuo followed by coevaporation with toluene (3 × 10 mL) to give 26.5 mg of the depropylidenated second intermediate. The second intermediate was dissolved in NaOMe (MeOH, 0.01 M, 10 mL) and stirred at room temperature for 45 min. The reaction mixture was neutralized with AcOH (aq, 10%), and solvents were



removed in vacuo. The residue was purified by flash chromatography over silica gel ( $\text{CH}_2\text{Cl}_2$ :MeOH:H<sub>2</sub>O 65:35:5) to give **2**. <sup>1</sup>H NMR ( $\text{D}_2\text{O}$ , 300 MHz):  $\delta$  4.30 (d, 1 H, *J* 7.7 Hz,  $\beta$ -H-1), 3.93–3.38 (m, 11 H, *H*-2 to *H*-6 +  $\text{OCH}_2$  +  $\text{CH}$  +  $\text{CH}_2\text{OH}$ ).

**5(6)-Carboxyfluorescein.** Resorcinol (40 g, 0.36 mol), 1,2,4-tricarboxylic anhydride (35 g, 0.18 mol, mortared), and  $\text{ZnBr}_2$  (60 g, 0.27 mol) were melted at 180 °C. The mixture solidified after 30 min, and the reaction mixture was allowed to cool after a total of 1 h of heating. A 1 N HCl solution (700 mL) was added to the flask, and the temperature was maintained at 110–120 °C for 1 h. The hot acidic solution was filtered and the filtrate saved. Trapped solids were put back in the flask with the remaining solids, and 1 N HCl solution (700 mL) was added, heated at 110–120 °C for 1 h, and filtered. The procedure was repeated a third time. Orange-brown solids precipitated quickly in the three filtrates. The solids were filtered off separately once the filtrates had reached rt, and each was washed with 1 N HCl solution (100 mL) and H<sub>2</sub>O (2  $\times$  100 mL) to give 5(6)-carboxyfluorescein in a total off 27.5 g (40%). The three crops contained different ratios of the 5- and 6-regioisomer.

**5- and 6-Dipivaloylfluoresceincarboxylate Diisopropylammonium Salt (3 and 5).** 5(6)-Carboxyfluorescein (6.3 g, 16.7 mmol) and pivaloyl anhydride (12.6 mL, 61.7 mmol) were refluxed under an Ar atmosphere for 2 h before the reaction mixture was allowed to reach rt. THF (20 mL) and H<sub>2</sub>O (10 mL) were added, and the mixture was stirred for 18 h at room temperature. Et<sub>2</sub>O (50 mL) was added, and the aqueous layer was removed followed by extraction of the organic layers with H<sub>2</sub>O (3  $\times$  25 mL), 1 N HCl solution (50 mL), and brine (50 mL). The organics were dried over  $\text{MgSO}_4$  and the solvents removed in vacuo. The residue was dissolved in EtOH (63 mL) and DIPA (6.3 mL) and kept at –20 °C for 2 h. The solids formed were filtered off and washed with cold EtOH (2  $\times$  10 mL, –20 °C – 10 °C) to give 2.76 g of the 6-regioisomer **5**. The mother liquor was concentrated in vacuo, and the residue was dissolved in EtOH (50 mL) and DIPA (5 mL) and stored at –20 °C. The solids were filtered off and washed with EtOH (15 mL, –20 °C – 10 °C) to give 0.4 g of the 6-isomer. Another crop of the 6-isomer was crystallized from EtOH (20 mL) and DIPA (5 mL) leaving only 6% of the 6-isomer in the mother liquor. The mother liquor was concentrated in vacuo, and the residue was redissolved in Et<sub>2</sub>O (50 mL) and washed with HCl (1 N, 50 + 3  $\times$  25 mL) and brine (50 mL). The Et<sub>2</sub>O phase was dried over  $\text{MgSO}_4$ , and the solvent was removed providing 2.45 g of **3**. Isolated yields based on 5(6)-carboxyfluorescein were thus 27% of **3** and 29% of **5**. <sup>1</sup>H NMR according to ref 12.

**5-Carboxyfluorescein (6).** 5-Dipivaloylcarboxyfluorescein (**3**) (300 mg, 0.55 mmol) was dissolved in MeOH (8.3 mL) and NaOH (aq, 1 N, 5.5 mmol) and stirred at room temperature for 50 min. A 1 N HCl solution (6.5 mmol) was added, and volatiles were removed in vacuo. The solids were filtered off and washed with H<sub>2</sub>O (2  $\times$  5 mL) and Et<sub>2</sub>O (2  $\times$  5 mL) to give 190 mg (92%) of **6**. <sup>1</sup>H NMR ( $\text{CD}_3\text{OD}$ , 300 MHz):  $\delta$  8.92 (d, *J* 1.3 Hz, *Ar* *H*-4), 8.48 (dd, *J*<sub>1</sub> 1.5 Hz, *J*<sub>2</sub> 7.9 Hz, *Ar* *H*-6), 7.57 (d, *J* 8.6 Hz, *Ar* *H*-7), 7.39 (d, *J* 9.1 Hz, *Ar*), 7.29 (d, *J* 2.0 Hz, *Ar*), 7.12 (dd, *J*<sub>1</sub> 2.1 Hz, *J*<sub>2</sub> 9.1 Hz, *Ar*). HR-ESI-QTOF calcd for  $\text{C}_{21}\text{H}_{11}\text{O}_7$  ( $\text{M} - \text{H}^+$ ) 375.0510, obsd 375.0502.

**6-Carboxyfluorescein (7).** 6-Dipivaloylfluoresceincarboxylate diisopropylethylammonium salt (**5**) (3.25 g, 5.04 mmol) was dissolved in MeOH (60 mL) and NaOH (aq, 1 N, 30.2 mmol) and stirred at room temperature for 1 h. A solution of hydrochloric acid (1 N, 40 mL) was added, and volatiles were removed in vacuo causing precipita-

tion. The solids were filtered off and washed with H<sub>2</sub>O (50 mL) and Et<sub>2</sub>O (2  $\times$  50 mL) to give 1.8 g (95%) of **7**. <sup>1</sup>H NMR ( $\text{CD}_3\text{OD}$ , 300 MHz):  $\delta$  8.46 (m, 2 H, *Ar* *H*-4 + *Ar* *H*-5), 8.04 (app. s, 1 H, *Ar* *H*-7), 7.47 (d, 2 H, *J* 9.2 Hz, *Ar*), 7.34 (d, 2 H, *J* 2.1 Hz, *Ar*), 7.17 (dd, 2 H, *J*<sub>1</sub> 2.3 Hz, *J*<sub>2</sub> 9.2 Hz, *Ar*). HR-ESI-QTOF calcd for  $\text{C}_{21}\text{H}_{11}\text{O}_7$  ( $\text{M} - \text{H}^+$ ) 375.0505; obsd 375.0511.

**6-(Carboxymethylaminocarbonyl)fluorescein (8a).** The reaction was carried out as in the general procedure for coupling with amino acids using glycine methyl ester hydrochloride to give 246 mg (78%) of **8a**. Purification by flash chromatography on silica gel using the same system as for **8b** but using dry packing due to the poor solubility of **8a**. <sup>1</sup>H NMR ( $\text{CD}_3\text{OD}$ , 300 MHz):  $\delta$  8.49 (app s, 1 H, *Ar* *H*-4), 8.25 (app d, 1 H, *J* 8.0 Hz, *Ar* *H*-6), 7.31 (d, 1 H, *J* 8.0 Hz, *Ar* *H*-7), 6.69 (d, 2 H, *J* 2.3 Hz, *Ar*), 6.61 (d, 2 H, *J* 8.7 Hz, *Ar*), 6.54 (dd, 2 H, *J*<sub>1</sub> 2.3 Hz, *J*<sub>2</sub> 8.7 Hz, *Ar*), 4.10 (s, 2 H,  $\text{C}(\text{O})\text{CH}_2\text{N}$ ). HR-ESI-QTOF calcd for  $\text{C}_{23}\text{H}_{14}\text{NO}_8$  ( $\text{M} - \text{H}^+$ ) 432.0734, obsd 432.0732.

**6-(2-Carboxyethylaminocarbonyl)fluorescein (8b).** The reaction was carried out as in the general procedure for coupling with amino acids using  $\beta$ -alanine methyl ester hydrochloride to give 372 mg (64%) of **8b**. <sup>1</sup>H NMR ( $\text{CD}_3\text{OD}$ , 300 MHz):  $\delta$  8.41 (d, 1 H, *J* 0.9 Hz, *Ar* *H*-4), 8.18 (dd, 1 H, *J*<sub>1</sub> 1.6 Hz, *J*<sub>2</sub> 8.1 Hz, *Ar* *H*-6), 7.29 (d, 1 H, *J* 7.9 Hz, *Ar* *H*-7), 6.68 (s, 2 H, *J* 2.2 Hz, *Ar*), 6.59 (d, 2 H, *J* 7.9 Hz, *Ar*), 6.53 (dd, 2 H, *J*<sub>1</sub> 2.3 Hz, *J*<sub>2</sub> 8.8 Hz, *Ar*), 3.68 (t, 2 H, *J* 6.8 Hz,  $\text{NCH}_2$ ), 2.67 (t, 2 H, *J* 6.7 Hz,  $\text{C}(\text{O})\text{-CH}_2$ ). HR-ESI-QTOF calcd for  $\text{C}_{24}\text{H}_{16}\text{NO}_8$  ( $\text{M} - \text{H}^+$ ) 446.0881, obsd 446.0892.

**6-(3-Carboxypropylaminocarbonyl)fluorescein (8c).** The reaction was carried out as in the general procedure for coupling with amino acids using GABA methyl ester hydrochloride to give 255 mg (76%) of **8c**. <sup>1</sup>H NMR ( $\text{CD}_3\text{OD}$ , 300 MHz):  $\delta$  8.42 (app s, 1 H, *Ar* *H*-4), 8.19 (dd, 1 H, *J*<sub>1</sub> 1.4 Hz, *J*<sub>2</sub> 8.0 Hz, *Ar* *H*-6), 7.29 (d, 1 H, *J* 8.1 Hz, *Ar* *H*-7), 6.68 (s, 2 H, *J* 2.2 Hz, *Ar*), 6.59 (d, 2 H, *J* 8.7 Hz, *Ar*), 6.53 (dd, 2 H, *J*<sub>1</sub> 2.3 Hz, *J*<sub>2</sub> 8.7 Hz, *Ar*), 3.48 (t, 2 H, *J* 6.9 Hz,  $\text{NCH}_2$ ), 2.42 (t, 2 H, *J* 6.7 Hz,  $\text{C}(\text{O})\text{-CH}_2$ ), 1.95 (app q, *J*<sub>1</sub> 7.3 Hz, *J*<sub>2</sub> 6.7 Hz,  $\text{CH}_2$ ). HR-ESI-QTOF calcd for  $\text{C}_{25}\text{H}_{18}\text{NO}_8$  ( $\text{M} - \text{H}^+$ ) 460.1037, obsd 460.1031.

**6-(Carboxymethylaminocarbonyl)fluorescein (9a).** The reaction was carried out as in the general procedure for coupling with amino acids using glycine methyl ester hydrochloride to give 100% yield of **9a**. <sup>1</sup>H NMR ( $(\text{CD}_3)_2\text{CO}$ , 300 MHz):  $\delta$  8.32 (bt, 1 H, *NH*), 8.23 (dd, 1 H, *J*<sub>1</sub> 7.9 Hz, *Ar* *H*-5), 8.05 (d, 1 H, *J* 8.0 Hz, *Ar* *H*-4), 7.74 (app s, 1 H, *Ar* *H*-7), 6.73 (d, 2 H, *J* 1.8 Hz, *Ar*), 6.68 (d, 2 H, *J* 8.6 Hz, *Ar*), 6.60 (dd, 2 H, *J*<sub>1</sub> 2.0 Hz, *J*<sub>2</sub> 8.6 Hz, *Ar*), 4.06 (d, 2 H, *J* 5.8 Hz,  $\text{CH}_2$ ). HR-ESI-QTOF calcd for  $\text{C}_{23}\text{H}_{14}\text{NO}_8$  ( $\text{M} - \text{H}^+$ ) 432.0719, obsd 432.0733.

**6-(2-Carboxyethylaminocarbonyl)fluorescein (9b).** The reaction was carried out as in the general procedure for coupling with amino acids using  $\beta$ -alanine methyl ester hydrochloride to give 253 mg (91%) of **9b**. <sup>1</sup>H NMR ( $(\text{CD}_3)_2\text{CO}$ , 300 MHz):  $\delta$  8.18 (dd, 1 H, *J*<sub>1</sub> 1.3 Hz, *J*<sub>2</sub> 7.9 Hz, *Ar* *H*-5), 8.03 (d, 1 H, *J* 7.9 Hz, *Ar* *H*-4), 7.70 (app s, 1 H, *Ar* *H*-7), 6.74 (d, 2 H, *J* 2.3 Hz, *Ar*), 6.66 (d, 2 H, *J* 8.6 Hz, *Ar*), 6.59 (dd, 2 H, *J*<sub>1</sub> 2.3 Hz, *J*<sub>2</sub> 8.7 Hz, *Ar*), 3.55 (m, 2 H,  $\text{NCH}_2$ ), 2.56 (t, 2 H, *J* 6.8 Hz,  $\text{C}(\text{O})\text{-CH}_2$ ). HR-ESI-QTOF calcd for  $\text{C}_{24}\text{H}_{16}\text{NO}_8$  ( $\text{M} - \text{H}^+$ ) 446.0876, obsd 446.0865.

**6-(3-Carboxypropylaminocarbonyl)fluorescein (9c).** The reaction was carried out as in the general procedure for coupling with amino acids using GABA methyl ester hydrochloride to give 95% yield of **9c**. <sup>1</sup>H NMR ( $\text{CD}_3\text{OD}$ , 300 MHz):  $\delta$  8.11 (dd, 1 H, *J*<sub>1</sub> 0.9 Hz, *J*<sub>2</sub> 7.9 Hz, *Ar* *H*-5), 8.05 (d, 1 H, *J* 8.0 Hz, *Ar* *H*-4), 7.61 (app s, 1 H, *Ar* *H*-7), 6.68 (d, 2 H, *J* 2.2 Hz, *Ar*), 6.59 (d, 2 H, *J* 8.6 Hz, *Ar*), 6.53 (dd, 2 H, *J*<sub>1</sub> 2.2 Hz, *J*<sub>2</sub> 8.7 Hz, *Ar*), 3.33 (t, 2 H, *J* 6.9

Hz,  $\text{NCH}_2$ ), 2.30 (t, 2 H,  $J$  7.3 Hz,  $\text{C}(\text{O})\text{CH}_2$ ), 1.81 (app. q, 2 H,  $\text{CH}_2$ ). HR-ESI-QTOF calcd for  $\text{C}_{25}\text{H}_{18}\text{NO}_8$  ( $\text{M} - \text{H}^+$ ) 460.1032, obsd 460.1039.

**Lactosylamine (10).** Lactose **1** (500 mg, 1.46 mmol) and  $\text{NH}_4\text{HCO}_3$  (115 mg, 1.46 mmol) were dissolved in  $\text{NH}_3$  (aq, 28%) and stirred in a stoppered flask at room temperature for 15 h. The reaction mixture was concentrated to ca. half volume in vacuo and lyophilized once.  $^1\text{H}$  NMR showed the major products to be lactosylamine **10** (46%) and lactosylcarbamate **11** (35%).  $^1\text{H}$  NMR ( $\text{D}_2\text{O}$ , 300 MHz):  $\delta$  5.05 (d, 0.10 H,  $J$  3.8 Hz,  $\alpha$   $\text{H}-1$ ), 4.55 (d, 0.36 H,  $J$  9.2 Hz,  $\beta$   $\text{H}-1$ ), 4.27 (d, 1 H,  $J$  7.7 Hz,  $\beta$   $\text{H}-1'$ ), 3.94 (d, 0.46 H,  $J$  8.8 Hz,  $\beta$   $\text{H}-1$ ), 3.90–3.05 (m, 12 H,  $\text{H}-2$  to  $\text{H}-6 + \text{H}-2'$  to  $\text{H}-6'$ ). HR-ESI-QTOF calcd for  $\text{C}_{12}\text{H}_{24}\text{NO}_{10}$  ( $\text{M} + \text{H}^+$ ) 342.1400, obsd 342.1405.

**Compound 12.** The reaction was carried out as in the general procedure for coupling with crude lactosylamine **10/11**, using **6** to give **12** in 24% isolated yield. However, impurities coluted with product, and repeated HPLC runs and a flash chromatography on silica gel were required to give pure product.  $^1\text{H}$  NMR ( $\text{CD}_3\text{OD}$ , 500 MHz):  $\delta$  8.55 (app s, 1 H,  $\text{Ar H}-4$ ), 8.18 (app d, 1 H,  $J$  7.9 Hz,  $\text{Ar H}-6$ ), 7.33 (d, 1 H,  $J$  8.0 Hz,  $\text{Ar H}-7$ ), 6.83 (d, 2 H,  $J$  9.6 Hz,  $\text{Ar}$ ), 6.68 (d, 2 H,  $J$  2.2 Hz,  $\text{Ar}$ ), 6.58 (dd, 2 H,  $J_1$  1.9 Hz,  $J_2$  8.9 Hz,  $\text{Ar}$ ), 5.80 (d, 0.15 H,  $J$ ,  $\alpha$   $\text{H}-1$ ), 5.20 (d, 1 H,  $J$  8.9 Hz,  $\beta$   $\text{H}-1$ ), 4.40 (d, 1 H,  $J$  9.6 Hz,  $\beta$   $\text{H}-1'$ ), 3.92–3.47 (m, 12 H,  $\text{H}-2$  to  $\text{H}-6 + \text{H}-2'$  to  $\text{H}-6'$ ). HR-ESI-QTOF calcd for  $\text{C}_{33}\text{H}_{34}\text{NO}_{16}$  ( $\text{M} + \text{H}^+$ ) 700.1872, obsd 700.1838.

**Compound 13.** The reaction was carried out as in the general procedure for coupling with crude lactosylamine **10/11**, using **7** to give **13** in 32% isolated yield.  $^1\text{H}$  NMR ( $\text{CD}_3\text{OD}$ , 500 MHz):  $\delta$  8.19 (app d, 1 H,  $J$  8.1 Hz,  $\text{Ar H}-5$ ), 8.07 (d, 1 H,  $J$  8.0 Hz,  $\text{Ar H}-4$ ), 7.73 (app s, 1 H,  $\text{Ar H}-7$ ), 6.68 (app. s, 2 H,  $\text{Ar}$ ), 6.62 (d, 2 H,  $J$  8.7 Hz,  $\text{Ar}$ ), 6.54 (app d, 2 H,  $J$  8.7 Hz,  $\text{Ar}$ ), 5.69 (d, 0.11 H,  $J$  5.6 Hz,  $\alpha$   $\text{H}-1$ ), 5.08 (d, 1 H,  $J$  9.1 Hz,  $\beta$   $\text{H}-1$ ), 4.33 (d, 1 H,  $J$  7.7 Hz,  $\beta$   $\text{H}-1'$ ), 3.80–3.30 (m, 12 H,  $\text{H}-2$  to  $\text{H}-6 + \text{H}-2'$  to  $\text{H}-6'$ ). HR-ESI-QTOF calcd for  $\text{C}_{33}\text{H}_{32}\text{NO}_{16}$  ( $\text{M} - \text{H}^+$ ) 698.1721, obsd 698.1702.

**Compound 14a.** The reaction was carried out as in the general procedure for coupling with crude lactosylamine **10/11**, using **8a** to give **14a** in 34% isolated yield.  $^1\text{H}$  NMR ( $\text{CD}_3\text{OD}$ , 500 MHz):  $\delta$  8.50 (app s, 1 H,  $\text{Ar H}-4$ ), 8.23 (d, 1 H,  $J$  8.00 Hz,  $\text{Ar H}-6$ ), 7.30 (d, 1 H,  $J$  8.0 Hz,  $\text{Ar H}-7$ ), 6.68 (d, 2 H,  $J$  2.3 Hz,  $\text{Ar}$ ), 6.63 (d, 2 H,  $J$  8.8 Hz,  $\text{Ar}$ ), 6.54 (dd, 2 H,  $J_1$  2.2 Hz,  $J_2$  8.7 Hz,  $\text{Ar}$ ), 5.58 (d, 0.07 H,  $J$  5.4 Hz,  $\alpha$   $\text{H}-1$ ), 4.99 (d, 1 H,  $J$  9.2 Hz,  $\beta$   $\text{H}-1$ ), 4.37 (d, 1 H,  $J$  7.7 Hz,  $\beta$   $\text{H}-1'$ ), 4.16 (d, 2 H,  $J$  3.8 Hz,  $\text{C}(\text{O})\text{CH}_2\text{N}$ ), 3.90–3.35 (m, 12 H,  $\text{H}-2$  to  $\text{H}-6 + \text{H}-2'$  to  $\text{H}-6'$ ). HR-ESI-QTOF calcd for  $\text{C}_{33}\text{H}_{37}\text{N}_2\text{O}_{17}$  ( $\text{M} + \text{H}^+$ ) 757.2086, obsd 757.2097.

**Compound 14b.** The reaction was carried out as in the general procedure for coupling with crude lactosylamine **10/11**, using **8b** to give **14b** in 51% of **14b**.  $^1\text{H}$  NMR ( $\text{CD}_3\text{OD}$ , 500 MHz):  $\delta$  8.41 (app s, 1 H,  $\text{Ar H}-4$ ), 8.16 (app d, 1 H,  $J$  7.8 Hz,  $\text{Ar H}-5$ ), 7.28 (d, 1 H,  $J$  8.0,  $\text{Ar H}-7$ ), 6.68 (d, 2 H,  $J$  1.9 Hz,  $\text{Ar}$ ), 6.61 (d, 2 H,  $J$  8.7 Hz,  $\text{Ar}$ ), 6.54 (dd, 2 H,  $J_1$  1.9 Hz,  $J_2$  8.6 Hz,  $\text{Ar}$ ), 5.58 (d, 0.08 H,  $J$  6.5 Hz,  $\alpha$   $\text{H}-1$ ), 4.96 (d, 1 H,  $J$  9.2 Hz,  $\beta$   $\text{H}-1$ ), 4.35 (d, 1 H,  $J$  10.6 Hz,  $\beta$   $\text{H}-1'$ ), 3.88–3.43 (m, 14 H,  $\text{H}-2$  to  $\text{H}-6 + \text{H}-2'$  to  $\text{H}-6' + \text{NCH}_2$ ), 2.61 (t, 2 H,  $J$  4.7 Hz,  $\text{C}(\text{O})\text{CH}_2$ ). HR-ESI-QTOF calcd for  $\text{C}_{36}\text{H}_{39}\text{N}_2\text{O}_{17}$  ( $\text{M} + \text{H}^+$ ) 771.2243, obsd 771.2282.

**Compound 14c.** The reaction was carried out as in the general procedure for coupling with crude lactosylamine **10/11**, using **8c** to give **14c** in 44% isolated yield.  $^1\text{H}$  NMR ( $\text{CD}_3\text{OD}$ , 500 MHz):  $\delta$  8.43 (app s, 1 H,  $\text{Ar H}-4$ ), 8.17 (dd, 1 H,  $J_1$  1.2 Hz,  $J_2$  7.9 Hz,  $\text{Ar H}-6$ ), 7.29 (d, 1 H,  $J$  8.0 Hz,

$\text{Ar H}-7$ ), 6.68 (d, 2 H,  $J$  2.3 Hz,  $\text{Ar}$ ), 6.63 (d, 2 H,  $J$  8.7 Hz,  $\text{Ar}$ ), 6.54 (dd, 2 H,  $J_1$  2.0 Hz,  $J_2$  8.7 Hz,  $\text{Ar}$ ), 5.56 (d, 0.10 H,  $J$  5.5 Hz,  $\alpha$   $\text{H}-1$ ), 4.95 (d, 1 H,  $J$  9.2 Hz,  $\beta$   $\text{H}-1$ ), 4.36 (d, 1 H,  $J$  7.7 Hz,  $\beta$   $\text{H}-1'$ ), 3.85–3.40 (m, 14 H,  $\text{H}-2$  to  $\text{H}-6 + \text{H}-2'$  to  $\text{H}-6' + \text{NCH}_2$ ), 2.38 (m, 2 H,  $\text{C}(\text{O})\text{CH}_2$ ), 1.97 (m, 2 H,  $\text{CH}_2$ ). HR-ESI-QTOF calcd for  $\text{C}_{37}\text{H}_{41}\text{N}_2\text{O}_{17}$  ( $\text{M} + \text{H}^+$ ) 785.2399, obsd 785.2417.

**Compound 15a.** The reaction was carried out as in the general procedure for coupling with crude lactosylamine **10/11**, using **9a** to give **15a** in 38% isolated yield.  $^1\text{H}$  NMR ( $\text{CD}_3\text{OD}$ , 500 MHz):  $\delta$  8.06 (dd, 1 H,  $J_1$  1.4 Hz,  $J_2$  8.1 Hz,  $\text{Ar H}-5$ ), 7.97 (d, 1 H,  $J$  8.0,  $\text{Ar H}-4$ ), 7.59 (app s, 1 H,  $\text{Ar H}-7$ ), 6.57 (d, 2 H,  $J$  2.4 Hz,  $\text{Ar}$ ), 6.52 (d, 2 H,  $J$  8.7 Hz,  $\text{Ar}$ ), 6.43 (dd, 2 H,  $J_1$  2.4 Hz,  $J_2$  7.1 Hz,  $\text{Ar}$ ), 5.38 (d, 0.09 H,  $J$  5.47,  $\alpha$   $\text{H}-1$ ), 4.79 ( $\beta$   $\text{H}-1$ ), 4.23 (d, 1 H,  $J$  7.63,  $\beta$   $\text{H}-1'$ ), 3.91 (s, 2 H,  $\text{C}(\text{O})\text{CH}_2\text{N}$ ), 3.80–3.30 (m, 12 H,  $\text{H}-2$  to  $\text{H}-6 + \text{H}-2'$  to  $\text{H}-6'$ ). HR-ESI-QTOF calcd for  $\text{C}_{35}\text{H}_{35}\text{N}_2\text{O}_{17}$  ( $\text{M} - \text{H}^+$ ) 755.1936, obsd 755.1909.

**Compound 15b.** The reaction was carried out as in the general procedure for coupling with crude lactosylamine **10/11**, using **9b** to give 20.3 mg (30%) of **15b**.  $^1\text{H}$  NMR ( $\text{CD}_3\text{OD}$ , 500 MHz):  $\delta$  8.11 (app d, 1 H,  $J$  8.0 Hz,  $\text{Ar H}-5$ ), 8.06 (d, 1 H,  $J$  8.0 Hz,  $\text{Ar H}-4$ ), 7.60 (app s, 1 H,  $\text{Ar H}-7$ ), 6.68 (app s, 2 H,  $\text{Ar}$ ), 6.63 (s, 2 H,  $J$  8.7 Hz,  $\text{Ar}$ ), 6.54 (dd, 2 H,  $J_1$  2.2 Hz,  $J_2$  8.7 Hz,  $\text{Ar}$ ), (d, 0.09 H,  $J$  5.5 Hz,  $\alpha$   $\text{H}-1$ ), 4.87 ( $\beta$   $\text{H}-1$ ), 4.60 (s, 0.21 H,  $\text{NH}$ ), 4.34 (d, 1 H,  $J$  7.6 Hz,  $\beta$   $\text{H}-1'$ ), 3.80–3.30 (m, 14 H,  $\text{H}-2$  to  $\text{H}-6 + \text{H}-2'$  to  $\text{H}-6' + \text{NCH}_2$ ), 2.51 (m, 2 H,  $\text{C}(\text{O})\text{CH}_2$ ). HR-ESI-QTOF calcd for  $\text{C}_{36}\text{H}_{37}\text{N}_2\text{O}_{17}$  ( $\text{M} - \text{H}^+$ ) 769.2092, obsd 769.2104.

**Compound 15c.** The reaction was carried out as in the general procedure for coupling with crude lactosylamine **10/11**, using **9c** to give **15c** in 26% isolated yield.  $^1\text{H}$  NMR ( $\text{CD}_3\text{OD}$ , 500 MHz):  $\delta$  8.09 (m, 2 H,  $\text{Ar H}-4 + \text{Ar H}-5$ ), 7.65 (app s, 1 H,  $\text{Ar H}-7$ ), 6.85 (d, 2 H,  $J$  8.8 Hz,  $\text{Ar}$ ), 6.69 (d, 2 H,  $J$  1.8 Hz,  $\text{Ar}$ ), 6.60 (dd, 2 H,  $J_1$  8.8 Hz,  $\text{Ar}$ ), 5.47 (d, 0.09 H,  $J$  5.5 Hz,  $\alpha$   $\text{H}-1$ ), 4.86 (d, 1 H,  $J$  9.5 Hz,  $\beta$   $\text{H}-1$ ), 4.62 (app s, 1 H,  $\text{NH}$ ), 4.34 (d, 1 H,  $J$  7.6 Hz,  $\beta$   $\text{H}-1'$ ), 3.90–3.30 (d, 14 H,  $\text{H}-2$  to  $\text{H}-6 + \text{H}-2'$  to  $\text{H}-6' + \text{NCH}_2$ ), 2.28 (m, 2 H,  $\text{C}(\text{O})\text{CH}_2$ ), 1.88 (m, 2 H,  $\text{CH}_2$ ). HR-ESI-QTOF calcd for  $\text{C}_{37}\text{H}_{39}\text{N}_2\text{O}_{17}$  ( $\text{M} - \text{H}^+$ ) 783.2249, obsd 783.2222.

**Compound 16.** The reaction was carried out as in the general procedure for coupling with crude glycosylamines of oligosaccharides, using lacto-*N*-triose to give **16** in 37% isolated yield.  $^1\text{H}$  NMR ( $\text{CD}_3\text{OD}$ , 400 MHz):  $\delta$  8.60 (app s, 1 H,  $\text{Ar H}-4$ ), 8.28 (dd, 1 H,  $J_1$  1.6 Hz,  $J_2$  8.1 Hz,  $\text{Ar H}-6$ ), 7.39 (d, 1 H,  $J$  7.9 Hz,  $\text{Ar H}-7$ ), 6.93–6.66 (m, 6 H,  $\text{Ar}$ ), 4.98 (d, 1 H,  $J$  9.0 Hz,  $\beta$   $\text{H}-1$ ), 4.63 (d, 1 H,  $J$  8.4 Hz,  $\beta$   $\text{H}$ ), 4.37 (d, 1 H,  $J$  7.3 Hz,  $\beta$   $\text{H}$ ), 4.16 (s, 2 H,  $\text{C}(\text{O})\text{CH}_2$ ), 4.04 (d, 1 H,  $J$  2.2 Hz,  $\text{H}-4$ ), 3.89–3.34 (m, 17 H,  $\text{H}-2$  to  $\text{H}-6 + \text{H}-2'$  to  $\text{H}-6' + \text{H}'-2$  to  $\text{H}'-6$ ), 1.99 (s, 3 H,  $\text{NAc}$ ). HR-ESI-QTOF calcd for  $\text{C}_{43}\text{H}_{50}\text{N}_3\text{O}_{22}$  ( $\text{M} + \text{H}^+$ ) 960.2880, obsd 960.2908.

**Compound 17.** The reaction was carried out as in the general procedure for coupling with crude glycosylamines of oligosaccharides, using lacto-*N*-neo-tetrose to give **17** in 44% isolated yield.  $^1\text{H}$  NMR ( $\text{CD}_3\text{OD}$ , 400 MHz):  $\delta$  8.60 (app s, 1 H,  $\text{Ar H}-4$ ), 8.28 (dd, 1 H,  $J_1$  1.6 Hz,  $J_2$  8.0 Hz,  $\text{Ar H}-6$ ), 7.39 (d, 1 H,  $J$  8.1 Hz,  $\text{Ar H}-7$ ), 6.93–6.66 (m, 6 H,  $\text{Ar}$ ), 4.94 (d, 1 H,  $J$  9.1 Hz,  $\beta$   $\text{H}-1$ ), 4.65 (d, 1 H,  $J$  8.3 Hz,  $\beta$   $\text{H}$ ), 4.37 (d, 2 H,  $J$  7.4 Hz,  $\beta$   $\text{H} + \beta$   $\text{H}$ ), 4.16 (s, 2 H,  $\text{C}(\text{O})\text{CH}_2$ ), 4.04 (d, 1 H,  $J$  2.5 Hz,  $\text{H}-4$ ), 3.90–3.33 (m, 23 H,  $\text{H}-2$  to  $\text{H}-6 + \text{H}-2'$  to  $\text{H}-6' + \text{H}'-2$  to  $\text{H}'-6 + \text{H}''-2$  to  $\text{H}''-6$ ), 1.99 (s, 3 H,  $\text{NAc}$ ). HR-ESI-QTOF calcd for  $\text{C}_{49}\text{H}_{60}\text{N}_3\text{O}_{27}$  ( $\text{M} + \text{H}^+$ ) 1122.3408, obsd 1122.3452.

**Recombinant Galectins.** Recombinant rat galectin-1 and human galectin-3 were produced in *E. coli* BL21 (pET1d and pET-3c vectors, respectively) and purified by chromatography on lactosyl-Sepharose as described (Cop-



per et al., 1991 for galectin-1; Massa et al., 1993, for galectin-3) (13, 14). The *N*-terminus of Gal-8 and thioredoxin was expressed as a fusion protein in *E. coli* BL21 (pET32 vector) and purified by chromatography on lactosyl-Sepharose as described (14). Before use, lactose was removed by dialysis against PBS (118 mM NaCl, 67 mM Na/K-phosphate, pH 7.2) and the galectin concentrated using CentriPrep concentrators (Millipore, Bedford, MA).

**Fluorescence Polarization Binding Assay.** To measure direct binding of fluorescent probe to galectin, FP was measured from above in 96-well microtiter plates (black polystyrene, Costar, Corning, NY) using a PolarStar instrument (BMG, Offenburg, Germany). The final sample volume in each well was 200  $\mu$ L. For direct binding a series of different concentrations of galectin-3 were prepared in a microtiter plate (100  $\mu$ L per well). Then 100  $\mu$ L fluorescent probe was added to a final concentration of 0.1 or 1.0  $\mu$ M, and the plate was incubated under slow rotary shaking in the dark for 5 min. Control wells containing only fluorescent probe or fluorescein were included. All dilutions and measurements were done in PBS.

The FP is measured by two photomultipliers (PMT1 and PMT2) receiving light through two perpendicularly polarized channels. The values are given as polarization units ( $P = \text{PMT1} - \text{PMT2} / (\text{PMT1} + \text{PMT2})$ ) (5, 17). The fluorescein containing well was used to balance the gain of the photomultipliers (setting the K factor, according to instrument manual) assuming that free fluorescein should give a value of 35 mP. The total fluorescence intensity was measured as the sum of the two PMT channels, to detect quenching of the bound probe (difference between probe only or probe with maximum amount of galectin).

The temperature was set to 24, 30, 35, 40, or 45 using the thermostat of the instrument. To measure at about 5  $^{\circ}$ C, the plate was cooled on ice for 5 min before FP-recording. The temperature in selected wells was measured before and after recording using a TEMP 4 Acorn Series thermistor temperature sensor (Oakton Instruments, Vernon Hills, IL).

Data plotting, regression analysis, and curve construction was done using Prism 3.0 (GraphPad Software, San Diego, CA).

## RESULTS AND DISCUSSION

### Structural Considerations for Design of Probes.

The probes described here were designed with consideration of the structural features of galectin-carbohydrate interaction (4, 7, 8, 15), even if they would be useful for many other carbohydrate binding proteins as well. As shown in Figure 1, a Gal residue is most tightly bound to the galectin carbohydrate recognition domain (CRD) via a number of hydrogen bonds (dotted lines above 1) and a hydrophobic stacking interaction with a Trp side chain (below 1). The Glc residue of lactose and the corresponding residue of other disaccharides (e.g. LacNAc) interact much less with the protein and only along one of its sides. This interaction, however, is important, as the binding affinity of Gal alone is about 100 fold lower compared to that of lactose. The fine specificity of galectins arises mainly from differential recognitions of additional saccharides or other modifications of the disaccharide at position Gal HO-3 (and lesser extent position HO-2) which project into an extended groove on the galectin. Another source of fine specificity is the differential recognition of saccharides where the 4Glc of lactose has been replaced by another residue (e.g.

4GlcNAc, 3GlcNAc, or 3GalNAc), which projects similar enough structural features toward the protein (6, 16). The fluorescent probe, therefore, should preserve the structure of the saccharide parts interacting with galectin, while the fluorophore should be sufficiently removed not to cause adverse interactions itself.

Previous studies indicate that if the Glc ring is opened, the binding affinity for galectin-1 becomes much lower, apparently because the steric restriction of the interacting groups are required (6). To test this further, 2 was synthesized as an analogue permitting exactly the same hydrogen bond interactions to the protein as lactose but lacking the restriction of the Glc pyranose ring. This compound bound galectins-1 and -3 by over 10-fold less well than lactose (data not shown). These results reaffirmed that it was highly desirable to derivatize the saccharides keeping the reducing residue ring closed. The commonly used reductive amination would open the ring and, hence, significantly alter the interaction with the protein.

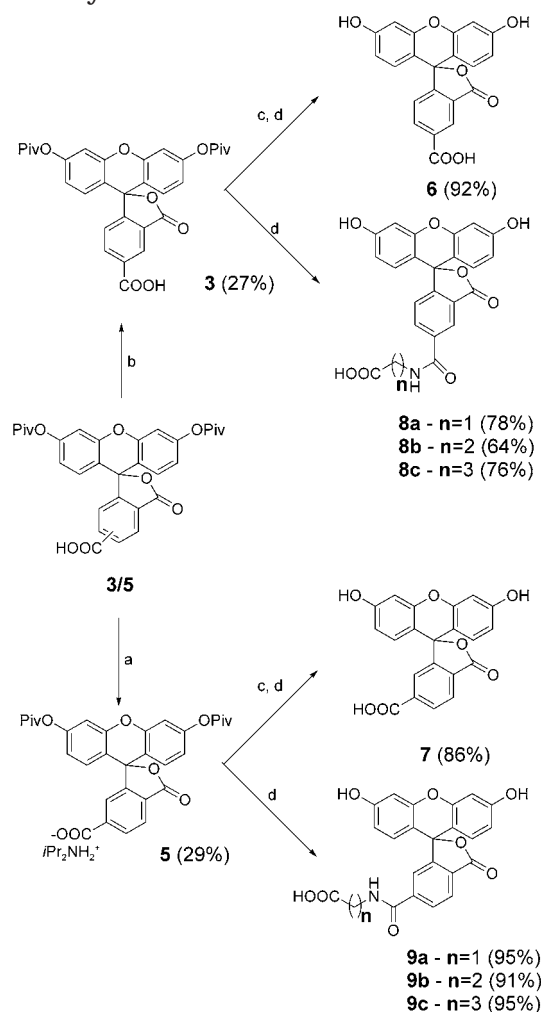
Another consideration is the tether length between the saccharide and the fluorescein moiety. As seen from Figure 1, the reducing end of lactose is not buried but is well exposed from the protein and points out into the solution. This made it likely that the tethers would not have to be very long and only limited interaction between the protein and fluorescein and tether was expected. On the other hand, a too long tether could lead to less optimal results in the FP assay due to movement of the fluorophore independent of the bound saccharide (17). Hence, we linked carboxyfluorescein to lactosylamine directly or via tethers consisting of glycine (three more atoms),  $\beta$ -alanine (four more atoms), or GABA (five more atoms).

Although carboxyfluorescein is synthesized and commonly used as mixture of two regioisomers, namely 5- and 6-carboxyfluorescein (6, 7) (18), we found it important to examine each isomer separately as they might differ in their interactions, albeit limited as mentioned above, with the protein. A few reports suggest differences in behavior and subsequent binding assays for the two isomers (19, 20). The two isomers have almost identical spectroscopic properties, making a direct comparison of lectin-binding properties possible (21). Working with single isomers also significantly simplified chromatographic separations and subsequent characterizations by NMR.

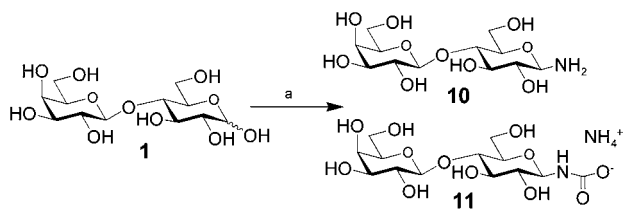
**Synthesis of Saccharide-Fluorescein Probes.** Due to the cost of commercial (21), regioisomerically pure 5- and 6-carboxyfluorescein (6, 7) in gram amounts, we synthesized the dipivaloyl-protected derivatives (mixture of 3 and 5), permitting separation by crystallization essentially as described (12, 22) (Scheme 1). Then 6 and 7, for untethered coupling to the glycosylamine, were obtained by direct deprotection by ester saponification of 3 and 5, respectively. The tethered derivatives 8a-c and 9a-c were obtained by coupling of 3 and 5, respectively, with the methyl esters of glycine,  $\beta$ -alanine, and GABA followed by the deprotection in a one-pot, two-step procedure. The yields of 9a-c were good to excellent, whereas the yields of 8a-c were only fair. We believe this is due to losses in the purification caused by the poor solubility of 6 and 8a-c, as compared to 7 and 9a-c, resulting in chromatographic difficulties.

Lactosylamine 10, was synthesized according to standard literature procedure (Scheme 2) (10). The reaction in Scheme 2 gives predominately a mixture of lactosylamine 10 and lactosylcarbamate 11.



**Scheme 1. Separation of 5- and 6-Carboxyfluorescein Followed by the Introduction of Tethers<sup>a</sup>**

<sup>a</sup> (a) Crystallization from EtOH/DIPA; (b) residual mother liquor after repeated crystallization of **5**; (c) HCl salt of the methyl esters of glycine ( $n=1$ ),  $\beta$ -alanine ( $n=2$ ), or GABA ( $n=3$ ), BOP/HOBt/DIPEA/ $\text{Me}_2\text{SO}$ ; (d) NaOH (aq, 1 M)/MeOH, rt, 30–60 min.

**Scheme 2. Introduction of Amine at the Reducing End of Lactose<sup>a</sup>**

<sup>a</sup> (a)  $\text{NH}_4\text{HCO}_3(\text{s})/\text{NH}_3(\text{aq, concentrated})$ , 42 °C, 15–24 h.

The crude lactosylamine/lactosylcarbamate **10/11** mixture was acylated with **6–9c** to give compounds (**12–15c**) in up to 65% yield after HPLC purification (Table 1, yields based on the combined amounts of **10** and **11**). It was expected that the lactosylcarbamate **11** would rapidly decarboxylate to **10** during the reaction. However, NMR of crude reaction mixture **10/11** showed lactosylcarbamate remaining after 3 days in  $\text{D}_2\text{O}$  solution at room temperature. Whether this affects the rates and yields in the coupling to **6–9c** remains to be studied.

A number of alternative coupling agents were investigated for the acylation reaction (EDC/NHS, EDC/HOBt, EDC/Pfp, DCC/HOBt, BTC, EEDQ,  $\text{COCl}_2$ , FDP, FDDP,

PyBOP, BOP, BOP/HOBt, HBTU). However, only the BOP-reagents, HBTU, and BTC gave observable product, with best yields for the BOP reagents. Accordingly, compounds **12–15c** were synthesized using the combination BOP/HOBt/DIPEA/ $\text{Me}_2\text{SO}$  (**23**) as shown in Table 1. We also note that a “standard” combination like EDC/NHS/DIPEA/ $\text{Me}_2\text{SO}$  gave good to excellent yields in coupling **6–9c** with noncarbohydrate amines such as the primary methyl esters of glycine,  $\beta$ -alanine, GABA, and also norephedrine (96% yield), the latter used as a structural mimic of the reducing end of a glycosylamines.

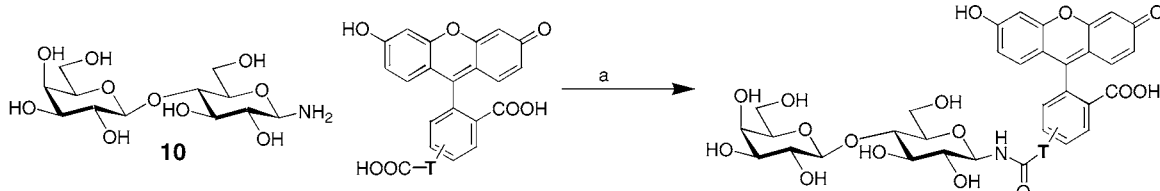
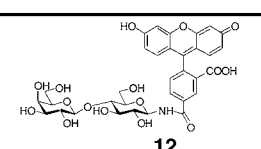
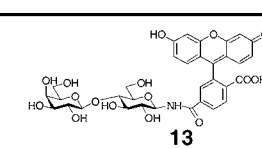
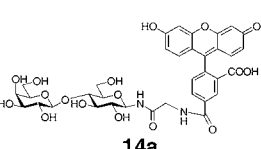
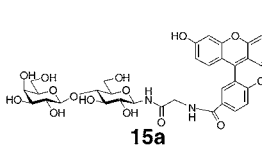
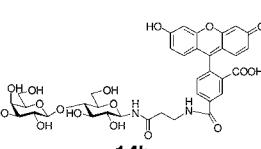
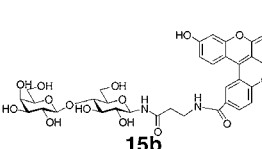
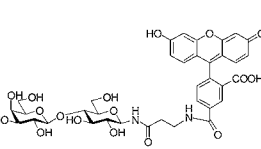
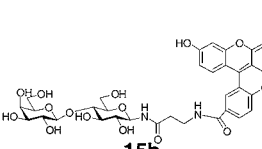
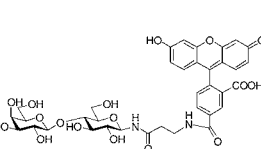
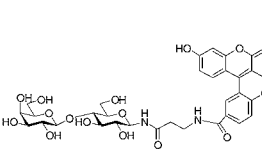
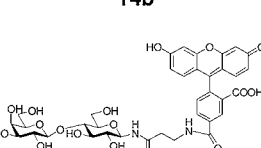
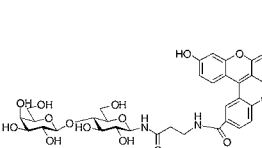
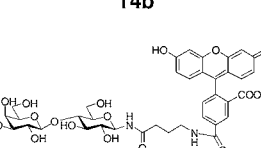
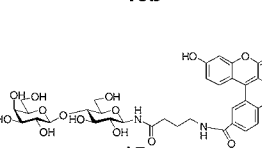
Having established the acylation conditions, the **10/11** mixture was reacted with the different relative amounts of carboxyfluorescein derivatives (Table 1). In most cases, the yields of purified saccharide derivative varied from about 30 to 65%. In all cases there was a competing formation of carboxyfluorescein amide, which was even observed as the major product in entry 10 (Table 1). This is due to significant amounts of ammonia remaining in the crude lactosylamine **10** after a single lyophilization. The residual ammonia can be removed with, for example, repeated lyophilizations, but at the expense of partial hydrolysis of **10**, which was highly undesirable in our synthetic approach, since for more complex saccharides, available in small amounts, the glycosylamine will be the limiting factor. Alternatively using an excess of the other reagents (e.g. **9b**/BOP/HOBt in entries 11–13) scavenged the ammonia and afforded good yield of the desired product vis-à-vis the glycosylamine.

**Binding of the Probes to Galectins in a Fluorescence Polarization Assay.** The saccharide–fluorescein conjugates (**12–15c**) were used as probes to test their binding to galectins-1, -3, and -8N by fluorescence polarization (Figure 2). A fixed amount of probe (0.1  $\mu\text{M}$ ) was mixed with different concentrations of galectin ( $X$ -axis) and FP was measured ( $Y$ -axis). A rise in the FP values with increasing galectin concentration indicates binding since the bound probe gives a higher FP value. All the data points agreed well, when fit by nonlinear regression, to curves corresponding to a simple one to one galectin–probe interaction. The position of the curves along the  $X$ -axis represents the affinity with lower  $K_d$  values the further left the curve is. The approached maximum value correlates with the size of the protein–probe complex but is abrogated by independent movements of the fluorophore (propeller effects). Large differences in the binding ability of the different probes for the different galectins are apparent.

The best probes were found among the 5-carboxyfluorescein derivatives (**14a–c**) whereas the corresponding 6-carboxyfluorescein (**15a–c**) bound more poorly to all the galectins. However, significant binding of **15b** and **15c** to galectin-8N showed that also the 6-carboxyfluorescein derivatives can bind to the appropriate protein, and hence, their apparent total lack of binding to galectins-1 and -3 is maybe due to steric hindrance and/or propeller effects. This surprising finding is of great practical importance thus implicating the importance of using pure fluorescein isomers. If such a difference was present also in earlier studies where the mixed isomers have been used it might have confounded the results.

The tether length also greatly affected binding. Both probes with direct amide linkage to carboxyfluorescein (**12**, **13**) bound poorly to galectins-3 and -8N, apparently due to severe steric repulsions with the galectin CRDs. Compound **14a** with a glycine tether is the best probe for galectin-3, **14c** with GABA tether is preferred by

**Table 1. Conjugation of Lactosylamine 10 to Various Carboxyfluorescein Derivatives (acid) with Different Relative Amounts of Reagents <sup>a,b</sup>**

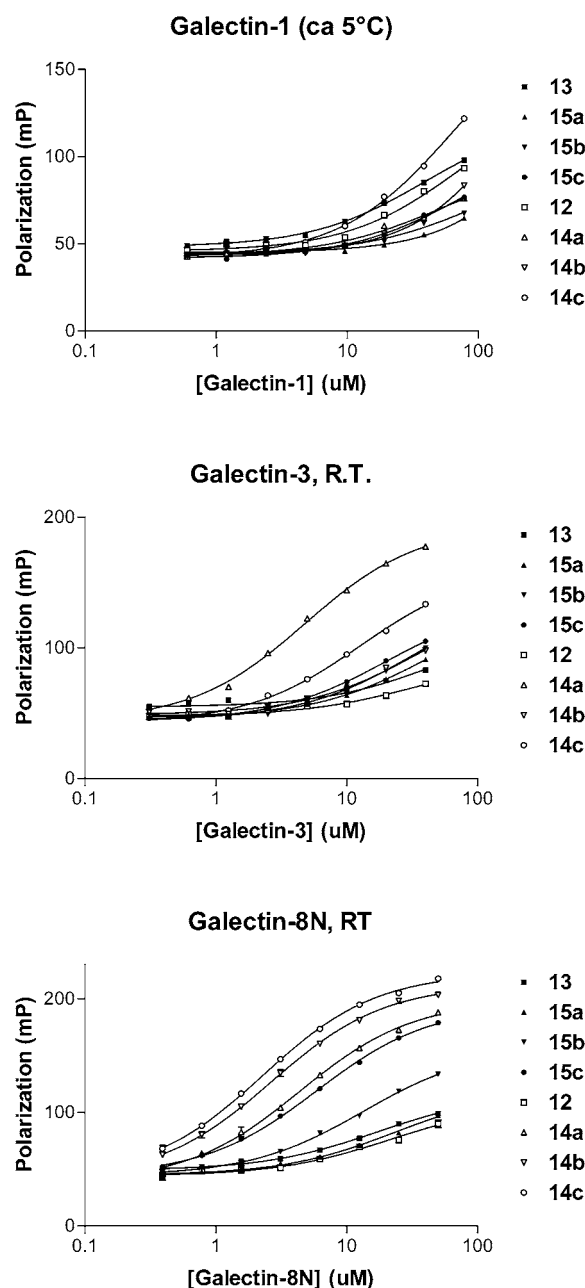
							
Entry	Acid. (eq.)	Product	Yield <sup>c</sup> (%)	Entry	Acid (eq.)	Product	Yield <sup>c</sup> (%)
1	<b>6</b> (2)	 <b>12</b>	24	8	<b>7</b> (2)	 <b>13</b>	32
2	<b>8a</b> (2)	 <b>14a</b>	34	9	<b>9a</b> (2)	 <b>15a</b>	38
3	<b>8b</b> (1)	 <b>14b</b>	46	10	<b>9b</b> (1)	 <b>15b</b>	<31
4	<b>8b</b> (2)	 <b>14b</b>	51	11	<b>9b</b> (2)	 <b>15b</b>	30
5	<b>8b</b> (4)	 <b>14b</b>	36	12	<b>9b</b> (4)	 <b>15b</b>	59
6	<b>8b</b> (8)	 <b>14b</b>	37	13	<b>9b</b> (8)	 <b>15b</b>	65
7	<b>8c</b> (2)	 <b>14c</b>	44	14	<b>9c</b> (2)	 <b>15c</b>	26

<sup>a</sup> Lactosylamine **10** (1 eq), acid ( $x$  equiv), BOP ( $x$  equiv), HOBT ( $x$  equiv), and DIPEA ( $2.5x$  equiv). Reaction 0.1 M (**10**) in Me<sub>2</sub>SO and stirred at room temperature for 2–12 h. <sup>b</sup> Capital T in top scheme represents the various tethers in the case of compounds **14a–c** and **15a–c** and a covalent bond for compounds **12** and **13**. <sup>c</sup> The yields are purified product as mol % of the crude **10/11** mixture.

galectin-1, and **14c** and **14b** (GABA and  $\beta$ -alanine tethers) are about equally good for galectin-8N.

**Application to Complex Saccharides.** To test our protocol on more complex, biologically interesting oligosaccharides, lacto-*N*-triose (LNT-2) and lacto-*N*-neo-

tetraose (LNT-3), were conjugated to structure **8a** to optimize for testing against galectin-3. In both cases 2 mg of oligosaccharide was reacted with 4 equiv of **8a** to result in 37% and 44% isolated yield of **16** and **17** (Figure 3), calculated on the reducing sugars. Thus, the fluores-



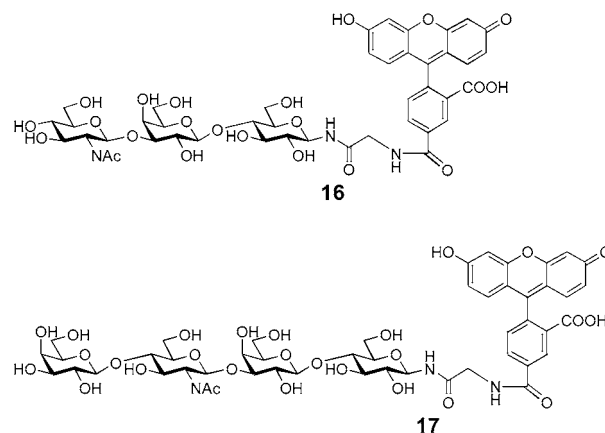
**Figure 2.** Binding curves of **12–15c** in the fluorescence polarization assay against galectins-1, -3, and -8N.

cein-labeling methodology optimized for lactose is clearly applicable on small amounts of larger and more complex oligosaccharides. Results from these and other labeled oligosaccharides in the fluorescence polarization assay will be reported elsewhere.

## CONCLUSION

The present results demonstrate a convergent procedure with a simple final step to conjugate different premade carboxyfluorescein derivatives to the reducing end of complex saccharides, available in limiting amounts, with conservation of the reducing sugar ring. The simplicity of our fluorescein-labeling procedure renders it ideal for use with small amounts of complex natural oligosaccharides.

The probes were shown to be applicable to probe galectin binding abilities in a FP assay. A dependence of



**Figure 3.** Fluorescent derivatives of LNT-2 and LNNt with tether optimized for galectin-3.

carboxyfluorescein isomer and tether length demonstrated the importance of selecting the optimal derivative for use with complex saccharides. The use of the same selected derivative with a large range of complex saccharides will create a probe library for defining lectin specificity. Even if the yields are only 30–50%, based on the saccharide, they are sufficient for generating useful amounts of probe even from small amounts of saccharide. This is because the FP assay is very sensitive; 1 mg probe suffices for about 50 000 assays with the 200  $\mu$ L assay volume used in this paper, and this can most likely be improved by minaturization.

We thank Angelina So, University of Waterloo, ON, Canada, and Alex Young, University of Toronto, ON, Canada, for HRMS analyses and Barbro Kahl-Knutsson, Lund University, for help with FP-analysis. E.F. thanks the Natural Science and Engineering Research Council of Canada and the University of Waterloo for financial support, and H.L. thanks the Swedish Research Council (grant 12165) for financial support. U.J.N. thanks the program “Glycoconjugates in Biological Systems” sponsored by the Swedish Strategic Research Foundation for financial support.

**Supporting Information Available:**  $^1\text{H}$  NMR spectra of compounds **2**, **6–9c**, **10/11**, **12–15c**, **16**, and **17**. This material is available free of charge via the Internet at <http://pubs.acs.org>.

## LITERATURE CITED

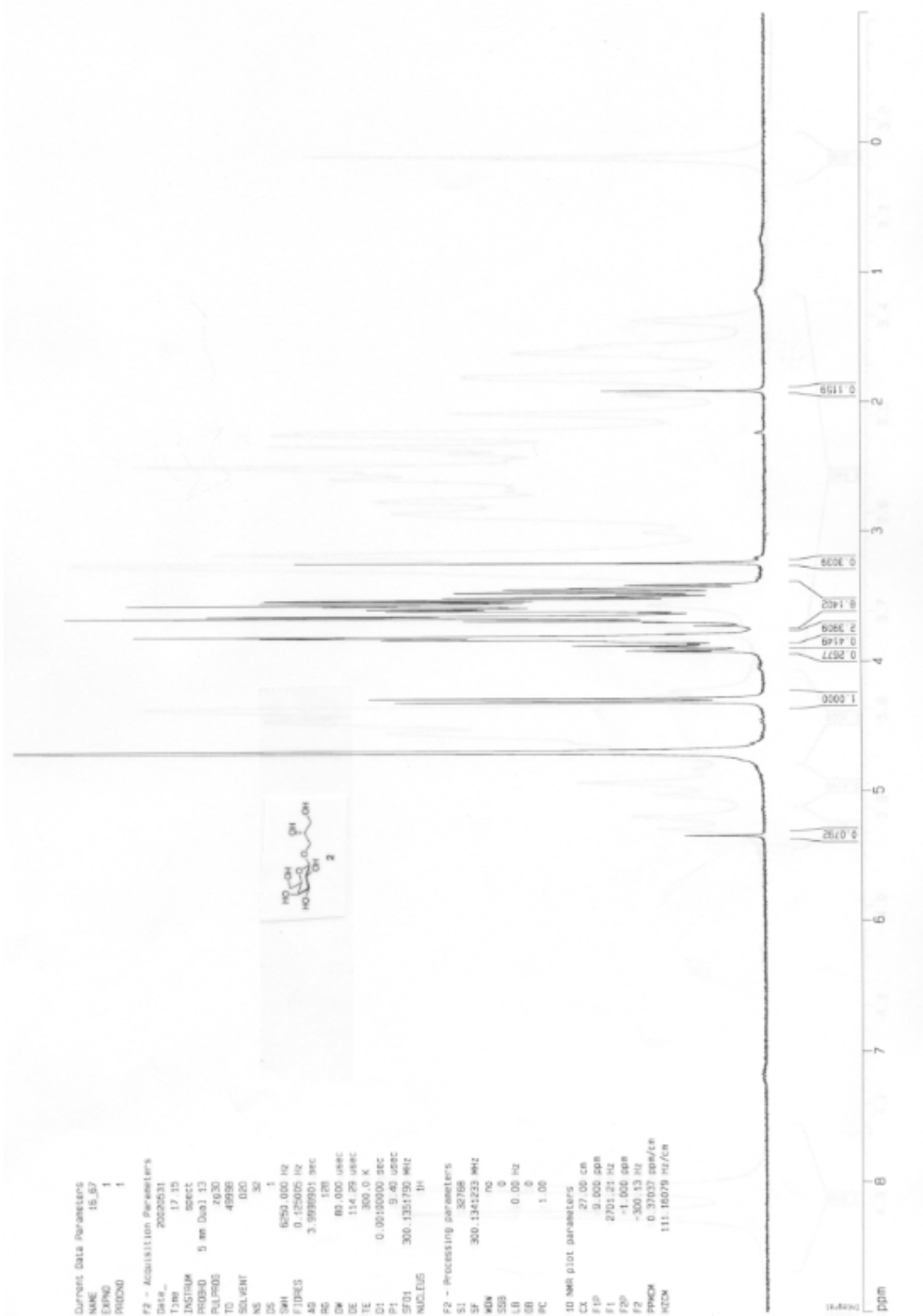
- (1) Cooper, D. N. W. (2002) Galectinomics: finding themes in complexity. *Biochem. Biophys. Acta* **1572**, 209–231.
- (2) Rabinovich, G. A., Rubinstein, N., and Fainboim, L. (2002) Unlocking the secrets of galectins: a challenge at the frontier of glyco-immunology. *J. Leukocyte Biol.* **71**, 741–752.
- (3) Rabinovich, G. A., Baum, L. G., Tinari, N., Paganelli, R., Natoli, C., Liu, F. T., and Iacobelli, S. (2002) Galectins and their ligands: amplifiers, silencers or tuners of the inflammatory response? *Trends Immunol.* **23**, 313–20.
- (4) Sörme, P., Qian Y., Nyholm, P., Leffler, H., and Nilsson, U. J. (2002) Low micromolar inhibitors of galectin-3 based on 3'-derivatization of *N*-acetylglucosamine. *ChemBioChem* **3**, 183–189.
- (5) Sörme, P., Kahl-Knutsson, B., Wellmar, U., Nilsson, U. J., and Leffler, H. (2003) Fluorescence polarization to study galectin-ligand interactions. *Methods Enzymol.* **362**, 504–512.
- (6) Lee, R. T., Ichikawa, Y., Allen, H. J., and Lee, Y. C. (1990) Binding characteristics of galactoside-binding lectin (galaptin) from human spleen. *J. Biol. Chem.* **265**, 7864–7871.
- (7) Barondes, S. H., Cooper, D. N. W., Gitt, M. A., and Leffler, H. (1994) Galectins. Structure and function of a large family of animal lectins. *J. Biol. Chem.* **269**, 20807–20810.

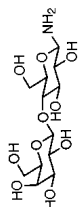


- (8) Rini, J. M., and Lobsanov, Y. D. (1999) New animal lectin structures. *Current Opin. Struct. Biol.* 9, 578–584.
- (9) Hirabayashi, J., Hashidate, T., Arata, Y., Nishi, N., Nakamura, T., Hirashima, M., Urashima, T., Oka, T., Futai, M., Muller, W. E. G., Yagi, F., and Kasai, K. (2002) Oligosaccharide specificity of galectins: a search by frontal affinity chromatography. *Biochim. Biophys. Acta* 1572, 232–254.
- (10) Lubineau, A., Augé J., and Drouillat, B. (1995) Improved synthesis of glycosylamines and a straightforward preparation of *N*-acylglycosylamines as carbohydrate-based detergents. *Carbohydr. Res.* 266, 211–219.
- (11) Miller, J. S., Dudkin, V. Y., Lyon, G. J., Muir, T. W., and Danishefsky, S. J. (2003) Toward fully synthetic *N*-linked glycoproteins. *Angew. Chem., Int. Ed.* 42, 431–434.
- (12) Rossi, M. R., Kao, J. P. Y. (1997) Practical Method for the Multigram Separation of the 5- and 6-Isomers of Carboxyfluorescein. *Bioconjugate Chem.* 8, 495–497.
- (13) Cooper, D. N., Massa, S. M., and Barondes, S. H. (1991) Endogenous muscle lectin inhibits myoblast adhesion to laminin. *J. Cell Biol.* 115, 1437.
- (14) Massa, S. M., Cooper, D. N., Leffler, H., and Barondes, S. H. (1993) L-29, an endogenous lectin, binds to glycoconjugate ligands with positive cooperativity. *Biochemistry* 32, 260.
- (15) Seetharaman, J., Kanigsberg, A., Slaaby, R., Leffler, H., Barondes, S. H., and Rini, J. M. (1998) X-ray crystal structure of the human galectin-3 carbohydrate recognition domain at 2.1-Å resolution. *J. Biol. Chem.* 273, 13047–13052.
- (16) Leffler, H., and Barondes, S. H. (1986) Specificity of binding of three soluble rat lung lectins to substituted and unsubstituted mammalian  $\beta$ -galactosides. *J. Biol. Chem.* 261, 10119–10126.
- (17) Nasir, M. S., Jollei, M. E. (1999) Fluorescence polarization, an analytical tool for immunoassay and drug discovery. *Comb. Chem. High Throughput Screening* 2, 177–190.
- (18) Two numbering schemes exist for naming carboxyfluorescein: One scheme is based on the lactone form of fluorescein where the spiro center is position 1 (adopted here). The second scheme is based on the ring open, free dicarboxylic acid, form in which the phenyl's point of attachment to the xanthene moiety is position 1.
- (19) Ajtai, K., Ringler, D., Toft, D., Hellen, E. H., Ilich, P. J., and Burghardt, T. P. (1992) Stereospecific reaction of muscle fiber proteins with the 5' or 6' iodoacetamido derivative of tetramethylrhodamine: Only the 6' isomer is mobile on the surface of S1. *Biophys. J.* 61, A287, Abstract 1647.
- (20) Buolamwini, J. K., Craik, J. D., Wiley, J. S., Robins, M. J., Gati, W. P., Cass, C. E., and Paterson, A. R. P. (1994) Conjugates of fluorescein and SAENTA (5'-*S*-(2-aminoethyl)-N<sup>6</sup>-(4-nitrobenzyl)-5'-thioadenosine): flow cytometry probes for the ES nucleoside transport elements of the plasma membrane. *Nucleosides Nucleotides* 13, 737–751.
- (21) Molecular Probes, Eugene, OR.
- (22) Chen, C., and Poenie, M. (1993) New Fluorescent Probes for Protein Kinase C. *J. Biol. Chem.* 268, 15812–15822.
- (23) The BOP reagent gives the cancer suspect/confirm HMPA as a byproduct; suitable protection is advisable. PyBOP has been developed as replacement for BOP, exhibiting similar function but without HMPA as byproduct.

BC034130J

## Supporting Information





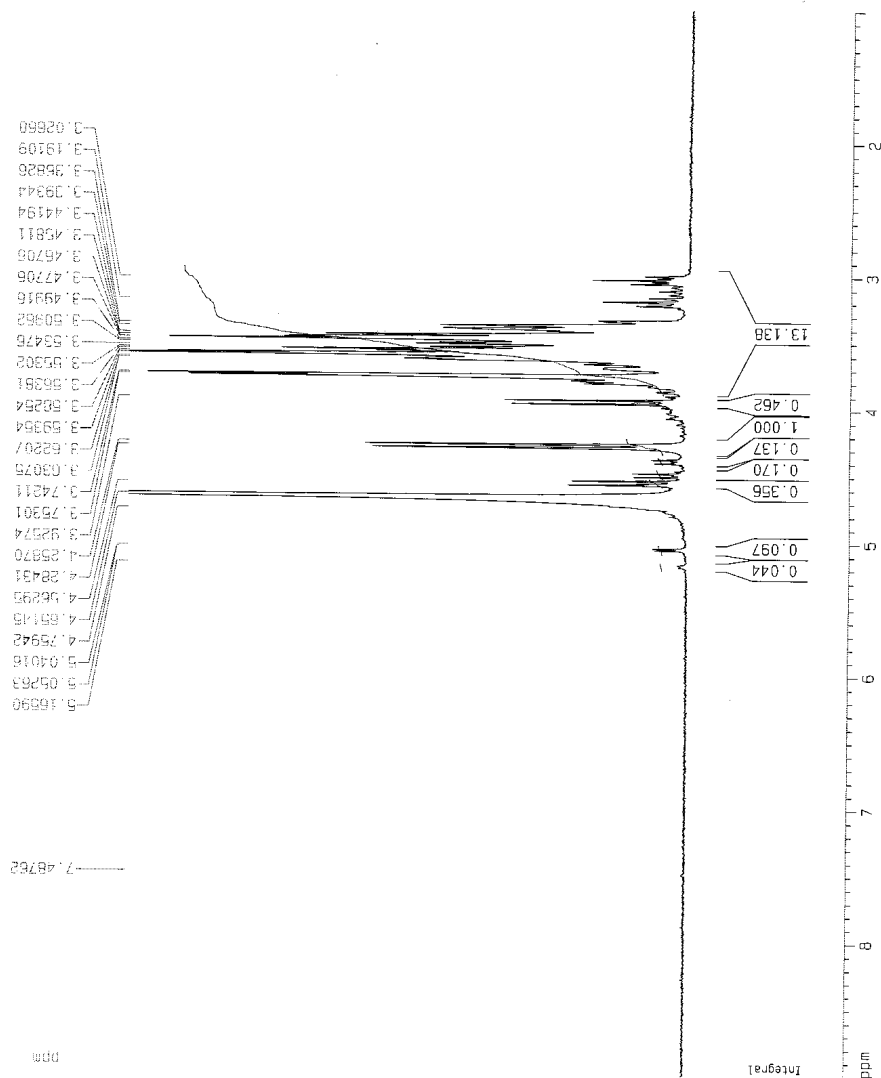
Current Data Parameters  
 NAME C015  
 EXPNO 1  
 PROCNO 1

F2 - Acquisition Parameters  
 Date\_ 20030108  
 Time 13.13  
 INSTRUM Avance300  
 PROBHD 5 mm QNP 1H/1  
 PULPROG zg30  
 TO 16384  
 SOLVENT CDCl3  
 NS 16  
 DS 2  
 SWH 4006.410 Hz  
 FIDRES 0.244532 Hz  
 AQ 2.044731 sec  
 RG 352  
 DW 124.800 usec  
 DE 6.00 usec  
 TE 300.0 K  
 D1 1.00000000 sec

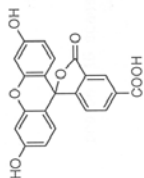
===== CHANNEL f1 =====  
 NUC1 1H  
 P1 12.00 usec  
 PL1 0.00 dB  
 SFO1 300.1318044 MHz

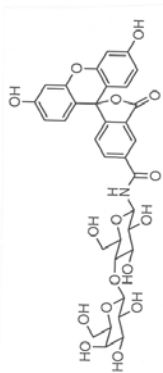
F2 - Processing parameters  
 SI 8192  
 SF 300.1300124 MHz  
 WDW EM  
 SSB 0  
 LB 0.30 Hz  
 GB 0  
 PC 1.00

1D NMR plot parameters  
 CX 20.00 cm  
 C1 194.24 cm  
 F1P 9.000 bpm  
 F1 2701.17 Hz  
 F2P 1.000 ppm  
 F2 300.13 Hz  
 PPMCM 0.40000 ppm/cm  
 HZCM 120.05200 Hz/cm

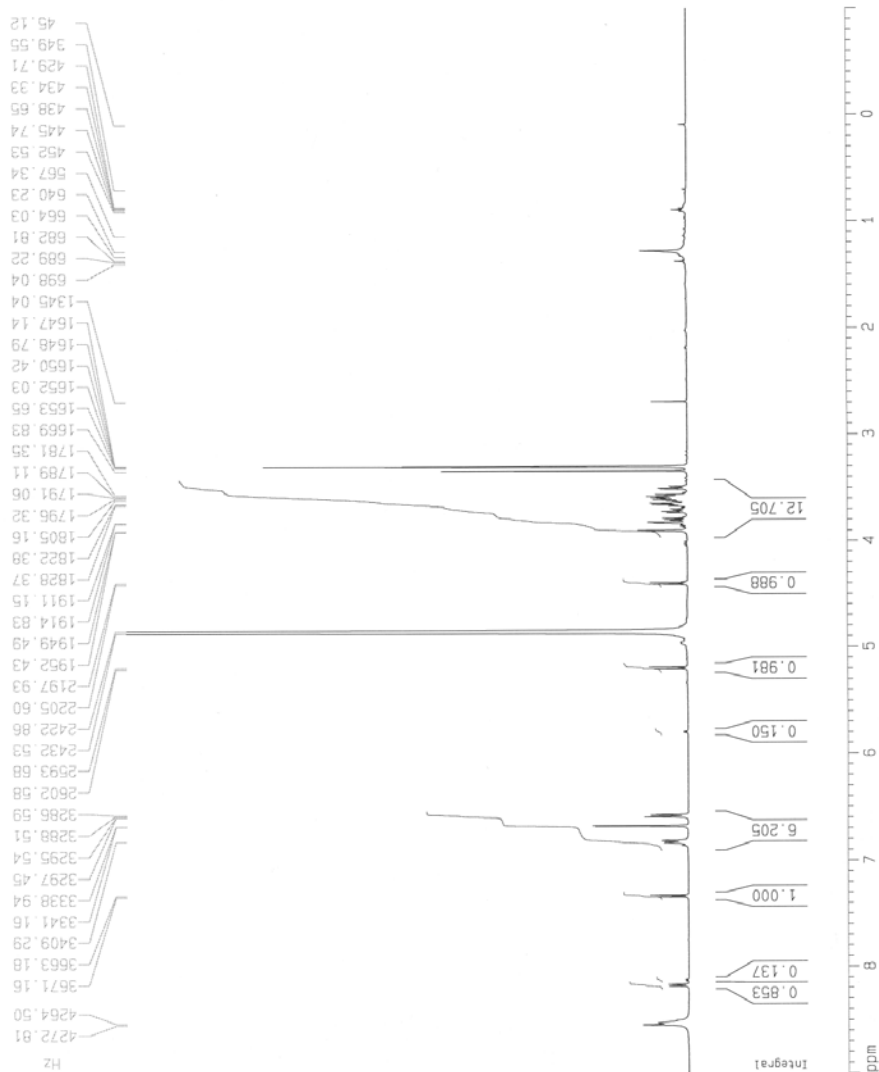




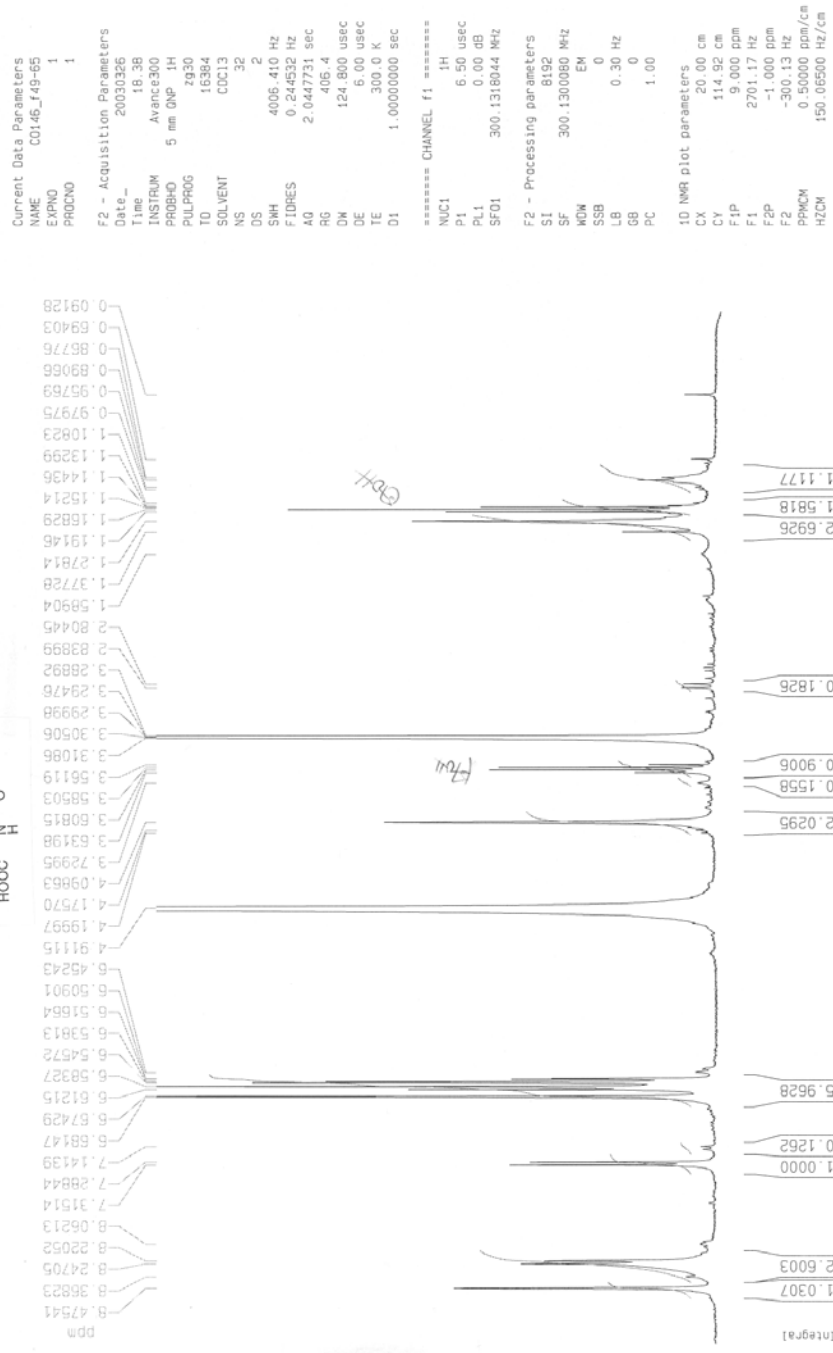
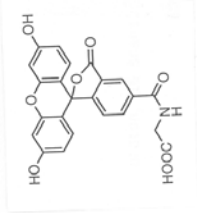




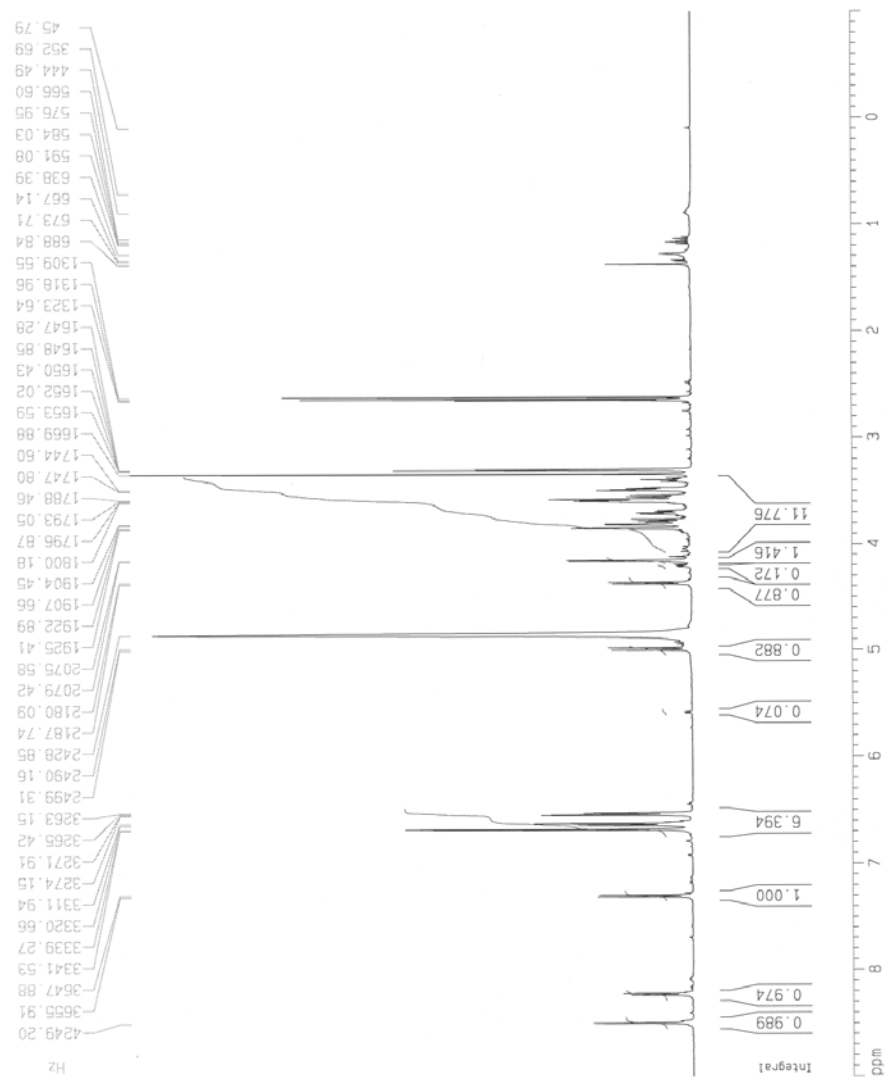
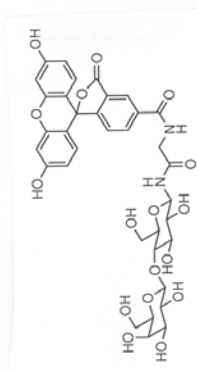
Current Data Parameters  
NAME C0157500 C0150-300  
EXPNO 1  
PROCNO 1  
F2 - Acquisition Parameters  
Date\_ 20030419  
Time 19.02  
INSTRUM drx500  
PROBHD 5 mm BBI 1H-BB  
PULPROG zg30  
TD 65536  
SOLVENT CDCl3  
NS 32  
DS 2  
SWH 10330.578 Hz  
FIDRES 0.157632 Hz  
AQ 3.1720407 sec  
RG 181  
DE 48.400 usec  
TE 300.0 K  
D1 1.00000000 sec  
===== CHANNEL f1 =====  
NUC1 1H  
P1 7.00 usec  
PL1 -3.00 dB  
SFO1 500.130085 MHz  
F2 - Processing parameters  
SI 32768  
SF 500.1300159 MHz  
WDW EM  
SSB 0  
LB 0.30 Hz  
GB 0  
PC 1.00  
1D NMR plot parameters  
CX 20.00 cm  
CY 12.50 cm  
FIP 9.000 ppm  
F1 4501.17 Hz  
F2 -1.000 ppm  
F2 -500.13 Hz  
PPMCM 0.50000 ppm/cm  
HZCM 250.06500 Hz/cm



⑤







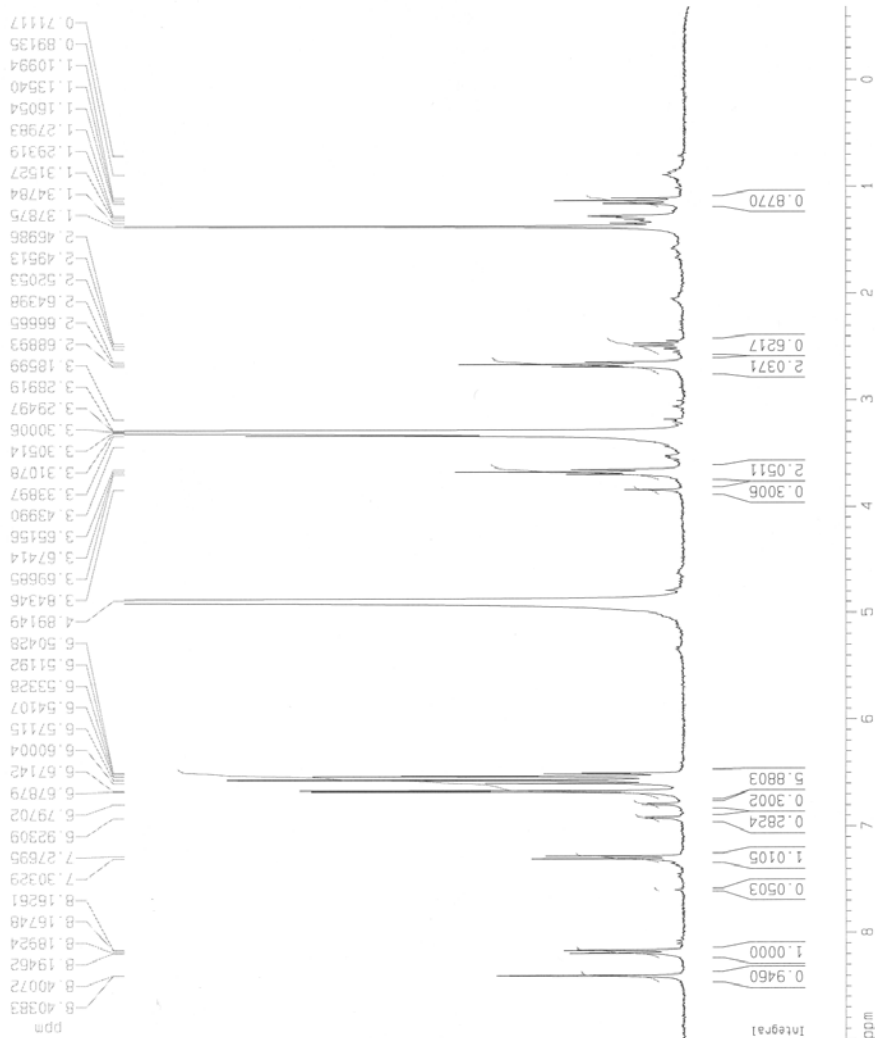
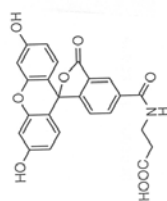
Current Data Parameters  
 NAME C0157\_500actual  
 EXPNO 1  
 PROCNO 1

F2 - Acquisition Parameters  
 Date\_ 20030419  
 Time 22.09  
 INSTRUM gn-500  
 PROBHD 5 mm BBI 1H-8B  
 PULPROG zg30  
 TD 65536  
 SOLVENT CCl3  
 NS 32  
 DS 2  
 SWH 10330.578 Hz  
 FIDRES 0.157632 Hz  
 AQ 3.1720407 sec  
 RG 128  
 DW 48.400 usec  
 DE 6.00 usec  
 TE 300.0 K  
 D1 1.00000000 sec

\*\*\*\*\* CHANNEL f1 \*\*\*\*\*  
 NUC1 1H  
 P1 7.00 usec  
 PL1 -3.00 dB  
 SFO1 500.1330885 MHz

F2 - Processing parameters  
 SI 32768  
 SF 500.1300159 MHz  
 MDW EM  
 SSB 0  
 LB 0.30 Hz  
 GB 0  
 PC 1.00

1D NMR plot parameters  
 CX 20.00 cm  
 CY 12.50 cm  
 FIP 9.000 ppm  
 F1 4501.17 Hz  
 F2P -1.000 ppm  
 F2 -500.13 Hz  
 PPMCM 0.50000 ppm/cm  
 HZCM 250.06500 Hz/cm



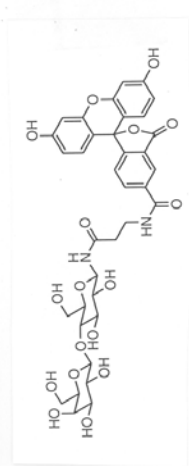
Current Data Parameters  
 NAME CO149\_2nd  
 EXPNO 1  
 PROCNO 1

F2 - Acquisition Parameters  
 Date\_ 20030403  
 Time 14.42  
 INSTRUM Avance300  
 PROBHD 5 mm QNP 1H  
 PULPROG zg30  
 TO 16364  
 SOLVENT CDCl3  
 NS 48  
 DS 2  
 SWH 4006.410 Hz  
 FIDRES 0.244532 Hz  
 AQ 2.0447731 sec  
 RG 724.1  
 DM 124.800 usec  
 DE 6.00 usec  
 TE 300.0 K  
 D1 1.00000000 sec

\*\*\*\*\* CHANNEL f1 \*\*\*\*\*  
 NUC1 1H  
 P1 6.50 usec  
 PL1 0.00 dB  
 SFO1 300.1318044 MHz

F2 - Processing parameters  
 SI 8192  
 SF 300.1300080 MHz  
 MDW EM  
 SSB 0  
 LB 0.30 Hz  
 GB 0  
 PC 1.00

1D NMR plot parameters  
 CX 20.00 cm  
 CY 143.09 cm  
 FIP 9.000 ppm  
 F1 2701.17 Hz  
 F2P -1.000 ppm  
 F2 -300.13 Hz  
 PPMCM 0.50000 ppm/cm  
 HZCM 150.06500 Hz/cm



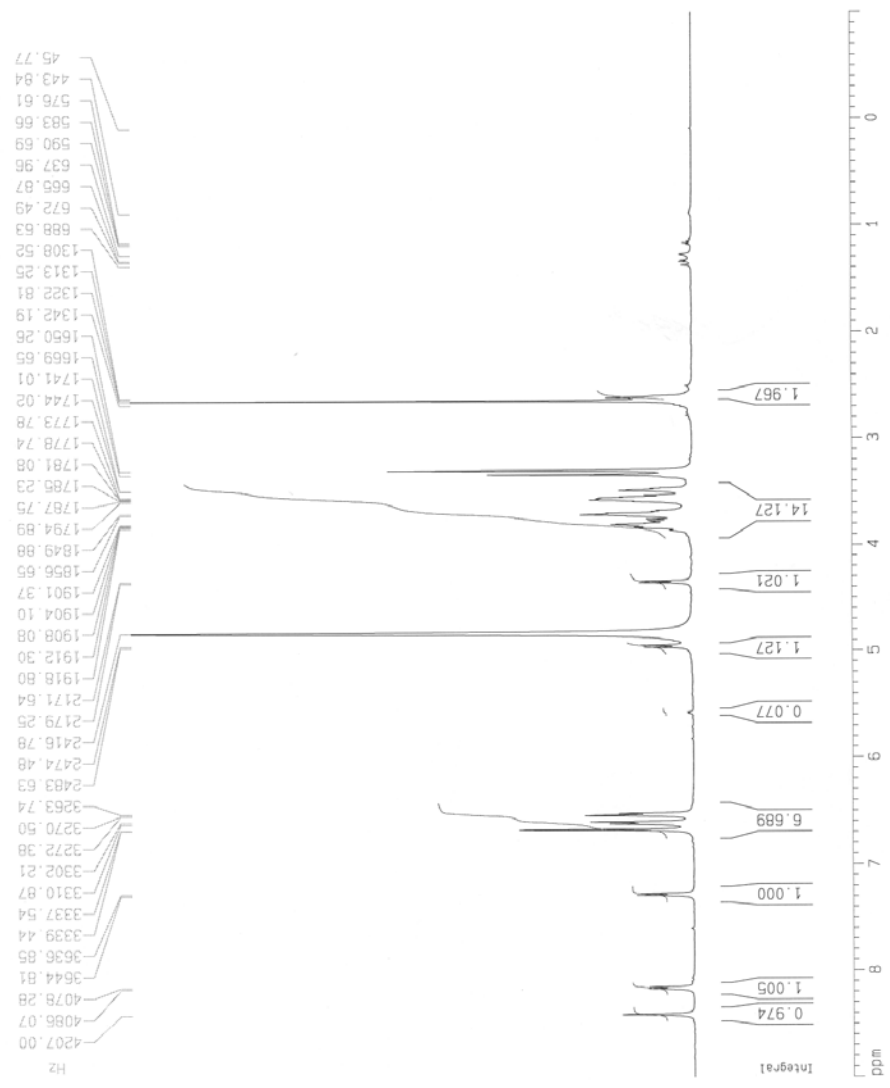
Current Data Parameters  
NAME C0152\_500  
EXPNO 1  
PROCNO 1

F2 - Acquisition Parameters  
Date\_ 20030419  
Time 21.56  
INSTRUM drx500  
PROBHD 5 mm BBI 1H-50  
PULPROG zgpg30  
TD 65536  
SOLVENT COC13  
NS 32  
DS 2  
SWH 10330.578 Hz  
FIDRES 0.157632 Hz  
AQ 3.1720407 sec  
RG 90.5  
DN 48.400 usec  
DE 6.00 usec  
TE 300.0 K  
D1 1.00000000 sec

===== CHANNEL f1 =====  
NUC1 1H  
P1 7.00 usec  
PL1 -3.00 dB  
SF01 500.1330885 MHz

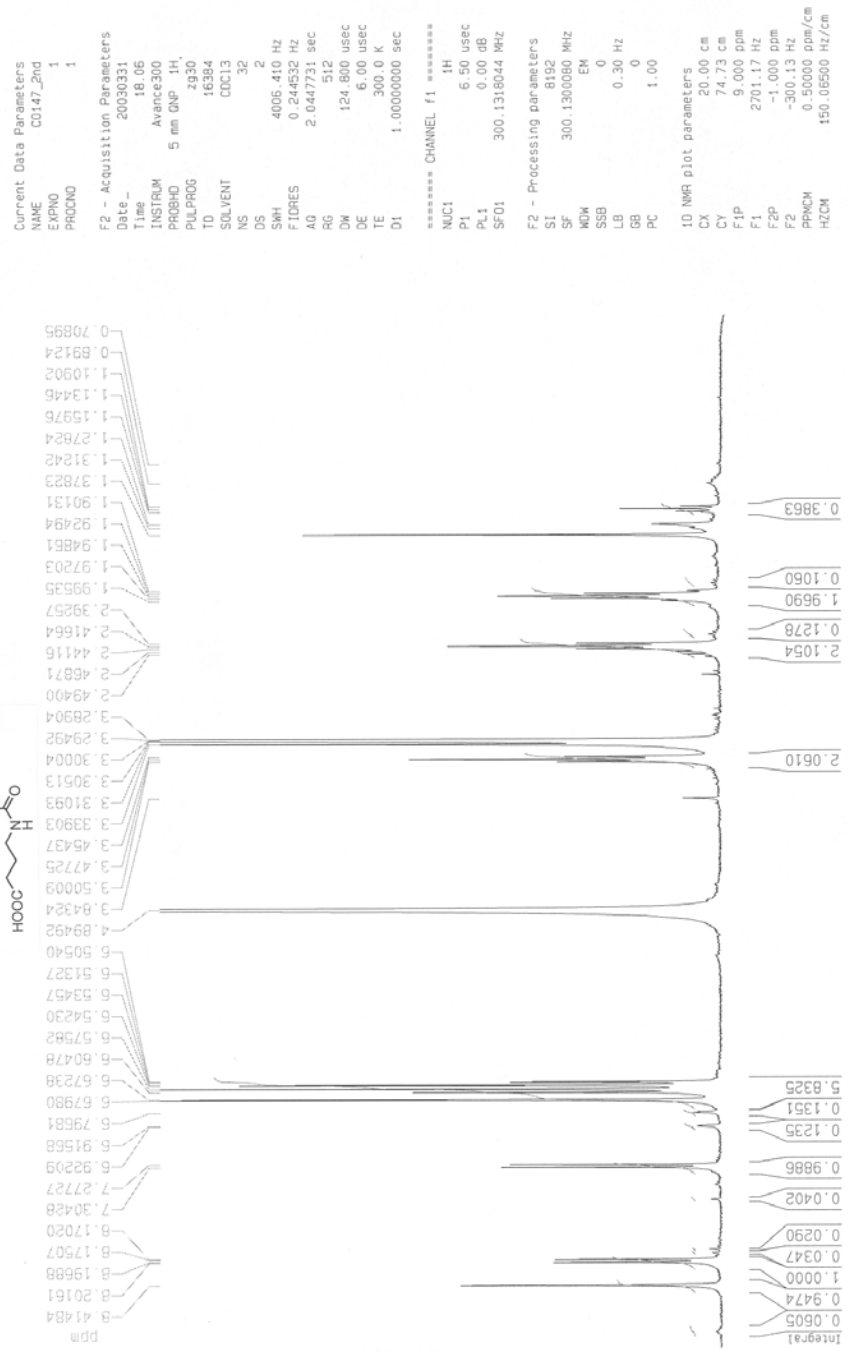
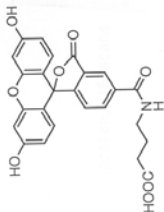
F2 - Processing parameters  
SI 32768  
SF 500.1300159 MHz  
WDW EM  
SSB 0  
LB 0.30 Hz  
GB 0  
PC 1.00

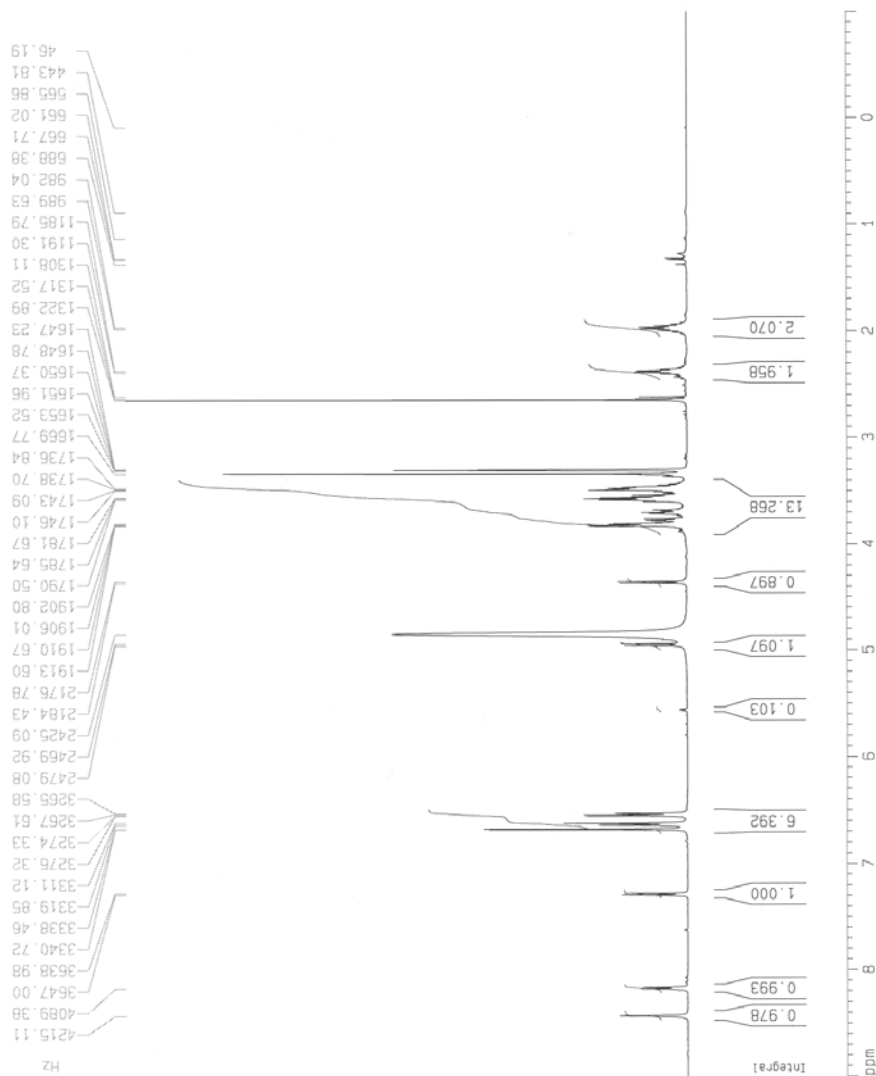
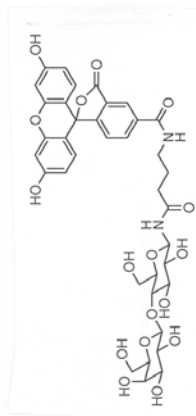
1D NMR plot parameters  
CX 20.00 cm  
CY 12.50 cm  
FIP 9.000 ppm  
F1 4501.17 Hz  
F2P -1.000 ppm  
F2 -500.13 Hz  
PPMCM 0.50000 ppm/cm  
HZCM 250.06500 Hz/cm





25





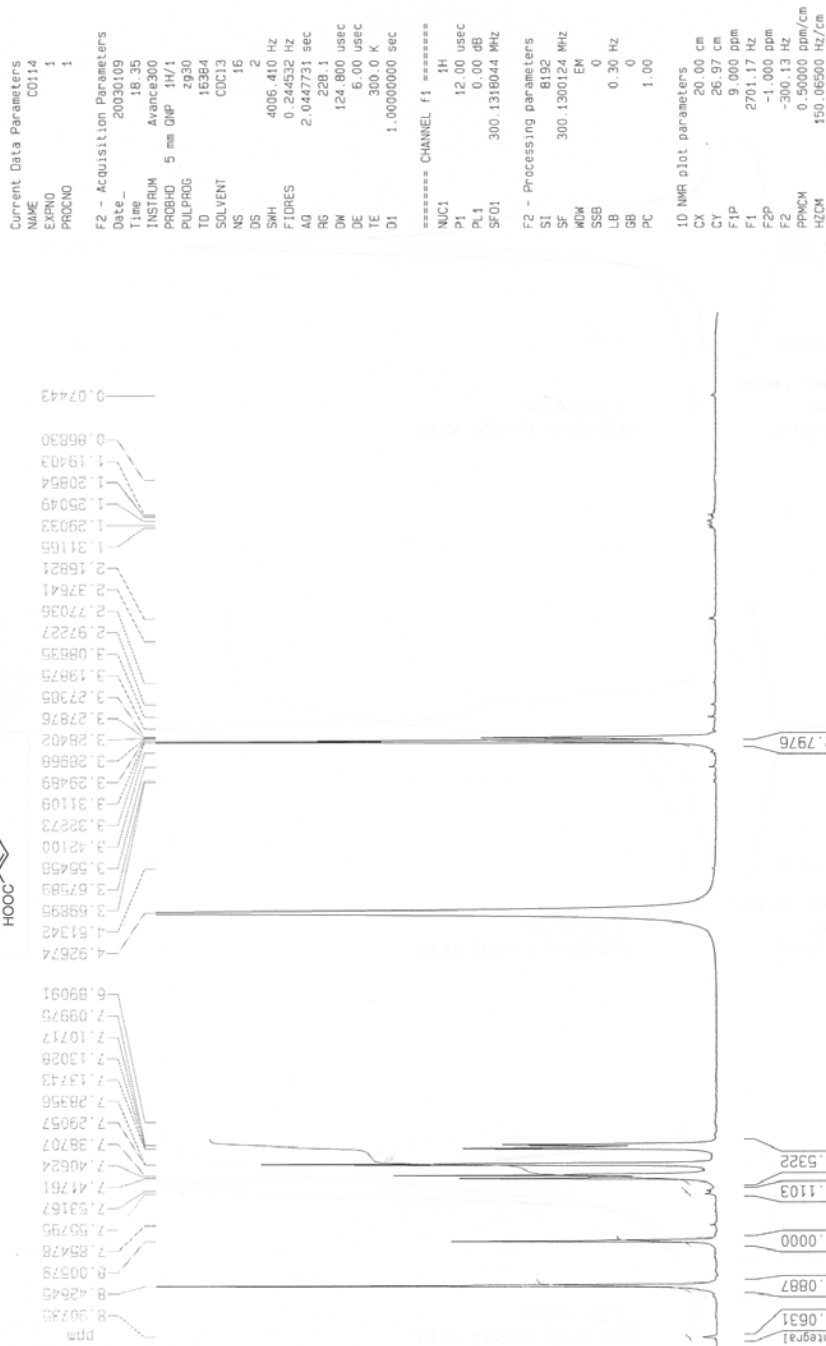
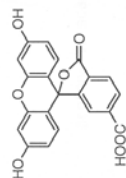
Current Data Parameters  
NAME C0153\_500  
EXPNO 1  
PROCNO 1

F2 - Acquisition Parameters  
Date\_ 20030419  
Time 21.46  
INSTRUM dfx500  
PROBHD 5 mm BBI 1H-BB  
PULPROG zg30  
TD 65536  
SOLVENT CDCl3  
NS 32  
DS 2  
SWH 10330.578 Hz  
FIDRES 0.157632 Hz  
AQ 3.1720407 sec  
RG 101.6  
DM 48.400 usec  
DE 6.00 usec  
TE 300.0 K  
D1 1.00000000 sec

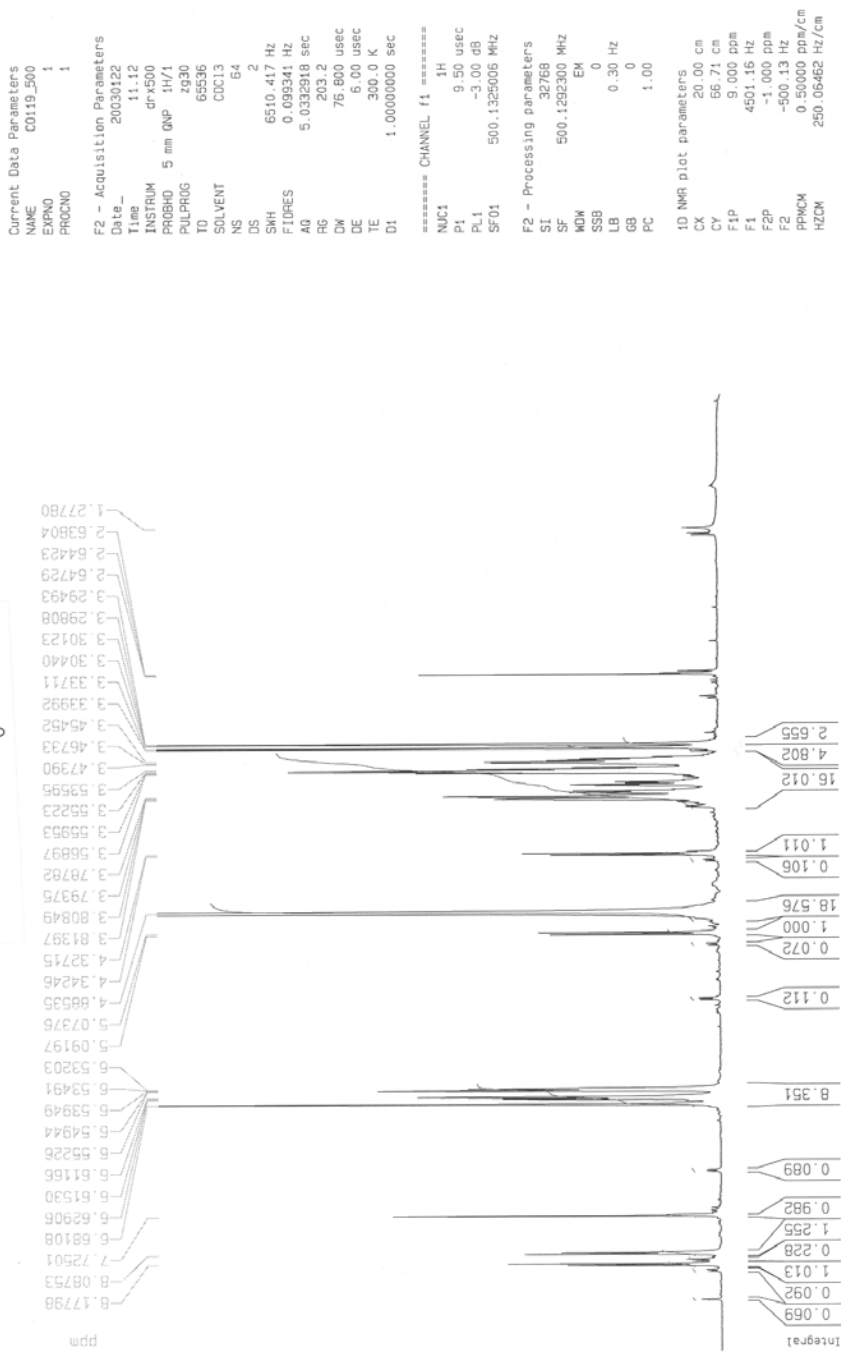
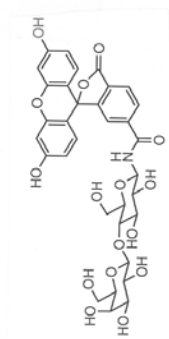
===== CHANNEL f1 =====  
NUC1 1H  
P1 7.00 usec  
PL1 -3.00 dB  
SFO1 500.1300885 MHz

F2 - Processing parameters  
SI 32768  
SF 500.1300159 MHz  
WDW EM  
SSB 0  
LB 0.30 Hz  
GB 0  
PC 1.00

1D NMR plot parameters  
CX 20.00 cm  
CY 12.50 cm  
F1P 9.000 ppm  
F1 4501.17 Hz  
F2P -1.000 ppm  
F2 -500.13 Hz  
PPMCM 0.50000 ppm/cm  
HZCM 250.06500 Hz/cm

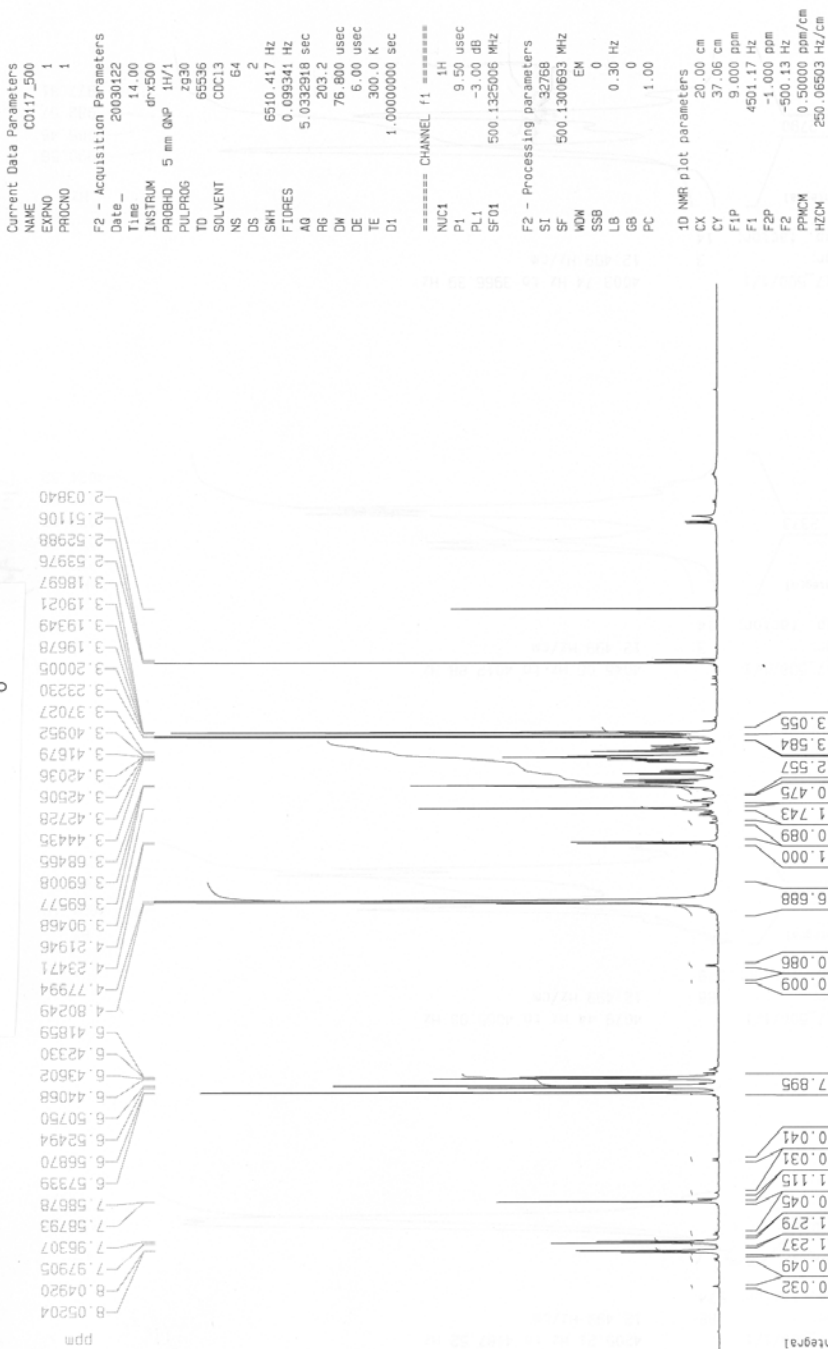
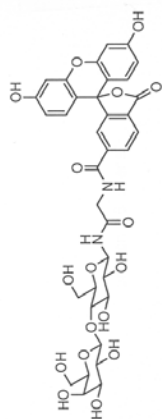




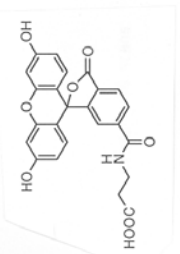


proton, 15 scans









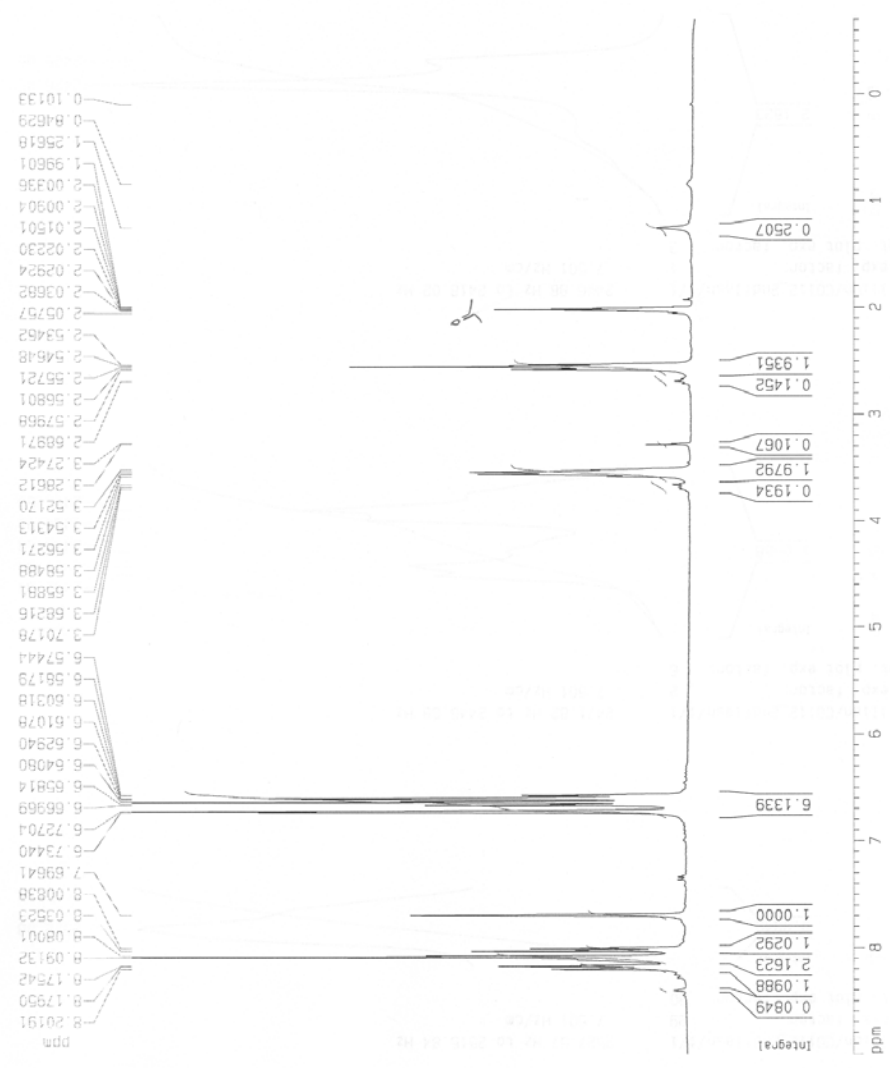
Current Data Parameters  
 NAME C0112\_2ndflash  
 EXPNO 1  
 PROCNO 1

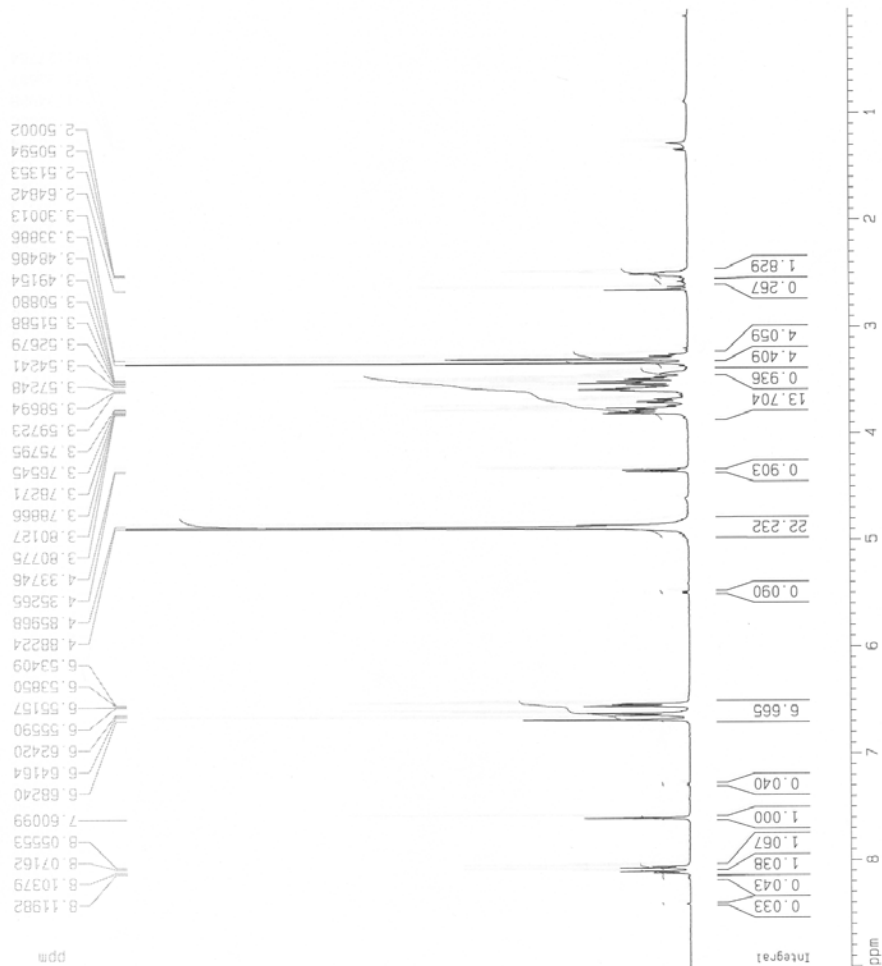
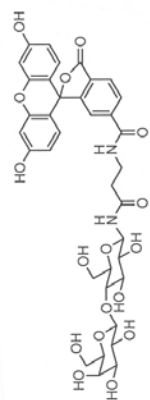
F2 - Acquisition Parameters  
 Date\_ 20030109  
 Time 18.45  
 INSTRUM Avance300  
 PROBHD 5 mm GNP 1H/1  
 PULPROG zg30  
 TO 16384  
 SOLVENT ~~CDCl3~~ *acetone*  
 NS 16  
 DS 2  
 SWH 4006.410 Hz  
 FIDRES 0.244532 Hz  
 AQ 2.0447731 sec  
 RG 228.1  
 DM 124.800 usec  
 DE 6.00 usec  
 TE 300.0 K  
 D1 1.00000000 sec

\*\*\*\*\* CHANNEL f1 \*\*\*\*\*  
 NUC1 1H  
 P1 12.00 usec  
 PL1 0.00 dB  
 SF01 300.1318044 MHz

F2 - Processing parameters  
 SI 8192  
 SF 300.1300124 MHz  
 WDW EM  
 SSB 0  
 LB 0.30 Hz  
 GB 0  
 PC 1.00

10 NMR plot parameters  
 CX 20.00 cm  
 CY 12.04 cm  
 F1P 9.000 ppm  
 F1 2701.17 Hz  
 F2P -1.000 ppm  
 F2 -300.13 Hz  
 PPMCM 0.50000 ppm/cm  
 HZCM 150.06500 Hz/cm





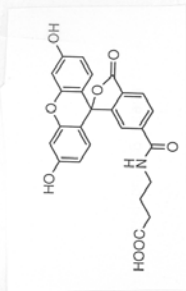
Current Data Parameters  
NAME C0118\_500  
EXPNO 1  
PROCNO 1

F2 - Acquisition Parameters  
Date\_ 20030122  
Time 10.47  
INSTRUM dr-500  
PROBHD 5 mm QNP 1H/1  
PULPROG zg30  
TD 65536  
SOLVENT MeOH  
NS 67  
DS 2  
SWH 6510.417 Hz  
FIDRES 0.098341 Hz  
AQ 5.0332918 sec  
RG 228.1  
DM 76.800 usec  
DE 6.00 usec  
TE 300.0 K  
D1 1.00000000 sec

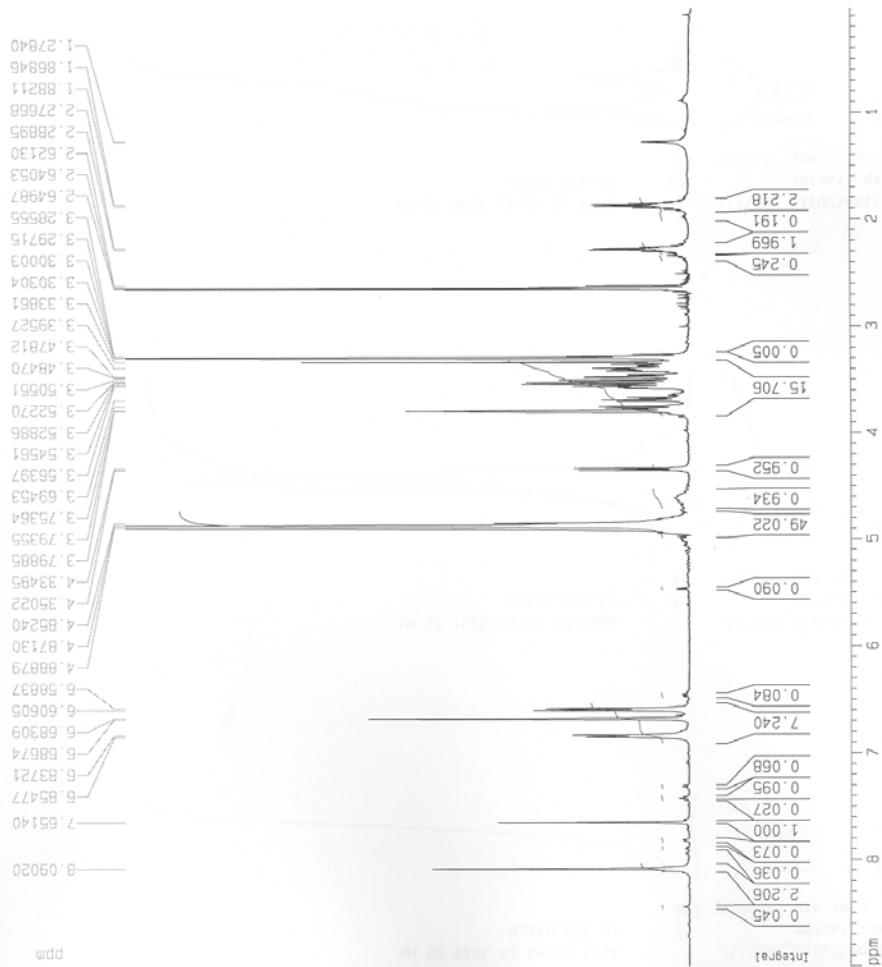
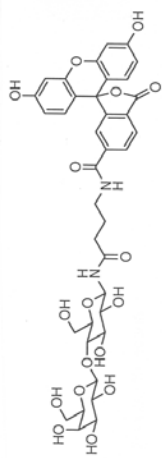
\*\*\*\*\* CHANNEL f1 \*\*\*\*\*  
NUC1 1H  
P1 9.50 usec  
PL1 -3.00 dB  
SF01 500.1325006 MHz

F2 - Processing parameters  
SI 32768  
SF 500.1292318 MHz  
WDW EM  
SSB 0  
LB 0.30 Hz  
GB 0  
PC 1.00

1D NMR plot parameters  
CX 20.00 cm  
CY 28.11 cm  
FIP 9.000 ppm  
F1 4501.16 Hz  
F2P -1.000 ppm  
F2 -500.13 Hz  
PPMCM 0.50000 ppm/cm  
HZCM 250.06462 Hz/cm







Current Data Parameters  
NAME C0116\_500  
EXPNO 1  
PROCNO 1

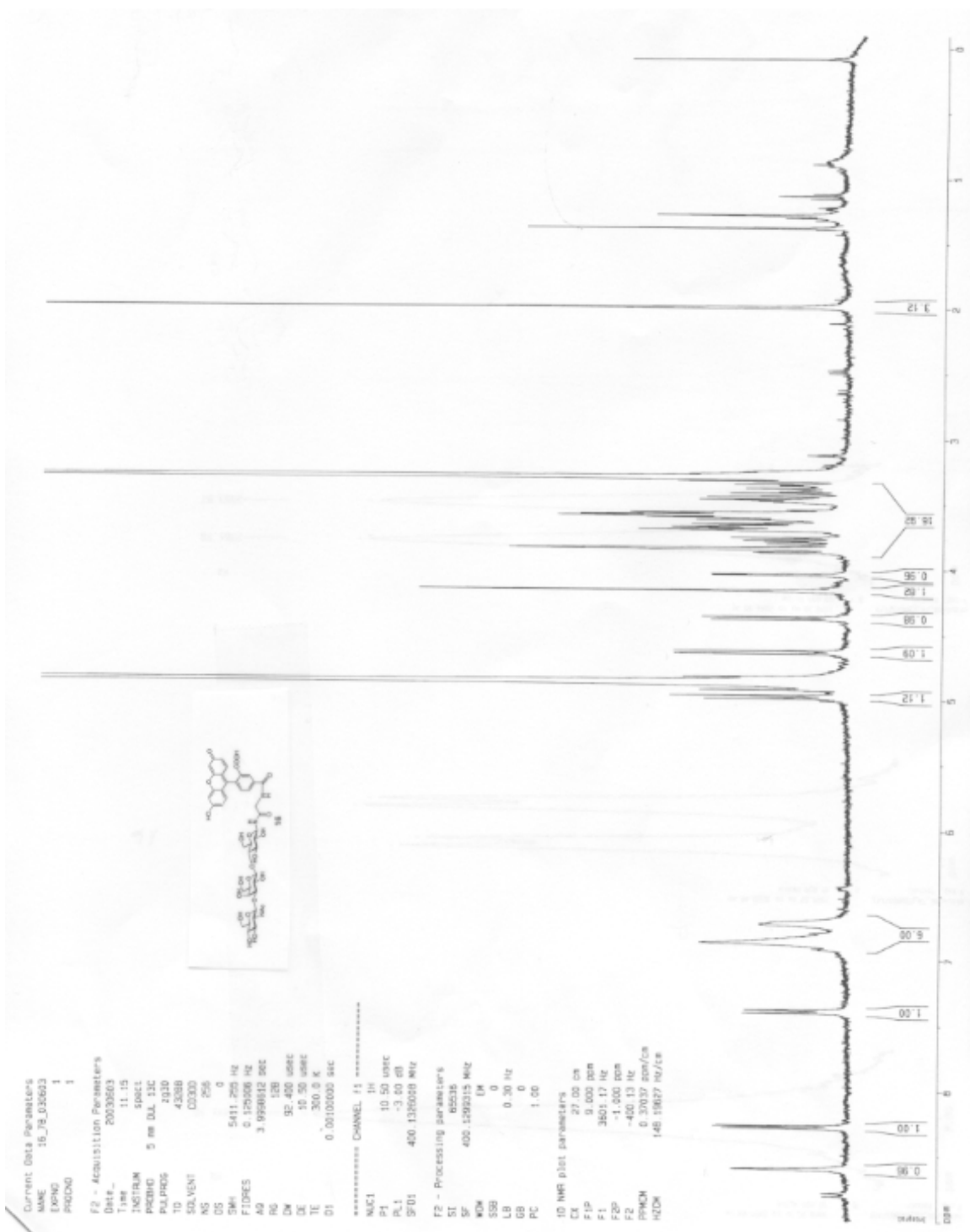
F2 - Acquisition Parameters  
Date\_ 20030122  
Time 14.19  
INSTRUM drx500  
PROBHD 5 mm QNP 1H/1  
PULPROG zgpg30  
TD 65536  
SOLVENT DMSO  
NS 64  
DS 2  
SMH 6510.417 Hz  
FIDRES 0.099341 Hz  
AQ 5.032918 sec  
RG 228.1  
DM 76.800 usec  
DE 6.00 usec  
TE 300.0 K  
D1 1.00000000 sec

===== CHANNEL f1 =====  
NUC1 1H  
P1 9.50 usec  
PL1 -3.00 dB  
SFO1 500.1325006 MHz

F2 - Processing parameters  
SI 32768  
SF 500.1292312 MHz  
WDW EM  
SSB 0  
LB 0.30 Hz  
GB 0  
PC 1.00

1D NMR plot parameters  
CX 20.00 cm  
CY 121.89 cm  
FIP 9.000 ppm  
F1 4501.16 Hz  
F2 -1.000 ppm  
F2 -500.13 Hz  
PPMCM 0.50000 ppm/cm  
HZCM 250.06462 Hz/cm







# Aryldiazomethanes for Universal Labeling of Nucleic Acids and Analysis on DNA Chips

Ali Laayoun,<sup>\*,†</sup> Mitsuharu Kotera,<sup>\*,‡</sup> Isabelle Sothier,<sup>†</sup> Emmanuelle Trévisiol,<sup>‡</sup> Eloy Bernal-Méndez,<sup>†</sup> Cécile Bourget,<sup>‡</sup> Lionel Menou,<sup>†</sup> Jean Lhomme,<sup>‡</sup> and Alain Troesch<sup>†</sup>

BioMérieux, Advanced Technology/Molecular Diagnostics, Chemin de l'Orme - 69280 Marcy l'Etoile, France, and LEDSS, UMR5616 CNRS - BP53, Université Joseph Fourier, 38041 Grenoble, France. Received July 31, 2003; Revised Manuscript Received October 3, 2003

DNA and RNA labeling and detection are key steps in nucleic acid-based technologies, used in medical research and molecular diagnostics. We report here the synthesis, reactivity, and potential of a new type of labeling molecule, *m*-(*N*-Biotinoylamino)phenylmethyldiazomethane (*m*-BioPMDAM), that reacts selectively and efficiently with phosphates in nucleotide monomers, oligonucleotides, DNA, and RNA. This molecule contains a biotin as detectable unit and a diazomethyl function as reactive moiety. We demonstrate that this label fulfills the requirements of stability, solubility, reactivity, and selectivity for hybridization-based analysis and especially for detection on high-density DNA chips.

## INTRODUCTION

In recent years, a vast amount of genetic information has been obtained from numerous genome sequencing projects. The availability of these data has boosted the development and use of nucleic acid-based technologies in biomedical research and in vitro diagnostics to identify and quantify organisms that are present in biological samples, study genome expression levels, and detect genetic mutations and polymorphisms.

A typical nucleic acid-based assay usually comprises different steps, i.e., target isolation, enzymatic amplification, and detection by hybridization onto specific complementary probe(s). The analysis of target/probe hybrids is a key step in this process and generally requires the use of reporter molecules to specifically label the nucleic acids. Depending on the test format, those reporter molecules are incorporated either in the target (during the enzymatic amplification or postsynthesis) or in the detection probes. It is essential that these labeling methods do not disrupt the base pairing capability which is critical for preserving specificity during enzymatic incorporation and the subsequent hybridization detection step. This requirement is particularly important for microarrays or DNA chips, which represent one of the most promising methods for assessing genetic diversity at a large scale and a high resolution. This technology is based on the hybridization of labeled nucleic acid targets onto large sets of oligonucleotide probes (1, 2). Enzymatic incorporation of the label, either during target amplification or postsynthetically, represents the most widely used labeling method in DNA chip analysis (3–5) but presents some drawbacks. The amplified product may become altered in the presence of modified, labeled nucleotides. Also, postsynthetic labeling methods make use of ad-

ditional enzymatic steps which require precise calibration of the enzyme activity to achieve a reproducible labeling yield. Moreover, because the enzymes used depend on the target type (DNA or RNA), no specific method is universally applicable to all nucleic acids. A more convenient alternative is to label the target chemically and a variety of chemical methods for direct modification and derivatization of nucleic acids with functional groups have been proposed (6–10). Chemical labeling generally occurs at the bases, thereby altering the hybridization properties.

We have previously described a strategy for labeling RNA molecules on their terminal phosphate (11, 12). This chemical labeling takes advantage of the fragmentation step, which is required for the hybridization to high-density DNA chips (3), to attach the reporter molecule 5-(bromomethyl)fluorescein (5-BMF) to the 3'-phosphate of cleaved RNA fragments. In our model experiments, we reported higher labeling densities than with enzymatic incorporation of labeled ribonucleotides (11). The hybridization efficiency was shown to be preserved, but labeling yields on single- and double-stranded DNA were poor (13). We now report a new type of labeling reagent, *m*-BioPMDAM (3) (*m*-(*N*-Biotinoylamino)phenylmethyldiazomethane), that selectively and more efficiently reacts on the phosphates of nucleic acid sequences. The molecule includes in its structure a biotin unit covalently linked to the reactive phenyldiazomethane moiety. Its synthesis is described. In a model study we show that *m*-BioPMDAM reacts selectively on the phosphate of a series of 3'-nucleotide monophosphates, and it can be used to label oligonucleotides and long DNA and RNA sequences, prior to their analysis on high-density DNA chips.

## EXPERIMENTAL PROCEDURES

All commercially available chemical reagents and solvents were used without purification. D-biotin was purchased from Lancaster Synthesis (Windham, NH) or Avocado Research Chemicals (Heysham, UK). MnO<sub>2</sub> and Celite-545 were purchased from Merck (Fontenay-sous-bois, France), molecular sieves (3 Å, powder) from Acros Organics (Noisy-le-Grand, France), boric acid from Eu-

\* To whom correspondence should be addressed. A.L.: Advanced Technology/Molecular Diagnostics, BioMérieux, S.A., Chemin de l'Orme - 69280 Marcy l'Etoile, France. Tel: +33 478 875 337. Fax: +33 478 875 340. E-mail: ali.laayoun@eu.biomerieux.com.

<sup>†</sup> BioMérieux.

<sup>‡</sup> Université Joseph Fourier.

robio (Les Ulis, France), and 3'-GMP from ICN Biomedicals (Costa Mesa, CA). All other nucleotides were from Sigma (Saint Quentin-Fallavier, France). TLC: Merck silica gel 60 F<sub>254</sub> plates. Preparative reverse phase column chromatography: Merck LiChroprep RP 18 silica gel (40–63  $\mu$ m). Mp: Electrothermal Serie IA9100 apparatus, uncorrected. UV: Perkin-Lambda 15UV/VIS. IR: Perkin-Elmer Impact 400 spectrophotometer. NMR: Bruker AC 200, Avance 300 spectrometers. For <sup>1</sup>H NMR, CDCl<sub>3</sub> as solvent,  $\delta_{\text{H}} = 7.24$ , DMSO-*d*<sub>6</sub> as solvent,  $\delta_{\text{H}} = 2.49$ ; for <sup>13</sup>C NMR, CDCl<sub>3</sub> as solvent,  $\delta_{\text{C}} = 77.5$ , DMSO-*d*<sub>6</sub> as solvent,  $\delta_{\text{C}} = 39.5$ . Mass spectra: Delsi-Nermag R10–10 or VG Platform (Micromass) spectrometers.

**Synthesis of *m*-BioPMDAM (3).** 3-(*N*-Biotinoylamino)acetophenone (**1**). To a solution of D-biotin (1.0 g, 4.1 mmol) in dry DMF (45 mL) cooled to 0 °C under argon were added successively *N*-methylmorpholine (590  $\mu$ L, 5.33 mmol) and isobutyl chloroformate (840  $\mu$ L, 6.60 mmol). The solution was stirred for 30 min, and then 3-aminoacetophenone (824 mg, 6.10 mmol) and *N*-methylmorpholine (480  $\mu$ L, 4.35 mmol) in 10 mL of DMF were added. The solution was stirred at 0 °C for 2 h, and then the solvent was removed under vacuum. The residue was dissolved in 3 mL of MeOH, and then 50 mL of water were added. The resulting precipitate was filtered, washed successively with water, CH<sub>2</sub>Cl<sub>2</sub>, and ether, and dried to give 1.2 g of crude **1**. Recrystallization from MeOH–water gave **1** (1.01 g, 70%) as a white powder. Mp 145 °C; IR (KBr):  $\nu = 3280, 2931, 2857, 1691, 1590, 1540, 1487, 1434, 1298, 1266 \text{ cm}^{-1}$ ; <sup>1</sup>H NMR (300 MHz, DMSO-*d*<sub>6</sub>):  $\delta = 1.3\text{--}1.7$  (m, 6H), 2.33 (t,  $J = 8 \text{ Hz}$ , 2H), 2.55 (s, 3H), 2.58 (d,  $J = 12 \text{ Hz}$ , 1H), 2.83 (dd,  $J = 12$  and  $5 \text{ Hz}$ , 1H), 3.13 (m, 1H), 4.15 (m, 1H), 4.31 (m, 1H), 6.34 (s, 1H), 6.41 (s, 1H), 7.44 (t,  $J = 8 \text{ Hz}$ , 1H), 7.64 (d,  $J = 8 \text{ Hz}$ , 1H), 7.85 (d,  $J = 8 \text{ Hz}$ , 1H), 8.17 (s, 1H), 10.05 (s, 1H). <sup>13</sup>C NMR (50 MHz, DMSO-*d*<sub>6</sub>):  $\delta = 197.5, 171.3, 162.6, 139.5, 137.1, 128.9, 123.3, 122.8, 118.0, 60.9, 59.0, 55.2, 39.6, 36.0, 28.0, 27.9, 26.5, 24.9$ ; MS (FAB/glycerol):  $m/z$  362 [M + H]<sup>+</sup>.

3-(*N*-Biotinoylamino)acetophenone Hydrazone (**2**). To a solution of **1** (500 mg, 1.38 mmol) in absol ethanol (8 mL) was added 200  $\mu$ L (4.15 mmol) of hydrazine monohydrate. The solution was refluxed for 2 h. After cooling, the white precipitate was filtered, washed with water and ether, and then dried to give **2** (385 mg, 74%) as a white powder. Mp 185 °C; IR (KBr):  $\nu = 3298, 2931, 2857, 1698, 1665, 1626, 1541, 1494, 1470, 1446, 1330, 1265 \text{ cm}^{-1}$ ; <sup>1</sup>H NMR (300 MHz, DMSO-*d*<sub>6</sub>):  $\delta = 1.3\text{--}1.7$  (m, 6H), 1.98 (s, 3H), 2.26 (t,  $J = 8 \text{ Hz}$ , 2H), 2.56 (d,  $J = 12 \text{ Hz}$ , 1H), 2.81 (dd,  $J = 12$  and  $5 \text{ Hz}$ , 1H), 3.11 (m, 1H), 4.13 (m, 1H), 4.29 (m, 1H), 6.39 (s, 3H), 6.42 (s, 1H), 7.22 (m, 2H), 7.50 (d,  $J = 8 \text{ Hz}$ , 1H), 7.84 (s, 1H), 9.82 (s, 1H). <sup>13</sup>C NMR (75 MHz, DMSO-*d*<sub>6</sub>):  $\delta = 171.6, 163.1, 142.2, 140.6, 139.5, 128.7, 120.0, 118.2, 115.9, 61.4, 59.6, 55.8, 40.2, 36.6, 28.6, 28.4, 25.5, 11.7$ ; MS (FAB/glycerol):  $m/z$  376 [M + H]<sup>+</sup>.

3-(*N*-Biotinoylamino)phenylmethyldiazomethane (**3**, *m*-BioPMDAM). To a solution of **2** (180 mg, 0.48 mmol) in DMF (2 mL) was added MnO<sub>2</sub> (340 mg, 3.9 mmol). After 30 min of stirring at room temperature, the reaction mixture was filtered through a Celite (0.5 cm thickness)–molecular sieves 3 Å (powder, 0.5 cm thickness) pad. The reaction mixture was concentrated in vacuo to 0.5 mL, and then 5 mL of ether was added. The resulting precipitate was filtered, washed with ether, and dried to give **3** (170 mg, 95%) as a pink powder. Mp 160 °C; IR (KBr):  $\nu = 3278, 2935, 2859, 2038, 1704, 1666, 1605, 1577, 1536, 1458, 1430, 1263 \text{ cm}^{-1}$ ; <sup>1</sup>H NMR (300 MHz,

DMSO-*d*<sub>6</sub>):  $\delta = 1.3\text{--}1.7$  (m, 6H), 2.11 (s, 3H), 2.28 (t,  $J = 8 \text{ Hz}$ , 2H), 2.57 (d,  $J = 12 \text{ Hz}$ , 1H), 2.81 (dd,  $J = 12$  and  $5 \text{ Hz}$ , 1H), 3.11 (m, 1H), 4.13 (m, 1H), 4.29 (m, 1H), 6.33 (s, 1H), 6.41 (s, 1H), 6.60 (m, 1H), 7.25 (m, 3H), 9.84 (s, 1H). <sup>13</sup>C NMR (75 MHz, DMSO-*d*<sub>6</sub>):  $\delta = 171.6, 163.1, 140.5, 132.8, 129.7, 116.4, 114.6, 111.7, 61.4, 59.6, 55.7, 51.7, 40.2, 36.6, 28.6, 28.4, 25.4, 9.8$ ; MS (FAB/thioglycerol):  $m/z$  346 [M + H – N<sub>2</sub>]<sup>+</sup>.

**Stability of *m*-BioPMDAM (3).** The purity of **3** was evaluated by <sup>1</sup>H NMR in DMSO-*d*<sub>6</sub> by the integration ratio between the multiplet signals at 6.60 ppm and at 4.13 ppm (relaxation delay: 10 s). The initial purity of *m*-BioPMDAM (**3**) prepared above was 80–90%. The stability was evaluated by the same manner using a DMSO-*d*<sub>6</sub> solution of **3** (30 mM).

**Alkylation of Nucleotide Monomers with *m*-BioPMDAM (3).** *Analytical.* Each nucleotide monomer (0.04 mM): 3'-UMP, 3'-AMP, 3'-CMP, or 3'-GMP was incubated with 2 mM of *m*-BioPMDAM in a mixture of DMSO:CH<sub>3</sub>CN:H<sub>2</sub>O (1:3:1, vol/vol/vol) containing 2 mM H<sub>3</sub>BO<sub>3</sub> (pH 7.3) at 60 °C. Reaction mixtures (250  $\mu$ L) were then washed with CH<sub>2</sub>Cl<sub>2</sub> and alkylation rates estimated using capillary electrophoresis.

*Capillary Electrophoresis (CE) Procedure.* CE experiments were performed with a Beckman P/ACE 5000 capillary electrophoresis instrument (Beckman Coulter, Fullerton, CA). An untreated fused silica capillary (75  $\mu$ m  $\times$  50 cm) was used. The applied voltage was 30 kV (normal polarity) and the capillary temperature maintained at 23 °C. The electrophoregrams were recorded at 254 nm. Borate buffer solution (0.1 M, pH 8.3) was prepared from boric acid by adjusting pH with NaOH solution and filtered through 0.2  $\mu$ m filter. Samples were injected by pressure (0.5 psi, 5 s). Before each run, the capillary was regenerated by using successively NaOH solution (0.1 N, 2 min), pure water (2 min), and borate buffer (2 min) by pressure (20 psi).

*Preparative Run (4).* A mixture of 9.3 mg (21  $\mu$ mol) of 3'-UMP (disodic salt tetrahydrated), 2 mL of H<sub>3</sub>BO<sub>3</sub> solution (0.1 M), 2 mL of CH<sub>3</sub>CN, 6 mL of methanol, and 75 mg (200  $\mu$ mol) of *m*-BioPMDAM (**3**) was stirred at room temperature for 2.5 h. To the resulting mixture were added CH<sub>2</sub>Cl<sub>2</sub> (30 mL) and H<sub>2</sub>O (3 mL). Aqueous phase was separated and further washed twice with CH<sub>2</sub>Cl<sub>2</sub> (30 mL) and then concentrated. The crude product was purified by reverse-phase silica gel chromatography (LiChroprep RP 18 silica gel, 40–63  $\mu$ m, eluant: 0–30% MeOH/H<sub>2</sub>O) to afford 10 mg (69%) of solid **4**. The designations "a" and "b" in the <sup>1</sup>H NMR data refer to the two sets of signals for two diastereoisomers. <sup>1</sup>H NMR (300 MHz, D<sub>2</sub>O):  $\delta = 1.35\text{--}1.75$  (m, 6H, CH<sub>2</sub>-biotin), 1.46 and 1.48 (2d,  $J = 7 \text{ Hz}$ , 3H, CH<sub>3</sub>), 2.36 and 2.37 (2t,  $J = 7 \text{ Hz}$ , CH<sub>2</sub>-biotin), 2.70 (d,  $J = 13 \text{ Hz}$ , 1H, CH<sub>2</sub>-biotin), 2.92 and 2.93 (2dd,  $J = 13$  and  $5 \text{ Hz}$ , 1H, CH<sub>2</sub>-biotin), 3.28 (m, 1H, CH-biotin), 3.33 (m, 1H, H<sub>a</sub>-2'), 3.47 and 3.57 (ABX,  $J = 13, 4$ , and  $2 \text{ Hz}$ , 2H, H<sub>b</sub>-5',5''), 3.69 and 3.80 (ABX,  $J = 13, 4$ , and  $3 \text{ Hz}$ , 2H, H<sub>a</sub>-5',5''), 3.84 (m, 1H, H<sub>b</sub>-4'), 3.99 (t,  $J = 5 \text{ Hz}$ , 1H, H<sub>b</sub>-2'), 4.06 (m, 1H, H<sub>a</sub>-4'), 4.10 (m, 1H, H<sub>a</sub>-3'), 4.19 (m, 1H, H<sub>b</sub>-3'), 4.36 (m, 1H, CH-biotin), 4.52 (m, 1H, CH-biotin), 5.23 (m, 1H, CHOP), 5.52 (d,  $J = 3 \text{ Hz}$ , 1H, H<sub>a</sub>-1'), 5.62 (d,  $J = 5 \text{ Hz}$ , 1H, H<sub>b</sub>-1'), 5.75 and 5.76 (2d,  $J = 8 \text{ Hz}$ , 1H, H-5), 7.13–7.22 (m, 1H), 7.24–7.34 (m, 2H), 7.44 (s broad, 1H), 7.65 and 7.68 (2d,  $J = 8 \text{ Hz}$ , 1H, H-6); <sup>31</sup>P NMR (81 MHz, D<sub>2</sub>O):  $\delta = -0.38, -0.52$ ; ESI-MS:  $m/z$  670 [M + H]<sup>+</sup>.

**Adducts 5–7.** These adducts were obtained by the same procedure as described above for **4**.

**Adduct 5:** yield 12 mg (60%). <sup>1</sup>H NMR (300 MHz, D<sub>2</sub>O):  $\delta = 1.3\text{--}1.7$  (m, 6H, CH<sub>2</sub>-biotin), 1.45 and 1.48 (2d,



$J = 7$  Hz, 3H, CH<sub>3</sub>), 2.37 (t,  $J = 7$  Hz, CH<sub>2</sub>-biotin), 2.70 (d,  $J = 13$  Hz, 1H, CH<sub>2</sub>-biotin), 2.92 and 2.93 (2dd,  $J = 13$  and 5 Hz, 1H, CH<sub>2</sub>-biotin), 3.20 (m, 1H, H<sub>a</sub>-2'), 3.27 (m, 1H, CH-biotin), 3.47 and 3.60 (ABX,  $J = 13$ , 4 and 2 Hz, 2H, H<sub>b</sub>-5',5''), 3.69 and 3.82 (ABX,  $J = 13$ , 4 and 2 Hz, 2H, H<sub>a</sub>-5',5''), 3.86 (m, 1H, H<sub>b</sub>-4'), 3.93 (t,  $J = 5$  Hz, 1H, H<sub>b</sub>-2'), 4.04 (m, 2H, H<sub>a</sub>-3' and H<sub>a</sub>-4'), 4.13 (m, 1H, H<sub>b</sub>-3'), 4.34 (m, 1H, CH-biotin), 4.52 (m, 1H, CH-biotin), 5.22 (m, 1H, CHOP), 5.52 (d,  $J = 3$  Hz, 1H, H<sub>a</sub>-1'), 5.65 (d,  $J = 5$  Hz, 1H, H<sub>b</sub>-1'), 5.90 and 5.91 (2d,  $J = 8$  Hz, 1H, H-5), 7.10–7.20 (m, 1H), 7.21–7.35 (m, 2H), 7.43 and 7.46 (2s broad, 1H), 7.58 and 7.61 (2d,  $J = 8$  Hz, 1H, H-6); <sup>31</sup>P NMR (121 MHz, D<sub>2</sub>O):  $\delta = -0.38, -0.49$ ; ESI-MS:  $m/z$  669 [M + H]<sup>+</sup>.

Adduct **6**: yield 14 mg (74%). <sup>1</sup>H NMR (300 MHz, D<sub>2</sub>O):  $\delta = 1.20$ – $1.63$  (m, 6H, CH<sub>2</sub>-biotin), 1.45 and 1.49 (2d,  $J = 7$  Hz, 3H, CH<sub>3</sub>), 2.27 and 2.29 (2t,  $J = 7$  Hz, CH<sub>2</sub>-biotin), 2.64 and 2.66 (2d,  $J = 13$  Hz, 1H, CH<sub>2</sub>-biotin), 2.83 and 2.85 (2dd,  $J = 13$  and 5 Hz, 1H, CH<sub>2</sub>-biotin), 3.34 (m, 1H, CH-biotin), 3.47 and 3.62 (ABX,  $J = 13$ , 3 and 2 Hz, 2H, H<sub>b</sub>-5',5''), 3.70 and 3.83 (ABX,  $J = 13$ , 4 and 2 Hz, 2H, H<sub>a</sub>-5',5''), 3.80 (t,  $J = 4$  Hz, 1H, H<sub>a</sub>-2') 3.96 (m, 1H, H<sub>b</sub>-4'), 4.18 (m, 1H, H<sub>a</sub>-4'), 4.24 (m, 1H, CH-biotin), 4.36 (m, 1H, H<sub>a</sub>-3'), 4.41–4.50 (m, 3H, H<sub>b</sub>-3', CH-biotin, H<sub>b</sub>-2'), 5.24 (m, 1H, CHOP), 5.62 (d,  $J = 5$  Hz, 1H, H<sub>b</sub>-1'), 5.65 (d,  $J = 4$  Hz, 1H, H<sub>a</sub>-1'), 7.06–7.20 (m, 2H), 7.28 (m, 1H), 7.34 and 7.42 (2s broad, 1H), 8.09 and 8.09 (2s, 1H, H-8), 8.12 (s, 1H, H-2); <sup>31</sup>P NMR (121 MHz, D<sub>2</sub>O):  $\delta = -0.27, -0.49$ ; ESI-MS:  $m/z$  693 [M + H]<sup>+</sup>.

Adduct **7**: yield 10 mg (65%). <sup>1</sup>H NMR (300 MHz, D<sub>2</sub>O):  $\delta = 1.24$ – $1.69$  (m, 6H, CH<sub>2</sub>-biotin), 1.46 and 1.49 (2d,  $J = 7$  Hz, 3H, CH<sub>3</sub>), 2.27 and 2.30 (2t,  $J = 7$  Hz, CH<sub>2</sub>-biotin), 2.64 and 2.67 (2d,  $J = 13$  Hz, 1H, CH<sub>2</sub>-biotin), 2.84 and 2.85 (2dd,  $J = 13$  and 4 Hz, 1H, CH<sub>2</sub>-biotin), 3.17 (m, 1H, CH-biotin), 3.50 and 3.62 (ABX,  $J = 13$ , 4 and 2 Hz, 2H, H<sub>b</sub>-5',5''), 3.70 and 3.82 (ABX,  $J = 13$ , 4 and 2 Hz, 2H, H<sub>a</sub>-5',5''), 3.71 (m, 1H, H<sub>a</sub>-2') 3.95 (m, 1H, H<sub>b</sub>-4'), 4.13 (m, 1H, H<sub>a</sub>-4'), 4.27 (m, 1H, CH-biotin), 4.37 (t,  $J = 5$  Hz, 1H, H<sub>b</sub>-2'), 4.45 (m, 1H, H<sub>a</sub>-3'), 4.48 (m, 1H, CH-biotin), 4.51 (m, 1H, H<sub>b</sub>-3'), 5.24 (m, 1H, CHOP), 5.50 (d,  $J = 3$  Hz, 1H, H<sub>a</sub>-1'), 5.51 (d,  $J = 5$  Hz, 1H, H<sub>b</sub>-1'), 7.12–7.23 (m, 2H), 7.26–7.29 (m, 1H), 7.38 and 7.49 (2s broad, 1H), 7.74 (s, 1H, H-8); <sup>31</sup>P NMR (121 MHz, D<sub>2</sub>O):  $\delta = -0.23, -0.34$ ; ESI-MS:  $m/z$  709 [M + H]<sup>+</sup>.

**Evaluation of Diazo Labeling of Oligonucleotides.** The three oligonucleotide sequences, fragments of the *Mycobacterium tuberculosis* (*Mtb*) 16S rRNA sequence, were 5'-ACACCTCTCAGGCCGCTACCCGTCGTCGCCTTGTTAGGCC-3'; 5'-CCGTCGTCGCCTTGTTAGGCCGTCACCCACCAACAAGCT-3', and 5'-GTCACCCACCAACAAGCTGATAGGCCGCGGGCTCATCCACACCG-3'. These DNA oligomers, bearing fluorescein at their 5'-end, were obtained from Eurogentec (Seraing, Belgium). Five picomoles of each oligonucleotide were treated with 2, 5, 10, and 20 mM *m*-BioPMDAM at 95 °C, in pure water, for 10 min. After the labeled targets were hybridized to the *Mycobacterium* DNA chip (15), the 5'-fluorescein label was detected and the emitted signal was denoted as S1. The chip was then stained for 10 min at room temperature, with 6  $\mu$ L (6  $\mu$ g) of an anti-biotin antibody (Rockland Immunochemical, Gilbertsville, PA) labeled with fluoresceins (two labels per antibody) and diluted in 0.05 M Tris pH 7, 0.5 M NaCl, 0.02% Tween-20, 500  $\mu$ g/mL BSA. After it was washed, the chip was scanned and the registered signal was noted as S2. In all cases, the background was deducted. The difference of signal intensities (taking into account the number of fluoresceins per anti-biotin anti-

body) was used to estimate the number of biotin labels per oligonucleotide.

**Nucleic Acid Targets Preparation.** Preparation and amplification of the *Mtb* 16S rRNA locus was carried out from freshly grown colonies, according to the procedure described by Troesch et al. (15) with the following modifications. PCR amplification was carried out in a 50  $\mu$ L reaction volume using the Fast Start Taq DNA polymerase (Roche Molecular Biochemicals, Mannheim, Germany), 200  $\mu$ M of each deoxyribonucleotide triphosphate (Promega, Madison, WI), and 0.3  $\mu$ M of primers. PCR was performed in a Perkin-Elmer 9700 thermal cycler with an initial denaturation step at 94 °C for 5 min and cycling conditions of 94 °C for 30 s, 68 °C for 30 s, 72 °C for 45 s for 35 cycles, and 72 °C for 7 min for the last cycle. The promoter-tagged PCR amplicons were used for generating single-stranded RNA targets by in vitro transcription. Each 20- $\mu$ L reaction mixture contained 8  $\mu$ L of PCR product (approximately 50 ng). Transcription was carried out using the in vitro transcription kit megascript (Ambion, Austin, TX). The reaction was performed at 37 °C for 2 h.

Genomic DNA from *Mtb* was extracted from a freshly grown liquid culture by universal lysis protocol (18) and using Genomic-tip 500/G (Qiagen, Venlo, The Netherlands), following the manufacturer's instructions.

**Labeling of RNA. Labeling During Cleavage (LDC).** Five microliters (0.04  $\mu$ g) of in vitro transcripts was incubated at 60 °C for 10 min in labeling buffer (I) containing 30 mM imidazole, 5 mM MnCl<sub>2</sub>, 2 mM *m*-BioPMDAM or at 60 °C for 30 min in labeling buffer (II) containing 6 mM imidazole, 60 mM MnCl<sub>2</sub>, 2 mM 5-(bromomethyl)fluorescein (5-BMF) (Molecular Probes, Eugene, OR).

**Labeling Plus Cleavage (LPC).** Conditions were the same as for LDC protocol, except that labeling and cleavage were done sequentially: 10 min at 60 °C for labeling with 2 mM *m*-BioPMDAM, followed by 10 min at 60 °C for cleavage with 30 mM imidazole, 5 mM MnCl<sub>2</sub> or 10 min at 60 °C for labeling with 2 mM 5-BMF, followed by 10 min at 60 °C for cleavage with 6 mM imidazole, 60 mM MnCl<sub>2</sub>.

**Labeling of DNA. Labeling During Cleavage (LDC).** Ten microliters of DNA amplicons (0.75  $\mu$ g) were incubated at 95 °C for 10 min in 3 mM HCl, 10 mM *m*-BioPMDAM or in 3 mM HCl, 10 mM 5-BMF.

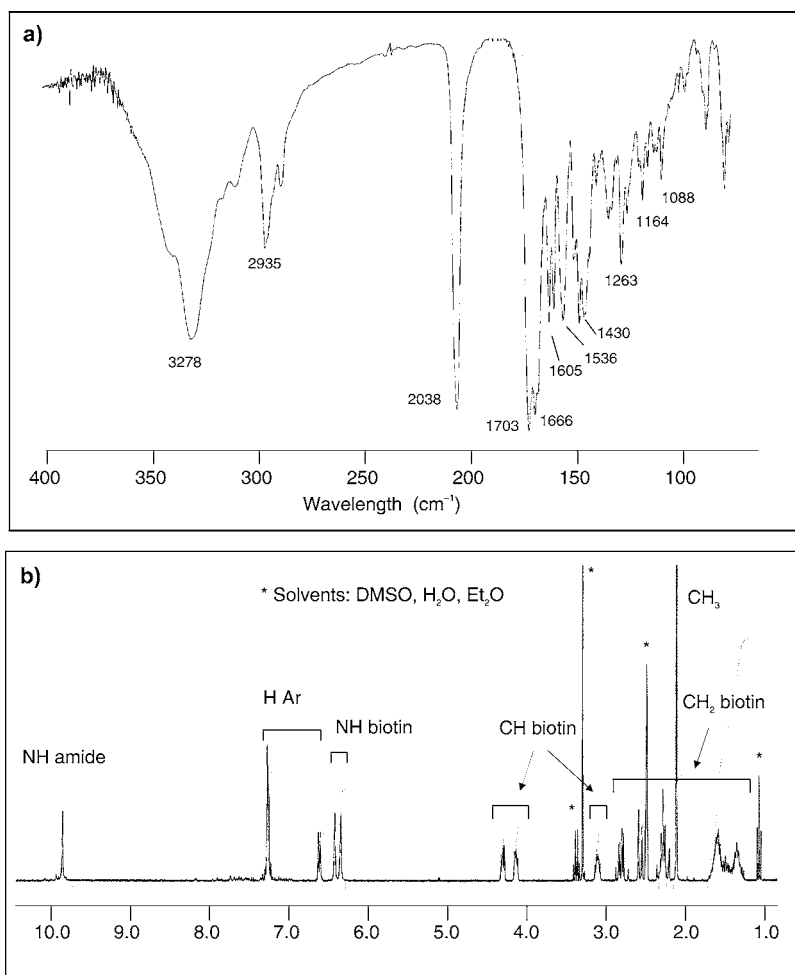
**Labeling Plus Cleavage (LPC).** For LPC of DNA, conditions were the same as for LDC, except that labeling and fragmentation were done sequentially: 10 min at 95 °C for labeling with 10 mM *m*-BioPMDAM or 10 mM 5-BMF, followed by 10 min at 95 °C for cleavage in 3 mM HCl. Labeling of 10  $\mu$ L DNA amplicons, in LPC procedure, with Biotin-Chem-Link distributed by Roche Molecular Biochemicals (Mannheim, Germany) and "Label IT Biotin" reagent from Mirus (Madison, WI) was carried out according to the supplier's instructions. The fragmentation was achieved in 3 mM HCl, 10 min at 95 °C.

**Labeling Plus Cleavage of Genomic DNA.** gDNA of *Mtb* (10  $\mu$ g) was labeled in 30 mM *m*-BioPMDAM at 95 °C for 25 min and then fragmented by 10 mM HCl at 95 °C for 5 min.

**Purification of Labeled Targets.** For all labeling protocols, unreacted label was removed prior to the hybridization step by means of silica membrane purification, 6S Qiavac columns (Qiagen, Venlo, The Netherlands), according to the manufacturer's instructions.

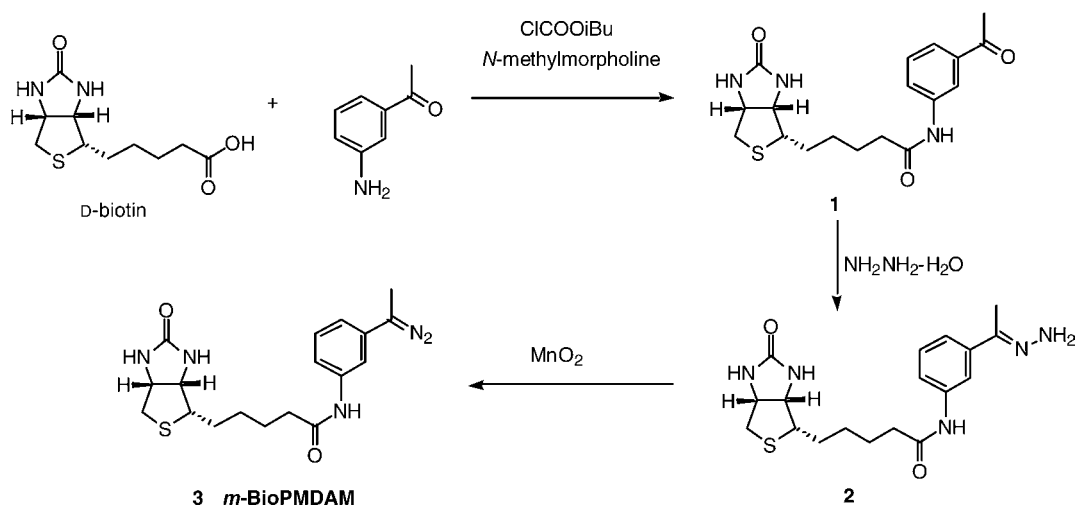
**Probe Array Hybridization and Analysis.** The *Mycobacterium* DNA chip (bioMerieux, Marcy-l'Etoile, France) is divided into 23000 specific 35 by 35  $\mu$ m





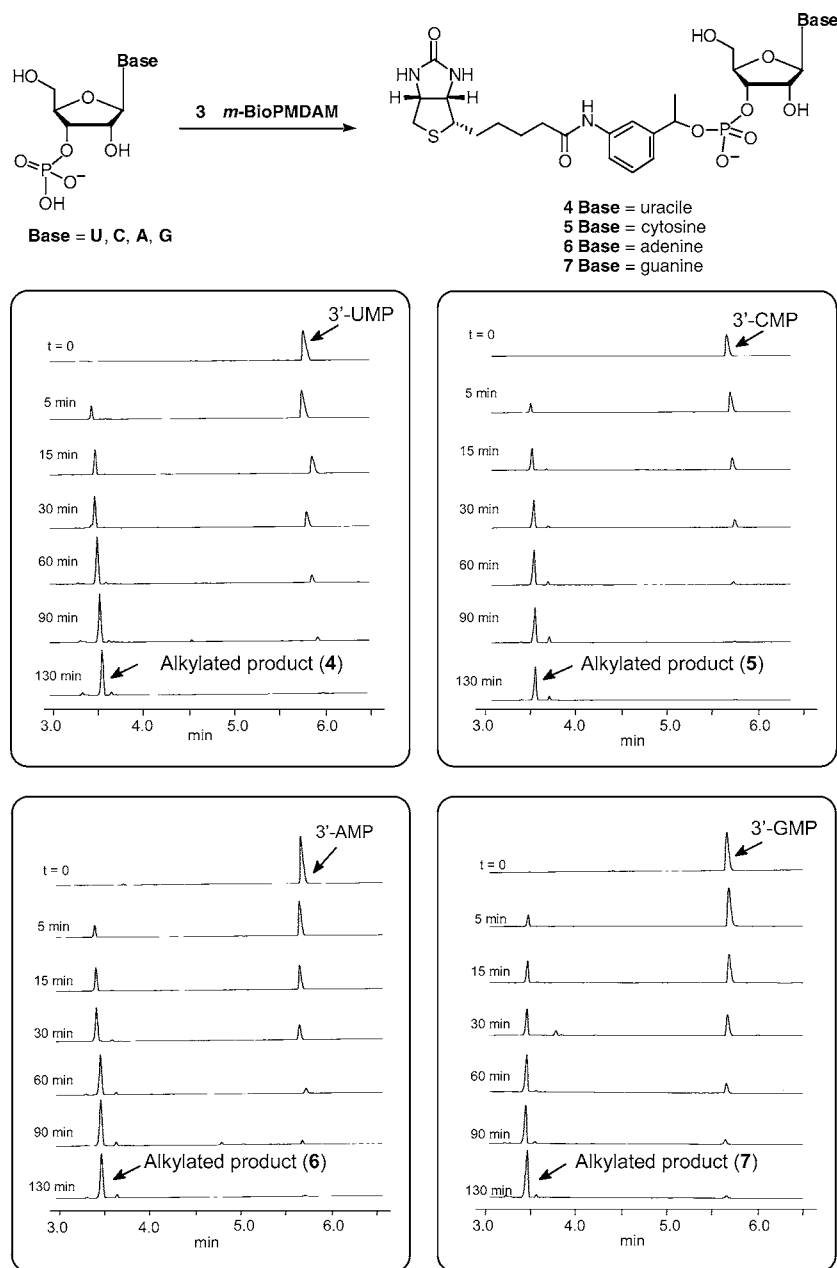
**Figure 1.** IR (a) and <sup>1</sup>H NMR (b) spectra of *m*-BioPMDAM (**3**).

**Scheme 1**



synthesis sites, over a 5.25- by 5.25-mm area. The four-probe interrogation strategy, similar to that described by Troesch et al. (15), was used to identify sequence variation in 16S rRNA and *rpoB* loci. Briefly, for every base interrogated within a given reference sequence, four probes of equal lengths are synthesized on the chip (usually 20mers). Those four probes are identical except at the interrogation position (centrally located within the probe), thus representing perfect hybridization match and the three possible mismatches. Base calls are determined by comparing the signal intensity of the labeled

target for the four probes. The DNA chips used in the study were manufactured by Affymetrix (Santa Clara, CA). One hundred microliters of the labeled and purified nucleic acid fragments were added to 400  $\mu$ L of hybridization buffer (15), containing 0.9 M NaCl, 60 mM NaH<sub>2</sub>PO<sub>4</sub> pH 7.4, 6 mM EDTA, 0.05% Triton X-100, 3 M betaine, 5 mM DTAB (dodecyl trimethylammonium bromide) and denatured at 95 °C for 10 min. DNA fragments labeled with "Label IT" Biotin reagent were denatured with denaturation buffers according to the supplier's protocol. Hybridization onto the *Mycobacterium*



**Figure 2.** Capillary electrophoresis (CE) study of the alkylation of the nucleotide monophosphates with *m*-BioPMDAM (**3**).

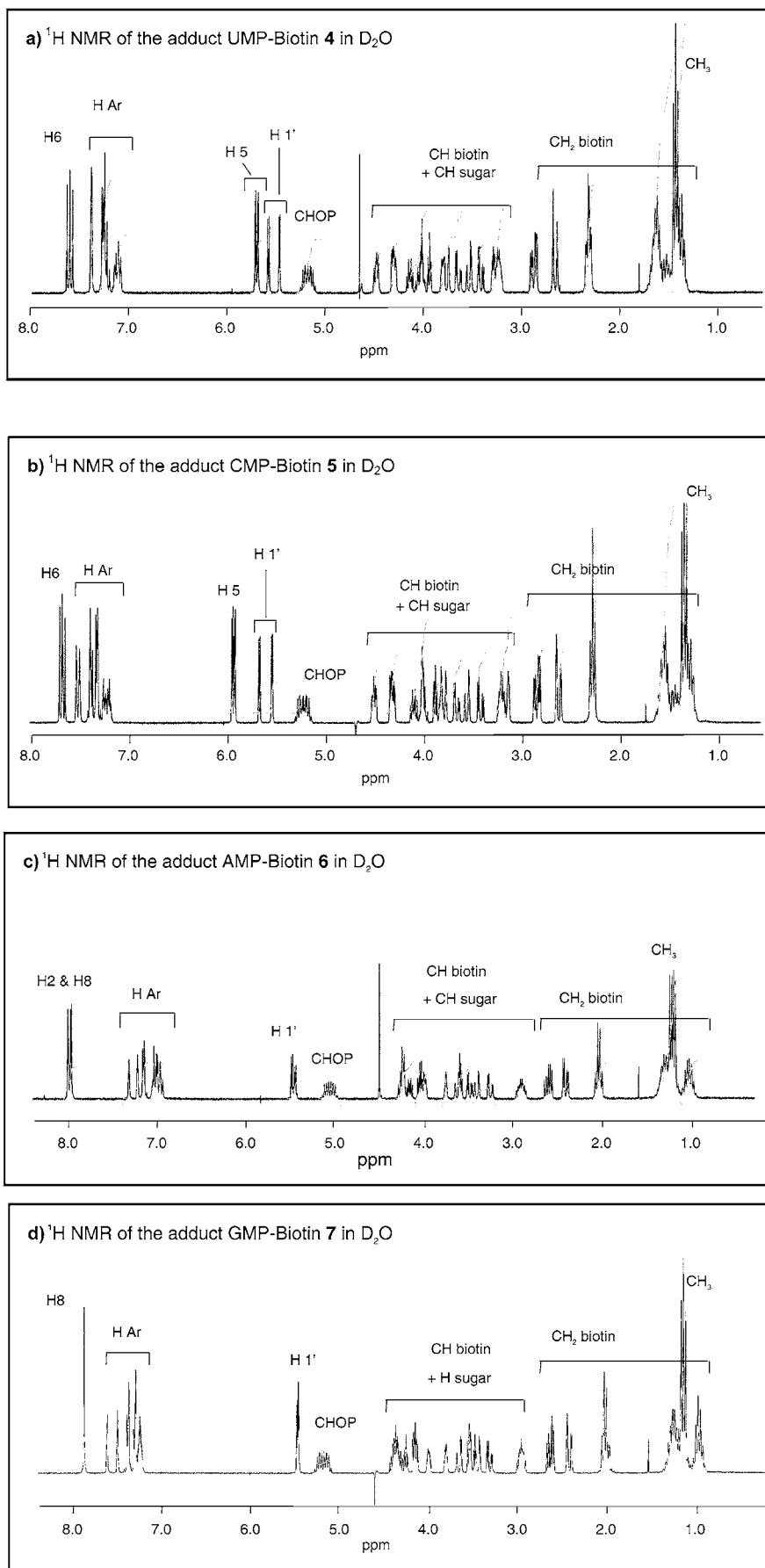
DNA chip was performed at 45 °C during 30 min and the chip was washed twice in 0.45 M NaCl, 30 mM NaH<sub>2</sub>PO<sub>4</sub>, 3 mM EDTA pH 7.4, 0.005% Triton X-100 at 30 °C (15). For biotinylated fragments, the DNA chip was stained for 10 min with a solution made of 600  $\mu$ L of 0.05 M Tris pH 7, 0.5 M NaCl, 0.02% Tween-20, 500  $\mu$ g/mL BSA and 6  $\mu$ L of Streptavidin-R-Phycoerythrin conjugate (300  $\mu$ g/mL; DakoCytomation, Glostrup, Denmark). After a washing step in 0.9 M NaCl, 0.06 M NaH<sub>2</sub>PO<sub>4</sub>, 6 mM EDTA pH 7.4, 0.05% Triton X-100, the fluorescent signal emitted by the target bound to the DNA chip was detected by a GeneArray scanner (Agilent, Palo Alto, CA), at a pixel resolution of 3  $\mu$ m. Probe array cell intensities, nucleotide base calls and reports were generated by functions available on the GeneChip software (Affymetrix, Santa Clara, CA).

## RESULTS AND DISCUSSION

Most electrophilic reagents, halides, sulfates, sulfonates, epoxid, etc, react with nucleotides and nucleic

acids essentially at the oxygen or nitrogen nucleophilic sites of the nucleobases (14). Design of the labeling reagent *m*-BioPMDAM was based on preliminary model studies which had shown that aryldiazomethanes did react at the phosphate group with nucleotide monophosphates (unpublished results). *m*-BioPMDAM (**3**) was thus prepared, that includes in its structure the reactive phenylmethyl diazomethane unit (PMDAM) covalently linked through an amide bond to the biotin (Bio) moiety.

**Synthesis of the *m*-BioPMDAM Reagent (**3**).** *m*-BioPMDAM **3** was prepared from commercial 3-aminoacetophenone and D-biotin with a 49% global yield (Scheme 1). Coupling of the two entities was accomplished in DMF using isobutyl chloroformate as coupling reagent in the presence of *N*-methylmorpholine (70% yield). The methyl ketone function of the resulting conjugate **1** was transformed into the hydrazone **2** by warming with hydrazine monohydrate in ethanol in 74% yield. MnO<sub>2</sub> oxidation of **2** yielded the diazo reagent *m*-BioPDAM **3** as a pink powder that was characterized notably by the <sup>1</sup>H and <sup>13</sup>C



**Figure 3.**  $^1\text{H}$  NMR spectra of the alkylation products with *m*-BioPMDAM (**3**) (a) of the 3'-UMP, (b) of the 3'-CMP, (c) of the 3'-AMP, and (d) of the 3'-GMP.



NMR spectrum (Figure 1a). It exhibited in the IR the characteristic vibration at 2038  $\text{cm}^{-1}$  (Figure 1b).

Simple alkyl diazoalkanes are unstable compounds. Substitution by aryl and electron-attracting groups generally increase the stability of the diazo function. It was thus essential to test the stability of the *m*-BioPMDAM reagent. Stability in solution was evaluated by  $^1\text{H}$  NMR spectroscopy. The half-life of *m*-BioPMDAM in DMSO- $d_6$  solution (30 mM) at room temperature is  $t_{1/2} = 3$  days.

**Reaction of *m*-BioPMDAM with 3'-Nucleotide Monophosphates.** To study the site selectivity of the reaction of *m*-BioPMDAM we examined its reaction with representative nucleotide phosphates that incorporate the four different nucleobases, i.e., 3'-AMP, 3'-GMP, 3'-CMP, 3'-UMP. Reactions were most conveniently monitored at the analytical stage using capillary electrophoresis. To dissolve both the charged hydrophilic nucleotides and the lipophilic *m*-BioPMDAM reagent, a homogeneous mixture of solvents (DMSO: $\text{CH}_3\text{CN}:\text{H}_2\text{O}$ ) was used. The reaction was run under buffered conditions at pH 7.3 using a large excess of *m*-BioPMDAM label. Figure 2 shows the evolution of the reactions run at 60 °C with the different nucleotides as monitored by capillary electrophoresis. The reaction profiles are quite similar for the four nucleotides examined. One very major (or unique) reaction product was formed and the kinetics of the reactions were quite comparable. In the experimental conditions used, the time required for 50% transformation of all nucleotides was about 15 min and transformation was complete after 130 min.

The reaction products were identified by running the reactions at the preparative scale (20  $\mu\text{mol}$ -scale). They were isolated and characterized by their analytical and spectroscopic data. The adducts were obtained in 70% average yield after purification, and they exhibited in  $^1\text{H}$  NMR spectra all peaks corresponding to the indicated structures (Figure 3). We note the presence of two diastereoisomers in a 1/1 ratio as reflected by the splitting of the sugar protons (H1', H2', H3', H4', H5'-5''). The CH proton vicinal to the phosphate appears at 5.2 ppm. The proton-decoupled phosphorus NMR spectra equally indicate the presence of two diastereoisomers giving rise to two peaks: at  $\delta = -0.23$  and  $-0.34$  ppm for the adduct with 3'-GMP, to be compared with the  $\delta = +4.0$  ppm value observed for 3'-GMP nucleotide. The same observation was done for all adducts.

**Reaction of *m*-BioPMDAM with Oligonucleotides.** Reaction of *m*-BioPMDAM with three synthetic oligodeoxyribonucleotides, fragments of a 16S rRNA *Mycobacterium tuberculosis* (*Mtb*) sequence containing a fluorescein label at their 5'-end, was studied. A mix of the three oligonucleotides was labeled with different concentrations of *m*-BioPMDAM, purified, and then hybridized onto a *Mycobacterium* DNA chip (15). Median intensity of fluorescence signals emitted by the hybridized oligonucleotides, before and after a "posthybridization" staining step (with anti-biotin antibody bearing fluoresceins), were measured (see Experimental Procedures). The comparison of the two intensity values showed that approximately 3 of every 10 phosphates were labeled in our model experiments, suggesting that selective alkylation by *m*-BioPMDAM occurred on internucleotidic phosphates as well. This is substantially more than the one label per nucleic acid fragment indicated as the best yield in prior work with 5-(bromomethyl)fluorescein and iodoacetamido-fluorescein as labeling reagents (11–13).

**Labeling of RNA and DNA with *m*-BioPMDAM.** We further evaluated the labeling efficiency on longer DNA and RNA targets generated by enzymatic amplifi-

**Table 1. Chip Analysis of DNA Amplicons and RNA Transcripts, from 16S rRNA *M. tuberculosis* Locus, Labeled with 5-BMF and *m*-BioPMDAM**

labeling procedure			chip results <sup>a</sup>		
			BC (%)	median intensity (rfu)	signal/background
RNA	LDC <sup>b</sup>	<i>m</i> -BioPMDAM	97.3	20968	43.0
		5-BMF	95.7	11058	31.0
	LPC <sup>c</sup>	<i>m</i> -BioPMDAM	96.8	13402	30.0
DNA	LDC	5-BMF	90.8	9312	13.0
		<i>m</i> -BioPMDAM	99.5	2538	4.5
	LPC	5-BMF	62.7	157	1.5
		<i>m</i> -BioPMDAM	100	4700	10.7
		5-BMF	0	18	0.2

<sup>a</sup> Chip results are given in terms of base call (BC) percentage (percent of homology between the experimentally derived sequence and the reference sequence tiled on the array), median signal intensity (relative fluorescence unit), and signal/background ratios.

<sup>b</sup> LDC: labeling during cleavage. <sup>c</sup> LPC: labeling plus cleavage.

**Table 2. Chip Analysis of DNA Amplicons Labeled with *m*-BioPMDAM and Two Existing Chemical Methods**

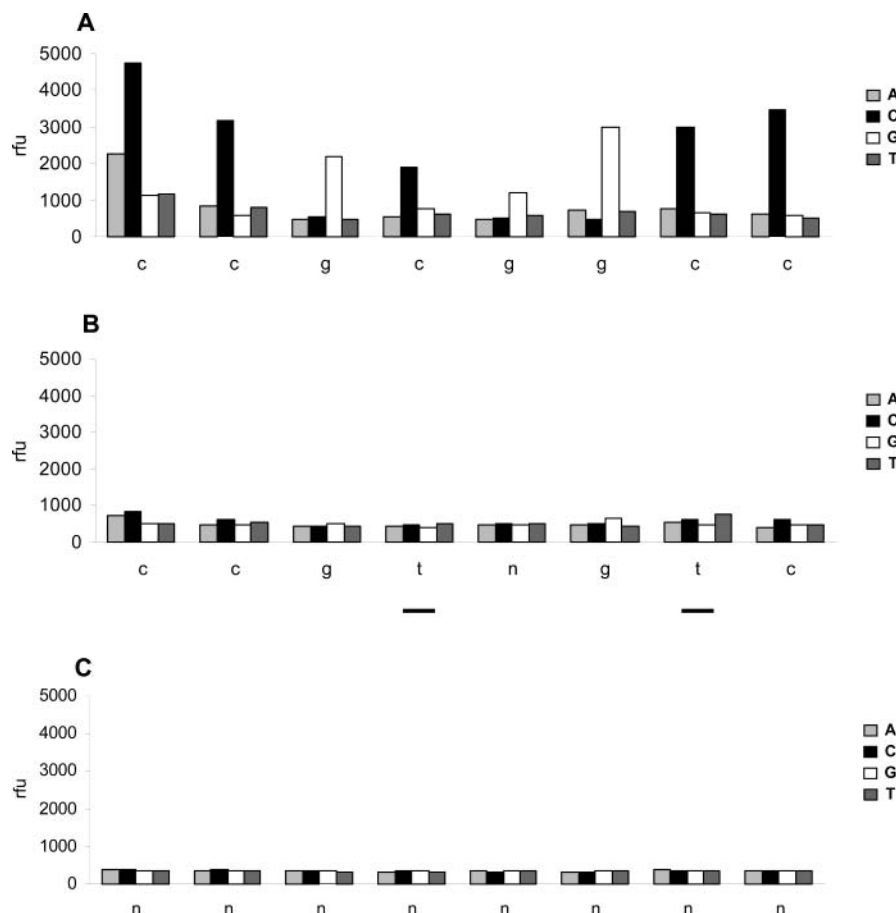
labeling procedure			chip results <sup>a</sup>		
			BC (%)	median intensity (rfu)	signal/background
DNA	LPC <sup>b</sup>	<i>m</i> -BioPMDAM	98.4	4274	13.0
		Biotin-Chem-Link	85.4	1175	3.2
		Label IT Biotin	38.4	87	3.5

<sup>a</sup> Chip results are given in terms of base call (BC) percentage (percent of homology between the experimentally derived sequence and the reference sequence tiled on the array), median signal intensity (relative fluorescence unit), and signal/background ratios.

<sup>b</sup> LPC: labeling plus cleavage.

cation (16S rDNA hypervariable region of *Mtb*, 202 nt) (15), prior to their hybridization to the *Mycobacterium* DNA chip. Cleavage of labeled DNA and RNA targets into smaller fragments is a prerequisite for improving the uniformity and specificity of hybridization onto the DNA chip (3). RNA targets were cleaved with  $\text{Mn}^{2+}$  and imidazole (16). The DNA targets were fragmented by acidic treatment that promoted random depurination and cleavage (17). Labeling was accomplished during or before the cleavage step, and the labeled fragments were then hybridized to the *Mycobacterium* DNA chip. Base-calling, that measures the percent of homology between the experimentally derived sequence and the ref 202 nt sequence tiled on the array, was accurate for all experiments conducted with *m*-BioPMDAM. The signal intensities were strong and the signal/background ratios high, all significantly better than with 5-(bromomethyl)fluorescein, determined for comparison (Table 1). This was especially true for DNA target labeling which was poor with the latter compound but gave good results with *m*-BioPMDAM.

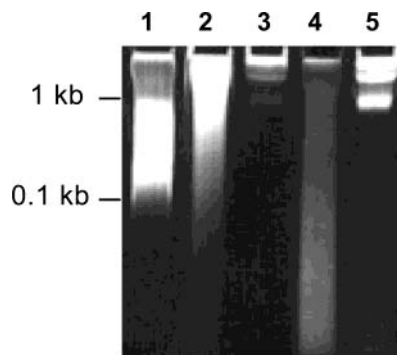
DNA amplicons labeling was also evaluated using two commercially available chemistries, used to label nucleic acids for DNA array analysis (Table 2). "Biotin-Chem-Link" is based on the use of monofunctional-platinum derivatives (10), that bind to nitrogen atom in guanine and adenine, whereas "Label IT Biotin" reagent uses a nondisclosed chemistry to covalently attach the label to nucleic bases in DNA. With these two technologies, targeting the nucleobases, signal intensities, and base call percentages were significantly lower compared to those obtained with phosphate labeling via diazo chemistry (Table 2). This is especially true in GC-rich region, as depicted in Figure 4. The data clearly corroborates that



**Figure 4.** Analysis of a GC-rich region of 16S rRNA *Mycobacterium tuberculosis* (5'CCGCGGCC). Targets were labeled with *m*-BioPMDAM (A), Biotin-Chem-Link (B), or LabelIT Biotin (C) and hybridized to a *Mycobacterium* DNA chip. Signal intensities for the four different probes at each interrogation position are shown on the y axis, and base-calling results are shown on the x axis. Underlined: incorrect nucleotide calls, n: undetermined. The graphs highlight the hybridization specificity and the good discrimination obtained with *m*-BioPMDAM labeled targets.

the label attachment on nucleic bases, via a covalent or noncovalent binding, alters the base-pairing efficiency and hybridization specificity, in particular in DNA chip applications requiring sequence calling at high resolution. *m*-BioPMDAM was also tested in other DNA chip applications requiring such resolution, like detection of antibiotic-resistant mutations in *Mtb* and of anti-retroviral drug mutations in HIV-1 (data not shown) or typing of *Staphylococcus aureus* strains (19), and the results confirmed the base-pairing specificity. Moreover, labeling was equally efficient for cleaved or uncleaved targets. This suggests that diazo labeling can be used for other detection systems that do not require target fragmentation before hybridization, e.g., low-density probes detection formats.

The potential of diazomethyl chemistry for labeling natural (not enzymatically amplified) nucleic acid targets was evaluated by labeling genomic DNA (gDNA) extracted from *Mtb*. Hybridization of directly labeled genomic DNA to high-density DNA chips would represent a simple mean to perform genome-wide scale analysis. SDS-PAGE showed that gDNA molecules were labeled (Figure 5). Indeed, a slight gel-shift was observed, after *m*-BioPMDAM treatment (lane 2) due to the neutralization of negative charges on the phosphodiester groups. Addition of neutravidin to the labeled sample shifted *Mtb* gDNA strongly toward higher molecular weights (lane 3). Interestingly, this shift was also observed with cleaved gDNA, showing that all fragments were labeled by biotin



**Figure 5.** *Mtb* gDNA labeled with *m*-BioPMDAM (3). Products were analyzed by SDS-PAGE and ethidium Bromide staining. Lane 1: sheared gDNA, not treated with *m*-BioPMDAM. Lane 2: gDNA labeled with *m*-BioPMDAM. Lane 3: 10 µL of labeled gDNA in lane 2 incubated for 5 min with 5 µL of 2 mg/mL neutravidin (Pierce) prior to electrophoresis. Lane 4: gDNA labeled with *m*-BioPMDAM (lane 2) and fragmented by 10 mM HCl at 95 °C for 5 min. Lane 5: 10 µL of labeled and cleaved gDNA in lane 4 incubated with 5 µL of 2 mg/mL neutravidin during 10 min.

(lanes 4 and 5). The base-calling accuracy obtained after analysis of the fragments on the chip (>90%, data not shown) shows that diazo labeling can be used to attach a detectable tag to a natural nucleic acid (the entire *Mtb* genome, in our experiment) before DNA chip analysis.

## CONCLUSION

The *m*-BioPMDAM reagent described here has been shown to selectively react on phosphates in nucleotide monomers and polynucleotides and has been successfully used to label RNA and DNA targets, of different sequence composition and length. The labeling reagent is stable and can be provided as a ready-to-use component. The highly reactive diazo function is used to obtain the rapid (15–30 min, depending on target type) and selective alkylation of both internucleotidic and terminal phosphates, with labeling of approximately 3 of every 10 phosphates in our model experiments. This represents a very high labeling density with no negative impact on base-pairing efficiency (as shown by the high base-calling percentage obtained in DNA chip analysis). Moreover, diazo labeling chemistry is not sensitive to buffer components or contaminants in a nucleic acid sample; the targets are labeled as such without any prior purification step (whereas purification is necessary with the approach using monofunctional-platinum derivatives). The final conjugate is very stable, even under heat-denaturing conditions and long hybridization time (overnight).

The labeling method described here requires a posthybridization staining step to introduce the fluorescent dye (via a streptavidin-fluorescent label conjugate). This step could be avoided, thus simplifying the experimental protocol, by using a diazo-compatible dye, where the fluorescent moiety is directly attached to the diazo reactive group. Our work on development of such fluorescent diazo compounds is currently in progress.

Overall, these features make diazo labeling particularly well-suited for conducting extensive analysis on DNA chips, such as whole genome RNA and DNA analysis and parallel testing of numerous targets in routine diagnosis.

## ACKNOWLEDGMENT

We thank C. Tora for technical assistance in the synthesis of the diazo compounds and F. Telles for her contribution to the gDNA experiments. E.B.M. acknowledges a Marie Curie Industry Host Fellowship (Quality of Life Program).

## LITERATURE CITED

- (1) Ramsay, G. (1998) DNA Chips: State-of-the-art. *Nature Biotechnol.* 16, 40–44.
- (2) Lockhart, D. J., and Winzler, E. A. (2000) Genomics, gene expression and DNA arrays. *Nature* 405, 827–836.
- (3) Chee, M., Yang, R., Hubbel, E., Berno, A., Huang, X. C., Stern, D., Winkler, J., Lockhart, D. J., Morris, M. S., and Fodor, S. P. A. (1996) Accessing genetic information with high-density DNA arrays. *Science* 274, 610–614.
- (4) Cho, R. J., Fromont-Racine, M., Wodicka, L., Feierbach, B., Stearns, T., Legrain, P., Lockhart, D. J., and Davis, R. W. (1998) Parallel analysis of genetic selections using whole genome oligonucleotide arrays. *Proc. Natl. Acad. Sci. U.S.A.* 95, 3752–3757.
- (5) Rosenow, C., Saxena, R. M., Durst, M., and Gingeras, T. R. (2001) Prokaryotic RNA preparation methods useful for high-density array analysis: comparison of two approaches. *Nucleic Acids Res.* 29, e112.
- (6) O'donnel, M. J., and McLaughlin, L. W. (1996) Reporter groups for the analysis of nucleic acid structure. In *Bioorganic Chemistry: Nucleic Acids* (Hecht, S. M., Ed.) pp 216–243, Oxford University Press, New York.
- (7) Kessler, C. (1995) Methods for nonradioactive labeling of nucleic acids. In *Nonisotopic probing, blotting, and sequencing* (Kricka, L. J., Ed.) pp 41–109, Academic Press, San Diego.
- (8) Hermanson, G. T. (1996) Nucleic acid and oligonucleotides modification and conjugation. In *Bioconjugate Techniques* (Hermanson, G. T., Ed.) pp 639–671, Academic Press, San Diego.
- (9) Hoewel, T., and Kubbies, M. (2002) Nonradioactive labeling and detection of mRNAs hybridized onto nucleic acid cDNA arrays. *Methods Mol. Biol.* 185, 417–23.
- (10) van Belkum, A., Linkels, E., Jelsma, T., Houthoff, H. J., van den Berg, F., and Quint, W. (1993) Application of a new, universal DNA labeling system in the PCR mediated diagnoses of *Chlamydia trachomatis* and human papillomavirus type 16 infection in cervical smears. *J. Virol. Methods* 45, 189–200.
- (11) Monnot, V., Tora, C., Lopez, S., Menou, L., and Laayoun, A. (2001) Labeling during cleavage (LDC), a new labeling approach for RNA. *Nucleosides, Nucleotides Nucleic Acids* 20, 1177–1179.
- (12) Laayoun, A. (2002) Process for labeling a ribonucleic acid, and labeled RNA fragments which are obtained thereby. United States Patent 6,376,179.
- (13) Browne, K. A. (2002) Metal ion-catalyzed nucleic acid alkylation and fragmentation. *J. Am. Chem. Soc.* 124, 7950–7962.
- (14) Mountzouris, J., and Hurley, L. H. (1996) Small Molecule-DNA Interaction. In *Bioorganic Chemistry: Nucleic Acids* (Hecht, S. M., Ed.) pp 288–323, Oxford University Press, New York.
- (15) Troesch, A., Nguyen, H., Miyada, C. G., Desvarenne, S., Gingeras, T. R., Kaplan, P. M., Cros, P., and Mabilat, C. (1999) *Mycobacterium* species identification and rifampin resistance testing with high-density DNA probe arrays. *J. Clin. Microbiol.* 37, 49–55.
- (16) Breslow, R., and Xu, R. (1993) Recognition and catalysis in nucleic acid chemistry. *Proc. Natl. Acad. Sci. U.S.A.* 90, 1201–1207.
- (17) Lhomme, J., Constant, J. F., and Demeunynck, M. (2000) Abasic DNA structure, reactivity, and recognition. *Biopolymers* 52, 65–83.
- (18) Broyer, P., Cleuziat, P., Colin, B., Jaravel, C., and Santoro, L. (2000) Improved device and method for lysis of microorganisms. PCT WO 00/05338.
- (19) van Leeuwen, W., Jay, C., Snijders, S., Durin, N., Lacroix, B., Verbrugh, H., Enright, M., Troesch, A., and van Belkum, A. (2003) *Staphylococcus aureus* multilocus sequence typing with DNA array technology. *J. Clin. Microbiol.* 41, 3323–3326.

BC0341371



## Site-Specific Cleavage of RNA and DNA by Complementary DNA–Bleomycin A5 Conjugates

Pavel E. Vorobjev,<sup>†</sup> Janet B. Smith,<sup>‡</sup> Inna A. Pyshnaya,<sup>†</sup> Asya S. Levina,<sup>†</sup> Valentina F. Zarytova,<sup>†</sup> and Eric Wickstrom<sup>§,\*</sup>

Laboratory of Nucleic Acid Chemistry, Institute of Bioorganic Chemistry, Russian Academy of Sciences, Novosibirsk 630090, Russia, and Department of Microbiology and Immunology, and Department of Biochemistry and Molecular Pharmacology, Kimmel Cancer Center, and Cardeza Foundation for Hematologic Research, Thomas Jefferson University, Philadelphia, Pennsylvania 19107 Received August 23, 2003

Bleomycin displays clinical chemotherapeutic activity, but is so nonspecifically toxic that it is rarely administered. It was therefore of interest to determine whether bleomycin could be directed to cleave RNA or DNA at a specific site by conjugation to a complementary oligonucleotide. A 15 nt *MYC* complementary oligodeoxynucleotide (HMYC55) bearing a 5' bleomycin A5 (Blm) residue was designed to base-pair with nt 7047–7061 of human *MYC* mRNA. Reactivity of the Blm–HMYC55 conjugate (and mismatch controls) with a *MYC* mRNA 30-mer, a *MYC* DNA 30-mer, and a *MYC* 2'-*O*-methyl RNA 30-mer, nt 7041–7070, was analyzed in 100  $\mu$ M FeNH<sub>4</sub>SO<sub>4</sub>, 50 mM  $\beta$ -mercaptoethanol, 200 mM LiCl, 10 mM Tris-HCl, pH 7.5, at 37 °C. Cleavage of the substrate RNA or DNA occurred primarily at the junction of the complementary DNA-target RNA duplex, 18–22 nt from the 5' end of the RNA. Reaction products with lower mobility than the target RNA or DNA also formed. Little or no reaction was observed with more than three mismatches in a Blm–oligodeoxynucleotide conjugate. Neither the short RNA or DNA cleavage fragments nor the low mobility products were observed in the absence of Fe(II), or the presence of excess EDTA. The target RNA was also cleaved efficiently by bleomycin within a hybrid duplex with a preformed single-nucleotide bulge in the RNA strand. New Blm–oligodeoxynucleotide conjugates containing long hexaethylene glycol phosphate based linkers between oligodeoxynucleotide and bleomycin were designed to target this bulge region. These conjugates achieved 8–18% cleavage of the target RNA, depending on the length of the linker. Blm–oligodeoxynucleotide conjugates thus demonstrated sequence specificity and site specificity against RNA and DNA targets.

### INTRODUCTION

The ability to turn off individual genes at will in growing cells provides a powerful tool for elucidating the role of a particular gene and for therapeutic intervention when that gene is overexpressed or mutated. Following the first suggestion that a complementary oligonucleotide could be prepared to target a naturally occurring nucleic acid sequence (1), an antisense oligonucleotide was first utilized successfully against Rous sarcoma virus (2). Since then, complementary oligonucleotides were first used to inhibit the expression of an activated oncogene, *MYC*, in human HL-60 promyelocytic leukemia cells (3). Antisense DNA inhibition has been applied to a wide variety of target genes in cells (4), animals (5), and humans (6).

Chemically reactive oligonucleotide derivatives on the complementarity principle underlie the design of a new generation of antiviral and antitumor therapeutic drugs (7). In particular, the chain scission antibiotic bleomycin A5 has been conjugated to complementary oligonucleotides to allow site-directed cleavage of DNA (8). Bleo-

mycin (Blm) is an antibiotic derived from the soil bacterium *Streptomyces verticillus* (9). The nonspecific cleavage of double stranded DNA or higher ordered tRNA by bleomycin results in antibacterial as well as antitumor activity (10). The bleomycins are glycopeptides with a molecular weight of approximately 1500 Da. Differences exist among bleomycin molecules due to differences in the composition of their terminal amines. There are four functional domains within the bleomycin structure (9) (Figure 1). Bleomycins are classified according to the different terminal amines attached to the bithiazole group at the C-terminus. It is the bithiazole residue and the C-terminal amine that are responsible for binding to DNA. Thus, the differences in the C-terminal amines in the various classes of bleomycin result in different binding affinities, with subsequent differences in cleavage efficiencies.

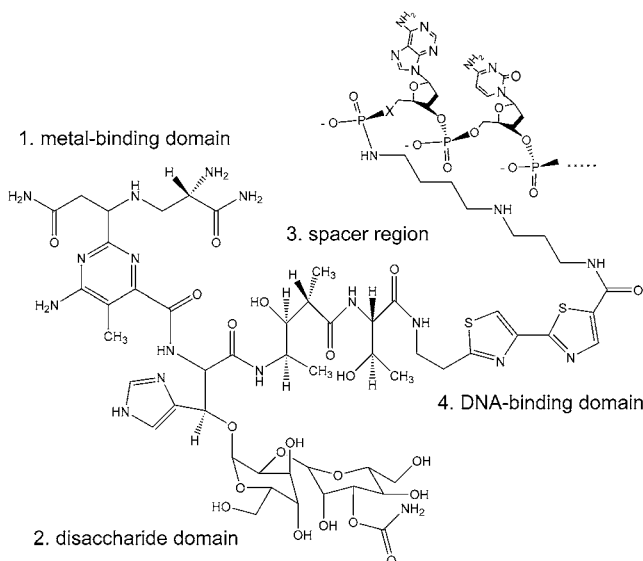
Bleomycins contain metal binding domains at the N-terminus, and binding of a divalent metal cation is thought to be necessary for this domain to become functional. Although Fe(II) is one of the most efficient ions that serve this function, other divalent cations may also form a complex with the N-terminal domain (10). Cleavage of yeast tRNA<sup>Phe</sup> by free bleomycin has been observed, dependent on the secondary and tertiary structure, as well as the primary sequence, of the tRNA, resulting in cleavage at numerous positions; the percentage of cleavage at each site was quite low (10). It is known that some RNAs serving different biological functions are

\* Corresponding author. Voice: 215-955-4578; fax: 215-955-4580. E-mail: eric@tesla.jci.tju.edu.

<sup>†</sup> Russian Academy of Sciences.

<sup>‡</sup> Department of Microbiology and Immunology, Thomas Jefferson University.

<sup>§</sup> Department of Biochemistry and Molecular Pharmacology, Thomas Jefferson University.



**Figure 1.** Bleomycin A5-oligonucleotide. The metal-binding domain (1) at the amino terminus of bleomycin is responsible for cleavage and also interacts with the nucleic acid target. The disaccharide domain (2) favors the binding of oxygen, which is necessary for oxidative cleavage of the nucleic acid. The structure of spacer region (3) plays a significant role in defining optimal conformation of the molecule, thus influencing the efficiency of DNA cleavage. The DNA-binding domain (4) at the C-terminal end of bleomycin forms a strong noncovalent complex with the nucleic acid.

efficiently cleaved by free bleomycin. In particular, the cleavage of 5S yeast ribosomal RNA occurs at U nucleotide residues in the 5'-GUA-3' sequences preceding single-nucleotide bulges (11). Apparently, these regions of the RNA structure serve as sites of the preferential binding of bleomycin in the conformation favorable for selective oxidation of the ribose residue.

We hypothesized that the cleavage activity of bleomycin could be targeted to a specific DNA or mRNA sequence by conjugation of bleomycin to the 5' end of a complementary oligodeoxynucleotide. We also hypothesized that the cleavage of the target RNA could be increased significantly by formation of one-nucleotide bulge motifs in the RNA:antisense duplex.

Previously we reported that a 15 nt antisense oligonucleotide, MMYC55, targeted to a C-terminal site in murine *c-myc* mRNA inhibited tumor growth in a mouse

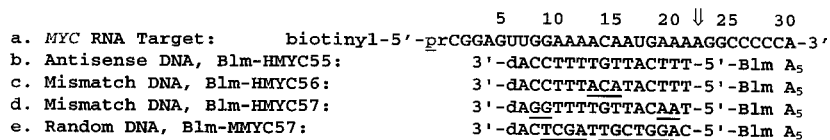
model of B-cell lymphoma (12), in agreement with earlier observations of inhibition of human *MYC* expression in human HL60 cells by the corresponding HMYC55 antisense 3'-N-phosphoramidate (13).

## EXPERIMENTAL PROCEDURES

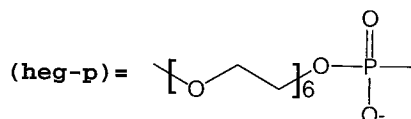
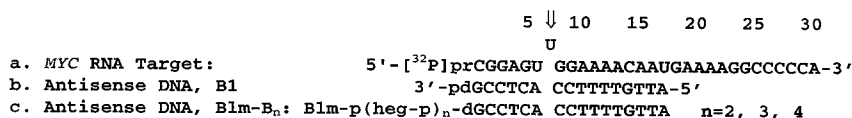
**Oligonucleotides.** The oligonucleotide portion of Blm-HMYC55 conjugate was designed to base-pair with the sense strand of the human *MYC* mRNA corresponding to those same nucleotides (Figure 2). The target sequence, nucleotides 7041–7070 (14), encodes 30 nucleotides encoding residues 382–391 of the C-terminal domain of Myc protein. Below the target RNA in Figure 2 are the three Blm-oligonucleotide reagents that were used in the experiments described. Three internal mismatches (underlined sequence) in HMYC56 disrupt continuous base-pairing to the target, allowing six base-pairs to form on either side of the mismatch zone. The random reagent includes 15 nucleotides that are unable to base-pair stably with the target RNA. We hypothesized that cleavage of the target RNA could occur at the junction of the 5' end of the Blm-HMYC55 antisense reagent and the RNA target, 21 nucleotides from the 5' end of the RNA target (blue arrow in Figure 2). Alternatively, we hypothesized that cleavage of the target RNA could occur at a single nucleotide bulge (blue arrow in Figure 3) created near the 5' end of the RNA upon formation of bulged hybrid duplexes with 3'-Blm-linker-oligonucleotide 16-mers (Figure 3).

Bleomycin A5 was obtained from the Institute of Organic Synthesis (Riga, Latvia). The *MYC* sense DNA and RNA 30-mer targets, DNA 15-mers HMYC55, HMYC56, HMYC57, MMYC57 (Figure 2), and DNA 16-mer B1, and its hexaethylene glycol-containing analogues (Figure 3) were synthesized by the phosphoramidite approach, then purified by ion exchange and reversed-phase HPLC. The hexaethylene glycol phosphoramidite synthon for Blm-B2–B4 oligonucleotides was synthesized as described previously (15). Bleomycin A5 was conjugated with oligonucleotides as described (16, 17). Oligonucleotides were activated with a mixture of triphenylphosphine and 2,2'-dipyridyl disulfide in the presence of (dimethylamino)pyridine *N*-oxide. Bleomycin A5 was attached to the activated 5'-phosphate of oligonucleotides through the terminal spermidine amino group.

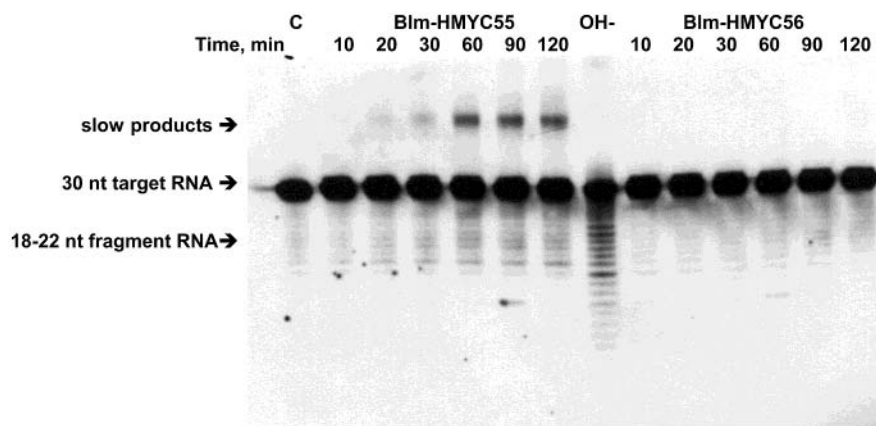
Analytical denaturing gel electrophoresis of Blm-DNA conjugates revealed single bands. MALDI-TOF mass



**Figure 2.** *MYC* RNA: Blm-DNA schematic. a. *MYC* RNA target, 30 nucleotides derived from the human *MYC* exon 3, nucleotides 7041–7070 (14); b. antisense Blm-oligodeoxynucleotide 15-mer; c, d. mismatch Blm-oligodeoxynucleotide 15-mers; e. random Blm-oligodeoxynucleotide 15-mer.



**Figure 3.** Bulged *MYC* RNA: Blm-DNA schematic. a. [<sup>32</sup>P] *MYC* RNA target with bulge at U7; b. B1, antisense oligodeoxynucleotide 16-mer lacking complement for U7; c. Blm-B<sub>n</sub>, antisense Blm-linker-oligodeoxynucleotide 16-mer with 2, 3, or 4 hexaethylene glycol phosphate linkers.



**Figure 4.** *MYC* RNA reactions with 10  $\mu$ M Blm–HMYC55 vs 10  $\mu$ M Blm–HMYC56. Each 10  $\mu$ L reaction mixture also contained 1  $\mu$ M *MYC* target RNA 30-mer, 50 mM  $\beta$ -mercaptoethanol, 200 mM LiCl, 10 mM Tris-HCl, pH 7.5. Bleomycin reactions were initiated by the addition of 100  $\mu$ M  $\text{Fe}(\text{NH}_4)_2(\text{SO}_4)_2$ , and were incubated at 37  $^\circ\text{C}$ . Lane C: *MYC* RNA in reaction conditions for 120 min; lane OH $^-$ : 0.2 M  $\text{NaHCO}_3$ , pH 8.9, 30 min. at 37  $^\circ\text{C}$ .

spectroscopy of the antisense Blm–linker-oligodeoxynucleotide 16-mer with 2, 3, or 4 hexaethylene glycol phosphate linkers (Figure 3c) was consistent with prediction: for  $n = 2$ , calculated 6985.8 Da, measured 6982.6 Da; for  $n = 3$ , calculated 7330.1 Da, measured 7330.7 Da; for  $n = 4$ , calculated 7674.4 Da, measured 7688.0 Da. Concentrations of oligonucleotides were measured spectrophotometrically. Calculated molar extinction coefficients at 260 nm were 149 300/M $\cdot$ cm for Blm–HMYC55, 156 000/M $\cdot$ cm for Blm–HMYC56, 163 700/M $\cdot$ cm for Blm–HMYC57, 159 600/M $\cdot$ cm for Blm–MMYC57, 157 400/M $\cdot$ cm for Blm–Bn, 305 500/M $\cdot$ cm for 30-mer target DNA, and 307 700/M $\cdot$ cm for 30-mer target RNA.

The 5'-biotinyl *MYC* sense RNA 30-mer and homologous 5'-biotinyl DNA were obtained from CyberSyn (Aston PA) following synthesis by the phosphoramidite approach and purified by gel electrophoresis. PAGE-purified RNA and DNA were desalted on a C<sub>18</sub> SepPak (Whatman). The *MYC* sense RNA and DNA 30-mer targets were also 5'-labeled with [ $\gamma$ -<sup>32</sup>P]ATP catalyzed by T4 polynucleotide kinase (20).

**Cleavage Reactions.** Unless otherwise noted, cleavage reactions contained 1  $\mu$ M target RNA or DNA, 10  $\mu$ M Blm–DNA, 100  $\mu$ M  $\text{Fe}(\text{NH}_4)_2(\text{SO}_4)_2$ , 50 mM  $\beta$ -mercaptoethanol, 200 mM LiCl, 10 mM Tris-HCl, pH 7.5. The total volume of each reaction was adjusted to 10  $\mu$ L with argon-saturated diethylpyrocarbonate-treated double-deionized water. The reaction was incubated at 37  $^\circ\text{C}$  for 2 h, unless otherwise noted. In some cases, reaction mixtures were treated subsequently with base (0.25 M hydrazine-HCl, pH 8.0, for RNA target, or 0.1 M *n*-butylamine, for DNA target) to hydrolyze unstable intermediate products and resolve low mobility complexes. RNA was incubated 30 min. at 37  $^\circ\text{C}$  in 0.2 M  $\text{NaHCO}_3$ , pH 8.9, to generate alkaline hydrolysis ladders.

**Electrophoretic Analysis.** Each reaction was terminated by addition of four volumes of gel loading buffer II (Ambion, Austin TX) (95% formamide, 18 mM EDTA, 0.025% NaDodSO<sub>4</sub>, 0.025% xylene cyanol FF, and 0.025% bromophenol blue) and stored at –20  $^\circ\text{C}$  until electrophoresis on a 20% denaturing polyacrylamide gel at 50 V/cm until the bromophenol blue dye reached  $\frac{3}{4}$  of the way into the gel. 5'-Biotinyl-RNA and DNA gels were electroblotted onto Zeta-probe nylon membrane (Bio-Rad) at 12 V for 33 min. The RNA or DNA was immobilized by UV-cross-linking using UV-transilluminator. Detection of the RNA and DNA, which were labeled at the 5' end with biotin, was performed using the Ambion Bright-

Star BioDetect Kit. The resulting chemiluminescence was recorded onto Kodak XOMAT film with a typical exposure time of 15 min. Quantitative estimations were made using [<sup>32</sup>P]RNA and [<sup>32</sup>P]DNA targets. Products of cleavage were separated by electrophoresis on 20% denaturing polyacrylamide gel. Gels were dried on a Fisher Biotech FB GD 45 gel drier and autoradiographed with Kodak XOMAT film. Developed films were quantitated on a Kodak 440CF imaging system.

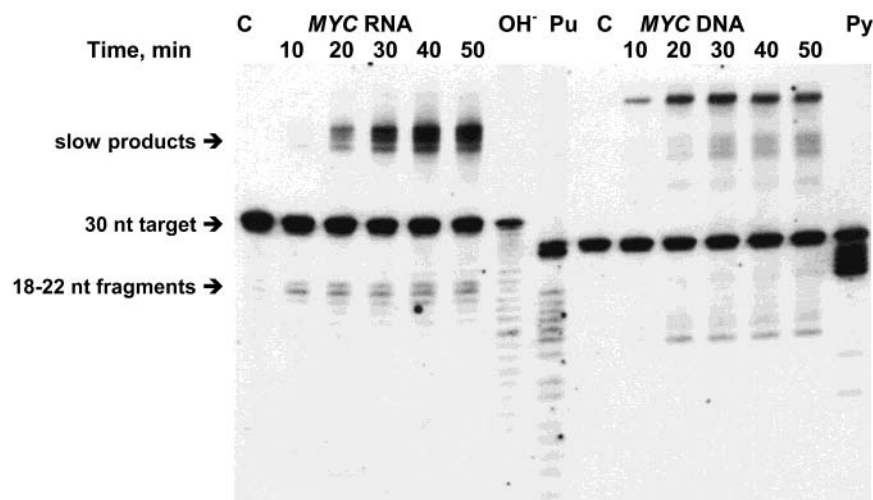
## RESULTS

**Sequence Dependence of RNA Reactions.** The time course of the reaction of *MYC* RNA 30-mer with Blm–HMYC55 vs Blm–HMYC56 was analyzed (Figure 4). The reactions were carried out as described in Materials and Methods above, initiated by the simultaneous addition of Fe(II) and  $\beta$ -mercaptoethanol. In the presence of conjugated Blm–HMYC55, cleavage of *MYC* RNA was observed, 18–22 nucleotides from the 5' end of the RNA. These sites correlated with the positioning of bleomycin by the antisense portion of the reagent (blue arrow in Figure 2). The same bands were observed in the presence of Blm–HMYC56 (3 nt mismatch) at much lower intensities. The reactions with Blm–HMYC55, but not Blm–HMYC56, also produced products that migrated more slowly than the original RNA target, suggesting an additional reaction mechanism more complex than cleavage.

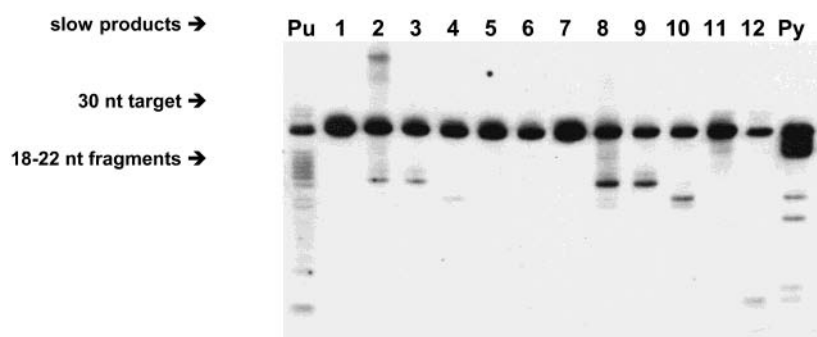
No reaction products were observed in the presence of HMYC55 plus free Blm, or Blm conjugated to a non-complementary MMYC57 15-mer (not shown). Treatment of reacted RNA samples with 0.25 M hydrazine-HCl, pH 8.0, for 30 min. at 37  $^\circ\text{C}$  did not change the band intensities (not shown).

**Sequence Dependence of DNA Reactions.** When a *MYC* DNA 30-mer was also reacted with Blm–HMYC55, and the time course compared for both the RNA and DNA targets, the same analogous low mobility products were seen, along with 18–22 nt DNA fragments (Figure 5). The cleavage product bands reached a plateau early in the 50 min incubation, but the slowly moving products increased linearly throughout the course of the reaction. Lower levels of the reaction products were also observed, in the case of the DNA target (Figure 6), with Blm–HMYC56 (3 mismatches), Blm–HMYC57 (2  $\times$  2 mismatches), but not with random Blm–MMYC57 (12 mismatches). Blm–MMYC57 produced a 5 nt DNA fragment which can be observed also in reaction with free

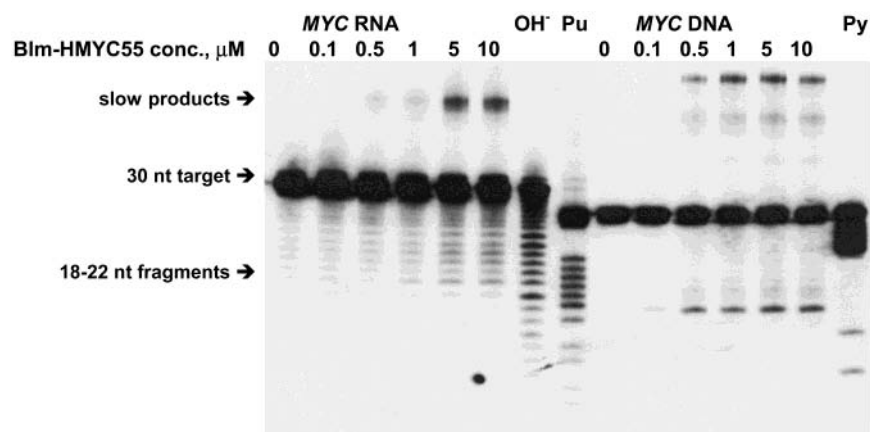




**Figure 5.** *MYC* RNA and *MYC* DNA reactions with 10  $\mu$ M Blm-HMYC55. Each 10  $\mu$ L reaction mixture also contained 1  $\mu$ M *MYC* target RNA 30-mer or DNA 30-mer, 50 mM  $\beta$ -mercaptoethanol, 200 mM LiCl, 10 mM Tris-HCl, pH 7.5. The reactions were initiated by the addition of 100  $\mu$ M  $\text{Fe}(\text{NH}_4)_2(\text{SO}_4)_2$ . Lane C: *MYC* target in reaction conditions for 50 min.; lane OH<sup>-</sup>: 0.2 M NaHCO<sub>3</sub>, Pu, Py: Maxam-Gilbert reactions at purine and pyrimidine residues, respectively.



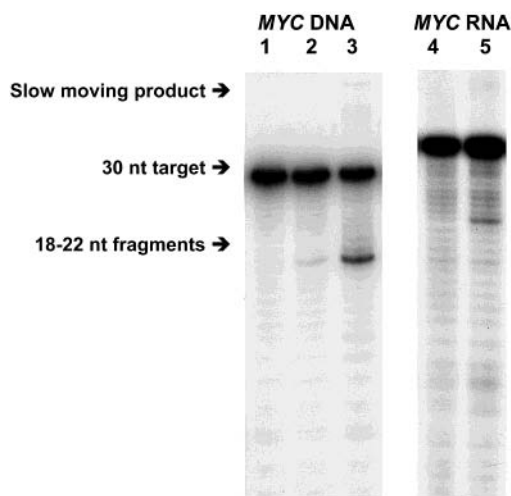
**Figure 6.** *MYC* DNA reactions with 10  $\mu$ M Blm-DNA conjugates. Each 10  $\mu$ L reaction mixture also contained 1  $\mu$ M *MYC* target DNA 30-mer, 50 mM  $\beta$ -mercaptoethanol, 200 mM LiCl, 10 mM Tris-HCl, pH 7.5. The reactions were initiated by the addition of 100  $\mu$ M  $\text{Fe}(\text{NH}_4)_2(\text{SO}_4)_2$ , and were incubated at 37 °C for 2 h. Lanes 1, 7: *MYC* DNA in reaction conditions; lanes 2, 8: Blm-HMYC55; lanes 3, 9: Blm-HMYC56; lanes 4, 10: Blm-HMYC57; lanes 5, 11: Blm-MMYC57; lanes 6, 12: Blm. Before analysis, the reactions in lanes 7–12 were treated with 0.1 M butylamine, 8 min., 95 °C. Lanes Pu, Py: Maxam-Gilbert reactions at purine and pyrimidine residues, respectively.



**Figure 7.** *MYC* RNA and DNA reactions with varying concentrations of Blm-HMYC55. Each 10  $\mu$ L reaction mixture also contained 1  $\mu$ M *MYC* target RNA 30-mer or DNA 30-mer, 50 mM  $\beta$ -mercaptoethanol, 200 mM LiCl, 10 mM Tris-HCl, pH 7.5. The reactions were initiated by the addition of 100  $\mu$ M  $\text{Fe}(\text{NH}_4)_2(\text{SO}_4)_2$ , and were incubated at 37 °C for 50 min. Lane OH<sup>-</sup>: 0.2 M NaHCO<sub>3</sub>; lanes Pu, Py: Maxam-Gilbert reactions at purine and pyrimidine residues, respectively.

bleomycin. Generally, the alkaline treatment reveals additional products of DNA cleavage by bleomycin. Samples of 2 h. DNA reactions were treated with 0.1 M *n*-butylamine for 8 min. at 95 °C before electrophoresis (Figure 6). Treatment with *n*-butylamine eliminated the slowly moving bands and increased the intensities of the cleavage bands.

**Concentration Dependence.** To examine the dependence of product formation on Blm-HMYC55 concentration, a ramp of concentrations from 0.1  $\mu$ M to 10  $\mu$ M, reacting with 1  $\mu$ M *MYC* RNA or DNA, was studied (Figure 7). This experiment revealed that as the Blm-HMYC55 concentrations increased, the extent of cleavage products and slowly migrating products after 50 min also



**Figure 8.** MYC [ $^{32}$ P]RNA and [ $^{32}$ P]DNA reactions with Blm–HMYC55. Each 10  $\mu$ L reaction mixture also contained 1  $\mu$ M MYC target RNA 30-mer or DNA 30-mer, 50 mM  $\beta$ -mercaptoethanol, 200 mM LiCl, 10 mM Tris-HCl, pH 7.5. The reactions were initiated by the addition of 100 mM  $\text{Fe}(\text{NH}_4)_2(\text{SO}_4)_2$ , and were incubated at 37  $^\circ\text{C}$  for 50 min. Lane 1: MYC DNA in reaction conditions; lane 2: 1  $\mu$ M of Blm–HMYC55 added; lane 3: 10  $\mu$ M of Blm–HMYC55 added; lane 4: MYC RNA in reaction conditions; lane 5: 10  $\mu$ M of Blm–HMYC55 added.

increased, reaching a plateau at 5  $\mu$ M for the RNA target, and 1  $\mu$ M for the DNA target. However, product yield remained low; in no case was all target RNA or DNA consumed. Quantitative estimations were made using [ $^{32}$ P]RNA and [ $^{32}$ P]DNA targets. For both targets the amount of slowly moving products did not exceed 3% (Figure 8). The maximum amount of rapidly moving products formed with the RNA target by 10  $\mu$ M Blm–HMYC55 was two times higher (6%). Under the same conditions, 25% of the DNA target was cleaved. Control reactions extended to 7 h revealed no slowly migrating products without bleomycin, with 1  $\mu$ M free bleomycin, with 1  $\mu$ M Blm–HMYC56, with 1  $\mu$ M Blm–HMYC55 but without mercaptoethanol, or with a mixture of 1  $\mu$ M free bleomycin and 1  $\mu$ M HMYC55 (not shown).

**Fe(II) Dependence.** The appearance of tRNA<sup>Phe</sup> cleavage products in the presence of free bleomycin,

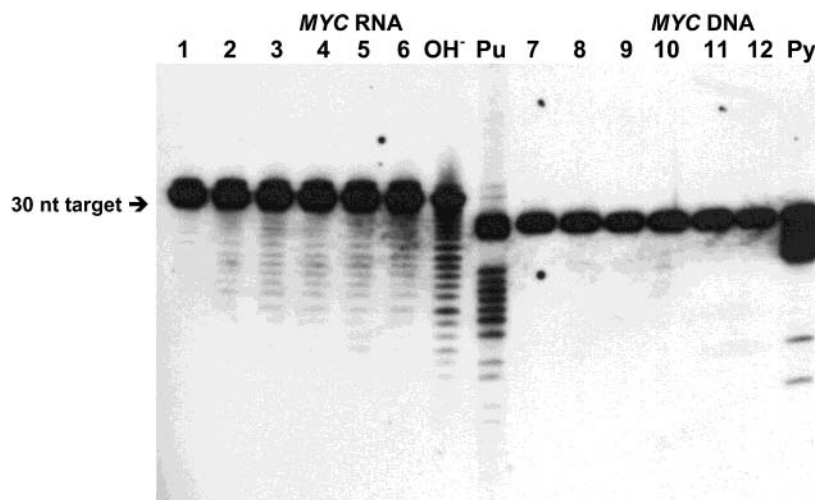
without free Fe(II) (10), invited a similar experiment with Blm–HMYC55 (Figure 9). Preincubation of RNA or DNA with 10 mM EDTA prior to adding Blm–DNA, without any subsequent addition of Fe(II), did not result in any of the slowly moving products or specific cleavage products seen before.

**2'-OH Dependence.** Considering the cleavage of RNA by Blm–HMYC55, one possible mechanism characteristic of RNA is self-hydrolysis by a 2'-OH, mediated by some general base moiety of adjacent bleomycin. Substitution of the MYC RNA target with MYC 2'-O-methyl RNA, suggested by Dr. Serge Beaucage, provided a simple test of that model. Without free Fe(II), no products were observed upon incubation of 1  $\mu$ M MYC 2'-O-methyl RNA with Blm–HMYC55. Both rapidly migrating and slowly migrating products were observed in the presence of Fe(II) (Figure 10).

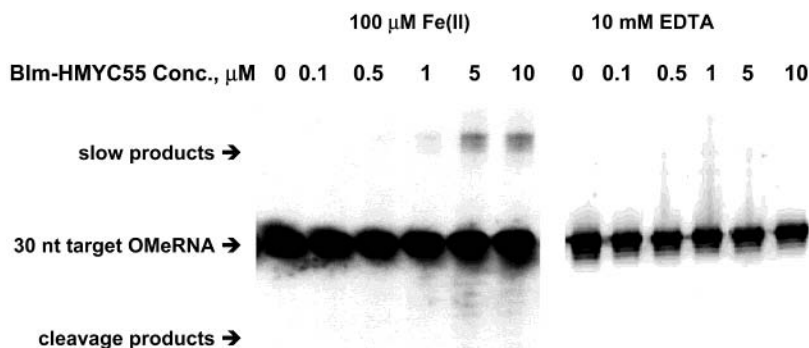
**Cleavage of the RNA by Free Bleomycin at a Bulged Site.** In the case of imperfect complementation between the 16-base oligodeoxynucleotide B1 (Figure 3) and the [ $^{32}$ P]RNA target, an imperfect duplex with a one-nucleotide bulge at U7 in the RNA chain was presumably formed. Efficient cleavage of the [ $^{32}$ P]RNA target by free bleomycin, 30% in 2 h, was observed at U6 adjacent to the presumed bulge at U7 (Figure 11).

**Cleavage of the RNA by Bleomycin–DNA Conjugate at a Bulged Site.** Analogous bulged duplexes of [ $^{32}$ P]RNA with Blm–(hexaethylene glycol phosphate)<sub>n</sub>–B1 DNA conjugates were studied. For the bleomycin residue that was attached to the 3'-terminus of B1 to reach the desired cleavage site, flexible linkers consisting of two, three, or four residues of hexaethylene glycol phosphate, respectively, were included in the Blm–DNA conjugates (Figure 3). Molecular modeling suggested that the lengths of all three linkers are larger than the distance between the 3'-terminal phosphate group of oligonucleotide B1 in conjugates Blm–B2, Blm–B3, and Blm–B4 and the cleaved U6 residue in the RNA target involved in the hybrid duplexes.

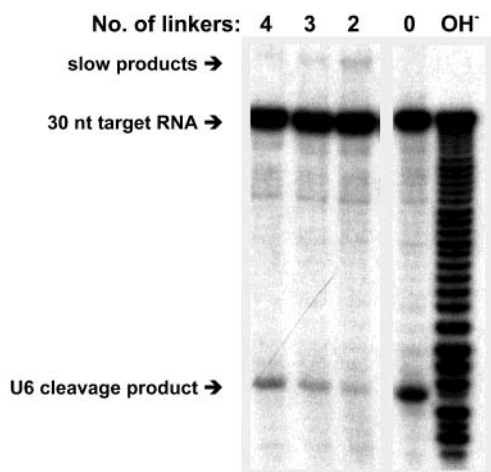
In the presence of conjugates Blm–B2, Blm–B3, and Blm–B4, cleavage of the RNA target occurred at U6 (Figure 11). The efficiency of cleavage in the complex depended on the length of the linker between the bleo-



**Figure 9.** MYC RNA and DNA reactions with 10  $\mu$ M Blm–DNA conjugates preincubated with EDTA. Each 10  $\mu$ L reaction mixture also contained 1  $\mu$ M MYC target RNA (lanes 1–6) or DNA (lanes 7–12) 30-mer, 50 mM  $\beta$ -mercaptoethanol, 200 mM LiCl, 10 mM Tris-HCl, pH 7.5, 10 mM EDTA. Reactions were initiated by the addition of the Blm–DNA conjugate, and were incubated at 37  $^\circ\text{C}$  for 2 h. Lane 1: MYC RNA, lane 7: MYC DNA in reaction conditions; lanes 2, 8: Blm–HMYC55; lanes 3, 9: Blm–HMYC56; lanes 4, 10: Blm–HMYC57; lanes 5, 11: Blm–MMYC57; lanes 6, 12: Blm; lane OH<sup>-</sup>: 0.2 M NaHCO<sub>3</sub>; lanes Pu, Py: Maxam–Gilbert reactions at purine and pyrimidine residues, respectively.



**Figure 10.** *MYC* 2'-*O*-methyl RNA reactions with increasing concentrations of Blm-HMYC55. Each 10  $\mu$ L reaction mixture contained 1  $\mu$ M *MYC* target 2'-*O*-methyl RNA 30-mer, Blm-HMYC55 at the concentrations shown, 50 mM  $\beta$ -mercaptoethanol, 200 mM LiCl, 10 mM Tris-HCl, pH 7.5. The reactions were initiated by the addition of 100  $\mu$ M  $\text{Fe}(\text{NH}_4)_2(\text{SO}_4)_2$ , and were incubated at 37  $^\circ\text{C}$  for 2 h.



**Figure 11.** *MYC* [ $^{32}\text{P}$ ]RNA reactions with 10  $\mu$ M Blm-(hexaethylene glycol phosphate) $_n$ -B1 DNA conjugates that induce a bulge in the RNA at U7. Each 10  $\mu$ L reaction mixture also contained 1  $\mu$ M *MYC* target RNA 30-mer, 50 mM  $\beta$ -mercaptoethanol, 200 mM LiCl, 10 mM Tris-HCl, pH 7.5. The reactions were initiated by the addition of 100  $\mu$ M  $\text{Fe}(\text{NH}_4)_2(\text{SO}_4)_2$ , and were incubated at 37  $^\circ\text{C}$  for 2 h. Lane 0: 10  $\mu$ M free bleomycin in the presence of 10  $\mu$ M B1 oligonucleotide;  $\text{OH}^-$ : 0.2 M  $\text{NaHCO}_3$ .

mycin residue and the oligonucleotide: 8% with Blm-B2, 12% with Blm-B3, and 18% with Blm-B4.

## DISCUSSION

These results reveal that targeted cleavage of RNA or DNA by antisense-conjugated bleomycin is possible. Bleomycin conjugated to HMYC55 cleaved the complementary *MYC* RNA or DNA target at the junction between the DNA:RNA duplex and the RNA single strand, the site to which the oligodeoxynucleotide portion of the reagent directed the bleomycin molecule (Figure 2). It was essential for the antisense oligodeoxynucleotide to be conjugated to bleomycin and fully base-paired in order for cleavage of the RNA target to occur (Figures 4, 6).

In addition, reaction of *MYC* RNA or DNA with Blm-HMYC55 yielded slowly migrating products. Considering the extent of formation of the slowly migrating products, it would be valuable to identify their composition and structure. Mild treatment of reacted RNA samples with hydrazine-HCl did not convert much of the slowly migrating bands to high mobility RNA fragments. On the other hand, more vigorous treatment of reacted DNA

samples with *n*-butylamine fully converted slowly migrating bands to high mobility cleavage fragments.

The slowly migrating products included less than 1% of total band intensity in those reactions that included the Blm-HMYC56 3-mismatch control, and none were detected in the presence of the Blm-HMYC57 4-mismatch control, Blm-random, or free Blm. Reactions in the absence of  $\text{Fe}(\text{II})$  (Figure 9) did not result in any of the slowly moving products or cleavage products, implying the absence of an  $\text{Fe}(\text{II})$ -independent cleavage mechanism. One of the conceivable routes for the formation of such cross-links is the interaction of primary or secondary amines on bleomycin with base labile lesions, which are formed on DNA or RNA as a consequence of oxidation by activated bleomycin (18).

The low extent of target RNA or DNA cleavage by Blm-HMYC55 might reflect a requirement for a rarely occurring conformation. In light of these considerations, it is possible that greater reactivity might result from the use of short tandem oligonucleotides (19), or some other oligonucleotide design, instead of a single completely complementary 15-nt oligonucleotide.

The experiments with Blm-(hexaethylene glycol phosphate) $_n$ -B1 DNA conjugates provided an interesting test of the latter suggestion. Considerably greater cleavage of the target RNA was achieved using conjugates that induce a single nucleotide bulge in the RNA strand of the hybrid duplex. The increase in the extent of cleavage with the lengthening of the linker probably indicates that a particular conformation is favored for efficient cleavage.

Further investigations will be necessary to determine whether complementary bleomycin-oligodeoxynucleotide conjugates exhibit greater antisense efficacy in cells than do complementary oligodeoxynucleotides alone and whether bleomycin-oligodeoxynucleotide conjugates are less toxic than free bleomycin in normal cells.

## ACKNOWLEDGMENT

We thank Dr. Serge Beaucage for suggesting the 2'-*O*-methyl RNA experiment. This work was supported by RFBR grant 99-04-49731a and 02-04-49597a to V.F.Z., Fogarty International Research Collaboration Award TW01094 to V.F.Z. and E.W., and NIH grant CA42960 to E.W.

## LITERATURE CITED

- (1) Belikova, A. M., Zarytova, V. F., and Grineva, N. I. (1967) *Tetrahedron Lett.* 37, 3557-62.



- (2) Zamecnik, P. C., and Stephenson, M. L. (1978) *Proc. Natl. Acad. Sci. U. S. A.* 75, 280–4.
- (3) Wickstrom, E. L., Bacon, T. A., Gonzalez, A., Freeman, D. L., Lyman, G. H., and Wickstrom, E. (1988) *Proc. Natl. Acad. Sci. U. S. A.* 85, 1028–32.
- (4) Wickstrom, E. (1991) *Prospects for Antisense Nucleic Acid Therapy of Cancer and AIDS*, Wiley-Liss, New York.
- (5) Agrawal, S. (1996) *Antisense Therapeutics*, Humana Press, Totowa, NJ.
- (6) Wickstrom, E. (1998) *Clinical Trials of Genetic Therapy with Antisense DNA and DNA Vectors*, Marcel Dekker, New York.
- (7) Knorre, D. G., Vlassov, V. V., Zarytova, V. F., Lebedev, A. V., and Fedorova, O. S. (1994) *Design and Targeted Reactions of Oligonucleotide Derivatives*, CRC Press, Boca Raton, FL.
- (8) Sergeyev, D. S., and Zarytova, V. F. (1996) *Russian Chemical Reviews* 65, 355–378.
- (9) Umezawa, H. (1976) *Prog. Biochem. Pharmacol.* 11, 18–27.
- (10) Keck, M. V., and Hecht, S. M. (1995) *Biochemistry* 34, 12029–37.
- (11) Holmes, C. E., and Hecht, S. M. (1993) *J. Biol. Chem.* 268, 25909–13.
- (12) Smith, J. B., and Wickstrom, E. (1998) *J. Natl. Cancer Inst.* 90, 1146–54.
- (13) Gryaznov, S., Skorski, T., Cucco, C., Nieborowska-Skorska, M., Chiu, C. Y., Lloyd, D., Chen, J. K., Koziolkiewicz, M., and Calabretta, B. (1996) *Nucleic Acids Res.* 24, 1508–14.
- (14) Gazin, C., Dupont de Dinechin, S., Hampe, A., Masson, J. M., Martin, P., Stehelin, D., and Galibert, F. (1984) *EMBO J.* 3, 383–7.
- (15) Pyshnaya, I. A., Pyshnyi, D. V., Ivanova, E. M., Zarytova, V. F., Bonora, G. M., Scalfi-Happ, C., and Seliger, H. (1998) *Nucleosides Nucleotides* 17, 1289–1297.
- (16) Zarytova, V. F., Sergeyev, D. S., and Godovikova, T. S. (1993) *Bioconjugate Chem.* 4, 189–93.
- (17) Sergeyev, D. S., Godovikova, T. S., and Zarytova, V. F. (1995) *Nucleic Acids Res.* 23, 4400–6.
- (18) Gavin, I. M., Melnik, S. M., Yurina, N. P., Khabarova, M. I., and Bavykin, S. G. (1998) *Anal. Biochem.* 263, 26–30.
- (19) Sergeyev, D. S., Vorobjev, P. E., and Zarytova, V. F. (1997) *Nucleosides Nucleotides* 16, 1575–1577.
- (20) Berkner, K. L., and Folk, W. R. (1977) *J. Biol. Chem.* 252, 3176–84.

BC034148U

# Chemoenzymatic Synthesis and Antibody Detection of DNA Glycoconjugates

Yingli Wang and Terry L. Sheppard\*

Department of Chemistry and The Robert H. Lurie Comprehensive Cancer Center, Northwestern University, 2145 Sheridan Road, Evanston, Illinois 60208-3113. Received August 20, 2003; Revised Manuscript Received October 14, 2003

A chemoenzymatic approach for the efficient synthesis of DNA–carbohydrate conjugates was developed and applied to an antibody-based strategy for the detection of DNA glycoconjugates. A phosphoramidite derivative of *N*-acetylglucosamine (GlcNAc) was synthesized and utilized to attach GlcNAc sugars to the 5'-terminus of DNA oligonucleotides by solid-phase DNA synthesis. The resulting GlcNAc–DNA conjugates were used as substrates for glycosyl transferase enzymes to synthesize DNA glycoconjugates. Treatment of GlcNAc–DNA with  $\beta$ -1,4-galactosyl transferase (GalT) and UDP–Gal produced *N*-acetylglucosamine-modified DNA (GlcNAc–DNA), which could be converted quantitatively to the trisaccharide Lewis X (LeX)–DNA conjugate by  $\alpha$ -1,3-fucosyltransferase VI (FucT) and GDP–Fuc. The facile enzymatic synthesis of LeX–DNA from GlcNAc–DNA also was accomplished in a one-pot reaction by the combined action of GalT and FucT. The resulting glycoconjugates were characterized by gel electrophoresis, matrix-assisted laser desorption/ionization time-of-flight mass spectrometry (MALDI-TOF MS), and glycosidase digestion experiments. Covalent modification of the 5'-terminus of DNA with carbohydrates did not interfere with the ability of DNA glycoconjugates to hybridize with complementary DNA, as indicated by UV thermal denaturation analysis. The trisaccharide DNA glycoconjugate, LeX–DNA, was detected by a dual DNA hybridization/monoclonal antibody (mAb) detection protocol ("Southwestern"): membrane-immobilized LeX–DNA was visualized by Southern detection with a radiolabeled complementary DNA probe and by Western chemiluminescence detection with a mAb specific for the LeX antigen. The efficient chemoenzymatic synthesis of DNA glycoconjugates and the Southwestern detection protocol may facilitate the application of glycosylated DNA to cellular targeting and DNA glycoconjugate detection strategies.

## INTRODUCTION

Cell surface glycoconjugates, composed of carbohydrates covalently linked to biomolecules such as lipids or proteins, are key elements in biological molecular recognition processes (1). Glycoconjugates have been implicated in cancer metastasis (2), immune response to pathogenic infection (3), and inflammation (4). For example, the Lewis X (LeX) blood group antigen (BGA) represents an important and well-characterized oligosaccharide in human biology (5). The LeX trisaccharide, Gal $\beta$ 1–4(Fuc $\alpha$ 1–3)GlcNAc, and its BGA analogues are involved in the infection of human cells by parasites (6) and bacteria (7). LeX antigens also serve as tumor markers, since their presence appears to correlate with the metastatic potential of tumor cells (8). The readout and response to cell surface glycoconjugates are performed largely by specific carbohydrate binding proteins, called lectins (9). In addition to naturally occurring lectins, monoclonal antibodies (mAb's) that bind specifically to oligosaccharide structures in glycoconjugates have been isolated. The availability of mAb's specific to carbohydrate antigens has enhanced the understanding of the biological roles of glycoconjugates (10) and formed the basis for antibody-based detection methods for cellular glycosylation states (11, 12). Because of the specificity inherent in protein–carbohydrate interactions, syn-

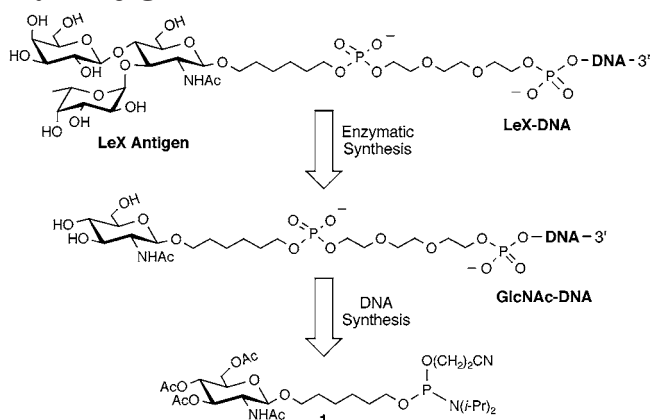
thetic carbohydrate mimics (13), carbohydrate-anchored liposomes (14), and carbohydrate-modified dendrimers (15, 16) have been prepared to investigate carbohydrate–lectin interactions and drug development applications.

In contrast to the abundance of glycosylated proteins and lipids in biological systems, few examples of glycosylated nucleic acids have been reported (17–19). An interesting counterexample was provided by Borst and co-workers, who discovered the existence of 5-( $\beta$ -D-glucosylhydroxymethyl)-2'-deoxyuridine, the "J" nucleoside, in the DNA of *Trypanosoma brucei* (20) and other kinetoplastids (21). Although the biological role of the J-base remains under investigation, it has been implicated in gene expression regulation (22, 23).

The discovery of glycosylated DNA and the importance of carbohydrates in cellular molecular recognition processes have spurred the design, synthesis, and evaluation of artificial DNA glycoconjugates that combine the desirable recognition properties of DNA and carbohydrates. Two main approaches for the conjugation of carbohydrate moieties to DNA recently have been developed: (1) incorporation of glycosylated phosphoramidite building blocks into DNA through solid-phase DNA synthesis (24–28) and (2) postsynthetic glycosylation of a reactive site on synthetic or plasmid DNA (29–31). Despite the reported successes for decoration of DNA with carbohydrates, all current methods require laborious chemical synthesis of a carbohydrate derivative suitable for conjugation to DNA. Although synthesis of monosaccharide derivatives is relatively straightforward, the attachment

\* To whom correspondence should be addressed. Tel: 847-467-7636; Fax: 847-491-7713; E-mail: t-sheppard@northwestern.edu.

### Scheme 1. Chemoenzymatic Synthesis of DNA Glycoconjugates



of complex carbohydrates to DNA is hampered by the synthetic effort required to prepare the oligosaccharide portion with appropriate stereo- and regiochemical control.

Chemoenzymatic synthesis was developed recently to streamline the synthesis of complex carbohydrates (32), glycopeptides (33), and glycopolymers (34). The approach involves the synthesis of a core carbohydrate that serves as a glycosyl acceptor for a glycosyl transferase enzyme. The glycosyl transferase, which utilizes a sugar–nucleotide donor, catalyzes the stereo- and regiospecific glycosylation of the acceptor sugar with the donor carbohydrate. The chemoenzymatic method was successfully employed for the synthesis of sialyl Lewis X (sLeX) BGA (35) and for conjugating sLeX antigens to glycoproteins (36, 37) and synthetic peptides (38). The chemoenzymatic method offers the advantages of enzymatic selectivity, rate acceleration, and compatibility with aqueous reaction media, while avoiding complex protection and deprotection strategies that are required for chemical synthesis of carbohydrates (32). Furthermore, the approach is quite general, provided that the glycosyltransferase enzymes with the desired carbohydrate specificity are available.

Herein we describe a chemoenzymatic approach for the synthesis of DNA glycoconjugates that combines the advantages of chemical synthesis of glycosylated DNA with the efficiency and selectivity conferred by glycosyl transferase enzymes. Our approach is outlined in Scheme 1. We selected **LeX–DNA** as our initial chemoenzymatic target because of the important role of LeX antigens in several biological recognition events. In addition, its sialylated derivative (sLeX) was synthesized previously by both conventional synthetic organic approaches (39, 40) and chemoenzymatic methods (35). Finally, the LeX antigen offers the potential for lectin or antibody-based detection of the LeX–trisaccharide conjugated to DNA. As illustrated in Scheme 1, the target LeX–trisaccharide antigen is tethered to the 5′-end of the DNA oligonucleotide through organic spacers designed to ensure independent functioning of the carbohydrate and DNA portions of the hybrid molecule. We envisaged that **LeX–DNA** would be derived from the sequential enzymatic glycosylation of a monosaccharide-derivatized, **GlcNAc–DNA**. The **GlcNAc–DNA** would be obtained by coupling of the GlcNAc phosphoramidite (**1**) to the 5′-end of a DNA oligonucleotide during solid-phase DNA synthesis. We now report the successful chemoenzymatic synthesis of DNA glycoconjugates, according to Scheme 1, and describe the properties of these hybrid bioconjugates. Our studies show that glycosylation of the 5′-end of DNA oligonucleotides does not interfere with the ability of

DNA glycoconjugates to base pair with complementary DNA. In addition, the **LeX–DNA** offers a new orthogonal detection method for glycosylated DNA, the “Southwestern” detection, in which the oligonucleotide domain is detected by hybridization with a complementary labeled DNA probe, and the LeX–trisaccharide is specifically recognized by an anti-LeX mAb and coupled to a chemiluminescence detection scheme.

### EXPERIMENTAL PROCEDURES

**General Procedures.** All glassware was oven-dried (140 °C). Anhydrous reagents were supplied by Aldrich in Sure-Seal bottles. N<sub>2</sub> was used as an inert atmosphere. All reagents were supplied by Aldrich and were used without further purification unless otherwise noted. Silica gel (40–63 μm, EM Science) was used for flash column chromatography. EM Science Kieselgel 60 F254 plates (0.25 mm) were used for analytical thin-layer chromatography (TLC). Compounds on TLC were visualized by staining with Verghn’s reagent (0.26 M ammonium molybdate, 6.0 mM ceric sulfate in 10% aqueous H<sub>2</sub>SO<sub>4</sub>) (41) followed by warming of the silica gel plate. <sup>1</sup>H and <sup>13</sup>C NMR spectra were recorded at 500 and 125 MHz, respectively, on a Varian 500 instrument, unless noted otherwise. Chemical shift values are reported in parts per million (ppm) in the following format: chemical shift (multiplicity, integration, coupling constant in Hertz, proton assignment). Proton assignments for <sup>1</sup>H spectra were determined using <sup>1</sup>H–<sup>1</sup>H NMR COSY data. <sup>31</sup>P NMR data were recorded at 162 MHz on a Varian 400 spectrometer and were referenced to an external standard of 85% phosphoric acid. Mass spectral data for small molecules were obtained by FAB on a Micromass 70SE–4F spectrometer with 3-nitrobenzyl alcohol or glycerol as the matrix. T4 polynucleotide kinase was obtained from US Biochemical (USB). Terminal deoxynucleotidyl transferase was purchased from Promega. [α-<sup>32</sup>P]-dATP (3000 Ci/mmol) and [γ-<sup>32</sup>P]-ATP (7000 Ci/mmol) were purchased from ICN. Radioactive bands in polyacrylamide gels were visualized using a Molecular Dynamics Storm Phosphorimager and quantitated using Molecular Dynamics ImageQuant software. LeX-conjugated bovine serum albumin (LeX–BSA), bovine recombinant β-1,4-galactosyltransferase expressed from *Spodoptera frugiperda*, human recombinant α-1,3-fucosyltransferase (VI) expressed from *Spodoptera frugiperda*, UDP-α-D-galactose disodium salt, GDP-β-L-fucose disodium salt, anti-LeX (mouse, 32.7 μg/mL), and anti-mouse IgM (goat, peroxidase conjugate, 1 mg/mL) were purchased from Calbiochem. Zeta-probe GT membrane was purchased from Biorad. ECL PLUS western blotting detection kit was purchased from Amersham. Molecular biology grade 4-(2-hydroxyethyl)-1-piperazineethanesulfonic acid (HEPES) was purchased from Sigma.

**6-Benzoyloxyhexyl 2-Acetamido-3,4,6-tri-O-acetyl-2-deoxy-β-D-glucopyranoside (3)** (42). 1-Chloro-2-acetamido-3,4,6-tri-O-acetyl-2-deoxy-α-D-glucopyranoside (**43**) (**2**) (1 g, 2.73 mmol) and 6-benzoyloxyhexanol (**44**) (700 mg, 3.31 mmol) were dissolved in anhydrous CH<sub>2</sub>Cl<sub>2</sub> (27 mL) under N<sub>2</sub>. AgOTf (912.3 mg, 3.55 mmol) was added, and the solution was stirred for 30 min at 25 °C in the dark. The reaction was filtered through a 1 cm Celite pad, and the pad was washed with EtOAc (200 mL). The filtrate was concentrated to 100 mL and washed consecutively with saturated aqueous NaHCO<sub>3</sub> (30 mL), H<sub>2</sub>O (30 mL) and saturated aqueous NaCl (30 mL). The organic layer was dried over MgSO<sub>4</sub>, filtered, concentrated, and purified by flash chromatography (30% hexane/EtOAc) to yield **3** (392.6 mg, 27%). <sup>1</sup>H NMR (CDCl<sub>3</sub>): δ 7.34 (m,



5H, Ar-*H*), 5.52 (d, 1H,  $J_{\text{NH},2} = 8.2$  Hz, NHAc), 5.31 (dd, 1H,  $J_{3,4} = 9.6$  Hz,  $J_{3,2} = 9.6$  Hz, H3), 5.07 (dd, 1H,  $J_{4,3} = 9.6$  Hz,  $J_{4,5} = 9.6$  Hz, H4), 4.68 (d, 1H,  $J_{1,2} = 8.8$  Hz, H1), 4.50 (s, 2H, ArCH<sub>2</sub>), 4.27 (dd, 1H,  $J_{6,5} = 4.5$  Hz,  $J_{6,6'} = 12.5$  Hz, H6), 4.13 (dd, 1H,  $J_{6',5} = 1.5$  Hz,  $J_{6',6} = 12.5$  Hz, H6'), 3.87 (m, 1H, H5), 3.78 (m, 1H, H2), 3.69 (m, 1H, OCH<sub>2</sub>(CH<sub>2</sub>)<sub>5</sub>OBn), 3.46 (t, 2H,  $J = 6.8$  Hz, CH<sub>2</sub>OBn), 3.43 (m, 1H, OCH<sub>2</sub>(CH<sub>2</sub>)<sub>5</sub>OBn), 2.09 (s, 3H, AcO), 2.05 (s, 3H, AcO), 2.03 (s, 3H, AcO), 1.93 (s, 3H, AcN), 1.60 (m, 4H, OCH<sub>2</sub>CH<sub>2</sub>(CH<sub>2</sub>)<sub>2</sub>CH<sub>2</sub>CH<sub>2</sub>OBn), 1.36 (m, 4H, O(CH<sub>2</sub>)<sub>2</sub>-(CH<sub>2</sub>)<sub>2</sub>(CH<sub>2</sub>)<sub>2</sub>OBn). <sup>13</sup>C NMR (CDCl<sub>3</sub>):  $\delta$  170.7, 170.6, 170.1, 169.3, 138.5, 128.3, 127.6, 127.5, 100.7, 73.0, 72.5, 71.8, 70.4, 69.9, 68.9, 62.3, 55.0, 29.9, 29.5, 26.1, 25.9, 23.5, 21.0, 21.0, 20.9. HRMS-FAB ( $m/z$ ): [M + Na]<sup>+</sup> calcd, 560.2472; found, 560.2473.

**6-Hydroxyhexyl 2-Acetamido-3,4,6-tri-*O*-acetyl-2-deoxy- $\beta$ -D-glucopyranoside (**4**)** (45). A solution of **3** (200 mg, 0.37 mmol) in 2 mL of 95% EtOH was stirred at RT under 250 psi H<sub>2</sub> in the presence of 10% Pd/C (35 mg) for 72 h. The solution was filtered, concentrated, and purified by flash chromatography to yield **4** (163.1 mg, 98%). <sup>1</sup>H NMR (CDCl<sub>3</sub>):  $\delta$  5.54 (d, 1H,  $J = 8.5$  Hz, NHAc), 5.30 (dd, 1H,  $J_{3,2} = 10$  Hz,  $J_{3,4} = 10$  Hz, H3), 5.08 (dd, 1H,  $J_{4,3} = 10$  Hz,  $J_{4,5} = 10$  Hz, H4), 4.68 (d, 1H,  $J_{1,2} = 8.0$  Hz, H1), 4.27 (dd, 1H,  $J_{6,5} = 4.5$  Hz,  $J_{6,6'} = 12.5$  Hz, H6), 4.13 (dd, 1H,  $J_{6',5} = 1.5$  Hz,  $J_{6',6} = 12.5$  Hz, H6'), 3.89 (m, 1H, H5), 3.83 (m, 1H, H2), 3.72 (m, 1H, OCH<sub>2</sub>(CH<sub>2</sub>)<sub>5</sub>OH), 3.65 (t, 2H,  $J = 6.4$  Hz, OCH<sub>2</sub>(CH<sub>2</sub>)<sub>4</sub>CH<sub>2</sub>-OH), 3.49 (m, 1H, OCH<sub>2</sub>(CH<sub>2</sub>)<sub>5</sub>OH), 2.10 (s, 3H, AcO), 2.04 (s, 3H, AcO), 2.03 (s, 3H, AcO), 1.96 (s, 3H, AcN), 1.58 (m, 4H, OCH<sub>2</sub>CH<sub>2</sub>(CH<sub>2</sub>)<sub>2</sub>CH<sub>2</sub>CH<sub>2</sub>OH), 1.38 (m, 4H, O(CH<sub>2</sub>)<sub>2</sub>(CH<sub>2</sub>)<sub>2</sub>(CH<sub>2</sub>)<sub>2</sub>OH). <sup>13</sup>C NMR (CDCl<sub>3</sub>):  $\delta$  170.8, 170.7, 170.4, 169.4, 100.8, 72.5, 71.8, 69.8, 68.9, 62.7, 62.4, 54.8, 32.8, 29.4, 25.9, 25.6, 23.5, 21.1, 21.0, 20.9. HRMS-FAB ( $m/z$ ): [M + Na]<sup>+</sup> calcd, 470.2002; found, 470.2003.

**6-*O*-(2-Cyanoethyl-*N,N*-diisopropylphosphoroamidyl)hexyl 2-Acetamido-3,4,6-tri-*O*-acetyl-2-deoxy- $\beta$ -D-glucopyranoside (**1**)**. 2-Cyanoethyl-*N,N*-tetraiso-propylphosphorodiamidite (92.4  $\mu$ L, 0.29 mmol) was added to a solution of **4** (100 mg, 0.22 mmol) and diisopropylammonium tetrazolidine (23 mg, 0.13 mmol) in anhydrous CH<sub>2</sub>Cl<sub>2</sub> (5.5 mL) under N<sub>2</sub>. The reaction was stirred at 25 °C for 30 min and quenched by addition of CH<sub>2</sub>Cl<sub>2</sub> (5.5 mL) and H<sub>2</sub>O (5.5 mL). The phases were separated, and the aqueous phase was back-extracted twice with CH<sub>2</sub>Cl<sub>2</sub> (5.5 mL). The combined organic layers were washed consecutively with saturated aqueous NaHCO<sub>3</sub> (2  $\times$  11 mL), H<sub>2</sub>O (2  $\times$  5.5 mL), and saturated aqueous NaCl (5.5 mL). The solution was dried over MgSO<sub>4</sub>, filtered, concentrated, and purified by flash chromatography (1% Et<sub>3</sub>N, 20% acetone/EtOAc) to yield **1** (111.1 mg, 77%). The final product was coevaporated with anhydrous acetonitrile and dried in vacuo for 12 h. Compound **1** was stored at -20 °C. <sup>1</sup>H NMR (CD<sub>3</sub>CN):  $\delta$  6.39 (d, 1H,  $J = 9.2$  Hz, NHAc), 5.12 (t, 1H,  $J_{3,4} = 10$  Hz, H3), 4.92 (t, 1H,  $J_{4,3} = 10$  Hz, H4), 4.84 (d, 1H,  $J = 8.0$  Hz, H1), 4.21 (dd, 1H,  $J_{5,6} = 4.0$  Hz,  $J_{6,6'} = 10.8$  Hz, H6), 4.13 (dd, 1H,  $J_{6',6} = 10.8$  Hz, H6'), 3.75 (m, 4H, H5, N[CH(CH<sub>3</sub>)<sub>2</sub>]<sub>2</sub>, OCH<sub>2</sub>CH<sub>2</sub>CN), 3.60 (m, 4H, H2, OCH<sub>2</sub>-(CH<sub>2</sub>)<sub>5</sub>OP, OCH<sub>2</sub>(CH<sub>2</sub>)<sub>4</sub>CH<sub>2</sub>OP), 3.48 (m, 1H, OCH<sub>2</sub>(CH<sub>2</sub>)<sub>5</sub>-OP), 2.16 (s, 3H, AcO), 2.13 (s, 3H, AcO), 2.01 (s, 3H, AcO), 1.80 (s, 3H, AcN), 1.58 (m, 4H, OCH<sub>2</sub>CH<sub>2</sub>(CH<sub>2</sub>)<sub>2</sub>CH<sub>2</sub>CH<sub>2</sub>OH), 1.35 (m, 4H, O(CH<sub>2</sub>)<sub>2</sub>(CH<sub>2</sub>)<sub>2</sub>(CH<sub>2</sub>)<sub>2</sub>OH), 1.17 (t, 12H,  $J = 6.5$  Hz, N[CH(CH<sub>3</sub>)<sub>2</sub>]<sub>2</sub>). <sup>13</sup>C NMR (CDCl<sub>3</sub>):  $\delta$  170.8, 170.5, 170.1, 170.0, 101.3, 73.3, 72.0, 70.2, 69.5, 64.1, 63.9, 62.7, 59.0, 58.8, 54.5, 43.6, 43.4, 31.8, 31.7, 29.9, 26.2, 26.1, 24.8, 24.7, 23.0, 20.9, 20.8, 20.8, 20.8,

20.7. <sup>31</sup>P NMR (CD<sub>3</sub>CN):  $\delta$  147.549 (s, P-1). HRMS-FAB ( $m/z$ ): [M + H]<sup>+</sup> calcd, 648.3261; found, 648.3263.

**DNA Synthesis, Deprotection, and Purification.** Unmodified DNA oligonucleotides were synthesized by Integrated DNA Technologies (Coralville, IA), purified by 20% denaturing polyacrylamide gel electrophoresis (dPAGE), and characterized by MALDI-TOF MS. Carbohydrate-modified DNA oligonucleotides were synthesized by automated methods on a Pharmacia Gene Assembler at the 1.3  $\mu$ mol scale. The triethyleneglycol phosphoramidite and natural nucleoside phosphoramidites, utilizing labile base protecting groups (Pac-dA-CE, Ac-dc-CE, *i*Pr-Pac-dG-CE and dT-CE), were obtained from Glen Research (Sterling, VA). Phosphoramidite **1** was used at a concentration of 0.1 M in anhydrous CH<sub>3</sub>-CN for DNA synthesis. After synthesis, the DNA-carbohydrate conjugates were deprotected in 28% ammonium hydroxide for 24 h at 37 °C. The ammonia solution was removed using a Speedvac concentrator, and the residue was redissolved in 200  $\mu$ L of TE Buffer (10 mM Tris, 1 mM EDTA, pH 7.5) and combined with 200  $\mu$ L of 2x gel loading buffer (2x GLB: 20% (v/v) sucrose, 0.1 M EDTA, 0.1% (w/v) SDS, 0.05% (w/v) bromophenol blue, 0.05% (w/v) xylene cyanol, 16 M Urea). The DNA glycoconjugates were purified using 20% dPAGE (29:1 acrylamide:bisacrylamide, 8 M urea, 89 mM Tris, 89 mM borate, 1 mM Na<sub>2</sub>EDTA) with 1x TBE (89 mM Tris, 89 mM borate, 1 mM Na<sub>2</sub>EDTA) as a running buffer. DNA in gels was imaged by short-wave UV shadowing, excised with a flame-sterilized razor blade, and eluted from the gel pieces with crush and soak buffer (10 mM Tris-HCl, 200 mM NaCl, 1 mM EDTA, pH 7.5) at 25 °C for 12 h. The eluent and the gel pieces were combined and filtered through a 0.2  $\mu$ m filter. NaOAc (3 M, pH 5.2, 0.1x v:v) and ethanol (3.0x v:v) were added into the filtrate, and the precipitation solution was incubated at -20 °C for 2 h. The supernatant was removed, and the pellets were dried on a Speedvac concentrator, redissolved in 500  $\mu$ L ddH<sub>2</sub>O, and desalted on a G-25 Sephadex column (NAP, Amersham). Purified DNA glycoconjugates were quantitated by UV absorption at 260 nm using extinction coefficients based on nearest-neighbors method (46).

**3'-Radiolabeling of DNA Glycoconjugates.** DNA glycoconjugate (~100 pmol) was incubated at 37 °C for 45 min with 50 units of terminal deoxytransferase (TDT) in a 20  $\mu$ L reaction containing 100 mM cacodylate pH 6.8, 0.1 mM DTT, 1 mM CoCl<sub>2</sub>, and 40 pmol [ $\alpha$ -<sup>32</sup>P]-dATP. 2x GLB (20  $\mu$ L) was added to the reaction, and the sample was purified by nondenaturing 20% PAGE (29:1 acrylamide:bisacrylamide, 89 mM Tris, 89 mM borate) with 1x TB (89 mM Tris, 89 mM borate) as running buffer. The gel was imaged onto film, and the band corresponding to radiolabeled DNA conjugate was excised with a flame-sterilized razor blade. The DNA was removed from the gel slices by elution into 300  $\mu$ L of ddH<sub>2</sub>O for 12 h at 4 °C.

**5'-Radiolabeling of DNA Oligonucleotides.** DNA oligonucleotide (100 pmol) was incubated at 37 °C for 40 min with 24.5 units of polynucleotide kinase (USB) in a 20  $\mu$ L reaction containing 10 mM Tris-acetate, 10 mM magnesium acetate, 50 mM potassium acetate, and 24 pmol (8.4 Ci/ $\mu$ L) of [ $\gamma$ -<sup>32</sup>P]-ATP (7000 Ci/mmol). 2x GLB (25  $\mu$ L) then was added to the reaction, and the sample was purified by nondenaturing 20% PAGE and isolated as described for 3'-radiolabeling.

**Synthesis of LacNAc-DNA by  $\beta$ -1,4-Galactosyltransferase-Catalyzed Glycosylation of GlcNAc-DNA.** GlcNAc-DNA (40 nmol) was incubated at 37 °C for 8 h with 0.1 unit of  $\beta$ -1,4-galactosyltransferase in a

60  $\mu$ L solution containing 50 mM HEPES pH 7.5, 20 mM Mn(OAc)<sub>2</sub>, 0.5 mg/mL  $\alpha$ -lactalbumin, and 0.13 mM Gal-UDP. 2x GLB (60  $\mu$ L) was added to the reaction, and the sample was purified by nondenaturing 20% PAGE with 1x TB as the running buffer. The DNA glycoconjugates were imaged by short-wave UV shadowing, excised with a flame-sterilized razor blade, and retrieved from the gel pieces by soaking in 300  $\mu$ L of ddH<sub>2</sub>O at 4  $^{\circ}$ C for 12 h. The purified DNA glycoconjugate was desalted by reverse phase HPLC (RP-HPLC).

**DNA Desalting by RP-HPLC.** Gel purified DNA glycoconjugates were desalted by RP-HPLC on a Waters series 600 HPLC system using an XTerra reverse-phase C-18 column (3.5  $\mu$ m, 4.6 mm  $\times$  50 mm). After injection of the oligonucleotide, a 30 min 100% water wash at 1 mL/min was used to elute buffer salts. The desalted DNA glycoconjugates then were eluted with 95% CH<sub>3</sub>CN/H<sub>2</sub>O. DNA-containing peaks (254 nm absorption) were collected and dried by lyophilization.

**Synthesis of LeX-DNA by  $\alpha$ -1,3-Fucosyltransferase (VI)-Catalyzed Glycosylation of LacNAc-DNA.** LacNAc-DNA (40 nmol) was incubated at 37  $^{\circ}$ C for 8 h with 1.4 mU of  $\alpha$ -1,3-fucosyltransferase (VI) in a 60  $\mu$ L solution containing 50 mM HEPES, pH 7.5, 20 mM Mn(OAc)<sub>2</sub>, 0.5 mg/mL  $\alpha$ -lactalbumin, and 0.13 mM Fuc-GDP. 2x GLB (60  $\mu$ L) was added to the reaction, and the sample was purified by a nondenaturing 20% PAGE with 1x TB as the running buffer. The glycoconjugates were recovered and desalted as described previously.

**Synthesis of LeX-DNA by  $\alpha$ -1,3-Fucosyltransferase (VI)- and  $\beta$ -1,4-Galactosyltransferase-Catalyzed Glycosylation of GlcNAc-DNA.** GlcNAc-DNA (40 nmol) was incubated at 37  $^{\circ}$ C for 8 h with 0.1 unit of  $\beta$ -1,4-galactosyltransferase and 1.4 mU of  $\alpha$ -1,3-fucosyltransferase (VI) in a 60  $\mu$ L solution containing 50 mM HEPES pH 7.5, 20 mM Mn(OAc)<sub>2</sub>, 0.5 mg/mL  $\alpha$ -lactalbumin, 0.13 mM Fuc-GDP, and 0.13 mM Gal-UDP. 2x GLB (60  $\mu$ L) was added to the reaction, and the sample was purified and isolated as described previously.

**MALDI-TOF MS.** Mass spectral data for oligonucleotides were obtained on a PerSeptive Biosystems, Inc. (Foster City, CA), Voyager-DE PRO Biospectrometry Workstation MALDI-TOF mass spectrometer. An N<sub>2</sub> laser was used (337 nm wavelength, 3 ns pulse). All spectra were acquired in the negative ion mode averaging 300 shots. Matrix for **GlcNAc-DNA-1**, **LacNAc-DNA-1**, and **LeX-DNA-1** was prepared by mixing 80  $\mu$ L of a 0.2 M solution of 2,4,6-trihydroxyacetophenone in 1:1 CH<sub>3</sub>CN:H<sub>2</sub>O and 10  $\mu$ L of 0.3 M aqueous ammonium citrate. Matrix for **GlcNAc-DNA-2**, **LacNAc-DNA-2**, and **LeX-DNA-2** was prepared by mixing 20  $\mu$ L of a 0.2 M solution of 2,4,6-trihydroxyacetophenone in 1:1 CH<sub>3</sub>CN:H<sub>2</sub>O, 10  $\mu$ L of a 0.2 M solution of 2,3,4-trihydroxyacetophenone in 1:1 CH<sub>3</sub>CN:H<sub>2</sub>O, and 10  $\mu$ L of 0.2 M aqueous ammonium citrate. Poly(dT)<sub>10</sub>, poly(dT)<sub>24</sub> and poly(dT)<sub>37</sub> were obtained from Integrated DNA Technologies and used for internal calibration. All observed masses were in agreement with calculated values (*m/z*): **GlcNAc-DNA-1**: calcd, 5084.39; found, 5084.15. **LacNAc-DNA-1**: calcd, 5246.53; found, 5247.15. **LeX-DNA-1**: calcd, 5392.67; found, 5389.94. **GlcNAc-DNA-2**: calcd, 9498.19; found, 9499.58. **LacNAc-DNA-2**: calcd, 9660.33; found, 9657.92. **LeX-DNA-2**: calcd, 9806.47; found, 9806.62.

**UV Thermal Denaturation Analysis.** Thermal denaturation data were acquired on a Cary 500 spectrophotometer equipped with a multicuvette thermoelectric controller in 10 mm quartz cuvettes. Duplex oligonucleo-

tides were prepared from 2  $\mu$ M of each strand in buffer consisting of 10 mM sodium phosphate, 0.1 mM EDTA, 150 mM NaCl, pH 7.0. Strands were annealed by heating to 95  $^{\circ}$ C for 15 min and cooling to 25  $^{\circ}$ C over 2 h. The samples were degassed under vacuum for 3 min prior to melting analysis. The absorbance was measured at 260 nm as the samples were heated from 25  $^{\circ}$ C to 98  $^{\circ}$ C at 0.5  $^{\circ}$ C/min. Melting temperatures (*T<sub>m</sub>*) were determined from plots of  $dA_{260}/dT$  vs *T* and are derived from replicate melting experiments using two independent samples.

**Membrane Blotting of DNA Glycoconjugates, DNA Oligonucleotides, and LeX-BSA.** A wet Zeta-probe GT membrane was placed on top of a moist 3MM Whatman filter paper, and all air bubbles were removed. DNA glycoconjugates (50 pmol), standard DNA oligonucleotides (50 pmol), and LeX-BSA (50 pmol) were spotted on the membrane by pipetting. The membrane then was heated at 80  $^{\circ}$ C for 45 min and cooled to RT.

**Detection of DNA Glycoconjugates with Anti-LeX Antibody.** Blotted membranes were incubated in 5% nonfat dry milk (NFDM) in TTBS (0.02 M Tris, 0.5 M NaCl, 0.05% Tween 20, pH 7.5) and shaken at 25  $^{\circ}$ C for 1 h to block nonspecific binding. The membrane was transferred to a solution of 5% NFDM/TTBS with anti-LeX antibody (mouse, 65.4 ng/mL) and incubated at 25  $^{\circ}$ C for 1 h. The membrane was washed with 0.2% NFDM/TTBS for 3  $\times$  5 min and incubated in a solution of anti-mouse IgM (goat, HRP conjugate, 200 ng/mL) in 5% NFDM/TTBS at 25  $^{\circ}$ C for 1 h. The membrane was washed 3 times for 5 min each in 0.2% NFDM/TTBS, then for 15 min with TBS (0.02 M Tris base, 0.5 M NaCl, pH 7.5). The membrane was developed for 5 min using an ECL PLUS western blotting detection kit. The wet membrane was wrapped with plastic wrap and exposed to film (KODAK O-XMAT-LS).

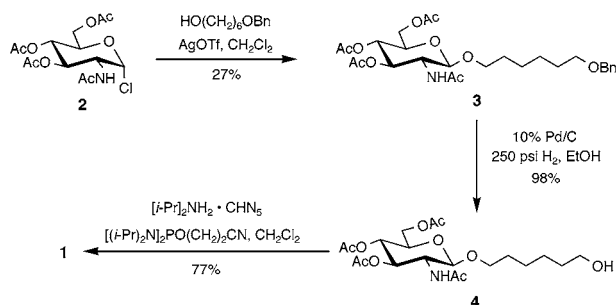
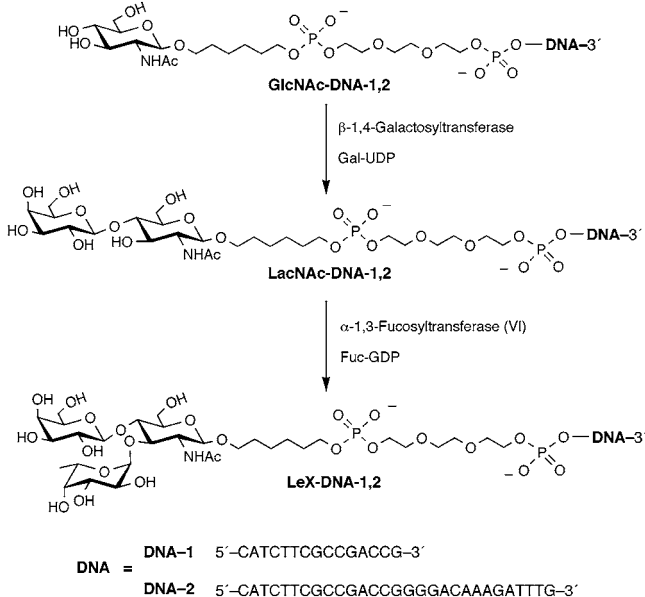
**Detection of DNA Glycoconjugates with Radiolabeled Complementary DNA Probes.** Blotted membranes were incubated in hybridization buffer (0.5 M phosphate buffer, 1 mM EDTA, 7% SDS, pH 7.2) at 65  $^{\circ}$ C for 30 min. The membrane was transferred to hybridization buffer containing radiolabeled (400 kcpm) complementary DNA oligonucleotide and incubated at 55  $^{\circ}$ C for 30 min. The membrane was washed consecutively with wash buffer I (40 mM phosphate, 1 mM EDTA, 5% SDS, pH 7.2) for 3 min at 55  $^{\circ}$ C, and wash buffer II (40 mM phosphate, 1 mM EDTA, 1% SDS, pH 7.2) for 3 min at 55  $^{\circ}$ C. The membrane was air-dried, wrapped with plastic, and imaged with a phosphor screen.

## RESULTS AND DISCUSSION

**Synthesis of GlcNAc Phosphoramidite (1).** The chemical component of the chemoenzymatic approach, outlined in Scheme 1, involved the synthesis of GlcNAc phosphoramidite (**1**) and preparation of **GlcNAc-DNA**. Our carbohydrate target (**1**) featured a GlcNAc sugar with a linker that originated at the glycosidic position of the sugar and terminated in a phosphoramidite group for use in standard solid-phase DNA synthesis. The glycosidic linker site was chosen for two major reasons. First, literature precedent (24, 47–49) suggested that stereocontrolled incorporation of linker groups at glycosidic sites would be accessible by standard glycosylation methods. Second, since our enzymatic approach relied on the availability of unmodified sugar hydroxyls for optimal activity of the glycosyl transferases, attachment of DNA to the nonreducing end of the glycoconjugate offered considerable advantages.

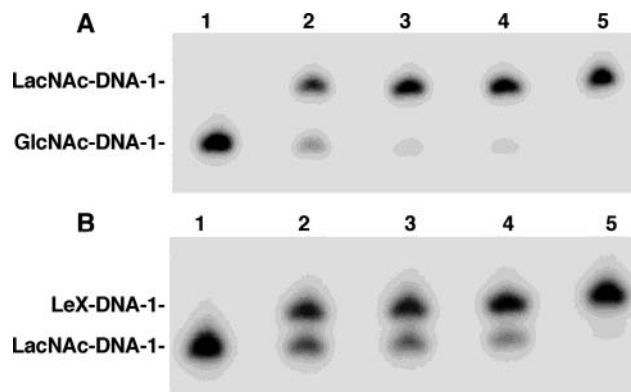
The GlcNAc phosphoramidite (**1**) was prepared using the route detailed in Scheme 2. The anomeric chloride



**Scheme 2. Synthesis of GlcNAc Phosphoramidite Derivative 1****Scheme 3. Chemoenzymatic Synthesis of LeX-DNA**

starting material (**2**) was synthesized from D-glucosamine in 76% yield as described (43). The known monobenzyl ether of 1,6-hexanediol (**44**) was glycosylated with GlcNAc donor **2** in the presence of silver triflate to form 6-benzyloxyhexyl 2-acetamido-3,4,6-tri-O-acetyl-2-deoxy-β-D-glucopyranoside (**3**) (24). The anomeric configuration for **3** was confirmed as β, based on the inferred trans diaxial orientation of H1 and H2 by  $^1\text{H}$  NMR experiments ( $J_{1,2} = 8.8$  Hz). Isomeric structures (such as ortho ester) were ruled out by  $^{13}\text{C}$  NMR chemical shift analysis. The benzyl group was removed from **3** by hydrogenolysis (50) using Pd/C catalyst to provide alcohol **4** in 98% yield. Finally, the protected GlcNAc derivative **4** was converted to the phosphoramidite target (**1**) by standard methods (51). All synthetic intermediates were characterized by  $^1\text{H}$  and  $^{13}\text{C}$  NMR and HRMS-FAB MS. Phosphoramidite **1** also was characterized by  $^{31}\text{P}$  NMR.

**Synthesis of GlcNAc-DNA Glycoconjugates.** The GlcNAc phosphoramidite (**1**) was used for the synthesis of GlcNAc-modified oligonucleotides by solid-phase DNA synthesis. Two sequences were synthesized, **GlcNAc-DNA-1** and **GlcNAc-DNA-2**, as shown in Scheme 3. A water-soluble and biologically compatible triethylene glycol linker was inserted between GlcNAc and the DNA sequence to prevent steric interference between the carbohydrate and the DNA oligonucleotide. After synthesis, oligonucleotides were deprotected in 28% aqueous ammonia for 24 h at 37 °C, which also removed the O-acetyl protecting groups from the GlcNAc precursor. The coupling yield of **1** during DNA synthesis could not be determined directly by standard assays, due to the



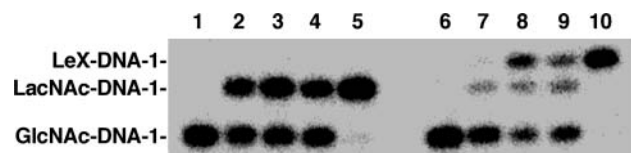
**Figure 1.** Stepwise enzymatic synthesis of LeX-DNA-1. (A) Galactosyl transfer to **GlcNAc-DNA-1**; lanes 2–5: GalT-catalyzed glycosylation of **GlcNAc-DNA-1** for 30 s, 1, 2, and 3 min; (B) Fucosyl transfer to **LacNAc-DNA-1**; lane 1: **LacNAc-DNA-1**; lanes 2–5: FucT-catalyzed glycosylation of **LacNAc-DNA-1** for 30 s, 1, 2, and 3 min.

lack of a dimethoxytrityl protecting group. However, in all cases, only one DNA product was observed during the gel electrophoresis purification of **GlcNAc-DNA**, indicating that the coupling efficiency of **1** was comparable to that of the natural nucleotides (>90%). **GlcNAc-DNA** was further characterized by matrix-assisted laser desorption/ionization time-of-flight mass spectrometry (MALDI-TOF MS). The DNA glycoconjugates gave the expected masses: **GlcNAc-DNA-1**,  $[M]^-$  calcd, 5084.39; found, 5084.15; **GlcNAc-DNA-2**,  $[M]^-$  calcd, 9498.19; found, 9499.58.

**Enzymatic Synthesis and Characterization of DNA Glycoconjugates.** The enzymatic conversion of **GlcNAc-DNA** into **LeX-DNA**, described in Scheme 3, proceeds by two sequential glycosyl transfer reactions:  $\beta$ -1,4-galactosyltransferase (GalT) catalyzed conversion of **GlcNAc-DNA** to **LacNAc-DNA** and  $\alpha$ -1,3-fucosyltransferase VI (FucT) mediated transformation of **LacNAc-DNA** to **LeX-DNA**. We envisaged two possible reaction sequences for the enzymatic synthesis of **LeX-DNA** from **GlcNAc-DNA**. The first was a stepwise route, in which **LacNAc-DNA** would be synthesized using GalT, and the disaccharide-DNA hybrid would be isolated and utilized in a FucT-catalyzed step to synthesize **LeX-DNA**. The sequence of these two reaction steps could not be exchanged because the substrate of FucT is **LacNAc-DNA** (52). A second approach, commonly used for the chemoenzymatic synthesis of glycosylated peptides and proteins (32), was a one-pot, two-step reaction sequence in which the two enzymes were incubated simultaneously with UDP-Gal, GDP-Fuc, and the **GlcNAc-DNA** substrate. In this approach, **LacNAc-DNA**, produced by the GalT reaction, would be glycosylated in situ by FucT to provide **LeX-DNA**. Both approaches proved successful for the enzymatic synthesis of **LeX-DNA** from **GlcNAc-DNA**.

The synthesis of **LacNAc-DNA** and **LeX-DNA** by stepwise action of GalT and FucT is detailed in Figure 1 for DNA glycoconjugates based on sequence **DNA-1** (Scheme 3). Enzymatic glycosylation reactions were performed on **GlcNAc-DNA-1** that had been labeled at its 3'-end with a  $^{32}\text{P}$  tracer, and were assayed by denaturing polyacrylamide gel electrophoresis (dPAGE). Figure 1A illustrates the time course for the conversion of **GlcNAc-DNA-1** (0.1  $\mu\text{M}$ ) to **LacNAc-DNA-1** at 37 °C (50 mM HEPES pH 7.5, 20 mM  $\text{Mn}(\text{OAc})_2$ , 0.5 mg/mL  $\alpha$ -lactalbumin, 2.5  $\mu\text{M}$  Gal-UDP, and 25 units/ $\mu\text{L}$





**Figure 2.** One-pot enzymatic synthesis of **LeX-DNA-1**. Lane 1: **GlcNAc-DNA-1**; lanes 2–5: GalT-catalyzed glycosylation of **GlcNAc-DNA-1** for 15 s, 45 s, 1 min, 10 min; lane 6: **GlcNAc-DNA-1**; lanes 7–10: GalT- and FucT-catalyzed one-pot glycosylation of **GlcNAc-DNA-1** for 15 s, 45 s, 1 min, 10 min.

GalT). Under these conditions, **GlcNAc-DNA-1** (lane 1) was transformed to a product with lower gel mobility (lanes 2–5). More than 50% of **GlcNAc-DNA-1** was converted to product in the first 30 s (lane 2), and the GalT-dependent reaction was >90% complete within 3 min (lanes 3–5). The product (top band, lanes 2–5) showed a mobility shift corresponding to an increase in molecular weight, which was consistent with the synthesis of **LacNAc-DNA-1**. To verify the identity of the lower mobility product, a preparative scale (40 nmole) GalT reaction was performed on unlabeled **GlcNAc-DNA-1** to provide adequate material for further characterization. The product was purified by nondenaturing PAGE, desalted by RP-HPLC, and analyzed by MALDI-TOF MS. The isolated product gave the expected mass for **LacNAc-DNA-1**:  $[M]^-$  calcd, 5246.53; found, 5247.15.

Purified **LacNAc-DNA-1**, which had been synthesized by enzymatic galactosyl transfer, was utilized as a substrate for the FucT-mediated conversion to **LeX-DNA-1**. The reaction mixture (0.1  $\mu$ M 3'-labeled **LacNAc-DNA-1**, 50 mM HEPES, 20 mM Mn(OAc)<sub>2</sub>, 0.5 mg/mL  $\alpha$ -lactalbumin, 2.5  $\mu$ M Fuc-GDP, and 0.35 units/ $\mu$ L FucT) was incubated at 37 °C. Reaction aliquots were removed at specific intervals across 30 s–3 min and analyzed by dPAGE. The results are shown in Figure 1B. The FucT reaction led to a fucosylated DNA product shown by a lower gel mobility band (top band, lanes 2–5), compared with **LacNAc-DNA-1** (lane 1). The reaction proceeded efficiently and was >90% complete in less than 3 min (lane 5). To demonstrate that the product of the FucT reaction was indeed **LeX-DNA-1**, a preparative scale (40 nmole) enzymatic fucosylation reaction was performed. The product was purified by nondenaturing PAGE/RP-HPLC and characterized by MALDI-TOF MS. As was the case for the GalT chemistry, the FucT reaction led to the expected product: **LeX-DNA-1** ( $[M]^-$  calcd, 5392.67; found, 5389.94).

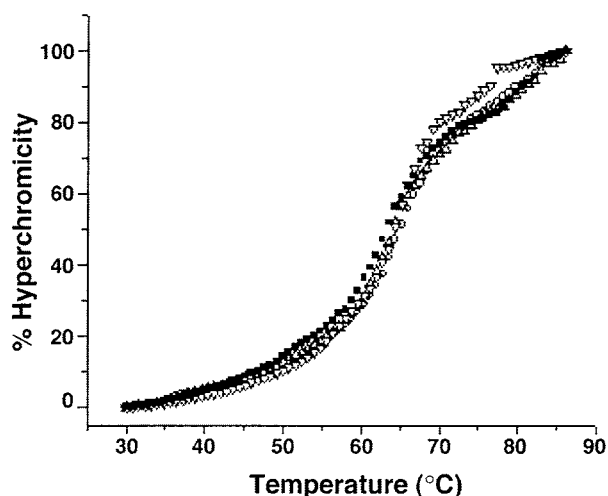
Having demonstrated the efficient stepwise synthesis of **LeX-DNA-1** from **GlcNAc-DNA-1**, we examined the potential for one-pot assembly of **LeX-DNA** by tandem action of GalT and FucT. The time course of the one-pot reaction was analyzed by dPAGE.

The left panel of Figure 2 (lanes 1–5) demonstrates the stepwise conversion of **GlcNAc-DNA-1** to **LacNAc-DNA-1**, which serves as a control for the one-pot reaction. The results of the one-pot tandem reaction are shown in the right panel of Figure 2 (lanes 6–10). Based on gel mobility shifts, the **GlcNAc-DNA-1** starting material (lane 6) was first transformed to **LacNAc-DNA-1** (lane 7). The resulting **LacNAc-DNA-1** underwent further conversion to **LeX-DNA-1** (lanes 8–10). The one-pot reaction led to complete conversion of **GlcNAc-DNA-1** to **LeX-DNA-1** within minutes. Consistent with the substrate specificity of FucT (52), incubation of **GlcNAc-DNA** with FucT produced no new products.

To assess the generality of enzymatic glycosylation of chemically synthesized DNA glycoconjugates, the GalT and FucT experiments were repeated for **GlcNAc-DNA-2**. **LacNAc-DNA-2**, obtained from a GalT reaction, and **LeX-DNA-2**, derived from a one-pot tandem reaction of **GlcNAc-DNA-2** with GalT and FucT, showed gel shift profiles (Supporting Information) similar to those observed for the **DNA-1** glycoconjugates (Figure 2). Preparative enzymatic glycosylations of **GlcNAc-DNA-2** produced DNA glycoconjugates that gave the expected masses by MALDI-TOF MS: **LacNAc-DNA-2** ( $[M]^-$  calcd, 9660.33; found, 9657.92); **LeX-DNA-2** ( $[M]^-$  calcd, 9806.47; found, 9806.62).

**Characterization of DNA Glycoconjugates by Glycosidase Digestion.** To further characterize the identity and specificity of glycosyl transfer reactions of DNA glycoconjugates, "on target" enzymatic digestion experiments (53) were performed. In this approach, DNA glycoconjugates were subjected to digestion by specific glycosidase enzymes on MALDI-TOF MS sample preparation plates. MALDI-TOF mass spectra were obtained for the DNA glycoconjugates before and after digestion with an exoglycosidase specific for a terminal sugar. Successful digestion of the terminal glycosidic bond would reveal the precursor DNA glycoconjugate by MALDI-TOF MS and validate the regiochemistry and stereochemistry of the glycosyl transfer reaction. For compatibility with the MALDI-TOF MS conditions, ammonium acetate (25 mM) was used as the digestion buffer. The on-target digestion of **GlcNAc-DNA-1** was carried out with  $\beta$ -N-acetylglucosaminidase, which specifically cleaves  $\beta$ -linked GlcNAc residues. Incubation of **GlcNAc-DNA-1** at 37 °C for 26 h and subsequent MALDI-TOF MS analysis showed conversion of **GlcNAc-DNA-1** to the **DNA-1** glycol linker conjugate (Supporting Information). The conversion of **GlcNAc-DNA-1** to the parent **DNA-1** structure validates the  $\beta$ -stereochemistry of GlcNAc attachment to the linker. The on-target digestion of **LacNAc-DNA-1** with  $\beta$ -1,4-galactosidase was performed at 37 °C for 14 h. The post-digestion MALDI-TOF MS revealed a peak with the same  $m/z$  as **GlcNAc-DNA-1**, which indicated that the galactose residue was attached to the 4-position of the GlcNAc sugar with  $\beta$ -stereochemistry. Taken together, "on target digestion" of DNA glycoconjugates supports our previous assignments of the identities of **GlcNAc-DNA** and **LacNAc-DNA**.

**Duplex Stability of DNA Glycoconjugates.** Applications of DNA glycoconjugates that take advantage of DNA's coding potential require that DNA glycosylation does not interfere with the base pairing properties of DNA. To assess the effect of carbohydrate modifications on DNA duplex stability, UV thermal denaturation analysis was undertaken with DNA duplexes containing **GlcNAc-DNA**, **LacNAc-DNA**, and **LeX-DNA** strands. The glycosylated DNA sequences were annealed with a complementary DNA strand (**DNA-1'**, Figure 3) at 95 °C for 15 min and cooled to RT over 2 h in a solution containing 2  $\mu$ M of each single strand, 10 mM phosphate buffer, 0.1 mM EDTA and 150 mM NaCl at pH 7.0. For comparison, unmodified **DNA-1** was annealed with **DNA-1'** under identical conditions. As demonstrated in Figure 3, UV thermal denaturation analysis of the unmodified **DNA-1/DNA-1'** (solid squares) duplex showed a cooperative denaturation profile, with a melting temperature ( $T_m$ ) of 63 °C. The duplexes comprised of **DNA-1** glycoconjugates with **DNA-1'** (open symbols, Figure 3) showed no significant destabilization of the duplex due to the carbohydrate modifications ( $T_m$  63–65 °C). Similarly,

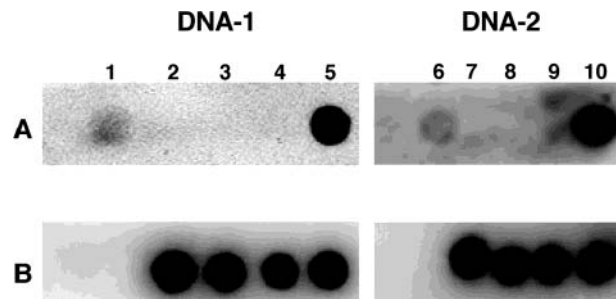


**Figure 3.** Thermal denaturation analysis of DNA-1 glycoconjugates. Conditions: 2  $\mu$ M each single strand, 10 mM sodium phosphate, 0.1 mM EDTA, 150 mM NaCl, pH 7.0. Heating rate: 0.5  $^{\circ}$ C/min. **DNA-1'**: 5' CCGTCGGCGAAGATG 3'. Legend: Solid squares: **DNA-1/DNA-1'**; Open circles: **GlcNAc-DNA-1/DNA-1'**; Open triangles: **LacNAc-DNA-1/DNA-1'**; Inverted triangles: **LeX-DNA-1/DNA-1'**.

thermal denaturation analysis of duplexes composed of **DNA-2** glycoconjugates and **DNA-2'** under the same conditions showed that carbohydrate modification leads to a small decrease in the cooperativity of the DNA melting transition, but the duplex thermal stability was relatively unperturbed (Supporting Information).

**Southwestern Detection of LeX-DNA.** DNA glycoconjugates represent bioconjugates that possess the properties of both DNA and carbohydrates. Because of the central importance of these two classes of biomolecules, numerous approaches for the detection of DNA or glycoconjugates have been developed. Hybridization assays such as the Southern blot (54), in which a radiolabeled complementary nucleic acid probe binds specifically to a target DNA sequence, have been invaluable for DNA detection. In glycobiology, mAb's have been used to detect the presence of specific carbohydrate antigens (55, 56). Much in the same way that mAb's are used to detect proteins in "Western blots," carbohydrate detection by antibodies involves readout of a primary mAb-carbohydrate binding event by a secondary labeled antibody. DNA glycoconjugates, by virtue of their carbohydrate and nucleic acid characteristics, offer a platform for orthogonal detection of either biomolecular component. To assess the feasibility of a combined "Southwestern" detection approach for DNA glycoconjugates, the **LeX-DNA** hybrid was used as a model system for antibody detection. DNA glycoconjugates were bound to nylon membranes and probed either with an antibody specific for the LeX trisaccharide or with a radiolabeled DNA probe complementary to the sequence of the DNA glycoconjugate.

An assay for the antibody-based detection of LeX antigens was developed using two types of antibodies: (1) a primary anti-LeX antibody (derived from mouse), which interacts specifically with the LeX antigen, and (2) a secondary anti-mouse antibody (derived from goat), which was conjugated to horseradish peroxidase (HRP). Binding of the secondary antibody to the primary antibody-LeX complex would localize HRP to membrane spots bearing LeX antigens. Membranes then would be visualized using a HRP-catalyzed chemiluminescence assay. To demonstrate the antibody-based detection strategy, DNA glycoconjugates were spotted on a membrane (see Figure



**Figure 4.** Southwestern detection of DNA glycoconjugates. (A) Anti-LeX detection by chemiluminescence using anti-LeX antibody and (B) DNA detection using radiolabeled complementary DNA strands. Spot 1: LeX-BSA; spot 2: unmodified **DNA-1**; spot 3: **GlcNAc-DNA-1**; spot 4: **LacNAc-DNA-1**; spot 5: **LeX-DNA-1**; spot 6: LeX-BSA; spot 7: unmodified **DNA-2**; spot 8: **GlcNAc-DNA-2**; spot 9: **LacNAc-DNA-2**; spot 10: **LeX-DNA-2**. **DNA-1'**: 5' CCGTCGGCGAAGATG 3'; **DNA-2'**: 5' CAAATCTTTGTCCCCGGTCGGCGAAGATG 3'.

4). A membrane was prepared for each DNA sequence (Figure 4, **DNA-1**, left panels; **DNA-2**, right panels). For each DNA series, unmodified DNA (spots 2 and 7), **GlcNAc-DNA** (spots 3 and 8), **LacNAc-DNA** (spots 4 and 9) and **LeX-DNA** (spots 5 and 10) were spotted on a Zeta-probe GT membrane. Figure 4A demonstrates the results of antibody detection of LeX antigens. As a positive control, LeX-conjugated bovine serum albumin protein (LeX-BSA) was spotted on each membrane (spots 1 and 6). As expected, spots containing materials with LeX trisaccharides, LeX-BSA (spots 1 and 6, Figure 4A) and **LeX-DNA** (spots 5 and 10, Figure 4A) were detected by chemiluminescence with the anti-LeX antibody. In contrast, unmodified DNA (spots 2 and 7) and glycosylated DNA that lacked the LeX antigen, **GlcNAc-DNA** (spots 3 and 8) and **LacNAc-DNA** (spots 4 and 9), were not detected by the antibody specific for LeX recognition (Figure 4A).

To assess whether the same membrane spots could be visualized by nucleic acid hybridization, a Southern detection experiment was performed. The membranes from Figure 4A were stripped to remove antibody and subsequently probed with radiolabeled complementary DNA strands. Due to the pairing properties of DNA glycoconjugates, it was expected that all spots containing nucleic acid would be visualized by phosphorimager analysis of bound probe. As demonstrated in Figure 4B, spots 2–5, which contained **DNA-1**, and spots 7–9, which contained **DNA-2**, gave strong signals in the presence of complementary DNA probe. In contrast, spots containing only protein and carbohydrate (LeX-BSA, spots 1 and 6, Figure 4B) produced no signals, because the protein cannot hybridize with radiolabeled DNA strands. The combined Southwestern detection of DNA glycoconjugates further validated the identity of the DNA glycoconjugate synthesized by the chemoenzymatic approach: sequence-specific DNA binding and LeX-specific antibody recognition were observed in the presence of the target, in both cases. Furthermore, the orthogonal blotting approach of DNA glycoconjugates by radiolabeled complementary strands or anti-LeX antibodies suggests that the DNA and the carbohydrate components of DNA glycoconjugates function independently. These studies demonstrate the potential for detection of specific DNA glycoconjugates by standard glycobiology and molecular biology methods.

Our future plans for DNA glycoconjugates synthesized by chemoenzymatic methods include nucleic acid delivery, targeting and DNA imaging. One direction includes



the application of chemoenzymatic synthesis of DNA glycoconjugates to antisense oligonucleotide delivery strategies. Specifically, antisense DNA oligonucleotides conjugated to cell-type specific antigens will be used for the selective targeting of DNA to cancer cells. Second, in combination with targeting, it may be possible to adapt our chemoenzymatic method to facilitate cellular uptake of DNA. Finally, the utility of the antibody-based DNA detection approach will be explored as an alternative to standard DNA detection strategies and applied toward the visualization of DNA compartmentalization in cells.

In conclusion, a new chemoenzymatic approach to the synthesis of DNA glycoconjugates was developed. **GlcNAc-DNA** was synthesized by solid-phase DNA synthesis using GlcNAc phosphoramidite derivative **1**. Oligosaccharide structures, such as LacNAc or LeX, were elaborated on the **GlcNAc-DNA** core by stepwise or one-pot glycosyl transferase enzyme reactions. The combination of chemical synthesis with the efficiency and specificity of enzymatic synthesis may allow for the rapid preparation of complex DNA glycoconjugates of biochemical or therapeutic interest. For example, it may be possible to extend the methodology to the synthesis of **sLeX-DNA**, in which the biologically important sLeX antigen (*4, 35*) would be synthesized from a simple DNA glycoconjugate. Alternatively, the approach may be applied to the synthesis of cell-specific carbohydrate antigens that may be used to target cellular delivery or uptake of DNA or antisense nucleic acid molecules (*57*). Finally, the combination of these chemoenzymatic methods with the demonstrated orthogonal DNA glycoconjugate detection approach may offer potential for in situ detection of these hybrid biomaterials for biochemical experiments or under cellular conditions.

#### ACKNOWLEDGMENT

This research was supported by a National Cancer Institute SPORE in Prostate Cancer Career Development Award to T.L.S., administered through The Robert H. Lurie Comprehensive Cancer Center of Northwestern University. The MALDI-TOF MS instrument was purchased with funds provided by a NIH Scientific Instrumentation grant (1-S10-RR13810). We acknowledge the use of instruments in the Keck Biophysics Facility at Northwestern University.

**Supporting Information Available:** Characterization data for **1**, mass spectrometric data for modified oligonucleotides, glycosylation assays, "on target" enzymatic digestion assays, and melting curve data. This material is available free of charge via the Internet at <http://pubs.acs.org/BC>.

#### LITERATURE CITED

- (1) Dwek, R. A. (1996) Glycobiology: Toward understanding the function of sugars. *Chem. Rev.* **96**, 683–720.
- (2) Gorelik, E., Galili, U., and Raz, A. (2002) On the role of cell surface carbohydrates and their binding proteins (lectins) in tumor metastasis. *Cancer Metastasis Rev.* **20**, 245–277.
- (3) Ritchie, G. E., Moffatt, B. E., Sim, R. B., Morgan, B. P., Dwek, R. A., and Rudd, P. M. (2002) Glycosylation and the complement system. *Chem. Rev.* **102**, 305–319.
- (4) McEver, R. P. (1997) Selectin-carbohydrate interactions during inflammation and metastasis. *Glycoconjugate J.* **14**, 585–591.
- (5) Feizi, T. (1997) Carbohydrate differentiation antigens II, SSEA-1 (Lex) and related structures. *New Compr. Biochem.* **29b**, 571–586.
- (6) Cummings, R. D., and Nyame, A. K. (1996) Glycobiology of schistosomiasis. *FASEB J.* **10**, 838–848.
- (7) Edwards, N. J., Monteiro, M. A., Faller, G., Walsh, E. J., Moran, A. P., Roberts, I. S., and High, N. J. (2000) Lewis X structures in the O antigen side-chain promote adhesion of *Helicobacter pylori* to the gastric epithelium. *Mol. Microbiol.* **35**, 1530–1539.
- (8) Garratty, G. (1995) Blood group antigens as tumor markers, parasitic/bacterial/viral receptors, and their association with immunologically important proteins. *Immunol. Invest.* **24**, 213–232.
- (9) Lis, H., and Sharon, N. (1998) Lectins: Carbohydrate-specific proteins that mediate cellular recognition. *Chem. Rev.* **98**, 637–674.
- (10) Singhal, A., and Hakomori, S. (1990) Molecular changes in carbohydrate antigens associated with cancer. *BioEssays* **12**, 223–230.
- (11) Van Dam, G. J., Bergwerff, A. A., Thomas-Oates, J. E., Rotmans, J. P., Kamerling, J. P., Vliegthart, J. F. G., and Deelder, A. M. (1994) The immunologically reactive O-linked polysaccharide chains derived from circulating cathodic antigen isolated from the human blood fluke *Schistosoma mansoni* have Lewis x as repeating unit. *Eur. J. Biochem.* **225**, 467–482.
- (12) Pan, J., Yeager, H., and Cutz, E. (2002) Neuronal developmental marker FORSE-1 identifies a putative progenitor of the pulmonary neuroendocrine cell lineage during lung development. *J. Histochem. Cytochem.* **50**, 1567–1578.
- (13) Sears, P., and Wong, C.-H. (1999) Carbohydrate mimetics: a new strategy for tackling the problem of carbohydrate-mediated biological recognition. *Angew. Chem., Int. Ed.* **38**, 2301–2324.
- (14) Sihorkar, V., and Vyas, S. P. (2001) Potential of polysaccharide anchored liposomes in drug delivery, targeting and immunization. *J. Pharm. Pharmaceut. Sci.* **4**, 138–158.
- (15) Cloninger, M. J. (2002) Biological applications of dendrimers. *Curr. Opin. Chem. Biol.* **6**, 742–748.
- (16) Stiriba, S.-E., Frey, H., and Haag, R. (2002) Dendritic polymers in biomedical applications: From potential to clinical use in diagnostics and therapy. *Angew. Chem., Int. Ed.* **41**, 1329–1334.
- (17) Lichtenstein, J., and Cohen, S. S. (1960) Nucleotides derived from enzymatic digests of nucleic acids of T2, T4, and T6 bacteriophages. *J. Biol. Chem.* **235**, 1134–1141.
- (18) Lehman, I. R., and Pratt, E. A. (1960) On the structure of the glucosylated hydroxymethylcytosine nucleotides of coliphages T2, T4, and T6. *J. Biol. Chem.* **235**, 3254–3259.
- (19) Ehrlich, M., and Ehrlich, K. C. (1981) A novel, highly modified, bacteriophage DNA in which thymine is partly replaced by a phosphoglucuronate moiety covalently bound to 5-(4', 5'-dihydroxypentyl)uracil. *J. Biol. Chem.* **256**, 9966–9972.
- (20) Gommers-Ampt, J. H., Vanleeuwen, F., Debeer, A. L. J., Vliegthart, J. F. G., Dizdaroğlu, M., Kowalak, J. A., Crain, P. F., and Borst, P. (1993)  $\beta$ -D-Glucosyl-hydroxymethyluracil – a novel modified base present in the DNA of the parasitic protozoan trypanosoma-brucei. *Cell* **75**, 1129–1136.
- (21) van Leeuwen, F., Taylor, M. C., Mondragon, A., Moreau, H., Gibson, W., Kieft, R., and Borst, P. (1998)  $\beta$ -D-glucosyl-hydroxymethyluracil is a conserved DNA modification in kinetoplastid protozoans and is abundant in their telomeres. *Proc. Natl. Acad. Sci. U.S.A.* **95**, 2366–2371.
- (22) Borst, P., and van Leeuwen, F. (1997)  $\beta$ -D-Glucosyl-hydroxymethyluracil, a novel base in African trypanosomes and other Kinetoplastida. *Mol. Biochem. Parasitol.* **90**, 1–8.
- (23) van Leeuwen, F., Kieft, R., Cross, M., and Borst, P. (2000) Tandemly repeated DNA is a target for the partial replacement of thymine by  $\beta$ -D-glucosyl-hydroxymethyluracil in *Trypanosoma brucei*. *Mol. Biochem. Parasitol.* **109**, 133–145.
- (24) Akhtar, S., Routledge, A., Patel, R., and Gardiner, J. M. (1995) Synthesis of monomannoside and dimannoside phosphoramidite derivatives for solid-phase conjugation to oligonucleotides. *Tetrahedron Lett.* **36**, 7333–7336.
- (25) de Kort, M., Ebrahimi, E., Wijsman, E. R., van der Marel, G. A., and van Boom, J. H. (1999) Synthesis of oligodeoxynucleotides containing 5-( $\beta$ -D-glycopyranosyloxymethyl)-2'-deoxyuridine, a modified nucleoside in the DNA of *Trypanosoma brucei*. *Eur. J. Org. Chem.*, 2337–2344.



- (26) Sheppard, T. L., Wong, C. H., and Joyce, G. F. (2000) Nucleoglycoconjugates: Design and synthesis of a new class of DNA-carbohydrate conjugates. *Angew. Chem., Int. Ed.* **39**, 3660–3663.
- (27) Matsuura, K., Hibino, M., Yamada, Y., and Kobayashi, K. (2001) Construction of glyco-clusters by self-organization of site-specifically glycosylated oligonucleotides and their cooperative amplification of lectin-recognition. *J. Am. Chem. Soc.* **123**, 357–358.
- (28) Dubber, M., and Frechet, J. M. J. (2003) Solid-phase synthesis of multivalent glycoconjugates on a DNA synthesizer. *Bioconjugate Chem.* **14**, 239–246.
- (29) Matsuura, K., Akasaka, T., Hibino, M., and Kobayashi, K. (2000) Facile synthesis of stable and lectin-recognizable DNA-carbohydrate conjugates via diazo coupling. *Bioconjugate Chem.* **11**, 202–211.
- (30) Dey, S., and Sheppard, T. L. (2001) Ketone-DNA: A versatile postsynthetic DNA decoration platform. *Org. Lett.* **3**, 3983–3986.
- (31) Charles, I., Xue, L. A., and Arya, D. P. (2002) Synthesis of aminoglycoside-DNA conjugates. *Bioorg. Med. Chem. Lett.* **12**, 1259–1262.
- (32) Koeller, K. M., and Wong, C. H. (2000) Synthesis of complex carbohydrates and glycoconjugates: Enzyme-based and programmable one-pot strategies. *Chem. Rev.* **100**, 4465–4493.
- (33) Davis, B. G. (2002) Synthesis of glycoproteins. *Chem. Rev.* **102**, 579–601.
- (34) Flitsch, S. L. (2000) Chemical and enzymatic synthesis of glycopolymers. *Curr. Opin. Chem. Biol.* **4**, 619–625.
- (35) Ichikawa, Y., Lin, Y. C., Dumas, D. P., Shen, G. J., Garciajunceda, E., Williams, M. A., Bayer, R., Ketcham, C., Walker, L. E., Paulson, J. C., and Wong, C. H. (1992) Chemical-enzymatic synthesis and conformational-analysis of sialyl Lewis-X and derivatives. *J. Am. Chem. Soc.* **114**, 9283–9298.
- (36) Seitz, O., and Wong, C. H. (1997) Chemoenzymatic solution- and solid-phase synthesis of *O*-glycopeptides of the mucin domain of MAdCAM-1. A general route to *O*-LacNAc, *O*-sialyl-LacNAc, and *O*-sialyl-Lewis-X peptides. *J. Am. Chem. Soc.* **119**, 8766–8776.
- (37) Halcomb, R. L., Huang, H. M., and Wong, C. H. (1994) Solution-phase and solid-phase synthesis of inhibitors of *Helicobacter-pylori* attachment and E-selectin-mediated leukocyte adhesion. *J. Am. Chem. Soc.* **116**, 11315–11322.
- (38) Matsuda, M. (2001) Heterobifunctional ligands: Practical chemoenzymatic synthesis of a cell adhesive glycopeptide that interacts with both selectins and integrins. *J. Med. Chem.* **44**, 715–724.
- (39) Danishefsky, S. J., Koseki, K., Griffith, D. A., Gervay, J., Peterson, J. M., McDonald, F. E., and Oriyama, T. (1992) Azaglycosylation of complex stannyl alkoxides with glycal-derived iodo sulfonamides: a straightforward synthesis of sialyl-Lewis X antigen and other oligosaccharide domains. *J. Am. Chem. Soc.* **114**, 8331–8333.
- (40) Danishefsky, S. J., Gervay, J., Peterson, J. M., McDonald, F. E., Koseki, K., Oriyama, T., Griffith, D. A., Wong, C. H., and Dumas, D. P. (1992) Remarkable regioselectivity in the chemical glycosylation of glycal acceptors: a concise solution to the synthesis of sialyl-Lewis X glycal. *J. Am. Chem. Soc.* **114**, 8329–8331.
- (41) Corey, E. J., and Roberts, B. E. (1997) Total synthesis of dysidiolide. *J. Am. Chem. Soc.* **119**, 12425–12431.
- (42) Pochet, S., Kansal, V., Destouesse, F., and Sarfati, S. R. (1990) Alkylglycoside carbonates of 3'-azido-3'-deoxythymidine. *Tetrahedron Lett.* **31**, 6021–6024.
- (43) Horton, D. (1973) 2-Acetamido-3,4,6-tri-*O*-acetyl-2-deoxy- $\alpha$ -D-glucopyranosyl chloride. *Organic Synthesis*, pp 1–5, Wiley, New York.
- (44) Bouzide, A., and Sauve, G. (1997) Highly selective silver-(I) oxide mediated monoprotection of symmetrical diols. *Tetrahedron Lett.* **38**, 5945–5948.
- (45) Zemlyakov, A. E., Kakayan, E. S., and Chirva, V. Y. (1989) Synthesis of  $\beta$ -( $\omega$ -aminoalkyl)glycosides of *N*-acetylmuramoyl-L-alanyl-D-isoglutamine. *Bioorg. Khim.* **15**, 1527–1533.
- (46) Richards, E. G. (1975) Use of tables in calculation of absorption, optical rotatory dispersion, and circular dichroism of polyribonucleotides. *Handbook of Biochemistry and Molecular Biology: Nucleic Acids*, 3rd ed., pp 596–603, CRC Press, Cleveland.
- (47) Bhattacharyya, B. R., Ramaswamy, K., and Crane, R. K. (1976) Synthesis of some  $\beta$ -D-glucopyranosides having a hydrophobic aglycon group terminated with a hydrophilic group. *Carbohydr. Res.* **47**, 167–171.
- (48) Charreyre, M. T., Boullanger, P., Pichot, C., Delair, T., Mandrand, B., and Llauro, M. F. (1993) Synthesis of a hexyl methacrylate-terminated disaccharide monomer and study of its radically initiated homo- and copolymerization with styrene. *Makromol. Chem.* **194**, 117–135.
- (49) Ren, T., Zhang, G., and Liu, D. (2001) Synthesis of bifunctional cationic compounds for gene delivery. *Tetrahedron Lett.* **42**, 1007–1010.
- (50) Heathcock, C. H., and Ratcliff, R. (1971) Stereoselective total synthesis of the guaiazulenic sesquiterpenoids  $\alpha$ -bulnesene and bulnesol. *J. Am. Chem. Soc.* **93**, 1746–1757.
- (51) Caruthers, M. H., Barone, A. D., Beaucage, S. L., Dodds, D. R., Fisher, E. F., McBride, L. J., Matteucci, M., Stabinsky, Z., and Tang, J. Y. (1987) Chemical synthesis of deoxyoligonucleotides by the phosphoramidite method. *Methods Enzymol.* **154**, 287–313.
- (52) Weston, B. W., Smith, P. L., Kelly, R. J., and Lowe, J. B. (1992) Molecular cloning of a fourth member of a human  $\alpha$ (1, 3)fucosyltransferase gene family. Multiple homologous sequences that determine expression of the Lewis x, sialyl Lewis x, and difucosyl sialyl Lewis x epitopes. *J. Biol. Chem.* **267**, 24575–24584.
- (53) Geyer, H., Schmitt, S., Wuhler, M., and Geyer, R. (1999) Structural analysis of glycoconjugates by on-target enzymatic digestion and MALDI-TOF-MS. *Anal. Chem.* **71**, 476–482.
- (54) Southern, E. M. (1975) Detection of specific sequences among DNA fragments separated by gel electrophoresis. *J. Mol. Biol.* **98**, 503–517.
- (55) Remoortere, A., Hokke, C. H., van Dam, G. J., van Die, I., Deelder, A. M., and van den Eijnden, D. H. (2000) Various stages of schistosoma express Lewis(x), LacdiNAc, GalNAc $\beta$ 1–4 (Fuc $\alpha$ 1–3)GlcNAc and GalNAc $\beta$ 1–4(Fuc $\alpha$ 1–2Fuc $\alpha$ 1–3)GlcNAc carbohydrate epitopes: detection with monoclonal antibodies that are characterized by enzymatically synthesized neoglycoproteins. *Glycobiology* **10**, 601–609.
- (56) Allendoerfer, K. L., Durairaj, A., Matthews, G. A., and Patterson, P. H. (1999) Morphological domains of Lewis-X/ FORSE–1 immunolabeling in the embryonic neural tube are due to developmental regulation of cell surface carbohydrate expression. *Dev. Biol.* **211**, 208–219.
- (57) Akhtar, S., Hughes, M. D., Khan, A., Bibby, M., Hussain, M., Nawaz, Q., Double, J., and Sayed, P. (2000) The delivery of antisense therapeutics. *Adv. Drug Delivery Rev.* **44**, 3–21.

BC034144P